

# Handbook of NOISE AND VIBRATION CONTROL



MALCOLM J. CROCKER

# HANDBOOK OF NOISE AND VIBRATION CONTROL



## EDITORIAL BOARD

---

**Malcolm J. Crocker**, *Editor-in-Chief*

**Robert J. Bernhard**, West Lafayette, Indiana, USA

**Klaus Brinkmann**, Braunschweig, Germany

**Michael Bockhoff**, Senlis, France

**David J. Ewins**, London, England

**George T. Flowers**, Auburn, Alabama, USA

**Samir N. Y. Gerges**, Florianopolis, Brazil

**Colin H. Hansen**, Adelaide, Australia

**Hanno H. Heller**, Braunschweig, Germany

**Finn Jacobsen**, Lyngby, Denmark

**Daniel J. Inman**, Blacksburg, Virginia, USA

**Nickolay I. Ivanov**, St. Petersburg, Russia

**M. L. Munjal**, Bangalore, India

**P. A. Nelson**, Southampton, England

**David E. Newland**, Cambridge, England

**August Schick**, Oldenburg, Germany

**Andrew F. Seybert**, Lexington, Kentucky, USA

**Eric E. Ungar**, Cambridge, Massachusetts, USA

**Jan W. Verheij**, Delft, The Netherlands

**Henning von Gierke**, Dayton, Ohio, USA

# HANDBOOK OF NOISE AND VIBRATION CONTROL

---

Edited by  
Malcolm J. Crocker



John Wiley & Sons, Inc.

This book is printed on acid-free paper. ∞

Copyright © 2007 by John Wiley & Sons, Inc. All rights reserved

Published by John Wiley & Sons, Inc., Hoboken, New Jersey  
Published simultaneously in Canada

Wiley Bicentennial Logo: Richard J. Pacifico.

No part of this publication may be reproduced, stored in a retrieval system, or transmitted in any form or by any means, electronic, mechanical, photocopying, recording, scanning, or otherwise, except as permitted under Section 107 or 108 of the 1976 United States Copyright Act, without either the prior written permission of the Publisher, or authorization through payment of the appropriate per-copy fee to the Copyright Clearance Center, Inc., 222 Rosewood Drive, Danvers, MA 01923, (978) 750-8400, fax (978) 750-4470, or on the Web at [www.copyright.com](http://www.copyright.com). Requests to the Publisher for permission should be addressed to the Permissions Department, John Wiley & Sons, Inc., 111 River Street, Hoboken, NJ 07030, (201) 748-6011, fax (201) 748-6008, or online at <http://www.wiley.com/go/permission>.

**Limit of Liability/Disclaimer of Warranty:** While the publisher and the author have used their best efforts in preparing this book, they make no representations or warranties with respect to the accuracy or completeness of the contents of this book and specifically disclaim any implied warranties of merchantability or fitness for a particular purpose. No warranty may be created or extended by sales representatives or written sales materials. The advice and strategies contained herein may not be suitable for your situation. You should consult with a professional where appropriate. Neither the publisher nor the author shall be liable for any loss of profit or any other commercial damages, including but not limited to special, incidental, consequential, or other damages.

For general information on our other products and services or for technical support, please contact our Customer Care Department within the United States at (800) 762-2974, outside the United States at (317) 572-3993 or fax (317) 572-4002.

Wiley also publishes its books in a variety of electronic formats. Some content that appears in print may not be available in electronic books. For more information about Wiley products, visit our web site at [www.wiley.com](http://www.wiley.com).

***Library of Congress Cataloging-in-Publication Data:***

Handbook of noise and vibration control / edited by Malcolm J. Crocker.

p. cm.

ISBN 978-0-471-39599-7 (Cloth)

1. Noise—Handbooks, manuals, etc. 2. Vibration—Handbooks, manuals, etc. 3. Noise control—Handbooks, manuals, etc.

I. Crocker, Malcolm J.

TD892.H353 2007

620.2'3—dc22

2007007042

Printed in the United States of America

10 9 8 7 6 5 4 3 2 1

For Ruth

# CONTENTS

---

<b>Foreword</b>	<b>xv</b>
<b>Preface</b>	<b>xvii</b>
<b>Contributors</b>	<b>xix</b>
1. Fundamentals of Acoustics, Noise, and Vibration <i>Malcolm J. Crocker</i>	1
<b>PART I. Fundamentals of Acoustics and Noise</b>	<b>17</b>
2. Theory of Sound—Predictions and Measurement <i>Malcolm J. Crocker</i>	19
3. Sound Sources <i>Philip A. Nelson</i>	43
4. Sound Propagation in Rooms <i>K. Heinrich Kuttruff</i>	52
5. Sound Propagation in the Atmosphere <i>Keith Attenborough</i>	67
6. Sound Radiation from Structures and Their Response to Sound <i>Jean-Louis Guyader</i>	79
7. Numerical Acoustical Modeling (Finite Element Modeling) <i>R. Jeremy Astley</i>	101
8. Boundary Element Modeling <i>D. W. Herrin, T. W. Wu, and A. F. Seybert</i>	116
9. Aerodynamic Noise: Theory and Applications <i>Philip J. Morris and Geoffrey M. Lilley</i>	128
10. Nonlinear Acoustics <i>Oleg V. Rudenko and Malcolm J. Crocker</i>	159
<b>PART II. Fundamentals of Vibration</b>	<b>169</b>
11. General Introduction to Vibration <i>Bjorn A. T. Petersson</i>	171
12. Vibration of Simple Discrete and Continuous Systems <i>Yuri I. Bobrovnikskii</i>	180
13. Random Vibration <i>David E. Newland</i>	205
14. Response of Systems to Shock <i>Charles Robert Welch and Robert M. Ebeling</i>	212

15. Passive Damping <i>Daniel J. Inman</i>	225
16. Structure-Borne Energy Flow <i>Goran Pavić</i>	232
17. Statistical Energy Analysis <i>Jerome E. Manning</i>	241
18. Nonlinear Vibration <i>Lawrence N. Virgin, Earl H. Dowell, and George Flowers</i>	255
<b>PART III. Human Hearing and Speech</b>	<b>269</b>
19. General Introduction to Human Hearing and Speech <i>Karl T. Kalveram</i>	271
20. The Ear: Its Structure and Function, Related to Hearing <i>Hiroshi Wada</i>	277
21. Hearing Thresholds, Loudness of Sound, and Sound Adaptation <i>William A. Yost,</i>	286
22. Speech Production and Speech Intelligibility <i>Christine H. Shadle</i>	293
<b>PART IV. Effects of Noise, Blast, Vibration, and Shock on People</b>	<b>301</b>
23. General Introduction to Noise and Vibration Effects on People and Hearing Conservation <i>Malcolm J. Crocker</i>	303
24. Sleep Disturbance due to Transportation Noise Exposure <i>Lawrence S. Finegold, Alain G. Muzet, and Bernard F. Berry</i>	308
25. Noise-Induced Annoyance <i>Sandford Fidell</i>	316
26. Effects of Infrasound, Low-Frequency Noise, and Ultrasound on People <i>Norm Broner</i>	320
27. Auditory Hazards of Impulse and Impact Noise <i>Donald Henderson and Roger P. Hamernik</i>	326
28. Effects of Intense Noise on People and Hearing Loss <i>Rickie R. Davis and William J. Murphy</i>	337
29. Effects of Vibration on People <i>Michael J. Griffin</i>	343
30. Effects of Mechanical Shock on People <i>A. J. Brammer</i>	354
31. Hearing Protectors <i>Samir N. Y. Gerges and John G. Casali</i>	364
32. Development of Standards and Regulations for Occupational Noise <i>Alice H. Suter</i>	377
33. Hearing Conservation Programs <i>John Erdreich</i>	383
34. Rating Measures, Descriptors, Criteria, and Procedures for Determining Human Response to Noise <i>Malcolm J. Crocker</i>	394

<b>PART V. Noise and Vibration Transducers, Analysis Equipment, Signal Processing, and Measuring Techniques</b>	<b>415</b>
35. General Introduction to Noise and Vibration Transducers, Measuring Equipment, Measurements, Signal Acquisition, and Processing <i>Malcolm J. Crocker</i>	417
36. Acoustical Transducer Principles and Types of Microphones <i>Gunnar Rasmussen and Per Rasmussen</i>	435
37. Vibration Transducer Principles and Types of Vibration Transducers <i>Colin H. Hansen</i>	444
38. Sound Level Meters <i>George S. K. Wong</i>	455
39. Noise Dosimeters <i>Chucri A. Kardous</i>	465
40. Analyzers and Signal Generators <i>Henrik Herlufsen, Svend Gade, and Harry K. Zaveri</i>	470
41. Equipment for Data Acquisition <i>Zhuang Li and Malcolm J. Crocker</i>	486
42. Signal Processing <i>Allan G. Piersol</i>	493
43. Noise and Vibration Measurements <i>Pedro R. Valletta and Malcolm J. Crocker</i>	501
44. Determination of Sound Power Level and Emission Sound Pressure Level <i>Hans G. Jonasson</i>	526
45. Sound Intensity Measurements <i>Finn Jacobsen</i>	534
46. Noise and Vibration Data Analysis <i>Robert B. Randall</i>	549
47. Modal Analysis and Modal Testing <i>David J. Ewins</i>	565
48. Machinery Condition Monitoring <i>Robert B. Randall</i>	575
49. Wavelet Analysis of Vibration Signals <i>David E. Newland</i>	585
50. Use of Near-Field Acoustical Holography in Noise and Vibration Measurements <i>Earl G. Williams</i>	598
51. Calibration of Measurement Microphones <i>Erling Frederiksen</i>	612
52. Calibration of Shock and Vibration Transducers <i>Torben Rask Licht</i>	624
53. Metrology and Traceability of Vibration and Shock Measurements <i>Hans-Jürgen von Martens</i>	633
<b>PART VI. Principles of Noise and Vibration Control and Quiet Machinery Design</b>	<b>647</b>
54. Introduction to Principles of Noise and Vibration Control <i>Malcolm J. Crocker</i>	649

55. Noise and Vibration Source Identification <i>Malcolm J. Crocker</i>	668
56. Use of Enclosures <i>Jorge P. Arenas and Malcolm J. Crocker</i>	685
57. Use of Sound-Absorbing Materials <i>Malcolm J. Crocker and Jorge P. Arenas</i>	696
58. Use of Barriers <i>Jorge P. Arenas</i>	714
59. Use of Vibration Isolation <i>Eric E. Ungar</i>	725
60. Damping of Structures and Use of Damping Materials <i>Eric E. Ungar</i>	734
61. Dynamic Vibration Absorbers <i>Leif Kari</i>	745
62. Rotor Balancing and Unbalance-Caused Vibration <i>Maurice L. Adams, Jr.</i>	753
63. Active Noise Control <i>Stephen J. Elliott</i>	761
64. Active Vibration Control <i>Christopher Fuller</i>	770
65. Microelectromechanical Systems (MEMS) Sensors for Noise and Vibration Applications <i>James J. Allen</i>	785
66. Design of Low-Noise Machinery <i>Michael Bockhoff</i>	794
67. Psychoacoustics and Product Sound Quality <i>Malcolm J. Crocker</i>	805
<b>PART VII. Industrial and Machine Element Noise and Vibration Sources—Prediction and Control</b>	<b>829</b>
68. Machinery Noise and Vibration Sources <i>Malcolm J. Crocker</i>	831
69. Gear Noise and Vibration Prediction and Control Methods <i>Donald R. Houser</i>	847
70. Types of Bearings and Means of Noise and Vibration Prediction and Control <i>George Zusman</i>	857
71. Centrifugal and Axial Fan Noise Prediction and Control <i>Gerald C. Lauchle</i>	868
72. Types of Electric Motors and Noise and Vibration Prediction and Control Methods <i>George Zusman</i>	885
73. Pumps and Pumping System Noise and Vibration Prediction and Control <i>Mirko Čudina</i>	897



## CONTENTS

xi

74. Noise Control of Compressors <i>Malcolm J. Crocker</i>	910
75. Valve-Induced Noise: Its Cause and Abatement <i>Hans D. Baumann and Mats Åbom</i>	935
76. Hydraulic System Noise Prediction and Control <i>Nigel Johnston</i>	946
77. Furnace and Burner Noise Control <i>Robert A. Putnam, Werner Krebs, and Stanley S. Sattinger</i>	956
78. Metal-Cutting Machinery Noise and Vibration Prediction and Control <i>Joseph C. S. Lai</i>	966
79. Woodworking Machinery Noise <i>Knud Skovgaard Nielsen and John S. Stewart</i>	975
80. Noise Abatement of Industrial Production Equipment <i>Evgeny Rivin</i>	987
81. Machine Tool Noise, Vibration, and Chatter Prediction and Control <i>Lars Håkansson, Sven Johansson, and Ingvar Claesson</i>	995
82. Sound Power Level Predictions for Industrial Machinery <i>Robert D. Bruce, Charles T. Moritz, and Arno S. Bommer</i>	1001

## **PART VIII. Transportation Noise and Vibration—Sources, Prediction, and Control**

**1011**

83. Introduction to Transportation Noise and Vibration Sources <i>Malcolm J. Crocker</i>	1013
84. Internal Combustion Engine Noise Prediction and Control—Diesel and Gasoline Engines <i>Thomas E. Reinhart</i>	1024
85. Exhaust and Intake Noise and Acoustical Design of Mufflers and Silencers <i>Hans Bodén and Ragnar Glav</i>	1034
86. Tire/Road Noise—Generation, Measurement, and Abatement <i>Ulf Sandberg and Jerzy A. Ejsmont</i>	1054
87. Aerodynamic Sound Sources in Vehicles—Prediction and Control <i>Syed R. Ahmed</i>	1072
88. Transmission and Gearbox Noise and Vibration Prediction and Control <i>Jiri Tuma</i>	1086
89. Jet Engine Noise Generation, Prediction, and Control <i>Dennis L. Huff and Edmane Envia</i>	1096
90. Aircraft Propeller Noise—Sources, Prediction, and Control <i>F. Bruce Metzger and F. Farassat</i>	1109
91. Helicopter Rotor Noise: Generation, Prediction, and Control <i>Hanno H. Heller and Jianping Yin</i>	1120
92. Brake Noise Prediction and Control <i>Michael J. Brennan and Kihong Shin</i>	1133

93.	Wheel–Rail Interaction Noise Prediction and Its Control <i>David J. Thompson</i>	1138
<b>PART IX. Interior Transportation Noise and Vibration Sources—Prediction and Control</b>		<b>1147</b>
94.	Introduction to Interior Transportation Noise and Vibration Sources <i>Malcolm J. Crocker</i>	1149
95.	Automobile, Bus, and Truck Interior Noise and Vibration Prediction and Control <i>Robert J. Bernhard, Mark Moeller, and Shaobo Young</i>	1159
96.	Noise Management of Railcar Interior Noise <i>Glenn H. Frommer</i>	1170
97.	Interior Noise in Railway Vehicles—Prediction and Control <i>Henrik W. Thrane</i>	1178
98.	Noise and Vibration in Off-Road Vehicle Interiors—Prediction and Control <i>Nickolay Ivanov and David Copley</i>	1186
99.	Aircraft Cabin Noise and Vibration Prediction and Passive Control <i>John F. Wilby</i>	1197
100.	Aircraft Cabin Noise and Vibration Prediction and Active Control <i>Sven Johansson, Lars Håkansson, and Ingvar Claesson</i>	1207
101.	Noise Prediction and Prevention on Ships <i>Raymond Fischer and Robert D. Collier</i>	1216
<b>PART X. Noise and Vibration Control in Buildings</b>		<b>1233</b>
102.	Introduction—Prediction and Control of Acoustical Environments in Building Spaces <i>Louis C. Sutherland</i>	1235
103.	Room Acoustics <i>Colin H. Hansen</i>	1240
104.	Sound Absorption in Rooms <i>Colin H. Hansen</i>	1247
105.	Sound Insulation—Airborne and Impact <i>Alfred C. C. Warnock</i>	1257
106.	Ratings and Descriptors for the Built Acoustical Environment <i>Gregory C. Tocci</i>	1267
107.	ISO Ratings and Descriptors for the Built Acoustical Environment <i>Heinrich A. Metzen</i>	1283
108.	Acoustical Design of Office Work Spaces and Open-Plan Offices <i>Carl J. Rosenberg</i>	1297
109.	Acoustical Guidelines for Building Design and Noise Control <i>Chris Field and Fergus Fricke</i>	1307
110.	Noise Sources and Propagation in Ducted Air Distribution Systems <i>Howard F. Kingsbury</i>	1316

## CONTENTS

xiii

111.	Aerodynamic Sound Generation in Low Speed Flow Ducts <i>David J. Oldham and David D. Waddington</i>	1323
112.	Noise Control for Mechanical and Ventilation Systems <i>Reginald H. Keith</i>	1328
113.	Noise Control in U.S. Building Codes <i>Gregory C. Tocci</i>	1348
114.	Sound Insulation of Residential Housing—Building Codes and Classification Schemes in Europe <i>Birgit Rasmussen</i>	1354
115.	Noise in Commercial and Public Buildings and Offices—Prediction and Control <i>Chris Field and Fergus Fricke</i>	1367
116.	Vibration Response of Structures to Fluid Flow and Wind <i>Malcolm J. Crocker</i>	1375
117.	Protection of Buildings from Earthquake-Induced Vibration <i>Andreas J. Kappos and Anastasios G. Sextos</i>	1393
118.	Low-Frequency Sound Transmission between Adjacent Dwellings <i>Barry M. Gibbs and Sophie Maluski</i>	1404
<b>PART XI. Community and Environmental Noise and Vibration Prediction and Control</b>		<b>1411</b>
119.	Introduction to Community Noise and Vibration Prediction and Control <i>Malcolm J. Crocker</i>	1413
120.	Exterior Noise of Vehicles—Traffic Noise Prediction and Control <i>Paul R. Donovan and Richard Schumacher</i>	1427
121.	Rail System Environmental Noise Prediction, Assessment, and Control <i>Brian Hemsworth</i>	1438
122.	Noise Attenuation Provided by Road and Rail Barriers, Earth Berms, Buildings, and Vegetation <i>Kirill Horoshenkov, Yiu W. Lam, and Keith Attenborough</i>	1446
123.	Ground-Borne Vibration Transmission from Road and Rail Systems: Prediction and Control <i>Hugh E. M. Hunt and Mohammed F. M. Hussein</i>	1458
124.	Base Isolation of Buildings for Control of Ground-Borne Vibration <i>James P. Talbot</i>	1470
125.	Aircraft and Airport Noise Prediction and Control <i>Nicholas P. Miller, Eugene M. Reindel, and Richard D. Horonjeff</i>	1479
126.	Off-Road Vehicle and Construction Equipment Exterior Noise Prediction and Control <i>Lyudmila Drozdova, Nickolay Ivanov, and Gennadiy H. Kurtsev</i>	1490
127.	Environmental Noise Impact Assessment <i>Marion A. Burgess and Lawrence S. Finegold</i>	1501
128.	Industrial and Commercial Noise in the Community <i>Dietrich Kuehner</i>	1509

129. Building Site Noise	1516
<i>Uwe Trautmann</i>	
130. Community Noise Ordinances	1525
<i>J. Luis Bento Coelho</i>	
<b>Reviewers List</b>	1533
<b>Glossary</b>	1537
<b>Index</b>	1557

## FOREWORD

---

When the term *noise control* became prevalent in the middle of the last century, I didn't like it very much. It seemed to me to regard all sound from products as undesirable, to be treated by the add-ons in the form of barriers, silencers, and isolators. Now I know that many practitioners of this art are more sophisticated than that, as a perusal of the material in this excellent book will show. Therefore, we have to be appreciative of the work by the editor and the assembly of expert authors he has brought together. They have shown that in order to make products quieter and even more pleasing to listen to, you have to attack the noise in the basic design process, and that requires understanding basic physics of sound generation and propagation. It also requires that we understand how people are affected by sounds in both undesirable and favorable ways.

The early chapters discuss fundamental ideas of sound, vibration, propagation, and human response. Most active practitioners in noise control will already have this background, but it is common for an engineer who has a background in, say, heat transfer to be asked to become knowledgeable in acoustics and work on product noise problems. Lack of background can be made up by attending one or more courses in acoustics and noise control, and this book can be a powerful addition in that process. Indeed, the first five major sections of the book provide adequate material for such an educational effort.

Most engineers will agree that if possible it is better to keep the noise from being generated in the first place rather than blocking or absorbing it after it has already been generated. The principles for designing quieter components such as motors, gears, and fans are presented in the next chapters. When noise is reduced by add-ons that increase product weight and size, or interfere with cooling and make material choices more difficult, the design and/or selection of quiet components becomes attractive. These chapters will help the design engineer to get started on the process.

The reliance on add-ons continues to be a large part of noise control activity, and that subject is covered here in chapters on barriers, sound absorbers, and vibration isolation and damping. The relatively new topic of active noise reduction is also here. These add-on treatments still have to be designed to provide the performance needed, and much of the time those responsible for reducing product sound do not have the ability to redesign a noisy component; so an add-on may be the only practical choice.

Transportation is a source of noise for the owner/user of vehicles and for bystanders as well. As users, most of us want quiet pleasing sounding interiors, and the technology for achieving that sound is widely employed. It is in this area in particular that ideas for sound quality—achieving the right sound for the product—have received the greatest emphasis.

The sound of a dishwasher in the kitchen directly impacts the owner/user of that product, but the owner/user also gets the benefit of the product. But in many cases, the effects of product noise are also borne by others who do not get the benefit. The sounds of aircraft, automobile traffic, trains, construction equipment, and industrial plants impact not only the beneficiaries of those devices but the bystanders as well. In these cases, national, state, and local governments have a role to play as honest brokers, trying to balance the costs and benefits of noise control alternatives. Should highway noise be mitigated by barriers or new types of road surfaces? Why do residents on one side of a street receive noise reduction treatments for aircraft noise at their house while those across the street do not, simply because a line

has to be drawn somewhere? And should aircraft noise be dealt with by insulating homes or by doing more research to make aircraft quieter? How is the balance to be struck between locomotive whistles that disturb neighbors and better crossing safety?

These policy issues are not easy, but to the credit of the editor and the authors, the book brings such issues to the fore in a final set of chapters. The editor and the authors are to be congratulated for tackling this project with professionalism and dedication, and bringing to all of us a terrific book on an important subject.

Richard H. Lyon

*Belmont, Massachusetts*

## PREFACE

---

This book is designed to fill the need for a comprehensive resource on noise and vibration control. Several books and journals on noise control, and others on vibration control already exist. So why another book and why combine both topics in one book? First, most books cover only a limited number of topics in noise or vibration and in many cases their treatment has become dated. Second is the fact that noise and vibration have a close physical relationship. Vibrating systems make noise, and noise makes structural systems vibrate. There are several other reasons to include both topics in one book. People are adversely affected by both noise and vibration and, if sufficiently intense, both noise and vibration can permanently hurt people. Also, structural systems, if excited by excessive noise and vibration over sufficient periods of time, can fatigue and fail. There are other reasons as well. Because noise and vibration are both dynamic processes, similar measurement systems, signal processing methods and data analysis techniques can be used to study both phenomena. In the prediction of noise and vibration, similar analytical and numerical approaches such as the finite element and boundary element methods and the statistical energy analysis approach can also be used for both.

Considerable progress has been made in recent years in making quieter machinery, appliances, vehicles and aircraft. This is particularly true for mass produced items for which development costs can be spread over a large production run and where sufficient expenditures on noise and vibration reduction can be justified. Significant progress has also been made in the case of some very expensive first cost machines such as passenger aircraft, in which large sums have been spent successfully to make them quieter. In many such cases, most of the simple noise and vibration reduction measures have already been taken and further noise and vibration reduction involves much more sophisticated experimental and theoretical approaches such as those described in some of the chapters in this book. Some problems such as those involving community noise, and noise and vibration control of buildings, can be overcome with well known and less sophisticated approaches as described in other chapters, provided the techniques are properly applied.

This book was conceived to meet the needs of many different individuals with varying backgrounds as they confront a variety of noise and vibration problems. First a detailed outline for the handbook was prepared and an editorial board selected whose members provided valuable assistance in refining the outline and in making suggestions for the choice of authors. By the time the authors were selected, the complete handbook outline, including the detailed contents for each chapter, was well advanced. This was supplied to each author. This approach made it possible to minimize overlap of topics, and to ensure adequate cross referencing.

To prevent the handbook becoming too long, each author was given a page allowance. Some chapters such as those on compressors, fans, and mufflers were given a greater page allowance because so many are in use around the world. Each author was asked to write at a level accessible to general readers and not just to specialists and to provide suitable, up-to-date references for readers who may wish to study the subject in more depth. I believe that most authors have responded admirably to the challenge.

The handbook is divided into 11 main parts and contains a total of 130 chapters. Three additional parts contain the glossary, index and list of reviewers. Each of the 11 main parts starts with a general review

chapter which serves as an introduction to that part and also at the same time helps in cross-referencing the topics covered in that part of the book and other relevant chapters throughout the handbook. These introductory review chapters also sometimes cover additional topics not discussed elsewhere in the book. It was impossible to provide extended discussion of all topics relating to noise, shock, and vibration in this volume. Readers will find many topics treated in more detail in my *Encyclopedia of Acoustics* (1997) and *Handbook of Acoustics* (1998), both published by John Wiley and Sons, New York. The first chapter in the handbook provides an introduction to some of the fundamentals of acoustics, noise, and vibration for those who do not feel it necessary to study the more advanced acoustics and vibration treatments provided in Parts 1 and 2 of the book.

The division of the chapters into 11 main parts of the book is somewhat arbitrary, but at the same time logical. Coverage includes fundamentals of acoustics and noise; fundamentals of vibration; human hearing and speech; effects of noise, blast, vibration and shock on people; noise and vibration analysis equipment, signal processing and measurements; industrial and machine element noise and vibration sources; exterior and interior transportation vehicle noise and vibration sources; noise and vibration control of buildings, and community noise and vibration. The book concludes with a comprehensive glossary and index and a list of the chapter reviewers. The glossary was compiled by Zhuang Li and the editor, with substantial and valuable inputs also from all of the authors of the book. In addition, although the index was mostly my own work with valuable assistance provided by my staff, again authors provided important suggestions for the inclusion of key words.

I am very much indebted to more than 250 reviewers who donated their time to read the first drafts of all of the chapters including my own and who made very valuable comments and suggestions for improvement. Their anonymous comments were supplied to the authors, to help them as they finalized their chapters. Many of the reviewers were members of the International Institute of Acoustics and Vibration, who were able to supply comments and suggestions from a truly international perspective. The international character of this handbook becomes evident when one considers the fact that the authors are from 18 different countries and the reviewers from over 30 countries.

In view of the international character of this book, the authors were asked to use metric units and recognized international terminology wherever possible. This was not always possible where tables or figures are reproduced from other sources in which the American system of units is still used. The acoustics and vibration terminology recommended by the International Standardization Organisation (ISO) has also been used wherever possible. So, for example, terminology such as sound level, dB(A) is replaced by A-weighted sound pressure level, dB; and sound power level, dB(A) is replaced by A-weighted sound power level, dB. This terminology, although sometimes more cumbersome, is preferred in this book because it reduces potential confusion between sound pressure levels and sound power levels and does not mix up the A-weighting with the decibel unit. Again it has not always been possible to make these changes in the reproduction of tables and figures of others.

I would like to thank all the authors who contributed chapters to this book for their hard work. In many cases the editorial board provided considerable help. Henning von Gierke, in particular, was very insistent that vibration be given equal weight to noise and I followed his wise advice closely. I wish to thank my assistants, Angela Woods, Elizabeth Green and especially Renata Gallyamova, all of whom provided really splendid assistance in making this book possible. I am also indebted to my students, in particular Zhuang Li and Cédric Béchet, who helped proofread and check the final versions of my own chapters and many others throughout this book. The editorial staff at Wiley must also be thanked, especially Bob Hilbert, who guided this *Handbook* to a successful conclusion. Last and not least, I should like to thank my wife Ruth and daughters Anne and Elizabeth for their support, patience and understanding during the preparation of this book.

MALCOLM J. CROCKER



## CONTRIBUTORS

---

**Mats Åbom**, The Marcus Wallenberg Laboratory for Sound and Vibration Research, KTH—The Royal Institute of Technology, SE-100 44 Stockholm, Sweden

**Maurice L. Adams, Jr.**, Mechanical & Aerospace Engineering, The Case School of Engineering, Case Western Reserve University, Cleveland, Ohio 44106–7222, United States

**Syed R. Ahmed**, German Aerospace Research Establishment (DLR) (retired), AS/TA, Lilienthalpl. 7, 38108, Braunschweig, Germany

**James J. Allen**, MEMS Devices and Reliability Physics, Sandia National Laboratories, Albuquerque, New Mexico 87185, United States

**Jorge P. Arenas**, Institute of Acoustics, Universidad Austral de Chile, Campus Miraflores, P.O. Box 567, Valdivia, Chile

**R. Jeremy Astley**, Institute of Sound and Vibration Research, University of Southampton, Southampton, SO17 1BJ, United Kingdom

**Keith Attenborough**, Department of Engineering, The University of Hull, Cottingham Road, Hull HU6 7RX, United Kingdom

**Hans D. Baumann**, 3120 South Ocean Boulevard, No. 3301, Palm Beach, Florida 33480, United States

**J. Luis Bento Coelho**, CAPS—Instituto Superior Técnico, 1049–001 Lisbon, Portugal

**Robert J. Bernhard**, School of Mechanical Engineering, Purdue University, West Lafayette, Indiana 47907, United States

**Bernard F. Berry**, Berry Environmental Ltd., 49 Squires Bridge Road, Shepperton, Surrey TW17 0JZ, United Kingdom

**Yuri I. Bobrovnikskii**, Department of Vibroacoustics, Mechanical Engineering Research Institute, Russian Academy of Sciences, Moscow 101990, Russia

**Michael Bockhoff**, Ingénierie Bruit et Vibrations, Centre Technique des Industries Mécaniques (CETIM), 60300 Senlis, France

**Hans Bodén**, The Marcus Wallenberg Laboratory for Sound and Vibration Research, Department of Aeronautical and Vehicle Engineering, KTH—The Royal Institute of Technology, SE-100 44, Stockholm, Sweden

**A. J. Brammer**, Ergonomic Technology Center, University of Connecticut Health Center, Farmington, Connecticut, United States, and Enviro-Health Solutions, Ottawa, Ontario, Canada

**Michael J. Brennan**, Institute of Sound and Vibration Research, University of Southampton, Southampton, SO17 1BJ, United Kingdom

**Norm Broner**, National Practice Leader—Acoustics, Sinclair Knight Merz, Melbourne 3143, Australia

**Robert D. Bruce**, CSTI Acoustics, 15835 Park Ten Place, Suite 105, Houston, Texas 77084-5131, United States

**Marion A. Burgess**, Acoustics and Vibration Unit, School of Aerospace, Civil and Mechanical Engineering, The University of New South Wales at the Australian Defence Force Academy, Canberra ACT 2600, Australia

**Arno S. Bommer**, CSTI Acoustics, 15835 Park Ten Place, Suite 105, Houston, Texas 77084-5131, United States

**John G. Casali**, Department of Industrial and Systems Engineering, Virginia Polytechnic Institute and State University, Blacksburg, Virginia 24061, United States

**Ingvar Claesson**, Department of Signal Processing, Blekinge Institute of Technology, S-372 25 Ronneby, Sweden

**Robert D. Collier**, Thayer School of Engineering, 8000 Commings Hall, Dartmouth College, Hanover, New Hampshire 03755, United States

**David C. Copley**, Sound and Cooling Research, Caterpillar Inc., Peoria, Illinois 61656, United States

**Malcolm J. Crocker**, Department of Mechanical Engineering, Auburn University, Auburn, Alabama 36849, United States

**Mirko Čudina**, Laboratory for Pumps, Compressors and Technical Acoustics, University of Ljubljana, Faculty of Mechanical Engineering, 1000 Ljubljana, Slovenia

**Rickie R. Davis**, National Institute for Occupational Safety and Health, 4676 Columbia Parkway, Cincinnati, Ohio 45226, United States

**Paul R. Donavan**, Illingworth and Rodkin Inc., 505 Petaluma Boulevard, South, Petaluma, California 94952-5128, United States

**Earl H. Dowell**, Department of Mechanical Engineering, Duke University, Durham, North Carolina 27708, United States

**Luydmila Drozdova**, Environmental Engineering Department, Baltic State Technical University, 1st Krasnourmeyskaya Street, 1, 190005, St. Petersburg, Russia

**Robert M. Ebeling**, Information Technology Laboratory, U.S. Army Engineer Research and Development Center, 3909 Halls Ferry Road, Vicksburg, Mississippi 39180, United States

**Jerzy A. Ejsmont**, Mechanical Engineering Faculty, Technical University of Gdansk, ul. Narutowicza 11/12, 80-952 Gdansk, Poland

**Stephen J. Elliot**, Signal Processing & Control Group, Institute of Sound and Vibration Research, University of Southampton, Southampton, SO17 1BJ, United Kingdom

**Edmane Envia**, Acoustics Branch, NASA Glenn Research Center, 21000 Brookpark Road, Cleveland, Ohio 44135, United States

**John Erdreich**, Ostergaard Acoustical Associates, 200 Executive Drive, West Orange, New Jersey 07052, United States

**David J. Ewins**, Mechanical Engineering Department, Imperial College London, London, SW7 2AZ, United Kingdom

**F. Farassat**, NASA Langley Research Center, Hampton, Virginia 23681-2199, United States

**Sanford Fidell**, Fidell Associates, Inc., 23139 Erwin Street, Woodland Hills, California 91367, United States

**Chris Field**, Arup Acoustics San Francisco, 901 Market Street, San Francisco, California 94103, United States

**Lawrence S. Finegold**, Finegold & So, Consultants, 1167 Bournemouth Court, Centerville, Ohio 45459-2647, United States

**Raymond Fischer**, Noise Control Engineering, Inc., Billerica, Massachusetts 01821, United States

**George Flowers**, Department of Mechanical Engineering, Auburn University, Auburn, Alabama 36849, United States

**Erling Frederiksen**, Danish Primary Laboratory of Acoustics (DPLA), and Brüel & Kjær, 2850 Naerum, Denmark

**Fergus R. Fricke**, Faculty of Architecture Design and Planning, University of Sydney, Sydney, New South Wales 2006, Australia

**Glenn H. Frommer**, Mass Transit Railway Corporation Ltd, Telford Plaza, Kowloon Bay, Kowloon, Hong Kong

**Christopher Fuller**, Department of Mechanical Engineering, Virginia Polytechnic Institute and State University, Blacksburg, Virginia 24061, United States

**Svend Gade**, Brüel & Kjær Sound & Vibration Measurement A/S, 2850 Nærum, Denmark

**Samir N. Y. Gerges**, Mechanical Engineering Department, Federal University of Santa Catarina (UFSC), Campus Universitário, Trindade, Florianópolis, Santa Catarina, Brazil, 88040-900

**Barry M. Gibbs**, Acoustics Research Unit, School of Architecture and Building Engineering, University of Liverpool, Liverpool, L69 3BX United Kingdom

**Ragnar Glav**, The Marcus Wallenberg Laboratory for Sound and Vibration Research, Department of Aeronautical and Vehicle Engineering, KTH—The Royal Institute of Technology, SE-100 44, Stockholm, Sweden

**Michael J. Griffin**, Human Factors Research Unit, Institute of Sound and Vibration Research, University of Southampton, Southampton SO17 1BJ, United Kingdom

**Jean-Louis Guyader**, Vibration and Acoustics Laboratory, National Institute of Applied Sciences of Lyon, Villeurbanne, France 69621

**Lars Håkansson**, Department of Signal Processing, Blekinge Institute of Technology, S-372 25 Ronneby, Sweden

**Roger P. Hamernik**, Department of Communication Disorders, State University of New York at Plattsburgh, Plattsburgh, New York 12901, United States

**Colin H. Hansen**, School of Mechanical Engineering, University of Adelaide, Adelaide, South Australia 5005, Australia

**Hanno H. Heller**, German Aerospace Center (DLR), Institute of Aerodynamics and Flow

Technologies (Technical Acoustics), D-38108 Braunschweig, Germany

**Brian Hemsworth**, Noise Consultant, 16 Whistlestop Close, Micklegate, Derby DE3 9DA, United Kingdom

**Donald Henderson**, Center for Hearing and Deafness, State University of New York at Buffalo, Buffalo, New York 14214, United States

**Henrik Herlufsen**, Brüel & Kjær Sound & Vibration Measurement A/S, 2850 Nærum, Denmark

**D. W. Herrin**, Department of Mechanical Engineering, University of Kentucky, Lexington, Kentucky 40506-0503, United States

**Richard D. Horonjeff**, Consultant in Acoustics and Noise Control, 81 Liberty Square Road 20-B, Boxborough, Massachusetts 01719, United States

**Kirill Horoshenkov**, School of Engineering, Design and Technology, University of Bradford, Bradford BD7 1DP, West Yorkshire, United Kingdom

**Donald R. Houser**, Gear Dynamics and Gear Noise Research Laboratory, The Ohio State University, Columbus, Ohio 43210, United States

**Dennis L. Huff**, NASA Glenn Research Center, 21000 Brookpark Road, Cleveland, Ohio 44135, United States

**Hugh E. M. Hunt**, Engineering Department, Cambridge University, Trumpington Street, Cambridge CB2 1PZ, United Kingdom

**Mohammed F. M. Hussein**, School of Civil Engineering, University of Nottingham, Nottingham, NG7 2RD, United Kingdom

**Daniel J. Inman**, Department of Mechanical Engineering, Virginia Polytechnic Institute and State University, Blacksburg, Virginia 24061, United States

**Nickolay I. Ivanov**, Department of Environmental Engineering, Baltic State Technical University, 1st Krasnoarmeyskaya Street, 1, 190005 St. Petersburg, Russia

**Finn Jacobsen**, Acoustic Technology, Ørsted DTU, Technical University of Denmark, DK-2800 Kgs. Lyngby, Denmark

**Sven Johansson**, Department of Signal Processing, Blekinge Institute of Technology, 5-372 25 Ronneby, Sweden

**Nigel Johnston**, Department of Mechanical Engineering, University of Bath, Bath, BA2 7AY, United Kingdom

**Hans G. Jonasson**, SP Technical Research Institute of Sweden, SE-501 15 Borås, Sweden

**Karl T. Kalveram**, Institute of Experimental Psychology, University of Duesseldorf, 40225 Duesseldorf, Germany

**Andreas J. Kappos**, Department of Civil Engineering, Aristotle University of Thessaloniki, 54124, Thessaloniki, Greece

**Chucri A. Kardous**, Hearing Loss Prevention Section, National Institute for Occupational Safety and Health, Cincinnati, Ohio 45226, United States

**Leif Kari**, The Marcus Wallenberg Laboratory for Sound and Vibration Research, KTH—The Royal Institute of Technology, SE-100 44 Stockholm, Sweden

**Reginald H. Keith**, Hoover & Keith, Inc., 11391 Meadowglen, Suite D, Houston, Texas 77082, United States

**Howard F. Kingsbury**, State College, Pennsylvania, United States

**Werner Krebs**, Siemens AG, PG G251, Mellinghofer Str. 55, 45473 Mülheim an der Ruhr, Germany

**Dietrich Kuehner**, de BAKOM GmbH, Bergstrasse 36, D-51519 Odenthal, Germany

**Gennadiy M. Kurtsev**, Environmental Engineering Department, Baltic State Technical University, 1st Krasnoarmeyskaya Street, 1, 190005 St. Petersburg, Russia

**K. Heinrich Kuttruff**, Institute of Technical Acoustics, RWTH Aachen University, D 52056 Aachen, Germany

**Joseph C. S. Lai**, Acoustics & Vibration Unit, School of Aerospace, Civil and Mechanical Engineering, The University of New South Wales at the Australian Defence Force Academy, Canberra, ACT 2600, Australia.

**Yiu W. Lam**, Acoustics Research Centre, School of Computing, Science and Engineering, University of Salford, Greater Manchester, M5 4WT, United Kingdom

**Gerald C. Lauchle**, Graduate Program in Acoustics, Pennsylvania State University, University Park, Pennsylvania 16802, United States

**Zhuang Li**, Spectra Quest, Inc., 8201 Hermitage Road, Richmond, Virginia 23228, United States

**Torben Rask Licht**, Brüel & Kjær, Skodborgvej 307, DK-2850 Naerum, Denmark

**Geoffrey M. Lilley**, School of Engineering Sciences, University of Southampton, SO17 1BJ, United Kingdom

**Sophie Maluski**, School of Computer Science and Engineering, University of Salford, Greater Manchester M5 4W1, United Kingdom

**Jerome E. Manning**, Cambridge Collaborative, Inc., 689 Concord Ave, Cambridge, Massachusetts 01742, United States

**Heinrich A. Metzen**, DataKustik GmbH, Gewerbering 5, 86926 Greifenberg, Germany

**F. Bruce Metzger**, Metzger Technology Services, Simsbury, Connecticut 06070, United States

**Mark Moeller**, Spirit AeroSystems, Wichita, Kansas, United States

**Nicholas P. Miller**, Harris Miller Miller & Hanson Inc., 77 South Bedford Street, Burlington, Massachusetts 01803

**Charles T. Moritz**, Blachford, Inc., West Chicago, Illinois 60185, United States

**Philip J. Morris**, Department of Aerospace Engineering, Pennsylvania State University, University Park, Pennsylvania 16802, United States

**William J. Murphy**, National Institute for Occupational Safety and Health, 4676 Columbia Parkway, Cincinnati, Ohio 45226-1998, United States

**Alain G. Muzet**, Centre d'Etudes de Physiologie Appliquée du CNRS, 21, rue Becquerel, F-67087 Strasbourg Cedex, France

**Philip A. Nelson**, Institute of Sound and Vibration Research, University of Southampton, Southampton, SO17 1BJ, United Kingdom

**David E. Newland**, Engineering Department, Cambridge University, Trumpington Street, Cambridge, CB2 1PZ, United Kingdom

**David J. Oldham**, Acoustics Research Unit, School of Architecture and Building Engineering, University of Liverpool, Liverpool, L69 3BX, United Kingdom

**Goran Pavić**, INSA Laboratoire Vibrations Acoustique (LVA), Batiment 303-20, Avenue Albert Einstein 69621, Villeurbanne Cedex, France

**Bjorn A. T. Petersson**, Institute of Fluid Mechanics and Engineering Acoustics, Technical University of Berlin, Einsteinufer 25, D-10587 Berlin, Germany

**Allan G. Piersol**, Piersol Engineering Company, 23021 Brenford Street, Woodland Hills, California 91364-4830, United States

**Robert A. Putnam**, Environmental Engineering Acoustics, Siemens Power Generation, Inc., Orlando, Florida 32826, United States

**Robert B. Randall**, School of Mechanical and Manufacturing Engineering, University of New South Wales, Sydney, New South Wales 2052, Australia

**Birgit Rasmussen**, SBI, Danish Research Institute, Dr. Neergaards Vej 15, DK-2970 Hørsholm, Denmark

**Gunnar Rasmussen**, G.R.A.S. Sound and Vibration, Skoulytoften 33, 2840 Holte, Denmark

**Per Rasmussen**, G.R.A.S. Sound and Vibration, Skoulytoften 33, 2840 Holte, Denmark

**Eugene M. Reindel**, Harris Miller Miller & Hanson Inc., 945 University Avenue, Suite 201, Sacramento, California 95825, United States

**Thomas E. Reinhart**, Engine Design Section, Southwest Research Institute, San Antonio, Texas 78228, United States

**Evgeny Rivin**, Wayne State University, Detroit, Michigan, United States

**Carl J. Rosenberg**, Acentech, 33 Moulton Street, Cambridge, Massachusetts 02138, United States

**Oleg V. Rudenko**, Institute of Technology, Campus Grasvik, 371 79 Karlskrona, Sweden

**Ulf Sandberg**, Department of Applied Acoustics, Chalmers University of Technology, Gothenburg, Sweden

**Stanley S. Sattinger**, Advanced Fossil Energy Systems, Siemens Power Generation, Pittsburgh, Pennsylvania 15235, United States

**Richard F. Schumacher**, Principal Consultant, R.S. Beratung LLC, 7385 Denton Hill Road, Fenton, Michigan, 48430, United States

**A. F. Seybert**, Department of Mechanical Engineering, University of Kentucky, Lexington, Kentucky 40506-0503, United States

**Anastasios Sextos**, Department of Civil Engineering, Aristotle University of Thessaloniki, 54124, Thessaloniki, Greece

**Christine H. Shadle**, Haskins Laboratories, 300 George Street, New Haven, Connecticut 06511, United States

**Kihong Shin**, School of Mechanical Engineering, Aandong National University, 388 Songchon-Dong, Andong, 760-749 South Korea

**Knud Skovgaard Nielsen**, AkustikNet A/S, DK 2700 Broenshoej, Denmark

**John S. Stewart**, Department of Mechanical and Aerospace Engineering, North Carolina State University, Raleigh, North Carolina, United States

**Alice H. Suter**, Alice Suter and Associates, Ashland, Oregon, United States

**Louis C. Sutherland**, Consultant in Acoustics, 27803 Longhill Dr., Rancho Palos Verdes, California 90275, United States

**James P. Talbot**, Atkins Consultants, Brunel House, RTC Business Park, London Road, Derby, DE1 2WS, United Kingdom

**David J. Thompson**, Institute of Sound and Vibration Research, University of Southampton, Southampton SO17 1BJ, United Kingdom

**Henrik W. Thrane**, Ødegaard & Danneskiold-Samsøe, 15 Titangade, DK 2200, Copenhagen, Denmark

**Gregory C. Tocci**, Cavanaugh Tocci Associates, Inc., 327F Boston Post Road, Sudbury, Massachusetts 01776, United States

**Uwe Trautmann**, ABIT Ingenieure Dr. Trautmann GmbH, 14513 Teltow/Berlin, Germany

**Jiri Tuma**, Faculty of Mechanical Engineering, Department of Control Systems and Instrumentation, VSB—Technical University of Ostrava, CZ 708 33 Ostrava, Czech Republic

**Eric E. Ungar**, Acentech Incorporated, 33 Moulton Street, Cambridge, Massachusetts 02138, United States

**Pedro R. Valletta**, interPRO, Acustica-Electroacustica-Audio-Video, Dr. R. Rivarola 147, Tors Buenos Aires, Argentina

**Lawrence N. Virgin**, Department of Mechanical Engineering, Duke University, Durham, North Carolina 27708, United States

**Hans-Jürgen von Martens**, Physikalisch-Technische Bundesanstalt PTB Braunschweig und Berlin, 10587 Berlin, Germany

**Hiroshi Wada**, Department of Bioengineering and Robotics, Tohoku University, Aoba-yama 01, Sendai 980–8579, Japan

**David C. Waddington**, Acoustics Research Centre, School of Computing, Science and Engineering, University of Salford, Greater Manchester M5 4WT 9NU, United Kingdom

**Alfred C. C. Warnock**, National Research Council, M59 IRC Acoustics, Montreal Road, Ottawa, Ontario, K1A 0R6, Canada

**Charles Robert Welch**, Information Technology Laboratory, U.S. Army Engineer Research and Development Center, 3909 Halls Ferry Road, Vicksburg Mississippi 39180, United States

**John F. Wilby**, Wilby Associates, 3945 Bon Homme Road, Calabasas, California 91302, United States

**Earl G. Williams**, Naval Research Laboratory, Washington, D.C. 20375–5350, United States

**George S. K. Wong**, Acoustical Standards, Institute for National Measurement Standards, National Research Council Canada, Canada K1A 0R6

**T. W. Wu**, Department of Mechanical Engineering, University of Kentucky, Lexington, Kentucky 40506–0503, United States

**Jianping Yin**, German Aerospace Center (DLR), Institute of Aerodynamics and Flow Technologies (Technical Acoustics), D-38108 Braunschweig, Germany

**William A. Yost**, Parmly Hearing Institute, Loyola University, 6525 North Sheridan Drive, Chicago, Illinois 60626, United States

**Shaobo Young**, Ford Motor Company, 2101 Village Road, Dearborn, Michigan, United States

**Harry K. Zaveri**, Brüel & Kjær Sound & Vibration Measurement A/S, 2850 Nærum, Denmark

**George Zusman**, IMI Sensors Division, PCB Piezotronics, Depew, New York 14043, United States

# CHAPTER 1

## FUNDAMENTALS OF ACOUSTICS, NOISE, AND VIBRATION

Malcolm J. Crocker

Department of Mechanical Engineering  
Auburn University  
Auburn, Alabama

### 1 INTRODUCTION

The vibrations in machines and structures result in oscillatory motion that propagates in air and/or water and that is known as sound. Sound can also be produced by the oscillatory motion of the fluid itself, such as in the case of the turbulent mixing of a jet with the atmosphere, in which no vibrating structure is involved. The simplest type of oscillation in vibration and sound phenomena is known as simple harmonic motion, which can be shown to be sinusoidal in time. Simple harmonic motion is of academic interest because it is easy to treat and manipulate mathematically; but it is also of practical interest. Most musical instruments make tones that are approximately periodic and simple harmonic in nature. Some machines (such as electric motors, fans, gears, etc.) vibrate and make sounds that have pure tone components. Musical instruments and machines normally produce several pure tones simultaneously. Machines also produce sound that is not simple harmonic but is random in time and is known as noise. The simplest vibration to analyze is that of a mass–spring–damper system. This elementary system is a useful model for the study of many simple vibration problems. Sound waves are composed of the oscillatory motion of air (or water) molecules. In air and water, the fluid is compressible and the motion is accompanied by a change in pressure known as sound. The simplest form of sound is one-dimensional plane wave propagation. In many practical cases (such as in enclosed spaces or outdoors in the environment) sound propagation in three dimensions must be considered.

### 2 DISCUSSION

In Chapter 1 we will discuss some simple theory that is useful in the control of noise and vibration. For more extensive discussions on sound and vibration fundamentals, the reader is referred to more detailed treatments available in several books.<sup>1–7</sup> We start off by discussing simple harmonic motion. This is because very often oscillatory motion, whether it be the vibration of a body or the propagation of a sound wave, is like this idealized case. Next, we introduce the ideas of period, frequency, phase, displacement, velocity, and acceleration. Then we study free and forced vibration of a simple mass–spring system and the influence of damping forces on the system. These vibration topics are discussed again at a more advanced level in Chapters 12, 15, and 60. In Section 5 we

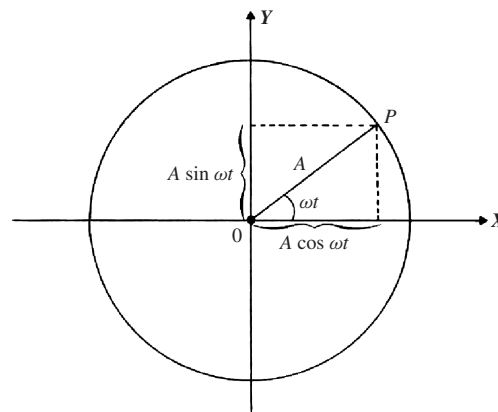
discuss how sound propagates in waves, and then we study *sound intensity* and *energy density*. In Section 6 we consider the use of decibels to express *sound pressure levels*, *sound intensity levels*, and *sound power levels*. Section 7 describes some preliminary ideas about human hearing. In Sections 8 and 9, we study frequency analysis of sound and frequency weightings and finally in Section 10 day–night and day–evening–night sound pressure levels.

In Chapter 2 we discuss some further aspects of sound propagation at a more intermediate level, including the radiation of sound from idealized spherical sources, standing waves, and the important ideas of *near*, *far*, *free*, and *reverberant* sound fields. We also study the propagation of sound in closed spaces indoors and outdoors. This has applications to industrial noise control problems in buildings and to community noise problems, respectively. Chapter 2 also serves as an introduction to some of the topics that follow in Part I of this handbook.

### 3 SIMPLE HARMONIC MOTION

The motion of vibrating systems such as parts of machines, and the variation of sound pressure with time is often said to be simple harmonic. Let us examine what is meant by simple harmonic motion.

Suppose a point  $P$  is revolving around an origin  $O$  with a constant angular velocity  $\omega$ , as shown in Fig. 1.



**Figure 1** Representation of simple harmonic motion by projection of the rotating vector  $A$  on the  $X$  or  $Y$  axis.

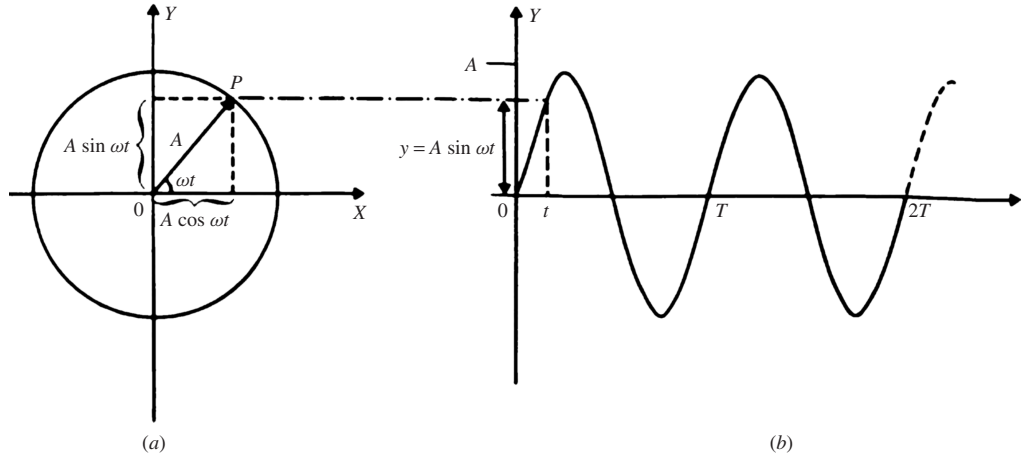


Figure 2 Simple harmonic motion.

If the vector  $OP$  is aligned in the direction  $OX$  when time  $t = 0$ , then after  $t$  seconds the angle between  $OP$  and  $OX$  is  $\omega t$ . Suppose  $OP$  has a length  $A$ , then the projection on the  $X$  axis is  $A \cos \omega t$  and on the  $Y$  axis,  $A \sin \omega t$ . The variation of the projected length on either the  $X$  axis or the  $Y$  axis with time is said to represent simple harmonic motion.

It is easy to generate a displacement vs. time plot with this model, as is shown in Fig. 2. The projections on the  $X$  axis and  $Y$  axis are as before. If we move the circle to the right at a constant speed, then the point  $P$  traces out a curve  $y = A \sin \omega t$ , horizontally. If we move the circle vertically upwards at the same speed, then the point  $P$  would trace out a curve  $x = A \cos \omega t$ , vertically.

### 3.1 Period, Frequency, and Phase

The motion is seen to repeat itself every time the vector  $OP$  rotates once (in Fig. 1) or after time  $T$  seconds (in Figs. 2 and 3). When the motion has repeated itself, the displacement  $y$  is said to have gone through one *cycle*. The number of cycles that occur per second is called the *frequency*  $f$ . Frequency may be expressed in cycles per second or, equivalently in hertz, or as abbreviated, Hz. The use of hertz or Hz is preferable because this has become internationally agreed upon as the unit of frequency. (Note cycles per second = hertz). Thus

$$f = 1/T \text{ hertz} \quad (1)$$

The time  $T$  is known as the *period* and is usually measured in seconds. From Figs. 2 and 3, we see that the motion repeats itself every time  $\omega t$  increases by  $2\pi$ , since  $\sin 0 = \sin 2\pi = \sin 4\pi = 0$ , and so on. Thus  $\omega T = 2\pi$  and from Eq. 1,

$$\omega = 2\pi f \quad (2)$$

The angular frequency,  $\omega$ , is expressed in radians per second (rad/s).

The motion described by the displacement  $y$  in Fig. 2 or the projection  $OP$  on the  $X$  or  $Y$  axes in Fig. 2 is said to be *simple harmonic*. We must now discuss something called the *initial phase angle*, which is sometimes just called *phase*. For the case we have chosen in Fig. 2, the phase angle is zero. If, instead, we start counting time from when the vector points in the direction  $OP_1$ , as shown in Fig. 3, and we let the angle  $XOP_1 = \phi$ , this is equivalent to moving the time origin  $t$  seconds to the right in Fig. 2. Time is started when  $P$  is at  $P_1$  and thus the initial displacement is  $A \sin \phi$ . The *initial phase angle* is  $\phi$ . After time  $t$ ,  $P_1$  has moved to  $P_2$  and the displacement

$$y = A \sin(\omega t + \phi) \quad (3)$$

If the initial phase angle  $\phi = 0^\circ$ , then  $y = A \sin \omega t$ ; if the phase angle  $\phi = 90^\circ$ , then  $y = A \sin(\omega t + \pi/2) \equiv A \cos \omega t$ . For mathematical convenience, complex exponential notation is often used. If the displacement is written as

$$y = A e^{j\omega t}, \quad (3a)$$

and we remember that  $A e^{j\omega t} = A(\cos \omega t + j \sin \omega t)$ , we see in Fig. 1 that the real part of Eq. (3a) is represented by the projection of the point  $P$  onto the  $x$  axis,  $A \cos \omega t$ , and of the point  $P$  onto the  $y$  or imaginary axis,  $A \sin \omega t$ . Simple harmonic motion, then, is often written as the real part of  $A e^{j\omega t}$ , or in the more general form  $A e^{j(\omega t + \phi)}$ . If the constant  $A$  is made complex, then the displacement can be written as the real part of  $A e^{j\omega t}$ , where  $A = A e^{j\phi}$ .

### 3.2 Velocity and Acceleration

So far we have examined the displacement  $y$  of a point. Note that, when the displacement is in the  $OY$  direction, we say it is positive; when it is in



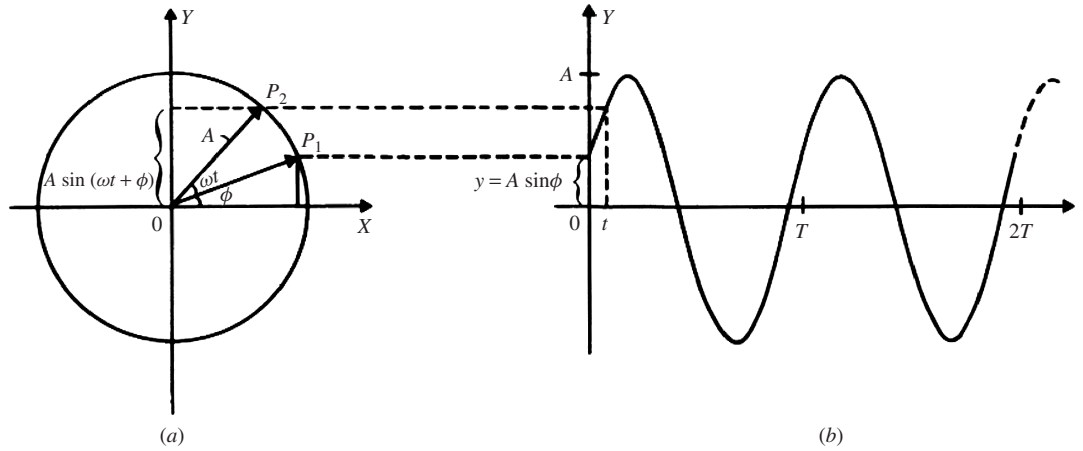


Figure 3 Simple harmonic motion with initial phase angle  $\phi$ .

the opposite direction to  $OY$ , we say it is negative. Displacement, velocity, and acceleration are really vector quantities in mathematics; that is, they have magnitude and direction. The velocity  $v$  of a point is the rate of change of position with time of the point  $x$  in metres/second. The acceleration  $a$  is the rate of change of velocity with time. Thus, using simple calculus:

$$v = \frac{dy}{dt} = \frac{d}{dt}[A \sin(\omega t + \phi)] = A\omega \cos(\omega t + \phi) \quad (4)$$

and

$$a = \frac{dv}{dt} = \frac{d}{dt}[A\omega \cos(\omega t + \phi)] = -A\omega^2 \sin(\omega t + \phi) \quad (5)$$

Equations (3), (4), and (5) are plotted in Fig. 4.

Note, by trigonometric manipulation we can rewrite Eqs. (4) and (5) as (6) and (7):

$$v = A\omega \cos(\omega t + \phi) = A\omega \sin\left(\omega t + \frac{\pi}{2} + \phi\right) \quad (6)$$

and

$$a = -A\omega^2 \sin(\omega t + \phi) = +A\omega^2 \sin(\omega t + \pi + \phi) \quad (7)$$

and from Eq. (3) we see that  $a = -\omega^2 y$ .

Equations (3), (6), and (7) tell us that for simple harmonic motion the *amplitude* of the velocity is  $\omega$  or  $2\pi f$  greater than the *amplitude* of the displacement, while the *amplitude* of the acceleration is  $\omega^2$  or  $(2\pi f)^2$

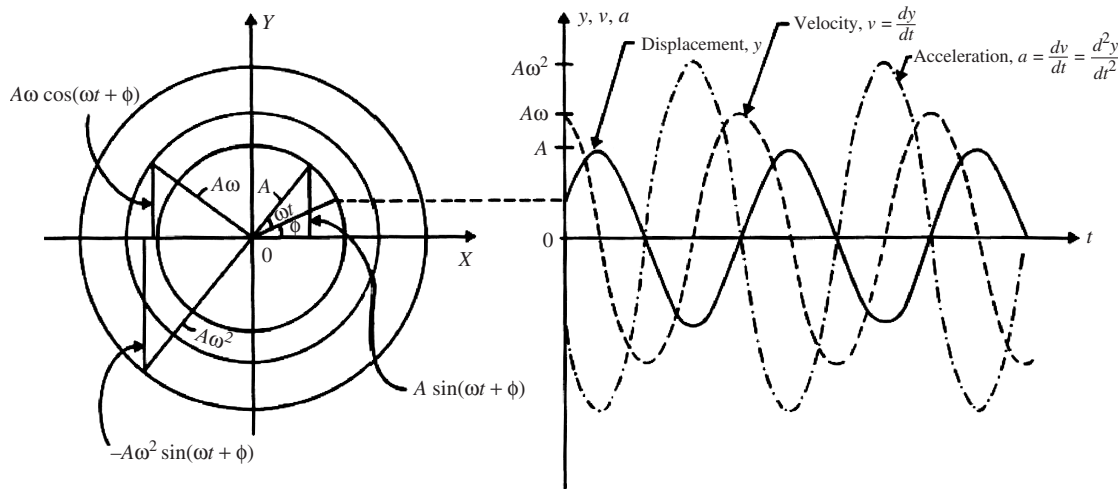


Figure 4 Displacement, velocity, and acceleration.

greater. The *phase* of the velocity is  $\pi/2$  or  $90^\circ$  ahead of the displacement, while the acceleration is  $\pi$  or  $180^\circ$  ahead of the displacement.

Note, we could have come to the same conclusions and much more quickly if we had used the complex exponential notation. Writing

$$y = Ae^{j\omega t}$$

then

$$v = Aj\omega e^{j\omega t} = j\omega y$$

and

$$a = A(j)^2 \omega^2 e^{j\omega t} = -A\omega^2 e^{j\omega t} = -\omega^2 y$$

## 4 VIBRATING SYSTEMS

### 4.1 Mass-Spring System

**A. Free Vibration – Undamped** Suppose a mass of  $M$  kilogram is placed on a spring of stiffness  $K$  newton-metre (see Fig. 5a), and the mass is allowed to sink down a distance  $d$  metres to its equilibrium position under its own weight  $Mg$  newtons, where  $g$  is the acceleration of gravity  $9.81 \text{ m/s}^2$ . Taking forces and deflections to be positive upward gives

$$-Mg = -Kd \quad (8)$$

thus the static deflection  $d$  of the mass is

$$d = Mg/K \quad (8a)$$

The distance  $d$  is normally called the *static deflection* of the mass; we define a new displacement coordinate system, where  $Y = 0$  is the location of the mass after the gravity force is allowed to compress the spring.

Suppose now we displace the mass a distance  $y$  from its equilibrium position and release it; then it will oscillate about this position. We will measure the deflection from the equilibrium position of the mass (see Fig. 5b). Newton's law states that force is equal to mass  $\times$  acceleration. Forces and deflections are again assumed positive upward, and thus

$$-Ky = M \frac{d^2 y}{dt^2} \quad (9)$$

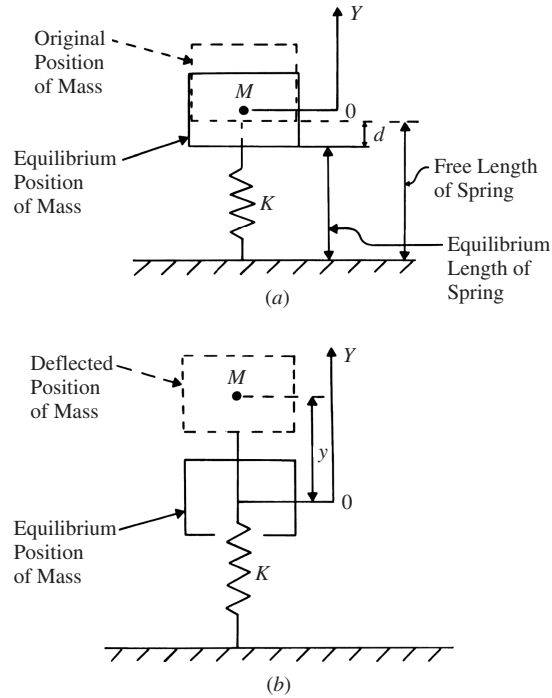
Let us assume a solution to Eq. (9) of the form  $y = A \sin(\omega t + \phi)$ . Then upon substitution into Eq. (9) we obtain

$$-KA \sin(\omega t + \phi) = M[-\omega^2 \sin(\omega t + \phi)]$$

We see our solution satisfies Eq. (9) only if

$$\omega^2 = K/M$$

The system vibrates with free vibration at an angular frequency  $\omega$  radians/second. This frequency,  $\omega$ , which is generally known as the *natural* angular frequency, depends only on the stiffness  $K$  and



**Figure 5** Movement of mass on a spring: (a) static deflection due to gravity and (b) oscillation due to initial displacement  $y_0$ .

mass  $M$ . We normally signify this so-called natural frequency with the subscript  $n$ . And so

$$\omega_n = \sqrt{K/M}$$

and from Eq. (2)

$$f_n = \frac{1}{2\pi} \sqrt{K/M} \text{ Hz} \quad (10)$$

The frequency,  $f_n$  hertz, is known as the *natural frequency* of the mass on the spring. This result, Eq.(10), looks physically correct since if  $K$  increases (with  $M$  constant),  $f_n$  increases. If  $M$  increases with  $K$  constant,  $f_n$  decreases. These are the results we also find in practice.

We have seen that a solution to Eq. (9) is  $y = A \sin(\omega t + \phi)$  or the same as Eq. (3). Hence we know that *any system that has a restoring force that is proportional to the displacement will have a displacement that is simple harmonic*. This is an alternative definition to that given in Section 3 for *simple harmonic motion*.

**B. Free Vibration – Damped** Many mechanical systems can be adequately described by the simple mass-spring system just discussed above. However, for some purposes it is necessary to include the effects of losses (sometimes called damping). This

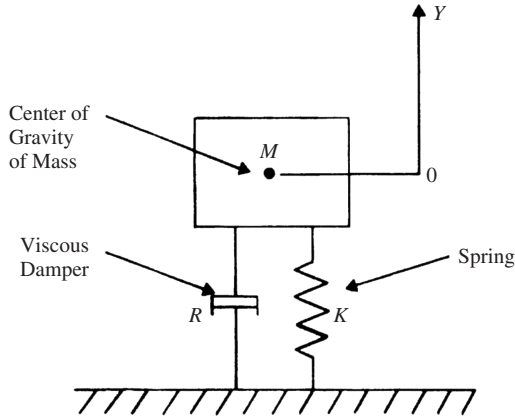


Figure 6 Movement of damped simple system.

is normally done by including a viscous damper in the system (see Fig. 6). See Chapters 15 and 60 for further discussion on passive damping. With viscous or “coulomb” damping the friction or damping force  $F_d$  is assumed to be proportional to the velocity,  $dy/dt$ . If the constant of proportionality is  $R$ , then the damping force  $F_d$  on the mass is

$$F_d = -R \frac{dy}{dt} \quad (11)$$

and Eq. (9) becomes

$$-R \frac{dy}{dt} - Ky = M \frac{d^2 y}{dt^2} \quad (12)$$

or equivalently

$$M \ddot{y} + R \dot{y} + Ky = 0 \quad (13)$$

where the dots represent single and double differentiation with respect to time.

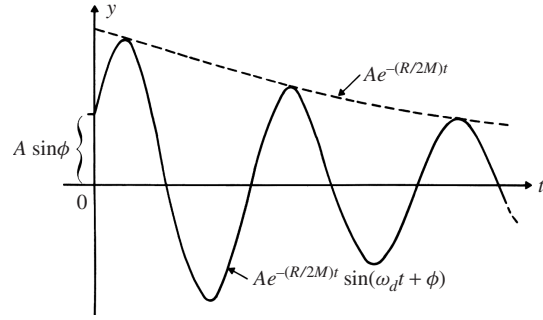
The solution of Eq. (13) is most conveniently found by assuming a solution of the form:  $y$  is the real part of  $A e^{j\lambda t}$  where  $A$  is a complex number and  $\lambda$  is an arbitrary constant to be determined. By substituting  $y = A e^{j\lambda t}$  into Eq. (13) and assuming that the damping constant  $R$  is small,  $R < (4MK)^{1/2}$  (which is true in most engineering applications), the solution is found that:

$$y = A e^{-(R/2M)t} \sin(\omega_d t + \phi) \quad (14)$$

Here  $\omega_d$  is known as the damped “natural” angular frequency:

$$\omega_d = \omega_n [1 - (R/2M)^2]^{1/2} \quad (15)$$

where  $\omega_n$  is the undamped natural frequency  $\sqrt{K/M}$ . The motion described by Eq. (14) is plotted in Fig. 7.

Figure 7 Motion of a damped mass-spring system,  $R < (4MK)^{1/2}$ .

The amplitude of the motion decreases with time unlike that for undamped motion (Fig. 3). If the damping is increased until  $R$  equals  $(4MK)^{1/2}$ , the damping is then called critical,  $R_{crit} = (4MK)^{1/2}$ . In this case, if the mass in Fig. 6 is displaced, it gradually returns to its equilibrium position and the displacement never becomes negative. In other words, there is no oscillation or vibration. If  $R > (4MK)^{1/2}$ , the system is said to be overdamped.

The ratio of the damping constant  $R$  to the critical damping constant  $R_{crit}$  is called the damping ratio  $\delta$ :

$$\delta = R/R_{crit} = R/(2M\omega) \quad (16a)$$

In most engineering cases the damping ratio,  $\delta$ , in a structure is hard to predict and is of the order of 0.01 to 0.1. There are, however, several ways to measure damping experimentally. (See Chapters 15 and 60.)

**C. Forced Vibration—Damped** If a damped spring-mass system is excited by a simple harmonic force at some arbitrary angular forcing frequency  $\omega$  (Fig. 8), we now obtain the equation of motion (16b):

$$M \ddot{y} + R \dot{y} + Ky = F e^{j(\omega t)} = |F| e^{j(\omega t + \phi)} \quad (16b)$$

The force  $F$  is normally written in the complex form for mathematical convenience. The real force acting is, of course, the real part of  $F$  or  $|F| \cos(\omega t)$ , where  $|F|$  is the force amplitude.

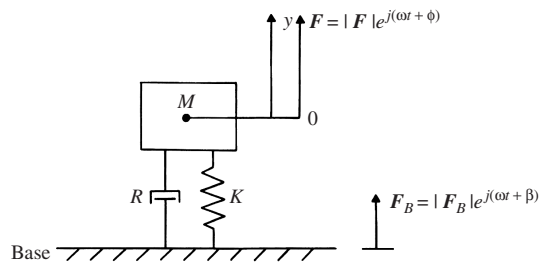


Figure 8 Forced vibration of damped simple system.

If we assume a solution of the form  $y = Ae^{j\omega t}$  then we obtain from Eq. (16b):

$$A = \frac{|F|}{j\omega R + K - M\omega^2} \quad (17)$$

We can write  $A = |A|e^{j\alpha}$ , where  $\alpha$  is the phase angle between force and displacement. The phase,  $\alpha$ , is not normally of much interest, but the amplitude of motion  $|A|$  of the mass is. The amplitude of the

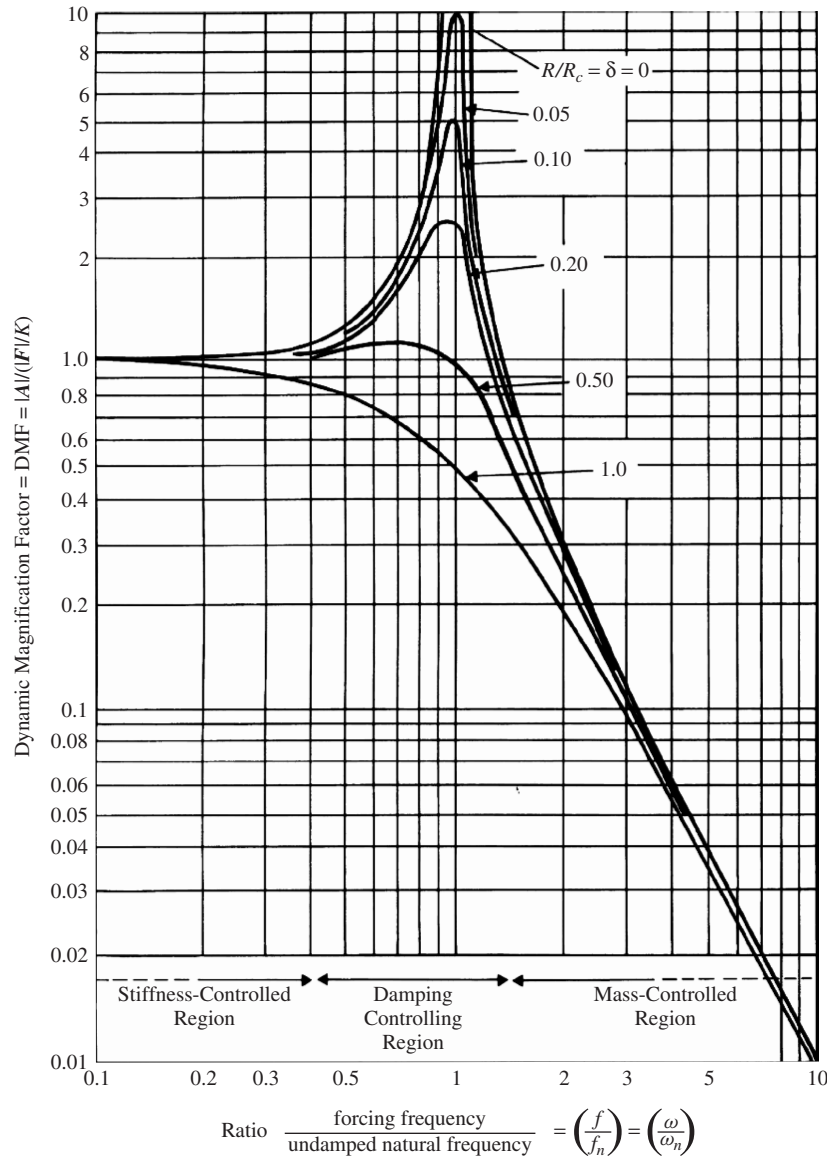
displacement is

$$|A| = \frac{|F|}{[\omega^2 R^2 + (K - M\omega^2)^2]^{1/2}} \quad (18)$$

This can be expressed in alternative form:

$$\frac{|A|}{|F|/K} = \frac{1}{[4\delta^2(\omega/\omega_n)^2 + (1 - (\omega/\omega_n)^2)^2]^{1/2}} \quad (19)$$

Equation (19) is plotted in Fig. 9. It is observed that if the forcing frequency  $\omega$  is equal to the natural



**Figure 9** Dynamic modification factor (DMF) for a damped simple system.

frequency of the structure,  $\omega_n$ , or equivalently  $f = f_n$ , a condition called resonance, then the amplitude of the motion is proportional to  $1/(2\delta)$ . The ratio  $|A|/(|F|/K)$  is sometimes called the *dynamic magnification factor* (DMF). The number  $|F|/K$  is the *static deflection* the mass would assume if exposed to a *constant* nonfluctuating force  $|F|$ . If the damping ratio,  $\delta$ , is small, the displacement amplitude  $A$  of a structure excited at its *natural* or *resonance* frequency is very high. For example, if a simple system has a damping ratio,  $\delta$ , of 0.01, then its dynamic displacement amplitude is 50 times (when exposed to an oscillating force of  $|F|$  N) its static deflection (when exposed to a static force of amplitude  $|F|$  N), that is, DMF = 50. Situations such as this should be avoided in practice, wherever possible. For instance, if an oscillating force is present in some machine or structure, the frequency of the force should be moved away from the natural frequencies of the machine or structure, if possible, so that resonance is avoided. If the forcing frequency  $f$  is close to or coincides with a natural frequency  $f_n$ , large amplitude vibrations can occur with consequent vibration and noise problems and the potential of serious damage and machine malfunction.

The force on the idealized damped simple system will create a force on the base  $F_B = R\dot{y} + Ky$ . Substituting this into Eq. (16) and rearranging and finally comparing the amplitudes of the imposed force  $|F|$  with the force transmitted to the base  $|F_B|$  gives

$$\frac{|F_B|}{|F|} = \left[ \frac{1 + 4\delta^2(\omega/\omega_n)^2}{4\delta^2(\omega/\omega_n)^2 + (1 - (\omega/\omega_n)^2)^2} \right]^{1/2} \quad (20)$$

Equation (20) is plotted in Fig. 10. The ratio  $|F_B|/|F|$  is sometimes called the *force transmissibility*  $T_F$ . The force amplitude transmitted to the machine support base,  $F_B$ , is seen to be much greater than one, if the exciting frequency is at the system resonance frequency. The results in Eq. (20) and Fig. 10 have important applications to machinery noise problems that will be discussed again in detail in Chapter 54. Briefly, we can observe that these results can be utilized in designing vibration isolators for a machine. The natural frequency  $\omega_n$  of a machine of mass  $M$  resting on its isolators of stiffness  $K$  and damping constant  $R$  must be made much less than the forcing frequency  $\omega$ . Otherwise, large force amplitudes will be transmitted to the machine base. Transmitted forces will excite vibrations in machine supports and floors and walls of buildings, and the like, giving rise to additional noise radiation from these other areas. Chapter 59 gives a more complete discussion on vibration isolation.

## 5 PROPAGATION OF SOUND

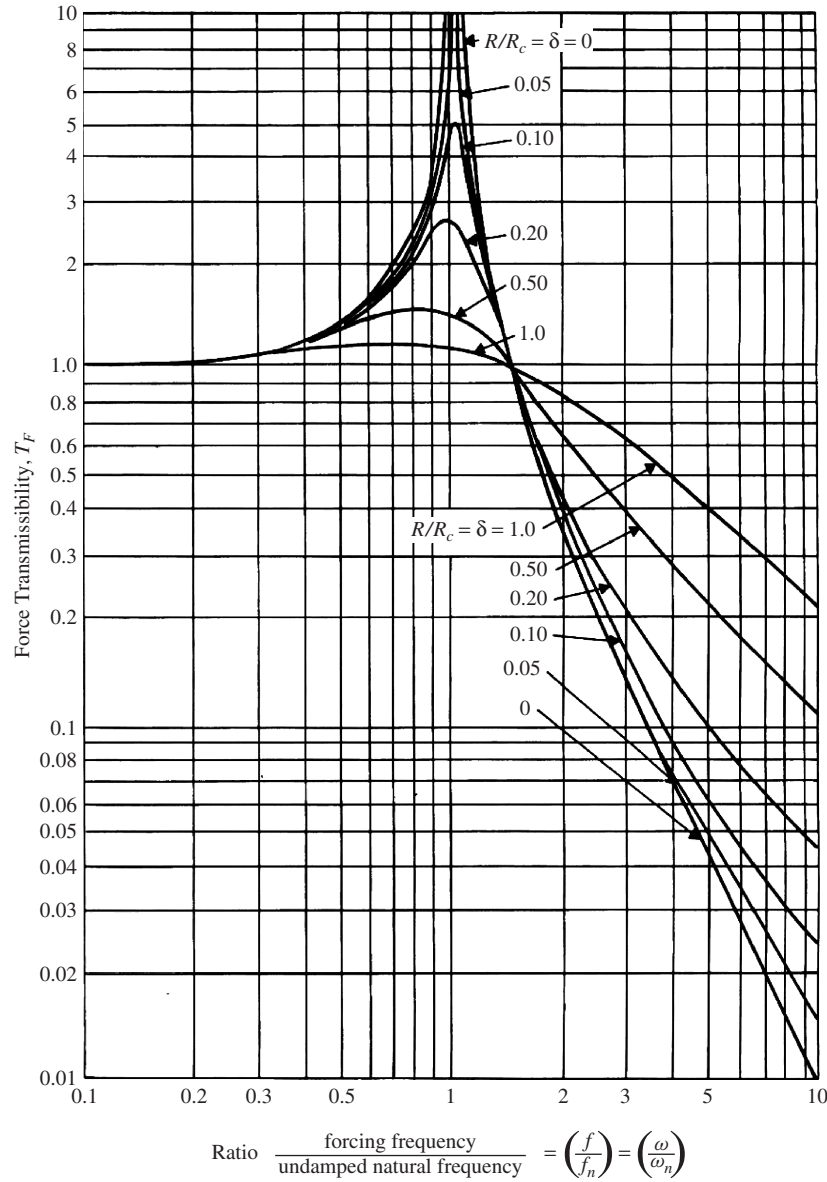
### 5.1 Plane Sound Waves

The propagation of sound may be illustrated by considering gas in a tube with rigid walls and having a rigid piston at one end. The tube is assumed to be infinitely long in the direction away from the piston.

We shall assume that the piston is vibrating with simple harmonic motion at the left-hand side of the tube (see Fig. 11) and that it has been oscillating back and forth for some time. We shall only consider the piston motion and the oscillatory motion it induces in the fluid from when we start our clock. Let us choose to start our clock when the piston is moving with its maximum velocity to the right through its normal equilibrium position at  $x = 0$ . See the top of Fig. 11, at  $t = 0$ . As time increases from  $t = 0$ , the piston straight away starts slowing down with simple harmonic motion, so that it stops moving at  $t = T/4$  at its maximum excursion to the right. The piston then starts moving to the left in its cycle of oscillation, and at  $t = T/2$  it has reached its equilibrium position again and has a maximum velocity (the same as at  $t = 0$ ) but now in the negative  $x$  direction. At  $t = 3T/4$ , the piston comes to rest again at its maximum excursion to the left. Finally at  $t = T$  the piston reaches its equilibrium position at  $x = 0$  with the same maximum velocity we imposed on it at  $t = 0$ . During the time  $T$ , the piston has undergone one complete cycle of oscillation. We assume that the piston continues vibrating and makes  $f$  oscillations each second, so that its frequency  $f = 1/T$  (Hz).

As the piston moves backward and forward, the gas in front of the piston is set into motion. As we all know, the gas has mass and thus inertia and it is also compressible. If the gas is compressed into a smaller volume, its pressure increases. As the piston moves to the right, it compresses the gas in front of it, and as it moves to the left, the gas in front of it becomes rarified. When the gas is compressed, its pressure increases above atmospheric pressure, and, when it is rarified, its pressure decreases below atmospheric pressure. The pressure difference above or below the atmospheric pressure,  $p_0$ , is known as the sound pressure,  $p$ , in the gas. Thus the sound pressure  $p = p_{\text{tot}} - p_0$ , where  $p_{\text{tot}}$  is the total pressure in the gas. If these pressure changes occurred at constant temperature, the fluid pressure would be directly proportional to its density,  $\rho$ , and so  $p/\rho = \text{constant}$ . This simple assumption was made by Sir Isaac Newton, who in 1660 was the first to try to predict the speed of sound. But we find that, in practice, regions of high and low pressure are sufficiently separated in space in the gas (see Fig. 11) so that heat cannot easily flow from one region to the other and that the adiabatic law,  $p/\rho^\gamma = \text{constant}$ , is more closely followed in nature.

As the piston moves to the right with maximum velocity at  $t = 0$ , the gas ahead receives maximum compression and maximum increase in density, and this simultaneously results in a maximum pressure increase. At the instant the piston is moving to the left with maximum negative velocity at  $t = T/2$ , the gas behind the piston, to the right, receives maximum rarefaction, which results in a maximum density and pressure decrease. These piston displacement and velocity perturbations are superimposed on the much greater random motion of the gas molecules (known as the Brownian motion). The mean speed of the molecular random motion in the gas depends on its absolute

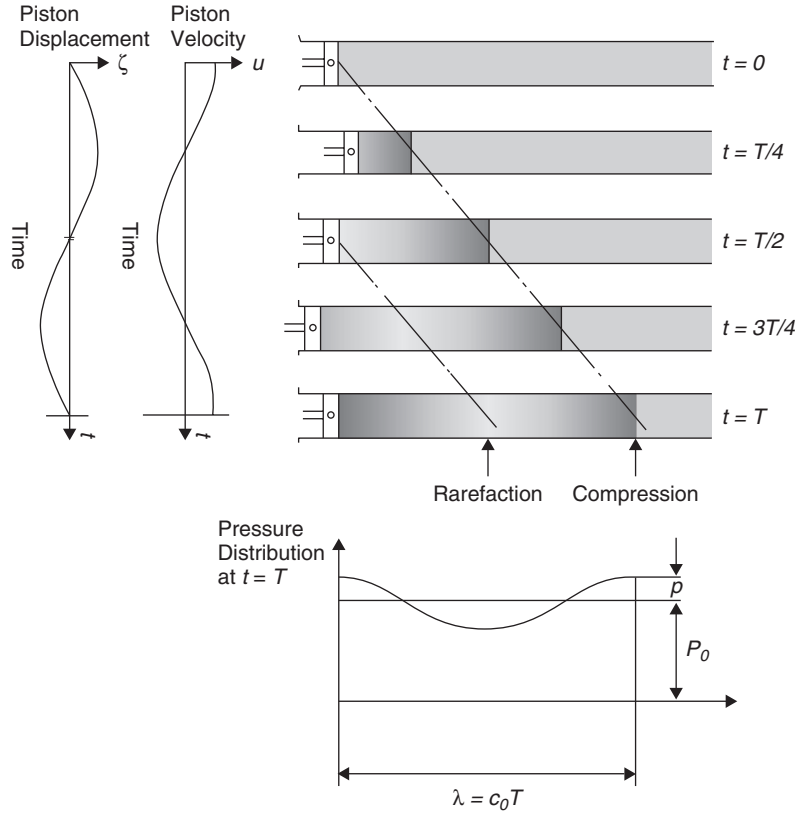


**Figure 10** Force transmissibility,  $T_F$ , for a damped simple system.

temperature. The disturbances induced in the gas are known as acoustic (or sound) disturbances. It is found that momentum and energy pulsations are transmitted from the piston throughout the whole region of the gas in the tube through molecular interactions (sometimes simply termed molecular collisions). The rate at which the motion is transmitted throughout the fluid depends upon its absolute temperature. The speed of transmission is known as the speed of sound,  $c_0$ :

$$c_0 = (\gamma RT)^{1/2} \quad \text{metres/second}$$

where  $\gamma$  is the ratio of specific heats,  $R$  is the gas constant of the fluid in the tube, and  $T$  is the absolute temperature (K). A small region of fluid instantaneously enclosing a large number of gas molecules is known as a particle. The motion of the gas particles "mimics" the piston motion as it moves back and forth. The velocity of the gas particles (superimposed on the random Brownian motion of the molecules) depends upon the velocity of the piston as it moves back and forth and is completely unrelated to the speed of the sound propagation  $c_0$ . For a given amplitude of vibration of



**Figure 11** Schematic illustration of the sound pressure distribution created in a tube by a piston undergoing one complete simple harmonic cycle of operation in period  $T$  seconds.

the piston,  $A$ , we know from Eq. (4) that the velocity amplitude is  $\omega A$ , which increases with frequency, and thus the piston only has a high-velocity amplitude if it is vibrated at high frequency.

Figure 11 shows the way that sound disturbances propagate along the tube from the oscillating piston. Dark regions in the tube indicate regions of high gas compression and high positive sound pressure. Light regions in the tube indicate regions of rarefaction and low negative sound pressure. Since the motion in the fluid is completely repeated periodically at one location and also is identically repeated spatially along the tube, we call the motion wave motion. At time  $t = T$ , the fluid disturbance, which was caused by the piston beginning at  $t = 0$ , will only have reached a distance  $c_0 T$  along the tube. We call this location, the location of the *wave front* at the time  $T$ . Figure 11 shows that at distance  $c_0 T$  along the tube, at which the motion starts to repeat itself. The distance  $c_0 T$  is known as the wavelength  $\lambda$  (metres), and thus

$$\lambda = c_0 T \quad \text{metres}$$

Figure 11 shows the location of the wave front for different times and the sound pressure distribution in

the tube at  $t = T$ . The sound pressure distribution at some instant  $t$  is given by

$$p = P \cos(2\pi x / \lambda)$$

where  $P$  is the sound pressure amplitude ( $\text{N/m}^2$ ). Since the piston is assumed to vibrate with simple harmonic motion with period  $T$ , its frequency of oscillation  $f = 1/T$ . Thus the wavelength  $\lambda$  (m) can be written

$$\lambda = c_0 / f$$

The sound pressure distribution,  $p$  ( $\text{N/m}^2$ ), in the tube at any time  $t$  (s) can thus be written

$$p = P \cos[2\pi(x/\lambda - t/T)]$$

or

$$p = P \cos[(kx - \omega t)]$$

where  $k = 2\pi/\lambda = \omega/c_0$  and  $\omega = 2\pi f$ . The parameter,  $k$ , is commonly known as the wavenumber, although the term wavelength parameter is better, since  $k$  has the dimensions of  $1/\text{m}$ .

## 5.2 Sound Pressure

With sound waves in a fluid such as air, the sound pressure at any point is the difference between the total pressure and normal atmospheric pressure. The sound pressure fluctuates with time and can be positive or negative with respect to the normal atmospheric pressure.

Sound varies in magnitude and frequency and it is normally convenient to give a single number measure of the sound by determining its time-averaged value. The time average of the sound pressure at any point in space, over a sufficiently long time, is zero and is of no interest or use. The time average of the square of the sound pressure, known as the mean square pressure, however, is not zero. If the sound pressure at any instant  $t$  is  $p(t)$ , then the mean square pressure,  $\langle p^2(t) \rangle_t$ , is the time average of the square of the sound pressure over the time interval  $T$ :

$$\langle p^2(t) \rangle_t = \frac{1}{T} \int_0^T p^2(t) dt \quad (21)$$

where  $\langle \rangle_t$  denotes a time average.

It is usually convenient to use the square root of the mean square pressure:

$$p_{\text{rms}} = \sqrt{\langle p^2(t) \rangle_t} = \sqrt{\frac{1}{T} \int_0^T p^2(t) dt}$$

which is known as the root mean square (rms) sound pressure. This result is true for all cases of continuous sound time histories including noise and pure tones. For the special case of a pure tone sound, which is simple harmonic in time, given by  $p = P \cos(\omega t)$ , the root mean square sound pressure is

$$p_{\text{rms}} = P/\sqrt{2} \quad (22)$$

where  $P$  is the sound pressure amplitude.

## 5.3 Particle Velocity

As the piston vibrates, the gas immediately next to the piston must have the same velocity as the piston. A small element of fluid is known as a *particle*, and its velocity, which can be positive or negative, is known as the *particle velocity*. For waves traveling away from the piston in the positive  $x$  direction, it can be shown that the particle velocity,  $u$ , is given by

$$u = p/\rho c_0 \quad (23)$$

where  $\rho$  = fluid density (kg/m<sup>3</sup>) and  $c_0$  = speed of sound (m/s).

If a wave is reflected by an obstacle, so that it is traveling in the negative  $x$  direction, then

$$u = -p/\rho c_0 \quad (24)$$

The negative sign results from the fact that the sound pressure is a scalar quantity, while the particle velocity is a vector quantity. These results are true for any type of plane sound waves, not only for sinusoidal waves.

## 5.4 Sound Intensity

The intensity of sound,  $I$ , is the time-averaged sound energy that passes through unit cross-sectional area in unit time. For a plane progressive wave, or far from any source of sound (in the absence of reflections):

$$I = p_{\text{rms}}^2/\rho c_0 \quad (25)$$

where  $\rho$  = the fluid density (kg/m<sup>3</sup>) and  $c_0$  = speed of sound (m/s).

In the general case of sound propagation in a three-dimensional field, the sound intensity is the (net) flow of sound energy in unit time flowing through unit cross-sectional area. The intensity has magnitude and direction

$$I = pu_r = \langle p \cdot u_r \rangle_t = \frac{1}{T} \int_0^T p \cdot u_r dt \quad (26)$$

where  $p$  is the total fluctuating sound pressure, and  $u_r$  is the total fluctuating sound particle velocity in the  $r$  direction at the measurement point. The total sound pressure  $p$  and particle velocity  $u_r$  include the effects of incident and reflected sound waves.

## 5.5 Energy Density

Consider the case again of the oscillating piston in Fig. 11. We shall consider the sound energy that is produced by the oscillating piston, as it flows along the tube from the piston. We observe that the wavefront and the sound energy travel along the tube with velocity  $c_0$  metres/second. Thus after 1 s, a column of fluid of length  $c_0$  m contains all of the sound energy provided by the piston during the previous second. The total amount of energy  $E$  in this column equals the time-averaged sound intensity multiplied by the cross-sectional area  $S$ , which is from Eq. (22):

$$E = SI = Sp_{\text{rms}}^2/\rho c_0 \quad (27)$$

The sound per energy unit volume is known as the energy density  $\epsilon$ ,

$$\epsilon = [Sp_{\text{rms}}^2/\rho c_0]/c_0 S = p_{\text{rms}}^2/\rho c_0^2 \quad (28)$$

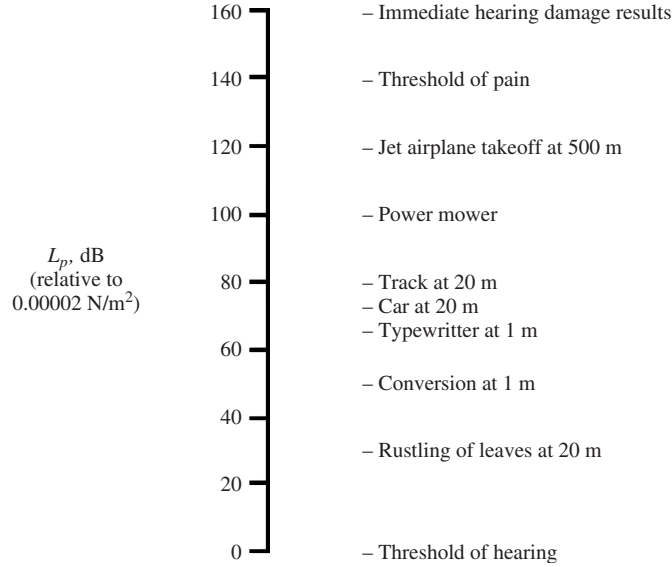
This result in Eq. (28) can also be shown to be true for other acoustic fields as well, as long as the total sound pressure is used in Eq. (28), and provided the location is not very close to a sound source.

## 5.6 Sound Power

Again in the case of the oscillating piston, we will consider the sound power radiated by the piston into the tube. The sound power radiated by the piston,  $W$ , is

$$W = SI \quad (29)$$





**Figure 12** Some typical sound pressure levels,  $L_p$ .

But from Eqs. (23) and (25) the power is

$$W = S(p_{\text{rms}} u_{\text{rms}}) \quad (29a)$$

and close to the piston, the rms particle velocity,  $u_{\text{rms}}$ , must be equal to the rms piston velocity. From Eq. (29a), we can write

$$W = S \rho c_0 v_{\text{rms}}^2 = 4\pi r^2 \rho c_0 v_{\text{rms}}^2 \quad (30)$$

where  $r$  is the piston and duct radius, and  $v_{\text{rms}}$  is the rms velocity of the piston.

## 6 DECIBELS AND LEVELS

The range of sound pressure magnitudes and sound powers of sources experienced in practice is very large. Thus, logarithmic rather than linear measures are often used for sound pressure and sound power. The most common measure of sound is the *decibel*. Decibels are also used to measure vibration, which can have a similar large range of magnitudes. The decibel represents a relative measurement or ratio. Each quantity in decibels is expressed as a ratio relative to a *reference sound pressure*, *sound power*, or *sound intensity*, or in the case of vibration relative to a *reference displacement*, *velocity*, or *acceleration*. Whenever a quantity is expressed in decibels, the result is known as a *level*.

The decibel (dB) is the ratio  $R_1$  given by

$$\log_{10} R_1 = 0.1 \quad 10 \log_{10} R_1 = 1 \text{ dB} \quad (31)$$

Thus,  $R_1 = 10^{0.1} = 1.26$ . The decibel is seen to represent the ratio 1.26. A larger ratio, the *bel*, is sometimes used. The bel is the ratio  $R_2$  given by

$\log_{10} R_2 = 1$ . Thus,  $R_2 = 10^1 = 10$ . The bel represents the ratio 10 and is thus much larger than a decibel.

### 6.1 Sound Pressure Level

The sound pressure level  $L_p$  is given by

$$\begin{aligned} L_p &= 10 \log_{10} \left( \frac{\langle p^2 \rangle_t}{p_{\text{ref}}^2} \right) = 10 \log_{10} \left( \frac{p_{\text{rms}}^2}{p_{\text{ref}}^2} \right) \\ &= 20 \log_{10} \left( \frac{p_{\text{rms}}}{p_{\text{ref}}} \right) \text{ dB} \end{aligned} \quad (32)$$

where  $p_{\text{ref}}$  is the reference pressure,  $p_{\text{ref}} = 20 \mu\text{Pa} = 0.00002 \text{ N/m}^2 (= 0.0002 \mu\text{bar})$  for air. This reference pressure was originally chosen to correspond to the quietest sound (at 1000 Hz) that the average young person can hear. The sound pressure level is often abbreviated as SPL. Figure 12 shows some sound pressure levels of typical sounds.

### 6.2 Sound Power Level

The sound power level of a source,  $L_W$ , is given by

$$L_W = 10 \log_{10} \left( \frac{W}{W_{\text{ref}}} \right) \text{ dB} \quad (33)$$

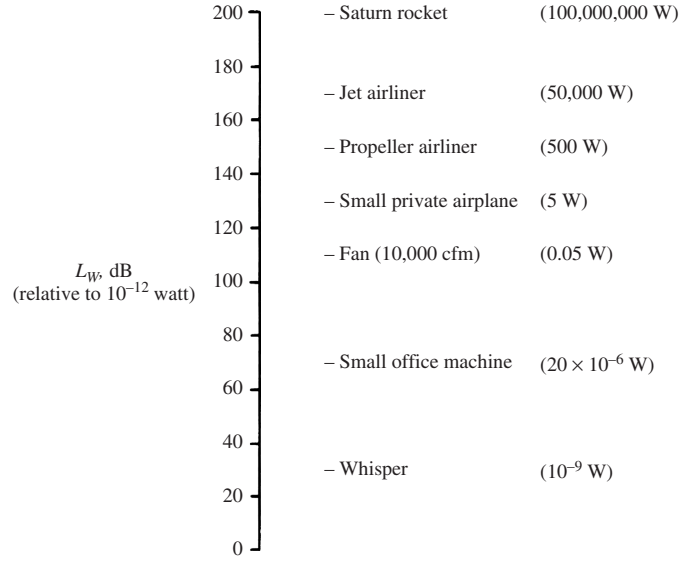
where  $W$  is the sound power of a source and  $W_{\text{ref}} = 10^{-12} \text{ W}$  is the reference sound power.

Some typical sound power levels are given in Fig. 13.

### 6.3 Sound Intensity Level

The sound intensity level  $L_I$  is given by

$$L_I = 10 \log_{10} \left( \frac{I}{I_{\text{ref}}} \right) \text{ dB} \quad (34)$$



**Figure 13** Some typical sound power levels,  $L_W$ .

where  $I$  is the component of the sound intensity in a given direction and  $I_{\text{ref}} = 10^{-12} \text{ W/m}^2$  is the reference sound intensity.

#### 6.4 Combination of Decibels

If the sound pressures  $p_1$  and  $p_2$  at a point produced by two independent sources are combined, the mean square pressure is

$$\begin{aligned}
 p_{\text{rms}}^2 &= \frac{1}{T} \int_0^T (p_1 + p_2)^2 dt = \langle p_1^2 + 2p_1p_2 + p_2^2 \rangle_t \\
 &= \langle p_1^2 \rangle_t + \langle p_2^2 \rangle_t + 2\langle p_1p_2 \rangle_t \equiv \overline{p_1^2} + \overline{p_2^2} \\
 &\quad + 2\overline{p_1p_2}, \quad (35)
 \end{aligned}$$

where  $\langle \rangle_t$  and the overbar indicate the time average  $\frac{1}{T} \int_0^T \langle \rangle dt$ .

Except for some special cases, such as two pure tones of the same frequency or the sounds from two correlated sound sources, the cross term  $2\langle p_1p_2 \rangle_t$  disappears if  $T \rightarrow \infty$ . Then in such cases, the mean square sound pressures  $\overline{p_1^2}$  and  $\overline{p_2^2}$  are additive, and the total mean square sound pressure at some point in space, if they are completely independent noise sources, may be determined using Eq. (35a).

$$p_{\text{rms}}^2 = \overline{p_1^2} + \overline{p_2^2} \quad (35a)$$

Let the two mean square pressure contributions to the total noise be  $p_{\text{rms}1}^2$  and  $p_{\text{rms}2}^2$  corresponding to sound pressure levels  $L_{p1}$  and  $L_{p2}$ , where  $L_{p2} = L_{p1} - \Delta$ . The total sound pressure level is given by

the sum of the individual contributions in the case of uncorrelated sources, and the total sound pressure level is given by forming the total sound pressure level by taking logarithms of Eq. (35a)

$$\begin{aligned}
 L_{pt} &= 10 \log[(p_{\text{rms}1}^2 + p_{\text{rms}2}^2)/p_{\text{ref}}^2] \\
 &= 10 \log(10^{L_{p1}/10} + 10^{L_{p2}/10}) \\
 &= 10 \log(10^{L_{p1}/10} + 10^{(L_{p1}-\Delta)/10}) \\
 &= 10 \log[10^{L_{p1}/10}(1 + 10^{-\Delta/10})] \\
 &= L_{p1} + 10 \log(1 + 10^{-\Delta/10}) \quad (35b)
 \end{aligned}$$

where,  $L_{pt}$  = combined sound pressure level due to both sources

$L_{p1}$  = greater of the two sound pressure level contributions

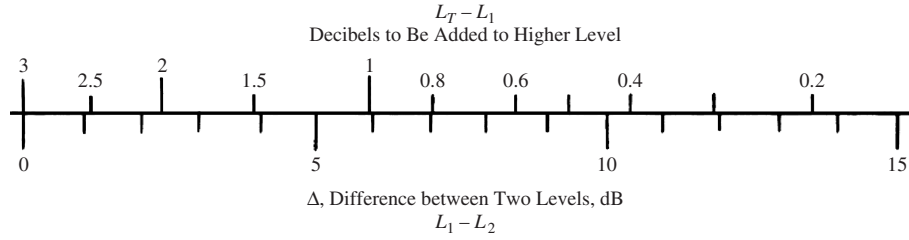
$\Delta$  = difference between the two contributions, all in dB

Equation (35b) is presented in Fig. 14.

**Example 1** If two independent noise sources each create sound pressure levels operating on their own of 80 dB, at a certain point, what is the total sound pressure level? *Answer:* The difference in levels is 0 dB; thus the total sound pressure level is  $80 + 3 = 83 \text{ dB}$ .

**Example 2** If two independent noise sources have sound power levels of 70 and 73 dB, what is the total level? *Answer:* The difference in levels is 3 dB; thus the total sound power level is  $73 + 1.8 = 74.8 \text{ dB}$ .

Figure 14 and these two examples do *not* apply to the case of two pure tones of the same frequency.



**Figure 14** Diagram for combination of two sound pressure levels or two sound power levels of uncorrelated sources.

*Note:* For the special case of two pure tones of the same amplitude and frequency, if  $p_1 = p_2$  (and the sound pressures are in phase at the point in space of the measurement):

$$L_{p_{\text{total}}} = 10 \log \left[ \frac{1}{T} \int_0^T (p_1 + p_2)^2 dt \right] \\ = L_{p_1} + 10 \log 4 \equiv L_{p_2} + 6 \text{ dB} \quad (36)$$

**Example 3** If  $p_1 = p_2 = 1 \text{ Pa}$  and the two sound pressures are of the same amplitude and frequency and in phase with each other, then the total sound pressure level

$$L_p(\text{total}) = 20 \log \left[ \frac{2}{20 \times 10^{-6}} \right] = 100 \text{ dB}$$

**Example 4** If  $p_1 = p_2 = 1 \text{ Pa}$  and the two sound pressures are of the same amplitude and frequency, but in opposite phase with each other, then the total sound pressure level

$$L_p(\text{total}) = 20 \log \left[ \frac{0}{20 \times 10^{-6}} \right] = -\infty \text{ dB}$$

For such a case as in Example 1 above, for pure-tone sounds, instead of 83 dB, the total sound pressure level can range anywhere between 86 dB (for in-phase sound pressures) and  $-\infty$  dB (for out-of-phase sound pressures). For the Example 2 above, the total sound power radiated by the two pure-tone sources depends on the phasing and separation distance.

## 7 HUMAN HEARING

Human hearing is most sensitive at about 4000 Hz. We can hear sound down to a frequency of about 15 or 16 Hz and up to about 15,000 to 16,000 Hz. However, at low frequency below about 200 Hz, we cannot hear sound at all well, unless the sound pressure level is quite high. See Chapters 19 and 20 for more details. Normal speech is in the range of about 100 to 4000 Hz with vowels mostly in the low- to medium-frequency range and consonants mostly in the high-frequency range. See Chapter 22. Music has a larger frequency range and can be at much higher sound pressure levels than the human voice. Figure 15 gives an idea of the approximate frequency and sound pressure level boundaries of speech, music, and the audible range

of human hearing. The lower boundary in Fig. 15 is called the threshold of hearing since sounds below this level cannot be heard by the average young person. The upper boundary is called the threshold of feeling since sounds much above this boundary can cause unpleasant sensations in the ear and even pain and, at high enough sound pressure levels, immediate damage to the hearing mechanism. See Chapter 21.

## 8 FREQUENCY ANALYSIS

Sound signals can be combined, but they can also be broken down into frequency components as shown by Fourier over 200 years ago. The ear seems to work as a frequency analyzer. We also can make instruments to analyze sound signals into frequency components.

Frequency analysis is commonly carried out using (a) constant frequency band filters and (b) constant percentage filters. The constant percentage filter (usually one-octave or one-third-octave band types) most parallels the way the human auditory system analyzes sound and, although digital processing has mostly overtaken analog processing of signals, it is still frequently used. See Chapters 40, 41, and 42 for more details about filters, signal processing, and data analysis.

The following symbol notation is used in Sections 8.1 and 8.2:  $f_L$  and  $f_U$  are the lower and upper cutoff frequencies, and  $f_C$  and  $\Delta f$  are the band center frequency and the frequency bandwidth, respectively. Thus  $\Delta f = f_U - f_L$ . See Fig. 16.

### 8.1 One-Octave Bands

For one-octave bands, the cutoff frequencies  $f_L$  and  $f_U$  are defined as follows:

$$f_L = f_C / \sqrt{2} \\ f_U = \sqrt{2} f_C$$

The center frequency (or geometric mean) is

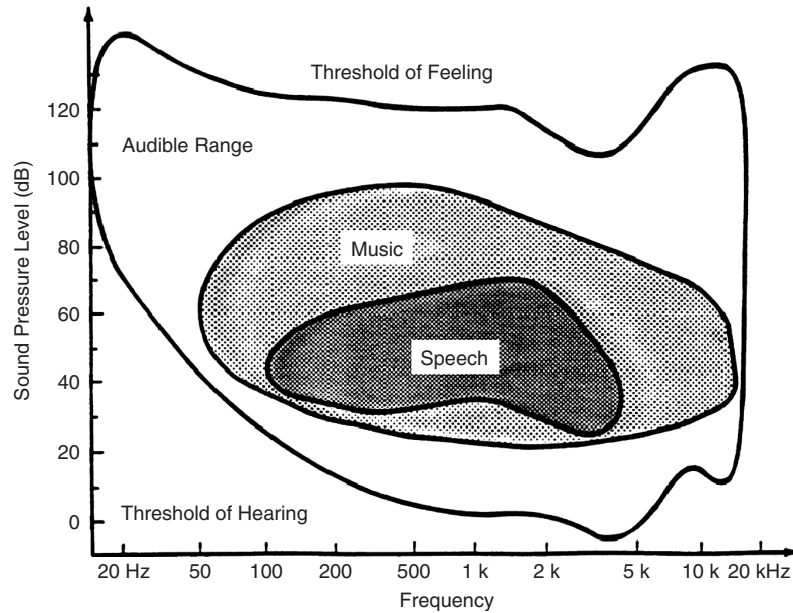
$$f_C = \sqrt{f_L f_U}$$

Thus

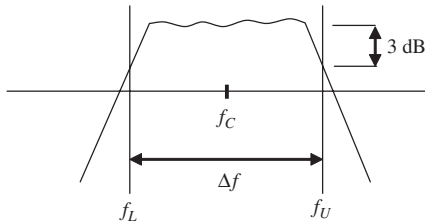
$$f_U / f_L = 2$$

The bandwidth  $\Delta f$  is given by

$$\Delta f = f_U - f_L = f_C(\sqrt{2} - 1/\sqrt{2}) = f_C/\sqrt{2}$$



**Figure 15** Sound pressure level versus frequency for the audible range, typical music range, and range of speech.



**Figure 16** Typical frequency response of a filter of center frequency  $f_C$  and upper and lower cutoff frequencies,  $f_U$  and  $f_L$ .

so

$$\Delta f \approx 70\%(f_C)$$

## 8.2 One-Third-Octave Bands

For one-third-octave bands the cutoff frequencies,  $f_L$  and  $f_U$ , are defined as follows:

$$f_L = f_C / \sqrt[6]{2} = f_C / 2^{1/6}$$

$$f_U = f_C 2^{1/6}$$

The center frequency (geometric mean) is given by

$$f_C = \sqrt{f_L f_U}$$

Thus

$$f_U / f_L = 2^{1/3}$$

The bandwidth  $\Delta f$  is given by

$$\Delta f = f_U - f_L = f_C (2^{1/6} - 2^{-1/6})$$

so

$$\Delta f \approx 23\%(f_C)$$

## NOTE

1. The center frequencies of one-octave bands are related by 2, and 10 frequency bands are used to cover the human hearing range. They have center frequencies of 31.5, 63, 125, 250, 500, 1000, 2000, 4000, 8000, 16,000 Hz.
2. The center frequencies of one-third octave bands are related by  $2^{1/3}$  and 10 cover a decade of frequency, and thus 30 frequency bands are used to cover the human hearing range: 20, 25, 31.5, 40, 50, 63, 80, 100, 125, 160, ... 16,000 Hz.

## 9 FREQUENCY WEIGHTING (A, B, C, D)

Other filters are often used to simulate the hearing system of humans. The relative responses of A-, B-, C-, and D-weighting filters are shown in Fig. 17. The most commonly used is the A-weighting filter. These filter weightings are related to human response to pure tone sounds, although they are often used to give an approximate evaluation of the loudness of noise as well. Chapter 21 discusses the loudness of sound in more detail.

## 10 EQUIVALENT SOUND PRESSURE LEVEL ( $L_{eq}$ )

The equivalent sound pressure level,  $L_{eq}$ , has become very frequently used in many countries in the last 20 to 25 years to evaluate industrial noise, community noise near airports, railroads, and highways. See Chapter 34

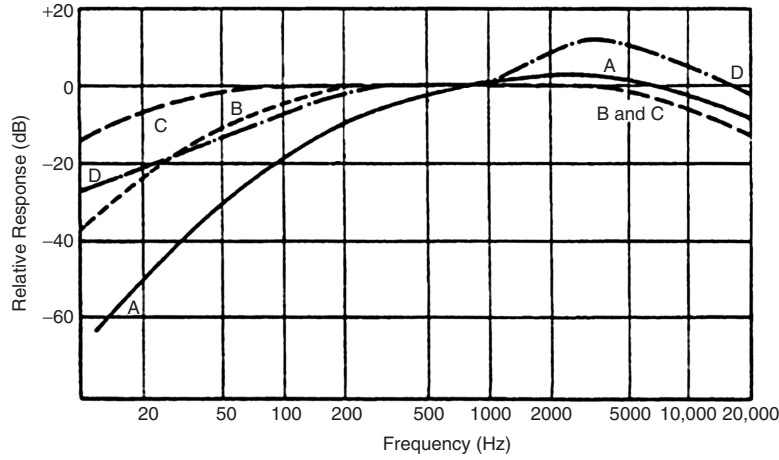


Figure 17 Frequency weightings.

for more details. The equivalent sound pressure level is defined by

$$L_{eq} = 10 \log \left[ \frac{\overline{p_{rms}^2}}{p_{ref}^2} \right] = 10 \log \frac{1}{T} \int_0^T 10^{L(t)/10} dt$$

$$= 10 \log \frac{1}{N} \sum_{i=1}^N 10^{L_i/10} \quad (37)$$

The averaging time  $T$  can be, for example, 1 h, 8 h, 1 day, 1 week, 1 month, and so forth.  $L(t)$  is the short-time average. See Fig. 18a.  $L_i$  can be a set of short-time averages for  $L_p$  over set periods. If the sound pressure levels,  $L_i$ , are values averaged over constant time periods such as one hour, then they can be summed as in Eq. (37). See Fig. 18b. The sound pressure signal is normally filtered with an A-weighting filter.

### 11 DAY-NIGHT SOUND PRESSURE LEVEL ( $L_{dn}$ )

In some countries, penalties are made for noise made at night. For instance in the United States the so-called day-night level is defined by

$$L_{dn} = 10 \log \left[ \frac{1}{24} \left\{ \int_{07:00}^{22:00} 10^{L_p/10} dt + \int_{22:00}^{07:00} 10^{(L_p+10)/10} dt \right\} \right] \quad (38)$$

The day-night level  $L_{dn}$  has a 10-dB penalty applied between the hours of 22:00 and 07:00. See Eq. (38).

The sound pressure level  $L_p$  readings (short time) used in Eq. (38) are normally A-weighted. The day-night descriptor can also be written

$$L_{dn} = 10 \log \left[ \frac{1}{24} \{ 15 \times 10^{L_{eqd}/10} + 9 \times 10^{(L_{eqn}+10)/10} \} \right] \quad (39)$$

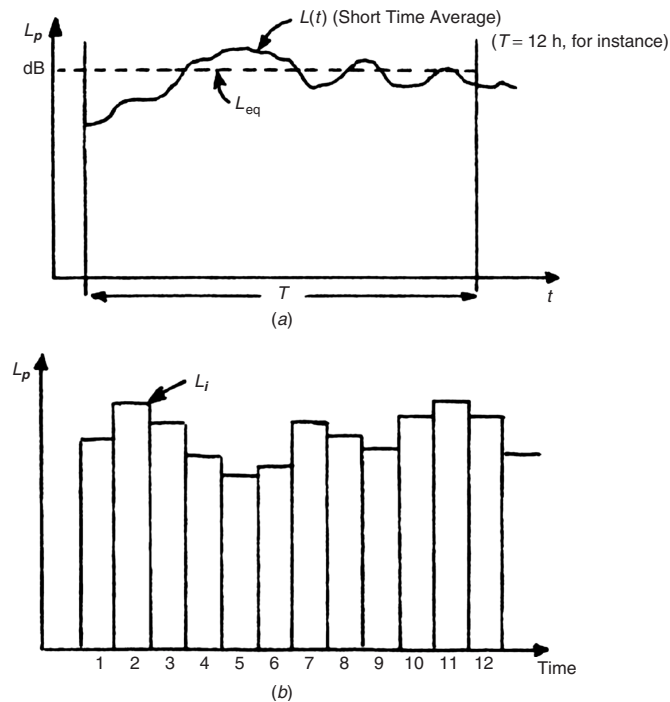
where  $L_{eqd}$  is the A-weighted daytime equivalent sound pressure level (from 07:00 to 22:00) and  $L_{eqn}$  is the night-time A-weighted sound pressure level (from 22:00 to 07:00).

### 12 DAY-EVENING-NIGHT SOUND PRESSURE LEVEL ( $L_{den}$ )

In some countries, separate penalties are made for noise made during evening and night periods. For instance, the so-called day-evening-night level is defined by

$$L_{den} = 10 \log \left[ \frac{1}{24} \left\{ \int_{07:00}^{19:00} 10^{L_p/10} dt + \int_{19:00}^{22:00} 10^{(L_p+5)/10} dt + \int_{22:00}^{07:00} 10^{(L_p+10)/10} dt \right\} \right] \quad (40)$$

The day-evening-night level  $L_{den}$  has a 5-dB penalty applied during the evening hours (here shown as 19:00 to 22:00) and a 10-dB penalty applied between the hours of 22:00 and 07:00. See Eq. (40). Local jurisdictions can set the evening period to be different



**Figure 18** Equivalent sound pressure level.

from 19:00 to 22:00, if they wish to do so for their community.

## REFERENCES

1. D. A. Bies and C. H. Hansen, *Engineering Noise Control—Theory and Practice*, 3rd ed., E & FN Spon, London, 2003.
2. L. H. Bell, *Industrial Noise Control—Fundamentals and Applications*, Marcel Dekker, New York, 1982.
3. D. E. Hall, *Basic Acoustics*, Wiley, New York, 1987.
4. L. E. Kinsler, A. R. Frey, A. B. Coppens and J. V. Sanders, *Fundamentals of Acoustics*, 4th ed., Wiley, New York, 1999.
5. F. J. Fahy and J. G. Walker (Eds.), *Fundamentals of Noise and Vibration*, E & FN Spon, London, 1998.
6. M. J. Lighthill, *Waves in Fluids*, Cambridge University Press, Cambridge, 1978.
7. A. D. Pierce, *Acoustics: An Introduction to Its Physical Properties and Applications*, McGraw-Hill, New York, 1981 (reprinted by the Acoustical Society of America, 1989).

**PART I**

---

**FUNDAMENTALS OF  
ACOUSTICS AND NOISE**

# CHAPTER 2

## THEORY OF SOUND – PREDICTIONS AND MEASUREMENT

Malcolm J. Crocker

Department of Mechanical Engineering  
Auburn University  
Auburn, Alabama

### 1 INTRODUCTION

The fluid mechanics equations, from which the acoustics equations and results may be derived, are quite complicated. However, because most acoustical phenomena involve very small perturbations from steady-state conditions, it is possible to make significant simplifications to these fluid equations and to linearize them. The results are the equations of linear acoustics. The most important equation, the wave equation, is presented in this chapter together with some of its solutions. Such solutions give the sound pressure explicitly as functions of time and space, and the general approach may be termed the wave acoustics approach. This chapter presents some of the useful results of this approach but also briefly discusses some of the other alternative approaches, sometimes termed ray acoustics and energy acoustics that are used when the wave acoustics approach becomes too complicated.

The first purpose of this chapter is to present some of the most important acoustics formulas and definitions, without derivation, which are used in the chapters following in Part I and in many of the other chapters of this handbook. The second purpose is to make some helpful comments about the chapters that follow in Part I and about other chapters as seems appropriate.

### 2 WAVE MOTION

Some of the basic concepts of acoustics and sound wave propagation used in Part I and also throughout the rest of this book are discussed here. For further discussion of some of these basic concepts and/or a more advanced mathematical treatment of some of them, the reader is referred to Chapters 3, 4, and 5 and later chapters in this book. The chapters in Part I of the *Handbook of Acoustics*<sup>1</sup> and other texts<sup>2–12</sup> are also useful for further discussion on fundamentals and applications of the theory of noise and vibration problems.

Wave motion is easily observed in the waves on stretched strings and as ripples on the surface of water. Waves on strings and surface water waves are very similar to sound waves in air (which we cannot see), but there are some differences that are useful to discuss. If we throw a stone into a calm lake, we observe that the water waves (*ripples*) travel out from the point where the stone enters the water. The ripples spread out circularly from the source at the

wave speed, which is independent of the wave height. Somewhat like the water ripples, sound waves in air travel at a constant speed, which is proportional to the square root of the absolute temperature and is almost independent of the sound wave strength. The wave speed is known as the speed of sound. Sound waves in air propagate by transferring momentum and energy between air particles. Sound wave motion in air is a disturbance that is imposed onto the random motion of the air molecules (known as Brownian motion). The mean speed of the molecular random motion and rate of molecular interaction increases with the absolute temperature of the gas. Since the momentum and sound energy transfer occurs through the molecular interaction, the sound wave speed is dependent solely upon the absolute temperature of the gas and *not* upon the strength of the sound wave disturbance. There is no net flow of air away from a source of sound, just as there is no net flow of water away from the source of water waves. Of course, unlike the waves on the surface of a lake, which are circular or two dimensional, sound waves in air in general are spherical or three dimensional.

As water waves move away from a source, their curvature decreases, and the *wavefronts* may be regarded almost as straight lines. Such waves are observed in practice as *breakers* on the seashore. A similar situation occurs with sound waves in the atmosphere. At large distances from a source of sound, the spherical wavefront curvature decreases, and the wavefronts may be regarded almost as plane surfaces.

Plane sound waves may be defined as waves that have the same acoustical properties at any position on a plane surface drawn perpendicular to the direction of propagation of the wave. Such plane sound waves can exist and propagate along a long straight tube or duct (such as an air-conditioning duct). In such a case, the waves propagate in a direction along the duct axis and the plane wave surfaces are perpendicular to this direction (and are represented by duct cross sections). Such waves in a duct are one dimensional, like the waves traveling along a long string or rope under tension (or like the ocean breakers described above).

Although there are many similarities between one-dimensional sound waves in air, waves on strings, and surface water waves, there are some differences. In a fluid such as air, the fluid particles vibrate back and forth in the same direction as the direction of wave propagation; such waves are known as longitudinal,



compressional, or sound waves. On a stretched string, the particles vibrate at right angles to the direction of wave propagation; such waves are usually known as transverse waves. The surface water waves described are partly transverse and partly longitudinal, with the complication that the water particles move up and down and back and forth horizontally. (This movement describes elliptical paths in shallow water and circular paths in deep water. The vertical particle motion is much greater than the horizontal motion for shallow water, but the two motions are equal for deep water.) The water wave direction is, of course, horizontal.

Surface water waves are not compressional (like sound waves) and are normally termed surface gravity waves. Unlike sound waves, where the wave speed is independent of frequency, long wavelength surface water waves travel faster than short wavelength waves, and thus water wave motion is said to be dispersive. Bending waves on beams, plates, cylinders, and other engineering structures are also dispersive (see Chapter 10). There are several other types of waves that can be of interest in acoustics: shear waves, torsional waves, and boundary waves (see Chapter 12 in the *Encyclopedia of Acoustics*<sup>13</sup>), but the discussion here will concentrate on sound wave propagation in fluids.

### 3 PLANE SOUND WAVES

If a disturbance in a thin cross-sectional element of fluid in a duct is considered, a mathematical description of the motion may be obtained by assuming that (1) the amount of fluid in the element is conserved, (2) the net longitudinal force is balanced by the inertia of the fluid in the element, (3) the compressive process in the element is adiabatic (i.e., there is no flow of heat in or out of the element), and (4) the undisturbed fluid is stationary (there is no fluid flow). Then the following equation of motion may be derived:

$$\frac{\partial^2 p}{\partial x^2} - \frac{1}{c^2} \frac{\partial^2 p}{\partial t^2} = 0 \quad (1)$$

where  $p$  is the sound pressure,  $x$  is the coordinate, and  $t$  is the time.

This equation is known as the one-dimensional equation of motion, or acoustic wave equation. Similar wave equations may be written if the sound pressure  $p$  in Eq. (1) is replaced with the particle displacement  $\xi$ , the particle velocity  $u$ , condensation  $s$ , fluctuating density  $\rho'$ , or the fluctuating absolute temperature  $T'$ . The derivation of these equations is in general more complicated. However, the wave equation in terms of the sound pressure in Eq. (1) is perhaps most useful since the sound pressure is the easiest acoustical quantity to measure (using a microphone) and is the acoustical perturbation we sense with our ears. It is normal to write the wave equation in terms of sound pressure  $p$ , and to derive the other variables,  $\xi$ ,  $u$ ,  $s$ ,  $\rho'$ , and  $T'$  from their relations with the sound pressure  $p$ .<sup>4</sup> The sound pressure  $p$  is the acoustic pressure

perturbation or fluctuation about the time-averaged, or undisturbed, pressure  $p_0$ .

The speed of sound waves  $c$  is given for a perfect gas by

$$c = (\gamma RT)^{1/2} \quad (2)$$

The speed of sound is proportional to the square root of the absolute temperature  $T$ . The ratio of specific heats  $\gamma$  and the gas constant  $R$  are constants for any particular gas. Thus Eq. (2) may be written as

$$c = c_0 + 0.6T_c \quad (3)$$

where, for air,  $c_0 = 331.6$  m/s, the speed of sound at  $0^\circ\text{C}$ , and  $T_c$  is the temperature in degrees Celsius. Note that Eq. (3) is an approximate formula valid for  $T_c$  near room temperature. The speed of sound in air is almost completely dependent on the air temperature and is almost independent of the atmospheric pressure. For a complete discussion of the speed of sound in fluids, see Chapter 5 in the *Handbook of Acoustics*.<sup>1</sup>

A solution to (1) is

$$p = f_1(ct - x) + f_2(ct + x) \quad (4)$$

where  $f_1$  and  $f_2$  are arbitrary functions such as sine, cosine, exponential, log, and so on. It is easy to show that Eq. (4) is a solution to the wave equation (1) by differentiation and substitution into Eq. (1). Varying  $x$  and  $t$  in Eq. (4) demonstrates that  $f_1(ct - x)$  represents a wave traveling in the positive  $x$  direction with wave speed  $c$ , while  $f_2(ct + x)$  represents a wave traveling in the negative  $x$  direction with wave speed  $c$  (see Fig. 1).

The solution given in Eq. (4) is usually known as the *general solution* since, in principle, any type of sound waveform is possible. In practice, sound waves are usually classified as impulsive or steady in time. One particular case of a steady wave is of considerable importance. Waves created by sources vibrating sinusoidally in time (e.g., a loudspeaker, a piston, or a more complicated structure vibrating with a discrete angular frequency  $\omega$ ) both in time  $t$  and space  $x$  in a sinusoidal manner (see Fig. 2):

$$p = p_1 \sin(\omega t - kx + \phi_1) + p_2 \sin(\omega t + kx + \phi_2) \quad (5)$$

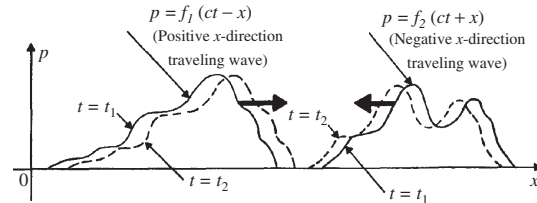


Figure 1 Plane waves of arbitrary waveform.

At any point in space,  $x$ , the sound pressure  $p$  is simple harmonic in time. The first expression on the right of Eq. (5) represents a wave of amplitude  $p_1$  traveling in the positive  $x$  direction with speed  $c$ , while the second expression represents a wave of amplitude  $p_2$  traveling in the negative  $x$  direction. The symbols  $\phi_1$  and  $\phi_2$  are phase angles, and  $k$  is the *acoustic wavenumber*. It is observed that the wavenumber  $k = \omega/c$  by studying the ratio of  $x$  and  $t$  in Eqs. (4) and (5). At some instant  $t$  the sound pressure pattern is sinusoidal in space, and it repeats itself each time  $kx$  is increased by  $2\pi$ . Such a repetition is called a wavelength  $\lambda$ . Hence,  $k\lambda = 2\pi$  or  $k = 2\pi/\lambda$ . This gives  $\omega/c = 2\pi/\lambda = 2\pi/\lambda$ , or

$$\lambda = \frac{c}{f} \quad (6)$$

The wavelength of sound becomes smaller as the frequency is increased. In air, at 100 Hz,  $\lambda \approx 3.5 \text{ m} \approx 10 \text{ ft}$ . At 1000 Hz,  $\lambda \approx 0.35 \text{ m} \approx 1 \text{ ft}$ . At 10,000 Hz,  $\lambda \approx 0.035 \text{ m} \approx 0.1 \text{ ft} \approx 1 \text{ in}$ .

At some point  $x$  in space, the sound pressure is sinusoidal in time and goes through one complete cycle when  $\omega$  increases by  $2\pi$ . The time for a cycle is called the period  $T$ . Thus,  $\omega T = 2\pi$ ,  $T = 2\pi/\omega$ , and

$$T = \frac{1}{f} \quad (7)$$

#### 4 IMPEDANCE AND SOUND INTENSITY

We see that for the one-dimensional propagation considered, the sound wave disturbances travel with a constant wave speed  $c$ , although there is no net, time-averaged movement of the air particles. The air particles oscillate back and forth in the direction of wave propagation ( $x$  axis) with velocity  $u$ . We may show that for any plane wave traveling in the positive  $x$  direction at any instant

$$\frac{p}{u} = \rho c \quad (8)$$

and for any plane wave traveling in the negative  $x$  direction

$$\frac{p}{u} = -\rho c \quad (9)$$

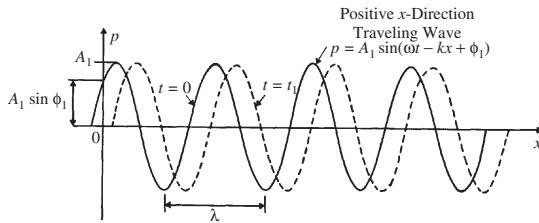


Figure 2 Simple harmonic plane waves.

The quantity  $\rho c$  is known as the characteristic impedance of the fluid, and for air,  $\rho c = 428 \text{ kg/m}^2 \text{ s}$  at  $0^\circ\text{C}$  and  $415 \text{ kg/m}^2 \text{ s}$  at  $20^\circ\text{C}$ .

The *sound intensity* is the rate at which the sound wave does work on an imaginary surface of unit area in a direction perpendicular to the surface. Thus, it can be shown that the *instantaneous* sound intensity in the  $x$  direction,  $I$ , is obtained by multiplying the *instantaneous* sound pressure  $p$  by the *instantaneous* particle velocity in the  $x$  direction,  $u$ . Therefore

$$I = pu \quad (10)$$

and for a plane wave traveling in the positive  $x$  direction this becomes

$$I = \frac{p^2}{\rho c} \quad (11)$$

The time-averaged sound intensity for a plane wave traveling in the positive  $x$  direction,  $\langle I \rangle_t$ , is given as

$$\langle I \rangle_t = \frac{\langle p^2 \rangle_t}{\rho c} \quad (12)$$

and for the special case of a sinusoidal (pure-tone) sound wave

$$\langle I \rangle_t = \frac{\langle p^2 \rangle_t}{\rho c} = \frac{\hat{p}^2}{2\rho c} \quad (13)$$

where  $\hat{p}$  is the sound pressure amplitude, and the mean-square sound pressure is thus  $\langle p^2 \rangle_t = p_{\text{rms}}^2 = \frac{1}{2}\hat{p}^2$ .

We note, in general, for sound propagation in three dimensions that the instantaneous sound intensity  $\mathbf{I}$  is a vector quantity equal to the product of the sound pressure and the instantaneous particle velocity  $\mathbf{u}$ . Thus  $\mathbf{I}$  has magnitude and direction. The vector intensity  $\mathbf{I}$  may be resolved into components  $\mathbf{I}_x$ ,  $\mathbf{I}_y$ , and  $\mathbf{I}_z$ . For a more complete discussion of sound intensity and its measurement see Chapter 45 and Chapter 156 in the *Handbook of Acoustics*<sup>1</sup> and the book by Fahy.<sup>9</sup>

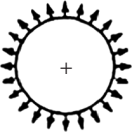
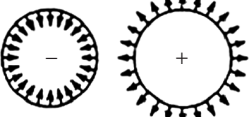
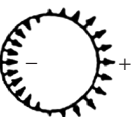


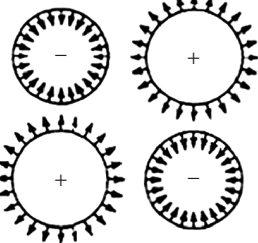
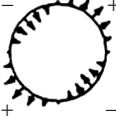



#### 5 THREE-DIMENSIONAL WAVE EQUATION

In most sound fields, sound propagation occurs in two or three dimensions. The three-dimensional version of Eq. (1) in Cartesian coordinates is

$$\frac{\partial^2 p}{\partial x^2} + \frac{\partial^2 p}{\partial y^2} + \frac{\partial^2 p}{\partial z^2} - \frac{1}{c^2} \frac{\partial^2 p}{\partial t^2} = 0 \quad (14)$$

This equation is useful if sound wave propagation in rectangular spaces such as rooms is being considered. However, it is helpful to recast Eq. (14) in spherical coordinates if sound propagation from sources of sound in free space is being considered. It is a simple mathematical procedure to transform Eq. (14) into spherical coordinates, although the resulting equation

**Table 1 Models of Idealized Spherical Sources: Monopole, Dipole, and Quadrupole<sup>a</sup>**

Monopole Distribution Representation	Velocity Distribution on Spherical Surface	Oscillating Sphere Representation	Oscillating Force Model
Monopole 			
Dipole 	Dipole 	Dipole 	Dipole 
Quadrupole (Lateral quadrupole shown) 	Quadrupole (Lateral quadrupole shown) 	Quadrupole (Lateral quadrupole shown) 	Quadrupole  Quadrupole 

<sup>a</sup> For simple harmonic sources, after one half-period the velocity changes direction; positive sources become negative and vice versa, and forces reverse direction with dipole and quadrupole force models.

is quite complicated. However, for propagation of sound waves from a spherically symmetric source (such as the idealized case of a pulsating spherical balloon known as an omnidirectional or monopole source) (Table 1), the equation becomes quite simple (since there is no angular dependence):

$$\frac{1}{r^2} \frac{\partial}{\partial r} \left( r^2 \frac{\partial p}{\partial r} \right) - \frac{1}{c^2} \frac{\partial^2 p}{\partial t^2} = 0 \quad (15a)$$

After some algebraic manipulation Eq. (15a) can be written as

$$\frac{\partial^2(rp)}{\partial r^2} - \frac{1}{c^2} \frac{\partial^2(rp)}{\partial t^2} = 0 \quad (15b)$$

Here,  $r$  is the distance from the origin and  $p$  is the sound pressure at that distance.

Equation (15a) is identical in form to Eq. (1) with  $p$  replaced by  $rp$  and  $x$  by  $r$ . The general and simple harmonic solutions to Eq. (15a) are thus the same as Eqs. (4) and (5) with  $p$  replaced by  $rp$  and  $x$  with  $r$ . The general solution is

$$rp = f_1(ct - r) + f_2(ct + r) \quad (16)$$

or

$$p = \frac{1}{r} f_1(ct - r) + \frac{1}{r} f_2(ct + r) \quad (17)$$

where  $f_1$  and  $f_2$  are arbitrary functions. The first term on the right of Eq. (17) represents a wave traveling outward from the origin; the sound pressure  $p$  is seen to be inversely proportional to the distance  $r$ . The second term in Eq. (17) represents a sound wave traveling inward toward the origin, and in most practical cases such waves can be ignored (if reflecting surfaces are absent).

The simple harmonic (pure-tone) solution of Eq. (15) is

$$p = \frac{A_1}{r} \sin(\omega t - kr + \phi_1) + \frac{A_2}{r} \sin(\omega t + kr + \phi_2). \quad (18)$$

We may now write that the constants  $A_1$  and  $A_2$  may be written as  $A_1 = \hat{p}_1 r$  and  $A_2 = \hat{p}_2 r$ , where  $\hat{p}_1$  and  $\hat{p}_2$  are the sound pressure amplitudes at unit distance (usually m) from the origin.

## 6 SOURCES OF SOUND

The second term on the right of Eq. (18), as before, represents sound waves traveling inward to the origin

and is of little practical interest. However, the first term represents simple harmonic waves of angular frequency  $\omega$  traveling outward from the origin, and this may be rewritten as<sup>6</sup>

$$p = \frac{\rho c k Q}{4\pi r} \sin(\omega t - kr + \phi_1) \quad (19)$$

where  $Q$  is termed the *strength of an omnidirectional (monopole) source* situated at the origin, and  $Q = 4\pi A_1 / \rho c k$ . The mean-square sound pressure  $p_{\text{rms}}^2$  may be found<sup>6</sup> by time averaging the square of Eq. (19) over a period  $T$ :

$$p_{\text{rms}}^2 = \frac{(\rho c k)^2 Q^2}{32\pi^2 r^2} \quad (20)$$

From Eq. (20), the mean-square pressure is seen to vary with the inverse square of the distance  $r$  from the origin of the source for such an idealized omnidirectional point sound source everywhere in the sound field. Again, this is known as the *inverse square law*. If the distance  $r$  is doubled, the sound pressure level [see Eq. (29) in Chapter 1] decreases by  $20 \log_{10}(2) = 20(0.301) = 6$  dB. If the source is idealized as a sphere of radius  $a$  pulsating with a simple harmonic velocity amplitude  $U$ , we may show that  $Q$  has units of volume flow rate (cubic metres per second). If the source radius is small in wavelengths so that  $a \leq \lambda$  or  $ka \leq 2\pi$ , then we can show that the strength  $Q = 4\pi a^2 U$ .

Many sources of sound are not like the simple omnidirectional monopole source just described. For example, an un baffled loudspeaker produces sound both from the back and front of the loudspeaker. The sound from the front and the back can be considered as two sources that are  $180^\circ$  out of phase with each other. This system can be modeled<sup>6,9</sup> as two out-of-phase monopoles of source strength  $Q$  separated by a distance  $l$ . Provided  $l \ll \lambda$ , the sound pressure produced by such a dipole system is

$$p = \frac{\rho c k Q l \cos \theta}{4\pi r} \left[ \frac{1}{r} \sin(\omega t - kr + \phi) + k \cos(\omega t - kr + \phi) \right] \quad (21)$$

where  $\theta$  is the angle measured from the axis joining the two sources (the loudspeaker axis in the practical case). Unlike the monopole, the dipole field is not omnidirectional. The sound pressure field is directional. It is, however, symmetric and shaped like a figure-eight with its lobes on the dipole axis, as shown in Fig. 7b.

The sound pressure of a dipole source has near-field and far-field regions that exhibit similar behaviors to the particle velocity near-field and far-field regions of a monopole. Close to the source (the near field), for some fixed angle  $\theta$ , the sound pressure falls

off rapidly,  $p \propto 1/r^2$ , while far from the source (the far field  $kr \geq 1$ ), the pressure falls off more slowly,  $p \propto 1/r$ . In the near field, the sound pressure level decreases by 12 dB for each doubling of distance  $r$ . In the far field the decrease in sound pressure level is only 6 dB for doubling of  $r$  (like a monopole). The phase of the sound pressure also changes with distance  $r$ , since close to the source the sine term dominates and far from the source the cosine term dominates. The particle velocity may be obtained from the sound pressure [Eq. (21)] and use of Euler's equation [see Eq. (22)]. It has an even more complicated behavior with distance  $r$  than the sound pressure, having three distinct regions.

An oscillating force applied at a point in space gives rise to results identical to Eq. (21), and hence there are many real sources of sound that behave like the idealized dipole source described above, for example, pure-tone fan noise, vibrating beams, un baffled loudspeakers, and even wires and branches (which sing in the wind due to alternate vortex shedding) (see Chapters 3, 6, 9, and 71).

The next higher order source is the quadrupole. It is thought that the sound produced by the mixing process in an air jet gives rise to stresses that are quadrupole in nature. See Chapters 9, 27, and 28. Quadrupoles may be considered to consist of two opposing point forces (two opposing dipoles) or equivalently four monopoles. (See Table 1.) We note that some authors use slightly different but equivalent definitions for the source strength of monopoles, dipoles, and quadrupoles. The definitions used in Sections 6 and 8 of this chapter are the same as in Crocker and Price<sup>6</sup> and Fahy<sup>9</sup> and result in expressions for sound pressure, sound intensity, and sound power, which although equivalent are different in form from those in Chapter 9, for example.

The expression for the sound pressure for a quadrupole is even more complicated than for a dipole. Close to the source, in the near field, the sound pressure  $p \propto 1/r^3$ . Farther from the sound source,  $p \propto 1/r^2$ ; while in the far field,  $p \propto 1/r$ .

Sound sources experienced in practice are normally even more complicated than dipoles or quadrupoles. The sound radiation from a vibrating piston is described in Chapter 3. Chapters 9 and 11 in the *Handbook of Acoustics*<sup>1</sup> also describe radiation from dipoles and quadrupoles and the sound radiation from vibrating cylinders in Chapter 9 of the same book.<sup>1</sup>

The discussion in Chapter 3 considers steady-state radiation. However, there are many sources in nature and created by people that are transient. As shown in Chapter 9 of the *Handbook of Acoustics*,<sup>1</sup> the harmonic analysis of these cases is often not suitable, and time-domain methods have given better results and understanding of the phenomena. These are the approaches adopted in Chapter 9 of the *Handbook of Acoustics*.<sup>1</sup>

## 7 SOUND INTENSITY

The radial particle velocity in a nondirectional spherically spreading sound field is given by Euler's equation

as

$$u = -\frac{1}{\rho} \int \frac{\partial p}{\partial r} dt \quad (22)$$

and substituting Eqs. (19) and (22) into (10) and then using Eq. (20) and time averaging gives the magnitude of the radial sound intensity in such a field as

$$\langle I \rangle_t = \frac{p_{\text{rms}}^2}{\rho c} \quad (23)$$

the same result as for a plane wave [see Eq. (12)]. The sound intensity decreases with the inverse square of the distance  $r$ . Simple omnidirectional monopole sources radiate equally well in all directions. More complicated idealized sources such as dipoles, quadrupoles, and vibrating piston sources create sound fields that are directional. Of course, real sources such as machines produce even more complicated sound fields than these idealized sources. (For a more complete discussion of the sound fields created by idealized sources, see Chapter 3 of this book and Chapters 3 and 8 in the *Handbook of Acoustics*.<sup>1</sup>) However, the same result as Eq. (23) is found to be true for any source of sound as long as the measurements are made sufficiently far from the source. The intensity is not given by the simple result of Eq. (23) close to idealized sources such as dipoles, quadrupoles, or more complicated real sources of sound such as vibrating structures. Close to such sources Eq. (10) must be used for the instantaneous radial intensity, and

$$\langle I \rangle_t = \langle pu \rangle_t \quad (24)$$

for the time-averaged radial intensity.

The time-averaged radial sound intensity in the far field of a dipole is given by<sup>6</sup>

$$\langle I \rangle_t = \frac{\rho c k^4 (Ql)^2 \cos^2 \theta}{32\pi^2 r^2}. \quad (25)$$

## 8 SOUND POWER OF SOURCES

### 8.1 Sound Power of Idealized Sound Sources

The *sound power*  $W$  of a sound source is given by integrating the intensity over any imaginary closed surface  $S$  surrounding the source (see Fig. 3):

$$W = \int_S \langle I_n \rangle_t dS \quad (26)$$

The normal component of the intensity  $I_n$  must be measured in a direction perpendicular to the elemental area  $dS$ . If a spherical surface, whose center coincides with the source, is chosen, then the sound power of an omnidirectional (monopole) source is

$$W_m = \langle I_r \rangle_t 4\pi r^2 \quad (27a)$$

$$W_m = \frac{p_{\text{rms}}^2}{\rho c} 4\pi r^2 \quad (27b)$$

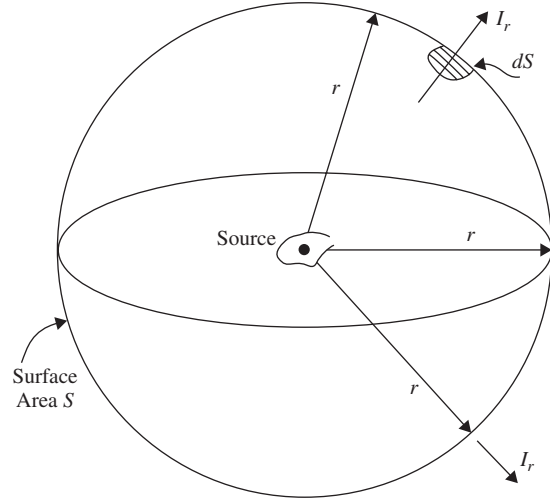


Figure 3 Imaginary surface area  $S$  for integration.

and from Eq. (20) the sound power of a monopole is<sup>6,9</sup>

$$W_m = \frac{\rho c k^2 Q^2}{8\pi} \quad (28)$$

It is apparent from Eq. (28) that the sound power of an idealized (monopole) source is independent of the distance  $r$  from the origin, at which the power is calculated. This is the result required by conservation of energy and also to be expected for all sound sources.

Equation (27b) shows that for an omnidirectional source (in the absence of reflections) the sound power can be determined from measurements of the mean-square sound pressure made with a single microphone. Of course, for real sources, in environments where reflections occur, measurements should really be made very-close to the source, where reflections are presumably less important.

The sound power of a dipole source is obtained by integrating the intensity given by Eq. (25) over a sphere around the source. The result for the sound power is

$$W_d = \frac{\rho c k^4 (Ql)^2}{24\pi} \quad (29)$$

The dipole is obviously a much less efficient radiator than a monopole, particularly at low frequency.

In practical situations with real directional sound sources and where background noise and reflections are important, use of Eq. (27b) becomes difficult and less accurate, and then the sound power is more conveniently determined from Eq. (26) with a sound intensity measurement system. See Chapter 45 in this book and Chapter 106 in the *Handbook of Acoustics*.<sup>1</sup>

We note that since  $p/u_r = \rho c$  (where  $\rho$  = mean air density kg/m<sup>3</sup> and  $c$  = speed of sound 343 m/s) for a plane wave or sufficiently far from any source,

that

$$I_r = \frac{1}{T} \int_0^T \frac{p^2(t)}{\rho c} dt = \frac{p_{\text{rms}}^2}{\rho c} \quad (30)$$

where Eq. (30) is true for random noise for a single frequency sound, known as a pure tone.

Note that for such cases we only need to measure the mean-square sound pressure with a simple sound level meter (or at least a simple measurement system) to obtain the sound intensity from Eq. (30) and then from that the sound power  $W$  watts from Eq. (26) is

$$W = \int_S \frac{p_{\text{rms}}^2}{\rho c} dS = 4\pi r^2 \frac{p_{\text{rms}}^2}{\rho c} \quad (31)$$

for an omnidirectional source (monopole) with no reflections and background noise. This result is true for noise signals and pure tones that are produced by omnidirectional sources and in the so-called far acoustic field.

For the special case of a pure-tone (single-frequency) source of sound pressure amplitude,  $\hat{p}$ , we note  $I_r = \hat{p}^2/2\rho c$  and  $W = 2\pi r^2 \hat{p}^2/\rho c$  from Eq. (31).

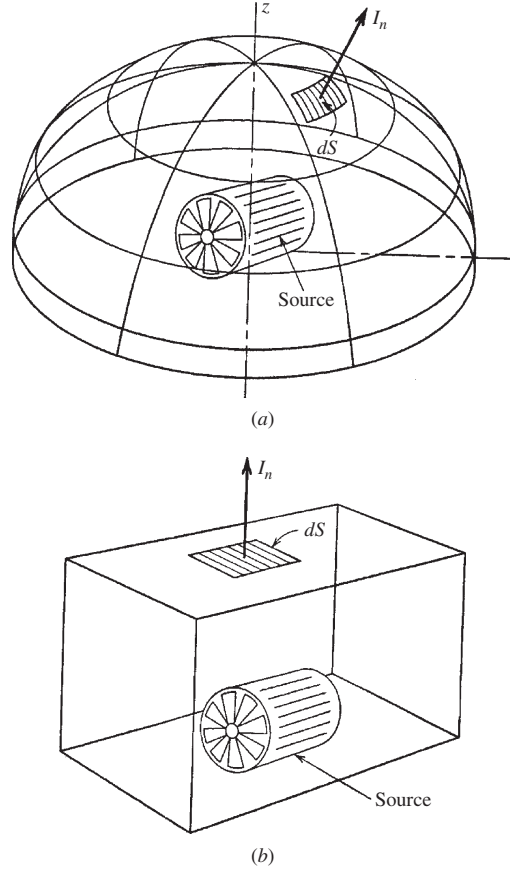
For measurements on a hemisphere,  $W = 2\pi r^2 p_{\text{rms}}^2/\rho c$  and for a pure-tone source  $I_r = \hat{p}^2/2\rho c$ , and  $W = \pi r^2 \hat{p}^2/\rho c$ , from Eq. (31).

Note that in the general case, the source is *not* omnidirectional, or more importantly, we must often measure quite close to the source so that we are in the *near* acoustic field, not the *far* acoustic field. However, if appreciable reflections or background noise (i.e., other sound sources) are present, then we *must* measure the intensity  $I_r$  in Eq. (26). Figure 4 shows two different enclosing surfaces that can be used to determine the sound power of a source. The sound intensity  $I_n$  must always be measured perpendicular (or normal) to the enclosing surfaces used. Measurements are normally made with a two-microphone probe (see Chapter 45). The most common microphone arrangement is the face-to-face model (see Fig. 5).

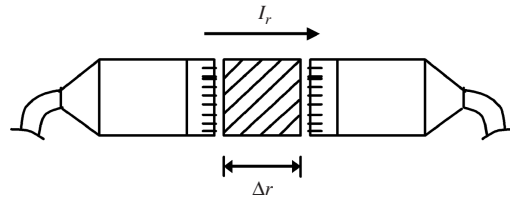
The microphone arrangement shown also indicates the microphone separation distance,  $\Delta r$ , needed for the intensity calculations. See Chapter 45. In the face-to-face arrangement a solid cylindrical spacer is often put between the two microphones to improve the performance.

**Example 1** By making measurements around a source (an engine exhaust pipe) it is found that it is largely omnidirectional at low frequency (in the range of 50 to 200 Hz). If the measured sound pressure level on a spherical surface 10 m from the source is 60 dB at 100 Hz, which is equivalent to a mean-square sound pressure  $p_{\text{rms}}^2$  of  $(20 \times 10^{-3})^2$  (Pa)<sup>2</sup>, what is the sound power in watts at 100 Hz frequency? Assume  $\rho = 1.21$  kg/m<sup>3</sup> and  $c = 343$  m/s, so  $\rho c = 415 \approx 400$  rayls:

$$p_{\text{rms}}^2 = (20 \times 10^{-3})^2 = 400 \times 10^{-6} \text{ (Pa)}^2$$



**Figure 4** Sound intensity  $I_n$ , being measured on (a) segment  $dS$  of an imaginary hemispherical enclosure surface and (b) an elemental area  $dS$  of a rectangular enclosure surface surrounding a source having a sound power  $W$ .



**Figure 5** Sound intensity probe microphone arrangement commonly used.

then from Eq. (31):

$$W = 4\pi r^2 (400 \times 10^{-6}) / \rho c$$

$$W = 4\pi (100 \times 400 \times 10^{-6}) / 400$$

$$\approx 4\pi \times 10^{-4} \approx 1.26 \times 10^{-3} \text{ watts}$$



**Example 2** If the sound intensity level, measured using a sound intensity probe at the same frequency, as in Example 1, but at 1 m from the exhaust exit, is 80 dB (which is equivalent to  $0.0001 \text{ W/m}^2$ ), what is the sound power of the exhaust source at this frequency?

From Eq. (26)

$$W = \int_S I_r dS = (0.0001) \times 4\pi(1)^2$$

(for an omnidirectional source). Then

$$W = 1.26 \times 10^{-3} \text{ watts}$$

(the same result as Example 1).

Sound intensity measurements do and should give the same result as sound pressure measurements made in a free field.

Far away from complicated sound sources, provided there is no background noise, and reflections can be ignored:

$$p_{\text{rms}}^2 = \rho c W / (4\pi r^2) \quad (32)$$

$$p_{\text{rms}}^2 / p_{\text{ref}}^2 = (W / W_{\text{ref}}) (1/r^2) \rho c W_{\text{ref}} / [p_{\text{ref}}^2 4\pi(1)^2] \quad (33)$$

And by taking 10 log throughout this equation

$$L_p = L_W - 20 \log r - 11 \text{ dB} \quad (34)$$

where  $L_p$  = sound pressure level

$L_W$  = source sound power level

$r$  = distance, in metres, from the source center

(Note we have assumed here that  $\rho c = 415 \cong 400$  rayls.)

If  $\rho c \cong 400$  rayls ( $\text{kg/m}^2\text{s}$ ), then since

$$I = p_{\text{rms}}^2 / \rho c \quad (35)$$

$$I / I_{\text{ref}} = (p_{\text{rms}}^2 / p_{\text{ref}}^2) (p_{\text{ref}}^2 / I_{\text{ref}} \rho c)$$

So,

$$L_I = L_p + 10 \log \left[ \frac{400 \times 10^{-12}}{1} \frac{1}{10^{-12} \times 400} \right] \quad (36)$$

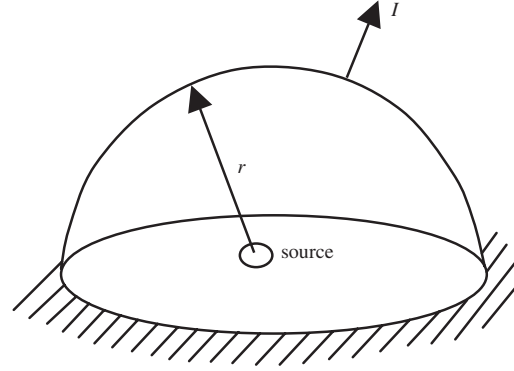
$$L_I = L_p + 0 \text{ dB}$$

## 9 SOUND SOURCES ABOVE A RIGID HARD SURFACE

In practice many real engineering sources (such as machines and vehicles) are mounted or situated on hard reflecting ground and concrete surfaces. If we can assume that the source of power  $W$  radiates only to a half-space solid angle  $2\pi$ , and no power is absorbed by the hard surface (Fig. 6), then

$$I = W / 2\pi r^2$$

$$L_p \cong L_I = L_W - 20 \log r - 8 \text{ dB} \quad (37)$$



**Figure 6** Source above a rigid surface.

where  $L_W$  is the sound power level of the source and  $r$  is the distance in metres.

In this discussion we have assumed that the sound source radiates the same sound intensity in all directions, that is, it is omnidirectional. If the source of sound power  $W$  becomes directional, the mean-square sound pressure in Eqs. (32) and (35) will vary with direction, and the sound power  $W$  can only be obtained from Eqs. (26) and (31) by measuring either the mean-square pressure ( $p_{\text{rms}}^2$ ) all over a surface enclosing the source (in the far acoustic field, the far field) and integrating Eq. (31) over the surface, or by measuring the intensity all over the surface in the *near* or *far* acoustic field and integrating over the surface [Eq. (26)]. We shall discuss source directivity in Section 10.

**Example 3** If the sound power level of a source is 120 dB (which is equivalent to 1 acoustical watt), what is the sound pressure level at 50 m (a) for radiation to whole space and (b) for radiation to half-space?

(a) For whole space:

$$I = 1/4\pi(50)^2 = 1/10^4 \pi (\text{W/m}^2), \text{ then}$$

$$L_I = 10 \log(10^{-4} / \pi 10^{-12})$$

$$(\text{since } I_{\text{ref}} = 10^{-12} \text{ W/m}^2)$$

$$= 10 \log 10^8 - 10 \log \pi$$

$$= 80 - 5 = 75 \text{ dB}$$

Since we may assume  $r = 50$  m is in the far acoustic field,  $L_p \cong L_I = 75$  dB as well (we have also assumed  $\rho c \cong 400$  rayls).


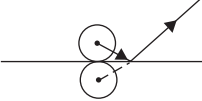
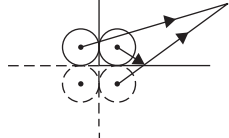

b) For half space:

$$I = 1/2\pi(50)^2 = 2/10^4 \pi (\text{W/m}^2), \text{ then}$$

$$L_I = 10 \log(2 \times 10^{-4} / \pi 10^{-12})$$

$$\text{since } I_{\text{ref}} = 10^{-12} \text{ W/m}^2$$

**Table 2 Simple Source Near Reflecting Surfaces<sup>a</sup>**

Intensity	Source	Condition	Number of Images	$p_{rms}^2$	Power	$D$	DI
$I$		Free field	None	$p_{rms}^2$	$W$	1	0 dB
$4I$		Reflecting plane	1	$4p_{rms}^2$	$2W$	4	6 dB
$16I$		Wall-floor intersection	3	$16p_{rms}^2$	$4W$	16	12 dB
$64I$		Room corner	7	$64p_{rms}^2$	$8W$	64	18 dB

<sup>a</sup>  $D$  and DI are defined in Eqs. (38), (43), and (45).

$$\begin{aligned}
 &= 10 \log 2 + 10 \log 10^8 - 10 \log \pi \\
 &= 80 + 3 - 5 = 78 \text{ dB}
 \end{aligned}$$

and  $L_p \cong L_I = 78 \text{ dB}$  also.

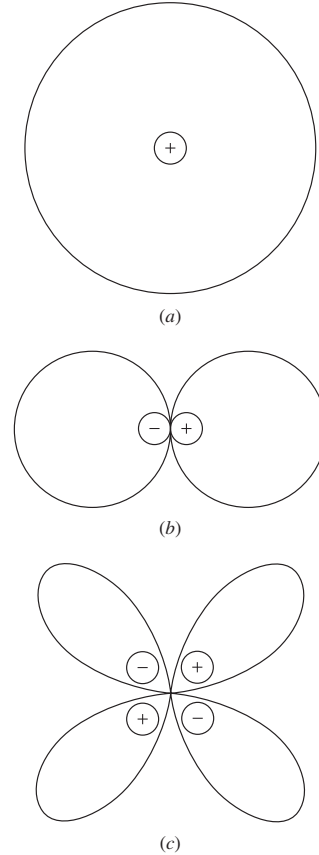
It is important to note that the sound power radiated by a source can be significantly affected by its environment. For example, if a simple constant-volume velocity source (whose strength  $Q$  will be unaffected by the environment) is placed on a floor, its sound power will be doubled (and its sound power level increased by 3 dB). If it is placed at a floor-wall intersection, its sound power will be increased by four times (6 dB); and if it is placed in a room corner, its power is increased by eight times (9 dB). See Table 2. Many simple sources of sound (ideal sources, monopoles, and real small machine sources) produce more sound power when put near reflecting surfaces, provided their surface velocity remains constant. For example, if a monopole is placed touching a hard plane, an image source of equal strength may be assumed.

## 10 DIRECTIVITY

The sound intensity radiated by a dipole is seen to depend on  $\cos^2\theta$ . See Fig. 7.

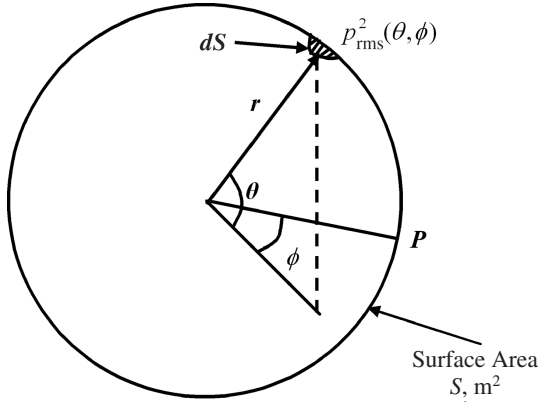
Most real sources of sound become directional at high frequency, although some are almost omnidirectional at low frequency (depending on the source dimension,  $d$ , they must be small in size compared with a wavelength  $\lambda$ , so  $d/\lambda \ll 1$  for them to behave almost omnidirectionally).

**Directivity Factor [ $D(\theta, \phi)$ ]** In general, a directivity factor  $D_{\theta, \phi}$  may be defined as the ratio of the radial



**Figure 7** Polar directivity plots for the radial sound intensity in the far field of (a) monopole, (b) dipole, and (c) (lateral) quadrupole.





**Figure 8** Geometry used in derivation of directivity factor.

intensity  $\langle I_{\theta, \phi} \rangle_t$  (at angles  $\theta$  and  $\phi$  and distance  $r$  from the source) to the radial intensity  $\langle I_s \rangle_t$  at the same distance  $r$  radiated from an omnidirectional source of the same total power (Fig. 8). Thus

$$D_{\theta, \phi} = \frac{\langle I_{\theta, \phi} \rangle_t}{\langle I_s \rangle_t} \quad (38)$$

For a directional source, the mean square sound pressure measured at distance  $r$  and angles  $\theta$  and  $\phi$  is  $p_{\text{rms}}^2(\theta, \phi)$ .

In the far field of this source ( $r \gg \lambda$ ), then

$$W = \int_S \frac{p_{\text{rms}}^2(\theta, \phi)}{\rho c} dS \quad (39)$$

But if the source were omnidirectional of the same power  $W$ , then

$$W = \int_S \frac{p_s^2}{\rho c} dS \quad (40)$$

where  $p_s^2$  is a constant, independent of angles  $\theta$  and  $\phi$

We may therefore write:

$$W = \frac{1}{\rho c} \int_S p_{\text{rms}}^2(\theta, \phi) dS = \frac{p_s^2}{\rho c} \int_S dS \quad (41)$$

and

$$p_{\text{rms}}^2 = p_s^2 = \frac{1}{S} \int_S p^2(\theta, \phi) dS \quad (42)$$

where  $p_s^2$  is the space-averaged mean-square sound pressure.

We define the directivity factor  $D$  as

$$D(\theta, \phi) = \frac{p_{\text{rms}}^2(\theta, \phi)}{p_s^2} \text{ or } D(\theta, \phi) = \frac{p_{\text{rms}}^2(\theta, \phi)}{p_{\text{rms}}^2} \quad (43)$$

as the ratio of the mean-square pressure at distance  $r$  to the space-averaged mean-square pressure at  $r$ , or the ratio of the mean-square sound pressure at  $r$  divided by the mean-square sound pressure at  $r$  for an omnidirectional sound source of the same sound power  $W$ , watts.

**Directivity Index** The directivity index DI is just a logarithmic version of the directivity factor. It is expressed in decibels.

A directivity index  $DI_{\theta, \phi}$  may be defined, where

$$DI_{\theta, \phi} = 10 \log D_{\theta, \phi} \quad (44)$$

$$DI(\theta, \phi) = 10 \log D(\theta, \phi) \quad (45)$$

Note if the source power remains the same when it is put on a hard rigid infinite surface  $D(\theta, \phi) = 2$  and  $DI(\theta, \phi) = 3$  dB.

Directivity factor:

$$D = \frac{p_{\text{rms}}^2(\theta, \phi)}{p_s^2} \quad (46)$$

Directivity index:

$$DI = 10 \log[D(\theta, \phi)] \quad (47)$$

### Numerical Example

1. If a constant-volume velocity source of sound power level of 120 dB (which is equivalent to 1 acoustic watt) radiates to whole space and it has a directivity factor of 12 at 50 m, what is the sound pressure level in that direction?

$$I = 1/4\pi(50)^2 = 1/10^4 \pi (W/m^2)$$

then

$$\langle L_I \rangle_S = 10 \log(10^{-4} / \pi 10^{-12})$$

$$(\text{since } I_{\text{ref}} = 10^{-12} \text{ W/m}^2)$$

$$= 10 \log 10^8 - 10 \log \pi = 75 \text{ dB}$$

But for the directional source  $L_p(\theta, \phi) = \langle L_p \rangle_S + DI(\theta, \phi)$ , then assuming  $\rho c = 400$  rayls,

$$L_p(\theta, \phi) = 75 + 10 \log 12$$

$$= 75 + 10 + 10 \log 1.2 = 85.8 \text{ dB}$$

2. If this constant-volume velocity source is put very near a hard reflecting floor, what will its sound pressure level be in the same direction?

If the direction is away from the floor, then

$$L_p(\theta, \phi) = 85.8 + 6 = 91.8 \text{ dB}$$

### 11 LINE SOURCES

Sometimes noise sources are distributed more like idealized *line sources*. Examples include the sound radiated from a long pipe containing fluid flow or the sound radiated by a stream of vehicles on a highway. If sound sources are distributed continuously along a straight line and the sources are radiating sound independently, so that the sound power/unit length is  $W'$  watts/metre, then assuming cylindrical spreading (and we are located in the far acoustic field again and  $\rho c = 400$  rayls):

$$I = W'/2\pi r \quad (48)$$

so,

$$L_I = 10 \log(I/I_{\text{ref}}) = 10 \log(W'/2 \times 10^{-12} \pi r)$$

then

$$L_p \cong L_I = 10 \log(W'/r) + 112 \text{ dB} \quad (49)$$

and for half-space radiation (such as a line source on a hard surface, such as a road)

$$L_p \cong L_I = 10 \log(W'/r) + 115 \text{ dB} \quad (50)$$

### 12 REFLECTION, REFRACTION, SCATTERING, AND DIFFRACTION

For a homogeneous plane sound wave at normal incidence on a fluid medium of different characteristic impedance  $\rho c$ , both reflected and transmitted waves are formed (see Fig. 9).

From energy considerations (provided no losses occur at the boundary) the sum of the reflected

intensity  $I_r$  and transmitted intensity  $I_t$  equals the incident intensity  $I_i$ :

$$I_i = I_r + I_t \quad (51)$$

and dividing throughout by  $I_i$ ,

$$\frac{I_r}{I_i} + \frac{I_t}{I_i} = R + T = 1 \quad (52)$$

where  $R$  is the *energy reflection coefficient* and  $T$  is the *transmission coefficient*. For plane waves at normal incidence on a plane boundary between two fluids (see Fig. 9):

$$R = \frac{(\rho_1 c_1 - \rho_2 c_2)^2}{(\rho_1 c_1 + \rho_2 c_2)^2} \quad (53)$$

and

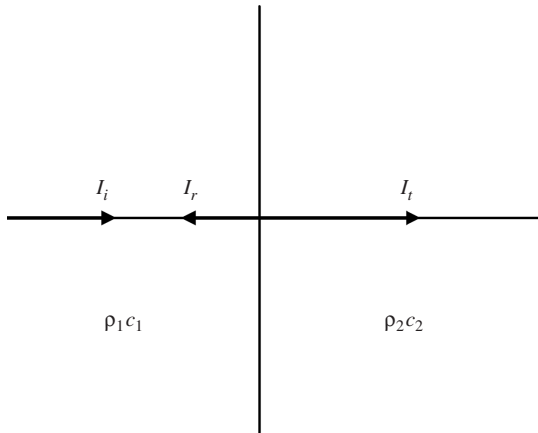
$$T = \frac{4\rho_1 c_1 \rho_2 c_2}{(\rho_1 c_1 + \rho_2 c_2)^2} \quad (54)$$

Some interesting facts can be deduced from Eqs. (53) and (54). Both the reflection and transmission coefficients are independent of the direction of the wave since interchanging  $\rho_1 c_1$  and  $\rho_2 c_2$  does not affect the values of  $R$  and  $T$ . For example, for sound waves traveling from air to water or water to air, almost complete reflection occurs, independent of direction, and the reflection coefficients are the same and the transmission coefficients are the same for the two different directions.

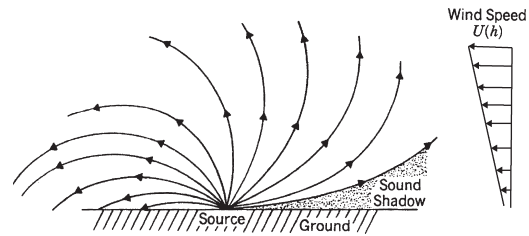
As discussed before, when the characteristic impedance  $\rho c$  of a fluid medium changes, incident sound waves are both reflected and transmitted. It can be shown that if a plane sound wave is incident at an oblique angle on a plane boundary between two fluids, then the wave transmitted into the changed medium changes direction. This effect is called *refraction*. Temperature changes and wind speed changes in the atmosphere are important causes of refraction.

Wind speed normally increases with altitude, and Fig. 10 shows the refraction effects to be expected for an idealized wind speed profile. Atmospheric temperature changes alter the speed of sound  $c$ , and temperature gradients can also produce sound shadow and focusing effects, as seen in Figs. 11 and 12.

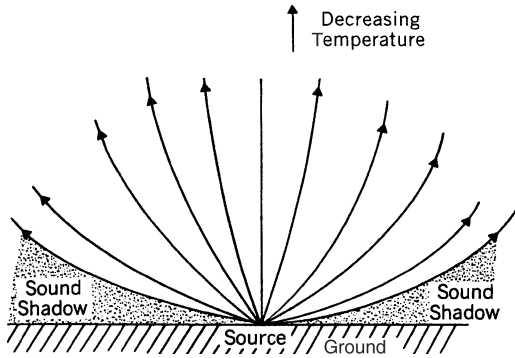
When a sound wave meets an obstacle, some of the sound wave is deflected. The *scattered* wave is defined to be the difference between the resulting



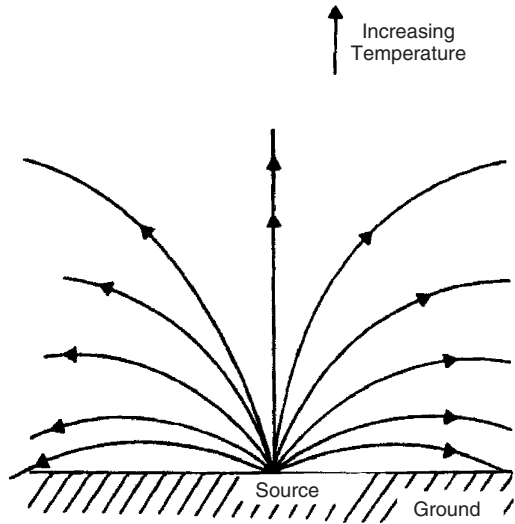
**Figure 9** Incident intensity  $I_i$ , reflected intensity  $I_r$ , and transmitted intensity  $I_t$  in a homogeneous plane sound wave at normal incidence on a plane boundary between two fluid media of different characteristic impedances  $\rho_1 c_1$  and  $\rho_2 c_2$ .



**Figure 10** Refraction of sound in air with wind speed  $U(h)$  increasing with altitude  $h$ .



**Figure 11** Refraction of sound in air with normal temperature lapse (temperature decreases with altitude).



**Figure 12** Refraction of sound in air with temperature inversion.

wave with the obstacle and the undisturbed wave without the presence of the obstacle. The scattered wave spreads out in all directions interfering with the undisturbed wave. If the obstacle is very small compared with the wavelength, no sharp-edged sound shadow is created behind the obstacle. If the obstacle is large compared with the wavelength, it is normal to say that the sound wave is *reflected* (in front) and *diffracted* (behind) the obstacle (rather than *scattered*). In this case a strong sound shadow is caused in which the wave pressure amplitude is very small. In the zone between the sound shadow and the region fully “illuminated” by the source, the sound wave pressure amplitude oscillates. These oscillations are maximum near the shadow boundary and minimum well inside the shadow. These oscillations in amplitude are normally termed *diffraction bands*. One of the most common examples of diffraction caused by a body is the diffraction of sound over the sharp edge of a

barrier or screen. For a plane homogeneous sound wave it is found that a strong shadow is caused by high-frequency waves where  $h/\lambda \geq 1$  and a weak shadow where  $h/\lambda \leq 1$ , where  $h$  is the barrier height and  $\lambda$  is the wavelength. For intermediate cases where  $h/\lambda \approx 1$ , a variety of interference and diffraction effects are caused by the barrier. Scattering is caused not only by obstacles placed in the wave field but also by fluid regions where the properties of the medium such as its density or compressibility change their values from the rest of the medium. Scattering is also caused by turbulence (see Chapters 5 and 28 in the *Handbook of Acoustics*<sup>1</sup>) and from rain or fog particles in the atmosphere and bubbles in water and by rough or absorbent areas on wall surfaces.

### 13 RAY ACOUSTICS

There are three main modeling approaches in acoustics, which may be termed wave acoustics, ray acoustics, and energy acoustics. So far in this chapter we have mostly used the wave acoustics approach in which the acoustical quantities are completely defined as functions of space and time. This approach is practical in certain cases where the fluid medium is bounded and in cases where the fluid is unbounded as long as the fluid is homogeneous. However, if the fluid properties vary in space due to variations in temperature or due to wind gradients, then the wave approach becomes more difficult and other simplified approaches such as the ray acoustics approach described here and in Chapter 3 of the *Handbook of Acoustics*<sup>1</sup> are useful. This approach can also be extended to propagation in fluid-submerged elastic structures, as described in Chapter 4 of the *Handbook of Acoustics*.<sup>1</sup> The energy approach is described in Section 14.

In the ray acoustics approach, rays are obtained that are solutions to the simplified eikonal equation [Eq. (55)]:

$$\left(\frac{\partial S}{\partial x}\right)^2 + \left(\frac{\partial S}{\partial y}\right)^2 + \left(\frac{\partial S}{\partial z}\right)^2 - \frac{1}{c^2} = 0 \quad (55)$$

The ray solutions can provide good approximations to more exact acoustical solutions. In certain cases they also satisfy the wave equation.<sup>8</sup> The eikonal  $S(x, y, z)$  represents a surface of constant phase (or wavefront) that propagates at the speed of sound  $c$ . It can be shown that Eq. (55) is consistent with the wave equation only in the case when the frequency is very high.<sup>7</sup> However, in practice, it is useful, provided the changes in the speed of sound  $c$  are small when measured over distances comparable with the wavelength. In the case where the fluid is homogeneous (constant sound speed  $c$  and density  $\rho$  throughout),  $S$  is a constant and represents a plane surface given by  $S = (\alpha x + \beta y + \gamma z)/c$ , where  $\alpha$ ,  $\beta$ , and  $\gamma$  are the direction cosines of a straight line (a ray) that is perpendicular to the wavefront (surface  $S$ ). If the fluid can no longer be assumed to be homogeneous and the speed of sound  $c(x, y, z)$  varies with position, the approach becomes approximate only. In this case some parts

of the wavefront move faster than others, and the rays bend and are no longer straight lines. In cases where the fluid has a mean flow, the rays are no longer quite parallel to the normal to the wavefront. This ray approach is described in more detail in several books and in Chapter 3 of the *Handbook of Acoustics*<sup>1</sup> (where in this chapter the main example is from underwater acoustics). The ray approach is also useful for the study of propagation in the atmosphere and is a method to obtain the results given in Figs. 10 to 12. It is observed in these figures that the rays always bend in a direction toward the region where the sound speed is less. The effects of wind gradients are somewhat different since in that case the refraction of the sound rays depends on the relative directions of the sound rays and the wind in each fluid region.

#### 14 ENERGY ACOUSTICS

In enclosed spaces the wave acoustics approach is useful, particularly if the enclosed volume is small and simple in shape and the boundary conditions are well defined. In the case of rigid walls of simple geometry, the wave equation is used, and after the applicable boundary conditions are applied, the solutions for the natural (eigen) frequencies for the modes (standing waves) are found. See Chapters 4 and 103, and Chapter 6 in the *Handbook of Acoustics*<sup>1</sup> for more details. However, for large rooms with irregular shape and absorbing boundaries, the wave approach becomes impracticable and other approaches must be sought. The ray acoustics approach together with the multiple-image-source concept is useful in some room problems, particularly in auditorium design or in factory spaces where barriers are involved. However, in many cases a statistical approach where the energy in the sound field is considered is the most useful. See Chapters 17 and 104 and also Chapters 60–62 in the *Handbook of Acoustics*<sup>1</sup> for more detailed discussion of this approach. Some of the fundamental concepts are briefly described here.

For a plane wave progressing in one direction in a duct of unit cross section area, all of the sound energy in a column of fluid  $c$  metres in length must pass through the cross section in 1 s. Since the intensity  $\langle I \rangle_t$  is given by  $p_{\text{rms}}^2/\rho c$ , then the total sound energy in the fluid column  $c$  metres long must also be equal to  $\langle I \rangle_t$ . The energy per unit volume  $\epsilon$  (joules per cubic metre) is thus

$$\epsilon = \frac{\langle I \rangle_t}{c} \quad (56)$$

or

$$\epsilon = \frac{p_{\text{rms}}^2}{\rho c^2} \quad (57)$$

The energy density  $\epsilon$  may be derived by alternative means and is found to be the same as that given in Eq. (56) in most acoustic fields, except very close to sources of sound and in standing-wave fields. In a room with negligibly small absorption in the air or at the boundaries, the sound field created by a

source producing broadband sound will become very reverberant (the sound waves will reach a point with equal probability from any direction). In addition, for such a case the sound energy may be said to be diffuse if the energy density is the same anywhere in the room. For these conditions the time-averaged intensity incident on the walls (or on an imaginary surface from one side) is

$$\langle I \rangle_t = \frac{1}{4} \epsilon c \quad (58)$$

or

$$\langle I \rangle_t = \frac{p_{\text{rms}}^2}{4\rho c} \quad (59)$$

In any real room the walls will absorb some sound energy (and convert it into heat).

The *absorption coefficient*  $\alpha(f)$  of the wall material may be defined as the fraction of the incident sound intensity that is absorbed by the wall surface material:

$$\alpha(f) = \frac{\text{sound intensity absorbed}}{\text{sound intensity incident}} \quad (60)$$

The absorption coefficient is a function of frequency and can have a value between 0 and 1. The *noise reduction coefficient* (NRC) is found by averaging the absorption coefficient of the material at the frequencies 250, 500, 1000, and 2000 Hz (and rounding off the result to the nearest multiple of 0.05). See Chapter 57 in this book and Chapter 75 in the *Handbook of Acoustics*<sup>1</sup> for more detailed discussion on the absorption of sound in enclosures.

#### 15 NEAR FIELD, FAR FIELD, DIRECT FIELD, AND REVERBERANT FIELD

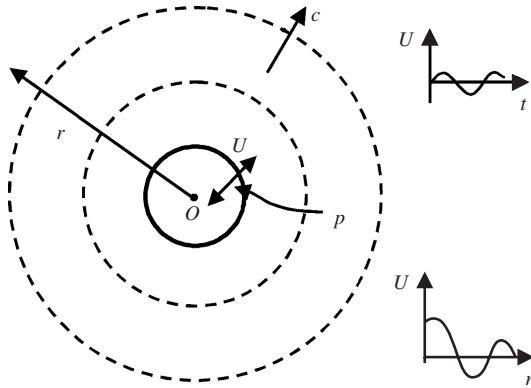
Near to a source, we call the sound field, the *near acoustic field*. Far from the source, we call the field the *far acoustic field*. The extent of the near field depends on:

1. The type of source: (monopole, dipole, size of machine, type of machine, etc.)
2. Frequency of the sound.

In the *near field* of a source, the sound pressure and particle velocity tend to be very nearly *out of phase* ( $\approx 90^\circ$ ).

In the *far field*, the sound pressure and particle velocity are very nearly in phase. Note, far from any source, the sound wave fronts flatten out in curvature, and the waves appear to an observer to be like plane waves. In plane progressive waves, the sound pressure and particle velocity are in phase (provided there are no reflected waves). Thus far from a source (or in a plane progressive wave)  $p/u = \rho c$ . Note  $\rho c$  is a real number, so the sound pressure  $p$  and particle velocity  $u$  must be in phase.

Figure 13 shows the example of a finite monopole source with a normal simple harmonic velocity amplitude  $U$ . On the surface of the monopole, the



**Figure 13** Example of monopole. On the monopole surface, velocity of surface  $U$  = particle velocity in the fluid.

surface velocity is equal to the particle velocity. The particle velocity decreases in inverse proportion to the distance from the source center  $O$ .

It is common to make the assumption that  $kr = 2\pi fr/c = 10$  is the boundary between the near and far fields. Note this is only one criterion and that there is no sharp boundary, but only a gradual transition. First we should also think of the type and the dimensions of the source and assume, say that  $r \gg d$ , where  $d$  is a source dimension. We might say that  $r > 10d$  should also be applied as a secondary criterion to determine when we are in the far field.

**Reverberation** In a confined space we will get reflections, and far from the source the reflections will dominate. We call this reflection-dominated region the *reverberant field*. The region where reflections are unimportant and where a doubling of distance results in a sound pressure drop of 6 dB is called the *free* or *direct* field. See Fig. 14.

**Sound Absorption** The sound absorption coefficient  $\alpha$  of sound-absorbing materials (curtains, drapes, carpets, clothes, fiber glass, acoustical foams, etc.), is defined as

$$\alpha = \frac{\text{sound energy absorbed}}{\text{sound energy incident}}$$

$$\alpha = \frac{\text{sound power absorbed}}{\text{sound power incident}}$$

$$\alpha = \frac{\text{sound intensity absorbed}}{\text{sound intensity incident}} = \frac{I_a}{I_i} \quad (61)$$

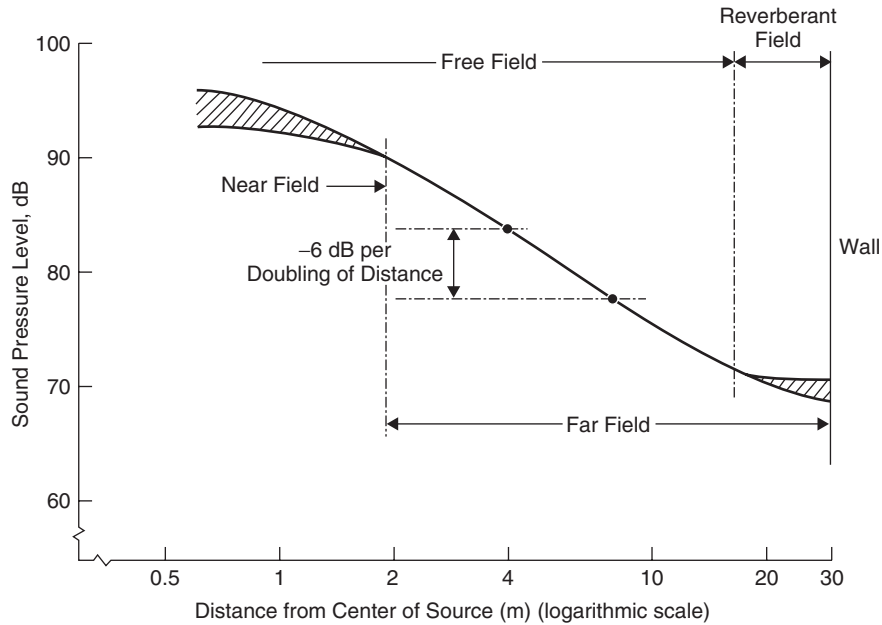
Note  $\alpha$  also depends on the angle of incidence. The absorption coefficient of materials depends on frequency as well. See Fig. 15.

Thicker materials absorb more sound energy (particularly important at low frequency).

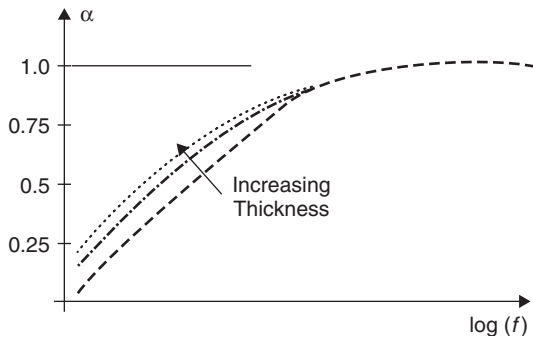
If all sound energy is absorbed,  $\alpha = 1$  (none reflected).  
If no sound energy is absorbed,  $\alpha = 0$ :

$$0 \leq \alpha \leq 1$$

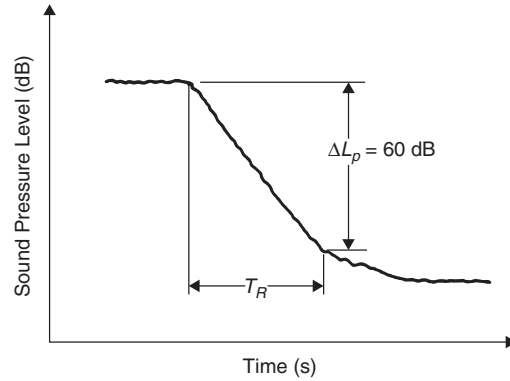
If  $\alpha = 1$ , the sound absorption is perfect (e.g., a window).



**Figure 14** Sound pressure level in an interior sound field.



**Figure 15** Sound absorption coefficient  $\alpha$  of typical absorbing materials as a function of frequency.



**Figure 16** Measurement of reverberation time  $T_R$ .

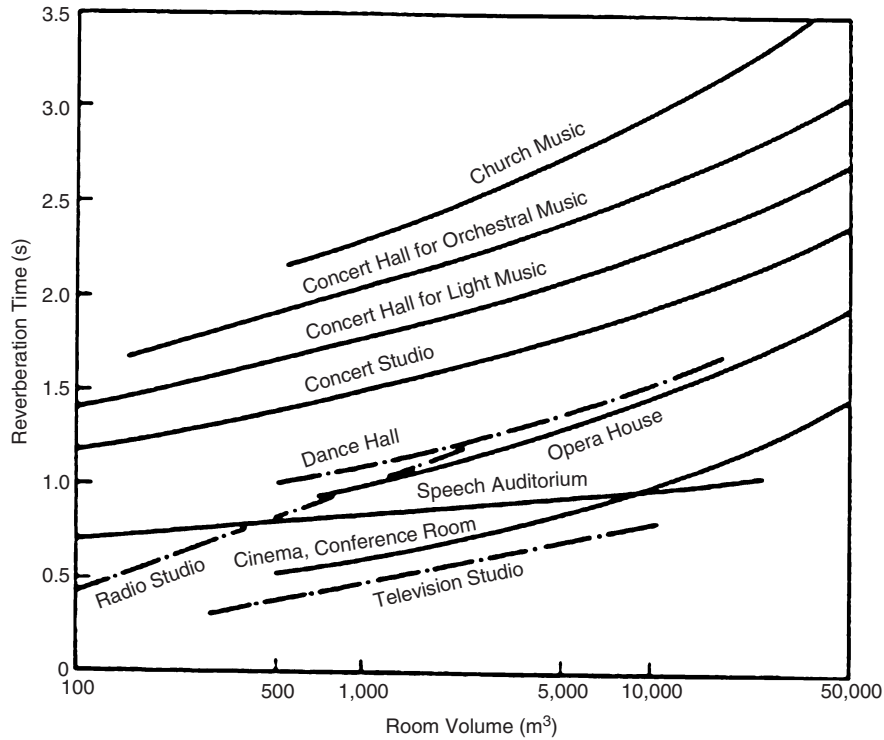
The behavior of sound-absorbing materials is described in more detail in Chapter 57.

**Reverberation Time** In a reverberant space, the reverberation time  $T_R$  is normally defined to be the time for the sound pressure level to drop by 60 dB when the sound source is cut off. See Fig. 16. Different reverberation times are desired for different types of spaces. See Fig. 17. The Sabine formula is often used,  $T_R = T_{60}$  (for 60 dB):

$$T_{60} = \frac{55.3V}{cS\bar{\alpha}}$$

where  $V$  is room volume ( $\text{m}^3$ ),  $c$  is the speed of sound ( $\text{m/s}$ ),  $S$  is wall area ( $\text{m}^2$ ), and  $\bar{\alpha}$  is the angle-averaged wall absorption coefficient, or

$$T_{60} = \frac{55.3V}{c \sum_{i=1}^n S_i \alpha_i} \quad (62)$$



**Figure 17** Examples of recommended reverberation times.

where  $S_i$  is  $i$ th wall area of absorption coefficient  $\alpha_i$ .

In practice, when the reverberation time is measured (see Fig. 16), it is normal practice to ignore the first 5-dB drop in sound pressure level and find the time between the 5-dB and 35-dB drops and multiply this time by 2 to obtain the reverberation time  $T_R$ .

**Example** A room has dimensions  $5 \times 6 \times 10 \text{ m}^3$ . What is the reverberation time  $T_{60}$  if the floor ( $6 \times 10 \text{ m}$ ) has absorbing material  $\bar{\alpha} = 0.5$  placed on it? We will assume that  $\bar{\alpha} = 0$  on the other surfaces (that are made of hard painted concrete.) (See Fig. 18.)

$$T = 55.3V/cS \bar{\alpha} = 55.3(5 \times 6 \times 10)/(343) \\ (6 \times 10)0.5 = 1.6 \text{ s}$$

**Noise Reduction Coefficient** Sometimes an average absorption coefficient is given for a material to obtain a single number measure for its absorption performance. This average coefficient is normally called its noise reduction coefficient (NRC). It is usually defined to be the average of the values of  $\alpha$  at 250, 500, 1000, and 2000 Hz:

$$\text{NRC} = (\alpha_{250} + \alpha_{500} + \alpha_{1000} + \alpha_{2000})/4 \quad (63)$$

**Example:** If  $\alpha_{250} = 0.25$ ,  $\alpha_{500} = 0.45$ ,  $\alpha_{1000} = 0.65$ , and  $\alpha_{2000} = 0.81$ , what is the NRC?

**Solution**  $\text{NRC} = (0.25 + 0.45 + 0.65 + 0.81)/4 = 0.54$ .

Notice that the Sabine reverberation time formula  $T_{60} = 0.16V/S \bar{\alpha}$  still predict a reverberation time as  $\bar{\alpha} \rightarrow 1$ , which does not agree with the physical world. Some improved formulas have been devised by Eyring and Millington-Sette that overcome this problem. Sabine's formula is acceptable, provided  $\bar{\alpha} \leq 0.5$ .

## 16 ROOM EQUATION

If we have a *diffuse* sound field (the same sound energy at any point in the room) and the field is also *reverberant* (the sound waves may come from any direction, with equal probability), then the sound intensity striking the wall of the room is found by integrating the plane wave intensity over all angles  $\theta$ ,  $0 < \theta < 90^\circ$ . This involves a weighting of each

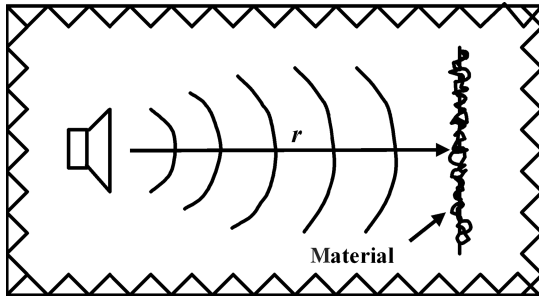


Figure 18 Sound source in anechoic room.

wave by  $\cos \theta$ , and the average intensity for the wall in a reverberant field becomes

$$I_{\text{rev}} = \frac{p_{\text{rms}}^2}{4\rho c} \quad (64)$$

Note the factor 1/4 compared with the plane wave case.

For a point in a room at distance  $r$  from a source of power  $W$  watts, we will have a direct field contribution  $W/4\pi r^2$  from an omnidirectional source to the mean-square pressure and also a reverberant contribution.

We may define the reverberant field as the field created by waves after the first reflection of direct waves from the source. Thus the energy/second absorbed at the first reflection of waves from the source of sound power  $W$  is  $W\bar{\alpha}$ , where  $\bar{\alpha}$  is the average absorption coefficient of the walls. The power thus supplied to the reverberant field is  $W(1 - \bar{\alpha})$  (after the first reflection). Since the power lost by the  $W$  reverberant field must equal the power supplied to it for steady-state conditions, then

$$S \bar{\alpha} \left( \frac{p_{\text{rms}}^2}{4\rho c} \right) = W(1 - \bar{\alpha}) \quad (65)$$

where  $p_{\text{rms}}^2$  is the mean-square sound pressure contribution caused by the reverberant field.

There is also the direct field contribution to be accounted for. If the source is a broadband noise source, these two contributions: (1) the direct term  $p_{\text{drms}}^2 = \rho c W / 4\pi r^2$  and (2) the reverberant contribution,  $p_{\text{revrms}}^2 = 4\rho c W(1 - \bar{\alpha}) / S \bar{\alpha}$ . So,

$$p_{\text{tot}}^2 = (\rho c W) \left[ \frac{1}{4\pi r^2} + \frac{4(1 - \bar{\alpha})}{S \bar{\alpha}} \right] \quad (66)$$

and after dividing by  $p_{\text{ref}}^2$ , and  $W_{\text{ref}}$  and taking 10 log, we obtain

$$L_p = L_w + 10 \log \left[ \frac{1}{4\pi r^2} + \frac{4}{R} \right] + 10 \log \left( \frac{\rho c}{400} \right) \quad (67)$$

where  $R$  is the so-called room constant  $S \bar{\alpha} / (1 - \bar{\alpha})$ .

**Critical Distance** The critical distance  $r_c$  (or sometimes called reverberation radius) is defined as the distance from the sound where the direct field and reverberant field contributions to  $p_{\text{rms}}^2$  are equal:

$$\frac{1}{4\pi r^2} = \frac{4}{R} \quad (68)$$

Thus,

$$r_c = \sqrt{\frac{R}{16\pi}} \quad (69)$$

Figure 19 gives a plot of Eq. (67) (the so-called room equation).



**Noise Reduction** If we are situated in the reverberant field, we may show from Eq. (67) that the noise level reduction,  $\Delta L$ , achieved by increasing the sound absorption is

$$\Delta L = L_{p1} - L_{p2} = 10 \log(4/R_1) - 10 \log(4/R_2) \quad (70)$$

$$\therefore \Delta L = 10 \log \left( \frac{R_2}{R_1} \right) \approx 10 \log \left( \frac{S_2 \bar{\alpha}_2}{S_1 \bar{\alpha}_1} \right) \quad (71)$$

Then  $A = S \bar{\alpha}$  is sometimes known as the absorption area,  $m^2$  (sabins). This may be assumed to be the area of perfect absorbing material,  $m^2$  (like the area of a perfect open window that absorbs 100% of the sound energy falling on it). If we consider the sound field in a room with a uniform energy density  $\epsilon$  created by a sound source that is suddenly stopped, then the sound pressure level in the room will decrease.

By considering the sound energy radiated into a room by a directional broadband noise source of sound power  $W$ , we may sum together the mean squares of the sound pressure contributions caused by the direct and reverberant fields and after taking logarithms obtain the sound pressure level in the room:

$$L_p = L_W + 10 \log \left( \frac{D_{\theta,\phi}}{4\pi r^2} + \frac{4}{R} \right) + 10 \log \left( \frac{\rho c}{400} \right) \quad (72)$$

where  $D_{\theta,\phi}$  is the directivity factor of the source (see Section 7) and  $R$  is the so-called room constant:

$$R = \frac{S \bar{\alpha}}{1 - \bar{\alpha}} \quad (73)$$

A plot of the sound pressure level against distance from the source is given for various room constants in Fig. 19. It is seen that there are several different

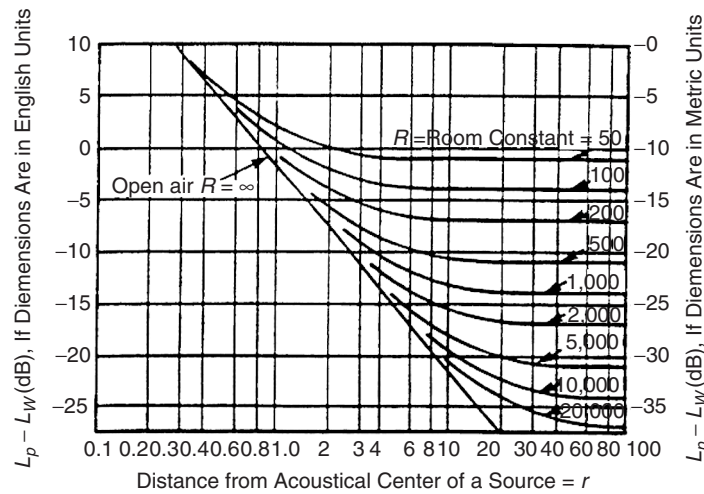
regions. The near and far fields depend on the type of source (see Section 11 and Chapter 3) and the free field and reverberant field. The free field is the region where the direct term  $D_{\theta,\phi}/4\pi r^2$  dominates, and the reverberant field is the region where the reverberant term  $4/R$  in Eq. (48) dominates. The so-called critical distance  $r_c = (D_{\theta,\phi} R / 16\pi)^{1/2}$  occurs where the two terms are equal.

## 17 SOUND RADIATION FROM IDEALIZED STRUCTURES

The sound radiation from plates and cylinders in bending (flexural) vibration is discussed in Chapter 6 in this book and Chapter 10 in the *Handbook of Acoustics*.<sup>1</sup> There are interesting phenomena observed with free-bending waves. Unlike sound waves, these are dispersive and travel faster at higher frequency. The bending-wave speed is  $c_b = (\omega \kappa c_l)^{1/2}$ , where  $\kappa$  is the radius of gyration  $h/(12)^{1/2}$  for a rectangular cross section,  $h$  is the thickness, and  $c_l$  is the longitudinal wave speed  $\{E/[\rho(1 - \sigma^2)]\}^{1/2}$ , where  $E$  is Young's modulus of elasticity,  $\rho$  is the material density, and  $\sigma$  is Poisson's ratio. When the bending-wave speed equals the speed of sound in air, the frequency is called the critical frequency (see Fig. 20). The critical frequency is

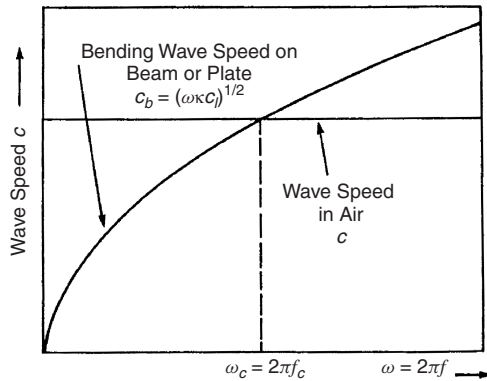
$$f_c = \frac{c^2}{2\pi \kappa c_l} \quad (74)$$

Above this frequency,  $f_c$ , the coincidence effect is observed because the bending wavelength  $\lambda_b$  is greater than the wavelength in air  $\lambda$  (Fig. 21), and trace wave matching always occurs for the sound waves in air at some angle of incidence. See Fig. 22. This has important consequences for the sound radiation from structures and also for the sound transmitted through the structures from one air space to the other.

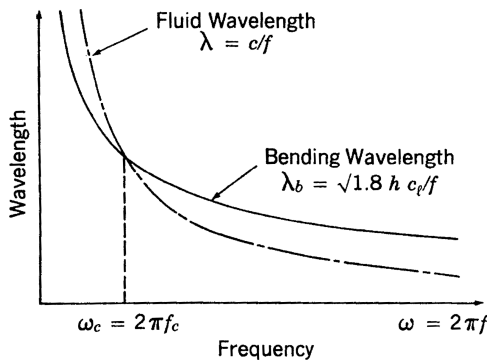


**Figure 19** Sound pressure level in a room (relative to sound power level) as a function of distance  $r$  from sound source.

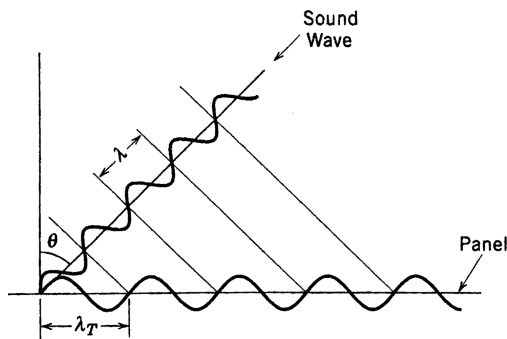




**Figure 20** Variation of frequency of bending wave speed  $c_b$  on a beam or panel and wave speed in air  $c$ .



**Figure 21** Variation with frequency of bending wavelength  $\lambda_b$  on a beam or panel and wavelength in air  $\lambda$ .



**Figure 22** Diagram showing trace wave matching between waves in air of wavelength  $\lambda$  and waves in panel of trace wavelength  $\lambda_T$ .

For free-bending waves on infinite plates above the critical frequency, the plate radiates efficiently, while below this frequency (theoretically) the plate cannot radiate any sound energy at all. (See Chapter 6.) For finite plates, reflection of the bending waves at the edges of the plates causes standing waves that

allow radiation (although inefficient) from the plate corners or edges even below the critical frequency. In the plate center, radiation from adjacent quarter-wave areas cancels. But radiation from the plate corners and edges, which are normally separated sufficiently in acoustic wavelengths, does not cancel. At very low frequency, sound is radiated mostly by corner modes, then up to the critical frequency, mostly by edge modes. Above the critical frequency the radiation is caused by surface modes with which the whole plate radiates efficiently (see Fig. 23). Radiation from bending waves in plates and cylinders is discussed in detail in Chapter 6 and Chapter 10 of the *Handbook of Acoustics*.<sup>1</sup> Figure 24 shows some comparisons between theory and experiment for the level of the radiation efficiencies for the sound radiation for several practical cases of simply supported and clamped panel structures with acoustical and point mechanical excitation.

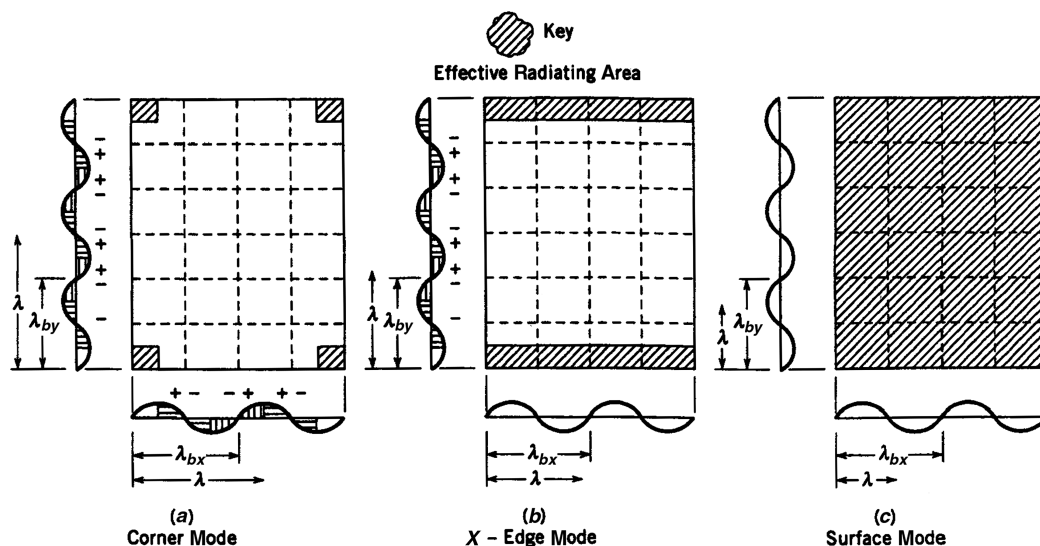
Sound transmission through structures is discussed in Chapters 56 and 105 of this book and Chapters 66, 76, and 77 of the *Handbook of Acoustics*.<sup>1</sup>

Figures 24a and 24b show the logarithmic value of the radiation efficiency  $10 \log \sigma$  plotted against frequency for stiffened and unstiffened plates. See Chapter 6 for further discussion on radiation efficiency  $\theta_{\text{rad}}$ , which is also known as radiation ratio.

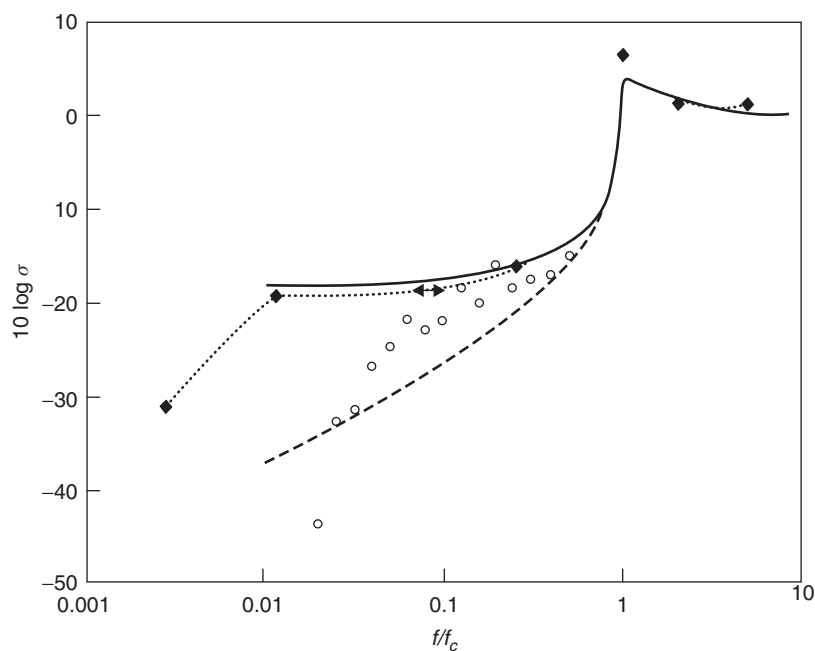
## 18 STANDING WAVES

Standing-wave phenomena are observed in many situations in acoustics and the vibration of strings and elastic structures. Thus they are of interest with almost all musical instruments (both wind and stringed) (see Part XIV in the *Encyclopedia of Acoustics*<sup>13</sup>); in architectural spaces such as auditoria and reverberation rooms; in volumes such as automobile and aircraft cabins; and in numerous cases of vibrating structures, from tuning forks, xylophone bars, bells and cymbals to windows, wall panels, and innumerable other engineering systems including aircraft, vehicle, and ship structural members. With each standing wave is associated a mode shape (or shape of vibration) and an eigen (or natural) frequency. Some of these systems can be idealized to simple one-, two-, or three-dimensional systems. For example, with a simple wind instrument such as a flute, Eq. (1) together with the appropriate spatial boundary conditions can be used to predict the predominant frequency of the sound produced. Similarly, the vibration of a string on a violin can be predicted with an equation identical to Eq. (1) but with the variable  $p$  replaced by the lateral string displacement. With such a string, solutions can be obtained for the fundamental and higher natural frequencies (overtones) and the associated standing-wave mode shapes (which are normally sine shapes). In such a case for a string with fixed ends, the so-called overtones are just integer multiples (2, 3, 4, 5, ...) of the fundamental frequency.

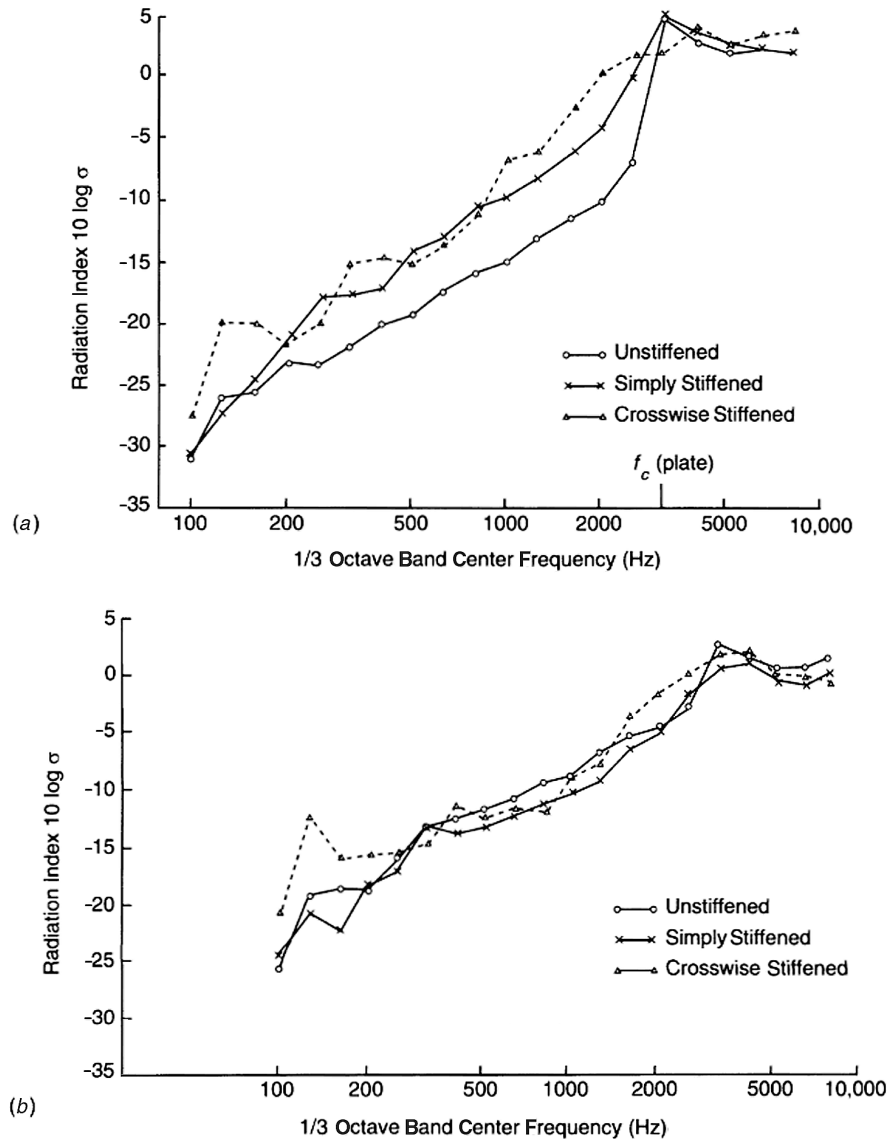
The standing wave with the flute and string can be considered mathematically to be composed of two waves of equal amplitude traveling in opposite



**Figure 23** Wavelength relations and effective radiating areas for corner, edge, and surface modes. The acoustic wavelength is  $\lambda$ ; while  $\lambda_{bx}$  and  $\lambda_{by}$  are the bending wavelengths in the  $x$  and  $y$ -direction, respectively. (See also the *Handbook of Acoustics*,<sup>1</sup> Chapter 1.)



**Figure 24** Comparison of theoretical and measured radiation ratios  $\sigma$  for a mechanically excited, simply supported thin steel plate ( $300 \text{ mm} \times 300 \text{ mm} \times 1.22 \text{ mm}$ ). (—) Theory (simply supported), (---) theory (clamped edges), (...) theory,<sup>14</sup> and (o) measured.<sup>15</sup> (See *Encyclopedia of Vibration*.<sup>16</sup>)



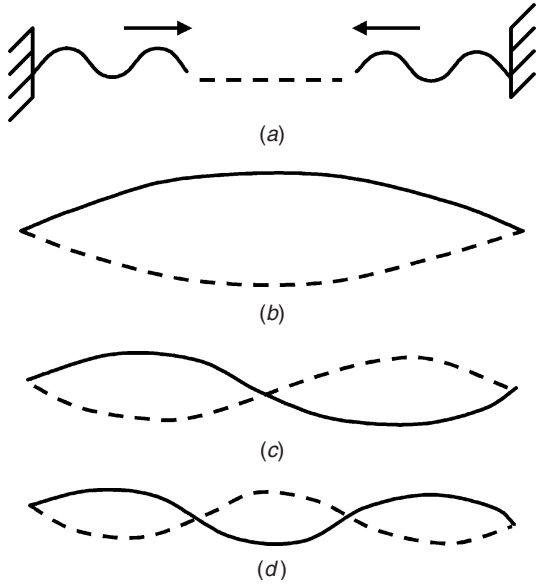
**Figure 25** Measured radiation ratios of unstiffened and stiffened plates for (a) point mechanical excitation and (b) diffuse sound field excitation. (Reproduced from Ref. 17 with permission. See *Encyclopedia of Vibration*.<sup>16</sup>)

directions. Consider the case of a lateral wave on a string under tension. If we create a wave at one end, it will travel forward to the other end. If this end is fixed, it will be reflected. The original (incident) and reflected waves interact (and if the reflection is equal in strength) a perfect standing wave will be created. In Fig. 26 we show three different frequency waves that have interacted to cause standing waves of different frequencies on the string under tension.

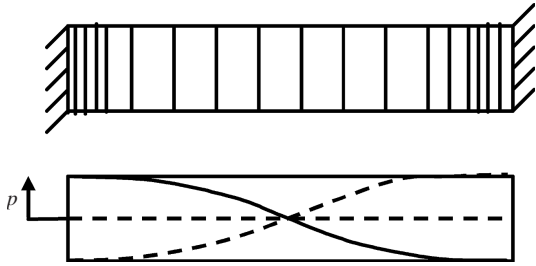
A similar situation can be conceived to exist for one-dimensional sound waves in a tube or duct. If the tube has two hard ends, we can create similar

standing one-dimensional sound waves in the tube at different frequencies. In a tube, the regions of high sound pressure normally occur at the hard ends of the tube, as shown in Fig. 27. See Refs. 18–20.

A similar situation occurs for bending waves on bars, but because the equation of motion is different (dispersive), the higher natural frequencies are not related by simple integers. However, for the case of a beam with simply supported ends, the higher natural frequencies are given by  $2^2, 3^2, 4^2, 5^2, \dots$ , or  $4, 9, 16, 25, \dots$ , and the mode shapes are sine shapes again.



**Figure 26** Waves on a string: (a) Two opposite and equal traveling waves on a string resulting in standing waves, (b) first mode,  $n = 1$ , (c) second mode,  $n = 2$ , and (d) third mode,  $n = 3$ .



**Figure 27** Sound waves in a tube. First mode standing wave for sound pressure in a tube.

The standing waves on two-dimensional systems (such as bending vibrations of plates) may be considered mathematically to be composed of four opposite traveling waves. For simply supported rectangular plates the mode shapes are sine shapes in each direction. For three-dimensional systems such as the air volumes of rectangular rooms, the standing waves may be considered to be made up of eight traveling waves. For a hard-walled room, the sound pressure has a cosine mode shape with the maximum pressure at the walls, and the particle velocity has a sine mode shape with zero normal particle velocity at the walls. See Chapter 6 in the *Handbook of Acoustics*<sup>1</sup> for the natural frequencies and mode shapes for a large number of acoustical and structural systems.

For a three-dimensional room, normally we will have standing waves in three directions with sound pressure maxima at the hard walls.

To understand the sound propagation in a room, it is best to use the three-dimensional wave equation in Cartesian coordinates:

$$\nabla^2 p - \frac{1}{c^2} \frac{\partial^2 p}{\partial t^2} = 0 \quad (75)$$

or

$$\frac{\partial^2 p}{\partial x^2} + \frac{\partial^2 p}{\partial y^2} + \frac{\partial^2 p}{\partial z^2} - \frac{1}{c^2} \frac{\partial^2 p}{\partial t^2} = 0 \quad (76)$$

This equation can have solutions that are “random” in time or are for the special case of a pure-tone, “simple harmonic” sound.

The simple harmonic solution is of considerable interest to us because we find that in rooms there are solutions only at certain frequencies. It may be of some importance now to mention both the sinusoidal solution and the equivalent solution using complex notation that is very frequently used in acoustics and vibration theory.

For a one-dimensional wave, the simple harmonic solution to the wave equation is

$$p = \hat{p}_1 \cos[k(ct - x)] + \hat{p}_2 \cos[k(ct + x)] \quad (77)$$

where  $k = \omega/c = 2\pi f/c$  (the wavenumber).

The first term in Eq. (77) represents a wave of amplitude  $\hat{p}_1$  traveling in the  $+x$  direction. The second term in Eq. (77) represents a wave of amplitude  $\hat{p}_2$  traveling in the  $-x$  direction.

The equivalent expression to Eq. (77) using complex notation is

$$p = \text{Re}\{\tilde{P}_1 e^{j(\omega t - kx)}\} + \text{Re}\{\tilde{P}_2 e^{j(\omega t + kx)}\} \quad (78)$$

where  $j = \sqrt{-1}$ ,  $\text{Re}\{\}$  means real part; and  $\tilde{P}_1$  and  $\tilde{P}_2$  are complex amplitudes of the sound pressure; remember  $k = \omega/c$ ;  $kc = 2\pi f$ . Both Eqs. (77) and (78) are solutions to Eq. (75).

For the three-dimensional case ( $x$ ,  $y$ , and  $z$  propagation), the sinusoidal (pure tone) solution to Eq. (76) is

$$p = \text{Re}\{\tilde{P} \exp(j[\omega t \pm k_x x \pm k_y y \pm k_z z])\} \quad (79)$$

Note that there are  $2^3$  (eight) possible solutions given by Eq. (79). Substitution of Eq. (79) into Eq. (76) (the three-dimensional wave equation) gives [from any of the eight ( $2^3$ ) equations]:

$$\omega^2 = c^2(k_x^2 + k_y^2 + k_z^2) \quad (80)$$

from which the wavenumber  $k$  is

$$k = \frac{\omega}{c} = \sqrt{(k_x^2 + k_y^2 + k_z^2)} \quad (81)$$

and the so-called direction cosines with the  $x$ ,  $y$  and  $z$  directions are  $\cos \theta_x = \pm k_x/k$ ,  $\cos \theta_y = \pm k_y/k$ , and  $\cos \theta_z = \pm k_z/k$  (see Fig. 28).

Equations (80) and (81) apply to the cases where the waves propagate in unbounded space (infinite space) or finite space (e.g., rectangular rooms).

For the case of rectangular rooms with hard walls, we find that the sound (particle) velocity (perpendicular) to each wall must be zero. By using these boundary conditions in each of the eight solutions to Eq. (27a), we find that  $\omega^2 = (2\pi f)^2$  and  $k^2$  in Eqs. (80) and (81) are restricted to only certain discrete values:

$$k^2 = \left(\frac{n_x \pi}{A}\right)^2 + \left(\frac{n_y \pi}{B}\right)^2 + \left(\frac{n_z \pi}{C}\right)^2 \quad (82)$$

or

$$\omega^2 = c^2 k^2$$

Then the room natural frequencies are given by

$$f_{n_x n_y n_z} = \frac{c}{2} \sqrt{\left(\frac{n_x}{A}\right)^2 + \left(\frac{n_y}{B}\right)^2 + \left(\frac{n_z}{C}\right)^2} \quad (83)$$

where  $A$ ,  $B$ ,  $C$  are the room dimensions in the  $x$ ,  $y$ , and  $z$  directions, and  $n_x = 0, 1, 2, 3, \dots$ ;  $n_y = 0, 1, 2, 3, \dots$  and  $n_z = 0, 1, 2, 3, \dots$ . Note  $n_x$ ,  $n_y$ , and  $n_z$  are the number of half waves in the  $x$ ,  $y$ , and  $z$  directions. Note also for the room case, the eight propagating waves add together to give us a standing wave. The wave vectors for the eight waves are shown in Fig. 29.

There are three types of standing waves resulting in three modes of sound wave vibration: axial, tangential, and oblique modes. Axial modes are a result of sound propagation in only one room direction. Tangential modes are caused by sound propagation in two directions in the room and none in the third direction. Oblique modes involve sound propagation in all three directions.

We have assumed there is no absorption of sound by the walls. The standing waves in the room can be excited by noise or pure tones. If they are excited by pure tones produced by a loudspeaker or a machine

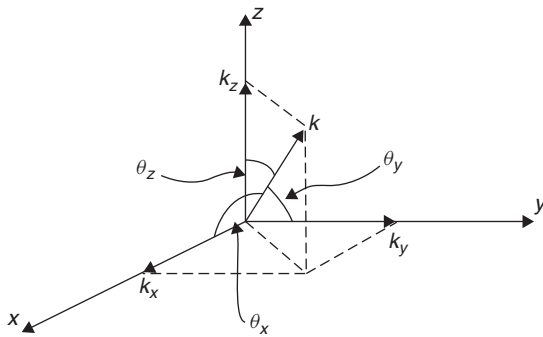


Figure 28 Direction cosines and vector  $k$ .

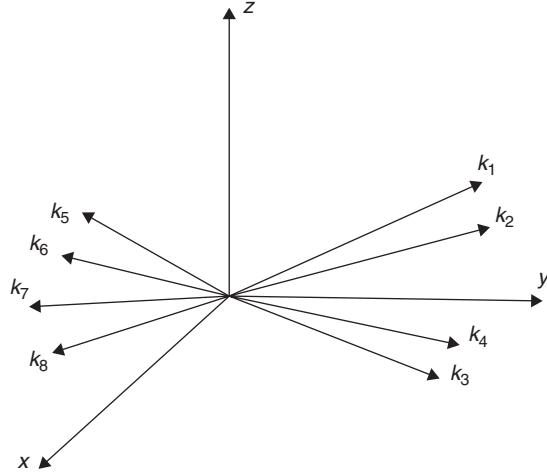


Figure 29 Wave vectors for eight propagating waves.

that creates sound waves exactly at the same frequency as the eigenfrequencies (natural frequencies)  $f_E$  of the room, the standing waves are very pronounced. Figures 30 and 31 show the distribution of particle velocity and sound pressure for the  $n_x = 1$ ,  $n_y = 1$ , and  $n_z = 1$  mode in a room with hard reflecting walls. See Chapters 4 and 103 for further discussion of standing-wave behavior in rectangular rooms.

## 19 WAVEGUIDES

Waveguides can occur naturally where sound waves are channeled by reflections at boundaries and by refraction. Even the ocean can sometimes be considered to be an acoustic waveguide that is bounded above by the air-sea interface and below by the ocean bottom (see Chapter 31 in the *Handbook of Acoustics*<sup>1</sup>). Similar channeling effects are also sometimes observed in the atmosphere. (See Chapter 5.) Waveguides are also encountered in musical instruments and engineering applications. Wind instruments may be regarded as waveguides. In addition, waveguides comprised

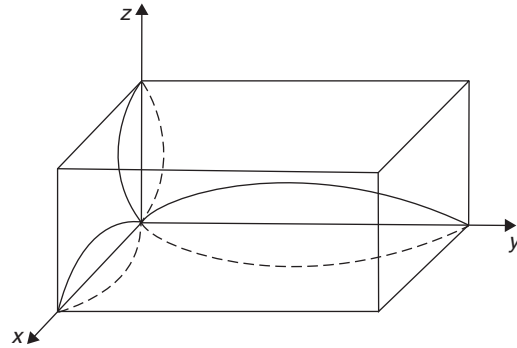
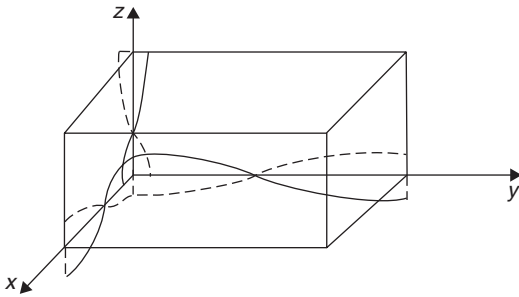


Figure 30 Standing wave for  $n_x = 1$ ,  $n_y = 1$ , and  $n_z = 1$  (particle velocity shown).



**Figure 31** Standing wave for  $n_x = 1$ ,  $n_y = 1$ , and  $n_z = 1$  (sound pressure shown).

of pipes, tubes, and ducts are frequently used in engineering systems, for example, exhaust pipes, air-conditioning ducts and the ductwork in turbines and turbofan engines. The sound propagation in such waveguides is similar to the three-dimensional situation discussed in Section 15 but with some differences. Although rectangular ducts are used in air-conditioning systems, circular ducts are also frequently used, and theory for these must be considered as well. In real waveguides, airflow is often present and complications due to a mean fluid flow must be included in the theory.

For low-frequency excitation only plane waves can propagate along the waveguide (in which the sound pressure is uniform across the duct cross section). However, as the frequency is increased, the so-called first cut-on frequency is reached above which there is a standing wave across the duct cross section caused by the first higher mode of propagation.

For excitation just above this cut-on frequency, besides the plane-wave propagation, propagation in higher order modes can also exist. The higher mode propagation in each direction in a rectangular duct can be considered to be composed of four traveling waves with a vector (ray) almost perpendicular to the duct walls and with a phase speed along the duct that is almost infinite. As the frequency is increased, these vectors point increasingly toward the duct axis, and the phase speed along the duct decreases until at very high frequency it is only just above the speed of sound  $c$ . However, for this mode, the sound pressure distribution across duct cross section remains unchanged. As the frequency increases above the first cut-on frequency, the cut-on frequency for the second higher order mode is reached and so on. For rectangular ducts, the solution for the sound pressure distribution for the higher duct modes consists of cosine terms with a pressure maximum at the duct walls, while for circular ducts, the solution involves Bessel functions. Chapter 7 in the *Handbook of Acoustics*<sup>1</sup> explains how sound propagates in both rectangular and circular guides and includes discussion on the complications created by a mean flow, dissipation, discontinuities, and terminations. Chapter 161 in the *Encyclopedia of Acoustics*<sup>13</sup> discusses the propagation of sound in another class of waveguides, that is, acoustical horns.

## 20 ACOUSTICAL LUMPED ELEMENTS

When the wavelength of sound is large compared to physical dimensions of the acoustical system under consideration, then the lumped-element approach is useful. In this approach it is assumed that the fluid mass, stiffness, and dissipation distributions can be “lumped” together to act at a point, significantly simplifying the analysis of the problem. The most common example of this approach is its use with the well-known Helmholtz resonator in which the mass of air in the neck of the resonator vibrates at its natural frequency against the stiffness of its volume. A similar approach can be used in the design of loudspeaker enclosures and the concentric resonators in automobile mufflers in which the mass of the gas in the resonator louvers (orifices) vibrates against the stiffness of the resonator (which may not necessarily be regarded completely as a lumped element). Dissipation in the resonator louvers may also be taken into account. Chapter 21 in the *Handbook of Acoustics*<sup>1</sup> reviews the lumped-element approach in some detail.

## 21 NUMERICAL APPROACHES: FINITE ELEMENTS AND BOUNDARY ELEMENTS

In cases where the geometry of the acoustical space is complicated and where the lumped-element approach cannot be used, then it is necessary to use numerical approaches. In the late 1960s, with the advent of powerful computers, the acoustical finite element method (FEM) became feasible. In this approach the fluid volume is divided into a number of small fluid elements (usually rectangular or triangular), and the equations of motion are solved for the elements, ensuring that the sound pressure and volume velocity are continuous at the node points where the elements are joined. The FEM has been widely used to study the acoustical performance of elements in automobile mufflers and cabins.

The boundary element method (BEM) was developed a little later than the FEM. In the BEM approach the elements are described on the boundary surface only, which reduces the computational dimension of the problem by one. This correspondingly produces a smaller system of equations than the FEM. BEM involves the use of a surface mesh rather than a volume mesh. BEM, in general, produces a smaller set of equations that grows more slowly with frequency, and the resulting matrix is full; whereas the FEM matrix is sparse (with elements near and on the diagonal). Thus computations with FEM are generally less time consuming than with BEM. For sound propagation problems involving the radiation of sound to infinity, the BEM is more suitable because the radiation condition at infinity can be easily satisfied with the BEM, unlike with the FEM. However, the FEM is better suited than the BEM for the determination of the natural frequencies and mode shapes of cavities.

Recently, FEM and BEM commercial software has become widely available. The FEM and BEM are described in Chapters 7 and 8 of this book and in Chapters 12 and 13 in the *Handbook of Acoustics*.<sup>1</sup>

## 22 ACOUSTICAL MODELING USING EQUIVALENT CIRCUITS

Electrical analogies have often been found useful in the modeling of acoustic systems. There are two alternatives. The sound pressure can be represented by voltage and the volume velocity by current, or alternatively the sound pressure is replaced by current and the volume velocity by voltage. Use of electrical analogies is discussed in Chapter 11 of the *Handbook of Acoustics*.<sup>1</sup> They have been widely used in loudspeaker design and are in fact perhaps most useful in the understanding and design of transducers such as microphones where acoustic, mechanical, and electrical systems are present together and where an overall equivalent electrical circuit can be formulated (see *Handbook of Acoustics*,<sup>1</sup> Chapters 111, 112, and 113). Beranek makes considerable use of electrical analogies in his books.<sup>11,12</sup> In Chapter 85 of this book and Chapter 14 in the *Handbook of Acoustics*<sup>1</sup> their use in the design of automobile mufflers is described.

## REFERENCES

1. M. J. Crocker (Ed.), *Handbook of Acoustics*, Wiley, New York, 1998.
2. M. J. Lighthill, *Waves in Fluids*, Cambridge University Press, Cambridge, 1978.
3. P. M. Morse and K. U. Ingard, *Theoretical Acoustics*, Princeton University Press, Princeton, NJ, 1987.
4. L. E. Kinsler, A. R. Frey, A. B. Coppens, and J. V. Sanders, *Fundamentals of Acoustics*, 4th ed., Wiley, New York, 1999.
5. A. D. Pierce, *Acoustics: An Introduction to Its Physical Principles and Applications*, McGraw-Hill, New York, 1981.
6. M. J. Crocker and A. J. Price, *Noise and Noise Control*, Vol. 1, CRC Press, Cleveland, OH, 1975.
7. M. J. Crocker and F. M. Kessler, *Noise and Noise Control*, Vol. II, CRC Press, Boca Raton, FL, 1982.
8. R. G. White and J. G. Walker (Eds.), *Noise and Vibration*, Halstead Press, Wiley, New York, 1982.
9. F. J. Fahy, *Sound Intensity*, 2nd ed., E&FN Spon, Chapman & Hall, London, 1995.
10. E. Skudrzyk, *The Foundations of Acoustics*, Springer, New York, 1971.
11. L. L. Beranek, *Acoustical Measurements*, rev. ed., Acoustical Society of America, New York, 1988.
12. L. L. Beranek, *Acoustics*, Acoustical Society of America, New York, 1986 (reprinted with changes).
13. M. J. Crocker, *Encyclopedia of Acoustics*, Wiley, New York, 1997.
14. I.L. Ver and C. I. Holmer, Chapter 11 in *Noise and Vibration Control*, L. L. Beranek (Ed.), McGraw-Hill, New York, 1971.
15. R. A. Pierri, Study of a Dynamic Absorber for Reducing the Vibration and Noise Radiation of Plate-like structures, M.Sc. Thesis, University of Southampton, 1977.
16. S. G. Braun, D. J. Ewins and S. S. Rao, *Encyclopedia of Vibration*, Academic, San Diego, 2001.
17. F. J. Fahy, *Sound and Structural Vibration—Radiation, Transmission and Response*, Academic, London, 1985.
18. F. J. Fahy and J. G. Walker (Eds.), *Fundamentals of Noise and Vibration*, E & FN Spon, London, 1998.
19. D. A. Bies and C. H. Hansen, *Engineering Noise Control—Theory and Practice*, 3rd ed., E & FN Spon, London, 2003.
20. F. J. Fahy, *Foundations of Engineering Acoustics*, Academic, London, 2000.

# CHAPTER 3

## SOUND SOURCES

Philip A. Nelson  
Institute of Sound and Vibration Research  
University of Southampton  
Southampton, United Kingdom

### 1 INTRODUCTION

This chapter will present an introduction to elementary acoustic sources and the sound fields they radiate. Sources of spherical waves at a single frequency are first described with reference to the concept of a pulsating sphere whose surface vibrations are responsible for producing sound radiation. From this idea follows the notion of the point monopole source. Of course, such idealized sources alone are not a good representation of many practical noise sources, but they provide the basic source models that are essential for the analysis of the more complex acoustic source distributions that are encountered in practical noise control problems. These simple models of spherical wave radiation are also used to discuss the ideas of acoustic power radiation, radiation efficiency, and the effect of interaction between different source elements on the net flow of acoustic energy. Further important elementary source models are introduced, and specific reference is made to the sound fields radiated by point dipole and point quadrupole sources. Many important practical problems in noise control involve the noise generated by unsteady flows and, as will be demonstrated in later chapters, an understanding of these source models is an essential prerequisite to the study of sound generated aerodynamically.

### 2 THE HOMOGENEOUS WAVE EQUATION

It is important to understand the physical and mathematical basis for describing the radiation of sound, and an introduction to the analysis of sound propagation and radiation is presented here. Similar introductions can also be found in several other textbooks on acoustics such as those authored by Pierce,<sup>1</sup> Morse and Ingard,<sup>2</sup> Dowling and Ffowcs Williams,<sup>3</sup> Nelson and Elliott,<sup>4</sup> Dowling,<sup>5</sup> Kinsler et al.,<sup>6</sup> and Skudrzyk.<sup>7</sup> Acoustic waves propagating in air generate fluctuations in pressure and density that are generally much smaller than the average pressure and density in a stationary atmosphere. Even some of the loudest sounds generated (e.g., close to a jet engine) produce pressure fluctuations that are of the order of 100 Pa, while in everyday life, acoustic pressure fluctuations vary in their magnitude from about  $10^{-5}$  Pa (about the smallest sound that can be detected) to around 1 Pa (typical of the pressure fluctuations generated in a noisy workshop). These fluctuations are much smaller than the typical average atmospheric pressure of about  $10^5$  Pa. Similarly, the density fluctuations associated with the propagation of some of the loudest sounds generated

are still about a thousand times less than the average density of atmospheric air (which is about  $1.2 \text{ kg m}^{-3}$ ). Furthermore, the pressure fluctuations associated with the propagation of sound occur very quickly, the range of frequencies of sounds that can be heard being typically between 20 Hz and 20 kHz (i.e., the pressure fluctuations occur on a time scale of between 1/20th of a second and 1/20,000th of a second). These acoustic pressure fluctuations can be considered to occur *adiabatically* since the rapid rate of change with time of the pressure fluctuations in a sound wave, and the relatively large distances between regions of increased and decreased pressure, are such that there is a negligible flow of heat from a region of compression to a region of rarefaction. Under these circumstances, it can be assumed that the density change is related only to the pressure change and not to the (small) increase or decrease in temperature in regions of compression or rarefaction. Furthermore, since these pressure and density fluctuations are very small compared to the average values of pressure and density, it can also be assumed that the fluctuations are *linearly* related. It turns out (see, e.g., Pierce,<sup>1</sup> pp. 11–17) that the acoustic pressure fluctuation  $p$  is related to the acoustic density fluctuation  $\rho$  by  $p = c_0^2 \rho$  where  $c_0$  is the speed of sound in air.

The sound speed  $c_0$  in air at a temperature of 20°C and at standard atmospheric pressure is about  $343 \text{ m s}^{-1}$  and thus it takes an acoustic disturbance in air about one third of a second to propagate 100 m. As sound propagates it also imparts a very small motion to the medium such that the pressure fluctuations are accompanied locally by a fluctuating displacement of the air. This small air movement can be characterized by the local *particle velocity*, a “particle” being thought of as a small volume of air that contains many millions of gas molecules. The typical values of particle velocity associated with the propagation of even very loud sounds are usually less than about  $1 \text{ m s}^{-1}$  and so the local velocity of the air produced by the passage of a sound wave is actually very much smaller than the speed with which the sound propagates.

Since the acoustic pressure, density, and particle velocity fluctuations associated with sound waves in air are usually relatively small, the equations governing mass and momentum conservation in a fluid continuum can be considerably simplified in order to relate these acoustical variables to one another. The general conservation equations can be *linearized* and terms that are proportional to the product of the acoustical variables can be discarded from the equations. The



equation of mass conservation in a homogeneous three-dimensional medium at rest reduces to

$$\frac{\partial \rho}{\partial t} + \rho_0 \left( \frac{\partial u_1}{\partial x_1} + \frac{\partial u_2}{\partial x_2} + \frac{\partial u_3}{\partial x_3} \right) = 0 \quad (1)$$

where  $u_1$ ,  $u_2$ , and  $u_3$  are the three components of the acoustic particle velocity in the  $x_1$ ,  $x_2$ , and  $x_3$  directions and  $\rho_0$  is the average density of the medium. This equation can be written more compactly in vector notation such that

$$\frac{\partial \rho}{\partial t} + \rho_0 \nabla \cdot \mathbf{u} = 0 \quad (2)$$

where  $\nabla \cdot \mathbf{u}$  is the divergence of the vector  $\mathbf{u}$  given by the scalar product of the del operator  $\mathbf{i}(\partial/\partial x_1) + \mathbf{j}(\partial/\partial x_2) + \mathbf{k}(\partial/\partial x_3)$  with the velocity vector  $\mathbf{i}u_1 + \mathbf{j}u_2 + \mathbf{k}u_3$  where  $\mathbf{i}$ ,  $\mathbf{j}$ , and  $\mathbf{k}$  are, respectively, the unit vectors in the  $x_1$ ,  $x_2$ , and  $x_3$  directions. Similarly, for an inviscid medium, the linearized equations of momentum conservation in these three coordinate directions reduce to

$$\begin{aligned} \rho_0 \frac{\partial u_1}{\partial t} + \frac{\partial p}{\partial x_1} &= 0 & \rho_0 \frac{\partial u_2}{\partial t} + \frac{\partial p}{\partial x_2} &= 0 \\ \rho_0 \frac{\partial u_3}{\partial t} + \frac{\partial p}{\partial x_3} &= 0 \end{aligned} \quad (3)$$

which can be written more compactly as

$$\rho_0 \frac{\partial \mathbf{u}}{\partial t} + \nabla p = 0 \quad (4)$$

where  $\mathbf{u}$  and  $\nabla p$  are, respectively, the vectors having components  $(u_1, u_2, u_3)$  and  $(\partial p/\partial x_1, \partial p/\partial x_2, \partial p/\partial x_3)$ . Taking the difference between the divergence of Eq. (4) and the time derivative of Eq. (2) and using the relation  $p = c_0^2 \rho$  leads to the wave equation for the acoustic pressure fluctuation given by

$$\nabla^2 p - \frac{1}{c_0^2} \frac{\partial^2 p}{\partial t^2} = 0 \quad (5)$$

where in rectangular Cartesian coordinates  $\nabla^2 p = \partial^2 p/\partial x_1^2 + \partial^2 p/\partial x_2^2 + \partial^2 p/\partial x_3^2$ . This equation governs the behavior of acoustic pressure fluctuations in three dimensions. The equation states that the acoustic pressure at any given point in space must behave in such a way to ensure that the second derivative of the pressure fluctuation with respect to time is related to the second derivatives of the pressure fluctuation with respect to the three spatial coordinates. Since the equation follows from the mass and momentum conservation equations, pressure fluctuations satisfying this equation also satisfy these fundamental conservation laws. It is only through finding pressure fluctuations that satisfy this equation that the physical implications of the wave equation become clear.

### 3 SOLUTIONS OF THE HOMOGENEOUS WAVE EQUATION

The simplest and most informative solutions of the wave equation in three dimensions are those associated with spherically symmetric wave propagation. If it can be assumed that the pressure fluctuations depend only on the radial coordinate  $r$  of a system of spherical coordinates, the wave equation reduces to (see Pierce,<sup>1</sup> p. 43)

$$\frac{1}{r^2} \frac{\partial}{\partial r} \left( r^2 \frac{\partial p}{\partial r} \right) - \frac{1}{c_0^2} \frac{\partial^2 p}{\partial t^2} = 0 \quad (6)$$

and this equation can, after some algebra, be written in the form

$$\frac{\partial^2(r p)}{\partial r^2} - \frac{1}{c_0^2} \frac{\partial^2(r p)}{\partial t^2} = 0 \quad (7)$$

It is easy to show that this equation has solutions given by  $r p = f(t - r/c_0)$  or by  $r p = g(t + r/c_0)$  where  $f(\ )$  or  $g(\ )$  means "a function of." Proof that these functions, of either  $t - r/c_0$  or of  $t + r/c_0$ , are solutions of Eq. (7) can be established by differentiating the functions twice with respect to both  $r$  and  $t$  and then demonstrating that the resulting derivatives satisfy the equation. It follows, therefore, that the solution for the radially dependent pressure fluctuation is given by

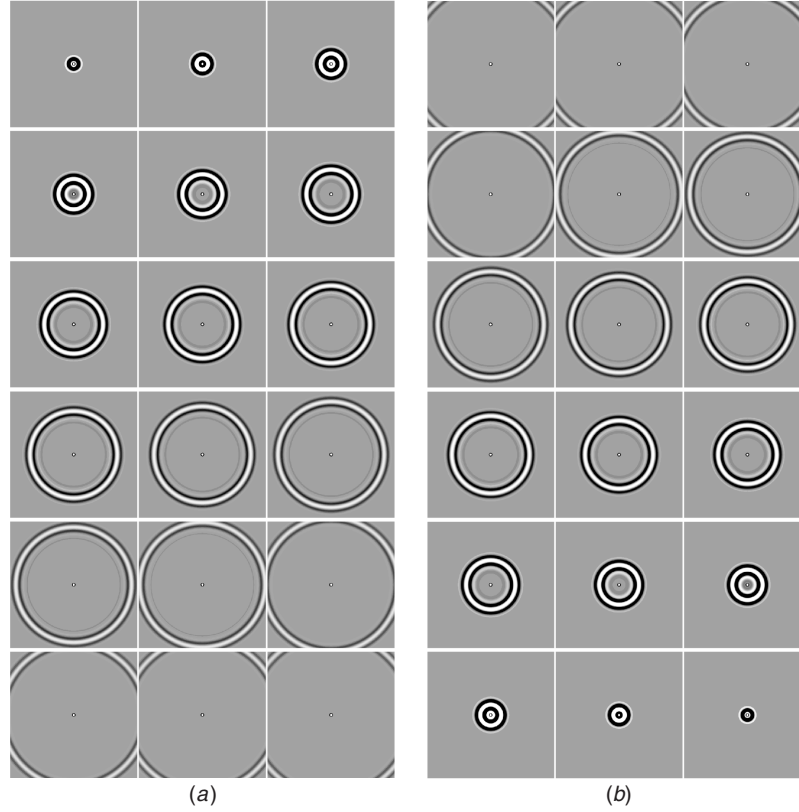
$$p(r, t) = \frac{f(t - r/c_0)}{r} + \frac{g(t + r/c_0)}{r} \quad (8)$$

The function of  $t - r/c_0$  describes waves that propagate outward from the origin of the coordinate system, and Fig. 1a illustrates the process of the outward propagation of a particular sound pulse. The figure shows a series of "snapshots" of the acoustic pressure pulse whose time history takes the form

$$f(t) = e^{-\pi(at)^2} \cos \omega_0 t \quad (9)$$

The figure shows that as the radial distance  $r$  from the origin is increased, the pressure pulse arrives at a later time; this relative time delay is described by the term  $t - r/c_0$ .

Also, as the wave propagates outward, the amplitude of the pulse diminishes as the waves spread spherically; this reduction in amplitude with increasing radial distance from the origin is described by the term  $1/r$ . Figure 1b also shows a series of snapshots of the acoustic pressure associated with waves propagating *inward* toward the origin, and this process is described by the function of  $t + r/c_0$ . In this case as the radial distance from the origin reduces, then the sound pulse associated with this inward traveling wave will arrive at a progressively later time, the pulses arriving at a radial distance  $r$  at a time  $r/c_0$  before the time  $t$  at which the pulse arrives at the origin. Obviously the



**Figure 1** Series of “snapshots” of the sound field associated with (a) outgoing and (b) incoming spherical acoustic waves.

pressure fluctuations also become greater in amplitude as they converge on the origin, this being again described by the term  $1/r$ . Inward propagating waves are legitimate solutions of the wave equation under certain circumstances (e.g., inside a spherical vessel; see Skudrzyk,<sup>7</sup> p. 354, for a discussion). However, it can be argued formally that the solution for inward coming waves is not tenable if one considers sound propagation in a free field since such waves would have to be generated at infinity at an infinite time in the past. The formal mathematical test for the validity of solutions of the wave equation is provided by the Sommerfeld radiation condition (see, e.g. Pierce,<sup>2</sup> p. 177).

#### 4 SIMPLE HARMONIC SPHERICAL WAVES

It is extremely useful in analyzing acoustical problems to be able to work at a single frequency and make use of complex exponential representations of acoustic wave propagation. For example, we may assume that the acoustic pressure everywhere has a dependence on time of the form  $e^{-j\omega t}$  where  $\omega$  is the angular frequency and  $j$  is the square root of  $-1$ . In such a case, the solution for the acoustic pressure as a function of time in the case of spherically symmetric radially

outward propagation can be written as

$$p(r, t) = \text{Re} \left\{ \frac{Ae^{j(\omega t - kr)}}{r} \right\} \quad (10)$$

where  $\text{Re}$  denotes the “real part of” the complex number in curly brackets and  $k = \omega/c_0$  is the wavenumber. The term  $A$  is a complex number that describes the amplitude of the wave and its relative phase. Thus, for example,  $A = |A|e^{j\phi_A}$  where  $|A|$  is the modulus of the complex number and  $\phi_A$  is the phase. The term  $e^{-jkr}$  also describes the change in phase of the pressure fluctuation with increasing radial distance from the origin, this phase change resulting directly from the propagation delay  $r/c_0$ . Taking the real part of the complex number in Eq. (10) shows that

$$p(r, t) = \frac{|A| \cos(\omega t - kr + \phi_A)}{r} \quad (11)$$

and this describes the radial dependence of the amplitude and phase of the single frequency pressure fluctuation associated with harmonic outgoing spherical

waves. It is also useful to be able to define a single complex number that represents the amplitude and phase of a single frequency pressure fluctuation, and in this case the complex pressure can be written as

$$p(r) = \frac{Ae^{-jkr}}{r} \quad (12)$$

where the real pressure fluctuation can be recovered from  $p(r, t) = \text{Re}\{p(r)e^{j\omega t}\}$ . It turns out that in general it is useful to describe the complex acoustic pressure  $p(\mathbf{x})$  as a complex number that depends on the spatial position (described here by the position vector  $\mathbf{x}$ ). This complex pressure must satisfy the single frequency version of the wave equation, or Helmholtz equation, that is given by

$$(\nabla^2 + k^2)p(\mathbf{x}) = 0 \quad (13)$$

It is very straightforward to verify that the complex pressure variation described by Eq. (12) satisfies Eq. (13). It is also useful to describe the other acoustic fluctuations such as density and particle velocity in terms of spatially dependent complex numbers. In the case of spherically symmetric wave propagation, the acoustic particle velocity has only a radial component, and if this is described by the radially dependent complex number  $u_r(r)$ , it follows that momentum conservation relationship given by Eq. (4) reduces to

$$j\omega\rho_0 u_r(r) + \frac{\partial p(r)}{\partial r} = 0 \quad (14)$$

Assuming the radial dependence of the complex pressure described by Eq. (12) then shows that the complex radial particle velocity can be written as

$$u_r(r) = \frac{A}{j\omega\rho_0} \left( \frac{jk}{r} + \frac{1}{r^2} \right) e^{-jkr} \quad (15)$$

The complex number that describes the ratio of the complex pressure to the complex particle velocity is known as the *specific acoustic impedance*, and this is given by

$$z(r) = \frac{p(r)}{u_r(r)} = \rho_0 c_0 \left( \frac{jkr}{1 + jkr} \right) \quad (16)$$

The modulus of the impedance thus describes the ratio of the amplitudes of the pressure and velocity fluctuations while the phase of the impedance describes the phase difference between the pressure and particle velocity fluctuations. First note that when  $kr$  becomes very much greater than unity, then the impedance  $z(r) \approx \rho_0 c_0$ , where  $\rho_0 c_0$  is known as the *characteristic acoustic impedance* of the medium. Since  $kr = 2\pi/\lambda$ , where  $\lambda$  is the acoustic wavelength, this condition occurs when the distance  $r$  is many wavelengths from the origin (where the source of the waves is assumed

to be located). Therefore, many wavelengths from the source, the pressure and velocity fluctuations are in phase with one another, and their amplitudes are related simply by  $\rho_0 c_0$ . This region is known as the *far field* of the source of the waves. However, when  $kr$  is very much smaller than unity, then the impedance  $z(r) \approx \rho_0 c_0(jkr)$ . This shows that, at distances from the source that are small compared to the wavelength, the particle velocity fluctuation becomes much larger relative to the pressure fluctuation than is the case at many wavelengths from the source. At these small distances, the pressure and particle velocity fluctuations are close to being  $90^\circ$  out of phase. This region is known as the *near field* of the source of the waves.

## 5 SOURCES OF SPHERICALLY SYMMETRIC RADIATION

A rigid sphere whose surface vibrates to and fro in the radial direction provides a simple conceptual model for the generation of spherical acoustic waves. Such a pulsating sphere can be assumed to have a mean radius  $a$  and to produce surface vibrations at a single frequency that are uniform over the surface of the sphere. If these radial vibrations are assumed to have a complex velocity  $U_a$  say, then the acoustic pressure fluctuations that result can be found by equating this velocity to the particle velocity of the outward going spherical waves generated. Since the pressure and particle velocity of the waves generated are related by the expression for the impedance given above, it follows that at the radial distance  $a$  from the origin upon which the sphere is centered, the complex acoustic pressure is given by

$$p(a) = \frac{Ae^{-jka}}{a} = \rho_0 c_0 \left( \frac{jka}{1 + jka} \right) U_a \quad (17)$$

This equation enables the complex amplitude  $A$  of the acoustic pressure to be expressed in terms of the radial surface velocity  $U_a$  of the pulsating sphere. It then follows that the radial dependence of the complex acoustic pressure can be written as

$$p(r) = \rho_0 c_0 a \left[ \frac{jka}{1 + jka} \right] \frac{U_a e^{-jk(r-a)}}{r} \quad (18)$$

The product of the radial surface velocity  $U_a$  and the total surface area of the sphere  $4\pi a^2$  provides a measure of the *strength* of such an acoustic source. This product, usually denoted by  $q = 4\pi a^2 U_a$ , has the dimensions of *volume velocity*, and the pressure field can be written in terms of this source strength as

$$p(r) = \rho_0 c_0 \left[ \frac{jk}{1 + jka} \right] \frac{q e^{-jk(r-a)}}{4\pi r} \quad (19)$$

The definition of the sound field generated by a *point monopole source* follows from this equation by

assuming that the radius  $a$  of the sphere becomes infinitesimally small but that the surface velocity of the sphere increases to ensure that the product of surface area and velocity (and thus source strength) remains constant. Therefore, as  $ka$  tends to zero, the expression for the pressure field becomes

$$p(r) = \rho_0 c_0 j k \frac{q e^{-jkr}}{4\pi r} \quad (20)$$

It is worth noting that this expression can be written in terms of the time derivative of the source strength defined by  $\dot{q} = j\omega q$  such that  $p(r) = \rho_0 \dot{q} e^{-jkr} / 4\pi r$ , and since the term  $e^{-jkr} = e^{-j\omega r/c_0}$  represents a pure delay of  $r/c_0$  in the time domain, then the expression for the acoustic pressure as a function of time can be written as

$$p(r, t) = \frac{\rho_0 \dot{q}(t - r/c_0)}{4\pi r} \quad (21)$$

This demonstrates that the acoustic pressure time history replicates exactly the time history of the *volume acceleration* of the source but, of course, delayed by the time that it takes for the sound to travel radially outward by a distance  $r$ .

## 6 ACOUSTIC POWER OUTPUT AND RADIATION EFFICIENCY

The *instantaneous acoustic intensity* defines the local instantaneous rate at which acoustic energy flows per unit surface area in a sound field. It is equal to the product of the local acoustic pressure and the local acoustic particle velocity. The time-averaged acoustic intensity is defined by the vector quantity

$$\mathbf{I}(\mathbf{x}) = \frac{1}{T} \int_{-T/2}^{T/2} p(\mathbf{x}, t) \mathbf{u}(\mathbf{x}, t) dt \quad (22)$$

where  $T$  denotes a suitably long averaging time in the case of stationary random fluctuations, or the duration of a period of a single frequency fluctuation. For single frequency fluctuations, this time integral can be written in terms of the complex pressure and particle velocity such that  $\mathbf{I}(\mathbf{x}) = (\frac{1}{2}) \text{Re}\{p(\mathbf{x})^* \mathbf{u}(\mathbf{x})\}$  where the asterisk denotes the complex conjugate. The acoustic power output of a source of sound is evaluated by integrating the sound intensity over a surface surrounding the source. Thus, in general

$$W = \int_S \mathbf{I}(\mathbf{x}) \cdot \mathbf{n} dS \quad (23)$$

where  $\mathbf{n}$  is the unit vector that is normal to and points outward from the surface  $S$  surrounding the source. In the particular case of the pulsating sphere of radius  $a$  where the pressure and particle velocity are uniform across the surface of the sphere, the acoustic power output is given by evaluating this

integral over the surface of the sphere. Thus, in this case

$$\begin{aligned} W &= 4\pi a^2 \frac{1}{2} \text{Re}\{p(a)^* U_a\} \\ &= 2\pi a^2 \rho_0 c_0 |U_a|^2 \frac{(ka)^2}{1 + (ka)^2} \end{aligned} \quad (24)$$

This calculation is of considerable assistance in explaining some basic features of the efficiency with which acoustic sources radiate sound. First, note that if the product  $ka = 2\pi a/\lambda$  is very large (i.e., the radius of the sphere is very large compared to the acoustic wavelength), then the sound power radiated is given by  $W \approx 2\pi a^2 \rho_0 c_0 |U_a|^2$ , while if the reverse is true, and  $ka$  is very small (i.e., the radius of the sphere is very small compared to the acoustic wavelength), the sound power radiated is approximated by the expression  $W \approx 2\pi a^2 \rho_0 c_0 |U_a|^2 (ka)^2$ . It is clear that, in the second case, since by definition  $ka$  is small, the efficiency with which surface velocity fluctuations are converted into sound power radiated is very much less than in the first case, where the radius of the sphere is very much greater than the acoustic wavelength. It turns out that this is a general characteristic of acoustic sources and more complex radiators of sound are often characterized by their *radiation efficiency* that is defined by the ratio

$$\sigma = \frac{W}{\rho_0 c_0 S (1/2) \langle |U|^2 \rangle} \quad (25)$$

where  $\langle |U|^2 \rangle$  denotes the squared modulus of the velocity fluctuation averaged over the surface area  $S$  of the body that radiates the acoustic power  $W$ . Most sources of sound follow the general trend of relatively inefficient radiation at low frequencies (where the wavelength is much greater than the dimensions of the radiator) and relatively efficient radiation ( $\sigma \approx 1$ ) at high frequencies (where the wavelength becomes smaller than the dimensions of the radiator). Obviously, the exact nature of the surface velocity distribution dictates the radiated sound field and of paramount importance is the interference produced in the sound field between neighboring elements of the effective distribution of source strength.

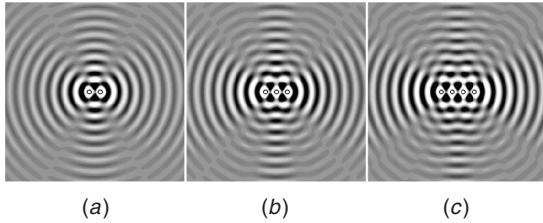
## 7 INTERFERENCE BETWEEN POINT SOURCES

The linearity of the wave equation leads to the *principle of superposition*, which in turn implies that the sound field generated by a number of acoustic sources is simply the sum at any instant of the sound fields generated by all of the sources individually (i.e., the sound fields generated by each of the sources when the strengths of all the others is set to zero). For single frequency sound fields, the total complex acoustic pressure is simply found by adding the complex pressures generated by each of the sources. Thus, for

example, if there are  $N$  point sources each of strength  $q_n$ , then the total complex pressure produced by these sources is given by

$$p(\mathbf{x}) = \frac{\rho_0 c_0 j k q_1 e^{-jkr_1}}{4\pi r_1} + \frac{\rho_0 c_0 j k q_2 e^{-jkr_2}}{4\pi r_2} + \dots + \frac{\rho_0 c_0 j k q_N e^{-jkr_N}}{4\pi r_N} \quad (26)$$

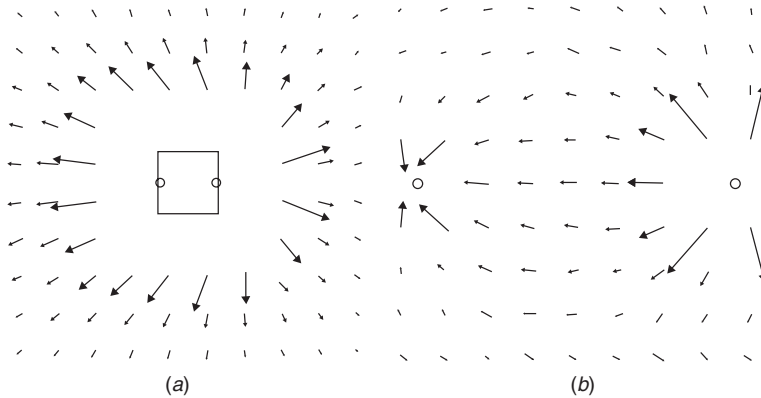
where the distances  $r_n = |\mathbf{x} - \mathbf{y}_n|$  are the radial distances to the vector position  $\mathbf{x}$  from the vector positions  $\mathbf{y}_n$  at which the sources are located. The net sound fields produced by the interference of these individual fields can be highly complex and depend on the geometric arrangement of the sources, their relative amplitudes and phases, and, of course, the angular frequency  $\omega$ . It is worth illustrating this complexity with some simple examples. Figure 2 shows the interference patterns generated by combinations of two, three, and four monopole sources each separated by one acoustic wavelength when all the source strengths are in phase. Regions of *constructive interference* are shown (light shading) where the superposition of the fields gives rise to an increase in the acoustic pressure



**Figure 2** Single frequency sound field generated by (a) two, (b) three, and (c) four point monopole sources whose source strengths are in phase and are separated by a wavelength  $\lambda$ .

amplitude, as are regions of *destructive interference* (dark shading) where the acoustic pressure amplitude is reduced.

It is also worth emphasizing that the energy flow in such sound fields can also be highly complex. It is perfectly possible for energy to flow out of one of the point sources and into another. Figure 3 shows the time-averaged intensity vectors when a source of strength  $q_2 = q_1 e^{j\phi}$  is placed at a distance  $d = \lambda/16$  apart from a source of strength  $q_1$  when the phase difference  $\phi = 4.8kd$ . The source of strength  $q_1$  appears to absorb significant power while the source of strength  $q_2$  radiates net power. The power that finds its way into the far field turns out to be a relatively small fraction of the power being exchanged between the sources. The possibility of acoustic sources being net absorbers of acoustic energy may at first sight be unreasonable. However, if one thinks of the source as a pulsating sphere, or indeed the cone of a baffled loudspeaker, whose velocity is prescribed, then it becomes apparent that the source may become a net absorber of energy from the sound field when the net acoustic pressure on the source is close to being out of phase with the velocity fluctuations of the surface. It turns out that the net acoustic power output of a point source can be written as  $W = (\frac{1}{2}) \text{Re}\{p^* q\}$ , and, if the phase difference between the pressure and volume velocity is given by  $\phi_{pq}$ , then we can write  $W = (\frac{1}{2}) |p| |q| \cos \phi_{pq}$ . It therefore follows that, if the phase difference  $\phi_{pq}$  is, for example,  $180^\circ$ , then the power  $W$  will be negative. Of course, a source radiating alone produces a pressure fluctuation upon its own surface, some of which will be in phase with the velocity of the surface and thereby radiate sound power. As shown by this example, however, if another source produces a net fluctuating pressure on the surface of the source that is out of phase with the velocity of the source, the source can become a net absorber of acoustic energy. The consequences of this for the energy used to drive the fluctuating velocity of



**Figure 3** Time-averaged intensity vectors generated by the superposition of the sound fields generated by two point monopole sources  $q_1$  (on the left) and  $q_2$  (on the right) where  $q_2 = q_1 e^{j\phi}$ ,  $|q_2| = |q_1|$ ,  $d = \lambda/16$ , and  $\phi = 108^\circ = 4.8kd$  rad. The dimension of one side of (a) is  $\lambda/2$  and one side of (b) is  $\lambda/10$ , which corresponds to the square depicted in (a).

the source surface can be understood by examination of the detailed electrodynamics of, for example, a moving coil loudspeaker (see Nelson and Elliott,<sup>4</sup> p. 140). It is concluded that, in practice, the power radiated as sound is generally a small fraction of that necessary to overcome the mechanical and electrical energy losses sustained in producing the requisite surface velocity of the source. Thus, when a loudspeaker acts as an absorber of acoustic energy, there will be a relatively small reduction (of typically a few percent) in the electrical energy consumed in order to produce the necessary vibrations of the loudspeaker cone.

## 8 THE POINT DIPOLE SOURCE

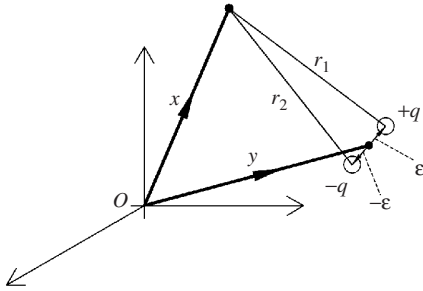
The sound field radiated by a point dipole source can be thought of as the field radiated by two point monopole sources of the same strength but of opposite phase that are placed very close together compared to the wavelength of the sound radiated. In fact, the point dipole field is exactly equivalent to the field of the two monopoles when they are brought infinitesimally close together in such a way as to keep constant the product of their source strength and their distance apart. Assume that, as illustrated in Fig. 4, one of the monopoles, of strength  $q$  say, is located at a vector position  $\mathbf{y} + \boldsymbol{\epsilon}$  while the other, of strength  $-q$ , is located at  $\mathbf{y} - \boldsymbol{\epsilon}$ . The sound field at the position  $\mathbf{x}$  can then be written as

$$p(\mathbf{x}) = \frac{\rho_0 c_0 j k q e^{-j k r_1}}{4 \pi r_1} - \frac{\rho_0 c_0 j k q e^{-j k r_2}}{4 \pi r_2} \quad (27)$$

where the distances from the sources to the field point are, respectively, given by  $r_1 = |\mathbf{x} - (\mathbf{y} + \boldsymbol{\epsilon})|$  and  $r_2 = |\mathbf{x} - (\mathbf{y} - \boldsymbol{\epsilon})|$ . On the assumption that the vector  $\boldsymbol{\epsilon}$  is small, one may regard the first term on the right side of Eq. (27) as a function of the vector  $\mathbf{y} + \boldsymbol{\epsilon}$  and make use of the Taylor series expansion:

$$f(\mathbf{y} + \boldsymbol{\epsilon}) = f(\mathbf{y}) + \boldsymbol{\epsilon} \cdot \nabla_{\mathbf{y}} f(\mathbf{y}) + \frac{1}{2} (\boldsymbol{\epsilon} \cdot \nabla_{\mathbf{y}})^2 f(\mathbf{y}) + \dots \quad (28)$$

where, for example,  $\nabla_{\mathbf{y}} f = \partial f / \partial y_1 \mathbf{i} + \partial f / \partial y_2 \mathbf{j} + \partial f / \partial y_3 \mathbf{k}$  such that  $\nabla_{\mathbf{y}}$  is the del operator in the  $y$  coordinates. Similarly, the second term on the right



**Figure 4** Coordinate system for the analysis of the dipole source.

side of Eq. (27) can be regarded as a function  $f(\mathbf{y} - \boldsymbol{\epsilon})$ , and, therefore, in the limit that  $\boldsymbol{\epsilon} \rightarrow 0$ , it is possible to make the following approximations:

$$\frac{e^{-j k r_1}}{4 \pi r_1} \approx \frac{e^{-j k r}}{4 \pi r} + \boldsymbol{\epsilon} \cdot \nabla_{\mathbf{y}} \left( \frac{e^{-j k r}}{4 \pi r} \right) \quad (29a)$$

$$\frac{e^{-j k r_2}}{4 \pi r_2} \approx \frac{e^{-j k r}}{4 \pi r} - \boldsymbol{\epsilon} \cdot \nabla_{\mathbf{y}} \left( \frac{e^{-j k r}}{4 \pi r} \right) \quad (29b)$$

where  $r = |\mathbf{x} - \mathbf{y}|$  and the higher order terms in the Taylor series are neglected. Substitution of these approximations into Eq. (27) then shows that

$$p(\mathbf{x}) = \rho_0 c_0 j k (q \mathbf{d}) \cdot \nabla_{\mathbf{y}} \left( \frac{e^{-j k r}}{4 \pi r} \right) \quad (30)$$

where the vector  $\mathbf{d} = 2\boldsymbol{\epsilon}$  and the product  $(q \mathbf{d})$  is the *vector dipole strength*. It is this product that is held constant as the two monopoles are brought infinitesimally close together. Noting that

$$\begin{aligned} \nabla_{\mathbf{y}} \left( \frac{e^{-j k r}}{4 \pi r} \right) &= (\nabla_{\mathbf{y}} r) \frac{\partial}{\partial r} \left( \frac{e^{-j k r}}{4 \pi r} \right) \\ &= -\frac{(\mathbf{x} - \mathbf{y})}{r} \frac{\partial}{\partial r} \left( \frac{e^{-j k r}}{4 \pi r} \right) \end{aligned} \quad (31)$$

and since  $(\mathbf{x} - \mathbf{y})/r = \mathbf{n}_r$  is the unit vector pointing from the source to the field point, the expression for the dipole field reduces to

$$p(\mathbf{x}) = -\rho_0 c_0 k^2 (q \mathbf{d}) \cdot \mathbf{n}_r \left( \frac{e^{-j k r}}{4 \pi r} \right) \left( 1 + \frac{1}{j k r} \right) \quad (32)$$

If  $\theta$  defines the angle between the vector  $\mathbf{n}_r$  and the axis of the dipole (defined by the direction of the vector  $\mathbf{d}$ ), then  $\mathbf{d} \cdot \mathbf{n}_r = d \cos \theta$ , and the strong directivity of the dipole source becomes apparent. It is also evident that when  $kr$  is small (i.e., the field point is a relatively small number of wavelengths from the source), then the “near-field” term given by  $1/jkr$  has an influence on the pressure fluctuations produced, but that this term vanishes in the far field (as  $kr \rightarrow \infty$ ). It can also be shown that this sound field is identical to that produced by a fluctuating point force  $\mathbf{f}$  applied to the medium where the force is given by  $\mathbf{f} = \rho_0 c_0 j k q \mathbf{d}$ . A simple practical example of a dipole source is that of an open-backed loudspeaker radiating sound whose wavelength is much greater than the loudspeaker dimensions. Such a source applies a fluctuating force to the surrounding medium without introducing any net fluctuating volume flow into the surrounding medium. The dipole source also has considerable utility in modeling the process of aerodynamic sound generation; it turns out that the sound generated by turbulence interacting with a rigid body at low Mach numbers can be modeled as if

the sound were generated by a distribution of dipole sources on the surface of the body. The strengths of these dipoles are given exactly by the fluctuations in force applied locally by the unsteady flow to the body.

### 9 POINT QUADRUPOLE SOURCES

The approach taken to deriving the field of the point dipole source can also be more generally applied to other arrangements of point monopole sources. Thus, for example, if there are  $N$  point monopoles of strength  $q_n$  clustered around a point defined by the position vector  $\mathbf{y}$  such that the  $n$ th source has a position vector  $\mathbf{y} + \mathbf{e}_n$ , the total field at  $\mathbf{x}$  can be written as

$$p(\mathbf{x}) = \sum_{n=1}^N \frac{\rho_0 c_0 j k q_n e^{-jkr_n}}{4\pi r_n} \quad (33)$$

where  $r_n = |\mathbf{x} - (\mathbf{y} + \mathbf{e}_n)|$ . Each of the terms in this summation can then be expanded as a Taylor series such that

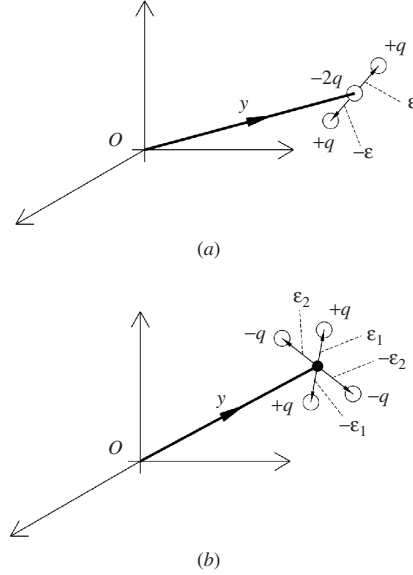
$$\begin{aligned} \frac{e^{-jkr_n}}{4\pi r_n} &\approx \frac{e^{-jkr}}{4\pi r} + \mathbf{e}_n \cdot \nabla_y \left( \frac{e^{-jkr}}{4\pi r} \right) \\ &+ \frac{1}{2} (\mathbf{e}_n \cdot \nabla_y)^2 \left( \frac{e^{-jkr}}{4\pi r} \right) + \dots \end{aligned} \quad (34)$$

where  $r = |\mathbf{x} - \mathbf{y}|$ . The total sound field can then be written as

$$\begin{aligned} p(\mathbf{x}) &= \left[ \sum_{n=1}^N q_n + \left( \sum_{n=1}^N q_n \mathbf{e}_n \right) \cdot \nabla_y \right. \\ &\quad \left. + \frac{1}{2} \sum_{n=1}^N q_n (\mathbf{e}_n \cdot \nabla_y)^2 + \dots \right] \\ &\quad \times \frac{\rho_0 c_0 j k e^{-jkr}}{4\pi r} \end{aligned} \quad (35)$$

where the right side of the equation represents a *multipole expansion* of the source distribution. The first two terms in this series describe, respectively, monopole and dipole sound fields, while the third term describes the radiation from a *quadrupole* source. Particular examples of quadrupole sources are illustrated in Fig. 5a that shows an arrangement of monopole sources that combine to produce a *longitudinal* quadrupole, and in Fig. 5b that shows a source arrangement that defines a *lateral* quadrupole source. In both of these cases the first two summation terms in the above series expansion are zero (this is readily seen by using the values of  $q_n$  and  $\mathbf{e}_n$  illustrated in Fig. 5). The third term then becomes the leading order term in the series and this can be written as

$$p(\mathbf{x}) = \sum_{\mu=1, v=1}^{\mu=3, v=3} Q_{\mu v} \frac{\partial^2}{\partial y_\mu \partial y_v} \left( \frac{\rho_0 c_0 j k e^{-jkr}}{4\pi r} \right) \quad (36)$$



**Figure 5** Coordinate system for the analysis of (a) longitudinal and (b) lateral quadrupole sources.

where the subscripts  $\mu$  and  $v$  define the three coordinate directions (taking the values 1, 2, 3), and the quadrupole strengths are given by

$$Q_{\mu v} = \frac{1}{2} \sum_{n=1}^N \epsilon_{n\mu} \epsilon_{nv} q_n \quad (37)$$

where  $\epsilon_{n\mu}$  and  $\epsilon_{nv}$  are the components of the vector  $\mathbf{e}_n$  in the three coordinate directions. There are nine possible combinations of  $\mu$  and  $v$  that define the strengths  $Q_{\mu v}$  of different types of quadrupole source; these are  $Q_{11}$ ,  $Q_{22}$  and  $Q_{33}$  all of which are longitudinal quadrupoles, and  $Q_{12}$ ,  $Q_{13}$ ,  $Q_{21}$ ,  $Q_{23}$ ,  $Q_{31}$ , and  $Q_{32}$ , which are lateral quadrupoles. Calculation of the sound field radiated involves undertaking the partial derivatives with respect to  $y_\mu$  and  $y_v$  in Eq. (36). It can be shown that in the case of the longitudinal quadrupole depicted in Fig. 5a, where the constituent monopoles lie in a line parallel to the  $x_1$  axis, the sound field reduces to

$$\begin{aligned} p(\mathbf{x}) &= -\frac{\rho_0 c_0 j k^3 e^{-jkr}}{4\pi r} Q_{11} \\ &\times \left[ \cos^2 \theta \left( 1 + \frac{3}{jkr} + \frac{3}{(jkr)^2} \right) - \frac{1}{jkr} - \frac{1}{(jkr)^2} \right] \end{aligned} \quad (38)$$

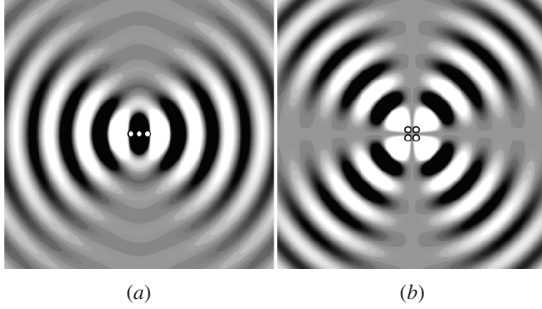
where  $Q_{11} = q\epsilon^2$  and  $\cos \theta = (x_1 - y_1)/r$ . The lateral quadrupole depicted in Fig. 5b has the sound field

$$\begin{aligned} p(\mathbf{x}) &= -\frac{\rho_0 c_0 j k^3 e^{-jkr}}{4\pi r} Q_{12} \\ &\times \left[ \cos \theta \sin \theta \cos \phi \left( 1 + \frac{3}{jkr} + \frac{3}{(jkr)^2} \right) \right] \end{aligned} \quad (39)$$



where again  $Q_{12} = q\epsilon^2$  and  $\sin\theta\cos\phi = (x_2 - y_2)/r$ , where  $(r, \theta, \phi)$  are spherical coordinates centred on the position of the source. The sound fields generated by harmonic lateral and longitudinal quadrupole sources are illustrated in Figs. 6a and 6b. Again, the near fields of the sources, as represented by the terms within the round brackets in Eqs. (38) and (39) that involve the reciprocal of  $jkr$ , vanish in the far field as  $kr \rightarrow \infty$ , and the directivity of the radiation evident in Figs. 6a and 6b is expressed by the terms  $\cos^2\theta$  and  $\cos\theta\sin\theta\cos\phi$  for longitudinal and lateral quadrupoles, respectively.

It should also be pointed out that, in general, any single point quadrupole source can be regarded as being comprised of nine components whose individual strengths are represented by the terms  $Q_{\mu\nu}$ . These components are often thought of the elements of a three-by-three matrix, and thus the quadrupole can be defined in terms of a “tensor” strength in much the same way as a point dipole has a three-component “vector” strength.



**Figure 6** Single frequency sound fields generated by (a) longitudinal and (b) lateral quadrupole sources.

A longitudinal quadrupole component can also be thought of as being comprised of two point dipoles of equal magnitude but opposite phase that thus apply a fluctuating direct stress to the medium. A simple practical example of such a source is that provided by the vibration of a tuning fork where the two prongs of the fork vibrate out of phase in order to apply a net fluctuating stress to the surrounding medium. No net force is applied and no net volume flow is produced. A lateral quadrupole component on the other hand can be thought of as being comprised of two out-of-phase point dipoles that act in parallel to apply a net fluctuating shear stress to the medium. As explained in more detail in later chapters, these source models form the basis for the analysis of sound generated by unsteady flows and are particularly important for describing the noise radiated by turbulent jets.

## REFERENCES

1. A. D. Pierce, *Acoustics: An Introduction to Its Physical Principles and Applications*, McGraw-Hill, New York, 1981.
2. P. M. Morse and K. U. Ingard, *Theoretical Acoustics*, McGraw-Hill, New York, 1968.
3. A. P. Dowling and J. E. Ffowcs Williams, *Sound and Sources of Sound*, Ellis Horwood, Chichester, 1983.
4. P. A. Nelson and S. J. Elliott, *Active Control of Sound*, Academic, London, 1992.
5. A. P. Dowling, Steady State Radiation from Sources, in *Encyclopedia of Acoustics*, M. J. Crocker (Ed.), Wiley, New York, 1997, Chapter 2.
6. L. E. Kinsler, A. R. Frey, A. B. Coppens, and J. V. Sanders, *Fundamentals of Acoustics*, Wiley, New York, 1982.
7. E. Skudrzyk, *The Foundations of Acoustics*, Springer, New York, 1971.



# CHAPTER 4

## SOUND PROPAGATION IN ROOMS

**K. Heinrich Kuttruff**  
Institute of Technical Acoustics  
RWTH Aachen University  
Aachen, Germany

### 1 INTRODUCTION

Sound propagation in closed rooms is of interest for several reasons. Not only the acoustical design of large performance halls is of concern but also the acoustical comfort of such environments where people spend most of their lifetimes, either at work in office spaces, workshops, or factories or in homes, hotels, and restaurants. Three different main approaches can be used to describe the complicated sound fields in rooms (Section 2 to 4). The most rigorous and abstract one is based on solutions of the acoustic wave equation, amended by certain conditions that include the shape and the properties of the room boundaries. Here, the sound field is conceived of as being composed of certain elements, named normal modes. Another, conceptually simpler approach to room acoustics, is the geometrical one; it starts with the sound ray and studies the propagation of many rays throughout the room. The acoustical properties of a room can also be discussed in terms of the energy flow. This last method is called the statistical approach. The final section of this chapter is devoted to sound absorption.

### 2 WAVE ACOUSTICS

#### 2.1 Normal Modes and Eigenfrequencies

The physically exact description of the sound field in a room<sup>1,2</sup> is based upon the acoustic wave equation. If we assume that the time dependence of the sound pressure  $p$  is according to  $\exp(j\omega t)$  with  $\omega$  denoting the angular frequency, this equation transforms into the Helmholtz equation:

$$\nabla^2 p + k^2 p = 0 \quad (1)$$

where  $k = \omega/c$  is the angular wave number.

Any solution of this equation has to comply with the acoustical properties of the boundary, that is, of the room walls. These properties can be expressed in terms of the wall impedance, which is defined as the ratio of the acoustic pressure  $p$  acting on a given point of the surface and the normal component  $v_n$  of the air velocity at the same point:

$$Z = \left( \frac{p}{v_n} \right)_{\text{boundary}} \quad (2)$$

This quantity is usually complex, which indicates that there is a phase difference between  $p$  and  $v_n$ .

Sometimes, the various elements of the surface react nearly independently from each other to the incident wave. Then the wall or boundary is said to be of the locally reacting type. In this case the normal velocity depends not on the spatial distribution, that is, on the direction of incidence of the primary wave.

The boundary condition can be expressed by the wall impedance  $Z$ :

$$Z \frac{\partial p}{\partial n} + j\omega\rho_0 p = 0 \quad (3)$$

In this equation,  $\rho_0$  ( $=1.2 \text{ kg/m}^3$  at normal conditions) denotes the density of air,  $\partial p/\partial n$  is the component of the sound pressure gradient in the direction of the outward-pointing boundary normal. It should be noted that the wall impedance depends usually on the frequency and may vary from one boundary point to another.

The Helmholtz equation (1) supplemented by the boundary condition (3) can only be solved for certain discrete values  $k_n$  of the angular wavenumber  $k$ , so-called eigenvalues. (The subscript  $n$  stands for three integers according to the three space coordinates.) These values are real if air attenuation (see Section 5.1) is neglected and the wall impedance is purely imaginary, that is, if all walls have mass or spring character, or if it is zero or infinite. Then each eigenvalue is related to a characteristic angular frequency  $\omega_n = ck_n$  and hence to a frequency

$$f_n = \frac{ck_n}{2\pi} \quad (4)$$

called the allowed frequency or the eigenfrequency. However, if the impedance of any wall portion has a real component indicating losses, the sound field cannot persist but must die out if there is no sound source making up for the losses. Therefore, the time dependence of the sound pressure must be governed by a factor  $\exp(j\omega t - \delta t)$  with  $\delta$  denoting some decay constant. Then the eigenvalues  $k_n$  turn out to be complex,  $k_n = (\omega_n + j\delta_n)/c$ .

Each eigenvalue is associated with (at least) one solution  $p_n(\mathbf{r})$  of Eq. (1) where the vector  $\mathbf{r}$  symbolizes the space coordinates. These solutions are called the eigenfunctions or characteristic functions of the room. They correspond to characteristic distributions of the sound pressure amplitude known as normal modes. Each of them can be conceived as a three-dimensional

standing wave with a typical pattern of maxima and minima of the sound pressure amplitude, the minima being situated on certain “nodal surfaces.” If there are no losses the pressure amplitude on these surfaces is zero. In all other cases the standing waves are less pronounced or may even vanish.

Once the eigenfunctions of an enclosure are known, the acoustical response of the room to any type of excitation can be expressed by them, at least in principle. However, the practical use of this formalism is rather limited because closed expressions for the eigenfunctions and eigenfrequencies can be worked out for simply shaped rooms only with rigid walls. In general, one has to resort to numerical methods such as the finite element method, and even then only small enclosures (in relation to the wavelength) can be treated in this way. For larger rooms, either a geometrical analysis based on sound rays (Section 3) or an energy-based treatment of the sound field (Section 4) is more profitable.

## 2.2 A Simple Example: The Rectangular Room

In this section we consider a rectangular room that is bounded by three pairs of parallel and rigid walls, the walls of each pair being perpendicular to the remaining ones. Expressed in Cartesian coordinates  $x$ ,  $y$ , and  $z$ , the room extends from  $x = 0$  to  $x = L_x$  in the direction of the  $x$  axis, from  $y = 0$  to  $y = L_y$  in  $y$  direction, and  $z = 0$  to  $z = L_z$  in  $z$  direction (see Fig. 1).

Since  $Z = \infty$  for rigid walls, the boundary condition (3) transforms into

$$\frac{\partial p}{\partial x} = 0 \text{ for } x = 0 \text{ and } x = L_x$$

and two similar equations for the  $y$  and the  $z$  direction. The Helmholtz equation in Cartesian coordinates reads

$$\frac{\partial^2 p}{\partial x^2} + \frac{\partial^2 p}{\partial y^2} + \frac{\partial^2 p}{\partial z^2} + k^2 p = 0 \quad (5)$$

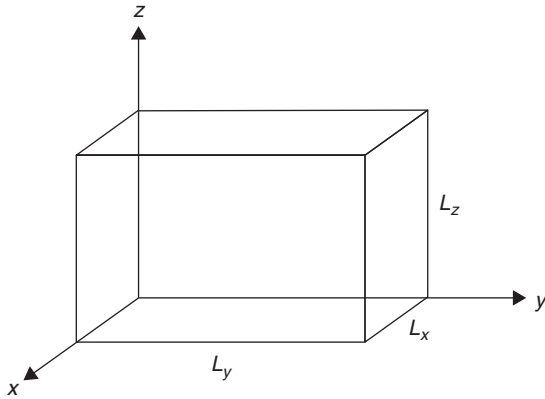


Figure 1 Rectangular enclosure.

Its solutions satisfying the boundary conditions are given by

$$p_{n_x n_y n_z}(x, y, z) = A \cos\left(\frac{n_x \pi x}{L_x}\right) \cos\left(\frac{n_y \pi y}{L_y}\right) \times \cos\left(\frac{n_z \pi z}{L_z}\right) \quad (6)$$

Here  $A$  is an arbitrary constant, and  $n_x$ ,  $n_y$ , and  $n_z$  are integers. The associated angular eigenfrequency  $\omega_{n_x n_y n_z}$  is  $ck_{n_x n_y n_z}$  with

$$k_{n_x n_y n_z} = \pi \sqrt{\left(\frac{n_x}{L_x}\right)^2 + \left(\frac{n_y}{L_y}\right)^2 + \left(\frac{n_z}{L_z}\right)^2} \quad (7)$$

According to Eq. (6) the nodal surfaces are equidistant planes parallel to the room walls.

Figure 2 shows curves of constant sound pressure amplitude ( $|p/p_{\max}| = 0.2, 0.4, 0.6$ , and  $0.8$ ) in the plane  $z = 0$  for  $n_x = 3$  and  $n_y = 2$ . The dotted lines are the intersections of two systems of equidistant nodal planes with the bottom  $z = 0$ , they separate regions in which the instantaneous sound pressure has opposite signs.

The number of eigenfrequencies within the frequency range from zero to an upper limit  $f$  can be estimated by

$$N_f \approx \frac{4\pi}{3} V \left(\frac{f}{c}\right)^3 + \frac{\pi}{4} S \left(\frac{f}{c}\right)^2 + \frac{L}{8} \left(\frac{f}{c}\right) \quad (8)$$

In this expression  $V$  and  $S$  are the volume of the room and the area of its boundary, respectively, and  $L = 4(L_x + L_y + L_z)$ . It is noteworthy that its first term is valid for any enclosure. The same holds for

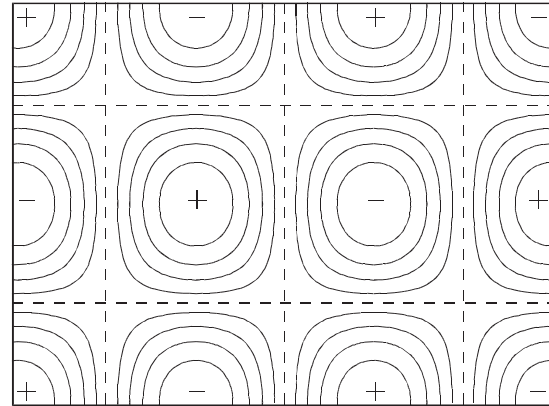


Figure 2 Normal mode in a rectangular enclosure (see Fig.1): Curves of equal sound pressure amplitude in a plane perpendicular to the  $z$  axis ( $n_x = 3, n_y = 2$ ).

the average spacing of adjacent eigenfrequencies as derived from that term:

$$\langle \delta f \rangle \approx \frac{c^3}{4\pi V f^2} \quad (9)$$

According to these equations, a room with a volume of 1000 m<sup>3</sup> has more than 100 million eigenfrequencies in the frequency range from 0 to 10,000 Hz; their average spacing at 1000 Hz is as small as about 0.003 Hz!

Of course, a rectangular room with perfectly rigid walls is never encountered in reality. Nevertheless, Eq. (6) is still a good approximation to the true pressure distribution even if there are losses, provided they are not too high. If the wall impedance is finite but purely imaginary, the eigenvalues  $k_n$  are still real but different from those in Eq. (7), particularly the lowest ones. Similarly, the nodal planes are still equidistant, but their locations are different from those of the rigid room.

To get an idea of the influence of losses we denote with  $Z_x$  the impedance of the walls perpendicular to the  $x$  axis, and similarly  $Z_y$  and  $Z_z$ , and we assume that these impedances are real and finite but still large compared to the characteristic impedance  $\rho_0 c$  of air ( $c$  = sound velocity). Then the eigenvalues are approximately

$$k_n \approx k'_n + j \frac{2\rho_0\omega}{k'_n} \left( \frac{1}{L_x Z_x} + \frac{1}{L_y Z_y} + \frac{1}{L_z Z_z} \right) \quad (10)$$

with  $k'_n \approx k_{n_x, n_y, n_z}$  after Eq. (7). As stated in Section 2.1, the imaginary part of  $k_n$  in Eq. (10) is related to the decay constant  $\delta_n$ .

### 2.3 Steady-State Sound Field

If all eigenvalues  $k_n = (\omega_n + j\delta_n)/c$  and the associated eigenfunctions  $p_n(\mathbf{r})$  are known for a given enclosure, the complex sound pressure amplitude in any inner point  $\mathbf{r}$  can be expressed in terms of them. Let us suppose that the room is excited by a point source at a location  $\mathbf{r}'$  operated at an angular frequency  $\omega$ . Then, under the assumption  $\omega_n \gg \delta_n$ , the complex sound pressure amplitude in  $\mathbf{r}$  can be represented by the expression

$$p_\omega(\mathbf{r}) = C \sum_{n=0}^{\infty} \frac{\omega p_n(\mathbf{r}) p_n(\mathbf{r}')}{K_n (\omega^2 - \omega_n^2 - 2j\delta_n \omega_n)} \quad (11)$$

The constant  $C$  is proportional to the strength of the sound source;  $K_n$  is a normalization constant. The function  $p_\omega(\mathbf{r})$  can be conceived as the transfer function of the room between the points  $\mathbf{r}$  and  $\mathbf{r}'$ . Each term of the sum represents a resonance of the enclosure with the angular resonance frequency  $\omega_n$ . Whenever the driving frequency  $\omega$  coincides with one of the eigenfrequencies  $\omega_n$ , the contribution of the corresponding term will reach its maximum.

Concerning the frequency dependence of the pressure amplitude, two limiting cases have to be distinguished: At low frequencies the mean spacing

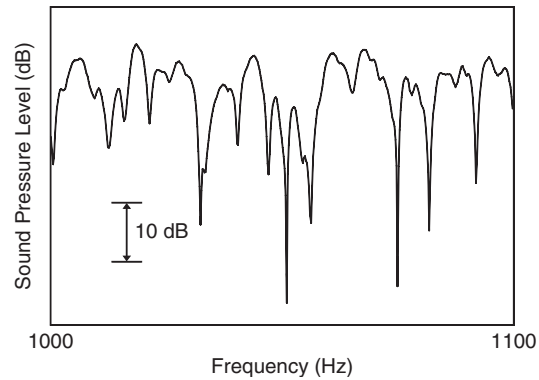
$\langle \delta f \rangle$  of eigenfrequencies after Eq. (9) is substantially larger than the average half-width  $\langle \Delta f \rangle = \langle \delta \rangle / 2\pi$  of the resonance curves with  $\langle \delta \rangle$  denoting an average decay constant. Then the transfer function  $p_\omega(\mathbf{r})$  of the enclosure consists of an irregular succession of well-separated resonance curves, accordingly each normal mode can clearly be observed. At high frequencies, however,  $\langle \delta f \rangle$  is much smaller than  $\langle \Delta f \rangle$ , hence many eigenfrequencies are lying within the half-width of each resonance curve. In other words, the resonance curves will strongly overlap and cannot be separated. When the room is excited with a sine tone, not just one but several or many terms of the sum in Eq. (11) will give significant contributions to the total sound pressure  $p_\omega(\mathbf{r})$ .

The characteristic frequency that separates both frequency regions is the so-called *Schroeder frequency*<sup>3</sup>:

$$f_s = \frac{5000}{\sqrt{V \langle \delta \rangle}} \approx 2000 \sqrt{\frac{T}{V}} \quad (12)$$

where  $T$  denotes the reverberation time of the room (see next subsection). For a living room with a volume  $V = 50$  m<sup>3</sup> and a reverberation time  $T = 0.5$  s, this frequency is about 200 Hz. We can conclude from this example that isolated modes will turn up only in small enclosures such as bathrooms, passenger cars, or truck cabins.

The more typical situation in room acoustics is that of strong modal overlap, characterized by  $f > f_s$ . In this case  $p_\omega(\mathbf{r})$  can be considered as a random function of the frequency with certain general properties, some of which will be described below. Logarithmic representations or recordings of  $|p_\omega(\mathbf{r})|$  are often referred to as *frequency curves* in room acoustics. Figure 3 shows a slice of such a frequency curve obtained in the range from 1000 to 1100 Hz. The irregular shape of this curve is typical for all rooms, no matter where the sound source or the receiving point is located; the only condition is that the distance between both points exceeds the reverberation distance [see Eq. (27)]. A frequency curve shows a maximum



**Figure 3** Portion of a frequency curve, ranging from 1000 to 1100 Hz.

whenever many contributions to the sum in Eq. (11) happen to have about the same phase. Similarly, a minimum appears if most of these contributions cancel each other. It can be shown<sup>3</sup> that the mean spacing between adjacent maxima of a frequency curve is about

$$\langle \delta f_{\max} \rangle \approx \frac{\langle \delta \rangle}{\sqrt{3}} \approx \frac{4}{T} \quad (13)$$

Furthermore, the magnitude  $|p|$  of the sound pressures in a room follows a Rayleigh distribution: Let  $q$  denote  $|p|$  divided by its average; then the probability that this quantity lies within the interval from  $q$  to  $q + dq$  is given by

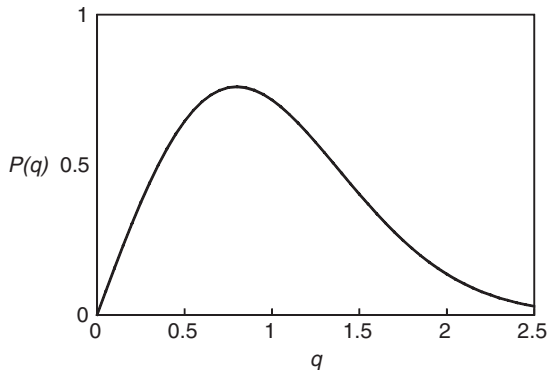
$$P(q) dq = \frac{\pi}{2} \exp\left(-\frac{\pi q^2}{4}\right) q dq \quad (14)$$

This distribution is plotted in Fig. 4. It should be pointed out that it holds not only for one particular frequency curve but as well for all levels encountered in a room at a given frequency. It tells us that about 70% of the levels are contained within a 10-dB range around their average value.

#### 2.4 Transient Response: Reverberation

As already noted in Section 2.1, any normal mode of an enclosure with complex wall impedance will decay unless a sound source compensates for the wall losses. Therefore, if a sound source is abruptly stopped at time  $t = 0$ , all excited normal modes will die out with their individual damping constants  $\delta_n$ . Accordingly, if we assume  $\omega_n \gg \delta_n$  as before, the sound pressure at any point can be expressed by

$$p(t) = \sum_{n=0}^{\infty} a_n e^{-\delta_n t} e^{j\omega_n t} \quad \text{for } t \geq 0 \quad (15)$$



**Figure 4** Rayleigh distribution, indicating the probability density of sound pressure amplitudes in a room. The abscissa is  $q = |p|/\langle |p| \rangle$ .

The complex coefficients  $a_n$  contain the eigenfunctions  $p_n(\mathbf{r})$  and depend on the location of the sound source and the signal it emits. Equation (15) describes what is called the reverberation of a room.

Very often the decay constants  $\delta_n$  are not too different from each other and may therefore be replaced without much error by their mean value  $\langle \delta \rangle$ . Then the energy density at a certain point of the sound field will decay at a uniform rate:

$$\varepsilon(t) = \varepsilon_0 e^{-2\langle \delta \rangle t} \quad \text{for } t \geq 0 \quad (16)$$

In room acoustics, the duration of sound decay is usually characterized by the *reverberation time*, or the *decay time*,  $T$ , defined as the time interval in which the sound energy or energy density drops to one millionth of its initial value, or the sound pressure level decreases by 60 dB. From Eq. (16) it follows that

$$T = \frac{3 \ln 10}{\langle \delta \rangle} \approx \frac{6.91}{\langle \delta \rangle} \quad (17)$$

The reverberation time is one of the most important quantities in room acoustics. It can be measured with good accuracy, and the available formulas (see Section 4.3) predict it quite well.

### 3 GEOMETRIC ACOUSTICS

Although the formal treatment as outlined in the preceding section yields many important insights into sound propagation in rooms, the geometrical approach is more closely related to our imagination. It is based not on the concept of waves but on the notion of sound rays, and it considers mere energy propagation. Accordingly, all phase effects such as interference or diffraction are neglected. This simplification is permissible if the sound signal is composed of many spectral components covering a wide frequency range. Then it can be assumed that all constructive or destructive phase effects cancel each other when two or more sound field components are superimposed at a point, and the total energy at it is simply obtained by adding their energies. Components with this property are often referred to as *incoherent*.

A sound ray can be thought of as a small sector subtending a vanishingly small solid angle that is cut out of a spherical wave. Usually, it is pictured as a straight line provided the medium is homogeneous. Along these lines the sound energy travels with constant velocity, and from the definition of a ray it follows that the total energy carried by it is independent on the distance it has traveled provided the medium is free of dissipation. The intensity along a sound ray, however, decreases proportionally to  $1/r^2$ , where  $r$  denotes the distance from the sound source.

Furthermore, we assume that all sound reflecting objects, in particular all walls of a room, are large compared to the acoustic wavelength. Then the reflection of sound obeys the same law as the reflection of light in geometrical optics. As an exception we shall

consider in Section 3.2 diffuse reflections from walls with many surface irregularities.

### 3.1 Sound Reflection and Image Sources

When a sound wave represented as a ray falls upon a plane and smooth wall of infinite extension, it will be “specularly” reflected from it. This means that the angle under which the reflected ray leaves the wall equals the angle of incidence where both angles are measured against the wall normal (see Fig. 5); furthermore, the incident ray, the reflected ray, and the wall normal are situated in the same plane. This law can also be applied to walls of finite size provided their dimensions are large compared to the acoustic wavelength so that diffraction effects from the edges can be neglected.

If the incident ray is emitted by a point source, the reflected ray can be thought of as originating from a virtual sound source that is the mirror image of the original source with respect to the reflecting wall as also shown in Fig. 5. This secondary source, which is assumed to emit the same signal as the original one, is called an *image source*. The idea of image sources is particularly useful for constructing the reflection of a ray bundle from a plane wall portion or for finding the sound path that connects a given source and receiving point, including reflection from a wall. Its full potential is developed, however, in the discussion of sound propagation in enclosures.

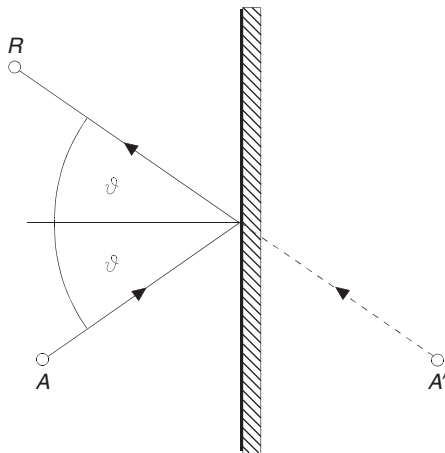
Because of the wall losses, only a fraction of the incident sound energy will be reflected from the wall. This can be accounted for by the absorption coefficient  $\alpha$  of the wall, defined as the fraction of incident sound energy absorbed by the wall. Accordingly, the reflection process reduces the energy of the sound ray by the factor  $1 - \alpha$ . This is tantamount to operating the image source at a power reduced by this factor. If the sound source has a certain directivity, the

symmetrically inverted directivity pattern must be assigned to the image source.

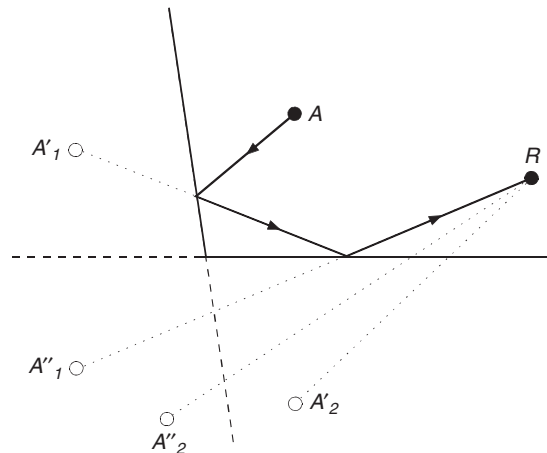
If a reflected sound ray strikes a second wall, the sound path can be found by repeating the mirroring process, that is, a second image source is constructed that is the mirror image of the first one with respect to the second wall. This is illustrated by Fig. 6, which depicts an edge formed by two adjacent plane walls. In addition to the two first-order image sources  $A'_1$  and  $A'_2$ , there are two second-order image sources  $A''_1$  and  $A''_2$ . It should be noted that there is no path connecting the source with the receiving point  $R$  via  $A''_2$  and some first-order image source. This example shows that certain image sources may turn out to be “invisible,” that is, they are not valid. This happens whenever a ray intersects the plane of a wall outside its physical extension.

A regular array of image sources is formed by two parallel infinite planes with distance  $h$  as depicted in Fig. 7. This “enclosure” can be regarded as a model of many factory spaces or of open-plan bureaus the height of which is small compared to their lateral dimensions. Since most points are not close to a side wall, the contributions of the latter can be neglected. The image sources of this flat room are arranged along a vertical line; they are equidistant, if the primary source lies exactly in the middle between the floor and the ceiling.

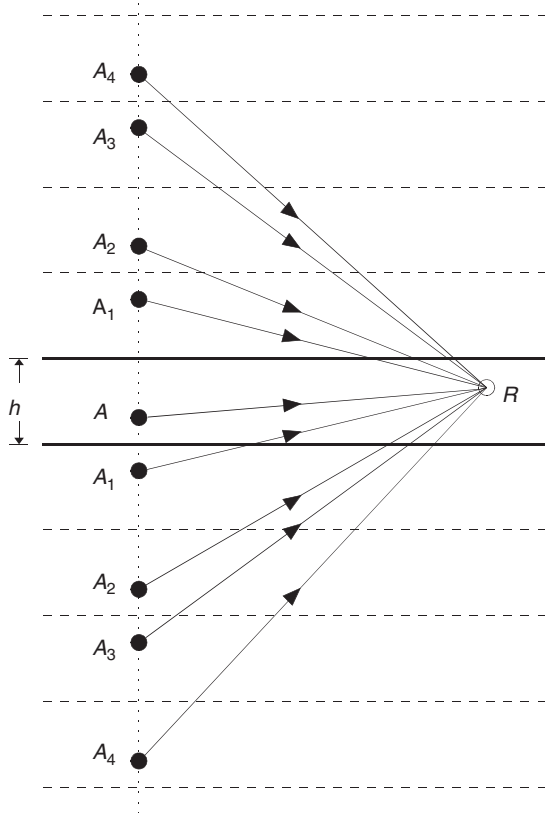
For a space that is completely surrounded by plane walls, mirroring may be repeated over and over, leading to images of increasing order. These images form a three-dimensional pattern that depends on the geometry of the enclosure. However, most of these image sources are invisible from a given observation point. Several algorithms have been developed by which the visibility or validity of image sources can be checked.<sup>4,5</sup> (An exception is the rectangular room, its image sources form a regular three-dimensional



**Figure 5** Sound reflection from a plane wall:  $A$  original source,  $A'$  image source,  $R$  receiving point.



**Figure 6** Sound reflections from an edge formed by two adjacent walls:  $A$  original sound source,  $A'$  first-order image sources,  $A''$  second-order image sources,  $R$  receiving point.



**Figure 7** Flat room with original sound source  $A$  and image sources  $A_n$ ;  $R$  receiving point.

pattern, and all of them are visible from all positions within the original enclosure.)

Once all valid images up to a certain order (or strength) are known, the boundary itself is no longer needed; the energy density at a certain point of the room is obtained just by adding the contributions of all visible image sources provided they are not too faint. The effect of air attenuation is easily included if desired (see Section 5.1).

In this way, not only the steady-state energy density but also transient processes can be studied. Suppose the original sound source would produce the energy density  $\varepsilon(t)$  at some point of the free space. In a room, each image source will emit a weaker replica of this energy signal, provided the absorption of the boundary is frequency independent. At a given receiving point, it will appear with some delay  $\tau_n$  depending on its distance from the image source. Thus the total energy signal observed at the receiving point is

$$\varepsilon'(t) = \sum_n b_n \varepsilon(t - \tau_n) \quad (18)$$

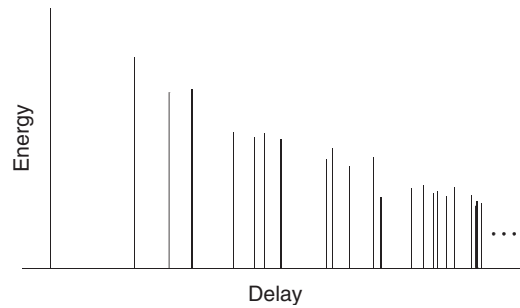
with the coefficients  $b_n$  characterizing the relative strengths of the different contributions.

If  $\varepsilon(t)$  is an impulse with vanishingly short duration, the result of this superposition is the energetic impulse response of the enclosure for a particular source–receiver arrangement as shown in Fig. 8. In this diagram, each contribution to the sum in Eq. (18) is represented by a vertical line the length of which is proportional to its energy. The first line marks the “direct sound component,” contributed by the original sound source. The abscissa in Fig. 8 is the delay of the reflected components with respect to the direct sound. Although this diagram is highly idealized, it shows that usually most of the sound energy received at some point in a room is conveyed by image sources, that is, by wall reflections. Experimentally obtained impulse responses differ from this simple scheme since real walls have frequency-dependent acoustical properties and hence change the form of the reflected signal. Generally, the impulse response can be regarded as the *acoustical fingerprint* of a room.

### 3.2 Enclosures with Curved or Diffusely Reflecting Walls

The concept of image sources is a valuable tool in the acoustical design of rooms, and several commercially available computer programs are based upon it. However, it cannot be applied to curved walls, although the laws of specular reflection are still valid for such surfaces as long as all their dimensions including the radius of curvature are large compared to the wavelength. In some cases, the laws of concave or convex mirrors as known from optics can be used to study the effect of such surfaces.<sup>2</sup> In general, however, the reflected sound rays must be found by constructing the wall normal in each wall point of interest and applying the reflection law separately to each them.

The idea of image sources fails too when the surface of a wall is not smooth but has a certain structure, which is quite often the case. If the dimension of the nonuniformities is comparable to the sound wavelength, the wall does not reflect the arriving sound according to the above-mentioned law but scatters it into different directions. About the same happens if a wall has nonuniform impedance. Walls with irregularly distributed nonuniformities produce what is called



**Figure 8** Energetic impulse response of a room (schematically).



*diffuse reflections* in room acoustics. It is obvious that diffusely reflecting walls make the sound field in a room much more uniform. This is believed to be one of the reasons why many old concert halls with their molded wall decorations, pillars, columns, statuettes, coffered ceilings, and the like are well-known for their excellent acoustics. In modern halls, walls are often provided with recesses, boxes, and the like in order to achieve similar effects. Particularly effective devices in this respect are *Schroeder* diffusers consisting of a series of wells the depths of which are chosen according to certain number-theoretic schemes.<sup>6</sup>

In the limit of very strong scattering it is admissible and convenient to apply Lambert's law, according to which the scattered intensity is proportional to the cosine of the scattering angle  $\vartheta$ , that is, the angle between the wall normal and the direction into which the sound is scattered:

$$dI(r, \vartheta) = P_s \frac{\cos \vartheta}{\pi r^2} \quad (19)$$

where  $P_s$  is the total power scattered by the reflecting wall element  $dS$ , and  $r$  is the distance from it.

If the boundary of an enclosure scatters the arriving sounds everywhere according to Eq. (19), an analytical method, the so-called radiosity method can be used to find the steady-state energy distribution in the enclosure as well as its transient behavior. This method is based on a certain integral equation and is described elsewhere.<sup>7,8</sup>

A more general way to determine the sound field in an enclosure the boundary of which produces at least partially diffuse reflections is *ray tracing*.<sup>9,10</sup> The easiest way to understand these techniques is by imagining hypothetical sound particles that act as the carriers of sound energy. These particles are emitted by the sound source, and they travel with sound velocity along straight lines until they arrive at a wall. Specularly reflected particles will continue their way according to the law of specular reflection. If a particle is scattered from the boundary, its new direction is determined by two computer-generated random numbers in such a way, that the azimuth angle is uniformly distributed while the distribution of the angle  $\vartheta$  must follow Eq. (19). In any case, wall absorption is accounted for by reducing the energy of a reflected particle by a factor  $1 - \alpha$  with  $\alpha$  denoting the absorption coefficient. The final result is obtained by adding the energies of all particles crossing a previously assigned counting volume considered as the "receiver." Classifying the arrival times of the particles yields the energetic impulse response for the chosen receiving position.

## 4 STATISTICAL ROOM ACOUSTICS

### 4.1 Diffuse Sound Field

In this section closed formulas for the energy density in an enclosure both at steady-state conditions and during

sound decay are presented. Such expressions are of considerable importance in practical room acoustics. They are used to predict noise levels in working environments or to assess the suitability of a room for the different types of performances.

The approach we are using here is based on the energy balance:

$$P(t) = \frac{d}{dt} \int_V \varepsilon dV + E_{\text{abs}} \quad (20)$$

where  $V$  is the room volume and  $E_{\text{abs}}$  denotes the energy that the boundary absorbs per second;  $P(t)$  is the power supplied to the room by some sound source, and  $\varepsilon$  is the energy density. This equation tells us that one part of the input energy is used to change the energy content of the room, whereas the other one is dissipated by the boundary.

Generally, the relation between the energy density and the absorbed energy  $E_{\text{abs}}$  is quite involved. It is simple, however, if the sound field in the room can be assumed as *diffuse*. This means that at each point inside the boundary the sound propagation is uniformly distributed over all directions. Accordingly, the total intensity vector in a diffuse field would be zero. In real rooms, however, the inevitable wall losses "attract" a continuous energy flow originating from the sound source; therefore, the intensity vector cannot completely vanish. At best we can expect that a sound field is sufficiently diffuse to permit the application of the properties to be outlined below.

Generally, the degree of sound field diffusion depends on the shape of the room. In an irregular polyhedron room there will certainly be stronger mixing of sound rays than in a sphere or another regularly shaped enclosure. Another important factor is the kind of boundary. The energy distribution—both spatial and directional—will be more uniform if the walls are not smooth but produce diffuse reflections by some scattering (see preceding subsection). And finally the degree of sound field diffusion is influenced by the amount and distribution of wall absorption. Usually, diffusion is the higher the smaller is the total absorption and the more uniformly it is distributed over the boundary. It should be emphasized that the condition of a diffuse sound field must be clearly distinguished from diffuse wall reflections; the latter usually increase the degree of sound field diffusion, but they do not guarantee it.

An important property of a diffuse sound field is the constancy of its energy density throughout the whole room. Furthermore, it can be shown that the energy  $B$  hitting the boundary per second and unit area is also constant along the boundary and is related to the energy density  $\varepsilon$  by

$$B = \frac{c}{4} \varepsilon \quad (21)$$

To give Eq. (20) a useful form, it is convenient to introduce the *equivalent absorption area* or the total

absorption of the room:

$$A = \iint_S \alpha dS \text{ or } A = \sum_i S_i \alpha_i \quad (22)$$

The latter expression is applicable if the boundary consists of several finite portions with constant absorption coefficients  $\alpha_i$ ; their areas are  $S_i$ . Since the sound field is assumed as diffuse, the absorption coefficient in this and the following expressions is identical with the absorption coefficient  $\alpha_d$  for random sound incidence to be defined in Eq. (35).

Now the total energy  $E_{\text{abs}}$  absorbed per second can be expressed as  $AB = (c/4)A\varepsilon$ . Then Eq. (20) becomes a simple differential equation of first order:

$$V \frac{d\varepsilon}{dt} + \frac{cA}{4}\varepsilon = P(t) \quad (23)$$

which is easily solved for any time-dependent power output  $P(t)$ .

The equivalent absorption area has the dimension of square metres and can be imagined as the area of a totally absorbing boundary portion, for instance, of an open window with area  $A$  in which the total absorption of the enclosure is concentrated.

#### 4.2 Stationary Energy Density

At first we consider a sound source with constant power output  $P$ ; accordingly the energy density will also be constant and the time derivative in Eq. (23) is zero. Hence the steady-state energy density  $\varepsilon_s = \varepsilon$  is

$$\varepsilon_s = \frac{4P}{cA} \quad (24)$$

For practical purposes it is convenient to convert the above relation into the logarithmic scale and thus to relate the sound pressure level  $L_p$  with the sound power level  $L_W = 10 \cdot \log_{10}(P/P_0)$  ( $P_0 = 10^{-12}$  W):

$$L_s = L_W - 10 \cdot \log_{10} \left( \frac{A}{1\text{m}^2} \right) + 6 \text{ dB} \quad (25)$$

This relation is frequently used to determine the total sound power output  $P$  of a sound source by measuring the stationary sound pressure level. The equivalent absorption area  $A$  of the enclosure is obtained from its reverberation time (see next section). Furthermore it shows to which extent the noise level in workshops, factory halls, or open-plan bureaus can be reduced by providing the ceiling and the side walls with some sound-absorbing lining.

Equations (24) and (25) represent the energy density and the sound pressure level in what is called the diffuse or the reverberant field. This field prevails when the distance  $r$  of the observation point from the sound source is relatively large. In the vicinity of the

sound source, however, the direct sound component is predominant. For a nondirectional sound source the energy density of this latter component is

$$\varepsilon_d = \frac{P}{4\pi cr^2} \quad (26)$$

In a certain distance, the so-called reverberation distance  $r_r$ , both components, namely the direct and the reverberant part of the energy density, are equal:

$$r_r = \frac{1}{4} \sqrt{\frac{A}{\pi}} \approx 0.057 \sqrt{\frac{V}{T}} \quad (27)$$

Here  $T$  is the reverberation time already introduced in Section 2.4. According to this formula, the reverberation distance  $r_r$  in a hall with a volume of 10,000 m<sup>3</sup> and a reverberation time  $T = 2$  s is about 4 m. The total energy density  $\varepsilon_t$  is given by

$$\varepsilon_t = \varepsilon_d + \varepsilon_s = \frac{P}{4\pi cr^2} \left( 1 + \frac{r^2}{r_r^2} \right) \quad (28)$$

The above relations should be applied with some caution. For signals with narrow frequency bandwidth they yield at best an average or expectation value of  $\varepsilon$  since we know from Section 2.3 that the stationary sound pressure amplitude in an enclosure is far from being constant but is distributed over a wide range. The same holds true for the energy density. Even for wide-band excitation, the energy density is usually not completely constant throughout the room. One particular deviation<sup>11</sup> is due to the fact that any reflecting wall enforces certain phase relations between incident and reflected waves no matter from which directions they arrive. As a consequence, the energy density in a diffuse field shows spatial fluctuations in the vicinity of a wall depending on its acoustical properties and on the frequency spectrum of the sound signal. Right in front of a rigid wall, for instance, the energy density is twice its average value far away from it. In the high-frequency limit, these deviations can be neglected.

#### 4.3 Sound Decay

For the discussion of decaying sound fields we imagine a sound source exciting the enclosure up to the time  $t = 0$  when it is abruptly stopped. (As an alternative, sound decay can be produced by a short impulse emitted at  $t = 0$ .) If the sound field is sufficiently diffuse, Eq. (23) can be applied with  $P = 0$ . The solution of this differential equation is

$$\varepsilon(t) = \varepsilon_0 \exp \left( -\frac{cA}{4V}t \right) \quad \text{for } t \geq 0 \quad (29)$$

which agrees with Eq. (16) if we set  $\langle \delta \rangle = cA/8V$ . The symbol  $\varepsilon_0$  denotes the initial energy density at  $t = 0$ . From this equation, the reverberation time  $T$  of the enclosure, that is, the time in which the energy density



has dropped by a factor of  $10^6$  (see Section 2.4) is easily obtained:

$$T = \frac{24 \cdot \ln 10}{c} \cdot \frac{V}{A} = 0.163 \frac{V}{A} \quad (30)$$

In these expressions all lengths must be expressed in metres.

Equation (30) is the famous Sabine reverberation formula<sup>12</sup> and is probably the most important relation in room acoustics. Despite its simplicity, its accuracy is sufficient for most practical purposes provided the correct value for the equivalent absorption  $A$  is inserted. However, it fails for enclosures with high absorption: for a perfectly absorbing boundary ( $A = S$ ) it still predicts a finite reverberation time although in this case there would be no reverberation at all.

A more rigorous derivation leads to another decay formula that is free of this defect:

$$T = 0.163 \frac{V}{-S \ln(1 - \langle \alpha \rangle)} \quad (31)$$

This relation is known as Eyring's formula,<sup>13</sup> although it was first described by *Fokker* (1924). It is obvious that it yields the correct reverberation time  $T = 0$  for a totally absorbing boundary. For  $\langle \alpha \rangle \ll 1$  it becomes identical with Sabine's formula, Eq. (30).

Sound attenuation in air can be taken into account by adding a term  $4mV$  to the denominator of Eq. (30) or (31), leading to

$$T = 0.163 \frac{V}{4mV + A} \quad (30a)$$

and

$$T = 0.163 \frac{V}{4mV - S \ln(1 - \langle \alpha \rangle)} \quad (31a)$$

In both expressions,  $m$  is the attenuation constant of air, which will be explained in more detail in Section 5.1, where numerical values of  $m$  will be presented.

The content of these formulas may be illustrated by a simple example. We consider a hall with a volume of  $V = 15000 \text{ m}^3$ , the total area  $S$  of its walls (including the ceiling and the floor) is  $4200 \text{ m}^2$ . The area occupied by the audience amounts to  $800 \text{ m}^2$ , its absorption coefficient is 0.9 (at medium sound frequencies, say 500 to 1000 Hz) while the absorption coefficient of the remaining part of the boundary is assumed to be 0.1. This leads to an equivalent absorption area  $A$  of  $1060 \text{ m}^2$ , accordingly the average absorption coefficient  $A/S = \langle \alpha \rangle$  is 0.252 and  $-\ln(1 - \langle \alpha \rangle) = 0.29$ . With these data Eq. (30) yields a reverberation time of 2.3 s. The decay time after Eyring's formula Eq. (31) is somewhat smaller, namely 2.0 s. Including air attenuation according to

Eq. (31a) with  $m = 10^{-3}$  would reduce the latter value to about 1.9 s.

It should be recalled that the derivation of all the formulas presented in this and the preceding section was based upon the assumption of diffuse sound fields. On the other hand, sound fields in real rooms fulfill this condition at best approximately as was pointed out in Section 4.1. Particularly strong violations of the diffuse field condition must be expected in very long or flat enclosures, for instance, or if the boundary absorption is nonuniformly distributed. A typical example is an occupied auditorium where most of the absorption is concentrated onto the area where the audience is seated. In fact, the (average) steady-state energy density in a fully occupied concert hall is not constant in contrast to what Eq. (24) or Eq. (28) predicts for  $r \gg r_r$ . Nevertheless, experience has shown that the reverberation formulas presented in this section yield quite reasonable results even in this case. Obviously, the decay process involves mixing of many sound components, and hence the relations derived in this subsection are less sensitive to violations of the diffuse field condition.

## 5 SOUND ABSORPTION

### 5.1 Air Attenuation

All sound waves are subject to attenuation by the medium in which they are propagated. In air, this effect is not very significant at audio frequencies, therefore it is often neglected. Under certain conditions, however, for instance, in large halls and at elevated frequencies, it becomes noticeable.

The attenuation by air has several reasons: heat conductivity and viscosity, and in particular certain relaxation processes that are caused by the molecular structure of the gases of which air consists.

A plane sound wave traveling along the  $x$  axis of a Cartesian coordinate system is attenuated according to

$$I(x) = I_0 \exp(-mx) \quad (32)$$

or, expressed in terms of the sound pressure level:

$$L(x) = L_0 - 4.34mx \quad (\text{dB}) \quad (33)$$

According to the various processes involved in attenuation, the attenuation constant  $m$  shows a complicated frequency dependence, furthermore it depends on the temperature and the humidity of the air. Table 1 lists some values of  $m$  in air.

### 5.2 Absorption Coefficient and Wall Impedance

In Section 3.1 the absorption coefficient of a boundary was introduced as the fraction of incident sound energy that is not reflected by it. Usually, this quantity depends on the frequency and on the incidence

**Table 1** Attenuation Constant of Air at 20°C and Normal Atmospheric Pressure, in  $10^{-3} \text{ m}^{-1}$ .

Relative Humidity (%)	Frequency (kHz)						
	0.5	1	2	3	4	6	8
40	0.60	1.07	2.58	5.03	8.40	17.71	30.00
50	0.63	1.08	2.28	4.20	6.84	14.26	24.29
60	0.64	1.11	2.14	3.72	5.91	12.08	20.52
70	0.64	1.15	2.08	3.45	5.32	10.62	17.91

After Ref. 14.

angle  $\vartheta$ . It is related to the more general wall impedance  $Z$  as defined in Eq. (2) by

$$\alpha(\vartheta) = 1 - \left| \frac{Z \cos \vartheta - \rho_0 c}{Z \cos \vartheta + \rho_0 c} \right|^2 \quad (34)$$

If the boundary reacts locally to an incoming wave (see Section 2.1), the wall impedance does not depend on the direction of sound incidence; hence the only angle dependence of  $\alpha(\vartheta)$  is that of the cosine function. If furthermore  $|Z| > \rho_0 c$  as is usually the case, the absorption coefficient grows at first when  $\vartheta$  is increased; after reaching a maximum it diminishes and finally becomes zero at grazing incidence ( $\vartheta = \pi/2$ ).

Since in most enclosures the sound field can be regarded as more or less diffuse, it is useful to assign an averaged absorption coefficient to the boundary, calculated according to *Paris'* formula:

$$\alpha_d = \int_0^{\pi/2} \alpha(\vartheta) \sin(2\vartheta) d\vartheta \quad (35)$$

For a locally reacting surface  $\alpha_d$  can be directly calculated after inserting Eq. (34). The result is presented in Fig. 9. This diagram shows contours of constant absorption coefficient  $\alpha_d$ . Its abscissa and ordinate are the phase angle  $\beta$  and the magnitude, respectively, of the "specific wall impedance"

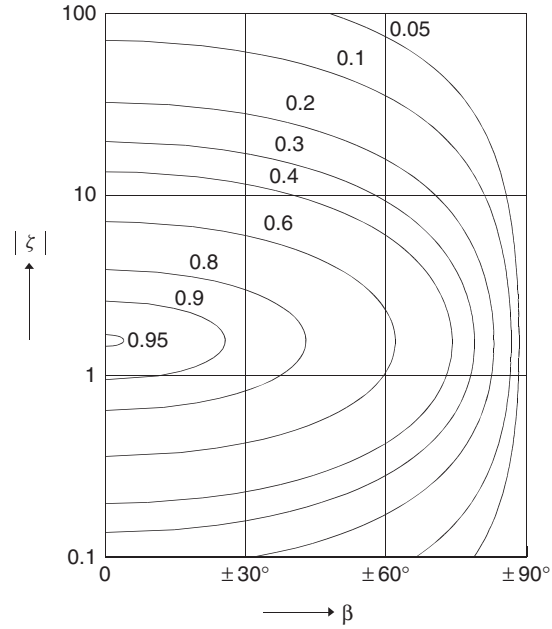
$$\zeta = |\zeta| \exp(j\beta) = \frac{Z}{\rho_0 c} \quad (36)$$

respectively. It is noteworthy that  $\alpha_d$  has an absolute maximum 0.951 for the specific impedance  $\zeta = 1.567$ , that is, it will never reach unity.

### 5.3 Types of Sound Absorbers

After this more formal description of sound absorption a brief account of the various sorts of sound-absorbing devices will be presented.

**5.3.1 Absorption by Yielding Walls** The simplest case of a sound-absorbing boundary is a wall that is set into motion as a whole by the pressure variations of the sound field in front of it. The wall emits



**Figure 9** Curves of equal absorption coefficient of a locally reacting surface for random sound incidence. The abscissa and the ordinate are the phase angle  $\beta$  and the magnitude, respectively, of the specific wall impedance  $\zeta = Z/\rho_0 c$ .

a secondary sound wave into the outer space; hence "absorption" is not caused by dissipation but by transmission. Therefore, the well-known mass law of sound transmission through walls applies according to which the absorption coefficient at normal sound incidence is:

$$\alpha(0) \approx \left( \frac{2\rho_0 c}{\omega m'} \right)^2 \quad (37)$$

Here  $m'$  is the "specific mass," that is, the mass per unit area of the boundary. This approximation is permissible if  $2\rho_0 c/\omega m'$  is small compared with unity, which is usually the case. At random sound incidence the absorption coefficient is about twice the above value.

Practically this type of absorption occurs only at low frequencies and with light walls such as thin windows or membranes.

**5.3.2 Absorption by Porous Materials** Commonly used sound absorbers comprise porous materials. The absorption is brought about by pressure differences or pressure gradients that enforce airflows within the pores. The losses are caused by internal friction (viscosity) and by heat conduction between the air and the pore walls. By both processes motional energy is irreversibly transformed into heat. The absorption depends on the sort, the dimensions of the material, and on the way it is exposed to the sound field.

At first we consider a thin porous sheet, a curtain, for instance. Suppose at both its sides are different pressures  $p$  and  $p'$ . Then the flow resistance characterizing the material is

$$r_s = \frac{p - p'}{v_s} \quad (38)$$

with  $v_s$  denoting the velocity of the airflow enforced by the pressure difference  $p - p'$ .

Another characteristic quantity is the specific mass  $m'$  of the sheet. If the curtain is exposed to a sound wave with an angular frequency well below  $\omega_s = r_s/m'$ , it will move as a whole and the airflow forced through the pores will be small. For frequencies much larger than  $\omega_s$ , however, the curtain stays at rest because of its inertia; the velocity at its surface is entirely due to the air passing the material. In the latter case, the absorption coefficient of the curtain may become quite noticeable even if the curtain is freely hanging; its maximum is 0.446 occurring when  $r_s = 3.14\rho_0 c$ .

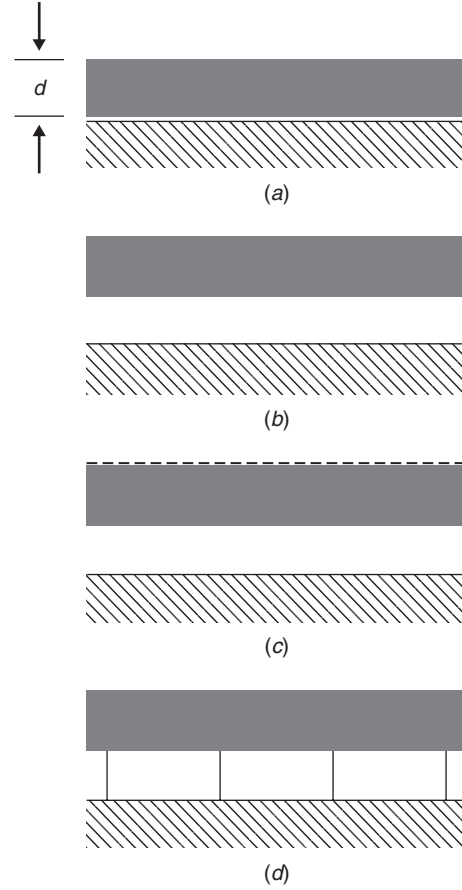
The situation is different when the curtain or the fabric is arranged in front of a rigid wall with some airspace in between. At normal sound incidence, a standing wave will be formed in the airspace with a velocity node at the wall. The absorption coefficient shows strong and regular fluctuations. It vanishes whenever the depth is an integer multiple of the sound wavelength. In the frequency range between two of these zeros it assumes a maximum:

$$\alpha_{\max} = \frac{4\rho_0 c r_s}{(r_s + \rho_0 c)^2} \quad (39)$$

The strong frequency of the absorption coefficient can be prevented by arranging the curtain in deep folds.

Most sound absorbers consist of a layer of porous materials, for instance, of rockwool, glass fiber, or plastic foam. Again, the properties of the layer is characterized by the flow resistance  $r_s$ . Another important parameter is the porosity  $\sigma$  defined as the volume fraction of the voids in the material.

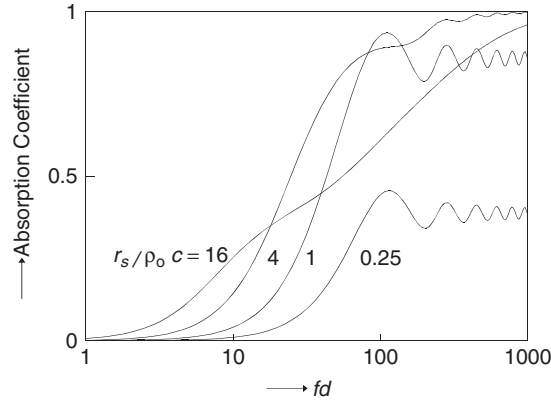
In Fig. 10a we consider a homogeneous layer of porous material right in front of a rigid wall. When a sound wave arrives perpendicularly at this arrangement, one portion of it is reflected from the



**Figure 10** Various types of porous absorbers. (a) Porous layer in front of a rigid wall, (b) same, with airspace behind the layer, (c) as in (b), with perforated panel in front of the layer, (d) as in (b), with airspace partitioned.

front face while the other one will intrude into the material. If the interior attenuation is high, this part will die out after a short traveling distance. Otherwise, a more or less pronounced standing wave will be formed in the material that leads to fluctuations of the absorption coefficient as in the case considered before. When the thickness  $d$  of the layer is small compared with the acoustic wavelength, that is, at low frequencies, its absorption coefficient is small because all the porous material is situated close to the velocity node next to the rigid wall.

This behavior is illustrated by Fig. 11, which shows the absorption coefficient for normal sound incidence of an arrangement after Fig. 10a. The active material is assumed to consist of many fine and equidistant channels in a solid matrix (Rayleigh model), the porosity  $\sigma$  is 0.95. The abscissa of the diagram is the product  $fd$  of the frequency and the thickness of the layer in metres, the parameter is the fraction  $r_s/\rho_0 c$ . High absorption coefficients are



**Figure 11** Absorption coefficient of a layer according to Fig. 15a (Rayleigh model,  $\sigma = 0.95$ , normal sound incidence).  $fd$  in Hz m, curve parameter:  $r_s/\rho_0 c$ . (From Ref. 2).

achieved if  $r_s/\rho_0 c$  is in the range of 1 to 4 and the product  $fd$  exceeds 30 Hz m.

The range of high absorption can be significantly extended toward lower frequencies by mounting the active layer in some distance from the rigid wall as shown in Fig. 10b, that is, by avoiding the region of low particle velocity.

In practical applications, a protective layer must be arranged in front of the porous material to keep humidity away from it and, at the same time, to prevent particles from polluting the air in the room. The simplest way to do this is by wrapping the porous material into thin plastic foils. Protection against mechanical damage is often achieved by a perforated facing panel made of metal, wood, or plastic (see Fig. 10c). In any case, the protective layer acts as a mass load that reduces the absorption of the whole arrangement at high frequencies.

At oblique sound incidence, sound waves can propagate within a porous material parallel to its surface. The same effect occurs in an air backing. Hence this type of absorber is generally not locally reacting. Its performance can be improved, however, by partitioning the airspace as shown in Fig. 10d.

**5.3.3 Resonance Absorbers** A panel arranged in front of a rigid wall with some airspace in between acts as a resonance absorber. The panel may be unperforated and must be mounted in such a way that it can perform bending vibrations under the influence of an arriving sound wave. The motion of the panel is controlled by its specific mass  $m'$  and by the stiffness of the air cushion behind it. (The bending stiffness of the panel is usually so small that its influence on the resonance frequency is negligible.) As an alternative, a sparsely perforated panel may be employed to which the specific mass

$$m' = \frac{\rho_0}{\sigma} \left( h + \frac{\pi}{2} a \right) \quad (40)$$

can be attributed. Here  $h$  is the thickness of the panel,  $a$  is the radius of the holes, and  $\sigma$  is their fractional area. In both cases the resonance frequency and hence the frequency, at which the absorber is most effective, is

$$f_0 \approx \frac{c}{2\pi} \sqrt{\frac{\rho_0}{m'D}} \quad (41)$$

with  $D$  denoting the thickness of the airspace. Sound absorption is caused by elastic losses in the panel if this is unperforated, or, for a perforated panel, by viscous losses in the apertures. It can be increased by arranging some porous material in the airspace.

Figure 12 shows an example of a panel absorber, along with the absorption coefficient measured in the reverberation chamber (see Section 5.4).

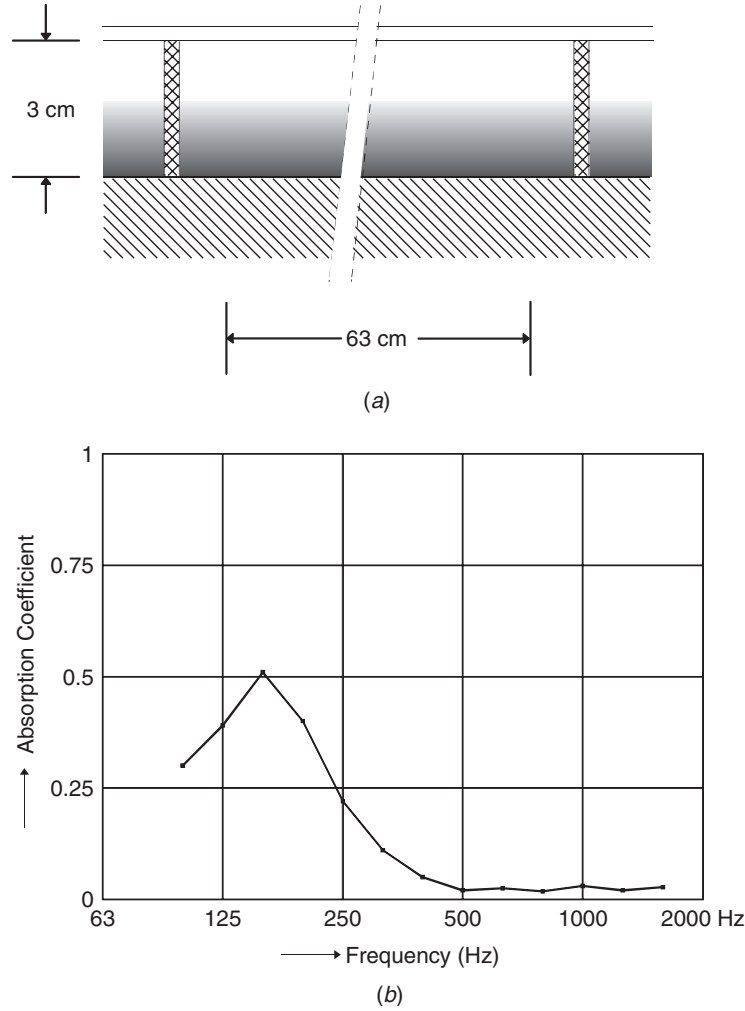
Resonance absorbers are very useful in room acoustics as well as in noise control since they offer the possibility to control the reverberation time within limited frequency ranges, in particular at low frequencies.

## 5.4 Measurement of Sound Absorption

A simple device for measuring the absorption coefficient of a boundary is the impedance tube or Kundt's tube in which a sinusoidal sound wave is excited at one end, whereas the test sample is placed at the other. Both waves, the original one and the wave reflected from the test specimen form a standing wave; the mutual distance of pressure maxima (and also of minima) is  $\lambda/2$  ( $\lambda$  = acoustic wavelength).

To determine the absorption coefficient the standing-wave ratio  $q = p_{\max}/p_{\min}$  is measured with a movable probe microphone where  $p_{\max}$  and  $p_{\min}$  are the maximum and minimum pressure amplitude in the standing wave. The absorption coefficient is obtained from

$$\alpha = \frac{4q}{(1+q)^2} \quad (42)$$



**Figure 12** Resonance absorber with panel. (a) Construction, the specific mass  $m_s$  of the panel is  $5 \text{ kg/m}^2$ . (b) Absorption coefficient.

For many practical purposes this information is sufficient. If the specific impedance is to be determined, the phase difference  $\chi$  between the sound pressures of the incident and the reflected sound wave at the surface of the test specimen is needed. It is obtained from the distance  $d_{\min}$  of the first pressure minimum from the specimen:

$$\chi = \pi \left( \frac{4d_{\min}}{\lambda} - 1 \right) \quad (43)$$

From  $\chi$  and  $q$ , the phase angle  $\beta$  and the magnitude of the specific impedance  $\zeta$  [see Eq. (36)] are calculated using the relations

$$\beta = \text{atn} \left( \frac{q^2 - 1}{2q} \sin \chi \right) \quad (44a)$$

$$|\zeta| = \sqrt{\frac{(q^2 + 1) + (q^2 - 1) \cos \chi}{(q^2 + 1) - (q^2 - 1) \cos \chi}} \quad (44b)$$

For locally absorbing materials the absorption coefficient at random incidence can be determined from these data by using Fig. 9.

As mentioned, the application of the impedance tube is limited to normal sound incidence and to materials for which a small sample can be considered representative for the whole lining. Furthermore, the frequency range is limited by the requirement that the diameter of the tube is smaller than  $0.586\lambda$ . If the cross section is rectangular, the wider side must be smaller than  $\lambda/2$ . More details on the construction of the tube and the measuring procedure may be looked up in the relevant international standard.<sup>15</sup>

**Table 2 Typical Absorption Coefficients of Various Wall Materials (Random Incidence)**

Material	Octave Band Center Frequency (Hz)					
	125	250	500	1000	2000	4000
Hard surfaces (concrete, brick walls, plaster, hard floors etc.)	0.02	0.02	0.03	0.04	0.05	0.05
Carpet, 5 mm thick, on solid floor	0.02	0.03	0.05	0.10	0.30	0.50
Slightly vibrating surfaces (suspended ceilings etc.)	0.10	0.07	0.05	0.04	0.04	0.05
Plush curtain, flow resistance 450 N s/m, deeply folded, distance from solid wall ca. 5 cm	0.15	0.45	0.90	0.92	0.92	0.95
Acoustical plaster, 10 mm thick, sprayed on solid wall	0.08	0.15	0.30	0.50	0.60	0.70
Polyurethane foam, 27 kg/m <sup>3</sup> , 15 mm thick on solid wall	0.08	0.22	0.55	0.70	0.85	0.75
Rockwool, 46.5 kg/m <sup>3</sup> , 30 mm thick, on concrete	0.08	0.42	0.82	0.85	0.90	0.88
Same as above, but with 50 mm airspace, laterally partitioned	0.24	0.78	0.98	0.98	0.84	0.86
Metal panels, 0.5 mm thick with 15% perforation, backed by 30 mm rockwool and 30 mm additional airspace, no partitions	0.45	0.70	0.75	0.85	0.80	0.60
Fully occupied audience, upholstered seats	0.50	0.70	0.85	0.95	0.95	0.90

Another important method of absorption measurement is based upon Eq. (30). It is carried out in a so-called reverberation chamber, a room with rigid and smooth walls and with a volume  $V$  of 150 to 300 m<sup>3</sup>. The reverberation time of the chamber is measured both with and without the test sample in it, usually with noise bands of third octave width. The results are  $T$  and  $T_0$ . Then the absorption coefficient of the test specimen is

$$\alpha = 0.163 \frac{V}{S'} \left( \frac{1}{T_0} - \frac{S - S'}{S} \frac{1}{T} \right) \quad (45)$$

with  $S$  and  $S'$  denoting the total wall area and the sample area, respectively.

The reverberation method is well suited for measuring the absorption of almost any type of absorber, wall lining, ceiling and so forth, but also that of single persons, blocks of seats, unoccupied or occupied, and the like. It has the particular advantage that the measurement is carried out under conditions that are typical for many practical application, that is, the procedure yields the absorption at random sound incidence, at least in principle. As the impedance tube method, it is internationally standardized.<sup>16</sup>

Special precautions must be taken to provide for a diffuse sound field in a reverberation chamber. This is relatively easy for the empty room, but not so easy if a heavily absorbing test specimen is placed in the room. One way to achieve sound field diffusion is to avoid parallel wall pairs in the design of the measuring chamber. It can be improved by “acoustically rough” walls, the irregularities of which scatter the sound waves. A commonly used alternative is the use of

volume scatterers such as bent shells of plastic or wood that are suspended from the ceiling.

Theoretically, the absorption coefficient determined with this method should agree with  $\alpha_d$  from Eq. (35); for a locally reacting boundary it should never exceed 0.951. Instead absorption coefficients in excess of 1 are often observed when highly absorbing materials are examined. Such results that are in contradiction with the very meaning of the absorption coefficient may have several reasons. At first, it should be noted that application of the more correct Eyring formula (31) would yield slightly lower coefficients. A more important source of error is lack of sound field diffusion. Finally, systematic errors may be induced by the so-called edge effect: Sound diffraction at the edges of the test specimen increases its effective area.

Table 2 lists the absorption coefficients of some commonly used materials, wall linings, and the like as measured with the reverberation method.

## REFERENCES

1. P. M. Morse and K. U. Ingard, *Theoretical Acoustics*, McGraw-Hill, New York, 1968.
2. H. Kuttruff, *Room Acoustics*, 4th ed. Spon Press, London, 2000.
3. M. R. Schroeder and H. Kuttruff, On Frequency Response Curves in Rooms. Comparison of Experimental, Theoretical and Monte Carlo Results for the Average Spacing between Maxima, *J. Acoust. Soc. Am.*, Vol. 34, 1962, pp. 76–80.
4. J. Borish, Extension of the Image Source Model to Arbitrary Polyhedra, *J. Acoust. Soc. Am.*, Vol. 75, 1978, pp. 1827–1836.
5. M. Vorländer, Simulation of the Transient and Steady-State Sound Propagation in Rooms Using a New Combined Ray-Tracing/Image Source Algorithm, *J. Acoust. Soc. Am.*, Vol. 86, 1989, pp. 172–178.

6. M. R. Schroeder, *Number Theory in Science and Communications*, 2nd ed., Springer, Berlin, 1989.
7. W. B. Joyce, Effect of Surface Roughness on the Reverberation Time of a Uniformly Absorbing Spherical Enclosure, *J. Acoust. Soc. Am.*, Vol. 64, 1978, pp. 1429–1436.
8. R. N. Miles, Sound Field in a Rectangular Enclosure with Diffusely Reflecting Boundaries, *J. Sound Vib.*, Vol. 92, 1984, pp. 203–213.
9. A. Krokstad, S. Strøm, and S. Sørsdal, Calculating the Acoustical Room Response by the Use of the Ray Tracing Techniques *J. Sound Vib.*, Vol. 8, 1968, pp. 118–124.
10. A. M. Ondet and J. L. Barbry, Modeling of Sound Propagation in Fitted Workshops Using Ray Tracing. *J. Acoust. Soc. Am.*, Vol. 85, 1989, pp. 787–192.
11. R. V. Waterhouse, Interference Patterns in Reverberant Sound Fields, *J. Acoust. Soc. Am.*, Vol. 27, 1955, pp. 247–258.
12. W. C. Sabine, *The American Architect*, 1900; see also *Collected Papers on Acoustics*, No. 1, Harvard University Press, Cambridge, 1923. Reprinted by Dover Publications, New York, 1964.
13. C. F. Eyring, Reverberation Time in “Dead” Rooms, *J. Acoust. Soc. Am.*, Vol. 1, 1930, pp. 217–241; Methods of Calculating the Average Coefficient of Sound Absorption, *J. Acoust. Soc. Am.*, Vol. 4, 1933, pp. 178–192.
14. H. E. Bass, L. C. Sutherland, A. J. Zuckerwar, D. T. Blackstock, and D. M. Hester, Atmospheric Absorption of Sound: Further Developments, *J. Acoust. Soc. Am.*, Vol. 97, 1995, pp. 680–683.
15. ISO 10534, Acoustics—Determination of Sound Absorption Coefficient and Impedance in Impedance tubes, International Organisation for Standardisation, Geneva, Switzerland, 2006.
16. ISO 354, Acoustics—Measurement of Sound Absorption in a Reverberation Room, International Organisation for Standardisation, Geneva, Switzerland, 2003.

# CHAPTER 5

## SOUND PROPAGATION IN THE ATMOSPHERE

Keith Attenborough  
Department of Engineering  
The University of Hull  
Hull, United Kingdom

### 1 INTRODUCTION

Knowledge of outdoor sound propagation is relevant to the prediction and control of noise from land and air transport and from industrial sources. Many schemes for predicting outdoor sound are empirical and source specific. At present, methods for predicting outdoor noise are undergoing considerable assessment and change in Europe as a result of a recent European Community (EC) Directive and the associated requirements for noise mapping. The attenuation of sound outdoors is the sum of the reductions due to geometric spreading, air absorption, interaction with the ground, barriers, vegetation, and atmospheric refraction. This chapter details the physical principles associated with the sources of attenuation and offers some guidance for assessing their relative importance. More details about the noise reduction caused by barriers, trees, and buildings are to be found in Chapter 122.

### 2 SPREADING LOSSES

Distance alone will result in wavefront spreading. In the simplest case of a sound source radiating equally in all directions, the intensity  $I$  ( $\text{W m}^{-2}$ ) at a distance  $r$  (m) from the source of power  $W$  (W) is given by

$$I = \frac{W}{4\pi r^2} \quad (1)$$

This represents the power per unit area on a spherical wavefront of radius  $r$ . In logarithmic form the relationship between sound pressure level  $L_p$  and sound power  $L_W$  may be written

$$L_p = L_W - 20 \log r - 11 \text{ dB} \quad (2)$$

From a point sound source, this means a reduction of  $20 \log 2$  dB, that is, 6 dB, per distance doubling in all directions. Most sources appear to be point sources when the receiver is at a sufficient distance from them. A point source is omnidirectional. If the source is directional, then (2) is modified by inclusion of the directivity index (DI).

$$L_p = L_W + \text{DI} - 20 \log r - 11 \text{ dB} \quad (3)$$

The directivity index is  $10 \log \text{DF}$  dB where DF is the directivity factor, which is the ratio of the actual intensity in a given direction to the intensity of an omnidirectional source of the same power output. Such directivity is either inherent or location induced.

A simple case of location-induced directivity arises if the point source, which would normally create spherical wavefronts of sound, is placed on a perfectly reflecting flat plane. Radiation from the source is thereby restricted to a hemisphere. The directivity factor for a point source on a perfectly reflecting plane is 2 and the directivity index is 3 dB. For a point source at the junction of a vertical perfectly reflecting wall with a horizontal perfectly reflecting plane, the directivity factor is 4 and the directivity index is 6 dB. It should be noted that these adjustments ignore phase effects and assume incoherent reflection.<sup>1</sup>

From an infinite line source, the wavefronts are cylindrical; so wavefront spreading means a reduction of 3 dB per distance doubling. Traffic noise may be modeled by a line of incoherent point sources on an acoustically hard surface. If a line source of length  $l$  consists of contiguous omnidirectional incoherent elements of length  $dx$  and source strength  $W dx$ , the intensity at a location halfway along the line and at a perpendicular distance  $d$  from it, so that  $dx = rd\theta/\cos\theta$  where  $r$  is the distance from any element at angle  $\theta$  from the perpendicular, is given by

$$I = \int_{-l/2}^{l/2} \frac{W}{2\pi r^2} dx = \frac{W}{2\pi d} \left[ 2 \tan^{-1} \left( \frac{l}{2d} \right) \right]$$

This results in

$$L_p = L_W - 10 \log d - 8 + 10 \log \left[ 2 \tan^{-1} \left( \frac{l}{2d} \right) \right] \text{ dB} \quad (4)$$

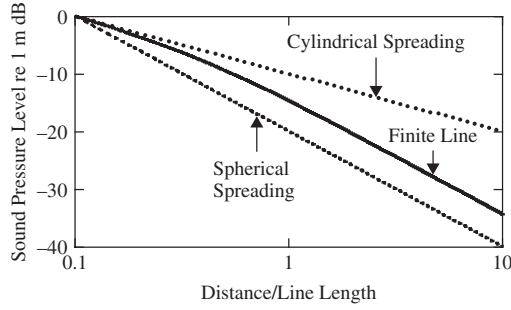
Figure 1 shows that attenuation due to wavefront spreading from the finite line source behaves as that from an infinite line at distances much less than the length of the source and as that from a point source at distances greater than the length of the source.

### 3 ATTENUATION OF OUTDOOR SOUND BY ATMOSPHERIC ABSORPTION

A proportion of sound energy is converted to heat as it travels through the air. There are heat conduction losses, shear viscosity losses, and molecular relaxation losses.<sup>2</sup> The resulting air absorption becomes significant at high frequencies and at long range, so air acts as a low-pass filter at long range. For a plane wave, pressure  $P$  at distance  $x$  from a position where the pressure is  $P_0$  is given by

$$P = P_0 e^{-\alpha x/2} \quad (5)$$





**Figure 1** Comparison of attenuation due to geometrical spreading from point, infinite line, and finite line sources.

The attenuation coefficient  $\alpha$  for air absorption depends on frequency, humidity, temperature, and pressure and may be calculated using Eqs. (6) to (8).<sup>3</sup>

$$\alpha = f^2 \left[ \left( \frac{1.84 \times 10^{-11}}{\left( \frac{T_0}{T} \right)^{1/2} \frac{p_s}{p_0}} \right) + \left( \frac{T_0}{T} \right)^{2.5} \right] \times \left( \frac{0.10680 e^{-3352/T} f_{r,N}}{f^2 + f_{r,N}^2} + \frac{0.01278 e^{-2239.1/T} f_{r,O}}{f^2 + f_{r,O}^2} \right) \frac{\text{nepers}}{\text{m} \cdot \text{atm}} \quad (6)$$

where  $f_{r,N}$  and  $f_{r,O}$  are relaxation frequencies associated with the vibration of nitrogen and oxygen molecules, respectively, and are given by

$$f_{r,N} = \frac{p_s}{p_0} \left( \frac{T_0}{T} \right)^{1/2} \left( 9 + 280 H e^{-4.17[(T_0/T)^{1/3} - 1]} \right) \quad (7)$$

$$f_{r,O} = \frac{p_s}{p_0} \left( 24.0 + 4.04 \times 10^4 H \frac{0.02 + H}{0.391 + H} \right) \quad (8)$$

where  $f$  is the frequency,  $T$  is the absolute temperature of the atmosphere in kelvins,  $T_0 = 293.15$  K is the reference value of  $T$  (20°C),  $H$  is the percentage molar concentration of water vapor in the atmosphere =  $\rho_{\text{sat}} r_h p_0 / p_s$ ,  $r_h$  is the relative humidity (%), and  $p_s$  is local atmospheric pressure and  $p_0$  is the reference atmospheric pressure (1 atm =  $1.01325 \times 10^5$  Pa);  $\rho_{\text{sat}} = 10^{C_{\text{sat}}}$ , where  $C_{\text{sat}} = -6.8346(T_0/T)^{1.261} + 4.6151$ . These formulas give estimates of the absorption of pure tones to an accuracy of  $\pm 10\%$  for  $0.05 < H < 5$ ,  $253 < T < 323$ ,  $p_0 < 200$  kPa. It should be noted that use of local meteorological data is necessary when calculating the atmospheric absorption.<sup>4</sup> Moreover outdoor air absorption varies through the day and the year.<sup>5</sup>

#### 4 DIFFRACTION OVER BARRIERS

Obstacles such as noise barriers that intercept the line of sight between source and receiver and that are large compared to the incident wavelengths reduce the sound at the receiver. As long as the transmission loss through the barrier material is sufficiently high, the performance of a barrier is dictated by the geometry (see Fig. 2).

The total sound field in the vicinity of a semi-infinite half-plane depends on the relative position of source, receiver, and the thin plane. The total sound field  $p_T$  in each of three regions shown in Fig. 2 is as follows:

$$\text{In front of the barrier: } p_T = p_i + p_r + p_d \quad (9a)$$

$$\text{Above the barrier: } p_T = p_i + p_d \quad (9b)$$

$$\text{In the shadow zone: } p_T = p_d \quad (9c)$$

Fresnel numbers of the source and image source are denoted, respectively, by  $N_1$  and  $N_2$  are defined as follows:

$$N_1 = \frac{R' - R_1}{\lambda/2} = \frac{k}{\pi} (R' - R_1) \quad (10a)$$

$$N_2 = \frac{R' - R_2}{\lambda/2} = \frac{k}{\pi} (R' - R_2) \quad (10b)$$

where  $R_1$  and  $R_2$  are defined in Fig. 2,  $R' = r_s + r_r$  is the shortest path source–edge–receiver, and  $k$  the wavenumber corresponding to wavelength  $\lambda$  in air, =  $2\pi/\lambda$ .

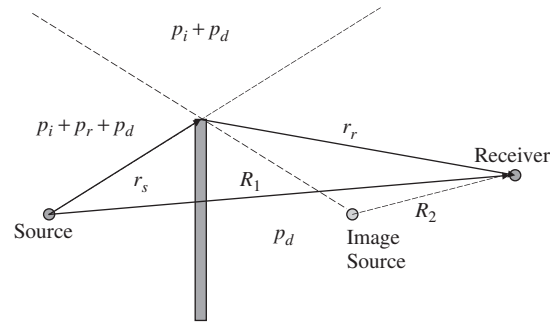
The attenuation (Att dB) of the screen (or sometimes known as the insertion loss, IL, dB) is often used to assess the acoustical performance of the barrier (see also Chapter 122). It is defined as follows:

$$\text{Att} = \text{IL} = 20 \log \left( \left| \frac{p_w}{p_{w/o}} \right| \right) \quad (11)$$

where  $p_w$  and  $p_{w/o}$  is the total sound field with or without the presence of the barrier.

Maekawa<sup>6</sup> described the attenuation of a screen using an empirical approach based on the Fresnel number  $N_1$  associated with the source. Hence

$$\text{Att} = 10 \log(3 + 20N_1) \quad (12)$$



**Figure 2** Diffraction of sound by a thin barrier.

The Maekawa curve can be represented mathematically by<sup>7</sup>

$$\text{Att} = 5 + 20 \log \frac{\sqrt{2\pi N_1}}{\tanh \sqrt{2\pi N_1}} \quad (13)$$

Menounou<sup>8</sup> has modified the Kurze–Anderson empirical formula<sup>7</sup> by using both Fresnel numbers [Eqs. (10)]. The improved Kurze–Anderson formula is given by

$$\text{Att} = \text{Att}_s + \text{Att}_b + \text{Att}_{sb} + \text{Att}_{sp} \quad (14a)$$

where

$$\text{Att}_s = 20 \log \frac{\sqrt{2\pi N_1}}{\tanh \sqrt{2\pi N_1}} - 1 \quad (14b)$$

$$\text{Att}_b = 20 \log \left[ 1 + \tanh \left( 0.6 \log \frac{N_2}{N_1} \right) \right] \quad (14c)$$

$$\text{Att}_{sb} = (6 \tanh \sqrt{N_2} - 2 - \text{Att}_b)(1 - \tanh \sqrt{10N_1}) \quad (14d)$$

$$\text{Att}_{sp} = -10 \log \frac{1}{(R'/R_1)^2 + (R'/R_1)} \quad (14e)$$

The term  $\text{Att}_s$  is a function of  $N_1$ , which is a measure of the relative position of the receiver from the source. The second term depends on the ratio of  $N_2/N_1$ , which depends on the proximity of either the source or the receiver to the half-plane. The third term is only significant when  $N_1$  is small and depends on the proximity of the receiver to the shadow boundary. The last term, a function of the ratio  $R'/R_1$ , accounts for the diffraction effect due to spherical incident waves.

These formulas only predict the amplitude of sound and do not include wave interference effects. Such interference effects result from the contributions from different diffracted wave paths in the presence of ground.

Consider a source  $S_g$  located at the left side of the barrier, a receiver  $R_g$  at the right side of the barrier, and  $O$  is the diffraction point on the barrier edge (see Fig. 3). The sound reflected from the ground surface can be described by an image of the source,  $S_i$ . On the receiver side sound waves will also be reflected from

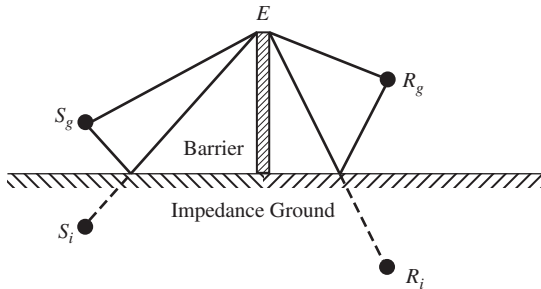


Figure 3 Diffraction by a barrier on impedance ground.

the ground. This effect can be considered in terms of an image of the receiver,  $R_i$ . The pressure at the receiver is the sum of four terms that correspond to the sound paths  $S_g E R_g$ ,  $S_i E R_g$ ,  $S_g E R_i$ , and  $S_i E R_i$ .

If the surface is a perfectly reflecting ground, the total sound field is the sum of the diffracted fields of these four paths:

$$P_T = P_1 + P_2 + P_3 + P_4 \quad (15a)$$

where

$$P_1 = P(S_g, R_g, E) \quad P_2 = P(S_i, R_g, E)$$

$$P_3 = P(S_g, R_i, E) \quad P_4 = P(S_i, R_i, E)$$

$P(S, R, E)$  is the diffracted sound field due to a thin barrier for given positions of source  $S$ , receiver  $R$ , and the point of diffraction at the barrier edge  $E$ . If the ground has finite impedance (such as grass or a porous road surface), then the pressure corresponding to rays reflected from these surfaces should be multiplied by the appropriate spherical wave reflection coefficient(s) to allow for the change in phase and amplitude of the wave on reflection as follows:

$$P_r = P_1 + Q_s P_2 + Q_R P_3 + Q_s Q_R P_4 \quad (16)$$

where  $Q_s$  and  $Q_R$  are the spherical wave reflection coefficients for the source and receiver side, respectively. The spherical wave reflection coefficients can be calculated according to Eq. (27) for different types of ground surfaces and source/receiver geometries.

For a given source and receiver position, the acoustical performance of the barrier on the ground is normally assessed by use of either the excess attenuation (EA) or the insertion loss (IL). They are defined as follows:

$$\text{EA} = \text{SPL}_f - \text{SPL}_b \quad (17)$$

$$\text{IL} = \text{SPL}_g - \text{SPL}_b \quad (18)$$

where  $\text{SPL}_f$  is the free field noise level,  $\text{SPL}_g$  is the noise level with the ground present, and  $\text{SPL}_b$  is the noise level with the barrier and ground present. Note that, in the absence of a reflecting ground, the numerical value of EA (which was called Att previously) is the same as IL. If the calculation is carried out in terms of amplitude only, then the attenuation  $\text{Att}_n$  for each sound path can be directly determined from the appropriate Fresnel number  $F_n$  for that path. The excess attenuation of the barrier on a rigid ground is then given by

$$A_T = 10 \log \left( 10^{-\left| \frac{\text{Att}_1}{10} \right|} + 10^{-\left| \frac{\text{Att}_2}{10} \right|} + 10^{-\left| \frac{\text{Att}_3}{10} \right|} + 10^{-\left| \frac{\text{Att}_4}{10} \right|} \right) \quad (19)$$

The attenuation for each path can either be calculated by empirical or analytical formulas depending on the complexity of the model and the required accuracy. Lam and Roberts<sup>9</sup> have suggested a simple approach capable of modeling wave effects in which the phase of the wave at the receiver is calculated from the path length,  $r_r$ , via the top of the screen, assuming a  $\pi/4$  phase change in the diffracted wave. This phase change is assumed to be constant for all source–barrier–receiver geometries. For example, the diffracted wave along the path  $S_g ER_g$  would be given by

$$P_1 = \text{Att}_1 e^{i[k(r_0+r_r)+\pi/4]} \quad (20)$$

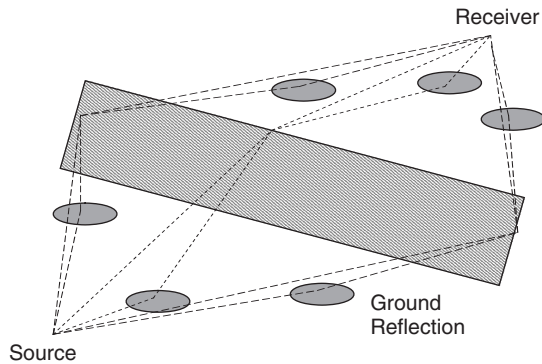
This approach provides a reasonable approximation for the many situations of interest where source and receiver are many wavelengths from the barrier and the receiver is in the shadow zone.

### 5 ATTENUATION CAUSED BY FINITE BARRIERS AND BUILDINGS

All noise barriers have finite length and, for certain conditions, sound diffracting around the vertical ends of the barrier may be significant. This will be the case for sound diffracting around buildings also. Figure 4 shows the eight diffracted ray paths contributing to the total field behind a finite-length barrier situated on finite impedance ground. In addition to the four “normal” ray paths diffracted at the top edge of the barrier (see Fig. 3), four more ray paths are diffracted at the vertical edges, that is, two rays at either edge being, respectively, the direct diffracted ray and the diffracted-and-reflected ray.

The reflection angles of the two diffracted-and-reflected rays are independent of the barrier position. Rays reflect either at the source side or on the receiver side of the barrier, depending on the relative positions of the source, receiver, and barrier. The total field is given by

$$P_T = P_1 + Q_S P_2 + Q_R P_3 + Q_S Q_R P_4 + P_5 + Q_R P_6 + P_7 + Q_R P_8 \quad (21)$$



**Figure 4** Ray paths around a finite length barrier or building on the ground.

where  $P_1$  to  $P_4$  are those given earlier for the diffraction at the top edge of the barrier.

Although accurate diffraction formulas may be used to compute  $P_i$  ( $i = 1, \dots, 8$ ), a simpler approach is to assume that each diffracted ray has a constant phase shift of  $\pi/4$  regardless the position of source, receiver, and diffraction point. Further detail on barrier attenuation will be found in Chapter 122.

### 6 GROUND EFFECTS

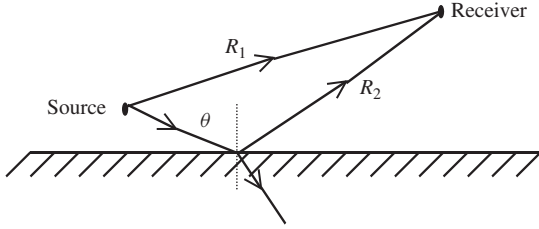
Ground effects (for elevated source and receiver) are the result of interference between sound traveling directly from source to receiver and sound reflected from the ground when both source and receiver are close to the ground. Sometimes the phenomenon is called ground absorption but, since the interaction of outdoor sound with the ground involves interference, there can be enhancement as well as attenuation. Above ground, such as nonporous concrete or asphalt, the sound pressure is doubled more or less over a wide range of audible frequencies. Such ground surfaces are described as *acoustically hard*. Over porous surfaces, such as soil, sand, and snow, enhancement tends to occur at low frequencies since the larger the sound wave the less able it is to penetrate the pores. The presence of vegetation tends to make the surface layer of ground including the root zone more porous. The layer of partly decayed matter on the floor of a forest is highly porous. Snow is significantly more porous than soil and sand. Porous ground surfaces are sometimes called *acoustically soft* or may be referred to as *finite impedance* ground surfaces.

### 7 BOUNDARY CONDITIONS AT THE GROUND

Typically, the speed of sound in the ground is much slower than that in the air, that is,  $c \gg c_1$ . The propagation of sound in the air gaps between solid particles is impeded by viscous friction. This in turn means that the index of refraction in the ground,  $n_1 = c/c_1 \gg 1$ , and any incoming sound ray is refracted toward the normal as it propagates from air and penetrates the ground. This type of ground surface is called *locally reacting* because the air–ground interaction is independent of the angle of incidence of the incoming waves. The acoustical properties of locally reacting ground may be represented simply by its relative normal incidence surface impedance ( $Z$ ), or its inverse (the relative admittance  $\beta$ ), and the ground is said to form an impedance boundary. A perfectly hard ground has infinite impedance (zero admittance). A perfectly soft ground has zero impedance (infinite admittance). If the ground is not locally reacting, that is, it is externally reacting, then there are two separate boundary conditions governing the continuity of pressure and the continuity of the normal component of air particle velocity.

### 8 ATTENUATION OF SPHERICAL ACOUSTIC WAVES OVER THE GROUND

The idealized case of a point (omnidirectional) source of sound at height  $z_s$  and a receiver at height  $z$  and



**Figure 5** Sound propagation from a point source to a receiver above a ground surface.

horizontal distance  $r$  above a finite impedance plane (admittance  $\beta$ ) is shown in Fig. 5.

Between source and receiver there is a direct sound path of length  $R_1$  and a ground-reflected path of length  $R_2$ . With the restrictions of long range ( $r \approx R_2$ ), high frequency [ $kr \gg 1$ ,  $k(z + z_s) \gg 1$ ], where  $k = \omega/c$  and  $\omega = 2\pi f$  ( $f$  being frequency) and with both the source and receiver located close ( $r \gg z + z_s$ ) to a relatively hard ground surface ( $|\beta|^2 \ll 1$ ), the total sound field at  $(x, y, z)$  can be determined from

$$p(x, y, z) = \frac{e^{ikR_1}}{4\pi R_1} + \frac{e^{ikR_2}}{4\pi R_2} + \Phi_p + \Phi_s \quad (22)$$

where

$$\Phi_p \approx 2i\sqrt{\pi} \left(\frac{1}{2}kR_2\right)^{1/2} \beta e^{-w^2} \text{erfc}(-iw) \frac{e^{ikR_2}}{4\pi R_2} \quad (23)$$

and  $w$ , sometimes called the numerical distance, is given by

$$w \approx \frac{1}{2}(1+i)\sqrt{kR_2}(\cos\theta + \beta) \quad (24)$$

In (22),  $\Phi_s$  represents a surface wave and is small compared with  $\Phi_p$  under most circumstances. It is included in careful computations of the complementary error function  $[\text{erfc}(x)]$ .<sup>10,11</sup>

After rearrangement, the sound field due to a point monopole source above a locally reacting ground becomes

$$p(x, y, z) = \frac{e^{ikR_1}}{4\pi R_1} + [R_p + (1 - R_p)F(w)] \frac{e^{ikR_2}}{4\pi R_2} \quad (25)$$

where  $R_p$  is the plane wave reflection coefficient and  $F(w)$ , sometimes called the boundary loss factor, is given by

$$F(w) = 1 + i\sqrt{\pi}w \exp(-w^2) \text{erfc}(-iw) \quad (26)$$

where  $F(w)$  results from the interaction of a spherical wavefront with a ground of finite impedance. The term in the square bracket of (25) may be interpreted as the spherical wave reflection coefficient:

$$Q = R_p + (1 - R_p)F(w) \quad (27)$$

If the plane wave reflection coefficient is used in (25) instead of the spherical wave reflection coefficient, it leads to the prediction of zero sound pressure when both source and receiver are on the ground ( $R_p = -1$  and  $R_1 = R_2$ ). The contribution of the second term of  $Q$  to the total field allows for the fact that the wavefronts are spherical rather than plane and has been called the *ground wave*, in analogy with the corresponding term in the theory of AM radio reception.<sup>12</sup> If the wavefront is plane ( $R_2 \rightarrow \infty$ ), then  $|w| \rightarrow \infty$  and  $F \rightarrow 0$ . If the surface is acoustically hard, then  $|\beta| \rightarrow 0$ , which implies  $|w| \rightarrow 0$  and  $F \rightarrow 1$ . If  $\beta = 0$ , the sound field consists of two terms: a direct wave contribution and a specularly reflected wave from the image source, and the total sound field may be written

$$p(x, y, z) = \frac{e^{ikR_1}}{4\pi R_1} + \frac{e^{ikR_2}}{4\pi R_2}$$

This has a first minimum corresponding to destructive interference between the direct and ground-reflected components when  $k(R_2 - R_1) = \pi$ , or  $f = c/2(R_2 - R_1)$ . Normally this destructive interference is at too high a frequency to be of importance in outdoor sound prediction. The higher the frequency of the first minimum in the ground effect, the more likely that it will be destroyed by turbulence.

For  $|\beta| \ll 1$  but at grazing incidence ( $\theta = \pi/2$ ), so that  $R_p = -1$  and

$$p(x, y, z) = 2F(w)e^{ikr}/r \quad (28)$$

The numerical distance,  $w$ , is given by

$$w = \frac{1}{2}(1+i)\beta\sqrt{kr} \quad (29)$$

Equation (25) is the most widely used analytical solution for predicting the sound field above a locally reacting ground in a homogeneous atmosphere. There are many other accurate asymptotic and numerical solutions available but no significant numerical differences between various predictions have been revealed for practical geometries and typical outdoor ground surfaces.

Although it is numerically part of the calculation of the complementary error function, the surface wave is a separate contribution propagating close to and parallel to the porous ground surface. It produces elliptical motion of air particles as the result of combining motion parallel to the surface with that normal to the surface in and out of the pores. The surface wave decays with the inverse square root of range rather than inversely with range as is true for other components. At grazing incidence on a plane with high impedance such that  $|\beta| \rightarrow 0$ , the condition for the existence of a surface wave is simply that the imaginary part of the ground impedance (the reactance) is greater than the real part (the resistance). Surface waves due to a point source have been generated and studied extensively in laboratory experiments over

cellular or lattice surfaces placed on smooth hard surfaces.<sup>13-16</sup> The outdoor ground type that most likely produce measurable surface waves is a thin layer of snow over a frozen ground, and such waves over snow have been observed using blank pistol shots.<sup>17</sup>

There are some cases where it is not possible to model the ground surface as an impedance plane, that is,  $n_1$  is not sufficiently high to warrant the assumption that  $n_1 \gg 1$ . In this case, the refraction of sound wave depends on the angle of incidence as sound enters into the porous medium. This means that the apparent impedance depends not only on the physical properties of the ground surface but also, critically, on the angle of incidence. It is possible to introduce an *effective* admittance,  $\beta_e$ , defined by

$$\beta_e = \zeta_1 \sqrt{n_1^2 - \sin^2 \theta} \quad (30)$$

where  $\zeta_1$  is the density ratio of air to ground,  $\zeta_1 = \rho/\rho_1 \ll 1$ . This allows use of the same results as before but with admittance replaced by the effective admittance (30) for a semi-infinite nonlocally reacting ground.<sup>18</sup> There are some situations where there is a highly porous surface layer above a relatively nonporous substrate. This is the case with forest floors consisting of partly decomposed litter layers above relatively high flow resistivity soil, with freshly fallen snow on a hard ground or with porous asphalt laid on a nonporous substrate. The minimum depth,  $d_m$ , for such a multiple layer ground to be treated as a semi-infinite externally reacting ground to satisfy the above condition depends on the acoustical properties of the ground and the angle of incidence, but we can consider two limiting cases. Denoting the complex wavenumber or propagation constant within the surface layer of the ground by  $k_1 = k_r + ik_x$ , and for normal incidence, where  $\theta = 0$ , the required condition is simply

$$d_m > 6/k_x \quad (31)$$

For grazing incidence where  $\theta = \pi/2$ , the required condition is

$$d_m > 6 \left[ \sqrt{\frac{(k_r^2 - k_x^2 - 1)^2}{4} + k_r^2 k_x^2} - \frac{k_r^2 - k_x^2 - 1}{2} \right]^{1/2} \quad (32)$$

It is possible to derive an expression for the effective admittance of a ground with an arbitrary number of layers. However, sound waves can seldom penetrate more than a few centimetres in most outdoor ground surfaces. Lower layers contribute little to the total sound field above the ground and, normally, consideration of ground structures consisting of more than two layers is not required for predicting outdoor sound. Nevertheless, the assumption of a double layer structure<sup>18</sup> has been found to enable improved agreement with data obtained over snow.<sup>19</sup> It has been shown that, in cases where the surface

impedance depends on angle, replacing the normal surface impedance by the grazing incidence value is sufficiently accurate for predicting outdoor sound.<sup>20</sup>

## 9 ACOUSTIC IMPEDANCE OF GROUND SURFACES

For most outdoor sound predictions, the ground may be considered to be a porous material with a rigid, rather than elastic, frame. The most important characteristic of a ground surface that affects its acoustical character is its flow resistivity or air permeability. Flow resistivity is a measure of the ease with which air can move in and out of the ground. It represents the ratio of the applied pressure gradient to the induced volume flow rate per unit thickness of material and has units of  $\text{Pa s m}^{-2}$ . If the ground surface has a high flow resistivity, it means that it is difficult for air to flow through the surface. Flow resistivity increases as porosity decreases. For example, conventional hot-rolled asphalt has a very high flow resistivity (10 million  $\text{Pa s m}^{-2}$ ) and negligible porosity, whereas drainage asphalt has a volume porosity of up to 0.25 and a relatively low flow resistivity ( $< 30,000 \text{ Pa s m}^{-2}$ ). Soils have volume porosities of between 10 and 40%. A wet compacted silt may have a porosity that can be as low as 0.1 and a rather high flow resistivity (4 million  $\text{Pa s m}^{-2}$ ). Newly fallen snow has a porosity of around 60% and a fairly low flow resistivity ( $< 10,000 \text{ Pa s m}^{-2}$ ). The thickness of the surface porous layer also is important and whether or not it has acoustically hard substrate.

A widely used model for the acoustical properties of outdoor surfaces involves a single parameter, the "effective" flow resistivity,  $\sigma_e$ , to characterize the ground.<sup>21</sup> According to this single-parameter model, the propagation constant,  $k$ , and normalized characteristic impedance,  $Z$ , are given by

$$\frac{k}{k_1} = \left[ 1 + 0.0978 \left( \frac{f}{\sigma_e} \right)^{-0.700} + i0.189 \left( \frac{f}{\sigma_e} \right)^{-0.595} \right] \quad (33a)$$

$$Z = \frac{\rho_1 c_1}{\rho c} = 1 + 0.0571 \left( \frac{f}{\sigma_e} \right)^{-0.754} + i0.087 \left( \frac{f}{\sigma_e} \right)^{-0.732} \quad (33b)$$

This model may be used for a locally reacting ground as well as for an extended reaction surface. On occasion, better agreement with grassland data<sup>22</sup> has been obtained by assuming that the ground surface is that of a hard-backed porous layer of thickness  $d$  such that the surface impedance  $Z_s$  is given by

$$Z_s = Z \coth(-ikd) \quad (34)$$

A model based on an exponential change in porosity with depth has been suggested.<sup>23,24</sup> Although this model is suitable only for a high flow resistivity (i.e., locally reacting) ground, for many outdoor ground surfaces, it has enabled better agreement with measured data than obtained using Eq. (33b). The two adjustable parameters are the effective flow resistivity ( $\sigma_e$ ) and the effective rate of change of porosity with depth ( $\alpha_e$ ). The impedance of the ground surface is predicted by

$$Z = 0.436(1 + i) \sqrt{\frac{\sigma_e}{f}} + 19.74i \frac{\alpha_e}{f} \quad (35)$$

More sophisticated analytical models for the acoustical properties of rigid-porous materials introduce porosity, the tortuosity (or “twistiness”) of the pores, factors related to pore shape,<sup>25</sup> and multiple layering. Models that introduce the viscous and thermal characteristic dimensions of pores<sup>26</sup> are based on a formulation by Johnson et al.<sup>27</sup> Recently, it has been shown possible to obtain explicit relationships between the characteristic dimensions and grain size by assuming a specific microstructure of identical stacked spheres.<sup>28</sup> Other developments allow for a log-normal pore size distribution, while assuming pores of identical shape.<sup>29–30</sup> On occasion it is important to include multiple layering also. A standard method for obtaining ground impedance is the template method based on short-range measurements of excess attenuation.<sup>31</sup> It should be noted that parameters deduced from data according to (33) to (35) show that there can be a wide range of parameter values for “grassland”.

## 10 EFFECTS OF SMALL-SCALE ROUGHNESS

There have been advances also in methods of obtaining surface admittance directly.<sup>32</sup> Measurements obtained over uncultivated grassland,<sup>33</sup> using this direct impedance-fitting method, indicate that the surface impedance tends to zero above 3 kHz. Reflection involving incoherent scatter from a randomly rough porous surface may be used to explain these measurements. The assumed flow resistivity and porosity are within the expected range for a soil. However, small-scale roughness must be included to provide a reasonable fit to these grassland data. For grazing incidence on a hard surface containing randomly distributed two-dimensional (2D) roughness normal to the roughness axes, the effective admittance may be written<sup>34</sup>

$$\beta = \left( \frac{3V^2 k^3 b}{2} \right) \left( 1 + \frac{\delta^2}{2} \right) - iVk(\delta - 1) \quad (36)$$

where  $V$  is the roughness volume per unit area of surface (equivalent to mean roughness height),  $b$  is the mean center-to-center spacing,  $\delta$  is an interaction factor depending on the “shape” and “concentration” of the roughness and, as before,  $k$  is the wavenumber in air. An interesting consequence of (36) is that a surface that would be acoustically hard if smooth has, effectively, a finite impedance when rough. The real part

of the admittance allows for incoherent scatter from the surface and varies with the cube of frequency and the square of the roughness volume per unit area. The same approach can be extended to give the effective normalized surface admittance of a porous surface containing 2D roughness.<sup>33,35</sup> It is possible to obtain the following approximation for the impedance of a randomly rough porous surface near grazing incidence<sup>36</sup>:

$$Z_r \approx Z_s - \left( \frac{\langle H \rangle R_s}{\gamma \rho_0 c_0} \right) \left( \frac{2}{v} - 1 \right) \quad [\text{Re}(Z_r) \geq 0] \quad (37)$$

where  $v = 1 + \frac{2}{3}\pi \langle H \rangle$  and  $\langle H \rangle$  is the root-mean-square roughness height.

Cultivation practices intended to break up soil compaction beneath the ground surface caused, for example, by repeated passage of heavy vehicles, have important influences on ground effect since they change the surface properties. Aylor<sup>37</sup> noted a significant change in the excess attenuation at a range of 50 m over a soil after disking without any noticeable change in the meteorological conditions. Plowing turns the soil surface over to a depth of about 0.15 m. Measurements taken over cultivated surfaces before and after subsoiling and plowing have been shown to be consistent with predicted effects of the resulting changes in surface roughness and flow resistivity.<sup>38</sup>

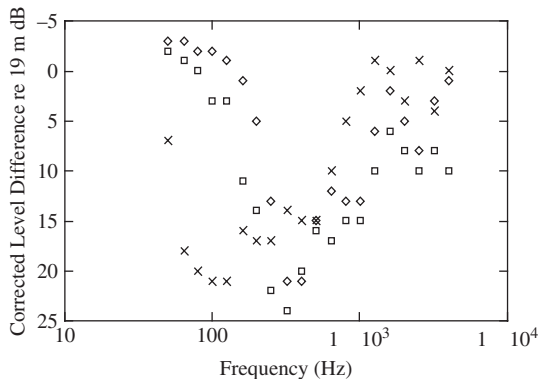
## 11 EXAMPLES OF GROUND ATTENUATION UNDER WEAKLY REFRACTING CONDITIONS

Pioneering studies of the combined influences of the ground surface and meteorological conditions were carried out using a fixed Rolls Royce Avon jet engine as a source (nozzle-center height 1.82 m) at two grass-covered airfields (Radlett and Hatfield).<sup>39,40</sup> Examples of the resulting data, quoted as the difference between sound pressure levels registered by microphones at 1.5 m height and horizontal distances of 19 m (the reference location) and 347 m, corrected for the decrease expected from spherical spreading and air absorption, are shown in Fig. 6.

The data over grass cover were obtained with a positive vector wind (from source to receiver) of 1.27 m/s (5 ft/s). The ground attenuation at Hatfield, although still a major propagation factor, that is, over 15 dB near 400 Hz, was less than that at Radlett, and its maximum value occurred at a higher frequency. Snowfall during the period of these measurements also enabled study of the influence of several centimetres of snow with a comparable positive vector wind of 1.52 m/s (6 ft/s). These data revealed the large effect at low frequencies, that is, over 20 dB attenuation in the 63- and 125-Hz third-octave bands, over snow.

Noise measurements have been made to distances of 3 km during aircraft engine runups with the aim of defining noise contours in the vicinity of airports.<sup>41</sup> Measurements were made for a range of power settings during several summer days under near to calm weather conditions (wind speed < 5 m/s, temperature between 20 and 25°C). Between 7 and 10 measurements were made at every measurement station

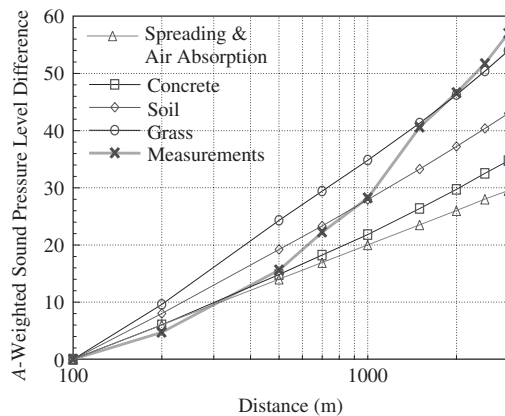




**Figure 6** Data for the level difference between microphones at 19 and 347 m from a fixed jet engine source with a positive vector wind between source and receiver of 1.27 m/s (5 ft/s) corrected for wavefront spreading and air absorption.  $\square$  represent data at Radlett;  $\diamond$  represent data at Hatfield;  $\times$  represent data obtained over approximately 0.15 m thick (6–9 in.) snow at Hatfield.

(in accordance with ICAO Annex 16 requirements) and the results have been averaged. Example results are shown in Fig. 7. It can be shown that these data are consistent with nearly acoustically neutral conditions.<sup>41</sup> Note that at 3 km, the measured levels are more than 30 dB less than would be expected from wavefront spreading and air absorption only.

At distances of less than between 500 and 700 m from the engine, the data suggest attenuation rates near to the “concrete” or “spherical spreading plus air absorption” predictions. Beyond 700 m the measured



**Figure 7** Measured differences between the A-weighted sound pressure level at 100 m and those measured at ranges up to 3 km during an Il-86 aircraft’s engine test in the direction of the maximum jet noise generation ( $\sim 40^\circ$  from exhaust axis) and predictions for levels due to a point source at the engine center height assuming spherical spreading plus air absorption and various types of ground.

attenuation rate is nearer to the “soil” or between the “soil” and “grass” predictions. This is the result of the fact that the runups took place over the concrete surface of an apron and further away (i.e., between 500 and 700 m in various directions) the ground surface was “soil” and/or “grass.”

## 12 ATTENUATION THROUGH TREES AND FOLIAGE

Ignoring meteorological effects, a mature forest or woodland may have three types of influence on sound. First is ground effect. This is particularly significant if there is a thick litter layer of partially decomposing vegetation on the forest floor. In such a situation the ground surface consists of a thick highly porous layer with rather low flow resistivity thus giving a primary excess attenuation maximum at lower frequencies than observed over typical grassland. This is consistent with the data collected over ranges of 500 m<sup>42</sup> and is similar to the effect, mentioned earlier, over snow. Second, the trunks and branches scatter the sound out of the path between source and receiver. Third, the foliage attenuates the sound by viscous friction.

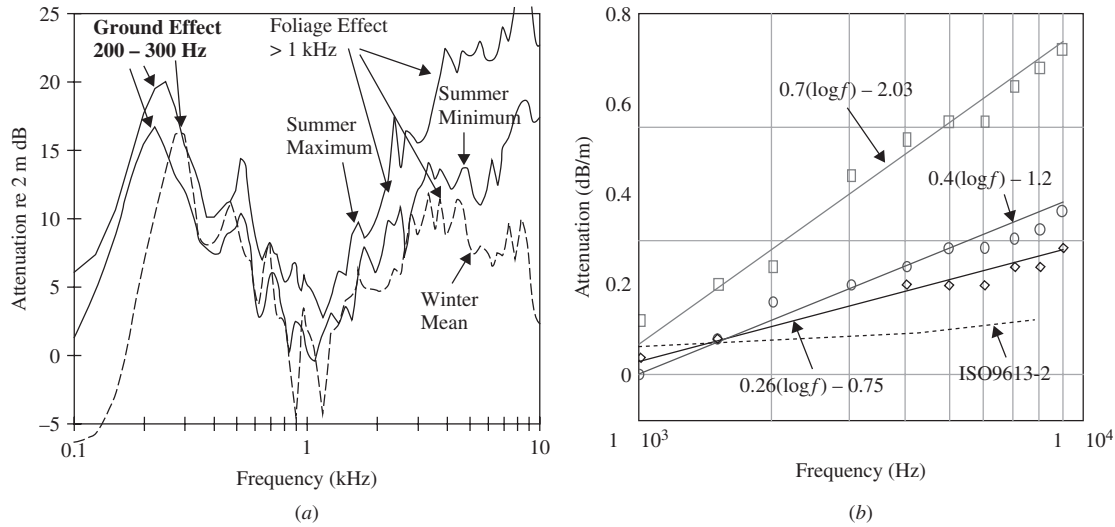
Predictions of the total attenuation through woodland, in qualitative agreement with measurements made during conditions with little or no wind and small temperature gradients, have been obtained by adding the contributions to attenuation for large cylinders (representing trunks), small cylinders (representing foliage), and the ground.<sup>43</sup> But it is necessary to adjust several parameters to obtain quantitative agreement. Foliage has the greatest effect above 1 kHz and the foliage attenuation increases approximately in a linear fashion with frequency. Figure 8 shows a typical variation of attenuation with frequency and linear fits to the foliage attenuation.

## 13 WIND AND TEMPERATURE GRADIENT EFFECTS ON OUTDOOR SOUND PROPAGATION

The atmosphere is constantly in motion as a consequence of wind shear and uneven heating of Earth’s surface (Fig. 9). Any turbulent flow of a fluid across a rough solid surface generates a boundary layer. Most interest, from the point of view of outdoor sound prediction, focuses on the lower part of the meteorological boundary layer called the surface layer. In the surface layer, turbulent fluxes vary by less than 10% of their magnitude, but the wind speed and temperature gradients are largest. In typical daytime conditions the surface layer extends over 50 to 100 m. Usually it is thinner at night. Turbulence may be modeled in terms of a series of moving eddies or “turbules” with a distribution of sizes.

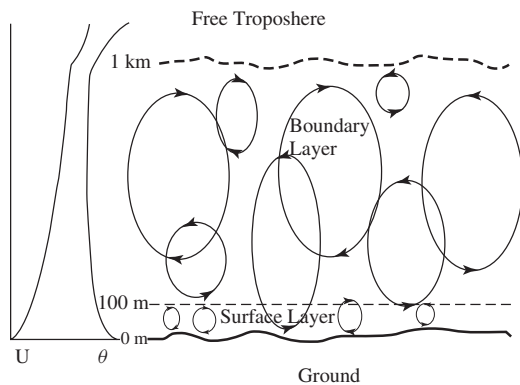
In most meteorological conditions, the speed of sound changes with height above the ground. Usually, temperature decreases with height (the adiabatic lapse condition). In the absence of wind, this causes sound waves to bend, or refract, upward. Wind speed adds or subtracts from sound speed.

When the source is downwind of the receiver the sound has to propagate upwind. As height increases,



**Figure 8** (Left) Measured attenuation through alternate bands of Norway spruce and oak (planted in 1946) with Hawthorn, roses, and honeysuckle undergrowth; visibility less than 24 m. (Right) Linear fits to attenuation above 1 kHz in mixed conifers (squares), mixed deciduous summer (circles), and spruce monoculture (diamonds). Also shown is the foliage attenuation predicted according to ISO 9613-2.

the wind speed increases and the amount being subtracted from the speed of sound increases, leading to a negative sound speed gradient. Downwind, sound pressure refracts downward. Wind effects tend to dominate over temperature effects when both are present. Temperature inversions, in which air temperature increases up to the inversion height, cause sound waves to refract downward below that height. Under inversion conditions, or downwind, sound pressure levels decrease less rapidly than would be expected from wavefront spreading alone.



**Figure 9** Schematic representation of the daytime atmospheric boundary layer and turbulent eddy structures. The sketch graph on the left shows the mean wind speed ( $U$ ) and the potential temperature profiles ( $\theta = T + \gamma_d z$ , where  $\gamma_d = -0.098^\circ\text{C/km}$  is the dry adiabatic lapse rate,  $T$  is the temperature and  $z$  is the height).

In general, the relationship between sound speed profile  $c(z)$ , temperature profile  $T(z)$ , and wind speed profile  $u(z)$  in the direction of sound propagation is given by

$$c(z) = c(0) \sqrt{\frac{T(z) + 273.15}{273.15}} + u(z) \quad (38)$$

where  $T$  is in degrees Celsius and  $u$  is in metres/second.

#### 14 SHADOW ZONES

A negative sound gradient means upward refraction and the creation of a sound shadow at a distance from the source that depends on the gradient. The presence of a shadow zone means that the sound pressure level decreases faster than would be expected from distance alone. A combination of slightly negative temperature gradient, strong upwind propagation, and air absorption has been observed, in carefully monitored experiments, to reduce sound pressure levels, 640 m from a 6-m-high source over relatively hard ground, by up to 20 dB more than expected from spherical spreading.<sup>44</sup> Since shadow zones can be areas in which there is significant excess attenuation, it is important to determine their boundaries.

For a source close to the ground, assuming circular ray paths, the distance to the shadow zone is given approximately by

$$x = \left[ 2c_0 / \left( -\frac{dc}{dz} \right) \right]^{1/2} (\sqrt{h_s} + \sqrt{h_r}) \quad (39)$$



where  $h_s$  and  $h_r$  are heights of source and receiver, respectively, and  $dc/dz$  must be negative for a temperature-induced shadow zone.

When a wind is present, the combined effects of temperature lapse and wind will tend to enhance the shadow zone upwind of the source, since wind speed tends to increase with height. Downwind of the source, however, the wind will counteract the effect of temperature lapse, and the shadow zone will be destroyed. In any case, an acoustic shadow zone is never as complete as an optical one would be, as a result of diffraction and turbulence. In the presence of wind with a wind speed gradient of  $du/dz$ , the formula for the distance to the shadow zone boundary is given by

$$x = \left[ 2c_0 \left/ \frac{du}{dz} \cos \beta - \frac{dc}{dz} \right. \right]^{1/2} (\sqrt{h_s} + \sqrt{h_r}) \quad (40)$$

where  $\beta$  is the angle between the direction of the wind and the line between source and receiver.

Note that there will be a value of the angle  $\beta$ , (say  $\beta_c$ ), given by

$$\frac{du}{dz} \cos \beta_c = \frac{dc}{dz}$$

or

$$\beta_c = \cos^{-1} \left( \frac{dc}{dz} \left/ \frac{du}{dz} \right. \right) \quad (41)$$

at and beyond which there will not be a shadow zone. This represents the critical angle at which the effect of wind counteracts that of the temperature gradient.

## 15 ATMOSPHERIC TURBULENCE

Shadow zones due to atmospheric refraction are penetrated by sound scattered by turbulence, and this sets a limit of the order of 20 to 25 dB to the reduction of sound pressure levels within the sound shadow.<sup>45,46</sup> Another consequence of atmospheric turbulence is a fluctuation of the amplitude of outdoor sound at any given receiver. The extent of this fluctuation caused by turbulence initially increases with increasing distance of propagation, sound frequency, and strength of turbulence but reaches a limiting value fairly quickly. This means that the fluctuation in overall sound pressure levels from distant sources (e.g., line-of-sight from an aircraft at a few kilometres) may have a standard deviation of no more than about 6 dB.<sup>46</sup>

Turbulence destroys the coherence between direct and ground-reflected sound and consequently reduces the destructive interference in ground effect. Equation (25) may be modified to obtain the mean-squared pressure at a receiver in a turbulent but *acoustically neutral* (no refraction) atmosphere<sup>47</sup>

$$\langle p^2 \rangle = \frac{1}{R_1^2} + \frac{|Q|^2}{R_2^2} + \frac{2|Q|}{R_1 R_2} \cos[k(R_2 - R_1) + \theta] C \quad (42)$$

where  $\theta$  is the phase of the reflection coefficient, ( $Q = |Q|e^{i\theta}$ ),  $C$  is the coherence factor determined

by the turbulence effect,  $R_1$  is the direct sound path length, and  $R_2$  is the ground-reflected path length.

Hence the sound pressure level,  $P$ , is given by

$$P = 10 \log_{10}(\langle p^2 \rangle) \quad (43)$$

Most recent calculations of turbulence effects on outdoor sound have relied on estimated or best-fit values, rather than measured values, of turbulence parameters. Although assumption of a Gaussian spectrum provides a poor overall description of the spectrum of atmospheric turbulence, it allows many results to be obtained in simple analytical form.<sup>48</sup> Typically, the high wavenumber part of the spectrum is the main contributor to turbulence effects on sound propagation. So the assumption of a Gaussian spectrum results in best-fit parameter values that are rather less than those that are measured. For a Gaussian turbulence spectrum, the coherence factor,  $C$ , is given by<sup>49</sup>

$$C = e^{-\sigma^2(1-\rho)} \quad (44)$$

where  $\sigma^2$  is the variance of the phase fluctuation along a path and  $\rho$  is the phase covariance between adjacent paths (e.g., direct and reflected).

$$\sigma^2 = A \sqrt{\pi} \langle \mu^2 \rangle k^2 R L_0 \quad (45)$$

of the index of refraction, and  $L_0$  is the outer (inertial) scale of turbulence.

The coefficient  $A$  is given by

$$A = 0.5 \quad R > k L_0^2 \quad (46a)$$

$$A = 1.0 \quad R < k L_0^2 \quad (46b)$$

The parameters  $\langle \mu^2 \rangle$  and  $L_0$  may be determined from field measurements or estimated.

The phase covariance is given by

$$\rho = \frac{\sqrt{\pi}}{2} \frac{L_0}{h} \operatorname{erf} \left( \frac{h}{L_0} \right) \quad (47)$$

where  $h$  is the maximum transverse path separation and  $\operatorname{erf}(x)$  is the error function defined by

$$\operatorname{erf}(x) = \frac{2}{\sqrt{\pi}} \int_0^x e^{-t^2} dt \quad (48)$$

For a sound field consisting *only* of direct and reflected paths (which will be true at short ranges) in the absence of refraction, the parameter  $h$  is the mean propagation height given by

$$\frac{1}{h} = \frac{1}{2} \left( \frac{1}{h_s} + \frac{1}{h_r} \right) \quad (49)$$

where  $h_s$  and  $h_r$  are the source and receiver heights, respectively. Daigle<sup>49</sup> uses half this value to obtain better agreement with data.

Near grazing incidence, if  $h \rightarrow 0$ , then  $\rho \rightarrow 1$  and  $C \rightarrow 1$ . For greatly elevated source and/or receiver,  $h \rightarrow$  large and  $C \rightarrow$  maximum. The mean-squared refractive index may be calculated from the measured instantaneous variation of wind speed and temperature with time at the receiver. Specifically

$$\langle \mu^2 \rangle = \frac{\sigma_w^2 \cos^2 \alpha}{C_0^2} + \frac{\sigma_T^2}{4T_0^2}$$

where  $\sigma_w^2$  is the variance of the wind velocity,  $\sigma_T^2$  is the variance of the temperature fluctuations,  $\alpha$  is the wind vector direction, and  $C_0$  and  $T_0$  are the ambient sound speed and temperature, respectively. Typical values of best-fit mean-squared refractive index are between  $10^{-6}$  for calm conditions and  $10^{-4}$  for strong turbulence. A typical value of  $L_0$  is 1 m but in general a value equal to the source height should be used.

## 16 CONCLUDING REMARKS

During the last few years there have been considerable advances in numerical and analytical methods for outdoor sound prediction.<sup>50,51</sup> Details of these are beyond the scope of this work, but a review of recent progress may be found in Berengier et al.<sup>52</sup> As mentioned in the introduction, methods for predicting outdoor noise are undergoing considerable assessment and change in Europe as a result of a recent EC Directive<sup>53</sup> and the associated requirements for noise mapping. At the time of this writing, a European project HARMONOISE<sup>54</sup> is developing a comprehensive source-independent scheme for outdoor sound prediction. As in NORD2000,<sup>55</sup> various relatively simple formulas predicting the effect of topography, for example, are being derived and tested against numerical predictions.

## REFERENCES

1. K. M. Li and S. H. Tang, "The Predicted Barrier Effects in the Proximity of Tall Buildings," *J. Acoust. Soc. Am.*, Vol. 114, 2003, pp. 821–832.
2. H. E. Bass, L. C. Sutherland, and A. J. Zuckewar, "Atmospheric Absorption of Sound: Further Developments," *J. Acoust. Soc. Am.*, Vol. 97, No. 1, 1995, pp. 680–683.
3. D. T. Blackstock, *Fundamentals of Physical Acoustics*, Wiley, Hoboken, NJ, 2000.
4. C. Larsson, "Atmospheric Absorption Conditions for Horizontal Sound Propagation," *Appl. Acoust.*, Vol. 50, 1997, pp. 231–245.
5. C. Larsson, "Weather Effects on Outdoor Sound Propagation," *Int. J. Acoust. Vib.*, Vol. 5, No. 1, 2000, pp. 33–36.
6. Z. Maekawa, "Noise Reduction by Screens," *Appl. Acoust.*, Vol. 1, 1968, pp. 157–173.
7. U. J. Kurze and G. S. Anderson, "Sound Attenuation by Barriers," *Appl. Acoust.*, Vol. 4, 1971, pp. 35–53.
8. P. Menounou, "A Correction to Maekawa's Curve for the Insertion Loss behind Barriers," *J. Acoust. Soc. Am.*, Vol. 110, 2001, pp. 1828–1838.
9. Y. W. Lam and S. C. Roberts, "A Simple Method for Accurate Prediction of Finite Barrier Insertion Loss," *J. Acoust. Soc. Am.*, Vol. 93, 1993, pp. 1445–1452.
10. M. Abramowitz and I. A. Stegun, *Handbook of Mathematical Functions with Formulas, Graphs, and Mathematical Tables*, Dover, New York, 1972.
11. F. Matta and A. Reichel, "Uniform Computation of the Error Function and Other Related Functions," *Math. Comput.*, Vol. 25, 1971, pp. 339–344.
12. A. Banos, in *Dipole Radiation in the Presence of Conducting Half-Space*, Pergamon, New York, 1966, Chapters 2–4. See also A. Banos, Jr., and J. P. Wesley, *The Horizontal Electric Dipole in a Conduction Half-Space*, Univ. Calif. Electric Physical Laboratory, 1954, S10 Reference 53–33 and 54–31.
13. R. J. Donato, "Model Experiments on Surface Waves," *J. Acoust. Soc. Am.*, Vol. 63, 1978, pp. 700–703.
14. C. H. Howorth and K. Attenborough, "Model Experiments on Air-Coupled Surface Waves," *J. Acoust. Soc. Am.*, Vol. 92, 1992, p. 2431(A).
15. G. A. Daigle, M. R. Stinson, and D. I. Havelock, "Experiments on Surface Waves over a Model Impedance Using Acoustical Pulses," *J. Acoust. Soc. Am.*, Vol. 99, 1996, pp. 1993–2005.
16. Q. Wang and K. M. Li, "Surface Waves over a Convex Impedance Surface," *J. Acoust. Soc. Am.*, Vol. 106, 1999, pp. 2345–2357.
17. D. G. Albert, "Observation of Acoustic Surface Waves in Outdoor Sound Propagation," *J. Acoust. Soc. Am.*, Vol. 113, No. 5, 2003, pp. 2495–2500.
18. K. M. Li, T. F. Waters-Fuller, and K. Attenborough, "Sound Propagation from a Point Source over Extended-Reaction Ground," *J. Acoust. Soc. Am.*, Vol. 104, 1998, pp. 679–685.
19. J. Nicolas, J. L. Berry, and G. A. Daigle, "Propagation of Sound above a Finite Layer of Snow," *J. Acoust. Soc. Am.*, Vol. 77, 1985, pp. 67–73.
20. J. F. Allard, G. Jansens, and W. Lauriks, "Reflection of Spherical Waves by a Nonlocally Reacting Porous Medium," *Wave Motion*, Vol. 36, 2002, pp. 143–155.
21. M. E. Delany and E. N. Bazley, "Acoustical Properties of Fibrous Absorbent Materials," *Appl. Acoust.*, Vol. 3, 1970, pp. 105–116.
22. K. B. Rasmussen, "Sound Propagation over Grass Covered Ground," *J. Sound Vib.*, Vol. 78 No. 25, 1981, pp. 247–255.
23. K. Attenborough, "Ground Parameter Information for Propagation Modeling," *J. Acoust. Soc. Am.*, Vol. 92, 1992, pp. 418–427. See also R. Raspet and K. Attenborough, "Erratum: Ground Parameter Information for Propagation Modeling," *J. Acoust. Soc. Am.*, Vol. 92, 1992, p. 3007.
24. R. Raspet and J. M. Sabatier, "The Surface Impedance of Grounds with Exponential Porosity Profiles," *J. Acoust. Soc. Am.*, Vol. 99, 1996, pp. 147–152.
25. K. Attenborough, "Models for the Acoustical Properties of Air-Saturated Granular Materials," *Acta Acust.*, Vol. 1, 1993, pp. 213–226.
26. J. F. Allard, *Propagation of Sound in Porous Media: Modelling Sound Absorbing Material*, Elsevier Applied Science, New York, 1993.
27. D. L. Johnson, T. J. Plona, and R. Dashen, "Theory of Dynamic Permeability and Tortuosity in Fluid-Saturated

- Porous Media," *J. Fluid Mech.*, Vol. 176, 1987, pp. 379–401.
28. O. Umnova, K. Attenborough, and K. M. Li, "Cell Model Calculations of Dynamic Drag Parameters in Packings of Spheres," *J. Acoust. Soc. Am.*, Vol. 107, No. 6, 2000, pp. 3113–3119.
  29. T. Yamamoto and A. Turgut, "Acoustic Wave Propagation through Porous Media with Arbitrary Pore Size Distributions," *J. Acoust. Soc. Am.*, Vol. 83, 1988, pp. 1744–1751.
  30. K. V. Horoshenkov, K. Attenborough, and S. N. Chandler-Wilde, "Padé Approximants for the Acoustical Properties of Rigid Frame Porous Media with Pore Size Distribution," *J. Acoust. Soc. Am.*, Vol. 104, 1998, pp. 1198–1209.
  31. ANSI S1 1999, Template Method for Ground Impedance, Acoustical Society of America, New York.
  32. S. Taherzadeh and K. Attenborough, "Deduction of Ground Impedance from Measurements of Excess Attenuation Spectra," *J. Acoust. Soc. Am.*, Vol. 105, 1999, pp. 2039–2042.
  33. K. Attenborough and T. Waters-Fuller, "Effective Impedance of Rough Porous Ground Surfaces," *J. Acoust. Soc. Am.*, Vol. 108, 2000, pp. 949–956.
  34. P. M. Boulanger, K. Attenborough, S. Taherzadeh, T. F. Waters-Fuller, and K. M. Li, "Ground Effect over Hard Rough Surfaces," *J. Acoust. Soc. Am.*, Vol. 104, 1998, pp. 1474–1482.
  35. K. Attenborough and S. Taherzadeh, "Propagation from a Point Source over a Rough Finite Impedance Boundary," *J. Acoust. Soc. Am.*, Vol. 98, 1995, pp. 1717–1722.
  36. K. Attenborough, unpublished report D3 for EC FP5 SOBER.
  37. D. E. Aylor, "Noise Reduction by Vegetation and Ground," *J. Acoust. Soc. Am.*, Vol. 51, 1972, pp. 197–205.
  38. K. Attenborough, T. F. Waters-Fuller, K. M. Li, and J. A. Lines, "Acoustical Properties of Farmland," *J. Agric. Engng. Res.*, Vol. 76, 2000, pp. 183–195.
  39. P. H. Parkin and W. E. Scholes, "The Horizontal Propagation of Sound from a Jet Close to the Ground at Radlett," *J. Sound Vib.*, Vol. 1, 1965, pp. 1–13.
  40. P. H. Parkin and W. E. Scholes, "The Horizontal Propagation of Sound from a jet Close to the Ground at Hatfield," *J. Sound Vib.*, Vol. 2, 1965, pp. 353–374.
  41. O. Zaporozhets, V. Tokarev, and K. Attenborough, "Predicting Noise from Aircraft Operated on the Ground," *Appl. Acoust.*, Vol. 64, 2003, pp. 941–953.
  42. G. A. Parry, J. R. Pyke, and C. Robinson, "The Excess Attenuation of Environmental Noise Sources through Densely Planted Forest," *Proc. IOA*, Vol. 15, 1993, pp. 1057–1065.
  43. M. A. Price, K. Attenborough, and N. W. Heap, "Sound Attenuation through Trees: Measurements and Models," *J. Acoust. Soc. Am.*, Vol. 84, 1988, pp. 1836–1844.
  44. V. Zoubhoff, Y. Brunet, M. Berengier, and E. Sechet, *Proc. 6th International Symposium on Long Range Sound Propagation*, D. I. Havelock and M. Stinson (Eds.) NRCC, Ottawa, 1994, pp. 251–269.
  45. T. F. W. Embleton, "Tutorial on Sound Propagation Outdoors," *J. Acoust. Soc. Am.*, Vol. 100, 1996, pp. 31–48.
  46. L. C. Sutherland and G. A. Daigle, "Atmospheric Sound Propagation," in *Handbook of Acoustics*, M. J. Crocker (Ed.), Wiley, New York, 1998, pp. 305–329.
  47. S. F. Clifford and R. T. Lataitis, "Turbulence Effects on Acoustic Wave Propagation over a Smooth Surface," *J. Acoust. Soc. Am.*, Vol. 73, 1983, pp. 1545–1550.
  48. D. K. Wilson, On the Application of Turbulence Spectral/Correlation Models to Sound Propagation in the Atmosphere, Proc. 8th LRSPS, Penn State, 1988.
  49. G. A. Daigle, "Effects of Atmospheric Turbulence on the Interference of Sound Waves above a Finite Impedance Boundary," *J. Acoust. Soc. Am.*, Vol. 65, 1979, pp. 45–49.
  50. K. Attenborough, H. E. Bass, X. Di, R. Raspet, G. R. Becker, A. Güdesen, A. Chrestman, G. A. Daigle, A. L'Espérance, Y. Gabillet, K. E. Gilbert, Y. L. Li, M. J. White, P. Naz, J. M. Noble, and H. J. A. M. van Hoof, "Benchmark Cases for Outdoor Sound Propagation Models," *J. Acoust. Soc. Am.*, Vol. 97, 1995, pp. 173–191.
  51. E. M. Salomons, *Computational Atmospheric Acoustics*, Kluwer Academic, Dordrecht, The Netherlands, 2002.
  52. M. C. Bérangier, B. Gavreau, Ph. Blanc-Benon, and D. Juvé, "Outdoor Sound Propagation: A Short Review on Analytical and Numerical Approaches," *Acta Acustica*, Vol. 89, 2003, pp. 980–991.
  53. Directive of the European Parliament and of the Council Relating to the Assessment and Management of Noise, 2002/EC/49, Brussels, Belgium, 25 June 2002.
  54. HARMONOISE contract funded by the European Commission IST-2000-28419, <http://www.harmonoise.org>, 2000.
  55. J. Kragh and B. Plovsing, Nord2000. Comprehensive Outdoor Sound Propagation Model. Part I-II. DELTA Acoustics & Vibration Report, 1849–1851/00, 2000 (revised 31 December, 2001).

# CHAPTER 6

## SOUND RADIATION FROM STRUCTURES AND THEIR RESPONSE TO SOUND

Jean-Louis Guyader

Vibration and Acoustics Laboratory  
National Institute of Applied Sciences of Lyon  
Villeurbanne, France

### 1 INTRODUCTION

Sound radiation from structures and their response to sound can be seen as the interaction of two subsystems: the structure and the acoustic medium, both being excited by sources, mechanical for the structure and acoustical in the fluid<sup>1-4</sup>. The interaction is generally separated into two parts: (1) the radiation describing the transmission from the structure to the acoustic medium and (2) the fluid loading that takes into account the effect of the fluid on the structure. The resolution of the problem in general is difficult, and it is preferable, in order to predict and understand the underlying phenomena, to study separately 1) acoustic radiation from structures and 2) structural excitation by sound. Even with the separation into two problems, simple explanations of the phenomena are difficult to make, and for the sake of simplicity the case of plane structures is used as a reference.

#### 1.1 Chapter Contents

The chapter begins with an explanation of radiation from simple sources, monopoles and dipoles, and a discussion on indicators like radiation factors used in more complicated cases. The generalization to multipolar sources is then presented which leads to the concept of equivalent sources to predict radiation from structures. In Section 2 wave analysis of radiation from planar sources is presented and this permits the separation of structural waves into radiating and nonradiating components; this approach explains why the reduction of vibration does not introduce in general an equivalent decrease of noise radiated.

The integral equation to predict radiation from structures is presented in Section 3. The application to finite, baffled plates is described using modal expansion for the plate response. For modal frequencies below the critical frequency, the radiation is poor because of acoustical short circuiting. Physically, only the edges or corners of the plate are responsible for noise emission. Finally the excitation of structures by sound waves is studied. The presence of acoustic media produces added mass and additional damping on structures. For heavy fluids, the effect is considerable. With light fluids only slight modifications of modal mass and modal damping are observed.

The plate excitation by propagating acoustic waves depends on the acoustic and mechanical wavelengths; for infinite plates the phenomenon of coincidence is described, which appears also in finite plates when resonant modes with maximum joint acceptance are excited.

### 2 ELEMENTARY SOURCES OF SOUND RADIATION

Acoustic fields associated with elementary sources are of great interest 1) because they characterize some basic behaviors of radiating bodies; for example, one can introduce easily the concepts of radiation efficiency and directivity, and 2) because they can be used to express the radiation of complicated objects. The method to predict the radiated pressure of vibrating surfaces with multipole decomposition (or equivalent source decomposition) is briefly presented here. A second method that constitutes the standard calculation of the radiated field is the integral representation of the pressure field. In this method two elementary sources are of basic importance: the monopole and the dipole. This importance is due to the possibility of representing all acoustic sources associated with structural vibration by a layer of monopoles and a layer of dipoles. This approach is presented in Section 3.

#### 2.1 Sound Radiated by a Pulsating Sphere: Monopole

The sound radiated by a pulsating sphere of radius  $a$ , centered at point  $M_0$ , and having a radial surface velocity  $V$  is a spherical wave having the well-known expression :

$$p(M, M_0) = V \rho_0 c \frac{jka^2}{1 + jka} \exp(jka) \frac{\exp(-jkr)}{r} \quad (1)$$

where  $r = |MM_0|$  is the distance between points  $M$  and  $M_0$ ,  $c$  is the speed of sound, and  $\rho_0$  is the mass density of the acoustic medium. The expression for the sound pressure radiated is only valid outside the sphere, namely when  $r > a$ .

The acoustic radiation can be characterized through energy quantities, in particular the sound power radiated and the radiation factor.

The radial velocity  $V_r$  and radial sound intensity  $I_r$  of the spherical wave are, respectively,

$$V_r = V \frac{ka^2}{1 + jka} \frac{1 + jkr}{kr^2} \exp(jka) \exp(-jkr) \quad (2)$$

$$I_r = V^2 \frac{k^2 a^2}{1 + k^2 a^2} \frac{a^2}{r^2} \rho_0 c \quad (3)$$

The acoustic field radiated by a pulsating sphere is nondirectional. This is, of course, due to the spherical symmetry of the source. The radiated power  $\Pi_{\text{rad}}$  can be calculated on the sphere's surface or on a sphere at a distance  $r$ , the result being the same and given by

$$\Pi_{\text{rad}} = 4\pi V^2 \frac{k^2 a^2}{1 + k^2 a^2} a^2 \rho_0 c \quad (4)$$

An important parameter to describe the radiation from the vibrating object is the radiation factor  $\sigma$ . It is defined as the ratio of the sound power radiated to the square of the velocity of the source times the acoustic impedance  $\rho_0 c$ . It is nondimensional and indicates the radiation efficiency of the vibration field. In the present case one has

$$\sigma = \frac{k^2 a^2}{1 + k^2 a^2} \quad (5)$$

The radiation efficiency of a pulsating sphere depends on the nondimensional frequency  $ka$ . For small values of  $ka$ , the efficiency is low and tends to unity when  $ka$  increases. This means also that, at a given frequency, a large sphere is a better radiator than a small one. This tendency is true in general; a small object is not an efficient radiator of noise at low frequency.

The monopole is the limiting case of a pulsating sphere when its radius tends to zero; however, to have a nonzero pressure field, the amplitude of the sphere's vibration velocity must increase as the inverse of the radius squared. Thus, it tends to infinity when  $r \rightarrow 0$ . A major conclusion is that a monopole is an ideal model and not a real physical source because it is not defined mathematically when  $r = 0$ .

The sound pressure field radiated by a monopole has the form given by Eq. (1) but is characterized by its strength  $S$ :

$$p(M, M_0) = S \frac{\exp(-jkr)}{r} = S 4\pi g(M, M_0) \quad (6)$$

where

$$g(M, M_0) = \frac{\exp(-jkr)}{4\pi r}$$

is called the Green's function for a free field. (It is the basic tool for integral representation of radiated sound pressure fields (see Section 4).)

## 2.2 Sound Radiated by Two Pulsating Spheres in Opposite Phase, Dipole

A second elementary source consists of two equal out-of-phase pulsating spheres separated by a distance  $2d$ .

Because the problem is linear, the total sound pressure radiated is the sum of that radiated independently by each pulsating sphere:

$$p(M, M_0) = V \rho_0 c \frac{jka^2}{1 + jka} \exp(jka) \times \left[ \frac{\exp(-jkr_1)}{r_1} - \frac{\exp(-jkr_2)}{r_2} \right] \quad (7)$$

where  $M_1$  and  $M_2$  are the centers of the two spheres;  $r_1 = |MM_1|$  and  $r_2 = |MM_2|$  are the distances from those centers to point  $M$ , and  $M_0$  is the point located at middistance from the centers of the two spheres.

The dipole is the limiting case of this physical problem. One first assumes that the pulsating spheres are monopoles of opposite strength of the form  $S = D/2d$ . The sound pressure is thus given by

$$p(M, M_0) = D \left\{ \left[ \frac{\exp(-jkr_1)}{r_1} - \frac{\exp(-jkr_2)}{r_2} \right] / 2d \right\} \quad (8)$$

The dipole is the limiting case when the distance  $d$  tends to zero, that is, by using the definition of the derivative in the direction  $\overrightarrow{M_1 M_2}$ :

$$\begin{aligned} p(M, M_0) &= D 4\pi \frac{\partial g(M, M_0)}{\partial d} \\ &= D \left\{ \frac{\partial}{\partial x} \left[ \frac{\exp(-jkr)}{r} \right] d_x \right. \\ &\quad + \frac{\partial}{\partial y} \left[ \frac{\exp(-jkr)}{r} \right] d_y \\ &\quad \left. + \frac{\partial}{\partial z} \left[ \frac{\exp(-jkr)}{r} \right] d_z \right\} \quad (9) \end{aligned}$$

where  $(d_x, d_y, d_z)$  are the components of the unit vector of direction  $\overrightarrow{M_1 M_2}$ , which indicates the axis of the dipole. The dipole source strength is  $D$ .

The dipole is a theoretical model only and not a real physical source because it consists of two monopoles.

An elementary calculation leads to another expression for the sound pressure radiated by a dipole:

$$\begin{aligned} p(M, M_0) &= D \frac{\partial}{\partial r} \left[ \frac{\exp(-jkr)}{r} \right] \\ &\quad \times \left( \frac{\partial r}{\partial x} d_x + \frac{\partial r}{\partial y} d_y + \frac{\partial r}{\partial z} d_z \right) \quad (10) \end{aligned}$$

The sound pressure field has now a strong directivity. In particular, in the plane normal to the axis of the dipole the radiated pressure is zero and in the direction of the axis the pressure is maximum.

### 2.3 Multipoles

Let us consider the pressure field of a monopole. It satisfies the homogeneous Helmholtz equation in the entire space, except at the source point:

$$\Delta g(M, M_0) + k^2 g(M, M_0) = 0 \quad \text{for all points } M \neq M_0 \quad (11)$$

where  $\Delta$  is the Laplacian operator.

One can derive this equation and obtain the following result:

$$\frac{\partial^{n+m+q}}{\partial x^n \partial y^m \partial z^q} [\Delta g(M, M_0) + k^2 g(M, M_0)] = 0 \quad \text{for all points } M \neq M_0 \quad (12)$$

Because the order of derivation is not important, this equation can also be written as

$$\Delta g_{nmq}(M, M_0) + k^2 g_{nmq}(M, M_0) = 0 \quad \text{for all points } M \neq M_0 \quad (13)$$

where

$$g_{nmq}(M, M_0) = \frac{\partial^{n+m+q}}{\partial x^n \partial y^m \partial z^q} g(M, M_0) \quad \text{for all points } M \neq M_0 \quad (14)$$

All the functions  $g_{nmq}(M, M_0)$ , are solutions of the homogeneous Helmholtz equation, except at the source point  $M_0$ . They constitute a set of elementary solutions that can be used to represent radiated sound fields. If  $n = m = q = 0$ , the corresponding solution is a monopole. The first derivative corresponds to dipole pressure fields; for example,  $n = 1, m = q = 0$ , is the pressure field created by a dipole of axis  $x$ , the two others by dipoles of axis  $y$  and  $z$  (the dipole described in Section 1.2 is a linear combination of these three elementary dipoles). The second derivatives are characteristic of quadrupoles and higher derivatives of multipole pressure fields characterized by more and more complicated directivity patterns.

### 2.4 Equivalent Source Decomposition Technique

The functions  $g_{nmq}(M, M_0)$  constitute an infinite number of independent pressure field solutions of the Helmholtz equation in whole space, except at the point source  $M_0$  and verify the Sommerfeld conditions at an infinite distance from the source point. This set of functions can be used to express the sound radiated by vibrating objects. This is commonly called the *equivalent sources decomposition* technique. Let us consider a closed vibrating surface and study the sound pressure radiated into the surrounding external acoustic medium.

The solution is calculated as the linear combination of multipole contributions:

$$p(M) = \sum_{n=0}^{\infty} \sum_{m=0}^{\infty} \sum_{q=0}^{\infty} A_{nmq} g_{nmq}(M, M_0) \quad (15)$$

where  $M_0$  is located inside the vibrating surface and the coefficients  $A_{nmq}$  of the expansion must be adjusted in order to agree with the normal velocity of the vibrating surface.

Equation (15) satisfies the Helmholtz equation and the radiation conditions at infinity because it is the sum of functions verifying these conditions. To be the solution of the problem, it has also to verify the velocity continuity on the vibrating surface:

$$\frac{-1}{j\omega\rho} \frac{\partial p}{\partial n}(Q) = V_n(Q) \quad (16)$$

where  $\partial p / \partial n$  is the normal derivative and  $V_n(Q)$  is the normal velocity of the point  $Q$  of the vibrating surface.

Substituting Eq. (15) into Eq. (16) one obtains

$$\sum_{n=0}^{\infty} \sum_{m=0}^{\infty} \sum_{q=0}^{\infty} A_{nmq} \frac{\partial g_{nmq}}{\partial n}(Q, M_0) = -j\omega\rho V_n(Q) \quad (17)$$

Numerically, only a finite number of functions can be considered in the evaluation of Eq. (17), and, thus, a finite number of equations is necessary to calculate the unknown amplitudes  $A_{nmq}$ . The simplest possibility is to verify Eq. (17) at a number of points on the surface equal to the number of terms of the expansion:

$$\sum_{n=0}^N \sum_{m=0}^M \sum_{q=0}^Q A_{nmq} \frac{\partial g_{nmq}}{\partial n}(Q_i, M_0) = -j\omega\rho V_n(Q_i) \quad \text{for } i = 0, 1, 2, \dots, N + M + Q \quad (18)$$

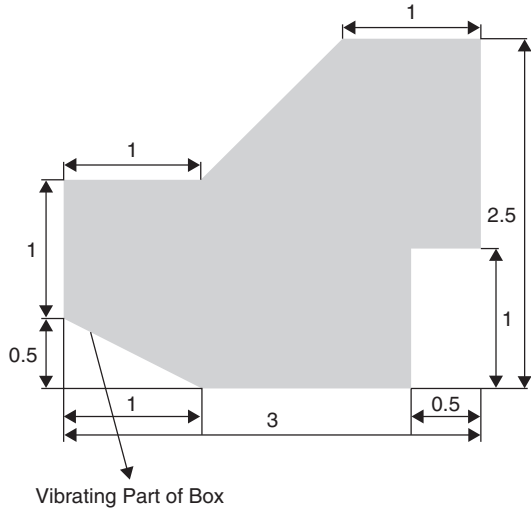
This is a linear system that can be solved to obtain the unknown term  $A_{nmq}$ . Introducing the corresponding values in Eq. (15) allows one to calculate the radiated sound pressure field.

The equivalent source technique has been applied in several studies<sup>5-12</sup> in the form presented or in other forms. Among different possibilities one can use several monopoles placed at different locations inside the vibrating surface instead of multipoles located at one point source. A second possibility is to adapt the sources to a particular geometry, for example, cylindrical harmonics to predict radiation from cylinders.

As an example the following two-dimensional case is presented (see Fig. 1). The calculations were made by Pavic.<sup>12</sup> For low wavenumbers the reconstructed velocity field shows some small discrepancies at the corners, particularly when they are close to the vibrating part of the box. (See Fig 2.)

### 3 WAVE APPROACH

The analysis presented in this section treats a particular case that is quite different from real structures. However, it is a fruitful approach because basic radiation phenomenon can be demonstrated analytically. In particular, the fundamental notion of radiating and nonradiating structural vibration waves presented here is essential for a good understanding of sound radiation phenomena.



**Figure 1** Box-type structure geometry (dimensions in metres).

### 3.1 Radiation from a Traveling Wave on an Infinite Vibrating Plane

Let us consider an infinite plane where a propagating wave is traveling, creating a velocity field in the

$z$  direction, of the form

$$V_z(x, y) = A \exp(j\lambda x + j\mu y) \quad (19)$$

where  $V_z(x, y)$  is the velocity in the  $z$  direction (normal to the plane),  $A$  is the amplitude of the velocity, and  $\lambda, \mu$  are the wavenumbers in the  $x$  and  $y$  directions. A physical illustration of the problem is the velocity field produced by a plate in bending vibration, located in the plane  $z = 0$ .

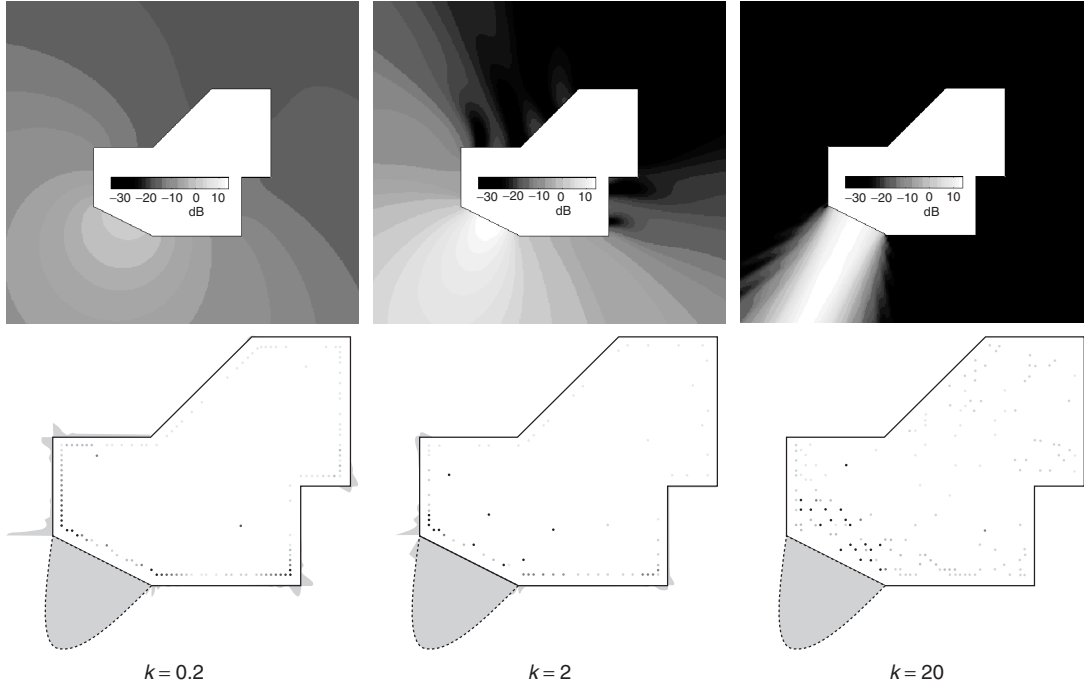
Let us study the sound pressure created by this source, in the infinite medium located in the half space  $z > 0$ . The sound pressure  $p(x, y, z)$  must satisfy the Helmholtz equation in the half space [Eq. (20)] and the continuity of acoustic velocity in the  $z$  direction and the velocity field (1) [Eq. (21)]:

$$\Delta p + k^2 p = 0 \quad (20)$$

where  $k = \omega/c$  is the acoustic wave number,  $\omega$  is the angular frequency, and  $c$  is the speed of sound.

$$V_z(x, y) = \frac{j}{\omega \rho_0} \frac{\partial p}{\partial z}(x, y, 0) \quad (21)$$

where  $\rho_0$  is the fluid density.



**Figure 2** Calculated radiated sound pressure at three wavenumbers (top) and reconstructed velocity field on the boundary (bottom). High-pressure level corresponds to white and low to black. The equivalent source positions are indicated by points inside the box, their strengths are indicated by the darkness. (From Pavic.<sup>12</sup>)

The velocity continuity over the plane implies a sound pressure field having the same form in the  $x$  and  $y$  directions as the propagating wave Eq. (19):

$$p(x, y, z) = F(z) \exp(j\lambda x + j\mu y) \quad (22)$$

Using Eqs. (20)–(22), one can obtain the following equations for  $F(z)$ :

$$\frac{d^2 F}{dz^2}(z) + (k^2 - \lambda^2 - \mu^2)F(z) = 0 \quad (23)$$

$$\frac{dF}{dz}(0) = -j\omega\rho_0 A \quad (24)$$

The solution of Eqs. (23) and (24) has two different forms depending on the frequency. Let us first define the cutoff frequency  $\omega_{co}$ :

$$\omega_{co} = c\sqrt{\lambda^2 + \mu^2} \quad (25)$$

If  $\omega > \omega_{co}$ , the solution is

$$F(z) = -\frac{\omega\rho_0}{k_z} A \exp(-jk_z z) \quad (26)$$

$$\text{and} \quad k_z = \sqrt{k^2 - \lambda^2 - \mu^2} \quad (27)$$

The sound pressure in the acoustic medium can be obtained from Eq. (22):

$$p(x, y, z) = -\frac{\omega\rho_0}{k_z} A \exp(j\lambda x + j\mu y - jk_z z) \quad (28)$$

If  $\omega < \omega_{co}$ , the solution is

$$F(z) = j\frac{\omega\rho_0}{\gamma_z} A \exp(-\gamma_z z) \quad (29)$$

$$\text{and} \quad \gamma_z = \sqrt{-k^2 + \lambda^2 + \mu^2} \quad (30)$$

The sound pressure is given by

$$p(x, y, z) = j\frac{\omega\rho_0}{\gamma_z} A \exp(j\lambda x + j\mu y - \gamma_z z) \quad (31)$$

Equation (28) indicates that the sound pressure wave propagates in the  $z$  direction, while the solution given by Eq. (31) diminishes with the distance from the plane. This is of major importance and indicates that a vibration wave propagating on a plane can produce two types of acoustic phenomena, which depend on frequency. In the first case noise is emitted far from the plate as opposed to the second case where the sound pressure amplitude decreases exponentially with the distance from the plane. This basic result is of great importance for understanding radiation phenomena.

### 3.2 Radiating and Nonradiating Waves

A transverse vibration wave traveling on a plane can produce two types of acoustic waves, commonly called radiating waves and nonradiating waves for reasons explained in this section.

**3.2.1 Radiating Waves** The sound pressure is of the type given in Eq. (28). It is a wave propagating in directions  $x$ ,  $y$ , and  $z$ . The dependence of the wavenumbers  $\lambda$ ,  $\mu$  and  $k_z$  on the angles  $\theta$  and  $\varphi$  can be written as

$$\begin{aligned} \lambda &= k \sin(\varphi) \sin(\theta) \\ \mu &= k \cos(\varphi) \sin(\theta) \\ k_z &= k \cos(\theta) \end{aligned} \quad (32)$$

where  $\varphi = \arctan(\lambda/\mu)$  and  $\theta = \arccos(\sqrt{1 - \omega_{co}^2/\omega^2})$ .

When  $\theta = 0$ , the sound wave is normal to the plane; when  $\theta = \pi/2$ , it is grazing. Using the expression for  $\theta$  versus frequency, one can see that just above the cutoff frequency,  $\theta = \pi/2$  ( $k_z = 0$ ) and the radiated wave is grazing, then the propagation angle  $\theta$  decreases with frequency and finally reaches 0 at high frequency, meaning that the sound wave tends to be normal to the plane. Directivity gives a first description of the radiation phenomenon. A second one characterizing energetically the noise emitted is also of interest. The intensity propagated by a sound wave given in Eq. (33) is the basic quantity. However, in order to have a nondimensional quantity, the radiation factor  $\sigma$  given in Eq. (34) is generally preferred to indicate radiation strength. Due to the infinite nature of the vibrating surface, the radiation factor is calculated for a unit area; the ratio of the sound power radiated and the square of the velocity of a unit area times the acoustic impedance  $\rho_0 c$ , reduces to the ratio of the sound intensity component in the  $z$  direction and the square of the modulus of the vibration wave velocity amplitude. It indicates the efficiency of the vibration field to radiate noise far from the vibrating object:

$$\mathbf{I} = \begin{Bmatrix} I_x \\ I_y \\ I_z \end{Bmatrix} = \frac{1}{2} |A|^2 \frac{\omega\rho_0}{k_z^2} \begin{Bmatrix} -\lambda \\ -\mu \\ k_z \end{Bmatrix} \quad (33)$$

$$\sigma = \frac{I_z}{\rho_0 c |A|^2} \quad (34)$$

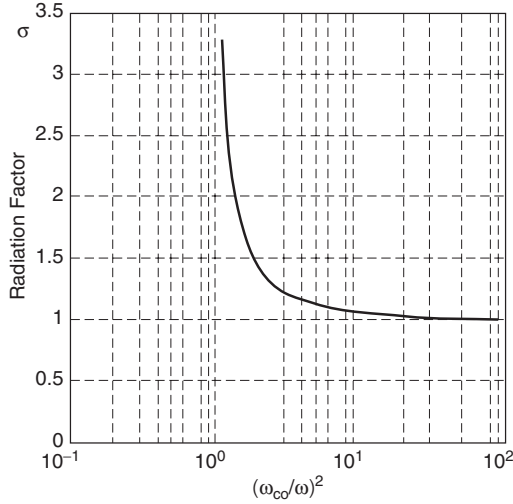
The sound intensity vector shows that the sound wave follows the propagation of the vibration wave in the  $(x, y)$  directions but also propagates energy in the  $z$  direction.

After calculation, the radiation factor can be expressed simply as

$$\sigma = \frac{1}{\sqrt{1 - \omega_{co}^2/\omega^2}} \quad (35)$$

Figure 3 presents the radiation factor versus frequency. Just above the cutoff frequency it tends to infinity;





**Figure 3** Radiation factor  $\sigma$  versus frequency ratio  $(\omega_{c0}/\omega)^2$ .

then it decreases and tends to unity at high frequency. Of course, an infinite radiation factor is not realistic. Since fluid loading has not been considered in this standard analysis, the vibration wave amplitude is not affected by the sound pressure created. In reality, just above the cutoff frequency the radiated pressure tends to be infinite and blocks the vibration of the plane. Consequently, when the radiation efficiency tends to infinity, the wave amplitude tends to zero and the radiated sound pressure remains finite.

It is interesting to notice the relation between the angle of the radiated wave and the radiation efficiency:

$$\theta = \arccos\left(\frac{1}{\sigma}\right) \quad (36)$$

So, for high values of the radiation factor, grazing waves are radiated, and for values close to unity the radiation is normal to the plane. This tendency is quite general and remains true in more complicated cases like finite plates.

**3.2.2 Nonradiating Waves** Nonradiating waves are also called evanescent waves in the literature. The pressure is of the form given in Eq. (31) that corresponds to frequencies below the cutoff frequency. The intensity vector of the sound wave can be calculated easily:

$$\mathbf{I} = \begin{Bmatrix} I_x \\ I_y \\ I_z \end{Bmatrix} = \frac{1}{2} |A|^2 \frac{\omega \rho_0}{\gamma_z^2} \exp(-2\gamma_z z) \begin{Bmatrix} -\lambda \\ -\mu \\ 0 \end{Bmatrix} \quad (37)$$

The sound wave generated is different from those observed in the radiating wave case. Sound intensity still propagates along the plane but no longer in the  $z$  direction. Having the intensity component in the  $z$  direction equal to zero does not mean an absolute

silence exists in the fluid medium but that the pressure amplitude decreases exponentially with distance from the plane. To hear the acoustic effect of the vibration wave, one has to listen in the vicinity of the plane.

Obviously, the radiation factor is equal to zero, and no directivity of the sound field can be defined because of the vanishing nature of the radiated wave.

### 3.3 Radiation from a Baffled Plane Vibration Field

**3.3.1 Plane Wave Decomposition of a Vibration Field** The previous results can be extended to finite vibrating plane surfaces very easily. Let us consider a vibration field on an infinite plane of the form:

$$V_z(x, y) = \begin{cases} 0 & \text{if } (x, y) \notin S \\ V_p(x, y) & \text{if } (x, y) \in S \end{cases} \quad (38)$$

where  $V_p(x, y)$  is the transverse velocity of surface  $S$ .

The following analysis is based on the two-dimensional space Fourier transform of the vibration field (38):

$$\tilde{V}_z(\lambda, \mu) = \iint_S \exp[-j(\lambda x + \mu y)] V_p(x, y) dx dy \quad (39)$$

Because the transverse velocity is zero except on the surface  $S$ , the integral over the infinite plane reduces to the integral over the surface  $S$ .

Calculating the inverse transform gives the velocity vibration field on the whole plane:

$$V_z(x, y) = \int_{-\infty}^{+\infty} \int_{-\infty}^{+\infty} \frac{\tilde{V}_z(\lambda, \mu)}{4\pi^2} \times \exp[j(\lambda x + \mu y)] d\lambda d\mu \quad (40)$$

This expression demonstrates that each vibration field defined on the surface  $S$  can be decomposed in an infinite number of propagating waves having the same form used in Eq. (19), where  $A = \tilde{V}_z(\lambda, \mu)/4\pi^2$ .

**3.3.2 Sound Pressure Radiated** Because the problem is linear, the sound pressure radiated by a group of waves traveling on the plane is the sum of the pressures radiated by each wave separately. Section 4 demonstrates that two types of waves exist which depend on frequency: radiating waves and nonradiating waves. Thus, the radiated sound pressure can be calculated by separating the vibration waves into two groups:  $p_R(x, y, z)$ , the pressure due to radiating waves, and  $p_{NR}(x, y, z)$ , the pressure due to nonradiating waves. Then, the total sound pressure radiated is the sum of the two terms:

$$p(x, y, z) = p_R(x, y, z) + p_{NR}(x, y, z) \quad (41)$$

where

$$p_{NR}(x, y, z) = \iint_{\sqrt{\lambda^2 + \mu^2} > \omega/c} \frac{j\omega\rho_0}{\sqrt{\lambda^2 + \mu^2 - (\omega/c)^2}} \times \frac{\tilde{V}_z(\lambda, \mu)}{4\pi^2} \exp[j\lambda x + j\mu y - \sqrt{\lambda^2 + \mu^2 - (\omega/c)^2} z] d\lambda d\mu \quad (42)$$

$$p_R(x, y, z) = \iint_{\sqrt{\lambda^2 + \mu^2} < \omega/c} \frac{\omega\rho_0}{\sqrt{(\omega/c)^2 - \lambda^2 - \mu^2}} \times \frac{\tilde{V}_z(\lambda, \mu)}{4\pi^2} \exp[j\lambda x + j\mu y - j\sqrt{(\omega/c)^2 - \lambda^2 - \mu^2} z] \times d\lambda d\mu \quad (43)$$

Several interesting points can be understood from Eqs. (42) and (43):

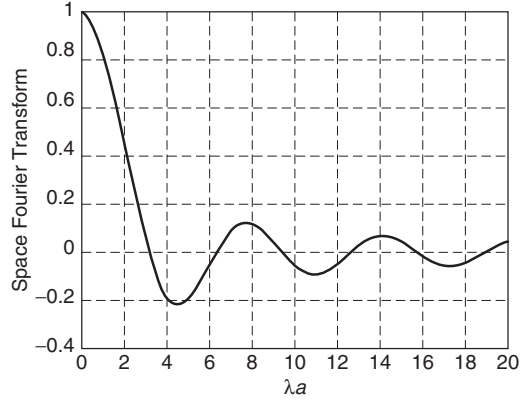
1. The pressure due to the radiating waves is easier to calculate than the one due to nonradiating waves because the integration domain is finite in Eq. (43) and infinite in Eq. (42).
2. If one is interested in the sound pressure in the far field of the radiating surface, the part due to nonradiating waves can be neglected because of its exponential decay with  $z$ .
3. In the near field of the radiating surface both types of waves contribute to the pressure.
4. To reduce the sound power radiated by the vibration field one has to decrease the amplitude of the radiating wave. This explains why reducing the vibration level can have a very small effect on the radiated sound.

**3.3.3 Wave Decomposition of the Vibration Field of a Piston** Let us consider a rectangular piston of length  $2a$  and width  $2b$ . The vibration field of the baffled piston is given by Eq. (44):

$$V_z(x, y) = \begin{cases} 1 & \text{if } (x, y) \in [-a, +a] \times [-b, +b] \\ 0 & \text{if } (x, y) \notin [-a, +a] \times [-b, +b] \end{cases} \quad (44)$$

A simple calculation gives the two-dimensional space Fourier transform:

$$\tilde{V}_z(\lambda, \mu) = 4 \frac{\sin(\lambda a)}{\lambda} \frac{\sin(\mu b)}{\mu} \quad (45)$$



**Figure 4** Space Fourier transform  $\left[\tilde{V}_z(\lambda, 0)/4ab = \sin(\lambda a)/\lambda a\right]$  of the rectangular piston vibration field versus  $\lambda a$ .

Figure 4 presents the variation with  $\lambda a$  of the function

$$\frac{\tilde{V}_z(\lambda, 0)}{4ab} = \frac{\sin(\lambda a)}{\lambda a}$$

It can be concluded that the waves of greatest amplitude are those with low values of  $\lambda a$ . Of course, the same tendency applies for  $\tilde{V}_z(0, \mu)/4ab$ , and it can be concluded that waves dominating the piston motion are those with small values of  $\lambda a$  and  $\mu b$ .

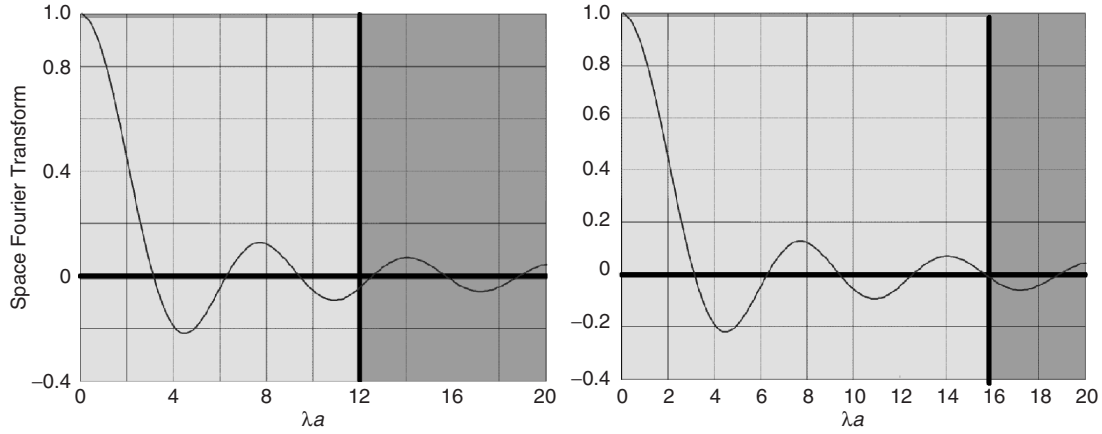
Substituting Eq. (45) into Eqs. (42) and (43) and calculating the integral leads to the sound pressure field radiated by the rectangular piston. However, our goal here is not to carry out this calculation but to use wave decomposition to understand the phenomenon.

The radiating waves are frequency dependent and have wavenumbers located in a circle given by

$$\lambda^2 + \mu^2 < (\omega/c)^2 \quad (46)$$

This circle decomposes the wavenumber plane into two domains: inside the circle are located wavenumber components of radiating waves, and outside are located those of nonradiating waves. All wavenumber components participate in the vibration field, but only the radiating wave components contribute to sound power radiation. One can conclude that the proportion of radiating waves is a good indicator of the radiation efficiency of the piston.

At low frequency the radius of the circle is small and the proportion of radiating waves is small compared to that of nonradiating waves. As a consequence, the radiation efficiency is much less than one. When the frequency increases the radius of the circle does the same, and more and more wavenumber components become radiating, leading to a greater radiation efficiency of the piston. Finally due to the decrease of wave amplitude with wavenumber [see Eq. (45)], at a sufficiently high frequency all nonradiating components



**Figure 5** Radiating (light grey) and nonradiating (dark grey) wavenumber components of the piston vibration field. The left figure shows a lower frequency than the right figure.

have very low amplitudes and do not contribute significantly to the vibration field and sound radiation. This means that all wave components which participate significantly in the vibration field radiate noise and the radiation factor tends toward unity. This point is illustrated in Fig. 5, however, for the sake of simplicity, only the one-dimensional representation is presented. The radiating components are located in the light grey wavenumber region and the nonradiating in the dark grey region; when the frequency increases the light grey part increases too.

The wave analysis of vibration fields described here for the rectangular piston can be extended directly to all planar baffled sources. It demonstrates quite simply a fundamental property of radiation phenomena. Reduction of vibration levels is not equivalent to reduction of radiated noise. If the decrease of vibration velocity is due to that of nonradiating wave components, the sound power radiated remains unchanged.

### 3.4 Sound Radiated by an Infinite Plate

Up to now the velocity of vibration waves was defined independently of the mechanical structure. Of course, in real cases one has to take into account the structure where the propagation takes place. Let us consider a thin plate; the equation of motion is

$$-\omega^2 MW(x, y) + D \left( \frac{\partial^4 W}{\partial x^4} + 2 \frac{\partial^4 W}{\partial x^2 \partial y^2} + \frac{\partial^4 W}{\partial y^4} \right) = 0 \quad (47)$$

where  $M$  is the mass per unit area of the plate,  $D$  is the bending stiffness, and  $W(x, y)$  is the transverse displacement.

If a propagating wave in Eq. (48) is traveling on the plate, it must satisfy the equation of motion Eq. (47). That is to say:

$$W(x, y) = B \exp(j\lambda x + j\mu y) \quad (48)$$

$$[-\omega^2 M + D(\lambda^2 + \mu^2)] B \times \exp(j\lambda x + j\mu y) = 0 \quad (49)$$

To be satisfied, Eq. (49) introduces a relation between  $\omega$  and  $(\lambda, \mu)$ :

$$\omega = \sqrt{\frac{D}{M}} (\lambda^2 + \mu^2) \quad (50)$$

When Eq. (50) is satisfied, the propagating wave corresponds to a natural bending wave in the plate. To fit with the calculation of the sound radiation from a velocity propagating wave made in Section 2, one can calculate the vibration velocity associated with the bending displacement, Eq. (48):

$$V_z(x, y) = j\omega B \exp(j\lambda x + j\mu y) \quad (51)$$

Calculations made in Section 2.3 can be used here by replacing the wave amplitude  $A$  by  $j\omega B$ ; however, the cutoff frequency limiting the frequency domain of radiating and nonradiating waves must take into account Eq. (50).

The cutoff frequency depends on wavenumbers  $\lambda$  and  $\mu$  through Eq. (25):

$$\omega_{co} = c\sqrt{\lambda^2 + \mu^2}$$

In addition at each frequency and in particular at the cutoff frequency,  $\omega_{co}$ , the wavenumbers  $(\lambda, \mu)$  must also satisfy Eq. (50):

$$\omega_{co} = \sqrt{\frac{D}{M}} (\lambda^2 + \mu^2)$$

Both relations can be verified simultaneously at only one frequency:

$$\omega_{co} = \omega_c = c^2 \sqrt{\frac{M}{D}}$$

where  $\omega_c$  is the critical frequency. This frequency depends on the plate characteristics and speed of sound. With standard expressions of mass per unit area of the plate and bending stiffness, the critical frequency can be written

$$\omega_c = c^2 \sqrt{\frac{\rho_p(1-\nu^2)12}{E}} \frac{1}{h} \quad (52)$$

where  $\rho_p$  is the mass per unit volume,  $E$  the Young's modulus,  $\nu$  the Poisson ratio, and  $h$  the thickness of the plate.

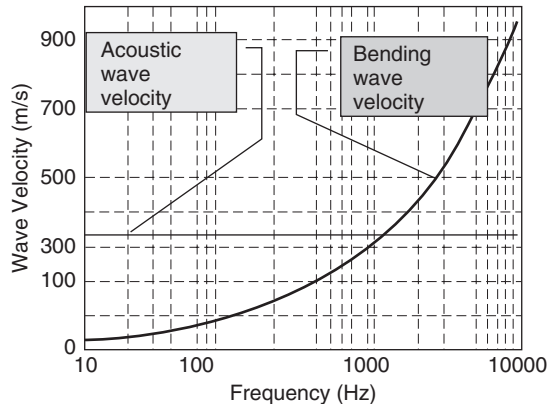
Thus, radiation from an infinite plate in bending motion is characterized by one cutoff frequency, called the critical frequency. For  $\omega < \omega_c$  the sound wave is of the form in Eq. (31), it is evanescent in the  $z$  direction and the vibration wave is nonradiating. For  $\omega > \omega_c$  the acoustic wave is of the form in Eq. (28); it is propagating in the  $z$  direction, and the vibration wave is radiating.

The radiation factor of an infinite plate has the form given in Fig. 4; below the critical frequency it is equal to zero, just above it tends to infinity and is asymptotic to one at high frequency. It is shown later that this trend is realistic to describe the sound radiation from finite plates.

To give a second explanation for the phenomenon, one can compare the velocity of bending waves  $c_B$  in the plate [Eq. (53)] and the speed of sound (see Fig. 6):

$$c_B = \sqrt{\omega} \sqrt[4]{\frac{D}{M}} \quad (53)$$

Let us consider a propagating acoustic wave generated by the vibration wave in the plate. Due to the continuity of plate and acoustic velocities, the projection of



**Figure 6** Acoustic and bending wave velocities versus frequency. The intersection of the two curves occurs at the critical frequency.

the acoustic wavelength on the plane of the plate must be equal to the bending wavelength:

$$\frac{c_B}{\omega} = \frac{c}{\omega} \sin(\theta) \Rightarrow \sin(\theta) = \frac{c}{c_B} \quad (54)$$

where  $\theta$  is the angle between the direction of propagation of the acoustic wave and the normal to the plane of the plate. From Eq. (54) it is easy to see that this angle only exists when  $c_B > c$ , that is, when bending waves are supersonic. For  $c_B < c$  (subsonic bending waves), the sound wave no longer propagates in the  $z$  direction.

Finally using Eq. (53) for the bending wave speed, one can conclude that below the critical frequency bending waves are subsonic while above they are supersonic. A parallel can be established between supersonic and radiating waves and also between subsonic and non-radiating waves.

#### 4 INTEGRAL EQUATION FOR NOISE RADIATION

In this section the main method used for the prediction of the sound pressure radiated by the vibrating object is presented. It is based on the concept of Green's function; that is, an elementary solution of the Helmholtz equation used to calculate the radiated sound field from the vibrating objects. The method is related to Huygens' principle where objects placed in an acoustic field appear as secondary sources.

##### 4.1 Kirchhoff Integral Equation

Let us consider the following acoustical problem. Acoustic sources  $S(M)$  are emitting noise in an infinite acoustic medium. An object is placed in this medium, which occupies the volume  $V$  inside the surface  $\bar{V}$ .

The sound pressure has to satisfy the following equations:

$$\Delta p(M) + k^2 p(M) = S(M) \quad (55)$$

where  $M$  is a point in the infinite space outside the object of surface  $\bar{V}$ .

At each point  $Q$  on the surface  $\bar{V}$  the acoustic normal velocity must be equal to that of the vibrating object  $v_n(Q)$  (in the following the outer normal to the fluid medium is considered):

$$v_n(Q) = \frac{j}{\omega \rho} \frac{\partial p}{\partial n}(Q) \quad (56)$$

where  $\partial/\partial n$  is the derivative of the sound pressure normal to the surface  $\bar{V}$  at point  $Q$ .

Let us also consider the following problem that characterizes the sound pressure field created by a point source located at  $M_0$ :

$$\Delta g(M, M_0) + k^2 g(M, M_0) = \delta(M - M_0) \quad (57)$$

where  $\delta(M - M_0)$  is the Dirac delta function.

This is the fundamental equation satisfied by the Green's function. It has also to satisfy the Sommerfeld condition at infinity;  $g(M, M_0)$  is named the Green's function in infinite space. It corresponds to the pressure field of a monopole of strength  $1/4\pi$  placed at point  $M_0$ .

$$g(M, M_0) = \frac{\exp(-jkr)}{4\pi r} \quad \text{where } r = |M - M_0| \quad (58)$$

Using the previous equations one can write

$$\begin{aligned} & \iiint_{R^3-V} [\Delta p(M) + k^2 p(M)] g(M, M_0) dM \\ &= \iiint_{R^3-V} S(M) g(M, M_0) dM \end{aligned} \quad (59)$$

Then transforming the integral of the left hand side of the equation by use of the Ostrogradsky formula, one obtains

$$\begin{aligned} & \iiint_{R^3-V} [\Delta g(M, M_0) + k^2 g(M, M_0)] p(M) dM \\ &= \iiint_{R^3-V} S(M) g(M, M_0) dM \\ & \quad - \iint_{\bar{V}} \frac{\partial p}{\partial n}(Q) g(Q, M_0) - \frac{\partial g}{\partial n}(Q, M_0) p(Q) dQ \end{aligned}$$

Finally taking into account the fundamental equation verified by the Green's function and the property of the Dirac delta function, the sound pressure at point  $M_0$  can be expressed as follows:

$$\begin{aligned} p(M_0) &= \iiint_{R^3-V} S(M) g(M, M_0) dM \\ & \quad - \iint_{\bar{V}} \frac{\partial p}{\partial n}(Q) g(Q, M_0) \\ & \quad - \frac{\partial g}{\partial n}(Q, M_0) p(Q) dQ \end{aligned} \quad (60)$$

This expression is known as the Kirchhoff integral equation. Two terms appear: the first is the direct field; the second is the diffracted the field. The direct field can be interpreted as the superposition of monopoles located at source points in the volume occupied by the fluid medium; the sound source amplitude being the monopole strength. The diffracted field is the superposition of monopoles of strength  $\partial p / \partial n(Q)$  and dipoles of strength  $p(Q)$  located on the surface of the object. The presence of the object in the sound field of the sound source

produces secondary sources of monopole and dipole types responsible for the diffraction of the sound.

To calculate the sound pressure at point  $M_0$  in the volume, it is necessary to know the boundary sound pressure and velocity on the surface  $\bar{V}$ . In our case the velocity is given, but the pressure is unknown. The general expression, Eq., (60) reduces to

$$\begin{aligned} p(M_0) &= \iiint_{R^3-V} S(M) g(M, M_0) dM \\ & \quad - \iint_{\bar{V}} -j\omega\rho v_n(Q) g(Q, M_0) \\ & \quad - \frac{\partial g}{\partial n}(Q, M_0) p(Q) dQ \end{aligned} \quad (61)$$

To determine the sound pressure at the boundary one can use the previous integral equation for point  $Q_0$  situated on the surface. However, in this case, due to the presence of the Dirac delta function on the boundary surface, the expression for the pressure is modified:

$$\begin{aligned} \frac{p(Q_0)}{2} &= \iiint_{R^3-V} S(M) g(M, Q_0) dM \\ & \quad - \iint_{\bar{V}} \frac{\partial p}{\partial n}(Q) g(Q, Q_0) \\ & \quad - \frac{\partial g}{\partial n}(Q, Q_0) p(Q) dQ \end{aligned} \quad (62)$$

or for a given normal velocity on the object:

$$\begin{aligned} \frac{p(Q_0)}{2} &= \iiint_{R^3-V} S(M) g(M, Q_0) dM \\ & \quad - \iint_{\bar{V}} -j\omega\rho v_n(Q) g(Q, Q_0) \\ & \quad - \frac{\partial g}{\partial n}(Q, Q_0) p(Q) dQ \end{aligned} \quad (63)$$

This equation is generally solved numerically by the collocation technique in order to obtain the boundary pressure, which is then used in Eq (61) to calculate the sound pressure in the fluid medium. The Kirchhoff integral equation presents a problem in the prediction of the radiated sound pressure, known as singular frequencies, where the calculation is not possible. The singular frequencies correspond to the resonance frequencies of the acoustic cavity having the volume  $V$  of the object responsible for diffraction. Different methods can be used to avoid the problem of singular frequency; some of them are described in the literature.<sup>32-36</sup>

The same approach can be used for internal cavity problems. The Kirchhoff integral equation has the form of Eqs. (64) and (65) for points, respectively, inside the cavity of volume  $V$  and on the boundary surface  $\bar{V}$ :

$$p(M_0) = \iiint_V S(M)g(M, M_0) dM - \iint_{\bar{V}} -j\omega\rho v_n(Q)g(Q, M_0) - \frac{\partial g}{\partial n}(Q, M_0)p(Q) dQ \quad (64)$$

$$\frac{p(Q_0)}{2} = \iiint_V S(M)g(M, Q_0) dM - \iint_{\bar{V}} -j\omega\rho v_n(Q)g(Q, Q_0) - \frac{\partial g}{\partial n}(Q, Q_0)p(Q) dQ \quad (65)$$

In this case, the problem of singular frequency is physically realistic and corresponds to resonances of the cavity.

#### 4.2 Rayleigh Integral Equation

Other Kirchhoff-type integral equations can be obtained using the modified Green's functions. For example, let us consider the Green's function  $g_0(M, M_0)$  that satisfies

$$\Delta g_0(M, M_0) + k^2 g_0(M, M_0) = \delta(M - M_0) \quad (66)$$

$$\text{and} \quad \frac{j}{\omega\rho} \frac{\partial g_0}{\partial n}(Q, M_0) = 0 \quad \forall Q \in \bar{V} \quad (67)$$

Using this new Green's function in Eq. (61) produces a modified integral equation:

$$p(M_0) = \iiint_V S(M)g_0(M, M_0) dM - \iint_{\bar{V}} -j\omega\rho v_n(Q)g_0(Q, M_0) dQ \quad (68)$$

This integral equation is much simpler than Eq. (61) because it is explicit, and the radiated sound pressure can be directly calculated without previous calculation of boundary unknowns. Several other integral equations derived from the basic Kirchhoff integral can be obtained by modification of the Green's function. One has to notice, as a general rule, that the simplification of the integral equation is balanced by the

difficulty of calculation of the modified Green's function. However, in one particular case, one can simplify the integral equation and keep a simple Green's function; it is the case of a planar radiator, which leads to the Rayleigh integral equation. In this case the Green's function is  $g_R(M, M_0)$ , and it satisfies Eqs. (69) and (70):

$$\Delta g_R(M, M_0) + k^2 g_R(M, M_0) = \delta(M - M_0) + \delta(M - M_0^{im}) \quad (69)$$

$$\text{and} \quad \frac{j}{\omega\rho} \frac{\partial g_R}{\partial n}(Q, M_0) = 0 \quad \forall Q \in \bar{V} \quad (70)$$

In this problem the surface  $\bar{V}$  is the plane  $z = 0$ , and the point  $M_0^{im}$  is the symmetrical point of  $M_0$  relative to the plane  $\bar{V}$ . The Green's function is thus the sound pressure created by a monopole placed at  $M_0$  and by its image source, which is a second monopole placed at point  $M_0^{im}$ . This Green's function is the superposition of both sound pressure fields:

$$g_R(M, M_0) = \frac{\exp(-jkr)}{4\pi r} + \frac{\exp(-jkr_{im})}{4\pi r_{im}} \quad \text{where } r = |M - M_0| \text{ and } r_{im} = |M - M_0^{im}| \quad (71)$$

The sound pressure field in the half space  $z > 0$  can be calculated with the following integral equation:

$$p(M_0) = \iiint_V S(M)g_R(M, M_0) dM - \iint_{\bar{V}} -j\omega\rho v_n(Q)g_R(Q, M_0) dQ \quad (72)$$

When no volume sources are present, the equation reduces to

$$p(M_0) = \iint_{\bar{V}} j\omega\rho v_n(Q)g_R(Q, M_0) dQ \quad (73)$$

In addition, because point  $Q$  is located on the plane, one has  $r = r_{im}$  and the Rayleigh Green's function is written as

$$g_R(Q, M_0) = \frac{\exp(-jkr)}{2\pi r}$$

Finally, the Rayleigh integral equation, Eq. (74), is obtained (Rayleigh first integral formula),

$$p(M_0) = \iint_{\bar{V}} j\omega\rho v_n(Q) \frac{\exp(-jkr)}{2\pi r} dQ \quad (74)$$

This equation is quite simple both in the integral equation and in the Green's function expression. The Raleigh integral equation relies on the concept of image sources and is restricted to planar radiators. Physically it demonstrates that the radiated sound pressure is the effect of the superposition of monopoles whose strength is proportional to the vibration velocity of the object.

One important point is that the equation is also valid for point  $Q_0$  on the plate, which is different from the general Kirchhoff integral where a factor of  $1/2$  must be introduced in the integral equation for points on the boundary surface.

## 5 SOUND RADIATION FROM FINITE PLATES AND MODAL ANALYSIS OF RADIATION<sup>13-30</sup>

### 5.1 Plate Vibration Modes and Modal Expansion of the Radiated Pressure and Power

The plate under study is rectangular and simply supported. It is a simple case where the vibration modes are well known. The natural frequencies  $\omega_{il}$  and the mode shapes  $f_{il}(x, y)$  are given by

$$\omega_{il} = \sqrt{\frac{D}{M}} \left[ \left( \frac{i\pi}{a} \right)^2 + \left( \frac{l\pi}{b} \right)^2 \right] \quad (75)$$

$$f_{il}(x, y) = \sin \left( \frac{i\pi}{a} x \right) \sin \left( \frac{l\pi}{b} y \right) \quad (76)$$

where  $D$  and  $M$  are the bending stiffness and mass per unit area of the plate, and  $a$  is the width and  $b$  the length.

The response of the plate can be calculated as a modal response superposition:

$$W(x, y) = \sum_{i=1}^{\infty} \sum_{l=1}^{\infty} a_{il} f_{il}(x, y) \quad (77)$$

Assuming the plate is baffled, the sound pressure radiated can be calculated using the Rayleigh integral approach or the radiating and nonradiating wave decomposition technique. Here the Rayleigh integral approach is used. The normal velocity can be obtained from the plate displacement:

$$v_n(x, y) = \sum_{i=1}^{\infty} \sum_{l=1}^{\infty} j\omega a_{il} f_{il}(x, y) \quad (78)$$

Substituting this expression in Eq. (74), the radiated sound pressure is

$$\begin{aligned} p(x_0, y_0, z_0) &= \sum_{i=1}^{\infty} \sum_{l=1}^{\infty} j\omega \rho a_{il} \\ &\times \int_0^a \int_0^b f_{il}(x, y) \\ &\times g_R(x, y, 0; x_0, y_0, z_0) dx dy \quad (79) \end{aligned}$$

where

$$\begin{aligned} g_R(x, y, 0; x_0, y_0, z_0) &= \frac{\exp(-jkr)}{2\pi r} \text{ and} \\ r &= \sqrt{(x - x_0)^2 + (y - y_0)^2 + (z_0)^2} \quad (80) \end{aligned}$$

The sound radiation is generally characterized by the sound power radiated  $\Pi_{\text{rad}}$  in order to have a global quantity. The calculation can be made integrating the sound intensity normal to the plate on the plate surface. After calculation one obtains

$$\begin{aligned} \Pi_{\text{rad}} &= \frac{1}{2} \sum_{i=1}^{\infty} \sum_{l=1}^{\infty} \sum_{s=1}^{\infty} \sum_{r=1}^{\infty} \omega^2 \rho \operatorname{Re} \left\{ a_{rs}^* a_{il} \right. \\ &\times \int_0^a \int_0^b \int_0^a \int_0^b f_{il}(x, y) g_R(x, y, 0; x_0, y_0, 0) \\ &\times f_{sr}(x_0, y_0) dx dy dx_0 dy_0 \left. \right\} \end{aligned}$$

this expression can be concisely written by introducing the radiation impedances  $Z_{ilrs}$ :

$$\Pi_{\text{rad}} = \frac{1}{2} \sum_{i=1}^{\infty} \sum_{l=1}^{\infty} \sum_{s=1}^{\infty} \sum_{r=1}^{\infty} \omega^2 \operatorname{Re} \{ a_{rs}^* a_{il} Z_{ilrs} \} \quad (81)$$

where

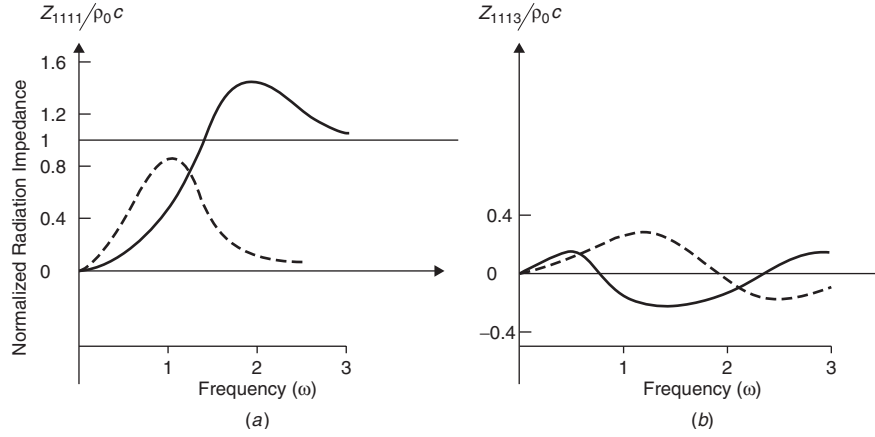
$$\begin{aligned} Z_{ilrs} &= \int_0^a \int_0^b \int_0^a \int_0^b \rho f_{il}(x, y) \\ &\times g_R(x, y, 0; x_0, y_0, 0) f_{sr}(x_0, y_0) \\ &\times dx dy dx_0 dy_0 \quad (82) \end{aligned}$$

Radiation impedances are complex quantities, and they are often separated into two parts, radiation resistances  $R_{ilrs}$  and radiation reactances  $X_{ilrs}$ :

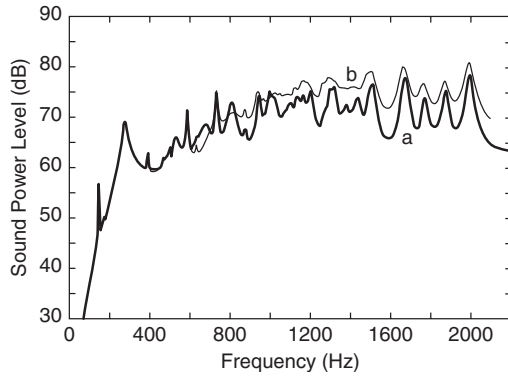
$$Z_{ilrs} = R_{ilrs} + jX_{ilrs} \quad (83)$$

When two different modes  $(i, l)$  and  $(r, s)$  are considered,  $Z_{ilrs}$  is known as the modal cross-radiation impedance. When the same mode  $(i, l)$  is considered,  $Z_{ilil}$  is known as the mode radiation impedance.

In Fig. 7 an example is presented. The first tendency that appears is that the cross-radiation resistance and reactance oscillate around zero when the frequency is varied, as opposed to the direct radiation resistance and reactance, which remain positive at all frequencies. However, the radiation reactance tends to be negligible at high frequencies, as opposed to radiation resistance which tends to the fluid acoustic impedance.



**Figure 7** Radiation impedance of rectangular plate modes versus frequency. (a) Mode radiation resistance (solid line) and reactance (dashed line) for mode (1,1). (b) Modal cross-radiation resistance (dashed line) and reactance (solid line) for modes (1,1) and (1,3). (From Sandman.<sup>15</sup>)



**Figure 8** Sound power level radiated by a baffled cylinder in water versus frequency. (a) Calculation with modal cross-radiation impedances and (b) calculation without modal cross-radiation impedances. (From Guyader and Laulagnet.<sup>23</sup>)

In Fig. 8 the influence of neglecting cross-modal radiation impedance is presented. The case considered is extreme in the sense that the fluid is water and has an acoustic impedance more than a thousand times greater than air.

It can be seen in Fig. 8, that the general trend does not change when cross-modal radiation impedances are neglected. However, the power radiated by the cylinder can be modified by up to 10 dB at higher frequencies. This result is related to the heavy fluid loading of the structure. For light fluid loading the influence of cross-modal radiation impedances is quite small, and in general the cross-modal contributions are neglected. An approximate expression for the radiated sound power can be found:

$$\Pi_{\text{rad}} = \frac{1}{2} \sum_{i=1}^{\infty} \sum_{l=1}^{\infty} \omega^2 |a_{il}|^2 R_{ilil} \quad (84)$$

To a first approximation the radiated sound power of the plate is the sum of the power radiated by each mode separately. The modal radiation is characterized by the modal resistance.

Modal resistances (or mode radiation factor  $\sigma_{mn}$ ,

$$\sigma_{mn} = \frac{R_{mnmn}}{\rho c N_{mn}}$$

where  $N_{mn}$  is the norm of the mode) of rectangular simply supported plates have been calculated in different studies using the Rayleigh integral approach or wave decomposition. The expressions of Wallace<sup>14</sup> are given in Table 1, and Fig. 4 presents some typical results.

The main trends that can be observed in Fig. 9 are the radiation properties of plate modes below and above the mode critical frequency

$$\omega_c^{mn} = c \left[ \left( \frac{n\pi}{b} \right)^2 + \left( \frac{m\pi}{a} \right)^2 \right]^{0.5}$$

Below  $\omega_c^{mn}$  the radiation factor is small and decreases with frequency, while above it is equal to unity. In addition, depending on the mode shape, the radiation factor below  $\omega_c^{mn}$  is small. This is due to the acoustic short-circuit effect. The short-circuit strength is larger for plate modes of high orders than low orders and also for odd mode orders rather than even ones.

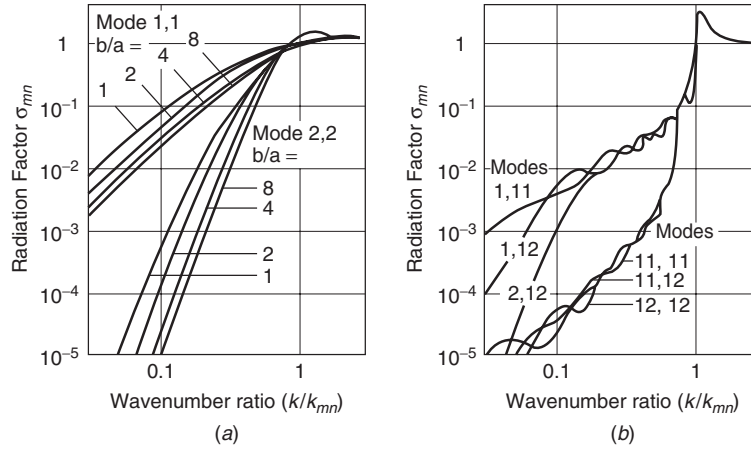
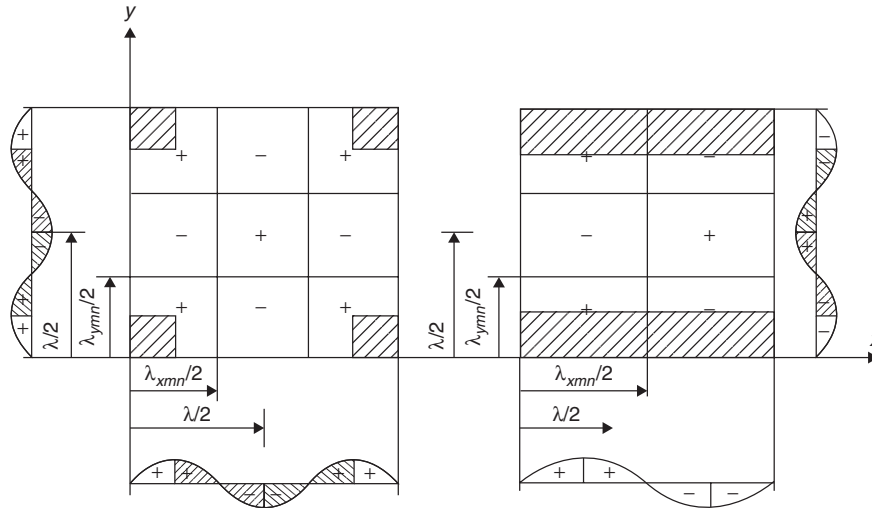
To explain the phenomenon, let us consider the mode shape of Fig 10. When some parts of the plate are pushing the fluid (positive contribution), the other parts are pulling it (negative contribution). Both

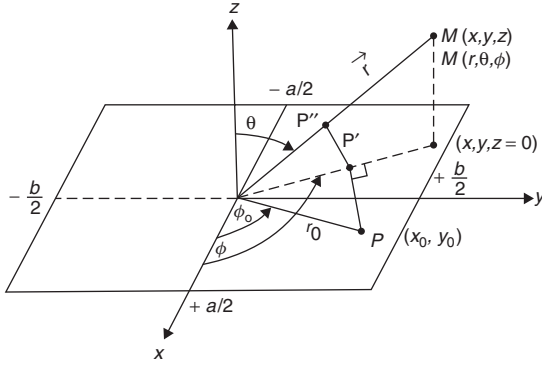


**Table 1** Radiation Factor  $\sigma_{mn}$  for Modes of Rectangular Simply Supported Plate

$k < k_{mn}$ and $k_x < k < k_y$	$\sigma_{mn} = \frac{k(k_x^2 + k_{mn}^2 - k^2)}{ak_x(k_{mn}^2 - k^2)^{3/2}}$
$k < k_{mn}$ and $k_x > k > k_y$	$\sigma_{mn} = \frac{k(k_y^2 + k_{mn}^2 - k^2)}{bk_y(k_{mn}^2 - k^2)^{3/2}}$
$k < k_{mn}$ and $k_x > k$ and $k_y > k$	$\sigma_{mn} = \frac{8k^2}{abk_x^2k_y^2} \left\{ 1 - (-1)^m \frac{\sin(ak)}{ak} - (-1)^n \frac{\sin(bk)}{bk} + (-1)^{m+n} \frac{\sin[k(a^2 + b^2)^{0.5}]}{k(a^2 + b^2)^{0.5}} \right\}$
$k < k_{mn}$ and $k_x < k$ and $k_y < k$	$\sigma_{mn} = k \left[ \frac{k_x^2 + k_{mn}^2 - k^2}{ak_x(k_{mn}^2 - k^2)^{1.5}} + \frac{k_y^2 + k_{mn}^2 - k^2}{bk_y(k_{mn}^2 - k^2)^{1.5}} \right]$
$k > k_{mn}$	$\sigma_{mn} = \frac{k}{(k^2 - k_{mn}^2)^{0.5}}$
$k \approx k_{mn}$	$\sigma_{mn} = \frac{k}{3\pi} \left( \frac{a}{\sqrt{m}} + \frac{b}{\sqrt{n}} \right)$

Approximate values after Maidanik.<sup>13</sup>  $n$  and  $m$  are mode indices,  $k_{mn} = \left[ \left( \frac{m\pi}{a} \right)^2 + \left( \frac{n\pi}{b} \right)^2 \right]^{0.5}$ ,  $k_x = \frac{m\pi}{a}$ , and  $k_y = \frac{n\pi}{b}$ .

**Figure 9** Radiation factor  $\sigma_{mn}$  of plate modes versus ratio of acoustic and plate mode wavenumbers: (a) modes (1,1) and (2,2) for different values of the length to width ratio of the plate and (b) high-order modes. (From Wallace.<sup>14</sup>)**Figure 10** Acoustical short circuit, edge, and corner radiation modes. (From Lesueur et al.<sup>4</sup>)



**Figure 11** Polar coordinates used for plate sound radiation in the far field.

contributions cancel when the acoustic wavelength is greater than the flexural one. Physically the effect is equivalent to the case of a long boat (here the acoustic medium) excited by water waves of short wavelengths (the plate motion). The boat remains almost motionless (the radiated sound pressure is small). The importance of the short circuit depends on the mode shape. As a general rule the acoustical short circuit implies radiation of plate modes essentially produced by the boundary. Edge radiation modes exist when  $k < k_{mn}$  and  $k_x < k < k_y$  or  $k < k_{mn}$  and  $k_x > k > k_y$ , and corner radiation modes when  $k < k_{mn}$  and  $k_x > k$  and  $k_y > k$ . See Fig 10.

## 5.2 Directivity of the Radiated Pressure Field

One important result concerning the radiated sound pressure in the far field of the plate is given here without derivation. Introducing polar coordinates for the acoustic medium  $(R, \theta, \phi)$  where  $R$  is the distance from the central point of the plate to a listening point in the far field, one has the geometry shown in Fig 11.

The radiated sound pressure in the far field of the plate is given by Eq. (85), and for a complete derivation one can consult Junger and Feit.<sup>1</sup>

$$p(R, \theta, \Phi) = \rho \omega^2 \tilde{W} [-k \sin(\theta) \sin(\Phi), -k \sin(\theta) \cos(\Phi)] \frac{\exp(-jkR)}{R} \quad (85)$$

where  $\tilde{W}(\lambda, \mu)$  is the double space Fourier transform of the plate displacement

$$\tilde{W}(\lambda, \mu) = \frac{1}{2\pi} \int_{-\infty}^{\infty} \int_{-\infty}^{\infty} \exp(-j\lambda x - j\mu y) \times W(x, y) dx dy \quad (86)$$

The application of this expression to plate modes of a simply supported rectangular plate is quite

elementary and gives the directivity of the sound pressure field radiated by the modes:

$$\tilde{W}_{rs}(\lambda, \mu) = \frac{2}{\pi} \frac{(r\pi/a)(s\pi/b)}{\left(\lambda^2 - \left(\frac{r\pi}{a}\right)^2\right) \left(\mu^2 - \left(\frac{s\pi}{b}\right)^2\right)} \times d(\lambda, \mu) \quad (87)$$

where

$$d(\lambda, \mu) = \begin{cases} \cos\left(\frac{\lambda a}{2}\right) \cos\left(\frac{\mu b}{2}\right), & r = \text{odd}, s = \text{odd} \\ -\cos\left(\frac{\lambda a}{2}\right) \sin\left(\frac{\mu b}{2}\right), & r = \text{odd}, s = \text{even} \\ -\sin\left(\frac{\lambda a}{2}\right) \cos\left(\frac{\mu b}{2}\right), & r = \text{even}, s = \text{odd} \\ \sin\left(\frac{\lambda a}{2}\right) \sin\left(\frac{\mu b}{2}\right), & r = \text{even}, s = \text{even} \end{cases} \quad (88)$$

The phenomena associated with the directivity of the modal radiated sound pressure in the far field are complicated. First, the symmetry and antisymmetry of plate modes produce symmetrical or antisymmetrical sound pressure fields. Consequently, the radiated sound pressure normal to the plate midpoint is zero if one index of the plate mode is even. To this effect one has to add the influence of the plate area. For a given frequency the number of radiation lobes increases with the plate dimensions (or for a given size of the plate the number of directivity lobes increases with frequency). Finally a maximum of the radiated sound pressure appears at an angle  $\hat{\theta}$ , which depends on the frequency and mode order as given by Eq. (89):

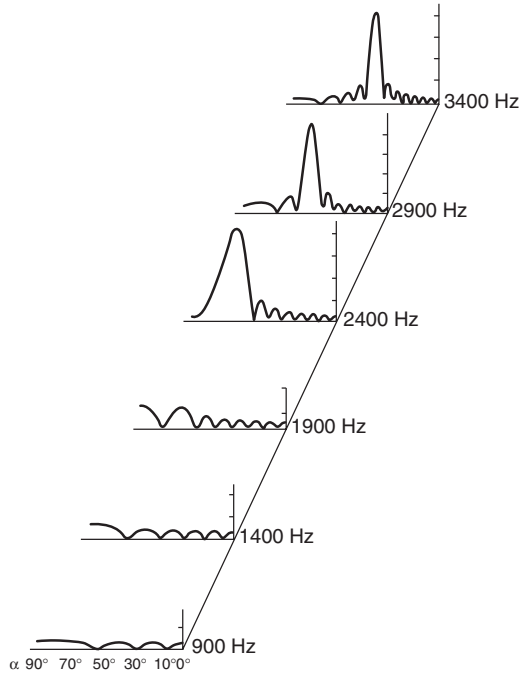
$$\hat{\theta} = \arcsin \left[ \frac{c}{\omega} \sqrt{\left(\frac{r\pi}{a}\right)^2 + \left(\frac{s\pi}{b}\right)^2} \right] \quad (89)$$

The angle of maximum sound radiation exists only for frequencies above  $c\sqrt{(r\pi/a)^2 + (s\pi/b)^2}$ .

Figure 12 presents the phenomenon described here for the case of mode (15,15); the angle  $\hat{\theta}$  of maximum radiation can be seen for frequencies above 2400 Hz.

## 5.3 Frequency Averaged Radiation from Plates Subjected to Rain on the Roof Excitation

For this type of excitation all the modes are equally excited, and the resonant modes in a frequency band of excitation have the same responses ( $\langle \omega^2 |a_{il}|^2 \rangle$  constant for all resonant modes). The radiated sound power



**Figure 12** Directivity of the sound pressure radiated in the far field by rectangular plate mode (15,15), for different frequencies. (From Guyader and Laulagnet.<sup>23</sup>)

of the plate is the superposition of resonant mode radiation:

$$\begin{aligned} \langle \Pi_{\text{rad}} \rangle &= \sum_{i=\text{resonant}} \sum_{l=\text{resonant}} \rho \langle \omega^2 |a_{il}|^2 \rangle \langle R_{ilil} \rangle \\ &= \rho \langle \omega^2 |a_{il}|^2 \rangle \sum_{i=\text{resonant}} \sum_{l=\text{resonant}} \langle R_{ilil} \rangle \quad (90) \end{aligned}$$

where  $\langle \rangle$  indicates frequency averaging over a frequency band centered at  $f$ .

Defining the plate radiation factor  $\bar{\sigma}$  as the ratio of radiated sound power and the plate velocity squared times the acoustic impedance, one has

$$\begin{aligned} \bar{\sigma} &= \frac{\langle \Pi_{\text{rad}} \rangle}{\rho c \langle V^2 \rangle} \\ &= \frac{\langle \omega^2 |a_{il}|^2 \rangle \sum_{i=\text{resonant}} \sum_{l=\text{resonant}} \langle R_{ilil} \rangle}{\rho c \langle \omega^2 |a_{il}|^2 \rangle \sum_{i=\text{resonant}} \sum_{l=\text{resonant}} N_{il}} \\ &= \frac{1}{N_{\text{res}}} \sum_{i=\text{resonant}} \sum_{l=\text{resonant}} \langle \sigma_{il} \rangle \quad (91) \end{aligned}$$

where  $N_{\text{res}}$  is the number of resonant modes.

The plate radiation factor  $\bar{\sigma}$  has been estimated (see reference 13 and the correction in reference 31), and

**Table 2** Radiation Factor  $\bar{\sigma}$  for Rectangular Simply Supported Plate of Length  $a$  and Width  $b$

$$\begin{aligned} f < f_c & \quad \bar{\sigma} = \frac{2\lambda_a \lambda_c}{ab} \frac{f}{f_c} g_1 + \frac{2(a+b)\lambda_c}{ab} g_2 \\ f \approx f_c & \quad \bar{\sigma} = \sqrt{\frac{a}{\lambda_c}} + \sqrt{\frac{b}{\lambda_c}} \\ f > f_c & \quad \bar{\sigma} = \frac{1}{\sqrt{f_c/f}} \end{aligned}$$

Sources: After Refs. 6 and 31.

analytical expressions obtained are given in Table 2. It permits one to quickly get an approximate value for the radiated sound power from a knowledge of the plate mechanical response. The major phenomenon is the low radiation below the critical frequency of the plate  $f_c = c^2 \sqrt{M/D}$ , because of the acoustical short circuit, and a radiation factor equal to unity above. The maximum efficiency occurs at the critical frequency. The expressions given in Table 2 are approximations and may differ from those of different authors.

In Table 2,  $\lambda$  is the acoustic wavelength, and  $\lambda_c$  is the acoustic wavelength at the critical frequency. The two coefficients  $g_1$  and  $g_2$  characterize the sound radiation from the corners and the edges of the plate. One has

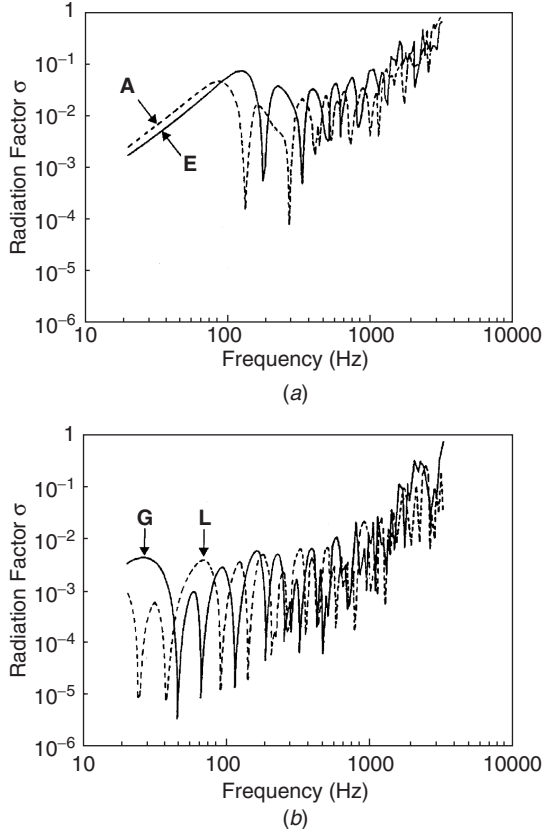
$$\begin{aligned} g_1 &= \begin{cases} \frac{4(1-2f/f_c)}{\pi^4 \sqrt{f/f_c - f^2/f_c^2}} & \text{when } f < f_c/2 \\ 0 & \text{when } f > f_c/2 \end{cases} \\ g_2 &= \frac{1}{\pi^2} \frac{1-f/f_c}{(1-f/f_c)^{1.5}} \log \left( \frac{1+\sqrt{f/f_c}}{1-\sqrt{f/f_c}} + 2\sqrt{f/f_c} \right) \end{aligned}$$

The influence of boundary conditions on the radiation factor is not negligible. Following the results presented in Fig. 13 and demonstrated in Berry et al.,<sup>22</sup> one can conclude that translational and rotational boundary stiffness modify the radiation efficiency. However, the main influence is associated with the translational one. Below the critical frequency the radiation factor of a rectangular plate having free or guided boundary conditions is much smaller than the radiation factor of the same plate simply supported or clamped. This indicates that blocking the translational motion of the plate boundary strongly increases the radiation efficiency. On the other hand, clamped or simply supported plates (resp. guided or free) have approximately the same radiation efficiency, indicating that blocking the rotational motion at the boundaries is not so important. Above the critical frequency the radiation factor tends to unity whatever the boundary conditions of the plate.

## 6 RESPONSE OF STRUCTURES TO SOUND EXCITATION

### 6.1 Infinite Plate Excited by a Plane Wave

A basic case to understand the phenomena of structural excitation by field pressure a sound is the infinite plate excited by a plane wave. The advantage of this case



**Figure 13** (a) Radiation factor  $\sigma$  of a rectangular plate for different types of boundary conditions. A simply supported, E clamped. (b) Radiation factor of a rectangular plate for different types of boundary conditions. G guided, L free. (From Berry et al.<sup>22</sup>)

is the simplicity of the structural response calculation, which permits one to clearly explain the governing mechanisms.

Let us consider an infinite plate separating an acoustic medium into two parts. In the first one a plane incident wave is reflected by the plate, while in the second a plane wave is transmitted.

The sound pressure in the emitting half-space is given by

$$p_1(x, y, z) = \exp[-jk \sin(\theta) \sin(\phi)x - jk \sin(\theta) \cos(\phi)y] \{ \exp[-jk \cos(\theta)z] + B \exp[jk \cos(\theta)z] \} \quad (92)$$

The sound pressure in the receiving half-space is given by

$$p_2(x, y, z) = \exp[-jk \sin(\theta) \sin(\phi)x - jk \sin(\theta) \cos(\phi)y] \times \{ A \exp[-jk \cos(\theta)z] \} \quad (93)$$

The plate displacement has the form

$$W(x, y) = C \exp[-jk \sin(\theta) \sin(\phi)x - jk \sin(\theta) \cos(\phi)y] \quad (94)$$

The verification of velocity continuity of the plate and the acoustic normal velocity and of the plate equation of motion allows us to find the amplitudes of sound pressures and plate waves:

$$C = \frac{2}{\left\{ -\omega^2 M + D(1 + j\eta)[k^4 \sin^4(\theta)] + 2j\omega[\rho c / \cos(\theta)] \right\}} \quad (95)$$

$$B = 1 - j\omega \frac{\rho c}{\cos(\theta)} C \quad (96)$$

$$A = j\omega \frac{\rho c}{\cos(\theta)} C \quad (97)$$

The amplitude  $C$  of the plate vibration depends, of course, on its mass and bending stiffness. These effects are quite different and depend on frequency. Figure 14 presents the plate velocity level versus frequency for different angles of incidence.

At the angular coincidence frequency  $\omega_{coi}$ , the plate amplitude is maximum:

$$C = \frac{2}{M(j\eta)\omega_{coi}^2 + 2j\omega_{coi}[\rho c / \cos(\theta)]} \quad (98)$$

where

$$\omega_{coi} = \frac{c^2}{\sin^2(\theta)} \sqrt{\frac{M}{D}} \quad (99)$$

This maximum plate response is due to the coincidence phenomenon, which appears when the projection of the acoustic wavelength is equal to the plate natural bending wavelength. This situation is only possible at the coincidence frequency. If, in addition, the plate damping loss factor  $\eta$  is equal to zero the plate does not modify the sound propagation. One has  $B = 0$  and  $A = 1$ , which indicates no reflection by the plate.

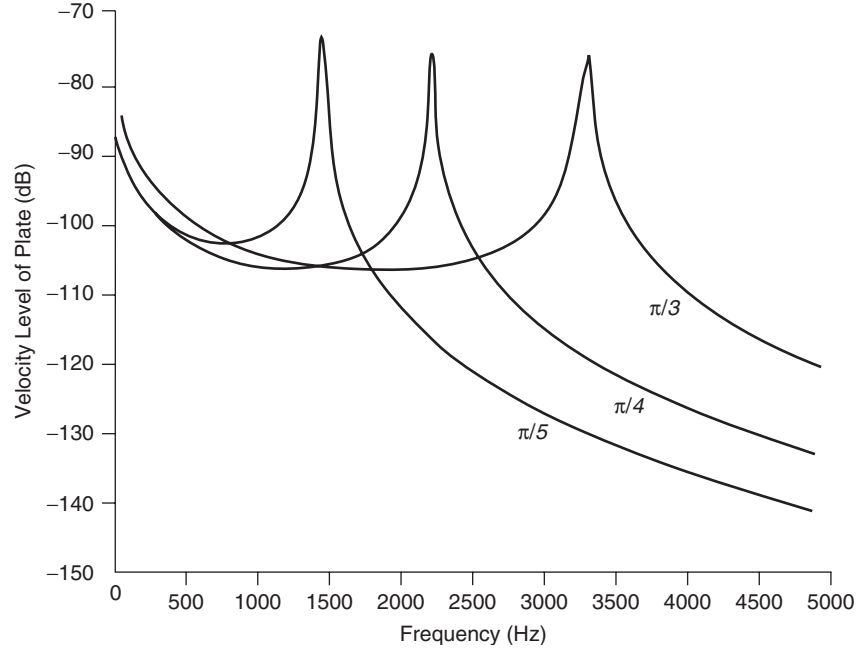
At low frequency,  $\omega < \omega_{coi}$ , the plate response is governed by its mass; the plate amplitude of vibration is equal to

$$C \approx \frac{2}{-M\omega^2}$$

At high frequency,  $\omega > \omega_{coi}$ , the plate response is governed by the stiffness effect; the plate amplitude is equal to

$$C \approx \frac{2}{D[k^4 \sin^4(\theta)]}$$

The presence of the fluid appears like additional damping for the plate. When the plate is in vacuum, the damping effect is associated with the term  $D(j\eta)(k^4 \sin^4(\theta))$ , and when it is immersed in



**Figure 14** Plate velocity level be consistent,  $L_v$ , versus frequency (Hz) for three angles of incidence ( $\pi/3$ ,  $\pi/4$ ,  $\pi/5$ ). Steel plate of 0.01 m thickness and damping loss factor equal to 0.01.

the fluid it is associated with  $D(j\eta)[k^4 \sin^4(\theta)] + 2j[\rho c / \cos(\theta)]$ . Thus, one can define an equivalent plate loss factor  $\eta_{eq}$  including dissipation in the plate and acoustic emission from the plate:

$$\eta_{eq} = \eta + \frac{2[\rho c / \cos(\theta)]}{D[k^4 \sin^4(\theta)]} \quad (100)$$

To summarize, one can say that the level of vibration induced by acoustic excitation is controlled by the mass of the plate below the coincidence frequency. Then the maximum appears with the coincidence effect, and the plate amplitude is limited by damping due to internal dissipation but also to sound re-radiation by the plate (see Fig. 15). At higher frequency the plate velocity level is controlled by the bending stiffness. It decreases with increasing frequency. The coincidence phenomenon appears at the coincidence frequency and depends on the incidence angle; see Fig. 14. Its minimum value is obtained for grazing incidence waves and is equal to the critical frequency as was discussed in Section 5.2 as the frequency limit of radiation from infinite plates. The coincidence frequency tends to infinity for normal incidence, meaning that the coincidence phenomenon does not exist anymore.

The excitation of the infinite plate by a reverberant sound field can be studied by summing the effect of plane waves of different angles of incidence. (see Fig. 16.) The square of the velocity of a plate excited by a sound diffuse field can be calculated adding plate

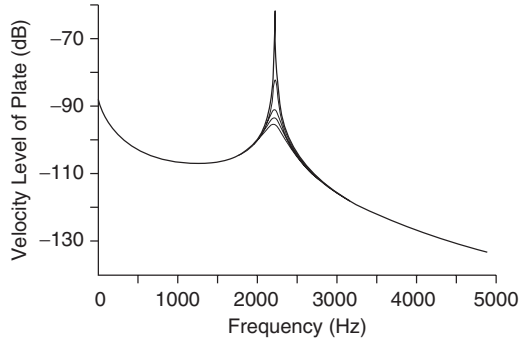
squared velocities created by each wave of the diffuse field, and the following result can be obtained:

$$\begin{aligned} \int_0^{2\pi} \int_0^{\pi/2} \omega^2 |W(x, y)|^2 d\theta d\phi &= 2\pi \int_0^{\pi/2} |C|^2 d\theta \\ &\int_0^{\pi/2} \{ (8\pi\omega^2) / [1 - \omega^2 M + D[k^4 \sin^4(\theta)]]^2 \\ &+ \{ D\eta[k^4 \sin^4(\theta)] \\ &+ 2\omega[\rho c / \cos(\theta)]^2 \} \sin \theta d\theta \end{aligned} \quad (101)$$

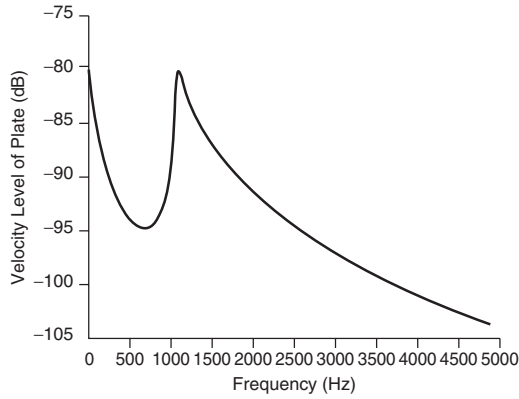
For diffuse field excitation the averaging effect does not change the general trends observed for oblique incidence. The maximum of the plate response appears at the critical frequency  $\omega_c = c^2 \sqrt{M/D}$ , and the peak of maximum velocity is not so sharp as it is for a single angle of incidence.

## 6.2 Sound Excitation of Finite Baffled Plates

Let us consider a finite rectangular simply supported plate mounted in an infinite rigid baffle, separating the surrounding acoustic medium into two parts, the emitting and receiving half-spaces. An incident plane wave excites the plate, assumed to be and the resulting vibrations produce reflected and transmitted



**Figure 15** Plate velocity level,  $L_v$ , versus frequency (Hz) for various values of damping loss factor. Steel plate of 0.01 m thickness and angle of incidence of  $45^\circ$ . At the coincidence frequency the curves corresponds from top to bottom to damping loss factors equal to 0.001, 0.021, 0.041, 0.061, 0.081, and 0.101.



**Figure 16** Plate velocity level versus frequency (Hz), for diffuse field excitation. Steel plate of 0.01 m thickness with damping loss factor equal to 0.02.

sound waves. Classically, the reflected sound wave is assumed to be decomposed into a reflected plane wave, assuming that the plate is motionless, and a radiated wave due to the plate vibration. The sound pressures in the emitting and receiving half-space, have the following form:

$$p_1(x, y, z) = p_1^{\text{blocked}}(x, y, z) + p_1^{\text{rad}}(x, y, z) \quad (102)$$

$$p_2(x, y, z) = p_2^{\text{rad}}(x, y, z) \quad (103)$$

where the blocked and radiated sound pressures are given by Eqs. (104) and (105), respectively. The blocked sound pressure is the superposition of incident and reflected plane waves when the plate is

motionless:

$$p_1^{\text{blocked}}(x, y, z) = \exp(-jk \sin \theta \sin \phi x - jk \sin \theta \cos \phi y) [\exp(-jk \cos \theta z) + \exp(jk \cos \theta z)] \quad (104)$$

The expression for the radiated sound pressure has been derived in Section 4, taking into account the modal expansion of the plate response:

$$p_m^{\text{rad}}(x, y, z) = \sum_{i=1}^{\infty} \sum_{l=1}^{\infty} j \omega \rho a_{il} \times \int_0^a \int_0^b f_{il}(x_0, y_0) g_R^m(x_0, y_0, 0; x, y, z) \times dx dy, \quad m = 1, 2 \quad (105)$$

To calculate sound pressure fields one has to solve the plate equation of motion:

$$-\omega^2 MW(x, y) + D \left( \frac{\partial^4 W}{\partial x^4} + 2 \frac{\partial^4 W}{\partial x^2 \partial y^2} + \frac{\partial^4 W}{\partial y^4} \right) \times (x, y) = p_1(x, y, 0) - p_2(x, y, 0) \quad (106)$$

The solution of this equation is obtained by modal decomposition, with resonance frequencies  $\omega_{il}$  and mode shapes  $f_{il}(x, y)$  given by

$$\omega_{il} = \sqrt{\frac{D}{M}} \left[ \left( \frac{i\pi}{a} \right)^2 + \left( \frac{l\pi}{b} \right)^2 \right],$$

$$f_{il}(x, y) = \sin \left( \frac{i\pi}{a} x \right) \sin \left( \frac{l\pi}{b} y \right) \quad (107)$$

where  $D$  is the bending stiffness and  $M$  is the mass per unit area of the plate,  $a$  is the width and  $b$  is the length.

The plate response is calculated by expanding it in its in vacuo plate modes.

$$W(x, y) = \sum_{i=1}^{\infty} \sum_{l=1}^{\infty} a_{il} f_{il}(x, y) = \sum_{i=1}^{\infty} \sum_{l=1}^{\infty} a_{il} \sin \left( \frac{i\pi}{a} x \right) \times \sin \left( \frac{l\pi}{b} y \right) \quad (108)$$

After substitution of the modal expansion into the plate equation of motion and use of orthogonality properties, the modal amplitudes are found to satisfy Eq. (109):

$$\begin{aligned}
& -\omega^2 M_{nm} a_{nm} + K_{nm}(1 + j\eta) a_{nm} \\
& = P_{nm} - \sum_{r=1}^{\infty} \sum_{s=1}^{\infty} j\omega a_{nm} (Z_{nmrs}^1 + Z_{nmrs}^2) N_{nm} \quad (109)
\end{aligned}$$

where  $a_{nm}$  is the plate mode  $(n, m)$  amplitude,  $M_{nm}$  is the generalized mass,  $K_{nm}$  is the generalized stiffness of mode  $(n, m)$  and  $\eta$  the damping loss factor of the plate.

In the right hand side of the equation, two terms appear. The first one

$$\begin{aligned}
P_{nm} &= \int_0^a \int_0^b p_1^{\text{blocked}}(x, y, 0) \\
&\quad \times \sin\left(\frac{n\pi}{a}x\right) \sin\left(\frac{m\pi}{b}y\right) dx dy \quad (110)
\end{aligned}$$

is the generalized force due to the acoustic excitation. The second represents the influence of the plate radiation on the response. It can be calculated as in Section 5.1. The term is characterized by modal responses of two modes  $(n, m)$  and  $(r, s)$  and

$$\begin{aligned}
Z_{nmrs}^i &= \frac{1}{N_{rs}} \int_0^a \int_0^b \int_0^a \int_0^b \sin\left(\frac{n\pi}{a}x\right) \sin\left(\frac{m\pi}{b}y\right) \\
&\quad \times g_R^i(x, y, 0; x_0, y_0, 0) \sin\left(\frac{r\pi}{a}x_0\right) \\
&\quad \times \sin\left(\frac{s\pi}{b}y_0\right) dx dy dx_0 dy_0 \quad (111)
\end{aligned}$$

their radiation impedance in the fluid medium  $i$ .

A first conclusion that can be drawn concerning the influence of the fluid surrounding the plate is the coupling of in vacuum modes through the radiation impedances. For heavy fluids like water this coupling cannot be ignored, and in vacuum resonance frequencies and mode shapes are completely different when the plate is fluid loaded. On the other hand for light fluids the structural behavior is not strongly modified by fluid loading, and the modal response can be approximated by neglecting modal cross coupling.

$$\begin{aligned}
& -\omega^2 M_{nm} a_{nm} + K_{nm}(1 + j\eta) a_{nm} \\
& = P_{nm} - j\omega a_{nm} (Z_{nmnm}^1 + Z_{nmnm}^2) N_{nm} \quad (112)
\end{aligned}$$

The radiation impedance of mode  $(n, m)$  is a complex quantity, so one can separate modal resistance and reactance into real and imaginary part, respectively:

$$Z_{nmnm}^i = R_{nmnm}^i + jX_{nmnm}^i$$

The amplitude of mode  $(n, m)$  is then governed by the following equation :

$$\begin{aligned}
& -\omega^2 [M_{nm} + (X_{nmnm}^1 + X_{nmnm}^2)/\omega N_{nm}] a_{nm} \\
& + K_{nm} \{1 + j(\eta + [R_{nmnm}^1 + R_{nmnm}^2]/K_{nm} \\
& \times \omega N_{nm})\} a_{nm} = P_{nm} \quad (113)
\end{aligned}$$

Physically, one can see that radiation reactances produce an effect of added modal mass, and the resonance frequencies of panels tend to decrease when they are fluid loaded. The radiation resistances introduce an additional damping compared to the in vacuo situation. In fact, the additional losses of one plate mode are equal to the power it radiates into both fluid media.

In the case of an infinite plate, the fluid loading introduces only additional damping and no additional mass on the plate. This is due to the type of sound wave created: Only propagating waves exist for infinite plates compared to the finite plate vibration case which produces both propagating and evanescent waves. Propagating waves are responsible for additional damping; evanescent waves are responsible for additional mass.

The generalized force takes into account the excitation of plate modes by the blocked pressure:

$$\begin{aligned}
P_{nm} &= 2 \int_0^a \int_0^b \exp[-jk \sin(\theta) \sin(\phi)x] \\
&\quad \times -jk \sin(\theta) \cos(\phi)y] \sin\left(\frac{n\pi}{a}x\right) \\
&\quad \times \sin\left(\frac{m\pi}{b}y\right) dx dy \quad (114)
\end{aligned}$$

The calculation of the generalized force shows the important phenomenon of joint acceptance. After calculation one has

$$\begin{aligned}
P_{nm} &= \frac{64 \left(\frac{n\pi}{a}\right)^2 \left(\frac{m\pi}{b}\right)^2}{\left\{ \left[ (k \sin \theta \sin \phi)^2 - \left(\frac{n\pi}{a}\right)^2 \right]^2 \right.} \\
&\quad \times \left. \left[ (k \sin \theta \cos \phi)^2 - \left(\frac{m\pi}{b}\right)^2 \right]^2 \right\}} \\
&\quad \times \left\{ \begin{aligned} & \cos^2 \left( k \sin \theta \sin \phi \frac{a}{2} \right) \\ & \times \cos^2 \left( k \sin \theta \cos \phi \frac{b}{2} \right) \\ & \cos^2 \left( k \sin \theta \sin \phi \frac{a}{2} \right) \\ & \times \sin^2 \left( k \sin \theta \cos \phi \frac{b}{2} \right) \\ & \sin^2 \left( k \sin \theta \sin \phi \frac{a}{2} \right) \\ & \times \cos^2 \left( k \sin \theta \cos \phi \frac{b}{2} \right) \\ & \sin^2 \left( k \sin \theta \sin \phi \frac{a}{2} \right) \\ & \times \sin^2 \left( k \sin \theta \cos \phi \frac{b}{2} \right) \end{aligned} \right\} \quad (115)
\end{aligned}$$

In Eq. (115), four cases are possible: from top to bottom they corresponds to (odd, odd), (odd, even), (even, odd), and (even, even) modes.

Because of the singularity of the denominator in Eq. (115), one can see that modes satisfying Eqs. (116) and (117) are highly excited; their joint acceptances are large:

$$\omega = \left(\frac{n\pi}{a}\right) \frac{c}{\sin \theta \sin \phi} \quad (116)$$

$$\omega = \left(\frac{m\pi}{b}\right) \frac{c}{\sin \theta \cos \phi} \quad (117)$$

However, a high level of excitation is not sufficient to produce a high level of response of the mode. It is also necessary to excite it at its resonance frequency, and thus to satisfy Eq. (118).

$$\omega = \omega_{nm} = \sqrt{\frac{D}{M}} \left[ \left(\frac{n\pi}{a}\right)^2 + \left(\frac{m\pi}{b}\right)^2 \right] \quad (118)$$

The fulfilment of these three conditions is only possible at one frequency, the coincidence frequency:

$$\omega_{\text{coin}} = \sqrt{\frac{M}{D}} \frac{c^2}{(\sin \theta)^2} \quad (119)$$

For infinite plates the coincidence frequency already exists and is characterized by a high amplitude of vibration due to the coincidence of the acoustics and plate natural wavenumbers. For finite plates a second interpretation of the same phenomenon can be made, the high level of vibration being due to resonant modes having maximum joint acceptance values.

## 7 CONCLUSIONS

In this section the basic phenomenon of sound radiation from structures has been presented on the case of plates. Of course, more complicated structures have specific behavior, but the major trends remain close to plates. In particular an acoustic short circuit appears for frequencies below the critical frequency, and the radiation efficiency is low, meaning that structural vibrations have difficulty to produce noise. Modal decomposition and wave decomposition of the vibration fields have been used to describe the radiation phenomenon leading to concepts of radiating and nonradiating waves or modal radiation efficiency. The influence of structural boundary conditions is important below the critical frequency. However, blocking the translational motion has a stronger influence than blocking the rotational motion.

The classical approach to predict sound radiation is based on integral equations. The method has been described here and different possibilities presented based on Kirchhoff or Rayleigh integrals. A second possibility is presented that consists of replacing the structure by equivalent acoustic sources located inside the volume that is occupied by the structure and which produce the same vibration field.

Finally, the excitation of structures by a sound field has been presented. The major tendency that appears is the reciprocity of the radiation of sound from structures and the structural response excited by sound. Many studies have been made during the past three decades and numerical tools have been developed for prediction of radiated sound pressure by industrial structures. The remaining problems are associated with time-consuming calculations and dispersion of experimental results. This leads the research in this field toward energy methods and frequency averaging to predict the sound radiation from structures. These new trends can be found in the literature.<sup>37-41</sup>

## REFERENCES

1. M. Junger and D. Feit, *Sound, Structures and Their Interaction*, 2nd ed., M.I.T. Press, Cambridge, Massachusetts, 1985.
2. F. Fahy, *Sound and Structural Vibration, Radiation Transmission and Response*, Academic, New York, 1985.
3. L. Cremer, M. Heckl, and E. Ungar, *Structure Borne Sound*, Springer, Berlin 1973.
4. C. Lesueur, *Rayonnement acoustique des structures* (in French) Eyrolles, Paris, 1988.
5. W. Williams, D. A. Parke, A. D. Moran, and C. H. Sherman, Acoustic Radiation from a Finite Cylinder, *J. Acoust. Soc. Am.*, Vol. 36, 1964, pp. 2316-2322.
6. L. Cremer, Synthesis of the Sound Field of an Arbitrary Rigid Radiator in Air with Arbitrary Particle Velocity Distribution by Means of Spherical Sound Fields (in German), *Acustica*, Vol. 55, 1984, pp. 44-47.
7. G. Koopman, L. Song, and J. B. Fahnline, A Method for Computing Acoustic Fields Based on the Principle of Wave Superposition, *J. Acoust. Soc. Am.*, Vol. 88, 1989, pp. 2433-2438.
8. M. Ochmann, Multiple Radiator Synthesis—An Effective Method for Calculating the Radiated Sound Field of Vibrating Structures of Arbitrary Source Configuration (in German), *Acustica*, Vol. 72, 1990, pp. 233-246.
9. Y. I. Bobrovnikskii and T. M. Tomilina, Calculation of Radiation from Finite Elastic Bodies by Method of Equivalent Sources, *Sov. Phys. Acoust.*, Vol. 36, 1990, pp. 334-338.
10. M. Ochmann, The Source Simulation Technique for Acoustic Radiation Problem, *Acustica*, Vol. 81, 1995, pp. 512-527.
11. M. Ochmann, The Full-Field Equations for Acoustic Radiation and Scattering, *J. Acoust. Soc. Am.*, Vol. 105, 1999, pp. 2574-2584.
12. G. Pavic, Computation of Sound Radiation by Using Substitute Sources, *Acta Acustica united with Acustica* Vol. 91, 2005, pp. 1-16.
13. G. Maidanik, Response of Ribbed Panels to Reverberant Acoustic Fields, *J. Acoust. Soc. Am.*, Vol. 34, 1962, pp. 809-826.
14. C. E. Wallace, Radiation Resistance of a Rectangular Panel, *J. Acoust. Soc. Am.*, Vol. 53, No. 3, 1972, pp. 946-952.
15. B. E. Sandman, Motion of Three-Layered Elastic-Viscoelastic Plate Under Fluid Loading, *J. Acoust. Soc. Am.*, Vol. 57, No. 5, 1975, pp. 1097-1105.
16. B. E. Sandman, Fluid Loading Influence Coefficients for a Finite Cylindrical Shell, *J. Acoust. Soc. Am.*, Vol. 60, No. 6, 1976, pp. 1503-1509.



17. G. Maidanik, The Influence of Fluid Loading on the Radiation from Orthotropic Plates, *J. Sound Vib.*, Vol. 3, No. 3, 1966, pp. 288–299.
18. G. Maidanik, Vibration and Radiative Classification of Modes of a Baffled Finite Panel, *J. Sound Vib.*, Vol. 30, 1974, pp. 447–455.
19. M. C. Gomperts, Radiation from Rigid Baffled, Rectangular Plates with General Boundary Conditions, *Acustica*, Vol. 30, 1995, pp. 320–327.
20. A. S. Nikiforov, Radiation from a Plate of Finite Dimension with Arbitrary Boundary Conditions, *Sov. Phys. Acoust.*, Vol. 10, No. 2, 1964, pp. 178–182.
21. A. S. Nikiforov, Acoustic Interaction of the Radiating Edge of a Plate, *Sov. Phys. Acoust.* Vol. 27, No. 1, 1981.
22. A. Berry, J.-L. Guyader, J. and J. Nicolas, A General Formulation for the Sound Radiation from Rectangular, *J. Acoust. Soc. Am.*, Vol. 37, No. 5, 1991, pp. 93–102.
23. J.-L. Guyader and B. Laulagnet, ‘Structural Acoustic Radiation Prediction: Expanding the Vibratory Response on Functional Basis, *Appl. Acoust.*, Vol. 43, 1994, pp. 247–269.
24. P. R. Stepanishen, Radiated Power and Radiation Loading of Cylindrical Surface with Non-uniform Velocity Distributions, *J. Acoust. Soc. Am.*, Vol. 63, No. 2, 1978, pp. 328–338.
25. P. R. Stepanishen, Modal Coupling in the Vibration of Fluid Loaded Cylindrical Shells, *J. Acoust. Soc. Am.*, Vol. 71, No. 4, 1982, pp. 818–823.
26. B. Laulagnet and J.-L. Guyader, Modal Analysis of Shell Acoustic Radiation in Light and Heavy Fluids, *J. Sound Vib.*, Vol. 131, No. 3, 1989, pp. 397–415.
27. B. Laulagnet and J.-L. Guyader, Sound Radiation from a Finite Cylindrical Ring Stiffened Shells, *J. Sound Vib.*, Vol. 138, No. 2, 1990, pp. 173–191.
28. B. Laulagnet and J.-L. Guyader, Sound Radiation by Finite Cylindrical Shell Covered with a Compliant Layer, *ASME J. Vib. Acoust.*, Vol. 113, 1991, pp. 173–191.
29. E. Rebillard and J.-L. Guyader, Calculation of the Radiated Sound from Coupled Plates, *Acta Acustica*, Vol. 86, 2000, pp. 303–312.
30. O. Beslin and J.-L. Guyader, The Use of “Ectoplasm” to Predict Radiation and Transmission Loss of a Holed Plate in a Cavity, *J. Sound Vib.*, Vol. 204, No. 2, 2000, pp. 441–465.
31. M. J. Crocker and Price, Sound Transmission Using Statistical Energy Analysis, *J. Sound Vib.*, Vol. 9, No. 3, 1969, pp. 469–486.
32. M. N. Sayhi, Y. Ousset, and G. Verchery, Solution of Radiation Problems by Collocation of Integral Formulation in Terms of Single and Double Layer Potentials, *J. Sound Vib.*, Vol. 74, 1981, pp. 187–204.
33. H. A. Schenk, Improved Integral Formulation for Acoustic Radiation Problems, *J. Acoust. Soc. Am.* Vol. 44, 1967, pp. 41–58.
34. G. Chertock, Solutions for Sound Radiation Problems by Integral Equations at the Critical Wavenumbers, *J. Acoust. Soc. Am.*, Vol. 47, 1970, pp. 387–388.
35. K. A. Cunefare, G. Koopman, and K. Brod, A Boundary Element Method for Acoustic radiation Valid for all Wavenumbers, *J. Acoust. Soc. Am.*, 85, 1989, pp. 39–48.
36. A. J. Burton and G. F. Miller, The Application of Integral Equation Methods to the Numerical Solution of Some Exterior Boundary Value Problems, *Proc. Roy. Soc. Lond.*, Vol. 323, 1971, pp. 201–210.
37. J.-L. Guyader, and Th. Loyau, The Frequency Averaged Quadratic Pressure: A Method for Calculating the Noise Emitted by Structures and for Localizing Acoustic Sources, *Acta Acustica*; Vol. 86, 2000, pp. 1021–1027.
38. J. K. Kim and J. G. Ih, Prediction of Sound Level at High Frequency Bands by Mean of Simplified Boundary Element Method, *J. Acoust. Soc. Am.*, Vol. 112, 2002, pp. 2645–2655.
39. J. K. Kim and J. G. Ih, Prediction of Sound Level at High Frequency Bands by Mean of Simplified Boundary Element Method, *J. Acoust. Soc. Am.*, Vol. 112, 2002, pp. 2645–2655.
40. L. P. Franzoni, D. B. Bliss, and J. W. Rouse, An Acoustic Boundary Element Method Based on Energy and Intensity Variables for Prediction of High Frequency Broadband Sound Fields, *J. Acoust. Soc. Am.* Vol. 110, 2001, pp. 3071–3080.
41. J.-L. Guyader, Integral Equation for Frequency Averaged Quadratic Pressure, *Acta Acustica*, Vol. 90, 2004, pp. 232–245.

# CHAPTER 7

## NUMERICAL ACOUSTICAL MODELING (FINITE ELEMENT MODELING)

R. Jeremy Astley  
Institute of Sound and Vibration Research  
University of Southampton  
Southampton, United Kingdom

### 1 INTRODUCTION

The finite element (FE) method has become a practical technique for acoustical analysis and solution of noise and vibration problems. In recent years, the method has become relatively accessible to practicing engineers and acousticians through specialized acoustical codes or as an adjunct to larger general-purpose FE programs. The intention here is not to educate the reader in programming the finite element method for acoustics but rather to present the essential features of the method and to indicate the types of analysis for which it can be used. The accuracy and limitations that may be expected from current models will also be discussed. More advanced FE formulations, which are the subject of research rather than industrial application, will also be reviewed.

### 2 FINITE ELEMENT METHOD

The finite element method emerged in the early 1960s as one of several computer-based techniques competing to replace traditional analytic and graphical methods of structural analysis. It rapidly achieved a position of dominance and spread to other branches of continuum mechanics and engineering physics.

The first indication that the FE approach could be applied to acoustics came with pioneering work by Gladwell, Craggs, Kagawa, and others in the late 1960s and early 1970s.<sup>1</sup> The boundary element (BE) technique was also being developed at this time, and the first commercial computer code to focus specifically on acoustics and vibration embodied both methods.\* The further development of specialized codes for acoustics† and the inclusion of more extensive acoustical capabilities in general-purpose FE codes‡ has continued to the present day.

Accurate prediction of noise has become increasingly important in many areas of engineering design as environmental considerations play a larger role in defining the public acceptance and commercial viability of new technologies. In the aircraft and automotive industries, for example, acceptable levels of interior noise and exterior community noise are critical factors in determining the viability of new engine and airframe

concepts. The need for precise acoustical predictions for such applications acts as a driving force for current developments in BE and FE methods for acoustics.

The question of whether BE or FE methods are the more effective for acoustical computations remains an open one. BE models that discretize only the bounding surface require fewer degrees of freedom but are nonlocal in space. FE models require many more variables but are local in space and time, which greatly reduces the solution time for the resulting equations.<sup>2</sup> In the case of homogeneous, uncoupled problems, it is generally true that BE methods produce a faster solution; certainly this is the case for “fast multipole” BE methods,<sup>3</sup> which are currently unassailable as regards efficiency for scattering computations in homogeneous media. The strength of FE models lies in their general robustness and in their ability to treat inhomogeneous media and to take advantage of the sparse nature of structural discrete models in coupled acoustical-structural computations.<sup>4</sup>

### 3 AN ACOUSTICAL FE MODEL

The FE method is “domain-based”.§ It is based on the notion of polynomial interpolation of acoustic pressure over small but finite subregions of an acoustical domain. A typical¶ FE acoustical model is illustrated in Fig. 1. This shows a three-dimensional FE model for an acoustical muffler of fairly complex geometry||. The FE *mesh* is formed by dividing the interior of the muffler into a large number of nonoverlapping *elements*. These are subregions of finite extent, in this case tetrahedra. A finite number of *nodes* define the topology of each element. These are placed on the vertices, edges, or surfaces of the element or at interior points. In the current instance, the nodes are placed at the four vertices of the tetrahedron. The FE method facilitates the use of an *unstructured*

\*SYSNOISE, released by Dynamic Engineering in 1988.

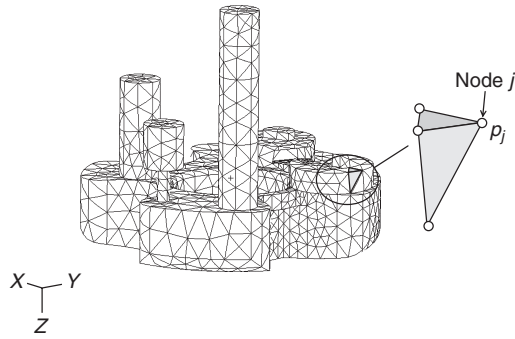
†For example, SYSNOISE, ACTRAN, and COMET.

‡For example, MSC/NASTRAN, ANSYS, and ABAQUS.

§It is based on a discrete model for the entire solution domain. It differs in this regard from the Boundary Element Method (BEM) which involves a discretization only of the bounding surfaces of the region.

¶The model is “typical” in that it represents the sort of acoustical problem that can be treated in a routine fashion by commercially available FE acoustical codes.

||Courtesy of Free Field Technologies S. A. (FFT). The mesh shown was used for an acoustical study using MSC-Actran.



**Figure 1** Acoustical finite element mesh and topology of a single element (enlarged).

mesh, in that elements can vary arbitrarily in size and position provided that contiguous elements are joined node for node in a “compatible” way. This in turn facilitates automatic mesh generation for arbitrarily shaped domains, an important practical consideration. The FE model differs in this regard from low-dispersion finite difference (FD) schemes,<sup>5</sup> which have also been applied to acoustical problems but which rely upon a “structured” mesh in which grid points are aligned in regular rows or planes.\*

In the FE formulation, the acoustic pressures at each node— $p_j$ , say, at node  $j$ —become the *degrees of freedom* of a discrete model. For problems of linear acoustics, the resulting equations are linear in the unknown nodal pressures. They must then be solved at each instant in time in the case of a transient solution or for each frequency of interest in the case of time harmonic excitation. The approximate FE solution exists not just at the nodes but at all points throughout the elements. The nature of the interpolation used within an element is central to the FE concept. It leads to the notion of *shape functions*, which define the variation of the dependent variable in terms of nodal values. The ability of the mesh to accurately represent the physical solution depends upon the complexity of the shape functions and the size of the elements. Central to estimates of accuracy in acoustical problems is the relationship between the node spacing and the characteristic wavelength of the solution, often characterized as a target figure for “nodes per wavelength.”

The following types of analysis can be performed by current FE acoustical codes, some more routinely than others:

- Calculation of the natural frequencies and eigenmodes of acoustical enclosures
- Calculation of the response of interior acoustic volumes to structural excitation and/or distributed acoustic sources

- Coupled acoustical-structural analysis of types 1 and 2
- Propagation through porous media and absorption by acoustically treated surfaces
- Radiation and scattering in unbounded domains
- Transmission in ducts and waveguides
- The analysis of acoustic propagation on mean flows

Not *all* of these capabilities are available in *all* program. Indeed, they have been listed roughly in order of increasing complexity. The first two or three will be found in many general-purpose, predominantly structural FE codes while the remainder are progressively the preserve of codes that specialize in acoustics and vibration. Most of these analyses are performed in the frequency domain.

The remainder of this chapter is organized in the following way. The field equations and boundary conditions of linear acoustics are introduced in Section 4. A derivation of the discrete FE equations is given in Section 5, followed by a discussion of the types of discrete analysis that can then be performed. Element interpolation and its impact on accuracy and convergence are detailed in Section 6. Applications to ducts and waveguides are dealt with in Section 7, and the use of FE models for unbounded problems is covered in Section 8. FE models for flow acoustics are discussed in Section 9. The particular issues involved in the solution of very large sets of FE equations are reviewed in Section 10, along with current attempts to reduce problem size by using functions other than polynomials as a basis for FE models. Some general comments follow in Section 11.

## 4 EQUATIONS OF ACOUSTICS

### 4.1 Acoustic Wave Equation and the Helmholtz Equation

The acoustic pressure  $P(\mathbf{x}, t)$  at location  $\mathbf{x}$  and time  $t$  in a quiescent, compressible, lossless medium is governed by the linearized wave equation

$$\rho_0 \nabla \cdot \left( \frac{1}{\rho_0} \nabla P \right) - \frac{1}{c_0^2} \frac{\partial^2 P}{\partial t^2} = S(\mathbf{x}, t) \quad (1)$$

where  $\rho_0(\mathbf{x})$  and  $c_0(\mathbf{x})$  are the local density and sound speed, and  $S(\mathbf{x}, t)$  is a distributed acoustic source<sup>†</sup>. The corresponding acoustic velocity  $\mathbf{U}(\mathbf{x}, t)$  is related to the acoustic pressure by the linearized inviscid momentum equation

$$\frac{\partial \mathbf{U}}{\partial t} = -\frac{1}{\rho_0} \nabla P \quad (2)$$

In the case of time harmonic disturbances of radian frequency  $\omega$ , for which  $P(\mathbf{x}, t) = p(\mathbf{x})e^{i\omega t}$ , the resulting

\*There are greater similarities between finite element and finite volume schemes, see subsequent comments in Section 9.2.

<sup>†</sup>Often expressed in terms of monopole, dipole, and quadrupole components.

complex pressure amplitudes  $p$  and velocity amplitude  $\mathbf{u}^*$  satisfy

$$\rho_0 \nabla \cdot \left( \frac{1}{\rho_0} \nabla p \right) + k^2 p = s \quad \text{where} \quad i\omega \mathbf{u} = -\frac{1}{\rho_0} \nabla p \quad (3)$$

where  $k$  is the characteristic wavenumber ( $= \omega/c_0$ ). Equation (1) or (3) form the starting point for most FE acoustical models. If the acoustic medium is homogeneous ( $\rho_0, c_0$  constant) Eq. (3) reduces to the standard Helmholtz equation.

#### 4.2 Acoustical Boundary Conditions

Acoustical boundary conditions applied on a bounding surface  $\Gamma$  with a unit outward normal  $\hat{\mathbf{n}}$  include the following “standard” cases:

**A Rigid Impervious Boundary** The normal component of the acoustic velocity is zero on such a boundary. From Eq. (2) this gives

$$\nabla P \cdot \hat{\mathbf{n}} = 0 \quad \text{or} \quad \nabla p \cdot \hat{\mathbf{n}} = 0 \quad (4)$$

**A Locally Reacting Boundary (Frequency Domain)** The performance of a locally reacting acoustical surface is characterized by a frequency-dependent normal impedance  $z(\omega)$ , such that  $p(\omega) = z(\omega)u_n(\omega)$  where  $u_n = \mathbf{u} \cdot \hat{\mathbf{n}}$ . By using the second of equations (3) this can be written as a “Robin” boundary condition on acoustic pressure, that is,

$$\nabla p \cdot \hat{\mathbf{n}} = -ikA(\omega)p \quad (5)$$

where  $A(\omega)$  is the nondimensional admittance [ $= \rho_0 c_0 / z(\omega)$ ]. A zero admittance corresponds to rigid impervious boundary [cf. (5) and (4)].

**A Locally Reacting Boundary (Time Domain).** A locally reacting boundary in the time domain is more difficult to define. The inverse Fourier transform of the frequency-domain impedance relationship,  $p(\omega) = z(\omega)u_n(\omega)$ , gives a convolution integral

$$P(t) = \int_{-\infty}^{+\infty} Z(\tau)U_n(t - \tau) d\tau \quad (6)$$

where  $Z(t)$  is the inverse Fourier transform of  $z(\omega)$ . Equation (6) is difficult to implement in practice since it requires the time history of  $U_n(t)$  to be retained for all subsequent times. Also, the form of  $z(\omega)$  must be such that  $Z(t)$  exists and is causal, which is not necessarily the case for impedance models defined empirically in the frequency domain.

\*In the remainder of this chapter, time-domain quantities are denoted by upper-case variables  $P, U, S \dots$  and corresponding frequency-domain quantities by lower case variables  $p, u, s, \dots$ .

A time-domain impedance condition based on expression (6) but suitable for FE implementation has been proposed by Van den Nieuwenhof and Coyette.<sup>6</sup> It gives stable and accurate solutions provided that the impedance can be approximated by a rational expression

$$\frac{z(\omega)}{\rho_0 c_0} = r_1 + \frac{r_2 - r_1}{1 + i\omega r_3} + \frac{i\omega r_4}{1 + i\omega r_5 - \omega^2 / r_6^2} + i\omega r_7 \quad (7)$$

where the constants  $r_1, \dots, r_7$  must satisfy stability constraints. Alternatively, and this has only been implemented in finite difference (FD) models to date rather than FE models, one-dimensional elements can be attached to the impedance surface to explicitly represent the effect of cavity liners.<sup>7</sup>

**A Prescribed Normal Displacement** If the bounding surface experiences a prescribed, structural displacement, continuity of normal acceleration at the surface gives

$$\nabla P \cdot \hat{\mathbf{n}} = \rho_0 \ddot{W} \quad \text{or} \quad \nabla p \cdot \hat{\mathbf{n}} = -\omega^2 \rho_0 w \quad (8)$$

where  $W(\mathbf{x}, t) = w(\mathbf{x})e^{i\omega t}$  is the normal displacement into the acoustical domain.

**The Sommerfeld Radiation Condition** At a large but finite radius  $R$  from an acoustical source or scattering surface, an unbounded solution of the Helmholtz equation must contain only outwardly propagating components. This constraint must be included in any mathematical statement of the problem for unbounded domains. The Sommerfeld condition, that

$$\frac{\partial p}{\partial r} + ikp = o(R^{-\alpha}), \quad (9)$$

ensures that this is the case where  $\alpha = \frac{1}{2}$  or 1 for two-dimensional (2D) and three-dimensional (3D) problems, respectively.

The Sommerfeld condition can be approximated on a distant but finite cylinder (2D) or sphere (3D) by specifying a  $\rho c$  impedance—or unit nondimensional admittance  $A(\omega) = 1$ . This is a *plane damper*, which is transparent to plane waves propagating normal to the boundary. More accurate *spherical* and *cylindrical* dampers, transparent to cylindrical and spherically symmetric waves, are obtained by setting  $A(\omega)$  equal to  $(ik + R^{-1})$  and  $(ik + \frac{1}{2}R^{-1/2})$ , respectively.

Higher order nonreflecting boundary conditions (NRBCs), which can be applied closer to the scattering surface, have also been derived. Many involve higher order radial derivatives, which are difficult to accommodate in a weak Helmholtz sense. The second-order NRBC proposed by Bayliss, Gunzberger, and Turkel<sup>8</sup> is, however, widely used and can be imposed weakly by replacing the admittance  $A(\omega)$  of Eq. (5) by a differential operator involving only first-order radial derivatives.

Many *nonlocal* approximations for the far-field boundary have also been developed but are generally less attractive for FE implementation. These include the DtN approach of Givoli and Keller, mode matching, and coupling to boundary integral schemes. A general review of these methods is found in Givoli's monograph.<sup>9</sup>

## 5 GENERAL FINITE ELEMENT FORMULATION FOR INTERIOR PROBLEMS

Consider an acoustical region  $\Omega$  bounded by a surface  $\Gamma$ . Such an arrangement is illustrated in two dimensions in Fig. 2. The bounding surface  $\Gamma$  is divided into nonoverlapping segments that correspond to an acoustically *hard* segment ( $\Gamma_h$ ), a locally reacting *soft* segment ( $\Gamma_z$ ), and a *structural* boundary ( $\Gamma_{st}$ ) on which a normal displacement  $w$  is prescribed. These are modeled by boundary conditions (4), (5), and (8). The solution domain  $\Omega$  is divided into a discrete number of finite elements. In Fig. 2 these take the form of two-dimensional triangles defined by corner nodes. Many other element topologies are possible (see Section 6).

### 5.1 Trial Solution and Shape Functions

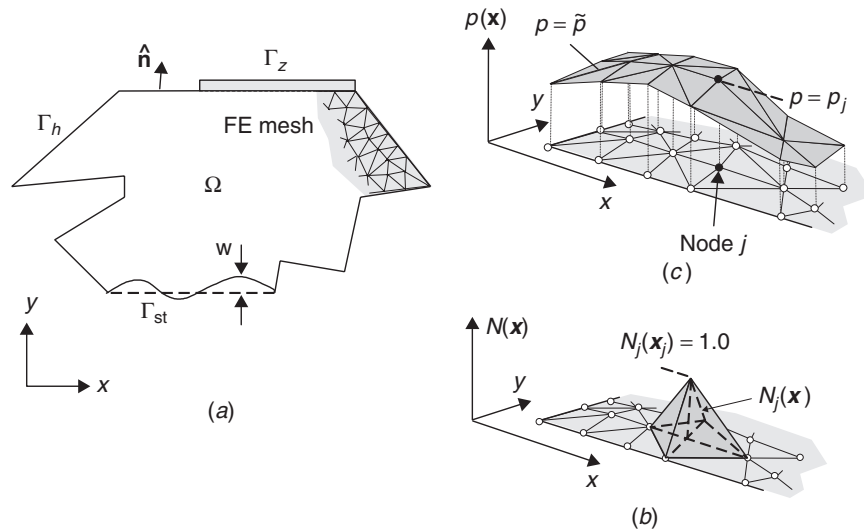
The acoustic pressure  $P(\mathbf{x}, t)$ —or the acoustic pressure amplitude  $p(\mathbf{x}, \omega)$  in the time-harmonic case—are approximated by trial solutions  $\tilde{P}$  or  $\tilde{p}$  of the form

$$\begin{aligned}\tilde{P}(\mathbf{x}, t) &= \sum_{j=1}^n P_j(t) N_j(\mathbf{x}) \quad \text{and} \\ \tilde{p}(\mathbf{x}, \omega) &= \sum_{j=1}^n p_j(\omega) N_j(\mathbf{x})\end{aligned}\quad (10)$$

where  $P_j$  or  $p_j$  denotes nodal values of pressure or pressure amplitude at node  $j$ , and  $n$  is the total number of nodes. The function  $N_j(\mathbf{x})$  is termed a *shape* function. It takes the value of unity at node  $j$  and zero at all other nodes.\* The shape functions act globally as interpolation functions for the trial solution but are defined locally within each element as polynomials in physical or mapped spatial coordinates. For example, the shape functions of the triangular elements shown in Fig. 2a are formed from the basis set  $\{1, x, y\}$ . Within each triangle they take the form  $(a_1 + a_2x + a_3y)$  where  $a_1$ ,  $a_2$ , and  $a_3$  are constants chosen so that the trial solution within the element takes the correct value at each node. This means that the number of polynomial terms in the basis set must be the same as the number of nodes in the element topology (three in this case).

The element shape functions defined in this way combine to form a global shape function  $N_j(\mathbf{x})$  that itself takes a value of unity at node  $j$  and zero at all other nodes. This is indicated by the “hat shaped” function in Fig. 2b. The trial solution itself, which is given by expression (10), is then a summation of these functions weighted by the nodal values of pressure. In the case of the model illustrated in Fig. 2, this gives a trial solution that can be visualized as a piecewise continuous assembly of plane facets when plotted as a surface over the  $x$ - $y$  plane, as shown in Fig. 2c. Although the notion of a global trial solution and of global shape functions are useful in a conceptual sense, all of the operations required to form the finite element equations are performed at the element level.

\*This is not strictly true in the case of hierarchical elements where shape functions are associated with edges or faces rather than with nodes.



**Figure 2** The FE model. (a) Geometry, mesh, and boundary conditions. (b) Global shape function  $N_j(\mathbf{x})$ . (c) Trial solution.

A definition of the shape functions within each element is therefore all that is needed in practice.

## 5.2 Weak Variational Formulation

Consider the problem posed by Eq. (3) subject to boundary conditions (4), (5), and (8). By multiplying Eq. (3) by a test function  $f(\mathbf{x})$ , integrating over  $\Omega$  and applying the divergence theorem, we obtain an equivalent integral statement that

$$\begin{aligned} \int_{\Omega} \frac{1}{\rho_0} [\nabla f \cdot \nabla \tilde{p} - \frac{\omega^2}{c_0^2} f \tilde{p}] d\Omega + i\omega \int_{\Gamma_z} \frac{A(\omega)}{\rho_0 c_0} f \tilde{p} d\Gamma \\ + \int_{\Gamma_{st}} \omega^2 f w_n d\Gamma + \int_{\Omega} \frac{1}{\rho_0} f s d\Omega = 0 \end{aligned} \quad (11)$$

where  $f$  is continuous and differentiable.\* The second and third terms in the above expression are obtained by assuming that the normal derivatives of pressure on  $\Gamma_z$  and  $\Gamma_{st}$  satisfy Eqs. (5) and (8). This integral statement therefore embodies a *weak* expression of these boundary conditions. Note also that when the admittance is zero, the integral over  $\Gamma_z$  disappears, so that the default *natural* boundary condition on an external surface—if no other condition is specified—is that of a hard acoustical surface.

## 5.3 Discrete Equations

When the trial solution of expression (10) is substituted into the integral relationship (11), a linear equation is obtained in the unknown coefficients  $p_j(\omega)$ . By using a complete set of test functions,  $f_k$  say ( $k = 1, 2, \dots, n$ ), a complete set of linear equations is generated. This requires the selection of suitable test functions that satisfy appropriate continuity requirements. The shape functions  $N_j(x)$  are a natural choice. By setting  $f_k(\mathbf{x}) = N_k(\mathbf{x})$ , ( $k = 1, \dots, n$ ), we obtain a symmetric system of linear equations:

$$[\mathbf{K} + i\omega\mathbf{C} - \omega^2\mathbf{M}]\{\mathbf{p}\} = \{\mathbf{f}_{st}\} + \{\mathbf{f}_s\} \quad (12)$$

where  $\mathbf{M}$ ,  $\mathbf{K}$ , and  $\mathbf{C}$  are acoustic *mass*, *stiffness*, and *damping* matrices given by

$$\begin{aligned} M_{jk} &= \int_{\Omega} \frac{N_j N_k}{\rho_0 c_0^2} d\Omega, & K_{jk} &= \int_{\Omega} \frac{\nabla N_j \cdot \nabla N_k}{\rho_0} d\Omega, \\ C_{jk} &= \int_{\Gamma_z} \frac{A(\omega)}{\rho_0 c_0} N_j N_k d\Gamma \end{aligned} \quad (13)$$

and the vectors  $\{\mathbf{f}_{st}\}$  and  $\{\mathbf{f}_s\}$  are forcing terms due to structural excitation and acoustic sources. They are given by

$$\begin{aligned} \{f_{st}\}_j &= - \int_{\Gamma_w} \omega^2 N_j w_n d\Gamma \quad \text{and} \\ \{f_s\}_j &= - \int_{\Omega} \frac{1}{\rho_0} N_j s d\Omega \end{aligned} \quad (14)$$

The above integrals are evaluated element by element and *assembled* to form the global matrices  $\mathbf{K}$ ,  $\mathbf{C}$ , and  $\mathbf{M}$  and the forcing vectors  $\mathbf{f}_s$  and  $\mathbf{f}_{st}$ . The *assembly* procedure is common to all FE models and is described elsewhere.<sup>10</sup> Numerical integration is generally used within each element.

## 5.4 Types of Analysis

**Frequency Response** The solution of Eq. (12) over a range of frequencies gives the forced acoustical response of the system. The presence of bulk absorbing materials within such a system is accommodated quite easily since continuity of normal particle velocity is weakly enforced at any discontinuity of material properties within  $\Omega$ . Inhomogeneous reactive regions within the finite element model are, therefore, treated by using different material properties— $c_0$  and  $\rho_0$ —within different elements. Absorptive materials can be modeled in the same way by using complex values of sound speed and density. Empirical models for rigid-porous materials that express  $c_0$  and  $\rho_0$  in terms of a nondimensional parameter  $(\sigma/\rho_0 f)$  where  $\sigma$  is the flow resistivity and  $f$  the frequency<sup>11</sup> are commonly used. Elastic-porous materials can also be modeled, but here additional FE equations for the displacement of the elastic frame must be used to supplement the acoustic equations.<sup>12,13</sup>

**Normal Mode Analysis** When the forcing term is removed from Eq. (12) and if no absorption is present, the undamped acoustic modes of the enclosure are solutions of the eigenvalue problem:

$$[\mathbf{K} - \omega^2\mathbf{M}]\{\mathbf{p}\} = 0 \quad (15)$$

The eigenmodes obtained in this way are useful in characterizing the system but can also be used as a reduced basis with which to calculate its frequency response using Eq. (12), as in analogous structural models.<sup>10</sup>

**Acousto-structural Coupling** Structural coupling can be included by supplementing Eq. (12) with an equivalent set of FE equations for the structural displacement on  $\Gamma_{st}$ . This allows the effect of the acoustical loading on the structure to be modelled and *vice versa*. If the trial solution of the structural FE model is analogous to expression (10), but with

\*More formally,  $f \in H^1(\Omega)$  where  $H^1(\Omega) = \{q: \int_{\Omega} [|\nabla q|^2 + |q|^2] d\Omega < \infty\}$ .

nodal displacements  $w_j$  ( $j = 1, 2, \dots, n_{st}$ ) as degrees of freedom, a coupled system of equations results of the form

$$\begin{bmatrix} \mathbf{K} & \mathbf{0} \\ -\mathbf{A}^T & \mathbf{K}_{st} \end{bmatrix} + i\omega \begin{bmatrix} \mathbf{C} & \mathbf{0} \\ \mathbf{0} & \mathbf{C}_{st} \end{bmatrix} - \omega^2 \begin{bmatrix} \mathbf{M} & -\rho\mathbf{A} \\ \mathbf{0} & \mathbf{M}_{st} \end{bmatrix} \begin{bmatrix} \mathbf{p} \\ \mathbf{w} \end{bmatrix} = \begin{bmatrix} \mathbf{f}_s \\ \mathbf{f}_{ext} \end{bmatrix} \quad (16)$$

where  $\mathbf{K}_{st}$ ,  $\mathbf{C}_{st}$ , and  $\mathbf{M}_{st}$  are stiffness, damping, and mass matrices for the structure, and  $\mathbf{A}$  is a coupling matrix that contains integral products of the acoustical and structural shape functions over  $\Gamma_{st}$ . The vector  $\mathbf{f}_{ext}$  contains external nodal forces and moments applied to the structure. The unsymmetric nature of the coupled mass and stiffness matrices can be inconvenient. If so, Eq. (16) can be symmetrized. This is most simply achieved by using the velocity potential rather than the pressure to describe the acoustic field, but other methods are also used.<sup>14</sup>

**Transient Response** Provided that the acoustic damping matrix is frequency independent, the inverse Fourier transform of Eq. (12) yields an equivalent set of transient equations:

$$[\mathbf{K}]\dot{\mathbf{P}} + [\mathbf{C}]\dot{\mathbf{P}} + [\mathbf{M}]\ddot{\mathbf{P}} = \{\mathbf{F}_{st}\} + \{\mathbf{F}_s\} \quad (17)$$

where  $\mathbf{F}_{st}$  and  $\mathbf{F}_s$  are obtained from time-domain versions of expressions (14).<sup>\*</sup> The above equations can be integrated in time by using a numerical time-stepping

scheme. Implicit schemes, such as Newmark- $\beta$ , are favored for their accuracy and stability, but explicit and indirect implicit schemes are used for large problems, being less memory intensive and more suited to parallel implementation.<sup>15,16</sup> In cases where frequency-dependent acoustic damping is present, the derivation of suitable time-domain equations is less straightforward. When the damping arises from a frequency-dependent local admittance, for example, a suitable transient impedance boundary condition, along the lines of those discussed in Section 4.2, must be incorporated in to the discrete problem. An example of such a treatment is given in Ref. 6.

## 6 ELEMENT ORDER, ACCURACY, AND CONVERGENCE

### 6.1 Types of Element

The elements commonly used for acoustical analysis—and indeed for general FE application—are based on polynomial shape functions of physical or mapped coordinates. Some elements of this type are shown in Fig. 3. Triangular and quadrilateral elements for two-dimensional analysis are shown in the first two columns of the figure, and analogous tetrahedral and hexahedral elements for three dimensions are shown in the last two columns. In the case of the 2D quadrilateral and 3D hexahedral elements the shape functions are obtained in terms of mapped coordinates  $(\zeta, \eta)$  and  $(\zeta, \eta, \xi)$  rather than Cartesian coordinates  $(x, y, z)$ . Details of the shape functions for such elements are given in general FE texts<sup>17</sup> and will not be repeated here. In Fig. 3 the appropriate polynomial basis set is indicated under each element. Note that the number of polynomial terms in each case is equal to the number of nodes. It is simple also to

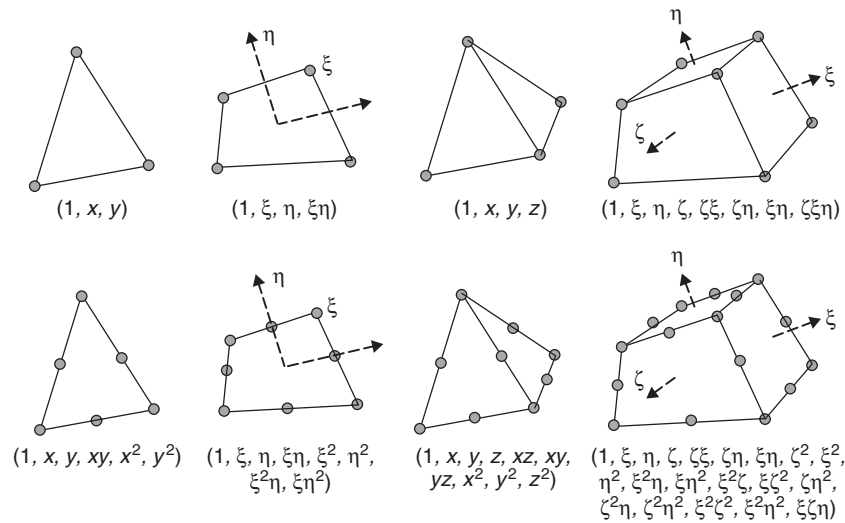


Figure 3 Element topologies.

<sup>\*</sup>A similar set of time-domain equations can be obtained from Eq. (16) for the coupled structural-acoustical problem.

verify that by holding  $x$  or  $y$  or  $z$  (or  $\zeta$  or  $\eta$  or  $\xi$ ) constant, the trial solution within each element varies linearly with the other variables for elements in the top row of Fig. 3 and quadratically for those in the bottom row. The polynomial order  $p$  of these elements is  $p = 1$  and  $p = 2$ , respectively. Elements of arbitrary polynomial order can be formulated quite easily, but in practice elements of orders  $p > 2$  are not common in general-purpose FE codes. The use of  $p$  elements of higher order is, however, attractive as a means of combatting pollution error in acoustics (see Section 6.2). High-order *spectral elements*, which substitute orthogonal polynomials for node-based Lagrangian shape functions, are also used. The reader is referred elsewhere<sup>18</sup> for a more complete discussion of such elements.

## 6.2 Numerical Error

The error present in the FE solution derives from two sources: *approximability* error and *pollution* error. The approximability error is a measure of the *best approximation*, which can be achieved for a given spatial interpolation. The pollution error is associated with the numerical representation of phase or dispersion and depends on the variational statement itself.

**Approximability** The best approximation that can be achieved by representing a sinusoidal, time-harmonic disturbance by piecewise continuous polynomial interpolation gives a global error that is proportional to  $(kh)^p$  where  $k$  is the wavenumber,  $h$  is the node spacing, and  $p$  is the polynomial order of the shape functions. This is the approximability error of the discrete solution.

In terms of the characteristic wavelength  $\lambda$  of a solution, the approximability error decreases as  $(\lambda/h)^{-p}$  where  $\lambda/h$  can be interpreted in a physical sense as the number of nodes that are used to model a single wavelength. The error will decrease more rapidly for higher order elements than for lower order ones due to the index  $p$ . An absolute lower limit is  $\lambda/h = 2$  (2 nodes per wavelength), which corresponds to an alternating sawtooth pattern in the discrete solution at successive nodes. Larger values of  $\lambda/h$  are clearly needed for any reasonable FE representation using polynomial shape functions. A rule of thumb that is often used is *ten nodes per wavelength*. This is adequate at low frequencies when few wavelength variations are present within the computational domain. It should be used with great caution at higher frequencies for reasons that will become apparent shortly.

**Pollution Effect** The pollution error in the FE solution is significant when the wavelength of the disturbance is small compared to the dimensions of the computational domain. The magnitude of the pollution effect depends on the underpinning variational statement. It is associated with the notion of numerical dispersion. Small phase differences between the exact and computed solution may not contribute significantly to numerical error over a single

wavelength but accumulate over many wavelengths to give a large global error. The pollution error therefore varies not only with the mesh resolution (nodes per wavelength) but also with the absolute value of frequency. The overall global error for a conventional variational FE solution of the type discussed so far takes the form<sup>19</sup>

$$\epsilon = C_1(kh)^p + C_2kL(kh)^{2p} \quad (18)$$

where  $L$  is a geometric length scale,  $p$  is the element order, and  $C_1$  and  $C_2$  are constants. The first term represents the approximability error, the second the pollution effect. This can be appreciable even for modest values of  $kL$ . This is illustrated by the data in Table 1, which is obtained for linear ( $p = 1$ ) one-dimensional elements.\* The numbers of nodes per wavelength required to achieve a global error  $\epsilon^\dagger$  of less than 10% are tabulated for increasing values of  $kL$ . In multidimensional situations the pollution effect is further complicated by considerations of element orientation with respect to wave direction.<sup>20</sup>

Given the form of expression (18), the accuracy of a solution at a given frequency can be improved either by refining the mesh and reducing  $h$  for a fixed value of  $p$  ( $h$  refinement) or by retaining the same mesh and increasing the order of the elements ( $p$  refinement) or by some selective application of both techniques ( $h$ - $p$  refinement).<sup>18</sup>  $h$  refinement remains the most common approach in acoustical applications, although the use of second-order elements rather than linear or bilinear ones is widely recognized as being worthwhile if they are available. Higher order *spectral* elements (typically  $p \sim 5$ ) have, however, been shown to be effective for short-wave problems,<sup>21</sup> and high-order elements of this type ( $p \sim 10 - 15$ ) have been used in transient FE modeling of seismic wave propagation.<sup>22</sup> A difficulty encountered in using very high order elements is that the conditioning of the equations deteriorates as the order increases, particularly when Lagrangian shape functions are used. This is reduced by the use of orthogonal polynomials as shape functions, but the degrees of freedom then relate to edges or faces rather than nodes (for details see Ref. 18). More radical methods for combatting pollution error by using nonpolynomial interpolation will be discussed in Section 10.3.

**Table 1 Mesh Resolution Required to Ensure Global Solution Error  $\epsilon$  Does Not Exceed 10%<sup>a</sup>**

$kL$	10	50	100	200	400	800
Nodes/ $\lambda$	16	25	38	57	82	107

<sup>a</sup>1D uniform duct.  $p = 1$ .

\*This table contains selected data from Ref. 19.

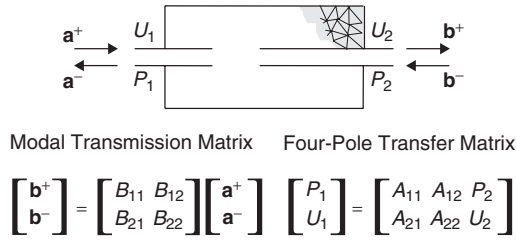
$\epsilon = \frac{1}{L} \int_0^L |p_c - p_{ex}| dx$ ,  $p_c$  computed solution,  $p_{ex}$  exact solution.



## 7 DUCTS AND WAVEGUIDES

### 7.1 Transmission in Nonuniform Ducts

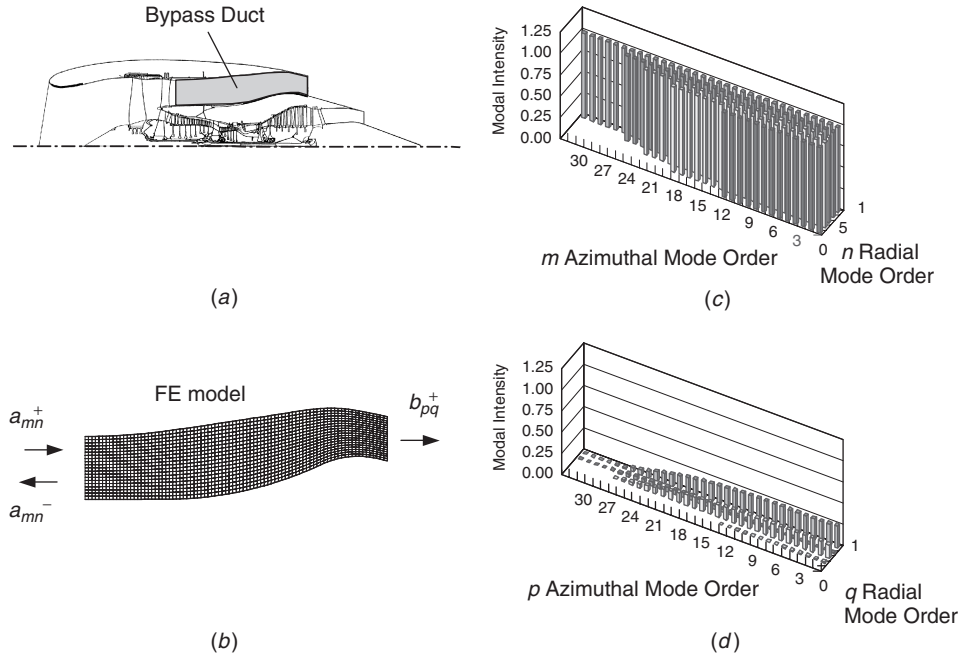
FE models for transmission in nonuniform ducts differ from those for general interior problems only in their treatment of boundary conditions at the inlet and outlet planes. Often it is possible to neglect higher order modes at the inlet and outlet, and in such cases the most straightforward approach is to use the *four-pole* method proposed by Young and Crocker.<sup>23</sup> This characterizes the transmission properties of an arbitrary duct by means of a transfer matrix that relates arbitrary inlet values of pressure and volume velocity,  $P_1$  and  $U_1$ , to equivalent outlet values,  $P_2$  and  $U_2$  (see Fig. 4). The four terms in the transfer matrix are obtained by solving an FE problem for two



**Figure 4** Characterization of acoustical transmission in a nonuniform duct.

different combinations of inlet and outlet parameters. This method can also be applied to systems with mean flow<sup>24</sup> and to more complex branched systems by combining transfer matrices for individual components arranged either in series or in parallel.<sup>25</sup> A modification proposed by Craggs permits the behavior of a limited number of higher order modes to be modeled in a similar way.<sup>26</sup>

Such models do not, however, deal accurately with systems where an incident mode is scattered into multiple higher order modes by nonuniform geometry or the presence of liners. Modal boundary conditions should then be used. These involve matching the FE solution at the inlet and outlet planes to truncated series of positively and negatively propagating modes. This yields a set of equations that contains both nodal values of pressure within the duct and modal coefficients at the end planes as unknown variables. The solution of these equations gives a transmission matrix  $\mathbf{B}$  —see Fig. 4 —that relates vectors of the modal coefficients at the inlet ( $\mathbf{a}^+$  and  $\mathbf{a}^-$ ) to those at the outlet ( $\mathbf{b}^+$  and  $\mathbf{b}^-$ ). Such models have been used extensively for propagation in turbofan inlet and bypass ducts where many modes are generally cut-on.<sup>27</sup> A solution for propagation in a lined axisymmetric bypass duct is shown in Fig. 5.<sup>28</sup> The power in each cut-on mode is plotted against azimuthal and radial mode order at the inlet and exhaust planes. Equipartition of incident modal power is assumed at the inlet. The selective effect of the acoustical treatment in attenuating specific modes is evident in the solution. Although intended for



**Figure 5** FE computation of transmission in a turbofan bypass duct.<sup>28</sup> (a) Duct geometry, (b) FE mesh and modal variables, (c) incident modal powers, and (d) transmitted modal powers.

multimode solutions, the modal approach can also be applied to exhaust and induction systems where only one mode is cut-on.<sup>29</sup>

## 7.2 Eigenmodes in Uniform Ducts

The acoustic field in a prismatic duct of constant cross section can be expressed as a sum of discrete eigenmodes. These are solutions of the homogeneous acoustic wave equation [see Eq. (1)], which take the form

$$P(\mathbf{x}, t) = \psi(x, y)e^{i\omega t - ik\lambda z} \quad (19)$$

where  $z$  is the duct axis,  $\psi(x, y)$  is a transverse eigenmode and  $\lambda$  is a nondimensional axial wavenumber. The attenuation per unit length along the duct is proportional to the imaginary part of  $k\lambda$ . Substitution of expression (19) into the homogeneous version of (1) gives a two-dimensional Helmholtz equation of the form

$$\rho_0 \nabla_2 \left( \frac{1}{\rho_0} \nabla_2 p \right) + k^2 (1 - \lambda^2) p = 0 \quad (20)$$

where  $\nabla_2 = (\partial/\partial x, \partial/\partial y)$ . A finite element discretization in two dimensions analogous to that of Section 5 then gives an algebraic eigenvalue problem of the form

$$[\mathbf{K} + i\omega\mathbf{C} - \omega^2\mathbf{M}]\{\psi\} = -\lambda^2\omega^2[\mathbf{M}]\{\psi\} \quad (21)$$

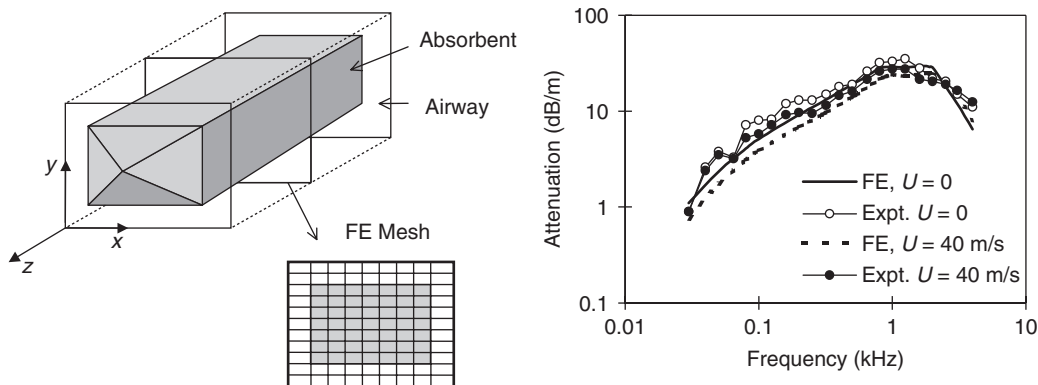
where  $[\mathbf{K}]$ ,  $[\mathbf{C}]$ , and  $[\mathbf{M}]$  are two-dimensional equivalents of expressions (13) obtained by integrating over the duct cross section and around its perimeter. Eigenproblems of this type can be formed for local and bulk lined ducts and can include also structural coupling with the duct walls. The inclusion of mean flow in the airway of such ducts leads to a higher order problem in  $\lambda$ .<sup>30</sup> Results obtained from such a study are shown in Fig. 6. This shows an FE model for one cell of a “bar silencer” and includes a comparison of

measured and predicted axial attenuations. Such models have proven to be reliable predictors of the *least attenuated* mode that often dominates observed behavior. A similar approach has been applied in a modified form to predict attenuation in the capillary pores of automotive catalytic converters.<sup>31</sup>

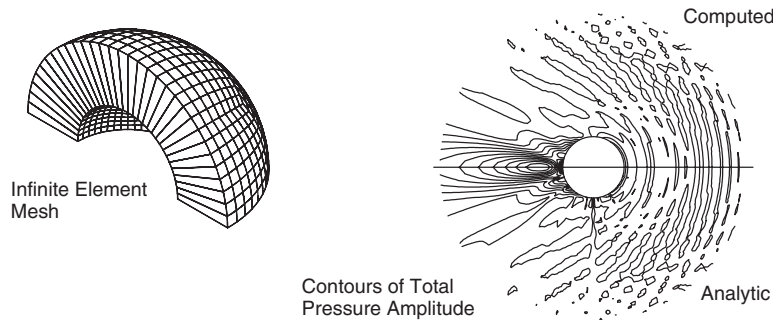
## 8 UNBOUNDED PROBLEMS

New issues arise when FE methods are applied to unbounded problems. First, how to construct an artificial outer boundary to the FE domain, which will be transparent to outgoing disturbances, and second, how to reconstruct a far-field solution, which lies beyond the computational domain. Both issues are resolved by BE schemes that require no truncation surface and that embody an exact far-field representation. However, the BE approach is restricted in practice to problems for which an analytic free field Green’s function exists—in effect homogeneous problems. With this proviso, BE method schemes, particularly those based on *fast multipole* and associated methods<sup>3,32</sup> currently offer the most efficient solution for homogeneous exterior problems. The case for traditional BE method is less conclusive.<sup>2</sup> Domain-based FE methods are important, however, in situations where the exterior field is inhomogeneous—due to temperature gradients or convective terms, for example—or at lower frequencies in situations where problem size is less important than ease of implementation and robustness, particularly in terms of coupling to structural models.

Many methods have been used to terminate the computational domain of exterior FE models. A comprehensive review of them lies beyond the scope of this chapter. Many are described in Refs. 33 and 34. They divide broadly into schemes that are local and non-local on the truncation boundary. *Nonlocal* methods include traditional mode matching, FE-DtN, and FE-BE models in which the FE domain is matched to a BE model at the truncation boundary. *Local* methods are generally preferable, especially for larger problems. FE



**Figure 6** FE model for bar silencer eigenmodes and comparison with measured values of axial attenuation. (Reprinted from *Journal of Sound and Vibration*, Vol. 196, R. J. Astley and A. Cummings, Finite Element Computation of Attenuation, in Bar-Silencers and Comparison with Experiment, 1995, pp. 351–369, with permission from Elsevier.)



**Figure 7** IE model for scattering by a rigid sphere ( $kD = 20$ , element order = 10). (Reprinted with permission from R. J. Astley et al., *Journal of the Acoustical Society of America*, Vol. 103, 1998, pp. 49–63. Copyright 1998, Acoustical Society of America.)

implementation of the first- or second-order boundary conditions of Bayliss, Gunzberger, and Turkel<sup>8</sup> have been used extensively. Local conditions developed by Engquist and Majda and by Feng have also been used. Both are reviewed and summarized in Ref. 35. Absorbing and perfectly matched layers (PMLs) are also used, as are infinite element (IE) schemes. The latter have proved the most robust of all these methods for commercial exploitation and are implemented in major commercial codes such as SYSNOISE, ACTRAN, ABAQUS, and COMET. They have the advantage of being simple to integrate within conventional FE programs while offering a variable, high-order nonreflecting boundary condition. The order of the boundary treatment can be increased indefinitely subject only to conditioning issues at high orders.<sup>36</sup> The use of relatively high-order elements (typically in the range 10 to 15) means that an anechoic termination can be applied very close to the radiating or scattering body. The far-field directivity is given directly by such formulations and does not necessitate a Kirchhoff or Ffowcs-Williams Hawkins integration. The effectiveness of high-order infinite elements in resolving complex exterior fields is illustrated in Fig. 7. This shows a comparison of the exact and computed sound pressure amplitude for a plane wave scattered by a rigid sphere of diameter  $D$  for  $kD = 20$ . The exterior region is modeled entirely by infinite elements. These are shown on the left of the figure, truncated at  $r = D$ . Such models can also be used in the time domain<sup>37</sup> and extended to spheroidal and elliptical coordinate systems.<sup>38</sup>

## 9 ACOUSTIC PROPAGATION ON MEAN FLOWS

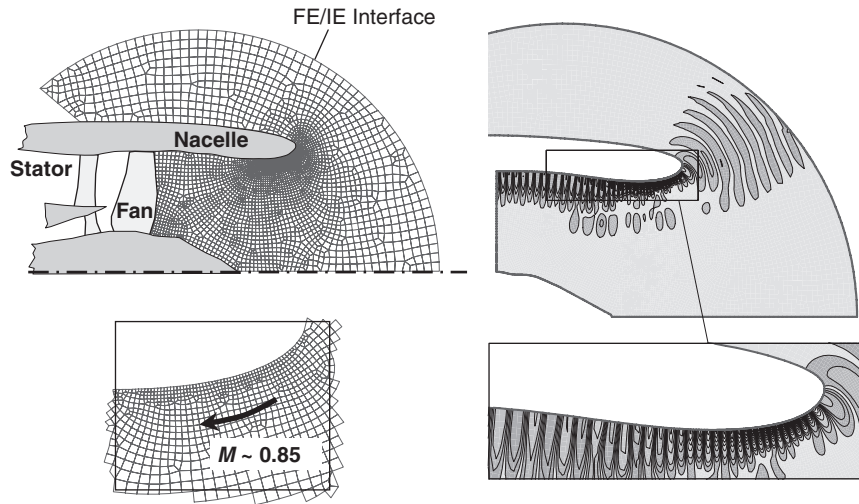
### 9.1 Irrotational Mean Flow

When mean flow is present, the propagation of an acoustical disturbance is modified by convection. When the mean flow is irrotational, the convective effect can be modeled by formulating the acoustical problem in terms of the acoustic velocity potential and by solving a convected form of the wave equation or Helmholtz equation. FE and IE models based on

this approach have been used quite extensively to predict acoustic propagation in aeroengine intakes.<sup>28,39</sup> A solution of this type is illustrated in Fig. 8. This shows the FE mesh and solution contours for a high-order spinning mode that is generated on the fan plane of a high bypass ratio turbofan engine and propagates to the free field. Increased resolution is required in the FE mesh in the near-sonic region close to the lip of the nacelle to capture the wave shortening effect of the adverse mean flow. The solution shown was obtained using the ACTRAN-AE code with quadratic finite elements and infinite elements of order 15. High-order spectral elements have been applied to similar three-dimensional problems with flow.<sup>21</sup>

### 9.2 Rotational Mean Flow

When the mean flow is rotational, the acoustical disturbance is coupled to vortical and entropy waves. The linearized Euler equations (LEE) must then be used. Structured, high-order, dispersion relation preserving (DRP) finite difference schemes<sup>5</sup> are the method of choice for such problems, but FE time-domain schemes based on the discontinuous Galerkin method (DGM) have also proved effective. These combine low numerical dispersion with an unstructured grid.<sup>40</sup> Time-domain DGM is also well suited to parallel implementation. As with other time-domain LEE methods, DGM has the disadvantage, however, of introducing shear flow instabilities that must be damped or filtered to preserve the acoustical solution.<sup>41</sup> Frequency-domain FE models based on the LEE formulation avoid these problems but are known to be unstable when a conventional Bubnov–Galerkin formulation is used with continuous test functions. A streamwise upwind Petrov Galerkin (SUPG) FE model has been proposed to remedy this deficiency.<sup>42</sup> Alternatively, the Galbrun equations, which pose the flow acoustical problem in terms of Lagrangian displacements, can be used as the basis for a stable frequency-domain mixed FE model for propagation on shear flows.<sup>43</sup> Many uncertainties remain, however, regarding the treatment of shear instabilities and time-domain impedance boundary conditions in rotational flows.



**Figure 8** FE/IE solution for radiation from an engine intake with mean flow. FE mesh (left). Contours of instantaneous sound pressure (right). A spinning mode of azimuthal order 26 and radial order 1 is incident at the fan.  $kR = 34$ ,  $M_{\max} = 0.85$ .

## 10 SOLVING LARGE PROBLEMS

Practical difficulties arise in solving the FE equations at high frequencies, particularly for three-dimensional problems where very large numbers of nodes are needed for *short-wavelength* solutions. This situation arises when the computational domain is much larger than the characteristic acoustic wavelength. Such problems are not uncommon in application areas such as medical ultrasound, aeroacoustics, underwater structural acoustics, and outdoor propagation. For two-dimensional or axisymmetric problems, the situation is tenable. If the *10 nodes per wavelength* rule is applied in two dimensions to a solution domain that extends for 10 acoustic wavelengths in each direction, the required mesh contains approximately 10,000 nodes. Such problems can be solved relatively easily using a direct solver and require only seconds or minutes of CPU time on a single 32-bit processor. An equivalent three-dimensional model of the same dimensions and with a similar acoustic wavelength and mesh resolution contains approximately 1,000,000 nodes. This poses an altogether different computational challenge. The direct solution of such a problem scales poorly with problem size,\* and requires very many CPU hours and unacceptable memory requirements. Different approaches must, therefore, be adopted for such problems. Several strategies exist.

### 10.1 Indirect Solvers

The use of indirect solvers allows fully condensed storage to be used for the assembled coefficient matrices

\*Technically, the scaling is as the third power of the matrix dimension for conventional direct solvers, but better performance is observed when advanced sparse solvers are used.

and greatly reduces overall storage requirements. Iterative solvers can also exploit fast vector operations and lend themselves to efficient parallel computation. However, the rate of convergence of standard iterative solvers<sup>†</sup> is poor for discrete Helmholtz problems and deteriorates with frequency. Diagonal and incomplete LU preconditioning leads to some improvement for problems of modest size,<sup>44</sup> but effective and robust general preconditioners for the Helmholtz problem have yet to be developed. An interesting variant here is the fictitious domain method<sup>45</sup> in which a regular rectangular mesh is used over most of the domain, adjusted only at domain boundaries to accommodate irregular shapes. The regularity of the mesh permits the construction of a highly effective preconditioner and permits the solution of very large homogeneous Helmholtz problems using an indirect parallel solver.

### 10.2 Domain Decomposition

Irrespective of whether iterative or direct methods are used, the key to developing a practical FE acoustical code for large problems lies currently in efficient parallelization on a distributed memory system such as a PC cluster. By distributing the solution over  $N$  processors the required CPU time can in theory be reduced by a factor  $1/N$ . This sharing of the solution across a number of processors is commonly achieved by domain decomposition whereby the physical solution domain is subdivided into overlapping or nonoverlapping subregions within which the solution is localized and dealt with by a single processor. Communication between processors is necessary and the extent to which this can be reduced tends to dominate the

<sup>†</sup>GMRES, QMR, and BiCGstab, for example.<sup>48</sup>

relative efficiency of different domain decomposition approaches. General tools such as METIS\* and PETSc† are available to assist the user in putting together combinations of solver and domain segmentation that balance the load on each processor and optimize parallel speedup. The reader is referred elsewhere for a full treatment of domain decomposition.<sup>46</sup> In the frequency domain, the finite element tearing and integration method (FETI) has been applied quite extensively to large Helmholtz problems, particularly in underwater scattering,<sup>47</sup> while more straightforward Schur-type methods have been applied to problems in aeroacoustic propagation.<sup>21</sup> In both cases, problem sizes of the order  $10^6$  to  $10^7$  degrees of freedom are solved, albeit with some effort. In the case of Ref. 21, for example, 2.5 days of process time was required on 192 processors to solve a Helmholtz problem with  $6.7 \times 10^6$  degrees of freedom. An equivalent time-domain DGM parallel formulation with  $22 \times 10^6$  discretization points required comparable effort (10 days on 32 processors). While specialized acoustical FE codes such as SYS-NOISE and ACTRAN offer limited parallel capability at the time of writing, a truly efficient and robust, parallel acoustical FE code has yet to appear in the commercial domain.

A sort of domain decomposition which is widely used for large structural models but equally applicable to FE acoustics is automated multilevel substructuring (AMLS).<sup>49</sup> Here the problem size is reduced by projecting the FE solution vector onto a smaller set of eigenmodes. These are calculated not for the model as a whole but for substructures obtained by using an automated domain decomposition procedure (such as METIS). This reduces a large and intractable eigenvalue problem to a series of smaller problems of reduced dimensions. While AMLS is routinely used for structural problems—within the automated component mode synthesis (ACMS) facility of MSC/NASTRAN, for example—its potential for purely acoustical problems has not yet been realized.

### 10.3 Alternative Spatial Representations

As an alternative—or adjunct—to the use of more efficient solvers to reduce solution times for large problems, the number of equations itself can be reduced prior to solution by more effective discretization. The constraint here in conventional FE codes is the *nodes per wavelength* requirement, exacerbated by pollution error at high frequencies. A possible remedy for this *impasse* is the use of nonpolynomial bases that are able to capture more accurately the wavelike character of the solution. More specifically, an argument can be made that the inclusion of approximate or exact *local* solutions of the governing equations within the

trial solution will improve spatial resolution. This concept underpins several contemporary approaches to FE computation of wave problems. In the case of the Helmholtz equation, local plane wave solutions are used for this purpose. It then becomes possible, in theory, to accurately represent many wavelengths of the solution within a single element, eliminating the nodes per wavelength requirement altogether.

The partition of unity (PUM) approach proposed initially by Babuska and Melenk and developed by Bettess and Laghrouche<sup>50</sup> provides a simple illustration of this philosophy. In an FE implementation of the PUM for the Helmholtz problem, the trial solution of Eq. (10) is replaced by one in which each nodal shape function is “enriched” by a set of discrete plane waves. This gives a trial solution of the form

$$\tilde{p}(\mathbf{x}, \omega) = \sum_{j=1}^n \sum_{l=1}^m q_{jl}(\omega) \psi_{jl}(\mathbf{x}) \quad \text{where} \quad \psi_{jl}(\mathbf{x}) = N_j(\mathbf{x}) e^{-i\mathbf{k}_{lj}(\mathbf{x}-\mathbf{x}_j)} \quad (22)$$

The numerical solution is, therefore, defined by  $m \times n$  unknown parameters ( $q_{jl}$ ,  $j = 1, \dots, n$ ,  $l = 1, \dots, m$ ,) where each node has  $m$  degrees of freedom. Each of these represents the amplitude of a plane wave propagating with a discrete wavenumber  $\mathbf{k}_{lj}$ . In the case of an inhomogeneous or anisotropic medium the magnitude and direction of the wavenumber  $\mathbf{k}_{lj}$  can be chosen so that it represents an exact or approximate local solution at node  $j$ . In this sense the basis functions,  $\psi_{jl}(\mathbf{x})$ , have been enriched by the inclusion of information about the local solution. The construction of  $\psi_{jl}(\mathbf{x})$  as the product of a conventional nodal shape function and a local wave approximation is illustrated in Fig. 9.

In all other respects the PUM variational formulation is the same as that of a conventional FE model, although element integrations become more time consuming since the basis functions are highly oscillatory within each element. If the true solution corresponds to a plane wave propagating in one of the discrete wave directions, the numerical solution will represent it without approximation. In real cases, where a spectrum of wave components are present, the PUM solution will attempt to fit these to an ensemble of discrete waves modulated by the conventional element shape functions.

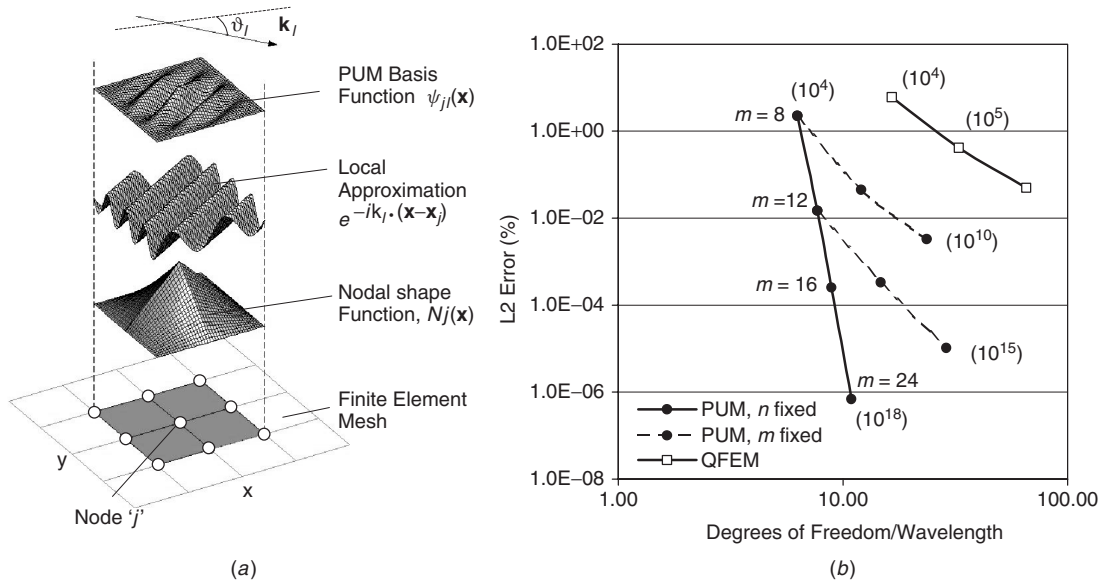
The accuracy of PUM and conventional FE models are compared in Fig. 9b. Mesh resolution is characterized by the number of degrees of freedom per wavelength.<sup>‡</sup> Figure 9 shows the  $L_2$  error for the computed acoustic field in a 2D lined duct. A prescribed set of positive and negative running modes are injected at one end of the duct and a compatible impedance

\*See METIS homepage, <http://www-users.cs.umn.edu/karypis/metis>.

†Portable Extensible Toolkit for Scientific computation, see <http://www.mcs.anl.gov/petsc>.

‡This is obtained for an unstructured 2D mesh by multiplying the square root of the number of degrees of freedom per unit area by the characteristic acoustic wavelength  $\lambda = 2\pi/k$ .





**Figure 9** (a) The PUM basis function. (b) PUM and quadratic FEM (QFEM) solution error as a function of mesh resolution. 2D uniform lined duct,  $kL = 40$ ,  $M = 0.25$ . Condition number indicated in parentheses ( $10^n$ ) for selected data points.

condition is applied at the other. The comparison is made for a mean flow of Mach number 0.25. The percentage  $L_2$  error is plotted against mesh resolution for a number of PUM meshes with different numbers of wave directions at each node, and for coarse, medium, and fine conventional FE meshes based on quadratic polynomial elements (QFEM). The PUM meshes are characterized by the number of wave directions,  $m$ . It is clear that the accuracy of the PUM solution can be improved either by refining the mesh (dashed line) or by increasing the number of wave directions (solid line), the latter being the more effective. In the case of the conventional scheme, the first option only is available. In all cases, however, the PUM is clearly more accurate for a given number of degrees of freedom than the conventional QFEM. The only obstacle to improving accuracy indefinitely is one of conditioning. The condition number of the coefficient matrix for the PUM model becomes large as the number of waves increases or as the frequency decreases. This is undesirable and mitigates against any use of iterative solution methods. The order of magnitude of the condition number for selected data points is indicated in parentheses in Fig. 9b.

The PUM approach is by no means alone in using a plane wave basis to improve resolution. The same philosophy underpins a number of recent FE formulations. These include the discontinuous enrichment method<sup>51</sup> and the ultraweak variational formulation.<sup>52</sup> A similar concept is implicit in recent meshless methods proposed for the Helmholtz problem.<sup>53</sup>

## 11 CONCLUDING COMMENTS

The application of finite elements in acoustics is now a relatively mature technology. Robust commercial

codes are available that deal well with standard linear analyses and permit accurate predictions to be made for acoustical and acoustical-structural problems that include the effects of absorption and radiation. Acoustic propagation on mean flows is also becoming available to general users and this trend will continue as the demand for accurate aeroacoustic modeling grows for turbomachinery, automotive, and other applications. FE acoustical analysis is restricted at the current time mainly to low and moderate frequency cases. This is a practical rather than a theoretical limitation and will diminish in the years to come as more effective parallel acoustical codes are developed and as new more efficient element formulations are improved and refined. The principal advantages of the finite element approach remain its ability to model arbitrarily shaped acoustical domains using unstructured meshes and its inherent capacity for dealing with material and other inhomogeneities in a seamless fashion.

## REFERENCES

1. A. Craggs, The Use of Simple Three-Dimensional Acoustic Finite Elements for Determining the Natural Modes and Frequencies of Complex Shaped Enclosures, *J. Sound Vib.*, Vol. 23, No. 3, 1972, pp. 331–339.
2. I. Harari and T. J. R. Hughes, Cost Comparison of Boundary Element and Finite Element Methods for Problems of Time Harmonic Acoustics, *Comput. Methods Appl. Mech. Eng.*, Vol. 97, 1992, pp. 77–102.
3. L. Greengard, J. Huang, V. Rokhlin, and S. Wandzura, Accelerating Fast Multipole Methods for the Helmholtz Equation at Low Frequencies, *IEEE Computa. Sci. Eng.*, Vol. 5, 1998, pp. 32–47.
4. D. S. Burnett, A Three-Dimensional Acoustic Infinite Element Based on a Prolate Spheroidal Multipole

- Expansion, *J. Acoust. Soc. Am.*, Vol. 96, 1994, pp. 2798–2816.
5. C. K. W. Tam and J. C. Webb, Dispersion Preserving Finite Difference Schemes for Computational Acoustics, *J. Comput. Phys.*, Vol. 107, 1993, pp. 262–281.
  6. B. Van den Nieuwenhof and J.P. Coyette, Treatment of Frequency Dependent Admittance Boundary Conditions in Transient Acoustic Finite/Infinite Element Models, *J. Acoust. Soc. Am.*, Vol. 110, 2001, pp. 1743–1751.
  7. L. Sbardella, B. J. Tester, and M. Imregun, A Time-Domain Method for the Prediction of Sound Attenuation in Lined Ducts, *J. Sound Vib.*, Vol. 239, 2001, pp. 379–396.
  8. A. Bayliss, M. Gunzberger, and E. Turkel, Boundary Conditions for the Numerical Solution of Elliptical Equations in Exterior Regions, *SIAM J. Appl. Math.*, Vol. 42, 1982, pp. 430–450.
  9. D. Givoli, *Numerical Methods for Problems in Infinite Domains*, Elsevier, Amsterdam, 1992.
  10. M. Petyt, *Introduction to Finite Element Vibration Analysis*, Cambridge University Press, Cambridge, England, 1998.
  11. F. P. Mechel, *Formulas of Acoustics —Section G.11*, Springer, Berlin, 2002.
  12. O. C. Zienkiewicz and T. Shiomi, Dynamic Behaviour of Saturated Porous Media. The Generalized Biot Formulation and Its Numerical Implementation, *Int. J. Numer. Meth. Eng.*, Vol. 8, 1984, pp. 71–96.
  13. N. Atalla, R. Panneton, and P. Debergue, A Mixed Displacement–pressure formulation for poroelastic materials, *J. Acoust. Soc. Am.*, Vol. 104, 1998, pp. 1444–1452.
  14. X. Wang and K. L. Bathe, Displacement/Pressure Based Mixed Finite Element Formulations for Acoustic Fluid-Structure Interaction Problems, *Int. J. Numer. Meth. Eng.*, Vol. 40, 1997, pp. 2001–2017.
  15. G. Seriani, A Parallel Spectral Element Method for Acoustic Wave Modeling, *J. Comput. Acoust.*, Vol. 5, No. 1, 1997, pp. 53–69.
  16. J. A. Hamilton and R. J. Astley, Acoustic Propagation on Irrotational Mean Flows Using Time-Domain Finite and Infinite Elements, in AIAA paper 2003-3208, 9th AIAA/CEAS Aeroacoustics Conference, 12–14 May 2003 Hilton Head, SC, 2003.
  17. O. C. Zienkiewicz and R. L. Taylor, *The Finite Element Method*, 5th ed., Vol. 1, McGraw-Hill, London, 1990, Chapters 8 and 9.
  18. S. B. Szabo and I. Babuska, *Finite Element Analysis*, Wiley, New York, 1991.
  19. F. Ihlenburg, *Finite Element Analysis of Acoustic Scattering*, Springer, New York, 1998.
  20. A. Deraemaeker, I. Babuska, and P. Bouillard, Dispersion and Pollution of the FEM Solution for the Helmholtz Equation in One, Two and Three Dimensions, *Int. J. Numer. Meth. Eng.*, Vol. 46, 1999, pp. 471–499.
  21. M. Y. Hussaini, D. Stanescu, J. Xu, and F. Farassat, Computation of Engine Noise Propagation and Scattering Off an Aircraft, *Aeroacoustics*, Vol. 1, 2002, pp. 403–420.
  22. G. Seriani, 3-D Large-Scale Wave Propagation Modeling by Spectral Element Method on Cray T3E Multiprocessor, *Comput. Methods Appl. Mech. Eng.*, Vol. 164, 1998, pp. 235–247.
  23. C. J. Young and M. C. Crocker, Prediction of Transmission Loss in Mufflers by the Finite Element Method, *J. Acoust. Soc. Am.*, Vol. 57, 1975, pp. 144–148.
  24. K. S. Peat, Evaluation of Four Pole Parameters for Ducts with Flow by the Finite Element Method, *J. Sound Vib.*, Vol. 84, 1982, pp. 389–395.
  25. P. S. Christiansen and S. Krenk, Recursive Finite Element Technique for Acoustic Fields in Pipes with Absorption, *J. Sound Vib.*, Vol. 122, 1988, pp. 107–118.
  26. A. Craggs, Application of the Transfer Matrix and Matrix Condensation Methods with Finite Elements to Duct Acoustics, *J. Sound Vib.*, Vol. 132, 1989, pp. 393–402.
  27. R. J. Astley and J. A. Hamilton, Modelling Tone Propagation from Turbofan Inlets—The Effect of Extended Lip Liners, in AIAA paper 2002-2449, 8th AIAA/CEAS Aeroacoustics Conference, 17–19 June 2002 Breckenridge, CO, 2002.
  28. R. Sugimoto, R. J. Astley, and A. J. Kempton, Prediction of Multimode Propagation and Attenuation in Aircraft Engine Bypass Ducts, in Proceedings of 18th ICA, Kyoto, April 2004, abstract 00456, 2004.
  29. W. Eversman, Systematic Procedure for the Analysis of Multiply Branched Acoustic Transmission Lines, *Stress Reliability Design ASME J. Vibr. Acoust.*, Vol. 109, 1986, pp. 168–177.
  30. R. J. Astley and A. Cummings, Finite Element Computation of Attenuation in Bar-Silencers and Comparison with Experiment, *J. Sound Vib.*, Vol. 196, 1995, pp. 351–369.
  31. R. J. Astley and A. Cummings, Wave Propagation in Catalytic Converters, Formulation of the Problem and Finite Element Solution, *J. Sound Vib.*, Vol. 188, 1995, pp. 635–657.
  32. A. A. Ergin, B. Shankar, and E. Michielssen, Fast Transient Analysis of Acoustic Wave Scattering from Rigid Bodies Using a Two-Level Plane Wave Time Domain Algorithm, *J. Acoust. Soc. Am.*, Vol. 106, 1999, pp. 2405–2416.
  33. R. J. Astley, K. Gerdes, D. Givoli, and I. Harari (Eds.), *Finite Elements for Wave Problems, Special Issue, Journal of Computational Acoustics*, Vol. 8, No. 1, World Scientific, Singapore, 2000.
  34. D. Givoli and I. Harari (Eds.), *Exterior Problems of Wave Propagation, Special Issue, Computer Methods in Applied Mechanics and Engineering*, Vol. 164, Nos. 1–2, pp. 1–226, North Holland, Amsterdam, 1998.
  35. J. J. Shirron and I. Babuska, A Comparison of Approximate Boundary Conditions and Infinite Element Methods for Exterior Helmholtz Problems, *Comput. Methods Appl. Mech. Eng.*, Vol. 164, 1998, pp. 121–139.
  36. R. J. Astley and J. P. Coyette, Conditioning of Infinite Element Schemes for Wave Problems, *Comm. Numer. Meth. Eng.*, Vol. 17, 2000, pp. 31–41.
  37. R. J. Astley and J. A. Hamilton, Infinite Elements for Transient Flow Acoustics, in Proceedings 7th AIAA/CEAS Aeroacoustics Conference, 28–30 May 2001 Maastricht, The Netherlands, AIAA paper 2001-2171, 2001.
  38. D. S. Burnett and R. L. Holford, Prolate and Oblate Spheroidal Acoustic Infinite Elements, *Comput. Methods Appl. Mech. Eng.*, Vol. 158, 1998, pp. 117–141.
  39. W. Eversman, Mapped Infinite Wave Envelope Elements for Acoustic Radiation in a Uniformly Moving Medium, *J. Sound Vib.*, Vol. 224, 1999, pp. 665–687.

40. P. R. Rao and P. J. Morris, Application of a Generalised Quadrature Free Discontinuous Galerkin Method in Aeroacoustics, in AIAA paper 2003-3120, 9th AIAA/CEAS Aeroacoustics Conference, 12–14 May, Hilton Head, SC, 2003.
41. A. Agarwal, P. J. Morris, and R. Mani, Calculation of Sound Propagation in Non-uniform Flows: Suppression of Instability Waves. *AIAA J.*, Vol. 42, pp. 80–88, 2004.
42. P. P. Rao and P. J. Morris, Some Finite Element Applications in Frequency Domain Aeroacoustics, AIAA paper 2004-2962, 2004.
43. F. Treysède, G. Gabard, and M. Ben Tahar, A Mixed Finite Element Method for Acoustic Wave Propagation in Moving Fluids Based on an Eulerian-Lagrangian Description, *J. Acoust. Soc. Am.*, Vol. 113, No. 2, 2003, pp. 705–716.
44. J. A. Eaton and B. A. Regan, Application of the Finite Element Method to Acoustic Scattering Problems, *AIAA J.*, Vol. 34, 1996, pp. 29–34.
45. E. Heikkola, T. Rosi, and J. Toivanen, A Parallel Fictitious Domain Method for the Three Dimensional Helmholtz Equation, *SIAM J. Sci. Comput.*, Vol. 24, No. 5, 2003, pp. 1567–1588.
46. B. F. Smith, P. E. Bjorstad, and W. D. Gropp, *Domain Decomposition, Parallel Multilevel Methods for Elliptic Partial Differential Equations*, Cambridge University Press, Cambridge, 1996.
47. R. Djellouli, C. Farhat, A. Macedo, and R. Tezaur, Finite Element Solution of Two-dimensional Acoustic Scattering Problems Using Arbitrarily Shaped Convex Artificial Boundaries, *J. Comput. Acoust.*, Vol. 8, No. 1, 2000, pp. 81–99.
48. Y. Saad, *Iterative Methods for Sparse Linear Systems*, PWS, Boston, 1996.
49. J. K. Bennighof and R. B. Lehoucq, An Automated Multilevel Substructuring Method for Eigenspace Computation in Linear Elastodynamics, *SIAM J. Sci. Comput.*, Vol. 25, 2003, pp. 2084–2106.
50. O. Laghrouche, P. Bettess, and R. J. Astley, Modelling of Short Wave Diffraction Problems Using Systems of Plane Waves, *Int. J. Numer. Meth. Eng.*, Vol. 54, 2002, pp. 1501–1533.
51. C. Farhat, I. Harari, and U. Hetmaniuk, A Discontinuous Galerkin Method with Lagrange Multipliers for the Solution of Helmholtz Problems in the Mid frequency Range, *Comput. Methods Appl. Mech. Eng.*, Vol. 192, 2003, pp. 1389–1419.
52. O. Cessenat and B. Despres, Application of an Ultra Weak Variational Formulation of Elliptic PDEs to the Two-Dimensional Helmholtz Problem, *SIAM J. Numer. Anal.*, Vol. 35, 1998, pp. 255–299.
53. S. Suleau, A. Deraemaeker, and P. Bouillard, Dispersion and Pollution of Meshless Solutions for the Helmholtz Equation, *Comput. Methods Appl. Mech. Eng.*, Vol. 190, 2000, pp. 639–657.



# CHAPTER 8

## BOUNDARY ELEMENT MODELING

D. W. Herrin, T. W. Wu, and A. F. Seybert  
Department of Mechanical Engineering  
University of Kentucky  
Lexington, Kentucky

### 1 INTRODUCTION

Both the boundary element method (BEM) and the finite element method (FEM) approximate the solution in a piecewise fashion. The chief difference between the two methods is that the BEM solves the acoustical quantities on the boundary of the acoustical domain (or air) instead of in the acoustical domain itself. The solution within the acoustical domain is then determined based on the boundary solution. This is accomplished by expressing the acoustical variables within the acoustical domain as a surface integral over the domain boundary. The BEM has been used to successfully predict (1) the transmission loss of complicated exhaust components, (2) the sound radiation from engines and compressors, and (3) passenger compartment noise.

In this chapter, a basic theoretical development of the BEM is presented, and then each step of the process for conducting an analysis is summarized. Three practical examples illustrate the reliability and application of the method to a wide range of real-world problems.

### 2 BEM THEORY

An important class of problems in acoustics is the propagation of sound waves at a constant frequency  $\omega$ . For this case, the sound pressure  $\hat{P}$  at any point fluctuates sinusoidally with frequency  $\omega$  so that  $\hat{P} = pe^{i\omega t}$  where  $p$  is the complex amplitude of the sound pressure fluctuation. The complex exponential allows us to take into account sound pressure magnitude and phase from point-to-point in the medium.

The governing differential equation for linear acoustics in the frequency domain for  $p$  is the Helmholtz equation:

$$\nabla^2 p + k^2 p = 0 \quad (1)$$

where  $k$  is the wavenumber ( $k = \omega/c$ ). The boundary conditions for the Helmholtz equation are summarized in Table 1.

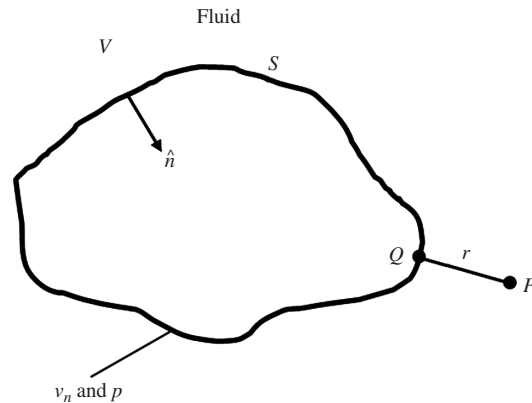
For exterior problems, the boundary integral equation<sup>1</sup>

$$C(P)p(P) = \int_S \left( \frac{\partial p}{\partial n} G(r) - p \frac{\partial G(r)}{\partial n} \right) dS \quad (2)$$

can be developed using the Helmholtz equation [Eq. (1)], Green's second identity, and the Sommerfeld

**Table 1** Boundary Conditions for Helmholtz Equation

Boundary Condition	Physical Quantity	Mathematical Relation
Dirichlet	Sound pressure ( $p_e$ )	$p = p_e$
Neumann	Normal velocity ( $v_n$ )	$\frac{\partial p}{\partial n} = -i\omega\rho v_n$
Robin	Acoustic impedance ( $Z_a$ )	$\frac{\partial p}{\partial n} = -i\omega\rho \frac{1}{Z_a} p$



**Figure 1** Schematic showing the variables for the direct boundary element method.

radiation condition.<sup>1-3</sup> The variables are identified in Fig. 1. If complex exponential notation is adopted, the kernel in Eq. (2) or the Green's function is

$$G(r) = \frac{e^{-ikr}}{4\pi r} \quad (3)$$

where  $r$  is the distance between the collocation point  $P$  and the integration point  $Q$  on the surface. Equation (3) is the expression for a point monopole source in three dimensions. The lead coefficient  $C(P)$  in Eq. (2) is a constant that depends on the location of the collocation point  $P$ . For interior problems, the direct BEM formulation is identical to that shown in Eq. (2) except that the lead coefficient  $C(P)$  is replaced by  $C^0(P)$ , which is defined differently.<sup>1,2</sup> Table 2 shows how both lead coefficients are defined

**Table 2 Lead Coefficient Definitions at Different Locations**

Location of $P$	$C(P)$	$C^0(P)$
In acoustical domain $V$	1	1
Outside acoustical domain $V$	0	0
Smooth boundary	$\frac{1}{2}$	$\frac{1}{2}$
Corners/edges	$1 - \int_S \frac{\partial}{\partial n} \left( \frac{1}{4\pi r} \right) dS$	$-\int_S \frac{\partial}{\partial n} \left( \frac{1}{4\pi r} \right) dS$

depending on whether the problem is an interior or exterior one.

For direct or collocation approaches,<sup>1-19</sup> the boundary must be closed, and the primary variables are the sound pressure and normal velocity on the side of the boundary that is in contact with the fluid. The normal velocity ( $v_n$ ) can be related to the  $\partial p / \partial n$  term in Eq. (2) via the momentum equation that is expressed as

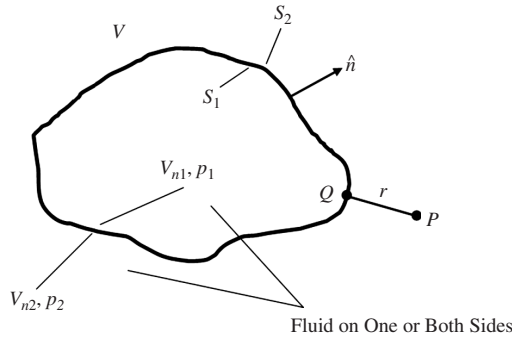
$$\frac{\partial p}{\partial n} = -i\rho\omega v_n \quad (4)$$

where  $\rho$  is the mean density of the fluid.

When using the direct BEM, there is a distinction between an interior and exterior problem. However, there is no such distinction using indirect BEM approaches.<sup>20-28</sup> Both sides of the boundary are considered simultaneously even though only one side of the boundary may be in contact with the fluid. As Fig. 2 indicates, the boundary consists of the inside ( $S_1$ ) and outside surfaces ( $S_2$ ), and both sides are analyzed at the same time.

In short, boundary integral equations like Eq. (2) can be written on both sides of the boundary and then summed resulting in an indirect boundary integral formulation that can be expressed as

$$p(P) = \int_S \left[ G(r) \delta p - \frac{\partial G(r)}{\partial n} \delta p \right] dS \quad (5)$$

**Figure 2** Schematic showing the variables for the indirect boundary element method.

In Eq. (5), the primary variables are the single- ( $\delta p$ ) and double-layer ( $\delta p$ ) potentials. The single-layer potential ( $\delta p$ ) is the difference in the normal gradient of the pressure and can be related to the normal velocities ( $v_{n1}$  and  $v_{n2}$ ), and the double-layer potential ( $\delta p$ ) is the difference in acoustic pressure ( $p_1$  and  $p_2$ ) across the boundary of the BEM model. Since  $S_1$  is identical to  $S_2$ , the symbol  $S$  is used for both in Eq. (5) and the normal vector is defined as pointing away from the acoustical domain.

Table 3 summarizes how the single- and double-layer potentials are related to the normal velocity and sound pressure. If a Galerkin discretization is adopted, the boundary element matrices will be symmetric, and the solution of the matrices will be faster than the direct method provided a direct solver is used.<sup>21</sup> Additionally, the symmetric matrices are preferable for structural-acoustical coupling.<sup>25</sup> The boundary conditions for the indirect BEM are developed by relating the acoustic pressure, normal velocity, and normal impedance to the single- and double-layer potentials.

More thorough descriptions for the direct and indirect BEM are presented by Wu<sup>3</sup> and Vlahopoulos,<sup>27</sup> respectively. It should be mentioned that the differences between the so-called direct and indirect approaches have blurred recently. In fact, high-level studies by Wu<sup>29</sup> and Chen et al.<sup>30,31</sup> combine both procedures into one set of equations. Chen et al. developed a direct scheme using Galerkin discretization, which generated symmetric matrices. However, these state-of-the-art approaches are not used in commercial software at the time of this writing.

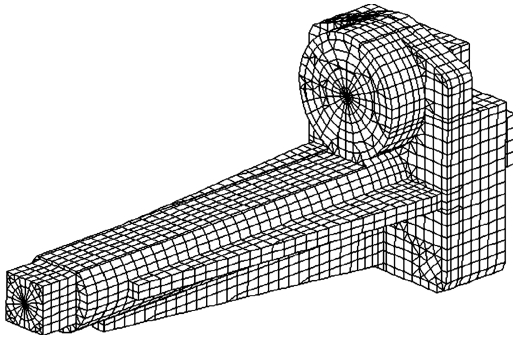
### 3 MESH PREPARATION

Building the mesh is the first step in using the BEM to solve a problem. Figure 3 shows a BEM model used for predicting the sound radiation from a gear housing. The geometry of the housing is represented by a BEM mesh, a series of points called nodes on the surface of the body that are connected to form elements of either quadrilateral or triangular shape.

Most commercially available pre- and postprocessing programs developed for the FEM may also be used for constructing BEM meshes. In many instances, a solid model can be built, and the surface of the solid can be meshed automatically creating a mesh representative of the boundary. Alternatively, a wire frame or surface model of the boundary could be created using computer-aided design (CAD) software and then meshed. Regardless of the way the mesh is prepared, shell elements are typically used in the finite element

**Table 3 Relationship of Single- and Double-Layer Potentials to Boundary Conditions**

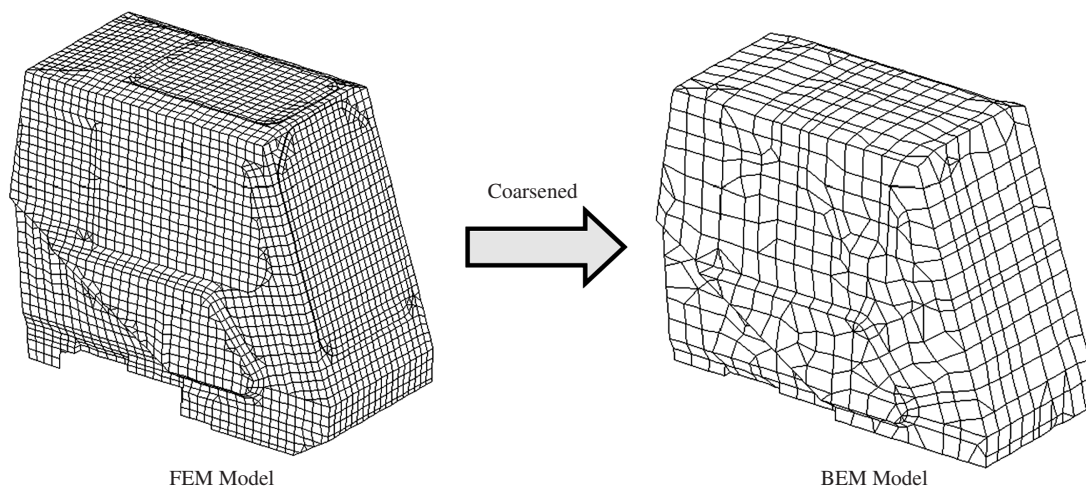
Potential	Symbol	Mathematical Relation
Single layer	$\delta p$	$\frac{\delta p_1}{\delta n} - \frac{\delta p_2}{\delta n}$
Double layer	$\delta p$	$p_1 - p_2$



**Figure 3** Boundary element model of a gear housing.

preprocessor, and the nodes and elements are transferred to the boundary element software. The material properties and thickness of the elements are irrelevant since the boundary elements only bound the domain.

Sometimes a structural finite element mesh is used as a starting point for creating the boundary element mesh. Sometimes a boundary element mesh can be obtained by simply “skinning” the structural finite element mesh. However, the structural finite element mesh is often excessively fine for the subsequent acoustical boundary element analyses, leading to excessive CPU (central processing unit) time. Commercially available software packages have been developed to skin and then coarsen structural finite element meshes.<sup>32,33</sup> These packages can automatically remove one-dimensional elements like bars and beams, and skin three-dimensional elements like tetrahedrons with two-dimensional boundary elements. Then, the skinned model can be coarsened providing the user with the desired BEM mesh. An example of a skinned and coarsened model is shown in Figure 4.



**Figure 4** Schematic showing a boundary element model that was created using the finite element model as a starting point.

It is well known that the BEM can be CPU intensive if the model has a large number of nodes (i.e., degrees of freedom). The solution time is roughly proportional to the number of nodes cubed for a BEM analysis, although iterative solvers may reduce the solution time. Nevertheless, if solution time is an issue and it normally is, it will be advantageous to minimize the number of nodes in a BEM model.

Unfortunately, the accuracy of the analysis depends on having a sufficient number of nodes in the model. Thus, most engineers try to straddle the line between having a mesh that will yield accurate results yet can be solved quickly. The general rule of thumb is that six linear or three parabolic elements are needed per acoustic wavelength. However, these guidelines depend on the geometry, boundary conditions, desired accuracy, integration quadrature, and solver algorithm.<sup>34,35</sup> Therefore, these guidelines should not be treated as strict rules.

One notable exception to the guidelines is the case where the normal velocity or sound pressure on the boundary is complicated. Accordingly, the boundary mesh and the interpolation scheme will need to be sufficient to represent the complexity of this boundary condition. This may require a much finer mesh than the guidelines would normally dictate. Regardless of the element size, the shape of the element appears to have little impact on the accuracy of the analysis, and triangular boundary elements are nearly as accurate as their quadrilateral counterparts.<sup>34</sup>

One way to minimize the number of nodes without losing any precision is to utilize symmetry when appropriate. The common free space Green's function [Eq. (3)] was used for the derivation earlier in the chapter. However, the Green's function can take different forms if it is convenient to do so. For example, the half-space Green's function could be used for modeling a hemisphere radiation problem.

Similarly, different Green's functions can be used for the axisymmetric and two-dimensional cases.<sup>2</sup> Symmetry planes may also be used to model rigid floors or walls provided that the surface is infinite or can be approximated as such.

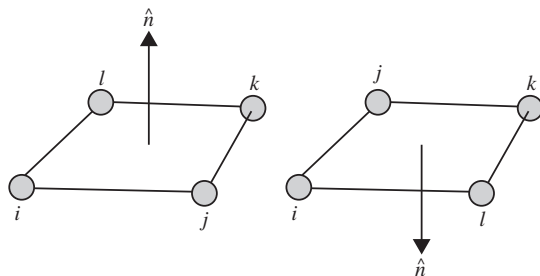
The direction of the element normal to the surface is another important aspect of mesh preparation. The element normal direction is determined by the sequence of the nodes defining a particular element. If the sequence is defined in a counterclockwise fashion, the normal direction will point outward. Figure 5 illustrates this for a quadrilateral element. The element normal direction should be consistent throughout the boundary element mesh. If the direct BEM is used, the normal direction should point to or away from the acoustical domain depending on the convention used by the BEM software. In most instances, adjusting the normal direction is trivial since most commercial BEM software has the built-in smarts to reverse the normal direction of a mesh or to make the normal direction consistent.

#### 4 FLUID PROPERTY SPECIFICATION

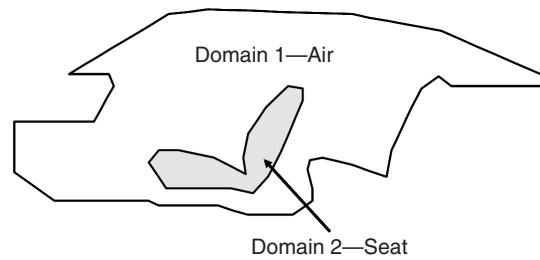
After the mesh is defined, the fluid properties for the acoustical domain can be specified. The BEM assumes that the fluid is a homogeneous ideal fluid in the linear regime. The fluid properties consist of the speed of sound and the mean density.

In a BEM model, a sound-absorbing material can be modeled as either locally reacting or bulk reacting. In the local reacting case, the surface impedance is used as a boundary condition (see Table 1). In the bulk-reacting case, a multidomain<sup>36,37</sup> or direct-mixed body BEM<sup>38</sup> analysis should be performed, using bulk-reacting properties to model the absorption. Any homogeneous sound-absorbing material can be described in terms of its bulk properties. These bulk properties include both the complex density and speed of sound for a medium<sup>39</sup> and provide an ideal mechanism for modeling the losses of a sound-absorbing material. Bulk-reacting properties are especially important for thick sections of sound-absorbing materials.

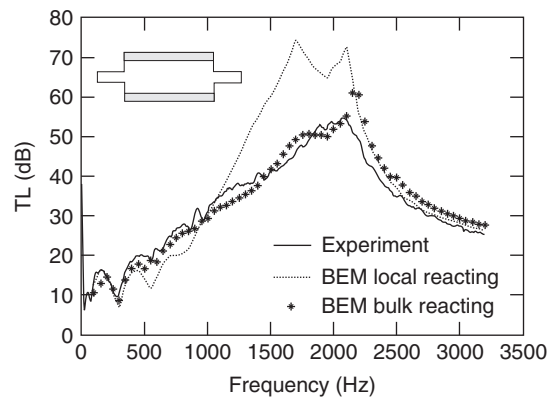
As mentioned previously, the BEM assumes that the domain is homogeneous. However, a nonhomogeneous domain could be divided into several smaller



**Figure 5** Manner in which the normal direction is defined for a boundary element.



**Figure 6** Passenger compartment modeled as two separate acoustical domains.



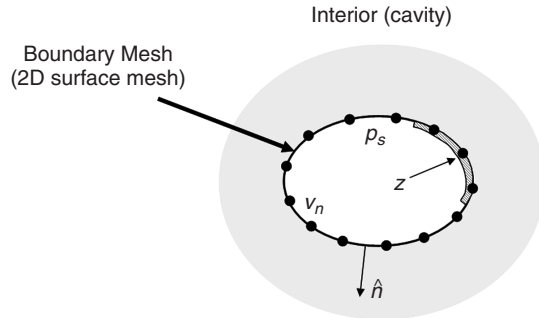
**Figure 7** Comparison of the transmission loss for a lined expansion chamber using local and bulk reacting models.

subdomains having different fluid properties. Where the boundaries are joined, continuity of particle velocity and pressure is enforced. For example, the passenger compartment shown in Figure 6 could be modeled as two separate acoustical domains, one for the air and another for the seat. The seat material properties would be the complex density and speed of sound of the seat material. Another application is muffler analysis with a temperature variation. Since the temperature variations in a muffler are substantial, the speed of sound and density of the air will vary from chamber to chamber. Using a multidomain BEM, each chamber can be modeled as a separate subdomain having different fluid properties.

The advantage of using a bulk-reacting model is illustrated in Figure 7. BEM transmission loss predictions are compared to experimental results for a packed expansion chamber with 1-inch-thick sound-absorbing material.<sup>38</sup> Both locally and bulk-reacting models were used to simulate the sound absorption. The results using a bulk-reacting model are superior, corresponding closely to the measured transmission loss.

#### 5 BOUNDARY CONDITIONS

The boundary conditions for the BEM correspond to the Dirichlet, Neumann, and Robin conditions for



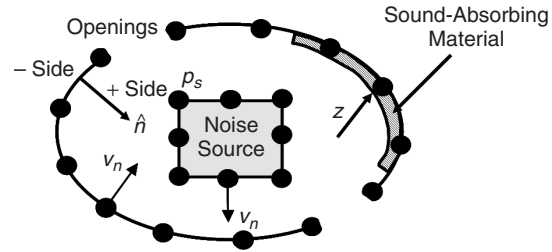
**Figure 8** Schematic showing the boundary conditions for the direct BEM.

Helmholtz equation (as shown in Table 1). Figure 8 shows a boundary element domain for the direct BEM. The boundary element mesh covers the entire surface of the acoustical domain. At each node on the boundary, a Dirichlet, Neumann, or Robin boundary condition should be specified. In other words, a sound pressure, normal velocity, or surface impedance should be identified for each node. Obtaining and/or selecting these boundary conditions may be problematic. In many instances, the boundary conditions may be assumed or measured. For example, the normal velocity can be obtained by a FEM structural analysis, and the surface impedance can be measured using a two-microphone test.<sup>40</sup> Both the magnitude and the phase of the boundary condition are important. Most commercial BEM packages select a default zero normal velocity boundary condition (which corresponds to a rigid boundary) if the user specifies no other condition.

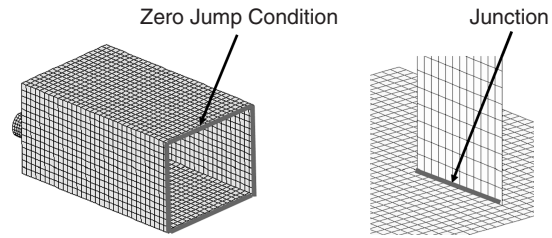
The normal velocity on the boundary is often obtained from a preliminary structural finite element analysis. The frequency response can be read into BEM software as a normal velocity boundary condition. It is likely that the nodes in the FEM and BEM models are not coincident with one another. However, most commercial BEM packages can interpolate the results from the finite element mesh onto the boundary element mesh.

For the indirect BEM, the boundary conditions are the differences in the pressure, normal velocity, and surface impedance across the boundary. Figure 9 illustrates the setup for an indirect BEM problem. Boundary conditions are applied to both sides of the elements. Each element has a positive and negative side that is identified by the element normal direction (see Fig. 9). Most difficulties using the indirect BEM are a result of not recognizing the ramifications of specifying boundary conditions on both sides of the element.

To model an opening using the indirect BEM, a zero jump in pressure<sup>27,28</sup> should be applied to the edges of the opening in the BEM mesh (Fig. 10). Most commercial BEM software has the ability to locate nodes around an opening so that the user can easily apply the zero jump in pressure. Additionally,



**Figure 9** Schematic showing the boundary conditions for the indirect BEM.

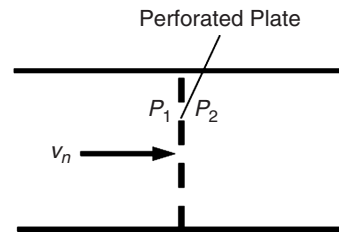


**Figure 10** Special boundary conditions that may be used with the indirect BEM.

special treatment is important when modeling three or more surfaces that intersect (also illustrated in Fig. 10). Nodes must be duplicated along the edge and compatibility conditions must be applied.<sup>27,28</sup> Though this seems complicated, commercial BEM software can easily detect and create these junctions applying the appropriate compatibility conditions.

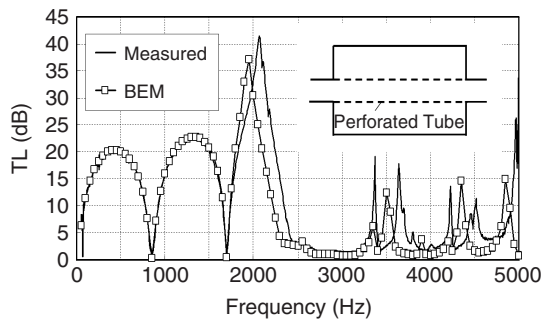
Many mufflers utilize perforated panels as attenuation mechanisms, and these panels may be modeled by specifying the transfer impedance of the perforate.<sup>41,42</sup> The assumption is that the particle velocity is continuous on both sides of the perforated plate but the sound pressure is not. For example, a perforated plate is shown in Fig. 11. A transfer impedance boundary condition can be defined at the perforated panel and expressed as

$$Z_{tr} = \frac{p_1 - p_2}{v_n} \quad (6)$$



**Figure 11** Schematic showing the variables used to define the transfer impedance of a perforate.





**Figure 12** Transmission loss for a concentric tube resonator with a perforate.

where  $Z_{tr}$  is the transfer impedance,  $p_1$  and  $p_2$  are the sound pressures on each side of the plate, and  $v_n$  is the particle velocity. The transfer impedance can be measured or estimated using empirical formulas. In these empirical formulas, the transfer impedance is related to factors like the porosity, thickness, and hole diameter of a perforated plate.<sup>43,44</sup> Figure 12 shows the transmission loss results computed using the BEM results for an expansion chamber with a perforated tube.

Another useful capability is the ability to specify acoustic point sources in a BEM model. Noise sources can be modeled as a point source if they are acoustically small (i.e., the dimensions of a source are small compared to an acoustic wavelength) and omnidirectional. Both the magnitude and the phase of the point source should be specified.

## 6 SPECIAL HANDLING OF ACOUSTIC RADIATION PROBLEMS

The BEM is sometimes preferred to the FEM for acoustic radiation problems because of the ease in meshing. However, there are some solution difficulties with the BEM for acoustic radiation problems. Both the direct and indirect methods have difficulties that are similar but not identical. With the direct BEM, the exterior boundary integral equation does not have a unique solution at certain frequencies. These frequencies correspond to the resonance frequencies of the airspace interior to the boundary (with Dirichlet boundary conditions). Though the direct BEM results will be accurate at most frequencies, the sound pressure results will be incorrect at these characteristic frequencies.

The most common approach to overcome the nonuniqueness difficulty is to use the combined Helmholtz integral equation formulation, or CHIEF, method.<sup>11</sup> A few overdetermination or CHIEF points are placed inside the boundary, and CHIEF equations are written that force the sound pressure to be equal to zero at each of these points. Several CHIEF points should be identified inside the boundary because a CHIEF point that falls on or near the interior nodal surface of a particular eigenfrequency will not provide

a strong constraint since the pressure on that interior nodal surface is also zero for the interior problem. As the frequency increases, the problem is compounded by the fact that the eigenfrequencies and the nodal surfaces become more closely spaced. Therefore, analysts normally add CHIEF points liberally if higher frequencies are considered. Although the CHIEF method is very effective at low and intermediate frequencies, a more theoretically robust way to overcome the nonuniqueness difficulty is the Burton and Miller method.<sup>5</sup>

Similarly, for an indirect BEM analysis, there is a nonexistence difficulty associated with exterior radiation problems. Since there is no distinction between the interior and exterior analysis, the primary variables of the indirect BEM solution capture information on both sides of the boundary.<sup>27</sup> At the resonance frequencies for the interior, the solution for points on the exterior is contaminated by large differences in pressure between the exterior and interior surfaces of the boundary. The nonexistence difficulty can be solved by adding absorptive planes inside or by specifying an impedance boundary condition on the interior surface of the boundary.<sup>27</sup>

The lesson to be learned is that exterior radiation problems should be approached carefully. However, excellent acoustical predictions can be made using the BEM, provided appropriate precautions are taken.

## 7 BEM SOLUTION

Even though BEM matrices are based on a surface mesh, the BEM is often computationally and memory intensive. Both the indirect and direct procedures produce dense matrices that are not sparse, as is typical of finite element matrices. For realistic models, the size of the matrix could easily be on the order of tens of thousands. The memory storage of an  $N \times N$  matrix is on the order of  $N^2$ , while the solution time using a direct solver is on the order of  $N^3$ . As the BEM model grows, the method sometimes becomes impractical due to computer limitations.

One way to overcome the solution time difficulty is to use an iterative solver<sup>45</sup> with some appropriate preconditioning.<sup>46,47</sup> Iterative solvers are much faster than conventional direct solvers for large problems.<sup>48</sup> Also, there is no need to keep the matrix in memory, although the solution is slower in that case.<sup>49</sup> Additionally, BEM researchers have been working on different variations of the so-called fast multipole expansion method based on the original idea by Rokhlin<sup>50-53</sup> in applied physics.

## 8 POSTPROCESSING

Boundary element results can be viewed and assessed in a number of different ways. The BEM matrix solution only computes the acoustical quantities on the surface of the boundary element mesh. Thus, only the sound pressure and/or normal velocity is computed on the boundary using the direct method, and only the single- and/or double-layer potentials are computed using the indirect BEM. Following this, the acoustical

quantities at points in the field can be determined from the boundary solution by integrating the surface acoustical quantities over the boundary, a process requiring minimal computer resources. As a result, once an acoustical BEM analysis has been completed, results can be examined at any number of field points in a matter of minutes. This is a clear advantage of using numerical approaches like the BEM over the time-intensive nature of experimental work. However, the numerical results in the field are only as reliable as the calculated acoustical quantities on the boundary, and the results should be carefully examined to assure they make good engineering sense.

To help evaluate the results, commercial software includes convenient postprocessing capabilities to determine and then plot the sound pressure results on standard geometric shapes like planes, spheres, or hemispheres in the sound field. These shapes do not have to be defined beforehand, making it very convenient to examine results at various locations of interest in the sound field. Furthermore, the user can more closely inspect the solution at strategic positions. For example, Fig. 13 shows a sound pressure contour for the sound radiated by an engine cover. A contour plot of the surface vibration is shown under the engine cover proper, and the sound pressure results are displayed on a field point mesh above the cover and give a good indication of the directivity of the sound at that particular frequency.

Additionally, the sound power can be computed after the matrix solution is completed. One advantage of the direct BEM is that the sound power and radiation efficiency can be determined from the boundary solution directly. This is a direct result of only one side of the boundary being considered for the solution. However, determining the sound power using the indirect BEM is a little more problematic. Normally, the user defines a sphere or some other geometric shape that encloses the sound radiator. After the sound pressure and particle velocity are computed on the

geometric shape, the sound power can be determined by integrating the sound intensity over the area of the shape. Results are normally better if the field points are located in the far field.

Another possible use of BEM technology can be to identify the panels that contribute most to the sound at a point or to the sound field as a whole. For instance, a BEM mesh was painted onto a diesel engine and then vibration measurements were made at each node on the engine surface. The measured vibrations were used as the input velocity boundary condition for a subsequent BEM calculation. The sound power contributions (in decibels) from the oil pan and the front cover of a diesel engine are shown in Fig. 14. As the figure indicates, the front cover is the prime culprit at 240 Hz. This example illustrates how the BEM can be used as a diagnostic tool even after a prototype is developed.

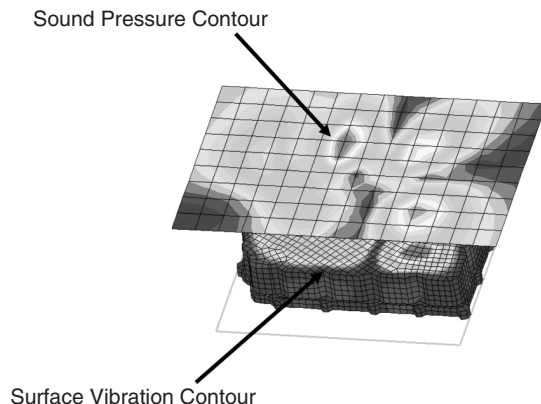
Boundary element method postprocessing is not always a turnkey operation. The user should carefully examine the results first to judge whether confidence is warranted in the analysis. Furthermore, unlike measurement results, raw BEM results are always on a narrow-band basis. Obtaining the overall or A-weighted sound pressure or sound power may require additional postprocessing depending on the commercial software used. Also, the transmission loss for a muffler or a plenum system cannot be exported directly using many BEM software packages. This requires additional postprocessing using a spreadsheet or mathematical software.

## 9 EXAMPLE 1: CONSTRUCTION CAB

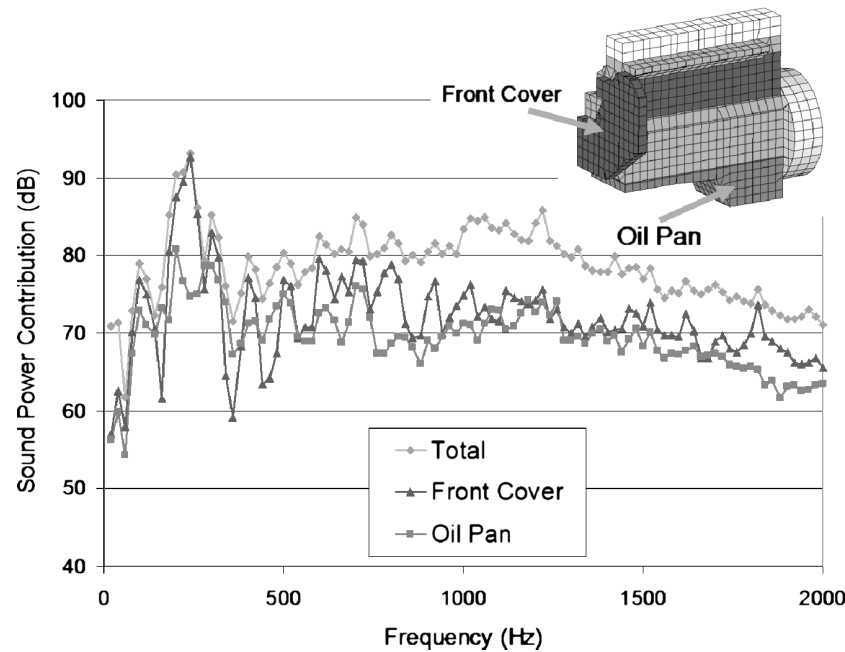
A construction cab is an example of an interior acoustics problem. The construction cab under consideration is  $1.9 \times 1.5 \times 0.9 \text{ m}^3$ . Due to the thickness of the walls, and the high damping, the boundary was assumed to be rigid. A loudspeaker and tube were attached to the construction cab, and the sound pressure was measured using a microphone where the tube connects to the cab. All analyses were conducted at low enough frequencies so that plane waves could be assumed inside the tube. Medium-density foam was placed on the floor of the cab.

First, a solid model of the acoustical domain was prepared, and the boundary was meshed using shell elements. A commercial preprocessor was used to prepare the mesh, which was then transferred into BEM software. In accordance with the normal convention for the commercial BEM software in use, the element normal direction was checked for consistency and chosen to point toward the acoustical domain. For the indirect BEM, the normal direction must be consistent, pointing toward the inside or outside.

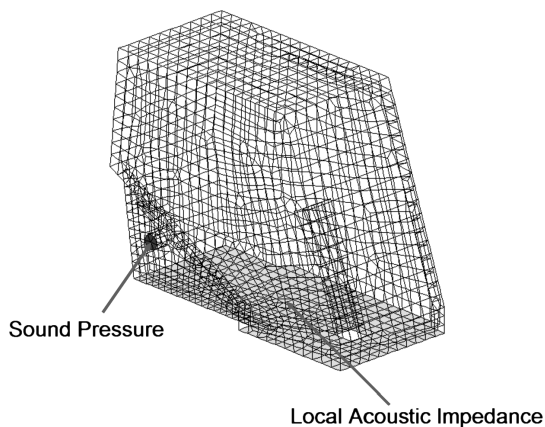
In this case, both the direct and indirect BEM approaches were used. For the indirect BEM, the boundary conditions are placed on the inner surface, and the outer surface is assumed to be rigid (normal velocity of zero). For both approaches, the measured sound pressure at the tube inlet was used as a boundary condition, and a surface impedance was applied to the floor to model the foam. (The surface impedance of the foam was measured in an impedance tube.<sup>40</sup>) All



**Figure 13** Contour plot showing the sound pressure variation on a field point plane located above an engine cover.



**Figure 14** BEM predicted sound power contributions from the oil pan and front cover of a diesel engine.



**Figure 15** Schematic showing the BEM mesh and boundary conditions for the passenger compartment of a construction cab.

other surfaces aside from the floor were assumed to be rigid. The boundary conditions are shown in Fig. 15.

Since the passenger compartment airspace is modally dense, a fine frequency resolution of 5 Hz was used. The sound pressure results are compared at a point in the interior to measured results in Fig. 16. The results demonstrate the limits of the BEM. Although the boundary element results do not exactly match the measured results, the trends are predicted well and the overall sound pressure level is quite close. Determining

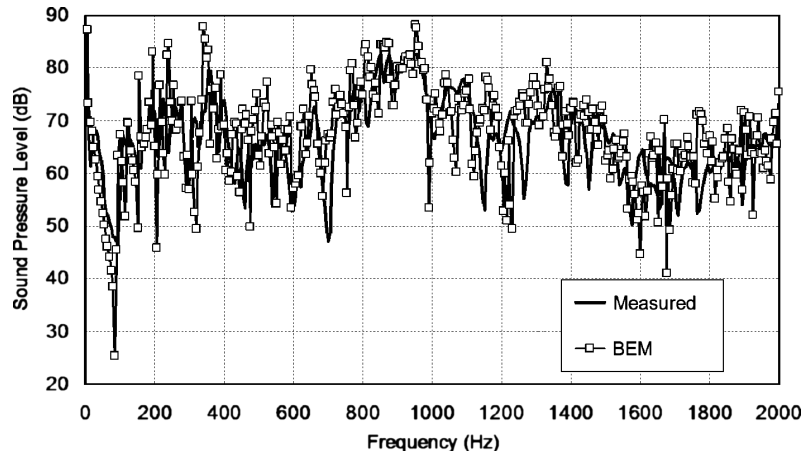
the pressure at a single point is arguably the most challenging test for a boundary element analysis. The BEM fares better when the sound power is predicted since the sound pressure results are used in an overall sense.

## 10 EXAMPLE 2: ENGINE COVER IN A PARTIAL ENCLOSURE

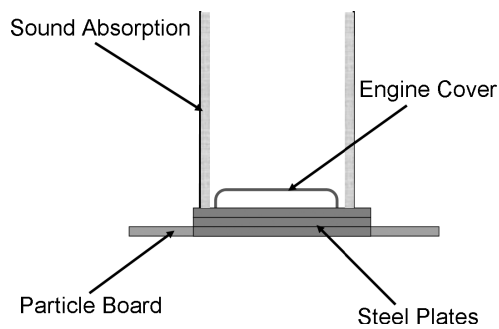
The sound radiation from an aluminum engine cover in a partial enclosure was predicted using the indirect BEM.<sup>54</sup> The experimental setup is shown in Fig. 17. The engine cover was bolted down at 15 locations to three steel plates bolted together ( $\frac{3}{4}$  inches thick each). The steel plates were rigid and massive compared to the engine cover and were thus considered rigid for modeling purposes. A shaker was attached to the engine cover by positioning the stinger through a hole drilled through the steel plates, and high-density particleboard was placed around the periphery of the steel plates. The experiment was designed so that the engine cover could be assumed to lie on a rigid half space. The engine cover was excited using white-noise excitation inside a hemianechoic chamber.

To complicate the experiment, a partial enclosure was placed around the engine cover. The plywood partial enclosure was 0.4 m in height and was lined with glass fiber on each wall. Although the added enclosure is a simple experimental change, it had a significant impact on the sound radiation and the way in which the acoustical system is modeled. This problem is no longer strictly exterior or interior since the enclosure is open, making the model unsuitable for the direct BEM; the indirect BEM was used.





**Figure 16** Sound pressure level comparison at a point inside the construction cab. (The overall A-weighted sound pressure levels predicted by BEM and measured were 99.7 dB and 97.7 dB respectively.)



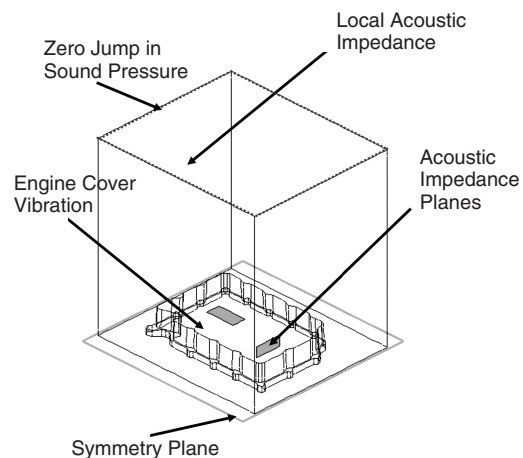
**Figure 17** Schematic showing the experimental setup of an engine cover located inside a partial enclosure.

the vibration results from the structural finite element model onto the surface of the boundary element mesh.

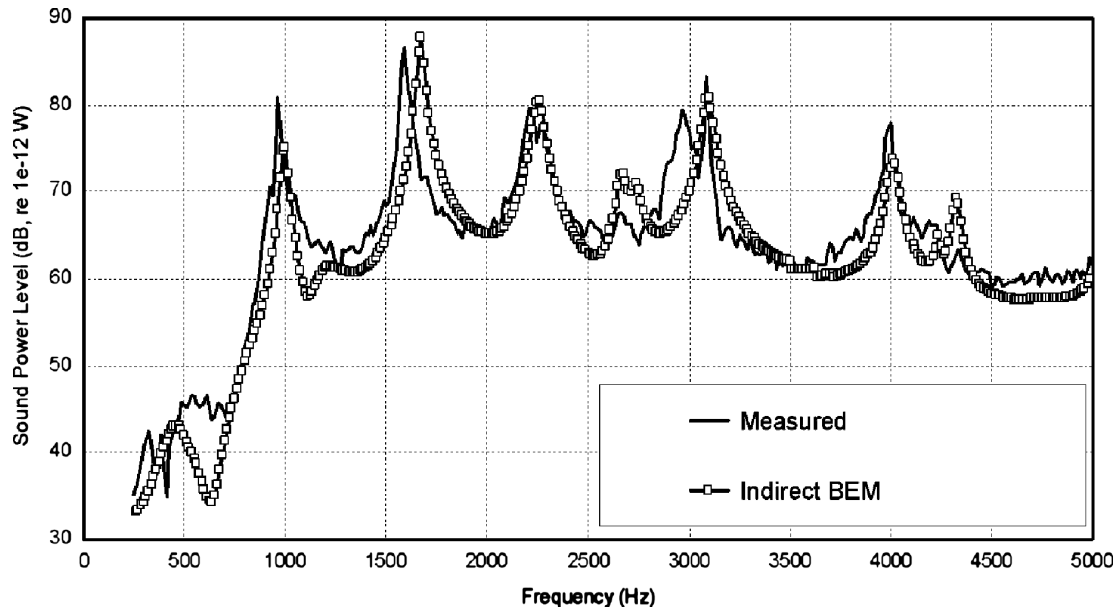
A symmetry plane was placed at the base of the engine cover to close the mesh. Since this is an acoustic radiation problem, precautions were taken to avoid errors in the solution due to the nonexistence difficulty for the indirect BEM discussed earlier. Two rectangular planes of boundary elements were positioned at right angles to one another in the space between the engine cover boundary and the symmetry plane (Fig. 18). An impedance boundary condition was applied to each side of the planes. Since the edges of each plane are free, a zero jump in pressure was applied along the edges.

A structural finite element model of the cover was created from a solid model of the engine cover. The solid model was automatically meshed using parabolic tetrahedral finite elements, and a frequency response analysis was performed. The results of the finite element analysis were used as a boundary condition for the acoustical analysis that followed.

Using the same solid model as a starting point, the boundary element mesh was created by meshing the outer surface of the solid with linear quadrilateral elements. The boundary element mesh is simpler and coarser than the structural finite element mesh. Since features like the small ribs have dimensions much less than an acoustic wavelength, they have a negligible effect on the acoustics even though they are significant structurally. Those features were removed from the solid model before meshing so that the mesh was coarser and could be analyzed in a timely manner. The boundary condition for the engine cover is the vibration on the cover (i.e., the particle velocity). The commercial BEM software used was able to interpolate



**Figure 18** Schematic showing the boundary conditions that were assumed for a vibrating engine cover inside a partial enclosure.



**Figure 19** Comparison of the sound power from the partial enclosure. Indirect BEM results are compared with those obtained by measurement. (The overall A-weighted sound power levels predicted by BEM and obtained by measurement were both 97.6 dB.)

The thickness of the partial enclosure was neglected since the enclosure is thin in the acoustical sense (i.e., the combined thickness of the wood and the absorptive lining is small compared to an acoustic wavelength). A surface impedance boundary condition was applied on the inside surface of the elements, and the outside surface was assumed to be rigid (zero velocity boundary condition). As indicated in Fig. 18, a zero jump in pressure was applied to the nodes on the top edge.

As Fig. 19 shows, the BEM results compared reasonably well with the experimental results. The closely matched A-weighted sound power results are largely a result of predicting the value of the highest peak accurately. The differences at the other peaks can be attributed to errors in measuring the damping of the engine cover. A small change in the damping will have a large effect on the structural FEM analysis and a corresponding effect on any acoustic computational analysis that follows. Measuring the structural damping accurately is tedious due to data collection and experimental setup issues involved.

## 11 CONCLUSION

The objective of this chapter was to introduce the BEM, noting some of the more important developments as well as the practical application of the method to a wide variety of acoustic problems. The BEM is a tool that can provide quick answers provided that a suitable model and realistic boundary conditions can be applied. However, when the BEM is looked at objectively, many practitioners find that it is not quite

what they had hoped for. Today, many problems are still intractable using numerical tools in a purely predictive fashion. For example, forces inside machinery (i.e., engines and compressors) are difficult to quantify. Without realistic input forces and damping in the structural FEM model, numerical results obtained by a subsequent BEM analysis should be considered critically. Certainly, the BEM may still be useful for determining the possible merits of one design over another. Nevertheless, it is hard to escape the suspicion that many models may not resemble reality as much as we would like.

## REFERENCES

1. A. F. Seybert, B. Soenarko, F. J. Rizzo, and D. J. Shippy, "An Advanced Computational Method for Radiation and Scattering of Acoustic Waves in Three Dimensions," *J. Acoust. Soc. Am.*, Vol. 77, 1985, pp. 362–368.
2. A. F. Seybert, B. Soenarko, F. J. Rizzo, and D. J. Shippy, "Application of the BIE Method to Sound Radiation Problems Using an Isoparametric Element," *ASME Trans. J. Vib. Acoust. Stress Rel. Des.*, Vol. 106, 1984, pp. 414–420.
3. T. W. Wu, The Helmholtz Integral Equation, in *Boundary Element Acoustics, Fundamentals and Computer Codes*, T. W. Wu (Ed.), WIT Press, Southampton, UK, 2000, Chapter 2.
4. R. J. Bernhard, B. K. Gardner, and C. G. Mollo, "Prediction of Sound Fields in Cavities Using Boundary Element Methods," *AIAA J.*, Vol. 25, 1987, pp. 1176–1183.

5. A. J. Burton and G. F. Miller, "The Application of Integral Equation Methods to the Numerical Solutions of Some Exterior Boundary Value Problems," *Proc. Roy. Soc. London*, Vol. A 323, 1971, pp. 201–210.
6. L. H. Chen, and D. G. Schweikert, "Sound Radiation from an Arbitrary Body," *J. Acoust. Soc. Am.*, Vol. 35, 1963, pp. 1626–1632.
7. G. Chertock, "Sound Radiation from Vibrating Surfaces," *J. Acoust. Soc. Am.*, Vol. 36, 1964, pp. 1305–1313.
8. L. G. Copley, "Integral Equation Method for Radiation from Vibrating Bodies," *J. Acoust. Soc. Am.*, Vol. 44, 1967, pp. 41–58.
9. K. A. Cunefare, G. H. Koopmann, and K. Brod, "A Boundary Element Method for Acoustic Radiation Valid at All Wavenumbers," *J. Acoust. Soc. Am.*, Vol. 85, 1989, pp. 39–48.
10. O. von Estorff, J. P. Coyette, and J-L. Migeot, Governing Formulations of the BEM in Acoustics, in *Boundary Elements in Acoustics: Advances and Applications*, O. von Estorff (Ed.), WIT Press, Southampton, UK, 2000, Chapter 1.
11. H. A. Schenck, "Improved Integral Formulation for Acoustic Radiation Problem," *J. Acoust. Soc. Am.*, Vol. 44, 1968, pp. 41–58.
12. A. F. Seybert, and C. Y. R. Cheng, "Applications of the Boundary Element Method to Acoustic Cavity Response and Muffler Analysis," *ASME Trans. J. Vib. Acoust. Stress Rel. Des.*, Vol. 109, 1987, pp. 15–21.
13. A. F. Seybert, B. Soenarko, F. J. Rizzo, and D. J. Shippy, "A Special Integral Equation Formulation for Acoustic Radiation and Scattering for Axisymmetric Bodies and Boundary Conditions," *J. Acoust. Soc. Am.* Vol. 80, 1986, pp. 1241–1247.
14. A. F. Seybert and T. W. Wu, Acoustic Modeling: Boundary Element Methods, in *Encyclopedia of Acoustics*, M. J. Crocker (Ed.), Wiley, New York, 1997., pp. 173–184.
15. S. Suzuki, S. Maruyama, and H. Ido, "Boundary Element Analysis of Cavity Noise Problems with Complicated Boundary Conditions," *J. Sound Vib.*, Vol. 130, 1989, pp. 79–91.
16. T. Terai, "On the Calculation of Sound Fields Around Three-Dimensional Objects by Integral Equation Methods," *J. Sound Vib.*, Vol. 69, 1980, pp. 71–100.
17. W. Tobacman, "Calculation of Acoustic Wave Scattering by Means of the Helmholtz Integral Equation, I," *J. Acoust. Soc. Am.*, Vol. 76, 1984, pp. 599–607.
18. W. Tobacman, "Calculation of Acoustic Wave Scattering by Means of the Helmholtz Integral Equation, II," *J. Acoust. Soc. Am.*, Vol. 76, 1984, pp. 1549–1554.
19. P. C. Waterman, "New Formulation of Acoustic Scattering," *J. Acoust. Soc. Amer.*, Vol. 45, 1969, pp. 1417–1429.
20. P. J. T. Filippi, "Layer Potentials and Acoustic Diffraction," *J. Sound Vib.*, Vol. 54, 1977, pp. 473–500.
21. M. A. Hamdi, "Une Formulation Variationnelle par Equations Integrales pour la Resolution de L'equation de Helmholtz avec des Conditions aux Limites Mixtes," *Comtes Rendus Acad. Sci. Paris*, Vol. 292, Ser. II, 1981, pp. 17–20.
22. M. A. Hamdi, and J. M. Ville, "Development of a Sound Radiation Model for a Finite-Length Duct of Arbitrary Shape," *AIAA J.*, Vol. 20, No. 12, 1982, pp. 1687–1692.
23. M. A. Hamdi and J. M. Ville, "Sound Radiation from Ducts: Theory and Experiment," *J. Sound Vib.*, Vol. 107, 1986, pp. 231–242.
24. C. R. Kipp and R. J. Bernhard, "Prediction of Acoustical Behavior in Cavities Using Indirect Boundary Element Method," *ASME Trans. J. Vib. Acoust. Stress Rel. Des.*, Vol. 109, 1987, pp. 15–21.
25. J. B. Mariem and M. A. Hamdi, "A New Boundary-Finite Element Method for Fluid-Structure Interaction Problems," *Intl. J. Num. Meth. Engr.*, Vol. 24, 1987, pp. 1251–1267.
26. S. T. Raveendra, N. Vlahopoulos, and A. Glaves, "An Indirect Boundary Element Formulation for Multi-Valued Impedance Simulation in Structural Acoustics," *App. Math. Modell.*, Vol. 22, 1998, pp. 379–393.
27. N. Vlahopoulos, Indirect Variational Boundary Element Method in Acoustics, in *Boundary Element Acoustics, Fundamentals and Computer Codes*, T. W. Wu (Ed.), WIT Press, Southampton, UK, 2000, Chapter 6.
28. N. Vlahopoulos and S. T. Raveendra, "Formulation, Implementation, and Validation of Multiple Connection and Free Edge Constraints in an Indirect Boundary Element Formulation," *J. Sound Vib.*, Vol. 210, 1998, pp. 137–152.
29. T. W. Wu, "A Direct Boundary Element Method for Acoustic Radiation and Scattering from Mixed Regular and Thin Bodies," *J. Acoust. Soc. A.*, Vol. 97, 1995, pp. 84–91.
30. Z. S. Chen, G. Hofstetter, and H. A. Mang, "A Symmetric Galerkin Formulation of the Boundary Element Method for Acoustic Radiation and Scattering," *J. Computat. Acoust.*, Vol. 5, 1997, pp. 219–241.
31. Z. S. Chen, G. Hofstetter, and H. A. Mang, "A Galerkin-type BE-FE Formulation for Elasto-Acoustic Coupling," *Comput. Meth. Appl. Mech. Engr.*, Vol. 152, 1998, pp. 147–155.
32. *SFE Mecosa User's Manual*, SFE, Berlin, Germany, 1998.
33. *LMS Virtual.Lab User's Manual*, LMS International, 2004.
34. S. Marburg, "Six Boundary Elements per Wavelength. Is that Enough?" *J. Computat. Acoust.*, Vol. 10, 2002, pp. 25–51.
35. S. Marburg and S. Schneider, "Influence of Element Types on Numeric Error for Acoustic Boundary Elements," *J. Computat. Acoust.*, Vol. 11, 2003, pp. 363–386.
36. C. Y. R. Cheng, A. F. Seybert, and T. W. Wu, "A Multi-Domain Boundary Element Solution for Silencer and Muffler Performance Prediction," *J. Sound Vib.*, Vol. 151, 1991, pp. 119–129.
37. H. Utsuno, T. W. Wu, A. F. Seybert, and T. Tanaka, "Prediction of Sound Fields in Cavities with Sound Absorbing Materials," *AIAA J.*, Vol. 28, 1990, pp. 1870–1876.
38. T. W. Wu, C. Y. R. Cheng, and P. Zhang, "A Direct Mixed-Body Boundary Element Method for Packed Silencers," *J. Acoust. Soc. Am.*, Vol. 111, 2002, pp. 2566–2572.
39. H. Utsuno, T. Tanaka, T. Fujikawa, and A. F. Seybert, "Transfer Function Method for Measuring Characteristic Impedance and Propagation Constant of Porous Materials," *J. Acoust. Soc. Am.*, Vol. 86, 1989, pp. 637–643.
40. ASTM Standard, E1050-98, "Standard Test Method for Impedance and Absorption of Acoustical Material

- Using a Tube, Two Microphones and a Digital Frequency Analysis System," ASTM, 1998.
41. C. N. Wang, C. C. Tse, and Y. N. Chen, "A Boundary Element Analysis of a Concentric-Tube Resonator," *Engr. Anal. Boundary Elements*, Vol. 12, 1993, pp. 21–27.
  42. T. W. Wu and G. C. Wan, "Muffler Performance Studies Using a Direct Mixed-Body Boundary Element Method and a Three-Point Method for Evaluating Transmission Loss," *ASME Trans. J. Vib. Acoust.*, Vol. 118, 1996, pp. 479–484.
  43. J. W. Sullivan and M. J. Crocker, "Analysis of Concentric-Tube Resonators Having Unpartitioned Cavities," *J. Acoust. Soc. Am.*, Vol. 64, 1978, pp. 207–215.
  44. K. N. Rao and M. L. Munjal, "Experimental Evaluation of Impedance of Perforates with Grazing Flow," *J. Sound Vib.*, Vol. 108, 1986, pp. 283–295.
  45. Y. Saad and M. H. Schultz, "GMRES-A Generalized Minimal Residual Algorithm for Solving Nonsymmetric Linear Systems," *SIAM J. Sci. Statist. Comput.*, Vol. 7, 1986, pp. 856–869.
  46. S. Marburg and S. Schneider, "Performance of Iterative Solvers for Acoustic Problems. Part I. Solvers and Effect of Diagonal Preconditioning," *Engr. Anal. Boundary Elements*, Vol. 27, 2003, pp. 727–750.
  47. M. Ochmann, A. Himm, S. Makarov, and S. Semenov, "An Iterative GMRES-based Boundary Element Solver for Acoustic Scattering," *Engr. Anal. Boundary Elements*, Vol. 27, 2003, pp. 717–725.
  48. S. Schneider and S. Marburg, "Performance of Iterative Solvers for Acoustic Problems. Part II: Acceleration by ilu-type Preconditioner," *Engr. Anal. Boundary Elements*, Vol. 27, 2003, pp. 751–757.
  49. S. N. Makarov and M. Ochmann, "An Iterative Solver for the Helmholtz Integral Equation for High Frequency Scattering," *J. Acoust. Soc. Am.*, Vol. 103, 1998, pp. 742–750.
  50. L. Greengard and V. Rokhlin, "A New Version of the Fast Multipole Method for the Laplace Equation in Three Dimensions," *Acta Numer.*, Vol. 6, 1997, pp. 229–270.
  51. V. Rokhlin, "Rapid Solution of Integral Equations of Classical Potential Theory," *J. Comput. Phys.*, Vol. 60, 1985, pp. 187–207.
  52. T. Sakuma and Y. Yasuda, "Fast Multipole Boundary Element Method for Large-Scale Steady-State Sound Field Analysis, Part I: Setup and Validation," *Acustica*, Vol. 88, 2002, pp. 513–515.
  53. S. Schneider, "Application of Fast Methods for Acoustic Scattering and Radiation Problems," *J. Computat. Acoust.*, Vol. 11, 2003, pp. 387–401.
  54. D. W. Herrin, T. W. Wu, and A. F. Seybert, "Practical Issues Regarding the Use of the Finite and Boundary Element Methods for Acoustics," *J. Building Acoust.*, Vol. 10, 2003, pp. 257–279.

# CHAPTER 10

## NONLINEAR ACOUSTICS

Oleg V. Rudenko\*  
Blekinge Institute of Technology  
Karlskrona, Sweden

Malcolm J. Crocker  
Department of Mechanical Engineering  
Auburn University  
Auburn, Alabama

### 1 INTRODUCTION

In many practical cases, the propagation, reflection, transmission, refraction, diffraction, and attenuation of sound can be described using the linear wave equation. If the sound wave amplitude becomes large enough, or if sound waves are transmitted over considerable distances, then nonlinear effects occur. These effects cannot be explained with linear acoustics theory. Such nonlinear phenomena include waveform distortion and subsequent shock front formation, frequency spreading, nonlinear wave interaction (in contrast to simple wave superposition) when two or more waves intermingle, nonlinear attenuation, radiation pressure, and streaming. Additionally in liquids, cavitation and “water hammer” and even sonoluminescence can occur.

### 2 DISCUSSION

In most noise control problems, only a few nonlinear effects are normally of interest and these occur either first in intense noise situations, for example, close to jet or rocket engines or in the exhaust systems of internal combustion engines, or second in sound propagation over great distances in environmental noise problems. The first effect—the propagation of large amplitude sound waves—can be quite pronounced, even for propagation over short distances. The second, however, is often just as important as the first, and is really the effect that most characterizes nonlinear sound propagation. In this case nonlinear effects occur when small, but finite amplitude waves travel over sufficiently large distances. Small local nonlinear phenomena occur, which, by accumulating effects over sufficient distances, seriously distort the sound waveform and thus its frequency content. We shall mainly deal with these two situations in this brief chapter. For more detailed discussions the reader is referred to several useful and specialized books or book chapters on nonlinear acoustics.<sup>1–9</sup>

The second effect described, waveform distortion occurring over large distances, has been known for a long time. Stokes described this effect in a paper<sup>10</sup> in

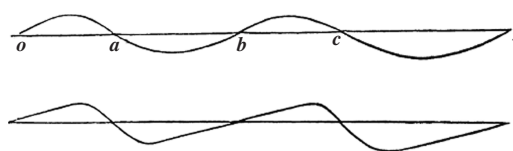


Figure 1 Wave steepening predicted by Stokes.<sup>10</sup>

1848 and gave the first clear description of waveform distortion and steepening. See Fig. 1.

More recent theoretical and experimental results show that nonlinear effects cause any periodic disturbance propagating through a nondispersive medium to be transformed into a sawtooth one at large distances from its origin. In its travel through a medium, which is quadratically nonlinear, the plane wave takes the form of a “saw blade” with triangular “teeth.” The transformation of periodic wave signals into sawtooth signals is shown in Fig. 2a. As the distance,  $x$ ,

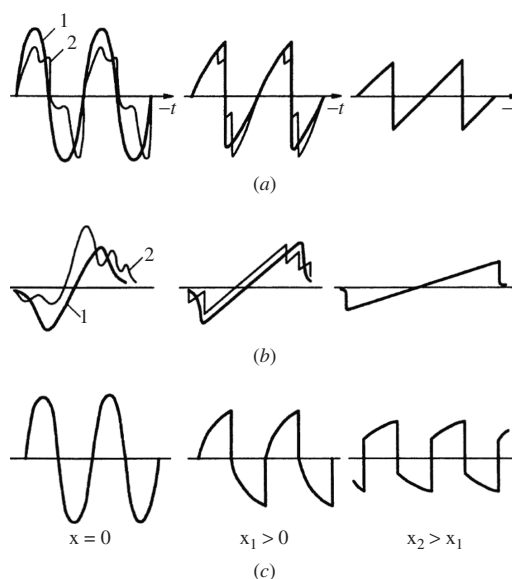


Figure 2 Examples of wave steepening from Rudenko.<sup>22</sup>

\*Present address: Department of Acoustics, Physics Faculty, Moscow State University, 119992 Moscow, Russia.

from the origin of the sound signal increases, any fine details in the initial wave profile become smoothed out through dissipation, during the wave propagation. The final wave profile is the same for both a simple harmonic signal (curve 1) and a more complicated complex harmonic signal (curve 2) at some distance from the source ( $x = x_2$  in Fig. 2a).

A single impulsive sound signal becomes transformed into an N-wave (Fig. 2b) at large distances from its origin if the medium is quadratically nonlinear. Note that the integral of the time history of the function tends to zero as  $x \rightarrow \infty$  as a result of diffraction.

In cubically nonlinear media the teeth of the saw blade have a trapezoidal form (Fig 2c). Each wave period has two shocks, one compression and the other rarefaction. The existence of sawtooth-shaped waves other than those shown in Fig. 2 is possible in media with more intricate nonlinear dissipative and dispersive behaviors. The disturbances shown in Fig. 2, however, are the most typical.

These effects shown in Fig. 2 can be explained using very simple physical arguments.<sup>11</sup> Theoretically, the wave motion in a fluid in which there is an infinitesimally small disturbance, which results in a sound pressure fluctuation field,  $p$ , can be described by the well-known wave equation:

$$\frac{\partial^2 p}{\partial x^2} - \frac{1}{c_0^2} \frac{\partial^2 p}{\partial t^2} = 0 \quad (1)$$

Theoretically, sound waves of infinitesimally small amplitude travel without distortion since all regions of the waveform have the same wave speed  $dx/dt = c_0$ . However, even in a lossless medium (one theoretically without the presence of dispersion), progressive waves of small but finite amplitude become distorted with distance and time. This is because, in the regions of the wave with positive sound pressure (and thus positive particle velocity), the sound wave travels faster than in the regions with negative sound pressure (and thus particle velocity). This effect is caused by two phenomena<sup>11</sup>:

1. The sound wave is traveling through a velocity field consisting of the particle velocity  $u$ . So with waves of finite amplitude, the wave speed (with respect to a fixed frame of reference) is

$$dx/dt = c + u \quad (2)$$

where  $c$  is the speed of sound with respect to the fluid moving with velocity  $u$ .

2. The sound speed  $c$  is slightly different from the equilibrium sound speed  $c_0$ . This is because where the particle velocity is positive (so is the sound pressure) the gas is compressed and the absolute temperature  $T$  is increased. Where the particle velocity is negative (and the sound pressure is too) then the temperature is decreased. An increased temperature results in a slightly higher sound speed  $c$  and a decreased temperature results in a slightly decreased sound speed  $c$ .

Mathematically we can show that the speed of sound is given by

$$c = c_0 + [(\gamma - 1)/2]u \quad (3)$$

where  $\gamma$  is the ratio of specific heats of the gas. We can also show that the deviation of  $c$  from  $c_0$  can be related to the nonlinearity of the pressure–density relationship. If Eqs. (2) and (3) are combined, we obtain

$$dx/dt = c_0 + \beta u \quad (4)$$

where  $\beta$  is called the coefficient of nonlinearity and is given by

$$\beta = (\gamma + 1)/2 \quad (5)$$

The fact that the sound wave propagation speed depends on the local particle velocity as given by Eq. (4) shows that strong disturbances will travel faster than those of small magnitude and provides a simple demonstration of the essential nonlinearity of sound propagation.

We note in Fig. 3 that  $u_p$  is the particle velocity at the wave peak, and  $u_v$  is the particle velocity at the wave valley. The time used in the bottom figure of Fig. 3 is the retarded time  $\tau = t - x/c_0$ , which is used to present all of the waveforms together for comparison. The distance  $\bar{x}$  in Fig. 3c is the distance needed for the formation of a vertical wavefront.

Mathematically, nonlinear phenomena can be related to the presence of nonlinear terms in analytical models, for example, in wave equations. Physically, nonlinearity leads to a violation of the superposition principle, and waves start to interact with each other. As a result of the interaction between frequency components of the wave, new spectral regions appear and the wave energy is redistributed throughout the frequency spectrum. Nonlinear effects depend on the “strength” of the wave; they are well-defined if the intensity of the noise, the amplitude of the harmonic signal, or the peak pressure of a single pulse is large enough.

The interactions of intense noise waves can be studied by the use of statistical nonlinear acoustics.<sup>1,4,14,16</sup> Such studies are important because different sources of high-intensity noise exist both in nature and engineering. Explosive waves in the atmosphere and in the ocean, acoustic shock pulses (sonic booms), noise generated by jets, and intense fluctuating sonar signals are examples of low-frequency disturbances for which nonlinear phenomena become significant at large distances. There also exist smaller noise sources whose spectra lie in the ultrasonic frequency range. These include, for instance, ordinary electromechanical transducers whose field always contains fluctuations, and microscopic sources like bubble (cavitation) noise and acoustic emission created during growth of cracks. Finally, intense noise of natural origin exists, such as thunder and seismic waves. There are obvious links between statistical nonlinear acoustics and “nonwave”

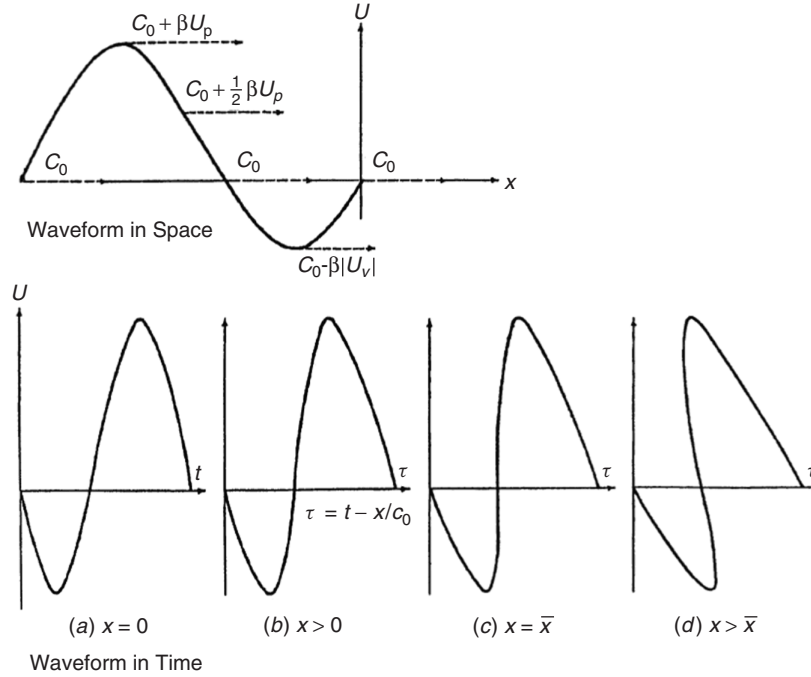


Figure 3 Wave steepening predicted by Eq. (4).<sup>20</sup>

problems—turbulence, aeroacoustic interactions, and hydrodynamic instabilities.

### 3 BASIC MATHEMATICAL MODELS

#### 3.1 Plane Waves

We shall start by considering the simple case of a plane progressive wave without the presence of reflections. For waves traveling only in the positive  $x$  direction, we have from Eq. (1), remembering that  $p/u = \rho_0 c_0$ ,

$$\frac{\partial^2 u}{\partial x^2} - \frac{1}{c_0^2} \frac{\partial^2 u}{\partial t^2} = 0 \quad (6)$$

Equation (6) may be integrated once to yield a first-order wave equation:

$$\frac{\partial u}{\partial x} + \frac{1}{c_0} \frac{\partial u}{\partial t} = 0 \quad (7)$$

We note that the solution of the first-order Eq. (7) is  $u = f(t - x/c_0)$ , where  $f$  is any function. Equation (7) can also be simplified further by transforming it from the coordinates  $x$  and  $t$  to the coordinates  $x$  and  $\tau$ , where  $\tau = t - x/c_0$  is the so-called retarded time. This most simple form of equation for a linear traveling wave is  $\partial u(x, \tau)/\partial x = 0$ . This form is equivalent to the form of Eq. (7).

The model equation containing an additional nonlinear term that describes source-generated waves of

finite amplitude in a lossless fluid is known as the Riemann wave equation:

$$\frac{\partial u}{\partial x} - \frac{\beta}{c_0^2} u \frac{\partial u}{\partial \tau} = 0 \quad (8)$$

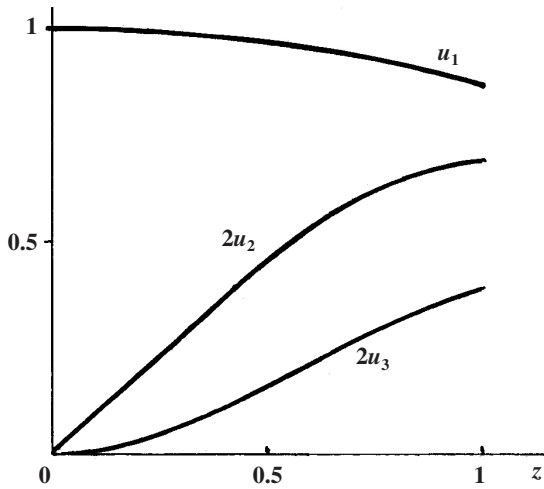
Physically, its general solution is  $u = f(\tau + \beta u x / c_0^2)$ .

For sinusoidal source excitation,  $u = u_0 \sin(\omega t)$  at  $x = 0$ , the solution is represented by the Fubini series<sup>1,2</sup>:

$$\frac{u}{u_0} = \sum_{n=1}^{\infty} \frac{2}{n z} J_n(n z) \sin(n \omega \tau) \quad (9)$$

Here  $z = x/\bar{x}$  is the normalized coordinate (see Fig. 3), and  $\bar{x} = c_0^2 / (\beta \omega u_0)$  is the shock formation distance. As shown in Fig. 4, at the distance  $z = 1$ , or at  $x = \bar{x}$ , the amplitude of the second and third harmonics reach correspondingly 0.35 and 0.2 of the initial amplitude of the fundamental harmonic. Consequently, at distances  $x \approx \bar{x}$  nonlinearity comes into particular prominence.

For example, if an ultrasonic wave having an intensity of 10 W/cm<sup>2</sup> and a frequency of 1 MHz propagates in water ( $\beta \approx 4$ ), the shock formation distance is about 25 cm. For a sound wave propagating in the air ( $\beta \approx 1.2$ ) and having a sound pressure level of 140 dB (relative to the root-mean-square pressure



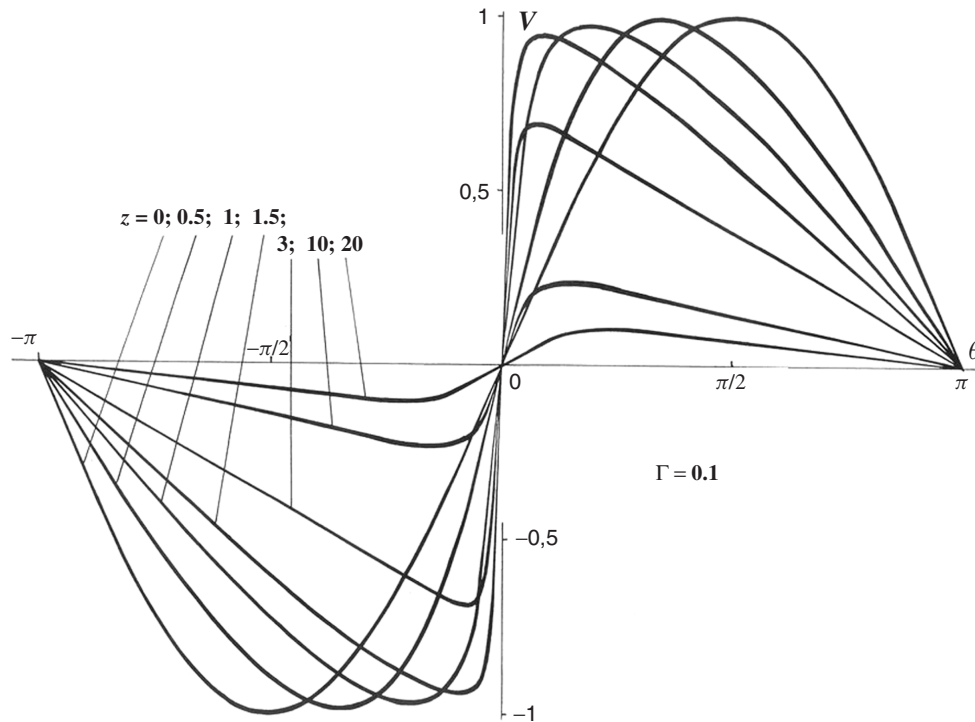
**Figure 4** Schematic of energy "pumping" to higher frequencies predicted by the Fubini solution.

$2 \times 10^{-5}$  Pa) and at a frequency 3.3 kHz, one can estimate that  $\bar{x} \approx 6$  m.

Many of the physical phenomena accompanying high-intensity wave propagation can compete with the

nonlinearity and weaken its effect. Phenomena such as dissipation, diffraction, reflection, and scattering decrease the characteristic amplitude  $u_0$  of the initial wave and, consequently, increase the shock formation distance  $\bar{x}$ . The influence of dissipation can be evaluated by use of an inverse acoustical Reynolds number  $\Gamma = \alpha \bar{x}$ ,<sup>1</sup> where  $\alpha$  is the normal absorption coefficient of a linear wave. Numerical studies (Rudenko<sup>23</sup>) show that nonlinearity is clearly observed at  $\Gamma \leq 0.1$ . The absorption predominates at high values of  $\Gamma$ , and nonlinear transformation of the temporal profile and spectrum is weak. For two examples given above, the parameter  $\Gamma$  is equal to 0.0057 (water) and 0.0014 (air), and conditions to observe nonlinear distortion are very good.

The competition between nonlinearity and absorption is shown in Fig. 5. In the first stage, for distances  $x < \bar{x}$ , the distortion of the initial harmonic wave profile goes on in accordance with the Fubini solution [Eq. (9)]. Thereafter, during the second stage,  $\bar{x} < x < 2/\alpha$ , a leading steep shock front forms inside each wavelength, and the wave profile takes on a sawtooth-shaped form. The nonlinear absorption leads to the decay of the peak disturbance, and after considerable energy loss has occurred, at distances  $x > 2/\alpha$ , the wave profile becomes harmonic again. So, in this third stage  $x > 2/\alpha$ , the propagation of the impaired wave is described by the linear wave equation.



**Figure 5** Transformation of one period of harmonic initial signal in the nonlinear and dissipative medium.<sup>23</sup> Normalized variables are used here:  $V = u/u_0$  and  $Z = x/\bar{x}$ .



### 3.2 General Wave Equation for Nonlinear Wave Propagation

The general equation that describes one-dimensional propagation of a nonlinear wave is

$$\frac{\partial p}{\partial x} + \frac{p}{2} \frac{d}{dx} \ln S(x) - \frac{\beta}{c_0^3 \rho_0} p \frac{\partial p}{\partial \tau} - \frac{b}{2c_0^3 \rho_0} \frac{\partial^2 p}{\partial \tau^2} = 0 \quad (10)$$

Here  $p(x, \tau)$  is the acoustic pressure, which depends on the distance  $x$  and the retarded time  $\tau = t - x/c_0$ , which is measured in the coordinate system accompanying the wave and moves with the sound velocity  $c_0$ ;  $\beta$ ,  $b$  are coefficients of nonlinearity and effective viscosity,<sup>1</sup> and  $\rho_0$  is the equilibrium density of the medium. Equation (1) can describe waves traveling in horns or concentrators having a cross-section area  $S(x)$ . If  $S = \text{const}$ , Eq. (10) transforms to the ordinary Burgers equation for plane waves.<sup>1</sup> If  $S \sim x$ , Eq. (10) describes cylindrical waves, and if  $S \sim x^2$ , it describes spherical ones. Equation (10) is applicable also as a transfer equation to describe waves propagating through media with large inhomogeneities if a nonlinear geometrical approach is used; for such problems,  $S(x)$  is the cross-section area of the ray tube, and the distance  $x$  is measured along the central curvilinear ray. Using new variables

$$V = \frac{p}{p_0} \sqrt{\frac{S(x)}{S(0)}} \quad \theta = \omega_0 \tau,$$

$$z = \omega_0 p_0 \int_0^x \frac{\beta}{c_0^3 \rho_0} \sqrt{\frac{S(0)}{S(x')}} dx'$$

one can reduce Eq. (10) to the generalized Burgers equation

$$\frac{\partial V}{\partial z} - V \frac{\partial V}{\partial \theta} = \Gamma(z) \frac{\partial^2 V}{\partial \theta^2} \quad (11)$$

whose properties are described in the literature.<sup>1,17</sup> Here  $p_0$  and  $\omega_0$  are typical magnitudes of the initial acoustic pressure and frequency, and

$$\Gamma(z) = \left[ \frac{b\omega_0}{2\beta p_0} \sqrt{\frac{S(x)}{S(0)}} \right]_{x=x(z)} \quad (12)$$

is the normalized effective viscosity.

Next a one-dimensional model can be derived to describe nonlinear waves in a hereditary medium (i.e., a medium with a memory)<sup>1</sup>:

$$\frac{\partial p}{\partial x} - \frac{\beta}{c_0^3 \rho_0} p \frac{\partial p}{\partial \tau} - \frac{m}{2c_0} \frac{\partial}{\partial \tau} \int_{-\infty}^{\tau} K(\tau - \tau') \frac{\partial p}{\partial \tau'} d\tau' = 0 \quad (13)$$

Here  $m$  is a constant that characterizes the “strength of memory,” and the kernel  $K(t)$  is a decaying function that describes the temporal weakening of the memory. In relaxing fluids  $K(t) = \exp(-t/t_r)$ , where  $t_r$  is the relaxation time. Such an exponential kernel is valid for atmospheric gases; it leads to the appearance of dispersion and additional absorption, which is responsible for shock front broadening during the propagation of a sonic boom. For solids, reinforced plastics and biological tissues  $K(t)$  has a more complicated form.

If it is necessary to describe the behavior of acoustical beams and to account for diffraction phenomena, the following equation can be used:

$$\frac{\partial}{\partial \tau} [\hat{\Pi}(p)] = \frac{c_0}{2} \Delta_{\perp} p \quad (14)$$

where  $\Delta_{\perp}$  is the “transverse” Laplace operator acting on coordinates in the cross section of the acoustical beam;  $\hat{\Pi}(p) = 0$  is one of the one-dimensional equations that is to be generalized [e.g. Eqs. (10) or (13)]. The Khokhlov–Zabolotskaya–Kuznetsov Eq. (15)<sup>5,9</sup>:

$$\frac{\partial}{\partial \tau} \left[ \frac{\partial p}{\partial x} - \frac{\beta}{c_0^3 \rho_0} p \frac{\partial p}{\partial \tau} - \frac{b}{2c_0^3 \rho_0} \frac{\partial^2 p}{\partial \tau^2} \right] = \frac{c_0}{2} \Delta_{\perp} p \quad (15)$$

is the most well-known example; it generalizes the Burgers equation for beams and takes into account diffraction, in addition to nonlinearity and absorption.

## 4 NONLINEAR TRANSFORMATION OF NOISE SPECTRA

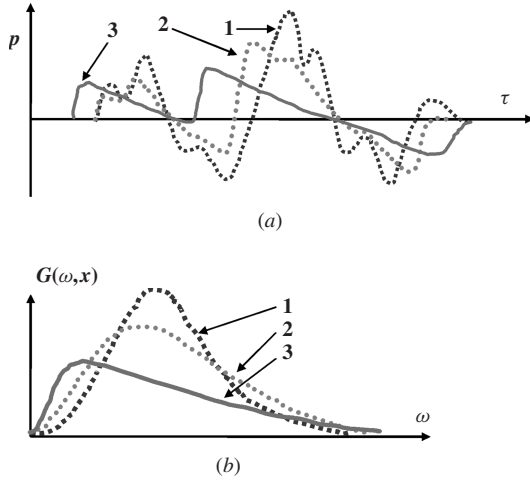
The following are examples and results obtained from numerical or analytical solutions to the models listed above. All tendencies described below have been observed in laboratory experiments or in full-scale measurements, for example, jet and rocket noise (see details in the literature<sup>1,14,16</sup>).

### 4.1 Narrow-Band Noise

Initially, a randomly modulated quasi-harmonic signal generates higher harmonics  $n\omega_0$ , where  $\omega_0$  is the fundamental frequency. At short distances in a Gaussian noise field the mean intensity of the  $n$ th harmonic is  $n!$  times higher than the intensity of the  $n$ th harmonic of a regular wave. This phenomenon is related to the dominating influence of high-intensity spikes caused by nonlinear wave transformations. The characteristic width of the spectral line of the  $n$ th harmonic increases with increases in both the harmonic number  $n$  and the distance of propagation  $x$ .

### 4.2 Broadband Noise

During the propagation of the initial broadband noise (a segment of the temporal profile of the waveform is shown by curve 1 in Fig. 6a) continuous distortion occurs. Curves 2 and 3 are constructed for successively



**Figure 6** (a) Nonlinear distortion of a segment of the temporal profile of initial broadband noise  $p$ . Curves 1, 2, and 3 correspond to increasing distances  $x_1 = 0, x_2 > 0, x_3 > x_2$ . (b) Nonlinear distortion of the spectrum  $G(\omega, x)$  of broadband noise. Curves 1, 2, and 3 correspond to the temporal profiles shown in (a).

increasing distance and display two main tendencies. The first one is the steepening of the leading fronts and the formation of shock waves; it produces a broadening of the spectrum toward the high-frequency region.

The second tendency is a spreading out of the shocks, collisions of pairs of them and their joining together; these processes are similar to the adhesion of absolutely inelastic particles and lead to energy flow into the low-frequency region.

Nonlinear processes of energy redistribution are shown in Fig. 6b. Curves 1, 2, and 3 in Fig. 6b are the mean intensity spectra  $G(\omega, x)$  of random noise waves 1, 2, and 3 whose retarded time histories are shown in Fig. 6a.

The general statistical solution of Eq. (10), which describes the transformation of high-intensity noise spectra in a nondissipative medium, is known for  $b = 0^1$ :

$$G(\omega, x) = \frac{\exp\left[-\left(\frac{\varepsilon}{c_0^3 \rho_0} \omega \sigma x\right)^2\right]}{2\pi \left(\frac{\varepsilon}{c_0^3 \rho_0} \omega \sigma x\right)^2} \times \int_{-\infty}^{\infty} \left\{ \exp\left[\left(\frac{\varepsilon}{c_0^3 \rho_0} \omega x\right)^2 R(\theta)\right] - 1 \right\} \times \exp(-i\omega\theta) d\theta \quad (16)$$

Here  $R(\theta = \theta_1 - \theta_2) = \langle p(\theta_1)p(\theta_2) \rangle$  is the correlation function of an initial stationary and Gaussian random

process, and  $\sigma^2 = R(0)$ . For simplicity, the solution, Eq. (16), is written here for plane waves; but one can easily generalize it for arbitrary one-dimensional waves [for any cross-section area  $S(x)$ ] using the transformation of variables. See Eq. (12).

### 4.3 Noise-Signal Interactions

The initial spectrum shown in Fig. 7a consists of a spectral line of a pure tone harmonic signal and broadband noise. The spectrum, after distortion by nonlinear effects, is shown in Fig. 7b.

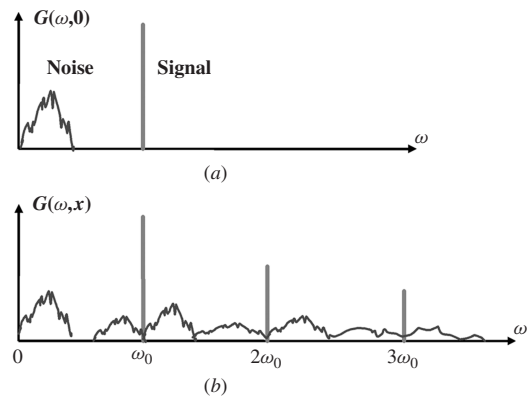
As a result of the interaction, the intensity of the fundamental pure tone wave  $\omega_0$  is decreased, due to the transfer of energy into the noise component and because of the generation of the higher harmonics,  $n\omega_0$ . New spectral wave noise components appear in the vicinity  $\omega = n\omega_0$ , where  $n = 1, 2, 3, \dots$ . These noise components grow rapidly during the wave propagation, flow together, and form the continuous part of the spectrum (see Fig. 7b).

In addition to being intensified, the noise spectrum can also be somewhat suppressed. To observe this phenomenon, it is necessary to irradiate noise with an intense signal whose frequency is high enough so that the initial noise spectrum, and the noise component generated near to the first harmonic, do not overlap.<sup>14</sup>

Weak high-frequency noise can be also partly suppressed due to nonlinear modulation by high-intensity low-frequency regular waves. Some possibilities for the control of nonlinear intense noise are described in the literature.<sup>8,14</sup>

The attenuation of a weak harmonic signal due to nonlinear interaction with a noise wave propagating in the same direction occurs according to the law

$$p = p_0 \exp\left[-\frac{1}{2} \left(\frac{\varepsilon}{c_0^3 \rho_0} \omega_0 \sigma x\right)^2\right] \quad (17)$$



**Figure 7** Nonlinear interaction of spectra of the tone signal and broadband noise. Initial spectrum (a) corresponds to the distance  $x = 0$ . Spectrum (b) measured at the distance  $x > 0$  consists of higher harmonics  $n\omega_0$  and new broadband spectral areas.

here  $\sigma^2 = \langle p^2 \rangle$  is the mean noise intensity. The dependence of the absorption with distance  $x$  in Eq. (17) is given by  $\exp(-\beta x^2)$ , which does not depend on either the location of the noise or the signal spectrum. The standard dependence  $\exp(-\alpha x)$  takes place if a deterministic harmonic signal propagates in a spatially isotropic noise field. Here<sup>21</sup>

$$\alpha = \frac{\pi \varepsilon^2}{4 c_0^5 \rho_0^2} \left[ \int_0^{\omega_0} \frac{\omega_0^2 + \omega^2}{\omega} G(\omega) d\omega + 2\omega_0 \int_{\omega_0}^{\infty} G(\omega) d\omega \right] \quad (18)$$

where  $G(\omega)$  is the spectrum of the noise intensity:

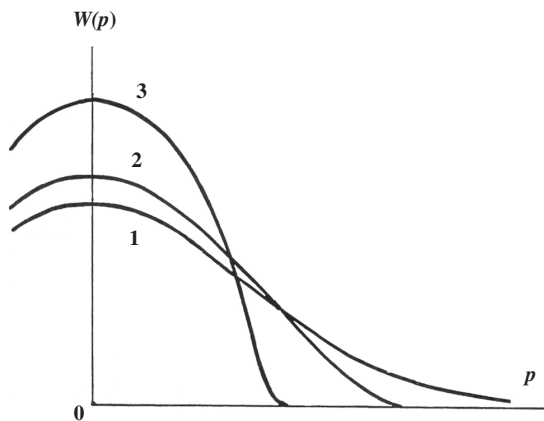
$$\sigma^2 = \int_0^{\infty} G(\omega) d\omega$$

## 5 TRANSFORMATION OF STATISTICAL DISTRIBUTION

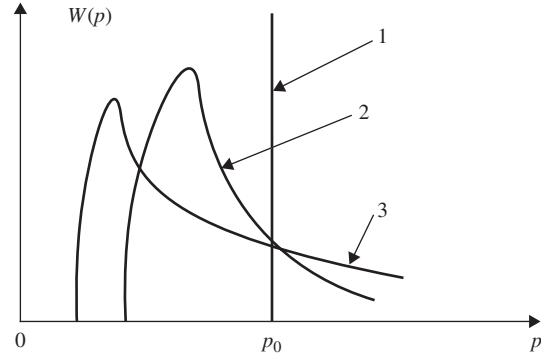
The nonlinear distortion of the probability distribution for nonlinear quasi-harmonic noise is illustrated in Fig. 8. Curve 1 shows the initial Gaussian distribution. Because of shock wave formation and subsequent nonlinear absorption, the probability of small values of the acoustic pressure  $p$  increases owing to the decrease in the probability of large high-peak pressure jumps (curves 2 and 3).

A regular signal passing through a random medium gains statistical properties. Typical examples are connected with underwater and atmospheric long-range propagation, as well as with medical devices using shock pulses and nonlinear ultrasound in such an inhomogeneous medium as the human body.

A sonic boom (N-wave) generated by a supersonic aircraft propagates through the turbulent boundary



**Figure 8** Nonlinear distortion of the probability of detection  $W(p)$  of the given value of acoustic pressure  $p$ . Curves 1, 2, and 3 correspond to increasing distances  $x_1 = 0, x_2 > 0$ , and  $x_3 > x_2$ .



**Figure 9** Nonlinear distortion of the statistical distribution of the peak pressure of a sonic boom wave passed through a turbulent layer. Line 1 is the initial distribution, curves 2 and 3 correspond to distances  $x_1, x_2 > x_1$ .

layers of the atmosphere. Transformation of the statistical distribution of its peak pressure is shown in Fig. 9.<sup>18</sup> Initial distribution is a delta-function (line 1), peak pressure is pre-determined and is equal to  $p_0$ .

At increasing distances (after passing through the turbulent layer, curves 2 and 3), this distribution broadens; the probability increases that both small- and large-amplitude outbursts are observed. So, turbulence leads to a decrease in the mean peak pressure, but fluctuations increase as a result of random focusing and defocusing caused by the random inhomogeneities in the atmosphere.

Nonlinear propagation in media containing small inhomogeneities responsible for wave scattering is governed by an equation like Eq. (10), but one which contains a fourth-order dissipative term instead of a second-order one<sup>19</sup>:

$$-\frac{b}{2c_0^3 \rho_0} \frac{\partial^2 p}{\partial \tau^2} \Rightarrow +\beta \frac{\partial^4 p}{\partial \tau^4} \quad \beta = \frac{8\langle \mu^2 \rangle a^3}{c_0^4} \quad (19)$$

Here  $\langle \mu^2 \rangle$  is the mean square of fluctuations of the refractive index, and  $a$  is the radius of correlation. Scattering losses are proportional to  $\omega^4$  instead of  $\omega^2$  in viscous media. Such dependence has an influence on the temporal profile and the spectrum of the nonlinear wave; in particular, the increase of pressure at the shock front has a nonmonotonic (oscillatory) character.

## 6 SAMPLE PRACTICAL CALCULATIONS

It is of interest in practice to consider the parameter values for which the nonlinear phenomena discussed above are physically significant. For instance, in measuring the exhaust noise of a commercial airliner or of a spacecraft rocket engine at distances of 100 to 200 m, is it necessary to consider nonlinear spectral distortion or not? To answer this question we evaluate the shock formation distance for wave propagation in air in more detail than in Section 3.

For a plane simple harmonic wave, the shock formation distance is equal to

$$\bar{x}_{\text{pl}} = \frac{c_0^2}{\beta \omega u_0} = \frac{c_0^3 \rho_0}{2\pi \beta f p_0} \quad (20)$$

where  $p_0$  is the amplitude of the sound pressure, and  $f = \omega/2\pi$  is the frequency. For a spherical wave one can derive the shock formation distance using Eqs. (10) and (11):

$$\bar{x}_{\text{sph}} = x_0 \exp\left(\frac{c_0^3 \rho_0}{2\pi \beta f p_0 x_0}\right) \quad (21)$$

Here  $x_0$  is the radius of the initial spherical front of the diverging wave. In other words,  $x_0$  is the radius of a spherical surface surrounding the source of intense noise, at which the initial wave shape or spectrum is measured.

Let the sound pressure level of the noise measured at a distance of  $x_0 = 10$  m be 140 dB, and the typical peak frequency  $f$  of the spectrum be 1 kHz. Evaluating the situation for propagation in air using the parameters:

$$\beta = 1.2 \quad c_0 = 330 \text{ m/s} \quad \rho_0 = 1.3 \text{ kg/m}^3$$

gives the following values for the shock formation distances:

$$\bar{x}_{\text{pl}} \sim 20 \text{ m} \quad \bar{x}_{\text{sph}} \sim 80 \text{ m}$$

So in this situation, shocks form in spherical wave propagation at a greater distance than in plane wave propagation because the spherical spreading decreases the wave intensity and, consequently, nonlinear phenomena accumulate more slowly in the spherical than in the plane wave propagation case.

In all practical cases, the real shock front formation length  $\bar{x}$  obeys the inequality

$$\bar{x}_{\text{pl}} < \bar{x} < \bar{x}_{\text{sph}}$$

At distances, for which  $x \sim \bar{x}$ , nonlinear distortion is significant.

During experiments performed by Pestorius and Blackstock,<sup>25</sup> which used a long tube filled with air, strong nonlinear distortion of the noise spectrum was observed at distances between as little as 2 to 10 m, for sound pressure levels of 160 dB. This result agrees with predictions made using Eq. (20) for a frequency  $f$  of about 1 kHz. Morfey<sup>26</sup> analyzed several experiments and observed nonlinear distortion in the spectra of four-engine jet aircraft at distances between 262 and 501 m, for frequencies between  $f = 2$  and 10 kHz. He also analyzed the noise spectrum of an Atlas-D rocket engine at distances of 1250 to 5257 m, at frequencies in the range of  $f = 0.3$  to 2.4 kHz. These observations correspond to the

analytical case of spherically diverging waves. See Eq. (21).

Extremely strong noise is produced near the rocket exhausts of large spacecraft during launch. For example, assume that the sound pressure level is 170 dB at 10 m from a powerful space vehicle such as the *Saturn V* or the space shuttle. The shock formation distance is predicted from Eq. (21) to be a further distance of  $\bar{x}_{\text{sph}} \approx 13$  m for a frequency of 500 Hz. The approximate temporal duration  $t_{\text{fr}}$  of the shock front at a distance  $x$  can be calculated using Eq. (22), which is found in Rudenko and Soluyan<sup>1</sup>:

$$t_{\text{fr}} = \frac{1}{\pi^2 f} \frac{\bar{x}_{\text{pl}}}{\bar{x}_{\text{abs}}} \frac{x}{x_0} \left[ 1 + \frac{x_0}{\bar{x}_{\text{pl}}} \ln\left(\frac{x}{x_0}\right) \right] \quad (22)$$

where  $\bar{x}_{\text{abs}} = \alpha^{-1} = (4\pi^2 f^2 \delta)^{-1}$  is the absorption length, and the value of  $\delta = 0.5 \times 10^{-12} \text{ s}^2/\text{m}$  is assumed for air. For the assumed sound pressure level of 170 dB and the frequency 500 Hz, we substitute the values  $\bar{x}_{\text{pl}} = x_0 = 10$  m and evaluate the width of the shock front  $l_{\text{fr}} = c_0 t_{\text{fr}}$  at small distances of 25 to 30 m from the center of the rocket exhaust nozzles. This shock width being of the order of  $l_{\text{fr}} \approx 0.01 - 0.1$  mm is much less than the wavelength,  $\lambda \approx 67$  cm. Such a steep shock front is formed because of strong nonlinear effects. As the sound wave propagates, the shock width increases and reaches  $l_{\text{fr}} \approx 7$  cm at distances of about 23 km. It is evident that nonlinear phenomena will be experienced at large distances from the rocket. That is the reason why it is possible to hear the "crackling sound" standing far from the launch position. However, the value of 23 km for the distance at which the shock disappears is realistic only if the atmosphere is assumed to be an unlimited and homogeneous medium. In reality, due to reflection from the ground and the refraction of sound rays in the real inhomogeneous atmosphere, the audibility range for shocks can be somewhat less. To describe nonlinear sound propagation in the real atmosphere, the numerical solution of the analysis of more complicated mathematical models such as Rudenko<sup>22</sup> needs to be undertaken.

It is necessary to draw attention to the strong exponential dependence of nonlinear effects on the frequency  $f_0$ , the sound wave amplitude  $p_0$ , and the initial propagation radius  $x_0$ , for spherical waves. From Eq. (21) we have

$$\bar{x}_{\text{sph}} = x_0 \exp\left(\frac{\text{const}}{f p_0 x_0}\right)$$

Consequently, the shock formation distance  $\bar{x}_{\text{sph}}$  is very sensitive to the accuracy of measurement of these parameters. Other numerical examples concerning nonlinear noise control are given in the literature.<sup>8,14,16</sup>

Consider now a sonic boom wave propagating as a cylindrical diverging wave from a supersonic aircraft.

The shock formation distance for this case is

$$\bar{x}_{\text{cyl}} = x_0 \left( 1 + \frac{c_0^3 \rho_0}{4\pi \beta f p_0 x_0} \right)^2 \quad (23)$$

At small distances from the aircraft, for example, at 50 m, the peak sound pressure is about 3000 Pa and the pulse duration  $t_0 = f^{-1} \sim l/v$ , where  $l$  is the length of the aircraft fuselage, and  $v > c_0$  is the speed of supersonic flight. For the parameters of aircraft length and speed,  $l = 10$  m,  $v = 1.3c_0$ , evaluation of Eq. (23) gives  $\bar{x}_{\text{cyl}} \sim 100$  m. This means that at several hundred metres from the aircraft, the multiple collisions of shocks generated by singularities of the aerodynamic profile come to an end, and the sonic boom wave changes into an N-wave, as shown in Fig. 2b.

At greater distances, the peak pressure of the N-wave decreases, and the value of the distance  $\bar{x}_{\text{cyl}}$  increases. For a peak pressure of 200 Pa measured at  $x_0 = 1$  km, and for a pulse duration  $t_0 = f^{-1} = 0.05$  s we obtain a distance of  $\bar{x}_{\text{cyl}} \sim 3$  km, according to Eq. (23). So, for a distance of  $x_0 = 1$  km from the aircraft, an additional distance  $\bar{x}_{\text{cyl}} - x_0 = 2$  km will produce a significant change in the shape of the N-wave due to the nonlinear wave propagation effects.

Nonlinear phenomena appear also near to the sharp tips of bodies and orifices in the high-speed streamlines of an oscillating fluid. These nonlinearities are caused by the large spatial gradients in the hydrodynamic field and are related to the convective term  $(\mathbf{u} \nabla) \mathbf{u}$  in the equation of motion of the fluid, in the form of the Navier–Stokes or Euler equations. This effect is quite distinct from the more common nonlinear phenomena already described. Nonlinear wave distortion cannot build up during wave propagation since the effect only has a “local” character. To determine the necessary sound pressure level at which we can observe these phenomena in an oscillating flow, we evaluate the velocity gradients. (Note that in the case of harmonic vibrations in the streamlines around an incompressible liquid, higher harmonics will appear.) We assume that the gradient is of the order of  $u / \max(r_0, \delta)$ , where  $\delta = \sqrt{\nu/\omega}$  is the width of the acoustical boundary layer,  $r_0$  is the minimum radius of the edge of the body,  $u$  is the vibration velocity, and  $\nu = \eta/\rho_0$  is the kinematic viscosity. The width is the dominating factor for sharp edges, if  $r_0 < \delta$ . This “boundary nonlinearity” is significant at Reynolds numbers of  $\text{Re} \sim 1$ , which are proportional to the ratio of the terms in the Navier–Stokes or Euler equations of motion of the fluid:

$$\text{Re} \sim \left| (\mathbf{u} \nabla) \mathbf{u} \left( \frac{\partial \mathbf{u}}{\partial t} \right)^{-1} \right| \sim \frac{u}{\sqrt{\omega \nu}} = \sqrt{\frac{2I}{c \omega \eta}} \quad (24)$$

As can be determined by Eq. (24), this nonlinearity manifests itself in air at a sound pressure level of 120 dB, at a frequency of about 500 Hz. If vortices form near to the edge of a body immersed in an oscillating flow, nonlinearity in such a flow can be

observed even at a sound pressure level as low as 90 dB. Boundary layer nonlinearity is significant in the determination of the resonance frequency of sound absorbers, which contain Helmholtz resonators with sound-absorbing material in their necks. This nonlinearity can detune the resonance condition at the frequency given by linear approximations. It can even have the opposite effect of enhancing the dissipation of acoustic energy by the absorber, if it is excited off resonance, according to the linear approximations.<sup>8</sup>

## 7 FURTHER COMMENTS AND CONCLUSIONS

Only common nonlinear events occurring in typical media have been discussed. However, nonlinear phenomena of much more variety can occur. Nonlinearity manifests itself markedly in conditions of resonance, if the standing waves that form in spatially limited systems have a high  $Q$  factor. Using high- $Q$  resonators, it is possible to accumulate a considerable amount of acoustic energy and provide conditions for the clear manifestation of nonlinear phenomena even in the case of weak sound sources.<sup>23</sup>

Some structures (such as components of the fuselage of an aircraft) can have huge nonlinearities caused by special types of inhomogeneous inclusions (in cases such as the delamination of layered composites, with cracks and grain boundaries in metals, and with clamped or impacting parts, etc.). These nonlinear phenomena can be used to advantage in sensitive nondestructive tests.

It is necessary to mention a nonlinear device known as a “parametric array.” Its use is common in underwater acoustics.<sup>9</sup> Recently, it has also been put to use in air in the design of parametric loudspeakers.<sup>27,28</sup>

The difference between linear and nonlinear problems is sometimes only relative. For example, aerodynamic sound generation can be referred to as a linear problem; but some people say that this is a nonlinear phenomenon described by the nonlinear terms in the Lighthill equation. Both viewpoints are true. Chapter 9 in this book, which is written by Morris and Lilley, is devoted to the subject of aerodynamic sound. The aerodynamic exhaust noise generated by turbojet and turbofan engines is discussed by Huff and Envia in Chapter 89 of this book. Lighthill, Powell and Ffowcs Williams also discuss jet noise generation in Chapters 24, 25, and 26 in the *Handbook of Acoustics*.<sup>29</sup>

## REFERENCES

1. O. V. Rudenko and S. I. Soluyan, *Theoretical Foundations of Nonlinear Acoustics*, Plenum, Consultants Bureau, New York, 1977.
2. R. T. Beyer, *Nonlinear Acoustics in Fluids*, Van Nostrand Reinhold, New York, 1984; *Nonlinear Acoustics*, Acoustical Society of America, American Institute of Physics, New York, 1997.
3. K. A. Naugol'nykh and L. A. Ostrovsky (Eds.), *Non-Linear Trends in Physics*, American Institute of Physics, New York, 1994.
4. K. Naugolnykh and L. Ostrovsky, *Non-Linear Wave Processes in Physics*, Cambridge University Press, Cambridge, 1998.

5. M. F. Hamilton and D. T. Blackstock, *Nonlinear Acoustics*, Academic, San Diego, 1998.
6. O. V. Rudenko, Nonlinear Acoustics, in *Formulas of Acoustics*, F. P. Mechel (Ed), Springer, 2002.
7. L. Kinsler, Frey et al., *Fundamentals of Acoustics*, 4th ed., Wiley, New York, 2000.
8. O. V. Rudenko and S. A. Rybak (Eds.), *Noise Control in Russia*, NPK Informatica, 1993.
9. B. K. Novikov, O. V. Rudenko, and V. I. Timoshenko, *Nonlinear Underwater Acoustics* (trans. R. T. Beyer), American Institute of Physics, New York, 1987.
10. G. C. Stokes, On a Difficulty in the Theory of Sound, *Philosophical Magazine*, Ser. 3, Vol. 33, 1848, pp. 349–356.
11. D. T. Blackstock and M. J. Crocker, in *Handbook of Acoustics*, M. J. Crocker (Ed.), Wiley, New York, 1998, Chapter 15.
12. D. T. Blackstock, in *Handbook of Acoustics*, M. J. Crocker (Ed.), Wiley, New York, 1998, Chapter 16.
13. D. G. Crighton, in *Handbook of Acoustics*, M. J. Crocker (Ed.), Wiley, New York, 1998, Chapter 17.
14. O. V. Rudenko, Interactions of Intense Noise Waves, *Sov. Phys. Uspekhi*, Vol. 29, No. 7, 1986, pp. 620–641.
15. S. N. Gurbatov, A. N. Malakhov, and A. I. Saichev, *Nonlinear Random Waves and Turbulence in Nondispersive Media: Waves, Rays, Particles*, Wiley, New York, 1992.
16. S. N. Gurbatov, and O. V. Rudenko, Statistical Phenomena, in *Nonlinear Acoustics*, M. F. Hamilton and D. T. Blackstock (Eds.), Academic, New York, 1998, pp. 377–398.
17. B. O. Enflo and O. V. Rudenko, To the Theory of Generalized Burgers Equations, *Acustica–Acta Acustica*, Vol. 88, 2002, pp. 155–162.
18. O. V. Rudenko and B. O. Enflo, Nonlinear N-wave Propagation through a One-dimensional Phase Screen, *Acustica–Acta Acustica*, Vol. 86, 2000, pp. 229–238.
19. O. V. Rudenko and V. A. Robsman, Equation of Nonlinear Waves in a Scattering Medium, *Doklady-Physics (Reports of Russian Academy of Sciences)*, Vol. 47, No. 6, 2002, pp. 443–446.
20. D. T. Blackstock, Nonlinear Acoustics (Theoretical), in *American Institute of Physics Handbook*, 3rd ed. D. E. Gray (Ed.), McGraw-Hill, New York, 1972, pp. 3-183–3-205.
21. P. J. Westervelt, Absorption of Sound by Sound, *J. Acoust. Soc. Am.*, Vol. 59, 1976, pp. 760–764.
22. O. V. Rudenko, Nonlinear Sawtooth-shaped Waves, *Physics–Uspekhi*, Vol. 38, No 9, 1995, pp. 965–989.
23. O. A. Vasil'eva, A. A. Karabutov, E. A. Lapshin, and O. V. Rudenko, *Interaction of One-Dimensional Waves in Nondispersive Media*, Moscow State University Press, Moscow, 1983.
24. B. O. Enflo, C. M. Hedberg, and O. V. Rudenko, Resonant Properties of a Nonlinear Dissipative Layer Excited by a Vibrating Boundary: Q-factor and Frequency Response, *J. Acoust. Soc. Am.*, Vol. 117, No. 2, 2005, pp. 601–612.
25. F. M. Pestorius and D. T. Blackstock, in *Finite-Amplitude Wave Effects in Fluids*, IPC Science and Technology Press, London, 1974, p. 24.
26. C. L. Morfey, in Proc. 10 International Symposium on Nonlinear Acoustics, Kobe, Japan, 1984, p. 199.
27. T. Kite, J. T. Post, and M. F. Hamilton, Parametric Array in Air: Distortion Reduction by Preprocessing, in *Proc. 16th International Congress on Acoustics*, Vol. 2, P. K. Kuhl and L. A. Crum (Eds.), New York, ASA, 1998, pp. 1091–1092.
28. F. J. Pompei, The Use of Airborne Ultrasonics for Generating Audible Sound Beams, *J. Audio Eng. Soc.*, Vol. 47, No. 9, 1999.
29. M. J. Crocker (Ed.), *Handbook of Acoustics*, Wiley, and New York, 1998, Chapters 23, 24, and 25.

# CHAPTER 9

## AERODYNAMIC NOISE: THEORY AND APPLICATIONS

Philip J. Morris and Geoffrey M. Lilley\*  
Department of Aerospace Engineering  
Pennsylvania State University  
University Park, Pennsylvania

### 1 INTRODUCTION

This chapter provides an overview of *aerodynamic noise*. The theory of aerodynamic noise, founded by Sir James Lighthill,<sup>1</sup> embraces the disciplines of acoustics and unsteady aerodynamics, including turbulent flow. Aerodynamic noise is generated by the unsteady, nonlinear, turbulent flow. Thus, it is self-generated rather than being the response to an externally imposed source. It is sometimes referred to as *flow noise*, as, for instance, in duct acoustics, and is also related to the theory of hydrodynamic noise. In its applications to aeronautical problems we will often mention *aeroacoustics* in referring to problems of both sound propagation and generation. The source of aerodynamic noise is often a *turbulent flow*. So some description of the characteristics of turbulence in jets, mixing regions, wakes, and boundary layers will give the reader sufficient information on the properties of turbulent flows relevant to noise prediction.

### 2 BACKGROUND

In 1957, Henning von Gierke<sup>2</sup> wrote:

Jet aircraft, predominating with military aviation, create one of the most powerful sources of man-made sound, which by far exceeds the noise power of conventional propeller engines. The sound [pressure] levels around jet engines, where personnel must work efficiently, have risen to a point where they are a hazard to man's health and safety and are now at the limit of human tolerance. Further increase of sound [pressure] levels should not be made without adequate protection and control; technical and operational solutions must be found to the noise problem if it is not to be a serious impediment to further progress in aviation.

In spite of tremendous progress in the reduction of aircraft engine noise (see Chapters 89 and 90 of this handbook), the issues referred to by von Gierke continue to exist. Aircraft noise at takeoff remains an engine noise problem. However, for modern commercial aircraft powered by high bypass ratio

turbofan engines, during the low-level approach path of all aircraft to landing, it is found that engine and airframe make almost equal contributions to the total aircraft noise as heard in residential communities close to all airports. Thus, the physical understanding of both aircraft engine and airframe noise, together with their prediction and control, remain important challenges in the overall control of environmental pollution.

In this chapter, following a brief introduction into the theory of linear and nonlinear acoustics, the general theory of aerodynamic noise is presented. The discussion is then divided between the applications of the theory of Lighthill<sup>1,3</sup> to the noise generation of free turbulent flows, such as the mixing region noise of a jet at subsonic and supersonic speeds, and its extension by Curle,<sup>4</sup> referred to as the theory of Lighthill–Curle, to the noise generation from aircraft and other bodies in motion. The other major development of Lighthill's theory, which is discussed in this chapter, is its solution due to Ffowcs Williams and Hawkings<sup>5</sup> for arbitrary surfaces in motion. Lighthill's theory as originally developed considered the effects of convective amplification, which was later extended to include transonic and supersonic jet Mach numbers by Ffowcs Williams.<sup>6</sup> It is referred to as the Lighthill–Ffowcs Williams *convective amplification theory*. In its application, Lighthill's theory neglects any interaction between the turbulent flow and the sound field generated by it. The extension of Lighthill's theory to include *flow-acoustical interaction* was due to Lilley.<sup>7</sup> This is also described in this chapter, along with a more general treatment of its practical application, using the linearized Euler equations with the nonlinear sources similar to those found in Lighthill's theory, and the adjoint method due to Tam and Auriault.<sup>8</sup>

In the discussion on the applications to *jet noise*, the noise arising from turbulent mixing is shown to be enhanced at supersonic speeds by the presence of a shock and expansion cell structure in the region of the jet potential core. This results in both broadband shock associated noise and tonal components called screech. The noise sources revert to those associated with turbulent mixing only downstream of the station where the flow velocity on the jet axis has decayed to the local sonic velocity.

The practical application of the combined theory of generation and propagation of aerodynamic noise is introduced in Section 8, which discusses *computational aeroacoustics* (CAA). This relatively new

\*Present address: School of Engineering Sciences, University of Southampton, Southampton, SO17 1BJ, United Kingdom and NASA Langley Research Center, Mail Stop 128, Hampton, Virginia, 23681, United States of America.

field uses the computational power of modern high-performance computers to simulate both the turbulent flow and the noise it generates and radiates.

The final sections of this chapter consider applications of aerodynamic noise theory to the noise radiated from turbulent boundary layers developing over the wings of aircraft and their control surfaces. The two major developments in this field are the Lighthill–Curle<sup>4</sup> theory applicable to solid bodies and the more general theory due to Ffowcs Williams and Hawkings<sup>5</sup> for arbitrary surfaces in motion. The theory has applications to the noise from closed bodies in motion at sufficiently high Reynolds numbers for the boundary layers to be turbulent. The theory applies to both attached and separated boundary layers around bluff bodies and aircraft wings at high lift. Noise radiation is absent from steady laminar boundary layers but strong noise radiation occurs from the unsteady flow in the transition region between laminar and turbulent flow. A further important aspect of the noise from bodies in motion is the diffraction of sound that occurs at a wing trailing edge. The theory of *trailing edge noise* involves a further extension of Lighthill's theory and was introduced by Ffowcs Williams and Hall.<sup>9</sup> In aeronautics today, one of the major applications of *boundary layer noise* is the prediction and reduction of noise generated by the airframe, which includes the wings, control surfaces, and the undercarriage. This subject is known as *airframe noise*. Its theory is discussed with relevant results together with brief references to methods of noise control.

Throughout the chapter simple descriptions of the physical processes involving noise generation from turbulent flows are given along with elementary scaling laws. Wherever possible, detailed analysis is omitted, although some analysis is unavoidable. A comprehensive list of references has been provided to assist the interested reader. In addition, there are several books that cover the general areas of acoustics and aeroacoustics. These include, Goldstein,<sup>10</sup> Lighthill,<sup>11</sup> Pierce,<sup>12</sup> Dowling and Ffowcs Williams,<sup>13</sup> Hubbard,<sup>14</sup> Crighton et al.,<sup>15</sup> and Howe.<sup>16</sup> Additional reviews are contained in Ribner,<sup>17</sup> and Crocker.<sup>18,19</sup> In this chapter we do not discuss problems where aerodynamic noise is influenced by the vibration of solid surfaces, such as in fluid–structure interactions, where reference should be made to Cremer, Heckl, and Petersson<sup>20</sup> and Howe.<sup>16</sup>

### 3 DIFFERENCES BETWEEN AERODYNAMIC NOISE AND LINEAR AND NONLINEAR ACOUSTICS

The theory of linear acoustics is based on the linearization of the Navier–Stokes equations for an inviscid and isentropic flow in which the propagation of weak acoustic waves are small perturbations on the fluid at rest. The circular frequency,  $\omega$ , of the acoustic, or sound, waves is given by

$$\omega = kc \quad (1)$$

where  $k = 2\pi/\lambda$  is the wavenumber,  $\lambda$  is the acoustic wavelength, and  $c$  is the speed of sound. The frequency in hertz,  $f = \omega/2\pi$ . Linear acoustics uses the linearized Euler equations, derived from the Navier–Stokes equations, incorporating the thermodynamic properties of a perfect gas at rest. The properties of the undisturbed fluid at rest are defined by the subscript zero and involve the density  $\rho_0$ , pressure  $p_0$ , and enthalpy  $h_0$ , with  $p_0 = \rho_0 h_0(\gamma - 1)/\gamma$ , and the speed of sound squared,  $c_0^2 = \gamma p_0/\rho_0 = (\gamma - 1)h_0$ . The relevant perturbation conservation equations of mass and momentum for a fluid at rest are, respectively,

$$\frac{\partial \rho'}{\partial t} + \rho_0 \theta' = 0 \quad \frac{\partial \rho_0 \mathbf{v}'}{\partial t} + \nabla p' = 0 \quad (2)$$

where  $\theta' = \nabla \cdot \mathbf{v}'$  is the fluctuation in the rate of dilatation, and  $\mathbf{v}'$  is the acoustic particle velocity. In the propagation of plane waves  $p' = \rho_0 c_0 v'$ . Since the flow is isentropic  $p' = c_0^2 \rho'$ .

From these governing equations of linearized acoustics we find, on elimination of  $\theta'$ , the *unique* acoustic wave equation for a fluid at rest, namely

$$\left( \frac{\partial^2}{\partial t^2} - c_0^2 \nabla^2 \right) \rho' = 0 \quad (3)$$

When the background fluid is in motion, with the uniform velocity  $\mathbf{V}_0$ , the linear operator following the motion is  $D_0/Dt \equiv \partial/\partial t + \mathbf{V}_0 \cdot \nabla$ , and we obtain the *Galilean invariant* convected acoustic wave equation,

$$\left( \frac{D_0^2}{Dt^2} - c_0^2 \nabla^2 \right) \rho' = 0 \quad (4)$$

Problems in acoustics can be solved by introducing both volume and surface distributions of sound sources, which are classified by type as monopole, dipole, quadrupole, and so on, representing, respectively, a single simple source, and two and four simple sources in close proximity, and are similar to the point sources in ideal potential flow fluid dynamics. The inhomogeneous acoustic wave equations are obtained by adding the distribution of acoustic sources,  $A(\mathbf{x}, t)$ , to form the right-hand side of the homogeneous convection equation (4):

$$\left( \frac{D_0^2}{Dt^2} - c_0^2 \nabla^2 \right) \rho' = A(\mathbf{x}, t) \quad (5)$$

and similarly for the unique wave equation (3).

The energy conservation equation is obtained by multiplying, respectively, the above conservation of mass and momentum equations by  $p'$  and  $\mathbf{v}'$  to give

$$\begin{aligned} \frac{1}{2\rho_0 c_0^2} \frac{\partial (p')^2}{\partial t} &= -\theta' p' \\ \frac{\partial \rho_0 (v')^2/2}{\partial t} &= -\nabla \cdot p' \mathbf{v}' + \theta' p' \end{aligned} \quad (6)$$



By elimination of  $p'/\theta'$  we find the energy conservation equation in linear acoustics, namely

$$\frac{\partial w}{\partial t} + \nabla \cdot \mathbf{I} = 0 \quad (7)$$

where  $w = \rho_0(v')^2/2 + (\frac{1}{2})(p')^2/(\rho_0 c_0^2)$  is the sum of the acoustic kinetic and potential energies and  $\mathbf{I} = p'\mathbf{v}'$  is the acoustic intensity.

When the acoustic waves are of finite amplitude, we must use the complete Navier–Stokes equations. However, on the assumption that the diffusive terms have negligible influence on wave propagation at high Reynolds numbers, we find that for acoustic waves of finite amplitude propagating in one dimension only, the following exact nonlinear inhomogeneous acoustic wave equation can be obtained:

$$\frac{D^2 \chi}{Dt^2} - \frac{\partial}{\partial x} \left( c^2 \frac{\partial \chi}{\partial x} \right) - \left( \frac{D\chi}{Dt} \right)^2 = 0 \quad (8)$$

where  $\chi = \ln \rho/\rho_0$ ,  $D/Dt \equiv \partial/\partial t + u\partial/\partial x$  is the nonlinear convective operator following the motion, and the variable sound speed  $c^2 = c_0^2 \exp[(\gamma - 1)\chi]$ . The nonlinearity is shown by the addition of  $(D\chi/Dt)^2$  to the linear acoustic wave equation, together with the dependence of the speed of sound on the amplitude  $\chi$ . Problems in nonlinear acoustics require the solution of the corresponding nonlinear inhomogeneous equation incorporating the distribution of acoustic source multipoles on the right-hand side of the above homogeneous equation. A simpler approach is to use the Lighthill–Whitham<sup>21</sup> theory whereby the linear acoustical solution is obtained and then its characteristics are modified to include the effects of the finite amplitude wave motion and the consequent changes in the sound speed. It is also found from the Navier–Stokes equations, including the viscous terms, that in one dimension, and using the equation for  $\chi$ , the nonlinear equation for the particle velocity,  $u$ , is given approximately, due to the vanishingly small rate of dilatation inside the flow, by Burgers equation,

$$\frac{Du}{Dt} = \nu \nabla^2 u \quad (9)$$

which explains the nonlinear steepening arising in the wave propagation plus its viscous broadening. It has an exact solution based on the Cole–Hopf transformation. The fluid’s kinematic viscosity is  $\nu$ . The solutions to Burgers equation in the case of inviscid flow are equivalent to the method of Lighthill–Whitham. The latter method was extended to the theory of “bunching” of multiple random shock waves by Lighthill<sup>22</sup> and Puneekar et al.<sup>23</sup> using Burgers equation. Additional information on nonlinear acoustics is given in Chapter 10 of this handbook.

We now turn to *aerodynamic noise*, the science of which was founded by Lighthill.<sup>1</sup> It is based on the

exact Navier–Stokes equations of compressible fluid flow, which apply equally to both viscous and turbulent flows. However, all mathematical theories need to be validated by experiments, and it was fortunate that such verification—that turbulence was the source of noise—was available in full from the earlier experiments on jet noise, begun in 1948, by Westley and Lilley<sup>24</sup> in England and Lassiter and Hubbard<sup>25</sup> in the United States. The theory and experiments had been motivated by the experience gained in measuring the jet noise of World War II military aircraft, the wider certain noise impact on residential areas, due to the rapid growth of civil aviation, and the introduction of jet propulsion in powering commercial aircraft. At the time of the introduction of Lighthill’s theory, a range of methods for jet noise reduction had already been invented by Lilley, Westley, and Young,<sup>24</sup> which were later fitted to all commercial jet aircraft from 1960 to 1980, before the introduction of the quieter turbofan bypass engine in 1970.

Aerodynamic noise problems differ from those of classical acoustics in that the noise is self-generated, being derived from the properties of the unsteady flow, where the intensity of the radiated sound, with its broadband frequency spectrum and its total acoustic power, are a small by-product of the kinetic energy of the unsteady flow. At low Mach numbers, the dominant wavelength of the sound generated is typically much larger than the dimensions of the flow unsteadiness. In this case we regard the sound source as compact. At high frequencies and/or higher Mach numbers the opposite occurs and the source is noncompact.

The frequency  $\omega$  and wavenumber  $k$  are the parameters used in the Fourier transforms of space–time functions used in defining the wavenumber/frequency spectrum in both acoustics and turbulence analysis. Apart from the Doppler changes in frequency due to the source motion relative to a receiver, the wavenumber and frequency in the sound field generated by turbulent motion must equal the same wavenumber and frequency in the turbulence. But here we must add a word of caution since, in turbulence, the dynamic processes are nonlinear and the low wavenumber section of the turbulent energy wavenumber spectrum receives contributions from all frequencies. Thus, in a turbulent flow, where the source of noise is an eddy whose length scale is very small compared with the acoustic wavelength for the same frequency, the matching acoustic wavenumber will be found in the low wavenumber end of the turbulent energy spectrum, referred to as the acoustical range. At low Mach numbers its amplitude will be very small compared with that of wavenumbers in the so-called convective range of the turbulent energy spectrum corresponding to the same frequency in the acoustical spectrum. This may at first cause confusion, but it must be remembered that turbulent eddies of all frequencies contribute to the low wavenumber end of the energy spectrum. There is no difficulty in handling these problems in aerodynamic noise theory if we remember that  $\omega$  and  $k$  always refer to the acoustic field external to the turbulent flow, with  $\omega/k = c$ , the speed of sound, and  $\lambda = 2\pi/k$ ,

is the sound wavelength. The amplitude is measured by its intensity  $\mathbf{I} = \mathbf{n}(c_\infty^3/\rho_\infty)\langle(\rho')^2\rangle$ , where  $\rho'$  is the density perturbation due to the sound waves. The normal to the wave front is  $\mathbf{n}$ . On the other hand, the properties of the turbulence are defined by the turbulent kinetic energy,\*  $k_T = (\frac{1}{2})\langle(v')^2\rangle = u_0^2$ , its integral length scale,  $\ell_0$ , and the corresponding frequency of the sound generated,  $\omega_0$ , satisfying the Strouhal number  $s_T = \omega_0\ell_0/u_0$ . In most turbulent flows  $s_T \approx 1$  to 1.7. If we follow these simple rules and use relevant frequency spectra for both the acoustics and turbulence problems, the use of the wavenumber spectrum in the turbulence becomes unnecessary. This in itself is a useful reminder since the wavenumber spectrum, in the important low wavenumber acoustic region, is rarely measured, at least to the accuracy required in aeroacoustics. It is important to recognize that almost the same compressible flow wavenumber spectrum appears in the turbulence analysis for an incompressible flow, where no noise is generated. In many applications of Lighthill's theory we may put the acoustic wavenumber in the turbulence equal to zero, which is its value in an incompressible flow where the propagation speed is infinite. There are, however, many aerodynamic noise problems of interest in the field of aeroacoustics at low Mach numbers, where the equivalent acoustic sources are compact. In such cases the fluid may be treated as though it were approximately an unsteady incompressible flow.

There is no unique method available to describe the equations of aerodynamic noise generated by a turbulent flow. The beauty of Lighthill's approach, as discussed below, is that it provides a consistent method for defining the source of aerodynamic noise and its propagation external to the flow as an acoustic wave to a far-field observer. It avoids the problem of nonlinear wave propagation within the turbulent flow and ensures that the rate of dilatation fluctuations within the flow are accounted for exactly and are not subject to any approximation. Thus, it is found possible in low Mach number, and high Reynolds number, flows for many practical purposes to regard the turbulent flow field as almost incompressible. The reason for this is that both the turbulent kinetic energy and the rate of energy transfer across the turbulent energy spectrum in the compressible flow are almost the same as in an incompressible flow. It follows that, in those regions of the flow where diffusive effects are almost negligible and the thermodynamic processes are, therefore, quasi-isentropic, the density and the rate of dilatation fluctuations in the compressible flow are directly related to the fluctuations in the pressure, turbulent kinetic energy, and rate of energy transfer in the incompressible flow. They are obtained by introducing a finite speed of sound, which replaces the infinite propagation speed in the case of the incompressible flow.

\*The turbulent kinetic energy is often denoted simply by  $k$ .  $k_T$  is used here to avoid confusion with the acoustic wavenumber.

The theory of aerodynamic noise then becomes simplified since the effects of compressibility, including the propagation of sound waves, only enter the problem in the uniform flow external to the unsteady almost incompressible sound sources replacing the flow. It is found that the unsteady flow is dominated by its unsteady vorticity,  $\boldsymbol{\omega} = \nabla \times \mathbf{v}$ , which is closely related to the angular momentum in the flow. The dimensions of the vorticity are the same as those of frequency. The noise generated is closely related to the cutting of the streamlines in the fluid flow by vortex lines, analogous to the properties of the lines of magnetic force in the theory of electricity and magnetism. A large body of experience has been built on such models, referred to as the *theory of vortex-sound* by Howe,<sup>26</sup> based on earlier work by Powell.<sup>27</sup> These methods require the distribution of the unsteady vorticity field to be known. (The success of the method is very much in the skill of the mathematician in finding a suitable model for the unsteady vortex motion.) It then follows that, based on the assumption of an inviscid fluid, that the given unsteady vorticity creates a potential flow having an unsteady flow field based on the Biot-Savart law. As shown by Howe,<sup>16</sup> the method is exact and is easily applied to a range of unsteady flows, including those with both solid and permeable boundaries and flows involving complex geometries. Some simple acoustic problems involving turbulent flow can also be modeled approximately using the theory of vortex-sound.

The problems first considered by Lighthill were of much wider application and were applicable to turbulent flows. Turbulence is an unsteady, vortical, nonlinear, space-time random process that is self-generated. Although some compact turbulent flows at low Mach numbers can be treated by the theory of vortex-sound, the broader theory embracing the multiscale characteristics of this highly nonlinear turbulent motion, requires the treatment proposed by Lighthill, extended to higher Mach numbers by Ffowcs Williams,<sup>6</sup> and by Lilley,<sup>7</sup> Goldstein,<sup>10</sup> and others to include the effects of flow-acoustic interaction.

Lighthill's theory, based on the exact compressible Navier-Stokes equations, considers the equations for the fluctuations in pressure, density, and enthalpy within an isolated domain of turbulent flow, which is being convected with the surrounding compressible and irrotational fluid, and on which it feeds to create the unsteady random vortical motion. Within the turbulent fluid of limited extent, the equations for the unsteady pressure, and the other flow variables, are all nonlinear. However, Lighthill was able to show that beyond a certain distance from the flow, of the order of an acoustic wavelength, the sound waves generated by the turbulent motion satisfy the standard linear wave equation and are thus propagating outward at the speed of sound in the uniform medium external to the flow. In Lighthill's original work the uniform medium external to the flow was at rest.

Lighthill realized that much of the unsteadiness within the flow and close to its free boundaries, related to nonlinear turbulent fluid dynamics, with

the influence of the turbulence decaying rapidly with distance from the flow. Moreover, an extremely small fraction of the compressible flow kinetic energy escapes from the flow as radiated sound. In the near field of the source of noise, the surging to and fro of the full flow energy produces almost no net transport of energy along the sound ray from the source to far-field observer. Lighthill devised a method by which this small fraction of the kinetic energy of the nonlinear turbulent motion, escaping in the form of radiated sound, could be calculated without having first to find the full characteristics of the nonlinear wave propagation within the flow. Lighthill was concerned that the resulting theory should not only include the characteristics of the turbulent flow but also the corresponding sound field created within the flow and the interaction of the turbulence on that sound field as it propagated through the flow field before escaping into the external medium. But all these effects contributing to the amplitude of the noise sources within the flow were, of course, unknown a priori. Lighthill thus assumed that, for most practical purposes, the flow could be regarded as devoid of all sound effects, so that at all positions within the flow, sound waves and their resulting sound rays generated by the flow unsteadiness, would travel along straight lines between each source and a stationary observer in the far acoustic field in the medium at rest. Such an observer would receive packets of sound waves in phase from turbulence correlated zones, as well as packets from uncorrelated regions, where the latter would make no contribution to the overall sound intensity. Thus Lighthill reduced the complex nonlinear turbulent motion and its accompanying noise radiation, into an equivalent linearized acoustical problem, or *acoustical analogy*, in which the complete flow field, together with its uniform external medium at rest, was replaced by an equivalent distribution of moving acoustic sources, where the sources may move but not the fluid. The properties of this equivalent distribution of moving acoustic sources has to be determined a priori from calculations based on simulations to the full Navier–Stokes equations or from experiment.

Therefore, we find that *Lighthill's inhomogeneous wave equation* includes a left-hand side, the propagation part, which is the homogeneous wave equation for sound waves traveling in a uniform medium at rest, and a right-hand side, the generation part, which represents the distribution of *equivalent acoustic sources* within what was the flow domain. The latter domain involves that part of the nonlinear turbulent motion that generates the sound field. As written, Lighthill's equation is exact and is as accurate as the Navier–Stokes equations on which it is based. In its applications, its right-hand side involves the best available database obtained from theory or experiment. Ideally, this is a time-accurate measurement or calculation of the properties of the given compressible turbulent flow, satisfying appropriate boundary and initial conditions. In general, this flow would be measured or calculated on the assumption that the sound field present in the flow has a negligible back reaction on the turbulent flow.

However, Ffowcs Williams and Hawkings<sup>5</sup> found a solution to Lighthill's equation, which can be used to find the far-field sound intensity, directivity, and spectrum, once the time-dependent properties of the turbulent flow, together with its acoustic field, are known on any arbitrary moving permeable surface within the flow, called the Ffowcs Williams–Hawkings acoustical data surface, and embracing the dominant noise sources within the flow. Volume sources external to the Ffowcs Williams–Hawkings surface have to be calculated separately. It should be noted that in all computer simulations, the required information on the data surface is rarely available. The exception is direct numerical simulation (DNS); see Section 8. The data are normally unresolved at high frequencies that are well within the range of interest in aeronautical applications.

Earlier in this section, the theory of nonlinear acoustics was introduced along with the Lighthill–Whitham theory, with its application to derive the pattern of shock waves around a body, such as an aircraft, traveling at supersonic speeds. Shock waves are finite-amplitude sound waves. Their speed of propagation is a function of their strength, or pressure rise, and therefore they travel at speeds greater than the speed of sound. Shock waves are absent from aircraft flying at subsonic speeds. The acoustical disturbances generated by the passage of subsonic aircraft travel at the speed of sound, and the sound waves suffer attenuation with distance from the aircraft due to spherical spreading. The noise created by subsonic aircraft is discussed in Section 9.4. An aircraft flying at supersonic speeds at constant speed and height creates a pattern of oblique shock waves surrounding the aircraft, which move attached to the aircraft while propagating normal to themselves at the speed of sound. These shock waves propagate toward the ground and are heard as a double boom, called the sonic boom, arising from the shock waves created from the aircraft's nose and tail. The pressure signature at ground level forms an *N*-wave comprising the overpressure of the bow shock wave followed by an expansion and then the pressure rise due to the tail wave. The strength of the sonic boom at ground level for an aircraft the size of the Concorde flying straight and level at  $M = 2$  is about  $96 \text{ N/m}^2$  or  $2 \text{ lbf/ft}^2$ . An aircraft in accelerated flight flying at supersonic speeds, such as in climbing flight from takeoff to the cruising altitude, develops a superboom, or focused boom. The shock waves created from the time the aircraft first reached sonic speed pile up, since the aircraft is flying faster than the waves created earlier along its flight trajectory. The superboom has a strength at ground level many times that of the boom from the aircraft flying at a constant cruise Mach number. The flight of supersonic aircraft over land over towns and cities is presently banned to avoid minor damage to buildings and startle to people and animals. The theory of the sonic boom is given by Whitham.<sup>21</sup> Further references are given in Schwartz.<sup>28</sup>

#### 4 DERIVATION OF Lighthill's EQUATION FOR AERODYNAMIC NOISE

The exact equations governing the flow of a compressible fluid are the nonlinear Navier–Stokes equations. These equations for the conservation of mass, momentum, and heat energy are, respectively,

$$\begin{aligned} \frac{D\rho}{Dt} + \rho \nabla \cdot \mathbf{v} &= 0 & \rho \frac{D\mathbf{v}}{Dt} + \nabla p &= \nabla \cdot \boldsymbol{\tau} \\ \rho \frac{Dh}{Dt} - \frac{Dp}{Dt} &= \nabla \cdot \mathbf{q} + \boldsymbol{\tau} : \nabla \mathbf{v} \end{aligned} \quad (10)$$

where the conservation of entropy is represented by  $\rho T Ds/Dt \equiv \rho Dh/Dt - Dp/Dt$ . The heat flux vector is  $\mathbf{q}$ , the viscous stress tensor (dyadic\*) is  $\boldsymbol{\tau}$ ,  $\gamma = C_p/C_v$  is the ratio of the specific heats, and  $s$  is the specific entropy. The nonlinear operator following the motion is  $D/Dt \equiv \partial/\partial t + \mathbf{v} \cdot \nabla$ . We see that, with the diffusive terms included, the thermodynamic processes are nonisentropic. The equation of state for a perfect gas is  $p = (\gamma - 1)\rho h/\gamma$ , and the enthalpy,  $h = C_p T$ , where  $T$  is the absolute temperature. These are six equations for the six unknowns  $\rho$ ,  $p$ ,  $h$ , and  $\mathbf{v}$ .

To clarify the generation of aerodynamic noise by turbulence, defined as random unsteady vortical motion, we consider the special case of a finite cloud of turbulence moving with an otherwise uniform flow of velocity,  $\mathbf{V}_0$ . In the uniform mean flow all flow quantities are described by the subscript zero. The fluctuations of all quantities are denoted by primes. Internal to the flow, primed quantities will be predominately turbulent fluctuations since the fluctuations due to sound waves are relatively very small. External to the turbulent flow, the flow is irrotational and includes not only the unsteady sound field but also the entrainment induced by the turbulent flow and on which the turbulent flow feeds. The characteristics of the entrainment are an essential part of the characteristics of the turbulent flow, but its contribution to the radiated noise is known to be small and will be neglected in our analysis. We introduce the linear operator following the uniform mean motion,  $D_0/Dt \equiv \partial/\partial t + \mathbf{V}_0 \cdot \nabla$ , which is equivalent to a coordinate frame moving with the mean flow velocity  $\mathbf{V}_0$ . In many turbulent flows the density fluctuations, internal to the turbulent flow, do not greatly influence the structure of the turbulent flow and, except in the case of high-temperature and/or high-velocity

flows, are small in comparison with the mean flow density. Here we shall neglect, for convenience only, the product  $\rho'\mathbf{v}'$  and  $\rho'h'$  compared with  $\rho_0\mathbf{v}'$  and  $\rho_0h'$ , respectively. Thus, our simplified conservation equations for mass, momentum, heat energy, and turbulent kinetic energy for a turbulent flow, noting that the derivatives of all quantities appear as their fluctuations only become, respectively<sup>†</sup>

$$\frac{D_0\rho'}{Dt} + \nabla \cdot \rho_0\mathbf{v}' = 0 \quad (11)$$

$$\frac{D_0}{Dt}(\rho_0\mathbf{v}') + \nabla \cdot (\rho_0\mathbf{v}'\mathbf{v}' - \boldsymbol{\tau}') + \nabla p' = 0 \quad (12)$$

$$\begin{aligned} \frac{D_0\rho_0h'}{Dt} + \nabla \cdot \rho_0\mathbf{v}'h' - \frac{D_0p'}{Dt} - \mathbf{v}' \cdot \nabla p' \\ = \nabla \cdot \mathbf{q}' + \boldsymbol{\tau}' : \nabla \mathbf{v}' \end{aligned} \quad (13)$$

$$\begin{aligned} \frac{D_0\rho_0(v')^2/2}{Dt} + \frac{\nabla \cdot \rho_0\mathbf{v}'(v')^2}{2} + \mathbf{v}' \cdot \nabla p' \\ = \nabla \cdot (\boldsymbol{\tau}' \cdot \mathbf{v}') - \boldsymbol{\tau}' : \nabla \mathbf{v}' \end{aligned} \quad (14)$$

where at high Reynolds numbers, except in the region close to solid boundaries, the viscous diffusion term,  $\nabla \cdot (\boldsymbol{\tau}' \cdot \mathbf{v}')$ , can be neglected. However, the viscous dissipation function,  $\boldsymbol{\tau}' : \nabla \mathbf{v}' = \rho_0 \epsilon'_{\text{diss}}$  is always finite and positive in a turbulent flow. The heat flux,  $\nabla \cdot \mathbf{q}'$ , also contains a diffusion part, which is negligible at high Reynolds numbers except close to solid boundaries, plus a dissipation part, which must be added to  $\boldsymbol{\tau}' : \nabla \mathbf{v}'$  in the heat energy equation. In the section below describing the characteristics of turbulent motion, we will discuss how the dissipation function equals the rate of energy exchange across the turbulent energy spectrum. Turbulent flow processes are never completely isentropic, but since energy dissipation only occurs in the smallest scales of turbulence, the rate of energy transfer is almost

\*We have chosen to use vector notation throughout this chapter for consistency. In order to accommodate tensor forms, it is necessary to introduce dyadics.<sup>29</sup> Thus, the shear stress tensor is represented by the dyadic  $\boldsymbol{\tau}$  and has nine components. The operation  $\nabla \cdot \boldsymbol{\tau}$  is equivalent to  $\partial \tau_{ij}/\partial x_j$  and gives a vector. The colon denotes a scalar or inner product of two dyadics and gives a scalar. For example,  $\boldsymbol{\tau} : \nabla \mathbf{v}$  is equivalent to  $\tau_{ij}\partial v_i/\partial x_j$ . The dyadic or tensor product of two vectors gives a tensor. For example,  $\mathbf{v}\mathbf{v}$  (sometimes  $\mathbf{v} \otimes \mathbf{v}$ ) is equivalent to  $u_i u_j$ . The identity dyadic, equivalent to the Kronecker delta, is denoted by  $\boldsymbol{\mathcal{I}}$ .

<sup>†</sup>In this set of equations there is no flow-acoustics interaction since the mean velocity is a constant everywhere and no gradients exist. In a nonuniform flow, gradients exist and additional terms arise involving products of mean velocity gradients and linear perturbations. These additional terms, which have zero mean, are not only responsible for flow-acoustics interaction, but play an important role in the properties of the turbulence structure, and the turbulence characteristics. They do not control the generation of aerodynamic noise. Lighthill, in his original work, assumed their bulk presence could be regarded as an effective source of sound, but this interpretation was incorrect since their contribution to the generated sound must be zero. *Flow-acoustic interaction could be considered after the solution to Lighthill's equation has been performed for the given distribution of noise sources.* The alternative is to include the mean velocity and temperature gradients in the turbulent flow as modifications to the propagation in Lighthill's equation, but not the generation terms. The latter proposal is the extension to Lighthill's theory introduced by Lilley.<sup>7</sup>

constant from the largest to the smallest eddies. From the time derivative of the equation of continuity and the divergence of the equation of motion, we find, respectively, two equations for the time variation of the rate of dilatation:

$$\begin{aligned} \frac{D_0}{Dt}(\rho_0\theta') &= -\frac{D_0^2\rho'}{Dt^2} - \frac{D_0}{Dt}(\rho_0\theta') \\ &= -\nabla \cdot \nabla \cdot (\rho_0\mathbf{v}'\mathbf{v}' - \boldsymbol{\tau}') - \nabla^2 p' \quad (15) \end{aligned}$$

These equations for the fluctuations in  $\theta'$  show that inside the turbulent flow the fluctuations in the rate of dilatation are almost negligible compared with the dominant terms on the right-hand side. Nevertheless if they were zero there would be no density fluctuations and therefore no noise would be radiated from the flow.

*This was a most significant feature of Lighthill's theory of aerodynamic noise, in that although  $\theta'$  is an extremely small quantity, and is almost impossible to measure, it must never be put equal to zero in a compressible flow. Its value\*  $\theta' = O(\varepsilon'_T/c_0^2)$ , where†  $\varepsilon'_T \approx \varepsilon'_{diss}$ , and shows the relative smallness of the rate of loss of energy relating to noise radiation from the turbulent kinetic energy and the rate of energy transfer in the nonlinear turbulent energy cascade.*

Hence, on eliminating  $D_0/Dt(\rho_0\theta')$  between the two equations, we find Lighthill's Galilean invariant, convected wave equation for the fluctuating pressure:

$$\begin{aligned} \left(\frac{1}{c_\infty^2} \frac{D_0^2}{Dt^2} - \nabla^2\right) p' &= \nabla \cdot \nabla \cdot (\rho_0\mathbf{v}'\mathbf{v}' - \boldsymbol{\tau}') \\ &+ \frac{1}{c_\infty^2} \frac{D_0^2}{Dt^2} (p' - c_\infty^2\rho') \quad (16) \end{aligned}$$

and for the fluctuating density, as was shown earlier by both Lilley<sup>7</sup> and Dowling et al.,<sup>30</sup>

$$\left(\frac{D_0^2}{Dt^2} - c_\infty^2 \nabla^2\right) \rho' = \nabla \cdot \nabla \cdot \boldsymbol{\mathcal{T}} \quad (17)$$

where Lighthill's stress tensor is  $\boldsymbol{\mathcal{T}} = \rho_0\mathbf{v}'\mathbf{v}' - \boldsymbol{\tau}' + \mathcal{I}(p' - c_\infty^2\rho')$ . We note the different right-hand sides to these wave equations for  $p'$  and  $\rho'$ . However, their solutions lead to the same value for the acoustic intensity in the radiation field.

The turbulent energy conservation equation is important in all work involving turbulent flow and

aeroacoustics. If we assume  $p' = c_0^2\rho'$ , as in linear acoustics above, we find

$$\begin{aligned} \frac{D_0}{Dt} \left[ \frac{\rho_0(v')^2}{2} + \frac{(p')^2}{2\rho_0 c_0^2} \right] + \nabla \cdot \mathbf{v}' \left[ p' + \frac{\rho_0(v')^2}{2} \right] \\ = -\rho_0 \varepsilon'_{diss} \quad (18) \end{aligned}$$

which is the turbulent kinetic energy conservation equation. This may be written in a similar form to that of the corresponding equation in linear acoustics given above, namely

$$\frac{D_0 w}{Dt} + \nabla \cdot \mathbf{I} = -\rho_0 \varepsilon'_{diss} \quad (19)$$

where in the turbulent flow  $w = [\rho_0(v')^2/2 + (p')^2/(2\rho_0 c_0^2)]$  and  $\mathbf{I} = \mathbf{v}' [p' + \rho_0(v')^2/2]$ . Within the turbulent flow the velocity and pressure fluctuations are dominated by the turbulent fluctuations, but external to the turbulent cloud  $\rho_0 \varepsilon'_{diss}$  is effectively zero and  $p'$  and  $\mathbf{v}'$  are then just the acoustical fluctuations arising from the propagating sound waves generated by the turbulence in the moving cloud. In the acoustic field external to the flow,  $\rho_0(v')^2/2 \ll |p'|$ . Within the turbulent flow the fluctuating pressure,  $p' = O[\rho_0(v')^2]$ . In Lighthill's convected wave equation for aerodynamic noise, when the flow variable is  $p'$ , the source includes  $(1/c_\infty^2)(D_0^2/Dt^2)(p' - c_\infty^2\rho')$  and was called by Lighthill the nonisentropic term. For flows at near ambient temperature this term can be neglected. However, we can show, following Lilley,<sup>7</sup> by neglecting the diffusion terms in high Reynolds number flows in the equation for the conservation of stagnation enthalpy, that

$$\begin{aligned} \frac{1}{c_\infty^2} \frac{D_0}{Dt} (p' - c_\infty^2\rho') &= -\frac{\gamma-1}{2c_\infty^2} \frac{D_0}{Dt} \rho_0(v')^2 \\ &- \frac{\gamma-1}{2c_\infty^2} \nabla \cdot \rho_0\mathbf{v}'(v')^2 - \nabla \cdot \rho_0\mathbf{v}' \left( \frac{h'}{h_\infty} \right) \quad (20) \end{aligned}$$

noting  $c_\infty^2 = (\gamma-1)h_\infty$ . All the equivalent acoustic source terms in Lighthill's equation are nonlinear in the fluctuations of the turbulence velocity and enthalpy or temperature. In most turbulent flows at high Reynolds number the fluctuations in the viscous stress tensor,  $\boldsymbol{\tau}'$ , can be neglected compared with the fluctuations in the Reynolds stress tensor  $\rho_0\mathbf{v}'\mathbf{v}'$ , but the fluctuations in the dissipation function,  $\rho_0 \varepsilon'_{diss}$  are always finite. In an incompressible flow, generating zero noise,  $\nabla^2 p' = -\nabla \cdot \nabla \cdot (\rho_0\mathbf{v}'\mathbf{v}')$ , and in a compressible flow this same relation almost holds, where the difference is entirely due to the removal of the rate of dilatation constraint,  $\nabla \cdot \mathbf{v}' = 0$ . It was shown by Lighthill that the effective strength of the equivalent noise sources could be obtained by writing  $\nabla \approx -(1/c_\infty)D_0/Dt$ , multiplied by the direction cosine of the position of

\*Since  $c_0^{-2}D_0 p'/Dt = D_0 \rho'/Dt = -\rho_0\theta'$ , we find,  $D_0 p'/Dt = -\rho_0 c_0^2 \theta' = O(\rho_0 \omega_0 u_0^2)$ , which confirms the value given.

† $\varepsilon'_T$  is the rate of energy transfer from the large to the small eddies, which almost equals the rate of energy dissipation,  $\varepsilon'_{diss}$  in both compressible and incompressible flow.  $\varepsilon'_T \approx O(u_0^3/\ell_0) \approx O(u_0^2\omega_0)$ .

the observer relative to that of the source. Thus for the far-field noise

$$\left( \frac{D_0^2}{Dt^2} - c_\infty^2 \nabla^2 \right) \rho' \sim \frac{1}{c_\infty^2} \frac{D_0^2 \mathcal{T}_{xx}}{Dt^2} \quad (21)$$

where

$$\begin{aligned} \mathcal{T}_{xx} = c_\infty^2 \left[ \frac{\rho_0(v'_x)^2}{c_\infty^2} - \frac{\gamma-1}{2} \frac{\rho_0(v')^2}{c_\infty^2} \right. \\ \left. + \frac{\gamma-1}{2} \frac{\rho_0 v'_x(v')^2}{c_\infty^3} + \rho_0 \frac{v'_x}{c_\infty} \frac{h'}{h_\infty} \right] \quad (22) \end{aligned}$$

and the subscript  $x$  refers to components resolved in the direction between source and observer. The first term was derived from a double divergence and is an acoustic quadrupole source. It equals the fluctuations in the normal components of the turbulence Reynolds stress in the direction of the observer, since in turbulent flows of ambient temperature  $\mathcal{T}_{xx} = \rho_0(v'_x)^2$ . The second is a monopole having the same strength as a quadrupole. The third and fourth terms were derived from a single divergence and are therefore dipole. The two dominant sources are the first and the last. The first term leads to a far-field acoustic intensity proportional to the eighth power of the turbulent velocity, while the last term is proportional to the sixth power of the turbulent velocity. In an unheated flow the last term is absent, but in a heated flow at low Mach numbers it exceeds the first in magnitude.

The special case, originally considered by Lighthill, was for a cloud of turbulence moving at a constant convection speed through an external medium at rest. This case can be recovered by putting  $\mathbf{V}_0 = 0$ . The solution to Lighthill's unique wave equation in the coordinates of the observer in the far field at rest is given by the convolution of the source terms with the free space Green's function. If the acoustic wavelength is assumed to be much greater than the characteristic dimension of the source region, a compact source distribution, then the far-field density fluctuation is given approximately by

$$\rho'(\mathbf{x}, t) \sim \frac{1}{4\pi c_\infty^4 R} \int_{\mathcal{V}} \frac{\partial^2 \mathcal{T}_{xx}}{\partial \tau^2} \left( \mathbf{y}, t - \frac{R}{c_\infty} \right) d^3 \mathbf{y} \quad (23)$$

where  $R = |\mathbf{x}| \simeq |\mathbf{x} - \mathbf{y}|$ , and  $\mathcal{V}$  denotes the flow volume containing the equivalent noise sources. The retarded time,  $\tau = t - R/c_\infty$ , is equal to the source, or emission time. The observer time is  $t$ .

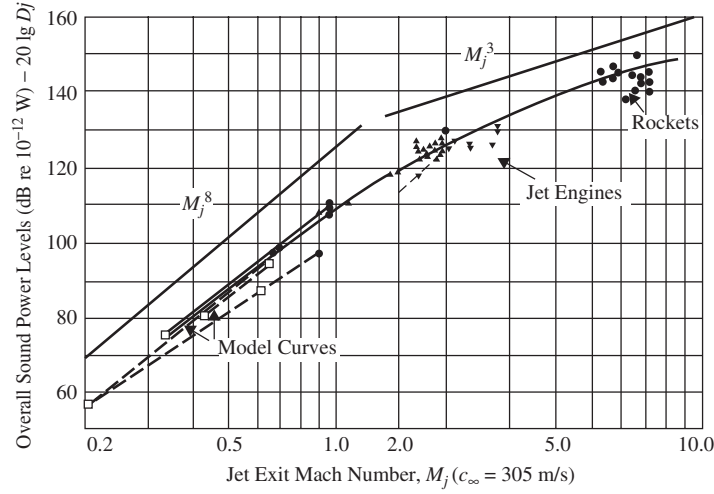
Here the distribution of the equivalent sound sources is given by  $\mathcal{T}_{xx} = \mathcal{T}_{ij} x_i x_j / x^2$ , which is also Lighthill's fluctuating normal stress in the direction of the observer at  $\mathbf{x}$ , and the variation with observer location  $\partial/\partial x_i$  has been replaced by  $-(1/c_\infty)(x_i/x) \partial/\partial t$ . Equation (23) shows that the far-field density is given by the integral over the source volume of the second

time derivative of the Lighthill stress tensor evaluated at the emission, or retarded time,  $\tau = (t - R/c_\infty)$ .

Lighthill considered the emission of sound from each moving source as it crossed a fixed point,  $\mathbf{y}$ , in the coordinates at rest at the retarded time,  $\tau = t - |\mathbf{x} - \mathbf{y}|/c_\infty$  where the observer's coordinates are  $(\mathbf{x}, t)$ . If the velocity of each source relative to the observer at rest is  $V_c$ , then the frequency of the sound received by the observer,  $\omega = \omega_0/C_\theta$ , where  $\omega_0$  is the frequency of the source at emission in the moving frame, and

$$C_\theta = \sqrt{(1 - M_c \cos \theta)^2 + (\omega_0 \ell_1 / c_\infty)^2 \times (\cos^2 \theta + (\ell_\perp / \ell_1)^2 \sin^2 \theta)} \quad (24)$$

is the generalized Doppler factor, which is finite even when  $M_c \cos \theta = 1$ . The different integral turbulence length scales  $\ell_1$  and  $\ell_\perp$ , which are in the directions of the mean motion and transverse, respectively, are discussed later.  $M_c = V_c/c_\infty$  is the "acoustical" convection Mach number. The equivalent acoustic source in the moving frame has the same strength per unit volume, namely  $\mathcal{T}$ , as discussed above involving the non-linear turbulence fluctuations alone. Lighthill's model is always a "good" first approximation even though it neglects flow-acoustical interaction, caused by refraction and diffraction effects on sound emitted by the sources and then traveling through a nonuniform mean flow. Although it is permitted to use different convection speeds according to the local distribution of mean velocity in a free shear or boundary layer flow, it is normally found sufficient to use an averaged convection speed for any cross section of the moving "cloud" of turbulence. The convection theory of aerodynamic noise is referred to as the Lighthill-Ffowcs Williams convection theory and is applicable to all Mach numbers. The success of this theory is seen by the results shown in Fig. 1 obtained from experiment over an extended range of subsonic and supersonic jet exit Mach numbers from jet aircraft and rockets. The solid line in this figure is simply an empirical curve connecting the theoretical asymptotic limits of jet noise proportionality of  $V_j^8$  at moderate to high subsonic jet exit Mach numbers, with  $V_j^3$  at high supersonic speeds. The full extent of confirmation between experiment and theory cannot be obtained by comparison with one single curve since the theory is dependent on both the values of jet exit Mach number and jet exit temperature and applies to shock-free jets only. A more relevant comparison is shown in Figs. 3 and 4 for jets of various temperature ratios at subsonic to low supersonic speeds, where the "acoustical" convection Mach number,  $M_c = V_c/c_\infty$ , is less than unity, and the jets are therefore free of shocks. The theoretical curve in these figures is that calculated from the Lighthill-Ffowcs Williams formula and is shown also in Fig. 2 for the single jet temperature ratio of unity. It is based on the generalized Doppler factor,  $C_\theta$ , given by Eq. (24) for a constant turbulence Strouhal number,  $s_T$ , a characteristic turbulence velocity,  $u_0$ , proportional to the jet



**Figure 1** Variation of sound power levels from Chobotov and Powell.<sup>31</sup> •, Rocket; ▼, turbojet (afterburning); ▲, turbojet (military power); ■, exit velocity  $> M_j = 0.8$ ; □, air model (exit velocity  $< M_j = 0.8$ ).  $D_j$  is the exit diameter in inches. (Adapted from Ffowcs Williams.<sup>6</sup>)

constant nozzle exit area is given by

$$P_{ac} = \text{constant} \times M_j^8 \left( \int_0^\pi C_\theta^{-5/2} \sin \theta d\theta \right) \quad (26)$$

Publisher's Note:

Permission to reproduce this image online was not granted by the copyright holder. Readers are kindly requested to refer to the printed version of this chapter.

**Figure 2** Lighthill–Ffowcs Williams convective amplification theory of jet noise. Sound power level as a function of jet exit Mach number,  $M_j$ . —, including flow–acoustical interaction; - - -, convective amplification theory, Eq. (26).

exit velocity  $V_j$ , and a mean convection velocity  $V_c$  proportional to  $V_j$ , such that

$$C_\theta = \sqrt{(1 - M_c \cos \theta)^2 + \alpha^2 M_c^2} \quad (25)$$

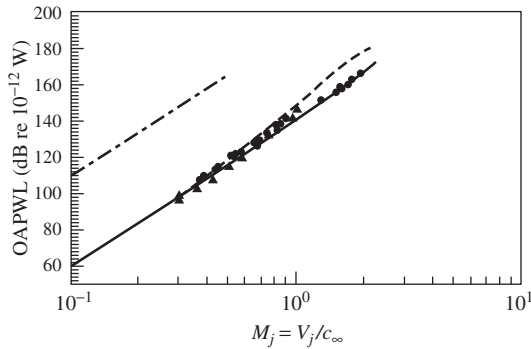
exists for all values of  $M_j$ , for shock-free conditions in the jet. In Fig. 1.2  $\alpha$  has the value of  $\frac{1}{2}$  and  $V_c/V_j = 0.62$ . The total acoustic power for such an ideal jet operating at ambient temperature and for a

Equation (26) shows that when  $M_j \ll 1$ , the total acoustic power varies as  $M_j^8$ . In the limit of  $M_j \gg 1$ , the total acoustic power varies as  $M_j^3$ , but this limit is not reached until  $M_j = 3$ .

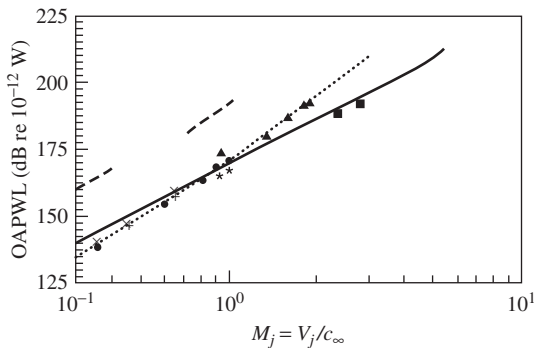
The constant is a function of the jet exit temperature ratio. The theoretical curve is for one temperature ratio only. Therefore, it is not possible to compare this theoretical result with experimental results for a range of temperature ratios in one figure with a single curve. However, the spread of results with temperature ratio, except at low jet Mach numbers, is far less important than with the variation in jet velocity. Thus, Fig. 2 demonstrates the change in velocity dependency of the total jet acoustic power that occurs as the jet exit velocity changes from subsonic to supersonic speeds, with respect to the ambient speed of sound. In particular, the velocity power law changes from  $V_j^8$  at low subsonic Mach numbers to  $V_j^3$  at high supersonic Mach numbers. But a remarkable feature of this comparison between the convective amplification theory and experiment, is that it clearly shows that in the experiments the departure from the  $V_j^8$  law at high subsonic Mach numbers is not present. The explanation is simply that although the convective amplification theory is correct in respect of sound amplitude, the directivity of the propagated sound is modified as a result of flow–acoustical interaction. The latter is clearly demonstrated in the downstream

direction of a jet by the almost complete zone of silence, especially at high frequencies, present in an angular range around the jet centerline. Thus, we find for much of the subsonic range, for jets at ambient temperatures or for heated jets, except at low jet Mach numbers, the noise intensity varies as  $V_j^8$ , and similarly for much of the supersonic and hypersonic regime, the variation is with  $V_j^3$ . This is also shown in Figs. 3 and 4.

When the flow is supersonic and shock waves appear inside the turbulent flow, models need to be introduced to include the effects of shock and expansion waves on the turbulent shear layer development. The theory is modified when turbulence is in the presence of solid walls, and when the turbulence is scattered as it crosses the trailing edge of a wing in flowing to form the wing wake. All these separate cases are considered below, and in each case the Lighthill stress



**Figure 3** Overall sound power level (OAPWL) for a cold jet. Nozzle exit area  $0.000507 \text{ m}^2$ ,  $\gamma_\infty = \gamma_j = 1.4$ .  $\blacktriangle$ , Lush<sup>37</sup>;  $\bullet$ , Olsen et al.<sup>38</sup>; —, with refraction; - - -, refraction neglected; - · - ·,  $V_j^8$ . (From Lilley.<sup>39</sup>)



**Figure 4** Overall sound power level (OAPWL) for a hot jet. Nozzle exit area  $1.0 \text{ m}^2$ ,  $\gamma_\infty = 1.4$ ,  $\gamma_j = 1.4$ . —,  $V_j^8$ ; - - -,  $V_j^8$ ,  $T_{\text{stagj}}/T_\infty$  values: [subsonic, Hoch et al.<sup>40</sup>  $\times$ , 1.2;  $+$ , 1.4;  $\cdot$ , 2.0 (theory)]; [supersonic, Tanna<sup>41</sup>.  $\blacktriangle$ , 2.0;  $\blacksquare$ , 6.25; —, 6.25 (theory)]. (From Lilley.<sup>39</sup>)

tensor,  $\mathcal{T}$ , provides the major characteristics of the equivalent source of noise per unit volume, but whose value must be obtained from experiment or from models based on solutions to the Navier–Stokes equations.

The case of turbulent flows, where the mean flow is nonuniform, presents a special case. In Lighthill's original work the turbulent flow Mach numbers were small and sound sources were compact with the acoustic wavelength exceeding the dimensions of the flow. Lighthill argued that the flow fluctuations should include not only the turbulent flow fluctuations but also the fluctuations arising from the sound field created by the turbulence in the flow. Nevertheless, it had to be assumed when considering the propagation of the sound that no sound existed inside the flow. However, it also had to be assumed that the sound, generated at a source within the flow, traveled at the speed of sound along the ray following the straight line joining the emission point  $y$  with the observer at  $x$ , in the external ambient medium at rest. In this model there was no flow-acoustical interaction.

Early measurements showed flow-acoustics interaction was important with respect to the directivity of the far-field sound intensity. The investigations of pressure fluctuations by Lilley<sup>32</sup> within a turbulent flow suggested that the wavenumber spectrum was dominated by two dominant processes, one was called the mean shear interaction and the other was called the turbulence–turbulence interaction. The former process dominated the lower frequencies, including the peak in the spectrum, and most of the inertial range. The latter dominated the higher frequencies and wavenumbers. The resultant models for the mean square of the turbulent pressure fluctuations fitted the available experimental data, confirming that the linear products in the complete Reynolds stress tensor were responsible for the dominant characteristics of turbulent mixing. But this presented a conflict since, if the same models were used in Lighthill's stress tensor, it implied that it should include linear terms involving products of mean and turbulent velocity components. But, as derived above, we found that Lighthill's stress tensor must only include products of turbulent velocity fluctuations, and measurements had confirmed that the amplitude of the radiated sound depended on the product of the turbulent velocity components in the fluctuations of the Reynolds stress tensor, which dominate Lighthill's stress tensor.

Lilley<sup>7</sup> and Goldstein<sup>10</sup> showed that all linear fluctuations in the conservation equations were responsible for flow-acoustic interactions, which is part of propagation, and only nonlinear fluctuations were responsible for noise generation. It was demonstrated that the linear perturbation terms in the Euler equations were responsible for flow-acoustic interaction and modified the propagation section of Lighthill's wave equation, which became an exact generalized third-order linear wave equation for the simple case of a parallel mean shear turbulent flow. Its homogeneous form is known as the Pridmore-Brown equation.<sup>33</sup> The generation part of the equation was also modified and



included a modified form of Lighthill's source function plus an additional contribution from a product term, involving the local mean shear times components of the nonlinear Lighthill stress tensor. Other authors have tried to replace Lilley's third-order inhomogeneous equation with approximate second-order equations, claiming these can include the effects of both generation and flow-acoustical interaction. However, all these attempts have failed as can easily be seen from inspection of the complete Euler equations, from which Lilley's equation was derived.\* These equations, written as linearized Euler equations with the nonlinear source terms similar to the components of Lighthill's stress tensor, can be solved using the adjoint method introduced by Tam and Auriault.<sup>8</sup> The solution to Lilley's equations involves Green's functions expressed in Airy functions and is similar to the solution of equations found by Brekhovskikh<sup>34</sup> in wave propagation in multilayered media. The theory of acoustical-flow interaction shows the importance

\*Howe<sup>26</sup> derived an exact second-order nonlinear wave equation for aerodynamic noise in the flow variable  $B = h + v^2/2$ :

$$\frac{D}{Dt} \left( \frac{1}{c^2} \frac{DB}{Dt} \right) - \nabla^2 B + \frac{\nabla h \cdot \nabla B}{c^2} = -\nabla \cdot (\mathbf{v} \times \boldsymbol{\omega}) + \frac{\mathbf{v} \times \boldsymbol{\omega}}{c^2} \cdot \frac{D\mathbf{v}}{Dt} \quad (27)$$

which only has simple analytic solutions when both the nonlinear operators and source terms are linearized. Most of the terms discarded in the linearization in applications to turbulent flows, are turbulent fluctuating quantities, which should rightly be included in the noise generating terms. *The resultant approximate equation is, therefore, not applicable for turbulent flows and problems involving flow-acoustic interaction.* Its merit is in showing that a "good" approximation to Lighthill's stress tensor is  $\nabla \cdot (\mathbf{v} \times \boldsymbol{\omega})$ , which is known to be important in the theory of vortex-sound and in the structure of turbulent flows. The claim that the convected wave equation based on the stagnation enthalpy,  $B$ , provides the true source of aerodynamic noise is, we believe, an overstatement because unless all convective terms are removed from the source terms and all turbulent fluctuations are removed from the propagation it is impossible to judge the true nonlinear qualities of the source. This has been achieved with our presentation of Lighthill's theory and the generalized theory of Lilley presented below. Indeed the starting point of the latter work was the second-order equation

$$\left( \frac{D^2}{Dt^2} - \nabla(c^2 \nabla) \right) \chi = \nabla \mathbf{v} : \nabla \mathbf{v} \quad (28)$$

where  $\chi = \ln \rho$ , which is an even simpler nonlinear equation than that derived by Howe. But the expanded version of this equation reduces to a third-order generalized inhomogeneous wave equation, where its left-hand side involves only a linear operator. The expanded form of Howe's equation required in turbulent shear flows also reduces to a third-order equation.

of sound refraction within the flow especially in the higher frequencies of sound generation within the turbulence. In the case of jet noise, high-frequency sound waves propagating in directions close to the jet axis are refracted by the flow and form a zone of silence close to the jet boundary. Figure 3 shows how sound refraction almost cancels the convective amplification effects of the Lighthill-Ffowcs Williams theory in the case of the total acoustic power from "cold," or ambient, jet flows at high subsonic and low supersonic Mach numbers. Figure 4 shows similar results for the total acoustic power of hot jets showing that, at high Reynolds numbers, hot jets at low Mach numbers radiate proportional to  $M_j^6$ , while at Mach numbers greater than about  $M_j = 0.7$  they radiate proportional to  $M_j^8$ . Reference should also be made to Mani.<sup>35</sup> For recent experiments on heated jet noise, reference should also be made to Viswanathan.<sup>36</sup>

Before using these results to obtain scaling laws for the noise radiated by jets, some discussion of the characteristics of the structure of turbulent shear flows is given.

## 5 STRUCTURE OF TURBULENT SHEAR FLOWS

Before considering the special properties of the turbulent structure of a turbulent jet at high Reynolds numbers, we will first discuss some general properties of turbulent shear flows.

The experimental work of Townsend<sup>42</sup> and others over the past 50 years have provided details of the mean structure of turbulent shear flows and have enabled models to be developed for the mean velocity and pressure distributions in both incompressible and compressible flows. However, in aerodynamic noise calculations we require not only the details of the averaged structure of the turbulent shear flow but also the time-accurate properties of the flow, involving the fluctuations in all the physical variables. Such details are difficult to obtain experimentally, both in respect of the instrumentation required, and that the time for measurements having the required accuracy is normally prohibitive. Even with today's large supercomputers, and with the use of computer clusters, it is still impossible to simulate turbulent flows at high Reynolds number with meaningful data to predict the full-scale noise characteristics from turbulent jets and boundary layers. Direct numerical simulation (DNS) has produced results at low Reynolds numbers, but such calculations are very expensive and time consuming. Moreover, important changes in the structure of jets and boundary layers, including attached and separated flows, occurs with increases in Reynolds number, so that noise prediction is heavily reliant on accumulated full-scale experimental data, including noise measurements involving phased arrays, and particle image velocimetry (PIV) and laser Doppler velocimetry (LDV) within the flow. However, the use of approximate results for the determination of the noise generation from turbulent shear flows, based largely on a knowledge of the averaged turbulent

structure, has produced results that have helped in the formulation of approximate methods, which can then be calibrated against the full-scale flow and far-field noise databases.

It is from flow visualizations, using smoke, schlieren, and shadowgraph, that a qualitative understanding is obtained of the global features of the turbulent flow field, as well as many of its time-dependent features. Moreover, such results can usually be obtained quickly and always help in planning more quantitative follow-on experiments. At sufficiently high Reynolds numbers, the mixing between two or more adjacent fluids flowing at different speeds, and/or temperatures, generates a shear layer of finite thickness, where the perturbation fluctuations are unstable and the mixing, which is initially laminar, eventually passes through a transition zone and becomes turbulent. Turbulence is described as a random eddying motion in space and time and possesses the property vorticity,  $\omega = \nabla \times \mathbf{v}$ , relating to the development of spatial velocity gradients in the flow, typical of the vortices seen in flow visualizations. Outside any turbulent flow the motion is irrotational. All turbulent flow feeds on the external irrotational motion and the vorticity in the turbulent motion cannot be sustained without entrainment of the irrotational ambient fluid. The entrainment into a turbulent flow may be at a lower velocity than the turbulent flow, but its rate of mass flow, in general, far exceeds that of the primary turbulent flow. Important changes such as stretching and distortion occur to the flow as it crosses the boundary, known as the superlayer, between the irrotational and turbulent motion. The generation of sound in a compressible turbulent flow relates to its density fluctuations, corresponding to its pressure fluctuations, which are almost adiabatic, as well as local changes in volume, relating to the rate of dilatation in the turbulent fluid, where the latter are zero in an incompressible flow, where sound waves do not exist.

Townsend<sup>42</sup> showed that although turbulence contains a very broad range of length scales and frequencies, its structure can be represented approximately in terms of three scales. These include a large-scale structure, the order of the local width of the shear layer, and a smaller scale structure containing the bulk of the kinetic energy in the turbulence. The third scale had been suggested earlier by Kolmogorov<sup>43</sup> as the scale of the very small dissipating eddies, whereby the energy of the turbulence is lost in transformation into heat. Kolmogorov proposed that, whereas the large-scale turbulent motion was dependent on the initial and boundary conditions for the flow and therefore was flow dependent and anisotropic, the small-scale motion was so far removed from the large-scale and energy-containing scales, that its dynamics were the same for all flows and should be locally isotropic. The hypothesis was introduced that the small-scale structure of turbulence was in almost universal equilibrium. An energy cascade was visualized, whereby energy was exchanged nonlinearly between the large-scale eddies and those containing most of the energy and followed by further nonlinear energy exchange from one scale

to the next smaller, finally down to the Kolmogorov dissipation scale. Remarkably, it has been shown that the rate of energy transferred in the energy cascade is almost lossless, even though the detailed physical processes involved are not fully understood. Work by Gaster et al.<sup>44</sup> and Morris et al.<sup>45</sup> has shown that the large-scale motion in shear flow turbulence is structured on the instability of the disturbed motion and can be calculated on the basis of the eigenmodes of linear instability theory. The full motion is nonlinear. (That the large-scale structure of shear flow turbulence could be calculated from the eigenmodes of linear instability theory was a surprising deduction, but a highly important one in the theory of turbulence. It is consistent with the notion that the structure of turbulent flows is dominated by solutions to the nonlinear inhomogeneous unsteady diffusion equation, which involve the eigenmodes of the linear homogeneous equation. The uncovering of the complexity of this nonlinear theory of turbulent mixing and evaluation of its time-accurate properties is the goal of all turbulent flow research.)

In a jet at high Reynolds number, the turbulent mixing region immediately downstream of the nozzle exit grows linearly with distance, with its origin close to the nozzle exit. The conical mixing region closes on the nozzle centerline approximately five jet diameters from the nozzle exit for a circular nozzle. This region is known as the potential core of the jet since the velocity along the nozzle centerline remains constant and equal to the jet exit velocity. Beyond the potential core, for a circular jet, the centerline velocity varies inversely with axial distance and the jet expands linearly. The variation of jet geometry with distance from the nozzle exit varies with the shape of the nozzle. Similar changes occur in both the density and temperature distributions. For the jet discharging into an ambient medium at rest, the mean pressure distribution remains almost constant everywhere, although, arising from the strong turbulent intensity in the turbulent mixing regions, the mean pressure in these mixing regions is slightly lower than ambient when the jet velocity is subsonic. When the jet velocity is supersonic the structure of the jet is controlled by a pattern of expansion and shock waves. It is only when the supersonic field of flow has decayed to subsonic velocities that the jet mixing region recovers the form of the subsonic jet.

Returning to the subsonic jet, the discussion so far has related to the mean rate of growth of the mixing regions upstream and downstream of the end of the potential core. The boundary of the turbulent jet is far from uniform and undulates randomly as it embraces the entrainment of irrotational flow from the ambient medium. The large eddy structure in the outer region of the jet reflects this entrainment, which increases linearly with distance downstream of the nozzle exit. Nevertheless in a frame of reference moving with the local averaged mean velocity, referred to as the mean convection velocity, we find it is sufficient to define averaged turbulent characteristic velocities and length scales,  $u_0$  and  $\ell_0$ , respectively, which become only functions of the distance downstream of the nozzle

exit. These quantities can then be used to define the strength of the equivalent sound sources within the mixing layers. More complete data can be obtained by computing the distributions of  $k_T$  and  $\varepsilon_T$ , which are, respectively, the averaged turbulent kinetic energy and the rate of turbulent energy transfer, using steady flow RANS (Reynolds averaged Navier–Stokes equations) throughout the flow. Here we have put  $k_T = u_0^2$  and  $\varepsilon_T = u_0^3/\ell_0 = \omega_0 u_0^2$ .

Under an assumption of flow similarity, which is supported by experimental observations in a high Reynolds number jet,  $u_0$  becomes proportional to the local centerline mean velocity, and  $\ell_0$  becomes proportional to the local width of the mixing layer. Density fluctuations within the flow are normally neglected as they are small and have little influence on the properties of the mean flow. However, the effect of temperature fluctuations can never be neglected in heated turbulent flows. Even when the motion is supersonic and Mach waves are generated, which as described below can be analyzed by linear theory, the generation of sound still involves nonlinear processes. Lighthill's theory of aerodynamic noise describes the input required in order to evaluate the generation of noise in such a turbulent flow.

When the mixing regions are fully turbulent at a sufficiently high Reynolds number, for any given jet Mach number, and the flow is self-preserving, its average structure becomes independent of the jet Reynolds number, based on the nozzle diameter, and the jet velocity at the nozzle exit. Experiment suggests this jet Reynolds number, based on the jet exit conditions and the jet diameter, must exceed about 500,000 for turbulent flow independence to be achieved. This is a stringent condition, especially for hot jets in a laboratory simulation, since the high jet temperature generates a low jet density and increased molecular viscosity, with the result that the Reynolds number, for a given jet Mach number, is lowered. For details of recent laboratory experiments on the far-field noise of hot jets reference should be made to Viswanathan.<sup>36</sup>

## 6 SIMPLE JET NOISE SCALING FORMULAS

The far-field pressure and density fluctuations are related by  $p'(\mathbf{x}, t) = c_\infty^2 \rho'(\mathbf{x}, t)$ . The acoustic intensity  $I(\mathbf{x})$  is the average flux of acoustic power per unit area. It is given by

$$I(\mathbf{x}) = \frac{\langle p'^2 \rangle}{\rho_\infty c_\infty} = \frac{c_\infty^3}{\rho_\infty} \langle \rho'^2 \rangle \quad (29)$$

where  $\langle \dots \rangle$  denotes the time average of a quantity. The source region is characterized by velocity and length scales  $u_0$  and  $\ell_0$ , respectively, which are assumed to be functions of the distance downstream from the jet exit only. Lighthill's stress tensor is given by  $\mathcal{T}_{xx} \sim \rho_0 u_0^2$  and the characteristic frequency  $\omega_0$  is determined from the turbulence Strouhal number,  $s_T = \omega_0 \ell_0 / u_0$ , which has a value based on measurements of about 1.7.

From Lighthill's solution, the sound intensity per unit volume of flow at a distance  $R$  from the nozzle exit is of the order

$$i(\mathbf{x}) \sim \frac{1.7^4}{16\pi^2 R^2 \ell_0 C_\theta^5} \frac{\rho_0^2}{\rho_\infty} u_0^3 m_0^5 \quad (30)$$

where the turbulence Mach number, with respect to the ambient speed of sound, is  $m_0 = u_0/c_\infty$ .

Consider first the early mixing region of a circular jet of diameter  $D_J$ , extending to the end of the potential core. The annular mixing region has nearly zero width at the nozzle exit and grows linearly over the potential core of length  $L$ . Its width at an axial distance  $y_1 = L$  is assumed to be  $D_J$ . The average turbulent velocity fluctuation,  $u_0$ , remains constant over the distance  $L$ , since  $u_0$  is proportional to the mean velocity difference across the initial mixing region, which equals  $V_J$ , when the jet is exhausting into a medium at rest, having the density,  $\rho_\infty$ , and speed of sound,  $c_\infty$ . The average length scale of the turbulence,  $\ell_0$ , is proportional to the local width of the mixing region,  $b(y_1)$ . So  $b(y_1) = y_1 D_J / L$  and we put  $K = b/\ell_0$ . In order to determine the total intensity Eq. (30) must be integrated over the average mixing region volume from  $y_1 = 0$  to  $L$ . Since a slice of the mixing region has a volume of approximately  $\pi D_J b(y_1) dy_1$ ,

$$I(\mathbf{x}) \sim \frac{1.7^4 K D_J^2}{16\pi R^2 C_\theta^5} \frac{\rho_0^2}{\rho_\infty} u_0^3 m_0^5 \frac{L}{D_J} \quad (31)$$

A similar integration is required for the jet downstream of the potential core, where the mixing region is growing linearly with  $y_1$ , and the centerline velocity is decreasing inversely with  $y_1$ . A constant property mixing region of approximate length  $2D_J$  between the end of the potential core and the decaying jet downstream is also included. The contributions from the three regions are then added to obtain

$$I(\mathbf{x}) \sim \frac{1.7^4 K D_J^2}{16\pi R^2} \rho_J u_L^3 m_L^5 \left( \frac{L}{D_J} + 2 \right) \times \left( C_\theta^{-5} + \frac{1}{6} \frac{T_J}{T_\infty} \right) \quad (32)$$

where in the initial mixing region and the transition region we have assumed  $\rho_0^2/\rho_\infty = \rho_\infty T_\infty / T_J$ , and in the decaying region  $\rho_0^2/\rho_\infty = \rho_\infty$ . Then  $u_L$  and  $m_L$  are the values, respectively, of  $u_0$  and  $m_0$  at the end of the potential core and within the transitional region.

In this simple analysis the directivity is based on the effect of convective amplification on the radiated sound. The effects of refraction can be included approximately by using Snell's law, and assuming the existence of a zone of silence extending in the downstream direction to an angle  $\theta_{cr}$ , from the jet axis. An approximate result for the total acoustic power in

watts,  $P$  is found from the integration of  $I(\mathbf{x})$  over a sphere of radius  $R$ , leading to

$$P \sim \frac{1.7^4 K (\pi D_J^2/4)}{2} \rho_J u_L^3 m_L^5 \left( \frac{L}{D_J} + 2 \right) \times \int_{\theta_{cr}}^{\pi} \left( C_{\theta}^{-5} + \frac{1}{6} \frac{T_J}{T_{\infty}} \right) \sin \theta d\theta \quad (33)$$

Alternatively,

$$\frac{P}{L_P} = \frac{K 1.7^4}{\pi} \left( \frac{u_L}{V_J} \right)^8 \left( \frac{L}{D_J} + 2 \right) \times \int_{\theta_{cr}}^{\pi} \left( C_{\theta}^{-5} + \frac{1}{6} \frac{T_J}{T_{\infty}} \right) \sin \theta d\theta \quad (34)$$

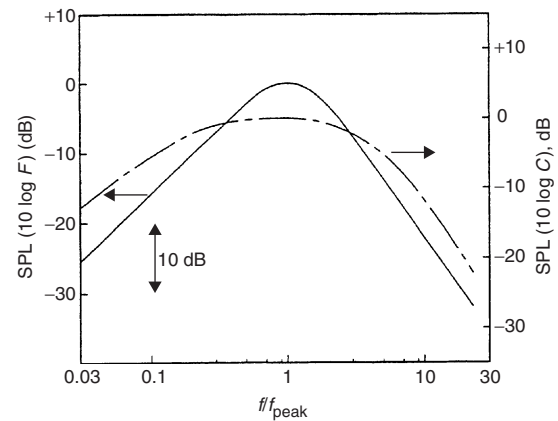
where the jet operating conditions are expressed in the Lighthill parameter,  $L_P = (\pi D_J^2/4) [(\frac{1}{2}) \rho_J V_J^3] M_J^5$ , which is the mean energy flux at the jet exit multiplied by  $M_J^5$ . The right-hand side embraces the mean geometry of the jet mixing region and its flow parameters.

The total acoustic power in decibels is given by  $N(\text{dB re } 10^{-12} \text{ W}) = 120 + 10 \log_{10} P$ . As an example, the total acoustic power from a jet of diameter  $D_J = 0.025$  m, exhausting at  $V_J = 340$  m/s, and a static temperature of 288 K, equals approximately  $N(\text{dB}) = 132 \text{ dB re } 10^{-12} \text{ W}$ , where it has been assumed that  $K = 4.8$ ,  $u_L/V_J = 0.2$ , and  $L/D_J = 5$ . The half-angle of the zone of silence is  $\theta_{cr} = 52^\circ$ . The Lighthill parameter in this case is  $L_P = 1.182 \times 10^4 \text{ W}$ .

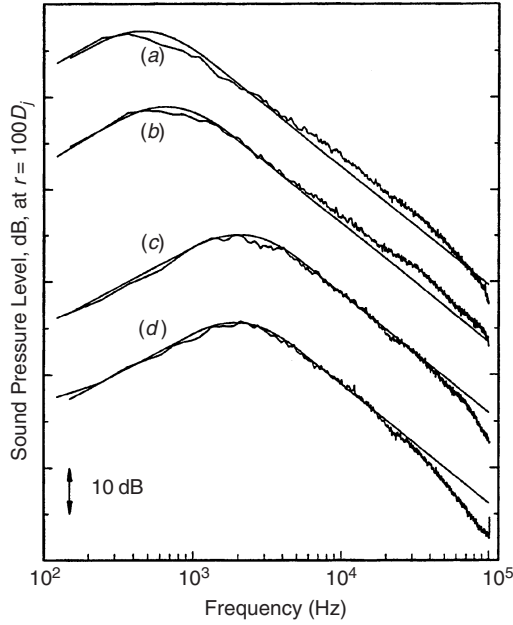
Estimates can also be made for the axial source strength distribution and the shape of the spectrum for the acoustic power. The axial source strength, the power emitted per unit axial distance,  $dP(W)/dy_1$ , can be found by multiplying the source intensity per unit volume by the source cross-sectional area, which, as given above, is  $\pi D_J b(y_1)$  in the early mixing region and by  $\pi b^2(y_1)$  in the jet downstream region. The source strength is constant in the initial mixing region and decays rapidly with seven powers of the axial distance in the downstream jet region. The acoustic power spectral density, the acoustic power per unit frequency, can be obtained by dividing the power per unit length of the jet by the rate of change of characteristic frequency with axial distance. That is  $dP/d\omega = dP/dy_1 / |d\omega/dy_1|$ . In the initial mixing region the characteristic frequency is inversely proportional to axial distance and in the downstream jet is inversely proportional to the square of axial distance. The acoustic power spectral density for the far-field noise from the entire jet is found in the low frequencies to increase as  $\omega^2$  and in the high frequencies to fall as  $\omega^{-2}$ . These useful results show that the major contribution to the overall noise is generated in the

region just beyond the end of the potential core. In addition, the bulk of the high frequency noise generation comes from the initial mixing region and correspondingly the bulk of the low-frequency noise is generated downstream of the potential core, where the axial velocity is decaying to small values compared with the nozzle exit velocity. Of course, this refers to the dominant contributions to the noise generation, it being understood that at all stations in the jet the noise generation is broadband and covers the noise from both large- and small-scale energy-containing eddies.

These simple scaling laws form the basis for empirical jet noise prediction methods such as the SAE Aerospace Recommended Practice 876<sup>46</sup> and the methods distributed by ESDU International.<sup>47</sup> These methods include predictions for single and dual stream jets including the effects of forward flight and jet heating. To obtain the overall sound pressure level (OASPL) and one-third octave spectra for different observer angles, interpolation from an experimental database is used. An important contribution to the prediction of full-scale shock-free jet noise over a wide range of jet velocity and temperature, was made by Tam et al.<sup>48</sup> who showed, from a wide experimental database, that the jet noise spectrum at most angles to the jet axis could be represented by a combination of two universal spectra shown in Fig. 5. Figures 6 and 7 show how well these two spectra fit the experiments for a wide range of operating conditions near the peak noise directions ( $\chi \approx 150^\circ$ ) and in the sideline direction ( $\chi \approx 90^\circ$ ) where  $\chi$  is the polar angle measured from the jet inlet axis. At intermediate angles the measured spectra can be fitted by a weighted combination of these two spectra. Tam et al.<sup>48</sup> used this excellent correlation as justification for the existence of two noise sources for



**Figure 5** Similarity spectra for the two components of turbulent mixing noise. —, large turbulence structures/instability waves noise,  $F(f/f_{\text{peak}})$ ; ---, fine-scale turbulence noise,  $G(f/f_{\text{peak}})$ . (From Tam et al.<sup>48</sup>)



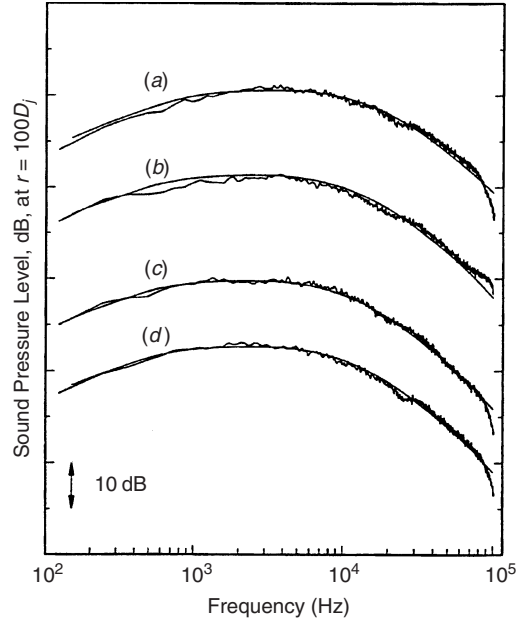
**Figure 6** Comparison of the similarity spectrum of large-turbulence structure/instability waves noise and measurements:

- (a)  $M_j = 2.0$ ,  $T_r/T_\infty = 4.89$ ,  $\chi = 160.1^\circ$ ,  
SPL<sub>max</sub> = 124.7 dB
- (b)  $M_j = 2.0$ ,  $T_r/T_\infty = 1.12$ ,  $\chi = 160.1^\circ$ ,  
SPL<sub>max</sub> = 121.6 dB
- (c)  $M_j = 1.96$ ,  $T_r/T_\infty = 1.78$ ,  $\chi = 138.6^\circ$ ,  
SPL<sub>max</sub> = 121.0 dB
- (d)  $M_j = 1.49$ ,  $T_r/T_\infty = 1.11$ ,  $\chi = 138.6^\circ$ ,  
SPL<sub>max</sub> = 106.5 dB

(From Tam et al.<sup>48</sup>) All levels referenced to  $2 \times 10^{-5}$  N/m<sup>2</sup>, 122-Hz bandwidth.

jet noise: a “large-scale” structure source and a “fine-scale” structure source. Though, as discussed below, this is likely to be a reasonable assumption at high speeds, its validity for subsonic jets has yet to be established. Additional comparisons of these similarity spectra with jet noise measurements, for both subsonic as well as supersonic jets, are given by Viswanathan.<sup>36</sup>

The turbulent jet noise far-field acoustical spectra receive contributions from all regions of the jet with the major contributions being generated by the scales of turbulence near the energy-containing ranges. These scales range from extremely small close to the nozzle exit to extremely large far downstream. The acoustical spectrum for the complete jet is therefore very different from that generated locally at any downstream station of the jet, where it has many of the characteristics of local anisotropic or even isotropic turbulence. In the latter case, in the range of high frequencies far beyond the peak in the spectra, and therefore of the contribution made by the energy



**Figure 7** Comparison of the similarity spectrum of fine-scale turbulence and measurements:

- (a)  $M_j = 1.49$ ,  $T_r/T_\infty = 2.35$ ,  $\chi = 92.9^\circ$ ,  
SPL<sub>max</sub> = 96 dB
- (b)  $M_j = 2.0$ ,  $T_r/T_\infty = 4.89$ ,  $\chi = 83.8^\circ$ ,  
SPL<sub>max</sub> = 107 dB
- (c)  $M_j = 1.96$ ,  $T_r/T_\infty = 0.99$ ,  $\chi = 83.3^\circ$ ,  
SPL<sub>max</sub> = 95 dB
- (d)  $M_j = 1.96$ ,  $T_r/T_\infty = 0.98$ ,  $\chi = 120.2^\circ$ ,  
SPL<sub>max</sub> = 100 dB

(From Tam et al.<sup>48</sup>) All levels referenced to  $2 \times 10^{-5}$  N/m<sup>2</sup>, 122-Hz bandwidth.

containing eddies, the laws for the decay of high-frequency noise can be represented by universal laws based on the local equilibrium theory of turbulence as found by Lilley.<sup>49</sup> To predict the noise radiation in more detail, additional analysis is needed. The details are beyond the scope of this chapter. They can be found in the original papers by Lighthill,<sup>1,3</sup> Ffowcs Williams,<sup>6</sup> and a review of classical aeroacoustics, with applications to jet noise, by Lilley.<sup>50</sup> The spectral density of the pressure in the far field is given by the Fourier transform of the autocorrelation of the far-field pressure. The instantaneous pressure involves an integral over the source region of the equivalent source evaluated at the retarded time,  $\tau = t - R/c_\infty$ . Thus the autocorrelation of the pressure must be related to the cross correlation of the source evaluated at emission times that would contribute to the pressure fluctuations at the observer at the same time. Since the Fourier transform of the source cross correlation is the source wavenumber–frequency spectrum, it is not surprising that it is closely related to the far-field spectral density. In fact, a rather simple relationship exists. Based on

Lighthill's acoustical analogy,

$$S(\mathbf{x}, \omega) = \frac{\pi \omega^4}{2 \rho_\infty c_\infty^5 R^2} \int_V H\left(\mathbf{y}, \frac{\omega \mathbf{x}}{c_\infty R}, \omega\right) d^3 \mathbf{y} \quad (35)$$

where  $S(\mathbf{x}, \omega)$  is the spectral density at the observer location  $\mathbf{x}$  and frequency  $\omega$ .  $H(\mathbf{y}, \mathbf{k}, \omega)$  is the wavenumber–frequency spectrum at the source location  $\mathbf{y}$  and acoustic wavenumber  $\mathbf{k}$ . This apparently complicated mathematical result has a simple physical explanation.

The wavenumber–frequency representation of the source is a decomposition into a superposition of waves of the form  $\exp[i(\mathbf{k} \cdot \mathbf{y} - \omega t)]$ . To follow a point on one wave component, such as a wave crest,  $\mathbf{k} \cdot \mathbf{y} - \omega t = \text{constant}$ . The phase velocity of the wave is  $d\mathbf{y}/dt$ . But, from Eq. (35), only those wavenumber components with  $\mathbf{k} = \omega \mathbf{x}/(c_\infty R)$  contribute to the radiated noise. The phase velocity in the direction of the observer is  $(\mathbf{x}/R) \cdot (d\mathbf{y}/dt)$ . Thus, only those waves whose phase velocity in the direction of the observer is equal to the ambient speed of sound ever escape the source region and emerge as radiated noise.

To proceed further it is necessary to provide a model for the source statistics. This can be a model for the two-point cross-correlation or the cross spectral density (see, Harper-Bourne<sup>51</sup>). The former is most often used. Detailed measurements of the two-point cross-correlation function of the turbulence sources have been attempted, but usually they are modeled based on measurements of correlations of the axial velocity fluctuation.\* A typical measurement is shown

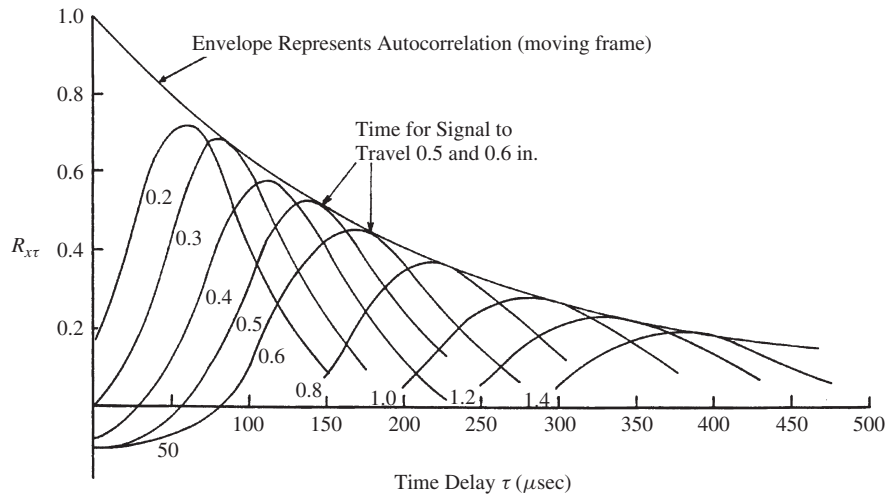
in Fig. 8. Each curve represents a different axial separation. As the separation distance increases, so the maximum correlation decreases. If the separation distances are divided by the time delays for the maximum correlation a nearly linear relationship is found. This gives the average convection velocity of the turbulence,  $U_c = M_c c_\infty$ . The envelope of the cross correlation curves represents the autocorrelation in a

$T_{xx}$  and the wavenumber-frequency spectrum of the source. In their nondimensional form these space/time covariances were used to obtain the far-field acoustic intensity per unit flow volume in the mixing regions of the jet. The corresponding radiated power spectral density per unit volume of flow is then given by

$$p_{ac} = \left(\frac{4}{15} \pi\right) (\rho_\infty \langle u'^2 \rangle \omega^4 / c_\infty^5) \int_0^\infty r^4 dr \times \int_0^\infty \cos \omega \tau (\partial f(r, \tau) / \partial r)^2 d\tau \quad (36)$$

where  $f(r, \tau)$  is the longitudinal velocity correlation coefficient in isotropic turbulence. Here  $r$  and  $\tau$  are, respectively, the two-point space and retarded time separation variables. This model of the turbulence was used to calculate the total acoustic power from jets over a wide range of jet velocity and temperature using the distribution of turbulent kinetic energy,  $k_T$ , and the rate of energy transfer,  $\epsilon_T$ , as determined by experiment and RANS calculations. The results of these computations are shown in Figs. 3 and 4 in comparison with experimental data. The numerical results for the total acoustic power thus differ slightly from those obtained from the simple scaling laws discussed above and the approximations using the Gaussian forms.

\*In isotropic turbulence Lilley<sup>39</sup> used the DNS data of Sarkar and Hussaini<sup>52</sup> to find the space/retarded time covariance of



**Figure 8** Cross correlation of axial velocity fluctuations with downstream wire separation. Numbers on curves represent separation (in.).  $Y/D = 0.5$ ,  $X/D = 1.5$  (fixed wire). 1.0 in. = 2.54 cm. (From Davies et al.)<sup>53</sup>

reference frame moving at the convection velocity. Various analytic functions have been used to model the cross-correlation function. The analysis is simplified if the temporal and spatial correlations are assumed to have a Gaussian form. But other functions provide a better fit to the experimental data.

The far-field spectral density is then found to be given by

$$S(\mathbf{x}, \omega) = \frac{1}{32\pi c_\infty^4 R^2} \int \rho_0^2 u_0^2 \ell_1 \ell_\perp^2 \omega_0^3 \frac{\omega^4}{\omega_0^4} \times \exp\left(-\frac{C_\theta^2 \omega^2}{4\omega_0^2}\right) d\mathbf{y} \quad (37)$$

For a compact source,  $\omega_0 \ell_1 / c_\infty \ll 1$ , and the modified Doppler factor reduces to the Doppler factor. However, at high speeds, this term cannot be neglected and is important to ensure that the sound field is finite at the Mach angle,  $\cos^{-1}(1/M_c)$ .

The OASPL directivity for the intensity is obtained by integration with respect to frequency, giving

$$I(x, \theta) = \frac{\langle (p')^2 \rangle(R, \theta)}{\rho_\infty c_\infty} = \frac{3}{4\sqrt{\pi} \rho_\infty c_\infty^5 R^2} \int \frac{\ell_1 \ell_\perp^2 \rho_0^2 u_0^4 \omega_0^4}{C_\theta^5} d\mathbf{y} \quad (38)$$

If  $\ell_1$  and  $\ell_\perp$  are assumed to scale with  $\ell_0$ , then the intensity per unit volume of the turbulence is given by

$$i(x, \theta) \sim \frac{\rho_0^2}{\rho_\infty} \left(\frac{\ell_0}{R}\right)^2 \frac{u_0^5 m_0^3}{\ell_0^3} C_\theta^{-5} \quad (39)$$

which is in agreement with Eq. (30).  $C_\theta^{-5}$  is called the convective amplification factor. It is due to the apparent change in frequency of the source, the Doppler effect, as well as effective change in the spatial extent of the source region. This latter effect is associated with the requirement that sources closer to the observer must radiate sound later than those farther from the observer to contribute to sound at the same time. During this time the convecting sources change their location relative to the observer. The net effect is that the sound is amplified if the sources are convecting toward the observer. This effect is described in detail by Ffowcs Williams.<sup>6</sup>

At  $90^\circ$  to the jet axis there is no convective amplification. Thus, a comparison of the noise spectra at any observer angle should be related to the  $90^\circ$  spectrum, when a Doppler frequency shift is also applied, through the convective amplification factor. Measurements (see, e.g., Lush<sup>37</sup>) show this to be reasonably accurate at low frequencies, though there is generally an underprediction of the levels at small observer angles to the jet downstream axis. However, the peak frequency in the spectrum actually decreases

with decreasing observer angle (relative to the jet downstream axis), and convective amplification is apparently completely absent at high frequencies. The measurements show a “zone of silence” for observers at small angles to the jet downstream axis.

The zone of silence is due to mean flow/acoustical interaction effects. That is, sound that is radiated in the downstream direction is refracted away from the jet’s downstream axis. This is because the propagation speed of the wavefronts is the sum of the local sound speed and the local mean velocity. Thus, points on the wavefronts along the jet centerline travel faster than those away from the axis, and the wavefronts are bent away from the downstream direction. A similar effect, described by Snell’s law, is observed in optics. Though, in principle, Lighthill’s acoustical analogy accounts for this propagation effect, it relies on subtle phase variations in the equivalent sources that are difficult, if not impossible, to model. Lilley<sup>7,54</sup> showed that linear propagation effects can be separated from sound generation effects if the equations of motion are rearranged so that the equivalent sources are at least second order in the fluctuations about the mean flow. This emphasizes the nonlinear nature of the sound generation process. Then, in the limit of infinitesimal fluctuations, the acoustical limit, the homogeneous equation describes the propagation of sound through a variable mean flow. Lilley showed that such a separation can be achieved for a parallel mean flow. That is, one in which the mean flow properties vary only in the cross stream direction. This is a good approximation to both free and bounded shear flows at high Reynolds numbers. The resulting acoustical analogy, which has been derived in many different forms, is known as Lilley’s equation. Its solution forms the basis for jet noise prediction methods that do not rely on empirical databases (see, e.g., Khavaran et al.<sup>55</sup>).

In recent years, different versions of the acoustical analogy have been formulated. Goldstein<sup>56</sup> rearranged the Navier–Stokes equations into a set of inhomogeneous linearized Euler equations with source terms that are exactly those that would result from externally imposed shear stress and energy flux perturbations. He introduced a new dependent variable to simplify the equations and considered different choices of base flow. Morris and Farassat<sup>57</sup> argued that a simple acoustical analogy would involve the inhomogeneous linearized Euler equations as the sound propagator. This also simplifies the equivalent source terms. Morris and Boluriaan<sup>58</sup> derived the relationship between Green’s function of Lilley’s equation and Green’s functions for the linearized Euler equations. In a slight departure from the fundamental acoustical analogy approach, Tam and Auriault<sup>59</sup> argued that the physical sources of sound are associated with fluctuations in the turbulent kinetic energy that causes local pressure fluctuations. Then the gradient of the pressure fluctuations are the acoustic sources. Again, the sound propagation was calculated based on the linearized Euler equations. It is expected that new versions of the original acoustical



analogy will be developed. This is because the acoustical analogy approach offers a relatively inexpensive method of predicting the radiated noise from a limited knowledge of the turbulent flow, such as a steady Computational Fluid Dynamics (CFD) solution. However, it has yet to be shown that these approaches can be used with confidence when subtle changes in the flow are made, such as when “chevrons” or “serrations” are added to the jet nozzle exhaust. In such cases, either extensive measurements or detailed CAA (as described below) may be necessary.

## 7 SUPERSONIC JET NOISE

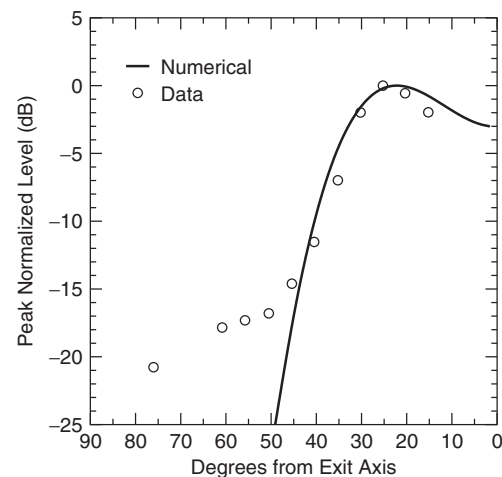
As the speed of the jet increases, both the structure of the jet and the noise radiation mechanisms change. Ffowcs Williams<sup>6</sup> used Lighthill’s acoustical analogy to show that the eighth velocity power law scaling for the intensity changes to a velocity cubed scaling when the jet velocity significantly exceeds the ambient speed of sound, as shown in Fig. 1. However, at these high speeds, two new phenomena become important for noise generation and radiation. The first is related to the supersonic convection of the turbulent large-scale structures and the second is related to the presence of shock cells in the jet when operating off-design. The physical mechanism of turbulent shear layer-shock interaction and the consequent generation of shock noise is complex. Contributions to its understanding have been given experimentally by Westley and Wooley<sup>60</sup> and Panda,<sup>61</sup> and theoretically by Ribner<sup>62</sup> and Manning and Lele.<sup>63</sup> A review of supersonic jet noise is provided by Tam.<sup>64</sup>

### 7.1 Noise from Large-Scale Structures/Instability Waves

The experiments of Winant and Browand<sup>65</sup> and Brown and Roshko<sup>66</sup> were the first to demonstrate that the turbulent mixing process in free shear flows is controlled by large-scale structures. These large eddies engulf the ambient fluid and transport it across the shear layer. Similarly, high-speed fluid is moved into the ambient medium. This is different from the traditional view of turbulent mixing involving random, small eddies, performing mixing in a similar manner to molecular mixing. Though it was first thought that these large-scale structures were an artifact of low Reynolds number transitional flows, subsequent experiments by Papamoschou and Roshko,<sup>67</sup> Lepicovsky, et al.,<sup>68</sup> and Martens et al.,<sup>69</sup> demonstrated their existence for a wide range of Reynolds and Mach numbers. Experiments (see, e.g., Gaster et al.<sup>44</sup>) also showed that the characteristics of the large-scale structures were related to the stability characteristics of the mean flow. A turbulence closure scheme based on this observation was developed by Morris et al.<sup>45</sup> Such so-called instability wave models have also been used to describe the large-scale turbulence structures in shear layers and jets and their associated noise radiation (see, e.g., Tam<sup>70</sup> and Morris<sup>71</sup>).

A complete analysis of the noise radiation by large-scale turbulence structures in shear layers and

jets at supersonic speeds, and comparisons with measurements, is given by Tam and Morris<sup>72</sup> and Tam and Burton.<sup>73</sup> The analysis involves the matching of a near-field solution for the large-scale structures with the radiated sound field using the method of matched asymptotic expansions. However, the basic physical mechanism is easily understood in terms of a “wavy wall analogy.” It is well known that if a wall with a small-amplitude sinusoidal oscillation in height is moved parallel to its surface then, if the speed of the surface is less than the ambient speed of sound in the fluid above the wall, the pressure fluctuations decay exponentially with distance from the wall. However, if the wall is pulled supersonically, then Mach waves are generated and these waves do not decay with distance from the wall (in the plane wall case). These Mach waves represent a highly directional acoustic field. The direction of this radiation, relative to the wall, is given by  $\theta = \cos^{-1}(1/M)$ , where  $M$  is the wall Mach number. This is another manifestation of the requirement that for sound radiation to occur the source variation must have a phase velocity with a component in the direction of the observer that is sonic. In the case of the turbulent shear flow, the large-scale structures, that are observed to take the form of a train of eddies, generate a pressure field that is quasi-periodic in space and convects with a velocity of the order of the mean flow velocity. At low speeds, the pressure fluctuations generated by the wave train are confined to the near field. However, when the convection velocity of the structures is supersonic with respect to the ambient speed of sound, they radiate sound directly to the far field. The result is a highly directional sound radiation pattern. Figure 9 shows a comparison



**Figure 9** Comparison of predicted far-field directivity calculations for a cold Mach 2 jet with measured data. Predictions based on an instability wave model for the large-scale structures and their radiated noise. Strouhal number = 0.2. (From Dahl<sup>75</sup> with permission. Data from Seiner and Ponton.<sup>74</sup>)



of the predicted directivity, based on an instability wave model, with measurements. The agreement is excellent in the peak noise direction. At larger angles to the downstream axis the predictions fall below the measurements. At these angles, the subsonic noise generation mechanisms are more efficient than the instability wave radiation.

Though the evidence is strongly in favor of large-scale structure or instability wave radiation at supersonic convection velocities being the dominant noise source, it does not provide a true prediction capability. This is because the analysis to this time has been linear. So absolute noise radiation levels are not predicted: just the relative levels. An aeroacoustics problem that has been fully represented by an instability wave model is the excitation of jets by sound. Tam and Morris<sup>76</sup> modeled the acoustical excitation of a high Reynolds number jet. The complete model includes a "receptivity" analysis, which determines to what level the instability wave is excited by the sound near the jet exit, the calculation of the axial development of the instability wave, based on linear instability analysis, and the interaction between the finite amplitude instability wave and the small-scale turbulence. The agreement with experiment was excellent, providing strong support for the modeling of the large-scale structures as instability waves.

## 7.2 Shock-Associated Noise

The large-scale structures, modeled as instability waves, also play an important role in shock-associated noise. Shock-associated noise occurs when a supersonic jet is operating "off-design." That is, the pressure at the nozzle exit is different from the ambient pressure. For a converging nozzle, the exit pressure is always equal to the ambient pressure when the pressure ratio (the ratio of the stagnation or reservoir to the ambient pressure) is less than the critical value of  $[1 + (\gamma - 1)/2]^{1/(\gamma - 1)}$ , where  $\gamma$  is the specific heat ratio. The ratio is 1.893 for air at standard temperature. Above this pressure ratio the converging nozzle is always "under expanded." Converging-diverging nozzles can be either under- or overexpanded. When a jet is operating off-design, a shock cell system is established in the jet plume. This diamond-shaped pattern of alternating regions of pressure and temperature can often be seen in the jet exhaust flow of a military jet aircraft taking off at night or in humid air conditions.

Pack<sup>77</sup> extended a model first proposed by Prandtl that describes the shock cell structure, for jets operating close to their design condition, with a linear analysis. If the jet is modeled by a cylindrical vortex sheet, then inside the jet the pressure perturbations satisfy a convected wave equation. The jet acts as a waveguide that reflects waves from its boundary. This is a steady problem in which the waveguide is excited by the pressure mismatch at the nozzle exit. This simple model provides a very good approximation to the shock cell structure. Tam et al.<sup>78</sup> extended the basic model to include the effects of the finite thickness of the jet shear layer and its growth in the axial direction.

They showed excellent agreement with measurements of the shock cell structure. Morris et al.<sup>79</sup> applied this model to jets of arbitrary exit geometry.

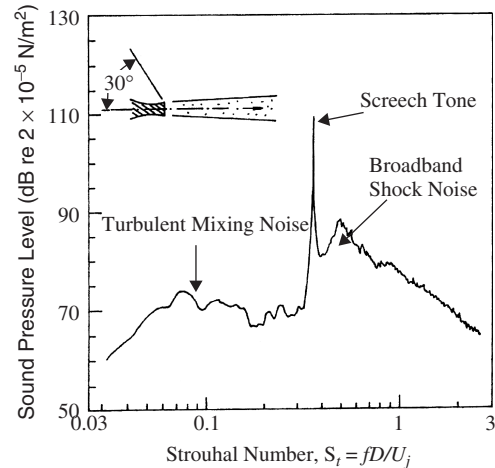
Fig. 10 shows a jet noise spectrum measured at 30° to the jet inlet direction. Three components are identified. The jet mixing noise occurs at relatively low frequencies and is broadband with a peak Strouhal number of approximately  $S_t = 0.1$ . Also identified are broadband shock noise and screech. These noise mechanisms and models for their prediction are described next.

The first model for shock-associated noise was developed by Harper-Bourne and Fisher.<sup>81</sup> They argued that it was the interaction between the turbulence in the jet shear layer and the quasi-periodic shock cell structure that set a phased array of sources at the locations where the shock cells intersected the shear layer. Tam and Tanna<sup>82</sup> developed a wave model for this process. Let the axial variation of the steady shock cell structure pressure  $p_s$  in the jet be modeled, following Pack,<sup>77</sup> in terms of Fourier modes. The amplitude of the modes is determined by the pressure mismatch at the jet exit. That is, let

$$p_s = \sum_{n=0}^{\infty} a_n \exp(ik_n x) + \text{complex conjugate} \quad (40)$$

where  $2\pi/k_n$  is the wavelength of the  $n$ th mode. So,  $2\pi/k_1$  gives the fundamental shock cell spacing,  $L_1$ . Let the pressure perturbations  $p_t$ , associated with the shear layer turbulence, be represented by traveling waves of frequency  $\omega$  and wavenumber  $\alpha$ . That is,

$$p_t = b_n \exp[i(\alpha x - \omega t)] + \text{complex conjugate} \quad (41)$$



**Figure 10** Typical far-field narrow-band supersonic jet noise spectrum level showing the three components of supersonic jet noise: turbulent mixing noise, broadband shock-associated noise, and screech 1-Hz bandwidth. (From Tam.<sup>64</sup>) (Data from Seiner.<sup>80</sup>)

A weak interaction between the steady and traveling wave patterns generates an interference pattern  $p_i \sim p_s \times p_t$ , where

$$\begin{aligned} p_i \sim & a_n b_n \exp\{i[(\alpha + k_n)x - \omega t]\} \\ & + a_n b_n^* \exp\{-i[(\alpha - k_n)x - \omega t]\} \\ & + \text{complex conjugate} \end{aligned} \quad (42)$$

The phase velocity of the traveling wave given by the first term in (42) is given by  $\omega/(\alpha + k_n)$ . Thus, this pattern travels more slowly than the instability wave and will only generate sound at very high jet velocities. The wave represented by the second term has a phase velocity of  $\omega/(\alpha - k_n)$ . Clearly, this is a very fast wave pattern and can even have a negative phase velocity so that it can radiate sound to the forward arc.

As noted before, for sound radiation to occur, the phase velocity of the source must have a sonic component in the direction of the observer. Let the observer be at a polar angle  $\theta$  relative to the downstream jet axis. Then, for sound radiation to occur from the fast moving wave pattern,

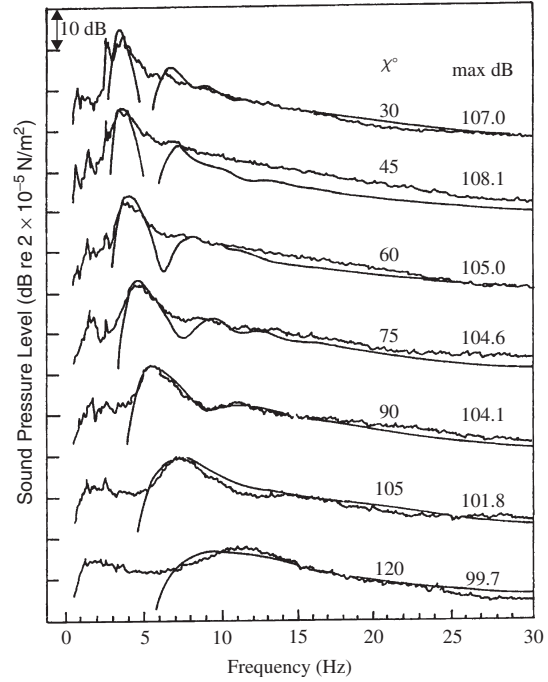
$$\frac{\omega \cos \theta}{\alpha - k_n} = c_\infty \quad (43)$$

If the phase velocity of the instability wave or large-scale turbulence structures is  $u_c = \omega/\alpha$ , then the radiated frequency is given by

$$f = \frac{u_c}{L_1 (1 - M_c \cos \theta)} \quad (44)$$

where  $M_c = u_c/c_\infty$ . It should be remembered that the turbulence does not consist of a single traveling wave but a superposition of waves of different frequencies moving with approximately the same convection velocity. Thus, the formula given by (44) represents how the peak of the broadband shock-associated noise varies with observer angle. Based on this modeling approach, Tam<sup>83</sup> developed a prediction scheme for broadband shock-associated noise. It includes a finite frequency bandwidth for the large-scale structures. An example of the prediction is shown in Fig. 11. The decrease in the peak frequency of the broadband shock-associated noise with increasing angle to the jet downstream axis is observed. Note that the observer angles in the figure are measured relative to the jet inlet axis: a procedure used primarily by aircraft engine companies. As the observer moves toward the inlet, the width of the shock-associated noise spectrum decreases, in agreement with the measurements. Also noticeable is a second oscillation in the noise spectrum at higher frequencies. This is associated with the interaction of the turbulence with the next Fourier mode representing the shock cell structure.

Screech tones are very difficult to predict. Though the frequency of the screech tones are relatively easy to predict, their amplitude is very sensitive to the details of the surrounding environment. Screech tones were first observed by Powell.<sup>85,86</sup> He recognized that the



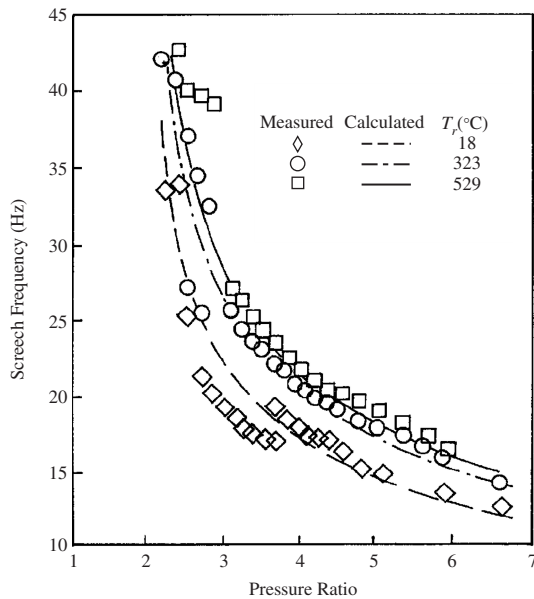
**Figure 11** Comparison between calculated broadband shock noise spectrum levels and measurements of Norum and Seiner.<sup>84</sup> Predictions based on stochastic model for broadband shock-associated noise of Tam,<sup>83</sup> 40-Hz bandwidth. (From, Tam.<sup>64</sup>)

tones were associated with a feedback phenomenon. The components of the feedback loop involve the downstream propagation of turbulence in the jet shear layer, its interaction with the shock cell structure, which generates an acoustic field that can propagate upstream, and the triggering of shear layer turbulence due to excitation of the shear layer at the nozzle lip. Tam et al.<sup>87</sup> suggested a link between broadband shock-associated noise and screech. It was argued that the component of broadband shock-associated noise that travels directly upstream should set the frequency of the screech. Thus, from (1.44), with  $\theta = \pi$ , the screech frequency  $f_s$  is given by

$$f_s = \frac{u_c}{L_1} \frac{1}{1 + M_c} \quad (45)$$

An empirical frequency formula, based on  $u_c \approx 0.7$  and accounting for the fact the shock cell spacing is approximately 20% smaller than that given by the vortex sheet model, is given by Tam.<sup>64</sup>

$$\begin{aligned} \frac{f_s d_j}{U_j} = & 0.67 (M_j^2 - 1)^{-1/2} \left[ 1 + 0.7 M_j \right. \\ & \left. \times \left( 1 + \frac{\gamma - 1}{2} M_j^2 \right)^{-1/2} \left( \frac{T_r}{T_\infty} \right)^{1/2} \right]^{-1} \end{aligned} \quad (46)$$



**Figure 12** Comparisons between measured<sup>88</sup> and calculated<sup>87</sup> screech tone frequencies at different total temperature  $T_r$ . (From Tam.<sup>64</sup>)

where  $T_r$  and  $T_\infty$  are the jet reservoir and the ambient temperature, respectively. Figure 12 shows a comparison of the calculated screech tone frequencies based on (46) and the measurements by Rosfjord and Toms<sup>88</sup> for different temperature jets. The agreement is very good. Tam<sup>89</sup> extended these ideas to give a formula for screech frequency tones in a rectangular jet. Morris<sup>90</sup> included the effects of forward flight on the shock cell spacing and screech frequencies, and Morris et al.<sup>79</sup> performed calculations for rectangular and elliptic jets. In all cases the agreement with experiment was good.

Full-scale hot jets show less ability to screech than laboratory cold jets at similar pressure ratios. This was observed on the Concorde. However, screech tones can occur at full scale and be so intense that they can result in structural damage. Intense pressure levels have been observed in the internozzle region of twin supersonic jets. This is the configuration found in the F-15 jet fighter. Seiner et al.<sup>91</sup> describe the resulting sonic fatigue damage. They also conducted model experiments. Tam and Seiner<sup>92</sup> and Morris<sup>93</sup> studied the instability of twin supersonic jets as a way to understand the screech mechanisms.

Numerical simulations of jet screech have been performed by Shen and Tam.<sup>94,95</sup> They examined the effect of jet temperature and nozzle lip thickness on the screech tone frequencies and amplitude. Very good agreement was achieved with measurements by Ponton and Seiner.<sup>96</sup> These simulations are an example of the relatively new field of computational aeroacoustics

(CAA). A very brief introduction to this area is given in the next section.

Military aircraft powered by jet engines and rocket motors, the launchers of space vehicles, and supersonic civil transports, can have a jet exit Mach number sufficiently large for the eddy convection Mach number to be highly supersonic with respect to the ambient medium. Such very high speed jets generate a phenomenon known as “crackle.” This arises due to the motion of supersonic eddies that, during their lifetime, create a pattern of weak shock waves attached to the eddy, having the character of a sonic boom as discussed in Section 3. Thus, in the direction normal to the shock waves, the propagating sound field external to the jet comprises an array of weak sonic booms and is heard by an observer as a crackle. Further details of this phenomenon are given by Ffowcs Williams et al.<sup>97</sup> and Petitjean et al.<sup>98</sup>

## 8 COMPUTATIONAL AEROACOUSTICS

With the increased availability of high-performance computing power, the last 15 years have seen the emergence of the field of computational aeroacoustics (CAA). This involves the direct numerical simulation of both the unsteady turbulent flow and the noise it generates. Excellent reviews of this new field have been given by Tam,<sup>99</sup> Lele,<sup>100</sup> Bailly and Bogey,<sup>101</sup> Colonius and Lele,<sup>102</sup> and Tam.<sup>103</sup> In addition, an issue of the *International Journal of Computational Fluid Dynamics*<sup>104</sup> is dedicated to issues and methods in CAA.

There are several factors that make CAA far more challenging than traditional computational fluid dynamics (CFD). First, the typical acoustic pressure fluctuation is orders of magnitude smaller than the mean pressure or the fluctuations in the source region. Second, acoustic wave propagation is both nondispersive and nondissipative (except when atmospheric absorption effects are included). The range of frequencies generated in, for example, jet noise, cover at least two decades. Also, aeroacoustics is a multiscale phenomenon, with the acoustic wavelengths being much greater than the smallest scales of the turbulence. This is especially important, as most aeroacoustic problems of practical interest involve turbulence at high Reynolds numbers. Finally, acoustic radiation usually occurs in unbounded domains, so nonreflecting boundary treatments are essential.

The requirements of high accuracy and low dispersion and dissipation have resulted in the use of high-order discretization schemes for CAA. Spectral and pseudospectral schemes have been widely used for turbulence simulation in simple geometries. They have also been used in CAA<sup>105</sup> to compute the near field with the far field being calculated with an acoustical analogy formulation. Finite element methods have also been used. In particular, the discontinuous Galerkin method<sup>106,107</sup> has become popular. The advantage of this method is that the discretization is local to an individual element and no global matrix needs to be constructed. This makes their implementation on parallel computers particularly efficient. The most popular

methods for spatial discretization have been finite difference methods. These include compact finite difference methods<sup>108</sup> and the dispersion-relation-preserving (DRP) schemes introduced by Tam and Webb.<sup>109</sup> The latter method optimizes the coefficients in a traditional finite-difference scheme to minimize dispersion and dissipation. CAA algorithms are reviewed by Hixon.<sup>110</sup>

Boundary conditions are very important as the slightest nonphysical reflection can contaminate the acoustical solution. In addition, nonreflecting boundary conditions must allow for mean entrainment of ambient fluid by the jet. Without this, the axial evolution of the jet would be constrained. An overview of boundary conditions for CAA is given by Kurbatskii and Mankbadi.<sup>111</sup> Boundary conditions can be either linear or nonlinear in nature. Among the linear methods, there are characteristic schemes such as a method for the Euler equations by Giles,<sup>112</sup> and methods based on the form of the asymptotic solution far from the source region, such as given by Bayliss and Turkel<sup>113</sup> and Tam and Webb.<sup>109</sup> The perfectly matched layer (PML) was first introduced in electromagnetics by Berenger<sup>114</sup> and adapted to the linearized Euler equations by Hu.<sup>115</sup> Hu<sup>116</sup> has made recent improvements to the method's stability. The PML involves a buffer domain around the computational domain in which the outgoing sound waves are damped. Nonlinear methods include the approximate multidimensional characteristics-based schemes by Thompson,<sup>117,118</sup> as well as buffer zone techniques, originally introduced by Israeli and Orszag,<sup>119</sup> and also implemented by Freund<sup>120</sup> and Wasistho et al.<sup>121</sup> among many others. Absorbing boundary conditions are reviewed by Hu.<sup>122</sup>

Finite difference discretization of the equations of motion generally yields two solutions. One is the longer wavelength solution that is resolved by the grid. The second is a short wavelength solution that is unresolved. The short wavelength solutions are called spurious waves. These waves can be produced at boundaries, in regions of nonuniform grid, and near discontinuities such as shocks. They can also be generated by the nonlinearity of the equations themselves, such as the physical transfer of energy from large to small scales in the Navier-Stokes equations, and by poorly resolved initial conditions. Various approaches have been taken to eliminate these spurious waves. These include the use of biased algorithms,<sup>123</sup> the application of artificial dissipation,<sup>109,124</sup> and explicit or implicit filtering.<sup>125</sup> Whatever method is used, care must be taken not to dissipate the resolved, physical solution.

Many of the difficulties faced in CAA stem from the turbulent nature of source region. Clearly, if the turbulence cannot be simulated accurately, the associated acoustic radiation will be in error. The direct numerical simulation (DNS) of the turbulence is limited to relatively Reynolds numbers as the ratio of largest to the smallest length scales of the turbulence is proportional to  $Re^{3/4}$ . Thus the number of grid points required for the simulation of one large-scale eddy is at least  $Re^{9/4}$ .

Freund<sup>126</sup> performed a DNS of a  $Re_D = 3.6 \times 10^3$  jet at a Mach number of 0.9 and used  $25.6 \times 10^6$  grid points. To simulate higher Reynolds turbulent flows either large eddy simulation (LES) or detached eddy simulation (DES) has been used. In the former case, only the largest scales are simulated and the smaller, subgrid scales are modeled. Examples include simulations by Bogey et al.,<sup>127</sup> Morris et al.,<sup>128</sup> and Uzun et al.<sup>129</sup> DES was originally proposed for external aerodynamics problems by Spalart et al.<sup>130</sup> This turbulence model behaves like a traditional Reynolds-averaged Navier-Stokes (RANS) model for attached flows and automatically transitions to an LES-like model for separated flows. The model has been used in cavity flow aeroacoustic simulations,<sup>131</sup> and in jet noise simulations.<sup>132,133</sup> All of these simulations involve large computational resources and the computations are routinely performed on parallel computers. A review of parallel computing in computational aeroacoustics is given by Long et al.<sup>134\*</sup>

Early studies in CAA emphasized the propagation of sound waves over large distances to check on the dispersion and dissipation characteristics of the algorithms. However, more recent practical applications have focused on a detailed simulation of the turbulent source region and the near field. The far field is then obtained from the acoustical analogy developed by Ffowcs Williams and Hawkins.<sup>5</sup> This analogy was developed with applications in propeller and rotorcraft noise in mind. It extends Lighthill's acoustic analogy to include arbitrary surfaces in motion. Its application in propeller noise is described in Chapter 90 of this handbook. The source terms in the Ffowcs Williams-Hawkins (FW-H) equation include two surface sources in addition to the source contained in Lighthill's equation (17). In propeller and rotorcraft noise applications these are referred to as "thickness" and "loading noise." However, the surfaces need not correspond to physical surfaces such as the propeller blade. They can be permeable. The advantage of the permeable surface formulation is that if all the sources of sound are contained within the surface, then the radiated sound field is obtained by surface integration only. Brentner and Farassat<sup>135</sup> have shown the

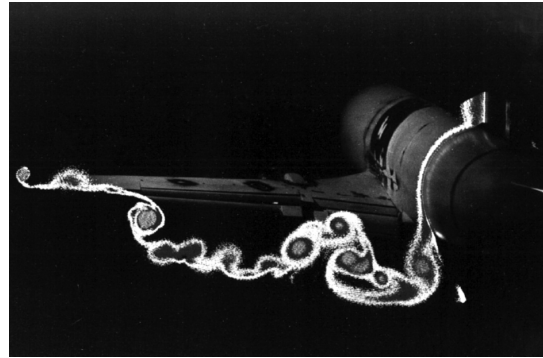
\*The attempts to find time-accurate calculations of a turbulent flow at moderate to high Reynolds numbers for noise predictions have shown that, outside the range of DNS calculations, the range of frequencies covered is restricted, arising from computer limitations, when compared with the noise spectra from the aircraft propulsion engines in flight. It appears that the turbulence model equations used for the averaged properties in a steady flow are less reliable when used for the unsteady time-accurate properties and calibration of unsteady methods poses many difficult problems. Hence the need continues to exist for acoustical models based on the steady-state averaged turbulence quantities in noise prediction methods, where the methods need to be carefully calibrated against experimental data. Emphasis should also be placed on modeling the noise generated by the unresolved scales of turbulence in LES and DES.

general relationship between the FW–H equation and the Kirchhoff equation (see Farassat and Myers<sup>136</sup>). di Franciscantonio<sup>137</sup> implemented the permeable surface form of the FW–H equation for rotor noise prediction. The advantage of the FW–H equation, clearly demonstrated by Brentner and Farassat, is that it is applicable to any surface embedded in a fluid that satisfies the Navier–Stokes equations. On the other hand, the Kirchhoff formulation relies on the wave equation being satisfied outside the integration surface. Brentner and Farassat<sup>135</sup> show examples where noise predictions based on the Kirchhoff formulation can be in error by orders of magnitude in cases where nonlinear effects are present outside the integration surface. Examples include situations where a wake crosses the surface, such as in calculations of noise radiated by a cylinder in uniform flow, or in the presence of shocks, such as occur in transonic flow over a rotor blade. Most recent CAA noise predictions have used the FW–H formulation.

## 9 BOUNDARY LAYER NOISE

In this section, the noise radiated from external surface boundary layers is discussed. The noise radiated from internal boundary layers in ducts is a separate problem and reference should be made to later chapters in this handbook. Here applications of aerodynamic noise theory to the noise radiated from the boundary layers developing over the upper and lower surfaces of aircraft wings and control surfaces are considered. This forms a major component of airframe noise, which together with engine noise contribute to aircraft noise as heard on the ground in residential communities close to airports. At takeoff, with full engine power, aircraft noise is dominated by the noise from the engine. But, on the approach to landing at low flight altitudes, airframe and engine noise make roughly equal contributions to aircraft noise. Thus, in terms of aircraft noise control it is necessary to reduce both engine and airframe noise for residents on the ground to notice a subjective noise reduction. Methods of airframe noise control are not discussed in detail in this section and the interested reader should refer to the growing literature on this subject. A review of airframe noise is given by Crighton.<sup>138</sup> The complexity of the various boundary layers and their interactions on an aircraft forming its wake is shown in Fig. 13.

The structure of the turbulent compressible boundary layer varies little from that of the boundary layer in an incompressible layer. The distribution of the mean flow velocity, however, changes from that in an incompressible flow due to the variation of the mean temperature and mean density for a given external pressure distribution. At low aircraft flight Mach numbers the boundary layer density fluctuations relate directly to the pressure fluctuations. The presence of sound waves represents a very weak disturbance in turbulent boundary layers and does not greatly modify the structure of the pressure fluctuations as measured in incompressible flows. The wall pressure fluctuations under a turbulent boundary layer are often referred to as boundary layer noise, or pseudonoise, since they are measured



**Figure 13** Structure of the wake downstream of high-lift extended flaps (photograph using the Wake Imaging System). (From Crowder.<sup>139</sup>)

by pressure transducers and microphones. However, they are defined here as flow pressure fluctuations and not noise. Turbulent boundary layer noise refers to the propagation of noise emerging out of a boundary layer and radiated to an observer in the acoustic far field. Steady flow laminar boundary layers do not generate noise, but this is not true of the region of transition between laminar and fully developed turbulent flow, where the flow is violently unsteady. Here, only the case where the turbulence in the boundary layer commences at the wing leading edge is considered. Let us first consider the radiation from the region of the boundary layer remote from the leading and trailing edges, where it can be assumed that the boundary layer is part of an idealized infinite flat plate having no edges.

### 9.1 Noise Radiation from an Infinite Flat Plate

For a rigid flat plate the governing wave equation for this theoretical problem is called the Lighthill–Curle equation. In this case the radiated sound field is shown to be a combination of quadrupole noise generated by the volume distribution of the Reynolds stresses in  $\mathcal{T}_{ij}$ , and the dipole noise generated by the distribution of surface stresses  $p_{ij}$ . For the infinite plate, the source distribution resulting from a turbulent flow is clearly noncompact. For the infinite plate it was found by Phillips<sup>140</sup> and Kraichnan<sup>141</sup> that the strength of the total dipole noise was zero due to cancellation by the image sound field. The quadrupole noise is, however, doubled by reflection from the surface, as found by Powell.<sup>142</sup> It has been shown by Crighton<sup>143</sup> and Howe<sup>144</sup> that, for upper surface sources not close to the edge of a half-plane, the sound radiation is upward and quadrupole, similar to that occurring with the infinite plate. Equivalent sound sources in a boundary layer on the lower surface radiate downward, and the radiation is quadrupole, for sources not close to the edge. Thus, for an aircraft, the sound radiation from the normal surface pressure fluctuations over the wing are negligible, in spite of the large surface wing area, compared with (i) the noise radiated from the jet of

the propulsion engines, since in the jet the turbulence intensity is much greater, and (ii) the diffracted noise radiated from the wing trailing edge, as will be shown below.

## 9.2 The Half-Plane Problem

The propagation of sound waves from sources of sound close to a sharp edge behave differently from sound propagating from the equivalent sources of sound in free turbulence. The pressure field close to a sound source, and within a wavelength of that source, becomes amplified by the proximity to the edge. The edge then becomes the origin for a diffracted sound field, which is highly amplified compared with that generated by free turbulence. In the pioneering work of Ffowcs Williams and Hall,<sup>9</sup> the aeroplane wing is replaced by a half-plane with its sharp trailing edge representing the scattering edge. The theory is similar to that in electromagnetic diffraction theory introduced by Macdonald.<sup>145</sup> In this representation of the theory there is no flow. However, subsequent work by Crighton<sup>143</sup> and Howe<sup>144</sup> and others has shown that the theory can be applied to moving sources crossing the edge, which can be interpreted as representing turbulence crossing the wing trailing edge from the boundary layer into the wake. Therefore, Lighthill's theory, as used in the theory of free turbulence, as modified in the Lighthill–Curle theory to include the flow over a plane surface, and now further modified by Ffowcs Williams and Hall<sup>9</sup> to include the effect of the finite wing trailing edge, can be used. The theory is similar to that of Lighthill, but instead of the free-field Green's function a special Green's function is used that has its normal derivative zero on the half-plane, and represents an outgoing wave in the far field. It is found that with this Green's function the surface contribution to the far-field noise involves only viscous stresses and at high Reynolds numbers their contribution is negligible. In most applications to aircraft noise the lower surface boundary layer is much thinner than the upper surface boundary layer and hence the greater contribution to the noise below the aircraft arises from the upper surface boundary layer as its pressure field is scattered at the wing trailing edge, and the sound radiated is diffracted to the observer. Thus following Goldstein<sup>10</sup> the acoustic field is given by,

$$(\rho - \rho_\infty)(\mathbf{x}, t) \sim \frac{1}{c_\infty^2} \int \frac{\partial^2 G}{\partial y_i \partial y_j} \mathcal{T}_{ij}^* dy + \frac{1}{c_\infty^2} \int \frac{\partial G}{\partial y_i} f_i^* dS(\mathbf{y}) \quad (47)$$

where  $dy$  represents an elemental volume close to the edge of the half-plane,  $f_i$  are the unsteady forces acting on the surface  $S(\mathbf{y})$ , and the asterisk denotes evaluation at the retarded or emission time,  $t - R/c_\infty$ . The distribution of sound sources per unit volume is proportional to  $\mathcal{T}_{ij}$ , but their contribution to the far-field sound is now enhanced compared with that in free turbulence, since (i) they no longer appear with

derivatives, and (ii) the term involving the derivatives of the Green's function is singular at the edge.

The Green's function,  $G$  for the half-plane, satisfies the boundary condition that  $\partial G / \partial y_2 = 0$  on  $y_1 > 0$  and  $y_2 = 0$ . The outgoing wave Green's function for the Helmholtz equation  $G_\omega$  is related to the Green's function  $G$  by (see Goldstein,<sup>10</sup> page 63):

$$G(\mathbf{x}, t | \mathbf{y}, \tau) = \frac{1}{2\pi} \int_{-\infty}^{\infty} \exp[-i\omega(t - \tau)] G_\omega(\mathbf{x}, \mathbf{y}) d\omega \quad (48)$$

Its far-field expansion is given by

$$G_\omega = \frac{1}{4\pi} \left[ \frac{e^{ikx}}{x} F(a) + \frac{e^{ikx'}}{x'} F(a') \right] \quad (49)$$

where  $x$  and  $x'$  are, respectively, the distances between the stationary observer at  $\mathbf{x}$  and the stationary source at  $\mathbf{y}$  above the plane and its image position  $\mathbf{y}'$  below the plane.  $k = \omega/c_\infty$  is the free space wavenumber.  $F(a)$  is the Fresnel integral,\* and since acoustic wavenumbers are small for typical frequencies of interest in problems of aircraft noise, it follows that the Fresnel integral is approximately equal to  $a/\sqrt{\pi}$ . Note that this special Green's function is simply the sum of two free-field Green's functions, each weighted by Fresnel integrals. It follows that the diffracted sound field below an aircraft has a distinct radiation pattern of cardioid shape, which is almost independent of the turbulent sound sources.

The solution to Lighthill's integral in the frequency domain is

$$\tilde{\rho} = \frac{1}{c_\infty^2} \int \frac{\partial^2 G_\omega}{\partial y_i \partial y_j} \tilde{\mathcal{T}}_{ij} dy \quad (52)$$

where  $\tilde{\mathcal{T}}_{ij}$  is the Fourier transform of  $\mathcal{T}_{ij}$ . On introducing the approximation to the Fresnel integrals

---

\*The Fresnel integral is given by

$$F(a) = \frac{1}{2} + \frac{e^{i\pi/4}}{\sqrt{\pi}} \int_a^\infty e^{iu^2} du \quad (50)$$

where the diffraction parameters for the source and its image are, respectively,

$$a = (2kr_0 \sin \theta)^{1/2} \cos\left[\frac{1}{2}(\phi - \phi_0)\right] \\ a' = (2kr_0 \sin \theta)^{1/2} \cos\left[\frac{1}{2}(\phi + \phi_0)\right] \quad (51)$$

The source position is given in cylindrical coordinates  $(r_0, \phi_0)$  relative to the edge, while the line from the origin on the edge to the observer is given in terms of the angles  $(\theta, \phi)$ . For sources close to the plane the differences between  $R$  and  $R'$  in the far field can be ignored.

for small values of  $a$ , and noting that for a given frequency  $\omega$

$$a + a' = \frac{(2\omega \sin \theta)^{1/2}}{c_\infty^{1/2}} r_0^{1/2} \cos\left(\frac{\phi}{2}\right) \cos\left(\frac{\phi_0}{2}\right) \quad (53)$$

where the distance from the edge to the sound source at  $\mathbf{y}$  is  $r_0 = \sqrt{y_1^2 + y_2^2}$  and  $\tan \phi_0 = y_2/y_1$ , it is found that for all frequencies of the turbulent fluctuations, the Fourier transform of the far-field density has a proportionality with  $\omega^{1/2}$ . When the averaged values of the  $T_{ij}$  covariance are introduced, the far-field sound intensity per unit flow volume is accordingly

$$i(\mathbf{x}) \sim \frac{1}{2\pi^3} \frac{\rho_\infty \omega_0 u_0^4}{c_\infty^2 R^2} \left(\frac{\ell_0}{r_0}\right)^2 \sin \theta \cos^2\left(\frac{\phi}{2}\right) \quad (54)$$

Clearly, the distance of the source from the edge,  $r_0$  is of the order of the scale of the turbulence,  $\ell_0$ . However, it should be recalled that the turbulence covers a wide range of scales and frequencies and all such sources are compact with  $\ell_0/\lambda \ll 1$ , even when  $\ell = \delta$ , the boundary layer thickness, where the acoustic wavelength,  $\lambda = 2\pi c_\infty/\omega$ . The theory is valid when  $kr_0 \ll 1$ . If the scale of the turbulence is  $\ell_0$ , equal to the integral scale, which is assumed to be the scale of the energy containing eddies, then  $\omega \ell_0/u_0 = s_T$ , where the turbulence Strouhal number,  $s_T = 1.7$ , approximately. It is found that, for all frequencies of interest in aircraft noise problems,  $kr_0 \ll 1$ .

### 9.3 Frequency Spectrum of Trailing Edge Noise

From dimensional reasoning, the high-frequency local law of decay can be found in the inertial subrange of the turbulence. First, the acoustic power spectral density per unit volume of turbulence,  $\tilde{p}_s$ , is given by

$$\tilde{p}_s \sim \frac{2}{\pi^2} \frac{\rho_\infty}{c_\infty^2} F(\varepsilon_T, \omega) \quad (55)$$

since the spectral density at high frequencies depends only on the frequency,  $\omega$ , and the rate of energy transfer,  $\varepsilon_T$ . It follows that  $F(\varepsilon_T, \omega)$  has the dimensions of the fourth power of the velocity. Dimensional analysis shows that

$$F(\varepsilon_T, \omega) = \beta \left(\frac{\varepsilon_T}{\omega}\right)^2 \quad (56)$$

But since  $\varepsilon_T = v\omega_s^2$  with  $\omega_s = u_s/\ell_s$  and  $u_s \ell_s/v = 1$  (where the subscript  $s$  denotes the smallest scales of the turbulence), it follows that with  $\beta$ , a dimensionless constant,

$$F(\varepsilon_T, \omega) = \beta \left(\frac{u_s^2}{\omega/\omega_s}\right)^2 \quad (57)$$

Also since  $\varepsilon_T = u_0^3/\ell_0$ , and experiment shows that the power spectral density continues smoothly from

its value in the inertial subrange into the energy-containing range, it is found that

$$\tilde{p}_s(\omega) \sim \left(\frac{u_0^2}{\omega/\omega_0}\right)^2 \quad (58)$$

and this same law applies for the total power spectral density. This result can be compared with that found by Meecham<sup>146</sup> for isotropic free turbulence where  $\tilde{p}(\omega) \sim [u_0^2/(\omega/\omega_0)]^{7/2}$ . When the acoustic power is measured in octave, one-third octave or any  $(1/n)$ th octave bands, the above decay law becomes  $(\omega/\omega_0)^{-1}$ , a result of considerable importance in respect of measurements of airframe subjective noise in terms of perceived noise levels.

### 9.4 Noise from Aircraft Flying in “Clean” Configuration

Now, consider the special case of an aircraft flying at an altitude of  $H$  past a stationary observer on the ground. Here it is assumed that the aircraft is flying in its “clean” configuration at an aircraft lift coefficient of order  $\overline{C}_L = 0.5$ . By flying clean, it is meant that the aircraft is flying with wheels up and flaps and slats retracted. This flying configuration exists before the aircraft is approaching an airport at its approach speed where it flies in its high-lift or “dirty” configuration. The noise from this latter aircraft configuration is not considered here, since it goes beyond the scope of this chapter centered on that part of aeroacoustics devoted to jet and boundary layer noise. The flight speed is  $V_\infty$ . The wing mean chord is  $\bar{c}$ . We assume that over both the upper and lower surfaces the boundary layers are fully turbulent from the leading to the trailing edge and are attached. However, due to the adverse pressure gradient over the wing upper surface, corresponding to a given flight lift coefficient, the thickness of the upper surface boundary layer is considerably thicker than that over the under surface. The structure of the turbulent boundary layer is usually considered in coordinates fixed in the aircraft, and in this frame of reference it is easily demonstrated that the flow in the boundary layers evolves through a self-generating cycle, which convects the large-scale eddies in the outer boundary layer past the wing surface at a speed,  $V_c$ , slightly less than that of the freestream. The structure of the outer region of the boundary layer is governed by the entrainment of irrotational fluid from outside the boundary layer and its conversion to turbulence in crossing the superlayer, plus the diffusion of the small-scale erupting wall layer, containing a layer of longitudinal vortices, which were earlier attached to the wall. On leaving the trailing edge both the outer and inner regions combine and form the wake, which trails downstream of the trailing edge.

In the corresponding case of the aircraft in motion, the stationary observer, a distance  $H$  below the aircraft, sees the outer boundary layer of the aircraft wing and its wake moving very slowly, following the aircraft, at a speed,  $V_\infty - V_c$ . The merging of the wake



and the turbulent boundary layers becomes smeared and irregular. The wake decays slowly in time.

In Section 9.2 it was shown that the turbulence in the upper surface boundary layer, as it approaches the wing trailing edge, creates a pressure field that is amplified and scattered at distances close to the trailing edge, but small compared with the acoustic wavelength, corresponding to the frequency of the turbulence. It was shown that the scattered pressure field generates a strong diffracted sound field centered on the wing trailing edge, having an intensity per unit flow volume of

$$i(\mathbf{x}) \sim \frac{1}{2\pi^3} \frac{\rho_\infty \omega_0 u_0^4}{c_\infty^2 R^2} \left( \frac{\ell_0}{r_0} \right)^2 \sin \theta \cos^2 \left( \frac{\phi}{2} \right) \quad (59)$$

To find the sound intensity, or sound pressure level, at a ground observer, it is necessary to determine the fraction of the flow volume embracing the sound sources in the upper surface boundary layer that are within an acoustic wavelength of the wing trailing edge and which approach the trailing edge in their passage to form the wing's wake. First, it is noted that the upper surface boundary layer is almost at rest in the atmosphere following its formation by the moving aircraft. Indeed it is seen by the stationary observer as a layer of near stagnant air surrounding the aircraft and forming its wake. It is assumed that the mean chord of the wing, or control surface, is small compared with the height of the aircraft, so that the observer viewing the passage of the aircraft along any slant distance defined by  $(x, \phi)$  directly below its flight trajectory, sees the trailing edge move a distance  $\bar{c}$  as the aircraft crosses the observer's line of sight. The total sound intensity, including the sound of all frequencies, received along the conical ray joining the aircraft to the observer, equals the sound emitted by sound sources within approximately a volume  $V_e = \bar{c} \times b \times \delta$ , where  $b$  is the wing span and  $\delta$  is the upper surface boundary layer thickness at the wing trailing edge.\* These sources emit from the near stagnant turbulent fluid as the trailing edge sweeps by, although the origin of the diffracted sound is moving with the trailing edge. Since the flight Mach numbers of interest are small, the Doppler effect on the frequency between the emitted sound and that received by the observer is neglected. The wind tunnel experiments of Brooks and Hodgson<sup>147</sup> on the trailing edge noise from an airfoil showed good agreement with the theoretical predictions.

The flight parameters of the aircraft, apart from its wing geometry,  $b, \bar{c}$ , and wing area,  $S = b \times \bar{c}$ , involve its vertical height,  $H$ , and slant height and angle  $(x, \phi)$ , the flight speed  $V_\infty$ , and the Mach number with respect to the ambient speed of sound,  $M_\infty$ . The all-up weight

of the aircraft can be written  $W = (\frac{1}{2})\rho_\infty V_\infty^2 \bar{C}_L S$ , where  $\bar{C}_L$  is the aircraft lift coefficient. The total sound intensity in  $W/m^2$  is given by

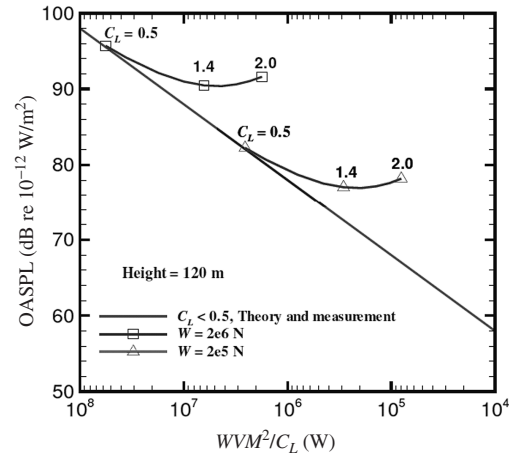
$$I(W/m^2) = \frac{1.7}{2\pi^3} \frac{\rho_\infty S V_\infty^3 M_\infty^2}{R^2} \left( \frac{u_0}{V_\infty} \right)^5 \left( \frac{\ell_0}{r_0} \right)^3 \times \left( \frac{\delta}{\ell_0} \right)_{TE} \cos^2 \left( \frac{\phi}{2} \right) \quad (60)$$

when  $\theta = 90^\circ$ ;  $\ell_0$  is assumed equal to the upper surface boundary layer displacement thickness, based on experimental evidence relating to the peak frequency in the far-field noise spectrum. Hence,

$$I(W/m^2) = \frac{1.7}{\pi^3} \frac{W V_\infty M_\infty^2}{\bar{C}_L R^2} \left( \frac{u_0}{V_\infty} \right)^5 \left( \frac{\ell_0}{r_0} \right)^3 \times \left( \frac{\delta}{\ell_0} \right)_{TE} \cos^2 \left( \frac{\phi}{2} \right) \quad (61)$$

which is the value used for the lower bound estimates of the airframe noise component for an aircraft flying in the clean configuration at a  $\bar{C}_L = 0.5$ , as shown in Fig. 14 as well as for the hypothetical clean aircraft flying on the approach at a  $\bar{C}_L = 2$ , as shown in Fig. 15.

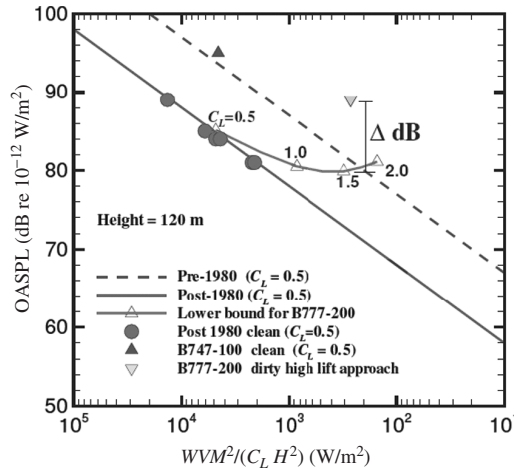
The interest in an aircraft flying in the clean configuration is that it provides a baseline value for the lowest possible noise for an aircraft flying straight and level of given weight and speed. Indeed, from flight tests, it has been demonstrated that the airframe noise component of all aircraft satisfies the simple  $V_\infty^5$



**Figure 14** Lower bound for overall sound pressure level (OASPL) for clean pre-1980 aircraft flying at the approach  $\bar{C}_L$ ; aircraft height,  $H = 120$  m and  $\bar{C}_L = 0.5$ .  $W$  = All-up weight,  $V$  = flight velocity,  $M$  = flight Mach number  $= V/c_\infty$ . (From Lockard and Lilley.<sup>148</sup>)

\*The true volume of sound sources may be somewhat less, but experiments confirm that all three quantities are involved in the determination of the sound intensity at ground level during an aircraft's flyover.





**Figure 15** Lower bound for OASPL for clean post-1980 aircraft flying at the approach  $\overline{C}_L$ ; aircraft height,  $H = 120$  m.  $W =$  All-up weight,  $V =$  flight velocity,  $M =$  flight Mach number  $= V/c_\infty$ . (From Lockard and Lilley.<sup>148</sup>)

relationship derived above. The clean configuration noise law applies also to gliders and birds, with the exception of the owl, which flies silently.<sup>†</sup> This demonstrates that the mechanism for airframe noise generation on all flying vehicles is the scattering of the boundary layer unsteady pressure field at the wing trailing edge and all control surfaces. In the clean configuration the aircraft is flying with wheels up, and trailing edge flaps and leading edge slats retracted. It is assumed that the aircraft lift coefficient, flying in this configuration, is of the order  $\overline{C}_L = 0.5$ .

An aircraft on its approach to landing has to fly at 1.3 times the stalling speed of the aircraft, and hence its lift coefficient has to be increased to about  $\overline{C}_L = 2.0$ . For a CTOL (conventional takeoff and landing) aircraft, such low speeds and high lift coefficients can only be achieved by lowering trailing edge flaps and opening leading edge slats. In addition, the undercarriage is lowered some distance from an airport to allow the pilot time to trim the aircraft for safe landing. The

aircraft is now flying in what is referred to as the dirty configuration. The undercarriage, flaps, and slats all introduce regions of highly separated turbulent flow around the aircraft and thus the airframe noise component of the aircraft noise is greatly increased. This noise is of the same order as the noise of the engine at its approach power. This is greater than the power required to fly the aircraft in its clean configuration due to the increase in drag of the aircraft flying in its dirty, or high-lift, configuration. Noise control of an aircraft is, therefore, directed toward noise reduction of both the engine and the high-lift configuration. The specified noise reduction imposes in addition the special requirement that this must be achieved at no loss of flight performance.

It is, therefore, important to establish not only a lower bound for the airframe noise component for the aircraft flying in its clean configuration, but also a lower bound for the airframe noise component when the aircraft is flying in its approach configuration. For this second lower bound, the assumption is made of a hypothetical aircraft that is able to fly at the required approach  $\overline{C}_L$  and speed for the aircraft at its required landing weight, with hush kits on its flaps and slats so that they introduce no extra noise to that of an essentially clean aircraft. For this second lower bound it is assumed the undercarriage is stowed. The approach of this hypothetical aircraft to an airport would therefore require that the undercarriage be lowered just before the airport was approached so that its increased noise would be mainly confined to within the airport and would not be heard in the residential communities further away from the airports boundary fence. The estimated increase in noise with increase in aircraft lift coefficient and consequent reduction in aircraft speed has been obtained by and Lockard and Lilley<sup>148</sup> from calculations of the increased boundary layer thickness at the wing trailing edge and the increase in the turbulent intensity as a result of the increased adverse pressure gradient over the upper surface of the wing.

## 9.5 Noise of Bluff Bodies

The aerodynamic noise generated by the turbulent wake arising from separated flow past bluff cylindrical bodies is of great practical importance. On aircraft it is typified by the noise from the landing gear with its assembly of cylinders in the form of its oleo strut, support braces, and wheels. From the Lighthill–Curle theory of aerodynamic noise it is shown that the fluctuations in aerodynamic forces on each cylindrical component can be represented as equivalent acoustical dipoles with a noise intensity proportional to  $V_\infty^6$ . No simple formula exists for landing gear noise, and reference should be made to Crighton<sup>138</sup>. A procedure for estimating landing gear noise is given in the Aircraft Noise Prediction Program (ANOPP)<sup>149</sup>. For detailed description of the complex flow around a circular cylinder, for a wide range of Reynolds numbers and Mach numbers, reference should be made to Zdravkovich.<sup>150,151</sup>

<sup>†</sup>The almost silent flight of the owl through its millions of years of evolution is of considerable interest to aircraft designers since it establishes that strictly there is no lower limit to the noise that a flying vehicle can make. In the case of the owl, its feathers, different from those of all other birds, have been designed to eliminate scattering from the trailing edge so that its noise is proportional to  $V_\infty^6$  and not  $V_\infty^5$ . This amounts to a large noise reduction at its low flight speed. But the other remarkable feature of the owl's special feathers is that they eliminate sound of all frequencies above 2 kHz. Thus, the owl is able to approach and capture its prey, who are unaware of that approach, in spite of their sensitive hearing to all sounds above 2 kHz. This is the reason that we can claim that the owl is capable of silent flight.

## 9.6 The Noise Control of Aircraft

This is an important area of aeroacoustics which is considered in detail in later chapters of this handbook. But a few remarks on this important subject need to be made in this chapter dealing with aerodynamic noise and, in particular, jet noise and boundary layer noise. In all these subjects the noise generated from turbulent flows in motion has been shown to be a high power of the mean speed of the flow. Hence the most important step in seeking to reduce noise comes from flow speed reduction. But, in considering boundary layer noise, it has been shown that the mechanism for noise generation is the result of scattering of the boundary layer's pressure field at the trailing edge resulting in a sound power proportional to  $M_\infty^5$ . Thus, a prime method for noise reduction is to eliminate the trailing edge scattering, resulting in a sound power proportional to  $M_\infty^6$ . A number of methods have been proposed to achieve this noise reduction. These include trailing edge serrations or brushes and the addition of porosity of the surface close to the trailing edge.

## REFERENCES

1. M. J. Lighthill, "On Sound Generated Aerodynamically: I. General Theory," *Proc. Roy. Soc. London, Series A*, Vol. 211, 1952, pp. 564–587.
2. H. von Gierke, *Handbook of Noise Control*, McGraw-Hill, New York, 1957, Chapters 33 and 34, pp. 33–1.
3. M. J. Lighthill, "On Sound Generated Aerodynamically. II. Turbulence as a Source of Sound," *Proc. Roy. Soc. London, Series A*, Vol. 222, 1954, p. 1–32.
4. N. Curle, "The Influence of Solid Boundaries upon Aerodynamic Sound," *Proc. Roy. Soc. London, Series A*, Vol. 231, No. 1187, 1955, pp. 505–514.
5. J. E. Ffowcs Williams and D. L. Hawkings, "Sound Generation by Turbulence and Surfaces in Arbitrary Motion," *Phil. Trans. Roy. Soc. of London, Series A*, Vol. 264, 1969, pp. 321–342.
6. J. E. Ffowcs Williams, "The Noise from Turbulence Convected at High Speed," *Phil. Trans. Roy. Soc. of London, Series A*, Vol. 255, 1963, pp. 469–503.
7. G. M. Lilley, "On the Noise from Jets," *Noise Mechanisms*, AGARD-CP-131, 1973.
8. C. K. W. Tam and L. Auriault, "Mean Flow Refraction Effects on Sound Radiated from Localized Sources in a Jet," *J. Fluid Mech.*, Vol. 370, 1998, pp. 149–174.
9. J. E. Ffowcs Williams and L. H. Hall, "Aerodynamic Sound Generation by Turbulent Flows in the Vicinity of a Scattering Half Plane," *J. Fluid Mech.*, Vol. 40, 1970, pp. 657–670.
10. M. E. Goldstein, *Aeroacoustics*, McGraw-Hill, New York, 1976.
11. M. J. Lighthill, *Waves in Fluids*, Cambridge University Press, Cambridge, 1978.
12. A. D. Pierce, *Acoustics: An Introduction to Its Physical Principles and Applications*, Acoustical Society of America, Woodbury, NY, 1989.
13. A. P. Dowling and J. E. Ffowcs Williams, *Sound and Sources of Sound*, Ellis Horwood, Chichester, 1983.
14. Hubbard, H. H. *Aeroacoustics of Flight Vehicles, Vol. 1, Noise Sources, Vol. 2, Noise Control*, Acoustical Society of America, Woodbury, NY, 1995.
15. D. G. Crighton, A. P. Dowling, J. E. Ffowcs Williams, M. Heckl, and F. G. Leppington, *Modern Methods in Analytical Acoustics*, Springer, London, 1992.
16. M. S. Howe, *Acoustics of Fluid-Structure Interactions*, Cambridge University Press, Cambridge, 1998.
17. H. S. Ribner, "The Generation of Sound by Turbulent Jets," *Adv. Appl. Mech.*, Vol. 8, 1964, pp. 103–182.
18. M. J. Crocker (Ed.), *Encyclopedia of Acoustics*, Wiley, New York, 1997.
19. M. J. Crocker (Ed.), *Handbook of Acoustics*, Wiley, New York, 1998.
20. L. Cremer, M. Heckl, and B. Petersson, *Structure-Borne Sound: Structural Vibrations and Sound Radiation at Audio Frequencies*, Springer, Berlin, 2005.
21. G. B. Whitham, "Nonlinear Dispersive Waves," *Proc. Roy. Soc. London, Series A*, Vol. 283, 1952, pp. 238–261.
22. M. J. Lighthill, "Some Aspects of the Aeroacoustics of Extreme-Speed Jets," *Symposium on Aerodynamics and Aeroacoustics*, F.-Y. Fung (Ed.), World Scientific, Singapore, 1994.
23. J. N. Punekar, G. J. Ball, G. M. Lilley, and C. L. Morfey, "Numerical Simulation of the Nonlinear Propagation of Random Noise," *15th International Congress on Acoustics*, Trondheim, Norway, 1995.
24. R. Westley, and G. M. Lilley, "An Investigation of the Noise Field from a Small Jet and Methods for Its Reduction," Report 53, College of Aeronautics Cranfield (England), 1952.
25. L. W. Lassiter and H. H. Hubbard, "Experimental Studies of Noise from Subsonic Jets in Still Air," NACA TN 2757, 1952.
26. M. S. Howe, "Contributions to the Theory of Aerodynamic Sound with Applications to Excess Jet Noise and Its Theory of the Flute," *J. Fluid Mech.*, Vol. 71, 1975, pp. 625–973.
27. A. Powell, "Theory of Vortex Sound," *J. Acoust. Soc. Am.*, Vol. 36, No. 1, 1964, pp. 177–195.
28. Schwartz, I. R. "Third Conference on Sonic Boom Research," NASA SP-255, 1971.
29. P. M. Morse and H. Feshbach, Dyadics and Other Vector Operators, in *Methods of Theoretical Physics, Part I*, McGraw-Hill, New York, 1953, pp. 54–92.
30. A. P. Dowling, J. E. F. Williams, and M. E. Goldstein, "Sound Production in a Moving Stream," *Phil. Trans. Roy. Soc. London, Series A*, Vol. 288, 1978, pp. 321–349.
31. V. Chobotov and A. Powell, "On the Prediction of Acoustic Environments from Rockets," Tech. Rep. E. M.-7-7, Ramo-Wooldridge Corporation Report, 1957.
32. G. M. Lilley, "On the Noise from Air Jets," Tech. Rep. 20376, Aeronautical Research Council, 1958.
33. D. C. Pridmore-Brown, "Sound Propagation in a Fluid Flowing Through an Attenuating Duct," *J. Fluid Mech.*, Vol. 4, 1958, pp. 393–406.
34. L. M. Brekhovskikh, *Waves in Layered Media* (trans. Robert T. Beyer), 2nd ed., Academic, New York, 1980.
35. R. Mani, "The Influence of Jet Flow on Jet Noise," *J. Fluid Mech.*, Vol. 80, 1976, pp. 753–793.
36. K. Viswanathan, "Aeroacoustics of Hot Jets," *J. Fluid Mech.*, Vol. 516, 2004, pp. 39–82.
37. P. A. Lush, "Measurements of Jet Noise and Comparison with Theory," *J. Fluid Mech.*, Vol. 46, 1971, pp. 477–500.

38. W. A. Olsen, O. A. Gutierrez, and R. G. Dorsch, "The Effect of Nozzle Inlet Shape, Lip Thickness, and Exit Shape and Size on Subsonic Jet Noise," Tech. Rep. NASA TM X-68182, 1973.
39. G. M. Lilley, "The Radiated Noise from Isotropic Turbulence with Applications to the Theory of Jet Noise," *J. Sound Vib.*, Vol. 190, No. 3, 1996, pp. 463–476.
40. R. Hoch, J. P. Duponchel, B. J. Cocking, and W. D. Bryce, "Studies of the Influence of Density on Jet Noise," *J. Sound Vib.*, Vol. 28, 1973, pp. 649–688.
41. H. K. Tanna, "An Experimental Study of Jet Noise, Part 1: Turbulent Mixing Noise," *J. Sound Vib.*, Vol. 50, 1977, pp. 405–428.
42. A. A. Townsend, *The Structure of Turbulent Shear Flow*, 2nd ed., Cambridge University Press, Cambridge, 1976.
43. A. N. Kolmogorov, "Energy Dissipation in a Locally Isotropic Turbulence," *Doklady Akademii Nauk SSSR*, Vol. 32, No. 1, 1941, pp. 19–21 (English trans. in: *Am. Math. Soc. Transl.*, Series 2, Vol. 8, p. 87, 1958, Providence, RI).
44. M. Gaster, E. Kit, and I. Wygnanski, "Large-Scale Structures in a Forced Turbulent Mixing Layer," *J. Fluid Mech.*, Vol. 150, 1985, pp. 23–39.
45. P. J. Morris, M. G. Giridharan, and G. M. Lilley, "On the Turbulent Mixing of Compressible Free Shear Layers," *Proc. Roy. Soc. London, Series A*, Vol. 431, 1990, pp. 219–243.
46. SAE International, *SAE ARP876, Revision D. Gas Turbine Jet Exhaust Noise Prediction*, SAE International, Warrendale, PA, 1994.
47. ESDU, "ESDU Aircraft Noise Series," 2005, <http://www.esdu.com>.
48. C. K. W. Tam, M. Golebiowski, and J. M. Seiner, "On the Two Components of Turbulent Mixing Noise from Supersonic Jets," AIAA Paper 96-1716, State College, PA, 1996.
49. G. M. Lilley, "The Acoustic Spectrum in the Sound Field of Isotropic Turbulence," *Int. J. Aeroacoust.*, Vol. 4, No. 1+2, 2005, pp. 11–20.
50. G. M. Lilley, Jet Noise Classical Theory and Experiments, in *Aeroacoustics of Flight Vehicles, Vol. 1; Noise Sources*, H. H. Hubbard (ed.), Acoustical Society of America, 1995, pp. 211–290.
51. M. Harper-Bourne, "Jet Noise Turbulence Measurements," AIAA Paper 2003-3214, Hilton Head, SC, 2003.
52. S. Sarkar, and M. Y. Hussaini, "Computation of the Sound Generated by Isotropic Turbulence," Report 93-74, ICASE, 1993.
53. P. O. A. L. Davies, M. J. Fisher, and M. J. Barratt, "The Characteristics of the Turbulence in the Mixing Region of a Round Jet," *J. Fluid Mech.*, Vol. 15, 1963, pp. 337–367.
54. G. M. Lilley, "Generation of Sound in a Mixing Region," in *Aircraft engine noise reduction—Supersonic Jet Exhaust Noise*, Tech. Rep. AFAPL-TR-72-53 Vol. IV, Aero Propulsion Laboratory, Ohio, 1972.
55. A. Khavaran and J. Bridges, "Modelling of Fine-Scale Turbulence Mixing Noise," *J. Sound Vib.*, Vol. 279, 2005, pp. 1131–1154.
56. M. E. Goldstein, "A Generalized Acoustic Analogy" *J. Fluid Mech.*, Vol. 488, 2003, pp. 315–333.
57. P. J. Morris and F. Farassat, "Acoustic Analogy and Alternative Theories for Jet Noise Prediction," *AIAA J.*, Vol. 40, No. 4, 2002, pp. 671–680.
58. P. J. Morris and S. Boluriaan, "The Prediction of Jet Noise From CFD Data," AIAA Paper 2004-2977, Manchester, England, 2004.
59. C. K. W. Tam and L. Auriault, "Jet Mixing Noise from Fine-Scale Turbulence," *AIAA J.*, Vol. 37, No. 2, 1999, pp. 145–153.
60. R. Westley and J. H. Woolley, "The Near Field Sound Pressures of a Choked Jet When Oscillating in the Spinning Mode," AIAA Paper 75-479, Reston, VA, 1975.
61. J. Panda, "An Experimental Investigation of Screech Noise Generation," *J. Fluid Mech.*, Vol. 376, 1999, pp. 71–96.
62. H. S. Ribner, "Convection of a Pattern of Vorticity through a Shock Wave," NACA Report 1164, 1954.
63. T. Manning and S. K. Lele, "Numerical Simulations of Shock-Vortex Interactions in Supersonic Jet Screech," AIAA Paper 98-0282, Reston, VA, 1998.
64. C. K. W. Tam, "Supersonic Jet Noise," *Ann. Rev. Fluid Mech.*, Vol. 27, 1995, pp. 17–43.
65. C. D. Winant and F. K. Browand, "Vortex Pairing: The Mechanism of Turbulent Mixing-Layer Growth at Moderate Reynolds Number," *J. Fluid Mech.*, Vol. 63, 1974, pp. 237–255.
66. G. L. Brown and A. Roshko, "On Density Effects and Large Structure in Turbulent Mixing Layers," *J. Fluid Mech.*, Vol. 64, 1974, pp. 775–816.
67. D. Papamoschou and A. Roshko, "The Compressible Turbulent Shear Layer: An Experimental Study," *J. Fluid Mech.*, Vol. 197, 1988, pp. 453–477.
68. J. Lepicovsky, K. K. Ahuja, W. H. Brown, and P. J. Morris, "Acoustic Control of Free Jet Mixing," *J. Propulsion Power*, Vol. 2, No. 4, 1986, pp. 323–330.
69. S. Martens, K. W. Kinzie, and D. K. McLaughlin, "Measurements of Kelvin-Helmholtz Instabilities in a Supersonic Shear Layer," *AIAA J.*, Vol. 32, 1994, pp. 1633–1639.
70. C. K. W. Tam, "Supersonic Jet Noise Generated by Large Scale Disturbances," *J. Sound Vib.*, Vol. 38, 1975, pp. 51–79.
71. P. J. Morris, "Flow Characteristics of the Large-Scale Wavelike Structure of a Supersonic Round Jet," *J. Sound Vib.*, Vol. 53, No. 2, 1977, pp. 223–244.
72. C. K. W. Tam and P. J. Morris, "The Radiation of Sound by the Instability Waves of a Compressible Plane Turbulent Shear Layer," *J. Fluid Mech.*, Vol. 98, No. 2, 1980, pp. 349–381.
73. C. K. W. Tam and D. E. Burton, "Sound Generation by the Instability Waves of Supersonic Flows. Part 2. Axisymmetric Jets," *J. Fluid Mech.*, Vol. 138, 1984, pp. 273–295.
74. J. M. Seiner and M. K. Ponton, "Aeroacoustic Data for High Reynolds Number Supersonic Axisymmetric Jets," Tech. Rep. NASA TM-86296, 1985.
75. M. D. Dahl, The Aerosacoustics of Supersonic Coaxial Jets, Ph.D. Thesis, Pennsylvania State University, Department of Aerospace Engineering, University Park, PA, 1994.
76. C. K. W. Tam and P. J. Morris, "Tone Excited Jets, Part V: A Theoretical Model and Comparison with Experiment," *J. Sound Vib.*, Vol. 102, 1985, pp. 119–151.
77. D. C. Pack, "A Note on Prandtl's Formula for the Wavelength of a Supersonic Gas Jet," *Quart. J. Mech. App. Math.*, Vol. 3, 1950, pp. 173–181.
78. C. K. W. Tam, J. A. Jackson, and J. M. Seiner, "A Multiple-Scales Model of the Shock-Cell Structure

- of Imperfectly Expanded Supersonic Jets," *J. Fluid Mech.*, Vol. 153, 1985, pp. 123–149.
79. P. J. Morris, T. R. S. Bhat, and G. Chen, "A Linear Shock Cell Model for Jets of Arbitrary Exit Geometry," *J. Sound Vib.*, Vol. 132, No. 2, 1989, pp. 199–211.
  80. J. M. Seiner, "Advances in High Speed Jet Aeroacoustics," AIAA Paper 84-2275, Reston, VA, 1984.
  81. M. Harper-Bourne and M. J. Fisher, "The Noise from Shock Waves in Supersonic Jets," *Noise Mech.*, AGARD-CP-131, 1973.
  82. C. K. W. Tam and H. K. Tanna, "Shock-Associated Noise of Supersonic Jets from Convergent-Divergent Nozzles," *J. Sound Vib.*, Vol. 81, 1982, pp. 337–358.
  83. C. K. W. Tam, "Stochastic Model Theory of Broadband Shock-Associated Noise from Supersonic Jets," *J. Sound Vib.*, Vol. 116, 1987, pp. 265–302.
  84. T. D. Norum and J. M. Seiner, "Measurements of Static Pressure and Far Field Acoustics of Shock-Containing Supersonic Jets," NASA TM 84521, 1982.
  85. A. Powell, "On the Mechanism of Choked Jet Noise," *Proc. Phys. Soc. London*, Vol. 66, 1953, pp. 1039–1056.
  86. A. Powell, "The Noise of Choked Jets," *J. Acoust. Soc. Am.*, Vol. 25, 1953, pp. 385–389.
  87. C. K. W. Tam, J. M. Seiner, and J. C. Yu, "Proposed Relationship between Broadband Shock Associated Noise and Screech Tones," *J. Sound Vib.*, Vol. 110, 1986, pp. 309–321.
  88. T. J. Rosjford and H. L. Toms, "Recent Observations Including Temperature Dependence of Axisymmetric Jet Screech," *AIAA J.*, Vol. 13, 1975, pp. 1384–1386.
  89. C. K. W. Tam, "The Shock Cell Structure and Screech Tone Frequency of Rectangular and Nonaxisymmetric Jets," *J. Sound Vib.*, Vol. 121, 1988, pp. 135–147.
  90. P. J. Morris, "A Note on the Effect of Forward Flight on Shock Spacing in Circular Jets," *J. Sound Vib.*, Vol. 122, No. 1, 1988, pp. 175–178.
  91. J. M. Seiner, J. C. Manning, and M. K. Ponton, "Dynamic Pressure Loads Associated with Twin Supersonic Plume Resonance," *AIAA J.*, Vol. 26, 1988, pp. 954–960.
  92. C. K. W. Tam and J. M. Seiner, "Analysis of Twin Supersonic Plume Resonance," AIAA Paper 87-2695, Sunnyvale, CA, 1987.
  93. P. J. Morris, "Instability Waves in Twin Supersonic Jets," *J. Fluid Dynamics*, Vol. 220, 1990, pp. 293–307.
  94. H. Shen and C. K. W. Tam, "Effects of Jet Temperature and Nozzle-Lip Thickness on Screech Tones," *AIAA J.*, Vol. 38, No. 5, 2000, pp. 762–767.
  95. H. Shen and C. K. W. Tam, "Three-Dimensional Numerical Simulation of the Jet Screech Phenomenon," *AIAA J.*, Vol. 40, No. 1, 2002, pp. 33–41.
  96. M. K. Ponton and J. M. Seiner, "The Effects of Nozzle Exit Lip Thickness on Plume Resonance," *J. Sound and Vib.*, Vol. 154, No. 3, 1992, pp. 531–549.
  97. J. E. Ffowcs Williams, J. Simson, and V. J. Virchis, "Crackle: An Annoying Component of Jet Noise," *J. Fluid Mech.*, Vol. 71, 1975, pp. 251–271.
  98. B. P. Petitjean, K. Viswanathan, and D. K. McLaughlin, "Acoustic Pressure Waveforms Measured in High Speed Jet Noise Experiencing Nonlinear Propagation," AIAA Paper 2005-0209, Reston, VA, 2005.
  99. C. K. W. Tam, "Computational Aeroacoustics: Issues and Methods," *AIAA J.*, Vol. 33, No. 10, 1995, pp. 1788–1796.
  100. S. K. Lele, "Computational Aeroacoustics: A Review," AIAA Paper 97-0018, Reston, VA, 1997.
  101. C. Bailly and C. Bogey, "Contributions of Computational Aeroacoustics to Jet Noise Research and Prediction," *Int. J. Computat. Fluid Dynamics*, Vol. 18, No. 6, 2004, pp. 481–491.
  102. T. Colonius and S. K. Lele, "Computational Aeroacoustics: Progress on Nonlinear Problems of Sound Generation," *Prog. Aerosp. Sci.*, Vol. 40, 2004, pp. 345–416.
  103. C. K. W. Tam, "Computational Aeroacoustics: An Overview of Computational Challenges and Applications," *Int. J. Computat. Fluid Dynamics*, Vol. 18, No. 6, 2004, pp. 547–567.
  104. "Computational Aeroacoustics," *Int. J. Computat. Fluid Dynamics*, Vol. 18, No. 6, 2004.
  105. E. J. Avital, N. D. Sandham, and K. H. Luo, "Mach Wave Sound Radiation by Mixing Layers. Part I: Analysis of the Sound Field," *Theoret. Computat. Fluid Dynamics*, Vol. 12, No. 2, 1998, pp. 73–90.
  106. B. Cockburn, G. Karniadakis, and C.-W. Shu (Eds.), *Discontinuous Galerkin Methods: Theory, Computation, and Applications*, Springer, Berlin, 2000.
  107. H. L. Atkins and C.-W. Shu, "Quadrature-Free Implementation of Discontinuous Galerkin Method for Hyperbolic Equations," *AIAA J.*, Vol. 36, 1998, pp. 775–782.
  108. S. K. Lele, "Compact Finite Difference Schemes with Spectral-like Resolution," *J. Computat. Phys.*, Vol. 103, No. 1, 1992, pp. 16–42.
  109. C. K. W. Tam and J. C. Webb, "Dispersion-Relation-Preserving Difference Schemes for Computational Aeroacoustics," *J. Computat. Phys.*, Vol. 107, No. 2, 1993, pp. 262–281.
  110. D. R. Hixon, "Radiation and Wall Boundary Conditions for Computational Aeroacoustics: A Review," *Int. J. Computat. Fluid Dynamics*, Vol. 18, No. 6, 2004, pp. 523–531.
  111. K. A. Kurbatskii and R. R. Mankbadi, "Review of Computational Aeroacoustics Algorithms," *Int. J. Computat. Fluid Dynamics*, Vol. 18, No. 6, 2004, pp. 533–546.
  112. M. B. Giles, "Nonreflecting Boundary Conditions for Euler Equation Calculations," *AIAA J.*, Vol. 28, No. 12, 1990, pp. 2050–2057.
  113. A. Bayliss and E. Turkel, "Radiation Boundary Conditions for Wave-like Equations," *Commun. Pure Appl. Math.*, Vol. 33, No. 6, 1980, pp. 707–725.
  114. J. P. Berenger, "A Perfectly Matched Layer for the Absorption of Electromagnetic Waves," *J. Computat. Phys.*, Vol. 114, No. 2, 1994, pp. 185–200.
  115. F. Q. Hu, "On Absorbing Boundary Conditions for Linearized Euler Equations by a Perfectly Matched Layer," *J. Computat. Phys.*, Vol. 129, No. 1, 1996, pp. 201–219.
  116. F. Q. Hu, "A Stable, Perfectly Matched Layer for Linearized Euler Equations in Unsplit Physical Variables," *J. Computat. Phys.*, Vol. 173, 2001, pp. 455–480.
  117. K. W. Thompson, "Time-Dependent Boundary Conditions for Hyperbolic Systems," *J. Computat. Phys.*, Vol. 68, 1987, pp. 1–24.

118. K. W. Thompson, "Time-Dependent Boundary Conditions for Hyperbolic Systems, II," *J. Computat. Phys.*, Vol. 89, 1990, pp. 439–461.
119. M. Israeli and S. A. Orszag, "Approximation of Radiation Boundary Conditions," *J. Computat. Phys.*, Vol. 41, 1981, pp. 115–135.
120. J. B. Freund, "Proposed Inflow/Outflow Boundary Condition for Direct Computation of Aerodynamic Sound," *AIAA J.*, Vol. 35, 1997, pp. 740–742.
121. B. Wasistho, B. J. Geurts, and J. G. M. Kuerten, "Simulation Techniques for Spatially Evolving Instabilities in Compressible Flow over a Flat Plate," *Comput. Fluids*, Vol. 26, 1997, pp. 713–739.
122. F. Q. Hu, "Absorbing Boundary Conditions," *Int. J. Computat. Fluid Dynamics*, Vol. 18, No. 6, 2004, pp. 513–522.
123. D. R. Hixon and E. Turkel, "Compact Implicit MacCormack-type Schemes with High Accuracy," *J. Computat. Phys.*, Vol. 158, No. 1, 2000, pp. 51–70.
124. D. P. Lockard and P. J. Morris, "A Parallel Implementation of a Computational Aeroacoustics Algorithm for Airfoil Noise," *J. Computat. Acoust.*, Vol. 5, 1997, pp. 337–353.
125. M. R. Visbal and D. V. Gaitonde, "High-Order-Accurate Methods for Complex Unsteady Subsonic Flows," *AIAA J.*, Vol. 37, 1999, pp. 1231–1239.
126. J. B. Freund, "Noise Sources in a Low Reynolds Number Turbulent Jet at Mach 0.9," *J. Fluid Mech.*, Vol. 438, 2001, pp. 277–305.
127. C. Bogey, C. Bailly, and D. Juve, "Noise Investigation of a High Subsonic, Moderate Reynolds Number Jet Using a Compressible LES," *Theoret. Computat. Fluid Dynamics*, Vol. 16, No. 4, 2003, pp. 273–297.
128. P. J. Morris, L. N. Long, T. E. Scheidegger, and S. Boluriaan, "Simulations of Supersonic Jet Noise," *Int. J. Aeroacoustics*, Vol. 1, No. 1, 2002, pp. 17–41.
129. A. Uzun, G. A. Blaisdell, and A. S. Lyrintzis, "3-D Large Eddy Simulation for Jet Aeroacoustics," AIAA Paper 2003-3322, Hilton Head, SC, 2003.
130. P. R. Spalart, W. H. Jou, W. H. Strelets, and S. R. Allmaras, "Comments on the Feasibility of LES for Wings and on a Hybrid RANS/LES Approach," *Proceedings of the First AFOSR International Conference on DNS/LES*, Greyden Press, Columbus, OH, 1997.
131. C. M. Shieh and P. J. Morris, "Comparison of Two- and Three-Dimensional Turbulent Cavity Flows," AIAA Paper 2001-0511, Reno, NV, 2001.
132. M. Shur, P. R. Spalart, and M. K. Strelets, "Noise Prediction for Increasingly Complex Jets," *Computational Aeroacoustics: From Acoustic Sources Modeling to Far-Field Radiated Noise Prediction*, Colloquium EUROMECH 449, Chamonix, France, Dec. 9–12 2003.
133. U. Paliath and P. J. Morris, "Prediction of Noise from Jets with Different Nozzle Geometries," AIAA Paper 2004-3026, Manchester, England, 2004.
134. L. N. Long, P. J. Morris, and A. Agarwal, "A Review of Parallel Computation in Computational Aeroacoustics," *Int. J. Computat. Fluid Dynamics*, Vol. 18, No. 6, 2004, pp. 493–502.
135. K. S. Brentner, and F. Farassat, "Analytical Comparison of Acoustic Analogy and Kirchhoff Formulation for Moving Surfaces," *AIAA J.*, Vol. 36, No. 8, 1998, pp. 1379–1386.
136. F. Farassat and M. K. Myers, "Extension of Kirchhoff's Formula to Radiation from Moving Surfaces," *J. Sound Vib.*, Vol. 123, No. 3, 1988, pp. 451–461.
137. P. di Francesantonio, "A New Boundary Integral Formulation for the Prediction of Sound Radiation," *J. Sound Vib.*, Vol. 202, No. 4, 1997, pp. 491–509.
138. D. G. Crighton, "Airframe Noise," in *Aeroacoustics of Flight Vehicles, Vol. 1; Noise Sources*, H. H. Hubbard (Ed.), Acoustical Society of America, Woodbury, NY, 1995, pp. 391–447.
139. J. P. Crowder, "Recent Advances in Flow Visualization at Boeing Commercial Airplanes," *5th International Symposium on Flow Visualization—Prague, Czechoslovakia*, Hemisphere Publishing, New York, 1989.
140. O. M. Phillips, "On the Aerodynamic Surface Sound from a Plane Turbulent Boundary Layer," *Proc. Roy. Soc. London. Series A*, Vol. 234, 1956, pp. 327–335.
141. R. H. Kraichnan, "Pressure Fluctuations in Turbulent Flow Over a Flat Plate," *J. Acoust. Soc. Am.*, Vol. 28, 1956, pp. 378–390.
142. A. Powell, "Aerodynamic Noise and the Plane Boundary," *J. Acoust. Soc. Am.*, Vol. 32, No. 8, 1960, pp. 982–990.
143. D. G. Crighton and F. G. Leppington, "On the Scattering of Aerodynamic Noise," *J. Fluid Dynamics*, Vol. 46, No. 3, 1971, pp. 577–597.
144. M. S. Howe, "A Review of the Theory of Trailing Edge Noise," *J. Sound Vib.*, Vol. 61, No. 3, 1978, pp. 437–465.
145. H. M. MacDonald, "A Class of Diffraction Problems," *Proc. London Math. Soc.*, Vol. 14, No. 410–427, 1915, pp. 410–427.
146. W. C. Meecham and G. W. Ford, "Acoustic Radiation from Isotropic Turbulence," *J. Acoust. Soc. Am.*, Vol. 30, 1958, pp. 318–322.
147. T. F. Brooks and T. H. Hodgson, "Trailing Edge Noise Prediction from Measured Surface Pressures," *J. Sound Vib.*, Vol. 78, 1981, pp. 69–117.
148. D. P. Lockard and G. M. Lilley, "The Airframe Noise Reduction Challenge," *Tech. Rep. NASA/TM2004213013*, 2004.
149. W. E. Zorowski, "Aircraft Noise Prediction Program. Theoretical Manual," *Tech. Rep., NASA TM 83199*, 1982.
150. M. M. Zdravkovich, *Flow around Circular Cylinders. Fundamentals*, Vol. 1, Oxford University Press, Oxford, 1997.
151. M. M. Zdravkovich, *Flow around Circular Cylinders. Applications*, Vol. 2, Oxford University Press, Oxford, 2003.

## **PART II**

---

# **FUNDAMENTALS OF VIBRATION**

# CHAPTER 11

## GENERAL INTRODUCTION TO VIBRATION

**Bjorn A. T. Petersson**

**Institute of Fluid Mechanics and Engineering Acoustics  
Technical University of Berlin  
Berlin, Germany**

### 1 INTRODUCTION

An important class of dynamics concerns linear and angular motions of bodies that respond to applied disturbances in the presence of restoring forces. Examples are building structure response to an earthquake, unbalanced axle rotation, flow-induced vibrations of a car body, and the rattling of tree leaves. Owing to the importance of the subject for engineering practice, much effort has been and is still spent on developing useful analysis and predictive tools, some of which are detailed in subsequent chapters. Mechanical vibrations denote oscillations in a mechanical system. Such vibrations not only comprise the motion of a structure but also the associated forces resulting or applied. The vibration is characterized by its frequency or frequencies, amplitude, and phase. Although the time history of vibrations encountered in practice usually does not exhibit a regular pattern, the sinusoidal oscillation serves as a basic representation. The irregular vibration, then, can be decomposed in several frequency components, each of which has its own amplitude and phase.

### 2 BASIC CONCEPTS

It is customary to distinguish between deterministic and random vibrations. For a process of the former type, future events can be described from knowledge of the past. For a random process, future vibrations can only be probabilistically described. Another categorization is with respect to the stationarity of the vibration process. Hereby, a stationary process is featured by time-invariant properties (root mean square (rms) value, frequency range), whereas those properties vary with time in a nonstationary process.

Yet a third classification is the distinction between free and forced vibrations. In a free vibration there is no energy supplied to the vibrating system once the initial excitation is removed. An undamped system would continue to vibrate at its natural frequencies forever. If the system is damped, however, it continues to vibrate until all the energy is dissipated. In contrast, energy is continuously supplied to the system for a forced vibration. For a damped system undergoing forced vibrations the vibrations continue in a steady state after a transient phase because the energy supplied compensates for that dissipated. The forced vibration depends on the spectral form and spatial distribution of the excitation as well as on the dynamic characteristics of the system.

Finally, it is necessary to distinguish between linear and nonlinear vibrations. In this context, focus is on the former, although some of the origins of nonlinear processes will be mentioned. In a linear vibration, there is a linear relationship between, for example, an applied force and the resulting vibratory response. If the force is doubled, the response, hence, will be doubled. Also, if the force is harmonic of a single frequency, the response will be harmonic of the same frequency. This means that the principle of superposition is generally applicable for linear vibrations. No such general statements can be made for nonlinear vibrations since the features are strongly dependent on the kind of nonlinearity.

Encompassed in this section of the handbook is also the area of fatigue. It can be argued that the transition from linear to nonlinear vibration takes place just in the area of fatigue. Although short-time samples of the vibration appear linear or nearly linear, the long-term effects of very many oscillations are irreversible.

The analysis of an engineering problem usually involves the development of a physical model. For simple systems vibrating at low frequencies, it is often possible to represent truly continuous systems with discrete or lumped parameter models. The simplest model is the mass–spring–damper system, also termed the single-degree-of-freedom system since its motion can be described by means of one variable. For the simple mass–spring–damper system, exposed to a harmonic force excitation, thus, the motion of the mass will have the frequency of the force, but the amplitude will depend on the mass, spring stiffness, and damping. Also the phase of the motion, for example, relative that of the force, will depend on the properties of the system constituents. If, on the other hand, the simple system is exposed to random excitation, the motion of the mass cannot be described by its value at various time instances but is assessed in terms of mean values and variances or spectra and correlation functions. It is important to note that a random process is a mathematical model, not the reality. Finally, a sudden, nonperiodic excitation of the mass such as an impact or shock usually leads to a strong initial response with a gradual transition to free vibrations. Depending upon the severity of the shock, the response can be either linear or nonlinear. The motion of the mass–spring–damper system, therefore, includes both the frequencies of the shock and the natural frequency of the system. Accordingly, it is common to describe the motion in terms of a response spectrum, which depicts the maximum acceleration, velocity, or

displacement experienced by the simple system as a function of time, normalized with respect to the period of its natural vibration.

Common for all types of vibration is that the mass gives rise to an inertia force, the spring an elastic restoring force, and the damping acts as a converter of mechanical energy into some other form, most commonly heat. Additionally, an increase of the mass lowers the natural frequency, whereas an increase of the spring stiffness elevates it. The reduction of the natural frequency resulting from an increase of the damping can practically most often be neglected.

More complicated systems can be seen as composed of multiple mass–spring–damper systems termed multiple-degree-of-freedom systems. Such models like the simple mass–spring–damper system are usually only applicable for low frequencies.

As the frequency or the complexity of the system increases, it becomes necessary to consider the system as continuous, that is, the system parameters such as mass, stiffness, and damping are distributed. Simultaneously, analytical mathematical descriptions are usually substituted by numerical analysis methods such as finite element or boundary element methods. Alternatively, the vibrations can be described in terms of averages for the flow between and storage of energy in various parts of the complex system by means of statistical energy analysis.

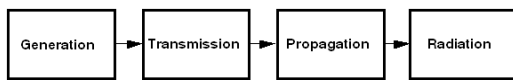
The mechanical vibration process can be subdivided into four main stages as depicted in Fig. 1. The first stage—generation—comprises the origin of an oscillation, that is, the mechanism behind it. The second—transmission—covers the transfer of oscillatory energy from the mechanisms of generation to a (passive) structure. In the structure, be it the passive part of the source or an attached receiving structure, the third stage—propagation—is recognized whereby energy is distributed throughout this structural system. Fourth, any structural part vibrating in a fluid environment (air) will impart power to that fluid—radiation—that is perceived as audible sound.

This subdivision also serves as a basis for the activities in control of mechanical vibrations. Typical problems relating to generation are:

- Unbalances
- Misalignments
- Rolling over rough surfaces
- Parametric excitation
- Impacts
- Combustion

They are of great importance in noise control. Transmission entails problems such as:

- Shock and vibration isolation



**Figure 1** Mechanical vibration as a process.

- Structural design (mismatch of structural dynamic characteristics)
- Machine monitoring and diagnosis

They are often the best compromise for noise and vibration control activities in view of cost and practicability. Prominent examples of problems belonging to propagation are:

- Ground vibrations
- Nondestructive testing
- Measurement of material properties
- Damping

Herein both wave theoretical approaches and modal synthesis can be employed. Finally, in the radiation phase are encountered problems like:

- Sound transmission
- Sound radiation

Most of the areas mentioned above will be treated in more detail in subsequent chapters.

### 3 BASIC RELATIONSHIPS AND VALIDITY

For small-scale mechanical vibrations, the process most often can be considered linear and the underlying equations are Newton's second law and Hooke's law. For lumped parameter systems consisting of masses  $m$  and massless springs of stiffnesses  $s$ , these laws read

$$m \frac{\partial^2 \xi_i}{\partial t^2} = F_i \quad i \in N \quad (1)$$

and

$$F_i = s \Delta \xi_i \quad i \in N \quad (2)$$

The two equations describe the inertia and elastic forces, respectively, required for the existence of elastic waves. The terms  $\xi_i$  are the displacement components of the masses;  $F_i$  denote the force components acting on the masses, and  $\Delta \xi_i$  are the changes in lengths of the springs due to the forces  $F_i$ . Two approximations underlie Eqs. (1) and (2), the first of which is the replacement of the total derivative by the partial. This means that any convection is neglected and large amplitudes cannot be handled. The second approximation is that the spring is considered to behave linearly. The equations are frequently employed in Chapter 12 to derive the equations of motion for single- and multidegree-of-freedom systems.

For continuous systems, Eq. (1) and (2) have to be modified slightly. The masses must be replaced by a density  $\rho$ , the forces by stresses  $\sigma_{ij}$ , and the changes



in length are substituted by strains  $\partial\xi/\partial x$ . In such a way, the equations turn into<sup>1,2</sup>

$$\rho \frac{\partial^2 \xi_i}{\partial t^2} = \frac{\partial \sigma_{ij}}{\partial x_j} + \beta_i \quad i, j \in [1, 2, 3] \quad (3)$$

$$\sigma_{ij} = G \left[ \frac{2\mu}{1-2\mu} \left( \frac{\partial \xi_k}{\partial x_k} \right) \delta_{ij} + \left( \frac{\partial \xi_i}{\partial x_j} + \frac{\partial \xi_j}{\partial x_i} \right) \right] \quad i, j, k \in [1, 2, 3] \quad (4)$$

for the practically important case with a homogeneous, isotropic material of shear modulus  $G$  and Poisson's ratio  $\mu$ . In Eqs. (3) and (4), use is made of the summation convention for tensors, that is, summation has to be made for repeated indices. The  $\beta_i$  are any body forces present. Alternatively, Eq. (4) can also be written in terms of the shear modulus  $G$  and Young's modulus  $E$ , which are related as  $E = G(1 + 2\mu)$ .

For a rod, subject to an axial force, for instance, the primary motion is, of course, in the axial direction, but there occurs also a contraction of the cross section. This contraction, expressed in terms of the axial strain amounts to  $\varepsilon_2 = \varepsilon_3 = -\mu\varepsilon_1$ .

The main difference between waves in fluids and elastic solids is that while only longitudinal or compressional waves exist in fluids in the absence of losses, also shear waves occur in solids. In the one-dimensional case, compressional waves are governed by the wave equation

$$\left( \frac{d^2}{dx_1^2} - k_C^2 \right) \xi_1 = F'(x_1) \quad (5)$$

whereas shear waves, with the displacement in direction 3, perpendicular to the propagation direction 1, obey

$$\left( \frac{d^2}{dx_1^2} - k_S^2 \right) \xi_3 = T'(x_1) \quad (6)$$

for harmonic processes. In Eqs. (5) and (6),  $k_C^2 = \omega^2 \rho / E$  and  $k_S^2 = \omega^2 \rho / G$  are the wavenumbers of the compressional and shear waves, respectively, where  $\omega = 2\pi f$  is the angular frequency.  $F'$  and  $T'$  are the axial and transverse force distributions, respectively. Other wave types such as bending, torsion, and Rayleigh waves can be interpreted as combinations of compressional and shear waves.

Owing to its great practical importance with respect to noise, however, the bending wave equation is given explicitly for the case of a thin, isotropic, and homogeneous plate:

$$(\nabla^4 - k_B^4) \xi_3 = \frac{12(1-\mu^2)}{Eh^3} \sigma_e \quad (7)$$

Herein,  $k_B^4 = 12(1-\mu^2)\rho\omega^2/(Eh^2)$  is the bending wavenumber, where  $h$  is the plate thickness.  $\xi_3$  is

the displacement normal to the plate surface and  $\sigma_e$  is the externally applied force distribution. This wave equation, which is based on Kirchhoff's plate theory, can normally be taken as valid for frequencies where the bending wavelength is larger than six times the plate thickness.

The equation is also applicable for slender beams vibrating in bending. The only modifications necessary for a beam of rectangular cross section are the removal of the factor  $1-\mu^2$  in Eq. (7) as well as in the bending wavenumber and insertion of the beam width  $b$  in the denominator of the right-hand side. Also, the force distribution changes to a force per unit length  $\sigma'_e$ .

Linear mechanical vibrations are often conveniently described in exponential form:

$$\xi(t) = \text{Re}[Ae^{j\omega t}] \quad (8)$$

where  $A$  is an amplitude, which is complex in general, that is, it has a phase shift relative to some reference. This enables the description of vibrations in terms of spectra, which means that the time dependence is written as a sum or integral of terms in the form of Eq. (8), all with different amplitudes, phases, and frequencies.

For the assessment of, for instance, the merit of design or vibration control measures, there is a growing consensus that this should be undertaken with energy- or power-based quantities. Hereby, nonstationary processes such as vibrations resulting from impacts encompassing a finite amount of energy are assessed by means of

$$\begin{aligned} E &= \int_0^{T_p} F(t) \xi(t) dt = \int_0^{T_p} \text{Re}[\hat{F}e^{j\omega t}] \text{Re}[\hat{\xi}e^{j\omega t}] dt \\ &= \frac{1}{2} \text{Re}[\hat{F}\hat{\xi}^*] \end{aligned} \quad (9)$$

while those that can be considered stationary, such as, for example, the fuselage vibration of a cruising aircraft, are appropriately assessed by means of the power averaged over time:

$$\begin{aligned} \overline{W} &= \lim_{T \rightarrow \infty} \frac{1}{T} \int_0^T F(t) \frac{\partial \xi(t)}{\partial t} dt \\ &= \lim_{T \rightarrow \infty} \frac{1}{T} \int_0^T \text{Re}[\hat{F}e^{j\omega t}] \text{Re}[\hat{\xi}e^{j\omega t}] dt \\ &= \frac{1}{2} \text{Re}[\hat{F}\hat{\xi}^*] \end{aligned} \quad (10)$$

In the two expressions above, the two latter forms apply to harmonic processes. Moreover, the vector nature of force, displacement, and velocity is

herein suppressed such that collinear components are assumed. The advantage of using energy or power is seen in the fact that the transmission process involves both kinematic (motion) and dynamic (force) quantities. Hence, observation of one type only can lead to false interpretations. Furthermore, the use of energy or power circumvents the dimensional incompatibility of the different kinematic as well as dynamic field variables. The disadvantages lie mainly in the general need of a phase, complicating the analysis as well as the measurements.

As mentioned previously, the vibration energy in a system undergoing free vibrations would remain constant in the absence of damping. One consequence of this would be that the vibration history of the system would never fade. Since such behavior contradicts our experience, the basic equations have to be augmented to account for the effect of the inevitable energy losses in physical systems. The conventional way to account for linear damping is to modify the force–displacement or stress–strain relations in Eq. (2) or (4). The simplest damping model is a viscous force, proportional to velocity, whereby Eq. (2) becomes

$$F = s \Delta \xi + C \frac{\partial}{\partial t} (\Delta \xi) \quad (11)$$

in which  $C$  is the damping constant. For continua, a similar viscous term has to be added to Eq. (4). This expression appropriately describes dampers situated in parallel with the springs but do not correctly describe the behavior of materials with inner dissipative losses. Other models with a better performance, provided the parameters are chosen properly, can be found in Zener.<sup>3</sup> One such is the Boltzmann model, which can be represented by

$$F(t) = s_0 \Delta \xi(t) - \int_0^\infty \Delta \xi(t - \tau) \varphi(\tau) d\tau \quad (12)$$

In this expression,  $\varphi(\tau)$  is the so-called relaxation function, consisting of a sum of terms in the form  $(D/\tau_R) \exp(-\tau/\tau_R)$  where  $D$  is a constant and  $\tau_R$  the relaxation time. The relaxation time spans a wide range, from  $10^{-9}$  up to  $10^5$  seconds. The model represents a material that has memory such that the instantaneous value of the viscous force  $F(t)$  not only depends on the instantaneous value of the elongation  $\Delta \xi(t)$  but also on the previous history  $\Delta \xi(t - \tau)$ .

Additional loss mechanisms are dry or Coulomb friction at interfaces and junctions between two structural elements and radiation damping, caused by waves transmitted to an ambient medium. Here, it should be noted that while the latter can be taken as a linear phenomenon in most cases of practical interest, the former is a nonlinear process.

Although Eq. (12) preserves linearity because no product or powers of the field quantities appear, it yields lengthy and intractable expressions when employed in the derivation of the equations of

motion. In vibroacoustics, therefore, this is commonly circumvented by introducing complex elastic moduli for harmonic motion<sup>4</sup>

$$E = E_0(1 + j\eta) \quad G = G_0(1 + j\eta) \quad (13)$$

where  $E_0$  and  $G_0$  are the ordinary (static) Young's and shear moduli, respectively. The damping is accounted for through the loss factor  $\eta = E_{\text{diss}}/(2\pi E_{\text{rev}})$ , that is, the ratio of the dissipated-to-reversible energy within one period. In many applications, the loss factor can be taken as frequency independent. The advantage of this formalism is that loss mechanisms are accounted for simply by substituting the complex moduli for the real-valued ones everywhere in the equations of motion. It must be observed, however, that complex moduli are mathematical constructs, which are essentially applicable for harmonic motion or superimposed harmonic motions. Problematic, therefore, is often a transformation from the frequency domain to that of time when assumed or coarsely estimated loss factors are used.

The relations described above can be used to develop the equations of motion of structural systems. With the appropriate boundary and initial conditions, the set of equations can be used in many practical applications. There remain, however, situations where their application is questionable or incorrect and the results can become misleading. Most often, this is in conjunction with nonlinear effects or when parameters vary with time. Some important causes of nonlinearities are:

- Material nonlinearities, that is, the properties  $s$ ,  $E$ ,  $G$ , and  $C$  are amplitude dependent as can be the case for very large scale vibrations or strong shocks.
- Frictional forces that increase strongly with amplitude, an effect that is often utilized for shock absorbers.
- Geometric nonlinearities, which occur when a linear relationship no longer approximates the dynamic behavior of the vibrating structure. Examples of this kind of nonlinearity are when the elongation of a spring and the displacement of attached bodies are not linearly related, Hertzian contact with the contact area changing with the displacement,<sup>5</sup> and large amplitude vibrations of thin plates and slender beams such that the length variations of the neutral layer cannot be neglected.<sup>6</sup>
- Boundary constraints, which cannot be expressed by linear equations such as, for example, Coulomb friction or motion with clearances.<sup>7</sup>
- Convective forces that are neglected in the inertia terms in Eqs. (1) and (3).

Slight nonlinearities give rise to harmonics in the response that are not contained in the excitation. For strong nonlinearities, a chaotic behavior may occur.

Examples of parametric changes in time or space are:

- Changes in a pendulum length.
- Stiffness changes due to variations of the point of contact, for example, a tooth in a gear wheel is considered as a short cantilever beam, for which the forcing point is continuously moving.
- Impedance variations as experienced by a body moving on a spatially varying supporting system such as a wheel on a periodically supported rail.

#### 4 ENERGY-BASED PRINCIPLES

An alternative approach for developing the equations of motion for a vibrating system is established via the energies. The most powerful method of this kind is based on Hamilton's principle:

$$\int_{t_1}^{t_2} [\delta(E_{\text{kin}} - E_{\text{pot}}) + \delta V] dt \quad (14)$$

which states that “for an actual motion of the system, under influence of the conservative forces, when it is started according to any reasonable initial conditions, the system will move so that the time average of the difference between kinetic and potential energies will be a minimum (or in a few cases a maximum).”<sup>8</sup> In Eq. (14),  $E_{\text{kin}}$  and  $E_{\text{pot}}$  denote the total kinetic and potential energies of the system and the symbol  $\delta$  indicates that a variation has to be made. For dissipative systems, either the variation in Eq. (14) is augmented by a dissipation function involving quadratic expressions of relative velocities<sup>9,10</sup> or the loss factor is simply introduced. External excitation or sinks can be incorporated by also including the virtual work done  $\delta V$ . Accordingly, all kinds of linear, forced vibrations can be handled. Hamilton's principle is highly useful in vibroacoustics. It can be seen as the starting point for the finite element method,<sup>10,11</sup> be used for calculating the vibrations of fluid loaded as well as coupled systems,<sup>12</sup> and to determine the phase speed of different wave types.<sup>13–15</sup>

A special solution to Eq. (14) is  $\overline{E_{\text{kin}}} = \overline{E_{\text{pot}}}$  where the overbar, as before, denotes time average. This special solution is known as Rayleigh's principle,<sup>15</sup> which states that the time averages of the kinetic and potential energies are equal at resonance. Since

$$\overline{E_{\text{kin}}} \propto \overline{\left(\frac{\partial \xi_i}{\partial t}\right)^2} \propto \omega^2 \overline{\xi_i^2}$$

the principle realizes a simple method to estimate resonance frequencies using assumed spatial distributions of the displacements, required for establishing the energies. Hereby, it should be noted that provided the boundary conditions can be satisfied, a first-order error

in the assumed distribution only results in a second-order one in the frequencies. In any case, Rayleigh's principle always renders an upper bound for the resonance frequency. An extension of this principle is the so-called Rayleigh–Ritz method, which can be applied to assess higher resonance frequencies as well as mode shapes.<sup>14,15</sup> In Mead,<sup>16</sup> Rayleigh's principle is employed to calculate the first pass- and stop-bands of periodic systems.

With respect to calculations of resonance frequencies, mode shapes, impulse or frequency responses, and the like for multidegree-of-freedom systems, Lagrange's equations of the second type

$$\frac{d}{dt} \left\{ \frac{\partial(E_{\text{kin}} - E_{\text{pot}})}{\partial \dot{\xi}_n} - \frac{\partial(E_{\text{kin}} - E_{\text{pot}})}{\partial \xi_n} \right\} = 0 \quad (15)$$

constitute a practical means. In these equations,  $\dot{\xi}_n$  and  $\xi_n$  are the  $n$ th velocity and displacement coordinates, respectively. In cases with external excitation  $F_n$ , the forces have to be included in the right-hand side.

Most differential equations describing linear mechanical vibrations are symmetric or self-adjoint. This means that the reciprocity principle is valid.<sup>17</sup> The principle is illustrated in Fig. 2 in which a beam is excited by a force  $F_A$  at a position  $A$  and the response  $\xi_B$  is observed at the position  $B$  in a first realization. In the second, reciprocal realization, the beam is excited at position  $B$  and the response is observed at  $A$ . The reciprocity now states that

$$F_A \xi'_A = F'_B \xi_B \Leftrightarrow \frac{F_A}{\xi_B} = \frac{F'_B}{\xi'_A} \quad (16)$$

which means that excitation and response positions can be interchanged as long as the directions of  $F_A$  and  $\xi'_A$  as well as  $F'_B$  and  $\xi_B$  are retained. The principle is also valid for other pairs of field variables, provided their product results in an energy or power quantity such as, for example, rotations and moments. An extension of the reciprocity principle, invoking the superposition principle, is termed the law of mutual energies.<sup>18</sup>

The reciprocity of linear systems has proven a most useful property in both theoretical and experimental work.<sup>19–21</sup> If, for example,  $F_A$  is cumbersome to compute directly or position  $A$  is inaccessible in

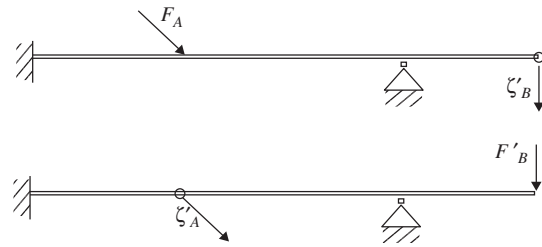


Figure 2 Illustration of reciprocity.

a measurement, the reciprocal realization can be employed to indirectly determine the force sought.

## 5 DESCRIPTIONS OF VIBRATIONS

As mentioned previously, mechanical vibrations are commonly represented in the frequency domain by means of spectral functions. The functions are usually ratios of two complex variables having the same time dependence, for example,  $e^{j\omega t}$ . The most common spectral functions are frequency response functions and transfer functions. Typical examples of the former kind are defined as:

- Input mobility

$$Y_{\xi F}(x_S|x_S) = \dot{\xi}(x_S)/F(x_S)$$

$$Y_{\dot{\theta} M}(x_S|x_S) = \dot{\theta}(x_S)/M(x_S)$$

- Transfer mobility

$$Y_{\xi F}(x_R|x_S) = \dot{\xi}(x_R)/F(x_S)$$

$$Y_{\dot{\theta} M}(x_R|x_S) = \dot{\theta}(x_R)/M(x_S)$$

- Cross-transfer mobility

$$Y_{\dot{\theta} F}(x_R|x_S) = \dot{\theta}(x_R)/F(x_S)$$

$$Y_{\xi M}(x_R|x_S) = \dot{\xi}(x_R)/M(x_S)$$

In these expressions,  $\dot{\xi}$  is the velocity in the direction of the force  $F$  whereas  $\dot{\theta}$  is the rotational velocity directed as the moment  $M$ ;  $x_S$  and  $x_R$  are the positions of the excitation and some observation point, removed from the excitation, respectively. The mobility thus represents the response of a structure due to a unit excitation. In the literature, other forms of frequency response functions are also found, such as receptance ( $R = \xi/F$ ), acceleration ( $A = \dot{\xi}/F$ ), and mechanical impedance ( $Z = F/\dot{\xi}$ ). A significant advantage of frequency response functions is that they can be used to predict the response of structures to arbitrary excitations in practical applications. The input mobility is particularly important since it is intimately associated with the power, for example,

$$W = \frac{1}{2} \text{Re}[Y_{\xi F}] |F|^2 \quad W = \frac{1}{2} \text{Re}[Y_{\dot{\theta} M}] |M|^2 \quad (17)$$

which describe the power transmitted to a structure by a point force and moment excitation, respectively.

Transfer functions, on the other hand, are normally ratios between two observations of the same field variable, such as, for instance,  $H_{12} = \xi(x_1)/\xi(x_2)$ , where the displacement at position  $x_1$  is compared with that at  $x_2$ . Both kinds of spectral functions are today conveniently measured by means of multichannel signal analysers; see Chapter 40.

A representation of the vibrating system in the time domain can be achieved by means of the impulse response function or Green's function  $g$ . This time-dependent function is the solution to the equation

$$\left( \frac{\partial^2}{\partial x^2} - \frac{1}{c_L^2} \frac{\partial^2}{\partial t^2} \right) g(x, t|x_S, t_0) = \delta(x - x_S) \delta(t - t_0) \quad (18)$$

in the one-dimensional case and represents the vibrational response at a position  $x$  and a time instant  $t$  due to a unit impulse, described by Dirac's delta function  $\delta$ , at a position  $x_S$  at time  $t_0$ . Similar impulse response function can be defined for two- and three-dimensional systems as well as coupled systems by substituting the adequate set of differential equations for that within parenthesis on the left-hand side. The impulse response function can be said to be a solution to the equation of motion for a special excitation. A set of impulse response functions for various positions, thus, can give all the information required about the vibrating system.

This approach has the advantage in transient analyses that the response to an arbitrary excitation is obtained directly from the convolution integral:

$$\xi(x, t) = \int F'(x_S, t_0) g(x, t|x_S, t_0) dx_S dt_0 \quad (19)$$

In this form, the vibration response is expressed as a sum of many very short and concentrated impulses. Owing to this, impulse response functions are often used for numerical computations of response time histories such as those due to shocks, but they are also suitable when nonlinear devices are attached or applied to linearly vibrating systems.<sup>22</sup>

There is a strong relationship between the impulse response function and the frequency response function in that the Fourier transform of either yields the other, save some constant. This relationship is often used to develop the impulse response function.

As an alternative to the wave theoretical treatment of vibrations dealt with above, a modal description of the vibrations can be employed for finite structures. As mentioned previously, a finite system responds at preferred frequencies, the natural frequencies or eigenfrequencies  $\omega_n$ , when exposed to a short, initial disturbance. Associated with those eigenfrequencies are preferred vibrational patterns, the natural vibrations or eigenfunctions  $\phi_n(x)$ . The modal description draws upon the fact that the vibrations can be expressed as a sum of eigenfunctions or (normal) modes.<sup>23</sup> In a one-dimensional case this means that

$$\xi(x) = \sum_{n=1}^{\infty} \hat{\xi}_n \phi_n(x) \quad (20)$$

where  $\xi$  is the displacement but can, of course, be any other field variable.  $\hat{\xi}_n$  are the modal amplitudes. The eigenfunctions are the solutions to the homogeneous

equation of motion and have to satisfy the boundary conditions. By employing this representation, it is possible to express forced vibration through the modal expansion theorem:

$$\xi(x) = \sum_{n=1}^{\infty} \frac{\phi_n(x)}{\Lambda_n[\omega_n^2(1 + j\eta_n) - \omega^2]} \times \int_L F'(x)\phi_n(x) dx \quad (21)$$

where  $\Lambda_n = \int_L m'(x)\phi_n^2(x) dx$  is the so-called norm and  $F'(x)$  is a harmonic force distribution. The damping of the system is accounted for through the modal loss factors  $\eta_n$ , which have to be small. The theorem states that the response of a system to some excitation can be expressed in terms of the eigenfunctions and the eigenfrequencies of the system.<sup>24</sup> A sufficient condition for the validity is that the system is “closed,” that is, no energy is leaving it. Otherwise, the orthogonality of the eigenfunctions must be verified. Such modal expansions are practically useful mainly for problems involving low or intermediate frequencies since the number of modes grows rapidly with frequency in the general case. For high frequencies, the modal summation in Eq. (21) can be approximated by an integral and a transition made to spatially averaged descriptions of the vibration.

Equation (21) can also be used for free vibrations in the time domain, for example, for response calculations from short pulses or shocks. The corresponding expression, obtained by means of a Fourier transform, can be written as<sup>24</sup>

$$\xi(x, t) = \sum_{n=1}^{\infty} \frac{I_n}{\omega_n} \phi_n(x) e^{-j\eta_n \omega_n t/2} \cos \omega_n t \quad t > 0 \quad (22)$$

wherein  $I_n$  are functions of the excitation and its position. The expression shows that the free vibration is composed of decaying modes where the number of significant modes is strongly dependent on the duration of the exciting pulse. For short impulses, the number of significant modes is generally quite substantial, whereas only the first few might suffice for longer pulses such as shocks.

When the number of modes in a frequency band (modal density) gets sufficiently large, it is often more appropriate and convenient to consider an energetic description of the vibration. The primary aim is then to estimate the distribution of energy throughout the vibrating system. The energy is taken to be the long-term averaged sum of kinetic and potential energy, from which the practically relevant field variables can be assessed. Such a description with spatially averaged energies is also justified from the viewpoint that there is always a variation in the vibration characteristics of nominally equal systems such that a fully deterministic description becomes less meaningful. The uncertainty

of deterministic predictions, moreover, increases with system complexity and is also related to wavelength, that is, to the frequency since small geometrical deviations from a nominal design have a stronger influence as their dimensions approach the wavelength. As in room acoustics, therefore, statistical formulations such as statistical energy analysis (SEA)<sup>25</sup> are widely employed in mechanical vibrations where subsystems are assumed drawn from a population of similar specimens but with random parameters.

The energy imparted to a structure leads to flows of energy between the subsystems, which can be obtained from a power balance whereby also the losses are taken into account. This is most simply illustrated for two coupled subsystems, as depicted in Fig. 3 where power is injected in subsystem 1  $W_{1in}$ . This is partially transmitted to subsystem 2  $W_{21}$  and partially dissipated  $W_{1diss}$ . Similarly, the power transmitted to subsystem 2 is partially retransmitted to subsystem 1  $W_{12}$  and partially dissipated  $W_{2diss}$ . This means that the power balance for the system can be written as

$$\begin{aligned} W_{1in} + W_{12} &= W_{21} + W_{1diss} \\ W_{21} &= W_{12} + W_{2diss} \end{aligned} \quad (23)$$

For linear subsystems, the power transmitted between them is proportional to the energy of the emitting subsystem and, hence, to the average mean square velocity, where the equality of kinetic and potential energies for resonantly vibrating systems is invoked. A spatial average is denoted by  $\langle \rangle$  enclosing the variable. Accordingly, the energy flows can formally be written as

$$W_{21} = C_{21} \langle |\dot{\xi}_1|^2 \rangle \quad W_{12} = C_{12} \langle |\dot{\xi}_2|^2 \rangle \quad (24)$$

where  $C_{21}$  and  $C_{12}$  are coefficients that are dependent on the spatial and temporal coupling of the two vibration fields. The main advantages of SEA are the “analysis philosophy,” transparency of the approach and that it swiftly can furnish results, which give good guidance to important parameters, also for rather

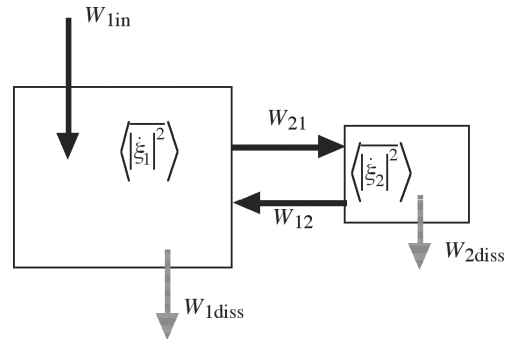


Figure 3 Energy flows in two coupled subsystems.

**Table 1 Material Properties**

Material	$\rho$ (kg/m <sup>3</sup> )	$E$ (GPa)	$G$ (GPa)	$\mu$ —	$c_C$ (m/s)	$c_S$ (m/s)
Aluminum	2700	72	27	0.34	5160	3160
Brass	8400	100	38	0.36	3450	2100
Copper	8900	125	48	0.35	3750	2300
Gold	19300	80	28	0.43	2030	1200
Iron	7800	210	80	0.31	5180	3210
Lead	11300	16	5.6	0.44	1190	700
Magnesium	1740	45	17	0.33	5080	3100
Nickel	8860	200	76	0.31	4800	2960
Silver	10500	80	29	0.38	2760	1660
Steel	7800	200	77	0.3	5060	3170
Tin	7290	54	20	0.33	2720	1670
Zinc	7140	100	41	0.25	3700	2400
Perspex	1150	5.6	2.1	0.35	2200	1300
Polyamid	1100–1200	3.6–4.8	1.3–1.8	0.35	1800–2000	1100–1200
Polyethylene	≈900	3.3	—	—	1900	540
Rubber						
30 shore	1010	0.0017	0.0006	≈0.5	41	24
50 shore	1110	0.0023	0.0008	≈0.5	46	27
70 shore	1250	0.0046	0.0015	≈0.5	61	35
Asphalt	1800–2300	7–21	—	—	1900–3100	
Brick						
Solid	1800–2000	≈16	—	0.1–0.2	2600–3100	1700–2000
Hollow	700–1000	3.1–7.8	—	0.1–0.2		
Concrete						
Dense	2200–2400	≈26	—	0.1–0.2	3400	2200
Light	1300–1600	≈4.0	—	0.1–0.2	1700	1100
Porous	600–800	≈2.0	—	0.1–0.2	1700	1100
Cork	120–250	0.02–0.05	—	—	430	
Fir	540	1.0–16.0	0.07–1.7	—	1400–5000	350–1700
Glass	2500	40–80	20–35	0.25	4800	3100
Gypsum board	700–950	4.1	—	—	2000–2500	
Oak	500–650	1.0–5.8	0.4–1.3	—	1200–3000	800–1400
Chipboard	600–750	2.5–3.5	0.7–1.0	—	2000–2200	1000–1200
Plaster	≈1700	≈4.3	—	—	≈1600	
Plywood	600	2.5	0.6–0.7	—	2000	1000

complicated systems. In Chapter 17, the topic is given a comprehensive treatment.

## 6 LIST OF MATERIAL PROPERTIES

Table 1 lists the most important material properties in relation to mechanical vibrations. Regarding data on loss factors, the reader is referred to Chapter 15.  $c_C$  and  $c_S$  are the compressional and shear wave speeds, respectively.

## REFERENCES

1. L. Brekhovskikh and V. Goncharov, in *Mechanics of Continua and Wave Dynamics*, Springer, Berlin, 1985, Chapters 1–4.
2. J. D. Achenbach, *Wave Propagation in Elastic Solids*, North-Holland, Amsterdam, 1973.
3. C. Zener, *Elasticity and Anelasticity of Metals*, University of Chicago Press, Chicago, 1948.
4. A. D. Nashif, D. I. G. Jones, and J. P. Henderson, *Vibration Damping*, Wiley, New York, 1985.
5. K. L. Johnson, *Contact Mechanics*, Cambridge University Press, Cambridge, 1985, Chapters 4 and 7.
6. S. P. Timoshenko and S. Woinowsky-Krieger, *Theory of Plates and Shells*, McGraw-Hill, New York, 1959, Chapter 13.
7. V. I. Babitsky, Dynamics of Vibro-Impact Systems, *Proceedings of the Euromech Colloquium*, 15–18 September 1998, Springer, Berlin, 1999.
8. P. M. Morse and H. Feshbach, *Methods of Theoretical Physics*, Vol. 1, McGraw-Hill, New York, 1953, Chapter 3.
9. J. W. Rayleigh, *Theory of Sound*, Vol. I, Dover, New York, 1945, Sections 81 and 82.
10. M. Petyt, *Introduction to Finite Element Vibration Analysis*, Cambridge University Press, Cambridge, 1990, Chapter 2.
11. O. Zienkiewicz, *The Finite Element Method*, McGraw-Hill, London, 1977.
12. M. C. Junger and D. Feit, *Sound, Structures and Their Interaction*, Acoustical Society of America, 1993, Chapter 9.
13. L. Cremer, M. Heckl, and B. A. T. Petersson, *Structure-Borne Sound*, 3rd ed., Springer, Berlin, 2005, Chapter 3.

14. L. Meirowitch, *Elements of Vibration Analysis*, McGraw-Hill, New York, 1986.
15. R. E. D. Bishop and D. C. Johnson, *The Mechanics of Vibration*, Cambridge University Press, London, 1979, Chapters 3, 5, and 7.
16. D. J. Mead, A General Theory of Harmonic Wave Propagation in Linear Periodic Systems with Multiple Coupling, *J. Sound Vib.*, Vol. 27, 1973, pp. 235–260.
17. Y. I. Belousov and A. V. Rimskii-Korsakov, The Reciprocity Principle in Acoustics and Its Application to the Calculation of Sound Fields of Bodies, *Sov. Phys. Acoust.*, Vol. 21, 1975, pp. 103–106.
18. O. Heaviside, *Electrical Papers*, Vols. I and II, Maximillan, 1892.
19. L. L. Beranek, *Acoustic Measurements*, Wiley, New York, 1949.
20. M. Heckl, Anwendungen des Satzes von der wechselseitigen Energie, *Acustica*, Vol. 58, 1985, pp. 111–117.
21. B. A. T. Petersson and P. Hammer, Strip Excitation of Slender Beams, *J. Sound Vib.*, Vol. 150, 1991, pp. 217–232.
22. M. E. McIntyre, R. T. Schumacher, and J. Woodhouse, On the Oscillations of Musical Instruments, *J. Acoust. Soc. Am.*, Vol. 74, 1983, pp. 1325–1345.
23. R. Courant and D. Hilbert, *Methods of Mathematical Physics*, Vol. I, Wiley Interscience, New York, 1953, Chapter V.
24. L. Cremer, M. Heckl, and B. A. T. Petersson, *Structure-Borne Sound*, 3rd ed., Springer, Berlin, 2005, Chapter 5.
25. R. H. Lyon and R. G. DeJong, *Theory and Application of Statistical Energy Analysis*, 2nd ed., Butterworth-Heinemann, Boston, 1995.

# CHAPTER 12

## VIBRATION OF SIMPLE DISCRETE AND CONTINUOUS SYSTEMS

Yuri I. Bobrovnikskii

Department of Vibroacoustics  
Mechanical Engineering Research Institute  
Russian Academy of Sciences  
Moscow, Russia

### 1 INTRODUCTION

Both free and forced vibration models of simple linear discrete and continuous vibratory mechanical systems are widely used in analyzing vibrating engineering structures. In discrete systems (also called lumped-parameter systems), the spatial variation of the deflection from the equilibrium position is fully characterized by a finite number of different amplitudes. In continuous systems (or distributed parameter systems), the deflection amplitude is defined by a continuous function of the spatial coordinates. Mathematically, the difference between the two types of vibratory systems is that vibrations of discrete systems are described by ordinary differential equations, while vibrations of continuous systems are described by partial differential equations, which are much more difficult to solve. Physically, the difference means that, in discrete systems, the most simple (elementary) motion is sinusoidal in time oscillation of inertia elements, while in continuous systems the elementary motion is wave motion that can travel along the system. In engineering practice, continuous systems are often replaced, for example, using the finite element method, by discrete systems.

#### 1.1 Single-Degree-of-Freedom System

A system with single degree of freedom (SDOF system) is the simplest among the vibratory systems. It consists of three elements: inertia element, elastic element, and damping element. Its dynamic state is fully described by one variable that characterizes deflection of the inertia element from the equilibrium position. For illustration, some SDOF systems are presented in Table 1, where indicated they are all three elements and the corresponding variable.

The role of SDOF systems in vibration theory is very important because any linear vibratory system behaves like an SDOF system near an isolated natural frequency and as a connection of SDOF systems in a wider frequency range.<sup>1</sup>

It is commonly accepted to represent a general SDOF system as the mass–spring–dashpot system shown in Table 1 as number one. Therefore, all the results are presented below for this SDOF system. To apply the results to physically different SDOF systems, the parameters  $m$ ,  $k$ ,  $c$ , and the displacement  $x$  should be replaced by the corresponding quantities as done in

Table 1. Usually, the inertia and elastic parameters are identified from the physical consideration, while the damping coefficient is estimated from measurement.

The ordinary differential equation that describes vibration of the mass–spring–dashpot system is obtained from Newton's second law and has the form

$$m\ddot{x}(t) + c\dot{x}(t) + kx(t) = f(t) \quad (1.1)$$

where  $x(t)$  is the displacement of the mass from the equilibrium position, and  $f(t)$  is an external force applied to the mass. The three terms in the left-hand side of the equation represent the force of inertia, dashpot reaction force, and the force with which the spring acts on the mass.

#### 1.2 Free Vibration

Free or unforced vibration of the SDOF system corresponds to zero external loading,  $f(t) = 0$ ; it is described by solutions of homogeneous Eq. (1.1) and uniquely determined by the initial conditions. If  $x_0 = x(0)$  and  $\dot{x}_0 = \dot{x}(0)$  are the displacement and velocity at the initial moment  $t = 0$ , the general solution for free vibration at time  $t > 0$  is

$$x(t) = x_0 e^{-\zeta\omega_0 t} \cos \omega_d t + \frac{\dot{x}_0 + \zeta\omega_0 x_0}{\omega_d} e^{-\zeta\omega_0 t} \sin \omega_d t \quad (1.2)$$

Here  $\zeta$  is the *damping ratio*,  $\omega_0$  is the *undamped natural frequency*, and  $\omega_d$  is the natural frequency of the damped system:

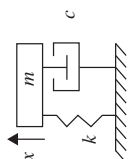
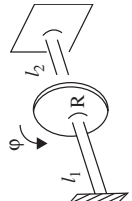
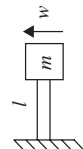
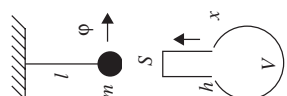
$$\omega_0 = \sqrt{k/m} \quad \zeta = c/2m\omega_0 \quad \omega_d = \omega_0 \sqrt{1 - \zeta^2} \quad (1.3)$$

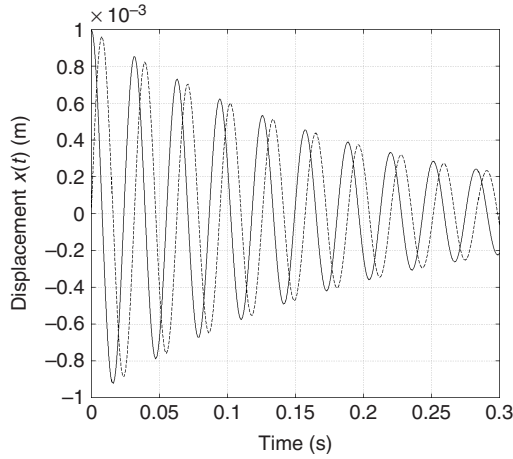
Further, it is assumed that the amount of damping is not very large, so that  $1 > \zeta$  and the natural frequency  $\omega_d$  is real valued. (When damping is equal to or greater than the critical value,  $\zeta \geq 1$  or  $c^2 \geq 4mk$ , the system is called overdamped and its motion is aperiodic.)

The time history of the vibration process (1.2) is shown in Fig. 1. It is seen from Eq. (1.2) and Fig. 1 that the free vibration of a SDOF system, that is its response function to any initial excitation  $x_0$  and  $\dot{x}_0$ , is always harmonic oscillation with natural frequency  $\omega_d$  and exponentially decaying amplitude. The rate of decay is characterized by the damping ratio  $\zeta$ . Sometime, instead of  $\zeta$ , other characteristics of decay



**Table 1 Examples of SDOF System**

Vibratory System		Inertia Element	Elastic Element	Damping Element	Variable
	Mass–spring–dashpot system	Mass, $m$ (kg)	Spring with stiffness $k$ (N m <sup>-1</sup> )	Dashpot with damping coefficient $c$ (kg s <sup>-1</sup> )	Linear displacement $x$ (m)
		Moment of the disc inertia $\frac{mR^2}{2}$ (kg m <sup>2</sup> )	Static torsional stiffness of the shaft $G \frac{\pi a^4}{2} \left( \frac{1}{l_1} + \frac{1}{l_2} \right)$ (N m) $G$ = shear modulus $a$ = radius of the shaft	Losses in shaft material	Angular displacement of the disc $\varphi$ (rad)
	Cantilever beam with a mass at the end	Mass, $m$ (kg)	Static flexural stiffness of the beam $\frac{3EI}{l^3}$ (N m <sup>-1</sup> ) $E$ = Young's modulus $I$ = moment of inertia	Losses in beam material	Linear displacement of the mass $w$ (m)
	Pendulum	Moment of inertia $ml^2$ (kg m <sup>2</sup> )	Angular stiffness due to gravity $g = 9.8$ (m s <sup>-2</sup> ) $mgI$ (N m)	Friction in suspension axis	Angular displacement $\varphi$ (rad)
	Helmholtz resonator (long-necked open vessel)	Mass of the fluid in the neck $\rho Sh$ (kg) $\rho$ = density $S$ = cross-sectional area	Static stiffness of the fluid in the vessel $\frac{\rho_0 S^2}{V}$ (N m <sup>-1</sup> ) $p_0$ = atmospheric pressure $V$ = vessel volume	Viscous losses at the neck walls and radiation losses	Linear displacement of the fluid in the neck $x$ (m)



**Figure 1** Free vibration of a mass–spring–dashpot system with initial conditions:

$$x_0 = 10^{-3} \text{ m}; \dot{x}_0 = 0 \text{ (solid line),}$$

$$x_0 = 0; \dot{x}_0 = 0.2 \text{ ms}^{-1} \text{ (dashed line).}$$

are introduced. These are the logarithmic decrement and loss factor  $\eta$ —see Section 1.4 and Chapter 15.

### 1.3 Forced Harmonic Vibration

If, beside the initial condition, an SDOF system is acted upon by external force  $f(t)$ , its motion is the superposition of two components: free vibration (1.2)

and the vibration caused by  $f(t)$  and called forced vibration. In the simplest case the force is harmonically varying in time and represented, for the sake of convenience, in the complex form as

$$f(t) = \text{Re}(f e^{-i\omega t}) \quad (1.4)$$

where  $\omega$  is an arbitrary frequency and  $f$  is the complex amplitude (details of the complex representation see in Chapter 11); the forced component of the system response is also a harmonic function of the same frequency  $\omega$ . When represented in the similar complex form, this component is characterized by the complex-valued displacement amplitude  $x$ , which is equal to

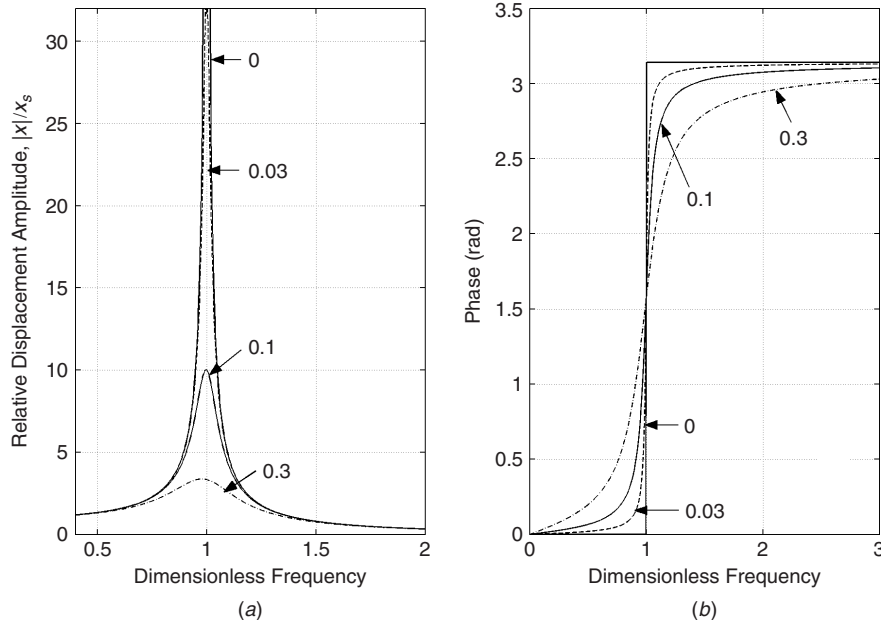
$$x = f/k(\omega) \quad k(\omega) = k - m\omega^2 - i\omega c$$

$$= k[e(1 - \varepsilon^2) - i\eta_0\varepsilon] \quad (1.5)$$

where  $\varepsilon = \omega/\omega_0$ ,  $k(\omega)$  is the complex-valued *dynamic stiffness* of the system,  $\eta_0$  being the resonance value of the loss factor given by

$$\eta_0 = \frac{c}{m\omega_0} = 2\zeta \quad (1.6)$$

Figure 2 presents the absolute value and phase of the displacement amplitude (1.5) of the SDOF-system for different rates of damping. The curves in Fig. 2a are

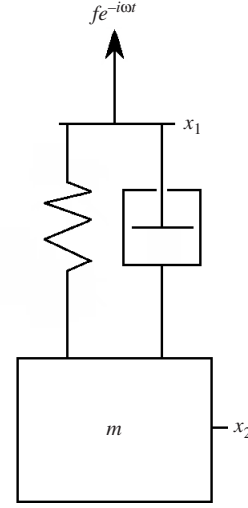


**Figure 2** (a) Displacement amplitude normalized with the static displacement  $x_s = f/k$  and (b) phase vs. dimensionless frequency  $\omega/\omega_0$  for different values of the resonant loss factor  $\eta_0 = 0; 0.03; 0.1; 0.3$ .

commonly referred to as the *frequency response functions*, or FRFs. It is seen from Fig. 2 that the displacement FRF is maximum at frequency  $\omega_0\sqrt{1-\eta_0^2}/2$ . The phenomenon when a system response has maximum values is called *resonance*. Resonance is also observed in the velocity and acceleration responses of the SDOF system. However, they reach maximum values at different frequencies. The resonance frequency of the velocity response is equal to the undamped natural frequency  $\omega_0$ , the acceleration amplitude reaches its maximum value at frequency  $\omega_0/\sqrt{1-\eta_0^2}/2$ , while none of the physical variables resonates at the damped natural frequency  $\omega_d = \omega_0\sqrt{1-\eta_0^2}/4$ . Note that for small damping, all these frequencies are about equal. The amplitude of the system response at the resonance frequency is inversely proportional to the loss factor  $\eta_0$ .

In an SDOF system, one can also observe *antiresonance*—the phenomenon when the system response is minimum. Consider the case of an external force that is applied to the spring–dashpot connection point while the mass is free from an external loading, as shown in Fig. 3. Figure 4 presents the amplitude and phase of the velocity response at the driving point normalized with  $f/m\omega_0$  as a function of frequency for various rates of damping. The antiresonance frequency is very close to undamped natural frequency  $\omega_0$  (although not exactly equal). At this frequency, the velocity amplitude at the driving point is minimum while the amplitude of the mass velocity is maximum.

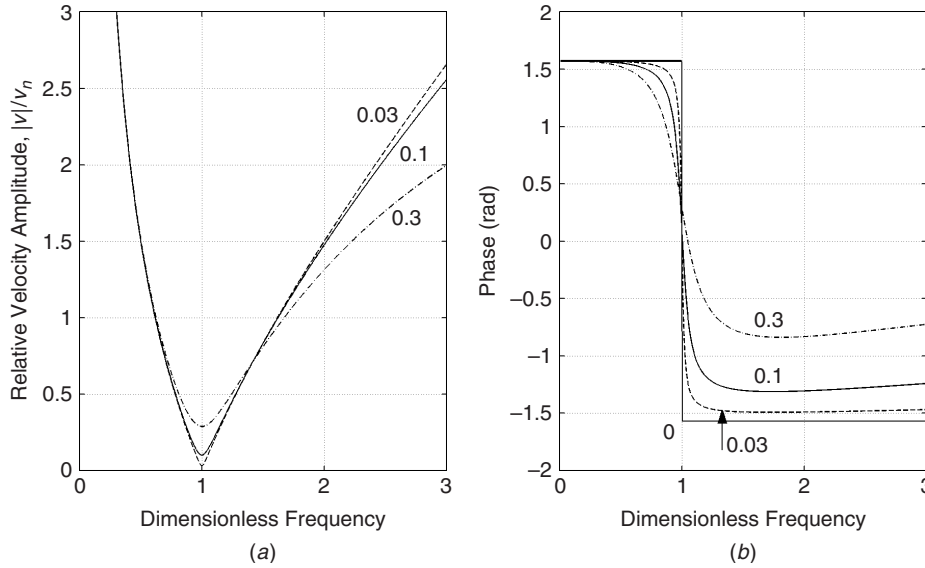
The displacement and acceleration at the driving point also manifest antiresonance. However, their



**Figure 3** SDOF system with an external force applied to the spring–dashpot connection point.

antiresonance frequencies slightly differ from that of the velocity response—higher for the displacement and lower for the acceleration, the difference being proportional to  $\eta_0^2$ . The amplitude of the response at the antiresonance frequency is proportional to the loss factor  $\eta_0$ .

From analysis of Figs. 2 and 4 one can conclude that the phenomena of resonance and antiresonance observed in forced vibration are closely related to free



**Figure 4** Driving point (a) velocity amplitude normalized with  $v_n = f/m\omega_0$  and (b) phase vs. frequency  $\omega/\omega_0$  for different values of loss factor  $\eta_0 = 0; 0.03; 0.1; 0.3$ .

vibration of the SDOF system at its natural frequency. Their occurrence depends on the point the external force is applied to and on what kind of response is considered. These two phenomena are likely the main features of the frequency response functions of all known linear vibratory systems.

#### 1.4 Energy Characteristics

For an SDOF system executing harmonic vibration under the action of external force (1.4), applied to the mass, the time-average kinetic energy  $T$ , potential energy  $U$ , and the power  $\Phi$  dissipated in the dashpot are equal to

$$\begin{aligned} T &= \frac{1}{4} m |\dot{x}|^2 = \frac{|f|^2}{4k} \frac{\varepsilon^2}{(1 - \varepsilon^2)^2 + \eta_0^2 \varepsilon^2} \\ U &= \frac{1}{4} k |x|^2 = \frac{|f|^2}{4k} \frac{1}{(1 - \varepsilon^2)^2 + \eta_0^2 \varepsilon^2} \\ \Phi &= \frac{1}{2} c |\dot{x}|^2 = \frac{|f|^2}{2m\omega_0} \frac{\eta_0 \varepsilon^2}{(1 - \varepsilon^2)^2 + \eta_0^2 \varepsilon^2} \end{aligned} \quad (1.7)$$

where  $\varepsilon = \omega/\omega_0$ . At low frequencies ( $\omega < \omega_0$ ) the potential energy is greater than the kinetic energy. At high frequencies ( $\omega > \omega_0$ ), on the contrary, the kinetic energy dominates. The only frequency where they are equal to each other is the natural undamped frequency  $\omega_0$ .

The *loss factor*  $\eta(\omega)$  of the system is defined at frequency  $\omega$  as the ratio of the vibration energy dissipated in the dashpot during one period  $T = 2\pi/\omega$  to the time average total energy  $E = T + U$  of the system:

$$\eta(\omega) = \frac{\Phi}{\omega E} = \eta_0 \frac{2\varepsilon}{1 + \varepsilon^2} \quad (1.8)$$

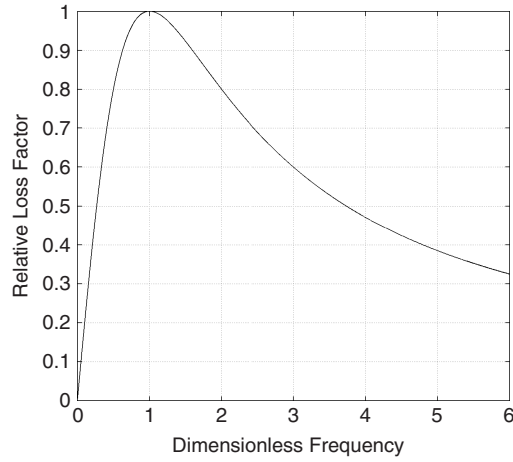
where  $\eta_0$  is the maximum value (1.6) of the loss factor.

The graph of the loss factor as a function of frequency is shown in Fig. 5. It is seen from the figure that the loss factor is small at low and high frequencies. It reaches the maximum value at the undamped natural frequency  $\omega_0$ .

Direct measurement of the dissipated power (1.7) and loss factor (1.8) is practically impossible. However, there are some indirect methods for obtaining  $\eta(\omega)$ , one of which is the following. When an external harmonic force (1.4) acts on the system, one can measure, for example, with the help of an impedance head, the complex amplitude  $f$  of the force and the complex velocity amplitude  $\dot{x}$  at the driving point, and compute the complex power flow into the system:

$$P = \frac{1}{2} \dot{x}^* f = I + iQ. \quad (1.9)$$

where the asterisk denotes the complex conjugate. The real part of  $P$ , called *the active power flow*, is the time-average vibration power injected into the system by the external source. Due to the energy conservation law,



**Figure 5** The loss factor, Eq. (1.8), normalized with the resonance value  $\eta_0 = c/m\omega_0$  vs. dimensionless frequency  $\omega/\omega_0$ .

this power should be equal to the power dissipated in the system so that the equality takes place:

$$I = \Phi \quad (1.10)$$

If, using the measured velocity amplitude  $\dot{x}$ , one can compute the total energy of the system  $E$ , one also can obtain the loss factor (1.8).

The imaginary part  $Q$  of the complex power flow (1.9), called *the reactive power flow*, does not relate to dissipation of energy. It satisfies the equation

$$Q = 2\omega(U - T) \quad (1.11)$$

and may be regarded as a measure of closeness of the system vibration to resonance or antiresonance. Note that Eqs. (1.10) and (1.11) hold for any linear vibratory system.

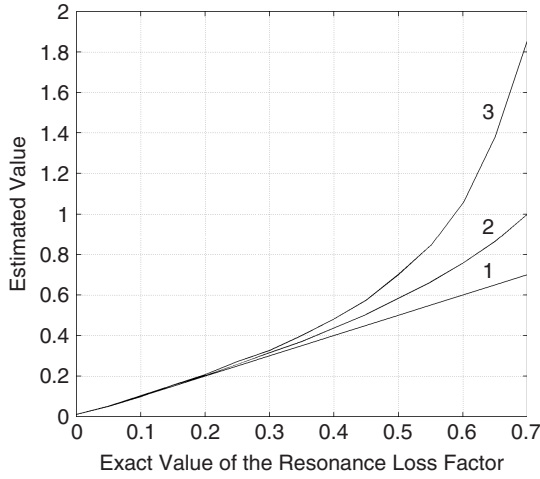
Another indirect method of measuring the loss factor (more exactly its resonance value  $\eta_0$ ) is based on analysis of the velocity FRF. If  $\omega_1$  and  $\omega_2$  are the frequencies where the velocity amplitude is equal to 0.707 of its maximum value at  $\omega_0$ , then the following equation takes place:

$$\eta_0 = \frac{\Delta\omega}{\omega_0} \quad (1.12)$$

where  $\Delta\omega = \omega_2 - \omega_1$ . It should be emphasized, however, that this method is valid only for the velocity FRF. For the displacement and acceleration frequency response functions, Eq. (1.12) gives overestimated values of the resonant loss factor  $\eta_0$ —see Fig. 6. More details about measurement of the damping characteristics can be found in Chapter 15.

#### 1.5 Nonharmonic Forced Vibration

Vibration of real structures is mostly nonperiodic in time. In noise and vibration control, there are two



**Figure 6** Estimates of the resonance value of the loss factor of SDOF system using Eq. (1.12) and (1) the velocity FRF, (2) displacement FRF, and (3) acceleration FRF.

main approaches in the analysis of nonharmonic forced vibration—one in frequency domain and another in time domain. The frequency-domain analysis is based on the representation, with the help of the Fourier transform, of any time signal as the superposition of harmonic signals. The general procedure of the analysis is the following. First, the external excitation on the system is decomposed into the sum of time-harmonic components. Then, the response of the system to a harmonic excitation component is obtained. And at last, all the harmonic responses are collected into the final nonharmonic response, which may then be used for solving the needed control problems.

Apply now this procedure to the SDOF system under study acted upon by a nonharmonic external force  $f(t)$  and described by Eq. (1.1). Assume that the force is deterministic and square integrable and, therefore, may be represented as the Fourier integral with the spectral density  $F(\omega)$ :

$$f(t) = \int_{-\infty}^{\infty} F(\omega) e^{i\omega t} d\omega$$

$$F(\omega) = \frac{1}{2\pi} \int_{-\infty}^{\infty} f(t) e^{-i\omega t} dt \quad (1.13)$$

(For details of the Fourier transform and how to compute the spectral density, e.g., by the FFT, see Chapter 42. The case of random excitation is considered in Chapter 13.) Representing in a similar manner displacement  $x(t)$  as a Fourier integral and using the response (1.5) of the system to harmonic excitation, one can obtain the following general

equation for the displacement response to arbitrary external force:

$$x(t) = \frac{1}{m} \int_{-\infty}^{\infty} \frac{F(\omega) e^{i\omega t} d\omega}{\omega_0^2 - \omega^2 + 2i\zeta\omega\omega_0} \quad (1.14)$$

where  $\omega_0$  and  $\zeta$  are given in Eq. (1.3).

As an example consider the response of the SDOF system to a very short impulse that acts at moment  $t = t_0$  and that mathematically can be written as the Dirac delta function,  $f(t) = \delta(t - t_0)$ . Solution (1.14) gives in this case the following response, which is known as the *impulse response function*, or *IRF*, and is usually denoted by  $h(t - t_0)$ :

$$h(t - t_0) = \begin{cases} 0 & \text{for } t < t_0 \\ \frac{1}{m\omega_d} e^{-\zeta\omega_0(t-t_0)} \sin \omega_d(t - t_0) & \text{for } t \geq t_0 \end{cases} \quad (1.15)$$

One can easily verify that IRF (1.15) corresponds to the free vibration (1.2) of the SDOF system with initial condition  $x_0 = 0, \dot{x}_0 = 1/m$ .

The other approach in the analysis of nonharmonic forced vibration is based on consideration in time domain and employs the impulse response function (1.15):

$$x(t) = \int_{-\infty}^{\infty} f(t_0) h(t - t_0) dt_0 \quad (1.16)$$

Physical meaning of this general equation is the following. An external force may be represented as the superposition of infinite number of  $\delta$  impulses:

$$f(t_0) = \int_{-\infty}^{\infty} f(\tau) \delta(\tau - t_0) d\tau$$

Since the response to the impulse  $f(\tau) \delta(\tau - t_0)$  is equal to  $f(t_0) h(t - t_0)$ , the superposition of the responses to all the impulses is just the response (1.16). Equation (1.16) is also called the integral of Duhamel.

As an example consider again forced harmonic vibration of the SDOF system, but this time assume that the harmonic force, say of frequency  $\omega_0$ , begins to act at  $t = 0$ :

$$f(t) = \begin{cases} 0 & \text{for } t < 0 \\ f_0 \cos \omega_0 t & \text{for } t \geq 0 \end{cases}$$

Assume also that before  $t = 0$  the system was at rest. Then, with the help of the integral of Duhamel (1.16), one obtains the displacement response as

$$x(t) = \frac{f_0}{c\omega_0} \left( \sin \omega_0 t - \frac{\omega_0}{\omega_d} e^{-\zeta\omega_0 t} \sin \omega_d t \right)$$

This response consists of two components. The first component,  $(f_0/c\omega_0) \sin \omega_0 t$ , presents the steady-state forced vibration (1.5) at frequency  $\omega_0$ . The second component is free vibration at natural frequency  $\omega_d$  caused by the sudden application of the external force. At the initial moment  $t = 0$ , both components have comparable amplitudes. As time increases the free vibration component decreases exponentially, while the amplitude of the steady-state component remains unchanged. For example, if the resonance loss factor of the system is  $\eta_0 = 0.05$  (as in Fig. 1), the free vibration amplitude becomes less than 5% of the steady-state amplitude after 19 periods passed ( $t \geq 19T$ , where  $T = 2\pi/\omega_d$ ) and less than 1% for  $t \geq 30T$ .

## 2 MULTI-DEGREE-OF-FREEDOM SYSTEMS

Multi-degree-of-freedom systems (designated here as NDOF systems) are linear vibratory systems that require more than one variable to completely describe their vibrational behavior. For example, vibration of a machine on resilient supports is a combination of its motions in various directions. If the machine may be considered as a rigid body (this is the case of low frequencies), one needs six variables (three translational and three rotational deflections from the equilibrium position) to describe the current position of the machine. This machine-isolator system is said to have six degrees of freedom (DOFs). The minimum number of variables needed for the description of a vibratory system defines its number of DOFs.

In this section, discrete vibratory systems with finite numbers of DOFs are considered. Many modern methods of vibration analysis of engineering structures, such as the finite element method, modal analysis, and others, are based on vibration analysis of NDOF systems. The number of DOFs of such a system depends on the structure as well as on the frequency range. The machine mentioned above might undergo deformations at higher frequencies, and this will require additional variables for adequate description. However, it is not reasonable to increase the number  $N$  of DOFs beyond a certain limit, since computational efforts increase, in general case, as  $N^3$ . Other methods of analysis, for example, the use of continuous models having infinite number of DOFs, may often be more appropriate.

Many properties of vibratory NDOF systems are identical to those of SDOF systems: NDOF system has  $N$  natural frequencies, free vibrations are exponentially decaying harmonic motions, forced vibration may demonstrate resonance and antiresonance, and the like. There are also specific properties that are absent in SDOF system vibration being the consequence of the multi-DOF nature. These are the existence of normal modes of vibration, their orthogonality, decomposition of arbitrary vibration into normal modes, and related properties that constitute the basis of modal analysis.

### 2.1 Equations of Motion

Consider a general mass-spring-dashpot system with  $N$  degrees of freedom vibration that is completely

described by  $N$  displacements, which, for simplicity, are written as one displacement vector:

$$\mathbf{x}(t) = [x_1(t), x_2(t), \dots, x_N(t)]^T \quad (2.1)$$

where the upper index  $T$  means transposition. Vibration of the system is governed by the well-known set of  $N$  linear ordinary differential equations:

$$\mathbf{M}\ddot{\mathbf{x}}(t) + \mathbf{C}\dot{\mathbf{x}}(t) + \mathbf{K}\mathbf{x}(t) = \mathbf{f}(t) \quad (2.2)$$

where

$$\mathbf{f}(t) = [f_1(t), f_2(t), \dots, f_N(t)]^T \quad (2.3)$$

is the vector of external forces acting on the masses,  $\mathbf{M} = [m_{jn}]$  is a symmetric ( $m_{jn} = m_{nj}$ ) positive definite inertia matrix of order  $N$ ,  $\mathbf{C} = [c_{jn}]$  is a symmetric nonnegative damping  $N \times N$  matrix, the square stiffness matrix  $\mathbf{K} = [k_{jn}]$  is also assumed symmetric and nonnegative. The assumption of symmetry means that, in the system, there are no gyroscopic elements that are described by antisymmetric matrices ( $c_{jn} = -c_{nj}$ ). The symmetry of the matrices also means that the Maxwell-Betti reciprocity theorem is valid for the system. (The theorem states<sup>2</sup>: the dynamic response, i.e., the displacement amplitude and phase, of  $j$ th mass to a harmonic external force applied to  $n$ th mass is equal to the dynamic response of  $n$ th mass to the same force applied to  $j$ th mass.) A more general case of NDOF systems with nonsymmetric matrices is discussed in Section 2.4.

**Example** 2DOF system (Fig. 7) consists of two masses  $m_1$  and  $m_2$  moving in vertical direction, two springs of stiffness  $k_1$  and  $k_2$ , and two dashpots with damping coefficients  $c_1$  and  $c_2$ . The two variables for description of system vibration are displacements  $x_1(t)$  and  $x_2(t)$  of the two masses. External force  $f_1(t)$  acts on the first mass while the second mass is free of loading. The system vibration is governed by the set of ordinary differential equations (2.2) with system matrices

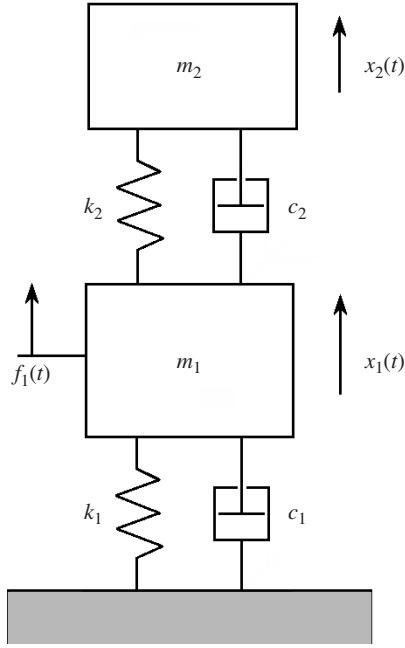
$$\mathbf{M} = \begin{bmatrix} m_1 & 0 \\ 0 & m_2 \end{bmatrix} \quad \mathbf{C} = \begin{bmatrix} c_1 + c_2 & -c_2 \\ -c_2 & c_2 \end{bmatrix} \quad \mathbf{K} = \begin{bmatrix} k_1 + k_2 & -k_2 \\ -k_2 & k_2 \end{bmatrix} \quad (2.4)$$

and vector (2.3) that has two components,  $f_1(t) \neq 0$  and  $f_2(t) = 0$ .

### 2.2 Free Vibration

Free vibration of NDOF systems corresponds to solutions of a homogeneous set of linear equations (2.2) with  $\mathbf{f}(t) = 0$ . As the coefficients of the equations are assumed independent of time, the solutions are sought in the form

$$\mathbf{x}(t) = \text{Re}(\mathbf{x}e^{j\omega t}) \quad (2.5)$$



**Figure 7** Example of a two-degree-of-freedom system. Arrows indicate the positive direction of the force and displacements.

where  $\mathbf{x} = [x_1, x_2, \dots, x_N]^T$  is the vector of the complex amplitudes of the mass displacements.

**Undamped System** Consider first the undamped system for which matrix  $\mathbf{C}$  is the null matrix. Substitution of (2.5) into Eq. (2.2) leads to the following set of algebraic equations with respect to the complex amplitudes:

$$(\mathbf{K} + \gamma^2 \mathbf{M})\mathbf{x} = 0 \quad (2.6)$$

In linear algebra, this problem is known as the generalized eigenvalue problem.<sup>3</sup> A solution to Eq. (2.6) exists only for certain values of parameter  $\gamma$  that are the roots of the characteristic equation  $\det(\mathbf{K} + \gamma^2 \mathbf{M}) = 0$ . For matrices  $\mathbf{M}$  and  $\mathbf{K}$  with the special properties indicated above, all the roots of the characteristic equation are pure imaginary:

$$\gamma_n^{(1,2)} = \pm i\omega_{0n} \quad n = 1, 2, \dots, N \quad (2.7)$$

where the real-valued nonnegative *undamped natural frequencies*

$$\{\omega_{01}, \omega_{02}, \dots, \omega_{0N}\} \quad (2.8)$$

constitute the *spectrum* of the system. Corresponding to each natural frequency  $\omega_{0n}$ , the eigenvector  $\mathbf{x}_n$  of the problem (2.6) exists. Its components are real valued and equal to the amplitudes of the mass displacements when the system is vibrating at frequency  $\omega_{0n}$ . The pair

$\{\omega_{0n}, \mathbf{x}_n\}$  defines the *n*th *natural* or *normal mode* of vibration, the vector  $\mathbf{x}_n$  being termed the *mode shape*.

**Orthogonality Relations** The theory<sup>3</sup> says that the mode shapes are  $\mathbf{M}$ -orthogonal and  $\mathbf{K}$ -orthogonal, that is, orthogonal with weights  $\mathbf{M}$  and  $\mathbf{K}$ , so that

$$\mathbf{x}_j^T \mathbf{M} \mathbf{x}_n = \delta_{jn} \quad \mathbf{x}_j^T \mathbf{K} \mathbf{x}_n = \omega_{0n}^2 \delta_{jn} \quad (2.9)$$

where  $\delta_{jn}$  is the symbol of Kroneker that equals to unity if  $j = n$  and to zero if  $j \neq n$ .

Mathematically, orthogonality relations (2.9) mean that two symmetric matrices,  $\mathbf{M}$  and  $\mathbf{K}$ , may be simultaneously diagonalized by the *congruence transformation* with the help of the *modal matrix*  $\mathbf{X} = [\mathbf{x}_1, \dots, \mathbf{x}_N]$ , composed of the mode shape vectors  $\mathbf{x}_n$ :

$$\mathbf{X}^T \mathbf{M} \mathbf{X} = \mathbf{I} \quad \mathbf{X}^T \mathbf{K} \mathbf{X} = \mathbf{\Omega}_0^2 = \text{diag}(\omega_{01}^2, \dots, \omega_{0N}^2) \quad (2.10)$$

(Note that the modal matrix also diagonalizes matrix  $\mathbf{M}^{-1}\mathbf{K}$  by the *similarity transformation*:  $\mathbf{X}^{-1}(\mathbf{M}^{-1}\mathbf{K})\mathbf{X} = \mathbf{\Omega}_0^2$ ). As a consequence, the transition from displacement variables (2.5) to the *modal coordinates*  $\mathbf{q} = [q_1, \dots, q_N]^T$

$$\mathbf{x} = \mathbf{X} \mathbf{q} \quad (2.11)$$

transforms the set of equations (2.6) into the following set:

$$(\mathbf{\Omega}_0^2 + \gamma^2 \mathbf{I})\mathbf{q} = 0 \quad (2.12)$$

the matrix of which is diagonal, and  $\mathbf{I}$  is the identity matrix. Set (2.12) principally differs from set (2.6): in Eqs. (2.12), the modal coordinates are uncoupled, while in Eqs. (2.6), the displacement coordinates are coupled. Therefore, each equation of set (2.12) may be solved with respect to the corresponding modal coordinate independently from other equations.

Physically, the orthogonality relations (2.9), (2.10) together with Eqs. (2.12) mean that the normal modes are independent from each other. If a normal mode of certain natural frequency and mode shape exists at a given moment, it will exist unchanged all the later time without interaction with other modes. In other words, an NDOF system is equivalent to  $N$  uncoupled SDOF systems.

**Free Vibration** If  $\mathbf{x}_0 = \mathbf{x}(0)$  and  $\dot{\mathbf{x}}_0 = \dot{\mathbf{x}}(0)$  are initial values of the displacements and velocities, the time history of free vibration is described by the sum of the normal modes

$$\mathbf{x}(t) = \sum_{n=1}^N \left( a_n \cos \omega_{0n} t + \frac{b_n}{\omega_{0n}} \sin \omega_{0n} t \right) \mathbf{x}_n \quad (2.13)$$

where the decomposition coefficients are obtained using the orthogonality relation (2.9) as

$$a_n = \mathbf{x}_n^T \mathbf{M} \mathbf{x}_0 \quad b_n = \mathbf{x}_n^T \mathbf{M} \dot{\mathbf{x}}_0$$

It is seen from these equations that in order to excite a particular normal mode, say  $j$ th mode, apart from other modes, the initial disturbances  $\mathbf{x}_0$  and/or  $\dot{\mathbf{x}}_0$  should be equal exactly to  $j$ th mode shape.

### NDOF System with Proportional Damping

When the NDOF system is damped, its free vibration amplitudes satisfy the following set of linear algebraic equations:

$$(\mathbf{M}\gamma^2 + \mathbf{C}\gamma + \mathbf{K})\mathbf{x} = \mathbf{0} \quad (2.14)$$

The simplest for analysis is the case of the so-called *proportional damping*, or Rayleigh damping, when the damping matrix is a linear combination of the mass and stiffness matrices:

$$\mathbf{C} = 2\alpha\mathbf{M} + 2\beta\mathbf{K} \quad (2.15)$$

Equation (2.14), in this case, can be transformed into

$$(\mathbf{K} + \mu^2\mathbf{M})\mathbf{x} = \mathbf{0} \quad \mu^2 = \gamma^2 \frac{1 + 2\alpha/\gamma}{1 + 2\beta\gamma}$$

This equation coincides with Eq. (2.6) for undamped system. Hence, the parameter  $\mu^2$  may be equal to one of  $N$  real-valued quantities  $\mu_n^2 = -\omega_{0n}^2$ —see Eq. (2.7), while the parameter  $\gamma$  is complex valued:

$$\begin{aligned} \gamma_n^{(1,2)} &= -\zeta_n\omega_{0n} \pm i\omega_n \quad n = 1, 2, \dots, N \\ \zeta_n &= \alpha/\omega_{0n} + \beta\omega_{0n} \quad \omega_n = \omega_{0n}\sqrt{1 - \zeta_n^2} \end{aligned} \quad (2.16)$$

The mode shapes  $\mathbf{x}_n$  coincide with the undamped mode shapes, that is, they are real valued and  $\mathbf{M}$ -orthogonal and  $\mathbf{K}$ -orthogonal.

Free vibration of the damped NDOF system is the superposition of  $N$  undamped normal modes, amplitudes of which exponentially decrease with time. The time history of free vibration is described by

$$\begin{aligned} \mathbf{x}(t) = \sum_{n=1}^N e^{-\zeta_n\omega_{0n}t} &\left( a_n \cos \omega_n t \right. \\ &\left. + \frac{b_n + \zeta_n\omega_{0n}a_n}{\omega_n} \sin \omega_n t \right) \mathbf{x}_n \end{aligned} \quad (2.17)$$

where coefficients  $a_n$  and  $b_n$  are obtained from the initial conditions as in Eq. (2.13), modal damping ratios  $\zeta_n$  and natural frequencies being given in Eq. (2.16). Note that if a system is undamped or it has a Rayleigh damping, all its inertia elements move, during free vibration, in phase or in counterphase as seen from Eqs. (2.13) and (2.17).

### NDOF System with Nonproportional Damping

When damping in the NDOF system is nonproportional, the characteristic equation of set (2.14),  $\Delta(\gamma) = \det(\gamma^2\mathbf{M} + \gamma\mathbf{C} + \mathbf{K} = 0)$ , has  $N$  complex-conjugate

pairs of roots (2.16), just as in the case of proportional damping, though with more complicated expressions for the damping ratios  $\zeta_n$  and natural frequencies  $\omega_n$ . The main difference from the case of proportional damping is that the eigenvectors of the problem (2.14) are complex valued and constitute  $N$  complex-conjugate pairs. Physically, it means that each mass of the system has its own phase of free vibration, which may differ from 0 and  $\pi$ . Another difference is that these complex eigenvectors do not satisfy the orthogonality relations (2.9). This makes the solution (2.17) incorrect and requires more general approaches to treating the problem. Two such approaches are outlined in what follows.

The first and often used approach is based on conversion of  $N$  equations of the second order (2.2) into a set of  $2N$  equations of the first order. This can be done, for example, by introducing the state-space  $2N$  vector  $\mathbf{s}(t) = [\mathbf{x}^T(t), \dot{\mathbf{x}}^T(t)]^T$ . Set (2.2) is then cast into

$$\begin{aligned} \mathbf{A}\dot{\mathbf{s}}(t) + \mathbf{B}\mathbf{s}(t) &= \mathbf{g}(t) \\ \mathbf{A} &= \begin{bmatrix} \mathbf{I} & \mathbf{0} \\ \mathbf{0} & \mathbf{M} \end{bmatrix} \quad \mathbf{B} = \begin{bmatrix} \mathbf{0} & -\mathbf{I} \\ \mathbf{K} & \mathbf{C} \end{bmatrix}, \\ \mathbf{g}(t) &= \begin{bmatrix} \mathbf{0} \\ \mathbf{f}(t) \end{bmatrix} \end{aligned} \quad (2.18)$$

Seeking a solution of homogeneous equations (2.18) in the form  $\mathbf{s}(t) = \mathbf{s} \exp(\gamma t)$ , one can obtain  $2N$  complex eigenvalues and  $2N$  eigenvectors  $\mathbf{s}_n$ . Simultaneously, it is necessary to consider the adjoint to (2.18) set of  $2N$  equations:

$$-\mathbf{A}^*\dot{\mathbf{r}}(t) + \mathbf{B}^*\mathbf{r}(t) = \mathbf{0} \quad (2.19)$$

and to find its eigenvectors  $\mathbf{r}_n$ . The asterisk denotes the Hermitian conjugate, that is, complex conjugate and transposition. The eigenvectors of the two adjoint problems,  $\mathbf{s}_n$  and  $\mathbf{r}_n$ , are biorthogonal with weight  $\mathbf{A}$  and weight  $\mathbf{B}$

$$r_j^* \mathbf{A} \mathbf{s}_m = \delta_{jm} \quad \mathbf{r}_j^* \mathbf{B} \mathbf{s}_m = \gamma_m \delta_{jm} \quad (2.20)$$

Decomposing the initial  $2N$  vector  $\mathbf{s}_0 = \mathbf{s}(0)$  into eigenvectors  $\mathbf{s}_n$  and using the orthogonality relations (2.20), one can obtain the needed equation for the free vibration. This equation is mathematically exact, although not transparent physically. More details of this approach can be found elsewhere.<sup>4</sup>

Another approach is physically more familiar but is approximate mathematically. The solution of Eq. (2.2) is sought as the superposition of the undamped natural modes, that is, in the form (2.17). The approximation is to neglect those damping terms that are nonproportional and retain the proportional ones. The accuracy of the approximation depends on how the actual damping is close to the Rayleigh damping. In the illustrative example of the next subsection, both



approaches will be used for treating forced vibration of a 2DOF system.

### 2.3 Forced Vibration

Forced vibration of NDOF systems corresponds to solutions of inhomogeneous equation (2.2) with a nonzero excitation force,  $\mathbf{f}(t) \neq 0$ .

Consider first the harmonic excitation  $\mathbf{f}(t) = \text{Re}[\mathbf{f} \exp(-i\omega t)]$ . The steady-state response of the system is also a vector time function of the same frequency,  $\mathbf{x}(t) = \text{Re}[\mathbf{x} \exp(-i\omega t)]$ . The vector of the complex displacement amplitudes  $\mathbf{x}$  is determined from Eq. (2.2):

$$\mathbf{x} = [\mathbf{K}(\omega)]^{-1} \mathbf{f} = \mathbf{G}(\omega) \mathbf{f} \quad (2.21)$$

$$\mathbf{K}(\omega) = \mathbf{K} - \omega^2 \mathbf{M} - i\omega \mathbf{C}$$

where the  $N \times N$  matrix  $\mathbf{G}(\omega)$  of the dynamic flexibilities is the inverse of the dynamic stiffness matrix  $\mathbf{K}(\omega)$ . For a given external force vector  $\mathbf{f}$ , solution (2.21) gives the amplitudes and phases of all the mass displacements. As each element of the flexibility matrix is the ratio of two polynomials of frequency  $\omega$ , the denominator being equal to the characteristic expression  $\det \mathbf{K}(\omega)$ , the frequency response functions (2.21) demonstrate maxima near the system natural frequencies (resonance) and minima between them (antiresonance)—see, for example, Fig. 8.

When the number of DOFs of the mechanical system is not small, *modal analysis* is more appropriate in practice for analyzing the system vibration. It is

based on the representation of solution (2.21) in a series of the undamped normal modes and decoupling the NDOF system into  $N$  separate SDOF systems. The basic concepts of the modal analysis are the following (its detailed presentation is given in Chapter 47).

Let  $\{\omega_{0n}, \mathbf{x}_n\}$  be the undamped normal modes,  $n = 1, 2, \dots, N$ —see the previous subsection. Transforming the physical variables  $\mathbf{x}(t)$  into modal coordinates  $\mathbf{q}(t) = [q_1(t), \dots, q_N(t)]^T$  as in Eq. (2.11) and using the orthogonality relations (2.10), one can obtain from Eq. (2.2) the following  $N$  ordinary differential equations:

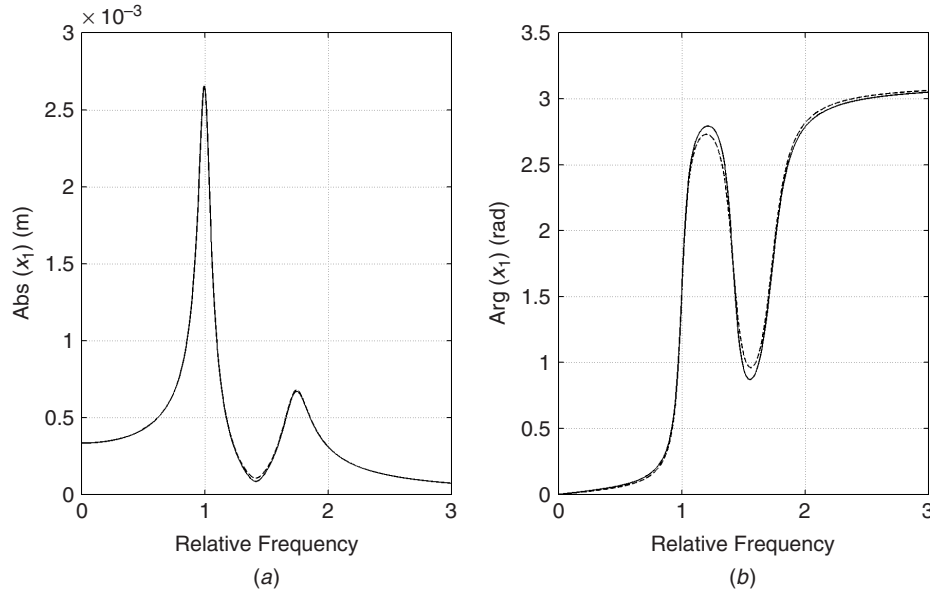
$$\ddot{\mathbf{q}}(t) + \mathbf{D}\dot{\mathbf{q}}(t) + \mathbf{\Omega}_0^2 \mathbf{q}(t) = \mathbf{X}^T \mathbf{f}(t) \quad (2.22)$$

where  $\mathbf{D} = \mathbf{X}^T \mathbf{C} \mathbf{X}$ .

If damping is proportional, the matrices  $\mathbf{D}$  and  $\mathbf{\Omega}_0^2$  are both diagonal, all the equations (2.22) are independent, and the modal variables are decoupled. The vibration problem for the NDOF system is thus reduced to the problem for  $N$  separate SDOF systems. One can obtain in this case the following equation for the flexibility matrix (2.21) decomposed into the modal components:

$$\mathbf{G}(\omega) = \mathbf{X}(\mathbf{\Omega}_0^2 - \omega^2 \mathbf{I} - 2i\omega \mathbf{D})^{-1} \mathbf{X}^T$$

$$= \sum_{n=1}^N \frac{\mathbf{x}_n \mathbf{x}_n^T}{\omega_{0n}^2 - \omega^2 - 2i\omega \omega_{0n} \zeta_n} \quad (2.23)$$



**Figure 8** (a) Amplitude–frequency curves and (b) phase–frequency curves for the displacement of the first mass of 2DOF system (Fig. 7): exact solution (2.21)—solid lines; approximate solution with the proportional damping—dashed lines; dimensionless frequency is  $\omega/\omega_1$ .

It is instructive to compare solution (2.21), (2.23) with similar solution (1.5) for an SDOF system. It is seen from Eq. (1.5) that to put an SDOF system into resonance, *one condition* should be met—the excitation frequency should be close to the system natural frequency. For NDOF systems it is not sufficient. To put an NDOF system into resonance, *two conditions* should be met as it follows from Eq. (2.23): beside the closeness of the frequencies, the shape of the external force should be close to the corresponding mode shape. If the force shape is orthogonal to the mode shape,  $\mathbf{x}_n^T \mathbf{f} = 0$ , the response is zero even at the resonance frequency.

The response of the NDOF system to a non-harmonic excitation can be obtained from the harmonic response (2.21), (2.23) with the help of the Fourier transformation as is done for SDOF system in Section 1.4. In particular, if the external force is an impulsive function  $\mathbf{f}(t) = \mathbf{f} \delta(t - t_0)$ , the system response is described by the impulse response matrix function, which is the Fourier transform of the flexibility matrix

$$\mathbf{H}(t - t_0) = \begin{cases} \mathbf{0} & \text{if } t < t_0 \\ \sum_{n=1}^N e^{-\zeta_n \omega_{0n}(t-t_0)} \frac{\sin \omega_n(t-t_0)}{\omega_n} \mathbf{x}_n \mathbf{x}_n^T & \text{if } t \geq t_0 \end{cases} \quad (2.24)$$

The time response to an arbitrary excitation  $\mathbf{f}(t)$  can then be computed as

$$\mathbf{x}(t) = \int_{-\infty}^{\infty} \mathbf{H}(t - t_0) \mathbf{f}(t_0) dt_0 \quad (2.25)$$

Equations (2.24) and (2.25) completely solve the problem of forced nonharmonic vibrations of undamped and proportionally damped NDOF systems.

If damping is not proportional, the coordinate transformation (2.11) diagonalizes only the inertia and stiffness matrices [see Eqs. (2.10)] but not the damping matrix. In this case, Eq. (2.22) is coupled through the nondiagonal elements of matrix  $\mathbf{D}$ , and the NDOF system cannot be represented as  $N$  independent SDOF systems. One commonly used approach to treating the problem is to obtain the approximate solution by neglecting the off-diagonal elements of matrix  $\mathbf{D}$  and retaining only its diagonal elements, which correspond to the proportional damping components and using Eqs. (2.23) to (2.25).

Another approach is to use the *complex modal analysis* based on introducing the state-space coordinates—see Eqs. (2.18) to (2.20). This approach leads to exact theoretical solutions of the problem, but it is more laborious than the approximate classical modal analysis (because of doubling the space dimension) and difficult for practical implementation.<sup>4</sup>

**Example** Consider forced harmonic vibration of the 2DOF system in Fig. 7 under the action of force  $f_1 =$

$1 \cdot \exp(-i\omega t)$  applied to the first mass. Let the parameters (2.4) be  $m_1 = 0.5$  kg,  $m_2 = 0.125$  kg,  $k_1 = 3 \times 10^3$  Nm<sup>-1</sup>,  $k_2 = 10^3$  Nm<sup>-1</sup>,  $c_1 = 5$  Ns m<sup>-1</sup>, and  $c_2 = 1$  Ns m<sup>-1</sup>. The eigenvalues of the undamped problem,  $\omega_{01}^2 = 4 \times 10^3$  s<sup>-2</sup> and  $\omega_{02}^2 = 1.2 \times 10^4$  s<sup>-2</sup>, correspond to the undamped natural frequencies, 10 and 17 Hz. The normal mode shapes are  $\mathbf{x}_1 = [1, 2]^T$ ,  $\mathbf{x}_2 = [-1, 2]^T$ . Since the damping of the system is not proportional, matrix  $\mathbf{D}$  in Eq. (2.22) is not diagonal:

$$\mathbf{D} = \mathbf{X}^T \mathbf{C} \mathbf{X} = \begin{bmatrix} 6 & -2 \\ -2 & 14 \end{bmatrix}$$

Figure 8 presents the amplitude and phase of the first mass displacement as functions of frequency. Solid lines correspond to the exact solution (2.21), while the dashed lines correspond to the approximate solution obtained by neglecting off-diagonal terms of matrix  $\mathbf{D}$ . Though the difference between the exact (non-proportional) and approximate (proportional) damping is about 20%,  $\|\Delta \mathbf{C}\|/\|\mathbf{C}\| = 0.2$ , where  $\|\mathbf{C}\|$  is the Euclidean matrix norm,<sup>3</sup> the difference between the solutions is noticeable only at the natural frequencies being less than 0.4% at the resonance frequencies and 20% at the antiresonance frequency.

## 2.4 General Case

In practice, a linear vibratory system may contain gyroscopic (rotating) elements, parts of nonmechanical nature, control devices, and the like. As a result, its mass, damping, and stiffness matrices in Eq. (2.2) may be nonsymmetric and not necessarily positive definite. For such systems, the classical modal analysis, based on simultaneous diagonalization of mass and stiffness symmetric matrices by the congruence transformation (2.10), is not valid. One general approach to treating the problem in this case is to use the complex modal analysis in  $2N$ -dimensional state space<sup>4</sup>—see Eqs. (2.18) to (2.20). However, for large  $N$ , it may be more appropriate to use a simpler and physically more transparent method of analysis in  $N$ -dimensional “Lagrangian” space. This method is based on simultaneous diagonalization of two square matrices by the so-called *equivalent transformation*.<sup>3</sup> It represents a direct extension of the classical modal analysis and may be applied to practically every real situation. In what follows, the basic concepts of this method, which may be termed as *generalized modal analysis*, are briefly expounded. A detailed description can be found in the literature.<sup>5</sup>

Let  $\mathbf{M}$  be a square inertia matrix of order  $N$  that, without loss of generality, is assumed nonsingular and  $\mathbf{K}$  be a stiffness  $N \times N$  matrix. They are generally nonsymmetric, and their elements are real valued. For equation of motion (2.2), define two adjoint algebraic generalized eigenvalue problems [compare with Eq. (2.6)]:

$$\mathbf{K} \mathbf{x} = \lambda \mathbf{M} \mathbf{x} \quad \mathbf{K}^T \mathbf{y} = \lambda \mathbf{M}^T \mathbf{y} \quad (2.26)$$

These problems have identical eigenvalues  $\lambda_n$  but different eigenvectors  $\mathbf{x}_n$  and  $\mathbf{y}_n$ ,  $n = 1, 2, \dots, N$ . (Note that in the literature they are sometimes called the right and left eigenvectors.) By assuming that  $N$  eigenvectors  $\mathbf{x}_n$  are linearly independent or that the eigenvalues  $\lambda_n$  are distinct, one can derive from Eq. (2.26) the following biorthogonality relations:

$$\mathbf{Y}^T \mathbf{M} \mathbf{X} = \mathbf{I} \quad \mathbf{Y}^T \mathbf{K} \mathbf{X} = \mathbf{\Lambda} \quad (2.27)$$

where

$$\mathbf{\Lambda} = \text{diag}(\lambda_1, \dots, \lambda_N)$$

$$\mathbf{X} = [\mathbf{x}_1, \dots, \mathbf{x}_N] \quad \mathbf{Y} = [\mathbf{y}_1, \dots, \mathbf{y}_N]$$

Equations (2.27) mean that the mass and stiffness matrices,  $\mathbf{M}$  and  $\mathbf{K}$ , may be simultaneously diagonalized by the equivalence transformation with the help of two nonsingular matrices  $\mathbf{X}$  and  $\mathbf{Y}$ . Hence, the variable transformation

$$\mathbf{x}(t) = \mathbf{X} \mathbf{q}(t) \quad (2.28)$$

completely decouples Eq. (2.2) with  $\mathbf{C} = 0$ :

$$\ddot{\mathbf{q}}(t) + \mathbf{\Lambda} \mathbf{q}(t) = \mathbf{Y}^T \mathbf{f}(t) \quad (2.29)$$

The eigenvectors  $\mathbf{x}_n$  and  $\mathbf{y}_n$  may be termed *natural modes* and *adjoint modes*. When eigenvalue  $\lambda_n$  is real positive, the free system motion is harmonic, square root  $\sqrt{\lambda_n}$  is the natural frequency, and the corresponding mode shape  $\mathbf{x}_n$  has real-valued components (i.e., all masses move in phase or counterphase).

If square matrices  $\mathbf{M}$  and  $\mathbf{K}$  are symmetric, the eigenvalue problems (2.26) are identical and the problem (2.2) is self-adjoint. In this case, the adjoint eigenvectors  $\mathbf{y}_n$  coincide with  $\mathbf{x}_n$  and the equivalence transformation (2.27) becomes the congruence transformation (2.10). The classical modal analysis is thus a particular case of the generalized modal analysis based on eqs. (2.26) to (2.29).

It should be noted that the equivalence transformation cannot diagonalize simultaneously three matrices unless the damping matrix  $\mathbf{C}$  is a linear combination of  $\mathbf{M}$  and  $\mathbf{K}$ . Therefore, in general case the transformation (2.28) reduces equation (2.2) into  $N$  equations:

$$\ddot{\mathbf{q}}(t) + \mathbf{D} \dot{\mathbf{q}}(t) + \mathbf{\Lambda} \mathbf{q}(t) = \mathbf{Y}^T \mathbf{f}(t) \quad (2.30)$$

that are coupled through off-diagonal elements of matrix  $\mathbf{D} = \mathbf{Y}^T \mathbf{C} \mathbf{X}$ . An approximate solution to Eq. (2.30) may be obtained by neglecting off-diagonal terms of  $\mathbf{D}$ .

### 3. CONTINUOUS ONE-DIMENSIONAL SYSTEMS

Continuous vibratory systems are used as models of comparatively large vibrating engineering structures and structure elements of uniform or regular geometry.

Beams, plates, and shells are examples of continuous systems. In the systems, the inertia, elastic, and damping parameters are continuously distributed, and the number of degrees of freedom is infinite even if the system size is limited.

Wave motion is the main phenomenon in continuous vibratory systems. Any free or forced vibration of such a system can always be expanded in terms of elementary wave motions. Therefore, in this and following sections, considerable attention is devoted to the properties of waves.

Mathematical description of vibration in continuous systems is based rather on "theory-of-elasticity" and "strength-of-materials" consideration than on mechanical consideration of case of discrete systems. However, the governing equations of motion for most of the existing continuous systems do not originate from the exact equations of elasticity. They are obtained, as a rule, by making certain simplifying assumptions on the kinematics of deformation and using Hamilton's variational principle of least action.

In this section, one-dimensional (1D) continuous vibratory systems are considered in which two of three dimensions are assumed as small compared to the wavelength. A vibration field in a 1D system depends on time and one space coordinate. Examples of 1D systems are thin straight or curved beams (rods, bars, columns, thin-walled members), taut strings (ropes, wires), fluid-filled pipes, and the like. Most attention is paid to waves and vibration in an elastic beam—a widely used element of engineering structures.

#### 3.1 Longitudinal Vibration in Beams

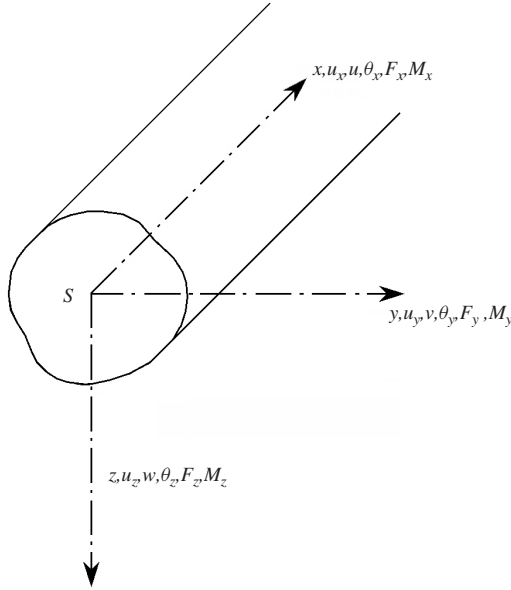
Consider a straight uniform thin elastic beam of cross-sectional area  $S$ . Let axis  $x$  be directed along the beam and pass through the cross-section centroid (Fig. 9). The main assumptions of the simplest (engineering) theory of longitudinal vibration are the following: plane cross sections remain plane during deformation; the axial displacement  $u_x$  and stress  $\sigma_{xx}$  are uniform over cross section, and the lateral stresses are zero. Mathematically, these can be written as

$$\begin{aligned} u_x(x, y, z, t) &= u(x, t) & u_y(x, y, z, t) &= -\nu y u'(x, t) \\ u_z(x, y, z, t) &= -\nu z u'(x, t) \\ \sigma_{xx}(x, y, z, t) &= E u'(x, t) & \sigma_{yy} &= 0 & \sigma_{zz} &= 0 \end{aligned} \quad (3.1)$$

where prime denotes the derivative with respect to  $x$ ,  $E$  and  $\nu$  are Young's modulus and Poisson's ratio. Equation for the axial stress follows from Hooke's law.<sup>2</sup> Nonzero lateral displacements,  $u_y$  and  $u_z$ , are allowed due to the Poisson effect.

#### Governing Equation and Boundary Conditions

To obtain the governing equation of longitudinal vibration, one should compute the kinetic and potential energies that correspond to hypothesis (3.1) and then employ Hamilton's variational principle. (For a detailed description of the principle see Chapter 11.)



**Figure 9** Frame of references and positive direction of the displacement  $u_j$  and force  $F_j$ , angle of twist  $\theta_j$  and moment  $M_j$  round axis  $j$  in a beam of cross-section  $S$ ,  $j = x, y, z$ .

The kinetic energy of the beam of length  $l$  is

$$T = \frac{1}{2} \rho \int_0^l \iint_S (\dot{u}_x^2 + \dot{u}_y^2 + \dot{u}_z^2) dx dS$$

$$= \frac{1}{2} \rho \int_0^l (S \dot{u}^2 + v^2 I_p \dot{u}^2) dx \quad (3.2)$$

where  $\rho$  is the density of the beam material,  $I_p = \iint_S (y^2 + z^2) dS$  is the polar moment of the cross section, and the overdot designates the time derivative. The first term of Eq. (3.2) describes the kinetic energy of axial movement and the second term—of the lateral movement. The potential energy of the beam is equal to

$$U = \frac{1}{2} \int_0^l \iint_S \left( \frac{\sigma_{xx}^2}{E} + \frac{\sigma_{xy}^2 + \sigma_{xz}^2}{G} \right) dx dS$$

$$= \frac{1}{2} \int_0^l (E S u'^2 + v^2 G I_p u''^2) dx \quad (3.3)$$

Here  $G$  is the shear modulus. The first term of Eq. (3.3) represents the energy of the axial deformation, while

the second term relates to the shear deformation. If only the first terms of Eqs. (3.2) and (3.3) are retained, the following equation can be obtained from the variational principle:

$$E S u''(x, t) - \rho S \ddot{u}(x, t) = -f_x(x, t) \quad (3.4)$$

where  $f_x(x, t)$  is the linear density of external axial load. This equation is called the *Bernoulli equation*. Formally, it coincides with the wave equations that describe wave motions in many other structures and media (strings, fluids, solids), but differs from them by the coefficients and physical content.

Vibration of continuous systems should also be described by boundary conditions. For longitudinally vibrating beams, the simplest and most frequently used end terminations are the fixed and free ends with the following boundary conditions:

$$u(l, t) = 0 \quad (\text{fixed end})$$

$$F_x(l, t) = 0 \quad (\text{free end}) \quad (3.5)$$

where  $l$  is the end coordinate, and

$$F_x(x, t) = \iint_S \sigma_{xx} dS = E S u'(x, t) \quad (3.6)$$

is the axial force that is transmitted in the beam through cross section  $x$ .

**Harmonic Wave Motion** Consider an elementary longitudinal wave motion in the beam of the form

$$u(x, t) = \text{Re} [u \exp(ikx - i\omega t)]$$

$$= u_0 \cos(kx - \omega t + \varphi) \quad (3.7)$$

Here  $k = 2\pi/\lambda$  is the *wave number* or *propagation constant*,  $\lambda$  is the *wavelength*;  $u_0$  is the wave amplitude,  $(kx - \omega t + \varphi)$  is the phase of the wave,  $\varphi$  is the initial phase;  $u = u_0 \exp(i\varphi)$  is the complex wave amplitude. The wave motion (3.7) is harmonic in time and space coordinates. Any vibration motion of the beam is a superposition of the elementary wave motions of the type (3.7).

One of the most useful characteristics of a wave is its *dispersion*  $k(\omega)$ , that is, the dependence of the wave number on frequency. To a great extent, dispersion is responsible for the spectral properties of finite continuous systems, and it usually needs to be studied in detail. Substitution of (3.7) into the Bernoulli equation (3.4) yields the *dispersion equation*:

$$k^2 - k_E^2 = 0 \quad k_E = \omega \sqrt{\frac{\rho}{E}} = \frac{\omega}{c_E} \quad (3.8)$$

which just relates the wavenumber to frequency. Equation (3.8) has two roots,  $k_{1,2} = \pm k_E$ , which

correspond to the waves (3.7) propagating in positive (sign +) and negative (sign -) directions;  $k_E$  and  $c_E$  are called the longitudinal wavenumber and velocity. It is seen that the wavenumber is a linear function of frequency.

Three types of velocities are associated with a wave. Each phase of the wave  $kx - \omega t + \phi = \text{constant}$  propagates with the *phase velocity*

$$c_{\text{ph}} = \frac{\omega}{k} = \sqrt{\frac{E}{\rho}} = c_E \quad (3.9)$$

If the wave amplitude  $u$  is a smooth function of  $x$ , the envelope  $u(x)$  propagates with the *group velocity*<sup>6</sup>:

$$c_{\text{gr}} = \frac{\partial \omega}{\partial k} \quad (3.10)$$

which, for the beam, is equal to the phase velocity  $c_{\text{ph}}$ . One more velocity is the *energy velocity*. It is defined as the ratio of the time-average power flow across a cross section,  $P(x) = \text{Re}(-F_x \dot{u}^*)$  to the linear density of the time-average total energy  $E(x)$ ,  $c_{\text{en}} = P(x)/E(x)$ . It can be shown that for longitudinal wave (3.7) the velocity of energy propagation is equal to the group velocity,  $c_{\text{en}} = c_{\text{gr}}$ . In fact, the equivalence of the group and energy velocities takes place for all known systems and media.<sup>7</sup> Note that the dispersion (3.8) can also be interpreted as independence of the three longitudinal velocities on frequency.

Consideration of propagation of waves (3.7) allows one to solve some practical problems. As an example, consider the wave reflection at the beam end. Since the phase velocity (3.9) does not depend on frequency, a disturbance of any shape propagates along the beam without distortion. For example, if at moment  $t = 0$  there is an impulse of the space shape  $u(x, 0) = \psi(x)$  propagating in positive direction, it will continue to propagate at later time with speed  $c_E$  pertaining its shape,  $u(x, t) = \psi(x - c_E t)$ . When such an impulse meets the fixed end, it reflects with the same shape but with opposite sign [because of boundary condition (3.5)]. Therefore, the stresses of the reflected impulse are identical to those of the incident impulse giving the *double* stress values at the fixed beam termination. When the impulse meets the free end [see boundary condition (3.5)], its shape pertains but the doubling is observed for displacement, and the reversal is associated with the stresses: Compression reflects as tension and vice versa. This explains, for example, the phenomenon when a part of a beam made of a brittle material may be torn at the free end due to tensile fracture. The phenomenon is known in ballistic and sometimes used in material strength tests.

**Free Vibration of a Finite Beam** Consider now a beam of length  $l$ . Free harmonic vibration is a

combination of elementary waves (3.7):

$$u(x, t) = \text{Re}[(ae^{ik_E x} + be^{-ik_E x})e^{-i\omega t}]$$

where  $a$  and  $b$  are the complex wave amplitudes that are determined from the boundary conditions at the ends. Let both ends be fixed,  $u(0, t) = u(l, t) = 0$ . Then one can obtain the *characteristic equation*

$$\frac{\sin k_E l}{k_E l} = 0 \quad \text{or} \quad k_E l = \pi n \quad n = \pm 1, \pm 2, \dots$$

and the relation between the amplitudes,  $a + b = 0$ . The positive roots of the characteristic equation determine an infinite (countable) number of the normal modes of the beam

$$\{\omega_{0n}, u_n(x)\}_{n=1}^{\infty} \quad (3.11)$$

with undamped natural frequencies  $\omega_{0n} = \pi n c_E / l$  and mode shapes  $u_n(x) = (l/2)^{-1/2} \sin(\pi n x / l)$ . The main properties of the normal modes of the beam (3.11) are very similar to those of NDOF systems: The spectrum is discrete; in each mode all the beam points move in phase or counterphase; the modes are orthogonal:

$$\int_0^l u_m(x) u_n(x) dx = \delta_{mn} \quad (3.12)$$

Free vibration of a finite beam is a superposition of the normal modes (3.11) with the amplitudes that are determined from initial conditions with the help of the orthogonality relation (3.12) just like for NDOF systems—see Eqs. (2.9) and (2.13).

**Forced Vibration of a Finite Beam** Analysis of forced vibration of beams is also very similar to that of NDOF system vibration. When an external force is harmonic in time,  $f_x(x, t) = f_x(x) \exp(-i\omega t)$ , the solution is obtained as the expansion in the normal modes (3.11):

$$u(x, t) = \frac{1}{\rho S} \sum_{n=1}^{\infty} \frac{f_{xn} u_n(x) \exp(-i\omega t)}{\omega^2 - \omega_{0n}^2} \quad (3.13)$$

$$f_{xn} = \int_0^l f_x(x) u_n(x) dx$$

If the excitation frequency approaches one of the natural frequencies and the force shape is not orthogonal to the corresponding mode shape, the beam resonance occurs. When the external force is not harmonic in time, the problem may first be cast into the frequency domain by the Fourier transform, and the final result may be obtained by integrating solution (3.13)

over all the frequencies—see also Eqs. (2.23) to (2.25).

**Damped Beams** There are three main types of losses of the vibration energy in elastic bodies.<sup>8</sup> The first type is associated with transmission of the vibration energy to the ambient medium by viscous friction or/and by sound radiation from the beam surface. These losses are proportional to the velocity and lead to the additional term  $[-2d\dot{u}(x, t)]$  in the Bernoulli equation (3.4),  $d$  being the damping coefficient. As a consequence, the free longitudinal wave (3.7) attenuates in space,  $k = k_E + i\delta/c_E$ ,  $\delta = d/\rho S$ , the natural frequencies of a finite beam become complex,  $\omega_n = -i\delta \pm \sqrt{\omega_{0n}^2 - \delta^2}$ , and the denominators of each term in solution (3.13) change into  $\omega^2 - \omega_{0n}^2 + 2i\omega\delta$ .

Losses of the second type are the contact losses at junctions of the beam with other structures. The third type constitutes the internal losses in the beam material. They may be taken into consideration if the axial stress of the beam is assumed to be related to the axial strain as  $\sigma_{xx} = E(1 + 2\varepsilon\partial/\partial t)\partial u/\partial x$ . This gives the additional term  $2\varepsilon\partial^3 u/\partial x^2 \partial t$  in the wave equation (3.4) and leads to complex natural frequencies of the finite beam, and to the solution (3.13) with denominators  $\omega^2 - \omega_{0n}^2(1 - 2i\varepsilon\omega)$ .

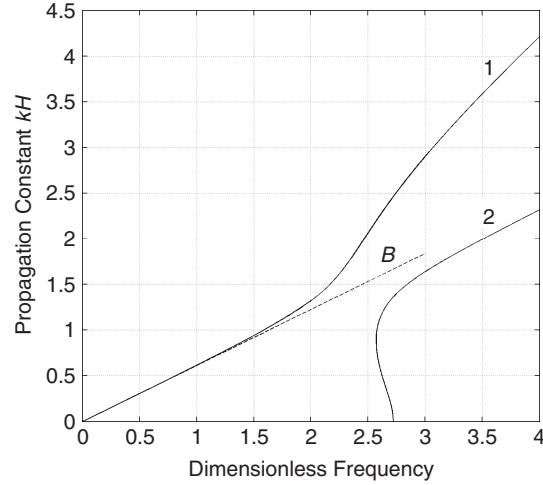
**Nonuniform Beams** When a beam is nonuniform, for example, has a variable cross-sectional area  $S(x)$ , the equation of motion is

$$\frac{\partial}{\partial x} \left( ES \frac{\partial u}{\partial x} \right) - \rho S \frac{\partial^2 u}{\partial t^2} = -f(x, t) \quad (3.14)$$

For some functions  $S(x)$  this equation may be solved analytically. For example, if  $S(x)$  is a linear or quadratic function of  $x$ , solutions of Eq. (3.14) are the Bessel functions or spherical Bessel functions. For arbitrarily varying cross section, no analytical solutions exist, and Eq. (3.14) is solved numerically, for example, by the finite element method (FEM).

**Improved Theories of Longitudinal Vibrations in Beams** A beam may be treated as a three-dimensional body using the exact equations of linear theory of elasticity, that is, avoiding assumptions (3.1). Such exact solutions have been obtained for a circular cylinder and others.<sup>9</sup>

The exact theory says that, in a beam, an infinite number of waves of type (3.7) exist at any frequency. They differ from each other by the values of the propagation constant and shape of cross-section vibrations and are called as the *normal modes* or *normal waves*. At low frequencies, the first normal wave of the symmetric type is a propagating wave with a real propagation constant, while all other normal waves are evanescent waves, that is, have complex propagation constants and therefore attenuate with distance. The Bernoulli longitudinal wave with the propagation constant (3.8) describes only the first normal wave.



**Figure 10** Dispersion of normal modes of a narrow beam of rectangular cross section (of height  $2H$  and width  $2h$ ,  $H/h = 10$ ) according to the exact theory (solid lines 1 and 2) and to the Bernoulli equation (dashed line B); dimensionless frequency is equal to  $k_t H$ , where  $k_t = \omega(\rho/G)^{1/2}$  is the shear wavenumber and  $G$  is the shear modulus of the beam material.

Figure 10 presents the dispersion curves of the normal waves according to the exact theory (solid lines) and the dispersion (3.8)—dashed line B. It is seen that the Bernoulli equation (3.4) provides good description of dispersion and, hence, spectral properties of finite beams in rather wide low-frequency range up to the frequency at which the diameter of the beam cross section is equal to a half of the shear wavelength.

One may try to improve the equation of Bernoulli (3.4) by taking into account new effects of deformation. If, for example, in Eq. (3.2), the kinetic energy of lateral displacement is taken into account, this will add the term  $\rho v^2 I_p \ddot{u}''$  to Eq. (3.4). If, in addition, the second term of Eq. (3.3) is taken into account, one more term  $v^2 G I_p u^{IV}$  will appear in Eq. (3.4). However, the improvements in the accuracy of vibration analysis caused by these and similar attempts turn out insignificant. The Bernoulli equation (3.4) remains the simplest and the best among the known governing equations of the second and the fourth orders for longitudinal vibration of thin beams.

### 3.2 Torsional Vibration in Beams

Low-frequency torsional waves and vibration are also described by the wave equations of the type (3.4) or (3.14). According to the theory of Saint-Venant,<sup>2</sup> the simplest of the existing theories, torsion of a straight uniform beam is composed of two types of deformation: rotation of the cross sections as rigid bodies and deplanation, that is, the axial displacement of the cross-sectional points. Mathematically, this can

be written as the following kinematic hypothesis:

$$u_x(x, y, z, t) = \theta'(x, t)\varphi(y, z)$$

$$u_y(x, y, z, t) = -z\theta(x, t)$$

$$u_z(x, y, z, t) = y\theta(x, t)$$

where  $\theta$  is the angle of twist about the axis  $x$ ,  $\varphi(y, z)$  is the torsional function that satisfies equation  $\Delta\varphi = 0$  and boundary condition  $\partial\varphi/\partial n = 0$  on the contour of the beam cross section. Taking into account only the kinetic energy of rotation and the potential energy of shear deformations, one can obtain, using the variational principle, the *equation of Saint-Venant* for torsional vibration:

$$GI_S\theta''(x, t) - \rho I_p\ddot{\theta}(x, t) = -m_x(x, t) \quad (3.15)$$

Here,  $m_x$  is the linear density of an external torque,  $I_p$  is the polar moment of inertia,  $G$  and  $\rho$  are the shear modulus and density of the material;  $GI_S$  is the torsional stiffness. The quantity  $I_S$  depends on the torsional function  $\varphi$ . For a beam of a ring cross section ( $R_1$  and  $R_2$  being the outer and inner radii), it is equal to  $I_S = (R_1^4 - R_2^4)\pi/2$ ; for an elliptic cross section ( $a$  and  $b$  being the semi-axes)  $I_S = \pi a^3 b^3 / (a^2 + b^2)$ ; for a thin-walled beam of open cross section (of length  $L$  and thickness  $h$ ), it equals to  $I_S = Lh^3/3$ , and so forth.<sup>2</sup>

The boundary conditions for torsional vibration at end  $x = l$  are

$$\begin{aligned} \theta(l, t) &= 0 \quad (\text{fixed end}), \\ M_x(l, t) &= 0 \quad (\text{free end}), \end{aligned} \quad (3.16)$$

where  $M_x$  is the torque in cross-section  $x$ . It is equal to the moment of the shear stresses:

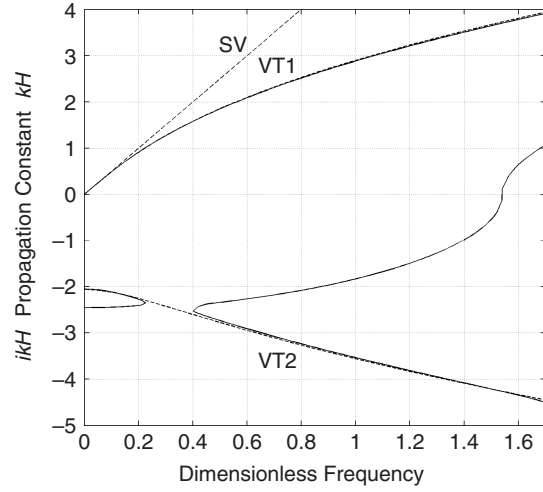
$$M_x(x, t) = GI_S\theta'(x, t)$$

As the equation of Saint-Venant (3.15) and boundary conditions (3.16) are mathematically identical to the equation of Bernoulli (3.4) and boundary conditions (3.5) for longitudinal waves and vibration, all results obtained in the previous subsection are valid also for torsional waves and vibration and therefore are omitted here.

There are several improved engineering theories of torsional vibrations. Taking account of the potential energy of deformation yields the equation of Vlasov–Timoshenko<sup>10</sup>:

$$EI_\varphi\theta^{IV} - GI_S\theta'' + \rho I_\varphi\ddot{\theta}'' + \rho I_p\ddot{\theta} = m_x$$

$$I_\varphi = \iint_S \varphi^2 dS$$



**Figure 11** Real and imaginary branches of dispersion of the torsional normal modes in the narrow beam as in Fig. 10 according to the exact theory (solid lines), the Saint-Venant theory (dashed line SV), and Vlasov–Timoshenko equation (dashed lines VT); dimensionless frequency is  $k_t H$ .

It contains the fourth derivative with respect to  $x$  and therefore describes two normal waves. Figure 11 presents the dispersion curves of the torsional normal waves in a narrow beam as in Fig. 10 computed according to the exact theory of elasticity (solid lines) as well as to the Saint-Venant theory (dashed line SV) and to the Vlasov–Timoshenko equation (two dashed lines VT). It is seen that the Saint-Venant equation (3.15) describes adequately the first propagating normal wave in low-frequency range. The equation of Vlasov and Timoshenko describes this wave much more accurately. However, it fails to describe properly the evanescent normal waves with pure imaginary propagation constants. That is why the Saint-Venant equation is preferable in most practical low-frequency problems.

### 3.3 Flexural Vibration in Beams

Transverse motion of thin beams resulting from bending action produces flexural (or bending) waves and vibration. Their governing equations, even in the simplest case, contain the space derivative of the fourth order thus describing two normal waves at low frequencies. Widely used are two engineering equations of flexural vibration—the classical equation of Bernoulli–Euler and the improved equation of Timoshenko.

Consider a straight uniform thin beam (see Fig. 9) that performs flexural vibration in the plane  $xz$  (this is possible when the beam cross section is symmetric with respect to plane  $xz$ ). The main assumption of the Bernoulli–Euler theory is the following: The plane cross sections initially perpendicular to the axis of the beam remain plane and perpendicular to the



neutral axis in bending; the lateral stresses are zero. Mathematically, the assumption can be written as

$$\begin{aligned} u_x(x, y, z, t) &= -zw'(x, t) & u_y(x, y, z, t) &= 0 \\ u_z(x, y, z, t) &= w(x, t) & \sigma_{xx} &= E\partial u_x/\partial x \end{aligned} \quad (3.17)$$

Computing the kinetic and potential energies as in Eqs. (3.2) and (3.3) and using the variational principle, one can obtain from (3.17) the *Bernoulli–Euler equation* for the lateral displacement  $w(x, t)$  of the beam:

$$EI_y w^{IV}(x, t) + \rho S \ddot{w}(x, t) = f_z(x, t) \quad (3.18)$$

where  $f_z$  is the linear density of external force,  $EI_y$  is the bending stiffness,  $I_y$  is the second moment of beam cross section with respect to axis  $y$ . Since Eq. (3.18) is of fourth order, there must be two boundary conditions at each end. Typically, they are written as the equalities to zero of two of the following quantities—displacement  $w$ , slope  $w'$ , bending moment  $M_y$ , and shear force  $F_z$ :

$$\begin{aligned} M_y(x, t) &= M_y(x=0, t) = -EI_y w''(x, t) \\ F_z(x, t) &= -EI_y w'''(x, t) & I_y &= \iint_S z^2 dS \end{aligned} \quad (3.19)$$

Examples of boundary conditions are presented in Table 2.

The elementary flexural wave motion has the same form as that of other waves [see Eq. (3.7)]:

$$w(x, t) = \text{Re}[w \exp(ikx - i\omega t)] \quad (3.20)$$

After substitution of this into a homogeneous equation (3.18), one obtains the dispersion equation

$$k^4 = \omega^2(\rho S/EI_y) = k_0^4 \quad (3.21)$$

that relates the wavenumber  $k$  to frequency  $\omega$ , and  $k_0$  is called the flexural wavenumber. Equation (3.21) has four roots,  $\pm k_0$  and  $\pm ik_0$ . Hence, two different types of waves (3.20) exist in the Bernoulli–Euler beam (positive and negative signs mean positive and negative directions of propagation or attenuation along axis  $x$ ). The first type, with real-valued wavenumbers, corresponds to flexural waves propagating without attenuation. The second type, with imaginary wavenumbers, corresponds to evanescent waves that exponentially decay with the space coordinate  $x$ .

The phase velocity of the propagating flexural wave depends on frequency:

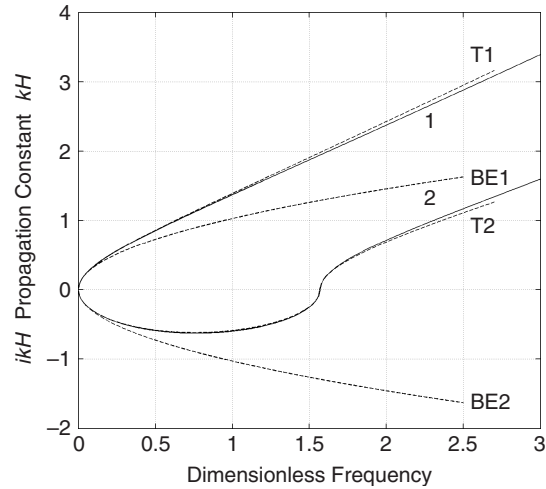
$$c_{ph} = \frac{\omega}{k} = \omega^{1/2} \left( \frac{EI_y}{\rho S} \right)^{1/4}$$

The higher the frequency the greater is the phase velocity. The group velocity and, hence, the energy velocity, is twice the phase velocity,  $c_{gr} = \partial\omega/\partial k = 2c_{ph}$ . Dependence  $c_{ph}$  on frequency leads to distortion of impulses that may propagate along the beam. Let, for example, a short and narrow impulse be excited at moment  $t = 0$  near the origin  $x = 0$ . Since the impulse has a broad-band spectrum, an observer at point  $x_0$  will detect the high-frequency components of the impulse practically immediately after excitation, while the low-frequency components will be arriving at  $x_0$  for a long time because of their slow speed. The impulse, thus, will be spread out in time and space due to dispersive character of flexural wave propagation in beams.

In reality, the phase and group velocities cannot increase without limit. The Bernoulli–Euler theory of flexural vibration is restricted to low frequencies and to smooth shapes of vibration. Comparison against exact solutions shows that the frequency range of the theory validity is limited to the frequency at which the shear wavelength of the beam material is 10 times the dimension  $D$  of the beam cross section, and the flexural wavelengths should not be shorter than approximately  $6D$ —see Fig. 12.

**Timoshenko Equation** An order of magnitude wider is the frequency range of validity of the Timoshenko theory for flexural vibration of beams. The theory is based on the following kinematic hypothesis:



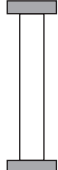

$$\begin{aligned} u_x(x, y, z, t) &= z\theta_y(x, t) & u_y(x, y, z, t) &= 0 \\ u_z(x, y, z, t) &= w(x, t) \end{aligned} \quad (3.22)$$



**Figure 12** Real and imaginary branches of dispersion of the flexural normal modes in the narrow beam as in Fig. 10 according to the exact theory (solid lines), the Bernoulli–Euler theory (dashed lines *BE*), and to the Timoshenko equation (dashed lines *T*); dimensionless frequency is  $k_t H$ .



**Table 2 Natural Frequencies of Flexurally Vibrating Bernoulli–Euler Beams**  $\left( \xi = kl, f_n [\text{Hz}] = \frac{\xi_n^2}{2\pi l^2} \left( \frac{EI}{\rho S} \right)^{1/2} \right)$

Beam	Boundary Conditions	Characteristic Equation	First Four Roots of the Characteristic Equation ( $n = 1, 2, 3, 4$ )	Asymptotic Roots of the Characteristic Equation ( $n > 4$ )
Free 	$F(0) = 0$ $M(0) = 0$ $F(l) = 0$ $M(l) = 0$	$\xi^4 (1 - \cosh \xi \cdot \cos \xi) = 0$	0 4.730 7.853 10.996	$\pi n - \frac{\pi}{2}$
Pinned 	$w(0) = 0$ $M(0) = 0$ $w(l) = 0$ $M(l) = 0$	$\frac{\sin \xi}{\xi} = 0$	3.142 6.283 9.425 12.566	$\pi n$
Clamped 	$w(0) = 0$ $w'(0) = 0$ $w(l) = 0$ $w'(l) = 0$	$\frac{1 - \cosh \xi \cdot \cos \xi}{\xi^4} = 0$	4.730 7.853 10.996 14.137	$\pi n + \frac{\pi}{2}$
Cantilever 	$w(0) = 0$ $w'(0) = 0$ $F(l) = 0$ $M(l) = 0$	$1 + \cosh \xi \cdot \cos \xi = 0$	1.875 4.694 7.855 10.996	$\pi n - \frac{\pi}{2}$

Here,  $\theta_y$  is the angle of rotation about axis  $y$ , which is not generally equal to  $(-w')$  as in the Bernoulli–Euler theory—see Eq. (3.17). This means that plane cross-sections initially perpendicular to the beam axis, remain plane, but they are no longer perpendicular to the neutral axis during bending. In other words, the shear deformations are possible in the Timoshenko beam. Computing the kinetic energy of the lateral and rotational movement and the potential energy of pure bending and shear deformation one can obtain, with the help of the variational principle, the *Timoshenko equations*:

$$\begin{aligned}\rho S \ddot{w}(x, t) &= qGS(w'' + \theta_y') + f_z(x, t) \\ \rho I_y \ddot{\theta}_y(x, t) &= EI_y \theta_y'' - qGS(w' + \theta_y)\end{aligned}\quad (3.23)$$

Function  $f_z$  in Eq. (3.23) is the linear density of an external force. The boundary conditions are the same as for the Bernoulli–Euler equation, but the bending moment and shear force are defined by the equations:

$$\begin{aligned}M_y(x, t) &= EI_y \theta_y'(x, t) \\ F_z(x, t) &= qGS[w'(x, t) + \theta_y(x, t)]\end{aligned}\quad (3.24)$$

From the point of view of linear theory of elasticity, there exists a contradiction between the two assumptions of the Timoshenko theory, namely between the plane cross-section hypothesis (3.22) and existence of shear stresses  $\sigma_{xz}$ . For that reason, Timoshenko introduced the *shear coefficient*  $q$  replacing elastic modulus  $G$  by  $qG$ .<sup>11</sup> This coefficient, together with the rotatory inertia taken into account, considerably improves the spectral properties of beams and makes Eqs. (3.23) the most valuable in flexural vibration theory.

In Fig. 12 presented are the dispersion curves of a beam of the rectangular cross section ( $H/h = 10$ ). Curves 1 and 2 are computed on the basis of linear theory of elasticity, curves *BE* correspond to dispersion (3.21) of the Bernoulli–Euler beam, and curves *T* are described by the equations

$$2k_{1,2}^2 = k_E^2 + \frac{k_t^2}{q} \pm \left[ \left( k_E^2 - \frac{k_t^2}{q} \right) + 4k_0^4 \right]^{1/2} \quad (3.25)$$

that are obtained from Eqs. (3.23) for wave (3.20). The shear coefficient value  $q = \pi^2/12$  is chosen from the coincidence of the cutoff frequencies in the real beam and its model. It is seen from Fig. 12 that the frequency range of validity of the Timoshenko theory is much wider than that of the Bernoulli–Euler theory. It is valid even at frequencies where the shear wavelength of the beam material is comparable with the dimension of the beam cross section.

As for free and forced flexural vibrations of finite beams, their analysis is very similar to that of NDOF systems and longitudinal vibrations of beams. The common procedure is the following.<sup>12</sup> First,

the undamped normal modes are determined. For that, the general solution of homogeneous Eq. (3.18) or Eqs. (3.23), that is, a superposition of the free waves (3.21), that satisfies the boundary conditions (3.19), should be found. As a result, one obtains the characteristic equation and normalized mode shapes as well as the orthogonality relation. Substitution of the dispersion (3.21) or (3.25) into the characteristic equation gives also the discrete spectrum of the natural frequencies. The characteristic equations and natural frequencies for several beams are presented in Table 2. The next step of the analysis is decomposition of the free or forced vibrations into the normal modes and determination of the unknown mode amplitudes from the initial conditions and external force.

Note that the orthogonality relation for the *BE* beam is the same as in (3.12). For the Timoshenko beam, it is more complicated and includes the weighted products of the displacements and slopes<sup>13</sup>:

$$\int_0^l [w_m(x)S w_n(x) + \theta_{ym}(x)I_y \theta_{yn}(x)] dx = \delta_{mn} \quad (3.26)$$

### 3.4 Nonsymmetric and Curved Beams

Uncoupled longitudinal, flexural, and torsional vibrations in a beam are possible only if it is straight and its cross section is symmetric with respect to planes  $xy$  and  $xz$  (Fig. 9). For arbitrary beam geometry, all these types of vibration are coupled and should be treated simultaneously.

#### Beam with a Nonsymmetric Cross Section

Engineering equations for coupled vibration of a thin straight uniform beam with a nonsymmetric cross section can be obtained with the help of the variational principle starting from the same assumptions that were made above for each type of motion separately. Namely, the beam cross section is assumed to have a hard undeformable contour in the  $yz$  plane (see Fig. 9) but has the ability to move in the  $x$  direction during torsion (i.e., depplanation is possible). Mathematically, it can be written as the following kinematics hypothesis:

$$\begin{aligned}u_x(x, y, z, t) &= u(x, t) + z\theta_y(x, t) \\ &\quad - y\theta_z(x, t) + \varphi(y, z)\theta'(x, t) \\ u_y(x, y, z, t) &= v(x, t) - z\theta(x, t) \\ u_z(x, y, z, t) &= w(x, t) + y\theta(x, t)\end{aligned}\quad (3.27)$$

Motion of a beam element  $dx$  is characterized by six independent quantities (or DOFs)—displacements  $u, v, w$  and angles  $\theta, \theta_y, \theta_z$ . Angles  $\theta_y$  and  $\theta_z$  do not coincide with  $-w'$  and  $v'$ , thus, allowing additional shear deformation in bending (as in a Timoshenko

beam). Deplanation is described by the torsional function  $\varphi$ , which should be found from the boundary value problem as in Saint-Venant theory—see Eq. (3.15).

After writing the kinetic and potential energies and using the variational principle, one can obtain, from Eqs. (3.27), the set of six governing equations, each of the second order. There should be imposed six boundary conditions at each end. The equations as well as the expressions for the forces and moments at cross-section  $x$  can be found elsewhere.<sup>13</sup>

If the beam has arbitrary cross-section geometry, one of the equations, namely the equation of Bernoulli (3.4) of longitudinal vibration, is independent. Other five equations are coupled. If the beam cross section has a plane of symmetry, like in  $\Pi$  or T beams, flexural vibration in this plane becomes uncoupled and described by the Timoshenko equations (3.23). If the cross section has two planes of symmetry, like, for example, in a box beam, flexural vibration in both symmetry planes and torsional vibration are uncoupled and may be analyzed independently.

**Curved Beams** A curved beam is one more 1D model where various types of beam vibration may be coupled even if the cross section is symmetric. Geometrically, a curved beam is characterized by a local curvature and twist. In the general case of twisted beam, for example, in a helical spring, all the wave types are coupled including the longitudinal one. In a curved beam of symmetric cross section with no twist (the beam lies in a plane), for example, in a ring, there are two independent types of motion: coupled longitudinal-flexural vibration in the plane of the beam, and torsional-flexural vibration out of the plane. Governing equations for both types can be found in the literature.<sup>2,14</sup>

#### 4 CONTINUOUS TWO-DIMENSIONAL SYSTEMS

Two-dimensional (2D) continuous systems are models of engineering structures one dimension of which is small compared to two other dimensions and to the wavelength. A vibration field in a 2D system depends on time and two space coordinates. Examples of such systems are membranes, plates, shells, and other thin-walled structures. In this section, vibrations of the most used 2D systems—plates and cylindrical shells—are considered. Thin plates are models of flat structural elements. There are two independent types of plate vibrations—flexural and in-plane vibrations. Flexural vibrations of finite plates have comparatively low natural frequencies, they are easily excited (because of low stiffness) and play the key role in radiation of sound into environment. The in-plane vibrations of plates are “stiff” and radiate almost no sound, but they store a lot of the vibration energy and easily transport it to distant parts of elastic structures. Shells model curved thin 2D structural elements, like hulls, tanks, and the like. Generally, all types of vibration are coupled in shells due to the surface curvature.

##### 4.1 Flexural Vibration of Thin Plates

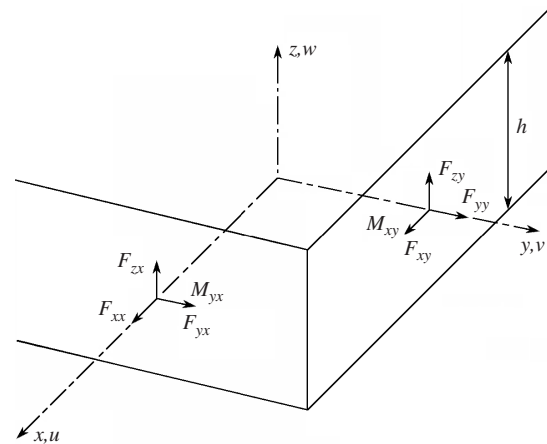
Consider a uniform elastic plate of small thickness  $h$  made of an isotropic material with the Young's modulus  $E$  and Poisson's ratio  $\nu$ . When the plate is bent, its layers near the convex surface are stretched, while the layers near the concave surface are compressed. In the middle, there is a plane, called the neutral plane, with no in-plane deformation. Let  $xy$  plane of Cartesian coordinates coincide with the neutral plane and axis  $z$  be perpendicular to it, so that  $z = \pm h/2$  are the faces of the plate (Fig. 13).

The main assumption of the classical theory of flexural vibration of thin plates is the following: plane cross sections that are perpendicular to the middle plane before bending remain plane and perpendicular to the neutral plane after bending. It is equivalent to the kinematic hypothesis concerning distribution of the displacements  $u_x$ ,  $u_y$ , and  $u_z$  over the plate:

$$\begin{aligned} u_x(x, y, z, t) &= -z \frac{\partial w}{\partial x} \\ u_y(x, y, z, t) &= -y \frac{\partial w}{\partial y} \\ u_z(x, y, z, t) &= w(x, y, t) \end{aligned} \quad (4.1)$$

where  $w$  the lateral displacement of the neutral plane. Besides, it is assumed that the normal lateral stress  $\sigma_{zz}$  is zero not only at the free planes  $z = \pm h/2$  but also inside the plate.

Starting from Eq. (4.1) and Hook's law, one can compute strains and stresses, the kinetic and potential energy and obtain, with the help of the variational principle of the least action, the classical *equation of Germin–Lagrange* of flexural vibration on thin



**Figure 13** Cartesian coordinates and the positive direction of the displacements, bending moments, and forces acting at the cross sections perpendicular to axes  $x$  and  $y$ .

plates<sup>15</sup>:

$$D\Delta\Delta w(x, y, t) + \rho h \ddot{w}(x, y, t) = p_z(x, y, t) \quad (4.2)$$

Here  $D = Eh^3/12(1 - \nu^2)$  is the flexural stiffness,  $\rho$  is the mass density,  $p_z$  is the surface density of external forces,  $\Delta = \partial^2/\partial x^2 + \partial^2/\partial y^2$  is the Laplacian operator. The equation is of the fourth order with respect to the space coordinates, therefore two boundary conditions should be imposed at each edge that are similar to those of the flexurally vibrating beam. The expressions for the bending moments and effective shear forces are the following:

At the edge  $x = \text{const.}$

$$\begin{aligned} M_{yx} &= -D \left( \frac{\partial^2 w}{\partial x^2} + \nu \frac{\partial^2 w}{\partial y^2} \right) \\ F_{zx} &= -D \left[ \frac{\partial^3 w}{\partial x^3} + (2 - \nu) \frac{\partial^3 w}{\partial x \partial y^2} \right] \end{aligned} \quad (4.3)$$

and at the edge  $y = \text{const.}$

$$\begin{aligned} M_{xy} &= D \left( \frac{\partial^2 w}{\partial y^2} + \nu \frac{\partial^2 w}{\partial x^2} \right) \\ F_{zy} &= -D \left[ \frac{\partial^3 w}{\partial y^3} + (2 - \nu) \frac{\partial^3 w}{\partial x^2 \partial y} \right] \end{aligned} \quad (4.4)$$

Double index notation for the moments and forces is adopted just in the same manner as for the stress components in theory of elasticity: The first index designates the component and the second index indicates the area under consideration. For example,  $M_{yx}$  is the  $y$  component of the moment of stresses at the area perpendicular to  $x$  axis—see Fig. 13.

The assumptions underlying the Germin–Lagrange equation (4.2) are identical to those of the Bernoulli–Euler equation (3.18). Moreover, these equations coincide if the wave motion on the plate does not depend on one of the space coordinates. Therefore, the general properties of flexural waves and vibration of plates are very similar to those of beams.

Consider a straight-crested time-harmonic flexural wave of frequency  $\omega$  and complex displacement amplitude  $w_0$  propagating at the angle  $\psi$  to the  $x$  axis:

$$w(x, y, t) = \text{Re} \{ w_0 \exp[ik(x \cos \psi + y \sin \psi) - i\omega t] \} \quad (4.5)$$

Substitution of this into Eq. (4.2) gives the dispersion equation

$$k^4 = k_p^4 = \frac{\rho h \omega^2}{D} \quad (4.6)$$

relating the wavenumber  $k$  to frequency  $\omega$ . The equation has roots  $\pm k_p, \pm ik_p$ . Hence, there are two types of the plane waves in plates—propagating and

evanescent. The real-valued wavenumbers correspond to the propagating wave:

$$w_1 e^{ik_p(x \cos \psi + y \sin \psi) - i\omega t}$$

Its amplitude  $|w_1|$  is constant everywhere on the plate. The imaginary-valued wavenumbers correspond to the evanescent wave:

$$w_2 e^{-k_p(x \cos \psi + y \sin \psi) - i\omega t}$$

Its amplitude changes along the plate. The steepest change takes place in the  $\psi$  direction, while along the straight line  $\psi + \pi/2$  it remains constant. The graph of dispersion (4.6) is identical to curves  $BE$  in Fig. 12.

It follows from Eq. (4.6) that the phase velocity of the propagating wave is proportional to the square root of frequency. The group and energy velocities are twice the phase velocity, just as for the propagating flexural wave in a beam. This causes the distortion of the shape of disturbances that propagate on a plate.

Beside plane waves (4.5) with linear fronts, other types of the wave motion are possible on the plate as a 2D continuous system. Among them the axisymmetric waves with circular wavefronts are the most important. Such waves originate from local disturbances. In particular, if a time-harmonic force

$$p_z(x, y, t) = p_0 \delta(x - x_0) \delta(y - y_0) \exp(-i\omega t)$$

is applied to point  $(x_0, y_0)$  of an infinite plate, the flexural wave field is described by

$$\begin{aligned} w(x, y, t) &= p_0 g(x, y; x_0, y_0) = \frac{p_0}{8Dk_p^2} \\ &\times \left[ H_0(k_p r) - \frac{2}{\pi} K_0(k_p r) \right] \\ r &= [(x - x_0)^2 + (y - y_0)^2]^{1/2} \end{aligned} \quad (4.7)$$

Here  $H_0$  and  $K_0$  are Hankel's and McDonald's cylindrical functions.<sup>6</sup> The Green's function  $g$  of an infinite plate consists of the outgoing (propagating) circular wave  $H_0(k_p r)$  and the circular evanescent wave described by the function  $K_0(k_p r)$ . When distance  $r$  is large ( $k_p r \gg 1$ ), the response amplitude decreases as  $r^{-1/2}$ . For  $r = 0$ , Eq. (4.7) gives the input impedance of an infinite plate:

$$z_p = p_0 / \dot{w}(x_0, y_0, t) = 8\sqrt{Dm}$$

with  $m = \rho h$ . The impedance is real valued. Physically, this means that the power flow from the force source into the plate is pure active, and no reactive field component is excited in the plate.

The forced flexural vibrations of an infinite plate under the action of arbitrary harmonic force  $p_z(x, y, t)$

can be computed with the help of Green's function (4.7):

$$w(x, y, t) = \iint_{\Omega} g(x, y; x_0, y_0) p_z(x_0, y_0, t) dx_0 dy_0 \quad (4.8)$$

where integration is performed over the area  $\Omega$  where the external force is applied. If the force is not harmonic in time, the solution for the forced vibration can be obtained by integration of solution (4.8) over the frequency range.

As for the analysis of vibrations of finite plates, the general approach is the same as that for finite beams and NDOF systems. A finite plate of any geometry has an infinite countable number of the normal modes. The mode shapes are orthogonal and constitute a complete set functions, so that any free or forced vibrations of the finite plate can be decomposed into normal modes and found from the initial conditions and the prescribed force.

It is worth noting that the normal modes of most finite plates cannot be found analytically. For example, a rectangular plate admits the analytical solution only if a pair of opposite edges are simply supported [ $w = M_{yx} = 0$  or  $w = M_{xy} = 0$ —see Eqs. (4.3) and (4.4)] or sliding ( $\partial w/\partial x = F_{zx} = 0$  or  $\partial w/\partial y = F_{zy} = 0$ ). For a free plate ( $M_{yx} = F_{zx} = 0$  and  $M_{xy} = F_{zy} = 0$ ), clamped plate (displacements and slopes are zero at four edges) and for all other edge conditions analytical solutions are not found yet. However, the natural frequencies and mode shapes have been obtained numerically (by Ritz' method) for most practically important geometries.<sup>16</sup>

The range of validity of the Germin–Lagrange equation is restricted to low frequencies. Similar to the Bernoulli–Euler equation for beams, it is valid if the shear wavelength in the plate material is 10 times greater than the thickness  $h$  and the flexural wavelength is  $6h$  or greater. In the literature, there are several attempts to improve the Germin–Lagrange equation. The best of them is the theory of Uflyand<sup>17</sup> and Mindlin.<sup>18</sup> It relates to the classical theory of Germin–Lagrange just as the Timoshenko theory of beams relates to the Bernoulli–Euler theory: The shear deformations and rotatory inertia are taken into account. As a result, the frequency range of its validity is an order of magnitude wider than that of the classical equation (4.2).

## 4.2 In-Plane Vibration of Plates

In-plane waves and vibration of a plate are symmetric with respect to the midplane and independent from its flexural (antisymmetric) vibrations. In the engineering theory of in-plane vibrations, which is outlined in this subsection, it is assumed that, due to small  $h$  compared to the shear wavelength, all the in-plane displacement and stresses are uniform across the thickness and that the lateral stresses are zero not only at the faces but also inside the plate:

$$\sigma_{xz} = \sigma_{yz} = \sigma_{zz} = 0 \quad (4.9)$$

Mathematically, these assumptions can be written as

$$\begin{aligned} u_x(x, y, z, t) &= u(x, y, t) \\ u_y(x, y, z, t) &= v(x, y, t) \\ u_z(x, y, z, t) &= -\frac{vz}{1-\nu} \left( \frac{\partial u}{\partial x} + \frac{\partial v}{\partial y} \right) \end{aligned} \quad (4.10)$$

Computing from (4.9) and (4.10) the kinetic and potential energies, one can obtain, using the variational principle of the least action, the following equations<sup>15</sup>:

$$\begin{aligned} K_l \frac{\partial^2 u}{\partial x^2} + K_t \frac{\partial^2 u}{\partial y^2} + \Delta K \frac{\partial^2 v}{\partial x \partial y} - \rho h \ddot{u} &= -p_x(x, y, t) \\ K_t \frac{\partial^2 v}{\partial x^2} + K_l \frac{\partial^2 v}{\partial y^2} + \Delta K \frac{\partial^2 u}{\partial x \partial y} - \rho h \ddot{v} &= -p_y(x, y, t) \end{aligned} \quad (4.11)$$

where  $u$  and  $v$  are the displacements in  $x$  and  $y$  directions (see Fig. 13); the thin plate longitudinal and shear stiffnesses are equal to

$$\begin{aligned} K_l &= \frac{Eh}{1-\nu^2} \quad K_t = Gh = \frac{Eh}{2(1+\nu)} \\ \Delta K &= K_l - K_t = \frac{Eh}{2(1-\nu)} \end{aligned} \quad (4.12)$$

and  $p_x, p_y$  are the surface densities of external forces. Two boundary conditions should be prescribed at each edge, and the following force–displacement relations take place:

$$\begin{aligned} F_{xx} &= K_l \left( \frac{\partial u}{\partial x} + \nu \frac{\partial v}{\partial y} \right) \\ F_{xy} = F_{yx} &= K_t \left( \frac{\partial v}{\partial x} + \frac{\partial u}{\partial y} \right) \\ F_{yy} &= K_l \left( \frac{\partial v}{\partial y} + \nu \frac{\partial u}{\partial x} \right) \end{aligned} \quad (4.13)$$

Elementary in-plane wave motions have the form of a time-harmonic plane wave propagating at angle  $\psi$  to  $x$  axis:

$$\begin{bmatrix} u(x, y, t) \\ v(x, y, t) \end{bmatrix} = \begin{bmatrix} u \\ v \end{bmatrix} \exp[ik(x \cos \psi + y \sin \psi) - i\omega t]$$

It satisfies homogeneous equations (4.11) and the following dispersion equation:

$$(k^2 - k_l^2)(k^2 - k_t^2) = 0 \quad (4.14)$$

where  $k_l = \omega/c_l$ ,  $k_t = \omega/c_t$ . It is seen that two types of plane waves exist on the plate. The first is the longitudinal wave

$$A_l \begin{bmatrix} \cos \psi \\ \sin \psi \end{bmatrix} \exp[ik_l(x \cos \psi + y \sin \psi) - i\omega t]$$

that propagates with the phase velocity  $c_l = (K_l/\rho h)^{1/2}$  in which the plate particles move in the direction of wave propagation. The second is the shear wave

$$A_t \begin{bmatrix} -\sin \psi \\ \cos \psi \end{bmatrix} \exp[ik_t(x \cos \psi + y \sin \psi) - i\omega t]$$

that propagates with the phase velocity  $c_t = (K_t/\rho h)^{1/2}$  in which the plate particles displacements are perpendicular to the direction of wave propagation. Both waves are propagating ones at all frequencies. Their group and energy velocities are equal to the phase velocity and do not depend on frequency. For that reason, any in-plane disturbance propagates along the plate without distortion.

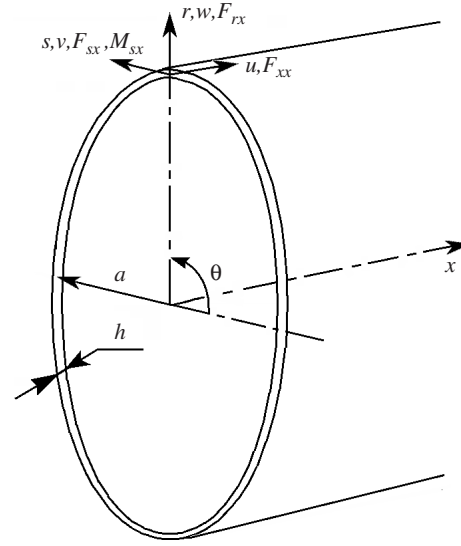
As in case of flexural vibration, problems of free or forced in-plane vibration of a finite plate are seldom solvable analytically. For example, for rectangular plates analytical solutions exist only if at a pair of the opposite edges the so-called mixed boundary conditions are prescribed (the mixed conditions at an edge normal to  $x$  axis are  $F_{xx} = v = 0$  or  $F_{yx} = u = 0$ ; at an edge normal to the  $y$  axis they are  $F_{xy} = v = 0$  or  $F_{yy} = u = 0$ ). For all other boundary conditions, the natural frequencies and modal shapes should be computed numerically.<sup>16</sup>

The frequency range of validity of Eqs. (4.11) is rather wide—the same as that of the Bernoulli equation (3.4) of longitudinal vibration in beams (see Fig. 10). They are valid even if the shear wavelength is comparable with the plate thickness  $h$ .

### 4.3 Vibration of Shells

Shells are models of curved thin-walled elements of engineering structures such as ship hulls, fuselages, cisterns, pipes, and the like. Most theories of shell vibration are based on Kirchhoff–Love’s hypothesis that is very similar to that of flat plates. Since flexural and in-plane vibrations are coupled in shells, the corresponding engineering equations are rather complicated even in the simplest cases: The total order of the space derivatives is eight. In this subsection, waves and vibration of a uniform closed circular cylindrical shell are briefly documented. Results of more detailed analysis of vibration of this and other shells can be found elsewhere.<sup>19</sup>

According to Kirchhoff–Love’s hypothesis, the shell thickness  $h$  is small compared to the shear wavelength, to other two dimensions, and to the smaller radius of curvature. Therefore, the transverse normal stresses are assumed zero, and plane cross sections perpendicular to the undeformed middle surface remain plane and perpendicular to the deformed middle surface. These may be written as a kinematic hypothesis, which is a combination of hypotheses (4.1) and (4.10). After computing, with the help of Hook’s law and surface theory relations, the strains and stresses, kinetic and potential energy, one can obtain from the variational principle the following



**Figure 14** Circular cylindrical shell and the positive direction of the displacements, forces, and moments at  $x$  cross section.

engineering equations known as *Donnell–Mushtari equations*<sup>19</sup>:

$$\rho h \ddot{\mathbf{u}}(x, s, t) - \mathbf{L} \mathbf{u}(x, s, t) = \mathbf{q}(x, s, t) \quad (4.15)$$

where  $s = a\theta$  (see Fig. 14),  $a$  and  $h$  are the radius and thickness of the shell,  $\mathbf{u} = [u, v, w]^T$  is the displacement vector,  $\mathbf{q}$  is the vector of the external force densities,  $\mathbf{L}$  is the  $3 \times 3$  matrix of the differential operators:

$$\begin{aligned} L_{11} &= K_l \frac{\partial^2}{\partial x^2} + K_t \frac{\partial^2}{\partial s^2} \\ L_{12} &= L_{21} = \Delta K \frac{\partial^2}{\partial x \partial s} \\ L_{13} &= -L_{31} = \nu K_l \frac{1}{a} \frac{\partial}{\partial x} \\ L_{22} &= K_t \frac{\partial^2}{\partial x^2} + K_l \frac{\partial^2}{\partial s^2} \\ L_{23} &= -L_{32} = K_l \frac{1}{a} \frac{\partial}{\partial s} \\ L_{33} &= K_l \frac{1}{a^2} + D \Delta^2 \end{aligned} \quad (4.16)$$

Here  $K_l$ ,  $K_t$ , and  $D$  are the longitudinal, shear, and flexural thin-plate stiffnesses—see Eqs. (4.2) and (4.12),  $\Delta = \partial^2/\partial x^2 + \partial^2/\partial s^2$ . Four boundary conditions should be prescribed at each edge. The

forces and moments at cross-section  $x = \text{const.}$  are

$$\begin{aligned} F_{xx} &= -K_l \left( \frac{\partial u}{\partial x} + \nu \frac{\partial v}{\partial s} + \nu \frac{w}{a} \right) \\ F_{sx} &= -K_t \left( \frac{\partial u}{\partial s} + \frac{\partial v}{\partial x} \right) \\ F_{rx} &= -D \left[ \frac{\partial^3 w}{\partial x^3} + (2 - \nu) \frac{\partial^3 w}{\partial x \partial s^2} \right] \\ M_{sx} &= -D \left( \frac{\partial^2 w}{\partial x^2} + \nu \frac{\partial^2 w}{\partial s^2} \right) \end{aligned} \quad (4.17)$$

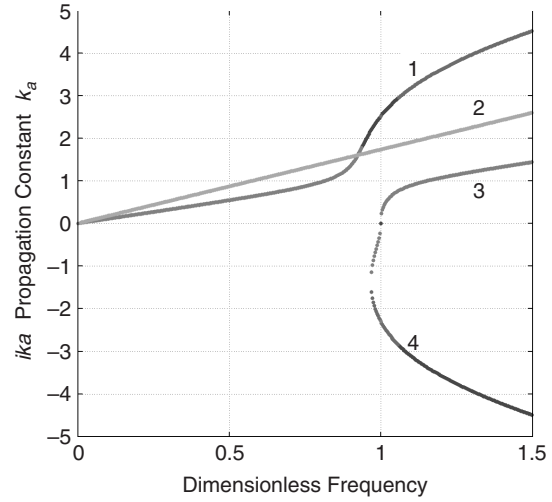
Among a large number of thin-shell engineering theories, Eqs. (4.15) are the simplest that describe coupled flexural and in-plane vibration. When radius  $a$  of the shell tends to infinity, these two types of vibration become uncoupled: Eqs. (4.15) reduce to Eqs. (4.11) for in-plane vibration and to the classical Germin–Lagrange equation (4.2). The matrix operator  $\mathbf{L}$  in (4.15) is self-adjoint, and, hence, the reciprocal Maxwell–Betti theorem is valid in the Donnell–Mushtari shell.

From the wave theory point of view, a thin cylindrical shell is a 2D solid waveguide.<sup>9</sup> At each frequency, there exist, in such a waveguide, an infinite (countable) number of the normal modes of the form

$$\mathbf{u}_m(x, s, t) = \mathbf{u}_m(s) \exp(ikx - i\omega t) \quad (4.18)$$

where  $k$  and  $\mathbf{u}_m(s)$  are the propagation constant and shape of the normal mode,  $m = 0, 1, 2, \dots$ . For a closed cylindrical shell, the shape function  $\mathbf{u}_m(s)$  is a periodic function of  $s$  with period  $2\pi a$  and, hence, can be decomposed into the Fourier series. For circumferential number  $m$  the shapes are  $[u_m \cos \psi_m, v_m \sin \psi_m, w_m \cos \psi_m]^T$  or  $[u_m \sin \psi_m, -v_m \cos \psi_m, w_m \sin \psi_m]^T$ ,  $\psi_m = ms/a$ ;  $u_m, v_m, w_m$  are the complex amplitudes of the displacement components. Substitution of (4.18) into Eq. (4.15) leads to the dispersion relation in the form of a polynomial of the fourth order with respect to  $k^2$ . Hence, for each circumferential number  $m$ , there are four root pairs  $\pm k_j$ ,  $j = 1 \div 4$ , that correspond to four types of the normal modes.

Consider axisymmetric normal modes,  $m = 0$ . The real and imaginary branches of dispersion are shown in Fig. 15. One real-valued root of the dispersion equation is  $k = \pm k_t$  (curve 2). It corresponds to the propagating torsional wave. Another real-valued root at low frequencies is  $k = \pm k_l$ . It corresponds to the longitudinal propagating wave. The remaining low-frequency roots of the dispersion equation are complex and correspond to complex evanescent waves. The frequency  $\text{rf}$  for which  $k_l a = f/\text{rf} = 1$  is called *the ring frequency*. At this frequency, the infinite shell is pulsating in the radial direction while the tangential and axial displacements are zero. Near the ring frequency, two complex waves transform into



**Figure 15** First four real and imaginary branches of dispersion of the axisymmetric ( $m = 0$ ) normal modes of the Donnell–Mushtari closed cylindrical shell:  $h/a = 0.02$ ; frequency is normalized with the ring frequency.

one propagating wave and one evanescent wave. At high frequencies, the four shell normal waves are indiscernible from two flexural and two in-plane waves of the flat plate.

Very similar behavior demonstrates dispersion of normal modes with higher circumferential numbers  $m$ . For  $m \geq 2$ , all low-frequency roots of the dispersion equation are complex, and the corresponding normal modes are complex evanescent waves. At higher frequencies, they transform into imaginary evanescent and propagating waves. And at very high frequencies the dispersion of the shell normal modes tends to dispersion of the plate waves (4.6) and (4.14).

Analysis of finite shell vibrations is very similar to that of other elastic systems: Free or forced vibrations are decomposed in the normal modes. The natural frequencies and mode shapes are obtained from solution of Eqs. (4.15) with four boundary conditions at each edge. The most simple is the case of the so-called Navier conditions at both edges  $x = 0, l$ . These are mixed conditions [e.g.,  $M_{sx} = w = F_{xx} = v = 0$ —see Eq. (4.17)]. The shell normal modes do not interact at such edges reflecting independently. Finite shells with other boundary conditions are analyzed numerically.<sup>19</sup>

The range of validity of the Donnell–Mushtari theory, as well as of other theories based on the Kirchhoff–Love hypothesis, is restricted to low frequencies. Their energy errors are estimated as  $\max\{(kh)^2, h/a\}$ .

The theory of Donnell–Mushtari admits one important simplification. When a shell is very thin and, hence, very soft in bending, the flexural stiffness may be neglected,  $D = 0$ , and Eqs. (4.15) become of the fourth order. This case corresponds to *the membrane theory*. On the contrary, when a shell is thick, more

complicated theories are needed to take into account the additional shear deformations and rotatory inertia (as in the Timoshenko beam theory) as well as other effects.<sup>14,19</sup>

## REFERENCES

1. E. J. Skudrzyk, *Simple and Complex Vibratory Systems*, Penn State University Press, University Park, PA, 1968.
2. A. E. H. Love, *Treatise on the Mathematical Theory of Elasticity*, Dover, New York, 1944.
3. R. A. Horn and C. R. Johnson, *Matrix Analysis*, Cambridge University Press, Cambridge, 1986.
4. D. E. Newland, "On the Modal Analysis of Non-conservative Linear Systems," *J. Sound Vib.*, Vol. 112, 1987, pp. 69–96.
5. T. K. Caughey and F. Ma, "Analysis of Linear Nonconservative Vibrations," *ASME J. Appl. Mech.*, Vol. 62, 1995, pp. 685–691.
6. P. M. Morse and K. Uno Ingard, *Theoretical Acoustics*, Princeton University Press, Princeton, NJ, 1986.
7. M. A. Biot, "General Theorems on the Equivalence of Group Velocity and Energy Transport," *Phys. Rev.*, Vol. 105, Ser. 2, 1957, pp. 1129–1137.
8. A. D. Nashif, D. I. G. Jones, and J. P. Henderson, *Vibration Damping*, Wiley, New York, 1985.
9. M. Redwood, *Mechanical Waveguides*, Pergamon, New York, 1960.
10. S. P. Timoshenko, "Theory of Bending, Torsion, and Stability of Thin-Walled Beams of Open Cross-sections," (1945), in *The Collected Papers*, McGraw-Hill, New York, 1953.
11. S. P. Timoshenko, "On the Correction for Shear of the Differential Equation for Transverse Vibrations of Prismatic Bars," (1921), in *The Collected Papers*, McGraw-Hill, New York, 1953.
12. R. D. Blevins, *Formulas for Natural Frequencies and Mode Shapes*, Van Nostrand Reinold New York, 1979.
13. Yu. I. Bobrovnikskii and K. I. Maltsev, "Engineering Equations for Beam Vibration," *Soviet Phys. Acoust.*, Vol. 29, No. 4, 1983, pp. 351–357.
14. K. F. Graff, *Wave Motion in Elastic Solids*, Ohio State University Press, Columbus, OH, 1975.
15. L. D. Landau and E. M. Lifshitz, *Theory of Elasticity*, 2nd ed., Pergamon, Oxford, 1986.
16. A. W. Leissa, *Vibration of Plates*, ASA Publications, Columbus, OH, 1993.
17. Ya. S. Uflyand, "Wave Propagation under Transverse Vibrations of Beams and Plates," *Appl. Math. Mech.*, Vol. 12, 1948, pp. 287–300.
18. R. D. Mindlin, "Influence of Rotatory Inertia and Shear on Flexural Motion of Isotropic Elastic Plates," *ASME J. Appl. Mech.*, Vol. 18, 1951, pp. 31–38.
19. A. W. Leissa, *Vibration of Shells*, ASA Publications, Columbus, OH, 1993.

## BIBLIOGRAPHY

- Achenbach, J. D., *Wave Propagation in Elastic Solids*, North-Holland, New York, 1984.
- Bolotin, V. V., *Random Vibration of Elastic Structures*, Martinus Nijhoff, The Hague, 1984.
- Braun, S. G., Ewins, D. J., and Rao S. S. (Eds.), *Encyclopedia of Vibration*, 3 vol; Academic, San Diego, 2002.
- Cremer, L., Heckl, M., and Ungar, E. E. *Structure-Borne Sound*, Springer, New York, 1973.
- Crocker, M. (Ed.), *Encyclopedia of Acoustics*, Wiley, New York, 1997.
- Inman, J. J., *Engineering Vibrations*, Prentice-Hall, Englewood Cliffs, NJ, 1995.
- Meirovitch, L., *Fundamentals of Vibrations*, McGraw-Hill, New York, 2001.
- Rao, S. S., *Mechanical Vibrations*, 3rd ed, Addison-Wesley, Reading, MA, 1995.
- Rayleigh, Lord, *Theory of Sound*, Dover, New York, 1945.
- Soedel, W., *Vibration of Shells and Plates*, 2nd ed, Marcel Dekker, New York, 1993.



# CHAPTER 13

## RANDOM VIBRATION

David E. Newland  
Engineering Department  
Cambridge University  
Cambridge, United Kingdom

### 1 INTRODUCTION

Random vibration combines the statistical ideas of random process analysis with the dynamical equations of applied mechanics. The theoretical background is substantial, but its essence lies in only a few fundamental principles. Familiarity with these principles allows the solution of practical vibration problems. Random vibration includes elements of probability theory, correlation analysis, spectral analysis, and linear system theory. Also, some knowledge of the response of time-varying and nonlinear systems is helpful.

### 2 SUMMARY OF STATISTICAL CONCEPTS

Random vibration theory seeks to provide statistical information about the severity and properties of vibration that is irregular and does not have the repetitive properties of deterministic (nonrandom) harmonic motion. This statistical information is represented by probability distributions.

#### 2.1 First-Order Probability Distributions

*Probability distributions* describe how the values of a random variable are distributed. If  $p(x)$  is the *probability density function* for a random variable  $x$ , then  $p(x)dx$  is the probability that the value of  $x$  at any chosen time will lie in the range  $x$  to  $x + dx$ . For example, if  $p(x)dx = .01$ , then there is a 1 in 100 chance that the value of  $x$  at the selected time will lie in the chosen band  $x$  to  $x + dx$ . Since there must be some value for  $x$  between  $-\infty$  and  $+\infty$ , it follows that

$$\int_{-\infty}^{\infty} p(x) dx = 1 \quad (1)$$

The *average (or mean) value* of  $x$  is expressed as  $E[x]$  and is given by the equation

$$E[x] = \int_{-\infty}^{\infty} x p(x) dx \quad (2)$$

The *ensemble average* symbol  $E$  indicates that the average has been calculated for infinitely many similar situations. The idea is that an experiment is being conducted many times, and that the measured value is recorded simultaneously for all the ongoing similar experiments. This is different from sampling the same experiment many times in succession to calculate a *sample average*. Only if the random process is

*stationary* and *ergodic* will the sample average be the same as the ensemble average.

A process is said to be *stationary* if its statistical descriptors do not change with time. It is also *ergodic* if every sample function has the same sample averages.

#### 2.2 Higher-Order Probability Distributions

This idea of distributions is extended to cases when there are more than one random variable, leading to the concept of *second-order probability density functions*,  $p(x_1, x_2)$ . Corresponding to (1), these have to be normalized so that

$$\int_{-\infty}^{\infty} \int_{-\infty}^{\infty} p(x_1, x_2) dx_1 dx_2 = 1 \quad (3)$$

and the ensemble average of the product of random variables  $x_1 x_2$  is then given by

$$E[x_1 x_2] = \int_{-\infty}^{\infty} \int_{-\infty}^{\infty} x_1 x_2 p(x_1, x_2) dx_1 dx_2 \quad (4)$$

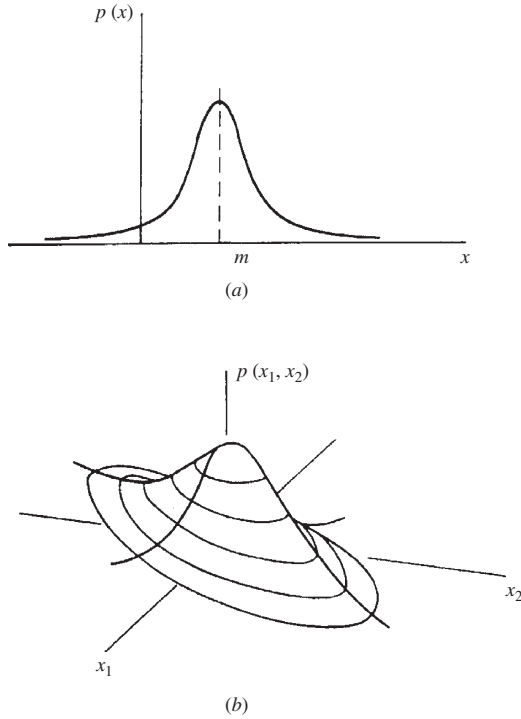
If all the higher-order probability density functions  $p(x_1, x_2, x_3, \dots)$  of a random process are known, then its statistical description is complete. Of course, they never are known because an infinite number of measurements would be needed to measure them, but it is often assumed that various simplified expressions may be used to define the *probability distribution* of a random process.

#### 2.3 Commonly Assumed Probability Distributions

The most common assumption is that a random variable has a normal or *Gaussian distribution* (Fig. 1). Then  $p(x)$  has the familiar bell-shaped curve, and there are similar elliptical bell shapes in higher dimensions. Equations for the Gaussian bell are given, for example, in Newland.<sup>1</sup>

A second common assumption is the *Rayleigh distribution* (Fig. 2a). This is often used to describe how peaks are distributed (every peak is assumed to have an amplitude somewhere between zero and infinity, therefore  $p(x)$  is zero for  $x < 0$ ).

A more general but similar distribution is defined by the *Weibull function* (Fig. 2b). This has been found to represent some experimental situations quite well and is often used. Equations for Rayleigh and Weibull distributions are also given in Newland.<sup>1</sup>



**Figure 1** (a) First-order Gaussian probability density function and (b) second-order Gaussian probability surface.

## 2.4 Autocorrelation and Spectral Density

In order to describe the statistical frequency of random processes, the concept of *spectral density* is used. The idea is that, although a random signal will have no harmonics (as a periodic signal would have), its energy will be distributed continuously across the frequency spectrum from very low or zero frequency to very high frequencies. Because a stationary random signal has no beginning or ending (in theory), its Fourier transform does not exist. But if the signal is averaged to compute its *autocorrelation function*  $R_{xx}(\tau)$  defined by

$$R_{xx}(\tau) = E[x(t)x(t + \tau)] \quad (5)$$

this function decays to zero for  $\tau$  large (Fig. 3).

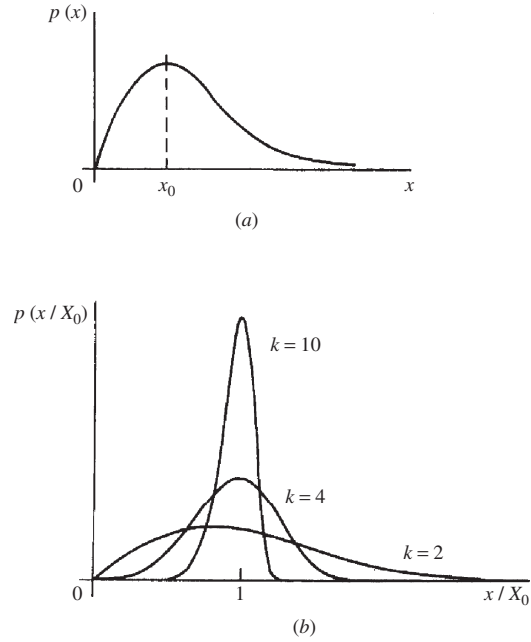
The graph becomes asymptotic to the square of the mean value  $m^2$  and is confined between upper and lower limits  $m^2 \pm \sigma^2$  where  $\sigma$  is the standard deviation defined by

$$\sigma^2 = E[x^2] - m^2 \quad (6)$$

and  $m$  is the mean value defined by

$$m = E[x] \quad (7)$$

The Fourier transform of  $R_{xx}(\tau)$  is the mean-square *spectral density* of the random process  $x(t)$ . Its formal



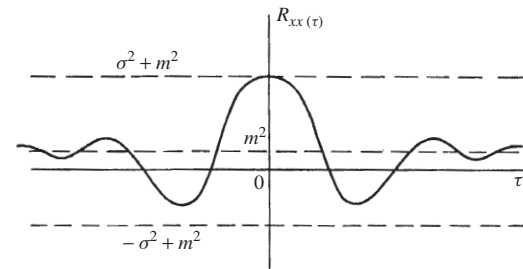
**Figure 2** (a) Rayleigh probability density function and (b) Weibull probability density functions (different choices of the parameter  $k$  are possible).

definition is

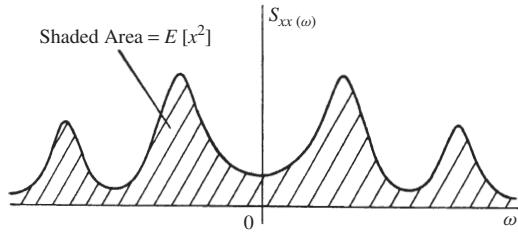
$$S_{xx}(\omega) = \frac{1}{2\pi} \int_{-\infty}^{\infty} R_{xx}(\tau) e^{-i\omega\tau} d\tau \quad (8)$$

In this formula  $\omega$  is the angular frequency (units of radians/second) and, to allow the complex exponential representation to be used, must run from minus infinity to plus infinity. However  $S_{xx}(\omega)$  is symmetrical about the  $\omega = 0$  position (Fig. 4).

It can be shown that  $S_{xx}(\omega)$  is always real and positive and the area under the graph in Fig. 4 is numerically equal to the signal's mean-square value  $E[x^2]$  (see Newland<sup>1</sup>).



**Figure 3** Typical autocorrelation function for a stationary random process.



**Figure 4** Typical spectral density function plotted as a function of angular frequency.

By computing the inverse Fourier transform of  $S_{xx}(\omega)$ , the autocorrelation function  $R_{xx}(\tau)$  can be recovered.

### 2.5 Cross Correlation and Cross Spectral Density

Similar relationships hold for cross-correlation functions in which sample functions from two different random processes are averaged, and these lead to the theory of *cross correlation* and the *cross-spectral density function*  $S_{xy}(\omega)$  where the subscripts  $x$  and  $y$  indicate that samples from two different random variables  $x(t)$  and  $y(t)$  have been processed. A selection of relevant source literature is included in Refs. 1 to 9.

There are specialist *fast Fourier transform (FFT)* algorithms for computing spectral densities. These are routinely used for practical calculations (see Newland,<sup>1</sup> Press et al.,<sup>10</sup> and Chapter 42 of this handbook).

## 3 SUMMARY OF APPLIED MECHANICS CONCEPTS

Applied mechanics theory (see, e.g., Newland<sup>11</sup>) provides the system response properties that relate response and excitation. Therefore, applied mechanics theory allows the input–output properties of dynamical systems to be calculated and provides the connection between random vibration excitation and the random vibration response of deterministic systems.

### 3.1 Frequency Response Function

For time-invariant linear systems with an input  $x(t)$  and a response  $y(t)$ , if the input is a harmonic forcing function represented by the complex exponential function

$$x(t) = e^{i\omega t} \quad (9)$$

the response is, after starting transients have decayed to zero,

$$y(t) = H(i\omega)e^{i\omega t} \quad (10)$$

where  $H(i\omega)$  is the complex *frequency response function* for the system.

### 3.2 Impulse Response Function

Corresponding to the frequency response function is its (inverse) Fourier transform

$$h(t) = \frac{1}{2\pi} \int_{-\infty}^{\infty} H(i\omega)e^{i\omega t} d\omega \quad (11)$$

which is called the *impulse response function*. It can be shown (see Newland<sup>1</sup>) that  $h(t)$  describes the response of the same system when a unit impulsive hammer blow is applied to the input with the system initially quiescent.

## 4 INPUT–OUTPUT RESPONSE RELATIONSHIPS FOR LINEAR SYSTEMS

### 4.1 Single-Input, Single-Output (SISO) Systems

There are two key input–output relationships.<sup>1</sup> The first relates the *average value* of the response of a linear time-invariant system when excited by stationary random vibration to the average value of the excitation. If  $x(t)$  is the input (or excitation) with ensemble average  $E[x]$  and  $y(t)$  is the output (or response) with ensemble average  $E[y]$ , and if  $H(i0)$  is the (real) value of the frequency response function  $H(i\omega)$  at zero frequency,  $\omega = 0$ , then

$$E[y] = H(i0)E[x] \quad (12)$$

For linear systems, the mean level of excitation is transmitted as if there were no superimposed random fluctuations. Since, for many systems, there is no response at zero frequency, so that  $H(i0) = 0$ , it follows that the mean level of the response is zero whether the excitation has a zero mean or not.

The second and key relationship is between the *spectral densities*. The input spectral density  $S_{xx}(\omega)$  and the output spectral density  $S_{yy}(\omega)$  are connected by the well-known equation

$$S_{yy}(\omega) = |H(i\omega)|^2 S_{xx}(\omega) \quad (13)$$

This says that the spectral density of the output can be obtained from the spectral density of the input by multiplying by the magnitude of the frequency response function squared. Of course, all the functions are evaluated at the same frequency  $\omega$ . It is assumed that the system is linear and time invariant and that it is excited by random vibration whose statistical properties are stationary.

### 4.2 Multiple Input, Multiple Output (MIMO) Systems

For Eq. (13), there is only one input and one output. For many practical systems there are many inputs and several outputs of interest. There is a corresponding result that relates the spectral density of each output to the spectral densities of all the inputs and the cross-spectral densities of each pair of inputs (for every input paired with every other input). The result is conceptually similar to (13) and is usually expressed in matrix form<sup>1,8</sup>:

$$S_{yy}(\omega) = H^*(\omega)S_{xx}(\omega)H^T(\omega) \quad (14)$$

where now the functions are matrices. For example, the function in the  $m$  th row and  $n$  th column of  $S_{yy}(\omega)$

is the cross-spectral density between the  $m$ th and  $n$ th outputs. The asterisk in (14) denotes the complex conjugate of  $H(\omega)$  and the  $T$  denotes the transposition of  $H(\omega)$ .

There are similar matrix relationships between all the input and output statistics for time-invariant, linear systems subjected to stationary excitation. There is an extension for the general case of continuous systems subjected to distributed excitation, which is varying randomly in space as well as time, and simplifications when modal analysis can be carried out and results expressed in terms of the response of normal modes. These are covered in the literature, for which a representative sample of relevant reference sources is given in the attached list of references.

## 5 INPUT-OUTPUT RESPONSE RELATIONSHIPS FOR OTHER SYSTEMS

### 5.1 General

The theoretical development is much less cut-and-dried when the system that is subjected to random excitation is a nonlinear system or, alternatively, is a linear system with parametric excitation.<sup>12</sup> The responses of such systems have not yet been reduced to generally applicable results. Problems are usually solved by approximate methods. Although, in principle, exact solutions for the response of any dynamical system (linear or nonlinear) subjected to white Gaussian excitation can be obtained from the theory of *continuous Markov processes*, exact solutions are rare, and approximate methods have to be used to find solutions. This puts Markov analysis on the same footing as other approximate methods. *Perturbation techniques* and *statistical linearization* are two approximate methods that have been widely used in theoretical analysis.

### 5.2 Perturbation Techniques

The basic idea is to expand the solution as a power series in terms of a small scaling parameter. For example, the solution of the weakly nonlinear system

$$\ddot{y} + \eta \dot{y} + \omega^2 y + \varepsilon f(y, \dot{y}) = x(t) \quad (15)$$

where  $|\varepsilon| \ll 1$ , is assumed to have the form

$$y(t) = y_0(t) + \varepsilon y_1(t) + \varepsilon^2 y_2(t) + \cdots \quad (16)$$

After substituting (16) into (15) and collecting terms, the coefficients of like powers of  $\varepsilon$  are then set to zero. This leads to a hierarchy of linear second-order equations that can be solved sequentially by linear theory.

Using these results, it is possible to calculate approximations for  $R_{yy}(\tau)$  from (5) and then for the spectral density  $S_{yy}(\omega)$  from the transform equation (8). Because of their complexity, in practice results have generally been obtained to first-order accuracy only. The method can be extended to multi-degree-of-freedom systems, but there may then be

huge algebraic complexity. A general proof of convergence is not currently available.

### 5.3 Statistical Linearization

This method involves replacing the governing set of differential equations by a set of linear differential equations that are “equivalent” in some way. The parameters of the equivalent system are obtained by minimizing the equation difference, calculated as follows. If a linear system

$$\ddot{y} + \eta_e \dot{y} + \omega_e^2 y = x(t) \quad (17)$$

is intended to be equivalent to the nonlinear system (15), the equation difference is obtained by subtracting one equation from the other to obtain

$$e(y, \dot{y}) = \varepsilon f(y, \dot{y}) + (\eta - \eta_e) \dot{y} + (\omega^2 - \omega_e^2) y \quad (18)$$

where  $\eta_e$  and  $\omega_e^2$  are unknown parameters. They are chosen so as to minimize the mean square of the equation difference  $e(y, \dot{y})$ .

This requires the probability structure of  $y(t)$  and  $\dot{y}(t)$  to be known, which usually it is not. Instead it is assumed that the response variables have a Gaussian distribution. Even if  $x(t)$  is not Gaussian, it has been found that this will be approximately true for lightly damped systems.

There has been considerable research on the statistical linearization method,<sup>13,14</sup> and it has been used to analyze many practical response problems, including problems in earthquake engineering with hysteretic damping that occurs due to slipping or yielding.

### 5.4 Monte Carlo Simulation

This is the direct approach of numerical simulation. Random excitation with the required properties is generated artificially, and the response it causes is found by numerically integrating the equations of motion. Provided that a sufficiently large number of numerical experiments are conducted by generating new realizations of the excitation and integrating its response, an ensemble of sample functions is created from which response statistics can be obtained by averaging across the ensemble. This permits the statistics of nonstationary processes to be estimated by averaging data from several hundred numerically generated sample functions.

For numerical predictions, either Monte Carlo methods, or the analytical procedures developed by Bendat<sup>15</sup> are generally used.

## 6 APPLICATIONS OF RANDOM VIBRATION THEORY

### 6.1 General

For the wide class of dynamical systems that can be modeled by linear theory, it is possible to calculate all the required statistical properties of the response, provided that sufficient statistical detail is given about the

excitation. In practice, far-ranging assumptions about the excitation are often made, but it is nevertheless of great practical importance to be able to calculate statistical response data and there are many applications.

## 6.2 Properties of Narrow-Band Random Processes

When a strongly resonant system responds to broadband random excitation, its response spectral density falls mainly in a narrow band of frequencies close to the resonant frequency. Since this output is derived by filtering a broadband process, many nearly independent events contribute to it. Therefore, on account of the central limit theorem,<sup>4</sup> the probability distribution of a narrow-band response process approaches that of a Gaussian distribution even if the excitation is not Gaussian.

This is an important result. If the response spectral density of a narrow-band process  $S_{yy}(\omega)$  is known, because it is (assumed) to be Gaussian, all the other response statistics can be derived from  $S_{yy}(\omega)$ .

For any stationary random process  $y(t)$ , it can be shown<sup>1</sup> that the response displacement  $y(t)$  and response velocity  $\dot{y}(t)$  are uncorrelated, so that their joint probability density function  $p(y, \dot{y})$  can be expressed as the product of the two first-order probability density functions  $p(y)$  and  $p(\dot{y})$  for  $y(t)$  and  $\dot{y}(t)$  so that

$$p(y, \dot{y}) = p(y)p(\dot{y}) \quad (19)$$

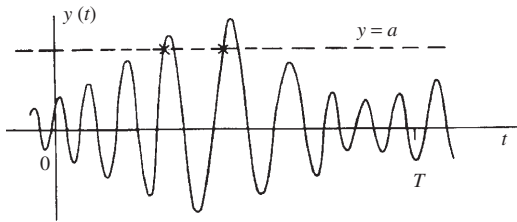
This is important in the development of crossing analysis (see below).

## 6.3 Crossing Analysis

Figure 5 shows a sample function from a stationary narrow-band random process.

The ensemble average number of up-crossings (crossings with positive slope) of the level  $y = a$  in time  $T$  will be proportional to  $T$ , and this leads to the concept of an average frequency for up-crossings, which is usually denoted by the symbol  $v^+(a)$ . For a linear system subjected to Gaussian excitation with zero mean, it can be shown that  $v^+(a)$  is given by

$$v^+(a = 0) = \frac{1}{2\pi} \left[ \frac{\int_{-\infty}^{\infty} \omega^2 S_{yy}(\omega) d\omega}{\int_{-\infty}^{\infty} S_{yy}(\omega) d\omega} \right]^{1/2} \quad (20)$$



**Figure 5** Up-crossings of a sample function from a narrow-band process  $y(t)$ .

This is the ensemble average frequency of zero crossings for the  $y(t)$  process. It is only the same as the average frequency along the time axis if the process is ergodic.

## 6.4 Distribution of Peaks

For a narrow-band process that has one positive peak for every zero crossing, the proportion of cycles whose peaks exceed  $y = a$  is  $v^+(a)/v^+(0)$ . This is the probability that any peak chosen at random exceeds  $a$ . For Gaussian processes, it leads to the result that<sup>1</sup>

$$p_p(a) = \frac{a}{\sigma_y^2} \exp\left(-\frac{a^2}{2\sigma_y^2}\right) \quad (21)$$

for  $a \geq 0$ , which is the Rayleigh distribution shown in Fig. 2a.

This result depends on the assumption that there is only one positive peak for each zero crossing. An expression can be calculated for the frequency of maxima of a narrow-band process, and this assumption can only be valid if the frequency of zero crossings and the frequency of maxima are the same. It turns out that they are the same only if the spectral bandwidth is vanishingly small, which of course it never is. So in practical cases, irregularities in the narrow-band waveform in Fig. 5 give rise to additional local peaks not represented by the Rayleigh distribution (21). A more general (and more complicated) expression for the distribution of peaks can be calculated that incorporates a factor that is the ratio of the average number of zero crossings divided by the average number of peaks. For a broadband random process, there are many peaks for each zero crossing. In the limiting case, the distribution of peaks is just a Gaussian distribution that is the same as the (assumed) Gaussian amplitude distribution.

## 6.5 Envelope Properties

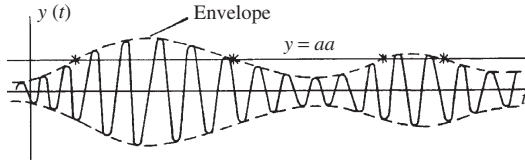
The envelope  $A(t)$  of a random process  $y(t)$  may be defined in various different ways. For each sample function it consists of a smoothly varying pair of curves that just touches the extremes of the sample function but never crosses them. The differences in definition revolve around where the envelope touches the sample function. This can be at the tips of the peaks or slightly to one side of each peak to give greater smoothness to the envelope.

One common definition is to say that the envelope is the pair of curves  $A(t)$  and  $-A(t)$  given by

$$A^2(t) = y^2(t) + \frac{\dot{y}^2(t)}{v^+(0)^2} \quad (22)$$

where  $v^+(0)$  is the average frequency of zero crossings of the  $y(t)$  process.

When  $y(t)$  is stationary and Gaussian, it can then be shown that this definition leads to the following



**Figure 6** Envelope of a sample function from a narrow-band process  $y(t)$ .

envelope probability distribution:

$$p(A) = \frac{A}{\sigma_y^2} \exp\left(-\frac{A^2}{2\sigma_y^2}\right) \quad A \geq 0 \quad (23)$$

which is the same as the probability distribution for the peaks of a narrow band, stationary, Gaussian process (21). However, the two distributions differ if the process  $y(t)$  is not both narrow and Gaussian.

### 6.6 Clumping of Peaks

The response of a narrow-band random process is characterized by a slowly varying envelope, so that peaks occur in clumps. Each clump of peaks greater than  $a$  begins and ends by its envelope crossing the level  $y = a$  (Fig. 6). For a process with a very narrow bandwidth, the envelope is very flat and clumps of peaks become very long.

It is possible to work out an expression for the average number of peaks per clump of peaks exceeding level  $y = a$ , subject to necessary simplifying assumptions. This is important in some practical applications, for example, fatigue and endurance calculations, when a clump of large peaks can do a lot of harm if it occurs early in the duration of loading.

### 6.7 Nonstationary Processes

One assumption that is inherent in the above results is that of stationarity. The statistical properties of the random process, whatever it is, are assumed not to change with time. When this assumption cannot be made, the analysis becomes much more difficult. A full methodology is given in Piersol and Bendat.<sup>7</sup>

If the probability of a nonstationary process  $y(t)$  remains Gaussian as it evolves, it can be shown that its peak distribution is close to a Weibull distribution. The properties of its envelope can also be calculated.<sup>8</sup>

### 6.8 First-Passage Time

The first-passage time for  $y(t)$  is the time at which  $y(t)$  first crosses a chosen level  $y = a$  when time is measured forward from some specified starting point. A stationary random process has no beginning or ending, but the idea that a stationary process can be “turned on” at  $t = 0$  is used to predict the time of failure if this occurs when  $y(t)$  first crosses the  $y = a$  level.

Subject to important simplifying assumptions, the probability density function for first-passage time is

$$p(T) = v^+(a) \exp(-v^+(a)T) \quad T > 0 \quad (24)$$

from which the mean and variance of the first-passage time can be calculated to be

$$E[T] = \frac{1}{v^+(a)} \quad \text{and} \quad \text{var}[T] = \frac{1}{[v^+(a)]^2} \quad (25)$$

A general exact solution for the first-passage problem has not yet been found. The above results are only accurate for crossings randomly distributed along the time axis. Because of clumping, the intervals between clumps will be longer than the average spacing between crossings and the probability of a first-passage excursion will, therefore, be less than indicated by the above theory.

### 6.9 Fatigue Failure under Random Vibration

The calculation of fatigue damage accumulation is complex and there are various different models. One approach is to assume that individual cycles of stress can be identified and that each stress cycle advances a fatigue crack. When the crack reaches a critical size, failure occurs. One cycle of stress of amplitude  $S$  is assumed to generate  $1/N(S)$  of the damage needed to cause failure.

For a stationary, narrow-band random process with average frequency  $v^+(0)$ , the number of cycles in time  $T$  will be  $v^+(0)T$ . If the probability density for the distribution of peaks is  $p_p(S)$ , then the average number of stress cycles in the range  $S$  to  $S + dS$  will be  $v^+(0)T p_p(S) dS$ . The damage done by this number of stress cycles is

$$v^+(0)T p_p(S) dS \frac{1}{N(S)} \quad (26)$$

and so the average damage  $D(T)$  done by all stress cycles together will be

$$E[D(T)] = v^+(0)T \int_0^\infty \frac{1}{N(S)} p_p(S) dS \quad (27)$$

Failure is assumed to occur when the accumulated damage  $D(T)$  is equal to one.

The variance of the accumulated fatigue damage can also be calculated, again subject to simplifying assumptions.<sup>2</sup> It can be shown that, when there is a substantially narrow-band response, an estimate of the average time to failure can be made by assuming that this is the value of  $T$  when  $E[D(T)] = 1$ .

It has been found that (27) tends to overestimate fatigue life, sometimes by an order of magnitude, even for narrow-band processes. Generally, “peak counting” procedures have been found more useful for numerical predictions (see, e.g., Ref. 16).

Of course the practical difficulty is that, although good statistical calculations can be made, the fracture model is highly idealistic and may not represent what really happens adequately.

## REFERENCES

1. D. E. Newland, *An Introduction to Random Vibrations, Spectral and Wavelet Analysis*, 3rd ed., Pearson Education (formerly Longman), 1993, reprinted by Dover, New York, 2005.
2. S. H. Crandall and W. D. Mark, *Random Vibration in Mechanical Systems*, Academic, New York, 1963.
3. G. M. Jenkins and D. G. Watts, *Spectral Analysis and Its Applications*, Holden-Day, San Francisco, 1968.
4. W. B. Davenport, Jr., and W. L. Root, *An Introduction to the Theory of Random Signals and Noise*, McGraw-Hill, New York, 1958.
5. M. Ohta, K. Hatakeyama, S. Hiromitsu, and S. Yamaguchi, "A Unified Study of the Output Probability Distribution of Arbitrary Linear Vibratory Systems with Arbitrary Random Excitation," *J. Sound Vib.*, Vol. 43, 1975, pp. 693–711.
6. J. S. Bendat and A. G. Piersol, *Random Data Analysis and Measurement Procedures*, 3rd ed., Wiley, New York, 2000.
7. A. G. Piersol and J. S. Bendat, *Engineering Applications of Correlation and Spectral Analysis*, 2nd ed., Wiley, New York, 1993.
8. N. C. Nigam, *Introduction to Random Vibrations*, MIT Press, Cambridge, MA, 1984.
9. N. C. Nigam and S. Narayanan, *Applications of Random Vibrations*, Springer, Berlin, 1994.
10. W. H. Press, B. P. Flannery, S. A. Teukolsky, and W. T. Vetterling, *Numerical Recipes*, Cambridge University Press, New York, 1986; also subsequent editions for specific computer languages.
11. D. E. Newland, *Mechanical Vibration Analysis and Computation*, Pearson Education (formerly Longman), 1989, reprinted by Dover, New York, 2005.
12. R. A. Ibrahim, *Parametric Random Vibration*, Research Studies Press and Wiley, New York, 1985.
13. J. B. Roberts and P. D. Spanos, "Stochastic Averaging: An Approximate Method for Solving Random Vibration Problems," *Int. J. Non-Linear Mech.*, Vol. 21, 1986, pp. 111–134.
14. J. B. Roberts and P. D. Spanos, *Random Vibration and Statistical Linearization*, Wiley, New York, 1990.
15. J. S. Bendat, *Nonlinear Systems: Techniques and Applications*, Wiley, New York, 1998.
16. *SAE Fatigue Design Handbook*, AE-22, 3rd ed., Society of Automotive Engineers, Warrendale, PA, 1997.

# CHAPTER 14

## RESPONSE OF SYSTEMS TO SHOCK

**Charles Robert Welch and Robert M. Ebeling**  
Information Technology Laboratory  
U.S. Army Engineer Research and Development Center  
Vicksburg, Mississippi

### 1 INTRODUCTION

Shock loading is a frequent experience. The slamming shut of a door or window, the dropping of a package and its impact onto a hard surface, and the response of a car suspension system to a pothole are everyday examples of shock loading. Less common examples include the explosive loading of structures, the impact of water waves onto piers and marine structures, and the response of targets to high-velocity projectiles.

This chapter treats the response of mechanical systems to shock loading. The nature of shock loading is discussed, and references are provided that give details of some common and uncommon loading functions, such as impact and explosion-induced air blast and water shock. The mechanical systems are simplified as single-degree-of-freedom (SDOF), spring-mass-dashpot systems. A unified treatment is provided that treats the response of these SDOF systems to a combination of directly applied forces and to motions of their supporting bases. SDOF systems fall naturally into one of four categories: undamped, underdamped, critically damped, and overdamped. We describe these categories and then treat the response of undamped and underdamped systems to several loading situations through the use of general methods including the Duhamel integral, Laplace transforms, and shock spectra methods. Lastly, examples of shock testing methods and equipment are discussed.

### 2 NATURE OF SHOCK LOADING AND ASSOCIATED REFERENCES

Shock loading occurs whenever a mechanical system is loaded faster than it can respond. Shock loading is a matter of degree. For loading rates slower than the system's response the system responds to the time-dependent details of the load, but as the loading rate becomes faster than the system's ability to respond, the system's response gradually changes to one that depends on only the total time integral, or impulse, of the loading history.

Undamped and underdamped mechanical systems respond in an oscillatory fashion to transient loads. Associated with this oscillatory behavior is a characteristic natural frequency. Another way of describing

shock loading is that, as the frequency content of the loading history increases beyond the natural frequency of the system, the system's response becomes more impulsive, until in the limit the response becomes pure shock response.

There is an equivalency between accelerating the base to which the SDOF system is attached and applying a force directly to the responding SDOF mass. Hence, shock loading also occurs as the frequency content of the base acceleration exceeds the system's natural frequency.

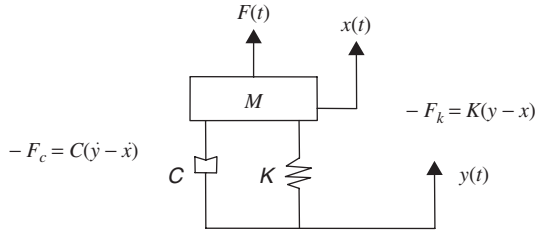
The quintessential historic reference on the response of mechanical systems to transient loads is Lord Rayleigh,<sup>1</sup> which treats many classical mechanical systems such as vibrating strings, rods, plates, membranes, shells, and spheres. A more recent comprehensive text on the topic is Graff,<sup>2</sup> which includes the treatment of shock waves in continua. Meirovitch<sup>3</sup> provides an advanced treatment of mechanical response for the mathematically inclined, while Burton<sup>4</sup> is a very readable text that covers the response of mechanical systems to shock. Harris and Piersol<sup>5</sup> are comprehensive and include Newmark and Hall's pioneering treatment of the response of structures to ground shock. Den Hartog<sup>6</sup> contains problems of practical interest, such as the rolling of ships due to wave action. The history of the U.S. Department of Defense and U.S. Department of Energy activities in shock and vibration is contained in Pusey.<sup>7</sup>

References on the shock loading caused by different phenomena are readily available via government and academic sources. Analytic models for air blast and ground shock loading caused by explosions can be found in the U.S. Army Corps of Engineers publication.<sup>8</sup> The classic reference for explosively generated watershock is Cole.<sup>9</sup> Goldsmith<sup>10</sup> and Rinehart<sup>11</sup> cover impact phenomena, and a useful closed-form treatment of impact response is contained in Timoshenko and Goodier.<sup>12</sup>

References on vibration isolation can be found in Mindlin's classical work on packaging,<sup>13</sup> Sevin and Pilkey,<sup>14</sup> and Balandin, Bolotnik, and Pilkey.<sup>15</sup>

Treatments of shock response similar to this chapter can be found in Thomson and Dahleh,<sup>16</sup> Fertis,<sup>17</sup> Welch and White,<sup>18</sup> and Ebeling.<sup>19</sup>





**Figure 1** Single-degree-of-freedom (SDOF) system exposed to a transient force  $F(t)$  and base motion  $y(t)$ .

### 3 SINGLE-DEGREE-OF-FREEDOM SYSTEMS: FORCED AND BASE-EXCITED RESPONSE

Consider the mass–spring–dashpot systems shown in Fig. 1 in which a transient force  $F(t)$  is applied to the mass  $M$ . Such a system is called a single-degree-of-freedom system because it requires a single coordinate to specify the location of the mass. Let the equilibrium position of the mass (the position of the mass absent all forces) relative to an inertial reference frame be given by  $x(t)$ ; let the location of the base to which the spring and dashpot are attached be given by  $y(t)$ ; and let the force due the spring and the dashpot be given by  $F_k$  and  $F_c$ , respectively. Vector notation is not being used for the various quantities for simplicity and because we are dealing in only one dimension. For a linear elastic spring, with spring constant  $K$ , and a dashpot with viscous dampening constant  $C$ , the spring and dashpot forces are given by

$$-F_k = K(y - x) \quad -F_c = C(\dot{y} - \dot{x}) \quad (1)$$

where a dot over a variable indicates differentiation with respect to time. Employing Newton's second law produces

$$M\ddot{x} = F(t) - F_c - F_k$$

or

$$M\ddot{x} + C(\dot{x} - \dot{y}) + K(x - y) = F(t) \quad (2)$$

Let

$$u = x - y \quad \dot{u} = \dot{x} - \dot{y} \quad \ddot{u} = \ddot{x} - \ddot{y} \quad (3)$$

Employing Eqs. 3 in 2 produces

$$\ddot{u} + \frac{C}{M}\dot{u} + \frac{K}{M}u = \frac{F(t)}{M} - \ddot{y}(t) \quad (4)$$

Equation (4) states that for the SDOF system's response, a negative acceleration of the base,  $-\ddot{y}$ , is equivalent to a force  $F(t)/M$  applied to the mass. This is an important result.

For reasons that will become obvious shortly, define

$$\omega_n^2 = \frac{K}{M} \quad \rho = \frac{C}{2\sqrt{KM}} \quad (5)$$

where  $\omega_n$  is the natural frequency in radians/second and  $\rho$  is the damping ratio. Using Eqs. (5) in (4) produces

$$\ddot{u} + 2\rho\omega_n\dot{u} + \omega_n^2u = \frac{F(t)}{M} - \ddot{y}(t) \quad (6)$$

The complete solution to Eq. 6 (see Spiegel<sup>20</sup>) consists of the solution of the homogeneous form of Eq. (6), added to the particular solution:

$$\ddot{u} + 2\rho\omega_n\dot{u} + \omega_n^2u = 0 \quad (\text{homogeneous equation}) \quad (7)$$

$$\ddot{u} + 2\rho\omega_n\dot{u} + \omega_n^2u = \frac{F(t)}{M} - \ddot{y}(t) \quad (\text{particular equation}) \quad (8)$$

Single-degree-of-freedom systems exhibit four types of behavior dependent on the value of  $\rho$  (see Thomson and Dahleh<sup>16</sup>). To illustrate these, assume there is no applied force [ $F(t) = 0$ ] and no base acceleration ( $\ddot{y} = 0$ ), but that the SDOF system has initial conditions of displacement and velocity given by

$$u(0) = u_1 \quad \dot{u}(0) = \dot{u}_1 \quad (9)$$

Under these conditions, the particular solution is zero, and the system's response is given by solutions to the homogeneous equation [Eq. (7)]. Such a response is termed "free vibration response" (see Chapter 12). The four types of SDOF systems, and their corresponding free vibration response, are given by<sup>16,20</sup>:

For  $\rho = 0$  (undamped oscillatory system):

$$u(t) = u_1 \cos \omega_n t + \frac{\dot{u}_1}{\omega_n} \sin \omega_n t \quad (10)$$

For  $0 < \rho < 1$  (underdamped oscillatory system):

$$u(t) = e^{-\rho\omega_n t} \left( u_1 \cos \omega_D t + \frac{\dot{u}_1 + \rho\omega_n u_1}{\omega_D} \sin \omega_D t \right) \quad (11)$$

For  $\rho = 1$  (critically damped system):

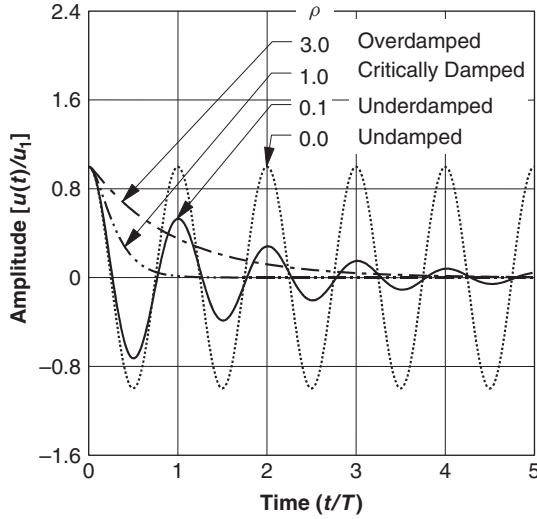
$$u(t) = e^{-\omega_n t} [u_1 + (\dot{u}_1 + \omega_n u_1)t] \quad (12)$$

For  $\rho > 1$  (overdamped systems):

$$u(t) = e^{-\rho\omega_n t} \left\{ \frac{1}{2} \left[ u_1 \left( 1 + \rho \frac{\omega_n}{\omega_D} \right) + \frac{\dot{u}_1}{\omega_D} \right] e^{\omega_D t} + \frac{1}{2} \left[ u_1 \left( 1 - \rho \frac{\omega_n}{\omega_D} \right) - \frac{\dot{u}_1}{\omega_D} \right] e^{-\omega_D t} \right\} \quad (13)$$

where  $\omega_D = \omega_n \sqrt{1 - \rho^2}$  (damped natural frequency).  $\omega_n$  (14)

In Fig. 2, the displacement responses of the four systems for  $u(0) = u_1$ ,  $\dot{u}(0) = 0$  are shown plotted in scaled or normalized fashion as  $u(t)/u_1$ . Time is scaled



**Figure 2** Response of undamped, underdamped, critically damped, and overdamped SDOF systems to an initial displacement  $u_1$ .

by  $t/T$  where  $T$  is the natural period of the oscillatory systems and is given by

$$T = 1/f_n \quad (15)$$

where  $f_n$  is the natural frequency in cycles/second (or hertz) of the oscillatory SDOF systems and is given by

$$f_n = \omega_n/2\pi \quad (16)$$

It is clear from Fig. 2 that the first two systems exhibit oscillatory behavior, and the second two systems do not. The underdamped homogeneous solution converges to the undamped solution for  $\rho = 0$  [Eqs. (11), (12), and (15)]. The SDOF systems encountered most often are either undamped ( $\rho = 0$ ) or underdamped ( $\rho(1)$ ), and from this point forward only these systems will be considered.

In Fig. 2 the natural period of the two oscillatory systems becomes apparent. Shock loading occurs when the duration, rise time, or other significant time variations of  $F(t)$  or  $\ddot{y}(t)$  are small as compared to the natural period of the system. These features manifest themselves as frequency components in the forcing functions or the base accelerations that are higher than the natural or characteristic frequency of the SDOF system (see next section). When pure shock loading occurs, the system responds impulsively by which the time integrals of the force or acceleration history determine the system response.

Shock loading is a matter of degree. Transient forces or accelerations whose rise time to peak are, say, one third of the system's characteristic frequency are less impulsive than forcing phenomena that are 1/100 of the system's response, but impulsive behavior begins when the forcing function  $F(t)$ , or base acceleration  $\ddot{y}(t)$ , has significant time-dependent

features shorter than the system's characteristic or natural period.

#### 4 DUHAMEL'S INTEGRAL AND SDOF SYSTEM RESPONSE TO ZERO RISE TIME, EXPONENTIALLY DECAYING BASE ACCELERATION

The response of an underdamped or undamped SDOF system to an abrupt arbitrary force,  $F(t)$ , or to an abrupt arbitrary base acceleration,  $\ddot{y}(t)$ , can be treated quite generally using Duhamel's integral.<sup>5,16,17</sup> This technique is also applicable to nonshock situations.

Impulse  $I(t)$  is defined as the time integral of force,

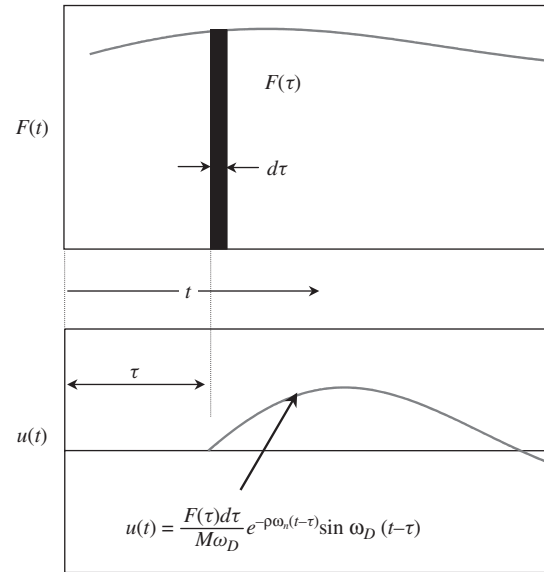
$$I(t) = \int_0^t F(t) dt$$

From Newton's second law,

$$F(t) = M \frac{dv}{dt} \text{ or } dv = \frac{F(t) dt}{M}$$

where  $v$  is the velocity of the mass,  $M$ . This indicates that the differential change in velocity of the mass is equal to the differential impulse divided by the mass.

Now consider the arbitrary force history as shown at top of Fig. 3 that acts on the mass of an SDOF system. At some time,  $\tau$ , into the force history we can identify a segment  $\delta\tau$  wide with amplitude  $F(\tau)$ . This segment will cause a change in velocity of the SDOF mass, but in the limit as  $\delta\tau$  tends toward zero, there will be no time for the system to undergo any displacement. If this segment is considered by itself, then this is



**Figure 3** Arbitrary force history,  $F(t)$ , and an SDOF system's response to a segment  $d\tau$  wide.

equivalent to initial conditions on the SDOF system at  $t = \tau$  of:

$$u(\tau) = 0 \quad \dot{u}_1(\tau) = \frac{F(\tau) d\tau}{M} \quad (17)$$

From Eq. (12) we would expect the response of an underdamped SDOF system to be

$$u(t) = e^{-\rho\omega_n(t-\tau)} \left[ \frac{F(\tau) d\tau}{M\omega_D} \sin \omega_D(t - \tau) \right]$$

The system's response to this segment alone of the force history is shown notionally in the bottom of Fig. 3. The SDOF systems considered thus far are linear systems. An important property of linear systems is that their response to multiple forces can be determined by adding their responses to each of the forces. Hence, to determine the response of the SDOF to the complete force history we can integrate over time, thus

$$u(t) = \frac{1}{M\omega_D} \int_0^t F(\tau) e^{-\rho\omega_n(t-\tau)} \sin \omega_D(t - \tau) d\tau \quad (18)$$

Equation (18) is known variously as Duhamel's integral, the convolution integral, or the superposition integral for an underdamped SDOF system subjected to a force  $F(t)$ . For  $\rho = 0$ , hence  $\omega_D = \omega_n$ , Eq. (18) reduces to the response of an undamped system to an arbitrary force. Because of the superposition property of linear systems, the response of an SDOF system to other forces or initial conditions can be found by adding these other responses to the response given by Eq. (18).

The general form of Duhamel's integral is

$$u(t) = \int_0^t F(\tau) H(t - \tau) d\tau$$

where  $H(t - \tau)$  is the system's response to a unit impulse.

Referring to Eq. (8), we see that a force  $F(t)/M$  is equivalent to acceleration  $-\ddot{y}(t)$ . Thus from Eq. (18) the Duhamel integral can be written immediately for an arbitrary base acceleration history as

$$u(t) = \frac{-1}{\omega_D} \int_0^t \ddot{y}(\tau) e^{-\rho\omega_n(t-\tau)} \sin \omega_D(t - \tau) d\tau \quad (19)$$

Equations (18) and (19) treat the general loading of underdamped and undamped SDOF systems, including that caused by shock loading. Consider now the response of an SDOF system to a shocking base acceleration, specifically an abrupt (zero rise time), exponentially decaying base acceleration of the form:

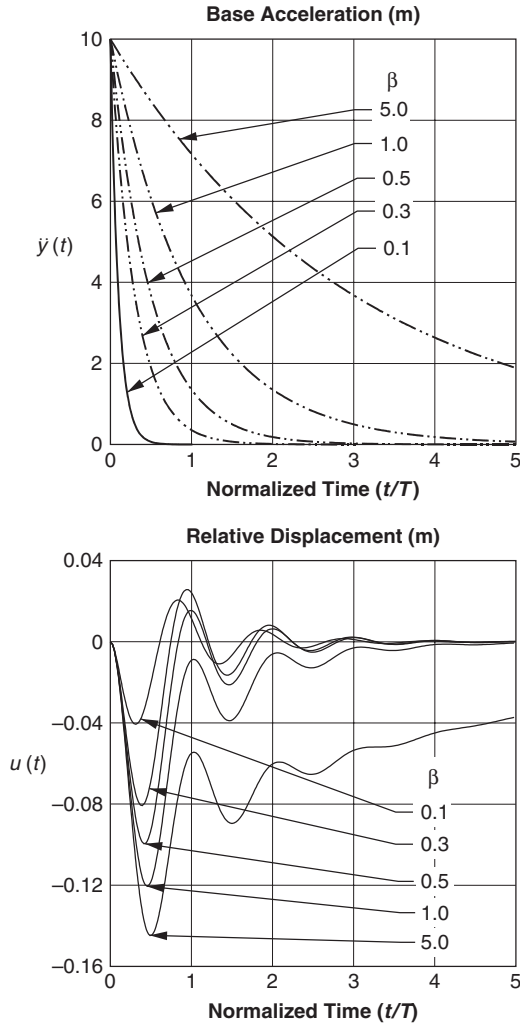
$$\ddot{y}(t) = A_m e^{-t/\beta T} \quad (20)$$

in which the acceleration begins abruptly at  $t = 0$ , with magnitude  $A_m$ , time decay constant  $\beta$ , and  $T$  is the undamped period of the SDOF system. Thus,

$$\beta T = \beta \frac{1}{f_n} = \frac{2\pi\beta}{\omega_n} \quad (21)$$

In Fig. 4  $\ddot{y}(t)$  is shown plotted as a function of normalized time ( $t/T$ ) for several values of the decay constant  $\beta$ . Using Eq. (20) in Eq. (19) produces

$$u(t) = -\frac{A_m}{\omega_D} \int_0^t e^{-\tau/\beta T} e^{-\rho\omega_n(t-\tau)} \sin \omega_D(t - \tau) d\tau \quad (22)$$



**Figure 4** Response of SDOF system to exponential base acceleration of various decay constants ( $A_m = 10 \text{ m/s}^2$ ,  $\omega_n = 10 \text{ rad/s}$ ,  $\rho = 0.2$ ).

Letting

$$\omega_e = \omega_n \left( \frac{1}{2\pi\beta} - \rho \right)$$

Eq. (22) can be expressed as

$$u(t) = -\frac{A_m}{\omega_D} e^{-\rho\omega_n t} \int_0^t e^{-\omega_e \tau} \sin \omega_D(t - \tau) d\tau$$

Carrying out the integration and placing in the limits of integration produces

$$u(t) = \frac{A_m}{\omega_e^2 + \omega_D^2} e^{-\rho\omega_n t} \times \left( \cos \omega_D t - \frac{\omega_e}{\omega_D} \sin \omega_D t - e^{-\omega_e t} \right) \quad (23)$$

Double integrating Eq. (20) with respect to time produces

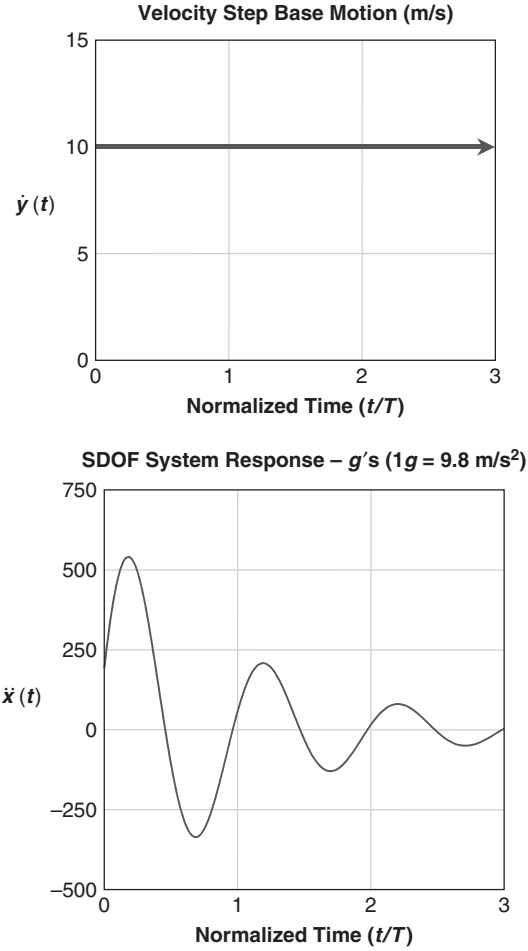
$$y(t) = A_m [(\beta T)t + (\beta T)^2 (e^{-t/\beta T} - 1)] \quad (24)$$

and from Eq. (3), the motion of the mass is given by  $x(t) = u(t) + y(t)$ . The relative displacement  $u(t)$  from Eq. (24) of the SDOF system is shown plotted versus  $(t/T)$  at the bottom of Fig. 4 for several values of the decay constant  $\beta$ . The SDOF system in Fig. 4 has a natural frequency  $\omega_n$  of 10 rad/s, damping  $\rho = 0.2$ , and has a peak base acceleration  $A_m$  of 10 m/s<sup>2</sup>.

## 5 LAPLACE TRANSFORMS AND SDOF SYSTEM RESPONSE TO A VELOCITY STEP FUNCTION

One approach for estimating the response of an SDOF system to an abrupt (shock) base motion is to assume that the base motion follows that of a zero-rise-time permanent change in velocity, that is, a velocity step function (top of Fig. 5). This type of motion contains very high frequency components because of the zero-rise-time nature of the pulse (hence infinite acceleration), and significant low-frequency characteristics because of the infinite duration of the pulse. For many cases in which the base acceleration is not well quantified but is known to be quite large, while the maximum change in velocity of the base is known with some certainty, assuming this type of input provides a useful upper bound on the acceleration experienced by the SDOF mass. It is also useful in the testing of small SDOF systems because for these systems, simulating this type of input is relatively easy in the laboratory.

There are some situations in which the base motion contains frequencies of significant amplitude close to or equal to the natural frequency of the SDOF system. In these cases, the velocity step function input may not be an upper-bound estimate of the acceleration.



**Figure 5** SDOF system response to a base motion consisting of a velocity step ( $f_n = 100$  Hz,  $\rho = 0.15$ ).

For a velocity step function, the base velocity is

$$\dot{y}(t) = V_0 \underline{H}(t - \xi) \quad \xi = 0 \quad (25)$$

where  $V_0$  is the amplitude of the velocity change ( $V_0 = 10$  m/s in Fig. 5), and  $\underline{H}(t - \xi)$  is the modified Heaviside unit step function defined as

$$\begin{aligned} \underline{H}(t - \xi) &= 0 & \text{for } t \leq \xi \\ &= 1 & \text{for } t > \xi \end{aligned}$$

While the velocity of the base is  $V_0$  for  $t > 0$ , the base velocity and displacement at  $t = 0$  are given by

$$y(0) = 0 \quad \dot{y}(0) = 0 \quad (26)$$

As mentioned previously, the velocity step function exposes the SDOF system to infinite accelerations at  $t = 0$  regardless of the magnitude of the velocity.

This is because this change in velocity occurs in zero time. Differentiating Eq. (25) to obtain the acceleration gives

$$\ddot{y}(t) = \frac{d[V_0 H(t - \xi)]}{dt} = V_0 \delta(t - \xi) \quad \xi = 0 \quad (27)$$

where  $\delta(t - \xi)$  is the Dirac delta function whose properties are

$$\begin{aligned} \delta(t - \xi) &= \begin{cases} 0 & \text{for } t \neq \xi \\ \infty & \text{for } t = \xi \end{cases} \\ \int_{-\infty}^{\infty} \delta(t - \xi) dt &= 1 \\ \int_{-\infty}^{\infty} \delta(t - \xi) F(t) dt &= F(\xi) \end{aligned}$$

Equation (27) states that the base of the SDOF system experiences an acceleration that is infinite at  $t = 0$  and zero at all other times, and that the integral of the acceleration is exactly the velocity step function of Eq. (25).

We will assume that the SDOF system mass is stationary at  $t = 0$ , with initial conditions:

$$x(0) = 0 \quad \dot{x}(0) = 0 \quad (28)$$

Using Eqs. (26) and (27) in Eq. (3) results in the initial condition of  $u(t)$ :

$$u(0) = 0 \quad \dot{u}(0) = 0 \quad (29)$$

Laplace transforms can be used to solve the differential equation of motion for this shock problem. Laplace transforms are one of several types of integral transforms (e.g., Fourier transforms) that transform differential equations into a corresponding set of algebraic equations.<sup>20-22</sup> The algebraic equations are then solved, and the solution is had by inverse transforming the algebraic solution. For Laplace transforms the initial conditions are incorporated into the algebraic equations.

If  $g(t)$  is defined for all positive values of  $t$ , then its Laplace transform,  $L[g(t)]$ , is defined as

$$L[g(t)] = \int_0^{\infty} e^{-st} g(t) dt = \bar{g}(s)$$

where  $s$  is called the Laplace transform variable, and  $\bar{g}$  is used to indicate the Laplace transform of  $g$ . Similarly, letting  $L[u(t)] = \bar{u}(s)$  designate the Laplace transform of  $u$ , the Laplace transform of Eq. (8), with  $F(t) = 0$ , becomes

$$L[\ddot{u}(t)] + L[2\rho\omega_n \dot{u}(t)] + L[\omega_n^2 u(t)] = L[-\ddot{y}(t)]$$

or

$$L[\ddot{u}(t)] + 2\rho\omega_n L[\dot{u}(t)] + \omega_n^2 L[u(t)] = -L[V_0 \delta(t)]$$

Employing the definition of the Laplace transform in the above produces

$$\begin{aligned} [s^2 \bar{u} - s u(0) - \dot{u}(0)] + 2\rho\omega_n [s \bar{u} - u(0)] \\ + \omega_n^2 \bar{u} = -V_0 \end{aligned}$$

in which the initial conditions for  $u$  show up explicitly. Using Eq. (29) in the above produces

$$\bar{u} = \frac{-V_0}{s^2 + 2\rho\omega_n s + \omega_n^2} \quad (30)$$

Equation (30) can be rewritten as

$$\begin{aligned} \bar{u} &= \frac{-V_0}{(s + \rho\omega_n)^2 + \omega_n^2 - \rho^2 \omega_n^2} \\ &= \frac{-V_0}{(s + \rho\omega_n)^2 + \omega_D^2} \end{aligned} \quad (31)$$

where we have used  $\omega_D = \omega_n(1 - \rho^2)^{1/2}$ . The inverse transform of Eq. (31) (see Churchill<sup>22</sup>) is

$$u(t) = \frac{-V_0}{\omega_D} e^{-\rho\omega_n t} \sin(\omega_D t) \quad (32)$$

which provides the displacement of the SDOF mass relative to the base on which it is mounted. After  $t = 0$ ,  $\dot{y}(t)$  is a constant, and the acceleration of the mass is given by

$$\ddot{x}(t) = \ddot{u}(t) + \ddot{y}(t) = \ddot{u}(t) \quad \text{for } t > 0$$

and the acceleration of the SDOF mass can be had by differentiating Eq. (32) twice with respect to time to get

$$\begin{aligned} \ddot{x}(t) &= V_0 e^{-\rho\omega_n t} [2\rho\omega_n \cos(\omega_D t) \\ &\quad + (1 - 2\rho^2)\omega_n^2/\omega_D \sin(\omega_D t)] \end{aligned} \quad (33)$$

Using the fact that

$$A \sin(\omega t + \phi) = B \sin(\omega t) + C \cos(\omega t)$$

where

$$\begin{aligned} A &= (C^2 + B^2) \\ \phi &= \arctan(C/B) \end{aligned}$$

Equation (33) becomes

$$\begin{aligned} \ddot{x}(t) &= \frac{V_0 \omega_n}{(1 - \rho^2)^{1/2}} e^{-\rho\omega_n t} \sin(\omega_D t + \phi) \\ \phi &= \arctan \left[ \frac{2\rho(1 - \rho^2)^{1/2}}{(1 - 2\rho^2)} \right] \end{aligned} \quad (34)$$

At the bottom of Fig. 5,  $\ddot{x}(t)$  (in units of acceleration due to gravity,  $g = 9.8 \text{ m/s}^2$ ) from Eq. (34) is shown plotted as a function of normalized time,  $t/T$ , for an SDOF system that has characteristics  $\omega = 2\pi 100 (f_n = 100 \text{ Hz})$ ,  $\rho = 0.15$ , and input base velocity  $V_0 = 10 \text{ m/s}$ .

We will now derive several approximate expressions for the peak acceleration experienced by an SDOF system undergoing a velocity step shock to its base (see Welch and White<sup>18</sup>). These approximations apply to SDOF systems whose dampening ratio is  $\rho < 0.4$ . Differentiating Eq. (34) with respect to time and setting the result equal to zero produces

$$\ddot{x}(t) = 0 = \frac{V_0 \omega_n}{(1 - \rho^2)^{1/2}} e^{-\rho \omega_n t} \times [-\rho \omega_n \sin(\omega_D t + \phi) + \omega_D \cos(\omega_D t + \phi)]$$

Solving for  $t = t_p$ , the time to peak acceleration, in the above and using Eqs. (15) and (34) produces

$$t_p = \frac{1}{\omega_D} \left\{ \arctan \left[ \frac{(1 - \rho^2)^{1/2}}{\rho} \right] - \arctan \left[ \frac{2\rho(1 - \rho^2)^{1/2}}{(1 - 2\rho^2)} \right] \right\} \quad (35)$$

For  $\rho < 0.4$ :

$$\begin{aligned} \arctan \left[ \frac{(1 - \rho^2)^{1/2}}{\rho} \right] &\approx \frac{\pi}{2} - \rho \\ \arctan \left[ \frac{2\rho(1 - \rho^2)^{1/2}}{(1 - 2\rho^2)} \right] &\approx 2\rho \end{aligned} \quad (36)$$

or

$$t_p \approx \frac{1}{\omega_D} \left( \frac{\pi}{2} - 3\rho \right) = \frac{1}{(1 - \rho^2)^{1/2} 2\pi f_n} \left( \frac{\pi}{2} - 3\rho \right) \quad (37)$$

which can be further simplified:

$$t_p \approx \frac{1}{4f_n} - \frac{3\rho}{2\pi f_n} \quad (38)$$

Equation (38) provides reasonable estimates of the time to peak acceleration for SDOF systems that have  $\rho < 0.4$ . It indicates that the time to peak acceleration decreases with increasing dampening and will occur at  $t_p = 0$  for

$$\frac{1}{4f_n} = \frac{3\rho}{2\pi f_n}$$

or,

$$\rho = \frac{2\pi}{12} \approx 0.52$$

The actual value of  $\rho$  for  $t_p = 0$  can be found from Eq. (35):

$$\arctan \left[ \frac{(1 - \rho^2)^{1/2}}{\rho} \right] = \arctan \left[ \frac{2\rho(1 - \rho^2)^{1/2}}{1 - 2\rho^2} \right]$$

or

$$\rho = 0.50$$

We will now develop a simplified approximate equation for the peak acceleration. For  $\rho < 0.4$ , using the second of Eqs. (34) and (36) we have

$$\phi = \arctan \left[ \frac{2\rho(1 - \rho^2)^{1/2}}{1 - 2\rho^2} \right] \approx 2\rho \quad (39)$$

Using Eqs. (38) and (39) in the first of Eq. (34) produces for the peak acceleration  $\ddot{x}_p$ :

$$\begin{aligned} \ddot{x}_p &\approx \frac{V_0 \omega_n}{(1 - \rho^2)^{1/2}} \exp \frac{-\rho \omega_n}{\omega_D} \left( \frac{\pi}{2} - 3\rho \right) \\ &\quad \sin \left( \frac{\pi}{2} - 3\rho + 2\rho \right) \\ &= V_0 f_n \left[ \frac{2\pi}{(1 - \rho^2)^{1/2}} \exp \left[ \frac{-\rho}{(1 - \rho^2)^{1/2}} \right] \right. \\ &\quad \left. \left( \frac{\pi}{2} - 3\rho \right) \cos(\rho) \right] \end{aligned} \quad (40)$$

Equation (40) can be further simplified by realizing that the term within the large brackets is fairly constant over the range  $0 < \rho < 0.4$ , and, to 25% accuracy, Eq. (40) can be approximated by

$$\ddot{x}_p \approx 5.5 V_0 f_n \quad (41)$$

Equation (41) states that the peak acceleration experienced by an SDOF system with  $\rho < 0.4$  as a result of a velocity step to its base is directly proportional to the change in the base velocity and the SDOF's natural frequency. Equation (41) can be used for rough analysis of SDOF systems subjected to shocks generated by drop tables (see Section 7) and for estimating the maximum acceleration an SDOF system experiences as a result of a shock.

## 6 SHOCK SPECTRA

This section describes the construction of shock spectra, which are graphs of the maximum values of acceleration, velocity, and/or displacement response of an infinite series of linear SDOF systems with constant damping ratio  $\rho$  shaken by the same acceleration history  $\ddot{y}(t)$  applied at its base (Fig. 1). Each SDOF system is distinguished by the value selected for its undamped natural cyclic frequency of vibration  $f_n$  (units of cycles/second, or hertz), or equivalently, its undamped natural period of vibration  $T$  (units of seconds).

**Table 1** Definition of Earthquake Response Spectrum Terms

Symbols	Definition	Description
$S_D = SD$	$ u(t) _{\max}$	Relative displacement response spectrum or spectral displacement
SV	$ \dot{u}(t) _{\max}$	Relative velocity response spectrum
SA	$ \ddot{x}(t) _{\max} =  \ddot{u}(t) + \ddot{y}(t) _{\max}$	Absolute acceleration response spectrum
$S_V = PSV$	$= \omega_n S_D = 2 \pi f_n S_D$	Spectral pseudovelocity
$S_A = PSA$	$= \omega_n S_V = (\omega_n)^2 S_D = 4 \pi^2 f_n S_D$	Spectral pseudoacceleration

Note:  $\omega_n = \sqrt{\frac{K}{M}}$ ;  $\omega_n = 2 \pi f_n$ ;  $\omega_n = \frac{2 \pi}{T}$ ; and  $f_n = \frac{1}{T}$

In the civil engineering field of structural dynamics, an acceleration history is assigned to  $\ddot{y}(t)$  in Fig. 1. This  $\ddot{y}(t)$  is either an earthquake history recorded during an earthquake event or a synthetic accelerogram. The shock spectra generated using this  $\ddot{y}(t)$  is referred to as response spectra (Ebeling<sup>19</sup>). Response spectra are useful not only in characterizing a design earthquake event but are directly used in the seismic design of a building by allowing for the computation of maximum displacements and internal forces.

The construction of the response spectrum plots a succession of peak response values for SDOF systems with constant damping ratio  $\rho$  and natural frequencies  $f_n$  ranging from near zero to values of tens of thousands of hertz. For each SDOF system of value  $f_n$  the dynamic response is computed using a numerical procedure like the central difference method. The dynamic response of the Fig. 1 SDOF system is expressed in terms of either the relative response or the total response of the SDOF system. Response spectrum values are the maximum response values for each of five types of SDOF responses for a system of frequency  $f_n$  and damping  $\rho$ . These five response parameters are listed in Table 1.

The value assigned to each of the five Table 1 dynamic response terms for an SDOF system is the peak response value computed during the shock. The relative displacement response spectrum,  $S_D$ , or SD, is the maximum absolute relative displacement value  $|u(t)|_{\max}$  computed using numerical methods for each of the SDOF systems analyzed. The relative velocity response spectrum, SV, is the maximum absolute value of the computed relative velocity time history  $|\dot{u}(t)|_{\max}$  and computed using numerical methods. The absolute acceleration response spectrum, SA, is the maximum absolute value of the sum of the computed relative acceleration time history  $\ddot{u}(t)$  for the SDOF system (also computed using numerical methods) plus the ground (i.e., Fig. 1 base) acceleration history  $\ddot{y}(t)$ . The spectral pseudovelocity,  $S_V$ , or PSV, of the acceleration time history is computed using  $S_D$  for each SDOF system analyzed. The spectral pseudoacceleration,  $S_A$ , or PSA, of the acceleration time history  $\ddot{y}(t)$  is computed using the value for  $S_D$  for each SDOF system analyzed.

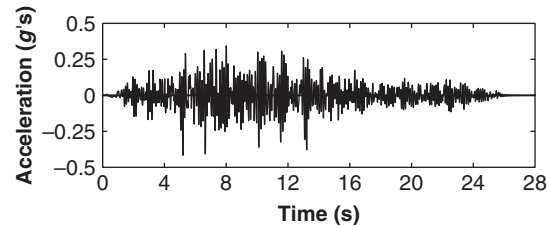
The term  $S_V$  is related to the maximum strain energy stored within the linear spring portion of the SDOF system when the damping force is neglected. The

pseudovelocity values of  $S_V$  for a SDOF system of frequency  $f_n$  are not equivalent to the relative velocity value SV, as shown in Ebeling.<sup>19</sup> This is especially true at low frequency (see Fig. 6.12.1 in Chopra<sup>23</sup>). The prefix *pseudo* is used because  $S_V$  is not equal to the peak of the relative velocity  $\dot{u}(t)$ .

The  $S_A$  is distinguished from the absolute acceleration response spectrum SA. The pseudoacceleration values  $S_A$  for an SDOF system of frequency  $f_n$  are equal to the absolute acceleration value SA only when  $\rho = 0$  (Ebeling<sup>19</sup>). For high-frequency, stiff SDOF systems values for  $S_A$  and SA approach the value for the peak acceleration  $|\ddot{y}(t)|_{\max}$ . As the frequency  $f_n$  approaches zero, the values for  $S_A$  and SA approach zero.

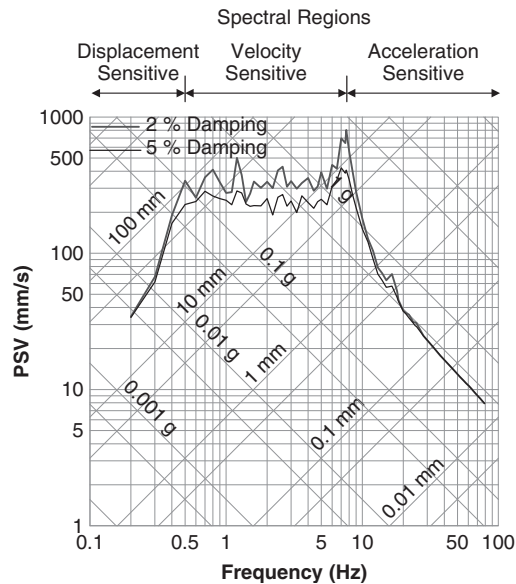
The following paragraph discusses an example construction of a response spectrum for an infinite series of linear SDOF systems shaken by the Fig. 6 acceleration history. Figure 6 is the top of powerhouse substructure (total) acceleration history response to a synthetic accelerogram representing a design earthquake in the Ebeling et al.<sup>24</sup> seismic evaluation of Corps of Engineers' powerhouse substructures. Peak ground (i.e., at base) acceleration is 0.415g.

In practical applications, each of the five response spectrum values is often plotted as the ordinate versus values of system frequencies  $f_n$  along the abscissa for a series of SDOF systems of constant damping  $\rho$ . Alternatively, a compact four-way plot that replaces three of these plots (of  $S_D$ ,  $S_V$ , and  $S_A$ ) with a single plot is the tripartite response spectra. Figure 7 shows the tripartite response spectra plot for the Fig. 6 acceleration history  $\ddot{y}(t)$  for 2 and 5% damping. A log-log scale is used with  $S_V$  plotted along the ordinate



**Figure 6** Acceleration time history computed at the top of an idealized powerhouse substructure. (From Ebeling et al.<sup>24</sup>)





**Figure 7** Response spectra for a top of powerhouse substructure amplification study acceleration time history;  $\rho = 2\%$  and  $5\%$ . (From Ebeling et al.<sup>24</sup>)

and  $f_n$  along the abscissa. Two additional logarithmic scales are shown in Fig. 7 for values of  $S_D$  and  $S_A$  and sloping at  $-45^\circ$  and  $+45^\circ$ , respectively, to the  $f_n$  axis. Another advantage of the tripartite response spectra plot is the ability to identify three spectral regions in which ranges in natural frequencies of SDOF systems are sensitive to acceleration, velocity, and displacement, respectively, as identified in Fig. 7.

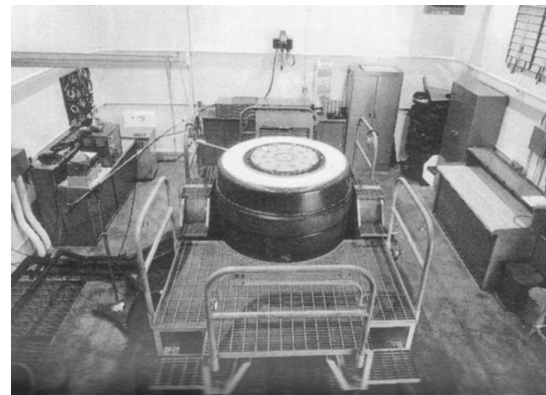
We observe that for civil engineering structures with high frequency, say  $f_n$  greater than 30 Hz,  $S_A$  for all damping values approaches the peak ground acceleration of  $0.415g$  and  $S_D$  is very small. For a fixed mass, a high-frequency SDOF system is extremely stiff or essentially rigid; its mass would move rigidly with the ground (i.e., the base). Conversely, for the left side of the plot for low-frequency systems and for a fixed mass, the system is extremely flexible; the mass would be expected to remain essentially stationary while the ground below moves and its absolute and relative accelerations will approach zero.

## 7 SHOCK TESTING METHODS AND DEVICES

The theoretical developments described thus far assume that the physical characteristics of the mechanical systems and the forcing functions or base motions are known. These kinds of data are gathered through experimental methods. There are four primary types of testing devices for determining the characteristics of mechanical systems: load deflection devices, harmonically oscillating shaker machines, impact testing machines, and programmable hydraulic-actuator machines.

Load deflection devices are used to determine the spring–force deflection curves for mechanical systems. For a linear spring, the slope of the force–deflection curve is equal to the spring constant  $K$ . Load deflection devices can be of a variety of types. Weights can be used to load the mechanical systems, in which case the load is equivalent to the weight used, or hydraulic or screw-type presses can be used to load the mechanical system in which case the load is measured using commercial load cells. Commercial load cells usually consist of simple steel structures in which one member is strain gaged using foil or semiconductor strain gages (see Perry and Lissner<sup>25</sup>). The deformation of the strain-gaged member is calibrated in terms of the load applied to the load cell. A simple load cell is a moderately long (length-to-diameter ratio of 4 or more), circular cross-section column loaded parallel to its axis. Axial and Poisson strains recorded near its midpoint are directly related to the load applied through the Young's modulus and Poisson's ratio of the load cell material. The resultant deflection of the mechanical system is monitored using commercially available deflection sensors such as linear-variable displacement sensors, magnetic displacement sensors, or optical sensors. While load deflection devices provide data on the spring forces of a mechanical system, they provide no information on its dampening characteristics.

Harmonic motion shaker machines range in size from a few pounds to several tons (Fig. 8). The shaker machines are of two types: piezoelectric driven and electromagnetic driven. Their purpose is to derive the frequency response characteristics of the mechanical system under test normally by driving the base of the mechanical system with a harmonic motion that is swept in frequency (see Frequency Response Functions, Chapter 12). The piezoelectric crystal machines use the piezoelectric effect to drive the mechanical system. The piezoelectric effect is manifested in some crystalline structures in which a voltage applied to opposite surfaces of the crystal causes the crystal to



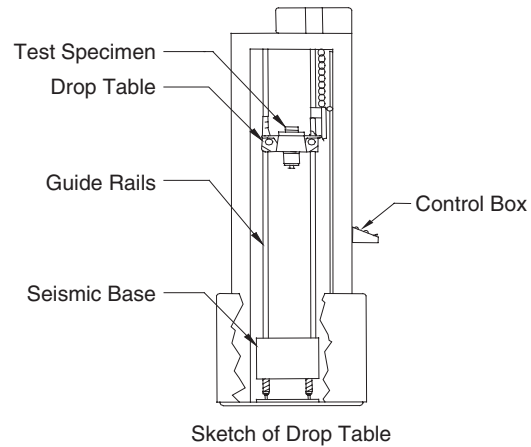
**Figure 8** Early Los Alamos National Laboratory electrodynamic shaker capable of generating peak forces of 22,000 lb. (From Pusey.<sup>7</sup>)





**Figure 9** Los Alamos National Laboratory 150-ft drop tower. (From Pusey.<sup>7</sup>)

change its dimensions. Alternatively, if the crystal is compressed or elongated, a voltage will be produced on these surfaces; thus this piezoelectric effect can also be used as a sensing method. Electromagnetic shakers use a magnet-in-wire coil structure similar to an electromagnetic acoustical speaker. A voltage applied to the coil causes the magnet to displace. Piezoelectric shakers are capable of higher frequencies but



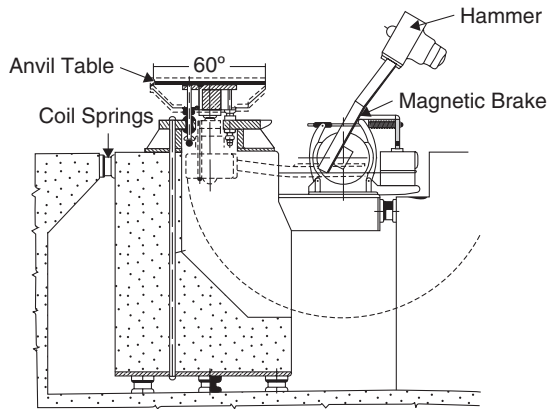
Sketch of Drop Table



Photograph of Drop Table

**Figure 10** Photo and cross section of commercial drop table.

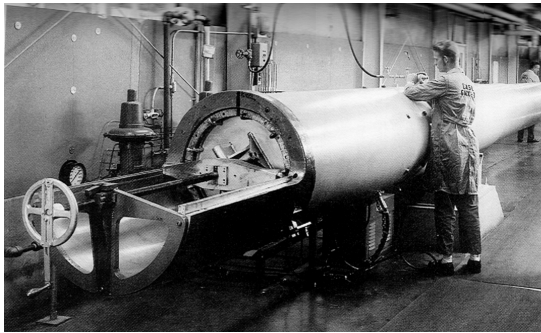
have lower peak displacements than electromagnetic shakers. While shakers are usually used to produce harmonic motion of the base of the mechanical system, they can also be used to generate random vibratory or short impulsive input. The frequency response and damping characteristics in all cases are determined by comparing the input base motion at particular frequencies to the resultant motion of the mechanical system at the same frequency. The input and response motions are often monitored via commercially available accelerometers. For the random or impulse case, the frequency content and phase of the input and



**Figure 11** U.S. Navy medium-weight shock machine. (From Pusey.<sup>7</sup>)

mechanical system response are derived by performing fast Fourier transforms (Hamming<sup>26</sup>) on the associated signals. The frequency and phase data are then used to derive the frequency response functions (Chapter 13).

Impact testing lends itself to a multitude of test methods. The simplest form of impact testing is the drop test in which the mechanical system under study is dropped from a known distance onto a rigid surface. The mechanical system's response is monitored through impact to derive its response characteristics. Mindlin<sup>13</sup> provides additional information and is a classic reference on drop testing. An extreme case of drop testing device built by the Lawrence Livermore National Laboratory is the 150-ft drop tower shown in Fig. 9 (page 221). To provide more precise control of the drop test, commercially available drop tables are used, an example of which is shown in Fig. 10. In the drop table test machine, a falling test platform is constrained in its ballistic fall by two or more guide bars. The item under test is rigidly attached to the test platform. The test platform is coupled to the guide bars through sleeve or roller bearings to ensure consistent and smooth operation. The falling platform impacts a controlled surface either directly or through

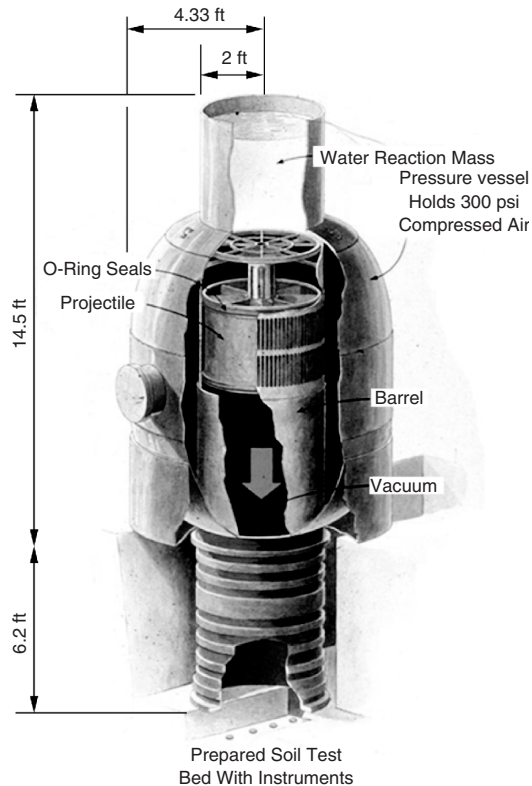


**Figure 12** Los Alamos National Laboratory 24-inch bore gas gun. (From Pusey.<sup>7</sup>)

an impacting material such as an engineered crushable foam or expanded metal structure. The control surface may be rigid or may itself be mounted through a spring-mass-dashpot system to a rigid surface. By using a drop table, the orientation of the test sample, the contact surfaces, and the velocity at impact are controlled.

Several types of impact test machines were developed by the U.S. Navy (Pusey<sup>7</sup>). These include the light-weight and medium-weight shock machines (Fig. 11). The two types of machines are of similar design, with the light-weight machine being used to shock test lighter equipment than the medium-weight machine. For both machines the test specimen is mounted on an anvil table of prescribed mass and shape. For the medium-weight shock machine a large (3000-lb) hammer is dropped through a circular arc section and impacts from below a 4500-lb anvil table containing the test item.

Another type of impact device is the gas gun. A familiar and small form of a gas gun is a pellet or BB rifle. Gas guns use compressed air to accelerate a test article to a maximum velocity, and then the article is allowed to impact a prescribed surface. The item under test is sometimes the projectile and sometimes the target being impacted. Figure 12 shows a 24-inch bore



**Figure 13** A 4-ft-diameter vertical gas gun developed at the U.S. Army Engineer Waterways Experiment Station (WES). (From White et al.<sup>27</sup>)

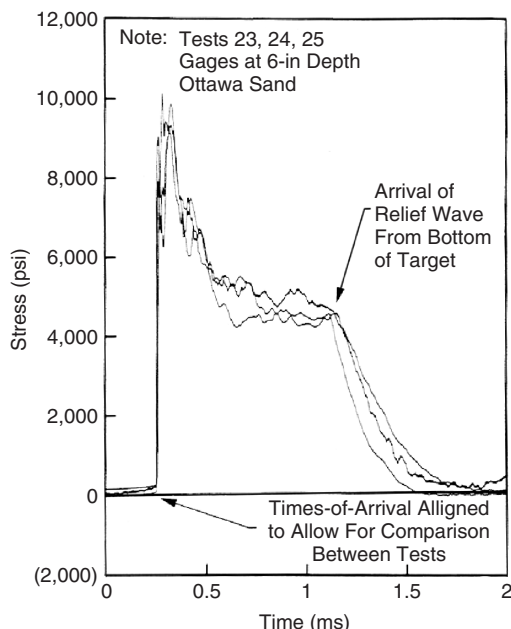
horizontal gas gun developed from a 16-inch naval gun by the Los Alamos National Laboratory. Using 3000-psi compressed air, it was capable of accelerating a 200-lb test article to velocities of 1700 ft/s. Figure 13 shows the 4-ft-diameter vertical gas gun developed by the U.S. Army Corps of Engineers (White et al.<sup>27</sup>). The device is capable of accelerating a 4-ft-diameter, 3500-lb projectile to velocities of 210 ft/s. It was used to generate shock waves in soils and to shock test small buried structures such as ground shock instruments. Sample soil stress waveforms produced by the gun in Ottawa Sand are shown in Fig. 14 (White<sup>28</sup>).

Programmable hydraulic actuator machines consist of one or more hydraulic actuators with one end affixed to a test table or structure and the other end affixed to a rigid and stationary surface. The forces and motions delivered to the test table by the actuators are normally controlled via digital feedback loops. The position and orientation of the actuators allow the effects of several directions of motion to be tested simultaneously. Test specimens can be accommodated on the larger devices that range from a few pounds to several thousands of pounds. The input from the actuators is prescribed and controlled through digital computers. Programmable hydraulic actuator machines have been used to simulate the effects of earthquakes on  $\frac{1}{4}$ -scale reinforced concrete multistory structures, the effects of launch vibrations on a U.S. space shuttle, the effects of nuclear-generated ground shock on underground shelter equipment, and other loading environments. Hydraulic actuators can provide for

large displacements and precisely controlled loading conditions.

## REFERENCES

1. L. Rayleigh, *The Theory of Sound*, Vols. I and II, Dover, New York, 1945.
2. K. Graff, *Wave Motion in Elastic Solids*, Dover, New York, 1991.
3. L. Meirovitch, *Computational Methods in Structural Dynamics*, Kluwer Academic, 1980.
4. R. Burton, *Vibration and Impact*, Dover, New York, 1968.
5. C. Harris and A. G. Piersol, *Shock and Vibration Handbook*, 5th ed., McGraw-Hill, New York, 2001.
6. J. P. Den Hartog, *Mechanical Vibrations*, Dover, New York, 1985.
7. H. C. Pusey (Ed.), *Fifty Years of Shock and Vibration Technology*, SVM15, Shock and Vibration Information Analysis Center, U.S. Army Engineer Research and Development Center, Vicksburg, MS, 1996.
8. H. C. Pusey (Ed.), *Fundamentals of Protective Design for Conventional Weapons*, TM 5-855-1, Headquarters, Department of the Army, 3 Nov. 1986.
9. R. H. Cole, *Underwater Explosions*, Princeton University Press, Princeton, NJ, 1948.
10. W. Goldsmith, *Impact: The Theory and Physical Behavior of Colliding Solids*, Dover, New York, 2001.
11. J. S. Rinehart, *Stress Transients in Solids*, HyperDynamics, Santa Fe, NM, 1975.
12. S. P. Timoshenko and J. N. Goodier, *Theory of Elasticity*, 3rd ed., McGraw-Hill, New York, 1970.
13. R. D. Mindlin, "Dynamics of Package Cushioning," *Bell Systems Tech. J.*, July, 1954, pp. 353-461.
14. E. Sevin and W. D. Pilkey, *Optimum Shock and Vibration Isolation*, Shock and Vibration Information Analysis Center, U.S. Army Engineer Research and Development Center, Vicksburg, MS, 1971.
15. D. V. Balandin, N. N. Bolotnik, and W. D. Pilkey, *Optimal Protection from Impact, Shock, and Vibrations*, Gordon and Breach Science, 2001.
16. W. T. Thomson and M. D. Dahleh, *Theory of Vibrations with Applications*, 5th ed., Prentice-Hall, Englewood Cliffs, NJ, 1997.
17. D. G. Fertis, *Mechanical and Structural Vibrations*, Wiley, New York, 1995.
18. C. R. Welch and H. G. White, "Shock-Isolated Accelerometer Systems for Measuring Velocities in High-G Environments," Proceedings of the 57th Shock and Vibration Symposium, Shock and Vibration Information Analysis Center, U.S. Army Engineer Research and Development Center, Vicksburg, MS, October 1986.
19. R. M. Ebeling, *Introduction to the Computation of Response Spectrum for Earthquake Loading*, Technical Report ITL-92-4, U.S. Army Engineer Waterways Experiment Station, Vicksburg, MS, 1992. <http://libweb.wes.army.mil/uhtbin/hyperion/TR-ITL-92-4.pdf>.
20. M. R. Spiegel, *Applied Differential Equations*, 3rd ed., Prentice-Hall, Englewood Cliffs, NJ, 1980.
21. G. Arfken, W. Hans, and H. J. Weber, *Mathematical Methods for Physicists*, 2nd ed., Academic, New York, 2000.
22. R. V. Churchill, *Operational Mathematics*, 3rd ed., McGraw-Hill, New York, 1971.



**Figure 14** Soil stress waveforms generated in test bed impacted by the 4-ft (1.22-m)-diameter gas gun projectile. (From White.<sup>28</sup>) (Note: 1 psi = 6894 N/m<sup>2</sup>)

23. A. K. Chopra, *Dynamics of Structures, Theory and Applications to Earthquake Engineering*, Prentice-Hall, Englewood Cliffs, NJ, 1995.
24. R. M. Ebeling, E. J. Perez, and D. E. Yule, *Response Amplification of Idealized Powerhouse Substructures to Earthquake Ground Motions*, ERDC/ITL TR-06-1, U.S. Army Engineer Research and Development Center, Vicksburg, MS, 2005.
25. C. C. Perry and H. R. Lissner, *The Strain Gage Primer*, 2nd ed., McGraw-Hill, New York, 1962.
26. R. W. Hamming, *Numerical Methods for Scientists and Engineers*, 2nd ed., Dover, New York, 1987.
27. H. G. White, A. P. Ohrt, and C. R. Welch, Gas Gun and Quick-Release Mechanism for Large Loads, U.S. Patent 5,311,856, U.S. Patent and Trademark Office, Washington, DC, 17 May 1994.
28. H. G. White, *Performance Tests with the WES 4-Ft-Diameter Vertical Gas Gun*, Technical Report SL-93-11, U.S. Army Engineer Research and Development Center, Vicksburg, MS, July 1993.

## BIBLIOGRAPHY

- Lelanne, C., *Mechanical Vibration and Shock, Mechanical Shock*, Vol. II, Taylor & Francis, New York, 2002.

# CHAPTER 15

## PASSIVE DAMPING

**Daniel J. Inman**  
 Department of Mechanical Engineering  
 Virginia Polytechnic Institute and State University  
 Blacksburg, Virginia

### 1 INTRODUCTION

Damping involves the forces acting on a vibrating system so that energy is removed from the system. The phenomenon is caused through a variety of mechanisms: impacts, sliding or other friction, fluid flow around a moving mass (including sound radiation), and internal or molecular mechanisms that dissipate energy through heat (viscoelastic mechanisms). Damping, unlike stiffness and inertia, is a dynamic quantity that is not easily deduced from physical logic and cannot be measured using static experiments. Thus, it is generally more difficult to describe and understand. The concept of damping is introduced in vibration analysis to account for energy dissipation in structures and machines. In fact, viscous damping, the most common form of damping used in vibration analysis, is chosen for modeling because it allows an analytical solution of the equations of motion rather than because it models the physics correctly. The basic problems are: modeling the physical phenomena of energy dissipation in order to produce predictive analytical models, and creating treatments, designs, and add-on systems that will increase the damping in a mechanical system in order to reduce structural fatigue, noise, and vibration.

### 2 FREE VIBRATION DECAY

Most systems exhibit some sort of natural damping that causes the vibration in the absence of external forces to die out or decay with time. As forces proportional to acceleration are inertial and those associated with stiffness are proportional to displacement, viscous damping is a nonconservative force that is velocity dependent. The equation of motion of a single degree of freedom system with a nonconservative viscous damping force is of the form:

$$m\ddot{x}(t) + c\dot{x}(t) + kx(t) = F(t) \quad (1)$$

Here  $m$  is the mass,  $c$  is the damping coefficient,  $k$  is the stiffness,  $F(t)$  is an applied force,  $x(t)$  is the displacement, and the overdots denote differentiation with respect to the time  $t$ . To start the motion in the absence of an applied force, the system and hence Eq. (1) is subject to two initial conditions:

$$x(0) = x_0 \text{ and } \dot{x}(0) = v_0$$

Here the initial displacement is given by  $x_0$  and the initial velocity by  $v_0$ . The model used in Eq. (1)

is referred to as *linear viscous damping* and serves as a model for many different kinds of mechanisms (such as air damping, strain rate damping, various internal damping mechanisms) because it is simple, easy to solve analytically, and often gives a good approximation of measured energy dissipation.

The single-degree-of-freedom model of Eq. (1) can be written in terms of the dimensionless damping ratio by dividing (1) by the mass  $m$  to get

$$\ddot{x}(t) + 2\zeta\omega_n\dot{x}(t) + \omega_n^2x(t) = f(t) \quad (2)$$

where the natural frequency is defined as  $\omega_n = \sqrt{k/m}$  (in radians per second), and the dimensionless *damping ratio* is defined by  $\zeta = c/2\sqrt{km}$ . The nature of the solutions to Eqs. (1) and (2) depend entirely on the magnitude of the damping ratio. If  $\zeta$  is greater or equal to 1, then no oscillation occurs in the free response [ $F(t) = 0$ ]. Such systems are called *critically damped* ( $\zeta = 1$ ) or *overdamped* ( $\zeta > 1$ ). The unique value of  $\zeta = 1$  corresponds to the critical damping coefficient given by

$$c_{cr} = 2\sqrt{km}$$

However, the most common case occurs when  $0 < \zeta < 1$ , in which case the system is said to be *underdamped* and the solution is a decaying oscillation of the form:

$$x(t) = Ae^{-\omega_n\zeta t} \sin(\omega_d t + \phi) \quad (3)$$

Here  $A$  and  $\phi$  are constants determined by the initial conditions, and  $\omega_d = \omega_n\sqrt{1 - \zeta^2}$  is the damped natural frequency. It is easy to see from the solution given in Eq. (3) that the larger the damping ratio is, the faster any free response will decay.

Fitting the form of Eq. (3) to the measured free response of a vibrating system allows determination of the damping ratio  $\zeta$ . Then knowledge of  $\zeta$ ,  $m$ , and  $k$  allow the viscous damping coefficient  $c$  to be determined.<sup>1</sup> The value of  $\zeta$  can be determined experimentally in the underdamped case from the logarithmic decrement. Let  $x(t_1)$  and  $x(t_2)$  be measurements of unforced response of the system described by Eq. (1) made one period apart ( $t_2 = t_1 + 2\pi/\omega_d$ ). Then the *logarithmic decrement* is defined by

$$\delta = \ln \frac{x(t_1)}{x(t_2)} = \ln e^{\zeta\omega_n(2\pi/\omega_d)} = \frac{2\pi\zeta}{\sqrt{1 - \zeta^2}} \quad (4)$$



**Table 1 Some Common Nonlinear Damping Models<sup>a</sup>**

Coulomb damping	$\mu \text{ mg sgn}(\dot{x})$
Air damping	$a \text{ sgn}(x)\dot{x}^2$
Material damping	$d \text{ sgn}(\dot{x})x^2$
Structural damping	$b \text{ sgn}(\dot{x}) x $

<sup>a</sup> Sgn is the signum function that takes the sign of the argument and the constants  $a$ ,  $b$ , and  $d$  are coefficients of the respective damping forces.

The logarithmic decrement is determined by measurements, from the left side of Eq. (4) and provides a measurement of  $\zeta$  through the right-hand side of Eq. (4). This yields

$$\zeta = \frac{\delta}{\sqrt{4\pi^2 + \delta^2}} \quad (5)$$

Unfortunately, this simple measurement of damping does not extend to more complex systems.<sup>2</sup>

The simple single-degree-of-freedom model given in Eq. (2) forms a basis for discussing damping in much more complex systems. By decoupling the equations of motion of multiple-degree-of-freedom systems and distributed mass systems (using modal analysis), the damping ratio is used to discuss damping in almost all linear systems. In addition, insight into nonlinear damping effects can be obtained by analyzing Eq. (1) numerically with the velocity term replaced with various models such as those listed in Table 1.

The presence of nonlinear damping mechanisms greatly changes the nature of the response and the behavior of the system. In general, the concept of a single static equilibrium position associated with the linear system of Eq. (1) gives way to the concept of multiple or even infinite equilibrium points. For example, with Coulomb damping, a displaced particle will oscillate with linear, rather than exponential, decay and come to rest, not at the starting equilibrium point, but rather anywhere in a region defined by the static friction force (i.e., any point in this region is an equilibrium point). In general, analytical solutions for systems with the damping mechanisms listed in Table 1 are not available and hence numerical solutions must be used to simulate the response. Joints and other connection points are often the source of nonlinear damping mechanisms.<sup>3</sup>

### 3 EFFECTS ON THE FORCED RESPONSE

When the system described by Eq. (1) is subjected to a harmonic driving force,  $F(t) = F_0 \cos(\omega t)$ , the phenomenon of resonance can occur. Resonance occurs when the displacement response of the forced system achieves its maximum amplitude. This happens if the driving frequency  $\omega$  is at or near the natural frequency  $\omega_n$ . In fact, without damping, the response is a sinusoid with ever-increasing amplitude, eventually causing the system to respond in its nonlinear region and/or break. The presence of damping, however,

removes the solution of ever-increasing amplitude and renders a solution of the form [for  $F(t) = F_0 \cos \omega t$ ]:

$$x(t) = \underbrace{Ae^{-\zeta\omega_n t} \sin(\omega_d t + \phi)}_{\text{transient}} + \underbrace{X \cos(\omega t - \theta)}_{\text{steady state}} \quad (6)$$

Here  $A$  and  $\phi$  are constants of integration determined by the initial conditions,  $X$  is the steady-state magnitude and  $\theta$  is the phase shift of the steady-state response. The displacement magnitude and phase of the steady-state response are given by

$$X = \frac{F_0}{\sqrt{(\omega_n^2 - \omega^2)^2 + (2\zeta\omega_n\omega)^2}}, \quad \theta = \tan^{-1} \left( \frac{2\zeta\omega_n\omega}{\omega_n^2 - \omega^2} \right) \quad (7)$$

Equation (7) shows that the effect of damping on the response of a system to a harmonic input is to reduce the amplitude of the steady-state response and to introduce a phase shift between the driving force and the response.

Through the use of Fourier analysis and the definition of linearity, the response of a linear damped system to a general force will be some combination of terms such as those given in (6) with a transient term that dies out (quickly if  $\zeta$  is large) and a steady-state term with amplitude dependent on the inverse of the damping ratio. Thus it is easy to conclude that increasing the damping in a system generally reduces the amplitude of the response of the system. With this as a premise many devices and treatments have been invented to provide increased damping as a mechanism for reducing unwanted vibration.

### 4 COMPLEX MODULUS

The concept of complex modulus includes an alternative representation of damping related to the notion of complex stiffness. A complex stiffness can be derived from Eq. (1) by representing a harmonic input force as a complex exponential:  $F(t) = F_0 e^{j\omega t}$ . Using this complex function representation of the harmonic driving force introduces a complex function response in the equation of motion, and it is the real part of this response that is interpreted as the physical response of the system. Substitution of this form into Eq. (1) and assuming the solution is of the complex form  $X(t) = X e^{j\omega t}$  yields

$$\left[ -m\omega^2 + \underbrace{k \left( 1 + \frac{\omega c}{k} j \right)}_{k^*} \right] X = F_0 \quad (8)$$

Here  $k^*$  is called the complex stiffness and has the form

$$k^* = k(1 + \bar{\eta}j) \quad \bar{\eta} = \frac{c}{k}\omega \quad (9)$$

where  $\bar{\eta}$  is called the *loss factor*, another common way to characterize damping. Note that the complex

stiffness is just an alternative way to represent the viscous damping appearing in Eq. (1). However, the concepts of loss factor and complex modulus actually carry deeper notions of temperature dependence, frequency dependence, and hysteresis as discussed in the following (see Chapter 60 for details).

Note from the form of the loss factor given in Eq. (9) that its value depends on the driving frequency. Also note that this form of describing the damping also depends on the system being driven harmonically at a single frequency. This notion of complex stiffness is sometimes referred to as Kelvin–Voigt damping and is often used to represent the internal damping of certain materials. Viscoelastic materials (rubberlike materials) are often modeled using the notion of loss factor and complex stiffness.<sup>4,5</sup>

The concept of complex modulus is similar to that of complex stiffness. Let  $E^*$  denote the complex modulus of a material and  $E$  denote its elastic modulus. The complex modulus is defined by

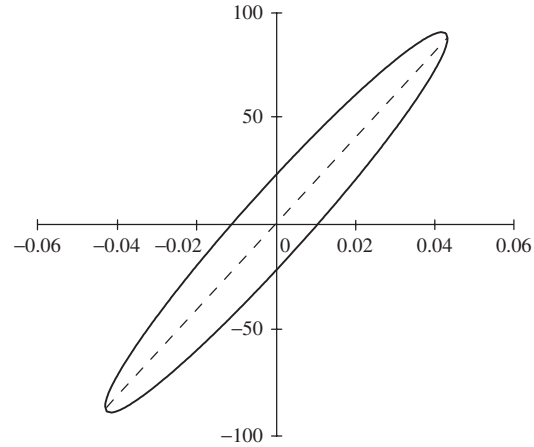
$$E^* = E(1 + j\eta) \quad (10)$$

where  $\eta$  is the loss factor of the viscoelastic material. The loss factor is determined experimentally by driving a material coupon harmonically at a single frequency and fixed temperature, then measuring the energy lost per cycle. This procedure is repeated for a range of frequencies and temperatures resulting in plots of  $\eta(\omega)$  for a fixed temperature ( $T$ ) and  $\eta(T)$  for a fixed frequency. Unfortunately, such models are not readily suitable for transient vibration analysis or for broadband excitations, impulsive loads, and the like.

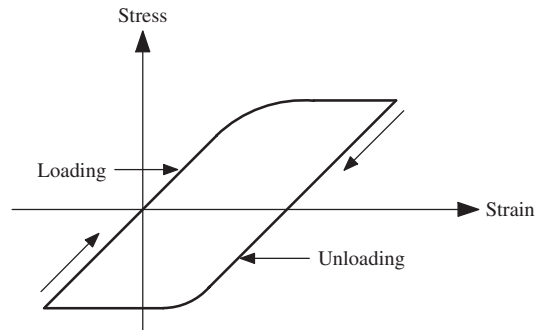
Since the stiffness of an object is easily related to the modulus of the material it is made of, the notions of complex stiffness and complex modulus give rise to an equivalent value of the loss factor so that  $\eta = \bar{\eta}$  (provided the elastic system consists of a single material and is uniformly strained). In the event that the system is driven at its natural frequency, the damping ratio and the loss factor are related by  $\eta = 2\zeta$ , providing a connection between the viscous damping model and the complex modulus and loss factor approach.<sup>2,4</sup>

The complex modulus approach is also associated with the notion of hysteresis and hysteretic damping common in viscoelastic materials.<sup>6</sup> Hysteresis refers to the notion that energy dissipation is modeled by a hysteresis loop obtained from plotting the stress versus strain curve for a sample material while it undergoes a complete cycle of a harmonic response. For damped systems the stress–strain curve under cyclic loading is not single valued (as it is for pure stiffness) but forms a loop. This is illustrated in Fig. 1, which is a plot of  $F(t) = c\dot{x}(t) + kx(t)$  versus  $x(t)$ .

The area inside the hysteresis loop corresponds to the energy dissipated per cycle. Materials are often tested by measuring the stress (force) and strain (displacement) under carefully controlled steady-state harmonic loading. For linear systems with viscous



**Figure 1** Plot of force  $[c\dot{x}(t) + kx(t)]$  versus displacement, defining the hysteresis loop for a viscously damped system.



**Figure 2** Sample experimental stress versus strain plot for one cycle of a harmonically loaded material in steady state illustrating a hysteresis loop for some sort of internal damping.

damping the shape of the hysteresis loop is an ellipse as indicated in Fig. 1. For all other damping mechanisms of Table 1, the shape of the hysteresis loop is distorted. Such tests produce hysteresis loops of the form shown in Fig. 2. Note that, for increasing strain (loading), the path is different than for decreasing strain (unloading). This type of damping is often called hysteretic damping, solid damping, or structural damping.

## 5 MULTIPLE-DEGREE-OF-FREEDOM SYSTEMS

Lumped mass systems with multiple degrees of freedom provide common models for use in vibration and noise studies, partially because of the tremendous success of finite element modeling (FEM) methods. Lumped mass models, whether produced directly by the use of Newton's law or by use of FEM,

result in equations of motion of the form (see also Chapter 12):

$$M\ddot{\mathbf{x}}(t) + C\dot{\mathbf{x}}(t) + K\mathbf{x}(t) = \mathbf{F}(t) \quad (11)$$

Here  $M$  is the mass matrix,  $K$  is the stiffness matrix (both of dimension  $n \times n$  where  $n$  is the number of degrees of freedom),  $\mathbf{x}(t)$  is the  $n$  vector of displacements, the overdots represent differentiation with respect to time,  $\mathbf{F}(t)$  is an  $n$  vector of external forces, and the  $n \times n$  matrix  $C$  represents the linear viscous damping in the structure or machine being modeled. Equation (11) is subject to the initial conditions:

$$\mathbf{x}(0) = \mathbf{x}_0 \quad \dot{\mathbf{x}}(0) = \dot{\mathbf{x}}_0$$

In general, the matrices  $M$ ,  $C$ , and  $K$  are assumed to be real valued, symmetric, and positive definite (for exceptions see Inman<sup>5</sup>). As in the single-degree-of-freedom case, the choice of damping force in Eq. (11) is more one of convenience than of one based on physics. However, solutions to Eq. (11) closely resemble experimental responses of structures rendering Eq. (11) useful in many modeling situations.<sup>2</sup>

The most useful form of Eq. (11) is when the damping matrix  $C$  is such that the equations of motion can be decoupled by an eigenvalue-preserving transformation (usually called the modal matrix, as it consists of the eigenvectors of the undamped system). The mathematical condition that allows the decoupling of the equations of motion into  $n$  single-degree-of-freedom equations identical to Eq. (2) is simply that  $CM^{-1}K = KM^{-1}C$ , which happens if and only if the product  $CM^{-1}K$  is a symmetric matrix.<sup>7</sup> In this case the mode shapes of the undamped system are also modes of the damped system. This gives rise to calling such systems "normal mode systems." In addition, if this matrix condition is not satisfied and the system modes are all underdamped, then the mode shapes will not be real but rather complex valued, and such systems are called *complex mode systems*. A subset of damping matrices that satisfies the matrix condition are those that have damping matrix made up of a linear combination of mass and stiffness, that is,  $C = \alpha M + \beta K$ , where  $\alpha$  and  $\beta$  are constant scalars. Such systems are called *proportionally damped* and also give rise to real normal mode shapes.

Let the matrix  $L$  denote the Cholesky factor of the positive definite matrix  $M$ . A Cholesky factor<sup>1</sup> is a lower triangular matrix such that  $M = LL^T$ . Then premultiplying Eq. (11) by  $L^{-1}$  and substituting  $\mathbf{x} = L^{-T}\mathbf{q}$  yields a mass normalized stiffness matrix  $\tilde{K} = L^{-1}KL^{-T}$ , which is both symmetric and positive definite if  $K$  is. From the theory of matrices, the eigenvalue problem for  $\tilde{K}$ ,  $\tilde{K}\mathbf{u}_i = \lambda_i\mathbf{u}_i$ , is symmetric and thus yields real-valued eigenvectors forming a basis, and positive real eigenvalues  $\lambda_i$ . If the eigenvectors  $\mathbf{u}$  are normalized and used as the columns of a matrix  $P$ , then  $P^T P = I$  the identity

matrix and  $P^T \tilde{K} P = \text{diag}[\omega_i^2]$ . Furthermore, if the damping matrix causes  $CM^{-1}K$  to be symmetric, then  $P^T \tilde{C} P = \text{diag}[2\zeta_i\omega_i]$ , which defines the modal damping ratios  $\zeta_i$ . In this case the equations of motion decouple into  $n$  single-degree-of-freedom systems, called *modal equations*, of the form:

$$\ddot{r}_i(t) + 2\zeta_i\omega_i\dot{r}_i(t) + \omega_i^2 r_i(t) = f_i(t) \quad (12)$$

These modal equations are compatible with modal measurements of  $\zeta_i$  and  $\omega_i$  and form the basis for modal testing.<sup>2</sup>

If, on the other hand, the matrix  $CM^{-1}K$  is not symmetric, the equations of motion given in Eq. (11) will not decouple into modal equations such as (12). In this case, state-space methods must be used to analyze the vibrations of a damped system. The state-space approach transforms the second-order vector differential equation given in (11) into the first-order form:

$$\dot{\mathbf{y}} = A\mathbf{y} + B\mathbf{F}(t) \quad (13)$$

Here the state matrix  $A$  and input matrix have the form:

$$A = \begin{bmatrix} 0 & I \\ -M^{-1}K & -M^{-1}C \end{bmatrix} \quad B = \begin{bmatrix} 0 \\ M^{-1} \end{bmatrix} \quad (14)$$

The state vector  $\mathbf{y}$  has the form:

$$\mathbf{y} = \begin{bmatrix} \mathbf{x} \\ \dot{\mathbf{x}} \end{bmatrix} \quad (15)$$

This first-order form of the equations of motion can be solved by appealing to the general eigenvalue problem  $A\mathbf{v} = \lambda\mathbf{v}$  to compute the natural frequencies and mode shapes. In addition Eq. (11) can be numerically simulated to produce the time response of the system. If each mode is underdamped, then from the above arguments the eigenvalues of the state matrix  $A$  will be complex valued, say  $\lambda = \alpha + \beta j$ . Then the natural frequencies and damping ratios are determined by

$$\omega_i = \sqrt{\alpha_i^2 + \beta_i^2} \quad \text{and} \quad \zeta_i = \frac{-\alpha_i}{\sqrt{\alpha_i^2 + \beta_i^2}} \quad (16)$$

In both the proportional damping case and the complex mode case the damping ratio can be measured using modal testing methods if the damping matrix is not known. The above formulas can be used to determine modal damping if the damping matrix is known.

In the preceding analysis, it was assumed that each mode was underdamped. This is usually the case, even with highly damped materials. If the damping matrix happens to be known numerically, then the condition



that each mode is underdamped will follow if the matrix  $4\tilde{K} - \tilde{C}^2$  is positive definite.<sup>8</sup>

In general, finite element methods are used to produce very accurate mass and stiffness matrices. However, when it comes to determining a damping matrix for a given machine or structure, the choice is not clear, nor does the choice follow from a sophisticated procedure. Many research articles have been written about methods of determining the damping matrix, but, in practice,  $C$  is developed in an ad hoc manner, usually in an attempt to model the response with classical normal modes.

Several approaches have been developed to relate the complex modulus and frequency-dependent loss factor models to FEM.<sup>9</sup> Many damping treatments are designed based on distributed mass models of basic structural elements such as bars, beams, plates, and shells. The basic equations of motion can be represented and best understood in operator notation (similar to the matrix notation used for lumped mass systems<sup>10</sup>). The modal decoupling condition is similar to the matrix case and requires that the damping and stiffness operators commute.<sup>11</sup> Examples of the form that the damping and stiffness operators take on are available in the literature.<sup>12</sup>

The complex eigenvalue analysis given in Eq. (16) forms a major method for use in the analysis and design of damping solutions for structures and machines. The solution is modeled, and then an eigenvalue analysis is performed to see if the modal damping has increased to an acceptable level. An alternate and more illuminating method of design is called the *modal strain energy* (MSE)<sup>13,14</sup> method. In the MSE method the modal damping of a structure is approximated by

$$\eta(r) = \sum_{j=1}^M \eta_j \frac{SE_j(r)}{SE(r)} \quad (17)$$

Here  $SE_j(r)$  is the strain energy in the  $j$ th material when deformed in the  $r$ th mode shape,  $SE(r)$  is the strain energy in the  $r$ th mode and  $\eta_j$  is the material loss factor for  $j$ th material. The MSE approach is valuable for determining placement of devices and layers, for determining optimal parameters, and for understanding the general effects of proposed damping solutions.<sup>14</sup>

## 6 SURFACE DAMPING TREATMENTS

Many systems and structures do not have enough internal or natural damping to limit vibrations to acceptable levels. Most structures made of sheet metal, for instance, have damping ratios of the order of 0.001 and will hence ring and vibrate for unacceptable lengths of time at unacceptable magnitudes. A simple fix for such systems is to coat the surface of the structure with a damping material, usually a viscoelastic material (similar to rubber). In fact, every automobile body produced is treated with a surface

damping treatment to reduce road and engine noise transmitted into the interior.

Adding a viscoelastic layer to a metal substrate adds damping because as the host structure bends in vibration, it strains the viscoelastic material in shear causing energy to be dissipated by heat. This notion of layering viscoelastic material onto the surface of a sheet of metal is known as a *free-layer damping treatment*. By adding a third layer on top of the viscoelastic that is stiff (and often thin). The top of the boundary of the viscoelastic material tries not to move, increasing the shear and causing greater energy dissipation. Such treatments are called *constrained layer damping treatments*.

The preliminary analysis of layered damping treatments is usually performed by examining a pinned-pinned beam with a layer of viscoelastic material on top of it. A smeared modulus formula for this sandwich beam is derived to produce a composite modulus in terms of the modulus, thickness, and inertia of each layer. Then the individual modulus value of the viscoelastic layer is replaced with its complex modulus representation to produce a loss factor for the entire system. In this way thickness, percent coverage and modulus can be designed from simple algebraic formulas.<sup>4</sup> This forms the topic of Chapter 60.

Other interesting surface damping treatments consist of using a piezoceramic material usually in the form of a thin patch layered onto the surface of a beam or platelike structure.<sup>15</sup> As the surface bends, the piezoceramic strains and the piezoelectric effect causes a voltage to be produced across the piezoceramic layer. If an electrical resistor is attached across the piezoceramic layer, then energy is dissipated as heat and the system behaves exactly like a free layer viscoelastic damping treatment (called a *shunt damper*). In this case the loss factor of the treated system can be shown to be

$$\eta(\omega) = \frac{\rho k^2}{(1 - k^2) + \rho^2} \quad (18)$$

where  $k$  is the electromechanical coupling coefficient of the piezoceramic layer and  $\rho = RC\omega$ . The value of  $R$  is the added resistance (ohms) and  $C$  is the value of the capacitance of the piezoceramic layer in its clamped state. In general, for a fixed amount of mass, a viscoelastic layer provides more damping, but the piezoceramic treatment is much less temperature sensitive than a typical viscoelastic treatment. If an inductor is added to the resistor across the piezoceramic, the system behaves like a vibration absorber or tuned mass damper. This inductive shunt is very effective but needs large inductance values requiring synthetic inductors, which may not be practical.

## 7 DAMPING DEVICES

Damping devices consist of vibration absorbers, tuned mass dampers, shock absorbers, eddy current dampers, particle dampers, strut mechanisms, and various other inventions to reduce vibrations. Vibration isolators are an effective way to reduce unwanted

**Table 2 Some Design Considerations for Various Add-on Damping Treatments**

	Layered Damping	Tuned Mass Damper	PZT <sup>a</sup> Resistive Shunt	PZT <sup>a</sup> Inductive Shunt	Shocks Struts Links
Target modes	Bending extension	Any	Bending extension	Bending Extension	Global
Design approach	MSE <sup>b</sup>	Complex eigenvalues	MSE <sup>b</sup>	Complex eigenvalues	MSE <sup>b</sup>
Feature	Wide band	Narrow band	Wide band	Narrow band	Removable
Design constraints	Area thickness temperature	Weight, rattle space	Wires and resistor	Inductance size	Stroke length

<sup>a</sup> Piezoceramic layer.<sup>b</sup> Modal strain energy.<sup>13</sup>

Source: From Ref. 14.

vibration also. However, isolators are not energy-dissipating (damping) devices but rather are designed around stiffness considerations to reduce the transmission of steady-state magnitudes. Isolators often have damping characteristics and their damping properties may greatly affect the isolation design. Isolators are designed in the load path of a vibrating mass and in the case of harmonic disturbances are designed by choosing the spring stiffness such that either the transmitted force or displacement is reduced (See Chapter 59).

Vibration absorbers and tuned mass dampers on the other hand are add on devices and do not appear in the load path of the disturbance. Again, basic absorber design for harmonic inputs involves stiffness and mass and not damping. However, damping plays a key role in many absorber designs and is usually present whether desired or not.

Eddy current dampers consist of devices that pass a metallic structural component through a magnetic field. They are very powerful and can often obtain large damping ratios. Particle dampers work by dissipating energy through impacts of the particles against the particles' container and are also very effective. However, neither of these methods are commercially developed or well analyzed. Shock absorbers and strut dampers are energy dissipation devices that are placed in the load path (such as an automobile shock absorber). Shocks are often oil-filled devices that cause oil to flow through an orifice giving a viscous effect, often modeled as a linear viscous damping term. However, they are usually nonlinear across their entire range of travel. Table 2 indicates the analysis considerations often used for the design of various add-on damping treatments.

## REFERENCES

1. D. J. Inman, *Engineering Vibrations*, 3rd ed., Prentice Hall, Upper Saddle River, NJ, 2007.
2. D. J. Ewins, *Modal Testing: Theory, Practice and Application*, 2nd ed., Research Studies Press, Hertfordshire, England, 2000.
3. L. Gaul and R. Nitsche, The Role of Friction in Mechanical Joints, *Appl. Mech. Rev.*, Vol. 54, No. 2, 2001, pp. 93–106.

4. A. D. Nashif, D. I. G. Jones, and J. P. Henderson, *Vibration Damping*, Wiley, New York, 1985.
5. D. J. Inman, *Vibrations with Control*, Wiley, Chichester 2007.
6. R. M. Christensen, *Theory of Viscoelasticity: An Introduction*, 2nd ed., Academic, New York, 1982.
7. T. K. Caughey and M. E. J. O'Kelly, Classical Normal Modes in Damped Linear Dynamic Systems, *ASME J. Appl. Mech.*, Vol. 132, 1965, pp. 583–588.
8. D. J. Inman and A. N. Andry, Jr., Some Results on the Nature of Eigenvalues of Discrete Damped Linear Systems, *ASME J. Appl. Mech.*, Vol. 47, No. 4, 1980, pp. 927–930.
9. A. R. Johnson, Modeling Viscoelastic Materials Using Internal Variables, *Shock Vib. Dig.*, Vol. 31, 1999, pp. 91–100.
10. D. J. Inman and A. N. Andry, Jr., The Nature of the Temporal Solutions of Damped Linear Distributed Systems with Normal Modes, *ASME J. Appl. Mech.*, Vol. 49, No. 4, 1982, pp. 867–870.
11. H. T. Banks, L. A. Bergman, D. J. Inman, and Z. Luo, On the Existence of Normal Modes of Damped Discrete Continuous Systems, *J. Appl. Mech.*, Vol. 65, No. 4, 1998, pp. 980–989.
12. H. T. Banks and D. J. Inman, On Damping Mechanisms in Beams, *ASME J. Appl. Mech.*, Vol. 58, No. 3, September, 1991, pp. 716–723.
13. E. E. Unger and E. M. Kerwin, Loss Factors of Viscoelastic Systems in Terms of Energy Concepts, *J. Acoust. Soc. Am.*, Vol. 34, No. 7, 1962, pp. 954–958.
14. C. D. Johnson, Design of Passive Damping Systems, *Special 50th Anniversary Design Issue of ASME J. Vibration and Acoustics*, Vol. 117(B), 1995, pp. 171–176.
15. G. A. Lesiutre, Vibration Damping and Control Using Shunted Piezoelectric Materials, *Shock Vibration Dig.*, Vol 30, No. 3, 1998, pp. 187–195.

## BIBLIOGRAPHY

- Korenev, B. G. and L. M. Reznikov, *Dynamic Vibration Absorbers: Theory and Technical Applications*, Wiley, Chichester, UK, 1993.
- Lazan, B. J., *Damping of Materials and Structures*, Pergamon, New York, 1968.
- Macinante, J. A., *Seismic Mountings for Vibration Isolation*, Wiley, New York, 1984.

- Mead, D. J., *Passive Vibration Control*, Wiley, Chichester, UK, 1998.
- Osinski, Z. (Ed.), *Damping of Vibrations*, Balkema Publishers, Rotterdam, Netherlands, 1998.

- Rivin, E. I. *Stiffness and Damping in Mechanical Design*, Marcel Dekker, New York, 1999.
- Sun, C. T. and Y. P. Lu, *Vibration Damping of Structural Elements*, Prentice Hall, Englewood Cliffs, NJ, 1995.

# CHAPTER 16

## STRUCTURE-BORNE ENERGY FLOW

Goran Pavić

INSA Laboratoire Vibrations Acoustique (LVA)  
Villeurbanne, France

### 1 INTRODUCTION

Structure-borne vibration produces mechanical energy flow. The flow results from the interaction between dynamic stresses and vibratory movements of the structure. The energy flow at any single point represents the instantaneous rate of energy transfer per unit area in a given direction. This flow is called the structure-borne intensity. Following its definition, the intensity represents a vector quantity. When integrating the normal component of intensity across an area within the body, the total mechanical energy flow rate through this area is obtained.

The intensity vector changes both its magnitude and direction in time. In order to compare energy flows at various locations in a meaningful way, it is the time-averaged (net) intensity that should be analyzed. Thus, the intensity concept is best associated with stationary vibration fields.

Experimental measurements of vibration energy flow through a structure enables identification of the positions of vibratory sources, vibration propagation paths, and absorption areas. Energy flow information is primarily dedicated to source characterization, system identification, and vibration diagnostics. Information provided by energy flow cannot be assessed by simply observing vibration levels. The structure intensity or energy flow in structures can be obtained either by measurement or by computation, depending on the nature of the problem being considered. Measurements are used for diagnostic or source identification purposes, while computation can be a valuable supplementary tool for noise and vibration prediction during the design stage.

### 2 ENERGY FLOW CONCEPTS

From the conceptual point of view, the energy flow (EF) carried by structure-borne vibration can be looked upon in three complementary ways:

1. The basic way to look at energy flow is via the intensity concept, where the structure-borne intensity (SI), that is, the energy flow per unit area, is used in a way comparable to using stress data in an analysis of structural strength. This concept is completely analogous to acoustic intensity. An SI analysis is, however, limited to computation only, as any measurement of practical use made on an object of complex shape has to be restricted to the exterior surfaces.
2. Structures of uniform thickness (plates, shells) can be more appropriately analyzed by integrating SI across the thickness. In this way, a unit

energy flow (UEF), that is, the flow of energy per unit length in a given direction tangential to the surface, is obtained. If the energy exchange between the outer surfaces and the surrounding medium is small in comparison with the flow within the structure, as it is usually for objects in contact with air, then the UEF vector lies in the neutral layer. For thin-walled structures where the wavelengths are much larger than the thickness, UEF can be expressed in terms of outer-surface quantities, which are readily measurable. The UEF concept is best utilized for source localization.

3. Structural parts that form waveguides or simple structural joints are most easily analyzed by means of the concept of total energy flow (TEF). Some parts, such as beams and elastic mountings, possess a simple enough shape to allow straightforward expression of the EF in terms of surface vibration. The TEF in more complex mechanical waveguides, such as fluid-filled pipes, can be evaluated by more elaborate procedures, such as the wave decomposition technique.

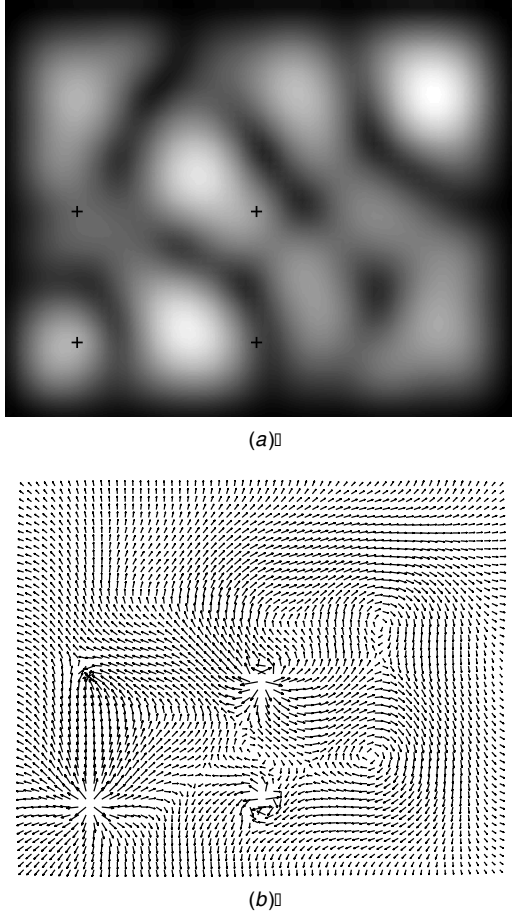
The structure-borne intensity (SI) is a vector quantity. The three components of an SI vector read<sup>1</sup>

$$I = -\sigma \dot{u} \quad (1)$$

where  $I = [I_x, I_y, I_z]^T$  is the column of  $x$ ,  $y$ , and  $z$  intensity components,  $\sigma$  is the  $3 \times 3$  matrix of dynamic stress,  $\dot{u}$  is the column of particle velocity components (a dot indicates time derivative), and superscript T indicates transpose. The negative sign in (1) is the consequence of sign convention: The compression stresses are considered negative. Since the shear stress components obey reciprocity,  $\sigma_{xy} = \sigma_{yx}$ , and so on, the complete SI vector is built up of nine different quantities, six stresses and three velocities. Each of the three SI components is a time-varying quantity, which makes both the magnitude and direction of the SI vector change in time.

The SI formula (1) is more complex than that for acoustic intensity. Each SI component consists of three terms instead of a single one because the shear stresses in solids, contrary to those in gases and liquids, cannot be disregarded. Sound intensity is thus simply a special case of (1) when shear effects vanish.

Figure 1 shows the computed vibration level and vectorial UEF of a flat rectangular  $1 \text{ m} \times 0.8 \text{ m} \times$



**Figure 1** Vibration of a clamped plate with lossy boundaries. (a) Vibration amplitude, and (b) UEF.

9 mm steel plate with clamped but lossy boundaries. Excitation is provided at four points via connections transmitting both forces and moments to the plate. The base frequency of excitation is 50 Hz to which the harmonics 2, 3, and 4 are added. The energy flow field displays strong divergence around the excitation points, which input energy to the plate, and convergence around points, which take the energy away. Vibration propagation paths are clearly visible. The map of vibration amplitudes shown in parallel cannot reveal any of these features.

### 3 GOVERNING FORMULAS FOR ENERGY FLOW

Using the basic SI formula (1) the expressions for UEF or TEF can be evaluated for some simple types of structures. As a rule, a different governing formula will apply to each type of structure. This section lists governing EF formulas for rods, beams, plates, shells, and mounts. The formulas are given in terms of surface strains and velocities, that is, the quantities that can be

measured. In order to obtain a particular governing formula, some modeling is required of the internal velocity and stress-strain distribution. For structures such as rods, beams, plates, and shells, simple linear relationships can express internal quantities in terms of external ones, as long as the wavelengths of the vibration motion are much larger than the lateral dimensions of the object. The latter condition limits the applicability of the formulas presented.

It is useful to present the governing formulas in a form suitable for measurement. As stresses cannot be measured in a direct way, stress-strain relationships are used instead. For homogeneous and isotropic materials behaving linearly, such as metals, the stress-strain relationships become fairly simple. These relationships contain only two independent material constants such as Young's and shear moduli.<sup>2</sup>

#### 3.1 Rods, Beams, and Pipes

At not too high frequencies, vibration of a rod can be decomposed in axial (longitudinal), torsional, and bending movements. If the rod is straight and of symmetric cross section, these three type of movements are decoupled. The energy flow can therefore be represented as a sum of longitudinal, torsional, and bending flows.

**3.1.1 Longitudinally Vibrating Rod** In longitudinal rod vibration, only the axial component of the stress in a rod differs from zero. This stress equals the product of the axial strain  $\epsilon$  and the Young's modulus  $E$ . The SI distribution in the cross section is uniform. The TEF  $P$  is obtained by multiplying the intensity with the area of the cross section  $S$ :

$$P_x = -SE\epsilon_{xx}\dot{u}_x = -SE\frac{\partial u_x}{\partial x}\dot{u}_x \quad (2)$$

**3.1.2 Torsionally Vibrating Rod** Torsion in a rod produces shear stresses, which rise linearly from the center of the rod, as does the tangential vibration velocity. The product of the two gives the SI in the axial sense. At a distance  $r$  from the center of torsion, the axial SI is proportional to  $r^2$ . If the rod is of a circular or annular cross section, the shear stresses are the only stresses in the rod. In such a case, the EF through the rod obtained by integrating the SI through the cross section reads

$$P = -G\Theta\frac{\partial\theta}{\partial x}\dot{\theta} \quad (3)$$

Here,  $\Theta$  denotes the polar moment of inertia of the cross section,  $\theta$  the angular displacement, and  $G$  the shear modulus. For a rod of annular cross section having the outer radius  $R_o$  and the inner radius  $R_i$ , the polar moment of inertia equals  $\Theta = \pi(R_o^4 - R_i^4)/2$ . The angular displacement derivative can then be replaced by the shear strain at the outer radius  $R_o$ ,  $\partial\theta/\partial x = \epsilon_{x\theta}/R_o$ . Likewise, the angular velocity  $\dot{\theta}$  can be replaced by the tangential velocity divided by the outer radius,  $\dot{u}_o/R_o$ .

If the rod is not of circular cross section, Eq. (3) applies still but, in addition to torsional motions, axial motions and stresses take place, which can generate the flow of energy. These depend on the shape of the cross section and should be analyzed separately in each individual case.

**3.1.3 Beam Vibrating in Flexure** In flexural vibration, two components of stress exist: the axial normal stress  $\sigma_{xx}$  and the lateral shear stress  $\sigma_{xz}$ . The axial stress varies linearly with distance from the neutral plane, while the variation of the shear stress depends on the cross-section shape. The axial component of particle velocity  $\dot{u}_x$  exhibits the same variation as the axial stress, while the lateral component  $\dot{u}_z$  remains constant across the beam thickness. Since the axial and lateral displacements are coupled through a simple expression  $u_x = -z \partial u_z / \partial x$ , two formulations of the EF are possible:

$$\begin{aligned} P_x &= \frac{JE}{\delta^2} \left( \delta \frac{\partial \varepsilon_{xx}}{\partial x} \dot{u}_z - \varepsilon_{xx} \dot{u}_x \right) \\ &= JE \left( \frac{\partial^3 u_z}{\partial x^3} \dot{u}_z - \frac{\partial^2 u_z}{\partial x^2} \frac{\partial \dot{u}_z}{\partial x} \right) \end{aligned} \quad (4)$$

where  $J$  is the area moment of inertia about the bending axis and  $\delta$  the distance from the neutral plane to the outer surface, to which the stresses and axial displacement refer. The first formulation contains strains, axial, and lateral velocities<sup>3</sup>; the second one contains lateral displacements and velocities only.<sup>4</sup>

**3.1.4 Straight Pipe** At not too high frequencies, three simple types of pipe vibration dominate the pipe motion: longitudinal, torsional, and flexural. At frequencies higher than a particular limiting frequency  $f_{\text{lim}}$  other, more complex, vibrations may take place. The limiting frequency is given by

$$f_{\text{lim}} = \frac{6h}{d\sqrt{15+12\mu}} f_{\text{ring}} \quad f_{\text{ring}} = \frac{c}{\pi d} \quad (5)$$

where  $f_{\text{ring}}$  is the pipe ring frequency,  $h$  is the wall thickness,  $d$  is the mean diameter,  $\mu$  is the mass ratio of the contained fluid and the pipe wall,  $c$  is the velocity of longitudinal waves in the wall,  $c = \sqrt{E/\rho}$ , and  $\rho$  is the pipe mass density. The three types of motion contribute independently to the total energy flow. This enables straightforward measurements.<sup>5</sup> The three contributions should be evaluated separately, using the formulas (2), (3), and (4), and then be added together.

### 3.2 Thin Flat Plate

The normal and in-plane movements of a vibrating flat thin plate are decoupled and thus can be considered independently. The UEF can be split in two orthogonal components, as shown in Fig. 2.

**3.2.1 Longitudinally Vibrating Plate** In a thin plate exhibiting in-plane motion only, the intensity is constant throughout the thickness. The UEF is obtained by

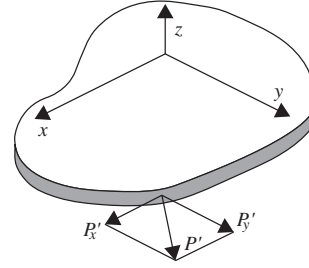


Figure 2 Components of energy flow in a thin plate.

simply multiplying the intensity with the plate thickness  $h$ . The UEF component in the  $x$  direction reads<sup>3</sup>:

$$\begin{aligned} P'_x &= hD_p \left( \varepsilon_{xx} \dot{u}_x + \frac{1-\nu}{2} \varepsilon_{xy} \dot{u}_y \right) \\ &= hD_p \left( \frac{\partial u_x}{\partial x} \dot{u}_x + \frac{1-\nu}{2} \frac{\partial u_y}{\partial x} \dot{u}_y \right) \end{aligned} \quad (6)$$

where  $D_p$  is the plate elasticity modulus,  $D_p = E/(1-\nu^2)$ ,  $\nu$  being the Poisson's coefficient. An analogous expression applies for the  $y$  direction, obtained by interchanging the  $x$  and  $y$  subscripts. The expression is similar to that for a rod (2), the difference being an additional term that is due to shear stresses carrying out work on motions perpendicular to the observed direction.

**3.2.2 Flexurally Vibrating Plate** The stress distribution across the thickness of a thin plate vibrating in flexure is similar to that of a beam. However, the plate stresses yield twisting in addition to bending and shear. Consequently, the intensity distribution across the plate thickness is analogous to that for the beam, with the exception of an additional mechanism: that of intensity of twisting. The plate terms depend on two coordinates,  $x$  and  $y$ . The UEF in the  $x$  direction reads

$$\begin{aligned} P'_x &= \frac{Eh}{3(1-\nu^2)} \left[ \frac{\partial(\varepsilon_{xx} + \varepsilon_{yy})}{\partial x} \dot{u}_z + (\varepsilon_{xx} + \nu\varepsilon_{yy}) \dot{u}_x \right. \\ &\quad \left. + \frac{1-\nu}{2} \varepsilon_{xy} \dot{u}_y \right] \end{aligned} \quad (7)$$

where  $\varepsilon$  stands for surface strain. The UEF in the  $y$  direction is obtained by an  $x$ - $y$  subscript interchange. As for the flexurally vibrating beam, the normal component of vibration of a flexurally vibrating plate is usually of a much higher level than the in-plane component. This makes it appropriate to give the intensity expressions in terms of the normal component  $u_z$  at the cost of increasing the order of spatial derivatives involved<sup>4</sup>:

$$\begin{aligned} P'_x &= \frac{Eh^3}{12(1-\nu^2)} \left[ \frac{\partial(\Delta u_z)}{\partial x} \dot{u}_z - \left( \frac{\partial^2 u_z}{\partial x^2} + \nu \frac{\partial^2 u_z}{\partial y^2} \right) \frac{\partial \dot{u}_z}{\partial x} \right. \\ &\quad \left. - (1-\nu) \frac{\partial^2 u_z}{\partial x \partial y} \frac{\partial \dot{u}_z}{\partial y} \right] \end{aligned} \quad (7a)$$

where  $\Delta$  is a Laplacian,  $\Delta = \partial^2/\partial x^2 + \partial^2/\partial y^2$ . The UEF formula (7a) is the one most frequently used.

### 3.3 Thin Shell

Due to the curvature of the shell, the in-plane and the normal motions are coupled. The UEF expressions for the shell become very complex.<sup>6</sup> If the shell is either cylindrical or spherical, the expressions for the UEF along the wall of the shell are the same as for a flat plate with the addition of a curvature-dependent UEF term  $P'_c$ :

$$P'_{\text{shell}} = (P'_{\text{in-plane}} + P'_{\text{flexural}})_{\text{plate}} + P'_c \quad (8)$$

The first two terms in brackets are given by Eqs. (6) and (7). The curvature term is fairly complex and contains many terms. In the case of thin shells, it can be simplified.

**3.3.1 Circular Cylindrical Shell** Let the shell be positioned axially in the  $x$  direction with the local  $x$ - $y$ - $z$  coordinate system attached to the observation point such that  $y$  is in tangential and  $z$  in radial direction. The axial and tangential components of the simplified curvature term read

$$\begin{aligned} P'_{c,x} &\approx -\frac{Eh^3}{12(1-\nu^2)} \frac{\nu}{a} u_z \dot{u}_x \\ P'_{c,y} &\approx -\frac{Eh^3}{12(1-\nu^2)} \frac{1}{a} u_z \dot{u}_y \end{aligned} \quad (9)$$

**3.3.2 Spherical Shell** If the shell is thin, the curvature-dependent term is approximately equal to<sup>8</sup>

$$P'_{c,x} \approx -\frac{Eh^3}{12(1-\nu^2)} \frac{1+\nu}{a} u_z \dot{u}_x \quad (10)$$

In this case, the curvature terms in  $x$  and  $y$  directions are the same since the shell is centrally symmetrical about the normal to the surface.

### 3.4 Resilient Mount

Beams (rods), plates, and shells usually represent generic parts of builtup mechanical assemblies. The energy flow in typical builtup structures can be found by using the expressions given in the preceding sections. These expressions refer to local energy flow and can be applied to any point of the part analyzed. Resilient mounts used for vibroisolation transmit energy flow, too. As mounts usually serve as a link between vibration sources and their support, all the vibratory energy flows through mounts.

**3.4.1 Unidirectional Motion of Mount Ends** At low frequencies, a mount behaves as a spring. The internal force in the mount is then approximately proportional to the difference of end displacements,  $F \approx \zeta(u_1 - u_2)$ . The input energy flow  $P_{\text{in}}$  and that leaving the mount  $P_{\text{out}}$  can be obtained by<sup>9</sup>

$$\begin{aligned} P_{\text{in}} &= F \dot{u}_1 \approx \zeta(u_1 - u_2) \dot{u}_1 \\ P_{\text{out}} &= F \dot{u}_2 \approx \zeta(u_1 - u_2) \dot{u}_2 \end{aligned} \quad (11)$$

where  $\zeta$  denotes the stiffness of the mount in the given direction.

**3.4.2 General Motion Conditions** In a general case, the movements of endpoints of a mount will not be limited to a single direction only. The direction of the instantaneous motion will change in time, while translations will be accompanied by rotations. The displacement of each endpoint can be then decomposed into three orthogonal translations and three orthogonal rotations (Fig. 3). The single internal force has to be replaced by a generalized internal load consisting of three orthogonal forces and three orthogonal moments. Each of these will depend on both end displacements, thus leading to a matrix expression of the following form:

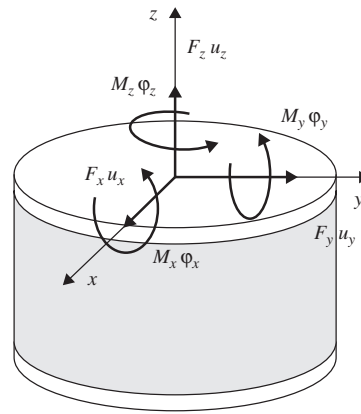
$$\{Q\} \approx [K_1]\{u_1\} - [K_2]\{u_2\} \quad (12)$$

where  $\{Q\} = \{F_x, F_y, F_z, M_x, M_y, M_z\}^T$  represents the internal generalized load vector (comprising the forces and moments), while  $\{u_1\} = \{u_{x1}, u_{y1}, u_{z1}, \phi_{x1}, \phi_{y1}, \phi_{z1}\}^T$  and  $\{u_2\} = \{u_{x2}, u_{y2}, u_{z2}, \phi_{x2}, \phi_{y2}, \phi_{z2}\}^T$  are the generalized displacement vectors of endpoints 1 and 2. Each of the stiffness matrices  $K$  in (12) contains  $6 \times 6 = 36$  stiffness components that couple six displacement components to six load components. Due to reciprocity, some of the elements of  $K$  are equal, which reduces the number of cross stiffness terms.

The total energy flow through the mount reads

$$\begin{aligned} P_{\text{in}} &\approx \{Q\}^T \{\dot{u}_1\} = (\{u_1\}^T [K_1]^T - \{u_2\}^T [K_2]^T) \{\dot{u}_1\} \\ P_{\text{out}} &\approx \{Q\}^T \{\dot{u}_2\} = (\{u_1\}^T [K_1]^T - \{u_2\}^T [K_2]^T) \{\dot{u}_2\} \end{aligned} \quad (13)$$

Equation (13), giving the instantaneous energy flow entering and leaving the mount, is valid as long as the inertial effects in the mount are negligible, that is, at low frequencies. The stiffness components appearing in Eq. (12) are assumed to be constant, which corresponds to the concept of a massless mount. With increase in frequency, these simple conditions change, as described in the next section.



**Figure 3** Movements and loading of a resilient element contributing to energy flow.

#### 4 MEAN ENERGY FLOW AND FLOW SPECTRUM

The governing formulas for energy flow given in the preceding chapter refer to the instantaneous values of intensity. It is useful to operate with time-averaged values of intensity and energy flow. This value is obtained by time averaging each of the terms appearing in the given governing formula.

The terms to be averaged are, without exception, the products between two time-dependent variables. The time-averaged product of two variables,  $q_1(t)$  and  $q_2(t)$ , can be represented in the frequency domain by the one-sided cross spectral density function of the two variables  $G_{12}(\omega)$ . The spectral density concept can be readily applied to the energy flow<sup>10</sup>:

$$\overline{q_1(t)q_2(t)} = \text{Re} \int_0^\infty G_{12}(\omega) d\omega \quad (14)$$

Here, the horizontal bar denotes time averaging, while  $\text{Re}$  denotes the real part of a complex variable.

Time-averaged EF represents net energy flow at the observed point. It is termed *active* because it refers to the portion of total energy flow that flows out of a given region. The remaining portion of the energy flow, which fluctuates to and fro but has zero mean value, is accordingly termed *reactive*. It is usually represented by the imaginary part of the cross spectral density of flow.

##### 4.1 Vibration Waves and Energy Flow

Vibration can be represented in terms of waves. Such a representation is particularly simple in the case of a vibrating rod or a beam because the wave motion takes place in an axial direction only. The parameters of wave motion can be easily computed or measured.

At any frequency, the vibratory motion of a rod can be given in terms of velocity amplitudes of two waves,  $V_1$  and  $V_2$ , traveling along the rod in opposite directions. The TEF in the rod then equals

$$P = \frac{1}{2}C(V_1^2 - V_2^2) \quad (15)$$

with  $C = S\sqrt{E\rho}$  for longitudinal vibration and  $C = (\Theta/R_o^2)\sqrt{G\rho}$  for torsional vibration.

In a beam vibrating in flexure, the two traveling waves of amplitudes  $V_1$  and  $V_2$  are accompanied by two evanescent waves. The latter contribute to energy flow, too. The contribution of evanescent waves depends on the product of their amplitudes as well as on the difference of their phases  $\psi_+$  and  $\psi_-$ . While the amplitudes of evanescent waves  $V_{e1}$  and  $V_{e2}$ , unlike those of traveling waves, vary along the beam, their product remains the same at any position. The phase difference between the evanescent waves is also invariant with respect to axial position. The TEF

in the beam, given in terms of vibration velocities, reads<sup>11</sup>

$$P = (\rho S)^{3/4}(JE)^{1/4}\sqrt{\omega}[V_1^2 - V_2^2 - V_{e1}V_{e2}\sin(\psi_+ - \psi_-)] \quad (16)$$

##### 4.1.1 Simplified Governing Formulas for Flexurally Vibrating Beams and Plates

At beam positions that are far from terminations, discontinuities, and excitation points, called the far field, the contribution of evanescent waves can be neglected. The notion of a far field applies to both beams and plates. The far-field range distance depends on frequency. It is approximately given for a beam by  $d = (\pi/\sqrt{\omega})(JE/\rho S)^{1/4}$ , where  $J$  is the area moment of inertia and  $S$  the cross-section area. For a plate, this distance is approximately  $d = (\pi/\sqrt{\omega})[h^2E/12\rho(1 - \nu^2)]^{1/4}$ , where  $h$  is the thickness and  $\nu$  the Poisson coefficient.

The far-field plate vibration is essentially a superposition of plane propagating waves. In such regions, a simplified formula applies to the spectral density of EF in flexural motion<sup>12</sup>:

$$G_P = -C/\text{Im}\{G_{vux}\} \quad (17)$$

where  $G_{vux}$  is the cross spectral density between the vibration velocity and its  $x$  derivative, while  $C$  is a constant depending on the cross section, mass density  $\rho$ , and Young's modulus  $E$ . For a beam  $C = 2\sqrt{SJE\rho}$ , for a plate  $C = 0.577h^2\sqrt{E\rho/(1 - \nu^2)}$ .

##### 4.2 Energy Flow in a Resilient Mount at Higher Frequencies

As the frequency increases, the mass of the mount becomes nonnegligible. The internal forces in the mount are no longer proportional to the relative displacements of the mount; neither are these forces the same at the two terminal points. The relationship between the forces and the vibration velocities at the terminal points is frequency dependent. It is usually expressed in terms of the direct and transfer stiffness of each of the two points. Due to inevitable internal losses in the element, the input EF must be larger than the output EF.

By assuming pure translational motion in the direction of the mount axis, four dynamic stiffness components of the mount can be defined,  $K_{11}$ ,  $K_{22}$ ,  $K_{12}$ , and  $K_{21}$ , such that

$$K_{mn} = j\omega \frac{F_m}{V_n} e^{j\zeta_{mn}} \Big|_{V_{k \neq n} = 0} \quad m, n, k = 1, 2 \quad (18)$$

Here,  $F$  and  $V$  stand for the force and velocity amplitudes, respectively, and  $\zeta_{mn}$  stands for the phase shift between the force and velocity while  $j = \sqrt{-1}$ . Each stiffness component  $K_{mn}$  thus becomes a complex, frequency-dependent quantity, which depends purely on mount properties. Given the end velocity amplitudes  $V_1$  and  $V_2$  and the phase shift between the



vibration of the points 1 and 2  $\varphi_{12}$ , the TEF at the mount endpoints 1 and 2 reads

$$P_1 = \frac{1}{2\omega} [V_1^2 |K_{11}| \sin(\zeta_{11}) + V_1 V_2 |K_{12}| \sin(\zeta_{12} - \varphi_{12})]$$

$$P_2 = \frac{1}{2\omega} [V_2^2 |K_{22}| \sin(\zeta_{22}) + V_1 V_2 |K_{21}| \sin(\zeta_{21} + \varphi_{12})]$$
(19)

Due to reciprocity, the two cross stiffness components are mutually equal,  $K_{21} = K_{12}$ . If the mount is made symmetrical with respect to two endpoints, the direct stiffness components are equal too,  $K_{11} = K_{22}$ .

When the mount exhibits motion of a more general nature than simple translation in one direction, the evaluation of energy flow through the mount becomes increasingly difficult. The basic guideline for the computation of the TEF in such a case is the following:

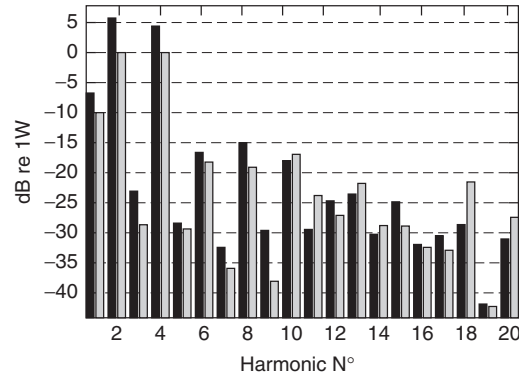
- Establish the appropriate stiffness matrix (i.e., relationships between all the relevant forces + moments and translation + angular displacements).
- Reconstruct the force + moment vectors at the endpoints from the known motions of these points.
- The TEF is obtained as the scalar product of the resultant force vector and the translational velocity vector plus the product of the resultant moment vector and the angular velocity vector. This applies to each of the endpoints separately.

Most resilient mounts, for example, those made of elastomers, have mechanical properties that depend not only on frequency but also on static preloading, temperature, and dynamical strain. Dynamic stiffness of the mount can sometimes be modeled as a function of operating conditions.<sup>13</sup> If the mount is highly nonlinear in the operating range, or if the attachments cannot be considered as points (e.g., rubber blocks of extended length, sandwiched between steel plates), the approach outlined above becomes invalid.

Figure 4 shows the total energy flow across all of the 4 resilient mounts of a 24-kW reciprocating piston compressor used in a water-chiller refrigeration unit. As the vibrations have essentially a multiharmonic spectrum, only the harmonics of the base frequency of 24 Hz are shown. Each harmonic is represented by the value of energy flow entering (dark columns) and leaving (light columns) the mounts. Absolute values are shown, to accommodate the decibel scale used. This explains seemingly conflicting results at some higher harmonics where the flow that leaves the mounts gets higher values than that entering the mounts.

## 5 MEASUREMENT OF ENERGY FLOW

Governing formulas for energy flow can be expressed in different ways using either stresses (strains), displacements (velocities, accelerations), or combinations



**Figure 4** Energy flow through compressor mounts. (Dark columns) flow entering the mounts and (light columns) flow leaving the mounts. Absolute values are shown.

of these. As a general rule, the formulations based solely on vibration displacements (velocities, accelerations) are preferred by vibration specialists.

Each governing formula contains products of time-varying field variables that need to be measured simultaneously. Spectral representation of energy flow can be obtained by replacing product averages by the corresponding spectral densities.

The energy flow governing formulas, except in the case of resilient mounts, contain spatial derivatives of field variables. Measurement of spatial derivatives represents a major problem. In practice, the derivatives are substituted by finite difference approximations. Finite difference approximations lead to errors that can be analytically estimated and sometimes kept within acceptable limits by an appropriate choice of parameters influencing the measurement accuracy. A way of circumventing the measurement of spatial derivatives consists of establishing a wave model of the structure analyzed and fitting it with measured data. This technique is known as wave decomposition approach.<sup>3,14</sup> The decomposition approach enables the recovery of all the variables entering the governing formulas.

### 5.1 Transducers for Measurement of Energy Flow

Measurement of energy flow requires the use of displacement (velocity, acceleration) or strain sensors or both. Structure-borne vibrations at a particular point generally consist of both normal and in-plane (tangential) components, which can be translational and/or rotational. Measurement of SI or EF requires separate detection of some of these motions without any perceptible effect from other motions. This requirement poses the major problem in practical measurements. Another major problem results from the imperfect behavior of individual transducers, which gives a nonconstant relationship between the physical quantity measured and the electrical signal that represents it. Both effects can severely degrade accuracy since the measured quantities make up the product(s) where these effects matter a lot.

**5.1.1 Seismic Accelerometer** An accelerometer is easy to mount and to use but shows some negative features where SI (EF) is concerned:

- *Cross sensitivity:* An accelerometer always possesses some cross sensitivity, typically up to a few percent. Nonetheless, this effect can still be significant, especially in cases where a given motion is measured in the presence of a strong component of cross motion.
- *Positioning:* Due to its finite size, the sensitivity axis of an accelerometer used for in-plane measurement can never be placed at the measurement surface. Thus, any in-plane rotation of the surface corrupts the accelerometer output. Compensation can be effected by measuring the rotation of the surface.
- *Dynamic loading:* An accelerometer loads the structure to which it is attached. This effect is of importance for SI measurement on lightweight structures.

**5.1.2 Strain Gauge** Strain gauges measure normal strain, that is, elongation. Shear strain at the free surface can be measured by two strain gauges placed perpendicularly to each other. Resistive strain gauges exhibit few of the drawbacks associated with accelerometers: cross sensitivity is low and the sensitivity axis is virtually at the surface of the object, due to extremely small thickness of the gauge, while dynamic loading is practically zero. However, the conventional gauges exhibit low sensitivity where typical levels of strain induced by structure-borne vibration are concerned, which means that typical signal-to-noise values could be low. Semiconductor gauges have a much higher sensitivity than the conventional type, but high dispersion of sensitivity makes the semiconductor gauges unacceptable for intensity work.

**5.1.3 Noncontact Transducers** Various non-contact transducers are available for the detection of structure motion such as inductive, capacitive, eddy current, light intensity, and light-modulated transducers. The majority of such transducers are of a highly nonlinear type. Optical transducers that use the interference of coherent light such as LDV (laser Doppler velocimeter) are well suited for SI work.<sup>15</sup> The most promising, however, are optical techniques for whole-field vibration detection, such as holographic or speckle-pattern interferometric methods.<sup>16</sup> Applications of these are limited, for the time being, to plane surfaces and periodic signals only. Another interesting approach of noncontact whole-field SI measurement of simple-shaped structures consists of using acoustical holography.<sup>17,18</sup>

## 5.2 Transducer Configurations

In some cases of the measurement of energy flow, more than one transducer will be needed for the detection of a single physical quantity:

- When separation of a particular type of motion from the total motion is required

- When detection of a spatial derivative is required
- When different wave components need to be extracted from the total wave motion

The first case arises with beams, plates, and shells where longitudinal and flexural motions take place simultaneously. The second case occurs when a direct measurement implementation of SI or EF governing equations is performed. The third case applies to waveguides—beams, pipes, and the like—where the wave decomposition approach is used.

**5.2.1 Separation of Components of Motion** In a beam or a rod all three types of vibration motion, that is, longitudinal, torsional, and flexural, can exist simultaneously. The same applies to longitudinal and flexural vibrations in a flat plate. The problem here is that both longitudinal and flexural vibrations produce longitudinal motions. In order to apply intensity formulas correctly to a measurement, the origin of the motion must be identified. This can be done by connecting the measuring transducers in such a way as to suppress the effects of a particular type of motion, for example, by placing two identical transducers at opposite sides of the neutral plane and adding or subtracting the outputs from the transducers.

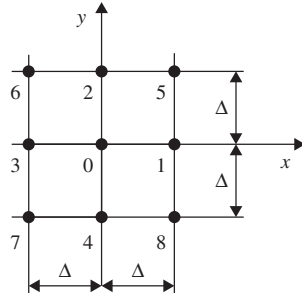
In the case of shells, the in-plane motions due to bending must be separated from the extensional motions before shell governing formulas can be applied. Corrections for the effect of bending, which affects longitudinal motion measured at the outer surface, apply for thin shells in the same way as for thin plates.

**5.2.2 Measurement of Spatial Derivatives** Formulas for energy flow contain spatial derivatives. The usual way of measuring spatial derivatives is by using finite difference concepts. The spatial derivative of a function  $q$  in a certain direction, for example, the  $x$  direction, can be approximated by the difference between the values of  $q$  at two adjacent points, 1 and 2, located on a straight line in the direction concerned:

$$\frac{\partial q}{\partial x} \approx \frac{q(x + \Delta x/2) - q(x - \Delta x/2)}{\Delta x} \quad (20)$$

The spacing  $\Delta x$  should be small in order to make the approximation (20) valid. The term “small” is related to the wavelength of vibration. Using the principle outlined, higher order derivatives can be determined from suitable finite difference approximations. Referring to the scheme in Fig. 5, the spatial derivatives appearing in the EF formulas can be determined from the finite difference approximations listed below.

$$\begin{aligned} \frac{\partial q}{\partial y} &\approx \frac{q_2 - q_4}{2\Delta} & \frac{\partial^2 q}{\partial x^2} &\approx \frac{q_1 - 2q_0 + q_3}{\Delta^2} \\ \frac{\partial^2 q}{\partial y^2} &\approx \frac{q_2 - 2q_0 + q_4}{\Delta^2} & \frac{\partial^2 q}{\partial x \partial y} &\approx \frac{q_5 - q_6 + q_7 - q_8}{4\Delta^2} \end{aligned} \quad (21)$$



**Figure 5** Transducer configuration for measurement of spatial derivatives.

Errors in measurement of higher order derivatives, such as those appearing in the expressions for plate and shell flexural vibration, increase exponentially with the order of derivative. For these reasons, measurement of higher order spatial derivatives should be avoided. Simplified measurement techniques, such as the two-transducer method described, may seem far more suitable for practical purposes. These, however, have to stay limited to far-field conditions, that is, locations far from sources or discontinuities.

### 5.3 Wave Decomposition Technique

This approach is suitable for waveguides, for example, rods, beams, and pipes, where the vibration field can be described by a simple wave model in frequency domain. The velocity amplitude  $V_n$  of longitudinal or torsional (i.e., nondispersive) vibration can be represented by two oppositely propagating waves, those of

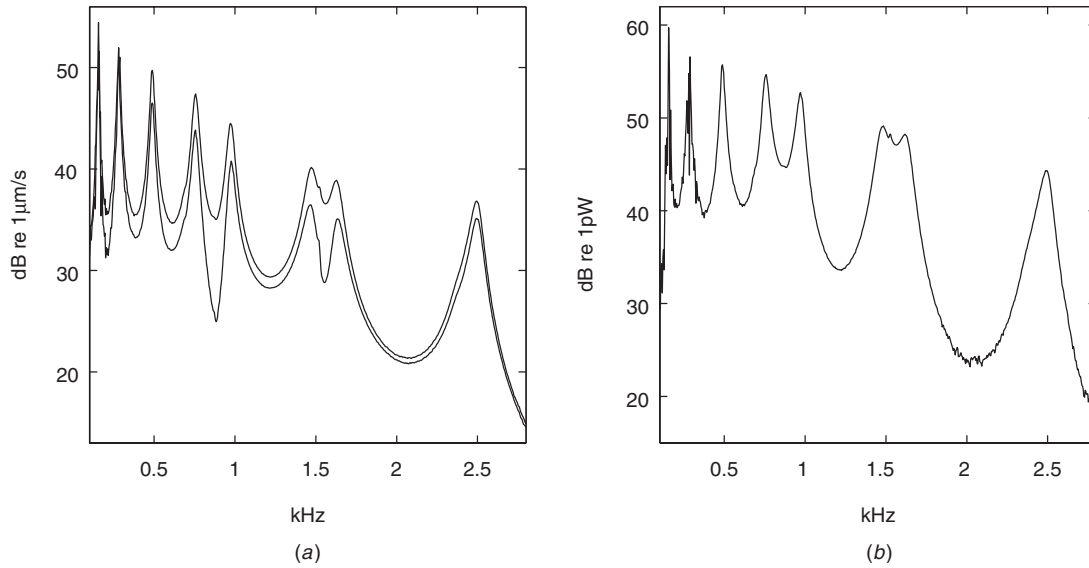
flexural (dispersive) vibration  $V_d$  by four waves:

$$V_n(x, \omega) = \sum_{i=1}^2 V_i e^{j\varphi_i} e^{j(-1)^i k x}$$

$$V_d(x, \omega) = \sum_{i=1}^4 V_i e^{j\varphi_i} e^{(-j)^i k x} \quad (22)$$

In such a representation the wave amplitudes  $V_i$  as well as the phases  $\varphi_i$  of these waves are unknown. The wavenumber  $k$  is supposed to be known. By measuring complex vibration amplitudes  $V_n$  at two positions,  $x_1$  and  $x_2$ , the unknown wave amplitudes can be easily recovered. Likewise, the measurement of complex vibration amplitudes  $V_d$  at four positions,  $x_1, \dots, x_4$ , can recover the four related amplitudes by some basic matrix manipulations. Once these are known, the energy flow is obtained from Eq. (15) or (16).

Figure 6 shows the application of the wave decomposition technique to a 1-mm-thick steel beam. The 28-cm-long, 1.5-cm-wide beam was composed of two parts joined by a resilient joint. The spacing between measurement points was 2 cm. The measurements were done using a scanning laser vibrometer. The signal from the vibration exciter driving the beam was used as a reference to provide the phase relationship between different measurement signals that could not be simultaneously recorded. The left plot shows the amplitudes of two propagating waves while the right plot shows the TEF evaluated by using the amplitude data via Eq. (16).



**Figure 6** TEF measured in a 1-mm-thick steel beam incorporating a resilient joint. (a) Amplitudes of propagating flexural waves: thick line, positive direction; thin line, negative direction. (b) TEF.

#### 5.4 Measurement Errors

Measurements of energy flow are very sensitive to various types of errors. An electrical signal from the transducer may be subjected to distortion and noise, which can greatly affect the resulting intensity readings. Equally damaging can be the inaccurate positioning and cross sensitivity of transducers.

**5.4.1 Instrumentation Error** The most significant source of signal distortion where SI (EF) is concerned is the phase shift between the physical quantity measured and the conditioned electrical signal that represents it. This effect becomes particularly significant in connection with finite difference representation of field variables.<sup>19</sup> It can be shown that the error due to phase shift  $\Delta\phi$  in the measurement of spatial derivatives has the order of  $1/(k\Delta)^n$ , where  $\Delta$  is the distance between transducers and  $n$  the derivative order.

To keep the phase mismatch error small, the instrumentation phase matching between channels must be extremely good because the product  $k\Delta$  has itself to be small in order to make the finite difference approximation valid.

Another important error that can affect measurement accuracy can be caused by the transducer mass loading.<sup>20</sup> The transducer mass should be kept well below the value of the structural apparent mass.

**5.4.2 Finite Difference Convolution Error** By approximating spatial derivatives with finite differences, systematic errors are produced that depend on the spacing between the transducers. Thus, the finite difference approximation of the first spatial derivative will produce an error equal to

$$\varepsilon \approx -\frac{1}{24}(k\Delta)^2 \quad (23)$$

This error is seen to be negative: That is, the finite difference technique underestimates the true value. The finite difference error of the second derivative is approximately twice the error of the first derivative. The errors of higher order derivatives rise in proportion to the derivative order, in contrast to the instrumentation errors, which exhibit an exponential rise.

**5.4.3 Wave Decomposition coincidence error** The technique of wave decomposition is essentially a solution to an inverse problem. At particular "coincidence" frequencies, which occur when the transducer spacing matches an integer number of half the wavelength, the solution is badly conditioned, making the error rise without limits. This error can be avoided by changing the spacing and repeating the measurements.

#### REFERENCES

1. W. Maysenhölder, *Energy of Structure-Borne Sound* (in German), Hirzel, Stuttgart/Leipzig, 1994.
2. S. P. Timoshenko and J. N. Goodier, *Theory of Elasticity*, McGraw-Hill, New York, 1970.
3. G. Pavić, Determination of Sound Power in Structures: Principles and Problems of Realisation, Proc. 1st Int. Congress on Acoustical Intensity, Senlis, 1981, pp. 209–215.
4. D. Noiseux, Measurement of Power Flow in Uniform Beams and Plates, *J. Acoust. Soc. Am.*, Vol. 47, 1970, pp. 238–247.
5. G. Pavić, Vibroacoustical Energy Flow Through Straight Pipes, *J. Sound Vib.*, Vol. 154, 1992, pp. 411–429.
6. C. R. Fuller and F. J. Fahy, Characteristics of Wave Propagation and Energy Distribution in Cylindrical Elastic Shells Filled with Fluid, *J. Sound Vib.*, Vol. 81, 1982, pp. 501–518.
7. G. Pavić, Vibrational Energy Flow in Elastic Circular Cylindrical Shells, *J. Sound Vib.*, Vol. 142, 1990, pp. 293–310.
8. I. Levanat, Vibrational Energy Flow in Spherical Shell, Proc. 3rd Congress on Intensity Techniques, Senlis, 1990, pp. 83–90.
9. G. Pavić and G. Oresković, Energy Flow through Elastic Mountings, Proc. 9th Int. Congress on Acoustics, Madrid, 1977, Vol. 1, p. 293.
10. J. W. Verheij, Cross-Spectral Density Methods for Measuring Structure-Borne Power Flow on Beams and Pipes, *J. Sound Vib.*, Vol. 70, 1980, pp. 133–139.
11. G. Pavić, Measurement of Structure-Borne Wave Intensity, Part 1: Formulation of Methods, *J. Sound Vib.*, Vol. 49, 1976, pp. 221–230.
12. P. Rasmussen and G. Rasmussen, Intensity Measurements in Structures, Proc. 11th Int. Congress on Acoustics, Paris, 1983, Vol. 6, pp. 231–234.
13. L. Kari, On the Dynamic Stiffness of Preloaded Vibration Isolators in the Audible Frequency Range: Modeling and Experiments, *J. Acoust. Soc. Am.*, Vol. 113, 2003, pp. 1909–1921.
14. C. R. Halkyard and B. R. Mace, A Wave Component Approach to Structural Intensity in Beams, Proc. 4th Int. Congress on Intensity Techniques, Senlis, 1993, pp. 183–190.
15. T. E. McDevitt, G. H. Koopmann, and C. B. Burroughs, Two-Channel Laser Vibrometer Techniques for Vibration Intensity Measurements, Part I. Flexural Intensity, *J. Vib. Acoust.*, Vol. 115, 1993, pp. 436–440.
16. J. C. Pascal, X. Carniel, V. Chalvidan, and P. Smigiel-ski, Energy Flow Measurements in High Standing Vibration Fields by Holographic Interferometry, Proc. Inter-Noise 95, Newport Beach, 1995, Vol. 1, pp. 625–630.
17. E. G. Williams, H. D. Dardy, and R. G. Fink, A Technique for Measurement of Structure-Borne Intensity in Plates, *J. Acoust. Soc. Am.*, Vol. 78, 1985, pp. 2061–2068.
18. J. C. Pascal, T. Loyau, and J. A. Mann III, Structural Intensity from Spatial Fourier Transform and Bahim Acoustic Holography Method, Proc. 3rd Int. Congress on Intensity Techniques, Senlis, August 1990, pp. 197–206.
19. G. P. Carroll, Phase Accuracy Considerations for Implementing Intensity Methods in Structures, Proc. 3rd Congress on Intensity Techniques, Senlis, 1990, pp. 241–248.
20. R. J. Bernhard and J. D. Mickol, Probe Mass Effects on Power Transmission in Lightweight Beams and Plates, Proc. 3rd Congress on Intensity Techniques, Senlis, 1990, pp. 307–314.

# CHAPTER 17

## STATISTICAL ENERGY ANALYSIS

**Jerome E. Manning**  
Cambridge Collaborative, Inc.  
Cambridge, Massachusetts

### 1 INTRODUCTION

Statistical energy analysis (SEA) is commonly used to study the dynamic response of complex structures and acoustical spaces. It has been applied successfully in a wide range of industries to assist in the design of quiet products. SEA is most useful in the early stages of design when the details of the product are not known and it is necessary to evaluate a large number of design changes. SEA is also useful at high frequencies where the dynamic response is quite sensitive to small variations in the structure and its boundary conditions.

A statistical approach is used in SEA to develop a prediction model. The properties of the vibrating system are assumed to be drawn from a random distribution. This allows great simplifications in the analysis, whereby modal densities, average mobility functions, and energy flow analysis can be used to obtain response estimates and transfer functions.

Statistical energy analysis combines statistical modeling with an energy flow formulation. Using SEA, the energy flow between coupled subsystems is defined in terms of the average modal energies of the two subsystems and coupling factors between them. Equations of motion are obtained by equating the time-average power input to each subsystem with the sum of the power dissipated and the power transmitted to other subsystems. Over the past 10 years SEA has grown from an interesting research topic to an accepted design analysis tool.

### 2 STATISTICAL APPROACH TO DYNAMIC ANALYSIS

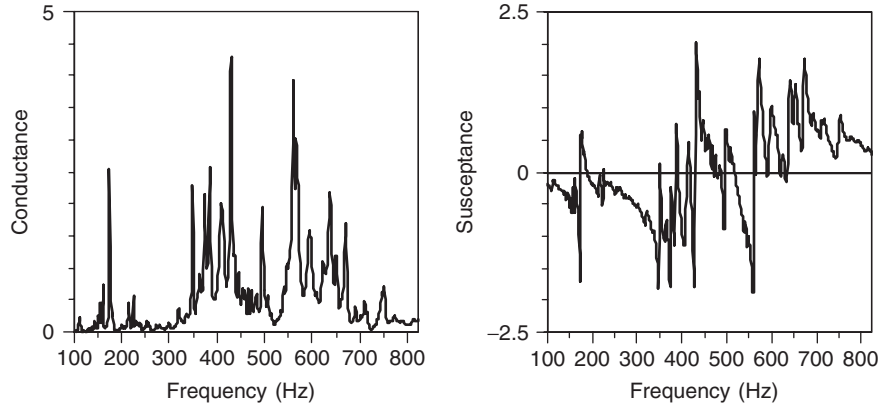
Earlier chapters of this handbook have presented a variety of techniques to study the dynamic response of complex structural and acoustical systems. By and large, these techniques have used a deterministic approach. In the analytical techniques, it has been assumed that the system being studied can be accurately defined by an idealized mathematical model. Techniques based on the use of measured data have assumed that the underlying physical properties of the system are well defined and time invariant. Although the excitation of the system was considered to be a random process in several of the earlier sections, the concept that the system itself has random properties was not pursued.

The most obvious source of randomness is manufacturing tolerances and material property variations. Although variations in geometry may be small and have a negligible effect on the low-frequency dynamics of the system, their effect at higher frequencies cannot be neglected. Another source of randomness is uncertainty in the definition of the parameters needed to

define a deterministic model. For example, the geometry and boundary conditions of a room will change with the arrangement of furnishings and partitions. Vehicles will also change due to different configurations of equipment and loadings. Finally, during the early phases of design, the details of the product or building being designed are not always well defined. This makes it necessary for the analyst to make an intelligent guess for the values of certain parameters. If these parameters do not have a major effect on the response being predicted, the consequences of a poor guess are not serious. On the other hand, if the parameters do have a major effect, the consequences of a poor guess can be catastrophic. Although deterministic methods of analysis have the potential to give exact solutions, they often do not because of errors and uncertainties in the definition of the required parameters.

The vibratory response of a dynamic system may be represented by the response of the modes of vibration of the system. Both theoretical and experimental techniques to obtain the required mode shapes and resonance frequencies exist. A statistical approach will now be followed in which resonance frequencies and mode shapes are assumed to be random variables. This approach will result in great simplifications where average mobility functions and power inputs from excitation sources can be defined simply in terms of the modal density and structural mass or acoustical compliance of the system. Modal densities in turn can be expressed in terms of the dimensions of the system and a dispersion relation between wave number and frequency.

If the properties describing a dynamic system can be accurately defined, the modes of the system can be found mathematically in terms of the eigenvalues and eigenfunctions of a mathematical model of the system, or they can be found experimentally as the resonance frequencies and response amplitudes obtained during a modal test. The availability of finite element models and computer software makes it possible today to determine the modes of very complex and large structures. Although it might be argued that the computational cost to determine a sufficient number of modes to analyze acoustical and structural systems at high frequencies is too high, that cost is dropping each year with the development of faster and less expensive computers. Thus, many vibration analysts believe that analysis based on modes determined from a finite element model can provide them with the answers they need. Similarly, many engineers who are more inclined toward the use of measured data believe that analysis based on modes determined from a modal test will suffice.



**Figure 1** Drive point conductance and susceptance for a typical structure.

The accuracy of a modal analysis depends on the accuracy with which the modal parameters can be determined and on the number of modes that are included in the analysis. Since the modes form a mathematically complete set of functions, a high degree of accuracy can be obtained by including a large number of modes in the analysis. In practice, the accuracy with which the modal parameters can be determined decreases for the higher order modes. Thus, the accuracy of the modal analysis depends to a large extent on the number of modes needed to describe the vibration of the system. At low frequencies, for lightly damped systems, the response can be accurately described in terms of the response of a few modes. On the other hand, at high frequencies and for highly damped systems, a large number of modes are required, and the accuracy of the modal analysis decreases. In this case, a statistical description of the system is warranted. Using a statistical description avoids the need for an accurate determination of the resonance frequencies and mode shapes, thereby eliminating the main source of error in the modal analysis. Of course, in using a statistical description, the ability to determine the exact response at specific locations and frequencies is lost. Instead, a statistical description of the response is obtained.

## 2.1 Mobility Formulation

To illustrate the use of modal analysis and the application of a statistical approach, the response of a linear system to a point excitation with harmonic  $e^{j\omega t}$  time dependence is considered. For a structural system, the ratio of the complex amplitude of the response velocity to the complex amplitude of the excitation force is defined as the point mobility for the system. A transfer mobility is used if the location of the response point is different than that of the excitation point. A drive point mobility is used if the locations of the response and drive points are the same. The drive point mobility at coordinate location  $x$  can be written as a

summation of modal responses,

$$Y_{pt}(x, \omega) = \sum_{i=1}^{\infty} \frac{1}{M_i} \frac{j\omega\psi_i^2(x)}{(\omega_i^2 - \omega^2) + j\omega\omega_i\eta_i} \quad (1)$$

where  $Y_{pt}(x, \omega)$  is the drive point mobility for the structure,  $M_i$  is the modal mass,  $\psi_i(x)$  is the mode shape for the  $i$ th mode,  $\omega$  is the radian frequency of excitation,  $\omega_i$  is the resonance frequency of the  $i$ th mode,  $\eta_i$  is the damping loss factor,  $j$  equals the square root of  $-1$ , and the summation is over all modes of the system. The mobility consists of a real part—the conductance—and an imaginary part—the susceptance. The conductance is often of greater interest since the product of the conductance and the mean-square force is the input power to the system. The conductance and susceptance for a typical lightly damped system are shown in Fig. 1.

For light damping, the conductance as a function of frequency shows a large peak at each resonance frequency. The amplitude of the peak is governed by the damping and by the value of the mode shape at the drive point. Since the resonance frequencies and mode shapes are assumed to be random, the conductance as a function of frequency is analogous to a random time series of pulses. Fortunately, the statistics of such a random process has been extensively studied.

**2.1.1 Frequency Averages** A frequency-averaged conductance is found by integrating the real part of the mobility over frequency and dividing by the bandwidth:

$$\langle G_{pt}(x, \omega) \rangle_{\Delta\omega} = \frac{1}{\Delta\omega} \int_{\Delta\omega} \text{real}\{Y_{pt}(x, \omega)\} \Delta\omega \quad (2)$$

where  $\langle \rangle$  signifies an average,  $\text{real}\{ \}$  signifies the real part of a complex number, and the integral is over the frequency band,  $\Delta\omega$ . For any particular frequency band, the average conductance is largely determined by the number of modes with resonance frequencies

within the band. For light damping, the contribution to the integral in Eq. (2) from a single mode with a resonance frequency within the band is approximately  $(\pi/2)\psi_i^2/M_i$ . If the resonance frequency of the mode is outside of the band,  $\Delta\omega$ , the contribution to the integral is very small and can be ignored. Thus, the frequency-averaged conductance is given by

$$\langle G_{\text{pt}}(x, \omega) \rangle_{\Delta\omega} = \frac{1}{\Delta\omega} \frac{\pi}{2} \sum_{\substack{i \\ \text{modes} \\ \text{in } \Delta\omega}} \frac{\psi_i^2(x)}{M_i} \quad (3)$$

where the summation is over all modes with resonance frequencies in the band. Note that the frequency-averaged conductance does not depend on the precise values for the resonance frequencies or the damping, but only on the number of modes within the band and their mode shapes at the drive point.

**2.1.2 Spatial Averages** The statistical approach can be extended one step further by averaging the conductance over the spatial extent of the system. For a homogeneous system, the spatial-average value of the mode shape squared is equal to the modal mass divided by the physical mass of the system,  $M_i/M$ . Thus, the drive point conductance averaged both over a band of frequencies and over the spatial extent of the system is given by

$$\langle G_{\text{pt}}(x, \omega) \rangle_{\Delta\omega, x} = \frac{\pi}{2M} \frac{N_{\Delta\omega}}{\Delta\omega} \quad (4)$$

where  $N_{\Delta\omega}$  is the number of modes with resonance frequencies in the band  $\Delta\omega$ —the “resonant mode count”—and  $M$  is the physical mass of the structure. Equation (4) applies only to homogeneous structures. However, it can also be used for the general case, if we replace  $M$  in Eq. (4) by the dynamic mass,  $M_d$ , where

$$M_d(\omega) = \frac{1}{N_{\Delta\omega}} \sum_{\substack{i \\ \text{modes} \\ \text{in } \Delta\omega}} \frac{\langle \psi_i^2(x) \rangle_x}{M_i} \quad (5)$$

The definition of a dynamic mass allows the expression given in Eq. (4) to be used for the average conductance of both homogeneous structures and nonhomogeneous structures, such as framed plates and structures loaded with components.

**2.1.3 Acoustical Systems** The formulation above is for a structural system in which the equations of motion are formulated in terms of a response variable such as displacement. For an acoustic system, the equations of motion are typically formulated in terms of pressure, a stress variable. In this case, a similar formulation can be carried out. However, the acoustical

resistance—pressure divided by volume velocity—is obtained rather than the conductance, and the structural mass is replaced by the bulk compliance of the acoustical space,

$$\langle R_{\text{pt}}^A(x, \omega) \rangle_{\Delta\omega, x} = \frac{\pi}{2} \frac{N_{\Delta\omega}}{\Delta\omega} \frac{1}{C_a} \quad (6)$$

where  $R_{\text{pt}}^A$  is the point acoustical resistance for the acoustical space and  $C_a$  is the bulk compliance of the space ( $V/\rho c^2$  for a space with rigid walls).

**2.1.4 Ensemble Averages** An ensemble-averaged conductance is found by averaging the real part of the mobility over a large number of individual products drawn from a random distribution. For example, an ensemble of products may be defined as the vehicles coming off a production line. Alternatively, an ensemble may be defined as the vehicles of a specific model with random configurations for passenger load, interior trim, and road conditions. The ensemble average has the advantage that it can be useful both for random excitation and for single frequency excitation.

If an ensemble of systems is defined such that the resonance frequencies are distributed as a Poisson random process and the mode shapes are uniformly distributed, the ensemble average is given by

$$\langle G_{\text{pt}}(x, \omega) \rangle_{\text{ens}} = \frac{\pi}{2} \frac{n(\omega)}{M_d} \quad (7)$$

where  $n(\omega)$  is the modal density for the system—the ensemble-average number of modes per unit radian frequency.

It is common in SEA to assume that ensemble averages are equal to frequency averages. This is analogous to the ergodic assumption for a random time series in which ensemble averages are equal to time averages. The validity of the SEA ergodic assumption depends on the underlying validity of the assumed probability distributions for resonance frequencies and mode shapes. An extensive amount of work is required to validate these distributions. Thus, the SEA ergodic assumption is often accepted as a “best available” estimate. It should, however, be used with caution.

The susceptance or imaginary part of the mobility can also be determined from a modal summation. However, since the imaginary part of each term in the summation exhibits both positive and negative values, the number of terms that must be included in the summation to obtain a good estimate of the susceptance is much greater than were required to obtain a good estimate of the average conductance.

## 2.2 Modal Density

The previous section shows how the use of a statistical description of a dynamic system can lead to a great simplification in the determination of the average structural conductance or acoustical resistance. The exact resonance frequency and mode shape for each



individual mode are no longer needed. Instead, the resonant mode count or modal density can be used. The distinction between these two variables is often quite subtle. The term *mode count* is used to describe the number of modes with resonance frequencies within a given frequency band. The modal density, on the other hand, is a mathematical quantity that gives a statistical estimate of the average number of resonant modes per unit frequency for an ensemble of systems. If we define an ensemble of system for which the geometry and material parameters vary randomly within manufacturing tolerances or design limits, the mode count will vary from system to system within the ensemble. The average mode count over the ensemble can be estimated from the modal density:

$$N_{\Delta\omega} = \int_{\omega_1}^{\omega_2} n(\omega) d\omega \quad (8)$$

where  $\omega_1$  and  $\omega_2$  are the lower and upper frequencies of the band,  $\Delta\omega$ . In many cases the modal density will be a fairly smooth function of frequency. The average mode count can then be obtained simply as the product of the modal density at the band center frequency and the frequency bandwidth.

**2.2.1 Asymptotic Modal Densities** In most cases, the mode count or modal density can be determined analytically using asymptotic modal densities that are valid at high frequencies where many resonant modes exist even in narrow bands of frequency. The general use of these asymptotic modal densities to obtain the mode count has led to the idea that statistical modeling can only be used at high frequencies. This is indeed a misconception. As long as correct values are used for the modal density and the dynamic mass, the statistical modeling can be extended to low frequencies where the number of modes is small. However, at these low frequencies the variance of the estimates may become quite large, so that the average value is not a good estimate for any individual structure.

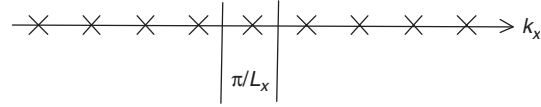
**One-Dimensional System** The modes of a one-dimensional system have mode shapes that are functions of a single spatial coordinate. For a system with uniform properties, the mode shapes at interior positions away from any boundary are in the form of a sinusoid,

$$\psi_i(x) = A_i \sin(k_i x + \varphi_i) \quad (9)$$

where  $k_i$  is a wavenumber describing the rate of variation of the mode shape with the spatial coordinate,  $x$ , and  $\varphi_i$  is a spatial phase factor that depends on boundary conditions. The wavenumber for a mode is related to the number of half-wavelengths within the length of the system,

$$k_i = \frac{\pi}{L}(i + \delta) \quad (10)$$

where  $L$  is the length of the system,  $i$  is an integer, and  $\delta$  is a small constant,  $(-\frac{1}{2} \leq \delta \leq \frac{1}{2})$  whose value



**Figure 2** Wavenumber space for a one-dimensional system.

depends on the boundary conditions at each end of the system.

The modes can be represented graphically in wavenumber space. For a one-dimensional system, wavenumber space is a single axis. Each mode can be represented by a point along the axis at the value  $k_i$ , as shown in Fig. 2. If the value of  $\delta$  is constant from mode to mode, as would be the case for clamped or free boundary conditions, the spacing between modes in wavenumber space,  $\Delta k$ , is simply the ratio  $\pi/L$ . If on the other hand, the value of  $\delta$  is random due, for example, to a random boundary condition, the average spacing between modes is also  $\pi/L$ . Although the exact position of a mode in wavenumber space depends on the value of  $\delta$ , each mode will “occupy” a length of the wavenumber axis defined by the average spacing,  $\Delta k$ .

To determine the modal density, a relationship between wavenumber and frequency is needed. This relationship is the dispersion relation or characteristic equation for the system. For a simple one-dimensional acoustical duct the dispersion relation is  $k = \omega/c$ , where  $c$  is the speed of sound. For bending deformations of a one-dimensional beam (without shear deformations or rotational inertia) the dispersion relation is  $k^4 = \omega^2 m/EI$ , where  $m$  is the mass per unit length,  $E$  is Young’s modulus for the material, and  $I$  is the bending moment of inertia. The dispersion relation allows mapping of the frequency range,  $\Delta\omega$ , to the corresponding wavenumber range,  $\Delta k$ . The average value of the mode count is then obtained by dividing  $\Delta k$  by  $\Delta\omega$ . The modal density can now be written as the limit,

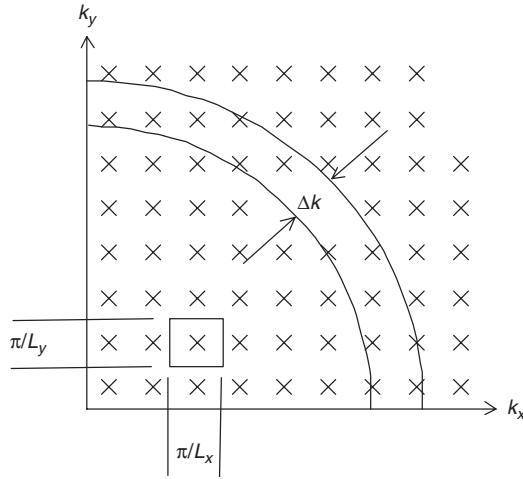
$$n(\omega) = \lim_{\Delta\omega \rightarrow 0} \frac{\Delta k}{\Delta\omega} \frac{1}{\delta k} \quad (11)$$

The ratio  $\Delta k/\Delta\omega$ , in the limit as the frequency range approaches zero, becomes the derivative of the wavenumber with respect to frequency. This derivative is the inverse of  $d\omega/dk$ , which is the group speed for the system. Thus, the modal density for the general one-dimensional system becomes

$$n(\omega) = \frac{L}{\pi c_g} \quad (12)$$

The modal density of the general one-dimensional system is simply related to the length of the system and the group speed. In this asymptotic result, which becomes exact as the number of modes increases, boundary conditions are not important. For the lower order modes, it is possible to correct the modal density for specific types of boundary conditions. However, the increase in accuracy may not be worth the effort.





**Figure 3** Wavenumber space for a two-dimensional system.

The general result shows that the modal density depends on the group speed. Thus, the modal density of a one-dimensional acoustical lined duct should take into account the effect of the lining on the group speed. If the acoustical media is a fluid, the wall compliance can have a significant effect on the group speed and should be considered.

**Two-Dimensional System** The modes of a two-dimensional system have mode shapes that vary along two spatial coordinates. Like the one-dimensional system, the modes of the two-dimensional system can be represented graphically in wavenumber space. However, wavenumber space becomes a plane defined by two axes. Each mode can be represented by a point on the plane, so that the modes of the system can be represented by a lattice of points as shown in Fig. 3. For a rectangular system, the lattice forms a rectangular grid of points. The average spacing between the points along the  $k_x$  axis is  $\pi/L_x$ , and the spacing between the points along the  $k_y$  axis is  $\pi/L_y$ , where  $L_x$  and  $L_y$  are the dimensions of the system. Thus, a mode occupies a small area in wavenumber space equal to  $\pi^2/A$ , where  $A$  is the area of the panel.

The dispersion relation for a two-dimensional system relates the frequency to the two wavenumber components,  $k_x$  and  $k_y$ . For a simple rectangular acoustical layer, the dispersion relation is  $k_x^2 + k_y^2 = \omega^2/c^2$ , where  $c$  is the speed of sound. For bending deformations of a rectangular plate (without shear deformations or rotational inertia) the dispersion relation is  $(k_x^2 + k_y^2)^2 = \omega^2 m/EI'$ , where  $m$  is the mass per unit area and  $I'$  is the bending moment of inertia of the plate. The dispersion relation allows lines of constant frequency to be drawn in wavenumber space for the upper and lower frequencies of the band,  $\Delta\omega$ . For the simple systems above, these lines are quarter-circles forming an annular region as shown

in Fig. 3. The average value of the mode count is obtained by dividing the area of this region by the area occupied by a single mode. The modal density can now be written as the limit

$$n(\omega) = \lim_{\Delta\omega \rightarrow 0} \frac{\Delta k}{\Delta\omega} \frac{kA}{2\pi} \quad (13)$$

where  $k^2 = k_x^2 + k_y^2$ .

The modal density for the general two-dimensional system becomes

$$n(\omega) = \frac{kA}{2\pi c_g} \quad (14)$$

Both the wavenumber and the group speed can be found from the dispersion relation.

The formulation of modal density using wavenumber space allows extension of the results to more complicated systems. For example, the modal density for bending modes of a fluid-loaded plate can be obtained by adjusting the group speed to account for the fluid loading. Similarly, the modal density for bending modes, including the effects of transverse shear deformations and rotary inertia, can be obtained by adjusting the group speed to account for these effects. The modal densities for cylindrical shells and orthotropic plates can be obtained using wavenumber space. For these cases, however, the lines of constant frequency will not be circular.

**Three-Dimensional System** The modes of a three-dimensional system have mode shapes that vary along three spatial coordinates. In this case, wavenumber space becomes a volume defined by three axes. Like the one-dimensional and two-dimensional systems, each mode can be represented by a point in wavenumber space, so that the modes of the system form a lattice of points in three dimensions. Each mode occupies a small volume in wavenumber space equal to  $\pi^3/V$ , where  $V$  is the volume of the system. The exact location of the mode within this volume will depend on the exact boundary conditions.

The dispersion relation for the three-dimensional system gives the frequency as a function of three wavenumbers. For a uniform acoustical space the dispersion relation is

$$\omega = c\sqrt{k_x^2 + k_y^2 + k_z^2} \quad (15)$$

where  $c$  is the speed of sound. The dispersion relation allows two-dimensional surfaces of constant frequency to be drawn in wavenumber space. The average cumulative mode count can now be obtained by dividing the total volume under these surfaces by the average volume occupied by a single mode. The dispersion relation for the uniform acoustical space results in spherical surfaces with a volume of  $k^3/2$  (one-eighth sphere with radius  $k$ ). Each mode occupies

a volume equal to  $\pi^3/V$ , so that the cumulative mode count becomes

$$N(\omega) = \frac{k^3 V}{6\pi^2} \quad (16)$$

The modal density is found from the derivative of the cumulative mode count:

$$n(\omega) = \frac{k^2 V}{2\pi^2 c_g} \quad (17)$$

The asymptotic modal density of the general three-dimensional space gives an accurate estimate of the mode count at high frequencies where many modes occur. It can also be used at lower frequencies as the ensemble average for systems with random boundary conditions. In room acoustics, the walls are commonly assumed to be rigid. In this case corrections to the asymptotic modal density can be introduced that improve the accuracy of the mode count at low frequencies. However, these corrections are only valid for a space in which the assumption of rigid walls is valid. Such an assumption would not be valid, for example, for a fluid-filled tank.

Table 1 provides a summary of the asymptotic modal densities and cumulative mode counts.

**2.2.2 Finite Element Modeling** Finite element models show great potential as a means to determine the correct mode count for complex structures and acoustical spaces at lower frequencies. Although these models may lose some accuracy in defining the resonance frequencies of the higher order modes, their use to determine the number of modes within defined frequency bands is justified. Two procedures can be used for determining a mode count from a finite element model. In the first an eigenvalue analysis is used to obtain the resonance frequencies. The mode count is obtained by dividing the frequency range of interest into bands and counting the number of resonance frequencies in each band. In the second technique, the resonance frequencies are used to determine the frequency spacing between modes. The average frequency spacing is found by averaging over a set number of spacing intervals rather than over a set frequency band. Finally, the modal density is

obtained from the inverse of the average spacing. Although the first technique is commonly used, the second technique is preferred, since it provides an estimate of the average modal density with a constant statistical accuracy.

In SEA the modes of a structural element are often subdivided into groups of modes with similar properties. For example, the modes of a plate element may be divided into *bending* and *in-plane* subsystems. When using a finite element model to determine modal densities some type of sorting based on mode shape may be required. For thin structural elements the number of bending modes in a band of frequency greatly outnumbers the in-plane compression and shear modes. It is then reasonable to use the modal density from the finite element model to determine the modal density for the bending subsystem. An example is shown in Fig. 4. In this example the modes for a section of the floor of a passenger vehicle are determined for different boundary conditions and used to obtain the modal density for the floor SEA bending subsystem.

Engineering judgment is needed to decide whether to use the modal density for a single boundary condition or to assume a random boundary condition and average the modal densities obtained from the finite element model over the different boundary conditions. The average over boundary conditions is often a more reliable estimate.

### 3 SEA ENERGY FLOW METHOD

Since its introduction in the early 1960s, statistical energy analysis, or SEA as it is commonly called, has gained acceptance as a method of analysis for structural-acoustical systems.<sup>1</sup> SEA draws on many of the fundamental concepts from statistical mechanics, room acoustics, wave propagation, and modal analysis.<sup>2-9</sup> At first, SEA appears to be a very simple method of analysis. However, because of the diversity of concepts used in formulating the basic SEA equations, the method quickly becomes very complex. For this reason, analysts have recommended caution in using SEA. However, when used properly, SEA is a powerful method of vibration and acoustical analysis.

In SEA, the system being analyzed is divided into a set of coupled subsystems. Each subsystem represents a group of modes with similar characteristics. The SEA subsystems can be considered to be "control volumes" for vibratory or acoustic energy flow. Under steady-state conditions, the time-average power input to a subsystem from external sources and from other connected subsystems must equal the sum of the power dissipated within the subsystem by damping and the power transmitted to the connected subsystems.

Consider, for example, a piece of machinery located within an enclosure in a large equipment room as shown in Fig. 5. The noise in the equipment room due to operation of the machine is of concern. A simple SEA model for this problem is shown in Fig. 6. In this model three subsystems are used: one for

**Table 1 Cumulative Mode Count and Modal Density for Homogeneous Subsystems**

Subsystem	Cumulative Mode Count $N(\omega)$	Modal Density $n(\omega)$
One dimensional	$\frac{kL}{\pi}$	$\frac{L}{\pi c_g}$
Two dimensional	$\frac{k^2 A}{4\pi}$	$\frac{kA}{2\pi c_g}$
Three dimensional	$\frac{k^3 V}{6\pi^2 c_g}$	$\frac{k^2 V}{2\pi^2 c_g}$

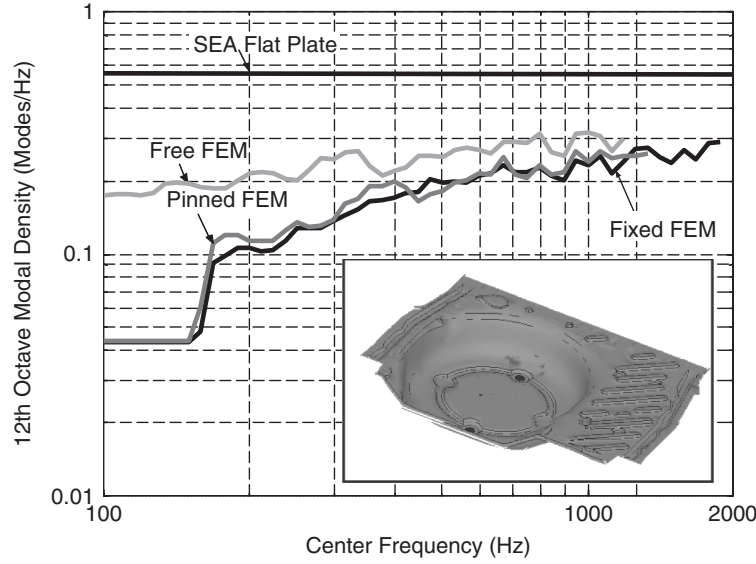


Figure 4 Modal density from finite element analysis.

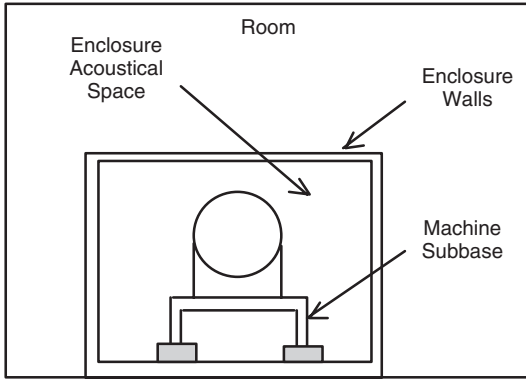


Figure 5 Machinery noise problem.

the acoustic modes of the interior space within the enclosure, one for bending modes of the enclosure walls, and one for the acoustic modes of the exterior space in the equipment room. The airborne and structure-borne noise from the machine are specified as power inputs to the model. The input power to the enclosure acoustical space,  $W_a^{\text{in}}$ , is taken to be the airborne noise radiated by the machine, which can be determined using acoustic intensity measurements. The input power to the enclosure wall,  $W_s^{\text{in}}$ , is determined from the vibration of the machine at its attachment to the enclosure base. The time-average power dissipated within each subsystem is indicated by the terms  $W_a^{\text{diss}}$ ,  $W_s^{\text{diss}}$ , and  $W_r^{\text{diss}}$ .

Following the usual definition of the damping loss factor, the time-average power dissipated within the subsystem can be written in terms of the time-average

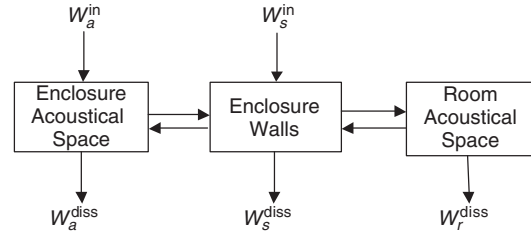


Figure 6 Simple three-element SEA model of equipment enclosure.

energy of the system and the radian frequency of vibration:

$$W_s^{\text{diss}} = \omega \eta_{s;\text{diss}} E_s \quad (18)$$

where  $\omega$  is the radian frequency (typically, a one-third octave-band center frequency),  $\eta_{s;\text{diss}}$  is the damping loss factor for subsystem  $s$ , and  $E_s$  is the time-average energy for subsystem  $s$ .

The energy transmitted between the connected subsystems can also be assumed to be proportional to the energy in each system. By analogy to the dissipated power, the factor of proportionality for transmitted power is called the coupling loss factor. However, since energy flow between the two systems can be in either direction, two coupling loss factors must be identified, so that the net energy flow between two connected subsystems is given by

$$W_{a;s}^{\text{trans}} = \omega \eta_{a;s} E_a - \omega \eta_{s;a} E_s \quad (19)$$

where  $\eta_{a;s}$  and  $\eta_{s;a}$  are the coupling loss factors between subsystem  $a$  and  $s$  and between  $s$  and  $a$ .

These two coupling loss factors are not equal. A power balance can now be performed on each subsystem to form a set of linear equations relating the energies of the subsystems to the power inputs:

$$\omega \begin{bmatrix} \eta_{a;d} + \eta_{a;s} + \eta_{a;r} & -\eta_{s;a} \\ -\eta_{a;s} & \eta_{s;d} + \eta_{s;a} + \eta_{s;r} \\ -\eta_{a;r} & -\eta_{s;r} \\ -\eta_{r;a} \\ -\eta_{r;s} \\ \eta_{r;d} + \eta_{r;a} + \eta_{r;s} \end{bmatrix} \begin{bmatrix} E_a \\ E_s \\ E_r \end{bmatrix} = \begin{bmatrix} W_a^{\text{in}} \\ W_s^{\text{in}} \\ W_r^{\text{in}} \end{bmatrix} \quad (20)$$

Note that the subscript notation typically used in SEA is not conventional matrix notation. Also note that the loss factor matrix is not symmetric.

### 3.1 SEA Reciprocity

The coupling loss factors used in SEA are generally not reciprocal, that is,  $\eta_{s;r} \neq \eta_{r;s}$ . If it is assumed, however, that the energies of the modes in a given subsystem are equal—at least within the concept of an ensemble average—and that the responses of the different modes are uncorrelated, a reciprocity relationship can be developed. The assumptions for this relationship are more restrictive than required for a general statement of reciprocity, so that the term SEA reciprocity should be used.

Statistical energy analysis reciprocity requires that the coupling loss factors between two subsystems be related by the modal densities:

$$n(\omega)_s \eta_{s;r} = n(\omega)_r \eta_{r;s} \quad (21)$$

Using this relationship, a new coupling factor,  $\beta$ , can be introduced that allows the energy balance equations to be written in a symmetric form:

$$\begin{bmatrix} \beta_{a;d} + \beta_{a;s} + \beta_{a;r} & -\beta_{a;s} \\ -\beta_{a;s} & \beta_{s;d} + \beta_{s;a} + \beta_{s;r} \\ -\beta_{a;r} & -\beta_{s;r} \\ \beta_{r;d} + \beta_{r;a} + \beta_{r;s} \end{bmatrix} \begin{bmatrix} E_a/n(\omega)_a \\ E_s/n(\omega)_s \\ E_r/n(\omega)_r \end{bmatrix} = \begin{bmatrix} W_a^{\text{in}} \\ W_s^{\text{in}} \\ W_r^{\text{in}} \end{bmatrix} \quad (22)$$

where

$$\beta_{s;r} = \omega \eta_{s;r} n(\omega)_s = \omega \eta_{r;s} n(\omega)_r = \beta_{r;s} \quad (23)$$

The ratio of total energy to modal density has the units of power and can be called *modal power*.

### 3.2 Coupling Loss Factor Measurement

The coupling loss factors or coupling factors cannot be measured directly. However, a power injection technique can be used to infer the coupling factor from measured values of power input and

response energy. Using this technique each subsystem is excited in turn with a unit power input, and the response energy of the subsystems is measured to form a matrix of measured energies. Each column in the matrix corresponds to the measured response energies when one subsystem is excited. For example, the second column contains the measured energies when the second subsystem is excited. The coupling loss factor matrix is determined by inverting the matrix of measured subsystem energies:

$$[\eta] = [E]^{-1} \quad (24)$$

The off-diagonal terms are the negative values of the coupling loss factors, while the sum of terms for each row give the damping loss factors. This measurement technique has been successfully used to “measure” in situ coupling and damping loss factors. However, errors in the energy measurement can result in large errors in the measured loss factors. Systems containing highly coupled subsystems will result in energy matrices that are poorly conditioned since two or more columns will be nearly equal. Thus, the success of the measurement technique requires careful identification of the subsystems. The best results are obtained for light coupling, when the coupling loss factors are small compared to the damping loss factors, so that the loss factor matrix is diagonally dominant.

The measurement of subsystem energy is particularly difficult for subsystems with in-plane compression and shear modes. Because of the high stiffness of the in-plane modes a small amount of motion results in a large amount of energy. The measurement of subsystem energy is also difficult for subsystems in which the mass is nonuniformly distributed. For these subsystems an effective or dynamic mass must be determined at each measurement point.

### 3.3 Coupling Loss Factor Theory

Coupling loss factors can be predicted analytically using wave and mode descriptions of the subsystem vibrations. Waves are used when the number of dimensions of the subsystem is greater than the number of dimensions of the connection: for example, a beam connected at a point, a plate connected at a point or along a line, and an acoustical space connected at a point, line, or area. Modes are used when the number of dimensions of the subsystem is equal to the number of dimensions of the connection: for example, a beam connected along a line and a plate connected over an area.

When a wave description can be used for all subsystems at the connection, the coupling loss factor between subsystems can be written in terms of a power transmission coefficient. For a point connection between beams, the coupling factor between subsystem  $s$  and subsystem  $r$  can be written

$$\beta_{s;r} = \omega \eta_{s;r} n_s(\omega) = \frac{1}{2\pi} \tau_{s;r} \quad (25)$$

where  $\tau_{s,r}$  is the power transmission coefficient. The power transmission coefficient must take into account energy transmitted by all degrees of freedom at the connection: three translational degrees of freedom and three rotational degrees of freedom. For a point connection with a single degree of freedom (all other degrees of freedom are constrained), the transmission coefficient is given by

$$\tau_{s,r} = \frac{4R_s R_r}{|Z_j|^2} \quad (26)$$

where  $R$  is the subsystem resistance (real part of the impedance) for the unconstrained degree of freedom and  $Z_j$  is the junction impedance—the sum of the impedances of all subsystems connected at the point. The coupling factor given by Eqs. (25) and (26) can also be used for two- and three-dimensional subsystems connected at a point with a single degree of freedom, as long as the correct impedances are used. For point connections with multiple degrees of freedom, an estimate of the coupling factor can be obtained by summing the power transmission coefficients for each degree of freedom.

The coupling factor between two-dimensional subsystems connected along a line of length  $L$  can also be written in terms of a power transmission coefficient. However, for this case an integration must be performed over all angles of incidence. The coupling factor is given in terms of the angle-averaged transmission coefficient as

$$\beta_{s,r} = \omega \eta_{s,r} n_s(\omega) = \frac{1}{2\pi} \frac{k_s L}{\pi} \overline{\tau_{s,r}} \quad (27)$$

where  $k_s$  is the wavenumber of the source subsystem and  $\overline{\tau_{s,r}}$  is given by

$$\overline{\tau_{s,r}} = \frac{1}{2} \int_{-\pi/2}^{+\pi/2} \tau_{s,r}(\theta_s) \cos(\theta_s) d\theta_s \quad (28)$$

and  $\theta_s$  is the angle of incidence for a wave in the source subsystem. The parameter  $k_s L/\pi$  is the effective number of points for the line connection. For a line connection, the power transmission coefficient must take into account the energy transmitted by 4 degrees of freedom: three translational and one rotational. For a single degree of freedom, the transmission coefficient for an incident angle,  $\theta_s$ , can be expressed in terms of the line impedances of the source and receiver subsystems as

$$\tau_{s,r}(\theta_s) = \frac{4R_s(k_t)R_r(k_t)}{|Z_j(k_t)|^2} \quad (29)$$

where  $k_t$  is the trace wavenumber given by  $k_s \cos(\theta_s)$ , and  $R(k_t)$  is the real part of the line impedance for the unconstrained degree of freedom.

The formulation above can also be used to predict the coupling loss factor between three-dimensional subsystems coupled along a line, if the integration is performed over all solid angles of incidence. For this case, the angle-averaged transmission coefficient is written as

$$\overline{\tau_{s,r}} = \int_{-\pi/2}^{+\pi/2} \tau_{s,r}(\theta_s) \sin(\theta_s) \cos(\theta_s) d\theta_s \quad (30)$$

For an area connection between three-dimensional subsystems, the coupling factor is given in terms of the angle-averaged transmission coefficient as

$$\beta_{s,r} = \omega \eta_{s,r} n_s(\omega) = \frac{1}{2\pi} \frac{k_s^2 S}{4\pi} \overline{\tau_{s,r}} \quad (31)$$

where  $S$  is the area of the connection. The effective number of points for the area connection is given by the parameter,  $k_s^2 S/4\pi$ .

When the number of dimensions of a subsystem is equal to the number of dimensions of the coupling, modes are used to calculate the coupling loss factor. For example, the coupling loss factor between a two-dimensional system such as a plate or shell and a three-dimensional system such as an acoustical space is obtained by calculating the radiation efficiency for each mode of the plate, and averaging over all modes with resonance frequencies in the analysis bandwidth,

$$\eta_{s,r} = \frac{\rho_r c_r S}{\omega M_s} \frac{1}{N_s} \sum_i \sigma_i^{\text{rad}} \quad (32)$$

where  $\rho_r c_r$  is the characteristic impedance of the acoustical space,  $M_s$  is the mass of the plate,  $N_s$  is the mode count for the plate, and  $\sigma_i^{\text{rad}}$  is the radiation efficiency for mode  $i$  of the plate. Approximations to the summation can be made by grouping the modes into “edge” and “corner” modes.<sup>10</sup>

The power transmission coefficients and radiation efficiencies can be calculated with great accuracy. However, the relationship between these parameters and the SEA coupling loss factors requires that some assumptions be made regarding the vibration fields in the connected subsystems. First, the vibrations of the two subsystems are assumed to be uncorrelated. Second, the vibrations of the two subsystems are assumed to be “diffuse”—waves are incident on a point within the subsystem from all angles with equal intensity. Although these assumptions are difficult to prove, even for idealized structures and acoustical spaces, they are generally valid for lightly coupled systems at high frequencies, where many modes participate in the vibration response. The validity of the assumptions for highly coupled subsystems is open to question. Fortunately, the errors incurred using the above equations for highly coupled subsystems are generally small. The assumptions are also open to

question at low frequencies, where only a few modes participate in the response. At these frequencies, the equations above may predict coupling loss factors that are too large. However, it is difficult to quantify the error. In spite of the limited validity of the assumptions, the equations above provide useful estimates of the coupling loss factors, even for highly coupled subsystems at low frequencies.

### 3.4 Wave versus Modal Approaches

The earliest development of SEA was based on a study of coupled modes. The coupling factor between two coupled modes or oscillators was extended to study the coupling between two subsystems—each with a large number of modes. However, for many types of coupling the proper identification of the subsystem modes is difficult. For example, two plates coupled along one edge may be considered. Use of a clamped boundary condition at the coupling results in modes that allow no displacement at the connection and thus no energy flow. A free boundary condition results in no forces at the connection and again no energy flow. The problem of applying boundary conditions when the coupling between subsystems is at a boundary is difficult to resolve. For this reason, a wave approach is commonly used to compute SEA coupling factors. Following this approach the dynamic response of a subsystem is represented by a series of traveling waves. The wave field is assumed to be diffuse with incoherent waves incident from all directions. The assumption of a diffuse field allows a simple calculation of the SEA coupling factors in terms of wave transmission coefficients. The assumption of a diffuse field can be supported for an ensemble of dynamic systems with modes drawn from a random distribution of resonant frequencies and mode shapes. However, many systems of practical interest do not support this statistical model. For example, a cylindrical structure with periodic stiffeners exhibits strong frequency and wavenumber filtering. The assumption of a diffuse field loses its validity as the vibration propagates along the length of the cylinder. This problem may be alleviated by partitioning the waves (or modes) into different groups according to the direction of propagation. In general, great care must be taken in applying SEA to systems that are not very “random.”

### 3.5 Damping Loss Factor Theory

The damping loss factors can be predicted analytically for free-layer and constrained-layer treatments. The analysis approach is described in other chapters of this handbook. The damping for an acoustic space is often specified by the average absorption coefficient for the space rather than a damping loss factor. The power dissipated within the acoustical space can be written in terms of the time-average energy and the absorption coefficient as

$$W_a^{\text{diss}} = \omega \frac{S_a}{4k_a V_a} \alpha_{a;\text{diss}} E_a = \omega \eta_{a;\text{diss}} E_a \quad (33)$$

where  $S_a$  is the area of the absorbing surface,  $V_a$  is the volume of the acoustical space, and  $k_a$  is the acoustic wavenumber. It follows that the damping loss factor for an acoustical space can be obtained from the average absorption coefficient by the relation

$$\eta_{a;\text{diss}} = \frac{S_a}{4k_a V_a} \alpha_{a;\text{diss}} \quad (34)$$

where the constant  $4V/S$  is commonly referred to as the mean-free path.

### 3.6 Energy and Response

The SEA power balance equations can be solved to obtain the modal energy or modal power of each subsystem. The final step in the analysis is to relate these variables to the subsystem response. For structural subsystems, the spatial-average mean-square velocity is calculated from the kinetic energy. For resonant vibrations, the time-average kinetic energy is equal to the time-average potential energy. Thus, the average mean-square velocity in a band of frequencies is given by

$$\langle v^2 \rangle_{x,t} = \frac{E}{M} \quad (35)$$

where  $E$  is the total energy of all modes in the band and  $M$  is the mass of the subsystem. For acoustical subsystems, the spatial-average mean-square sound pressure is calculated from the potential energy,

$$\langle p^2 \rangle_{x,t} = \frac{E}{C_a} \quad (36)$$

where  $C_a$  is the compliance of the subsystem,  $V/\rho c^2$ , for an acoustical space with rigid walls.

The equations above are adequate for large, homogeneous subsystems. However, for small subsystems and for subsystems with significant spatial variations in element stiffness or mass, these equations lose accuracy. When the drive point conductance at the response point is known, either from measurement or from a finite element model, the conversion from energy to response can be carried out with greater accuracy. Since the average conductance is related to the modal density and mass of the system, see Eq. 7, the average mean-square velocity can be written in terms of the modal power as

$$\langle v^2 \rangle_{x,t} = \frac{2}{\pi} \langle G_{\text{pt}}(x, \omega) \rangle_{x, \Delta\omega} \varphi \quad (37)$$

A similar expression can be written for acoustical subsystems

$$\langle p^2 \rangle_{x,t} = \frac{2}{\pi} \langle R_{\text{pt}}(x, \omega) \rangle_{x, \Delta\omega} \varphi \quad (38)$$

where  $R$  is the point acoustical resistance. Equations (37) and (38) can also be used to obtain the response at single points within the subsystem rather than spatial averages. This removes a common criticism

of SEA—that the method can only calculate spatial averages of the response.

### 3.7 Variance

Statistical energy analysis provides a statistical description of the subsystem response. However, in many cases, SEA is used only to obtain an estimate of the mean. Although the mean provides the “best estimate” of the response, this estimate may differ significantly from the response measured for a single member of the ensemble of dynamic systems. The variance or standard deviation of the response provides a measure to quantify the expected confidence intervals for the SEA prediction. When the variance is high, the confidence intervals will be large, and the mean does not provide an accurate estimate of the response.

Using SEA in design requires that a confidence interval be established for the response prediction, so that an upper bound or “worst-case” estimate can be compared with design requirements. If the mean response is used for design, half the products produced will fail to meet the design requirements. Use of the mean plus two or three times the standard deviation (square root of the variance) provides a reasonable upper bound for the response prediction.

Methods to predict the variance of the SEA prediction are not well established, although work is continuing in this area. Often an empirical estimate of the variance or confidence interval is used. In other cases, an estimate based on the modal overlap parameter, the frequency bandwidth of the analysis, and a loading distribution factor is used.<sup>11,12</sup> The modal overlap parameter,  $M_{\text{overlap}}$ , is the ratio of the average damping bandwidth for an individual mode to the average spacing between resonance frequencies. This parameter can be written in terms of the damping loss factor and the modal density as

$$M_{\text{overlap}} = \frac{\pi}{2} \omega \eta_d n(\omega) \quad (39)$$

where  $\eta_d$  is the effective total damping loss factor for the subsystem. Large values of the product of the modal overlap parameter and the analysis bandwidth result in low variance and a narrow confidence interval. In this case, the mean is a good estimate of the response. Small values of the product result in high variance and wide confidence intervals. In this case, the mean does not give a good estimate of the response, and the variance should be determined so that an upper bound to the prediction can be obtained.

Failure to include an estimate of the variance in the SEA leads to some misunderstandings regarding the capabilities of SEA. First, SEA is not limited to high frequencies and high modal densities. However, at low frequencies and for low modal densities, the confidence interval for the SEA predictions will be large, so that an estimate of the variance must be made. Second, SEA is not limited to broadband noise analysis. However, for a single-frequency or narrow-band analysis, the confidence interval for the SEA

predictions will be larger than for a one-third octave or octave-band analysis.

### 4 EXAMPLE

Two examples are presented to illustrate the use of SEA. The first is a simplified model of a ship consisting of a machinery platform, a bulkhead, a deck, and a hull structure, as illustrated in Fig. 7.

This model was originally used to demonstrate the importance of in-plane modes in transmitting vibrational energy. The SEA model consists of seven plates, each with a bending and in-plane subsystem. The in-plane subsystem may be subdivided into in-plane compression and in-plane shear modes. However, these in-plane modes are generally strongly coupled and can be included in a single subsystem. Three line connections are used to connect the plate elements, as shown in Fig. 8.

The first step in the SEA is to set up the coupling matrix for the energy flow equations as shown in Eqs. (22) and (23). The modal densities for each plate are determined using the asymptotic two-dimensional modal density in Table 1. This expression can be used for both the bending and in-plane subsystems by using the correct wavenumber and group speed. The modal density for the in-plane subsystem is determined by summing the modal densities of compressional and shear modes. Each structural connection requires calculation of several coupling factors between the bending and in-plane subsystems of the connected plates. For the upper line connection between the platform and bulkhead plates, five coupling factors are needed: platform bending to bulkhead bending, platform bending to bulkhead in-plane, platform bending to platform in-plane, platform in-plane to bulkhead bending, platform in-plane to bulkhead in-plane, and bulkhead bending to bulkhead in-plane. For each coupling factor a wave approach is used to compute first a power transmission coefficient using Eqs. (28) and (29). The coupling factors are then computed using Eq. (27). The damping factors are computed from the damping loss factors and modal

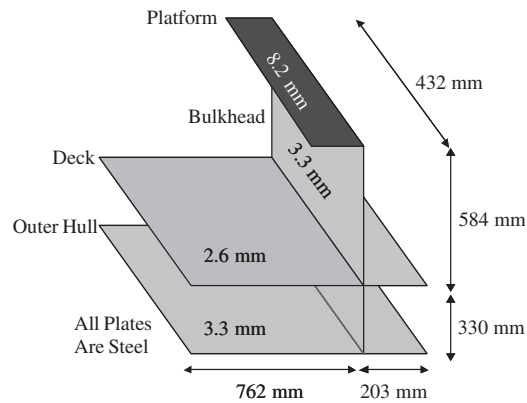


Figure 7 Simplified ship structure.

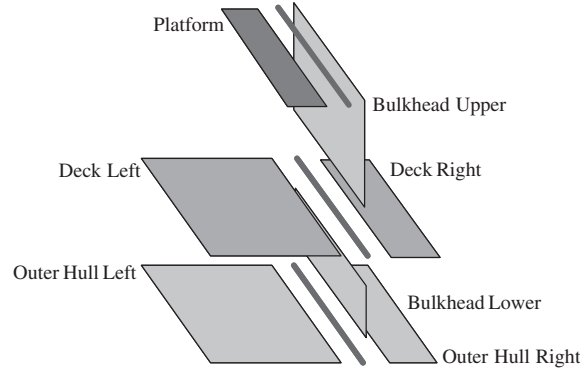


Figure 8 SEA ship model.

densities using Eq. (40):

$$\beta_{s;\text{damp}} = \omega \eta_{s;\text{damp}} n_s(\omega) \quad (40)$$

where  $\beta_{s;\text{damp}}$  is the damping factor,  $\eta_{s;\text{damp}}$  is the damping loss factor, and  $n_s(\omega)$  is the modal density of subsystem  $s$ . Damping loss factors are often based on empirical estimates or in some cases on measured data. They may also be computed analytically for free-layer and constrained-layer damping treatments. However, the damping loss factor must be calculated for the type of mode being considered. Bending modes often have significantly higher damping than in-plane compression and shear modes. The coupling and damping factors are now assembled to form the coupling matrix for the power balance equations. Each row of this matrix results from power balance for a single subsystem. For row  $s$  the diagonal term is the damping factor for subsystem  $s$  plus the sum of all coupling factors from subsystem  $s$  to other connected subsystems. The off-diagonal terms are the negative values of the coupling factor between subsystem  $s$  and the other connected subsystems. The linear matrix equation is then solved to obtain transfer functions between input power and response energy,

$$\text{PTF}_{s;r} = \frac{E_r/n(\omega)_r}{W_s^{\text{in}}} = \frac{\varphi_r}{W_s^{\text{in}}} \quad (41)$$

where  $\text{PTF}_{s;r}$  is the transfer function between input power to subsystem  $s$  and response modal power for subsystem  $r$ .

The second step in the SEA is to relate the modal power to the vibration response. The mean-square velocity is given in terms of the modal power by Eq. (37). The mean-square acceleration in a band of frequencies is simply obtained by dividing the mean-square velocity by the band-center radian frequency squared. For subsystem  $r$  the mean-square acceleration is given by

$$\langle a_r^2 \rangle_{x,t} = \frac{2}{\pi} \frac{\varphi_r}{\omega_c^2} \langle G_{r;\text{pt}}(x, \omega) \rangle_{x, \Delta\omega} \quad (42)$$

where  $\omega_c$  is the band center frequency and  $\langle a_r^2 \rangle$  is the mean-squared acceleration response of subsystem  $r$  in the band  $\Delta\omega$ . The average power spectral density in the band is obtained by dividing the mean-square acceleration by the frequency bandwidth. Typically, when calculating the power spectral density (PSD) the bandwidth should be expressed in hertz rather than radians per second.

The third step in the SEA is to compute the power input to the subsystems. In some cases when the input loads are localized and can be represented by point forces, the power input can be determined from force and velocity measurements. Measurement of the power input from applied moments may also be possible but is much more difficult. In other cases when only the applied forces are known, the power input can be determined from the frequency-average conductance at the excitation point,  $x_s$ ,

$$W_s^{\text{in}} = \langle F_s^2 \rangle \langle G_{s;\text{pt}}(x_s, \omega) \rangle_{\Delta\omega} \quad (43)$$

The results above can be combined to give a transfer function relating the mean-square response of subsystem ' $r$ ' at point  $x_r$  to an applied point force on subsystem ' $s$ ' at point  $x_s$ ,

$$\frac{\langle A_r^2 \rangle}{\langle F_s^2 \rangle} = \frac{2}{\pi} \frac{\langle G_{s;\text{pt}}(x_s, \omega) \rangle_{\Delta\omega} \langle G_{r;\text{pt}}(x_r, \omega) \rangle_{\Delta\omega}}{\omega_c^2} \text{PTF}_{s;r} \quad (44)$$

Predictions obtained from this SEA ship model are compared with measured data in Fig. 9. Also shown are an upper limit set at the mean plus two times the predicted SEA standard deviation. The lower plot shows predictions from a typical SEA model in which statistical estimates of the average conductance are used in Eq. (44). The upper plot shows predictions from a hybrid SEA model in which the SEA transfer functions are combined with measured values of



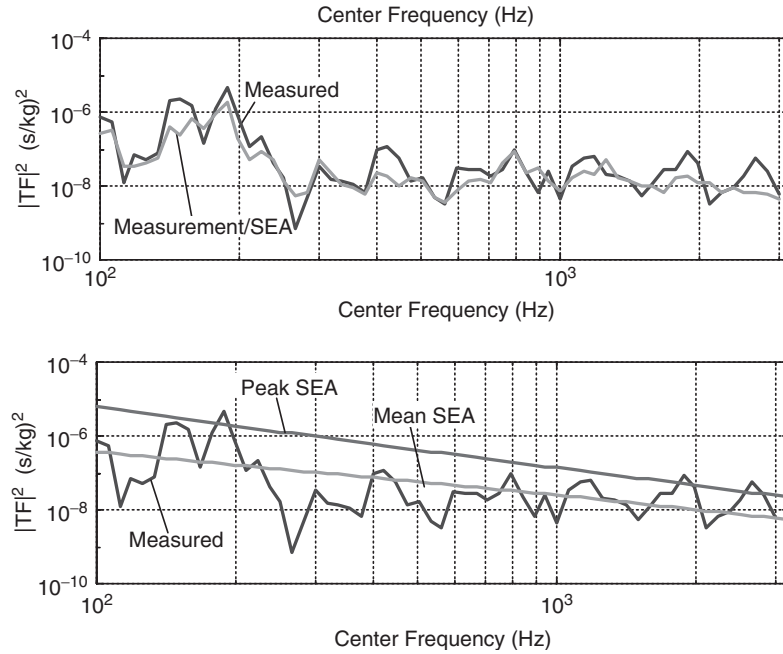


Figure 9 Ship model response.

the conductance. Use of measured conductance data improves the accuracy of the SEA prediction.

The second example is a structural-acoustical model of an automobile. The model is simplified to predict the interior cabin noise from airborne noise sources including the engine, tires, exhaust, and wind noise. The vehicle body is divided into a number of plate and shell elements as shown in Fig. 10. Acoustical elements are added both outside and inside the vehicle. The interior acoustical space is divided into 8 to 27 subspaces with either 2 or 3 sections in the vertical, transverse, and fore-aft directions. A smaller number of subspaces may be used for smaller compact vehicles while a larger number of subspaces would be used for larger sedans, wagons, and SUVs. The exterior acoustical space is also divided into subspaces with a near-field space the same size as the connected body structural element and a far-field space.

The in-plane modes of the body panels do not play a significant role in the sound transmission from the outer acoustical spaces. Thus, for this simplified model a single bending subsystem is used for each panel. The modal density for these bending subsystems is determined from Eq. (14). The modal densities for the acoustical spaces is determined from Eq. (17). Note that in both cases the modal densities are extensive properties so that the modal density of a sum of elements is equal to the sum of the modal densities of the individual elements. Under this condition subdividing the acoustical space does not introduce additional modes to the system. The damping of the acoustical spaces is determined from absorption coefficients for the surfaces within and at the edges of the space. The damping loss factor for the space is determined using Eq. (34) and then used in Eq. (40) to compute the damping factor. The coupling

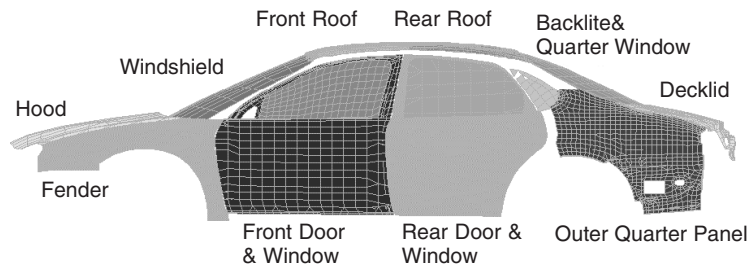


Figure 10 Vehicle SEA model body elements.

factors between resonant modes of the body panels and the acoustical spaces are computed in terms of the radiation efficiency from Eqs. (32) and (40). The coupling factors between connected acoustic spaces are computed by setting the average transmission coefficient to one in Eq. (31). Finally, coupling factors to account for the sound transmission by mass-law response of the body panels are computed by using the mass-law sound transmission coefficient in Eq. (31).

For this example the power input is determined for the external acoustic spaces from sound pressure level measurements in each space. Transfer functions between the input power to the external near-field acoustic spaces and their acoustic response mean-square sound pressure level are used to determine the required acoustic power input to match the measured acoustic levels.

After solving the SEA power flow equations the mean-square sound pressure level at the operator's ear position is determined from the modal power using Eq. (38). Parameter studies are performed in which the body panel damping loss factor is changed by introduction of damping treatments; the interior absorption coefficient is changed by introducing sound-absorbing headliners and seats; the sound transmission coefficient for the body panels is changed by introducing sound barriers on floor, door, and dash panel structures. Sound transmission through small penetrations in the dash structure and door seals is often shown to be a dominant sound transmission path.

## REFERENCES

1. R. H. Lyon and R. G. DeJong, *Theory and Application of Statistical Energy Analysis*, 2nd ed., Butterworth-Heinemann, Newton, MA, 1995.
2. F. J. Fahy, Statistical Energy Analysis, in R. G. White and J. G. Walker, Eds., *Noise and Vibration*, Ellis Horwood, Chichester, UK, 1982, Chapter 7.
3. C. H. Hodges and J. Woodhouse, Theories of Noise and Vibration Transmission in Complex Structures, *Reports Progress Phys.*, Vol. 49, 1986, pp. 107–170.
4. K. H. Hsu and D. J. Nefske, Eds., *Statistical Energy Analysis*, Vol. 3, American Society of Mechanical Engineers, New York, 1987.
5. E. E. Ungar, Statistical Energy Analysis, in *Structure-Borne Sound*, 2nd ed., L. Cremer, M. Heckl, and E. E. Ungar, Eds., Springer, Berlin, 1988, Section V.8.
6. M. P. Norton, Statistical Energy Analysis of Noise and Vibration, in *Fundamentals of Noise and Vibration Analysis for Engineers*, Cambridge University Press, Cambridge, UK, 1989, Chapter 6.
7. I. L. Ver, Statistical Energy Analysis, in *Noise and Vibration Control Engineering: Principles and Applications*, L. L. Beranek and I. L. Ver, Eds., Wiley, New York, 1992, Section 9.8.
8. A. J. Keane and W. G. Price, Eds., *Statistical Energy Analysis—An Overview, with Applications in Structural Dynamics*, Cambridge University Press, Cambridge, UK, 1994.
9. B. R. Mace, Statistical Energy Analysis: Coupling Loss Factors, Indirect Coupling and System Modes, *J. Sound Vib.*, Vol. 278, 2005, pp. 141–170.
10. G. Maidanik, Response of Ribbed Panels to Reverberant Acoustic Fields, *J. Acoust. Soc. Am.*, Vol. 34, 1962, pp. 809–826.
11. R. H. Lyon, Statistical Analysis of Power Injection and Response in Structures and Rooms, *J. Acoustic. Soc. Am.*, Vol. 45, 1969, pp. 545–565.
12. R. S. Langley and A. W. M. Brown, The Ensemble Statistics of the Energy of a Random System Subjected to Harmonic Excitation, *J. Sound Vib.*, Vol. 275, 2004, pp. 823–846.

# CHAPTER 18

---

## NONLINEAR VIBRATION

**Lawrence N. Virgin and Earl H. Dowell**  
Department of Mechanical Engineering  
Duke University  
Durham, North Carolina

**George Flowers**  
Department of Mechanical Engineering  
Auburn University  
Auburn, Alabama

### 1 INTRODUCTION

There have been great advances in the modeling and analysis of physical phenomena in recent years. These have come in spite of the fact that most physical problems have at least some degree of nonlinearity. Nonlinear effects may take a variety of forms, but they fall into three basic categories. They may be due to (1) geometric and kinematic effects, as with a simple pendulum undergoing large amplitude motion, (2) nonlinear elements (such as a hardening spring or a hydraulic damper), or (3) elements that are piecewise linear (such as bearing with a dead-band clearance region, looseness, and friction). The potential influence of nonlinearities on the overall dynamic behavior of a system depends very strongly on its specific category.

### 2 NONLINEAR FREE VIBRATION

Simplifying assumptions are often employed to reduce the complexity of nonlinear problems to allow them to be represented by linear expressions that can be solved in a relatively straightforward manner. Such linearization is an almost automatic part of solving many engineering problems. This is due to two basic reasons. First, problems in nonlinear mechanical vibration are considerably more difficult to analyze than their linear counterparts. Second, linearized models capture the essence of many physical problems and offer considerable insight into the dynamic behaviors that are to be expected.

However, this is not always the case. The presence of nonlinear forces in many physical systems results in a considerable number of possible behaviors even for relatively simple models. Mechanisms of instability and sudden changes in response are of fundamental importance in the behavior of nonlinear systems. The closed-form solutions familiar from linear vibration theory are of limited value and give little sense of the complexity and sometimes unpredictability of typical nonlinear behavior.

Solutions to the governing nonlinear equations of motion are obtained using either approximate analytical methods or numerical simulation guided by dynamical systems theory. Due to the inherent complexity of nonlinear vibration, the use of the

geometric, qualitative theory of ordinary differential equations plays a central role in the classification and analysis of such systems.

This chapter is divided into three main sections. The first describes the effects of nonlinear stiffness and damping on free oscillations resulting in multiple equilibria, amplitude-dependent frequencies, basins of attraction, and limit cycle behavior. The second describes the effects of external periodic forcing resulting in nonlinear resonance, hysteresis, subharmonics, superharmonic, and chaos. Low-order, archetypal examples with relevance to mechanical and electrical oscillators are used to illustrate the phenomena. Finally, some more complex examples of systems in which nonlinear effects play an important role are described.

#### 2.1 Autonomous Dynamical Systems

Nonlinear free vibration problems are generally governed by sets of  $n$  first-order ordinary differential equations of the form<sup>1</sup>

$$\dot{\mathbf{x}} = \mathbf{f}(\mathbf{x}) \quad (1)$$

In single-degree-of-freedom oscillators position and velocity are the two state variables. Often the stiffness terms are a function of displacement only and can be derived from a potential energy function. Many mechanical systems have the property that for small displacements this function will be linear in  $x$ , and furthermore the damping is often assumed to be governed by a simple, viscous energy dissipation giving linear terms in  $\dot{x}$ . In this case, standard vibration theory (see Chapter 12) can be used to obtain exact closed-form solutions giving an exponentially decaying (sinusoidal or monotonic) response.<sup>2,3</sup> Linear algebra techniques and modal analysis can be used for multi-degree-of-freedom systems. For systems where the induced nonlinearity is small, linearization and certain approximate analytical techniques can be used, but if no restriction is placed on nonlinearity, then numerical methods must generally be used to solve Eq. (1). Some specific examples in the following paragraphs illustrate typical transient behavior.

## 2.2 The Simple Pendulum

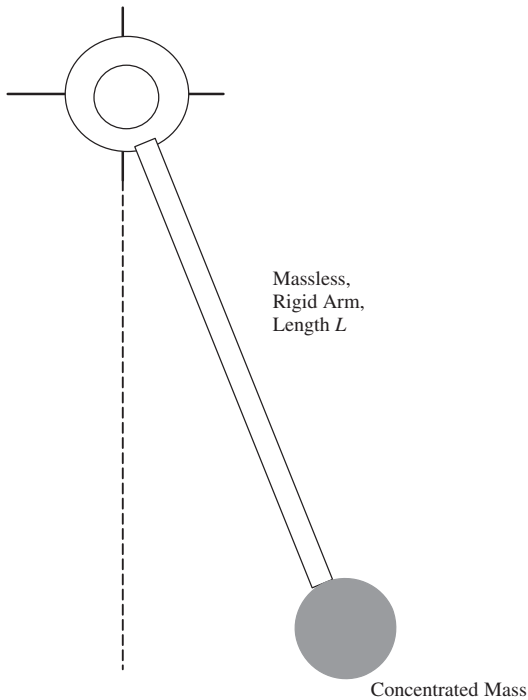
**Small-Amplitude Linear Behavior** As an introduction to typical nonlinear behavior consider the simple rigid-arm pendulum shown schematically in Fig. 1. It is a simple matter, using Newton's laws or Lagrange's equations,<sup>6</sup> to derive the governing equation of motion

$$\ddot{\theta} + b\dot{\theta} + (g/L)\sin\theta = 0 \quad (2)$$

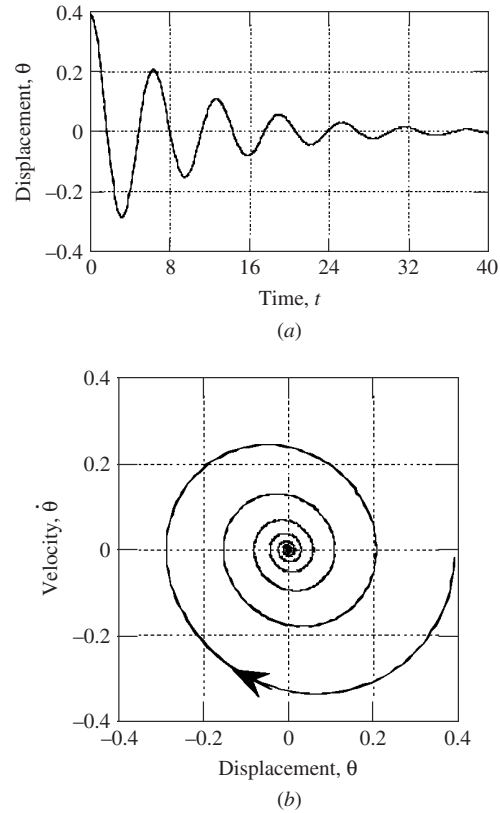
where  $b$  is the (viscous) damping coefficient. Note that the linear, undamped natural frequency is a constant  $\omega_0 = \sqrt{g/L}$ . For small angles,  $\sin\theta \cong \theta$ , and given the two initial conditions,  $\theta_0$  and  $\dot{\theta}_0$ , the pendulum will undergo an oscillatory motion that decays with a constant (damped) period as  $t \rightarrow \infty$  coming to rest at  $\theta = 0$ , the position of static stable equilibrium (Fig. 2a). This equilibrium position acts as a point attractor for all local transients.

It is very useful in nonlinear vibrations to look at phase trajectories in a plot of displacement against velocity. This is shown in Fig. 2b for the pendulum started from rest at  $\theta_0 = \pi/8$ . The near elliptical nature of these curves (indicating sinusoidal motion) is apparent as the motion evolves in a clockwise direction.

The motion of the pendulum can be thought to be occurring within the potential energy well shown



**Figure 1** Schematic diagram of the simple rigid-arm pendulum.

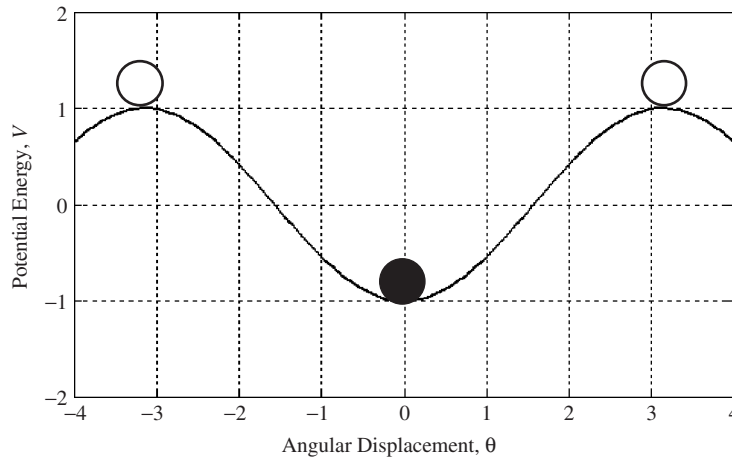


**Figure 2** Small-amplitude swings of the damped pendulum illustrating linear motion: (a) times series and (b) phase portrait. ( $\theta_0 = \pi/8$ ,  $\omega_0 = 1$ ,  $b = 0.1$ .)

in Fig. 3, that is, the integral of the restoring force. The assumption of small angles effectively means that the restoring force is assumed to be linear about the origin (Hooke's law), with a locally parabolic potential energy well. Using the analogy of a ball rolling on this surface, it is easy to visualize the motion shown in Fig. 2.

**Large-Amplitude Nonlinear Behavior** For large-angle swings of the pendulum the motion is no longer linear. The restoring force induces a softening spring effect. The natural frequency of the system will now be a function of amplitude as the unstable equilibrium at  $\theta = \pi$  comes into effect. Linear theory can also be used about an unstable equilibrium, and local trajectories will tend to diverge away from a saddle point. Physically, this is the case of the pendulum balanced upside down. The process of linearization involves the truncation of a power series about the equilibrium positions and characterizes the local motion. Often this information can then be pieced together to obtain a qualitative impression of the complete phase portrait.<sup>4</sup>

Consider the undamped ( $b = 0$ ) pendulum started from rest at  $\theta(0) = 0.99\pi$  and shown as a velocity



**Figure 3** Underlying potential energy for the pendulum showing the analogy of a rolling ball. The black ball represents stable equilibrium.

time response in Fig. 4a based on direct numerical simulation. These oscillations are far from sinusoidal. The pendulum slows down as it approaches its inverted position, with a natural period of approximately 3.5 times the linear natural period of  $2\pi$ .

### 2.3 Duffing's Equation

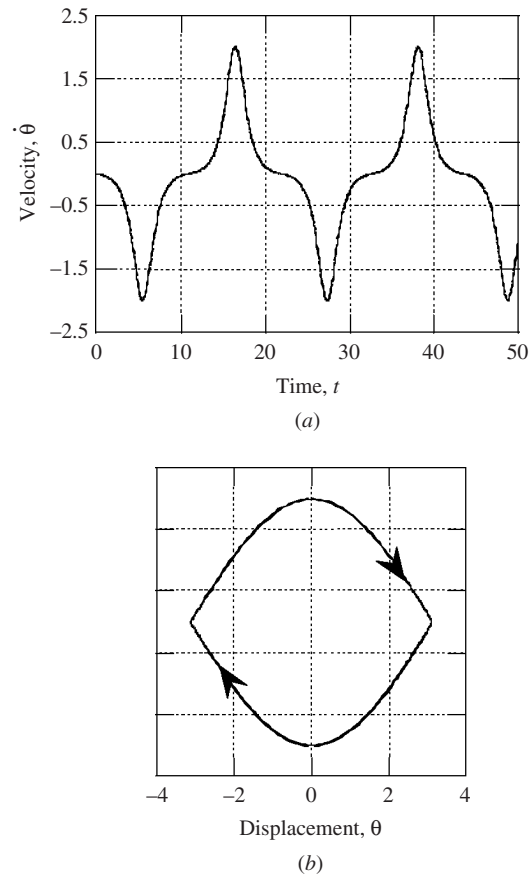
Another common example of an oscillator with a nonlinear restoring force is an autonomous form of Duffing's equation:

$$\ddot{x} + b\dot{x} + \alpha x + \beta x^3 = 0 \quad (3)$$

which can, for example, be used to study the large-amplitude motion of a pre- or postbuckled beam<sup>6</sup> or plate, or the moderately large-amplitude motion of the pendulum. The free vibration of a beam loaded axially beyond its elastic critical limit can be modeled by Eq. (4) with negative linear and positive cubic stiffness. In this case the origin (corresponding to the straight configuration) is unstable with two stable equilibrium positions at  $x = \pm 2$ , for example, when  $\alpha = -1$  and  $\beta = 4$ . Now, not only does the natural period depend on initial conditions but so does the final resting position as the two stable equilibria compete to attract transients. Each equilibrium is surrounded by a domain of attraction. These interlocking domains, or catchment regions, are defined by the separatrix, which originates at the saddle point. It is apparent that some transients will traverse the (double) potential energy well a number of times before sufficient energy has been dissipated and the motion is contained within one well. Clearly, it is difficult to predict which long-term resting position will result given a level of uncertainty in the initial conditions.<sup>6,7</sup>

### 2.4 Van der Pol's Oscillator

In the previous section the nonlinearity in the stiffness resulted in behavior dominated by point attractors

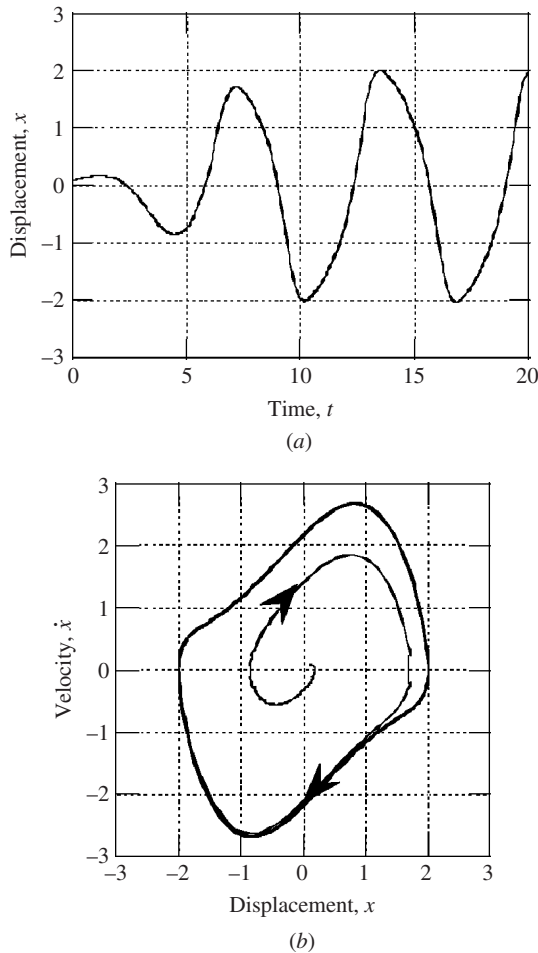


**Figure 4** Large undamped swings of the undamped pendulum: (a) velocity time series and (b) phase portrait. ( $\theta_0 = 0.99\pi$ ,  $\omega_0 = 1$ .)

(equilibria). Periodic attractors (limit cycles) are also possible in autonomous dynamical systems with nonlinear damping. A classical example relevant to electric circuit theory is Van der Pol's equation<sup>1,8</sup>

$$\ddot{x} - h(1 - x^2)\dot{x} + x = 0 \quad (4)$$

where  $h$  is a constant. Here, the damping term is positive for  $x^2 > 1$  and negative for  $x^2 < 1$ , for a positive  $h$ . When  $h$  is negative, local transient behavior simply decays to the origin rather like in Fig. 2. However, for positive  $h$ , a stable limit cycle behavior occurs where the origin is now unstable and solutions are attracted to a finite-amplitude steady-state oscillation. This is shown in Fig. 5, for  $h = 1$  and  $x_0 = \dot{x}_0 = 0.1$ , as a time series in Fig. 5a and a phase portrait in Fig. 5b. Initial conditions on the



**Figure 5** Stable limit cycle behavior exhibited by Van der Pol's equation: (a) time series and (b) phase portrait. ( $x_0 = 0.1, \dot{x}_0 = 0.1, h = 1.0$ .)

outside of this limit cycle would be similarly attracted. This phenomenon is also known as a self-excited or relaxation oscillation.<sup>8,9</sup> Related physical examples include mechanical chatter due to dry friction effects between a mass and a moving belt (stick-slip),<sup>10</sup> and certain flow-induced aeroelastic problems including galloping and flutter.<sup>11</sup>

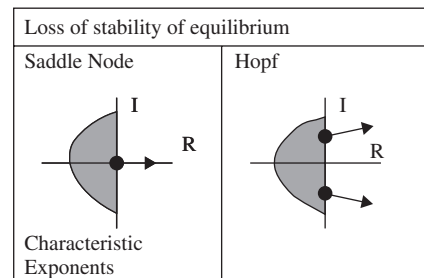
## 2.5 Instability

Nonlinear free vibration problems are generally dominated by the influence of equilibria on transient behavior. There are several definitions of stability, but generally if a small perturbation causes the system to move away from equilibrium, then this is a locally unstable state. This is familiar from linear vibration theory where transient behavior is described by the characteristic eigenvalues of the system. For example, the linear oscillator in Fig. 2 has two complex conjugate characteristic eigenvalues with negative real parts. A linearization about the inverted position for the pendulum would lead to one positive real eigenvalue resulting in divergence. Similarly, behavior in the vicinity of equilibrium for the Van der Pol oscillator ( $h > 0$ ) is characterized by complex conjugate eigenvalues but with positive real parts and hence a growth of unstable oscillations. The amplitude of the oscillation in this case is limited by nonlinear effects.

Such systems tend to be sensitive to certain control parameters, for example,  $h$  in Eq. (5). More generally a system of the form

$$\dot{\mathbf{x}} = \mathbf{f}(\mathbf{x}, \boldsymbol{\mu}) \quad (5)$$

must be considered where the external parameters  $\boldsymbol{\mu}$  allow a very slow (quasi-static) evolution of the dynamics. In nonlinear dynamic systems such changes in these parameters may typically result in a qualitative change (bifurcation) in behavior, and for systems under the operation of one control parameter these instabilities take place in one of two well-defined, generic ways. Both of these instability mechanisms have been encountered in the previous sections. The loss of stiffness is associated with the passage of an eigenvalue into the positive half of the complex plane, as shown in Fig. 6. This stability transition is known



**Figure 6** Two generic instabilities of equilibria under the operation of a single control.

as the saddle node but is also referred to as a fold bifurcation and is encountered, for example, in limit-point snap-through buckling in structural mechanics.<sup>6</sup> The loss of damping is associated with the passage of a pair of complex conjugate eigenvalues into the positive half of the complex plane. This instability mechanism is known as a Hopf bifurcation.<sup>12,13</sup>

It is also possible for the nonlinearity to determine stability of motion in the neighborhood of an equilibrium point. In such situations, a nonlinear analysis must be employed. For example, consider the dynamic system represented by the differential equations:

$$\begin{aligned}\dot{x} &= x^2y - x^5 \\ \dot{y} &= -y + x^2\end{aligned}$$

One equilibrium point is (0,0). The linearized equations about this point are

$$\begin{aligned}\dot{x} &= 0 \\ \dot{y} &= -y\end{aligned}$$

and the eigenvalues are 0, and  $-1$ . Since one of the eigenvalues has a zero real part [the (0,0) equilibrium point is not hyperbolic], one cannot draw any conclusions with regard to the stability of the equilibrium point from the eigenvalues of the linearized system. In order to properly analyze this system, one can employ center manifold theory,<sup>30,32</sup> which states that the flow in the center manifold determines the stability of a dynamic system operating in the neighborhood of a nonhyperbolic equilibrium point. A detailed analysis shows that the dynamics behavior of this example system operating on the center manifold is

$$\dot{z} = z^4 + \text{higher-order terms} \quad (6)$$

Examination of this equations shows that this system will be unstable in the neighborhood of  $z = 0$ , which then indicates that the original system is unstable in the neighborhood of the (0,0) equilibrium point.

### 3 NONLINEAR FORCED VIBRATION

#### 3.1 Nonautonomous Dynamical Systems

When a dynamic system is subjected to external excitation a mathematical model of the form

$$\ddot{\mathbf{x}} = \mathbf{f}(\mathbf{x}, t) \quad (7)$$

results. This system can be made equivalent to Eq. (1) by including the dummy equation  $\dot{t} = 1$  to give an extra phase coordinate. In forced nonlinear vibration primary interest is focused on the case where the input (generally force) is assumed to be a periodic function. For a single-degree-of-freedom oscillator the forcing phase effectively becomes the third state variable. If the system is linear, then the solution to Eq. (7) will

consist of a superposition of a complementary function that governs the transient free-decay response, and a particular integral that governs the steady-state forced response (see Chapter 12). The steady-state oscillation generally responds with the same frequency as the forcing and acts as a periodic attractor to local transient behavior.

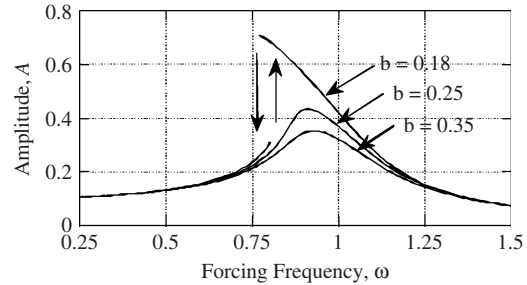
If Eq. (7) is nonlinear, then it is generally not possible to obtain an exact analytical solution. A number of choices are available: (1) linearize about the static equilibria and obtain solutions that are valid only in a local sense, (2) use an approximate analytical method and assume relatively small deviation from linearity, for example, use a perturbation scheme,<sup>14</sup> and (3) simulate the equation of motion using numerical integration.<sup>15</sup> The first of these approaches leads to the familiar resonance results from standard vibration theory (see Chapter 12). A large body of research has been devoted to the second approach.<sup>1,14,16,17</sup> However, due to recent advances in, and the availability of, digital computers and sophisticated graphics, the third approach has achieved widespread popularity in the study of nonlinear vibrations. Furthermore the numerical approach has been enhanced by the development of the qualitative insight of dynamical systems theory.<sup>18</sup>

#### 3.2 Nonlinear Resonance

The steady-state response of nonlinear vibration problems modeled by Eq. (7) with external forcing of the form

$$G \sin(\omega t + \phi) \quad (8)$$

exhibit some interesting differences from their linear counterparts. Consider the harmonically forced Duffing equation, that is, Eq. (8) added to the right-hand side of Eq. (4). For sufficiently large  $G$  the cubic nonlinearity is induced, and a typical resonance amplitude response is plotted as a function of forcing frequency in Fig. 7 for  $G = 0.1$  and three different damping levels. These curves were obtained using the method of harmonic balance<sup>1,7</sup> and illustrate several nonlinear features. For relatively small amplitudes, that is, in a system with relatively small external forcing, or



**Figure 7** Nonlinear resonance illustrating the jump in amplitude. This steady-state motion occurs about the offset static equilibrium position. ( $b = 0.18, 0.25, 0.35$ ,  $\alpha = -1$ ,  $\beta = 1$ ,  $G = 0.1$ .)



heavy damping, and generally away from resonance, the response is not significantly different from the linear case. However, for larger amplitudes the softening spring effect causes a bending over of the curves. This is related to the lengthening effect of amplitude on the natural period of the underlying autonomous system and causes the maximum amplitude to occur somewhat below the natural frequency, and for some frequencies multiple solutions are possible. For example, for the case  $b = 0.18$ , there are three steady-state solutions near  $\omega = 0.8$ . Two are stable and they are separated by an unstable solution (not shown). The two stable steady-state cycles are periodic attractors and compete for the capture of transient trajectories, that is, in this region different initial conditions lead to different persistent behavior. The jump phenomenon is observed by gradually (quasi-statically) changing the forcing frequency  $\omega$  while keeping all the other parameters fixed. Starting from small  $\omega$  and slowly increasing, the response will suddenly exhibit a finite jump in amplitude and follow the upper path. Now starting with a large  $\omega$  and gradually reducing, the response will again reach a critical state resulting in a sudden jump down to the small-amplitude solution. These jumps occur at the points of vertical tangency and bound a region of hysteresis.

A hardening spring exhibits similar features except the resonance curves bend to the right. A physical example of this type of behavior can be found in the large-amplitude lateral oscillations of a thin elastic beam or plate. In this case the induced in-plane (stretching) force produces a hardening (cubic) nonlinearity in the equations of motion, that is,  $\alpha$  and  $\beta$  both positive, and for certain forcing frequencies the beam can be perturbed from one type of motion to another. The domains of attraction often consist of interlocking spirals, and hence it may be difficult to determine which solution will persist given initial conditions to a finite degree of accuracy in a similar manner to the unforced case.

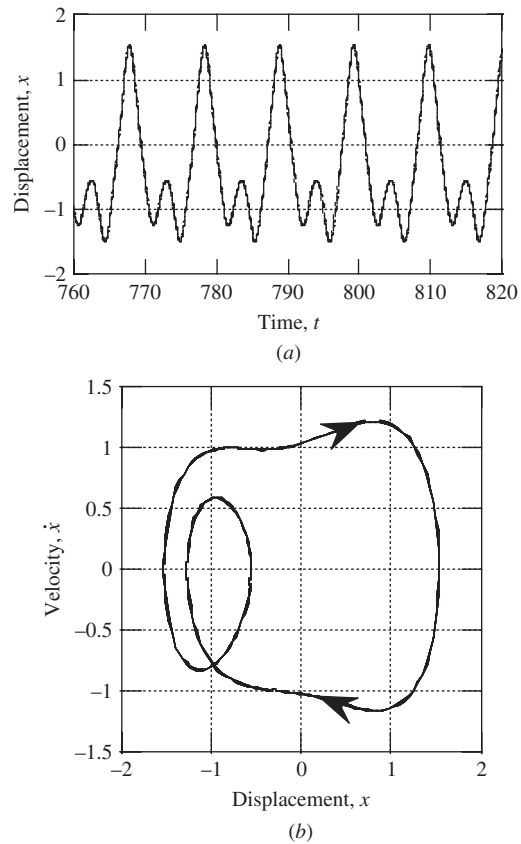
### 3.3 Subharmonic Behavior

Periodic solutions to ordinary differential equations need not necessarily have the same period as the forcing term. It is possible for a system to exhibit subharmonic behavior, that is, the response has a period of  $n$  times the forcing period. Subharmonic motion can also be analyzed using approximate analytical techniques.<sup>1,14,16</sup>

Figure 8 illustrates a typical subharmonic of order 2 obtained by numerically integrating Duffing's equation:

$$\ddot{x} + b\dot{x} + \alpha x + \beta x^3 = G \sin \omega t \quad (9)$$

for  $b = 0.3$ ,  $\alpha = -1$ ,  $\beta = 1$ ,  $\omega = 1.2$ , and  $G = 0.65$ . Subharmonic behavior is generally a nonlinear feature and is often observed when the forcing frequency is close to an integer multiple of the natural frequency. Also, subharmonics may result due to a bifurcation from a harmonic response and thus may complicate the



**Figure 8** Subharmonic oscillations in Duffing's equation: (a) time series and (b) phase projection. ( $b = 0.3$ ,  $\alpha = -1$ ,  $\beta = 1$ ,  $\omega = 1.2$ ,  $G = 0.65$ .)

approximate scenario shown in Fig. 7. Superharmonics corresponding to a response that repeats itself a number of times within each forcing cycle are also possible especially at low excitation frequencies.

### 3.4 Poincaré Sampling

A useful qualitative tool in the analysis of periodically forced nonlinear systems is the Poincaré section.<sup>4</sup> This technique consists of stroboscopically sampling the trajectory every forcing cycle or at a defined surface of section in the phase space. The accumulation of points will then reflect the periodic nature of the response. A fundamental harmonic response appears as a single point simply repeating itself. The location of this point on the phase trajectory and hence in the  $(x, \dot{x})$  projection depends on the initial conditions. For example, consider the subharmonic response of Fig. 8. The forcing period is  $T = 2\pi/\omega = 5.236$ , and if the response is inspected whenever  $t$  is a multiple of  $T$ , then 2 points are visited alternately by the trajectory as shown by the dots in Fig. 8b. The Poincaré sampling describes a mapping and can



also be used to study the behavior of transients and hence stability. Further refinements to this technique have been developed including the reconstruction of attractors using time-delay sampling.<sup>4</sup> This is especially useful in experimental situations where there may be a lack of information about certain state variables, or in autonomous systems where there is no obvious sampling period.

### 3.5 Quasi-periodicity

Another possible response in forced nonlinear vibration problems is the appearance of quasi-periodic behavior. Although the superposition of harmonics, including the beating effect, is commonly encountered in coupled linear oscillations, it is possible for nonlinear single-degree-of-freedom systems to exhibit a relatively complicated response where two or more incommensurate frequencies are present. For a two-frequency response local transients are attracted to the surface of a toroidal phase space, and hence Poincaré sampling leads to a continuous closed orbit in the projection because the motion never quite repeats itself. Although a quasi-periodic time series may look complicated, it is predictable. The fast Fourier transform (FFT) is a useful technique for identifying the frequency content of a signal and hence distinguishing quasi-periodicity from chaos.

### 3.6 Piecewise Linear Systems

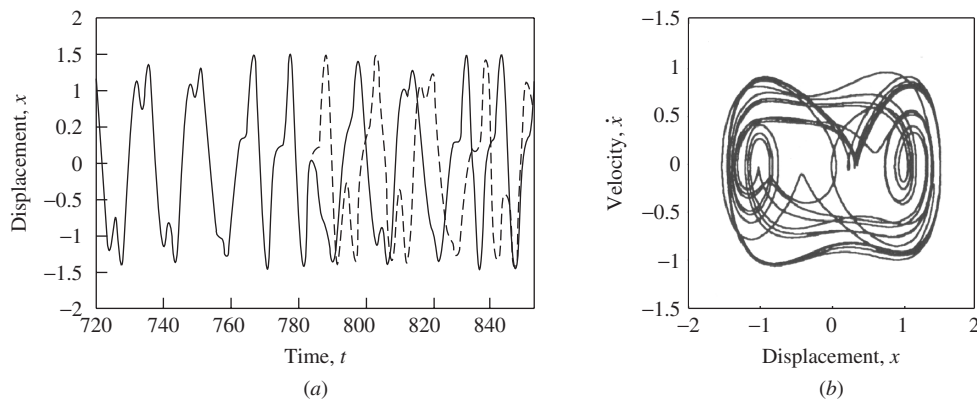
There are many examples in mechanical engineering where the stiffness of the system changes abruptly, for example, where a material or component acts differently in tension and compression, or a ball bouncing on a surface. Although they are linear within certain regimes, the stiffness is dependent on position and their behavior is often strongly nonlinear. If such systems are subjected to external excitation, then a complex variety of responses are possible.<sup>19,20</sup> Related problems include the backlash phenomenon in gear mechanisms where a region of

free play exists.<sup>6</sup> Nonlinearity also plays a role in some Coulomb friction problems including stick-slip where the discontinuity is in the relative velocity between two dry surfaces.<sup>1</sup> Feedback control systems often include this type of nonlinearity.<sup>21</sup>

### 3.7 Chaotic Oscillations

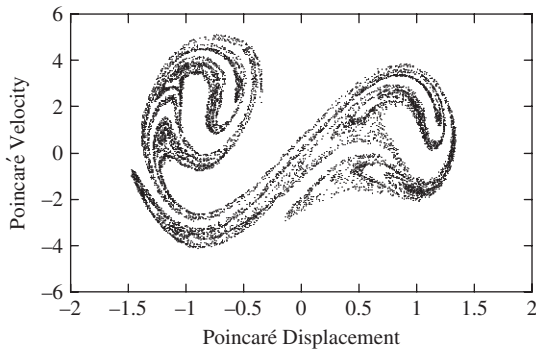
The possibility of relatively simple nonlinear systems exhibiting extremely complicated (unpredictable) dynamics was known to Poincaré about 100 years ago and must have been observed in a number of early experiments on nonlinear systems. However, the relatively recent ability to simulate highly nonlinear dynamical systems numerically has led to a number of interesting new discoveries with implications for a wide variety of applications, especially chaos, that is, a fully deterministic system that exhibits randomlike behavior and an extreme sensitivity to initial conditions. This has profound implications for the concept of predictability and has stimulated intensive research.<sup>22</sup>

Figure 9 shows a chaotic time series obtained by the numerical integration of Eq. (9) for appropriately selected  $b$ ,  $\alpha$ ,  $\beta$ ,  $G$ , and  $\omega$  using a fourth-order Runge–Kutta scheme.<sup>14</sup> Here, transient motion is allowed to decay leaving the randomlike waveform shown [Fig. 9a]. This response, which traverses both static equilibria ( $x_e = \pm 1$ ), may be considered to have an infinite period. An important feature of chaos, in marked contrast to linear vibration, is a sensitive dependence on initial conditions, and this figure also shows (dashed line) how initially adjacent chaotic trajectories diverge (exponentially on the average) with time. Given a very small difference in the initial conditions, that is, a perturbation of 0.001 in  $x$  at time  $t = 750$ , the mixing nature of the underlying (chaotic) attractor leads to a large difference in the response. Figure 9b shows the data for the original time series as a phase projection. Although the response remains bounded, the loss of predictability for increasing time is apparent.



**Figure 9** Chaotic response of Duffing's equation including exponential divergence of initially close trajectories; parameters same as Fig. 8,  $G = 0.5$ . (a) Time series, the initial separation in  $x$  is 0.001 at time  $t = 750$ , and (b) phase projection.

However, unlike truly random systems, the randomness of a chaotic signal is not caused by external influences but is rather an inherent dynamic (deterministic) characteristic. Poincaré sampling can be used effectively to illustrate the underlying structure of a chaotic response. A number of experimental investigations of chaos have been made in a nonlinear vibrations context including the buckled beam,<sup>6</sup> although early work on nonlinear circuits made a significant contribution.<sup>7</sup> Consider the example of a physical analog of the twin-well potential system described by Eq. (9), that is, a small cart rolling on a curved surface.<sup>23</sup> A chaotic attractor based on experimental data is shown in Fig. 10 where 10,000 Poincaré points, that is, forcing cycles, are plotted in the phase projection. A similar pattern is obtained by taking a Poincaré section on



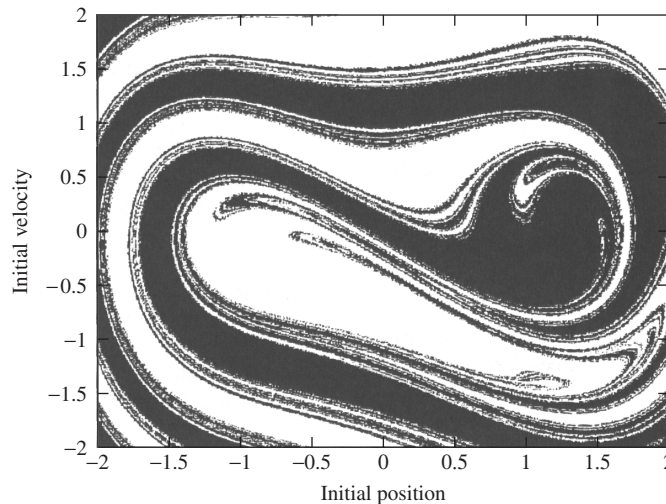
**Figure 10** Poincaré section of the chaotic attractor exhibited by an experimental (mechanical) analog<sup>23</sup> of Eq. (9).

the data of Fig. 9. The evolution of the trajectory follows a stretching and folding pattern, exhibiting certain fractal characteristics<sup>6</sup> including a noninteger dimension and can be shown to give a remarkably close correlation with numerical simulation.<sup>23</sup>

For certain parameter ranges catchment regions in forced oscillations also have fractal boundaries, that is, self-similarity at different length scales, although these can occur for periodic attractors. An example is given in Fig. 11 based on numerical integration of Eq. (9) with  $b = 0.168$ ,  $\alpha = -0.5$ ,  $\beta = 0.5$ ,  $G = 0.15$ , and  $\omega = 1$ . Here a fine grid of initial conditions is used to determine the basins of attraction for two periodic oscillations, one located within each well. Investigation of all initial conditions is a daunting task, especially for a higher-order system, but certain efficient techniques have been developed.<sup>24</sup> A relatively rare analytical success used to predict the onset of fractal basin boundaries based on homoclinic tangencies is Melnikov theory.<sup>18</sup>

A further remarkable feature of many nonlinear systems is that they follow a classic, universal route to chaos. Successive period-doubling bifurcations can occur as a system parameter is changed, and these occur at a constant geometric rate, often referred to as Feigenbaum's ratio. This property is exhibited by a large variety of systems including simple difference equations and maps.<sup>4,13,18</sup> Other identified routes to chaos include quasi-periodicity, intermittency and crises, and chaotic transients and homoclinic orbits.<sup>13</sup>

Two major prerequisites for chaos are (1) the system must be nonlinear and (2) the system must have at least a three-dimensional phase space. A number of diagnostic numerical tools have been developed to characterize chaotic behavior, other than the Poincaré map. The randomlike nature of a chaotic



**Figure 11** Fractal basin boundary for Duffing's equation based on numerical simulation ( $b = 0.168$ ,  $\alpha = -0.5$ ,  $\beta = 0.5$ ,  $\omega = 1$ ,  $G = 0.15$ ). The black (white) regions represent initial conditions that generate a transient leading to the periodic attractor in the right (left) hand well.

signal is reflected in a broadband power spectrum with all frequencies participating.<sup>25</sup> The widespread availability of fast Fourier transform software makes power spectral techniques especially attractive in an experimental situation. Also, the divergence of adjacent trajectories can be measured in terms of Lyapunov exponents.<sup>26</sup> The autocorrelation function also has been used to illustrate the increasing loss of correlation with time lag. Various measures of dimension have been developed as well to establish the relation between fractals, chaos, and dynamical behavior.

### 3.8 Instability

Analogous to the instability of (static) equilibria under the operation of one control parameter, periodic (dynamic) cycles also lose their stability in a small number of generic ways. Figure 12 summarizes the typical stability transitions encountered in nonlinear forced vibration problems. Here, Poincaré sampling is used to obtain information on local transient behavior in terms of characteristic multipliers that describe the rate of decay of transients onto a periodic attractor, and hence, in the complex plane characterizes the stability properties of a cycle. This is familiar as the root locus in control theory based on the  $z$  transform.<sup>21</sup> Slowly changing a system parameter may cause penetration of the unit circle and hence the local growth of perturbations. The cyclic fold is the underlying mechanism behind the resonant amplitude jump phenomenon, and the flip bifurcation leads to subharmonic motion and may initiate the period-doubling sequence.

The Neimark bifurcation is much less commonly encountered in mechanical vibration. Also, other types of instability are possible for nongeneric systems, for example, a perfectly symmetric, periodically forced pendulum may exhibit a symmetry-breaking pitchfork bifurcation.<sup>18</sup>

Again these instability phenomena can also be analyzed using approximate analytical techniques. Small perturbations about a steady-state solution are used to obtain a variational (Mathieu-type) equation, the stability of which can then be determined using Floquet theory or the Routh–Hurwitz criteria.<sup>1,14,16</sup>

### 3.9 Nonlinear Normal Modes

The technique of nonlinear normal modes (NNM) can be thought of as an extension of classical linear modal methods. Unlike linear systems, there may be more nonlinear modes than there are degrees of freedom for a given system. For example, bifurcations may occur that produce modes not predicted by a linearized analysis. Also, the principle of superposition does not, in general, apply to NNM as it does to linear modes.

This technique has been successfully used to analyze a number of complex problems, including nonlinear resonances and localization phenomena associated with the vibration of rotating bladed disk assemblies and nonlinear isolation systems. For situations where the nonlinearities have a strong influence on the system response, NNM can be a very powerful analysis tool. It can be used as a model reduction technique, allowing for the development of approximate models that neglect effects that do not substantially influence the phenomena being analyzed. Vakakis et al.<sup>31</sup> provide a comprehensive discussion of nonlinear normal modes.<sup>30</sup>

## 4 EXAMPLES IN PRACTICE

The preceding discussion has been aimed at acquainting the reader with the basic phenomena that may occur in nonlinear dynamical systems and with the basic tools that are used to analyze such systems. The reader must first ask the basic question: Are the nonlinearities an important component in the dynamical behavior of my system? That is, can the system behavior be adequately explained with a linear model? This question can be answered by posing the following questions:

- Is there more than one equilibrium point in the system?
- Do any of the eigenvalues of the linearized system about the equilibrium points have zero real parts?
- Does a frequency analysis of the steady-state vibration response show significant components at frequencies other than those that are driving the system? This may include sub- and superharmonics of the driving frequency.

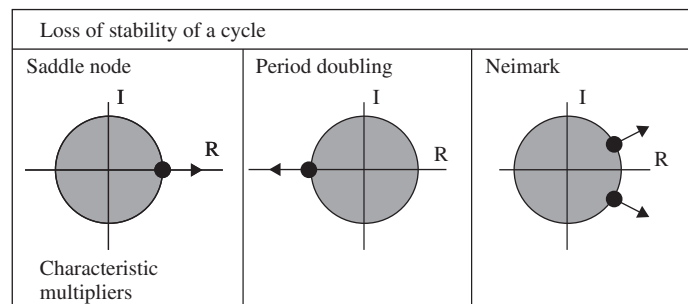


Figure 12 Generic instabilities of cycles under the operation of a single control.

If the answer to any of these questions is “yes,” then a nonlinear analysis is required. The nonlinearities are significant and must be considered in the dynamical analysis. The following paragraphs provide some examples of nonlinear systems and discuss the significance of the nonlinear terms with regard to the overall dynamics.

#### 4.1 Example 1: Rotor with Rubbing

**Instability Driven by Nonlinear Effects** Rubbing is common in rotating mechanical systems. There has been considerable debate over the years as to the true significance of rubbing as a destabilizing phenomena. Certainly, there is no doubt that many rotor systems experience rubbing regularly with no detrimental effects. On the other hand, there are numerous documented cases of high-amplitude rotor whirl driven by friction-induced contact resulting from rubbing. Childs<sup>29</sup> gives a good discussion of this topic for most rotor systems. For such systems, the stability may depend upon the amplitude of the disturbance away from the nominal “zero” location.

In order to gain some basic insight, consider a simple Jeffcott-type rotor model interacting across a

clearance,  $\delta$ , with a stationary housing, as shown in Fig. 13.

$$m\ddot{x} + c\dot{x} + kx + F_T \cos(\phi) - F_N \sin(\phi) = 0$$

$$m\ddot{y} + c\dot{y} + ky + F_N \cos(\phi) - F_T \sin(\phi) = 0$$

$$F_N = k_c(R - \delta)\Psi$$

$$F_T = \mu F_N \text{sign}(v_c)$$

$$\Psi = 1 \quad \text{if } R - \delta > 0$$

$$\Psi = 0 \quad \text{if } R - \delta < 0$$

where  $\mu$  is the friction coefficient between the rotor and the housing,  $k_c$  is the contact stiffness,  $v_c$  is the relative velocity at the contact point,  $F_N$  and  $F_T$  are the normal and tangential forces at the contact point, and  $\phi$  is the contact angle.

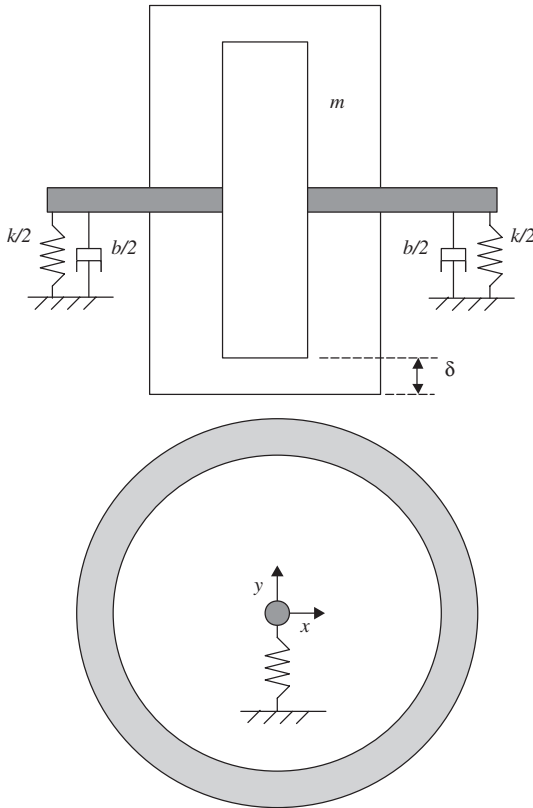
Two response cases are shown in Fig. 14. If the initial condition is sufficiently small such that the rotor does not contact the housing, then the vibration simply dies out to a zero steady-state level (Fig. 14a). However, for a certain running speed range and sufficiently large initial condition, the rotor will whirl in a limit cycle, as shown in Fig. 14b.

#### 4.2 Example 2: Systems with Clearance and Looseness

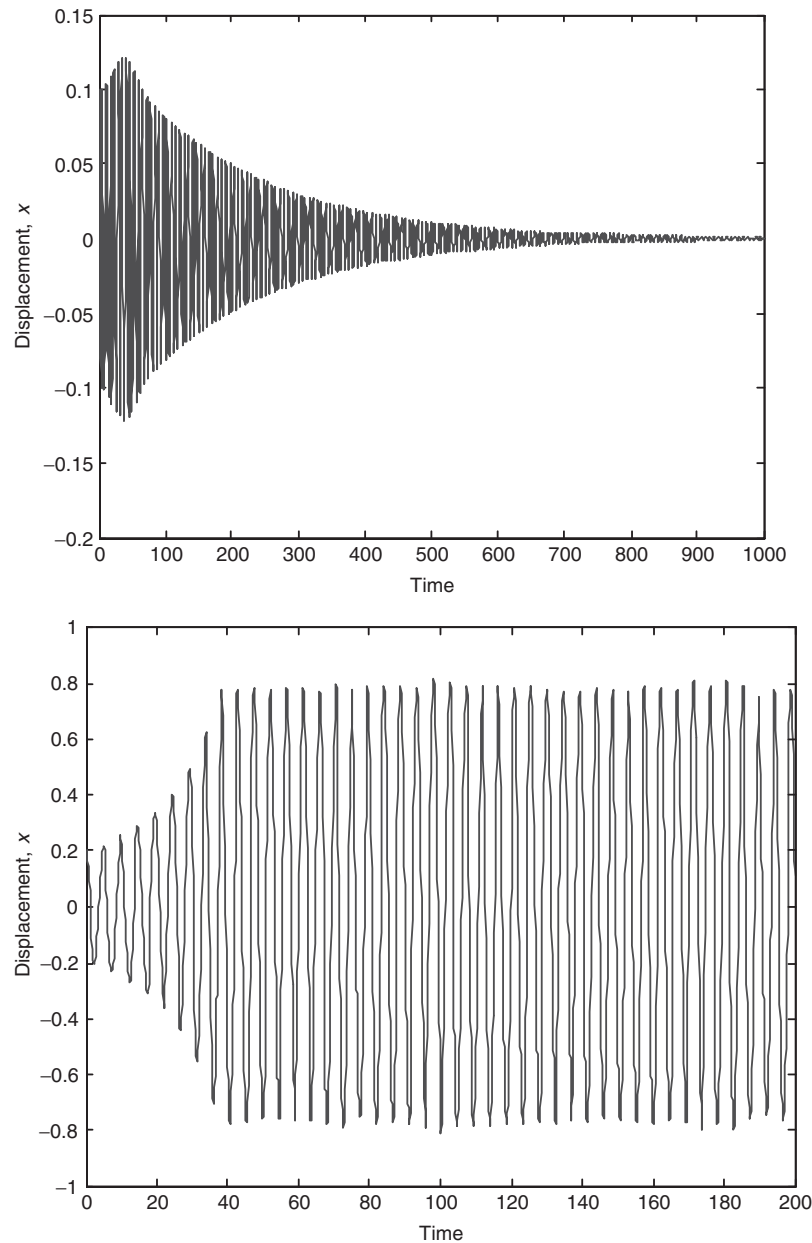
**Superharmonic Vibrations and Chaos** Looseness-type nonlinearities are common in mechanical systems. In fact, a certain amount of clearance is generally required between mechanical components if they are to be mated together and later separated. Often, this requirement is mitigated by employing press-fits and shrink-fits to mate and unmate the components. However, loosening and clearances may still appear as a result of temperature effects, centrifugal forces, wear, and the like. On Occasion, clearance is a fundamental design aspect. For example, impact and friction dampers require looseness in order to function.

One common indicator of the presence of such effects is the presence of significant frequency components at integer multiples of the running speed during steady-state operation. It should be noted that the presence of radial nonsymmetry due to support stiffness, rotating inertia, and so forth tends to exacerbate the influence of nonlinearities. Chaotic behavior has even been observed in such systems.

From a practical perspective, vibration signals are often analyzed for the purpose of monitoring the health of a structure or machine. There are a number of approaches, but they all basically compare the vibration signatures of the subject structure to that of a healthy structure of the same type. Often, deterioration is associated with effects that have a nonlinear influence on dynamic behavior, with small changes producing an amplified effect that is more readily discernible than would be the case if the influence was linear in nature. For example, the presence of a crack introduces a nonlinear feature as the crack



**Figure 13** Diagram of rotor with a clearance: (a) frontal view and (b) side view.

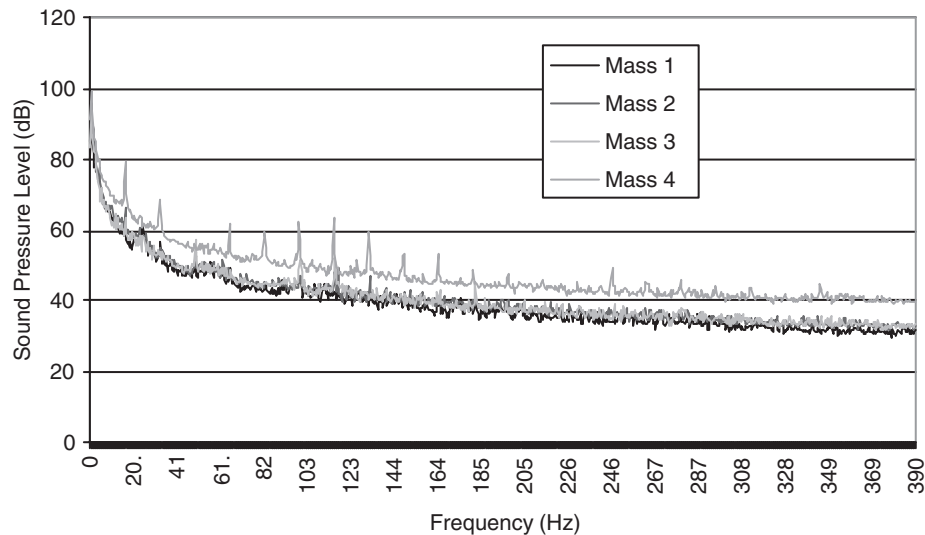


**Figure 14** Rotor response of two different initial conditions: (a) low-amplitude initial condition (no casing contact) and (b) higher amplitude initial condition (casing is contacted).

opens and closes. Also, bearing and joint wear results in increased clearances and looseness. So, identifying and quantifying such effects and their influence on vibration characteristics has widely shown to be a useful tool for health and condition monitoring.<sup>28,29</sup>

A practical example of such systems is the sound pressure levels produced by a fan with different levels

of imbalance. The noise was measured after different magnitude masses (4.636, 7.043, 16.322, and 32.089 g) were placed on one blade of the centrifugal fan in the unit. The microphone position used was 36 inches from the front of the unit (the same side of the unit as the door to the anechoic room) and centered at the front of the air-conditioning unit. Figure 15



**Figure 15** Narrow-band sound pressure level measured at 0.9 m from a fan with various imbalance masses added to the blower wheel (400-Hz frequency range).<sup>34</sup>

shows the narrow-band results for the cabinet sound pressure levels. The frequency range for these measurements was chosen to be in the low-frequency range of 0 to 400 Hz. This is because the added masses mainly cause low-frequency force excitation. Note that the masses create pure tone noise at the fundamental rpm/60 of the wheel and multiples (i.e., about 18.5 Hz and integer multiples). These pure tones become more and more pronounced as the out-of-balance mass is increased. They occur because of nonlinearities in the air-conditioning system caused by structural looseness and rattling. This phenomenon causes distortion of the sine wave shape of the fundamental pure tone out-of-balance force. This distortion effect causes harmonic multiples of the force to be created. There is an increase in noise of almost 10 dB when the largest out-of-balance mass is attached to the wheel. This increased noise (which is mainly low frequency as might be expected) was very evident to people present near the unit being tested. This low-frequency out-of-balance noise is quite unpleasant subjectively for people since it can be felt also as vibration by the human body.

## 5 SUMMARY

The field of nonlinear vibration has made substantial progress in the last two decades, developing tools and techniques for the analysis of complex systems. These years have seen the development and maturation of such areas as chaos and bifurcation analysis. However, substantial progress in a number of areas is still needed. For example, the analysis of high-order, nonlinear dynamical systems is still a difficult proposition.

The preceding discussion is meant to provide an overview of the field, including vibration phenomena that is uniquely nonlinear (such as limit cycles and

chaos) and analysis techniques that can be used to study such systems. References are provided to allow for more detailed information on specialized topics.

## REFERENCES

1. D. W. Jordan and P. Smith, *Nonlinear Ordinary Differential Equations*, Clarendon Press, Oxford, UK, 1987.
2. R. E. D. Bishop, *Vibration*, Cambridge University Press, Cambridge, UK, 1979.
3. W. T. Thomson, *Theory of Vibration with Applications*, Prentice-Hall, Englewood Cliffs, NJ, 1981.
4. J. M. T. Thompson and H. B. Stewart, *Nonlinear Dynamics and Chaos*, Wiley, Chichester, UK, 1986.
5. J. L. Singe and B. A. Griffith, *Principles of Mechanics*, McGraw-Hill, New York, 1942.
6. F. C. Moon, *Chaotic and Fractal Dynamics*, Wiley, New York, 1993.
7. C. Hayashi, *Nonlinear Oscillations in Physical Systems*, McGraw-Hill, New York, 1964.
8. B. Van der Pol, On Relaxation Oscillations, *Phil. Mag.*, Vol. 7, No. 2, 1926, pp. 978–992.
9. J. W. S. Rayleigh, *The Theory of Sound*, Dover, New York, 1896.
10. J. P. Den Hartog, *Mechanical Vibrations*, McGraw-Hill, New York, 1934.
11. E. H. Dowell, Flutter of a Buckled Plate as an Example of Chaotic Motion of a Deterministic Autonomous System, *J. Sound Vib.*, Vol. 147, 1982, pp. 1–38.
12. A. B. Pippard, *Response and Stability*, Cambridge University Press, Cambridge, UK, 1985.
13. A. J. Lichtenberg and M. A. Lieberman, *Regular and Chaotic Dynamics*, Springer, New York, 1992.
14. A. H. Nayfeh and D. T. Mook, *Nonlinear Oscillations*, Wiley, New York, 1979.
15. C. W. Gear, *Numerical Initial-Value Problems in Ordinary Differential Equations*, Prentice-Hall, Englewood Cliffs, NJ, 1971.



16. N. Minorsky, *Nonlinear Oscillations*, Van Nostrand, Princeton, NJ, 1962.
17. J. J. Stoker, *Nonlinear Vibrations*, Interscience, New York, 1950.
18. J. Guckenheimer and P. J. Holmes, *Nonlinear Oscillations, Dynamical Systems and Bifurcations of Vector Fields*, Springer, New York, 1983.
19. S. W. Shaw and P. J. Holmes, A Periodically Forced Piece-wise Linear Oscillator, *J. Sound Vib.*, Vol. 90, 1983, pp. 129–144.
20. P. V. Bayly and L. N. Virgin, An Experimental Study of an Impacting Pendulum, *J. Sound Vib.*, Vol. 164, 1993, pp. 364–374.
21. A. I. Mees, *Dynamics of Feedback Systems*, Wiley, Chichester, UK, 1981.
22. Y. Ueda, Steady Motions Exhibited by Duffing's Equation: A Picture Book of Regular and Chaotic Motions, in *New Approaches to Nonlinear Problems in Dynamics*, P. J. Holmes, Ed., Society for Industrial and Applied Mathematics, Philadelphia, PA, 1980, pp. 311–322.
23. J. A. Gottwald, L. N. Virgin, and E. H. Dowell, Experimental Mimicry of Duffing's Equation, *J. Sound Vib.*, Vol. 158, 1992, pp. 447–467.
24. C. S. Hsu, *Cell-to-Cell Mapping*, Springer, New York, 1987.
25. D. E. Newland, *An Introduction to Random Vibrations and Spectral Analysis*, 2nd ed., Longman, London, 1984.
26. A. Wolf, J. B. Swift, H. L. Swinney, and J. Vastano, Determining Lyapunov Exponents from a Time Series, *Phys. D*, Vol. 16, 1985, pp. 285–317.
27. E. Ott, C. Grebogi, and J. A. Yorke, Controlling Chaos, *Phys. Rev. Lett.*, Vol. 64, 1990, pp. 1196–1199.
28. G. Genta, *Vibrations of Structures and Machines: Practical Aspects*, 2nd ed., Springer, New York, 1995.
29. D. Childs, *Turbomachinery Rotordynamics: Phenomena, Modeling, and Analysis*, Wiley, New York, 1993.
30. F. C. Moon, *Chaotic and Fractal Dynamics: An Introduction for Applied Scientists and Engineers*, Wiley, New York, 1992.
31. A. F. Vakakis, L. I. Manevitch, Y. V. Mikhlin, V. N. Pilipchuck, and A. A. Zevin, *Normal Modes and Localization in Nonlinear Systems*, Wiley, New York, 1996.
32. N. S. Rasband, *Chaotic Dynamics of Nonlinear Systems*, Wiley, New York, 1990.
33. T. Yamamoto and Y. Ishida, *Linear and Nonlinear Rotordynamics*, Wiley, New York, 2001.
34. M. J. Crocker, personal communication, July 10, 2006.

## **PART III**

---

# **HUMAN HEARING AND SPEECH**



# CHAPTER 19

## GENERAL INTRODUCTION TO HUMAN HEARING AND SPEECH

Karl T. Kalveram  
Institute of Experimental Psychology  
University of Duesseldorf  
Duesseldorf, Germany

### 1 INTRODUCTION

This chapter discusses the way we hear, how sounds impair behavior, and how noise or hearing loss affect speech communication. Sound waves reaching the outer ear are physically characterized by frequency, intensity, and spectrum. As physiological acoustics points out, these physical variables are coded by hair cells in the inner ear into nerve impulses that our brains interpret as pitch, loudness, and timbre. Psychoacoustics deals with the quantitative relationship between the physical properties of sounds and their psychological counterparts. Noisiness and annoyance caused by sounds can also be subsumed to psychoacoustics, although they strongly depend also on the nonauditory context of the sounds. Speech recognition mirrors a particular aspect of auditory processing. Here, the continuous sonic stream is first partitioned into discrete sounds: vowels and consonants. These *phonemes* are then compiled to words, and the words to sentences, and so on. Therefore, speech recognition is hampered by background noise, which masks frequency bands relevant for phoneme identification, by damage to hair cells through intense noise or aging, which code for these relevant frequency bands, and by distortion or absence of signals necessary to delimit chunks on different levels of speech processing.

### 2 PHYSIOLOGICAL ACOUSTICS

**Physiological acoustics** tells us that the sound is converted by the eardrum into vibrations after passing through the outer ear canal. The vibrations are then transmitted through three little bones in the middle ear (hammer, anvil, and stirrup) into the cochlea in the inner ear (see Fig. 1, right side) via the oval window. In the fluid of the cochlea the basilar membrane is embedded, which when uncoiled resembles a narrow trapezoid with a length of about 3.5 cm, with the small edge pointing at the oval window. The incoming vibrations cause waves to travel along the basilar membrane. Sensors called inner hair cells and outer hair cells, which line the basilar membrane, transmute the vibrations into nerve impulses according to the bending of the hair cell's cilia.<sup>1,2</sup> **Place theory** links the pitch we hear with the place on the basilar membrane where the traveling waves achieve a maximal displacement. A pure tone generates one maximum, and a complex sound generates several maxima according to its spectral components. The closer the group of the maxima is placed to the

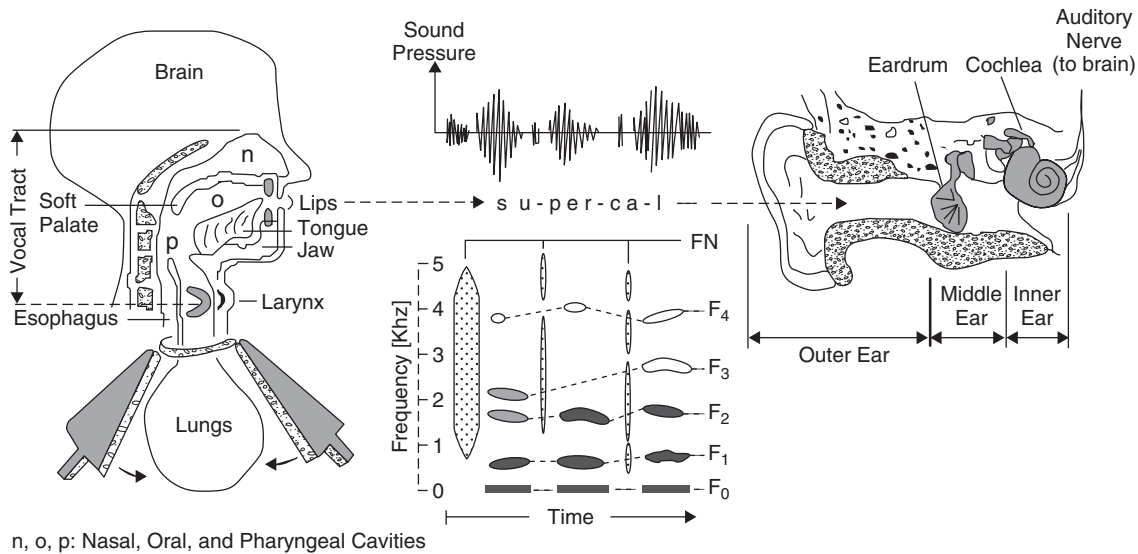
oval window, the higher the pitch, whereas the configuration of the maxima determines the timbre. The loudness of a sound seems to be read by the brain according to the number of activated hair cells, regardless of their location on the basilar membrane. While the inner hair cells primarily provide the afferent input into the acoustic nerve, the outer hair cells also receive efferent stimulation from the acoustic nerve, which generates additional vibrations of the basilar membrane, and leads to otoacoustic emissions. (See Fig. 18 of Chapter 20. Do not confuse with tinnitus.) These vibrations seem to modulate and regulate the sensitivity and gain of the inner hair cells. **Temporal theory** assumes that the impulse rate in the auditory nerve correlates to frequency, and therefore, also contributes to pitch perception (for details, see Chapter 20).

The ear's delicate structure makes it vulnerable to damage. **Conductive hearing loss** occurs if the mechanical system that conducts the sound waves to the cochlea loses flexibility, for instance, through inflammation of the middle ear. **Sensorineural hearing loss** is due to a malfunctioning of the inner ear. For instance, prolonged or repeated exposure to tones and/or sounds of high intensity can temporarily or even permanently harm the hair cell receptors (see Table 2 of Chapter 21 for damage risk criteria). Also, when people grow older, they often suffer a degeneration of the hair cells, especially of those near to the oval window, which leads to a hearing loss especially regarding sound components of higher frequencies.

### 3 PSYCHOLOGICAL ACOUSTICS

**Psychological acoustics** is concerned with the physical description of sound stimuli and our corresponding perceptions. Traditional psychoacoustics and *ecological psychoacoustics* deal with different aspects in this field.

**Traditional psychoacoustics** can further be subdivided into two approaches: (1) The **technical approach** concerns basic capabilities of the auditory system, such as the *absolute threshold*, the *difference threshold*, and the *point of subjective equality* with respect to different sounds. The psychological attributes, for instance, pitch, loudness, noisiness, and annoyance, which this approach refers to, are assumed to be quantifiable by so-called technical indices. These are values derived from physical measurements, for instance, from frequency, sound pressure, and duration



**Figure 1** Speaking and hearing. (Left side) Vocal tract, generating “supercalifragilisticexpialidocious.” (Middle part) Corresponding sound pressure curve and the sonogram of the first three syllables. (Right side) Ear, receiving the sonic stream and converting it to nerve impulses that transmit information about frequency, intensity, and spectrum via the auditory nerve to the brain, which then extracts the meaning. The figure suggests that production and perception of speech sounds are closely adapted to each other.

of sounds, which are then taken as the reaction of an average person. The special scaling of these measurements is extracted from the exploration of a number of normally sensing and feeling subjects. (2) The **psychological approach** uses such indices as the metric base but relates them with explicit measurements of the corresponding psychological attributes. This requires a specification of these attributes by appropriate psychological measurement procedures like *rating* or *magnitude scaling*.<sup>2</sup> The psychological approach principally provides, besides of the mean, also the scattering (standard deviation) among the individual data.

The **absolute threshold** denotes the minimum physical stimulation necessary to detect the attribute under consideration. A sound stimulus  $S$  described by its (physical) intensity  $I$  is commonly expressed by the **sound pressure level**  $L = 20 \log p/p_0 = 10 \log I/I_0$ , see Eq. (36) in Chapter 2. Thereby,  $I_0$  refers to the intensity of the softest pure tone one can hear, while  $p$  and  $p_0$  refer to the sound pressure. Conveniently,  $p_0 = 20 \mu\text{Pa}$ , and  $p$  can be measured by a calibrated microphone. Although  $L$  is a dimensionless number, it is given the unit **decibel (dB)**. Methodically, the absolute hearing threshold is defined as that sound pressure level of a pure tone that causes a detection with a probability of 50%. The thresholds are frequency dependent, whereby the minimal threshold resides between 1 and 5 kHz. This is that frequency domain that is most important for speech. As can be seen in Fig. 1 of Chapter 20, at the left and the right of the minimal value, the hearing

thresholds continuously increase, leaving a range of approximately 20 to 20,000 Hz for auditory perception in normal hearing persons. A person's **hearing loss** can be quantified through determination of the frequency range and the amount by which the absolute hearing thresholds in this range are elevated. The top of Figure 1 of Chapter 20 indicates the saturation level, where an increase of intensity has no effect on perceived loudness. This level, which is located at about 130 dB, is experienced as very uncomfortable or even painful. **Masking** labels a phenomenon by which the absolute threshold of a tone is raised if a sound more or less close in frequency, called the masker, is added. Thus, an otherwise clearly audible tone can be made inaudible by another sound. *Simultaneous masking* refers to sounds that occur in synchrony, and *temporal masking* to sounds occurring in succession. Thereby, *forward masking* means that a (weak) sound following the masker is suppressed, whereas in *backward masking*, a (weak) sound followed by the masker is suppressed. To avoid beats in an experimental setup, the masker is often realized as narrow-band noise. Tones that are higher in frequency than the center frequency of the masker are considerably more strongly suppressed than those below the center frequency. Enhancing the masker's intensity even broadens this asymmetry toward the tones whose frequency exceeds the center frequency. Simultaneous and temporal masking allow to sparsely recode sound signals without a recognizable loss of quality—as performed, for instance, in the **audio compression format MP3** for music. Here, a computer algorithm quickly calculates those parts of the audio input that will be inaudible and cancels them

in the audio signal to be put out. Also broadband noise and pink noise added to the auditory input can impair sound recognition by masking. This is of importance especially in speech perception.

The **difference threshold**, also called the **just noticeable difference (JND)**, describes the minimum intensity  $\Delta I$  by which a variable test stimulus  $S$  (comparison stimulus) must deviate from a standard stimulus  $S_0$  (reference stimulus) to be recognized as different from  $S_0$ . Both stimuli are usually presented as pairs, either simultaneously if applicable, or sequentially.  $\Delta I$  is, like the absolute threshold, statistically defined as that intensity difference by which a deviation between both stimuli is recognized with a probability of 50%. Regarding pure tones of identical frequency, the difference thresholds roughly follow **Weber's law**,  $\Delta I/I_0 = k = \text{const.}$ , where  $I_0$  refers to intensity of  $S_0$ , and  $k$  approximates 0.1. **Fechner's law**,  $E = \text{const} \log I/I_0$ , is assumed to hold for all kinds of sensory stimulation fulfilling Weber's law.<sup>2</sup> Here,  $E$  means the strength of the experienced loudness induced by a tone of intensity  $I$ , and  $I_0$  the absolute threshold of that tone. Both diminishing and enhancing loudness by 3 dB roughly correspond to the JND. Fechner's law is the starting point of a **loudness scale** that is applicable to sounds with arbitrary, but temporally uniform, distributions of spectral intensity. To account for the frequency-dependent sensitivity of the human ear, the sound pressure measurements pass an appropriate filter. Mostly, a filter is chosen whose characteristic is inversely related to the 40-phon contour sketched in Fig. 2 of Chapter 21 (40 phon—for definition see below—characterizes a clearly audible, but very soft sound). We call this the **A-weighted sound pressure level**. It provides a technical loudness index with the unit dB.

The **point of subjective equality (PSE)** refers to cases where two physically different stimuli appear as equal with respect to a distinct psychological attribute, here the experienced loudness. Considered statistically, the PSE is reached at that intensity, where the test stimulus is judged louder than the standard with a probability of 50%. The concept allows to construct an alternative **loudness scale with the unit phon**, the purpose of which is to relate the loudness of tones with diverse frequencies and sound pressure levels to the loudness of 1-kHz tones. The scaling procedure takes a pure tone of 1 kHz at variable sound pressure levels as standards. Test stimuli are pure tones, or narrow-band noise with a clear tonal center, which are presented at different frequencies. The subject's task is to adjust the intensity of the test stimulus such that it appears as equally loud compared to a selected standard. Figure 2 of Chapter 21 shows the roughly U-shaped dependency of these sound pressure levels on frequency. All sounds fitting an equal-loudness contour are given the same value as the standard to which they refer. However, the unit of this scale is renamed from dB into phon. In other words, all sounds relabeled to  $x$  phon appear as equally loud as a pure tone of 1 kHz at a sound pressure level of  $x$  dB.

The **quantitative specification of a psychological attribute** requires one to assume that the subjects assign scaleable perceived strengths  $E$  to the physical stimuli  $S$  to which they are exposed. In rating, typically a place between two boundaries that represent the minimal and the maximal strength has to be marked. The boundaries are given specific numbers, for instance, 0 and 100, and the marked place is then converted into a corresponding number assumed to mirror  $E$ . In **magnitude scaling**, typically a physical standard  $S_0$  is additionally provided that induces the perceptual strength  $E_0$  to be taken as the internal standard respective unit. Then, the subject is given a number  $0 < x < \infty$  and instructed to point at that stimulus  $S$ , which makes the corresponding perceived strength  $E$  equal to  $x$  times the perceived strength  $E_0$  of the standard  $S_0$ . Or, loosely speaking,  $S$  is considered as *subjectively equal* to  $x$  times  $S_0$ . Both rating and magnitude scaling principally provide psychophysical dose-response curves, where  $E$  is plotted against  $S$ .

**Pitch** can be measured on the **mel scale** by magnitude scaling. Here, a pure tone of 1 kHz at a sound pressure level of 40 dB is taken as the standard that is assigned the pitch value of 1000 mel. A test tone of arbitrary frequency, which appears as  $x$  times higher in pitch than the standard tone's pitch, is assigned the value of  $x1000$  mel ( $0 < x < \infty$ ). Experiments reveal that the mel scale is monotonically, but not completely linearly, related to the logarithm of the tone's frequency, and that pitch measured in mel slightly depends on the intensity of the test tones.

**Loudness** can, aside from the rather technical A-weighted dB and phon scales, be measured also by psychological magnitude scaling. This yields the **sone scale**.<sup>2</sup> The standard stimulus is a tone of 1 kHz at a sound pressure level of 40 dB, which is assigned the loudness of 1 sone. A test stimulus can be a steady-state sound of arbitrary spectral intensity distribution. The listener's task is analogous to that in the *mel* scale: A sound is given the loudness  $x$  sone if it appears as  $x$  times as loud as the standard. The sone scale differs from the phon scale in that all judgments are referred to one standard, not to many standards of different intensities among the tones of 1 kHz, in that the demand of tonality is relinquished, and in that psychological scaling is required (for details, see Chapter 21). The sone scale approximately corresponds to **Stevens' power law**,  $E = \text{const}(I/I_0)^b$ , where  $b$  is a constant value, here about 0.3. Notice that Fechner's law and Stevens' law cannot produce coinciding curves because of the different formulas.

**Noisiness** is an attribute that may be placed between loudness and annoyance. It refers to temporally extended sounds with fluctuating levels and spectra. An adequate physical description of those stimuli is provided by the **equivalent continuous A-weighted sound pressure level** ( $L_{pAeq,T}$ ). Here, the microphone-based A-weighted sound pressure level is converted into intensity, temporally integrated, and the result averaged over the measurement period  $T$ . The

finally achieved value is again logarithmized and multiplied by 10. The unit is called dB. A refinement of the sound pressure's weighting as applied in the "perceived noise level" yields dB measurements the unit of which is called noy.

**Annoyance caused by noise** refers, as noisiness, to unwanted and/or unpleasant sounds and is mostly attributed to temporally extended and fluctuating sounds emitted, for instance, by traffic, an industrial plant, a sports field, or the activity of neighboring residents. Mainly, the  $L_{pAeq,T}$ , or other descriptors highly correlating with the  $L_{pAeq,T}$  (see Chapter 25), are taken as the metric base, whereby the measurement periods  $T$  can range from hours to months. Annoyance with respect to the noise exposition period is explicitly measurable by rating. Sometimes also the percentage of people who are highly annoyed when exposed to a specific sound in a specific situation during the specified temporal interval is determined (for details, see Chapter 25). To achieve dose-response relationships (e.g., mean annoyance ratings in dependency on the related  $L_{pAeq,T}$  measurements) of reasonable linearity and minimal error, it is recommended that the annoyance judgments be improved, for instance, by a refinement of the categories offered to the listeners.<sup>3</sup> Annoyance quantified in this manner depends, however, besides the sound's intensity, spectral composition, and temporal fluctuation, especially on the nonacoustical context. So, the coefficient of correlation between annoyance ratings from field studies and the corresponding  $L_{pAeq,T}$  values seldom exceeds  $\frac{1}{2}$ . That is to say, the relative part of the variance of annoyance ratings cleared up by physical sound characteristics as given in the  $L_{pAeq,T}$  is mostly less than  $\frac{1}{4}$ . This results in a broad "error band" around the mean dose-response curve. Nevertheless, technical and also political agencies usually assess community reactions to noise exposure solely by the microphone-based  $L_{pAeq,T}$  or related descriptors. However, because most of these descriptors correlate with each other close to 1, it does not make much sense to prefer one of them to the others.<sup>4</sup> It must also be taken as a matter of fact that individual annoyance cannot validly be measured by such an index and that community annoyance is captured by these indices solely through a high degree of aggregation. **Nonauditory context variables influencing sound-induced annoyance** include the time of day the sound occurs, the novelty and meaning the sound carries, and cultural<sup>5</sup> as well as past personal experiences with that sound. Current theories of annoyance that claim to explain these context effects refer either to the psychological or the biological function of audition. The **psychological function** of the acoustical signals includes (1) feedback related to an individual's sensorimotor actions, (2) identification, localization, and the controllability of sound sources, (3) nonverbal and verbal communication, (4) environmental monitoring, and (5) the tendency to go on alert through inborn or learned signals. Acoustical signals incompatible with, or even severely disturbing, control of

behavior, verbal communication, or recreation, relaxation, and sleep, enforce to break the current behavior. This is considered as the primary effect of noise exposure, followed by annoyance as the psychological reaction to the interruption.<sup>6</sup> Regarding the **biological function**, the respective theory assumes that annoyance is a **possible loss of fitness signal** (PLOF-signal), which indicates that the individual's Darwinian fitness (general ability to successfully master life and to reproduce) will decrease if she or he continues to stay in that situation. Therefore, especially residents should feel threatened by foreigners who are already audible in the habitat, because that may indicate that there are intruders that are going to exploit the same restricted resources in the habitat. This explains why sounds perceived as man-made are likely to evoke more annoyance than sounds of equal level and spectral composition, but attributed to non-man-made, respectively, natural sources.<sup>7</sup> Thus, annoyance is considered as the primary effect of noise exposure, which is followed by a distraction of attention from the current activity. That in turn frees mental resources needed for behavioral actions toward the source of the sound. Possible actions are retreating from the source, tackling the source, standing by and waiting for the opportunity to select an appropriate behavior, or simply coping with the annoyance by adapting to the noise.<sup>8</sup>

**Ecological psychoacoustics** deals, in contrast to traditional psychoacoustics, with real-world sounds that usually vary in frequency, spectral composition, intensity, and rhythm. The main topics can be called auditory analysis and auditory display. Both are restricted to the nonspeech and nonmusic domain.

**Auditory analysis** treats the extraction of semantic information conveyed by sounds and the construction of an auditory scenery from the details extracted by the listener. Experiments reveal that the incoming sonic stream is first segregated into coherent and partly or totally overlapping discernible auditory events, each identifying and characterizing the source that contributes to the sonic stream. Next, these events are grouped and establish the auditory scene.<sup>9</sup> A prominent but special example is the discovery that detection and localization of a (moving) source exploits (1) the temporal difference of the intensity onsets arriving at the ears, (2) different prefiltering effects on the sonic waves before they reach the eardrums due to shadowing, diffraction, and reflection properties of the head, auricles, torso, and environment, and (3) the variation of the spectral distribution of intensity with distance.<sup>2</sup> To acquire such sophisticated skills, infants may need up to 12 years, a fact that should be taken into account if an unattended child below this age is allowed, or even urged, to cross, cycle, or play in the vicinity of places with road traffic.

**Auditory display** concerns how artificial sounds can be generated to induce a desired auditory scene in the listener. The term covers (1) *auditory icons* suitable for alerts or for the representation of ongoing processes in systems (e.g., in computers and machines), (2) *audification* of originally inaudible periodic signals by frequency shifting into the audible range for humans

(e.g., seismic records), (3) *sonification* of originally nonauditory and nonperiodic events (e.g., radioactivity measured by a Geiger counter), and (4) also *sonic qualification* of nonauditory events or facts (e.g., auditory accentuation of particular visual scenes in movies, or auditory identification of defects in mechanical machines).<sup>10</sup>

#### 4 SPEECH COMMUNICATION

The basic capabilities of generation, processing, segregation, and grouping of sonic streams include, as Fig.1 suggests, also **speech production** and **speech perception**. The complicated structure of speech makes this kind of communication susceptible to disturbances at different locations in the transmission path. Instances of such disturbances are *background noise*, *hearing loss*, and *disturbed auditory feedback*.

**Speech production** can be described as hierarchically organized **multiple parallel-to-serial transformations**.<sup>11</sup> Consider, for instance, a keynote speaker trying to transmit an idea. She/he then serializes the idea into sentences, each sentence into words, each word into syllables, each syllable into special speech sounds (phonemes) called vowels (V) and consonants (C), and each phoneme into a particular stream of sound pressure fluctuations, as indicated in the left and middle of Fig.1. Vowels have the character of tones with a low fundamental frequency (men: ~80–160 Hz, women ~170–340 Hz). They are generated by air flowing through adducted vocal folds, which makes them vibrate through the Bernoulli effect, while the vocal tract (pharyngeal plus oral plus nasal cavities) is relatively “open.” This gesture is called *voicing* or *phonation*. The vocal tract forms an acoustic resonator, the shape of which is controlled by the speaker in a manner that concentrates the sound energy into four narrow frequency bands called **formants**. Vowels then differ with respect to the distribution of energy in these formants. Consonants originate if the articulators (lips, tongue, jaw, soft palate) form narrow gaps in the vocal tract while air flows through. This causes broadband turbulence noise reaching relatively high frequencies. Consonants can be voiced or unvoiced, depending on whether or not the broadband signal is accompanied by phonation.<sup>12</sup> General American English includes, for instance, 16 vowels and 22 consonants. In each syllable, a vowel is mandatory that can, but must not, be preceded and/or followed by one or more consonants. Commonly, a person’s speech rate ranges between 4 to 6 syllables per second (see Chapter 22).

In general, a **linguistic stress** pattern is superimposed upon the syllables of an utterance. Stress is realized mainly by enhancing the loudness but can also be expressed by lucidly lengthening or shortening the duration of a syllable or by changing the fundamental frequency. It is the vowel that is manipulated to carry the stress in a stressed syllable. Usually, a string of several words is uttered in a fixed rhythm, whereby the beat coincides with the vowel of the stressed syllables. Linguistic pronouncement (prosody, stress) sustains speech recognition but carries also nonverbal

information, for example, cues informing the receiver about the emotional state of the speaker. An erroneous integration of linguistic stress into an utterance while serializing syllables into strings of phonemes is possibly the origin of stammering.<sup>11</sup>

**Speech perception** is inversely organized with respect to speech production and can be described as chained **serial-to-parallel transformations**. Thereby, serial-to-parallel transformation means that a temporal sequence of bits is constricted to an equivalent byte of information that is coded spatially without using the dimension of time. To get back the keynote, the listener, therefore, has at first to constrict distinct parts of the auditory stream into vowels and consonants that have subsequently to be concatenated to syllables. Now, words have to be assembled from the syllables, sentences from the words, and finally the keynote from the sentences. On each processing level, such a **segmentation** has to take place in order to get the units of the next level in the hierarchy. In the flow of speech, therefore, delimiter signals must be embedded that arrange the correct grouping of units on one level into a superunit on the next higher level. In communication engineering, such signals are provided by clock pulses or busy/ready signals. On the word and sentence levels, pauses and the raising/lowering of the fundamental frequency can be used for segmentation. To get syllables from phonemes, the vowel onset, though it is positioned in the middle of a syllable, provides a ready signal because each syllable has just one vowel. Grammatical constraints that generate redundancies, or the rhythm associated with a string of stressed syllables, can additionally be exploited for segmentation on this level. Hence, a distortion in paralleling serial events on an arbitrary level in ongoing speech can seriously hamper the understanding of speech. Referring to written language, it may be that such a deficit is responsible for dyslexia.

**Background noise and hearing loss** both impair the understanding of speech (see Chapter 22): The noise lowers the signal-to-noise ratio, and also a raised hearing threshold can be considered as equivalent to a lowered signal-to-noise ratio. However, an amplification of the unfiltered speech signal, which just compensates for the noise or the hearing loss, does not suffice to reestablish understandability. The reason is that speech roughly occupies the frequency range between 500 Hz and 5 kHz, but in vowels the sonic energy is almost entirely concentrated in the frequency band below 3 kHz, whereas in voiceless and voiced consonants energy is present also above 3 kHz. It is especially this higher frequency part of the spectrum that is necessary for the discrimination of consonants. Thus, low-pass filtering of speech signals hampers the discrimination of consonants much more than the discrimination of vowels. Since the number of consonants exceeds the number of vowels, and because of the basic C-V-C structure of the syllable, consonants transmit considerably more information than vowels. It follows that high-frequency masking noise, or age-related hearing loss with elevated hearing thresholds especially at the higher frequencies, or cutting off higher

frequencies by a poor speech transmission facility, must severely deteriorate speech recognition since in all three cases nearly exclusively the discrimination of consonants is impaired. A linear increase of an amplifier's gain in a transmission circuit cannot solve the problem. This enhances the intensity also in the low-frequency domain, which in turn broadens and shifts simultaneous and temporal masking toward the higher frequencies. So, the result is even a further decrease of understandability. Therefore, in order to overcome the noise, or the age-related hearing loss, or to help conference participants who often have problems to distinguish the consonants when listening to an oral presentation held in a foreign language in a noisy conference room, the frequencies above 3 kHz should considerably be more amplified than the lower frequencies. Modern hearing aids can even be attuned to meet individual deficits. This is performed by scaling the gain according to the elevation of the hearing thresholds at different frequencies. To avoid a disproportionate loudness recruitment (see Chapter 21), however, the gain must be scaled down, when the intensity attained through the amplification outreaches the threshold intensity.

**Disturbed auditory feedback** of one's own speech, for instance, through any kind of acoustical noise, or by delayed or frequency-shifted auditory feedback, affects speaking. An immediate reaction to those disturbances is that we usually increase loudness and decrease speech rate. Research, however, revealed that further effects can be observed: If the speech sound is fed back with a delay ranging from 200 to 300 ms (that corresponds to the duration of a syllable), artificial stutter is produced.<sup>13</sup> Delays in the range from 10 to 50 ms, although not noticed by the speaker, induce a lengthening of the vowel duration of linguistically stressed long syllables of about 30 to 80% of the delay time, whereas vowels of stressed short syllables and of unstressed syllables, and also all consonants, are left unaffected by the delayed feedback. This reveals that linguistic stressing imposes a strong **audio-phonatory coupling**, but solely upon the respective vowel.<sup>11</sup> However, the fundamental frequency when stripped of all harmonics by rigorous low-pass filtering does not have any influence on the timing of speech in a delayed feedback setup. In contrast, auditory feedback of the isolated fundamental frequency does influence phonation when the frequency is artificially shifted: It changes the produced frequency with a latency of about 130 ms in the opposite direction, such that at least an incomplete compensation for the artificial frequency shift is reached.<sup>14</sup>

All the effects of disturbed auditory feedback reported in the last paragraph indicate that speech production is embedded in different low-level control loops that use different channels hidden in the self-generated sound. We are yet far away from an understanding of the physiological base of these processes.

**Acknowledgement** The author thanks Nicole Pledger for language assistance.

## REFERENCES

1. D. G. Myers, *Psychology*, Worth, New York, 2004.
2. H. R. Schiffman, *Sensation and Perception. An Integrated Approach*, Wiley, New York, 1982.
3. S. Namba and S. Kuwano, Environmental Acoustics: Psychological Assessment of Noise, in *Ecological Psychoacoustics*, J. G. Neuhoff, Ed., Elsevier, New York, 2004, pp. 175–190.
4. K. T. Kalveram, The Theory of Mental Testing, and the Correlation between Physical Noise Level and Annoyance, *J. Acoustic. Soc. Am.*, Vol. 101, No. 5, 1997, p. 3171.
5. S. Kuwano, S. Namba, H. Fastl, M. Florentine, A. Schick, D. R. Zheng, H. Hoege, and R. Weber, A Cross-Cultural Study of the Factors of Sound Quality of Environmental Noise, in *Proceedings of the 137th Meeting of the Acoustical Society of America, and the 25th Meeting of the German Acoustics Association*, Technische Universität, Berlin, 1999, pp. CD, 4 pages.
6. D. C. Glass and J. E. Singer, Experimental Studies of Uncontrollable and Unpredictable Noise, *Representative Res. Social Psychol.*, Vol. 4, No. 1, 1973, pp. 165–183.
7. K. T. Kalveram, J. Dassow, and J. Vogt, How Information about the Source Influences Noise Annoyance, in *Proceedings of the 137th Meeting of the Acoustical Society of America, and the 25th German Acoustics Association*, Technische Universität, Berlin, 1999, pp. CD, 4 pages.
8. R. Lazarus, Thoughts on the Relations between Cognition and Emotion, *Amer. Psychol.*, Vol. 37, 1980, pp. 1019–1024.
9. A. S. Bregman, *Auditory Scene Analysis*, MIT Press, Cambridge, MA, 1990.
10. B. N. Walker and G. Kramer, Ecological Psychoacoustics and Auditory Display. Hearing, Grouping, and Meaning Making, in *Ecological Psychoacoustics*, J. G. Neuhoff, Ed., Elsevier, New York, 2004, pp. 149–174.
11. K. T. Kalveram, Neurobiology of Speaking and Stuttering. Proceedings of the Third World Congress of Fluency disorders in Nyborg, Denmark, in *Fluency Disorders: Theory, Research, Treatment and Self-help*, H. G. Bosshardt, J. S. Yaruss, and H. F. M. Peters, Eds., Nijmegen University Press, 2001, pp. 59–65.
12. G. Fant, Analysis and Synthesis of Speech Processes, in *Manual of Phonetics*, B. Malmberg, Ed., North Holland, Amsterdam, 1968, pp. 173–277.
13. B. S. Lee, Effects of Delayed Speech Feedback, *J. Acoustic. Soc. Am.*, Vol. 22, 1950, pp. 824–826.
14. U. Natke, T. M. Donath, and K. T. Kalveram, Control of Voice Fundamental Frequency in Speaking versus Singing, *J. Acoustic. Soc. Am.*, Vol. 113, No. 3, 2003, pp. 1587–1593.

# CHAPTER 20

## THE EAR: ITS STRUCTURE AND FUNCTION, RELATED TO HEARING

Hiroshi Wada

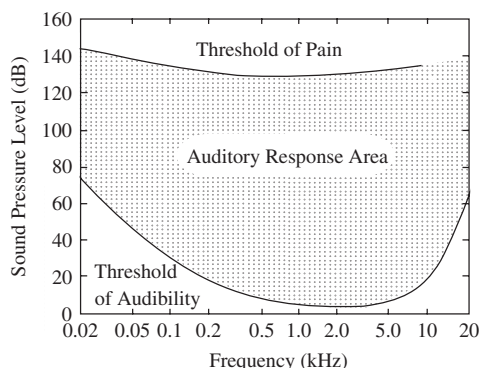
Department of Bioengineering and Robotics  
Tohoku University  
Sendai, Japan

### 1 INTRODUCTION

The ears are paired sense organs that collect, transmit, and detect acoustical impulses. Each of them is comprised of three main parts: the outer ear, middle ear, and inner ear. Sound waves are focused into the external auditory canal by the fleshy external part of the ear, or pinna. The sound waves in the auditory canal cause vibration of the tympanic membrane, which results in motion of the three small bones, or ossicles, in the middle ear. The motion of the ossicles is transmitted to the cochlea of the inner ear, where it is transformed into vibration of the organ of Corti. This vibration is amplified by the motion of outer hair cells located in this organ. The mechanical motion of the organ of Corti is then transduced into encoded nerve signals by inner hair cells, which are also situated in the organ of Corti, these signals subsequently being transmitted to the brain. For a good understanding of the function of the ear and human hearing, knowledge of the anatomy of the main parts of the hearing organ is required, as is interpretation of how all of these parts function together. Intense noise is of concern because it can cause permanent damage to the hearing mechanism, particularly the hair cells.

### 2 REMARKABLE SENSITIVITY OF THE EAR

Sound is energy that is transmitted by pressure waves in air and is the objective cause of the sensation of hearing.

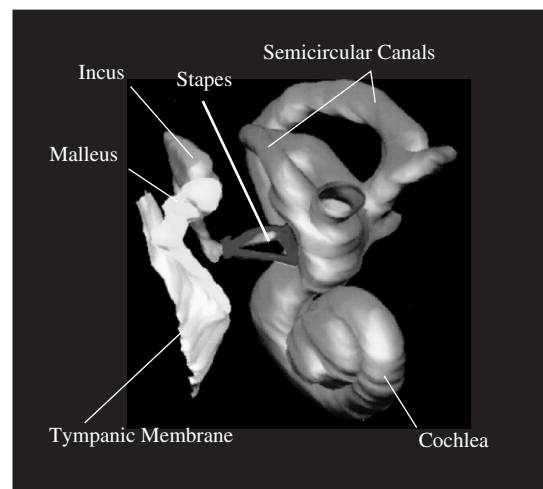


**Figure 1** Auditory response area for humans. Sound within the dotted area is audible. This area is bounded on one side by the limits of tolerability of sound and on the other side by the limits of detectability. The difference between the two thresholds is quite wide.

Figure 1 shows the auditory response area for humans.<sup>1,2</sup> Sound within the dotted area is bounded on one side by the threshold of pain and on the other by the threshold of audibility as a function of frequency. The sound pressure level (SPL) difference between these thresholds, that is, the dynamic range, is quite wide, nearly 130 dB at a frequency of 4.0 kHz. High-end recording equipment has a dynamic range of 90 dB. This means that our ears are much more sensitive than such equipment.

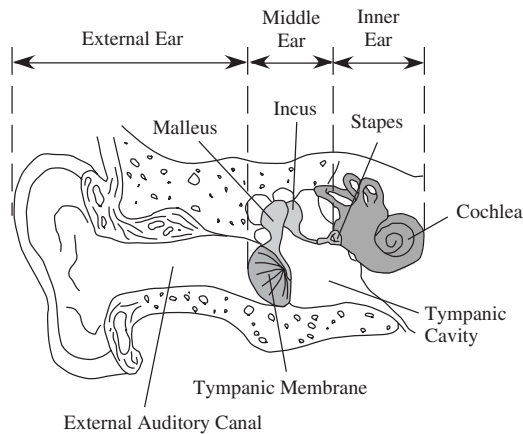
### 3 OVERVIEW OF PERIPHERAL ANATOMY: OUTER, MIDDLE, AND INNER EARS

Figure 2 displays a computer-aided reconstruction of the human middle and inner ears, which was obtained from a fixed temporal bone extracted from a fresh cadaver. The relationship of size and location among the various components of the peripheral auditory system can be clearly understood. In humans, as shown in Fig. 3, the external auditory canal with a diameter of 7 mm and a length of 30 mm, which is slightly bent and elliptical, is terminated by a conical-shaped tympanic membrane with a diameter



**Figure 2** Computer-aided reconstruction of the human middle and inner ear, which was obtained from the temporal bone extracted from a fresh cadaver. The relationship of size and location among the various components can be clearly understood.

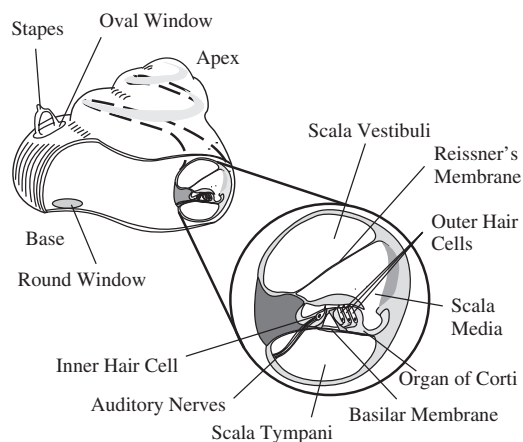




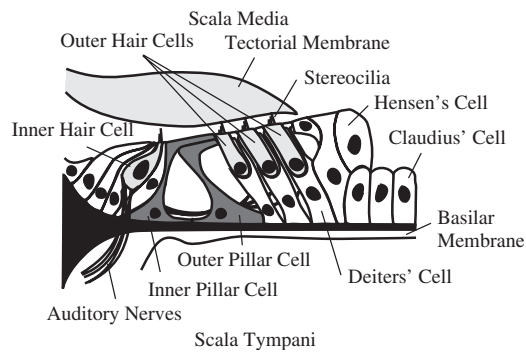
**Figure 3** Human peripheral auditory system. Mammals always have three ossicles, namely the malleus, the incus, and the stapes.

of 10 mm and a thickness of 0.1 mm. Three ossicles, namely the malleus, incus, and stapes, are located in the tympanic cavity. The malleus is attached to the tympanic membrane, the incus lies between the malleus and the stapes, and the stapes is connected to the cochlea.

Figure 4 depicts the human cochlea with a length of 35 mm, which is spiral shaped and has three fluid-filled compartments, that is, the scala vestibuli, the scala media, and the scala tympani. They are separated by Reissner's membrane and the basilar membrane. The scala vestibuli and scala tympani contain perilymph, and the scala media contains endolymph. At the basal end, the scala vestibuli has an oval window, and the scala tympani has a round window. The



**Figure 4** Human cochlea and its cross section. The cochlea has three fluid-filled compartments, which are divided by Reissner's membrane and the basilar membrane.



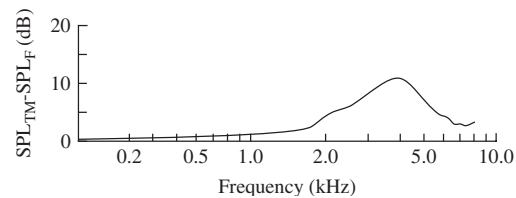
**Figure 5** Structure of the organ of Corti. This organ sits on the basilar membrane. Two types of sensory cells, i.e., the inner hair cells and the outer hair cells are located in this organ.

base of the stapes, called the footplate, is sealed by a flexible ligament, and the footplate transmits the vibration of the middle ear to the fluid in the scala vestibuli.

As shown in Fig. 5, the organ of Corti sits on the basilar membrane and contains two types of hair cells, that is, the inner hair cells and the outer hair cells. There are approximately 3,500 inner hair cells and 12,000 outer hair cells in humans.<sup>3</sup> Hairlike structures, that is, stereocilia, extend from the top of these cells. The organ of Corti is covered by the tectorial membrane and given rigidity by the pillar cells. There are three types of supporting cells, namely, Deiters', Hensen's, and Claudius' cells.

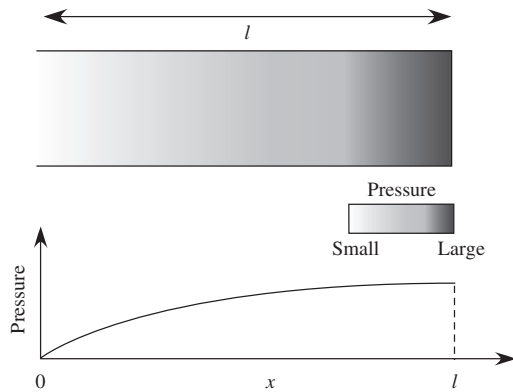
#### 4 ACOUSTICAL PROPERTIES OF THE OUTER AND MIDDLE EARS

As shown in Fig. 6,<sup>4</sup> sound pressure amplification at the tympanic membrane is greatest when the frequency is around 4.0 kHz. This amplification is caused by standing waves in the external auditory canal. Figure 7 depicts a simplified model of the external auditory



**Figure 6** External auditory canal resonance observed in human subjects. Plotted along the ordinate is the decibel difference between the sound pressure level at the tympanic membrane and that in the sound field at the entrance of the external auditory canal (F). The difference between them is largest at around  $f = 4.0$  kHz. [From Weiner and Ross.<sup>4</sup> Copyright © 1946 by The Acoustical Society of America (ASA). Reprinted by permission of American Institute of Physics (on behalf of ASA).]





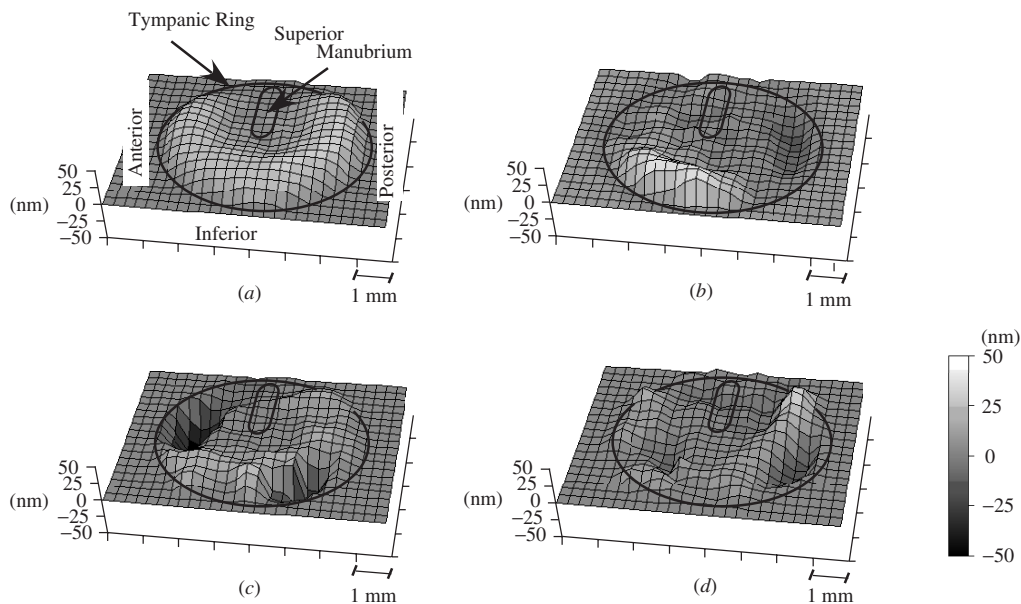
**Figure 7** Pressure variation in a pipe with one end open and the other end closed when  $f_0 = c/4l$ , where  $f_0$  is the fundamental resonance frequency,  $c$  is the velocity of the air, and  $l$  is the length of the pipe.

canal, that is, a pipe with one end open and the other end closed, with pressure variation along the pipe at the fundamental resonance frequency,  $f_0$ . Sound pressure amplification at the end of the pipe is noticeable. Due to this phenomenon, the threshold of audibility is

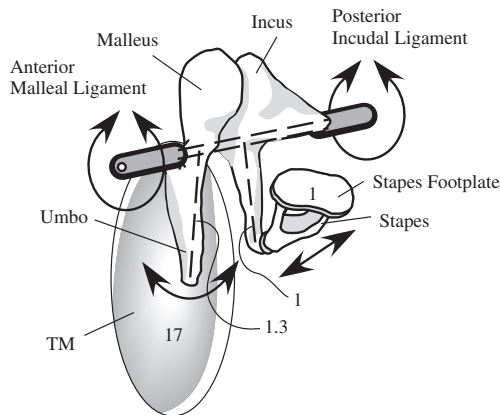
believed to be the smallest at the resonance frequency of the external auditory canal, which is shown in Fig. 1.

An attempt was made to measure the vibratory responses of guinea pig tympanic membranes using time-averaged electric speckle pattern interferometry.<sup>5</sup> Figure 8 shows perspective plots of the displacement distribution of the left tympanic membrane vibrations when the displacement at each point reaches its maximum value. The amplitude of tympanic membrane vibrations is of nanometer order of two digits, that is, 10 to 99 nm, when the sound pressure level of the stimulation is between 70 and 85 dB.

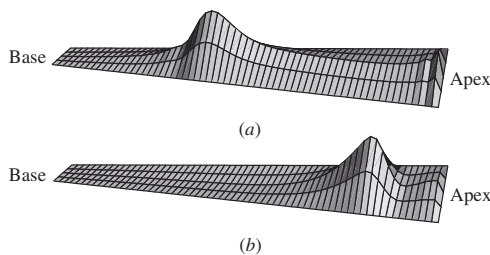
The three ossicles transmit sound vibrations from the tympanic membrane to the oval window of the cochlea. The main role of the middle ear is to match the low impedance of the air in the external auditory canal to the high impedance of the cochlear fluids. In other words, the middle ear is an impedance transformer. Without this function, much of the sound energy would be reflected. As shown in Fig. 9, when the tympanic membrane vibrates, the ossicles basically rotate around the axis between the anterior malleal ligament and the posterior incudal ligament, and the umbo and stapes have a pistonlike movement.<sup>6,7</sup> The area of the tympanic membrane is much larger than that of the stapes footplate. The forces collected by the tympanic



**Figure 8** Perspective plots of the displacement distribution of the left tympanic membrane vibrations when the displacement at each point reaches its maximum value: (a) frequency  $f = 1.0$  kHz and sound pressure level SPL = 85 dB, (b)  $f = 2.5$  kHz and SPL = 70 dB, (c)  $f = 3.0$  kHz and SPL = 75 dB, and (d)  $f = 4.0$  kHz and SPL = 75 dB. At the frequency of 1.0 kHz, the whole tympanic membrane vibrates in phase. The maximum displacement amplitude is about 30 nm. At the frequency of 2.5 kHz, the tympanic membrane has two local maxima, one in the posterior portion and the other in the inferior portion. The number of the peaks increases and the vibration mode becomes complicated with an increase in the frequency. [From Wada et al.<sup>5</sup> Copyright © 2002 by The Acoustical Society of America (ASA). Reprinted by permission of American Institute of Physics (on behalf of ASA).]



**Figure 9** Dynamic behavior of the middle ear. Arrows indicate the directions of the movements. The ratio of the area of the tympanic membrane to that of the stapes is 17 : 1, and the ratio of the arm of the malleus to that of the incus is 1.3 : 1.0.

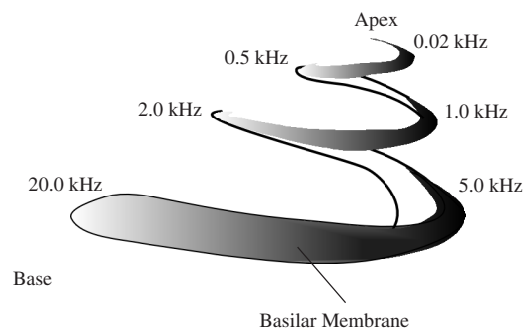


**Figure 10** Traveling waves on the basilar membrane obtained from the finite element method model: (a) input stimulus frequency  $f = 6.0$  kHz, and (b)  $f = 2.0$  kHz. Traveling waves on the basilar membrane have a peak near the base when high-frequency sound enters the cochlea, while low-frequency sound develops the traveling waves on the basilar membrane, which have a peak near the apex.

membrane, therefore, increase the pressure at the oval window. The arm of the malleus is larger than that of the incus, and this produces leverage, which increases the pressure and decreases the velocity at the stapes. By this mechanism, more than 30% of the sound energy reaches the cochlea.

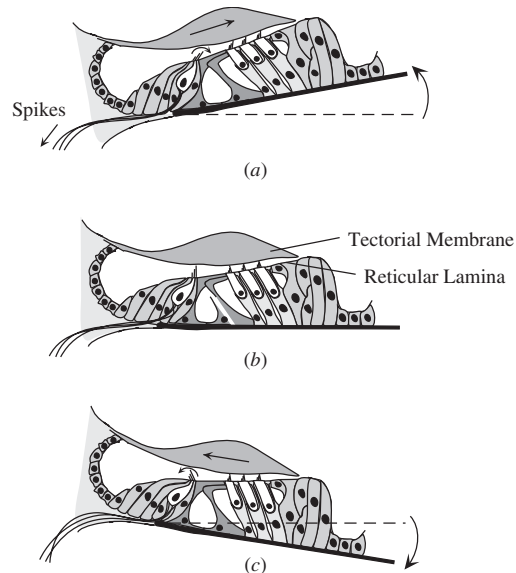
##### 5 COCHLEAR FUNCTION: TRAVELING WAVES ALONG THE COCHLEAR PARTITION, THE MECHANO-RECEPTOR-TRANSDUCTION ROLE OF HAIR CELLS, RECENT DISCOVERY OF HAIR CELL MOTILITY, AND THE "COCHLEAR AMPLIFIER" AND OTOACOUSTIC EMISSIONS

Vibrations of the stapes generate movement of the cochlear fluids that interacts with the basilar membrane, the stiffness of which decreases from base to



**Figure 11** Place-characteristic frequency map for humans. High- and low-frequency components of sound are analyzed in the basal and apical regions of the cochlea, respectively.

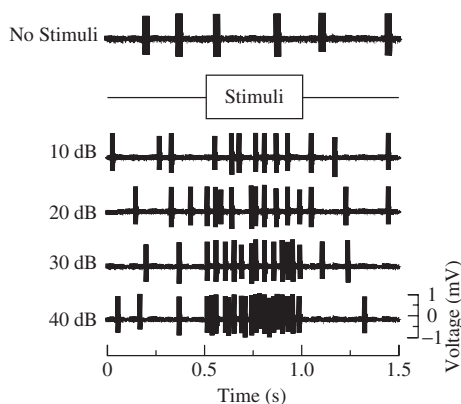
apex. This interaction produces progressive traveling waves on the basilar membrane,<sup>8</sup> which are similar to waves beating upon a seashore. Figure 10 depicts these traveling waves.<sup>9</sup> When sound is transmitted to the basilar membrane, the position of the maximum displacement amplitude of its vibration is related to the frequency of the sound. In other words, each position along the basilar membrane has a maximum displacement amplitude at a specific frequency called the characteristic frequency. Figure 11 is a frequency map for



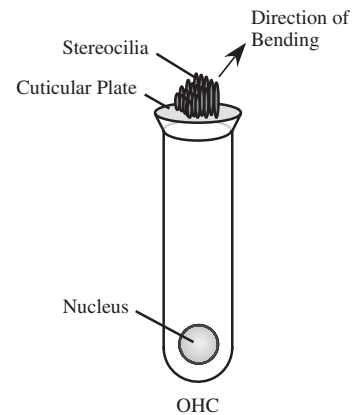
**Figure 12** Vibration mode of the organ of Corti: (a) displacement toward the scala vestibuli, (b) resting position, and (c) displacement toward the scala tympani. The inner hair cell stereocilia are deflected by the flow of fluid caused by shear motion between the tectorial membrane and the reticular lamina. [From Wada et al.<sup>11</sup> Copyright © 2002 by Elsevier. Reprinted by permission of Elsevier.]

humans showing characteristic frequencies at different positions in the ear.<sup>10</sup> As shown in Fig. 12, when sound enters the ear, the organ of Corti, which sits on the basilar membrane, undergoes a rocking motion. Although the details of cochlear operation are unclear, one possible mechanism is that basilar membrane displacement toward the scala vestibuli produces shear motion between the tectorial membrane and the reticular lamina and induces the flow of fluid in the direction of the arrow, which leads to the deflection of the free-standing inner hair cell stereocilia in the same direction as the flow.<sup>11</sup> This deflection induces the opening of ion channels and an influx of ions into the inner hair cell, thus releasing the transmitter. As a result, pulses are generated in the auditory nerve fibers, as shown in Fig. 13. Because of this mechanism, we can hear sound.

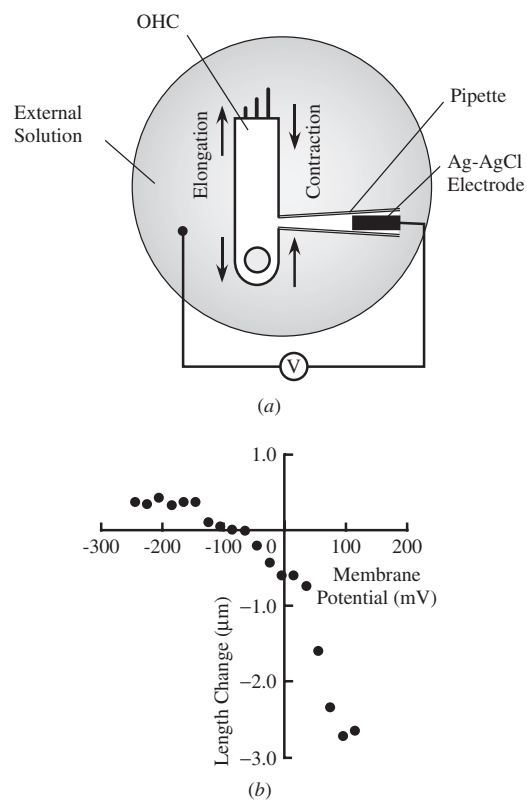
As depicted in Fig. 14, the mammalian outer hair cell is cylindrical shaped with a radius of 4 to 5  $\mu\text{m}$  and a length of 30 to 90  $\mu\text{m}$ . It is capped by the cuticular plate with stereocilia at one end and by the synaptic membrane at the other end. When the stereocilia bend in the direction of the arrow,  $\text{K}^+$  ions flow into the cell and depolarize the membrane potentials. At the same time, the outer hair cell contracts. By contrast, when the stereocilia bend in the direction opposite that of the arrow, the membrane potentials are hyperpolarized and the outer hair cell elongates.<sup>12</sup> Figure 15 depicts an experiment where, instead of bending stereocilia, intracellular potentials are changed by the whole-cell voltage-clamped technique. Experiments reveal that the input-output function of the outer hair cell is not expressed by a straight line but a curved one, that is, the function is nonlinear, which is responsible for compressive nonlinear responses of the basilar membrane<sup>13</sup> and the cochlea.<sup>14</sup> Moreover, the outer hair cells are under efferent control.<sup>15</sup>



**Figure 13** Response in the auditory nerve fiber. The upper waveform is an example of spontaneous activity. When a stimulus tone is delivered to the external auditory canal, the spike rate rises with an increase in the stimulus level.



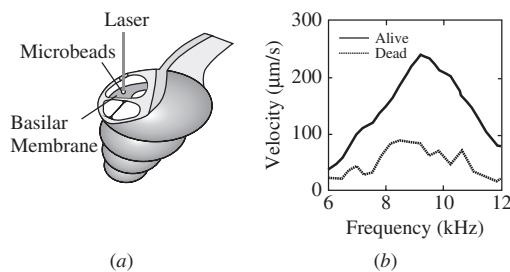
**Figure 14** Schematic diagram of the outer hair cell. The polarity is the same as that of Fig. 12. The cell is capped by the cuticular plate with stereocilia, which have a V- or W-shaped formation.



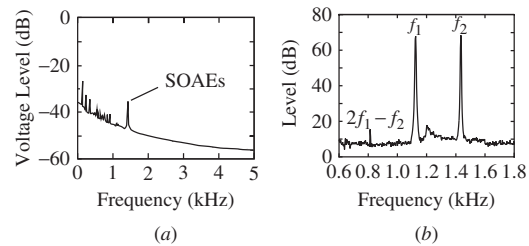
**Figure 15** Measurement of outer hair cell motility. (a) Whole-cell voltage clamp technique. To elicit mechanical movements of the outer hair cells, step and sinusoidal voltage stimuli are given to the isolated outer hair cells. (b) Length change of the outer hair cell in response to step voltage stimuli. The positive and negative directions show cell elongation and contraction, respectively.

As shown in Fig. 12, when the organ of Corti is deflected toward the scala vestibuli, the outer hair cell stereocilia bend due to the shear motion between the tectorial membrane and the reticular lamina because the tallest outer hair cell stereocilia adhere to the tectorial membrane. Simultaneously, the outer hair cells contract. Deflection of the organ of Corti toward the scala tympani leads to elongation of the outer hair cells. This repeated contraction and elongation of the outer hair cells, that is, the motility of the outer hair cells, magnifies the deflection of the organ of Corti. To confirm this cochlear amplification, an attempt was made to directly measure the basilar membrane vibrations in both living and dead guinea pigs by a laser Doppler velocimeter.<sup>16</sup> Figure 16 clearly shows that amplification of the basilar membrane vibrations occurs when an animal is alive. The magnified deflection of the organ of Corti leads to increases in the movement of the fluids in the space near the stereocilia of the inner hair cells and in the deflection of the inner hair cell stereocilia. Owing to the mechanism mentioned above, our auditory system is characterized by high sensitivity, sharp tuning, and compressive nonlinearity.<sup>17–19</sup>

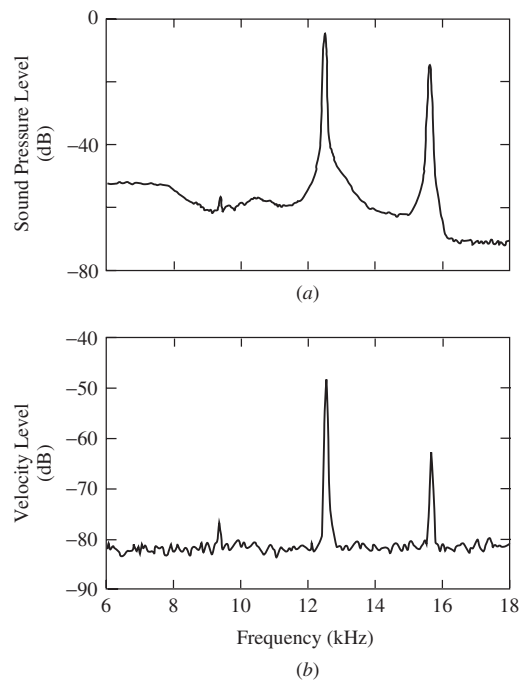
Recently, an interesting phenomenon, termed otoacoustic emissions, that is, sound that comes from the healthy ear, was discovered.<sup>20</sup> Otoacoustic emissions are low-intensity sound generated within the normal cochlea and emitted to the external auditory canal, either spontaneously or in response to acoustical stimulation. Figure 17 shows examples. As shown in Fig. 18, simultaneous measurement of distortion product otoacoustic emissions and basilar membrane velocity was carried out.<sup>16</sup> Clear peaks can be seen on both the spectrograms of the acoustical and basilar membrane velocity measurement at  $f = 2f_1 - f_2 = 9.40$  kHz. This result confirms that otoacoustic emissions sensitively reflect the dynamic behavior of the basilar membrane. The origin of otoacoustic emissions is thought



**Figure 16** Direct measurement of basilar membrane vibrations in a guinea pig. (a) Measurement procedure. A hole with a diameter of 0.5 mm is opened at the bony wall of the cochlea, and glass microbeads with a diameter of 20  $\mu\text{m}$  are placed on the basilar membrane in order to increase reflections of the laser beam. (b) The basilar membrane velocity responses to periodic tone. SPL = 75 dB. The basilar membrane vibrations are amplified when an animal is alive.



**Figure 17** Examples of otoacoustic emissions. (a) Spontaneous otoacoustic emissions of a guinea pig. Narrow-band signal at 1.43 kHz disappears 50 s after the respirator is stopped and reappears 2 min after the end of hypoxia. (b) Distortion-product otoacoustic emissions of a human. When two primary stimuli at levels  $\text{SPL}_1 - \text{SPL}_2 = 70$  dB and  $f_1 = 1125$  Hz and  $f_2 = 1434$  Hz are given to the external auditory canal, a cubic distortion product at the frequency  $2f_1 - f_2 = 816$  Hz is detected. It is believed that the nonlinear characteristics of the outer hair cell motility are responsible for generating such distortion. Interestingly, the level of the cubic distortion is greatest when the frequency ratio among  $2f_1 - f_2$ ,  $f_2$ , and  $f_1$  is equal to that of a chord, e.g., do, mi, and so.



**Figure 18** Frequency analysis of the outputs: (a) acoustical signal, and (b) basilar membrane velocity. Stimulus levels  $\text{SPL}_1$  and  $\text{SPL}_2$  of the primaries were 75 and 65 dB, respectively, and stimulus frequencies were  $f_1 = 12.55$  kHz,  $f_2 = 15.70$  kHz and  $2f_1 - f_2 = 9.40$  kHz. Peaks are clearly seen in both the acoustical signal and basilar membrane velocity at 9.40 kHz. [From Wada et al.<sup>16</sup> Copyright © 1997 by World Scientific Publishing. Reprinted by permission of World Scientific Publishing.]

to be the motility of the outer hair cells.<sup>21</sup> Recently, this technique has been applied to neonatal hearing screening.<sup>22</sup>

## 6 BRIEF SUMMARY OF CENTRAL AUDITORY NERVOUS SYSTEM: ANATOMY AND FUNCTION

Figure 19 shows the ascending auditory pathways. Although their functions remain unclear, some of them are introduced as follows: The cochlear nucleus is comparable to a switchboard and distributes auditory information to several different areas in the auditory pathways; the nucleus of the superior olive compares differences in the timing and loudness of the sound in each ear, and this function is essential for determining the location of sound; the inferior colliculus analyzes changes in the spectrum of sound such as amplitude and frequency modulation and contributes to the quality of sound.<sup>23</sup>

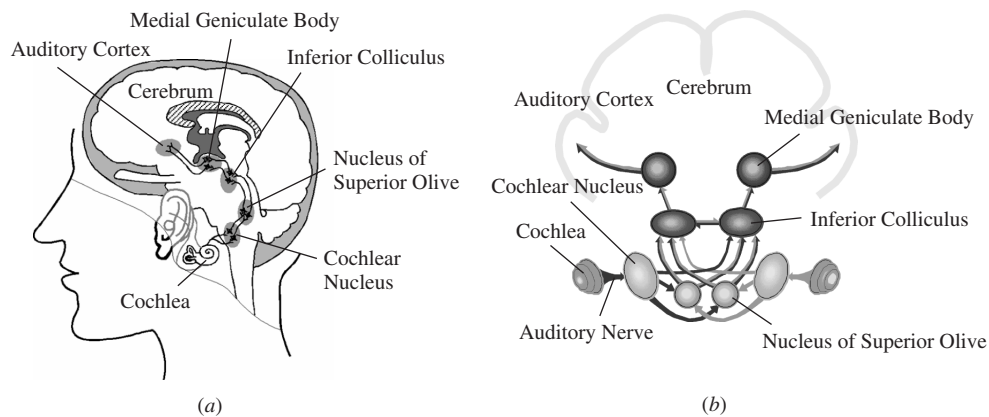
Efferent auditory pathways parallel the afferent pathways and descend from the cortex to the hair cells.

Although their functions are still not well understood, they are thought to improve the detection of signals in noise, protect our auditory system from noise damage, and be involved in attention.<sup>24</sup>

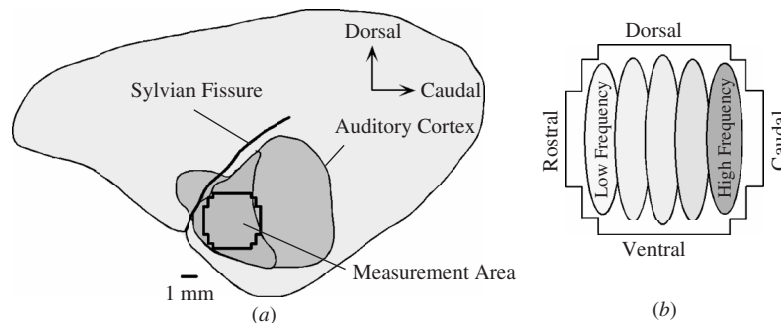
As displayed in Fig. 20, an impressive feature of the auditory cortex is its tonotopic organization, that is, information about the vibrations at different locations along the basilar membrane is relayed to the auditory cortex by fibers. Although the general functions of the auditory cortex are still uncertain, it is particularly sensitive to transients in acoustical signals and thus is considered to be necessary for short-term memory and the analysis of complex sound.<sup>25</sup>

## 7 NOISE-INDUCED HEARING LOSS

Noise-induced hearing loss is correlated with noise exposure and is the by-product of modernization. Exposure to moderate loud noise causes temporal hearing loss, which is later recovered. By contrast, exposure to severe loud noise causes permanent hearing loss. There is a consensus that the risk of

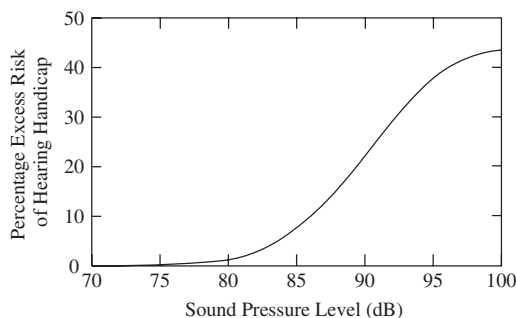


**Figure 19** Auditory pathways of the brainstem: (a) lateral view and (b) anterior view. Fibers from the cochlea ascend to the cochlear nucleus, the nucleus of the superior olive, the inferior colliculus, and the medial geniculate body, and terminate in the auditory cortex.

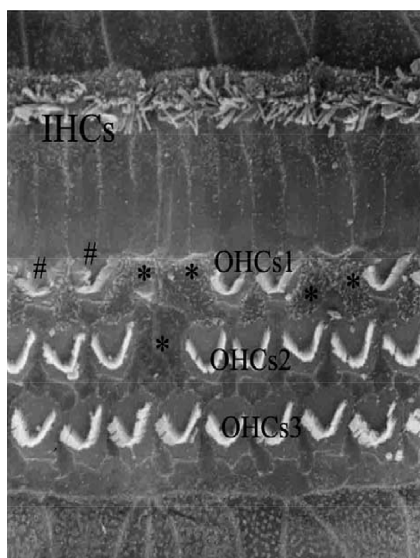


**Figure 20** Tonotopic organization of the auditory cortex in guinea pigs: (a) measurement area, and (b) schematic representation of the layout of the isofrequency areas. Low and high best frequencies are represented rostrally and caudally, respectively, and isofrequency lines are organized at right angles to the line showing the increase in frequency.



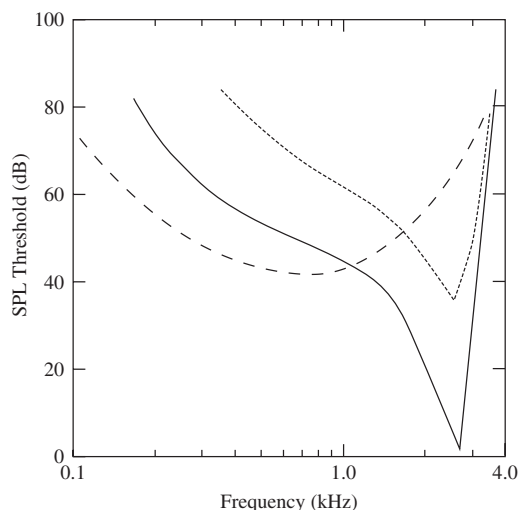


**Figure 21** Excess risk as a function of sound pressure level for subjects 65 years of age with an exposure duration of 45 years. Excess risk is defined as the percentage of individuals with hearing handicap among individuals exposed to daily 8-h occupational noise exposure. [From Prince et al.<sup>28</sup> Copyright © 1997 by The Acoustical Society of America (ASA). Reprinted by permission of American Institute of Physics (on behalf of ASA).]



**Figure 22** Scanning electron microscope study of missing and disarrayed outer hair cell stereocilia of the guinea pig after noise exposure at an SPL of 100 dB SPL for 8 h per day for 3 consecutive days: \*, missing; #, disarrayed. Not only sporadic missing outer hair cell stereocilia but also disarrayed outer hair cell stereocilia are observed. By contrast, no loss of the inner hair cell stereocilia is apparent. [From Hou et al.<sup>30</sup> Copyright © 2003 by Elsevier. Reprinted by permission of Elsevier.]

noise-induced hearing loss significantly increases with chronic exposure to noise above A-weighted 8-h time-weighted average sound pressure level of 85 dB (Fig. 21).<sup>26–28</sup> The degree of hearing loss depends not only on the intensity of the noise but also on



**Figure 23** Relationship between the tuning curve of auditory nerve fibers and the damage of outer and inner hair cells. —, both cells are intact; ---, total loss of the outer hair cells; ···, disarray of the inner hair cell stereocilia. Damage to the outer hair cells results in both elevation of threshold and loss of the tuning-curve tip. On the contrary, damage to the inner hair cell stereocilia results in only elevation of the threshold.

the duration of noise exposure. It also has individual variations.<sup>29</sup>

When sensory cells are exposed to moderate noise, the stereocilia of the outer hair cells are more easily damaged than those of the inner hair cells, which is shown in Fig. 22.<sup>30</sup> Furthermore, severe noise destroys the hair cells. As shown in Fig. 23, high sensitivity and sharp tuning of our hearing are lost when the outer hair cells are damaged, while sensitivity is reduced when stereocilia of the inner hair cells are partially damaged.<sup>31</sup> When the inner hair cells are completely destroyed, we become almost deaf.

## 8 CONCLUSIONS

An anatomical and functional overview of the human auditory system was herein presented, the main conclusions being as follows: High sensitivity and sharp tuning of our auditory system originate in the motility of the outer hair cells located in the organ of Corti in the cochlea, and the input–output function of the outer hair cell motility governs the nonlinearity of our auditory system. For those who would like to know more about our auditory system, well-written textbooks<sup>32–35</sup> are recommended. Furthermore, conference proceedings<sup>36–38</sup> are recommended for those who are interested in recent developments in this area.

## REFERENCES

1. W. M. Robinson and R. S. Dadson, A Redetermination of the Equal Loudness Relations for Pure Tones, *Br. J. Appl. Phys.*, Vol. 7, 1956, pp. 166–181.

2. R. L. Wegel, Physical Data and Physiology of Excitation of the Auditory Nerve, *Ann. Otol. Rhinol. Laryngol.*, Vol. 41, 1932, pp. 740–779.
3. L. Ulehlova, L. Voldrich, and R. Janisch, Correlative Study of Sensory Cell Density and Cochlea Length in Humans, *Hear. Res.*, Vol. 28, 1987, pp. 149–151.
4. F. M. Wiener and D. A. Ross, The Pressure Distribution in the Auditory Canal in a Progressive Sound Field, *J. Acoust. Soc. Am.*, Vol. 18, 1946, pp. 401–408.
5. H. Wada, M. Andoh, M. Takeuchi, H. Sugawara, T. Koike, T. Kobayashi, K. Hozawa, T. Gemma, and M. Nara, Vibration Measurement of the Tympanic Membrane of Guinea Pig Temporal Bones Using Time-Averaged Speckle Pattern Interferometry, *J. Acoust. Soc. Am.*, Vol. 111, 2002, pp. 2189–2199.
6. W. F. Decraemer and S. M. Khanna, New Insights into Vibration of the Middle Ear, in *The Function and Mechanics of Normal, Diseased and Reconstructed Middle Ears*, J. J. Rosowski and S. N. Merchant, Eds., Kluwer, The Hague, 2000, pp. 23–38.
7. T. Koike, H. Wada, and T. Kobayashi, Modeling of the Human Middle Ear Using the Finite-Element Method, *J. Acoust. Soc. Am.*, Vol. 111, 2002, pp. 1306–1317.
8. G. V. Békésy, *Experiments in Hearing*, McGraw-Hill, New York, 1960, pp. 452–455.
9. Wada Laboratory, Dynamic animation of the basilar membrane, available at [http://www.wadalab.mech.tohoku.ac.jp/FEM\\_BM-e.html](http://www.wadalab.mech.tohoku.ac.jp/FEM_BM-e.html), accessed February 14, 2007.
10. G. V. Békésy, *Experiments in Hearing*, McGraw-Hill, New York, 1960, pp. 441–443.
11. H. Wada, A. Takeda, and T. Kawase, Timing of Neural Excitation in Relation to Basilar Membrane Motion in the Basal Region of the Guinea Pig Cochlea During the Presentation of Low-Frequency Acoustic Stimulation, *Hear. Res.*, Vol. 165, 2002, pp. 165–176.
12. W. E. Brownell, C. R. Bader, D. Bertrand, and Y. de Ribaupierre, Evoked Mechanical Responses of Isolated Cochlear Outer Hair Cells, *Science*, Vol. 227, 1985, pp. 194–196.
13. L. Robles, M. A. Ruggero, and N. C. Rich, Basilar Membrane Mechanics at the Base of the Chinchilla Cochlea, *J. Acoust. Soc. Am.*, Vol. 80, 1986, pp. 1364–1374.
14. A. Cohen and M. Furst, Integration of Outer Hair Cell Activity in a One-Dimensional Cochlear Model, *J. Acoust. Soc. Am.*, Vol. 115, 2004, pp. 2185–2192.
15. E. Murugasu and I. J. Russell, The Effect of Efferent Stimulation on Basilar Membrane Displacement in the Basal Turn of the Guinea Pig Cochlea, *J. Neurosci.*, Vol. 16, 1996, pp. 1306–1317.
16. H. Wada, Y. Honnma, S. Takahashi, T. Takasaka, and K. Ohyama, Simultaneous Measurement of DPOAEs and Basilar Membrane Vibration by Acoustic Probe and Laser Doppler Velocimeter, in *Diversity in Auditory Mechanics*, E. R. Lewis et al., Eds., World Scientific, Singapore, 1997, pp. 284–290.
17. J. O. Pickles, *An Introduction to the Physiology of Hearing*, Academic, London, 1988, pp. 136–157.
18. C. D. Geisler, *From Sound to Synapse*, Oxford University Press, New York, 1998, pp. 125–138.
19. J. L. Goldstein, Auditory Nonlinearity, *J. Acoust. Soc. Am.*, Vol. 41, 1967, pp. 676–689.
20. D. T. Kemp, Stimulated Acoustic Emissions from within the Human Auditory System, *J. Acoust. Soc. Am.*, Vol. 64, 1978, pp. 1386–1391.
21. D. T. Kemp, Exploring Cochlear Status with Otoacoustic Emissions, the Potential for New Clinical Applications, in *Otoacoustic Emissions: Clinical Applications*, M. S. Robinette and T. J. Glatcke, Eds., Thieme Medical, New York, 2002, pp. 1–47.
22. B. A. Prieve, Otoacoustic Emissions in Neonatal Hearing Screening, in *Otoacoustic Emissions: Clinical Applications*, M. S. Robinette and T. J. Glatcke, Eds., Thieme Medical, New York, 2002, pp. 348–374.
23. J. O. Pickles, *An Introduction to the Physiology of Hearing*, Academic, London, 1988, pp. 163–204.
24. J. J. Guinan, Jr., Physiology of Olivocochlear Efferents, in *The Cochlea*, P. Dallos, A. N. Popper, and R. R. Fay, Eds., Springer, New York, 1996, pp. 435–502.
25. D. A. Hall, H. C. Hart, and I. S. Johnsrude, Relationships between Human Auditory Cortical Structure and Function, *Audiol. Neurotol.*, Vol. 8, 2003, pp. 1–18.
26. *Noise-Induced Hearing Loss*, American College of Occupational and Environmental Medicine, ACOEM Evidence-based Statement, 2002, available at <http://www.acoem.org/guidelines.aspx?id=846#>, accessed February 14, 2007.
27. *American National Standard: Determination of Occupational Noise Exposure and Estimation of Noise-Induced Hearing Impairment*, ANSI S3.44–1996, American National Standards Institute, New York, 1996.
28. M. M. Prince, L. T. Stayner, R. J. Smith, and S. J. Gilbert, A re-examination of Risk Estimates from the NIOSH Occupational Noise and Hearing Survey (ONHS), *J. Acoust. Soc. Am.*, Vol. 101, 1997, pp. 950–963.
29. A. R. Møller, *Hearing*, Academic, San Diego, 2000, pp. 404–419.
30. F. Hou, S. Wang, S. Zhai, Y. Hu, W. Yang, and L. He, Effects of  $\alpha$ -Tocopherol on Noise-Induced Hearing Loss in Guinea Pigs, *Hear. Res.*, Vol. 179, 2003, pp. 1–8.
31. M. C. Liberman and L. W. Dodds, Single-Neuron Labeling and Chronic Cochlear Pathology. III. Stereocilia Damage and Alterations of Threshold Tuning Curves, *Hear. Res.*, Vol. 16, 1984, pp. 55–74.
32. J. D. Durrant and J. H. Lovrinic, *Bases of Hearing Science*, Williams & Wilkins, Baltimore, MD, 1984.
33. J. O. Pickles, *An Introduction to the Physiology of Hearing*, Academic, London, 1988.
34. P. Dallos, A. N. Popper, and R. R. Fay, Eds., *The Cochlea*, Springer, New York, 1996.
35. C. D. Geisler, *From Sound to Synapse*, Oxford University Press, New York, 1998.
36. E. R. Lewis et al., Eds., *Diversity in Auditory Mechanics*, World Scientific, Singapore, 1997.
37. H. Wada et al., Eds., *Recent Developments in Auditory Mechanics*, World Scientific, Singapore, 2000.
38. A. W. Gummer, Ed., *Biophysics of the Cochlea*, World Scientific, Singapore, 2003.

# CHAPTER 21

## HEARING THRESHOLDS, LOUDNESS OF SOUND, AND SOUND ADAPTATION

**William A. Yost**  
Parmly Sensory Sciences Institute  
Loyola University  
Chicago, Illinois

### 1 INTRODUCTION

This chapter covers three important aspects of auditory perception: thresholds of hearing, loudness, and sound adaptation. Thresholds of hearing represent an estimate of the softest sounds the average human can detect, and these thresholds form the basis of the fundamental measure of hearing loss, the audiogram. Thresholds of hearing vary as a function of signal frequency and signal duration. Changes in many different physical aspects of sound may lead to the perception that the sound's loudness has changed. Loudness level measured in phons and based on equal loudness contours and loudness measured in sones using subjective scaling procedures are the two most common measures of subjective loudness. Sounds that are presented for long periods exhibit several perceptual phenomena including threshold shifts and various forms of adaptation. Long-duration, intense sounds can cause either a temporary or a permanent loss of hearing as measured by an increase in the threshold for detecting sound. The loudness or other perceptual aspects of sound can change as a function of prior exposure to sounds of long duration leading to various forms of auditory adaptation.

### 2 THRESHOLDS OF HEARING

A fundamental measure of the auditory system is the determination of the softest sounds that a person can detect. The threshold of hearing is measured as a function of the frequency of pure tones presented to subjects asked to detect tones that are presented at levels that are just detectable in a quiet and calibrated test environment. Thresholds of hearing are often used to determine a test subject's hearing loss and the frequency region in which that hearing loss occurs. When thresholds of hearing are used to determine hearing loss, the threshold measurements are often referred to as the audiogram.

In general, thresholds of hearing are measured by determining the sound pressure level of a tone presented at a specified frequency (often octaves of 125 Hz) that a subject indicates renders the tone just barely noticeable or detectable. The behavioral method for obtaining thresholds of hearing, the methods for calibrating the sound pressure level presented to the subject, and the hearing thresholds have been standardized [see American National Standards Institute (ANSI) and the International Organization

for Standardization (ISO) standards listed in the reference section]. The test tones can be presented over headphones of different types (e.g., supraaural and insert) or from a loudspeaker in the free field. A supraaural headphone has a cushion that fits over the pinna and the headphone speaker rests on the outside of the outer-ear canal. An insert phone has its earphone loudspeaker located within the outer-ear canal, usually in a pliable mold that seals the outer-ear canal. In all cases accurate estimates of the thresholds of hearing require that the test environment be as noise free as possible and conform to the specifications of the ANSI standard for American National Standard Maximum Permissible Ambient Noise Levels for Audiometric Test Rooms (1999).

If the thresholds of hearing are measured in the free field when the tones are presented from a loudspeaker, the thresholds are referred to as minimal audible field (MAF) thresholds. For a MAF estimate of the thresholds of hearing, the loudspeaker is located on the same plane as the listener's pinna, directly in front of the listener, 1 m from the location of the listener's pinna, and the listener uses both ears (binaural listening) in the detection task. The level of the tone at each frequency is calibrated using a microphone placed at the location of the listener's tympanic membrane (eardrum), but with the listener not in the room.

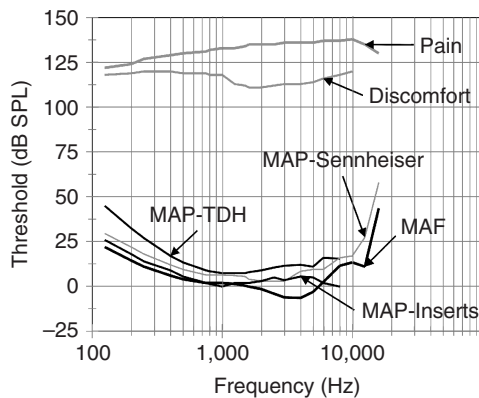
If the thresholds are measured via headphone presentations, then the thresholds are referred to as minimal audible pressure (MAP) thresholds. The level of the tones in the MAP procedure is calibrated by measuring the sound pressure level at each test frequency within an acoustic coupler fitted to the headphone. The acoustic coupler is standardized [ANSI 3.7–1995 (R2003), ANSI 3.25–1989 (R2003)] to provide a reasonable approximation of the acoustic properties of the outer ear so that the sound pressure level provided by the headphone is that which would occur at the tympanic membrane of an average listener. Acoustic couplers for supraaural phones measure the sound pressure in a volume of 6 mL, which is the approximate average volume of the outer-ear canal. Acoustic couplers for insert phones measure the sound pressure level in a volume of 2 mL, since 2 mL is the approximate average ear canal volume between the tip of the insert earphone and the tympanic membrane. Several different headphone and acoustic coupler combinations can be used to calibrate thresholds in MAP procedures. Such thresholds are referred to as



reference equivalent threshold sound pressure levels (RETSPLs).

A standardized psychophysical procedure is required to obtain accurate estimates of thresholds [ANSI 3.21–1978 (R1997)]. The accepted method is a method of limits procedure in which the level of the tone starts well above the threshold level, and then the level is decreased until the listener indicates that the tone is no longer detectable. Then the tonal level is increased and decreased from this initial estimate of threshold to estimate the final threshold level that would yield the tone as detectable 50% of the time. This procedure is repeated for each tonal frequency that is tested. Several other psychophysical procedures have also been used to measure thresholds of hearing [ANSI 3.21–1978 (R1997)].

Figure 1 and Table 1 present average standardized thresholds of hearing for listeners with normal hearing for the MAF and MAP procedures (ANSI S3.6–1996). The thresholds are expressed as MAF or MAP RETSPL thresholds of the sound pressure level (SPL, dB). The reference sound pressure for measuring decibels of sound pressure level is 20  $\mu$ Pa. Thus, as can be seen in Fig. 1 and Table 1, thresholds of hearing are lowest in the frequency region between 500 and 4000 Hz at about 0 dB, so that 20  $\mu$ Pa is approximately the smallest sound pressure detectable by the human auditory system. At this small pressure, it has been estimated that the tympanic membrane



**Figure 1** Thresholds of hearing in decibels of sound pressure level (dB SPL) are shown as a function of frequency (Hz) for six conditions: RETSPL minimal audible field (MAF) thresholds, RETSPL-MAP thresholds for a supraaural phone and 6-mL coupler, RETSPL-MAP thresholds for a supraaural phone and an artificial ear, RETSPL-MAP thresholds for an insert phone and a Zwischlocki coupler, thresholds for pain, and thresholds for discomfort. The RETSPL measures are from ANSI 3.6–1996. The thresholds for pain and discomfort represent estimates of the upper limits of sound pressure level that humans can tolerate. See Table 1 for additional details about the headphones and couplers used for these thresholds. (Based on ANSI standards and adapted from Yost.<sup>12</sup> Reprinted by permission.)

**Table 1** Thresholds of Audibility for a Number of Testing Condition

Frequency (Hz)	MAF <sup>a</sup>	Thresholds—RETSPL (dB SPL)		
		Supra-aural <sup>b</sup>	Circumaural <sup>c</sup>	Insert <sup>d</sup>
125	22	45	29.5	26
200	14.5	32.5	—	18
250	11	27	18	14
400	6	17	12	9
500	4	13.5	9.5	5.5
750	2	9	6.5	2
800	2	8.5	—	1.5
1,000	2	7.5	6.5	0
1,250	1.5	7.5	—	2
1,500	0.5	7.5	5.5	2
1,600	0	8	—	2
2,000	−1.5	9	3	3
2,500	−4	10.5	—	5
3,000	−6	11.5	3	3.5
4,000	−6.5	12	8.5	5.5
5,000	−3	11	9.5	5
6,000	2.5	16	9.5	2
8,000	11.5	15.5	16	0
10,000	13.5	—	21.5	—
12,500	11	—	27.5	—
16,000	43.5	—	58	—

<sup>a</sup> Binaural listening, free-field, 0° incidence.

<sup>b</sup> TDH type.

<sup>c</sup> Sennheiser HDA2000, IEC 318 with type 1 adaptor.

<sup>d</sup> HA-2 with rigid tube.

Source: From American National Standard ANSI 3.6–1996-Specifications for Audiometers.

is displaced a distance equal to approximately the diameter of a hydrogen atom. The thresholds of hearing indicate that human listeners can detect tones over the frequency region from approximately 20 to 20,000 Hz, but the thresholds are elevated for low and high frequencies relative to those in the middle frequencies within this range. The loss of sensitivity at the low and high frequencies is partially attributable to the transfer function of the outer and middle ears as well as limitations placed on the transduction of sound pressure and vibration into neural impulses that occurs within the inner ear.

Figure 1 and Table 1 indicate that the actual thresholds of hearing differ depending on how the tones are presented, that is, if they are presented over loudspeakers or from different headphone types. These differences exist despite the attempt to provide calibration procedures that might be thought of as ensuring that the thresholds represent the actual sound pressure level being delivered to the auditory system (i.e., to the tympanic membrane). However, differences in the measured thresholds exist despite the calibration procedures. Almost all of the differences in thresholds of hearing obtained across the various MAF and MAP procedures can be explained by taking into account the diffraction of sound around the head and pinna that occurs in several of the procedures and the exact

resonant and impedance properties of the outer ear.<sup>1</sup> Making exact estimates of the thresholds of hearing at frequencies higher than approximately 8000 Hz are complicated by the resonance properties of the outer-ear canal.

The thresholds of hearing also depend on the duration of the tone being presented. The thresholds in Fig. 1 and Table 1 represent thresholds in dB SPL for tones whose durations are 500 ms or longer. The thresholds of hearing increase as the duration of the tones decrease, and the exact nature of the increase in the thresholds of hearing with decreasing duration is frequency specific. For tonal frequencies less than approximately 1000 Hz, thresholds of hearing increase about 10 dB for each 10-fold decrease in tone duration below about 200 to 300 ms (i.e., maintaining the tonal level at threshold at approximately constant energy). However, the rate of increase in thresholds as duration decreases for tones whose frequencies are greater than 1000 Hz is less than that for tones whose frequencies are less than 1000 Hz.<sup>2</sup>

As the sound pressure level increases to large values human listeners will experience discomfort or pain, indicating that the levels are reaching the upper limit that the auditory system can tolerate. The upper curves in Fig. 1 indicate various estimates of the upper limit of audibility such that tones presented at these frequencies and levels will produce pain or discomfort. The decibel difference between the thresholds of hearing and the upper limits of audibility suggest that the dynamic range for hearing can be as large as 130 dB in the 1000-Hz region of the audible spectrum, and the dynamic range decreases as frequency increases or decreases from this region.

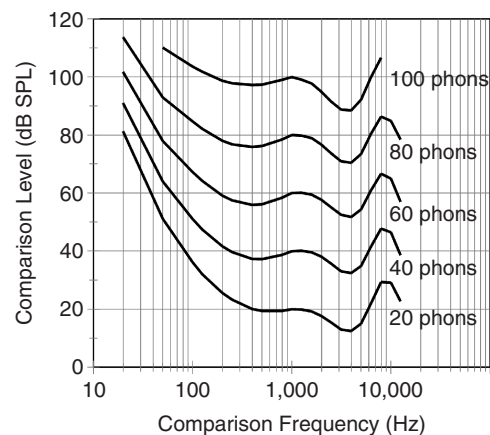
The auditory system can be stimulated either via sound traveling through the outer-ear canal and middle ear to the inner ear or via sound causing the skull to vibrate, which in turn stimulates inner-ear structures to signal the presence of sound. Thus, vibration of the skull (bone vibration), which bypasses the outer and middle ears, can lead to the sensation of sound. Since sound produced by bone vibration bypasses the normal air conduction means of delivering sound to the inner ear, differences between the thresholds of hearing for air conduction as opposed to bone conduction are used to diagnosis problems in the outer and, especially, the middle ear. Just as there are standardized methods and thresholds for air-conducted sound, so are there standardized methods and thresholds for bone-conducted sound [ANSI 3.6–1996 and ANSI 3.13–1987 (R2002)]. The level of sounds necessary to yield bone-conducted thresholds are considerably higher (60 dB or higher) than those obtained for air-conducted thresholds.

### 3 LOUDNESS OF SOUND

As the level of a sound changes, one usually reports that its loudness has changed. The standard definition of loudness [ANSI 3.20–1995 (R2003)] is: “Loudness is that attribute of auditory sensation in terms of which sounds may be ordered on a scale extending from soft to loud.” As such loudness is a subjective

attribute of a sound’s magnitude, as opposed to sound pressure level that is an objective or physical measure of sound magnitude. While the loudness of a sound varies as a function of changes in sound pressure level, loudness can also vary when other physical properties of a sound are changed such as frequency or duration. That is, subjective sound loudness is correlated with sound pressure level, but also with many other physical aspects of sound (e.g., frequency, bandwidth, duration).

Loudness is measured in two ways: as loudness level in phons and loudness in sones. Loudness level is measured in a loudness matching procedure in which two sounds are presented: the standard sound, which is a 1000-Hz tone presented at a particular level expressed in dB SPL, and the comparison (test) sound, presented at a particular tonal frequency (or a noise presented with a particular bandwidth). The listener adjusts the level of the comparison sound so that it is judged equal in subjective loudness to that of the standard sound. Figure 2 shows a few standardized equal-loudness contours obtained using this loudness matching procedure for different levels of the standard, 1000-Hz tone, and different tonal frequencies of the comparison sound (ISO 226:2003 Acoustics). All comparison tones presented at the level and frequency shown on an equal-loudness contour are judged equal in loudness and equal in loudness to a 1000-Hz tone presented at the level shown on the equal-loudness contour. If the level of the 1000-Hz standard was 40 dB SPL, then all of the comparison tones shown on the equal-loudness contour are judged equally loud to this 40-dB, 1000-Hz standard tone, and they are defined as having a loudness level of 40 phons. Thus, the loudness level of a sound of  $x$  phons



**Figure 2** Equal loudness contours showing the level of a comparison tone required to match the perceived loudness of a 1000-Hz standard tone presented at different levels (20, 40, 60, 80, and 100 dB SPL). Each curve is an equal loudness contour. [Based on ISO standard (ISO 226:2003 Acoustics) and adapted from Yost.<sup>12</sup> Reprinted by permission.]

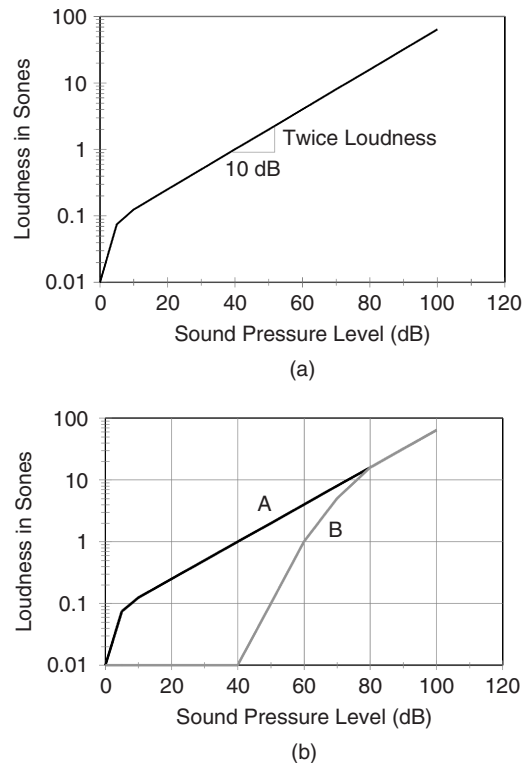
is the level of the sound required for that sound to be judged equally loud to a 1000-Hz tone presented at  $x$  dB SPL. A sound with a loudness level of 40 phons would be judged very soft. There are standard methods and calculations for determining the loudness level of tones and noises [ISO 226:2003 Acoustics and ANSI S3.4-1980 (R 1997)].

The 40-dB equal-loudness contour (i.e., 40-phon contour) is the basis of the weighting used in the definition of the A-weighted sound pressure level measure. If a sound is filtered by a filter whose transfer function is similar to the inverse of the 40-phon contour, the overall sound pressure level in decibels at the output of this filter when referenced to 20  $\mu$ Pa is defined as the A-weighted sound pressure level. That is, the overall level of a sound whose spectral components are weighted (filtered) so the high and low frequencies are attenuated as indicated by the inverse of the 40-phon equal-loudness contour known as the A-weighted sound pressure level. The 70-dB equal-loudness contour is used in the same way to determine the weightings for the C-weighted sound pressure level [see ANSI S1.8-1989 (R 2001)].

The loudness of a sound measured on the sone scale is determined from a loudness scaling procedure. While this procedure has not been standardized like that for the phon scale, the loudness of sounds has been measured in many different studies using different scaling procedures.<sup>3</sup> In a scaling procedure used to measure sones, a standard tone of 1000 Hz and 40 phons is compared to a comparison (test) sound. The listener in the loudness scaling task is asked to determine the level of the comparison sound in terms of a ratio, namely by judging the comparison sound as  $x$  times ( $0 \leq x \leq \infty$ ) as loud as the standard tone. By anchoring the resulting scale at 1 sone when the comparison sound is judged equal in loudness to the 40-phon standard, a numerical scale of loudness is obtained (see Fig. 3). Thus, a sound of  $y$  sones is one judged to be  $y$  times as loud as a sound that has a loudness of 40 phons (e.g., a sound with a loudness of 3 sones would be judged to be three times as loud as a 40-phon sound).

Above a given threshold value, there is a relatively linear relationship between log sones and level in decibels. The sone scale at 1000 Hz indicates that an increase or decrease in sound pressure level of 10 dB results in a judgment of that sound being twice or half as loud, respectively, that is, a doubling or halving of loudness equals an approximately 10-dB change in sound pressure level. In other contexts<sup>3,4</sup> the growth of loudness is expressed as a power function of sound intensity, for example,  $L = I^{0.3}$ , where  $L$  equals perceived loudness,  $I$  equals sound intensity (e.g., in  $\text{W}/\text{m}^2$ ), and the common exponent for such a loudness relationship is approximately 0.3.

When sounds are presented to both ears (sounds presented binaurally), loudness often increases over that measured when the sound is presented to only one ear. In this case, there is evidence for binaural loudness summation. Binaural loudness summation can vary from essentially no binaural summation up to 10 dB, depending on the stimulus and measurement conditions.<sup>5,6</sup>



**Figure 3** (a) Schematic depiction of loudness in sones of a 1000-Hz tone as a function of the level of the tone (dB SPL). The slope of the function indicates that approximately a 10-dB change in level is required to double loudness. 3.(b) Curve A represents the loudness curve from (a) curve B represents the perceived loudness of a 1000-Hz tone masked by a wideband noise (for a person with a hearing loss). Curve B with the steeper slope shows loudness recruitment. (Adapted from Yost<sup>12</sup> and Steinberg and Gardner.<sup>13</sup> Reprinted by permission)

#### 4 LOUDNESS RECRUITMENT

If a person has a hearing loss or is listening to a sound masked by other sounds, then the threshold for detecting that sound will be elevated as compared to that measured for a person without a hearing loss or in the absence of the interfering sounds. Yet, in these types of conditions the level of the sound judged to be painful or uncomfortable will be the same as that obtained for a person without a hearing loss or without the presence of interfering sounds. Thus, the growth of loudness between threshold and the upper limit of audibility as indicated by the thresholds for pain or discomfort will be steeper for the person with a hearing impairment or detecting tones in the presence of interfering sounds as compared to a person without a hearing loss or detecting a sound in the absence of interfering sounds (see Fig. 3). The increase in the slope of loudness in these circumstances is often referred to as "loudness recruitment" and most

people with a sensorineural hearing loss show such a recruitment of loudness.

Since the measurement of recruitment involves the determination of the thresholds of hearing, a theoretical issue concerning the slope of the recruitment function arises in terms of what the loudness of a sound is at its hearing threshold.<sup>7</sup> One argument is that the loudness of sound at its threshold is zero. However, other theoretical arguments and measurements suggest that while the loudness of a sound at its threshold is low, it is not exactly zero.<sup>7</sup>

## 5 PERMANENT AND TEMPORARY THRESHOLD SHIFTS

Long exposure to sound has several different effects on auditory function and on perception. Such exposure to sound can elevate the thresholds of hearing permanently or temporarily, or the exposure can influence the subjective loudness and perception of the sound or other sounds.

Exposure to very intense sounds or somewhat less intense sounds of long duration can cause an elevation of the thresholds of hearing after the intense sound has ceased. A permanent hearing loss results when these elevated thresholds become permanent. But even if exposure to loud sounds does not cause a permanent hearing loss or a permanent threshold shift (PTS), such exposures may lead to a temporary elevation of the thresholds of hearing or a temporary threshold shift (TTS). TTS can exist for just a few minutes after exposure to intense sound, or such threshold shifts can exist for days if not weeks. However, the hearing thresholds of someone experiencing TTS will eventually recover to the thresholds existing prior to the exposure, as long as the person is not exposed to other intense sounds in the intervening period. The length of recovery is directly related to the nature of the noise exposure in the recovery period.

With respect to PTS, there is a trade-off between the level of the exposing sound and its duration. The levels and durations that can cause auditory damage and, thus, lead to PTS are referred to as damage risk criteria (DRC). Table 2 indicates the DRC from the National Research Council's (NRC) Committee on Hearing, Bioacoustics, and Biomechanics (CHABA). The NRC-DRC indicates that if a person is exposed repeatedly (over the course of years) to sounds of these levels and duration, they will most likely experience PTS. Organizations such as the Occupational Safety and Health Administration (OSHA) use various DRCs to limit noise exposure in the workplace. PTS is usually associated with the loss of hair cells in the inner ear. Inner-ear hair cells transduce the pressure and vibrations of the inner ear into the neural-electrical signals used by the auditory system. Other standards have been generated to estimate the levels of sound that may lead to PTS [e.g., ISO 1999: 1990 and ANSI S3.44-1996 (R2001)].

Several variables affect the amount and duration of TTS that one experiences following loud sound exposure. The greatest amount of TTS occurs when the frequency of the sound used to measure TTS is the same or slightly higher than the frequency

**Table 2 Damage Risk Criteria (DRC) from the Committee on Hearing, Bioacoustics, and Biomechanics (CHABA) of the National Research Council (NRC)<sup>a,b</sup>**

Duration in Hours	A-weighted Sound Pressure Level
8	90
6	92
4	95
3	97
2	100
1	105
1/2	110
1/4 or less	115

<sup>a</sup> Repeated exposure to these sound pressure levels for these durations would lead to a permanent threshold shift.

<sup>b</sup> Note: When the daily noise exposure is composed of two or more periods of noise exposure at different levels, their combined effect should be considered, rather than the individual effect of each. If the sum of  $C_1/T_1 + C_2/T_2 + \dots + C_n/T_n$  exceeds unity, then the mixed exposure should be considered to exceed a permissible DRC.  $C_n$  indicates the total time exposure at a specified noise level, and  $T_n$  indicates the total time of exposure permitted at that level according to the DRC listed in the table. For instance, if one was exposed to 6 h ( $C_1$ ) at 95 dB and 2 h ( $C_2$ ) at 100 dB, the permissible time periods were 4 h ( $T_1$ ) and 2 h ( $T_2$ ). The sum is  $6/4 + 2/2 > 1.0$ , so this combined exposure exceeds the DRC.

of the exposing sounds. In general, the longer the exposing sound is, the greater the TTS is and the longer the recovery time from TTS. If one is exposed to a wideband sound, then most TTS occurs in the frequency region between 2000 and 6000 Hz, except when the exposure is at high levels and then TTS is greatest for all frequencies above about 2000 Hz. The occurrence of TTS is highly correlated with damage to various structures within the inner ear, but an exact cause of TTS is not known. Because of the difficulty of studying PTS directly in human subjects, measures of TTS are often used to infer or predict what type of sound exposures may cause permanent hearing loss.

## 6 LOUDNESS ADAPTATION

There are several perceptual effects that occur when one is exposed to an intense sound (but not a sound intense enough to produce TTS or PTS) for periods of many seconds to minutes. Loudness adaptation or perstimulatory fatigue occurs when the subjective loudness of a sound decreases as the exposure to the sound increases. That is, if one is exposed to a moderately intense sound for a few minutes, the loudness of the sound may fade. Such loudness adaptation is usually measured by asking listeners to match the loudness of a test sound to that of exposing sound that has been presented for several seconds or longer. The alternating binaural loudness balance (ABLB) procedure is a typical method used to measure loudness adaptation. The exposing sound at

one ear alternates over time with the comparison sound presented to the other ear. The listener adjusts the level of the test sound at one ear to match the subjective loudness of the exposing sound at the other ear. After presenting the exposing sound for several seconds or longer, the level of the test sound judged to be equal in loudness to the exposing sound decreases. The decrease in the test sound indicates that the loudness of the exposing sound decreases over time, suggesting that the auditory system adapts to the continuous presentation of the exposing sound. The decrease in loudness (i.e., loudness adaptation) ranges from a few decibels to 20 or more depending on the parameters of the exposing sound.

In some cases involving high-frequency tones (frequencies higher than 8000 Hz), loudness adaptation can be complete (leading to complete tone decay) in that after being exposed to the high-frequency tone for a few minutes the tone is no longer perceived as being present.<sup>8</sup> In such cases, any small change in the exposure is likely to restore the sensation of the high-frequency tone. In most other cases, the loudness of a sound may decrease from a few decibels to 20 or more as a function of loudness adaptation and the decrease in loudness is greater the longer the exposure (adaptation).

Such adaptation effects can determine the perceived loudness of sounds measured in different contexts. One such contextual effect on loudness is loudness recalibration.<sup>9</sup> Loudness recalibration can be either a perception of increased loudness (loudness enhancement) or decreased loudness (loudness assimilation) due to the context of other sounds presented around the same time as the sound whose loudness is being judged. For instance, if an intense tone of one frequency ( $f_1$ ) is followed by relatively less intense tones: one at the same frequency ( $f_1$ ) and another at a different frequency ( $f_2$ ), the resulting loudness perception is that the less intense tone at  $f_1$  is softer than if it had not been preceded by the intense sound.<sup>10</sup> This is like loudness adaptation in that intense sounds make less intense sounds softer, but less intense sounds do not make intense sounds louder. Such recalibration effects exist even when the recalibrating sounds are not of long duration (as occurs for perstimulatory fatigue). These contextual effects make the estimate of the loudness of sounds complicated in that loudness estimates appear to depend on the acoustical context in which a sound's loudness is to be judged.

Other forms of sound adaptation lead to auditory illusions. Such illusions occur when listeners are exposed to an adapting stimulus for a long period (a few minutes). Following the adaptation exposure, the listeners are presented a test stimulus, and the test stimulus is perceived as having attributes that are not a part of the physical stimulus. For instance, in the "enhancement effect/illusion"<sup>11</sup> the adapting stimulus is a wideband noise with a flat amplitude spectrum except in a narrow spectral region where there is a spectral notch (the flat-spectrum, wideband noise is filtered such that a narrow region of the spectrum is removed), and the test stimulus is the same wideband

noise presented with a flat-amplitude spectrum without the spectral notch (i.e., all spectral components within the bandpass of the noise are presented at the same average level). After a few minutes of exposure to the adapting stimulus with the spectral notch, a clear pitch corresponding to the region of the spectral notch is perceived as being present during the delivery of the following test stimulus, which has a flat amplitude spectrum. That is, the adapting exposure stimulus produced an illusory pitch in the test stimulus, since without such an adaptation process a flat-spectrum noise does not produce a pitch sensation, especially a sensation with a specific pitch.

Thus, one's perception of a particular sound can be significantly influenced by the acoustic context in which that sound occurs, especially when the contextual sounds have durations of seconds or minutes. Such effects of sound adaptation affect the auditory system's ability to process the sounds from the many possible sound sources in one's acoustic environment.

**Acknowledgment** This chapter was written with the assistance of grant support (Program Project Grant) from the National Institute on Deafness and Other Communication Disorders (NIDCD).

## REFERENCES

### STANDARDS REFERENCED

- ANSI S1.8-1989 (R 2001), *American National Standard Reference Quantities for Acoustical Levels*.
- ANSI S3.1-1999, *American National Standard Maximum Permissible Ambient Noise Levels for Audiometric Test Rooms*.
- ANSI S3.4-1980 (R 1997), *American National Standard Procedure for the Computation of Loudness of Noise*.
- ANSI S3.6-1996, *American National Standard Specification for Audiometers*.
- ANSI S3.7-1995 (R2003), *American National Standard Method for Coupler Calibration of Earphones*.
- ANSI 3.13-1987 (R2002), *American National Standard Mechanical Coupler for Measurement of Bone Vibrators*.
- ANSI 3.20-1995 (R2003), *American National Standard of Bioacoustical Terminology*.
- ANSI 3.21-1978 (R1997), *American National Standard Methods for Manual and Pure-Tone Threshold Audiometry*.
- ANSI 3.25-1989 (R2003), *American National Standard for an Occluded Ear Simulator*.
- ANSI S3.44-1996 (R2001), *American National Standard Determination of Occupational Noise Exposure and Estimation of Noise-Induced Hearing Impairment*.
- ISO 226:2003 **Acoustics**, *Normal Equal-Loudness-Level Contours*.
- ISO 1999:1990 **Acoustics**, *Determination of Occupational Noise Exposure and Estimate of Noise-Induced Hearing Impairment*.

### NUMBERED REFERENCES

1. W. A. Yost and M. C. Killion, Quiet Absolute Thresholds, in *Handbook of Acoustics*, M. Crocker, Ed., Wiley, New York, 1993.
2. C. S. Watson, C. S., and R. W. Gengel, Signal Duration and Signal Frequency in Relation to Auditory

- Sensitivity, *J. Acoust. Soc. Am.*, Vol. 46, 1969, pp. 989–997.
3. S. S. Stevens, *Psychophysics*, G. Stevens, Ed., Wiley, New York, 1975.
  4. S. S. Stevens, Neural Events and the Psychophysical Law, *Science*, Vol. 170, 1970, pp. 1043–1050.
  5. H. Fletcher and W. A. Munson, Loudness: Its Definition, Measurement, and Calculation, *J. Acoust. Soc. Am.*, Vol. 75, 1933, pp. 82–108.
  6. L. E. Marks, Binaural versus Monaural Loudness: Suprasummation of Tone Partially Masked by Noise, *J. Acoust. Soc. Am.*, Vol. 81, 1987, pp. 122–128.
  7. S. Buus, H. Müsch, and M. Florentine, On Loudness at Threshold, *J. Acoust. Soc. Am.*, Vol. 104, 1998, pp. 399–410.
  8. H. Huss and B. C. J. Moore, Tone Decay for Hearing Impaired Listeners with and without Dead Regions in the Cochlea, *J. Acoust. Soc. Am.*, Vol. 114, 2003, pp. 3283–3294.
  9. L. E. Marks, Recalibrating the Auditory System: The Perception of Loudness, *J. Exp. Psychol.*, Vol. 20, 1994, pp. 382–396.
  10. D. Mapes-Riordan and W. A. Yost, Loudness Recalibration as a Function of Level, *J. Acoust. Soc. Am.*, Vol. 106, 1999, pp. 3506–3511.
  11. N. F. Viemeister and S. P. Bacon, Forward Masking by Enhanced Components in Harmonic Complexes, *J. Acoust. Soc. Am.*, Vol. 71, 1982, pp. 1502–1507.
  12. W. A. Yost, *Fundamentals of Hearing: An Introduction*, 5th ed., Academic, San Diego, 2006.
  13. J. C. Steinberg and M. B. Gardner, The Dependence of Hearing Impairment on Sound Intensity, *J. Acoust. Soc. Am.*, Vol. 9, 1937, pp. 11–23.

# CHAPTER 22

## SPEECH PRODUCTION AND SPEECH INTELLIGIBILITY

Christine H. Shadle  
Haskins Laboratories  
New Haven, Connecticut

### 1 INTRODUCTION

Production of speech involves a chain of processes: cognitive, motor, aerodynamic, and acoustic. Perception of speech is similarly complex. In this chapter we discuss the difference between our underlying knowledge of a language (the phonology) and the articulatory and acoustic realization of it (the phonetics). We then describe vocal tract anatomy in order to make clear the phonetic classification of speech sounds by manner, place, and voicing.

In the source-filter theory of speech production, the output of sound sources is filtered by the resonant properties of the vocal tract. We describe the main sound sources: laryngeal vibration, which generates an efficient quasi-periodic source, and noise sources. Means of describing the filtering properties of the vocal tract by use of circuit analogs, and the limitations thereof, are then covered. Finally, acoustic cues for the major manner classes are described as well as the ways in which speech perception can be influenced by background noise or transmission distortion. Differences between intelligibility and quality, and means of testing speech samples for each, are covered briefly.

### 2 PHONETIC CLASSIFICATION OF SPEECH SOUNDS

Speech can be thought of as consisting of a meaningful sequence of sounds. The meaning derives from the cognitive processes in both speaker and listener; the sound is produced by issuing motor commands to control the shape of the vocal tract and the amount of air passing through it. The sounds that make up speech are classified according to the articulatory characteristics of their production, which affect their acoustic characteristics. The contrasts between sounds that can signal differences in meaning and the ways in which they can be combined are governed by phonology, our deep understanding of a language's sound structure. The minimal sound units that affect meaning are called phonemes. However, the articulatory gestures for adjacent phonemes overlap and cause the acoustic characteristics to overlap also, a phenomenon called coarticulation. The actual sounds that result are called phones, and study of the speech as opposed to language characteristics is called phonetics.<sup>1,2</sup>

Figure 1 shows a diagram of the lungs and vocal tract. Though the first use of these is for breathing, a person can deliberately control their lung pressure and the time-varying shape of their vocal tract in order to

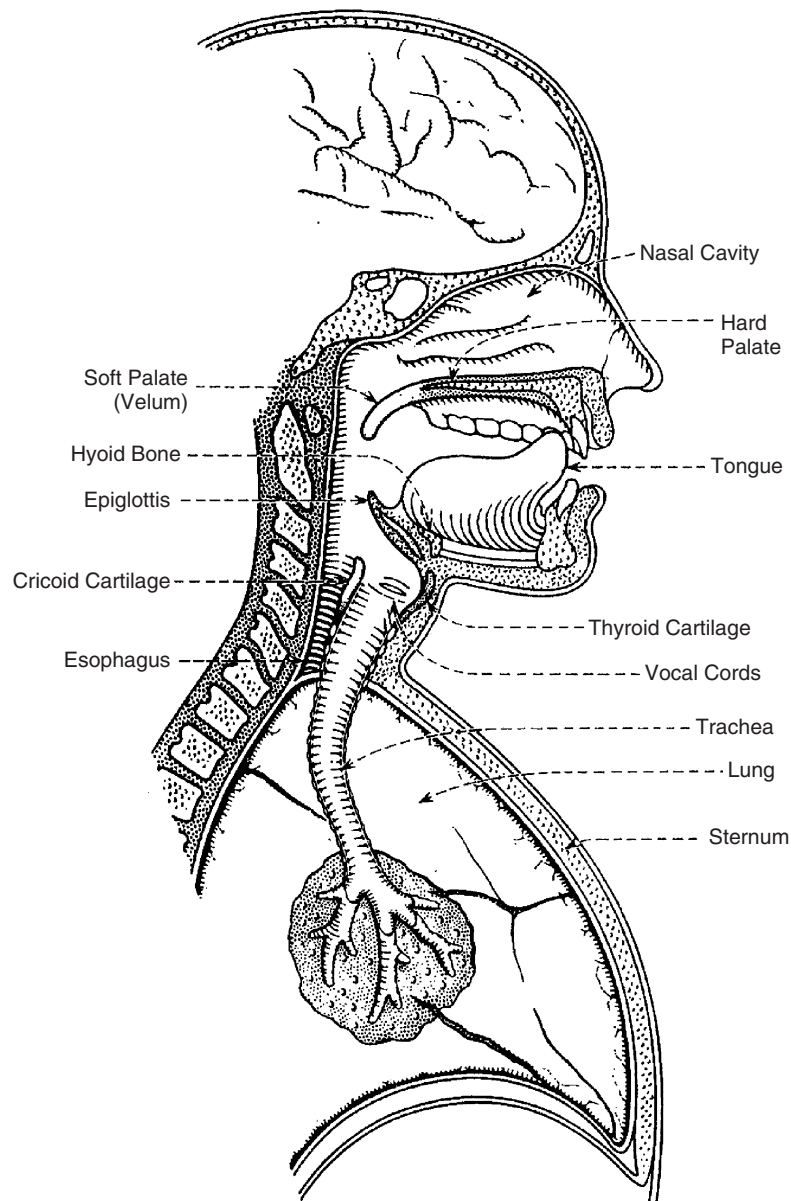
produce a sound sequence recognizable as speech. The air pressure is controlled by six sets of muscles affecting lung volume: abdominal, diaphragm, and four sets of rib muscles. Air passes from the lungs through the trachea and glottis (the space between the vocal folds), the first possible location for significant sound generation. The air continues on up the pharynx; if the velum (soft palate) is down, it splits between oral and nasal cavities, allowing both cavities to resonate. The tongue is the most mobile and significant articulator, but the lower jaw, lips, and velum can all affect the vocal tract shape as well. Any variation in tract shape affects its resonances; if the vocal tract gets constricted enough anywhere along its length, sound generation results.

Speech sounds are generally classified according to how much the vocal tract is constricted (the *manner*), where along the tract the point of greatest constriction is (the *place*), and whether or not the vocal folds are vibrating (the *voicing*). The manner classes with the least constriction anywhere along the vocal tract include the *vowels*, *semivowels* (sounds like /j,w/ as in yell, wool), and *liquids* (most versions of r and l); for these the most constricted region may have a cross-sectional area of approximately 1.0 cm<sup>2</sup>. The *nasals* have a complete constriction somewhere in the oral tract, and the velum is down; the place of a nasal depends on where in the oral tract the constriction is (at the lips for /m/, at the alveolar ridge just behind the teeth for /n/, or near the velum for /ŋ/, as in "sing"). For all of these manners the phonemes are voiced, meaning that a quasi-periodic sound is being produced by the vibration of the vocal folds.<sup>3</sup>

For the next three manners, in which the constriction is small enough that noise is generated along the tract, the phonemes may be voiced or voiceless. For *fricatives* a constriction is formed that is small enough (cross-sectional area from 0.03 to 0.20 cm<sup>2</sup>) for turbulence to be generated; the place of the constriction varies in English from lower lip and upper teeth for /f, v/, to the front part of the hard palate (just behind the alveolar ridge) for /ʃ, ʒ/, as in "shoo, azure"; /h/ is termed a glottal fricative, although the place at which the most turbulence noise is generated may not be at the glottis. Other places (e.g., pharynx, uvula; see Fig. 1) can be used to produce fricatives in other languages.<sup>4</sup>

For *stops*, the vocal tract is completely closed somewhere along its length, allowing pressure to build up. The constriction is then released, causing a brief burst of sound. There are six stops in English, listed





**Figure 1** Diagram of the vocal tract. (Reprinted with permission from Flanagan,<sup>12</sup> p. 10.)

in voiceless–voiced pairs at three places: /p,b, t,d, k,g/, as in *Pooh, boo, too, do, coo, goo*. Additional sounds may be produced after the release, during the transition to the next phoneme. These are referred to by the mechanism thought to generate that part of the transitory noise: *frication*, while the area of the opening constriction is in the range of 0.03 to 0.20 cm<sup>2</sup>, and then *aspiration*, thought to be produced by turbulence noise generated near the glottis. The aspiration phase typically only occurs for voiceless

stops during the time when the vocal folds are being adducted (brought together) for the following voiced sound; the glottis is small enough to generate turbulence noise, but too large still for phonation to occur.

Finally, *affricates* are intermediate between stops and fricatives. Initially there is complete closure as for a stop; the constriction is released more slowly than for a stop, however, producing a long interval of frication noise. In English there are only two affricates,

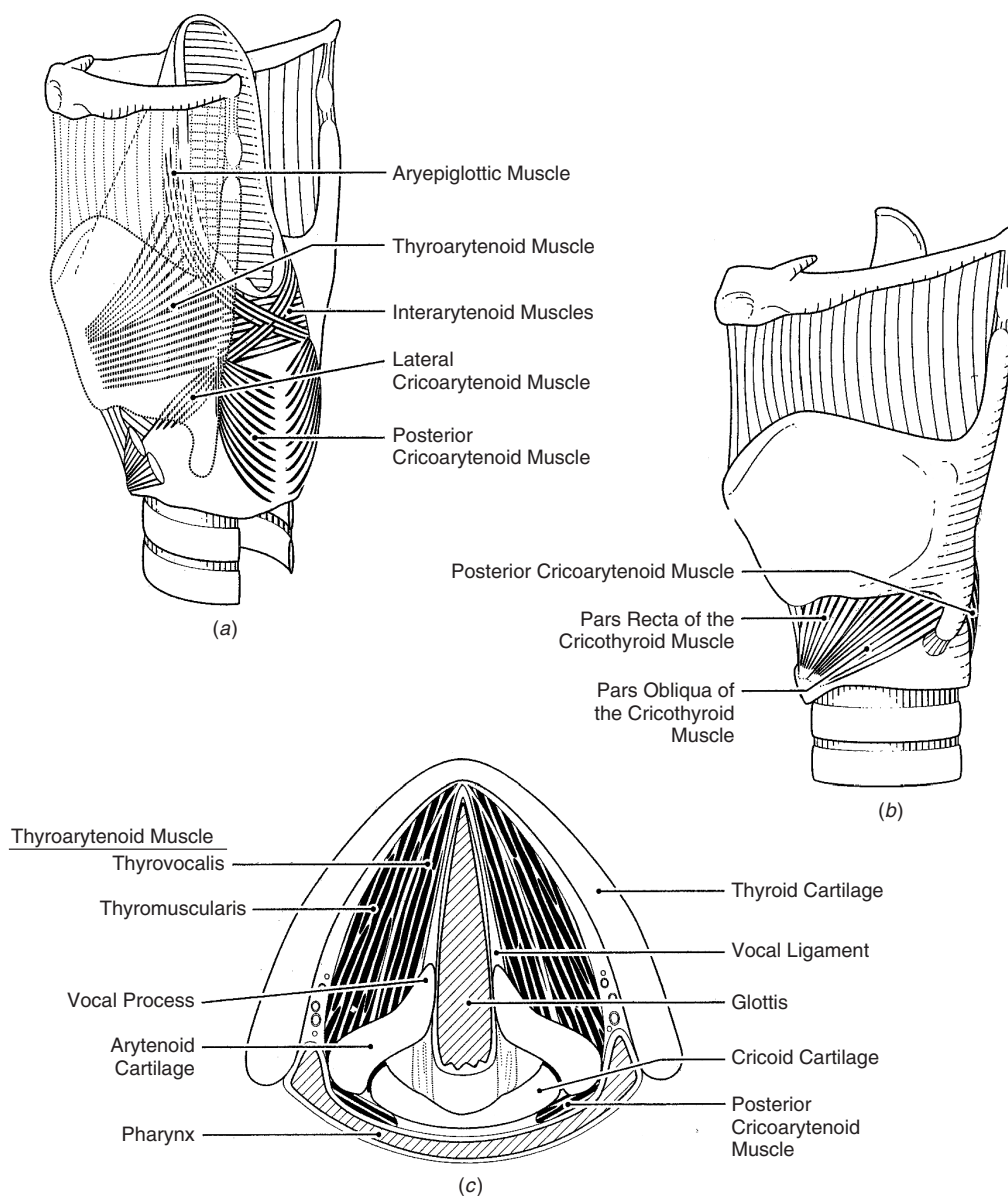


a voiceless–voiced pair with the same place: /tʃ, dʒ/ as in *Cheech* and *judge*.

### 3 ANATOMY, PHYSIOLOGY, AND SOUND PRODUCTION OF THE VOCAL FOLDS

Figure 2 shows a diagram of the vocal folds and surrounding structures. They consist of small muscles (the vocalis) with a cover of mucosal tissue. They are attached at the front to the inside of the thyroid cartilage (the Adam's apple), and at the back, to the arytenoid

cartilages, which sit on top of and can rotate with respect to the cricoid cartilage, which itself is hinged to the thyroid cartilage. Altogether, this means that there are many ways to control the vocal fold length and position with respect to each other. The tension on the folds results both from the distance between their endpoints (related to how the cartilages are positioned) and the degree to which the vocalis muscles are tensed. For the vocal folds to vibrate (also called *voicing*), the folds need to be positioned close to each other (to give a small glottal

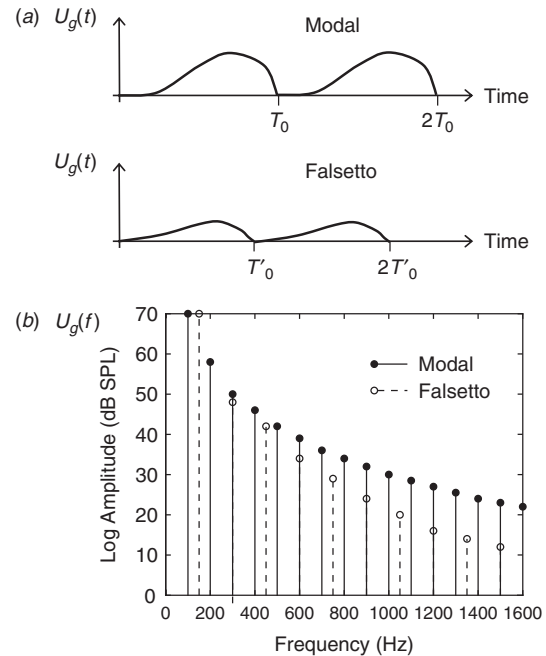


**Figure 2** Three views of the larynx and vocal folds: (a) posterior-lateral, (b) anterior-lateral, (c) superior view (transverse section at level of the vocal folds). (Reprinted with permission from Titze,<sup>5</sup> p. 12.)

rest area), the folds must be tensioned above a threshold, and the transglottal pressure (the pressure drop across the glottis, i.e., from just below to just above the vocal folds) must be above a threshold. In the classic myoelastic theory, as the air flows through the glottis the Bernoulli force pulls the folds together. The muscle tension of the folds exerts a restoring force, and when these forces are balanced the folds begin to oscillate. When they are close enough together, the folds touch during the oscillation, closing the glottis mostly or completely. Air pressure then builds up until the folds are blown apart and the cycle resumes. More recent theories indicate that the Bernoulli force plays a role only during part of the cycle, and some form of asymmetry is needed for sound to be generated, as discussed by Titze.<sup>5</sup> The closed phase of the cycle cuts the steady stream of air from the lungs into puffs, generating a periodic sound with a fundamental frequency (F0) that matches that of the mechanical oscillation, and a range of higher harmonics. The folds need not touch in order to generate a harmonic sound, however.<sup>5</sup>

The amount of energy in the harmonics and the subglottal pressure (the pressure below the glottis, at the upper end of the trachea) and volume velocities during voicing depend on the voice register being used. Voice registers exist in both speech and singing, though different terminology is used for each domain. Each register has a perceptibly different sound to it, which can be related to a different mode of vocal fold vibration caused by a different “setting” of laryngeal positioning and vocal fold tension. For instance, in modal voice (normal speaking voice) the entire muscle part of the vocal folds vibrates, and there is a significant closed phase that begins when the lower parts of the folds (nearest the trachea) slap together and ends when they peel apart from the bottom up. This results in a vertical wave traveling through the mass of the vocal fold and a complex vibration pattern that leads to the most energy in higher harmonics. In falsetto, the muscle mass is abducted (pulled apart) and only the mucosal cover vibrates, sometimes leading to incomplete closure along the length of the folds. This allows the vocal folds to vibrate at higher frequency, and there is noticeably less energy in the higher harmonics, as shown in Fig. 3.<sup>5,6</sup>

The rest length and mass of the vocal folds, which are not under the control of the speaker, determine the fundamental frequency (F0) range; longer folds with more mass will tend to vibrate with lower F0. Typical vocal fold lengths are 17 to 24 mm for adult men and 13 to 17 mm for adult women.<sup>2</sup> The positioning and tension of the folds, and the subglottal pressure, determine the instantaneous F0 value within the range possible for the speaker and are under the speaker's control. In general, the entire F0 range is available for singing, but only the lower part of that range is used for speech. The average F0 in speaking is 125 Hz for adult men, 200 Hz for adult women, and 300 Hz or more for children, and yet adult women can range from 110 Hz (for altos) to 1400 Hz (for sopranos) and adult men from 30 to 900 Hz.<sup>5</sup>



**Figure 3** Graphs showing (a) idealized waveforms of volume velocity through the glottis and (b) corresponding source spectra for modal and falsetto voice qualities.

The subglottal pressure can range from 3 to 30 cm H<sub>2</sub>O during voicing. Within a particular register the range may be smaller: For midvoice, subglottal pressure ranges from 10 to 30 cm H<sub>2</sub>O, and the airflow rate is at least 60 cm<sup>3</sup>/s, whereas for falsetto, subglottal pressure ranges from 2 to 15 cm H<sub>2</sub>O, and airflow is at least 70 cm<sup>3</sup>/s. For breathy voice, where the vocal folds might not contact each other at all though they are vibrating, airflow may be as high as 900 to 1000 cm<sup>3</sup>/s.<sup>3</sup>

#### 4 NOISE SOURCES

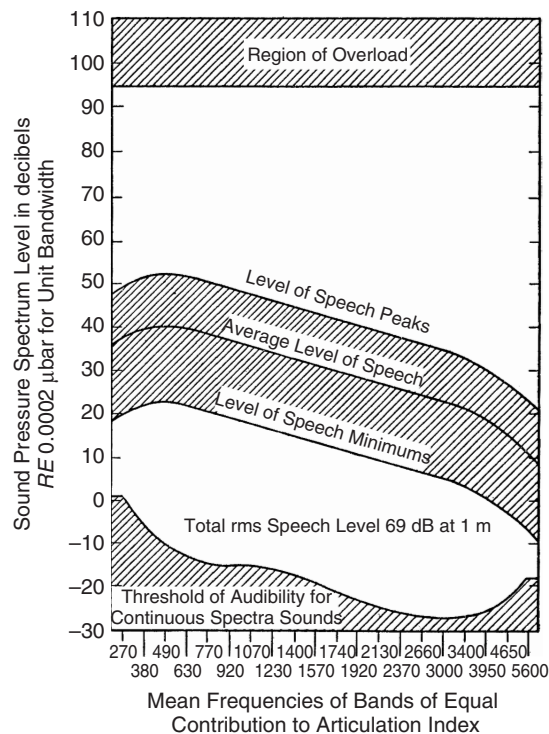
During voiceless consonants the vocal folds are abducted (pulled apart), enlarging the glottis to an area ranging from 1.0 to 1.4 cm<sup>2</sup>. Although this is smaller than the glottal area during breathing, it is significantly larger than the supraglottal constrictions for fricatives, which range from 0.03 to 0.2 cm<sup>2</sup>. During the steady-state part of a fricative, the supraglottal constriction typically has a pressure drop across it of 6 to 8 cm H<sub>2</sub>O and volume flow rate through it of 200 to 400 cm<sup>3</sup>/s. In the transitions into and out of the voiceless fricative, the glottis typically opens before the supraglottal constriction fully constricts, leading to higher volume velocities momentarily and giving the volume-velocity waveform a characteristic double-peaked profile. For /h/, with no significant supraglottal constriction, volume velocity can be as high as 1000 to 1200 cm<sup>3</sup>/s.<sup>7</sup>

For voiced fricatives, the vocal folds are abducted somewhat (pulled apart slightly) so that a slight peaking of the volume velocity can be observed in the transitions. In order to maintain voicing while still producing turbulence noise at the constriction, there must be pressure drops across both glottis and constriction.<sup>7</sup> If either pressure drop ceases to be sufficient to maintain sound generation, a fricative either loses voicing (so that a particular token of a voiced fricative is referred to as *having devoiced*) or loses noise generation (as happens more often with the weak fricatives /v, ð/, as in *vee, the*). In voiced stops, during the closed phase the air continues to pass through the glottis, increasing the pressure in the oral cavity; this can decrease the transglottal pressure drop enough so that voicing ceases. However, the vocal folds maintain their adducted (pulled-together) position, so that as soon as the closure is released and the oral pressure drops, voicing restarts quickly. The time between closure release and voicing onset is known as the voice onset time (VOT); it differs significantly between voiced and voiceless stops (typically, from 0 to 30 ms and from 70 to 120 ms, respectively), and is one of the strong perceptual cues to the voicing of the stop.<sup>8</sup>

The Reynolds number is a dimensionless parameter that has been used in aerodynamics to scale systems with similar geometry. It is defined as  $Re = VD/\nu$ , where  $V$  and  $D$  are, respectively, a characteristic velocity and dimension of the system, and  $\nu = 0.17 \text{ cm}^2/\text{s}$  is the kinematic viscosity of air. As  $Re$  increases, the flow changes from laminar to turbulent, often progressing through a transition region.<sup>9</sup> For fricatives the constriction in the vocal tract is treated as an orifice in a pipe would be, and  $Re$  is defined using the mean velocity in the constriction for  $V$  and the constriction diameter for  $D$ . For synthesis one would then only need to determine the critical Reynolds number at which turbulence begins. However, one difficulty has been to determine the area of the constriction so that the characteristic velocity through it can be determined from the more easily measurable volume velocity. A few studies have shown that  $Re_{crit}$  ranges from 1700 to 2300 for speech; the relation of acoustic source strength to  $Re$  has been the subject of much research.<sup>7,8</sup>

The acoustic output for speech varies over a wide range of amplitude and frequency, with vowels having a higher amplitude than voiceless consonants, especially at low frequencies. The long-term total root-mean-square (rms) speech sound pressure level for a male speaker using raised voice is, on average, 69 dB measured at 1 m directly in front of the speaker. Normal voice is about 6 dB less, loud voice about 6 dB more.

The long-term spectrum peaks at about 500 Hz for men, somewhat higher for women. The peak sounds range about 12 dB above the average level, and the minimum sounds about 18 dB below the average, as shown in Fig. 4.<sup>10</sup>



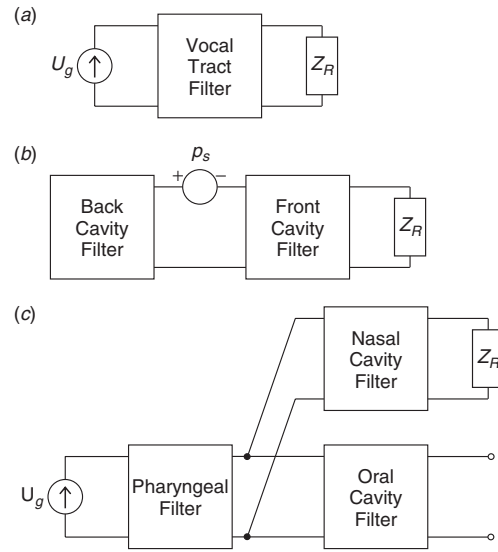
**Figure 4** Graph of sound pressure spectrum level showing the regions corresponding to speech (of raised voice of a male speaker), the threshold of audibility for young ears, and the region of overload. (Reprinted with permission from Beranek,<sup>10</sup> p. 408.)

## 5 SOURCE-FILTER THEORY OF SPEECH PRODUCTION

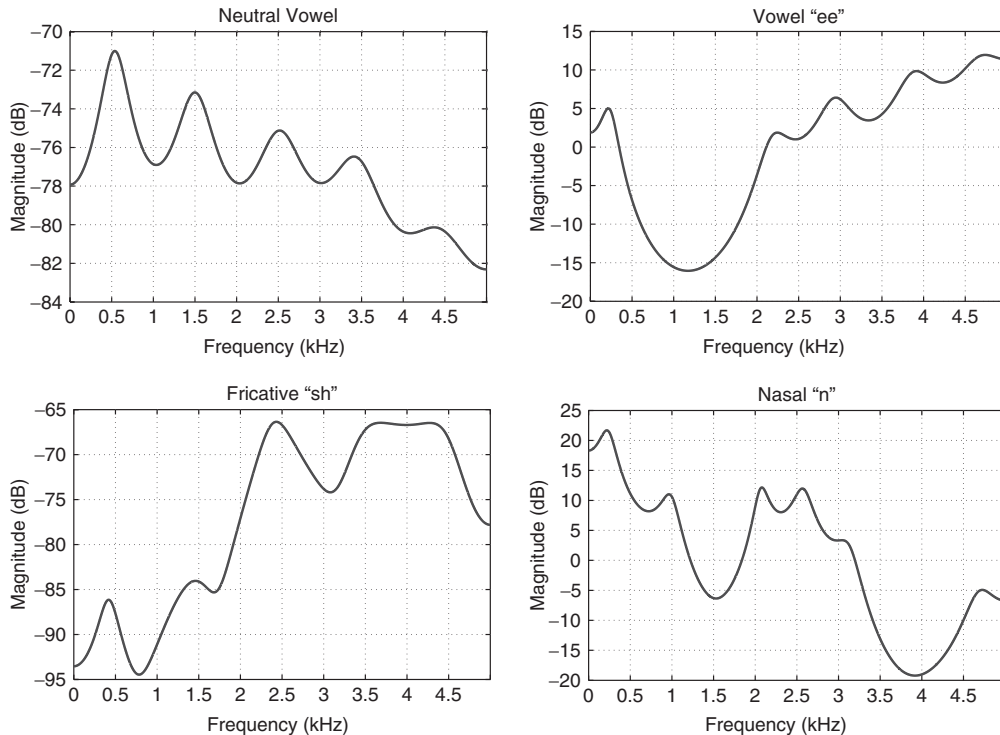
As a first approximation, the sound sources can be treated as independent of the filtering effects of the vocal tract. This, together with an assumption of plane-wave propagation in the tract, allows a circuit analogy to be used in which acoustic pressure is analogous to voltage and acoustic volume velocity to current. In the resulting transmission line analog, each section contains elements whose inductance, capacitance, or resistance depend on the cross-sectional area of the tract and the length of that section. Circuit theory can be used to derive the poles and zeros of the electrical system, which occur at the same frequencies as the acoustic resonances and antiresonances. Losses can be incorporated; the main source of loss is radiation at the lip opening, which can be modeled as an inductor and resistor in series.<sup>10</sup> Other sources of loss include yielding walls (the vocal tract is lined with soft tissue except at the hard palate and teeth), and viscosity and heat conduction; these are modeled with extra elements within each section of the transmission line. The transmission line can be converted to digital form, as a digital delay line.<sup>8,11</sup>

Because the tongue and other articulators move slowly relative to the vocal folds, the vocal tract filter can be treated as static during a single pitch period (vocal fold cycle). The vocal tract transfer function is defined to be the ratio of the “output,” typically the volume velocity at the lips, to the “input,” the source characteristic. Its poles are always the natural resonances of the entire system; its zeros depend on the topology of the system. If the source is at one end, the output is at the other end, and there are no parallel branches, there are no zeros; this is the case for nonnasalized vowels, as shown in Fig. 5a. If the source is intermediate (i.e., a supraglottal source, as for noise-excited consonants), there will be zeros corresponding to the resonances of the back cavities, which may destructively interfere with the system resonances (see Fig. 5b). Likewise, if the tract has any side branches, as, for instance, in nasals, there will be zeros corresponding to the resonances of the side branch (see Fig. 5c).<sup>8</sup>

Within these general characteristics, the vocal tract shape and especially the place of greatest constriction determine the frequencies of each resonance and antiresonance. Vowels can be distinguished by the first two resonances; the first three resonances distinguish liquids (/l and r/) also. Figure 6 shows idealized transfer functions for two vowels, the fricative “sh,” and



**Figure 5** Block diagrams of source-filter model of speech production for (a) vowel, (b) fricative or stop, and (c) nasal. The glottal voicing source is indicated by a volume-velocity source analogous to a current source,  $U_g$ . The noise source is indicated by a pressure source analogous to a voltage source,  $p_s$ .



**Figure 6** Typical transfer functions ( $U_L/U_g$ ,  $U_L/p_s$ , or  $U_n/U_g$ ) for the major classes of speech sounds. (Top) Vowels—neutral vowel schwa (as in “the”) and /i/ (as in “he”). (Lower left) The fricative “sh.” (Lower right) The nasal /n/.

the nasal /n/. The vowels have all-pole transfer functions, with the pole frequency differing according to the vocal tract shape. The fricative and nasal transfer functions have zeros as well as poles determined by the source location and oral cavity length, respectively. The transfer function for a stop is fricative-like immediately after release, becoming vowel-like (though noise excited) in the aspiration phase.

Two classic source models that work well and so continue to be used in synthesizers are the two-mass model of vocal fold vibration and a series pressure source located in the vicinity of the most constricted region for turbulence noise sources.<sup>12</sup> The former models each vocal fold as a combination of two masses and three springs, allowing mass, tension, and coupling to be set, as well as glottal rest area. The input parameter is subglottal pressure; it outputs volume velocity. Other models have been developed, including 16-mass models, ribbon and beam models, and finite element models of each vocal fold.<sup>5</sup> There have also been studies showing that there is interaction of the vocal fold vibration with the vocal tract acoustic impedance, and studies of the aeroacoustic effects of the vocal fold vibration.

Noise sources have long been modeled as acoustic pressure sources, analogous to voltage sources, placed in series. The location of such a source in the tract model affects the frequencies of the antiresonances (and thus the zeros of the transfer function) significantly. The overall source strength and how it changes in time, and the spectral characteristic of the source, also affect the predicted radiated sound. Some solutions used in synthesis include placement of the source according to the phoneme being synthesized,<sup>13</sup> or at a set distance downstream of a constriction<sup>12</sup>; in Flanagan and Cherry's noise source model the source strength is controlled by the Reynolds number of the upstream constriction, and the spectral characteristic consists of high-pass-filtered white noise (pp. 253–259 in Ref. 12). More recent results indicate that all aspects of turbulence noise generation—spatial and temporal distribution and spectral characteristics—depend strongly on the geometry of the tract downstream of the constriction, which is not fully specified in a model based on the cross-sectional areas along the tract.<sup>7</sup> Models that differ for each phoneme offer some improvement,<sup>8</sup> but any source generated by or pasted into a circuit analog will never accurately represent flow noise sources.

## 6 ENGINEERING ASPECTS OF SPEECH PERCEPTION

Speech perception encompasses the subset of auditory perception that allows us to understand speech and simultaneously deduce background acoustic characteristics and the speaker's age, gender, dialect, and mood. Some aspects of speech perception are innate; others are learned as part of learning a language. Various speech technologies attempt to replicate some part of human speech perception, exploiting current knowledge to do so. Thus, speech transmission and coding

seek to capture only the parts of the speech signal that are most vital for communication; speech recognition aims to produce written text from a speech signal, ignoring or neutralizing information about the speaker; speaker identification and verification ignore the segmental information but seek to correctly identify the speaker, or verify that the speaker's acoustic characteristics match their other characteristics such as an identity card presented to the computer.

Different speech sounds are distinguished from each other by differing sets of acoustic cues. For vowels, the frequencies of the lowest two or three resonances are most important, sufficient to deserve another name: The resonances are referred to as *formants* and numbered from lowest frequency on up. The first three vowel formants range between 200 and 3000 Hz for adults. The most sensitive part of our hearing is from 500 to 5000 Hz. The telephone capitalizes on these facts, having a bandwidth of 300 to 3400 Hz. This means that the fundamental frequency  $F_0$  is usually filtered out before transmission over the telephone; our auditory systems are able to deduce it from the harmonics that are transmitted.<sup>11</sup> Studies have been done to try to establish the bandwidth holding the “essential information” of speech. But intelligibility degrades only slightly when a large part of the spectrum is filtered out: For instance, low-pass filtering at 1800 Hz results in approximately 65% intelligibility (meaning that 65% of the phonemes could be correctly transcribed on average), but high-pass filtering at 1800 Hz yields about the same intelligibility. Clearly, there is a lot of redundancy in speech signals.<sup>14</sup> Mobile phones exploit more subtle aspects of auditory perception such as masking in order to compress the signal, thus minimizing the bandwidth needed for transmission.

In order to measure the success of such compression algorithms, and also to evaluate speech synthesizers, a variety of objective and subjective measures have arisen. A distinction must be made between speech intelligibility and quality. Simply stated, intelligibility measures the likelihood that the speech will be understood; speech quality measures naturalness and ease of listening. These concepts are equally valid for considering human speech with background noise, human speech that has been distorted or degraded by its method of recording or transmission, and computer-synthesized speech.<sup>11</sup> Both dimensions are important because it is possible to improve the speech quality and yet worsen its intelligibility, and vice versa; speech enhancement algorithms usually aim to improve both dimensions.

Normally, speech needs to be approximately 6 dB higher in level than background noise to be intelligible,<sup>14</sup> so many enhancement algorithms focus on improving the signal-to-noise ratio (SNR). However, SNR is a poor guide to the perceptual effects of a particular kind of noise. Also, it is well known that speakers will speak differently in the presence of background noise, changing duration, intensity, spectral tilt, among other parameters; these effects are not easily corrected for.<sup>15,16</sup> Consonants affect intelligibility of speech more than vowels and tend also

to have distinguishing acoustic cues that are noisy themselves and range over higher frequencies. An early study investigated consonant confusion patterns that occurred at different levels of background noise and with different filters applied; the weak fricatives were most readily confused.<sup>17</sup> More recently, the Diagnostic Rhyme Test (DRT)<sup>18</sup> was devised so that intelligibility could be tested feature by feature, for six features such as nasality, voicing, sonorance, and so on. The effect of a particular kind of distortion or background noise can be delineated. Speech quality can similarly be quantified using the Diagnostic Acceptability Measure (DAM).<sup>18–20</sup> These DRT and DAM measures, based on formal listening tests using human subjects, are termed subjective tests; many objective tests that do not use human subjects have been developed, in particular to evaluate mobile phone compression and coding algorithms.<sup>21</sup>

**Acknowledgment** Preparation of this chapter was supported by NIH grant NIDCD R01 DC 006705.

## REFERENCES

1. D. Crystal, *A Dictionary of Linguistics and Phonetics*, 3rd ed., Blackwell, Oxford, 1991.
2. G. J. Borden, K. S. Harris, and L. J. Raphael, *Speech Science Primer*, 4th ed., Lippincott Williams & Wilkins, Baltimore, MD, 2003.
3. J. C. Catford, *Fundamental Problems in Phonetics*, Indiana University Press, Bloomington, IN, 1977.
4. P. Ladefoged and I. Maddieson, *The Sounds of the World's Languages*, Blackwell, Oxford, 1996.
5. I. R. Titze, *Principles of Voice Production*, Prentice-Hall, Englewood Cliffs, NJ, 1994.
6. J. Sundberg, *The Science of the Singing Voice*, Northern Illinois University Press, DeKalb, IL, 1987.
7. C. H. Shadle, The Aerodynamics of Speech, in *Handbook of Phonetics*, W. J. Hardcastle and J. Laver, Eds., Blackwell, Oxford, 1997, pp. 33–64.
8. K. N. Stevens, *Acoustic Phonetics*, MIT Press, Cambridge, MA, 1998.
9. B. S. Massey, *Mechanics of Fluids*, 5th ed., Van Nostrand Reinhold, Wokingham, UK, 1983.
10. L. L. Beranek, *Acoustics*, McGraw-Hill Book, New York, 1954. Reprinted by American Institute of Physics for the Acoustical Society of America, New York, 1986.
11. D. O'Shaughnessy, *Speech Communications*, 2nd ed., IEEE Press, New York, 2000.
12. J. L. Flanagan, *Speech Analysis Synthesis and Perception*, 2nd ed. Springer, New York, 1972.
13. G. Fant, *Acoustic Theory of Speech Production*, Mouton, The Hague, 1970.
14. B. J. Moore, *Introduction to the Psychology of Hearing*, 3rd ed., Academic, London, 1989.
15. Y. Gong, Speech Recognition in Noisy Environments: A Review, *Speech Commun.*, Vol. 16, 1995, pp. 261–291.
16. J.-C. Junqua, The Influence of Acoustics on Speech Production: A Noise-Induced Stress Phenomenon Known as the Lombard Reflex, *Speech Commun.*, Vol. 20, 1996, pp. 13–22.
17. G. A. Miller and P. E. Nicely, An Analysis of Perceptual Confusions Among Some English Consonants, *J. Acoust. Soc. Am.*, Vol. 27, 1955, pp. 338–352.
18. W. Voiers, Diagnostic Acceptability Measure for Speech Communication Systems, Proc. IEEE ICASSP, Hartford, CT, 1997, pp. 204–207.
19. W. Voiers, Diagnostic Evaluation of Speech Intelligibility, in *Benchmark Papers in Acoustics*, M. E. Hawley, Ed., Dowden, Hutchinson and Ross, Stroudberg, PA, 1977, pp. 374–387.
20. S. Quackenbush, T. Barnwell, and M. Clements, *Objective Measures of Speech Quality*, Prentice-Hall, Englewood Cliffs, NJ, 1988.
21. L. Hanzo, F. C. A. Somerville, and J. P. Woodard, *Voice Compression and Communications*, IEEE Press, Wiley-Interscience, New York, 2001.

## **PART IV**

---

# **EFFECTS OF NOISE, BLAST, VIBRATION, AND SHOCK ON PEOPLE**



# CHAPTER 23

## GENERAL INTRODUCTION TO NOISE AND VIBRATION EFFECTS ON PEOPLE AND HEARING CONSERVATION

Malcolm J. Crocker

Department of Mechanical Engineering  
Auburn University  
Auburn, Alabama

### 1 INTRODUCTION

Noise and vibration may have undesirable effects on people. At low sound pressure levels, noise may cause annoyance and sleep disturbance. At increased levels, noise begins to interfere with speech and other forms of communication; at still higher levels that are sustained over a long period of time in industrial and other occupational environments, noise can cause permanent hearing damage. Loud impulsive and impact noise are known to cause immediate hearing damage. Similarly, whole-body vibration experienced at low levels may cause discomfort, while such vibration at higher levels can be responsible for a variety of effects including reduced cognitive performance and interference with visual tasks and manual control. Undesirable vibration may be experienced in vehicles and in buildings and can be caused by road forces, unbalanced machinery forces, turbulent boundary layer pressure fluctuations, and wind forces. High levels of sustained vibration experienced by operators of hand-held machines can cause problems with circulation and neuropathy of the peripheral nerves and can result in chronic diseases of the hand and arm. This introductory chapter summarizes some of the main effects of noise and vibration on people. For more in-depth discussion, the reader should consult the chapters following in Part IV of this book.

### 2 SLEEP DISTURBANCE

It is well known that noise can interfere with sleep. Not only is the level of the noise important for sleep interference to occur, but so is its spectral content, number and frequency of occurrences, and other factor. Even very quiet sounds such as dripping taps, ticking of clocks, and snoring of a spouse can disturb sleep. One's own whispered name can elicit wakening as reliably as sounds 30 or 40 dB higher in level. Common sources of noise in the community that will interfere with sleep are comprised of all forms of transportation, including road and rail traffic, aircraft, construction, and light or heavy industry. Some airports restrict night time aircraft movements. Road traffic is normally reduced at night and is less disturbing but is still potentially a problem. Noise interferes with sleep in two main ways: (1) it can result in more disturbed, lower quality sleep, and (2) it

can awaken the sleeper. Unfortunately, although there has been a considerable amount of research into sleep interference caused by noise, there is no internationally accepted way of evaluating the sleep interference that it causes or indeed of the best techniques to adopt in carrying out research into the effects of noise on sleep. Also, little is known about the cumulative long-term effects of sleep disturbance or sleep deprivation caused by noise. Fortunately, despite the lack of in-depth knowledge, sufficient noise-induced sleep interference data are available to provide general guidance for land-use planning, environmental impact statements for new highways and airports, and sound insulation programs for housing. Chapter 24 provides an overview of knowledge about sleep disturbance caused by noise.

### 3 ANNOYANCE

Noise consists of sounds that people do not enjoy and do not want to hear. However, it is difficult to relate the annoyance caused by noise to purely acoustical phenomena or descriptors. When people are forced to listen to noise against their will, they may find it annoying, and certainly if the sound pressure level of the noise increases as they are listening, their annoyance will likely increase. Louder sounds are usually more annoying, but the annoyance caused by a noise is not determined solely by its loudness. Very short bursts of noise are usually judged to be not as loud as longer bursts at the same sound pressure level. The loudness increases as the burst duration is increased until it reaches about  $\frac{1}{8}$  to  $\frac{1}{4}$  s, after which the loudness reaches an asymptotic value, and the duration of the noise at that level does not affect its judged loudness. On the other hand, the annoyance of a noise at a constant sound pressure level may continue growing well beyond the  $\frac{1}{4}$  s burst duration as the noise disturbance continues.

Annoyance caused by noise also depends on several other factors apart from the acoustical aspects, which include its spectral content, tonal content, cyclic or repetitive nature, frequency of occurrence, and time of day. Nonacoustical factors include biological and sociological factors and such factors as previous experience and perceived malfeasance. We are all aware of the annoyance caused by noise that we cannot easily control, such as that caused by barking dogs, dripping taps, humming of fluorescent lights, and the



like. The fact that the listener does not benefit from the noise, cannot stop the noise, and/or control it is important. For instance, the noise made by one's own automobile may not be judged very annoying while the noise made by other peoples' vehicles, motorcycles, lawnmowers, and aircraft operations at a nearby airport, even if experienced at lower sound pressure levels, may be judged much more disturbing and annoying. Chapter 25 reviews the annoyance of noise in detail and provides references for further reading.

#### 4 INFRA SOUND, LOW-FREQUENCY NOISE, AND ULTRASOUND

So far we have described the disturbing effects that are produced by noise within the frequency range of human hearing from about 20 to 16,000 Hz. But noise above and below this frequency range can also cause disturbance to people. Very low frequency noise or *infrasound* (usually considered to be at frequencies below 20 Hz) may be very intense although "inaudible" in the traditional sense of hearing; but nevertheless it may cause a sensation of pressure or presence in the ears. Low-frequency noise (LFN) between about 20 and 100 Hz, which is within the normally audible range, is usually more disturbing than infrasound. Low-frequency noise in the region of 20 to 50 Hz seems to be the worst problem and more disturbing than infrasound. Sources of infrasound and LFN noise include (1) air-conditioning systems in buildings with variable air volume controls or with large-diameter slow-speed fans and blowers and long ductwork in which low-frequency standing waves can be excited, (2) oil and gas burners, (3) boilers, and (4) diesel locomotives and truck and car cabins. Ultrasound covering the range 16,000 to 40,000 Hz is generated in many industrial and commercial devices and processes.

Chapter 26 reviews the known effects of infrasound, LFN, and ultrasound in more detail. Currently, our best information is that infra- and ultrasound can be tolerated at high sound pressure levels up to 140 dB for very short exposure times, while at levels between 110 and 130 dB, infra- and ultrasound can be tolerated for periods as long as 24 hours without apparent permanent physiological or psychological effects. There is no current evidence that levels of infrasound, LF, or ultrasound lower than 90 to 110 dB lead to permanent physiological or psychological damage or other side effects.

#### 5 IMPULSIVE AND IMPACT NOISE

High levels of impulsive and impact noise pose special threats to human hearing. These types of noise can also be very annoying. It is well known now that high levels of such noise damage the cochlea and its hair cells through mechanical processes. Unfortunately, there is currently no commonly accepted definition or recognized standard for what constitutes impulsive noise. Impulsive noise damage cannot be simply related to knowledge of the peak sound pressure level. The duration, number of impulsive events, impulse

waveform, and initial rise time are also all important in predicting whether impulsive or impact noise is likely to result in immediate hearing damage. Impulse noise damage also does not seem to correlate with the noise energy absorbed by the ear. It is known that hearing damage caused by a combination of impulsive noise events during steady background noise cannot be judged by simply adding the noise energy contained in each and may indeed be greater than simple addition would suggest.

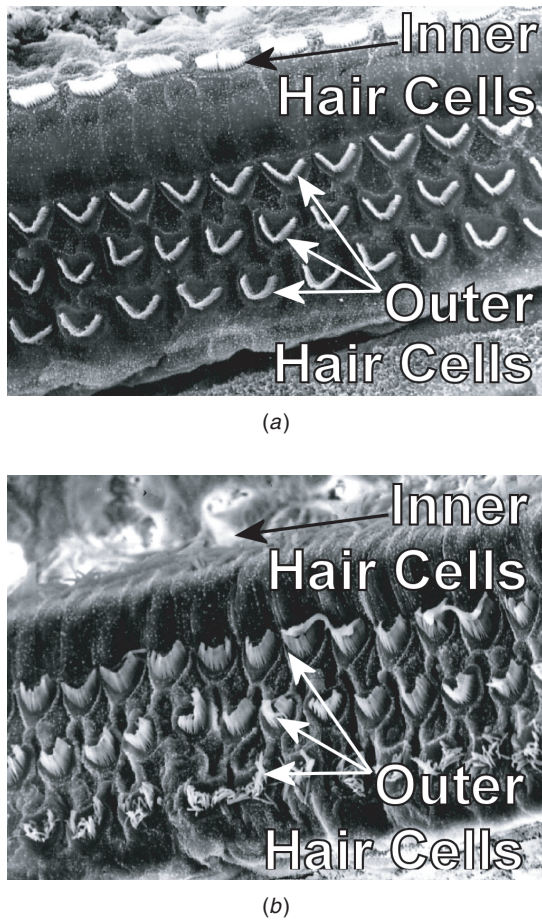
There is a huge variation in the characteristics of impulsive and impact noise to which people may be exposed. Peak sound pressure levels can be from 100 dB to as much as 185 dB, and impulse durations may vary from as little as a few microseconds to as much as hundreds of milliseconds. Impulses can be comprised of single events or multiple or repeated events. Cole has classified impulse and impact noise into two main types: (1) single nonreverberant impulses (termed A waves) and (2) reverberant impact noise (termed B waves) (see Chapter 27).

Explosions and the blast waves they create (often commonly called Friedlander waves) can be classified as A waves in Cole's system. They can have peak sound pressure levels of over 150 dB. They are really shock waves and are not purely sound waves. Riveting and punch press and forge forming and other machining processes in industry can result in reverberant noise caused by ringing of the manufactured parts. Such ringing noise is classified as B waves in this system. Although Cole's system includes the effects of peak sound pressure level, duration, and number of impulsive events, it is not completely comprehensive since it neglects the rise times, spectral contents, and temporal patterns of the impulses. Bruel has shown that crest factors as high as 50 dB are common in impulsive noises (see Chapter 27). Unfortunately, there is still no real consensus on how to predict and treat the damaging effects of impulsive noise compared to continuous intense noise. Chapter 27 discusses impulsive and impact noises in more detail.

#### 6 INTENSE NOISE AND HEARING LOSS

Continuous intense noise at much lower sound pressure levels than discussed in Section 5 can also produce hearing loss. The level needed to produce the hearing loss is much lower than the peak impulsive noise levels required to produce immediate damage. Protective mechanisms exist in the middle ear, which reduce the damaging effect of continuous intense noise. These mechanisms, however, only reduce the noise levels received by the cochlea by about 5 dB and are insufficient to protect the cochlea against most continuous intense noise. The hearing loss caused by continuous intense noise is described in detail in Chapter 28.

Hearing loss can be classified into two main types and is normally measured in terms of the shift of the following hearing threshold shifts (see Chapter 28): (1) Temporary threshold shift (TTS) is the shift in hearing threshold caused by noise that returns to normal after periods of 24 to



**Figure 1** Electron microscope image of the hair cells in the cochlea (a) hair cells before noise exposure and (b) damaged hair cells after intense noise exposure. (Courtesy of Pierre Campo, INRS, Departement PS, Vandoeuvre, France.)

48 hours. (2) Permanent threshold shift (PTS) is the shift in hearing threshold that is nonrecoverable even after extended periods of rest. PTS caused by exposure to intense noise over extended periods produces permanent irrecoverable damage to the cochlea. Figure 1 shows the destruction of the hair cells in a cochlea of a rat caused by intense noise.

Some people have hearing mechanisms that are more sensitive than other people's and are more prone to damage from continuous intense noise and to suffer PTS. Because harmful noise can be quite different in frequency content, often A-weighted sound pressure level is used as a measure of the intense noise for the prediction of hearing impairment (PTS). Continuous A-weighted sound pressure levels above 75 dB can produce hearing loss in people with the most sensitive hearing if experienced for extended periods of some years. As the A-weighted level increases,

an increasing fraction of the workforce experiences PTS. The PTS expected at different levels has been predicted by several organizations including the International Organization for Standardization (ISO), the Occupational Safety and Health Administration (OSHA), and the National Institute for Occupational Safety and Health (NIOSH) (see Table 1).

Some countries have hearing regulations that restrict the amount of daily noise exposure a person should be allowed to experience at different A-weighted sound pressure levels. Most countries use the 3-dB trading ratio (also known as the exchange rate) as the A-weighted level is changed. This assumes a linear relationship between noise energy absorbed and hearing loss. If the level increases by 3 dB it is assumed that the noise dose will be the same for an exposure period of half the time. In the United States, a 5-dB trading ratio (also known as the exchange rate) is used before the allowable exposure time is halved, which assumes that a worker get some breaks from the intense noise during the day's noise. Table 2 shows the time-weighted average (TWA) noise level limits promulgated by OSHA.

## 7 EFFECTS OF VIBRATION ON PEOPLE

Vibration has unwanted effects on people.<sup>2</sup> People are also very sensitive to vibration.

Undesired vibration can be experienced in vehicles, aircraft, buildings, and other locations. Vibration is normally measured in terms of acceleration levels. With low vibration levels, people may experience discomfort such as motion sickness. The amount of discomfort depends not only upon the magnitude but on the frequency of vibration and its direction and

**Table 1** Estimated Excess Risk of Incurring Material Hearing Impairment<sup>a</sup> as a Function of Average Daily Noise Exposure over a 40-year Working Lifetime<sup>b</sup>

Reporting Organization	Average Daily A-weighted Noise Level Exposure (dB)	Excess Risk (%) <sup>c</sup>
ISO	90	21
	85	10
	80	0
EPA <sup>d</sup>	90	22
	85	12
	80	5
NIOSH	90	29
	85	15
	80	3

<sup>a</sup> For purposes of comparison in this table, material hearing impairment is defined as an average of the Hearing Threshold Levels for both ears at 500, 1000, and 2000 Hz that exceeds 25 dB.

<sup>b</sup> Adapted from 39 *Fed. Reg.* 43802 [1974b].

<sup>c</sup> Percentage with material hearing impairment in an occupational-noise-exposed population after subtracting the percentage who would normally incur such impairment from other causes in an unexposed population.

<sup>d</sup> EPA = Environmental Protection Agency.

Source: From Ref. 1.

**Table 2 Time-Weighted Average (TWA) Noise Level Limits as a Function of Exposure Duration**

Duration of Exposure (h/day)	A-Weighted Sound Pressure Level (dB)		
	ACGIH	NIOSH	OSHA
16	82	82	85
8	85	85	90
4	88	88	95
2	91	91	100
1	94	94	105
1/2	97	97	110
1/4	100	100	115 <sup>a</sup>
1/8	103	103	—

<sup>a</sup> No exposure to continuous or intermittent A-weighted sound pressure level in excess of 115 dB.

<sup>b</sup> Exposure to impulsive or impact noise should not exceed a peak sound pressure level of 140 dB.

<sup>c</sup> No exposure to continuous, intermittent, or impact noise in excess of a C-weighted peak sound pressure level of 140 dB.

duration as well. As vibration levels increase, cognitive performance can be affected, and interference with visual tasks and manual control can occur. Vibration can be classified as whole body or part of the body such as an organ or limb. High levels of sustained vibration over an extended period of time can cause neuromuscular damage for hand-held machine operators and vascular and articular disorders. See Chapter 29 for more detailed discussion of this topic.

## 8 EFFECTS OF MECHANICAL SHOCK

Vibration caused by suddenly applied forces is normally classified as a shock.<sup>2</sup> With a shock, the maximum force is usually experienced in a few tenths of a second, and the duration of the applied forces is normally less than one second. Shocks can cause discomfort, but if of great enough magnitude, they can cause injury and if of sufficient magnitude, death. Like vibration, the effect of shocks upon people depends upon several factors including their magnitude, direction, frequency content, and whether or not impacts occur in conjunction with the shocks. Survivability of intense shocks and impacts depends to a large extent on whether or not the human body is restrained. Both experimental and theoretical models of human shock phenomena are used to study the effects of shock. Chapter 30 discusses the effects of mechanical shock and impact on people in detail.

## 9 HEARING PROTECTORS

It is best practice to reduce noise through: (1) the use of passive engineering controls such as use of enclosures, sound-absorbing materials, barriers, vibration isolators, etc., and then (2) using administrative measures such as restricting the exposure of personnel by limiting duration, proximity to noise sources, and the like. In cases where it is not practical or economical to reduce noise exposure to sound pressure levels that cause hearing hazards or annoyance, then hearing protectors should

be used.<sup>1</sup> Hearing protector devices (HPDs) can give noise protection of the order of 30 to 40 dB, depending on frequency, if used properly. Unfortunately, if they are incorrectly or improperly fitted, then the attenuation they can provide is significantly reduced. There are four main types of HPDs: earplugs, earmuffs, semi inserts, and helmets. Earplugs are generally low-cost, self-expanding types that are inserted in the ear canal and must be fitted correctly to achieve the benefit. Custom-molded earplugs can be made to fit an individual's ear canals precisely. Some people find earplugs uncomfortable to wear and prefer earmuffs.

Earmuffs use a seal around the pinna to protect it and a cup usually containing sound absorbing material to isolate the ear further from the environment. If fitted properly, earmuffs can be very effective. Unfortunately, earmuffs can be difficult to seal properly. Hair and glasses can break the seals to the head causing leaks and resulting in a severe degradation of the acoustical attenuation they can provide. In addition they have the disadvantage that they can become uncomfortable to wear in hot weather. The use of earmuffs simultaneously with earplugs can provide some small additional noise attenuation, but not as much as the two individual HPD attenuations added in decibels. Semi inserts consist of earplugs held in place in the ear canals under pressure provided by a metal or plastic band. These are convenient to wear but also have the tendency to provide imperfect sealing of the ear canal. If the plug portion does not extend into the ear canal properly, the semi insert HPD provide little hearing protection and can give the user a false sense of security.

Helmets usually incorporate semi inserts and in principle can provide slightly greater noise attenuation than the other HPD types. Attenuation is provided not only for noise traveling to the middle and inner ear through the ear canal, but for noise reaching the hearing organ through skull bone conduction. Helmets also provide some crash and impact protection to the head in addition to noise attenuation and are often used in conditions that are hazardous not only for noise but potential head injury from other threats. Unfortunately, the hearing protection they provide is also reduced if the semi inserts are improperly sealed in the ear canals. Chapter 31 contains more detailed discussion on hearing protectors.

## 10 NUMBERS OF PEOPLE EXPOSED

Large numbers of workers involved in manufacturing, utilities, transportation, construction, agriculture, and mining work in noisy conditions, which present hazards to hearing. In 1981, OSHA estimated that 7.9 million people in the United States working in manufacturing were exposed occupationally, to daily A-weighted sound pressure levels at or above 80 dB. In the same year, the U.S. Environment Protection Agency (EPA) estimated that more than 9 million U.S. workers were exposed occupationally to daily A-weighted levels above 85 dB. More than half of these workers were involved in manufacturing and utilities. Chapter 32 gives estimates for the number

of people working in hazardous noise conditions in other countries as well as the United States. Many governments require or mandate hearing conservation programs for workers in industries and in other occupations in which hazardous noise conditions exist. These are described in Chapter 33.

## 11 HEARING CONSERVATION PROGRAMS

Hearing conservation programs are designed to protect workers from the effects of hazardous noise environments. Protection can be provided not only by use of engineering controls designed to reduce the emission of noise sources, control of noise and vibration paths, and the provision of HPDs, but by the limitation of personnel exposure to noise as well. For instance, arranging for a machine to be monitored with a control panel that is located at some distance from a machine, instead of right next to it, can reduce personnel noise exposure. The rotation of personnel between locations with different noise levels during a workday can ensure that one person does not stay in the same high noise level throughout the workday. Chapter 33 describes hearing conservation programs and, in addition, some legal issues including torts, liabilities, and occupational injury compensation.

## 12 NOISE AND VIBRATION CRITERIA

Various noise and vibration environments have produced the requirements for different criteria to reduce

annoyance, discomfort, speech and sleep interference, and to reduce their hazardous effects. This has resulted in different rating measures being devised to account for these effects. For instance, it has been found impossible to use one noise measure to account for the effects of noise on speech interference, sleep interference, and air-conditioning noise in buildings, although sometimes the A-weighted 8-h equivalent sound pressure level is used. This measure, however, is obviously not suitable for hazardous impact noise and to assess the impact of time-varying noise such as aircraft movements at airports. The main reason is that this measure does not allow for variations in level and for night versus daytime exposure and the need to have a lower noise environment at night. Chapter 34 reviews the most common noise and vibration level criteria and rating measures in use in 2007.

## REFERENCES

1. Criteria for a Recommended Standard, Occupational Noise Exposure, Revised Criteria 1998, U.S. Department of Health and Human Services, <http://www.cdc.gov/niosh/98-126.html>.
2. M. J. Griffin, *Handbook of Human Vibration*, Academic, London, 1996.

# CHAPTER 24

## SLEEP DISTURBANCE DUE TO TRANSPORTATION NOISE EXPOSURE

Lawrence S. Finegold  
Finegold & So, Consultants  
Centerville, Ohio

Alain G. Muzet  
Centre d'Etudes de Physiologie Appliquée du CNRS  
Strasbourg, France

Bernard F. Berry  
Berry Environmental Ltd.  
Shepperton, Surrey, United Kingdom

### 1 INTRODUCTION

Sleep disturbance is a common effect of exposure to community noise, especially for transportation noise, such as that from aircraft, road traffic, and railways. Protection of sleep is necessary for a good quality of life,<sup>1,2</sup> as daytime well-being often depends on the previous night's sleep quality and efficiency. Sleep disturbance research has produced a considerable variability of results and little concrete guidance on how to assess potential sleep disturbance in a community. The absence of one internationally accepted exposure–effect (or dose–response) relationship is largely due to the lack of one “best choice” research technique, as well as the complex interactions of the many factors that influence sleep disturbance. Little is known about the *long-term, cumulative effects* of intermittent sleep disturbance from community noise exposures and only a handful of large-scale field studies have been conducted over the past decade. In spite of these limitations, current scientific data on noise-induced sleep disturbance can be used to support transportation-related environmental noise impact analyses, land-use planning, housing sound insulation programs, and related environmental noise management activities. This chapter provides information on noise exposure metrics, human response measures, dose–response curves, and recommended noise exposure criteria for predicting and assessing sleep disturbance at the community level.

### 2 WHY IS PREDICTION OF SLEEP DISTURBANCE IMPORTANT?

Most community development, such as a new highway or a new commuter rail line, projects result in an increase in community noise. The environmental impact analysis process and related environmental noise management activities should involve the prediction of future sleep disturbances due to the

expected increase in noise levels when increased nighttime noise exposures are expected. When a community development project involves nighttime noise exposure, it is important to consider the major impacts expected, including both sleep disturbance and community annoyance.

### 3 NOISE EXPOSURE – DIFFERENT METRICS AND NOISE CHARACTERISTICS

The sleep disturbance field study database described below consists largely of data from aircraft noise studies, although there are some data points from studies of road and rail traffic. This limitation should be considered when predicting sleep disturbance from the latter two sources. Different indices have been used to describe various community noise exposures, and there is no general agreement on which should be preferred among the many various available noise indices. The choice of noise metrics for establishing exposure criteria depends on both the particular type of noise source and the particular effect being studied. Even for sleep disturbance due to transportation noise exposure, there is no single noise exposure metric or measurement approach that is generally agreed upon. One important review of the sleep disturbance literature by Pearsons et al.<sup>3</sup> showed that, overall, sound exposure level (SEL) was a better predictor of sleep disturbance across the various studies included in their metaanalysis than was the maximum frequency–weight sound pressure level ( $L_{AFmax}$ ). However, other reviews of the literature showed that measures of peak sound pressure level are better predictors of disturbances during sleep than measures of average sound pressure level.<sup>4</sup> The community noise guidelines recently published by the World Health Organization (WHO<sup>1</sup>) allow the use of either  $L_{AFmax}$  or SEL. Thus, there is still no consensus on the best metric to use.

## 4 SLEEP DISTURBANCE

### 4.1 How to Assess Sleep Disturbance — Objective Evaluation of Sleep Disturbance

A variety of different techniques have historically been used in sleep disturbance research. Some studies are conducted in research laboratories using simulated noise exposures,<sup>5,6</sup> while other studies are conducted in “field settings”—that is, in people’s own homes—using actual community noises. The effects of noise on sleep can be measured immediately or evaluated afterwards—at the end of the night or during the following day. Immediate effects are mainly measured by objective data recorded during sleep, and they show how the sleeper is reacting to noise, either in terms of changes in sleep stage architecture or behaviorally indicated awakenings. Sleep stage architecture measurements include the following:

**Sleep Architecture** The stage and cycle infrastructure of rapid eye movement (REM) and non-REM sleep, as these relate to each other for the individual.

**Sleep Structure** Similar to sleep architecture. However, sleep structure—in addition to encompassing sleep stage and cycle relationships—assesses the within-stage qualities of the electroencephalogram (EEG) and other physiological attributes.

Aftereffects are measured in the morning by subjective evaluations of sleep quality or by objective biochemical data (such as levels of stress hormones, including adrenalin, noradrenalin, and cortisol)<sup>7–9</sup> or by performance levels during the following day.<sup>10,11</sup>

Because of the differences in research techniques used in sleep disturbance studies, it is not surprising that the results of various studies are quite different from each other, especially conclusions about the number of sleep stage changes and awakenings. Many published field studies present limited noise exposure data and limited sleep disturbance indices, mainly because the choice of measurement methods and sleep disturbance indicators are still controversial. This is particularly the case for studies using either behavioral awakening, as indicated by pushing a button when awakened,<sup>12</sup> and/or body motility (i.e., body movement as measured by an actimeter) as indicators of nocturnal awakening.<sup>13,14</sup> However, changes in sleep architecture, including both sleep stage changes and short-lasting awakenings as determined by EEG recordings, are more subtle and would often be totally missed by both the button-press and the actimetry research techniques. In addition, EEG recordings provide considerable data on a variety of sleep-related parameters. This technique is most useful for new research to increase our knowledge about the basic mechanisms of sleep.

Electroencephalographic studies provide the most detailed information about changes in sleep architecture in response to intruding noises and involve well-established research techniques for improving our understanding of the mechanisms of sleep, but the

long-term effects of the observed EEG responses are not known. Thus, it is difficult to determine practical noise exposure criteria using these data. Although physiological indicators of awakening would ideally provide the best data, usable conclusions from research using EEG and other physiological parameters, especially data from field research studies, are not yet ready for use in establishing noise exposure policies. Thus, guidelines for nighttime noise exposure are presently based on behavioral measures, either awakenings or bodily movements.

Each measurement approach has its own advantages and disadvantages. Behavioral awakening studies provide a clear and unambiguous indicator of awakening. However, there could be human responses to nighttime noise intrusions that do not result in sufficient awakening for the person to push the test button. Body motility studies provide a considerable amount of data on bodily movements that could indicate a stress response, but there is no way to determine whether or not a person was awakened by the noise, which would be a more clear indicator of an effect. In addition, body movements during sleep are quite normal physiological events. Only a small amount of them result in behavioral awakenings and only some of these could be attributed to noise; most nighttime body movements do not result in awakening.<sup>14</sup> Therefore, measuring bodily movement by actimetric techniques during sleep has limitations as a technique for predicting awakenings. However, it is a valuable research technique that can be used in people’s homes and is relatively inexpensive. The EEG recording technique provides some of the most detailed and useful information about sleep disturbance, but the results of EEG studies in the laboratory need real-world confirmation and validation in field studies, which are very expensive and quite difficult to perform.

## 5 IMMEDIATE EFFECTS

The following list includes some of the various objective physiological, biochemical, and behavioral measures used to assess the immediate effects of nighttime noise:

- Electroencephalograph arousal responses
- Sleep stage changes
- Nocturnal awakenings
- Total waking time
- Autonomic responses

## 6 AFTEREFFECT MEASURES

Chronic partial sleep deprivation induces marked tiredness, increases a low vigilance state, and reduces both daytime performance and the overall quality of life.<sup>1,15</sup> Other measures made after nighttime noise exposure include a variety of daytime task performance tests and tests of cognitive functioning, and the excretion of stress hormones in the morning urine flow can be measured by researchers to evaluate the impact

of overall noise exposure at night.<sup>16,17</sup> However, all of these types of measurements are quite difficult to perform in field situations and only a few studies have included them in recent years.

## 7 HEALTH EFFECTS

The goal of the scientific community is to be able to link sleep disturbance from noise exposure with long-term health impacts. Of particular interest is the possible relationship between noise and the stress responses it produces. These stress responses have the potential to be linked to hypertension, cardiovascular disease, and other severe medical problems.<sup>18–26</sup> However, it is difficult to separate out the effects of just the noise exposure because undisturbed sleep, as a prerequisite to good health, requires an environment with all of the following:

- Adequate noise environment
- Clean room air
- Adequate room temperature
- Adequate atmospheric humidity
- Adequate darkness

Thus, protection of sleep in community populations requires a broader health perspective. The combination of many different types of community noise sources, in conjunction with many nonnoise environmental factors, can have a significant impact on sleep quality and overall health. There is also a need to protect sensitive groups and shift workers who sleep during the day.<sup>27</sup>

## 8 SUBJECTIVE EVALUATION OF SLEEP DISTURBANCE

Recordings of objective sleep disturbance data can be too costly and too difficult to use with large samples of the population or when research funding is scarce, while subjective evaluation of sleep quality using a morning-after questionnaire is an easier and less costly way of collecting field data. Sleep disturbance can be assessed from complaints about bad sleep quality, nocturnal awakenings, often accompanied by impaired quality of the subsequent daytime period with increased tiredness, daytime sleepiness, and need for compensatory resting periods. However, the use of subjective complaints is quite different than an assessment based on objective (instrumental) measures. There are many factors that influence people's subjective evaluations of their own sleep quality. It has been very difficult for researchers to find a clear relationship between subjective complaints and actual noise exposure levels. In general, however, subjective self-reports of awakenings do not correlate well with more objective measures of sleep disturbance.<sup>28–30</sup> In the Netherlands Organization for Applied Scientific Research (TNO) analysis by Passchier-Vermeer, et al.,<sup>29</sup> no relationship could be established between a measure of the total night's exposure, the nighttime, 8-h, equivalent continuous A-weighted sound pressure

level ( $L_{Aeq,8h}$ ) (defined as  $L_{night}$ ) and self-reported sleep disturbance on the basis of the analysis of aircraft noise surveys. Thus, future use of self-reports of movement, awakenings, or other sleep-related effects, needs serious reconsideration because of the questionable validity of self-report data for predicting actual responses to noise events.

## 9 LABORATORY VERSUS IN-HOME FIELD STUDIES

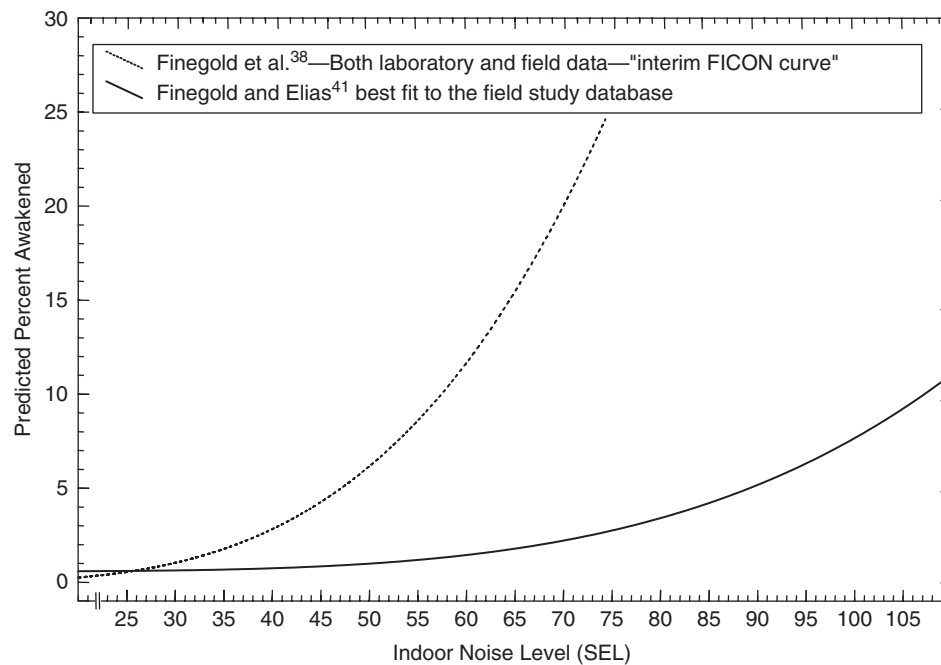
Survey of the literature shows large differences between results obtained in numerous laboratory studies and those issued from epidemiological or experimental studies made in real in-home situations. In the Pearsons et al.<sup>3</sup> metaanalysis, a comprehensive database representing over 25 years of both laboratory and field research on noise-induced sleep disturbance was compiled and analyzed. Those researchers firmly established the rather large differences observed between laboratory and in-home field studies, with nocturnal awakenings being much greater in laboratory studies. It would certainly be the case that a certain degree of habituation occurs in people's own homes for the number of noise-induced awakenings they experience. On the other hand, modifications in sleep stage architecture, especially the relationships between the time spent in the various sleep stages, show little habituation with time, while purely autonomic responses, such as heart rate, breathing rate, and systolic blood pressure, do not habituate at all over extended periods of time.<sup>31–34</sup>

## 10 CURRENT EXPOSURE-RESPONSE RELATIONSHIPS FOR SLEEP DISTURBANCE

### 10.1 Position of the European Commission

In July 2002 the European Commission (EC) published the "EU Directive on the Assessment and Management of Environmental Noise" (END).<sup>35</sup> This document specifies  $L_{night}$  as the indicator for sleep disturbance, although a response measure for sleep disturbance has not yet been selected. As part of developing the END, the European Commission contracted with TNO to derive exposure-response relationships between  $L_{night}$  and sleep disturbance for transportation noise, which will be included in a future Annex to the END and will most likely use motility (i.e., body movements) as the response (more information on the proposed EC approach can be found in Passchier-Vermeer et al.<sup>29</sup> and Miedema et al.<sup>36</sup>). TNO recognized that outdoor nighttime noise exposure at the most exposed facade of a dwelling (in terms of  $L_{night}$ ) is not the only acoustical factor that influences sleep disturbance. Therefore, attention is being given to the role of other factors, notably the actual noise exposure at the facade of the bedroom and the difference between outdoor and indoor noise levels (sound insulation) of bedrooms. There is also concern about whether using only a metric that describes the whole night exposure, such as  $L_{night}$ , is sufficient or whether an individual event metric is also needed. Vallet<sup>37</sup> has argued for a





**Figure 1** Finegold and Elias<sup>41</sup> sleep disturbance prediction curve and earlier FICON<sup>39</sup> interim curve.

supplementary indicator,  $L_{\max}$ , to be used in addition to  $L_{\text{night}}$ .

## 10.2 Sleep Disturbance Exposure–Response Relationships in the United States

In an early but quite important study, Pearsons et al.<sup>3</sup> compiled a comprehensive database representing over 25 years of both laboratory and field research on noise-induced sleep disturbance due to a variety of noise sources. This database was the basis for an interim curve recommended by Finegold et al.<sup>38</sup> to predict the percent of exposed individuals awakened as a function of indoor A-weighted sound exposure level (ASEL). This curve was adopted by the U.S. Federal Interagency Committee on Noise (FICON)<sup>39</sup> as an “interim” sleep disturbance curve with the caveat that additional research was needed. Since the publication of the FICON report, a series of additional field studies were conducted in the United States to further investigate noise-induced sleep disturbance from transportation noise sources, primarily aircraft noise, in various residential settings. Based on this series of field studies, BBN Laboratories developed an exposure–response relationship, which was recommended in the U.S. ANSI Standard S12.9, Part 6, Methods for Estimation of Awakenings Associated with Aircraft Noise Events Heard in Homes.<sup>40</sup> The BBN Laboratories metaanalysis was redone with some changes in the metaanalysis approach, as described in Finegold and Elias.<sup>41</sup> The results of this new metaanalysis are

shown in Fig. 1. The 1992 FICON curve is also shown in this figure for comparison purposes.

Three of the eight studies included in this database contained data on road traffic noise exposure, and thus it is deemed at least minimally sufficient to use this curve in predicting sleep disturbance due to road traffic noise. Six of the eight studies included data from aircraft noise exposures, but only one study contributed data on railway noise. Thus, sleep disturbance due to railway noise is the weakest part of the database. However, the final predictive curve averages together the responses to all transportation noise sources, making it, on average, reasonably applicable to all three transportation noise source categories: aircraft, road traffic, and railways. However, the Finegold and Elias<sup>41</sup> predictive curve only accounts for about 22% of the overall variance in the data. This means that sleep disturbance researchers are still not able to make very accurate predictions of sleep disturbance, especially at the community level. The reason for this is that there are many nonacoustic factors that affect people’s responses to noise during sleep in addition to the level and spectral properties of the intruding noise.

Figure 1 can be used to predict the level of sleep disturbance expected as a result of community development projects, such as adding an additional runway at an airport or changing a two-lane road into a major thoroughfare, where the future noise exposure can be modeled or otherwise estimated. For projects such as these that involve government funding, an environmental impact analysis is typically required. Noise issues, such as community annoyance



and sleep disturbance, are often highly controversial components of such an analysis. Accurate prediction of the effects of noise on affected communities is the foundation of informed noise management decisions and is a critical component of the environmental impact analysis process (see Chapter 127 of this handbook for a discussion of this topic).

## 11 EXPOSURE CRITERIA FOR ASSESSING SLEEP DISTURBANCE

The most common metrics for assessing the impacts of community noise, such as the day–night average sound pressure level (DNL), already contain a strong 10-dB penalty for nighttime noises, and community noise exposure policies typically do not include separate criteria for sleep disturbance. However, there are circumstances where a separate analysis of the impacts of nighttime noise is warranted. The World Health Organization<sup>1</sup> recommends that the indoor sound pressure levels should not exceed 45 dB  $L_{AFmax}$  more than 10 to 15 times per night for individual intrusive events and should not exceed an 8-h, equivalent continuous A-weighted sound pressure level ( $L_{Aeq,8h}$ ) of 30 dB for continuous total-night noise exposure in order to avoid negative effects on sleep, especially for transportation noise sources. WHO allows the use of either  $L_{AFmax}$  or SEL as the exposure metric. For intermittent events that approximate aircraft noise, with an effective duration of 10 to 30 s, values of 55 to 60 dB SEL correspond to an  $L_{AFmax}$  value of 45 dB. These criteria, however, do not take into account the practicality of achieving these goals. This understanding is important to efforts to implement the recommended criteria at the community level. According to WHO,<sup>1</sup> “the evaluation of (noise) control options must take into account technical, financial, social, health and environmental factors. . . . Cost-benefit relationships, as well as the cost-effectiveness of the control measures, must be considered in the context of the social and financial situation of each country.” WHO intended that these criteria be used as part of an environmental noise management decision-making process for which the environmental noise impact analysis process is one of the central issues, for managing impacts such as sleep disturbance. Most countries, including the United States, do not yet have noise exposure criteria specifically to address potential sleep disturbances in communities, although many European Union countries are considering taking this step, especially in the vicinity of large airports with numerous nighttime flight operations. Of course, it is true that assumptions about average attenuation value of housing sound insulation to meet indoor noise exposure criteria are only valid with the windows closed, even though this reduces the overall air quality in the bedroom.

In an environmental impact analysis or other use of the WHO criteria, it is important to remember that the exposure criteria is just one point along an exposure–response curve, and that these criteria are only “guidelines” not regulations. The overall environmental noise decision-making process should also consider

the cost and technical trade-offs involved in attempting to meet any particular exposure criterion. This allows some flexibility in addressing the engineering and financial issues involved in trying to meet the recommended exposure goals, rather than simply strictly applying exposure criteria without these considerations being taken into account.

## 12 SUMMARY

Although the most common metrics for assessing the impacts of community noise, day–night average sound pressure level (DNL) and day–evening–night average sound pressure level (DENL), already contain a 10-dB penalty for nighttime noises, there are circumstances where a separate analysis of the impacts of nighttime transportation noise is warranted, particularly in environmental impact analyses and related efforts. There are, however, different definitions of sleep disturbance and different ways to measure it, different exposure metrics that can be used, and consistent differences in the results of laboratory versus field studies. At the present time, very little is known about how, why, and how often people are awakened during the night, although it is generally acknowledged that the “meaning of the sound” to the individual, such as a child crying, is a strong predictor of awakening. More importantly, very little is known about the *long-term, cumulative effects* of intermittent sleep disturbance from community noise exposures.

This chapter briefly discussed the various approaches used in sleep disturbance research and presented the best information currently available to describe the exposure–response relationship between transportation noise exposure and sleep disturbance, although existing sleep disturbance databases for transportation noise sources contain considerably more data for aircraft noise exposure than for exposure to road traffic or railway noise. There are large differences between communities in their responses to community noises. Some of the reasons for this include differences in the characteristics of the noise itself, differences in individual sensitivities, differences in attitudinal biases toward the noise source, and the context of the living environment. Current exposure–response relationships use either “awakenings” or “body movements” to describe sleep disturbance.

Finally, this chapter also briefly discussed the issue of noise exposure criteria for sleep disturbance and how to use existing criteria in making community noise management decisions. The World Health Organization<sup>1</sup> has recommended that nighttime indoor sound pressure levels should not exceed approximately 45 dB  $L_{AFmax}$  more than 10 to 15 times per night. For intermittent events similar to aircraft overflights, with an effective duration of 10 to 30 s, this corresponds to indoor values of 55 to 60 dB SEL. According to WHO, either  $L_{AFmax}$  or SEL may be used if the noise is not continuous. For total night exposure, a criterion of 30 dB  $L_{Aeq,8h}$  was recommended for use in combination with the single event criterion ( $L_{AFmax}$  or SEL). At the present time, the WHO exposure criteria are

recommended for general transportation noise sources. It needs to be pointed out, however, that the criteria recommended by WHO are long-term targets and do not take into consideration the cost or technical feasibility of meeting their recommended ideal maximum exposure levels. WHO intended that these criteria be used as part of a noise management decision-making process, for which environmental noise impact analysis is the central issue. The Finegold and Elias<sup>41</sup> exposure-response curve allows consideration of the different levels of impact predicted at various levels of exposure and is recommended for use in predicting sleep disturbance in communities due to exposure to transportation noise, particularly aircraft noise.

## REFERENCES

1. World Health Organization (WHO), *Guidelines for Community Noise*, B. Berglund, T. Lindvall, D. Schwela, and K-T Goh, Eds., Geneva, WHO, 2000 (also available from the Internet at <http://whqlibdoc.who.int/hq/1999/a68672.pdf> or, <http://www.who.int/docstore/peh/noise/guidelines2.html>).
2. J. A. Hobson, *Sleep*, Scientific American Library, W.H. Freeman, New York, 1989.
3. K. Pearsons, D. S. Barber, B. Tabachnick, and S. Fidell, Predicting Noise-Induced Sleep Disturbance, *J. Acoust. Soc. Am.*, Vol. 97, 1995, pp. 331–338.
4. B. Berglund, T. Lindvall, and S. Nordin, Adverse Effects of Aircraft Noise, *Environ. Int.*, Vol. 16, 1990, pp. 315–338.
5. M. Basner, H. Buess, D. Elmenhorst, A. Gerlich, N. Luks, H. Maaß, L. Mawet, E.-W. Müller, G. Plath, J. Quehl, A. Samel, M. Schulze, M. Vejvoda, and J. Wenzel, Effects of Nocturnal Aircraft Noise (Vol. 1): Executive Summary (DLR report FB 2004-07/E), Cologne, German Aerospace Center (DLR) Institute of Aerospace Medicine, 2004 (also available on the Internet at <http://www.dlr.de/me/Institut/Abteilungen/Flugphysiologie/Fluglaerm/>).
6. A. Samel, M. Basner, H. Maaß, U. Müller, G. Plath, J. Quehl, and J. Wenzel, Effects of Nocturnal Aircraft Noise—Overview of the DLR Human Specific Investigations, in *Proceedings of INTER-NOISE 2004*, O. Jiricek and J. Novak, Eds., CD-ROM, 22–25 August, Prague, Czech Republic, 2004 (available for purchase on the Internet at <http://www.atlasbooks.com/marktplc/00726.htm>).
7. N. L. Carter, Transportation Noise, Sleep, and Possible After-Effects, *Environ. Int.*, Vol. 22, 1996, pp. 105–116.
8. C. Maschke, Noise-Induced Sleep Disturbance, Stress Reactions and Health Effects,” in *Protection Against Noise, Vol. 1: Biological Effects*, D. Prasher and L. Luxon, Eds., London, Whurr Publishers for the Institute of Laryngology and Otology, 1998.
9. C. Maschke, J. Harder, H. Ising, K. Hecht, and W. Thierfelder, Stress Hormone Changes in Persons Exposed to Simulated Night Noise, *Noise & Health*, Vol. 5; No. 17, 2002, pp. 35–45.
10. A. P. Smith, Noise, Performance Efficiency and Safety, *Int. Arch. Occupat. Environ. Health*, Vol. 62, 1990, 1–5.
11. R. T. Wilkinson and K. B. Campbell, Effects of Traffic Noise on Quality of Sleep: Assessment by EEG, Subjective Report, or Performance Next Day, *J. Acoust. Soc. Am.*, Vol. 75, 1984, pp. 468–475.
12. S. Fidell, K. Pearsons, B. Tabachnick, R. Howe, L. Silvati, and D. S. Barber, Field Study of Noise-Induced Sleep Disturbance, *J. Acoust. Soc. Am.*, Vol. 98, No. 2, 1995, pp. 1025–1033.
13. S. Fidell, K. Pearsons, B. G. Tabachnick, and R. Howe, Effects on Sleep Disturbance of Changes in Aircraft Noise near Three Airports, *J. Acoust. Soc. Am.*, Vol. 107, 2000, pp. 2535–2547.
14. J. A. Horne, F. L. Pankhurst, L. A. Reyner, K. Hume, and I. D. Diamond, A Field Study of Sleep Disturbance: Effect of Aircraft Noise and Other Factors on 5,742 Nights of Actimetrically Monitored Sleep in a Large Subject Sample, *Sleep*, Vol. 17, 1994, pp. 146–159.
15. E. Öhrström and B. Griefahn, Summary of Team 5: Effects of Noise on Sleep, in *Proceedings of the 6th International Congress on Noise as a Public Health Problem: Noise & Man '93*, M. Vallet, Ed., Nice, France, 5–9 July 1993, Institut National de Recherche sur les Transport et leur Sécurité, Nice, 1993, Vol. 3, pp. 393–403.
16. N. L. Carter, S. N. Hunyor, G. Crawford, D. Kelly, and A. J. Smith, Environmental Noise and Sleep—A Study of Arousals, Cardiac Arrhythmia and Urinary Catecholamines, *Sleep*, Vol. 17, 1994, pp. 298–307.
17. C. Maschke, S. Breinl, R. Grimm and H. Ising, The Influence of Nocturnal Aircraft Noise on Sleep and on Catecholamine Secretion, in *Noise and Disease*, H. Ising and B. Kruppa, Eds., Gustav Fischer, Stuttgart, 1993, pp. 402–407.
18. N. L. Carter, P. Ingham, K. Tran, and S. Huynor, A Field Study of the Effects of Traffic Noise on Heart Rate and Cardiac Arrhythmia During Sleep, *J. Sound Vib.*, Vol. 169, No. 2, 1994, pp. 221–227.
19. N. L. Carter, Cardiovascular Response to Environmental Noise During Sleep, in *Proceedings of 7th International Congress on Noise as a Public Health Problem*, Vol. 2, Sydney, Australia, 1998, pp. 439–444.
20. J. Di Nisi, A. Muzet, J. Ehrhart, and J. P. Libert, Comparison of Cardiovascular Responses to Noise During Waking and Sleeping in Humans, *Sleep*, Vol. 13, 1990, pp. 108–120.
21. B. Griefahn, Noise-Induced Extraaural Effects, *J. Acoust. Soc. Jpn. (E)*, Vol. 21, 2000, pp. 307–317.
22. B. Griefahn, Sleep Disturbances Related to Environmental Noise, *Noise and Health*, Vol. 4, No. 15, 2002, pp. 57–60.
23. C. Maschke, Epidemiological Research on Stress Caused by Traffic Noise and Its Effects on High Blood Pressure and Psychic Disturbances, in *Proceedings of ICBEN 2003: 8th International Congress on Noise as a Public Health Problem*, R. de Jong, Ed., CD-ROM, 29 June–3 July, 2003, Rotterdam, The Netherlands, 2003.
24. S. A. Stansfeld and P. Lercher, Non-Auditory Physiological Effects of Noise: Five Year Review and Future Directions, in *Proceedings of ICBEN 2003: 8th International Congress on Noise as a Public Health Problem*, R. de Jong, Ed., CD-ROM, 29 June–3 July, 2003, Rotterdam, The Netherlands, 2003.
25. W. Passchier-Vermeer, *Noise and Health*, Health Council of the Netherlands, The Hague (Publication No A93/02E), TNO Institute of Preventive Health Care, Leiden, 1993.
26. W. Passchier-Vermeer, Effects of Noise and Health, Report on Noise and Health Prepared by a Committee

- of the Health Council of The Netherlands, *Noise/News Int.*, 1996, pp. 137–150.
27. N. Carter, R. Henderson, S. Lal, M. Hart, S. Booth, and S. Hunyor, Cardiovascular Autonomic Response to Environmental Noise During Sleep in Night Shift Workers, *Sleep*, Vol. 25, 2002, pp. 457–464.
  28. A. Muzet, Noise Exposure from Various Sources—Sleep Disturbance, Dose-Effects Relationships on Adults (Paper 5038933-2002/6), Report to World Health Organization (WHO) Technical Meeting on Exposure-Response Relationships of Noise on Health, 19–21 September 2002, Bonn, Germany. Strasbourg, France: CEPA-CNRS, 2002. (May also be requested from WHO Regional Office for Europe, Bonn. See: <http://www.euro.who.int/noise/>.)
  29. W. Passchier-Vermeer, H. Vos, J. H. M. Steenbekkers, F. D. van der Ploeg, and K. Groothuis-Oudshoorn, Sleep Disturbance and Aircraft Noise, Exposure-Effect Relationships (Report nr 2002.027), Leiden, TNO-PG, 2002.
  30. W. Passchier-Vermeer, Night-Time Noise Events and Awakening (TNO INRO report 2003-32), Delft, The Netherlands; Netherlands Organisation for Applied Scientific Research (TNO), 2003.
  31. B. Griefahn, Long-Term Exposure to Noise. Aspects of Adaptation, Habituation and Compensation, *Waking & Sleeping*, Vol. 1, 1977, pp. 383–386.
  32. A. Muzet and J. Ehrhart, Habituation of Heart Rate and Finger Pulse Responses to Noise During Sleep. in *Proceedings of the Third International Congress on Noise as a Public Health Problem*, J. V. Tobias, Ed., ASHA Reports (No. 10), Rockville, Maryland, 1980, pp. 401–404.
  33. A. Muzet, J. Ehrhart, R. Eschenlauer, and J. P. Lienhard, Habituation and Age Differences of Cardiovascular Responses to Noise During Sleep, *Sleep*, Vol. 3, 1980, 212–215.
  34. E. Öhrström, and M. Björkman, Effects of Noise-Disturbed Sleep—A Laboratory Study on Habituation and Subjective Noise Sensitivity, *J. Sound Vib.*, Vol. 122, 1988, pp. 277–290.
  35. European Commission, *EU Directive on the Assessment and Management of Environmental Noise (END)*, The European Parliament and the Council of the European Union, 2002 (also available for download on the Internet at [http://europa.eu.int/eur-lex/pri/en/oj/dat/2002/l\\_189/l\\_18920020718en00120025.pdf](http://europa.eu.int/eur-lex/pri/en/oj/dat/2002/l_189/l_18920020718en00120025.pdf)).
  36. H. M. E. Miedema, W. Passchier-Vermeer, and H. Vos, Elements for a Position Paper on Night-time Transportation Noise and Sleep Disturbance (TNO Inro Report 2002-59), Delft, Netherlands Organisation for Applied Scientific Research, 2003 (also available on the Internet as a European Commission Position Paper at <http://europa.eu.int/comm/environment/noise/pdf/noisesleepdisturbance.pdf>).
  37. M. Vallet, Lmax at Night: A Supplementary Index to the EU Directive on Noise, in *Proceedings of ICBEN 2003: 8th International Congress on Noise as a Public Health Problem*, R. de Jong, Ed., CD-ROM, 29 June–3 July 2003, Rotterdam, The Netherlands, 2003.
  38. L. S. Finegold, C. S. Harris, and H. E. von Gierke, Community Annoyance and Sleep Disturbance: Updated Criteria for Assessing the Impacts of General Transportation Noise on People, *Noise Control Eng. J.*, Vol. 42, No. 1, 1994, pp. 25–30.
  39. Federal Interagency Committee on Noise (FICON), *Federal Agency Review of Selected Airport Noise Analysis Issues*, FICON, Washington, DC, 1992.
  40. American National Standards Institute (ANSI), Quantities and Procedures for Description and Measurement of Environmental Sound—Part 6: Methods for Estimation of Awakenings Associated with Aircraft Noise Events Heard in Homes (ANSI S12.9.-2000/Part 6), 2000. Available from the Standards Secretariat, Acoustical Society of America, Melville, NY.
  41. L. S. Finegold and B. Elias, A Predictive Model of Noise Induced Awakenings from Transportation Noise Sources, in *Proceedings of INTER-NOISE 2002* (CD-ROM), 19–21 August 2002, Dearborn, MI. (available for purchase on the Internet from <http://www.atlasbooks.com/marktplc/00726.htm>).

## BIBLIOGRAPHY

- Berglund, B. and T. Lindvall, Eds., Community Noise, Document prepared for the World Health Organization, Univ. of Stockholm, *Archives of the Center for Sensory Research*, Vol. 2, 1995, pp. 1–195. This document can be downloaded from the Internet at: <http://www.who.int/phe>.
- Berglund, B. Community Noise in a Public Health Perspective, in *Proceedings of INTER-NOISE 98, Sound and Silence: Setting the Balance*, V. C. Goodwin and D. C. Stevenson, Eds., Vol. 1, New Zealand Acoustical Society, Auckland, New Zealand, 1998, pp. 19–24.
- Cole, R. J., D. F. Kripke, W. Gruen, D. J. Mullaney, and J. C. Gillin, Automatic Sleep/Wake Identification from Wrist Activity, *Sleep*, Vol. 15, 1992, pp. 461–469.
- Griefahn, B., Noise and Sleep—Present State (2003) and Further Needs, in *Proceedings of ICBEN 2003: 8th International Congress on Noise as a Public Health Problem*, R. de Jong, Ed., CD-ROM, 29 June–3 July, 2003, Rotterdam, The Netherlands.
- Griefahn, B., C. Deppe, P. Mehnert, R. Moog, U. Moehler, and R. Schuemer, What Nighttimes Are Adequate to Prevent Noise Effects on Sleep? in *Noise as a Public Health Problem* (Noise Effects '98), Vol. 2, N. L. Carter and R. F. S. Job, Eds., Noise Effects '98 PTY Ltd., Sydney, Australia, 1998, pp. 445–450.
- Griefahn, B., A. Schuemer-Kohrs, R. Schuemer, U. Moehler, and P. Mehnert, Physiological, subjective, and Behavioural Responses to Noise from Rail and Road Traffic, *Noise & Health*, Vol. 3, 2000, 59–71.
- Ising, H. and M. Ising, Chronic Cortisol Increases in the First Half of the Night Caused by Road Traffic Noise, *Noise & Health*, Vol. 4, 2002, 13–21.
- Maschke, C., J. Harder, K. Hecht, and H. U. Balzer, Nocturnal Aircraft Noise and Adaptation, in *Proceedings of the Seventh International Congress on Noise as a Public Health Problem*, Vol. 2, N. Carter & R. F. S. Job, Eds., Noise Effects '98 Pty Ltd., Sydney, Australia, 1998, pp. 433–438.
- Maschke, C., K. Hecht, and U. Wolf, Nocturnal Awakenings Due to Aircraft Noise. Do Wake-up Reactions Begin at Sound Level 60 dB(A)? *Noise & Health*, Vol. 6, 24, 2004, pp. 21–33.
- Öhrström, E., A. Agge, and M. Björkman, Sleep Disturbances before and after Reduction in Road Traffic Noise, in *Proceedings of the Seventh International Congress on Noise as a Public Health Problem*, Vol. 2, N. Carter and R. F. S. Job, Eds., Noise Effects '98 Pty Ltd., Sydney, Australia, 1998, pp. 451–454.

- Öhrström E., and H. Svensson, Effects of Road Traffic Noise on Sleep, in *Proceedings of ICBEN 2003: 8th International Congress on Noise as a Public Health Problem*, R. de Jong, Ed., CD-ROM, 29 June–3 July, 2003, Rotterdam, The Netherlands.
- Passchier-Vermeer, W., Aircraft Noise and Sleep: Study in the Netherlands, in *Proceedings of ICBEN 2003: 8th International Congress on Noise as a Public Health Problem*, R. de Jong, Ed., CD-ROM, 29 June–3 July, 2003, Rotterdam, The Netherlands.
- Pearsons, K. S., Recent Field Studies in the United States Involving the Disturbance of Sleep from Aircraft Noise, in *Proceedings of INTER-NOISE 96: Noise Control—The Next 25 Years*, Vol. 5, F.A. Hill and R. Lawrence, Eds. Institute of Acoustics, St. Albans, UK, 1996, pp. 2271–2276.
- Pearsons, K. S., Awakening and Motility Effects of Aircraft Noise, in *Proceedings of the Seventh International Congress on Noise as a Public Health Problem*, vol. 2, N. Carter and R. F. S. Job, Eds., Noise Effects '98 Pty Ltd., Sydney, Australia, 1998, pp. 427–32.
- Stansfeld, S. A. and P. Lercher, Non-auditory Physiological Effects of Noise: Five Year Review and Future Directions, in *Proceedings of ICBEN 2003: 8th International Congress on Noise as a Public Health Problem*, R. de Jong, Ed., CD-ROM, 29 June–3 July, 2003, Rotterdam, The Netherlands.
- Vallet, M., J. M. Gagneux, and F. Simonnet, Effects of Aircraft Noise on Sleep: An in situ Experience, In *Proceedings of the Third International Congress on Noise as a Public Health Problem*, J. V. Tobias, Ed., ASHA Reports (No. 10), Rockville, MD, 1980, pp. 391–396.
- Vallet, M., J. M. Gagneux, V. Blanchet, B. Favre, and G. Labiale, Long Term Sleep Disturbance Due to Traffic Noise, *J. Sound Vib.*, Vol. 90, 1983, pp. 173–191.
- Vallet, M., J. M. Gagneux, J. M. Clairet, J. F. Laurens, and D. Letisserand, Heart Rate Reactivity to Aircraft Noise after a Long Term Exposure, in *Proceedings of the Fourth ICBEN Congress on Noise as a Public Health Problem*, G. Rossi, Ed., Turin, Italy, 21–25 June 1983, Centro Ricerche E Studi Amplifon, Milano, 1983, pp. 965–971.
- van Kempen, E. E. M. M., H. Kruize, H. C. Boshuizen, C. B. Ameling, B. A. M. Staatsen, and A. E. M. de Hollander, The Association between Noise Exposure and Blood Pressure and Ischemic Heart Disease: A Meta-Analysis, *Environ. Health Perspectives*, Vol. 110, No. 3, 2002, 307–315.

# CHAPTER 25

## NOISE-INDUCED ANNOYANCE

Sanford Fidell  
Fidell Associates, Inc.  
Woodland Hills, California

### 1 INTRODUCTION

Annoyance is the adverse attitude that people form toward sounds that distract attention from or otherwise interfere with ongoing activities such as speech communication, task performance, recreation, relaxation, and sleep. With respect to annoyance, noise is not merely *unwanted sound*, but rather unbidden sound that someone *else* considers too inconvenient to control. No matter how sophisticated methods for predicting annoyance from purely acoustic variables become, annoyance remains at root a property of an unwilling listener. It is a listener engaged in ongoing activities, not a sound level meter or a computational algorithm, that is annoyed by noise.

Annoyance differs from loudness in its dependence on duration and context. Once a sound attains a duration of about a quarter of a second, it grows no louder. The annoyance of a sound, however, continues to grow in direct proportion to its duration. Further, although the loudness of a sound is fully determined by its acoustic content, the annoyance of a sound may vary considerably with the activity in which a listener is engaged at the time of its occurrence, and with its meaning. Great individual and contextual differences in sensitivity to the annoyance of sounds are more the rule than the exception.

### 2 ABSOLUTE ANNOYANCE OF INDIVIDUAL SOUNDS

The basic acoustic correlates of the annoyance of sounds are their level, duration, spectral content, frequency of occurrence, and—particularly in a community noise setting—time of day of occurrence. As a generality, higher level, longer duration, more frequently occurring, and higher frequency sounds tend to be more annoying than lower level, shorter duration, less frequently occurring, and lower frequency sounds. Second-order properties of the character of sounds (e.g., tonality, impulsiveness, phase, complexity, and harmonic structure) can also contribute to their annoyance, as can nonacoustic factors such as novelty, fear, economic dependence, attitudes of misfeasance and malfeasance, learned associations and aversions, and the like.

As a further generality, sounds that are more readily noticed in the presence of commonplace ambient noise environments (such as those with prominent tonal, narrow-band, high-frequency, or otherwise distinctive spectral content; cyclical or repetitive sounds; and sounds that are less masked by background noise) are likely to be considered more annoying than the

complementary sorts of sounds. A level of audibility roughly an order of magnitude greater than that required for simple detection of sounds in an attentive listening task is required for sounds to reliably intrude upon the awareness of people absorbed in unrelated ongoing activities.<sup>1</sup>

Note, however, that intermittent and unexpected sounds of relatively low level occurring in low-level indoor noise environments (e.g., dripping faucets, a key in a doorknob, or a footfall in a quiet bedroom at night, mechanical squeaks and rattles, heel clicks, or indistinct conversation in adjacent living quarters) can also be highly annoying.<sup>2,3</sup> The annoyance of such low-level sounds is related to their bandwidth-adjusted signal-to-noise ratio (“noticeability”) but exacerbated by nonacoustic factors such as their unexpectedness, novelty, and meaning. In fact, the annoyance of even higher level noise events (e.g., barking dogs, children playing, or motorcycle drivebys) may be more greatly influenced by nonacoustic and contextual factors than by their physical properties.

### 3 RELATIVE INFLUENCES OF ACOUSTICAL AND NONACOUSTICAL FACTORS ON ANNOYANCE JUDGMENTS

Laboratory studies provide the strongest evidence of the predictive utility of frequency-weighting procedures for assessments of noise-induced annoyance. The judgments of people asked under controlled listening conditions to compare the annoyance of artificial or meaningless sounds such as tones and bands of noise are generally well predicted by spectral weighting procedures. For example, A-level is consistently found to be superior to unweighted (overall) noise metric as a predictor of annoyance<sup>4,5</sup> and measures such as effective perceived noise level<sup>6</sup> account well for the effects of signal duration on annoyance. Note, however, that sounds of identical equivalent level and power spectra but different phase spectra, which are indistinguishable to a sound level meter, can vary greatly in their judged annoyance.<sup>7</sup>

More complex metrics such as loudness level<sup>8,9</sup> that are level- as well as frequency-dependent are yet better predictors of laboratory annoyance judgments.<sup>10</sup> In applications such as prediction of automotive sound quality, attributes such as “harshness,” or “roughness,” and even more elaborate descriptors are commonplace. These descriptors, which are sensitive to higher order acoustical properties such as harmonic and phase structures of individual sounds, have gained popularity for evaluations of the sound quality of mechanical

sources, including gear, pump, air intake and exhaust, electric motor, chassis and suspension, and door slam.<sup>11</sup>

Outside of controlled laboratory settings, accurate prediction of the annoyance of cumulative, long-term noise exposure has proven more elusive. Sounds of relatively low signal-to-noise ratio are sometimes judged to be disproportionately annoying,<sup>2,12</sup> while sounds of relatively high absolute level (e.g., those of rail and road traffic) may be considered less annoying than sounds of comparable A-weighted level produced by aircraft.<sup>13–15</sup> No population-level dosage–response relationship for predicting the prevalence of annoyance from cumulative, long-term noise exposure has yet accounted for the better part of the variance in annoyance prevalence rates in communities.<sup>15–17</sup>

The contrast between the utility of frequency-weighted noise metrics as descriptors of noise-induced annoyance in laboratory settings on the one hand and their obvious shortcomings in everyday circumstances of environmental noise exposure on the other has given rise to persistent doubts<sup>18</sup> about the practical utility of noise descriptors that are based on complex frequency-weighting methods. These doubts extend to the rationale for interpreting the tolerability of environmental noise exposure via noise metrics that are better predictors in laboratory than residential settings.

Much uncertainty continues to surround (1) the nature and number of acoustical parameters that could arguably improve the adequacy of noise descriptors as predictors of annoyance in residential settings; (2) the necessity of accounting for context dependency of annoyance judgments; (3) the relative influences of nonacoustic factors on annoyance judgments (e.g., time of day, frequency and regularity of noise intrusions, attitudes and situation-dependent expectations about noise sources and their operators, locus of control over exposure, and demographic factors); and (4) parsimonious ways to accommodate additional predictive parameters.

#### 4 NATURE OF NOISE METRICS INTENDED TO PREDICT ANNOYANCE

Most descriptors of individual and multiple noise events used to predict annoyance correlate more highly with one another than with annoyance judgments. No amount of specification of the spectral content, level, crest factor, harmonic complexity, dynamic range, or bandwidth-adjusted signal-to-noise ratio of individual noise events guarantees a precise account of the likelihood or degree to which an individual will judge them to be annoying.

Two types of acoustical descriptors have been developed to predict the annoyance of sounds: Those intended to account for source-specific judgments of the annoyance of individual events and those intended for use in assessments of environmental noise impacts. The former descriptors are more complex, detailed, and expensive to measure or calculate and, hence, most appropriately used in a few applications where their costs are justifiable. For

example, for purposes of aircraft noise certification, Part 36 of the U.S. Federal Aviation Regulations requires elaborately controlled measurements of tone- and duration-corrected perceived noise levels.

For larger scale analyses, such as gauging community-level reaction to prospective transportation noise exposure, less complex, A-weighted noise level descriptors such as day–night average sound pressure level, are commonplace.<sup>19,20</sup> These measures of cumulative noise exposure combine into a single index—and thus inextricably confound—all of the primary characteristics of noise events that could plausibly give rise to noise-induced annoyance. Regulatory efforts to predict community annoyance from acoustical measurements alone are typically driven by administrative convenience, expedience, and commercial interest, rather than by theory-based, scientific understanding of causes and mechanisms of annoyance. The rationale for combining level, duration, spectral content, and frequency and time of occurrence, and for ignoring all of the secondary and nonacoustic determinants of annoyance, is provided by the *equal-energy hypothesis*—the notion that sounds of identical energy content are equally annoying. This is a simplification adopted for the sake of tractable analyses of the complexity and variability of community noise exposure.

#### 5 DIRECT MEASUREMENT OF THE ANNOYANCE OF SOUNDS

Most empirical procedures for direct measurement of the annoyance of individual sounds are adaptations of classical psychophysical techniques such as the methods of limits and of adjustment. The most readily interpretable of these methods solicit direct comparisons of the annoyance of pairs of sequentially presented sounds. In adaptive paired comparison experimental designs, for example, test participants typically listen to a pair of sounds (one constant and one variable) within a given trial and judge which of the pair is the more annoying before the start of the next trial. Presentation levels (or durations, or spectral content, or any other manipulable signal property) of the variable signal are adjusted according to test protocols on successive presentations to yield estimates of points of subjective equality of annoyance, or other specifiable points on psychometric functions.

Less direct procedures for gauging the annoyance of sounds are also common, including variants of magnitude estimation (in which numbers are assigned in proportion to the judged intensity of sensations), semantic differential (in which judgments are solicited of the degree to which sounds possess variously described qualities), cross-modality matching (in which the annoyance of sounds is matched to some other perceptual quantity), and absolute judgment techniques (in which test category labels are assigned to the annoyance of sounds). In community settings, procedures for conventional social survey and questionnaire design are also well established.<sup>21</sup>

## 6 COMMON SOURCES OF NOISE-INDUCED ANNOYANCE IN COMMUNITY AND OTHER SETTINGS

In motorized urban society, transportation-related sources are by far the most pervasive and annoying sources of community noise exposure.\* Airport-related noise is the highest level and the most extensively studied form of transportation noise, even though it consequentially annoys only a small proportion of the urban population worldwide. Noise created by aircraft en route is a common source of annoyance throughout many suburban and rural areas, albeit at cumulative exposure levels considerably lower than in the vicinity of airport runways.

In high population density urban life, characterized by extensive indoor living, noises created in adjacent dwelling units (heel clicks, door slams, plumbing and high-volume air handling noise, household appliances, electronic entertainment, indistinct conversation, etc.) and street sounds (including emergency vehicle warning signals, garbage collection, and crowd noise) are salient sources of noise-induced annoyance, even when not heard at absolute levels as great as those characteristic of outdoor transportation sources. Rattling sounds produced as secondary emissions by household paraphernalia and by doors, windows, ducts, and other light architectural elements excited by low-frequency noise or vibration from remote sources are also common sources of annoyance in residences.<sup>3</sup>

## 7 ANNOYANCE AS THE BASIS OF U.S. FEDERAL POLICY ON SIGNIFICANCE OF COMMUNITY NOISE IMPACTS

Despite the limited success of efforts to predict annoyance from exclusively physical measures of noise exposure, annoyance remains the summary measure of environmental noise effects favored by U.S. federal agencies. According to the Federal Interagency Committee on Noise,<sup>22</sup> “the percent of the [noise] exposed population expected to be Highly Annoyed (%HA) [is] the most useful metric for characterizing or assessing noise impact on people.” The prevalence of a consequential degree of annoyance in a community (percentage highly annoyed, or %HA) is simply 100 times the number of people who describe themselves as highly annoyed when their opinions are directly solicited in a social survey, divided by the total number of people interviewed. In this context, the distinction between “individual annoyance” and “community annoyance” is merely one of level of aggregation.

\*In typical residential settings and on a nationwide basis, noise produced by industrial activities (including electrical power production and distribution, refinery and manufacturing noise, automotive repair, quarry blasting, etc.), by construction, by military training operations, and by a large miscellany of other sources are more localized and affect far fewer people than transportation noise.

FICON<sup>22</sup> has not only adopted annoyance as its preferred “summary measure of the general adverse reaction of people to noise” for assessment of community-level environmental noise effects, but also endorsed a specific fitting function as its preferred dosage–effect relationship:

$$\%HA = 100 / (1 + e^{11.13 - 0.141L_{dn}})$$

Although officially endorsed, FICON’s dosage–effect relationship accounts for only 19% of the variance in aircraft noise annoyance data and is not a reliable source of accurate or precise predictions of the annoyance of transportation noise exposure. Miedema and Vos<sup>15</sup> have suggested alternate, source-specific fitting functions for road, rail, and airborne noise sources. Fidell<sup>17</sup> and Fidell and Silvati<sup>23</sup> have documented large errors of prediction and other limitations of FICON’s relationship.

A major attraction of a dosage–effect relationship between cumulative noise and annoyance is that it permits treatment of community-level noise effects in acoustical terms and serves as an ostensible underpinning for “land-use compatibility” recommendations expressed in units of decibels. Such recommendations provide the form, if not the substance, of a rationale for gauging the “acceptability” of noise in residential and other circumstances of exposure.<sup>17</sup>

## 8 RELATIONSHIP BETWEEN ANNOYANCE AND COMPLAINTS IN COMMUNITY SETTINGS

Because annoyance is a covert mental process, self-report in response to a structured interview is its only direct measure. Complaints are an unsolicited form of self-report of dissatisfaction with noise exposure. Although the attitude of annoyance and the behavior of complaining are both manifested through self-report, they are not synonymous, and annoyance may not be the sole cause of complaints. Both forms of reaction to noise exposure are affected by acoustical and nonacoustical factors and thus reflect the combined influences of “true” sensitivity to physical characteristics of exposure and of response bias.<sup>†</sup> FICON<sup>22</sup> observes that “annoyance can exist without complaints and, conversely, complaints may exist without high levels of annoyance” and concludes that annoyance is a more reliable indication of environmental noise impacts than complaints. It is equally true, however, that high levels of noise-induced annoyance can exist at low levels of noise exposure, and that low levels of annoyance can exist at high levels of noise exposure. Thus, lack of a

<sup>†</sup>Signal detection theory<sup>24,25</sup> Green and Swets, 1966; offers a systematic framework for analyzing the independent contributions of sensitivity and response bias to any decision process. Viewing a self-report of the form “I’m highly annoyed by the noise of that aircraft flyover” as the product of a decision-like process provides a theory-based avenue to analysis of the annoyance of community noise exposure.

simple relationship between noise exposure and its effects is not a persuasive rationale for a narrow focus on annoyance, to the exclusion of complaints, as a meaningful indication of community response to noise.<sup>17</sup>

In practical reality, it makes no more sense to ignore noise complaints because they may or may not be closely related to annoyance than to ignore annoyance because it may or may not be closely related to complaints. Whether reports of adverse consequences of noise exposure are solicited or unsolicited is of importance more for administrative reasons than for evaluating actual noise impacts. Geographic distributions of complaint densities (complaints per unit time per unit area) can also yield important clues about reactions to community noise exposure that are not apparent from simple annoyance prevalence rates.<sup>17</sup>

## REFERENCES

1. M. Sneddon, K. Pearsons, and S. Fidell, Laboratory Study of the Noticeability and Annoyance of Sounds of Low Signal-to-Noise Ratio, *Noise Control Eng. J.*, Vol. 51, No. 5, 2003, pp. 300–305.
2. S. Fidell, S. Teffeteller, R. Horonjeff, and D. Green, Predicting Annoyance from Detectability of Low Level Sounds, *J. Acoust. Soc. Am.*, Vol. 66, No. 5, 1979, pp. 1427–1434.
3. S. Fidell, K. Pearsons, L. Silvati, and M. Sneddon, Relationship between Low-Frequency Aircraft Noise and Annoyance Due to Rattle and Vibration, *J. Acoust. Soc. Am.*, Vol. 111, No. 4, 2002, pp. 1743–1750.
4. Ricarda Bennett and Karl Pearsons, Handbook of Aircraft Noise Metrics, NASA Contractor Report 3406, 1981.
5. B. Scharf and R. Hellman, How best to predict human response to noise on the basis of acoustic variables. In *Noise As a Public Health Problem*, J. V. Tobias, G. Jansen, and W. D. Ward, eds., ASHA Report No. 10, Rockville, MD, pp. 475–487 1980.
6. K. D. Kryter and K. S. Pearsons, Some Effects of Spectral Content and Duration on Perceived Noise Level, *J. Acoust. Soc. Am.*, Vol. 35, 1963, pp. 866–883.
7. S. Fidell, M. Sneddon, K. Pearsons, and R. Howe, Insufficiency of Spectral Information as a Primary Determinant of the Annoyance of Environmental Sounds, *Noise Control Eng. J.*, Vol. 50, No. 1, 2002, pp. 12–18.
8. S. Stevens, perceived Level of Noise by Mark VII and Decibels (E) *J. Acoust. Soc. Am.*, Vol. 51, No. 2, 1972, pp. 575–601.
9. E. Zwicker, Procedure for Calculating Loudness of Temporally Variable Sounds, *J. Acoust. Soc. Am.*, Vol. 62, No. 2, 1977, pp. 675–682.
10. K. Pearsons, R. Howe, M. Sneddon, L. Silvati, and S. Fidell, Comparison of Predictors of the Annoyance of Commuter, Stage II and Stage III Aircraft Overflights as Heard Outdoors, NASA Contractor Report 1997-205812, NASA Langley Research Center, Hampton, Virginia, May 1977.
11. E. Zwicker and H. Fastl, *Psychoacoustics Facts and Models*, Springer, Berlin, 1999.
12. S. Fidell, L. Silvati, B. Tabachnick, R. Howe, K. S. Pearsons, R. C. Knopf, J. Gramann, and T. Buchanan, Effects of Aircraft Overflights on Wilderness Recreationists, *J. Acoust. Soc. Am.*, Vol. 100, No. 5, 1996, pp. 2909–2918.
13. F. Hall, S. Birnie, M. Taylor, and J. Palmer, Direct Comparison of Community Response to Road Traffic Noise and to Aircraft Noise, *J. Acoust. Soc. Am.*, Vol. 70, No. 6, 1981, pp. 1690–1698.
14. J. M. Fields and J. G. Walker, Comparing the Relationships between Noise Level and Annoyance in Different Surveys: A Railway Noise vs. Aircraft and Road Traffic Comparison, *J. Sound and Vib.*, Vol. 81, No. 1, 1982, pp. 51–80.
15. H. Miedema and H. Vos, Exposure-Response Relationships for Transportation Noise, *J. Acoust. Soc. Am.*, Vol. 104, No. 6, 1998, pp. 3432–3445.
16. Job, R. F. S. (1988). “Community Response to Noise: A Review of Factors in Influencing the Relationship between Noise Exposure and Reaction,” *J. Acoust. Soc. Am.*, Vol. 83, No. 3, 1981, pp. 991–1001.
17. S. Fidell, The Schultz Curve 25 Years Later: A Research Perspective, *J. Acoust. Soc. Am.*, Vol. 114, No. 6, 2003, pp. 3007–3015.
18. J. Botsford, Using Sound Levels to Gauge Human Response to Noise, *Sound Vib.*, Vol. 3, No. 10, 1969, pp. 16–28.
19. American National Standards Institute, *Quantities and Procedures for Description and Measurement of Environmental Sound—Part 4: Noise Assessment and Prediction of Long-term Community Response*, Standards Secretariat, Acoustical Society of America, New York, 1996.
20. International Organization for Standardization (ISO), *Acoustics—Description and Measurement of Environmental Noise—Part 3: Application to Noise Limits*, Geneva, Switzerland, 1987.
21. J. M. Fields, R.G. De Jong, T. Gjestland, I.H. Flindell, R.F.S. Job, S. Kurra, P. Lercher, M. Vallet, T. Yano, R. Guski, U. Felscher-Suhr, and R. Schumer, Standardized General-Purpose Noise Reaction Questions for Community Noise Surveys: Research and Recommendation, *J. Sound Vib.*, Vol. 242, No. 4, 2001, pp. 641–679.
22. Federal Interagency Committee on Noise (FICON), Federal Agency Review of Selected Airport Noise Analysis Issues, *Final Report: Airport Noise Assessment Methodologies and Metrics*, FICON, Washington, DC, 1992.
23. S. Fidell and L. Silvati, Parsimonious Alternatives to Regression Analysis for Characterizing Prevalence Rates of Aircraft Noise Annoyance, *Noise Control Eng. J.*, Vol. 52, No. 2, March–April, 2004, pp. 56–68.
24. D. M. Green and J. A. Swets, *Signal Detection Theory and Psychophysics*, Wiley, New York, 1966.
25. D. M. Green and S. Fidell, Variability in the Criterion for Reporting Annoyance in Community Noise Surveys, *J. Acoust. Soc. Am.*, Vol. 89 No. 1, 1991, pp. 234–243.



# CHAPTER 26

## EFFECTS OF INFRASOUND, LOW-FREQUENCY NOISE, AND ULTRASOUND ON PEOPLE

Norm Broner  
Sinclair Knight Merz  
Melbourne, Australia

### 1 INTRODUCTION

Infrasound, low-frequency noise, and ultrasound have different effects on people. Infrasound is sound below 20 Hz, which is often inaudible, while low-frequency noise (LFN) is in the range of 20 to 100 Hz and audible. Ultrasound, on the other hand, includes noise in the high-frequency range above 16 kHz. Many of the effects attributed to infrasound are actually due to low-frequency noise in the region of 20 to 100 Hz.

In general, for sound pressure levels that occur in our everyday life, the low-frequency effects are not found to be significant in terms of causing long-term physiological damage. However, short-term changes in physiological responses and in performance can occur following exposure. Annoyance due to infrasonic, low-frequency, and ultrasonic exposure can also result from longer duration exposures (hours to days). Recent studies seem to show that low-frequency noise in the region of 20 to 50 Hz has a more significant effect on people than either infrasound or ultrasound at normal exposure levels.

### 2 INFRASOUND

Infrasound is generally considered to be sound at frequencies below 20 Hz. Many sources of infrasound and LFN have been identified, including air-conditioning systems, oil and gas burners, boilers, and noise inside transportation.<sup>1-4</sup> Many of these sources exhibit a spectrum that shows a general decrease in sound pressure level (SPL) with increase in frequency, and it is now apparent that the spectrum imbalance is a major source of subjective annoyance due to exposure to this type of sound. Subjective reports of disorientation, headache, and unpleasantness have been reported even where the A-weighted sound pressure level is relatively low.

In the 1960s and the 1970s and occasionally since, sensationalized reports of the “dangerous” nature of infrasound were reported, creating “panic” among some. Brain tumors, cot death, and “mashed intestines” were all “blamed” on infrasound in particular.<sup>1,3</sup> These reports have not been validated and have been the cause of misinformation and unnecessary angst by some members of the public.

Levels of infrasound, up to 150 dB, have been found to be tolerable for shorter exposures, and 24-h exposures up to 120 to 130 dB were found to be “safe” from a physiological point of view.<sup>1,3</sup> At these levels, the infrasound was generally considered quite

unpleasant subjectively, however, at levels at which infrasound normally occurs, that is, 90 to 110 dB (depending on frequency), the sound is generally potentially annoying only with relatively low potential for side effects.

### 2.1 Hearing Threshold

Many studies have been conducted to determine the infrasonic and low-frequency hearing threshold and loudness curves, and there is a general consistency among the results<sup>5</sup> (see Fig. 1). First, it appears that below around 15 Hz, there is a change in response to that of “sensation” or “presence” rather than that of “hearing.” ISO 226<sup>6</sup> provides equal-loudness-level contours based on pure tones under free-field listening conditions. This revised standard considered various research work, particularly since 1983 and as recent as 2002, and specifies contours, including the hearing threshold from 20 Hz up to 12,500 Hz. With respect to low-frequency noise, the work of Watanabe and Moller<sup>7</sup> was considered (see Fig. 1). This work gives the threshold as 107 dB at 4 Hz, 97 dB at 10 Hz, and 79 dB at 20 Hz, which coincides very nearly with the ISO 226<sup>6</sup> threshold curve at 20 Hz. Note that at about 15 Hz, there is a change of the threshold slope from approximately  $-20$  dB/octave at higher frequencies to  $-12$  dB/octave at lower frequencies. This change seems to reflect the change from a “hearing” perception above 15 Hz to one of “pressure,” particularly at higher SPLs. Note also that the hearing thresholds are mean values and that the standard variation about the mean is not insignificant.<sup>5</sup> This means that, on an individual basis, the threshold could be up to say, 5 to 10 dB lower or higher than the mean. For example, Frost<sup>9</sup> compared two subjects, one of whom was 15 dB more sensitive at 40 Hz than the other but had similar audiograms at 250, 500, and 1000 Hz.

Note that at low and particularly infrasonic frequencies, the loudness contours are much closer together so that for a given change in SPL (increase or decrease), the change in loudness is much greater at low frequencies than the same SPL change at high frequencies. For example, the difference between the 20- and 80-phon curves is 60 dB at 1000 Hz but only 15 dB at 8 Hz. Thus, the fluctuations in perceived loudness as a result of the level fluctuations will be considerably larger than at higher frequencies. This could be the explanation for the increased reported annoyance due to LFN and infrasound.

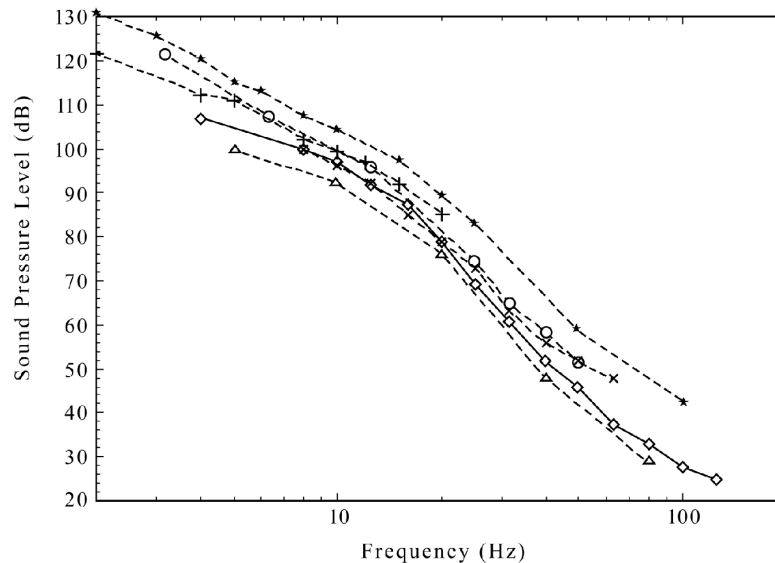


Figure 1 Comparison of threshold data. (From Watanabe and Moller.<sup>7</sup> Reprinted by permission.)

In addition, the thresholds for low-frequency complex noises appear to be *lower* than the pure-tone thresholds.<sup>5,10,11</sup> Thus, it appears there is an increased sensitivity to complex LFN such as heating, ventilation, and air-conditioning (HVAC) noise as compared to pure tones.

## 2.2 Temporary Threshold Shift (TTS)

A quantitative relationship between human exposure to infrasound and hearing loss is not well established, and this is partly due to the inability to produce infrasound exposures without audible overtones. It appears that (1) only small, if any, TTS can be observed following exposure to moderate and intense infrasonics, and (2) recovery to preexposure levels is rapid when TTS does occur. Similarly, it appears that LFN will produce TTS in some subjects after short exposure, but that recovery is rapid and complete. However, there is an indication that long-term exposure to very high levels may cause permanent hearing loss.<sup>1-3</sup>

## 2.3 Threshold of Pain

Low-frequency noise and infrasound at a higher level is less likely to result in hearing loss as compared to higher frequency sound at a similar level. The threshold of pain appears to be about 135 dB around 50 Hz, 140 dB around 20 Hz, increasing to about 162 dB at 2 Hz and 170 to 180 dB for static pressure.<sup>12</sup>

## 2.4 Annoyance

The primary effect due to infrasound and LFN appears to be annoyance. It can be said that the effects of infrasound and LFN are broadly similar to those of high-frequency noise in the sense that any unwanted sound is potentially annoying. However,

LFN and infrasound often exhibits itself in the form of “rumble” and “pressure,” and the sound pressure level fluctuations can exacerbate the annoyance reaction when compared to higher frequency noise.<sup>13,14</sup>

Broner and Leventhall<sup>15</sup> found that unless the conditions are optimized for differentiating sounds with respect to loudness and annoyance, subjects treated them in approximately the same way. It seems that for sound with “tonal” low-frequency content below 50 Hz and for infrasound, particularly where the sound pressure level is perceptibly fluctuating or throbbing, annoyance and loudness are treated differently and that this difference may increase with time.<sup>16</sup> As the loudness adapts more rapidly with time than the annoyance (i.e., the perceived loudness decreases more rapidly with time than the perceived annoyance), the effect is to effectively increase the annoyance with time. This effect would be worse for infrasound where the sound is not so much heard but is perceived rather as a feeling and sensation of pressure.

## 2.5 Annoyance Assessment

Assessment and prediction of annoyance due to infrasound and LFN is not simple. What is very clear is that the A-weighted SPL alone is **not** successful in assessing the response to infrasound and LFN.<sup>1-3</sup> A review of case histories indicates that very annoying sounds often have rather low A-weighted SPL but nevertheless cause significant annoyance. This is due to the presence of an unbalanced spectrum, which additionally may have an amplitude and/or temporal fluctuating characteristic.

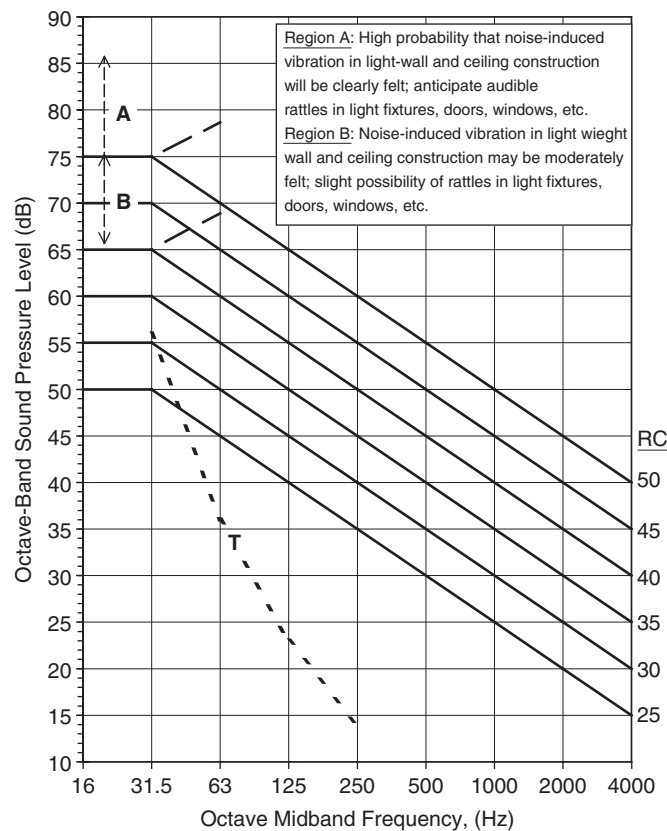
Empirical evidence shows that where the imbalance is such that the difference between the linear and A-weighted SPL is at least 25 dB, the sound is likely

to cause annoyance. Broner and Leventhall<sup>15</sup> and DIN 45680-1997<sup>17</sup> suggested that a difference of 20 dB can result in an unbalanced spectrum that could lead to LFN annoyance. Others suggested that a difference of only 15 dB was a good rule of thumb to identify a potential infrasound LFN problem situation.<sup>14,18</sup> In general, it seems that the (C—A) level difference is appropriate metric for indicating a potential LFN problem but that its predictive ability is of limited value.<sup>8</sup>

The perception of annoyance is particularly dependent on the degree of amplitude modulation and spectral balance,<sup>19,20</sup> and, as a result, it is considered that there is a significant limitation in the long-term averaging of infrasonic and LFN noise levels, as this approach results in the loss of information on fluctuations.<sup>15,21</sup>

Broner and Leventhall<sup>15</sup> recognized the problem of spectrum imbalance for assessment of infrasound and LFN complaints and proposed the low-frequency noise rating (LFNR) curves. These significantly reduced the infrasonic and low-frequency energy allowed by the noise rating (NR) curves. Further attempts at diagnostic assessment of room noise incorporated

elements of sound quality. Blazier<sup>22</sup> used 16 years of practical experience and data from Broner<sup>23</sup> to refine the earlier RC (room criterion) procedure for rating HVAC system-related noise in buildings developed by Blazier.<sup>24</sup> The refinement included a modification to the shape of the RC reference curves in the 16-Hz octave band (see Fig. 2), an improvement in the procedure for assessment of sound quality and the development of a scale to estimate the magnitude of subjective response as a function of spectrum imbalance, the “quality assessment index” (QAI). The method was designated the RC Mark II and this method allows the calculation of spectrum quality by calculating the balance of low, mid, and high frequencies. This method is preferred by the American Society of Heating, Refrigeration, and Air Conditioning Engineers (ASHRAE).<sup>25</sup> Note that the America National Standards Institute (ANSI) S12.2-1995<sup>26</sup> included both the RC method and the balanced noise criteria (NCB) method developed by Beranek.<sup>27</sup> This author feels strongly, based on empirical evidence,<sup>15</sup> that the NCB curves, which apply to occupied spaces, are much too lenient in the



**Figure 2** Family of room criterion (RC Mark II) reference curves. (Originally published by Warren E. Blazier.<sup>22</sup> Reprinted by permission.)

16 and 31.5-Hz octave bands and that the LFNR and RC Mark II methods are much preferred.

The G-weighting (ISO 7196-1995<sup>28</sup>) was specifically designed for assessment of infrasound, falling off rapidly below 1 Hz and above 20 Hz at 24 dB/octave. Between 1 and 20 Hz, it follows a slope of 12 dB/octave, thus each frequency is weighted in accordance with its relative contribution to the perception. Note that this feature may result in an underestimation of loudness at frequencies between about 16 and 20 Hz.<sup>29</sup> A G-weighted sound pressure level of 95 to 100 dB is close to perception level, while G-weighted levels below 85 to 90 dB are not normally significant for human perception. Note also that (1) due to the combined effect of individual differences in perception threshold and the steep rise in sensation above the threshold, the same infrasonic noise may appear loud and annoying to some people, while others may hardly perceive it.<sup>28</sup> (2) This weighting has a limited application in practice, and care should be taken not to put too much reliance on this metric as it may divert attention away from problems at higher frequencies. In practice, for commonly occurring noise levels, LFN in the range of 30 to 80 Hz is more likely to be a problem in terms of annoyance.<sup>3</sup>

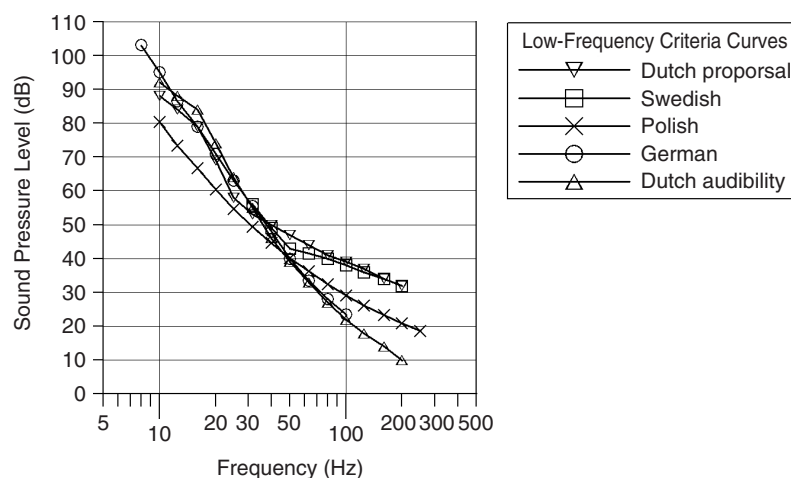
## 2.6 European Assessment Criteria

A number of different European methods have also been suggested for assessment of infrasound and LFN, all based on measured indoor noise levels. These are the Danish,<sup>29</sup> Swedish, German, Polish, and Dutch methods (Poulsen<sup>30</sup> and Leventhall<sup>8</sup> compare all of these). Each of these has different criteria for the allowed noise level, and the administrative procedures used in the individual countries to enforce the criteria are very different. Figure 3 shows a comparison of the various criteria curves.<sup>30</sup> Some of these methods also address the issue of fluctuations in level that have

been identified as a major cause of annoyance due to LFN, for example, DIN 45680.<sup>13</sup> A Working Group CEN/TC 126/WG1 linked to ISO/TC 43/SC 2 "Building Acoustics" is also working on two new European standards concerning the methods of measuring noise from service equipment in buildings.<sup>31</sup>

## 2.7 Performance Effects

Over the last few years, due to the prevalence of infrasonic and LFN sources such as ventilation/air conditioning, pumps, diesel engines, and compressors and due to the growing body of data showing the prevalence of low-frequency noise problems/effects, there has been interest in their impact in the workplace.<sup>14,32-34</sup> In terms of performance, infrasound and LFN is reported to cause drowsiness, fatigue, and headaches and can result in performance effects, possibly due to information processing overload. Low-frequency ventilation noise has been shown to affect a mentally demanding verbal reasoning task and work efficiency, and quality was found to be impaired. Further, LFN has been found to impair performance on tasks with high and moderate demands on cognitive processing when performed under high workload. LFN has also impaired performance on some of the low-demand tasks and a moderately demanding verbal task under low workload.<sup>33</sup> Thus the impact of LFN on performance is demonstrable under certain circumstances, and the significance of the impact is dependent on the nature of the work and the circumstances of that work, just as for higher frequency noise impact. It is likely that complex tasks and a long exposure would result in a measurable performance effect similar to the impact of higher frequency noise. Available evidence also suggests that infrasound even at very intense exposure levels is not detrimental to human performance.<sup>12</sup>



**Figure 3** Comparison of criteria curves from the different assessment methods. (From Poulsen.<sup>30</sup> Reprinted by permission.)

## 2.8 Physiological Effects

Physiological responses have been observed including cardiac rhythm and respiration rate [measured by electrocardiogram (EKG) recordings, pulse counts, and impedance pneumography], vasoconstriction and vasodilation, change of systolic rhythm, blood and endocrine changes, changes in cortisol levels, and disturbances to the central nervous system. The data suggests that any of these effects are unlikely to be of any practical importance except under extreme occupational exposure.<sup>34–36</sup>

## 2.9 Sleep Effect

There is some evidence that exposure to LFN results in reduced wakefulness or increased tiredness and a feeling of fatigue. The practical significance of this may be a reduced reaction time, which may be important in some situations, for example, driving on a freeway.<sup>37,38</sup>

## 3 ULTRASOUND

Ultrasound usually is considered to cover sound in the range of 16 to 40 Hz. There are many industrial and commercial sources of infrasound, for example, ultrasonic cleaners, welders, atomizers, and electroplaters. Due to the very high frequency, the wavelength of ultrasound is very small, of the order of 5 to 20 mm. Because of this, ultrasound is readily absorbed in the air and is readily attenuated by distance from the source and by normal building materials. Also, due to the impedance mismatch with the human body, the ear is usually the primary channel for transmitting airborne ultrasound to a person. Therefore, people who do not “hear” in the ultrasonic region usually do not display any of the subjective symptoms.

### 3.1 Ultrasonic Levels and Subjective Effects

Exposure to industrial ultrasonic devices rarely exceeds 120 dB, and exposure to commercial devices designed to emit ultrasound rarely exceeds 110 dB. Commercial devices that incidentally emit ultrasound, such as video display terminals, rarely exceed 65 dB at the operator's ear.<sup>39</sup> Note that many industrial and commercial processes that generate high levels of ultrasound also generate high levels of subharmonics, that is, sound at “sonic” frequencies. These sonic exposures cannot be ignored in considering the hazards of industrial ultrasonic exposure as it is often the sonic frequencies that are more hazardous for equivalent SPLs and that are the cause of the subjectively reported effects such as fullness of the ear, tinnitus, fatigue, dizziness, and headache.<sup>40</sup>

It appears that direct contact exposure to high-level ultrasound may cause a sharp pain or possibly a “burn,” but documented cases of actual tissue damage are rare. In any case, direct contact is usually due to an accident or carelessness. More normal is exposure to airborne ultrasound via the ear.

### 3.2 Hearing

The average threshold of hearing increases rapidly and monotonically with frequency at a rate of the

order of 12 dB/Hz between 14 and 20 Hz leading to a threshold of 100 dB at 20 Hz and 125 dB at 25 Hz. There are some reports that a temporary hearing loss may occur due to high-level ultrasound (>140 dB), but recovery seems to be complete and rapid. SPLs lower than 120 dB have not been demonstrated to cause hearing losses. Physiological effects (e.g., disturbance of neuromuscular coordination, dizziness, loss of equilibrium) appear to occur only at SPLs greater than that which causes TTS.

### 3.3 Criteria

The data indicates that when people are subjected to ultrasound without the audible components, no complaints are received. To avoid subjective affects for the unprotected ear, Acton<sup>41</sup> recommended criterion limits of 75 dB from 16 to 20 Hz and less than 110 dB for frequencies greater than 20 to 50 Hz, and these criteria seem to have been generally adopted. For frequencies between 10 and 20 Hz, the Occupational Safety and Health Administration (OSHA)<sup>42</sup> recommends a ceiling value of 105 dB to prevent subjective annoyance and discomfort, especially if the sounds are tonal in nature. It is noted, however, that subjective annoyance and discomfort may occur in some individuals at levels between 75 and 105 dB. Health Canada<sup>39</sup> also recommends a limit of 137 dB in the ultrasonic range to avoid the potential of mild heating effects. Occupational health and safety procedures are similar to those used for audible noise with the objective to ensure that ambient SPLs do not exceed the recommended maximum permissible exposure level.

## REFERENCES

1. N. Broner, The Effects of Low Frequency Noise on People—A Review, *J. Sound Vib.*, Vol. 58, No. 4, 1976, pp. 483–500.
2. B. Berglund, P. Hassmen, and R. F. Soames Job, Sources and Effects of Low-Frequency Noise, *J. Acoust. Soc. Am.*, Vol. 99, No. 5, 1996, pp. 2985–3002.
3. H. G. Leventhall, P. Pelmear, and S. Benton, *A Review of Published Research on Low Frequency Noise and Its Effects*, Dept of Environment, Food and Rural Affairs, London, 2003.
4. W. Tempest, Infrasound in Transportation, In *Infrasound and Low Frequency Vibration*, W. Tempest, Ed., Academic, London, 1976.
5. H. Moller, and C. S. Pedersen, Hearing at Low and Infrasonic Frequencies, *Noise & Health*, Vol. 6, No. 23, 2004, pp. 37–57.
6. ISO 226–2003 *Acoustics—Normal Equal-Loudness-Level Contours*, International Organization for Standardization, Geneva, Switzerland, 2003.
7. T. Watanabe and H. Moller, Low Frequency Hearing Thresholds in Pressure Field and in Free-Field, *J. Low Freq. Noise Vib.*, Vol. 9, No. 3, 1990, pp. 106–115.
8. G. Leventhall, Assessment and Regulation of Low Frequency Noise, ASHRAE Symposium, Orlando, Jan. 2005.
9. G. P. Frost, An Investigation into the Microstructure of the Low Frequency Auditory Threshold and of the Loudness Function in the Near Threshold Region, *J. Low Freq. Noise Vib.*, Vol. 6, No. 1, 1987, pp. 34–39.

10. T. Watanabe and S. Yamada, Study on Perception of Complex Low Frequency Tones, *J. Low Freq. Noise, Vib. Active Control*, Vol. 21, No. 3, 2002, pp. 123–130.
11. Y. Matsumoto, et al., An Investigation of the Perception Thresholds of Band-Limited Low Frequency Noises: Influence of Bandwidth, *J. Low Freq. Noise Vib.*, Vol. 22, No. 1, 2003, pp. 17–25.
12. H. E. Von Gierke and C. Nixon, Effects of Intense Infrasound on Man, In *Infrasound and Low Frequency Vibration*, W. Tempest, Ed., Academic, London, 1976.
13. H. G. Leventhall, Low Frequency Noise and Annoyance, *Noise & Health*, Vol. 6, No. 23, 2004, pp. 59–72.
14. K. Persson-Waye, Adverse Effects of Moderate Levels of Low Frequency Noise in the Occupational Environment, ASHRAE Symposium, Orlando, Jan. 2005.
15. N. Broner and H. G. Leventhall, Low Frequency Noise Annoyance Assessment by Low Frequency Noise Rating (LFNR) Curves, *J. Low Freq. Noise Vib.*, Vol. 2, No. 1, 1983, pp. 20–28.
16. R. P. Hellman and N. Broner, Relation Between Loudness and Annoyance over Time: Implications for Assessing the Perceived Magnitude of Low-Frequency Noise Presented at the Acoust. Soc. of Amer. 75th Anniversary Meeting, New York, May, 2004.
17. DIN 45680, Messung und Bewertung tieffrequenter Geräuschemissionen in der nachbarschaft (Measurement and Assessment of Residential Low Frequency Sound Emission) + Beiblatt: "hinweise zur Beurteilung bei Gewerblichen Anlagen" (in German), 1997.
18. Kjellberg, A., Tesarz, M., Holberg, K., and Landström, U., Evaluation of Frequency-Weighted Sound Level Measurements for Prediction of Low Frequency Noise Annoyance, *Env. Intl.*, Vol. 23, 1997, pp. 519–527.
19. J. Bengtsson, K. Persson-Waye, and A. Kjellberg, Sound Characteristics in Low Frequency Noise and their Relevance for Performance Effects, Inter-Noise 2002, Dearborn, MI, 2002, Paper 298.
20. J. S. Bradley, Annoyance Caused by Constant Amplitude and Amplitude Modulated Sounds Containing Rumble, *Noise Control Eng.*, Vol. 42, 1994, pp. 203–208.
21. W. E. Blazier and C. E. Ebbing, Criteria for Low Frequency HVAC System Noise Control in Buildings, InterNoise 92, Toronto, Canada, 1992, pp. 761–766.
22. W. E. Blazier, RC Mark II: A Refined Procedure for Rating Noise of Ventilating and Air Conditioning (HVAC) Systems in Buildings, *Noise Control Eng.*, Vol. 45, 1997, pp. 243–250.
23. N. Broner, Determination of the Relationship Between Low-Frequency HVAC Noise and Comfort in Occupied Spaces—Objective Phase, ASHRAE 714, prepared by Vipac Engineers & Scientists Ltd., Report 38114, Melbourne, Australia 1994.
24. W. E. Blazier, Revised Noise Criteria for Applications in the Acoustical Design and Rating of (HVAC) Systems, *Noise Control Eng.*, Vol. 16, No. 2, 1981, pp. 64–73.
25. Sound and Vibration Control, in *ASHRAE Applications Handbook*, Atlanta, GA, 2003, Chapter 47.
26. ANSI S12.2–1995, *Criteria for Evaluating Room Noise*, American National Standards Institute, New York, 1995.
27. L. L. Beranek, Balanced Noise Criterion (NCB) Curves, *J. Acoust. Soc. Am.*, Vol. 86, No. 2, 1989, pp. 650–664.
28. ISO 7196–1995(E), *Acoustics—Frequency Weighting Characteristics for Infrasound Measurements*, International Organization for Standardization, Geneva, Switzerland, 1995.
29. J. Jakobsen, Danish Guidelines on Environmental low Frequency Noise, Infrasound and Vibration, *J. Low Freq. Noise, Vib. Active Control*, Vol. 20, No. 3, 2001, pp. 141–148.
30. T. Poulsen, Comparison of Objective Methods for Assessment of Annoyance of Low Frequency Noise with Results of a Laboratory Listening Test, *J. Low Freq. Noise, Vib. Active Control*, Vol. 22, No. 3, 2003, pp. 117–131.
31. M. Mirowska, Problems of Measurement and Evaluation of Low-Frequency Noise in Residential Buildings in the Light of Recommendations and the New European Standards, *J. Low Freq. Noise Vib.*, Vol. 22, No. 4, 2003, pp. 203–208.
32. J. Bengtsson and K. Persson-Waye, Assessment of Low Frequency Complaints Among the Local Environmental Health Authorities and a Follow-up Study 14 Years Later, *J. Low Freq. Noise Vib.*, Vol. 22, No. 1, 2003, pp. 9–16.
33. K. Persson-Waye, Effects of Low Frequency Noise in the Occupational Environment—Present Knowledge Base, InterNoise 2002, Dearborn, MI, 2002.
34. M. Schust, Effects of Low Frequency Noise up to 100 Hz, *Noise & Health*, Vol. 6, No. 23, 2004, pp. 73–85.
35. M. J. Evans, Physiological and Psychological Effects of Infrasound at Moderate Intensities, in *Infrasound and Low Frequency Vibration*, W. Tempest, Ed., Academic, London, 1976.
36. C. Y. H. Qibai and H. Shi, An Investigation on the Physiological and Psychological Effects of Infrasound on Persons, *J. Low Freq. Noise, Vib. Active Control*, Vol. 23, No. 1, 2004, pp. 71–76.
37. M. E. Bryan and W. Tempest, Does Infrasound Make Drivers Drunk? *New Scientist*, Vol. 53, 1972, pp. 584–586.
38. K. Persson Weye, Effects of Low Frequency Noise on Sleep, *Noise & Health*, Vol. 6, No. 23, 2004, pp. 87–91.
39. Health Canada Guidelines for the Safe Use of Ultrasound: Part II—Industrial & Commercial Applications—Safety Code 24, 2002; [www.hc-sc.gc.ca/hecs-secs/ccrpb/publication/safety\\_code24/toc.htm](http://www.hc-sc.gc.ca/hecs-secs/ccrpb/publication/safety_code24/toc.htm).
40. L. L. Beranek and I. Ver, *Noise and Vibration Control Engineering: Principles and Applications*, Wiley, New York, 1992.
41. W. I. Acton, Exposure Criteria for Industrial Ultrasound, *Ann. Occup. Hyg.*, Vol. 18, 1978, pp. 267–268.
42. OSHA U.S. Dept of Labor, Technical Manual, Section III: Chapter 5, V, 2003; [www.osha.gov/dts/osta/otm/otm\\_iii/otm\\_iii\\_5.html](http://www.osha.gov/dts/osta/otm/otm_iii/otm_iii_5.html).

# CHAPTER 27

## AUDITORY HAZARDS OF IMPULSE AND IMPACT NOISE

**Donald Henderson**

Center for Hearing and Deafness  
State University of New York at Buffalo  
Buffalo, New York

**Roger P. Hamernik**

Department of Communication Disorders  
State University of New York at Plattsburgh  
Plattsburgh, New York

### 1 INTRODUCTION

High-level transient noise presents a special hazard to the auditory system. First, impulse noise may damage the cochlea by direct mechanical processes. Second, damage risk criteria evaluate impulse noise in terms of levels, duration, and number, but parameters such as temporal pattern, waveform, and rise time are also important in the production of a hearing loss. Third, the effects of impulse noise are often inconsistent with the principle of the equal energy hypothesis. Fourth, impulse noise can interact with background noise.

### 2 DEFINITION OF IMPULSE NOISE

The term impulse noise is used in this chapter as a generic term that includes all forms of high-intensity short-duration sounds, that is, from the most common industrial impacts to the intense blast waves associated with military operations. The range of parameters defining an impulse is large. Impulse durations may vary from tens of microseconds for small arms fire to several hundred milliseconds for a sonic boom or a reverberant industrial impact. Intensities for these impulses may vary from less than 100 dB to in excess of 185 dB peak sound pressure level (SPL). The energy of an impulse is usually broadly distributed, but spectral concentrations of energy can occur at various frequencies throughout the audible range. The number of occurrences of impulse noise in industry or the military may vary from one impulse or less per hour to several per second with no fixed interval of time between impulses. In addition to the physical parameters of the impulse, other environmental conditions associated with the exposure can seriously affect the outcome of an exposure, that is, a free field or reverberant enclosure, angle of incidence, or the presence of other noise or vibrations, drugs, and the like.

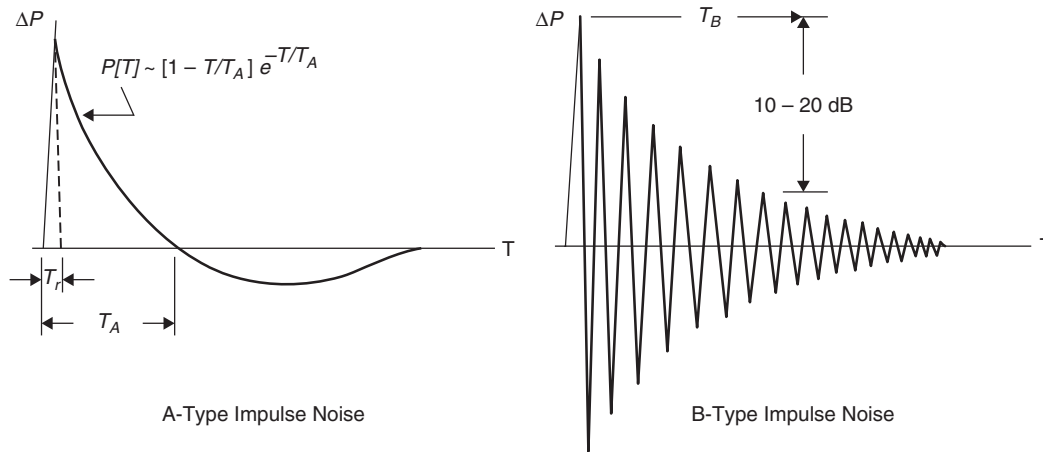
The waveforms or signatures of impulse noise can be very different. One extreme is industrial impact noise. Impact noise is reverberant (ringing), and its physical behavior generally conforms to the laws of acoustics. At the other extreme are blast waves. They

can have peaks of 150 dB or greater and are, in fact, shock waves that are governed by physical principles that are different from the laws of acoustics.<sup>1</sup>

Coles et al.<sup>2</sup> described two basic types of impulses: a nonreverberant A-wave and a reverberant B-wave (Fig. 1). This scheme characterizes the impulse in terms of peak level, duration, and number of impulses, but neglects a number of other potentially important variables, that is, rise time ( $T$ ),<sup>3</sup> spectrum,<sup>4</sup> and temporal pattern.<sup>5,6</sup> Additional working definitions of impulse noise can be found in the American National Standards Institute (ANSI) Standard S1.13 (1971), and a detailed exposition, which extends the definition,<sup>2</sup> can be found in Pfander<sup>7</sup> and Pfander et al.<sup>8</sup> Pfander considers the temporal specification of an impulse to include both the rarefaction and condensation phases as well as the duration of the impulse and the total number impulses.

The physical specification of the impulse is further complicated when the impulses are mixed with a continuous noise. The combination of impulse and continuous noise is very common in industrial settings. In fact, Bruel<sup>9</sup> showed that crest factors of 50 dB are common. The complexity of evaluation of the hazards to hearing of a complex noise environment is currently being evaluated using kurtosis as a descriptive metric. Thus, in some circumstances, it is difficult to establish when an exposure contains impulsive components that need to be evaluated separately. Certain studies<sup>10</sup> report a slight reduction in temporary threshold shift (TTS) produced by either agent alone. However, it is clear that under certain conditions, high-level impulses riding on a background noise produce greater injuries to the organ of Corti than either the impulse or the continuous noise alone.<sup>11</sup>

In summary, there is not a consensus on how to describe the various types of impulse noise. It is not clear what combinations of impulse and continuous noise will present hearing hazards that are different from those presented by a continuous noise exposure. However, the following review of the biological and audiological effects of impulse noise shows that



**Figure 1** Schematic representation of the two basic impulse noise pressure-time profiles, following the simplification of Coles et al.<sup>2</sup>

impulse noise can affect the auditory system differently than lower levels of continuous noise. Consequently, impulse noises may require special consideration when establishing future noise standards.

### 3 MEASUREMENT OF THE IMPULSE

There is general agreement that the best approach to measuring an isolated impulse is to record the pressure-time history of the impulse. However, because of the extreme limits of various impulse noise parameters (rise times can be as short as a few microseconds and intensities as high as 185 dB SPL), care must be given to the response properties of the measuring device. The time constant of some current impulse sound level meter (SLM) is approximately 30 to 40 ms; however, some of the shorter impulses, for example, gunfire, may last only a few hundred of a microsecond. Therefore, the limitations of the measurement system may seriously underestimate peak levels or other parameters of the impulse. However, for typical industrial types of impacts whose durations may last 200 ms or more, many of the current precision SLMs may be suitable measuring instruments.

Basically, the same considerations for a measurement system apply to impulse noise as apply to other physical systems, and general reviews can be found in Pfeiffer<sup>12</sup> and Nabelek.<sup>13</sup> A compilation of several studies dealing with measurements can be found in Ivarsson and Nilsson.<sup>14</sup> A suggestion was to develop computer-based instrumentation (digital techniques) to record and measure the cumulative distribution of sound pressure over the exposure period of interest.<sup>9</sup> From such measurements, various methods are available to calculate total or weighted energy levels of the stimulus for application to energy-based damage risk criteria.<sup>15</sup> While the greatest focus of measurement activity appears to be in estimating peak levels and total energies of exposure, there are other parameters, for example, presence of reflections, rise time,

and temporal pattern, that are important in determining the hazards of exposure.

Finally, there has been interest in developing instrumentation to produce a single number index of the hazards of an exposure containing impulsive components.<sup>15,16</sup> These dosimeters are usually based upon some weighted measure of total energy, and generally conform to the analytical model discussed by Martin.<sup>17</sup> While the potential value of such an instrument cannot be denied, it may be premature to adopt a measurement scheme that completely ignores a variety of potentially relevant parameters such as rise time, repetition rate, frequency content, and background noise.

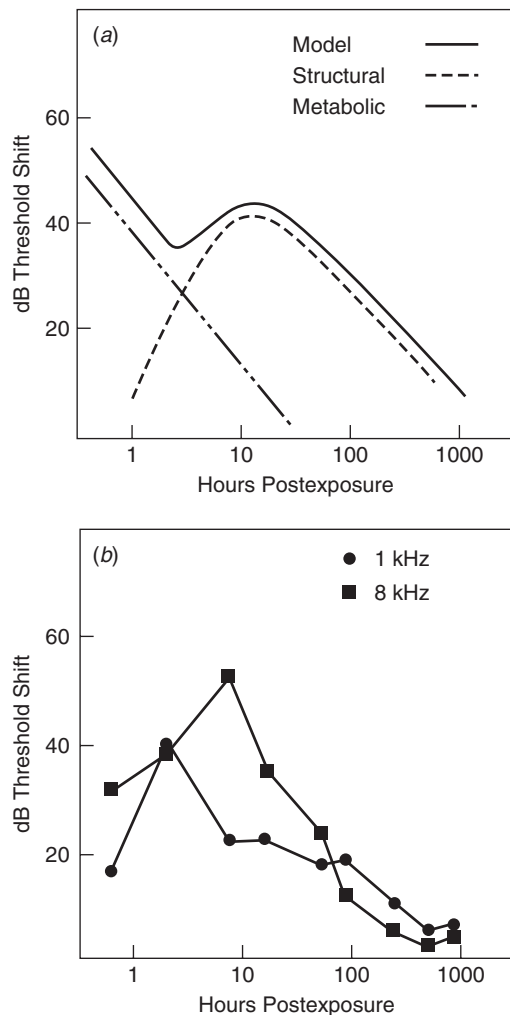
### 4 AUDIOMETRIC EFFECTS OF IMPULSE

Experiments on monkeys,<sup>18</sup> humans,<sup>19</sup> and chinchillas<sup>20,21</sup> have shown that the recovery from impulse noise often follows a nonmonotonic pattern, that is, there is a growth to a maximum level of TTS, as much as 10 h after exposure (Fig. 2). This pattern of recovery is much different from the typical linear (in log time) recovery pattern seen following a continuous noise exposure.<sup>22</sup>

Furthermore, exposures that produce the nonmonotonic recovery curves usually have a prolonged period of recovery and, in most of the cases examined, have both permanent threshold shifts (PTS) and losses of sensory cells.<sup>21,23,24</sup> Two investigations have developed comprehensive models of hearing loss using the results from TTS experiments. Kraak<sup>25</sup> proposed that PTS from a given exposure could be predicted by the time-integrated amount of TTS.

If subjects are exposed to a noise for a relatively long period of time, that is, on the order of days, hearing sensitivity decreases over an 8- to 48-h period and then stabilizes at an asymptotic level.<sup>26,27</sup> In contrast to many of the TTS results from short-duration exposures, asymptotic threshold shift (ATS)





**Figure 2** (a) Hypothetical threshold recovery curves illustrating the metabolic and structural recovery process for TTS associated with a model proposed by Luz and Hodge.<sup>62</sup> (b) The actual TTS recovery curves for chinchillas exposed to fifty 1-ms A-duration impulses at 155 dB. Note the growth of TTS between 1- to 10-h postexposure.

is a more orderly phenomenon with reduced amounts of intersubject variability.<sup>27</sup> The dynamics of the cochlear processes underlying ATS are beginning to be described.<sup>28</sup> If ATS is truly an asymptote, then it is likely that the level of ATS will represent the upper limit of PTS one can expect from prolonged exposure to the noise.

Although comparatively little data on impulse-noise-induced ATS currently exists,<sup>24,29,30</sup> there appear to be differences in the manner in which ATS develops following prolonged exposures to continuous and impulse noise. From the limited data available (Fig. 3),

the following tentative conclusions can be drawn: (1) A long duration series of impulses produce a stable level of asymptotic threshold shift with prolonged exposure times. (2) For a given level of ATS, the exposure time required to reach the ATS level can be much shorter for impulse noise than for continuous noise. (3) The rate of growth to asymptote is a strong function of impulse peak level, that is, at peak levels of 99 dB, 4 to 7 days are required to reach an ATS but at peak levels of 120 dB, only 1 h is required. (4) Variations in preexposure sensitivity do not contribute to the hearing loss caused by the noise exposure. (5) The function relating impulse noise level to the level of ATS is not simple. At impulse levels below about 110 dB, ATS grows at a rate of between 0.7 and 1 dB for each decibel increase in impulse level, while above 110 dB the slope increases to between 2.6 and 5 dB of ATS per decibel increase in impulse level. The change in the slope of the ATS function may signal a transition from a primarily metabolic mode of damage to a primarily mechanical mode and may be related to the idea of a *critical intensity*.<sup>31-33</sup> In summary, there are significant differences between the results of ATS exposures to continuous and impulse noise.

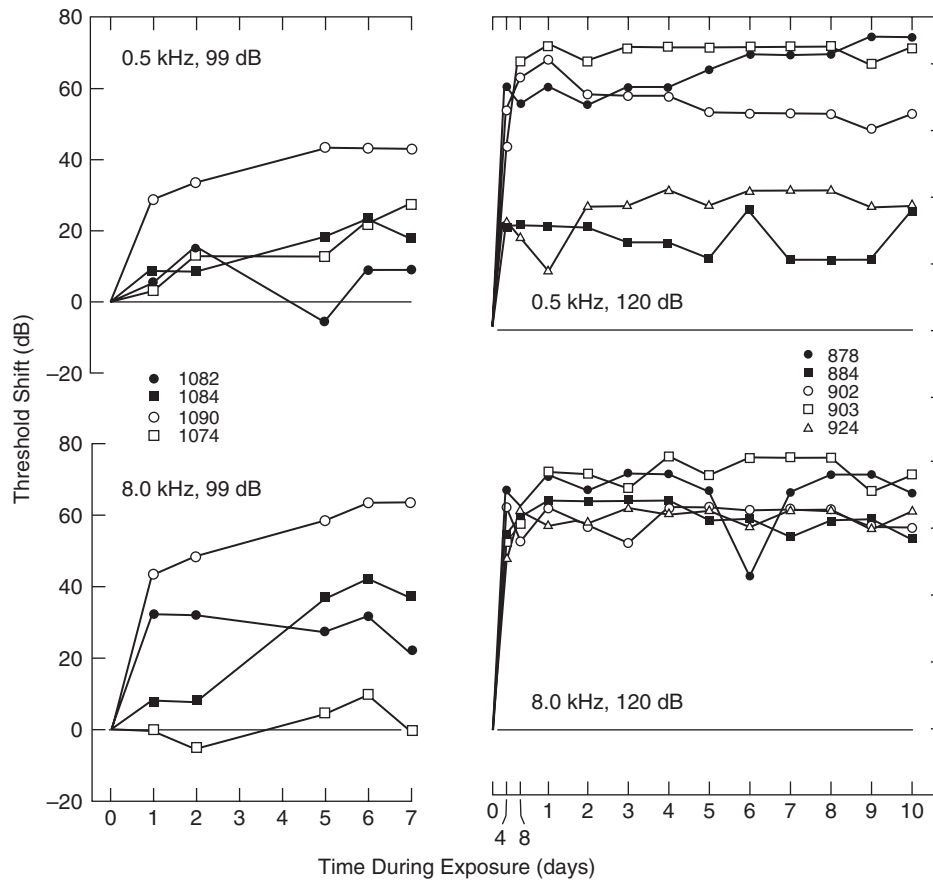
There is extreme variability in the audiometric changes that are produced by exposure to impulse noise. For the same conditions of exposure, variability across individuals can exceed 70 dB.<sup>30,34</sup> The tympanic membrane may account for part of this variability. At high levels of exposure (i.e., >160 dB for the chinchilla) the tympanic membrane (TM) can rip, which in turn leads to poorer transmission of energy through the middle ear and eventually smaller hair cell losses and less hearing loss.

There are other data<sup>30</sup> that show differences in TTS of 60 dB or more for subjects given the same exposure. Figure 3 shows individual animal data from chinchillas exposed to reverberant impulses at either 99- or 120-dB peak SPL. In the 120-dB exposure group there is a 60-dB range in the level of ATS measured at 0.5 kHz, while in the same animals tested at 8 kHz the range of the data is only about 20 dB. At the lower exposure level, one animal tested at 8 kHz did not develop ATS, while animal 1090 developed more than a 60-dB shift.

The extent of the variability in animal and controlled human studies has its parallels in demographic survey data. For example, Taylor and Pelmear,<sup>35</sup> from a carefully controlled survey in the drop forging industry, found variability so large as to preclude any meaningful description of data trends. Some typical data from the Taylor and Pelmear study illustrate the problem and are presented in Fig. 4.

## 5 ANATOMICAL AND PHYSIOLOGICAL CORRELATES

Hawkins<sup>36</sup> has made the case that the morphology of cochlear sensory cell lesion appears the same regardless of whether the lesion was induced by drugs, aging, or noise. However, this generalization does



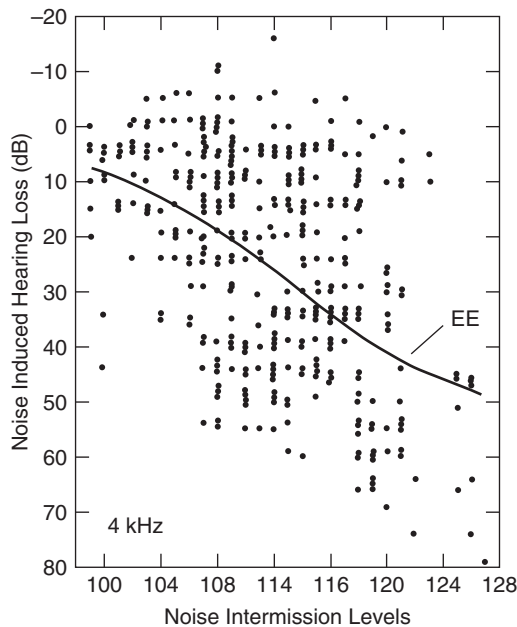
**Figure 3** Asymptotic threshold shift at 0.5 kHz and 8.0 kHz in individual chinchillas exposed to two different levels of reverberant B-type impulses.<sup>30</sup>

not cover some of the effects caused by impulse noise. Spoendlin<sup>37</sup> discussed the intensity levels of continuous and impulse noise required to cause direct mechanical damage to the organ of Corti and concludes that a critical level for the guinea pig for both continuous and impulse noise stimulation occurs at about 130 dB SPL. A graphic demonstration of the type of severe mechanical damage that can be seen following impulse noise exposure is shown in Fig. 5.

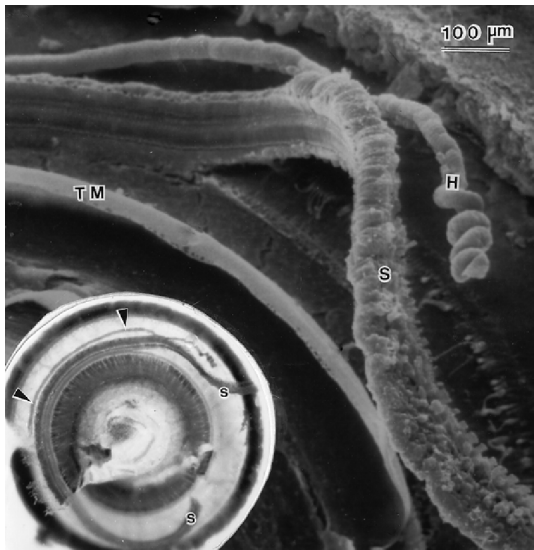
Figure 5 shows a scanning electron micrograph of the first turn of a chinchilla cochlea.<sup>38</sup> The animal was sacrificed within minutes of exposure. The figure illustrates the ripping of the organ of Corti from its attachments to the basilar membrane that can occur after a very brief but intense stimulation (approximately 100 impulses, at a rate of two impulses/minute at 160 dB SPL; the impulse has a 1.5-ms A duration). This type of damage is different from that observed following exposure to lower level continuous noise. This progression of changes that follow such severe mechanical damage (Fig. 5) is also probably different.<sup>39</sup> For exposure to continuous noise of a high level (above

120 dB) there are data showing "mechanically induced lesion,"<sup>40</sup> such as breaking of tight cell junctions, ripping of membrane, and so forth. Presumably, a severe metabolic disturbance in the cochlea results from the intermixing of perilymph and endolymph; and this disturbance to the biochemical balance leads to additional morphological changes. A similar set of conclusions was drawn by Schmeidt et al.,<sup>41</sup> who studied the disturbance of peroxidase in guinea pig cochlea following exposure to 164-dB impulses. Some insight into the progression of damage following impulse noise exposure can be obtained from the results of Kellerhals,<sup>42</sup> who exposed guinea pigs to gunfire, and Hamernik and Henderson,<sup>20</sup> who exposed guinea pigs to 50 impulses of approximately 161 dB per SPL. Both studies showed that sensory cells were lost over a period of up to 30 days.

A somewhat unusual set of result was obtained by Reinis,<sup>43</sup> who observed bleeding in the scala tympani of mice exposed to long-duration (120-ms) impulses. The occurrence of bleeding increased with peak levels of the impulse between 143 and 179 Pa



**Figure 4** Age-corrected individual noise-induced permanent threshold shifts in decibels at 4 kHz for workers exposed to impulse noise in the drop forging industry.<sup>35</sup> The solid line represents the predictions of the EEH.



**Figure 5** Scanning electron micrograph showing extensive tearing of the organ of Corti following blast wave exposures at 160 dB. The animal was sacrificed immediately after exposure. Outer and inner hair cells and their supporting elements (s) are torn loose from the basilar membrane. TM = tectorial membrane, H = Hensen cells. The insert shows an entire turn of the fractured organ of Corti.

(i.e., approximately 139 dB re: 20  $\mu$ Pa). Detailed histology of the cochlea was not presented.

The difference audiological and anatomical effects produced by exposure to impulse or continuous noise are primarily a function of the intensity of the noise, that is, high-level continuous noise (greater than an A-weighted sound pressure level of 120 dB) may also produce mechanical damage. However, the point of this section is that in practice it is unusual to find widespread exposures of humans to continuous noise levels in excess of 120 dB, while the contrary is true for impulse noise exposures.

## 6 PARAMETERS OF AN IMPULSE AND THEIR RELATIONS TO NIPTS

An understanding of the relationship between the various parameters of an impulse and the resultant noise induced permanent threshold shift (NIPTS) is essential to the development of noise standards for impulse noise exposures. In the United States, Canada, and the United Kingdom, the most accepted damage risk criteria (DRC) for impulse noise were developed in a joint effort with U.S and British scientists.<sup>2</sup> This DRC reflected a synthesis of the relatively few experimental results and observations that were available at the time. A 10-dB correction for a 100-fold change in the number of impulses was suggested and was incorporated in the Committee on Hearing and Bioacoustics (CHABA)<sup>44</sup> recommendations. For the purposes of this review, the Coles et al.<sup>2</sup> DRC provides a framework for organizing the results of a diverse set of experiments. The DRC developed by Smoorenburg<sup>45</sup> or Pfander<sup>8</sup> could also serve this purpose.

The following sections review the data from various parametric studies that considered the parameters of amplitude, duration, number of impulses, repetition rates, and rise time. The insights from this review are more applicable as guidelines for research rather than data for noise standards because it is difficult to compare the results of experimental animal studies, human TTS experiments, and demographic data and arrive at definitive conclusions.

### 6.1 Amplitude

The peak amplitude of an impulse noise exposure is a primary consideration in many of the available damage risk criteria (DRC).<sup>2,8,46</sup> However, there is not a simple relationship between the amplitude of an impulse and either cochlear damage or hearing loss.

Impulse noise experiments on human subjects using TTS are ethically limited to exposures that will produced only mild levels of TTS (i.e., 20 to 25 dB). In a systematic study by Tremolieres and Hetu<sup>47</sup> subjects were exposed to impact noise ranging from 107 to 137 dB. Over the 30-dB intensity range of the exposure, the average TTS increased about 15 dB or 0.5 dB per decibel of noise. Tremoliers and Hetu<sup>47</sup> hypothesized that the growth of TTS with exposure level was related to a power law. The Tremoliers and Hetu results build on the observation of McRobert

and Ward<sup>33</sup> who reported that a given impulse had a critical level, and that exposures to a few impulses above the critical level produced a considerable effect while exposure to a large number of impulses below the critical level had little effect.

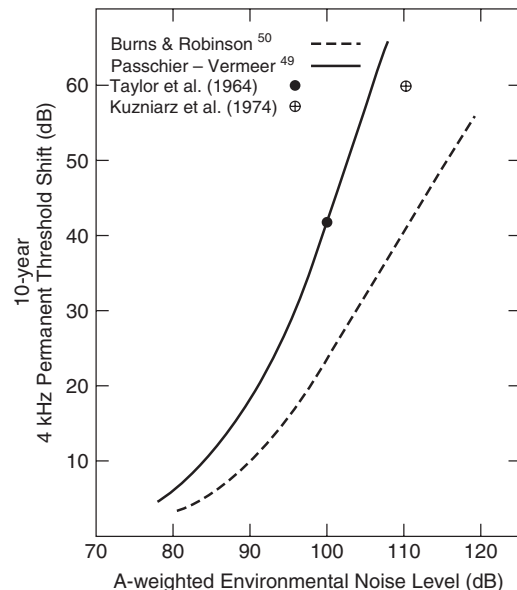
Systematic data for humans are not available, but some insight can be gained from animal experiments.<sup>30</sup> Four groups of chinchillas were exposed for a week to reverberant impulses (150-ms B duration) of 99, 106, 113, or 120 dB. Figure 7 shows that the level of ATS grows considerably slower than from 113 to 120 dB. Furthermore, there was significantly more PTS and cochlear damage in the 120-dB group. The break in the function shown in Fig. 9 might reflect a change in the cochlear processes underlying noise-induced hearing loss.

There are trends in the human demographic data that parallel the rapid growth of hearing loss following exposure to impulse noise or noise environments containing impulsive components. Ceypek et al.<sup>48</sup> reported the permanent threshold shift of workers who developed a large hearing loss (approximately 50 dB) at 4 and 6 kHz within 1 to 2 years. The level of the loss was stable for many years and only spread to lower frequencies. Taylor and Pelmear<sup>35</sup> performed a careful demographic study of Scottish workers exposed to a combination of impact and background noise. Aside from the extreme variability, one noteworthy aspect of their results is that for a change of 20 dB in the noise exposure there is an average change of 50 dB in the observed hearing loss (Fig. 4).

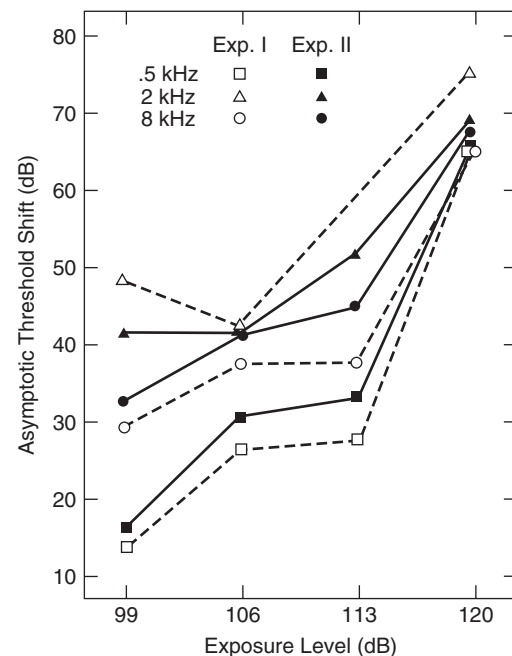
Finally, when one compares two commonly cited demographic studies that relate the A-weighted sound pressure level of exposure to hearing level, for example, the data of Passchier-Vermeer<sup>49</sup> and Burns and Robinson,<sup>50</sup> the former has a considerably steeper slope and greater hearing loss for presumably the same exposure (Fig. 6). However, in the Burns and Robinson<sup>50</sup> data, the exposures were devoid of impulsive components, while the Passchier-Vermeer<sup>49</sup> results are from heterogeneous noise conditions. The data from the Taylor and Pelmear<sup>35</sup> and Kuzniarz<sup>51</sup> studies are also plotted in Fig. 7. These studies are based on workers exposed to noise environments containing impulses; and in both cases, the Passchier-Vermeer curve is a better predictor of eventual hearing loss. Interpretation of the Ceypek et al.,<sup>48</sup> Taylor and Pelmear,<sup>35</sup> and Passchier-Vermeer<sup>49</sup> surveys is made difficult by the variability of the demographic studies, but they are in agreement with controlled laboratory experiments that show that the rate of growth of hearing loss may be accelerated when individuals are exposed to noise environments that contain impulsive noise, as compared to the acquisition of hearing loss with exposure to continuous noise alone.

## 6.2 Duration

The Coles et al.<sup>2</sup> DRC (Fig. 1) specifies two durations; that is, the A duration is the duration of the first overpressure in a Friedlander or blast wave, and the B duration is the time between the peak of



**Figure 6** Average NIHL at 4 kHz for two populations of workers from the demographic studies of Burns and Robinson<sup>50</sup> and Passchier-Vermeer.<sup>49</sup>



**Figure 7** Average ATS at three test frequencies from exposure to impact noise ranging from 99 to 120 dB.<sup>30</sup>

an impact and the point 20 dB down on the decay of a reverberant impulse waveform. An implicit assumption in the Coles et al.<sup>2</sup> DRC, as well as later

formulations by Pfander<sup>7</sup> and Pfander et al.,<sup>8</sup> is the longer duration impulses are more dangerous than the shorter duration impulses. While there is experimental support for this relationship, it is difficult to separate the importance of the impulse duration from the spectral content of an impulse. For A-type impulses, the duration is directly related to the spectrum of the impulse. Thus short-duration impulses have spectra that contain predominantly high-frequency energy and are inefficiently transmitted by the middle ear system. For longer duration impulses (1 ms), the DRC line for A-duration waves plateaus with increasing duration because the distribution of acoustic energy in the impulse is changed with the addition of lower frequencies. Price<sup>52</sup> has suggested modifying the DRC to account for the resonant characteristic of the external meatus, which could enhance the transmission of an A-duration impulse in the range of 100  $\mu$ s. The B-duration criterion line continues downward because the overall energy of the impulse at audible frequencies increases in proportion to the duration of the impulse.

There are very few systematic tests of the validity of the Coles et al.<sup>2</sup> DRC, but limited data from humans and chinchillas show that the duration of an impulse is related to the traumatic effects of the exposure, and the general slope of the line seems to be reasonable. Two recent human studies support the amplitude/duration trade-off. Tremolieres and Hetu<sup>47</sup> exposed subjects to impact noise ranging in amplitude from 107 to 137 dB with durations of 20 to 200 ms (the duration is the time from the impulse B-weighted peak level to the 8.7 dB down point). Yamamura et al.<sup>53</sup> exposed subjects to B-type impulses of either 100 or 105 dB with B durations of either 10, 50, or 100 ms. Both of these studies limited the TTS of the subjects to low levels (approximately 20 dB), but the trend was clear; for equal amplitudes, longer duration impulses produce more TTS. These results were confirmed by Hamernik and Henderson.<sup>54</sup>

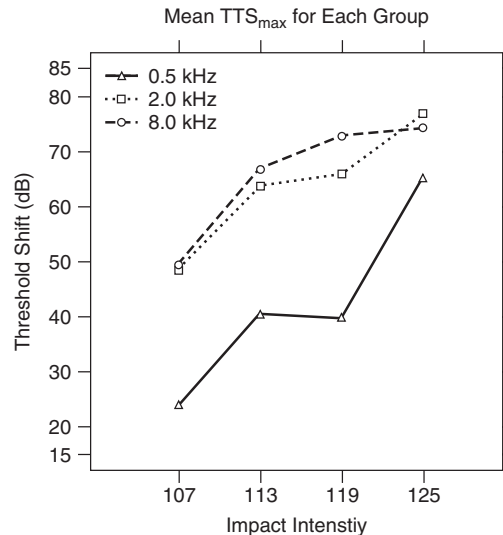
We do not have enough data (i.e., different signatures or varied numbers) to develop an empirical relation between the number of impulses and the resulting hearing loss. None of the presently proposed DRC treats the rate of presentation, or the temporal pattern of an impulse noise exposure as a critical variable. The literature suggests two important factors that vary with time: the acoustical reflex and the rate of recovery of cochlear homeostasis following the presentation of an impulse. There results are consistent with earlier studies by Ward et al.,<sup>32</sup> Perkins et al.,<sup>6</sup> Price,<sup>55</sup> and Hynson.<sup>5</sup>

## 7 EQUAL ENERGY HYPOTHESIS

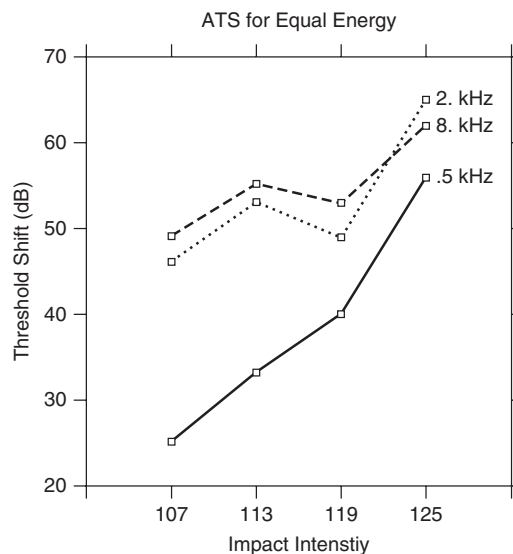
The equal energy hypothesis (EEH) has been expanded from the Eldred et al.<sup>56</sup> principal of *constant energy* and developed as a generalized scheme for evaluating most exposures where the total energy of an exposure (power  $\times$  time) is used as a predictor of hearing loss. Recently, a direct test of the EEH for impulse noise was performed using "realistic" exposures. In the first experiment,<sup>24</sup> chinchillas were exposed for 5 days

to one of four conditions: four impulses/second at 107 dB, one impulse/second at 113 dB, one impulse every four seconds at 119 dB, and one impulse every 16 seconds at 125 dB (Fig. 8).

In the second experiments (Fig. 9), chinchillas were exposed to the same class of impulse as in Fig. 8,



**Figure 8** Average ATS for exposure to impulse noise (B duration = 170 ms) ranging from 107 to 125 dB SPL. The rate of presentation was varied from 4/s to 1/16s; thus each exposure has the same amount of sound energy.<sup>24</sup>



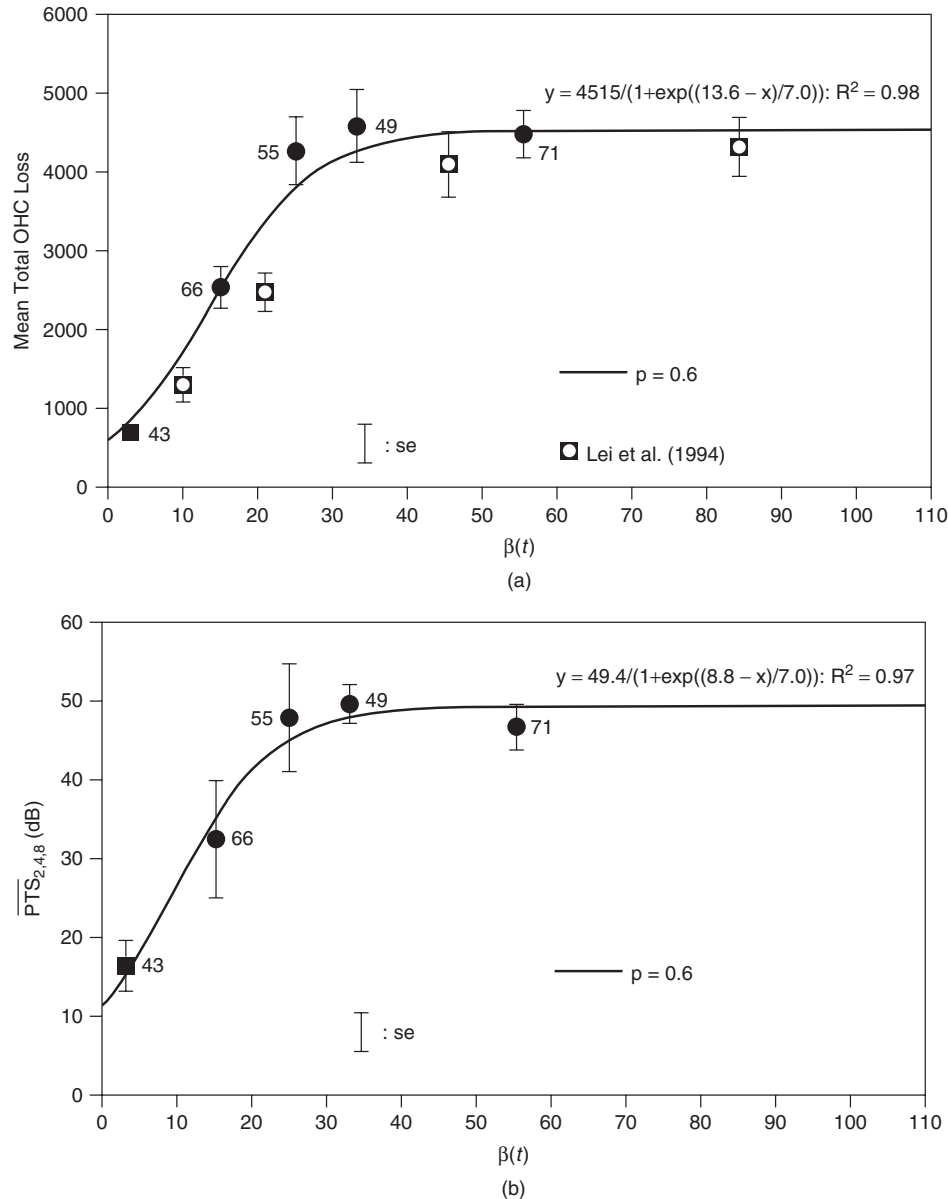
**Figure 9** Average maximum TTS for exposure to the same impulses as described in Fig. 8, but for these data the rate of impulse presentation was held constant and the duration of the exposure was varied to maintain equal energy.<sup>61</sup>

but the rate of presentation was held constant at one impulse/second and the duration of the exposure varied. All these exposures had the same acoustic energy but, if hearing loss was dependent on the total energy, then all groups should have the same levels of ATS. However, in both experiments there is an especially large increase in hearing loss (30 to 40 dB) when the level of noise is increased from 119 to

125 dB, and this large increment may reflect a change in the underlying mechanism of the hearing loss.

## 8 INTERACTION OF IMPULSE AND CONTINUOUS NOISE

Impulse/impact noise also presents a heightened risk when they occur with background noise (approximately an A-weighted sound pressure level of 85 to 95



**Figure 10** (a) Group mean total number of outer hair cells (OHC) and (b) the group mean permanent threshold shift averaged at the 2.0, 4.0, and 8.0 kHz test frequencies ( $\overline{PTS}_{2,4,8}$ ) as  $\beta(t)$  is increased.  $\square$  = the broadband class of non-Gaussian noise exposures;  $\bullet$  = the standard error.



dB). Experimental studies have shown that exposure to combinations of relatively benign impact and continuous noise can lead to multiplicative interactions with hearing loss and cochlear damage with the effects of the combination exposure being greater than the simple additive effects of impulse or continuous noise.

The interaction may be a factor in demographic studies. For example, the workers in the Passchier-Vermeer study<sup>57</sup> had substantially more hearing loss than workers in the Burns and Robinson study,<sup>50</sup> who were exposed to nominally the same amount of acoustic energy. Interestingly, the subjects of Passchier-Vermeer<sup>57</sup> were exposed to noise that had combinations of impact and continuous noise, while the subjects of Burns and Robinson<sup>50</sup> were exposed to more stationary continuous noise. The enhanced danger associated with combination noise exposures may be quantified by measuring the kurtosis of a noise exposure. Lei et al.<sup>58</sup> have shown that the kurtotic values of a noise, as well as the energy of the exposure, are important predictors of hearing loss. Lei et al.<sup>58</sup> showed that non-Gaussian noise exposures would produce more trauma than energy and spectrally equivalent Gaussian exposures. The non-Gaussian character of the noise was produced by the insertion of high-level noise bursts or impact transients into the otherwise Gaussian noise. They showed that the increased trauma was related to the kurtosis,  $\beta(t)$ , of the non-Gaussian signal (Fig. 10). These and other animal model experiments<sup>59</sup> as well as industrial epidemiological data<sup>60</sup> suggest limitations on the use of energy-based metrics such as the  $L_{eq}$ , which are the foundation of current international standards.

In summary, exposure to certain blast and impact noise of different parameters, for example, level, duration, and temporal pattern, produces conditions of TTS and PTS that are frequently inconsistent with the EEH. However, at lower levels of exposure, there are combinations of certain parameters of impact noise that do produce results consistent with the EEH.<sup>61</sup> Unfortunately, we simply do not have enough systematic data to delineate the range of conditions where the EEH is appropriate. For practical reasons, it is important to learn the boundary conditions of the EEH because the basic ideas behind the EEH are easy to incorporate into measurement schemes and noise standards.

**Acknowledgments** This review was partially supported by the following grants: National Institute of Occupational Safety and Health, grant Nos. 1-ROH-OH-00364, 1-RO1-OH-1518, and 2-R01-002317 also NIH contract NO1-NS-1-2381.

## REFERENCES

1. I. I. Glass, *Shock waves and man*, University of Toronto, Institute for Aerospace Studies, Toronto, Canada, 1974.
2. R. R. Coles, G. R. Garinther, D. C. Hodge and C. G. Rice, Hazardous Exposure to Impulse Noise, *J. Acoust. Soc. Am.*, Vol. 43, 1968, pp. 336–343.
3. I. G. Walker and A. Behar, Limitations in the Use of Tape-Recording for Impulse Noise Measurement and TTS Studies, *Proceedings of the 7th International Congress on Acoustics*, Akademia Kiado, Budapest, 1971.
4. G. R. Price, Mechanisms of Loss for Intense Sound Exposures, in *Hearing and Other Senses*, R. R. Ray and G. Gourwithc, Eds., Amphora, Groton, CT, 1983.
5. K. Hynson, R. P. Hamernik and D. Henderson, B-Duration Impulse Definition: Some Interesting Results, *J. Acoust. Soc. Am.*, Vol. Suppl. 1, 1976, p. S30.
6. C. Perkins, R. P. Hamernik, and D. Henderson, The Effect of Interstimulus Interval on the Production of Hearing Loss from Impulse Noise, *J. Acoust. Soc. Am.*, Vol. Suppl. 1, 1975, p. S1.
7. F. Pfander, *Das Knalltrauma*, Springer, Berlin, 1975.
8. F. Pfander, H. Bongartz, H. Brinkmann, and H. Kietz, Danger of Auditory Impairment from Impulse Noise: A Comparative Study of the CHABA Damage-Risk Criteria and Those of the Federal Republic of Germany, *J. Acoust. Soc. Am.*, Vol. 67, 1980, pp. 628–633.
9. P. V. Bruel, The Influence of High Crest Factor Noise on Hearing Damage, *Scand. Audiol. Suppl.*, Vol. 12, 1980, pp. 25–32.
10. A. Okada, K. Fukuda, and K. Yamamura, Growth and Recovery of Temporary Threshold Shift at 4 kHz Due to a Steady State Noise and Impulse Noises, *Int. Z. Angew. Physiol.*, Vol. 30, 1972, pp. 105–111. K. Yamamura, H. Takashima, H. Miyake, and A. Okada, Effect of Combined Impact and Steady State Noise on Temporary Threshold Shift (TTS), *Med. Lav.*, Vol. 65, 1974, pp. 215–223. S. Arlinger and P. Mellberg, A Comparison of TTS Caused by a Noise Band and by Trains of Clicks, *Scand. Audiol. Suppl.*, Vol. 12, 1980, pp. 242–248.
11. R. P. Hamernik and D. Henderson, Impulse Noise Trauma. A Study of Histological Susceptibility, *Arch. Otolaryngol.*, Vol. 99, 1974, pp. 118–121.
12. R. R. Pfeiffer, Consideration of the Acoustic Stimulus, in *Handbook of Sensory Physiology*, W. D. Keidel and D. Neff, Eds., Springer, Berlin, 1974, pp. 9–38.
13. I. V. Nabelek, Advances in Noise Measurement Schemes, in *New Perspectives on Noise Induced Hearing Loss*, R. P. Hamernik, D. Henderson, and R. Salvi, Eds., Raven, New York, 1982, pp. 491–509.
14. A. Ivarsson and P. Nilsson, Advances in Measurement of Noise and Hearing, *Acta Otolaryngol.*, Vol. 366, 1980, pp. 1–67.
15. G. R. Atherley and A. M. Martin, Equivalent-Continuous Noise Level as a Measure of Injury from Impact and Impulse Noise, *Ann. Occup. Hyg.*, Vol. 14, 1971, pp. 11–23.
16. H. Hakanson, B. Erlandsson, A. Ivarsson, and P. Nilsson, Differences in Noise Doses Achieved by Simultaneous Registrations from Stationary and Ear-Borne microphones, *Scand. Audiol. Suppl.*, Vol. 12, 1980, pp. 47–53.
17. A. Martin, The Equal Energy Concept Applied to Impulse Noise, in *The Effects of Noise on Hearing*, D. Henderson, R. P. Hamernik, D.S. Dosanjh, and J. Mills, Eds., Raven, New York, 1976, pp. 421–453.
18. G. A. Luz, Recovery from Temporary Threshold Shift in Monkeys Exposed to Impulse Noise: Evidence for Diphasic Recovery Process, *J. Acoust. Soc. Am.*, Vol. 48, 1970, pp. 96(A).

19. J. L. Fletcher, Temporary Threshold Shift Recovery from Impulse and Steady State Noise Exposure, *J. Acoust. Soc. Am.*, Vol. 48, 1970, pp. 96(A).
20. D. Henderson and R. P. Hamernik, Impulse Noise: The Effects of Intensity and Duration on the Production of Hearing Loss, 8th Int. Congr. on Acoust., London, 1974.
21. J. H. Patterson, I. M. Lomba-Gautier, and D. L. Curd, The Effect of Impulse Intensity and the Number of Impulses on Hearing and Cochlear Pathology in the Chinchilla, USAARL Rpt. No. 85-3, 1985.
22. W. D. Ward, A. Gloring, and D. L. Sklar, Temporary Threshold Shift from Octave Band Noise: Application to Damage Risk Criteria, *J. Acoust. Soc. Am.*, Vol. 31, 1959, pp. 522-528.
23. D. Henderson, R. P. Hamernik, and R. W. Sittler, Audiometric and Histological Correlates of Exposure to 1-msec Noise Impulses in the Chinchilla, *J. Acoust. Soc. Am.*, Vol. 56, 1974, pp. 1210-1221.
24. D. Henderson, R. J. Salvi, and R. P. Hamernik, Is the Equal Energy Rule Applicable to Impact Noise? *Scand. Audiol. Suppl.*, Vol. 16, 1982, pp. 71-82.
25. W. Kraak, Investigations on Criteria for the Risk of Hearing Loss Due to Noise, *Hearing Research and Theory*, in J. Tobias and E. D. Schubert, Eds., Academic, New York, 1981, pp. 189-305.
26. H. M. Carder and J. D. Miller, Temporary Threshold Shifts from Prolonged Exposure to Noise, *J. Speech Hear. Res.*, Vol. 15, 1972, pp. 603-623.
27. J. H. Mills, Threshold Shifts Produced by a 90-Day Exposure to Noise, in *The Effects of Noise on Hearing*, D. Henderson, R. P. Hamernik, D. S. Dosanjh, and J. H. Mills, Eds., Raven, New York, 1976, pp. 265-275.
28. B. A. Bohne and W. W. Clark, Growth of Hearing Loss and Cochlear Lesion with Increasing Duration of Noise Exposure, in *New Perspectives on Noise Induced Hearing Loss*, R. P. Hamernik, D. Henderson, and R. Salvi, Eds., Raven, New York, 1982, pp. 283-302.
29. E. A. Blakeslee, K. Hynson, R. P. Hamernik, and D. Henderson, Asymptotic Threshold Shift in Chinchillas Exposed to Impulse Noise, *J. Acoust. Soc. Am.*, Vol. 63, 1978, pp. 876-882.
30. D. Henderson and R. P. Hamernik, Asymptotic Threshold Shift from Impulse Noise, in *New Perspectives on Noise Induced Hearing Loss*, R. P. Hamernik, D. Henderson, and R. J. Salvi, Eds., Raven Press, New York, 1982, p. 265.
31. W. D. Ward Effect of Temporal Spacing on Temporary Threshold Shift from Impulses, *J. Acoust. Soc. Am.*, Vol. 34, 1962, pp. 1230-1232. D. Henderson and R. P. Hamernik, Impulse Noise-Induced Hearing Loss: An Overview, *Noise and Audiology*, in D. M. Lipscomb, Ed., University Park, Baltimore, MD, 1978, pp. 143-166.
32. W. D. Ward, W. Selters, and A. Gloring, Exploratory Studies on Temporary Threshold Shift from Impulses, *J. Acoust. Soc. Am.*, Vol. 33, 1961, pp. 781-793.
33. H. McRobert and W. D. Ward, Damage-Risk Criteria: The Trading Relation between Intensity and the Number of Nonreverberant Impulses, *J. Acoust. Soc. Am.*, Vol. 53, 1973, pp. 1297-1300.
34. K. D. Kryter and G. R. Garinther, Auditory Effects of Acoustic Impulses from Firearms, *Acta Otolaryngol.*, Vol. Suppl. 211, 1966.
35. W. Taylor and P. L. Pelmar, Noise Levels and Hearing Thresholds in the Drop Forging Industry, Med. Res. Council Project Rep., Grant G972/784/C, London, England, 1976.
36. J. E. Hawkins, Jr., Comparative Otopathology: Aging, Noise, and Ototoxic Drugs, *Adv. Otorhinolaryngol.*, Vol. 20, 1973, pp. 125-141.
37. H. Spoendlin, Anatomical Changes Following Various Noise Exposures, in *Effects of Noise on Hearing*, D. Henderson, R. P. Hamernik, D. S. Dosanjh, and J. Mills, Eds., Raven, New York, 1976, pp. 69-90.
38. R. P. Hamernik, G. Turrentine, M. Roberto, R. Salvi, and D. Henderson, Anatomical Correlates of Impulse Noise-Induced Mechanical Damage in the Cochlea, *Hear. Res.*, Vol. 13, 1984, pp. 229-247.
39. R. P. Hamernik, G. Turrentine, and C. G. Wright, Surface Morphology of the Inner Sulcus and Related Epithelial Cells of the Cochlea Following Acoustic Trauma, *Hear. Res.*, Vol. 16, 1985, pp. 143-160.
40. H. A. Beagley, Acoustic Trauma in the Guinea Pig. I, *Acta Otolaryngol.*, Vol. 60, 1965, pp. 437-451. H. A. Beagley, Acoustic Trauma in the Guinea Pig. II, *Acta Otolaryngol.*, Vol. 60, 1965, pp. 479-495. L. Voldrich, Experimental Acoustic Trauma. I, *Acta Otolaryngol.*, Vol. 74, 1972, pp. 392-327. L. Voldrich and L. Ulehlova, Correlation of the Development of Acoustic Trauma to the Intensity and Time of Acoustic Overstimulation, *Hear. Res.*, Vol. 6, 1982, pp. 1-6.
41. H. P. Schmidt, M. Biedermann, and G. Geyer, Peroxidase Distribution Pattern and Cochlear Microphonics in the Impulse-Noise Exposed Cochlea of the Guinea Pig (author's transl), *Anat. Anz.*, Vol. 144, 1978, pp. 383-392.
42. B. Kellerhals, Pathogenesis of Inner Ear Lesions in Acute Acoustic Trauma, *Acta Otolaryngol.*, Vol. 73, 1972, pp. 249-253.
43. S. Reinis, Acute Changes in Animal Inner Ears Due to Simulated Sonic Booms, *J. Acoust. Soc. Am.*, Vol. 60, 1976, pp. 133-138.
44. CHABA, Proposed Damage-Risk Criterion for Impulse Noise (Gunfire), Rep. of Working Group 57, NAS-NRC Comm. on Hearing Bioacoustics and Biomechanics, Washington, DC, 1968.
45. G. F. Smoorenburg, Damage Risk Criteria for Impulse Noise, in *New Perspectives on Noise Induced Hearing Loss*, R. P. Hamernik, D. Henderson, and R. Salvi, Eds., Raven, New York, 1982, pp. 471-490.
46. K. D. Kryter, Evaluation of Exposures to Impulse Noise, *Arch. Environ. Health*, Vol. 20, 1970, pp. 624-635.
47. C. Tremolieres and R. Hetu, A Multi-parametric Study of Impact Noise-Induced TTS, *J. Acoust. Soc. Am.*, Vol. 68, 1980, pp. 1652-1659.
48. T. Ceypek, J. Kuzniarz, and A. Lipowczan, The Development of Permanent Hearing Loss Due to Industrial Percussion Noise (Polish), *Med. Pr.*, Vol. 2, 1975, pp. 53-59.
49. W. Passchier-Vermeer, Hearing Loss Due to Continuous Exposure to Steady-State Broad-band Noise, *J. Acoust. Soc. Am.*, Vol. 56, 1974, pp. 1585-1593.
50. W. Burns and D. W. Robinson, An Investigation of the Effects of Occupational Noise on Hearing, in *Sensorineural Hearing Loss*, G. E. W. Wlstenholme and J. Knight, Eds., Williams and Wilkins, Baltimore, MD, 1970.
51. J. Kuzniarz, Z. Swiercznski, and A. Lipowczan, Impulse Noise Induced Hearing Loss in Industry and the



- Energy Concept: A Field Study. Proceedings of 2nd Conference, Southampton, England, 1976.
52. G. R. Price, Loss of Auditory Sensitivity Following Exposure to Spectrally Narrow Impulses, *J. Acoust. Soc. Am.*, Vol. 66, 1979, pp. 456–465.
  53. K. Yamamura, K. Aoshima, S. Hiramatsu, and T. Hikichi, An Investigation of the Effects of Impulse Noise Exposure on Man: Impulse Noise with a Relatively Low Peak Level, *Eur. J. Appl. Physiol. Occup. Physiol.*, Vol. 43, 1980, pp. 135–142.
  54. R. P. Hamernik and D. Henderson, The Potentiation of Noise by Other Ototraumatic Agents, in *Effects of Noise on Hearing*, D. Henderson, R. P. Hamernik, D. S. Dasanji, and J. H. Mills, Eds., Raven Press, New York, 1976, pp. 291–307.
  55. G. R. Price, Effect of Interrupting Recovery on Loss in Cochlear Microphonic Sensitivity, *J. Acoust. Soc. Am.*, Vol. 59, 1976, pp. 709–712.
  56. K. M. Eldred, W. Gannon, and H. E. von Gierke, Criteria for Short Time Exposure of Personnel to High Intensity Jet Aircraft Noise, WADCTN55–355, 1955.
  57. W. Passchier-Vermeer and W. Passchier, Environmental Noise Exposure, *Environ. Health Perspect.*, Vol. 106, 1998, pp. A527–528.
  58. S. F. Lei, W. A. Ahroon, and R. P. Hamernik, The Application of Frequency and Time Domain Kurtosis to the Assessment of Hazardous Noise Exposures, *J. Acoust. Soc. Am.*, Vol. 96, 1994, pp. 1435–1444.
  59. R. Lataye and P. Campo, Applicability of the  $L_{eq}$  as a Damage-Risk Criterion: An Animal Experiment, *J. Acoust. Soc. Am.*, Vol. 99, 1996, pp. 1621–1632.
  60. L. Thiery and C. Meyer-Bisch, Hearing Loss Due to Partly Impulsive Industrial Noise Exposure at Levels between 87 and 90 dB(A), *J. Acoust. Soc. Am.*, Vol. 84, 1988, pp. 651–659.
  61. M. Roberto, R. P. Hamernik, R. J. Salvi, D. Henderson, and R. Milone, Impact Noise and the Equal Energy Hypothesis, *J. Acoust. Soc. Am.*, Vol. 77, 1985, pp. 1514–1520.
  62. G. A. Luz and D. C. Hodge, Recovery from Impulse-Noise Induced TTS in Monkeys and Men: A Descriptive Model, *J. Acoust. Soc. Am.*, Vol. 49, 1971, pp. 1770–1777.

# CHAPTER 28

## EFFECTS OF INTENSE NOISE ON PEOPLE AND HEARING LOSS

Rickie R. Davis and William J. Murphy  
National Institute for Occupational Safety and Health  
Cincinnati, Ohio

### 1 INTRODUCTION

The purpose of this chapter is to provide an overview of the effects of noise on people and their hearing. Noise is a universal problem that damages hearing and impacts quality of life. Most industrial environments have noise as a component. This chapter will provide an introduction to the functioning of the peripheral auditory system, protective mechanisms of the ear, noise damage and how it is assessed, and some discussion of how noise regulations are determined.

### 2 NOISE AND THE EAR

A number of works have reviewed the interaction of the ear and noise<sup>1,2</sup> and other information resources such as websites (e.g., [www.cdc.gov/niosh/topics/noise](http://www.cdc.gov/niosh/topics/noise)) are available.

Noise is most commonly defined as unwanted sound or acoustic energy. However, acoustical descriptions usually characterize noise by its intensity, its frequency spectrum, and its temporal signature. Common terms are *wideband noise*, *white noise*, *pink noise*, and *octave-band noise*.<sup>3</sup> These terms refer to the width and shape of the frequency spectrum. Temporal signatures are *impact* and *impulse noise* and *intermittent* and *continuous noise*.

The mammalian ear is anatomically divided into three parts: the outer ear or pinna and ear canal, which ends at the *tympanic membrane* (or eardrum), the air-filled middle ear containing three bones or *ossicles*, and the inner ear or *cochlea*. The cochlea is fluid-filled and, in mammals, is shaped like a snail shell. The cochlea contains the outer and inner sensory hair cells and the basilar membrane. The outer and inner sensory hair cells differ in their shape, structural support, VIII<sup>th</sup> nerve innervation patterns, and function. The hair cells are so-called because they have tiny structures, *stereocilia*, on their apical surface consisting of stiff actin rods that resemble hairs. The hair cells are arranged in four rows the length of the cochlea: one row of inner hair cells and three rows of outer hair cells. The stereocilia of the third row of outer hair cells are embedded in an overlying gelatinous membrane called the tectorial membrane.

Acoustical vibrations in air set the tympanic membrane into motion and the vibrations are transmitted through the middle ear bones (the ossicles). These bones serve as an impedance-matching transformer between the gas medium of the atmosphere and the liquid medium of the cochlea and provide about 30

dB of gain. These vibrations then set the fluid of the cochlea into motion. The fluid acts upon the basilar membrane and the hair cells. Low-level vibrations are enhanced through active negative damping of the outer hair cells. Vibrations are then transduced to electrochemical energy by the inner hair cells and are transmitted as action potentials via the acoustical nerve to the brain. Each inner hair cell represents a place on the basilar membrane and each place represents a particular acoustic frequency. The reader is referred to Dallos,<sup>4</sup> Pickles,<sup>5</sup> and other writings on the ear for a more complete exposition.

The average human cochlea is insensitive to acoustic energy below about 20 Hz and above 20 kHz. Below 20 Hz humans often feel high-level acoustic energy as whole-body vibration. Above the high-frequency limit of the human (about 20 kHz in young ears), there is usually no sensation associated with the acoustic energy.

Depending upon the frequency of the sound, the ear is capable of detecting sounds less than 0 dB SPL (sound pressure level, dB referenced to 20  $\mu$ Pa). (Often youngsters can hear certain pure tones at  $-10$  or even  $-20$  dB SPL in the 1 to 3 kHz frequency range.) The threshold of pain for the ear is somewhere around 130 dB. Since the decibel scale is logarithmic, this represents an extremely wide dynamic physical range of sound intensity with a ratio of quietest stimulus to the threshold of pain of more than 1 trillion.

**Protective Mechanisms** The cochlea can be permanently damaged by high levels of sound. The auditory periphery has several mechanisms that provide some protection against loud sounds. These mechanisms include the malleus-incus joint, the stapedal annular suspensory ligament, the middle ear muscles (or the acoustical reflex), the olivocochlear pathway, and cellular scavengers of reactive oxygen species.

The ossicles consist of the malleus (or hammer), incus (or anvil), and stapes (or stirrup) bones. The joint between the malleus and the incus is held together by a ligament. Normally this joint is tightly held together so the malleus and incus move as a unit. At very high acoustical levels this joint allows the two bones to slip against each other, reducing transmission of acoustic energy through the ossicular chain. In addition, Price<sup>6</sup> has documented that the stapes bone is held against the oval window membrane of the cochlea by the annular suspensory ligament. This ligament acts as a nonlinear

spring, limiting the inward motion of the stapes and energy to the cochlea.

Located within the middle ear are two tiny muscles: the *tensor tympani* muscle is attached to the long process of the malleus and the *stapedius* muscle attached to the protuberance of the stapes—two of the bones of the ossicular transmission chain. In humans, contraction of the stapedius muscle, activated by the acoustical reflex arc, causes a stiffening of the ossicular chain transmission path and an increase in acoustic impedance. This leads to a reduction of acoustic energy presented to the cochlea. Unfortunately, the contraction requires tens of milliseconds,<sup>30</sup> adapts after a few seconds, and reduces the input by only 10 to 15 dB mainly in sounds below 1500 Hz. Thus the acoustical reflex is not a good substitute for an ear plug or muff in an industrial environment. A small percentage of the population does not exhibit an acoustical reflex.

A second reflex arc, which changes the gain of the outer hair cells, may play a protective role in the ear.<sup>7</sup> The efferent olivocochlear bundle of nerve fibers originate from cell bodies in the pons of the midbrain. These efferent fibers synapse on the outer hair cells. These fibers derive their functional input from the auditory nerve. As the level of stimulation increases, the feedback to the outer hair cells changes the outer hair cell stiffness and reduces the input to the inner hair cells. In a population there are differing levels of outer hair cell drive from the olivocochlear bundle. Maison and Liberman<sup>8</sup> showed in guinea pigs that those individuals possessing strong levels of olivocochlear bundle effect had decreased vulnerability to noise-induced hearing loss. Those individuals who had lower levels of olivocochlear bundle drive sustained a permanent threshold shift up to 40 dB greater than an individual with strong olivocochlear reflex drive. Normally, the olivocochlear bundle feedback functions at relatively low levels of sound producing a minor 0.5- to 1.5-dB attenuation when electrically stimulated under normal conditions. The purpose of the olivocochlear feedback loop is still controversial, and some authors argue against a protective role in high-level acoustical stimulation.<sup>9</sup>

The hair cells of the cochlea are prodigious consumers of oxygen. By-products of high oxygen use are the free-radical, reactive oxygen species.<sup>10</sup> Once generated, these extremely reactive versions of oxygen immediately interact with DNA (deoxyribonucleic acid), lipids and proteins. These interactions lead to damage of cellular components. This damage can result in death of the hair cell through *apoptosis* (programmed cell death).<sup>11,12</sup> Animal studies have shown that providing scavengers for free-radical oxygen species prior to and just after noise exposure can reduce the level of hearing threshold change.<sup>13,14</sup> Free-radical scavengers are the local protection accorded the cochlea against insult by a high-level noise. Presently companies are marketing over-the-counter compounds for use by noise-exposed people to prevent noise-induced hearing loss. There is presently no human evidence of prophylactic effects for any compound or food supplement to prevent or reduce noise-induced

hearing loss, but this evidence may be forthcoming. In 2004 the U.S. Army funded a double-blind study in human volunteers looking for these protective effects.<sup>15</sup>

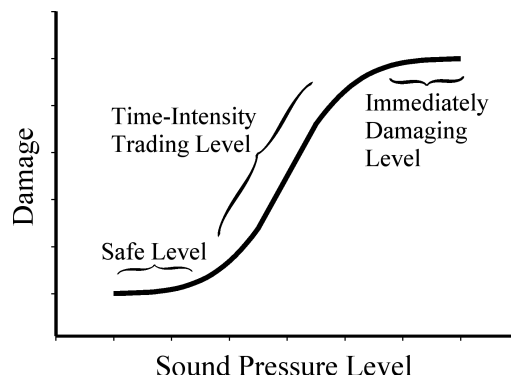
Although all of these mechanisms work in concert to reduce damage to the ear, they are inadequate for long-term protection in an industrial or military environment. Only by reducing exposure to noise can hearing be preserved.

### 3 AUDITORY AFTEREFFECTS OF NOISE

Figure 1 is a simple model of how the ear reacts to noise. The left-hand portion of the curve is the safe zone of the ear—noises in this range cause no measurable damage in normal people. Most people live in this range on a day-to-day basis.

*Temporary threshold shift (TTS)* is a change in absolute hearing threshold due to exposure to a higher level noise that resolves to *no measurable threshold shift* after some period of time. This recovery time can be from minutes to days. An intense noise exposure results in a combined threshold shift (CTS) that contains both TTS and permanent threshold shift components.

Noise of sufficient intensity and appropriate frequency can produce a permanent reduction of sensitivity of the ear to sound, also known as a *permanent threshold shift*, or *PTS*. This area of risk is represented in the right-hand portion of the curve of Fig. 1. Noise at this level can cause immediate damage to the sensory cells and supporting cells of the cochlea. This damage results in loss of outer hair cells due to *necrosis* or death due to mechanical overstimulation. Using microscopic carbon particles in chinchilla ears, Ahmad<sup>16</sup> showed that tiny holes were developed in the reticular lamina (upper surface of the organ of Corti) of the noise-damaged cochlea. These tiny holes allowed



**Figure 1** Theoretical noise damage curve. X axis is increasing sound pressure level. Y axis is increasing damage (may be shift in audiometric threshold or damage to hair cells). Left side of curve shows little or no damage due to noise. The middle section shows damage linearly increasing with noise exposure. The right section of the curve shows effect of extremely high noise exposures that asymptote with higher noise levels.

for the movement of the carbon particles from the fluid space at the tops of the hair cells to the fluid space around the hair cells. Presumably, this also allowed for the mixing of the fluids contained in these spaces (endolymph and perilymph). These fluids are very different in chemical composition and their mixing leads to death of the hair cells, or necrosis.

An intermediate level of sound can produce either TTS or PTS—the linear, central portion of Fig. 1. Currently there is little understanding of how TTS progresses to PTS or even if they are related. Detailed light and electron microscopy of the cochlea<sup>17</sup> has found no consistent changes in either inner or outer hair cells, which correlate with the psychophysical and electrophysiological changes measured in the auditory threshold.

The regulatory community accepts that TTS is an early predictor or a process of PTS. However, TTS has proven to be a poor predictor of PTS both in animal and epidemiologic studies of humans exposed to noise.<sup>18</sup> The underlying mechanisms for TTS and PTS are not likely the same. New techniques and research may provide a better understanding of this complex problem.

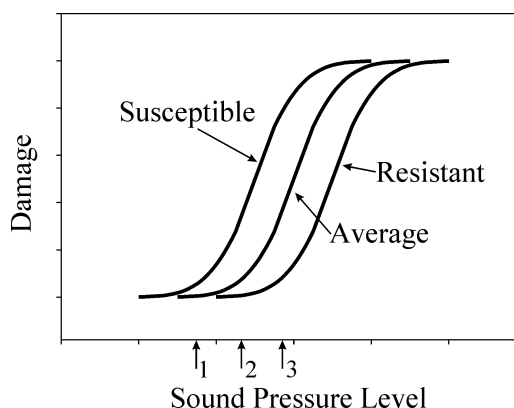
Within this linear portion of the graph (Fig. 1) the *equal-energy hypothesis (EEH)* tends to function well for continuous noise. In effect, this hypothesis says that equivalent hearing losses (generally PTS) can be produced by a low-level noise exposure over a long time and a high-level noise exposure over a short time. This hypothesis assumes that the ear integrates acoustic energy over some time period—usually 24 h. Thus, from the ear's perspective, a 1-h exposure at some sound intensity is equivalent to exposure to a sound intensity that is 3 dB less for 2 h. This is called a time–intensity trading ratio or simply trading ratio.

In the United States the linear range of this function is declared by regulations to have A-weighted sound pressure levels in the range of 90 to 120 dB. Table 1 demonstrates the difference in exposure times permitted between a 5-dB time–intensity trading ratio and a 3-dB ratio. Rather than using a physics-based 3 dB as the doubling rate, U.S. government regulators use 5 dB, under the assumption that workers will get breaks from

the noise during the day, allowing for recovery. Most countries today use a 3-dB trading ratio.

Determining the maximum acoustic energy a worker may be exposed to is a tricky political and scientific exercise. There are workers in the population so susceptible to noise that reduction of noise exposure would be economic and technologically infeasible. Subjecting normal workers to such abatement procedures would result in communication difficulties. On the other hand by setting the maximum exposure level higher indicates the amount of workers' hearing society is willing to sacrifice. Regulations are a compromise of economics, science, and politics.

The model in Fig. 1 is a reasonable first approximation for one person. However, in populations there are people for whom the entire curve may be displaced to the left (equal damage occurs at lower energy levels; labeled Sensitive in Fig. 2) or displaced to the right (exposure to higher energy levels causes less damage to the ear; labeled Resistant in Fig. 2). Currently, there is no way of predicting the sensitivity of a particular person's ears to noise. Only post hoc analysis can tell us if someone has particularly vulnerable (glass) or particularly resistant (iron) ears.



**Figure 2** Three theoretical noise damage curves as in Fig. 1. The left most curve demonstrates the effects of noise on a susceptible individual. The middle curve demonstrates the effects of noise on someone with normal susceptibility to noise (most of the population). The right curve shows the effects on a person resistant to noise. On the X axis arrow 1 points to the most protective noise exposure level—virtually everyone is protected from noise-induced hearing loss. Arrow 2 points to the most economically feasible noise exposure level—at least from the noise control view. The most susceptible workers in the population would receive large hearing losses, the normal (most) workers would receive a small hearing loss and the resistant would receive little or no hearing loss. Arrow 3 points to a compromise level—some of the most susceptible individuals would still receive a hearing loss, only a small portion of the normal (most) workers would sustain a hearing loss, yet it would not require as large of investment in engineering controls or hearing conservation as level 1.

**Table 1** Demonstration of Differences in Permissible Exposure Times for a 5-dB Trading Ratio versus a 3-dB Trading Ratio

Time of Permissible Unprotected Exposure <sup>a</sup>	5-dB Intensity/Time Trading Ratio (dB)	3-dB Intensity/Time Trading Ratio (dB)
8 h	90	90
4 h	95	93
2 h	100	96
1 h	105	99
30 min	110	102
15 min	115	105
7.5 min	120	108

<sup>a</sup> Current U.S. OSHA regulations.

The arrows on the  $x$  axis of Fig. 2 show how difficult it is to set a noise exposure fence. A regulation designed to protect the maximum number of workers would enact the level denoted by arrow 1. Even the most susceptible workers would be protected at this level. However, this would be burdensome to employers in requiring massive layouts in noise control. It would also be burdensome to employees in that the normal or resistant workers would be overprotected. Communication and safety signal recognition may suffer. Database analyses such as the International Organization for Standardization (ISO) 1999 indicate that even at 80 dB SPL some members of a population may incur a noise-induced hearing loss. Arrow 3 denotes the most economic level. At this level society is willing to sacrifice the hearing of a small number of the normal workers and most of the susceptible workers. A compromise is denoted by arrow 2 in which the hearing of a certain proportion of the normal and susceptible population is sacrificed.

The EEH is a reasonable first approximation as long as the acoustic energy remains within the linear region of the ear. Additional assumptions are that the ear integrates the noise over a 24-h period. Schneider<sup>19</sup> showed that the actin in the stereocilia of the hair cells is completely replaced over a 2-day period, which might indicate that sound exposure should be integrated over 2 days rather than a single 24-h day as is currently the practice. They also showed that the actin is replaced from the tip of the stereocilia rather than the base as one would guess.

Noise exposure can also result in *tinnitus*—a ringing or buzzing in the ears. Tinnitus can be thought of as the ear's pain response. Tinnitus can be present temporarily or, with continued noise exposure, it can become permanent. Current research places the generator of tinnitus in the central nervous system.<sup>20</sup> A working hypothesis is that cochlear input to the central nervous system is removed as a result of damage, and the brain produces a stimulus to replace that missing input. Generally, the subjective experience of tinnitus does not correlate with any sounds produced by the ear. Tinnitus may also be caused by exposure to chemicals (e.g., aspirin).

Susceptibility to noise-induced hearing loss is known to be specific to the individual. Workers with "tender" ears may be damaged by a particular noise while their co-workers who seem to have "tough" ears experience no damage. This effect is also seen in experimental animals. Animal research indicates that there are genetic predispositions to noise-induced hearing loss.<sup>21</sup> In the human population, no specific genes have been directly linked to susceptibility to noise-induced hearing loss. However, hearing disorders such as Usher's syndrome have a genetic basis.

One of the dangers of noise is that it may mask important signals for the worker. In the previous edition of this chapter Ward<sup>22</sup> presented a very complete discussion of masking by noise. In general terms, low-frequency noises are able to mask high-frequency noises by the "upward spread of masking." In work settings the most important signals that are masked

are co-worker speech and safety/warning signals. (The reduction of speech intelligibility by noise is complex and requires a book of its own.) The use of hearing protection and/or possession of a hearing loss, along with masking noises significantly complicates the acoustical environment and isolates the worker. Workers commonly maintain that their inability to hear speech, machinery, warning signals, and environmental sounds (e.g., "roof-talk" for underground mining) is a barrier to the use of hearing protection devices.<sup>23</sup> The increased masking with increasing noise level coupled with the TTS produced by noise exposure invalidates such claims. The masking by noise and the benefits of hearing protector use to reduce masking and TTS must be demonstrated to workers to overcome their reluctance to effectively use hearing protection.

#### 4 NONAUDITORY EFFECTS—NOISE AND THE BODY

Extremely loud blasts, usually encountered only in a military setting, can produce enough acoustic energy to damage internal organs. The ear, the gastrointestinal tract, the upper respiratory tract, and the lungs are particularly susceptible to blast damage because they are air filled.<sup>24</sup> Generally, the rank order of susceptibility to damage is the ears, the lungs and the gastrointestinal tract, which is least susceptible of the three systems. Fifty percent of normal human tympanic membranes will rupture in the 57- to 345-kPa peak pressure range (190 to 200 dB SPL peak pressure).<sup>25</sup>

Blast overpressure injury of the lungs can result in air emboli that can travel throughout the circulatory system. Even contusions of the lungs by blast can be life threatening. Blast overpressure lung injury may be enhanced by body armor. Foam material may more effectively couple the body to the acoustical event and increase injury.<sup>26</sup>

In the civilian sector most nonauditory effects of loud noise are related to psychological stress. Noise is considered stressful if the person cannot control it nor can they habituate to it.<sup>27</sup> At low levels unsignaled noise causes an orienting response. As the level becomes louder, the person startles with an increase in blood pressure and muscular contractions. These reactions last a few seconds, with an interruption of ongoing activities. At high enough levels sleep can be compromised, impacting quality of life. With chronic exposure a stress reaction results in release of the corticosteroids, which are part of the *fight-or-flight* system.<sup>27</sup> Researchers have noted statistically significant increases in blood pressure for workers exposed to noise greater than an A-weighted sound pressure level of 75 dB.<sup>28</sup>

#### 5 RISK ANALYSIS—NOISE AND THE POPULATION

In the occupational noise setting, risk analysis attempts to determine the shape of the noise-exposure response curve for the entire worker population. If Fig. 1 is generalized to the population, the analysis attempts to

determine levels at which the population is relatively safe and how much hearing damage will be produced at various levels of noise exposure. Due to individual susceptibility to noise and the inconsistent use of hearing protection, this is never a straightforward exercise. Risk analysis is very important for setting government regulations and can have significant impact on costs associated with protecting workers. In order to protect the most susceptible segment of the population, costs of hearing loss prevention programs may be doubled or tripled.

Risk analysis of occupational hearing loss is an important field of study and readers are referred to Prince<sup>29</sup> as a starting point.

## REFERENCES

1. D. Henderson, D. Prasher, R. Kopke, R. Salvi, and R. Hamernik, *Noise-Induced Hearing Loss: Basic Mechanisms, Prevention and Control*, Noise Research Network Publications, London, 2001.
2. E. Borg, B. Canlon, and B. Engström, Noise-Induced Hearing Loss. Literature Review and Experiments in Rabbits. *Scandinavian Audiol.*, Suppl. 40, 1995 pp. 1–147.
3. ANSI, S1.1–1999 Acoustical and Electroacoustical Terminology. American National Standards Institute, New York, 1999.
4. P. Dallos, A. N. Popper, R. R. Fay, Eds. *The Cochlea*, Springer Verlag, New York, 1996.
5. J. O. Pickles, *An Introduction to the Physiology of Hearing*, 2nd ed., Academic, New York, 1988.
6. G. R. Price, Upper Limit to Stapes Displacement: Implications for Hearing Loss, *J. Acoust. Soc. Am.*, Vol. 56, 1974, pp. 195–197.
7. X. Y. Zheng, D. Henderson, B. H. Hu, and S. L. McFadden, The influence of the Cochlear Efferent System on Chronic Acoustic Trauma, *Hearing Res.*, Vol. 107, 1997, pp. 147–159.
8. S. F. Maison, and M. C. Liberman, Predicting Vulnerability to Acoustic Injury by a Noninvasive Assay of Olivocochlear Reflex Strength, *J. Neurosci.*, Vol. 20, 2000, pp. 4701–4707.
9. E. C. Kirk and D. W. Smith, Protection from Acoustic Trauma Is Not a Primary Function of the Medial Olivocochlear Efferent System, *J. Assoc. Res. Otolaryngol.*, Vol. 4, 2003, pp. 445–465.
10. K. K. Ohlemiller, J. S. Wright, and L. L. Dugan, Early Elevation of Cochlear Reactive Oxygen Species Following Noise Exposure, *Audiol. Neurotol.*, Vol. 4, 2003, pp. 299–236.
11. B. H. Hu, W. Guo, P. Y. Wang, D. Henderson, and S. C. Jiang, Intense Noise-Induced Apoptosis in Hair Cells of Guinea Pig Cochlea, *Acta Otolaryngol.*, Vol. 120, 2000, pp. 19–24.
12. B. H. Hu, D. Henderson, and T. M. Nicotera, Involvement of Apoptosis in Progression of Cochlear Lesion Following Exposure to Intense Noise, *Hearing Res.*, Vol. 166, 2002, pp. 62–71.
13. D. Henderson, S. L. McFadden, C. C. Liu, N. Hight, and X. Y. Zheng, The Role of Antioxidants in Protection from Impulse Noise, *Ann. N.Y. Acad. Sci.*, Vol. 884, 1999, pp. 368–380.
14. R. D. Kopke, J. K. M. Coleman, X. Huang, P. A. Weiskopf, R. L. Jackson, J. Liu, M. E. Hoffer, K. Wood, J. Kil, and T. R. Van De Water, Novel Strategies to Prevent and Reverse Noise-Induced Hearing Loss, in *Noise-Induced Hearing Loss: Basic Mechanisms, Prevention and Control*, D. Henderson, D. Prasher, R. Kopke, R. Salvi, and R. Hamernik, Eds., Noise Research Network Publications, London, 2001.
15. Noise Regulation Report, Drugs Show Promise for Preventing Noise-Induced Hearing Loss, *Noise Regulation Rep.*, Vol. 31, No. 2, 2004, p. 18.
16. M. Ahmad, B. A. Bohne, and G. W. Harding, An in vivo Tracer Study of Noise-Induced Damage to the Reticular Lamina, *Hearing Res.*, Vol. 175, 2003, pp. 82–100.
17. N. Schmitt, K. Hsu, B. A. Bohne, and G. W. Harding, Hair-Cell-Membrane Changes in the Cochlea Following Noise, Association for Research in Otolaryngology Abstracts, 2004, p.132, Abstract 393. Abstract available at [http://www.aro.org/archives/2004/2004\\_16.html](http://www.aro.org/archives/2004/2004_16.html).
18. K. D. Kryter, W. D. Ward, J. D. Miller, and D. H. Eldredge, Hazardous Exposure to Intermittent and Steady-State Noise, *J. Acoust. Soc. Am.*, Vol. 39, 1966, pp. 451–464.
19. M. E. Schneider, I. A. Belyantseva, R. B. Azevedo, and B. Kachar, Rapid Renewal of Auditory Hair Cell Bundles, *Nature*, Vol. 418, 2002, pp. 837–838.
20. J. A. Kaltenbach, M. A. Zacharek, J. Zhang, and S. Frederick, Activity in the Dorsal Cochlear Nucleus of Hamsters Previously Tested for Tinnitus Following Intense Tone Exposure, *Neurosci. Lett.*, Vol. 355, Nos. 1–2, 2004, pp. 121–125.
21. L. C. Erway, Y-W. Shiao, R. R. Davis, and E. Krieg, Genetics of Age-Related Hearing Loss in Mice: III. Susceptibility of Inbred and F1 Hybrid Strains to Noise-Induced Hearing Loss, *Hearing Res.*, Vol. 93, 1996, pp. 181–187.
22. W. D. Ward, Effects of High Intensity Sound, in *Handbook of Acoustics*, M. J. Crocker, Ed., Wiley, New York, 1997.
23. T. C. Morata, C. L. Themann, R. F. Randolph, B. L. Verbsky, D. Byrne, and E. Reeves, Working in Noise with a Hearing Loss: Perceptions from Workers, Supervisors, and Hearing Conservation Program Managers, *Ear Hear.*, Vol. 26, 2005, pp. 529–545.
24. M. A. Mayorga, The pathology of primary blast overpressure injury, *Toxicology*, Vol. 121, 1997, pp. 17–28.
25. D. R. Richmond, E. R. Fletcher, J. T. Yelverton, and Y. Y. Phillips, Physical Correlates of Eardrum Rupture, *Ann. Otol. Rhinol. Laryngol.*, Vol. 98, 1989, pp. 35–41.
26. M. A. Mayorga, The Pathology of Blast Overpressure Injury, *Toxicology*, Vol. 121, 1997, pp. 17–28.
27. R. Rylander, Physiological Aspects of Noise-Induced Stress and Annoyance, *J. Sound Vib.*, Vol. 277, 2004, pp. 471–478.
28. T-Y. Chang, R-M. Jain, C-S. Wang, and C-C. Chan, Effects of Occupational Noise Exposure on Blood Pressure, *J. Occup. Environ. Med.*, Vol. 45, No. 12, 2003, pp. 1289–1296.
29. M. M. Prince, Distribution of Risk Factors for Hearing Loss: Implications for Evaluating Risk of Occupational Noise-Induced Hearing Loss, *J. Acoust. Soc. Am.*, Vol. 112, 2002, pp. 557–567.
30. S. A. Gelfand, The Acoustic Reflex, in *Handbook of Clinical Audiology*, 5th ed., J. Katz, R. F. Burkhard, and L. Medwetsky, Eds., Lippincott, Williams and Wilkins, Baltimore, MD, 2002, pp. 205–232.

**SUGGESTED ADDITIONAL READING**

NIOSH, Health Hazard Evaluations: Noise and Hearing Loss, National Institute for Occupational Safety and Health, Centers for Disease Control and Prevention, Cincinnati, OH, Publication #99-106, 1999. Available online at <http://www.cdc.gov/niosh/99-106pd.html>.

NIOSH, Criteria for a Recommended Standard, Hearing Loss, National Institute for Occupational Safety and Health, Centers for Disease Control and Prevention, Cincinnati,

OH, Publication #98-126, 1998. Available online at <http://www.cdc.gov/niosh/98-126.html>.

NIOSH, *Hearing Loss Prevention: A Practical Guide*, J. R. Franks, M. R. Stephenson, and C. J. Merry, Eds., National Institute for Occupational Safety and Health, Centers for Disease Control and Prevention, Cincinnati, OH, Publication #96-110, 1996. Available online at <http://www.cdc.gov/niosh/96-110.html>.

# CHAPTER 29

## EFFECTS OF VIBRATION ON PEOPLE

**Michael J. Griffin**  
Human Factors Research Unit  
Institute of Sound and Vibration Research  
University of Southampton  
Southampton, United Kingdom

### 1 INTRODUCTION

Human responses to vibration determine the acceptability of vibration in many environments. There are three categories of human exposure:

**Whole-Body Vibration** Where the body is supported on a vibrating surface (e.g., sitting on a seat that vibrates, standing on a vibrating floor, or lying on a vibrating surface).

**Motion Sickness** Caused by real or illusory movements of the body or the environment at low frequency (usually less than 1 Hz).

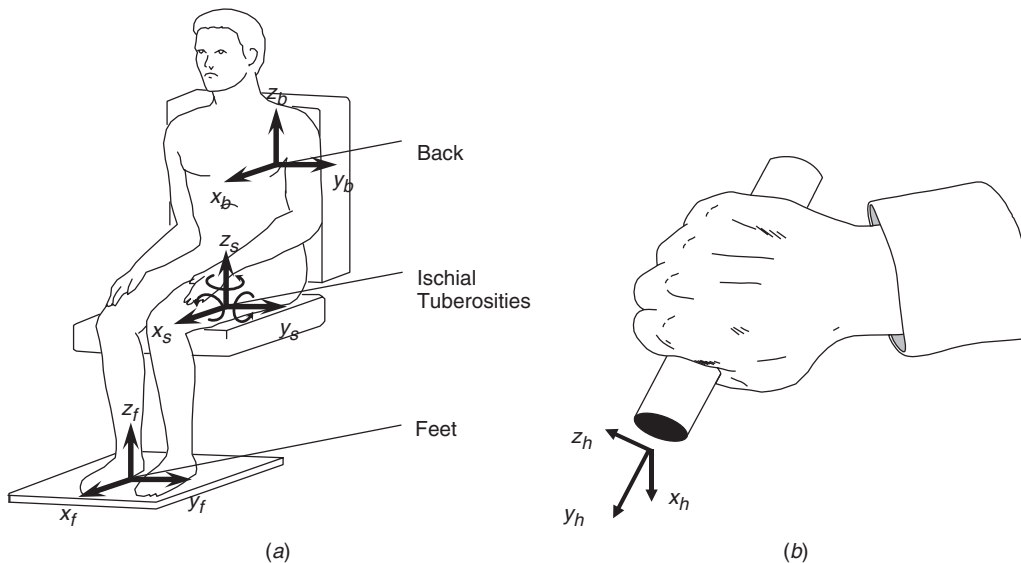
**Hand-Transmitted Vibration** Caused by processes in industry, agriculture, mining, construction, and transport where vibrating tools or workpieces are grasped or pushed by the hands or fingers.

This chapter identifies the principal human responses to vibration, summarizes methods of measuring, evaluating, and assessing exposures to vibration, and minimizing effects of vibration.

The vibration to which the human body is exposed is usually measured with accelerometers and expressed in terms of the acceleration, in metres per second per second (i.e.,  $\text{m s}^{-2}$ , or  $\text{m/s}^2$ ). The vibration is measured at the interface between the body and the surface in contact with the body (e.g., on the seat beneath the ischial tuberosities for a seated person; on a handle held by the hand).

Some human responses to vibration depend on the duration of exposure. The duration of measurement of vibration may affect the measured magnitude of the vibration when the conditions are not statistically stationary. The root-mean-square (rms) acceleration is often used, but it may not provide a good indication of vibration severity if the vibration is intermittent, contains shocks, or otherwise varies in magnitude from time to time.

The responses of the body differ according to the direction of the motion (i.e., axes of vibration). The three directions of whole-body vibration for seated and standing persons are fore and aft ( $x$  axis), lateral ( $y$  axis), and vertical ( $z$  axis). Figure 1 illustrates the translational and rotational axes for a seated person and the axes of hand-transmitted vibration.



**Figure 1** Axes of vibration used to measure exposures to (a) whole-body vibration and (b) hand-transmitted vibration.



## 2 WHOLE-BODY VIBRATION

Vibration of the whole body is produced by transport (road, off-road, rail, sea, and air), by some industrial machinery, and occurs in buildings. Whole-body vibration can affect human comfort as well as the performance of activities and health. An understanding of these effects and means of minimizing unwanted effects can be assisted by knowledge of the biodynamics of the body.

### 2.1 Biodynamics

The human body is a complex mechanical system that does not, in general, respond to vibration in the same manner as a rigid mass: There are relative motions between the body parts that vary with the frequency and the direction of the applied vibration. The dynamics of the body affect all human responses to vibration. However, the discomfort, the interference with activities, and the health effects of vibration cannot be predicted solely by considering the body as a mechanical system.

**2.1.1 Transmissibility of the Human Body** The resonances of the body vary with the direction of excitation, where the vibration is measured, as well as the posture of the body and the individual. For seated persons, there are resonances to the head at frequencies in the range 4 to 12 Hz for vertical vibration below 4 Hz with *x*-axis vibration, and below 2 Hz with lateral vibration.<sup>1,2</sup> A seat back can alter the transmission of vibration to the head and upper body of seated people, and bending of the legs affects the transmission of vibration to standing persons.

**2.1.2 Mechanical Impedance of the Human Body** Point mechanical impedance of the seated human shows a principal resonance for vertical vibration at about 5 Hz and, sometimes, a second resonance in the range 7 to 12 Hz.<sup>3</sup> This response means the body cannot usually be represented by a rigid mass when measuring (or predicting) the vibration transmitted through seats. The mechanical impedance of the body is generally nonlinear: The resonance frequency reduces when the vibration magnitude increases.

**2.1.3 Biodynamic Models** A simple model with one or two degrees of freedom can represent the point mechanical impedance of the body, and dummies may be constructed to represent this impedance for seat testing. The transmissibility of the body is affected by many more variables and requires more complex models reflecting the posture of the body and the translation and rotation associated with the various modes of vibration.

### 2.2 Vibration Discomfort

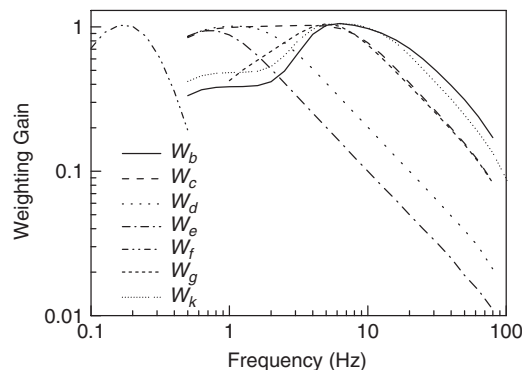
Vibration discomfort depends on various factors in addition to the characteristics of the vibration. It is often sufficient to predict the relative discomfort of different motions and not necessary to predict the absolute acceptability of vibration.

**2.2.1 Vibration Magnitude** The absolute threshold for the perception of vertical whole-body vibration in the frequency range of 1 to 100 Hz is, very approximately,  $0.01 \text{ m s}^{-2}$  rms; a magnitude of  $0.1 \text{ m s}^{-2}$  will be easily noticeable; magnitudes around  $1 \text{ m s}^{-2}$  rms are usually considered uncomfortable; magnitudes of  $10 \text{ m s}^{-2}$  rms are usually dangerous. The precise values depend on vibration frequency and the exposure duration, and they are different for other axes of vibration.

For some common motions, doubling the vibration magnitude approximately doubles the sensation of discomfort.<sup>4</sup> Halving a vibration magnitude can therefore produce a considerable reduction in discomfort. For some motions, the smallest detectable change in vibration magnitude (the difference threshold) is about 10%.<sup>5</sup>

**2.2.2 Effects of Vibration Frequency and Direction** Frequency weightings take account of the different sensitivity of the body to different frequencies. British Standard 6841<sup>6</sup> and International Standard 2631<sup>7</sup> define similar procedures for predicting vibration discomfort. Figure 2 shows frequency weightings  $W_b$  to  $W_f$  as defined in British Standard 6841; International Standard 2631 suggests the use of  $W_k$  in place of the almost identical weighting  $W_b$ . Table 1 shows how the weightings should be applied to the 12 axes of vibration illustrated in Fig. 1a. The weightings  $W_g$  and  $W_f$  are not required to predict vibration discomfort:  $W_g$  has been used for assessing interference with activities and is similar to the weighting for vertical vibration in ISO 2631<sup>8</sup>;  $W_f$  is used to predict motion sickness caused by vertical oscillation.

Some frequency weightings are used for more than one axis of vibration, with different *multiplying factors* allowing for overall differences in sensitivity between axes (Table 1). The frequency-weighted acceleration should be multiplied by the multiplying factor before the component is compared with components in other axes, or included in any summation over axes. The rms value of this acceleration (i.e., after



**Figure 2** Acceleration frequency weightings for whole-body vibration and motion sickness as defined in BS 6841<sup>6</sup> and ISO 2631.<sup>7</sup>

**Table 1 Application of Frequency Weightings for the Evaluation of Vibration with Respect to Discomfort**

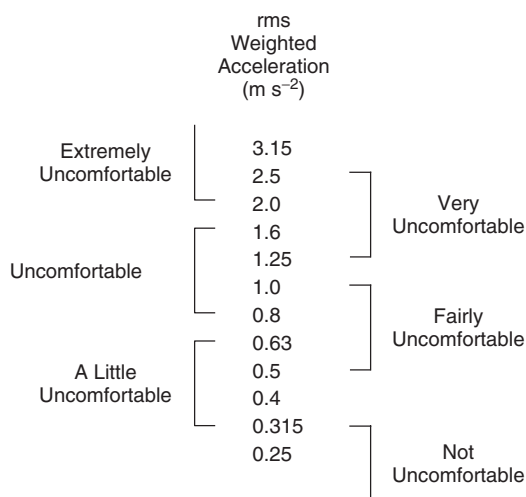
Input Position	Axis	Frequency Weighting	Axis Multiplying Factor
Seat	x	$W_d$	1.0
	y	$W_d$	1.0
	z	$W_b$	1.0
	$r_x$ (roll)	$W_e$	0.63
	$r_y$ (pitch)	$W_e$	0.40
Seat back	$r_z$ (yaw)	$W_e$	0.20
	x	$W_c$	0.80
	y	$W_d$	0.50
	z	$W_d$	0.40
	x	$W_b$	0.25
Feet	y	$W_b$	0.25
	z	$W_b$	0.40

frequency weighting and after being multiplied by the multiplying factor) is called a *component ride value*. In order to obtain an *overall ride value*, the *root-sums-of-squares* of the component ride values is calculated:

$$\text{Overall ride value} = \left[ \sum (\text{component ride values})^2 \right]^{1/2}$$

Overall ride values from different environments can be compared with each other, and overall ride values can be compared with Fig. 3 showing the ranges of vibration magnitudes associated with varying degrees of discomfort.

**2.2.3 Effects of Vibration Duration** The rate of increase in discomfort with increase in vibration duration may depend on many factors, but a simple fourth-power time dependency is used to approximate the change from the shortest possible shock to a

**Figure 3** Scale of vibration discomfort from British Standard 6841<sup>6</sup> and International Standard 2631.<sup>7</sup>**Table 2 Vibration Dose Values at Which Various Degrees of Adverse Comment May Be Expected in Buildings**

Place	Low Probability of Adverse Comment	Adverse Comment Possible	Adverse Comment Probable
Critical working areas	0.1	0.2	0.4
Residential	0.2–0.4	0.4–0.8	0.8–1.6
Office	0.4	0.8	1.6
Workshops	0.8	1.6	3.2

Source: Based on International Standard 2631 Part 2 (1989) and British Standard 6472 (1992)<sup>4,9,10</sup>

full day of vibration exposure [i.e., (acceleration)<sup>4</sup> × duration = constant, see Section 2.4.2].

**2.2.4 Vibration in Buildings** Acceptable magnitudes of vibration in some buildings are close to vibration perception thresholds. The acceptability of vibration in buildings depends on the use of the building in addition to the vibration frequency, direction, and duration. Using the guidance in ISO 2631 Part 2,<sup>9</sup> it is possible to summarize the acceptability of vibration in different types of buildings in a single table of vibration dose values (see BS 6472; Table 2<sup>10</sup>). The vibration dose values in Table 2 are applicable irrespective of whether the vibration occurs as a continuous vibration, intermittent vibration, or repeated shocks.

## 2.3 Interference with Activities

Vibration can interfere with the acquisition of information (e.g., by the eyes), the output of information (e.g., by hand or foot movements), or the complex central processes that relate input to output (e.g., learning, memory, decision making).

**2.3.1 Effects of Vibration on Vision** Reading a book or newspaper in a vehicle may be difficult because the paper is moving, the eye is moving, or both the paper and the eye are moving. There are many variables affecting visual performance in these conditions: It is not possible to adequately represent the effects of vibration on vision without considering the effects of these variables.<sup>4</sup>

**2.3.2 Manual Control** Writing and other complex control tasks involving hand control activities can also be impeded by vibration. The characteristics of the task and the characteristics of the vibration combine to determine effects of vibration on performance: A given vibration may greatly affect one type of control task but have little affect on another. The effects of vertical whole-body-vibration on spilling liquid from a hand-held cup are often greatest close to 4 Hz; the effects of vibration on writing speed and writing difficulty are most affected by vertical vibration in the range 4 to 8 Hz.<sup>11</sup> Although 4 Hz is a sensitive frequency for both drinking and the writing tasks, the dependence on

frequency of the effects of vibration are different for the two activities.

International Standard 2631 offered a *fatigue-decreased proficiency* boundary as a means of predicting the effects of vibration on activities.<sup>8</sup> A complex time-dependent magnitude of vibration was said to be “a limit beyond which exposure to vibration can be regarded as carrying a significant risk of impaired working efficiency in many kinds of tasks, particularly those in which time-dependent effects (“fatigue”) are known to worsen performance as, for example, in vehicle driving.” Vibration may influence “fatigue,” but there is, as yet, little evidence justifying the complex fatigue-decreased proficiency boundary presented in this standard.

**2.3.3 Cognitive Performance** Simple cognitive tasks (e.g., simple reaction time) appear to be unaffected by vibration, other than by changes in arousal or motivation or by direct effects on input and output processes. This may also be true for some complex cognitive tasks. However, the scarcity of experimental studies and the diversity of findings allows the possibility of real and significant cognitive effects of vibration.

## 2.4 Health Effects

Disorders have been reported among persons exposed to vibration in occupational, sport, and leisure activities. The studies do not agree on the type or the extent of disorders, and the findings have not always been related to appropriate measurements of vibration exposure. However, it is often assumed that disorders of the back (back pain, displacement of intervertebral disks, degeneration of spinal vertebrae, osteoarthritis, etc.) may be associated with vibration exposure.<sup>4,12</sup> There may be several alternative causes of any increase in disorders of the back among persons exposed to vibration (e.g., poor sitting postures, heavy lifting). It is often not possible to conclude confidently that a back disorder is solely, or primarily, caused by vibration.<sup>13</sup>

**2.4.1 Evaluation of Whole-Body Vibration** The manner in which the health effects of oscillatory motions depend upon the frequency, direction, and duration of motion is currently assumed to be similar to that for vibration discomfort. However, it is assumed that the *total* exposure, rather than the *average* exposure, is important.

**2.4.2 Assessment of Whole-Body Vibration** British Standard 6841<sup>6</sup> and International Standard 2631<sup>7</sup> give guidance on the severity of exposures to whole-body vibration. There are similarities between the two standards, but the methods within ISO 2631 are internally inconsistent.<sup>14</sup>

**British Standard 6841** British Standard 6841 defines an *action level* for vertical vibration based *vibration dose values*.<sup>6</sup> The vibration dose value uses a *fourth-power* time dependency to accumulate vibration

severity over the exposure period from the shortest possible shock to a full day of vibration:

$$\text{Vibration dose value} = \left[ \int_{t=0}^{t=T} a^4(t) dt \right]^{1/4}$$

where  $a(t)$  is the frequency-weighted acceleration. If the exposure duration ( $t$ , seconds) and the frequency-weighted rms acceleration ( $a_{\text{rms}}$ ,  $\text{m s}^{-2}$  rms) are known for conditions in which the vibration characteristics are statistically stationary, it can be useful to calculate the *estimated vibration dose value*, eVDV:

$$\text{Estimated vibration dose value} = 1.4a_{\text{rms}}t^{1/4}$$

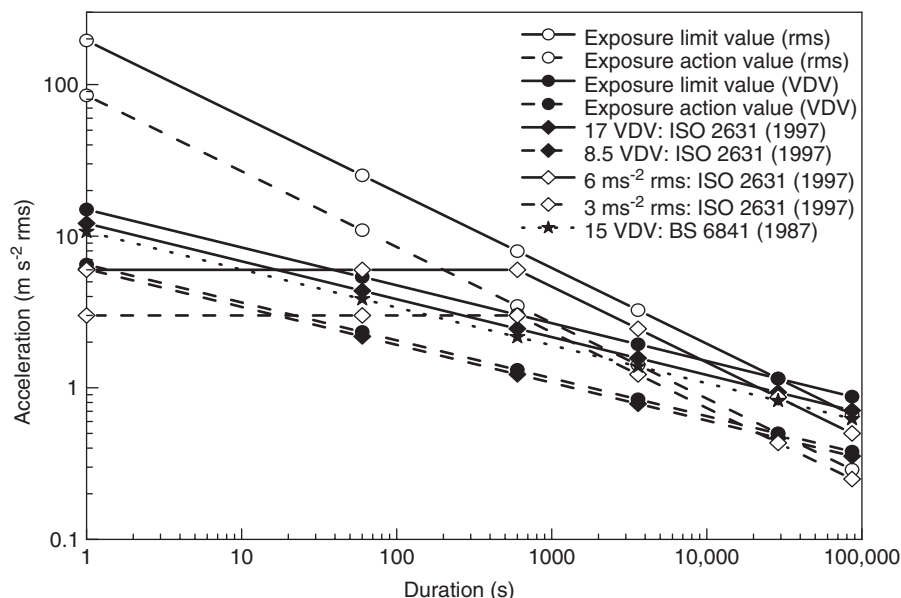
The eVDV is not applicable to transients, shocks, and repeated shock motions in which the crest factor (peak value divided by the rms value) is high.

No precise limit can be offered to prevent disorders caused by whole-body vibration, but British Standard 6841<sup>6</sup> (p. 18) offers the following guidance:

High vibration dose values will cause severe discomfort, pain and injury. Vibration dose values also indicate, in a general way, the severity of the vibration exposures which caused them. However there is currently no consensus of opinion on the precise relation between vibration dose values and the risk of injury. It is known that vibration magnitudes and durations which produce vibration dose values in the region of  $15 \text{ m s}^{-1.75}$  will usually cause severe discomfort. It is reasonable to assume that increased exposure to vibration will be accompanied by increased risk of injury (p. 18).

An action level might be set higher or lower than  $15 \text{ m s}^{-1.75}$ . Figure 4 shows this action level for exposure durations from one second to one day.

**International Standard 2631** International Standard 2631<sup>7</sup> offers two different methods of evaluating vibration severity with respect to health effects, and for both methods there are two boundaries. When evaluating vibration using the vibration dose value, it is suggested that below a boundary corresponding to a vibration dose value of  $8.5 \text{ m s}^{-1.75}$  “health risks have not been objectively observed,” between 8.5 and  $17 \text{ m s}^{-1.75}$  “caution with respect to health risks is indicated,” and above  $17 \text{ m s}^{-1.75}$  “health risks are likely.” The two boundaries define a *VDV health guidance caution zone*. The alternative method of evaluation in ISO 2631 uses a time dependency in which the acceptable vibration does not vary with duration between 1 and 10 min and then decreases in inverse proportion to the square root of duration from 10 min to 24 h. This method suggests an *rms health guidance caution zone*, but the method is not fully defined in the text, it allows very high accelerations at short durations, it conflicts with the vibration dose



**Figure 4** Comparison between the health guidance caution zones for whole-body vibration in ISO 2631-1 (1997) (3 to  $6 \text{ m s}^{-2} \text{ rms}$ ; 8.5 to  $17 \text{ m s}^{-1.75}$ ),  $15 \text{ m s}^{-1.75}$  action level implied in BS 6841 (1987), the exposure limit values and exposure action values for whole-body vibration in the EU Physical Agents (Vibration) Directive.<sup>6,7,15</sup>

value method and cannot be extended to exposure durations below 1 min (Fig. 4).

With severe vibration exposures, prior consideration of the fitness of the exposed persons and the design of adequate safety precautions may be required. The need for regular checks on the health of routinely exposed persons may also be considered.

**2.4.3 EU Machinery Safety Directive** The Machinery Safety Directive of the European Community (89/392/EEC) states that machinery must be designed and constructed so that hazards resulting from vibration produced by the machinery are reduced to the lowest practicable level, taking into account technical progress and the availability of means of reducing vibration.<sup>16</sup> The instruction handbooks for machinery causing whole-body vibration must specify the equivalent acceleration to which the body is exposed where this exceeds some stated value (for whole-body vibration this is currently a frequency-weighted acceleration of  $0.5 \text{ m s}^{-2} \text{ rms}$ ). The relevance of any such value will depend on the test conditions to be specified in other standards. Many work vehicles exceed this value at some stage during an operation or journey. Standardized procedures for testing work vehicles are being prepared; the values currently quoted by manufacturers may not always be representative of the operating conditions in the work for which the machinery is used.

**2.4.4 EU Physical Agents Directive (2002)** In 2002, the Parliament and Commission of the European Community agreed on "minimum health and safety requirements" for the exposure of workers to the risks

arising from vibration.<sup>15</sup> For whole-body vibration, the directive defines an 8-h equivalent *exposure action value* of  $0.5 \text{ m s}^{-2} \text{ rms}$  (or a vibration dose value of  $9.1 \text{ m s}^{-1.75}$ ) and an 8-h equivalent *exposure limit value* of  $1.15 \text{ m s}^{-2} \text{ rms}$  (or a vibration dose value of  $21 \text{ m s}^{-1.75}$ ). Member states of the European Union were required to bring into force laws to comply with the directive by 6 July 2005.

The directive says that workers shall not be exposed above the exposure limit value. If the exposure action values are exceeded, the employer shall establish and implement a program of technical and/or organizational measures intended to reduce to a minimum exposure to mechanical vibration and the attendant risks. The directive says workers exposed to vibration in excess of the exposure action values shall be entitled to appropriate health surveillance. Health surveillance is also required if there is any reason to suspect that workers may be injured by the vibration even if the exposure action value is not exceeded.

The probability of injury arising from occupational exposures to whole-body vibration at the exposure action value and the exposure limit value cannot be estimated because epidemiological studies have not yet produced dose-response relationships. However, it seems clear that the Directive does not define *safe exposures* to whole-body vibration since the rms values are associated with extraordinarily high magnitudes of vibration (and shock) when the exposures are short: These exposures may be assumed to be hazardous (see Fig. 4<sup>17</sup>). The vibration dose value procedure

suggests more reasonable vibration magnitudes for short-duration exposures.

## 2.5 Seating Dynamics

Seating dynamics can greatly influence the vibration responsible for discomfort, interference with activities, and injury. Most seats exhibit a resonance at low frequencies resulting in higher magnitudes of vertical vibration occurring on the seat than on the floor. At high frequencies, there is usually attenuation of vertical vibration. The principal resonance frequencies of common vehicle seats are usually in the region of 4 Hz. The variations in transmissibility between seats are sufficient to result in significant differences in the vibration experienced by people supported by different seats.

The transmissibility of a seat is dependent on the mechanical impedance of the human body, so the transmissibility of a seat measured with a mass supported on the seat will be different from that with a human body sitting in the seat. The nonlinearity of the body mechanical impedance results in seat transmissibilities that vary with changes in vibration magnitude and vibration spectra entering the seat. Measurements of seat transmissibility can be undertaken on laboratory simulators with volunteer subjects, but safety and ethical precautions are required to protect subjects.<sup>18</sup> Measurements may also be performed in vehicles. Anthropodynamic dummies are being developed to represent the average mechanical impedance of the human body so that laboratory and field studies can be performed without exposing people to vibration. Seat transmissibility may be predicted from the dynamic stiffness of a seat and the apparent mass of the human body.

The suitability of a seat for a specific vibration environment depends on: (1) the vibration spectra present in the environment, (2) the transmissibility of the seat, and (3) the sensitivity of the human body to the different frequencies of vibration. These three functions of frequency are contained within a simple numerical indication of the isolation efficiency of a seat called the *seat effective amplitude transmissibility* (SEAT).<sup>4</sup> In concept, the SEAT value compares the vibration severity on a seat with the vibration severity on the floor beneath the seat:

$$\text{SEAT}(\%) = \frac{\text{ride comfort on seat}}{\text{ride comfort on floor}} \times 100$$

A SEAT value greater than 100% indicates that, overall, the vibration on the seat is *worse* than the vibration on the floor beneath the seat; SEAT values below 100% indicate that the seat has provided some useful attenuation. Seats should be designed to have the lowest SEAT value compatible with other constraints. In common cars, SEAT values are often in the range of 60 to 80%. In railway carriages the SEAT value for vertical vibration is likely to be greater than 100% because conventional seats cannot provide any attenuation of the low-frequency vibration that is normally present in such vehicles. The optimization of

the seating dynamics can be the most effective method of improving vehicle ride.

The SEAT value may be calculated from either the frequency-weighted rms values (if the vibration does not contain transients) or the vibration dose values of the frequency-weighted acceleration on the seat and the floor:

$$\text{SEAT}(\%) = \frac{\text{vibration dose value on seat}}{\text{vibration dose value on floor}} \times 100$$

The SEAT value is influenced by the vibration input and not merely by the dynamics of the seat: Different values are obtained with the same seat in different vehicles. The SEAT value indicates the suitability of a seat for attenuating a particular type of vibration.

Conventional seating (comprising some combination of foam, rubber, or metal springing) usually has a resonance at about 4 Hz and, therefore, provides no attenuation at frequencies below about 6 Hz. Attenuation can be provided at frequencies down to about 2 or 3 Hz using a separate suspension mechanism beneath the seat pan. In such suspension seats, used in some off-road vehicles, trucks, and coaches, there are low-resonance frequencies (often below about 2 Hz). This is beneficial if the dominant vibration is at higher frequencies, but of no value if the dominant motion is at very low frequencies. Standards for testing the suitability of suspension seats for specific classes of work vehicles have been prepared (see International Standards ISO 5007,<sup>19</sup> ISO 7096,<sup>20</sup> and ISO 10326-1<sup>21</sup>). The suspension mechanism (comprising a spring and damper mechanism) has a limited travel, often 50 to 100 mm. If the relative motion of the suspension reaches this limit, there will be an impact that might cause more discomfort or hazard than would have been present with a conventional seat. Suspension seats are nonlinear (having friction affecting response with low magnitude motions, and hitting end-stops with high magnitudes), and their full response requires consideration of the dynamic response of the cushion and the impedance of the human body in addition to the idealized response of the damper and spring.

## 3 MOTION SICKNESS

Illness (e.g., vomiting, nausea, sweating, color changes, dizziness, headaches, and drowsiness) is a normal response to motion in fit and healthy people. Translational and rotational oscillation, constant speed rotation about an off-vertical axis, Coriolis stimulation, movements of the visual scene, and various other stimuli producing sensations associated with movement of the body can cause sickness.<sup>22</sup> However, motion sickness is neither explained nor predicted solely by the physical characteristics of motion.

Motion sickness arises from motions at frequencies associated with normal postural control of the body, usually less than 1 Hz. Laboratory studies with vertical oscillation and studies of motion sickness in ships led to the formulation of a frequency weighting,

$W_f$  (Fig. 2), and the *motion sickness dose value* for predicting sickness caused by vertical oscillation:

$$\text{Motion sickness dose value(MSDV)} = a_{\text{rms}} t^{1/2}$$

where  $a_{\text{rms}}$  is the root-mean-square value of the frequency-weighted acceleration ( $\text{m s}^{-2}$ ) and  $t$  is the exposure period (seconds).<sup>6,7,23</sup> The percentage of unadapted adults who are expected to vomit is given by  $1/3$  MSDV. These relationships have been derived from exposures in which up to 70% of persons vomited during exposures lasting between 20 min and 6 h.

Vertical oscillation is not the principal cause of sickness in road vehicles or trains, so the above expression should not be assumed to be applicable to the prediction of sickness in all environments.

#### 4 HAND-TRANSMITTED VIBRATION

Exposure of the fingers or the hands to vibration or repeated shock can give rise to various signs and symptoms. Five types of disorder may be identified: (1) circulatory disorders, (2) bone and joint disorders, (3) neurological disorders, (4) muscle disorders, and (5) other general disorders (e.g., central nervous system).<sup>4</sup> More than one disorder can affect a person at the same time, and it is possible that the presence of one disorder facilitates the appearance of another. The onset of each disorder is dependent on the vibration characteristics, individual susceptibility to damage, and other aspects of the environment. The term *hand-arm vibration syndrome* (HAVS) is sometimes used to refer to an unspecified combination of one or more of the disorders.

##### 4.1 Sources of Hand-Transmitted Vibration

The vibration on tools varies greatly depending on tool design and method of use, so it is not possible to categorize individual tool types as *safe* or *dangerous*. Table 3 lists some tools and processes that are common causes of vibration-induced injury.

##### 4.2 Effects of Hand-Transmitted Vibration

**4.2.1 Vascular Disorders** Vibration-induced white finger (VWF) is characterized by intermittent whitening (i.e., blanching) of the fingers. The fingertips are usually the first to blanch, but the affected area may extend to all of one or more fingers with continued vibration exposure. Attacks of blanching are precipitated by cold and therefore often occur in cold conditions or after contact with cold objects. The blanching lasts until the fingers are rewarmed and vasodilation allows the return of the blood circulation. Many years of vibration exposure often occur before the first attack of blanching is noticed. Affected persons often have other signs and symptoms, such as numbness and tingling. Cyanosis and, rarely, gangrene, have also been reported.

The severity of the effects of vibration are recorded by reference to the *stage* of the disorder. The staging of vibration-induced white finger is based on verbal

**Table 3 Tools and Processes Potentially Associated with Vibration Injuries<sup>a</sup>**

Category of Tool	Examples of Tool
Percussive metal-working tools	Powered percussive metal-working tools, including powered hammers for riveting, caulking, hammering, clinching, and flanging. Hammer swaging.
Percussive tools used in stone working, quarrying, construction, etc.	Percussive hammers, vibratory compactors, concrete breakers, pokers, sanders, and drills used in mining, quarrying, demolition, and road construction.
Grinders and other rotary tools	Pedestal grinders, hand-held portable grinders, flex-driven grinders and polishers, and rotary burring tools.
Timber and woodworking machining tools	Chain saws, brush cutters (clearing saws), hand-held or hand-fed circular saws, electrical screwdrivers, mowers and shears, hardwood cutting machines, barking machines, and strimmers.
Other processes and tools	Pounding machines used in shoe manufacture, drain suction machines, nut runners, concrete vibro-thickeners, and concrete levelling vibro-tables.

<sup>a</sup> The Health and Safety Executive suggest that for all workers using these vibratory tools health surveillance is likely to be appropriate.

Source: From Health and Safety Executive, 1994.<sup>24</sup>

statements made by the affected person. In the Stockholm workshop staging system, the staging is influenced by the frequency of attacks of blanching and the areas of the digits affected by blanching (Table 4).

A *scoring system* is used to record the areas of the digits affected by blanching (Fig. 5).<sup>4</sup> The scores correspond to areas of blanching on the digits commencing with the thumb. On the fingers a score of 1 is given for blanching on the distal phalanx, a score of 2 for blanching on the middle phalanx, and a score of 3 for blanching on the proximal phalanx. On the thumbs the scores are 4 for the distal phalanx and 5 for the proximal phalanx. The blanching scores for each finger, which are formed from the sums of the scores on each phalanx, may be based on statements from the affected person or on the visual observations of a designated observer.

**4.2.2 Neurological Disorders** Numbness, tingling, elevated sensory thresholds for touch, vibration, temperature, and pain, and reduced nerve conduction velocity are now considered to be separate effects of vibration and not merely symptoms of vibration-induced white finger. A method of reporting the extent of vibration-induced neurological effects of vibration



**Table 4 Stockholm Workshop Scale for Classification of Vibration-Induced White Finger<sup>a</sup>**

Stage	Grade	Description
0	—	No attacks
1	Mild	Occasional attacks affecting only the tips of one or more fingers
2	Moderate	Occasional attacks affecting distal and middle (rarely also proximal) phalanges of one or more fingers
3	Severe	Frequent attacks affecting all phalanges of most fingers
4	Very severe	As in stage 3, with trophic skin changes in the finger tips

<sup>a</sup> If a person has stage 2 in two fingers of the left hand and stage 1 in a finger on right hand, the condition may be reported as 2L(2)/1R(1). There is no defined means of reporting the condition of digits when this varies between digits on the same hand. The scoring system is more helpful when the extent of blanching is to be recorded.

Source: From Ref.<sup>25</sup>

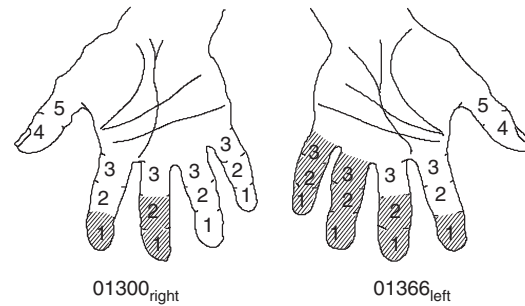
**Table 5 Proposed Sensorineural Stages of the Effects of Hand-Transmitted Vibration**

Stage	Symptoms
0 <sub>SN</sub>	Exposed to vibration but no symptoms
1 <sub>SN</sub>	Intermittent numbness with or without tingling
2 <sub>SN</sub>	Intermittent or persistent numbness, reduced sensory perception
3 <sub>SN</sub>	Intermittent or persistent numbness, reduced tactile discrimination and/or manipulative dexterity

Source: From Ref. 26.

has been proposed (see Table 5). This staging is not currently related to the results of any specific objective test: The *sensorineural stage* is a subjective impression of a physician based on the statements of the affected person or the results of any available clinical or scientific testing. Neurological disorders are sometimes identified by screening tests using measures of sensory function, such as the thresholds for feeling vibration, heat, or warmth on the fingers.

**4.2.3 Muscular Effects** Workers exposed to hand-transmitted vibration sometimes report difficulty with their grip, including reduced dexterity, reduced grip strength, and locked grip. Many of the reports are derived from symptoms reported by exposed persons, rather than signs detected by physicians, and could be a reflection of neurological problems. Muscle activity may be of great importance to tool users since a secure grip can be essential to the performance of the job and the safe control of the tool. The presence of vibration on a handle may encourage the adoption of a tighter grip than would otherwise occur; a tight grip may also increase the transmission of vibration to the hand and reduce the blood flow within the fingers. If the chronic



**Figure 5** Method of scoring the areas of the digits affected by blanching.<sup>4</sup> The blanching scores for the hands shown are 01300<sub>right</sub> and 01366<sub>left</sub>.

effects of vibration result in reduced grip, this may help to protect operators from further effects of vibration but interfere with both work and leisure activities.

**4.2.4 Articular Disorders** Surveys of the users of hand-held tools have found evidence of bone and joint problems, most often among men operating percussive tools such as those used in metal-working jobs and mining and quarrying. It is speculated that some characteristic of such tools, possibly the low-frequency shocks, is responsible. Some of the reported injuries relate to specific bones and suggest the existence of cysts, vacuoles, decalcification, or other osteolysis, degeneration, or deformity of the carpal, metacarpal, or phalangeal bones. Osteoarthritis and olecranon spurs at the elbow and other problems at the wrist and shoulder are also documented.<sup>4</sup> There is not universal acceptance that vibration is the cause of articular problems, and there is currently no dose–effect relation predicting their occurrence. In the absence of specific information, it seems that adherence to current guidance for the prevention of vibration-induced white finger may provide reasonable protection.

**4.2.5 Other Effects** Hand-transmitted vibration may not only affect the fingers, hands, and arms: Studies have reported an increased incidence of problems such as headaches and sleeplessness among tool users and have concluded that these symptoms are caused by hand-transmitted vibration. Although these are real problems to those affected, they are “subjective” effects that are not accepted as real by all researchers. Some current research is seeking a physiological basis for such symptoms. It would appear that caution is appropriate, but the adoption of modern guidance to prevent vibration-induced white finger may also provide some protection from any other effects of hand-transmitted vibration within, or distant from, the hand.

### 4.3 Standards for the Evaluation of Hand-Transmitted Vibration

There are various standards for the measurement, evaluation, and assessment of hand-transmitted vibration.

**4.3.1 Vibration Measurement** International Standards 5349-1<sup>27</sup> and 5349-2<sup>28</sup> give recommendations on methods of measuring the hand-transmitted vibration on tools and processes. Guidance on vibration measurements on specific tools is given elsewhere (e.g., ISO 8662).<sup>29</sup> Care is required to obtain representative measurements of tool vibration with appropriate operating conditions. There can be difficulties in obtaining valid measurements using some commercial instrumentation (especially when there are high shock levels). It is wise to determine acceleration spectra and inspect the acceleration time histories before accepting the validity of any measurements.

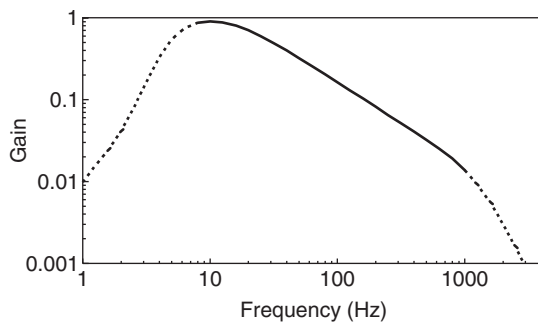
**4.3.2 Vibration Evaluation** All current national and international standards use the same frequency weighting (called  $W_h$ ) to evaluate hand-transmitted vibration over the approximate frequency range of 8 to 1000 Hz (Fig. 6).<sup>30</sup> This weighting is applied to measurements of vibration acceleration in each of the three axes of vibration at the point of entry of vibration to the hand. More recent standards suggest the overall severity of hand-transmitted vibration should be calculated from root-sums-of-squares of the frequency-weighted acceleration in the three axes. The standards imply that if two tools expose the hand to vibration for the same period of time, the tool having the lowest frequency-weighted acceleration will be least likely to cause injury or disease.

Occupational exposures to hand-transmitted vibration can have widely varying daily exposure durations—from a few seconds to many hours. Often, exposures are intermittent. To enable a daily exposure to be reported simply, the standards refer to an equivalent 8-h exposure:

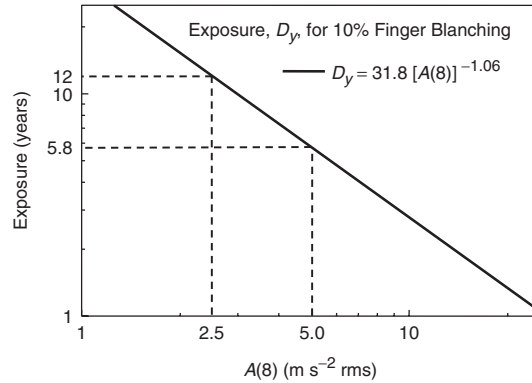
$$a_{hw(eq,8h)} = A(8) = a_{hw} \left[ \frac{t}{T_{(8)}} \right]^{1/2}$$

where  $t$  is the exposure duration to an rms frequency-weighted acceleration,  $a_{hw}$ , and  $T_{(8)}$  is 8 h (in the same units as  $t$ ).

**4.3.3 Vibration Assessment According to ISO 5349** In an informative annex of ISO 5349-1<sup>27</sup> there is a suggested relation between the lifetime



**Figure 6** Frequency weighting  $W_h$  for the evaluation of hand-transmitted vibration.



**Figure 7** Relation between daily  $A(8)$  and years of exposure expected to result in 10% incidence of finger blanching according to ISO 5349 (2001). A 10% probability of finger blanching is predicted after 12 years at the EU exposure action value and after 5.8 years at the EU exposure limit value.<sup>15,27</sup>

exposure to hand-transmitted vibration,  $D_y$  (in years), and the 8-h energy-equivalent daily exposure  $A(8)$  for the conditions expected to cause 10% prevalence of finger blanching (Fig. 7):

$$D_y = 31.8[A(8)]^{-1.06}$$

The percentage of affected persons in any group of exposed persons will not always correspond to the values shown in Fig. 7: The frequency weighting, the time dependency, and the dose–effect information are based on less than complete information, and they have been simplified for practical convenience. Additionally, the number of persons affected by vibration will depend on the rate at which persons enter and leave the exposed group. The complexity of the above equation implies far greater precision than is possible: A more convenient estimate of the years of exposure (in the range 1 to 25 years) required for 10% incidence of finger blanching is

$$D_y = \frac{30.0}{A(8)}$$

This equation gives the same result as the equation in the standard (to within 14%), and there is no information suggesting it is less accurate.

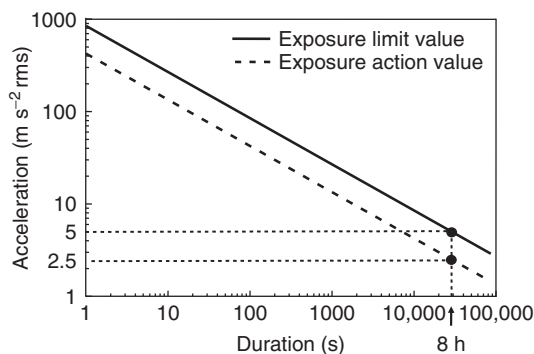
The informative annex to ISO 5349 (2001, Ref. 27, pp. 15–17) states: “Studies suggest that symptoms of the hand-arm vibration syndrome are rare in persons exposed with an 8-h energy-equivalent vibration total value,  $A(8)$ , at a surface in contact with the hand, of less than 2 m/s<sup>2</sup> and unreported for  $A(8)$  values less than 1 m/s<sup>2</sup>.” However, this sentence should be interpreted with caution in view of the very considerable doubts over the frequency weighting and time dependency in the standard.<sup>31</sup>



**4.3.4 EU Machinery Safety Directive** The Machinery Safety Directive of the European Community (89/392/EEC) requires that instruction handbooks for hand-held and hand-guided machinery specify the equivalent acceleration to which the hands or arms are subjected where this exceeds a stated value (currently a frequency-weighted acceleration of  $2.5 \text{ m s}^{-2} \text{ rms}$ ).<sup>16</sup> Very many hand-held vibrating tools can exceed this value. Standards defining test conditions for the measurement of vibration on many tools (e.g., chipping and riveting hammers, rotary hammers and rock drills, grinding machines, pavement breakers, chain saws) have been defined (e.g., ISO 8662<sup>29</sup>).

**4.3.5 EU Physical Agents Directive (2002)** For hand-transmitted vibration, the EU Physical Agents Directive defines an 8-h equivalent exposure action value of  $2.5 \text{ m s}^{-2} \text{ rms}$  and an 8-h equivalent, exposure limit value of  $5.0 \text{ m s}^{-2} \text{ rms}$  (Fig. 8).<sup>15</sup> The directive says workers shall not be exposed above the exposure limit value. If the 'exposure action values are exceeded, the employer shall establish and implement a program of technical and/or organizational measures intended to reduce to a minimum exposure to mechanical vibration and the attendant risks. The directive requires that workers exposed to mechanical vibration in excess of the exposure action values shall be entitled to appropriate health surveillance. However, health surveillance is not restricted to situations where the exposure action value is exceeded: health surveillance is required if there is any reason to suspect that workers may be injured by the vibration, even if the action value is not exceeded.

According to ISO 5349-1,<sup>27</sup> the onset of finger blanching would be expected in 10% of persons after 12 years at the EU exposure action value and after 5.8 years at the exposure limit value. The exposure action value and the exposure limit value in the directive do not define *safe exposures* to hand-transmitted vibration.<sup>17</sup>



**Figure 8** Hand-transmitted vibration exposure limit value [ $A(8) = 5.0 \text{ m s}^{-2} \text{ rms}$ ] and exposure action value [ $A(8) = 2.5 \text{ m s}^{-2} \text{ rms}$ ] in the EU Physical Agents (Vibration) Directive.<sup>15</sup>

#### 4.4 Preventative Measures

When there is reason to suspect that hand-transmitted vibration may cause injury, the vibration at tool-hand interfaces should be measured. It may then be possible to predict whether the tool or process is likely to cause injury and whether any other tool or process could give a lower vibration severity. The duration of exposure to vibration should also be quantified. Reduction of exposure time may include the provision of exposure breaks during the day and, if possible, prolonged periods away from vibration exposure. For any tool or process having a vibration magnitude sufficient to cause injury, there should be a system to quantify and control the maximum daily duration of exposure of any individual. The risks cannot be assessed accurately from vibration measurements: They contribute to an assessment of risk but may not always be the best way of predicting risk. Risk may also be anticipated from the type of work and knowledge that the same or similar work has caused problems previously.

When evaluating the risks using the frequency weightings in current standards, most commonly available gloves would *not* normally provide effective attenuation of the vibration on most tools.<sup>32</sup> Gloves and "cushioned" handles may reduce the transmission of high frequencies of vibration, but current standards imply that these frequencies are not usually the primary cause of disorders. Gloves may help to minimize pressure on the fingers, protect the hand from other forms of mechanical injury (e.g., cuts and scratches), and protect the fingers from temperature extremes. Warm hands are less likely to suffer an attack of finger blanching, and some consider that maintaining warm hands while exposed to vibration may also lessen the damage caused by the vibration.

Workers exposed to vibration known or suspected to cause injury should be warned of the possibility of vibration injuries and educated on the ways of reducing the severity of their vibration exposures. They should be advised of the symptoms to look out for and told to seek medical attention if the symptoms appear. There should be preemployment medical screening wherever a subsequent exposure to hand-transmitted vibration may reasonably be expected to cause vibration injury. Medical supervision of each exposed person should continue throughout employment at suitable intervals, possibly annually.

#### REFERENCES

1. G. S. Paddan and M. J. Griffin, The Transmission of Translational Seat Vibration to the Head. 1. Vertical Seat Vibration, *J. Biomech.*, Vol. 21, No. 3, 1988, pp. 191–197.
2. G. S. Paddan and M. J. Griffin, The Transmission of Translational Seat Vibration to the Head. II. Horizontal Seat Vibration, *J. Biomech.*, Vol. 21, No. 3, 1988, pp. 199–206.
3. T. E. Fairley and M. J. Griffin, The Apparent Mass of the Seated Human Body: Vertical Vibration, *J. Biomech.*, Vol. 22, No. 2, 1989, pp. 81–94.
4. M. J. Griffin, *Handbook of Human Vibration*, Academic, London, 1990.

5. M. Morioka and M. J. Griffin, Difference Thresholds for Intensity Perception of Whole-Body Vertical Vibration: Effect of Frequency and Magnitude, *J. Acoust. Soc. Am.*, Vol. 107, No. 1, 2000, pp. 620–624.
6. British Standards Institution, *Measurement and Evaluation of Human Exposure to Whole-Body Mechanical Vibration and Repeated Shock*, British Standard, BS 6841, London, 1987.
7. International Organization for Standardization, *Mechanical Vibration and Shock—Evaluation of Human Exposure to Whole-Body Vibration. Part 1: General Requirements*, International Standard, ISO 2631-1, Geneva, Switzerland, 1997.
8. International Organization for Standardization, *Guide for the Evaluation of Human Exposure to Whole-Body Vibration*, International Standard, ISO 2631 (E), Geneva, Switzerland, 1974.
9. International Organization for Standardization, *Evaluation of Human Exposure to Whole-Body Vibration. Part 2: Continuous and Shock-Induced Vibration in Buildings*, International Standard, ISO 2631-2, Geneva, Switzerland, 1989.
10. British Standards Institution, *Evaluation of Human Exposure to Vibration in Buildings (1 Hz to 80 Hz)*, British Standard, BS 6472, London, 1992.
11. C. Corbridge and M. J. Griffin, Effects of Vertical Vibration on Passenger Activities: Writing and Drinking, *Ergonomics*, Vol. 34, No. 10, 1991, pp. 1313–1332.
12. M. Bovenzi and C. T. J. Hulshof, An Updated Review of Epidemiologic Studies on the Relationship between Exposure to Whole-Body Vibration and Low Back Pain (1986–1997), *Int. Arch. Occupat. Environ. Health*, Vol. 72, No. 6, 1999, pp. 351–365.
13. K. T. Palmer, D. N. Coggon, H. E. Bednall, B. Pannett, M. J. Griffin, and B. Haward, *Whole-Body Vibration: Occupational Exposures and Their Health Effects in Great Britain*, Health and Safety Executive Contract Research Report 233/1999, HSE Books, London, 1999.
14. M. J. Griffin, A Comparison of Standardized Methods for Predicting the Hazards of Whole-Body Vibration and Repeated Shocks, *J. Sound Vib.*, Vol. 215, No. 4, 1998, pp. 883–914.
15. The European Parliament and the Council of the European Union, On the Minimum Health and Safety Requirements Regarding the Exposure of Workers to the Risks Arising from Physical Agents (vibration), Directive 2002/44/EC, *Official J. European Communities*, 6th July 2002; L177/13–19.
16. Council of the European Communities (Brussels), On the Approximation of the Laws of the Member States Relating to Machinery, Council Directive (89/392/EEC), *Official J. European Communities*, June, 9–32, 1989.
17. M. J. Griffin, Minimum Health and Safety Requirements for Workers Exposed to Hand-Transmitted Vibration and Whole-Body Vibration in the European Union; A Review. *Occupat. Environ. Med.*, Vol. 61, 2004, pp. 387–397.
18. International Organization for Standardization, *Mechanical Vibration and Shock—Guidance on Safety Aspects of Test and Experiments with People. Part 1: Exposure to Whole-Body Mechanical Vibration and Repeated Shock*, International Standard, ISO 13090–1, Geneva, Switzerland, 1998.
19. International Organization for Standardization, *Agricultural Wheeled Tractors—Operator's Seat—Laboratory Measurement of Transmitted Vibration*, International Standard, ISO 5007, Geneva, Switzerland, 1990.
20. International Organization for Standardization, *Earth-Moving Machinery—Laboratory Evaluation of Operator Seat Vibration*, International Standard, ISO 7096, Geneva, Switzerland, 2000.
21. International Organization for Standardization, *Mechanical Vibration—Laboratory Method for Evaluating Vehicle Seat Vibration. Part 1: Basic Requirements*, International Standard, ISO 10326–1, Geneva, Switzerland, 1992.
22. M. J. Griffin, Physical Characteristics of Stimuli Provoking Motion Sickness, in *Motion Sickness: Significance in Aerospace Operations and Prophylaxis*, AGARD Lecture Series LS—175, North Atlantic Treaty Organization, Brussels, Belgium, 1991.
23. A. Lawther and M. J. Griffin, Prediction of the Incidence of Motion Sickness from the Magnitude, Frequency, and Duration of Vertical Oscillation, *J. Acoust. Soc. Am.*, Vol. 82, No. 3, 1987, pp. 957–966.
24. Health and Safety Executive, *Hand-Arm Vibration*. Health and Safety Executive, HS(G) 88, London, 1994.
25. G. Gemne, I. Pyykko, W. Taylor, and P. Pelmear, The Stockholm Workshop Scale for the Classification of Cold-Induced Raynaud's Phenomenon in the Hand-Arm Vibration Syndrome (Revision of the Taylor-Pelmear Scale), *Scand. J. Work, Environ. Health*, Vol. 13, No. 4, 1987, pp. 275–278.
26. A. J. Brammer, W. Taylor, and G. Lundborg, Sensorineural Stages of the Hand-Arm Vibration Syndrome, *Scand. J. Work, Environ. Health*, Vol. 13, No. 4, 1987, pp. 279–283.
27. International Organization for Standardization, *Mechanical Vibration—Measurement and Evaluation of Human Exposure to Hand-Transmitted Vibration. Part 1: General Requirements*, International Standard, ISO 5349–1 E, Geneva, Switzerland, 2001.
28. International Organization for Standardization, *Mechanical Vibration—Measurement and Evaluation of Human Exposure to Hand-Transmitted Vibration. Part 2: Practical Guidance for Measurement at the Workplace*. International Standard, ISO 5349–2:2001 E, Geneva, Switzerland, 2002.
29. International Organization for Standardization, *Hand-Held Portable Tools—Measurement of Vibration at the Handle. Part 1: General*, International Standard ISO 8662–1, Geneva, Switzerland, 1988.
30. M. J. Griffin, Measurement, Evaluation and Assessment of Occupational Exposures to Hand-Transmitted Vibration, *Occupat. Environ. Med.*, Vol. 54, No. 2, 1997, pp. 73–89.
31. M. J. Griffin, M. Bovenzi, and C. M. Nelson, Dose-Response Patterns for Vibration-Induced White Finger, *Occupat. Environ. Med.*, Vol. 60, 2003, pp. 16–26.
32. M. J. Griffin, Evaluating the Effectiveness of Gloves in Reducing the Hazards of Hand-Transmitted Vibration, *Occupat. Environ. Med.*, Vol. 55, No. 5, 1998, pp. 340–348.

# CHAPTER 30

## EFFECTS OF MECHANICAL SHOCK ON PEOPLE

A. J. Brammer

Ergonomic Technology Center  
University of Connecticut Health Center  
Farmington, Connecticut  
and  
Envir-O-Health Solutions  
Ottawa, Ontario, Canada

### 1 INTRODUCTION

A mechanical shock is a nonperiodic, time-varying disturbance of a mechanical or biological system characterized by suddenness and severity with, for the human body (or body segment, e.g., hand and arm or head), the maximum forces occurring within a few tenths of a second and a total duration on the order of a second. Like vibration, the long-term average of shock motion will tend to zero, although it may include translations, or rotations, or both (e.g., vertical motion experienced by passengers during aircraft turbulence). There is no clearly definable or accepted boundary for the transition from transient *vibration* to a mechanical *shock*.

An impact occurs when the human body, or a body part, collides with an object. An impact may be distinguished from a shock by the following example. An individual seated in an automobile subjected to an upward vertical *shock* acceleration in excess of that due to gravity (e.g., traversing a speed bump) will momentarily lose contact with the seat cushion and subsequently suffer an *impact* with the seat on landing. Posture, contact area, muscle tension, and the relative internal motion and stresses of body parts may differ between these situations. Thus, when considering the injury potential or discomfort of a shock or impact, the size and shape of the object in contact with, or impacting, the body or body part (e.g., hand, or head) is important, as is the posture. The direction of application of the shock or impact to the body is equally important. Orthogonal coordinate axes are commonly specified at the seat for a seated person, with reference commonly made to *headward* [i.e., directed toward the head, i.e., in the  $+z$  direction of the coordinate system defined in International Organization for Standardization (ISO) standard 2631-1<sup>1</sup>—see Chapter 29], *tailward* (directed toward the feet, or  $-z$  direction), *spineward* (directed from chest toward the spine, or  $-x$  direction), or *sternumward* (directed from back toward the chest, or  $+x$  direction) forces and accelerations. A separate, standardized, orthogonal coordinate system with primary ( $z_h$ ) axis along on the third metacarpal is used to describe motions at the hand (ISO 5349-1<sup>2</sup>—see Chapter 29).

### 2 MEASUREMENTS AND METRICS

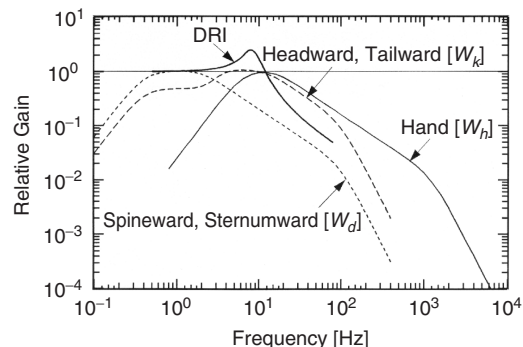
Uniaxial sensors, usually accelerometers, are employed to record instantaneous accelerations that vary with time  $t$ , as  $a(t)$ , with orthogonal component

accelerations commonly being combined by vector addition. Care must be taken to avoid exciting mechanical resonances within, or mechanical overloading sensors used to record large magnitude stimuli, such as those produced by some hand-held power tools (e.g., pneumatic hammers, impact drills). A common solution is to insert a mechanical filter between the accelerometer and the tool handle (see ISO 5349-2<sup>3</sup>).

### 2.1 Frequency Weighting

Human response to shock and impact depends on the frequency content of the stimulus, as well as the magnitude. Studies have been conducted to determine vibration magnitudes at different frequencies with an equal probability of causing a given human response. The biomechanic and biodynamic responses of the human body to external forces and accelerations can be expected to depend nonlinearly on the magnitude of the stimulus, and so any weighting of different frequencies will be applicable to a limited range of shock or impact magnitudes.

Equinoxious frequencies may be estimated, in principle, from epidemiological studies of health effects in human populations or, more commonly in practice, from the response of human subjects, animals, cadavers, or biodynamic models to the stimuli



**Figure 1** Frequency weightings for whole-body and hand-transmitted shocks.  $W_k$  is for headward and tailward whole-body shocks, and  $W_d$  is for spineward, sternumward, and side-to-side whole-body shocks.  $W_h$  is for all directions of shocks entering the hand.

of interest. The frequency weightings employed for hand-transmitted shocks, and small whole-body shocks influencing ride comfort in transportation vehicles, are those used for vibration (ISO 5349-1<sup>2</sup>; ISO 2631-1<sup>1</sup>), and are shown in Fig. 1. The range of frequencies is from 0.5 to 80 Hz for whole-body shocks and from 5.6 to 1400 Hz for shocks entering the hand. For a seated or standing person, the frequency weighting employed for the third orthogonal coordinate axis (from “side to side”) is also  $W_d$ . Frequency weightings for whole-body shocks likely to cause spinal injury are implicit in the biodynamic models used for their evaluation. The frequency weighting for the dynamic response index (DRI), which has been used extensively to evaluate headward whole-body shocks, is shown by the thick continuous line in Fig. 1. The frequency weightings are applied to acceleration–time histories,  $a(t)$ , by means of electronic filters or, implicitly, by the application of a biodynamic model as described in Section 4.

## 2.2 Characterizing the Magnitude of Shocks

The magnitude of a shock may be characterized by second, and higher, even-order mean values of the time history of the acceleration or by the output of biodynamic models. In the former case, the time history is commonly frequency weighted to equate the hazard at different frequencies,  $a_w(t)$ , that is, the mean value is

$$a_{RM} = \left[ \frac{1}{T} \int_0^T [a_w(t)]^m dt \right]^{1/r} \quad (1)$$

where the integration is performed for a time  $T$ , and  $m$  and  $r$  are constants describing the moment and root of the function. The higher order moments provide progressively greater emphasis to the components of the motion with larger amplitudes compared to the *root-mean-square* (rms) acceleration  $a_{rms}$ , which is obtained from Eq. (1) with  $m = r = 2$  and is the primary magnitude metric for human response to vibration. More appropriate metrics for shocks include the *root-mean-quad* (rmq) acceleration  $a_{rmq}$ , with  $m = r = 4$ ,<sup>4</sup> and metrics with higher even-order moments, such as with  $m = r = 6$ .

## 2.3 Characterizing Exposure to Shocks

A generalized expression for exposure during a time  $T$  to a stimulus function that has often been frequency weighted to equate the hazard at different frequencies, or transformed to estimate the internal motion of a body part,  $F(a_w(t))$  may be written

$$E(a_w, T)_{m,r} = \left[ \int_0^T [F(a_w(t))]^m dt \right]^{1/r} \quad (2)$$

As already noted,  $F(a_w(t))$  may be expected to be a nonlinear function of  $a_w(t)$ , and the function may be based on the output of a biodynamic model.

Within this family of exposure functions, generally only those with *even* integer values of the moment  $m$  are of interest. The *vibration dose value* (VDV) for which  $F(a_w(t)) \equiv a_w(t)$  and  $m = r = 4$ , may be used generally for characterizing exposure to small shocks,<sup>4</sup> that is,

$$\text{VDV} = E(a_w, T)_{4,4} = \left[ \int_0^T [a_w(t)]^4 dt \right]^{1/4} \quad (3)$$

Higher, even-order moment metrics (e.g.,  $m = r = 6$ ) have been proposed for exposure to repeated shocks (e.g., ISO 2631-5<sup>5</sup>). A related function, the severity index, for which  $F(a_w(t)) \equiv a_w(t)$ , moment  $m = 2.5$  and root  $r = 1$ , is sometimes used for the assessment of head impact, although it cannot be applied to long-duration acceleration–time histories owing to the noninteger value of  $m$ . The *head injury criterion* (HIC), which was developed as an alternative to the severity index, is used to assess the deceleration of instrumented crash test dummies or anthropomorphic manikins (see Section 4.3):

$$\text{HIC} = \left| (t_2 - t_1) \left[ \frac{1}{t_2 - t_1} \int_{t_1}^{t_2} a(t) dt \right]^{2.5} \right|_{\max} \quad (4)$$

where  $t_1$  and  $t_2$  are the times between which the HIC attains its maximum value, and  $a(t)$  is measured at the location of the center of gravity of the “head.”

## 3 QUANTIFYING HUMAN RESPONSE TO SHOCKS

Human subjects cannot be subjected to injurious shocks for ethical reasons, and so only responses to small-amplitude shocks are obtainable from laboratory experiments. The tolerance of the human body to large single shocks has been studied in the past: Such experiments are, however, unlikely to be replicated. Some information has been obtained from studies of accidents, although in most cases the input acceleration–time histories are poorly known. An exception is the single shocks powering the ejection seats of high-speed aircraft. Establishing the characteristics of shocks or impacts that result in injury to humans thus relies primarily on studies conducted with human surrogates (animal and cadavers) and predictions from theoretical models.

### 3.1 Experiments with Human Subjects

Human subjects have been exposed to whole-body mechanical shocks in the vertical and, most often separately, horizontal directions when sitting on a seat attached to the moving platform of a vibration exciter. For headward shocks the VDV has been shown to characterize the discomfort produced by either single or repeated shocks.<sup>6</sup> A single frequency weighting function may be used in the range of

shock magnitudes with peak accelerations up to about  $15 \text{ m} \cdot \text{s}^{-2} (W_k)$ . However, a nonlinear relationship may be required to extend the characterization of shocks to magnitudes in which impacts may occur if the subject is not restrained by a seat harness.<sup>7</sup> For the multiple whole-body shocks encountered in most commercial transportation, and industrial, settings, where exposures commonly also involve ongoing vibration, the preferred metric is the VDV calculated with a fixed frequency weighting [Eq.(3)]. The metric does not appear to be particularly sensitive to the precise form of the frequency weighting function when used to assess discomfort.<sup>8</sup>

The tolerance of the body to large single shocks has been studied in experiments conducted with a human subject seated on a rocket-propelled sled that is braked at the end of a test track. The subjects wore safety belts and harnesses to restrain motion during deceleration. Experiments have also been conducted using a drop tower for single tailward shocks.

The response of the hand and arm to shocks, as opposed to nonstationary random or periodic vibration, has received comparatively little attention.<sup>9</sup> While it has been suggested that acute and chronic health effects may be influenced by shocks, the results of experiments are contradictory. It has been demonstrated that the total mechanical energy absorbed by the hand and arm, as well as the forces exerted by the hands to grip and control the power tool, are increased by exposure to shocks when compared with exposure to continuous vibration.<sup>10</sup> The responses of the hand and arm to shocks are, however, considered at present to be defined by the same metric as used for vibration, namely the energy-equivalent rms exposure [i.e.,  $F(a_w(t)) = a_w(t)$  and  $m = r = 2$  in Eq. (2)].

### 3.2 Experiments with Human Surrogates

The boundary between the onset of injury and survivability of exposure to single whole-body shocks has been explored by a combination of experiments involving human subjects exposed to less hazardous shocks than those believed to define the boundary and animals (chimpanzee and hog) exposed to shocks at, or exceeding, the expected boundary. The animals were positioned on the rocket-propelled sled previously described either in a seated position, for exposure to spineward and sternunward shocks, or supine, for exposure to headward and tailward shocks. The animals were instrumented with, in some cases, accelerometers surgically embedded in the back. The efficacy of various forms of restraining devices in preventing or reducing injury was also studied (e.g., lap belts, shoulder straps, and thigh straps).

The onset and extent of injury from single impacts to the head have been studied using human cadavers and animals. A rotary hammer was used to simulate impact with a hard unyielding surface to determine the acceleration-time relationship for concussion in live dogs. In related experiments, cadavers with instrumented heads were positioned horizontally and dropped so that the head impacted a steel block. The research led to the Wayne State Concussion Tolerance

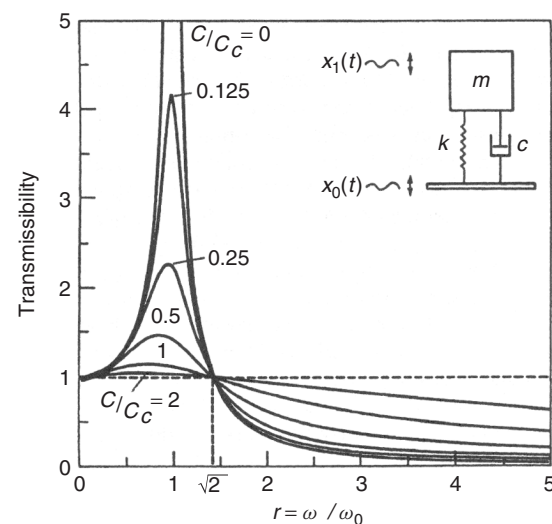
Curve for impact of the forehead on a hard, flat surface,<sup>11</sup> which has had considerable influence on motor vehicle passenger compartment design. The severity index describes the relationship between peak acceleration and impact duration from about 2.5 to 50 ms.

With changing ethics regarding animal and human experimentation, it is unlikely that the historical studies on the onset of injury from single shocks or impacts will be extended or repeated. Anthropomorphic manikins have now been developed as human surrogates for evaluating "human" response to extreme shock and impact environments (e.g., crash test dummies). More complete responses can be obtained, in principle, by computer models that simulate both the shock or impact environment and the "human."

## 4 SIMULATION OF HUMAN RESPONSE

### 4.1 Single-Degree-of-Freedom Biodynamic Model: Dynamic Response Index

The biodynamic response of the human body, or a body part, can be represented by the motion of a collection of masses, springs, and mechanical dampers for frequencies up to several hundred hertz.<sup>12</sup> The simplest model consists of a mass  $m$ , which represents the mass of the upper body of a seated person, supported by a spring with stiffness  $k$ , representing the spine and associated musculature, and a damper, which is excited at its base, as sketched in Fig. 2.



**Figure 2** Single-degree-of-freedom, lumped-parameter, biodynamic model (see text). The mass  $m$  is supported by a spring with stiffness  $k$  and viscous damper with resistance  $c$ . The transmissibility of motion to the mass is shown as a function of the frequency ratio,  $r (= \omega / \omega_0)$ , when the base is subjected to a displacement  $x_0(t)$ . The response of the mass is taken to represent spinal motion. (After Griffin.<sup>4</sup> Reprinted with permission.)

The transmissibility of this simple model, that is, the motion of the mass relative to that of the base ( $x_1/x_0$ ), is plotted in the diagram as a function of the ratio of the angular excitation frequency,  $\omega$ , to the (angular) resonance frequency,  $\omega_0 = (k/m)^{1/2}$ . It can be seen that for excitation frequencies less than the resonance frequency (i.e.,  $r = \omega/\omega_0 \ll 1$ ) the motion of the mass is essentially equal to that of the base. At angular frequencies greater than the resonance frequency (i.e.,  $r > \sqrt{2}$ ), however, the motion of the mass becomes progressively less than that of the base, forming a low-pass mechanical filter. At angular excitation frequencies close to the resonance frequency, the motion of the mass exceeds that of the base by an amount that depends on the damping ratio, labeled  $c/c_c$  in the diagram.

This single degree-of-freedom (DOF) biodynamic model has been used extensively to simulate the response of the spine to shocks. For headward shocks, the DRI estimates the potential for spinal injury from the maximum deflection of the spring,  $|x_1(t) - x_0(t)|_{\max}$ , which is calculated for a known input acceleration–time history. The metric relates the maximum compressive force of the spring,  $k|x_1(t) - x_0(t)|_{\max}$ , to the peak stress on the spine by assuming the cross-sectional area of the spine is proportional to the model mass, that is, by  $[k/m]|x_1(t) - x_0(t)|_{\max}$ . The DRI is then defined as  $(\omega_0)^2|x_1(t) - x_0(t)|_{\max}/g$ , where the natural frequency is 52.9 rad/s (thus making  $f_0 = 8.42$  Hz), the damping ratio is 0.224, and  $g$  is the acceleration of gravity ( $9.81 \text{ m s}^{-2}$ ). The model has been used to predict the spinal injury rate for input acceleration–time histories corresponding to those employed in rocket-driven ejection seats for high-speed aircraft. Its success has led to its adoption for specifying ejection seat performance, and its extension to a metric for exposure to repeated shocks<sup>13,14</sup> and to shocks in three dimensions.<sup>5,15</sup>

## 4.2 Complex Biodynamic Models

Numerous, more complex biodynamic models have been developed to incorporate more realistic descriptions of individual body parts and to predict the motion of one body part relative to another.<sup>16,17</sup> The mathematical dynamical model (MADYMO), which employs a combination of rigid bodies, joints, springs, and dampers to represent the human, or in some cases anthropomorphic manikin, is a comprehensive computer model for predicting the response to whole-body shocks. A MADYMO typically employs 15 ellipsoidal segments with masses and moments of inertia determined from anthropomorphic data for adults and children. The connections between these segments are flexible and possess elastic and resistive properties that are characteristic of human joints. The environment to be simulated may include the interior surfaces of vehicles or cockpits (e.g., seats and dashboard) and occupant restraints. The model may also simulate wind forces to estimate pilot motion after ejection from an aircraft.

There does not appear to be a biodynamic model specifically designed to predict the response of the

hand and arm to the shocks experienced while operating hand-held impact power tools. MADYMO models have been developed to predict the detailed response of some body parts to a simulated environment using finite elements (FEs), which can interact with the multibody model elements. Examples of human body subsystems that have been modeled with FEs include the spine, to estimate forces on the lumbar vertebral disks,<sup>18</sup> and to predict the injury potential of vertebral compression and torsional loads,<sup>19</sup> and the head and neck, to predict forward rotation loads during rapid horizontal deceleration.<sup>17</sup>

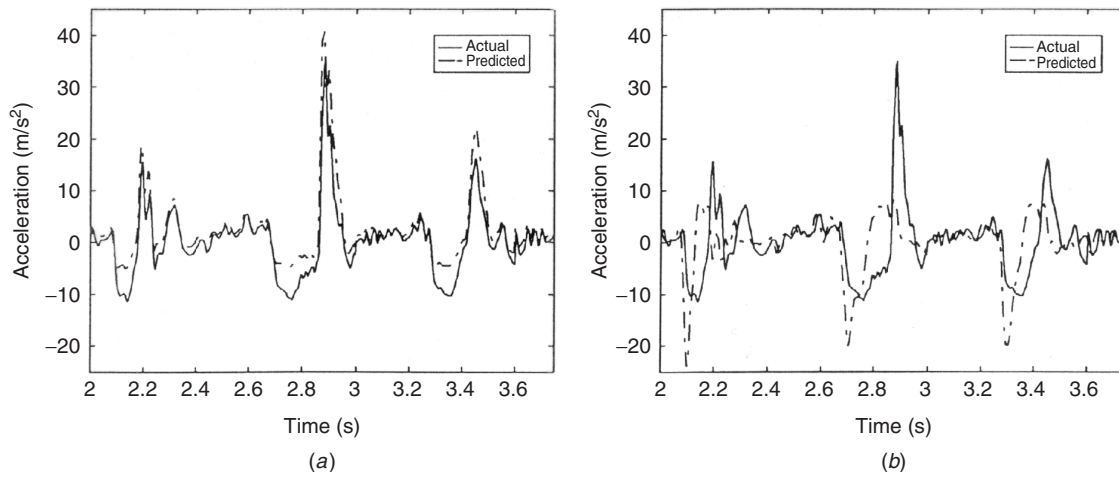
The nonlinear response of the spine to shocks has also been modeled using an artificial neural network.<sup>20</sup> The network is first trained with human responses to known input acceleration–time functions and is then capable of predicting spinal motion in response to arbitrary input accelerations that fall within the boundaries of magnitude and frequency set by the training data. The success of a neural network in predicting the motion recorded by an accelerometer placed over the L4 vertebral spinal process when a subject was exposed to tailward shocks and impacts is shown in Fig. 3. For comparison, the spinal motion predicted by the simple biodynamic model with parameters of the DRI is shown in Fig. 3. The output of the simple biodynamic model is obtained by linear filtering using the DRI frequency weighting of Fig. 1. It would appear from these results that a nonlinear model is required to reproduce spinal motion when the input acceleration–time history includes impacts.

## 4.3 Anthropomorphic Manikins

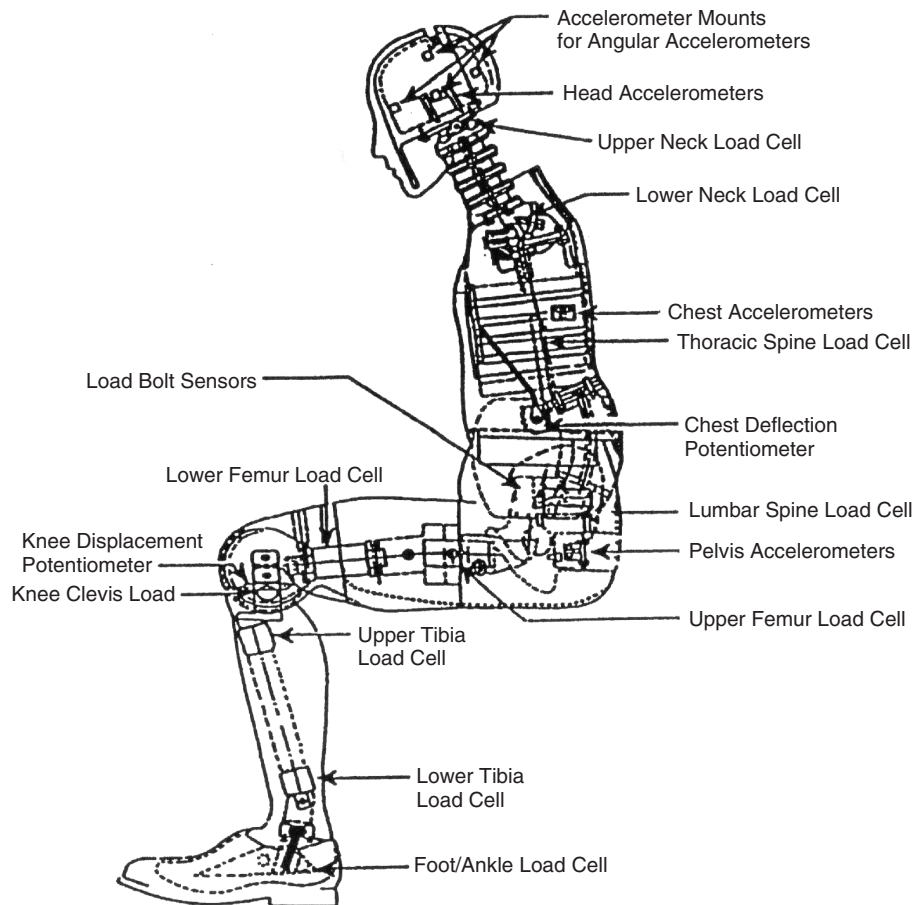
Manikins that mimic the shape, weight, and some biodynamic properties of humans are used extensively for motor vehicle crash testing and for evaluating aircraft escape systems and seating.<sup>21</sup> The Hybrid III manikin has become the de facto standard for simulating the response of motor vehicle occupants to frontal collisions and for tests of occupant safety systems (i.e., seat belts and air bags). The manikin approximates the size, shape, mass, and weight of the 50th-percentile North American adult male and consists of metal parts to provide structural strength and define the overall geometry (see Fig. 4).

The “skeleton” is covered with foam and an external vinyl skin to replicate the shape of the 50th-percentile male. The manikin possesses a rubber lumbar spine, curved to mimic a sitting posture. The head, neck, chest, and leg responses are intended to replicate human head acceleration resulting from forehead and side-of-the-head impacts; fore-and-aft, and lateral, bending of the neck; deflection of the chest to distributed forces on the sternum, and impacts to the knee, during rapid deceleration.<sup>22</sup> Instrumentation to record these responses as well as other parameters are indicated in Fig. 4. Hybrid III dummies are available for small (5th percentile) adult females and large (95th percentile) adult males, as well as for infants and children. A related side impact dummy has been developed.

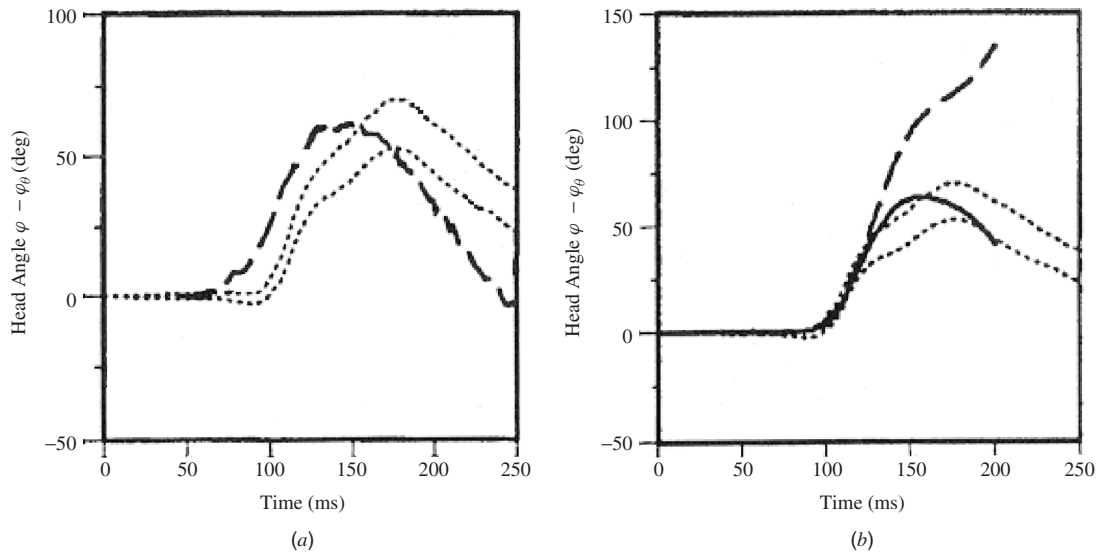




**Figure 3** Comparison between the measured (continuous line) and predicted (dashed lines) response of the spine (above L4) to shocks and impacts: (a) nonlinear neural network model and (b) DRI model. (From Nicol et al.<sup>20</sup> Reprinted with permission.)



**Figure 4** Sketch of Hybrid III anthropomorphic dummy designed for use in motor vehicle frontal crash tests, showing elements of construction and sensors. (From AGARD-AR-330.<sup>21</sup> Reprinted with permission.)



**Figure 5** Comparison between the response of human volunteers (dotted lines), a manikin, and a mathematical biodynamic model of the head and neck to  $150 \text{ m} \cdot \text{s}^{-2}$  spineward deceleration. (a) Response of Hybrid III head and neck (dashed line) and (b) response of three-dimensional MADYMO model of the head and neck with passive neck muscles (dashed line) and active neck muscles (continuous line). (From RTO-MP-20.<sup>17</sup> Reprinted with permission.)

Manikins have also been developed by the Air Force for use with aircraft ejection systems. The Advanced Dynamic Anthropomorphic Manikin (ADAM) is conceptually similar to that of the Hybrid III dummy and, in addition, attempts to replicate human joint motion, soft tissue, and the response of the spine to vertical accelerations for both small-amplitude vibration and large impacts. The spine consists of a mechanical spring-damper system (see Section 4.1) that is mounted within the torso.

The potential limitations of mechanical models for predicting nonlinear human responses to shock and impact may be overcome, in principle, by introducing active control systems. At present, only simple active biodynamic models have been demonstrated for use in seat testing.<sup>23</sup>

#### 4.4 Biofidelity of Biodynamic Models and Human Surrogates

Knowledge of the biofidelity of a biodynamic model or human surrogate is essential in order to relate the results to those expected with human subjects. This inevitably requires human subjects to be exposed to the same stimulus as the model or surrogate and hence limits comparisons to noninjurious shocks and impacts. Nevertheless, it is instructive to compare the time histories of some responses. A comparison between the responses of human volunteers, the range of which is shown by dotted lines, with those of the Hybrid III manikin and of a three-dimensional head and neck MADYMO model to a sternward deceleration are shown in Figs. 5a and 5b, respectively.

Inspection of Fig. 5a reveals that forward rotation of the head of the Hybrid III does not fall within the values defined by the human subjects, although the manikin does reproduce the maximum angular rotation of the head but at the wrong time after the onset of the shock. The MADYMO model also predicts head rotation that falls outside the range of values defined by human subjects when muscle behavior is not included. The inaccuracy can be overcome in this case by including muscle tension in the computer model (continuous line in Fig. 5b). It may be inferred from these results that the intrinsic mechanical damping of the neck of Hybrid III does not closely replicate the human response, and active “muscle” forces are necessary.

Employing the results of experiments with live animals to predict biodynamic responses in humans introduces uncertainties associated with interspecies differences. Of particular concern are the differences in size and mass of body parts and organs, which influence resonance frequencies. For this reason, most animal research has employed mammals of roughly similar size and mass to humans (i.e., hogs and chimpanzees).

As with manikins, human cadavers lack appropriate mechanical properties for tissues and muscle tension. The latter is important for obtaining realistic human responses, as has already been noted.

#### 5 HEALTH, COMFORT, AND INJURY CRITERIA

There is an extensive literature on the effects of shock and impact on humans.<sup>4,24</sup> For small-amplitude whole-body shocks, the primary response is of reduced comfort in transportation vehicles. The ability to perform



common tasks (e.g., writing, reading, drinking from a cup) is also impeded. Large-amplitude headward and tailward whole-body shocks can injure the spine when seated, and headward shocks can also injure the feet and ankles when standing. The response and injury potential will depend on the peak magnitude of the shock acceleration and its time history. The response to shocks in all directions will be influenced by the effectiveness of body restraints in restricting the relative displacement of body parts (e.g., “flailing” of arms and legs and “torpedoing” of torso through harness) and in preventing impacts with surrounding structures. The combination of extreme shock and impact can cause bone fracture and soft tissue (e.g., organ) injury. Fatal injury may result from exposure to large shocks or impacts. The consequences of impacts to body parts are influenced by the velocity, duration, area of impact, and transfer of momentum (e.g., bullet versus basketball) and, for the head, may involve fatal or nonfatal concussion, contusions, skull fracture, and axonal brain injury. Hand-transmitted shocks have not been conclusively demonstrated to lead to more rapid onset or extreme symptoms of the hand–arm vibration syndrome, even though this is suspected, and so are currently assessed by the criteria used for hand-transmitted vibration that are described in Chapter 29. The criteria described here are for discomfort and injury and survivability from exposure to whole-body shocks. There are, however, no universally accepted procedures or metrics.<sup>25</sup> Unfortunately, even consensus standards prepared for the same application (e.g., discomfort) contain significant incompatibilities.<sup>26</sup>

### 5.1 Discomfort – No Impacts

Exposure to shocks of insufficient magnitude to cause severe health effects may influence ride comfort in vehicles, aircraft, and boats. The VDV is correlated with subjective assessments of discomfort from

exposure to shocks, with the expected rating for motions judged to produce “severe discomfort” listed in Table 1. The acceleration–time histories are frequency weighted by  $W_k$  or  $W_d$  depending on the direction of the shocks relative to the body (see Fig. 1). The VDV is an acceptable metric for motions involving whole-body vibration as well as shocks and is suggested here for “small” shocks with peak accelerations up to about  $15 \text{ m} \cdot \text{s}^{-2}$ , provided the person is restrained.<sup>27</sup> The risk of injury should be considered for exposures involving shocks of greater magnitude (see Section 5.2).

The VDV provides a linear measure of the motion and may therefore not serve as an appropriate metric for nonlinear motions, such as those involving impacts (see Fig. 3). It should also be noted that motions considered unpleasant in most circumstances may in others be considered acceptable and even exhilarating (e.g., fairground rides).

### 5.2 Risk of Injury from Multiple Shocks and Impacts

A general method for assessing the risk of injury to a healthy seated person from exposure to multiple shocks and impacts has recently been proposed.<sup>31</sup> The method consists of three parts: a dynamic response model to predict the transmission of the motion from the seat to the spine; identification of acceleration peaks and their accumulation to form the dose at the spine; and an injury risk model for assessing the probability of adverse health effects based on the cumulative fatigue failure of repeatedly stressed biological materials.<sup>32</sup> The dynamic response model employs the nonlinear biodynamic model described in Section 4.2 for headward and tailward shocks and impacts, and (linear) single-degree-of-freedom biodynamic models for the other directions (see Section 4.1). The inputs to the

**Table 1 Health, Comfort, and Injury Criteria for Healthy Adults**

Human Response	Metric	Weighting, Model, or Manikin	Value	Source
<b>Discomfort (severe) – no impacts</b>				
Small shocks, any direction	VDV	$W_k$ , or $W_d$	$15 \text{ m/s}^{1.75}$	BSI 6841 <sup>27</sup>
<b>Risk of injury from shocks and impacts (up to <math>40 \text{ m} \cdot \text{s}^{-2}</math>)</b>				
Many shocks, any direction	$E(\Sigma a_{\text{peak}})_{6,6} \Rightarrow$ compress spine	Nonlinear (4.2) and single DOF (4.1) models	$>0.5 \text{ MPa}$	ISO 2631-5 <sup>5</sup>
<b>Risk of injury from shocks – subject restrained, no impacts</b>				
Large shocks, headward, tailward <sup>a</sup>	$E(\text{DRI}_q, n_q)$	DRI model	9.0	ASCC 61/25 <sup>28</sup>
<b>Survivable single shock, or impact</b>				
To body, headward shock <sup>a</sup>	DRI	DRI model	18	After von Gierke <sup>12</sup>
To body, spineward shock <sup>a</sup>	Peak acceleration		See Fig. 6	Eiband <sup>29</sup>
Head impact (manikin)	HIC	Hybrid III	1000	NHTSA <sup>30</sup>
To neck, flexion (manikin)	Moment	Hybrid III	190 N.m	NHTSA <sup>30</sup>
To neck, extension (manikin)	Moment	Hybrid III	57 N.m	NHTSA <sup>30</sup>

<sup>a</sup>When body restrained.

dynamic response models are the seat motions measured in the three orthogonal directions ( $x$ ,  $y$ , and  $z$ ). The acceleration dose is constructed separately from the peak acceleration of each shock at the spine that causes compression, or lateral motion,  $a_{\text{peak}}(t)$ , as calculated from the output of the appropriate biodynamic model using Eq. (2) with  $F(a_w(t)) \equiv a_{\text{peak}}(t)$  and  $m = r = 6$ . The combined acceleration dose applicable to an average working day is converted into an equivalent *static* compressive stress, which may then be assessed by a Palmgren–Miner model for fatigue failure of the vertebral end plates.<sup>31</sup> The calculation takes into account the reducing strength of the vertebrae with age. A lifetime exposure to a static stress of less than 0.5 MPa is associated with a low probability of an adverse health effect, whereas lifetime exposure to a static stress in excess of 0.8 MPa has a high probability of spinal injury.<sup>5</sup> The nonlinear biodynamic model is based on human responses to peak accelerations of up to  $40 \text{ m s}^{-2}$ , and so the method should not be applied to shocks and impacts of larger magnitude. This restriction has limited practical consequences, as such motions are unlikely to be tolerated in commercial transportation systems.

### 5.3 Risk of Injury from Large Shocks When Subject Restrained

For “large” single or multiple shocks in the headward or tailward direction, that is, with peak accelerations greater than about  $40 \text{ m s}^{-2}$ , the method proposed by Allen<sup>13</sup> and adopted by the Air Standardization Coordinating Committee,<sup>28</sup> which is conceptually

similar to that just described, is recommended for single or multiple shocks (no impacts). It is based on the DRI (see Section 4.1), which is extended to include multiple shocks and used to estimate the risk of spinal injury in healthy young men, using the theory of cumulative material fatigue damage. The model is applicable to persons who are seated and restrained by seat harnesses. The metric depends on the number of shocks experienced and is presented in the form described by Payne.<sup>14</sup> For exposures consisting of multiple shocks of differing magnitude, if there are  $n_q$  shocks of magnitude  $\text{DRI}_q$ , where  $q = 1, 2, 3, \dots, Q$ , then the dose can be expressed as

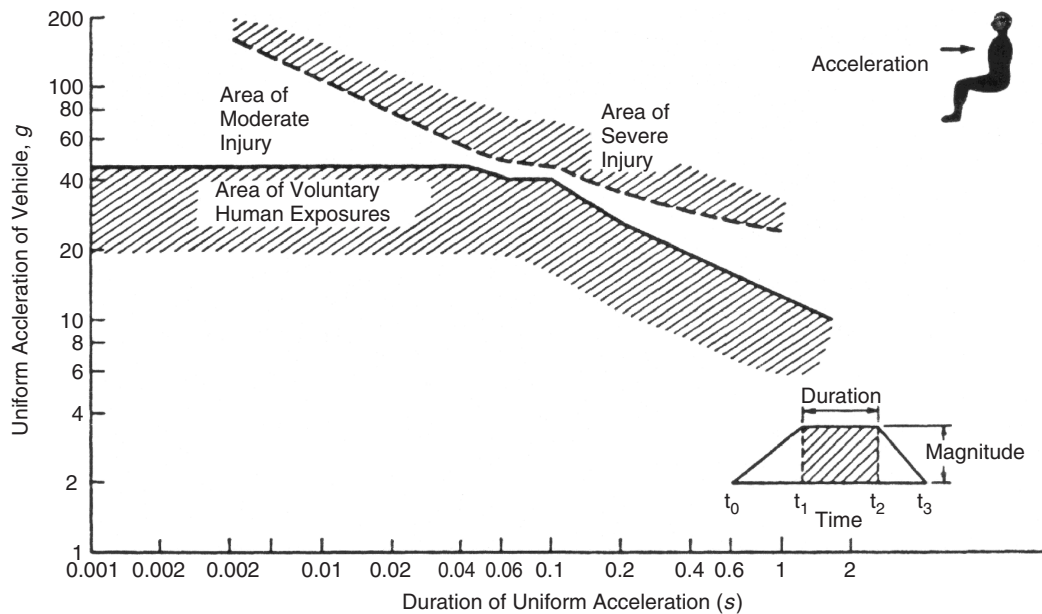
$$E(\text{DRI}_q, n_q) = \left[ \sum_{q=1}^Q n_q (\text{DRI}_q)^8 \right]^{1/8} \quad (5)$$

The metric is applied here to the shocks experienced during a “day,” normally expected to be no more than 8 h so that there is time for recovery between exposures. As the maximum value listed in Table 1 is applicable to healthy young men, it is to be expected that a more conservative value should be used when applying the procedure to older persons.

### 5.4 Survivable Single Shocks or Impacts

Estimates for *survivable* exposures of humans to single shocks are given for headward acceleration in Table 1 and for spineward deceleration in Fig. 6.

For headward acceleration, the accumulated operational experience with nonfatal aircraft ejections from



**Figure 6** Human tolerance of single, spineward shocks expressed as a function of the magnitude and duration of seat deceleration. (After Eiband.<sup>29</sup> Reprinted with permission.)

military aircraft suggests that a DRI of 18 is associated with a tolerable rate of spinal injury (<10%) among healthy, young male pilots who are restrained in their seats by conventional flying harnesses.<sup>12</sup> For spineward acceleration, the most reliable estimate is from the rapid deceleration of human volunteers and animals seated on a test sled with body restraints and is summarized in Fig. 6.<sup>29</sup> The limit of human tolerance is indicated by the boundary of severe injury, which depends on the duration of the peak acceleration and the rate of onset of the deceleration. The curve is a composite of injurious exposures to animals and extrapolations from exposures involving human subjects.

An alternative approach is to specify tolerance limits for measurements conducted on anthropomorphic manikins subjected to single shocks or impacts. The HIC has been applied to the motion of the center of gravity of the head of the Hybrid III manikin in motor vehicle crash tests prescribed by the U.S. National Highway Traffic Safety Administration (NHTSA), using a time interval ( $t_2 - t_1$ ) of 36 ms [see Eq.(4)]. The value in Table 1 is the maximum allowable by the NHTSA for frontal collisions and is considered to represent a "concussion tolerance level."<sup>33</sup> Values are also listed in the Table for the most common neck injury ("whiplash").<sup>34</sup> Survivable fracture limits for the pelvis, patella, and femur in frontal and side impacts have also been proposed for manikins.<sup>22</sup> Caution must be exercised in applying these data to humans, however. In particular, the rank ordering of the severity of head injuries in humans by the HIC values recorded on the Hybrid III has been questioned<sup>35,36</sup> and may reflect its biofidelity (see Section 4.4).

## REFERENCES

1. ISO 2631-1, *Mechanical Vibration and Shock—Evaluation of Human Exposure to Whole Body Vibration—Part 1: General Requirements*, 2nd ed., International Organization for Standardization, Geneva, 1997.
2. ISO 5349-1, *Mechanical Vibration—Measurement and Evaluation of Human Exposure to Hand-Transmitted Vibration—Part 1: General Guidelines*, International Organization for Standardization, Geneva, 2001.
3. ISO 5349-2, *Mechanical Vibration—Measurement and Evaluation of Human Exposure to Hand-Transmitted Vibration—Part 2: Practical Guidance for Measurement at the Workplace*, International Organization for Standardization, Geneva, 2002.
4. M. J. Griffin, *Handbook of Human Vibration*, Academic, London, 1990.
5. ISO 2631-5, *Mechanical Vibration and Shock—Evaluation of Human Exposure to Whole Body Vibration—Part 5: Method for Evaluation of Vibration Containing Multiple Shocks*, International Organization for Standardization, Geneva, 2004.
6. H. V. C. Howarth, and M. J. Griffin, Subjective Reaction to Vertical Mechanical Shocks of Various Waveforms, *J. Sound Vib.*, Vol. 147, 1991, pp. 395–408.
7. B. J. Cameron, J. B. Morrison, D. G. Robinson, A. V. Vukusic, G. Roddan, and S. H. Martin, Development of a Standard for the Health Hazard Assessment of Mechanical Shock and Repeated Impact in Army vehicles, Final Report DAMD 17-91-C-1115, BC Research Inc., Vancouver, Canada, 1997.
8. N. J. Mansfield, P. Holmlund, and R. Lundström, Comparison of Subjective Responses to Vibration and Shock with Standard Analysis Methods and Absorbed Power, *J. Sound Vib.*, Vol. 230, 2000, pp. 477–491.
9. N. Schafer, H. Dupuis, and E. Hartung, Acute Effects of Shock-Type Vibration Transmitted to the Hand-Arm System, *Int. Arch. Occup. Environ. Health*, Vol. 55, 1984, pp. 49–59.
10. L. Burström, and A. Sörensson, The Influence of Shock-Type Vibrations on the Absorption of Mechanical Energy in the Hand and Arm, *Int. J. Ind. Ergonomics*, Vol. 23, 1999, pp. 585–594.
11. L. M. Patrick, H. R. Lissner, and E. S. Gurdjian, Survival by Design—Head Protection, Proc. 7th Stapp Car Crash Conf., Detroit, 1965, pp. 483–499.
12. H. E. von Gierke, Biodynamic Models and Their Applications, *J. Acoust. Soc. Am.*, Vol. 50, 1970, pp. 1397–1413.
13. G. Allen, The Use of a Spinal Analogue to Compare Human Tolerance to Repeated Shocks with Tolerance to Vibration, in AGARD-CP-253, *Models and Analogues for the Evaluation of Human Biodynamic Response, Performance and Protection*, North Atlantic Treaty Organization, Neuilly Sur Seine, France, 1978.
14. P. R. Payne, A Unification of the ASCC and ISO Ride Comfort Methodologies, Unpublished Report 377–3, Payne Associates, Severna Park, MD, 1991.
15. J. W. Brinkley, L. J. Specker, and S. E. Mosher, Development of Acceleration Exposure Limits for Advanced Escape Systems, in AGARD-CP-472, *Implications of Advanced Technologies for Air and Spacecraft Escape*, North Atlantic Treaty Organization, Neuilly Sur Seine, France, 1990.
16. H. Seidel and M. J. Griffin, Modelling the Response of the Spinal System to Whole-Body Vibration and Repeated Shock," *Clin. Biomech.*, Vol. 16 (Suppl. 1), 2001, pp. S3–S7.
17. RTO-MP-20, *Models for Aircrew Safety Assessment: Uses, Limitations and Requirements*, North Atlantic Treaty Organization, Neuilly Sur Seine, France, 1999.
18. S. Pankoke, B. Buck, and H. P. Woelfel, Dynamic FE Model of Sitting Man Adjustable to Body Height, Body Mass, and Posture Used for Calculating Internal Forces in the Lumbar Vertebral Disks, *J. Sound Vib.*, Vol. 215, 1998, pp. 827–839.
19. H. E. von Gierke, To Predict the Body's Strength, *Aviat. Space & Environ. Med.*, Vol. 59, 1988, pp. A107–115.
20. J. Nicol, J. Morrison, G. Roddan, and A. Rawicz, Modelling the Dynamic Response of the Human Spine to Shock and Vibration Using a Recurrent Neural Network, Heavy Vehicle Systems, Special Series, *Int. J. Vehicle Design*, Vol. 4, 1997, pp. 145–165.
21. AGARD-AR-330, *Anthropomorphic Dummies for Crash and Escape System Testing*, North Atlantic Treaty Organization, Neuilly Sur Seine, France, 1997.
- AGARD-CP-597, *Impact Head Injury: Responses, Mechanisms, Tolerance, Treatment and Countermeasures*, North Atlantic Treaty Organization, Neuilly Sur Seine, France, 1997.
22. H. J. Mertz, Anthropometric Test Devices, in *Accidental Injury—Biomechanics and Prevention*, A. M. Nahum and J. W. Melvin Eds., Springer, New York, 1993, Chapter 4.

23. C. H. Lewis and M. J. Griffin, Evaluating the Vibration Isolation of Soft Cushion Seats Using an Active Anthropodynamic Dummy, *J. Sound Vib.*, Vol. 253, 2002, pp. 295–311.
24. H. E. von Gierke and A. J. Brammer, Effects of Shock and Vibration on Humans, in Harris' Shock and Vibration Handbook, 5th, ed., C. M. Harris and A. G. Piersol, Eds., McGraw-Hill, New York, 2002, Chapter 42.
25. A. J. Brammer, and D. E. Peterson, Vibration, Mechanical Shock, and Impact, in *Standard Handbook of Biomedical Engineering and Design*, M. Kutz, Ed., McGraw-Hill, New York, 2003, Chapter 10.
26. M. J. Griffin, A Comparison of Standardized Methods for Predicting the Hazards of Whole-Body Vibration and Repeated Shocks, *J. Sound Vib.*, Vol. 215, 1998, pp. 883–914.
27. BSI 6841, Measurement and Evaluation of Human Exposure to Whole-Body Mechanical Vibration and Repeated Shock, British Standards Institute, London, 1987.
28. ASCC ADV PUB 61/25, Human Tolerance to Repeated Shock, Air Standardization Coordinating Committee, Washington, DC, 1982.
29. A. M. Eiband, Human Tolerance to Rapidly Applied Accelerations: A Summary of the Literature, NASA Memo 5-19-59E, National Aeronautics and Space Administration, Washington, DC, 1959.
30. NHTSA, Federal Motor Vehicle Safety Standard 208. U.S. National Highway Traffic Safety Administration, Washington, DC.
31. J. B. Morrison, S. H. Martin, D. G. Robinson, G. Roddan, J. J. Nicol, M. J-N. Springer, B. J. Cameron, and J. P. Albano., Development of a Comprehensive Method of Health Hazard Assessment for Exposure to Repeated Mechanical Shocks, *J. Low Freq. Noise Vib.*, Vol. 16, (1997), pp. 245–255.
32. J. Sandover, The Fatigue Approach to Vibration and Health: Is It a Practical and Viable Way of Predicting the Effects on People? *J. Sound Vib.*, Vol. 215, (1998), pp. 699–721.
33. SAE J885, *Human Tolerance to Impact Conditions as Related to Motor Vehicle Design*, Society of Automotive Engineers, Warrendale, PA, 1986.
34. K. H. Digges, Injury Measurements and Criteria, in RTO-MP-20, *Models for Aircrew Safety Assessment: Uses, Limitations and Requirements*, North Atlantic Treaty Organization, Neuilly Sur Seine, France, 1999, pp. K2-1–K2-5.
35. E. R. Welbourne, Use of the Head Injury Criterion as a Measure of Vehicle Occupant Protection Performance, Proc. Joint Conf. AAAM and IRCOB, (1994), pp. 151–162.
36. H. J. Mertz, P. Prasad, and G. Nusholtz, *Head injury risk assessment for forehead impacts*, SAE 96099, Society of Automotive Engineers, Detroit, MI, 1996.

#### BIBLIOGRAPHY

- A. M. Nahum and J. W. Melvin, Eds., *Accidental Injury—Biomechanics and Prevention*, Springer, New York, 1993.

# CHAPTER 31

---

## HEARING PROTECTORS

**Samir N. Y. Gerges**  
Mechanical Engineering Department  
Federal University of Santa Catarina  
Trindade, Florianopolis, Santa Catarina, Brazil

**John G. Casali**  
Department of Industrial and Systems Engineering  
Virginia Polytechnic Institute and State University  
Blacksburg, Virginia

### 1 INTRODUCTION

In many industrial and military situations, it is not practical or economical to reduce the noise to levels that do not present either a hazard to hearing or annoyance. In these situations, personal hearing protection devices are capable of reducing the noise by up to about 45 dB, depending on their design and the sound frequency. A properly selected and fitted personal hearing protection device or a combination of them (e.g., earmuffs worn over earplugs) usually can establish sufficient reduction of noise at the ear, if not to a pleasant level at least to a harmless one. Certain types of hearing protectors can also reduce noise-induced annoyance and improve speech communication, signal detection, and audibility of desirable sounds, such as machine cues, in certain situations as described in the following. A personal hearing protection device (HPD) should be used for the whole time that one is in a noise area. If one removes the protector even for a small percentage of time, such as 5 to 10 min in a whole workday, the protection is sharply reduced.

### 2 HEARING PROTECTOR TYPES

Hearing protection devices can be divided into four categories according to their position relative to the ear: earplugs, semiinserts, earmuffs, and helmets.

*Earplugs* are inserted into the ear canal and remain there without any additional means of support. *Semiinserts*, also called supraaural HPDs, close the entrance to the ear canal without being deeply inserted into it and are supported by a head or chin band. These may be used as hearing protector and are also commonly designed as lightweight earphone systems for sound production. *Earmuffs* cover the entire outer ear with a cuplike shell, the edge of which is covered with a compliant cushion that presses and seals against the flesh. Muffs may be held in place by a headband, suspended from a hard hat via clamping arms or mounted inside a helmet. *Helmets* cover most of the head surface. They are not commonly used for ear protection alone; usually they combine this function with protection of the head against cold, impact hazards, and/or weapons threats such as gunshots.

Helmets may act also as a support for earphones or earmuffs, and if their design covers most of the head, may offer added hearing protection against the bone conduction pathway for noise that flanks the other types of HPDs.

Figure 1 shows examples of the four basic kinds of ear protectors. Each has advantages and disadvantages compared with the others.

Many other more sophisticated HPDs and special features for communications and other enhancements have arisen over the past decade, and these are typically embodied as augmentations of the basic HPD types mentioned in this section. These so-called augmented HPDs, due to their radical design departures from conventional protectors, are covered in a separate section (Section 12) herein.

### 3 BASIC REQUIREMENTS FOR HEARING PROTECTORS

Every HPD, irrespective of type, must comply with the requirements of (1) sound attenuation, (2) comfort, and (3) absence of adverse effects on human tissue. In addition there are three other requirements whose importance depends on the conditions of use: (4) conservation of speech intelligibility and hearing of signals, (5) ease of handling, and (6) durability.

1. The first requirement, sound attenuation, is obvious. It determines the amount of protection from noise that is afforded to the ear. The degree of sound attenuation necessary depends on the sound pressure, the kind of noise, and the duration of exposure. The exact nature of these interrelationships is somewhat obscure, but it can be stated quite generally that the amount of sound attenuation provided by an HPD should be sufficient to keep the noise level below the established safety limit (either government legislation, consensus standards, or prescribed safety practices in industry or elsewhere). All HPD will not be capable of attaining this limit. Even the best ear protectors do not attenuate more than 45 dB on the average, while an attenuation of 40 to 50 dB may be advisable under some circumstances. Limiting factors may be leakage around the HPD, sound transmission through the HPD, vibration of the HPD, and/or bone conduction of the

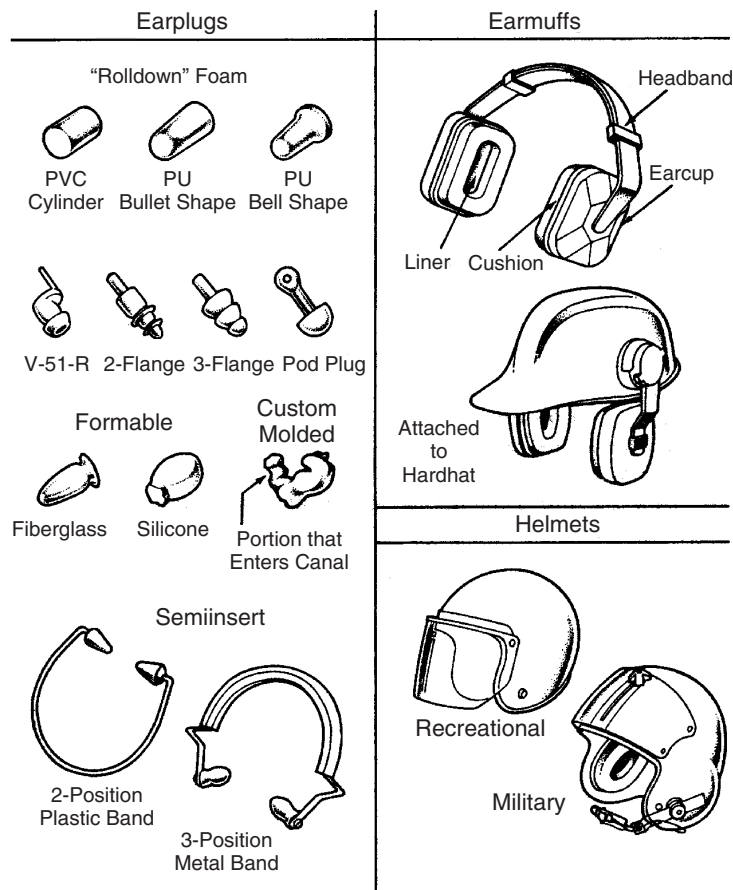


Figure 1 Four basic types of HPDs. (From Berger.<sup>1</sup>)

sound around the HPD.<sup>2</sup> All of these are referred to as “flanking paths.”

2. Although comfort may appear to be a secondary requirement at first glance, it must be realized that an uncomfortable HPD becomes intolerable after prolonged wear and is typically removed, negating any protective benefit it may have. The annoyance produced by noise of very high sound pressure, to some extent, may distract the discomfort caused by ear protectors. Consequently, the requirement of comfort is most acute in a noise of moderate sound pressure, where HPDs are used for psychological rather than for physiological reasons, for example, to eliminate the distraction caused by irregular noise, to reduce noise annoyance, or to facilitate sleep.

3. A third factor, which in itself justifies discarding otherwise satisfactory ear protectors, is a toxic or allergic effect on the skin. An HPD may lead to inflammations that cannot be controlled except by discontinuing its use. Fortunately, by careful selection of materials that contact the skin, nontoxicity is the easiest requirement to fulfill.

4. Whenever the noise level is low enough to permit speech communication and/or hearing of signals, the acoustical performance of the HPD should be such as to assure the highest possible speech intelligibility and audibility. Special devices designed to meet this requirement are discussed in Section 12 herein.

5. Ear protectors are effective only when used correctly. This is more easily achieved when their application is simple, and when they are properly selected for the individual user based on anthropometric size and fit. Sizing and fit issues are commonly encountered with “one size fits all” or multisized earplugs, but also the proper fit of earmuffs depends heavily on their design, such as headband height, width, and compression force on the cushions. If HPDs are difficult to handle and apply, the probability of incorrect use increases, and with it the variability of their protective performance.

6. The durability of an HPD is an economic factor and becomes important when large quantities are purchased. In general, more durable devices are more economical in the long run.

#### 4 COMFORT AND OTHER REQUIREMENTS

**Pressure** Pressure exerted by an HPD on the skin and underlying tissue and bone is probably the most direct cause of discomfort. If the pressure is strong and continues for a relatively long period of time, the pain may become intolerable. Two factors are involved, the total force of the ear protector against the skin and the distribution of the pressure.

The total force exerted by an earplug results from the ratio of its cross-sectional dimensions, the corresponding dimensions of the ear canal, and material density. For instance, a small-diameter earplug is generally more comfortable than a large-diameter one, unless, of course, the smaller earplug is inserted too deeply into the bony part of the ear canal or if it feels unstable as if it will fall out of the ear. The pressure exerted by earmuffs and semi-inserts varies proportionally with the force applied by their supporting means. A helmet creates a more complicated situation, and the total force depends partly on size, weight, and the distribution of head contact points of the helmet's liner cushion.

When the total force is distributed over a large area, the resulting pressure is smaller than when it is concentrated on a few spots. For this reason an earplug shaped to fit the contours of the auditory canal and made of a soft, conformable material that permits individual adaptation is more comfortable than a poorly shaped or noncompliant plug. The same is true for the sealing cushion of an earmuff or a semiinsert. In order to ensure a large area of contact with the skin, earmuffs and semiinserts should not only be of a size and shape compatible with the anatomy, but they should also be made of a compliant material.

When the area of contact between the ear protector and the skin is large, the total force acting on the flesh lining must be limited to a value that permits proper circulation of the blood. A certain amount of pressure on the skin is necessary to hold the ear protector in place and to provide sound attenuation. As the pressure diminishes, the impedance of the skin decreases and the vibration of the ear protector as a rigid body increases. With too little pressure air leaks may be created.

It is difficult to specify the maximum pressure acceptable for earplugs. Experience shows that, on the average, three to five sizes are sufficient to fit most ears, and a few earplugs (e.g., the venerable V-51R), are available in up to five sizes. The largest size that can be tolerated affords the maximum sound attenuation. Most earplugs, however, are designed to be one size fit most, and this quality can be reasonably established with multiflanged polymer earplugs or user-molded foam, wax, or spun fiber devices.

There are several investigators that have studied the effects of pressure and cushion force on comfort, including limits on those parameters (e.g., see the review in Casali and Grenell,<sup>3</sup> but little empirically derived design information currently exists. Pressure on the very sensitive pinna should be avoided as far as possible. Pressure limits have not been specified for semiinserts, but pressure just sufficient to hold

the semiinsert in place (and *not* as the basis for establishing a pneumatic seal) seems to be adequate.

**Weight** The weight of an HPD affects comfort directly because the force of gravity presses the device against the skin and indirectly because the force required to hold the device in place increases as the weight increases. The following weights are suggested: an earplug should weigh on the order of 1 to 5 g, an earmuff or an earphone mounted in a socket below 350 g, and a semiinsert assembly around 18 g. Too little weight is not advisable since sound attenuation, at least for most materials, becomes lower as the weight decreases.

**Temperature** Ambient temperature can affect both the acoustical performance and the comfort of an HPD. Some materials, such as waxes, become very soft at high temperatures, and air leaks and increased sound conduction through the material may result. In other devices, a moderate softening of the material at body temperature may improve the conformability, thus improving the seal and comfort.

Temperature may raise more serious problems with large hearing protectors, such as earmuffs and helmets, than with small ones. By providing heat insulation, they tend to raise the temperature of the head. In a cold climate this may be welcome but in a hot climate it becomes annoying. In addition to the discomfort caused by heat, evaporation of perspiration is almost impossible and buildup of humidity under the HPD occurs. Muff cushions made in part of absorbent materials improve this situation. They have other disadvantages, however.

They typically cannot be disassembled and washed, and if they are not changed frequently they may become unhygienic. Consequently, earmuffs should cover the smallest possible area of the head surface while still accommodating the pinnae; the area of contact with the skin of helmets should also be kept to a minimum; and if possible, ventilation can be provided, especially in the case of muffs with helmet.

**Wearing Time and Comfort** The longer discomfort exists, the more annoying it becomes and the more likely the HPD will be removed. For a short period of time, even hard, poorly shaped earplugs can be tolerated. On the other hand, HPDs that seem quite comfortable during the first minute may become intolerable after a half hour or so. Some particularly high-attenuation earplugs can be tolerably worn during short periods of exposure to intense noise, but only a few are sufficiently comfortable to wear for an 8-h period or during a whole day or night. In addition to the direct discomfort caused by pressure, long wearing periods accentuates the adverse effects of temperature and toxicity.

**Toxicity** Some materials affect the skin chemically and cause inflammation or other allergic reactions. As a matter of fact, any material can probably cause skin irritation under a given set of circumstances. Toxic effects cannot be eliminated completely because

some are the result of an allergy. Materials are available, however, that cause allergy only in rare cases and are otherwise practically free from toxic effects on the skin, even over long periods of use. Polymerized chloroprenes (neoprene) and polyvinyl chloride copolymers (vinylite) are generally nontoxic when compounded with nontoxic plasticizers. Since the testing of new materials takes a great deal of time, it seems advisable, at least for the present, to use these and other materials known from experience to be chemically neutral to the skin.

**Washability** If an ear protector is designed for repeated use, it should be washable. It should be resistant to damage not only due to water and soap but also to antiseptics, such as alcohol. Smooth surfaces of impermeable material lend themselves better to cleaning than do absorbent materials such as chamois or porous materials such as sponge rubber.

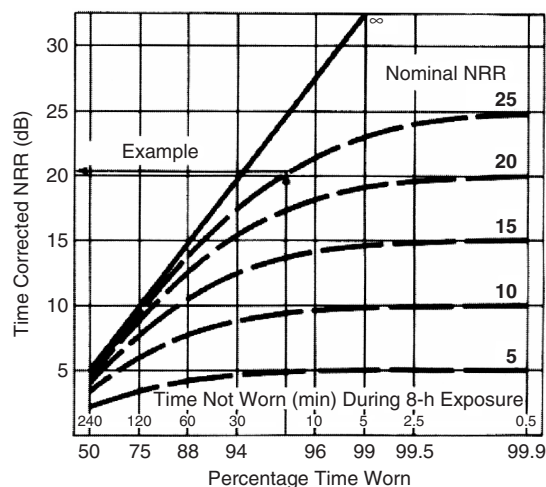
The requirement of washability should not be applied indiscriminately, however. Some earplugs are intended to be thrown away after one use and do not require washing. For some purposes, such as in the food processing industry, disposable earplugs are more readily accepted than "permanent" washable ones. Earmuffs are too expensive to be used only once, but they can be isolated from the skin by a disposable tissue or other inexpensive material, though such materials may impact attenuation.

**Durability** Durability, like washability, is not a universal requirement; for example, it is superfluous for very inexpensive earplugs designed to be used only once. "Permanent" devices, however, which may be less costly in the long run, should last as long as possible. Consequently, they should be reasonably rugged and made of a material resistant to aging. Many factors can speed up the aging process, but the most important seem to be ear wax, perspiration, humidity, light, ozone, and even some active chemicals contained in the air. Materials of the neoprene or vinylite type, when compounded with appropriate ingredients, are resistant to most of these influences and may last for 2 or more years without objectionable changes. Most of the soft resilient materials, however, show a tendency either to contract and harden with time or to expand and become too soft; in either case, the distortion of shape and material breakdown degrades attenuation.

**Ease of Handling** Ease of handling is often slighted; yet it contributes a lot to the performance of an HPD. A complicated device or one that has to be applied with precision may give excellent results in the laboratory but thereafter fail in the field because of incorrect use. The way in which an HPD is to be applied should be as obvious as practicable; its performance should not depend heavily on instructions that dictate precise placement. Three properties facilitate easy placement: mechanical simplicity, symmetry, and adaptability.

## 5 SELECTING HEARING PROTECTION

A correctly selected hearing protector should provide enough noise reduction to remove the risk of hearing



**Figure 2** Effect of percentage of time typical hearing protection is worn on the effective noise reduction experienced by the wearer, conserving 5-dB exchange rate. (From Berger.<sup>1</sup>)

damage (as discussed below), and at the same time allow communication with others and hearing of signals while ensuring reasonable comfort. The selection and the acceptance of an HPD is strongly linked to the comfort it affords. The users should participate in the selection of HPDs. This selection should be based on several pointed aspects, but it should also include the final user opinion.

It should be emphasized that the HPD should be used for the whole time that one is in a noise area. If one removes the protector even for a small percentage of time, such as 5 to 10 min in a whole workday, the protection is sharply reduced, as shown in Fig. 2.

## 6 EVALUATION OF HEARING PROTECTORS

In most countries, the required tests concern primarily noise attenuation, although in some areas, mechanical tests, comfort, and toxicity are also addressed by the testing standards. In all cases known to the authors, evaluation tests comprise in-laboratory tests. In some cases, field tests are used for validation purposes.

### 6.1 Attenuation Tests

Of the various tests on ear protectors, those of sound attenuation at the ear are the most widely known. These tests are still not entirely satisfactory because: (1) the reproducibility of the data from one laboratory to another with sufficient agreement is often lacking, and (2) the results from most test protocols, with the exception of all but the most recent standards (e.g., ANSI S12.6-1997—Method B<sup>4</sup>), are not representative of actual attenuation achieved in the industrial or military workplace.

Most present-day tests use human subjects and psychophysical (listening-based) methods, but efforts continue to develop microphone-based "objective" tests



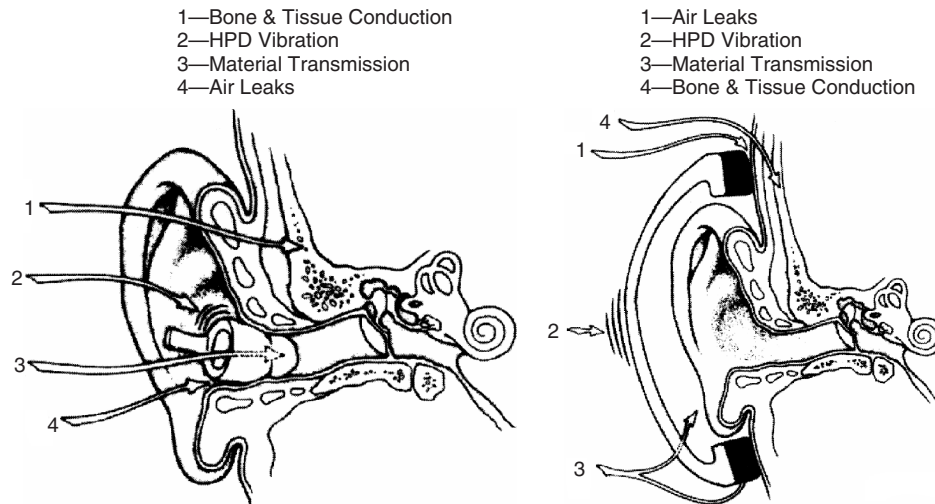


Figure 3 Sound flanking pathways for hearing protectors. (From Berger.<sup>1</sup>)

that can replace the psychophysical-based “subjective” methods. These efforts have largely failed for the following reasons. These include the fact that the sound attenuation provided by an HPD is dependent at least in part on the anatomical and mechanical properties of the human head and ear and how these structures behave when an HPD is applied. Furthermore, the objective tests do not accommodate the real influences of human variability in head/ear size and anthropometry, which greatly affect the performance of the HPD as worn.

## 6.2 Hearing Protector Attenuation

The maximum protection offered by an HPD is dependent on the frequency of the noise; in the most basic sense, the attenuation is much more limited at the low frequencies than the high. Despite the presence of an HPD, noise can still reach the inner ear of the person wearing the hearing protector by one or more of the following pathways (see Fig. 4):

1. Leakage around the protector’s contact with the head (for muffs) or ear canal (for earplug)
2. Vibration of the protector causing sound generation in the outer ear canal
3. Sound transmission through protector materials
4. Bone and tissue conduction through of the head

The four leakage pathways set practical limits to the noise attenuation provided by any ear protector (Fig. 3). The maximum possible attenuation of the protector is unlikely to be achieved for various reasons, for example, protector–wearer coupling seal, but approximate values for wearers of both plugs and muffs are between 40 to 60 dB depending on the frequency bands.<sup>5</sup>

The noise attenuation of a hearing protector is best represented by the *insertion loss* (IL), which is the difference between the sound pressure levels at the outer ear canal with and without the hearing protector.

Working environments are generally semireverberant fields characterized by broad or narrow-band frequencies. Therefore, any test method for measurement of hearing protector attenuation must reasonably represent this situation.

## 6.3 Hearing Protector Attenuation Measurements

Several national and international standards are available for the laboratory determination of hearing protector noise attenuation, mainly the American National Standards Institute (ANSI) standard used in the United States and International Organization for Standardization (ISO) and other recommendations and standards such as EN, OSHA, and NIUSH (see references at end of this chapter) used in Europe.

The method specified by the U.S. Environmental Protection Agency (EPA) for determining (and labeling) the amount of noise attenuation that an HPD provides is based on subjective tests of protectors as worn by listeners rather than objective tests from an electromechanical device. The actual test method is called the real-ear attenuation at threshold (REAT) test, and the techniques for measuring REAT, as presently required by the EPA, are specified in ANSI S3.19–1974,<sup>6</sup> which requires auditory thresholds be obtained from a panel of 10 normal-hearing listeners sitting in diffuse random-incidence sound field. The test signals are pulsed on one-third-octave bands of noise, which have center frequencies of 125, 250, 500, 1000, 2000, 3150, 4000, 6300, and 8000 Hz. Thresholds are determined with listener’s ears open and with their ears occluded by the hearing protector under test, and this is an important point—with the protector fit by an experimenter to obtain an optimal seal. The decibel difference between the open-ear threshold and the occluded-ear threshold at each frequency is the REAT in decibels for that frequency. Each listener is tested

three times with his or her ears open and three times with the ears occluded. Open and occluded tests should be counterbalanced. The REAT values for all 10 listeners are arithmetically summed, and the mean attenuation is calculated for each test frequency. Since there are three REAT values at each frequency for 10 listeners, the average calculated by dividing the grand total by 30 to obtain the grand mean. The standard deviation is also calculated for each test frequency using the number 29 (using  $n - 1$  from the formula for the standard deviation of a sample, where  $n$  is the number of samples) as the denominator, as if 30 separate subjects had provided one REAT each per test frequency.

When a REAT is being determined for the purpose of labeling hearing protectors according to EPA labeling requirements, the protector is fitted into the ear or placed on the head by the experimenter in order to obtain maximum protector performance. Technically, the experimenter-fit described in ANSI S3.19-1974<sup>6</sup> and adopted by the EPA does permit the test subjects to fit the protector themselves (using a fitting noise to adjust the device for maximum attenuation) provided that the experimenter personally checks each installation for good fit and acoustical seal and reinserts or readjusts the protector as necessary. In practice, however, experimenter-fit is generally taken to mean that the experimenter always personally fits the device under the test.

The European community also relies upon REAT for determining hearing protector attenuation (EN 24869<sup>7</sup> and EN 352<sup>8</sup>). However, there are differences in methods between the ISO and ANSI standards. The number of subjects required in ISO 4869-1<sup>9</sup> is 16 rather than 10, and each subject is tested only once with ears open and once with ears occluded to produce one REAT at each test frequency. In addition, ISO 4869-1 relies upon a subject-fit in which the listeners fit the hearing protectors using a fitting noise to adjust the protectors for best perceived attenuation but without feedback from the experimenter. Because of the lack of intervention by the experimenter in fitting the protector on the test subject, when hearing protectors are tested for European markets, the reported REATs are usually lower than when they are tested for distribution in the United States under ANSI S3.19-1974, Experimenter-Fit.<sup>6</sup>

In 1997, a new ANSI standard was approved (ANSI S12.6-1997<sup>4</sup> [Method A and B]). Method B, subject-fit protocol utilizes audiometrically qualified subjects who are trained and experienced in psychophysical threshold testing but *naïve with respect to use of hearing protectors*. These subjects fit the protectors on themselves after reading *only* the manufacturer's instruction, and they receive no assistance whatsoever from the experimenter. Method B has been demonstrated to provide data that approximate the protection that can be attained by a group of informed users in the workplace within a well-managed and well-supervised hearing conservation program.<sup>10</sup> The octave band results measured using the new standard can be converted to a single number called noise reduction ratio for subject fit (NRRsf).<sup>11</sup> This number is the single-number rating (SNR) for 84% of the population (see ISO 4869-2<sup>9</sup>)

less 5 dB. The NRRsf may be subtracted from the A-weighted sound pressure level (or  $L_{eq}$ ) exposure to give directly the protected level for 84% of the users.<sup>12</sup>

#### 6.4 Single-Number Ratings of Attenuation

The mean attenuation and standard deviations as reported by HPD suppliers have been used to calculate all ratings of protectors' performance according to the various methods in a compendium published by the National Institute for Occupational Safety and Health (NIOSH).<sup>13</sup>

The NRR is a single-number rating method that attempts to describe an HPD based on how much the overall (broadband) noise level is reduced by the device. The NRR is described in 40 CFR part 211 EPA Product Noise Labeling Law, subpart B hearing protective devices<sup>14</sup> and was adopted by the EPA from Method 2 in the first NIOSH compendium.<sup>15</sup>

The NRR is intended to be used for calculating the exposure under the HPD by subtracting it from the C-weighted environmental noise exposure level. Thus, if a protector has an NRR of 17 dB and it is used in an environmental noise level of 95 dB time-weighted average for an 8-h day, the noise level entering the ear could be expected to be 78 dB or lower in 98% of the cases. An alternative use of the NRR is with A-weighted noise level exposure measurements, wherein the NRR can be applied if 7 dB is first subtracted from its value. Thus, for the same protector above, if it is used at an environmental A-weighted noise level of 90 dB, then the A-weighted noise level entering the ear is  $90 - (17 - 7) = 80$  dB.

In Europe, rating systems (ISO/DIS 4869-1992<sup>9</sup>) have been adopted using a single number rating (SNR), the high-middle-low (HML) rating, and the assumed protection value (APV). These methods are based on REAT values measured according to ISO 4869-pt.1-1992<sup>9</sup> for one-third-octave bands in octave steps from 63 to 8000 Hz (when data for 63 Hz are not present, the summation occurs from 125 to 8000 Hz). All of these methods provide the user with the option of selecting a protection performance value, which is an indication of the percentage of test subjects who achieved the specified level of noise reduction.

#### 6.5 Headband Force of Earmuffs

As discussed above, with earmuffs, comfort will suffer if the head band force is too large. However, sufficient force is necessary for a quality fit of the hearing protector, which is in turn needed for establishing sufficient sound attenuation. Therefore, it is necessary to measure the headband force and also to use the measured force for quality control and other muff evaluations, such as useful work life. ANSI S3.19-1974<sup>6</sup> shows a mechanical device for headband force measurements. The EN 352-1,<sup>8</sup> 1993, standard shows a more accurate, mechanical/electric device. There is between 2 and 5% variation in the measured force. The applied pressure is actually more important than the headband force for acceptability comfort.<sup>3</sup> Hearing protectors with broad cushions will give less pressure with the same force.

### 6.6 Simultaneous Use of Two HPDs (Double Hearing Protection)

Many noise situations exist where the use of a single protector is not sufficient, particularly in the military and in a few industries. In these cases the use of "combined" protection (earmuff worn over earplugs) should be considered. However, because such noise exposures are usually very severe, extreme care is required and the performance of the combination should be known before use. Tests have shown that the performance of combination protection is not the arithmetic sum of the protectors' attenuation but instead, is something on the order of 5 to 15 dB more than the performance of the better of the two HPDs involved (EN 458).<sup>16</sup>

Berger et al. (page 321)<sup>17</sup> showed that at and above 2 kHz most earplug-plus-muff combinations provided attenuation that is approximately limited by the bone conduction flanking path (see Fig. 10.20 in Berger et al.<sup>18</sup>). Any extra attenuation gained varied between 0 and 15 dB for the better of the individual devices. The increase in NRR is between 3 and 10 dB when compared with the higher of the two individual protectors.

## 7 CONSIDERATIONS IN THE SELECTION AND USE OF HEARING PROTECTORS

Although the demonstrated noise reduction capability is arguably the most important factor to consider in the selection of hearing protection devices, several other points are also very important. Studies by Casali<sup>19</sup> and Riko and Alberti<sup>20</sup> on the effectiveness of hearing protectors suggest that workers are most likely to demonstrate consistent wearing of devices that are comfortable and easy to insert, regardless of the amount of attenuation they provide. Additional thought must be given to the worker's physical limitations, including concurrent use of safety glasses or eyeglasses, the need for the worker to hear warning signals, and the need to communicate verbally. The environmental conditions of the workplace, such as temperature, confined working spaces, or the wearing of additional personal protective devices (hardhats, safety glasses, respirators, etc.), also warrant consideration. The durability (shelf life or useful life) and hygienic issues posed by each type of HPD, as well as the length of time it will be worn, are also factors that should not be overlooked. Custom-molded earplugs are a viable HPD option for many individuals, but it is important to ensure both the expertise of those who will obtain the impression as well as those who will manufacture the final earplug.

To ensure that a worker receives the most effective attenuation from the use of an HPD, the worker should be trained in the use, care, and maintenance of the device. All HPDs, including user-molded earplugs and adjustable earmuffs, require good instruction. This training should be updated on a regular basis and should be provided by appropriately trained personnel.

Comfort is a personal matter. Many users would say that HPDs, as a class of personal protection equipment

(PPE), are generally uncomfortable. But with careful selection, fitting, and consideration of the environment of use, acceptable HPDs can in fact be matched to users. It is generally reasonable advice that a choice of HPDs that are adequate for the exposures faced should be provided to each worker. In fact, this is required by the OSHA hearing conservation amendment.<sup>21</sup>

Hearing protectors cannot be depended upon for complete protection unless they are selected properly and worn adequately and properly throughout the time of exposure. But, comfort can work against protection achieved; for example, small earplugs or weak headband springs on earmuffs may be more comfortable but offer low noise attenuation.

## 8 REAL-WORLD ATTENUATION

Standard laboratory methods (ANSI S3.19–1974,<sup>6</sup> ANSI S12.6–1984,<sup>22</sup> and ISO 4869 Pt 1–1992<sup>9</sup>) were developed to produce a measurement of attenuation for an optimum-fit condition. Since the late 1970s, researchers in various laboratories around the world<sup>13</sup> have been investigating the amount of attenuation workers typically receive. They found workers generally received much less attenuation than the optimum-fit laboratory methods predict. The magnitude of the difference was from 22 to 84% less attenuation for the real-world setting than for laboratory setting. Researchers of the ANSI working group have worked with researchers from other laboratories to develop and test laboratory methods that give measurements of hearing protector attenuation, which are more reflective of real-world performance and remain consistent from laboratory to laboratory. The new method provides very consistent interlaboratory results, much more consistent than those possible using the methods of ANSI S3.19–1974.<sup>6</sup> This latest standard, ANSI S12.6–1997 (B),<sup>4</sup> provides mean attenuation values that are much lower than optimum-fit attenuation and more in accord with real-world results, while maintaining a reasonable standard deviation.

## 9 PROBLEMS WITH HEARING PROTECTORS

Comfort, wearability, and durability are just as important, if not more important, than a few decibels more attenuation. Provided that the attenuation is reasonable, human factors issues usually make the difference in HPD selection. Some of these factors include hygiene, discomfort, effects on communication, effect on directional localization and distance of warning sounds, and safety in general. In particular, many workers complain that HPDs compromise their ability to hear fellow workers, public address system announcements, warning and other signals, and auditory cues from their machines (which they may rely on for carrying out their work). This is one of the major reasons for the development of augmented HPDs, which are discussed in Section 12.

## 10 COSTS OF HEARING PROTECTORS

The cost of hearing conservation by means of personal hearing protection should consider the following factors:

1. Initial cost of muffs and/or plugs
2. Management and administrative costs of ordering, documentation, storage, issuing, fitting, training, and assessment of effectiveness in a hearing conservation program
3. Replacement of the worn parts
4. Education in and encouragement toward the use of hearing protectors, correctly and consistently, using videos, lectures, posters, audiometric feedback, and the like

These costs can be compared with other methods of engineering noise reduction, say for the period of a 5- or 10-year hearing conservation program.

## 11 REPORTING PROTECTIVE FAILURES

Every employee should learn to be personally responsible for reporting HPD failures or other related noise exposure problems, which may include:

- Damaged HPDs
- Inflammation of the ear that may be due to HPD usage
- Overly compromised hearing of necessary workplace signals or speech
- Changes in conditions of machinery and equipment because of wear or lack of maintenance
- Any change in the perceived noise exposure due to moving of machines, new machines, and/or altered working methods and work practices

Ultimate responsibility for documenting these problems should be given to the health and safety representatives, to foremen and supervisors, and/or to the management staff. Direct and prompt action should be taken to mitigate or correct the failures or problems within the company's noise plan. Of course, reporting protective failures must not affect the worker's social status, job assignment, or compensation in the workplace.

## 12 AUGMENTED VERSUS CONVENTIONAL PASSIVE HPDs

So-called *conventional* HPDs constitute the vast majority of HPDs, and these devices have been the primary subject of this chapter to this point. These devices achieve attenuation of noise strictly by passive means without the use of dynamic mechanical elements or electronic circuitry and are effective protection against nearly all industrial noises and many military noises, if properly selected and worn. However, due to the very nature of the attenuation that conventional HPDs provide, signals and speech are attenuated no differently than noise of the same frequencies. Furthermore and by design, conventional HPDs reduce noise at the ear solely by passive means, and the attenuation provided is the same regardless of the incident sound pressure level, that is, the devices are *level independent* or *amplitude insensitive*. Although the devices are currently tested at the threshold of hearing using REAT

standards (e.g., ANSI S3.19–1974; Experimenter-Fit in the U.S.<sup>6</sup>), the attenuation achieved at threshold remains the same (or linear) throughout most of the dynamic range of noises normally encountered in industry and other settings. Exceptions include extremely high impulses of noise that may excite the HPD on the human head, an example being the separation of an earmuff cushion from the side of the head as an explosion's blast passes it. It is also noteworthy that most conventional HPDs have spectral attenuation curves that increase (more attenuation) nonlinearly as a function of sound frequency as described above.

A major impetus for the development of augmented HPDs has been the sometimes negative influence that conventional HPDs have on the hearing ability of users.<sup>23</sup> They have often been implicated in compromised auditory perception, degraded signal detection, and reduced speech communication abilities. Depending upon situational demands, these effects can create hazards for the wearer, or at the very least, resistance to use by those in need of hearing protection.

### 12.1 HPD Effects on Hearing Speech and Signals

Users may reject hearing protection if it compromises their hearing to an extent where sounds no longer appear natural, signals cannot be detected, and/or speech cannot be understood. In some cases, too much attenuation may be provided by an HPD for a particular noise situation, with the concomitant effect that the user's hearing is unnecessarily degraded. In very lay terms. This is commonly referred to as *overprotection*.

Overall, the research evidence on normal hearers generally suggests that conventional passive HPDs have little or no degrading effect on the wearer's understanding of external speech and signals in ambient A-weighted sound pressure levels above about 80 dB and may even yield some improvements with a crossover between disadvantage to advantage between 80 and 90 dB.<sup>23</sup> However, HPDs do often cause increased misunderstanding and poorer detection (as compared to unprotected conditions) in lower sound pressure levels, where HPDs are not typically needed for hearing protection anyway but may be applied for reduction of annoyance. In intermittent noise, HPDs may be worn during quiet periods so that when a loud noise occurs, the wearer will be protected. However, during those quiet periods, the conventional passive HPDs typically reduce hearing sensitivity.

Noise- and age-induced hearing losses generally occur in the high-frequency regions first, and for those so impaired, the effects of HPDs on speech perception are not clear-cut. Due to their already elevated thresholds for mid- to high-frequency speech sounds being further raised by the protector, hearing-impaired individuals are usually disadvantaged in their hearing by conventional HPDs. Although there is no consensus across studies, certain reviews have concluded that sufficiently hearing-impaired individuals will usually experience additional reductions in communication abilities with conventional HPDs worn in noise.<sup>24</sup>

Conventional passive HPDs cannot differentiate and selectively pass speech or nonverbal signal (or speech) energy versus noise energy at a given frequency. Therefore, conventional HPDs do not improve the speech/noise ratio in a given frequency band, which is the most important factor for achieving reliable detection or intelligibility. Since conventional HPDs attenuate high-frequency sound more than low-frequency sound, thereby attenuating the power of consonant sounds that are important for word discrimination, which lie in the higher frequency range, while also allowing low-frequency noise through, they enable an associated upward spread of masking to occur if the penetrating noise levels are high enough.

Since some of the high-frequency binaural cues (especially above about 4000 Hz) that depend on the pinnae are altered by HPDs, judgments of sound direction and distance may be compromised. Earmuffs, which completely obscure the pinnae, radically interfere with localization in the vertical plane and also tend to cause horizontal plane errors in both left-to-right and front-to-back judgments.<sup>24</sup> Earplugs may result in some front-back judgment errors but generally cause fewer localization problems than muffs, although exceptions do exist.

The safety professional often faces a dilemma in selecting HPDs for the workforce that provides adequate attenuation for the noise threat at hand, but also that does not provide so much attenuation that the worker cannot hear important signals and/or speech communications. This is the dilemma of *underprotection* versus *overprotection*.

To reduce worker complaints, and to some extent mitigate the underprotection versus overprotection dilemma, certain features have been developed and integrated into HPDs, as follows.

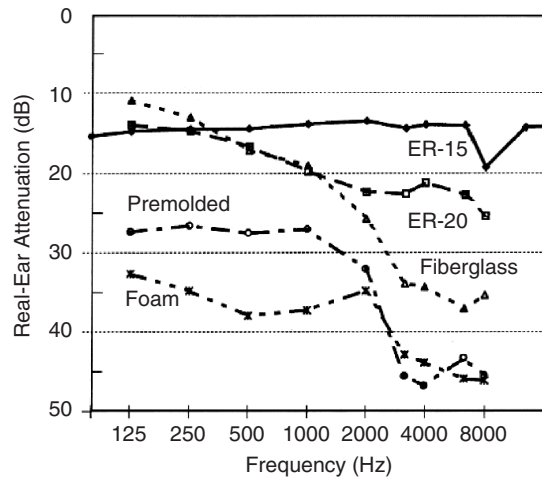
### 12.2 Uniform (Flat) Attenuation HPDs

Conventional HPDs generally increase attenuation profile as a function of frequency and, therefore, create a frequency imbalance from the listener's perspective. This is because the relative amplitudes of different frequencies are heard differently than they would be without the HPD, and, thus, broadband acoustical signals are heard as spectrally different from normal; in other words, usually as more *bassy*. Thus, the spectral quality of a sound is altered, and sound interpretation, which is important in certain jobs (e.g., machining, mining, and performing music), that relies on auditory inspection, may suffer as a result.

In an attempt to counter these effects, flat- or uniform-attenuation HPDs such as the ER-15 Musician's earplug or the ER-20 Hi-Fi earplug have been developed.<sup>23</sup> These devices utilize acoustical networks to provide essentially flat attenuation over the range of frequencies from 125 to 8000 Hz (see Fig. 4).

### 12.3 Level-Dependent HPDs

Level-dependent (also sometimes called *amplitude-sensitive*) HPDs are designed to intentionally change their attenuation characteristics as the incident noise level changes (increasing attenuation as noise level

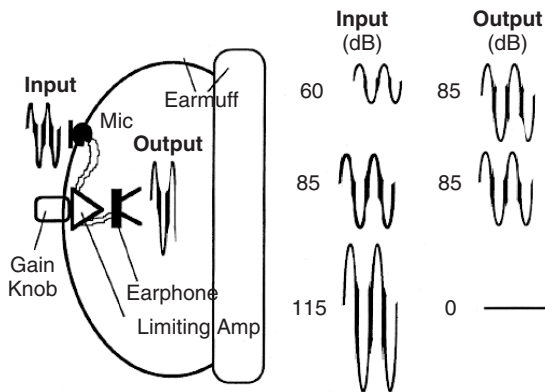


**Figure 4** Attenuation characteristics of two flat-attenuation earplugs and for standard premolded, fiberglass, and foam earplug. (From Berger.<sup>1</sup>)

increases). Such devices may be passive (relying on acoustical networks or mechanical valves for their unique attenuation characteristics) or electronic. While most of these devices are based on earmuff designs (e.g., the EAR Ultra 9000), a few level-dependent earplugs exist (e.g., the Gunfender and the U.S. Army's Combat Arms Earplug). Typically, these devices offer little or no attenuation at low to moderate noise levels; however, as ambient noise levels increase, their attenuation increases to some maximum level. The Army's Combat Arms Earplug reduces impulse noise levels of a howitzer (170 dB Peak to an acceptable level) while permitting normal speech and commands to be understood.

**Passive Level-Dependent HPDs** In passive level-dependent HPDs, a valve or sharp-edged orifice provides a controlled leakage path into the HPD. At low noise levels, the passive attenuation of the device behaves as that of a *leaky protector*, offering minimal attenuation below about 1000 Hz. This minimal attenuation is all that is available to protect the wearer's hearing at sound pressure levels below about 110 dB. Since such devices are intended to be used primarily in intermittent impulsive noise, this should not be a problem as long as the *off* periods are relatively quiet (e.g., below about an A-weighted sound pressure level of 85 dB). At elevated sound pressure levels (above about 110 to 120 dB, as might occur during a gunshot), the flow through the orifice changes from laminar to turbulent, effectively closing the orifice, thus increasing the attenuation of the device. An additional advantage is that some orifice-based devices offer roughly flat attenuation.<sup>25</sup>

**Electronic Level-Dependent HPDs** These battery-powered electronic HPDs are typically earmuff based and incorporate a microphone and output-limiting



**Figure 5** Example operating characteristics of an electronic level-dependent sound transmission earmuff (input is the ambient A-weighted sound pressure level in the environment and output is the earphone output).

amplifier to transmit external sounds to earphones mounted within the earcups. The electronics can be designed to pass and boost only certain sounds, such as the critical speech band or critical warning signal frequencies. Typically, the limiting amplifier maintains a predetermined (in most cases user-adjustable) gain, often limiting the earphone output to about an A-weighted sound pressure level of 82 to 85 dB, unless the ambient noise reaches a cutoff A-weighted sound pressure level of 115 to 120 dB, at which point the electronics cease to function (Fig. 5). At this point, the device essentially becomes a passive HPD.

Ideally, a level-dependent sound transmission HPD should exhibit flat frequency response and distortion-free amplification (without spurious electronic noise) across its passband, as well as high signal-to-noise (S/N) ratios at levels below its predetermined cutoff level. The cutoff level itself should be safe (to ensure that transmitted sound does not overexpose the wearer), achieved quickly (i.e., with little or no delay), and have a sharp attenuation transition without transients or oscillations. The passband of the electronics should be adequate to accommodate desired signals but not so wide as to pass unnecessary and undesirable noise to the listener. The external microphones (two, one for each ear to permit dichotic listening to aid in sound localization) should be minimally affected by wind or normal movement of the head. Such devices have the potential for improving the hearing of *hearing-impaired* listeners in quiet or moderate noise levels, acting much like a user-adjustable hearing aid. However, normal-hearing listeners may not realize similar benefits due to the potential for the residual electronic noise to mask desired signals. Like their passive counterparts, some of these devices are well suited for impulsive noise, but less so for sounds with long on durations, which can produce objectionable distortions.

Two example studies on electronic level-dependent earmuffs<sup>26,27</sup> have, respectively, demonstrated that (1)

several example devices exhibited adequate protection against most gunfire noise exposures, and (2) user-preferred settings of the volume control did not result in an appreciable increase in noise exposure dose over that experienced with the electronics turned off. More research on level-dependent HPDs is needed on the issues of protection from sharp transient impulses, such as high-caliber weapons and pile drivers, and on the efficacy of these devices in improving hearing ability in low-to-moderate level noises. On the issue of testing these HPDs against sharp impulse noise of very high levels, REAT testing is not applicable, so acoustical manikins exposed to noises produced by special apparatus for producing shock waves are necessary.<sup>28,29</sup>

## 12.4 Active Noise Reduction (ANR) HPDs

Active noise reduction relies on the principle of destructive interference of equal amplitude, about 180° out-of-phase sound waves at a given point in space; in the case of hearing protectors, the cancellation is established at, or very near, the outer ear. ANR has been incorporated into two types of at-the-ear systems: (1) those designed solely for hearing protection and (2) those designed for one- or two-way communications. Both types are further dichotomized into open-back (or supraaural) and closed-back (or circumaural earmuff) variations. In the former, a lightweight headband connects ANR microphone/earphone assemblies that are surrounded by foam pads that rest on the pinnae. In that there are no earmuff cups to afford passive protection, the open-back devices provide only active noise reduction. If there is an electronic failure, no protection is provided by the open-back device. Closed-back devices, which represent most ANR-based HPDs, are typically based on a passive noise-attenuating earmuff that houses the ANR transducers and, in some cases, the ANR signal processing electronics. If backup attenuation is needed from an ANR HPD in the event of an electronic failure of the ANR circuit, the closed-back HPD is advantageous due to the passive attenuation established by its earcup.

**Analog and Digital ANR HPDs** Detailed descriptions of the technology behind ANR electronic feedback/feedforward control systems are beyond the scope of this chapter but may be found in Casali and Robinson.<sup>30</sup> Basically, in a typical analog device, a closed-loop, feedback system is used that receives input from a sensing microphone that detects the noise that has penetrated the passive barrier posed by an earmuff. The signal is then fed back through a phase compensation filter, which reverses the phase, to an amplifier that provides the necessary gain, and finally is output as an *antinoise* signal through an earphone loudspeaker to effect cancellation inside the earcup. Digital technology, with its advances in speed, power, reliability, and miniaturization of signal processing components, has demonstrated strong promise for improving the capabilities of ANR-based HPDs, particularly in regard to precise tuning of the control system via software for optimizing the cancellation of specific sound frequencies.



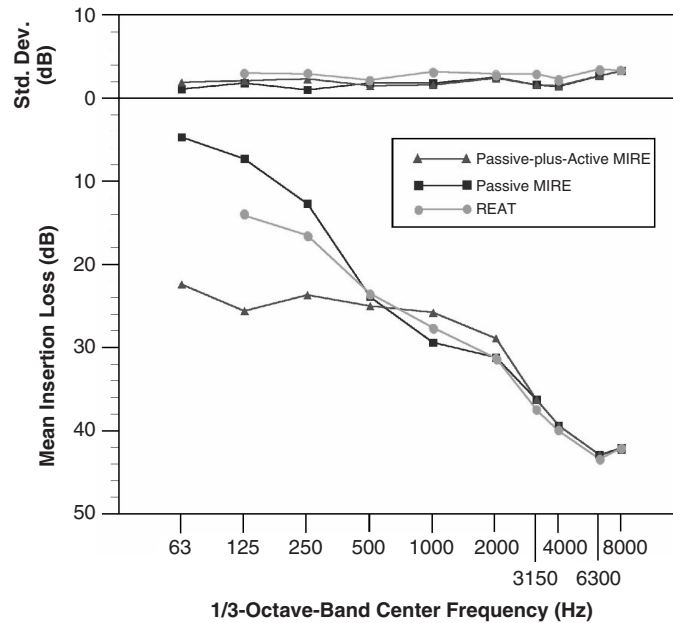


Figure 6 Attenuation of the NCT PA-3000 closed-back ANR headset. (From Casali and Robinson.<sup>33</sup>)

Due to the phase shifts that can be attributed to transducer (i.e., microphone, earphone) location differences, as well as the possibility of throughput delays in signal processing, establishing the correct phase relationship of the cancellation signal and noise becomes more difficult as the bandwidth of the noise increases; therefore, ANR has typically been most effective against *low-frequency* noise.

In certain types of noises, especially those characterized by high overall levels and/or frequency content that is heavily skewed toward frequencies of less than 1000 Hz, ANR-based hearing protectors may offer some warning signal detection advantages over HPDs with weaker low-frequency attenuation; however, these improvements are likely to be very user- and HPD-specific.<sup>31</sup> Part of the reason for the potential advantage is that in severe low-frequency noise, the ANR may serve to prevent the upward spread of noise masking into the warning signal's bandwidth.

**ANR HPD Attenuation and Testing/Labeling Issues** At present, standardized attenuation data and NRR ratings are not available for ANR hearing protectors. Microphone-in-real-ear (MIRE) testing (e.g., using ANSI S12.42-1995<sup>32</sup>) can be used to measure the passive (ANR off) and total (ANR on) attenuation of the device. The active component of the attenuation can then be computed using the following relationship, with each term measured in decibel attenuation:

$$\text{Active component} = \text{MIRE total} - \text{MIRE passive}$$

REAT or MIRE testing can be used to quantify, for performance testing purposes, the passive component

of the total attenuation, but the choice of method can affect the data. For example, MIRE attenuation at low frequencies is lower than REAT attenuation due to the physiological noise masking effects on occluded thresholds that occur in REAT testing. In addition, MIRE, unlike REAT, does not account for the bone conduction flanking path. Finally, passive attenuation is often decreased in the middle frequencies (from about 1000 to 3000 Hz) when the ANR circuit is turned on (i.e., the electronics produces and/or amplifies noise, which increases the noise level under the protector).

Typical REAT and MIRE attenuation for an earmuff-based ANR HPD is shown in Fig. 6. Readily apparent in the figure is the difference between the MIRE and REAT attenuation at 125 and 250 Hz. This difference is likely due to physiological noise masking the test stimulus during the REAT test. Also evident in the figure is the slight reduction in total attenuation at 1000 and 2000 Hz when the ANR device is turned on. In general, the depicted ANR muff has enhanced low-frequency attenuation and good mid range and high-frequency performance as well. However, even a well-designed large-volume ANR earmuff such as the one in Fig. 5 cannot typically outperform, on a purely attenuation basis, a well-fitted (and less expensive) foam earplug covered by a quality passive earmuff.<sup>23</sup> Consequently, some manufacturers of ANR-based devices distinguish their products by features and parameters other than attenuation performance, such as comfort and frequency response.

**Current ANR HPD Applications** Although ANR devices cannot currently be sold in the United States

under EPA labeling regulations as *hearing protectors* (except as to their passive attenuation only) due to the lack of appropriate ANR testing standards and labeling regulations, they are being used for various purposes in both the public and private sector. ANR headsets are sold to reduce noise annoyance (airline passenger and personal stereo headsets), as communications headsets for commercial, military, and civilian aviation, and used to combat severe noise environments in the military (particularly in armored vehicles). Special-purpose ANR devices are also (or have been) commercially available for telephone operators and telemarketers, to reduce patient noise exposure in magnetic imaging machines, and even to reduce siren noise for emergency vehicle crews. There is some disagreement in the hearing protection scientific community as to the potential for the application of ANR HPDs to industrial noise markets (for which low-frequency noise is *not* the norm) and, therefore, whether an NRR-like rating is really necessary.

### 12.5 Adjustable Attenuation HPDs

To help overcome the problem of overprotection in moderate noise environments, earplug designs have recently been developed that allow the user some level of control over the amount of attenuation achieved. These devices incorporate a leakage path that is adjustable via the setting of a valve that obstructs a tunnel or "vent" cut through the body of the plug, or via selection from a choice of available filters or dampers that are inserted into the vent.

The Dutch Ergotec Varifone is an example of an adjustable-valve design that is constructed from an acrylic custom-molded impression of the user's ear canal. According to the manufacturer's data, below 500 Hz the attenuation adjustment range is approximately 20 to 25 dB, with a maximum attenuation of about 30 dB at 500 Hz. At higher frequencies, the range of adjustment decreases, while the maximum attenuation attainable increases slightly. An example of a selectable-damper design is the Sonomax SonoCustom, manufactured in Canada. The Sonomax device has a variety of different attenuation dampers that provide the opportunity for discretely variable attenuation in a single device. Furthermore, the SonoCustom HPD is sold as a system with a probe tube microphone test apparatus that verifies the amount of attenuation achieved via MIRE techniques on each user as they are fit with the product.

There are two important distinctions between passive adjustable-attenuation HPDs and passive level-dependent HPDs discussed earlier. The former require user setting to effect attenuation changes, and the attenuation, once selected, is essentially independent of incident sound pressure level. Level-dependent devices, on the other hand, react automatically to changes in incident sound pressure levels, and the user typically has no control over the change in attenuation.

The adjustable attenuation class of HPD affords much flexibility in product design/development in that they can be fitted with *modular* augmentations, and

this is a major advantage in that these relatively expensive and personalized (i.e., custom- or semi-custom-molded) earplugs can be adapted to changing user needs and different noise environments. Filter-based devices can be tuned for specific environments or tuned to pass speech or other critical bands necessary for specific jobs. As this technology matures, the potential exists that additional electronic augmentations can also be incorporated into the devices (e.g., noise suppression, electronic filtering, closed-loop attenuation control, hearing assistive circuits, automatic gain control, etc.). This capability offers promise for improving the hearing ability of HPD users in noise environments over that which would be attained with conventional HPDs alone. Furthermore, there is much promise for "tuning" this type of HPD to optimize its characteristics for the individual user.

### REFERENCES

1. E. H. Berger, Hearing Protection Devices, in *The Noise Manual*, 5th ed., E. H. Berger, L. H. Royster, J. D. Royster, D. P. Driscoll, and M. Layne, Eds., American Industrial Hygiene Association, Fairfax, VA, 2000, pp. 379–454.
2. E. H. Berger and J. G. Casali, Hearing Protection Devices, in M. Valente, H. Hosford-Dunn, and R. J. Roeser, Eds., *Audiology: Diagnosis, Treatment Strategies, and Practice Management*, Thieme Medical, New York, 2000, pp. 669–689.
3. J. G. Casali and J. F. Grenell, Noise-Attenuating Earmuff Comfort: A Brief Review and Investigation of Band-Force, Cushion, and Wearing-Time Effects, *Appl. Acoust.*, Vol. 29, 1990, pp. 117–138.
4. American National Standards Institute, ANSI S12.6–1997, *Methods for Measuring the Real-Ear Attenuation of Hearing Protectors*, ANSI, New York, 1997.
5. E. H. Berger, W. D. Ward, J. C. Morrill, and L. H. Royster, *Noise and Hearing Conservation Manual*, American Industrial Hygiene Association (AIHA), Fairfax, VA, 1986.
6. American National Standards Institute, ANSI S3.19–1974, *Method for the Measurement of Real-Ear Protection of Hearing Protectors and Physical Attenuation of Earmuffs*, ANSI, New York, 1974.
7. EN 24869 Pt. 1, Sound Attenuation of Hearing Protectors—Part 1—Subjective Method of Measurement. EN 24869 Pt. 2, Estimation of Effective A-Weighted Sound Level of Hearing Protectors When Worn. EN 24869 Pt. 3, Measurement of Insertion Loss. EN 24869 Pt. 4, Measurement of the Sound Attenuation of Amplitude Sensitive Muff.
8. EN 352 Part 1, Hearing Protectors—Safety Requirements & Testing—Part 1: EarMuffs. EN 352 Part 2, Hearing Protectors—Safety Requirements & Testing—Part 2: Earplugs. EN 352 Part 3, Hearing Protectors—Safety Requirements & Testing—Part 3: Earmuff Attached to Industrial Safety Helmet. EN 352 Part 4, Hearing Protectors—Safety Requirements & Testing—Part 4: Level Dependent Earmuffs.
9. International Organization for Standardization, ISO 4869-1, *Acoustics, Measurement of Sound Attenuation of Hearing Protectors—Subjective Method*, Geneva, Switzerland.
10. E. H. Berger, J. R. Franks, A. Behar, J. G. Casali, C. Dixon-Ernst, R. W. Kieper, C. J. Merry, B. T. Mozo, C.



- W. Nixon, D. Ohlin, J. D. Royster, and L. H. Royster, Development of a New Standard Laboratory Protocol for Estimating the Field Attenuation of Hearing Protection Devices, Part III: The Validity of Using Subject-Fit Data," *J. Acoust. Soc. Am.*, Vol. 103, No. 2, 1998, pp. 665–672.
11. E. H. Berger and L. H. Royster, In Search of Meaningful Measures of Hearing Protector Effectiveness, 21st Annual Conference of the NHCA, San Francisco, CA, 1996.
  12. S. N. Y. Gerges, *Protetores Auditivos* (in Portuguese), NR Editora, Florianopolis, Santa Catarina, Brazil, 2003.
  13. J. R. Franks, C. R. Themann, and C. Sherris, *The NIOSH Compendium of Hearing Protection Devices*, U.S. Department Of Health and Human Services, Public Health Services, Center for Disease Control and Prevention, Atlanta, GA, 1994.
  14. Environmental Protection Agency, 40 CFR Part 211-Product Noise Labeling, Subpart B, Hearing Protective Devices, 44 *Fed. Reg.* 56139–56147, 1979.
  15. P. Kroes, R. Fleming, and B. Lempert, List of Personal Hearing Protectors and Attenuation Data, NIOSH Technical Report, HEW Publication No. 76–120, 1975.
  16. EN 458, Hearing Protectors—Recommendation for the Selection, Use, Care and maintenance—Guidance Document.
  17. E. H. Berger, Laboratory Attenuation of Earmuffs and Earplugs Both Singly and in Combination, *Am. Ind. Hyg. Assoc. J.*, Vol. 44, No. 5, 1983, pp. 321–329.
  18. E. H. Berger, L. H. Royster, J. D. Royster, D. P. Driscoll, and M. Layne, *The Noise Manual*, 5th ed., American Industrial Hygiene Association (AIHA), Fairfax, VA, 2000.
  19. J. G. Casali, Comfort: The "Other" Criterion for Hearing Protector Design and Selection, in *Proceedings of the 1992 Hearing Conservation Conference*, National Hearing Conservation Alliance, Greenwood Village, CO, pp. 47–53.
  20. S. M. Abel, P. W. Alberti, and K. Riko, User Fitting of Hearing Protectors: Attenuation Results, in *Personal Hearing Protection in Industry*, P. W. Albert, Ed., Raven Press, New York, 1982, pp. 315–322.
  21. OSHA, 29CFR1910.95, Occupational Noise Exposure; Hearing Conservation Amendment; Final Rule, Occupational Safety and Health Administration, Code of Federal Regulations, Title 29, Chapter XVII, Part 1910, Subpart G, 48 FR 9776–9785, Washington, DC, *Fed. Reg.*, 1983.
  22. American National Standards Institute, ANSI S12.6–1994, *Methods for Measuring the Real-Ear Attenuation of Hearing Protectors*, ANSI, New York, 1984.
  23. J. G. Casali, and E. H. Berger, Technology Advancements in Hearing Protection: Active Noise Reduction, Frequency/Amplitude-Sensitivity, and Uniform Attenuation, *Am. Ind. Hyg. Assoc. J.*, Vol. 57, 1996, pp. 175–185.
  24. A. H. Suter, The Effects of Hearing Protectors on Speech Communication and the Perception of Warning Signals, (AMCMS Code 611102.74A0011), U.S. Army Human Engineering Laboratory, Aberdeen Proving Ground, MD, 1989.
  25. C. H. Allen and E. H. Berger, Development of a Unique Passive Hearing Protector with Level-Dependent and Flat Attenuation Characteristics, *Noise Control Eng. J.*, Vol. 34, No. 3, 1990, pp. 97–105.
  26. W. J. Murphy and J. R. Franks, Do Sound Restoration Earmuffs Provide Adequate Protection for Gunshot Noise? *J. Acoust. Soc. Am.*, Vol. 112, No. 5, pt 2, 2002, p. 2294.
  27. J. G. Casali and W. H. Wright, Do Amplitude-Sensitive Hearing Protectors Improve Detectability of Vehicle Backup Alarms in Noise? in *Proceedings of the Human Factors and Ergonomics Society 39th Annual Meeting*, Human Factors and Ergonomics Society, San Diego, CA, Oct, 7–11, 1995, pp. 994–998.
  28. F. Vergara, S. N. Y. Gerges, and R. S. Birch, Objective Measurements for the Assessment of Hearing Protector Attenuation at High Level Impulsive Noise, *J. Acoust. Soc. Am.*, Vol. 112, No. 5, pt 2, 2002, p. 2317.
  29. J. Zera, Attenuation of High-Level Acoustic Impulses by Hearing Protectors, *J. Acoust. Soc. Am.*, Vol. 112, No. 5, pt 2, 2002, p. 2318.
  30. J. G. Casali and G. S. Robinson, Narrow-Band Digital Active Noise Reduction in a Siren-Canceling Headset: Real-Ear and Acoustic Manikin Insertion Loss, *Noise Control Eng. J.*, Vol. 42, No. 3, 1994, pp. 101–115.
  31. J. G. Casali, G. S. Robinson, E. C. Dabney, and D. Gauger, Effect of Electronic ANR and Conventional Hearing Protectors on Vehicle Backup Alarm Detection in Noise, *Human Factors*, Vol. 46, No. 1, 2004, pp. 1–10.
  32. American National Standards Institute, ANSI S12.42–1995, *Microphone-in-Real-Ear and Acoustic Test Fixture Methods for the Measurement of Insertion Loss of Circumaural Hearing Protection Devices*, ANSI, New York, 1995.
  33. J. G. Casali and G. S. Robinson, Empirical Determination of Insertion Loss for the NCT PA-3000 Active Noise Reduction Headset, Blacksburg, Virginia, (Technical Report Number 9511, Audio Lab 9/29/95-5-HP), Virginia Tech, Auditory Systems Laboratory, Blacksburg VA, 1995.

## BIBLIOGRAPHY

- D. L. Johnson and C. W. Nixon, Simplified Methods for Estimating Hearing Protector Performance, *Sound Vib.*, Vol. 8, No. 6, 1974, pp. 20–27.

# CHAPTER 32

## DEVELOPMENT OF STANDARDS AND REGULATIONS FOR OCCUPATIONAL NOISE

Alice H. Suter  
Alice Suter and Associates  
Ashland, Oregon

### 1 INTRODUCTION

Millions of people throughout the world are exposed to hazardous levels of noise. Because of lack of knowledge or lack of concern, a substantial portion of those exposed are losing their hearing. Occupational noise is not adequately dealt with by marketplace incentives. Worker compensation for hearing loss, at least in the United States, is relatively insignificant as a motivation for noise control. If workers' hearing is to be conserved, it is almost always up to government bodies to inform and regulate employers through necessary standards and regulations. It is important for safety and health professionals to be informed about the standards and regulations that apply to their companies in order to protect employees.

The regulatory process is not a simple one since several weighty decisions need to be made, including the amount of hearing and the percentage of the noise-exposed population to be protected. Thus it is not surprising that standards and regulations for noise exposure vary among the different nations, although recent trends are toward uniformity. Noise exposure regulations in the United States, however, seem to be lagging behind the other industrialized nations, both in terms of the degree of protection and the implementation of noise control measures.

### 2 NEED FOR STANDARDS AND REGULATIONS RELATED TO OCCUPATIONAL NOISE

In the United States, an estimated 9 million workers are exposed to average A-weighted sound pressure levels of 85 dB and above. The number of noise-exposed workers in various types of occupations is described in Table 1. Although these data are now more than 20 years old (with the exception of mining), no surveys

**Table 1 Number of American Workers Exposed to A-Weighted Sound Pressure Levels of 85 dB or above**

Sector	Number of Workers
Agriculture	323,000
Mining	218,400
Construction	513,000
Manufacturing and utilities	5,124,000
Transportation	1,934,000
Military	976,000
Total	9,088,400

Source: From Refs. 1–3.

**Table 2 Noisiest Manufacturing Industries, Listed in Descending Order According to Percentage of Workers Exposed to A-Weighted Sound Pressure Levels above 90 dB**

SIC Code	Industry
24	Lumber and Wood
22	Textiles
29	Petroleum and Coal
33	Primary metals
49	Utilities
26	Paper
28	Chemicals
27	Printing and publishing
34	Fabricated metals
20	Food
35	Machinery (except electrical)
37	Transportation equipment
25	Furniture and fixtures
30	Rubber and plastics
21	Tobacco
32	Stone, clay, and glass
36	Electrical machinery
23	Apparel
31	Leather

Source: Adapted from Ref. 4.

of noise exposure have effectively replaced them. One could hope that noise control programs could have reduced these numbers, but there is little evidence to that effect in the United States.

Table 2 shows the noisiest types of U.S. manufacturing industries stated in terms of Standard Industrial Code (SIC), arranged in descending order according to the percentage of workers exposed to A-weighted sound pressure levels above 90 dB. Although this ranking is based on data from U.S. industries, the relative noise hazards of other industries throughout the world is likely to be similar.

The reader should bear in mind that the information given in Tables 1 and 2 is not sufficiently conservative according to more recent damage–risk criteria, which show that a certain percentage of workers will incur material hearing impairment at daily average exposure levels below 85 dB (the criterion used in Table 1) and well below 90 dB (the criterion used in Table 2).

### 3 TERMINOLOGY

In the field of occupational noise, the terms *regulation*, *standard*, and *legislation* are often used

interchangeably, even though technically they may have slightly different meanings. In the United States, a regulation is a rule or order prescribed by a government authority and is usually more formal than a standard. A standard is a codified set of rules or guidelines, much like a regulation, but can be developed under the auspices of a consensus group, such as the International Organization for Standardization (ISO) or in the United States the American National Standards Institute (ANSI). Legislation consists of laws prescribed by legislating authorities or by local governing bodies.

In some countries national standards are called *legislation*. Some official bodies use the terms standards and regulations as well. The European Union (EU) issues *directives*. All members of the European Community needed to "harmonize" their noise standards (regulations or legislation) with the 1986 directive on occupational noise exposure by the year 1990.<sup>5</sup> This means that the noise standards and regulations of the member countries had to be at least as protective as the EU's directive. In 2003 the EU issued an updated directive for noise exposure<sup>6</sup> with which the member nations must comply no later than February 2006.

Some nations have a *code of practice*, which is somewhat less formal. For example, the Australian national standard for occupational exposure to noise consists of two short, mandatory paragraphs, followed by a 35-page code of practice, which provides practical guidance on how the standard should be implemented. Codes of practice usually do not have the legal force of regulations or legislation.

Another term that is used occasionally is *recommendation*, which is more like a guideline than a mandatory rule and is not enforceable. Examples of recommendations issued by a U.S. governmental body would be criteria developed by the National Institute for Occupational Safety and Health (NIOSH),<sup>7,8</sup> which are often considered recommendations for "best practice."

#### 4 CONSENSUS STANDARDS

At least in the United States, the advent of federal standards for occupational noise exposure was preceded by a series of consensus standards, issued by such organizations as the American Standards Association (the predecessor of ANSI), the National Research Council Committee on Hearing and Bioacoustics (CHABA), and the Intersociety Committee,<sup>9</sup> a group comprised of members from several professional organizations concerned with noise and hearing. Although these bodies reflected an ever increasing level of knowledge by the professional community, there was a need for uniformity. The U.S. federal government satisfied that need with the promulgation of a noise standard in 1969<sup>10</sup> under the authority of the Walsh-Healey Contracts Act of 1935. The same is happening currently in Europe under the direction of the European Union. In addition to ANSI, several international consensus organizations are currently active in noise standardization, particularly the ISO and the International Electrotechnical Commission (IEC). These organizations have been involved in

the standardization of criteria for exposure to noise, as well as standards for instruments and measurement methodologies.

The ISO's technical committee TC43, Acoustics, is made up of members from 27 countries. ISO Subcommittee SC1, Noise, is primarily concerned with noise exposure, emission, and measurement, as well as hearing conservation and machinery noise.

One of the most widely used noise standards is ISO 1999, Acoustics: Determination of Occupational Noise Exposure and Estimate of Noise-Induced Hearing Impairment,<sup>11</sup> which has a counterpart in the United States as ANSI S3.44.<sup>12</sup> Both of these standards may be used to predict the amount of hearing loss expected to occur in various centiles of the exposed population at various audiometric frequencies as a function of exposure level and duration, age, and sex.

#### 5 DAMAGE-RISK CRITERIA

The term *damage-risk criteria* refers to the risk of hearing impairment from various levels of noise. Many factors enter into the development of these criteria and standards in addition to the data describing the amount of hearing loss resulting from a certain amount of noise exposure. There are both technical and policy considerations operating in the development of criteria and their application to standards and regulations.

The following questions are good examples of policy considerations: What proportion of the noise-exposed population should be protected, and how much hearing loss constitutes an acceptable risk? Should we protect even the most sensitive members of the exposed population against any loss of hearing, or should we protect only against a compensable hearing handicap? The answers to these questions are directly related to the hearing loss formula that is used, and different governmental bodies and consensus organizations have varied widely in their selections.

In earlier years, regulatory decisions were made that allowed substantial amounts of hearing loss as an acceptable risk. The most common definition used to be an average hearing threshold level (or "low fence") of 25 dB or greater at the audiometric frequencies 500, 1000, and 2000 Hz. Since that time, the definitions of *hearing impairment* or *hearing handicap* have become more restrictive, with different nations or consensus groups advocating different definitions. For example, one U.S. government agency now uses a 25-dB average at 1000, 2000, and 3000 Hz,<sup>4</sup> and another uses the same low fence averaged over the frequencies 1000, 2000, 3000, and 4000 Hz.<sup>8</sup> Other definitions may incorporate a low fence of 20 or 30 dB and may include a different frequency combination or a broader range of frequencies.

In general, as definitions include higher frequencies and lower fences or hearing threshold levels, the acceptable risk becomes more stringent, and a higher percentage of the exposed population will appear to be at risk from given levels of noise. If there is to be no risk of any hearing loss from noise exposure, even in the more sensitive members of the exposed population, the permissible 8-h exposure limit would

have to be as low as an A-weighted sound pressure level of 75 dB. In fact, the EU has established an equivalent A-weighted sound pressure level ( $L_{eq}$ ) of 75 dB as the level at which the risk is negligible, and this level has also been put forward as a goal for Swedish production facilities.<sup>13</sup>

Overall, the prevailing thought on this subject is that it is acceptable for a noise-exposed workforce to lose a small amount of hearing, but not too much. As for how much is too much, there is no consensus at this time. In all probability, most nations draft standards and regulations that attempt to keep the risk at a minimum level while taking technical and economic feasibility into account, but without coming to consensus on such matters as the frequencies, fence, or percentage of the population to be protected.

## 6 PRESENTING THE DAMAGE-RISK CRITERIA

Criteria for noise-induced hearing loss may be presented in either of two ways: noise-induced permanent threshold shift (NIPTS) or percentage risk. NIPTS is the amount of permanent threshold shift in decibels remaining in a population after subtracting the threshold shift that would occur "normally" from causes other than occupational noise. The percentage risk is the percentage of a population with a given amount of noise-induced hearing impairment *after* subtracting the percentage of a similar population *not* exposed to occupational noise that would exceed that same impairment due to aging and other causes. This concept is sometimes called *excess risk*. Unfortunately, neither method is without problems.

The problem with using NIPTS alone is that it is difficult to summarize the effects of noise on hearing. The data are usually set out in a large table showing noise-induced threshold shift for each audiometric frequency as a function of noise level, years of exposure, and population centile. The concept of percentage risk is more attractive because it uses single numbers and appears to be easy to understand. But the problem with percentage risk is that it can vary enormously, depending on a number of factors, particularly the height of the hearing threshold level fence and the frequencies used to define hearing impairment (or handicap).

With both methods, the user needs to be sure that the exposed and nonexposed populations are well matched for such factors as age, nonoccupational noise exposure, and the fence and audiometric frequencies used to define hearing impairment (or handicap). For example, ISO 1999 offers two databases for use in predicting hearing loss from noise. Database A presents hearing threshold data from a European population, which has had minimal noise exposure. Database B gives hearing levels of a U.S. population with greater amounts of nonoccupational noise exposure plus some small amounts of occupational exposure. Both databases are at least 40 years old at this time, and nowadays it is difficult to find subjects in industrialized nations that have had no exposure to noise.

**Table 3 Example of a Population at Risk from Noise Exposure**

---

A-weighted noise exposure level: 90 dB
Sex: Male
Age: 50
Years of exposure: 30
Nonnoise population: Database A
Frequencies: average at 1000, 2000, 4000 Hz
Fence: 27 dB
Risk from aging: 3%
Risk from noise + aging: 16%
Percent risk: 13%

---

Source: From Ref. 11.

**Table 4 Example of a Population at Risk from Noise Exposure**

---

A-weighted noise exposure level: 90 dB
Sex: Male
Age: 60
Years of exposure: 40
Nonnoise population: Database A
Frequencies: average at 1000, 2000, 4000 Hz
Fence: 27 dB
Risk from aging: 15.5%
Risk from noise + aging: 35%
Percent risk: 19.5%

---

Source: From Ref. 11.

Table 3 shows an example of the percentage risk method taken from ISO 1999, Annex D.<sup>11</sup> According to the ISO data and method, the risk in a male population due to noise at an average A-weighted sound pressure level of 90 dB after 30 years of exposure is 13%, using the frequencies 1000, 2000, and 4000 Hz and a fence of 27 dB.

Using the same data and method, but changing just a few parameters, the risk becomes 19.5%, as in Table 4. By examining hearing impairment at age 60 instead of age 50, with 40 years of exposure instead of 30, the risk has been increased considerably.\* Moreover, the risk from aging alone has increased from 3 to 15.5% within 10 years.

Likewise, any change in the level of the fence or the selected frequencies would also change the outcome in terms of percentage risk. It is up to the policymakers to decide these parameters, as well as the predicted duration of noise exposure (a working lifetime of 30 or 40 years), in determining how much loss is to be prevented.

## 7 NOISE STANDARDS OF VARIOUS NATIONS

Table 5 gives some of the main features of the noise exposure standards of several nations. Most of the information is current as of this publication, but some

---

\*These figures are slightly different from those that would be obtained using the example in ISO Annex D. In the ISO example, the user makes a small adjustment to the NIPTS values, whereas it is more correct to make this adjustment to the hearing loss from aging, as has been done here.

**Table 5 Permissible Exposure Limits (PEL), Exchange Rates, and Other Requirements for Noise Exposure According to Nation**

Nation Date (if available)	PEL $L_{av}$ (8-h) (A-weighted average sound pressure level in dB)	Exchange Rate (dB)	$L_{max}$ (dB) $L_{peak}$ (dB)	Level Eng. Control (A-weighted average sound pressure level in dB)	Level Audio. Test (A-weighted average sound pressure level in dB)	Comments
Argentina, 2003	85	3	115 <sup>a</sup>	85	85	Note 1
Australia, 2000	85	3	140 <sup>b</sup> peak	85	85	Note 2
Brazil, 1992	85	5	115 <sup>a</sup> 130 peak or 120 <sup>b</sup>	85		
Canada, 1991	87	3		87	84	Note 3
Chile, 2000	85	3	115 <sup>a</sup> 140 <sup>b</sup> peak			Note 4
China, 1985	85	3	115 <sup>a</sup>	85		
Colombia, 1990	85	5	115 <sup>a</sup> 140 peak			
Denmark	85	3	See note			Note 5
EU, 2003	87	3	140 <sup>b</sup> 137 <sup>b</sup> 135 <sup>b</sup>	85	85 80	Note 6a Note 6b
Finland, 1982	85	3		85		
France, 1990	85	3	135 peak		85	
Germany, 1990	85	3	140 peak	90	85	Note 7
Hungary	55,70	3	125 <sup>a</sup> 140 peak	90		
India, 1989	90	5	115 <sup>a</sup> 140 peak			Note 8
Israel, 1984	85	5	115 <sup>a</sup> 140 peak			
Italy, 1990	85	3	140 peak	90	85	
Mexico, 2001	85	3	105 <sup>a</sup>	90	80	
Netherlands, 1987	80	3	140 peak	85		Note 9
New Zealand, 1995	85	3	140 peak	85	85	
Norway, 1982	85	3	110 <sup>a</sup>		80	Note 10
Spain, 1989	55,70	3	140 peak	90	80	
Sweden, 1992	85	3	115 <sup>a</sup> 135, 135, 135	85	85	Note 11
United Kingdom, 1989	85	3	140 peak	90	85	
United States, 1983	90	5	115 <sup>a</sup> 140 peak	90	85	Note 12
Uruguay, 1988	85	3		85	85	
Venezuela	85	3	140 peak			

<sup>a</sup>A-weighted sound pressure level.<sup>b</sup>C-weighted sound pressure level. No designation presumes unweighted.

Note 1. Argentine standard 295/2003 states that no work is allowed for sound pressure levels greater than 135 dB even for workers wearing hearing protectors.

Note 2. Each of the Australian states and territories has its own legislation for noise. All have now adopted the 8-h A-weighted  $L_{eq}$  of 85 dB and most have a standard of 140-dB peak C-weighted sound pressure level for impulses.Note 3. There is some variation among the individual Canadian provinces: Ontario and Quebec use an A-weighted sound pressure level of 90 dB with a 5-dB exchange rate; Alberta, British Columbia, New Brunswick, Newfoundland, Nova Scotia, Saskatchewan, and Yukon use 85 dB with a 3-dB exchange rate; and Northwest Territories uses 85 dB with a 5-dB exchange rate. All require engineering controls to the level of the PEL, at least for new equipment, processes, or worksites. Manitoba requires certain hearing conservation practices above an A-weighted level of 80 dB, hearing protectors and training on request above 85 dB, and engineering controls above 90 dB. The federal standard, effective July 1991, has no requirements for  $L_{max}$  or  $L_{peak}$ .

Note 4. Chilean standard DS 594/99 of April 2000 requires a maximum C-weighted sound pressure level of 95 dB for an 8-h exposure to impulse noise, measured at the worker's ear using a 3-dB exchange rate.

Table 5 (continued)

Note 5. In Denmark, a correction of 5 dB must be added to the measured A-weighted sound pressure level if the noise is impulsive. A noise is defined as impulsive if the peak A-weighted or C-weighted sound pressure level (on the peak-hold setting) exceeds 115 dB more than once per minute. The person measuring the noise has the option of using either A- or C-weighting.

Note 6a. European Union (Directive 2003/10/EC)<sup>6</sup> puts forward three exposure values: an A-weighted exposure limit value of  $L_{eq}$  87 dB and a peak C-weighted sound pressure level of 140 dB; an "upper action" A-weighted sound pressure level of 85 dB and a peak C-weighted sound pressure level of 137 dB; and a "lower action" A-weighted sound pressure level of 80 dB and a peak C-weighted sound pressure level of 135 dB. The attenuation of hearing protectors may be taken into account when assessing the exposure limit value, but not for requirements driven by the upper and lower action values. At no time shall employees' noise exposures exceed the exposure limit value. When exposures exceed the upper action level, the employer must implement a program of noise reduction, taking into account technology and availability of control measures.

Note 6b. EU continued.<sup>6</sup> Hearing protectors must be made available when exposures exceed the lower action A-weighted sound pressure level of 80 dB. Hearing protectors must be used by workers whose exposures equal or exceed the upper action value of 85 dB. Audiometric testing must be available to workers whose exposures exceed the upper action value, and when noise measurements indicate a risk to health these measures must be available at the lower action value.

Note 7. The German standard (UVV Lärm-1990) states that it is not possible to give a precise limit for the elimination of hearing hazard and the risk of other health impairments from noise. Therefore the employer is obliged to reduce the noise level as far as possible, taking technical progress and the availability of control measures into account.

Note 8. India: Recommendation.

Note 9. The Netherlands' noise legislation requires engineering noise control at an A-weighted sound pressure level or 85 dB "unless this cannot be reasonably demanded." Hearing protection must be provided above 80 dB and workers are required to wear it at levels above 90 dB.

Note 10. Norway requires an A-weighted PEL of 55 dB for work requiring a large amount of mental concentration, 70 dB for work requiring verbal communication or great accuracy and attention, and 85 dB for other noisy work settings. Recommended limits are 10 dB lower. Workers exposed to average A-weighted sound pressure levels greater than 85 dB should wear hearing protectors.

Note 11. In accordance with the new EU directive, Sweden uses the same 85-dB upper and 80-dB lower exposure values but reduces the limit value from 87 to 85 dB. The C-weighted peak sound pressure levels are also 135 for the upper, lower, and limit values, which is more conservative than the EU directive. In addition, Sweden adds a requirement for a maximum A-weighted sound pressure level (presumably for continuous noise) of 115 dB.

Note 12. These levels apply to the OSHA noise regulation<sup>16</sup> covering workers in general industry and maritime. The U.S. military services require standards that are somewhat more stringent. The U.S. Air Force and the U.S. Army both use an 85-dB PEL and a 3-dB exchange rate.

#### Sources:

Jorge P. Arenas, Institute of Acoustics, Universidad Austral de Chile, Valdivia, Chile. Paper presented at the 129th meeting of the Acoustical Society of America, 1995. Also via personal communication, Feb. 2005; updated information on noise standards of Latin American nations: Argentine Std. 295/2003; Chilean Std. DS 594/99, April 2000; Colombian Std. Res. 1792/90, May 1990; Mexican Std. NOM-011-STPS-2001; Uruguayan Std. Dec. 406/1988, June, 1988; Venezuelan Std. COVENIN 1565:1995.

Pamela Gunn, WorkSafe Division of the Department of Consumer and Employment Protection, Perth, Western Australia (personal communication, March 2005).

Tony F. W. Embleton, I-INCE Publication 97-1: Final Report—Technical Assessment of Upper Limits on Noise in the Workplace. Approved by the Board of Directors of I-INCE on 1997.08.23 and published in *Noise/News International*, Vol. 5, 1997, pp. 203–216.

Christine Harrison, Worker Compensation Board, British Columbia (personal communication, March 2005).

ILO, *Noise Regulations and Standards*, CIS database, International Labour Office, Geneva, Switzerland (summaries), 1994. Published standards of various nations.

standards may have been recently revised. Readers are advised to consult the newest versions of the individual nations' standards.

## 8 OTHER FEATURES OF NATIONS' NOISE STANDARDS

In addition to their requirements to protect workers against hearing loss, several nations include provisions for preventing other adverse effects of noise. Some nations state the need to protect against the extraauditory effects of noise in their regulations. Both the EU directive and the German standard acknowledge

that workplace noise involves a risk for the health and safety of workers beyond hearing loss, but that current scientific knowledge of the extraauditory effects does not enable precise safe levels to be set.

The Norwegian standard includes a requirement that noise levels must not exceed an A-weighted sound pressure level of 70 dB in work settings where speech communication is necessary. The German standard advocates noise reduction for the prevention of accident risks, and both Norway and Germany require a maximum A-weighted noise level of 55 dB to enhance concentration and prevent stress during mental tasks.

Some countries have special noise standards for different kinds of workplaces. For example, Finland and the United States have noise standards for commercial vehicle cabs, and Germany and Japan specify noise levels for offices. Others include noise as one of many regulated hazards in a particular process. Still other standards apply to specific types of equipment or machines, such as air compressors, chain saws, and construction equipment.

In addition, some nations have promulgated separate standards for hearing protection devices (e.g., the EU, Netherlands, and Norway) and for hearing conservation programs (e.g., France, Norway, Spain, Sweden, and the United States).

Some nations use innovative approaches to attack the occupational noise problem. For example, the Netherlands has a separate standard for newly constructed workplaces, and Australia and Norway give information to employers for instructing manufacturers to provide quieter equipment.

There is little information about the degree to which these standards and regulations are enforced. Some specify that employers "should" take certain actions (as in codes of practice or guidelines), while most specify that employers "shall." Standards that use "shall" are more apt to be mandatory, but individual nations vary widely in their ability and inclination to enforce. Even within the same nation, enforcement of occupational noise standards may vary considerably with the government in power.

## 9 FURTHER INFORMATION

Readers may consult the following publications for further information on standards and regulations for occupational noise exposure:

B. Goelzer, C. H. Hansen, and G. A. Sehrndt, Eds., *Occupational Exposure to Noise: Evaluation, Prevention, and Control*, Special Report S 64, published on behalf of the World Health Organization, Dortmund/Berlin, 2001.

NIOSH, *Criteria for a Recommended Standard: Occupational Noise Exposure; Revised Criteria*, National Institute for Occupational Safety and Health, U.S. Dept. HHS, report DHHS (NIOSH), Cincinnati, OH, 1998.

A. H. Suter, Standards and Regulations, in *Encyclopaedia of Occupational Health and Safety*, Vol. IV, 2nd. ed., J. M. Stellman, Ed., International Labour Office, Geneva, Switzerland, 1998.

A. H. Suter, Standards and Regulations, in *The Noise Manual* (rev. 5th ed.), E. H. Berger, L. H. Royster, J. D. Royster, D. P. Driscoll, and M. Layne, Eds., American Industrial Hygiene Assoc., Fairfax, VA, 2003, pp. 639–668.

**Acknowledgment** The author wishes to thank several colleagues for their contributions to the information on international standards, including Jorge Arenas,

Bernard Berry, Pamela Gunn, Christine Harrison, Roger Higgenson, Bengt Johansson, and Hans Lazarus.

## REFERENCES

1. M. Simpson and R. Bruce, *Noise in America: The Extent of the Noise Problem*, U.S. Environmental Protection Agency, EPA report no. 550/9-81-101, Washington, DC, 1981.
2. MSHA, Health Standards for Occupational Noise Exposure; Final Rule. U.S. Dept. of Labor, Mine Safety and Health Administration, 30 CFR Part 62. 64 *Fed. Reg.*, 1999, pp. 49548–49634, 49636–49637.
3. J. P. Seiler and D. A. Giardino, The Effect of Threshold on Noise Dosimeter Measurements and Interpretation of Their Results. Informational Report IR1224. U.S. Dept. Labor, Mine Safety and Health Administration, Pittsburgh, PA, 1994.
4. U.S. Dept. Labor, Occupational Safety and Health Administration, Occupational Noise Exposure: Hearing Conservation Amendment, 46 *Fed. Reg.*, 1981, pp. 4078–4179.
5. Council Directive of 12 May 1986 on the protection of workers from the risks related to exposure to noise at work. Council of European Communities, 86/188/EEC.
6. European Union, Directive 2003/10/EC of the European Parliament and of the Council on the Minimum Health and Safety Requirements Regarding the Exposure of Workers Arising from Physical agents (noise). (Seventeenth individual Directive within the meaning of Article 16(1) of Directive 89/391/EEC), 2003.
7. NIOSH, Criteria for a Recommended Standard: Occupational Exposure to Noise. National Institute for Occupational Safety and Health, U.S. Dept. HEW, report HSM 73–11001, Cincinnati, OH, 1972.
8. NIOSH, Criteria for a Recommended Standard: Occupational Noise Exposure; Revised Criteria. National Institute for Occupational Safety and Health, U.S. Dept. HHS, report DHHS (NIOSH) 98–126, Cincinnati, OH, 1998.
9. Intersociety Committee, "Guidelines for noise exposure control." *J. Occup. Med.*, Vol. 12, pp. 276–281, 1970.
10. U.S. Dept. Labor, Bu. Labor Standards, "Occupational Noise Exposure," 34 *Fed. Reg.* pp. 7948–7949, 1969.
11. International Organization for Standardization, ISO 1999, Acoustics: Determination of occupational noise exposure and estimate of noise-induced hearing impairment. Geneva, Switzerland, 1990.
12. American National Standard Determination of Occupational Noise Exposure and Estimation of Noise-Induced Hearing Impairment, ANSI S3-44–1996, New York.
13. T. Kihlman, Sweden's Action Plan against Noise, *Noise/News Int.*, Vol. 1, No. 4, 1993, pp. 194–208.
14. T. F.W. Embleton, I-INCE Publication 97-1: Final Report—Technical Assessment of Upper Limits on Noise in the Workplace, Approved by the Board of Directors of I-INCE on 1997.08.23 and published in *Noise/News Int.*, Vol. 5, 1997, pp. 203–216.
15. ILO, *Noise Regulations and Standards*, CIS database, International Labour Office, Geneva, Switzerland, 1994.
16. U.S. Code of Federal Regulations, Section 1910.95, Occupational Noise Exposure.

# CHAPTER 33

## HEARING CONSERVATION PROGRAMS

**John Erdreich**  
Ostergaard Acoustical Associates  
West Orange, New Jersey

### 1 INTRODUCTION

Hearing conservation programs have evolved from their original purpose of simply screening employee hearing. With increasingly sophisticated analyses of growing databases of employee audiometric data, of more detailed exposure records, and industry strategies to control noise exposure, the hearing conservation program has become the basis not only by which to protect worker hearing, but it is also a powerful tool with which to limit employer exposure to liability for nonoccupationally caused hearing impairments. Hearing conservation programs are, in essence, an educational tool for both the employer and the employee.

#### 1.1 Purpose of Hearing Conservation Programs

The essential components of a hearing conservation program (HCP) are as follows:

- Selection of a “key person” with responsibility and authority to coordinate all facets of the HCP for both worker and employer.
- Education of both parties regarding the effects of noise exposure on hearing.
- Annual audiometric screening of noise-exposed employees.
- Identification of locations and processes contributing to noise exposures.
- A program of noise control where exposures exceed a selected criterion level.
- Selection of the criterion noise exposure acceptable to management.
- Annual reviews of hearing losses to identify cause.

**1.1.1 Protection of Employee Hearing** Early hearing conservation programs were implemented in several industries following World War II. Primary among these were aircraft, petrochemical, and some railroads. In 1950, Kryter<sup>1</sup> published the original version of his monograph that described the relation between noise exposure and occupational hearing loss. This was further clarified by Glorig et al.<sup>2</sup> and by Burns and Robinson<sup>3</sup> in their studies of noise in American and British industry.

By the mid-1960s it was clear that noise-induced hearing loss (NIHL) was a serious problem and that workers needed to protect their hearing. In the United States regulations were promulgated mandating

acceptable noise exposures. At this writing, the United States, the European Union, and many other countries have promulgated similar regulations to protect and conserve worker hearing.

**1.1.2 Limitation of Employer Liability** Although early in the twentieth century there was little recourse an employee had to be compensated for occupational injuries or diseases, major changes began to evolve after World War II. In 1948 New York State workman’s compensation law was expanded to include coverage for noise-induced hearing loss (*Slawinsky vs. J. H. Walters and Company*). In the period between 1948 and 1962 other states adopted similar positions in which noise-induced hearing loss, although it develops over time, was considered a compensable occupational injury.

Workman’s compensation laws set schedules for compensation for occupational injuries and diseases. The employer is protected, to a degree in the United States, by its insurance coverage through the workers compensation system. However, for noise-induced hearing loss the employee can overcome the limited compensation payments if negligence on the part of his employer can be demonstrated. In that case, the injury is treated under tort law and is not adjudicated under the workman’s compensation system. Nor is it likely covered by the employer’s insurance. A comprehensive hearing conservation program will not only protect employee hearing but also will demonstrate that there is no negligence. Furthermore, it will document the hearing levels and progression of hearing impairment, if any, in the employee and others with similar exposures. This record is the best defense in tort litigation.

#### 1.2 Relation of the Hearing Conservation Program (HCP) to Regulations

**1.2.1 Occupational injury compensation** In the United States, a system of compensation for occupational injury has developed since the midtwentieth century. Workman’s compensation programs attempt to provide for this compensation in an environment that creates a buffer between the employee and the employer by establishing a uniform procedure for the injured employee to receive compensation for an injury. These programs impose three general requirements upon the claimant:

The existence of an injury must be established.  
Occupational causality must be demonstrated.  
Economic impact of the injury must be determined.



The existence of a hearing impairment is evaluated in the annual audiometric screening that is part of the HCP. This will be discussed subsequently.

For a determination of occupational causality for a noise-induced hearing impairment, demonstration of employee noise exposure sufficient to produce the measured impairment is required. Records of sound surveys conducted as part of the HCP can establish, in conjunction with an employee work history, the noise exposure of the individual during the period of employment. In this regard, a proper HCP provides a strong basis for adjudicating a claim for compensation for an occupational hearing impairment. An otologic examination is also recommended to preclude the existence of hearing impairments arising from nonoccupational causes.

Some jurisdictions require that the employee comply with the requirements of the HCP implemented by the employer. If the employer can demonstrate that the employee has not properly used the hearing protection provided, then the claim may be disallowed. For example, the New Jersey Workman's Compensation Statute (34:15-35.22)<sup>4</sup> states:

No compensation shall be payable for loss of hearing caused by hazardous noise...if an employer can properly document that despite repeated warnings, an employee willfully fails to properly and effectively utilize suitable protective device or devices provided by the employer capable of diminishing loss of hearing due to occupational exposure to hazardous noise.

Economic impact of a hearing impairment is assumed in all American workman's compensation regulations, although the schedule of compensation varies by jurisdiction and from federal to state plans. This is unrelated to the facts of exposure documented in the HCP.

**1.2.2 Torts** Although a system of compensation exists for occupational NIHL, the schedule of compensation is limited and does not protect the employer from litigation under the tort statutes. Generally, if the employee can demonstrate negligence on the part of the employer or a defect on the part of the manufacturer of the tools used in the course of employment, then it is possible to claim compensation unrestricted by the schedules set forth in the workman's compensation statutes.

In addition to employee audiometric data and noise surveys, HCP documentation should include company memoranda that describe the history of the HCP as well as the individuals responsible for its implementation. These are important instruments in the defense of these claims. For companies with several facilities the HCP should follow similar guidelines at each location to establish that corporate management has committed to the safety of its employees.

**1.2.3 Exposure Limitation** Permissible employee noise exposure in the United States is promulgated under the Occupational Safety and Health Act

(OSHA), CFR 1910.29.<sup>5</sup> In 1981 a dual limit was established by the Hearing Conservation Amendment to the act that established a threshold exposure at which hearing conservation is mandatory (the action level) and a higher threshold (the permissible exposure level, PEL), which defined the limit of exposure. These criteria are based on a 5-dB exchange rate (every 5-dB increase in level requires a halving of exposure time) and an 8-h exposure (Table 1).

Permissible time of exposure ( $t$ , in hours) at any level may be calculated as

$$t = \frac{8 \text{ h}}{2^{(L-90)/5}}$$

where  $L$  is the level of the sound to which the employee is exposed, 5 represents the exchange rate, and 90 is the 8-h PEL. Similar calculations may be carried out for a 3-dB exchange rate by replacing the 5 with 3.

**Table 1 Allowable Time (T) of Exposure in Minutes for 5- and 3-dB Exchange Rate at Different Levels**

Level	T at 5 dB	T at 3 dB
80	1920	4838
81	1671	3840
82	1455	3048
83	1267	2419
84	1103	1920
85	960	1524
86	836	1210
87	728	960
88	633	762
89	551	605
90	480	480
91	418	381
92	364	302
93	317	240
94	276	190
95	240	151
96	209	120
97	182	95
98	158	76
99	138	60
100	120	48
101	104	38
102	91	30
103	79	24
104	69	19
105	60	15
106	52	12
107	45	9
108	40	8
109	34	6
110	30	5
111	26	4
112	23	3
113	20	2
114	17	2
115	15	1

Noise dose ( $D$ ) is defined in terms of the 90 dB A-weighted sound pressure level 8-h limit that represents (OSHA) 100% dose. For a given exposure and duration ( $T_i$ ) the dose may be calculated as

$$D = \frac{T_i}{t} \times 100$$

$$= \frac{2^{(L-90)/5}}{8} \times T_i \times 100$$

Doses comprised of exposures at different levels are calculated by adding the individual doses. The OSHA action level is simply 50% of the 5 dB-exchange dose.

In some cases the employee exposure is reported in terms of the time weighted average level. This is the 8-h exposure equivalent to the calculated dose. Time weighted average is calculated as

$$D = \left( \frac{T_1}{t_1} + \frac{T_2}{t_2} + \frac{T_3}{t_3} + \dots + \frac{T_n}{t_n} \right) \times 100$$

$$\text{TWA} = 16.61 \log(D) + 90$$

Where exposures cannot be reduced by engineering controls, hearing protection is required to reduce exposures below 100% dose for those employees who have not suffered an occupational hearing loss, or a standard threshold shift (STS). Calculation of the STS is discussed in Section 2.5. For those employees who have suffered an STS, hearing protection must be worn when the exposure dose reaches 50% or 85 dB TWA.

Countries other than the United States use an exchange rate of 3 dB/doubling, which is the equivalent average level ( $L_{eq}$ ). This is defined in Chapter 127. Dose is calculated as above using 3 for the exchange rate in place of 5. Table 2 illustrates the difference between doses calculated on the basis of a 3-dB and a 5-dB exchange rate for all sound equal to or greater than 80 dB A-weighted sound pressure level for an 8-h exposure.

## 2 COMPONENTS OF THE HEARING CONSERVATION PROGRAM

The key individual, discussed in a later section, is responsible for the implementation of the HCP elements including:

- Initial site noise exposure survey
- Audiometric testing and assessment
- Notification of worker and employer
- Training and education
- Recordkeeping
- Noise control program
- Hearing conservation program evaluation

### 2.1 Site Noise Survey

A site noise survey is needed to determine whether a hearing conservation program is required at a particular facility. If such a survey reveals exposures above the criterion level, then the next step is to conduct individual dosimetry on a representative sample of employees. This sample should include all job functions that are potentially exposed above the selected criterion noise level. The results of the dosimeter will demonstrate several things: those employees who must be included in hearing conservation program, those areas and processes that contribute to the overexposure, and the tasks that are carried out by employees that cause the overexposures. For a hearing conservation program to be effective it is important to understand how an employee's dose accumulates to identify those tasks that could be subject to engineering controls.

**2.1.1 Initial Walk-through** The most important purpose of the initial walk-through is to gain an understanding of the facility and the work processes that are carried out. These will strongly influence the sound exposures of employees who are assigned to different job functions. This should include discussions with both management and employee representatives. Frequently, the employee representatives will offer different explanations of job functions than will management. After gaining an understanding of job functions and the layout of the facility, a sound survey comprising measurements of A-weighted sound pressure levels may be started.

Ideally, each job function in each area of the facility should be delineated, tabulated, and a short sample of the sound pressure level at each position should be measured. Based on the job functions and facility layout, the surveyor should determine the maximum sound levels to which employees are exposed and also a representative estimate of the TWA exposures. If the walk-through survey reveals few measured sound pressure levels above the [85 dB A-weighted sound pressure level] criterion and no estimated time weighted averages above the action level, there is no need for a hearing conservation program. Measured sound pressure levels should be documented and a summary prepared showing the monitoring locations and the results for future documentation of potential employee exposures.

In some cases the selected criterion above which the employee should not be exposed may be selected by management to be lower than a governmentally mandated level. In that case the company criterion is substituted for the regulatory limit.

**Table 2 Comparison of Dose for an 8-h Exposure at Level,  $L$ , for a 3 and a 5-dB Exchange Rate Including All Contributions to Exposure at or Above 80 dB**

A-weighted Sound Pressure Level (dB)	5-dB Exchange Dose	3-dB Exchange Dose
80	0.25	0.10
85	0.50	0.31
90	1.00	1.00
95	2.00	3.17
100	4.00	10.08
105	8.00	32.00
110	16.00	101.59
115	32.00	322.54

**2.1.2 Individual Dosimetry** Noise dosimeters integrate the instantaneous sound exposures to which the worker is subjected over the duration of the measurement—a full or a partial shift. These instruments are capable of employing selected exchange rates depending on the jurisdiction for which the exposure is evaluated. Dosimetry will reveal typical work shift exposures for each job function. Although many audio dosimeters exist that will monitor and calculate a single dose, these instruments are of limited benefit since they serve only to identify the overall level at which the individual is exposed. Using simple dosimeters can provide only an estimate of the number of people to be included in hearing conservation programs. Further, some instruments will produce a single value corresponding to the dose accumulated during the measurement period while others will produce a time history that depicts the moment-by-moment accumulation of the dose.

**Single Dose** Exposure measurements that produce a single-number dose are useful to demonstrate compliance with regulations. In the event that measurements reveal an employee overexposure, these results cannot provide information that supports further efforts to mitigate those overexposures. With the exception of a task in which the employee is subjected to a source of constant noise emission, there is no means to identify the process responsible for the majority of the accumulated dose without a time history of the exposure.

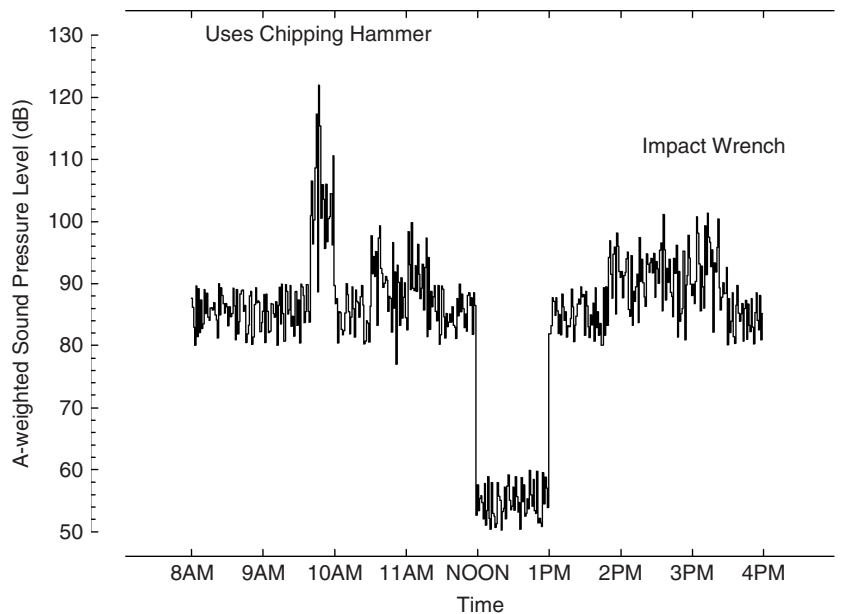
**Time History** Using time history dosimeters provides substantially more useful information. In addition to demonstrating the worker exposure, if the individual is instructed to keep a log of job tasks during the

monitoring, or if the surveyor keeps such a record, comparison of the log with the dosimeter time history can reveal those tasks that are responsible for the majority of the workers exposure. This is useful in planning either an engineering noise control or administrative program to reduce exposure.

As an example, Fig. 1 shows an employee exposure throughout a work shift. From noon to 1 p.m. exposures are low during the lunch break. Using a chipping hammer on a truck muffler from 9:30 a.m. to 10 a.m. produces the highest exposures during the shift. An impact wrench produces an increased exposure in the afternoon. Overall, the chipping hammer alone comprises 56% of this daily exposure of 128% (by the OSHA 5-dB exchange). Modifying this single task (e.g., by using a cutting torch instead of a chipping hammer) could reduce the exposure to 72% or a TWA of 88 dB from 92 dB.

#### **Octave-Band Measurements for Noise Control**

Effective noise control engineering requires detailed understanding of the mechanism of noise production of each contributing source as well as a detailed characterization of the spectrum and level of the contributions. Although the details of measurements for noise control are beyond the scope of this chapter, several American and international standards provide guidance for these measurements. Among these, International Organization for Standardization (ISO) 3746:1995<sup>6</sup> can provide data for both noise remediation and for prediction of noise levels that will be produced when equipment is placed into a facility. Similarly, American National Standards Institute (ANSI) S12.16–1992<sup>7</sup> is useful in this context.



**Figure 1** Single-shift exposure time history.

Following identification of the processes that contribute to the exceedance of the criterion noise dose, octave-band measurements should be taken to provide the basis on which to implement noise mitigation. Sound pressure levels must be sampled over the entire equipment duty cycle to define those components of the process that are responsible for the major contribution. This will enable the noise control engineer to develop optimal methods for reduction.

## 2.2 Employee Assessment and Testing

Evaluation of audiologic health in the industrial environment presents challenges different from the traditional diagnostic/rehabilitation setting. Not infrequently, audiometric evaluation is conducted to determine hearing handicap for the purposes of financial compensation of occupational hearing loss. In this adversarial situation the employee has an incentive to maximize the apparent impairment, while the employer is similarly motivated to demonstrate minimal impairment or nonoccupational causality. Accurate evaluation of employee hearing requires care by the audiometric technician to assure accurate results.

A critical aspect of any hearing conservation program is the baseline audiogram. At a minimum it serves as the benchmark against which future audiograms are compared. More importantly, the baseline audiogram establishes the hearing level of the employee at the start of his or her occupational noise exposure for the new employer. Some state compensation laws are structured such that the last employer of record is responsible for the full compensation burden for a hearing impairment unless the prior employer and the employee have been notified of a preexisting hearing impairment within a short period following new employment. Unless this notification is undertaken with the preemployment audiogram as its basis, a company with an effective hearing conservation program can find itself liable for a previous employer's ineffective program.

**2.2.1 Audiometric Test Procedures** Basic audiometric evaluations have been described in Chapter 120 of the *Encyclopedia of Acoustics*<sup>8</sup> to which the reader is referred. Initial screening of the employee is conducted with a pure-tone audiogram including the audiometric test frequencies of 500, 1000, 2000, 3000, 4000, and 6000 Hz. Industrial audiometry differs from diagnostic audiometry in several aspects. First, the individual being tested may not be cooperative. In instances where there is labor unrest or where there is incentive for financial gain through one of several injury compensation programs, the results of testing may be biased. Second, the technician must be vigilant that the worker being tested has not been exposed to levels of noise prior to the evaluation that could elevate the hearing threshold and produce an artifactual threshold elevation.

**Certification of the Technician** Technicians who conduct the audiometric screening of employees must be trained to recognize certain pathological conditions

such as an ear canal occluded by wax or a perforated eardrum. They must also recognize an employee who has difficulty performing an audiogram for whatever reason. In United States, audiometric technicians may be certified through the Council for Accreditation in Occupational Hearing Conservation (CAOHC). This organization conducts training courses for instructors who then conduct classes to train the audiometric technicians.

For a discussion of basic audiometry refer to Chapter 120 in the *Encyclopedia of Acoustics*.<sup>8</sup>

**2.2.2 Additional Audiometric Evaluation** The tests described below are carried out by licensed audiologists. They are beyond the purview of the audiometric technician.

**Pseudohypacusis** To evaluate cases of pseudohypacusis, or malingering, special audiometric tests are available. Several of these do not rely on cooperation of the patient while others exploit the compromised perception of sound if one ear is substantially less sensitive than the other.

Perhaps the most telling indication of malingering is inconsistency of thresholds produced on successive test-retest audiograms. The judgment required to maintain a sound at a constant suprathreshold level is much more difficult than the judgment of whether a sound is heard. One method of maintaining sound at a constant level is to ignore the sound entirely and simply depress and release the switch indicating "heard" and "not heard" with a regular rhythm. This produces a small range tracing on an automated tracking audiogram. Another technique is for the listener to set the criterion for "heard" versus "not heard" relatively high and low, respectively, resulting in large, atypical, threshold variations.

**Comparison of Speech Reception Threshold (SRT) and Pure-Tone Thresholds** Since the majority of information in speech is carried in the frequencies between 500 and 2000 Hz, it is reasonable to expect the speech reception threshold (SRT) to closely approximate the pure tone average (PTA) of 500, 1000, and 2000 Hz. A large difference between the SRT and the PTA in a listener is suggestive of non-organic hearing impairment. Extensive experience<sup>9</sup> with patients with confirmed pseudohypacusis showed that 70% exhibited SRTs at least 12 dB lower than the PTA. This discrepancy is one indication of malingering.

**Delayed Auditory Feedback** All speakers rely on feedback to modulate the level of their voice. This feedback is evidenced by the automatic increase or decrease of vocal effort depending on the level of background noise in which they speak. If a masking noise is applied as a listener reads aloud, the person's voice level will increase. This is known as the Lombard effect.

Although the Lombard effect itself can be used as a test for pseudohypacusis, a more dramatic

demonstration may be produced by presenting the listener's own speech as the masking sound. In a normal hearing individual auditory feedback is always present. Delaying the feedback, by presentation through a suitable electronic device, disrupts the normal processing of speech by the listener. The individual exhibits a change in speech rate and potentially vocal level. A normal hearing listener will take longer to read the same passage with 200-ms delayed feedback than with undelayed feedback.

The test is conducted by presenting the delayed speech initially at 0 dB HL (normal hearing threshold) subsequently raising it in 10-dB increments. The hearing-impaired individual will be unaffected until the delayed speech exceeds the true hearing threshold while the normal hearing individual will be affected at lower levels.

### 2.3 Employee and Management Feedback (Key Individual)

To maintain commitment to the goals of the HCP periodic review of program effectiveness and individual employee hearing status is crucial. For the program to be effective a key individual should be designated to whom the employee can direct questions about any aspect of the program, especially the use of hearing protective devices (HPDs) and the results of annual audiometric evaluations. The key individual should be educated in the details of hearing conservation to the extent of being able to accurately answer those questions. This person should occupy a place in the sociology of the company that engenders the respect of both labor and management. The key individual should also be in the position of addressing questions about the program from management including operational details, program effectiveness, and costs. Motivation and support is the key to continued HCP efficacy.

**2.3.1 Notification** Almost without exception, an employee will ask, "How did I do?" at the completion of the audiogram. While it is not the responsibility of the audiometric technician to provide feedback, with the advent of computerized audiometry and databases, feedback can be provided at that point that there is or is not a change from the previous test.

If changes are noted, it is appropriate to schedule a retest at a later date. The employee can be advised of the need to retest and that a written notification of the audiometric results will follow. This will also provide the supervising medical personnel an opportunity to determine if an otologic referral is appropriate.

In addition to providing individual employees notification of the results of their test, it is advisable

to provide management with annual summaries of the program results. By reporting the data shown in Table 3, any problem area in a facility can be identified by comparing the number of standard threshold shifts found with those in other departments. Furthermore, examination of the number of individuals exhibiting improved thresholds and those exhibiting worse thresholds in any year is an indication of the reliability of the testing procedures.

**2.3.2 Medical Referral** Referral to an otologist for a complete otologic workup is recommended for any employee who exhibits hearing loss on the baseline examination. Especially in the case where a worker has either never had a hearing test or where that evaluation was several years earlier, a medical exam frequently reveals underlying auditory pathology unrelated to noise exposures that could result in serious health consequences. Furthermore, such an evaluation may obviate claims for compensation at a later date. If an otologic examination is warranted, the physician will communicate the results of the exam to the employee.

### 2.4 Training and Education

Proper use and fitting of hearing protectors and the effects of noise on hearing are two topics that should be included in the employee education phase of the HCP. In companies that hold regular safety meetings this is most efficiently accomplished during one of those safety meetings. Material that can be used for the education and training is available from several sources, including the manufacturers of HPDs, professional industrial hygiene organizations, and the federal government. An excellent source of information on specific educational and training strategies is *The Noise Manual*.<sup>10</sup>

### 2.5 Recordkeeping

Maximum benefit to the employee and the employer occurs when full records of the HCP are maintained. OSHA requires only that after comparison of the current audiogram with the baseline audiogram, if an STS of 10 dB or more (average change at 2000, 3000, and 4000 Hz) has occurred, it must be recorded on the OSHA recordkeeping forms provided that, in addition, the average hearing threshold at those frequencies in the same ear is 25 dB or greater. All thresholds are referred to audiometric zero. If a threshold shift is determined to be nonoccupationally related, it need not be reported on the OSHA form. An excellent summary of recordkeeping rules may be found on the CAOHC website at [www.caohc.org/oshafinal.html](http://www.caohc.org/oshafinal.html).

**Table 3 Sample Database to Report Annual Summaries to Management**

Department	Number Employees Screened	Number STS Identified	Number Cases Worse by 10 dB	Number Cases Better by 10 dB	Number Referred to Otologist	Number STS Classified Occupational	Average Department Exposure Dose

This said, it is important that the employer document both the threshold shift and the determination of nonoccupational causation in the event of future tort claims. Additionally, HCP records should include noise surveys and should document mitigation that was carried out as part of the company effort to reduce employee noise exposure. This information forms the basis for the defense of any litigation related to hearing loss within the company.

## 2.6 Exposure Reduction

**2.6.1 Personal Protection** Hearing protection devices are covered in Chapter 31 to which the reader is referred.

**2.6.2 Engineering Controls** Reduction of source noise levels is the preferred method of employee exposure protection. The sound survey carried out in the facility can serve as the basis for source level reduction if it has included both time history dosimetry and one-third octave-band sound pressure level measurements. With these data the offending equipment or process responsible for the employee overexposures can be identified and appropriate engineering measures may be implemented. The detailed protocol for a noise control program is beyond the scope of this chapter and may be found in other sections of this handbook.

**2.6.3 Administrative Controls** Where engineering controls are not feasible, the remaining choice is to administratively limit employee noise exposure duration. This can be accomplished by rotating employees in and out of the high noise exposure areas throughout the work shift, taking care to limit the overall dose to the permissible exposure level. As this may have

implications for production goals, it is often the least desirable of options.

## 3 EVALUATION OF THE HEARING CONSERVATION PROGRAM

### 3.1 Statistical Review of the Company Database

On a facilitywide basis, occupational NIHL may be considered a public health issue and treated as such. The effectiveness of the intervention strategy, the hearing conservation program, can be evaluated in the same manner as any other public health program. Comparison of pre- and postintervention rates of “disease” within the facility and with expected rates of the “disease” with normative dose–response data are typical metrics appropriate for this evaluation. In this case, the dose–response relationship for development of NIHL is known from the ISO 1999<sup>11</sup> databases. Evaluation of the HCP is a statistical exercise similar to studying the epidemiology of the disease.<sup>12,13</sup>

Procedures for the calculation of expected NIHL can be found in ANSI S3.44–1996,<sup>14</sup> Section 6.3, to which the reader is referred for detailed information. Predicted values over a limited number of exposures are shown in Fig. 2.

Two different aspects of a hearing conservation program should be evaluated: quality and effectiveness. The *effectiveness* of a program is judged by the rate of new cases of occupational NIHL that develop. This rate may be biased by program errors that increase or decrease the rate from one test cycle to the next. The quality of the program relates to the consistency of test results and to the other factors such as training

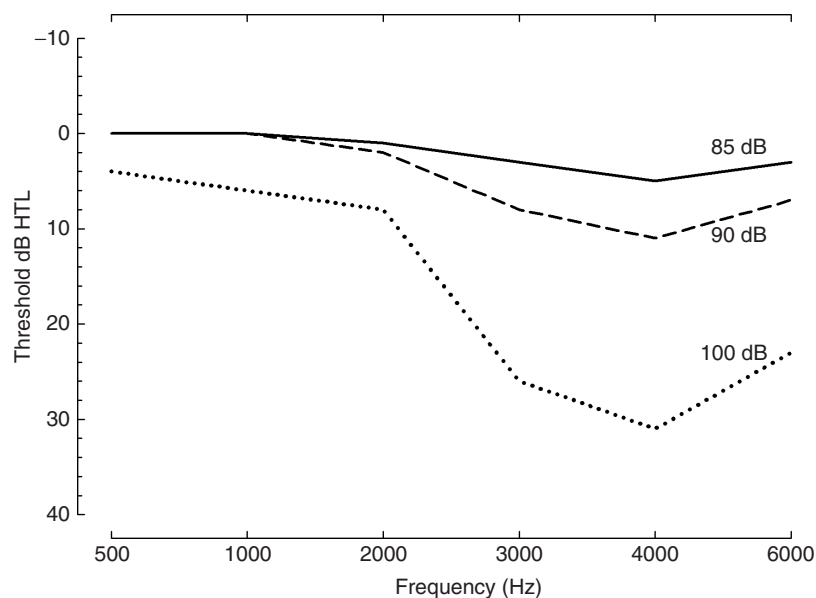


Figure 2 ISO 1999 30-year-old male hearing thresholds.

and feedback that affect the compliance of employees with the requirements of the HCP.

A preliminary gauge of program effectiveness may be determined from annual summaries of HCP monitoring results. Rates of NIHL lower than those predicted from the ANSI/ISO dose-response predictions are suggestive of an effective program if the data are reliable. Indicators of data quality are small variations between years using a metric of the percent of individual thresholds better or worse or the percent worse in sequential years of testing. Details of the technique of comparison can be found in the AIHA *Noise Manual*.<sup>9</sup> Although there is some controversy of the validity of details of the use of database comparisons, the overall concept can provide useful insights into the quality of an HCP.

### 3.2 Comparison with Normative Data (ISO 1999/ANSI S3.44)

Additionally, hearing threshold level data for groups in an HCP may be compared with the referenced databases in ISO 1999<sup>11</sup>/ANSI S3.44.<sup>14</sup> A higher threshold for a particular age cohort with a known exposure in comparison to the referenced databases suggests reason for review of the HCP effectiveness. Comparison of populations in different departments within the facility is also instructive.

An HCP with effective hearing protection should exhibit similar trends of hearing threshold changes across departments with different exposures because the HPDs should reduce all exposures to below the PEL. The department exhibiting higher mean threshold shifts than others should be reviewed for adequacy of the HCP implementation.

## 4 EVALUATING CAUSALITY

### 4.1 Patterns of Noise-Induced Hearing Loss

Sounds of different frequency are distributed spatially within the cochlea. The classical pattern of noise-induced hearing loss begins with a decrease of thresholds in the frequencies corresponding to that place in the cochlea at which 4 kHz sounds are localized. As the hearing impairment progresses, the "4 kHz notch" deepens and extends to higher and lower frequencies. Typical progressions of NIHL, based on the ISO 1999<sup>11</sup> male database, are shown in Figs. 2 and 3.

For a typical 30-year-old male exposed to 85 dB over his working life, there is a small threshold deficit at 4 kHz. A cohort of the same age but exposed to 95 dB TWA for the same duration exhibits a pronounced threshold deficit at 4 kHz and the adjacent frequencies. The individual exposed at 100 dB TWA for that same period exhibits the pronounced hearing loss shown in Fig. 2.

That exposure level is more important than duration is seen by comparison with Fig. 3.

This shows population thresholds for males aged 30 to 60 years exposed at 90 dB TWA over their working lives. The difference between the 30-year-old cohort and the 60-year-old cohort is only about 5 dB at the most affected frequency of 4 kHz.

### 4.2 Comparison of Individual NIHL with Population Databases

Although it is not possible to predict an individual's NIHL based on level and duration of exposure, comparison of an employee's threshold with the population can be instructive. Figure 4 illustrates a

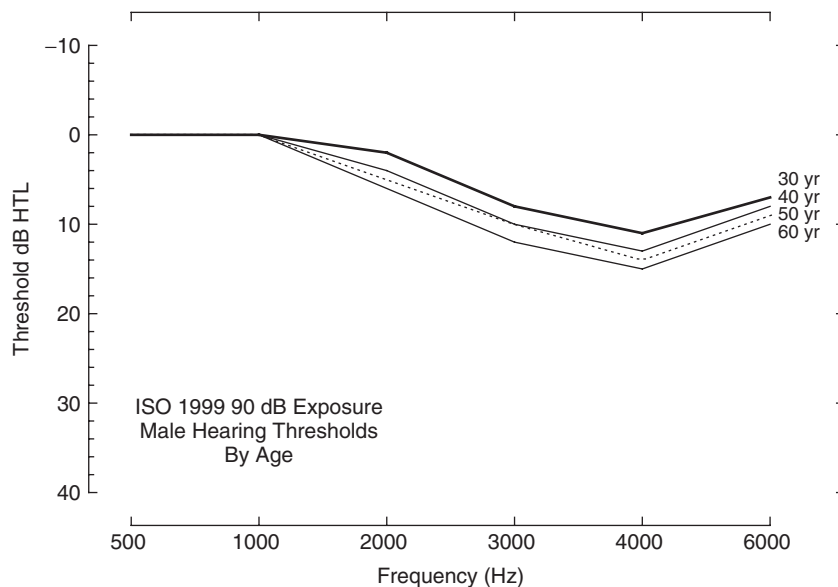


Figure 3 ISO 1999 90-dB exposure male hearing thresholds by age.

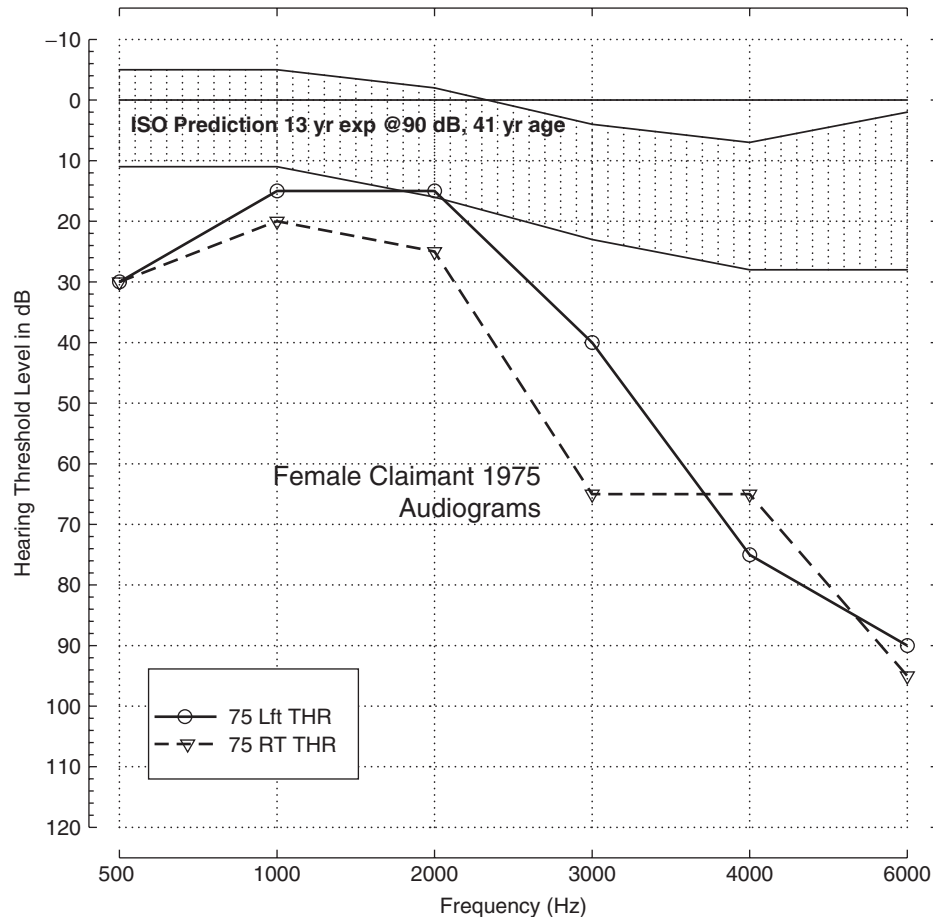


Figure 4 Female claimant 1975 audiograms.

range of hearing thresholds for female population exposed to 90 dB TWA for 13 years and for an individual similarly exposed. Predicted 90th and 10th percentile thresholds are shown. An individual exhibiting poorer thresholds than expected for the most sensitive subgroup is either exposed at levels higher than 90 dB TWA or may have hearing impairment of nonoccupational origin.

In this case, for a 13-year exposure at 90 dB, the hearing thresholds for a person claiming occupational NIHL at all frequencies other than 2 kHz are poorer than the predicted thresholds for the 10th percentile of the population. Furthermore, the pattern of hearing loss is atypical of NIHL; there is a low-frequency component and a substantial impairment at high frequencies. Twenty-two years after the first audiogram (Fig. 5) the new hearing profile for this person exhibits similar impairments at 4 and 6 kHz with a worsening of thresholds of as much as 40 dB in the lower frequencies. This is clear evidence of nonoccupational etiology of the impairment.

The audiometric profile in 1975 should have been cause for an otologic referral because of the departure from the normative thresholds.

#### 4.3 Retrospective Exposure Assessment Based On Current Hearing Levels

Given these possibilities, a retrospective noise survey database is invaluable. The combination of hearing impairments inconsistent with dose-response functions in the ISO/ANSI standards in support of previous exposure levels from past noise surveys is powerful evidence that the hearing impairment was not the result of occupational noise exposure.

#### 4.4 Role of the Otologist

At this point, referral to an otologist for a complete otologic examination is indicated. The otologist should be experienced in the evaluation of occupational hearing loss. A battery of tests included in this examination can definitively determine the cause of the threshold deficit.



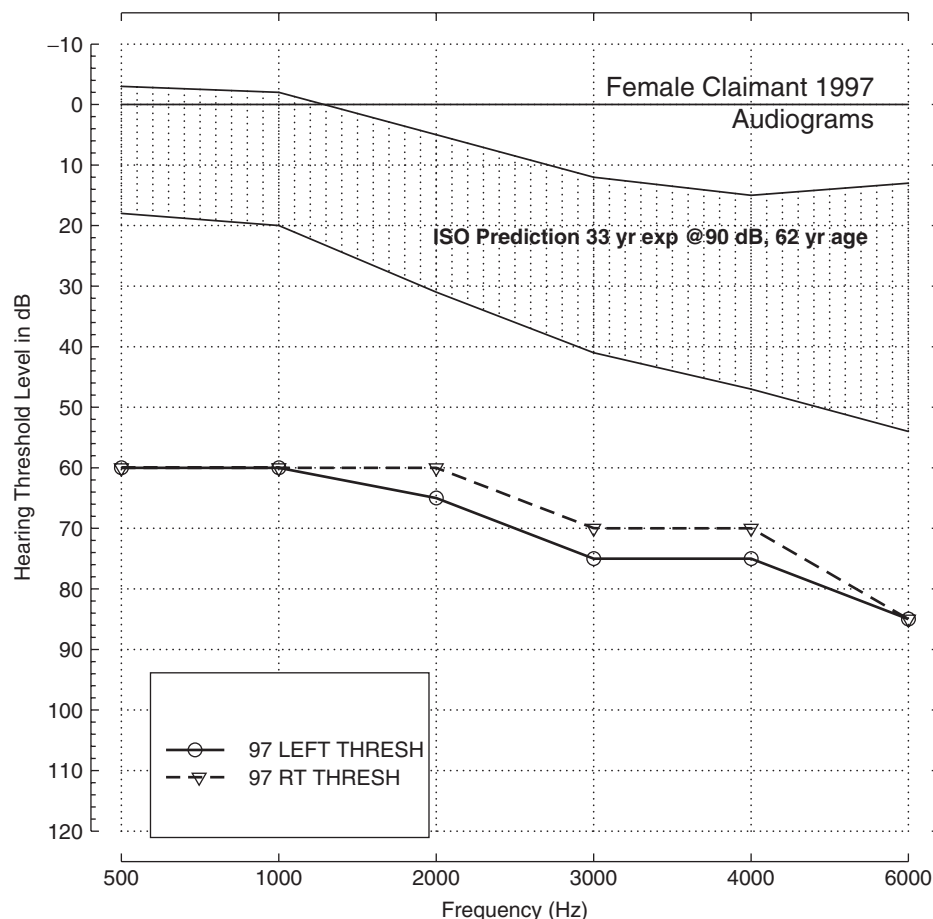


Figure 5 Female claimant 1997 audiograms.

#### 4.5 Nonoccupational Causes of Hearing Loss

Recent evidence in animal models as well as some epidemiologic studies has suggested that certain industrial chemicals may potentiate the effect of noise exposure by producing oxidative stress in the cochlea.<sup>15,16</sup> These substances include, among others, acrylonitrile, organic solvents, aminoglycoside antibiotics, and others. For this reason, it is recommended that the employee occupational history include summaries of chemical exposures as well as noise exposure.

#### REFERENCES

1. K. D. Kryter, *Physiological, Psychological, and Social Effects of Noise*. NASA reference publication RP-1115, 1984.
2. A. Glorig, W. D. Ward, and C. Nixon, Damage Risk Criteria and Noise-Induced Hearing Loss, *Arch. Otolaryngol.*, Vol. 74, 1961, pp. 413-423.
3. W. Burns and D. W. Robinson, *Hearing and Noise in Industry*, Her Majesty's Stationery Office, London, 1970.
4. New Jersey Permanent Statutes, Title 34 Labor and Workman's Compensation 34:15-35.10, Occupational Hearing Loss.
5. Occupational Safety and Health Administration, *Occupational Noise Exposure; Proposed Requirements and Procedures*, 39 *Fed. Reg.* 37773 [1974], (codified at 29 CFR 1910).
6. ISO (International Organization for Standardization), 3746:1995(E), *Acoustics—Determination of Sound Power Levels of Noise Sources Using Sound Pressure—Survey Method Using an Enveloping Measurement Surface over a Reflecting Plane*, (ISO, Geneva, Switzerland, 1995. 1, Geneva, Switzerland, 1995).
7. ANSI, American National Standard Institute, *Guidelines for the Specification of Noise of New Machinery* American National Standards Institute, New York, ANSI S12.16-1992.
8. M. J. Crocker, *Encyclopedia of Acoustics*, Wiley, New York, 1997.
9. I. M. Ventry, and J. B. Chaiklin, Evaluation of Pure-Tone Audiogram Configurations Used in Identifying

- Adults with Functional Hearing Loss, *J. Aud. Res.*, Vol. 5, 1965, pp. 212–218.
10. E. H. Berger, L. H. Royster, J. D. Royster, D. P. Driscoll, and M. Layne, Eds., *The Noise Manual*, AIHA Press, Alexandria, VA, 2000.
  11. ISO (International Organization for Standardization), *Acoustics—Determination of Occupational Noise Exposure and Estimation of Noise-Induced Hearing Impairment*, 2nd ed., ISO, Geneva, Switzerland, reference No. ISO 1999 (1990 E).
  12. J. Erdreich and L. S. Erdreich, Epidemiologic Strategies to Understanding Noise-Induced Hearing loss, in *New Perspectives in Noise-Induced Hearing Loss*, R. P. Hamernick, D. Henderson, and R. Salvi, eds., Raven Press, New York, 1982, pp. 439–460.
  13. J. Royster, and L.H. Royster, Evaluating Hearing Conservation Program Effectiveness, *The Noise Manual*, 5th ed., in E. Berger, et al., Eds., AIHA Press, Alexandria, VA, 2000.
  14. ANSI, American National Standard Institute, *Determination of Occupational Noise Exposure and Estimation Noise-Induced Hearing Impairment*, American National Standards Institute, New York, ANSI S3.44–1996.
  15. L. D. Fechter, S. F. L. Klis, N. A. Shirwany, T. G. Moore, and D. B. Rao, Acrylonitrile Produces Transient Cochlear Function Loss and Potentiates Permanent Noise-Induced Hearing Loss, *Toxicol. Sci.*, Vol. 75, 2003, pp. 117–123.
  16. T. C. Morata, D. E. Dunn, L. W. Kretschmer, G. K. Lemasters, and R. W. Keith, Effects of Occupational Exposure to Organic Solvents and Noise on Hearing, *Scand. J. Work Environ. Health*, Vol. 19, 1993, pp. 245–54.

## BIBLIOGRAPHY

- J. Fosbroke, Practical Observations on the Pathology and Treatment of Deafness, No. II, *The Lancet*, Vol. 1, —1831, pp. 645–648.
- D. L. Johnson, Prediction of NIPTS Due to Continuous Noise Exposure, Joint EPA/Air Force study, Wright-Patterson Air Force Base, OH, U.S. Air Force Aerospace Research Laboratory, Report No. AMRL-TR-73-91, 1973.

# CHAPTER 34

## RATING MEASURES, DESCRIPTORS, CRITERIA, AND PROCEDURES FOR DETERMINING HUMAN RESPONSE TO NOISE

Malcolm J. Crocker

Department of Mechanical Engineering  
Auburn University  
Auburn, Alabama

### 1 INTRODUCTION

People are exposed to noise during daytime and nighttime hours. During the day the noise can interfere with various activities and cause annoyance, and at night it can affect sleep. Very intense noise can even lead to hearing damage (see Chapters 19, 20, 27 to 29, and 33). In the daytime the activities most affected are communications that involve speech between individuals, speech in telephone communications, and speech and music on radio and television. If the noise is more intense, it is normally more annoying, although there are a number of other attitudinal and environmental factors that also affect annoyance. There are many different ways to measure and evaluate noise, each normally resulting in a different noise measure, descriptor, or scale. The various measures and descriptors mainly result from the different sources (aircraft, traffic, construction, industry, etc.) and the different researchers involved in producing them. From these measures and descriptors, criteria have been developed to decide on the acceptability of the noise levels for different activities. These criteria are useful in determining whether noise control efforts are warranted to improve speech communication, reduce annoyance, and lessen sleep interference. This chapter contains a review and discussion of some of the most important noise measures and descriptors. In the past 20 to 30 years these measures and descriptors have undergone some evolution and change as researchers have attempted to find descriptors that best relate to different human responses and are more easily measurable with improved instrumentation. For completeness this evolution is traced and some measures and descriptors are described that are no longer in use, since knowledge of them is needed in the study of the results of various noise studies reported in the literature.

### 2 LOUDNESS AND ANNOYANCE

As the level of the noise is increased, it is accompanied by an apparent increase in loudness. Loudness may be considered to be the subjective evaluation of the intensity of a noise when this evaluation is divorced from all the attitudinal, environmental, and emotional factors that may affect the listener's assessment of the annoying properties of the noise. Chapter 21

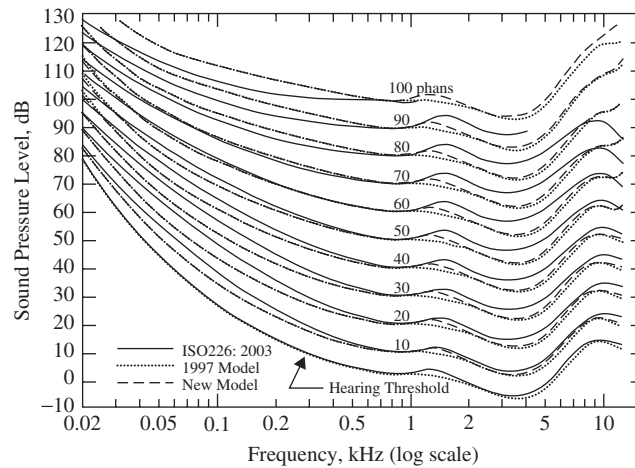
contains a detailed discussion on the loudness of noise. Generally, if a noise is louder, it is judged to be more annoying and vice versa, although there are exceptions. Table 1 shows some of the acoustical and nonacoustical factors that can contribute to the annoyance caused by noise. Some of the factors shown in Table 1 are also important in considerations of the effects of noise on speech communication (see Sections 6 and 7) and on sleep (see Section 15.1 and Chapter 24). The annoyance caused by noise is discussed further in Section 15.2 and in detail in Chapter 25.

### 3 LOUDNESS AND LOUDNESS LEVEL

As discussed in Chapter 21, which contains an in-depth description of the loudness of sound, and Chapter 67, the human ear does not have a uniform sensitivity to sound as its frequency is varied. Figure 2 in Chapter 21 and Fig. 2 in Chapter 67 show equal-loudness-level contours. These contours connect together pure-tone sounds that appear equally loud to the average listener. Recently, slightly modified contours have been proposed by Moore and co-workers.<sup>1-3</sup> See Fig. 1. In 2005, a new American National Standards Institute (ANSI) standard (ANSI S3.4-2005)<sup>4</sup> for the calculation of the loudness of steady sounds was published. This 2005 ANSI standard<sup>4</sup> is based on the loudness model of Moore et al.<sup>1</sup> The model in ANSI S3.4-2005 gives reasonably accurate predictions of a wide range of data on loudness perception.<sup>1</sup> However, the equal-loudness contours predicted by the model shown as the dotted

**Table 1 Some Acoustical and Nonacoustical Factors That Contribute to Annoyance Caused by Noise**

Acoustical Factors	Nonacoustical Factors
Sound pressure level	Time of day
Frequency spectrum	Time of year
Duration	Necessity for noise
Pure-tone content	Community attitudes
Impulsive character	Past experience
Fluctuation in level	Economic dependence on source



**Figure 1** The bottom curves (marked Hearing Threshold) show the absolute thresholds (free field, frontal incidence, binaural listening) predicted by the original (1997) model<sup>1</sup> (dotted line), the modified model (dashed line), and as published in ISO 389-7 (2005),<sup>7</sup> (solid line). The other curves show equal-loudness contours as predicted by the original model, the modified model, and as published in ISO 226 (2003)<sup>8</sup> (dotted, dashed, and solid lines, respectively).

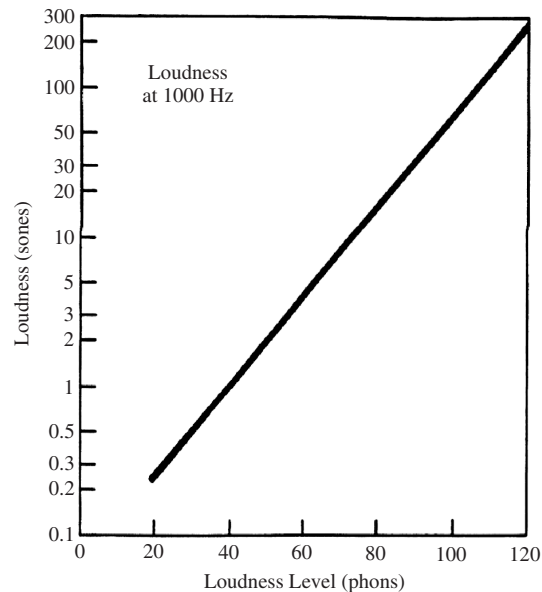
lines in Fig. 1 differ substantially from those in the International Organization for Standardization (ISO) standard that was applicable at the time (ISO 226, 1987),<sup>5</sup> which in turn were based on the 1956 data of Robinson and Dadson.<sup>6</sup>

Similar contours have been determined experimentally for bands of noise instead of pure tones. The unit of (linear) loudness is the *sone*. A sone is defined as the loudness of a pure tone, which has a sound pressure level of 40 dB at 1000 Hz. A sound that is twice as loud is said to have a loudness of 2 sones and so on. The loudness level of a 1000-Hz pure tone of 40 dB is defined as 40 *phons*. If the 1000-Hz pure tone is raised in level by 10 dB, it appears to be about twice as loud to the average listener. Thus a doubling of the loudness has been defined to be equivalent to an increase in loudness level of 10 phons. The relationship between loudness  $S$  and loudness level  $P$  (for both pure tones and bands of noise) is thus given by Eq. (1) and shown in Fig. 2:

$$S = 2^{(P-40)/10} \quad (1)$$

The preceding discussion has concerned the loudness of pure tones. Equal loudness contours for bands of noise were determined experimentally and independently by Stevens and Zwicker and standardized.<sup>9-12</sup> These can be used to evaluate the loudness (in sones) of noise sources. The procedure used in the Stevens mark VI method is to plot the noise spectrum in either octave or one-third-octave bands onto the loudness index contours. The loudness index (in sones) is determined for each octave (or one-third-octave) band and the total loudness  $S$  is then given by

$$S = S_{\max} + 0.3 \left( \sum S - S_{\max} \right) \quad (2)$$



**Figure 2** Relationship between the loudness (in sones) and the loudness level (in phons) of a sound.

where  $S_{\max}$  is the maximum loudness index and  $\sum S$  is the sum of all the loudness indices. The 0.3 constant (used for octave bands) in Eq. (2) is replaced by 0.15 for one-third-octave bands. The Stevens method assumes that the sound field is diffuse and does not contain any prominent pure tones. The Zwicker method is based on the critical band concept and, although more complicated than the Stevens method,

can be used either with diffuse or frontal sound fields. Complete details of the procedures are given in the ISO standard,<sup>12</sup> and Kryter<sup>13</sup> has discussed the critical band concept in his book. See also the updated ANSI standard, ANSI S3.4-2005.<sup>4</sup> This is based on the Zwicker method<sup>10,11</sup> but uses the more recent data of Glasberg and Moore.<sup>1,3</sup> In recent years the Zwicker method<sup>10,11</sup> has become more widely used than the Steven's method because it appears to relate better to the physiological response of the human auditory system.

#### 4 NOISINESS AND PERCEIVED NOISE LEVEL

##### 4.1 Noisiness

Although the level of noise or its loudness is very important in determining the annoyance caused by noise, there are other acoustical and nonacoustical factors that are also important. In laboratory studies, people were asked to rate sounds of equal duration in terms of their noisiness, annoyance, or unacceptability.<sup>16,17</sup> Using octave bands of noise, Kryter and others have produced *equal noisiness index* contours. These equal

noisiness contours are similar to those for equal loudness, except that at high frequency less sound energy is needed to produce equal noisiness and at low frequency more is needed. The unit of noisiness index is the *noy*  $N$ . Equal noisiness index curves are shown in Fig. 3. The procedure to determine the logarithmic measure, the *perceived noise level* (PNL), is quite complicated and has been standardized.<sup>18</sup> It has also been described in several books.<sup>19-21</sup> (See also Chapter 43.) Briefly, it may be stated as follows. Tabulate the octave band (or one-third-octave band) sound pressure levels of the noise. Calculate the noisiness index in noys for each band in Fig. 3.

Then calculate the total noisiness index  $N$ , from

$$N_t = N_{\max} + 0.3 \left( \sum N - N_{\max} \right) \quad (3)$$

where  $N_{\max}$  is the maximum noisiness index and  $\sum N$  is the sum of all the noisiness indices. If one-third-octave bands are used, the constant 0.3 for octave bands in Eq. (3) is replaced by 0.15.

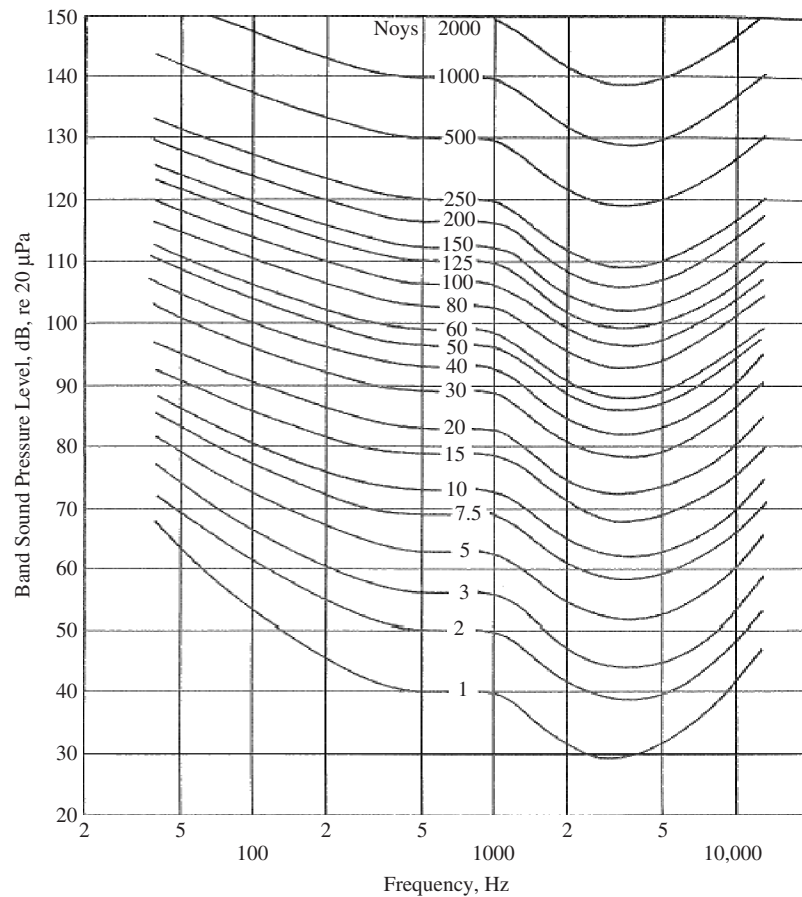


Figure 3 Contours of perceived noisiness.

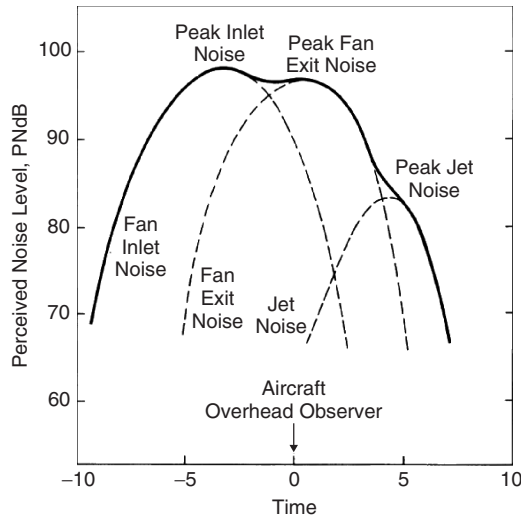
The total perceived noisiness index  $N_t$  (summed over all frequency bands) is converted to the PNL or  $L_{PN}$  from

$$L_{PN} = 40 + (33.22) \log N_t \quad (4)$$

The procedure is similar to that for calculating loudness level (phons) from loudness (sones). Some have questioned the usefulness of this procedure since listeners in laboratory experiments do not seem to be able to distinguish between (1) loudness and (2) noisiness and (3) annoyance. Despite this, the procedure has been widely used in assessing single-event aircraft noise. In the United States the Federal Aviation Administration (FAA) has adopted the effective perceived noise level for the certification of new aircraft. As an example, the noisiness of the spectra given in Fig. 6 of Chapter 119 can be calculated. The takeoff noise shown by the upper dashed line of Fig. 6 of Chapter 119 has a noisiness of 170 noys and a perceived noise level of 114 PNdB. Perceived noise level has received wide acceptance in many countries as a measure of aircraft noisiness with and without tone corrections.

#### 4.2 Effective Perceived Noise Level

Although PNL can be used to monitor the peak noise level of an aircraft passby (or flyover or flyby), this measure does not take into account the variation of the noise or its duration. Experiments have shown that annoyance and noisiness increase both with the magnitude and with the duration of a noise event. Noise that is of long duration is normally judged to be more annoying than noise of short duration. Figure 4 shows a PNL time history of a flyover of a typical fanjet aircraft. As the airplane approaches, the discrete



**Figure 4** Typical noise history of a fanjet aircraft flyover.<sup>12</sup>

frequency whine caused by fan and compressor noise radiated from the engine inlets is very evident. When the airplane is overhead, the noise is dominated by that from the fan exit and is again mostly whine. When the plane has passed, the low-frequency jet rumble is heard. The peaks for each source occur at different times since each source is very directional. The inlet noise is mainly “beamed” forward in the flight direction, while the jet noise is mainly radiated backward about 45° to the jet exhaust direction.

In addition to the effects of noise level and duration, the effects of tonal content must be considered. If the noise contains pure tones along with the broadband noise spectrum, it is also judged to be noisier than without such tones. To account for these effects the effective perceived noise level (EPNL) or  $L_{EPN}$  has been defined as

$$L_{EPN} = L_{PN,max} + C + D \quad (5a)$$

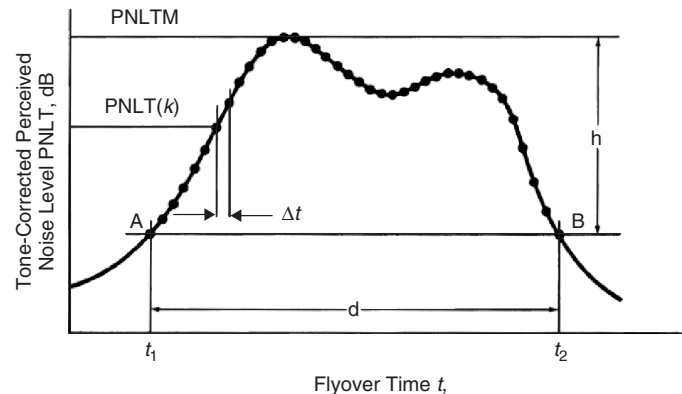
where  $C$  is the correction factor for pure tones (between 0 and 6 dB, depending on frequency and the tone magnitude in relation to the broadband noise in adjacent frequency bands) and  $D$  is a correction for duration.<sup>17-19</sup> EPNL is simply a time integration of the tone-corrected perceived noise level. Equation (5a) does not directly reveal the time integration. However, EPNL is defined in Federal Aviation Regulations (FAR) Part 36, and also International Civil Aviation Organization (ICAO) Annex 16 as

$$L_{EPN} = 10 \log \{ \text{sum} [ 10^{L_{PN}(k)/10} \Delta t ] \} - 10 \quad (5b)$$

where  $L_{PN}(k)$  is the perceived noise level plus the tone correction of the  $k$ th sample in the time history. There are some complexities regarding the maximum value of  $L_{PN}(k)$  also known as  $PNLT(k)$  if the tone correction at that moment is not as large as the average tone correction for the two preceding and two succeeding samples in which case this average replaces the tone correction value for sample  $k$ . But essentially Eq. (5b) states the summation process that is actually taking place, just as in any time-integrated measure of noise level.

The EPNL takes into account tonal content, duration, and the level of the noise by integrating the tone-corrected PNL over the duration of the event. An example of how the tone-corrected PNL varies with an aircraft flyover is shown in Fig. 5. For aircraft certification purposes  $h$  is equal to 10 PNdB,  $\Delta t$  is equal to 0.5 s, and the duration,  $d$ , is determined by the 10-dB down points shown as A and B in Fig. 5.

The procedure for calculating  $L_{EPN}$  is quite complicated, and its description is beyond the scope of this chapter. It is fully described in standards<sup>16,21,22</sup> and in some other books.<sup>17-19</sup> There is a useful, approximate relationship between A-weighted sound pressure level,  $L(A)$  and PNL. For aircraft noise spectra this is generally taken to be  $PNL = L(A) + 13$ , and  $EPNL = SEL + 3$  (SEL is sound exposure level). The A-weighting filter and A-weighted sound pressure level are discussed in the next section.

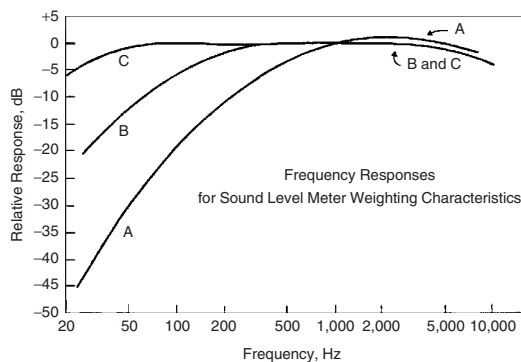


**Figure 5** How tone-corrected perceived noise level may vary in an aircraft flyover, showing some of the labeling used in the calculation of effective perceived noise level.<sup>20</sup>

## 5 WEIGHTED SOUND PRESSURE LEVELS

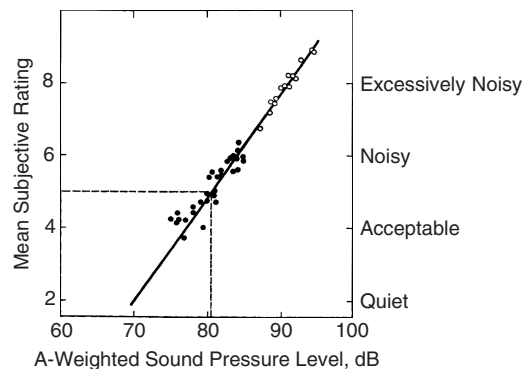
Figure 1 in this chapter and Fig. 2 in Chapter 21 show that the ear is most sensitive to sounds in the mid-frequency range around 1000 to 4000 Hz. It has a particularly poor response to sound at low frequency. It became apparent to scientists in the 1930s that electrical filters could be designed and constructed with a frequency response approximately equal to the inverse of these equal loudness curves. Thus A-, B-, and C-weighting filters were constructed to approximate the inverse of the 40-, 70-, and 90-phon contours (i.e., for low-level, moderate, and intense sounds), respectively. (See Fig. 1.) In principle, then, these filters, if placed between the microphone and the meter display of an instrument such as a sound level meter, should give some indication of the loudness of a sound (but for pure tones only).

The levels measured with the use of the filters shown in Fig. 6 are commonly called the A-, B-, and C-weighted sound levels. The terminology A-, B-, and C-weighted sound pressure levels is preferred by ISO to reduce any confusion with sound power level and will be used wherever possible



**Figure 6** A-, B-, and C-weighting filter characteristics used with sound level meters.

throughout this handbook. The A-weighting filter has been much more widely used than either the B- or C-weighting filter, and the A-weighted sound pressure level measured with it is still simply termed by ANSI as the sound level or noise level (unless the use of some other filter is specified). Because it is simple, giving a single number, and it can be measured with a low-cost sound level meter, the A-weighted sound pressure level has been used widely to give an estimate of the loudness of noise sources such as vehicles, even though these produce moderate to intense noise. Beranek and Ver have reviewed the use of the A-weighted sound pressure level as an approximate measure of loudness level.<sup>23</sup> The A-weighted sound pressure levels are often used to gain some approximate measure of the loudness levels of broadband sounds and even of the acceptability of the noise. Figure 7 shows that there is reasonable correlation



**Figure 7** Relation between subjective response and A-weighted sound pressure level for diesel engine trucks undergoing an acceleration test; •, values measured in 1960, ○, values measured in 1968. (From C. H. G. Mills and D. W. Robinson, *The Subjective Rating of Motor Vehicle Noise*, *The Engineer*, June 30, 1961; Ref. 39; and T. Priede, *Origins of Automotive Vehicle Noise*, *J. Sound Vib.*, Vol. 15, No. 1, 1971, pp. 61–73.)



between the subjective response of people to vehicle noise and A-weighted sound pressure levels for vehicle noise. The A-weighted sound pressure level forms the basis of many other descriptors described later in this chapter and of the SEL, single-event noise exposure level (SNEL), equivalent continuous sound pressure level  $L_{Aeq}$ , day-night level (DNL) ( $L_{dn}$ ), and day-evening-night level (DENL) discussed in Chapters 1 and 119. The A-weighted sound pressure level descriptor is also used as a limit for new vehicles (Chapter 119) and noise levels in buildings (see Chapter 97 in the *Encyclopedia of Acoustics*) in several countries. Although the A-weighting filter was originally intended for use with low-level sounds of about 40 dB, it is now commonly used to rate high-level noise such as in industry where A-weighted sound pressure levels may exceed 90 dB. At such high levels the A-weighted sound pressure level and the loudness level are normally in disagreement.

## 6 ARTICULATION INDEX AND SPEECH INTELLIGIBILITY INDEX

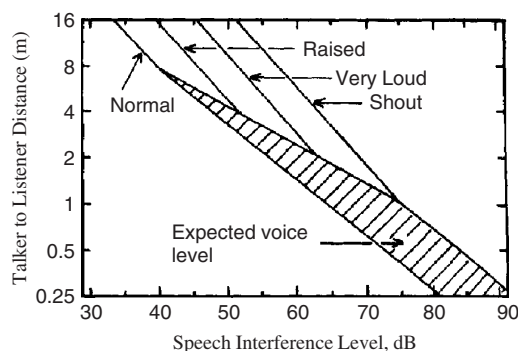
The articulation index (AI) is a measure of the intelligibility of speech in a continuous noise. The AI was first proposed by French and Steinberg<sup>24</sup> and was extended later by Beranek and Ver.<sup>23</sup> Speech has a dynamic range of about 30 dB in each one-third-octave band from 200 to 6000 Hz, and the long-term root-mean-square (rms) overall sound pressure level at the speaker's lips is about 65 dB. In speech, vowels and consonants are joined together to produce not only words but sounds that have a distinctive personal nature as well. The vowels usually have greater energy than consonants and give the speech its distinctive characteristics. This is because vowels have definite frequency spectra with superimposed short-duration peaks. The articulation index ranges from AI = 0 to 1.0 corresponding to 0 and 100% intelligibility, respectively. If the AI is less than about 0.3, speech communication is unsatisfactory (only about 30% of monosyllabic words understood); while if the AI is greater than about 0.6 or 0.7, speech communication is generally satisfactory (with more than 80% of monosyllabic words understood). Methods to calculate the AI are somewhat complicated and are given in American National Standard (ANSI S3.5–1969)<sup>25</sup> and explained in several books.<sup>17,20</sup> Since the calculation of AI is complicated, it will not be explained in detail here. The calculation of AI is also described briefly in Chapter 106. In 1997 the ANSI S3.5–1969 standard was updated and then further revised in 2002.<sup>26</sup> In this later standard, the AI has been renamed as the speech intelligibility index (SII). As before, the SII is calculated from acoustical measurements of speech and noise. The reader is referred to the new standard for the changes from AI to SII and complete details of the calculation of this index.<sup>26</sup> Because of the complication in the calculation of AI and SII, many favor the use of the speech interference level (SIL), which is easier to calculate. SIL is described in the next section of this chapter.

## 7 SPEECH INTERFERENCE LEVEL

The speech interference level is a measure used to evaluate the effect of background noise on speech communication.<sup>23</sup> The speech interference level is the arithmetic average of the sound pressure levels of the interfering background noise in the four octave bands with center frequencies of 500, 1000, 2000, and 4000 Hz [see ANSI S3.14–1977(R-1986)]. If the SIL of the background noise is calculated, then this may be used in conjunction with Fig. 8 to predict the sort of speech required for satisfactory face-to-face communication with male voices (i.e., for at least 95% sentence intelligibility). As an example, if the SIL is 40 dB and the speakers are males, they should be able to communicate with normal voices at 8 m. If the SIL increases to 50, raised voices must be used at 8 m. For females the SIL should be decreased by 5 dB (or the  $x$  axis moved to the right by 5 dB.) The shaded area of Fig. 8 shows the range of speech levels that normally occur as people raise their voices to overcome the background noise. Speech interference level is also discussed in Chapter 106. Because it is simpler to measure than the SIL, the A-weighted sound pressure level is sometimes used as a measure of speech interference, but with somewhat less confidence. Webster has produced a comprehensive diagram (see Fig. 9) that summarizes speech levels required for communication (at various distances) with 97% intelligibility of sentences for both outdoor and indoor situations.<sup>27</sup> Figure 9 is similar to Fig. 8 but contains some additional information concerning voice levels in different situations. With noise levels above 50 dB, people tend to raise their voice levels as shown by the “expected line” (at the left) for nonvital communication and the “communicating line” (at the right) of the diagonal shaded area for essential communication.

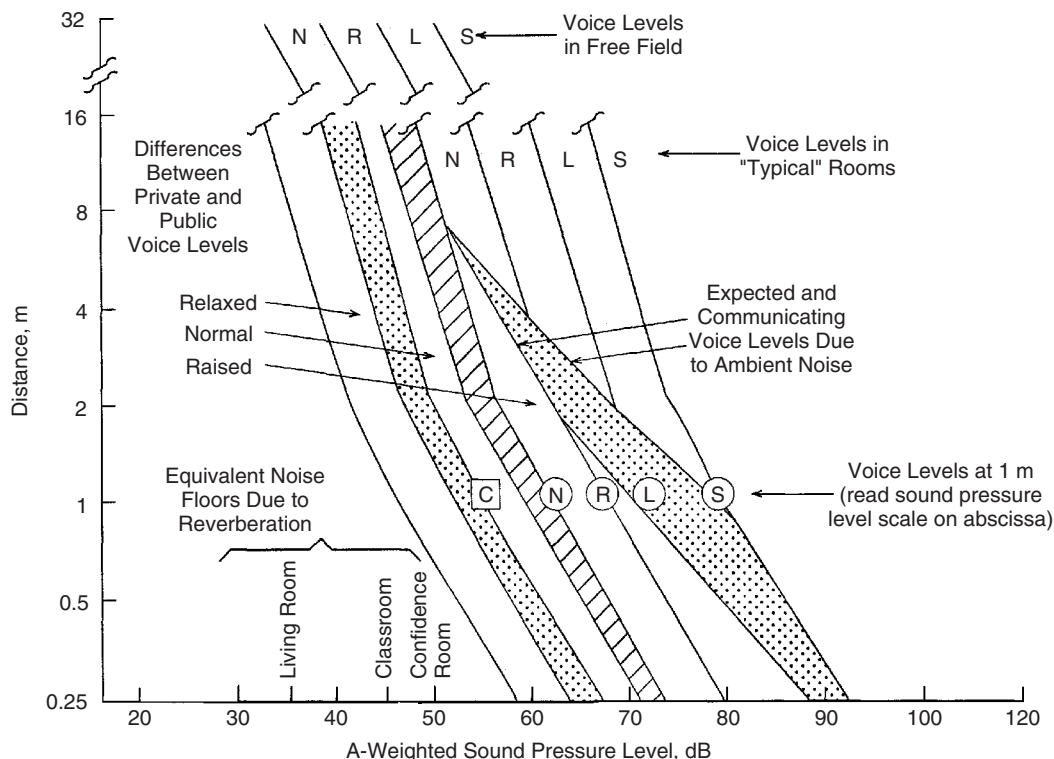
## 8 INDOOR NOISE CRITERIA

The speech interference level is mainly used to evaluate the effect of noise on speech in situations outdoors



**Figure 8** Talker-to-listener distances (m) for male speech communication to be just reliable. (Reprinted from American Standard ANSI S3.14–1977.)





**Figure 9** Comprehensive diagram summarizing speech levels for communication (at various distances) for 97% intelligibility of sentences on first presentation to listeners for both outdoors (free field) and indoor situations.<sup>27</sup>

or indoors where the environment is not too reverberant. The A-weighted sound pressure level can be used as a guide for the acceptability of noise in indoor situations, but it gives no indication about which part of the frequency spectrum is of concern. A number of families of noise-weighting curves have been devised to evaluate the acceptability of noise in indoor situations. These include *noise criterion (NC) curves*, *noise rating (NR) curves*, *room criterion (RC) curves*, and *balanced noise criterion (NCB) curves*. The curves have resulted from the need to either specify acceptable noise levels in buildings or determine the acceptability of noise in existing building spaces. A major concern has been to determine the acceptability of air-conditioning noise. Beranek and co-workers<sup>28-31</sup> has been a major contributor to the development of the NC and NCB noise criterion curves. Beranek and co-workers<sup>28-31</sup> and Blazier<sup>32</sup> were mainly responsible for the development of the RC room criterion curves. NR curves were devised by Kosten and van Os<sup>33</sup> and are similar to the NC curves. They have been standardized and adopted by the ISO. These noise-weighting curves are now reviewed briefly.

### 8.1 Noise Criterion Curves

The NC curves (Fig. 10) were developed from the results of a series of interviews with people in offices,

public spaces, and industrial spaces.<sup>28,29</sup> These results showed that the main concern was the interference of noise with speech communication and listening to music, radio, and television. In order to determine the NC rating of the noise under consideration, the octave-band sound pressure levels of the noise are measured, and these are then plotted on the family of NC curves (Fig. 10). The noise spectrum must not exceed the particular NC curve specified in any octave band in order for it to be assigned that particular NC rating.<sup>23</sup> NC curves are also discussed in Chapter 106.

### 8.2 Noise Rating Curves

The NR curves are similar to the NC curves (see Fig. 10). They were originally produced to develop a procedure to determine whether noise from factories heard in adjacent apartments and houses is acceptable.<sup>33</sup> The noise spectrum is measured and plotted on the family of NR curves (Fig. 11) in just the same way as with the NC curves. One difference from the NC curves, however, is the use of corrections for time of day, intermittency, audible pure tones, fraction of time the noise is heard, and type of neighborhood. These corrections are made to the final NR rating and not to the octave band levels used to determine the NR. It has been found that in the range of NR or NC

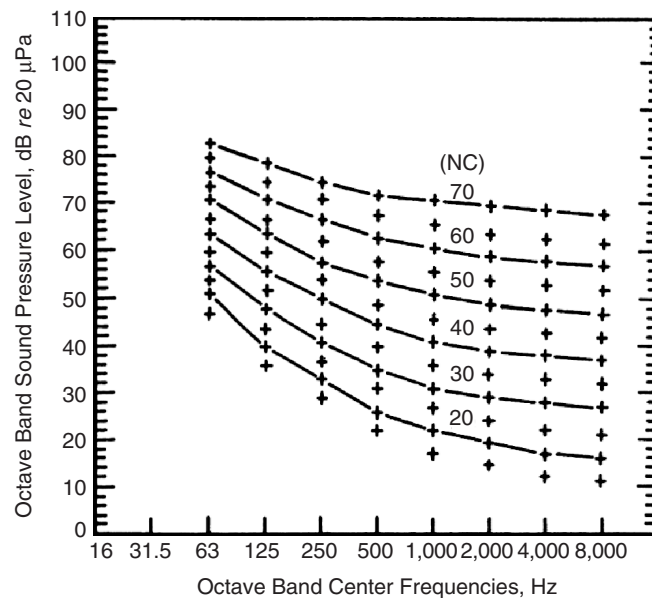


Figure 10 Noise criterion (NC) curves.

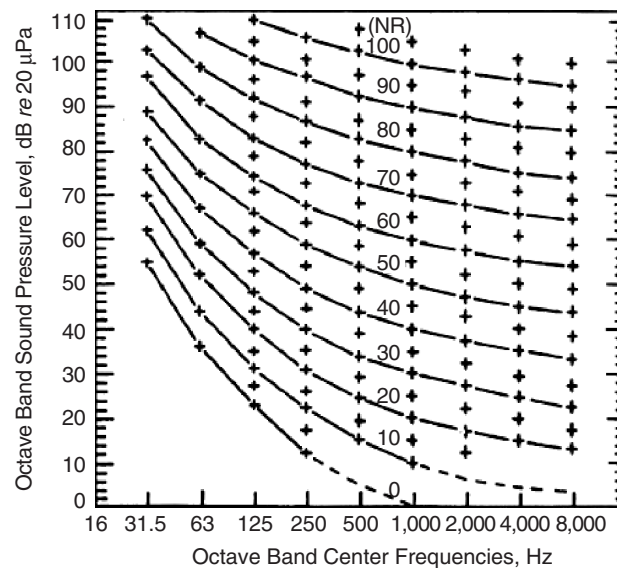


Figure 11 Noise rating (NR) curves.

of 20 to 50 there is little difference between the results obtained from the two approaches.

### 8.3 Room Criterion Curves

Noise Criterion curves are not defined in the low-frequency range (16- and 31.5-Hz octave bands) and are also generally regarded as allowing too much noise in the high-frequency region (at and above

2000 Hz). Blazier based his derivation of the RC curves on an extensive study conducted for the American Society of Heating, Refrigeration, and Air Conditioning Engineers (ASHRAE) by Goodfriend of generally acceptable background spectra in 68 unoccupied offices.<sup>32</sup> The A-weighted sound pressure levels were mostly in the range of 40 to 50 dB. Blazier<sup>32</sup> found that the curve that he obtained from

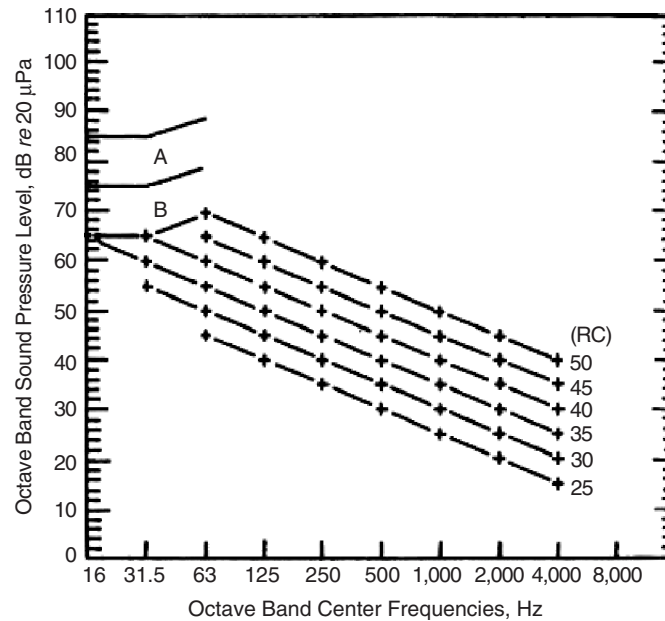


Figure 12 Room criterion (RC) curves.

the measured data had a slope of about  $-5$  dB/octave, and he thus drew a family of straight lines with this slope (see Fig. 12). He also found that intense low-frequency noise with a level of 75 dB or more in region A is likely to cause mechanical vibrations in lightweight structures (including rattles), while noise in region B has a low probability to cause such vibration. The value of the RC curve is the arithmetic average of the levels at 500, 1000, and 2000 Hz. Since these curves were obtained from measurements made with air-conditioning noise, they are mostly useful in rating the noise of such systems. RC curves are also discussed in Chapter 106.

#### 8.4 Balanced Noise Criterion Curves

In 1989, Beranek<sup>30,31</sup> modified the NC curves to include the 16- and 31.5-Hz octave bands and changed the slope of the curves so that it is now  $-3.33$  dB/octave between 500 and 8000 Hz. He also incorporated the A and B regions as specified by Blazier<sup>32</sup> in the RC curves. The rating number of a *balanced noise criterion* NCB curve is the arithmetic average of the octave band levels with midfrequencies of 500, 1000, 2000, and 4000 Hz. The result is a set of rating curves that are useful to rate air-conditioning noise in buildings (see Fig. 13). As an example of its use, a background noise spectrum from air-conditioning is plotted (as the dashed curve) in Fig. 13. The NCB is calculated from the formula  $NCB = \frac{1}{4}(44 + 42 + 37 + 33)$  dB. Thus this background noise spectrum can be assigned a rating of NCB 39 dB. Such a noise spectrum might be just acceptable in a general office, and barely acceptable in a bedroom and living room in a house, but not acceptable

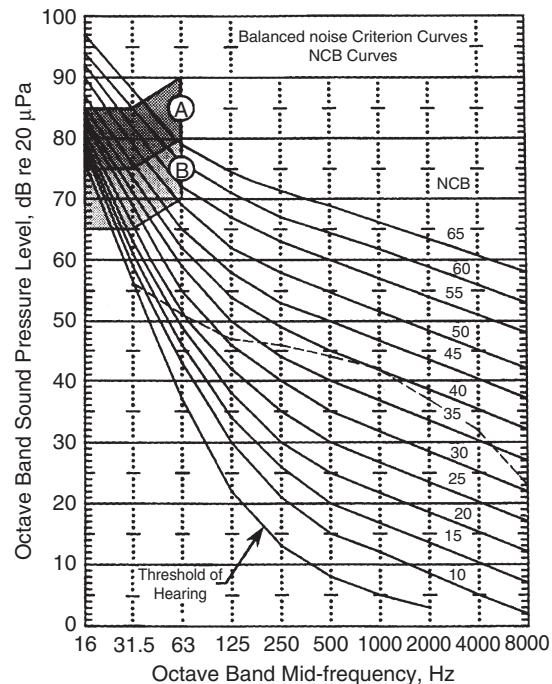


Figure 13 Balanced noise criterion (NCB) curves.

at all in a church, concert hall, or theater. NCB curves are also described in Chapter 106.

## 9 EQUIVALENT CONTINUOUS SOUND PRESSURE LEVEL

For noise that fluctuates in level with time it is useful to define the *equivalent continuous sound pressure level*  $L_{Aeq}$ , which is the A-weighted sound pressure level averaged over a suitable period  $T$ . This average A-weighted sound pressure level is also sometimes known as the *average sound level*  $L_{AT}$  in ANSI documents, so that  $L_{Aeq} = L_{AT}$ . The equivalent sound pressure level is given by

$$L_{Aeq} = 10 \log \left( \frac{1}{T} \int_0^T p_A^2 dt / p_{ref}^2 \right) \text{ dB} \quad (6)$$

where  $p_A$  is the instantaneous sound pressure measured using an A-weighting frequency filter and  $p_{ref}$  is the reference sound pressure 20  $\mu\text{Pa}$ . The averaging time  $T$  can be specified as desired to range from seconds to minutes or hours.

The average sound pressure level (or the equivalent continuous sound pressure level  $L_{Aeq}$ ) can be conveniently measured with an integrating sound level meter or some other similar device. Since it accounts both for magnitude and the duration,  $L_{Aeq}$  has become one of the most widely used measures for evaluating community (environmental) noise from road traffic, railways, and industry.<sup>34-36</sup>  $L_{Aeq}$  has also been found to be well correlated with the psychological effects of noise.<sup>37,38</sup> For community noise, a long-period  $T$  is usually used (often 24 h). In the literature  $L_{Aeq}$  is often abbreviated to  $L_{eq}$ .

## 10 DAY-NIGHT EQUIVALENT SOUND PRESSURE LEVEL

In the United States during the 1970s, the Environmental Protection Agency developed a measure, from the equivalent sound pressure level, known as the *day-night equivalent level* (DNL) or  $L_{dn}$  that accounts for the different response of people to noise during the night.<sup>38</sup>

$$L_{dn} = 10 \log \frac{15(10^{L_d/10}) + 9(10^{(L_n+10)/10})}{24} \quad (7)$$

where  $L_d$  is the 15-h daytime A-weighted equivalent sound pressure level (from 07:00 to 22:00) and  $L_n$  is the 9-h nighttime equivalent sound pressure level (from 22:00 to 07:00). The nighttime noise level is subjected to a 10-dB penalty because noise at night is deemed to be much more disturbing than noise during the day. This 10-dB nighttime penalty is analogous to the 10-dB nighttime penalty applied in both the composite noise rating (CNR) and the noise exposure forecast (NEF), as described in Section 12. The day-night equivalent level has become increasingly used in the United States and some other countries to evaluate community noise and in particular airport noise.<sup>36,39</sup> In 1980 the U.S. Federal Interagency Committee on Urban Noise (FICON) adopted  $L_{dn}$  as the appropriate descriptor of environmental noise in

residential situations.<sup>36-40</sup> Its use is also discussed in Chapter 106, where it is termed day-night average sound pressure level.

## 11 PERCENTILE SOUND PRESSURE LEVELS

The equivalent sound pressure level discussed above accounts for the fluctuation in noise level of an unsteady noise by forming an average sound pressure level to find an equivalent steady A-weighted sound pressure level. There is, however, some evidence that unsteady noise (e.g., from noise sources such as passing road vehicles or aircraft movements) is more disturbing than steady noise. To try to better account for fluctuations in noise level and the intermittent character of some noises, *A-weighted percentile sound pressure levels* are used in some measures, in particular those for community and traffic noise.<sup>34,41,42</sup> The level  $L_n$  is defined to represent the sound pressure level exceeded  $n\%$  of the time, and thus  $L_{10}$ , for example, represents the sound pressure level exceeded 10% of the time.

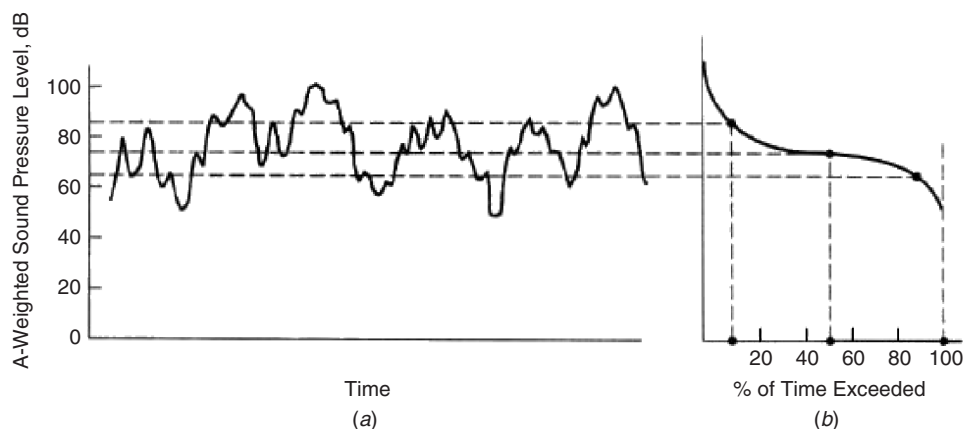
Figure 14 gives an example of  $L_{10}$ ,  $L_{50}$ , and  $L_{90}$  levels and a cumulative distribution. It is seen in this schematic example figure that the A-weighted level exceeded 10% of the time  $L_{10}$  is 85 dB, while  $L_{50}$  is sometimes termed the *median* noise level, since for half the time the fluctuating noise level is greater than  $L_{50}$  and for the other half it is less.  $L_{50}$  is used in Japan for road traffic noise. Levels such as  $L_1$  or  $L_{10}$  are used to represent the more intense short-duration noise events.  $L_{10}$  is used in Australia and the United Kingdom (over an 18-h 06:00 to 24:00 period) as a target value for new roads and for insulation regulations for new roads. Levels such as  $L_{90}$  or  $L_{99}$  are often used to represent the minimum noise level, the residual level from a graphic level recorder, or the average minimum readings observed when reading a sound level meter. Figure 15 shows the outdoor A-weighted sound pressure levels recorded in 1971 at 18 locations in the United States. Values of  $L_{99}$ ,  $L_{90}$ ,  $L_{50}$ ,  $L_{10}$ , and  $L_1$  are shown for the period 07:00 to 19:00.<sup>34,39</sup> The small range in levels in recordings 1 and 4 (urban situations) and the large range in levels in recordings 6, 11, 13, and 18 (situations involving aircraft overflights) are very evident. Obviously road traffic usually creates more steady noise, while aircraft movements lead to more extreme variations in noise levels. Percentile sound pressure levels are also discussed in Chapter 106.

## 12 EVALUATION OF AIRCRAFT NOISE

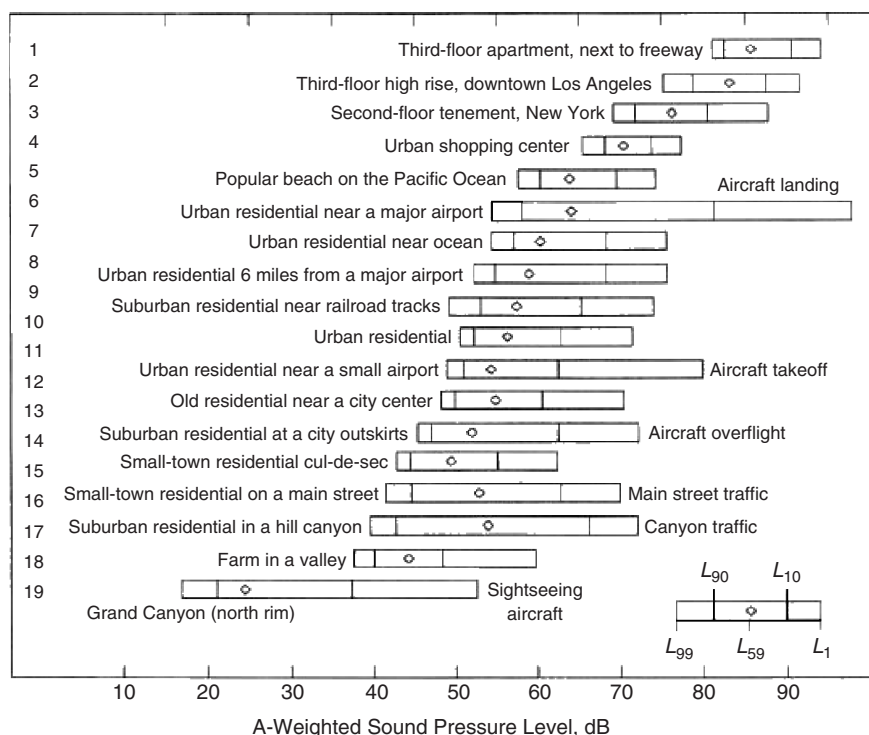
The noise levels around airports are of serious concern in many countries. Several attempts have been made to produce measures to predict and assess the annoyance caused by aircraft noise in the community. A study of rating measures in 1994 showed 11 different measures in use in the 16 countries studied.<sup>36</sup> The following measures merit brief discussion.

### 12.1 Composite Noise Rating

The CNR has a long history dating back to the early 1950s.<sup>43-45</sup> Originally, the basic measure it used was the level rank—a set of curves placed



**Figure 14** (a) Percentile levels and (b) cumulative probability distribution function of percentile levels.



**Figure 15** A-weighted sound pressure levels measured in 1971 at 18 locations in the United States. Values of the percentile levels  $L_{99}$ ,  $L_{90}$ ,  $L_{50}$ ,  $L_{10}$ , and  $L_1$ , where  $L_n$  is A-weighted sound pressure level exceeded  $n$  percent of the time are shown for the period 0700–1900 h. (From Refs. 34, 35, and 39)

about 5 dB apart in the midfrequency range, rather similar to the NC and NR curves described earlier. The level rank was obtained by plotting the noise spectrum on the curves and finding the highest zone into which the spectrum protruded. The rank found initially plus the algebraic addition of corrections

gave the CNR. The corrections<sup>43</sup> were for spectrum character, peak factor, repetitive character, level of background noise, time of day, adjustment to exposure, and public relations. The value of CNR obtained was associated with a range of community annoyance categories found from case histories—ranging from no

annoyance, through mild annoyance, mild complaints, strong complaints, and threats of legal action, to vigorous community response.

In the late 1950s, the CNR was adapted to apply to the noise of military jet aircraft<sup>46</sup> and later of commercial aircraft.<sup>47</sup> The calculation was further modified later when applied to commercial aircraft by using the PNL instead of the level rank or the sound pressure level (SPL) just referred to. More details on the calculation of CNR are given in the *Handbook of Acoustics*, Chapter 64.

The final version of CNR does not contain any corrections for background noise, previous experience, public relations, or other factors such as the presence of pure tones. Although CNR is no longer used, it is discussed here for completeness and because it has formed the basis for some of the other noise measures and descriptors, such as NEF, which follow.

## 12.2 Noise Exposure Forecast

The NEF is a similar measure to CNR, but it uses the effective perceived noise level instead of PNL.<sup>48,49</sup> Thus NEF automatically takes account of the annoying effects of pure tones and the duration of the flight events. The use of NEF has been superseded in the United States and most other countries by the day–night level  $L_{dn}$  or the day–evening–night level  $L_{den}$ .

## 12.3 Noise and Number Index

The *noise and number index* (NNI) is a subjective measure of aircraft noise annoyance first developed and used in the United Kingdom. The NNI was the outcome of surveys in 1961 and 1967 of noise in the residential districts within 10 miles of London (Heathrow) Airport.<sup>50,51</sup> NNI is based on a summation of  $\langle \text{PNL} \rangle_N$  terms weighted by aircraft movements.  $\langle \text{PNL} \rangle_N$  is the average peak noise level of all aircraft operating during a day, and  $N$  is the number of aircraft movements. Here PNL is the peak perceived noise level produced by an individual aircraft during the day and  $N$  is the number of aircraft operations of that type over a 24-h period.

In 1988 NNI was superseded in the United Kingdom by a measure based on the A-weighted  $L_{eq}$ . The  $L_{eq}$  is determined over the period 07:00 to 23:00. Noise at night is evaluated in terms of the size of the 90 SEL footprint of individual aircraft movements, or, less commonly, using  $L_{eq}$  determined over the period 23:00 to 07:00.

## 12.4 Equivalent A-weighted Sound Pressure Level $L_{eq}$ , Day–Night Level $L_{dn}$ , and Day–Evening–Night Level $L_{den}$

In recent years some countries have continued to use NEF or NNI or similar noise measures or descriptors related to those that include a weighting based on the number of aircraft movements.<sup>36</sup> However, because they are much simpler to measure and seem to give adequate correlation with subjective response, there has been a move in several countries toward the

use of  $L_{eq}$  and  $L_{dn}$ .<sup>36</sup> In Germany, Luxembourg, and the United Kingdom  $L_{eq}$  has been adopted: (1) in Germany and Luxembourg with day (06:00 to 22:00) and night (22:00 to 06:00) periods, and (2) in the United Kingdom with an 18-h period only (07:00 to 23:00) (because nighttime flights are normally restricted). The European Union has specified the use of  $L_{den}$  to evaluate aircraft noise, which includes three periods: day, evening, and night, from which  $L_{den}$  is calculated. See Chapters 1, 114, and 119.

In the United States since publication of the Environmental Protection Agency's (EPA) *Levels document*<sup>38</sup> and other similar publications, the use of CNR and NEF has been superseded by the day–night equivalent level DNL ( $L_{dn}$ ) for the assessment of the potential impacts of noise and for planning recommendations and land-use management near civilian and military airports.

## 13 EVALUATION OF TRAFFIC NOISE

### 13.1 Traffic Noise Index

In an attempt to develop acceptability criteria for traffic noise from roads in residential areas, Griffiths and Langdon<sup>57</sup> produced a unit for rating traffic noise, the *traffic noise index* (TNI). They measured A-weighted traffic noise at 14 sites in the London area and interviewed 1200 people at these sites in the process. Griffiths and Langdon excluded sites with noise sources other than traffic. They then used regression analysis to fit curves to the data. This indicated that  $L_{10}$  was better at predicting dissatisfaction than  $L_{50}$  or  $L_{90}$ , and that TNI was also superior to  $L_{10}$ ,  $L_{50}$ , and  $L_{90}$ .

Use of the traffic noise index has not been widespread. The index attempts to make an allowance for the noise variability since fluctuating noise is commonly assumed to be more annoying than steady noise.

Some doubt has been cast on the conclusions of Griffiths and Langdon, and it has been suggested that the very short sample times (100 s in each hour) used may have resulted in underestimates of  $L_{10}$  and overestimates of  $L_{90}$ .<sup>52</sup> TNI is not considered today to be significantly superior to either  $L_{10}$  or  $L_{eq}$  and has not been widely used.

Instead of TNI, the British government has adopted the A-weighted  $L_{10}$ , averaged over 18 h from 06:00 to 24:00, as the noise index to be used to implement planning and remedial measures to reduce the impact on people of road traffic noise.<sup>53–55</sup> In addition the British government uses a 16-h  $L_{eq}$  and an 8-h  $L_{eq}$  for the case of land used for residential development.

### 13.2 Noise Pollution Level

In a later survey, Robinson<sup>56</sup> again concluded that, with fluctuating noise,  $L_{eq}$ , the equivalent continuous A-weighted sound pressure level on an energy basis, was an insufficient descriptor of the annoyance caused by fluctuating noise. He included another term in his *noise pollution level* (NPL) or  $L_{NP}$ .

Robinson examined the available Griffiths and Langdon data.<sup>57</sup> He then examined the aircraft noise

experiments of Pearsons<sup>58</sup> and found that  $L_{NP}$  predicted very well Pearsons's data points and the trade-off between duration and level for individual flyover events. A-weighted levels were used in  $L_{NP}$  with traffic noise, and perceived noise levels (PNdB) were used with aircraft noise. The superiority of  $L_{NP}$  over all other forms of noise rating has not been proved in practice, and it has not been widely used.

### 13.3 Equivalent Sound Pressure Level

Figure 16 shows the annoyance results of Pearsons and co-workers, using six different noise ratings:  $L_1$ ,  $L_{10}$ ,  $L_{50}$ ,  $L_{90}$ ,  $L_{eq}$ , and  $L_{NP}$ .<sup>59</sup> As expected for all of the noise measures, annoyance increases with level. (See Chapter 25.) The shapes of the curves, however, do vary considerably when the annoyance is less than very annoying. In particular, the  $L_{10}$  and  $L_{eq}$  measures exhibit a very steep rise in annoyance from the categories of *slightly* to *moderately annoying* for no increase in noise level, presumably one of their drawbacks. However, except for the case of  $L_{NP}$  in the *extremely annoying* category, the standard deviation of  $L_{eq}$  for a specified response category was in all cases less than or equal to the standard deviation of the other noise measures. This is an advantage in the use of  $L_{eq}$  since there is more confidence in the annoyance scores predicted. There is one clear advantage of  $L_{eq}$  over  $L_{10}$ , however, in the case of noise containing short-duration, high-level single events. If the events do not occur for more than 10% of the time, then  $L_{10}$  will be relatively insensitive to these high-level events and will tend to represent the "background" noise. In fact, for a noise measure  $L_n$  to be useful, the intruding noise events must be present for *more than n%* of the time. This suggests that  $L_{10}$  would be unsuitable as a

measure of aircraft noise annoyance and that it might be a possible source of error in Griffiths and Langdon's results<sup>57</sup> for low traffic flows.

The A-weighted equivalent sound pressure level (often now denoted as  $L_{eq}$ ) has become the measure most commonly used to assess and regulate road traffic (and railroad noise).<sup>36</sup> In the United States  $L_{dn}$  (a similar measure) is used for road traffic noise assessment.

### 14 EVALUATION OF COMMUNITY NOISE

In some community noise measures, corrections are applied to community noise levels to account for pure-tone components or impulsive character, seasonal corrections (summer or winter when windows are always closed), type of district (rural, normal suburban, urban residential, noisy urban, very noisy urban), and for previous exposure (such corrections are similar to those for NR).

Figure 17 gives three examples of the A-weighted sound pressure levels measured in a community over a 24-h period.<sup>34</sup> The triangles in the three figures are the maximum levels read from a graphic level recorder. The continuous lines are percentile levels measured for hour-long periods throughout the 24 h. The highest percentile measure  $L_1$  does not represent the maximum levels well, which are presumably mostly higher level, short-duration sounds (occurring less than 1% of the time). It is observed in Fig. 17a and 17b that although the day-night levels  $L_{dn}$  are only 3 dB different (86 and 83), there is a much greater fluctuation in sound pressure level with time in Fig. 17b. This example is for a location near a major airport, and the fluctuation in level would suggest that the noise environment in location 6 would be much more annoying than in location 1 (near a freeway). Figure 17c illustrates

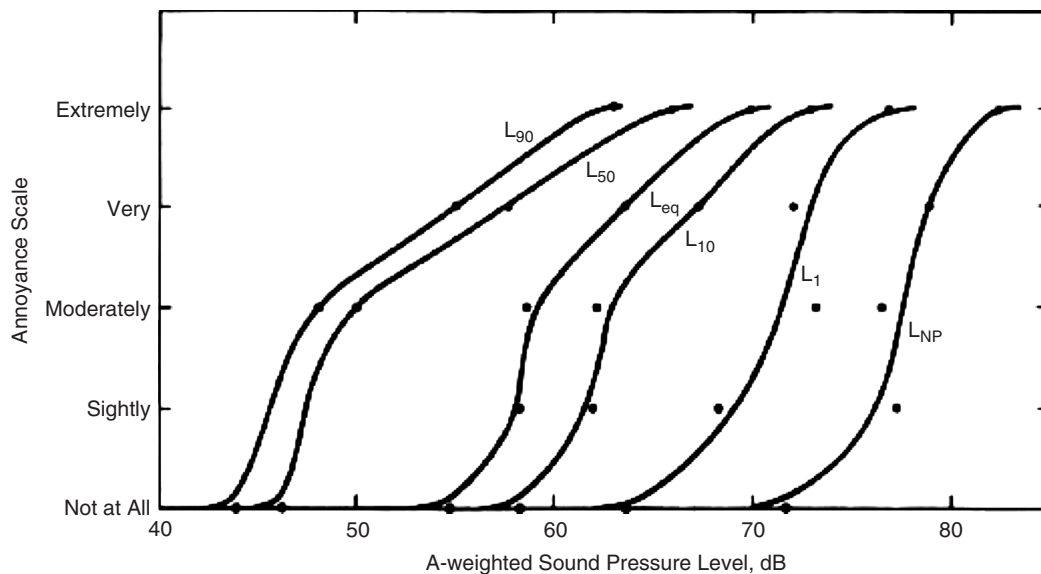
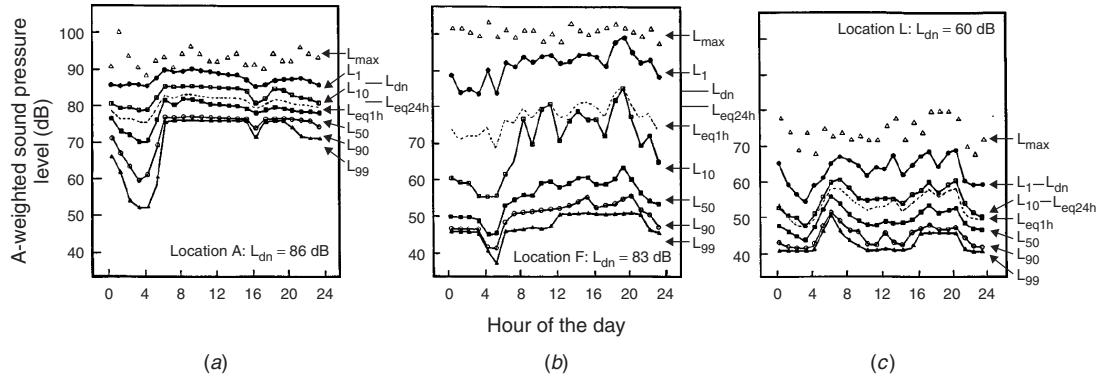


Figure 16 Annoyance as a function of noise level. (From Ref. 59)





**Figure 17** Variation of percentile levels throughout 24 h periods recorded at three residential locations (numbers 1, 6, and 12) in Los Angeles in 1971. (a) third-floor apartment near freeway, (b) urban residential location near major airport, and (c) old residential location near city center. The values of  $L_n$  represent the A-weighted sound pressure levels exceeded  $n$  percent of the time during 1-h periods. Hourly maximum levels  $L_{\max}$ , 1-h and 24-h values of  $L_{eq}$ , and the day-night level  $L_{dn}$  are also shown. (From Refs. 34 and 39.)

another quite different distribution of A-weighted sound pressure levels with time.

In the United States, the A-weighted  $L_{eq}$  and  $L_{dn}$  are normally used to characterize community noise. However, the Department of Housing and Urban Development (HUD) also recognizes the usefulness of  $L_{10}$  in some instances. In other countries the A-weighted  $L_{eq}$  is mainly used for community noise studies rather than  $L_{dn}$ . International standards on the description and measurement of environmental noise<sup>60</sup> recommend the use of A-weighted  $L_{eq}$  and rating levels (which are A-weighted  $L_{eq}$  values to which tone and impulse adjustments have been made). These standards also recommend that in some circumstances it may be useful to determine the distribution of A-weighted sound pressure levels by determining percentile levels such as  $L_{95}$ ,  $L_{50}$ , and  $L_5$ .

In California, some state legislation requires the use of the *community noise exposure level* (CNEL) rather than the day-night level  $L_{dn}$ . The two descriptors are similar except that the CNEL ( $L_{CN}$ ) like  $L_{den}$  has three periods instead of two. Besides the night penalty of 10 dB, an evening penalty of 5 dB is applied with CNEL. CNEL is defined<sup>61</sup> as

$$L_{CN} = 10 \log \frac{12(10^{L_d/10}) + 3(10^{(L_e+5)/10}) + 9(10^{(L_n+10)/10})}{24} \quad (8)$$

where  $L_d$  is the average 12-h day HNL (hourly noise level),  $L_e$  is the average 3-h evening HNL, and  $L_n$  is the average 9-h night HNL.

The hourly noise level is given by

$$HNL = 10 \log \frac{\int 10^{L/10} dt}{3600} \quad (9)$$

where  $L$  is the instantaneous A-weighted sound pressure level, and  $t$  is the time in seconds. The integral

is calculated and summed. HNL is usually computed electronically. As is discussed in Chapter 106, the CNEL has also been extensively used to evaluate airport noise in California.<sup>62</sup> In California it has also been used to assess environmental noise transmission into buildings (see Chapter 106).

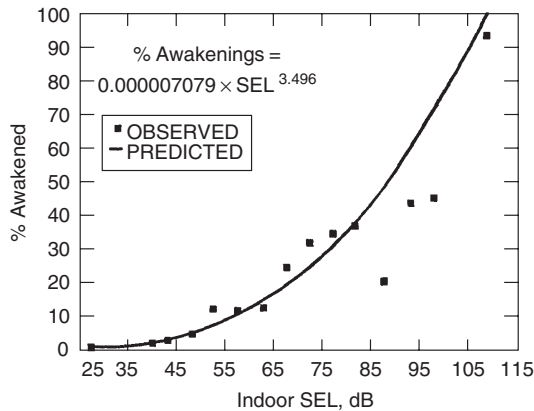
## 15 HUMAN RESPONSE

### 15.1 Sleep Interference

Various investigations have shown that noise disturbs sleep.<sup>63–69</sup> It is well known that there are several stages of sleep and that people progress through these stages as they sleep.<sup>63</sup> Noise can change the progression through the stages and if sufficiently intense can awaken the sleeper. Most studies have been conducted in the laboratory under controlled conditions using brief bursts of noise similar to aircraft flyovers or the passage of heavy vehicles. However, some have been conducted in the participants' bedrooms. Different measures have been used such as A-weighted *maximum sound pressure level*  $L_{A \max}$ , A-weighted *sound exposure level* (ASEL), *effective perceived noise level* (EPN dB), and *day-night sound pressure level* [DNL ( $L_{dn}$ )], and most studies have concentrated on the percentage of the subjects that are awakened. Pearsons et al.<sup>68</sup> have reassessed data from 21 sleep disturbance studies (drawn from the reviews of Lucas<sup>63</sup> and Griefhan<sup>64</sup> and seven additional studies). From these data, Finegold et al.<sup>69</sup> have proposed sleep disturbance criteria based on the indoor ASEL. In the reanalysis, because of the extremely variable and incomplete databases, the data were averaged in 5-dB intervals to reduce variability. A regression fit to these data gave the following expression (which is also shown graphically in Fig. 18):

$$\% \text{ Awakenings} = 7.1 \times 10^{-6} L_{AE}^{3.5} \quad (10)$$





**Figure 18** Proposed sleep disturbance curve based on data of Pearsons et al.<sup>68</sup> (From Ref. 69 with permission.) Curve represents percentage of subjects awakened against A-weighted sound exposure level ASEL.

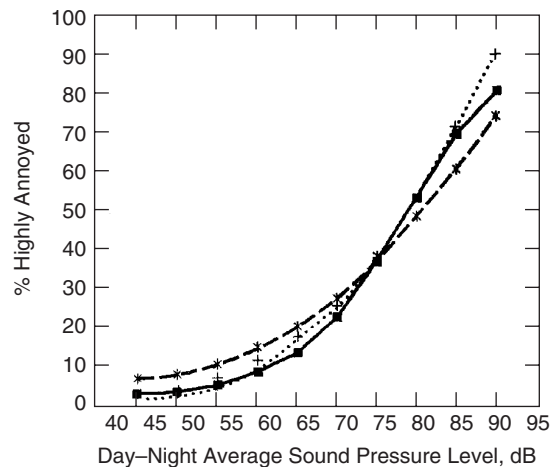
where  $L_{AE}$  is the indoor ASEL. Although the authors recognize that there are concerns with the existing data and there is a recognition that additional sleep disturbance data are needed, Finegold et al.<sup>69</sup> have proposed that Fig. 18 be used as a practical sleep disturbance curve until further data become available. Sleep disturbance caused by noise is discussed in more detail in Chapter 24.

## 15.2 Annoyance

In 1978 Schultz published an analysis of 12 major social surveys of community annoyance caused by transportation noise.<sup>70</sup> This Schultz analysis, which relates the percentage of the population that report they are “highly annoyed” by transportation noise to the A-weighted day–night average sound pressure level DNL ( $L_{dn}$ ), has become widely used all over the world as an important curve for describing the average community response to environmental noise. Since the Schultz curve was published, additional data have become available. Fidell et al.<sup>71</sup> used 453 exposure response data points compared to the 161 data points originally used by Schultz. This resulted in almost tripling the database for predicting noise annoyance from transportation noise. A later study by the U.S. Air Force eliminated 53 of these data points because there was insufficient correlation between the DNL and the percentage of the population that was highly annoyed, %HA.<sup>69</sup> The results of these two studies and the original Schultz curve are given in Fig. 19. Finegold et al.<sup>69</sup> recommend a logistic fit,

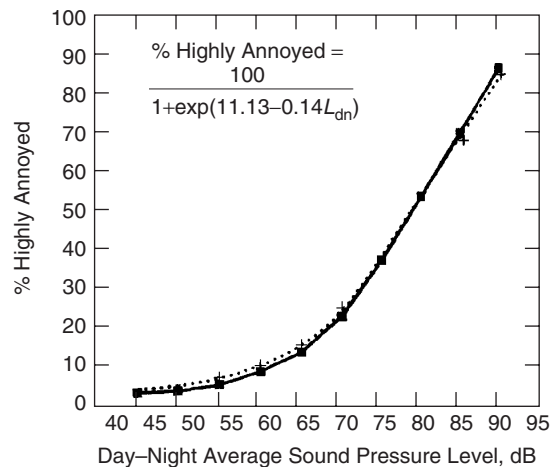
$$\%HA = \frac{100}{1 + \exp(11.13 - 0.14L_{dn})} \quad (11)$$

rather than the quadratic fit used by Fidell et al.<sup>71</sup> or the third-order polynomial fit used by Schultz.<sup>70</sup> This



**Figure 19** Curves representing the percentage of subjects that are highly annoyed by noise against A-weighted day–night average sound pressure level DNL ( $L_{dn}$ ): (—■—) New logistic USAF curve (400 data points), (...+...) Schultz<sup>70</sup> third-order polynomial (161 data points), and (---\*) Fidell et al.<sup>71</sup> quadratic curve (453 data points). (From Ref. 69 with permission.)

results in a very close agreement between the curve obtained with the 400 data points and the original 1978 Schultz curve.<sup>70</sup> See Fig. 20. The differences between the curves in Figs. 19 and 20 are not very significant; however, there are several advantages to the use of the logistic fit given in Eq. (11), including (1) the same predictive utility in both the original Schultz curve

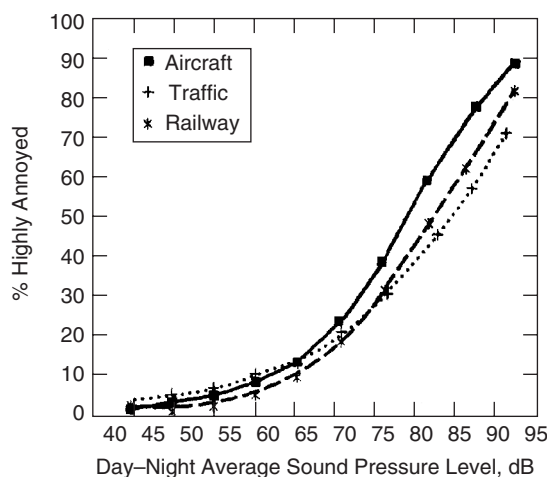


**Figure 20** Curves representing the percentage of subjects that are highly annoyed by noise against A-weighted day–night average sound pressure level DNL ( $L_{dn}$ ). (—■—) Logistic fit to 400 community annoyance social survey data points and (...+...) 1978 Schultz<sup>70</sup> curve. (From Ref. 69 with permission.)

and the Fidell et al. curve, (2) it allows prediction of annoyance to approach but does not reach 0 or 100%, (3) it approaches a 0% community annoyance prediction for a DNL ( $L_{dn}$ ) of approximately 40 dB rather than the anomaly of an increase in annoyance for levels of less than 45 dB as predicted by the Fidell et al. curve, (4) use of a logistic function has had a history of success with U.S. federal environmental impact analyses, and (5) it is based on the most defensible social survey database.<sup>69</sup>

Most community noise impact studies since the late 1970s have been based on a combination of aircraft and surface transportation noise sources. However, there has been a continuing controversy over whether all types of transportation should be combined into one general curve for predicting community annoyance to transportation noise.<sup>69,72-78</sup> Some researchers have suggested that people find aircraft noise more annoying than traffic noise or railroad noise for the same value of DNL.<sup>36,69,72,76</sup>

The differences have been discussed in the literature<sup>36,39,69</sup> and can perhaps be explained by a variety of causes such as (1) methodological differences, (2) variability in the criterion for reporting high annoyance, (3) inaccuracy in some of the acoustical measurements, (4) community response biases, and (5) aircraft noise entering homes through parts of the building structure with less transmission loss (such as the roof rather than the walls with aircraft noise). Figure 21 shows logistic fits to 400 final data points from a total of 22 different community annoyance surveys. It can be seen that aircraft noise appears to produce somewhat more annoyance than railroad or traffic noise particularly for the higher DNL ( $L_{dn}$ )



**Figure 21** Curves representing the percentage of subjects that are highly annoyed by noise against A-weighted day-night average sound pressure level DNL ( $L_{dn}$ ) for different sources: ■ Aircraft, ...+... traffic, and --\*-- railway. Curves based on data from Fidell et al.<sup>71</sup> (From Ref. 69 with permission.)

values. Miedema and Vos have made a reanalysis of data from selected social surveys that also shows that aircraft noise appears to cause more annoyance than other surface transportation noise sources.<sup>72</sup> However, the results from the Miedema and Vos study seem to suggest that for high values of DNL ( $L_{dn}$ ) (over 60 to 70 dB), although aircraft noise is by far the most annoying source, railroad noise is also more annoying than traffic noise (in contrast to the results of Finegold et al).<sup>69</sup>

If the five causes discussed above can be dismissed as responsible for the apparent greater annoyance of aircraft noise, then it may be that aircraft noise is more annoying than surface transportation noise for reasons such as: (1) the higher peak levels, (2) the greater variation in level with time, and (3) the different frequency spectra from other types of transportation noise sources. As already discussed in the text accompanying Fig. 17, aircraft noise does generally exhibit a much greater variation in level from traffic noise and other sources of surface transportation. If such variation is indeed more annoying and is one of the main causes of the difference in annoyance caused by these different forms of transportation noise, this suggests that it may be advisable to reexamine such measures that account for variation in level such as the TNI or the NPL discussed in Sections 13.1 and 13.2. The annoyance caused by noise is discussed in more detail in Chapter 25 and also briefly in Chapter 119.

## 16 NOISE CRITERIA AND NOISE REGULATIONS

Using some of the noise measures and descriptors discussed and surveys and human response studies, various criteria have been proposed so that noise environments can be determined that are acceptable for people, for speech communication, for different uses of buildings, for sleep, and for different land uses. In some countries such criteria are used to write noise regulations for new machinery, vehicles, traffic noise, railroad noise, aircraft and airport noise, community noise, and land use and planning. It is beyond the scope of this chapter to give a comprehensive summary of all these criteria and regulations. Instead just a few are described in this section. The interested reader is referred to the chapters in Part VIII and to the literature<sup>36,39,73</sup> for more complete summaries of criteria, regulations, and legislation. For instance, Chapter 120, provides information on limits for the noise of new vehicles in different countries (where acceleration noise tests are used). Such limits are based on results such as those presented in Fig. 7.

### 16.1 Noise Criteria

An example of noise criteria is given in Table 2, which is based on those suggested by Beranek and Ver<sup>23</sup> and gives recommended NCB curve values (and approximate A-weighted levels) for various indoor functional activity areas. The NCB curves are given in Fig. 13. For example, the air-conditioning unit

**Table 2 Recommended Values of NCB Curves for Different Uses of Spaces in Buildings<sup>a</sup>**

Type of Space (and Acoustical Requirements)	NCB Curve	Approximate $L_A$
Broadcast and recording studios	10	18
Concert halls, opera houses, and recital halls	10–15	18–23
Large auditoriums, large drama theaters, and large churches	<20	28
Broadcast, television, and recording studios	<25	33
Small auditoriums, small theaters, small churches, music rehearsal rooms, large meeting and conference rooms	<30	38
Bedrooms, sleeping quarters, hospitals, residences, apartments, hotels, motels, etc.	25–40	38–48
Private or semiprivate offices, small conference rooms, classrooms, and libraries	30–40	38–48
Living rooms and drawing rooms in dwellings	30–40	38–48
Large offices, reception areas, retail shops and stores, cafeterias, and restaurants	35–45	43–53
Lobbies, laboratory work spaces, drafting and engineering rooms, general secretarial areas	40–50	48–58
Light maintenance shops, industrial plant control, rooms, office and computer equipment rooms, kitchens, and laundries	45–55	53–63
Shops, garages, etc. (for just acceptable speech and telephone communication)	50–60	58–68
For work spaces where speech or telephone communication is not required, but where there must be <i>no risk</i> of hearing damage	55–70	63–78

Source: Based in part on Ref. 23.

<sup>a</sup>Also given are the approximate equivalent A-weighted sound pressure levels  $L_A$ .

chosen to supply air to bedrooms (used in residences, apartments, hotels, hospitals, etc.) should have a spectrum corresponding to no more than an NCB curve of 25 to 40 (or an A-weighted sound pressure level of no more than about 38 to 48 dB).

Another example of noise criteria are the guidelines recommended by EPA,<sup>38</sup> WHO,<sup>75</sup> FICON,<sup>40</sup> and various European road traffic regulating bodies. See Table 3. As already mentioned,  $L_{eq}$  is very widely used to evaluate road traffic, railroad, and even aircraft noise.<sup>36</sup> Interestingly, railroad noise has been found to be less annoying than traffic noise in several surveys.<sup>36,79,80</sup> This has resulted in noise limits (using  $L_{eq}$ ) that are 5 dB lower for railroad noise than road traffic noise in Austria, Denmark, Germany, and

Switzerland and 3 dB lower in The Netherlands.<sup>36</sup> Gottlob terms this difference the “railway bonus.”<sup>36</sup>

An example of national noise exposure criteria is the guidance given in the British government guidelines adopted in 1994 for land development given in Table 4. This table shows guidelines in A-weighted sound pressure levels  $L_{eq}$  for four noise exposure categories.<sup>81</sup> The noise exposure categories can be interpreted as follows<sup>82</sup>: (a) Noise need not be considered as a determining factor in granting planning permission, although the noise level at the high end of the category should not be regarded as a desirable level; (b) noise should be taken into account when determining planning applications, and where appropriate, conditions should be imposed

**Table 3 Guidelines from EPA,<sup>38</sup> WHO,<sup>75</sup> FICON,<sup>40</sup> and Various European Agencies for Acceptable Noise Levels**

Authority	Specified A-Weighted Sound Pressure Levels	Criterion
EPA levels	$L_{dn} \leq 55$ dB (outdoors)	Protection of public health and welfare with adequate margin of safety
Document <sup>38</sup>	$L_{dn} \leq 45$ dB (indoors)	
WHO	$L_{eq} \leq 50/55$ dB (outdoors; day)	Recommended guideline values
Document (1995) <sup>75</sup>	$L_{eq} \leq 45$ dB (outdoors; night)	
	$L_{eq} \leq 30$ dB (bedroom)	
	$L_{max} \leq 45$ dB (bedroom)	Considered generally compatible with residential development
U.S. Interagency Committee (FICON) <sup>40</sup>	$L_{dn} \leq 65$ dB	
	$65 \leq L_{dn} \leq 70$ dB	Residential use discouraged
Various European road traffic regulations <sup>36</sup>	$L_{eq} \geq 65$ or 70 dB (day)	Remedial measures required

Source: Based on Ref. 39.

**Table 4 Guidelines Used in the United Kingdom for A-Weighted Equivalent Sound Pressure Levels for Different Noise Exposure Categories**

Noise Source		Noise Exposure Category			
		A	B	C	D
Road traffic	(07.00–23.00)	<55	55–63	63–72	>72
	(23.00–07.00)	<45	45–57	57–66	>66
Rail traffic	(07.00–23.00)	<55	55–66	66–74	>74
	(23.00–07.00)	<45	45–59	59–66	>66
Air traffic	(07.00–23.00)	<57	57–66	66–72	>72
	(23.00–07.00)	<48	48–57	57–66	>66
Mixed sources	(07.00–23.00)	<55	55–63	63–72	>72
	23.00–07.00)	<45	45–57	57–66	>66

Source: Based on Ref. 81.

to ensure an adequate level of protection against noise; (c) planning permission should not normally be granted; where it is considered that permission should be given, for example, because there are no alternative quieter sites available, conditions should be imposed to ensure a commensurate level of protection against noise; and (d) planning permission should normally be refused.<sup>83,84</sup>

## 17 HUMAN VIBRATION CRITERIA

The effects of vibration on people are reviewed in Chapter 29. Different criteria are needed for vibration in buildings, vehicles, and that caused by the use of machine tools. Work continues on such effects of vibration on people and criteria for human comfort and protection.<sup>85–87</sup>

## REFERENCES

1. B. C. J. Moore, B. R. Glasberg, and T. Baer, A Model for the Prediction of Thresholds, Loudness and Partial Loudness, *J. Audio Eng. Soc.*, Vol. 45, 1997, pp. 224–240.
2. B. C. J. Moore, *An Introduction to the Psychology of Hearing*, 5th ed., Academic, San Diego, 2003.
3. B. R. Glasberg and B. C. J. Moore, Prediction of Absolute Thresholds and Equal-Loudness Contours Using a Modified Loudness Model (L), *J. Acoust. Soc. Am.*, Vol. 120, 2, 2006, pp. 585–588.
4. ANSI S3.4–2005, *Procedure for the Computation of Loudness of Steady Sounds*, American National Standards Institute, New York, 2005.
5. ISO 226, *Acoustics—Normal Equal-Loudness Contours*, International Organization for Standardization, Geneva, 1987.
6. D. W. Robinson and R. S. Dadson, A Re-determination of the Equal-Loudness Relations for Pure Tones, *Br. J. Appl. Phys.*, Vol. 7, 1956, pp.166–181.
7. ISO 389-7, *Acoustics—Reference Zero for the Calibration of Audiometric Equipment. Part 7: Reference Threshold of Hearing under Free-Field and Diffuse-Field Listening Conditions*, International Organization for Standardization, Geneva, 2005.
8. ISO 226, *Acoustics—Normal Equal-Loudness Contours*, International Organization for Standardization, Geneva, 2003.
9. S. S. Stevens, Procedure for Calculating Loudness: Mark VI, *J. Acoust. Soc. Am.*, Vol. 33, 1961, p. 1577.
10. E. Zwicker, Ein Verfahren zur Berechnung der Lautstärke (A Means for Calculating Loudness), *Acustica*, Vol. 10, 1960, p. 304.
11. E. Zwicker, Subdivision of the Audible Frequency Range into Critical Bands (Frequenzgruppen), *J. Acoust. Soc. Am.*, Vol. 33, 1961, p. 248.
12. ISO 532–1967, *Method for Calculating Loudness Level*, International Organization for Standardization, Geneva, 1967.
13. K. D. Kryter, *The Effects of Noise on Man*, 2nd ed., Academic, Orlando, FL, 1985.
14. K. D. Kryter, Scaling Human Reactions to the Sound from Aircraft, *J. Acoust. Soc. Am.*, Vol. 31, No. 11, 1959, pp. 1415–1429.
15. K. D. Kryter and K. S. Pearsons, Some Effects of Spectral Content and Duration on Perceived Noise Level, *J. Acoust. Soc. Amer.*, Vol. 35, No. 6, 1963, pp. 866–883.
16. ISO, *Procedure for Describing Aircraft Noise Heard on the Ground*, ISO 3891–1978, International Organization for Standardization, Geneva, 1978.
17. D. N. May, Basic Subjective Responses to Noise, in *Handbook of Noise Assessment*, D. N. May, Ed., Van Nostrand Reinhold, New York, 1978.
18. C. M. Harris, Ed., *Handbook of Acoustical Measurements and Noise Control*, 3rd ed., McGraw-Hill, New York, 1991, Chapter 47.
19. J. S. Anderson and M. Bratos-Anderson, *Noise, Its Measurement, Analysis, Rating, and Control*, Averbury Technical, Aldershot, UK, 1993.
20. M. J. Crocker, Noise of Air Transportation to Non-travellers, in *Handbook of Noise Assessment*, D. N. May, Ed., Van Nostrand Reinhold, New York, 1978.
21. Federal Aviation Regulation, FAR Part 36, Noise Standards: Aircraft Type and Airworthiness Certification, February 7, 2006. (See [www.faa.gov](http://www.faa.gov).)
22. International Civil Aviation Organization, ICAO, Annex 16 to the Convention on International Civil Aviation, Environmental Protection (Vol. I and II). (See [www.icao.int](http://www.icao.int).)
23. L. L. Beranek and I. L. Ver, *Noise and Vibration Control Engineering*, Wiley, New York, 1992.

24. N. R. French and J. C. Steinberg, Factors Governing the Intelligibility of Speech Sounds, *J. Acoust. Soc. Am.*, Vol. 19, 1947, pp. 90–119.
25. ANSI, *Methods for the Calculation of the Articulation Index*, ANSI S3.5–1969 (R1976), American National Standards Institute, New York, 1976.
26. ANSI S3.5–1997 (R2002), *Methods for the Calculation of the Speech Intelligibility Index*, American National Standards Institute, New York, 2002.
27. J. C. Webster, Communicating in Noise in 1978–1983, in E. Rossi, Ed, *Proceedings of the 4th International Congress on Noise as a Public Health Problem*, Torino, Italy, Vol. I, 1983, pp. 411–424.
28. L. L. Beranek, Revised Criteria for Noise Control in Buildings, *Noise Control*, Vol. 3, 1957, pp. 19–27.
29. L. L. Beranek, W. E. Blazier, and J. J. Figiver, *J. Acoust. Soc. Am.*, Vol. 50, 1971, pp. 1223–1228.
30. L. L. Beranek, Balanced Noise Criterion (NCB) Curves, *J. Acoust. Soc. Am.*, Vol. 86, pp. 650–664.
31. L. L. Beranek, Applications of NCB Noise Criterion Curves, *Noise Control Eng. J.*, Vol. 33, 1989, pp. 45–56.
32. W. E. Blazier, Revised Noise Criteria for Application in the Acoustical Design and Rating of HVAC Systems, *Noise Control Eng. J.*, Vol. 16, 1981, pp. 64–73.
33. C. W. Kosten and G. J. van Os, *Community Reaction Criteria for External Noise, in the Control of Noise*, NPL Symposium No. 12, HMSO, London, 1962, pp. 373–382.
34. EPA, *Community Noise*, Report No. NTID 330.3, U.S. Environmental Protection Agency, Washington, DC, 1971.
35. K. M. Eldred, Assessment of Community Noise, *Noise Control Eng. J.*, Vol. 3, No. 2, 1974, pp. 88–95.
36. D. Gottlob, Regulations for Community Noise, *Noise/News Int.*, Vol. 3, No. 4, 1995, pp. 223–236.
37. EPA, *Public Health and Welfare Criteria for Noise*, Report No. 550/9-73-002, U.S. Environmental Protection Agency, Washington, DC, 1973.
38. EPA, *Information on Levels of Environmental Noise Requisite to Protect Public Health and Welfare with an Adequate Margin of Safety*, Report No. 550/9-74-004, U.S. Environmental Protection Agency, Washington, DC, 1974.
39. E. A. G. Shaw, Noise Environments Outdoors and the Effects of Community Noise Exposure, *Noise Control Eng. J.*, Vol. 44, No. 3, 1996, pp. 109–119.
40. Federal Interagency Committee on Urban Noise, *Guidelines for Considering Noise in Land Use Planning and Control*, Document 1981-338-006/8071, U.S. Government Printing Office, Washington, DC, 1980.
41. W. E. Scholes and G. H. Vulkan, *Appl. Acoust.*, Vol. 2, 1967, pp. 185–197.
42. T. J. Schultz, *Community Noise Ratings*, 2nd ed., Applied Science, London, 1982.
43. W. A. Rosenblith, K. N. Stevens, and the staff of Bolt, Beranek, and Newman Inc., *Handbook of Acoustic Noise Control, Vol 2, Noise and Man*, WADC TR-52-204, Wright Air Development Center, Wright Patterson Air Force Base, Ohio, 1953, pp. 181–200.
44. K. N. Stevens, W. A. Rosenblith, and R. H. Bolt, A Community's Reaction to Noise: Can It Be Forecast? *Noise Control*, Vol. 1, 1955, pp. 63–71.
45. W. J. Galloway and D. E. Bishop, *Noise Exposure Forecasts: Evolution, Evaluation, Extensions, and Land Use Interpretations*, BBN Report No. 1862 for the FAA/DOT Office of Noise Abatement, Washington, DC, December 1969.
46. K. N. Stevens, A. C. Pientrasanta, and the staff of Bolt, Beranek, and Newman Inc., *Procedures for Estimating Noise Exposure and Resulting Community Reactions from Air Base Operations*, WADC TN-57-10, Wright Air Development Center, Wright Patterson Air Force Base, Ohio, 1957.
47. Bolt, Beranek, and Newman Inc., *Land Use Planning Relating to Aircraft Noise*, FAA Technical Report, October, 1964; also issued as Report No. AFM86-5, TM-5-365, NAVDOCKS P-38, U.S. Department of Defense, Washington, DC, 1964.
48. D. E. Bishop and R. D. Horonjeff, *Procedures for Developing Noise Exposure Forecast Areas for Aircraft Flight Operations*, FAA Report DS-67-10, Department of Transportation, Washington, DC, August 1967.
49. D. E. Bishop, *Community Noise Exposure Resulting from Aircraft Operations: Application Guide for Predictive Procedure*, AMRL-TR-73-105, November 1974, Bolt Beranek and Newman Inc., Canoga Park, California.
50. Committee on the Problem of Noise, *Noise—Final Report*, HMSO, London, 1963.
51. *Second Survey of Aircraft Noise Annoyance around London Heathrow Airport*, HMSO, London, 1971.
52. T. J. Schultz, Some Sources of Error in Community Noise Measurement, *J. Sound Vib.*, Vol. 6, No. 2, 1972, pp. 18–27.
53. Department of the Environment, *Motorway Noise and Dwellings*, Digest 153, Building Research Establishment, Garston, Watford, England, May 1973.
54. Department of Transport, *Calculation of Road Traffic Noise*, HMSO, London, 1988.
55. P. G. Abbott and P. M. Nelson, The Revision of Calculation of Road Traffic Noise 1988, *Acoust. Bull.* (Institute of Acoustics), Vol. 14, No. 1, 1989, pp. 4–9.
56. D. W. Robinson, The Concept of Noise Pollution Level, NPL Aero Report AC 38, National Physical Laboratory, Aerodynamics Division, Teddington, Middlesex, UK, March 1969. (See [www.npl.co.uk](http://www.npl.co.uk).)
57. I. D. Griffiths and F. J. Langdon, Subjective Response to Road Traffic Noise, *J. Sound Vib.*, Vol. 8, No. 1, 1968, pp. 16–33.
58. K. S. Pearsons, *The Effects of Duration and Background Level on Perceived Noisiness*, Report FAA ADS-78, Washington, DC, April 1966.
59. Bolt, Beranek, and Newman, Inc. *Establishment of Standards for Highway Noise Levels (Final Report)*, Vol. 5, Prepared for Transportation Research Board, National Cooperative Highway Research Program, National Academy of Sciences, NCHRP 3-7/3, Washington, DC, November 1974.
60. ISO, *Acoustics—Description, Measurement and Assessment of Environmental Noise—Part 1: Basic Quantities and Assessment Procedures*, ISO 1996-1:2003; *Part 2: Basic Quantities and Assessment Procedures*, ISO 1996-2:1987; *Part 3: Application to Noise Limits*, ISO 1996-3:1987, International Organization for Standardization, Geneva, Switzerland, 1996.
61. *Noise Standards for California Airports*, California Administrative Code, Title 4, Subchapter 6.
62. J. Goldstein, Descriptors of Auditory Magnitude and Methods of Rating Community Noise, in *Community*

- Noise, R. J. Peppin and C. W. Rodman, Eds., ASTM, Philadelphia, 1979, pp. 38–72.
63. J. S. Lucas, Noise and Sleep: A Literature Review and a Proposed Criterion for Assessing Effect, *J. Acoust. Soc. Am.*, Vol. 58, No. 6, 1975, pp. 1232–1242.
  64. B. Griefahn, Research on Noise-disturbed Sleep since 1973, *Proceedings of the Third International Congress on Noise as a Public Health Problem*, ASHA Report No. 10, 1980.
  65. C. J. Jones and J. B. Ollerhead, Aircraft Noise and Sleep Disturbance: A Field Study, in *Proceedings of EURO-NOISE '92*, R. Lawrence, Ed., London, 1992, pp. 119–127. (See [www.european-acoustics.org](http://www.european-acoustics.org).)
  66. J. B. Ollerhead et al., Report of a Field Study of Aircraft Noise and Sleep Disturbance, Civil Aviation Authority, London, England, December 1992.
  67. K. S. Pearsons, D. S. Barber, B. G. Tabachnik, and S. Fidell, Predicting Noise-induced Sleep Disturbance, *J. Acoust. Soc. Am.*, Vol. 97, 1995, pp. 331–338.
  68. K. S. Pearsons, D. S. Barber, and B. G. Tabachnik, Analyses of the Predictability of Noise-induced Sleep Disturbance, Technical Report HSD-TR-89-029, Human Science Division (HSDY/YAH U.S. Air Force Systems Command), Brooks Air Force Base, TX, October 1989.
  69. L. S. Finegold, C. S. Harris, and H. E. von Gierke, Community Annoyance and Sleep Disturbance: Updated Criteria for Assessment of the Impacts of General Transportation Noise on People, *Noise Control Eng. J.*, Vol. 42, No. 1, 1994, pp. 25–30.
  70. T. J. Schultz, Synthesis of Social Surveys on Noise Annoyance, *J. Acoust. Soc. Am.*, Vol. 64, 1978, pp. 377–405.
  71. S. Fidell, D. S. Barber, and T. J. Schultz, Updating a Dosage Effect Relationship for the Prevalence of Annoyance Due to General Transportation Noise, *J. Acoust. Soc. Am.*, Vol. 89, 1991, pp. 221–233.
  72. H. M. E. Miedema and H. Vos, Exposure Response Functions for Transportation Noise, *J. Acoust. Soc. Am.*, Vol. 104, pp. 3432–3445.
  73. H. E. Von Gierke and K. Eldred, Effects of Noise on People, *Noise/News Int.*, Vol. 1, No. 2, 1993, pp. 67–89.
  74. W. Passchier-Vermeer, *Noise and Health*, Publication No. A93/02, Health Council of Netherlands, The Hague, 1993.
  75. B. Berglund, T. Lindvall, and D. H. Schwela, Guidelines for Community Noise, World Health Organization, Geneva, Switzerland, 1999.
  76. K. D. Kryter, Community Annoyance from Aircraft and Ground Vehicle Noise, *J. Acoust. Soc. Am.*, Vol. 72, No. 4, 1982, pp. 1222–1242.
  77. T. J. Schultz, Comments on K. D. Kryter's Paper, Community Annoyance from Aircraft and Ground Vehicle Noise, *J. Acoust. Soc. Am.*, Vol. 72, No. 4, 1982, pp. 1243–1252.
  78. K. D. Kryter, Rebuttal by Karl D. Kryter to Comments by T. J. Schultz, *J. Acoust. Soc. Am.*, Vol. 72, No. 4, 1982, pp. 1253–1257.
  79. U. Mohler, Community Response to Railway Noise: A Review of Social Surveys, *J. Sound Vib.*, Vol. 120, 1988, pp. 321–332.
  80. J. Lang, Schallimmission von Schienenverkehrstrecken. Forschungsarbeiten aus dem Verkehrswesen, Vol. 23, Vienna, Austria, 1989.
  81. British Government Planning Policy Guidance PPG, *Planning and Noise*, London, September 1994. HM, London, UK.
  82. Private communication with Rupert Thornely-Taylor, April 29, 1996.
  83. Directive 2002/49/EC of the European Parliament and of the Council of 25 June 2002 Relating to Management of Environmental Noise. (See [www.imagine-project.org/bestarden/2002-49-EC.pdf](http://www.imagine-project.org/bestarden/2002-49-EC.pdf).)
  84. IEC 60268-16, *Sound System Equipment—Part 16, Objective Rating of Speech Intelligibility by Speech Transmission Index*.
  85. A. Ebrahimpour and R. L. Sack, A Review of Vibration Serviceability Criteria for Floor Structures, *Computers & Structures*, Vol. 83, Nos. 28–30, November 2005, pp. 2488–2494.
  86. M. Demić, J. Lukić, and Ž. Milić, Some Aspects of the Investigation of Random Vibration Influence on Ride Comfort, *J. Sound Vib.*, Vol. 253, No. 1, 2002, pp. 109–128.
  87. S. Rakheja, J. Z. Wu, R. G. Dong, A. W. Schopper, and P.-É. Boileau, A Comparison of Biodynamic Models of the Human Hand-Arm System for Applications to Hand-Held Power Tools, *J. Sound Vib.*, Vol. 249, No. 1, 2002, pp. 55–82.

**PART V**

---

**NOISE AND VIBRATION  
TRANSDUCERS, ANALYSIS  
EQUIPMENT, SIGNAL  
PROCESSING, AND MEASURING  
TECHNIQUES**

# CHAPTER 35

## GENERAL INTRODUCTION TO NOISE AND VIBRATION TRANSDUCERS, MEASURING EQUIPMENT, MEASUREMENTS, SIGNAL ACQUISITION, AND PROCESSING

Malcolm J. Crocker  
Department of Mechanical Engineering  
Auburn University  
Auburn, Alabama

### 1 INTRODUCTION

In the measurement of noise and vibration fields, it is necessary to sense the sound or vibration disturbance with a transducer. The transducer converts some physical property of the sound and vibration field into an electrical signal. This signal is then amplified, attenuated, or transformed in some way so that it can be analyzed and/or processed to provide the data of particular interest. For some cases such as simple measurements of the A-weighted sound pressure level, only limited amounts of processing are needed. In other cases with more sophisticated measurements, special analysis and processing is required. Such examples include modal analysis, sound intensity, wavelet analysis, machinery condition monitoring, and acoustical holography, with which quite complicated signal analysis and processing may be needed. In all cases considerable care should be taken to ensure that the transducers together with their measurement systems are calibrated and checked periodically to make sure they are working properly. Part V of this book contains 19 chapters concerned with the basic design principles of noise and vibration transducers, analysis equipment, signal processing, and simple and advanced measurement techniques for various noise and vibration measurements, including those for source and path identification.

### 2 TYPICAL MEASUREMENT SYSTEMS

It may be necessary to measure noise and/or vibration for various different reasons. Before beginning any measurement program, the objectives should be defined. For instance, it may be desired to measure noise to determine if a noise problem exists, whether the noise output of a machine is within its specifications, to determine the main sources of noise on a machine or in a vehicle or building. In the case of vibration, the reasons for measurement can include determining whether vibration of structures may result in unwanted sound generation, or in the case of intense vibration, machine wear and condition, and even the danger of structural fatigue and failure. The basis of all noise and vibration measurement systems is the transducer. The microphone is the main transducer

used to measure sound, while the accelerometer is the main transducer used to measure vibration. Specialized transducer systems have been developed to measure sound intensity in air and vibration intensity of structural systems. In addition, measurement procedures have been formulated to determine the modes of vibration of structures. Special rooms and systems such as anechoic and reverberant rooms and impedance tubes (see Chapter 43) are now widely used for sound power and noise source identification measurements of machines and the measurement of the acoustical impedance of materials. With any measurement, calibration of the system is essential to obtain reliable results that can be compared with results obtained by others.

Since about 1920, most sound and vibration measurement systems have made extensive use of electrical networks. From that time, the electrical amplification of signals has made possible several measurement techniques that were previously impossible to use. When measurements are made of noise or vibration, it is usually necessary to combine several different types of instruments into one measurement system. The individual components of the measuring system utilized will depend on the particular measurements needed. A generalized system is shown in Fig. 1. To design a system to make useful measurements, it is desirable for one to have a good understanding of the phenomena being investigated and to have a reasonable understanding of the functioning of the instrumentation and signal processing. The chapters in Part V of this book are designed to help with these requirements. Chapter 43 reviews some of the noise and vibration measurements in common use, uncertainty concerns with the measured results, and some of the more specialized procedures for measuring the passby noise of vehicles and the flyby noise of aircraft.

The first item in any noise or vibration measuring system is the *transducer*. As its name implies, this instrument converts a signal in one physical form into another, that is, a transducer converts a sound pressure signal or a vibration signal into an electrical signal. Normally, the electrical signal obtained from a transducer is not suitable for direct analysis or readout, and a *signal conditioner* is then used to amplify,



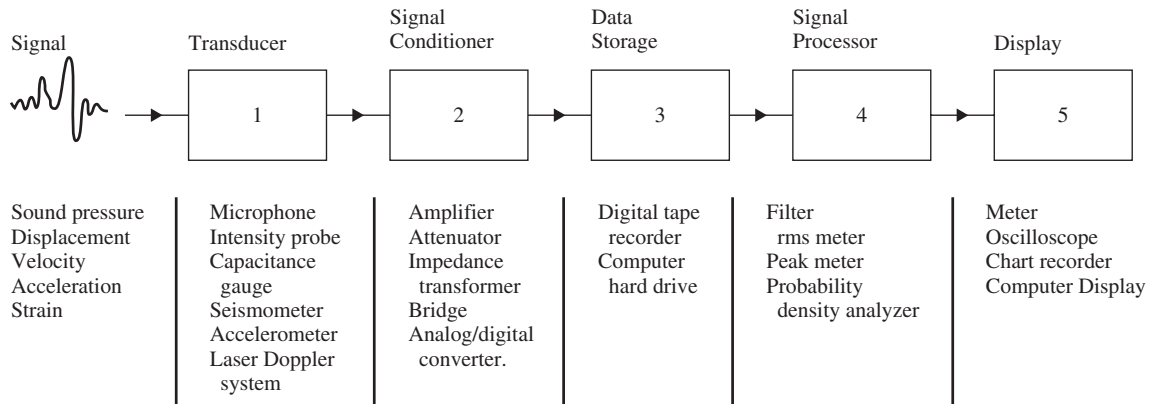


Figure 1 Idealized noise or vibration measuring system.

attenuate, or transform the signal using analog-to-digital (A/D) conversion. It is optional at this stage to include a *data storage* item in the system before the signal is passed to a *signal processor*. (See Fig. 1.) The signal processor may consist of a narrow-or wide-band filter, a root-mean-square (rms) detector, a probability density analyzer, and the like. See Chapter 40 for more details of signal analysis equipment and systems. The last item in the system is usually the *display unit*, a read-out unit, or a digital computer, which is used to perform some postprocessing of the signal. Analog and/or digital meters, oscilloscopes, and other units can all be used to display signals. Also a data storage item or data distribution system can be included in the main measurement system at this stage instead of earlier, so that the data can be analyzed or shared with others later. (See Chapter 41.)

### 3 TRANSDUCERS

Transducers and their associated measuring systems generally suffer from two major shortcomings:

1. A transducer will normally respond to other variables in addition to its response to the variable of interest. For example, a microphone, although being most sensitive to sound pressure, may also be slightly sensitive to variations in temperature, humidity, magnetic fields, and vibration.
2. It is difficult, and in many cases not possible, to introduce a transducer into the measurement medium without disturbing the medium in some way. The transducer will extract some energy from the medium or structural system. In addition, other disturbances will be caused. An accelerometer will add mass to the system and alter the structure's vibration. A pitot tube or hot-wire anemometer will disturb the flow. A microphone will reflect, diffract, and refract the incident sound wave. Some noncontacting vibration transducers and systems will not

directly interfere with the vibration of the system to be measured, but they will interfere with any associated sound field generated by the vibrating body.

#### 3.1 Transducer Characteristics

An ideal sound or vibration transducer should have the following characteristics<sup>1</sup>:

1. It should cause negligible diffraction of the sound field or structural vibration field (i.e., its dimensions should be small compared with the smallest sound or vibration wavelength of interest).
2. It should have a high acoustical or mechanical (driving point) impedance compared with the fluid medium or structure so that little energy is extracted from the field.
3. It should have low electrical noise.
4. Its output should be independent of temperature, humidity, magnetic fields, static pressure, and wind velocity, and it should be rugged and stable with time.
5. Its sensitivity should be independent of sound pressure or vibration level magnitudes.
6. Its frequency response should be flat.
7. It should introduce a zero phase shift between the sound pressure or structural vibration and the electrical output signal.

No transducer can meet all of the above criteria, and thus different types of transducers and vibration sensors are preferred for different measurements. The microphone is by far the most common form of acoustical transducer, and the piezoelectric accelerometer is the most widely used vibration transducer. Because of their importance the next section of this chapter concerns these devices. But it should be noted that other specialized noise and vibration transducers are used for measurements. For instance, sound intensity probes of

different designs can be used for noise source identification and sound power measurements of a source in situ (see Chapters 36 and 45), and several other types of vibration-measuring transducers such as strain gauges and laser Doppler interferometer systems are also in use, as described in Chapter 37.

### 3.2 Sensitivity

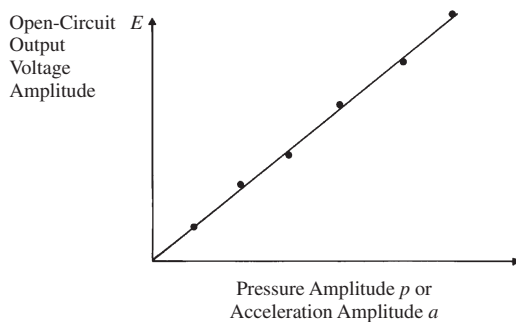
An ideal microphone (or accelerometer) together with its measurement system should have an output voltage amplitude  $E$  that is proportional to the exciting pressure amplitude  $p$  (or acceleration amplitude  $a$ ) (see Fig. 2). The ratio of open-circuit output voltage to input pressure (or acceleration) is normally called the sensitivity  $M_p$ :

$$M_p = E/p \quad \text{or} \quad M_p = E/a \quad (1)$$

The transducer sensitivity [V/(N/m<sup>2</sup>) or V/(m/s<sup>2</sup>)] depends on the microphone (or accelerometer) design. (Different types are discussed in Chapters 36 and 37 and later in Sections 4.1, 5.1, and 5.2 of this chapter.)

In the case of noise measurements with very low sound pressure amplitudes, electrical noise will exceed the voltage signal generated by the microphone, and this will govern the lower signal amplitude limit for measurements. With very high sound pressure amplitudes, the diaphragm displacement may become so large that the voltage generated is no longer proportional to the displacement. Nonlinearity then sets the upper amplitude use limit. See Chapter 36. For sound pressures somewhat above the nonlinear limit, physical damage to the microphone can occur.

The situation is similar for vibration measurements made with seismic mass accelerometers. For very high vibration amplitudes, the accelerometer displacement may become so large that the voltage generated is no longer proportional to the displacement. Nonlinearity again sets an upper use limit. For displacements above the nonlinear limit, physical damage to the accelerometer can occur. Large accelerometers are normally more sensitive than small ones, and this is advantageous in many applications; but large heavy accelerometers cause more mass loading problems



**Figure 2** Sensitivity of (1) an ideal microphone or accelerometer \_\_\_\_\_ and (2) an actual transducer •.

to start to occur at a lower frequency than small lightweight accelerometers.<sup>1</sup>

If Fig. 2 is plotted on a logarithmic scale, Fig. 3 is obtained. The reference voltage  $E_{\text{ref}}$  is normally taken as 1 V, while the reference sound pressure  $p_{\text{ref}}$  is usually taken as 20  $\mu\text{Pa}$ , and the reference acceleration is normally taken as 1  $\mu\text{m/s}^2$ .

A microphone or accelerometer has a usable range of operation between its upper and lower amplitude limits. Thus, at any frequency the *microphone or accelerometer response magnitude* is normally given by subtracting the  $X$  from the  $Y$  axis in Fig. 3, and the range  $\Delta R$  in which the microphone or accelerometer response  $R$  is constant is known as the dynamic range:

$$\begin{aligned} R &= 20 \log \left( \frac{E/p}{E_{\text{ref}}/p_{\text{ref}}} \right), \text{ dB} \\ &= 20 \log \left( \frac{E/E_{\text{ref}}}{p/p_{\text{ref}}} \right), \text{ dB} \end{aligned} \quad (2a)$$

or

$$\begin{aligned} R &= 20 \log \left( \frac{E/a}{E_{\text{ref}}/a_{\text{ref}}} \right), \text{ dB} \\ &= 20 \log \left( \frac{E/E_{\text{ref}}}{a/a_{\text{ref}}} \right), \text{ dB} \end{aligned} \quad (2b)$$

### 3.3 Dynamic Range

It is seen for the microphone (or accelerometer) shown in Fig. 3 that the dynamic range is about 100 dB. Most good-quality microphones have a dynamic range of about 100 to 120 dB (interestingly enough about the same as the human ear). See Chapter 36. As the microphone diaphragm diameter (or accelerometer mass) is increased, the transducer sensitivity is normally increased as well so that electrical noise is less of a problem and the lower signal amplitude limit for measurements is decreased. In the case of a microphone, however, a larger diaphragm diameter usually results in a larger deflection for a given sound pressure and a reduced upper sound pressure level limit because of nonlinearity problems. Thus between the upper and lower amplitude limits the microphone has a usable range of operation.

Small-diameter microphones are not very sensitive but can be used for high-amplitude sound pressures without distortion; their electronic noise floor is quite high, however. (Different types are discussed briefly in this chapter. The fundamentals of the operation of the main types of microphone are described in more detail in Chapter 36.) Large-diameter microphones are normally more sensitive and can be used for lower level noise than small-diameter microphones. Their noise floor is lower, but larger diameter microphones experience more diffraction problems at low frequencies than small-diameter microphones.<sup>1</sup> Figure 4 shows the inherent noise floor plotted against upper limiting frequency for four microphone diameters.<sup>2</sup> Because of the dynamic range problems, the small-diameter microphones cannot be

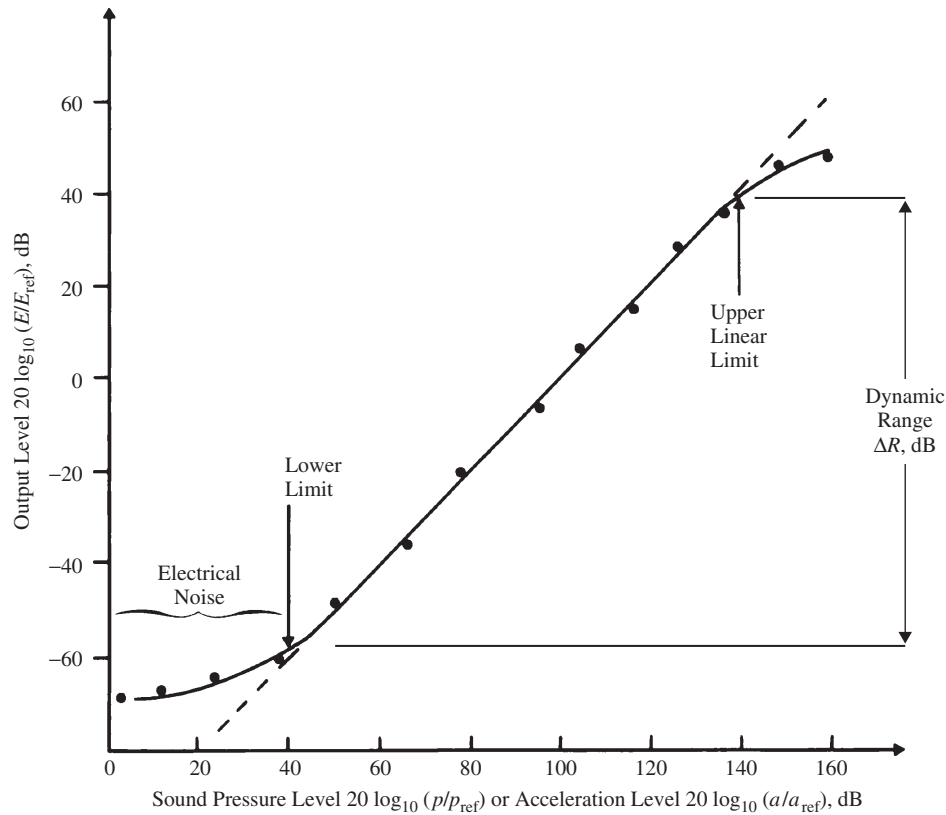


Figure 3 Sensitivity of an ideal microphone or accelerometer showing upper and lower limits.

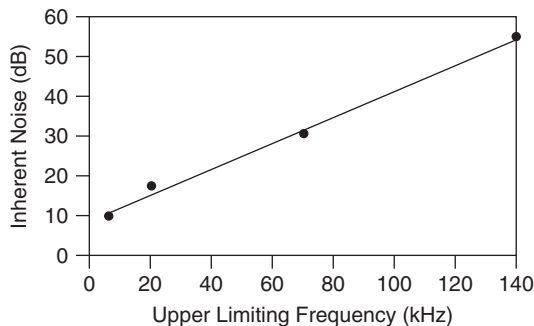


Figure 4 Inherent noise floor against upper limiting sound pressure level for four different diameter microphones. The four dots represent the four sizes of microphone (1 in.,  $\frac{1}{2}$  in.,  $\frac{1}{4}$  in., and  $\frac{1}{8}$  in.) in order from 1 in. (bottom left) to  $\frac{1}{8}$  in. (top right).<sup>2</sup>

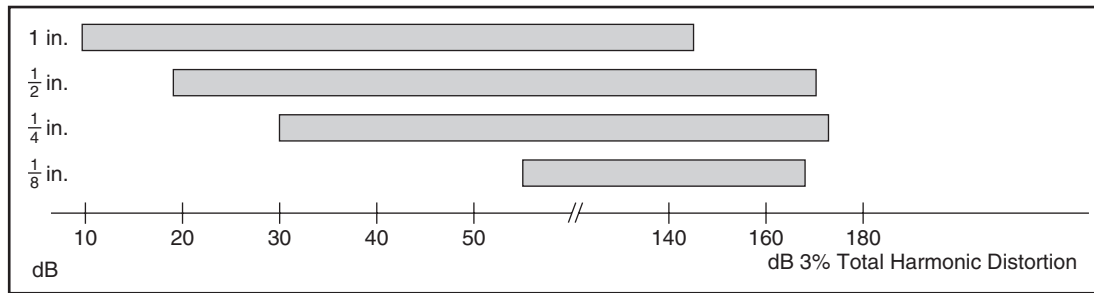
used for very “quiet” sounds, and the large-diameter microphones cannot be used for intense noise.

Figure 5 shows the dynamic range for four commercially available microphones. The lower level limit is given in terms of the A-weighted sound pressure

level of the internal noise floor of the microphone and associated preamplifier. The upper level limit is set by the sound pressure level at which 3% dynamic distortion occurs. It is observed that the 1-in. and  $\frac{1}{2}$ -in. diameter microphones have the greatest dynamic ranges of about 150 dB. The  $\frac{1}{4}$ -in. microphone has a dynamic range of about 140 dB, while the  $\frac{1}{8}$ -in. diameter microphone has a dynamic range of only about 100 dB.<sup>2</sup>

### 3.4 Frequency Response

The *magnitude of the frequency response*,  $R(f)$ , of an ideal microphone is given by Eq. (2a) as the frequency of the sound pressure  $p$  is changed. The *magnitude of the frequency response*,  $R(f)$ , of an ideal accelerometer is given by Eq. (2b) as the frequency of the vibration  $a$  is changed. Figure 6 shows the frequency response of an ideal microphone used for noise measurements or an ideal accelerometer used for vibration measurements. In practice microphones and accelerometers can only approach the ideal frequency response in Fig. 6. Resonance peaks of the diaphragm of the microphone or the inertial mass of the accelerometer are usually observed in the high-frequency range. These peaks are normally



**Figure 5** Comparison of the dynamic ranges of the same four condenser microphones as shown in Fig. 4. The lower limit is A-weighted sound pressure level. The upper limit is given in decibels at which 3% total harmonic distortion occurs.<sup>2</sup>

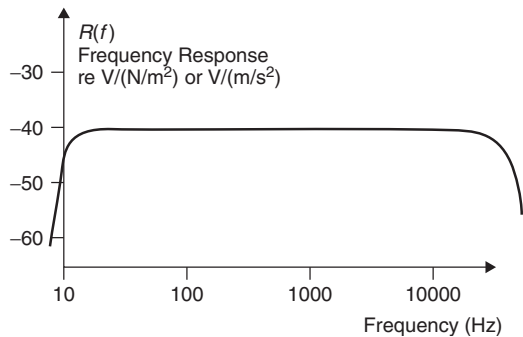
suppressed by the addition of damping or some other means at the transducer design stage. Note that for some measurements (e.g., explosive blasts with a microphone and shock events with an accelerometer) knowledge of the phase frequency response of the transducer is also important. For such measurements of impulsive phenomena, the additional requirements of zero or linear phase shift with frequency are needed for microphones and accelerometers, respectively.

Figure 7 shows the frequency response range of four different diameter condenser microphones.<sup>2</sup> It is

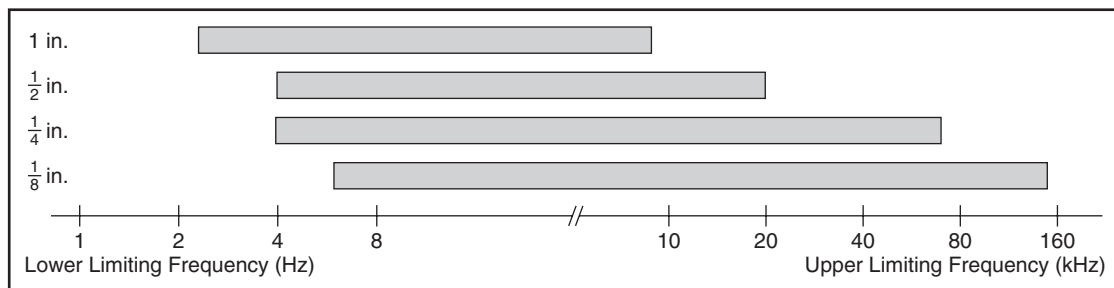
observed that the smaller diameter microphones have the largest usable frequency range. The  $\frac{1}{8}$ -in. diameter microphone has a usable range from about 5 Hz to about 150 kHz. The 1-in. microphone on the other hand has a much more restricted usable frequency range from about 2 Hz to only about 10 kHz.

#### 4 NOISE MEASUREMENTS

Since the human hearing range extends from about 20 to 20,000 Hz, it is desirable that the frequency response of microphones and noise measurement systems should be “flat” between these limits as shown in Fig. 6. For certain types of measurements (e.g., for measurement of sonic booms or explosive blasts), it may be necessary to measure sounds that contain frequencies lower than about 20 Hz. For scale-model studies or for the measurement of noise environments or structures subject to fatigue, it may be necessary to measure to frequencies higher than 20,000 Hz. We will first discuss the different types of microphones used in noise measurements and their acoustical properties and then methods by which microphones are calibrated. More details about microphones are given in Chapter 36 and of their calibration in Chapter 51. Chapter 57 in the *Handbook of Acoustics*<sup>3</sup> also has detailed information about microphone calibration.



**Figure 6** Frequency response of an ideal microphone or accelerometer.



**Figure 7** Comparison of the frequency response ranges of four different diameter condenser microphones [lower limiting frequency (Hz) and upper limiting frequency (kHz)]. Microphone diameters:  $\frac{1}{8}$  in.,  $\frac{1}{4}$  in.,  $\frac{1}{2}$  in., and 1 in.<sup>2</sup>

#### 4.1 Types of Microphones for Noise Measurements

An acoustical transducer is a device that converts some property of a sound field into an electrical signal. The most common device is the microphone designed to measure sound pressure. Some transducers have been designed, however, to measure sound particle velocity, sound pressure gradient, and sound intensity.

Microphones may be divided into three main classes: communication, studio, and measurement microphones. (See Chapter 36 for more details.) The discussion here mainly concerns noise measurement microphones. There are three main types of microphone used for noise measurements: (1) polarized condenser microphones, (2) prepolarized condenser microphones (sometimes called electret microphones), and (3) piezoelectric microphones. The polarized condenser microphone possesses a thin diaphragm under tension and must be provided with an external polarizing voltage that is applied between the diaphragm and the backplate. On the other hand, the prepolarized condenser (electret) microphone avoids the need for a polarizing voltage by the provision of a thin layer of electrically charged material, which is normally deposited on the backplate during manufacture.

Condenser microphones, because of their stability and well-defined mechanical impedance, are the ones mostly preferred for noise measurements. They do have drawbacks of fragility and sensitivity to humidity, however. Piezoelectric microphones are more robust than condenser microphones. They possess a stiff diaphragm that is coupled to a piezoelectric crystal or ceramic element.

Microphones may be divided into directional and nondirectional (or omnidirectional) types. In some cases, directional microphones may be useful, such as in the localization of noise sources. Most noise measurements are made with nominally omnidirectional microphones, although even these types become somewhat directional at high frequency, at which the dimensions of the microphone become comparable with the acoustic wavelength.

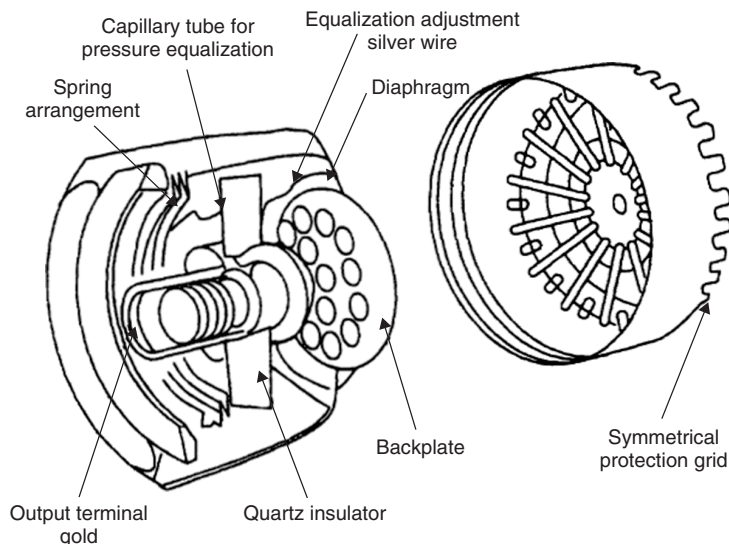
Microphones may be further subdivided into three main types: (1) free-field, (2) pressure-field, and (3) diffuse-field microphones. The frequency responses of these microphones are adjusted so that they have an essentially flat frequency response when placed in these different sound fields. Today TEDS (transducer electronic data sheet) microphones with built-in sensitivity are also available. These microphones have built-in information about the response required in different sound fields. So such TEDS microphones can be used in all of the three sound fields described above if they are used in conjunction with information loaded into the operating system of the associated analyzer. Chapter 36 describes the design and principles of operation of the main types of microphones and furthermore explains how the microphone parameters, physical properties, and design may be chosen to obtain the required microphone sensitivity, frequency response, and dynamic range. Chapter 43 also addresses some of the same considerations with respect to noise measurements.

**4.1.1 Condenser Microphones** The introduction, in the 1920s, of the condenser microphone with its uniform sensitivity, low distortion, and portability revolutionized electroacoustics, and it soon became an integral part of any high-quality sound system. However, although the polarized condenser microphone has significant advantages, it also suffers from some disadvantages: specifically its rather low sensitivity, high internal impedance, and the need for a polarizing voltage. These shortcomings led to the development of other microphone designs such as piezoelectric and prepolarized types, which will be discussed shortly and also in more detail in Chapter 36. The very large, almost distortionless electronic signal amplification that can now be achieved has made the lack of sensitivity of the condenser microphone unimportant, and, because of its smooth sensitivity over a very wide frequency range and its well-defined geometry, the condenser microphone is still preferred for use in many noise measurement applications.<sup>4</sup>

Figure 8 shows a diagram of a 1-in. condenser microphone. The condenser microphone consists of a thin metal diaphragm stretched under tension and spaced a short distance from an insulated backplate. The diaphragm and backplate constitute the electrodes of the condenser. Holes are drilled in the backplate to provide the required air damping for the diaphragm. A small hole is provided to equalize the static pressure across the diaphragm, provided that it changes slowly. This hole usually determines the lower cutoff frequency of the microphone. Some discussion of the electrical circuit of the system and the theory, design, and construction of condenser microphones is given in Chapter 36 and in Chapters 110 and 112 of the *Handbook of Acoustics*.<sup>3</sup> Other authors have also discussed the electrical theory in some detail.<sup>5-7</sup> It is normally necessary to remove the protection grid during microphone calibration (see Chapter 51).

**4.1.2 Prepolarized (Electret) Microphones** In the 1970s, a new type of precision microphone became commercially available. This microphone is basically a condenser microphone; however, no direct current (dc) polarization voltage is needed since the electret foil diaphragm and/or the backplate is permanently polarized during manufacture. The polarization voltage is created by embedding and aligning static electrical charges into a thin layer of material, which is deposited on the microphone diaphragm or backplate.

The first electret microphones used diaphragms made from an insulating material that carried the permanent electrical charge. The diaphragms of electret microphones made in this way have to be quite heavy in order to carry the permanent electrical charge material. Heavy diaphragms have several disadvantages and result in a low resonance frequency peak. Most high-quality electret microphones used for noise studies now have the permanently charged material attached to the stationary backplate instead of the diaphragm. In this way, much thinner diaphragms can be used, made of the same metal-coated plastic material used in condenser microphones. Such microphones have a



**Figure 8** Cross section through a 1-in. condenser microphone.

high resonance frequency peak and an overall performance almost rivaling the best condenser microphone. The thin diaphragm and the perforated backplate comprise the two plates of the condenser. Preamplifiers are still needed, and in some recent electret microphones miniature preamplifiers are built into the microphones themselves. See Chapter 36 and Chapters 110 and 112 of the *Handbook of Acoustics*.<sup>3</sup> Figure 9 shows a cross-sectional diagram of a typical electret microphone.<sup>8</sup>

The electret microphone has the following advantages: (a) no polarization voltage needed, (b) rugged construction, (c) large capacitance (about 500 pF), and hence, loading is a lesser problem than with the condenser microphone), and (d) low cost.<sup>6,9,10</sup>

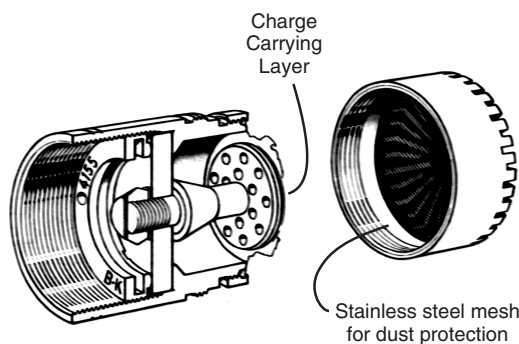
**4.1.3 Piezoelectric Microphones** The design and construction of piezoelectric transducers is discussed in Chapter 36 and in Chapters 110 and 112 in

the *Handbook of Acoustics*<sup>3</sup> and in varying detail by several other authors.<sup>11,12</sup>

Piezoelectric crystals may be cut and used in many different orientations. If a slice is cut from a piezoelectric crystal and pressures applied to the opposite faces of the slice causing a deformation, then equal and opposite charges are produced on the opposite faces of the slice with an electric potential developed between the faces. Crystals are often directly exposed to liquids (e.g., as hydrophones) where the high mechanical impedance of the liquid is not a disadvantage. In gases, the large acoustical/mechanical impedance mismatch is a disadvantage, and piezoelectric materials are usually used in conjunction with a diaphragm. See Chapter 36.

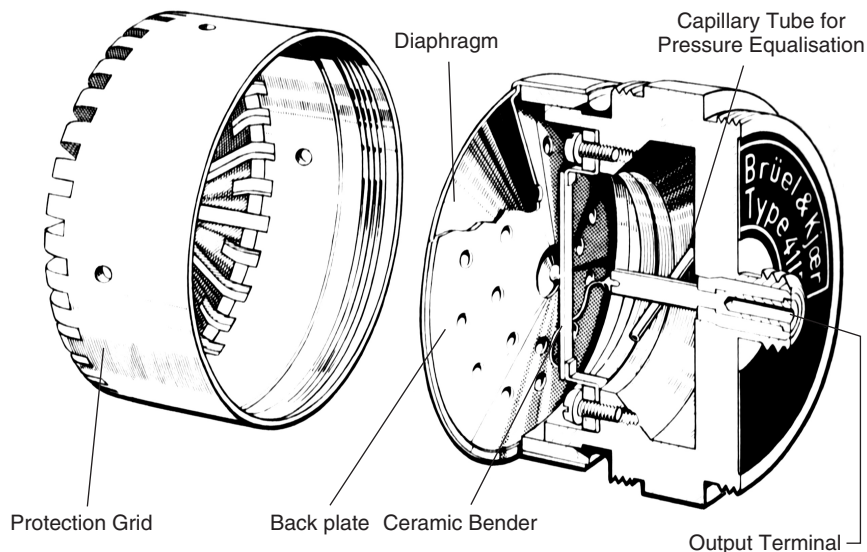
Figure 10 shows a cross-sectional view of a commercial piezoelectric microphone. Much thicker diaphragms are normally used with piezoelectric than condenser microphones (usually about 50 times greater). This inevitably leads to a lower resonance frequency for the diaphragm (assuming the density of the diaphragm material is the same) [consider Eq. (10) in Chapter 1]. To obtain a flat free-field response, it is necessary to damp this resonance overcritically. Hence the upper frequency response is poorer than with a condenser microphone because the mass-controlled region is entered at a lower frequency (see Fig. 9 in Chapter 1 and Chapter 36).

The diaphragm is connected to a ceramic bender element. A bimorph simply supported bender element is most often used, although sometimes cantilever benders are used.<sup>11,12</sup> The force needed to produce a voltage from a crystal or ceramic slice in pure compression is quite large. However, if a thin bar or beam is cut from a crystal in a suitable orientation, a voltage is produced across the beam as it is bent.<sup>1</sup> Metal foil is usually cemented to the outside surfaces



**Figure 9** Electret microphone using a thin electret polymer layer deposited on the perforated backplate.





**Figure 10** Cross-sectional view of piezoelectric microphone.

of the crystal, and the two foils with the crystal in between form a condenser of the solid dielectric type. It is usual to use two bars in conjunction to produce a *bimorph*. Electrical connections may be applied in two ways to the bimorph to produce either parallel or series connections.<sup>1</sup>

Other microphones are used for many communication purposes but not normally for precision noise measurements. The moving coil microphone has been in use for many years but is less valuable in noise work since its frequency response is not very smooth and is poor at high frequencies. Also its sensitivity is low. However, it does have some advantages that make it ideal for some applications. (See Chapter 36.)

## 4.2 Directivity

At low frequencies, for example, below about 1000 Hz, the frequency response of a microphone is independent of the angle of incidence of the sound waves. However, at higher frequencies, as the microphone dimensions and the wavelength of the sound become comparable, *diffraction* effects become important and the frequency response of a microphone is strongly dependent on the angle of incidence of the sound. See Fig. 11. The effect of *directivity* is discussed in detail in Chapter 36 and Chapter 3 in Ref 1.

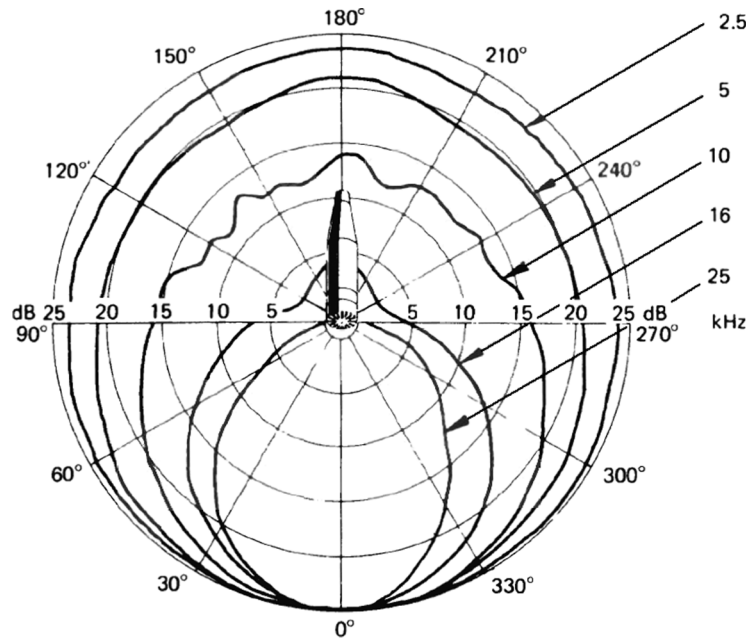
Microphones can be designed to have a flat frequency response when exposed to a free progressive wave sound field. They are usually known as free-field microphones. Other microphones can be designed to have a flat frequency response to grazing incidence sound waves and are normally known as pressure-field microphones. Still other microphones are designed to have a flat frequency response to random incidence sound and are known as diffuse-field incidence microphones. (See Chapters 36 and 43.) Care must be made

in ensuring that the right type is used. Figure 12 illustrates the use of different types.

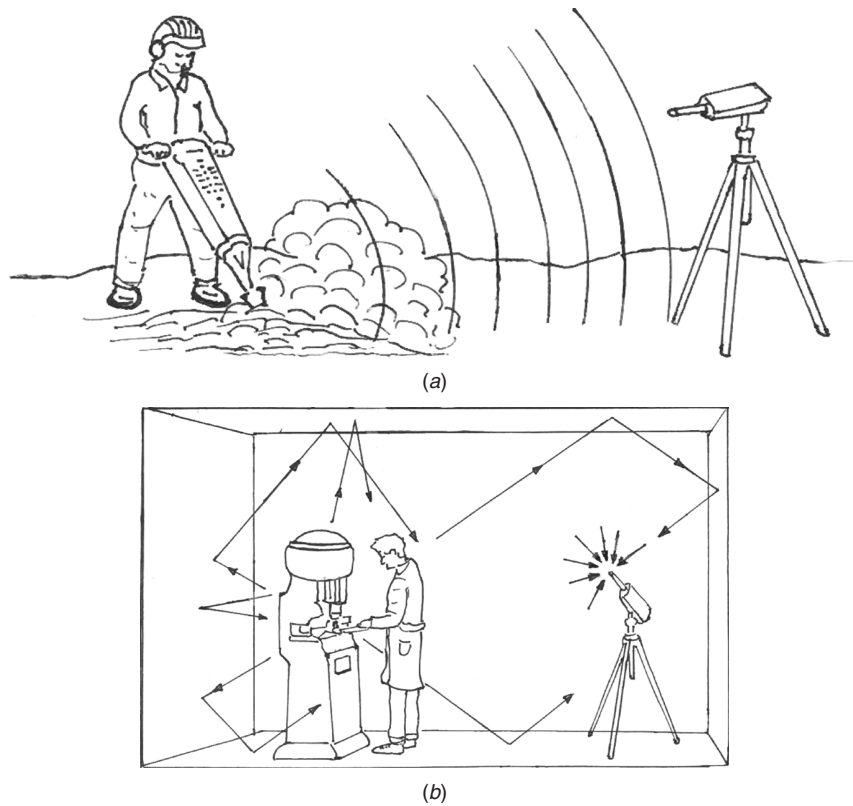
## 4.3 Transducer Calibration

It is important to calibrate transducers used for sound, shock, and vibration to ensure the accuracy of measurements made with them. Proper calibration also ensures that the results measured with the transducers are comparable with the results measured by others. The accuracy of the calibration must also be known. The transducer system and the calibration method used must perform the calibration with a known accuracy. If these conditions are met, then the calibration is termed as traceable. It should be noted, however, that this traceability is not an indication necessarily of highly accurate measurements, but simply that if the uncertainty is known, the measurements can then be compared with valid measurements made by others, which have also been made using proper calibration procedures. Thus measurements made with transducers and calibration procedures are of no use unless the associated uncertainty in measurement is also known. New and upgraded international standards now provide a variety of calibration methods together with their suitability for ensuring traceability.

Transducers should be calibrated on site before and after each measurement or set of measurements and periodically at service centers or national metrology laboratories. Chapter 51 describes calibration procedures for microphones and sound intensity systems. Chapter 52 discusses the calibration of shock and vibration transducers. Chapters 51 and 52 also describe the traceability of sound and vibration measurements, and Chapter 53 describes the traceability of shock and vibration measurements to national and international standards in detail.



**Figure 11** Directivity of a microphone with a protection grid at different frequencies.



**Figure 12** Noise measurements using (a) free-field microphone and (b) diffuse-field microphone.



Microphones, calibrators, and sound level meters all need to be calibrated. The most common requirement is the calibration of microphones for their sound pressure response, but calibrations for sound intensity, sound power, and acoustic impedance measurements are also commonly needed. Chapter 51 discusses the calibration of microphones in detail. Nedelitsky in Chapter 108 of the *Handbook of Acoustics*<sup>3</sup> and others have also discussed the problems of calibrating microphones. When a microphone is introduced into a sound field, it causes undesirable reflections and hence changes the sound field. This effect is more pronounced at high frequency. Ideally we should like to measure the sound pressure in the unperturbed or “free field,” but this is difficult. It is extremely important that manufacturers and users calibrate microphones accurately. Unfortunately, some users do not calibrate microphones sufficiently frequently to ensure the accuracy of sound pressure level readings. As already discussed, microphones may be designed to have three flat frequency responses. As mentioned before, TEDS microphones with built-in sensitivities are also available. TEDS microphones can be used to obtain all of the three flat frequency responses. The two main types of microphones in use are the *free-field* type (primarily used for outdoors measurements) and the *diffuse-field* type (mainly used for indoors measurements). Pressure-field microphones are mostly used for coupler measurements, except for the recently developed flat surface microphone.

As regards calibration of microphones, the pressure response may be considered to be the response of the microphone to a uniform pressure applied over its diaphragm. This is the response of an ideal microphone of *zero size* introduced into a free progressive plane wave field. However, when an actual finite size microphone is introduced into such a field, reflection and diffraction are caused, which give a different microphone response called the *free-field* response. See Chapter 36. Because the microphone can be oriented at any arbitrary angle in the plane wave field, perhaps the pressure response is more fundamental. There are several ways of measuring the pressure response of a microphone:<sup>13,14</sup> (a) pistonphone, (b) driven-diaphragm-type calibrator, (c) electrostatic actuator, (d) reciprocity method, and (e) substitution method. The only absolute method of calibration is the reciprocity method. This is somewhat complicated and time consuming; and the other four methods, although not giving absolute calibration, are more convenient and normally sufficiently accurate. See Chapter 51 in this handbook and Chapter 108 in the *Handbook of Acoustics*.<sup>3</sup>

**4.3.1 Pistonphones** The pistonphone is a very accurate, reliable, and simple device for calibrating a microphone that is convenient for use in the field. The principle of operation is quite simple. A small battery-powered electric motor drives a shaft on which is mounted a cam disk. The cam disk drives two pistons symmetrically. The cam gives the pistons a sinusoidal motion at four times the shaft rotational speed. The

stroke of the pistons (or peak amplitude from mean position) is thus one quarter of the difference in maximum and minimum diameters of the cam. The pistons vary the cavity volume sinusoidally in time and since for pistonphones a low frequency (e.g., 250 Hz) is normally chosen (for mechanical reasons), a corresponding sinusoidal variation in pressure occurs. (See Chapter 51 and Chapter 3 in Ref. 1 for the theory and further details of its operation.)

Provided the piston stroke is carefully controlled, the sound pressure level produced can be accurately predicted. Good sealing should be maintained when the microphone is fitted into the coupler opening. In principle, this type of pistonphone can be used to calibrate any microphone provided that good sealing is maintained. If microphones of different diameters are to be calibrated with the pistonphone, and different coupler connections are used to keep the volume unchanged, the sound pressure level is unchanged. If a different volume results, the change in sound pressure level can be predicted. (See Ref. 1 for the theory.) A change in atmospheric pressure will alter the calibration, but a correction is simply made by the use of a barometer provided by the manufacturer.

**4.3.2 Driven-Diaphragm Calibrators** Somewhat simpler, lower cost calibrators are also available that work on the driven-diaphragm principle. Some commercially available types produce 114 dB at 1000 Hz. A stabilized 1000-Hz oscillator feeds a piezoelectric driven element that vibrates the metallic diaphragm creating a pressure in the front coupling. The diaphragm is driven by an oscillator powered by a 9-V battery. Some calibrators generate five selected frequencies: 125, 250, 500, 1000, and 2000 Hz at 94 dB. With such calibrators, corrections should normally be made for changes in ambient temperature and pressure (altitude). Newer types of calibrator have a built-in microphone that measures and controls the sound pressure generated in the coupler cavity via a feedback loop. See Chapter 51 for more details of such driven-diaphragm-type calibrators.

**4.3.3 Sound Intensity Probe Calibration** When two phase-matched microphones are used together to form a sound intensity probe, then the two-microphone intensity probe can be calibrated by fitting an intensity coupler attached to the pistonphone. See Chapter 51. The coupler normally consists of two chambers (upper and lower) connected by a coupling element. When the pistonphone is connected to the coupler, a phase difference is created between the two sound pressures generated in the upper and lower chambers. The sound pressure amplitudes are the same, however, in both chambers. Thus the propagation of a plane progressive sound wave in a free field is simulated. If one microphone of the intensity pair is fitted to the upper chamber and the other is fitted to the lower chamber, then the simulated sound wave produced by the sound in the two chambers can be used for the calibration of the intensity probe for the measurement of both sound intensity and particle velocity. The

intensity coupler and pistonphone can also be used for the sound pressure sensitivity calibration of the two microphones. For this measurement, the two microphones are connected to the upper chamber of the coupler. They are then automatically exposed to the same sound pressure, and the amplitude and phase difference between the two microphones can be measured and checked to see that it is within acceptable limits. If a sound source, which can generate broadband sound, is attached to the coupler, then the pressure residual-intensity index spectrum can be measured as well. This index is used to determine the accuracy of the sound intensity measurements made with the probe. See Chapters 45, 51, and 86.

## 5 VIBRATION MEASUREMENTS

A vibration sensor is a device that converts some property of the vibration of a structure into an electrical signal. While a vibration generator works on the opposite principle of converting an electrical signal into a mechanical vibration. Both vibration sensors and generators may be termed transducers, since they convert one physical variable into another. (See Chapter 37.)

Vibration sensors can be made to work using several different principles and to measure surface displacement, velocity, acceleration, and strain. They may be arbitrarily designated as contacting or noncontacting devices. Contacting sensors are often convenient to use since they can measure vibration at a specific location on a structure. They do have the disadvantage, however, that they can change the vibration of the structure by adding mass and damping. This is particularly a problem if the structure is lightweight.

There are three quantities of most interest in vibration studies.<sup>1</sup> These are *displacement*, *velocity*, and *acceleration*. A fourth quantity, *strain*, is also frequently measured. In the early 1900s, most vibration measurements were made using *mechanical or optical devices*. Such devices are still used satisfactorily for low—frequency measurements (a few hertz). With the advent of electronics in the 1920s, transducers that converted mechanical into electrical signals were developed. Before about 1960, displacement and particularly velocity-sensitive transducers were utilized, especially when higher frequency measurements were needed. However, since that time acceleration-sensitive transducers (accelerometers) have become preferred. The reason for this is mainly because excellent lightweight accelerometers were developed to measure very high frequency vibrations (5000 Hz or more) in aircraft and spacecraft. Most velocity-sensitive transducers have an upper limiting frequency of about 1000 Hz, while piezoelectric accelerometers can be made to have an upper limiting frequency of 40,000 Hz or more.<sup>1</sup>

For many measurements it is unimportant whether displacement, velocity, or acceleration is measured. For simple harmonic motion, the amplitudes of these three quantities are simply related to each other by multiplying or dividing by the angular frequency  $\omega$

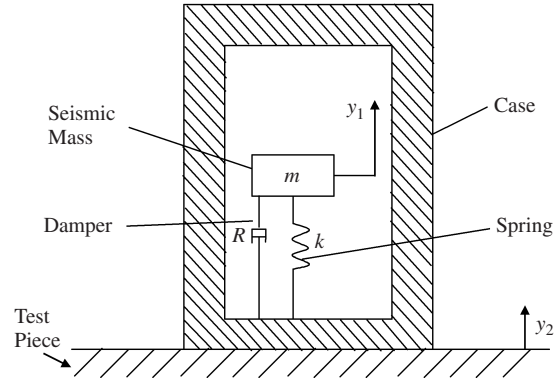


Figure 13 Idealized diagram of vibration transducer.

(see Chapters 1 and 43). Even if the vibration is random in nature, if frequency filtration is used, this principle can still be applied. Alternatively, the conversion from acceleration to velocity and displacement may be made by using electronic integration.

### 5.1 Principle of Seismic Mass Transducers

Modern-day piezoelectric accelerometers and some of the earlier displacement transducers<sup>15</sup> work on the same principle: A seismic mass  $m$  is supported on a spring of stiffness  $k$  and the whole is enclosed in a case (Fig. 13). The damping constant  $R$  in most applications is small, and it is neglected for simplicity in the following analysis (although it could easily be included).

If the vibrating member (test piece) is undergoing a time-dependent displacement,  $y_2(t)$ , and the mass experiences a time-dependent displacement,  $y_1(t)$ , then considering the forces acting on the mass  $m$ ,

$$k(y_2 - y_1) = m\ddot{y}_1 \quad (3)$$

The situation is identical to that studied in Section 4.1C of Chapter 1, except that there is no external force applied to the mass, and instead the test piece receives a displacement input,  $y_2(t)$ .

The easiest variable to measure is the relative displacement  $y_2 - y_1$ . We will assume the test piece experiences simple harmonic motion:

$$y_2 = B e^{i\omega t} \quad (4)$$

and, consequently in steady-state conditions, the mass experiences simple harmonic motion,  $y_1$  at the same angular frequency  $\omega$ :

$$y_1 = A e^{i\omega t} \quad (5)$$

Note that  $A$  and  $B$  are written as complex quantities because  $y_1$  and  $y_2$  will not generally be in phase (see

Section 4.1C in Chapter 1). From Eqs. (3), (4), and (5) we obtain (noting that  $i^2 = -1$ )

$$k(\mathbf{B} - \mathbf{A})e^{i\omega t} = -m\omega^2 \mathbf{A}e^{i\omega t} \quad (6)$$

$$\mathbf{B} - \mathbf{A} = -(m\omega^2/k)\mathbf{A} \quad (7)$$

Rearranging Eq. (7) gives

$$\mathbf{A} = -\left(\frac{k}{m\omega^2 - k}\right)\mathbf{B} \quad (8)$$

and substituting Eq. (8) into Eq. (7) gives

$$\mathbf{B} - \mathbf{A} = \frac{m\omega^2}{m\omega^2 - k}\mathbf{B} \quad (9)$$

It is easy to see how this result can be used to design displacement, velocity, or acceleration transducers.

**5.1.1 Seismic Mass Displacement and Velocity Transducers** Seismic mass displacement and velocity transducers were widely used until the 1950s. They required a large seismic mass and a soft spring (between about 0.5 and 3 Hz) and were operated well above the system's natural frequency to obtain a flat frequency response curve. They were heavy and only suitable for use on heavy machinery.<sup>16</sup> The soft spring gave a low resonance frequency between about 0.5 and 3 Hz, but the upper frequency limit was normally about 100 Hz due to limitations in the mechanical linkages used to measure the motion of the mass relative to the system's case. There are now several other displacement and velocity transducers available that do not suffer from this very limited frequency range. For example, the laser Doppler system can be used to measure dynamic displacement and velocity with a very high degree of precision.

#### 5.1.2 Seismic Mass Acceleration Transducers

To measure acceleration conveniently with the seismic mass, the system shown in Fig. 13 must be used as follows. The ratio of relative displacement amplitude  $|\mathbf{B} - \mathbf{A}|$  to test piece acceleration amplitude  $\omega^2|\mathbf{B}|$  is from Eq. (9)

$$\frac{|\mathbf{B} - \mathbf{A}|}{\omega^2|\mathbf{B}|} = \frac{1}{|\omega^2 - \omega_n^2|} = \frac{1/\omega_n^2}{|1 - (\omega^2/\omega_n^2)|} \quad (10)$$

Except for the constant  $(1/\omega_n^2)$  in the numerator, the right-hand side of Eq. (10) is identical to that of Eq. (19) in Chapter 1 with  $\delta = 0$ . If we had included damping in our model, the result would have again been identical to Eq. (19) in Chapter 1, except for the constant. Thus, we can make use of the results of Fig. 9 in Chapter 1. This figure shows that we should like to operate the instrument in the stiffness-controlled region, where  $\omega/\omega_n \ll 1$ .

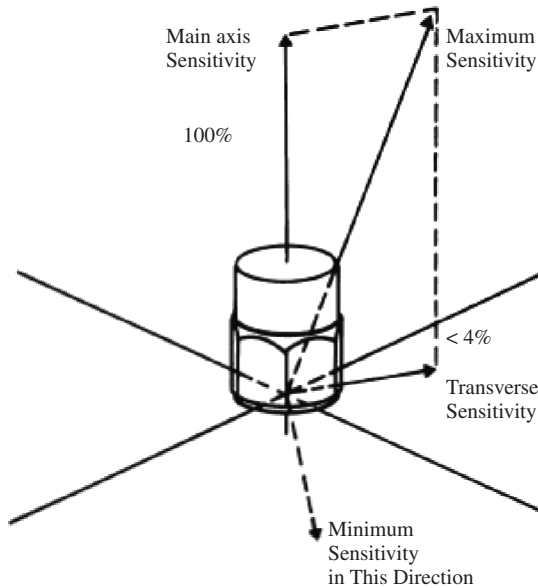
Again this is obvious from Eq. (10), since, if  $\omega/\omega_n \ll 1$ , the right-hand side becomes a constant (equal to  $1/\omega_n^2$ ). To obtain a flat frequency response over a wide frequency range,  $\omega_n$  should be made large. But note that in this case the sensitivity decreases, since it is approximately proportional to  $1/\omega_n^2$ . To obtain a large value of the frequency  $\omega_n$ , it is necessary to use a very stiff spring and a small mass, which is opposite to what is needed for seismic mass displacement and velocity transducers discussed above.<sup>1</sup>

It is possible to measure the relative displacement by attaching a strain gauge to the spring and calibrating the instrument by the change in resistance produced. This is the principle of the *strain gauge* accelerometer, which is normally used with a Wheatstone bridge. Such accelerometers will usually be found to have an upper frequency limit of about 1000 or 2000 Hz. Provided that the accelerometer is dc coupled, it is easy to calibrate the accelerometer by inverting it. If the strain gauge accelerometer is placed horizontally, there is no signal; placed vertically in one direction it gives a constant resistance change equivalent to +1 g and placed in the opposite vertical position the change is equivalent to -1 g. If the accelerometer is alternating current (ac) coupled, such calibration is not possible. However, the most commonly used type of accelerometer is now the *piezoelectric accelerometer*.<sup>17,18</sup>

#### 5.2 Piezoelectric Accelerometers

The piezoelectric accelerometer is a seismic mass type of accelerometer that works on the principle described above. The main types include the following: compression, delta shear, planar shear, theta shear, annular shear, and ortho shear. These are all designed to accentuate certain advantages that are useful in different environmental conditions and are described in more detail in Chapter 37 and Section 12 of Chapter 43. As already discussed, the heavier accelerometers have the greatest sensitivity but the lowest resonance frequency and vice versa.

Several characteristics of piezoelectric accelerometers need to be considered. The piezoelectric accelerometer produces a charge after deformation. After the signal is passed through a charge converter (incorporated in modern piezoelectric accelerometers), it can be considered as a voltage source. Hence, the sensitivity is given in  $\text{mV/ms}^{-2}$ . Besides being sensitive to acceleration in the longitudinal axis, the accelerometer is also slightly sensitive to vibration in the transverse axis due to irregularities in construction and alignment of the piezoelectric disks. See Fig. 14. Good accelerometers should have a *lateral sensitivity* less than 5% of the longitudinal (or main axis) sensitivity. The transverse sensitivity will vary in the base plane having maximum and minimum values in certain directions. The sensitivity of an accelerometer will be somewhat temperature dependent (one should always consult the manufacturer's instructions), however, provided the maximum (Curie point) temperature is not exceeded, the piezoelectric material will not be damaged and will retain its properties.



**Figure 14** Transverse and longitudinal sensitivity of accelerometer.

Piezoelectric accelerometers produce some output signal when subjected to acoustical signals or base strains. Normally the *acoustical sensitivity* is low (producing a false response output of less than 1 g for a sound pressure level input of 160 dB). As the test object vibrates, it will induce strain in the accelerometer base with a consequent output signal. Most accelerometer bases are made thick and rigid to reduce this effect.

As was discussed above (also see Chapter 37) all accelerometers exhibit a fundamental resonance frequency. The *frequency range* of an accelerometer is usually assumed to be bounded by an upper frequency limit of one third of the resonance frequency for less than 1-dB error or one fifth the resonance frequency for less than 0.5-dB error. This assumes that the accelerometer design has low damping. The upper frequency limit is extended in some accelerometer designs by using high damping. Today TEDS accelerometers are also available with built-in amplitude response information, so that the upper frequency limit is increased by about 50% to about one half of the resonance frequency.

The lower limiting frequency depends on the type of preamplifier used to follow the accelerometer. Two types may be used and are commercially available. If the preamplifier is designed so that the output voltage is proportional to the input voltage, it is called a voltage amplifier. If the output voltage is proportional to the input charge, it is called a charge amplifier. When a voltage amplifier is used, the accelerometer output voltage is very sensitive to cable capacitance. This is because typically the capacitance of a piezoelectric accelerometer is several hundred

picofarads (usually between 100 and 1000 pF). This is somewhere between the very low capacitance of a condenser microphone and the higher capacitance of a piezoelectric microphone (see Sections 4.1.1 and 4.1.3). When a charge amplifier is used, the output voltage is not sensitive to changes in cable length. Broch<sup>19</sup> describes the reasons for this in some detail. If a voltage amplifier is used, the lower limiting frequency (3-dB down point) is given by

$$f_l = \frac{1}{2\pi RC} \quad (11)$$

where  $R$  is the input resistance of the voltage preamplifier and  $C$  is the effective circuit capacitance:

$$C = \frac{(C_A + C_L)C_C}{C_A + C_L + C_C} \quad (12)$$

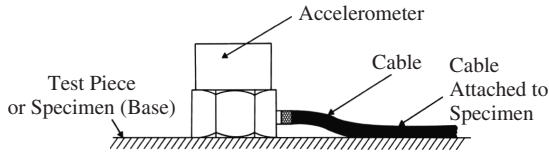
where  $C_A$ ,  $C_L$ , and  $C_C$  are the accelerometer, cable, and preamplifier capacitances, respectively.

The dynamic range of the piezoelectric accelerometer is determined by the lower limiting frequency set by electrical noise in the system and the upper limiting frequency governed by the preloading of the accelerometer and the mechanical strength of the piezoelectric element. Smaller accelerometers usually have a higher upper limit. (See Chapter 37.) It should also be noted that accelerometers have a main direction of sensitivity. See Fig. 14.

### 5.3 Measurement Difficulties

It should be noted that poor *mounting techniques* can have a marked effect on the frequency response above 2000 or 3000 Hz. Below this frequency, the mounting technique is not important as long as the accelerometer is fixed directly onto the specimen. The best technique is to attach the accelerometer to the specimen with a threaded steel stud. When this mounting method cannot be used, cement is also acceptable, and wax can be used with small to medium size accelerometers (up to 20 to 30 g).<sup>17</sup> At low frequencies, magnets may be used. *Ground loops* must be avoided, in particular, when low acceleration levels are measured. With higher acceleration levels, ground loops can also cause problems. Measurement errors of 50% or more may be caused by ground loops with acceleration amplitudes of 100 m/s<sup>2</sup> or more. In such cases the accelerometer should be electrically isolated from the specimen and attached with a nonconducting stud or cemented to a mica washer, which is in turn cemented to the specimen. Cable “whip” can produce electrical noise, and cables should be attached to the specimen as shown in Fig. 15.

In the case of the measurement of high-frequency vibration of thin metal plates, considerable care should be taken when using an accelerometer because of the *mass loading* effect. Well below its resonance frequency, the accelerometer can be assumed to act as a pure mass. The velocity of the test piece  $u_0$



**Figure 15** Mounting of an accelerometer to reduce cable whip noise.

can be assumed reduced to  $u_1$  by the addition of the accelerometer<sup>20</sup>

$$\frac{u_1}{u_0} = \frac{Z}{Z + i\omega m} \quad (13)$$

where  $Z$  = mechanical impedance of test piece at the attachment point,  $\omega$  = angular frequency, and  $m$  is the accelerometer mass.

The input point impedance for a metal plate can be assumed to be

$$Z = \frac{4}{\sqrt{3}} \rho c_L h^2 \quad (14)$$

where  $\rho$  = plate density,  $c_L$  = longitudinal wave speed in plate, and  $h$  = plate thickness.

Substituting Eq. (14) in Eq. (13) and assuming  $|Z| = |i\omega m|$ , which gives a 3-dB reduction in velocity amplitude (from Eq. 13), gives the frequency  $f_{3dB}$  at which the 3-dB reduction occurs as

$$f_{3dB} = \frac{2\rho c_L h^2}{\sqrt{3}\pi m} \quad (15)$$

Equation (15) is plotted in Fig. 16. This figure suggests that even lightweight accelerometers will “load” thin metal plates (e.g., a 10-g accelerometer will mass “load” a 3.2-mm ( $\frac{1}{8}$ -in.) aluminum plate at frequencies above about 4000 Hz).

To overcome such mass loading problems, various types of noncontacting gauges have been produced and still are widely used. Particular examples of where noncontacting gauges are invaluable are in the study of the vibration of thin sandwich composite panels and of loudspeaker cones. Examples of noncontacting gauges are given in Chapter 37.

#### 5.4 Calibration, Metrology, and Traceability of Shock and Vibration Transducers

Vibration measurements of acceleration, velocity, and displacement can be classified in two main ways: (1) relative measurements made between two points with systems such as laser Doppler interferometers and (2) absolute measurements made with seismic mass transducers (mainly accelerometers). The calibration of transducers used for both types of measurement is described in detail in Chapter 52. Chapter 52 also describes the traceability of vibration measurements and Chapter 53 describes the traceability of shock and

vibration measurements to national and international standards in more detail. In many ways the traceability requirements and calibration concerns for shock and vibration transducers are similar to those of microphones.

### 6 SIGNAL ANALYSIS, DATA PROCESSING, AND SPECIALIZED NOISE AND VIBRATION MEASUREMENTS

#### 6.1 Signal Analysis and Data Processing

Sound and vibration signals produced by transducers are not normally in a suitable form for the study of noise and vibration problems. Frequency analysis is the most common approach used in the solution of such problems. This is because the human ear acts in many ways like a frequency analyzer (see Chapter 67) and also because frequency analysis can often be used to reveal information that can be related to the operation of machines, in particular rotating machinery and to the properties and the behavior of structures (see Chapter 68). Until the late 1970s, frequency analysis mostly was carried out with dedicated instruments that incorporated analog filters. Since that time, with the advent of the fast Fourier transform (FFT) algorithm, frequency analysis has been increasingly carried out using digital computers, either as part of a dedicated instrument or after appropriate conversion of the analog signal to digital form (known as A/D conversion). The analog signal is converted into a series of discrete values (also known as a time series). Dual and multichannel analyzers are also in common use for the parallel analysis of the signals from several transducers.

Besides carrying out frequency analysis of signals, analyzers have been made to calculate various other functions including cross-spectra, coherence between signals, and the like. Chapter 40 provides detailed explanations for the working of analyzers. Chapter 41 explains how measured noise and vibration data can be acquired, processed, shared, and stored using the power of modern digital computer systems. Chapter 42 deals with signal processing. This chapter summarizes the analog-to-digital conversion process, digital data storage and retrieval, basic computations used in noise and vibration data analysis, and errors associated with the various calculations. Important considerations in signal processing include sampling rate, sampling interval, resolution, and data format. The analog data must be sampled so that at least two sample values per cycle of the highest frequency of interest in the analog signal are obtained. The format of the data is also important, and it must be ensured that the data produced are in a form that they can be read directly by any computer program written in a common language such as C or FORTRAN.

#### 6.2 Sound Level Meters and Dosimeters

The sound level meter (SLM) is an instrument designed to measure sound pressure over a frequency range and a sound pressure level range similar to the human ear. The basic SLM consists of a microphone,

amplifier, frequency weighting circuit(s), detector averaging circuit, and an analog or digital read-out device.<sup>21-25</sup> Miniaturization of electrical circuits and components has allowed small lightweight SLMs to be built, which possess considerable sophistication and capabilities. Also standards for SLMs written by successive national and international standards committees have resulted in different requirements and additional changes in SLM design and manufacture so that there is a wide variety of SLMs in use. There are four main types of SLM: 0, 1, 2, and 3. Type 0 meters are the most accurate and type 3

the least. The tolerances for the different types are specified in these standards. The different SLM types are generally used for precision, laboratory, field, and survey measurements. Dosimeters are similar in design to SLMs, except that the time constant, threshold, and exponent circuits are omitted.<sup>15,26</sup> Dosimeters are worn on the person and are normally designed to measure the so-called noise dose, which is a percentage of a criterion exposure, where exposure is measured in pascal-squared hours. The noise dose calculated depends on the exchange rate used. In the United States, the Occupational Safety and Health

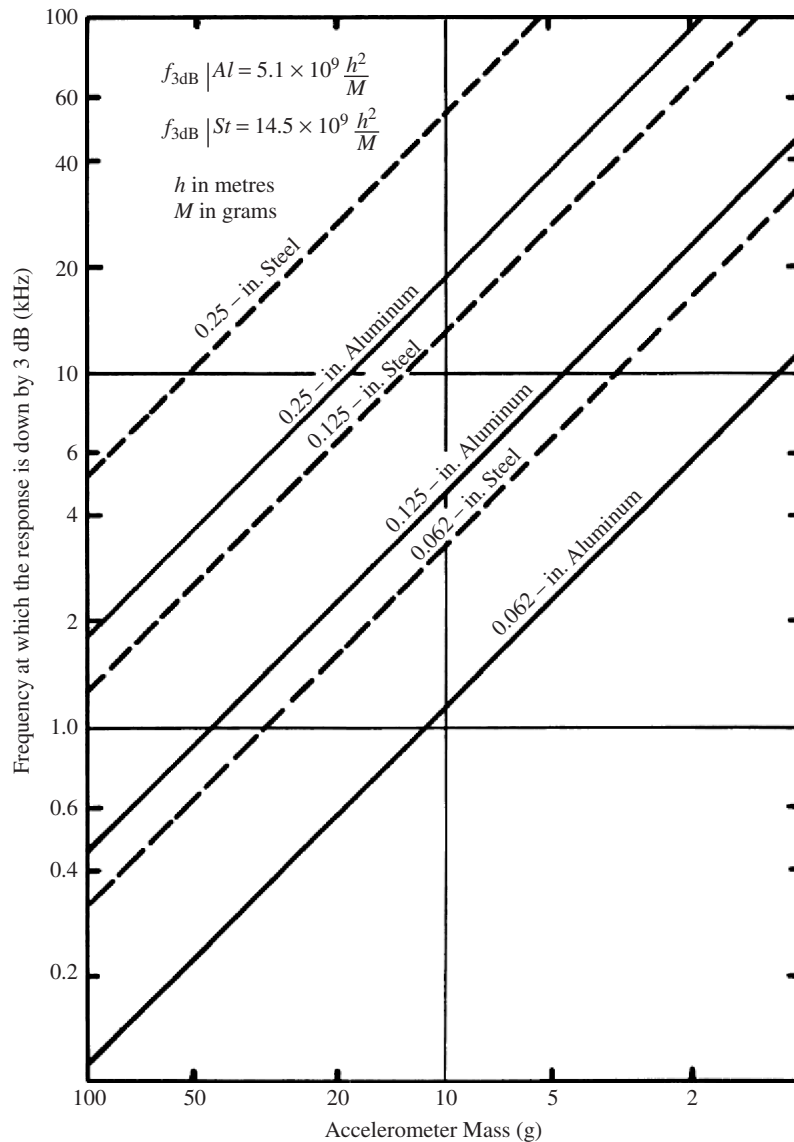


Figure 16 Effect of mass loading of an accelerometer on the vibration of a metal plate<sup>20</sup>.

Administration (OSHA) requires a 5-dB exchange rate while the National Institute for Occupational Safety and Health (NIOSH) and most other countries use the 3-dB (equal energy) exchange rate. Chapter 38 reviews the main aspects of SLM design and also briefly describes dosimeter design. Chapter 39 reviews dosimeters in more detail.

### 6.3 Noise and Vibration Measurements

Chapter 43 deals with basic noise and vibration measurements. The chapter describes proper measurement techniques, measurement uncertainties, and repeatability of measurements. Not only are routine noise and vibration measurements described, but also measurement procedures specifically designed to measure reverberation time, vehicle passby noise, airport noise monitoring, aircraft takeoff and landing noise, and measurements of the sound absorption coefficient and acoustic impedance of materials with the impedance tube technique. An example of the use of the impedance tube to measure the sound-absorbing properties of porous asphalt road surfaces is given in this chapter. Other books have useful chapters on noise measurements, such as Ref. 28.

### 6.4 Sound Power and Sound Intensity

Measurements of the sound power of machines are frequently needed. The European Union requires some machines to be provided with labels giving their sound power output. From knowledge of the sound power level, the sound pressure level can be calculated at a certain distance from a machine, either outside in free space or in a building, provided certain environmental conditions are known. Chapter 44 describes several methods that can be used and that have been standardized both nationally and internationally. Also measurement surfaces including the spherical and box surfaces are described. Reverberation time and comparison methods of measuring sound power are also reviewed in Chapter 44.

Sound intensity measurements described in Chapter 45 provide another method of determining the sound power output of sources, and this approach is particularly useful when the machine cannot be moved into a special facility such as an anechoic room or a reverberation room. In addition, the sound intensity approach can still be used to determine the sound power of a sound source when there is a hostile background noise present. Provided that the background noise is steady, good estimates of the sound power of a source can be made, even if the background noise level is very high. In such situations, the approaches described to obtain the sound power of sources in Chapter 44 normally fail.

Chapter 46 provides further in-depth discussion on data analysis with an emphasis on the use of such analysis to solve noise and vibration problems. Also some basic concepts including types of signals, probability distribution, and probability density are described. The chapter also describes techniques such as zoom analysis, practical FFT analysis, spectrum

averaging, and spectral analysis using filters, time-domain analysis, time synchronous averaging, and analysis of cyclo-stationary signals. Cyclo-stationary signal analysis has recently become the subject of increasing interest since it is now evident that many machine vibration signals are not purely periodic, since their vibrations possess amplitude modulations as well. This chapter explains how some of the data analysis techniques can be applied to vibration caused by worn roller bearings and diesel engine noise.

### 6.5 Modal Analysis

Modal analysis can be used to provide information concerning the natural frequencies, modal damping factors, and mode shapes of structures and machinery. This information can be obtained either from mathematical analysis of a structure's dynamic response derived from a set of equations and knowledge of its mass and stiffness distributions or from experimental measurements of the structure's response to excitation. Experimental modal analysis (often simply known as modal testing) is discussed in detail in Chapter 47. As explained in this chapter, however, modal testing cannot be divorced from mathematical models of the structure's dynamical behavior and the objective of modal testing in reality is an attempt to construct or validate a mathematical model of this behavior. Unfortunately, such mathematical models obtained through modal testing can never be quite complete because, in practice, the amount of experimental data obtained is inevitably limited. Usually, the mathematical model to be validated is a finite element model of the structure. Modal analysis is used for several main purposes. These include (a) monitoring the dynamic properties of a structure or machine to obtain early indications of structural deterioration or impending failure (often known as structural or machinery health monitoring), (b) modification of a structure's mass or stiffness distributions so as to change natural frequencies to avoid high-amplitude resonant vibration, the resulting structural fatigue and the possibility of failure, and (c) troubleshooting—the display of animated modes of vibration of the structure so that the dynamic behavior of certain critical areas of the structure can be understood, thus making possible practical solutions to vibration problems.

### 6.6 Condition Monitoring

Condition monitoring is discussed in Chapter 48. Such monitoring of machinery may give sufficient advance warning of wear and possible imminent breakdown and failure so that replacement parts can be obtained in time to avoid costly machine downtime and/or loss of production. Costs savings can be considerable, for instance, in the case of downtime of a city electrical power plant, where unexpected downtime losses can exceed several million U.S. dollars each day. The savings in avoiding unnecessary downtime costs often vastly exceed the costs of replacement machine parts. In cases such as aircraft power plants, predictive maintenance can even prevent the possibility



of catastrophic failure of the compressor blades and other components of the engines.

Chapter 48 describes two main approaches to condition monitoring: (1) monitoring the relative displacement of a rotating machine shaft or bearing with a proximity probe and (2) monitoring the vibration of the cover of a machine. Proximity probes are normally built into machines during manufacture; while, on the other hand, accelerometers can be placed on the cover of a machine at any time during service to monitor its vibration. Proximity probes are usually used to monitor changes in absolute shaft displacement and to measure so-called shaft orbits. Chapter 57 in the *Handbook of Acoustics*<sup>3</sup> also contains useful information concerning monitoring changes in shaft motion with the use of proximity probes. Chapter 48 is mainly concerned with vibration measurements of machine casings made with accelerometers. If a machine is monitored in its original new condition, measurements made later may reveal changes indicating wear and the possibility of failure. Faults related to the frequency of the shaft speed include: misalignment, imbalance, and cracks in the drive shaft. It is usually difficult to distinguish between these faults. Useful information is given in Chapter 48 about the changes in the vibration signature, which manifest themselves with electrical machines, gears, bearings, and reciprocating machinery such as internal combustion engines, pumps, compressors, and the like.

### 6.7 Advanced Noise and Vibration Analysis and Measurement Techniques

Wavelets are starting to become of practical use in the solution of noise and vibration problems, machinery diagnostics, and health monitoring. Wavelet analysis is concerned with the decomposition of time signals into short waves or *wavelets*. Any waveform may be used for such decomposition provided that it is localized at a particular time (or position). Chapter 49 provides an in-depth discussion of the basics of wavelet analysis of signals, and in this chapter time is taken as the independent variable, although, in practice, any physical variable can be used. The Fourier coefficients of a signal are obtained by averaging over the full length of the signal, and the result is that no information is provided about how the frequency content of the signal may be changing with time.

In principle, the short-time Fourier transform (STFT) does provide this needed frequency time variation information, by dividing the time record of the signal into sections, each of which is analyzed separately. The frequency coefficients of the signal computed by the STFT depend on the length and time (or position) of the short record that the calculation process assumes is one period of an infinitely long periodic signal (see Chapters 40, 42, and 46). The difficulty remains, however, that infinitely long harmonic functions are being used to decompose a transient signal. Wavelets are short functions that avoid this difficulty. A set of wavelet functions is used as the basis for the decomposition of transient time-history signal records.

Near-field acoustical holography is a technique that can be used to reconstruct the frequency spectrum of any sound field descriptor (i.e., sound pressure, particle velocity, and sound intensity) at any location in space, normal surface velocity/displacement, directivity patterns, and the total sound power of a source. This is achieved by making a sound pressure on a planar surface located near to the source's surface with either a scanning microphone (or hydrophone) or an array of microphones. If a scanning microphone is used, it should be robot controlled. The procedure essentially creates a near-field hologram and relies on the measurement of the phase relationship between all of the sensor elements in the array that is used. If a scanning microphone is used instead, then the phase relationship is obtained by comparisons with a reference signal, which is kept stationary throughout the measurement. The approach can be used both with sources that are random in nature (such as fluid flow or boundary layer noise sources) and with deterministic sources (such as those containing pure tones like noise from a propeller). Although the approach is not simple, it eliminates the need for costly facilities and relies on the use of software instead, some of which is becoming commercially available. Chapter 50 describes the theory behind this approach and also describes its use in practice to determine the in-flight sound pressure, normal surface velocity, and sound intensity on the interior fuselage surface and the floor of a passenger commuter aircraft.

### REFERENCES

1. M. J. Crocker and A. J. Price, *Noise and Noise Control*, Vol. I, CRC Press, Boca Raton, FL, 1975.
2. Brüel & Kjaer catalog, Naerum, Denmark, 2003.
3. M. J. Crocker, Ed., *Handbook of Acoustics*, Wiley, New York, 1998.
4. George S. K. Wong and Tony F. W. Embleton, Eds., *AIP Handbook of Condenser Microphones. Theory, Calibration, and Measurements*, American Institute of Physics, New York, 1995. Chapter 17.
5. A. Wood, *Acoustics*, Blackie & Son, London, 1940, Dover Reprint, New York, 1960, P. 513.
6. M. L. Gayford, *Electroacoustics, Microphones, Earphones and Loudspeakers*, American Elsevier, New York, 1971, P. 162.
7. L. L. Beranek, *Acoustics*, McGraw-Hill, New York, 1954, P. 157; reprinted by the Acoustical Society of America, New York, 1996.
8. G. M. Sessler and J. F. West, Foil Electret Microphones, *J. Acoust. Soc. Am.*, Vol. 40, 1966, P. 1433.
9. K. S. Hansen, *Details in the Construction of a Piezoelectric Microphone*, Brüel & Kjaer Tech. Rev. No. 1, Naerum, Denmark, 1969.
10. G. M. Sessler, and J. F., West, Foil Electret Microphones, *J. Acoust. Soc. Am.*, Vol. 40, 1973, pp. 1589–1600.
11. W. P. Mason, *Piezoelectric Crystals and Their Application to Ultrasonics*, Van Nostrand, New York, 1950.
12. L. E. Kinsler, and A. R. Frey, *Fundamentals of Acoustics*, 2nd ed., Wiley, New York, 1962, p. 325.
13. P. V. Brüel, and G. Rasmussen, *Free Field Response of Condenser Microphones*, Brüel & Kjaer Tech. Rev. No. 1, and Rev. No. 2, Naerum, Denmark, 1959.



14. American Standard ANSI S1.10-1966, American Standard for Calibration of Microphones.
15. Specification for Personal Noise Dosimeters, Acoustical Society of America, New York, 1991.
16. N. O. Myklestad, *Fundamentals of Vibration Analysis*, McGraw-Hill, New York, 1956, p. 101.
17. Brüel and Kjaer, *Piezo-electric Accelerometer and Vibration Preamplifier Handbook*, Naerum, Denmark, 1976.
18. ISO 5348-1998, Mechanical Vibration and Shock—Mechanical Mounting of Accelerometers, 1998.
19. J. T. Broch, *Mechanical Vibration and Shock Measurements*, Brüel & Kjaer Co., Naerum, Denmark, undated, pp. 66-68.
20. E. A. Starr, Sound and Vibration Transducers, in *Noise and Vibration Control*, L. L. Berane, Ed., McGraw-Hill, New York, 1971, Chapter 3. See also M. J. Crocker and A. J. Price, *Noise and Noise Control*, Volume 1, CRC Press, Cleveland, Ohio, 1975, Chapter 3.
21. IEC 60651-1979, Sound Level Meters, International Electrotechnical Commission, Geneva, Switzerland, 1979.
22. IEC 60804-1984, Integrating-averaging Sound Level Meters, International Electrotechnical Commission, Geneva, Switzerland, 1984.
23. IEC 61672-2, 2003, Electroacoustics-Sound Level Meters—Part 1: Specifications, International Electrotechnical Commission (IEC), Geneva, Switzerland, 2003.
24. ANSI S 1.4-1983 (R2001), Specification for Sound Level Meters, Acoustical Society of America, New York, 1983; ANSI S 1.4A -1985 (R2001), Amendment to ANSI S1.4-1983 Acoustical Society of America, New York, 1985.
25. ANSI S 1.25-1991 (R2002), Sound Level Meters—Part 1: Specifications.
26. IEC 61252-2002, Electroacoustics, Specifications for Personal Sound Exposure Meters, International Electrotechnical Commission, Geneva, Switzerland, 2002.6. IEC 61672-1, 2000.
27. C. M. Harris and A. G. Piersol, Eds. *Shock and Vibration Handbook*, 5th ed., McGraw-Hill, New York, 2001.

# CHAPTER 36

## ACOUSTICAL TRANSDUCER PRINCIPLES AND TYPES OF MICROPHONES

Gunnar Rasmussen and Per Rasmussen  
G.R.A.S. Sound & Vibration  
Holte, Denmark

### 1 INTRODUCTION

A microphone can be defined as a device that converts some property of an acoustic field into an electrical signal. The property of the sound field most often measured is the sound pressure, but other properties like pressure gradient or particle velocity may also be measured. The microphones may be broadly divided into three classes, according to their applications:

- *Communication microphones:* These are microphones for a wide range of applications, such as telephones, mobile telephones, dictaphones, walkie talkies, toys, hearing aids, and computer peripherals. The main factors for these applications are cost, size, and ruggedness.
- *Studio microphone:* A broad range of microphones for recording music and speech, such as on-stage performances and public address (PA) systems, and television. Some of the main factors for this class of microphones are performance, reliability, and design (appearance).
- *Measurement microphones:* For laboratory measurements, environmental measurements, type approval, and product labeling measurements. The main factors are precision, long-term stability, and calibration.

For each of the applications, the microphones may be developed to meet specifications for dynamic range, frequency range, size, and frequency response.

### 2 TYPES OF MICROPHONES

Different types of microphones may be divided according to the conversion principle used for converting the sound-field-related property to an electrical signal. In 1877, Thomas A. Edison invented the carbon lamp-black button microphone. This was one of the first practical microphones of the variable-resistor types. These microphones employed a diaphragm to convert the sound pressure signal into a mechanical force acting on carbon granulate. The force acting on the carbon granulate would change the electrical resistance of carbon and thereby modulate a bias current. This would provide a low output impedance signal that could be transmitted over considerable distances without amplification and was therefore quickly adopted for telephone use. The ability to be used without amplifying devices far outweighed its many disadvantages: poor temperature stability, sensitivity to humidity, and

problems with long-term as well as short-term stability and high noise floor. With the wide availability of amplifying devices and very high impedance input FETs (field-effect transistors), the carbon microphone is very seldom used today and will not be discussed further.

### 3 CONDENSER MICROPHONES

The most widely used microphone type today is the condenser-type microphone. This was invented in 1917 by E.C. Wentz and has since been developed further. The condenser-type microphone is available in the so-called externally polarized versions and in the prepolarized version, sometimes also called electret microphones. As the basic function of these types is almost the same, these will be handled together.

In a condenser microphone, a metallic or conducting diaphragm is placed close to and parallel with a backplate (Fig. 1), so that the diaphragm and the backplate form a capacitor. The capacity  $C_m$  of this capacitor is given by

$$C_m = \frac{\epsilon_0 \pi b^2}{h} \quad (1)$$

where  $\epsilon_0$  is the dielectric constant for air,  $b$  is the radius of the backplate, and  $h$  is the equilibrium distance between the backplate and the diaphragm. This capacitor is charged by a voltage source  $V_c$  through a large series resistor  $R_c$  so that the charge  $Q_c$  on the microphone becomes

$$Q_c = C_m V_c = V_c \frac{\epsilon_0 \pi b^2}{h} \quad (2)$$

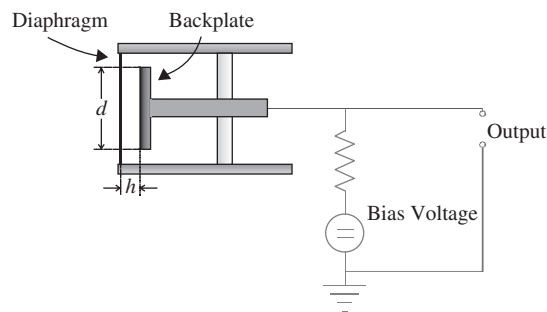


Figure 1 Condenser microphone principle.

If the pressure outside the microphone is different from the pressure inside the microphone, the diaphragm will be displaced from its equilibrium position. If the diaphragm is displaced by an amount  $x$ , this will, according to Eq. (1), cause a change in the microphone capacity:

$$C_{m,\Delta} = \frac{\epsilon_0 \pi b^2}{h+x} \quad (3)$$

The large series resistor  $R_c$  and a high input impedance preamplifier ensures that the charge  $Q_c$  in Eq. (2) is kept constant. The change in capacity will therefore result in a change in the voltage  $V_{out}$  across the microphone capacitor:

$$Q_c = C_m V_c = C_{m,\Delta} V_{out} = V_{out} \frac{\epsilon_0 \pi b^2}{h+x} \quad (4)$$

Combining Eqs. (2) and (4) gives

$$V_{out} = V_c \frac{h+x}{h} \quad (5)$$

A pressure difference  $p$  between the inside and the outside of the microphone will give a resulting diaphragm force  $F$  given by

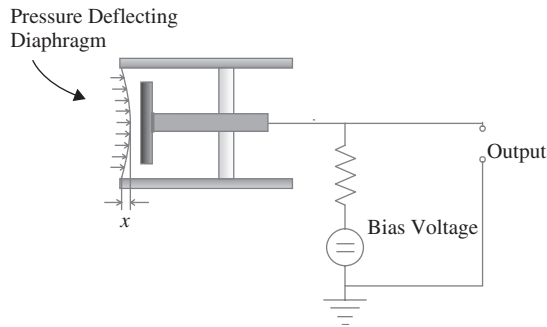
$$F = pA \quad (6)$$

where  $A$  is the effective diaphragm area. If  $Z_m$  is the mechanical impedance of the diaphragm, the resulting displacement of the diaphragm (Fig. 2) will be

$$x = \frac{F}{j\omega Z_m} = \frac{A}{j\omega Z_m} p \quad (7)$$

and the output signal from the microphone will be

$$V_{out} = V_c \frac{h + p(A/j\omega Z_m)}{h} \quad (8)$$



**Figure 2** Condenser microphone diaphragm deflection.

This equation shows that, for an overpressure outside the microphone, where the diaphragm is deflected toward the backplate (corresponding to a negative  $x$ ), the output signal will go down.

In general, the mechanical impedance of the diaphragm can be expressed as

$$Z_m = j\omega m_m + r_m + \frac{1}{j\omega c_m} \quad (9)$$

where  $m_m$  is the diaphragm mass,  $r_m$  is the damping in the microphone, and  $c_m$  is the stiffness of the diaphragm. It can be seen from Eq. (8) that in order to obtain a flat frequency response, the mechanical impedance of the diaphragm must be controlled by the diaphragm stiffness, and the contributions from mass and damping must be negligible:

$$Z_m \approx \frac{1}{j\omega c_m} \quad (10)$$

and if this is substituted in Eq. (8), the microphone output as a function of the input pressure is given by

$$V_{out} = V_c \frac{h + pAc_m}{h} \quad (11)$$

In practice, the microphone capacity is loaded by stray capacitance and the input impedance of the preamplifier, and this will lead to nonideal situations with limitations in performance and frequency range.

The prepolarized microphone, or electret-type microphone, is similar to the above-mentioned externally polarized microphone; only the polarization voltage is not established by an external voltage source. The polarization voltage is established by injecting an electrical charge into a thin layer of PTFE (polytetrafluoroethylene) or similar material, usually on the microphone backplate. Due to the high resistance of PTFE, the electrical charge decays only very slowly (decay rates from years to hundreds of years, depending on temperature).

#### 4 ELECTRODYNAMIC MICROPHONES

The electrodynamic microphone is, in principle, similar in build to an electrodynamic loudspeaker. However, instead of converting an electrical signal to sound, the sound pressure is converted to an electrical signal. The microphone (Fig. 3) consists of a stiff diaphragm loosely supported so that it can move freely. A coil is attached to the diaphragm, and the coil can be moved in a strong magnetic field caused by a permanent magnet.

A pressure difference  $p$  between the inside and the outside of the microphone will give a resulting diaphragm force  $F$  given by

$$F = pA \quad (12)$$

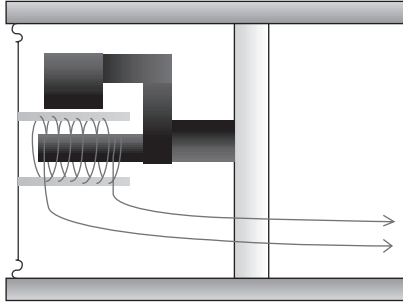


Figure 3 Dynamic microphone principle.

where  $A$  is the effective diaphragm area. If  $Z_m$  is the mechanical impedance of the diaphragm system, the resulting velocity  $v$  of the diaphragm and coil will be

$$v = \frac{pA}{Z_m} \quad (13)$$

As the coil is moving in the magnetic field  $B$ , this gives an output voltage  $V_{\text{out}}$  of

$$V_{\text{out}} = \frac{BlA}{Z_m} p \quad (14)$$

where  $l$  is the length of the wire in the coil.

Again, the diaphragm impedance is given as

$$Z_m = j\omega m_m + r_m + \frac{1}{j\omega c_m} \quad (15)$$

It can be seen from Eq. (14) that in order to obtain a flat frequency response, the mechanical impedance of the diaphragm must be controlled by the damping and the contributions from mass and stiffness must be negligible:

$$Z_m \approx r_m \quad (16)$$

and if this is substituted in Eq. (14), the microphone output as a function of the input pressure is given by

$$V_{\text{out}} = \frac{BlA}{r_m} p \quad (17)$$

so that in order for the microphone to give a flat frequency response, the diaphragm movement should be controlled by the damping.

## 5 PIEZOELECTRIC MICROPHONES

A wide variety of crystals and crystalline substances exhibit piezoelectric effects when mechanically deformed. This phenomenon is utilized in many types

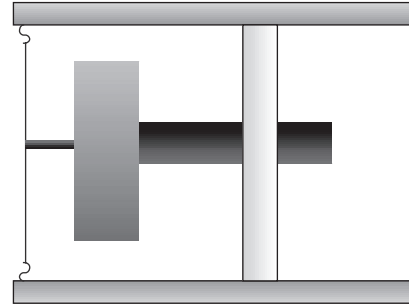


Figure 4 Piezoelectric microphone principle.

of transducers, including piezoelectric microphones and pressure transducers.

The piezoelectric microphone consists of a stiff diaphragm that is coupled to a piezoelectric crystal or ceramic substrate, as shown in Fig. 4. The output signal from the piezoelectric element is proportional to the mechanical displacement  $x$  of the element:

$$V_{\text{out}} = C_p x \quad (18)$$

where  $C_p$  is a constant for the piezoelectric element. A pressure difference  $p$  between the inside and the outside of the microphone will give a resulting diaphragm force  $F$  given by

$$F = pA \quad (19)$$

where  $A$  is the effective diaphragm area. If  $Z_m$  is the mechanical impedance of the piezoelectric element at the contact point with the diaphragm, the resulting displacement of the piezoelectric element will be

$$x = \frac{F}{j\omega Z_m} = \frac{A}{j\omega Z_m} p \quad (20)$$

and the output signal from the microphone will be

$$V_{\text{out}} = C_p \frac{A}{j\omega Z_m} p \quad (21)$$

Again, the diaphragm impedance is given as

$$Z_m = j\omega m_m + r_m + \frac{1}{j\omega c_m} \quad (22)$$

It can be seen from Eq. (21) that in order to obtain a flat frequency response, the mechanical impedance of the diaphragm must be controlled by the diaphragm stiffness and the contributions that form the mass and damping must be negligible:

$$Z_m \approx \frac{1}{j\omega c_m} \quad (23)$$

and if this is substituted in Eq. (21), the microphone output as a function of the input pressure is given by

$$V_{\text{out}} = C_p A c_m p \quad (24)$$

## 6 MICROPHONE DIRECTIVITY

Sound pressure is a scalar quantity and as such does not have any directional properties or information. However, a sound field may have a propagation direction, that is, the sound waves propagate in a certain direction. Different microphones may have different responses as a function of the orientation of the microphone relative to the orientation of the sound field. This may be expressed as

$$R(f, \theta) = \frac{V(f, \theta)}{V(f, 0^\circ)} \quad (25)$$

where  $V(f, \theta)$  is the output of the microphone as a function of frequency  $f$  for an angle  $\theta$  between the microphone and the propagation direction of the sound field, and  $V(f, 0^\circ)$  is the output of the microphone as a function of frequency  $f$  for an angle  $\theta = 0^\circ$  between the microphone and the propagation direction of the sound field ( $0^\circ$  incidence).

In general, microphones can be divided into directional microphones or omnidirectional microphones. Both types will eventually have a certain directionality, especially at higher frequencies where diffractions around the microphone start to change the acoustical field. While directional microphones are designed to obtain a certain directionality, omnidirectional microphones are designed to minimize directionality effects.

## 7 DIRECTIONAL MICROPHONES

Directionality microphones are designed so that both sides of the microphone diaphragm are exposed to the sound field, but with a delay in the sound signal from the front of the microphone to the back of the microphone.

For the microphone in a sound field (Fig. 5) the sound wave arrives first at the front of the microphone. Then the sound wave travels a distance  $l_1$  to the back of the microphone. This distance depends on the size

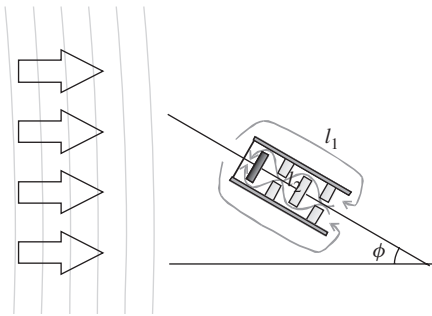


Figure 5 Directional microphone.

(diameter) of the microphone and on the angle  $\theta$  of the microphone relative to the propagation direction of the microphone:

$$l_1 = l_m \cos \theta \quad (26)$$

where  $l_m$  is a constant for the microphone depending on its size and geometry.

As the sound wave reaches the back of the microphone, it has to travel a further distance of  $l_2$ , which is independent of the angle  $\theta$ , but depends only on the design and geometry of the microphone. The total travel length  $l_t$  for the sound wave, therefore, becomes

$$l_t = l_1 + l_2 = l_m \cos \theta + l_2 \quad (27)$$

If the pressure of the incoming wave is  $p$  and the diaphragm area is  $S$ , the resulting force  $F$  on the diaphragm will be

$$\begin{aligned} F &= -dx \frac{\partial p}{\partial x} S = -l_t \frac{\partial p}{\partial x} S = -(l_m \cos \theta + l_2) \frac{\partial p}{\partial x} S \\ &= -(l_m \cos \theta + l_2) k p S \end{aligned} \quad (28)$$

Since the wave number  $k$  is proportional to the frequency  $f$ ,

$$k = \frac{2\pi f}{c} \quad (29)$$

the force  $F$  acting on the diaphragm will be proportional to the frequency. And to obtain a flat frequency response, the diaphragm impedance has either to be designed so that the output of the microphone is inversely proportional to the diaphragm force or it has to be corrected for electrically afterwards.

The actual directivity is independent of the frequency as long as the dimensions  $l_m$  and  $l_2$  are small compared to the wavelength. The directivity is given by Eqs. (25) and (28):

$$\begin{aligned} R(\theta) &= \frac{-(l_m \cos \theta + l_2) k p S}{-(l_m + l_2) k p S} = \frac{l_m \cos \theta + l_2}{l_m + l_2} \\ &= \frac{(l_m/l_2) \cos \theta + 1}{(l_m/l_2) + 1} \end{aligned} \quad (30)$$

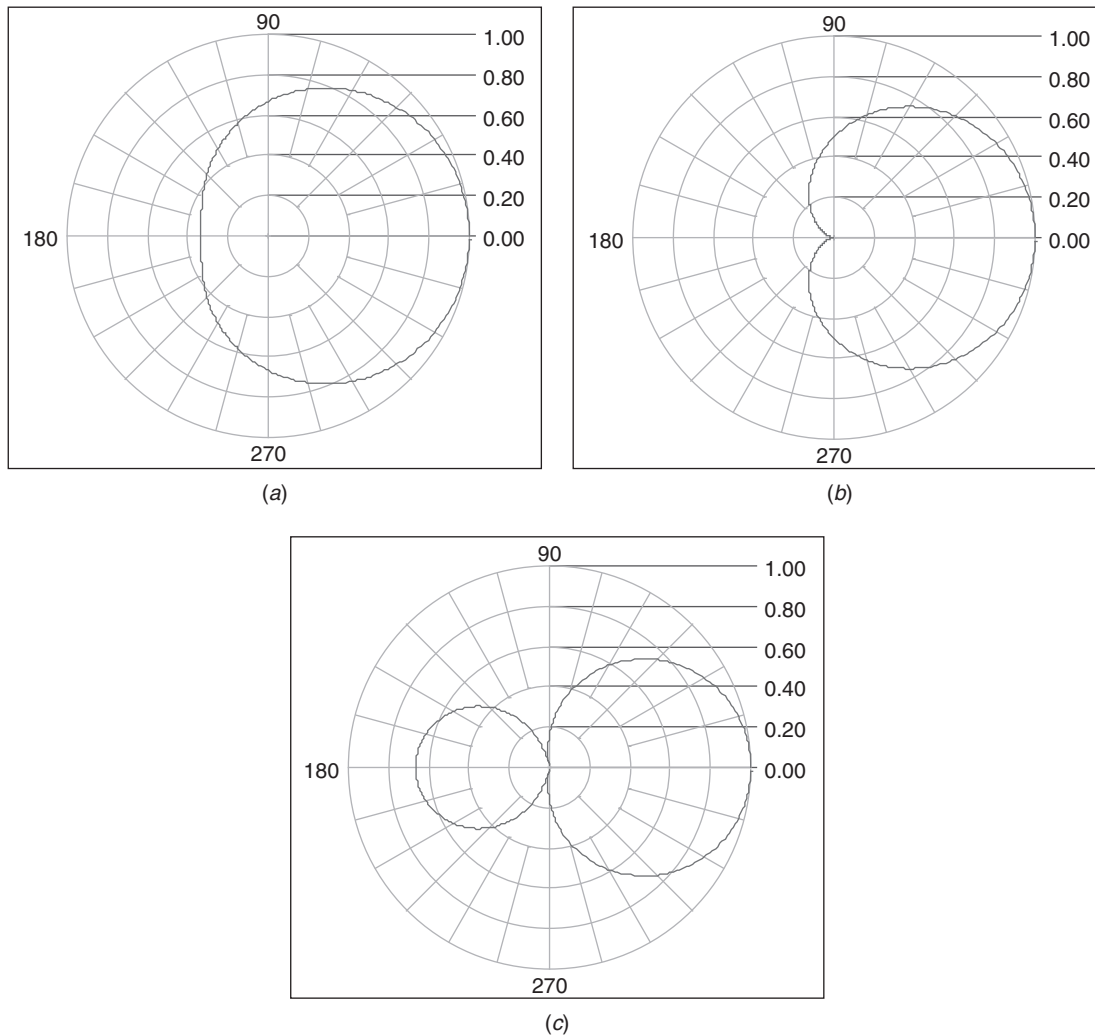
It can be seen that the directivity depends only on the ratio  $K$ :

$$K = \frac{l_m}{l_2} \quad (31)$$

Figure 6 shows some examples of the directivity plots for various ratios of  $K$ .

## 8 OMNIDIRECTIONAL MICROPHONE

As mentioned above, pressure is a scalar quantity and, as such, does not possess any directional information. Therefore, a pressure transducer is by definition an omnidirectional transducer.



**Figure 6** Microphone directivity for different  $K$  factors: (a)  $K = 0.5$ , (b)  $K = 1$ , and (c)  $K = 2$ .

This is true at low frequencies, but at higher frequencies, where the dimensions of the transducer become comparable to the wavelength, diffraction around the microphone will change the response.

In connection with the measurement of sound pressure, three types of microphones are used. These are: free-field microphones, pressure microphones, and random-incidence microphones. They are constructed to have different frequency characteristics in order to comply with different requirements.

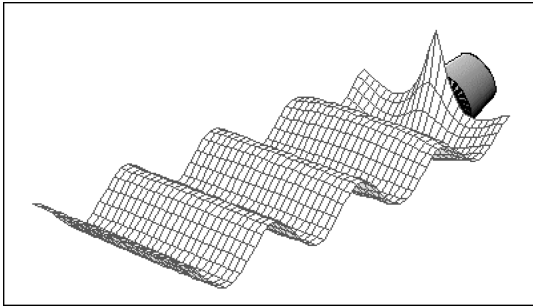
## 9 PRESSURE MICROPHONE

The pressure microphone is constructed to measure the actual sound pressure as it exists on the diaphragm. A typical application is the measurement of sound pressure in a closed coupler or the measurement of sound pressure at a boundary, such as a wall. In

this case, the microphone forms part of the wall and measures the sound pressure on the wall itself. The frequency response of this microphone should be flat over a wide-as-possible frequency range, taking into account that the sensitivity will decrease with increased frequency range. The acoustic damping in the air gap between the diaphragm and backplate is adjusted so that the frequency response is flat up to and a little beyond the resonant frequency.

## 10 FREE-FIELD MICROPHONE

The introduction of a microphone into a sound field will result in a pressure increase in front of the diaphragm (Fig. 7), depending on the wavelength. The free-field microphone is designed essentially to measure the sound pressure as it existed before the microphone was introduced into the sound field. At



**Figure 7** Pressure increase in front of microphone due to diffraction.

higher frequencies, the presence of the microphone in the sound field will change the sound pressure. Generally, the sound pressure around the microphone cartridge will increase due to reflections and diffraction. The free-field microphone is designed so that its frequency characteristics compensate for this pressure increase. The resulting output of the free-field microphone is a signal proportional to the sound pressure as it existed before the microphone was introduced into the sound field.

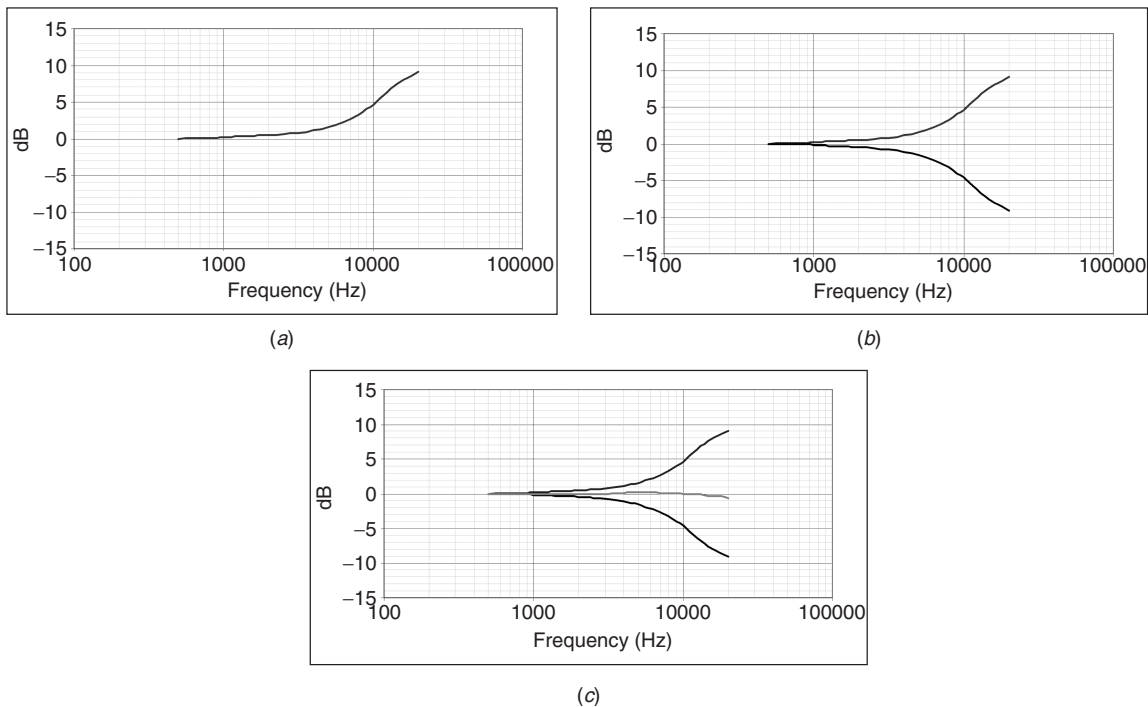
The free-field microphone should always point toward the sound source ( $0^\circ$  incidence) (Fig. 8a).

For a typical 0.5-in. microphone, the maximum pressure increase will occur at 26.9 kHz, where the wavelength of the sound coincides with the diameter of the microphone [ $\lambda = (342 \text{ m/s})/(26.9 \text{ kHz}) \approx 12.7 \text{ mm} \approx 0.5 \text{ in.}$ ]. The microphone then must be designed so that its sensitivity decreases by an amount that compensates for increased acoustic pressure in front of the diaphragm. This is done by increasing the internal acoustic damping in the microphone cartridge in order to obtain the desired frequency response (Fig. 8b) (see Section 12).

The result is an output from the microphone that is proportional to the sound pressure as it existed before the microphone was introduced into the sound field (Fig. 8c). The curve in Fig. 8a is also called the free-field correction curve for the microphone and must be added to the pressure frequency response of the microphone cartridge to obtain the acoustical characteristic of the microphone in a free field.

## 11 RANDOM-INCIDENCE MICROPHONE

In principle, the free-field microphone needs to be pointed toward the sound source in conditions where sound waves travel essentially in one direction. In some cases, for example, when measuring in a reverberation room or other highly reflecting surroundings, sound waves will not have a well-defined propagation direction but will arrive at the microphone from



**Figure 8** Frequency response of typical free field microphone: (a) Pressure increase in front of microphone due to diffraction. (b) Pressure response of microphone. (c) Resulting free-field response of microphone.



all directions simultaneously. The sound waves arriving at the microphone from the front will cause a pressure increase as described above for the free-field microphone, whereas sound waves arriving from the back of the microphone will cause a pressure decrease to a certain extent due to the shadowing effects of the microphone cartridge. The combined influence of the waves coming from different directions depends, therefore, on the distribution of sound waves from the different directions. For measurement microphones, a standard distribution has been defined, based on statistical considerations, resulting in a standardized random-incidence microphone.

## 12 MICROPHONE DESIGN PARAMETERS

The basic characteristics of a microphone are determined by factors such as size, diaphragm tension, distance between the diaphragm and the backplate, and the acoustic damping within the microphone. These factors will determine the frequency range of the microphone, its sensitivity, and its dynamic range. The sensitivity is described as the output voltage of the microphone for a given sound pressure excitation, and, in itself, is of little interest for the operation of the microphone, except for calibration purposes. However, the sensitivity of the microphone (together with the electrical impedance of its cartridge) also determines the lowest sound pressure level that can be measured with the microphone. The size of the microphone is the first parameter determining its sensitivity. Generally, the larger the diameter of the diaphragm, the more sensitive the microphone will be. There are, however, limits to how sensitive the microphone can be made simply by making it larger. The polarization voltage causes the diaphragm to be attracted, and deflected, toward the backplate. When the size of the microphone is increased, this deflection will also increase, and eventually the diaphragm will be deflected so much that it will actually touch the backplate. To avoid this, the distance between the diaphragm and the backplate can be increased or the polarization voltage can be lowered, in both cases leading to a decrease in sensitivity. The optimum practical size of a measurement microphone for use up to 20 kHz is very close to 0.5 inch (12.7 mm). In some special applications involving very low level measurements, 1-inch (25.4-mm) microphones may be required, but for the majority of applications, 0.5 inch or smaller is the better choice.

When the size of the microphone is decreased, the useful frequency range is increased. The frequency range obtainable is determined, in part, by the size of the microphone. At high frequencies, when the wavelength of sound waves becomes much smaller than the diameter of the diaphragm, the diaphragm will stop behaving like a rigid piston (the diaphragm is said to “break up”—not a destructive phenomenon). Different parts of the diaphragm will start to move with differing magnitude and phase, bringing about a change in the microphone’s frequency response. To avoid this, the upper limiting frequency is placed such that the sensitivity of the microphone drops off before

the diaphragm starts to break up. For a typical 0.5-inch microphone, the upper limiting frequency is placed in the range of 20 to 40 kHz, depending on diaphragm tension. If the diaphragm is tensioned, that is, made stiffer, its resonance frequency will be higher; on the other hand, the sensitivity of the microphone will be reduced because the diaphragm will deflect less for a given sound pressure level.

The frequency response of a microphone is determined by diaphragm tension, diaphragm mass, and the acoustic damping in the air gap between the diaphragm and backplate. This system can be represented by a simple mass–spring–damper system, as seen in Fig. 9. In this analogy, the mass represents the mass of the diaphragm, and the spring represents the tension in the diaphragm. Thus, if the diaphragm is tensioned to make it stiffer, the corresponding spring becomes stiffer. The damping element in the analogy represents the acoustic damping between the diaphragm and the backplate. This can be adjusted, for example, by drilling holes in the backplate, which will make it easier for the air to slip away from the air gap when the diaphragm is deflected, thereby decreasing damping.

This simple mechanical analogy of the microphone is a first-order mechanical system with a simple frequency response. At low frequencies (below resonant frequency), the response of the microphone is determined by the diaphragm tension (Fig. 10). If the diaphragm tension is increased, the output of the microphone will decrease, and if it is decreased, the output will increase. The tension and mass of the diaphragm determine the resonant frequency such that an increase in tension increases the resonant frequency, and an increase in mass decreases the resonant frequency. The response around the resonant frequency (Fig. 11) is determined by the acoustic damping, where an increase in damping will decrease the response. At higher frequencies, above the resonant frequency, the response of the microphone to sound pressure is determined by the mass of the diaphragm. The greater the mass of the diaphragm, the smaller will be the output signal from the microphone since the sound pressure has greater difficulty in moving the diaphragm.

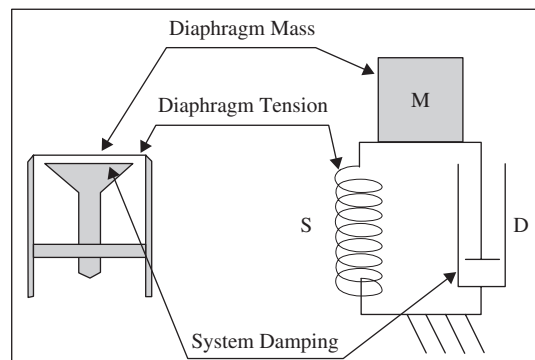


Figure 9 Microphone equivalent system.



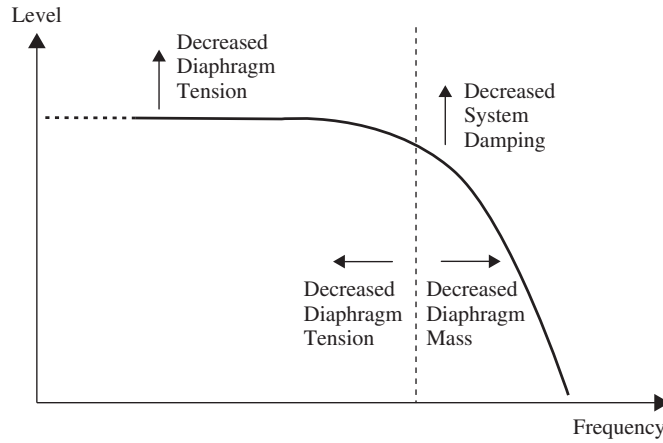


Figure 10 Microphone parameters.

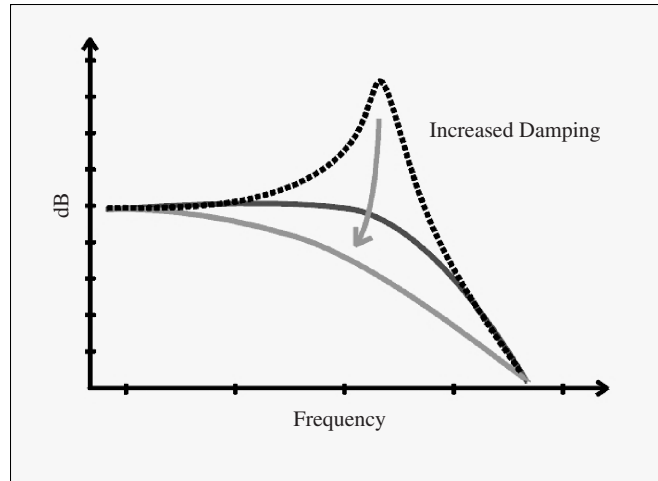


Figure 11 Microphone resonance damping.

### 13 DYNAMIC RANGE

The dynamic range of a microphone is the range between the highest and the lowest sound pressures that can be handled by the microphone. The highest level is determined by the distance between the backplate and the diaphragm, usually on the order of  $20\ \mu\text{m}$  ( $2 \times 10^{-5}\text{m}$ ). If the sound pressure is high enough, it will deflect the diaphragm so much that it will actually touch the backplate. In this situation, the microphone will become highly nonlinear. Thus, it is usual to limit the maximum deflection to about one-tenth of the distance between the backplate and the diaphragm. For a typical 0.5-inch measurement microphone, this will be around 140 dB (relative to  $2 \times 10^{-5}\text{ Pa}$ ). As the sound pressure is decreased, diaphragm movement is also decreased proportionally. Thus, at a sound pressure level of 20 dB (relative

to  $2 \times 10^{-5}\text{ Pa}$ ), the movement of the diaphragm is reduced by a factor of  $10^{-6}$  (120 dB), giving a diaphragm movement of around  $2 \times 10^{-12}\text{ m}$ .

The lowest level of sound pressure is determined by the inherent noise generated in the microphone itself and the conversion factor from pressure to voltage in connection with the preamplifier. The inherent noise generated by the microphone is associated with the damping in a simple mechanical model.<sup>1</sup> In an electrical analogy of this mechanical model, the damping is present in the form of a resistor  $R_A$ , and the Johnson noise from this resistor, expressed as power spectral density (PSD), is given by the Nyquist equation:

$$\text{PSD} = p_{\text{rms}}^2 / \Delta f = 4k_B T R_A \quad (32)$$

where  $k_B$  is the Boltzmann constant and  $T$  is the absolute temperature. It can be seen that this causes a frequency-independent thermal noise contribution proportional to the damping.

The Johnson noise contribution will be present on the output terminal of the microphone and is superimposed on the signal generated by the sound pressure on the diaphragm. This signal is given by the sound pressure  $p_i$  on the diaphragm and the sensitivity  $S_m$ . The sensitivity, or electromechanical coupling coefficient, is the ratio between the sound pressure and resulting output voltage. The total output  $V_o$  from the

microphone is therefore given by

$$V_o = N_s + p_i S_m \quad (33)$$

where  $N_s$  is the thermal noise contribution. It can be seen that the lower limit can be extended downward either by increasing the sensitivity or by decreasing the damping.

#### REFERENCE

1. G. S. K. Wong and T. F. W. Embleton, Eds., *AIP Handbook of Condenser Microphones*, AIP Press, Woodbury, NY, 1995.

# CHAPTER 37

## VIBRATION TRANSDUCER PRINCIPLES AND TYPES OF VIBRATION TRANSDUCERS

Colin H. Hansen  
School of Mechanical Engineering  
University of Adelaide  
Adelaide, South Australia, Australia

### 1 INTRODUCTION

Vibration transducers are used widely in noise, shock, and vibration control. There are two main types of vibration transducers: (1) vibration sensors, which convert vibration to an electrical signal (voltage or charge), and (2) generators, which work on the principle of converting an electrical voltage or current to a mechanical vibration.

There are several important properties that must be considered in the design and selection of a vibration transducer. The *sensitivity* of a measurement transducer represents the smallest quantity that it can measure. The term can also refer to the effect of various environmental parameters such as temperature, magnetic fields, and the like on the transducer output. The *dynamic range* represents the ratio of the largest to smallest quantities that can be measured and is usually expressed in decibels, while the *frequency range* is the range of frequencies to which a measurement transducer is sensitive or an actuator can excite. The electrical quantity that defines the electrical input or output of a transducer in terms of the relationship between voltage and current is known as the *input/output impedance*.

There are a number of Internet sites where more detailed information on vibration transducers is available. Two useful sites are [www.endevco.com](http://www.endevco.com) and [www.bk.dk](http://www.bk.dk). At the first site a handbook of dynamic measurement can be downloaded, and at the second a number of technical reviews are available that deal exclusively with vibration measurement. In addition to these sites, there are a number of useful handbooks that include vibration measurement information, including the one by Harris and Piersol.<sup>1</sup>

### 2 VIBRATION SENSORS

Prior to discussing vibration sensors in detail, it is useful to point out the relationships between the acceleration, velocity, and displacement of a vibrating object. For single frequencies or narrow bands of noise, the displacement  $d$ , velocity  $v$ , and acceleration  $a$  are related by the frequency  $\omega$  (rad/s), as  $d/\omega^2 = v/\omega = a$ . In terms of phase angle, velocity leads displacement by  $90^\circ$  and acceleration leads velocity by  $90^\circ$ . For narrow-band or broadband signals, velocity and displacement can also be derived from

acceleration measurements using electronic integrating circuits. On the other hand, deriving velocity and acceleration signals by differentiating displacement signals is generally not practical due primarily to the limited dynamic range of displacement transducers and secondarily to the cost of differentiating electronics.

### 2.1 Accelerometers

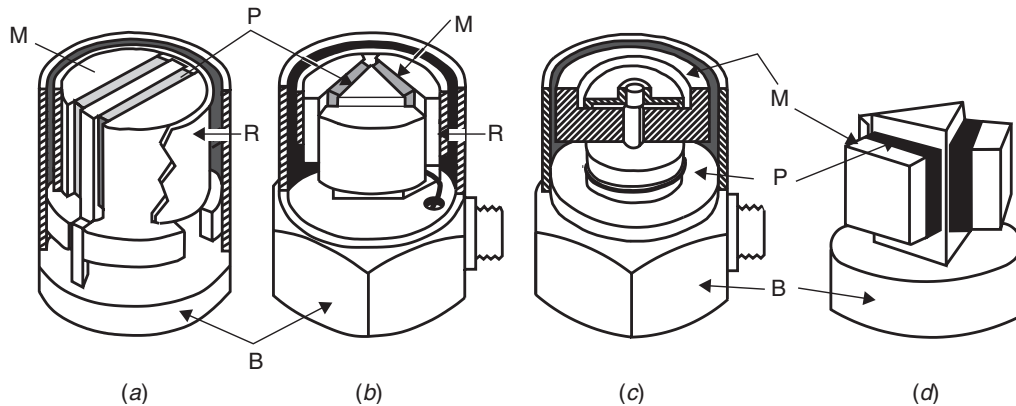
Vibratory motion is often sensed by using an accelerometer attached to the vibrating surface. These transducers, may be either piezoresistive or piezoelectric in nature.

Piezoelectric accelerometers consist of a small mass attached to a piezoelectric crystal. The inertia force due to acceleration of the mass causes stress in the crystal that in turn produces a voltage proportional to the stress (or acceleration of the mass). The mass may be mounted to produce either compressive/tensile stress or, alternatively, shear stress in the crystal. The latter arrangement allows a smaller (and lighter) accelerometer for the same sensitivity. It also results in less sensitivity to base strain and temperature.

Three piezoelectric accelerometer types are illustrated in Fig. 1a, 1b, and 1c and a schematic of the delta shear type is shown in Fig. 1d. All these figures are adapted from the Brüel and Kjær accelerometer handbook.<sup>2</sup> Piezoelectric accelerometers are by far the most commonly used.

Another type of piezoelectric accelerometer that is much less expensive is one made using piezoelectric polymer film (polyvinylidene fluoride, or PVDF) in place of the piezoelectric crystal. These accelerometers are used in mass production applications such as air bags in cars.

Piezoresistive accelerometers, which are a third type, rely on the measurement of resistance change in a piezoresistive element subjected to stress. The element is generally mounted on a beam, as in Fig. 2. They are less common than piezoelectric crystal accelerometers and generally less sensitive by an order of magnitude for the same size and frequency response. Also, they require a stable direct current (dc) power supply to excite the piezoresistive element (or elements). However, piezoresistive accelerometers are capable of measuring down to dc (or zero frequency), are easily calibrated at dc, and can be used effectively with low-impedance voltage amplifiers.



**Figure 1** Piezoelectric accelerometer configurations: (a) planar shear type, (b) delta shear type, (c) compression type, and (d) schematic of delta shear type. M = seismic mass, P = piezoelectric element, R = clamping ring, and B = base. (Adapted from Brüel and Kjær.<sup>2</sup>)

When choosing an accelerometer, some compromise must always be made between weight and sensitivity. Small accelerometers are more convenient to use, can measure higher frequencies, and are less likely to affect the vibration characteristics of the structure by mass loading it. However, they have low sensitivity, which puts a lower limit on the acceleration amplitude that can be measured. Accelerometers range in weight from miniature 0.2 g for high-level vibration amplitude (up to a frequency of 18 kHz) on light-weight structures to 500 g for low-level vibration measurement on heavy structures (up to a frequency of 1 kHz). Thus, prior to choosing an accelerometer, it is necessary to know approximately the range of vibration amplitudes and frequencies to be expected as well as detailed accelerometer characteristics, including the effect of various amplifier types. The latter information should be readily available from the accelerometer manufacturer.

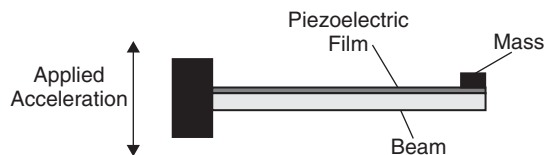
Accelerometers often have preamplifiers built into their casing so that their output can be fed into a standard voltage amplifier. When no in-built preamplifier exists, the signals are usually preconditioned by a charge amplifier before further amplification or connection to instrumentation such as a spectrum analyzer. Charge amplifiers act to virtually short circuit the accelerometer output and integrate the current running through this short circuit giving the resulting charge (coulomb = amperes  $\times$  seconds). This makes

them insensitive to cable capacitance (and thereby length) and to leakage resistance, which would modify the lower limiting frequency of a voltage amplifier. Charge amplifiers allow measurement of acceleration down to frequencies of 0.2 Hz, and they are insensitive to cable lengths up to 500 m. Many charge amplifiers also have the capability of integrating acceleration signals to produce signals proportional to velocity or displacement. Particularly at low frequencies, this facility should be used with care, as phase errors and high levels of electronic noise will be present, especially if double integration is used to obtain a displacement signal.

The minimum vibration level that can be measured by an accelerometer is dependent upon its sensitivity, and the preamplifier noise level can be as low as an equivalent  $10^{-4} \text{ ms}^{-2}$  for broadband measurements. The maximum level is dependent upon size and construction and can be as high as  $10^6 \text{ ms}^{-2}$  for small shock accelerometers. Most commercially available accelerometers at least cover the range  $10^{-2} \text{ ms}^{-2}$  to  $5 \times 10^4 \text{ ms}^{-2}$ . This range is then extended at one end or the other, depending upon accelerometer type.

The transverse sensitivity of an accelerometer is its maximum sensitivity in a direction at right angles to its main axis. The maximum value is usually quoted on calibration charts and should be less than 5% of the axial sensitivity. Clearly, this can affect acceleration readings significantly if the transverse vibration amplitude at the measurement location is an order of magnitude larger than the axial amplitude. Note that the transverse sensitivity is not the same in all directions; it varies from zero up to the maximum, depending on the direction of interest. Thus, it is possible to virtually eliminate the transverse vibration effect if the transverse vibration only occurs in one known direction.

Accelerometer base strain, due to the structure on which it is mounted undergoing strain variations, will generate vibration signals. These effects are reduced

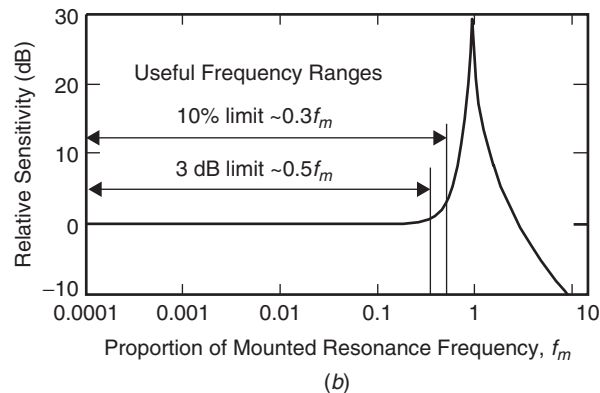
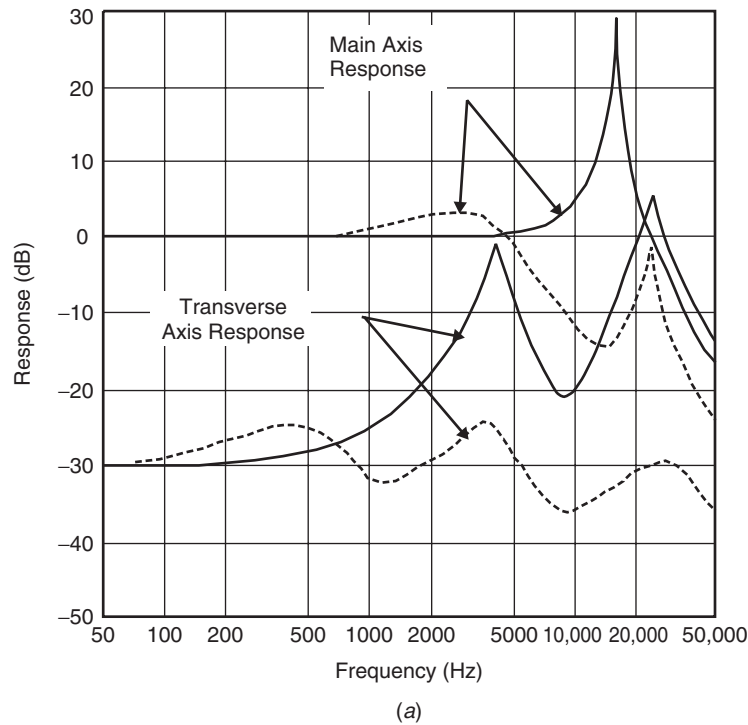


**Figure 2** Beam-type accelerometer using a PVDF film sensing element.

by using a shear-type accelerometer and are virtually negligible for piezoresistive accelerometers.

Magnetic fields generally have a negligible effect on an accelerometer, but large, varying fields may induce a spurious output. The effect of intense electric and magnetic fields can be minimized by using a differential preamplifier with two outputs from the same accelerometer such that voltages common to the two outputs are canceled out. This arrangement is generally necessary when using accelerometers near large generators or alternators.

Accelerometers are generally lightly damped and have a single-degree-of-freedom resonance (characterized by the seismic mass and piezoelectric crystal stiffness) well above the operating frequency range as shown in Fig. 3a. Care should be taken to ensure that high-frequency vibrations do not excite the accelerometer resonance and thus produce preamplifier or amplifier overloading or errors in measurements, especially when no frequency analysis is used. The effect of this resonance can be minimized by inserting a mechanical filter between the accelerometer and its mounting



**Figure 3** Typical frequency response of an accelerometer. Solid line is for an accelerometer bolted directly to a solid structure and the dashed line is the result of placing a mechanical filter between the accelerometer and solid structure. (Adapted from Brüel and Kjær.<sup>2</sup>)

point. This results in loss of accuracy at lower frequencies, effectively shifting the  $\pm 3$ -dB error point down in frequency by a factor of 5 (see Fig. 3b). However, the transverse sensitivity at higher frequencies is also much reduced.

The frequency response of an accelerometer is regarded as essentially flat over the frequency range for which its electrical output is proportional to within  $\pm 5$  to  $\pm 10\%$  of its mechanical input. The lower frequency limit has been discussed previously. The upper frequency limit is generally just less than one third (using the  $\pm 10\%$  limit) of the resonance frequency (see Fig. 3a). The resonance frequency is dependent upon accelerometer size and may be as low as 1000 Hz or as high as 180 kHz. In general, accelerometers with higher resonance frequencies are smaller in size and less sensitive.

There are numerous methods of attaching an accelerometer to a vibrating surface. Some are illustrated in ISO 5348<sup>3</sup> and Chapter 15 of Hansen and Snyder.<sup>4</sup> The method used will determine the upper frequency for which measurements will be valid.

Mounting the accelerometer by bolting it to the surface to be measured with a BeCu alloy stud is by far the best method and results in the resonance frequency quoted in the calibration chart. Best results are obtained if a thin layer of silicon grease is used between the accelerometer base and the structure, especially if the mounting surface is a little rough. If electrical isolation is desired, or if drilling holes in the surface is undesirable, a cementing stud may be used with little loss in performance. This stud is fixed to the surface using epoxy or cyanoacrylate adhesive. If electrical isolation is desired, a thin layer of epoxy can be spread on the surface and allowed to dry, and the stud then stuck to the dried layer. Alternatively, the accelerometer could be fixed to the surface directly using adhesive, but this can damage it superficially. An alternative method of electrical isolation if holes are allowed in the test surface is to use an isolated stud with a mica washer.

Beeswax can be used for fixing the accelerometer to the vibrating surface with little loss in performance up to temperatures of 40°C provided only a thin layer is used. Thin double-sided adhesive tape can also be used at the expense of reducing the usable upper frequency limit of the accelerometer by approximately 25%. Thick double-sided tape (0.8 mm) reduces the upper frequency limit by up to 80%. The use of a permanent magnet to mount the accelerometer also affects its performance, reducing its mounted resonance frequency by an amount highly dependent on magnet construction and surface properties. This mounting method is restricted to ferromagnetic materials.

For all accelerometers, the accelerometer cable should be fixed with tape to the vibrating surface to prevent the cable from excessive movement. This will minimize the effect of triboelectric noise, which results from the cable screen being separated from the insulation around the inner core of the cable. This separation creates a varying electric field that results in a minute current flowing into the screen that will be

superimposed on the accelerometer signal as a noise signal. For this reason low noise accelerometer cable should always be used.

Accelerometers generally have a flat zero degree phase between the mechanical input and electrical output signals at frequencies below about one third of the mounted resonance frequency. If accelerometers are heavily damped to minimize the resonance effect, then the phase error between the mechanical input and electrical output will be significant, even at low frequencies. This explains why commercially available accelerometers are usually lightly damped.

Temperatures above 100°C can result in small reversible changes in accelerometer sensitivity of up to 12% at 200°C. If the accelerometer base temperature is kept below 200°C using a heat sink and mica washer with forced air cooling, then it is possible to take measurements on surfaces as hot as 400°C. Without cooling, accelerometers cannot generally be used at temperatures in excess of 260°C. PVDF film accelerometers will not even tolerate this temperature and should not be used above 120°C.

If the test object is connected to ground, the accelerometer must be electrically isolated from it or an earth loop may result, producing a high-level hum in the resulting acceleration signal at the mains power supply frequency (50 or 60 Hz, depending on the country).

Accelerometers should not be dropped on hard surfaces (which can easily produce shocks in excess of 20,000 m/s<sup>2</sup>) or subjected to temperatures in excess of 260°C. Otherwise permanent damage (such as depolarization, cracking of the brittle piezoelectric element, or melting of the isolation materials), indicated by a significant change in accelerometer sensitivity, will result.

## 2.2 Velocity Transducers

Velocity transducers are generally one of two types. The least common type is the noncontacting magnetic-type consisting of a cylindrical permanent magnet on which is wound an insulated coil. A voltage is produced by the varying reluctance between the transducer and the vibrating surface. This voltage is proportional to the surface velocity and the mean distance between the transducer and the surface. When nonferrous vibrating surfaces are to be measured, a high permeability disk may be attached to the surface. This type of transducer is generally unsuitable for absolute measurements but is very useful for relative vibration velocity measurements such as needed for vehicle active suspension systems. Another device suitable for vehicle active suspension systems consists of a magnet fixed to the vehicle body and a coil fixed to the suspension. Relative motion between the two produces a coil voltage proportional to the velocity.<sup>5</sup> This type of device is a subset of the most common general type of velocity transducer consisting of a moving coil surrounding a permanent magnet. Inductive electromotive force (emf), which is proportional to the velocity of the coil with respect to the permanent magnet, is set up in the coil when it is vibrated. In the 10 Hz to 1 kHz frequency

range, for which the transducers are suitable, the permanent magnet remains virtually stationary and the resulting voltage is directly proportional to the velocity of the surface on which it is mounted. Outside of this frequency range, the velocity transducer electrical output is not proportional to its velocity. This type of velocity transducer is designed to have a low natural frequency (below its useful frequency range); thus, it is generally quite heavy and can significantly mass load light structures. Some care is needed in mounting but this is not as critical as for accelerometers, due to the relatively small upper frequency limit characterizing the basic transducer.

The velocity transducers discussed above generally cover the dynamic range of 1 to 100 mm/s. Some allow measurements down to 0.1 mm/s while others extend them to 250 mm/s. Sensitivities are generally of the order of 20 mV/mm s<sup>-1</sup>. Due to their limited dynamic range they are not as useful as accelerometers. Low impedance, inexpensive voltage amplifiers are suitable for amplifying the signal. Temperatures during operation or storage should not exceed 120°C.

Another type of velocity transducer is the laser Doppler velocimeter, which allows vibration velocity measurement without the need to fix anything to the vibrating surface. Commercially available systems focus a narrow beam of laser light on to a vibrating surface and measure the Doppler shift in the reflected light resulting from motion of the surface. Laser Doppler systems are available that scan surfaces very quickly and then display the entire surface motion on a computer screen. It is even possible to measure vibration along three Cartesian axes simultaneously. Torsional vibration can also be measured using a laser Doppler velocimeter with two laser beams that are directed at a rotating shaft. More details of the principles of operation of laser Doppler velocimeters are available from the manufacturers (e.g., Polytec in Germany). The dynamic range of these instruments has been improving steadily since the first versions became available. Minimum velocity levels that can be measured are approximately 0.01 mm/s and maximum velocities are about 20,000 mm/s peak to peak. Frequency ranges vary with the instrumentation type, but the upper range can be up to 1 MHz with the lower end 0 Hz.

### 2.3 Displacement Transducers

Although the dynamic range of displacement transducers is typically much smaller than it is for accelerometers, displacement transducers are often more practical at very low frequencies (0 to 10 Hz), where vibration amplitudes are measured in terms of tenths or hundredths of a millimetre, and where corresponding accelerations are small.

The most common type of displacement transducer is the proximity probe. Two types of proximity probes are available, the capacitance probe and the eddy current probe. The capacitance probe relies on the measurement of the change in electrical capacitance between the vibrating machine surface and the stationary probe. The eddy current probe relies on

the generation of a magnetic field at the probe tip by a high-frequency (>500 kHz) voltage applied to a coil of fine wire. This magnetic field induces eddy currents proportional to the size of the gap between the probe tip and machine surface. These currents oppose the high-frequency voltage and reduce its amplitude in proportion to the size of the gap. Typical gap ranges in which the amplitude is a linear function of gap size vary from between 1 and 4 mm for smaller diameter probes to between 2 and 20 mm for larger probes. The carrier amplitude signal is demodulated to give a low-impedance voltage output proportional to gap size over the linear range of the transducer.

Eddy current probes are more common and easier to use than capacitive-type pickups so further discussion will be restricted to the former type. When mounting an eddy current proximity probe to measure the vibration of a rotating shaft, the surface or shaft to be measured must be free of all irregularities such as scratches, corrosion, out-of-roundness, chain marks, and the like. Any irregularity will cause a change in probe gap that is not a shaft position change, resulting in signal errors. This is called mechanical runout.

The shaft material must be of uniform composition all the way round its surface so that the resistivity does not vary as the shaft rotates, resulting in an unwanted electronic noise signal. This is called electrical runout noise. Care should also be taken with the use of plated shafts, as thin plating can allow the eddy currents to penetrate to the main shaft material, resulting in two different material resistivities being detected as well as the rough interface surface between shaft and surface treatment. As probes are generally matched to a particular shaft material, this can lead to calibration problems, as well as electronic noise problems due to the rough interface.

Proximity probes require a power supply and low-impedance voltage amplifier, both of which are generally supplied in the same module. Note that the length of cable between the power supply and probe significantly affects the probe sensitivity.

The dynamic range of an eddy current proximity probe is typically 100:1, although some have a range of 150:1 and others 60:1. The resolution to which the probe can measure varies from 0.02 to 0.4 mm, depending upon the absolute range (2 to 25 mm). The limited dynamic range restricts its practical application to frequencies of less than 200 Hz.

Another commonly used displacement transducer is the linear variable differential transformer (LVDT). This is described in detail Hansen and Snyder.<sup>4</sup> A typical dynamic range for this type of transducer is about 100:1, with maximum displacements measurable ranging from 1 to 100 mm, depending on the transducer selected.

The frequency range characterizing most commercially available LVDT transducers is dc to 100 Hz. For long stroke ( $\pm 15$  to  $\pm 100$  mm) transducers, the diameter is typically between 12 and 20 mm, with a body length of about three times the maximum stroke (or displacement from center). Short stroke transducers usually have a fixed length not less than 30 to

50 mm. More detail on the principles of operation of these devices are available in publications from commercial suppliers.

A less commonly used displacement transducer is the linear variable inductance transducer (LVIT), which is used for measuring relative displacements, especially in vehicle suspension systems. It is described in detail by Hansen and Snyder<sup>4</sup> and Moore.<sup>6</sup>

## 2.4 Strain Sensors

When a structure vibrates either flexurally or longitudinally, its surface is subjected to cyclic strains that can be detected with a strain sensor. Three types of strain sensors will be considered here: conventional resistive strain gauges, PVDF film, and optical fibres.

**2.4.1 Resistive Strain Gauges** Resistive strain gauges are constructed of a thin, electrical-conducting wire, foil, or semiconductor sandwiched between two plastic sheets, as shown in Fig. 4a. Larger areas at the ends of the grid facilitate connection of cables. The plastic sheets bonded to the active element simplify handling and protect the element from mechanical damage.

Foil strain gauges are produced by photoetching a metallic foil (3 to 5  $\mu\text{m}$  thick). The material used for the metallic element is usually an alloy of nickel and copper (constantan), the exact composition of which is dependent upon the material on which the strain gauge is to be used. Some effort is made to match the temperature coefficient of expansion of the strain gauge with the material on which it is to be used.

Wire strain gauges are produced using metallic wire, 15 to 25  $\mu\text{m}$  in diameter. Foil gauges are easier to make if the gauge length is approximately 6 mm or less, whereas wire gauges are easier for lengths greater than approximately 6 mm. Wire gauges are also more suitable for high-temperature applications, as more suitable materials are available and better mounting techniques can be used.

Semiconductor strain gauges contain a semiconductor element a few hundred micrometres wide and 20 to 30  $\mu\text{m}$  thick, and their operation is based on the piezoresistive effect; that is, mechanical stress applied to a semiconductor will result in a change in resistance as a result of a change in electron mobility. This type of gauge is the most expensive and the least preferred type for most applications, unless a high sensitivity is needed.

The operation of metallic strain gauges is based on the principle that the electrical resistance of a metallic conductor changes if the conductor is subjected to an applied strain. The change in resistance of the strain gauge is partly due to the change in the geometry of the conductor and partly due to the change in the specific conductivity  $\rho$  of the conductor material due to changes in the material structure. The change in resistance  $\Delta R$  of a strain gauge as a fraction of the nominal resistance  $R_0$  for a cylindrical conductor is given by

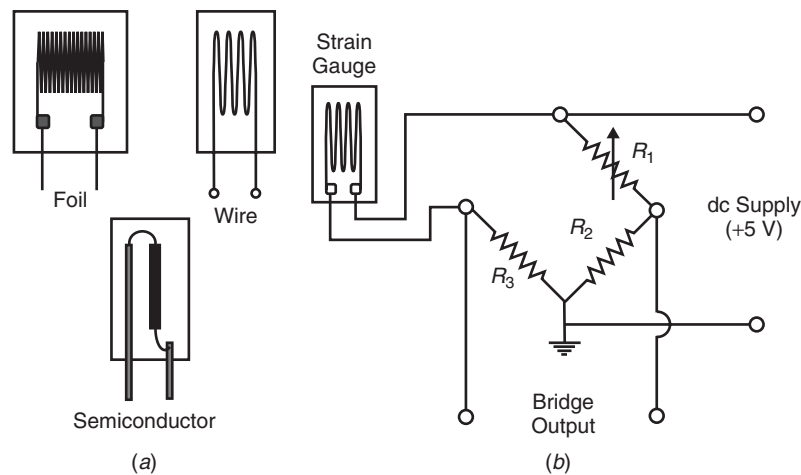
$$\frac{\Delta R}{R_0} = \varepsilon \left( 1 + 2\nu + \frac{1}{\rho} \frac{\partial \rho}{\partial \varepsilon} \right) \quad (1)$$

where  $\nu$  is Poisson's ratio,  $\varepsilon$  is the strain imposed on the strain gauge, and the first two terms in parentheses represent the geometrical component. The quantity in parentheses in Eq. (1) is a constant over a wide range of values of  $\varepsilon$  for materials such as constantan and shapes, which are used in strain gauges. Thus, Eq. (1) can be written as

$$\frac{\Delta R}{R_0} = K \varepsilon \quad (2)$$

where  $K$  is the gauge factor (usually in the vicinity of 2).

As the resistance change  $\Delta R$  is usually a very small value, it cannot be accurately measured directly. The



**Figure 4** (a) Strain gauge types and (b) Wheatstone bridge circuit.



most common means of determining  $\Delta R$  is to insert the strain gauge as one leg in a Wheatstone bridge (see Fig. 4b). The bridge is balanced by varying  $R_1$  to produce zero output, with the vibrating structure at rest. When the structure begins to vibrate, a voltage proportional to the strain (and thus structural vibration bending moment) will appear at the bridge output. Note that the bending moment is the double spatial derivative of the structural displacement.

The bridge output voltage  $V_0$  is related to the change in resistance  $\Delta R$  of the strain gauge, the bridge dc supply voltage  $V_s$ , and the structural strain as

$$\frac{V_0}{V_s} = \frac{\Delta R}{R} = K\varepsilon \quad (3)$$

As  $V_s$  is normally about 5 V and  $K$  is about 2, the output voltage  $V_0$  is about 10 times the strain level. Thus, 1  $\mu$ strain would produce 10  $\mu$ V. Clearly, a high-gain, low-noise operational amplifier is needed to amplify the voltage to a usable level if strains as low as a few microstrains are to be measured. Also, the dc power supply to the bridge must be characterized by very low noise levels; often batteries rather than regulated mains power are necessary. The dynamic range of a strain gauge and its associated electrical system is from 2 to 5  $\mu$ strain to 10,000  $\mu$ strain over a frequency range limited only by the amplifying electronics and the way the gauge is fixed to the structure. The frequency range of general interest is usually limited to dc to 1000 Hz, and this is easily covered with standard circuitry.

In some cases, the sensitivity of the measurement system can be increased by replacing resistances  $R_3$  or  $R_2$  in the Wheatstone bridge with a second strain gauge. If resistance  $R_2$  is replaced with a strain gauge, the two strain gauges in the bridge must be tensioned and compressed out-of-phase with one another for the two effects to add together. This is achieved, for example, by using two strain gauges on opposite sides of a beam to detect flexural vibration. This configuration has the added advantage of minimizing the dc drift in the output signal as a result of temperature changes occurring in the system being measured. If only one strain gauge is used (or if the second one replaces  $R_3$  in the Wheatstone bridge circuit), then a temperature change in the system being measured will cause the structure to expand differently to the strain gauge (as the coefficients of thermal expansion of the test structure and the strain gauge are not exactly matched in practice), thus resulting in a strain gauge output not related to stress in the structure. However, this is rarely a problem when strain gauges are used just to sense vibration, as the frequency of temperature fluctuations is generally well below the frequency range of interest.

When installing strain gauges on a surface for vibration measurement, many factors need to be considered such as adhesive selection, protection of the installed gauge from the environment, and selection of a gauge size appropriate for the task.

Larger gauges average the vibration over a larger surface area and are usually easier to install. Suitable adhesives include cyanoacrylate (superglue) provided the completed installation is covered with a waterproof compound. Other adhesives and protective compounds are available from strain gauge manufacturers.

**2.4.2 PVDF Film** When bonded to a surface, polyvinylidene difluoride (PVDF) film produces either a charge or a voltage proportional to the strain of the surface. The charge may be amplified by a high-impedance charge amplifier to produce a voltage proportional to the strain. The advantage offered by PVDF film when compared to strain gauges is its ability to act as a distributed sensor and to be shaped so that it senses particular vibration modes, or combinations of modes, if so desired.<sup>4</sup> For example, if it is desired to control sound radiation, then the sensor could be shaped so that it sensed the surface vibration distribution that contributed most to the sound radiation. When acting as a distributed sensor, PVDF film provides an output charge or voltage proportional to the surface strain integrated over the area covered by the sensor.

The PVDF film is an extremely flexible polymer that can be polarized across its thickness (usually between 9 and 110  $\mu$ m) by a strong electric field. It can act either as a sensor or an actuator. Once polarized, PVDF film will provide a charge or voltage when subjected to an applied tensile force or strain. Conversely, it will produce a strain when subjected to an applied voltage, but this must be well below its original polarization voltage. The maximum operating voltage is 30 V/ $\mu$ m thickness, and the breakdown voltage at which polarization is lost is 100 V/ $\mu$ m thickness. The polarization axis for PVDF film is usually normal to the surface, across the thickness. A detailed analysis of the output of a PVDF sensor as a result of vibration of the surface on which it is mounted is provided in Hansen and Snyder.<sup>4</sup>

Typical thicknesses of PVDF film range from 9 to 110  $\mu$ m. However, as shown by the analysis in Chapter 15 of Hansen and Snyder,<sup>4</sup> it can be seen that if the film is attached to a vibrating surface, the charge produced is independent of the film thickness, and only dependent upon the strain induced by the vibrating surface and the area of film used. On the other hand, the voltage produced is dependent on the thickness but not the area of film.

As a guide to the sensitivity of PVDF film compared to a strain gauge for measuring dynamic strain, a piece 10 mm  $\times$  10 mm will produce a charge of approximately 5.5 pC when subjected to 1  $\mu$ strain. A conventional charge amplifier noise floor is approximately 0.003 pC, so the strain detected can be as low as  $10^{-9}$ . This compares very favorably with a strain gauge that is limited to about  $10^{-6}$ . The upper limit of the dynamic strain that can be measured is governed by the tensile and compressive strength and is approximately 0.015, which is similar to a strain gauge.

**2.4.3 Optical Fibers** The use of optical fibres as strain sensors was first discussed by Butter and

Hocker.<sup>7</sup> Optical fiber sensing is expensive, requiring a laser and complex signal processing electronics, but for some applications it is the only feasible choice. Such applications include structures subjected to high-level electromagnetic fields, high temperatures and pressures, and/or harsh chemical environments. These sensors are described in detail in Hansen and Snyder.<sup>4</sup>

### 3 TRANSDUCERS FOR GENERATING VIBRATION

#### 3.1 Hydraulic Actuators

Hydraulic actuators generally consist of a piston in a hydraulic cylinder that has hydraulic fluid openings at each end. Introduction of high-pressure fluid into one end of the cylinder causes the piston to move to the other end, expelling fluid from the opening at that end. Switching the supply of high-pressure fluid to the other end of the cylinder causes the piston to move in the opposite direction.

The most common method to alternate the hydraulic supply from one end of the cylinder to the other is to use a servovalve, which consists of movable spool connected to a solenoid. Applying voltage to the solenoid coil causes the spool to move, which in turn results in the opening and closing of valves responsible for directing hydraulic fluid to either end of the hydraulic cylinder. Note that the servovalve spool is usually maintained in its inactive position with springs at either end. The operation of the servovalve is described in detail in Hansen and Snyder.<sup>4</sup>

One advantage of hydraulic actuators is their large displacement and high force generating capability for a relatively small size. Disadvantages include the need for a hydraulic power supply, which can be inherently noisy, and nonlinearities between the servovalve input voltage and the hydraulic actuator force or displacement output.

#### 3.2 Pneumatic Actuators

Pneumatic actuators are very similar in operation to hydraulic actuators, except that the hydraulic fluid is replaced by air. One advantage of active pneumatic actuators is that they can use the same air supply as passive air springs, which may be mounted in parallel with them. Pneumatic actuators may also be the

preferred option in cases where an existing compressed air supply is available. The major disadvantage of pneumatic actuators is their relatively low bandwidth (less than 10 Hz) due to the compressibility of the air.

#### 3.3 Proof Mass (or Inertial) Actuator

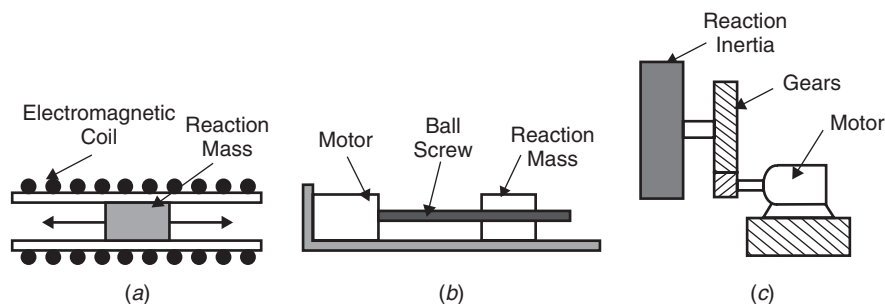
This type of actuator consists of a mass that is free to slide along a track or inside of a coil. The mass is accelerated using an electromagnetic field (see Fig. 5a), so in one sense this type of actuator is similar to an electrodynamic shaker, which will be described in the next section. In this case, the mass is a permanent magnet. The mass can also be accelerated by other means; for example, by connecting it to a ball screw (see Fig. 5b). The proof mass results in a reaction in the ball screw or electromagnetic stator that is attached to the structure to be controlled.

Another type of proof mass actuator is one that imparts moments rather than forces to a structure by control of a rotating mass, which results in reaction moments on the support structure (see Fig. 5c). One problem with linear proof mass actuators is the limited motion of the reaction mass, which becomes more serious when low-frequency vibration modes in a structure are to be controlled.

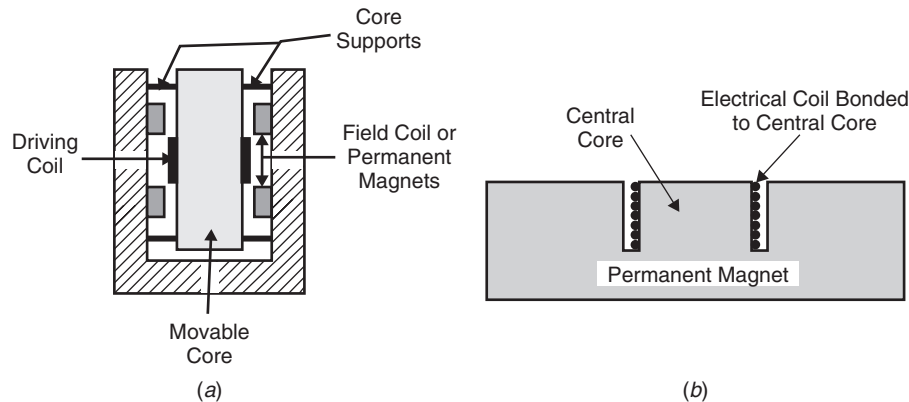
#### 3.4 Electrodynamic and Electromagnetic Actuators

Electrodynamic actuators or shakers consist of a movable core (or armature) to which is fixed a cylindrical electrical coil. The core and coil move back and forth in a magnetic field that is generated by a permanent magnet (smaller shakers) or by a direct current flowing through a second coil fixed to the stationary portion of the shaker (stator), as shown in Fig. 6a. The movable core is supported on mounts that are very flexible in the axial direction in which it is desired that the core move and rigid in the radial direction to prevent the core contacting the outer armature. To maximize lightness and stiffness, the core is usually constructed of high-strength aluminum alloy and is usually hollow. Mechanical stops are also usually provided to prevent the core from being over driven. In some cases, the driving coil is air cooled.

When a sinusoidal voltage is applied to the drive coil, the polarity and strength of the drive coil magnetic



**Figure 5** Proof mass (inertial) actuators: (a) linear, electromagnetic; (b) linear, ball screw; and (c) rotational.



**Figure 6** (a) Schematic of an electrodynamic shaker and (b) electromagnetic shaker.

field changes in phase with the applied voltage and so then does the force of attraction between the field coil (or permanent magnets) and the driving coil, resulting in axial movement of the core (or armature).

Electromagnetic actuators are similar in construction to electrodynamic shakers except that the inner core as well as the armature is fixed, (see Fig. 6b). It is constructed by surrounding an electrical coil with a permanent magnet. Supplying a sinusoidal voltage to the coil results in the production of a sinusoidally varying magnetic field that can be used to shake ferromagnetic structures, or structures made from other materials, if a thin piece of shim steel is bonded to them. Clearly, the electromagnetic actuator must be mounted on a rigid fixture, preferably not connected to the structure to be excited.

If the permanent magnet were not used, the attraction force between the coil and the structure being shaken would not vary sinusoidally but would appear like a rectified signal, with most of the excitation energy being at twice the coil driving frequency.

Electromagnetic drivers such as those just described are easily and cheaply constructed by bonding the coil from a loudspeaker driver into the core of the permanent magnet where it is normally located in its at rest condition.

### 3.5 Magnetostrictive Actuators

The most effective alloy used in these actuators is terfenol-D, with the composition  $\text{Tb}_{0.3} \text{Dy}_{0.7} \text{Fe}_{1.93}$ . The subscripts refer to the atomic proportions of each element (terbium, dysprosium, and iron). Multiplying these by the atomic weights gives the weight proportions (18, 42, and 40%, respectively). The notable properties of this material are its high strain ability (25 times that of nickel, the only other commonly used magnetostrictive material, and 10 times that of piezoelectric ceramics—see next section) and high-energy densities (100 times that of piezoceramics). Thus, terfenol-D can produce high force levels and high strains relative to other expanding materials. The maximum possible theoretical strain is 2440  $\mu\text{strain}$ ,

and 1400  $\mu\text{strain}$  are achievable in practice. The properties of terfenol are discussed in detail in the literature,<sup>4,8,9</sup> where a complete mathematical analysis is provided.

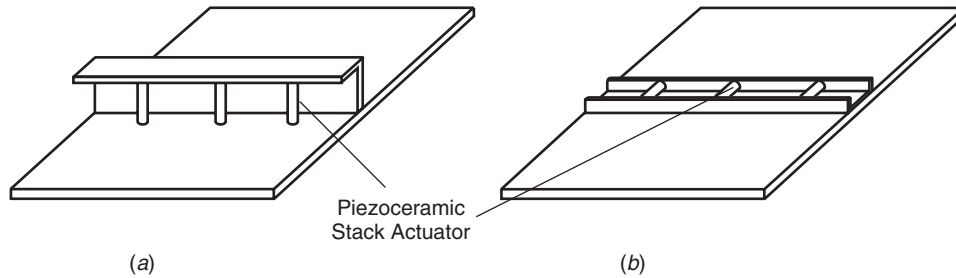
As an example, for an actuator containing a 50-mm long terfenol rod, the maximum possible displacement will be  $50 \times 10^{-3} \times 1400 \times 10^{-6}$  m or 70  $\mu\text{m}$ . In practice, actuators are generally limited to 1000  $\mu\text{strain}$  (or 50  $\mu\text{m}$  for a 50-mm-long Terfenol rod) to minimize nonlinearity.

As application of a magnetic field of any orientation will cause the terfenol rod to expand, a dc magnetic bias is necessary if the terfenol rod expansion and contraction is to follow an alternating current (ac) input signal into the coil. Thus, a dc magnetic bias supplied either with a dc voltage signal applied to the coil or with a permanent magnet, is required so that the terfenol rod expands and contracts about a mean strain (usually about 500  $\mu\text{strain}$ ). Use of a dc bias current introduces problems associated with drive amplifier design and transducer overheating; thus, it is more common to use a permanent magnet bias.

To optimize performance (maximize the strain ability of the actuator), it is necessary to apply a longitudinal prestress of between 7 and 10 MPa. The prestress ensures that the magnetically biased actuator will contract as much as it expands when a sinusoidal voltage is applied to the drive coil.

Terfenol actuators are usually characterized by a resonance frequency in the few kilohertz range and generally have a reasonably flat frequency response at frequencies below about half the resonance frequency. The actual resonance frequency depends on the mass driven and the stiffness of the terfenol rod. Longer, thinner drives and larger masses result in lower resonance frequencies.

The force output for a clamped actuator may be calculated using  $F = EA\Delta L/L$ , where  $E$  is the elastic modulus ( $3.5 \times 10^{10}$  N/m<sup>2</sup>),  $A$  is the cross-sectional area of the terfenol rod (m<sup>2</sup>), and  $\Delta L/L$  is the strain. Thus, a 6-mm-diameter rod operating in a magnetic



**Figure 7** Actuator configurations for applying a bending moment to a panel without a reaction mass.

field capable of producing  $\pm 500$   $\mu$ strain about, the bias value of  $+500$  can produce a force of  $\pm 500$  N.

Terfenol is very brittle and must be carefully handled. Its tensile strength is low (100 MPa), although its compressive strength is reasonably high (780 MPa). Another important disadvantage is the low displacement capability, which would be a problem in low-frequency vibration control (below 100 Hz). One way around this limitation is to use displacement expansion devices that rely on the lever principle to magnify the displacement at the expense of reduced force output. The main disadvantage associated with magnetostrictive actuators, however, is the hysteresis inherent in terfenol that results in a nonlinear actuation force for a linear voltage input. This results in excitation frequencies being generated that are not related to the voltage input frequencies.

The main advantage of terfenol is its high force capability for a relatively low cost. Electrodynamic shakers capable of the same force capability cost and weigh between 25 and 100 times as much and require a much larger driving amplifier. Thus, another advantage is small size and light weight, which makes the actuator ideal for use in situations where no reaction mass is necessary.

### 3.6 Shape Memory Alloy Actuators

A shape memory alloy is a material that when plastically deformed in its low-temperature (or martensitic) condition, and the external stresses removed, will regain its original (memory) shape when heated (to about  $60^\circ\text{C}$ ).<sup>10</sup> The process of regaining the original shape is associated with a phase change of the solid alloy from a martensite to an austenite crystalline structure. Restraining the material from regaining its memory shape can yield stresses of up to 500 MPa (for an 8% plastic strain and a temperature of  $180^\circ\text{C}$ ).<sup>11</sup> Thus if the temperature is cycled, a cyclic force can be generated and used for structural actuation. If the material, nitinol (56% nickel and 44% titanium) is used, it can be heated easily by passing a current through the material and cooled by turning off the current. However, the frequency response is very low; a maximum of 10 Hz can be expected. More details on how to use this material are provided by Hansen and Snyder.<sup>4</sup>

### 3.7 Piezoelectric Actuators

This type of actuator may be divided into two distinct categories; the thin plate or film type and the stack (shaker) type. The thin type may be further categorized into piezoceramic plates (PZT) or piezoelectric film (PVDF). The thin type is usually bonded to the structure it is to excite and generates excitation by imparting a bending moment to the structure. The thickness ranges from 0.25 to 6 mm. The stack type of actuator consists of many thin layers (about 100, each 0.25 to 1 mm thick) bonded together. It is used in a similar way to an electrodynamic shaker or magnetostrictive actuator, generally applying to the structure a force distributed over a small area.<sup>4</sup>

One problem with piezoelectric actuators (both the thin sheet type and stack type), which is also experienced by magnetostrictive actuators, is their hysteresis property, which means that the expansion as a function of a given applied electric field (or voltage) is dependent upon whether the field level is rising or falling. It is also a nonlinear function of the applied electric field in either direction. This results in nonlinear excitation of a structure attached to one of these actuator types. Thus, if the exciting voltage used to drive the actuator is sinusoidal, the resulting structure motion will contain additional frequencies.

### 3.8 Electrorheological Fluids

The most common type of electrorheological fluid being investigated commercially is the class of dielectric oils doped with semiconductor particle suspensions. On application of an electric field of sufficient strength, the particles form chains that link across the electrodes, resulting in an apparent change in viscosity (or resistance to flow). Perhaps the most obvious application of these types of fluid in active vibration control is to provide a variable damping force in a semiactive suspension system. Although it is possible to switch the fluids from their inactive to active state in 3 to 5 ms, it takes somewhat longer to reverse the process, thus severely restricting the useful frequency range of active dampers and isolators constructed from these materials. Other problems are associated with the relatively high-voltage requirements (2 to 10 kV) and separation of the fluid to solid particles when the fluid is in its inactive state.

### 3.9 Magnetorheological Fluids

Magnetorheological fluids (MRFs) are essentially non-colloidal suspensions consisting of a high concentration of magnetically polarizable particles dispersed in a nonmagnetic fluid carrier. The particles are usually iron oxides, and the carrier is usually silicon, oil, or glycerol. When a strong magnetic field is applied, the particles align and result in a large increase in the fluid stiffness. The fluid can respond to magnetic field variations at a rate of up to several hundred hertz, and they can operate in the temperature range of  $-50$  to  $+150^{\circ}\text{C}$ . These properties make them particularly suitable for use as an active element in vehicle suspension systems. The main disadvantage of these fluids is the settling out of suspension of the magnetic particles when the fluid is in its inactive state for an extended period of time.

## 4 SMART STRUCTURES

Smart structures contain sensors and/or actuators as an integral part. Passive smart structures contain only sensing elements that allow their state at any particular time to be determined. Such sensors could include piezoelectric film (PVDF) or optical fibers. Active smart structures contain in-built actuators as well as sensors, which enable them to respond automatically to correct some undesirable state detected by the sensors.

Actuators that have been used in laboratory experiments in the past include piezoelectric film or piezoceramic crystal or shape memory alloy. Magnetostrictive terfenol may also be useful for this purpose but is more likely to be bonded to the external surface of structures rather than embedded in them.

Structures that particularly lend themselves to the integration of sensors and actuators are carbon fiber and glass fiber composite structures, which are made by laminating the glass or carbon cloth with a suitable epoxy resin. However, other noncomposite structures can be made into smart structures by bonding actuators and sensors to their surface.

One interesting smart structure is a foam blanket in which small inertial actuators are embedded. The structure has vibration sensors on it that provide a signal to a control system that in turn drives the inertial actuators to minimize the vibration detected by the sensors. The actuators consist of small magnets contained in a plastic tube around which is wound a coil through which the control signal passes.

### 4.1 Novel Actuator Configurations

One problem with applying piezoceramic stacks, magnetostrictive rods, or hydraulic or electrodynamic actuators to a structure in the traditional way is

the need for a reaction mass and support for the actuator. The need for a reaction mass makes the application of active vibration control using these actuators impractical in many situations. However, the need for this reaction mass can be eliminated by using a more imaginative actuator configuration that applies control bending moments rather than control forces to the structure. For stiffened structures such as aircraft fuselages or submarine hulls, implementation of the actuator configurations is even more convenient.

Two possible actuator configurations that need no reaction mass are illustrated in Figs. 7a and 7b. The first figure illustrates the arrangement where stiffeners already existed on the panel, and the second figure shows an alternative arrangement that might be used if no prior stiffeners existed. The configurations shown for panel vibration control can easily be extended to cylindrical structures such as aircraft fuselages and submarine hulls.

## REFERENCES

1. C. M. Harris and A. G. Piersol, Eds., *Harris' Shock and Vibration Handbook*, 5th ed., McGraw-Hill, New York, 2001, Chapters 12–18.
2. Anonymous *Piezo-electric Brüel and Kjær, Accelerometer and Vibration Preamplifier Handbook*, Copenhagen, Denmark, 1976.
3. ISO5348—1998, Mechanical Vibration and Shock—Mechanical Mounting of Accelerometers, Geneva, Switzerland, 1998.
4. C. H. Hansen and S. D. Snyder, *Active Control of Sound and Vibration*, E&FN Spon, London, 1997.
5. P. T. Wolfe and M. R. Jolly, U.S. Patent 4,979,573, Velocity Transducer for Vehicle Suspension System, 1990.
6. J. H. Moore, Linear Variable Inductance Position Transducer for Suspension Systems, Proceedings of the Institution of Mechanical Engineers International Conference on Advanced Suspensions, London, 1988, pp. 75–82.
7. C. D. Butter and G. B. Hocker, Fibre Optics Strain Gauge, *Appl. Optics*, Vol. 17, 1978, pp. 2867–2869.
8. M. W. Hiller, M. D. Bryant, and L. Umega, Attenuation and Transformation of Vibration through Active Control of Magnetostrictive Terfenol, *J. Sound Vib.*, Vol. 134, 1989, pp. 507–519.
9. M. B. Moffett, A. E. Clark, M. Wun-Fogle, J. Linberg, J. P. Teter, and E. A. McLaughlin, Characterisation of Terfenol-D for Magnetostrictive Transducers, *J. Acoust. Soc. Am.*, Vol. 89, 1991, pp. 1448–1455.
10. Website, <http://www.nitinol.info/flash/index.html>.
11. C. A. Rogers, Active Vibration and Structural Acoustic Control of Shape Memory Alloy Hybrid Composites: Experimental Results, *J. Acoust. Soc. Am.*, Vol. 88, 1990, pp. 2803–2811.

# CHAPTER 38

## SOUND LEVEL METERS\*

George S. K. Wong  
Institute for National Measurement Standards  
National Research Council Canada  
Ottawa, Ontario, Canada

### 1 INTRODUCTION

Sound level meters are designed to measure sound over a range of frequencies and levels comparable to the range of the human ear. The human ear can sense sound in the frequency range from about 15 to 16,000 Hz and pressure changes in a range with a ratio in excess of 1 to  $1 \times 10^7$ . Sound level meters measure and display changes in sound pressures in a systematic manner. Sound pressures are compressed logarithmically so that the 1 to  $1 \times 10^7$  ratio range is expressed as 0 to 140 dB. The display, whether a ballistic meter movement or a digital display that updates only a few times a second, does not show sound pressure changes instantaneously. Instead, it averages the changes in one of several methods to produce a readable number. The two principal methods are exponential averaging and integrating averaging. Optional features that may be included in sound level meters (SLMs) include peak level, peak hold, maximum level, minimum level, noise dose, sound exposure, events, and exceedance levels with statistical distributions and time histories.

\*This chapter is based on Chapter 155, Sound Level Meters, by R.W. Krug, in Volume 4, pp. 1845–1854 of *Encyclopedia of Acoustics*, edited by Malcolm J. Crocker, Wiley, New York, 1997.

### 1.1 Principles of Operation

Exponential-averaging meters (see Fig. 1) measure sound pressure from a microphone. The microphone, amplifier, and weighting circuit limit the frequencies to a prescribed range. The signal is then squared, so positive and negative pressure changes are converted to the square of the input signal.

The time constant is a single-pole low-pass filter with an exponential time constant. The meter may be graduated directly in decibels (uneven scale), which compresses the low end of the scale and expands the high end, or the logarithm of the signal is taken to produce a linear display in decibels.

Integrating-averaging SLMs (see Fig. 2) detect, frequency weight, and square the sound pressure level similar to exponential-averaging SLMs. The squared signal is integrated. The logarithm of the integrated signal has the logarithm of time subtracted from it. Thus, the level is divided by time or averaged over a time period. The level is then displayed on a meter movement or digital display.

Apart from the microphone and amplifier (including preamplifier) shown in Figs. 1 and 2, a computer can emulate nearly all of the succeeding functions with a microprocessor or with a lap-top computer configured as sound pressure level measuring equipment.

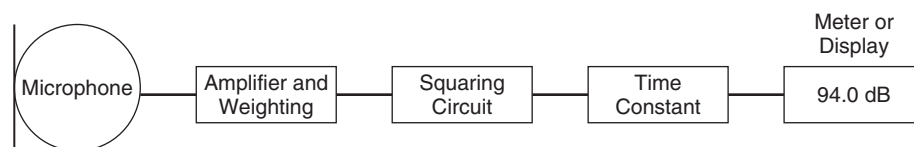


Figure 1 Exponential-averaging SLM.

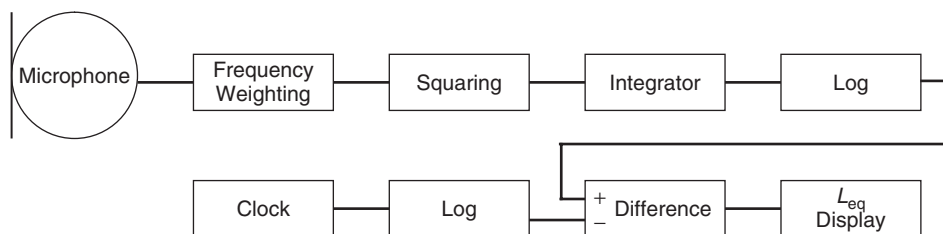


Figure 2 Integrating-averaging SLM.

## 1.2 National and International Standards

Standard specifications are required to ensure the sound is measured in a systematic and reproducible manner. Any number of frequency weightings, time constants, and integration methods could be used. Standards prescribe specific methods of measuring sound, and each generation of standards that have different tolerance limits for measurements, such as A-weighted levels, will make it difficult to correlate data on hearing conservation collected with older SLMs that satisfied the standards of the day. In view of the existence of a large number of older SLMs that are still operational and may be in use, it may be worthwhile to discuss briefly the requirements of some older standards. Some of the older and more recent SLM standards are listed below:

- ANSI S1.4-1983<sup>1</sup> and ANSI S1.4A-1985 Amendment to S1.4: Specification for sound level meters
- ANSI S1.25-1978, 1991<sup>2</sup>: Specification for personal noise dosimeters
- IEC 60651-1979<sup>3</sup>: Sound level meters
- IEC 60804-1984<sup>4</sup>: Integrating-averaging sound level meters
- IEC 61252-2002<sup>5</sup>: Specifications for personal sound exposure meters
- IEC 61672-1, 2002<sup>6</sup>: Sound level meters—Part 1: Specifications
- IEC 61672-2, 2003<sup>7</sup>: Sound level meters—Part 2: Pattern evaluation tests
- IEC 61672-3, 200X (under development): Sound level meters—Part 2: Periodic verification

The above International Electrotechnical Commission (IEC) 61672 series have superseded some of the older SLM standards, and the American National Standards Institute (ANSI) S1.4 is currently under revision. Terminology used in this chapter has been defined in the above standards.

The ANSI S1.4-1978 and the IEC 60651-1979 both specify exponential-averaging SLMs. They are similar except for the directional specifications of the microphone (see Section 2.2). Both specify three accuracy types of meters: type 0, type 1, and type 2. Type 0 instruments are the most accurate and are intended as laboratory standards. Type 1 instruments are intended for laboratory or field use where the acoustical environment can be closely specified and/or controlled. Type 2 SLMs are suitable for general field applications. Type 3 SLMs are specified in IEC 60651-1979. They are of low accuracy and are intended for sound surveys and with little capability to measure impulsive sounds.

The IEC 60804-1984 specifies type 0, type 1, type 2, and type 3 integrating-averaging SLMs. The ANSI S1.25-1991 personal noise dosimeter and the personal sound exposure meter specify instruments intended to be worn on a person to measure noise exposure. They specify only limited-range, single-frequency-weighting, type 2 instruments.

The IEC 61672-1, 2002, specifies class 1 and class 2 instruments. This relatively new standard eliminated

type 0 and type 3 instruments. Although the design goal of the A-weighting requirements are unchanged but the tolerance limits for class 1 SLMs has been changed to minus infinity at high frequency above 16 kHz (see Section 3.2). This reduces the capability to capture higher harmonics during measuring impulsive sounds.

## 2 MICROPHONES

Microphones are transducers that convert changes in sound pressure to an electrical signal. As is typical of many transducers, the microphone is likely to be the most critical, fragile, and expensive part of the instrument. Its response is likely to change with frequency, direction, temperature, absolute pressure, time, and several other factors. As such, it is important to appreciate the limitations and work with them to achieve accurate and reliable response. The selection of microphones<sup>8</sup> is very important for acoustical measurement. For critical applications it is important to understand that the sensitivity of condenser microphones varies with barometric pressure, and this variation that changes with frequency can be corrected.<sup>9,10</sup>

### 2.1 Types

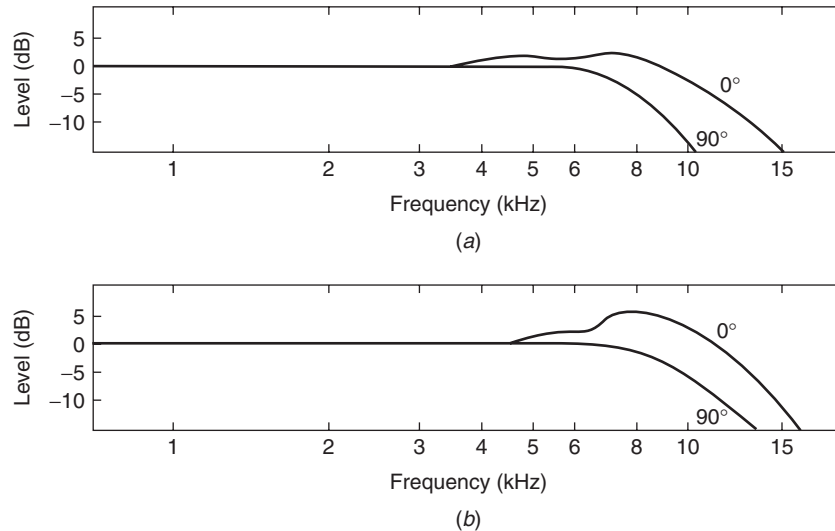
Sound level meters use several different microphone types. Three types are most commonly used: piezoelectric (ceramic) and two types of air condensers (polarized and electret). In view of the importance of potential hearing loss due to high-frequency sounds<sup>11</sup> the MEM (microelectromechanical) microphone may be used in future high-frequency SLMs that are under development in Germany.

**Ceramic** Ceramic microphones operate on the principle that piezoelectric materials will generate a voltage when subject to force changes. Ceramics are relatively low cost, have relatively low internal electrical noise, and, compared to other microphones, are quite rugged. They are quite sensitive to vibrations if not mounted properly. The frequency response of ceramic microphones is not as flat as other types, and, as a result, they are often only used with type 2 SLMs.

**Condenser** The capacitance will change if the separation between two plates is changed. Condenser or capacitor microphones are constructed with one plate of the capacitor made with a very light material that can move when subjected to changes in air pressure. A high voltage is connected via a high impedance to the other plate of the capacitor. Since charge on a capacitor is equal to the capacitance times the voltage, if the capacitance changes and the charge remains constant, the voltage also will change. Condenser microphones tend to be accurate and stable and have a wide, well-defined frequency bandwidth. They are relatively fragile and must be protected from hostile environments and high humidity.

*Polarized air condenser* microphones require an external voltage often in the range of 200 V. Sensitivity is a function of this voltage that must be well regulated.





**Figure 3** Examples of (a) free-field and (b) random-incidence half-inch microphones at 0° and 90° used in type 2 SLMs.

*Permanent charged or electret* microphones have permanent charge built into a plastic membrane. Response is similar to the polarized microphones.

**MEM** These microelectromechanical systems (MEMS) microphones have not been used in SLMs as such, but with their fast progress in development it is worth mentioning here to anticipate future possible application in miniaturization and special high-frequency sound level meters. MEMS are tiny microphones (as small as  $1.6 \times 2.8 \times 6$  mm) with their diaphragm edged from a single piece of silicon. With sophisticated chemical edging techniques, microphone backplate and possibly other electronics can be incorporated in a very small package and mass produced at a very low cost. There are many problems to be solved such as internal noise, frequency response, sensitivity stability, and dynamic range. Nonetheless, the development of a SLM the size of a matchbox may be closer than we anticipated.

## 2.2 Microphone Response

Microphone response changes with frequency. Microphones roll off below a couple of hertz to zero sensitivity at 0 Hz. At high frequencies the diameter of the microphone diaphragm is an appreciable part of a wavelength. As a result, the microphone rolls off at high frequencies and changes with the direction in which the microphone is pointed relative to the sound source. In general, microphones with smaller dimensions have better high-frequency response but also less sensitivity.

**Free Field** Free-field microphones are intended to measure sound in an open space free from reflections. The microphone should be pointed directly at the noise source at a 0° incidence. At 0° incidence the frequency

response is close to flat over the widest frequency range. High-frequency sound arriving from other angles may be somewhat attenuated (see Fig. 3). The IEC<sup>3,4,6,7</sup> specifies SLMs with free-field microphones.

**Random Incidence** Random-incidence microphones are intended to measure sound in a diffuse field where the sound is arriving from all directions such as inside a noisy plant or in an area with many reflections. Random-incidence microphones have the flattest response if pointed at about a 70° angle to the noise source. High-frequency noise arriving at angles less than 70° will cause the SLM to read somewhat higher, while angles greater than 70° will generally read somewhat lower (see Fig. 3). The ANSI specifies that SLMs shall use random-incidence microphones. (For more information on free-field and random-incidence measurement, see Chapters 6 and 17 in Ref. 8.)

**Pressure** Pressure microphones are intended to measure sound in a closed cavity. Its response is often similar to the response of a random-incidence microphone. SLMs are sometimes designed with special circuitry to correct a free-field microphone for random-incidence application.

## 3 FREQUENCY WEIGHTING

### 3.1 Standard Weightings

Frequency weightings have been standardized.<sup>12</sup> SLM standards IEC 60651-1979 and ANSI S1.4-1983 specify standard frequency-weighting networks such as A-, B-, and C-weighting (see Fig. 4).

**A-weighting** is intended to simulate the response of a nominal human ear at 40 phons. It is also considered by many regulations in many countries to be the best weighting for predicting hearing loss due to noise exposure. The SLMs, personal sound exposure meters,



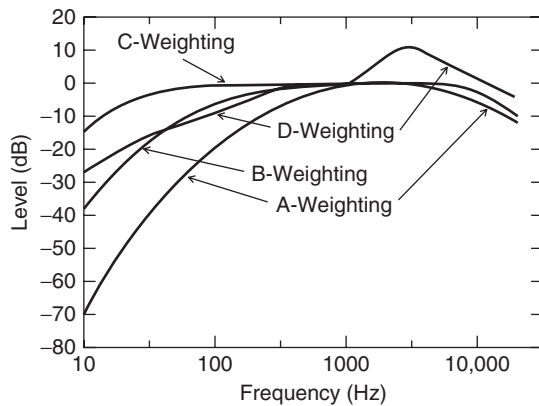


Figure 4 Frequency weighting curves.

and noise dosimeters use A-weighting to determine the effects of noise on humans. See Eq. (2).

**B-weighting** is intended to simulate the response of a nominal human ear at 70 phons. It is not widely used and has been omitted in the new standards.

**C-weighting** is intended to simulate the response of a nominal human ear at 100 phons. It is flat over most of the audible frequencies and is down 3 dB at 31.6

and 8000 Hz. Since it is flat over the audible range, it is often used to measure acoustical emission of machinery. It is also used to specify hearing protectors and to measure peak sound pressure level. See Eq. (1).

**D-weighting** was developed to measure noise from jet aircraft that have a perceived noise level that is higher than the level measured with A-weighting. It is not widely used and it has been dropped from current standards.

**Flat** or linear response is sometimes included in SLMs. Its frequency response is normally flat between two frequencies. The frequency response is very similar to C-weighting, with the response rolling off at the low end at a couple of hertz and at the high end at several tens of kilohertz. It has been replaced by the Z-weighting in current standards.

In IEC 61672, the A- and the C-weightings are specified, and the **Z-weighting** (or flat) defines a flat response with cutoff frequencies selected by the manufacturer of the SLM.

### 3.2 A-Weighting Tolerance Limits

In A-weighted level measurements it is important to understand the tolerance limits of an SLM. These tolerance limits play an important role in the indicated sound pressure level that may be quite different from the actual sound pressure level being measured. The class 2 tolerance limits (IEC 61672 and ANSI S1.4) are shown in Fig. 5. The design goal of the A-weighting

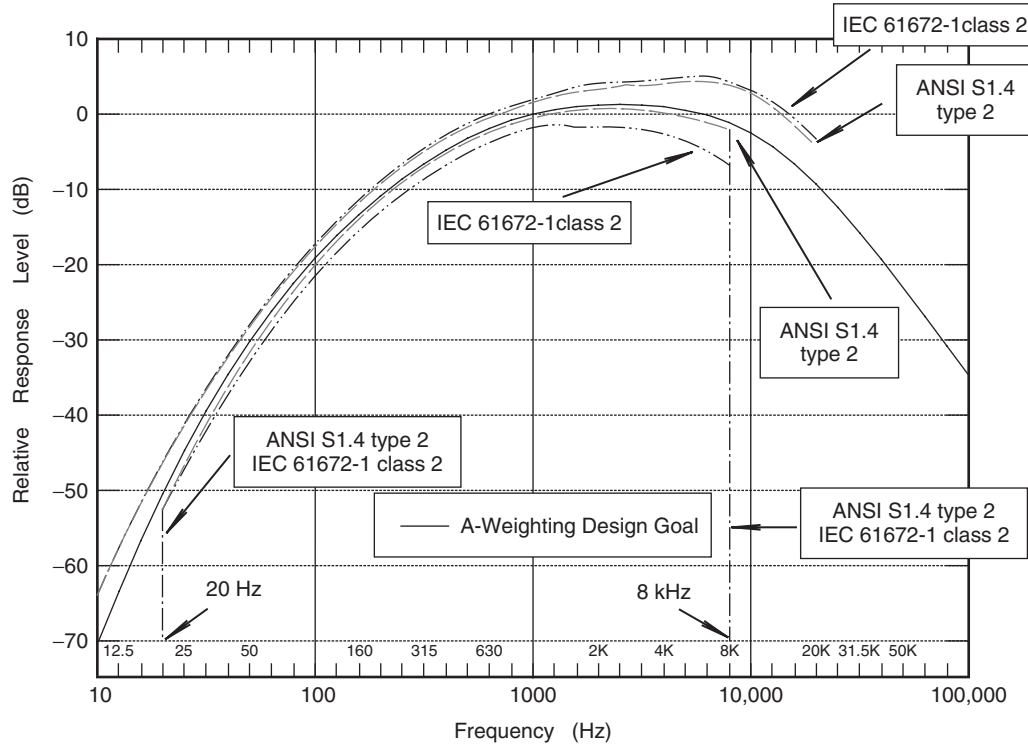


Figure 5 Class 2 (type 2) A-weighting tolerance limits.

is shown by the full line of the graph to 100 kHz. However, after 8 kHz the tolerance limit is at minus infinity. The sound energy above 8 kHz may be lost depending on the capability of the microphone and the electronic circuit. Since class 2 instruments are the workhorse of noise measurement related to hearing conservation and noise control program, one can imagine the result obtain with a class 2 instrument during the survey of factories and mines that usually have sounds of impulsive nature with harmonics that well exceed 8 kHz. The level measured by a class 2 instrument in an impulsive environment will be much lower. The A-weighting tolerance limits for class 1 instruments are shown in Fig. 6. For IEC 61672, after 16 kHz the tolerance limit is at minus infinity, which is an improvement from class 2 instruments. However, there is evidence<sup>11</sup> pointing to hearing loss due to high-frequency sounds. Removing the harmonics after 16 kHz is not helping hearing conservation programs that rely on SLMs to provide the correct sound pressure levels. It is important to point out that for ANSI S1.4A the A-weighted tolerance limits are much tighter, and it is capable of capturing sound energy beyond 20 kHz. See Fig. 6.

### 3.3 Weighting Equations

The equations for frequency responses for A- and C-weighting are

$$W_C(f) = 20 \log \left[ \frac{f_4^2 f^2}{(f^2 + f_1^2)(f^2 + f_4^2)} \right] - W_{C1000} \quad (1)$$

$$W_A(f) = 20 \log \left[ \frac{f_4^2 f^4}{(f^2 + f_1^2)(f^2 + f_2^2)^{1/2} \times (f^2 + f_3^2)^{1/2}(f^2 + f_4^2)} \right] - W_{A1000} \quad (2)$$

where  $W_{C1000}$  and  $W_{A1000}$  the normalization constants, rounded to the nearest 0.001 dB, are  $-0.062$  and  $-2.000$  dB, respectively, representing the attenuation necessary to provide frequency weighting of zero decibels at 1000 Hz for the C- and the A-weightings, respectively, and  $f_1 = 20.60$  Hz,  $f_2 = 107.7$  Hz,  $f_3 = 737.9$  Hz, and  $f_4 = 12194$  Hz.

### 4 SQUARING AND AVERAGING

The instantaneous level at the input of the squaring circuit is converted to a level proportional to the square of the level. It is interesting to note that if the input

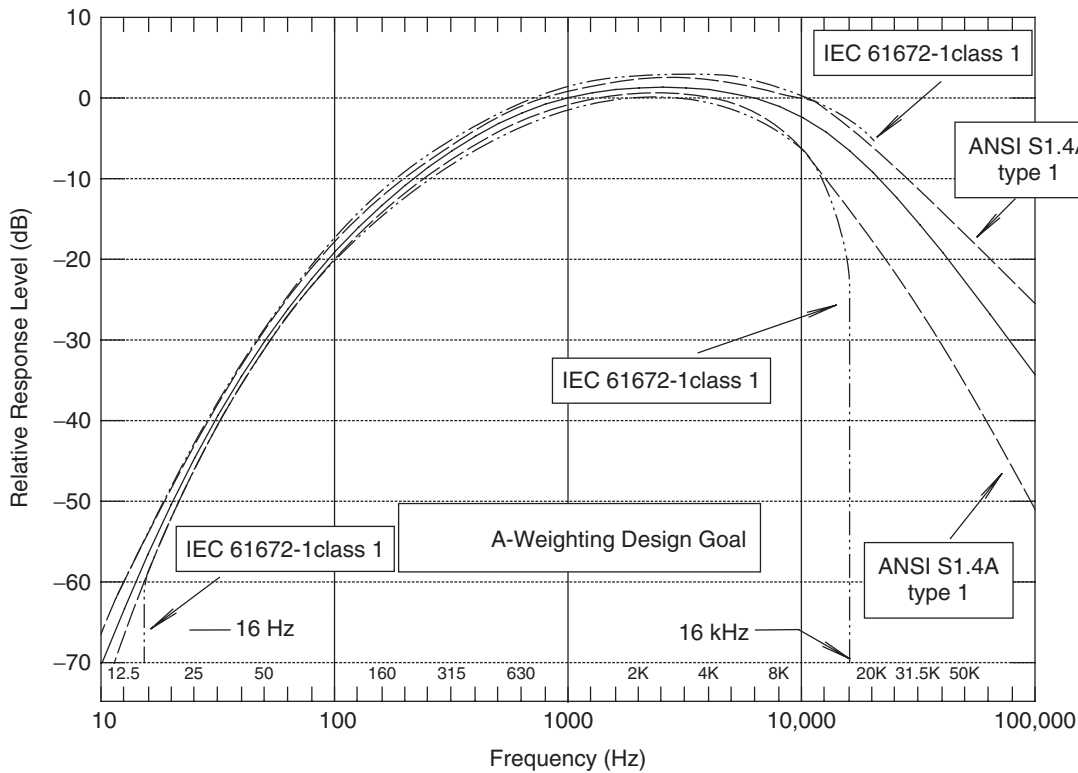


Figure 6 Class 1 (type 1) A-weighting tolerance limits.

pressure varies over 60 dB or 1000:1, the output must vary over a range of 1:  $1 \times 10^6$ .

The parameter  $p_a$  at the output of the squaring circuit can be found as

$$L_{\text{inst}} = 10 \log(p_a^2/p_o^2) \quad (3)$$

where  $L_{\text{inst}}$  is the instantaneous level in decibels and  $(p_a^2/p_o^2)$  is the ratio of the squared instantaneous A-weighted sound pressure to the squared reference sound pressure at 20  $\mu\text{Pa}$ .

#### 4.1 Exponential Averaging

A low-pass filter is placed after the squaring circuit to smooth out the instantaneous fluctuation and make it possible to read the level on a meter or digital display. Fast and slow responses are specified by several SLM standards and impulse response  $I$ , which is no longer specified in IEC 61672-1, but imbedded in many existing SLMs, can be found in IEC 60651-1979.

**Time Constants** *Slow (or S)* is specified as a 1-s time constant. Slow is used for measuring sound where an estimate of the average sound level is needed and the fluctuations are too fast to follow with a fast time constant. Slow is specified by the Occupational Safety and Health Administration (OSHA) and the Department of Defense (DOD) in the United States for measuring noise dose.

*Fast (or F)* is specified as a 0.125-s time constant. Fast follows fluctuations in sound levels better than slow but may fluctuate too much to be read. Fast is often used to measure transient noise such as vehicle passby noise.

*Impulse (or I)* is specified in IEC 60651-1979 as a 0.035-s time constant followed by a peak detector with a 1.5-s decay time such that the indicator will rise very rapidly to increasing levels but decay slowly when the level decreases. It is used primarily in Germany and a few other countries to measure highly impulsive noise.

#### 4.2 Peak, Maximum, or Minimum Hold

Sound level meters often include additional functions to measure the highest instantaneous level as well as the highest and lowest level after the time constant circuit. These functions can normally be reset to allow detection of the next level.

*Peak* is the highest instantaneous level. Peak is detected before the time constant circuit. It may have a different frequency weighting than the weighting used to calculate sound pressure level and other levels. Peak signals respond to pulses as short as 50  $\mu\text{s}$ . For a sine wave, the peak level is 3 dB higher than the root-mean-square (rms) level. The tone burst shown in Fig. 7 would have a peak reading of 103 dB.

*Maximum and minimum* levels are the highest and lowest levels detected after the time constant circuit. The tone burst shown in Fig. 7 has, after a few cycles, a fast maximum of 100 dB and a slow maximum of 96.6 dB. The minimum level for fast is 65.3 dB and for slow is 90.1 dB.

**Response to Tone Burst** On a logarithmic scale, the time constant will cause the display to change faster for an increase in level than for a decrease in level [see Eqs. (4) and (5)]. The maximum rates of decay for a big decrease in level are 4.34 dB/s for slow, 34.74 dB/s for fast, and 2.90 dB/s for impulse. The maximum response to a single tone burst relative to

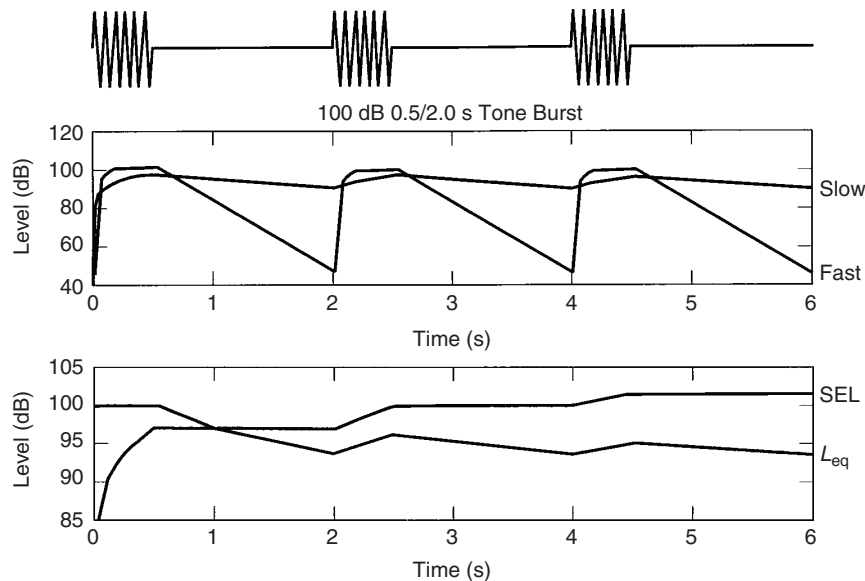


Figure 7 Slow, fast, SEL, and  $L_{\text{eq}}$  responses to tone burst.

the continuous level of the same tone is

$$L_{\text{on}} = L_{\text{tb}} - 10 \log(1 - e^{-T_1/\tau}) \quad (4)$$

The response when a tone is turned off is

$$L_{\text{off}} = L_{\text{on}} - 10 \log(1 - e^{-T_2/\tau})$$

$$L_{\text{off}} = L_{\text{on}} - 4.3429448 \frac{T_2}{\tau} \quad (5)$$

The integrated sound level of an integral number of tone bursts is

$$L_{\text{eq}} = L_{\text{tb}} - 10 \log\left(\frac{T_1}{T}\right) \quad (6)$$

where  $L_{\text{tb}}$  is the level of tone burst,  $T_1$  the duration of tone burst,  $T_2$  the time from the end of a continuous tone,  $T$  the time from the start of one tone burst to the start of the next tone burst ( $= 1$  per repetition frequency), and  $\tau$  an exponential time constant.

### 4.3 Integrating Averaging

**Equivalent Sound Pressure Level** Integrating SLMs, combine all the sound pressures between the start and end of an integration period. [See Eq. (7).] The equivalent sound pressure level ( $L_{\text{eq}}$ ) is the logarithmic average of the squared instantaneous pressures. While the exponential-averaging SLM display depends on what the sound level was immediately preceding the time it was read, integrating-averaging SLMs weigh equally all the sound from the start to the end of the integration time. As can be seen in Fig. 7, exponential-averaged SLMs keep changing when measuring discontinuous sound. Equivalent sound pressure level meters quickly settle to an average level. As a rule of thumb, the  $L_{\text{eq}}$  level should be within 0.1 dB of the final value after as many minutes as the time between impulses in seconds.

In theory, integrating do SLMs not have a time constant. In practice, some do exponentially average the squared pressure before doing the integration. If the integration time period is long compared to the time constant, the exponential circuit makes little difference. If a loud noise occurred shortly before the start time or shortly before the end time, part of that noise may be included or excluded:

$$L_{\text{eq}} = L_{\text{Aeq},T} = 10 \log \frac{1}{T} \int_{T_1}^{T_2} \frac{p_a^2(t)}{p_o^2} dt \quad (7)$$

$$\text{SEL} = L_{\text{EA},T} = 10 \log \int_{T_1}^{T_2} \frac{p_a^2(t)}{p_o^2} dt \quad (8)$$

where  $p_a$  is the instantaneous A-weighted sound pressure (for weighting other than A-weighting the subscript is changed) and  $T$  is the time between the

start and end times  $T_1$  and  $T_2$  (for the sound exposure level (SEL) the time is always in seconds).

**Sound Exposure Level** The SEL is similar to  $L_{\text{eq}}$  in that pressure is integrated over the measurement period [See Eq. (8).] The SEL measures the total energy and normalizes it to 1 s. The SEL is equal to  $L_{\text{eq}}$  after 1 s. If the  $L_{\text{eq}}$  is steady with time, the SEL will be 3 dB greater than  $L_{\text{eq}}$  after 2 s and 6 dB greater after 4 s, and increase by 3 dB whenever time doubles. The SEL is used to measure the total energy in an event independent of the time duration of the event.

**Short Equivalent Sound Pressure Level** Short  $L_{\text{eq}}$  is an  $L_{\text{eq}}$  value computed at very short intervals, perhaps every  $\frac{1}{8}$  or  $\frac{1}{16}$  s, and stored in memory for later analysis. Data in memory can then be used to calculate a number of sound descriptors such as  $L_{\text{eq}}$ , SEL, exposure, exceedance levels, sound pressure level, and maximum and minimum levels.

**Equivalent Sound Pressure Level per Day and Time-Weighted Average** The term  $L_{\text{ep},D}$  is the equivalent sound level per day, and TWA is the time-weighted average. Both  $L_{\text{ep},D}$  and TWA are similar to SEL except the integration is averaged over 8 h instead of 1 s. The level will be less than the  $L_{\text{eq}}$  level for time periods less than 8 h and greater than the  $L_{\text{eq}}$  level after 8 h. The  $L_{\text{ep},D}$  and TWA are used to measure worker noise exposure during a work day. It is assumed that workers who work less than 8 h can be exposed to higher noise levels during the time they are working without increasing their risk of noise-induced hearing loss. The parameter  $L_{\text{ep},D}$  is used in the European community while TWA is used in the United States. If the level is constant,  $L_{\text{ep},D}$  will increase by 3 dB if the time is doubled. Also,  $L_{\text{ep},D}$  is 44.59 dB less than SEL. The TWA may use different doubling or exchange rates. For OSHA compliance, it will increase by 5 dB if the time is doubled.

### 5 OPERATING RANGE

Ideally, an SLM should accurately measure all sounds from the noise floor to overload regardless of the temporal nature of the sound. While SLMs are available that accurately measure all sounds over a wide range, many SLMs that meet the older standards have very limited range, particularly when measuring transients.

In IEC 60651-1979 and ANSI S1.4-1983, the requirements for steady and transient response are very limited. Accurate steady-level response is only required over a 10-dB range, and transient response is only required for one tone burst. As many instruments made since these standards were issued barely meet the minimum requirements of the standards, much of the data taken with these instruments may be of little value.

The standards IEC 60651-1979 and ANSI S 1.4-1983 state that the accuracy of instruments shall be within  $\pm 0.4$ ,  $\pm 0.7$ , and  $\pm 1.0$  dB for types 0, 1, and 2 instruments, respectively. This accuracy is

required only for steady-tone sounds arriving from the reference direction under reference conditions of pressure, temperature, and humidity. Also, it is required only on one primary indicator range over a 10-dB span.

The SLM standards requirements for tone burst require only that type 1 and type 2 instruments be within tolerance at one point. On fast response only 0.2-s tone bursts and on slow response only 0.5-s tone bursts are required to be accurately measured. Unfortunately, there are many instruments on the market that only meet the standard for this one tone burst. If a noise burst is shorter than specified by the standard, the instruments read low or ignore the burst completely.

The standard IEC 60804-1984 expands the linearity range to 70, 60, and 50 dB for type 0, 1, and 2 instruments, respectively. It also requires tone bursts, as short as 0.001 s to be measured within  $\pm 0.5$ ,  $\pm 0.5$ , and  $\pm 1.0$  dB for type 0, 1, and 2 instruments, respectively. The standards for personal sound exposure meters and noise dosimeters follow the IEC 60804-1984 type 2 specifications. While this range may not be accurate for very short duration sound burst or for wide level changes, it is sufficient for most noise measurements.

The new IEC 61672-1 specifies only class 1 and class 2 instruments. The tolerance limits for performance include allowances for the expanded uncertainties of measurement that was tabulated for each requirement discussed in the standard. For example, at 250 Hz, the tolerance limits specified for weighted measurements for class 1 instruments is  $\pm 1.4$  dB. The corresponding expanded uncertainty allowed is 0.4 dB. (The corresponding tolerance limits specified in IEC 60651 is  $\pm 1.0$  dB without allowance for uncertainty of measurement). At 1 kHz (the reference frequency), the design goal for all frequency weightings is 0 dB with corresponding tolerance limits (with expanded uncertainties of measurements included) of  $\pm 1.1$  dB for class 1 and  $\pm 1.4$  dB for class 2 instruments.

### 5.1 Linearity Operating Range

The linearity range is specified for continuous sound pressure levels. Ideally the instrument should meet the linearity requirements on all ranges, although additional tolerance is allowed on ranges other than the primary indicator range. With IEC 60651, instruments are required to be linear over a range of frequencies from 31.5 Hz to 8 kHz.

In IEC 61672, level linearity applies over the total range for any frequency within the frequency of the sound level meter and for any frequency weighting or frequency response provided. At 1 kHz, on the reference level range the linear operating range shall be at least 60 dB, and the adjacent ranges shall overlap by at least 30 dB for SLMs that measure time-weighted sound levels, and at least 40 dB for SLMs that measure time-average sound levels or sound exposure levels. These new level linearity requirements have eliminated the discussion on dynamic range.

### 5.2 Dynamic Range

With previous standards such as IEC 60651 and IEC 60804, dynamic range, often called pulse range, determines the meter's performance when the sound level is not continuous. Ideally, it should be the same as the linearity range. Integrating SLMs are required to have 70, 60, or 50 dB pulse range for types 0, 1, and 2 meters, respectively. Exponential-averaging meters may be very limited in dynamic range capabilities.

### 5.3 Overload Indicators

Integrating-averaging SLMs and exponential-averaging SLMs are required to have overload detectors to indicate when an overload has occurred. The overload can occur at several places in the meter, and the overload detector may be required to measure several points. Different SLMs have their own implementation for overload indicators. It is best to consult the operating manual to obtain more details on their operation.

### 5.4 Noise Floor

The lowest level an instrument can read is determined by the noise floor. Noise may be generated in the microphone, its preamplifier, or the electronics of the meter. As a general rule, the lowest level an SLM can measure with 1-dB accuracy is 6 dB above the noise floor. For 0.1-dB accuracy the level must be 16 dB above the noise floor. If the noise floor is well behaved, it is possible to measure lower levels and calculate the actual noise level by logarithmically subtracting the noise from the signal on a mean-square basis. This technique is most useful when measuring sound that can be turned on and off, such as calibrating pure-tone audiometers [see Eq. (9)]:

$$L = 10 \log(10^{(L+N)/10} - 10^{N/10}) \quad (9)$$

where  $N$  is the noise floor,  $L + N$  the measured level including the noise, and  $L$  the level without the noise.

### 5.5 Threshold Circuits

It is sometimes desirable not to include sounds below a threshold level in the noise calculations. An example is excluding background noise when measuring the noise of an aircraft flyover. The OSHA regulations allow exclusion of noise below certain threshold levels.

Thresholds of noise dosimeters are placed after the time constant circuit and are well defined. Other threshold levels are not well defined, and the user must consult the meter-operating manual to determine exactly how the threshold works.

### 5.6 Reference Environmental Conditions

IEC 61672-1 specifies reference conditions for specifying of SLMs performance as:

Air temperature: 23°C,  
Static pressure: 101.325 kPa  
Relative humidity: 50%

## 6 DISPLAYS AND OUTPUTS

### 6.1 Analog and Digital

Conventional SLMs use an analog ballistic meter movement to display the sound level. Historically, the conversion to decibels was accomplished by scale graduations. This resulted in a scale with the numbers very close together on the left or lower end and separated on the high or upper end. Such scales were only useful over about a 20-dB range. When meter manufacturers included the logarithmic conversion in the meter electronics, analog meter scales of 30 or more decibels are possible with equal space per decibel. Although digital displays are now widespread, many users still prefer the analog display for ease of reading and detecting changes.

Digital displays offer wide range, and the numbers are easy to read down to a fraction of a decibel. These displays are difficult to read and interpret when used with exponential-averaging meters. If the sound level is not constant, the display will be different each time it updates. It is also necessary to consult the owner's manual to determine if the displayed number is the maximum level, the average level, or the level at the end of the update. Since a display that updates once a second can change 30 or more decibels during that second, it is important to know what is displayed.

### 6.2 Auxiliary Equipment

Auxiliary outputs are sometimes provided to connect the SLM to other equipment. Consult the operating manual before connecting to make sure the two pieces of equipment are compatible. In general, if a class 2 device such as a filter is connected to a class 1 SLM, the combination is considered as class 2.

## 7 CALIBRATION

It is recommended that SLMs be checked before and after every use with an acoustical calibrator. Manufacturers' recommendations should be followed. Normally, checking consists of removing the windscreen if any, carefully sliding the calibrator over the microphone, and reading the level. Care must be taken to ensure there is a good seal between the microphone and the calibrator or errors will result. If a calibration has changed by a few tenths of a decibel, it can normally be adjusted to the correct level.

Acoustical calibrators check only the reading at one or at a few frequencies and levels. It is possible for

a check to detect no change at one frequency and the SLM can be out of tolerance at another. If a microphone develops a pin hole air leak, the level may not change dramatically at 1000 Hz but may change considerably at other frequencies. Therefore, if daily checks require more than a few tenths of a decibel of corrections, it may be a sign of a much larger deviation at other frequencies. Good procedure recommends SLMs be calibrated at regular time intervals, such as yearly depending on the usage, by an accredited laboratory to ensure the instrument remains within the tolerance required by standards.

## 8 OTHER TYPES OF SOUND LEVEL METERS

### 8.1 Dosimeters and Personal Sound Exposure Meters

A special type of meter for measuring noise is the dosimeter or personal sound exposure meter. A block diagram of a noise dosimeter is shown in Fig. 8. An exposure meter would have a similar block diagram except the time constant, threshold, and exponent circuits would be omitted.

The instruments measure noise according to

$$E = \int_0^T p_a^2 dt \quad (10)$$

$$\text{DOSE} = \frac{100}{T_c} \int_0^T 2^{(L-L_c)/ER} dt \quad (11)$$

where  $E$  is exposure,  $p_a$  the A-weighted sound pressure,  $T_c$  the criterion time (normally 8 h),  $L_c$  the criterion level, and  $ER$  the exchange rate or doubling. In SI (International System units, exposure is measured in pascal-squared seconds ( $\text{Pa}^2 \cdot \text{s}$ ). For convenience, exposure in personal sound exposure meters is expressed in pascal-squared hours. Exposure to 85 dB for 8 h is approximately equal to one pascal-squared hour ( $\text{Pa}^2 \cdot \text{h}$ ).

Dose is another method of measuring noise exposure, with the results expressed as a percentage of a criterion exposure. In the United States, OSHA, defines 100% dose as the equivalent of a level of 90 dB for 8 h with a 5-dB exchange rate after the time constant. Other regulations may use different criterion levels and

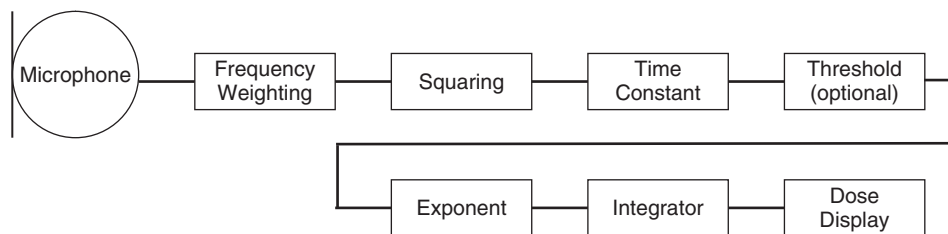


Figure 8 Noise dosimeter.

exchange rates. Since dose combines different levels with 5-dB (OSHA) or 4-dB (DOD) exchange rates, after the time constant circuit, the time constant will change the calculated dose. A slow time constant will produce a higher dose than a fast or no time constant if the sound level is not constant. While Eqs. (10) and (11) appear quite different, they are similar. If the exchange rate is 3 dB, the criterion level is 90 dB, and criterion time is 8 h, then 100% dose =  $3.2 \text{ Pa}^2 \cdot \text{h}$ .

## 9 OPTIONS

A number of additional devices may be built-in or connected to SLMs to expand their performance. Some of the measurements and options include acceleration, velocity, displacement, reverberation, signal analysis such as fast Fourier transform (FFT) and narrow band analysis, structural analysis, data acquisition, time capture, tracking filters, sound intensity, and sound power.

## REFERENCES

1. ANSI S 1.4-1983 (R2001), Specification for Sound Level Meters, Acoustical Society of America, New York, 1983. ANSI S 1.4A -1985 (R2001), Amendment to ANSI S1.4-1983, Acoustical Society of America, New York, 1985.
2. ANSI S 1.25-1991 (R2002), Specification for Personal Noise Dosimeters, Acoustical Society of America, New York, 1991.
3. IEC 60651-1979, Sound Level Meters, International Electrotechnical Commission, Geneva, Switzerland, 1979.
4. IEC 60804-1984, Integrating-Averaging Sound Level Meters, International Electrotechnical Commission, Geneva, Switzerland, 1984.
5. IEC 61252-2002, Electroacoustics, Specifications for Personal Sound Exposure Meters, International Electrotechnical Commission, Geneva, Switzerland, 2002.
6. IEC 61672-1, Sound level meters—Part 1: Specifications, International Electrotechnical Commission, Geneva, Switzerland, 2003.
7. IEC 61672-2, Sound level meters—Part 2: Pattern Evaluation Tests, International Electrotechnical Commission, Geneva, Switzerland, 2003.
8. G. S. K. Wong and Tony F. W. Embleton, Eds., *AIP Handbook of Condenser Microphones. Theory, Calibration, and Measurements*, American Institute of Physics, New York, 1995, Chapter 17.
9. G. S. K. Wong and L. Wu, Controlled Environment for Reciprocity Calibration of Laboratory Standard Microphones and Measurement of Sensitivity Pressure Correction, *Metrologia*, Vol. 36, 1999, pp. 275–280.
10. L. Wu, G. S. K. Wong, P. Hanes, and W. Ohm, Measurement of Sensitivity Level Pressure Corrections for LS2P Laboratory Standard Microphones, *Metrologia*, Vol. 42, 2005, pp. 45–48.
11. B. W. Lawton, Damage to Human Hearing by Airborne Sound of Very High Frequency or Ultrasonic Frequency, Contract Research Report 343/2001, Institute of Sound and Vibration Research for Health & Safety Executive, UK. Note: available at [http://www.hse.gov.uk/research/crr\\_pdf/2001/crr01343.pdf](http://www.hse.gov.uk/research/crr_pdf/2001/crr01343.pdf)
12. ANSI S1.42-2001, Design Response of Weighting Networks for Acoustical Measurements, Acoustical Society of America, New York, 2001.

# CHAPTER 39

## NOISE DOSIMETERS

**Chucui A. Kardous**  
Hearing Loss Prevention Section  
National Institute for Occupational Safety and Health  
Cincinnati, Ohio

### 1 INTRODUCTION

Noise-induced hearing loss is one of the most prevalent occupational illnesses in the world, but it is also the most preventable. Noise dosimeters have been used extensively over the past two decades to document noise exposures and ensure compliance with rules and regulations developed by various international organizations and regulatory agencies. In the United States, such dosimeters are required to comply with the American National Standards Institute (ANSI) Specification for Personal Noise Dosimeters S1.25–1991 (R1997), which states that dosimeters should be suitable for measurement of impulsive, intermittent, and continuous noise. Noise dosimeters measure and store sound pressure levels and, by integrating these measurements over time, provide a cumulative noise exposure reading for a given period. Dosimeters can function as personal or area noise monitors. In occupational settings, personal noise dosimeters are often worn on the body of a worker with the microphone mounted on the middle-top of the person's most exposed shoulder.

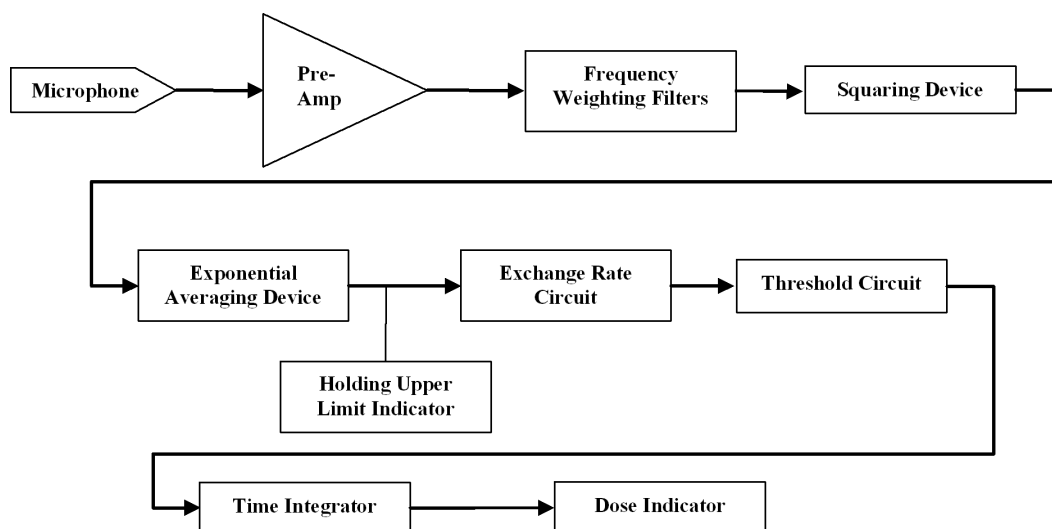
### 2 PRINCIPLE OF OPERATION

A dosimeter is a battery-powered, portable instrument, derived directly from sound level meters (SLM) to

automate the measurement and calculation of the percentage of the maximum permissible daily noise dose. It consists of a microphone that senses the sound pressure and produces an electrical signal. The output signal is amplified and fed into a frequency-weighting network (most typically, A-frequency weighting). The signal is then squared (sound pressure level is a function of pressure squared) and exponentially averaged with a specified time constant to establish a moving average window in time. The output sound level signal is fed into an integration section (an exponent circuit, threshold circuit, and integrator) that performs the algorithm necessary to compute the percentage criterion exposure (noise dose) according to a particular exchange rate, threshold level, and criterion sound level. The output is indicated as a percentage criterion exposure corresponding to the accumulated data at the completion of the measurement by the indicator circuit. The block diagram for the functional elements of the dosimeter is shown in Fig. 1.

#### 2.1 Noise Dose

Noise dosimeters compute a percentage criterion exposure or noise dose. Noise dose is the quantity that is expressed as a percentage of the maximum permissible daily exposure to noise. Noise dose is



**Figure 1** Block diagram of the essential elements of a noise dosimeter.



used in regulations to quantify exposure to noise in the workplace to protect against noise-induced hearing loss. ANSI S1.25 standard defines noise dose by the following mathematical equation:

$$D(Q) = \frac{100}{T_c} \int_0^T 10^{[(L_A(t) - L_c)/q]} dt \quad (1)$$

where  $D(Q)$  = noise dose for exchange rate  $Q$

$T_c$  = criterion sound duration = 8 h

$T$  = measurement duration in hours

$t$  = running time in hours

$L_A(t)$  = slow (or fast) A-weighted sound level in decibels (dB) when the sound level is greater than or equal to a user-selectable threshold sound level, or equals  $-\infty$  when the A-weighted sound level is less than the threshold level

$L_c$  = criterion sound level (in dB) specified by the manufacturer

$Q$  = exchange rate (in dB) (can be 3, 4, or 5 dB); and  $q = Q/\log(2)$  is parameter that determines the exchange rate

Exposure to a sound level that is equal to the criterion level  $L_c$  for a measurement time period equal to the criterion duration  $T_c$  yields a noise dose of 100%.

The Occupational Safety and Health Administration (OSHA) guidelines provide an alternate method for computing dose when the work shift noise exposure is composed of two or more discrete time periods of noise at varying levels. The total noise dose in percent is then defined by

$$D = 100 \left[ \frac{C_1}{T_1} + \frac{C_2}{T_2} + \cdots + \frac{C_i}{T_i} + \cdots + \frac{C_N}{T_N} \right] \quad (2)$$

where  $C_i$  is the total time of exposure at a specified A-weighted sound level, and  $T_i$  is the reference duration of noise exposure at that sound level that produces a dose of 100%.

The values for  $T_i$  are given in Table G-16a in Appendix A of the OSHA 29CFR 1910.95 regulations. A portion of Table G-16a is shown in Table 1. Table G-16a is derived from the following expression:

$$T_N = \frac{T_c}{2^{(L-L_c)/ER}}$$

or, for OSHA regulations

$$T_N = \frac{8}{2^{(L-90)/5}} \quad (3)$$

where  $L$  is the *slow* A-weighted sound level.  $L_c$  is the criterion or threshold level (90 dB), and ER is the exchange rate (5 dB).

**Table 1 Permissible A-weighted Noise Level Exposures**

Exposure Level, Slow (dB)	Duration per Day (h)
90	8
92	6
95	4
97	3
100	2
102	1.5
105	1
110	1.5
115	0.25 or less

From OSHA Table G-16, 29CFR 1910.95 (A).

## 2.2 Exchange Rate

Exchange rate is defined in ANSI S1.25 as “the change in sound level corresponding to a doubling or halving of the duration of sound level while a constant percentage of criterion exposure is maintained.” Dosimeters may be programmed to accept different exchange rates when performing their computations. OSHA requires the 5-dB exchange rate in its guidelines, while the National Institute for Occupational Safety and Health (NIOSH), the American Conference of Governmental Industrial Hygienists (ACGIH), and most international standards recommend the use of the 3-dB (equal-energy rule) exchange rate.<sup>1,2</sup>

## 2.3 Criterion Sound Pressure Level

Criterion sound level is the A-weighted sound level that corresponds to the maximum permitted daily exposure (dose of 100%) to noise if continually applied for the criterion time (typically 8 h). Criterion sound level also refers to occupational exposure limits specified by standards and regulations. The current OSHA permissible exposure limit (PEL) or criterion level is an A-weighted sound pressure level 90 dB. ACGIH and most international standards use the 85-dB criterion level, which is also the NIOSH recommended exposure limit (REL).

## 2.4 Threshold Sound Level

Threshold sound level, in decibels, is the sound level specified by the manufacturer of a noise dosimeter below which the instrument produces no dose accumulation. The current OSHA threshold level is set at 80 dB. The International Electrotechnical Commission (IEC) recommends a 40-dB threshold level.<sup>3</sup>

## 3 SOUND EXPOSURE MEASUREMENTS

Noise dosimeters are primarily used to measure workers' total noise exposure, especially when the noise levels are varying or intermittent, and the worker moves around frequently during the work shift. Dosimeters are also used to collect data for use in legal proceedings, development of engineering noise controls, and other industrial hygiene purposes.

When planning to conduct noise exposure measurements, steps must be taken to ensure that the dosimeters are calibrated and operated according to manufacturers' specifications. It is also necessary to understand

the properties of the acoustical environment, the main measurement objectives as they relate to determining the risk to hearing, and the limitations associated with the use of dosimeters.

### 3.1 Dosimeter Calibration

Dosimeter manufacturers recommend that the instrument be calibrated with an acoustical calibrator before and after each measurement to verify reliable operation. In addition to field calibration routines, the manufacturers recommend periodic comprehensive calibration and certification of the instrument by an accredited laboratory using traceable reference sources. Field calibration of contemporary dosimeters has been mostly automated through PC-based programs that run the calibration routine, document the time and date, and adjust for any offset in levels.

Figure 2 shows a Larson-Davis Model 706 dosimeter being calibrated at 114 dB sound pressure level (SPL) (1000 Hz) using the Larson-Davis CAL 150 Precision Acoustic Calibrator.

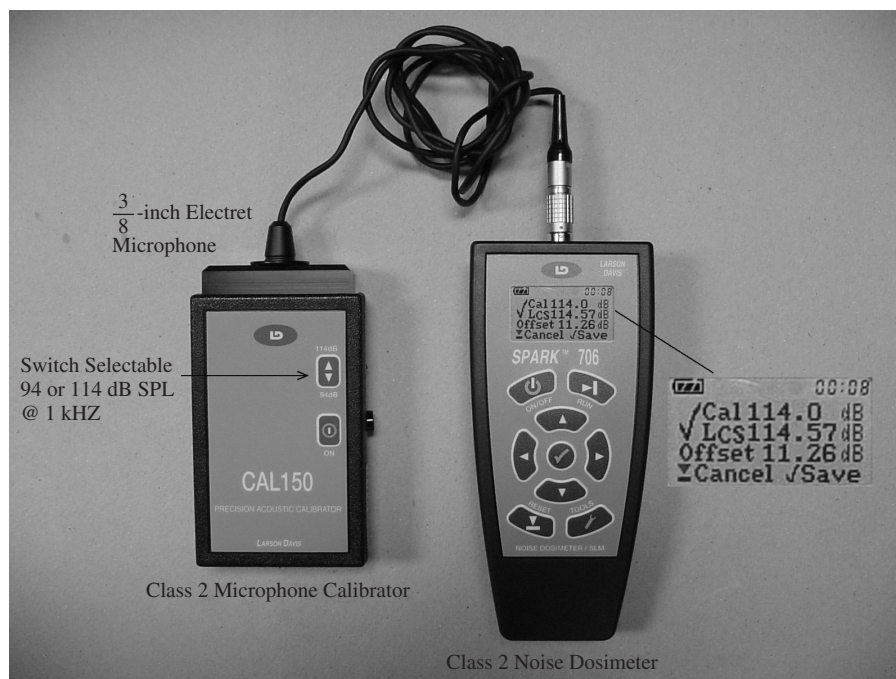
### 3.2 Operational Settings

Current dosimeters are designed to provide the user with parameters such as noise dose, time-weighted average, sound exposure level, as well as peak, maximum, and minimum sound pressure levels. Most dosimeters also generate statistical and graphical representations of the collected data. ANSI S1.25 specifies that dosimeters should at least provide the following parameters:

Frequency weighting: A or C  
Exponential averaging: F (fast); S (slow)  
Criterion level: 90, 85, 84, 80, or V (variable)  
Criterion duration: hours  
Threshold level: 90, 80, or V (variable)  
Exchange rate: 5, 4, or 3

### 3.3 Personal Exposure versus Area Monitoring

A dosimeter may be used as a personal dose meter or as an environmental area monitor. For personal noise monitoring, the instrument may be placed inside a pocket or clipped to a belt. OSHA requires the microphone of the dosimeter be placed in the “hearing zone” of the side of the worker facing the highest noise levels. The hearing zone is defined as hypothetical sphere of 300 mm radius enclosing the head of the wearer.<sup>4</sup> ANSI S12.19, Measurement of Occupational Noise Exposure, standard specifies that the microphone be located on the middle-top of the worker’s most exposed shoulder and that it be oriented approximately parallel to the plane of the shoulder, as shown in Fig. 3. However, studies have shown that placing the microphone on the person’s body can affect measurements by anywhere from an A-weighted sound pressure level of  $-1$  to  $+5$  dB.<sup>5,6</sup> The amount by which the human body affects measurements depends on the nature of the sound field, the frequency spectrum, the angle of incidence, the absorption of the clothing material, and the position of the microphone on the person. In most industrial settings, the A-weighted sound pressure level



**Figure 2** Calibration of a personal noise dosimeter with various components notated and highlighted.



**Figure 3** Microphone placement of a noise dosimeter on the shoulder of the wearer.

measurements are typically increased by 0.5 to 1.0 dB when the dosimeter is worn on a person compared with the measurements taken in the undisturbed field.<sup>7</sup>

To alleviate the limitations associated with workers' body distortion, minimize sound survey efforts, and provide better exposure estimates for groups of workers, measurement techniques such as profiling or task-based assessment can be used. The dosimeter's microphone can be mounted on a tripod and placed in the unoccupied worker position. A task-based noise assessment is accomplished by measuring noise varying over time and space for each defined work task.<sup>8</sup> Task-based measurements depend heavily on the accurate identification of the sound field at all points of the task area and the location of the worker versus time.

#### 4 DOSIMETER LIMITATIONS

In addition to the microphone distortions introduced by the worker head and torso, other environmental and electroacoustical factors can limit dosimeter capability and range of operation.

##### 4.1 Mechanical Vibration

Most microphones and dosimeters are sensitive to mechanical vibration, especially at very high SPLs (above 120 dB). Mechanical vibration may cause the

microphone or electronics to produce spurious signals in the dosimeter measurement and lead to an increase in the time-weighted average (TWA) and noise dose. To minimize the effects of vibration on the instrument, care must be taken to ensure that the microphone, cable, and dosimeter case are secured or isolated from the source of vibration. Dosimeter manufacturers test and report on the effects of mechanical vibrations by vibrating the entire instrument sinusoidally along the three mutually perpendicular axes at acceleration of  $0.98 \text{ m/s}^2$  and within the frequency range of 10 and 500 Hz.

##### 4.2 Impulse Noise

ANSI S1.25 specifies that noise dosimeters should be suitable for measurement of impulsive, intermittent, and continuous noise. OSHA regulations and NIOSH recommendations state that no exposure should be permitted above 140 dB peak sound pressure level. Nevertheless, dosimeters have been used for measurements of noise environments that have levels above 140 dB such as in construction, mining, and law enforcement firing ranges. It must be noted, however, that the OSHA regulations and the ANSI S1.25 standard require that dosimeters operate properly up to 140 dB.

NIOSH studies have found that personal noise dosimeters have inherent limitations and are susceptible to producing erroneous results when they are used in predominantly impulsive noise environments such as firing ranges.<sup>9</sup> These standard dosimeters "clipped" peak noise levels greater than the range of the instrument and acted as if they were at the maximum level of that specified range.

##### 4.3 Measurement Artifacts

Dosimeter microphones are susceptible to inadvertent or intentional tampering by the users. Such tampering may occur by tapping or rubbing the microphone, or by screaming or blowing into the microphone during measurements. Investigations into the potential sound-field contamination of such artifacts showed minimal impact (a fraction of a decibel for thumping and hollering to an A-weighted sound pressure level 1 to 2 dB for blowing with background noises of 85 and 90 dB) on the measured daily TWA when using the OSHA 5-dB exchange rule. However, the use of the International Organization for Standardization (ISO), NIOSH, or ACGIH noise exposure criteria showed much more significant increase (an A-weighted sound pressure level 2 to 5 dB) in the measured TWA.<sup>10</sup> To minimize the effect of such artifacts, most dosimeter microphones are provided with small windscreens that will guard against rubbing and touching, and some isolation against blowing. In addition to the windscreens, contemporary dosimeters are manufactured with built-in keypad locking and programmable automatic timers to reduce the potential for tampering. Finally, close examination of the time-history records can show if any abnormal or unexplained spurious events have occurred during the measurements.

#### 4.4 Wet and Humid Environments

Wet and humid environments present a challenge for collecting personal dosimetry measurements. The dosimeter instrument is typically water resistant and tested to withstand high levels of humidity. However, the microphone's frequency response is usually affected if the relative humidity is high or the temperature of the microphone is close to the dew point. Condensation may occur on the diaphragm of the microphone and can generate intermittent internal noise in the measurement.

When operating a dosimeter in a humid or rainy environment, appropriate all-weather microphones with shields must be selected to prevent water from affecting the diaphragm. Wrapping the microphone or enclosing it using makeshift material should be avoided because it can lead to serious errors in the measurements.

Dosimeter manufacturers test for variations of SPLs over some specified relative humidity range.

#### 4.5 Temperature

Current dosimeters are required to operate properly within ordinary indoor temperature ranges. Permanent damage can occur when they are operated or stored at extreme temperatures. The manufacturers are required to state temperature ranges over which the dosimeter, including the microphone, will meet national and international standards. Typically, dosimeters can be operated safely between  $-15$  and  $50^{\circ}\text{C}$  and can be stored (with the battery removed) at temperatures between  $-20$  and  $60^{\circ}\text{C}$ .

#### 4.6 Electromagnetic Interference

Current dosimeters are required to comply with national and international electromagnetic compatibility standards. Manufacturers test the performance of dosimeters to electromagnetic interference at power-line (50 or 60 Hz) frequencies. However, these standard dosimeters might be susceptible to electromagnetic and radio-frequency interference when operated near sources that generate strong electric and magnetic fields such as arc welders and furnaces, cellular and communications equipment, or induction heaters. ANSI S1.14-1998 (R2003) (Recommendations for Specifying and Testing the Susceptibility of Acoustical Instruments to Radiated Radio-Frequency Electromagnetic Fields, 25 MHz to 1 GHz) provides specification and testing for susceptibility radio-frequency and

electromagnetic fields.<sup>11</sup> To check for electromagnetic interference, the microphone might be replaced with a shielded capacitor (or "dummy microphone") with similar impedance. If electromagnetic interference is observed in the dosimeter reading, then action must be taken to shield the instrument.

#### REFERENCES

1. National Institute for Occupational Safety and Health, Criteria for a Recommended Standard—Occupational Noise Exposure (revised criteria 1998) DHHS (NIOSH) Pub. No. 98-126. NIOSH, Cincinnati, OH, 1998.
2. American Conference of Governmental Industrial Hygienists (ACGIH), TLV's and BEI's: Threshold Limit Values for Chemical Substances and Physical Agents, Biological Exposure Indices, Cincinnati, OH, ACGIH, 1997.
3. International Electrotechnical Commission (IEC), Electroacoustics Sound Level Meters—Part 1: Specifications, IEC 61672, Geneva, Switzerland, 2002.
4. ISO 1999:1990, Acoustics—Determination of Occupational Noise Exposure and Estimation of Noise-Induced Hearing Impairment, International Organization for Standardization, Geneva, Switzerland, 1990.
5. G. F. Kuhn and R. M. Guernsey, Sound Pressure Distribution about the Human Head and Torso, *J. Acoust. Soc. Am.*, Vol. 73, 1983, pp. 95-105.
6. G. F. Kuhn Comparisons between A-weighted Sound Pressure Levels in the Field and Those Measured on People or Manikins, *J. Acoust. Soc. Am.*, Vol. 79, suppl.1, 1986.
7. J. J. Earshen, Sound Measurement: Instrumentation and Noise Descriptors, in *The Noise Manual*, 5th ed., E. H. Berger, L. H. Royster, J. D. Royster, D. P. Driscoll, and M. Lane (Eds.), AIHA Press, American Industrial Hygiene Association, Fairfax, VA, 2000, Chapter 3.
8. N. S. Seixas, L. Sheppard, and R. Neitzel, Comparison of Task-Based Estimates with Full-Shift Measurements of Noise Exposure, *Am. Ind. Hyg. Assoc. J.*, Vol. 64, 2003, pp. 823-929.
9. C. A. Kardous and R. D. Willson, Limitations of Integrating Impulsive Noise When Using Dosimeters, *J. Occup. Env. Hyg.*, Vol. 1, 2004, pp. 456-462.
10. L. H. Royster, E. H. Berger, and J. D. Royster, Noise Surveys and Data Analysis, in *The Noise Manual*, 5th ed., E. H. Berger, L. H. Royster, J. D. Royster, D. P. Driscoll, and M. Lane Eds., 2000, Chapter 7.
11. ANSI S1.14-1998 (R2003), American National Standards Institute, Recommendations for Specifying and Testing the Susceptibility of Acoustical Instruments to Radiated Radio-Frequency Electromagnetic Fields, 25 MHz to 1 GHz, ANSI, New York, 2003.

# CHAPTER 40

## ANALYZERS AND SIGNAL GENERATORS

Henrik Herlufsen, Svend Gade, and Harry K. Zaveri

Brüel & Kjær

Sound & Vibration Measurement A/s

Naerum, Denmark

### 1 INTRODUCTION

An analyzer is a device that takes sound or vibration signals and extracts the various forms of information carried in the signals. An understanding of the basic concepts of signal analysis is important for correct use and setup of analyzers when dealing with the various types of noise and vibration signals encountered in practice. It is important to understand what analyzers can offer and provide. Frequency analysis is the most widely used method for solving noise and vibration problems. As the frequency content of the signal is generally related to a specific component of a given system, this method is often the key to a better understanding of the vibrational and acoustical phenomena. The filtering method and use of the fast Fourier transform (FFT) are common approaches for analysis of signals. Systems are often analyzed from measurements of their inputs and outputs. In contrast to a signal analyzer, a signal generator is a device used to generate sound and vibration signals for the purpose of the excitation of systems.

### 2 ANALYSIS CONCEPTS

#### 2.1 Basic Concepts, Signal Types, and Descriptors

Analysis of noise and vibration signals is performed in order to extract the various forms of information carried in the signals, which have been found to relate to the properties of a structure or a system under investigation. Different analysis techniques are used in order to acquire a specific type of information. The requirement is that the information should be extracted in a form that will make interpretation easier and communication and documentation simpler.

Different analyzers use different analysis techniques and are applied for the various applications. The most fundamental analysis is the determination of the amplitude characteristics and the spectral (frequency) distribution of the signal.

##### 2.1.1 Types of Signals and Spectral Units

The way we treat and analyze signals depends upon the type of signal. Signals can be divided into different categories, with the most basic division being stationary and nonstationary signals. Stationary signals are divided into deterministic and random signals, and nonstationary signals are divided into continuous and transient signals.<sup>1</sup> Examples of the various types in the time and frequency domains are illustrated in Fig. 1.

A unique descriptor for a continuous stationary signal is its root-mean-square (rms) value. It gives

information about the “power” in the signal in the following sense. If the signal is considered as an electrical voltage signal, the rms value is the constant voltage that will dissipate the same power (heat) in a resistor. It is a value in units of the measured quantity (such as pascals for sound measurements or metres per second squared for vibration measurements) and, thus, only a measure of the power in the above-described sense. The square of the rms value, that is, the mean square (MS) value, is related to power in the physical sense via an impedance.

*Stationary deterministic signals* are made of a combination of sinusoidal signals with different amplitudes and frequencies. The spectrum is characterized by content (power) at discrete frequencies (a line spectrum). This means they have a certain rms value (or MS value) at each of these frequencies and that the sum of the MS values at all the frequencies is the MS value of the signal (neglecting the random noise content, see below). Thus, it is natural to scale the spectra of these signals in terms of rms. In some vibration applications, the spectra are sometimes rescaled to the amplitude of the sine components (the peak value), which is  $\sqrt{2}$  rms or in the peak-to-peak value (i.e., twice the amplitude or  $2\sqrt{2}$  rms). Noise and vibration signals from rotating machinery with constant speed are examples of this type of signal.

*Stationary random signals* are described by their statistical properties, such as the mean value, standard deviation, amplitude probability, and so forth. In contrast to stationary deterministic signals, they have a continuous distribution of spectral content.

Random processes give rise to random signals, and all signals encountered in real life have a certain content of this kind of signal. Analysis of random data is a complete discipline in itself and has a wide range of applications. In analysis of deterministic signals, the random content is often referred to as the noise content, and methods are searched for to minimize its influence.

Due to the continuous distribution of spectral content, the natural way to scale the spectra is in terms of *power spectral density (PSD)*, and the power or MS value in a given frequency band is given by the integral of the PSD over the frequency band. The unit of PSD is  $\text{U}^2/\text{Hz}$ , where U is the unit of the measured signal. The square root of the PSD, often called the rms spectral density (rmsSD), has a unit of  $\text{U}/\sqrt{\text{Hz}}$ .

The spectrum of a random signal scaled in rms will thus change in accordance with the measurement bandwidth. This is observed, for example, when a

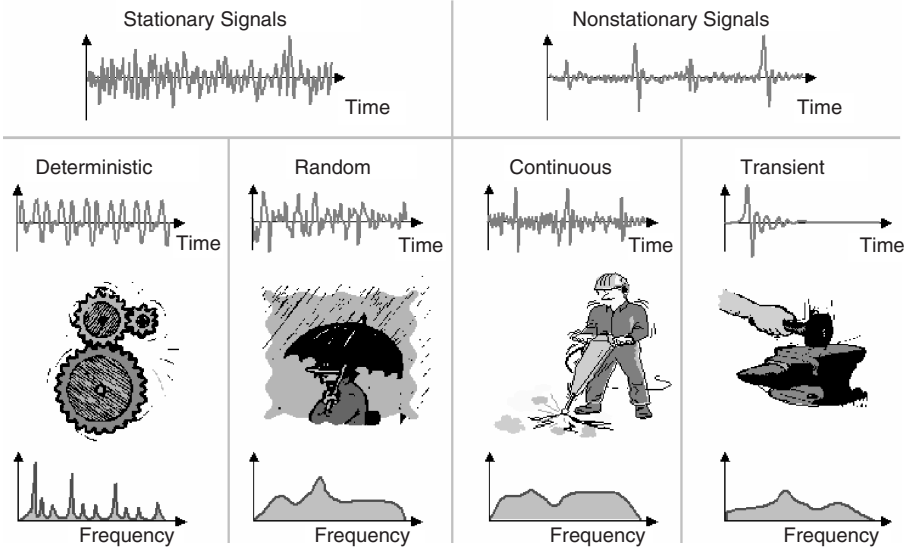


Figure 1 Examples of different types of signals and their spectral content.

deterministic signal contaminated with random noise is analyzed with different bandwidths. Decreasing the bandwidth will lower the rms value of the noise in the spectrum, whereas the rms values of the sine components remain the same (the sine components are assumed to be separated in different filter bands). A random signal with a flat (constant) power spectral density over a wide frequency range is called white noise, as it has the same spectral density at all frequencies.

*Transient signals* are signals of finite and relatively short duration. They are characterized by a certain amount of “energy” in the same way that continuous signals are characterized by a “power” value. Transient signals have spectral content continuously distributed with frequency, and the natural way to scale the spectra is therefore in terms of energy spectral density (ESD) ( $U^2s/Hz$ ), where  $U$  is the unit of the measured signal. The spectral units of the different types of signals are summarized in Table 1.

*Nonstationary continuous signals* are signals consisting of one or more of the following:

- Sine components with changing amplitudes and/or changing frequencies

- Random signals with statistical properties changing with time
- Transients appearing with varying intervals and with varying characteristics in time and frequency

2.2 Frequency Analysis – Filter and Detector

The purpose of frequency analysis is to estimate the spectral content of the signals.

A frequency analyzer consists of a set of filters and a detector, as shown in Fig. 2. Prior to analysis, the signal has to be conditioned in terms of level (gain/attenuation), and high- and/or low-pass filtering might be applied as well. In digital analyzers antialiasing filters (low-pass filters) are used in order to prevent aliasing, that is, the erroneous appearance of high frequencies as low frequencies in the subsequent analysis. The concepts and assets of digital processing are covered in Chapter 42 and not discussed further here.

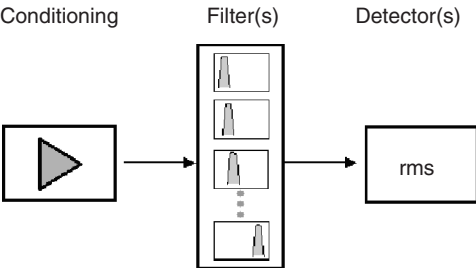


Figure 2 Block diagram of a frequency analyzer. The detector works for all the filters in case of a parallel filter bank.

Table 1 Spectral Scaling and Units for Different Signal Types <sup>a</sup>	
Signal Type	Spectral Scaling and Unit
Deterministic	rms ( $U$ ) or MS/Power ( $U^2$ )
Random	rmsSD ( $U/\sqrt{Hz}$ ) or PSD ( $U^2/Hz$ )
Transient	ESD ( $U^2s/Hz$ )

<sup>a</sup>  $U$  is the unit of the measured quantity (such as Pa or  $m/s^2$ ). MS is often referred to as “power.”

The *filter* is the frequency selective part that transmits those frequencies in the signal that are inside the passband of the filter. The *detector* detects the power in the transmitted signals in terms of its MS or rms value. In Fig. 2, only one detector is shown, and this is supposed to work as detector for all the filters in the situation of a parallel filter bank.

The filter in the frequency domain is described by its *frequency response function*. It is a complex function of frequency, having magnitude and phase, and defines the relationship between the input and output in the frequency domain as

$$H(f) = Y(f)/X(f) \quad (1)$$

where  $H(f)$  is the frequency response function of the filter and  $X(f)$  and  $Y(f)$  are the complex spectra (Fourier transforms) of the input signal and the output signal, respectively.

**2.2.1 Types of Filters** There exist four types of filters: low-pass filters, high-pass filters, bandpass filters, and bandstop (or band rejection) filters, as illustrated in Fig. 3. Figure 3 illustrates the filtering process and shows only the magnitude in the frequency domain. Low-pass, high-pass, and bandstop filters are often used in connection with signal conditioning or in preprocessing for other signal analysis applications.

*Bandpass filters* are used for frequency analysis and are characterized by a number of parameters. An ideal bandpass filter transmits frequencies in a given frequency band (the passband) and rejects frequencies outside the band. Practical (realizable) real-time filters have a frequency response function, as exemplified in Fig. 4, with a passband characterized by a ripple and a transition band with a finite slope. The frequency response function is complex, and Fig. 4 shows only the magnitude. The corresponding phase relates to the delay in the filter. The filter is characterized by

parameters, such as its *center frequency*, *bandwidth*, *ripple*, and *selectivity*.<sup>1</sup>

The passband is bounded by a lower limiting frequency  $f_1$  and an upper limiting frequency  $f_2$ , and the bandwidth of the filter,  $B = f_2 - f_1$ . Frequency  $f_0$  is the frequency in the “middle” (defined later) of the passband and is called the center frequency.

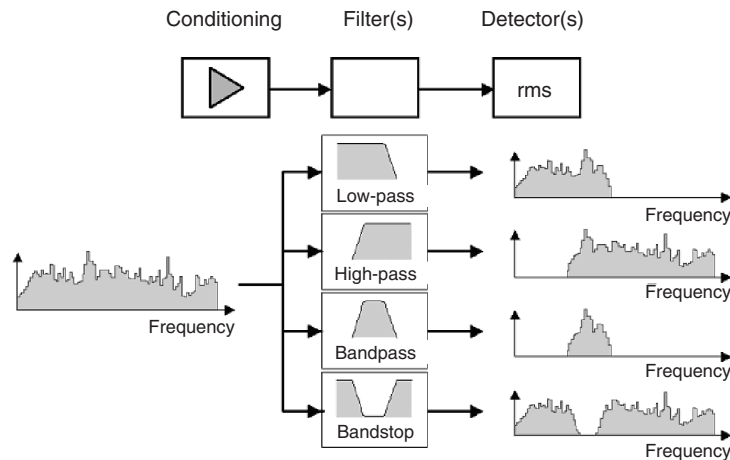
The definition of the bandwidth is not unique for a practical filter. The two most often traditionally used definitions are the 3-dB bandwidth and the “effective noise bandwidth” (sometimes referred to only as the noise bandwidth).

The *3-dB bandwidth* is the bandwidth where the lower and the upper limiting frequencies,  $f_1$  and  $f_2$ , are defined as the frequencies where only half of the power of the signal is transmitted, that is, the frequencies at which the signal is attenuated by 3 dB and the gain in the passband is assumed to be 1 (0 dB). The 3-dB bandwidth might be the relevant descriptor in the analysis of deterministic signals, that is, signals with content at discrete frequencies.

The *noise bandwidth* of a filter is the bandwidth of a corresponding ideal filter that transmits the same amount of power as the filter when both receive white noise as the input signal. The filters are assumed to have the same gain in the passband, which here is a gain of 1 (0 dB). The noise bandwidth relates to the transmission of broadband random signals and is therefore the bandwidth to be used when rescaling a detected MS (power) spectrum to a PSD spectrum for a random signal.

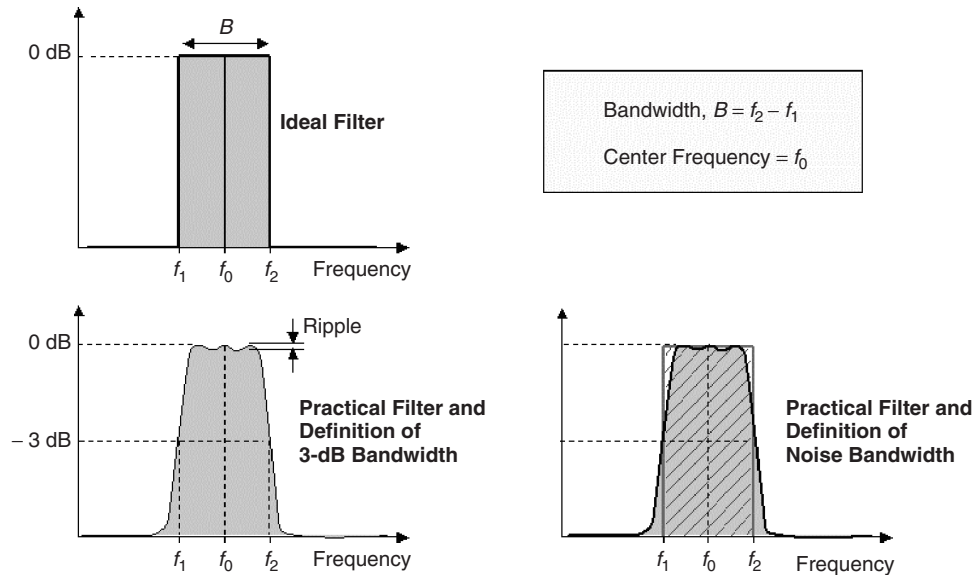
There exist two basic types of bandpass filters, namely constant bandwidth filters (also called absolute bandwidth filters) and constant percentage bandwidth filters (also called relative bandwidth filters).

*Constant bandwidth filters* have a bandwidth that is independent of the center frequency. Frequency analysis using constant bandwidth filters gives uniform resolution on a linear frequency scale and is the natural choice in analysis of deterministic signals containing



**Figure 3** Different types of filters. Low-pass, high-pass, bandpass, and bandstop.





**Figure 4** Filter characteristics of an ideal and a practical bandpass filter and definition of noise bandwidth, 3-dB bandwidth, and ripple in the passband.

harmonic components. For constant bandwidth filters the center frequency is defined as the arithmetic mean of  $f_1$  and  $f_2$ , that is,  $f_0 = (f_1 + f_2)/2$ , which is in the middle between  $f_1$  and  $f_2$  on a linear frequency scale.

*Constant percentage bandwidth (CPB)* filters have a bandwidth that is a fixed percentage of the center frequency. Octave and fractional-octave filters are examples of constant percentage bandwidth filters often used in acoustics. Octave filters have a bandwidth of approximately 71% and third-octave filters a bandwidth of approximately 23%.

Frequency analysis using constant percentage bandwidth filters gives uniform resolution on a logarithmic frequency scale and is often used when analyzing over a wide frequency range covering three or more decades.

Octave and fractional-octave filters are used extensively in acoustics, as they relate better than constant bandwidth filters do to the human perception of noise.

Other applications are monitoring or quality control measurements facing the following requirements: the bandwidth at low frequencies should be sufficiently narrow to separate the lower harmonic components of rotating elements (containing information about unbalance, misalignment, etc.), and at higher frequencies, the condition of bearings, gears, and the like should be detected in a few filters without the separation of individual components.

For constant percentage bandwidth filters the center frequency is defined as the geometric mean of  $f_1$  and  $f_2$ , that is,  $f_0 = \sqrt{f_1 f_2}$ , which is in the middle between  $f_1$  and  $f_2$  on a logarithmic frequency scale.

Figure 5 illustrates examples of characteristics of constant bandwidth filters and constant percentage

bandwidth filters. The *selectivity* describes the ability of the filter to separate closely spaced components with large differences in amplitude. For constant bandwidth filters, the bandwidth for 60-dB attenuation or the ratio of this bandwidth to the 3-dB bandwidth, called the shape factor, is used. For constant percentage bandwidth filters, the octave selectivity, which gives the attenuation one octave above and below the center frequency, is used.<sup>1</sup>

## 2.2.2 Filter Response Time and the Uncertainty Principle

So far the characteristics of a filter have been described only by its frequency response function, that is, in the frequency domain. They can be equally well described in the time domain via its *impulse response function*. The time domain and the frequency domain are mathematically related via the Fourier transform, and the impulse response function is the inverse Fourier transform of the frequency response function.

Equation (1) relates the input and the output of a filter in the frequency domain. In the time domain, the output signal  $y(t)$  is given by the convolution of the input signal  $x(t)$  and the impulse response function  $h(t)$  defined by the integral:

$$y(t) = \int_{-\infty}^{\infty} x(\tau)h(t - \tau) d\tau = x(t) * h(t) \quad (2)$$

where the symbol  $*$  represents convolution.

A consequence of the impulse response function and the frequency response function being Fourier transform pairs is that if one of them is narrow



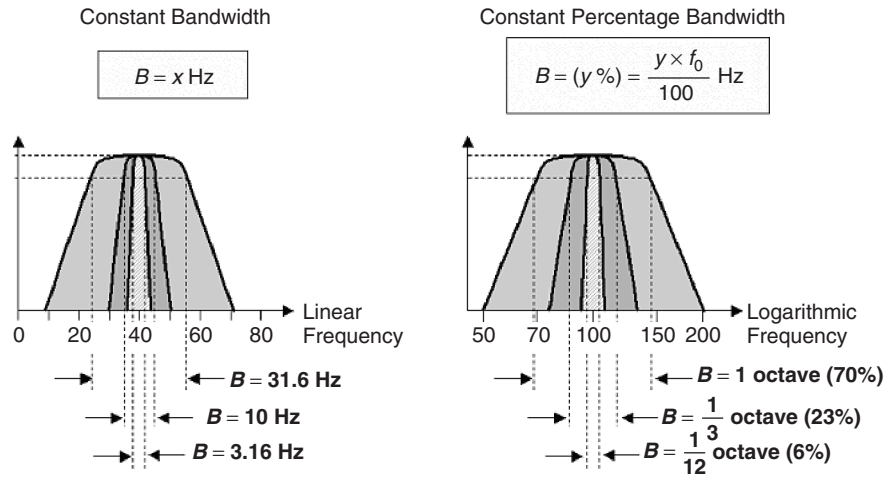


Figure 5 Examples of characteristics of constant bandwidth filters and constant percentage bandwidth filters.

(short), the other one will be wider (longer) than a corresponding minimum width (length). This can be formulated as

$$BT \geq 1 \quad (3)$$

where  $B$  is the width in frequency (bandwidth) and  $T$  is length in time. The relationship can include various constants depending upon the mathematical definition of  $B$  and  $T$ , but this is of less importance in this context. This fundamental principle, also known as the *uncertainty principle*, puts a limit to the corresponding resolutions (widths, accuracies) in the two domains and is a consequence of the mathematical formulation of frequency analysis (the Fourier transform). A more loose formulation is: Narrow in one domain means wide in the other domain.

The narrower the frequency response function is (i.e., the higher the resolution in the frequency domain), the longer the impulse response function will be (i.e., the longer it will take for the filter to respond). Figure 6 illustrates the response of a filter when a signal is applied at the input and the relationship between the rise (response) time  $T_R$  and the filter bandwidth  $B$ . This relationship is just an approximation, and the exact form of the response depends upon the design of the filter. For many practical filters, the time it takes for the filter to settle can be about four to six times the rise time  $T_R$ , where  $T_R \approx 1/B$ .

**2.2.3 The Detector** To determine the value of the signal after the filtering, a detector is required to estimate the power of the response signal from each of the filters. This is achieved by squaring

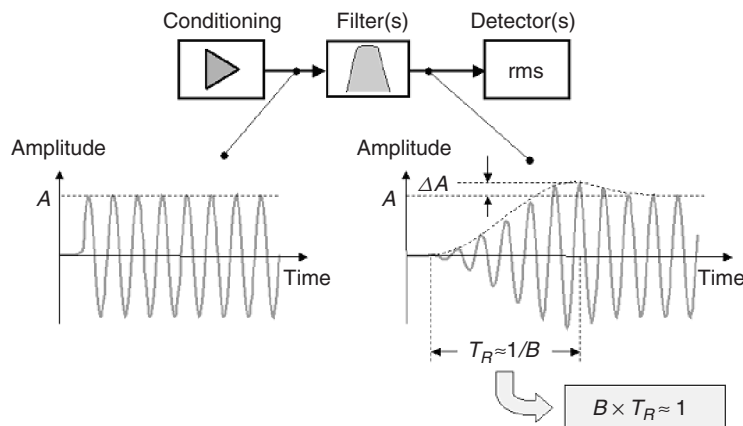


Figure 6 Illustration of the response of a filter and the approximate relationship between the rise time  $T_R$  and filter bandwidth  $B$ .

the response signals (giving instantaneous power) followed by averaging over time giving the mean value of the power or the MS value. Taking the square root of the MS value results in the rms value. Using linear averaging where all the time data within the averaging window are equally weighted, the rms value  $y_{\text{rms}}$  of a signal  $y(t)$  is given by

$$y_{\text{rms}} = \sqrt{\frac{1}{T_A} \int_{T_A} y^2(t) dt} \quad (4)$$

where  $T_A$  is the averaging time.

Another common way to average the signal is by using exponential averaging, where the present data is weighted higher than the previous data. This is illustrated in Fig. 7, which shows the detector, its elements, and the linear and exponential averaging functions (weighting on the squared signal).

The weighting for exponential averaging is given by  $1/\tau e^{t/\tau}$ ,  $t \leq 0$ , where  $\tau$  is the time constant. When analyzing a random signal, exponential averaging with a time constant  $\tau$  gives the same statistical accuracy as linear averaging of  $T_A = 2\tau$  and  $2\tau$  is said to be the equivalent averaging time for exponential averaging. Exponential averaging gives a continuous running average value, whereas linear averaging, in most implementations, is an averaging that stops after the elapsed averaging time.

In acoustics exponential averaging with time constants of 0.125 s (called fast) and 1 s (called slow) are often used. The required averaging time depends upon the type of signal to be analyzed.

For *stationary deterministic signals* averaging over 8 to 10 ripple periods of the squared signal (see Fig. 7)

gives reasonable accuracy. It should be noted that if there is more than one frequency component within the bandwidth, it is the ripple period of the lowest beat frequency that should be considered (the smallest difference in frequency between the components); see Ref. 1.

For *stationary random signals*, the relative standard deviation  $\varepsilon$  of the estimated rms value is given by

$$\varepsilon = \frac{1}{2\sqrt{BT_A}} \quad (5)$$

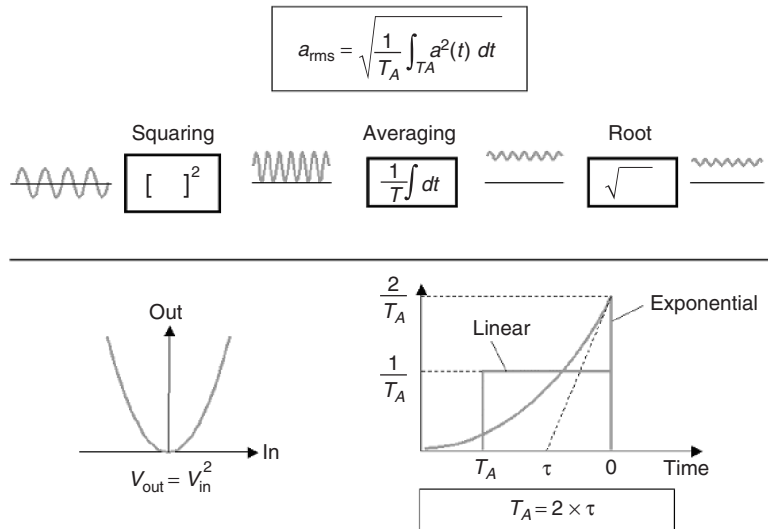
or in decibels

$$L_\varepsilon = \frac{4.34}{\sqrt{BT_A}} \text{ dB} \quad (6)$$

where  $B$  is the analysis bandwidth and  $BT_A$  is assumed  $\gg 1$ .

As an example, if  $BT_A = 100$ , then  $L_\varepsilon = 0.43$  dB, and there is approximately 68% probability of the level being within  $\pm 0.43$  dB around the mean value and approximately 95% probability of the level being within  $\pm 2L_\varepsilon = \pm 0.86$  dB around the mean value.

For a *transient signal*, the linear averaging time must be longer than the duration of the filtered transient, that is, longer than the length of the transient plus the length of the longest impulse response function of the filters. A trigger mechanism must be used as well, unless a running linear average with maximum hold is available. Exponential averaging with a time constant (averaging time) much longer (say at least 10 times) than the length of the filtered transient and with maximum hold can also be used. When the time constant is much longer than the filtered signal, the decay of the exponential weighting can be



**Figure 7** Schematic illustration of the rms detector and linear and exponential averaging (weighting on the squared signal).

neglected. The detected rms value, however, will be 3 dB too high, as the exponential weighting is twice as high as the linear weighting (with the same averaging time) at time  $t = 0$  (see Fig. 7) and this has to be corrected for.

The estimated MS spectrum can be rescaled to PSD (for random signals) by dividing by the analysis noise bandwidth and to ESD (for transient signals) by multiplying the PSD by the averaging time  $T_A$ . The averaged (detected) spectrum of a signal  $x(t)$  is also referred to as the autospectrum and denoted  $G_{XX}(f)$ .

For *nonstationary signals*, the averaging time will be a compromise between the ability to follow the changes in the signal and the accuracy in frequency, that is, a compromise between resolution in time and resolution in frequency. This will be discussed later.

Special detectors are used to measure peak values. This is normally done without any filtering, as the peak value is sensitive to filtering.

**2.2.4 Stepped, Swept, and Parallel Filter Analysis** In a stepped filter analyzer measurement in one filter band at a time is carried out. This is mainly used in analog, compact, low-cost field analyzers or level meters.

Swept filter analysis is performed by scanning a filter through the frequency range of interest. The analysis bandwidth and the averaging time put a limit on how fast the sweep can be performed. Stepped and swept filter analysis require the signal to be stationary, as only one frequency band is analyzed at a time.

Frequency analysis by using a bank of parallel filters and detectors allows for simultaneous analysis of the total signal in all the bands, also referred to as real-time analysis. This method opens the possibility for analysis of nonstationary signals. Most parallel filter analyzer implementations today are digital due to the advances in processing speed and capabilities in digital technology.

### 3 FREQUENCY ANALYSIS USING FFT

#### 3.1 Discrete Fourier Transform, Weighting and Averaging

Frequency analysis using the fast Fourier transform (FFT) is the most commonly used method for constant bandwidth analysis. The FFT is an algorithm for fast calculation of the discrete Fourier transform (DFT). The DFT is a special form of the Fourier transform working on a block (record) of discrete time samples. The assumption is that the record of time samples represents one period of an artificially periodic time signal having a line (discrete) spectrum, as illustrated in Fig. 8.

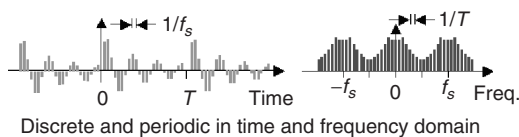


Figure 8 Discrete Fourier transform (DFT).

The time signal is sampled with an interval of  $\Delta t = 1/f_s$ , where  $f_s$  is the sampling frequency, and the record contains  $N$  samples giving a record length of  $T = N\Delta t$ . The resulting Fourier spectrum is conjugate even and has  $N/2 + 1$  (assuming  $N$  is even) complex spectral lines between 0 and  $f_s/2$  with a frequency spacing of  $\Delta f = 1/T$ . Due to the antialiasing filter, not all of the  $N/2 + 1$  frequency lines up to  $f_s/2$  (called the Nyquist frequency) are valid. In many practical implementations, the relation between the valid frequency span  $f_{span}$  and  $f_s$  is  $f_{span} = f_s/2.56$ , which means that a record of  $N$  time samples gives a complex spectrum with  $N/2.56 + 1$  valid lines. Thus, 2048 time samples gives 801 valid complex frequency lines (including a line at 0 Hz); 4096 time samples gives 1601 valid complex frequency lines, and so forth.

The assumption of the signal as being periodic with a period of  $T$  causes no “distortion” in the analysis for sinusoids having an integer number of periods in the record (see Fig. 9a). For other continuous signals not periodic with the record length, the periodic repetition causes distortion at the joints of the periods. This is illustrated in Fig. 9b. The resulting spectrum will be distorted correspondingly. The distortion in the estimated spectrum is also referred to as *leakage* since it appears that power at one frequency leaks out into other frequencies.

To avoid discontinuity at the joints, a smooth weighting function has to be applied on the time record. A very commonly used weighting is the *Hanning weighting*, which is one period of a cosine “lifted” such that it starts and ends at zero amplitude. This is illustrated in Figs. 9c and 9d. When no weighting is used, the weighting is often referred to as *rectangular weighting* or a *uniform weighting*.

For transient signals shorter than the record length, rectangular weighting should be used. For transient

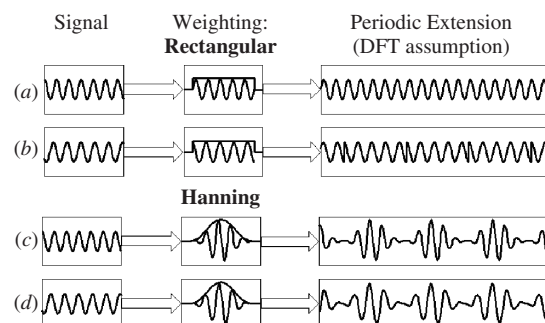


Figure 9 Assumption of periodic repetition in the DFT. An integer number of periods in the record length, (a) and (c). Continuous signal not periodic with the record length, (b) and (d). Rectangular weighting (no weighting) in (a) and (b) and Hanning weighting in (c) and (d). The Hanning weighting minimizes the distortion at the joints for continuous signals that are not periodic with the record length.

signals much shorter than the record length, a rectangular weighting shorter than the record length, with user-defined shift (positioning) and length, can be used. This is often referred to as a *transient weighting* and could in practice include a leading taper and a trailing taper at the edges, making a smooth transition from zero to unity and from unity back to zero inside the record length. The tapers are especially important if the signal contains a dc offset since they will eliminate sharp edges in the weighted signal and thus minimize the distortion in the frequency domain.

The response signal of a lightly damped system when excited by an impact will have a long decay (the system rings for a long time). If the response signal is longer than the record length, an *exponential weighting* can be applied on the signal in order to reduce the effect of the truncation at the end of the record. The exponential weighting is defined by a user-defined shift (perhaps with a leading taper) and a time constant. The extra artificial damping imposed by the exponential weighting can be compensated for subsequently in cases where the measured response signal itself contains exponentially decaying sinusoids (e.g., resonances with viscous damping).

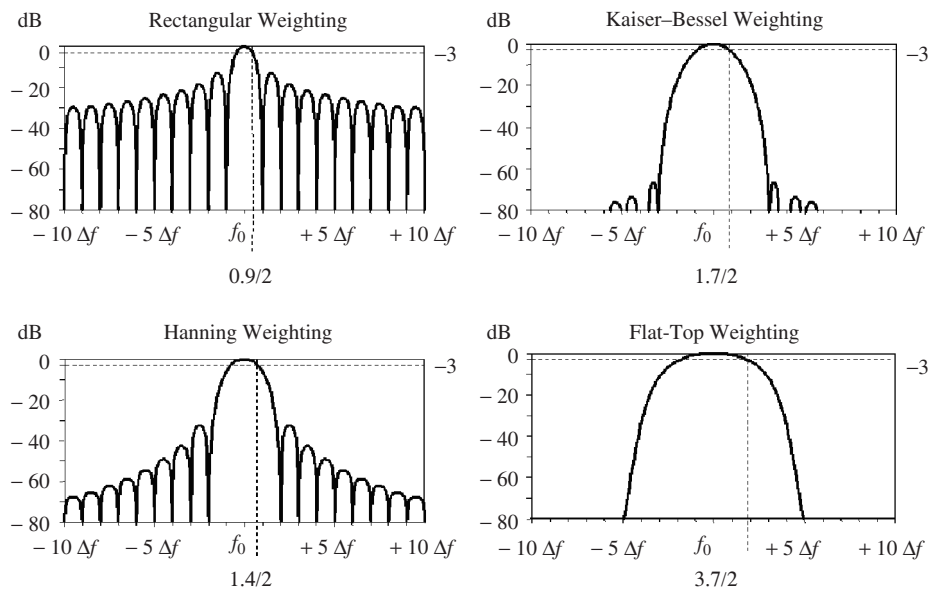
The DFT can also be considered as a filtering process in which each line (frequency) in the spectrum represents the output of a filter centered at that frequency. The weighting function determines the impulse response function of the filter, and the Fourier transform of the weighting function gives the corresponding frequency response function of the filter. Different weighting functions are used in order to optimize the characteristics of the filter. The most common general-purpose weighting function is the

Hanning weighting. This gives a good compromise between bandwidth, ripple in the passband, and selectivity. Of other weighting functions, the *flat-top* and the *Kaiser–Bessel* weighting functions should be mentioned. The flat-top weighting gives a filter with practically no ripple in the passband. It is used in situations in which unbiased estimates of the amplitude of sinusoids is of main interest, such as in the calibration of systems with a sinusoidal input signal. The word *flat* in flat-top refers to the characteristics in the frequency domain. The Kaiser–Bessel weighting is a weighting function that is optimized in terms of selectivity and bandwidth and can be used when closely spaced components with widely different amplitudes have to be separated.<sup>2,3</sup>

Figure 10 shows the characteristics in the frequency domain of the rectangular, Hanning, Kaiser–Bessel, and flat-top weighting functions, as they are defined in Gade and Herlufsen.<sup>2</sup> Considering the DFT as a filtering process the spectra (Fourier transforms) of the weighting functions determine the characteristics such as bandwidth, ripple, and selectivity, defined earlier.

Table 2 lists some of the most important filter characteristics for the rectangular, Hanning, flat-top, and Kaiser–Bessel weighting functions as defined in Gade and Herlufsen.<sup>2</sup> There exist different implementations of the Kaiser–Bessel and the flat-top weighting and the parameters might vary between different implementations. The parameters should therefore only be taken as guidelines for these weighting functions.

The autospectrum,  $S_{AA}(f)$ , of the signal  $a(t)$  is estimated by averaging the squared magnitude of the individual estimates of the complex spectra  $A_i(f)$  from each record, which for linear averaging



**Figure 10** Rectangular, Hanning, Kaiser–Bessel, and flat-top weighting functions, as they are defined in Ref. 2, in the frequency domain giving the frequency response functions of the filters.

**Table 2** Parameters Describing the Filter Characteristics of the Different Weighting Functions as Defined in Ref. 2.<sup>a</sup>

Weighting	Rectangular	Hanning	Kaiser-Bessel	Flat Top
Noise bandwidth	$1.0\Delta f$	$1.5\Delta f$	$1.8\Delta f$	$3.8\Delta f$
3-dB bandwidth	$0.9\Delta f$	$1.4\Delta f$	$1.7\Delta f$	$3.7\Delta f$
Ripple	3.9 dB	1.4 dB	1.0 dB	0.01 dB
Highest side lobe	-13 dB	-31 dB	-68 dB	-93 dB
Side-lobe slope per decade	20 dB	60 dB	20 dB	0 dB
60-dB bandwidth	$665\Delta f$	$13.3\Delta f$	$6.1\Delta f$	$9.1\Delta f$

<sup>a</sup> There exist different implementations of the Kaiser-Bessel and the flat-top weighting and the parameters might vary between different implementations, and they should therefore only be taken as guidelines for these weighting functions.

is

$$S_{AA}(f) = \frac{1}{N} \sum_{i=1}^N A_i^*(f) A_i(f) \quad (7)$$

where  $A_i^*(f)$  is the complex conjugate of  $A_i(f)$ , that is,  $A_i(f)$  with the phase inverted and  $N$  is the number of averages.  $A_i(f)$  and  $S_{AA}(f)$  have content at both positive and negative frequencies (see Fig. 8). The version of the autospectrum that only has content at nonnegative frequencies, that is, where the content at the negative frequencies is “transferred” to the corresponding positive frequencies, is called  $G_{AA}(f)$ ; see Refs. 4 to 6.

The  $BT_A$  product used for estimating the relative standard deviation of the estimated rms level in each frequency band, for stationary random signals [see Eqs. (5) and (6)] equals the number of averages of statistically independent records.

### 3.2 Overlap

Fast Fourier transform works on blocks of data. If the calculation time for a transform is shorter than the record length, it is possible to have overlap between the records (in “real-time” processing).

Applications of overlap analysis:

1. When analyzing random signals, a higher statistical accuracy for a given measurement time can be achieved. The  $BT_A$  product used for estimating the relative standard deviation of the estimated rms level depends upon the weighting and the overlap and is given by

$$BT_A = NBT_{\text{eff}} \quad (8)$$

where  $BT_{\text{eff}}$  is the effective  $BT$  product per record for the given weighting and overlap used and  $N$  is number of averages. Various  $BT_{\text{eff}}$  values<sup>2</sup> are given in Table 3. The numbers for the Kaiser-Bessel and the flat-top weighting might vary between different implementations.

From Table 3 it is seen that records with 50% overlap and Hanning weighting are almost statistically independent. This means that the same statistical

**Table 3**  $BT_{\text{eff}}$  for Different Weighting Functions and Different Overlap<sup>a</sup>

$BT_{\text{eff}}$ per Record	0% Overlap	50% Overlap	75% Overlap
Rectangular	1	0.660	0.363
Hanning	1	0.947	0.520
Kaiser-Bessel	1	0.989	0.628
Flat top	1	1.000	0.995

<sup>a</sup> The numbers for the Kaiser-Bessel and the flat-top weighting may vary between different implementations

accuracy can be obtained almost twice as fast using 50% overlap compared to 0% overlap.

2. Averaging using Hanning weighting with  $66\frac{2}{3}\%$  ( $\frac{2}{3}$ ), 75% ( $\frac{3}{4}$ ), 80% ( $\frac{4}{5}$ ) and so on overlap results in an overall weighting on the signal, which is flat (all samples are weighted equally). (See Ref. 2.)
3. In analysis of nonstationary signals, overlap facilitates the following of signal changes within the records.
4. When analyzing with low-frequency spans or with high resolution (zoom), where the records are relatively long, a faster display update rate can be achieved by using overlap.

### 3.3 Real-Time Analysis

In connection with FFT, real-time analysis is historically defined as the analysis of adjacent records, that is, with 0% overlap. This can be obtained when the calculation time equals the record length. The real-time frequency specifications of analyzers can thus be interpreted as a specification of the FFT processing speed.

From a more strict signal processing point of view, real-time analysis demands analysis of all the data all the time in all the frequency bands. When averaging using Hanning and  $66\frac{2}{3}\%$  overlap, all the samples are weighted equally, implying real-time analysis in the more strict sense.

#### 4 MULTICHANNEL APPLICATIONS

A number of important applications within signal and system analysis require the simultaneous measurement of multiple signals.

##### 4.1 System Analysis

System analysis is often based upon simultaneous measurements of the input(s) and the output(s) of the system. The single input–single output situation is illustrated in Fig. 11; See Refs. 4–6.

If the spectrum (Fourier transform) of the input signal is  $U(f)$ , the spectrum of the output is  $V(f)$ , and the frequency response function of the system is  $H(f)$ , then  $V(f) = H(f)U(f)$ . The measurement noise  $M(f)$  at the input is assumed to be uncorrelated with the input  $U(f)$ . Likewise,  $N(f)$  is the measurement noise at the output and is assumed to be uncorrelated with the output  $V(f)$ . The measured input is  $A(f) = U(f) + M(f)$ , and the measured output is  $B(f) = V(f) + N(f)$ . Notice that the noise at output  $N(f)$  could be due to other inputs not correlated with  $U(f)$ .

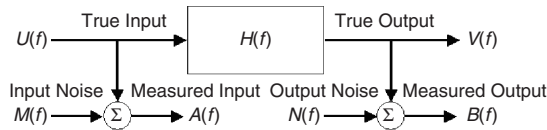
**4.1.1 Cross Spectrum** Together with the autospectra, the principal function for derivation of the system characteristics and quantification of the validity of the measurement is the *cross spectrum* between input and output.

Using FFT and linear averaging, the cross spectrum is estimated by

$$S_{AB}(f) = \frac{1}{N} \sum_{i=1}^N A_i^*(f) B_i(f) \quad (9)$$

where  $A_i(f)$  and  $B_i(f)$  are the complex spectra of the  $i$ th record,  $A_i^*(f)$  is the complex conjugate of  $A_i(f)$ , that is,  $A_i^*(f)$  with the phase inverted, and  $N$  is number of averages.

$A_i(f)$ ,  $B_i(f)$ , and  $S_{AB}(f)$  have content at both positive and negative frequencies (see Fig. 8). The version of the cross spectrum that only has content at nonnegative frequencies, that is, where the content



**Figure 11** System with a single input and single output.

at the negative frequencies is “transferred” to the corresponding positive frequencies, is called  $G_{AB}(f)$ ; see Refs. 4 to 6.

The averaging is performed on complex numbers, and the influence of the noise terms  $N(f)$  and  $M(f)$  will be reduced with averaging since they are uncorrelated with  $U(f)$  and  $V(f)$ . (This is because the phase between the noise signals and the input/output signals changes randomly from record to record.) Thus,  $G_{AB}(f) \rightarrow G_{UV}(f)$  as  $N \rightarrow \infty$ . This is the essence of cross-spectrum averaging. The correlated parts of the signals,  $U(f)$  and  $V(f)$ , are retained and the uncorrelated noise terms are reduced with averaging.

The phase of  $G_{UV}(f)$  is the phase of the system, that is, the phase of the frequency response function  $H(f)$ . The autospectrum can be considered as the cross spectrum of the signal with itself.

**4.1.2 Frequency Response Function** The frequency response function can be derived from the measured autospectra,  $G_{AA}(f)$  and  $G_{BB}(f)$ , and the cross spectrum  $G_{AB}(f)$ . Different estimators, such as  $H_1(f)$ ,  $H_2(f)$ , and  $H_3(f)$ , are used depending upon the measurement situation and the content of noise. Table 4 lists the estimators and their use in situations with noise at input, noise at output, and with the same amount of noise at both input and output. If there is noise only at the output,  $H_1(f)$  gives an unbiased estimate, and if there is noise only at the input,  $H_2(f)$  gives an unbiased estimate. The more uncorrelated noise there is in the signals, the more averaging is required in order to minimize the random error. Figures for the random errors are found in Ref. 4.

In situations where the measurement bandwidth is too wide compared to the width of the resonance peaks in the frequency response function, the estimators will also be biased, and the error is called *resolution bias error*. It turns out that  $H_2$  is less vulnerable to resolution bias errors at resonance peaks. Resolution bias is also referred to as *leakage*.

In the case of slightly nonlinear behavior, the  $H_1$  estimator gives the best linear approximation of the frequency response function for the given input (excitation) signal.

**4.1.3 Coherence** The coherence function  $\gamma^2(f)$  measures, on a scale from 0 to 1, the degree of linear relationship between the input and the output signals. The coherence is defined as

$$\gamma^2(f) = \frac{|G_{AB}(f)|^2}{G_{AA}(f)G_{BB}(f)} \quad (10)$$

**Table 4** Use of Frequency Response Function Estimators in Situations with Only Noise at Input, Only Noise at Output, and with Same Amount of Noise at Both Input and Output

Measurement Situation	$H_1 = \frac{G_{AB}}{G_{AA}}$	$H_2 = \frac{G_{BB}}{G_{BA}}$	$H_3 = \frac{G_{AB}}{ G_{AB} } \sqrt{\frac{G_{BB}}{G_{AA}}}$
Noise at input, $M(f)$		Unbiased	
Noise at output, $N(f)$	Unbiased		
Noise at input and output and $G_{MM} = G_{NN}$			Unbiased

A coherence of less than 1 can be due to one or more of the following situations:

1. Uncorrelated noise in the input and/or in the output signal
2. Insufficient resolution (resolution bias error or leakage)
3. Nonlinear behavior of the system (if the input signal is random)
4. Delay in the system not compensated for in the analysis
5. Time-varying system

The coherence gives an indication of the validity and the quality of the frequency response function measurement. The reason for a low coherence often has to be investigated further. Low coherence does not necessarily mean a bad measurement. The influence of noise at the input or at the output, for example, can be eliminated by using a sufficient number of averages. Low coherence due to insufficient resolution or due to delays not compensated for is an example of poor-quality measurements (bad measurements).

**4.1.4 Coherent Power, Noncoherent Power, and Signal-to-Noise Ratio** These functions are used in situations where the low coherence is due to noise at the output.

$$\text{Coherent power} = \gamma^2(f)G_{BB}(f)$$

is a measure of the output  $G_{VV}(f)$  of the system coherent with the input since there is no noise at the input [ $M(f) = 0$ ]. The

$$\text{Noncoherent power} = [1 - \gamma^2(f)]G_{BB}(f)$$

is a measure of the noise at the output  $G_{NN}(f)$ . The

$$\text{Signal-to-noise ratio} = \gamma^2(f)/[1 - \gamma^2(f)]$$

is a measure of  $G_{VV}(f)/G_{NN}(f)$ , that is, the signal-to-noise ratio at the output.

**4.1.5 Impulse Response Function** The impulse response function is calculated by taking the inverse Fourier transform of the frequency response function.  $H_1(f)$ ,  $H_2(f)$ , and  $H_3(f)$  give the estimates  $h_1(t)$ ,  $h_2(t)$ , and  $h_3(t)$ , respectively.

Other functions derived from the cross spectrum include

- Cross correlation
- Active intensity
- Phase-assigned spectrum

The phase-assigned spectrum of a signal is the autospectrum of the signal, with the phase of the cross spectrum between a reference signal and the signal

measured. It is, for example, used when determining the operating deflection shapes of vibrating structures.

## 5 ANALYSIS OF NONSTATIONARY SIGNALS

In the analysis of nonstationary signals, the resolution in both the time and the frequency domain is of importance. The resolution in the time domain should be fine enough to be able to follow the changes in the signal, and the resolution in the frequency domain should be sufficiently high to separate the different components in the spectrum.

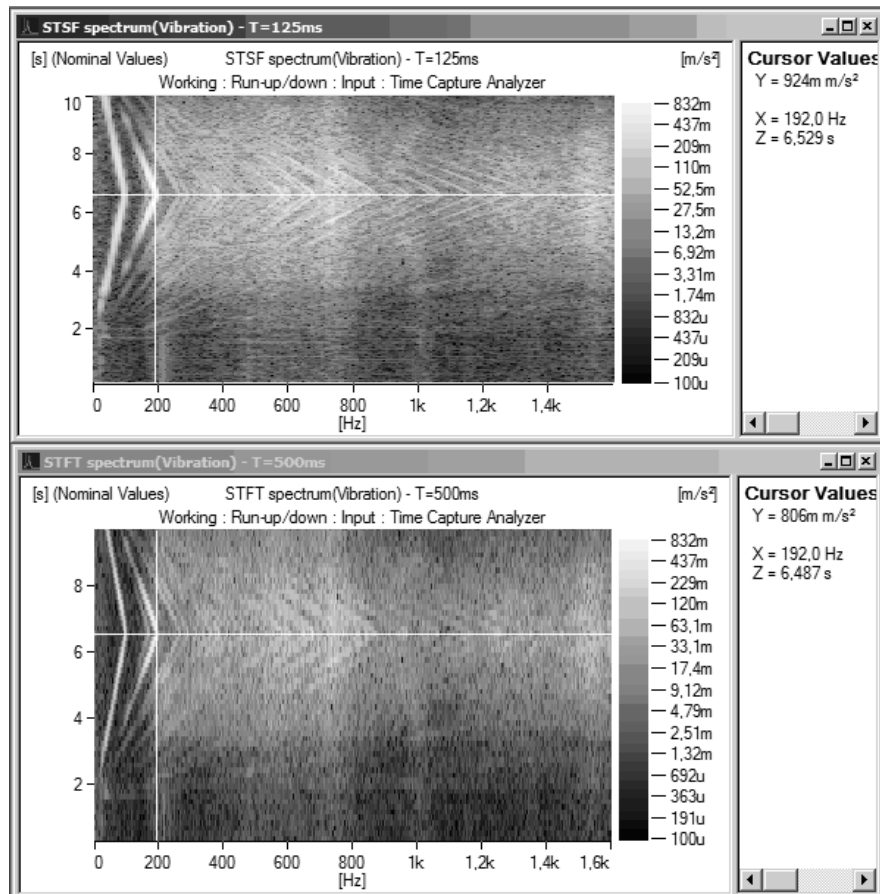
*Analysis using FFT* provides a constant bandwidth analysis in which the time and frequency resolution is governed by the relation  $T\Delta f = 1$ , where  $T$  is the record length and  $\Delta f$  the spacing between the frequency lines. When a weighting function, such as the Hanning weighting, is applied on the time signal, the effective length of the analyzed time signal is shortened and the (noise) bandwidth in the analysis correspondingly widened, that is,  $T_{\text{eff}}B \approx 1$  for each individual FFT (without averaging). The time resolution, given by  $T$ , or  $T_{\text{eff}}$ , is the same at all frequencies.

The individual FFT spectra, calculated with a certain overlap, can be stored in a multibuffer and displayed as a waterfall or contour plot. This is also referred to as short time Fourier transform (STFT). In Fig. 12, two analyses of a fast runup/down are shown. In the upper contour plot the record length  $T = 125$  ms, that is,  $\Delta f = 1/T = 8$  Hz, and in the lower contour plot the record length  $T = 500$  ms, that is,  $\Delta f = 2$  Hz. Hanning weighting and 66  $\frac{2}{3}$ % overlap is used. The rate of change of the fundamental frequency is approximately 18 Hz/s (1080 rpm/s; rpm = revolutions/minute). The record length of only 125 ms is short enough to follow the changes of the higher harmonics, and the different harmonic components (up to at least the 14th harmonic) are clearly detected, as seen in the upper plot. A record length of 500 ms, giving a higher frequency resolution ( $\Delta f = 2$  Hz), allows for a better detection of the lower harmonics and interharmonics (where the rate of change in frequency is lower), whereas the higher harmonics are more smeared.

Another very useful technique for analysis of nonstationary signals consisting of sinusoidal components with varying frequencies and amplitudes is the order tracking technique, which is discussed in Section 6.

*Wavelet analysis* is another analysis technique used for nonstationary signals. This provides constant percentage bandwidth analysis, with resolution in the time domain governed by the wavelet applied in the analysis.<sup>7</sup> The resolution in time increases with frequency corresponding to the increasing bandwidth. This is advantageous for signals having more rapid changes at the higher frequencies, as compared to the changes at the lower frequencies. Examples could be transient type response signals from systems with resonances having constant percentage damping. The more narrow resonances at low frequencies give longer responses to transient (impact) excitations than the





**Figure 12** Analysis using FFT (STFT) of a fast run-up/down. In the upper contour plot the record length  $T = 125$  ms, i.e.,  $\Delta f = 8$  Hz. In the lower contour plot the record length  $T = 500$  ms, i.e.,  $\Delta f = 2$  Hz.

wider resonances at higher frequencies. Location of transient events in the time domain could thus be improved at the higher frequencies. This technique is covered in Chapter 49 of this book and thus is not further discussed here.

Standardized *octave and fractional-octave filters* are mainly used within the acoustical applications of nonstationary signal analysis. The classical examples are reverberation time measurements, passby analysis, and flyover analysis. The resolution in the time domain is given by the effective duration of the impulse response function of the filter and the averaging time in the detector.

Standardized octave and fractional-octave filters have characteristics that are optimized in the frequency domain (magnitude of frequency response function), and the effective duration of the impulse response of the filters can be several times  $1/B$ , where  $B$  is the bandwidth of the filter. This puts a limit on how far down in frequency it is possible to follow changes in a nonstationary signal, since the filter bandwidth decreases with decreasing center frequency.

The detector is, in most cases, for nonstationary signal analysis set to (running) exponential averaging with a time constant  $\tau$  (corresponding to an equivalent averaging time of  $2\tau$ ) for all the filters. The averaging time puts a limit on how fast changes can be followed in all the filter bands. The compromise is that the averaging time should be short enough to follow the changes in the signal and long enough to give sufficient statistical accuracy.

Taking reverberation time as an example, the detector time constant  $\tau$  sets a limit on how short reverberation times can be measured. The minimum time constant of the system to be measured [i.e., the time it takes for the signal to decay a factor of  $e$  (or 8.7 dB)] is often set to  $4\tau$ , which means that the minimum reverberation time  $T_{60}$  is  $6.9 \times 4\tau = 27.6\tau$  ( $T_{60}$  is 6.9 times the time constant of the system, since 60 dB/8.7 dB = 6.9).

The exponential detector responds faster to an increasing signal than to a decreasing signal. Analysis of the time-reversed decaying signal has the advantage of lowering the minimum time constant of the system



to be measured to  $0.5\tau$ , or the minimum reverberation time  $T_{60}$  to  $6.9 \times 0.5\tau = 3.45\tau$ . This is discussed in Refs. 8–10.

## 6 ANALYSIS TECHNIQUES USED FOR SIGNALS FROM ROTATING MACHINERY

### 6.1 Order Tracking

Noise and vibration signals from rotating machinery with varying speeds contain sinusoidal components with varying frequencies and amplitudes. The rotating parts in the machinery give rise to components at the fundamental rotating frequency and its harmonics and, in some systems, also at its subharmonics and interharmonics. The harmonics are referred to as the harmonic orders or simply the orders. Order tracking is an analysis technique specially designed to extract the information about the harmonic components of signals.

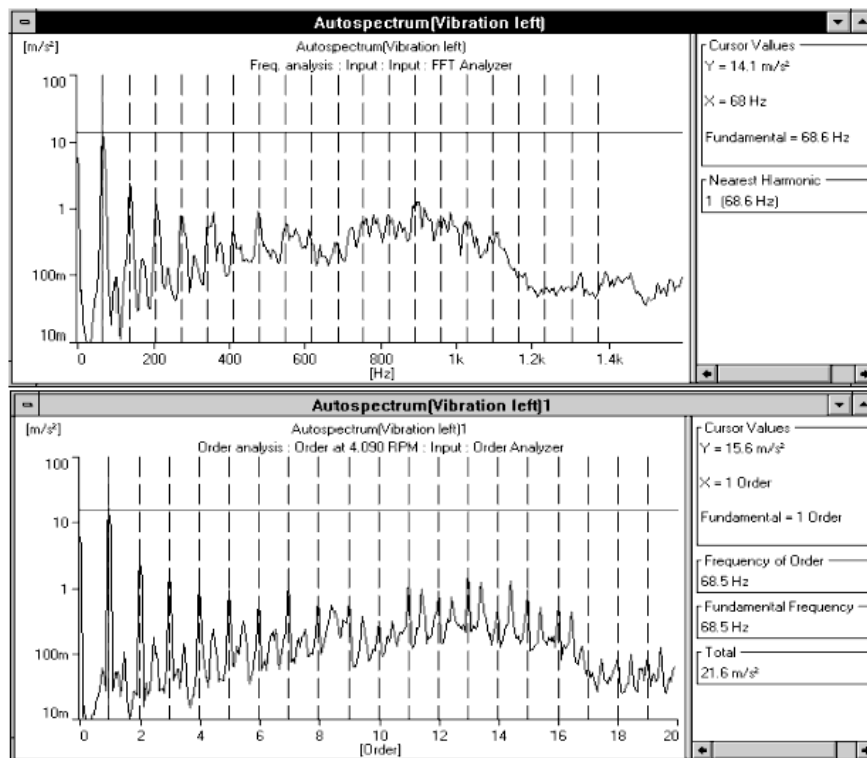
The instantaneous fundamental rotational frequency is typically measured by means of a tacho signal, and this is used to acquire signal values (samples) at times corresponding to *uniform shaft angle intervals* instead of at constant time intervals. Thus, there will be a fixed number of samples per shaft revolution independent of the rotational speed of the shaft, and an FFT will provide an *order spectrum* instead of a frequency spectrum. The orders will remain at fixed

positions in the order spectrum, independent of the rotational speed.<sup>11,12</sup>

An order tracking analysis is, in the spectral domain, specified in terms of an order span  $\text{Ord}_{\text{span}}$  and number of lines  $N_{\text{span}}$ , resulting in an order spacing between the spectral lines of  $\Delta\text{Ord} = \text{Ord}_{\text{span}}/N_{\text{span}}$ . The corresponding record length,  $T_{\text{rev}}$ , in number of revolutions, is given by the order spacing as  $T_{\text{rev}} = 1/\Delta\text{Ord}$ . This is similar to the way the record length,  $T$ , is given by the frequency line spacing,  $\Delta f$ , as  $T = 1/\Delta f$  for an ordinary FFT-based frequency analysis. An analyzer performing order tracking is often referred to as an order analyzer.

Figure 13 shows a frequency spectrum and an order spectrum measured on an electrical motor. The variation of the speed of the motor causes the frequency components to be smeared in the frequency spectrum (Fig. 13, top), and harmonic orders cannot be detected above 800 Hz. The order spectrum (Fig. 13, bottom) clearly reveals content in the harmonic orders and interharmonics up to order 20.

Order tracking is also used in the analysis of run-ups or run-downs (coast-downs) of machinery. Spectra are stored at predefined speed intervals, and the contour or waterfall plots of the spectra versus rotational speed give an overview of the content of harmonic orders and excitation of resonances during



**Figure 13** Measurements of frequency spectrum (*top*) and order spectrum (*bottom*) of the vibration from an electrical motor.

the run-up or run-down. Figure 14 shows the analysis of the vibration signal from an electrical motor during a run-up. Frequency and order tracking analysis is performed on the signal. The contour plots of the frequency spectra and the order spectra versus rotational speed are shown in the upper and the lower graph of Fig. 14, respectively.

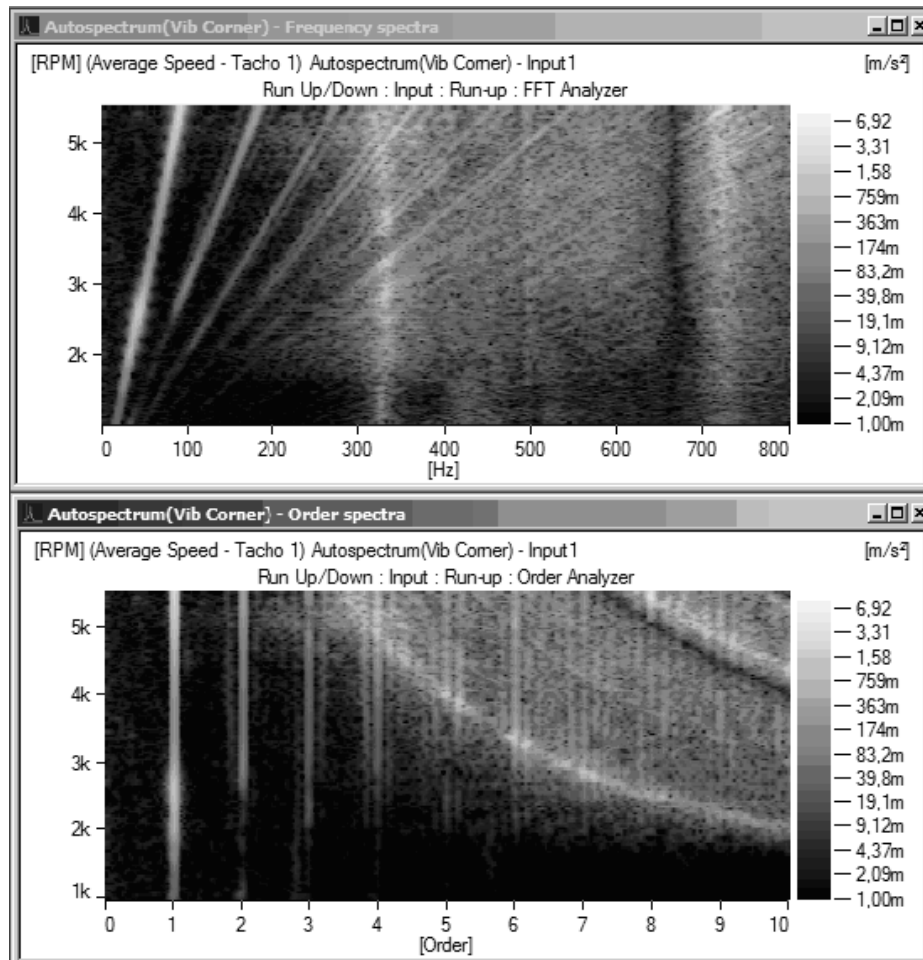
In the contour plot of the frequency spectra, the harmonic orders appear as oblique lines, while resonances (fixed frequencies) appear as vertical lines parallel to the rpm axis. In the plot of the order spectra, the orders appear parallel to the rpm axis, and resonances appear as hyperbolic curves.

In the frequency analysis, the time and the frequency resolution is constant during the run-up. In the above example, the record length of the FFT is  $T = 250$  ms, corresponding to a spacing between the frequency lines of  $\Delta f = 4$  Hz. In the order-tracking analysis each order spectrum is, in the above example,

based upon a record length of  $T_{\text{rev}} = 20$  revolutions, corresponding to a spacing between the order lines of  $\Delta \text{Ord} = 0.05$  orders. Thus, the records, measured in seconds, get shorter, and the bandwidths in the order spectra, measured in hertz, get wider, as the rpm increases. At each rpm (i.e., for each spectrum), the rms value of any order can be extracted and its variation as a function of rpm can be shown.

## 6.2 Signal Enhancement – Synchronous Time-Domain Averaging

This technique is used for extracting harmonic orders or periodic events buried in uncorrelated noise signals. It is used in connection with analysis using FFT and can be combined with order tracking. A synchronous trigger controls the recording of the time signals, and the averaging is performed in the time domain, resulting in an enhanced (averaged) time signal. The content



**Figure 14** Contour plots of frequency spectra (*upper graph*) and order spectra (*lower graph*) as a function of rotational speed of the vibration signal from an electrical motor during a run-up.

of the uncorrelated noise is reduced through averaging, whereas periodic events or orders harmonically related to the synchronous trigger are retained. If the speed of the machinery varies, order tracking should be used to have the time records based upon shaft revolutions (shaft angle). As this technique is covered in Chapter 46, it is not discussed further here.

### 6.3 Other Analysis Techniques

There exist a wide variety of other analysis techniques. Discussion of these is out of the scope of this chapter. Two of them are mentioned below.

*Cepstrum* For detection of periodicities in spectra. A harmonic or a sideband family, for example, appear as a periodicity in the spectrum.

*Envelope analysis* For detection of periodic impacts, for example, due to faults in roller element bearings.

## 7 SIGNAL GENERATION AND EXCITATION TECHNIQUES

In system analysis (Fig. 11), an externally generated signal is often used for provision of a proper excitation of the system either through a shaker or a loudspeaker. The signal should be adapted to the analysis. A signal generator, therefore, is often built into the analyzer. This facilitates setting up of the generator to correspond to the analysis parameters (or vice versa) and also facilitates possible synchronization between the two.

A wide variety of signals can be used. Choice of the signal depends upon many factors, such as available test time, required accuracy, application, dynamic behavior of the system, and content of uncorrelated noise in the measured input and output signals. (See Table 5.)

Description of the system characteristics in terms of the frequency response function and the impulse response function is based upon the assumption of linear behavior of the system. For an ideal linear system, any type of excitation signal can be used, as long as there is energy at all the frequencies of interest in the signal. Systems encountered in real life exhibit a certain degree of nonlinear behavior, and the choice of an excitation signal and its amplitude can influence the result.

In this chapter, only a brief introduction of the most commonly used signals followed by a tabular

overview of some of the main features is given. More information is found in the references, including Refs. 5, 13, and 14.

**Random** Continuous random signal, which can be band limited to fit the frequency range of the analysis. The amplitude and phase at each frequency varies randomly from record to record in the analysis using FFT, and the  $H_1$  estimator provides a best linear fit of the frequency response function in case of slightly nonlinear systems (see Refs. 4 and 5). White noise is most often used in connection with analysis using FFT.

In some acoustical applications where the analysis is performed using constant percentage bandwidth filters (fractional-octave filters), pink noise is often used. Pink noise has a power spectral density, which decreases proportionally with frequency (3 dB/octave), while the power in each of the filter bands is the same.

**Pseudorandom** Periodic repetition of a part of a random signal. As the period length is chosen to be equal to the record length in the FFT analysis, the signal has power only at frequencies coinciding with the frequency lines in the analysis. Rectangular weighting should be used and leakage is avoided in the analysis.

**Burst Random** Random signal gated with a user-definable gate width and repetition interval. With a gate (burst) sufficiently short to ensure the excitation and the response signals to be damped out at the end of the FFT record, rectangular weighting can be applied and leakage avoided in the analysis. A best linear fit of the frequency response function in case of a slightly nonlinear system can be obtained as for the random signal.

**Sine** Excitation at one frequency at a time. The amplitude can be controlled at different levels of excitation, facilitating analysis of the nonlinear behavior of systems. As the frequency is stepped or swept through the frequency range of interest, the test time usually becomes much longer than that for broadband signals.

**Fast Sine Sweep** A fast frequency sweep through a user-definable frequency range. By proper setting of the sweep rate the excitation and the response signals can be fitted into the record length of the FFT and leakage avoided in the analysis.

**Table 5 Overview of Some Main Features of Most Commonly Used Signals**

	Random	Pseudorandom	Burst Random	Sine	Fast Sine Sweep	Impulse
Control of frequency bandwidth	Yes	Yes	Yes	-	Yes	Limited
Leakage in analysis	Yes	Can be avoided	Can be avoided	Can be avoided	Can be avoided	Can be avoided
Best linear fit of slightly nonlinear systems	Yes	No	Yes	No	No	No
Crest factor	High	High	High	Low	Low	Very high
Signal-to-noise ratio	Fair	Good	Fair	Very good	Good	Poor
Test time	Short	Very short	Short	Long	Very short	Very short

**Impulse** A short-duration signal with a user-definable shape and length (and possibly repetition rate). The shape and the length of the pulse define the spectral content. The use of transient weighting on the response signal allows separation of the direct signal from the reflected signal in acoustical and electroacoustic systems.

## REFERENCES

1. R. B. Randall, *Frequency Analysis*, 3rd ed., Brüel & Kjær, Naerum, Denmark, 1987.
2. S. Gade and H. Herlufsen: Windows to FFT Analysis, *Brüel & Kjær Tech. Rev.*, No. 3 and No. 4, 1987.
3. F. J. Harris, On the Use of Windows for Harmonic Analysis with the Discrete Fourier Transform, *Proc. IEEE*, Vol. 66, No. 1, January 1978, pp. 51–83.
4. J. S. Bendat and A. G. Piersol, *Engineering Applications of Correlation and Spectral Analysis*, Wiley-Interscience, New York, 1980.
5. H. Herlufsen, Dual Channel FFT Analysis, *Brüel & Kjær Tech. Rev.*, No. 1 and No. 2, 1984.
6. J. S. Bendat and A. G. Piersol, *Random Data Analysis and Measurement Procedures*, Wiley, New York, 1986.
7. S. Gade and K. Gram-Hansen, Non-stationary Signal Analysis Using Wavelet Transform, Short-Time Fourier Transform and Wigner-Ville Distribution, *Brüel & Kjær Tech. Rev.*, No. 2, 1996.
8. F. Jacobsen, A Note on Acoustical Decay Measurements, *J. Sound Vib.*, Vol. 115, No. 1, 1987, pp. 163–170.
9. F. Jacobsen and J. H. Rindel, Letters to the Editor: Time Reversed Decay Measurements, *J. Sound Vib.*, Vol. 117 No. 1, 1987, pp. 187–190.
10. S. Gade and H. Herlufsen, Digital Filter Techniques vs. FFT Techniques for Damping Measurements, *Brüel & Kjær Tech. Rev.*, No. 1, 1994.
11. S. Gade, H. Herlufsen, H. Konstantin-Hansen, and N. J. Wismer, Order Tracking Analysis, *Brüel & Kjær Tech. Rev.*, No. 2, 1995.
12. R. Potter and M. Gribler, Computed Order Tracking Obsoletes Older Methods, SAE Noise and Vibration Conference, May 16–18, 1989, pp. 63–67.
13. D. J. Ewins, *Modal Testing: Theory, Practice and Applications*, 2nd ed., Research Studies Press, Baldock, UK, 2000.
14. D. Brown, G. Carbon, and K. Ramsey, Survey of Excitation Techniques Applicable to the Testing of Automotive Structures, Society of Automotive Engineers, Detroit, Feb.–March, 1977.

## BIBLIOGRAPHY

- E. O. Brigham, *The Fast Fourier Transform*, Prentice Hall Englewood Cliffs, NJ, 1974.
- K. Godfrey, *Perturbation Signals for System Identification*, Prentice Hall, Englewood Cliffs, NJ, 1993.
- S. M. Kay, *Modern Spectral Estimation: Theory and Applications*, Prentice Hall, Englewood Cliffs, NJ, 1986.
- L. D. Mitchell, Improved Methods for the FFT Calculation of the Frequency Response Function, *J. Mech. Des.*, April 1982, Vol. 104.
- A. V. Oppenheim and R. W. Schaffer, *Digital Signal Processing*, Prentice-Hall, Englewood Cliffs, NJ, 1975.
- P. D. Welch, The Use of Fast Fourier Transform for the Estimation of Power Spectra: A Method Based on Time Averaging over Short, Modified Periodograms, *IEEE Trans. Audio Electro. Acoust.*, Vol. II AU-15, June 1967, pp. 70–73.

# CHAPTER 41

## EQUIPMENT FOR DATA ACQUISITION

**Zhuang Li**  
Spectra Quest Inc.  
Richmond, Virginia

**Malcolm J. Crocker**  
Department of Mechanical Engineering  
Auburn University  
Auburn, Alabama

### 1 INTRODUCTION

Data acquisition is concerned with the gathering of information from measurement sources such as sensors and transducers, which are used to convert the physical variables of interest into electrical signals. For noise and vibration applications, data acquisition plays an important role in both real-time monitoring and control and post process and analysis. The data acquisition must be performed correctly on sound and vibration signals in order to obtain correct results. A variety of interfaces and bus technologies, through which data streams pass, are used to save the data on storage media. Because of rapidly changing technologies, network-based data acquisition systems are increasingly coming into use. Descriptions of general computer-based data acquisition systems for sound recording technologies are readily available.

### 2 GENERAL CONSIDERATIONS OF DATA ACQUISITION EQUIPMENT

Traditionally, instruments, for example, oscilloscopes and digital multimeters, have been designed to perform particular functions. So they have limited capabilities and flexibilities. Users are seldom able to adjust or customize instruments. With the development of computer technologies, traditional instruments are becoming replaced by computer-based instruments because of the processing, interfacing, and networking power of computers. Moreover, decreasing prices of computers as well as peripherals, such as memory and hard drives, are also helping make computers a central part of testing and control. For data acquisition, since computers have hard drives of huge data storage capabilities, computers have advantages over traditional data logging equipment. Figure 1 illustrates the basic components of computer-based measurement and control systems.

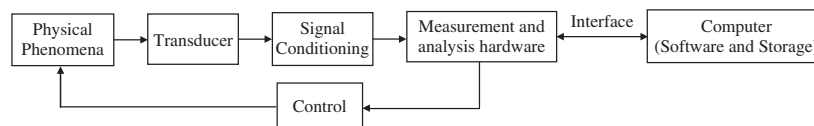
Transducers, for example, microphones, force transducers, accelerometers, and proximity probes, convert sound pressure, force, acceleration, and

displacement measurements into electrical signals. Sensor outputs must often be conditioned to provide signals suitable for the measurement devices. Signal conditioning generally includes power supply, signal amplification, filtering, and/or isolation. The reader is referred to Chapters 35 and 43 for further discussion on signal conditioning. Since most sound and vibration signals are in analog form, the measurement devices then digitize the signals based on the requirements of particular applications. For some real-time analyzers and portable instruments, analyses, such as the fast Fourier transform (FFT), are also performed by hardware because the processing speed of hardware is generally greater than that of software. However, developments in software technology and the processing speeds of CPUs (central processing units) have made software fast enough in many applications.

Measurement software is the interface between users and the measurement hardware. Users can develop their own programs to design instruments. Measurement software generally contains three elementary components: configuration utilities, application programming interfaces (API), and driver engines. Software is also used to manage the data stream to the storage media and may be used to integrate the measurement system into a network.

The basic aim of data acquisition is to obtain signals correctly and reduce noise as much as possible. The selection of appropriate measurement hardware is based on a proper understanding of the signal properties and system requirements.

For computer-based data acquisition, the analog signal needs to be converted to digital. The signal is not only sampled discretely in time but quantized as well with discrete amplitude values. Because of sampling, the digital system is limited in frequency, which may cause some problems, such as aliasing. Quantization noise is another disadvantage of the digital system because the analog amplitudes have to be represented and stored as finite binary numbers in a



**Figure 1** Basic components of computer-based measurement systems.

computer. So the sampling rate and resolution are two basic considerations of the analog-to-digital converter (ADC). To ensure correct data acquisition, one has to scrutinize the specifications of the measurement device, select an appropriate one and operate it carefully. The reader can refer to Ref. 1 for the related practical considerations in signal processing.

### 2.1 Sampling Rate

The well-known sampling theorem is usually stated as "the sampling rate must be at least twice the highest frequency." This statement is correct for baseband spectral analysis in which the bandwidth is from 0 Hz to the highest frequency limit. For better representation and reproduction of analog signals, a higher sampling rate, generally from three to five times the highest frequency, is recommended.

In more general cases, for example, zoom FFT, the bandwidth does not start from 0 Hz and can be narrow but in the high-frequency range. Then the statement in the last paragraph is not valid. A correct sampling rate should be defined based on the bandwidth rather than the highest frequency.<sup>2</sup> A sampling rate of 2.56 times the bandwidth is commonly used for zoom analysis.

### 2.2 Resolution

Resolution is the smallest amount of input signal change that an ADC can detect. Resolution can be represented by the number of bits of the ADC. After quantization, the analog values are rounded to finite possibilities determined by the resolution. These values are evenly distributed across the input range of the ADC. Obviously, the greater the number of bits used, the more accurate is the measurement. The signal-to-quantization noise ratio (SQNR) and the dynamic range also increase with the number of bits of the ADC.

There are two conventional analog-to-digital conversion methods: flash conversion and successive approximation. By involving the oversampling technique, the so-called sigma-delta ( $\Sigma\Delta$ ) conversion, sometimes referred to as delta-sigma conversion, has been widely used in recent years. This technique can obtain high resolution with a simple antialiasing filter.<sup>3,4</sup>

### 2.3 Input Range, Polarity, and Gain

The input range is the difference in voltage between the maximum and minimum voltage limits that can be measured by an analog input channel. The input range can be bipolar (for example,  $\pm 10$  V) or unipolar (for example, 0 to 5 V). The polarity of the output from the signal conditioner and the input of the measurement device must be matched. The gain is defined as the amplification or attenuation of the signal. Many measurement devices have multiple gains to select. A proper gain must be set to match the signal to the input range so that the best resolution can be obtained.

### 2.4 Analog Output

For use in modal analysis, we may need to generate white noise, pink noise, pure-tone, or swept-sine excitation. Active noise and vibration control applications also require the system to output voltage or current to

control the feedback loop. These can be done by the analog output channels on the measurement devices. Analog output is accomplished by using a digital-to-analog converter (DAC). Like the analog input, the resolution is determined by the number of bits. With techniques, such as FIFO (first in, first out) and DMA (direct memory access), high-speed updating can be obtained.

### 2.5 Digital Input/Output and Counter/Timer

Digital I/O (input/output) devices are commonly used in sound and vibration applications because some transducers output digital signals and the wide use of digital I/O in control systems. The common-mode noise and transient voltage spikes are two forms of interference in digital signals. If the signal is not properly conditioned, isolation is required on the data acquisition device. The voltage level is another consideration. Most digital I/O devices deal with 0- to 5-V TTL (transistor-transistor logic) and TTL-compatible CMOS (complementary metal-oxide-semiconductor) levels. Some devices work with 24-V levels, which are common in industrial applications.

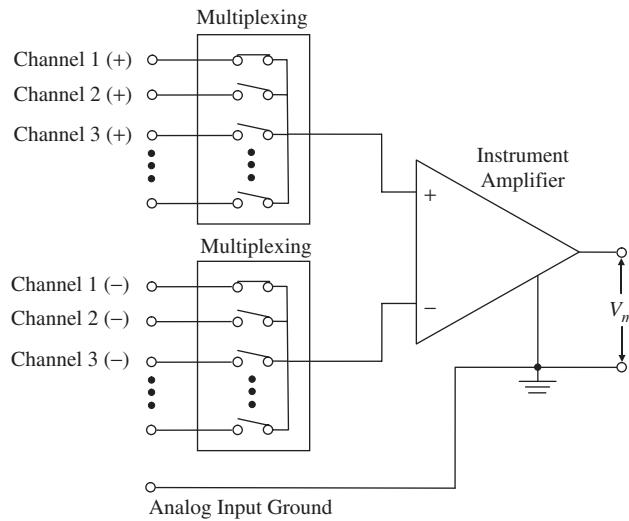
Counter/timer devices are used for a wide variety of applications, such as frequency measurements and position measurements. For rotating systems, a counter can be used to receive digital tachometer pulses. The counter size and the maximum source frequency are two major considerations for a counter. The counter size, which is the highest number that the counter can count, is determined by the number of bits. A large dynamic range requires a large number of bits. The maximum source frequency determines the resolution of a counter, which is the speed of the fastest signal that the counter can count. For example, a 20-MHz counter cannot catch pulses less than 50 ns.

### 2.6 Number of Input and Output Channels

The signal sources should be studied before the measurements are taken to make sure the number of input/output channels is sufficient. For example, a microphone array system may have a large number of microphones.

The differential measurement systems will double the number of input channels of single-ended measurement systems. The differential measurement systems are commonly used when the unwanted noise level is very high. Input channels exist in pairs, as shown in Fig. 2. One line is the positive (+) input and carries both the signal and the noise. The other is the reference, or negative (−) input, and only carries the noise. Ideally, the difference between the lines is then the real signal. In signal-ended measurements systems, the reference is the ground. So an input only occupies one channel.

Generally there are two methods for multichannel data acquisition. The first is that all input channels have their own sample-and-hold circuitries but share the same ADC. The digitizing circuitry scans the channels assigned by the software by a technique known as multiplexing or switching. So they have to have the same sampling rates. And the highest sampling rate capability of the ADC is divided by the number of



**Figure 2** Schematic of a differential measurement system.  $V_m$  is the measured voltage.

scanned channels. The other method, used especially for real-time analyzers, is that each channel has its own ADC. Then the sampling rate and bandwidth are preserved. The reader can also refer to Chapters 40 and 42 for discussion on multiple signal systems.

## 2.7 Triggering and Synchronization

Many noise and vibration applications require precision synchronization and timing for data acquisition. For example, with a rotating system, the use of two perpendicular proximity probes requires synchronization of the measurement. Timing and triggering of the signals help to make the measurement synchronized.

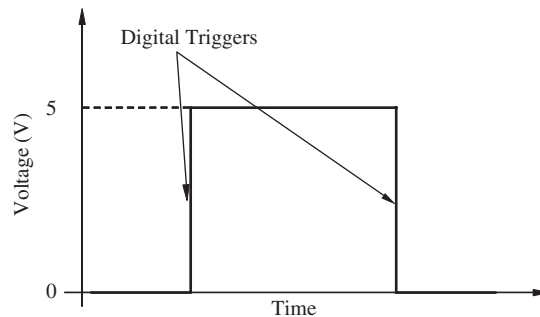
An external event, known as a trigger, can be used to start and/or stop the acquisition of data. The use of triggers ensures that the data are acquired only during the time of interest. This saves hardware bandwidth and storage.

Triggers fall into two main types: digital and analog. The rising or falling edge of a TTL signal can be used as a digital trigger, as shown in Fig. 3. The level and slope of an analog signal can be used as an analog trigger. The data acquisition device should satisfy the triggering conditions that the application requires. For example, some applications require synchronization of both the analog input and analog output.

Some advanced synchronization techniques have been used for more sophisticated data acquisition systems. For example, the PXI (PCI extensions for instrumentation, see Section 3.6 of this chapter) chassis can provide the same clock signal for synchronization between all devices plugged into the chassis.

## 3 INTERFACE AND BUS TECHNOLOGIES

The data acquired by the data acquisition devices stream to the computer memory or hard drive to be



**Figure 3** Rise and fall edges of a TTL signal.

analyzed, displayed, and stored through a certain interface, which is called a bus. Most traditional instruments have interfaces, such as the general-purpose interface bus (GPIB), RS-232, or the universal serial bus (USB), so that the data stored in these instruments can be transferred to computers. Data acquisition devices of different buses come in different forms and are suitable for different application requirements. For example, data acquisition boards plugged into desktop computers are used commonly in laboratories. However, PCMCIA (Peripheral Component MicroChannel Interconnect Architecture) cards for laptops and other portable equipment are more appropriate for measurements made in the field.

As modern computer technologies and fast buses, such as the USB, the FireWire bus, and the Ethernet, have entered the area of measurement and control, external devices have become easier to use than traditional internal personal computer (PC) buses. And the mixed I/O systems have begun to appear for use in

noise and vibration instrumentation. There are many textbooks available about buses.

When selecting data acquisition hardware, bus-related specifications, such as the transfer rate, the length of cable, and the extension capability, should be considered. Table 1 compares these features. The ISA/EISA (industry standard architecture/extended ISA) buses are not listed because they are no longer in use due to their low transfer rate. For new bus techniques, such as PCI-X, PCI Express, and 10 Gbit Ethernet, please consult Internet resources.

### 3.1 General-Purpose Interface Bus

The GPIB, or the Institute of Electrical and Electronics Engineers (IEEE) 488 bus, was developed originally to connect and control programmable instruments and provide a standard interface for communication between instruments from different manufacturers. GPIB is a digital 8-bit parallel communications interface capable of achieving data transfer of up to 8 Mbytes/s, through a shielded 24-line cable. The standard allows a maximum of 14 devices to be connected to a computer on the same bus. Many traditional instruments utilize a GPIB interface so that they can be connected together to establish a measurement and control network. There are three types of devices: listeners, talkers, and controllers. It is possible to have more than one controller on the bus, but only one can be active at a time. The reader can consult the literature<sup>5-8</sup> for more details, such as data lines, handshake lines, interface management lines, and higher performance GPIB.

### 3.2 Serial Communication

The serial port sends and receives data bit by bit. The data type transmitted through the serial port is ASCII (American Standard Code for Information Interchange). The reader can refer to books on serial communication for connector pin descriptions, on how to use the registers, and for related information.<sup>9,10</sup> However, note that the serial characteristics, including baud rate, data bits, stop bits, and parity, must match the ports that are connected.

Serial communication includes three standards: RS-232, RS-422, and RS-485. RS-232 is the most common serial standard, although it is being replaced by the USB. RS-422 and RS-485 use differential signals, as shown in Fig. 2, than the unbalanced signals

referenced to ground with the RS-232. So these two kinds of ports are less susceptible to noise. Table 1 shows that the RS-422 and RS-485 standards specify longer cables and wider bandwidths than those of the RS-232 and can be connected to multiple devices. Therefore, these two interfaces, especially the RS-485, are widely used to create networks in industrial applications that have more testing/control points and more serious environmental noise problems. And RS-232 works best for laboratory applications requiring a lower speed and less rugged connection.

The number of serial ports on a computer is limited. Generally a PC only has two RS-232 ports. If more serial ports are needed, a multiserial port board can be used to extend the capability of the system.

### 3.3 Universal Serial Bus

Although the USB was designed primarily to connect peripheral devices, such as keyboards, mice, printers, and digital cameras to PCs, it also provides an inexpensive but fast connection for data acquisition devices. The USB 1.1 specification has a maximum transfer rate of 12 Mbps. The USB 2.0 has a transfer rate of 480 Mbps. Devices that are connected through a USB port are external to PCs and hot pluggable, which means that it is convenient to add or remove a USB device without shutting down the computer. The bus is also capable of detecting a device automatically. That means that the user does not have to worry about configurations. This is called plug-and-play. The power supply available with the USB cable is an important benefit. Such devices automatically power down when not in use. Additionally, depending on the bus topology, up to 127 devices can communicate simultaneously through one USB port. By adding hubs, additional ports can be added to one host.<sup>11</sup>

The USB ports have some shortcomings, however. First, the USB cables are not industrially graded. This has the potential to cause errors in noisy environments. Also there is no latching mechanism for USB cables. So the cables can be disconnected easily by mistake. USB cables are generally 1 or 2 m long. With the use of USB extenders, longer cables can be put together. Some manufacturers offer cascaded extenders.

### 3.4 FireWire

Like the USB, the FireWire also supports hot-plug, plug-and-play, and cable power. The FireWire is able

**Table 1 Comparison of Buses**

	Maximum Transfer Rate	Maximum Number of Devices	Maximum Cable Length
GPIB	8 Mbyte/s	14	20 m
FireWire	3.2 Gbit/s	64	100 m
PCI/PXI	133 Mbyte/s (for 32-bit bus)	Depends on the slot number	—
PCMCIA	20 Mbyte/s	Depends on the slot number	—
RS-232	230 kbit/s	1	15 m
RS-422	10 Mbit/s	10	1.2 km
RS-485	10 Mbit/s	32	1.2 km
USB 2.0	480 Mbit/s	127	30 m
VXI	160 Mbyte/s	Depends on the slot number	—



to deliver data through either a synchronous or an asynchronous mode. Synchronous transport guarantees that a transmission is completed within a given amount of time, but it does not guarantee that the transmission is free of error. On the other hand, asynchronous transport guarantees accurate delivery, and devices with urgent messages can be given priority over all other devices. As the IEEE 1394 ports are not built into Intel's PC peripheral chip set, a separate IEEE 1394 controller, typically a PCI board, is required to communicate with IEEE 1394 devices. The reader can refer to the IEEE standard and the two amendments.<sup>12-14</sup>

### 3.5 Virtual Machine Environment (VME) and VEM Extensions for Instrumentation

The Virtual Machine Environment (VME) bus, or IEEE 1014, possesses an excellent backplane, which is a circuit board containing sockets into which other circuit boards can be plugged, for building instrument systems with high transfer rates up to 160 Mbytes/s.<sup>15,16</sup> The VXI bus (VME bus extensions for instrumentation) has been developed for portable applications and to provide a modular open standard for integration into the traditional GPIB test system and for stand-alone applications. A VXI system or subsystem consists of a VXI mainframe, an embedded controller, and VXI modules.

As the VME bus was designed specially for measurement purposes, VXI products are mainly used in high-end measurement applications, such as for military and aerospace tests. However, since the VME bus is not a part of modern computer architectures, VXI cannot take advantage of the developments in PC technologies. Its high price is another disadvantage for general-purpose test applications. For more information, the reader can consult the website of the VXI Bus Consortium, [www.vxi.org](http://www.vxi.org).

### 3.6 Peripheral Component Interconnect and PCI Extensions for Instrumentation

The PCI is a local bus for high-end computers made to replace the ISA and EISA buses. The PCI bus transfers 32- or 64-bit data at a clock speed of 33 MHz and offers a theoretical maximum transfer rate of 133 Mbytes/s.

The PXI is a modular instrumentation platform designed specifically for measurement and control applications. PXI systems benefit from features such as compact and rugged packaging, open standard, large selection of modules, and low cost. Like VXI systems, PXI systems are comprised of three basic components: the chassis, the system controller, and peripheral modules. The chassis provides the PXI backplane, which includes the 133-Mbyte/s PCI bus and timing and triggering buses for accurate synchronization without additional cabling. The chassis has an extended number of slots compared to desktop computers. So plenty of modules, such as data acquisition and the real-time analysis devices, can be integrated into a multifunctional system. The controller plugged into the chassis is actually a high-performance computer with an operating system installed. Generally, it has all the interface

capability that a PC has, such as floppy drive, serial ports, parallel port, USB port, Ethernet interface, and so on. Connecting the monitor, keyboard, and mouse, a PXI system can work as a stand-alone and portable measurement and control system. The controller also can work under the remote control of a PC.

For more information, the reader can consult the website of the PXI System Alliance, [www.pxisa.org](http://www.pxisa.org).

### 3.7 Peripheral Component MicroChannel Interconnect Architecture

The PCMCIA bus is designed for laptop computers. So the use of PCMCIA measurement devices is a good choice for portable applications. The PCMCIA 2.1 release in 1993 specified a 16-bit bus interface with a theoretical maximum transfer rate of 20 Mbytes/s. In 1995 the PCMCIA 2.1 was enhanced to provide 32-bit operation at a clock speed of 33 MHz, like that of the PCI bus. The PCMCIA bus can serve testing and control devices, as well as memory card, network connection, and bus interface.

### 3.8 Ethernet

Ethernet, which is specified by IEEE 802.3, is widely used not only for networks but also for communications between instruments and computers. The most common transfer rates are 10 Mbit/s and 100 Mbit/s. With new gigabit Ethernet cards, higher transfer rates can be achieved. Twisted cables, such as the CAT 5 cable, can be used to connect devices at distances up to 100 m. However, fibers can be used for longer distance communication.

The wireless Ethernet specified by IEEE 802.11 is another emerging standard for measurement and control. The transfer rate of wireless Ethernet is much lower and decreases as the distance between the instrument and the computer increases. For example, the transfer rate of 802.11g is 54 Mbit/s within 20 m, and is only 1 Mbit/s at a distance of 125 m. However, it is very convenient to use wireless equipment to avoid requiring cabling.

## 4 NETWORK-BASED DATA ACQUISITION

Network-based measurement and control systems are important for distributed systems and harsh or toxic environments that are not safe for human beings. The conventional network based on serial communication and GPIB have been described in the previous section. These interfaces have limitations in both performance and flexibility.<sup>17</sup> With the widespread adoption of technologies such as Ethernet, HTML (hypertext markup language), FTP (file transfer protocol), and wireless networks, along with software technologies, such as Visual Basic, Visual C++, and JAVA, measurements can be carried out over a local network, a company intranet, or the Internet.

For networked measurements, readers are recommended to study the seven-layer OSI (open systems interconnection) model.<sup>18</sup> The network is composed of modules that can be software or hardware. The client/server model is a widely used architecture for

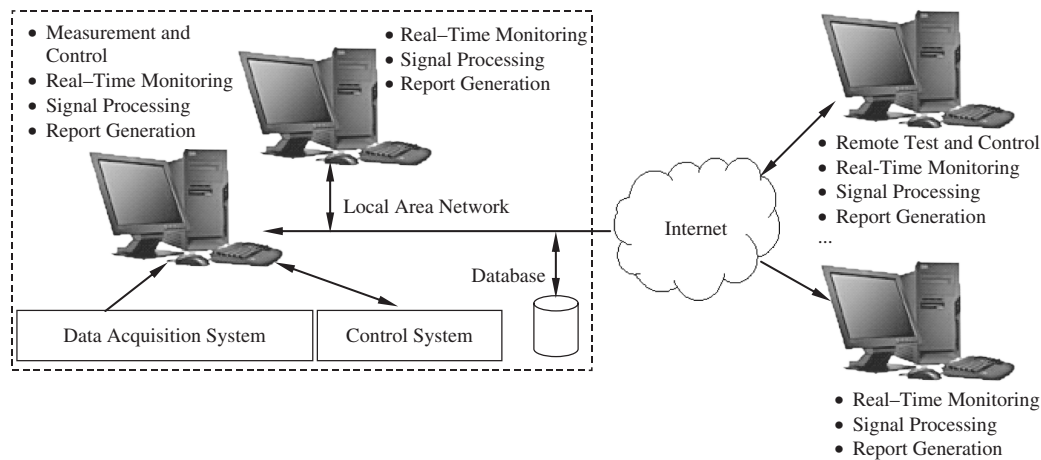


Figure 4 Client/server architecture for network-based test and control.

networked measurement and control and is illustrated in Fig. 4. The server can distribute data to clients. Clients can carry out remote control on the server. The other model is called peer to peer. At the measurement and control end, the data acquisition and control system can be connected to the server through different interfaces, such as PCI, GPIB, serial I/O, USB, IEEE 1394, and through wireless communication. Embedded systems are sometimes needed for certain measurement and control applications. An embedded system can be accessed from a host computer through the local area network (LAN). As the token ring network is now rarely used, Ethernet and wireless networks are becoming the most commonly used LAN architectures.

Some other LAN architectures may be appropriate for certain applications. For example, there are several kinds of industrial communication networks, such as Fieldbus and CAN (ISO 11898 Controller Area Network). They are designed for large-scale measurement and automation applications with multiple and distributed test and control points. The reader can consult the literature<sup>19,20</sup> for more information.

#### 4.1 Publishing and Sharing Data

Publishing data simply means generating a static Web report of test results so that the clients can access the report by using Web browsers. The most common method is to generate the report using HTML. Some corporations use a database to store the data and a Web interface for viewing the reports. Alternatively, the server can report the results by sending email. FTP is another way to access large files.

Sharing data is a dynamic process in which clients can access acquired data in real time. XML (extensible markup language) is a common standard for sharing data. XML generates a document that contains the acquired data. Because the document is built in a certain structure, it is easily accessible and readable by other applications through the network.<sup>21</sup> Another

method used is the National Instrument DataSocket. DataSocket is a new network programming technology for data streaming over a network and can respond to multiple users without the complexity of the low-level TCP (transmission control protocol) programming.

Since multiple PCs can visit the same data server, additional signal processing may be performed on remote computers without degrading the performance of the test and control system. Meanwhile, a single PC can be connected to multiple data servers, which is convenient with distributed measurement and control systems.

#### 4.2 Remote Control

With the data server running at the host computer, the control can be implemented from a remote computer on the network through a common Web browser. Although the acquisition is performed on the host computer, the remote user has complete control. The operation is the same as if the test were executed locally.

#### REFERENCES

1. J. C. Burgess, Practical Considerations in Signal Processing, in *Encyclopedia of Acoustics*, M. J. Crocker, Ed., Wiley, New York, 1997.
2. T. L. Lagö, Time and Frequency Consideration Using Heisenberg's Uncertainty Principle Applied in Mechanical and Acoustical Applications, Proceedings of Ninth International Congress on Sound and Vibration, Orlando, July 8–11, 2002.
3. J. W. Beauchamp and Robert C. Maher, Digital Audio, in *Encyclopedia of Acoustics*, M. J. Crocker, Ed., Wiley, New York, 1997.
4. S. K. Mitra, *Digital Signal Processing: A Computer-Based Approach*, McGraw-Hill, New York, 2001.
5. ANSI/IEEE Standard 488.1–1987, IEEE Standard Digital Interface for Programmable Instrumentation, Institute of Electrical and Electronics Engineers, New York, 1988.

6. IEEE Standard 488.2–1992, IEEE Standard Codes, Formats, Protocols, and Common Commands for Use with IEEE Std 488.1–1987, IEEE Standard Digital Interface for Programmable Instrumentation, Institute of Electrical and Electronics Engineers, New York, 1992.
7. IEEE Std 488–2003, IEEE Standard for Higher Performance Protocol for the Standard Digital Interface for Programmable Instrumentation, Institute of Electrical and Electronics Engineers, New York, 2003.
8. A. J. Caristi, *IEEE-488 General Purpose Instrumentation Bus Manual*, Academic, San Diego, 1989.
9. M. A. Miller, *Introduction to Digital and Data Communication*, West Publishing, St. Paul, MN, 1992.
10. J. Campbell, *The RS-232 Solution*, SYBEX Inc., San Francisco, 1989.
11. J. Hyde, *USB Design by Example: A Practical Guide to Building I/O Devices*, Wiley, New York, 1999.
12. IEEE Standard 1394–1995, IEEE Standard for a High Performance Serial Bus, Institute of Electrical and Electronics Engineers, New York, 1996.
13. IEEE Standard 1394a–2000, IEEE Standard for a High Performance Serial Bus—Amendment 1, Institute of Electrical and Electronics Engineers, New York, 2000.
14. IEEE Standard 1394–2002, IEEE Standard for a High-Performance Serial Bus—Amendment 2, Institute of Electrical and Electronics Engineers, New York, 2002.
15. ANSI/IEEEANSI/IEEE Standard 1014–1987, IEEE Standard for A Versatile Backplane Bus: VMEbus, Institute of Electrical and Electronics Engineers, New York, 1988.
16. S. Heath, *VMEbus User's Handbook*, CRC Press, Boca Raton, FL, 1989.
17. T. J. Reilly, Networked Vibration Testing and Analysis, *Sound Vibr. Mag.*, March 2002, pp. 14–17.
18. V. Boed, *Networking and Integration of Facilities Automation Systems*, CRC Press, Boca Raton, FL, 1999.
19. N. P. Mahalik, Ed, *Fieldbus Technology: Industrial Network Standards for Real-Time Distributed Control*, Springer, Berlin, 2003.
20. K. Etschberger, *Controller Area Network*, IXXAT Automation, Weingarten, Germany, 2001.
21. [www.xml.com](http://www.xml.com).

## BIBLIOGRAPHY

- J. Borwick, Ed, *Sound Recording Practice*, Oxford University Press, New York, 1994.
- M. Camras, Magnetic Recording Reproducing System, in *Encyclopedia of Acoustics*, M. J. Crocker, Ed., Wiley, New York, 1997.
- D. M. Huber and Robert E. Runstein, *Modern Recording Techniques*, 3rd ed., Howard W. Sams, Carmel, CA, 1989.
- K. C. Pohlmann, *Principles of Digital Audio*, McGraw-Hill, New York, 2000.

# CHAPTER 42

## SIGNAL PROCESSING

Allan G. Piersol  
Piersol Engineering Company  
Woodland Hills, California

### 1 INTRODUCTION

In general terms, signal processing is the science of extracting relevant information from measured data signals representing a phenomenon of interest. In the context of noise and vibration control, this usually means determining from measurements certain descriptive characteristics of the environment that will help identify the sources of the noise and vibration so that they can be reduced or controlled. The most important descriptive characteristic of common interest is the spectral content of the data, but other properties of the measured data may also be informative. Virtually all signal processing today is accomplished using digital instruments, but most transducers for measuring noise and vibration data produce analog voltage signals (see Chapters 38 through 41). Hence, the first step in digital signal processing is to translate the measured signals into a digital format for analysis. This chapter summarizes (a) analog-to-digital conversion procedures, (b) digital data storage and retrieval procedures, and (c) the basic digital computations involved in noise and vibration data analysis. The potential errors associated with all of these procedures and the computed results are also summarized.

### 2 ANALOG-TO-DIGITAL CONVERSION

An analog-to-digital converter (ADC) is a device that translates a continuous analog signal, which represents an uncountable set, into a series of discrete values (often called a time series), which represents a countable set. There are numerous types of ADC designs,<sup>1-4</sup> but the simplest type of ADC employs a sample-and-hold amplifier that translates the value of the analog signal at a specific sampling time into a constant voltage that is maintained until the

next sampling time. The series of constant-voltage steps are then compared to a repetitive ramp function produced by a sweep generator driven by a timing pulse generator or clock, and a binary counter is initiated at the start of each sweep cycle to produce a series of digital values representing the signal at discrete times.

Due to the merits of very high sampling rates relative to the highest frequency of interest in the data (oversampling to be discussed later), there is a movement toward ADCs with a different architecture that provide effective sampling rates in excess of  $10^5$  samples per second (sps). The most common type of ADC in this class is that referred to as the sigma-delta ( $\Sigma\Delta$ ) converter,<sup>1</sup> which is schematically illustrated in Fig. 1. The key features of a  $\Sigma\Delta$  converter are (a) the input of the analog signal through an integrator to a clock-driven comparator, which essentially acts as a one binary digit (one-bit) ADC, (b) the feedback of the one-bit comparator output through a one-bit digital-to-analog converter (DAC), which is then subtracted from the input analog signal, and (c) an averaging operation by a low-pass digital filter, which essentially increases the number of bits forming a digital value (the word size) in the digital output (see Refs. 4 to 6 for details on digital filters). Since the basic comparator and DAC operations are accomplished using a one-bit resolution, a very high initial sampling rate ( $>10^7$  sps) can be achieved. The digital filter is then set to provide an output sampling rate after decimation that is substantially less than the initial one-bit sampling rate, commonly by a ratio of 256:1.<sup>1</sup> The frequency range of the final digital data can be varied by one of two procedures. The first is to lock the cutoff frequency of the digital filter to the initial one-bit sampling rate of the comparator so that the final sampling rate is controlled by simply varying the comparator sampling

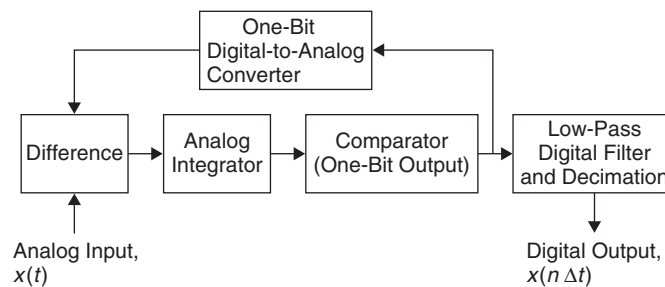


Figure 1 Schematic diagram of  $\Sigma\Delta$ -type analog-to-digital converter.<sup>3</sup>

rate. The second is to fix the initial sampling rate of the comparator and then control the frequency limit and sampling rate of the final digital data by varying the cutoff frequency of the digital filter and the degree of decimation. In either case, this process of oversampling followed by low-pass digital filtering and decimation can be interpreted as increasing the effective resolution of the digital output by suppressing the spectral density of the digital noise in the output. Further details are presented in Section 2.3

Some of the important general considerations associated with the use of an ADC may be summarized as follows:

1. **Format** Many ADCs are integrated into more general signal processing equipment where the natural binary output of the converter is easily accepted. However, some ADCs operate as independent instruments. In this case, the output of the instrument is usually in the ASCII (American Standard Code Information Interchange) format, which allows the ADC output to be read directly by any computer program written in a common language, such as C or FORTRAN, or to drive terminal and register displays directly.
2. **Resolution** The output of an ADC is a series of digital words, each composed of  $w$  bits, which determine the number of discrete levels that can be used to define the magnitude of the input analog signal at discrete times. Hence, there is a round-off error introduced by the conversion, to be discussed later.
3. **Sampling Interval** In most cases, an ADC samples the input analog signal with a fixed sampling interval  $\Delta t$ , as illustrated in Fig. 2. However, there are sometimes situations where a variable sampling interval might be desired, for example, the sampling of an otherwise sinusoidal signal with a time-varying frequency. To accommodate such situations, most ADCs allow the sampling rate to be varied continuously with time as desired.
4. **Sampling Rate** At least two sample values per cycle are required to define the highest frequency in an analog signal. Hence, the sampling rate of the ADC, denoted by  $R_s$ , imposes an upper frequency limit on the digital

data. More important, any frequency content in the analog signal above this upper frequency limit will fold back and sum with the digital data at frequencies below this limit to produce a serious error, called aliasing, to be discussed later.

5. **Multiple Signals** Consider the situation where it is desired to convert  $m$  independent analog signals simultaneously into a digital format. If the available ADC has a sampling rate of  $R_s \geq 2mf_c$ , where  $f_c$  is the highest frequency in the analog signals, then all  $m$  of the analog signals can be converted with a single ADC by sequentially sampling the signals (often referred to as time-domain multiplexing). Of course, sequential sampling introduces a time-delay error of  $\Delta t = 1/R_s$  from one signal to the next, but this time delay can be corrected when the digital sequence for each signal is recovered. On the other hand, because ADC devices are becoming relatively inexpensive, the use of parallel ADCs (one ADC for each analog signal) is becoming increasingly common.

## 2.1 Resolution

As mentioned before, the conversion of a continuous analog signal  $x(t)$  into a digital sequence with a finite number of possible values separated by a magnitude interval  $\Delta x$  clearly imposes a resolution problem in the form of a round-off error. The resolution of the ADC is a function of the word size  $w$  (the number of bits) used to form each digital value in the ADC output, and may be defined in several ways, as follows:

1. **Range of Counts** The range of counts (sometimes called the span) is defined as the total number of possible digital values provided by the ADC output. Excluding zero, the range of counts ( $S$ ) is given by

$$S = 2^w - 1 \quad (1)$$

2. **Dynamic Range** The dynamic range is defined as the ratio of the largest value (either plus or minus) to the smallest value provided by the ADC output. Assuming a mean value of zero and excluding the sign bit if used (one bit

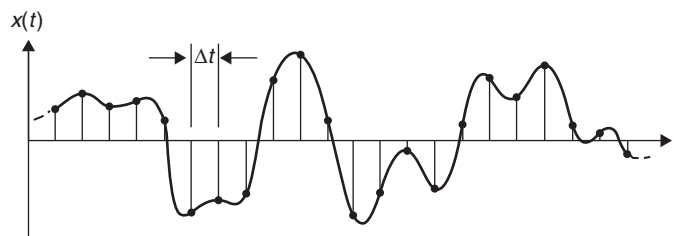


Figure 2 Sampling of analog signal with a constant sampling interval.<sup>2</sup>

to define the sign polarity), the dynamic range (DR) is given in decibels (dB) by

$$\text{DR(dB)} = 10 \log_{10}(2^w - 1)^2 \quad (2)$$

$$\approx 6w \text{ for } w > 5$$

3. *Peak Signal-to-Noise Ratio.* The peak signal-to-noise ratio is defined as the ratio of the largest value (either plus or minus) to the standard deviation of the digital noise in the output of the ADC. The standard deviation of the digital noise is given by<sup>2</sup>  $\sigma_n = \Delta x / \sqrt{12} = 0.289 \Delta x$ . Assuming a mean value of zero and excluding the sign bit if used, the peak signal-to-noise ratio (PS/N) is given in decibels (dB) by

$$\text{PS/N(dB)} = 10 \log_{10}[12(2^w - 1)^2] \quad (3)$$

$$\approx 6w + 11 \text{ for } w > 5$$

4. *Signal-to-Noise Ratio.* The signal-to-noise ratio is defined as the ratio of the maximum standard deviation of the signal without clipping to the standard deviation of the digital noise in the ADC output. It follows that the signal-to-noise ratio is a function of the ratio of the peak value to the standard deviation of the analog signal being converted. Specifically, the signal-to-noise ratio (S/N) is given in decibels (dB) by

$$\text{S/N(dB)} = \text{PS/N(dB)} - 10 \log_{10}(P/\sigma_s)^2 \quad (4)$$

where  $P$  is the peak value of the signal,  $\sigma_s$  is the standard deviation of the signal, and PS/N (dB) is defined in Eq. (3). For example, if the signal is a sine wave,  $(P/\sigma_s)^2 = 2$  (approximately 3 dB), so  $\text{S/N(dB)} = \text{PS/N(dB)} - 3$ . On the other hand, if the signal is random where clipping at three standard deviations is acceptable,  $(P/\sigma_s)^2 = 9$  (approximately 10 dB), so in this case  $\text{S/N(dB)} = \text{PS/N(dB)} - 10$ .

A summary of the values given by Eqs. (1) through (4) for various common word sizes is presented in Table 1. Of course, the values in Table 1 are theoretical maximum values. In reality, there are various possible errors in the ADC that can reduce the effective word

size by perhaps one or two bits.<sup>2</sup> Furthermore, the values in Table 1 assume the full range of the ADC is used to convert the signal to a digital format. If the full range of the ADC is not used, then the various values will be less. Finally, the values in Table 1 assume the mean value of the signal is zero, which is generally true of noise and vibration signals.

## 2.2 Sampling Rate

The appropriate sampling rate for the conversion of a continuous analog signal into a sequence of discrete values is governed by the sampling theorem.<sup>2</sup> Specifically, given an analog signal with a bandwidth of  $B$  hertz and a duration of  $T$  seconds, the number of equally spaced discrete values that will describe the signal is given approximately by  $n = 2BT$ . Assuming the bandwidth  $B$  is from zero to an upper cutoff frequency of  $f_c$ , it follows that  $n$  = twice the number of cycles, that is, at least two samples per cycle are required to describe the signal. This defines an upper frequency limit for the digital data, commonly referred to as the Nyquist frequency, given by

$$f_A = \frac{R_s}{2} = \frac{1}{2\Delta t} \quad (5)$$

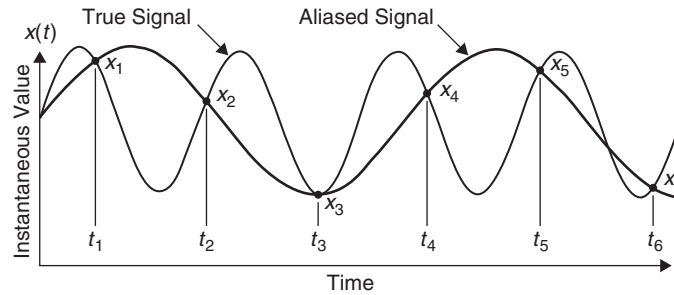
where  $R_s$  is the sampling rate in samples per second (sps), and  $\Delta t$  is the sampling interval in seconds. Any information in the analog signal at a frequency above the Nyquist frequency,  $f_A$ , will be interpreted as information at a frequency below  $f_A$ , as illustrated in Fig. 3. This phenomenon of information above  $f_A$  being folded back to frequencies below  $f_A$  is called aliasing. For data analyzed in terms of an auto- (power) spectral density function (to be defined later), the aliasing will distort the resulting spectrum of the data, as shown in Fig. 4. Note that there is no frequency limit on aliasing. Specifically, for any frequency  $f$  in the frequency range  $0 \leq f \leq f_A$ , the higher frequencies that will be aliased with  $f$  are defined by<sup>2</sup>

$$(2f_A \pm f), (4f_A \pm f), (6f_A \pm f), \dots \quad (6)$$

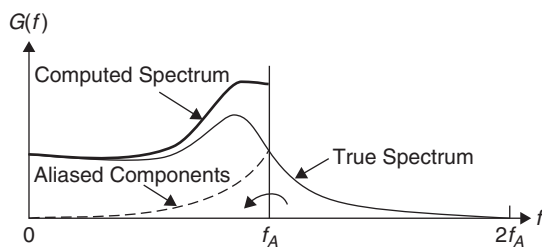
For example, if  $f_A = 100$  Hz (corresponding to a sampling rate of 200 sps), then the data at 170, 230, 370, 430 Hz, and so forth will fold back and appear at 30 Hz.

**Table 1 Range of Counts, Dynamic Range, and Signal-to-Noise Ratios for ADCs**

Word Size (excluding sign bit)	Range of Counts	DR (dB)	PS/N (dB)	S/N (dB) Sine Wave	S/N (dB) Random
10	1,023	60	71	68	61
12	4,095	72	83	80	73
14	16,383	84	95	92	85
16	65,535	96	107	104	97
18	262,143	108	119	116	109



**Figure 3** Frequency aliasing due to an inadequate sampling rate.<sup>2</sup>



**Figure 4** Illustration of aliasing in the computation of an autospectral density function.<sup>2</sup>

Aliasing is a particularly serious error because once the analog-to-digital conversion is complete, (a) it may not be obvious that aliasing occurred, and (b) even if it is known that aliasing occurred, it is generally not possible to correct the data for the resulting error. It is for these reasons that aliasing must be avoided by low-pass analog filtering of the input signal to the ADC. The appropriate cutoff frequency for the analog low-pass filter (commonly referred to as the antialiasing filter) is dependent on the roll-off rate of the filter. However, assuming a roll-off rate of at least 60 dB/octave, a cutoff frequency of  $f_c \approx 0.5f_A$  is desirable, although a cutoff frequency as high as  $f_c = 0.8f_A$  may be used if the filter has a very high cutoff rate or there is little high-frequency content in the analog signal.

### 2.3 Oversampling

As noted earlier, modern ADCs often have an initial sampling rate that provides a Nyquist frequency  $f_A$ , as defined in Eq. (5), which greatly exceeds the upper frequency of interest in the data. In such cases, a relative simple analog antialiasing filter can be used where the cutoff frequency is at perhaps only 10% of the Nyquist frequency for the initial sampling rate. A very sharp cutoff low-pass digital filter can then be applied to the output of the ADC with a cutoff frequency  $f_c$  that is consistent with the upper frequency limit of interest in the data. So as to limit the number of data values that must be processed, the resulting digital data are decimated to provide

a final sampling rate with a new Nyquist frequency consistent with the upper frequency limit fixed by the digital filter. In effect, the low-pass digital filter acts as the final antialiasing filter. For example, assume it is desired to analyze noise and vibration data up to a frequency of 10 kHz. Further assume the cutoff frequency of the low-pass digital filter is set at 80% of the final Nyquist frequency. It follows that a final sampling rate of 25 kps is required. Finally, assume an oversampling rate of 256:1 is employed. An initial sampling rate of 6.4 MHz is then required. This process of oversampling followed by digital filtering and decimation will dramatically enhance the signal-to-noise ratio of the data.<sup>7,8</sup> In the example above, even with only a one-bit initial conversion in the ADC, the effective word size of the final digital data values would be about  $w \approx 16$  bits.

## 3 DATA STORAGE AND RETRIEVAL

In some cases, noise and vibration data are analyzed online using a special-purpose instrument where the first input stage is an ADC. In this case, the output of the ADC goes directly into an analysis algorithm, such as a digital filtering algorithm<sup>4-6</sup> for instruments designed to compute  $\frac{1}{3}$  octave band spectra, or a FFT algorithm<sup>2,5</sup> for instruments designed to compute narrow bandwidth spectra. In other cases, however, the output of the ADC goes into some form of storage for later analysis. Furthermore, it is sometimes desired to retrieve the digital data from storage in an analog form.

### 3.1 Digital Storage

For digital data that will be analyzed in the near future, the most common approaches are to input the data into the random-access memory (RAM) or directly onto the hard disk (HD) of a digital computer. A direct input into RAM is generally the best approach if the number of data values is within the available RAM capacity. For those cases where the data analysis is to be performed at a later time, it is best to download the RAM into an HD, or record the data directly onto an HD. The speed that an HD can accept data is steadily increasing with time but is currently in excess of 40 Mbytes/s (for 16-bit sample values, 20 Msps). This is adequate to record the output of an ADC in real



time for most digitized noise and vibration signals. For long-term storage of digital data after the desired analyses have been performed, the data in RAM or HD can be downloaded into a removable storage medium such as a digital video disk (DVD) or a compact disk/read-only memory (CD-ROM). See Ref. 9 for details.

### 3.2 Digital-to-Analog Conversion

There are situations where it is desired to recover a continuous analog signal from stored digital data. This is accomplished using an digital-to-analog converter (DAC). A DAC is a relatively simple device where each digital value sequentially generates a fixed-level voltage signal, resulting ideally in a step function. In more advanced DAC designs, at least a linear interpolation routine is used to connect adjacent voltage values. In either case, there will be a discontinuity in the output voltage signal that produces a narrow bandwidth spurious signal at the sampling rate of the digital data and all harmonics thereof. These spurious signals, often called imaging errors,<sup>3</sup> must be suppressed by analog low-pass filtering, analogous to the low-pass filtering used to suppress aliasing errors in analog-to-digital conversion. Since the low-pass antialiasing filter removed all information in the digital data above the filter cutoff frequency  $f_c$ , it follows that the cutoff frequency for the antiimaging low-pass filter on the output of the DAC should be at  $f_c$  or less.

## 4 DIGITAL DATA ANALYSIS COMPUTATIONS

There are various data analysis procedures that are required for applications to the noise and vibration control procedures detailed in this handbook. The most important of these data analysis procedures are now summarized. For clarity, the basic definitions for the various data analysis functions are given in terms of continuous time and frequency variables, and the mean value of the signal being analyzed is assumed to be zero.

### 4.1 Definitions

The most important descriptive functions of data for noise and vibration control applications are as follows:

1. *Root-Mean-Square (rms) Value* The rms value is a measure of the total magnitude of a periodic or stationary random signal  $x(t)$ . It is given by

$$\sigma_x = \lim_{T \rightarrow \infty} \left[ \frac{1}{T} \int_0^T x^2(t) dt \right]^{1/2} \quad (7)$$

2. *One-Third Octave Band Levels* One-third octave band levels are given by the rms value, as defined by Eq. (7), of the output of a one-third octave bandwidth filter ( $B \approx 0.23 f_0$  where  $f_0$  is the filter center frequency), with the characteristics given by Ref. 10, versus the

filter center frequency. For acoustical data, the levels are usually presented in decibels (ref: 20  $\mu$ Pa).

3. *Fourier Transform* The Fourier transform over a finite time interval  $T$  is a frequency-domain function that provides the general frequency content of a periodic or stationary random signal  $x(t)$ . It is given by

$$X_T(f) = \int_0^T x(t) e^{-j2\pi ft} dt \quad (8)$$

Note that  $X_T(f)$  is defined for both positive and negative frequencies and for infinitely long time histories will usually approach an infinite value as  $T$  approaches infinity.

4. *Line Spectrum.* A line spectrum (also called a linear spectrum) is a frequency-domain function that defines the frequency content of a periodic signal  $x(t)$ . It is given by

$$L_x(f_i) = \frac{2}{T_P} |X_{T_P}(f_i)| \quad i = 1, 2, 3, \dots \quad (9)$$

where  $|X_{T_P}(f_i)|$  is the magnitude of the Fourier transform of  $x(t)$  computed ideally over the period  $T_P$  of the periodic signal, as defined in Eq. (8) with  $T = T_P$  and  $f = i/T_P$ ,  $i = 1, 2, 3, \dots$ . Note that  $L_x(f_i)$  and all other spectral functions to follow are defined for positive frequencies only.

5. *Autospectral Density Function* The autospectral density function (also called the power spectral density function, or simply the autospectrum or power spectrum) is a frequency-domain function that defines the spectral content of a stationary random signal  $x(t)$ . It is given by

$$G_{xx}(f) = \lim_{T \rightarrow \infty} \frac{2}{T} E[|X_T(f)|^2] \quad f > 0 \quad (10)$$

where  $|X_T(f)|$  is the magnitude of the Fourier transform of  $x(t)$  over the time interval  $T$ , as defined in Eq. (8), and  $E[\ ]$  denotes the expected value operator, which implies an averaging operation.<sup>2</sup>

6. *Cross-Spectral Density Function* The cross-spectral density function (also called the cross spectrum) is a frequency-domain function that defines the linear correlation and phase as a function of frequency between two stationary random signals  $x(t)$  and  $y(t)$ . It is given by

$$G_{xy}(f) = \lim_{T \rightarrow \infty} \frac{2}{T} E[X_T^*(f) Y_T(f)] \quad f > 0 \quad (11)$$



where  $X_T^*(f)$  is the complex conjugate of  $X_T(f)$ , and  $E[\ ]$  denotes the expected value operator, which implies an averaging operation.<sup>2</sup>

7. **Coherence Function** The coherence function (also called coherency squared) is a frequency-domain function that defines the normalized linear correlation (on a scale from zero to unity) as a function of frequency between two stationary random signals  $x(t)$  and  $y(t)$ . It is given by

$$\gamma_{xy}^2(f) = \frac{|G_{xy}(f)|^2}{G_{xx}(f)G_{yy}(f)} \quad f > 0 \quad (12)$$

where  $G_{xx}(f)$  and  $G_{yy}(f)$  are the autospectra of  $x(t)$  and  $y(t)$ , respectively, as defined in Eq. (10), and  $|G_{xy}(f)|$  is the magnitude of the cross spectrum between  $x(t)$  and  $y(t)$ , as defined in Eq. (11).

8. **Frequency Response Function** The frequency response function (also called the transfer function) is a frequency-domain function that defines the linear relationship as a function of frequency between two stationary random signals,  $x(t)$  and  $y(t)$ . It is given by

$$H_{xy}(f) = \frac{G_{xy}(f)}{G_{xx}(f)} = |H_{xy}(f)|e^{-j\phi_{xy}(f)} \quad f > 0 \quad (13)$$

where  $G_{xx}(f)$  is the autospectrum of  $x(t)$ , as defined in Eq. (10),  $G_{xy}(f)$  is the cross spectrum between  $x(t)$  and  $y(t)$ , as defined in Eq. (11), and  $|H_{xy}(f)|$  and  $\phi_{xy}(f)$  are the magnitude and phase, respectively, of  $H_{xy}(f)$ .

There are various other functions that can be helpful in some noise and vibration control problems, including:

1. Cross-correlation functions (given by the inverse Fourier transform of cross-spectral density functions), which can help locate noise and/or vibration sources<sup>2,11</sup>
2. Coherent output power functions, which can identify the spectrum at a given measurement location of the contribution a single noise and/or vibration source among many other sources<sup>2,11</sup>
3. Conditioned spectral functions, which can identify the correlated contributions of two or more noise and/or vibration sources<sup>2</sup>
4. Probability density functions, which can help identify the basic character of various noise and vibration sources<sup>2,12,13</sup> (also see Chapter 13)

5. Cepstrum functions that can be helpful in determining the nature and source of certain complex periodic noise and/or vibration sources<sup>12</sup>
6. Wavelet functions that can be useful in the analysis of nonstationary random signals<sup>13</sup> (also see Chapter 49).

## 4.2 Basic Digital Computations

The basic digital algorithms for the computations of the functions defined in the preceding section are summarized in the second column of Table 2. Note that the digital algorithms evolve directly from Eqs. (7) through (13) without the limiting operations and with  $x(t)$  replaced by  $x(n\Delta t)$ ;  $n = 0, 1, 2, \dots, N-1$ , where  $N$  is the number of sample values and  $\Delta t$  is the sampling interval given by  $\Delta t = 1/R_s$ . It follows that (a)  $T = N\Delta t$ , and (b)  $f = k\Delta f$ ;  $k = 1, 2, 3, \dots, N-1$ . Important factors associated with the spectral computations in Table 2 are as follows:

1. The hat (^) over the designation of the functions denotes that these are estimates that will vary from one measurement to the next for random noise and/or vibration environments<sup>2</sup>.
2. The digital form of the Fourier transforms,  $X_{N\Delta t}(k\Delta f)$  and  $Y_{N\Delta t}(k\Delta f)$ , in the various spectral computations is commonly referred to as the discrete Fourier transform (DFT) and is normally computed using a fast Fourier transform (FFT) algorithm, which provides a dramatic increase in computational efficiency. See Refs. 2, 5, and 13 for details on FFT algorithms.
3. The autospectrum and cross-spectrum computations are accomplished by dividing the available data record into  $n_d$  contiguous segments, each of duration  $T$ , and computing the spectral function over each segment. The spectral results from the  $n_d$  segments are then averaged to approximate the expected value operation in Eqs. (10) and (11).<sup>2</sup>
4. The basic spectral window produced by a Fourier transform has a  $\sin(x)/x$  characteristic with substantial side lobes that leak spectral components from one frequency to another. This leakage problem is commonly suppressed by tapering each segment of data prior to computing the transform. The process of tapering increases the effective bandwidth of the frequency resolution for spectral analysis, but this can be countered by the use of overlapped processing<sup>2,8,12</sup> (also see Chapter 46).
5. Since the duration of a noise and/or vibration measurement will rarely correspond to an integer multiple of the period of even a single periodic component (often called a tone) in a noise and vibration environment, the exact frequency and magnitude of the components in a line spectrum for periodic components (tones) will be somewhat blurred, even with a

**Table 2 Basic Digital Computations**

Function Being Estimated	Basic Computation	Normalized Random Error, $\varepsilon$ , or Standard Deviation, $\sigma$
rms value, $\hat{\sigma}_x$	$\left[ \frac{1}{N\Delta t} \sum_{n=0}^{N-1} x^2(n\Delta t) \right]^{1/2}$	Periodic data, none Random data, $1/(2\sqrt{B_s T})$
Fourier transform, $X_{N\Delta t}(k\Delta f)$	$\sum_{n=0}^{N-1} x(n\Delta t) \exp\left(\frac{-j2\pi kn}{N}\right);$ $k = 0, 1, 2, \dots, N-1$	—
Line spectrum, $S_x(k\Delta f)$ , for periodic signals (tones)	$\frac{2}{N\Delta t}  X_{N\Delta t}(k, \Delta f) ;$ $k = 1, 2, \dots, [(N/2) - 1]$	None
Autospectrum, $\hat{G}_{xx}(k\Delta f)$ , for random signals	$\frac{2}{(N\Delta t)n_d} \sum_{i=1}^{n_d}  X_{iN\Delta t}(k\Delta f) ^2;$ $k = 1, 2, \dots, [(N/2) - 1]$	$\varepsilon = \frac{1}{\sqrt{B_s T}} = \frac{1}{\sqrt{n_d}}$
Cross-spectrum, $\hat{G}_{xy}(k\Delta f)$ , for random signals	$\frac{2}{(N\Delta t)n_d} \sum_{i=1}^{n_d} X_{iN\Delta t}^*(k\Delta f) Y_{iN\Delta t}(k\Delta f);$ $k = 1, 2, \dots, [(N/2) - 1]$	Magnitude, $\varepsilon = \frac{1}{ \gamma_{xy}(k\Delta f) \sqrt{n_d}}$ Phase, $\sigma = \frac{(1 - \gamma_{xy}^2)^{1/2}}{ \gamma_{xy} \sqrt{2n_d}}$
Coherence function, $\hat{\gamma}_{xy}^2(k\Delta f)$ , for random signals	$\frac{ \hat{G}_{xy}(k\Delta f) ^2}{\hat{G}_{xx}(k\Delta f)\hat{G}_{yy}(k\Delta f)};$ $k = 1, 2, \dots, [(N/2) - 1]$	$\varepsilon = \frac{\sqrt{2}[1 - \hat{\gamma}_{xy}^2(k\Delta f)]}{ \hat{\gamma}_{xy}(k\Delta f) \sqrt{n_d}}$
Frequency response function, $\hat{H}_{xy}(k\Delta f)$ , for random signals	$\frac{\hat{G}_{xy}(k\Delta f)}{\hat{G}_{xx}(k\Delta f)};$ $k = 1, 2, \dots, [(N/2) - 1]$	Magnitude, $\varepsilon = \frac{[1 - \gamma_{xy}^2(k\Delta f)]^{1/2}}{ \gamma_{xy}(k\Delta f) \sqrt{2n_d}}$ Phase, $\sigma = \frac{(1 - \gamma_{xy}^2)^{1/2}}{ \gamma_{xy} \sqrt{2n_d}}$

tapering operation discussed in factor 4 above. However, there are algorithms that can be employed to extract the exact frequency and magnitude of each periodic component in a line spectrum.<sup>9</sup> Also, tracking analysis, where the sampling rate of the ADC is tied directly to the source of a periodic component, can yield highly accurate frequency and magnitude results.<sup>12</sup>

### 4.3 Computations for Nonstationary Data

The basic digital computational algorithms in Table 2 assume the noise or vibration data being analyzed are stationary over the analysis duration  $T = N\Delta t$ . However, it is common for the data of interest in noise and vibration control problems to have time-varying (nonstationary) characteristics. There are rigorous analytical procedures for the analysis of nonstationary noise and vibration data, for example, the Wigner distribution for deterministic data and the instantaneous spectrum for random data.<sup>2</sup> Nevertheless, it is more

common in practice for analysts to evaluate nonstationary noise and vibration data by assuming the data are piecewise stationary. Specifically, a measurement of duration  $T = N\Delta t$  is subdivided into a series of  $m$  contiguous segments, each of duration  $T_s = N_s\Delta t$  where  $T = mT_s$ . The desired functions from Table 2 can then be computed sequentially over the  $m$  segments or by a running average over the entire measurement with a linear averaging time  $T_s$ . Procedures are available to select a segment duration or a running averaging time  $T_s$  that will minimize the total mean square error in the results,<sup>2</sup> but it is more common for analysts to select an appropriate value for  $T_s$  based upon past experience or trial-and-error procedures.<sup>9,12</sup>

### 4.4 Statistical Sampling Errors

All of the computations for random signals summarized in Table 2 provide only estimates of the desired functions defined in Eqs. (7) through (13), as indicated by the hat (^) over the functions in Table 2. Specifically, the computed estimates, denoted generically as

$\hat{\phi}$ , will involve a statistical sampling (random) error that can be defined in terms of a normalized random error (also called the coefficient of variation) given by

$$\varepsilon = \frac{\sigma_{\hat{\phi}}}{\phi} \quad (15)$$

where  $\sigma_{\hat{\phi}}$  is the standard deviation of the estimate  $\hat{\phi}$ , and  $\phi$  is the true value of the function being estimated. The normalized random errors for the various computed estimates in Table 2 are summarized in the third column in Table 2. Note that for computed phase functions, the random error is better described simply by the standard deviation of the phase estimate without normalization. Further note that the bandwidth  $B_s$  is the “statistical bandwidth” given by

$$B_s = \frac{\left[ \int_0^\infty G_{xx}(f) df \right]^2}{\int_0^\infty G_{xx}^2(f) df} \quad (16)$$

For a uniform autospectrum over a bandwidth  $B$ , the statistical bandwidth is  $B_s = B$ .

The interpretation of the normalized random error is straightforward. Specifically, assuming the estimates have an approximately normal (Gaussian) distribution,<sup>2</sup> a normalized random error of  $\varepsilon = 0.1$  means that about 67% of the estimates will be within  $\pm 10\%$  of the true value of the function, and about 95% of the estimates will be within  $\pm 20\%$  of the true value of the function.

The computed frequency-dependent estimates in Table 2 may also involve a bias (systematic) error that is dependent on the resolution bandwidth,  $\Delta f$ , as well as other factors. See Refs. 2 and 11 for details on these potential bias errors.

## REFERENCES

1. E. O. Doebelin, *Measurement Systems: Application and Design*, 5th ed, McGraw-Hill, New York, 2004.
2. J. S. Bendat and A. G. Piersol, *Random Data: Analysis and Measurement Procedures*, 3rd ed., Wiley, New York, 2000.
3. M. A. Underwood, Applications of Digital Computers, in *Harris' Shock and Vibration Handbook*, 5th ed., C. M. Harris and A. G. Piersol, Eds., McGraw-Hill, New York, 2002, Chapter 27.
4. S. W. Smith, *The Scientist and Engineer's Guide to Digital Signal Processing*, California Technical Publishing, San Diego, CA, 2002 (online: <http://www.dspguide.com/pdfbook.htm>).
5. A. V. Oppenheimer and R. W. Schaffer, *Discrete-Time Signal Processing*, 2nd ed., Prentice-Hall, Upper Saddle River, NJ, 1999.
6. S. K. Mitra and J. F. Kaiser, *Handbook for Digital Signal Processing*, Wiley, New York, 1993.
7. M. W. Hauser, Principle of Oversampling A/D Conversion, *J. Audio Eng. Soc.*, Vol. 39, January/February 1991, p. 3.
8. J. C. Burgess, Practical Considerations in Signal Processing, in *Handbook of Acoustics*, M. J. Crocker Ed., Wiley, New York, 1998, Chapter 82.
9. H. Himelblau and A. G. Piersol, *Handbook for Dynamic Data Acquisition and Analysis*, 2nd ed., IEST-RD-DTE012.2, Institute of Environmental Sciences and Technology, Rolling Meadows, IL, 2006.
10. Anon., American National Standard, Specification for Octave-Band and Fractional-Octave-Band Analog and Digital Filters, ANSI Std S1.11-1998.
11. J. S. Bendat and A. G. Piersol, *Engineering Applications of Correlation and Spectral Analysis*, 2nd ed., Wiley, New York, 1993.
12. R. B. Randall, Vibration Analyzers and Their Use, in *Harris' Shock and Vibration Handbook*, 5th ed., C. M. Harris and A. G. Piersol, Eds., McGraw-Hill, New York, 2002, Chapter 14.
13. D. E. Newland, *Random Vibrations, Spectral and Wavelet Analysis*, 3rd ed., Wiley, New York, 1993.

# CHAPTER 43

## NOISE AND VIBRATION MEASUREMENTS

**Pedro R. Valletta**  
interPRO  
Acustica-Electroacustica-Audio-Video  
Buenos Aires, Argentina

**Malcolm J. Crocker**  
Department of Mechanical Engineering  
Auburn University  
Auburn, Alabama

### 1 INTRODUCTION

Noise and vibration measurements are needed for a variety of purposes, including source and path identification, noise and vibration reduction of machinery, measurement of interior and exterior noise and vibration of vehicles, aircraft, and ships to name just a few applications. Noise and vibration measurements also need to be made in buildings and of the acoustical materials used in them to determine their acceptability for various uses. Periodic calibration of measurement systems and of the transducers used for the sound and vibration measurements is essential. Not only should transducer systems be calibrated before and after each time they are used but also checked annually by organizations, whose results are traceable to national and international standards. Some years ago, almost all measurements were made with analog equipment. Many analog instruments are still in use around the world. However, by using analog-to-digital conversion, increasing use is now made of digital signal processing to extract the required data. This is done either in dedicated instruments or by transferring measurement results onto computers for later processing by software. Sound power level measurement of machines is now required for predictions of sound pressure level or for labeling or regulatory purposes in some countries. Such sound power measurements can be made in special facilities (in anechoic or reverberation rooms—see Chapter 44—or with sound intensity equipment—see Chapter 45.) Special noise measurements are also required for new aircraft and vehicles and for monitoring traffic noise in the community and aircraft noise around airports. (See Chapters 119–130.)

### 2 MEASUREMENT QUANTITIES

#### 2.1 Instantaneous Sound Pressure

Sound may be defined as a traveling disturbance in an elastic and inertial medium that can be perceived by a healthy human ear or instruments. It is important to consider that sound propagation is a three-dimensional process in space and that the sound disturbance varies with time. Thus, sound can be considered a four-dimensional field with several interrelated magnitudes that are dependant on the source, medium, and

boundary conditions. For the sake of simplicity, it is usually sufficient to assume a measurement process that involves the variation of the instantaneous pressure at a point in space; hence we will call this disturbance the instantaneous sound pressure  $p(t)$  (measured in pascals).

#### 2.2 Sound Pressure

The easiest measurable change of the medium is the variation in the local pressure from the ambient or undisturbed pressure. It is common practice to take its mean-square value and to calculate the root-mean-square (rms) pressure and call it the sound pressure  $\langle p \rangle$ . (See also Chapter 1.)

$$\langle p \rangle = \sqrt{\frac{1}{T} \int_0^T p^2(t) dt}, \quad (1)$$

where  $T$  is the time interval for the analysis or the period for periodic signals.

The sound pressure can be then expressed in decibels relative to a reference pressure  $p_0$  as the sound pressure level. See Chapter 1.

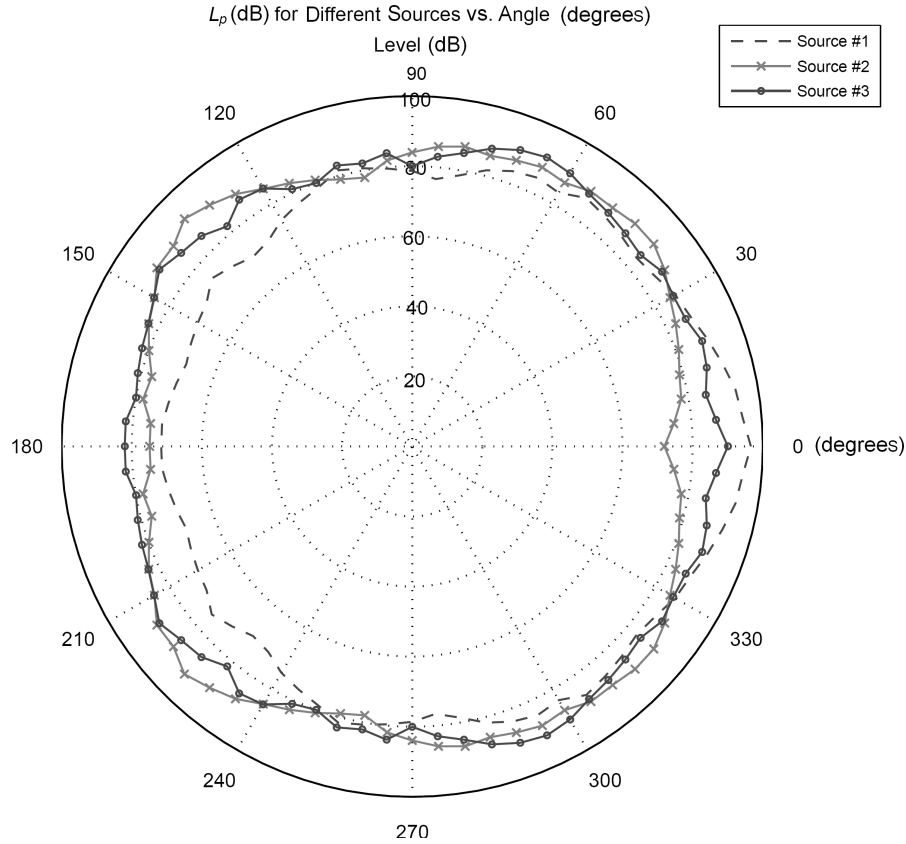
$$L_p = 20 \log_{10} \frac{\langle p \rangle}{p_0}, \quad (2)$$

where  $p_0$  is the reference pressure  $20 \times 10^{-6}$  Pa.

Along with this parameter of the signal under consideration, one more basic aspect has to be examined. That is, its level as a function of the frequency. With a simple approach this can be found by applying a Fourier transform to  $p(t)$ . However, more specific processes are generally applied to extract the pertinent data from the signal. (See Chapter 46 for more details on frequency analysis.)

#### 2.3 Sound Power Level

A traveling wave implies the existence of a source radiating sound power,  $P$ , into the medium. The sound



**Figure 1** Comparison of three sources with the same values of  $L_W$  but with different radiation patterns.

Note: The actual measurements were performed on one half of the circumference on the XY plane, and the overall sound power levels were adjusted to produce this comparison.

power level,  $L_W$ , is given in decibels by

$$L_W = 10 \log \left( \frac{P}{P_0} \right) \quad (3)$$

where  $P_0$  is the reference sound power,  $10^{-12}$  W.

The total sound power radiated by a source is independent of the directional characteristics of the source. These directional patterns are very important for noise control and noise propagation calculations because two sources with the same overall  $L_W$  may generate higher values of sound pressure level,  $L_p$ , in different directions as shown in Fig. 1. See Chapters 1, 44, and 45, for further discussion on directivity, sound pressure and vibration levels, and decibels.

## 2.4 Sound Intensity Level

The energy radiated by a source flows through a medium. The surface-normalized flow of this vector field in unit time represents the sound intensity, and normally the time-averaged intensity is the quantity

measured. The sound intensity  $\mathbf{I}$  is a vector quantity that is dependent on several factors, and it is simply related to the sound pressure  $p$  only under defined propagation conditions such as in a free field or in a reverberant field. This magnitude of the sound intensity  $\mathbf{I}$  is related to certain properties of the source, the medium, and the surroundings, and it can also be expressed in a logarithmic scale by

$$L_I = 10 \log \left( \frac{|\mathbf{I}|}{I_0} \right) \quad (4)$$

where  $I_0$  is the reference sound intensity,  $10^{-12}$  W/m<sup>2</sup>.

## 2.5 Acceleration-Velocity-Displacement

Pressure, force, acceleration, velocity, and displacement are physically related and therefore mathematically related also. The magnitudes of these variables and their logarithmic equivalents play an important role in sound and vibration. Even though sound may also be referred to as a vibration, this latter term has a

wider meaning and represents a separate phenomenon. The main quantities studied in vibration analysis are:

- Force,  $f(t)$
- Acceleration,  $a(t)$
- Velocity,  $v(t)$
- Displacement,  $x(t)$

The magnitudes of these variables can be assessed as instantaneous, peak, peak to peak, average, rms, as a function of frequency, or weighted or unweighted within a certain frequency bandwidth.

Their equivalent logarithmic expressions are given by:

- Force level

$$L_f = 20 \log \left( \frac{\langle f \rangle}{f_0} \right) \quad (5)$$

where  $\langle f \rangle$  is the rms value of the force (N), and  $f_0$  is the reference force ( $10^{-6}$  N).

- Acceleration level

$$L_A = 20 \log \left( \frac{\langle a \rangle}{a_0} \right) \quad (6)$$

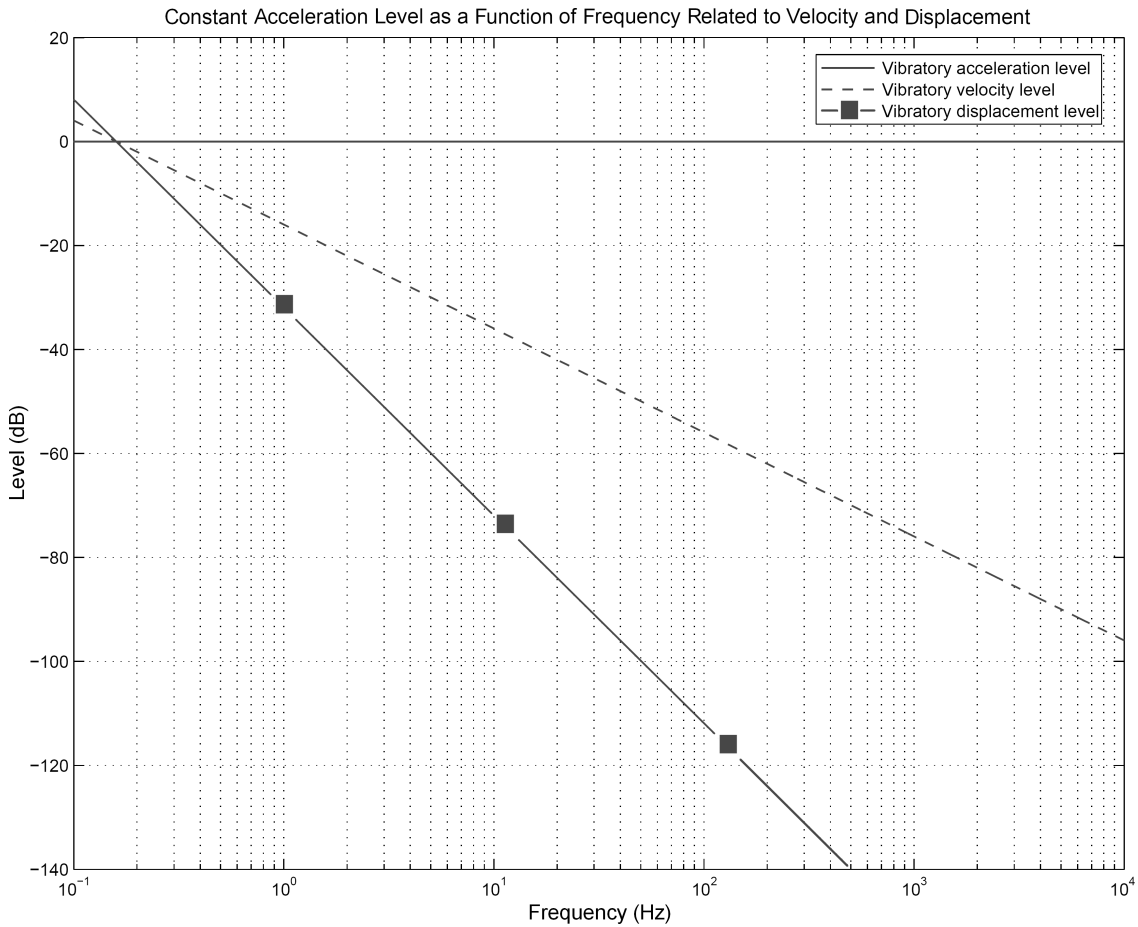
where  $\langle a \rangle$  is the rms value of the acceleration (in  $\text{m/s}^2$ ), and  $a_0$  is the reference acceleration,  $10^{-6} \text{ m/s}^2$ .

- Velocity level

$$L_A = 20 \log \left( \frac{\langle v \rangle}{v_0} \right) \quad (7)$$

where  $\langle v \rangle$  is the time-averaged velocity (in  $\text{m/s}$ ), and  $v_0$  is the reference velocity,  $10^{-9} \text{ m/s}$ .

By analyzing these magnitudes or levels along the frequency axis and without considering the phase



**Figure 2** Given an acceleration signal, a  $-20 \text{ dB/decade}$  low-pass filter can be applied to obtain the velocity, and a  $-40 \text{ dB/decade}$  low-pass filter to obtain displacement.

relationship between them, it is possible to correlate one magnitude with another, taking as a conversion factor the frequency of the signal under consideration (see Fig. 2).

We assume that  $a(t)$  and  $v(t)$  are defined as the acceleration and velocity, respectively. Consider their fast Fourier transforms (FFT):

$$\text{FFT}[a(t)] = A(\omega) \quad (8a)$$

$$\text{FFT}[v(t)] = V(\omega) \quad (8b)$$

$$V(\omega) = \frac{1}{j\omega} A(\omega) \quad (9)$$

At each frequency, the time-averaged and magnitude values of the velocity and acceleration are related by:

$$v(t) = \frac{1}{2\pi f} a(t) \quad (10)$$

In an analogous manner, we can write

$$x(t) = \frac{1}{(2\pi f)^2} a(t) \quad (11)$$

### 3 TYPES OF SIGNALS AND PROPER MEASUREMENT TECHNIQUES

Usually, it is not possible to directly measure any of the physical variables discussed above or their equivalent levels. However, it is possible to obtain equivalent representative electrical signals by means of the correct transformation of the sound and vibration events through the proper transducer mechanisms and algorithms, as shown in Chapters 35, 36, and 37. With carefully chosen transducers, these electrical signals will represent the scaled and transformed original magnitudes of the variables accurately.

The analysis must be carried out on a signal that will represent the actual magnitude under consideration, and some of the analysis transformation and domains are shown in Figs. 3 and 4. It is possible to apply different measurement techniques, which depend on several properties of the signal and which are adequately suited to extract the desired information. Processing techniques applied to the captured signal, whether in real time or postprocessed forms will include FFT, IFFT, convolution, de-convolution, filtering, cepstral techniques, correlation, and time-delay spectrometry. See Chapter 46 for a more detailed explanation of data analysis and signal classifications.

### 4 TYPICAL MEASUREMENT CHAIN

A typical measurement system block diagram is depicted in Fig. 5. In the digital era the measurement chain has evolved from (i) a quite complicated acquisition and processing system, which was always undergoing changes in hardware to (ii) a flexible and small processing unit fed by an analog transducer and

preamplifier or signal conditioner through an analog-to-digital (A/D) converter. Therefore, the original diagram has been replaced by a more straightforward and flexible digital signal processor (DSP) that performs different calculations with only the need to run a different binary code for each step of the measurement. There are three key parts in the diagram in Fig. 5.

**Transducer and Preamplifier** These are the most critical stages that affect the quality of the measurement and provide the basis for the accuracy, dynamic range, and noise floor of the system.

**A/D Converter** With a sampling rate (SR) and a conversion depth of  $N$  bits, this is the link between the analog continuous-time real-world and its digital discrete time representation. The continuously varying voltage across its input is correlated with a sampled and quantized signal in the digital domain. During this conversion the signal will be limited by the SR and the conversion depth or resolution,  $N$  bits, as follows (see Chapter 42):

The theoretical upper frequency range is

$$f_{\max} = \frac{\text{SR}}{2} \quad (12)$$

The actual frequency range will depend on the antialiasing filter used, and it may be reduced by as much as 20%.

The theoretical dynamic range (DR) is

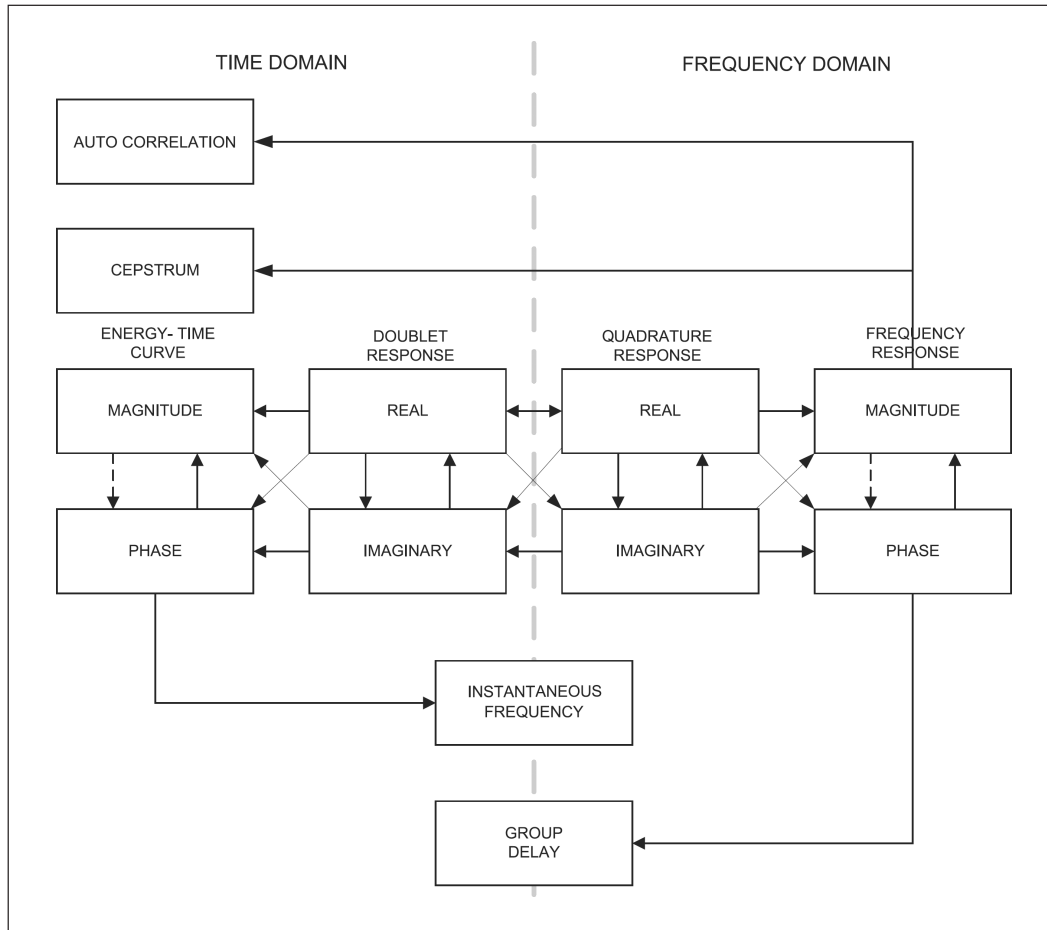
$$\text{DR} = 10 \log_{10}(2^{N \text{ bits}} - 1)^2 \quad (13)$$

With this process we will find that the conversion error is  $\pm \frac{1}{2}$  LSB (least significant bit), and this error is inherent in the use of an analog-to-digital converter. This fixed amount of uncertainty will have a greater affect on the lower than the higher level components of the signal. This implies that the precision will also be limited by the linear-to-log conversion process, and the variable error of this linear uncertainty will cause a large effect on the low levels of signals. The impact of this quantization error on a 16-bit A/D converter is shown in Fig. 6. More information on A/D converters can be found in Chapter 42.

**Digital Signal Processor** The digital signal processor needs to be properly programmed to comply with the parameters required in the particular measurement standard being used. The processor can be replaced by specific software running on a personal computer. Care must be taken to verify that the algorithm performs the required process effectively and accurately. Note that most software packages that are commercially available are expensive and specifically designed to operate with certain acquisition devices.

### 5 UNCERTAINTY AND REPEATABILITY

Taking a sound level meter as an example (Fig. 5, modified to use a microphone as a transducer), the signal will pass through several stages in the



**Figure 3** Measurement domains shown. Different transformations between time and frequency domains.

measurement chain. Every stage in this process will produce a certain uncertainty and, therefore, will increase the error in a particular measurement. A typical and expected uncertainty will occur with the class of instrument being used according to the standard being utilized [usually the International Electrotechnical Commission (IEC) or the American National Standards Institute (ANSI)]. However, there are other kinds of uncertainties that can be attributed to different causes in the measurement process and not to the instrument itself. In the case of a noise assessment with  $L_{Aeq}$  as the measured parameter, we can represent the final uncertainty  $\sigma_{tot}$  as

$$\sigma_{tot} = \sqrt{R^2 + X^2 + Y^2 + Z^2} \quad (14)$$

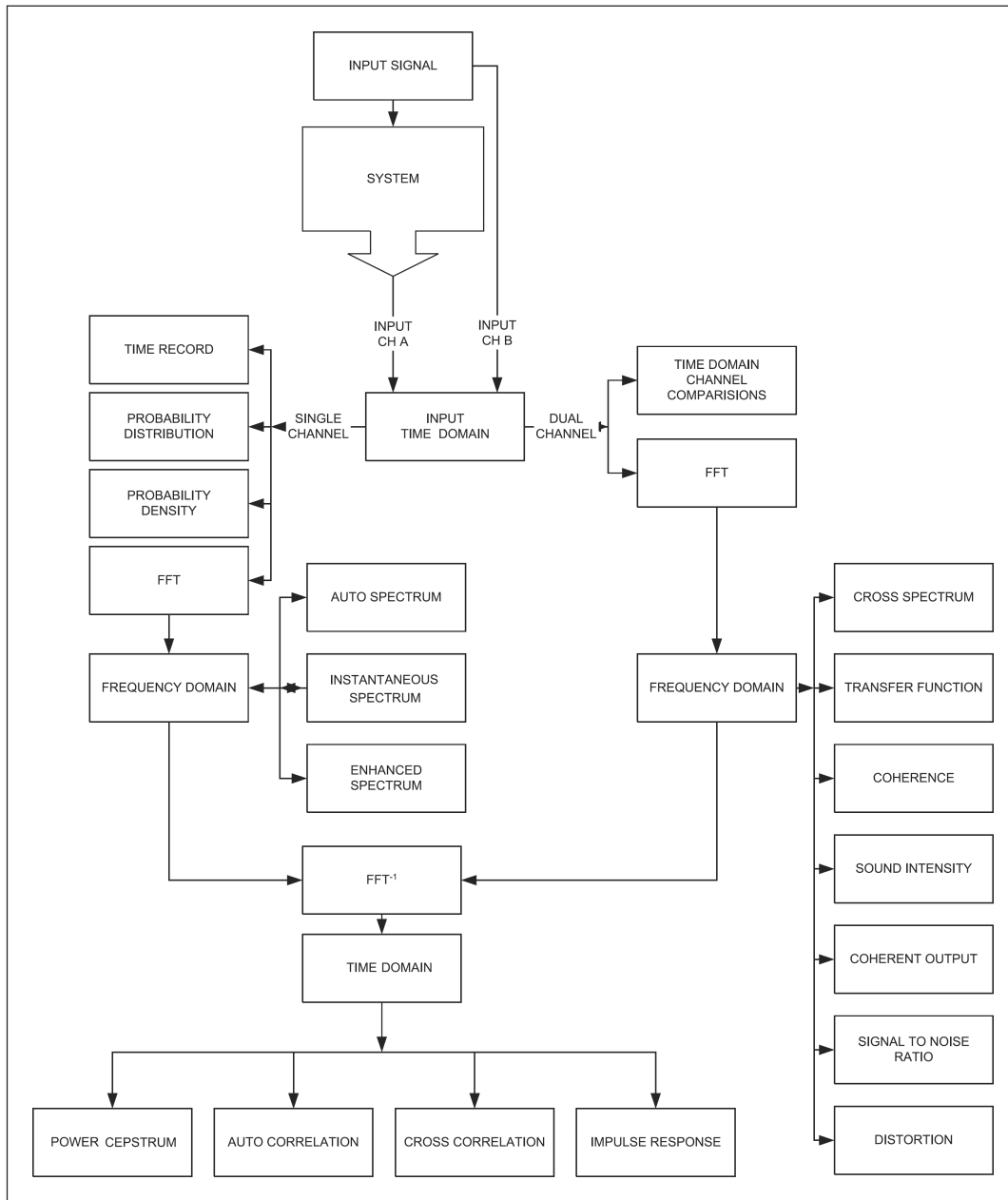
The final calculation, according to Table 1, yields  $\sigma = 1.5$  dB for class 1 instruments and  $\sigma = 2.25$  dB for class 2. As a consequence, measurements made of  $L_{Aeq}$  of a stable and continuous stationary random source, at close range to minimize propagation uncertainty

and with favorable meteorological conditions without residual noise, will represent the actual noise value within these uncertainty margins.

All this analysis is valid using a single parameter as a reference such as  $L_{Aeq}$ . In the case of a more complicated measurement environment, the accuracy of the measurement must be evaluated accordingly.

It is often required to evaluate energy sums instead of energy averages, for example, in the case of industrial noise dosage. In such a measurement, errors will accumulate creating an even higher uncertainty. A similar problem will arise when the spectrum has to be evaluated because of the linear distortion involved in the microphone and filter responses and variations in linearity as a function of frequency. All this is valid within a certain range of operation where a linear approximation can be applied, provided no overload occurs in the measurement chain. This procedure can be expanded to take into account more parameters, which are specifically related to the class of instrument, as can be seen in Table 2.





**Figure 4** Typical domain transformation and calculation options on a two-channel FFT.

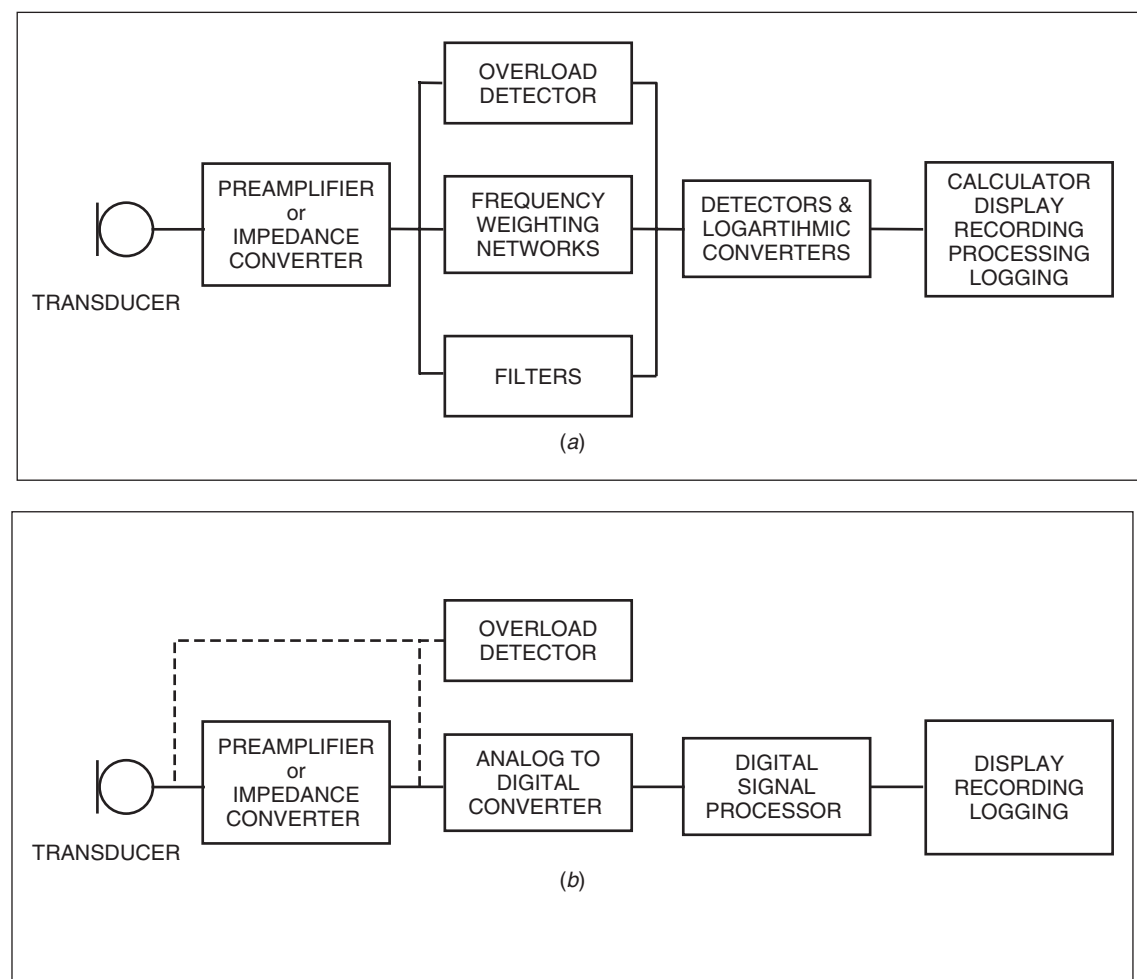
As a reference, the least attainable uncertainty with a laboratory-grade instrument will be, according to laboratory standards, within the uncertainty bounds of Table 3.

### 5.1 Other Factors

If we follow the correct calibration procedure and keep an updated and traceable calibration record every year

or two, we can be assured of obtaining proper readings with an instrument, within the accuracy established by the instrument classification (see Chapters 51 and 52).

Microphones are affected by environmental agents, electromagnetic interference, and vibration. Electronics are quite susceptible to thermal noise and electromagnetic fields. The extent to which these effects may



**Figure 5** (a) Block diagram of a typical analog measuring system. (b) In its digital counterpart, an analog-to-digital converter is implemented after the preamplifier or impedance converter and a DSP produces all of the measurement procedure.

**Table 1** Uncertainty of Measurement Based on Individual Uncertainties

Standard Deviation of Reproducibility <sup>a</sup> (dB)	Standard Uncertainty Due to Operating Conditions <sup>b</sup> (dB)	Standard Uncertainty Due to Weather & Ground Conditions <sup>c</sup> (dB)	Standard Uncertainty Due to Residual Sound <sup>d</sup> (dB)	Combined Standard Uncertainty $\sigma$ (dB)	Expanded Measurement Uncertainty (dB)
1.0	X	Y	Z	$\sqrt{1.0^2 + X^2 + Y^2 + Z^2}$	$\pm 2\sigma$

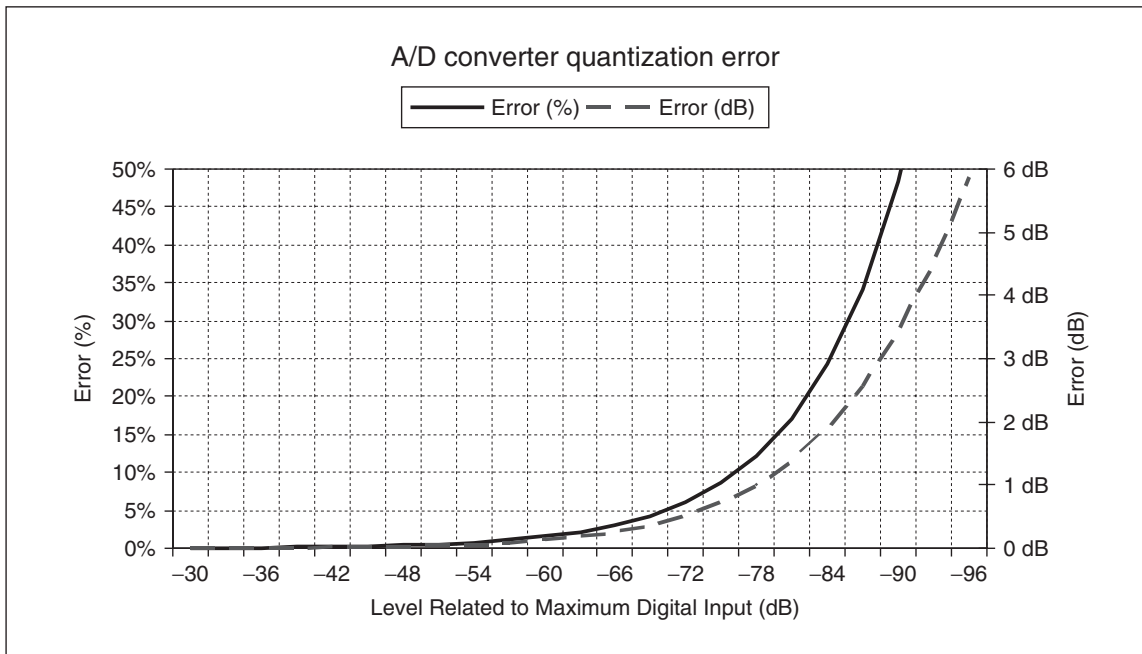
<sup>a</sup> Different operator, different equipment, same place, and everything else constant; see ISO 5725.<sup>1</sup> If class 2 sound level meters or directional microphones are used, the value will be larger.

<sup>b</sup> To be determined from at least 3, preferably 5, measurements under repeatability conditions (the same measurement procedure, the same instruments, the same operator, the same place), and at a position where variations in meteorological conditions have little influence on the results. For long-term measurements, more measurements will be required to determine a repeatable standard deviation.

<sup>c</sup> The value will vary depending upon the measurement distance and the prevailing meteorology. In this case  $Y = \sigma_m$ . For long-term measurements different weather categories will have to be dealt with separately and then combined together. For short-term measurements, these variations may add considerably to the measurement uncertainty.

<sup>d</sup> The value will vary depending on the difference between measured total values and the residual sound.

Source: Courtesy D. Manvell and E. Aflalo, of Bruel & Kjaer Sound & Vibration.



**Figure 6** Fixed error introduced by the quantization process. This error represents a larger percentage of the signal near the lowest levels on the logarithmic scale.

**Table 2** Uncertainty due to Several Factors for Short-Term Measurements Using IEC 61672<sup>2</sup> Class 1 and 2 Instruments.

Factor	IEC 61672 Class 1		IEC 61672 Class 2		Notes
	Specifications Minus Test	Expected Effect on Short-Term $L_{Aeq}$ Measurements	Specifications Minus Test	Expected Effect on Short-Term $L_{Aeq}$ Measurements	
Directional response	1.0	0.7	2.0	1.7	Estimated from different tolerances
Frequency weighting	1.0	1.0	1.8	1.8	Estimated from different tolerances
Level linearity	0.8	0.5	1.1	0.8	Estimated from different tolerances
Tone burst response	0.5	0.5	1.0	1.0	Long tones
Power supply voltage	0.1	0.1	1.0	0.2	From IEC 61672 <sup>2</sup>
Static pressure	0.7	0.0	1.0	0.0	Included in weather influence
Air temperature	0.8	0.0	1.3	0.0	Included in weather influence
Humidity	0.8	0.0	1.3	0.0	Included in weather influence
AC and radio frequency fields	1.3	0.0	2.3	0.0	Except near power systems
Calibrator	0.25	0.3	0.4	0.4	From calibrator standard
Windscreen	0.7	0.7	0.7	0.7	Estimated from different tolerances
<b>Combined Uncertainty (<math>\sigma</math>)</b>	<b>1.3</b>	<b>0.8</b>	<b>2.2</b>	<b>1.5</b>	
<b>Expanded Uncertainty (<math>2\sigma</math>)</b>	<b>2.6</b>	<b>1.6</b>	<b>4.5</b>	<b>2.9</b>	

Source: D. Manvell and E. Aflalo, Courtesy of Bruel & Kjaer Sound & Vibration.

**Table 3 Calibration Uncertainty**

Description	Measurement	Frequency Range	Least Uncertainties
<b>Microphones</b>			
	Absolute pressure sensitivity by wideband reciprocity method according to IEC 61094		
LS1, LS2, WS1, WS2		250 Hz, 500 Hz, 1 kHz	0.04 dB
LS1		20–24 Hz	0.1 dB
		25–49 Hz	0.08 dB
		50 Hz–4 kHz	0.04 dB
		4.1–6 kHz	0.05 dB
		6.1–8 kHz	0.06 dB
		8.1–10 kHz	0.08 dB
LS2		20–24 Hz	0.1 dB
		25–49 Hz	0.08 dB
		50 Hz–12.6 kHz	0.04 dB
		12.7–16 kHz	0.05 dB
		16.1–20 kHz	0.08 dB
		20.1–25 kHz	0.14 dB
		25.1–31.5 kHz	0.22 dB
	Free-field response by substitution (octave/third octave bands)		
Any		31.5 Hz	0.23 dB
		100 Hz	0.16 dB
		250–800 Hz	0.08
		10 kHz	0.24
		25 kHz	0.37
	Frequency response by electrostatic actuator method (range 20 Hz–20 kHz)		
WS1 (up to 20 KHz)			0.1 dB
WS2 (up to 10 KHz)			0.1 dB
	Frequency response for low-frequency microphones (range 1–250 Hz) using a large volume active coupler		
Low-frequency mics		0.1 Hz	0.18 dB
		16 Hz	0.13 dB
		125 Hz	0.17 dB
		250 Hz	0.37 dB
	Pressure sensitivity for $\frac{1}{2}$ in. microphones of types Bruel & Kjaer 4180, 4133, 4134, 4155, 4165, 519X, Rion UC53, and their equivalents by comparison using an active coupler (range 20 Hz–25 kHz)		
$\frac{1}{2}$ in. B&K, Rion & similar		20 Hz–4 kHz	0.06 dB
		4.1–15 kHz	0.07 dB
		15.1–20 kHz	0.10 dB
		20.1–23 kHz	0.18 dB
		23.1–25 kHz	0.26 dB
Other sizes		10 Hz	0.06
		16 Hz	0.05 dB
		31.6 Hz–500 Hz	0.04 dB
		1 kHz	0.07 dB
<b>Sound Level Meters</b>			
<b>Types 0, 1 and 2</b>	Including verification of statistical noise analysing function in sound level meters by the methods of AS 1259.1 and AS 1259.2 - 1990, IEC 651, IEC 804 and similar standards		
			0.1 dB or greater
<b>Band Pass Filters</b>			
	Attenuation according to AS/NZS 4476, IEC 61260 <sup>4</sup>		
		>50 dB ≤60 dB	0.1 dB
		>40 dB ≤50 dB	0.2 dB
		>60 dB ≤80 dB	0.3 dB

Table 3 (continued)

Description	Measurement	Frequency Range	Least Uncertainties
Acoustical Calibrators			
Types 0, 1 and 2	Including pistonphones and multifunction calibrators by IEC 60942 <sup>6</sup> method		
		Single frequency	0.06 dB
		31.5 Hz and 8 kHz	0.09 dB
		63 Hz and 4 kHz	0.08 dB
		125 Hz–2 kHz	0.07 dB
		12.5 kHz	0.15 dB
		16 kHz	0.23 dB
Vibration Transducers			
Vibration transducers	Absolute acceleration calibration by interferometry from 1 Hz–10 kHz by the ISO 16063-11 <sup>7</sup> methods. Voltage sensitivity or charge sensitivity		
		1–19.9 Hz	0.5%
		20–62.9 Hz	0.4%
		63 Hz–4.99 kHz	0.3%
		5–6.29 kHz	0.4%
		6.3–10 kHz	0.5%
Accelerometers of mass up to 1000 g	Voltage sensitivity or charge sensitivity by comparison with the ISO 16063-12 <sup>8</sup> methods		
		20 Hz–10 kHz acceleration from 10 m/s <sup>2</sup> to 980 m/s <sup>2</sup>	0.5%
Other Vibration Equipment			
Vibration analyzers			0.1%
Vibration filters			0.1%
Vibration calibrators			0.5%

Source: Data extracted from National Physics Laboratory, UK, 2006.

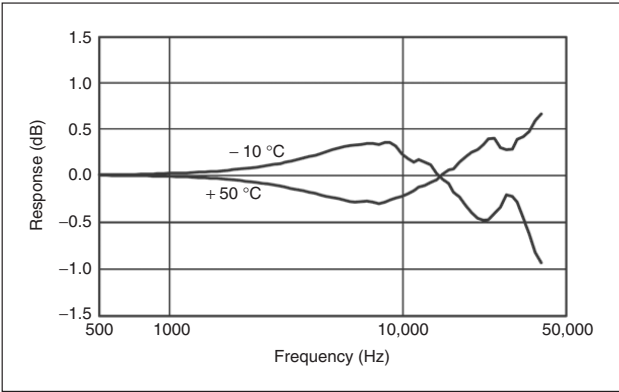


Figure 7 Effect of temperature variations on the sensitivity vs. frequency curve of a high-quality microphone. (Courtesy Bruel & Kjaer.)

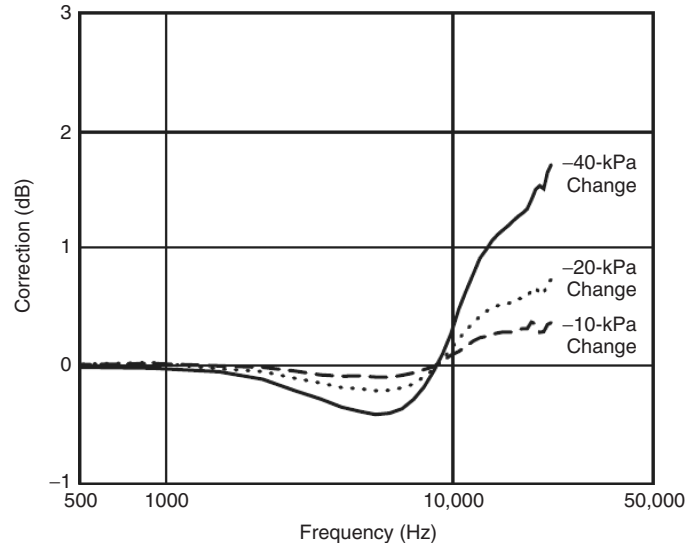
modify their performance depends on several factors. It is important to check the manufacturer’s specifications about these effects, which will vary from brand to brand. As a guideline, Figs. 7 and 8 show the temperature and the ambient pressure versus frequency sensitivity variations, which are typical of a commercial microphone.

6 REVERBERATION TIME MEASUREMENTS

The acoustical characteristics of a room are one of the main issues in noise control and architectural acoustics.

In the first case, we can focus on how these modify the amount of energy transmitted to the receiver, and in the second one we can include several measurable descriptors of a room to evaluate the quality of the perceived field. See Chapters 4 and 103 for more detailed information.

Among many of these parameters related to the acoustical quality of a room (see ISO 3382-1997<sup>9</sup>), the determination of the reverberation time (RT) is frequently the main goal of acoustical measurements. The reverberation time is defined as the time taken for the sound field energy to decrease to 1/1,000,000



**Figure 8** Effect of ambient atmospheric pressure variation on the sensitivity vs. frequency curve of a high-quality microphone. (Courtesy Bruel & Kjaer.)

of its original value, after the source has been turned off. It is useful to determine not only the most important characteristics of the acoustical environment but also to indirectly quantify the absorption coefficient measured in a reverberation chamber. This parameter—also known as the Sabine absorption coefficient—is widely used in architectural acoustics, noise control, and the acoustical characterization of material properties.

There are several methods available for the measurement of the RT. Each of these has differences compared with the others in terms of instrumentation, measurement time, and accuracy. There are two standard procedures:

1. Interrupted noise method
2. Integrated impulse response method

Some general considerations apply to both of these methods:

1. The standard frequency range of interest covers the octave or one-third octave bands beginning at 88 Hz and finishing at 5657 Hz. This range can be extended by one octave at the upper and lower frequency limits.\*
2. Both the source and the microphone have to be omnidirectional and comply with certain specifications.

\*Current laboratory test facilities for materials provide reliability and proper diffusion only to roughly 88 Hz and larger rooms should be constructed to allow this change to be globally representative, although there are some exceptions to this limit.

3. There should be no distortion or overload in the measurement chain.
4. All the characteristics of the instrument are clearly defined in the standard used.
5. There is a minimum distance from the source to the microphone as given by Eq. 15:

$$d_{\min} = 2\sqrt{\frac{V}{cT}}, \text{ m} \quad (15)$$

where  $V$  is the room volume,  $\text{m}^3$ ;  $T$  is the expected reverberation time, s, and  $c$  is the speed of sound in air, m/s.

6. The number of measurement points will influence the final result as well as the bandwidth and the RT. The uncertainties  $r_{20}$  and  $r_{30}$  can be evaluated for  $T_{20}$  and  $T_{30}$  with Eqs. (16) and (17), respectively (in accordance with ISO 5725-2<sup>1</sup>):

$$r_{20} = \frac{370}{\sqrt{BNT_{20}}} \% \quad (16)$$

$$r_{30} = \frac{200}{\sqrt{BNT_{30}}} \% \quad (17)$$

where  $B$  is the filter bandwidth (0.71 for octave and 0.23 for one-third octave band filters, multiplied by  $f_c$ ),  $N$  is the number of averages preformed,  $f_c$  is the center frequency of the measured values of  $T_{20}$  and  $T_{30}$ . See Table 4 for definitions.

7. The number of measurement positions will depend on the coverage method chosen and

**Table 4 Determination of RT Parameters from the Decay Curve**

Parameter	Starting Point	Finishing Point	Extrapolating to $T_{60}$
$T_{20}$	5 dB (below start of decay)	25 dB (below start of decay)	X 3
$T_{30}$	5 dB (below start of decay)	35 dB (below start of decay)	X 2

on the area or seating capacity in the case of an auditorium, and it should be selected as follows:

- Low coverage: in cases where only an assessment of the amount of room sound absorption is required for noise control purposes
  - Normal coverage: in cases where measurements are needed to verify whether the acoustical performance of a building meets specific design requirements
- Any special consideration regarding furniture, draperies, carpets, occupation, and the like should be clearly noted.
  - The temperature and humidity should be measured and recorded because they greatly affect the sound absorption of the air at high frequencies.

## 7 MEASUREMENT DESCRIPTORS FOR NOISE

It would be a great achievement to understand and represent noise signals and their underlying processes with a single index and to correlate this index with human perception of noise. Unfortunately, this is not the case, although there are a number of descriptors that are useful in evaluating the effects of noise. See Chapters 1, 34, and 106 for further discussion on measurement descriptors.

In the following definitions the word *signal* is understood to be a general term with a broad meaning ranging from sound to noise and including single, multiple, and complex noise sources, either fixed or moving.

**Instantaneous Sound Pressure— $p(t)$**  It is the most accurate descriptor of the signal under investigation, representing the variation of the sound pressure as a function of time. The definitions of the following parameters are based on this descriptor,  $p(t)$ .

**Time-weighted and Frequency-weighted Sound Pressure Level** This is the sound pressure level weighted in time and frequency with certain specific functions. The most common time weightings are slow, fast, and impulse. The most common frequency weightings are A, C, or no weighting.

**Peak Sound Pressure Level— $L_{\text{peak}}$**  This is the logarithmic expression of the frequency-weighted or unweighted maximum instantaneous value of the sound pressure  $p_{\text{max}}(t)$ .

$$L_{\text{peak}} = 10 \log_{10} \left( \frac{p_{\text{max}}}{p_0} \right)^2 \quad (18)$$

**Equivalent Continuous Sound Pressure Level— $L_{\text{Aeq}T}$**  This is denoted as  $L_{\text{Aeq}T}$  and represents the continuous steady-state A-weighted sound pressure level, which would have the same total mean energy as the signal under consideration in the same period of time  $T$ :

$$L_{\text{Aeq}T} = 10 \log_{10} \frac{1}{T} \int_0^T \left[ \frac{p_A(t)}{p_0} \right]^2 dt \quad (19)$$

where  $p_A(t)$  is the instantaneous A-weighted sound pressure,  $p_0$  is the reference sound pressure,  $20 \mu\text{Pa}$ , and  $T$  is the analysis time period.

**$N$  Percent Exceedance Level— $L_{K1K2N\%,T}$**  This is the time- and frequency-weighted sound pressure level exceeded for  $N\%$  of the time interval under consideration;  $K_1$  is the weighting filter of the instrument and  $K_2$  is the time weighting constant.  $L_{\text{AS}50,15 \text{ min}}$  is the A-weighted sound pressure level, slow time-averaged, exceeded 50% of the considered time of 15 min. See also Chapter 34.

**Sound Exposure Level (SEL)** This index applies to discrete noise events and is defined as the constant level that, if maintained during a 1-s interval, would deliver the same A-weighted sound energy to the receiver as the real time-varying event. We can understand this as a  $L_{\text{Aeq}T}$  normalized for  $T = 1 \text{ s}$ :

$$\text{SEL} = 10 \log_{10} \frac{1}{t_2 - t_1} \int_{t_1}^{t_2} \left[ \frac{p_A(t)}{p_0} \right]^2 dt \quad (20)$$

where  $p_A(t)$  is the instantaneous A-weighted sound pressure,  $p_0$  is the reference pressure of  $20 \mu\text{Pa}$ ,  $t_0$  is the reference time, in this case 1 s,  $t_2 - t_1$  is the time interval, which is made long enough to include the whole part of the event under consideration.

**Perceived Noise Level (PNL)** This index is based on perceived noisiness and applies to aircraft flyovers. The determination of the annoyance caused by aircraft noise is quite complicated and is explained in the aircraft noise measurement section of this chapter. See also Chapter 34.

**Specific Descriptors for Community Noise** The process of measuring and correlating noise with annoyance is a key issue in environmental impact studies. Descriptors are needed, not only to assess current situations but also to plan noise control measures and long-term noise impacts on the

population. This process encompasses not only the measurement of noise levels but also the understanding of the characteristics of noise events and the noise source in terms of level, frequency content, number of repetitions, and period of the day of occurrence. The noise events can be described in the following terms:

**Single Events** Events such as the passby of a motorcycle, the flyby of an aircraft, or a blast at a mining facility are defined as single events. These will be described in terms of sound exposure level with frequency weighting, maximum sound pressure level with time and frequency weighting, and peak sound pressure level with frequency weighting along with the event duration.

**Repetitive Single Events** These may be considered as the sum due to the reoccurrence of multiple individual events. In this case the measurement should be based on the descriptors for a single event plus the amount of repetitions that take place.

**Continuous Sound** The sound will be termed continuous when the sound pressure level generated is constant, fluctuating or slowly varying in the time interval of the analysis. A good descriptor for this category of noise is the A-weighted equivalent continuous sound pressure level.

If A-weighted sound pressure levels are not sufficient to assess the noise impact, more parameters need to be included to adjust and better correlate the measured event with annoyance. These parameters include corrections for period of day, tonality, low-frequency content, and impulsiveness. These adjustments should be consulted in the applicable standard or current legislation being used.

**Composite Whole-Day Rating Levels** Composite rating levels are used widely, and a substantial amount of research has been conducted, and standards and legislation have been written using this descriptor for guidance as the main assessed parameter. Two examples of this rating are the day–night rating level and day–evening–night rating level. See also Chapters 1, 34, and 106 for further discussion on these descriptors.

#### Day–Night Rating Level ( $L_{Rdn}$ )

$$L_{Rdn} = 10 \log \left[ \frac{d}{24} 10^{(L_{Rd} + K_d)/10} + \frac{24 - d}{24} 10^{(L_{Rn} + K_n)/10} \right] \quad (21)$$

#### Day–Evening–Night Rating Level ( $L_{Rden}$ )

$$L_{Rden} = 10 \log \left[ \frac{d}{24} 10^{(L_{Rd} + K_d)/10} + \frac{e}{24} 10^{(L_{Re} + K_e)/10} + \frac{24 - d - e}{24} 10^{(L_{Rn} + K_n)/10} \right] \quad (22)$$

where  $d$  is the number of daytime hours,  $e$  is the number of evening hours,  $L_{Rd}$  is the daytime rating level including adjustments for sources and characteristics,  $L_{Rn}$  is the nighttime rating level including adjustments for sources and characteristics,  $L_{Re}$  is the evening rating level including adjustments for sources and characteristics,  $K_d$  is the daytime adjustment,  $K_e$  is the evening time adjustment, and  $K_n$  is the nighttime adjustment.

The duration of each time period varies from country to country and both the period duration, and adjustment corrections for each period decided by the local noise authority must be used correctly.

## 8 VEHICLE NOISE MEASUREMENT

The measurement of noise and vibration in moving vehicles is a complicated process that involves several separate procedures (see Chapter 83). However, the emission of traffic noise produces an environmental impact in urban and suburban surroundings that can be measured. If the emission level of vehicles complies with certain established noise levels, the impact of this emission based on traffic density, street layout, and countermeasures can be evaluated and controlled beforehand. To evaluate this noise impact prior to the introduction of a new vehicle to the market, a reliable measurement method is needed. There are two main measurement methods used to establish the emission level of a vehicle considering it as a single source:

- Stationary
- Dynamic Accelerating

In general, these methods are not used to determine whether the noise is caused by aerodynamic, tire, engine, exhaust, gear box, or transmission sources.

Taking into account that in urban areas vehicles spend much of the time accelerating or decelerating, the standard procedure is to use engineering methods to obtain a quantitative measure of this emission level. The accelerating noise is often the peak noise output of many vehicles, and vehicle noise tests based on the full acceleration mode are commonly made. This procedure is covered fully in several national and international standards.

### 8.1 Measurement Instruments and Procedures

It is suggested to use an IEC 61672<sup>2</sup> type 1 sound level meter and to set the instrument detectors to A-weighting and fast time weighting. The required discrete-time interval to analyze the noise variation as a function of time is 30 ms. Critical distances and environmental conditions should be noted and reported as well as the vehicle speed with the precision stated in Table 5.

Special considerations are required to ensure hemispherical directivity with a divergence not more than  $\pm 1$  dB. To achieve this, ISO 10844<sup>10</sup> defines a specific procedure and ground plan to conduct the tests (see Fig. 9). Optimally, the A-weighted noise level floor should be not less than 10 dB below and if possible





by aircraft and airports, and (2) long-term influence of exposure to noise in residential zones nearby or affected by airports and its operations.

People are less tolerant of the noise generated by the flyover of an aircraft when they are indoors rather than outdoors, even if the same event with the same acoustical energy is involved. It does not seem to matter that sound pressure levels indoors are attenuated by the structure of the building. Therefore, the annoyance perceived by a listener is not a simple matter, and that is the reason for creating an accurate way to measure perceived noise levels.

### 9.1 Measurement Method and Calculation Procedure

To quantify the perceived noisiness, the noise generated (1) by single aircraft movements and (2) by multiple aircraft operations at airports are treated separately. In each case several international standards fully describe the recommended procedures for the noise measurements. See also Chapter 34.

The measurements of the noise generated by aircraft are made following these recommendations:

- A type 1 measurement device is required.
- The height of the microphone must be 1.2 m above the ground.
- The ground must be an acoustically hard surface.
- The microphone must be positioned in a straight line with the aircraft path.
- There must not be any obstacle in the area near the measurement station.
- At no time must the wind speed, measured 10 m above the ground, exceed 5 m/s, and the microphone must be properly protected from the wind.
- The measurement system must be calibrated before and after use.

The data obtained must be processed and preferably digitally recorded for later analysis to obtain the time history and spectrograms. To make a rough approximation to the perceived noise levels, it is only necessary to obtain the spectrum histories. To calculate an accurate result, however, which can be validated by international standards, it is necessary to obtain the time history as well. The frequency spectrum history must be obtained at least every 0.5 s throughout the measurement period. The results are analyzed in one-third octave bands from 50 to 10,000 Hz.

To calculate the perceived noise level (PNL), the sound pressure levels must first be converted into perceived noisiness (PN). The PN is given in “noys,” and the relationship between the sound pressure level  $L_p$ , PN, and PNL is shown in Fig. 10. The 1-noy curve is the minimum value of the sound pressure level  $L_p$  required to disturb a person’s tranquility. The PN or  $N$ , can be calculated with the following expression:

$$N = n_{\max} + 0.15 \left( \sum n - n_{\max} \right) \quad (23)$$

Once the PN value has been obtained, it is converted into PNL, which is a logarithmic expression relative to a reference PN value (2 noys in this case):

$$L_{PN} = 40 + \frac{10 \log_{10} N}{\log_{10} 2} \quad (24)$$

In the case that the spectrum curve obtained is not smooth and the differences between bands are greater than 3 dB, because of tonal components, a correction must be applied. This correction factor is called the tone correction  $C$  and is obtained by complicated calculations that are described in the relevant standard.

The PNL values corrected by this method are tone-corrected values and are named TCPNL. These corrections are shown in Fig. 11. However, TCPNL values are only spectrum corrected and do not take into account the fact that the annoyance caused by the noise depends not only on the frequency content of the event but also on the duration of the exposure. So a time correction should be applied as well. This time-corrected value  $L_{EPN}$  is defined as follows:

$$L_{EPN} = 10 \log_{10} \frac{1}{t_2 - t_1} \int_{t_1}^{t_2} 10^{L_{TPN}/10} dt \quad (25)$$

where  $L_{TPN}$  is the tone-corrected value of  $L_{PN}$ .

The effective perceived noise level, or EPNL, is the most accurate and accepted measurement unit for aircraft overall perceived noise level. However, PNL and TCPNL values will not always satisfy the need for a reliable noise figure. For the validation of the measurement, other variables such as aircraft conditions, the wind direction, and other meteorological aspects must be documented.

The equations given so far are only applicable to individual events. Equations (26) and (27) apply to multiple events through equivalent perceived noise levels (EQPNL) and A-weighted equivalent noise levels (EQANL):

$$L_{PNeq} = 10 \log_{10} \left( \frac{1}{T} \sum_i 10^{L_{EPN_i}/10} \right) \quad (26)$$

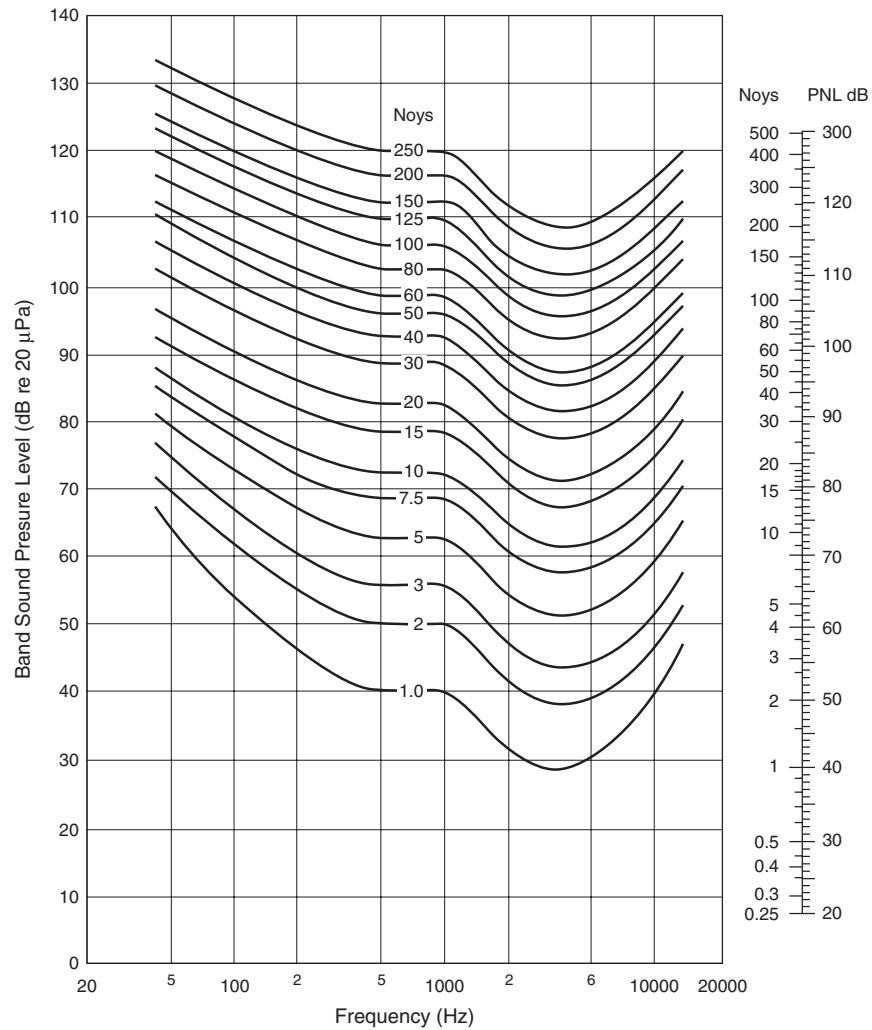
and

$$L_{AeqT} = 10 \log_{10} \left( \frac{1}{T} \sum_i 10^{L_{AX_i}/10} \right) \quad (27)$$

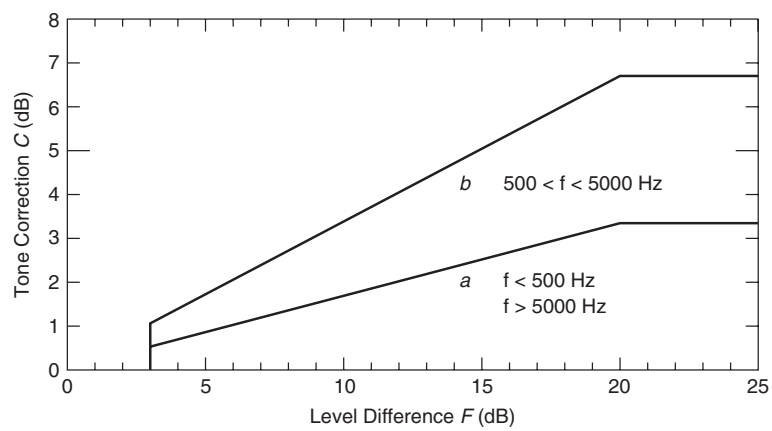
where  $i$  indicates the number of the event and  $T$  is the duration of the measurement in seconds.

### 9.2 Aircraft Noise Application Case

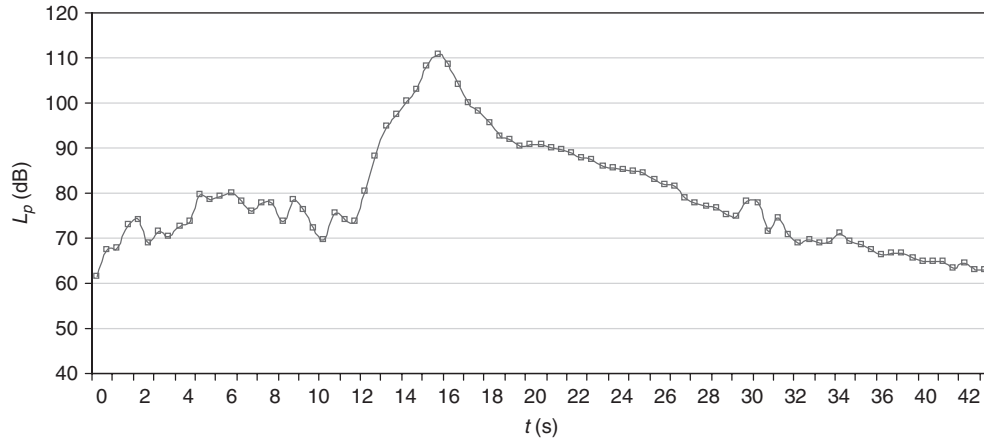
The calculation of EPNL requires a large amount of gathering and processing of data. In this example, measurements were made with a type 1 digital sound level meter capable of data recording, avoiding the need for an additional recorder. The time increment



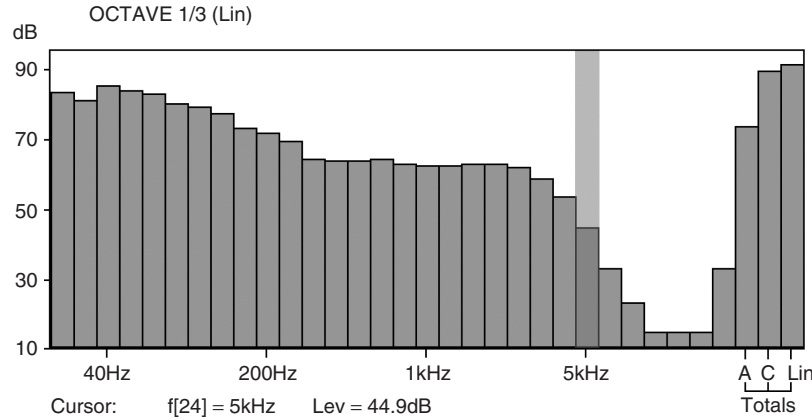
**Figure 10** Graph showing the relation between noys and PNL.



**Figure 11** Tone correction (C) for PNL used to obtain TCPNL values.



**Figure 12** A-weighted sound pressure level versus time data clearly showing the noise peak due to the aircraft flyover above the microphone location.



**Figure 13** Example of a nonsmooth aircraft noise spectrum where a tone correction must be applied.

( $k$ ) was taken as 0.5 s for a period of 43 s, which involved the aircraft takeoff. (See Figs. 12, 13, and 14.)

## 10 ACOUSTIC IMPEDANCE MEASUREMENTS

Impedance tubes are used to measure the acoustical properties of materials. Acoustic impedance is an important material characteristic directly related to the material sound absorption. The acoustic impedance can be measured quickly and evaluated with only a small sized sample of the material, without the need for a reverberation chamber. Impedance tube measurements are quite adequate for production tests and research and development measurements in the laboratory.

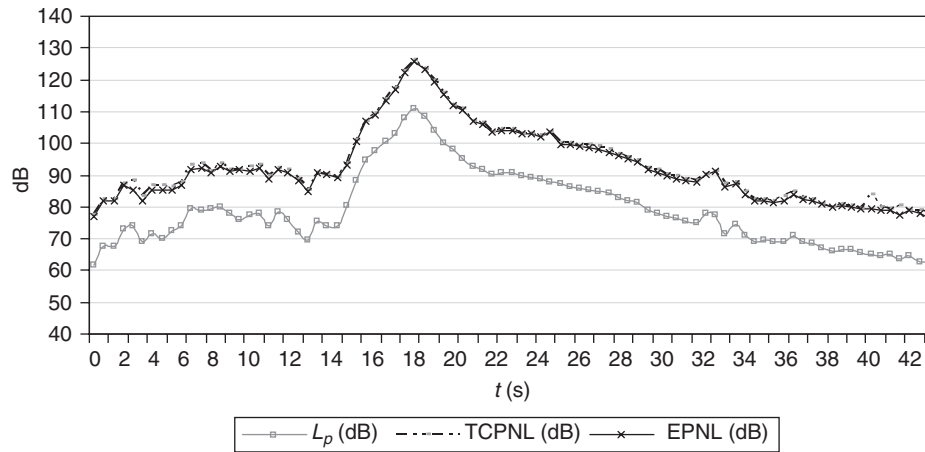
The setups of Figs. 15, 17, and 18 are used to determine the plane wave impedance of a material sample. The material impedance and the absorption and reflection coefficients can be determined by two main methods:

1. Measuring the standing-wave ratio with one microphone
2. Measuring the complex sound pressure transfer function between two microphones

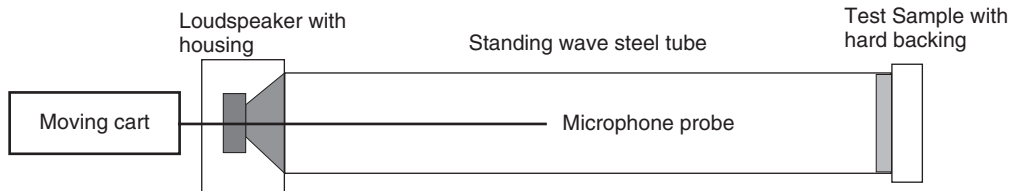
### 10.1 Standing Wave Ratio Method (One Moving Microphone)

Consider a pipe of cross-sectional area  $S$  and length  $L$ . Assume that the pipe is terminated at  $x = L$  by a mechanical impedance  $Z_m$  and is driven by a piston at  $x = 0$ . A movable probe microphone is used to measure the sound pressure of the standing-wave pattern inside the tube (Figs. 15 and 16). Provided the excitation is harmonic and of sufficiently low frequency to ensure only plane waves propagate, the following equation holds true for the pressure:

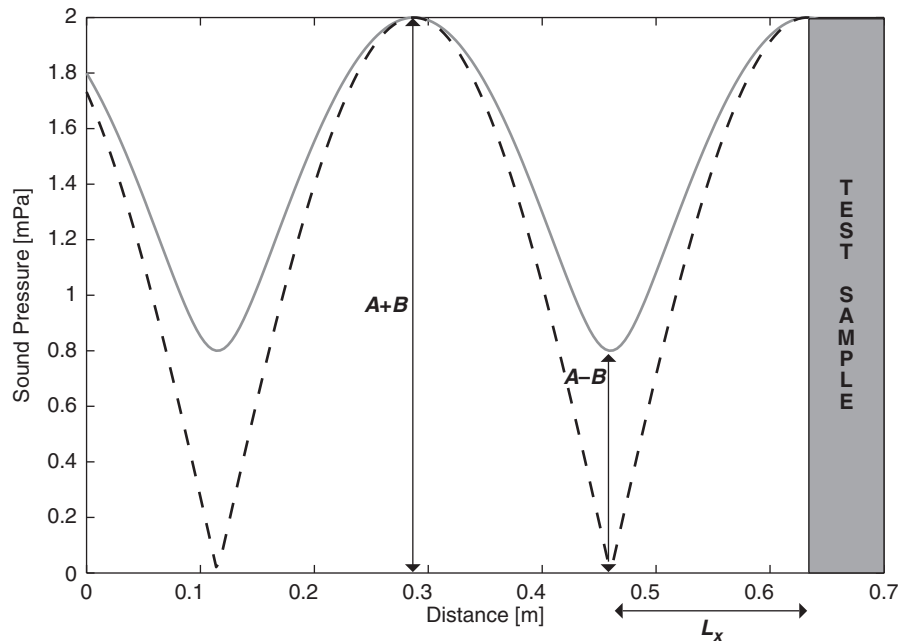
$$p(x, t) = A e^{j[\omega t + k(L-x)]} + B e^{j[\omega t - k(L-x)]} \quad (28)$$



**Figure 14** Difference between A-weighted  $L_p$  TCNLT, and EPNLT.



**Figure 15** Setup for measuring the normal incidence acoustic impedance of a material.



**Figure 16** Dashed line: Test sample has zero sound absorption. Solid line: test sample has sound absorption greater than zero. Notice that the sound pressure amplitude at an antinode is  $A + B$  and the sound pressure amplitude at a node is  $A - B$ .

where  $\mathbf{A}$  and  $\mathbf{B}$  are complex constants imposed by boundary conditions at the two ends of the pipe.

Therefore the particle velocity can be expressed as

$$\mathbf{u}(x, t) = \frac{1}{\rho c} (\mathbf{A} e^{j[\omega t + k(L-x)]} - \mathbf{B} e^{j[\omega t - k(L-x)]}) \quad (29)$$

and the acoustic impedance  $Z_A$  of the plane waves inside the tube is

$$Z_A(x) = \frac{\rho c}{S} \left\{ \frac{\mathbf{A} e^{j[\omega t + k(L-x)]} + \mathbf{B} e^{j[\omega t - k(L-x)]}}{\mathbf{A} e^{j[\omega t + k(L-x)]} - \mathbf{B} e^{j[\omega t - k(L-x)]}} \right\} \quad (30)$$

The mechanical load impedance at  $x = L$  can be expressed in terms of the acoustic impedance of the waves:

$$Z_m = S^2 Z_A = \rho c S \left( \frac{\mathbf{A} + \mathbf{B}}{\mathbf{A} - \mathbf{B}} \right) = \rho c S \left( \frac{1 + \mathbf{B}/\mathbf{A}}{1 - \mathbf{B}/\mathbf{A}} \right) \quad (31)$$

Rewriting  $\mathbf{A}$  and  $\mathbf{B}$  as follows:

$$\mathbf{A} = A, \quad \mathbf{B} = B e^{j\theta} \quad (32)$$

and substituting into Eq. (31) gives

$$Z_m = \rho c S \left[ \frac{1 + (B/A) e^{j\theta}}{1 - (B/A) e^{j\theta}} \right] \quad (33)$$

it is possible to extract from this equation the mechanical impedance, knowing the ratio of incident and reflected waves and the phase angle  $\theta$ . Substituting Eq. (32) into (28) and solving to obtain the modulus and average value of  $p(t)$ , we obtain

$$P = |p(t)| = \sqrt{(A+B)^2 \cos^2[k(L-x) - \frac{\theta}{2}] + (A-B)^2 \sin^2[k(L-x) - \frac{\theta}{2}]} \quad (34)$$

This sound pressure distribution along the  $x$ -axis is shown in Fig. 16 for two cases.

It is not possible to measure  $A$  and  $B$  separately but only  $A+B$  and  $A-B$ . Defining the standing-wave ratio (SWR) as

$$\text{SWR} = \frac{A+B}{A-B} \quad (35)$$

the sound power reflection coefficient  $R$  is

$$R = \frac{B}{A} = \frac{\text{SWR} + 1}{\text{SWR} - 1} \quad (36)$$

and it is possible to find a simple relation with the absorption coefficient for normal incidence:

$$\alpha_n = 1 - R^2 = \left( \frac{\text{SWR} + 1}{\text{SWR} - 1} \right)^2 \quad (37)$$

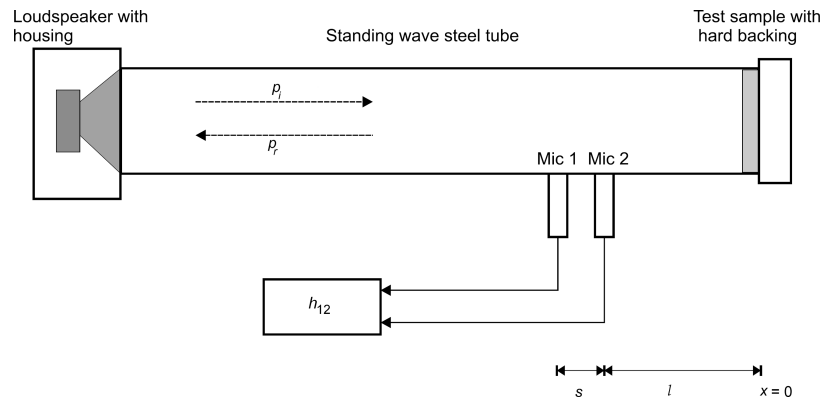
## 10.2 Transfer Function Method (Two Fixed Microphones)

This method (see Fig. 17) is based on the measured frequency response function between two microphones  $H_{12}$ , which implies separating the incident ( $p_i$ ) and reflected ( $p_r$ ) sound pressures and their respective Fourier transforms  $P_i$  and  $P_r$ , by computing the complex reflection coefficient,  $R$ , at the measurement surface. The complex impedance  $Z$  can be calculated from these data. The experimental setup for this procedure is shown in Fig. 18.

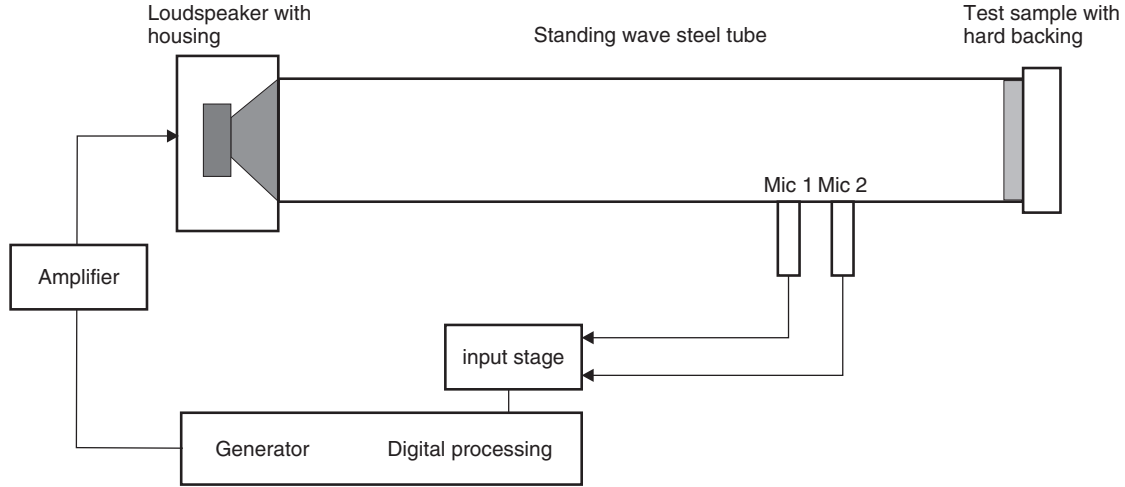
The frequency response function in the frequency domain,  $H_{12}$ , is defined as

$$H_{12} = \frac{P_2}{P_1} = \frac{P_{2i} + P_{2r}}{P_{1i} + P_{1r}} \quad (38)$$

where  $P$  is the Fourier transform of  $p(t)$ ,  $P_{ni}$  is the Fourier transform of the sound pressure due to the



**Figure 17** Impedance tube measurement setup. The microphones are located at positions 1 and 2, separated by a distance  $s$ . The sample is located at a distance  $\ell$  from microphone 2.



**Figure 18** Experimental setup for sound absorption measurement of material samples with tube, microphones A and B, and frequency analyzer.

incident waves ( $i$ ) at microphone  $n$ , and  $P_{nr}$  is the Fourier transform of the sound pressure due to the reflected waves ( $r$ ) at microphone  $n$ , where  $n$  is either 1 or 2 and refers to the microphone considered (see Fig.17).

Taking into account that

$$\begin{aligned} H_{12i} &= \frac{P_{2i}}{P_{1i}} & H_{12r} &= \frac{P_{2r}}{P_{1r}} \\ R_1 &= \frac{P_{1r}}{P_{1i}} & R_2 &= \frac{P_{2r}}{P_{2i}} \end{aligned} \quad (39)$$

For microphone 1 the following holds true:

$$R_1 = \frac{H_{12} - H_{12i}}{H_{12r} - H_{12}} \quad (40)$$

provided that only plane waves propagate in the tube and that the transfer functions  $H_{12i}$  and  $H_{12r}$  are  $e^{-jks}$  and  $e^{+jks}$ , respectively. Multiplying the calculated reflection coefficient by  $e^{j2k(l+s)}$  to calculate its value at  $x = 0$ ,  $R$  can be expressed as

$$R = e^{j2k(l+s)} R_1 = -e^{j2k(l+s)} \left( \frac{H_{12} - e^{-jks}}{H_{12} - e^{jks}} \right) \quad (41)$$

The normal incidence sound absorption coefficient is  $\alpha = 1 - |R|^2$ , and the surface-specific acoustic impedance ratio  $Z$  is

$$Z = \frac{Z_s}{\rho_0 c} = \frac{1 + R}{1 - R} \quad (42)$$

where  $Z_s$  is the specific acoustic impedance of the surface.

### 10.3 Application of Impedance Tube Measurements

The sound absorption and mechanical properties of several different road surfaces have been studied in a recent research project at Auburn University. The absorption coefficient of dense and porous road surfaces was measured in the laboratory using core samples with 10- and 15-cm diameter impedance tubes. The 15-cm tube allows the absorption of a large core sample surface to be determined, but only up to a frequency of about 1250 Hz. The 10-cm tube allows the absorption coefficient to be determined up to a frequency of about 1950 Hz. See the setup in Fig. 18. The two different diameter impedance tubes were also mounted vertically on some of the same pavement types and the absorption coefficient of these pavement types was measured in this way too.

The impedance tubes consist of a metal tube (of either 10- or 15-cm internal diameter) with a loudspeaker connected at one end and the test sample mounted at the other end. The loudspeaker is enclosed and sealed in a wooden box and is isolated from the tube to minimize structure-borne sound excitation of the impedance tube. Usually, a steel backing plate is fixed tightly behind the specimen to provide a hard sound reflecting termination. Plane waves are generated in the tube using broadband white noise from the noise generator of a Bruel & Kjaer PULSE system. The same tube can be used to measure the sound absorption coefficient of samples in situ. In such a case, the tube is mounted vertically to the surface under study and a seal is made with some sealant between a metal collar at the lower end of the tube and the sample.

Two identical microphones are mounted in the tube wall to measure the sound pressure at two longitudinal locations simultaneously. The PULSE

system is used to calculate the normal incidence absorption coefficient  $\alpha$  by processing an array of complex data from the measured frequency response function. Figure 19 illustrates the experimental setup for the test equipment.

The working frequency range is determined by the dimensions of the setup. The lower frequency limit depends on the microphone spacing. For frequencies lower than this limit, the microphone spacing is only a small part of the wavelength. Measurements at frequencies below this limit will cause unacceptable phase errors between the two microphones. The low-frequency limit was set at 200 Hz in these experiments. The upper frequency limit depends on the diameter of the tube:

$$f_u < \frac{Kc}{d} \quad \text{Hz} \quad (43)$$

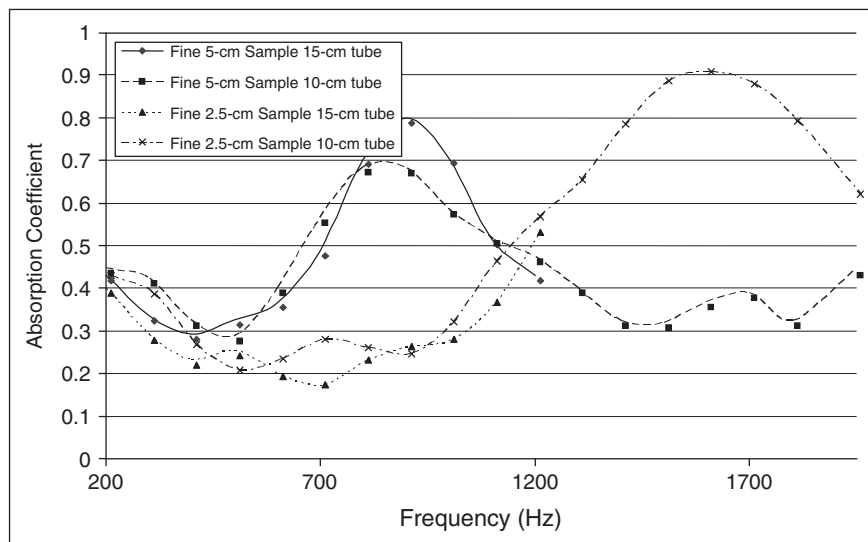
where  $c$  is the speed of sound (in m/s),  $d$  is the tube diameter (in m), and  $K$  is a constant equal to 0.586 in the International System (SI) of units.

For frequencies higher than  $f_u$ , the sound waves in the tube are no longer plane waves. For the 15-cm diameter tube, the theoretical upper frequency limit is 1318 Hz. However, the plane wave assumption did not appear valid for frequencies higher than 1250 Hz. So for these tests, the working frequency range was set to be from 200 to 1250 Hz. For the 10-cm diameter tube, the theoretical upper frequency limit for the tube is 1978 Hz. For some thin samples whose thicknesses were 2.54 and 3.84 cm, the first absorption peak occurs higher than 1250 Hz. So the smaller 10-cm tube can be used for thin samples. One result is shown in Fig. 20. It is observed that there is generally fair agreement between the results obtained with the two different diameter tubes. The larger diameter tube allows larger



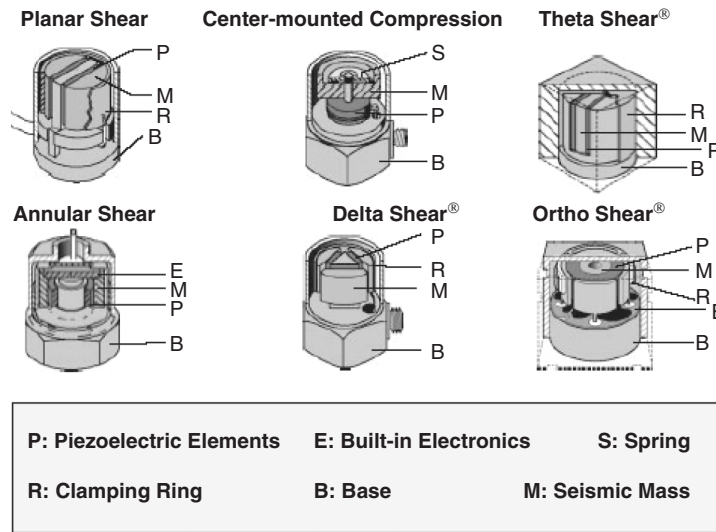
**Figure 19** Experimental setup for sound absorption measurements of asphalt road surface samples with impedance tube, microphones A and B, and frequency analyzer. Note the road surface samples and metal spacers. Two 10-cm diameter tubes lie horizontally on the table. One 15-cm diameter tube can be seen standing vertically on the left.

samples to be tested, which because of the non-uniform sample surfaces gives greater confidence in the measurements. The larger diameter tube, however, does not allow measurements to be made above about 1200 Hz. Since the A-weighted sound pressure level tire noise peaks at about 800 Hz for vehicles at highway speeds (see Chapter 86) porous road surfaces of the order of 4 to 5 cm in thickness would appear to be a good choice. Many more experimental results of the sound absorption measurements of road surface samples are presented in Ref. 11 and 12. Space limitations preclude their presentation here.



**Figure 20** Comparison of sound absorption coefficients of open graded fine core slabs measured by 15-cm and 10-cm tubes.



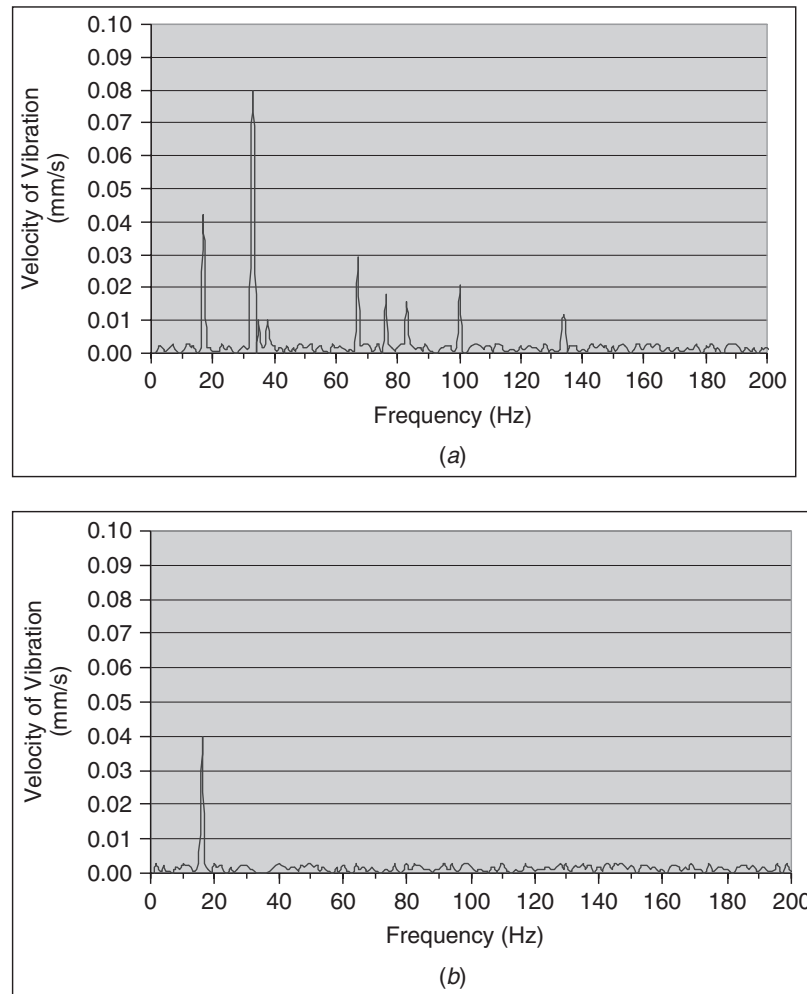


**Figure 21** Typical construction details and basic elements of the main types of piezoelectric seismic mass accelerometers.

**Table 6 Comparisons between Accelerometer and Preamplifier Types**

Stage	Type	Advantages	Disadvantages
<b>Transduction (piezoelectric sensor)</b>	Shear	<ul style="list-style-type: none"> <li>Temperature transient sensitivity is very low</li> <li>Base strain influence on measurement results is kept to a minimum</li> </ul>	<ul style="list-style-type: none"> <li>Because of its low sensitivity-to-mass ratio, very large and heavy units are needed for high sensitivities</li> </ul>
	Compression	<ul style="list-style-type: none"> <li>Robust unit, proper for heavy duty</li> <li>High sensitivities can be achieved with small seismic masses</li> </ul>	<ul style="list-style-type: none"> <li>Susceptible to temperature transients</li> <li>Base of the sensor is prone to strain influence</li> </ul>
<b>Preamplification</b>	External charge amplifier	<ul style="list-style-type: none"> <li>Allows the adjustment of sensitivity and time constant<sup>a</sup> of the preamplifier</li> <li>Better frequency response and lower noise levels</li> <li>Can be used with high-temperature vibrating samples</li> </ul>	<ul style="list-style-type: none"> <li>Very sensitive to triboelectric noise</li> <li>Low-noise cable must be used and it should not be longer than 10 m</li> <li>More expensive</li> </ul>
	Built-in charge amplifier	<ul style="list-style-type: none"> <li>Long cables are possible</li> <li>Regular cables can be used</li> <li>No need to use an external amplifier</li> <li>Economical signal conditioning</li> <li>Compatible output (voltage output) with several signal analysis systems</li> </ul>	<ul style="list-style-type: none"> <li>Time constant and preamplifier sensitivity are fixed and cannot be changed</li> </ul>

<sup>a</sup> The time constant defines, among other factors mentioned before, the low-end frequency response of the sensor, as well as the data output flow.



**Figure 22** Comparison of the vibration rms amplitudes measured on (a) the drive case and on (b) the concrete inertia base of a lifter motor.

## 11 ACCELEROMETER PRINCIPLES AND VIBRATION MEASUREMENTS

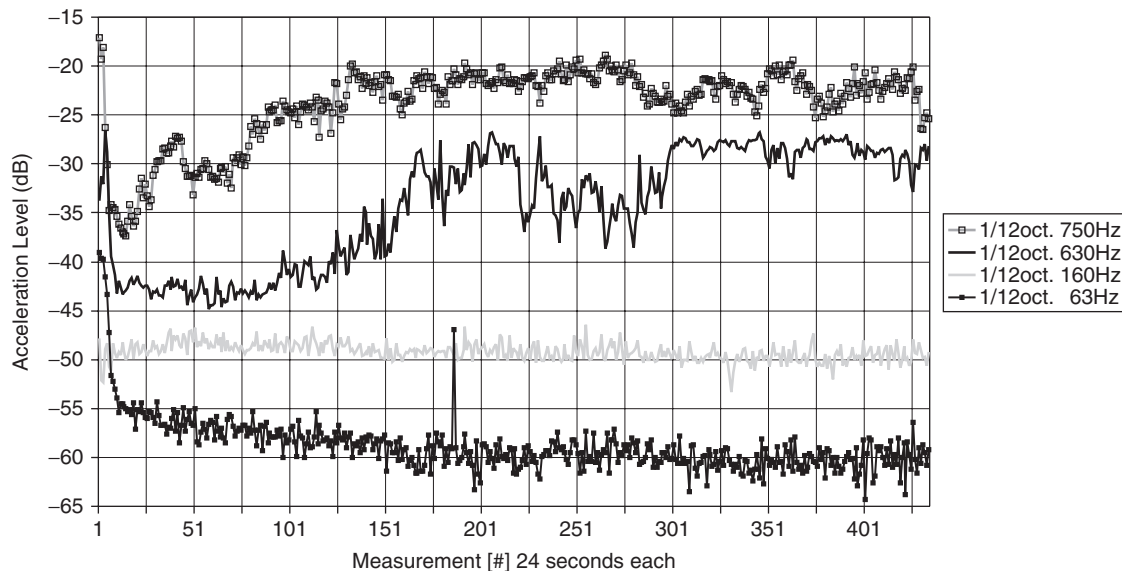
Accelerometers have become the most commonly used devices to measure vibration. (See Chapters 35 and 37.) The device mainly responsible for transforming the vibration into electrical signals is the piezoelectric accelerometer, which has an output proportional to the acceleration acting on its body. The key material used to build them is a piezoelectric crystal loaded by a seismic mass to enhance its sensitivity. Seismic mass theory is given in Chapter 35. Typical loading conditions are compression and shear as shown in Fig. 21.

The calculation of related velocity and displacement parameters can be done either in an analog electronic stage through integration or in the digital domain with algorithmic processing of the data gathered in almost real time. Taking into account that

acceleration, velocity, and displacement are mathematically related through derivatives and integrals (see Fig. 2 and Chapter 1), a typical measurement versus frequency graph will have a certain slope, and this slope will accentuate certain regions of the frequency plot. Therefore, it is usually common practice to select the vibration parameter that gives the flattest measured frequency response to optimize the dynamic range of the measurement chain.

There are three main characteristics of accelerometers that have to be carefully chosen in accordance with the particular measurement being made:

- **Mass.** If the accelerometer mass is large compared to the mass of the vibrating system, it will alter its natural frequency or load the system. The mass of the accelerometer should be



**Figure 23** Time history of 450 wiper runs,  $\frac{1}{12}$ th octave vibration testing of a small windshield wiper motor showing the burn-in settling and wear of the softer parts on the first runs reflected by the high variability of certain frequency bands. (Courtesy interPRO and Dakar Ingeniería Acústica.)

no more than one tenth of the vibrating system's mass. (See Fig. 16 in Chapter 35 and the related discussion there for a more complete description of the effects of mass loading of accelerometers.)

- **Charge Sensitivity** If the seismic mass of the accelerometer is increased, the resonance frequency will decrease and the charge sensitivity or output charge per acceleration unit applied will increase. Small mass units are capable of a wide range of frequency responses, and large mass units are optimum for measurement of small values of acceleration.
- **Mounted Resonance Frequency** The resonance frequency is directly proportional to the overall stiffness of the system. Consequently, the proper mounting method depends on the measurement objective and goals. As a general rule, the coupling between the sample and the accelerometer should be as stiff as possible to ensure unwanted resonances are avoided.

Additional factors should also be considered. Piezoelectric accelerometers are not immune to extreme environmental conditions, transverse motion, and magnetic field influences just to mention a few parameters that may affect the measurements. The manufacturer's data sheet should be consulted to ensure proper functioning conditions for the accelerometer.

A large variety of vibration measurement systems can be used, but for general purposes typical systems will be discussed. The transduction stage is performed by a piezoelectric sensor. Refer to Table 6 for a

comparison between different types of accelerometers. In this stage, the vibration of the sample is transmitted to the sensor, which converts it to an electrical signal proportional to the acceleration. The electrical signal from the sensor must be conditioned (i.e., amplified and impedance coupled). This is done by a charge-to-voltage converter.

The filtering stage, whose function is to reject undesired information, is done by electrical filtering of the output of the preamplifier. Note that this filtering stage only improves accuracy by omitting irregularities caused by the mechanical properties of the sensor (i.e., resonance frequency) or by simplifying the data gathered. However, to protect the accelerometer against excessive shock that could damage the device, mechanical filters may be needed, especially to protect it in the region near to and at its resonance frequency.

Sometimes the purpose of the measurement is not to determine the acceleration of an object but to measure its velocity or displacement. The integration stage makes this possible by integrating the acceleration. This is now generally done by a digital algorithm, but it can be done by analog integration.

The detection, linear to logarithm conversion, display, and logging are the final stages of the measurement chain. Before the detection phase, the signal processed is still an alternating current. A detector converts it to a direct current signal to produce the rms acceleration reading. Yet, due to the vast range of values, an additional process converts the rms acceleration values to acceleration levels in decibels referenced to  $10^{-6} \text{ m/s}^2$ . Then the results are finally displayed. The display can be analog or digital in

form. Several analysis tools are used for displaying the results (e.g., real-time frequency analyzers, printers, etc.). The results can also be recorded for later processing preferably in the digital domain.

Two actual vibration measurements are presented in Figs. 22 and 23. Figure 22 shows a decoupled lifter motor with measurements taken on the motor block and on the concrete inertia base. The decoupling is seen to work well above the strong first resonance at 18 Hz. Figure 23 shows measurements on a new windshield wiper motor undergoing its first 450 runs in a quality control test. The vibration levels generated during each run were measured by an accelerometer and analyzed in  $\frac{1}{12}$ th octave bands. It is clear that certain bands show an abrupt change in level during the first 20 runs (63 Hz, 160 Hz, 630 Hz, and 750 Hz). Since each run takes 24 s to complete, these frequency bands were found not to be useful for a pass-fail test for these small motors in which a quick detection of defective components is required.

**Acknowledgment** The authors would like to thank Antonio Sandoval Martinez for his assistance in the preparation of this chapter.

## REFERENCES

1. ISO 5725-2:1994, Accuracy (Trueness and Precision) of Measurement Methods and Results—Part 2: Basic Method for the Determination of Repeatability and Reproducibility of a Standard Measurement Method.
2. IEC 61672, Electroacoustics—Sound Level Meters.
3. IEC 61094-2, Measurement Microphones—Part 2: Primary Method for Pressure Calibration of Laboratory Standard Microphones by the Reciprocity Technique.
4. IEC 61260:1995, Electroacoustics-Octave-Band and Fractional-Octave-Band Filters.
5. ISO 532:1975, Acoustics—Method for Calculating Loudness Level.
6. IEC 60942, Electroacoustics—Sound Calibrators.
7. ISO 16063-11:1999, Methods for the Calibration of Vibration and Shock Transducers—Part 11: Primary Vibration Calibration by Laser Interferometry.
8. ISO 16063-12:2002, Methods for the Calibration of Vibration and Shock Transducers—Part 12: Primary Vibration Calibration by the Reciprocity Method.
9. ISO 3383-1997, Acoustics—Measurement of the Reverberation Time of Rooms with Reference to Other Acoustic Parameters.
10. ISO 10844:1994, Acoustics—Specification of Test Tracks for the Purpose of Measuring Noise Emitted by Road Vehicles.
11. M. J. Crocker, D. Hansen, and Z. Li. Measurement of the Acoustical and Mechanical Properties of Porous Road Surfaces and Tire/Road Noise, TRB Paper Number: 04-4816, and also *TRB J.* 2004.
12. M. J. Crocker, Z. Li, and J. P. Arenas, Measurements of Tyre/Road Noise and Acoustical Properties of Porous Road Surfaces, *Int. J. Acoust. Vib.* Vol. 10, No. 2, June 2005.

## BIBLIOGRAPHY

- K. B. Benson *Audio Engineering Handbook*, Mc-Graw Hill, New York, 1988.
- B. A. Blesser, Advanced Analog to Digital Conversion and Filtering: Data Conversion, in *Digital Audio*, Audio Engineering Society, New York, 1983.
- J. T. Broch, *Mechanical Vibration and Shock Measurements*, Bruel & Kjaer, Naerum, Denmark, 1984.
- IEC 268-1-1985, Sound System Equipment—Part 1: General Instructions and Applications for Standing Wave Apparatus Type 4002 and Frequency Analyzer Type 2107, Bruel & Kjaer, Naerum, Denmark, 1967.
- ISO 1996-1 Acoustics—Description, Measurement and Assessment of Environmental Noise—Part 1: Basic Quantities and Assessment Procedures.
- ISO 362-1998, Acoustics—Measurement of Noise Emitted by Accelerating Road Vehicles—Engineering Method.
- ISO 5130-1982, Acoustics, Measurement of Noise Emitted by Stationary Road Vehicles—Survey Method.
- B. F. G. Katz, Method to Resolve Microphone and Sample Location Errors in the Two-Microphone Duct Measurement Method, *JASA*, Vol. 108, No. 5, 2000.
- L. E. Kinsler, A. R. Frey, A. B. Coppens, and J. V. Sanders, *Fundamentals of Acoustics*, 3rd ed., Wiley, New York, 1982.
- H. Larsen, Reverberation Process at Low Frequencies, Bruel & Kjaer Technical Review No. 4, 1978.
- D. Manvell and E. Aflalo, Uncertainties in Environmental Noise Assessments—ISO 1996, Effects of Instrument Class and Residual Sound, Forum Acusticum, Budapest, 2005.
- Microphone Handbook* Vol. 1, Brüel & Kjaer, Naerum, Denmark, 1996.
- H. Myneke, The New Acoustics Laboratory of the Catholic University at Leuven, Paper E 5-11, Proc. 6th Int. Congr. Acoust., Tokyo, Japan, 1968.
- A. V. Oppenheim and A. S. Willsky, *Signals and Systems*, Prentice-Hall, Englewood Cliffs, NJ, 1997.
- D. Preis, Linear Distortion, *J. Audio Eng. Soc.*, Vol. 24, No. 5, June 1976, pp. 346–367.
- R. B. Randall, *Frequency Analysis*, Copenhagen, Bruel & Kjaer, Naerum, Denmark, rev. ed., 1987.
- D. Reynolds, *Engineering Principles of Acoustics: Noise and Vibration Control*, Allyn & Bacon, Boston, 1981.
- M. R. Schroeder, New Method of Measuring Reverberation Time, *J. Acoust. Soc. Am.*, Vol. 37, 1965, pp. 409–412.
- E. Zwicker, Scaling, in *Handbook of Sensory Physiology*, Part 2. Auditory System. Physiology (CNS): Behavioral studies in Psychoacoustics, W. D. Keidel and W. D. Neff, Eds., Springer, New York Vol. 5, 1975, pp. 401–448.

# CHAPTER 44

## DETERMINATION OF SOUND POWER LEVEL AND EMISSION SOUND PRESSURE LEVEL

Hans G. Jonasson

SP Technical Research Institute of Sweden  
Borås, Sweden

### 1 DETERMINATION OF SOUND POWER LEVEL USING SOUND PRESSURE

#### 1.1 Introduction

The noise emission from machinery is best described by the sound power level. Contrary to the sound pressure level, the sound power level is in principle independent of the acoustical properties of the room in which the machine is located. The sound power level is also the best quantity to use when calculating the sound pressure level in the reverberant field of the room in which the source is located. In addition to the sound power level, the emission sound pressure level, that is, the sound pressure level in a hemianechoic test environment, is used to describe the noise emission of machinery in the direct field of the source.

In many cases the sound power level will depend strongly on the mounting and operating conditions. In order to be able to compare the noise emission from similar machines from different manufacturers such conditions have to be standardized. This is done in machine-specific test codes (also called C-standards). These C-standards always use one or several of the basic measurement standards (also called B-standards) described in the following. Thus, before carrying out sound power measurements, it is essential to check if there is such a test code for the machine to be tested. In case there is no such test code, it is customary to select one or more of the following operating conditions: full load, no load (idling), conditions corresponding to maximum sound generation, representative operating conditions, or other specified operating conditions. Whichever conditions are used, they must be described carefully in the test report.

#### 1.2 Overview of Available Standards

The sound power level can be determined in many different ways. In principle all methods should give the same result,<sup>1,2</sup> although with different measurement uncertainties. Some of the methods are based on measurements of sound pressure and some on sound intensity. Here only the International Organization for Standardization (ISO) 3740 series<sup>3–9</sup> describing methods using sound pressure will be discussed. All these standards are also European standards and equivalent North American standards, and Japanese industrial standards are normally identical. The most suitable method to use in a given case is determined by the desired measurement uncertainty and by the available test environment and test equipment.

Sometimes the machine cannot be moved but must be measured in situ, and sometimes it is most practical to carry out the measurement in a dedicated laboratory.

In the ISO 3740 series the measurement uncertainty is divided into three different classes: grade 1, grade 2, and grade 3, also known as precision, engineering, and survey methods. Grade 1, which is the most accurate method, has a standard deviation of reproducibility less than 1 dB, whereas grade 2 and grade 3 are less than 2 and 3 dB, respectively.

The normal quantity to be measured is the time-averaged sound pressure level (also called equivalent continuous sound pressure level), but sometimes the single-event sound pressure level (also called sound exposure level) is also used. They are defined as

$$L_{p,eq,T} = 10 \log \left[ \frac{1}{T} \int_0^T 10^{0.1 L_p(t)} dt \right] \text{ dB} \quad (1)$$

$$\begin{aligned} L_{p,1s} &= 10 \log \left[ \frac{1}{T_0} \int_0^T 10^{0.1 L_p(t)} dt \right] \\ &= L_{p,eq,T} + 10 \log \left( \frac{T}{T_0} \right) \text{ dB} \end{aligned} \quad (2)$$

respectively, where  $T$  is the time interval for the measurement,  $T_0$  equals 1 s, and  $L_p(t)$  the instantaneous sound pressure level. In the ISO 3740 series  $L_{p,eq,T}$  is normally simply denoted  $L_p$ . Then  $L_p$  is used to calculate the sound power level and  $L_{p,1s}$  to calculate the sound energy level,  $L_J$ . The sound energy level is of particular interest for sources emitting single bursts of sound. It should be observed that nowadays it is recognized that  $L_J$  can be determined both in a hemianechoic and in a reverberant environment. If  $L_p$  is replaced by  $L_{p,1s}$  in the following formulas,  $L_W$  can be replaced by  $L_J$ .

Sometimes it is required to evaluate the presence of prominent tones. There are no objective methods to determine prominent tones in the basic sound power standards. However, there is one method in the test code ISO 7779<sup>10</sup> for information technology equipment.

A very simple overview of the different standards for determination of sound power levels is given in Table 1. The reproducibility standard deviation is a measure of the measurement uncertainty, see clause 1.6. More detailed guidance is given in ISO 3740.<sup>3</sup>

**Table 1 Selection of Measurement Method**

Standard ISO	Measurement Environment	Reproducibility Standard Deviation of the A-weighted Sound Power Level (dB)	Equipment in Addition to Sound Level Meter	Minimum Number of Microphone Positions	Background Noise Tolerance	Subclause
3741	Reverberation room	0.5	Equipment to determine reverberation time or a reference sound source	6	Poor	1.5
3743-1	Room with hard walls with $V \geq 40 \text{ m}^3$	1.5	Reference sound source, octave filter	3	Poor	1.4
3743-2	Special reverberation room with $V \geq 70 \text{ m}^3$	2.0		6	Poor	1.4
3744	Outdoors, large room, hemianechoic room with max environmental correction $K_2 = 2 \text{ dB}$	1.5		9	Good	1.5
3745	Hemianechoic room with maximum environmental correction $K_2 = 0.5 \text{ dB}$	0.5		20	Moderate	1.3
3746	Outdoors, <sup>a</sup> large room with maximum environmental correction $K_2 = 7 \text{ dB}$	3.0		4	Good	1.3
3747	Any indoor environment, which is a little reverberant	1.5	Reference sound source, octave filter	3	Poor	1.4

<sup>a</sup>ISO 3746 is the only standard that can be used on grass or soft earth.

### 1.3 Measurement Surface Methods

**1.3.1 General** The most basic method to determine the sound power level from a machine is to determine the mean sound pressure level on a measurement surface, that is, a hypothetical surface completely enclosing the machine under test and on which the measurement points are located. The sound power level is then given by

$$L_W = \overline{L_{pf}} + 10 \log \left( \frac{S}{S_0} \right) + C_1 \quad (3)$$

where  $\overline{L_{pf}}$  = mean sound pressure level on the (measurement surface dB)

$S$  = area of measurement surface ( $\text{m}^2$ )

$S_0 = 1 \text{ m}^2$

$$C_1 = -10 \log \left( \frac{B\sqrt{T_0}}{B_0\sqrt{T}} \right) \quad (4)$$

$B$  = static atmospheric pressure during the test

$T$  = temperature, in K

$B_0 = 1013.25 \text{ hPa}$

$T_0 = 313.15 \text{ K}$

Normally, the measurement surface is a box on the floor (= 5 sides) or a hemisphere as the source most often is located on a floor away from all other room boundaries. If the source is located close to a wall, the measurement surface is half a box on the floor (= 4 sides) or a  $\frac{1}{4}$  sphere. If the source is located in a corner, the measurement surface is  $\frac{1}{4}$  of a box on the floor (= 3 sides) or a  $\frac{1}{8}$  sphere, respectively. Whenever the source approaches a boundary surface the sound power output will be affected.<sup>11</sup> This effect is not properly taken into account in the ISO 3740 series. However, this effect is normally negligible for all but the lowest frequency bands.

Term  $C_1$  corrects the sound power level to actual meteorological conditions. The meteorological conditions will also affect the radiation from the source.<sup>12</sup> The latter will vary with the acoustic impedance of air, which in its turn varies with the atmospheric pressure and the temperature. To compensate for that, it has been decided to normalize measured sound power levels to the reference barometric pressure  $B_0$  and the temperature  $23^\circ\text{C}$  (= 296.15 K). This normalized sound power level,  $L_{W,N}$  is given by

$$L_{W,N} = \overline{L_{pf}} + 10 \log \left( \frac{S}{S_0} \right) + C_1 + C_2 \quad (5)$$

where

$$C_2 = -15 \log \left( \frac{BT_1}{B_0T} \right) \quad (6)$$

where  $T_1 = 296.15$  K. Up until now both  $C_1$  and  $C_2$  have been neglected in all standards except precision methods ISO 3741 and 3745. It is expected that similar corrections will be introduced in the future also into some other standards.

The mean sound pressure level on the measurement surface is given by

$$\overline{L_{pf}} = 10 \log \left( \frac{1}{n} \sum_{i=1}^n 10^{0.1L_{pi}} \right) \quad (7)$$

where  $L_{pi}$  is the sound pressure level in measurement position  $i$  on the measurement surface. In ISO 3744 the general principle is that each position must be associated with an equally large area on the measurement surface, and, if the difference between any two positions exceeds the number of positions, the number of positions has to be increased.

Equation (5) presumes that the intensity is measured along the normal to the measurement surface only. This is only obtained with a measurement of intensity, but for a sound pressure measurement it also fits well for a spherical or hemispherical measurement surface at a reasonably long distance. However, if the measurement surface is box shaped at a short distance, the sound will come from many different angles and not only along the normal. In that case  $L_{pi}$  will be overestimated<sup>13,14</sup> and we get a systematical overestimate of the sound power. This overestimate is normally rather small and ignored. However, to improve the reproducibility, it is recommended to use only one shape of reference surface for each type of machine.

Equation (5) is valid when there are no reflections from walls and ceiling. Some standards allow a correction,  $K_2$ , for such reflections, and we then get

$$L_W = \overline{L_{pf}} + 10 \log \left( \frac{S}{S_0} \right) + C_1 + C_2 - K_2 \quad (8)$$

where the environmental correction  $K_2$  is a correction to compensate for the increase in sound pressure level on the measurement surface due to reflections from walls, ceiling, and other reflecting objects in the vicinity, but excluding surfaces within the measurement surface, of the machine under test. Outdoors or in a hemianechoic room  $K_2 = 0$  dB. In other cases corrections have to be made. ISO 3744, which has the uncertainty of an engineering method, allows for corrections up to 2 dB, whereas the survey method ISO 3746 allows for corrections up to 7 dB. For ISO 3744 it has been proposed to increase the maximum allowable correction from 2 to 4 dB.

The term  $K_2$ , which describes the increase in sound pressure level on the measurement surface due to the

reverberant sound field in the room, is calculated from

$$K_2 = 10 \log \left( 1 + 4 \frac{S}{A} \right) \quad (9)$$

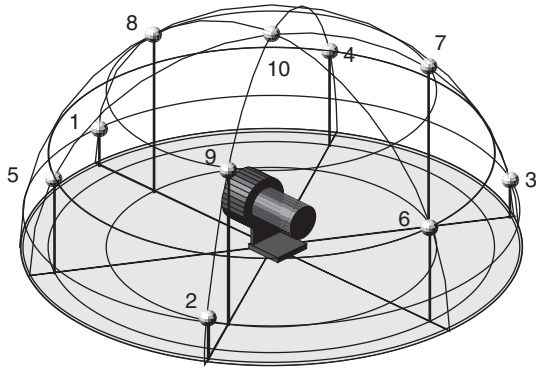
where  $A$  is the sound absorption area of the room estimated from:

$$A = \alpha S_v \quad (10)$$

where  $\alpha$  is the mean sound absorption coefficient of the room surfaces, which for A-weighted levels can be estimated from tables in the relevant standards;  $S_v$  is the total area of the boundary surfaces (walls, ceiling, and floor) of the test room, in meters squared;  $A$  can also be determined in frequency bands by measurements, for example, with a reference sound source or from reverberation time.

**1.3.2 The Sphere Method** The most accurate measurement surface method is the sphere method. In that case the measurement is a sphere or part thereof. At first the smallest possible imaginary box, the *reference box* is constructed, which completely encloses the source to be tested and all its important sound radiating parts. The reference box defines the size of the source with its characteristic distance  $d_0$ , the distance from the projection of the center of the reference box on the floor and one of the upper corners. Then a measurement distance, the radius  $R$ , of the hemispherical measurement surface, which is at least twice  $d_0$  is selected. For large sources  $d_0$  becomes large, and it is then often more practical to use a box-shaped measurement surface. The basic measurement positions on the hemispherical measurement surface are located as shown in Fig. 1. The engineering method ISO 3744 normally uses the 10 locations shown in the figure, whereas the survey method ISO 3746 only requires positions 4, 5, 6, and 10. Each position must represent an equally large area. If the largest difference in sound pressure level, in decibels, between any two positions exceeds the number of positions, then the number of positions must be increased. The precision method ISO 3745 requires 20 different positions, each at a different height. If the source under test emits stationary sound, it is also permissible to determine the surface sound pressure level using traversing microphone paths.

**1.3.3 The Box Method** The simplest and most popular measurement surface method is the box method, see Fig. 2. In this case the measurement surface is box shaped with each of the sides at the preferred measurement distance,  $d = 1.0$  m from the reference box. Alternatively, measurement distances shorter or longer than 1.0 m may be selected. Short distances require more microphone positions but improve the signal-to-noise ratio if the background noise is high. The basic microphone positions used in the engineering method ISO 3744 are on the middle of each side and in the four upper corners. More positions



**Figure 1** Basic microphone positions on a hemispherical measurement surface according to ISO 3744. The microphone heights are  $0.15R$ ,  $0.45R$ ,  $0.75R$ , and  $R$ , respectively.

are required for large sources. For survey-grade measurements the corner positions can be left out.

#### 1.4 The Comparison Method

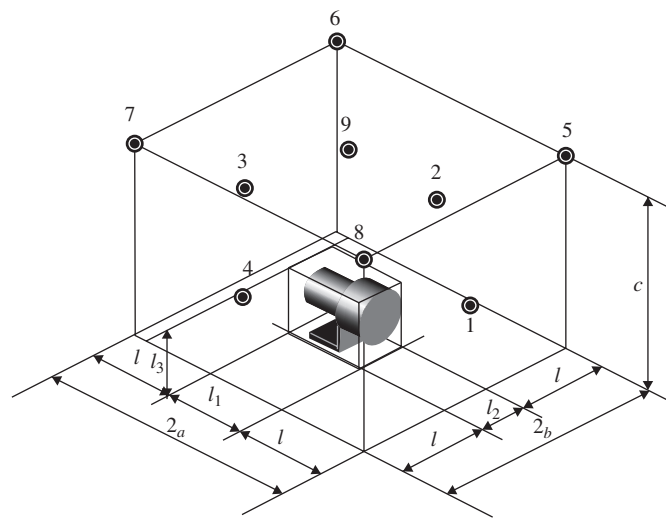
The comparison method is accurate, simple, and quick and is particularly suitable when one has no access to dedicated laboratories.<sup>14</sup> The principle is to compare the sound pressure level  $L_p$  from the source under test with the sound pressure level  $L_{pref}$  from a calibrated reference sound source with the known sound power level  $L_{Wref}$ . The unknown sound power level of the source under test is then given by

$$L_W = L_{Wref} + L_p - L_{pref} \quad (11)$$

To be accurate, the measurements have to be made in frequency bands and the A-weighted sound power level is then calculated. The comparison method is standardized in ISO 3743 and 3747 for in situ use. It is also an alternative for reverberation room measurements according to ISO 3741 and to determine the environmental correction  $K_2$  in ISO 3744 and 3746. The reference sound source must meet the requirements of ISO 6926.<sup>15</sup>

In ISO 3743-1, which is specifically designed to be used for small movable sources, the test environment must be a hard-walled room; that is, a room without major sound absorbing boundary surfaces, with a minimum volume of  $40 \text{ m}^3$  and at least 40 times the volume of the reference box. A sound absorbing surface is a surface with a sound absorption coefficient exceeding 0.20. At least three microphone positions, the same ones for both the source under test and the reference sound source, must be used, and the measurements are carried out in octave bands. The standard deviation of the reproducibility is in general 1.5 dB for the A-weighted sound power level. The method is a substitution method; that is, the source under test is moved and replaced by the reference sound source when the sound pressure generated by the latter is measured.

ISO 3747 is a true in situ method where it is assumed that the source under test is not movable. Normally, the reference sound source is located on top of the source under test. To guarantee grade 2 accuracy (engineering method), the test environment should be a little reverberant. The quality of the test environment is tested by carrying out a measurement of the excess of sound pressure level,  $DL_f$ , using the reference sound



**Figure 2** Basic microphone positions on a box-shaped measurement surface for a small source.



source.  $DL_f$  is given by

$$DL_f = L_{\text{pref}} - L_{W\text{ref}} + 11 + 20 \log \left( \frac{r}{r_0} \right) \quad (12)$$

where  $r$  is the distance between the reference sound source and the microphone;  $r_0 = 1$  m. To meet the accuracy requirements of a grade 2 method,  $r$  of the different microphone positions used must be selected such that  $DL_f \geq 7$  dB in each microphone position.

### 1.5 The Reverberation Method

This method is used in reverberant rooms. In order to meet the requirements for the standard ISO 3741, a special reverberation room has to be used. The most common size for such a room is 200 m<sup>3</sup>. It is then qualified for the frequency range of 100 to 10,000 Hz. If lower frequencies are of interest, the room should be larger. The measurements are carried out in  $\frac{1}{3}$  octave bands. Two methods are allowed. One is the comparison method and the other is the direct method. In the direct method the reverberation time and the mean sound pressure level in the room are measured. The sound power level is then given by

$$L_W = \overline{L_p} + 10 \log \left( \frac{A}{A_0} \right) + 10 \log \left( 1 + \frac{Sc}{8Vf} \right) + 4.34 \frac{A}{S} - 6 + C_1 + C_2 \quad (13)$$

where  $\overline{L_p}$  = mean sound pressure level in the room (dB)

$A$  = equivalent sound absorption area of the room (m<sup>2</sup>) determined from the reverberation time

$A_0 = 1$  m<sup>2</sup>

$S$  = total surface area of the reverberation room (m<sup>2</sup>)

$c$  = speed of sound at the temperature  $\theta$ ,  $c = 20.05 \sqrt{273 + \theta}$  m/s

$\theta$  = temperature (°C)

$V$  = volume of the room (m<sup>3</sup>)

$f$  = center frequency of the one-third octave band used for the measurement (Hz)

The term  $10 \log (1 + Sc/8 V/f)$  is a correction to compensate for the fact that the mean sound pressure level is not measured throughout the room volume but at least 1.0 m away from the boundary surfaces. As the energy density always is greatest close to the walls, this leads to a systematic underestimate of the true mean sound pressure level. The term  $4.34A/S$  accounts for the air absorption in the room.<sup>16</sup>  $C_1$  and  $C_2$  are the same corrections as for ISO 3745 with the difference that the reference condition for the normalized sound power level is that of  $\rho c = 400$  Ns/m<sup>3</sup> instead of standard barometric pressure and 23°C. It is recommended not to use this reference

condition of ISO 3741 but to use the reference condition of the most recent standard ISO 3745, that is,  $B = B_0$  and  $t = 23^\circ\text{C}$ , as this condition will be used in future standards:

$$A = \frac{55.26}{c} \left( \frac{V}{T_{\text{rev}}} \right) \quad (14)$$

The reverberation method is the most accurate and most convenient method to use for broadband noise sources provided that a reverberation room is available. The method is not as good for sources emitting narrow-band noise. To discover such problematic cases, ISO 3741 requires the use of six discrete microphone positions. For each measurement the standard deviation of these positions has to be evaluated. If it is too high, there are good reasons to assume that the source emits narrow-band noise, and it is then necessary to change the measurement procedure by using more source and/or microphone positions. There is also an option to avoid these additional positions by qualifying the room for narrow-band measurements by using rotating diffusors. However, this qualification procedure is quite difficult. To decrease the problems with tonal sounds, it is recommended not to have too long reverberation times as the modal overlapping improves with a higher sound absorption. When many microphone positions are required, it may be useful to use a moving microphone instead. The reverberation room method is standardized as a precision method in ISO 3741. The standard deviation of reproducibility of the A-weighted sound power level is 0.5 dB.

A special method in a special reverberation room is described in ISO 3743-2. That method was originally developed to make it possible to measure A-weighted sound pressure levels directly in a reverberant field. To make that possible the reverberation room has to be qualified to have a reverberation time following a specified frequency dependence. The development of modern instrumentation and better comparison methods has made this standard outdated.

### 1.6 Measurement Uncertainties

Traditionally, the measurement uncertainty in the ISO 3740 series is given in terms of the reproducibility standard deviation,  $\sigma_R$ . If a particular noise source were to be transported to each of a number of different test sites, and if at each test site the sound power level of that source were to be determined in accordance with the respective standard, but with different test personnel and different equipment, the results would show a scatter. Assuming that the variations in noise emission of the source were negligible, the maximum standard deviation of all these sound power level values is  $\sigma_R$ . The measurement uncertainty to be reported is the combined measurement uncertainty associated with a chosen coverage probability. By convention, a coverage probability of 95% is usually chosen, with an associated coverage factor of 2. This means that the result becomes  $L_{WA} \pm 2\sigma_R$ . The  $\sigma_R$  values of the different methods are given in Table 1.

In the near future, ISO plans to change to the format of ISO Guide to the Expression of Uncertainties in Measurements.<sup>17</sup> When it is implemented, it will be necessary to identify each source of error and the standard uncertainty,  $u_j$ , associated with it. Depending on the probability distribution, each error has a sensitivity coefficient  $c_j$ . A normal distribution has a sensitivity coefficient of 1. The combined standard uncertainty is then given by

$$u(L_W) = \sqrt{\sum_{j=1}^n (c_j u_j)^2} \quad (15)$$

### 1.7 Noise Declarations

Many sound power determinations are carried out on behalf of manufacturers who want to or have to declare the noise emission values of their products. For such declarations the measurement uncertainty and the standard deviation of production have to be taken into account. How this can be done is most simply described in ISO 4871<sup>18</sup> and, for computer and business equipment, in ISO 9296.<sup>19</sup> Both these standards are based on the more basic and more complicated standard ISO 7574.<sup>20</sup> Sometimes a noise test code may give additional information. ISO 4871 permits noise declarations either as declared single-number noise emission values or as declared dual-number noise emission values.

The declared single-number noise emission value for a production series of machines can be calculated from

$$L_d = \bar{L} + K \quad (16)$$

where  $\bar{L}$  is the mean value of a batch of the production, preferably from at least three different machines, and  $K$  is the expanded uncertainty.  $L$  is normally either the A-weighted sound power level  $L_{WA}$  or the A-weighted emission sound pressure level  $L_{pA}$ , but also other acoustical quantities can be declared accordingly. The value of  $K$ , in decibels, for a sample size of three machines is

$$K = 1.5s_t + 0.564(\sigma_M - s_t) \quad (17)$$

where the total standard deviation  $s_t$  is given by

$$s_t = \sqrt{s_R^2 + s_P^2} \quad (18)$$

Here  $s_P$  is the standard deviation of the production and  $s_R$  the standard deviation of the reproducibility. Values of  $s_t$  and  $\sigma_M$  may be given in the test code, but, if there is no such code available, the values given in Table 2 may be used. Only  $L_d$  is reported.

The declared single-number noise emission value is also called guaranteed value. The value of  $K$  determined above is based on ISO 7574-4 and results in a 5% risk of rejection for a sample of three machines. If a single machine out of batch is evaluated,

**Table 2 Estimated Default Values for  $s_t$  and  $\sigma_M$**

Accuracy Grade of Measurement Method	Estimated Values (dB)	
	$s_t$	$\sigma_M$
Engineering (grade 2)	2.0	2.5
Survey (grade 3)	3.5	4.0

the declared value is verified if the measured value is equal to or less than the declared value. A batch is verified if the mean value of three tested machines is at least 1.5 dB lower than the declared value. A dual-number declaration means that the measured value  $\bar{L}$  and the uncertainty  $K$  both are reported.

## 2 DETERMINATION OF EMISSION SOUND PRESSURE LEVEL

### 2.1 Introduction

The emission sound pressure level is defined as the sound pressure level in a specified location, the operator's position, if there is one, from a machine under standardized operating conditions in a test environment where the influence from all boundary surfaces, but the floor is negligible. It is best measured in a hemianechoic room.

In the ISO 11200 series<sup>21–26</sup> five different standards to determine the emission sound pressure level are described. One of the standards, ISO 11205,<sup>26</sup> uses the sound intensity level to approximate the emission sound pressure level. The quantities normally measured are  $L_{pAeq}$ ,  $L_{pA,1s}$  and  $L_{pCpeak}$ . A standing operator or bystander is specified to be located at the height  $1.55 \text{ m} \pm 0.075 \text{ m}$  above the floor. If there is a seat, the microphone must be located  $0.8 \pm 0.05 \text{ m}$  above the middle of the seat plane. If an operator is present, the microphone must be  $0.20 \pm 0.02 \text{ m}$  to the side of the center plane of the operator's head.

### 2.2 Laboratory Methods

The most common laboratory method for the determination of emission sound pressure level is ISO 11201.<sup>22</sup> This standard requires the same environment as ISO 3744,<sup>6</sup> which means that the environmental correction,  $K_2$ , at the measurement position may be up to 2 dB. However, contrary to ISO 3744 the standard does not allow any corrections. The measured value, corrected for background noise if relevant, is always the result. This is very unfortunate as this in principle means that room-dependent errors up to about 2 dB are accepted. Fortunately, most laboratories use hemianechoic rooms qualified according to ISO 3745,<sup>7</sup> which means that  $K_2 \leq 0.5 \text{ dB}$ . The operating conditions must be the same as those for the determination of sound power levels. Operating conditions are generally defined in machine-specific test codes.

In case there is no dedicated workplace, one either measures in the bystander positions in the middle of each side, 1 m from the sides of the reference box, or applies ISO 11203.<sup>24</sup> This standard calculates the

emission sound pressure level from the sound power level using the equation:

$$L_p = L_W - 10 \log \left( \frac{S}{S_0} \right) \quad (19)$$

where  $S$  is the box-shaped measurement surface on which the specified position is located. If there is no specified position, the distance is 1.0 m from the reference box.  $S_0$  is 1 m<sup>2</sup>.

### 2.3 In Situ Methods

For general field use ISO 11202<sup>23</sup> is the best method. Here the emission sound pressure level is given by

$$L_p = L'_p - K_3 \quad (20)$$

where  $L'_p$  is the measured sound pressure level, and the local environmental correction  $K_3$  is given by

$$K_3 = 10 \log \left( 1 + 4 \frac{S}{A} \right) \quad (21)$$

where  $S = 2\pi a^2$ , where  $a$  is the distance from the measurement point to the closest important sound source on the machine;  $A$  is the equivalent sound absorption area of the test room, which is estimated as prescribed in ISO 3746 for sound power measurements. In the present standard  $K_3$  is not allowed to be greater than 2.5 dB. However, investigations<sup>27</sup> have shown that more accurate results are achieved if  $K_3$  values up to 4 dB are allowed.

If a lower measurement uncertainty is desirable ISO 11204<sup>25</sup> can be applied. In that case either the sound power level has to be known or the sound pressure level has to be measured in several positions around the machine. The problem with this standard is that it is not always applicable. ISO 11205<sup>26</sup> is an interesting alternative in cases where the machine is located in a very reverberant environment.<sup>28</sup> In that case the sound intensity level is measured in the three Cartesian directions  $x$ ,  $y$ , and  $z$ . The emission sound pressure level  $L_p$  is given by

$$L_p = L_{Ixyz} + K_5 \quad (22)$$

where  $K_5 = 1$  dB and

$$L_{Ixyz} = 10 \log \sqrt{\left( 10^{\frac{L_{Ix}}{10}} \right)^2 + \left( 10^{\frac{L_{Iy}}{10}} \right)^2 + \left( 10^{\frac{L_{Iz}}{10}} \right)^2} \quad (23)$$

where  $L_{Ix}$ ,  $L_{Iy}$ , and  $L_{Iz}$  are the sound intensity levels determined in the three Cartesian directions.

When measuring  $L_{pCpeak}$  for impulsive sound sources reflections<sup>29,30</sup> from the boundary surfaces have less effect than is the case for  $L_p$ . Thus, no corrections are allowed for  $L_{pCpeak}$ . Peak values are

normally measured 10 times and the measurement result is the highest value.

### REFERENCES

1. ISO 12001:1996, Acoustics—Noise Emitted by Machinery and Equipment—Rules for the Drafting and Presentation of a Noise Test Code.
2. H. G. Jonasson and G. Andersen, Determination of Sound Power Levels Using Different Standards. An Internordic Comparison, *SP Report*, Vol. 9, 1996.
3. ISO 3740:2000, Acoustics—Determination of Sound Power Levels of Noise Sources. Guidelines for the Use of Basic Standards and for the Preparation of Noise Test Codes.
4. ISO 3741:1999, Acoustics—Determination of Sound Power Levels of Noise Sources Using Sound Pressure—Precision Methods for Reverberation Rooms
5. ISO 3743:1994, Acoustics—Determination of Sound Power Levels of Noise Sources Using Sound Pressure—Engineering Methods for Small, Movable Sources in Reverberant Fields. Part 1: Comparison Method in Hard-Walled Test Rooms. Part 2: Methods for Special Reverberation Test Rooms.
6. ISO 3744:1994, Acoustics—Determination of Sound Power Levels of Noise Sources Using Sound Pressure—Engineering Method in an Essentially Free Field over a Reflecting Plane.
7. ISO 3745:2003, Acoustics—Determination of Sound Power Levels of Noise Sources Using Sound Pressure—Precision Methods for Anechoic and Semi-anechoic Rooms.
8. ISO 3746:1995, Acoustics—Determination of Sound Power Levels of Noise Sources Using Sound Pressure—Survey Method Employing an Enveloping Measurement Surface over a Reflecting Plane.
9. ISO 3747:2000, Acoustics—Determination of Sound Power Levels of Noise Sources Using Sound Pressure—Comparison Method for Use in situ.
10. ISO 7779:1999, Acoustics—Measurement of Airborne Noise by Information Technology and Telecommunications Equipment.
11. H. G. Jonasson, Determination of Sound Power Level and Systematic Errors, *SP Report*, Vol. 39, 1998.
12. G. Hübner, Accuracy Consideration on the Meteorological Correction for a Normalized Sound Power Level, *Proc. Internoise*, 2000.
13. G. Hübner, Analysis of Errors in Measuring Machine Noise under Free-Field Conditions, *JASA*, Vol. 54, No. 4, 1973.
14. H. G. Jonasson, Sound Power Measurements in situ Using a Reference Sound Source, *SP Report*, Vol. 3, 1988.
15. ISO 6926:1999, Acoustics—Requirements for the Performance and Calibration of Reference Sound Sources Used for the Determination of Sound Power Levels.
16. M. Vorländer, Revised Relation between the Sound Power and the Average Sound Pressure Levels in Rooms and the Consequences for Acoustic Measurements, *Acustica* Vol. 81, 1995, pp. 332–343.
17. ISO, *Guide to the Expression of Uncertainties in Measurements (GUM)*, International Organization for Standardization, Geneva.
18. ISO 4871:1996, Acoustics—Declaration and Verification of Noise Emission Values of Machinery and Equipment.

19. ISO 9296:1988, Acoustics—Declared Noise Emission Values of Computer and Business Equipment.
20. ISO 7574:1985, Acoustics—Statistical Methods for Determining and Verifying Stated Noise Emission Values of Machinery and Equipment—Part 1: General Considerations and Definitions. Part 2: Methods for Stated Values of Individual Machines. Part 3: Simple (Transition) Method for Stated Values of Batches of Machines. Part 4: Methods for Stated Values for Batches of Machines.
21. EN ISO 11200:95, Noise Emitted by Machinery and Equipment—Guidelines for the Use of Basic Standards for the Determination of Emission Sound Pressure Levels at the Work Station and at Other Specified Positions.
22. ISO 11201:1995, Noise Emitted by Machinery and Equipment—Engineering Method for the Measurement of Emission Sound Pressure Level at the Work Station and at Other Specified Positions. Technical Corrigendum, 1:97.
23. ISO 11202:1995, Noise Emitted by Machinery and Equipment—Survey Method for the Measurement of Emission Sound Pressure Levels at the Work Station and at Other Specified Positions.
24. ISO 11203:1996, Noise Emitted by Machinery and Equipment—Determination of Emission Sound Pressure Levels at the Work Station and at Other Specified Positions from the Sound Power level.
25. ISO 11204:1996, Noise Emitted by Machinery and Equipment—Determination of Emission Sound Pressure Levels at the Work Station and at Other Specified Positions in situ. Technical Corrigendum, 1:97.
26. ISO 11205:2003, Acoustics—Determination of Sound Pressure Levels Using Sound Intensity.
27. H. G. Jonasson, Determination of Emission Sound Pressure Level and Sound Power Level in situ, *SP Report*, Vol. 18, 1999.
28. H. G. Jonasson and G. Andersen, Measurement of Emission Sound Pressure Levels Using Sound Intensity, *SP Report*, Vol. 75, 1995.
29. J. Olofsson and H. G. Jonasson, Measurement of Impulse Noise—An Inter-Nordic Comparison, *SP Report*, Vol. 47, 1998.
30. H. G. Jonasson and J. Olofsson, Measurement of Impulse Noise, *SP Report*, Vol. 38, 1997.

# CHAPTER 45

## SOUND INTENSITY MEASUREMENTS

Finn Jacobsen  
Acoustic Technology  
Technical University of Denmark  
Lyngby, Denmark

### 1 INTRODUCTION

Sound intensity is a measure of the flow of energy in a sound field. Sound intensity measurements make it possible to determine the sound power of sources without the use of costly special facilities such as anechoic and reverberation rooms. Other important applications of sound intensity include the identification and rank ordering of partial noise sources, visualization of sound fields, determination of the transmission losses of partitions, and determination of the radiation efficiencies of vibrating surfaces.

Measurement of sound intensity involves determining the sound pressure and the particle velocity at the same position simultaneously. The most common method employs two closely spaced pressure microphones and is based on determining the particle velocity using a finite difference approximation of the pressure gradient.

The sound intensity method is not without problems, and more knowledge is required in measuring sound intensity than in, say, using an ordinary sound level meter. The difficulties are mainly due to the fact that the accuracy of sound intensity measurements with a given measurement system depends very much on the sound field under study. Another problem is that the distribution of the sound intensity in the near field of a complex source is far more complicated than the distribution of the sound pressure, indicating that sound fields can be much more complicated than earlier realized.

### 2 SOUND FIELDS, SOUND ENERGY, AND SOUND INTENSITY

#### 2.1 Fundamental Relations

The instantaneous sound intensity  $\mathbf{I}(t)$  is a vector that describes the rate and direction of the net flow of sound energy per unit area as a function of time  $t$ . The dimensions of this quantity are energy per unit time per unit area ( $\text{W/m}^2$ ). The instantaneous sound intensity equals the product of the sound pressure  $p(t)$  and the particle velocity  $\mathbf{u}(t)$ ,<sup>1</sup>

$$\mathbf{I}(t) = p(t)\mathbf{u}(t) \quad (1)$$

By combining some of the fundamental equations that govern a sound field, the equation of conservation of mass, the adiabatic relation between changes in the sound pressure and in the density, and Euler's equation

of motion, one can derive the equation

$$\int_S \mathbf{I}(t) \cdot d\mathbf{S} = -\frac{\partial}{\partial t} \left( \int_V w(t) dV \right) = -\frac{\partial E(t)}{\partial t} \quad (2)$$

in which  $w(t)$  is the instantaneous total sound energy density,  $S$  is the area of a closed surface,  $V$  is the volume enclosed by the surface, and  $E(t)$  is instantaneous total sound energy within the surface.<sup>2</sup> The left-hand term is the net outflow of sound energy through the surface, and the right-hand term is the rate of change of the total sound energy within the surface. This is the equation of conservation of sound energy, which expresses the simple fact that the net flow of sound energy out of a closed surface equals the (negative) rate of change of the sound energy within the surface because the energy is conserved.

In practice, we are usually concerned with the time-averaged sound intensity in stationary sound fields:

$$\langle \mathbf{I}(t) \rangle_t = \langle p(t)\mathbf{u}(t) \rangle_t \quad (3)$$

For simplicity we use the symbol  $\mathbf{I}$  for this quantity rather than the more precise notation  $\langle \mathbf{I}(t) \rangle_t$ . If the sound field is harmonic with angular frequency  $\omega = 2\pi f$ , we can make use of the usual complex representation of the sound pressure and the particle velocity, which leads to the expression

$$\mathbf{I} = \frac{1}{2} \text{Re}\{p\mathbf{u}^*\} \quad (4)$$

where  $\mathbf{u}^*$  denotes the complex conjugate of  $\mathbf{u}$ .

It is possible to show from Eq. (2) that the integral of the time-averaged intensity over a surface that encloses a source equals the sound power emitted by the source  $P_a$ , that is,

$$\int_S \mathbf{I} \cdot d\mathbf{S} = P_a \quad (5)$$

irrespective of the presence of steady sources outside the surface.<sup>1,2</sup> This important equation is the basis of sound power determination using sound intensity. Another consequence of Eq. (2) is that the integral is zero:

$$\int_S \mathbf{I} \cdot d\mathbf{S} = 0 \quad (6)$$

when there is neither generation nor dissipation of sound energy within the surface, irrespective of the presence of steady sources outside the surface.

In a plane wave propagating in the  $r$  direction the sound pressure  $p$  and the particle velocity  $u_r$  are in phase and related by the characteristic impedance of air,  $\rho c$ , where  $\rho$  is the density of air and  $c$  is the speed of sound:

$$u_r(t) = \frac{p(t)}{\rho c} \quad (7)$$

Under such conditions the intensity is

$$\begin{aligned} I_r &= \langle p(t)u_r(t) \rangle_t = \langle p^2(t) \rangle_t \\ \rho c &= p_{\text{rms}}^2 \\ \rho c &= \frac{|p|^2}{2\rho c} \end{aligned} \quad (8)$$

where  $p_{\text{rms}}^2$  is the mean square pressure and  $p$  in the rightmost expression is the complex amplitude of the pressure in a plane wave in which the sound pressure is a sinusoidal function of time. In the particular case of a plane propagating wave, the sound intensity is seen to be simply related to the mean square sound pressure, which can be measured with a single microphone. Equation (8) is also valid in the important case of a simple spherical sound field generated by a monopole source under free-field conditions, irrespective of the distance to the source. A practical consequence of Eq. (8) is the following extremely simple relation between the sound intensity level (relative to  $I_{\text{ref}} = 1 \text{ pW/m}^2$ ) and the sound pressure level (relative to  $p_{\text{ref}} = 20 \text{ }\mu\text{Pa}$ ):

$$L_I \simeq L_p. \quad (9)$$

This is due to the fact that

$$\rho c \simeq \frac{p_{\text{ref}}^2}{I_{\text{ref}}} = 400 \text{ kg} \cdot \text{m}^{-2} \cdot \text{s}^{-1} \quad (10)$$

in air under normal ambient conditions. At a static pressure of 101.3 kPa and a temperature of 23°C, the error is about 0.1 dB.

However, in the general case the sound intensity is *not* simply related to the sound pressure, and both the sound pressure and the particle velocity must be measured simultaneously, and their instantaneous product time averaged as indicated by Eq. (3). This requires the use of a more complicated device than a single microphone. The sound intensity level is usually, although not always, lower than the sound pressure level.<sup>3</sup>

## 2.2 Active and Reactive Sound Fields

In spite of the diversity of sound fields encountered in practice, some typical sound field characteristics can be identified. For example, the sound field far

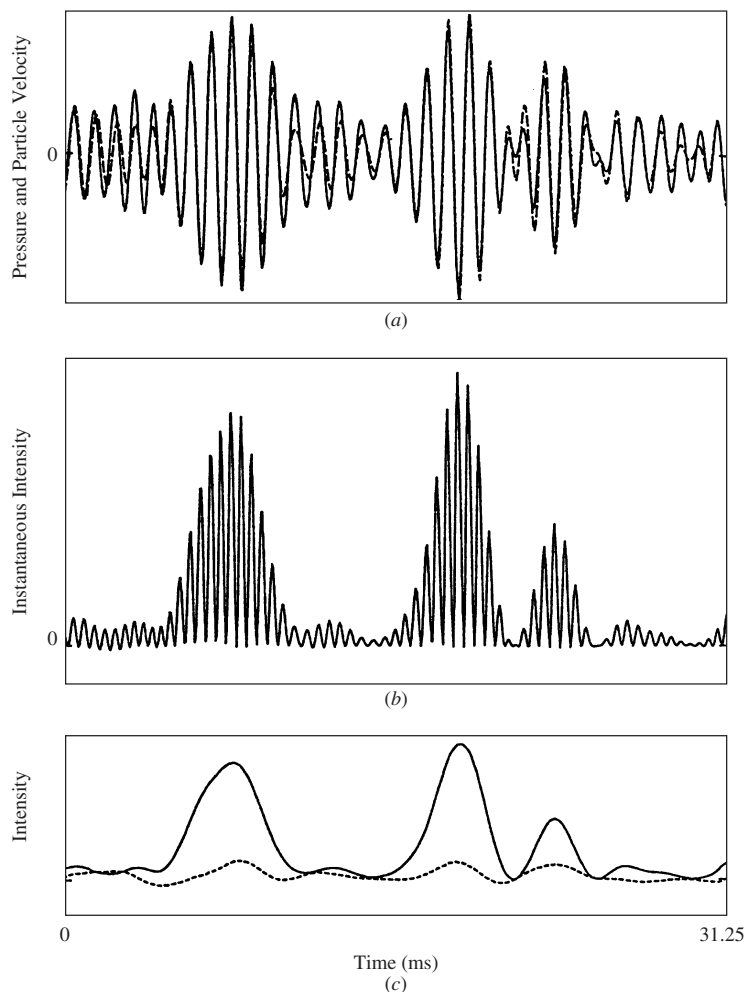
from a source under free-field conditions has certain well-known properties, the sound field near a source has other characteristics, and some characteristics are typical of a reverberant sound field.

It was mentioned above that the sound pressure and the particle velocity are in phase in a plane propagating wave. This is also the case in a free field, sufficiently far from the source that generates the field. Conversely, one of the characteristics of the sound field near a source is that the sound pressure and the particle velocity are partly out of phase. To describe such phenomena one may introduce the concept of active and reactive sound fields.

In a harmonic sound field the particle velocity may, without loss of generality, be divided into two components: one component in phase with the sound pressure and one component 90° out of phase with the sound pressure.<sup>4</sup> The instantaneous *active* intensity is the product of the sound pressure and the in-phase component of the particle velocity. This quantity has a nonzero time average: the time-averaged sound intensity, usually simply referred to as the sound intensity. The instantaneous *reactive* intensity is the product of the sound pressure and the out-of-phase component of the particle velocity. This quantity has a time average of zero, indicating that the sound energy is moving back and forth in the sound field without any net flow.

Very near a sound source the reactive field is usually stronger than the active field. However, the reactive field dies out rapidly with increasing distance to the source, and, even at a fairly moderate distance from the source, the sound field is dominated by the active field. The extent of the reactive field depends on the frequency, the dimensions, and the radiation characteristics of the sound source. In practice, the reactive field may usually be assumed to be negligible at a distance greater than, say, half a metre from the source.

Figures 1, 2, and 3 demonstrate the physical significance of the active and reactive intensities. Figure 1 shows the result of a measurement at a position about 30 cm (about one wavelength) from a small monopole source, an enclosed loudspeaker driven with a band of one-third octave noise. The sound pressure and the particle velocity (multiplied by  $\rho c$ ) are almost identical; therefore the instantaneous intensity is always positive: This is an *active* sound field. In Fig. 2 is shown the result of a similar measurement very near the loudspeaker (less than one tenth of a wavelength from the loudspeaker cone). In this case the sound pressure and the particle velocity are almost 90° out of phase, and as a result the instantaneous intensity fluctuates about zero, that is, sound energy flows back and forth, out of and into the loudspeaker. This is an example of a strongly *reactive* sound field. Finally Fig. 3 shows the result of a measurement in a reverberant room several metres from the loudspeaker generating the sound field. Here the sound pressure and the particle velocity appear to be uncorrelated signals. This is neither an active nor a reactive sound field; this is a *diffuse* sound field.



**Figure 1** Measurement in an active sound field. (a) solid line, instantaneous sound pressure; dashed line, instantaneous particle velocity multiplied by  $pc$ ; (b) instantaneous sound intensity; and (c) solid line, real part of complex instantaneous intensity; dashed line, imaginary part of complex instantaneous intensity. One-third octave noise with a center frequency of 1 kHz. (From Ref. 5. Reprinted with permission by Elsevier.)

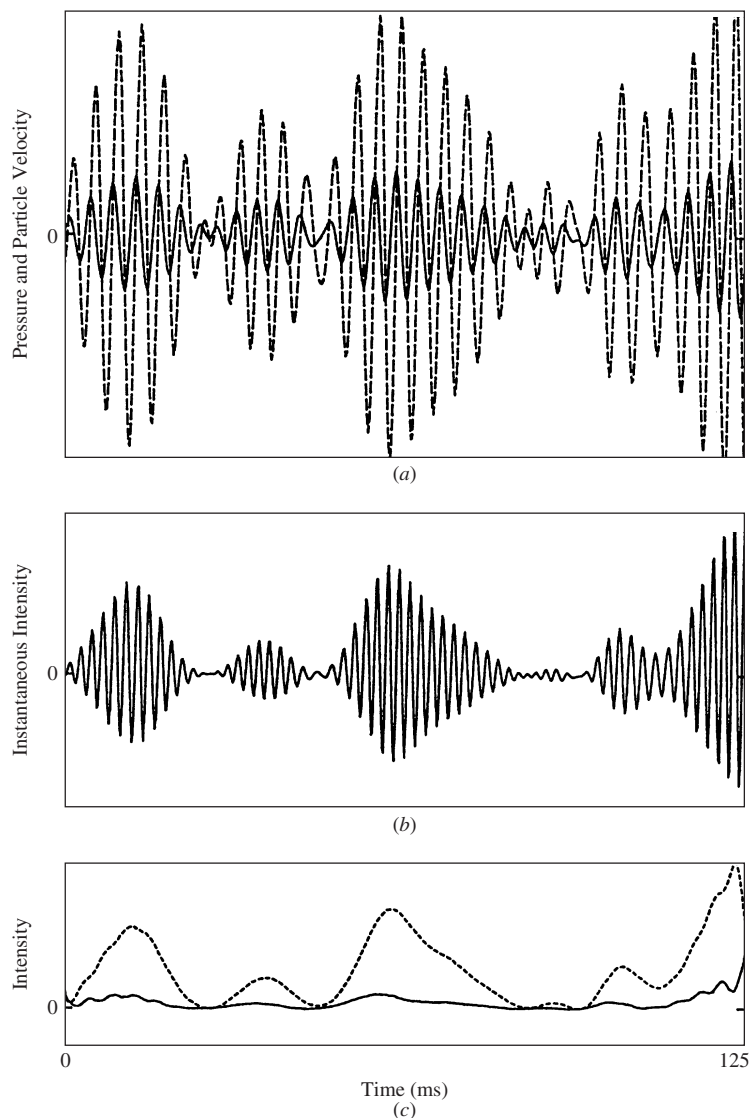
### 3 MEASUREMENT OF SOUND INTENSITY

Although acousticians have attempted to measure sound intensity since the 1930s, the first reliable measurements did not occur until the middle of the 1970s. Commercial sound intensity measurement systems came on the market in the beginning of the 1980s, and the first international standards for measurements using sound intensity and for instruments for such measurements were issued in the middle of the 1990s. A description of the history of the development of sound intensity measurement is given in Fahy's monograph *Sound Intensity*.<sup>1</sup>

The 50-year delay from when Olson submitted his application for a patent for an intensity meter in 1931 to when commercial measurement systems came on the

market in the beginning of the 1980s can be explained by the fact that it is far more difficult to measure sound intensity than to measure sound pressure. The problems are reflected in the extensive literature on the errors and limitations of sound intensity measurement and in the fairly complicated international and national standards for sound power determination using sound intensity, ISO 9614-1, ISO 9614-2, ISO 9614-3, and ANSI S12.12.<sup>6-9</sup>

Attempts to develop sound intensity probes based on the combination of a pressure transducer and a particle velocity transducer have occasionally been described in the literature, but this method has been hampered by the absence of reliable particle velocity transducers. However, a micromachined transducer called the Microflown has recently become available



**Figure 2** Measurement in a reactive sound field. Key as in Fig. 1. One-third octave noise with a center frequency of 250 Hz. (From Ref. 5. Reprinted with permission by Elsevier.)

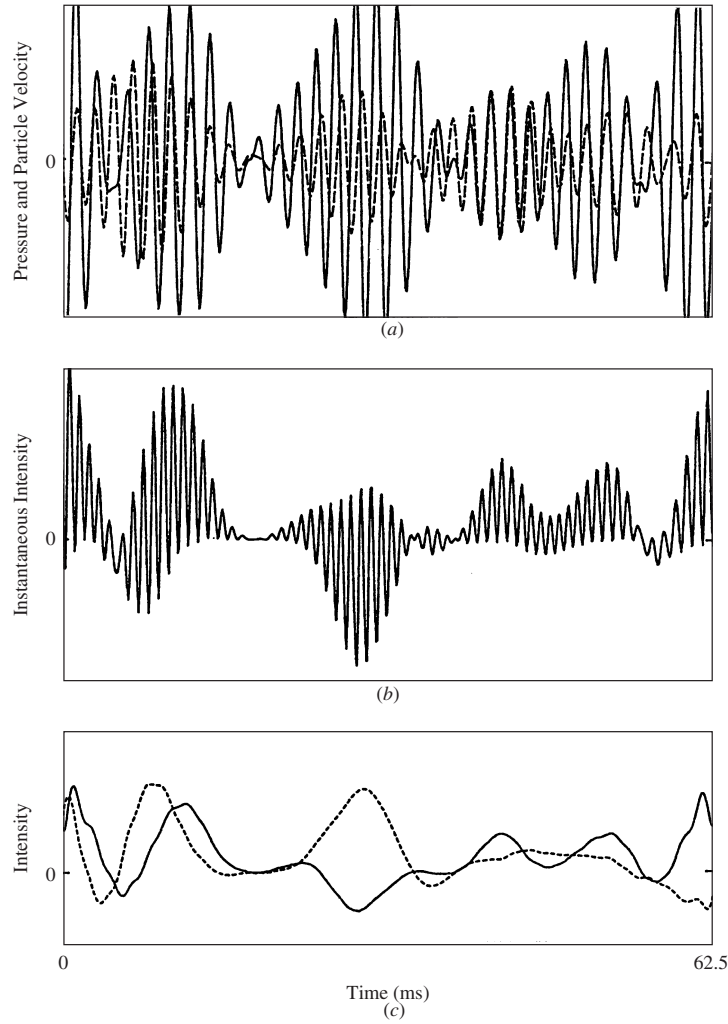
for measurement of the particle velocity, and a “low-cost intensity probe” based on this device is now in commercial production.<sup>10</sup> Recent results seem to indicate that it has potential.<sup>11</sup> However, one problem with any particle velocity transducer, irrespective of the measurement principle, is the strong influence of airflow. Another unresolved problem is how to determine the phase correction needed when two fundamentally different transducers are combined.

Apart from the Microflown intensity probe, all sound intensity measurement systems in commercial production today are based on the “two-microphone”

(or  $p$ - $p$ ) principle, which makes use of two closely spaced pressure microphones and relies on a finite difference approximation to the sound pressure gradient, and both the IEC 1043 standard on instruments for the measurement of sound intensity<sup>12</sup> and the corresponding North American ANSI standard<sup>13</sup> deal exclusively with the  $p$ - $p$  measurement principle. Therefore, all the considerations in this chapter concern this measurement principle.

Two pressure microphones are placed close to each other. The particle velocity component in the direction of the axis through the two microphones,  $r$ , is obtained through Euler’s equation of motion (Newton’s second





**Figure 3** Measurement in a diffuse sound field. Key as in Fig. 1. One-third octave noise with a center frequency of 500 Hz. (From Ref. 5. Reprinted with permission by Elsevier.)

law for a fluid):

$$\frac{\partial p(t)}{\partial r} + \rho \frac{\partial u_r(t)}{\partial t} = 0 \quad (11)$$

as

$$\hat{u}_r(t) = -\frac{1}{\rho} \int_{-\infty}^t \frac{p_2(\tau) - p_1(\tau)}{\Delta r} d\tau \quad (12)$$

where  $p_1$  and  $p_2$  are the signals from the two microphones,  $\Delta r$  is the microphone separation distance, and  $\tau$  is a dummy time variable. The caret indicates the finite difference estimate, which of course is an approximation to the real particle velocity. The sound

pressure at the center of the probe is estimated as

$$\hat{p}(t) = \frac{p_1(t) + p_2(t)}{2} \quad (13)$$

and the time-averaged intensity component in the  $r$  direction is

$$\hat{I}_r = \langle \hat{p}(t) \hat{u}_r(t) \rangle_t = \left\langle \frac{p_1(t) + p_2(t)}{2} \times \int_{-\infty}^t \frac{p_1(\tau) - p_2(\tau)}{\rho \Delta r} d\tau \right\rangle_t \quad (14)$$

Some sound intensity analyzers use Eq. (14) to measure the intensity in frequency bands (usually one-third octave bands). Another type calculates the intensity from the imaginary part of the cross spectrum of the two microphone signals,  $S_{12}(\omega)$ ,

$$\hat{I}_r(\omega) = -\frac{1}{\omega \rho \Delta r} \text{Im}\{S_{12}(\omega)\} \quad (15)$$

The time-domain formulation is equivalent to the frequency-domain formulation, and in principle Eq. (14) gives exactly the same result as Eq. (15) when the intensity spectrum is integrated over the frequency band of concern. The frequency-domain formulation, which makes it possible to determine sound intensity with a dual-channel fast Fourier transform (FFT) analyzer, was derived independently by Fahy and Chung in the late 1970s.<sup>14,15</sup>

The most common microphone arrangements are known as face-to-face and side-by-side microphones. The latter arrangement has the advantage that the diaphragms of the microphones can be placed very near a radiating surface but has the disadvantage that the microphones disturb each other acoustically. At high frequencies the face-to-face configuration with a solid spacer between the microphones is superior.<sup>16,17</sup> A sound intensity probe produced by Brüel & Kjær is shown in Fig. 4. The “spacer” between the microphones tends to stabilize the “acoustical distance” between them.<sup>16</sup>



**Figure 4** Sound intensity probe with the microphones in the “face-to-face” arrangement manufactured by Brüel & Kjær. (Courtesy Brüel & Kjær.)

#### 4 ERRORS AND LIMITATIONS IN MEASUREMENT OF SOUND INTENSITY

There are many sources of error in the measurement of sound intensity, and a considerable part of the sound intensity literature has been concerned with identifying and studying such errors. Some of the sources of error are fundamental, and others are associated with various technical deficiencies. One complication is that the accuracy depends very much on the sound field under study; under certain conditions even minute imperfections in the measuring equipment will have a significant influence. Another complication is that small local errors are sometimes amplified into large global errors when the intensity is integrated over a closed surface.<sup>18</sup>

The following is an overview of some of the most serious sources of error in the measurement of sound intensity. Those who make sound intensity measurements should know about the limitations imposed by

- The finite difference error<sup>19</sup>
- Errors due to scattering and diffraction<sup>17</sup>
- Instrumentation phase mismatch<sup>20</sup>

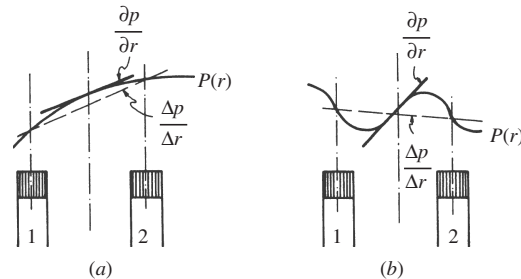
Other possible errors include

- Additive “false” low-frequency intensity signals caused by turbulent airflow<sup>21</sup>
- A random error caused by electrical noise in the microphones<sup>22</sup>

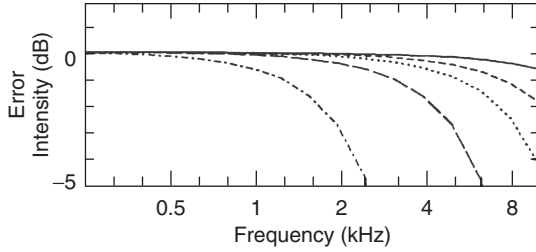
The latter is a problem only at fairly low sound pressure levels (say, below 40 dB relative to 20  $\mu$ Pa) and only at low frequencies (say, below 200 Hz).

##### 4.1 High-Frequency Limitations

The most fundamental limitation of the  $p$ - $p$  measurement principle is due to the fact that the sound pressure gradient is approximated by a finite difference of pressures at two discrete points. This obviously imposes an upper frequency limit that is inversely proportional to the distance between the microphones; see Fig. 5.



**Figure 5** Illustration of the error due to the finite difference approximation. (a) Good approximation at a low frequency and (b) poor approximation at a high frequency. (After Waser and Crocker.<sup>23</sup>)



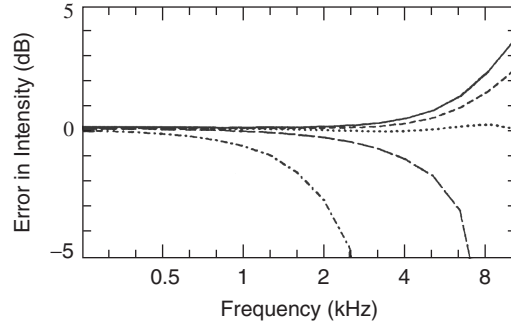
**Figure 6** Finite difference error of an ideal two-microphone sound intensity probe in a plane wave of axial incidence for different values of the separation distance: solid line, 5 mm; short dashed line, 8.5 mm; dotted line, 12 mm; long dashed line, 20 mm; dash-dotted line, 50 mm.

In the general case the finite difference error, that is, the ratio of the measured intensity  $\hat{I}_r$  to the true intensity  $I_r$ , depends on the sound field in a complicated manner.<sup>19</sup> In a plane sound wave of axial incidence the error can be shown to be<sup>16</sup>

$$\frac{\hat{I}_r}{I_r} = \frac{\sin k \Delta r}{k \Delta r} \quad (16)$$

where  $k = \omega/c$  is the wavenumber. This relation is shown in Fig. 6 for different values of the microphone separation distance. The upper frequency limit of intensity probes has generally been considered to be the frequency at which this error is acceptably small. With 12 mm between the microphones (a typical value) this gives an upper limiting frequency of about 5 kHz.

Equation (16) holds for an ideal sound intensity probe that does not in any way disturb the sound field. This is a good approximation if the microphones are small compared with the wavelength and the distance between them, but it is not a good approximation for a typical sound intensity probe such as the one shown in Fig. 4. The high-frequency performance of a real, physical probe is a combination of the finite difference error and the effect of the probe itself on the sound field. In the particular case of the face-to-face configuration, the two errors tend to cancel each other if the length of the spacer between the microphones equals their diameter; see Fig. 7. The physical explanation is that the resonance of the cavities in front of the microphones gives rise to a pressure increase that to some extent compensates for the finite difference error.<sup>17</sup> Thus, the resulting upper frequency limit of a sound intensity probe composed of half-inch microphones separated by a 12-mm spacer is 10 kHz, which is an octave above the limit determined by the finite difference error when the interference of the microphones on the sound field is ignored; compare Figs. 6 and 7. No similar canceling of errors occurs with the side-by-side configuration.



**Figure 7** Error of a sound intensity probe with half-inch microphones in the face-to-face configuration in a plane wave of axial incidence for different spacer lengths: solid line, 5 mm; short longdashed, 8.5 mm; dotted line, 12 mm; long dashed line, 20 mm; dash-dotted line, 50 mm.

#### 4.2 Instrumentation Phase Mismatch

Phase mismatch between the two measurement channels is the most serious source of error in the measurement of sound intensity, even with the best equipment that is available today. It can be shown that the estimated intensity, subject to a phase error  $\varphi_e$ , to a very good approximation can be written as

$$\hat{I}_r = I_r - \frac{\varphi_e}{k \Delta r} \frac{p_{\text{rms}}^2}{\rho c} \quad (17)$$

that is, phase mismatch in a given frequency band gives rise to a bias error in the measured intensity that is proportional to the phase error and to the mean square pressure and inversely proportional to the frequency and to the microphone separation distance.<sup>20</sup> In practice one must, even with state-of-the-art equipment, allow for phase errors ranging from about  $0.05^\circ$  at 100 Hz to  $2^\circ$  at 10 kHz. Both the physical phase difference in the sound field and the phase error between the microphones tend to increase with the frequency, from which it follows that this source of error is a potential problem in the entire frequency range—not just at low frequencies as often thought. Both the International Electrotechnical Commission (IEC) standard<sup>12</sup> and the North American ANSI National Standards Institute (ANSI) standard<sup>13</sup> on instruments for the measurement of sound intensity specify performance evaluation tests that ensure that the phase error is within certain limits.

Equation (17) is often written in the form

$$\hat{I}_r = I_r + \left( \frac{I_0}{p_0^2} \right) p_{\text{rms}}^2 = I_r \left( 1 + \frac{I_0}{p_0^2} \frac{p_{\text{rms}}^2}{I_r} \right) \quad (18)$$

where the *residual intensity*  $I_0$  and the corresponding sound pressure  $p_0$ ,

$$\frac{I_0}{p_0^2/\rho c} = -\frac{\varphi_e}{k\Delta r} \quad (19)$$

have been introduced. The residual intensity, which should be measured, for example, in one-third octave bands, is the “false” sound intensity indicated by the instrument when the two microphones are exposed to the same pressure  $p_0$ , for instance, in a small cavity. Under such conditions the true intensity is zero, and the indicated intensity  $I_0$  should obviously be as small as possible. The right-hand side of Eq. (18) demonstrates how the error caused by phase mismatch depends on the ratio of the mean square pressure to the intensity in the sound field—in other words on the sound field conditions.

Phase mismatch of sound intensity probes is usually described in terms of the so-called pressure-residual intensity index:

$$\delta_{pI_0} = 10 \log \left( \frac{p_0^2/\rho c}{I_0} \right) \quad (20)$$

which is just a convenient way of measuring and describing the phase error. With a microphone separation distance of 12 mm, the typical phase error mentioned above corresponds to a pressure-residual intensity index of 18 dB in most of the frequency range. The error due to phase mismatch is small provided that

$$\delta_{pI} \ll \delta_{pI_0} \quad (21)$$

where

$$\delta_{pI} = 10 \log \left( \frac{p_{\text{rms}}^2/\rho c}{I_r} \right) \simeq L_p - L_I \quad (22)$$

is the pressure-intensity index of the measurement. The inequality (21) is simply a convenient way of expressing that the phase error of the equipment should be much smaller than the phase angle between the two sound pressure signals in the sound field if measurement errors should be avoided. A more specific requirement can be expressed in the form<sup>7</sup>

$$\delta_{pI} < L_d = \delta_{pI_0} - K \quad (23)$$

where the quantity

$$L_d = \delta_{pI_0} - K \quad (24)$$

is called the *dynamic capability index* of the instrument and  $K$  is the *bias error index*. The dynamic capability index indicates the maximum acceptable value of the pressure-intensity index of the measurement for a given grade of accuracy. The larger the value of  $K$  the smaller is the dynamic capability index, the stronger and more restrictive is the requirement, and the smaller

is the error. The condition expressed by the inequality (23) and a bias error index of 7 dB guarantee that the error due to phase mismatch is less than 1 dB, which is adequate for most purposes. This corresponds to the phase error of the equipment being five times less than the actual phase angle in the sound field.

Most engineering applications of sound intensity measurements involve integrating the normal component of the intensity over a surface. The global version of Eq. (18) has the form<sup>20</sup>

$$\hat{P}_a = P_a \left[ 1 + \frac{I_0 \rho c}{p_0^2} \frac{\int_S (p_{\text{rms}}^2/\rho c) dS}{\int_S \mathbf{I} \cdot d\mathbf{S}} \right] \quad (25)$$

which shows that the global version of the inequality (23) can be written as

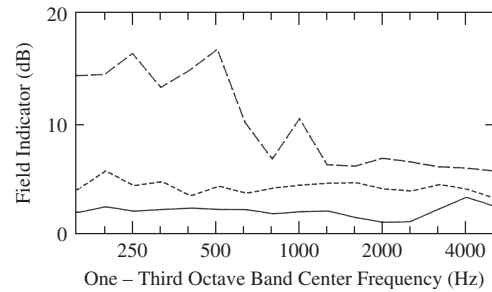
$$\Delta_{pI} < L_d = \delta_{pI_0} - K \quad (26)$$

where

$$\Delta_{pI} = 10 \log \left[ \frac{\int_S (p_{\text{rms}}^2/\rho c) dS}{\int_S \mathbf{I} \cdot d\mathbf{S}} \right] \quad (27)$$

is the global pressure-intensity index of the measurement. This quantity plays the same role in sound power estimation as the pressure-intensity index does in measurements at discrete points.

Figure 8 shows examples of the global pressure-intensity index measured under various conditions. It is obvious that the presence of noise sources outside the measurement surface increases the mean square pressure on the surface, and thus the influence of a given phase error; therefore a phase error, no matter how small, limits the range of measurement.



**Figure 8** The global pressure-intensity index  $\Delta_{pI}$  determined under three different conditions: solid line, measurement using a “reasonable” surface; dashed line, measurement using an eccentric surface; and dash-dotted line, measurement with strong background noise. (After Jacobsen.<sup>3</sup>)

In practice, one should examine whether the inequality (26) is satisfied or not when there is significant noise from extraneous sources. If the inequality is not satisfied, it can be recommended to use a measurement surface somewhat closer to the source than advisable in more favorable circumstances. It may also be necessary to modify the measurement conditions—to shield the measurement surface from strong extraneous sources, for example, or to increase the sound absorption in the room. All modern sound intensity analyzers can determine the pressure-intensity index concurrently with the actual measurement, so one can easily check whether phase mismatch is a problem or not. Some instruments automatically examine whether inequality (26) [or (23) in a point measurement] is satisfied or not and give warnings when this is not the case. It may well be impossible to satisfy the inequality in a frequency band with very little energy; this is, of course, of no concern.

## 5 CALIBRATION OF SOUND INTENSITY PROBES

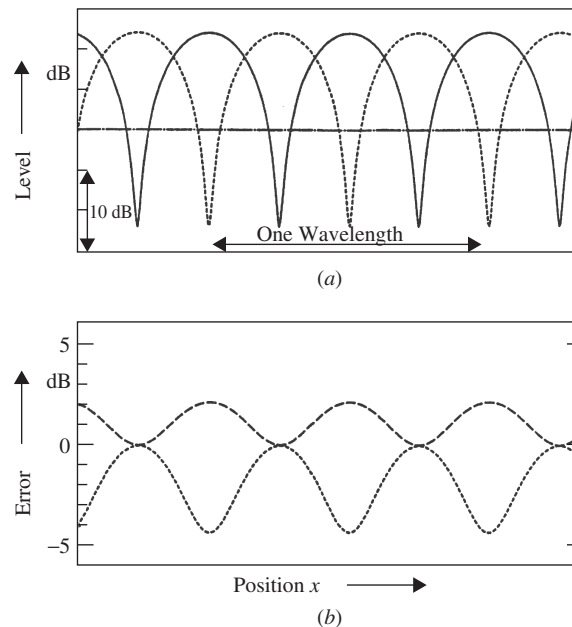
The purpose of the IEC standard for sound intensity instruments<sup>12</sup> and its North American counterpart<sup>13</sup> is to ensure that the intensity measurement system is accurate. Thus, minimum values of the acceptable pressure-residual intensity index are specified for the probe as well as for the processor, and according to the results of a test the instruments are classified as

being of “class 1” or “class 2.” The test involves subjecting the two microphones of the probe to identical pressures in a small cavity driven with wideband noise. As described in Section 4.2, the indicated pressure-intensity index equals the pressure-residual intensity index, which describes how well the two microphones are matched. A similar test of the processor involves feeding the same signal to the two channels.

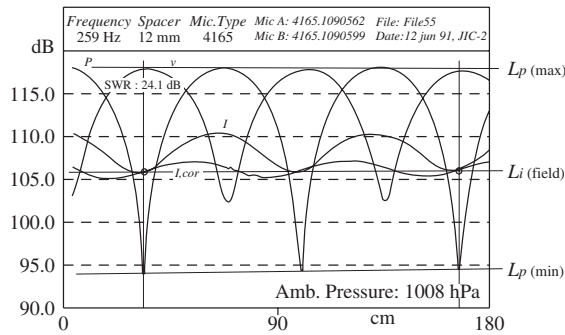
The pressure and intensity response of the probe should also be tested in a plane propagating wave as a function of the frequency, and the probe’s directional response is required to follow the ideal cosine law within a specified tolerance.

A special test is required in the frequency range below 400 Hz. According to this test the intensity probe should be exposed to the sound field in a standing-wave tube with a specified standing-wave ratio (24 dB for probes of class 1). When the sound intensity probe is drawn through this interference field, the sound intensity indicated by the measurement system should be within a certain tolerance.

Figure 9a illustrates how the sound pressure, the particle velocity, and the sound intensity vary with position in a one-dimensional interference field with a standing-wave ratio of 24 dB. It is apparent that the pressure-intensity index varies strongly with the position in such a sound field. Accordingly, the influence of a given phase error depends on the position, as shown in Fig. 9b. However, the test will



**Figure 9** (a) Sound pressure level (solid line), particle velocity level (dashed line), and sound intensity level (dash-dotted line) in a standing wave with a standing-wave ratio of 24 dB. (b) Estimation error of a sound intensity measurement system with a residual pressure-intensity index of 14 dB (positive and negative phase error). (From Ref. 24. Reprinted with permission by Elsevier.<sup>4</sup>)



**Figure 10** Response of a sound intensity probe exposed to a standing wave: sound pressure, particle velocity, intensity, and phase-corrected intensity. (After Frederiksen.<sup>25</sup>)

also reveal other sources of error than phase mismatch, for example, the influence of an unacceptably high vent sensitivity of the microphones.<sup>24,25</sup>

Figure 10 shows the measured pressure, particle velocity, intensity, and phase-corrected intensity in a standing-wave tube. The phase mismatch has been corrected by measuring the pressure-residual intensity index and subtracting the error term from the biased estimate given by Eq. (18). The remaining bias error is due to nonnegligible vent sensitivity of the particular microphones used in this test.<sup>25</sup> Note that the maximum error of the phase-corrected intensity does not occur at pressure maxima in the standing-wave field.

## 6 APPLICATIONS

Some of the most common practical applications of sound intensity measurements are now briefly discussed.

### 6.1 Sound Power Determination

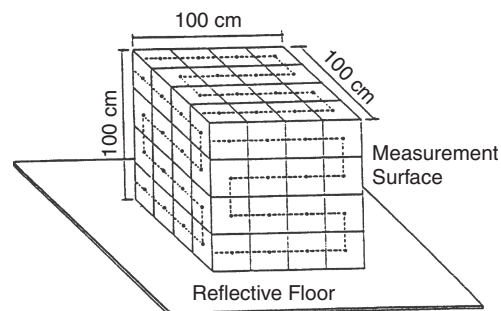
One of the most important applications of sound intensity measurements is the determination of the sound power of operating machinery in situ. Sound power determination using intensity measurements is based on Eq. (5), which shows that the sound power of a source is given by the integral of the normal component of the intensity over a surface that encloses the source, also in the presence of other sources outside the measurement surface. Neither an anechoic nor a reverberation room is required. The analysis of errors and limitations presented in Section 4 leads to the conclusion that the sound intensity method is suitable in the following instance:

- For stationary sources in stationary background noise provided that the global pressure-intensity index is within the dynamic capability of the equipment

The method is *not* suitable in the following instances:

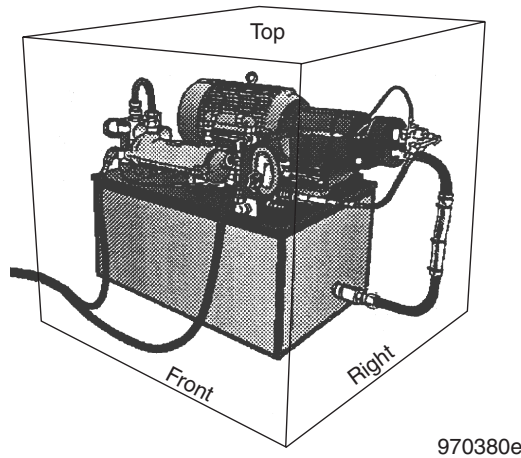
- For sources that operate in long cycles (because the sound field will change during the measurement)
- In nonstationary background noise (for the same reason)
- For weak sources of low-frequency noise (because of large random errors caused by electrical noise in the microphone signals)<sup>22</sup>

The surface integral can be approximated either by sampling at discrete points or by scanning manually or with a robot over the surface. With the scanning approach, the intensity probe is moved continuously over the measurement surface in such a way that the axis of the probe is always perpendicular to the measurement surface. A typical scanning path is shown in Fig. 11. The scanning procedure, which was introduced in the late 1970s on a purely empirical basis, was regarded with much skepticism for more than a decade<sup>27</sup> but is now generally considered to be more accurate and much faster and more convenient than the procedure based on fixed points.<sup>28,29</sup> A moderate scanning rate, say 0.5 m/s, and a “reasonable” scan line density should be used, say 5 cm between adjacent lines if the surface is very close to the source, 20 cm if it is further away. One cannot use the scanning



**Figure 11** Typical scanning path. (After Tachibana.<sup>26</sup>)





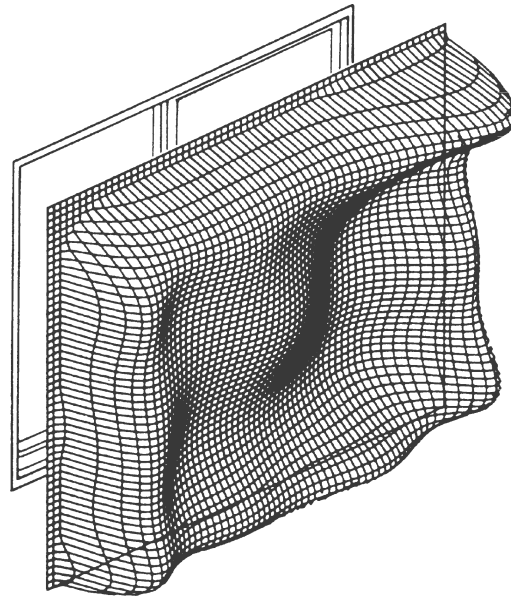
**Figure 12** Measurement surface divided into segments. (After Brüel & Kjær.<sup>30</sup>)

method if the source is operating in cycles; both the source under test and possible extraneous noise sources must be perfectly stationary. The procedure using fixed positions is used when the scanning method cannot be used, for example, because people are not allowed near an engine at full load.

Usually the measurement surface is divided into a number of segments, each of which will be convenient to scan; Fig. 12 shows a simple example. One will often determine the pressure-intensity index of each segment, and the accuracy of each partial sound power estimate depends on whether inequality (23) is satisfied or not, but it follows from inequality (26) that it is the global pressure-intensity index associated with the entire measurement surface that determines the accuracy of the estimate of the (total) radiated sound power. It may be impossible to satisfy inequality (23) on a certain segment, for example, because the net sound power passing through the segment takes a very small value because of extraneous noise; but, if the global criterion is satisfied, then the total sound power estimate will nevertheless be accurate.

Very near a large, complex source the sound field is often very complicated and may well involve regions with negative intensity, and far from a source background noise will usually be a problem, indicating the existence of an optimum measurement surface that minimizes measurement errors.<sup>31</sup> In practice, one uses a surface of a simple shape at some distance, say 25 to 50 cm, from the source. If there is a strong reverberant field or significant ambient noise from other sources, the measurement surface should be chosen to be somewhat closer to the source under study.

The three International Organization for Standardization (ISO) standards for sound power determination using intensity measurement<sup>6-8</sup> have been designed



**Figure 13** Distribution of normal intensity over a window transmitting in the 2-kHz one-third octave band. (After Tachibana.<sup>33</sup>)

for sources of noise in their normal operating conditions, which may be very unfavorable. In order to ensure accurate results under such general conditions, the user must determine a number of "indicators" and check whether various conditions are satisfied. The most important indicator is the global pressure-intensity index [Eq. (27)], and the most important condition is inequality (26). The standards also specify corrective actions when the requirements fail to be met. In addition ISO 9614-2 specifies a reproducibility test; each segment should be scanned twice with orthogonally oriented patterns, and the difference should be less than a specified value. Fahy, who was the convener of the working group that developed ISO 9614-1 and 9614-2, has described the rationale, background, and principles of the procedures specified in these standards.<sup>32</sup> The approach in the corresponding ANSI standard is quite different.<sup>9</sup> In this standard no less than 26 indicators are described, but it is optional to determine these quantities, and it is left to the user to interpret the data and decide what to do.

## 6.2 Noise Source Identification and Visualization of Sound Fields

This is another important application of the sound intensity method. A noise reduction project usually starts with the identification and ranking of noise sources and transmission paths, and sound intensity measurements make it possible to determine the partial sound power contribution of the various components

directly. Plots of the sound intensity normal to a measurement surface can be used in locating noise sources. Figure 13 shows an example of a plot of the normal intensity over a window transmitting sound. The dominant radiation of sound near edges and corners is clearly seen.

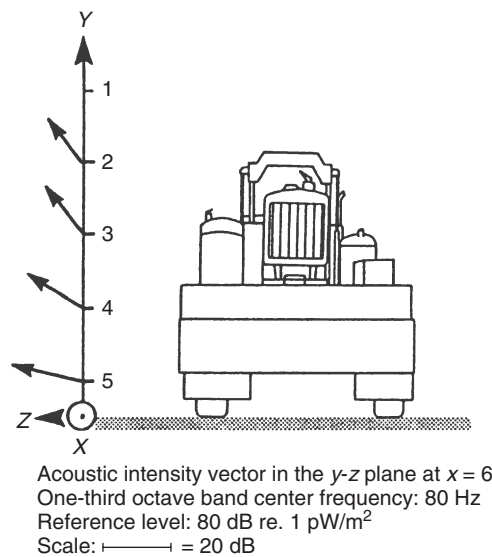
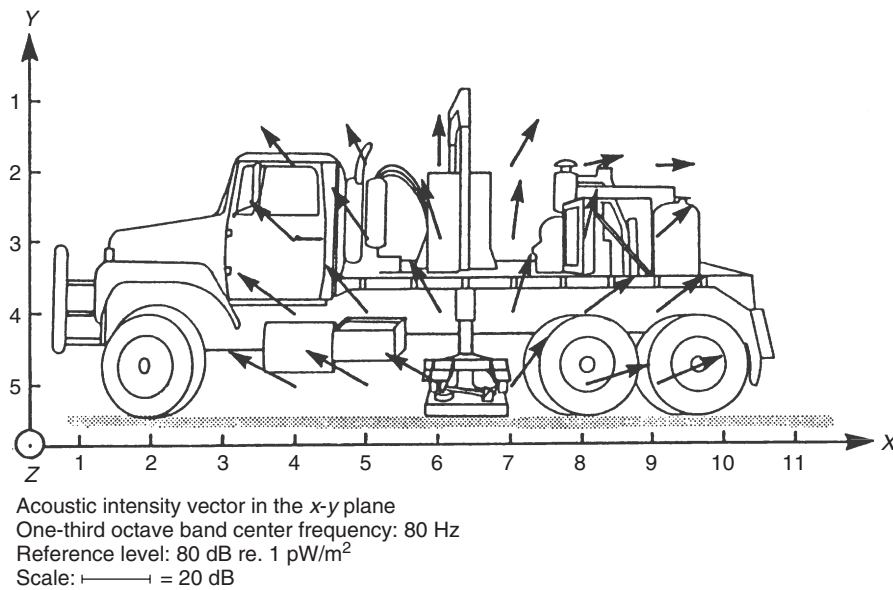
Visualization of sound fields, helped by modern computer graphics, contributes to our understanding of the sound radiation of complicated sources. Figure 14 shows vector plots near a seismic vibrator, and Fig. 15

shows the results of similar measurements near a musical instrument (a recorder).

### 6.3 Radiation Efficiency of Structures

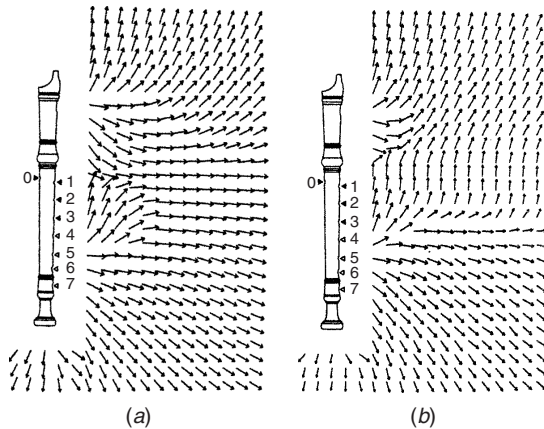
The radiation efficiency of a structure is a measure of how effectively it radiates sound. This dimensionless quantity is defined as

$$\sigma = \frac{P_a}{\rho c \langle v_n^2 \rangle S} \quad (28)$$



**Figure 14** Sound intensity vectors in the 80-Hz one-third octave band measured near a seismic vibrator. Components in (a) the x-y plane and (b) the y-z plane. (From Ref. 34. Reprinted with permission by Elsevier.)





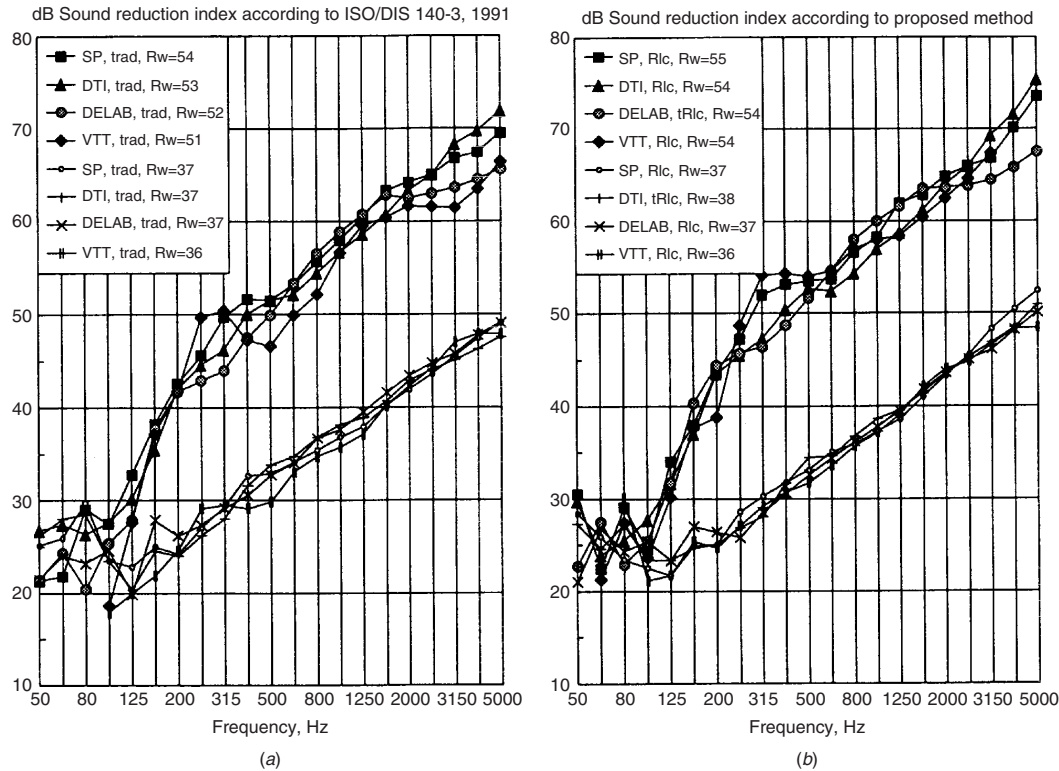
**Figure 15** Sound intensity distribution in the sound field generated by a recorder. (a) Fundamental (520 Hz) and (b) second harmonic (1040 Hz). (After Tachibana.<sup>35</sup>)

where  $P_a$  is the sound power radiated by the structure of surface area  $S$ ,  $v_n$  is normal velocity of the surface, and the angular brackets indicate averaging over time as well as space. The sound intensity method is

suitable for measuring the radiated sound power. In principle, one can also measure the surface velocity with an intensity probe since this quantity may be approximated by the normal component of the particle velocity near the radiating structure, which may be determined using Eq. (12).<sup>36</sup> The advantage is that the sound intensity and the velocity are determined at the same time. However, in practice, such a velocity measurement can be problematic, among other reasons because of its sensitivity to extraneous noise,<sup>37</sup> and a conventional measurement with accelerometers or a laser transducer may be a better option.

#### 6.4 Transmission Loss of Structures and Partitions

The conventional measure of the sound insulation of panels and partitions is the transmission loss (also called sound reduction index), which is the ratio of incident to transmitted sound power in logarithmic form. The traditional method of measuring this quantity requires a transmission suite consisting of two vibration-isolated reverberation rooms. The sound power incident on the partition under test in the source room is deduced from an estimate of the spatial average of the mean square sound pressure in the room on the assumption that the sound field is diffuse, and the



**Figure 16** Interlaboratory comparison for a single metal leaf window (lower curves) and for a double metal leaf window (upper curves): (a) conventional method and (b) intensity method. (From Ref. 38. Reprinted with permission by Elsevier.)

transmitted sound power is determined from a similar measurement in the receiving room where, in addition, the reverberation time must be determined. The sound intensity method, which is now standardized,<sup>39,40</sup> has made it possible to measure the transmitted sound power directly. In this case it is not necessary that the sound field in the receiving room is diffuse, which means that only one reverberation room, the source room, is necessary.<sup>41</sup> One cannot measure the incident sound power in the source room using sound intensity since the method gives the *net* sound intensity. Figure 16 shows the results of a round-robin investigation in which a single-leaf and a double-leaf construction were tested by four different laboratories using the conventional method and the intensity-based method.

The main advantage of the intensity method over the conventional approach is that it is possible to evaluate the transmission loss of individual parts of the partition. However, each sound power measurement must obviously satisfy the condition expressed by inequality (26).

There are other sources of error than phase mismatch. To give an example, the traditional method of measuring the sound power transmitted through the partition under test gives the transmitted sound power irrespective of the absorption of the partition, whereas the intensity method gives the net power.<sup>42</sup> If a significant part of the absorption in the receiving room is due to the partition, then the net power is less than the transmitted power because a part of the transmitted sound energy is reabsorbed/transmitted by the partition. Under such conditions one must increase the absorption of the receiving room; otherwise the intensity method will overestimate the transmission loss because the transmitted sound power is underestimated.

As an interesting by-product of the intensity method, it can be mentioned that deviations observed between results determined using the traditional method and the intensity method led several authors to reanalyze the traditional method in the 1980s<sup>43,44</sup> and point out that the Waterhouse correction,<sup>45</sup> well established in sound power determination using the reverberation room method, had been overlooked in the standards for measurement of transmission loss.

## 6.5 Other Applications

The fact that the sound intensity level is much lower than the sound pressure level in a diffuse sound field has led to the idea of replacing a measurement of the *emission sound pressure level* generated by machinery at the operator's position by a measurement of the sound intensity level, because the latter is less affected by diffuse background noise.<sup>46</sup> This method has recently been standardized.<sup>47</sup>

## REFERENCES

1. F. J. Fahy, *Sound Intensity* 2nd ed., E&FN Spon, London, 1995.
2. A. D. Pierce, *Acoustics: An Introduction to Its Physical Principles and Applications* 2nd ed., Acoustical Society of America, New York, 1989.
3. F. Jacobsen, Sound Field Indicators: Useful Tools, *Noise Control Eng. J.*, Vol. 35, 1990, pp. 37–46.
4. J. A. Mann III, J. Tichy, and A. J. Romano, Instantaneous and Time-Averaged Energy Transfer in Acoustic Fields, *J. Acoust. Soc. Am.*, Vol. 82, 1987, pp. 17–30.
5. F. Jacobsen, A Note on Instantaneous and Time-Averaged Active and Reactive Sound Intensity, *J. Sound Vib.*, Vol. 147, 1991, pp. 489–496.
6. ISO (International Organization for Standardization) 9614-1, Acoustics—Determination of Sound Power Levels of Noise Sources Using Sound Intensity—Part 1: Measurement at Discrete Points, 1993.
7. ISO (International Organization for Standardization) 9614-2, Acoustics—Determination of Sound Power Levels of Noise Sources Using Sound Intensity—Part 2: Measurement by Scanning, 1996.
8. ISO (International Organization for Standardization) 9614-3, Acoustics—Determination of Sound Power Levels of Noise Sources Using Sound Intensity—Part 3: Precision Method for Measurement by Scanning, 2002.
9. ANSI (American National Standards Institute) S12.12–1992, Engineering Method for the Determination of Sound Power Levels of Noise Sources Using Sound Intensity, 1992.
10. R. Raangs, W. F. Druyvesteyn, and H.-E. de Bree, A Low-Cost Intensity Probe, *J. Audio Eng. Soc.*, Vol. 51, 2003, pp. 344–357.
11. F. Jacobsen and H.-E. de Bree, A Comparison of Two Different Sound Intensity Measurement Principles, *J. Acoust. Soc. Am.*, Vol. 118, 2005, pp. 1510–1517.
12. IEC (International Electrotechnical Commission) 1043, Electroacoustics—Instruments for the Measurement of Sound Intensity—Measurements with Pairs of Pressure Sensing Microphones, 1993.
13. ANSI (American National Standards Institute) S1.9–1996, Instruments for the Measurement of Sound Intensity, 1996.
14. F. J. Fahy, Measurement of Acoustic Intensity Using the Cross-Spectral Density of Two Microphone Signals, *J. Acoust. Soc. Am.*, Vol. 62, 1977, pp. 1057–1059.
15. J. Y. Chung, Cross-Spectral Method of Measuring Acoustic Intensity without Error Caused by Instrument Phase Mismatch, *J. Acoust. Soc. Am.*, Vol. 64, 1978, pp. 1613–1616.
16. G. Rasmussen and M. Brock, Acoustic Intensity Measurement Probe, *Proc. Rec. Devel. Acoust. Intensity*, 1981, pp. 81–88.
17. F. Jacobsen, V. Cutanda, and P. M. Juhl, A Numerical and Experimental Investigation of the Performance of Sound Intensity Probes at High Frequencies, *J. Acoust. Soc. Am.*, Vol. 103, 1998, pp. 953–961.
18. J. Pope, Qualifying Intensity Measurements for Sound Power Determination, *Proc. Inter-Noise 89*, 1989, pp. 1041–1046.
19. U. S. Shirahatti and M. J. Crocker, Two-Microphone Finite Difference Approximation Errors in the Interference Fields of Point Dipole Sources, *J. Acoust. Soc. Am.*, Vol. 92, 1992, pp. 258–267.
20. F. Jacobsen, A simple and Effective Correction for Phase Mismatch in Intensity Probes, *Appl. Acoust.*, Vol. 33, 1991, pp. 165–180.
21. F. Jacobsen, Intensity Measurements in the Presence of Moderate Airflow, *Proc. Inter-Noise 94*, 1994, pp. 1737–1742.

22. F. Jacobsen, Sound Intensity Measurement at Low Levels, *J. Sound Vib.*, Vol. 166, 1993, pp. 195–207.
23. M. P. Waser and M. J. Crocker, Introduction to the Two-Microphone Cross-Spectral Method of Determining Sound Intensity, *Noise Control Eng. J.*, Vol. 22, 1984, pp. 76–85.
24. F. Jacobsen and E. S. Olsen, Testing Sound Intensity Probes in Interference Fields, *Acustica*, Vol. 80, 1994, pp. 115–126.
25. E. Frederiksen, *BCR Report: Sound Intensity Measurement Instruments. Free-field Intensity Sensitivity Calibration and Standing Wave Testing*, Brüel & Kjær, Nærum, 1992.
26. H. Tachibana and H. Yano, Changes of Sound Power of Reference Sources Influenced by Boundary Conditions Measured by the Sound Intensity Technique, *Proc. Inter-Noise 89*, 1989, pp. 1009–1014.
27. M. J. Crocker, Sound Power Determination from Sound Intensity—To Scan or Not to Scan, *Noise Contr. Eng. J.*, Vol. 27, 1986, p. 67.
28. U. S. Shirahatti and M. J. Crocker, Studies of the Sound Power Estimation of a Noise Source Using the Two-Microphone Sound Intensity Technique, *Acustica*, Vol. 80, 1994, pp. 378–387.
29. O. K. Ø. Pettersen and H. Olsen, On Spatial Sampling Using the Scanning Intensity Technique, *Appl. Acoust.*, Vol. 50, 1997, pp. 141–153.
30. Anon., *Sound Intensity Software BZ7205. User Manual*, Brüel & Kjær, Nærum, 1998.
31. F. Jacobsen, Sound Power Determination Using the Intensity Technique in the Presence of Diffuse Background Noise, *J. Sound Vib.*, Vol. 159, 1992, pp. 353–371.
32. F. J. Fahy, International Standards for the Determination of Sound Power Levels of Sources Using Sound Intensity Measurement: An Exposition, *Appl. Acoust.*, Vol. 50, 1997, pp. 97–109.
33. H. Tachibana, Applications of Sound Intensity Technique to Architectural Acoustics (in Japanese), *Proc. 2nd Symp. Acoust. Intensity*, 1987, pp. 103–114.
34. T. Astrup, Measurement of Sound Power Using the Acoustic Intensity Method—A Consultant's Viewpoint, *Appl. Acoust.*, Vol. 50, 1997, pp. 111–123.
35. H. Tachibana, Visualization of Sound Fields by the Sound Intensity Technique (in Japanese), *Proc. 2nd Symp. Acoust. Intensity*, 1987, pp. 117–126.
36. B. Forssen and M. J. Crocker, Estimation of Acoustic Velocity, Surface Velocity, and Radiation Efficiency by Use of the Two-Microphone Technique, *J. Acoust. Soc. Am.*, Vol. 73, 1983, pp. 1047–1053.
37. G. C. Steyer, R. Singh, and D. R. Houser, Alternative Spectral Formulation for Acoustic Velocity Measurement, *J. Acoust. Soc. Am.*, Vol. 81, 1987, pp. 1955–1961.
38. H. G. Jonasson, Sound Intensity and Sound Reduction Index, *Appl. Acoust.*, Vol. 40, 1993, pp. 281–293.
39. ISO (International Organization for Standardization) 15186-1, Acoustics—Measurement of Sound Insulation in Buildings and of Building Elements Using Sound Intensity—Part 1: Laboratory Measurements, 2000.
40. ISO (International Organization for Standardization) 15186-2, Acoustics—Measurement of Sound Insulation in Buildings and of Building Elements Using Sound Intensity—Part 2: Field Measurements, 2003.
41. M. J. Crocker, P. K. Raju, and B. Forssen, Measurement of Transmission Loss of Panels by the Direct Determination of Transmitted Acoustic Intensity, *Noise Contr. Eng. J.*, Vol. 17, 1981, pp. 6–11.
42. J. Roland, C. Martin, and M. Villot, Room to Room Transmission: What Is Really Measured by Intensity? *Proc. 2nd Intern. Congr. Acoust. Intensity*, 1985, pp. 539–546.
43. E. Halliwell and A. C. C. Warnock, Sound Transmission Loss: Comparison of Conventional Techniques with Sound Intensity Techniques, *J. Acoust. Soc. Am.*, Vol. 77, 1985, pp. 2094–2103.
44. B. G. van Zyl, P. J. Erasmus, and F. Anderson, On the Formulation of the Sound Intensity Method for Determining Sound Reduction Indices, *Appl. Acoust.*, Vol. 22, 1987, pp. 213–228.
45. R. V. Waterhouse, Interference Patterns in Reverberant Sound Fields, *J. Acoust. Soc. Am.*, Vol. 27, 1955, pp. 247–258.
46. H. G. Jonasson, Determination of Emission Sound Pressure Level and Sound Power Level in situ, SP Report 39, 1998.
47. ISO (International Organization for Standardization) 11205, Acoustics—Noise Emitted by Machinery and Equipment—Engineering Method for the Determination of Emission Sound Pressure Levels in situ at the Work Station and at Other Specified Positions Using Sound Intensity, 2003.

# CHAPTER 46

## NOISE AND VIBRATION DATA ANALYSIS

Robert B. Randall

School of Mechanical and Manufacturing Engineering  
The University of New South Wales  
Sydney, New South Wales, Australia

### 1 INTRODUCTION

Noise is often produced by the radiation of sound from vibrating surfaces. The noise can be related by a physical transfer function to the surface vibration. Analysis of the noise and vibration signals is usually done to extract parameters that best characterize the signals for the purpose of the practical application. These parameters often include root-mean-square (rms) values that can be used to assess signal strength or the potential of the noise or vibration to cause damage. In some cases, it is necessary to study the resonant response of excited structures or systems to which the signal is applied. In such cases, simple signal strength is not the only important factor but also how the noise and vibration is distributed with frequency. Hence, frequency analysis by fast Fourier transform (FFT) techniques and filters is often used.

In recognizing the impulsiveness of some noise and vibration signals, and their potential to cause and/or reveal damage to machinery, structures, and humans, a knowledge of statistical parameters such as kurtosis is valuable as a measure of impulsiveness. In addition, because the statistical distribution of local peak values is related to fatigue life of machinery and structures, methods of describing it are important. The relationship between two (or more) noise or vibration signals can be important, for example, to characterize the properties of a physical system by relating the applied excitation to the response of the system, or simply to determine if the signals are related. Thus methods of establishing such relationships, such as correlations, cross spectra, and frequency response functions, are of interest. Such noise and vibration signals being analyzed usually have wide frequency and dynamic ranges, and typical condenser microphones for noise signals and accelerometers for vibration signals must have suitable performance for their measurement.

### 2 SIGNAL TYPES

Many noise and vibration signals come from machines in operation. A simple machine such as a motor–pump set has a single rotating shaft (in sections joined by couplings), and some vibrations, such as those due to unbalance, are directly related to the shaft speed and phase locked to it. At constant speed the unbalance force will be sinusoidal, and the vibration response also largely at this same frequency. Because of nonlinearities in the structure and support, the response may contain sinusoidal components at higher harmonics (multiples) of the shaft speed, but will still be *periodic* with a period equal to one revolution. With two or

more independent shafts, such as with an aeroengine, the shaft-related signal will still be a sum of sinusoids, but no longer periodic. Such signals are known as *quasi-periodic*. In some other machines, for example, internal combustion engines, some vibration components, such as those due to combustion, are loosely tied to shaft speed, but not phase locked. Accordingly, there is an explosion in each cylinder every cycle, but the combustion events are not exactly repeatable. Such signals are known as *cyclostationary*. Yet other components, typically those associated with fluid flow, such as turbulent fluctuations and cavitation, are not tied to shaft speeds at all and are random, although they may be stationary; that is, their statistical properties are invariant with time. At this point it is also worth mentioning *pseudorandom* signals. These are formed by taking a section of random signal and repeating it periodically. Thus, over short time periods they appear random, but they are actually deterministic.

For constant operating conditions all the above signals may be considered stationary (at least if the various realizations are arranged with arbitrary zero times so that there is no reason why ensemble averages at one time should be different from those at other times), but in the more general case statistical parameters vary with time because of varying conditions, and the signals are then nonstationary. Typical examples are the noise from an aircraft flyover or the vibrations from a machine during run-up or coast-down. Such signals are typically analyzed by dividing them up into short quasi-stationary sections, and the changes in their parameters registered against time.

All the above signals are continuous and characterized by their local *power*, that is, the mean-square value averaged over a defined time interval, but a further class of signals can be categorized as *transients*, that is, single events starting and finishing with value (essentially) of zero. Transient signals are characterized by their *energy*, that is, the integral of their instantaneous power over their entire length, and it is important to recognize the different dimensions and units of their time and frequency representations. Shocks are of this type. Interpreting a squared signal as power requires explanation but can be seen by analogy with electrical power, the product of current and voltage. Thus power  $P = IV = I^2R = V^2/R$  (where  $I$  = current,  $V$  = voltage, and  $R$  = resistance), and so the physical power is related to the square of the current or voltage signal through a constant impedance or admittance parameter. In a similar manner, sound power is related to the square of sound pressure or

particle velocity, and vibration acceleration power is often represented in terms of  $g^2$  or  $(ms^{-2})^2$ .

Figure 1 shows how the above-mentioned signals may be classified, and Fig. 2 shows typical time- and frequency-domain representations of some signal types. *Stationary deterministic signals* are made up entirely of sinusoidal components, while *stationary random signals* have a spectrum distributed continuously with frequency. Sinusoids have a finite power concentrated at a single frequency, whereas the spectra of stationary random signals must be integrated over a finite frequency band to obtain finite power, and it is then appropriate to speak of a constant *power spectral density* (PSD) or power per hertz. Transients also have a spectrum distributed continuously with frequency, but as mentioned above the transient has finite energy

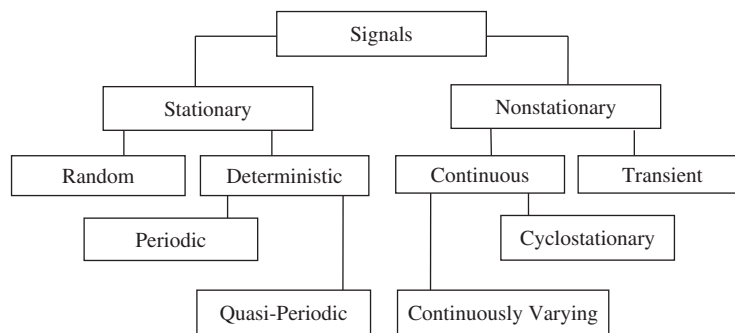
and the spectrum should be scaled in *energy spectral density* (ESD) or energy per hertz.

### 3 TIME-DOMAIN DESCRIPTIONS

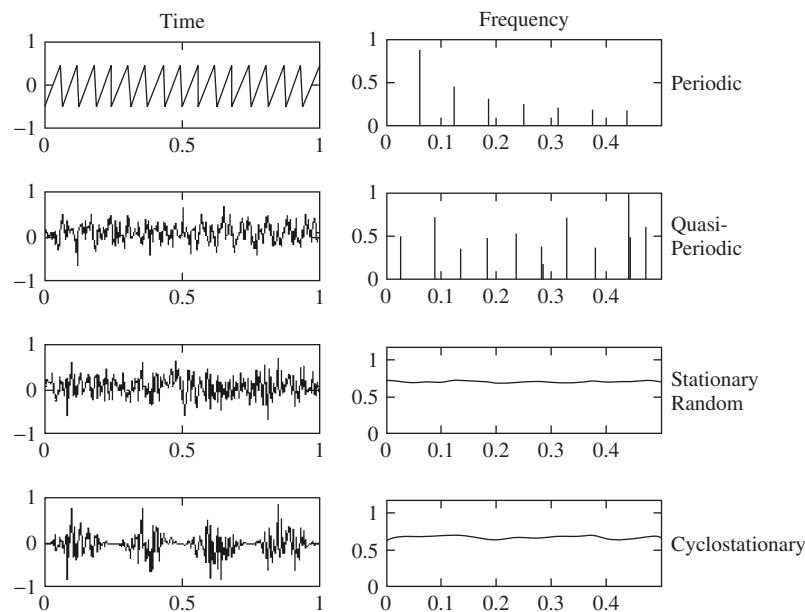
#### 3.1 Statistical Descriptors

Use can be made of basic statistics to extract characteristic parameters from the time signal directly. In the most general case we will be dealing with an ensemble of time signals arising from a random process, as illustrated in Fig. 3, and the statistical parameters are calculated as the “expected value,” or ensemble average, represented by the symbol  $E[\cdot]$ , at a given time.

This description can also be used for nonstationary signals. Thus the *mean value*, or simple average, is



**Figure 1** Division of signals into the main categories.



**Figure 2** Typical signals in the time and frequency domains.

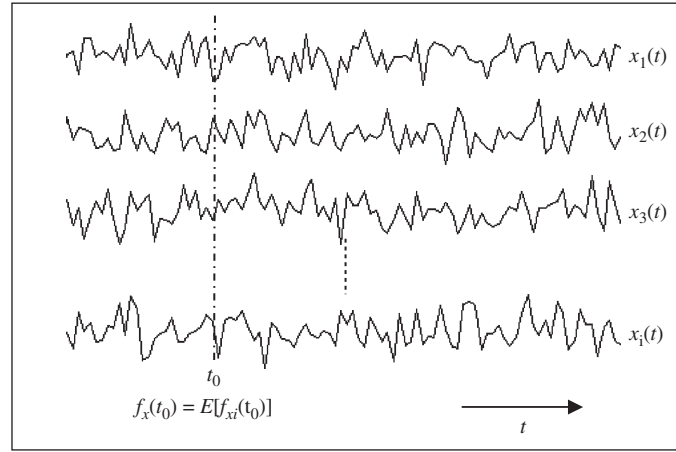


Figure 3 Illustration of ensemble averaging.

given by the formula

$$x_m(t) = E[x(t)] \quad (1)$$

However, for stationary signals, as mentioned above, the statistical parameters are independent of the time at which they are evaluated, and so  $x_m(t) = x_m$ , often represented as the constant  $\mu$ . As discussed in Chapter 13, provided the process is ergodic, the statistical parameters can be calculated from averages taken along the time record, so

$$\mu_T = \frac{1}{T} \int_0^T x(t) dt \quad (2)$$

which represents an average over  $T$  seconds, but the equivalence with the ensemble average applies as  $T \rightarrow \infty$ . Since the average is independent of time  $t$ , the integration can also be from  $-T/2$  to  $T/2$ . In what follows, until the case of nonstationary signals is considered, stationary signals will be assumed and all definitions will use time-domain averages.

If the squared value of the signal is averaged, this gives the *mean square value*, which is the averaged signal power. Thus,

$$x_{ms} = \frac{1}{T} \int_0^T x^2(t) dt \quad (3)$$

To obtain a parameter with the same dimensions and units as the original signal, it is normal to take the square root of the mean-square value to obtain the root-mean-square, or rms, value; thus;

$$x_{rms} = \sqrt{\frac{1}{T} \int_0^T x^2(t) dt} \quad (4)$$

It is also convenient to evaluate the parameters of the signal once the mean value or *direct current (dc) component* has been removed. The power of the remainder is the *variance*, given by

$$x_{var} = \sigma^2 = \frac{1}{T} \int_0^T (x(t) - \mu)^2 dt \quad (5)$$

and its square root is the *standard deviation*:

$$\sigma = \sqrt{\frac{1}{T} \int_0^T (x(t) - \mu)^2 dt} \quad (6)$$

### 3.2 Probability

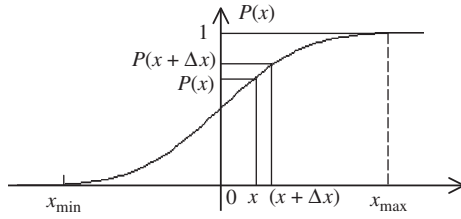
For the random signal  $x(t)$  (e.g., one of the realizations in Fig. 3), consider a number of samples at small uniform intervals. The fraction of samples that are less than a particular value of  $x$  can be used to define the *probability distribution*  $P(x)$ , which is the probability that the random variable  $x(t)$  is less than  $x$ . That is,

$$P(x) = \text{Pr}[x(t) < x] \quad (7)$$

where  $P(x)$  must have the form shown in Fig. 4, which states that  $x(t)$  is certain to be less than the maximum value  $x_{\max}$  [i.e.,  $P(x_{\max}) = 1$ ], and it can never be less than the minimum value  $x_{\min}$  [i.e.,  $P(x_{\min}) = 0$ ].  $P(x)$  can also be interpreted as the fraction of time  $x(t)$  is less than  $x$ . The probability that  $x(t)$  is between  $x + \Delta x$  and  $x$  is obviously  $P(x + \Delta x) - P(x)$ , as also shown in Fig. 4.

The *probability density*  $p(x)$  is defined as

$$p(x) = \lim_{\Delta x \rightarrow 0} \frac{P(x + \Delta x) - P(x)}{\Delta x} = \frac{dP(x)}{dx} \quad (8)$$



**Figure 4** Probability distribution for a random signal with maximum value  $x_{\max}$  and minimum value  $x_{\min}$ .

Since  $p(x) = dP(x)/dx$  and in the general case  $P(\infty) = 1$  while  $P(-\infty) = 0$ , it is evident that

$$\int_{-\infty}^{\infty} p(x) dx = \int_{-\infty}^{\infty} dP(x) = [P(\infty) - P(-\infty)] = 1$$

that is, the total area under the probability density curve must always be 1.

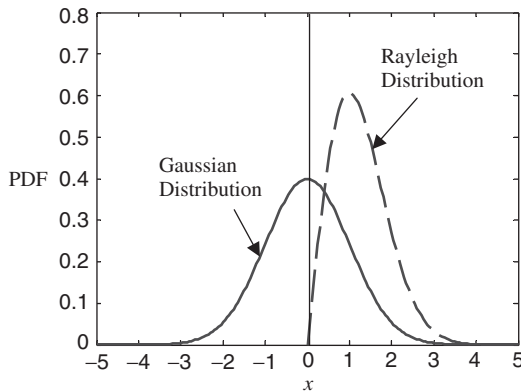
For so-called Gaussian random signals with a *normal distribution*, as discussed in Chapter 13, the probability density function is given by the formula

$$p(x) = \frac{1}{\sigma\sqrt{2\pi}} \exp\left(-\frac{(x - \mu)^2}{2\sigma^2}\right) \quad (9)$$

which is basically an  $e^{-x^2}$  curve centered on the mean value  $\mu$ , scaled in the  $x$  direction in terms of the standard deviation  $\sigma$ , and in the  $y$  direction so as to make the total integral unity. It is depicted in Fig. 5 (for zero mean value  $\mu$ ).

The statistical parameters of a signal can be obtained from the probability density function by taking various moments (see Chapter 13), for example,

$$\mu = \int_{-\infty}^{\infty} xp(x) dx \quad (10)$$



**Figure 5** Probability density functions for the Gaussian and Rayleigh distributions.

This is the first moment of the probability density function, and because the area under the curve is unity, it defines its center of gravity. It is obvious that for any symmetrical function, such as the Gaussian function of Eq.(9), the mean value will be at the line of symmetry.

Similarly, the variance is given by the second moment about the mean value, or

$$\sigma^2 = \int_{-\infty}^{\infty} [x - \mu]^2 p(x) dx \quad (11)$$

which corresponds to the *moment of inertia* about the mean value.

The third moment gives a parameter called the skewness, which is zero for symmetrical functions and large for asymmetrical functions, while the fourth moment (normalized by the square of the second moment to make it dimensionless) is called the kurtosis, and is large for “spiky” or impulsive signals because of the considerable weighting given to local spikes by taking the fourth power. The skewness and kurtosis are given by Eqs. (12) and (13), respectively:

$$S = \int_{-\infty}^{\infty} [x - \mu]^3 p(x) dx \quad (12)$$

$$K = \frac{\int_{-\infty}^{\infty} [x - \mu]^4 p(x) dx}{\sigma^4} \quad (13)$$

Note that in some references (e.g., Gardner<sup>1</sup>), the kurtosis is defined in terms of the fourth cumulant, rather than moment, in which case 3 is subtracted from the value obtained from Eq. (13). An  $n$ th-order cumulant is defined such that it contains no components of lower order, which is not the case for moments. For Gaussian signals all cumulants of higher than second order are equal to zero.

### 3.3 Statistics of Peak Values

In the analysis of fatigue failure of materials, the important factor determining fatigue life is the number of stress reversals at various stress levels, and the fatigue properties are characterized by so-called  $S-N$  curves (describing the number of stress reversals  $N$  at various stress levels  $S$ ). The data are often acquired using constant-amplitude sinusoidal stress fluctuations but are to be applied in more general stress versus time scenarios, and so it is necessary to determine the statistics of peak values (reversals) of a stress signal (or a vibration signal to which stress is proportional). Narrow-band Gaussian signals, as described in Chapter 13, have the appearance of a sinusoid with randomly varying amplitude. The probability density function of the signal itself is given by Eq.(9), but as described in Chapter 13, the

probability density of the peak values is given by the Rayleigh distribution (density) with the formula

$$p_p(x) = \frac{x}{\sigma^2} \exp\left(-\frac{x^2}{2\sigma^2}\right) \quad (14)$$

This is depicted in Fig. 5, along with the underlying normal density function.

#### 4 SPECTRAL ANALYSIS

From Fig. 2, it can be seen that the distinction between some signal types is much more apparent in the frequency than in the time domain, and moreover the frequency of a spectrum component will quite often localize its source, for example, the rate of tooth meshing of a particular pair of gears, so spectral analysis (frequency density analysis) will be considered in some detail.

##### 4.1 Fourier Analysis

The mathematical basis of frequency analysis is Fourier analysis. Fourier's original theorem stated that any periodic signal  $g(t)$ , repeating with period  $T$ , could be decomposed into a number, perhaps infinite, of sines and cosines with frequencies that are multiples of  $1/T$ , the fundamental frequency, that is,

$$g(t) = g(t + T) = \frac{a_0}{2} + \sum_{k=1}^{\infty} a_k \cos\left(\frac{k2\pi t}{T}\right) + \sum_{k=1}^{\infty} b_k \sin\left(\frac{k2\pi t}{T}\right) \quad (15)$$

The series decomposition is known as a Fourier series. The first (constant) term is the average value and is actually the cosine term for zero frequency. The scaling factor  $\frac{1}{2}$  is so that the same formula can be used for it as for the other cosine terms.

The  $a_k$  and  $b_k$  terms are determined by correlating the signal  $g(t)$  with the various sinusoids, and since the latter are all orthogonal, a nonzero result is only obtained for that part of  $g(t)$  corresponding to the sinusoid being correlated. Thus:

$$a_k = \frac{2}{T} \int_{-T/2}^{T/2} g(t) \cos(2\pi f_k t) dt \quad (16)$$

and

$$b_k = \frac{2}{T} \int_{-T/2}^{T/2} g(t) \sin(2\pi f_k t) dt \quad (17)$$

where  $f_k = k/T$ .

The total component at frequency  $f_k$  is thus  $a_k \cos(2\pi f_k t) + b_k \sin(2\pi f_k t)$ , which can also be expressed as  $C_k \cos(2\pi f_k t + \phi_k)$ , and can further be decomposed in terms of complex exponentials as

$$\frac{C_k}{2} \exp\{j(2\pi f_k t + \phi_k)\} + \frac{C_k}{2} \exp\{-j(2\pi f_k t + \phi_k)\}$$

Each sinusoidal component of amplitude  $C_k$  has thus been replaced by a pair of rotating vectors, one of amplitude  $C_k/2$  rotating at frequency  $f_k$  and with initial phase  $\phi_k$  and the other of the same amplitude rotating at  $-f_k$  and with initial phase  $-\phi_k$ . This leads to a two-sided spectrum with frequencies ranging from  $-\infty$  to  $+\infty$ . An alternative form for Eq. (15) is thus

$$g(t) = \sum_{k=-\infty}^{\infty} \frac{C_k}{2} \exp\{j(2\pi f_k t + \phi_k)\} = \sum_{k=-\infty}^{\infty} A_k \exp(j2\pi f_k t) \quad (18)$$

where each  $A_k$  value for negative  $k$  is the complex conjugate of the value for positive  $k$  and  $A_k$  represents the value of each rotating vector at time zero. The equivalent of Eqs. (16) and (17) is then

$$A_k = \frac{C_k}{2} \exp(j\phi_k) = \frac{1}{T} \int_{-T/2}^{T/2} g(t) \exp(-j2\pi f_k t) dt \quad (19)$$

Multiplication by the unit vector rotating at  $-f_k$  stops the component in  $g(t)$  originally rotating at  $f_k$ , at time zero, causing it to integrate to its correct value  $A_k$ , while all other components continue to rotate and integrate to zero over the periodic time.

Figure 6b depicts the harmonic spectrum of a periodically repeated transient signal, and Fig. 6a shows that if the repetition period  $T$  is allowed to tend to infinity, the harmonic spacing  $1/T$  approaches zero, and the spectrum becomes continuous. At the same time, the power approaches zero, but the energy is finite. The typical spectrum value at frequency  $f$  [by analogy with Eq.(19)] becomes

$$G(f) = \int_{-\infty}^{\infty} g(t) \exp(-j2\pi f t) dt \quad (20)$$

where there is no longer a division by  $T$  because the energy is finite, and the resulting time signal [by analogy with Eq.(18)] becomes

$$g(t) = \int_{-\infty}^{\infty} G(f) \exp(j2\pi f t) df \quad (21)$$

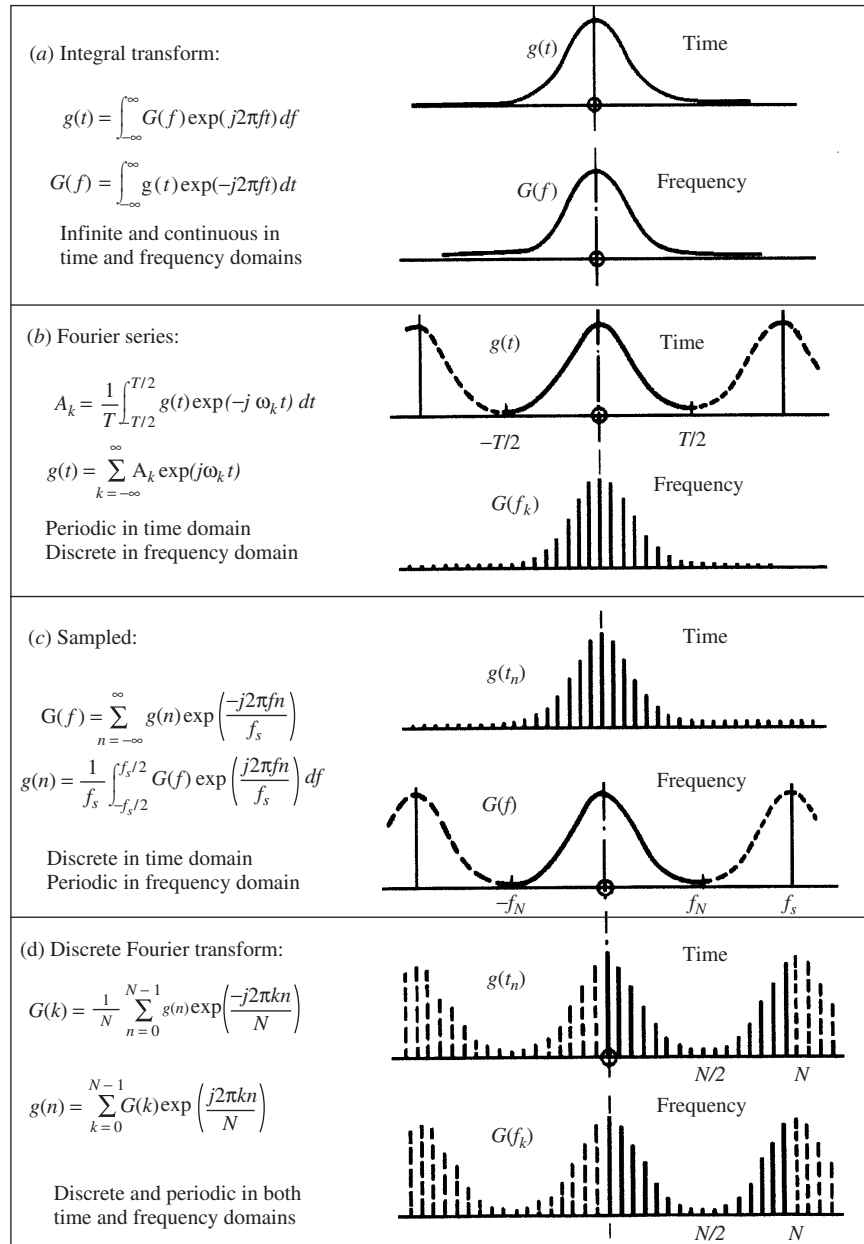
Equations (20) and (21) represent the forward and inverse *Fourier transforms*, respectively, for a transient. Note the relationship with the *Laplace transform*, which can be expressed as

$$G(s) = \int_0^{\infty} g(t) \exp(-st) dt \quad (22)$$



This is the same as Eq.(20) if  $g(t)$  is causal (e.g., any physical impulse response function, which must have zero value for negative time), and for  $s$  evaluated along the imaginary axis where  $s = j\omega = j2\pi f$ . Thus the Fourier transform can be interpreted as a special case of the Laplace transform. Because of the similarities of Eqs.(20) and (21) (only the sign of the exponent

is different), there is much symmetry between forward and inverse Fourier transforms, and, for example, Fig. 6c shows that for a discretely sampled time function, its spectrum is periodic (by analogy with Fig. 6b). Combining Figs. 6b and 6c we get what is known as the *discrete Fourier transform* (DFT), which is discrete in both domains, and can be calculated digitally from



**Figure 6** Various forms of the Fourier transform (a) Fourier integral transform, (b) Fourier series, (c) sampled functions, and (d) discrete Fourier transform.

a finite number of data. Note that it is also implicitly periodic in both domains, so that the frequency components in the second half of the spectrum equally represent the negative frequency components.

The equations for the forward and inverse DFT are as follows:

$$G(k) = \frac{1}{N} \sum_{n=0}^{N-1} g(n) \exp\left(-\frac{j2\pi kn}{N}\right) \quad (23)$$

and

$$g(n) = \sum_{k=0}^{N-1} G(k) \exp\left(\frac{j2\pi kn}{N}\right) \quad (24)$$

which gives  $N$  frequency values from  $N$  time samples, but for real-time signals there are only  $N/2$  independent (though complex) frequency components from zero to half the sampling frequency. As mentioned above, the second half of the spectrum (the negative-frequency components) are the complex conjugates of the corresponding positive-frequency components. This version corresponds most closely to the Fourier series in that the forward transform is divided by the length of record  $N$  to give correctly scaled Fourier series components. If the DFT is used with other types of signals, for example, transients or stationary random signals, the scaling must be adjusted accordingly as discussed below. Note that with the very popular signal processing package Matlab, the division by  $N$  is done in the inverse transform, which requires scaling in every case, as even though the forward transform is then closer to the Fourier integral, it still must be multiplied by the discrete equivalent of  $dt$ .

The forward DFT operation of Eq.(23) can be understood as the matrix multiplication:

$$\mathbf{G}_k = \frac{1}{N} \mathbf{W}_{kn} \mathbf{g}_n \quad (25)$$

where  $\mathbf{G}_k$  represents the vector of  $N$  frequency components, the  $G(k)$  of Eqs.(23) and (24), while  $\mathbf{g}_n$

represents the  $N$  time samples  $g(n)$ .  $\mathbf{W}_{kn}$  represents a square matrix of unit vectors  $\exp(-j2\pi kn/N)$  with angular orientation depending on the frequency index  $k$  (the rows) and time sample index  $n$  (the columns).

The so-called *fast Fourier transform*, or FFT, is just an extremely fast algorithm for calculating the DFT. It factorizes the matrix  $\mathbf{W}_{kn}$  into  $\log_2 N$  matrices, multiplication by each of which only requires  $N$  complex multiplications. The total number of multiplications is thus reduced from the order of  $N^2$  to  $N \log_2 N$ , a saving by a factor of more than 100 for a typical transform size of  $N = 1024 = 2^{10}$ .

## 4.2 Zoom FFT Analysis

The basic DFT transform of Eq.(23) extends in frequency from zero to the *Nyquist frequency* (half the sampling frequency) and has a resolution equal to the sampling frequency  $f_s$  divided by the number of samples  $N$ . Sometimes it is desired to analyze in more detail in a limited part of the frequency range, in which case use can be made of so-called *zoom analysis*. Since resolution  $\Delta f = f_s/N$ , the two ways to improve it are:

1. Increase the length of record  $N$ . In modern analyzers, and in signal processing packages such as Matlab, there is virtually no restriction on transform size, and so zoom can be achieved by performing a large transform and then viewing only part of the result.
2. Reduce the sampling frequency  $f_s$ . This can be done if the center of the desired zoom band is shifted to zero frequency so that the zoom band around the center frequency can be isolated by a low-pass filtration. The highest frequency is then half the zoom band, and the sampling frequency can be reduced accordingly without aliasing problems.

The latter process, known as *real-time zoom*, since the preprocessing normally has to be done in realtime, is illustrated in Fig. 7. The low-pass filtering and resampling process is usually done in octave (2:1)

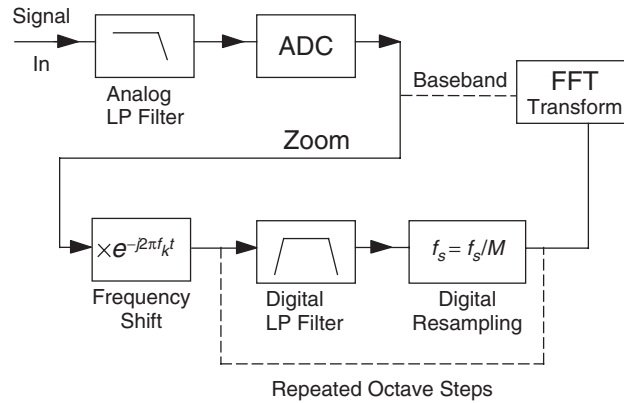
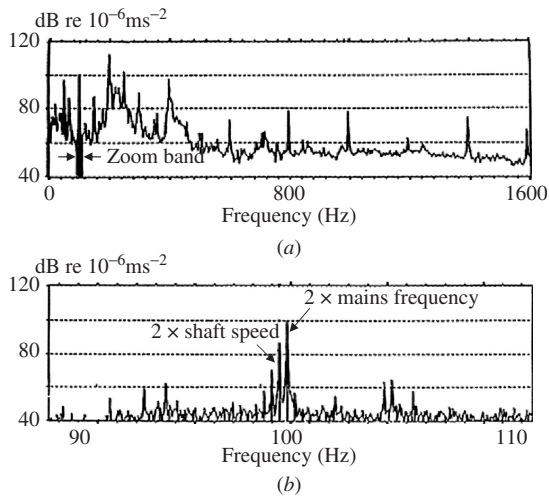


Figure 7 Schematic diagram of FFT zoom process.



**Figure 8** Use of FFT zoom to separate the harmonics of shaft speed from those of mains (line) frequency in an electric motor vibration spectrum. (a) Baseband spectrum with zoom band around 100 Hz highlighted and (b) zoom spectrum showing that twice mains frequency dominates over twice shaft speed.

steps, as a digital filter will always remove the highest octave, relative to the sampling frequency, and halving the sampling frequency simply means discarding every second sample (see discussion below of digital filters). If this is done in real-time by a specialized hardware processor, the sampling rate is reduced considerably before signals have to be stored, thus greatly conserving memory. Note that the time signal output from the zoom processor is complex, as the corresponding spectrum is not conjugate even.

Figure 8 shows an example of the use of zoom to separate the harmonics of shaft speed from those of mains frequency (U.S. line frequency) in the vibration signals from an induction motor. From the upper baseband spectrum it appears that the second harmonic of shaft speed is elevated. However, the lower zoom analysis centered on this frequency shows that it is the second harmonic of mains frequency that dominates (indicating an electrical rather than a mechanical fault), and the second harmonic of shaft speed is five times lower in level.

### 4.3 Practical FFT Analysis

The so-called *pitfalls* of the FFT are all properties of the DFT and result from the three stages in passing from the Fourier integral transform to the DFT. The first step is digitization of the time signal, which can give rise to *aliasing*; the second step is truncation of the record to a finite length, which can give rise to *leakage* or *window effects*; while the third results from discretely sampling the spectrum, which can give rise to the *picket fence effect*.

As explained in connection with Fig. 6, when a continuous time signal is sampled, it produces a

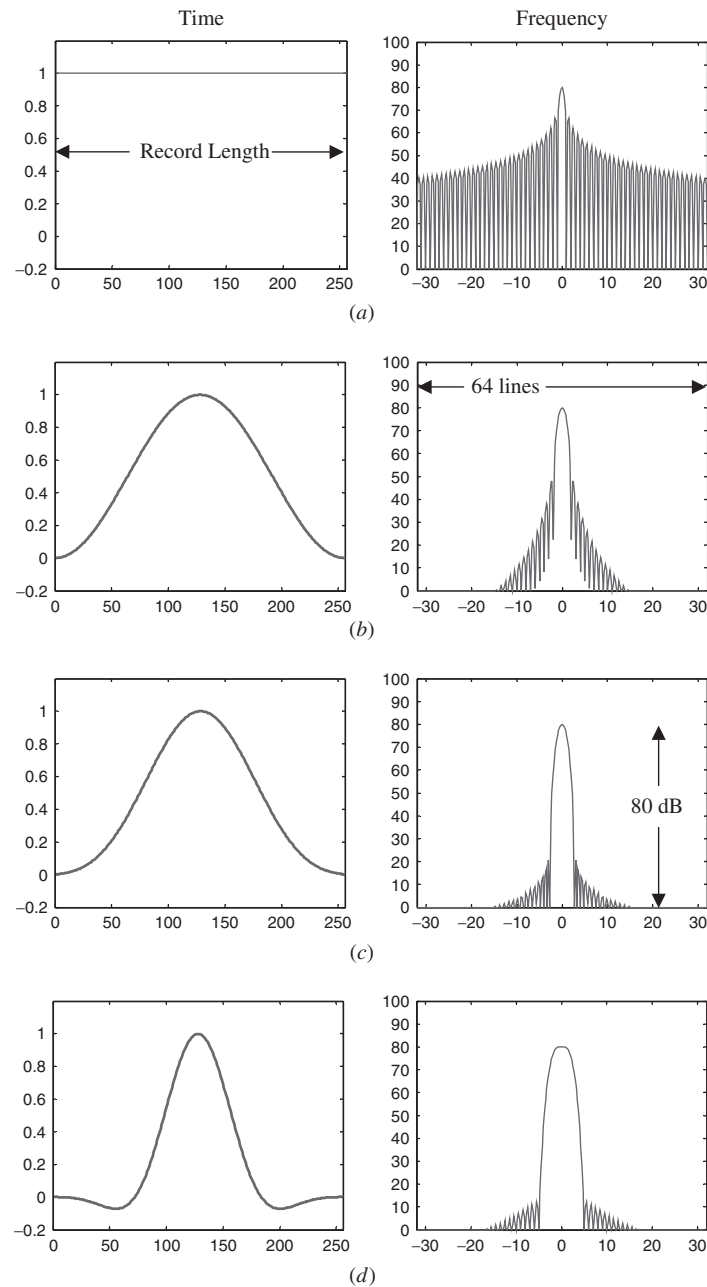
periodic spectrum with a period equal to the sampling frequency  $f_s$ . It can be seen that if the original signal contains any components outside the range  $\pm f_N$ , where  $f_N$  is the Nyquist frequency, then these will overlap with the true components giving “aliasing” (higher frequencies represented as lower ones). Once aliasing is introduced, it cannot be removed, so it is important to use appropriate analog low-pass filters before digitizing any time signal for processing. After initial correct digitization, digital low-pass filters can be used to permit resampling at a lower sampling rate.

With the DFT the signal is truncated to length  $T$ , which can be interpreted as multiplying it by a finite (rectangular) window of that length. By the convolution theorem, the spectrum is thus convolved with the Fourier transform of the window, which acts as a filter characteristic. Energy at a single frequency is spread into adjacent frequencies in the form of this characteristic, hence the term leakage. It can be advantageous to multiply the truncated segment with a different window function to improve its frequency characteristic and reduce leakage.

Finally, in the DFT the continuous spectrum is also discretely sampled in the frequency domain, which corresponds in the time domain to a periodic repetition of the truncated segment. The spectrum is not necessarily sampled at peaks, hence the term picket fence effect; it is as though the spectrum is viewed through the slits in a picket fence. Once again, use of another window function, other than rectangular, can reduce the picket fence effect, and in fact the so-called *flat-top* window virtually eliminates it.

### 4.4 Data Windows

A number of *data windows* (time windows when applied to time signals) have been developed for special purposes, depending on the type of signal being analyzed. As listed in Table 1, the main properties of the windows are their filter shape as characterized by their *noise bandwidth* (relative to the line spacing), the highest sidelobe, the rate of roll-off of the remaining sidelobes, and the maximum picket fence effect. The noise bandwidth is the width of an ideal (rectangular) filter that would transmit the same noise power for a white noise input, that is, having the same area under the amplitude squared characteristic. The table lists these properties for the most commonly used windows, and their time- and frequency-domain characteristics are shown in Fig. 9. The latter represent worst-case situations when the actual frequency is half way between two frequency lines. Otherwise, the sidelobes will not be sampled at their peaks. As an extreme example, when there is an integer number of periods in the record, the “ $\sin x/x$ ” characteristic of the rectangular window will be sampled at the zero crossings, and the sidelobes will not be apparent at all (thus corresponding to the fact that the periodic repetition will give an infinitely long sinusoid). Because of overlap, the frequency characteristics are also distorted when applied to a frequency near zero, or the Nyquist frequency. A good general-purpose window for continuous signals is the *Hanning* window,



**Figure 9** Data windows for continuous signals: (a) rectangular, (b) Hanning, (c) Kaiser-Bessel, and (d) flat top.

one period of a  $\sin^2$  function, as it has zero value and slope at each end and thus minimizes the discontinuity arising from joining the ends of the signal segment into a loop. Compared with a rectangular window, it has considerably improved filter characteristic, only slightly greater noise bandwidth, and much less picket fence error. The latter can easily be compensated for in

the case of sinusoidal components such as calibration signals.<sup>2</sup>

Where it is important to separate discrete frequency components, which are close together but of different levels, the *Kaiser-Bessel* window may be preferable to Hanning, but it has larger noise bandwidth. It should be kept in mind that separation of closely

spaced components may be better achieved using zoom analysis, as described above. For stationary deterministic signals, dominated by discrete frequency components, the best choice may be the flat-top window, mentioned above, as there is no need to compensate for picket fence error, also very valuable when using a calibration signal to calibrate the spectrum. Its noise bandwidth is very large, however, and so the discrete frequency components will not protrude so far from any noise in the spectrum (4 dB less compared with Hanning). This is because noise has a certain power spectral density, and the amount of noise power transmitted by a filter with larger bandwidth is greater, while the power in a sinusoidal component is independent of the filter bandwidth.

Windows are sometimes required in the analysis of transient signals also, such as in the hammer excitation of a structure for modal analysis purposes. The actual hammer force pulse will in general be very short, and it is common to place a short rectangular (so-called *transient*) window around it to remove noise in the rest of the record length. If the response vibration signals are shorter than the record length, there is no need to apply a window to the response acceleration traces. However, with lightly damped systems, the response may not decay to zero by the end of the (desired) record length. It is then necessary to either increase the record length (e.g., by zooming, which may require several analyses to cover the desired frequency range), or the signal can be forced to near zero at the end of the record by use of an *exponential* window. Multiplication by an exponential window corresponds to the addition of extra damping, which is known exactly, and so can be subtracted from the results of any measurements. A short taper, typically of a half-Hanning shape, can be added to both the leading and trailing edges of a transient window and to the leading edge of an exponential window, to make the transitions less abrupt.

#### 4.5 Scaling of FFT Spectra

For a typical sinusoidal component  $C_k \cos(2\pi f_k t + \phi_k)$  the instantaneous power is given by squaring it to

$$\begin{aligned} C_k^2 \cos^2(2\pi f_k t + \phi_k) \\ = C_k^2 \left\{ \frac{1}{2} + \frac{1}{2} \cos[2(2\pi f_k t + \phi_k)] \right\} \end{aligned}$$

and the average power or mean-square value is thus  $C_k^2/2$  since the sinusoidal part averages to zero. Since  $|A_k| = C_k/2$ , the mean-square value is also given by  $2|A_k|^2$  (i.e., the value obtained by adding the positive- and negative-frequency contributions) and the rms value by  $C_k/\sqrt{2}$  and  $\sqrt{2}|A_k|$ , respectively. This illustrates one aspect of *Parseval's theorem*, which states that the total power can be obtained by adding the mean-square values of all components in the time domain (because they are orthogonal, the square of the sum equals the sum of the squares), or the squared amplitudes of all components in the (two-sided) frequency domain.

When scaled as in Eq. (23), the  $G(k)$  resulting from the DFT (or FFT) is the  $A_k$  for the Fourier series of the periodically repeated signal segment. If the signal is genuinely made up of sinusoidal components, the measured  $|A_k|$  should be multiplied by  $\sqrt{2}$  to obtain the corresponding rms value or by 2 to obtain the sinusoidal amplitude. Most FFT analyzers would compensate for the reduction in power given by multiplication by a window (for Hanning this is achieved by scaling it to a maximum value of 2), although separate compensation may have to be made for picket fence error unless a flat-top window is used. A general way of determining the scaling effect of a window is to apply it to a sinusoid of known amplitude (with an integer number of periods in the record length), and scale the whole spectrum so that the maximum peak in the spectrum reads the correct value (possibly scaled to rms at the same time).

For stationary random signals, each record transformed will be treated by the DFT algorithm as a periodic signal, but the power in each spectral line can be assumed to represent the integral of the PSD over the frequency band of width  $\Delta f (= 1/T)$ , and thus the average PSD is obtained by multiplying the squared amplitude by  $T$ . The required averaging over a number of records does not change this scaling. How well the average PSD represents the actual PSD depends on the width of peaks (and valleys) in the spectrum. The width of such peaks is typically determined by the damping associated with a structural resonance excited by the broadband random signal, and the 3-dB bandwidth is given by twice the value of  $\sigma$  (expressed in Hz), where  $\sigma$  (expressed in rad/s) is the coefficient of exponential damping  $\exp(-\sigma t)$  for the resonance in question. The PSD will be sufficiently accurate if the 3-dB bandwidth is a minimum of five analysis lines. If a window such as Hanning has been used to reduce leakage, and if it is scaled so as to read the peak value of discrete frequency components (as recommended above), the calculated PSD value will have to be divided by the "noise bandwidth" indicated in Table 1 to compensate for the extra power given by the spectral sidebands.

Transient signals are also treated as being one period of a periodic signal, so not only does the power in a spectral line have to be converted to an average spectral density by dividing by  $\Delta f$ , but also the average power must be converted to energy per period by a further multiplication by  $T$ , altogether a multiplication by  $T^2$  to obtain a result scaled as ESD.

**Table 1 Properties of Various Windows**

Window	Noise Bandwidth	Highest Sidelobe (dB)	Sidelobe Roll-off (dB/decade)	Picket Fence Effect (dB)
Rectangular	1.0	-13	20	3.9
Hanning	1.5	-33	60	1.4
Kaiser-Bessel	1.8	-60	20	0.8
Flat top	3.8	-70	20	<0.1

Generally, transient signals will be shorter than the transform length, and thus a rectangular window will be used, and if the signal has decayed to near zero at the end of the record (possibly by using an exponential window), the signal bandwidth will be sufficiently greater than the analysis bandwidth for the average ESD to represent the true ESD. The extra damping given by an exponential window will genuinely give a reduction in signal energy.

#### 4.6 Spectrum Averaging

The need for averaging of FFT spectra is determined by whether the signal contains random components or not. Averaging should always be done in terms of signal power (i.e., amplitude squared) as it is this that is conserved independent of phase. The DFT spectra of discrete frequency components always have the same amplitude, and therefore little is achieved by averaging the squared amplitudes, although a small number of averages may be useful for clarifying which components are discrete frequency and which are random.

When meaningful spectra are to be obtained from random signals, which in mechanical signals are typically caused by fluid flow (turbulence, cavitation), road roughness, and the like, it is necessary to average a number of power spectrum estimates. The number of averages required is determined by the desired accuracy, as the standard deviation of the result (for Gaussian signals) is given by<sup>2</sup>

$$\varepsilon = \frac{1}{2\sqrt{n}} \quad (26)$$

where  $n$  is the number of independent averages. Thus, for  $n = 16$ ,  $\varepsilon = 12.5\%$  or 1 dB, meaning that there is a 68% probability that the result will be within  $\pm 1$  dB, 95% probability that it will be within  $\pm 2$  dB, and 99.7% probability that it will be within  $\pm 3$  dB. To halve the error it is necessary to make four times as many averages and so forth.

With a rectangular window, “independent” means nonoverlapping, but with other windows such as Hanning, advantage can be gained by overlapping, as information is lost near the two ends where the weighting is near zero. In fact, very little is lost statistically by overlapping 50%, and so this is recommended for stationary random signals, as twice as many effective averages can be obtained from a given length of signal. The overall weighting is not uniform in that case, but this gives no problem for stationary signals. To extract all information from a given length of record, in particular if it is nonstationary, it is advisable to overlap by a factor of at least  $\frac{2}{3}$ , although with typical FFT record lengths in powers of 2 it is often simpler to overlap by  $\frac{3}{4}$ . In the latter case the effective number of averages to insert in Eq. (26) is half the actual number. The Matlab function PSD performs overlap averaging, but the scaling should be checked by trial and error on a known signal.

#### 4.7 Spectral Analysis Using Filters

Before the advent of the FFT algorithm, most frequency analysis was done using analog filters to filter the signal in a series of contiguous filter bands, measuring the output of each filter with an rms detector.<sup>2</sup> Constant bandwidth filters were produced by a frequency shifting “heterodyne” process, but these have now been completely replaced by digital FFT analysis, at least in the audio frequency range. However, FFT spectra give constant resolution on a linear frequency scale, and this automatically gives a restriction in frequency range since the upper decade occupies 90% of the scale. Much frequency analysis for acoustical purposes is required to be octave-based on a logarithmic frequency axis since this better matches the response of the human ear. The ear interprets frequency intervals of one octave (ratio 2 : 1) as equal changes, and steps of one-third-octave (ratio  $2^{1/3}$  : 1) as significantly different for narrow-band noise. The  $1/n$  octave bands are *constant percentage bandwidth* (CPB), with equal resolution on a logarithmic axis, and allow depiction of a spectrum over a number of decades, for example, the nominal audio range of 20 Hz to 20 kHz. Since  $2^{10} = 1024$ , ten octaves are very close to three decades, and in fact the center frequencies of the standard one-third octave filters are adjusted slightly to correspond to one-tenth decades, with 10 filters between 100 Hz and 1 kHz, or between 1 kHz and 10 kHz. An octave band filter has bandwidth 70.7% (relative to the center frequency) and one-third octave 23.1%.

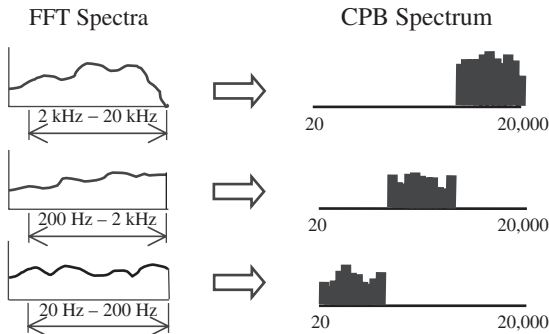
For filter bandwidth  $B$  in hertz, the filter response time is of the order of  $1/B$ , and thus it is necessary to wait at least this amount of time to obtain a result, even for deterministic signals. The resulting  $BT$  product of 1 corresponds to that for FFT analysis, where each spectrum of bandwidth  $B$  comes from a record length  $T = 1/B$ . For random signals, the  $BT$  product must be greater to give a spectrum value with reasonable confidence, and the equivalent of Eq. (26) is

$$\varepsilon = \frac{1}{2\sqrt{BT}} \quad (27)$$

where  $T$  represents the averaging time. Since the bandwidth of CPB filters increases with frequency, the standard error  $\varepsilon$  decreases correspondingly if the averaging time is constant. RMS detectors used with analog filters usually include the equivalent of  $RC$  smoothing circuits, with time constant equal to the product of circuit resistance  $R$  and capacitance  $C$ . As shown in Randall,<sup>2</sup> they give exponential averaging (by convolution with the exponentially decaying impulse response of the circuit) where the effective linear equivalent averaging time (on stationary signals) is  $2RC$ . However, their peak output for impulsive inputs is twice that of the running linear averager with the same averaging time, and account must be taken of this when frequency analyzing short transients.<sup>2</sup>

Digital filters can be designed to be similar to analog filters in that the output signal is convolved with the impulse response of the filter, and operate directly in the time domain on continuous (though sampled) signals (as opposed to the blockwise treatment of the FFT process). The coefficients that define the filter properties give a characteristic that is defined in relation to the sampling frequency. Thus, three sets of filter coefficients will define the one-third octave filters in one octave, but halving the sampling frequency will produce the equivalent filters one octave lower. Before halving the sampling frequency, the signal must be low-pass filtered by a filter that removes the upper octave of frequency information, but this can also be done by a digital filter with the same coefficients for every octave. When the sampling frequency is repeatedly halved for each octave, the total number of samples to be treated per unit time =  $M(1 + \frac{1}{2} + \frac{1}{4} + \frac{1}{8} + \dots) = 2M$  samples so that if the digital filter processor is capable of operating twice as fast as necessary for the highest octave, any number of lower octaves can be processed in real time. This feature was mentioned in conjunction with the zoom processor of Fig. 7.

Constant percentage bandwidth spectra can also be obtained by conversion from FFT spectra, as illustrated Fig. 10, where each decade is converted separately. The bandwidth of the individual lines in the original FFT spectra (including the effect of any window) must be less than the percentage bandwidth being converted to at the lowest frequency in the FFT band. The conversion is achieved by calculating the lower and upper cutoff frequencies of each constant percentage band, and then integrating up the power in the FFT lines (and parts of lines) between the limits. The method indicated in Fig. 10 gives a large change in filter characteristic at the junction between decades, and this can be a problem with acoustic spectra, which often have to satisfy standards with respect to filter characteristics. To reduce the latter problem, some FFT analyzers do the conversion on an octave rather than a decade basis.



**Figure 10** Conversion from FFT spectra to a CPB spectrum.

## 5 TIME-DOMAIN ANALYSIS

### 5.1 Correlation Functions

The *cross-correlation function* gives a measure of how well one signal correlates with a delayed version of the other, as a function of the delay (so-called *lag*). For random processes, the cross correlation is defined as an ensemble average, and for nonstationary processes is a function of evaluation time and time lag, namely

$$R_{xy}(t, \tau) = E[x(t - \tau/2)y(t + \tau/2)] \quad (28)$$

For stationary signals the result is independent of time  $t$ , and the average can be carried out over time, namely

$$R_{xy}(\tau) = \lim_{T \rightarrow \infty} \frac{1}{T} \int_{-T/2}^{T/2} x\left(t - \frac{\tau}{2}\right) y\left(t + \frac{\tau}{2}\right) dt \quad (29)$$

The *autocorrelation function* occurs when  $x(t)$  and  $y(t)$  are the same, giving the corresponding equations for nonstationary and stationary processes as

$$R_{xx}(t, \tau) = E\left[x\left(t - \frac{\tau}{2}\right)x\left(t + \frac{\tau}{2}\right)\right] \quad (30)$$

and

$$R_{xx}(\tau) = \lim_{T \rightarrow \infty} \frac{1}{T} \int_{-T/2}^{T/2} x\left(t - \frac{\tau}{2}\right)x\left(t + \frac{\tau}{2}\right) dt \quad (31)$$

or

$$R_{xx}(\tau) = \lim_{T \rightarrow \infty} \frac{1}{T} \int_{-T/2}^{T/2} x(t)x(t + \tau) dt \quad (32)$$

Strictly speaking, the Fourier transform of Eq. (20) is not defined for random signals, even though a procedure was given in the last section for estimating their PSD spectra by averaging the power spectra of a number of realizations of the signal obtained using the FFT. It can be shown (the so-called Wiener-Khinchin relations) that the power spectrum of a random signal is the Fourier transform [using Eq. (20)] of the autocorrelation function given by Eq. (31) or (32), and this provides another way of estimating it, though the FFT procedure is much more efficient. The autocorrelation function can be normalized to a maximum value of unity, by dividing the function by the value for  $\tau = 0$ , which will be seen to be the mean-square value.

The cross-correlation function can be used to determine to what extent one signal is a delayed version of another (if it is just that, the result will be the autocorrelation function with its peak at the delay time, while if it is similar but not identical there will



still be a peak but with a lower value of correlation). The autocorrelation function gives a measure of the *correlation length* of a signal, and will have peaks corresponding to the delay times of any echoes. Note that the effective length of an autocorrelation function is inversely proportional to its frequency bandwidth, so it is only for wideband signals that there will be distinct peaks in the correlation functions corresponding to the delays. The autocorrelation function for white noise (uniform PSD) is a delta function at zero time lag. Note that the cepstrum<sup>2</sup> in principle has delta functions corresponding to echo delay times, independent of the bandwidth, and is thus better than the autocorrelation for this purpose.

## 5.2 Time Synchronous Averaging

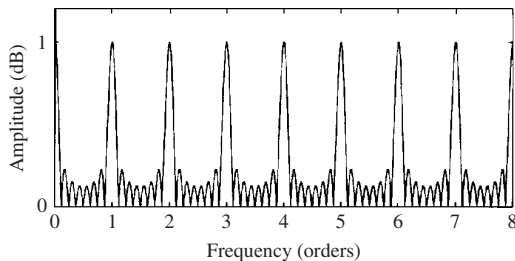
This is useful for extracting that part of a signal that is periodic with the same period as a trigger signal, for example, a once-per-revolution tacho signal from a shaft in a rotating machine. In practice, it is done by averaging together a series of signal segments each corresponding to one period of the synchronizing signal. Thus

$$y_a(t) = \frac{1}{N} \sum_{n=0}^{N-1} y(t + nT) \quad (33)$$

This can be modeled as the convolution of  $y(t)$  with a train of  $N$  delta functions displaced by integer multiples of the periodic time  $T$ , which corresponds in the frequency domain to a multiplication by the Fourier transform of this signal, which can be shown to be given by the expression<sup>3</sup>

$$C(f) = (1/N) \sin(N\pi T f) / \sin(\pi T f) \quad (34)$$

The filter characteristic corresponding to this expression is shown in Fig. 11 for the case where  $N = 8$  and is seen to be a comb filter selecting the harmonics of the periodic frequency. The greater the value of  $N$  the more selective the filter, and the greater the rejection of nonharmonic components. The noise bandwidth of the filter is  $1/N$ , meaning that the improvement in signal-noise ratio is  $10 \log_{10} N$  dB for additive random noise. For masking by discrete frequency signals, it



**Figure 11** Filter characteristic for eight averages. (From Ref. 3. Reprinted by permission of Elsevier.)

should be noted that the characteristic has zeros that move with the number of averages, so it is often possible to choose a number of averages that completely eliminates a particular masking frequency.<sup>3</sup>

For good results the synchronizing signals should correspond exactly with samples of the signal to be averaged, as one sample spacing corresponds to  $360^\circ$  of phase of the sampling frequency, and thus to  $144^\circ$  of phase at 40% of it, which is a typical maximum signal frequency. Moreover, even a 0.1% speed fluctuation would cause a jitter of the same order of the last sample in a (typical) 1000-sample record, with respect to the first, and thus an even greater loss of information at the end of the record, after averaging. Sampling the signal using a sampling frequency derived from the synchronizing (tacho) signal solves both these problems and is always to be recommended. The best method is to digitally resample each record based on the corresponding period of the tacho signal. This can be done in a number of ways, based on digital interpolation, for example, using cubic splines or the method of Ref. 4.

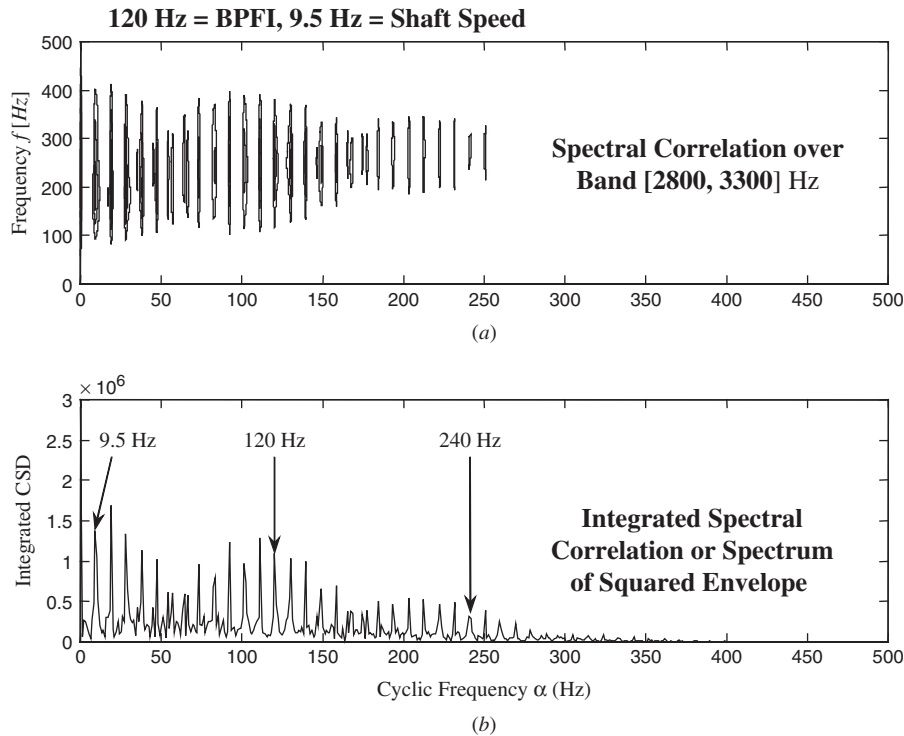
## 6 ANALYSIS OF CYCLOSTATIONARY SIGNALS

Cyclostationary signals are the subject of increasing interest in vibration analysis since it has been realized that many machine vibration signals are not simply periodic but cyclostationary. The definition of cyclostationarity at the  $n$ th order is that the  $n$ th order statistics are periodic. Thus, a first-order cyclostationary signal has periodic mean value, while a second-order cyclostationary signal has periodic autocorrelation function [this being defined by the time-varying ensemble average of Eq. (28)]. A typical second-order cyclostationary signal is amplitude modulated white noise, as shown in Fig. 2. It is obvious that an ensemble average of its variance (autocorrelation for  $\tau = 0$ ) will be periodic, and proportional to the square of the modulating function. A less obvious example of a second-order cyclostationary signal is frequency-modulated narrow-band noise, such as might arise as the response of a resonant system with periodically varying stiffness when excited by a white noise.

Many machine vibration signals are a mixture of first- and second-order cyclostationary components, such as the combustion pressure signal in each cylinder of an engine. There is an explosion every cycle, but not identical, so it can be divided up into the (ensemble) mean pressure (first-order cyclostationary) and the fluctuations around the mean, an amplitude-modulated noise (second-order cyclostationary) that averages to zero. In terms of noise generation these might be equally important. Another example is the vibrations generated by an extended spall in the inner race of a rolling element bearing, where the rollers are in a different position on the rough spalled surface for every rotation of the inner race. This can also be divided into first- and second-order components.

By definition, the autocorrelation function for a second-order cyclostationary signal is periodic with time  $t$ , though transient with time lag  $\tau$  (as for





**Figure 12** Spectral correlation and spectrum of squared envelope for a bearing fault signal.

any stochastic signal). Thus, if Fourier transforms are performed in the two directions, the transform in the  $\tau$  direction will give a continuous spectrum against normal frequency  $f$ , while that in the  $t$  direction (actually a Fourier series because of the periodicity) will give a discrete spectrum against so-called *cyclic frequency*  $\alpha$ . The result of the two-dimensional Fourier transform is the so-called *spectral correlation*. Figure 12a shows the spectral correlation for the vibration signal from a faulty bearing. It is seen to have the form of a second-order cyclostationary signal, being continuous against  $f$  while discrete against  $\alpha$ . Also shown in Fig. 12b is the integral of the spectral correlation over all  $f$ , which is shown in Ref. <sup>5</sup> to be the same as the spectrum of the squared envelope of the original time signal (i.e., the expected value of the square of the signal). This is useful for quantifying periodicity of a signal envelope, even where the signal has zero mean value. If the discrete frequency components are first removed from a signal, the spectral correlation calculated for specific cyclic frequencies can indicate whether second-order cyclostationarity exists at this frequency. The application of this to bearing diagnostics is explained in Chapter 48.

If only the first Fourier transform of the two-dimensional autocorrelation function from  $\tau$  to  $f$  is performed, the result is a time–frequency diagram related to the Wigner–Ville distribution (WVD), which

is for a single realization rather than an ensemble average. It is known as the Wigner–Ville spectrum, or instantaneous spectrum, and has the advantage that if only second-order cyclostationary components are present, the interference components that give problems with the WVD tend to average to zero since they come with random phase. The application of this to diesel engine vibration signals is illustrated in Chapter 48.

## 7 MULTIPLE-CHANNEL ANALYSIS

For system analysis, it is normally necessary to measure both input and output signals at the same time and process them in pairs to obtain transfer function information, such as frequency response functions (FRFs). With multiple inputs and/or outputs, it can be necessary to process more than two signals at a time, by matrix methods, but that will not be considered in detail here, as it is covered in other chapters.

## 8 THE CROSS SPECTRUM

The cross spectrum between two signals  $a(t)$  and  $b(t)$  is obtained by multiplying  $G_b(f)$ , the spectrum of the second, by the complex conjugate of  $G_a(f)$ , the spectrum of the first (this being considered as the input since the phase of the result has its phase as datum). As with the autospectrum, to which it reduces if the two signals are identical, for random signals

the individual estimates must be averaged to obtain meaningful results. Thus

$$G_{ab}(f) = E[G_a^*(f)G_b(f)] \quad (35)$$

By the Wiener–Khinchin relationship, the cross-spectrum is the Fourier transform of the cross correlation function between  $a(t)$  and  $b(t)$ , that is,

$$G_{ab}(f) = \mathfrak{F}\{R_{ab}(\tau)\} \quad (36)$$

This, of course, reverts to the power spectrum or autospectrum when the signals are identical, as mentioned in Section 5.1.

## 9 FREQUENCY RESPONSE FUNCTION

In the frequency domain the FRF is basically the ratio of output over input, or

$$H_{ab}(f) = \frac{G_b(f)}{G_a(f)} \quad (37)$$

but in the presence of noise, better estimates can be obtained by a process of least squares noise reduction. If noise is primarily located in the output signal (over which the experimentalist has less control), the procedure is modified by multiplying numerator and

denominator by the complex conjugate of the input spectrum, and averaging, to give

$$H_1(f) = \frac{E[G_b(f)G_a^*(f)]}{E[G_a(f)G_a^*(f)]} = \frac{G_{ab}(f)}{G_{aa}(f)} \quad (38)$$

since averaging reduces the effect of noise on the cross spectrum (and the input autospectrum is noise free).

If noise is primarily located in the input signal, a better estimate is given by

$$H_2(f) = \frac{E[G_b(f)G_b^*(f)]}{E[G_a(f)G_b^*(f)]} = \frac{G_{bb}(f)}{G_{ba}(f)} \quad (39)$$

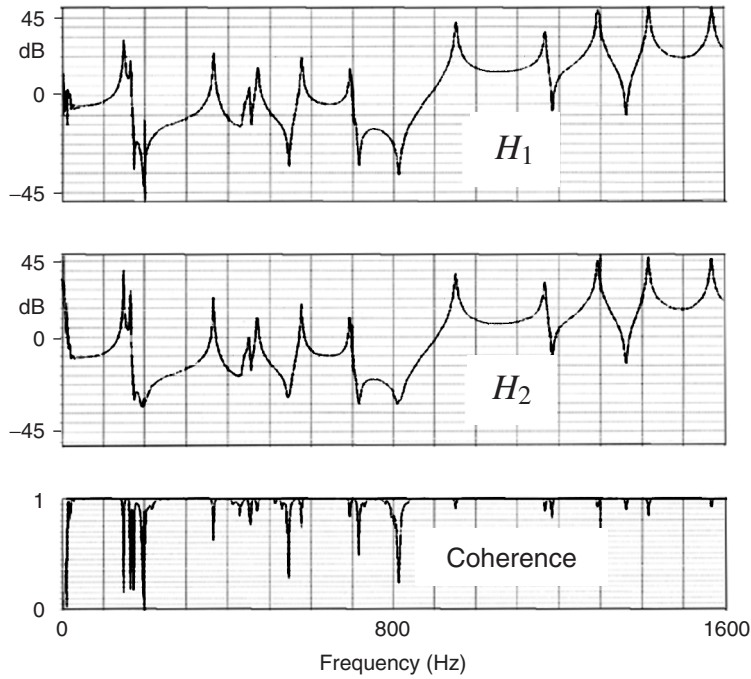
The system impulse response function can be obtained by inverse transformation of the FRF.

## 10 COHERENCE

The coherence gives a measure of the degree of linear relationship between two signals as a function of frequency. It is calculated by the formula

$$\gamma^2(f) = \frac{|G_{ab}(f)|^2}{G_{aa}G_{bb}} \quad (40)$$

This may be recognized as the square of the correlation coefficient between input and output spectral components at each frequency. It has values between



**Figure 13** Example of FRFs ( $H_1$  and  $H_2$ ) measured using random excitation with a shaker and the corresponding coherence.

zero and one depending on the degree of linearity. For a single estimate, it will always be one, since  $|G_{ab}| = |\bar{G}_a| \cdot |\bar{G}_b|$ . In the absence of noise and nonlinearity, each estimate of  $G_{ab}$  will have the same amplitude and orientation so that the average value will not change. However, in the presence of noise and/or nonlinearity the various estimates will change in length and particularly phase, so that the average obtained by vector summation will be less than if they were aligned and the value of the coherence drops below one. If there is no linear relationship, the various estimates will have random orientation and the average will tend to zero. It can be shown that the coherence is also given by

$$\gamma^2(f) = \frac{H_1(f)}{H_2(f)} \quad (41)$$

The coherence is very useful for judging the validity of FRFs and is much used in modal analysis (see Chapter 47).

An example of FRFs measured between two points on a rectangular brass plate is given in Fig. 13. It shows  $H_1$ ,  $H_2$ , and the coherence for measurements made with a shaker applying a random excitation (measured with a force transducer) and response measured using an accelerometer. Hanning windows were applied to both input and output signals. Also shown at the bottom is the coherence for this measurement. This is seen to be close to unity for most of the frequency range, but lower in the vicinity of resonance and antiresonances. The reason for the drop is different for the two cases. Near antiresonances, the coherence is low because the response signal is weak and masked by noise; thus  $H_1$  gives a good estimate in these regions. Near resonances, the coherence is reduced because of *resolution bias error*, basically a nonlinearity caused by leakage, since the resonance peaks are not sufficiently resolved by the Hanning window used. Because the width of resonance peaks tends to be proportional to the frequency (for constant relative damping), it is seen that the error is greater for the lower frequency resonances. Even so, for all resonances, a better estimate of their peak values would be given by  $H_2$ , as it can be shown that this is

less sensitive to resolution bias error.<sup>2</sup> Resolution bias error can be eliminated by zooming on the resonance peaks so that their width is greater than that of the Hanning window.

## REFERENCES

1. W. A. Gardner, *Introduction to Random Processes with Applications to Signals and Systems*, Macmillan, New York, 1986.
2. R. B. Randall, *Frequency Analysis*, rev. ed., Bruel & Kjaer, Copenhagen, 1987.
3. P. D. McFadden, A Revised Model for the Extraction of Periodic Waveforms by Time Domain Averaging, *Mech. Syst. Signal Process.*, Vol. 1, No. 1, 1987, pp. 83–95.
4. R. Potter and M. Gribler, Computed Order Tracking Obsolete Older Methods, SAE Paper 891131, Society of Automotive Engineers, Warrendale, PA, 1989.
5. R. B. Randall, J. Antoni, and S. Chobsaard, The Relationship between Spectral Correlation and Envelope Analysis in the Diagnostics of Bearing Faults and Other Cyclostationary Machine Signals, *Mech. Syst. Signal Process.*, Vol. 15, No. 5, 2001, pp. 945–962.

## BIBLIOGRAPHY

### Random Signals, Probability, Cyclostationarity

- J. S. Bendat and A. G. Piersol, *Random Data: Analysis and Measurement Procedures*, Wiley-Interscience, New York, 1971.
- A. Papoulis, *Probability, Random Variables and Stochastic Processes*, McGraw-Hill, New York, 1991.
- P. H. Wirsching, T. L. Paez, and K. Ortiz, *Random Vibrations, Theory and Practice*, Wiley-Interscience, New York, 1995.

### Correlation, Coherence

- J. S. Bendat and A. G. Piersol, *Engineering Applications of Correlation and Spectral Analysis*, Wiley-Interscience, New York, 1993.

### Fourier Analysis, FFT, Spectrum Analysis, Filter Analysis, and FRF

- E. O. Brigham, *The Fast Fourier Transform*, Prentice-Hall, Englewood Cliffs, NJ, 1974.
- A. Papoulis, *The Fourier Integral and Its Applications*, McGraw-Hill, New York, 1962.
- R. B. Randall, *Frequency Analysis*, rev. ed., Bruel & Kjaer, Copenhagen, 1987.

# CHAPTER 47

## MODAL ANALYSIS AND MODAL TESTING

David J. Ewins  
Mechanical Engineering Department  
Imperial College London  
London, United Kingdom

### 1 INTRODUCTION

Modal analysis is a term used to describe any of the processes employed to extract a structure's modal properties (natural frequencies, modal damping factors, and mode shapes) from information about the structure that is presented in a different format. When these properties are extracted from a theoretical analysis of the dynamic behavior, the modal analysis process involves computation of the modal properties from a set of equations of motion that have been written in terms of the individual mass and stiffness elements that make up the mathematical model of the structure (usually, a finite element model).

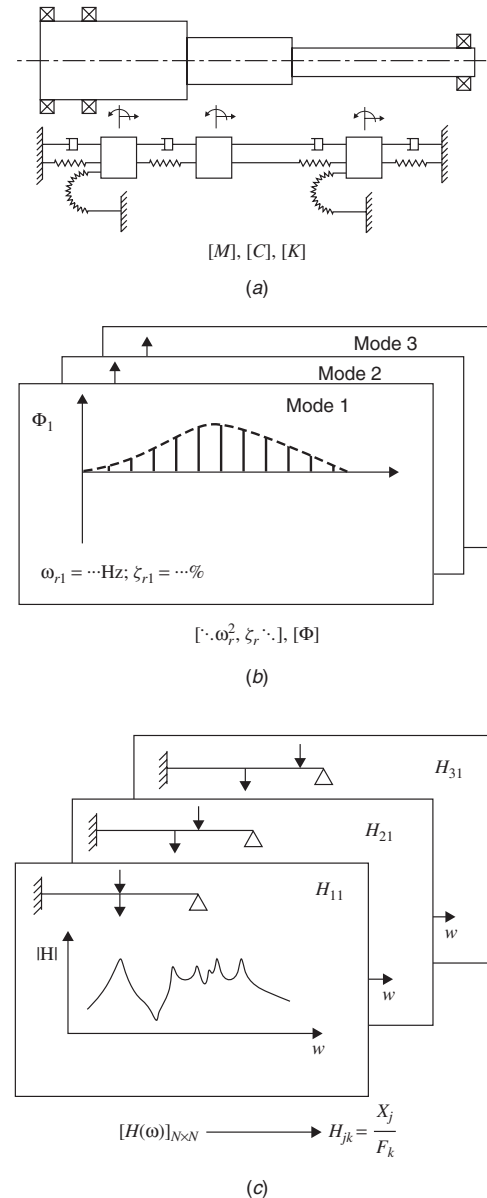
However, there is another important interpretation of the term modal analysis that is discussed here and that refers to the extraction of the same modal properties from measured data—usually response characteristics—rather than from a theoretical mathematical model. This approach is known as experimental modal analysis and is often referred to as modal testing, partly to avoid any confusion with theoretical modal analysis, but also to indicate quite clearly that it is concerned with measured data. So, *experimental* modal analysis is a methodology that enables a structure's modal properties to be determined from experimental observations of its dynamic response under test conditions. In fact, a more precise definition of modal testing is *the construction, using data measured on a test structure, of a mathematical model that describes the structure's dynamic behavior under a range of excitation conditions*. From this definition, it can be clearly deduced that the objective of experimental modal analysis is the construction of a mathematical model.

### 2 THEORETICAL BASIS

#### 2.1 Models for Structural Dynamics Analysis

In order to help set experimental modal analysis into perspective with respect to theoretical methods, it is helpful to discuss three different types of mathematical model that are used to describe a structure's dynamics and to show their interdependence (Fig. 1).

First is the *spatial model*, which describes the distribution in space of the mass, stiffness, and damping properties of the structure. Mathematically, the spatial model comprises three matrices: the mass matrix  $[M]$ , the stiffness matrix  $[K]$ , and—when the information is available—a damping matrix  $[C]$ . The unknown variables in the equations of motion written in terms of the spatial model are the time-varying displacements,  $\{x(t)\}$ , of the various degrees



**Figure 1** Types of mathematical models for dynamic analysis of structures: (a) spatial model, (b) modal model, and (c) response model.

of freedom (DOFs), which are used to describe the system's motion in response to a set of prescribed time-varying excitation forces,  $\{f(t)\}$ , applied at the same DOFs:

$$[M]\{x''(t)\} + [C]\{x'(t)\} + [K]\{x(t)\} = \{f(t)\} \quad (1)$$

The second type is the *modal model*, and this presents an alternative description of the dynamic behavior, expressed in terms of the fundamental (or "normal") vibration modes that represent the structure's natural (i.e., free or unforced) vibration behavior. This model comprises an eigenvalue matrix, containing the natural frequencies and modal damping factors,  $\text{diag}[\omega_r^2; \zeta_r]$ , and an eigenvector, or mode shape, matrix,  $[\Phi]$ . The equations of motion expressed using the modal model have as unknown quantities the magnitudes of response in each of the constituent modes,  $\{p(t)\}$ , resulting from the application of a set of modal excitation functions,  $\{P(t)\}$ :

$$[I]\{p''(t)\} + \text{diag}[2\zeta_r\omega_r]\{p'(t)\} + \text{diag}[\omega_r^2]\{p(t)\} = \{P(t)\} \quad (2)$$

The third model is the *response model*, and this describes the structure's dynamic behavior directly in terms of a specific characteristic response parameter, such as the frequency response function (FRF). Here, the equations of motion comprise a single matrix of FRFs,  $[H(\omega)]$ , with the harmonic responses at all DOFs as the unknown variables,  $\{X(\omega)\}$ , resulting from a matching set of harmonic excitation forces,  $\{F(\omega)\}$ . This response vector is sometimes referred to as an *operational deflection shape* and the corresponding equation is

$$[H(\omega)]\{F(\omega)\}e^{i\omega t} = \{X(\omega)\}e^{i\omega t} \quad (3)$$

The typical individual FRF is generally written as  $H_{jk}(\omega)$  and can be defined as  $X_j/F_k$ , where a single harmonic excitation force is applied at DOF  $k$  [ $f_k(t) = F_k e^{i\omega t}$ ;  $f_{1,2,3,\dots \neq k}(t) = 0$ ], and the resulting harmonic response at DOF  $j$  is  $x_j(t) = X_j e^{i\omega t}$ . This type of FRF is called a *receptance*, while other versions include *mobility* (when the response parameter is velocity rather than displacement) or *accelerance* when acceleration response is used.

## 2.2 Essential Theory of Experimental Modal Analysis

There are relatively simple mathematical expressions that interconnect these three models. Each model contains the same essential information as the others, unless there is a truncation (elimination) of certain data, in which case they provide different approximations to the structure that they all represent. In these circumstances, it is extremely important to understand the implications of such truncation. Because, in experimental activities, we are almost always obliged to

restrict the quantity of data that are measured, the probability of seeking to construct a mathematical model with incomplete data is relatively high. As a result, it is important that any discussion of modal testing is prefaced by an outline of the theoretical basis of the approach, and of the potential difficulties that may be encountered. The relevant mathematical relationships (subject to certain simplifying assumptions that are adopted here to retain a degree of simplicity in the expressions) are shown below:

$$[\Phi]^T[M][\Phi] = \text{diag}[I]; [\Phi]^T[K][\Phi] = \text{diag}[\omega_r^2] \quad (4)$$

$$[H(\omega)] = ([K] + i\omega[C] - \omega^2[M])^{-1} \quad (5)$$

$$[H(\omega)] = [\Phi]\text{diag}[(\omega_r^2 - \omega^2 + 2i\omega\omega_r\zeta_r)]^{-1}[\Phi]^T \quad (6)$$

$$H_{jk}(\omega) = \Sigma(\phi_{rj})(\phi_{rk})/(\omega_r^2 - \omega^2 + 2i\omega\omega_r\zeta_r) \quad (7)$$

Further details can be found in Refs. 1–4.

If it is required to determine a structure's modal properties from experimental measurements, then it is necessary to understand the theoretical basis of the processes used. The underlying theory for experimental modal analysis can be summarized by reference to the different mathematical models introduced in the previous section. In practice, the only parameters that can be measured directly are the time-varying quantities of excitation force and resulting response:  $\{f(t)\}$  and  $\{x(t)\}$ . The response model is the one that applies most directly to the situation in a modal test, and the most immediate output that is available from such a procedure will be a set of response functions. These will usually be FRFs as a result of the convenience of measuring and calculating responses to harmonic excitations. (However, it should be noted that a similar approach is possible with other types of standard response function, such as the impulse response function, or IRF.) Thus, in order to determine the natural frequencies and mode shapes, it is necessary to extract the required modal parameters from the measured response functions. This process is sometimes called *modal analysis* and sometimes *modal parameter extraction* and forms the heart of the postmeasurement stage of a modal test. In effect, we seek to construct a modal model by measuring data that allows us to "measure" a response model using the mathematical relationships shown above.

## 3 OBJECTIVES AND APPLICATIONS OF EXPERIMENTAL MODAL ANALYSIS

As mentioned in the previous section, the primary objective of modal testing is the construction of a mathematical model of the test structure from tests carried out under controlled conditions. Such a model is useful for a range of specific applications, including (but not limited to) those outlined below.

### 3.1 Model Validation

The most common application of a test-derived model is to validate a theoretical model, usually a finite

element description, that has been constructed for design purposes. This application involves a series of well-defined and interrelated steps that include:

1. Comparison of predicted and measured properties
2. Correlation of these properties to quantify their similarities/differences
3. Reconciliation of the two sets of results by identifying why they differ
4. Adjustment of one or other set of results so that they agree

At the conclusion of this last stage, the theoretical model can be deemed to have been validated, at least for further application in the range of frequencies and/or DOFs that have featured in the tests.

### 3.2 Diagnostics

In a similar vein, the same type of model can be used in a wide range of diagnostics applications, in particular to monitor changing patterns of behavior with continued running of a machine. The ability to interpret changes in behavior with the aid of a model of the structure means that sources of the changes can be identified, and early diagnosis of deterioration in the structure made.

### 3.3 Modification Design Using Test-Derived Model

Sometimes, it is impractical to construct a detailed and accurate mathematical model for a complex structure from theoretical considerations (even though it may be possible), and for these cases the construction of a model from tests can be very useful. A particular application here can be found in the evaluation of proposed structural modifications in an attempt to “tune” a structure’s dynamics. Tests on an existing structure, and especially those confined to the specific areas of interest, can be used to assess numerically the effect of making a series of alternative modifications (e.g., local changes of mass, stiffness, or damping) without the need to implement several variants of a basic idea on the actual structure. Parameter studies to

identify optimum values for certain key properties can be made by simulation, and only the final choice needs to be checked with further tests.

### 3.4 Troubleshooting

Lastly, there is a category of applications referred to as troubleshooting. In these cases, the ability to reconstruct and display the modes of vibration of an actual structure on the computer screen, to animate these in slow motion, and to inspect the details of this motion in critical areas of the structure can frequently provide a valuable insight into how the structure is actually moving. This insight, in the hands of a skilled engineer, can often be turned into an interpretation of what may well be very complex vibration behavior, and to explain why, even without the aid of a full mathematical model, thereby enabling the solution of a practical problem to be found.

## 4 PLANNING A MODAL TEST

### 4.1 Introduction

Before describing the techniques of data capture and analysis, we shall first discuss the overall concept and philosophy of the test procedure and identify those features critical to the effective and successful application of the process.

The essential components used in a modal test are well established (see Fig. 2). In addition to the items of specific hardware that are indicated on the schematic, there will generally be a software package used to manage the test, to collect and organize the various measurements, to process the measured data to reveal the required response functions, and, finally, to extract the underlying modal parameters from these response functions. The packages available for these activities are widely referred to as *modal analysis software*. For many of the items involved in planning the test, it is simply a question of selecting the unit with the most appropriate size or range. However, there are several other decisions to be made, mainly in respect of how to use the selected equipment, and these need an understanding of the underlying theory and philosophy of the method.

The basic concept of a modal test is that of measuring the response to a controlled and known

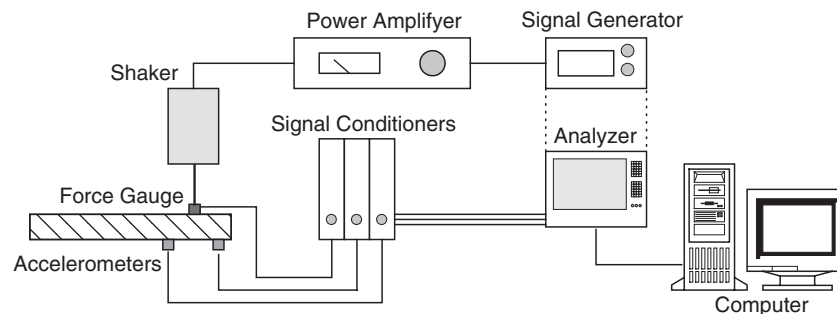


Figure 2 Basic components for a modal test setup.

applied excitation, and a number of key decisions in respect of this feature must be made early in the planning phase. The nature of the excitation device must be selected with care, as must the type of excitation signal that will be used to drive the structure. Another important decision is where the excitation(s) should be applied for maximum effect. Here we meet the common issue that the answers depend to some extent on the specific purpose and application of the test in question. In some applications, such as model validation, the accurate measurement of certain modes is more important than for others. In this case, a choice of excitation position can be made so as to maximize the visibility of the important modes and to suppress the response in unimportant ones. This will ensure a uniform accuracy of extracted modal data—a feature that is not always achieved without careful selection of excitation position.

Likewise, the type and location of response transducers demand careful selection as the failure to measure at sufficient points may make the ensuing results difficult to interpret. On the one hand, it is necessary to ensure sufficient spatial density of measurement points in order to be able to discriminate between two modes of similar form, while on the other, it is wasteful and unhelpful to so overspecify the number of response points that time is wasted in testing without matching benefits from the results. At the same time, the use of inappropriate transducers can bring about major systematic distortions in the resulting measurements—such as can be caused by mass-loading effects—for which it may be impossible to compensate in the post-measurement processing of the measured data.

#### 4.2 Test Planning and Virtual Testing

It is common practice nowadays for guidance on the test planning phase to be available from the modal analysis software used for the processing of measured data and extraction of the target modal parameters. When a modal test is undertaken for the purpose of validating a preexisting mathematical model, it is often possible to use the very model that is to be validated to help design the test itself. Specifically, with a model of the structure, extended to include the proposed test setup, it is possible and very effective to rehearse the planned tests in a numerical simulation, long before any hardware is produced or test program decided.

Careful planning of modal tests can pay handsome dividends by greatly reducing the possibility (a) of missing certain key data and/or (b) of overestimating the quantity of data that is required. With such information provided for the tester by this “virtual testing” concept, a near-optimal test schedule can be drawn up that delivers the best results possible in the time available for the test.

### 5 MEASUREMENT TECHNIQUES

#### 5.1 Introduction

In this section we summarize the main stages in the measurement phase of a modal test. There is

extensive literature addressing this important phase, and the reader is directed to Refs. 5 and 6, which include significant documents of a standards nature. Reference 5 is a multipart International Organization for Standardization (ISO) document on some of the fundamental measurement processes involved in modal testing, while Ref. 6 is a handbook of best practices that was prepared in the early 1990s under the auspices of the Dynamic Testing Agency (DTA) in the United Kingdom. In addition to these references, there are literally thousands of studies published in the past 40 years, many of which can be found or referenced in the conference proceedings of IMAC<sup>7</sup> and ISMA<sup>8</sup>. It should also be noted here that a number of the other chapters in this handbook deal in more detail with some of the individual items of equipment that are referred to below.

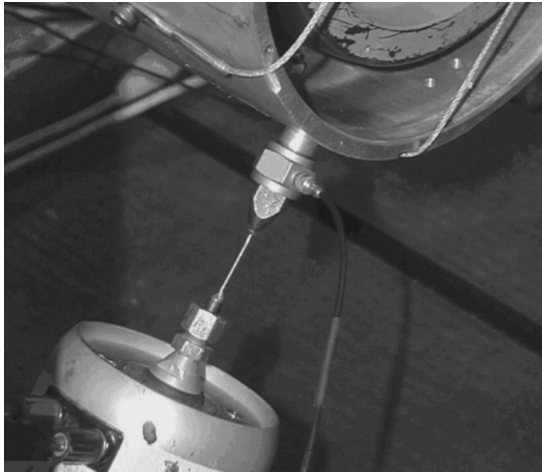
#### 5.2 Excitation Devices

There are several different types of device that are routinely used to generate the excitation necessary to conduct a modal test. These include:

- Electrodynamic exciters
- Electrohydraulic exciters
- Mechanical (rotating mass) devices
- Impactors and hammers
- Magnetic excitation
- Step-release devices
- Acoustic excitation

Each of these has particular advantages and drawbacks, the choice in each test usually being based on a balance between the degree of potential interference that attachment of the exciter causes on the structure against the ease of making accurate measurements of the actual forces exerted on the test structure. The noncontacting, and thus nonintrusive, excitation mechanisms carry with them a significant difficulty in measuring the forces they exert on the structure. On the other hand, direct physical connection of the moving part of an electrodynamic or electrohydraulic exciter risks contributing a significant influence on the motion of the structure we seek to measure. It is common practice to make the connections between exciter and structure by means of inserting a push-rod or “stinger,” such as the one illustrated in Fig. 3. The primary role of this device is to transmit an excitation force along the drive axis of the shaker while at the same time avoiding simultaneous application of secondary forces in any of the five other axes through which the two devices are connected. This issue of secondary forces is one that can give rise to significant errors, and considerable care must be taken in preparing a modal test to ensure that such effects are minimized.

There are other problems that can arise as a result of interactions between the test structure and the exciter. A properly located force transducer can help to ensure that such problems do not lead to significant errors in the measured response properties.



**Figure 3** Appropriate attachment of exciter to structure.

Finally, it is worth noting that there is growing interest in the use of “natural” excitation: excitation that comes from the environment in which the structure “operates” but that is such that it cannot be specifically identified or measured (referred to as “output-only modal analysis”).

### 5.3 Response Transducers

Another critical part of the measurement process is concerned with the effective transduction of the response levels, which must be measured at several points on the test structure. There are issues in selecting appropriate transducers that are centered around two main concerns:

1. The need to select sufficient measurement points so as to ensure adequate spatial coverage of the mode shapes and operation deflection shapes that are captured by the response transducers
2. The need to minimize the interference that the physical presence of transducers inevitably imposes on the test structure, thereby risking significant distortion of the vibration properties being measured

There are three primary transducer types in widespread use today:

1. Accelerometers (piezoelectric, piezoresistive, and other types)
2. Strain gauges
3. Laser-based devices, including scanning laser Doppler vibrometers and holography

Details of the actual devices available today can be found in other chapters of this handbook. However, it is worth noting here that when using accelerometers, or other similar attached transducers, and in situations

where it is required to obtain measurements at a large number of points, it is important to ensure that an efficient choice of measurement sites is made. The test planning methodology mentioned in Section 4.2 can also be applied to this critical aspect of the measurement process.

Some of the problems associated with the need to measure at many points on the structure can be avoided by using noncontacting optical “field” measurement methods and, in particular, the two laser-based techniques of scanning laser Doppler velocimetry (SLDV) and holography. The main limitation of response measurement using laser-based methods is the need for a clear line of sight to each of the degrees of freedom of interest. Nevertheless, these methods offer considerable advantages.

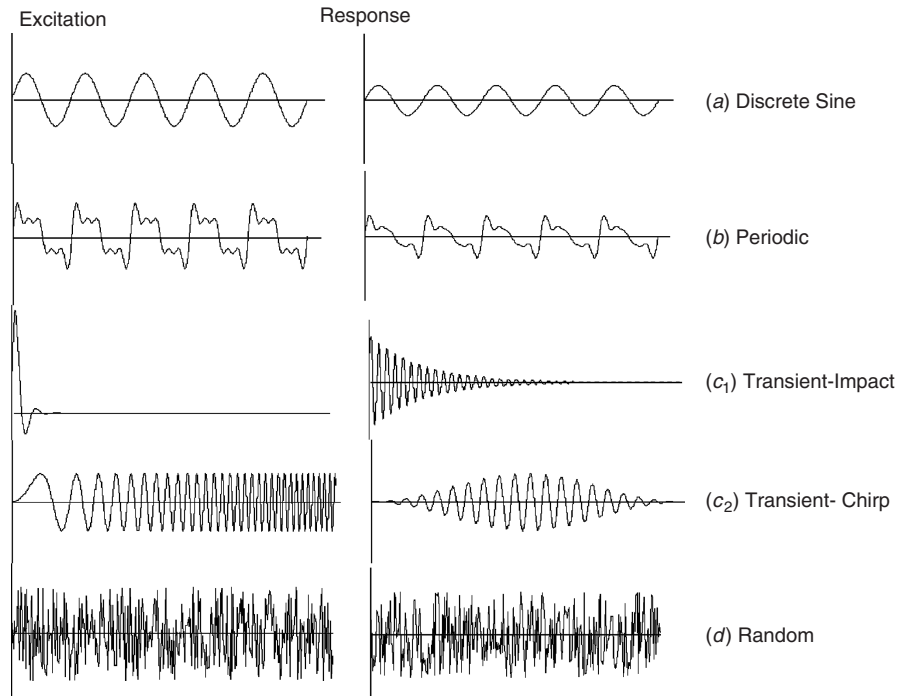
### 5.4 Excitation Signals for Modal Testing

A third issue to be addressed in planning a modal test is the question of what type of excitation signal will be used. There are essentially four categories of excitation signal in widespread use and, again, each has particular advantages and drawbacks. These are (i) sinusoidal, (ii) periodic, (iii) transient, and (iv) random and are illustrated schematically in Fig. 4.

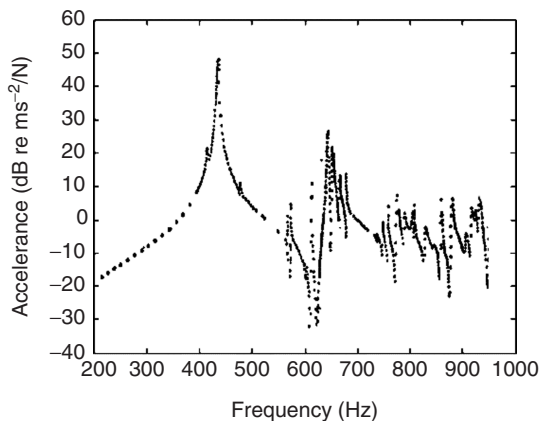
The first, and traditional, excitation signal is the simple sine wave. For this approach, the structure is excited at a specific frequency for long enough to capture measurements of the excitation force and all the response transducers before moving on (stepping rather than sweeping as in the past) to the next frequency where the same procedure is repeated, and so on until sufficient frequency points have been addressed. This approach tends to be slow, although it has a sometimes overlooked advantage that it allows the specific selection of each individual measurement frequency and does not demand, as do other methods, measurements at a fixed series of equally spaced frequencies spanning a chosen range. In practice, this means that it is possible to choose frequency steps that are close together near regions of resonance or antiresonance but that are more widely spaced in frequency regions where the response functions change more slowly (see Fig. 5). The sinusoidal excitation method is widely accepted as being the most precise and the most appropriate for cases where nonlinear behavior is expected or encountered.

The second commonly used excitation signal is periodic excitation. In this case, the structure is excited simultaneously at all the frequencies where measurements are required. In most current implementations where a discrete Fourier transform (DFT) type of spectral analysis procedure is used to analyze the measured data, a typical periodic excitation signal will contain components of every frequency in the analyzer spectrum. Typically, that might mean frequency components at 1-Hz intervals between 1 and 1600 Hz, for example. Such a signal has a clear advantage over the single-frequency sinusoidal excitation in that since all frequency points are measured simultaneously, the time required to acquire the necessary data to construct a response function should be much shorter than





**Figure 4** Common signal types used for modal tests: (a) sinusoidal, (b) periodic, (c) transient, and (d) random.



**Figure 5** Typical FRF measurement using sinusoidal excitation signal.

a method in which the frequency points are measured sequentially. However, the comparison is not quite so simple as this statement implies because, in practice, with a sinusoidal excitation many of the frequency points that find themselves away from regions of resonance or antiresonance might not need to be measured in a discrete sine test, and because of the relatively low signal strengths on each of the individual frequency components of the periodic signal, it is often necessary

to average for a reasonable period of time in order to filter out background noise.

The third common excitation type is transient. This comes in a number of specific types, with the impulse generated by an impact hammer or similar device being the most widely encountered. However, there are other transient signals that can be used with an attached shaker and these include: (a) controlled sine pulse, (b) single chirp, and (c) burst random and other continuous signals.

To avoid problems associated with the signal processing in each of these transient excitation signals (see Chapters 40, 42, and 46), it is necessary to arrange the test conditions such that not only has the excitation signal died away at the end of the finite measurement period but so also has the response signal. While transient excitation signals are deterministic, in the same way that sinusoidal and periodic signals are, the exact spectral transformation of such an aperiodic signal is a Fourier integral rather than the Fourier series, which is what is obtained when using a DFT analysis (as is almost always the case in modal testing). As a result of using the DFT analysis process, only an approximate indication of the structure's response function is obtained when using transient excitation signals. Considerable care must be exercised to keep these approximations to an acceptable level.

The fourth excitation signal, which has been used for a considerable time, is random excitation. This is the only nondeterministic signal used in modal

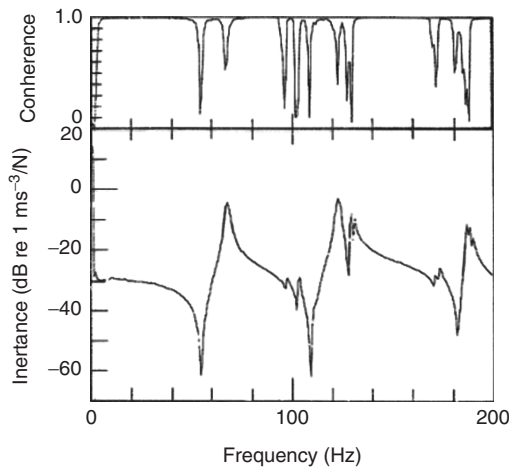
testing and in cases where a truly random excitation signal is used, such as is generated in a random noise generator, the signal processing and subsequent analysis necessary to obtain the required response functions for the structure's behavior involve more assumptions and need more care than is required for the deterministic signals. It is necessary to average both excitation and response signals for a considerable period of time to obtain statistically reliable results. Even then, there is only a finite probability of being acceptably close to the right answer, and this residual uncertainty can only be reduced by measuring data for longer and longer periods. As in the case of transient signals, this type of signal processing using the DFT incurs additional approximations to the resulting parameters and, in the case of random excitation, it is generally necessary to apply a windowing correction compensation procedure to all the measured signals to minimize the errors incurred. Figure 6 shows a typical frequency response function measured with a random excitation signal, including an indicator of quality (the coherence) on the response function.

The reader is referred to specialist texts for more detailed explanation and guidance in dealing with the problems associated with the measurement of the data required to carry out an experimental modal analysis. However, this section should serve to alert the modal tester to the more significant sources of potential errors that can generally be avoided by expert use of standard equipment.

## 6 PARAMETER EXTRACTION TECHNIQUES

### 6.1 Introduction

At the end of the measurement phase, it is customary to have acquired a set of measured response functions. The actual measurements taken are time histories of excitation forces and responses, but it is normal practice to convert these either to FRFs, for a



**Figure 6** Typical FRF measurement using multi-frequency excitation signal and DFT spectral analysis.

frequency-domain description, or to impulse response functions (IRFs), for those cases where a time-domain description is required. Nowadays, the vast majority of practical applications of experimental modal analysis provide the measured data in the form of FRFs. The next step in the process is to extract from these response functions a set of parameters that describe the underlying modal properties of the test structure. This is done using the basic theoretical relationship between the response model and the modal model and is usually carried out by fitting a theoretical curve of the correct form (but with initially unknown coefficient values) to the measured responses. Although application of these parameter extraction methods is increasingly a routine process, there are a number of subtleties and complexities that mean that it is appropriate to have a good understanding of the theoretical basis and assumptions on which the various algorithms are based. These will be outlined in this section.

### 6.2 Essential Principles

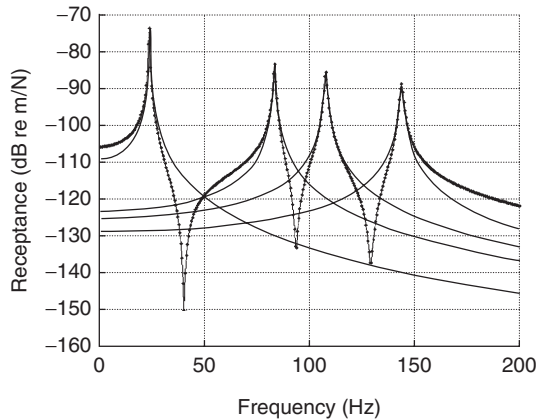
The basic theoretical expression for a typical FRF described in terms of modal parameters (response model from modal model) is given in Eq. (8). It is seen that the typical response function can be expressed by a summation of components from all of the modes of the structure, and that the relative importance or weighting of each modal component is related to the proximity of its natural frequency to the frequency at which the response function is defined. Figure 7a shows the essential construction of a frequency response function in terms of individual modal components. It can also be seen that within a narrow range of frequency in the immediate vicinity of each resonance, the frequency response function can be approximated by a single modal component plus two terms that represent approximately the effect of all the modes with lower and higher natural frequencies [Eq. (9) and Fig. 7b]. This expression is often further simplified to that shown in Eq. (10) with a single constant term to represent the combined effect of all other modes. Although this expression is not exact, it can be seen that if interest is confined to a very narrow range of frequencies around the natural frequency of one particular mode, it becomes a very good approximation and represents the underlying principle whereby the parameters of one mode can be extracted from analysis of a response function measured in the vicinity of the natural frequency of that mode:

$$H_{jk}(\omega) = \sum \frac{r A_{jk}}{\omega_r^2 - \omega^2 + 2i\omega\omega_r\zeta_r} \quad (8)$$

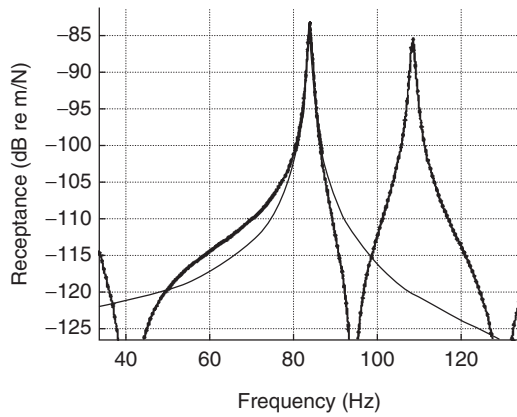
$$r A_{jk} = (\phi_{rj})(\phi_{rk})$$

$$H_{jk}(\omega)_{\omega_1 < \omega < \omega_2} \simeq \sum \frac{r A_{jk}}{\omega_r^2 - \omega^2 + 2i\omega\omega_r\zeta_r} - B_{jk}/\omega^2 + C_{jk} \quad (9)$$

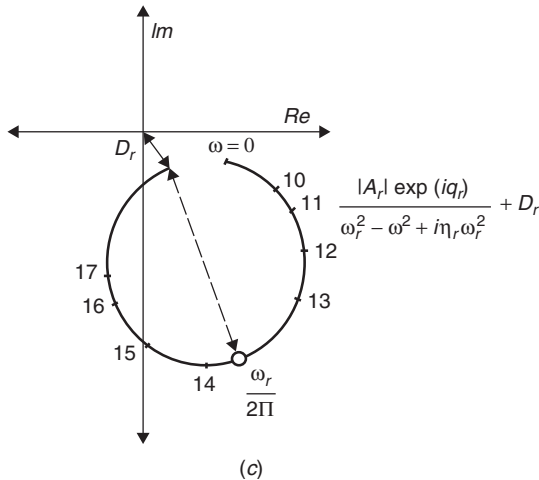
$$H_{jk}(\omega)_{\omega \sim \omega_s} \simeq \frac{s A_{jk}}{\omega_s^2 - \omega^2 + 2i\omega\omega_s\zeta_s} + s D_{jk} \quad (10)$$



(a)



(b)



(c)

**Figure 7** FRF curves in different formats: (a) construction of general FRF curve, (b) approximate FRF in vicinity of resonance, and (c) Nyquist plot of FRF in vicinity of resonance.

### 6.3 Single-Mode (SDOF) Modal Analysis

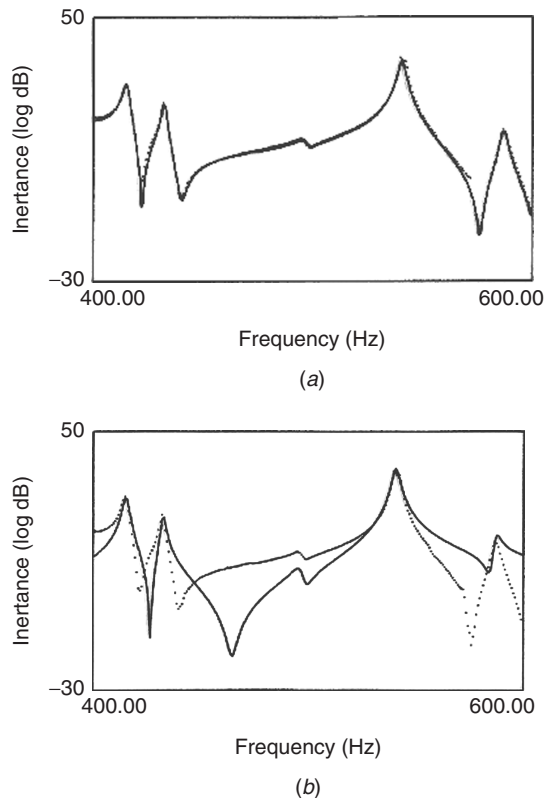
The FRF in the immediate vicinity of a natural frequency can also be examined in other presentation formats such as the Nyquist diagram in Fig. 7c. It can be seen that in this case the response function traces out a near-circular arc and that the underlying circle is displaced from the origin of the plot by a quantity,  $D$ . The properties of the circle contain the parameters of the mode in question, and the displacement of the circle from the origin represents the contribution of all the other modes and from a simple curve-fit analysis of a few response function data points, we can start to compile a table of modal parameters for the particular response function in question.

### 6.4 Multi-mode (MDOF) Modal Analysis

The previously described method is the most simple of those available, but with the widespread availability of extensive computation capacity, it is possible to undertake more ambitious and more accurate curve-fitting procedures. The first extension of the above approach, and one that relaxes any assumptions about single-mode dominance, is one in which the data points are fitted to a formula that contains not one but several modal components (so-called “MDOF” modal analysis). This is essentially a general curve-fitting process and there are several algorithms available for carrying it out. The result yields a table of best estimates of the modal parameters for the identified modes, plus any residual terms necessary to take account of the existence of other modes with natural frequencies outside the measured range—the so-called modal truncation effects. In this context, “best” is in the sense of a minimum least-squares error between the measured data points and corresponding points on the curve regenerated using the identified parameters themselves. Figure 8 illustrates the results from an MDOF modal analysis of a single FRF, clearly showing the importance of including the residual terms to account for the out-of-range modes.

### 6.5 Global Modal Analysis

Further extension of the generality in curve-fitting FRFs is possible by undertaking simultaneous analysis of several response functions relating to different points on the structure. If we have, say, a dozen frequency response functions that all share the same excitation point,  $k$ , but relate response levels at different points, such as  $j = 1, 2, 3, \dots$  (i.e., the FRFs in a single column of the FRF matrix), then there are certain features of which we can take advantage to speed up the parameter extraction process by analyzing all curves simultaneously. The modal constants would be different for each of the response functions, but the natural frequencies and damping factors must be the same because they relate to the same mode. Advantage can be taken of this feature by arranging a simultaneous analysis of all the response functions over a common frequency range and by building in the constraint that the eigenvalue part of the solution (natural frequency plus damping factor) has a unique



**Figure 8** Regenerated FRF curves and original measured data for single-FRF analyses: (a) MDOF curve fit, (b) MDOF omitting residual terms.

value and does not vary from curve to curve. Indeed, even greater generality is possible by using FRFs from several columns, or different excitations, in this analysis.

It is possible to use the MDOF analysis approach so that we can construct a table of all the eigenvalues for the modes that have been included in the measurement and as many of the individual elements from the eigenvectors as are covered by the set of measured response functions (in general, each FRF yields information on one DOF). These latter approaches to the parameter extraction task are usually referred to as “global” methods as they seek to provide a total solution to the modal model that is required and can be extended to include any set of FRFs in the “polyreference” version.

### 6.6 Parameter Extraction Algorithms

A large number of different numerical algorithms exist for the parameter extraction process. As we have described, they can be categorized into:

- One mode, one FRF (the SDOF method)
- One mode, several FRFs (global SDOF method)

- Several modes, one FRF (MDOF method)
- Several modes, several FRFs (global or polyreference MDOF method)

All these algorithms are based on the same underlying theoretical model, at least as far as the mass and stiffness are concerned. There are some variations as regards damping, reflecting the fact that, in reality, “damping” covers a wide range of different phenomena and mechanisms and is only ever represented approximately. However, each method attaches a different weighting to the measured data points with the result that each tends to give slightly different results to the others for real measured data that do not conform perfectly to the underlying linear assumptions. The reasons for this include:

- Slight nonlinearity in the structure
- Changes that can occur in the test structure’s properties during the test

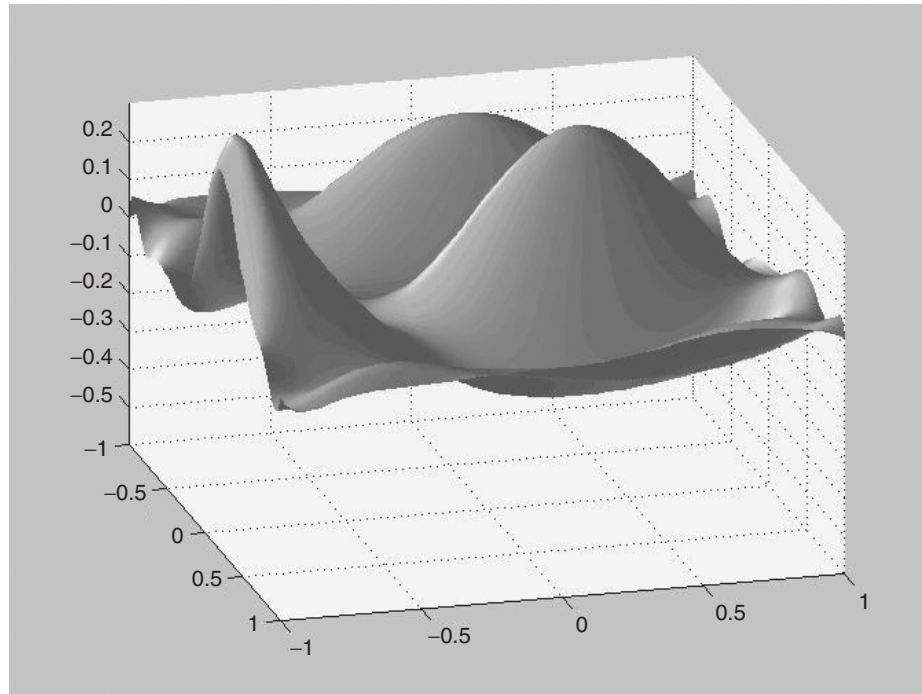
A significant factor in this respect results from the fact that many of the limitations to response function measurement are particularly significant near resonances, and these effects are most sensitive to the differences that exist between the different algorithms.

### 6.7 Construction of Mathematical Model from Modal Parameters

The preceding sections have been concerned with the extraction of individual modal parameters from measured responses. At the conclusion of such a process we shall have a table containing values for natural frequencies, damping factors, and individual eigenvector (mode shape) elements. These data comprise a modal model for the structure that has been tested, and an example of a typical mode shape from one such model, measured on an automotive panel, is shown in Fig. 9. In principle, the data contained in this model should be capable of reconstructing or regenerating the response functions that were measured and used to determine the modal properties. Ideally, they should also be capable of constructing a spatial model consisting of mass stiffness matrices. However, this transformation of information from one type of model to another is hampered by two practical effects.

The first of these issues is the obvious one in that the essential data that have been used to construct the model are *inaccurate*: They contain errors of measurement or of structural behavior. These errors, although small, will be propagated through a conversion from response to modal models, and back, and so will affect the quality of any subsequent model. Sometimes, the propagation has a deleterious effect in that small errors in the original data can escalate to large ones in the model.

The second limitation is more critical and stems from the fact that the data that have been measured, and the modal model that has been constructed from those measurements, are *incomplete*. It is clearly not possible to measure all the modes of a structure, nor



**Figure 9** Mode shape derived by modal analysis of scanning later measurements on an automobile panel.

to measure the mode shapes at all the degrees of freedom on a structure. As a result, a modal model that is constructed from a conventional modal test will include only a small fraction of the full properties. Examination of the formulas that link the modal model to the spatial model and the response model [see Eqs. (4), (5), and (6)] show that these are predicated on the assumption that each of those models is complete and that it contains information at all the degrees of freedom and for all the modes. This is clearly not possible for a practical structure and, as a result, although it is possible to construct a limited modal model from a set of measured frequency response functions, it is not possible to create a spatial model.

### 6.8 Determining the Number of Necessary Modes

The number of modes required in a mathematical model for a test structure depends strongly on the application of that model. If the model has been constructed to validate predictions from a theoretical model, and these predictions comprise a set of natural frequencies and mode shapes in a given frequency range, then a very useful application can be undertaken with only a limited set of modes. If, however, the application that is sought involves the need to use the model for calculating the response of the structure, then any restriction in the number of modes included in the model can present a significant limitation. To calculate accurately the response of a structure at a given frequency, it is

necessary to include components in the response from all the modes of vibration, including those whose natural frequencies are some distance from the frequency of the vibration of interest. The consequences of omitting the effect of modes “outside the range” of the modal test is demonstrated graphically in Fig. 8.

As a result of these considerations, it is as important to take due account of the number and choice of modes that are included in the model as it is to ensure that all the data and analyses provide accurate values for their respective parameters.

### REFERENCES

1. D. J. Ewins, *Modal Testing Theory, Practice and Application*, Research Studies Press, Baldock, UK, 1984, 2000.
2. N. Maia, et al., *Theoretical and Experimental Modal Analysis*, Research Studies Press, Baldock, UK, 1997.
3. W. Heylen, S. Lammens, and P. Sas, *Modal Analysis Theory and Testing*, Katholieke Universiteit Leuven, Leuven, Belgium, 1998.
4. J. He and Z. Fu, *Modal Analysis*, Butterworth Heinemann, Oxford, UK, 2001.
5. International Organization for Standardization (ISO), *Methods for the Experimental Determination of Mechanical Mobility*, Parts 1–5, 1986–1994.
6. Dynamic Testing Agency (UK), *Handbook on Guidelines to Best Practice*, Vol. 3. *Modal Testing*, Dynamic Testing Agency (DTA), London, 1993.
7. *Proc. IMAC*, Society of Experimental Mechanics, 1982–2005.
8. *Proc. ISMA*, Katholieke Universiteit Leuven, 1976–2004.

# CHAPTER 48

## MACHINERY CONDITION MONITORING

**Robert B. Randall**

School of Mechanical and Manufacturing Engineering  
The University of New South Wales  
Sydney, New South Wales, Australia

### 1 INTRODUCTION

The vibrations measured externally on operating machines contain much information as to their condition, as machines in normal condition have a characteristic *vibration signature*, while most faults change this signature in a well-defined way. Thus, vibration analysis is a way of getting information from the inside of operating machines without having to shut them down. Machine vibrations are measured in two fundamentally different ways: relative displacement of a shaft in its bearings using so-called proximity probes and absolute motion of the casing, usually at the bearings, using absolute motion transducers. The former must normally be designed into the machines and are typically used on high-speed turbomachines with fluid film bearings. They are used for permanent monitoring of relatively simple parameters such as peak-to-peak relative displacement and shaft orbits (in the bearing) and are primarily used to protect valuable and critical machines by shutting them down in the event of excessive vibration levels being developed. Only in a limited number of situations can long-term predictions be made, basically because incipient faults often show up first at high frequencies, to which the relative displacement measurements are not sensitive. This chapter is mainly concerned with measurements made with accelerometers (giving a signal proportional to vibration acceleration, possibly integrated to velocity), but proximity probe and other measurements (e.g., torsional vibration) are discussed where appropriate.

### 2 MACHINE VIBRATION SOURCES AND DIAGNOSTIC TECHNIQUES

#### 2.1 Related to Shaft Speed

A number of faults manifest themselves at a frequency corresponding to the speed of the shaft. Among these are unbalance, misalignment, and cracked shaft, and the problem is to distinguish between them. In general, misalignment tends to produce a stronger second harmonic of shaft speed and more axial motion, but the nonlinearity of components in the system (such as fluid film bearings) can distort the response to unbalance force, leading to higher harmonics, and moment unbalance gives rocking motions with axial components, so the division is not clear. Flexible couplings are often introduced to mitigate the effects of misalignment but introduce their own characteristics into the vibrations. Reference 1 describes how many types of couplings, for example, Hooke's joints and gear couplings, give even harmonics of shaft speed, primarily second order. It also shows how the

harmonics generated are related to coupling design. For constant unbalance distribution and alignment, cracks in shafts give changes at the low harmonics of shaft speed, though these may be more evident as a change in phase angle (relative to the phase of a once-per-revolution tacho signal) rather than in amplitude. Sophisticated rotor dynamic models are now being made of the most critical machines, and these provide the best possibilities for distinguishing between unbalance, misalignment, and shaft cracks, at least with the machine running at speed and load. Cracks can be detected during rundowns, not so much by a change in critical speed as by an increased response when harmonics of shaft speed pass through the critical speed(s).<sup>2,3</sup>

Other faults show up at subsynchronous frequencies, such as *oil whirl*, usually between 40 and 48% of shaft speed, caused by a resonant wave in the fluid film bearing. This can sometimes be confused with *hysteresis whirl*, due to hysteretic friction between components on the rotor. The friction forces are such that a self-excited whirl is generated on passing through the shaft critical speed and remains at this frequency as the shaft speed increases.<sup>4</sup> Since many machines run at about twice their first critical speed, this can sometimes be confused (and perhaps even merged) with oil whirl. When oil whirl combines with resonant shaft response, it is sometimes called *oil whip*. Exact subharmonics (e.g., one-half or one-third) can result from *parametric excitation*, variations in stiffness due to looseness, "rubs," and the like and can be distinguished by their exact subharmonic nature. Sudden changes in stiffness also increase the number of superharmonics, even in the absence of subharmonics.

A finely tunable harmonic/sideband cursor is useful to distinguish between exact and approximate subharmonics and between harmonics of shaft speed and mains frequency (see Section 2.2). Phase relationships between the two ends of a machine can distinguish between lateral and rocking motion. A phase difference of 90° between the horizontal and vertical transducer signals at one location indicates circular or elliptical orbits, while if they are in phase, motion must be along a straight line. Proximity probes are useful for fluid film bearings for a number of reasons as mentioned earlier. Determination of the position of the shaft in its bearing (and thus the point of minimum oil film thickness) helps to distinguish between unbalance, misalignment, and shaft cracks. The shape of the orbit, and whether it is precessing forward, or backward can help to distinguish between the different types of whirl,



for example, dry friction tends to excite backward precessing modes.<sup>4</sup> A useful source of information of the applications of proximity probes is the magazine *Orbit* produced by Bently Nevada Corporation.<sup>5</sup>

## 2.2 Electrical Machines

Electrical machines such as alternating current (ac) motors and generators generate vibrations due to electrical as well as mechanical forces.<sup>6</sup> Stator faults tend to give increases at twice mains frequency (line frequency in the United States), as this is the rate at which the poles of the rotating magnetic field are passing a fixed point (the anomaly) on the stator. For two-pole synchronous machines, this is the same as twice shaft speed, and thus it can be difficult to distinguish between a stator fault and misalignment. However, the electrical forces are strongly dependent on the load, and varying the load may allow the two effects to be separated. Switching off the power and tracking the second harmonic as it runs down in speed allows complete separation. For induction motors<sup>6</sup> the situation is easier in that the shaft speed is less than synchronous, and fast Fourier transform (FFT) zoom analysis allows separation of the harmonics of shaft speed from those of mains frequency. Figure 1 shows an example of a fault on the rotor of a four-pole induction motor (in the United States where the mains frequency is 60 Hz). The main effect is at the shaft speed (corresponding to the rate of rotation of the fault), but it can be distinguished from mechanical unbalance by virtue of the strong modulation sidebands that are clearly in evidence. The sideband cursor shows that these are spaced at 1.0 Hz, which is the number of poles times the slip frequency of 0.25 Hz (synchronous speed 30 Hz minus shaft speed 29.75 Hz). As explained in Ref. 6 this is the frequency at which the poles of the rotating field pass a given point (the anomaly) on the rotor.

## 2.3 Gears

Gears represent a typical component where the wide frequency range of accelerometers is needed. The basic vibration generating mechanism in gears is the

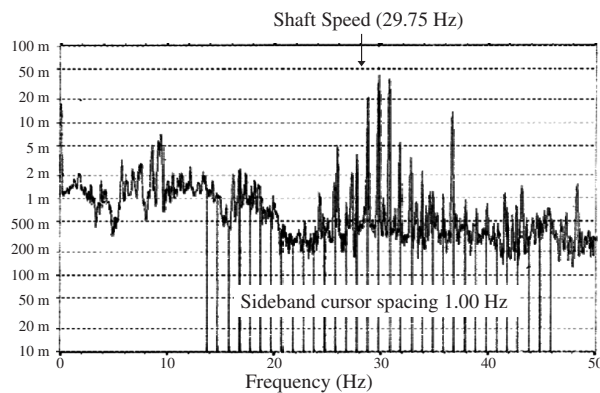
*transmission error* (TE), which can be understood as the relative torsional vibration of the two gears, corrected for the gear ratio. The TE results from a combination of geometric errors of the tooth profiles, and deflections due to tooth loading. Thus, even a gear with perfect involute profiles will have some TE under load, and it is important to make comparisons of gear vibration spectra under the same load to obtain information about changes in condition.

Gear vibration signals are dominated by two main types of phenomena<sup>7</sup>:

- Effects that are the same for each meshing tooth pair, such as the tooth deflection under load and the uniformly distributed part of initial machining errors and/or wear. These manifest themselves at the tooth-meshing frequency and its harmonics. Since there is a pure rolling action at the pitch circle, and sliding on either side, tooth wear tends to occur in two patches on each tooth, and thus wear is often first seen as an increase in the second harmonic of the tooth-meshing frequency.
- Variations between the teeth, which can be localized or distributed more uniformly around the gears. These manifest themselves at other harmonics of the gear rotational speeds for the gear on which they are located. Localized faults such as cracks and spalls tend to give a wide dispersion of harmonics and sidebands throughout the spectrum, whereas more slowly changing faults such as nonuniform wear tend to give stronger harmonics grouped around zero frequency and as sidebands around the harmonics of tooth-mesh frequency.

Since even with faults, the same geometric shapes always mesh in the same way, the signals produced by gears are basically deterministic, at least as long as the teeth remain in contact.

Most gear diagnostic techniques thus use time synchronous averaging (TSA) as a precursor to isolate



**Figure 1** Example of a rotor fault on an induction motor, showing modulation sidebands around the shaft speed component of 29.75 Hz (spacing 1 Hz).

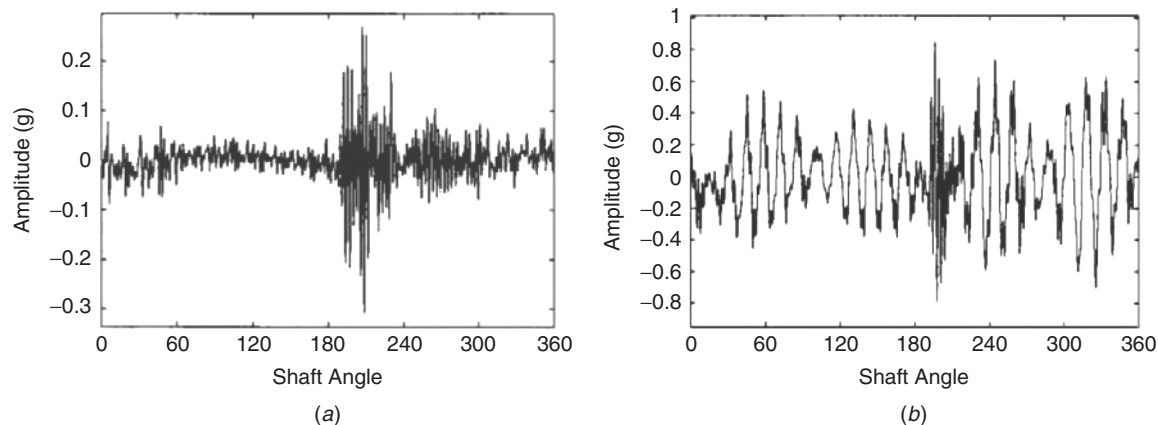
the vibrations from each individual gear. TSA is useful to extract that part of a signal that is periodic with the same period as a trigger signal, for example, a once-per-revolution tacho signal from a given shaft.<sup>8</sup> In practice, it is done by averaging together a series of signal segments each corresponding to one period of the synchronizing signal. To correct phase errors, it is necessary to first resample the signal to have a fixed number of samples per period, with the first lined up with the synchronizing signal. Such processing is called *order tracking* because the frequency axis can then be better scaled in harmonic orders rather than hertz. Order tracking can be done using a shaft encoder on a particular shaft to control the sampling clock, or by using a phase-locked loop tracking the tacho signal to generate a fixed number of sampling pulses per period of the locked frequency. Most modern analysis systems achieve the same effect by digitally resampling the signal at constant shaft phase increments, based on analysis of the tacho or shaft encoder signal.<sup>9</sup> This has the advantage that signals are available with both temporal and angular sampling, and transformation can be made between the two at any stage. Special techniques have been developed to get the averaged signature of sun and planet gears in a planetary gearbox, eliminating the effects of the varying distance of the planets to an external measurement point by capturing the signature of each tooth as it passes the measurement point.<sup>10</sup>

A general problem is to detect local faults on a gear once the averaged signature has been obtained. The effects of these are often obscured by the normal tooth-meshing pattern, so various techniques have been developed to remove the latter. The traditional way is to remove all harmonics of the tooth-meshing frequency in the frequency domain, inverse transforming back to the time domain to evaluate the result. The kurtosis (see Chapter 46) is a useful parameter for characterizing the severity of the residual

signal because it is a sort of normalized crest factor, and the local peak values are much greater than the background noise. A new method has recently been developed to obtain the residual signal using linear prediction.<sup>11</sup> An autoregressive (AR) parametric model is developed for the signal from an undamaged section of a gear using linear prediction, and when a damaged section of the gear enters the mesh, the actual value of the signal departs dramatically from the linearly predicted value, and the “error” gives a measure of the local change. Figure 2 compares the results of the two techniques for a typical case.

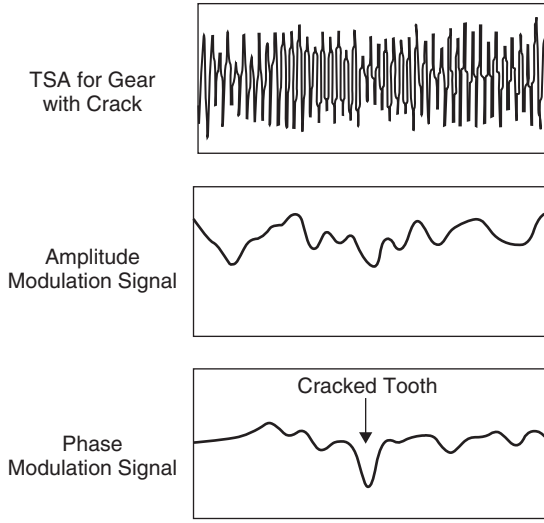
In some cases the presence of a local fault is not very clear, even after TSA, and a method has been developed to reveal a local fault by amplitude and phase demodulation of the tooth-meshing frequency of the signal using Hilbert transform techniques.<sup>12</sup> Figure 3 shows that the phase of the result revealed a crack long before it became evident in the amplitude of the signal. Attempts are currently being made to distinguish between the effects of cracks and spalls since the former would tend to give much more rapid failure.<sup>13</sup> Since spalls are a geometric error, while cracks give a change in stiffness, the symptoms of the latter are more load sensitive. In Chapter 88 an example is given of the detection of a local fault at light load.

Modulations of the gear-mesh signal give rise to sidebands around the gear-mesh harmonics and can often be revealed and quantified using the cepstrum, as described in Ref. 14. Another application of the cepstrum is in detecting echoes, and, in particular, it can be shown that an inverted echo makes all components in the cepstrum negative. Reference 15 shows how this can be used to locate spalls since these give rise to a negative echo in the acceleration signal as the mating tooth enters and leaves the spall.



**Figure 2** Enhancement of fault indications using AR modeling vs. harmonic removal: (a) residual signal (kurtosis, 11.14) obtained using linear prediction and (b) residual signal obtained (kurtosis, 3.03) by canceling harmonics of tooth-mesh frequency. (From Ref. 11. Reprinted by permission.)





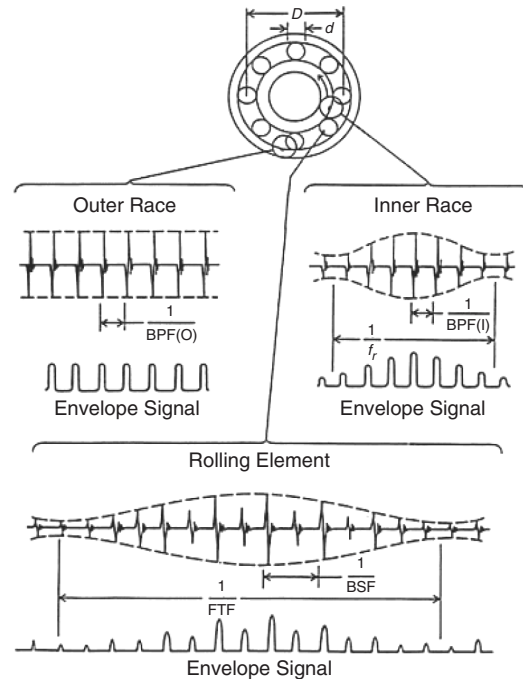
**Figure 3** Detection of a crack in a gear by demodulation of the tooth-meshing frequency after time synchronous averaging. (From Ref. 12. Reprinted by permission.)

## 2.4 Bearings

The discussion here is limited largely to rolling element bearings since with fluid film bearings in principle there should not be any metal-to-metal contact and consequent wear. There have been very few studies of detecting the wear of fluid film bearings from their vibration signals, but the operational faults that could give rise to such wear can be monitored by the techniques described in the section on shaft-related vibrations. This is one area where the use of oil analysis can aid vibration analysis, as bearing metals are quite distinctive in their chemical composition.

Figure 4 shows typical acceleration signals produced by localized faults in the various components of a rolling element bearing and the corresponding envelope signals produced by amplitude demodulation. It can be shown that analysis of the envelope signals gives more diagnostic information than analysis of the raw signals. The diagram illustrates that as the rolling elements strike a local fault on the outer or inner race, a shock is introduced that excites high-frequency resonances of the whole structure between the bearing and the response transducer. The same happens when a fault on a rolling element strikes either the inner or outer race. As explained in Ref. 16, the series of broadband bursts excited by the shocks is further modulated in amplitude by two factors:

- The strength of the bursts depends on the load borne by the rolling element(s), and this can be modulated by the rate at which the fault is passing through the load zone.
- Where the fault is moving, the transfer function of the transmission path varies with respect to the fixed positions of response transducers.



**Figure 4** Typical signals and envelope signals from local faults in rolling element bearings.

Figure 4 illustrates typical modulation patterns for unidirectional load on the bearing; shaft speed for inner race faults, and cage speed for rolling element faults. The formulas for the various frequencies shown in Fig. 4 are as follows:

Ballpass frequency, outer race:

$$\text{BPFO} = \frac{nf_r}{2} \left\{ 1 - \frac{d}{D} \cos \phi \right\} \quad (1)$$

Ballpass frequency, inner race:

$$\text{BPFI} = \frac{nf_r}{2} \left\{ 1 + \frac{d}{D} \cos \phi \right\} \quad (2)$$

Fundamental train frequency (cage speed):

$$\text{FTF} = \frac{f_r}{2} \left\{ 1 - \frac{d}{D} \cos \phi \right\} \quad (3)$$

Ballspin frequency:

$$\text{BSF} = \frac{Df_r}{2d} \left\{ 1 - \left( \frac{d}{D} \cos \phi \right)^2 \right\} \quad (4)$$

where  $f_r$  is the shaft speed,  $n$  is the number of rolling elements, and  $\phi$  is the angle of the load from the radial

plane. Note that the BSF is the frequency with which the fault strikes the same race (inner or outer), so that in general there are two shocks per basic period. Thus the even harmonics of BSF are often dominant.

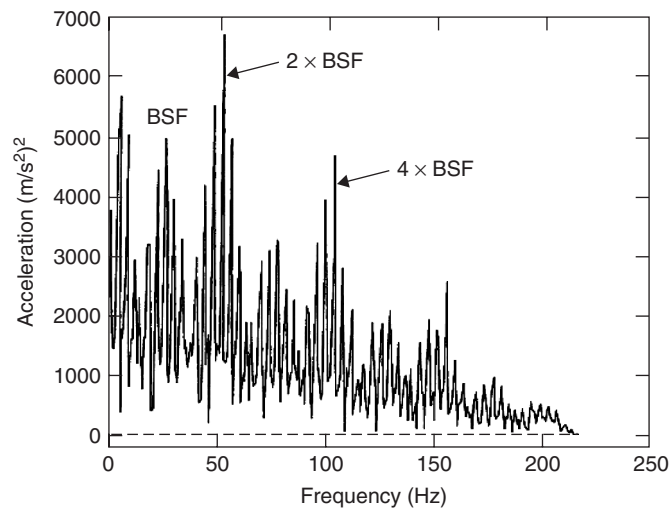
These are, however, the kinematic frequencies assuming no slip, and in actual fact there must virtually always be some slip for the following reason. The angle  $\phi$  varies with the position of each rolling element in the bearing, as the ratio of local radial to axial load changes, and thus each rolling element has a different effective rolling diameter and is trying to roll at a different speed. The cage ensures that the mean speed of all rolling elements is the same, by causing some random slip. This is typically of the order of 1 to 2%. This random slip, while small, does give a fundamental change in the character of the signal and is the reason why envelope analysis extracts diagnostic information not available from frequency analyses of the raw signal. It means that bearing signals can be considered as cyclostationary (see Chapter 46). This also allows bearing signals to be separated from gear signals<sup>17</sup> with which they are often mixed, as discussed below.

A very powerful technique for diagnosing bearing faults is using *envelope analysis*, as mentioned above. It can be shown that the spectrum of the raw signals (as depicted in Fig. 4) contains little diagnostic information as it is dominated by the high-frequency resonances excited and has only a small response at the actual characteristic frequencies given by Eqs. (1)–(4). Because of the small random fluctuation of the repetition frequencies, the higher harmonics of the bearing fault frequencies typically smear together in the vicinity of the resonance frequencies, giving the appearance of a noise spectrum. However, if the signal is bandpass filtered in a frequency band where there is a maximum (decibel) change in the spectrum caused

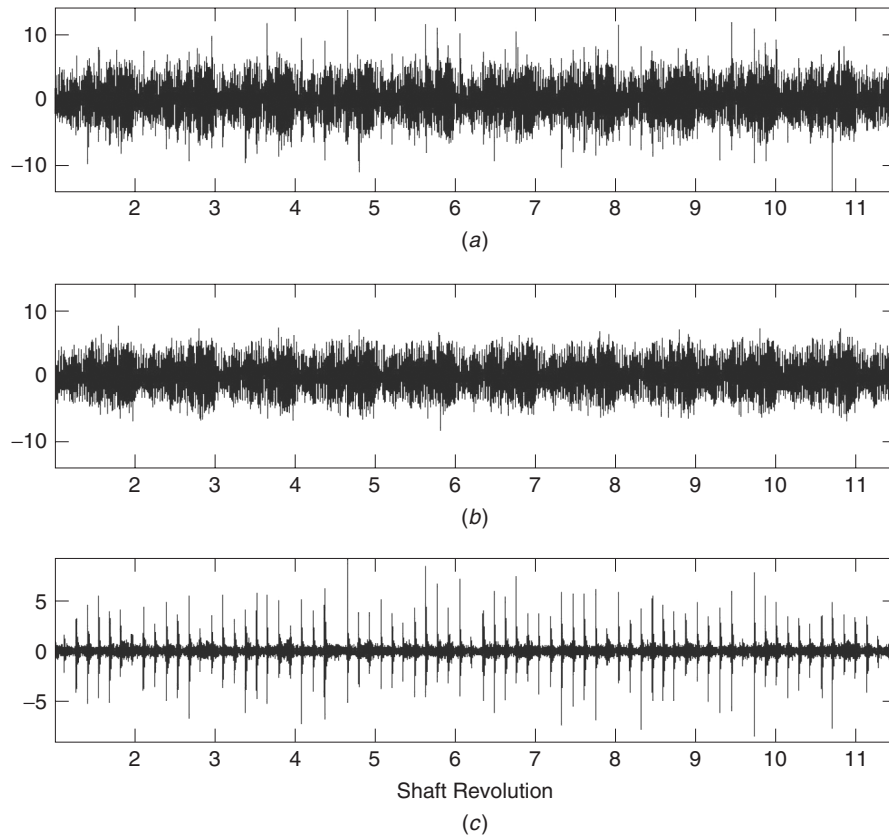
by the bearing fault, and then amplitude demodulated, the spectrum of the resulting envelope contains low harmonics of the fault frequencies (and any modulation sidebands), which are not appreciably smeared.

Figure 5 shows the envelope spectrum from measurements made on a gear test rig with and without a rolling element fault in a bearing. The major increases in the raw spectrum as a result of the fault were between 10 and 20 kHz, and there was negligible spectrum change below 8 kHz, even though the BSF was only 26 Hz. Figure 5 shows the spectrum of the square of the envelope, this having been shown in Ref. 18 to give better results than the spectrum of the envelope. This envelope spectrum is typical of a rolling element fault since it is dominated by harmonics of BSF (with the even harmonics more prominent) and with sidebands and low harmonics spaced at the cage frequency (the rate of passage of the fault through the load zone). Where the bearing signal is masked by discrete frequencies (often due to gears), it is possible to remove them before demodulation. This was originally achieved<sup>18</sup> by self-adaptive noise cancellation (SANC), making use of the fact that the random slip in the bearing signals makes their correlation length short in comparison with the deterministic gear signals. A later development called discrete/random separation (DRS), described in Ref. 19, achieves the same thing but much more efficiently since both the generation of the separation filter and its application by fast convolution are achieved using FFT methods. Figure 6 shows how DRS has been used to separate a faulty bearing signal from a normal gear vibration signal by which it was completely masked.

Occasionally, gear and bearing signals are combined multiplicatively rather than additively (when gear-mesh signals are modulated by the faulty bearing



**Figure 5** Spectrum of the squared envelope signal obtained by demodulating the signal in the band between 15 and 20 kHz. The dotted line at the base shows the envelope spectrum with no bearing fault.



**Figure 6** Separation of (additive) gear and bearing signals using DRS: (a) combined signal, (b) deterministic part (gear signal), and (c) stochastic (cyclostationary) part (bearing signal).

signal). The gear signal and first-order cyclostationary (periodic) part of the bearing signal can first be removed using DRS, after which the second-order cyclostationary part can reveal bearing faults and distinguish them from gear faults even though at the gear rotational frequency.<sup>17</sup> A second-order cyclostationary component at shaft speed, for example, would indicate a bearing inner race fault, at the same time separating this random component from stationary random noise.

## 2.5 Reciprocating Machines

Reciprocating machines, such as diesel engines and reciprocating compressors, also produce vibrations with both periodic and cyclostationary components. The latter are, for example, associated with combustion, which occurs every basic cycle, but not identically each time. Signals from reciprocating machines have a different character from those of simple rotating machines, as they consist of a series of impulsive events (combustion, piston slap, valves opening and closing, etc.), and so the most effective analysis techniques must take into account variations in both frequency and time (or crank angle). It is thus common

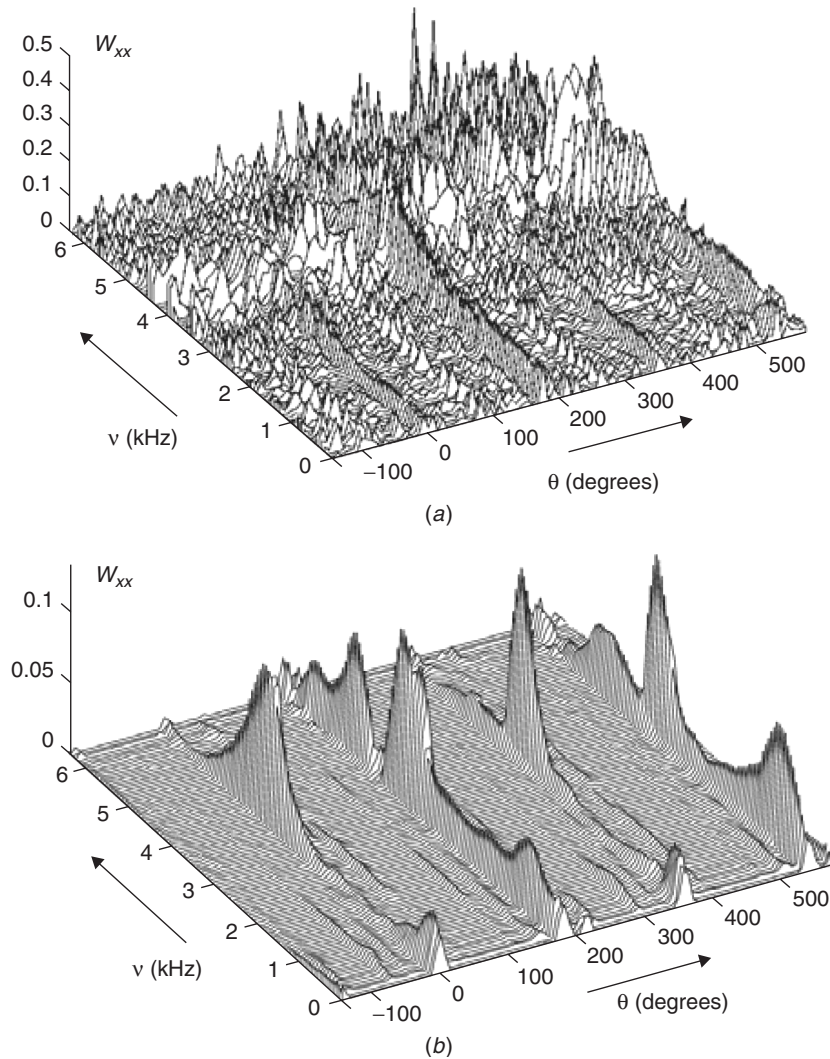
to use some form of time–frequency analysis to analyze the signals of reciprocating machines. This can be as simple as an STFT (short-time Fourier transform) analysis, where a window is moved along the record in overlapping steps and the spectrum determined for each window position. The result will be found to be more repeatable if the STFT diagram is averaged over several cycles (power spectrum average making it insensitive to phase variations). However, the STFT suffers from limitations in resolution given by the Heisenberg uncertainty principle, where the product of frequency and time resolutions is a constant. Obtaining a better time resolution (by a shorter window) gives a poorer frequency resolution and vice versa. The Wigner–Ville distribution (WVD) appears to give better simultaneous time–frequency resolution but suffers from nonphysical interference terms that are difficult to distinguish from the physically meaningful components. A range of smoothed versions have been developed<sup>20</sup> to reduce the interference while still retaining better simultaneous resolution, but these are all very onerous computationally. A relatively new development, which is very promising for internal combustion (IC) engine diagnostics, makes use

of the Wigner–Ville (or instantaneous) spectrum, an ensemble-averaged version of the WVD, which is ideal for second-order cyclostationary signals.

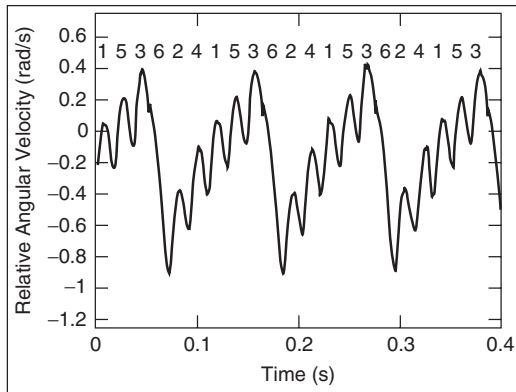
If the periodic part of the signal is first removed (e.g., by DRS), the interference terms in each realization of the WVD come with random phase and are canceled by averaging, leaving a time–frequency diagram with excellent resolution. Figure 7 compares the Wigner–Ville spectrum with the WVD for a typical diesel engine cycle.

Another diagnostic technique that has received some attention in the literature is the recovery of cylinder pressure signals from external measurements, of head/block acceleration, and/or crankshaft torsional vibration,<sup>22–24</sup> but generally applicable results have still not been achieved.

However, crankshaft torsional vibration, obtained by frequency demodulation of a shaft encoder signal, is a simple and very powerful tool for detecting misfires on an individual cylinder.<sup>25</sup> Figure 8 shows an example from a six-cylinder spark ignition engine, where there was no spark on one cylinder. The shaft encoder signal used was from a proximity probe detecting the passage of teeth on the ring gear. The first harmonic of the tooth passage frequency was first phase demodulated by Hilbert transform techniques, and the phase signal differentiated to frequency (angular velocity) by multiplying by  $j\omega$  in the frequency domain. Performing the differentiation this way allows a simultaneous bandpass filtration, the lower limiting frequency being just less than the basic cycle frequency, and the upper limiting frequency



**Figure 7** (a) WVD over one cycle of a diesel engine and (b) WVS averaged over 120 cycles. (From Ref.21.)



**Figure 8** Angular velocity (instantaneous crankshaft speed) for a spark ignition engine with a misfire on cylinder 6.

chosen to avoid amplifying high-frequency noise. The torsional vibration can alternatively be determined by using a high-frequency clock (e.g., 20 MHz) to time the intervals between the pulses, and this has the advantage that the same number of samples is obtained per cycle, independent of the speed. For some very localized faults it may be an advantage to further differentiate the signal to angular acceleration.

### 3 VIBRATION MONITORING SYSTEMS

The type of vibration monitoring system to be employed depends on the criticality of the machine being monitored and the economic driving factors. There is a basic division between permanent monitoring with fixed transducers and intermittent monitoring with portable equipment and offline analysis. The major economic benefits of condition monitoring usually come from predicting incipient faults well in advance, allowing repairs to be planned, spare parts to be acquired, and in particular avoiding losses in production, this often being a much more important economic factor than the damage to an individual machine.

Since an advance warning of several months is often required to minimize production loss, and it is now often possible using signal processing techniques to obtain this much lead time, intermittent monitoring is usually the most economical approach for the vast majority of machines. This is typically done using data collectors into which "route maps" can be downloaded, describing the measurement points on all machines to be monitored in a single excursion into the plant. Reference spectra and other data pertaining to each point can be downloaded at the same time as the route map, and standard analysis procedures can be implemented semiautomatically, such as spectrum comparisons and specific diagnostic procedures once a fault has been detected. Simple procedures can be done directly in the field, but data is usually stored and transferred back to a central computer,

allowing more detailed analysis to be done later if required. Monitoring intervals are typically weekly to monthly, depending on the anticipated leadtime and the criticality of the machine.

A small number of very critical machines often have permanently mounted transducers that can detect sudden changes in condition and initiate shutdown. Even though this automatically gives some loss in production, this may be minimal compared with what would result from an undetected catastrophic failure of the machine. Permanent monitoring is often performed with proximity probes, possibly supplemented with accelerometers, and is usually based on measuring simple parameters that allow rapid shutdown. Of course, if permanently mounted accelerometers are in place, detailed analysis can also be done, and would often be done at intervals of one day or so, giving more security than intermittent measurements at weekly or monthly intervals, and maximizing the lead-time after detection of change.

Whether for permanent or intermittent monitoring, accelerometers should typically be mounted on the bearings, where the dynamic loads are transmitted from internal rotating components to the casing. It is often sufficient to measure in one radial direction (vertical or horizontal) on radial bearings, and in the axial direction at thrust bearings, typically only at one end of a machine. The mounting point should be the same each time, usually by having a permanent mounting stud, and should be sufficiently rigid to give a repeatable frequency range up to at least 10 kHz. For intermittent monitoring, magnet mounting can be used if sufficiently rigid to give the required frequency range (e.g., rare-earth magnets) and if mounting points are sufficiently well defined (e.g., permanent magnet mounting pads).

### 4 FAULT DETECTION AND TREND ANALYSIS

As mentioned above, the use of accelerometers, possibly with integration to velocity, allows the measurement of signals with a frequency range of more than three decades, for example, 5 Hz to 5 kHz or 20 Hz to 20 kHz, with very good dynamic range, and such a range can be necessary to detect the full range of possible faults. These can extend down to 40% of shaft speed (e.g., oil whirl) up to the 400th harmonic of shaft speed (e.g., harmonics of gear-mesh and blade-pass frequencies). Rolling element bearings often have fault indications at frequencies of the order of 1000 or more times the shaft speed. Criteria exist for vibration severity, such as the International Organization for Standardization (ISO) Standard 2372 (developed from the German recommendation VDI-2056), and the so-called General Machinery Criterion Chart,<sup>26</sup> which was developed from the earlier Rathbone and Yates charts. These all represent equal velocity criteria, for a wide range of machine sizes and speeds, and can be expressed in terms of root-mean-square (rms) levels covering the frequency range 10 to 1000 Hz (where the only reason for the upper frequency limitation is the fact that much of the data on which they were based was obtained using velocity probes with that

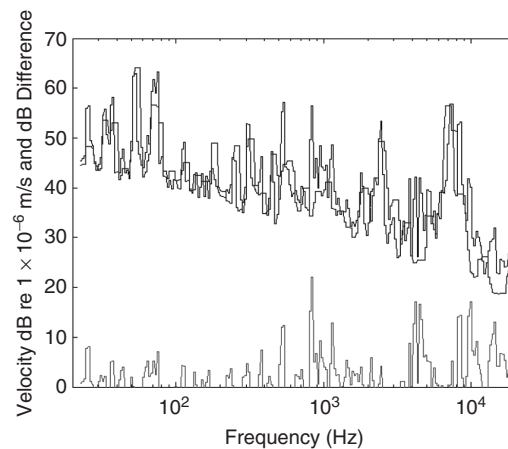


frequency range). Velocity best represents vibration severity because all vibrations represent an alternation between potential energy proportional to the square of strain and kinetic energy proportional to the square of velocity. Since design stress is largely independent of size and speed, vibration velocity tends to be fairly uniform over a range of machines and over a wide frequency range. However, an accelerometer with electronic integrator is the best velocity transducer, as it gives a much wider frequency and dynamic range in velocity than a direct velocity probe.

Even though the two standards mentioned above have different criteria for different machines, both are in agreement that equal changes in severity are represented by equal changes on a log amplitude scale and that a change of 20 dB (amplitude ratio 10:1) is serious. It can also be inferred that a change of 6 to 8 dB (ratio 2 to 2.5) is significant. Rather than using absolute criteria, a strong argument can be made for detecting faults based on the change from the normal levels at each measurement point, with 6 and 20 dB representing significant and serious changes, respectively. The use of velocity means that there is a better chance than otherwise that changes at any frequency will affect the rms levels, but it is still evident that monitoring of frequency spectra, rather than overall levels, will have a better chance of detecting changes at whatever frequency they should occur.

To compare digitized frequency spectra, it is common to make some kind of smeared "envelope" of the reference spectrum, to avoid problems with small speed changes, and the large changes in sample values along the steep flanks of discrete frequency peaks. A simple and very efficient way of doing this is to use constant percentage bandwidth (CPB) spectra, rather than FFT spectra, since their resolution is uniform on a logarithmic axis, and small speed changes can be compensated by a lateral shift. At the same time a CPB spectrum can cover a wide frequency range with a relatively small number of spectrum values. Figure 9 shows the application of this technique to signals from an auxiliary gearbox on a gas-turbine-driven oil pump.<sup>27</sup> It shows the comparison of a 4% bandwidth spectrum (180 values over three decades in frequency) with a mask formed from the original reference spectrum, and the resulting spectrum of exceedances. One of these exceeds 20 dB, but had stabilized, and in fact the machine was allowed to run under close supervision for a further 4 months before it was shut down for repair.

The positive spectrum changes detected by this procedure also provide a good way of trending changes in a condition as discussed in Ref. 28. Since equal changes in severity represent equal changes on a logarithmic amplitude axis, it is logical to plot the changes in decibel values, and a linear trend of decibel values would indicate a normal rate of change. If the severity of the fault feeds back on the rate of change of fault development, it might be better to fit an exponential curve to the dB values, to predict the time before they exceed a certain threshold, such as



**Figure 9** (Upper) Comparison of new spectrum with mask, velocity dB re  $1 \times 10^{-6}$  m/s and (lower) decibel difference spectrum.

20-dB change. It can be checked whether a linear or exponential trend gives the best fit to the data. It can be misleading to fit other curves, such as polynomials, to the data, as they are dangerous to use for extrapolation. The best prognostic methods use a failure model for the particular type of failure that has been diagnosed and fit the measured data to that model. This is advisable for cases such as rolling element bearings, where the symptoms may change in discrete steps as piecewise spalls develop (undetected below-surface cracking).

## REFERENCES

1. D. L. Dewell, and L. D. Mitchell, Detection of a Misaligned Disk Coupling Using Spectrum Analysis, ASME DET Conference, Mechanical Signature Analysis, Dearborn, MI, September, 1983, pp. 19–28.
2. J. Guillon, and A. Jaudet, The EDF Turbine Generator Fault Logging and Monitoring System, *Proc. EPRI 1982 Conference and Workshop*, Hartford, CT, August 25–27, 1982, pp. 2-66–2-87.
3. D. W. Perratt, Development of Condition Monitoring Equipment for C.E.G.B. Generating Plant, *Proc. EPRI 1982 Conference and Workshop*, Hartford, CT, August 25–27, 1982, pp. 2-88–2-102.
4. J. S. Sohre, Turbomachinery Problems: Causes and Cures, *Hydrocarbon Processing*, December, 1977, pp. 77–84.
5. Orbit, available on website <http://www.bently.com/search/orbitarchives.asp>.
6. J. H. Maxwell, Induction Motor Magnetic Vibration, *Proc. Vibration Institute*, Meeting, Houston, TX, April 19–21, 1983.
7. R. B. Randall, A New Method of Modeling Gear Faults, *ASME J. Mech. Design*, Vol. 104, 1982, pp. 259–267.
8. McFadden, PD (1987), A Revised Model for the Extraction of Periodic Waveforms by Time Domain Averaging, *Mech. Syst. & Signal Process.*, Vol. 1, No. 1, pp. 83–95.

9. R. Potter, and M. Gribler, Computed Order Tracking Obsoletes Older Methods, *SAE Paper 891131*, Society of Automotive Engineers, Warrendale, PA, 1989.
10. P. D. McFadden, Window Functions for the Calculation of the Time Domain Averages of the Vibration of the Individual Planet Gears and Sun Gear in an Epicyclic Gearbox, *ASME J. Vib. Acoust.*, Vol. 116, 1994, pp. 179–187.
11. W. Wang and A. K. Wong, Autoregressive Model-Based Gear Fault Diagnosis, *ASME J. Vib. and Acoust.*, Vol. 124, April, 2002, pp. 172–179.
12. P. D. McFadden, *ASME J. Vib., Acoust., Str., Rel. Des.*, Vol. 108, No. 2, 1986, pp. 165–170.
13. H. Endo, R. B. Randall, and C. Gosselin, Differential Diagnosis of Spalls vs Cracks in the Gear Tooth Fillet Region, *J. Failure Analysis Prevention*, Vol. 4, No. 5, 2004, pp. 57–65.
14. R. B. Randall, Cepstrum Analysis and Gearbox Fault Diagnosis, *Maintenance Management Int.*, Vol. 3, 1982–1983, pp. 183–208.
15. M. El Badaoui, J. Antoni, F. Guillet, and J. Daniere, Use of the Moving Cepstrum Integral to Detect and Localise Tooth Spalls in Gears, *Mech. Syst. Signal Process.*, Vol. 15, No. 5, 2001, pp. 873–885.
16. P. D. McFadden and J. D. Smith, Model for the Vibration Produced by a Single Point Defect in a Rolling Element Bearing, *J. Sound Vib.*, Vol. 96, No. 1, 1984, pp. 69–82.
17. J. Antoni and R. B. Randall, Differential Diagnosis of Gear and Bearing Faults, *ASME J. Vib. Acoust.*, Vol. 124, April, 2002, pp. 165–171.
18. D. Ho and R. B. Randall, Optimisation of Bearing Diagnostic Techniques Using Simulated and Actual Bearing Fault Signals *Mech. Syst. Signal Process.*, Vol. 14, No. 5, September, 2000, pp. 763–788.
19. J. Antoni and R. B. Randall, Unsupervised Noise Cancellation for Vibration Systems: Part II—A Novel Frequency Domain Algorithm, *Mech. Syst. Signal Process.*, Vol. 18, No. 1, 2004, pp. 103–118.
20. L. Cohen, *Time-Frequency Analysis*, Prentice-Hall, Englewood Cliffs, NJ, 1995.
21. J. Antoni, On the Benefits of the Wigner-Ville Spectrum for Analysing Certain Types of Vibration Signals, *Wespac 8 Conference*, Melbourne, 2003.
22. R. B. Randall, Y. Ren, and H. Ngu, Diesel Engine Cylinder Pressure Recovery, *Proc. 21st ISMA*, KU Leuven, Belgium, 1996, pp. 847–856.
23. F. Gu, P. J. Jacob, and A. D. Ball, A RBF Neural Network Model for Cylinder Pressure Reconstruction in Internal Combustion Engines, *Colloquium on Modelling and Signal Processing for Fault Diagnosis*, University of Leicester, December, 1996.
24. G. Zurita Villaroel, and A. Ågren, A New Approach to Diagnostics of the Combustion Process in Diesel Engines Using Vibration Measurements, Part 1: Reconstruction of Cylinder Pressure from Vibration Measurements, *Int. J. Acoust. Vib.*, Vol. 8, No. 2, 2003, pp. 68–76.
25. R. B. Randall, Diagnostics of IC Engines from Torsional Vibration Measurements, *Canadian Machinery Vibration Association Annual Conference*, Edmonton, Canada, August, 2001.
26. J. S. Mitchell, *Machinery Analysis and Monitoring*, PennWell, Tulsa, OK, 1981.
27. P. Bradshaw and R. B. Randall, Early Fault Detection and Diagnosis on the Trans Alaska Pipeline, *MSA Session, ASME Conf.*, Dearborn, 1983, pp. 7–17.
28. R. B. Randall, Computer Aided Vibration Spectrum Trend Analysis for Condition Monitoring, *Maintenance Manage. Int.*, Vol. 5, 1985, pp. 161–167.

# CHAPTER 49

## WAVELET ANALYSIS OF VIBRATION SIGNALS

David E. Newland  
Engineering Department  
Cambridge University  
Cambridge, United Kingdom

### 1 INTRODUCTION

A wavelet is a short wave. Wavelet analysis is concerned with the decomposition of the time histories of signals into short waves. Any waveform may be used for the decomposition provided that it is localized at a particular time (or position). For convenience in this chapter, time is taken to be the independent variable, so that localization results in concentration at a particular time, although any physical variable can be used. Wavelet analysis provides a valuable method of generating time–frequency (scale) maps of vibration signals. These allow the changing character of nonstationary vibration signals to be studied. Wavelets are becoming increasingly used in the analysis and solution of noise and vibration problems and in practical health monitoring of machinery.

### 2 WAVELET TRANSFORMS

#### 2.1 Wavelet Coefficients

If  $w(t)$  is the function of time  $t$  that describes a wavelet, and  $x(t)$  is the signal being studied, then the wavelet coefficient  $a_w(t)$  is defined by the correlation equation

$$a_w(t) = \int_{-\infty}^{\infty} x(\theta)w(t - \theta) d\theta \quad (1)$$

In effect  $a_w(t)$  is a correlation function. It provides information about the structure of  $x(t)$  and how it correlates with the shape of a wavelet  $w(t)$  positioned at time  $t$ . When  $x(t)$  correlates with  $w(t)$ , then  $a_w(t)$  will be large; when they do not correlate,  $a_w(t)$  will be small. Of course, more information is obtained if the correlation process is repeated with a different wavelet function,  $w_1(t)$ . Later in this chapter, the symbol  $x$  is used for the independent variable, instead of  $t$ , according to the usual notation of wavelet analysis.

#### 2.2 Properties of Wavelets

Wavelets are essentially local functions so that  $w(t) \rightarrow 0$  when  $|t| \rightarrow \infty$ . Therefore, in practical terms, the integral in (1) needs to extend over only a limited range of  $\theta$ , and  $a_w(t)$  gives information about  $x(\theta)$  in the vicinity of  $x(\theta = t)$ .

That is how wavelet analysis differs from Fourier analysis. Fourier transforms are calculated by the same equation (1) when the wavelet function  $w(t)$  is replaced by a harmonic function. In that sense, Fourier analysis may be thought of as an extreme case of wavelet analysis. In Fourier analysis, the requirement

that the wavelet should be a local function is ignored, and it is replaced by a wave that goes on forever.

Much of the theory of wavelet analysis is about *self-similar wavelets* (which are wavelets of the same shape but different length scales) spaced at discrete intervals along the time axis. It turns out that, just as a periodic signal may be represented by the (infinite) sum of its harmonics in Fourier analysis, so a transient signal may be represented by the (infinite) sum of the (weighted) amplitudes of its component wavelets. The component wavelets all belong to a doubly infinite set of self-similar wavelets: Each different wavelet is different both in scale and in position on the time axis.

#### 2.3 Comparison with the Short-Time Fourier Transform

Because Fourier coefficients are obtained by averaging over the full length of a signal, Fourier analysis provides no information about how frequency composition may be changing with time. To obtain *local* frequency data, a record must be divided into sections and each segment analyzed separately. The short-time Fourier transform (STFT) does this and is essential if the changing frequency composition of a transient signal is to be examined. Frequency coefficients computed by the STFT depend on the length and time (or position) of the short record that the calculation process assumes is one period of a periodic signal. Results computed by the STFT depend on how a record is subdivided, and making a good choice may be crucial. But the difficulty remains that infinitely long harmonic functions are being used to decompose a transient signal. It is usually better to employ a set of short functions as the basis for decomposing transient records. Wavelets are such short functions.

#### 2.4 Discrete Wavelet Transforms

The practical embodiment of wavelet transforms, as for the Fourier transform, requires a discrete calculation using sampled values of the continuous record  $x(t)$ . Just as the continuous Fourier transform is replaced by the discrete Fourier transform, so the continuous wavelet transform is replaced by the discrete wavelet transform.

If  $X(j)$ ,  $j = 1$  to  $N$ , are sampled values of the record  $x(t)$ , and  $A(k)$ ,  $k = 1$  to  $N$ , are sampled values of its wavelet transform (which are arranged in a logical order that takes account of the scale and position of the wavelet), then

$$A = WX \quad (2)$$



where  $W$  is an  $N \times N$  square matrix whose elements are determined by the chosen wavelet. Unless  $W$  is singular, the  $X$  numbers can always be regained from the  $A$  numbers, but, if  $W$  is an orthogonal matrix, it is not necessary to compute the inverse of  $W$  since  $W^{-1} = W^T$ , the transpose of  $W$ .

## 2.5 Orthogonal Wavelet Transforms

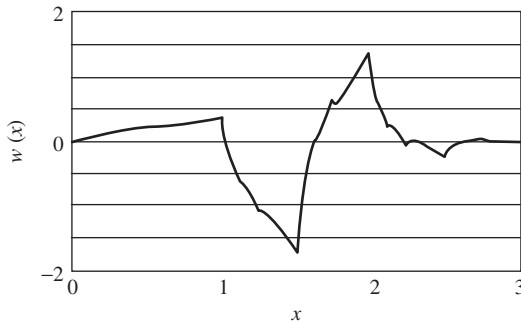
When reconstruction is needed, orthogonality of  $W$  is extremely important, so, for applications involving signal processing in which reconstruction is necessary, there has been tremendous interest in developing the theory of orthogonal wavelets. Even for orthogonal wavelets, efficient numerical algorithms are essential because numerical efficiency is extremely important. Any wavelet decomposition algorithm has to be judged against the fast Fourier transform (FFT) of Cooley and Tukey,<sup>1</sup> which for an  $N$  point sequence requires of the order  $N \log_2 N$  multiplications instead of  $N^2$  multiplications. Therefore, attention has focused on orthogonal wavelets with fast numerical algorithms.

## 3 DILATION WAVELETS

The first orthogonal wavelets to be developed for practical numerical computation, called dilation wavelets, arose from the pioneering work of Daubechies.<sup>2-5</sup> They depend on the theory of dilation equations, which form a special class of difference equation. There is an efficient numerical algorithm due to Mallat<sup>6</sup> for computing dilation wavelet transforms, and there are now various software toolboxes that implement his discrete dilation wavelet transform and its inverse. Dilation wavelets are compact in the time domain, which means that each wavelet has a definite beginning and a definite ending, and they are zero outside these limits. In the frequency domain they are not so restricted and necessarily cover an infinite frequency range, although being concentrated about a center frequency. A typical dilation wavelet is shown in Fig. 1. It begins at  $x = 0$  and finishes at  $x = 3$ .

### 3.1 Dilation Equations

With few exceptions, dilation wavelets cannot be expressed in functional form. Instead they are defined



**Figure 1** Dilation wavelet with four coefficients, derived from the scaling function in Fig. 2. (From Ref. 7.)

by a dilation equation that has to be solved by iteration or recursion. There are two steps in the definition. Step 1 defines a scaling function  $s(x)$  by an equation of the form

$$s(x) = c_0 s(2x) + c_1 s(2x - 1) + c_2 s(2x - 2) + c_3 s(2x - 3) \quad (3)$$

where the  $c$ 's are numerical (real) constants that may be either positive or negative. The wavelet  $w(x)$ , which corresponds to this scaling function, is defined by the corresponding equation

$$w(x) = -c_3 s(2x) + c_2 s(2x - 1) - c_1 s(2x - 2) + c_0 s(2x - 3) \quad (4)$$

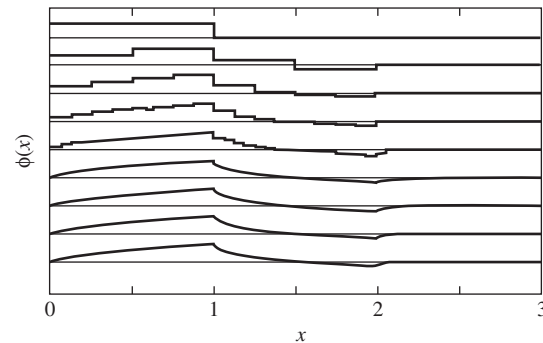
The same coefficients are used, but in reverse order and with alternate terms having their signs reversed. These equations contain four coefficients, and they may be extended following the same pattern to include any even number of coefficients.

Apart from a few simple cases, Eq. (3) cannot be solved directly to find the scaling function  $s(x)$ . Instead a solution is found by iteration. Each new approximation  $s_j(x)$  is computed from the previous approximation  $s_{j-1}(x)$  by the iterative scheme

$$s_j(x) = c_0 s_{j-1}(2x) + c_1 s_{j-1}(2x - 1) + c_2 s_{j-1}(2x - 2) + c_3 s_{j-1}(2x - 3) \quad (5)$$

with the process being continued until  $s_j(x)$  becomes indistinguishable from  $s_{j-1}(x)$ .

Figure 2 shows progressive stages in the generation of  $s(x)$  according to Eq. (5). The process begins by taking the starting function  $s_0(x)$  to be a box of length unity. This develops progressively into the shape that occupies the interval  $0 \leq x < 3$ . It has been computed for particular values of the coefficients  $c_0 = 0.6830$ ,  $c_1 = 1.1830$ ,  $c_2 = 0.3170$ , and  $c_3 = -0.1830$ ,



**Figure 2** Progressive stages in the generation of a dilation wavelet's scaling function, with four coefficients. (From Ref. 7.)

which have been chosen to ensure orthogonality and good convergence properties. Having found  $s(x)$ , the corresponding wavelet can be computed directly from Eq. (4), which leads to the shape shown in Fig. 1.

### 3.2 Mallat's Tree Algorithm

The iteration process represented in Eq. (5) can be carried out by a process of progressive multiplication. This was first implemented efficiently by Mallat<sup>6</sup> in his tree algorithm. The full theory is mathematically complicated (for a summary see Refs. 7 and 16), but the concept of its operation can be described as follows.

Suppose that a vibration record of finite length has been sampled at equally spaced intervals to generate the input sequence  $X(j)$ ,  $j = 1$  to  $N$ , where  $N = 2^n$ . Its dilation wavelet transform is computed by progressively filtering this sequence with two digital filters. At each stage of filtering, the sequence length is reduced by half. A low-pass filter generates the half-length sequence  $Y(k)$ ,  $k = 1$  to  $N/2$ , and a high-pass filter generates the half-length sequence  $Z(r)$ ,  $r = 1$  to  $N/2$ , according to the formulas

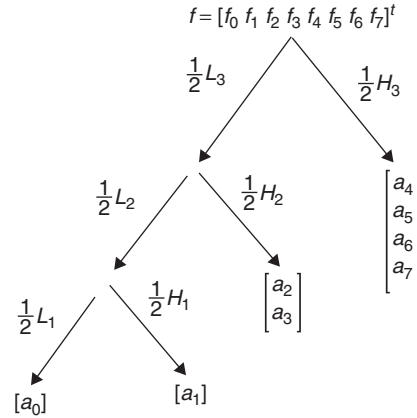
$$\begin{aligned} Y(N/2) &= L(N/2, N)X(N) \quad \text{and} \quad Z(N/2) \\ &= H(N/2, N)X(N) \end{aligned} \quad (6)$$

where the orders of the matrices are as shown. The low-pass filter is represented by the matrix  $L(N/2, N)$  and the high-pass filter by  $H(N/2, N)$ . This process is repeated with the  $Y$  vector (but not with the  $Z$  vector). The  $Z(N/2)$  vector from Eq. (6) is retained. The  $Y(N/2)$  vector is filtered by  $L(N/2, N/4)$  and  $H(N/2, N/4)$ . After the second set of matrix multiplications, a second  $Z(N/4)$  vector of length  $N/4$  is kept, while the new  $Y(N/4)$  vector is again subjected to a further decomposition. Eventually, the decomposition has continued until the orders of the final vectors are only one term each, and the transformation is complete.

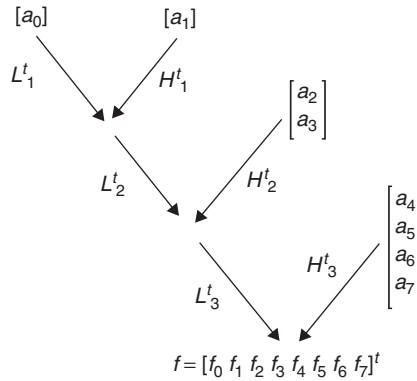
The repeated matrix multiplication process defined by this process is a discrete computation of the correlation integral (1) where the wavelet function  $w(t)$  is a dilation wavelet defined by the relevant coefficients  $c_0, c_1, c_2$ , and so on. This is because each step in the iteration process defined by the dilation equation (5) is represented by a matrix multiplication by  $L$ . Since the matrices operate on a column vector  $X$  whose elements are the sampled values of  $x(t)$  in (1), Mallat's tree algorithm gives a discrete approximation for the continuous integral in (1). This process is illustrated in Fig. 3 and the reverse transformation in Fig. 4.

### 4 MALVAR WAVELETS

A feature of the shape of the dilation wavelet in Fig. 1 is its irregular profile. Although dilation wavelets with more coefficients have a smoother shape, they do not have the familiar form of a smoothly windowed harmonic function. The use of windowed



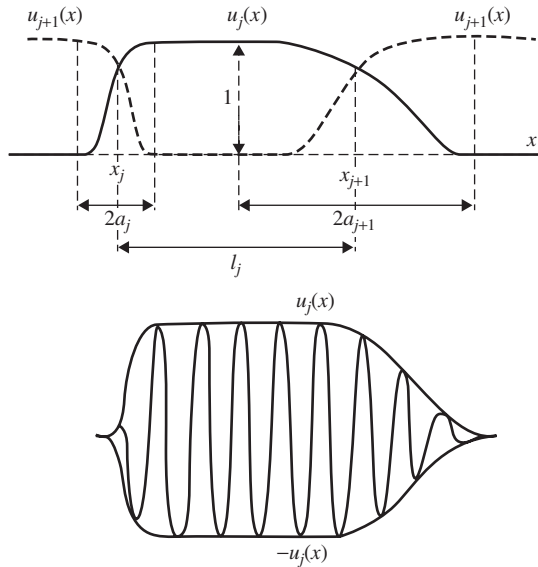
**Figure 3** Calculation of the dilation wavelet transform of an eight-term input sequence using  $N = 4$  wavelet coefficients. (After Mallat.<sup>6</sup>)



**Figure 4** Reverse calculation to find the inverse dilation wavelet transform of an eight-term sequence, using  $N = 4$  wavelet coefficients. (After Mallat.<sup>6</sup>)

harmonic wavelets has been developed by Malvar<sup>8</sup> and allows an arbitrarily chosen segment of a signal to be decomposed into a set of windowed harmonic functions. For each segment, the set of basis functions is exclusively either windowed cosine functions or windowed sine functions (Fig. 5).

For the frequency analysis of a measured signal this presents a problem. If there is a frequency component that is  $90^\circ$  out-of-phase with respect to Malvar's basis function at a given frequency, then the corresponding coefficient calculated by Eq. (1) will be very small. Without windowing, it would be zero. For example, if the basis functions are cosines, then a sine component at the frequency of one of the basis cosines will give an almost zero coefficient. Using the concept of *phase* from Fourier analysis, Malvar wavelets do not discriminate phase. For vibration analysis, this inability to represent phase is a disadvantage.



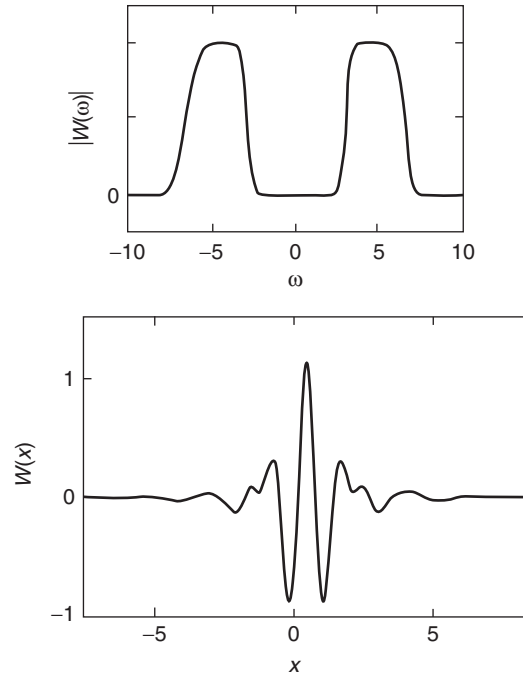
**Figure 5** Malvar wavelet. (From Malvar<sup>8</sup>; this diagram after Meyer,<sup>9</sup> Chapter 6.)

Another disadvantage is that the width of the window function,  $l_j = \alpha_j - \alpha_{j+1}$  in Fig. 5, is the same for all frequency components. Therefore, localization is much less precise at high frequencies than it is at low frequencies. If we want to know within a few cycles where a particular frequency component occurs, the segmentation of a signal into finite lengths that are independent of frequency is not helpful. The STFT suffers from the same drawback. As for dilation wavelets, Malvar wavelets are compact in the time domain and infinite in the frequency domain.

## 5 MEYER WAVELETS

In Chapter 6 of his book, Meyer<sup>9</sup> shows how he and Lemarié constructed an orthogonal set of time-scale wavelets by developing properties of Malvar's time-frequency wavelets. As Meyer pointed out, this is quite surprising because the Lemarié-Meyer wavelets constitute a "time-scale" algorithm, whereas the Malvar wavelets are a "time-frequency" algorithm. There is thus an incompatibility.

Instead of devising a wavelet by windowing a harmonic function by a tapered data window, as in Fig. 5, Meyer wavelets are defined in the frequency domain. By defining the wavelet's Fourier transform in a special way, it is possible to generate a complete set of orthogonal real wavelet functions of which an example is shown in Fig. 6. The magnitude of the defining Fourier transform is shown above, and the corresponding wavelet below. Because its Fourier transform is compact in the frequency domain, the wavelet itself extends over all time. Therefore Meyer's wavelets are less localized than dilation wavelets and



**Figure 6** Typical Meyer wavelet (lower view) with the modulus of its Fourier transform (upper view). (From Daubechies,<sup>5</sup> Chapter 4.)

Malvar wavelets, both of which have compact support in the time domain.

An advantage of Meyer's wavelets is that they can be computed by an algorithm using the FFT and mean Central Processing Unit (CPU) times may be comparable to, if not faster than, implementation of Mallat's pyramid algorithm for dilation wavelets. But for time-frequency analysis, Meyer wavelets have the same disadvantage in respect of phase discrimination as Malvar wavelets. Because all wavelets are self-similar, at each scale and each position, there is only one basis wavelet. This has the characteristic shape of the mother wavelet: it can be moved and it can be stretched or compressed, but its basic shape does not change. To recognize phase, at each level and each position, there have to be two wavelets with a 90° phase difference between them. This feature is provided by harmonic wavelets.

## 6 HARMONIC WAVELETS

Harmonic wavelets have their Fourier transform defined by

$$W_{m,n}(\omega) = 1/(n-m)(2\pi) \text{ for } m(2\pi) \leq \omega < n(2\pi) \\ = 0 \text{ elsewhere} \quad (7)$$

This is identically zero outside the band  $m(2\pi)$  to  $n(2\pi)$ , where  $m$  and  $n$  are real and positive but not

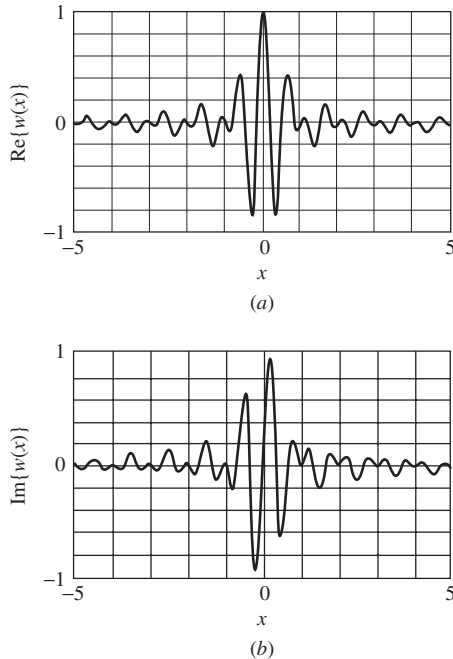
necessarily integer. Inside this band it has constant magnitude, normalized to ensure that the enclosed area is unity. The corresponding wavelet function, obtained by taking the inverse Fourier transform of  $W_{m,n}(\omega)$ , is

$$w_{m,n}(x) = \{\exp(i n 2\pi x) - \exp(im 2\pi x)\} / i 2\pi(n - m)x \quad (8)$$

The subscripts  $m, n$  define the wavelets' frequency scale or "level" in the frequency band  $m(2\pi)$  to  $n(2\pi)$  where  $n > m$ . To form a complete set of wavelets, adjacent wavelet levels must have Fourier transforms whose frequency bands touch each other, so that all values of  $\omega$  along the axis 0 to  $\infty$  are included. Figure 7 shows the real and imaginary parts of  $w(x)$  defined by Eq. (8) for the case when  $m = 1, n = 2$ . For harmonic wavelets, the (complex) wavelet amplitude  $a_{m,n,k}$  is the amplitude of the wavelet at level  $m, n$  and position  $k$ . This means that  $a_{m,n,k}$  is the amplitude of the wavelet at level  $m, n$  translated  $k$  steps at this level, which is  $\Delta x = k/(n - m)$  along the  $x$  axis. Because of orthogonality,  $a_{m,n,k}$  is given by

$$a_{m,n,k} = (n - m) \int_{-\infty}^{\infty} f(x) w_{m,n}^* \left( x - \frac{k}{n - m} \right) dx \quad (9)$$

where  $w^*$  denotes the complex conjugate of  $w$ .<sup>10,11</sup>



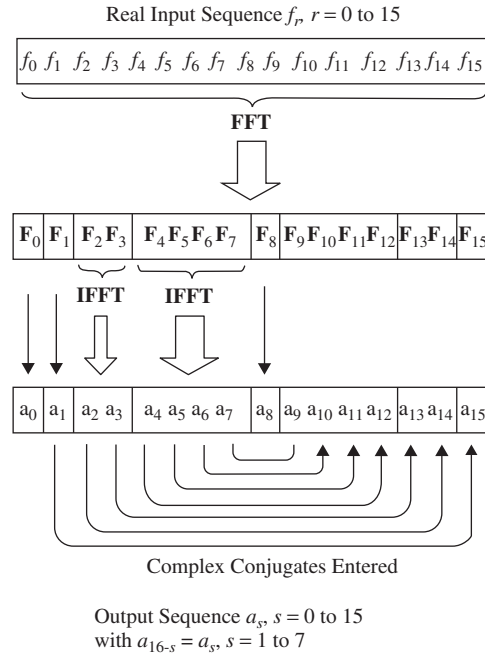
**Figure 7** (a) Real part and (b) imaginary part of the harmonic wavelet defined by (8) for the case when  $m = 1, n = 2$ . (From Newland,<sup>10</sup> Fig. 2.)

A disadvantage of harmonic wavelets is that their rate of decay is low (proportional to  $x^{-1}$ ) so that localization is not very precise. Their advantage is that since each wavelet is complex, with an even real part and an odd imaginary part (see Fig. 7), they can detect a harmonic frequency component whatever its phase. In other words, the ratio of the imaginary and real parts of harmonic wavelet coefficients provides a means of determining a position that interpolates between the locations of discrete wavelets.

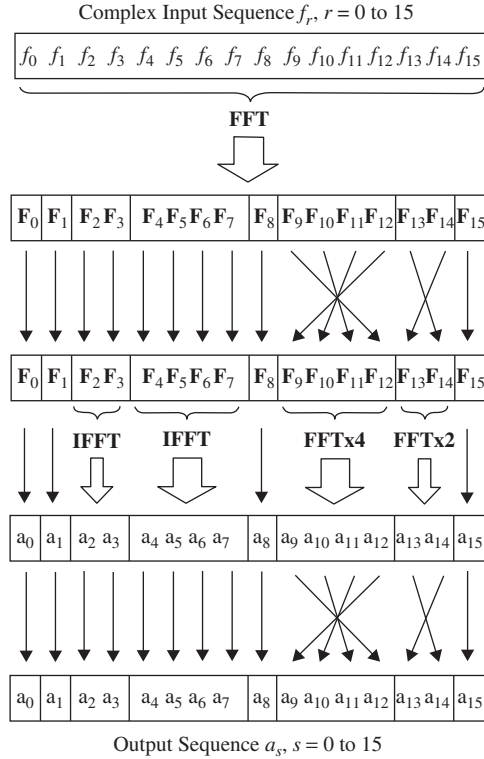
## 7 DISCRETE HARMONIC WAVELET TRANSFORM

It can be shown (see, e.g., Newland,<sup>7</sup> Chapter 17) that an algorithm for the computation of the  $a_{m,n,k}$  coefficients can be devised using two applications of the FFT as illustrated in Figs. 8 and 9. This is drawn for the case when  $n = 2m$  for all wavelet levels (with one exception, see below). The bandwidth of each wavelet level then doubles for each ascending level, so that the frequency scale increases in octaves.

There are two stages to the transform (Fig. 8). At stage 1, the FFT of the complete sequence  $f(r)$ ,  $r = 0$  to 15, is computed to generate the (complex) sequence of Fourier coefficients  $F(k)$ ,  $k = 0$  to 15. At stage 2, the  $F(k)$  are partitioned into octave blocks as shown, and the IFFT of partitioned blocks is computed separately. This generates the (complex) harmonic wavelet coefficients  $a(s)$ ,  $s = 0$  to 15. Symmetry of



**Figure 8** FFT algorithm to compute the harmonic wavelet transform for a real sequence of 16 terms for the case when  $n = 2m$  for all wavelet levels. (From Newland,<sup>10</sup> Fig. 6.)



**Figure 9** FFT algorithm to compute the harmonic wavelet transform for a complex sequence of 16 terms, also for the case when  $n = 2m$  for all wavelet levels. (From Newland,<sup>10</sup> Fig. 7.)

the calculation ensures that  $a(16 - s) = a^*(s), s = 1$  to 7 (the asterisk again denotes complex conjugate).

To prevent vanishingly small bandwidths,  $m$  is not allowed to become less than unity except for a zero-frequency band  $m = 0$  to  $n = 1$ . Thus the sequence of pairs  $(m, n)$  increase as (0,1), (1,2), (2,4), and so forth. The octave sequence is therefore complete except for a zero-frequency band  $0 \leq \omega < 2\pi$ .

A further major advantage of harmonic wavelets is that the speed of their computation is high. For a typical calculation, the discrete harmonic wavelet transform requires less than half the number of flops (floating point operations) of the dilation wavelet transform based on Mallat's algorithm with a dilation wavelet having 20 coefficients.<sup>10</sup> This is important for large calculations that, for vibration calculations, often involve plotting time-frequency maps.

An additional property of the harmonic wavelet transform (HWT) is that it is not necessary to use octave blocks when calculating the IFFTs in Figs. 8 and 9. Instead, any convenient partitioning can be used. Furthermore, to obtain maximum discrimination in a time-frequency map, the blocks of coefficients used for the IFFTs can overlap each other. This oversampling does not generate any new data but

interpolates between data points to achieve a resulting improvement in discrimination. An example is given in Section 10.

## 8 MEAN-SQUARE WAVELET MAPS

For harmonic wavelets, wavelet level defines a finite frequency band; for dilation wavelets, wavelet level is a measure of the center frequency of a localized but infinite band of frequencies. Therefore, wavelet level is interchangeable with frequency for harmonic wavelets and a measure of predominant frequency for dilation wavelets.

The mean-square map depends on the result that the mean-square value can be represented as a summation of the magnitudes of the wavelet coefficients squared. For discrete dilation wavelets, the summation is

$$\frac{1}{2^n} \sum_{r=0}^{2^n-1} x_r^2 = a_0^2 + \sum_{j=0}^{n-1} \frac{1}{2^j} \sum_{k=0}^{2^j-1} a_{2^j+k}^2 \quad (10)$$

while, for harmonic wavelets, it is

$$\frac{1}{2^n} \sum_{r=0}^{2^n-1} x_r^2 = a_0^2 + \sum_{j=0}^{n-2} \frac{1}{2^j} \sum_{k=0}^{2^j-1} \left\{ |a_{2^j+k}|^2 + |a_{2^n-2^j-k}|^2 \right\} + a_{N/2}^2 \quad (11)$$

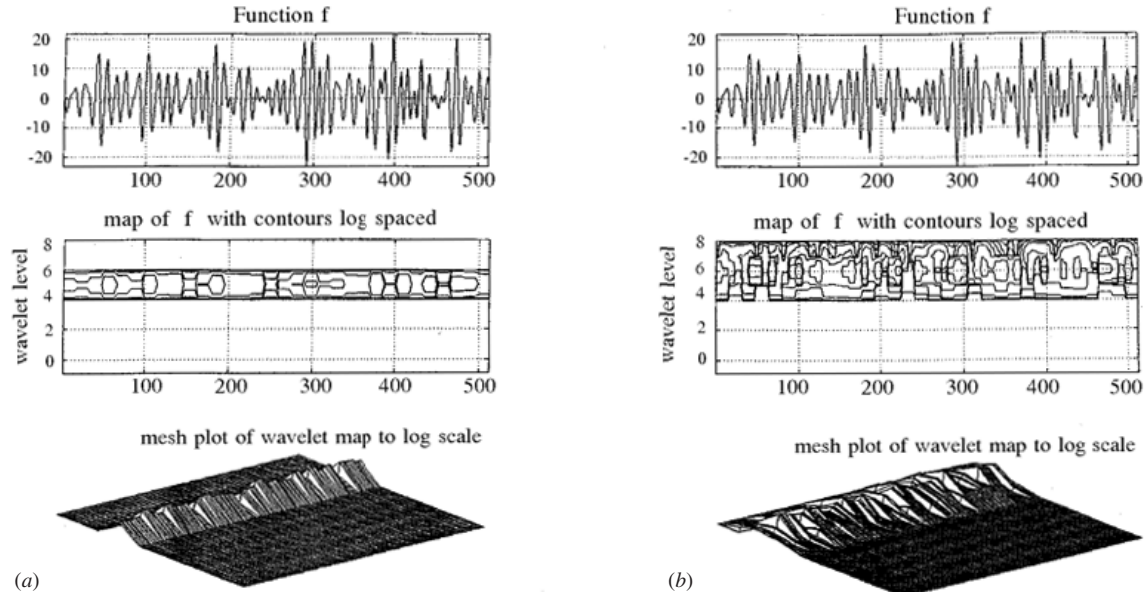
for the corresponding case when the frequency blocks cover octave bands.

If a three-dimensional graph is constructed with the moduli of wavelet amplitudes squared plotted on a base plane whose axes are wavelet level (represented by integer  $j$ ) in one direction and position (represented by integer  $k$ ) in the other (orthogonal) direction, the volume under the resulting surface can be normalized to be a measure of mean square. Where there are significant contributions to a signal's energy at particular frequencies and times, the mean-square surface will have localized peaks. Therefore, a contour plot of the mean-square surface will generate a two-dimensional map that illustrates the distribution of energy (i.e., mean-square value) over frequency and position.

### 8.1 Examples

Two examples are shown in Fig. 10. Wavelet maps of the same length of band-limited signal (shown) are drawn (a) for harmonic wavelets and (b) for dilation wavelets with  $N = 20$  wavelet coefficients. The signal is represented by the discrete function  $x_r, r = 0$  to 511, and the corresponding wavelet maps are shown immediately below this signal. Also, for clarification, mesh diagrams of the underlying shapes are drawn below each map. In the case of the harmonic wavelet map, it can be seen that the energy of the signal is confined to level 5 of the transform only. This is because  $x_r$  has been chosen to have a band-limited spectrum that falls within the frequency band of





**Figure 10** Discrete band-limited signal and its wavelet maps: (a) using harmonic wavelets and (b) using dilation wavelets with 20 coefficients. Mesh diagrams are drawn below each wavelet map. (From Newland.<sup>13</sup>)

level 5 of the harmonic wavelet transform. For dilation wavelets, the frequency spread is wider and is not band limited. Therefore, energy spreads over several levels of the dilation wavelet map as shown in Fig. 10b. The spacing of the contours and the vertical scale of the mesh diagrams in Fig. 10 are logarithmic, so the high peaks are relatively diminished in magnitude, but there is general correspondence between the location in time of the high peaks in  $x_r$  and the high peaks on the wavelet maps.

## 8.2 Applications

The use of mean-square wavelet maps to identify irregularities in otherwise smooth signals is shown in Figs. 11 and 12. The first shows a signal with a periodic local perturbation—almost invisible to the eye—and the corresponding harmonic wavelet map and mesh diagram with logarithmic scales. The identity and location of the peaks are now clearly visible. In Fig. 12, a harmonic signal has a single local higher frequency perturbation. The wavelet map and mesh diagram, again with logarithmic scales, allow this to be identified immediately. The identification of small, local perturbations on otherwise smoothly varying signals is one of the principal applications of wavelet analysis and offers considerable benefits in the field of vibration monitoring.

## 9 CONSTRUCTION OF TIME-FREQUENCY MAPS

### 9.1 Layout of Maps

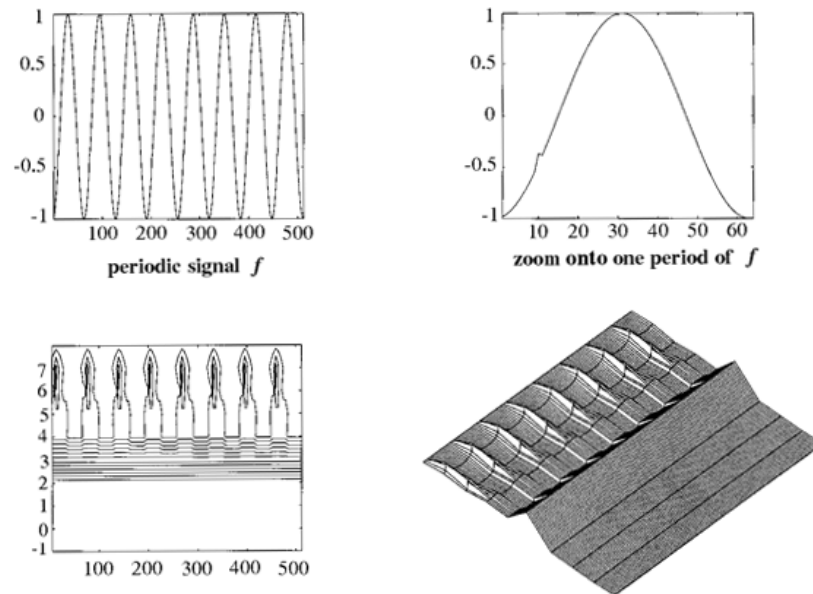
The detailed layout of mean-square maps<sup>12,13</sup> depends on which transform is used to compute the data that is

plotted. There are significant differences between the coordinate framework for HWT maps and STFT maps.

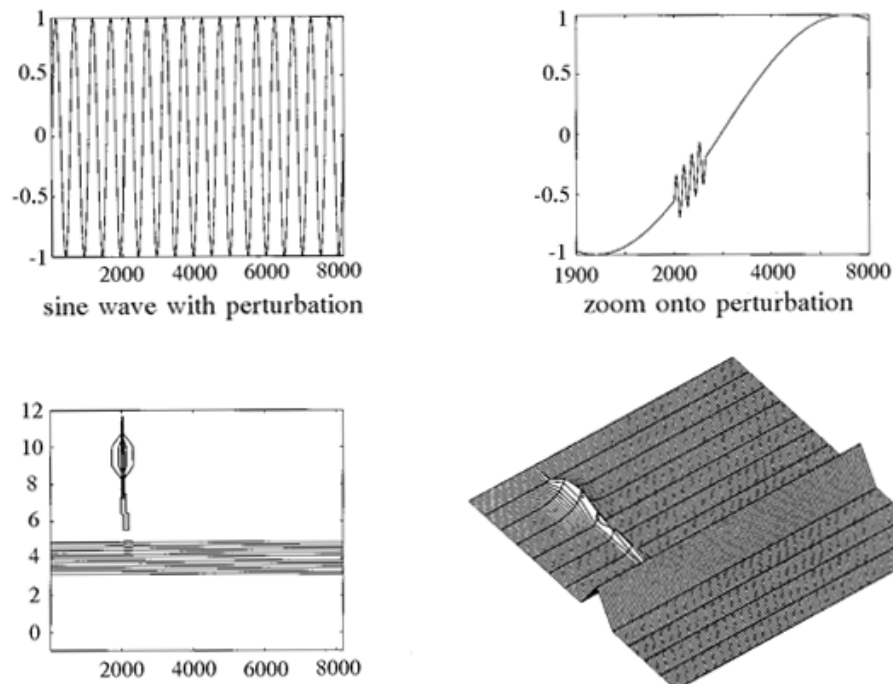
Begin with a (real) time history  $f(t)$  sampled to generate the discrete time series  $f(0)$  to  $f(31)$ . Let its harmonic wavelet representation be given by  $a(0)$  to  $a(31)$  and its short-time Fourier representation by  $b(0)$  to  $b(31)$ . Provided that there has not yet been any windowing to destroy data,  $f$ 's can be perfectly reconstructed from either  $a$ 's or  $b$ 's. The information contained in the input signal  $f(0)$  to  $f(31)$  has just been shifted around to appear in different forms.

Figure 13 shows the grid base for a mean-square map computed by the HWT for an input signal with 32 terms. The grid framework has axes that represent time (or position) horizontally on the page and frequency (or wavenumber) vertically. When drawn in this way, the volume enclosed by a surface through the points plotted is numerically equal to the mean-square value of the input signal. There is a minor proviso. The wavelet coefficient at the Nyquist frequency,  $a(N/2)$  (where for Fig. 13,  $N = 32$ ), has been taken to be zero (which in all practical cases it must be), otherwise the map has to have an additional row.

Similar information is generated by the STFT and may be plotted on a time-frequency map that has similar properties to a mean-square wavelet map. However, the computational process is different. In essence it is the following: Start with an input sequence of 32 (real) terms,  $f(r)$ ,  $r = 0$  to 31. Divide this, for example, into 4 adjoining sequences of 8 terms each,  $f(0)$  to  $f(7)$ ,  $f(8)$  to  $f(15)$ ,  $f(16)$  to  $f(23)$ , and  $f(24)$  to  $f(31)$ . Compute the FFT of each 8-term series and call these  $b(0)$  to  $b(7)$ ,  $b(8)$  to  $b(15)$ ,



**Figure 11** Discrete periodic signal  $f_r$ ,  $r = 0$  to 511, with its harmonic wavelet map and a corresponding mesh diagram of the map. The map contours are spaced logarithmically: Note how this accentuates the influence of the small local perturbations. (From Newland.<sup>13</sup>)



**Figure 12** Discrete periodic signal with a local higher frequency perturbation. The harmonic wavelet map again allows this to be identified clearly. (From Newland.<sup>13</sup>)

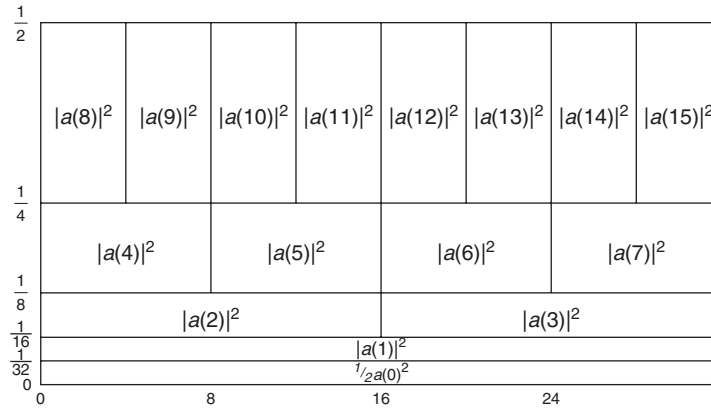


Figure 13 Grid base for plotting a harmonic wavelet map for a 32-term sequence.

$b(16)$  to  $b(23)$ , and  $b(24)$  to  $b(31)$ . Each of these 8-term series covers the full frequency range, with a middle term, for example,  $b(4)$ , being the Nyquist term. Hence  $b(5) = b^*(3)$ ,  $b(6) = b^*(2)$ , and  $b(7) = b^*(1)$  because of the symmetry of the FFT (see, e.g., Newland,<sup>7</sup> Chapter 10). To obtain a time–frequency map, the square of the moduli of the short-time Fourier coefficients are plotted on the grid base shown in Fig. 14. Again because of Parseval’s theorem, the sum of the squares of the Fourier coefficients is equal to the mean square of the input signal. Hence the total volume under a rectilinear surface constructed on the baseboard in Fig. 14, with the ordinates shown, is numerically equal to 4 times the mean-square value of the 32-term series  $f(0)$  to  $f(31)$ . The multiplier 4 arises because there are 4 subseries instead of one long series in the computation.

## 9.2 Lapped Transforms

Just as the  $f$ ’s may be processed in two different ways, they may also be processed more than once by the same basic method. Although this does not generate any new information, it allows the information that is there to be shown more clearly in a visual

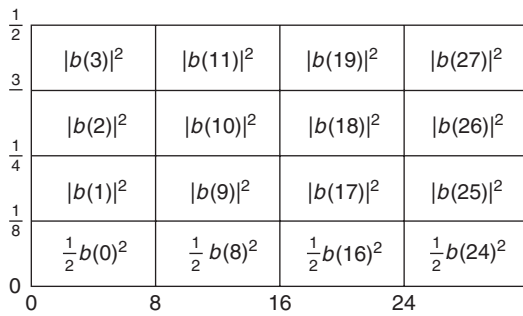


Figure 14 Grid base for plotting a STFT map for a 32-term sequence.

way. For the STFT, the time history is broken into different blocks before computing the discrete Fourier transform of each. By choosing the blocks differently, different Fourier coefficients are computed for the same time series. When these are plotted on one time–frequency plane, more detail is added to the resulting time–frequency map. For the HWT, the frequency series is partitioned into different blocks before their inverse FFTs are computed according to Fig. 8. This again generates more points for the time–frequency surface and so adds discrimination (but not extra accuracy) to the resulting graphical output.

## 9.3 Windowed Transforms

In discrete spectral analysis, it is customary to window the input sequence before computing its FFT. The input data is weighted by a *window function*. The window tapers at its edges, reducing to zero at the two ends of the data. Its purpose is to ensure that the end of the input data can be wrapped around to make a seamless joint with its beginning. This is because the FFT computes the Fourier transform of a periodic signal, one period of which is the length of data being analyzed. To prevent the introduction of spurious Fourier coefficients arising from discontinuities where one period joins the next period, the application of a tapered window ensures that the beginning and end of each period meet smoothly.

Because data is destroyed by the windowing operation, this leads to a reduction in the statistical reliability of the Fourier coefficients in the case of random data. However, it is more important to minimize the introduction of spurious high-frequency Fourier coefficients arising from wrap around, which is inherent in the FFT calculation (see, e.g., Newland,<sup>7</sup> Chapter 11), than to lose some statistical accuracy. The Hanning data widow (see, e.g., Bendat and Piersol<sup>15</sup>) of the form  $[1 - \cos(2\pi t/T)]/2$  where  $T$  is the record length, is one of the simplest windows and is often used for practical calculations.



In the case of the HWT, it is also advantageous to window the blocks of frequency coefficients before their IFFT is computed (see Fig. 8). In this case the reason is different. A typical harmonic wavelet for an octave block of frequency coefficients is shown in Fig. 15. The rate of decay of the wavelet with time is proportional only to  $1/t$ . Decay is slow and localization is poor. When, before the IFFT computation is made, the octave block of frequency coefficients is windowed with a Gaussian function, the modified wavelet is shown in Fig. 16. Its rate of decay away from its center is much improved. Since the harmonic wavelet transform calculates the coefficients of the decomposition of the input signal into a family of harmonic wavelets, better localization on the time–frequency map is achieved if the localization of the wavelets is improved. Therefore, it is desirable to window the blocks of frequency coefficients when computing mean-square harmonic wavelet maps. Since the frequency coefficients are generally complex, windowing in the HWT computation is applied only to the moduli of the complex coefficients.

Windowing destroys the orthogonality of the harmonic wavelet transform. This is a disadvantage when reconstruction is required. However, by overlapping the transform blocks, excessive information is produced,  $N$  pieces of input data producing more than  $N$  pieces of output data. Only some of this data is needed to achieve exact reconstruction of the original signal. Therefore, it is possible to devise an algorithm for computing the windowed HWT of an input signal

that allows perfect reconstruction, provided that the Fourier blocks in Figs. 8 and 9 are overlapped.

## 10 EXAMPLE OF TIME–FREQUENCY ANALYSIS

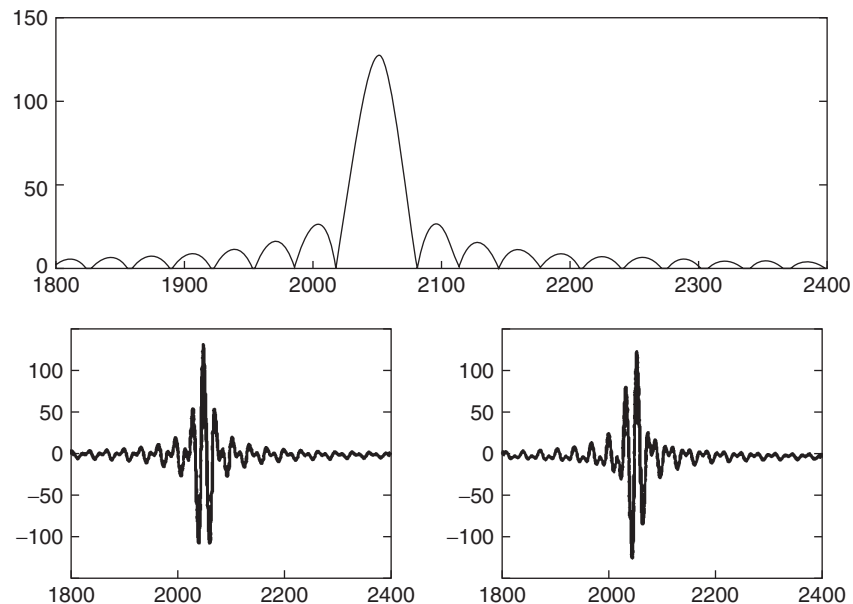
### 10.1 Experimental Data

In the following example calculations, experimental data is used.<sup>14</sup> This is the response of a long, thin steel beam when subjected to a transverse impulsive impact. The beam's transverse acceleration response close to the point of impact is shown in Fig. 17. This is in the form of a 1024-term series. The data sampling frequency was 4096 Hz. By using a soft-tipped impulse hammer, it was possible to ensure that significant aliasing did not occur as frequencies approaching the Nyquist frequency of 2048 Hz had been practically eliminated in the response.

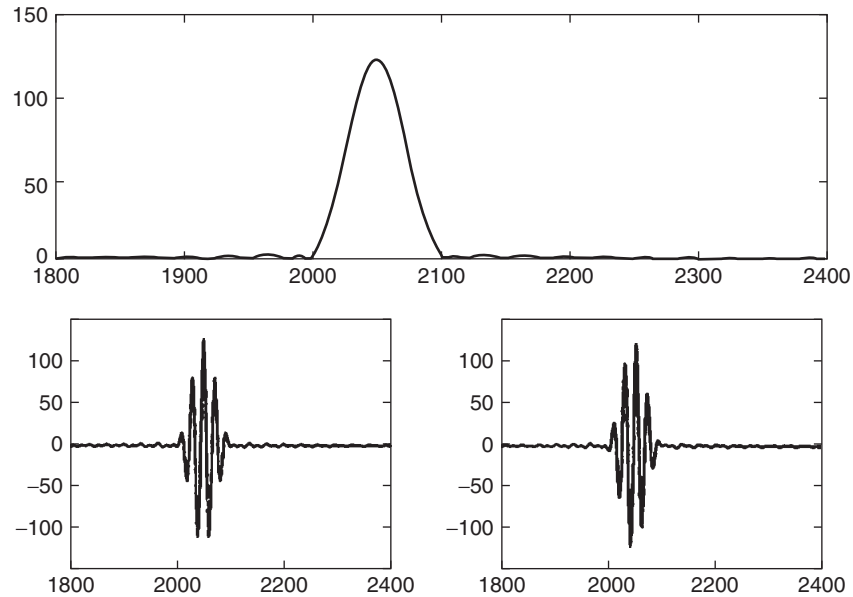
Bending waves emanate from the point of loading and travel along the beam away from the impact until the end of the beam is reached. They are then reflected and return to reach the measuring point, before this process repeats itself. The recorded acceleration should therefore show bursts of waves passing the measuring point as reflections continue until the vibrational energy is dissipated by damping.

### 10.2 STFT Time–Frequency Map

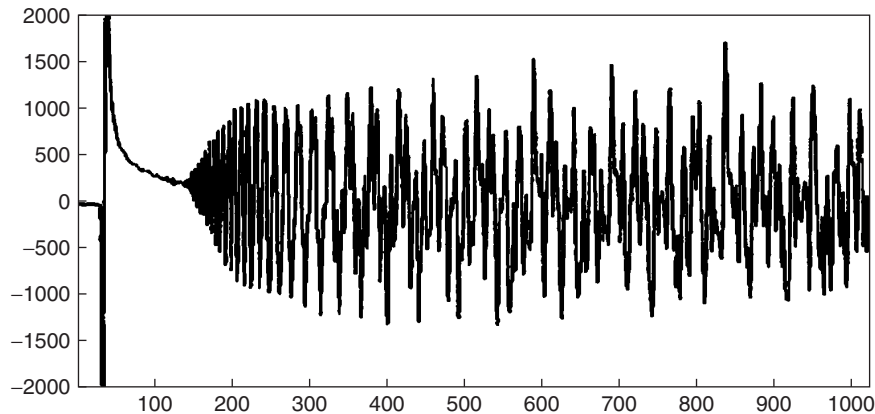
A time–frequency map constructed by applying the STFT is shown in Fig. 18. The input record has been divided into overlapping blocks of 128 terms each, with each new data block advanced 8 points with



**Figure 15** Modulus of a harmonic wavelet whose frequency band covers one octave (*upper view*) with the real part (*lower left*) and imaginary part (*lower right*) shown separately. The wavelet was computed for a 4096-term sequence  $F(k) = 0, k = 1$  to 4096 except for  $F(k) = 1$  for  $k = 129$  to 256.



**Figure 16** The same as Fig. 15 except that the moduli of the frequency coefficients  $F(k)$  in the octave band have been windowed by a Gaussian weighting function with its “standard deviation” set to one-fourth of an octave.



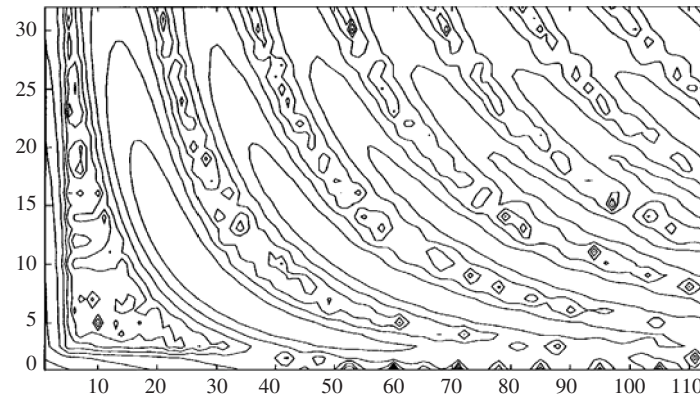
**Figure 17** Measured impulse response data; sequence length 1024. The time scale is horizontal, the frequency scale vertical.

respect to the last. Before computing the FFT of each block, the block is windowed by a Hanning weighting function of the form  $[1 - \cos(2\pi j/128)]/2$ ,  $j = 0$  to 127. The first block starts at the beginning of the 1024-term input data sequence, and there are 113 blocks with the last one finishing at the end of the input data. The presence of curved hills and valleys in Fig. 18 arises for the reason already explained. At any chosen frequency (on the vertical axis in Fig. 18), by drawing a horizontal line on the map, it can be seen that the mean-square response rises and falls as waves arrive from successive reflections and then pass

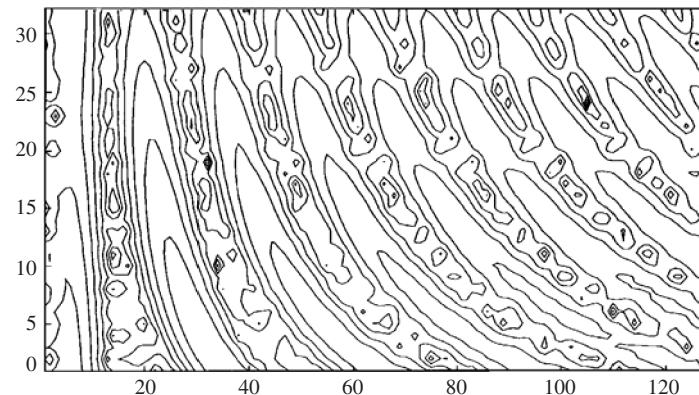
the measuring point. Knowing the dimensions of the beam and the position of the measuring point relative to the two ends, it is possible to estimate the group velocity of the waves and to determine its dependency on frequency from the time–frequency map.

### 10.3 HWT Time–Frequency Map

A second time–frequency map, for the same input data in Fig. 17 but computed by the HWT, is shown in Fig. 19. This has been computed by first calculating the FFT of the complete data sequence  $f(r)$ ,  $r = 0$  to 1023, as in Fig. 8. Then the IFFTs of



**Figure 18** Time–frequency map from the data shown in Fig. 17 when computed by the STFT. The time index is plotted horizontally, the frequency index vertically. Short data sequence length 128; each short segment advanced 8 points from the last; short data blocks windowed by a Hanning weighting function.



**Figure 19** Time–frequency map for the data in Fig. 17 when computed by the HWT. As for Fig. 18, the time index is plotted horizontally, and the frequency index vertically. Frequency block length 128; each frequency block advanced 8 points from the last; frequency blocks windowed by a Gaussian weighting function with a “standard deviation” of  $1/16$  of each block’s bandwidth.

overlapping blocks of 128 frequency coefficients have been calculated to generate the wavelet coefficients. Each new frequency block has been moved 8 places with respect to the last so that 49 separate frequency blocks are possible without overlapping either end of the frequency scale (the Nyquist frequency is term 513). These have been plotted to generate the map in Fig. 19. Each block of 128 frequency coefficients has been weighted by a window of the form  $\exp[-(j-64)^2/2\sigma^2]$ ,  $j = 0$  to 127, where in Fig. 19  $\sigma = 8$ , before its IFFT has been computed. Because each block is 128 terms long, it generates 128 wavelet coefficients corresponding to the wavelets whose centers are uniformly distributed along the time axis. Hence the horizontal axis in Fig. 19 runs from 1 to 128 (whereas that in Fig. 18 runs from 1 to 113 because 113 STFTs were computed). In this case the time base covers the full length of the input record. The

frequency scale is not the same as Fig. 18, however. This is because the middle frequency, of the first block of frequency coefficients is  $64/512$  of the Nyquist frequency, and the middle frequency of the last of the 49 frequency blocks is  $64/512$  below the Nyquist frequency. For the two graphs as plotted, Figs. 18 and 19, the frequency scales are therefore different. This difference may be reduced by using different block sizes but has been retained here to illustrate the difference between the two methods.

#### 10.4 Comments on These Results

Both the STFT method and the HWT method process the input time history to generate data for a time–frequency map. Comparable results can be achieved with each, but it can be shown that the wavelet method usually has advantages in speed of computation. The best choice of wavelet for a given

application is not obvious. But no method can overcome the fundamental uncertainty principle that to improve accuracy in frequency, it is necessary to reduce accuracy in time, and vice versa. This uncertainty does not allow a precise frequency to be identified from a short record length. If the standard deviation of a spectral estimate is to be equal to its predicted (mean) value, then frequency bandwidth  $B$  and record length  $T$  are related by the well-known equation (see, e.g., Newland,<sup>7</sup> Chapter 9)  $BT = 1$ . That is an unavoidable limitation that always applies.

## REFERENCES

1. J. W. Cooley and J. W. Tukey, An Algorithm for the Machine Calculation of Complex Fourier Series, *Math. Computation*, Vol. **19**, 1965, pp. 297–301. (Reprinted in *Papers on Digital Signal Processing*, A. V. Oppenheim, ED., MIT Press, Cambridge, MA, 1969.)
2. I. Daubechies, Orthonormal Bases of Compactly Supported Wavelets, *Comm. Pure Appl. Math.*, Vol. **XLI**, 1988, pp. 909–996.
3. I. Daubechies, Orthonormal Bases of Wavelets with Finite Support—Connection with Discrete Filters, in *Wavelets, Time-Frequency Methods and Phase Space*, J. M. Combes, A. Grossmann, Ph. Tchamitchian, Eds., Springer, Berlin, 1989.
4. I. Daubechies, The Wavelet Transform, Time-Frequency Localization and Signal Analysis, *I.E.E.E. Trans. Info. Theory*, Vol. **36**, 1990, pp. 961–1005.
5. I. Daubechies, *Ten Lectures on Wavelets*, CBMS-NSF Regional Conference Series in Applied Mathematics, SIAM, Philadelphia, 1992.
6. S. Mallat, A Theory for Multiresolution Signal Decomposition: The Wavelet Representation, *I.E.E.E. Trans. Pattern Analysis Machine Intell.*, Vol. **11**, 1989, pp. 674–693.
7. D. E. Newland, *Random Vibrations, Spectral and Wavelet Analysis*, 3rd ed., Dover, New York, 1993.
8. H. S. Malvar, *Signal Processing with Lapped Transforms*, Artech House, Boston, 1992.
9. Y. Meyer, *Wavelets: Algorithms & Applications* (trans. and rev. by R. D. Ryan), SIAM, Philadelphia, 1993.
10. D. E. Newland, Harmonic Wavelet Analysis, *Proc. R. Soc. Lond. A*, Vol. **443**, 1993, pp. 203–225.
11. D. E. Newland, Harmonic and Musical Wavelets, *Proc. R. Soc. Lond. A*, Vol. **444**, 1994, pp. 605–620.
12. D. E. Newland, Wavelet Analysis of Vibration, Part 1: Theory, *J. Vib. Acoust.*, *Trans. ASME*, Vol. **116**, 1994, pp. 409–416.
13. D. E. Newland, Wavelet Analysis of Vibration, Part 2: Wavelet Maps, *J. Vib. Acoust.*, *Trans. ASME*, Vol. **116**, 1994, pp. 417–425.
14. D. E. Newland, Practical Signal Analysis: Do Wavelets Make Any Difference? Proc. 1997 ASME Design Engineering Technical Conferences, Sacramento, Paper DETC97/VIB-4135, 1997.
15. J. S. Bendat and A. G. Piersol, *Engineering Applications of Correlation and Spectral Analysis*, Wiley, New York, 1980.
16. G. Strang and T. Nguyen, *Wavelets and Filter Banks*, Wellesley-Cambridge Press, Wellesley, MA, 1996.

# CHAPTER 50

## USE OF NEAR-FIELD ACOUSTICAL HOLOGRAPHY IN NOISE AND VIBRATION MEASUREMENTS

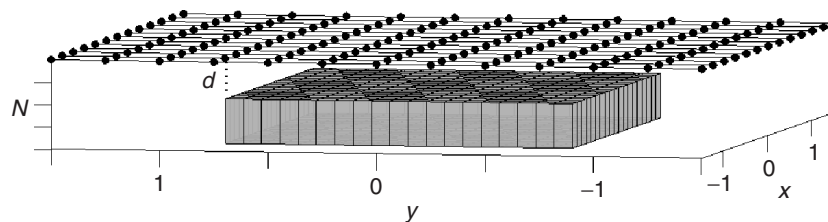
Earl G. Williams  
Naval Research Laboratory  
Washington, DC

### 1 INTRODUCTION

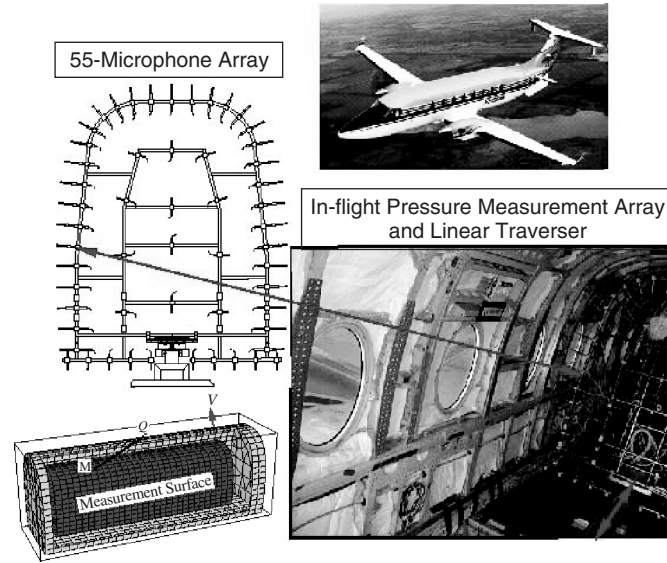
Since the first use of near-field acoustical holography (NAH) in 1980, there has been a rapid increase of research, development, and marketing with practical applications finding their way into many varied noise and vibration problems in industry and transportation. For example, near-field acoustical holography has been used to study the interior noise in aircraft and automobiles and the vibration and radiation from surface ships and submarines, as well as the noise problems in commercial products used in the home. Near-field acoustical holography is remarkable in its ability to thoroughly characterize a radiating source. This is because of the fact that it provides from a single experiment a frequency spectrum reconstruction of the total power radiated, directivity patterns, normal surface velocity and intensity, and the acoustic intensity vectors in the volume from the surface of the source to the far field. The reconstructed surface intensity is used to locate the sources of noise on the radiating structure, thus providing a powerful diagnostic tool for noise control problems. This recovery of the velocity, intensity, radiated power, and far-field directivity is carried out completely in software not hardware. Thus, the need for expensive hardware, such as vibrometers, intensity probes, anechoic chambers, and reverberation rooms can be eliminated. Furthermore, a single experiment achieves all these goals, minimizing the measurement time needed to characterize a source as well as uncertainties due to disparate measurements made in different facilities at different times.

### 2 FIELD OVERVIEW

At the core of NAH is the measurement of a near-field hologram. This consists of a broadband measurement of the pressure on a two-dimensional hypothetical surface with a scanning microphone/hydrophone or an array of sensors. This hypothetical surface is located near to the source surface and generally conformal to it, when possible. Figure 1 shows the experimental setup for a planar NAH experiment, in this case used to study a plate vibrator. The hypothetical measurement surface is made up of an array of microphones, and the conformal source surface is the parallel plane tangent to the top surface of the plate. One needs to procure microphone arrays and/or robot-controlled scanners to implement the pressure hologram measurement. The NAH approach is very attractive due to the state-of-the-art development of microphone technology and advances toward miniaturization (e.g., MEMS microphones) along with reduction of per unit cost. Critical to the NAH approach is the software package that provides the reconstruction of the various acoustical quantities of interest. Some software packages are now available commercially, and the development of a software package is not trivial. Aimed at providing an in-depth understanding of NAH and the software behind it, much of this chapter is dedicated to providing a “cookbook” recipe for a planar NAH system, incorporating the newest advances to date. The planar approach is emphasized here because a large number of noise sources can be studied with it. Furthermore it forms the template of the other NAH approaches, highlighted below, that can handle noise sources that do not fit a planar approach.



**Figure 1** Example of measurement of near field hologram using a microphone array shown above a rectangular plate vibrator.



**Figure 2** Experimental setup for measurement of interior hologram for IBEM using an array of 55 microphones. This array traversed the interior to produce a mailbox-like imaginary surface. Reconstruction surface was the fuselage and floor.

Also discussed is the most general form of NAH, which can be used to study sources of more complex surface geometry. This approach, which relies on the discretization of the Helmholtz integral equation, is called inverse boundary element methods (IBEM). Figure 2 shows an example of an experiment using IBEM to diagnose the interior noise on a Beechcraft airplane.<sup>1</sup> An array of 55 microphones in a vertical plane as shown in the figure was traversed through the cabin to acquire a broadband hologram on an imaginary mailbox-like surface as shown in the cutaway at the bottom left. IBEM was used to determine the pressure, normal velocity, and intensity on the fuselage surface and floor.

### 3 DEFINITION OF A NEAR-FIELD HOLOGRAM AND MEASUREMENT OF TIME-DOMAIN SIGNALS

Holography relies on the measurement of the phase relationship between all the sensor elements on the hologram surface. To put it another way, NAH requires acquisition of a spatially coherent sound field on an imaginary surface. For example, planar near-field acoustical holography requires instantaneous time snapshots of the pressure data  $\bar{s}(x, y, z = z_h, t)$  over a planar measurement array (see Fig. 1) where  $z = z_h$  represents the measurement plane. This requirement is satisfied by an array of microphones recording the sound field simultaneously. When a scanning microphone (or array) is used, then it is necessary to use stationary references recorded throughout the experiment. The reference signals may come from accelerometers attached to the source surface or microphones located close to the suspected radiation

sources. If this reference signal is denoted by  $\bar{r}(t)$ , the assumption that we are dealing with a linear system requires the following convolution relationship between the microphone signal and the reference (fixed in space) to be valid, where  $h(x, y, z_h, \tau)$  is the transfer function of the medium:

$$\bar{s}(x, y, z_h, t) = \int_{-\infty}^{\infty} h(x, y, z_h, \tau) \bar{r}(t - \tau) d\tau \quad (1)$$

This convolution relation exists whether or not the measurement surface is a plane.

The NAH measurements have historically broken into two camps that follow the types of time series present. These time series are either random or deterministic. The first deals with sources that are random in nature (such as flow noise) and the signal processing associated with the creation of holograms uses random data analysis procedures<sup>2</sup> relying on correlation theory. The second camp deals with deterministic sources (such as a swept sine wave shaker excitation). In both cases it is assumed that the excitation is stationary in space, although moving sources can be handled when the motion is known a priori. The following outline describes the characteristics of these two signal processing approaches, and the mathematical details are detailed in the sections below the outline.

- Random excitation of structure
  - Random noise excitation
  - Cross power spectral analysis with ensemble averaging

- Application to in situ machines operating with in situ excitation
- Deterministic (nonrandom) excitation
  - Temporal pulses (chirps) or swept sine wave excitation
  - Time-domain signal averaging and temporal Fourier transforms
  - Excellent laboratory tool using point force excitations as well as in situ machines with strong harmonic spectral lines

The very earliest experiments in NAH used deterministic sources done using sine wave excitation<sup>3,4</sup> to drive a structure of interest, such as a metal panel. Later the use of broadband pulses allowed for the acquisition of a wide band of frequencies from a single experiment.<sup>5</sup> Although this approach is excellent for controlled laboratory experiments and in situ machines with strong tonals, many commercial noise sources are randomly excited and have vibrations that are not deterministic. The signal-processing front end is handled by a different approach,<sup>6</sup> shown in the outline under random excitation. Important in this approach is the use of multiple references and its ability to deal with multiple excitation sources, often with the result that independent holograms are created for each source. This forms the essence of the STSF (special transformation of sound fields) procedure<sup>6</sup> that uses a signal-conditioning approach to orthogonalize multiple references and provide holograms for each reference. When the references are statistically independent, then orthogonalization is not necessary and standard cross-correlation techniques are easily applied.<sup>2</sup> Other procedures for partially correlated references have been and continue to be developed.<sup>7</sup> These signal-processing techniques are by no means trivial and with their careful application difficult noise sources can be tackled.

### 3.1 Deterministic Excitation

In the case of deterministic excitation, such as that created by a swept sine wave source, one can use the convolution theorem to obtain the frequency-domain unnormalized pressure  $s(x, y, z_h, \omega)$  from Eq. (1):

$$s(x, y, z_h, \omega) = H(x, y, z_h, \omega)r(\omega) \quad (2)$$

where  $s$ ,  $r$ , and  $H$  are the Fourier transforms of  $\bar{s}$ ,  $\bar{r}$ , and  $h$ , respectively. The *normalized pressure*  $p(x, y, z_h, \omega)$  representing the pressure coherent to the reference is determined from Eq. (2) and is defined as

$$p(x, y, z_h, \omega) \equiv s(x, y, z_h, \omega)/r(\omega) = H(x, y, z_h, \omega) \quad (3)$$

The normalized pressure is identical to the conjugate of the transfer function and has the units of pascals per unit of the reference. If the reference is a force signal, for example, the units are pascals per newton. The normalized pressure is used in Eq. (24) to compute the angular spectrum, which is the starting point for all of the NAH calculations.

The reference signal  $\bar{r}(t)$  fixed in space is measured simultaneously with each position of the microphone array, as Eq. (2) requires. Generally, signal averaging is used to reduce the noise in the microphone measurements. The frequency domain signal is derived from Eq. (17) (MatLab call **fft**). Starting time at  $t = 0$  using Eq. (10) where we redefine  $N$  as the number of time samples and  $q$  is replaced by  $j$  ( $j = 0, 1, \dots, N - 1$ ) we have at each measurement location  $(x_q, y_r)$

$$r(\omega_m) \approx \text{FFT}_j(\bar{r}(j\Delta t)) \quad (4)$$

$$s(x_q, y_r, 0, \omega_m) \approx \text{FFT}_j(\bar{s}(x_q, y_r, 0, j\Delta t)) \quad (5)$$

where FFT is fast Fourier transforms, and the first  $N/2$  frequency bins ( $f_m = \omega_m/2\pi$ , and  $j = 0$  corresponds to 0 Hz) are used and  $\Delta f = 1/(N\Delta t)$ .

### 3.2 Random Excitation

Again the objective is to determine the transfer function  $H(x, y, z_h, \omega)$ , which for random excitation, such as a shaker driven with a random time series, is determined using the auto and cross-spectral density functions between the reference and the microphone, denoted by  $S_{rr}(\omega)$  and  $S_{rs}(x, y, z_h, \omega)$ , respectively. In this case Eq. (1) becomes

$$S_{rs}(x, y, z_h, \omega) = H(x, y, z_h, \omega)S_{rr}(\omega) \quad (6)$$

Thus the transfer function is

$$H(x, y, z_h, \omega) = S_{rs}(x, y, z_h, \omega)/S_{rr}(\omega) \quad (7)$$

Random processing forms the basis of the spatial transformation of sound fields (STSF)<sup>6</sup> technique developed at Brüel and Kjaer. Once the front-end signal processing is accomplished, STSF uses NAH theory for the reconstruction of the normal surface velocity, pressure, and intensity. During the experiment the spectral density functions are determined using standard ensemble averaging. In the case of MatLab the spectral density function along with ensemble averaging is provided by the function **csd** in the signal-processing package. Since MatLab uses the engineering time convention, we use the complex conjugate of  $H$  due to the time dependence chosen for the NAH theory. Thus the normalized pressure in this case is

$$p(x, y, z_h, \omega) \equiv (S_{rs}(x, y, z_h, \omega)/S_{rr}(\omega))^* \\ = H(x, y, z_h, \omega)^* \quad (8)$$

This normalized pressure is used in Eq. (24) to compute the angular spectrum, the starting point for all the NAH calculations. Multiple incoherent excitations are processed in a straightforward manner.<sup>2,6,7</sup>

## 4 RECONSTRUCTION THEORY

The signal-processing procedures outlined above are used to create holograms that form the starting point



for NAH. Once the holograms are acquired, the main aim of NAH is to provide a reconstruction of the pressure, normal velocity, and intensity at the source boundary. There are three important theoretical approaches and they are summarized below: (1) characteristic eigenfunction expansion (NAH), (2) boundary element discretization of source surface (IBEM), and (3) approximate methods [Helmholtz least squares (HELS)].

#### 4.1 Characteristic Eigenfunction Expansion (NAH)

An overview of this approach is shown in the outline below, which can be used to compare with the outlines in the sections following.

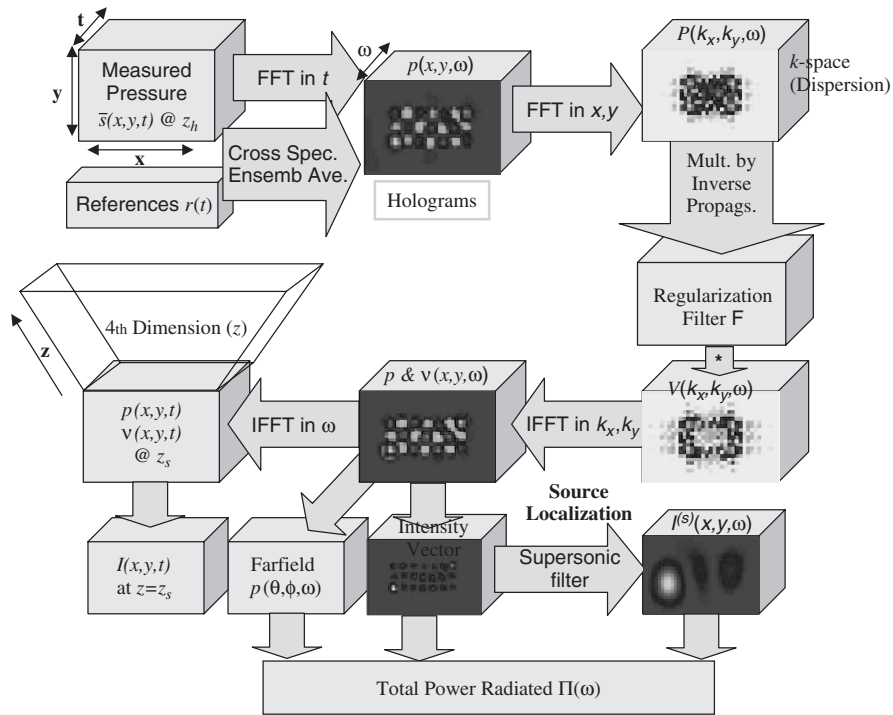
- Orthogonal eigenfunctions are chosen from one of the known separable solutions of the Helmholtz equation and are known analytically.
- The forward propagator (transfer function between the source surface normal velocity or pressure and the measurement surface) is known analytically.
- The reconstruction algorithm is very fast.
- Measurement and reconstruction surfaces must be constant coordinate surfaces of a separable coordinate system and must be conformal to one another.

- Eigenfunction expansion of the reconstructed field is always convergent without noise.
- Full aperture measurement (measurement surface forms a hypothetical closed surface) approach is very accurate.

Figure 3 displays a block diagram of the NAH approach including the signal-processing front end as well as the important postprocessing outputs that provide the noise analyst with ammunition to investigate noise sources. This approach is discussed in *Fourier Acoustics*,<sup>8</sup> although the regularization step was added later.<sup>9</sup> The postprocessing steps refer to the calculation of the acoustic intensity and the far-field pressure. Of particular significance is the use of the supersonic filter to localize hot spots of acoustic radiation on the surface of the vibrator. This quantity is often the key to locating the origins of sound. Finally the total power radiated from the structure radiated into the half-space for planar radiators, and into the full space for others, provides an important tool to discover noise problems in the vibrator.

#### 4.2 Boundary Element Discretization of Source Surface (IBEM)

The second approach to the reconstruction of the pressure and velocity fields on a vibrating structure is given by the inverse boundary element procedure



**Figure 3** Flowchart of the processing steps involved in NAH starting with the measured pressure field and references at the top left. Mathematical details of these steps for planar NAH are described in the text.



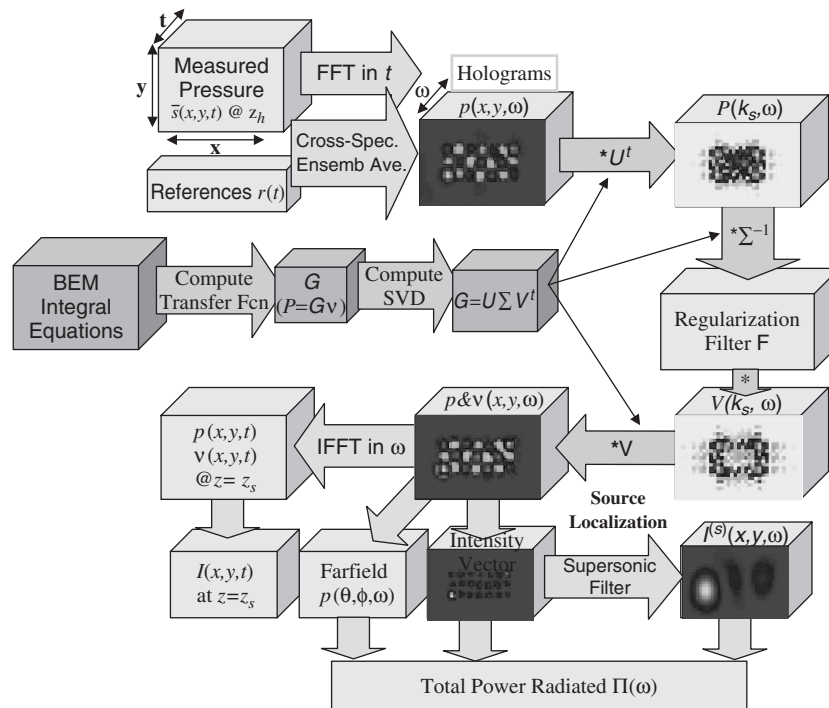
(IBEM).<sup>8,10</sup> An outline of this approach is provided below.

- Explicit methods are based on full Helmholtz integral equation.
- Implicit methods are based on single-layer potential, or double-layer potential, or a combination of both.
- Eigenfunctions are numerically determined.
- Forward propagator (transfer functions) is numerically determined.
- Reconstruction algorithm is slow.
- Measurement and reconstruction surfaces may have any shape.
- Full measurement aperture (measurement surface forms a hypothetical closed surface) approach is used.

This approach is illustrated in Fig. 4 and the important aspects are listed in the outline above. For comparison with Fig. 3 the added steps in the IBEM procedure are shown in a row (starting with BEM Integral Equations) just below the first row. Note that the signal-processing front end is identical in both cases. The coordinates  $(x, y, z)$  should be considered as generalized coordinates (not Cartesian) here, with the first two representing position in some sensible

fashion on the measurement surface and the third representing distance normal to the measurement surface. In this approach the pressure and velocity generally are represented by one-dimensional vectors. The transfer function between the measurement surface and the reconstruction surface is a matrix and is generated by using a BEM that discretizes the reconstruction surface using triangular or quadrilateral elements with a sufficient number of elements to represent the evanescent waves accurately (generally five to six points for the smallest evanescent wavelength of interest).<sup>11</sup>

The IBEM procedures break up into two different types, direct and indirect approaches. In the direct approach the full Helmholtz integral equation, the integrand contains both single- and double-layer potentials multiplied, respectively, by the surface normal velocity and surface pressure. The approach shown in Fig. 4 is the direct approach. The indirect approach uses just a single-layer potential multiplied by a source density term. Solving for the source density is an ill-posed inverse problem, and regularization is needed. Variants of this approach use double layer and combinations of single and double layers in the integrand. We use the single-layer approach, extensively as it is much faster and more accurate than the direct method. Furthermore, recent results<sup>12</sup> have shown that it does not fail at the eigenfrequencies for the interior problem, as previously thought,<sup>13</sup> but instead only suffers a slight



**Figure 4** Flowchart of the processing steps involved in IBEM starting with the measured pressure field and references at top left. Note that most of the steps are the same as in Fig. 3.

decrease in accuracy. For the indirect method an additional step is required to recover the normal velocity or pressure on the source surface, where these quantities are written in terms of integrals over the source density (a forward, well-posed problem).

What separates NAH and IBEM from holography and a multitude of image reconstruction techniques as well as the popular time-reversal approaches is the inclusion of evanescent pressure waves in the reconstruction (formation of the image). An example of an evanescent wave is shown in Fig. 5. These evanescent pressure waves decay rapidly away from the surface of the vibrating structure of interest and cannot be retrieved from measurements made far from the surface. These waves can only be captured from measurements made close to the structure, which accounts for the use of the word *near field* in NAH. The spatial resolution of the image reconstruction in this case is independent of the actual wavelength of the sound and is determined by the subwavelength evanescent waves.

Mathematically speaking, these evanescent waves present an ill-posed inverse problem when doing reconstructions because, due to measurement noise, small perturbations in the measured pressure can lead to large perturbations in the reconstructed quantities (such as the normal surface velocity). The reconstruction is stabilized by using a regularization procedure.<sup>9</sup> The velocity reconstruction is a more ill-posed problem than the pressure reconstruction and cannot be done without regularization.

Note that holograms can be made from any one of the three components of the fluid velocity instead of the acoustic pressure. Recent approaches have used normal velocity measurements to produce the hologram.<sup>14</sup> This approach has the advantage in encountering

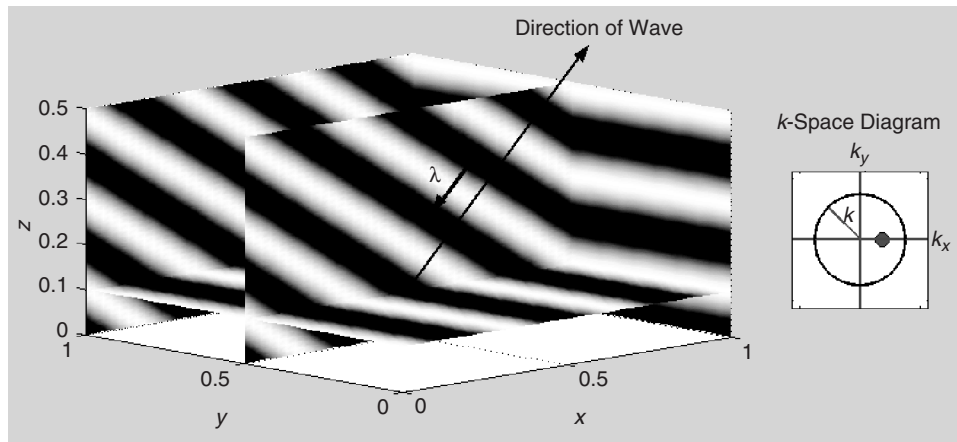
smaller errors in the velocity reconstruction compared with pressure measurement approaches. Direct measurement miniature velocity probes are now commercially produced.

#### 4.3 Approximate Methods (HELs)

The third method presented in the outline above is called HELs (Helmholtz least squares)<sup>15–17</sup> and is outlined below.

- Eigenfunctions (generally spherical harmonics) are chosen from one of the known separable solutions of the Helmholtz equation.
- Forward propagator is known analytically.
- Series expansion for the reconstructed field may be divergent after a certain number of terms even without noise.
- Reconstruction algorithm is very fast.

This method is based upon representing the measured data on an arbitrary surface by a series of spherical wavefunctions (made from spherical harmonics and the corresponding spherical Bessel or Hankel radial functions). Reconstructions are provided by reevaluation of the series at a different surface, and regularization is provided by a cross-validation procedure.<sup>18</sup> Since the measurement and reconstruction surfaces are not spherical in shape, this method differs from the NAH characteristic eigenfunction expansion approach discussed above. This method is referred to as an approximate method due to the fact that the series expansion of spherical wavefunctions may diverge (even without measurement noise) after a certain number of terms depending on the geometry of the surfaces<sup>19</sup> and on the complexity of the actual surface



**Figure 5** Snapshot at  $t = 0$  of a plane wave with  $k_x = k_{x0} \approx k/\sqrt{2}$  and  $k_y = 0$ . The sinusoidal variation of pressure along the two axes is shown gray scale coded, with white-gray representing positive pressure and black-gray negative pressure and the real part is plotted. The insert on the right shows the equivalent  $k$ -space ( $k_x, k_y$ ) representation. The trace wave along in the horizontal plane at  $z = 0.1$  axis is supersonic and lies within the radiation circle of radius  $k$ . Since  $k_y = 0$ , there is no variation in the  $y$  direction (infinite wavelength).

velocity. The reconstruction accuracy also depends upon the location of the origin for the wavefunction expansion, and only an ad hoc procedure exists at the present time for location of this origin. Optimization of the origin location is a problem yet to be solved. HELS has the same advantage of speed as the NAH approach, but, unlike NAH and like IBEM, it has the advantage that it does not require measurement and reconstruction surfaces to fall on a level coordinate of a separable coordinate system.

#### 4.4 Full and Patch Measurement Apertures

The theory for the NAH and IBEM approaches assume that the measurement and the reconstruction surfaces are complete closed surfaces. Although it is obvious from the statement of the integral equation that the source surface must be closed, it is not obvious that the measurement surface must also itself be closed. Some research has addressed the case of an open measurement surface<sup>20</sup> with a closed source surface. It is clear from this work, as well as being intuitive, that the evanescent waves cannot be recovered on the source surface outside the region represented by the normal projection of the measurement aperture down onto the source surface. In this case it would be better to eliminate the outside region completely from the problem, which reduces the size of the transfer matrices and reduces computation time significantly. This latter approach is called the partial aperture measurement approach and is shown in the second part of the outline below, which compares the full and the partial measurement aperture approaches.

- Full aperture measurement approaches:
  - Require overscanning for planar and cylindrical surfaces, closed measurement, and reconstruction surfaces for other coordinate systems such as spherical and spheroidal.
  - Time-consuming measurements and large data sets.
  - Smallest reconstruction errors.
  - Complete spatial reconstruction of the sound field is provided.
- Partial aperture measurement approaches:
  - Measurements done in a patch region, reconstruction obtained generally in a conformal reconstruction region directly below the patch.
  - Fast measurements and small data sets.
  - Larger reconstruction errors.
  - Only the acoustical quantities directly below the patch are obtained.

Patch-to-patch reconstruction is an area of current research. NAH deals with this problem by an intelligent guessing procedure to extend the measurement aperture with synthetic data (zero extension is not acceptable).<sup>21,22</sup> A promising approach, called SONAH (statistically optimal near-Field acoustical

holography), avoids the aperture extension problem.<sup>23</sup> Research is currently underway for the IBEM problem, although results have yet to be published. By virtue of its formulation HELS is a patch-to-patch procedure and thus has the practical advantages of patch holography built in.

We would like to emphasize the continued importance of the simplest NAH system—the planar array and planar NAH. In my experience many sources of interest can be measured with a planar system, thus reducing the complexity of the analysis to a minimum. Thus the rest of this chapter is dedicated to providing a “cookbook” recipe for planar NAH, including the newest advances. We hope this will provide the experimentalist and the entrepreneur with the tools to develop a self-contained measurement system. Furthermore, advancements in microphone array technologies with the reduction in costs underscore NAH and IBEM as timely technologies. The payoffs for the experimentalist and the entrepreneur can be huge.

### 5 COOKBOOK RECIPE FOR PLANAR NAH

Planar NAH provides one of the most comprehensive and fastest experimental tools for diagnosing noise. Although NAH has been developed to analyze vibrators of any shape, the planar form of NAH is by far the fastest and easiest to use. Although ideal for studying vibrators with planar surfaces, the boundaries of the source need not be planar, although the reconstruction plane is limited to a tangent plane not cutting into the source.

The remainder of this chapter is dedicated to planar NAH, and the formulas presented in this chapter are aimed at computer coding using MatLab or the equivalent. A flowchart of the processing is provided in Fig. 3 discussed above. These formulas are complete, taken from the author’s book<sup>8</sup> and journal publications (cited above) and his own operational MatLab code, so that the applications engineer will find it easy to develop his own or understand another’s NAH code for plane-to-plane reconstructions, for example, the STSF technique developed at Brüel & Kjaer.<sup>6</sup>

#### 5.1 Fourier Transforms

The theory of NAH is based on infinite Fourier transforms (FT) in both the space and time dimensions. These are approximated in practice using the fast Fourier transform algorithm, implemented in MatLab using the function `fft`. Whereas the time-domain Fourier transforms are straightforward, the space-domain transforms are implemented using weighting factors that guarantee that the angular spectrum given in Eq. (24), which forms the basis of all the NAH calculations, is computed as accurately as possible [using Eq. (26)].

#### 5.2 Space-Domain Infinite Fourier Transform

In Fig. 3 this step is shown by the arrow with the text “FFT in  $x, y$ ” in the top row. The infinite Fourier

transform,

$$F(k_x) = \int_{-\infty}^{\infty} f(x) e^{-ik_x x} dx \quad (9)$$

is implemented in software using a standard FFT (MatLab call **fft**), that is,

$$G_m = \text{FFT}_q[g_q] \equiv \sum_{q=0}^{M-1} g_q e^{-2\pi i q m / M} \quad (10)$$

To approximate Eq. (9) using the FFT defined in Eq. (10), given  $L_x$  is the length of the one-dimensional aperture defined by  $-L_x/2 \leq x \leq L_x/2$  and  $M$  the number of points, we use

$$F(k_{xm}) \approx \Delta x w_m \text{FFT}_q \left[ \underbrace{f((q - M'/2)\Delta x) w_q}_{g_q} \right] \quad (11)$$

where Table 1 gives the definition of the quantities needed for the fast Fourier transform. The weights arise from a careful discretization of the integral given in Eq. (9) and Eq. (14) (see Section 1.8.1 in

Ref. 8). For  $M$  even the weights are given by ( $m = 0, 1, \dots, M$ )

$$w_m \equiv (-1)^m \quad (12)$$

and for  $M$  odd

$$w_m = (-1)^m e^{-\pi i m / M} \quad (13)$$

### 5.3 Space-Domain Inverse Fourier Transform (IFT)

In Fig. 3 this step is shown by the arrow with the text “IFFT in  $k_x, k_y$ ” in the second row. The inverse of Eq. (9) is given by

$$f(x) = \frac{1}{2\pi} \int_{-\infty}^{\infty} F(k_x) e^{ik_x x} dk_x \quad (14)$$

and its implementation in software uses the inverse FFT (IFFT, MatLab call **ifft**):

$$g_q = \text{IFFT}_m[G_m] \equiv \frac{1}{M} \sum_{m=0}^{M-1} G_m e^{2\pi i q m / M} \quad (15)$$

**Table 1 Definition of Important Symbols Used in This Chapter**

Symbol	Description	Equation
$\equiv$	Definition	
$\mathbf{x}$	Position vector	$(x, y, z)$
$d$	Minimum distance to source	Fig. 1
$\ f(x, y)\ _2$	L2 norm	$\left( \sum_{q=1}^M \sum_{r=1}^N  f(x_q, y_r) ^2 \right)^{1/2}$
$k$	Wavenumber	$\omega/c$
$f$	Frequency (Hz)	$\omega/2\pi$
$M$	Number of points in $x$	
$N$	Number of points in $y$	
$\sigma$	Stand. dev. of noise	Eq. (27)
$\alpha$	Regularization parameter	Eq. (37)
$\Pi^{(\alpha)}$	$k$ -Space filter	Eq. (33), Eq. (34)
$\Delta x$	Microphone spacing in $x$	$\Delta x = L_x/M$
$\Delta y$	Microphone spacing in $y$	$\Delta y = L_y/N$
$L_x$ & $L_y$	Size of measurement aperture	
$x_q$	Lattice coordinate	$x_q = (q - M'/2)\Delta x$
$y_r$	Lattice coordinate	$y_r = (r - N'/2)\Delta y$
$\Delta k_x$	$k$ -Space spacing (FFT)	$\Delta k_x = 2\pi/L_x$
$\Delta k_y$	$k$ -Space spacing (FFT)	$\Delta k_y = 2\pi/L_y$
$k_{xm}$	$k$ -Space coordinates	$k_{xm} = (m - M'/2)\Delta k_x$
$k_{yn}$	$k$ -Space coordinates	$k_{yn} = (n - N'/2)\Delta k_y$
$q$ & $m = 0, 1, \dots, M-1$	Point indices	
$r$ & $n = 0, 1, \dots, N-1$	Point indices	
$M'$ or $N'$ ( $M$ or $N$ even)	Used above	$M' = M$ or $N' = N$
$M'$ or $N'$ ( $M$ or $N$ odd)	Used above	$M' = M-1$ or $N' = N-1$
$w_m$ & $w_n$	FFT weights in $x$ & $y$	Eq. (12) & Eq. (13)
$\bar{w}_m$ & $\bar{w}_n$	IFFT weights in $x$ & $y$	$w_m^*$ & $w_n^*$

To approximate Eq. (14) using the IFFT defined in Eq. (15) we use

$$f(x_q) \approx \frac{1}{\Delta x} \overline{w}_q \text{IFFT}_m \underbrace{[F((m - M'/2)\Delta k_x) \overline{w}_m]}_{G_m}, \quad (16)$$

where  $\overline{w}_q = w_q^*$  and  $\overline{w}_m = w_m^*$  (complex conjugate). Symbols are defined in Table 1.

#### 5.4 Time-Domain Infinite Fourier Transform

In Fig. 3 this step is shown by the arrow with the text “FFT in  $t$ ” in top row. As opposed to the standard engineering convention, NAH uses the following temporal Fourier transform definition:

$$s(\omega) = \int_{-\infty}^{\infty} \overline{s}(t) e^{i\omega t} dt \quad (17)$$

The use of  $e^{i\omega t}$  is the physics convention used in NAH and IBEM, whereas  $e^{-j\omega t}$  is the engineering convention used in MatLab. Note that the complex conjugate  $s(\omega)^*$  corresponds to the standard engineering convention (which uses  $e^{-i\omega t}$  when transforming time signals). The FFT implementation of Eq. (17) is given by the complex conjugate of Eq. (10) given a time sample of  $T$  points where  $g_q = \overline{s}(q\Delta t)$  and the data starts at  $t = 0$  with a sample spacing  $\Delta t$  seconds. The frequency bin width is given by  $\Delta f = 1/(T\Delta t)$  hertz.

#### 5.5 Time-Domain Inverse Fourier Transform

In Fig. 3 this step is shown by the arrow with the text “IFFT in  $\omega$ ” in the second row:

$$\overline{s}(t) = \frac{1}{2\pi} \int_{-\infty}^{\infty} s(\omega) e^{-i\omega t} d\omega \quad (18)$$

An example of the implementation using the IFFT is given in Eq. (41).

### 6 FUNDAMENTAL EQUATIONS IN RECTANGULAR COORDINATES

Near-field acoustical holography is based on the solutions to two fundamental equations, the Helmholtz equation and the Euler Equation.

#### 6.1 Helmholtz Equation

$$\nabla^2 p(\mathbf{x}, \omega) + k^2 p(\mathbf{x}, \omega) = 0 \quad \text{where} \quad \nabla^2 \equiv \frac{\partial^2}{\partial x^2} + \frac{\partial^2}{\partial y^2} + \frac{\partial^2}{\partial z^2} \quad (19)$$

where a source-free, homogeneous, nonviscous fluid of density  $\rho_0$  and constant sound speed  $c$  is assumed.

Define the *acoustic wavenumber*  $k = \omega/c$  and position vector  $\mathbf{x} \equiv (x, y, z)$ .

#### 6.2 Euler's Equation

$$i\omega\rho_0 \mathbf{v}(\mathbf{x}, \omega) = \nabla p(\mathbf{x}, \omega) \quad \text{where} \quad \nabla \equiv \frac{\partial}{\partial x} \hat{i} + \frac{\partial}{\partial y} \hat{j} + \frac{\partial}{\partial z} \hat{k} \quad (20)$$

and the velocity vector  $\mathbf{v}(\mathbf{x}, \omega)$  (Greek letter upsilon) is

$$\mathbf{v}(\mathbf{x}, \omega) = \dot{u}(\mathbf{x}, \omega) \hat{i} + \dot{v}(\mathbf{x}, \omega) \hat{j} + \dot{w}(\mathbf{x}, \omega) \hat{k} \quad (21)$$

$\hat{i}$ ,  $\hat{j}$ , and  $\hat{k}$  are unit vectors in the  $x$ ,  $y$ , and  $z$  directions, respectively. Convention: dot over a displacement quantity to indicate velocity. Displacements:  $u(\mathbf{x}, \omega)$ ,  $v(\mathbf{x}, \omega)$ , and  $w(\mathbf{x}, \omega)$ . Note Eq. (20) represents three scalar equations.

### 7 PLANE WAVE SOLUTIONS (FREQUENCY DOMAIN)

The plane wave solution of Eq. (19), assuming a time dependence of  $e^{-i\omega t}$  is

$$p(\mathbf{x}, \omega) = P(k_x, k_y, \omega) e^{i(k_x x + k_y y + k_z z)} \quad (22)$$

where  $P(k_x, k_y, \omega)$  is an arbitrary complex constant and

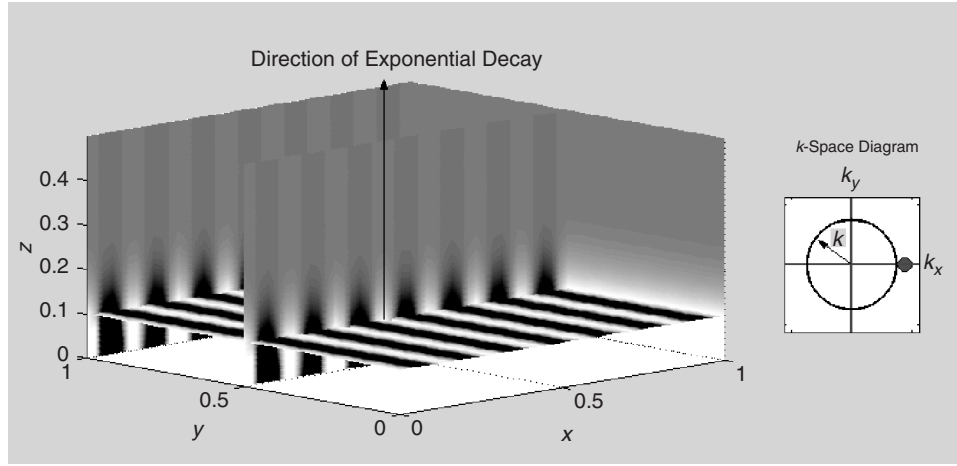
$$k^2 = k_x^2 + k_y^2 + k_z^2 \quad (23)$$

Since  $k$  is a constant, the three directional wavenumbers are not independent of one another. We choose  $k_z$  as the dependent variable and  $k_x$  and  $k_y$  as independent variables:

$$k_z^2 = k^2 - k_x^2 - k_y^2 \quad \text{where} \quad -\infty < k_x < \infty, \\ \text{and} \quad -\infty < k_y < \infty$$

#### 7.1 $k$ Space

In Fig. 3 this step is shown by the box labeled “ $P(k_x, k_y, \omega)$ ” on the top row. The  $k$  space is defined as the space using  $k_x$  and  $k_y$  for the horizontal and vertical axes, respectively, and where the amplitudes of the angular spectra functions  $P(k_x, k_y, \omega)$  given by Eq. (24) are plotted, generally using false color plots where the magnitude of  $P$  is correlated to a color spectrum. In this space an important curve is the radiation circle defined by the equation  $k_x^2 + k_y^2 = k^2$ , as shown in Figs. 5 and 6. The interior of this circle defines spectral components (see Fig. 5) that radiate to the far field, and the exterior defines components that are evanescent (see Fig. 6), decaying exponentially away from the vibrator and not reaching the far field.



**Figure 6** Evanescent wave ( $k_y = 0$ ) traveling in the direction of the  $x$  axis, decaying exponentially in the vertical direction. In  $k$ -space this wave falls outside the radiation circle, as shown by the large dot on the  $k_x$  axis. All evanescent waves lie outside the radiation circle and are subsonic in the horizontal plane. The wavelength in the horizontal plane at  $z = 0.1$  is smaller than the acoustic wavelength.

## 7.2 Examples of Solutions

**7.2.1 Plane Wave Solutions ( $k_x^2 + k_y^2 \leq k^2$ )** See the example with  $k_y = 0$ ,  $k_x < k$  in Fig. 5.

**7.2.2 Evanescent Wave ( $k_x^2 + k_y^2 > k^2$ )** See the example with  $k_y = 0$ ,  $k_x > k$  in Fig. 6.

## 7.3 Angular Spectrum

In Fig. 3 this step is shown by the box labeled “ $P(k_x, k_y, \omega)$ ” on the top row. The coefficient  $P(k_x, k_y, \omega)$  is called the angular spectrum of the pressure distribution in the measurement plane (defined to be at  $z = 0$ ) and is given by

$$P(k_x, k_y, \omega) = \int_{-\infty}^{\infty} dx \int_{-\infty}^{\infty} dy \times p(x, y, 0, \omega) e^{-i(k_x x + k_y y)} \quad (24)$$

$$= \mathcal{F}_x \mathcal{F}_y [p(x, y, 0, \omega)]$$

The angular spectrum forms the springboard for all NAH calculations, and it is critical that an accurate estimate of  $P(k_x, k_y, \omega)$  be obtained. Since a measurement array will not cover the infinite limits needed to calculate the angular spectrum, we require that the array is large enough to extend beyond the physical source being measured so that a finite approximation to Eq. (24) (limits in  $x$  replaced by  $-L_x/2$  and  $+L_x/2$  and limits in  $y$  by  $-L_y/2$  and  $+L_y/2$ ) is not severely in error. In practice, it is required that the pressure field at the edges of the array to have diminished by 30 dB in magnitude from the maximum pressure on the array. Typically, to satisfy

this condition, the array covers an area about twice the effective area of the source. Also a four- or eight-point Tukey spatial window is used to reduce the effects of wraparound error due to the FFT. Since the edges of the array are well beyond the source, the application of the Tukey window affects a small amount of the data. Zero padding can be added to the windowed data to further improve the reconstructions when the array is more than a couple of centimetres from the source. Table 2 gives the Tukey window values  $T(x_q)$  for an  $M$ -point data set in one of the coordinate directions. The Tukey window is applied to the second box labeled “ $p(x, y, \omega)$ ” in Fig. 3.

A second critical requirement for accurate estimation of the angular spectrum is the choice of the sample

**Table 2 Table of Tukey Window Values**

Sample Number ( $q$ )	4-Point Window ( $T(x_q)$ )	8-Point Window ( $T(x_q)$ )
1	0	0
2	0.1464	0.03806
3	0.5000	0.1464
4	0.8536	0.3087
5	1	0.5000
6	1	0.6913
7	1	0.8536
8	1	0.9619
...	1	1
N-6	1	0.9619
N-5	1	0.8536
N-4	1	0.6913
N-3	1	0.5000
N-2	0.8536	0.3087
N-1	0.5000	0.1464
N	0.1464	0.03806

spacing,  $\Delta x$  and  $\Delta y$ . To prevent spatial aliasing, one requires two samples per wavelength, where the wavelength is that of the highest wavenumber evanescent waves (see Fig. 6) that are measurable above the ambient noise level. As derived in my book [see Eq. (3.23) in Ref. 8] the required spacing is given by

$$\Delta x = \Delta y = \frac{\lambda_{x \min}}{2} = \frac{27.3}{\text{SNR}} d \quad (25)$$

where  $d$  is the minimum distance from the hologram plane to the source structure (see Fig. 1), and SNR is given by Eq. (28). The array spacing is generally the same in both directions.

**7.3.1 Implementation with the FFT** In Fig. 3 this step is shown by the box labeled “ $P(k_x, k_y, \omega)$ ” on the top row. Equation (24) is implemented using the four- or eight-point Tukey window above with spacing dictated by Eq. (25):

$$P(k_{xm}, k_{yn}, \omega) \approx \Delta x \Delta y w_m w_n \text{FFT}_p \times [w_p T(y_p) \text{FFT}_q [w_q T(x_q) p(x_q, y_p, 0, \omega)]] \quad (26)$$

where the two FFTs are implemented in MatLab using the function **fft2**.

#### 7.4 Estimate of Hologram Noise

Under the assumption that the noise in the pressure measurement is spatially incoherent and random (Gaussian), the standard deviation  $\sigma$  of the noise at frequency  $\omega$  is estimated by

$$\sigma \approx \sqrt{\frac{1}{Q} \sum_{m,n} |P(k_{xm}, k_{yn}, \omega)|^2} \quad (27)$$

where the values of  $m$  and  $n$  for  $(k_{xm}, k_{yn})$  are chosen to satisfy  $\sqrt{k_{xm}^2 + k_{yn}^2} > \max(|k_{xm}|, |k_{yn}|)$ , and  $Q$  is the number of points that satisfy this inequality. For Eq. (27) to be valid we must have that

$$e^{-d\sqrt{\max(|k_{mx}|, |k_{ny}|)^2 - k^2}} < \sigma/p_{\text{rms}}$$

where  $p_{\text{rms}} = p(x_q, y_p, 0, \omega)_2 / \sqrt{MN}$  is the root-mean-square (rms) measured pressure in the hologram, and  $d$  is the minimum distance between the hologram and the source boundary. The *signal-to-noise ratio* (SNR) in decibels is defined by

$$\text{SNR} = 20 \log_{10}(p_{\text{rms}}/\sigma) \quad (28)$$

### 8 GENERAL SOLUTION TO HELMHOLTZ EQUATION

The most general solution of Eq. (19) is a sum of an infinite number of plane and evanescent waves in different directions (all with possibly different complex

amplitudes  $P(k_x, k_y, \omega)$  at any given frequency  $\omega$ ). Given  $P(k_x, k_y, \omega)$  the field is completely determined in all free space above the vibrator,  $-d \leq z \leq \infty$ . The *reconstructed pressure* in this space is

$$p(\mathbf{x}, \omega) = \frac{1}{4\pi^2} \int_{-\infty}^{\infty} dk_x \int_{-\infty}^{\infty} dk_y \Pi^{(\omega)}(k_\rho, z) \times P(k_x, k_y, \omega) e^{i(k_x x + k_y y + k_z z)} \\ = \mathcal{F}_x^{-1} \mathcal{F}_y^{-1} [\Pi^{(\omega)}(k_\rho, z) P(k_x, k_y, \omega) e^{ik_z z}] \quad (29)$$

where  $k_\rho$  is defined in Eq. (33). The *reconstructed velocity vector* is

$$\mathbf{v}(\mathbf{x}, \omega) = \frac{1}{\rho_0 c k} \mathcal{F}_x^{-1} \mathcal{F}_y^{-1} [(k_x \hat{i} + k_y \hat{j} + k_z \hat{k}) \times \Pi^{(\omega)}(k_\rho, z) P(k_x, k_y, \omega) e^{ik_z z}] \quad (30)$$

where  $\Pi^{(\omega)}(k_\rho, z)$  is a  $k$ -space filter needed to remove noise when reconstructing the field close to the vibrator, that is,  $-d \leq z \leq 0$ .

#### 8.1 Implementation with the IFFT

In Fig. 3 this step is shown by the arrow with the text “IFFT in  $\omega$ ” on the second row:

$$p(x_q, y_p, z, \omega) \approx \frac{\bar{w}_q \bar{w}_p}{\Delta x \Delta y} \text{IFFT}_n [\bar{w}_n \text{IFFT}_m [\bar{w}_m \Pi^{(\omega)}(k_{\rho mn}, z) \times P(k_{xm}, k_{yn}, \omega) e^{ik_{zmn} z}]] \quad (31)$$

where  $k_{zmn} \equiv \sqrt{k^2 - k_{\rho mn}^2}$  and  $k_{\rho mn} \equiv \sqrt{k_{xm}^2 + k_{yn}^2}$ . The two inverse FFTs are implemented in MatLab using the function **ifft2**. The same implementation is used for the reconstruction of the velocity vector. The reconstruction of the normal velocity is

$$\dot{w}(x_q, y_p, z, \omega) \approx \frac{\bar{w}_q \bar{w}_p}{\rho_0 c k \Delta x \Delta y} \text{IFFT}_n [\bar{w}_n \text{IFFT}_m [\bar{w}_m \Pi^{(\omega)}(k_{\rho mn}, z) \times P(k_{xm}, k_{yn}, \omega) k_{zmn} e^{ik_{zmn} z}]] \quad (32)$$

The in-plane velocities  $\dot{u}$  and  $\dot{v}$  are obtained by replacing  $k_{zmn}$  in front of the exponent by  $k_{xm}$  and  $k_{yn}$ , respectively.

#### 8.2 $k$ -Space Tikhonov Filters

In Fig. 3 this step is shown by the box labeled “Regularization filter F” on the right column. These low-pass filters<sup>9,24</sup> stabilize the reconstruction and have the limiting values of 0 and 1 when  $k_\rho \rightarrow \infty$  and  $k_\rho \rightarrow 0$ , respectively. When  $z > 0$ , they are not

necessary since the reconstructions are stable, and we set  $\Pi^{(\alpha)} = 1$ . Otherwise when  $-d \leq z \leq 0$  the *standard Tikhonov filter* is given by

$$\Pi^{(\alpha)}(k_\rho, z) = \frac{|\lambda(k_\rho)|^2}{|\lambda(k_\rho)|^2 + \alpha} \quad k_\rho \equiv \sqrt{k_x^2 + k_y^2} \quad (33)$$

where  $\alpha$  is called the *regularization parameter* given by Eq. (37) or (38). An alternative filter, which appears to be a bit more accurate, is the *high-pass Tikhonov filter* and is given by

$$\Pi^{(\alpha)}(k_\rho, z) \equiv \frac{|\lambda(k_\rho)|^2}{(|\lambda(k_\rho)|^2 + \alpha(\alpha/(\alpha + |\lambda(k_\rho)|^2))^2)} \quad (34)$$

In both these filters the *eigenvalue*  $\lambda(k_\rho)$  for a pressure reconstruction Eq. (29) is

$$\lambda(k_\rho) \equiv e^{z\sqrt{k_\rho^2 - k^2}} \quad (35)$$

and for a velocity reconstruction Eq. (30) is

$$\lambda(k_\rho) \equiv \frac{\rho_0 c k}{i\sqrt{k_\rho^2 - k^2}} e^{z\sqrt{k_\rho^2 - k^2}} \quad (36)$$

Note that  $z = -d$  for the reconstruction closest to the source and when  $k_\rho^2 < k^2$  we use  $\sqrt{k_\rho^2 - k^2} = -i\sqrt{k^2 - k_\rho^2}$ .

### 8.3 Determination of Regularization Parameter $\alpha$

1. Determination using *Morozov discrepancy principle*. In this formula we need an estimate of the standard deviation of the noise in the hologram, given by Eq. (27). To solve for  $\alpha(\omega)$  we find the zero crossing of the following monotonic (in  $\alpha$ ) relationship ( $z$  held constant):

$$\|(1 - \Pi^{(\alpha)}(k_\rho, z))P(k_x, k_y, \omega)\|_2 - \sigma\sqrt{MN} = 0 \quad (37)$$

The value of  $\alpha$  corresponding to the zero crossing is found using the MatLab function **fzero**.

2. Determination using *generalized cross validation (GCV)*. We find the minimum of  $J(\alpha)$ :

$$J(\alpha) = \frac{\|(1 - \Pi^{(\alpha)}(k_\rho, z))P(k_x, k_y, \omega)\|_2^2}{\|1 - \Pi^{(\alpha)}(k_\rho, z)\|_1^2} \quad (38)$$

The value of  $\alpha(\omega)$  corresponding to the minimum is found using the MatLab function **fminbnd**.

### 8.4 Velocity Vector Angular Spectra above the Vibrator

The angular spectra at  $z$  corresponding to the velocity in the  $x$ ,  $y$ , and  $z$  directions are denoted by  $\dot{U}(k_x, k_y, z)$ ,  $\dot{V}(k_x, k_y, z)$ , and  $\dot{W}(k_x, k_y, z)$ , respectively, and are given by

$$\begin{aligned} & \dot{U}(k_x, k_y, z)\hat{i} + \dot{V}(k_x, k_y, z)\hat{j} + \dot{W}(k_x, k_y, z)\hat{k} \\ &= (k_x\hat{i} + k_y\hat{j} + k_z\hat{k}) \frac{P(k_x, k_y, \omega)}{\rho_0 c k} e^{ik_z z} \end{aligned} \quad (39)$$

They are computed by using Eq. (26). The angular spectrum of the normal velocity (and similarly for  $\dot{U}$  and  $\dot{V}$ ) is defined by

$$\dot{W}(k_x, k_y, z) \equiv \mathcal{F}_x \mathcal{F}_y [\dot{w}(x, y, z, \omega)] \quad (40)$$

## 9 RECOVERY OF TIME-DOMAIN SIGNALS

All computations are done in the frequency domain ( $\omega$ ). After all the frequency bins are processed, then the time-domain signals are reconstructed using Eq. (18) implemented using the IFFT given in Eq. (15). Since only positive frequencies are computed, the negative spectrum is recovered using  $s(-\omega) = s(\omega)^*$ . Once the negative spectrum is set, the necessary MatLab coding is

$$\overline{p}(\mathbf{x}, t) = \text{fftshift}(\text{ifft}(p(\mathbf{x}, \omega)^*)) \quad (41)$$

where the input is conjugated to account for the fact that NAH theory uses  $e^{-i\omega t}$  time convention. This operation guarantees that the resulting time-domain signal is purely real. A spectral window (Hanning or Kaiser-Bessel) is used on  $p(\mathbf{x}, \omega)$  before inverse transforming to the time domain to reduce artificial ringing in the time domain-signal, which arises from the sharp cutoffs of a rectangular window.

## 10 FAR-FIELD PROJECTION

In Fig. 3 this step is shown by the box labeled “Farfield  $p(\theta, \phi, \omega)$ ” on the bottom row:

$$p(r, \theta, \phi, \omega) = -i\rho_0 c k \frac{e^{ikr}}{2\pi r} \dot{W}(k_x, k_y, 0, \omega) \quad (42)$$

where  $k_x = k \sin \theta \cos \phi$  and  $k_y = k \sin \theta \sin \phi$  and  $(r, \theta, \phi)$  are standard spherical coordinates ( $\phi$  and  $\theta$  measured from the  $x$  and  $z$  axes, respectively, and  $r = \sqrt{x^2 + y^2 + z^2}$ ).  $\dot{W}(k_x, k_y, 0, \omega)$  is determined from Eq. (39) with  $z = 0$ . Generally,  $P(k_x, k_y, \omega)$  is interpolated first in  $k_x$  and  $k_y$  by adding a wide band of zeros around  $p(x, y, 0, \omega)$  and using Eq. (26). This is important at low frequencies where only a few  $k$ -space points fall within the radiation circle.

### 10.1 Directivity Function

Defined by

$$p(r, \theta, \phi, \omega) = \frac{e^{ikr}}{r} D(\theta, \phi, \omega) \quad (43)$$



the directivity function is

$$D(\theta, \phi, \omega) = \frac{-i\rho_0 c k}{2\pi} \dot{W}(k_x, k_y, 0, \omega) \quad (44)$$

The directivity function has the units of pascal-metres/(reference units).

### 11 ACTIVE AND REACTIVE INTENSITY

In Fig. 3 this step is shown by the box labeled “Intensity” on the bottom row. In Eq. (45)  $p$  and  $\mathbf{v}$  are calculated using Eqs. (29) and (30) for selected values of  $z \geq -d$ , and the resulting vector intensity field is plotted using the MatLab function `coneplot`.

$$\mathbf{I}(\mathbf{x}, \omega) = \frac{1}{2}(p(\mathbf{x}, \omega)\mathbf{v}(\mathbf{x}, \omega)^*) \quad (45)$$

where  $\text{Re}(\mathbf{I})$  is the active intensity and  $\text{Im}(\mathbf{I})$  the reactive intensity.

### 12 SUPERSONIC INTENSITY

In Fig. 3 this step is shown by the arrow with the text “Supersonic filter” on the bottom row. Often the active intensity on a surface has both ingoing and outgoing components, which obscure what areas of the surface actually radiate to the far field. In this case a new quantity was invented<sup>25,26</sup> that removes the ingoing components, providing an unambiguous map of the radiating regions of the source. Although the spatial resolution is reduced at the lower frequencies, this approach has proven to be very powerful in source identification problems. The supersonic intensity  $I_z^{(s)}$  is defined as

$$I_z^{(s)}(\mathbf{x}, \omega) \equiv \frac{1}{2}\text{Re}(p^{(s)}(\mathbf{x}, \omega)\dot{w}^{(s)}(\mathbf{x}, \omega)^*) \quad (46)$$

where  $p^{(s)}$  and  $\dot{w}^{(s)}$  are computed from Eqs. (31) and (32), respectively, with the a priori choice,  $k_p = k$ , in the  $k$ -space filter  $\Pi^{(w)}(k_p, z)$  (no regularization is required) that appears in these equations. Thus the cutoff of the filter is the acoustical circle (the circle of radius  $k$  shown in Figs. 5 and 6).

### 13 RADIATED POWER

In Fig. 3 this step is shown by the box labeled “Total Power Radiated” at the bottom. The total power radiated into the half-space  $z \geq -d$  is given by

$$\begin{aligned} \Pi(\omega) \approx & \frac{1}{2} \sum_{q=1}^M \sum_{r=1}^N \text{Re}[p(x_q, y_r, 0, \omega)\dot{w}^* \\ & \times (x_q, y_r, 0, \omega)] \Delta x \Delta y \end{aligned} \quad (47)$$

The radiated power, computed here at  $z = 0$ , is independent of  $z$ , however.

**Acknowledgments** This work was supported by the U.S. Office of Naval Research.

### REFERENCES

1. E. G. Williams, B. H. Houston, P. C. Herdic, S. T. Raveendra, and B. Gardner, Interior NAH in Flight, *J. Acoust. Soc. Am.*, Vol. 108, 2000, pp. 1451–1463.
2. J. S. Bendat and A. G. Piersol, *Random Data Analysis and Measurement Procedures*, 3rd ed., Wiley, New York, 2000.
3. E. G. Williams and J. D. Maynard, Holographic Imaging without the Wavelength Resolution Limit, *Phys. Rev. Lett.*, Vol. 45, 1980, pp. 554–557.
4. E. G. Williams, J. D. Maynard, and E. Skudrzyk, Sound Source Reconstructions Using a Microphone Array, *J. Acoust. Soc. Am.*, Vol. 68, 1980, pp. 340–344.
5. E. G. Williams, B. Houston, and J. A. Bucaro, Broadband Nearfield Acoustical Holography for Vibrating Cylinders, *J. Acoust. Soc. Am.*, Vol. 86, 1989, pp. 674–679.
6. J. Hald, STSF—A Unique Technique for Scan-Based Nearfield Acoustical Holography without Restriction on Coherence, Technical Report, *B&K Tech. Rev.*, No. 1, 1989.
7. H.-S. Kwon, Y.-J. Kim, and J. S. Bolton, Compensation for Source Nonstationarity in Multireference, Scan-Based Near-Field Acoustical Holography, *J. Acoust. Soc. Am.*, Vol. 113, 2003, pp. 360–368.
8. E. G. Williams, *Fourier Acoustics: Sound Radiation and Nearfield Acoustical Holography*, Academic, London, 1999.
9. E. G. Williams, Regularization Methods for Near-Field Acoustical Holography, *J. Acoust. Soc. Am.*, Vol. 110, 2001, pp. 1976–1988.
10. M. R. Bai, Application of BEM (Boundary Element Method)-Based Acoustic Holography to Radiation Analysis of Sound Sources with Arbitrarily Shaped Geometries, *J. Acoust. Soc. Am.*, Vol. 92, 1992, pp. 533–549.
11. A. F. Seybert, B. Soenarko, F. J. Rizzo, and D. J. Shippy, An Advanced Computational Method for Radiation and Scattering of Acoustic Waves in Three Dimensions, *J. Acoust. Soc. Am.*, Vol. 77, 1985, pp. 362–368.
12. N. Valdivia and E. G. Williams, Implicit Methods of Solution to Integral Formulations in Boundary Element Method Based Nearfield Acoustic Holography, *J. Acoust. Soc. Am.*, Vol. 116, 2004, pp. 1559–1572.
13. H. A. Schenck, Improved Integral Formulation for Acoustic Radiation Problems, *J. Acoust. Soc. Am.*, Vol. 44, 1968, pp. 41–58.
14. R. Visser, Acoustic Source Localization Based on Pressure and Particle Velocity Measurements, in *Proceedings Inter-Noise 2003*, Jeju, Korea, August 2003, pp. 665–670.
15. S. F. Wu and J. Yu, Reconstructing Interior Acoustic Pressure Field via Helmholtz Equation Least-Squares Method, *J. Acoust. Soc. Am.*, Vol. 104, 1998, pp. 2054–2060.
16. S. F. Wu, On Reconstruction of Acoustic Pressure Fields Using the Helmholtz Equation Least Squares Method, *J. Acoust. Soc. Am.*, Vol. 107, 2000, pp. 2511–2522.
17. S. F. Wu and X. Zhao, Combined Helmholtz Equation Least Squares Method for Reconstructing Acoustic Radiation from Arbitrarily Shaped Objects, *J. Acoust. Soc. Am.*, Vol. 112, 2002, pp. 179–188.

18. T. Semanova and S. f. Wu, The Helmholtz Equation Least-Squares Method and Rayleigh Hypothesis in Near-Field Acoustical Holography, *J. Acoust. Soc. Am.*, Vol. 115, 2004, pp. 1632–1640.
19. T. Semanova, *On the Behavior of the Helmholtz Equation Least-Squares Method Solutions for Acoustic Radiation and Reconstruction*, Ph.D. thesis, Wayne State University, Detroit, MI, June 2004.
20. A. Sarkissian, C. Gaumond, E. Williams, and B. Houston, Reconstruction of the Acoustic Field over a Limited Surface Area on a Vibrating Cylinder, *J. Acoust. Soc. Am.*, Vol. 93, 1993, pp. 48–54.
21. K. Saijyou and S. Yoshikawa, Reduction Methods of the Reconstruction Error for Large-Scale Implementation of Near-Field Acoustical Holography, *J. Acoust. Soc. Am.*, Vol. 110, 2001, pp. 2007–2023.
22. E. G. Williams, Continuation of Acoustic Near-Fields, *J. Acoust. Soc. Am.*, Vol. 113, 2003, pp. 1273–1281.
23. R. Steiner and J. Hald, Near-Field Acoustical Holography without the Errors and Limitations Caused by the Use of Spatial DFT, *Int. J. Acoust. and Vib.*, Vol. 6, 2001, pp. 83–89. 2001.
24. P. C. Hansen, *Rank-Deficient and Discrete Ill-Posed Problems*, SIAM, Philadelphia, 1998.
25. E. G. Williams, Supersonic Acoustic Intensity, *J. Acoust. Soc. Am.*, Vol. 97, 1995, pp. 121–127.
26. E. G. Williams, Supersonic Acoustic Intensity on Planar Sources, *J. Acoust. Soc. Am.*, Vol. 104, 1998, pp. 2845–2850.

# CHAPTER 51

## CALIBRATION OF MEASUREMENT MICROPHONES

Erling Frederiksen

Brüel & Kjær  
and

Danish Primary Laboratory of Acoustics (DPLA)  
Naerum, Denmark

### 1 INTRODUCTION

Calibration has been defined by international organizations as a “set of operations that establish, under specified conditions, the relationship between values of quantities indicated by a measuring instrument or system and the corresponding values realised by standards.”<sup>1</sup> In the field of acoustics this means: (1) determination of the difference between the level indicated by a sound level meter and the level of the sound applied to its microphone or (2) determination of the ratio between the output voltage of a microphone and the pressure of its exciting sound wave. The latter example, the sensitivity of a microphone, is a complex quantity. Depending on the application of the microphone, both magnitude and phase may have to be calibrated. To ensure that acoustical measurement and calibration results become correct and comparable with results obtained by others, the calibration of systems, microphones, and sound calibrators should be traceable to international standards.

### 2 TRACEABILITY

All calibrations of sound level meters, calibrators, and microphones should be linked to an unbroken chain of comparison calibrations, which via local and national standards goes back to international standards (see Fig. 1). All methods applied in the chain should be analyzed and evaluated in detail and their uncertainty should be specified. The resulting uncertainty, which depends on the composition of the chain, should be calculated and stated with the calibration result. In this way traceability ensures a known (but not necessarily a specifically low) uncertainty, which is important for evaluation and documentation of all measurement and calibration results.

### 3 CALIBRATION-RELATED MICROPHONE SUBJECTS

#### 3.1 Limitation of This Calibration Description

The sound field parameter of most common interest is the sound pressure, but the parameters sound intensity, sound power, and acoustic impedance are also frequently measured. Such measurements imply determination of both sound pressure and air-particle velocity. In principle, velocity can be directly measured with velocity-sensing microphones,<sup>2</sup> but it is most often determined indirectly with a set of pressure-sensing microphones, which simultaneously measure

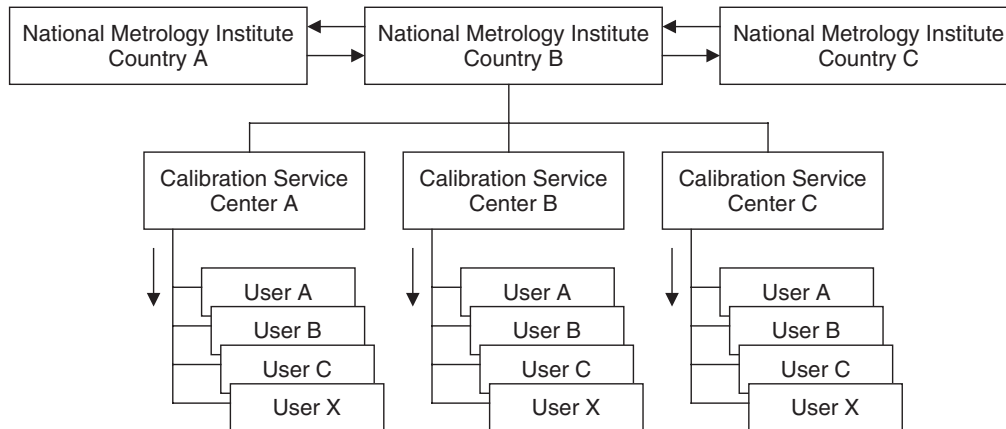
the sound pressure. As instruments using such microphones are most frequently applied, are covered by international standards, and can be most accurately calibrated, only the calibration of pressure-sensing microphones is described in the following. Essentially all measurement microphones have a cylindrical body and a metallic diaphragm, which is visible when its protection grid is dismantled. The simple shape of the body and the position of the diaphragm, at the end of the body, make these microphones well-suited for both calibration and for calculation of their acoustical properties. Traditional condenser microphones have these properties plus high and well-defined acoustical diaphragm impedance, which together have made these microphones the dominating type of measurement microphone.

#### 3.2 Microphone Standards

The International Electrotechnical Commission (IEC) has worked out and issued a series of measurement microphone and calibration standards under the common title and number Measurement Microphones—IEC 61094. Part 1 and Part 4 of the series specify required properties of laboratory standard microphones<sup>3</sup> and working standard microphones,<sup>4</sup> respectively. Laboratory standard microphones are mainly calibrated and kept as national standards but are also used as reference standards with comparison calibration systems, while working standard microphones are the microphones used for essentially all other kinds of acoustical measurements.

#### 3.3 Microphones and Sound Fields

The sensitivity and frequency response of a microphone depends on the type of sound field. The sensitivity is, therefore, generally specified for one of the following types of sound field: (a) a free field<sup>5</sup> with a plane wave, (b) a diffuse field,<sup>6,7</sup> and (c) a pressure field, that is, a field, where magnitude and phase of the pressure are independent of the position. At low frequencies, where the microphone diameter is small compared with the wavelength of the sound (say  $d < \lambda/30$ ), the sensitivity does not significantly depend on the type of field. The sensitivity of microphones less than 24 mm is thus the same for all field types up to about 500 Hz. As the frequency 250 Hz is well below this limit, it has become a commonly used sound calibrator and system calibration frequency that can be applied with all types of sound field. The



**Figure 1** Typical calibration hierarchy with service centers that ensure traceability to national and international standards.

field dependency increases with the diameter to wavelength ratio and thus with frequency. It is typically of the order 0.05 to 0.2 dB at 1000 Hz but may become as high as 10 to 15 dB at the highest operation frequencies (see Fig. 2). Therefore, specific models of microphone have been optimized, with respect to frequency response, for use in the different types of sound field. Prior to any acoustical measurement, both types of microphone and calibration should thus be selected in accordance with the type of sound field that occurs at the measurement site.

### 3.4 Open-Circuit and Loaded-Microphone Sensitivity

Typically, the capacitance of laboratory standard and measurement microphones is between 12 and 60 pF, but it can be as low as 3 pF for the smallest types of microphone. Due to the low capacitance, cables cannot be connected directly to the microphones without violating their function. A preamplifier with high-input and low-output impedance must, therefore, be connected to the output terminal of the microphone. Even such a preamplifier loads the microphone by its input capacitance and causes a sensitivity reduction that generally needs to be taken into

account. By most calibrations the nonloaded (open-circuit) sensitivity is determined and reported for the microphone. The loaded sensitivity might be measured, for specific microphone–preamplifier combinations, or it may be obtained by adding a predetermined nominal correction, valid for the types of microphone and preamplifier, to the open-circuit sensitivity.

The response of a microphone may be stated as sensitivity ( $M$ ) in volts per pascal (V/Pa) or in terms of sensitivity level ( $L_M$ ) in decibels related to the reference sensitivity ( $M_{\text{ref}}$ ), that is, 1 V/Pa;

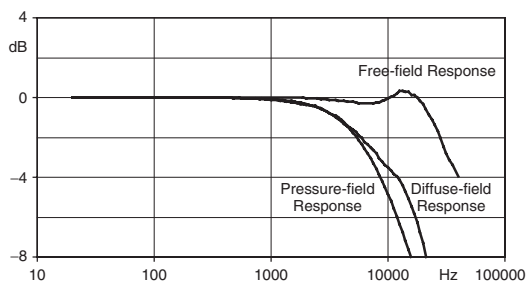
$$L_M = 20 \log \frac{M}{M_{\text{ref}}}$$

### 3.5 Microphone Preamplifiers

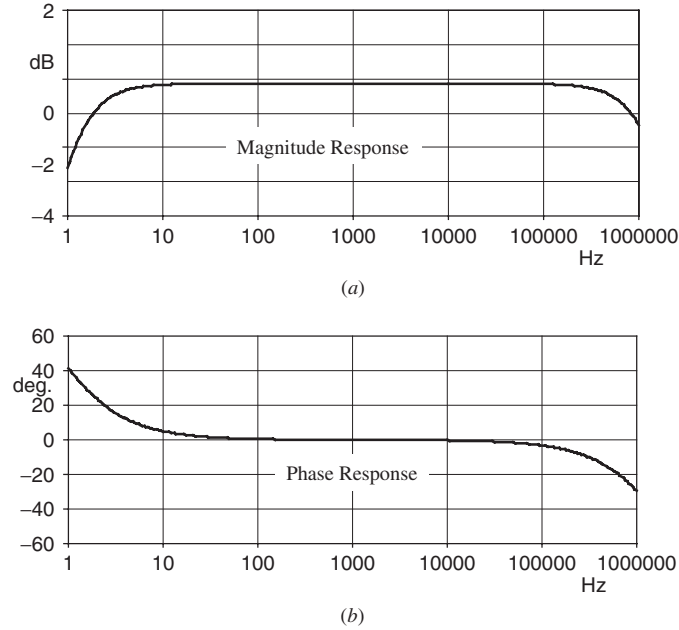
Modern preamplifiers have very high input impedance. The input resistance may be as high as  $10^{10}$  to  $10^{11} \Omega$  with a parallel capacitance as low as 0.1 to 0.2 F. The voltage gain of the amplifier built into the preamplifier unit is in most cases near to unity (1 or 0 dB). The electrical response of the microphone and preamplifier is essentially flat over the range from say 20 Hz to 100 kHz (Fig. 3). Therefore, its influence on the microphone frequency response is normally neglected in secondary microphone calibration. In connection with primary calibration and very precise measurements, the electrical response has to be measured.

### 3.6 Insert Voltage Technique

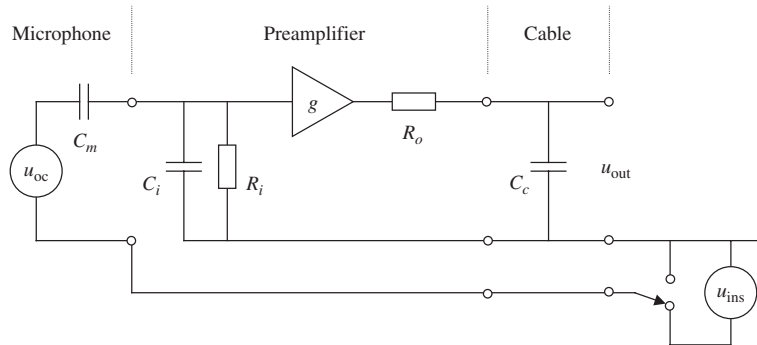
The insert voltage technique<sup>8</sup> is applied when measuring the electrical gain and frequency response of a microphone and its preamplifier with a possible influence of a loading cable (see Fig. 4). The principle is to measure the gain of the circuit with a voltage that is inserted directly into series with the microphone. During the measurement this voltage replaces the sound generated (open-circuit) signal ( $u_{\text{oc}}$ ) of the microphone. The gain ( $u_{\text{out}}/u_{\text{ins}}$ ) of the circuit, which



**Figure 2** Free-field, diffuse-field, and pressure-field frequency responses of a free-field microphone (12.7 mm) deviate from each other at higher frequencies.



**Figure 3** Electrical frequency responses of a typical measurement microphone ( $C = 18$  pF) and preamplifier ( $C_{in} = 0.2$  pF,  $R_{in} = 10$  G $\Omega$ ,  $R_{out} = 30$   $\Omega$ ) loaded with cable ( $C = 3000$  pF).



**Figure 4** Principle of insert voltage technique for measurement of electrical gain.

consists of microphone capacitance ( $C_m$ ), preamplifier input impedance ( $C_i \neq R_i$ ), amplifier gain ( $g$ ) and output resistance ( $R_o$ ), is measured with the loading of the cable capacitance ( $C_c$ ). Often the gain ( $G_{mp}$ ) is measured only at the preferred microphone calibration frequency and the reference frequency for the frequency response definition (often 250 Hz). This gain is used with the open-circuit sensitivity of a microphone to calculate its sensitivity in combination with a preamplifier. The gain in the midfrequency range is determined by

$$G_{mp}[\text{dB}] \cong 20 \log \frac{C_m}{C_m + C_i} + g[\text{dB}]$$

where  $G_{mp}$  = electrical gain of microphone and preamplifier at reference frequency (250 Hz)

$C_m$  = capacitance of microphone

$C_i$  = input capacitance of microphone preamplifier

$g$  = gain of voltage amplifier built into the preamplifier unit

The nominal gain valid for a specific combination of types of microphone and preamplifier is commonly used together with an individually measured microphone sensitivity to determine the sensitivity of a specific microphone and preamplifier combination:

$$M_{mp}[\text{dB re.1 V}] = M_{oc}[\text{dB re.1 V}] + G_{mp}[\text{dB}]$$

where  $M_{mp}$  = combined sensitivity of microphone and preamplifier

$M_{oc}$  = open-circuit sensitivity of microphone

$G_{mp}$  = electrical gain of microphone and preamplifier

The insert voltage technique is thus a method used in connection with other acoustical calibration techniques and is not a stand-alone method.

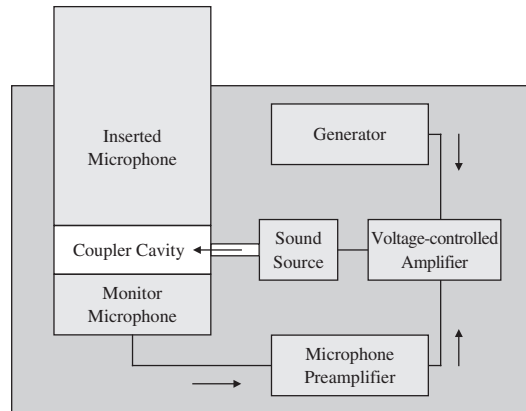
## 4 CALIBRATION METHODS

### 4.1 Sound Fields of Application and Calibration

**4.1.1 Selection of Calibration Method** The type of microphone and its calibration should be selected in accordance with the type of sound field at the measurement site. This means that the frequency response calibration should be valid for the relevant type of field but not necessarily be performed with that type of field. For any specific type of microphone there are essentially fixed ratios between the responses related to the three principal types of sound field. Therefore, if these ratios have once been determined and made generally available, all responses can be worked out after calibration of one of them. This fact is very important for calibration of common microphone types, as especially free-field and diffuse-field calibrations are technically difficult and costly to perform. Usually free-field and diffuse-field responses are thus determined by applying corrections, either to the pressure-field response or, most commonly, to the so-called electrostatic actuator response (see below), which is quite easily measured.

### 4.2 On-Site Calibration Methods

**4.2.1 Single-Frequency Calibration of Measurement System** On-site calibration of measurement systems is common and highly recommended. A system can be calibrated by analog gain adjustment or by data insertion according to the sensitivity stated on the microphone calibration chart or certificate. However, a system can also be calibrated by correcting its gain or settings until it displays the stated level of a connected sound calibrator. Any one of the two methods is fine with instruments that are frequently used and known to perform properly. However, it is recommended, especially in connection with critical and costly experiments, to apply both methods successively. This will reveal possible instrument defects or wrong settings and prevent that errors get "hidden" by a compensating but nonproper gain setting. Together the methods will, effectively, increase the confidence of correct system performance. Typically, the deviation between the two methods should not exceed a few tenths of a decibel. If the goal is met, one can subsequently either make no further correction or adjust the reading to match the level of the calibrator. The choice between the methods should depend on their uncertainties, which are generally of same order of magnitude.



**Figure 5** Principle of sound calibrator with integrated monitor microphone in pressure-controlling feedback loop.

Specifications of sound calibrators are given in national and international standards.<sup>9</sup> Most common types of sound calibrator are intended for calibration of measurement systems at one frequency only. Their operation frequency may be 250 Hz, but might also be 1000 Hz and comply with the requirements of national and international standards for sound level meters.<sup>10</sup> Older types of calibrator generally contained just an electrical generator and a sound source, while newer types have a built-in microphone that measures and controls the pressure generated in the coupler cavity via a feedback loop (see Fig. 5). The newer design leads to calibrators that are more stable and less dependent on ambient conditions because the sound pressure does not depend on a, generally, less stable sound source but rather on a more stable microphone. Furthermore, due to the feedback loop, such calibrators get lower acoustical output impedance and can be designed to become essentially independent of the load impedance made up by the inserted microphone.

These calibrators, which basically work with small coupler cavities, produce a pressure field. This means that no correction should be applied if the microphone to be calibrated is to be used in a pressure field, say, in a coupler used in the testing of hearing aids. However, if the microphone is part of a free-field sound level meter, one should be aware that its free-field sensitivity for 0° incidence is typically 0.1 to 0.3 dB higher (see microphone or instrument manual) than its pressure-field sensitivity at 1000 Hz. Therefore, to make the instrument read correctly under free-field conditions, the reading with the calibrator should be correspondingly lower than the stated calibrator level. As the diffuse- and pressure-field sensitivities of both one- and half-inch microphones are essentially equal at 1000 Hz, no such correction should be made, when calibrating systems for diffuse-field measurements.

#### 4.2.2 System Frequency Response Verification by Multifrequency Calibrator

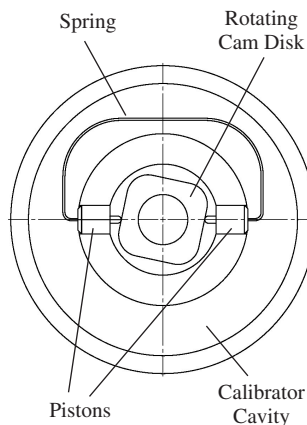
A multifrequency calibrator works at one frequency only, but the frequency can be changed in steps, usually by one octave over a range from say 31.6 Hz to 16 kHz. Generally, such calibrators apply the feedback principle (see above), which can work with coupler cavities so small that they can be operated at the highest mentioned frequency. This type of calibrator is widely used for sensitivity calibration at either 250 or 1000 Hz and for additional frequency response verification over its full range. At frequencies higher than 1000 Hz the pressure on the diaphragm of the inserted microphone differs from that of the calibrator cavity because of the influence of the diaphragm protection grid. Therefore, high-frequency verification of frequency response is only possible if corrections have been measured and are specified for the particular type of microphone. Without corrections this type of calibrator is used for checking stability of frequency response over time.

**4.2.3 Application of Pistonphones** Some types of sound calibrator, called pistonphones, are based on a mechanical operation principle. Pistonphones for use in the field are usually equipped with two pistons driven by a rotating cam disk in and out of the calibrator cavity, where the sound pressure is generated (see Fig. 6). The precisely controlled sinusoidal displacement of the pistons creates a well-defined sound pressure that can be calculated by

$$p \cong \gamma p_{\text{amb}} \frac{2Sd}{\sqrt{2}V}$$

where  $p$  = root-mean-square value of created sound pressure

$\gamma$  = ratio of specific heats of the gas in the cavity ( $\gamma = 1.402$  for dry air at 20°C)



**Figure 6** Principle of hand-held pistonphone. The cam disk in the center displaces the pistons into the surrounding cylindrical calibrator cavity.

$p_{\text{amb}}$  = ambient static pressure

$S$  = mean cross-sectional area of the pistons

$d$  = peak displacement of the pistons

$V$  = volume of coupler cavity (including volume of loading microphone)

The equation is fully valid for adiabatic compression conditions, but, in practice, a heat conduction effect that occurs at the wall of the cavity, especially at low frequencies, reduces the pressure slightly.<sup>8</sup> Typically, such pistonphones work at 250 Hz. As their sound pressure is proportional to the ambient pressure, a precision barometer must follow any pistonphone for accurate determination of its sound pressure. Pistonphones are generally very stable over time. Therefore, they are used as precision field calibrators and as reference standards for comparison calibration of other types of sound calibrator.

#### 4.2.4 Sound Intensity and Particle Velocity Calibration

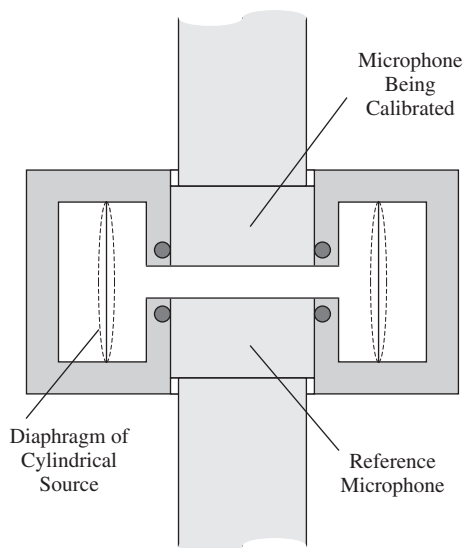
The uncertainty of sound intensity and particle velocity measurements is highly influenced by even small-phase deviations between the applied measurement channels. As microphones, preamplifiers, and amplifiers of the analyzer all contribute to the resulting phase difference, it is important to verify that a user-combined system meets his requirements. Any difference between the phase responses leads to a false intensity that may either add to or subtract from the measured intensity of the field. Therefore, IEC 61043<sup>11</sup> prescribes minimum requirements to pressure-residual intensity index, which is the difference between the pressure level and the residual (false) intensity level that are measured, when the microphones of the probe are exposed to the same pressure. Calibrators that cover the range from 20 Hz to 10 kHz have been designed and are commercially available for this purpose. Particle velocity measurements are also highly influenced by a possible gain difference. This type of error may be detected and reduced with the calibrator by making a minor gain adjustment in one of the channels.

Such calibrators are also designed for absolute pressure level calibration of probes and some even for calibration of intensity level. Intensity is simulated by two signals of controlled pressure and controlled phase difference. An intensity level uncertainty of about 0.12 to 0.16 dB is obtainable at 250 Hz.

### 4.3 Methods of Calibration Service Centers

**4.3.1 Secondary Calibration** A secondary calibration is the calibration of a secondary standard, whose value is assigned by comparison with a primary standard of the same quantity.<sup>1</sup> Such calibrations may be performed by national metrology institutes but are most often made by calibration service centers.

**4.3.2 Sensitivity Comparison Calibration** Sensitivity determination by comparing the output of an unknown microphone with that of a known reference standard is the most commonly used method. This type of calibration is generally made at one frequency only,



**Figure 7** Principle of comparison coupler with built-in source. Operation is possible up to 20 kHz due to its symmetry and the closely mounted diaphragms.

while calibration at other frequencies is performed as a measurement of the frequency response, which is normalized at the sensitivity calibration frequency (typically 250 Hz). The comparison calibration can either be performed by substitution or by simultaneous excitation of the unknown and known microphones. The latter method has the advantage that no uncertainty is related to the microphone loading of the sound source. However, in addition to a two-channel measurement system, the method requires an active two-port coupler (see Fig. 7) or a corresponding microphone mounting. IEC 61094-5<sup>12</sup> describes comparison calibration of microphones with active two-port couplers and mounting jigs.

The equation for the sensitivity calculation is shown below. As the sensitivity of a microphone depends on ambient conditions, it is common to state the calibration result at standard reference conditions [101.325 kPa, 23°C, 50% RH, (relative humidity)]. Therefore, corrections that account for the sensitivity difference between measurement and reference conditions are inserted in the equation. These corrections can only be performed, if sensitivity coefficients for static pressure, temperature, and relative humidity are available for both microphones:

$$\begin{aligned}
 M_X [\text{dB re. 1 V/Pa}] &= M_R [\text{dB re. 1 V/Pa}] \\
 &+ 20 \log \frac{u_X}{u_R} + 20 \log \frac{G_R}{G_X} \\
 &+ \text{Cor}_{\text{Ps}} + \text{Cor}_T + \text{Cor}_{\text{RH}}
 \end{aligned}$$

where  $M_X$  = sensitivity of microphone being calibrated

$M_R$  = sensitivity of reference microphone

$u_X$  = output voltage of microphone being calibrated

$u_R$  = output voltage of reference microphone

$G_X$  = electrical gain of channel with microphone being calibrated

$G_R$  = electrical gain of channel with reference microphone

$\text{Cor}_{\text{Ps}}$  = sensitivity correction for ambient pressure

$\text{Cor}_T$  = sensitivity correction for ambient temperature

$\text{Cor}_{\text{RH}}$  = sensitivity correction for ambient humidity

#### 4.3.3 Frequency Response Calibration by Electrostatic Actuator

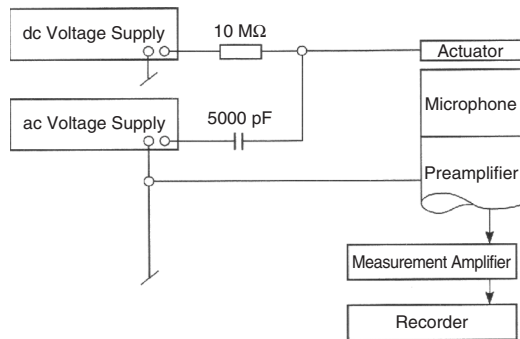
In calibration service centers and by manufacturers, where many measurement microphones are calibrated, the most commonly applied method for frequency response calibration is the electrostatic actuator method. This method is fast and it only requires “normal” laboratory conditions (no specific acoustical measurement rooms). An electrostatic actuator excites the diaphragm of the microphones by electrostatic forces. The sound, which under certain conditions can be heard during actuator calibration, is thus not generated by the actuator but by the excited microphone diaphragm. This diaphragm-generated sound is the reason that the measured actuator response differs from the pressure response of the microphone. The difference (in decibels), which is essentially zero at lower frequencies, is about +0.1 dB at 1 kHz and −1.5 dB at 10 kHz for highly sensitive microphones (1-inch pressure microphones with 50 mV/Pa) that have diaphragms with low acoustic impedance. For less sensitive microphones the difference is significantly smaller. However, the difference is essentially the same for all units of a given type or model of microphone. Therefore, corrections can be applied with actuator calibration results to determine free-field, diffuse-field, and also pressure-field responses. The actuator method is generally used between 20 Hz and 200 kHz. It may also be used at higher and lower frequencies, though with low-frequency calibration one should be aware that the actuator excites the microphone diaphragm only. This means that the low-frequency roll-off of the free- and diffuse-field responses, which is caused by the static pressure equalization vent of the microphone, cannot be measured by this method.

An actuator is a metallic plate placed in front of and in parallel with the microphone diaphragm that must consist of metal or have an electrically conducting layer on its external side. Actuators are typically driven with 30 to 100 V ac (alternating current) and 800 V dc (direct current) (see Fig. 8), and they generate an equivalent sound pressure level of 94 to 100 dB. For details, see Ref. 13 and IEC 61094-6.<sup>14</sup>

#### 4.3.4 Frequency Response Calibration by Small-Volume Active Coupler

Small-volume comparison calibration is an alternative method for





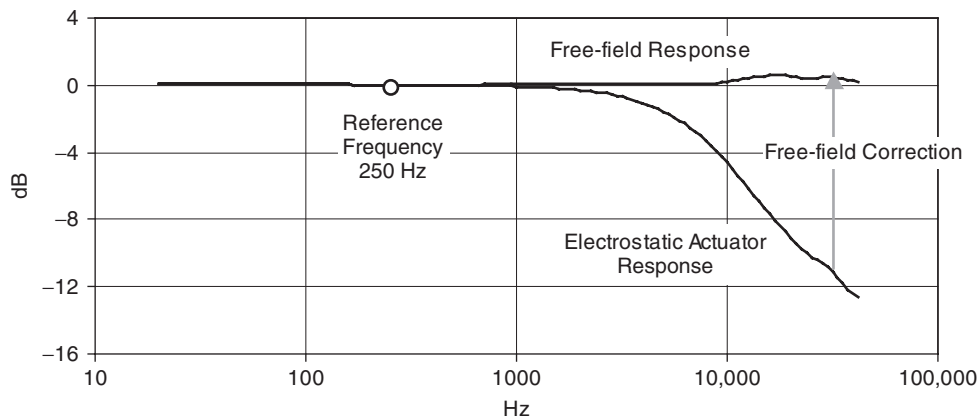
**Figure 8** Block diagram of electrostatic actuator calibration system.

frequency response calibration. Its major advantage over electrostatic actuator calibration is that microphones to be calibrated do not need to have electrically conducting diaphragms and that they can be calibrated without dismantling their diaphragm protection grids. The method implies thus less risk of destroying microphones and can be used under less controlled working conditions. Like the actuator method this method requires application of corrections to obtain frequency responses that are valid in the principal types of sound field. Disadvantages are that sound field corrections have not been measured and published to the same extent as for the actuator method and that the frequency range of the method is less wide, due to resonance phenomena in the applied couplers. The uncertainty that can be achieved with the method is very good (say 0.05 dB,  $k = 2$ ) at lower frequencies, but it increases significantly from about 4 up to 16 kHz, which is a typical upper limit for calibration of half-inch microphones. A sketch of a small-volume active coupler is shown in Fig. 7. IEC 61094-5<sup>12</sup> describes the method in greater detail.

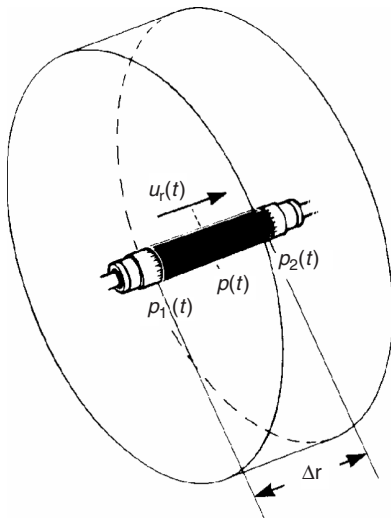
**4.3.5 Sound Field Corrections** Frequency responses that are measured with electrostatic actuator or with small-volume comparison couplers are generally not directly applicable. Corrections should be applied to the measured responses to obtain responses that are valid under free-field, diffuse-field, or pressure-field conditions. The measured responses are usually normalized at 250 Hz, where the influence of the type of sound field on the microphone sensitivity is essentially zero for microphones of diameter less than say 25 mm. The necessary sound field corrections may be worked out by acoustical metrology institutes or by leading manufacturers, who master primary calibration methods and have the necessary acoustical facilities. Free-field corrections depend on angle of sound incidence on the microphone body. Free-field microphones are generally optimized for and applied with axial sound incidence on the front of their diaphragms (called 0° incidence) and should also be calibrated for this incidence. The free- and diffuse-field corrections account for the change of sound pressure in the measurement point, which is due to the presence of the microphone body and is caused by diffraction and reflection of the sound. The correction is a function of microphone dimensions and shape of body and protection grid. A free-field response, obtained by adding the correction to the measured electrostatic actuator response, is shown in Fig. 9. More details and data can be found in the Brüel & Kjær Microphone Handbook.<sup>15</sup>

#### 4.3.6 Phase Response Comparison Calibration

Measurement of sound intensity is most often performed in accordance with an internationally standardized method<sup>11</sup> that is based on pressure measurements only. Intensity measurement probes intended for one-, two-, or three-dimensional measurements are equipped with a pair of pressure-sensing microphones for each dimension. The microphone pair measures the pressure at two points with predefined distance on the probe measurement axis (Fig. 10). The intensity is obtained



**Figure 9** Corrections added to a measured electrostatic actuator response to obtain the microphone response curve valid for free-field conditions.



**Figure 10** One-dimensional intensity measurement probe equipped with pressure-sensing microphones.

by multiplying pressure and air particle velocity, which are represented by functions of sum and difference of the measured pressure values, as shown in

$$\overline{I_r} = \frac{p_1(t) + p_2(t)}{2} \int \frac{p_1(t) - p_2(t)}{\Delta r_0 \rho_0} dt$$

where the bars indicate time average of intensity and  $p_1(t)$ ,  $p_2(t)$  = instantaneous sound pressure measured by microphones 1 and 2

$\Delta r_0$  = distance between pressure measurement points

$\rho_0$  = density of gas (air)

$t$  = Time

The method is only applicable if the phase response characteristics of the applied microphones are essentially equal. Even a small deviation between the phase responses can lead to a significant error of the measured velocity and thus also of the intensity.

IEC 61043 specifies minimum acceptable pressure-residual intensity indices for probes and measurement systems. The indices are differences between the levels of pressure and residual intensity that are measured by the system and related to probe and system, respectively, when the same signal is applied to the two microphones. The standard specifies indices for a fixed microphone distance (25 mm), which for the microphones can be converted to deviations between their phase responses (see Fig. 11). The conversion is made with the following equation below:

$$\Delta\phi \cong \frac{\Delta R f}{c} 360 \times 10^{-\text{Index}/10}$$

where  $\Delta\phi$  = maximum phase response deviation

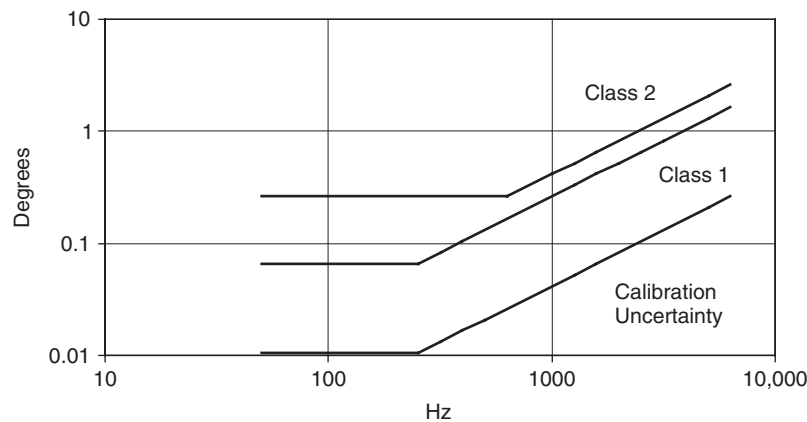
$\Delta R$  = nominal microphone distance (25 mm)

$f$  = frequency

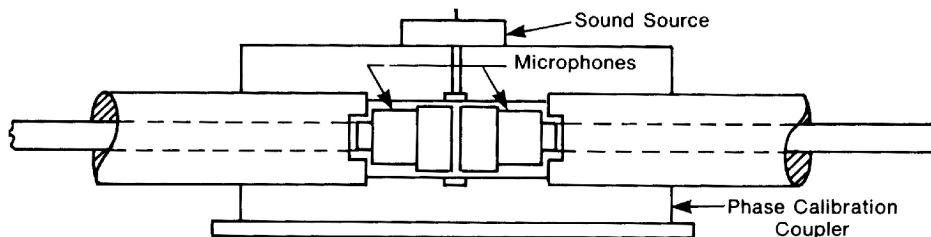
Index = minimum index specified by IEC61043

The uniformity requirements to phase responses are not met by randomly selected pairs of measurement microphones. Different microphone mechanisms cause phase deviations that are generally far too large, both at low and at high frequencies. Therefore, microphones are selected to form suitable matching pairs.

The pressure on the diaphragm and that at the static pressure equalization vent determine the low-frequency phase response of a microphone and thus also the phase response deviation between two microphones. Therefore, microphone pairs that are to be compared with respect to phase response deviation must be exposed to essentially the same pressure at both diaphragms and vents during the calibration.



**Figure 11** Upper limits (IEC 61043) of phase response deviation for pairs of intensity measurement microphone and related limit of phase calibration uncertainty.



**Figure 12** Phase response comparison coupler for selection and calibration of matched pairs of microphone.

To ensure sufficient pressure uniformity over a wide frequency range, the coupler (see Fig. 12) used with the measurement must be as small as possible and situate the microphones placed close to each other with their diaphragms “face to face.” This positioning gives pressure uniformity also at high frequencies, where only the pressure at the diaphragms is significant. This type of coupler can work from a few hertz up to about 6 kHz and 10 kHz with half-inch and quarter-inch microphones, respectively.<sup>16</sup> Couplers designed with two sound inlets can work at frequencies that are about 50% higher. The estimated calibration uncertainty ( $k = 2$ ) is less than 12% of the requirements in the standard.

**4.3.7 Low-Frequency Calibration** The low-frequency response of a microphone depends on the time constant of its static pressure equalization system and also on, whether the venting channel is exposed to the sound field or not. Typically, the response of a microphone rolls off by 3 dB at a frequency between 1 and 3 Hz, if the vent is exposed, while the response is essentially flat to dc if it is nonexposed. At frequencies lower than 10 times the  $-3$  dB frequency, it is important to choose a low-frequency calibration method that will expose the microphone diaphragm and vent to the sound in a way that corresponds to that existing on the intended measurement site.<sup>15</sup> Specially designed pistonphones and couplers with wall-mounted reference microphones are commonly used for low-frequency calibration.

#### 4.4 Methods of Microphone Testing

**4.4.1 Environmental Testing** The sensitivity of any measurement microphone is to some degree influenced by the ambient conditions.<sup>15,17</sup> The international standards for laboratory<sup>3</sup> and working standard microphones<sup>4</sup> require that the magnitudes of pressure, temperature, and relative humidity coefficients do not exceed certain limits. These coefficients are most often measured with electrostatic actuators, whose excitation of the microphone is essentially independent of the ambient parameters. It should be noted that the actuator measurement determines changes of microphone pressure sensitivity only—it does not measure changes of diffraction and reflection. Changes of free- and diffuse-field corrections are small and are generally ignored but may be estimated from changes

of speed of sound and their influence on the wavelength. This is influenced by temperature and, to a small degree, by the ambient pressure and humidity.

**4.4.2 Dynamic Range Testing** The dynamic range of condenser microphones is generally large compared with the range of commonly occurring and measured sound pressure levels. Sometimes measurements must be made near to the lower limit—the level of the inherent noise of the microphone—or near to the upper limit, which is usually determined by microphone distortion or by its preamplifier clipping of the signal.<sup>15</sup>

Inherent noise of a microphone can be measured by placing the microphone in a sound-isolating chamber.<sup>18</sup> This is typically a sealed metal cylinder with walls of 10- to 20-mm thickness and a volume of 1000 to 2000 cm<sup>3</sup>. Such a chamber can be used for broadband noise measurements down to less than 0 dB (threshold of hearing), if it is isolated from vibration.

High-level calibration or test devices have been designed with horn-drivers, shakers, pistonphones, and resonating tubes, which all work at relatively low frequencies.<sup>19</sup> Linearity is measured with such systems by comparing the device under test with selected high-level reference microphones. One example is a resonating tube system that at 500 Hz can measure level linearity and distortion from an SPL of 94 dB to 174 dB (0.1 bar) with uncertainty less than 0.025 dB and 0.5%, respectively, at the highest level.<sup>20,21</sup>

#### 4.5 Methods of National Metrology Institutes

**4.5.1 Primary Calibration** The sensitivity of measurement microphones is most often determined by comparison with that of a reference microphone, which is usually a laboratory standard microphone. Also this reference might have been calibrated by comparison; however, this is not possible for the upper microphone in the calibration hierarchy. It will have to be calibrated by a “primary calibration” method that determines microphone sensitivity based on nonacoustical, that is, physical, mechanical, and electrical, parameters.

Microphone reciprocity calibration is an example of a primary method. It was invented in the 1940s, and since then the method has become refined and standardized and is now the dominating primary method for both free-field<sup>22</sup> and pressure-field calibration.<sup>8</sup>

**Table 1 Uncertainty of Pressure Reciprocity Calibration of Leading National Metrology Institute**

Uncertainty ( $k = 2$ )		20 Hz	32 Hz	63 Hz–4 kHz	10 kHz	20 kHz	25 kHz
Pressure field	LS1	0.06 dB	0.04 dB	0.03 dB	0.08 dB	—	—
	LS2	0.08 dB	0.05 dB	0.04 dB	0.04 dB	0.08 dB	0.12 dB

The reciprocity calibration technique, which is considerably more complex and time consuming than comparison calibration techniques, is mainly applied by national metrology institutes and by leading microphone manufacturers.

**4.5.2 Principle of Reciprocity Calibration** The reciprocity calibration method<sup>23</sup> requires reciprocal transducers,<sup>24</sup> like condenser microphones, that are passive and can work both as sound sensors and sources. The calibration technique is based on the measurement of transfer functions for pairs of microphones that are operated as source and sensor, respectively. The microphones are coupled together in an acoustically well-defined way, while the overall transfer function, the ratio between sensor output voltage and source input current, is measured. From this ratio, called the electrical transfer impedance, and from the acoustical coupling or transfer impedance the microphone sensitivity product may be calculated:

$$M_1 M_2 = \left( \frac{Z_e}{Z_a} \right)_A$$

$M_1, M_2$  = sensitivities of microphones 1 and 2

$Z_e/Z_a$  = ratio of electrical and acoustical transfer impedance

By having three microphones (1, 2, 3) and by making three measurements (A, B, C) with the three possible microphone combinations (1–2, 1–3, 2–3), the sensitivities of the microphones can be calculated from values of measured electrical and calculated acoustical transfer impedance:

$$\begin{aligned} M_1 M_2 &= \left( \frac{Z_e}{Z_a} \right)_A & M_1 M_3 &= \left( \frac{Z_e}{Z_a} \right)_B \\ M_2 M_3 &= \left( \frac{Z_e}{Z_a} \right)_C \end{aligned}$$

Different microphone responses can be obtained by reciprocity calibration by applying different microphone coupling principles. The pressure-field responses are thus obtained by coupling the microphones with the

air (or gas) inside a small closed cavity, while the free-field responses are obtained with open-air coupling in a space that has no disturbing sound reflecting surfaces (an anechoic room).

**4.5.3 Pressure Reciprocity Calibration** Several national metrology institutes around the world offer a pressure reciprocity calibration<sup>8,25</sup> service for laboratory standard microphones. Typically, the frequency range is from 20 Hz to 10 kHz for 1-inch (LS1) and 20 Hz to 20 kHz for 0.5-inch (LS2) microphones, but some institutes have experience with calibration at both lower and higher frequencies. Standing waves in couplers determine the upper frequency limit of pressure reciprocity calibration. The wave problem can be reduced either by filling hydrogen, which has higher speed of sound than air, into the coupler or by shaping the couplers as “near ideal” acoustical transmission lines. This type of coupler, called a plane-wave coupler, performs in an analyzed and predictable way and is now applied for most primary pressure calibrations. Table 1 shows typical calibration uncertainty values.

#### 4.5.4 Free-field Reciprocity Calibration<sup>22,26</sup>

Only few laboratories offer a free-field reciprocity calibration service. The theory behind free-field reciprocity calibration is simpler than that of pressure reciprocity, but technically it is much more difficult to perform. The major reason is that condenser microphones are very weak sound sources, when applied in the open space. This leads to serious noise and cross-talk-related measurement problems. As this is the case especially at lower frequencies, the lower limit of free-field calibration services is generally about 1 to 3 kHz. Free-field calibration can be performed up to about 25 and 50 kHz for 1-inch and 0.5-inch microphones, respectively. Table 2 shows typical calibration uncertainty values.

#### 4.5.5 Free-Field Corrections of Laboratory Standard Microphones

Fortunately, there is, essentially, a fixed ratio between the free-field and the pressure-field sensitivities of any microphone or model of microphone. Therefore, if this ratio is known, the free-field sensitivity can be calculated by adding a correction to the pressure-field sensitivity, which

**Table 2 Uncertainty of Free-Field Reciprocity Calibration of Leading National Metrology Institute**

Uncertainty ( $k = 2$ )		1 kHz	2 kHz	4 kHz	8 kHz	10 kHz	20 kHz	40 kHz
Free field	LS1	0.10 dB	0.08 dB	0.07 dB	0.07 dB	0.08 dB	0.15 dB	—
	LS2	0.12 dB	0.10 dB	0.08 dB	0.07 dB	0.07 dB	0.09 dB	0.15 dB

is more easily and more accurately measured. Free-field corrections for the following laboratory standard microphones: Brüel & Kjær Type 4160 and Type 4180, Tokyo Rico Type MR103 and Type MR112, and Western Electric Type 640AA have been measured and calculated and are stated in the manufacturer specifications, standards, and research reports. Newer and internationally agreed free-field correction data have been published for Laboratory Standard Microphones types LS1 and LS2 in an IEC Technical Specification TS 61094-7. These corrections<sup>29</sup> are supported by several measurement results obtained with the B&K microphones Types 4160 and 4180.

#### 4.5.6 Determination of Diffuse-Field Frequency Response

Diffuse-field reciprocity calibration<sup>27</sup> is, in principle, possible, but it is associated with several problems that have presently not been sufficiently analyzed and described to make the method practically applicable.<sup>28</sup> Therefore, diffuse-field responses of microphones are generally calculated from free-field responses measured for different angles of sound incidence. The angles are typically spaced by  $10^\circ$  and cover the range from  $0^\circ$  to  $180^\circ$ . During the calculation a weighting factor is applied with the correction of each measured angle to account for its probability of occurrence in a diffuse sound field. This method of calculating the diffuse-field sensitivity from a series of free-field responses and the diffuse-field correction from a series of free-field corrections is standardized and is the commonly used method for determining diffuse-field responses. Diffuse-field corrections that are determined by this method are frequently applied with electrostatic actuator measurements by service centers for secondary microphone calibration.

#### 4.5.7 Calibration of Reference Sound

**Calibrators** The International Standard for Sound Calibrators IEC60942<sup>9</sup> specifies a laboratory standard calibrator named Class LS. This class of calibrator includes reference standard pistonphones that are mainly used by national metrology institutes and calibration service centers for comparison calibration of other types of calibrators. The sound pressure of pistonphones might be determined by calculation after measurement of their mechanical dimensions, speed of rotation, and ambient conditions. However, such laboratory sound standards are generally calibrated by measuring the sound pressure by one or more reference standard microphones, which are calibrated by the pressure reciprocity method. This method may lead to an uncertainty of less than 0.05 dB ( $k = 2$ ).

#### REFERENCES

1. ISO Guide 99, *International Vocabulary of Basic and General Terms in Metrology*, International Organization for Standardization, Geneva, Switzerland, 1996.
2. H.-E. de Bree, The Microphoflown: An Acoustic Particle Velocity Sensor, *Acoust. Australia*, Vol. 31, 2003, pp. 91–94.
3. IEC 61094-1, Measurement Microphones, Part 1: Specifications for Laboratory Standard Microphones, 2000.
4. IEC 61094-4, Measurement Microphones, Part 4: Specifications for Working Standard Microphones, 1995.
5. IEC 50, International Electrotechnical Vocabulary, Chapter 801: Acoustics and Electroacoustics, 801-23-28—Free Sound Field, 1994.
6. IEC 50, International Electrotechnical Vocabulary, Chapter 801: Acoustics and Electroacoustics, 801-23-31—Diffuse Sound Field, 1994.
7. IEC 61183, Electroacoustics—Random-Incidence and Diffuse-Field Calibration of Sound Level Meters, 1994.
8. IEC 61094-2, Measurement Microphones, Part 2: Primary Method for Pressure Calibration of Laboratory Standard Microphones by the Reciprocity Technique, 1992.
9. IEC 60942, Electroacoustics—Sound Calibrators, 2002.
10. IEC 61672-2, Electroacoustics—Sound Level Meters—Part 1: Specifications, 2005.
11. IEC 61043, Electroacoustics—Instruments for the Measurement of Sound Intensity Measurements with Pairs of Pressure Sensing Microphones, 1993.
12. IEC 61094-5, Measurement Microphones—Part 5: Methods for Pressure Calibration of Working Standard Microphones by Comparison, 2001.
13. E. Frederiksen, Electrostatic Actuator, in *AIP Handbook of Condenser Microphones*, G. S. K. Wong and T. F. W. Embleton, Eds., American Institute of Physics, New York, 1994, pp. 231–246.
14. IEC 61094-6, Measurement Microphones—Part 6: Electrostatic Actuators for Determination of Frequency Response, 2004.
15. Brüel & Kjær, *Microphone Handbook* (BA5105), *Theory* (Vol. 1) and *Data* (Vol. 2), Naerum, Denmark.
16. E. Frederiksen and O. Schultz, Pressure Microphones for Intensity Measurements with Significantly Improved Phase Properties, *Brüel & Kjær Tech. Rev.*, No. 4, 1986.
17. K. Rasmussen, The Influence of Environmental Conditions on the Pressure Sensitivity of Measurement Microphones, *Brüel & Kjær Tech. Rev.*, No. 1, 2001.
18. K. C. T. Ngo and A. J. Zuckerwar, Acoustic Isolation Vessel for Measurement of the Background Noise in Microphones, *J. Acoust. Soc. Am.*, Vol. 93, No. 5, 1993.
19. D. C. Aldridge, D. R. Jarvis, B. E. Jones, and R. T. Rakowski, A Method for Demonstrating the Linearity of Measurement Microphones at High Sound Pressures, *Acustica*, Vol. 84, 1998, pp. 1167–1171.
20. E. Frederiksen, System for Measurement of Microphone Distortion and Linearity from Medium to Very High Levels, *Brüel & Kjær Tech. Rev.*, No. 1, 2002.
21. E. Frederiksen, Verification of High-Pressure Linearity and Distortion of Measurement Microphones, Proceedings of the International Conference on Acoustics, Kyoto, Japan, 2004.
22. IEC 61094-3, Measurement Microphones—Part 3: Primary Method for Free-Field Calibration of Laboratory Standard Microphones by the Reciprocity Technique.
23. L. L. Beranek, Reciprocity Technique of Calibration, in *Acoustical Measurements*, American Institute of Physics, L. L. Beranek, Cambridge, MA, 1988, Chapter 42.
24. IEC 50(801), Vocabulary: Acoustics and Electroacoustics, 801-25-08—Reciprocal Transducer.
25. G. S. K. Wong, Primary Pressure Calibration by Reciprocity, in *AIP Handbook of Condenser Microphones*,

- G. S. K. Wong and T. F. W. Embleton, Eds., American Institute of Physics, New York, 1994, Chapter 4.
26. V. Nedzelitsky, Primary Method for Calibrating Free-Field Response, in *AIP Handbook of Condenser Microphones* G. S. K. Wong and T. F. W. Embleton, Eds., American Institute of Physics, New York, 1994, Chapter 5.
27. IEC 61183, Electroacoustics—Random-Incidence and Diffuse-Field Calibration of Sound Level Meters.
28. H. G. Diestel, Reciprocity Calibration of Microphones in a Diffuse Sound Field, *J. Acoust. Soc. Am.*, Vol. 33, No. 4, 1961.
29. IEC TS 61094-7, Measurement Microphones, Part 7: Values for the Difference between Free-Field and Pressure Sensitivity Levels of Laboratory Standard Microphones.

# CHAPTER 52

## CALIBRATION OF SHOCK AND VIBRATION TRANSDUCERS

Torben Rask Licht  
Brüel & Kjær  
Naerum, Denmark

### 1 INTRODUCTION

This chapter describes various methods used today for calibration of vibration and shock transducers. The general concepts of sensitivity, traceability, and hierarchy are briefly introduced. A short description of the general measurement principles is given, stressing the difference between relative and absolute measurement principles. The important features of the most common types of transducers and preamplifiers are described, as this is important knowledge to avoid errors in the calibration process. Over time many methods have been used and might still be useful, but this chapter is limited to the most important methods. As the range of frequencies and amplitudes covered by vibration transducers is very large, it will often be necessary to apply several methods to give a complete calibration of a transducer. The chapter describes calibrators, comparison to a reference transducer, and primary calibration methods. Typical attainable uncertainties are given to help the user to select the method most appropriate for a given measurement task.

### 2 SENSITIVITY AND TRACEABILITY

To calibrate a transducer is to determine its sensitivity, sometimes referred to as the calibration factor, in terms of units of electrical output (volts, amperes, etc.) per unit of the physical input parameter (pressure, acceleration, distance, etc.). In general, this includes both magnitude and phase information and is a complex quantity. The fundamental units provide a fixed reference, which is essential as it allows measurements, including calibrations, to be compared—measurements, which could have been made by different people, in different locations, and under different conditions. The units must be referred to in a known and agreed way that is well defined and monitored on an international basis in organizations like BIPM (Bureau International des Poids et Mesures). The accuracy of the calibration must also be known, that is, the device and method used to calibrate an accelerometer must perform the calibration with a known uncertainty.

If these conditions are fulfilled, the calibration is called traceable. It is important to note that traceability is not in itself an indication of high accuracy, but if the uncertainty is known, the calibration can then be compared with other valid measurements. Therefore, a calibration is not useful, unless the associated uncertainty is known. Chapter 53 has more details about traceability.

### 3 CALIBRATION HIERARCHY

To avoid the necessity for carrying out absolute (i.e., with direct link to the fundamental quantities) calibrations of each individual transducer, a hierarchy of reference standard transducers is established. International traceability and verification of uncertainties is obtained by performing international key comparisons of reference standard transducers between the national metrology institutes (NMIs) as required by the Consultative Committee for Acoustics, Ultrasound and Vibration (CCAUUV) under the International Bureau of Weights and Measures (BIPM). Regionally key comparisons including at least one NMI are used to ensure that the uncertainties stated are fulfilled. Chapter 53 has more details about calibration hierarchy.

### 4 GENERAL MEASUREMENT PRINCIPLES

#### 4.1 Description of Motion

To describe fully any motion of a solid body three linear and three rotational degrees of freedom need to be described. This makes vibration measurement and calibration different from the sound pressure, which is a parameter describing the properties at a point with only one degree of freedom. For measurement and calibration purposes it is normally desirable to create and measure only one degree of freedom at one time.

#### 4.2 Motion Measurement

There are two basically different ways of measuring motion:

1. *Relative* measurement between two points, where the motion of one of the points is considered sufficiently well known or unimportant
2. *Absolute* measurement with respect to an inertial system

An example of the first type is the motion of a shaft relative to the bearing, where the absolute motion often is less important. The second type of measurements uses practically only so-called seismic (or mass–spring) instruments, which use an internal seismic mass as reference.

#### 4.3 Relative Methods

A number of different principles are used to make relative measurements, some of which can also be used internally for seismic transducers. These methods

comprise capacitive, inductive, and reductive methods, but for calibration purposes a discussion of the most important methods follows.

**Interferometric Methods** Today the most widely used method to calibrate vibration transducers with high accuracy is the laser interferometric method. Several techniques exist, but basically a very well-defined laser wavelength is used as a gauge to measure the displacement. Often simple fringe counting can be used to determine the vibration amplitude with high accuracy.

**Doppler Effect** In interferometers and other similar instruments the Doppler effect is used directly to measure velocity. The basic physical law for wave propagation tells us that a wave reflected from an object moving with a velocity  $v$  relative to our combined transmitter and receiver will be frequency shifted according to the formula

$$\Delta f = \frac{2v}{\lambda}$$

where  $\lambda$  is the wavelength of the wave used. This may range from low-frequency sound in the metre range over radar in the centimetre range to lasers with less than  $1 \mu\text{m}$  wavelength. For vibration measurements the use of lasers is increasing due to the development of well-suited inexpensive lasers and detectors.

#### 4.4 Physical Principles Used for Absolute Measurements

All the transducers used for absolute measurements are using a seismic mass as built-in reference, and many different methods can be used for detection of the relative motion between the mass and the housing. To get a good feeling for what happens inside a seismic transducer, the model shown in Fig. 1 is used, where  $k$  is the stiffness of the spring and  $c$  is the damping. The ratio between the motion amplitude of the moving part and the relative motion of the mass with respect to the

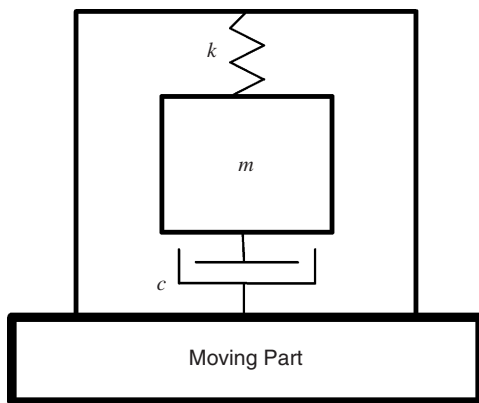


Figure 1 Seismic transducer model.

housing can be described in magnitude and phase by the formulas

$$R = \frac{(\omega/\omega_r)^2}{\sqrt{[1 - (\omega/\omega_r)^2]^2 + [2d(\omega/\omega_r)]^2}} \quad \text{and}$$

$$\theta = \tan^{-1} \frac{2d(\omega/\omega_r)}{1 - (\omega/\omega_r)^2}$$

where  $d$  is the fraction of critical damping ( $c = 2\sqrt{km} = 2m\omega_r$ ) and  $\omega_r = \sqrt{k/m}$  is the resonance angular frequency. Some typical curves showing the resulting internal relative displacements relative to different input parameters are shown in Fig. 2.

It is seen that the relation between input acceleration and relative displacement is close to unity (better than 10%) up to about one third of the resonance frequency for lightly damped transducers. The phase shift is less than half a degree in the same range. For damped transducers the range can be extended to 0.7 times the resonance frequency at the expense of a phase shift of up to  $60^\circ$ .

For acceleration-sensitive transducers with high resonance frequencies ( $>10 \text{ kHz}$ ) the damping is normally very low and the spring very stiff. For lower resonance frequencies the amplification at resonance tends to make transducers very fragile, and therefore they are often damped by air or silicone oil.

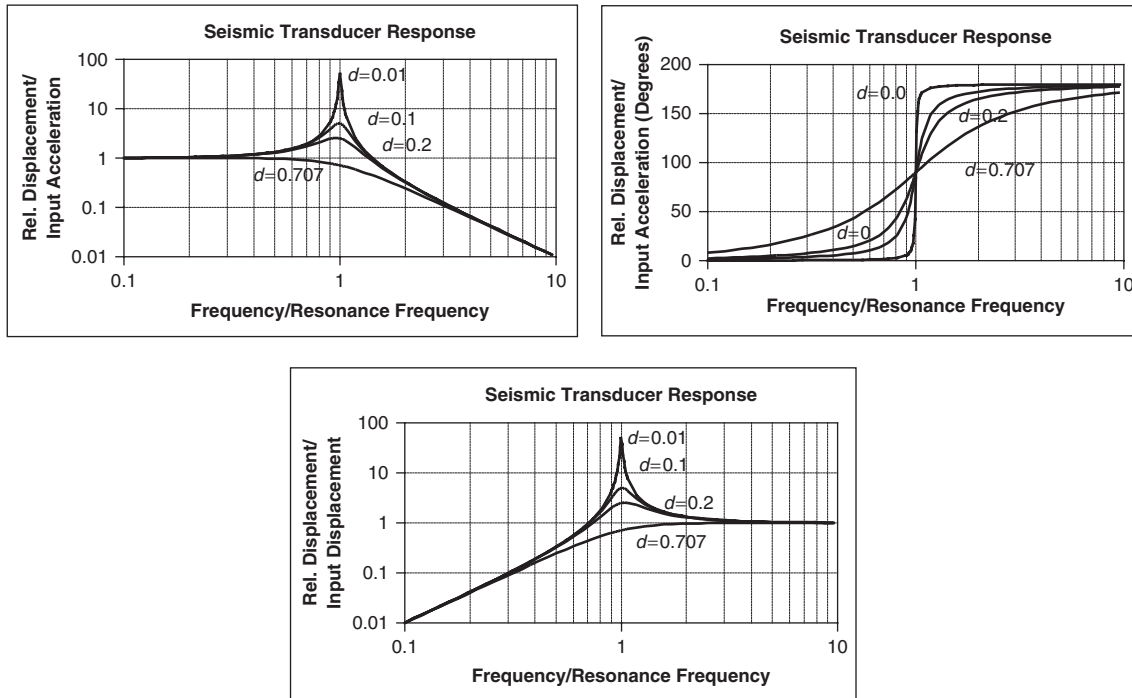
If the resonance frequency is made very low, that is, in the range 1 to 50 Hz, then the mass will remain virtually fixed in space while the housing will move together with the structure at frequencies well above resonance. This situation is shown on the third graph in Fig. 2, indicating a numerically close to unity relation between displacements when the frequency is above two to three times the resonance frequency. In most cases the transducers, mostly referred to as velocity pickups, but also including seismometers, are damped, giving large phase errors up to more than 10 times the resonance frequency.

## 5 VIBRATION AND SHOCK TRANSDUCERS

### 5.1 Standards

In contrast to the situation for microphones there are no international standards for the shape of or output from vibration transducers. However, a few properties have become common in industry for mid-size general-purpose accelerometers. The common mounting thread is 10-32 UNF and the common connector uses the same thread and is in general referred to as a 10-32-microdot connector after the manufacturer introducing this type of connectors. Most transducers using built-in electronics work with a constant-current supply on the same line as the signal. The common way of doing this is to use a 24-V supply with a constant-current diode in series. The diode gives between 4 and 20 mA current (the higher the longer cables to be driven) and the transducer delivers the vibration signal as an oscillating voltage around a constant bias of 8 to 12 V.





**Figure 2** Internal relative displacements relative to input parameters for seismic transducers.

Another area that lacks standards is the influence of the transducer on the measured parameter. The presence of the microphone alters the sound pressure measured in front of the microphone. Therefore free-field corrections are used. The presence of an accelerometer alters the vibration of the structure on which it is mounted. The stiffness and mass of the structure (i.e., its mechanical impedance) changes the mounted resonance frequency of the transducer. These phenomena will have to be taken into account by the users, but standards for doing this in the same way are not available. Guidelines for mounting of transducers can be found in Ref. 1.

## 5.2 Vibration Signal Types

The motion, which is the object of measurement in any measurement setup, can be described by various parameters. First of all the directional and rotational properties of the motion need to be known. For calibration it is normally desirable to have only one degree of freedom at one time, and most transducers are also only sensitive along or around one axis. In special cases transducers can have properties where the signal along one axis have great influence on the response along another axis. In such cases calibration using multi-axis excitation can be useful, but this is quite complicated to perform and only done at specialized laboratories and at relatively low frequencies. Even if such information is available, it does not mean that the transducer alone can be used to characterize the

motion. It can normally only be used to estimate errors. If information about the critical axis input is available from another transducer, this might be used to correct the measurements, but systems doing so are very rare.

For the remaining part of the chapter we are only treating rectilinear motion along or rotational motion around the so-called sensitive axis of a transducer. For calibration normally only two different types of signals along or around the sensitive axis are used, stationary vibration signals (sinusoidal or random) or transients normally referred to as shocks. Many transducers can be calibrated by both methods and used for both types of signals, but the calibration methods differ considerably.

## 5.3 Transducer Sensitivity

Apart from very specialized transducers giving frequency-modulated or optical outputs the outputs from the transducers are voltage, current, or charge signals proportional to acceleration, velocity, or displacement. Some transducers have intrinsic low-impedance output or built-in electronics providing suitable electrical output when the correct power supply is used. For transducers with high-impedance output a preamplifier or conditioner will normally be needed.

## 5.4 Preamplifiers

For the large fraction of stable and well-proven accelerometers based on piezoelectric ceramics or

quartz without built-in electronics, it is imperative to use a suitable preamplifier/conditioner to get reliable results in calibration. The output impedance is basically a capacitance varying from a few picofarads to several nanofarads. This implies that the output voltage and the lower limiting frequency will vary according to the capacitance of the cable used, the input impedance of the amplifier, and the leakage resistance of the cable and transducer. This makes the use of voltage preamplifiers "microphone style" impractical. The better solution for such transducers is to use a so-called charge amplifier. The charge amplifier is a virtual short-circuit of the transducer through which the current is integrated giving an output proportional to the generated charge, usually expressed in picocoulombs. (Note: The unit coulomb is defined as ampere times seconds corresponding to the integration of current.) This gives a result practically independent of cable capacitance and leakage resistance. For calibration purposes the properties in the form of the gain (normally expressed as mV/pC) as a function of frequency will have to be known. Frequency ranges are often from a fraction of a hertz to 100 kHz with gains from -40 to 80 dB relative to 1 mV/pC. Many charge amplifiers have a range of high- and low-pass filters, and some have facilities for analog integration to give outputs proportional to velocity or displacement with an accelerometer at the input.

For the transducers using bridge-type sensitive elements, for example, the so-called piezoresistive (semiconductor strain gauge) transducers, a well-controlled supply of 1 to 10 V is needed. Their output is proportional to the excitation voltage. These transducers have the property that they respond to a constant acceleration. This permits special calibration methods (e.g., based on earth's gravity) to be used.

## 6 CALIBRATION METHODS

### 6.1 On-site Calibration Methods

When setting up larger measurement systems, it is good practice to check that the different transducer channels are set up correctly. Depending on the available data and the total uncertainty for each channel, a small reference vibration source can be used either for calibration of the channel or as a check of the proper function of the channel. This is performed using so called calibrators. Their use is described in the International Organization for Standardization (ISO) standard ISO 16063-21.<sup>2</sup>

#### Calibrators or Vibration Reference Sources

These are small, handy, completely self-contained vibration reference sources intended for rapid calibration and checking of vibration measuring, monitoring, and recording systems. Often an acceleration level of  $10 \text{ m s}^{-2}$  at a frequency of 159.15 Hz ( $\omega = 1000 \text{ rad s}^{-1}$ ) is used, permitting the reference signal to be used also for velocity and displacement calibration at  $10 \text{ mm s}^{-1}$  and  $10 \text{ }\mu\text{m}$ , respectively. An example of the cross section of such a device is shown in Fig. 3. It shows the internal construction including an accelerometer that is used in a closed loop to maintain the defined level independent of the load and the support of the exciter (the relative motion between the body of the exciter and the moving element varies depending on the load and support of the exciter). The attainable uncertainty is typically 3 to 5% on the generated vibration magnitude.

If the requirements for a calibration are limited and suitable conditioning and readout instruments are available, a calibration can be performed at the vibration frequency and magnitude available from the exciter.

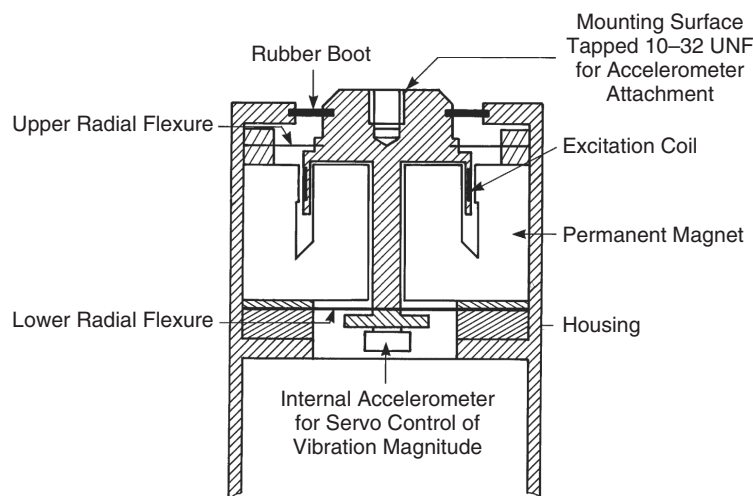
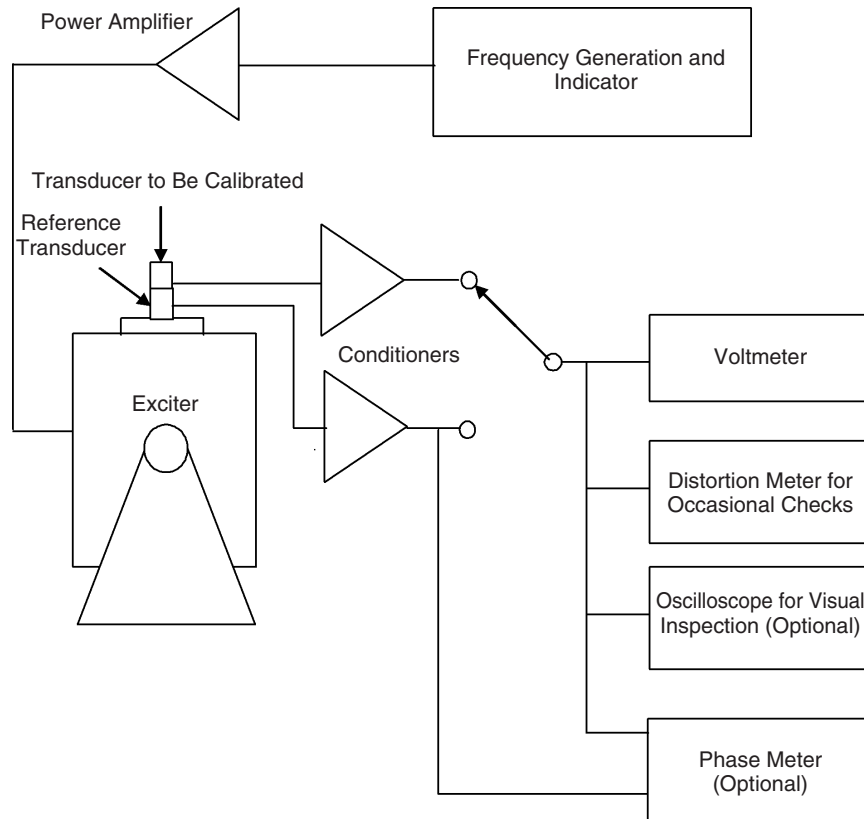


Figure 3 Cross section of calibration exciter. (Courtesy Brüel & Kjær, Sound & Vibration Measurement.)



**Figure 4** Example of a measuring system for vibration calibration by comparison to a reference transducer. (Adapted from ISO 16063-21.)

## 6.2 Calibration by Earth's Gravitation

For DC responding transducers the local gravitational constant can be used to give very accurate calibrations. By letting the transducer's sensitive axis be aligned with gravity, measure the DC output and then turn it exactly  $180^\circ$  and measure again. The difference, which is twice the gravitational constant (close to  $2g$ ), and its DC sensitivity can then be determined with quite high accuracy. The method is described in Ref. 3.

## 6.3 Calibration Service Methods

By far the largest number of transducer calibrations is made by what could be described as calibration service centers, ranging from the initial calibration at a production line over manufacturers' service centers to independent calibration centers and larger users' internal calibration departments.

**Comparison Methods, Vibration** The methods used are nearly always a comparison to a reference transducer supplied with a traceable calibration from, for example, a national metrology institute. This method of applying an exciter and vibration excitation is the most common method used to calibrate vibration

transducers over a frequency range. It is described in Ref. 2.

The standard provides detailed procedures for performing calibrations of rectilinear vibration transducers by comparison in the frequency range from 0.4 Hz to 10 kHz. The principle is shown in Fig. 4. An exciter is driven from a generator through a power amplifier. The moving element of the exciter is transmitting the generated motion to the two transducers mounted on top of it. The linear vibration generated at the common interface of the transducers is measured by the reference transducer and by the transducer to be calibrated. This is mounted firmly on the top of the reference or on a fixture containing the reference. In the case of stud-mounted transducers, a thin film of light oil, wax, or grease should be used between the mounting surfaces of the transducer(s) and exciter, particularly in the case of calibrations performed at high frequencies.<sup>1</sup> The two outputs are conditioned if necessary and compared. The measured ratio of their outputs reflects the ratio of their sensitivities when any amplification in the conditioners is taken into account. The simplest setup uses only one voltmeter and a selector. If the vibration magnitude is stable, this gives very precise calibrations also without absolute calibration of the voltmeter.

**Table 1** Uncertainties for Typical Transducer Using Different Methods

	Frequency Range	160 Hz	> 2 to 10 Hz	> 10 Hz to 2 kHz	> 2 to 4 kHz	> 4 to 7 kHz	> 7 to 10 kHz
Method	Reference calibration						
Vibration source	160-Hz calibrator	3–5					
Comparison best attainable	Best NMI multipoint calibration	0.4	0.4	0.5	0.5	0.8	1.0
Comparison typical	160 Hz ref. calibration	0.6	0.7	0.7	0.9	1.2	1.8
Best NMI laser interferometry on good reference transducer		0.2	0.2	0.2	0.3	0.4	0.4

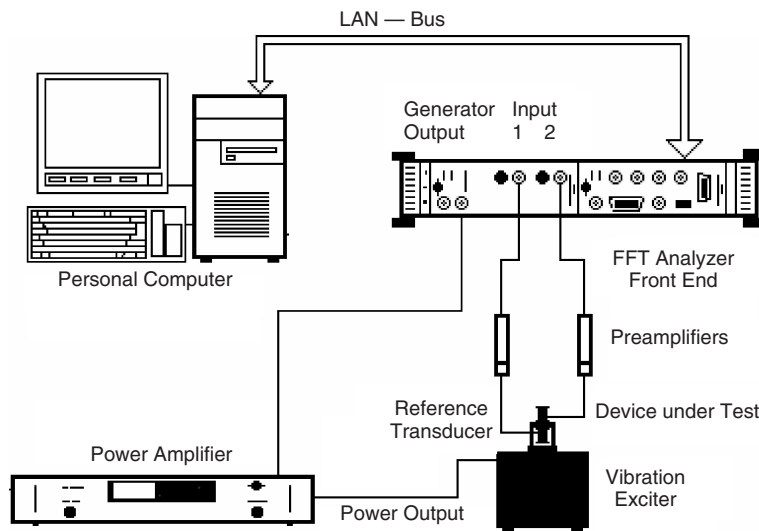
Only the sensitivity of the reference and the gain of the conditioners are needed. If phase is required, a phase meter can be added. An oscilloscope is practical for observing the process but is not a requirement. If transducers responding to different vibration parameters (e.g., a reference responding to acceleration and a velocity pickup to be calibrated) are tested, the distortion can be important and needs to be measured to evaluate the uncertainty. However, it is normally not needed for each measurement but only for getting data for the uncertainty calculations.

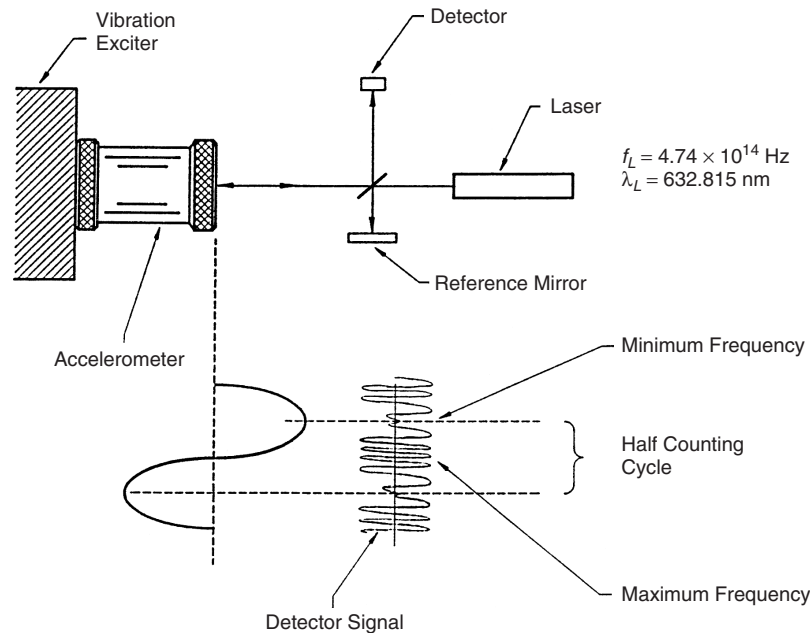
The standard contains detailed instructions for calculation of the total expanded uncertainties for such systems. The most important parts are the uncertainty of the reference, the determination of the ratio of the two outputs, and last but not least the effect of transverse, rocking, and bending motion combined with the transverse sensitivity of the transducers. The latter is often underestimated due to lack of information about the exciters used and the transverse sensitivity of the transducers. It is, for example, not unusual to find transverse and rocking motion in the order of 25% or more in certain frequency ranges. An example

of typical and best attainable uncertainties on a typical transducer on “spring guided” exciters is given in Table 1. The frequency range will normally require more than one exciter and the transverse sensitivity on the transducer is given as 5% maximum at low frequencies increasing to 10% at 10 kHz. The values are total estimated uncertainties for a coverage factor  $k = 2$ . They are somewhat lower than the values given in the standards that have rather conservative values.

In modern systems a two-channel fast Fourier transform (FFT) analyzer with a generator can replace most of the individual instruments, as shown in Fig. 5. In this case magnitude and phase are obtained automatically and distortion is unimportant but can also easily be measured.

**Comparison Methods, Shock** In general, the vibration exciters used can normally not deliver more than  $1000 \text{ m s}^{-2}$  (100g), and therefore shock methods are used to obtain peak magnitudes of  $100,000 \text{ m s}^{-2}$  (10,000g) to check linearity of transducers. A comprehensive standard was recently published: ISO 16063-22:2005, Methods for the Calibration of

**Figure 5** Example of vibration transducer calibration system used for comparison to a reference transducer.



**Figure 6** Principle of interferometer used for ratio counting.

Vibration and Shock Transducers—Part 22: Shock Calibration by Comparison to a Reference Transducer. The main difference from vibration calibration is that an impulsive excitation is used, mostly obtained by letting a piston or hammer mechanism hit an anvil on which the reference and unknown transducer is mounted. The peak magnitudes of the two time records are determined, and their ratio gives the ratio of the sensitivities just like for vibration. Often curve-fitting techniques are used to get a good determination of the maximum. FFT analysis can also be used to give a frequency response within the range of frequencies contained in the shock pulse spectrum.

**Comparison Methods, Angular Vibration** When angular vibration is measured, methods very similar to linear vibration can be used. The only difference being that the exciter will produce an angular vibration. A standard in the ISO 16063 series is under preparation as Part 23: Angular Vibration Calibration by Comparison to a Reference Transducer.

#### 6.4 Methods of National Metrology Institutes

At the NMIs a number of primary calibration methods are used. The goal is to get the unit [e.g.,  $\text{V}/(\text{m s}^{-2})$ ] determined by means as close to the fundamental units (V, m, and s) as possible. The methods are not limited to the NMIs, as other laboratories might use them if they have the need.

**Primary Vibration Calibration Methods** The most common method used today is the primary vibration calibration by laser interferometry. It is

described in Ref. 4. A reciprocity technique based on the same fundamental principles as for microphones has been used since the 1950s but is now less used because it is more complicated than the laser interferometry. The reciprocity method is described in Ref. 5.

A typical setup for vibration calibration by laser interferometry is shown in Fig. 6. It illustrates method 1 of the 3 methods described in the standard. This is the so-called fringe-counting method. The laser beam from a HeNe laser working in the TEM00 mode gives a beam with sufficient coherence length and well-defined wavelength. The beam is divided into two by a beam splitter. One beam reaches the fixed mirror and is reflected back onto the detector, the other is reflected from the surface of the moving accelerometer (or a mirror block attached to it) and then deflected by the beam splitter to the detector where it interferes with the other part. A motion of  $\lambda/4$  will change the path length by  $\lambda/2$  and thereby the phase between the two beams by  $180^\circ$ . This leads to the following relationship between the number of intensity shifts or fringes per vibration period  $R_f$  and the sinusoidal acceleration amplitude  $\hat{a}$ :

$$R_f = \frac{8\hat{a}}{\omega\lambda} = \frac{8a_{\text{rms}}\sqrt{2}}{(2\pi f)^2\lambda}$$

where  $\omega$  = angular vibration frequency

$f$  = vibration frequency

$\lambda$  = wavelength of the laser beam

$a_{\text{rms}}$  = root-mean-square (rms) value of the sinusoidal acceleration

By using a counter to count the fringes using the vibration frequency as reference, the ratio  $R_f$  is obtained directly. A very precise determination of the vibration amplitude is obtained by averaging over 100 or more periods. This method works well from the lowest frequencies and up to about 1000 Hz where the amplitude in the vibration only gives a few fringes.

The mathematical description of the detector signal shows that the frequency component at the vibration frequency becomes zero at certain values of the vibration amplitude given by the Bessel function of first kind and first order. This is described as method 2 in the standard, useful at frequencies from 800 Hz to 10 kHz. By varying the amplitude of the vibration, the zero points can be found as minima of the filtered detector signal and the transducer sensitivity can then be determined.

Method 3 of the standard is the so-called sine approximation method. The interferometer is now be configured to give two outputs in quadrature. These two signals will theoretically describe a point following the path of a circle if they were used to give the  $x$  and  $y$  deflections of an oscilloscope. Mathematically, the angle  $\hat{\phi}$  to the point on the circle, found as the  $\arctan$  of  $B/A$  (where  $B$  and  $A$  are the  $y$  and  $x$  values found for the point on the circle) gives the displacement (relative to  $\lambda$ ) leading to the relationship

$$\hat{a} = \pi \lambda f^2 \hat{\phi}$$

where  $\hat{\phi}$  is the modulation phase amplitude, the other symbols as above. This technique requires high-frequency analog-to-digital conversion of the detector signals and has, therefore, only been possible at reasonable cost recently. It can be used over the full frequency range provided a sufficient amount of fast memory is available and that conversion frequencies sufficient for the desired velocity can be used. It can also be used to determine the phase shift of the transducers.

For DC responding transducers primary DC calibration can be performed by different centrifuge-based methods. These are described in Refs. 6 and 7. The large installations needed imply that these methods are normally only used for inertial guidance-type transducers. These are considered outside the scope of this handbook.

**Primary Shock Calibration Methods** Although older methods, using velocity determination by two light beams being cut, might still be useful, the modern way is described in Ref. 8. It is basically identical to method 3 used for primary vibration but will require wider bandwidth if the full range of shock pulses is to be measured. The range covers shocks with peak accelerations of 100 to 100,000  $\text{m s}^{-2}$ . The shocks are generated by the same methods as used for comparison calibration. The attainable uncertainty is 1% at a reference peak value of 1000  $\text{m s}^{-2}$  and 2 ms duration and up to 2% at other values.

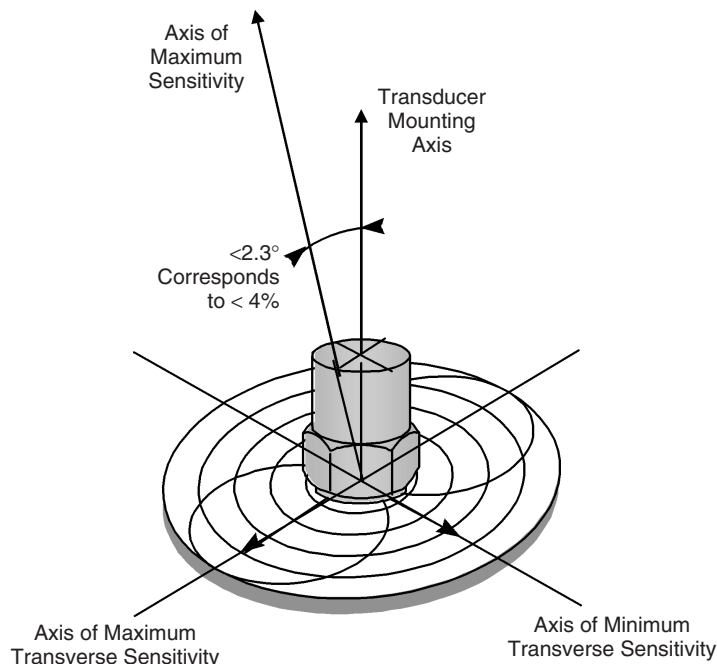
## 6.5 Transducer Test Methods

**Environmental Testing** For selection of transducers for specific measurement tasks it can be important

to know the performance under special environmental conditions. For these tests a number of ISO standards are available, some of them under revision:

- ISO 5347-11:1993, Part 11: Testing of Transverse Vibration Sensitivity (to become ISO 16063-31, Methods for the Calibration of Vibration and Shock Transducers—Part 31: Testing of Transverse Vibration Sensitivity)
  - ISO 5347-12:1993, Part 12: Testing of Transverse Shock Sensitivity
  - ISO 5347-13:1993, Part 13: Testing of Base Strain Sensitivity
  - ISO 5347-14:1993, Part 14: Resonance Frequency Testing of Undamped Accelerometers on a Steel Block
  - ISO 5347-15:1993, Part 15: Testing of Acoustic Sensitivity
  - ISO 5347-16:1993, Part 16: Testing of Torque Sensitivity
  - ISO 5347-17:1993, Part 17: Testing of Fixed Temperature Sensitivity
  - ISO 5347-18:1993, Part 18: Testing of Transient Temperature Sensitivity
  - ISO 5347-19:1993, Part 19: Testing of Magnetic Field Sensitivity
- Parts 12–19 of ISO 5347 were confirmed in 2004.

Only the concept and testing of transverse vibration sensitivity shall be described briefly as it is important for most calibrations. Figure 7 illustrates the concept. For any vibration transducer there exists one axis that provides maximum response to a vibration input. Due to small imperfections in the mechanical alignment and, for example, polarization direction of the piezoelectric elements in piezoelectric accelerometers, this axis is not perpendicular to the mounting surface. Therefore, as shown in the figure the maximum sensitivity vector will have a projection onto the plane of the mounting surface. This projection is referred to as the maximum transverse sensitivity of the transducer, and its value is normally stated in the calibration chart. The sensitivity to vibration in directions in the plane of mounting can be described as a figure of eight (i.e., two circles touching in a point). The direction of minimum transverse sensitivity is indicated on some transducers. This allows the transducer to be aligned in order to give minimum sensitivity to a specific direction of vibration. The testing has typically been made by low-frequency long-stroke ( $> 25$  mm) sliding tables with built-in turntables. The motion in the sensitive direction shall be below 0.1% of the in-plane motion. Operating the turntable permits the determination of minimum direction and maximum sensitivity. The frequencies used are typically 10 to 50 Hz. For higher frequencies vibrating long bars are used, excited by two perpendicular exciters for which the relative phase can be varied to give the desired motion. As mentioned when discussing vibration signal types, some transducers (especially “cantilever constructions”) have transverse sensitivities depending on the vibration in the main axis direction. To give a complete description of



**Figure 7** Transducer transverse sensitivity.

their behavior special setups are needed giving multi-axis excitation.<sup>9</sup>

## REFERENCES

1. ISO 5348:1998, Mechanical Vibration and Shock—Mechanical Mounting of Accelerometers, confirmed 2004, International Organization for Standardization, Geneva, Switzerland.
2. ISO 16063-21:2003, Methods for the Calibration of Vibration and Shock Transducers—Part 21: Vibration Calibration by Comparison to a Reference Transducer. International Organization for Standardization, Geneva, Switzerland.
3. ISO 5347-5:1993, Part 5: Calibration by Earth's Gravitation, confirmed 2004, International Organization for Standardization, Geneva, Switzerland.
4. ISO 16063-11:1999, Methods for the Calibration of Vibration and Shock Transducers—Part 11: Primary Vibration Calibration by Laser Interferometry, confirmed 2004, International Organization for Standardization, Geneva, Switzerland.
5. ISO 16063-12:2002, Methods for the Calibration of Vibration and Shock Transducers—Part 12: Primary Vibration Calibration by the Reciprocity Method. International Organization for Standardization, Geneva, Switzerland.
6. ISO 5347-7:1993, Part 7: Primary Calibration by Centrifuge, confirmed 2004, International Organization for Standardization, Geneva, Switzerland.
7. ISO 5347-8, Part 8: Primary Calibration by Dual Centrifuge, confirmed 2004, International Organization for Standardization, Geneva, Switzerland.
8. ISO 16063-13:2001, Methods for the Calibration of Vibration and Shock Transducers—Part 13: Primary Shock Calibration Using Laser Interferometry. International Organization for Standardization, Geneva, Switzerland.
9. T. Usuda, C. Weißenborn, and H.-J. von Martens, Theoretical and Experimental Investigation of Transverse Sensitivity of Accelerometers under Multiaxial Excitation, *Measurement Sci. Tech.*, Vol. 15, 2004, pp. 896–904.



# CHAPTER 53

## METROLOGY AND TRACEABILITY OF VIBRATION AND SHOCK MEASUREMENTS

Hans-Jürgen von Martens  
Physikalisch-Technische Bundesanstalt (PTB)  
Braunschweig and Berlin, Germany

### 1 INTRODUCTION

Traceability to the International System of Units (SI) is increasingly required for vibration and shock measurements as specified in international standards, recommendations, and regulations to ensure product quality, health, and safety. Metrology, known as the science of measurement, includes all aspects both theoretical and practical with reference to measurements, whatever their uncertainty. It is important to be aware of the metrological aspects of establishing traceability for measurements of rectilinear and angular motion quantities, including the evaluation of measurement uncertainty. New and upgraded ISO (International Organization for Standardization) standards provide a variety of calibration methods with respect to their suitability for ensuring traceability. Advanced traceability systems provide the generation and highly accurate measurement of rectilinear vibration and shock motion, as well as angular motion. National measurement standards in most countries constitute the top level of the traceability chain. Specifically developed national measurement standards are directly accessible for highly accurate measurements of metrological characteristics of rectilinear and angular transducers and vibrometers.

### 2 VIBRATION AND SHOCK FROM THE VIEW OF METROLOGY

#### 2.1 Realization of the SI Units of Motion Quantities

The terms *vibration* and *shock* are defined as special variations with time of the magnitude of a quantity, which is descriptive of the motion or position of a mechanical system (cf. ISO 2041<sup>1</sup>). The physical quantities widely used to describe vibration and shock motion in different applications are rectilinear acceleration, velocity, displacement and angular acceleration, angular velocity, and rotation angle (cf. Table 1). From the viewpoint of metrology, the units and associated scales of the six motion quantities have to be realized and disseminated with appropriate time dependencies (preferably sinusoidal and shock-shaped time histories).

To realize the SI units and associated scales of motion quantities such as acceleration and angular acceleration, adequate national measurement standards are needed. A *national (measurement) standard* is a standard recognized by a national decision to serve, in a country, as the basis for assigning values to other standards of the quantity concerned.<sup>2</sup> Such other standards are *primary standards*, *secondary standards*,

*reference standards*, *working standards*, and *transfer standards* (for definitions, see Ref. 2). The variety of motion quantities and their time histories to be realized and disseminated cannot be covered by a single standard device. An ensemble of seven national measurement standards covering the realization and dissemination of the six motion quantities in wide parameter ranges and with the highest accuracy achieved so far is described in Section 5.

#### 2.2 Dissemination of the SI Units of Motion Quantities

To disseminate the units and associated scales of motion quantities, calibrations of standard transducers or measuring instruments (see Section 2.1) are carried out. Three typical calibration situations (measuring instrument, calibrator, transducer) are shown in Fig. 1. In Fig. 1a the standard device consists of a generator, which produces the measurand  $x$ , and a standard measuring instrument, which measures  $x$ . The reading of the measuring instrument to be calibrated when supplied with the input  $x$  is compared with the indication of the standard device. The same arrangement is shown in Fig. 1b, however, standard and object to be calibrated have changed their role: The object to be calibrated is a calibrator consisting of generator and measuring instrument, and the standard is a single measuring instrument. In this case, the calibrator generates a specified quantity  $x$  that is indicated by the associated instrument. The reading is compared with the reading of the standard measuring instrument. The block diagram in Fig. 1c shows that the calibration of a transducer is similar to that of a measuring instrument, except that the transducer output signal must be measured by an additional standard measuring instrument [e.g., a root-mean-square (rms) voltmeter].

All three arrangements have in common that the generator produces disturbing quantities  $z_i(G)$ , in addition to the measurand (e.g., a purely sinusoidal vibration). These disturbing quantities  $z_i(G)$  act on both measuring instruments (e.g. harmonics from nonlinear distortion). Other disturbing quantities  $z_i(E)$  originate in the environment (e.g., temperature) and may also have correlated effects on the two instruments.

The variety of disturbing effects to be considered in the uncertainty evaluation will be demonstrated in Section 6. In the uncertainty evaluations, no distinction will any longer be made between  $z_i(G)$  and  $z_i(E)$ , which will be referred to as influence quantities  $z_i$ .



**Table 1 Rectilinear and Angular Motion Quantities (Sinusoidal, Shock-Shaped and Other Dependencies on Time)**

Motion			Dependence on Time	
Direction	Quantity	Unit	General	Sinusoidal
Linear	Displacement $s$	m	$s(t)$	$s(t) = \hat{s} \cos(\omega t + \varphi_s)$
	Velocity $v$	m/s	$v(t) = \frac{ds}{dt}$	$v(t) = \hat{v} \cos(\omega t + \varphi_v), \hat{v} = \omega \hat{s}, \varphi_v = \varphi_s + \frac{\pi}{2}$
	Acceleration $a$	m/s <sup>2</sup>	$a(t) = \frac{d^2s}{dt^2}$	$a(t) = \hat{a} \cos(\omega t + \varphi_a), \hat{a} = \omega^2 \hat{s}, \varphi_a = \varphi_s + \pi$
Angular	Rotation angle $\Phi$	rad	$\Phi(t)$	$\Phi(t) = \hat{\Phi} \cos(\omega t + \varphi_\Phi)$
	Angular velocity $\Omega$	rad/s	$\Omega(t) = \frac{d\Phi}{dt}$	$\Omega(t) = \hat{\Omega} \cos(\omega t + \varphi_\Omega), \hat{\Omega} = \omega \hat{\Phi}, \varphi_\Omega = \varphi_\Phi + \frac{\pi}{2}$
	Angular acceleration $\alpha$	rad/s <sup>2</sup>	$\alpha(t) = \frac{d^2\Phi}{dt^2}$	$\alpha(t) = \hat{\alpha} \cos(\omega t + \varphi_\alpha), \hat{\alpha} = \omega^2 \hat{\Phi}, \varphi_\alpha = \varphi_\Phi + \pi$

### 3 TRACEABILITY CONCEPTS

#### 3.1 Traceability of Vibration and Shock Measurements

*Traceability* is defined<sup>2</sup> as the property of the result of a measurement or the value of a standard whereby it can be related to stated references, usually national or international standards, through an unbroken chain of comparisons all having stated uncertainties. An unbroken chain of comparisons is called a *traceability chain*. No international measurement standard exists in the area of vibration and shock measurements. However, several countries—through their *national metrology institutes* (NMIs) and accreditation bodies—have related the measurements of rectilinear and angular motion quantities to the *national measurement standards* of another country after the latter had verified the best accuracy of calibrations within the framework of international and regional comparisons (see Section 5). The above definition of traceability given in Ref. 2 is a general one. For vibration and shock measurements, specific traceability concepts have been established, which will be described and discussed in the following.

#### 3.2 Requirements on Traceability

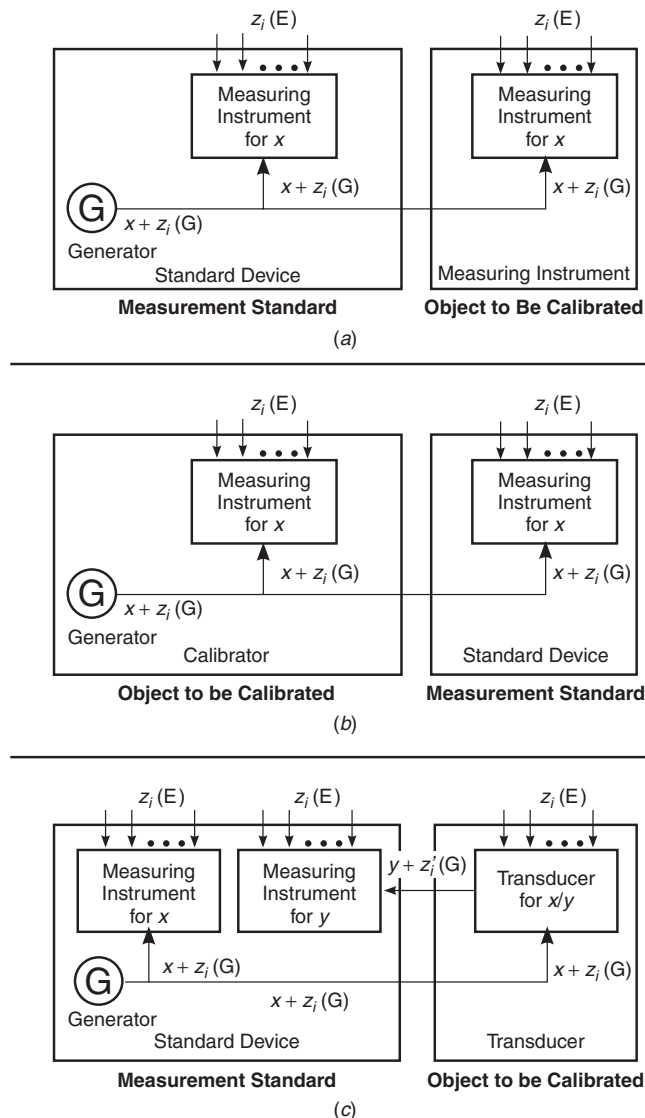
The SI units for physical quantities, such as metre per second squared (m/s<sup>2</sup>) for the quantity of acceleration, are realized by NMIs and disseminated to external clients through calibrations (cf. Fig. 2). The metrological infrastructure of a country is formed by accredited and nonaccredited calibration laboratories. All calibration laboratories (including NMIs) have to comply with the ISO/IEC Standard 17025<sup>3</sup> (IEC is the International Electrotechnical Commission). Section 5.6, Measurement Traceability, of this international standard gives specific requirements for establishing the traceability of measurement standards and measuring instruments to the SI units through an unbroken chain of calibrations or comparisons. The calibration certificates issued by calibration laboratories have to state the measurement results, including the measurement uncertainty and/or a statement of conformity with an equivalent metrological specification. The uncertainty

of measurement is to be evaluated and expressed in accordance with the *ISO Guide*.<sup>4</sup> To ensure compliance of the units realized by the NMIs, within well-specified uncertainties in accordance with their definition in the SI, key comparisons are carried out. Key comparisons carried out in the area of vibration organized under the auspices of the *Consultative Committee for Acoustics, Ultrasound and Vibration (CCAUV)* include a limited number of NMIs worldwide (e.g., 12 NMIs in CCAUV.V-K1, see Section 4.4). The key comparison reference values (KCRVs) as specified by the International Committee for Weights and Measures (CIPM) key comparisons are disseminated through various regional key comparisons to a great number of NMIs within the regional metrology organizations (RMOs), in particular the Asia Pacific Metrology Programme (APMP), Euro-Asian Cooperation of National Metrology Institutions (COOMET), European Collaboration in Measurement Standards (EUROMET), Southern African Development Community Cooperation in Measurement Traceability (SADCMET), and Sistema Inter-Americano de Metrologia (SIM, Inter-American System of Metrology).

#### 3.3 Traceability to Primary Methodologies

From the definition of traceability and the explanations given above, it should be clear that the chain of calibrations providing traceability has its origin in adequate national measurement standards.

One traceability system widely used is based on primary vibration calibration of an accelerometer standard by laser interferometry at the NMI level and secondary vibration calibration by the comparison method at the level of accredited calibration laboratories (cf. Fig. 2). After primary calibration, this accelerometer standard can be used in a calibration laboratory, both the accelerometer standard (reference accelerometer) and the transducer to be calibrated being subjected to the same motion and their output signals being compared. If that transducer is a working standard, it is used afterwards in a nonaccredited laboratory for the calibration of working transducers or vibrometers by comparison, too. The upgraded documentary standards recently developed for vibration calibration by laser



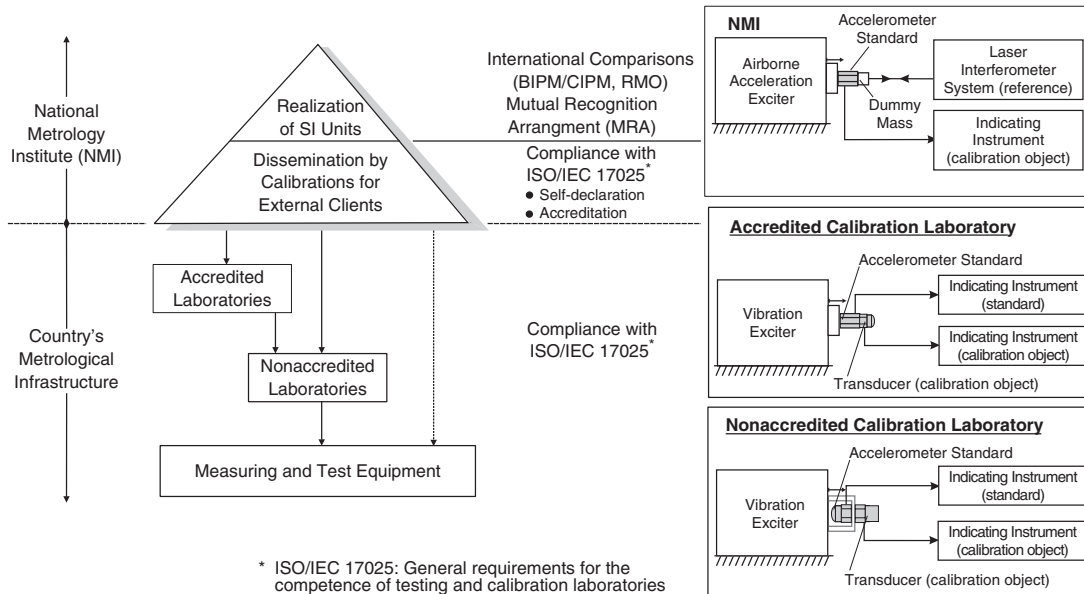
**Figure 1** Block schemes of typical calibration setups with measurand  $x$  and influence quantities  $z_i$ : (a) vibration measurement instrument, (b) vibration calibrator, and (c) transducer (e.g., accelerometer).

interferometry (ISO 16063-11<sup>5</sup>) and calibration by comparison to a reference transducer (ISO 16063-21<sup>6</sup>) reflect the need for calibration in the frequency range, which is representative for the conditions of application of the reference transducer or working transducer (specified frequency range 0.4 Hz to 10 kHz).

Vibration calibration is not representative for the behavior of a transducer used for shock measurements. As a normative basis to ensure traceability for shock acceleration measurements, the new standards ISO 16063-13<sup>7</sup> for primary shock calibration by laser interferometry and ISO 16063-22<sup>8</sup> for shock calibration by

comparison to a reference transducer have recently been developed. The standard<sup>8</sup> specifies to which degree and with which consequences a primary shock calibration of a reference transducer can be dispensed with:

1. "If the reference transducer has proved to be linear, the primary shock calibration may be replaced by primary vibration calibration in accordance with ISO 16063-11 or ISO 16063-12."<sup>5,9</sup>
2. "Hopkinson bar shock calibrators have operational ranges of high accelerations (peak values 1 km/s<sup>2</sup> to 2000 km/s<sup>2</sup>), which may be used to



**Figure 2** General traceability chain and application to vibration and shock measurements.

evaluate the performance of transducers. This part of ISO 16063 specifies the range from  $100 \text{ m/s}^2$  to  $100 \text{ km/s}^2$ , which has reference to primary methodologies (ISO 16063-13). Larger accelerations (peak values) and shorter pulse durations are possible but without reference to primary methodologies.”<sup>8</sup>

The term *primary methodologies* is used above as reference to those implemented ISO standard methods that are *adequate* for the primary calibration of standard transducers. This underlines that other primary calibration methods specified in ISO 5347-5:1993 (Calibration by Earth’s Gravitation), 5347-7:1993 (Primary Calibration by Centrifuge), and 5347-8:1993 (Primary Calibration by Dual Centrifuge) are *not adequate* for transducers intended to be used for measurements of shock-shaped or other time dependencies outside the scopes of these standards, and vice versa.

It is sometimes assumed that traceability to the SI unit of acceleration or other motion quantities can be established by any calibration laboratory by implementation of a primary calibration method (e.g., reciprocity method or laser interferometry in accordance with the relevant ISO standard), without link-up to an NMI. Primary calibration methods may well be used in an accredited or a nonaccredited calibration laboratory for some reasons. However, the implementation of a *primary calibration method* specified in the ISO standards does not necessarily lead to a *primary standard* which is by definition<sup>2</sup> a standard that is designed or widely acknowledged as having the highest metrological qualities and whose value is accepted

without reference to other standards of the quantity concerned. Such primary standards (national measurement standards) are usually established only in the NMI of the respective country by implementation of ISO primary calibration methods. The CIPM key comparison CCAUV.V-K1 revealed that the compliance with given uncertainty limits of calibration equipment used in calibration laboratories (primary calibration included) can only be verified by linkup to appropriate national measurement standards, which have specified uncertainties that have been validated in international or regional key comparisons or supplementary comparisons performed under the auspices of the *International Bureau of Weight and Measures (BIPM)* and the associated Consultative Committee, CCAUV: All 12 participating laboratories have used laser interferometry in accordance with ISO 16063-11<sup>5</sup> and demonstrated good results in the calibration of one of the two transfer standards, which was a reference accelerometer of back-to-back design, whose reference surface (top surface) was accessible to the laser light beam. However, for the other reference accelerometer that was of single-ended design, the calibration results of several laboratories showed significant systematic deviations (at 5 kHz greater than 1% up to 6%) due to significant relative motion in the kilohertz range between the laser light spot and the accelerometer reference surface (mounting surface).<sup>10</sup> For the variety of sources of error and uncertainty components to be considered in calibrations, see Section 6.

### 3.4 Traceability to National Measurement Standards

This subsection combines the general requirement of traceability to primary methodologies (see Section 3.3)

with the objective to provide motion quantities with adequate time histories by the national measurement standards.<sup>11,12</sup> Traceability for vibration and shock measurements can be ensured by generating at the NMI level the three linear and three angular motion quantities (cf. Table 1) with sinusoidal, shock-shaped, and other, user-defined time histories and by measuring them by laser interferometry. The latest developments in laser interferometry have made it possible to establish a uniform methodology for primary measurement, covering the variety of motion quantities, sinusoidal and shock-shaped time dependencies, and wide parameter ranges. The traceability chain described in Section 5 realizes and disseminates the units of the respective physical quantities at such time dependencies that reproduce, during calibration of any transducer (e.g., accelerometer) or measuring instrument (e.g., laser vibrometer), as closely as possible the conditions of use after calibration (i.e., shock measurement in the peak value acceleration range of 1 km/s<sup>2</sup> to 50 km/s<sup>2</sup> at defined shock shapes and pulse durations).<sup>13,14</sup>

### 3.5 Option of Direct Access to National Measurement Standards

As the measurement and calibration capabilities available at the NMI level go, in some cases, far beyond those available at lower levels of the traceability chain (i.e., in accredited calibration services and industrial calibration laboratories), the national measurement standards may be used directly to meet special demands from industry and elsewhere for investigations of the dynamic behavior of transducers and measuring instruments or for their accurate dynamic calibration (for examples see Section 5).

## 4 ESTABLISHMENT OF TRACEABILITY

### 4.1 Selection of ISO Standard Methods

Under the general title *Methods for the Calibration of Vibration and Shock Pick-ups*, a standard series, ISO 5347, was issued in the period between 1987 and 1997. A revision of the ISO 5347 series, renumbered to ISO 16063, was started in 1995, focusing on the specification of upgraded and new calibration methods needed at different levels of a traceability chain for the field of vibration and shock: methods for primary vibration calibration, secondary vibration calibration, primary shock calibration, and secondary shock calibration.

For primary vibration calibration by laser interferometry at the NMI level, ISO 16063-11:1999<sup>5</sup> has extended the frequency range (0.4 Hz to 10 kHz) and included absolute phase shift measurement. ISO 16063-13:2001<sup>7</sup> provides interferometric primary shock calibration (100 m/s<sup>2</sup> to 100 km/s<sup>2</sup>). ISO 16063-15<sup>15</sup> specifies primary angular vibration calibrations (magnitude and phase shift) in the frequency range from 0.4 Hz to 1.6 kHz. For rectilinear vibration and shock calibration at lower levels of the traceability chain, Parts 21 and 22 of ISO 16063 provide upgraded comparison methods, and ISO 16063-23 is the corresponding project for angular vibration calibration by comparison to a reference transducer.

### 4.2 Implementation of ISO Standard Methods

Hierarchies of measurement standards have been established and are operated in NMIs as well as in accredited and nonaccredited calibration laboratories, in compliance with the upgraded and new ISO standards (see Section 4.1). Most of the NMIs use commercial high-quality vibration and shock generators or even complete calibration equipment.

Alternatively, several NMIs have specifically developed vibration and shock generators (e.g., NIST Super Shaker,<sup>16</sup> PTB rectilinear and angular motion exciters,<sup>13,14</sup> see also Section 5) and laser interferometry.<sup>17–24</sup> Examples of specific national measurement standards are briefly described in Section 5. For other examples, see Refs. 25 to 34.

Accredited and nonaccredited calibration laboratories are in most cases equipped with commercial calibration devices that are available from several manufacturers in compliance with the respective ISO standards. Using the ISO methods specified, national measurement standards and calibration equipment for calibration laboratories provide many new and improved calibration and measurement capabilities and thus international traceability.

### 4.3 Calibration and Measurement Capabilities Available

Uncertainties for different methods on typical transducers using different methods are specified in Table 1 of Chapter 52 with reference to the ISO standards and to the calibration and measurement capabilities (CMCs) published at <http://www.bipm.org>. In the following, a more detailed survey is given.

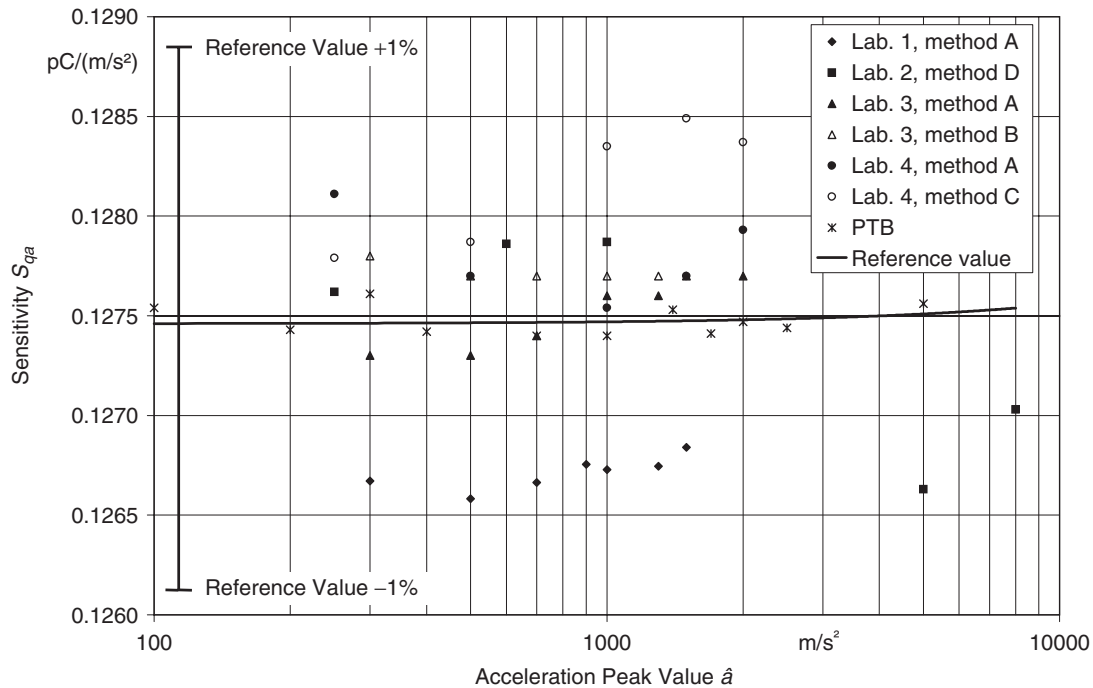
#### Capabilities of National Metrology Institutes

The NMIs equipped with primary and/or comparison calibration facilities have offered their CMCs in Appendix C of the Mutual Recognition Arrangement (MRA) (see <http://www.bipm.org>, Key Comparison Database). An example for the wide measurement ranges of vibration and shock parameters covered by primary calibration in an NMI using several national measurement standards is described in Section 5.

#### Capabilities of Accredited Calibration Laboratories

As most calibration laboratories accredited for vibration and shock measurements and calibrations (quantity of acceleration) are equipped with commercial high-quality calibration equipment, their calibration capabilities confirmed by the accreditation body of the respective country (e.g., UKAS in the United Kingdom, DKD in Germany, and NATA in Australia) also meet high demands. This is valid in particular if the reference standards of the calibration laboratory are periodically calibrated in an NMI providing high-level CMCs.

For example, the calibration capabilities of the calibration laboratories accredited by the Deutscher Kalibrierdienst (DKD) are specified at [www.dkd.info](http://www.dkd.info). Rectilinear vibration calibrations cover frequencies from 0.4 Hz to 20 kHz (including phase calibrations



**Figure 3** Results of an interlaboratory comparison of shock calibrations: method A: pendulum shock calibrator, method B: linear shock calibrator (air bearing), method C: pneumatic shock calibrator, and method D: drop ball calibrator.

up to 10 kHz), shock calibrations cover 50 m/s<sup>2</sup> to 100 km/s<sup>2</sup>, and angular calibrations are available, for example, in the frequency range from 8 Hz to 100 Hz for angular velocity transducers. The accreditation for best uncertainties of 0.25% (sinusoidal) and 1% (shock acceleration) was possible because of the highly accurate primary calibrations of the laboratories' reference transducers carried out at the NMI of Germany (PTB).

#### 4.4 Demonstration of CMCs by Comparisons

Though it might be expected that all calibration laboratories (NMIs included) establish uncertainty budgets in compliance with the *ISO Guide*,<sup>4</sup> the accuracy attained can be reliably assessed only by appropriate comparison measurements. Numerous international, regional, and national comparisons performed over the last two decades have largely contributed to the recognition of systematic deviations and their sources and to prove the uncertainty statements of any laboratory. In Ref. 13, the comparisons reported in Refs. 35 to 38 are discussed in detail. The first key comparison in the area of vibration<sup>39</sup> carried out between 12 NMIs worldwide, furnished highly accurate key comparison reference values that have been disseminated to many countries by regional key comparisons within the regional metrology organizations (e.g., Ref. 40). It was demonstrated that great experience and the application of advanced techniques are

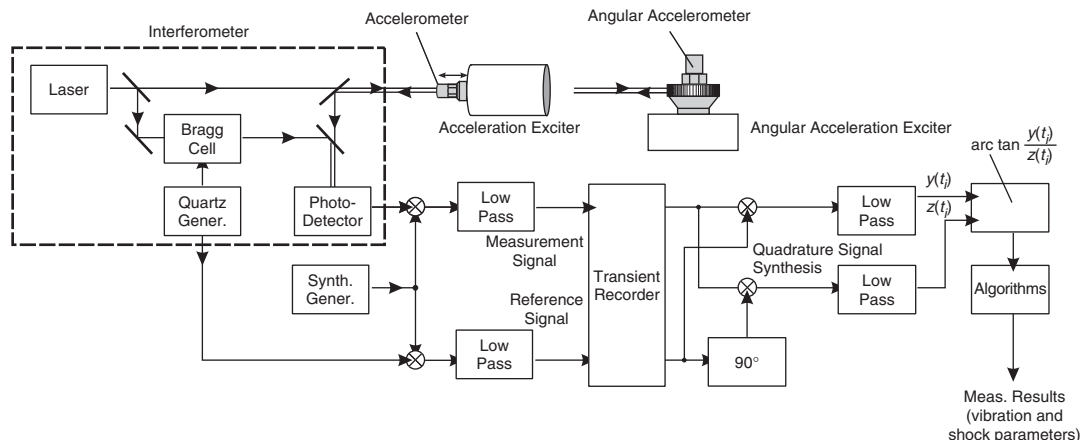
necessary to reach an expanded uncertainty (coverage factor  $k = 2$ ) of 0.5% at a reference frequency of 160 Hz and 1% at other frequencies in the range from 1 Hz to 10 kHz in accordance with the international standard.<sup>5</sup> The results and conclusions of the key comparison CCAUV.V-K1 are specified in detail in Ref. 39. In addition to the magnitude, the phase shift of the complex sensitivity of reference accelerometers has also been included in comparisons at the NMI level.<sup>41</sup>

As an example, Fig. 3 shows a result of the interlaboratory shock comparison of the DKD laboratories in Germany, performed in 2001. The relative deviations of the DKD laboratories results of the shock sensitivity of a reference accelerometer from the reference values measured at the PTB were less than 1% in all cases. This has demonstrated the reliability of the accredited best measurement uncertainty of 1%. For a European interlaboratory comparison see Ref. 42.

## 5 EXAMPLE OF AN ADVANCED TRACEABILITY CHAIN

### 5.1 Concept for Motion Generation and Measurement at the NMI Level

For the advanced state of the realization and dissemination (by primary calibration) of the units of motion quantities, the traceability chain established in Germany may be considered as a representative example<sup>13,14</sup>; see [www.ptb.de](http://www.ptb.de). An ensemble of seven different measuring standards have been developed



**Figure 4** Generation and measurement of linear and angular motion quantities, using exciters with air bearings, heterodyne interferometers with frequency conversion, and digital data processing.

at the PTB for the realization of the units of the six motion quantities (cf. Table 1) and the primary calibration of transducers of these motion quantities. Each measuring standard consists of a rectilinear or an angular acceleration exciter, a laser interferometer with signal measuring system, a system for measuring electrical output quantities of calibration objects (voltage or charge), a supply system, and a vibration isolation system. The motion exciters have been specially designed to generate the six motion quantities rectilinearly or around a fixed axis, with sinusoidal or defined shock-shaped time dependencies.

Laser interferometry, which is the preferred primary vibration calibration method at the NMI level, has been further developed at PTB in the last years as a uniform methodology and technique for the primary measurement of translational motion quantities (e.g., acceleration) and rotational motion quantities (e.g., angular acceleration) at sinusoidal, shock-shaped, and other, user-defined time histories.<sup>13,43–49</sup> Figure 4 shows the methods and techniques applicable to all the measurement standards, in accordance with ISO 16063-11<sup>5</sup> (sine-approximation method), ISO 16063-13<sup>7</sup> (shock signal processing; see Fig. 8), and ISO 16063-15<sup>15</sup> (sine-approximation method), respectively. Alternatively, for special measurements and calibrations, homodyne interferometry is used in specific modifications.<sup>50,51</sup>

The vibration isolation systems are specifically developed so that the reaction forces from the motion exciter are prevented from exciting any disturbing motion (e.g., resonance) in sensitive interferometer parts (e.g., beam splitter, reference reflector), and the interferometer is isolated from ground motion. Active vibration isolation control and position control is used to ensure efficient vibration isolation while keeping the interferometer adjusted.

To simulate in calibrations typical multiaxial excitation to which working transducers are frequently

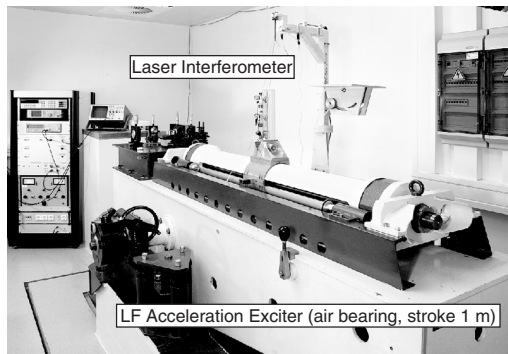
exposed, a standard measuring device has been developed to simultaneously generate and precisely measure motion quantities in up to three orthogonal directions ( $X, Y, Z$ ) and around a rotational axis ( $Z$ ), with user-defined time histories (see Section 5.3).

The primary calibration methods and techniques developed at PTB in compliance with the ISO standards and current standardization projects are used in Germany and Europe on the basis of three agreed EUROMET projects providing traceability for sinusoidal acceleration (Project Ref. No. 198), angular acceleration (Project Ref. No. 284), and shock acceleration (Project Ref. No. 368), cf. [www.EUROMET.org](http://www.EUROMET.org). Traceability is provided by primary calibrations of reference or transfer standards, which are later used in accredited calibration laboratories (calibration services) in Germany and other countries. The calibration capabilities achieved in accredited calibration laboratories are shown at [www.DKD.info](http://www.DKD.info) as an example.

## 5.2 Survey of National Measurement Standards Developed

The national measurement standards based on the concept of Section 5.1 are

1. Low-frequency acceleration standard 0.1 Hz to 20 Hz (sinusoidal vibration, max. displacement double amplitude 1 m, cf. Fig. 5)
2. Low-frequency acceleration standard 0.4 Hz to 63 Hz (sinusoidal vibration, max. acceleration amplitude 15 m/s<sup>2</sup>)
3. Medium-frequency acceleration standard (sinusoidal vibration, 10 Hz to 5 kHz)
4. High-frequency acceleration standard (sinusoidal vibration, 10 Hz to 20 kHz, min. displacement amplitude 1 nm; see Figs. 6 and 7)
5. Shock acceleration standard 50 m/s<sup>2</sup> to 5 km/s<sup>2</sup> (shock duration 0.8 ms to 10 ms)

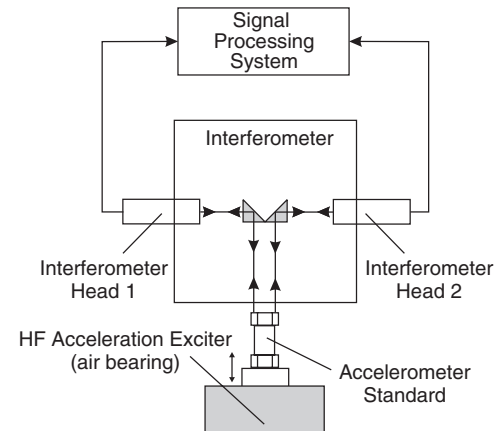


**Figure 5** Low-frequency acceleration measurement standard 0.1 Hz to 20 Hz.

6. Shock acceleration standard  $1 \text{ km/s}^2$  to  $100 \text{ km/s}^2$  (shock duration  $70 \mu\text{s}$  to  $300 \mu\text{s}$ ; cf. Fig. 8).
7. Angular acceleration standard (sinusoidal vibration, 0.4 Hz to 1 kHz)

The standard measuring devices are named acceleration standard and angular acceleration standard, respectively. However, at sinusoidal accelerations or angular accelerations free from distortion, the measurands velocity, displacement and angular velocity, and rotation angle, respectively, are generated at the same time so that, in connection with the laser interferometer, the units of the three rectilinear motion quantities (acceleration, velocity, and displacement) and of the three angular motion quantities (angular acceleration, angular velocity, and rotation angle) are realized. The measurement uncertainty stated for acceleration and angular acceleration is also valid for the two other translational or rotational motion quantities.

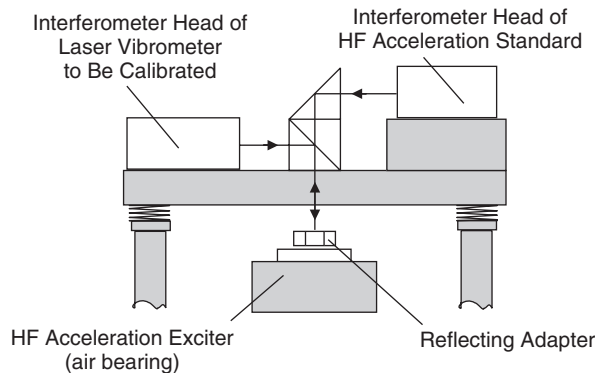
The amplitudes of sinusoidal accelerations, velocities, and displacements are measured with a relative measurement uncertainty of 0.1% to 0.2% at frequencies from 0.4 Hz to 20 kHz (frequency dependent). The complex sensitivity of precise accelerometers



**Figure 6** HF acceleration standard equipped with two-channel laser interferometry used for the calibration of accelerometers.

(reference and transfer standards) can be measured with a measurement uncertainty of 0.1% to 0.3% for the magnitude and of  $0.2^\circ$  to  $0.5^\circ$  for the phase shift in the frequency range from 0.4 Hz to 10 kHz (primary calibration in accordance with ISO 16063-11<sup>5</sup>). For frequencies higher than 10 kHz, a best measurement uncertainty of  $\leq 1\%$  up to 20 kHz is available for the calibration of reference accelerometers. For the calibration of reference laser vibrometers in compliance with ISO 16063-11, a best measurement uncertainty of 0.1% to 0.2% at frequencies from 0.4 Hz to 20 kHz is attainable to date. The CIPM key comparison CCAUV.V-K1 revealed that the PTB has kept the extremely low expanded uncertainty  $< 0.1\%$  (expanded uncertainty for coverage factor  $k = 2$ , see Ref. 4) at all 22 frequencies from 40 Hz to 5 kHz (one-third octave frequency series) covered by the key comparison.

For primary shock calibrations in compliance with ISO 16063-13,<sup>7</sup> a best measurement uncertainty of  $\leq 0.5\%$  to 1% is available at acceleration peak values from  $50 \text{ km/s}^2$  to  $100 \text{ km/s}^2$ . In addition to the shock



**Figure 7** HF acceleration standard modified for laser vibrometer calibrations.



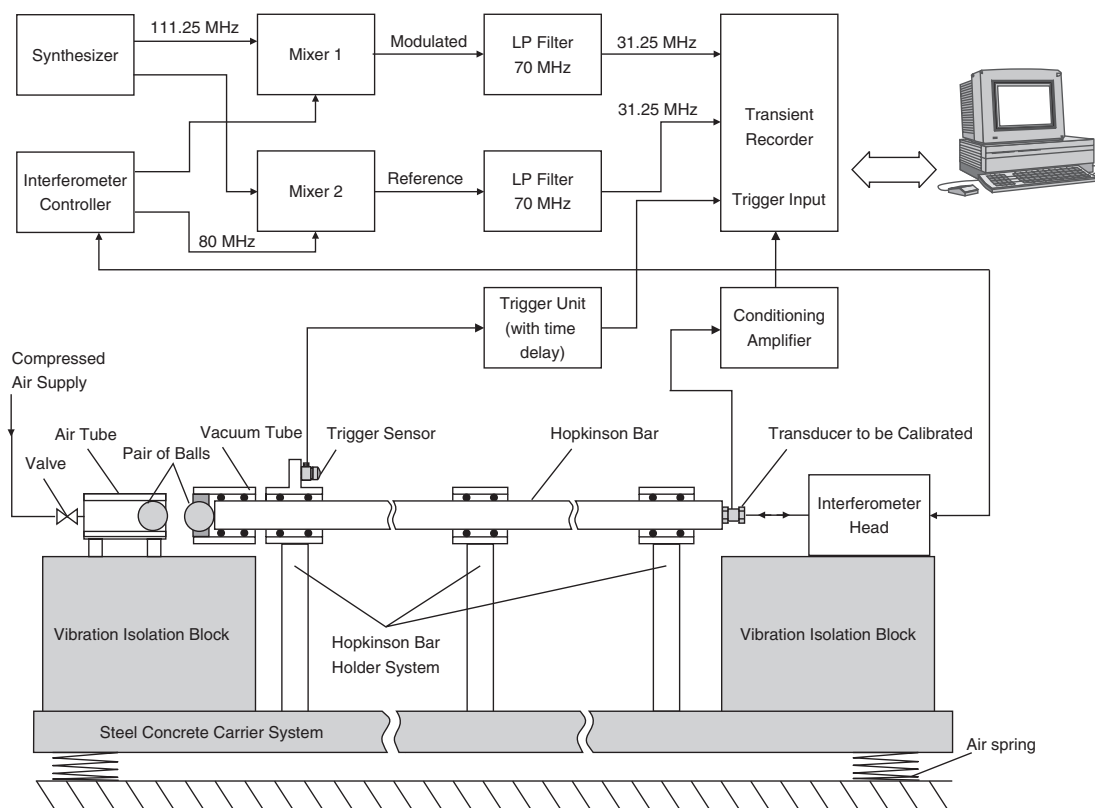


Figure 8 Shock acceleration measurement standard 1 km/s<sup>2</sup> to 100 km/s<sup>2</sup>.

sensitivity defined as the ratio of peak value of the output to peak value of the acceleration, the sensitivity for certain spectral frequencies of the shock spectrum can be measured with the same uncertainty, using the shock acceleration standard shown in Fig. 8.

The amplitudes of sinusoidal angular accelerations, angular velocities, and rotation angles are measured with a relative measurement uncertainty from < 0.3% to 0.5% (frequency dependent), using the angular acceleration standard. The complex sensitivity of precise angular accelerometers and angular velocity transducers (reference and transfer standards) can be measured with a measurement uncertainty ranging from < 0.3% to 0.5% for the magnitude and 0.5° for the phase shift.

The potential high accuracy (low uncertainty) of measurement of laser interferometry can be achieved only in conjunction with high-performance standard exciters, by efficient vibration isolation, and by data acquisition at a high sampling rate, with high resolution and large memory, and by sophisticated data processing procedures. Only small deviations from uniaxial, purely sinusoidal, or defined shock motion are tolerable. Relative motion between the transducer reference surface and the spot(s) sensed by the interferometer must be kept small or negligible. For

detailed descriptions and specifications, see Refs. 13 and 14, as well as [www.bipm.org](http://www.bipm.org) and [www.ptb.de](http://www.ptb.de).

To suppress the effect of deviations from rectilinear motion in accelerometer calibrations, the displacement is to be measured at four different points equally spaced on the top surface of a back-to-back (BB) accelerometer or on the base surface of a single-ended (SE) accelerometer. In the case of the high-frequency acceleration standard, which simultaneously senses the motion at two different points displaced by 180° (see Fig. 6), two measurement series have been successively carried out, changing the position of the laser light spots by 90°. The phase shift between the sinusoidal vibrations measured at the two positions shifted by 180° has been taken into account when calculating the “mean value” of the motion quantity acting on the transducer to be calibrated. Moreover, the position of mounting of the transducer to be calibrated is changed in angle steps of 90° to compensate the effects of transverse motion if any.

For the calibration of laser vibrometers (see Fig. 7), the effect of relative motion is eliminated by a special adaptor with a reflecting surface and an arrangement that leads the laser light beams from the interferometer of the national measurement standard and the laser vibrometer to be calibrated to the same reflecting point.



### 5.3 Simultaneous Multicomponent Motion Generation and Measurement

In normal applications, a transducer (e.g., accelerometer) is subjected to motion components in up to 6 degrees of freedom. The triaxial motion exciter is equipped with a measuring table on which the rotational exciter can be mounted. Both exciters can alternatively be used separately. The triaxial motion exciter consists of three electrodynamic vibration exciters that are coupled by a hydrostatic bearing. It can control the vibration parameters on three axes independently. The rotational exciter uses a brushless three-phase hollow-shaft motor that is electronically commutated and servo-controlled and is equipped with an air bearing. The motion quantities can be generated and measured by laser interferometry in the different axes simultaneously and with different user-defined time histories. First calibrations with simultaneous excitation of motion quantities in more than one axis revealed that some transducer designs cause interrelated effects that are not taken into account by the linear superposition principle.<sup>52</sup> In accelerometer designs using a bending beam, the transverse sensitivity measured without any vibration acting in the main sensitivity axis of the accelerometer may differ considerably from the transverse sensitivity measured in the presence of a vibration acting in the main axis (i.e., when the bending beam is deflected by a vibration to be measured). Triaxial vibration excitation allows, among other things, the transverse sensitivity to be determined with simultaneous excitation of a vibration in the main axis of the transducer, thus simulating application conditions

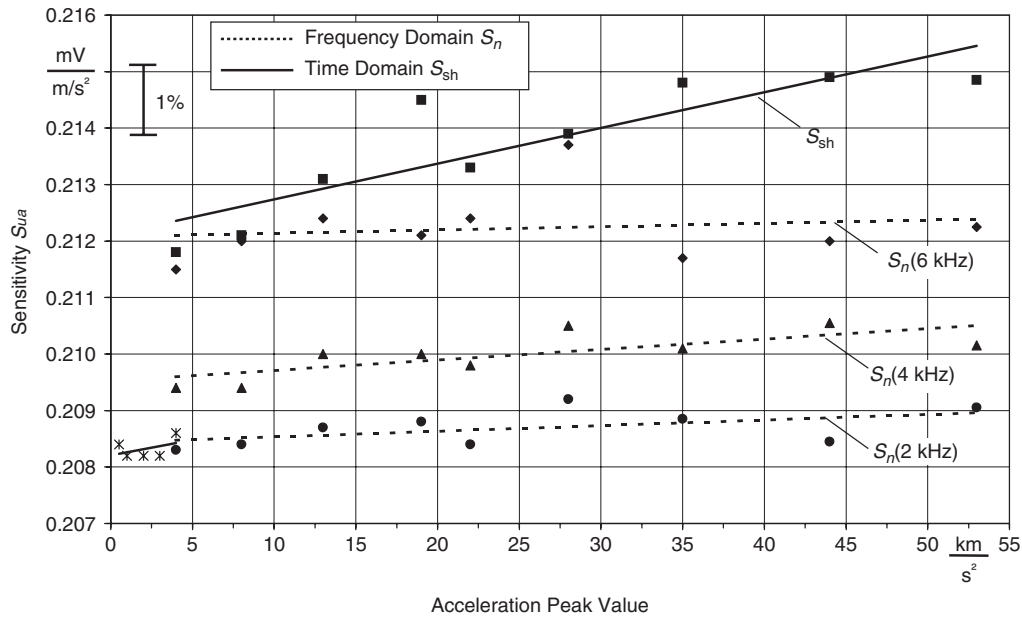
where the transducer is exposed to multiaxial vibration. The advantage of triaxial excitation for testing the transverse sensitivity of vibration transducers has been taken into account in the revision of ISO 5347-11 (to become ISO 16063-31).<sup>53</sup>

### 5.4 Application of National Measurement Standards – Identification of Dynamic Behavior of Transducers

High-quality generation and measurement of motion quantities is required to accurately identify the dynamic characteristics of rectilinear and angular transducers and measuring instruments (reference standards in particular). Some examples are:

- Highest measurement accuracy achieved in accelerometer calibrations so far<sup>39</sup>
- Comparison results of accurate phase calibrations<sup>41</sup>
- Long-term stability of reference accelerometers<sup>39</sup>
- Calibration of different digital laser vibrometers<sup>14</sup>
- Linearity of reference accelerometers (sinusoidal acceleration, dynamic range from 3 m/s<sup>2</sup> to 200 m/s<sup>2</sup>)<sup>39</sup>
- Linearity of reference accelerometers (shock acceleration, dynamic range from 50 m/s<sup>2</sup> to 100 km/s<sup>2</sup>)<sup>47</sup>

Figure 9 shows the results of a linearity test of a reference accelerometer, using the PTB techniques



**Figure 9** Linearity test of a piezoelectric accelerometer by shock excitation using the shock acceleration standards 5 km/s<sup>2</sup> and 100 km/s<sup>2</sup> (see Section 5.2).

and procedures of signal processing in the time domain and in the frequency domain. The sensitivity values obtained for several spectral frequencies of the shock spectrum (frequency domain) revealed that the reference accelerometer behaved linearly within the uncertainty of the investigation of better than 1% up to 50 km/s<sup>2</sup> at least. The need for such accurate linearity tests is demonstrated in Ref. 54. The shock sensitivity measured by definition in the time domain increases with the acceleration peak value because the shock duration becomes shorter and the shock spectrum shifts to higher frequencies.<sup>14,47</sup> Above 5 km/s<sup>2</sup>, the shock acceleration standard 100 km/s<sup>2</sup> was used (standard 6 in Section 5.2); below 5 km/s<sup>2</sup>, the shock acceleration standard 5 km/s<sup>2</sup> was used (standard 5 in Section 5.2). The leap in the shock sensitivity is caused by different shock durations of these standard devices.

## 6 EXPRESSION OF UNCERTAINTY IN MEASUREMENTS

### 6.1 Survey of Procedures of the ISO Guide

Over the last few decades, various concepts and procedures of uncertainty evaluation were proposed and discussed. With the publication of the *ISO Guide to the Expression of Uncertainty in Measurement* (GUM) in 1993, a unified method for the evaluation and expression of measurement uncertainties was accepted worldwide. The accuracy of a measurement is to be described by the expanded uncertainty  $U$  for a given coverage factor  $k$  or coverage probability  $P$ . The purpose of the expanded uncertainty  $U$  is to provide an interval  $y - U$  to  $y + U$  within which the value of  $Y$ , the specific quantity subjected to measurement or calibration and estimated by  $y$ , can be expected with high probability to lie. The NMIs have made efforts to confidently assert that  $y - U \leq Y \leq y + U$ . The GUM procedure can briefly be described by the following 6 steps:

Step 1 Establish the model of evaluation:

$$Y = f(X_1, X_2, \dots, X_N) \quad Y, X_i \text{ are random variables}$$

$$y = f(x_1, x_2, \dots, x_N) \quad y, x_i \text{ are estimates of } Y, X_i$$

Step 2 Determine the standard uncertainty  $u(x_i)$  of input estimate  $x_i$ . Example of rectangular distribution model:

$$u(x_i) = b/\sqrt{3} \quad \text{with} \\ b = (b_+ - b_-)/2 \quad E\{X_i\} = (b_+ + b_-)/2$$

Step 3 Determine the estimated covariance

$$u(x_i, x_j)$$

Step 4 Calculate the uncertainty contributions  $u_i(y)$ ,  $u(y_i, y_j)$ :

$$u_i(y) = c_i u(x_i) \quad c_i = \left( \frac{\partial f}{\partial X_i} \right)_{x_i}$$

$$u(y_i, y_j) = c_i c_j u(x_i, x_j)$$

Step 5 Calculate the combined uncertainty  $u_c(y)$ :

$$u_c(y) = \sqrt{\sum_{i=1}^N c_i^2 u^2(x_i) + 2 \sum_{i=1}^{N-1} \sum_{j=i+1}^N c_i c_j u(x_i, x_j)}$$

Step 6 Calculate the expanded uncertainty  $U(y)$  from  $u_c(y)$ :

$$U = k u_c \quad \frac{U}{y} = k \frac{u_c}{y} \quad (k \text{ is coverage factor, preferably } k = 2)$$

### 6.2 Tools for Uncertainty Evaluations in Vibration Measurements and Calibrations

In vibration and shock measurements and calibrations, the application of the GUM may be difficult and very time consuming unless some possibilities of simplification are used. In Refs. 55 and 56, a survey is given of the problems typically encountered in uncertainty calculations when vibrations are measured or accelerometers calibrated. It is shown how a model function of simple structure can be established for the usually complex relationship between the output quantity (e.g., sensitivity of an accelerometer), the quantity to be measured (e.g., acceleration), and various influence quantities (noise, transverse motion, base strain, etc.). Among other things, nonlinear effects such as the influences of distortion, hum, and noise can be properly taken into account.

A set of rules has been explained that allow the uncertainty components ("standard uncertainties") of the "input quantities  $X_i$ " to be estimated in dependence on the degree of information available about the uncertainty sources. Some of the methodical tools described in Refs. 55 and 56 are demonstrated in Annex C of ISO 16063-1<sup>57</sup> and in the example of Section 6.3. The propagation of the errors and uncertainties within a traceability chain has been described in detail.<sup>58</sup>

### 6.3 Example: Uncertainty Evaluation of an Accelerometer Calibration

Theoretical and experimental investigations into the errors and uncertainties of measurements of motion quantities ("vibration and shock measurements") at the NMI level have been reported in Refs. 50, 55, 56, and 58. On the basis of the cause-and-effect diagram shown in Fig. 10, detailed uncertainty budgets have been established.<sup>55</sup> The calibration task reflected by this cause-and-effect diagram is to determine the magnitude  $S$  of the complex charge sensitivity of an accelerometer, defined as the ratio of charge amplitude  $\hat{q}$  at its output to acceleration amplitude  $\hat{a}$  at its input,

$$S = \frac{\hat{q}}{\hat{a}} \quad (1)$$

For the example of interferometric calibration, the relationship

$$S = \frac{1}{(2\pi)^2} \frac{1}{f^2} \frac{\hat{u}}{\hat{s}} \frac{1}{S_A} \prod_i K_i \quad (2)$$

with

$$K_i = (1 - e_i^*) \quad (2a)$$

was derived from Eq. (1), thus expressing the magnitude  $S$  of the charge sensitivity of the accelerometer as a function of the measurands voltage amplitude  $\hat{u}$ , displacement amplitude  $\hat{s}$ , charge amplifier sensitivity (magnitude)  $S_A$ , vibration frequency  $f$ , and correction factors  $K_i$ , which take the relative error components  $e_i^*$  into account (for details, see Refs. 55 and 56).

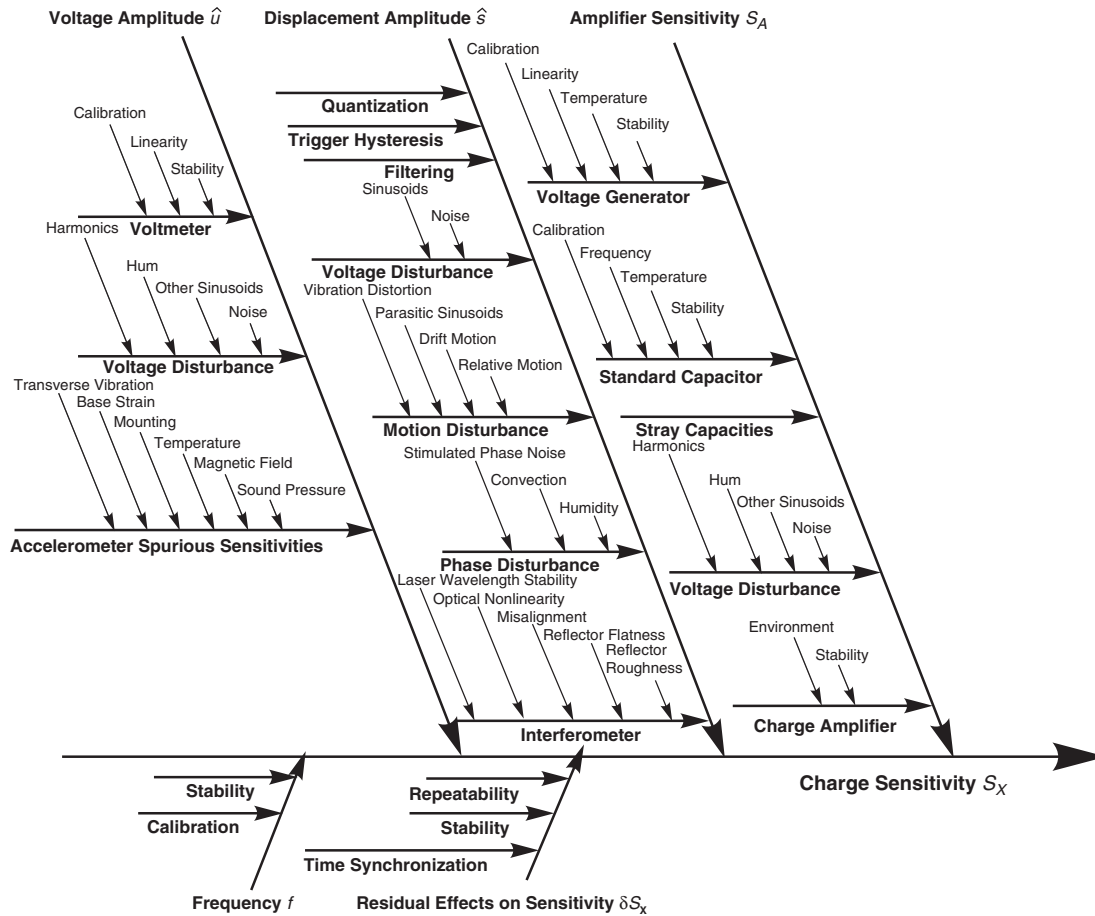
The logical structure of the cause-and-effect diagram of Fig. 10 subdivides the variety of error sources into groups affecting the measurement of voltage, displacement, charge amplifier sensitivity, and frequency. In addition to these four quantities, which are measurands of the indirect measurement of the output quantity  $S$ , a fifth path  $\delta S$  is included to take residual (combined) effects into account, which cannot be assigned to any of the four measurands of the indirect measurement.

For the mathematical model Eq. (2) with Eq. (2a) for the measurement of the magnitude of the complex sensitivity of the accelerometer, the expression for the relative combined standard uncertainty

$$\frac{u_c(S)}{S} = \sqrt{\left(\frac{u(\hat{u})}{\hat{u}}\right)^2 + \left(\frac{u(\hat{s})}{\hat{s}}\right)^2 + \left(\frac{2u(f)}{f}\right)^2 + \left(\frac{u(S_q)}{S_q}\right)^2 + \sum_{i=5}^N (u(K_i))^2} \quad (3)$$

can be applied, where  $u(x_i)$  is the standard uncertainty of the input estimate  $x_i$ ,  $i = 1, 2, \dots, N$ . The expanded uncertainty  $U$  is determined by multiplying  $u_c$  by a coverage factor  $k$  (normally  $k = 2$ , see Section 6.1, step 6).

The uncertainty evaluation described in detail in Ref. 55 is valid for the sensitivity measurement (magnitude) at a frequency of 800 Hz and an acceleration



**Figure 10** Cause-and-effect diagram for the measurement of the charge sensitivity of an accelerometer (method 1 specified in ISO 16063-11).<sup>5</sup>

amplitude of 50 m/s<sup>2</sup>. The expanded uncertainty  $U$  ( $k = 2$ ) of 0.065% resulting from the uncertainty budget<sup>55</sup> has been rounded to 0.1%, which is the best uncertainty stated by the PTB for vibration measurement and calibrations (e.g., in Ref. 39). The uncertainty evaluations that have been demonstrated for interferometric vibration measurements and primary calibrations of accelerometer standards with expanded uncertainties of  $\leq 0.1\%$  for a coverage factor  $k = 2$  were assessed by different international comparison measurements (see Ref. 39).

Various further specific uncertainty evaluations carried out for vibration and shock measurements and calibrations based on the GUM<sup>4</sup> have been published (e.g., Refs. 59 to 63).

## REFERENCES

1. ISO 2041, Vibration and Shock—Vocabulary, International Organization for Standardization (ISO), Geneva, Switzerland, 1990.
2. International Vocabulary of Basic and General Terms in Metrology, International Organization for Standardization (ISO), Geneva, Switzerland, 1993.
3. ISO/IEC 17025, General Requirements for the Competency of Testing and Calibration Laboratories, Geneva, Switzerland, 2005.
4. *ISO Guide to the Expression of Uncertainty in Measurement*, International Organization for Standardization (ISO), Geneva, Switzerland, 1995.
5. ISO 16063-11, Methods for the Calibration of Vibration and Shock Transducers—Part 11: Primary Vibration Calibration by Laser Interferometry, International Organization for Standardization (ISO), Geneva, Switzerland, 1999.
6. ISO 16063-21, Methods for the Calibration of Vibration and Shock Transducers—Part 21: Vibration Calibration by Comparison to a Reference Transducer, International Organization for Standardization (ISO), Geneva, Switzerland, 2003.
7. ISO 16063-13, Methods for the Calibration of Vibration and Shock Transducers—Part 13: Primary Shock Calibration Using Laser Interferometry, International Organization for Standardization (ISO), Geneva, Switzerland, 2001.
8. ISO 16063-22, Methods for the Calibration of Vibration and Shock Transducers—Part 22: Shock Calibration by Comparison to a Reference Transducer, International Organization for Standardization (ISO), Geneva, Switzerland, 2005.
9. ISO 16063-12, Methods for the Calibration of Vibration and Shock Transducers—Part 12: Primary Vibration Calibration by the Reciprocity Method, International Organization for Standardization (ISO), Geneva, Switzerland, 2002.
10. H.-J. von Martens, A. Link, H.-J. Schlaak, A. Täubner, W. Wabinski, and C. Weißenborn, Investigations to Assess the Best Accuracy Attainable in Accelerometer Calibrations, *SPIE*, Vol. 4827, 2002, pp. 258–276.
11. N. H. Clark, Traceable Vibration Measurements—Who Needs Them? *SPIE*, Vol. 3411, 1998, pp. 182–186.
12. H.-J. von Martens, ISO Standardization to Ensure Traceability of Vibration and Shock Measurements, Proceedings 1st Pan-American/Iberian Meeting on Acoustics, Cancun, Mexico, 2002.
13. H.-J. von Martens, Current State and Trends of Ensuring Traceability for Vibration Measurements, *Metrologia*, Vol. 36, 1999, pp. 357–373.
14. H.-J. von Martens, A. Link, H.-J. Schlaak, A. Täubner, W. Wabinski, and U. Göbel, Recent Advances in Vibration and Shock Measurements and Calibrations Using Laser Interferometry, *SPIE*, Vol. 5503, 2004, pp. 1–19.
15. ISO 16063-15, Methods for the Calibration of Vibration and Shock Transducers—Part 15: Primary Angular Vibration Calibration by Laser Interferometry, International Organization for Standardization, Geneva, Switzerland, 2006.
16. B. Payne, Laser Interferometer and Reciprocity Calibration of Accelerometers Using the NIST Super Shaker, *SPIE*, Vol. 3411, 1998, pp. 187–194.
17. C. S. Veldman, A Novel Implementation of the Sine-approximation Method for Primary Vibration Calibration by Laser Interferometry, *SPIE*, Vol. 4827, 2002, pp. 37–49.
18. T. Usuda, E. Furuta, A. Ohta and H. Nakano, Development of Laser Interferometer for Sine-approximation Method, *SPIE*, Vol. 4827, 2002, pp. 29–36.
19. B. Payne and D. J. Evans, Comparison of Results of Calibrating the Magnitude of the Sensitivity of Accelerometers by Laser Interferometry and Reciprocity, *Metrologia*, Vol. 36, 1999, pp. 391–394.
20. N. H. Clark, First-Level Calibrations of Accelerometers, *Metrologia*, Vol. 36, 1999, pp. 385–389.
21. K. Ueda, T. Usuda, T. Ishigami, and T. Kurosawa, The Current Status of Measurement Standards for Vibration and Shock in NRLM, *SPIE*, Vol. 4072, 2000, pp. 106–112.
22. F. Alasia, S. Baggia, G. Basile, G. Booth, and F. Mazzoleni, A Four-Reflection Interferometer Configuration for Vibration Calibration, *SPIE*, Vol. 4072, 2000, pp. 106–112.
23. T. Usuda, A. Ohta, T. Ishigami, O. Fuchiwaki, D. Misaki, H. Aoyama and S. Sato, The Current Progress of Measurement Standards for Vibration in NMII/AIST, *SPIE*, Vol. 5503, 2004, pp. 30–38.
24. G. Basile, D. Mari, and F. Mazzoleni, A Four Reflection Laser Interferometer for Vibration Measurements, Proceedings 6th International Conference on Vibration Measurements by Laser Techniques, Ancona, Italy, 2004.
25. R. D. Sill, Accelerometer Calibration to 50 kHz with a Quadrature Laser Interferometer, Proceedings NCSL, Workshop & Symposium, Session 7B, Atlanta GA, 1997, pp. 767–773.
26. M. Bauer, F. Ritter, and G. Siegmund, High-Precision Laser Vibrometers Based on Digital Doppler Signal Processing, *SPIE*, Vol. 4827, 2002, pp. 50–61.
27. L. Zhang and J. Peng, Primary Acceleration Calibration by Heterodyne Laser Interferometer and PXI Instrument, *SPIE*, Vol. 5503, 2004, pp. 588–597.
28. U. Bühn and H. Nicklich, Primary Vibration Calibration by Laser Interferometry—Requirements, Problems and First Experience with a New Calibration System, *SPIE*, Vol. 4827, 2002, pp. 62–73.
29. T. R. Licht and S. E. Salbol, Low Frequency Laser Calibration of Vibration Transducers Using Off-the-Shelf Laser Vibrometers and Counters, Proceedings 5th International Conference on Vibration Measurements by Laser Techniques, Ancona, Italy, 2002.

30. E. Sadikoglu, E. Bilgic, and B. Karaboce, Characterization of Commercial Type Vibration Exciters by Self-Mixing Interferometry, *SPIE*, Vol. 5503, 2004, pp. 598–601.
31. S. Chen, Accelerometer Sensitivity Calibration by Phase Differences of a Single Channel Laser Interferometer: Theory, *SPIE*, Vol. 5503, 2004, pp. 417–422.
32. S. Rojas-Ramires, A. Elias-Juarez, H.-J. Schlaak, and H.-J. von Martens, Shock Measurements with a Homodyne Interferometer for Accelerometer Calibration, *SPIE*, Vol. 4072, 2000, pp. 146–157.
33. Da-Hong Lian, Xiao-Mei Xu, and Xin-Liang Li, Accelerometer Shock Calibration Using Differential Grating Laser Interferometer from 100 m/s<sup>2</sup> to 1 000 000 m/s<sup>2</sup>, *SPIE*, Vol. 3411, 1998, pp. 239–251.
34. D. C. Robinson, M. R. Serbyn, and B. F. Payne, A Description of NBS Calibration Services in Mechanical Vibration and Shock, *NBS Tech. Note*, Vol. 1232, 1987, pp. 1–22.
35. M. R. Serbyn, Statistical Analysis of an Accelerometer Round Robin, *J. Acoust. Soc. Am.*, Vol. 87, 1990, p. 593(A).
36. CMEA Comparison of Accelerometer Calibration, Report CMEA, Ref-No. 01.752, 1989, pp. 17–87.
37. M. Fourcade, First European Comparison in Accelerometry, Using Two Standard Accelerometers, International Comparison, Final Report, *Metrologia*, Vol. 34, 1997, pp. 197–198.
38. S. Chen and H.-J. von Martens, APMP Regional Comparison of Standard Accelerometer, Final Report APMP-IC-4-9, 2001.
39. H.-J. von Martens, C. Elster, A. Link, A. Täubner, and W. Wabinski, Key Comparison CCAUV.V-K1 Final Report, [www.bipm.org/kcdb](http://www.bipm.org/kcdb), *Metrologia*, Vol. 40, Tech. Suppl. 09001, 2003.
40. Euromet-Project Ref.-No 579, European Comparison in Accelerometer Calibration EUROMET.AUV.V-K1, [www.EUROMET.org](http://www.EUROMET.org), 2003.
41. C. S. Veldman and H.-J. von Martens, Phase Calibration of Laboratory Standard Accelerometers Using Laser Interferometry, *SPIE*, Vol. 5503, 2004, pp. 403–416.
42. H.-J. von Martens, Final Report on the EA Interlaboratory Comparison A1—Acceleration, PTB, Berlin, 1998.
43. H.-J. von Martens, A. Täubner, W. Wabinski, A. Link, and H.-J. Schlaak, Laser Interferometry—Tool and Object in Vibration and Shock Calibrations, *SPIE*, Vol. 3411, 1998, pp. 195–206.
44. A. Link, J. Gerhardt, and H.-J. von Martens, Amplitude and Phase Calibration of Accelerometers in the Nanometer Range by Heterodyne Interferometry, *SPIE*, Vol. 2868, 1996, pp. 37–48.
45. W. Wabinski and H.-J. von Martens, Time Interval Analysis of Interferometer Signals for Measuring Amplitude and Phase of Vibrations, *SPIE*, Vol. 2868, 1996, pp. 166–177.
46. A. Link, H.-J. von Martens, and W. Wabinski, New Method for Absolute Shock Calibration of Accelerometers, *SPIE*, Vol. 3411, 1998, pp. 224–235.
47. A. Link, W. Wabinski, and H.-J. von Martens, Accelerometer Identification by High Shock Intensities Using Laser Interferometry, *SPIE*, Vol. 5503, 2004, pp. 580–587.
48. H.-J. von Martens and A. Täubner, Interferometric Low-Frequency Calibration of Translation and Rotation Quantity Transducers, Proceedings 7th International Meeting on Low Frequency Noise & Vibration, Edinburgh, Great Britain, 1993, pp. 77–82.
49. A. Täubner and H.-J. von Martens, Measurement of Angular Acceleration, Angular Velocities and Rotation Angles by Grating Interferometry, *Measurement*, Vol. 24, 1998, pp. 21–32.
50. H.-J. von Martens, Investigations into the Uncertainties of Interferometric Measurements of Linear and Circular Vibrations, *Shock Vib.*, Vol. 4, 1997, pp. 327–340.
51. H.-J. von Martens, Interferometric Counting Methods for Measuring Displacements in the Range 10<sup>−9</sup> to 1 m, *Metrologia*, Vol. 24, 1987, pp. 163–170.
52. T. Usuda, C. Weißenborn, and H.-J. von Martens, Theoretical and Experimental Investigation of Transverse Sensitivity of Accelerometers under Multiaxial Excitation, *Measurement Sci. Tech.*, Vol. 15, 2004, pp. 896–904.
53. ISO 5347-11, Methods for the Calibration of Vibration and Shock Pick-ups—Part 11: Testing of Transverse Vibration Sensitivity, International Organization for Standardization, Geneva, Switzerland, 1993.
54. D. J. Evans, Testing the Sensitivity of Accelerometers Using Mechanical Shock Pulses under NIST Special Publication 250 Special Test no. 24040S, ASME International Mechanical Engineering Congress & Exposition, San Francisco, 1995.
55. H.-J. v. Martens, Evaluation of Uncertainty in Interferometric Vibration Measurements, *SPIE*, Vol. 4072, 2000, pp. 82–101.
56. H.-J. von Martens, Evaluation of Uncertainty in Measurements—Problems and Tools, *Optics Lasers Eng.*, Vol. 38, 2002, pp. 185–206.
57. ISO 16063-1, Methods for the Calibration of Vibration and Shock Transducers—Part 1: Basic Concepts, International Organization for Standardization, Geneva, Switzerland, 1998.
58. H.-J. von Martens and P. Rogazewski, Representation and Transfer of the Units of Vibration Quantities in the GDR, *OIML Bull.*, Vol. 108, 1987, pp. 26–37.
59. G. Silva-Pineda and L. Ferrer-Argote, On the Estimation of Uncertainties for the Accelerometer Calibration Using Laser Interferometry, *SPIE*, Vol. 4072, 2000, pp. 137–145.
60. T. Usuda and T. Kurosawa, Calibration Methods for Vibration Transducers and Their Uncertainties, *Metrologia*, Vol. 36, 1999, pp. 375–383.
61. K. Ueda, A. Umeda, and H. Imai, Uncertainty Evaluation of a Primary Shock Calibration Method for Accelerometers, *Metrologia*, Vol. 37, 2000, pp. 187–197.
62. H. Nicklich and U. Bühn, Practical Experiences in Primary Vibration Calibration Using Laser Vibrometry—Measurement Uncertainties in Wide Frequency Range Applications, *SPIE*, Vol. 5503, 2004, pp. 442–445.
63. B. Payne and D. J. Evans, Errors in Accelerometer Calibration Using Laser Interferometry Due to Harmonic Distortion and Cross Motion in the Applied Motion, *SPIE*, Vol. 4072, 2000, pp. 102–105.

## **PART VI**

---

# **PRINCIPLES OF NOISE AND VIBRATION CONTROL AND QUIET MACHINERY DESIGN**

# CHAPTER 54

## INTRODUCTION TO PRINCIPLES OF NOISE AND VIBRATION CONTROL

Malcolm J. Crocker

Department of Mechanical Engineering  
Auburn University  
Auburn, Alabama

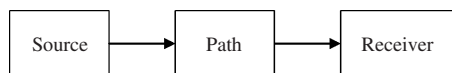
### 1 INTRODUCTION

Machines are used for a variety of purposes. The noise and vibration of appliances is often simply just annoying. The noise and vibration of machines in industry, however, can be intense enough to permanently hurt people. Although each machinery noise and vibration problem is somewhat different, a systematic approach and use of several well-known methods often produce sufficient reduction and acceptable conditions.<sup>1</sup> This chapter begins with a discussion of the source–path–receiver model, continues with a description of the most useful passive noise and vibration control approaches, and concludes with a discussion of the sources of noise and vibration in several important classes of machines and methods of identifying sources. Several individual worked examples are provided of the use of passive noise and vibration control approaches, and a specific example is given of how noise has been reduced on a mobile air compressor.

### 2 SYSTEMATIC APPROACH TO NOISE PROBLEMS

Noise control should always be incorporated at the design stage wherever possible because there are more low-cost options and possibilities than to make completed machines or installations quieter.<sup>1–3</sup> After machines are built or installations completed, noise control approaches can still be achieved through various modifications and add-on treatments, but these are frequently more difficult and expensive to implement. Several books deal with the fundamentals of noise control and with practical applications of noise control techniques.<sup>4–12</sup> Other books deal with acoustics and noise theory.<sup>13,14</sup>

Noise problems can be described using the simple *source–path–receiver* model<sup>4</sup> shown in Fig. 1. The *sources* are of two main types: (1) airborne sound sources caused by gas fluctuations (as in the fluctuating release of gas from an engine exhaust) or (2) structure-borne machinery vibration sources that in turn create



**Figure 1** Source–path–receiver model for noise problems.

sound fields (e.g., engine surface vibrations). Moreover, these sound pressure and vibration sources are of two types: (1) steady state and (2) impulsive. Both steady-state and impulsive vibrations (caused by impacting parts) are commonly encountered in machines. The *paths* may also be airborne or structure-borne in nature.

Source modifications are the best practice but are sometimes difficult to accomplish. Often changes in the path or at the *receiver* may be the only real options available. The model shown in Fig. 1 is very simple. In reality there will be many sources and paths. The dominant source should be treated first, then the secondary one, and so on. The same procedure can also be applied to the paths. Finally, when all other possibilities are exhausted, the receiver can be treated. If, as in most noise problems, the receiver is the human ear, earplugs or earmuffs or even complete personnel enclosures can be used.

Measurements, calculations, and experience all play a part in determining the dominant noise and vibration sources and paths. The dominant sources (and paths) can sometimes be determined from careful experiments. In some cases, parts of a machine can be turned off or disconnected to help identify sources. In other cases, parts of a machine can be enclosed, and then sequential exposure of machine parts can be used to identify major sources. Frequency analysis of machines can also be used as a guide to the causes of noise, as with the case of the firing frequency in engines, the pumping frequency of pumps and compressors, and the blade-passing frequency of fans. More sophisticated methods are also available involving the use of coherence, cepstrum, and intensity methods. Methods for determining the sources of noise and vibration in machinery are discussed in Chapter 55 of this book.

### 3 NOISE REDUCTION TECHNIQUES

A study of the literature reveals many successful well-documented methods used to reduce the noise of machines. These can be classified using the source–path–receiver model. Some of the most useful approaches can generally be used only at the source or in the path. Others, such as *enclosure*, can be adapted for use at any location. For instance, a small enclosure can be built inside a machine around a gear or bearing, or a larger enclosure or room can be built around a complete machine. Finally, an enclosure or personnel booth can be built for the use of a machine operator.

**Table 1** Passive Noise Control Approaches That May Be Considered for Source, Path, or Receiver

Source	Choose quietest machine source available Reduce force amplitudes Apply forces more slowly Use softer materials for impacting surfaces Balance moving parts Use better lubrication Improve bearing alignment Use dynamic absorbers Change natural frequencies of machine elements Increase damping of machine elements Isolate machine panels from forces Reduce radiating surface areas (by adding holes)
Path	Stagger time of machine operations in a plant Install vibration isolators Use barriers Install enclosures Use absorbing materials Install reactive or dissipative mufflers Use vibration breaks in ductwork Mismatch impedances of materials Use lined ducts and plenum chambers Use flexible ductwork Use damping materials
Receiver	Provide earplugs or earmuffs for personnel Construct personnel enclosures Rotate personnel to reduce exposure time Locate personnel remotely from sources

Table 1 summarizes a large number of approaches that have been found useful in practice.

#### 4 MAIN PASSIVE NOISE CONTROL APPROACHES

In this section the main passive noise control approaches are briefly summarized. These include the use of (1) vibration isolators, (2) acoustical absorbing material, (3) enclosures, (4) barriers, and (5) vibration damping material.

##### 4.1 Use of Vibration Isolators

Vibration isolation has been discussed frequently in the literature. Chapter 59 also presents a detailed review of vibration isolation theory and practice. Vibration isolators are used in two main situations: (1) where a machine source is producing vibration that it is desired to prevent vibration energy flowing to supporting structures and (2) where a delicate piece of equipment (such as an electronics package or precision grinder) must be protected from vibration in the structure. It is the first case that will receive attention here. Primary emphasis is placed on reducing the force transmitted from the machine source to the supporting structure, but a secondary consideration is to reduce the vibration of the machine source itself.

It is often found that machines are attached to metal decks, grills, and sometimes lightweight wood or concrete floors. The machine on its own is usually

incapable of radiating much noise (particularly at low frequency). The supporting decks, grills, and floors, however, tend to act like sounding boards, just as in musical instruments, and amplify the machine noise. Properly designed vibration isolators can overcome this noise problem.

Vibration isolators are of three main types: (1) spring, (2) elastomeric, and (3) pneumatic. Spring isolators are durable but have little damping. Elastomeric isolators are less durable and are subject to degradation due to corrosive environments. They have higher damping and are less expensive. Pneumatic isolators are used where very low frequency excitation is present.

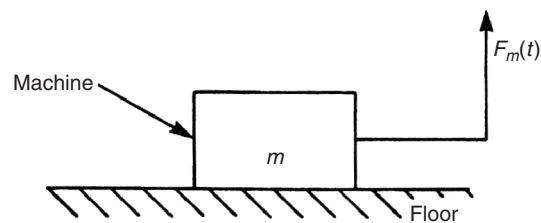
Often the exciting forces are caused by rotational out-of-balance forces in machines or machine elements or by magnetic or friction effects. Usually, these forces are simple harmonic in character. Such forces occur in electric motors, internal combustion engines, bearings, gears, and fans. Sometimes, however, the exciting forces may be impulsive in nature (e.g., in the case of punch presses, stamping operations, guillotines, tumblers, and any machines where impacts occur). The design of vibration isolators for a machine under the excitation of a simple harmonic force is considered below.

**Theory of Vibration Isolation** A machine may be considered, for simplicity, to be represented by a rigid mass  $m$ . If the machine is attached directly to a large rigid massive floor, as shown in Fig. 2, then all the periodic force  $F_m(t)$  applied to the mass is directly transmitted to the floor. We will assume that the force on the mass is vertical and  $F_m(t) = F_m \sin 2\pi ft$ , where  $F_m$  is the amplitude of this force, and  $f$  is its frequency (Hz).

If a vibration isolator is now placed between the machine and the floor, we can model this system with the well-known single-degree-of-freedom system shown in Fig. 3. The following discussion assumes that the isolators have a constant stiffness and that the damping is viscous in nature.

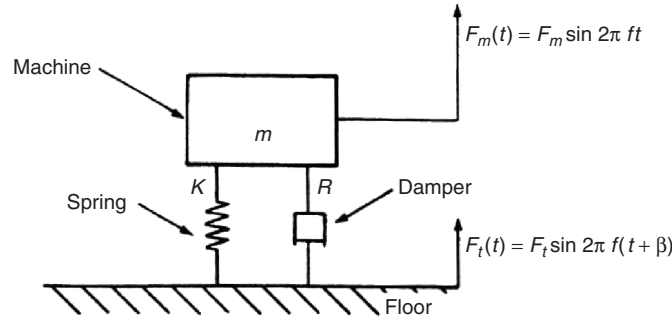
Suppose, for the moment, that the periodic force is stopped and that the mass  $m$  is brought to rest. If the mass  $m$  is displaced from its equilibrium position and released, then it will vibrate with a *natural frequency* of vibration  $f_n$  given by

$$f_n = \left( \frac{1}{2\pi} \right) \sqrt{\frac{K}{m}} \quad \text{Hz} \quad (1)$$



**Figure 2** Rigid machine of mass  $m$  attached to a rigid massive floor.





**Figure 3** Rigid machine of mass  $m$  separated from rigid massive floor by vibration isolator of stiffness  $K$  and damping  $R$ .

where, in International System (SI) units,  $K$  is the stiffness (N/m) and  $m$  is the mass (kg). See Chapter 1.

If the exciting force  $F_m(t)$  is now resumed, then a force  $F_t(t)$  will be transmitted to the rigid floor. This force  $F_t(t)$  will be out of phase with  $F_m(t)$ , but it is simple to show that the ratio of the amplitudes of the forces in the steady state is given by

$$T_F = \frac{F_t}{F_m} = \sqrt{\frac{1 + 4(f/f_n)^2(R/R_c)^2}{[1 - (f/f_n)^2]^2 + 4(f/f_n)^2(R/R_c)^2}} \quad (2)$$

where  $f$  is the frequency of the exciting force (Hz),  $f_n$  is the natural frequency of vibration of the mass  $m$  on the spring (Hz),  $R$  is the coefficient of damping (Vs/m), and  $R_c$  is the coefficient of critical damping ( $R_c = 2\sqrt{mK}$ ). See Chapter 1 for further discussion on vibration. The ratio  $F_t/F_m$  is known as the force transmissibility  $T_F$ .

The vibration amplitude  $A$  of the machine mass  $m$  is given by

$$\frac{A}{F_m/K} = \frac{1}{\{[1 - (f/f_n)^2]^2 + 4(f/f_n)^2(R/R_c)^2\}^{1/2}} \quad (3)$$

The ratio  $A/(F_m/K)$  is known as the *dynamic magnification factor* (DMF). This is because  $F_m/K$  represents the static displacement of the mass  $m$  if a static force of value  $F_m$  is applied, while  $A$  represents the dynamic displacement amplitude that occurs due to the periodic force of amplitude  $F_m$ . Note that the ratio  $R/R_c$  is known as the *damping ratio*  $\delta$ . If  $\delta = 1.0$ , the damping is called *critical damping*. With most practical vibration isolators,  $\delta$  may be in the range from about 0.01 to 0.2. Equations (2) and (3) are plotted in Figs. 4 and 5, respectively.

If the machine is run at the natural frequency  $f_n$ , we see from Fig. 4 that  $f/f_n$  is 1.0 and the force amplitude transmitted to the floor is very large, particularly if the damping in the isolator support is small. If the machine is operated much above the natural frequency, however, then the force amplitude transmitted to the floor will be very small.

**Example 1. Machine Isolation** Suppose we wish to isolate the 120-Hz vibration of an electric motor. If

we choose isolators so that the system has a natural frequency of 12 Hz, then the ratio  $f/f_n = 10$ . If the damping in the isolator system is  $R/R_c = 0.1$ , the force transmissibility will be only about 0.025, or 2.5%.

We define the efficiency  $\eta$  of the isolator as

$$\eta = (1 - T_F) \times 100\% \quad (4)$$

Thus in Example 1 the isolator efficiency is 97.5%.

To reduce the force transmissibility still further, we could use softer isolators and choose a still lower resonance frequency. There is some danger in doing this, however, because the static deflection of the machine will naturally increase if we use softer isolators. Since a large static deflection may be undesirable (it may interfere with the operation of the machine), this restricts the softness of the isolator and thus how low we can make the natural frequency  $f_n$ . The static deflection  $d$  produced in the isolator by the gravity force on the mass  $m$  is given by  $d = mg/K$ . We have already seen that the natural frequency is related to  $K$  and  $m$  by  $f_n = (1/2\pi)\sqrt{K/m}$ . Hence we can relate the static deflection  $d$  to the natural frequency  $f_n$ :

$$d = \frac{g}{4\pi^2 f_n^2} \quad (5)$$

where the static deflection  $d$  is given in centimetres (or inches) and  $g$  is the acceleration of gravity, 981 cm/s<sup>2</sup>.

The relationship given in Eq. (5) has been plotted in Fig. 6. The greatest static deflection  $d$  that can be allowed from operational considerations should be chosen. This will then allow a determination of the lowest allowable  $f_n$ . It should be noted that excessive static deflection may interfere with the operation of the machine by causing alignment problems. Also, using isolators with a small vertical stiffness usually means that they may have a small horizontal stiffness, and there will be stability problems. Both these considerations limit the lowest allowable  $f_n$ .

#### Simple Design Procedure and Worked Example

With springs, the damping is small (usually  $\delta < 0.1$ ), and we may use Eqs. (2) and (3) and Figs. 4 and

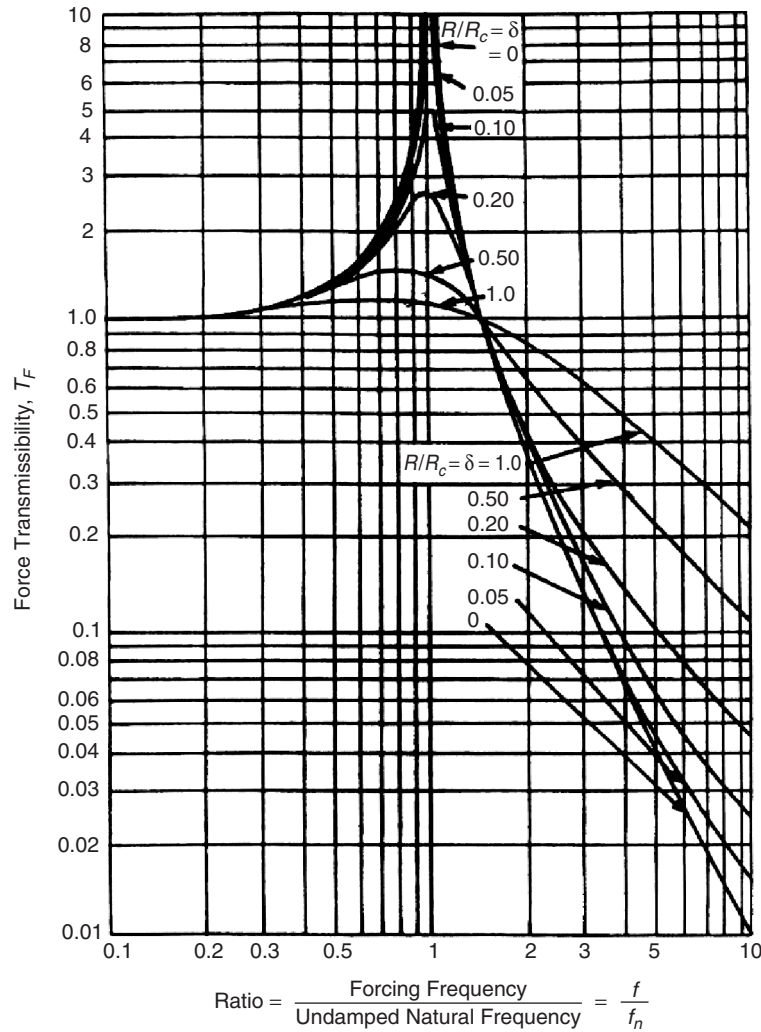


Figure 4 Force transmissibility  $T_F$  for the rigid machine–isolator–rigid floor system.

5, assuming that  $\delta = 0$ . With  $\delta = 0$  (or, equivalently,  $R = 0$ ), Eqs. (2) and (5) give

$$T_F = \frac{F_t}{F_m} = \frac{1}{1 - 4\pi^2 f^2 d/g} \quad (6)$$

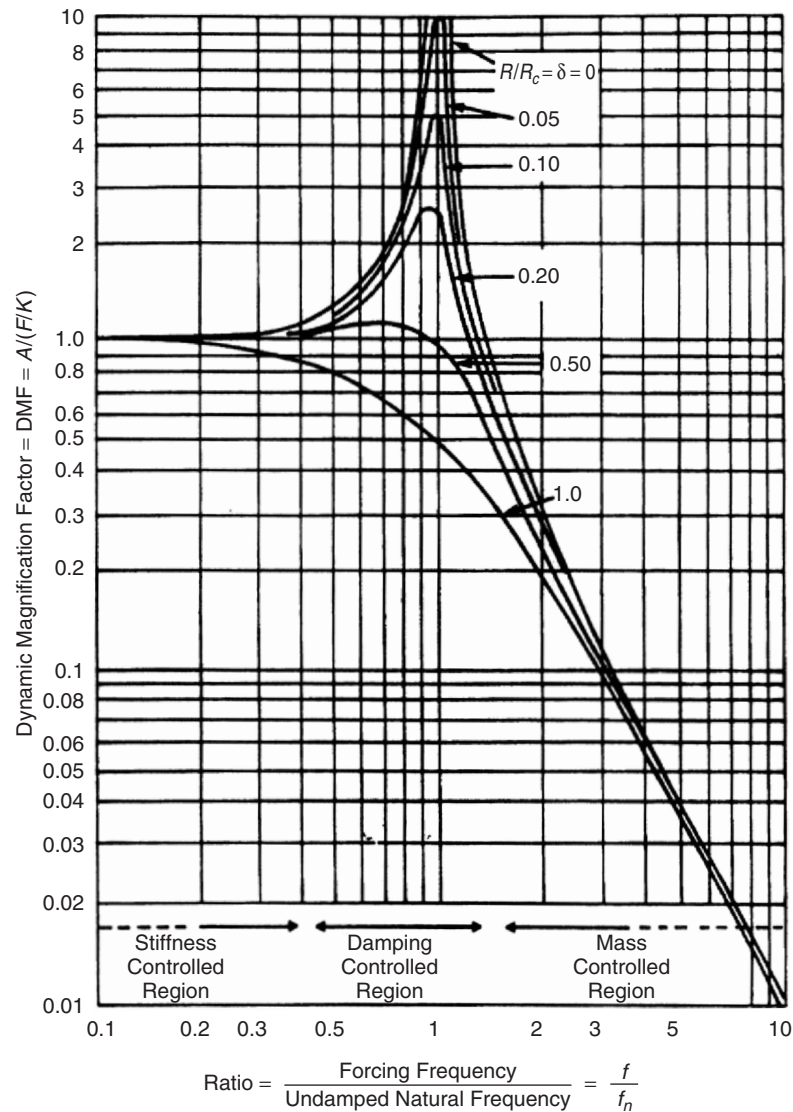
This result is plotted in Fig. 7. The suggested procedure is as follows.

1. Establish the total weight of the machine and the lowest forcing frequency experienced.
2. From Fig. 7 select the force transmissibility allowable (this determines the static deflection, given the lowest forcing frequency).
3. From the spring constants given by the manufacturer, the machine weight, and the static

deflection, choose the appropriate vibration isolator.

**Example 2. Machine Isolation** An electric motor of mass 100 kg and a reciprocating compressor of mass 500 kg are mounted on a common support. The motor runs at 2400 revolutions/minute (rpm) and by a belt drives the compressor at 3000 rpm. The vertical force fed to the support is thought to be excessive. Choose six equal spring mounts to provide a force transmissibility not exceeding 5%.

1. The total machine weight is 600 kg, and the lowest forcing frequency is 2400 rpm (or 40 Hz).
2. From Fig. 7, the static deflection required is 0.33 cm (0.13 in).

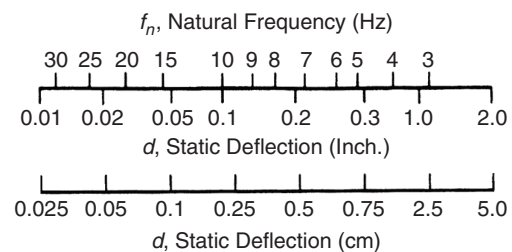


**Figure 5** Dynamic magnification factor (DMF) for the rigid machine-isolator-floor system.

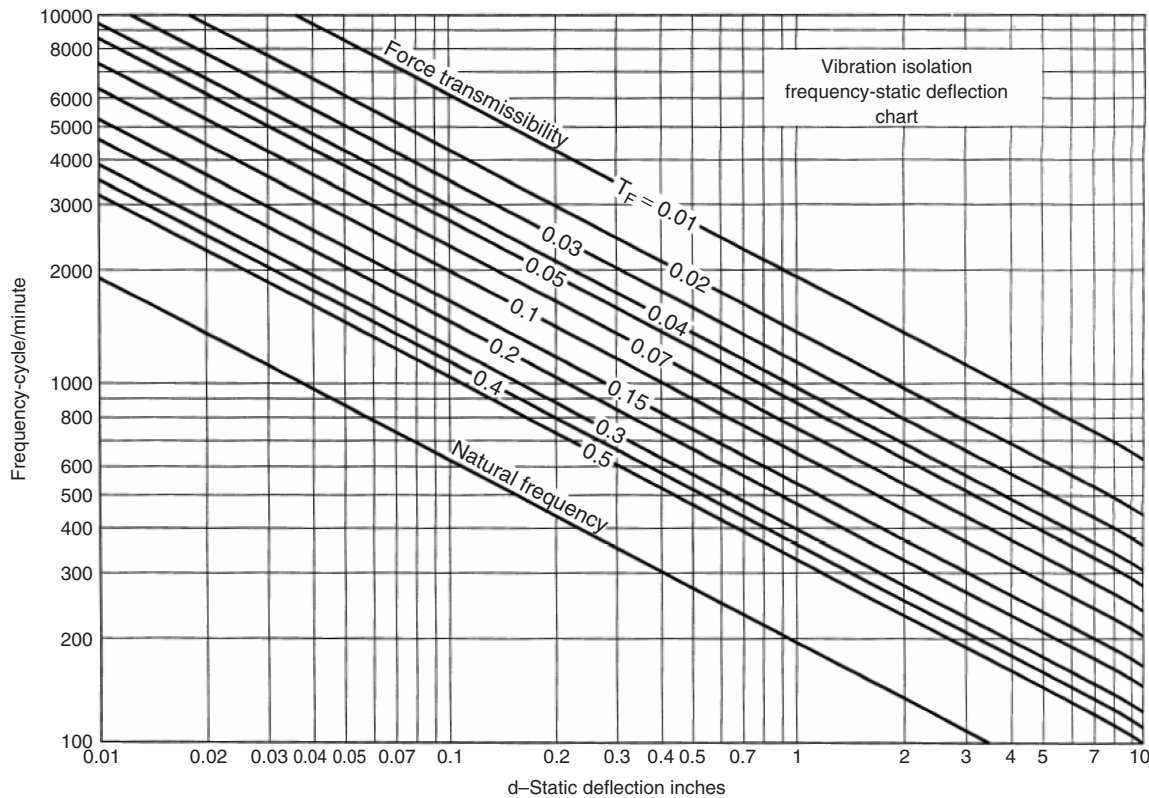
3. Thus, since there are six spring isolators, each must support a mass of 100 kg. This requires a spring constant for each isolator of  $981/0.33 = 3000 \text{ N/cm}$ .

As a check on the calculation, we see from Fig. 6 that a static deflection of 0.33 cm. requires a natural frequency of about 8.6 Hz. Thus, the ratio of forcing frequency to natural frequency  $f/f_n = 40/8.6 = 4.65$ . From Fig. 4, with zero damping,  $T_F = 0.05$ , which agrees with the design requirement.

**Machine Vibration** There are several other factors that should be considered in isolator design. First,



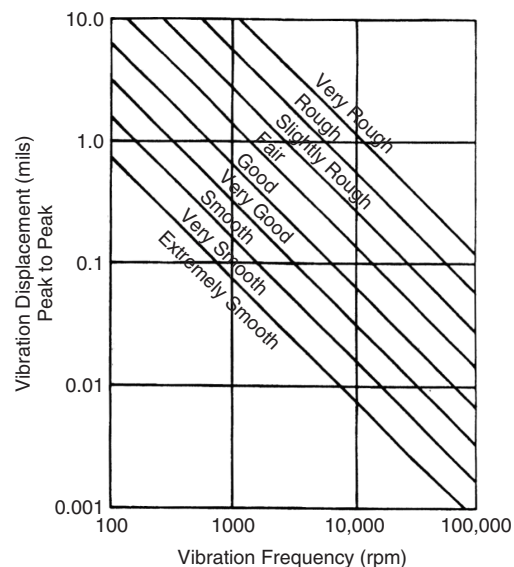
**Figure 6** Relationship between natural frequency  $f_n$  of machine-isolator-floor system and static deflection  $d$  of machine.



**Figure 7** Relationship (for a linear isolator) between forcing frequency  $f$ , force transmissibility  $T_F$ , and static deflection  $d$  of machine-isolator-floor system, without damping ( $R = 0$ ). (Note deflection given in inches. 1 inch = 2.54 cm.)

we notice from Figs. 4 and 5 that when a machine is started or stopped, it will run through the resonance condition and then, momentarily,  $f/f_n = 1$ . When passing through the resonance condition, large vibration amplitudes can exist on the machine, and the force transmitted will be large, particularly if the damping is small. Assuming viscous damping, to provide small force transmissibility at the operating speed, small damping is required; however, to prevent excessive machine vibration and force transmission during stopping and starting, large damping is needed. These two requirements are conflicting. Fortunately, some forces, such as out-of-balance forces, are much reduced during starting and stopping. However, it is normal to provide a reasonable amount of damping ( $\delta = 0.1$  to  $0.2$ ) in spring systems to reduce these starting and stopping problems. The severity of the machine vibration problem can be gauged from Fig. 8.

**Use of Inertia Blocks** Inertia blocks are normally made from concrete poured onto a steel frame. If the mass supported by the vibration isolators is increased by mounting a machine on an inertia block, the static deflection will be increased. If the isolator stiffness is correspondingly increased to keep the static deflection the same, then there is no change in the resonance



**Figure 8** Machine vibration severity chart showing peak-to-peak vibration (2A) mils (1 mil = 0.001 in. = 0.0254 mm).

frequency or the force transmissibility  $T_F$ . The use of an inertia block does, however, result in a reduced vibration amplitude of the machine mass. It also has additional advantages including (1) *improving stability* by providing vibration isolator support points that are farther apart, (2) *lowering the center of gravity* of the system, thus improving stability and reducing the effect of coupled modes and rocking natural frequencies, (3) producing more even weight distribution for machines often enabling the use of symmetrical vibration isolation mounts, (4) *functioning as a local acoustical barrier* to shield the floor of an equipment room from the noise radiated from the bottom of the machine and reducing its transmission to rooms below, and (5) *reducing the effect on the machine of external forces* such as transient loads or torques caused by operation of motors or fans or rapid changes in machine load or speed.

**Other Considerations** The performance of vibration isolators in the high-frequency range ( $f/f_n \geq 1$ ) is often disappointing. There are several possible reasons, but often they all result in an increase in force transmissibility  $T_F$  for  $f/f_n \geq 1$ . Usually, the reasons are deviations from the simple single-degree-of-freedom model as mentioned below.<sup>5</sup>

**(a) Support Flexibility** If the assumption that the support is rigid does not hold, then the support will also deflect (e.g., a flexible floor). If the isolator stiffness is similar in magnitude to that of the supporting floor, then additional resonances in the floor-machine system will occur for  $f/f_n > 1$ . It is normal practice to choose isolators (assuming a rigid support or floor) to have a natural frequency well below the fundamental natural frequency of the floor itself. (If possible there should not be any machine-exciting frequencies in the frequency range 0.8 to 1.3 times the floor fundamental natural frequency.) The fundamental natural frequency of a wood floor is usually in the 20 to 30-Hz frequency range, while that of a concrete floor is in the 30–100-Hz range.

**(b) Machine Resonances** Internal resonances in the machine structure will also increase the force transmissibility  $T_F$  in a similar manner to support

flexibility. Increasing the stiffness and/or the damping of machine members can help to reduce this effect.

**(c) Standing-Wave Effects** Standing-wave effects in the vibration isolators can significantly decrease their performance and increase force transmissibility for  $f/f_n \geq 1$ , but this typically occurs only at high frequency. This effect can be reduced by increasing the damping in the isolators. Springs particularly suffer from this problem because of their low inherent damping. Soft materials (such as felt or rubber) placed between the spring and the support can alleviate the problem. In elastometric isolators the effects of standing wave resonators are small because of their higher damping.

**(d) Shock Isolation** If the forces in the machine are impulsive in character (such as caused by repeated impacts), then the discussion for isolation of the single-degree-of-freedom model presented so far can still be used. It is normal practice to choose an isolator that provides a natural period  $T$  ( $T = 1/f_n$ ), which is much greater than the shock pulse duration but less than the period of repetition of the force.

**Example 3. Shock Isolation** A nail-making machine cuts nails five times each second ( $T = 0.2$  s). The shock pulse duration is approximately 0.015 s. What is a suitable choice of vibration isolator for the machine? Elastometric isolators that provide a natural period of vibration of 0.1 s (natural frequency of 10 Hz) would be a good choice. They have high damping.

## 4.2 Use of Sound-Absorbing Materials

Sound-absorbing materials have been found to be very useful in the control of noise. They are used in a variety of locations: close to sources of noise (e.g., close to sources in electric motors), in various paths, (e.g., above barriers or inside machine enclosures), and sometimes close to a receiver (e.g., inside earmuffs). When a machine is operated inside a building, the machine operator usually receives most sound through a direct path, while people situated at greater distances receive sound mostly through reflections (see Fig. 9).

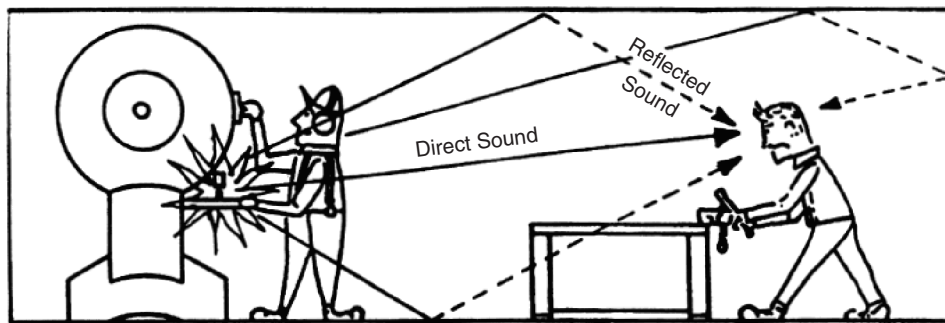


Figure 9 Paths of direct and reflected sound emitted by a machine in a building.

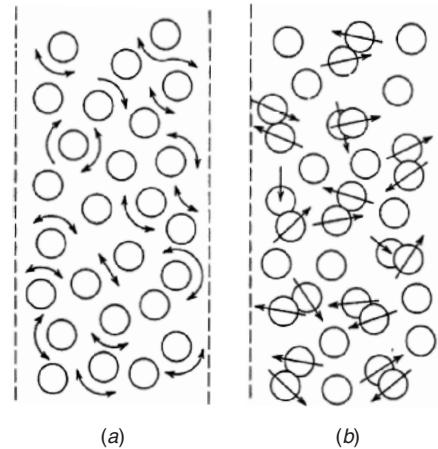


The relative contributions of the sound reaching people at a distance through direct and reflected paths are determined by how well the sound is reflected and absorbed by the walls in the building. The *absorption coefficient* of a material  $\alpha(f)$ , which is a function of frequency, has already been defined in Chapter 2:

$$\alpha(f) = \frac{\text{sound intensity absorbed}}{\text{sound intensity incident}} \quad (7)$$

Thus  $\alpha(f)$  is the fraction of incident sound intensity that is absorbed, and it can vary between 0 and 1. Materials that have a high value of  $\alpha$  are usually fibrous or porous. Fibrous materials include those made from natural or artificial fibers including glass fibers. Porous materials made from open-celled polyurethane foams are also widely used. The properties and use of sound-absorbing materials are discussed in more detail in Chapter 57.

It is believed that there are two main mechanisms by which the sound is absorbed in materials: (1) viscous dissipation of energy by the sound waves as they propagate in the narrow channels of the material and (2) energy losses caused by friction as the fibers of the material rub together under the influence of the sound waves. These mechanisms are illustrated in Fig. 10. In both mechanisms sound energy is converted into heat. The sound absorption coefficient of most acoustical materials increases with frequency (see Fig. 11), and coefficients of some common sound-absorbing materials and construction materials are shown in Tables 2 and 3. The noise reduction coefficient (NRC) of a sound-absorbing material is defined as the average of the absorption coefficients at 250, 500, 1000, and 2000 Hz (rounded off to the nearest multiple of 0.05).



**Figure 10** The two main mechanisms believed to exist in sound-absorbing materials: (a) viscous losses in air channels and (b) mechanical friction caused by fibers rubbing together.

In the case of machinery used in reverberant spaces, the reduction in sound pressure level  $L_p$  in the reverberant field caused by the addition of sound-absorbing material placed on the walls or under the roof (see Fig. 12) can be estimated for a source of sound power level  $L_W$  from the so-called room equation:

$$L_p = L_W + 10 \log \left( \frac{D}{4\pi r^2} + \frac{4}{R} \right) \quad (8)$$

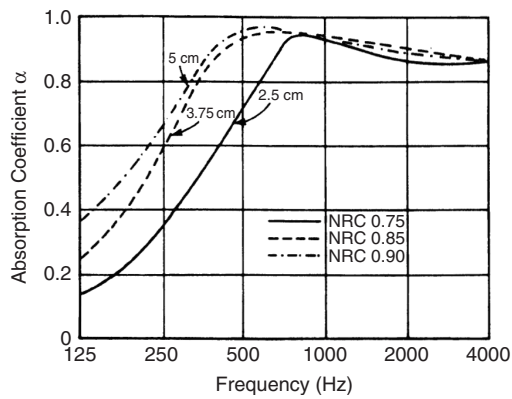
where  $R$  is the *room constant* and is given by  $R = S\bar{\alpha}/(1 - \bar{\alpha})$ ,  $\bar{\alpha}$  is the surface average absorption

**Table 2** Typical Sound Absorption Coefficients  $\alpha(f)$  of Common Acoustical Materials

Materials	Frequency (Hz)					
	125	250	500	1000	2000	4000
Fibrous glass (typically 65 kg/m <sup>3</sup> ) hard backing						
2.5 cm thick	0.07	0.23	0.48	0.83	0.88	0.80
5 cm thick	0.20	0.55	0.89	0.97	0.83	0.79
10 cm thick	0.39	0.91	0.99	0.97	0.94	0.89
Polyurethane foam (open cell)						
0.6 cm thick	0.05	0.07	0.10	0.20	0.45	0.81
1.2 cm thick	0.05	0.12	0.25	0.57	0.89	0.98
2.5 cm thick	0.14	0.30	0.63	0.91	0.98	0.91
5 cm thick	0.35	0.51	0.82	0.98	0.97	0.95
Hairfelt						
1.2 cm thick	0.05	0.07	0.29	0.63	0.83	0.87
2.5 cm thick	0.06	0.31	0.80	0.88	0.87	0.87

**Table 3 Sound Absorption Coefficient  $\alpha(f)$  of Common Construction Materials**

Material	Frequency $f$ (Hz)					
	125	250	500	1000	2000	4000
Brick						
Unglazed	0.03	0.03	0.03	0.04	0.04	0.05
Painted	0.01	0.01	0.02	0.02	0.02	0.02
Concrete block, painted	0.10	0.05	0.06	0.07	0.09	0.03
Concrete	0.01	0.01	0.015	0.02	0.02	0.02
Wood	0.15	0.11	0.10	0.07	0.06	0.07
Glass	0.35	0.25	0.18	0.12	0.08	0.04
Gypsum board	0.29	0.10	0.05	0.04	0.07	0.09
Plywood	0.28	0.22	0.17	0.09	0.10	0.11
Soundbox						
concrete block						
Type A (slotted), 15 cm	0.62	0.84	0.36	0.43	0.27	0.50
Type B, 15 cm	0.31	0.97	0.56	0.47	0.51	0.53
Carpet	0.02	0.06	0.14	0.37	0.60	0.66

**Figure 11** Sound absorption coefficient  $\alpha$  and noise reduction coefficient (NRC) for typical fiberglass form-board of different thicknesses.

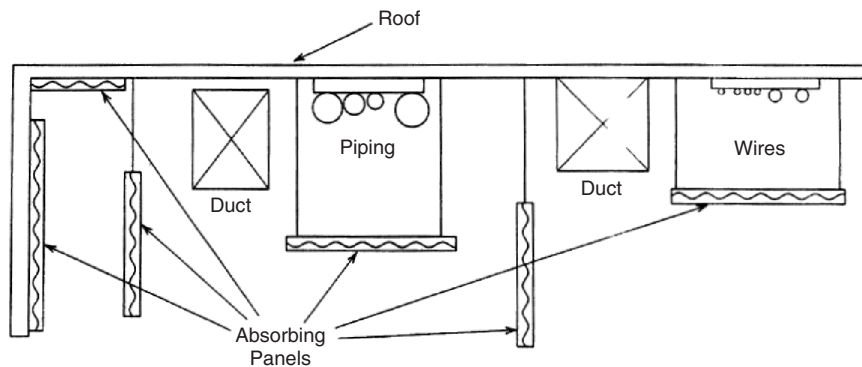
coefficient of the walls,  $D$  is the source directivity (see Chapter 1), and  $r$  is the distance in metres from the source. The surface average absorption coefficient  $\bar{\alpha}$  may be estimated from

$$\bar{\alpha} = \frac{S_1\alpha_1 + S_2\alpha_2 + S_3\alpha_3 + \dots}{S_1 + S_2 + S_3 + \dots} \quad (9)$$

where  $S_1, S_2, S_3, \dots$  are the surface areas of material with absorption coefficients  $\alpha_1, \alpha_2, \alpha_3, \dots$ . For the suspended absorbing panels shown in Fig. 12, both sides of the panel are normally included in the surface area calculation.

If the sound absorption is increased, then from Eq. (8) the change in sound pressure level  $\Delta L$  in the reverberant space (beyond the critical distance  $r_c$ ) (see Chapter 1) is

$$\Delta L = L_{p1} - L_{p2} = 10 \log \frac{R_2}{R_1} \quad (10)$$

**Figure 12** Sound-absorbing material placed on the walls and under the roof and suspended as panels in a factory building.

If  $\bar{\alpha} \ll 1$ , then the reduction in sound pressure level (sometimes called the *noise reduction*) is given by

$$\Delta L \approx 10 \log \frac{S_2 \bar{\alpha}_2}{S_1 \bar{\alpha}_1} \quad (11)$$

where  $S_2$  is the total surface area of the room walls, floor, and ceiling and any suspended sound-absorbing material,  $\bar{\alpha}_2$  is the average sound absorption coefficient of these surfaces after the addition of sound-absorbing material, and  $S_1$  and  $\bar{\alpha}_1$  are the area and the average sound absorption coefficient before the addition of the material. The terms  $S\bar{\alpha}$  are known as absorption areas.

**Example 4. Reverberant Noise Reduction Using Absorbing Materials.** A machine source operates in a building of dimensions 30 m  $\times$  30 m with a height of 10 m. Suppose the average absorption coefficient is  $\bar{\alpha} = 0.02$  at 1000 Hz. What would be the noise reduction in the reverberant field if 100 sound-absorbing panels with dimensions 1 m  $\times$  2 m each with an absorption coefficient of  $\bar{\alpha} = 0.8$  at 1000 Hz were suspended from the ceiling (assume both sides absorb sound)? The room surface area = 2(900) + 4(300) = 3000 m<sup>2</sup>; therefore  $R_1 = (3000 \times 0.02)/0.98 = 60/0.98 = 61.2$  sabins (m<sup>2</sup>). The new average absorption coefficient  $\bar{\alpha}_2 = (3000 \times 0.02 + 200 \times 2 \times 0.8)/3400 = 60 + 320 = 380/3400 = 0.11$ . The new room constant is  $(3400 \times 0.11)/0.89 = 420$  sabins (m<sup>2</sup>). Thus from Eq. (10) the predicted noise reduction  $\Delta L = 10 \log(420/61.2) = 8.3$  dB. This calculation may be repeated at each frequency for which absorption coefficient data are available. It is normal to assume that about 10 dB is the practical limit for the noise reduction that can be achieved by adding sound-absorbing material in industrial situations.

### 4.3 Acoustical Enclosures

*Acoustical enclosures* are used wherever containment or encapsulation of the source or receiver are a good, cost-effective, feasible solution. They can be classified in four main types: (1) large loose-fitting or room-size enclosures in which complete machines or personnel are contained, (2) small enclosures used to enclose small machines or parts of large machines, (3) close-fitting enclosures that follow the contours of a machine or a part, and (4) wrapping or lagging materials often used to wrap pipes, ducts, or other systems.

The performance of such enclosures can be defined in three main ways<sup>5</sup>: (1) *noise reduction* (NR), the difference in sound pressure levels between the inside and outside of the enclosure, (2) *transmission loss* (TL, or equivalently the *sound reduction index*), the difference between the incident and transmitted sound intensity levels for the enclosure wall, and (3) *insertion loss* (IL), the difference in sound pressure levels at the receiver point *without* and *with* the enclosure wall in place. The definitions for the NR, TL, and IL performance of an enclosure are similar to those for mufflers (Chapters 83 and 85) and barriers (Chapters 58 and 122). Enclosures can either be complete

or partial (in which some walls are removed for convenience or accessibility). Penetrations are also often necessary to provide access or cooling.

The transmission coefficient  $\tau$  of a wall may be defined as

$$\tau = \frac{\text{sound intensity transmitted by wall}}{\text{sound intensity incident on wall}} \quad (12)$$

and this is related to the TL (or sound reduction index) by

$$TL = 10 \log \frac{1}{\tau} \quad (13)$$

If the sound fields can be considered to be reverberant on the two sides of a complete enclosure, then

$$NR = L_{p1} - L_{p2} = TL + 10 \log \frac{A_2}{S_e} \quad (14)$$

where  $L_{p1}$  and  $L_{p2}$  are the sound pressure levels on the transmission and receiving sides of the enclosure.  $A_2 = S_2 \bar{\alpha}_2$  is the absorption area in square metres or feet in the receiving space material where  $\bar{\alpha}_2$  is the average absorption coefficient of the absorption material in the receiving space averaged over the area  $S_2$ , and  $S_e$  is the enclosure surface area in square metres or feet.

Equation (14) can be used to determine the TL of a partition of surface area  $S_e$  placed between two isolated reverberation rooms in which a noise source creates  $L_{p1}$  in the source room, and this results in  $L_{p2}$  in the receiving room. Also Eq. (14) can be used to design a personnel enclosure. If the enclosure is located in a factory building in which the reverberant level is  $L_{p1}$ , then the enclosure wall TL and interior absorption area  $A_2$  can be chosen to achieve an acceptable value for the interior sound pressure level  $L_{p2}$ . In the case that the surface area  $S_2$  of the interior absorbing material  $S_2 = S_e$ , the enclosure surface area, then Eq. (14) simplifies to

$$NR = TL + 10 \log \bar{\alpha}_2 \quad (15)$$

We see that normally the NR achieved is less than the TL. Also when  $\bar{\alpha}_2$ , the average absorption coefficient of the absorbing material in the receiving space, approaches 1, then  $NR \rightarrow TL$  (the expected result), although when  $\bar{\alpha}_2 \rightarrow 0$ , then the theory fails.

**Example 5. Personnel Enclosure** If the reverberant level in a factory space is 90 dB in the 1000-Hz one-third octave band, what values of TL and  $\bar{\alpha}$  should be chosen to ensure that the interior level inside a personnel enclosure is below 60 dB? Assuming that  $S_2 = S_e$ , then if TL is chosen as 40 dB and  $\bar{\alpha} = 0.1$ ,  $NR = 40 + 10 \log 0.1 = 40 - 10 = 30$  dB, and  $L_{p2} = 60$  dB. If  $\bar{\alpha}$  is increased to 0.2, then  $NR = 40 + 10 \log 0.2 = 40 - 7 = 33$  and  $L_{p2} = 57$  dB, meeting the requirement. Note that in general, since TL varies



with frequency [see Eq. (18)], then this calculation would have to be repeated for each one-third octave band center frequency of interest. At low frequency, since large values of TL and  $\bar{\alpha}$  are difficult to achieve, it may not be easy to obtain large values of NR.

When an enclosure is used to contain a source, it works by reflecting the sound field back toward the source causing an increase in the sound pressure level inside the enclosure. From energy considerations the insertion loss would be zero if there were no acoustical absorption inside. The buildup of sound energy inside the enclosure, however, can be reduced significantly by the placement of sound-absorbing material inside the enclosure. It is also useful to place sound-absorbing materials inside personnel protective booths for similar reasons. In general, it is difficult to predict the insertion loss of an enclosure. For one installed around a source with a considerable amount of absorbing material used inside to prevent *any* interior reverberant sound energy buildup, then from energy considerations:

$$IL \approx TL$$

if the receiving space is quite absorbent and if IL and TL are wide-frequency-band averages (e.g., at least one octave). If insufficient absorbing material is placed inside the enclosure, the sound pressure level will build up inside the enclosure by multiple reflections, and the enclosure effectiveness will be degraded. From energy considerations it is obvious that if there is no sound absorption inside ( $\bar{\alpha} = 0$ ), the enclosure will be useless, and its IL will be zero.

An estimate of the insertion loss of intermediate cases  $0 < \bar{\alpha} < 1$  can be obtained by assuming that the sound field inside the enclosure is reverberant and that the interior surface of the enclosure is lined with absorbing material of average absorption coefficient  $\bar{\alpha}$ . With the assumptions that (1) the average absorption coefficient in the room containing the noise source is not greater than 0.3 (which is true for most reverberant factory or office spaces), (2) the noise source does not provide direct mechanical excitation to the enclosure, and (3) the noise source occupies less than about 0.3 to 0.4 of the enclosure volume, then it may be shown that the insertion loss of a loose-fitting enclosure made to contain a noise source situated in a reverberant room is<sup>6</sup>

$$IL = L_{p1} - L_{p2} = TL + 10 \log \frac{A_e}{S_e} \quad (16)$$

where  $L_{p1}$  is the reverberant level in the room containing the noise source (without the enclosure),  $L_{p2}$  is the reverberant level at the same point (with the enclosure),  $A_e$  is the absorption area inside the enclosure  $S_i \bar{\alpha}_i$ , and  $\bar{\alpha}_i$  is the surface average absorption coefficient of this material. In the case that the surface area of the enclosure  $S_e = S_i$ , the area of the interior absorbing material, then Eq. (16) simplifies to

$$IL = TL + 10 \log \bar{\alpha}_i \quad (17)$$

It is observed that, in general, the insertion loss of an enclosure containing a source is less than the transmission loss. Also when  $\bar{\alpha}_i$  the average absorption coefficient of the internal absorbing material approaches 1, then  $IL \rightarrow TL$  (the expected result), although when  $\bar{\alpha}_i \rightarrow 0$ , then this theory fails.

**Example 6. Machine Enclosure** If the sound pressure level  $L_{p1}$  in a reverberant factory space caused by a machine source in the 1000-Hz one-third octave band is 85 dB, what values of TL and  $\bar{\alpha}$  should be chosen to ensure that the reverberant level is reduced to be below 60 dB? Assuming that  $S_i = S_e$ , then if TL is chosen to be 30 dB and  $\bar{\alpha} = 0.1$ ,  $IL = 30 + 10 \log 0.1 = 30 - 10 = 20$  dB and  $L_{p2} = 65$  dB. If  $\bar{\alpha}$  is increased to 0.2, then  $IL = 30 + 10 \log 0.2 = 30 - 7 = 23$  dB and  $L_{p2} = 62$  dB. If  $\bar{\alpha}$  is increased to 0.4, then  $IL = 30 + 10 \log 0.4 = 30 - 4 = 26$  dB and  $L_{p2} = 59$  dB, thus meeting the requirement. As in Example 5, we note that since TL varies with frequency  $f$  [see Eq. (18)], this calculation should be repeated at each frequency of interest. At low frequency, since large values of TL and  $\bar{\alpha}$  are hard to obtain, it may be difficult to obtain large values of IL.

Thus the transmission loss can be used as a rough guide to the IL of a sealed enclosure, only if allowance is made for the sound absorption inside the enclosure. The transmission loss of an enclosure is normally dominated by the mass/unit area  $m$  of the enclosure walls (except in the coincidence-frequency region). This is because the stiffness and damping of the enclosure walls are unimportant, the response is dominated by inertia  $m(2\pi f)$ , where  $f$  is the frequency in hertz. The transmission loss of an enclosure wall for sound arriving from all angles is approximately

$$TL = 20 \log(mf) - C \quad \text{dB} \quad (18)$$

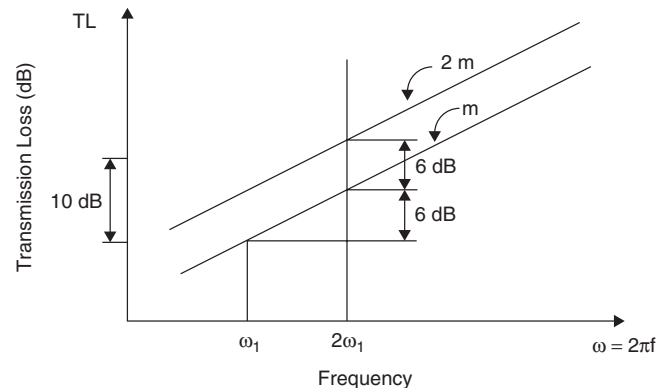
where  $m$  is the surface density (mass/unit area) of the enclosure walls and  $C = 47$  if the units of  $m$  are  $\text{kg/m}^2$  and  $C = 34$  if the units are  $\text{lb/ft}^2$ . Figure 13 shows that the transmission loss of a wall [given by Eq. (18)] theoretically increases by 6 dB for doubling of frequency or for doubling of the mass/unit area of the wall. If some areas of the enclosure walls have a significantly poorer TL than the rest; then this results in a degradation in the overall transmission loss of the enclosure. Where the enclosure surface is made of different materials (e.g., wood walls and window glass), then the average transmission loss  $TL_{\text{ave}}$  of the composite wall is given by

$$TL_{\text{ave}} = 10 \log 1/\bar{\tau} \quad (19)$$

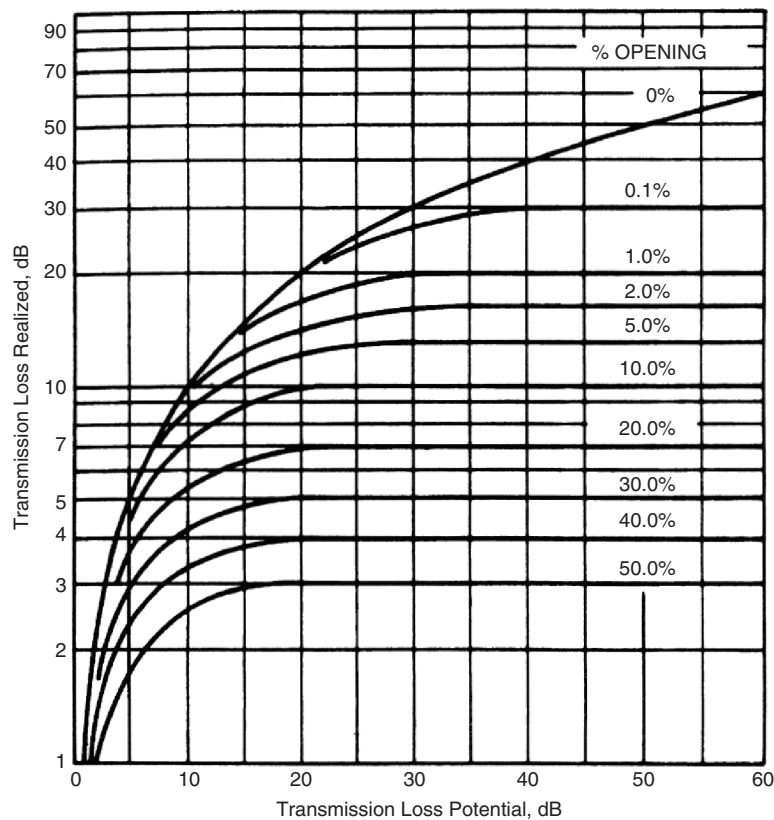
where the average transmission coefficient  $\bar{\tau}$  is

$$\bar{\tau} = \frac{S_1 \tau_1 + S_2 \tau_2 + \cdots + S_n \tau_n}{S_1 + S_2 + S_3 + \cdots + S_n} \quad (20)$$

where  $\tau_i$  is transmission coefficient of the  $i$ th wall element and  $S_i$  is the surface area of  $i$ th wall element



**Figure 13** Variation of mass law transmission loss (TL) of a single panel [see Eq. (18)].

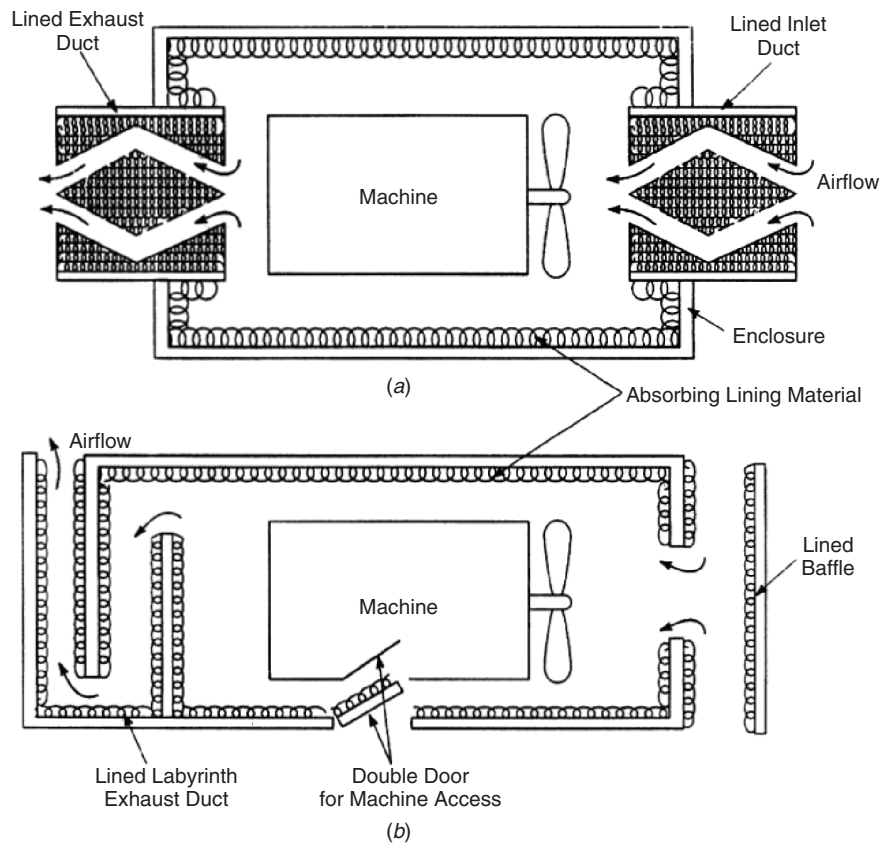


**Figure 14** Transmission loss of enclosure walls with holes as a function of transmission loss (TL) of enclosure wall without holes and percentage open area of holes

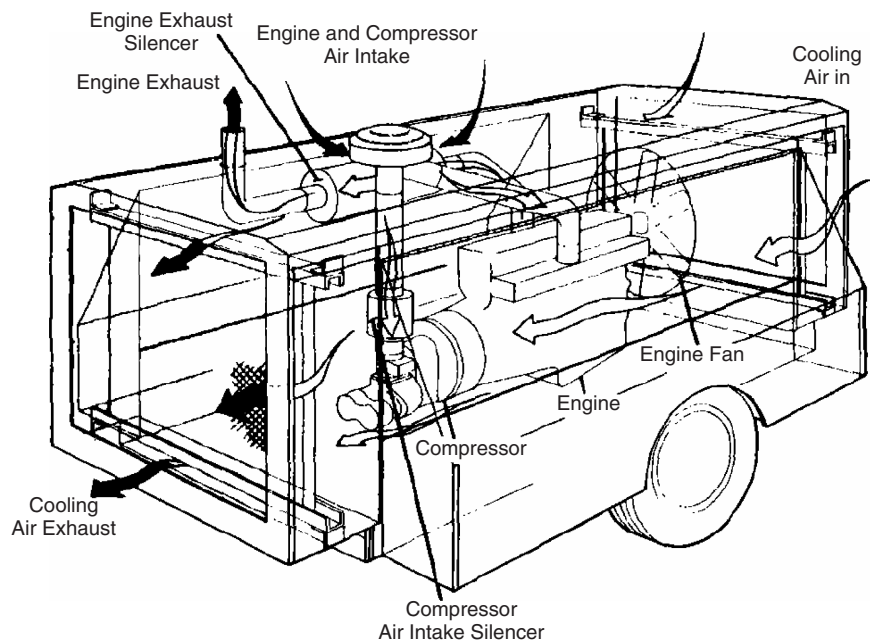
( $\text{m}^2$ ). If holes or leaks occur in the enclosure walls and if the TL of the holes is assumed to be 0 dB, then Fig. 14 shows the degradation in the average TL of the enclosure walls. If the penetrations in the enclosure walls are lined with absorbing materials, as shown in

Fig. 15, then the degradation in the enclosure TL is much less significant.

**Case History: Enclosure for a Mobile Compressor** Figure 16 shows an enclosure for a compressor driven by a diesel engine. In this design,



**Figure 15** Enclosures with penetrations (for cooling) lined with sound absorbing materials: (a) lined ducts and (b) lined baffles with double-door access provided to interior of machine.



**Figure 16** Major components and cooling airflow of an air compressor.<sup>15</sup>

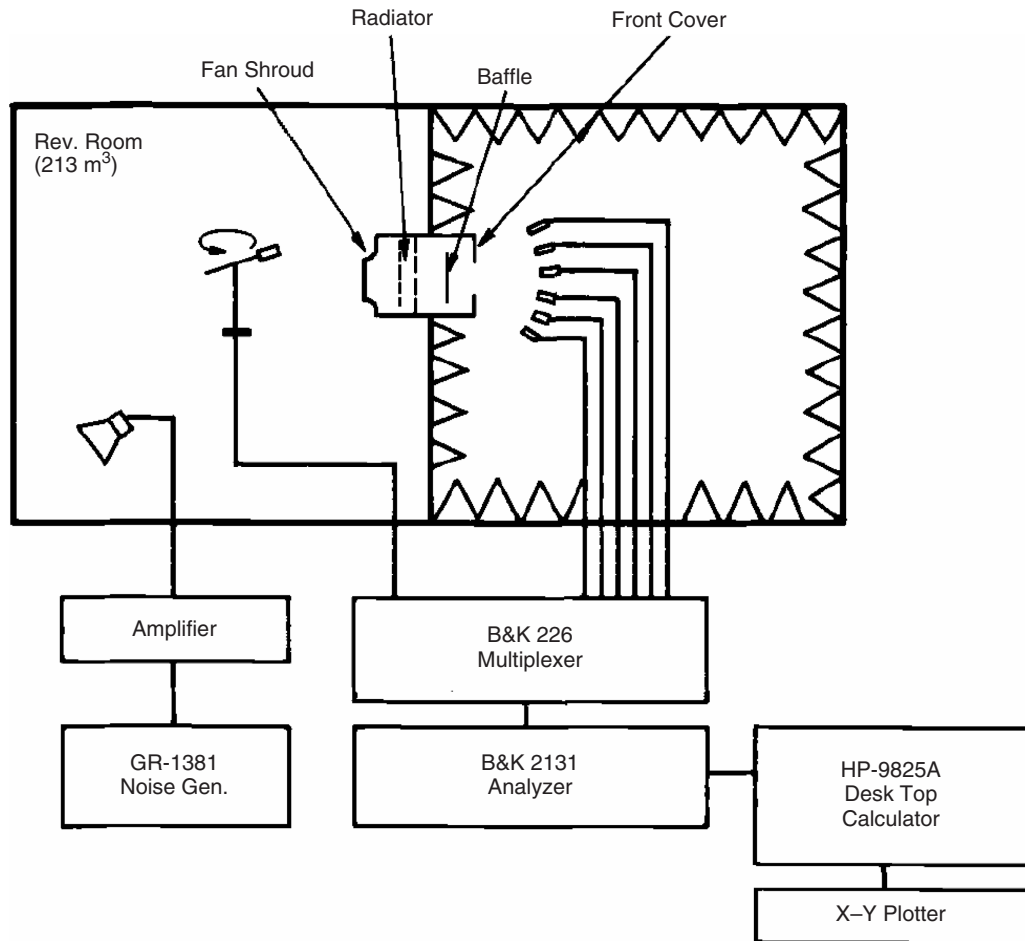


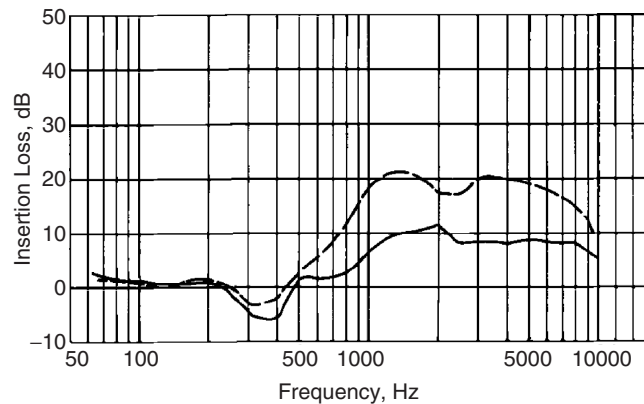
Figure 17 Experimental setup.<sup>15</sup>

sound-absorbing material is located inside the enclosure, and air paths are provided for the passage of cooling air. Reference 15 gives extensive details of a theoretical and experimental acoustical design study of the inlet cooling duct for the compressor enclosure. In this study, noise control approaches such as those shown in Fig. 15 had already been undertaken by the manufacturer. In the production unit, a baffle (a small crosswise barrier) was installed to reduce the noise of the cooling fan radiated out of the cooling air inlet. It was desired to reduce the overall noise of the compressor unit in production. An experimental test setup was built as shown in Fig. 17. The experiments showed that the insertion loss produced by the air inlet baffle could be increased only slightly with changes of baffle location; however, a significant insertion loss at frequencies above 500 Hz was achieved by lining the cooling air duct with sound-absorbing material. The sound absorbing material that was most effective was found to be 25.4-mm-thick fiberglass covered with

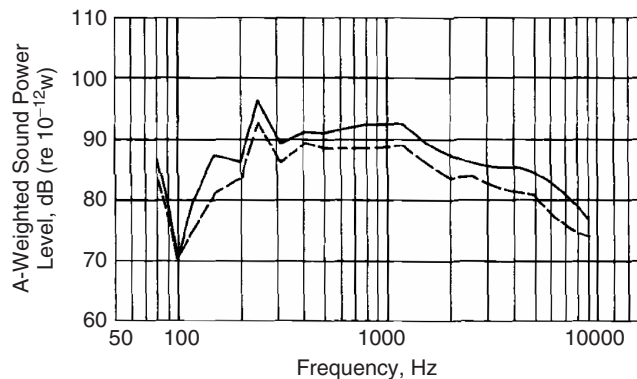
23% porosity metal sheet. The fiberglass had a density of  $48 \text{ kg/m}^3$ . Figure 18 shows the insertion loss measured on the test setup presented in Fig. 17: (1) with the polyurethane foam as installed in the original production unit and (2) with the 25.4-mm-thick  $48\text{-kg/m}^3$  fiberglass and perforated metal facing as the absorption material inlet duct lining used later in this study.

It was decided to make only two main improvements to the compressor unit to reduce its noise: (1) increasing the sound absorption coefficient of the cooling air duct lining and (2) replacing the silencer (muffler) on the engine/compressor air intake with one having a higher value of insertion loss. Figure 19 shows the effect of these two changes on the sound power level of the compressor unit.<sup>15</sup>

**Other Industrial Enclosures** Figure 20 shows an enclosure built for a band saw. A sliding window is provided that can be opened for access to controls. A sliding door is also provided that can be closed as much as possible around items fed to the band saw.



**Figure 18** Inlet duct insertion loss measured on the test setup with: —, polyurethane foam installed in production; - - -, fiberglass and perforated metal used as absorption material.<sup>15</sup>

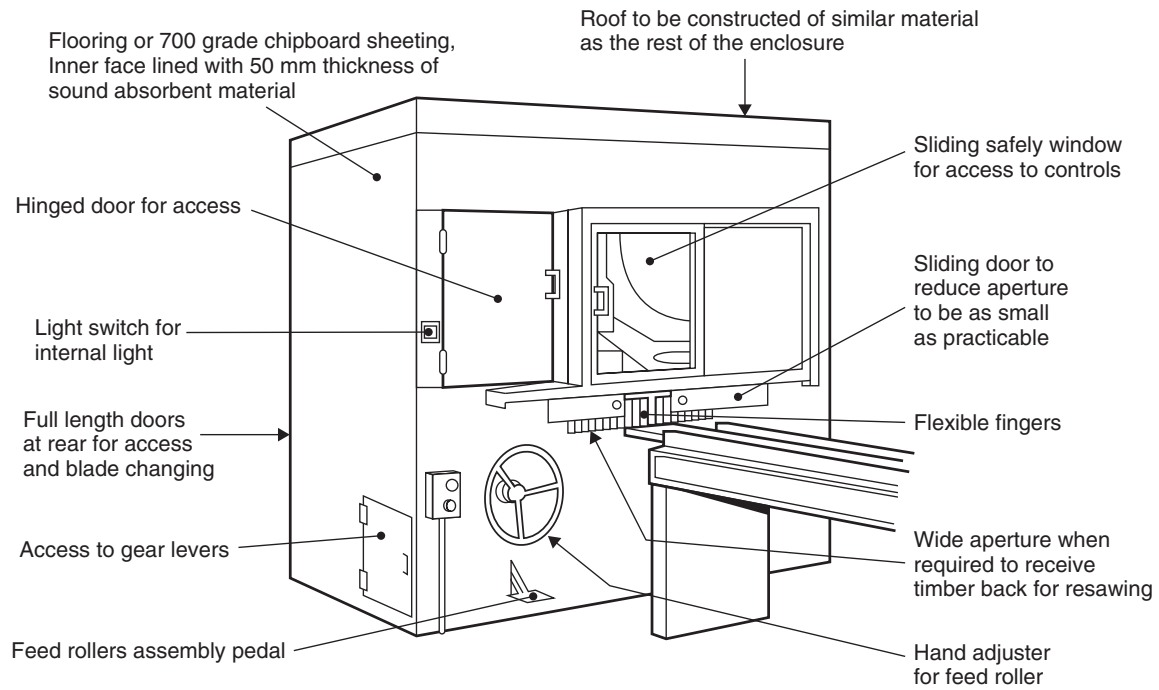


**Figure 19** A-weighted sound power level of the air compressor before and after modifications: —, before modification and - - - after modification.<sup>15</sup>

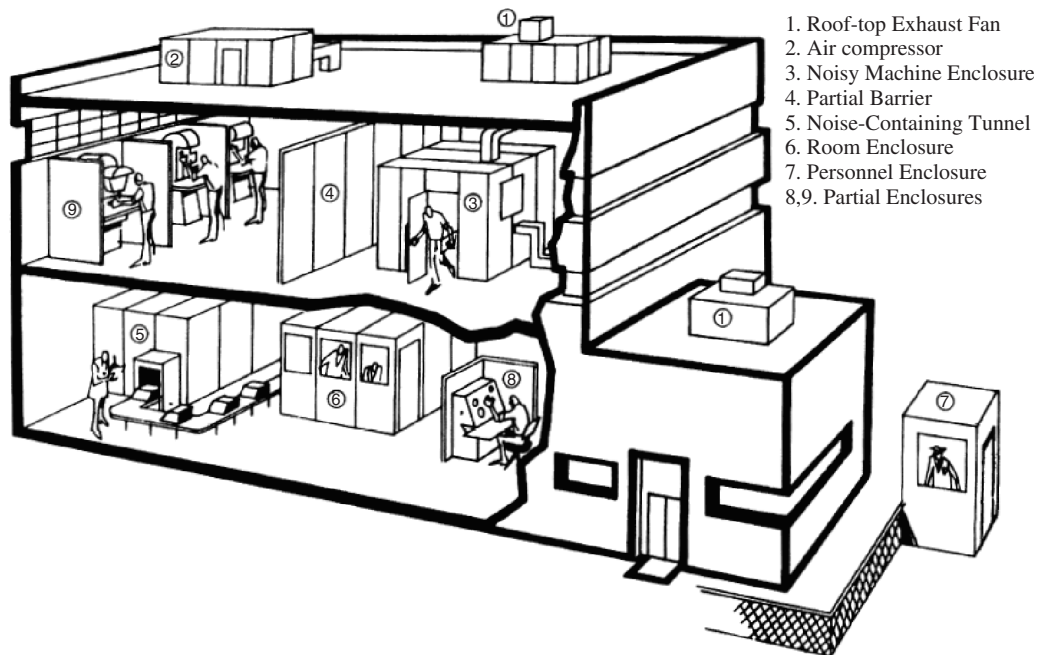
The interior of the enclosure is lagged with 50 mm of sound-absorbing material. Enclosures are available from manufacturers in a wide variety of ready-made modular panels (see Fig. 21). Figure 21 shows how these panels can be built into a variety of complete machine enclosures and partial and complete personnel enclosures.

**Close-Fitting Enclosures** If the noise source occupies no more than about one-third of the volume of a sealed enclosure, then the simple theory described by Eqs. (16) and (17) can be used. However, in many cases when machines are enclosed, it is necessary to locate the enclosure walls close to the machine surfaces, so that the resulting air gap is small. Such enclosures are termed *close-fitting enclosures*. In such cases the sound field inside the enclosure is not reverberant or diffuse and the theory discussed so far can be used only for a first approximation of the insertion loss of an enclosure. There are several effects that occur with close-fitting enclosures.

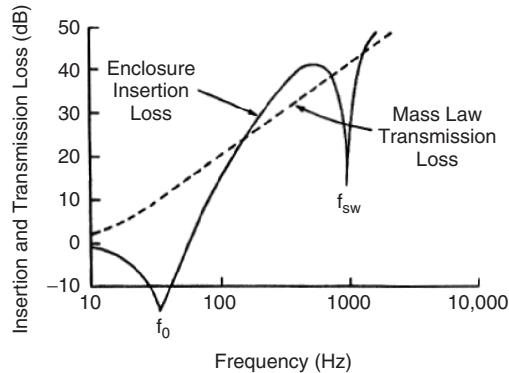
First, if the source is not a constant velocity source then in principle the close-fitting enclosure can “load” it so that it produces less sound power. However, in most machinery noise problems, the source behaves like a constant velocity source and the loading effect is negligible. Second, and more importantly, are the reductions in the insertion loss that occur at certain frequencies (when the enclosure becomes “transparent”). See the frequencies  $f_0$  and  $f_{sw}$  in Fig. 22. When an enclosure is close-fitting, then to a first approximation the sound waves approach the enclosure walls at normal incidence instead of random incidence. When the air gap is small, then a resonant condition at frequency  $f_0$  occurs where the enclosure wall mass is opposed by the wall and air gap stiffness. In addition standing-wave resonances can occur in the air gap at frequencies  $f_{sw}$ . These resonances can be reduced by the placement of sound-absorbing material in the air gap.<sup>16,17</sup> Jackson has produced simple theoretical models for close-fitting enclosures that assume a uniform air gap.<sup>16,17</sup> However, in practice,



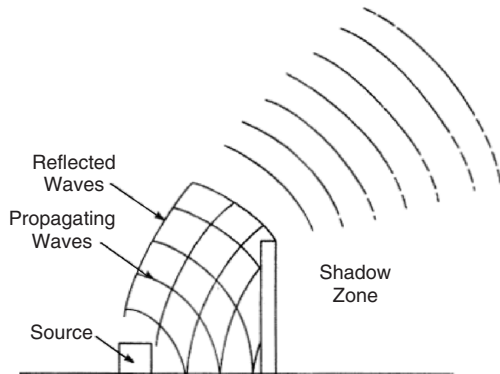
**Figure 20** Enclosure for a band saw.



**Figure 21** Ready-made modular materials used to make enclosures and barriers in a factory building. (Courtesy of Lord Corporation, Erie, PA.)



**Figure 22** Insertion loss and transmission loss of an enclosure, (mass/unit area =  $16 \text{ kg/m}^2$ , air gap =  $16 \text{ cm}$ ). (Reprinted from Ref. 17, Copyright 1962, with permission from Elsevier.)

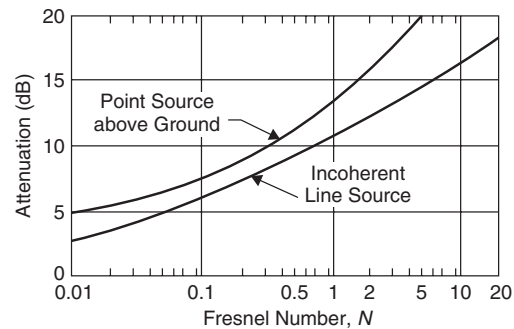
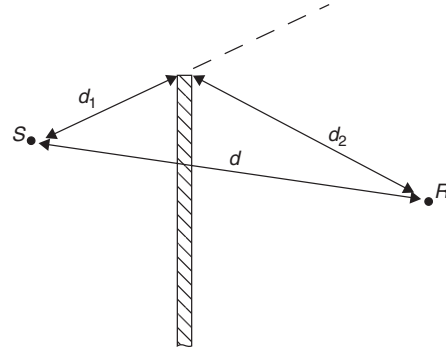


**Figure 23** Sound waves reflected and diffracted by barrier and acoustical shadow zone.

the air gap varies with real enclosures, and these simple theoretical models and some later ones can only be used to give some guidance of the insertion loss to be expected in practice. Finite element and boundary element approaches can be used to make insertion loss predictions for close-fitting enclosures with complicated geometries.

#### 4.4. Barriers

An obstacle placed between a noise source and a receiver is termed a *barrier* or *screen*, as explained in Chapter 58. When a sound wave approaches the barrier, some of the sound wave is reflected and some is transmitted past (see Fig. 23). At high frequency, barriers are quite effective, and a strong acoustical “shadow” is cast. At low frequency (when the wavelength can equal or exceed the barrier height), the barrier is less effective, and some sound is diffracted into the shadow zone. Indoors, barriers are usually partial walls. Outdoors, the use of walls, earth berms, and even buildings can protect residential



**Figure 24** Attenuation of a barrier as a function of Fresnel number  $N$  for point and incoherent line sources.

areas from traffic and industrial noise sources. (see Chapter 122.) Empirical charts are available to predict the attenuation of a barrier.<sup>4</sup> Figure 24 shows the *insertion loss* or reduction in sound pressure level expected after installation of a semiinfinite barrier in free space between a source and receiver. If barriers are used inside buildings, their performance is often disappointing because sound can propagate into the shadow zone by multiple reflections. To produce acceptable attenuation, it is important to suppress these reflections by the use of sound-absorbing material, particularly on ceilings just above the barrier. In Fig. 24,  $N$  is the dimensionless Fresnel number related to the shortest distance over the barrier  $d_1 + d_2$  and the straight line distance  $d$  between the source  $S$  and receiver  $R$ :

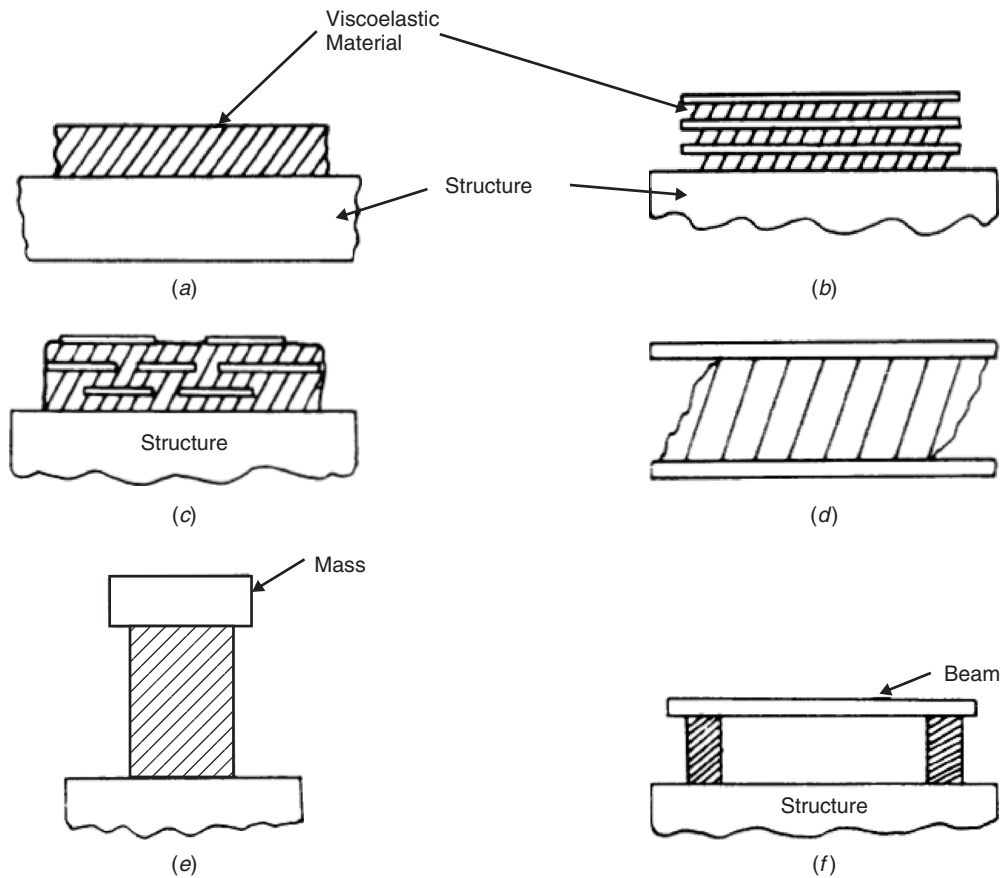
$$N = 2(d_1 + d_2 - d)/\lambda \quad (21)$$

where  $\lambda$  is the wavelength and  $d_1$  and  $d_2$  are shown in Fig. 24.

#### 4.5 Damping Materials

Load-bearing and non-load-bearing structures of a machine (panels) are excited into motion by mechanical machine forces resulting in radiated noise. Also, the sound field inside an enclosure excites its walls into vibration. When resonant motion dominates the vibration, the use of damping materials can result in





**Figure 25** Different ways of using vibration damping materials: (a) free layer, (b) multiple constrained layer, (c) multilayer tile spaced treatment, (d) sandwich panel, (e) tuned damper, and (f) resonant beam damper. Shaded elements represent viscoelastic material.

significant noise reduction. In the case of machinery enclosures, the motion of the enclosure walls is normally mass controlled (except in the coincidence-frequency region), and the use of damping materials is often disappointing. Damping materials are often effectively employed in machinery in which there are impacting parts since these impacts excite resonant motion.

Damping involves the conversion of mechanical energy into heat. Damping mechanisms include friction (rubbing) of parts, air pumping at joints, sound radiation, viscous effects, eddy currents, and magnetic and mechanical hysteresis. Rubbery, plastic, and tarry materials usually possess high damping. During compression, expansion, or shear, these materials store elastic energy, but some of it is converted into heat as well. The damping properties of such materials are temperature dependent. Damping materials can be applied to structures in a variety of ways. Figure 25 shows some common ways of applying damping materials and systems to structures. Chapter 60 describes damping mechanisms in

more detail and how damping materials can be used to reduce vibration in some practical situations.

## REFERENCES

1. R. H. Bolt and K. U. Ingard, System Considerations in Noise Control Problems, in *Handbook of Noise Control*, C. M. Harris, Ed., McGraw-Hill, New York, 1957, Chapter 22.
2. R. H. Lyon, *Machinery Noise and Diagnostics*, Butterworths, Boston, 1987.
3. D. A. Bies and C. H. Hansen, *Engineering Noise Control* 2nd ed., Chapman & Hall, London, 1996.
4. M. J. Crocker and A. J. Price, *Noise and Noise Control*, Vol. I, CRC Press, Cleveland, OH, 1975.
5. M. J. Crocker and F. M. Kessler, *Noise and Noise Control* Vol. II, CRC Press, Boca Raton, FL, 1982, Chapter 1.
6. I. Sharland, *Woods Practical Guide to Noise Control*, Woods of Colchester, Waterlow, London, 1972.
7. J. D. Irwin and E. R. Graf, *Industrial Noise and Vibration Control*, Prentice-Hall, Englewood Cliffs, NJ, 1979.



8. L. W. Bell and D. H. Bell, *Industrial Noise Control—Fundamentals and Applications*, 2nd ed., Marcel Dekker, New York, 1993.
9. R. F. Barron, *Industrial Noise Control and Acoustics*, Marcel Dekker, New York, 2003.
10. C. E. Wilson, *Noise Control*, rev. ed., Kreiger, Malabar, FL, 2006.
11. F. J. Fahy and J. G. Walker, Eds., *Fundamentals of Noise and Vibration*, E&FN Spon, Routledge Imprint, London, 1998.
12. I. L. Ver and L. L. Beranek, *Noise and Vibration Control Engineering—Principles and Applications*, 2nd ed., Wiley, Hoboken, NJ, 2005.
13. F. Fahy, *Foundations of Engineering Acoustics*, Academic, London, 2001.
14. L. E. Kinsler, A. R. Frey, A. B. Coppens, and J. V. Sanders, *Fundamentals of Acoustics*, Fourth Edition, Wiley, New York, 1999.
15. Y. Wang and J. W. Sullivan, Baffle-Type Cooling System: A Case Study, *Noise Control Eng. J.*, Vol. 22, No. 2, 1984, pp. 61–67.
16. R. S. Jackson, The Performance of Acoustic Hoods at Low Frequencies, *Acustica*, Vol. 12, 1962, p. 139.
17. R. S. Jackson, Some Aspects of the Performance of Acoustic Hoods, *J. Sound Vib.*, Vol. 3, No. 1, 1966, p. 82.

# CHAPTER 55

## NOISE AND VIBRATION SOURCE IDENTIFICATION

Malcolm J. Crocker

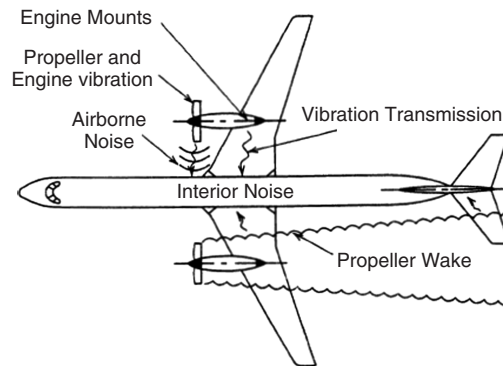
Department of Mechanical Engineering  
Auburn University  
Auburn, Alabama

### 1 INTRODUCTION

In most machinery noise and vibration control problems, knowledge of the dominant noise and vibration sources in order of importance is very desirable, so that suitable modifications can be made. In a complicated machine, such information is often difficult to obtain, and many noise and vibration reduction attempts are made based on inadequate data so that frequently expensive or inefficient noise and vibration reduction methods are employed. Machine noise and vibration can also be used to diagnose increased wear. The methods used to identify noise and vibration sources will depend on the particular problem and the time and resources (personnel, instrumentation, and money) and expertise available and on the accuracy required. In most noise and vibration source identification problems, it is usually the best practice to use more than one method to ensure greater confidence in the identification procedure. Well-tried methods are available and novel methods are under development.

### 2 SOURCE-PATH-RECEIVER

Noise and vibration source and path identification methods of differing sophistication have been in use for many years.<sup>1–29</sup> Some approaches are used in parallel with others to provide more information about sources and increased confidence in the results. In recent years, a considerable amount of effort has been devoted in the automobile industry to devise better methods of noise and vibration source and path identification.<sup>30–51</sup> Most effort has been expended on interior cabin noise and separating airborne<sup>30–35</sup> and structure-borne<sup>36–39</sup> paths. Engine and power train noise and vibration sources and paths<sup>40–45</sup> and tire noise<sup>46,47</sup> have also received attention. This effort has been expended not only to make the vehicles quieter but to give them a distinctive manufacturer brand sound. See Chapter 67. More recently these methods have been extended and adapted in a variety of ways to produce improved methods for source and path identification.<sup>54–75</sup> One example is the so-called transfer path analysis (TPA) approach<sup>69</sup> and variations of it, which to some extent are based on an elaborated version of the earlier coherence approach for source and path modeling.<sup>21–29</sup> See Sections 7 and 9 of this chapter. Commercial softwares are now available using the TPA and other related approaches for noise and vibration source and path identification. Pass-by exterior noise sources of automobiles and railroad vehicles has also been studied.<sup>48–53</sup>

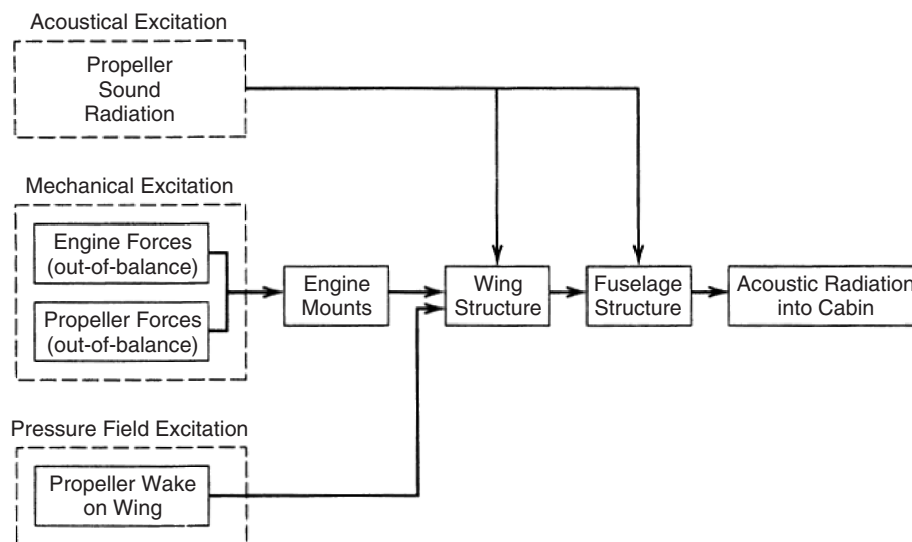


**Figure 1** Sources and paths of airborne and structure-borne noise and vibration resulting in interior noise in an airplane cabin.

As discussed in Chapter 54, noise and vibration energy must flow from a *source* through one or more *paths* to a *receiver* (usually the human ear). Figure 1 in Chapter 54 shows the simplest model of a *source–path–receiver* system. Noise sources may be *mechanical* in nature (caused by impacts, out-of-balance forces in machines, vibration of structural parts) or *aerodynamic* in nature (caused by pulsating flows, flow–structure interactions, jet noise, turbulence). Noise and vibration energy can flow through a variety of airborne and structure-borne paths to the receiver. Figure 1 shows an example of a propeller-driven airplane. This airplane situation can be idealized as the much more complicated source–path–receiver system shown in Fig. 2. In some cases the distinction between the source(s) and path(s) is not completely clear, and it is not easy to neatly separate the sources from the paths. In such cases, the sources and paths must be considered in conjunction. However, despite some obvious complications, the source–path–receiver model is a useful concept that is widely used. In this chapter we will mainly concern ourselves with machinery noise sources. We note that *cutting* or *blocking* one or more noise and/or vibration *paths* often gives invaluable information about the noise sources.

### 3 CLUES TO NOISE SOURCES

There are various characteristics of a sound field that give indications of the types of noise sources



**Figure 2** Source-path-receiver system showing airborne and structure-borne paths for a twin-engine propeller-driven airplane.

present and their spatial distribution. These include the frequency distribution of the sound pressure level, the directional properties of the sound field, and the variation of the sound pressure level with distance from the sources. Knowledge of the variation in the sound pressure level with time can also be instructive. For more sophisticated measurements it is useful to have some theoretical understanding of the propagation of sound from idealized sound source models—monopole, dipole, quadrupole, line source, piston—and the generation of sound caused by mechanical systems—mechanical impacts and vibrating beam and plates. See Chapters 1, 2, 3, and 6. Such theoretical understanding not only guides us in deciding which measurements to make but also aids in interpreting the results. In fact as the measurements made become more sophisticated, increasing care must be taken in their interpretation. There is a danger with sophisticated measurements of collecting large amounts of data and then either being unable to interpret them or reaching incorrect conclusions. With the advent of increasingly sophisticated signal processing equipment and software, knowledge of signal analysis and signal processing theory has become very important. See Chapters 40 and 42.

#### 4 CLASSICAL METHODS OF IDENTIFYING NOISE AND VIBRATION SOURCES

Some of the elementary or classical methods of identifying noise sources have been reviewed in detail in the literature<sup>1</sup> and do not require a profound theoretical understanding of sound propagation. They will only be briefly reviewed here.

*Subjective assessment* of noise is very useful because the human ear and brain can distinguish

between different sounds more precisely than the most sophisticated measurement system. With practice, an operator can tell by its sound if a machine is malfunctioning; a noise consultant can accurately estimate the blade passage frequency of a fan. In identifying sources, we should always listen to a machine first. To localize the sources and cut out extraneous noise, stethoscopes can be used or a microphone-amplifier-earphone system. Such a system also sometimes allows one to position the microphone near a source in an inaccessible or dangerous place where the human ear cannot reach. Chapter 67 discusses the subjective assessment of sound. In fact, humans can discern small differences in machine sounds that sometimes pose difficult tasks for sophisticated analysis equipment.

*Selective operation* of a complicated machine is often very useful. As long as the operation of a machine is not severely changed by disconnecting some of the parts sequentially, such a procedure can indicate the probable contribution of these parts to the total machine noise, when all parts are operating simultaneously. For instance, engine noise can be measured with and without the cooling fan connected, and this can then give an estimate of the fan noise. Note, however, that if the fan noise is lower in level than the engine noise, the accuracy of the estimate will be poor. The fan noise estimate can be checked by driving the fan separately by a “quieted” electric motor or other device. We should be aware that in some cases disconnecting some parts may alter the operation of the other parts of the machine and give misleading results. An example is an engine driving a hydraulic transmission under load. Disconnecting the transmission will give a measure of the engine-structure radiated noise, provided the inlet

and exhaust noise are piped out of the measuring room and the cooling fan is disconnected. But note that in such a situation the engine is now unloaded, and its noise may be different from the loaded case. Also an unfueled engine may be driven by a quieted electric motor so that the so-called engine mechanical noise is measured and the combustion noise is excluded. However, in this procedure the mechanical forces in the engine will be different from the normal fueled running situation, and we cannot say that this procedure will give the "true" mechanical noise.

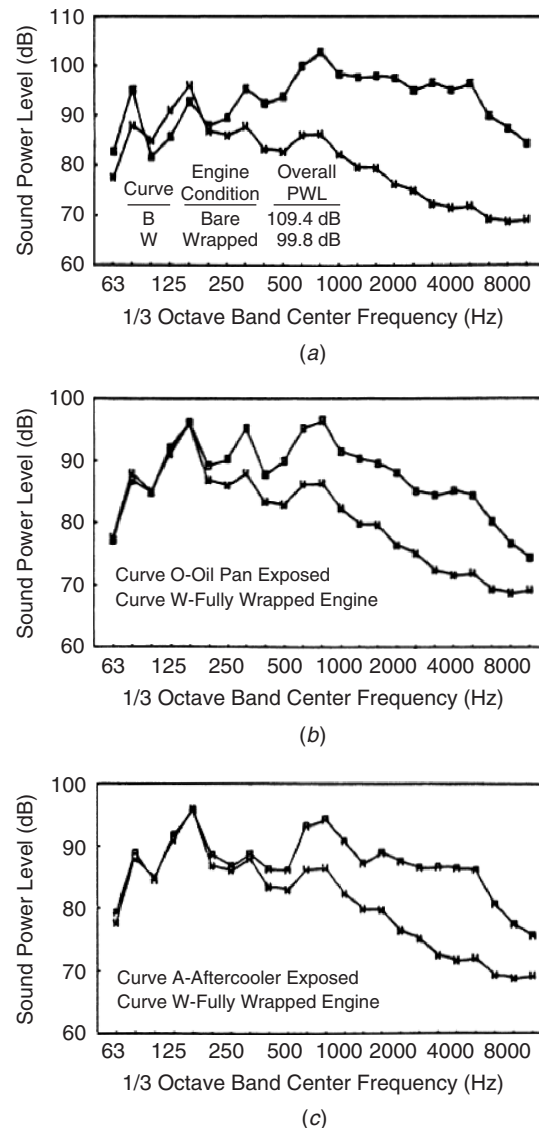
*Selective wrapping* or enclosure of different parts of a machine is a useful procedure often used. If the machine is completely enclosed with a tight-fitting sealed enclosure and the parts of the enclosure are sequentially removed exposing different machine surfaces, then, in principle, the noise from these different surfaces can be measured. This method has the advantage that it is not normally necessary to stop any part of the machine, and thus the machine operation is unchanged. However, some minor changes may occur if any damping of the machine surfaces occurs or because sound will now diffract differently around the enclosure.

Measurements of the sound power radiated from different surfaces of a diesel engine using this selective wrapping approach are discussed in Refs. 2 and 3. An array of 30 microphone positions on a spherical surface surrounding the engine was used for both the lead-wrapping and bare-engine sound measurements. Overall one-third octave sound pressure level data were gathered. These data were then converted to sound intensity estimates by assuming (1) spherical propagation, (2) no reflections, and (3) that the intensity is equal to the mean-square pressure divided by the air's characteristic impedance  $\rho c$ . Then the sound intensity data were integrated numerically over the surface of the spherical measuring surface enclosing the engine to obtain the sound power. The lead was wrapped on the engine so that later a particular surface, for example, the oil pan, could be exposed. The one-third octave band results for the fully wrapped engine compared with the results for the bare engine at the 1500 Revolutions/minute (rpm) engine speed, 542-Nm torque operating condition are shown in Fig. 3a. This comparison shows that the lead wrapping is ineffective at frequencies at and below the 250-Hz one-third octave band.<sup>2,3</sup>

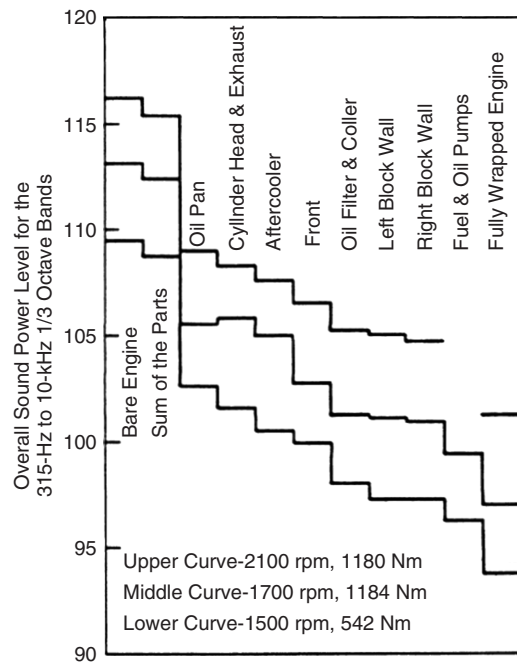
Eight individual parts of the engine were chosen for noise source identification and ranking purposes using the measurement technique with the spherical microphone array and the engine lead wrapped.<sup>2,3</sup> The measurements were made by selectively exposing each of the eight parts, one at a time, while the other seven parts were encased in the 0.8-mm foam-backed lead. Sound power level measurements were then made for each of the eight parts for three separate steady-state operating conditions.<sup>2,3</sup> One-third octave band comparisons with the fully wrapped engine are shown in Figs. 3b and 3c for two of the eight parts at the 1500 rpm operating condition. These plots show that the sound power measurements using lead wrapping

are not always accurate for the weaker parts until the frequency exceeds 1000 Hz. A plot of the noise source ranking using overall sound power levels for the eight parts under investigation for the 315-Hz to 10-kHz one-third octave bands is given in Fig. 4.

Similar selective wrapping techniques have been applied to a complete truck (Fig. 5). Exhaust noise was suppressed with an oversize muffler, the engine was wrapped, and even the wheel bearings were covered! The results of this investigation<sup>4</sup> are shown in Fig. 6a



**Figure 3** Sound power level of engine and parts at 1500 rpm and 542-Nm torque: (a) bare and fully wrapped engine, (b) oil pan and fully-wrapped engine, and (c) aftercooler and fully wrapped engine. (From Ref. 2.)



**Figure 4** Noise source ranking in terms of sound power levels from lead-wrapping far-field spherical array method for the 315-Hz to 10-kHz one-third octave bands. (From Ref. 2.)

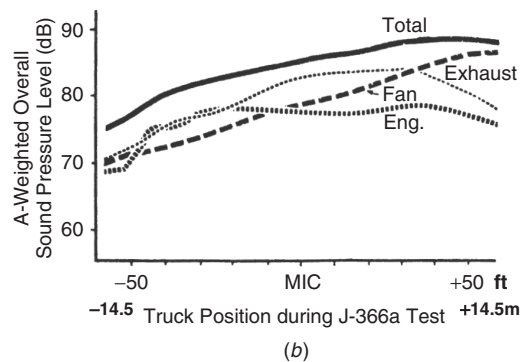
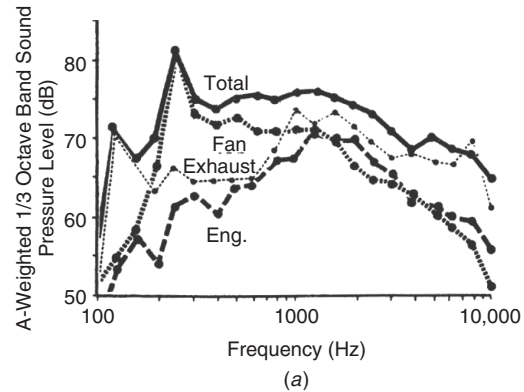
and 6b. Although the selective wrapping technique is very instructive, it is time consuming, and this has led to the search for other techniques that do not require complete enclosure, as described later.

## 5 FREQUENCY ANALYSIS

If the noise (or vibration) of either the complete machine or of some part (obtained by selective operation or sequential wrapping) is measured, then various analyses may be made of the data. The most



**Figure 5** Selective wrapping and oversize muffler used on a diesel engine truck.



**Figure 6** A-weighted sound pressure levels obtained from selective wrapping and selective operation techniques applied to truck in Fig. 5: (a) A-weighted one-third octave analysis and (b) A-weighted overall sound pressure level contributions of truck sources as a function of truck drive by position (in feet and metres). (From Ref. 4.)

common analysis performed is *frequency analysis*. The reason probably is because one of the most important properties of the ear is performing frequency analysis of sounds. Analog analyzers (filters) have been available for many years. These analog devices have now been largely overtaken by digital analyzers (filters). Real-time analyzers and fast Fourier transform (FFT) analyzers are now widely available.

Real-time and FFT analyzers speed up the frequency analysis of the data, but because of the analysis errors that are possible (particularly with the FFT) great care should be taken. With FFT analyzers, antialiasing filters can be used to prevent frequency folding; and if reciprocating machine noise is analyzed, the analysis period must be at least as long as the repetition period (or multiples) to incorrect frequencies being diagnosed. Chapter 42 deals in detail with signal processing, while Chapter 40 reviews the use of different types of filters and the FFT technique and other related topics. Chapter 43 reviews noise and vibration measurements.

Assuming the frequency analysis has been made correctly, then it can be an important tool in identifying



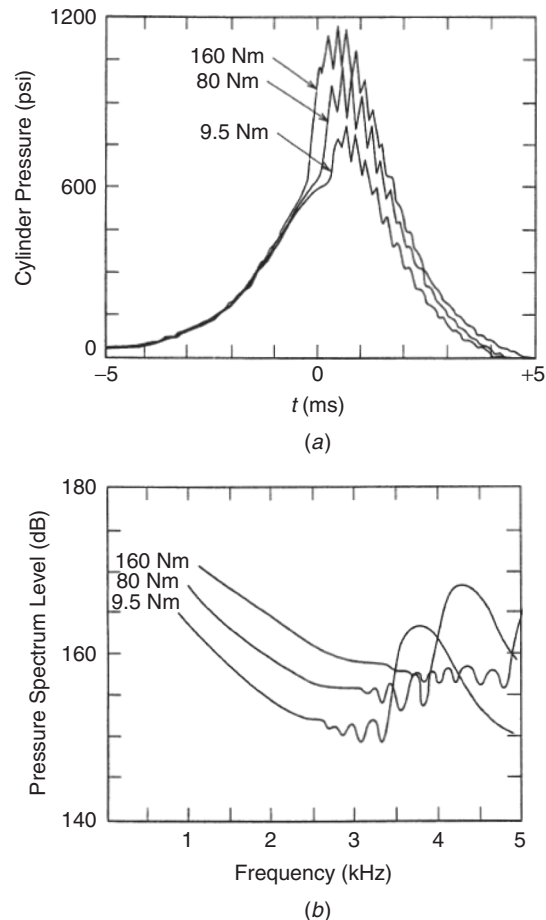
noise sources. With reciprocating and rotating machinery, pure tones are found that depend on the speed of rotation  $N$  in rpm, and geometrical properties of the systems. As discussed in Chapter 68, several frequencies can be identified with rolling-element bearings,<sup>5</sup> including the fundamental frequency  $N/60$  Hz, the inner and outer race flaw defect frequencies, and the ball flaw defect, ball resonance and the race resonance frequencies. Bearing noise is discussed further in Chapter 70. With gears, noise occurs at the tooth contact frequency  $tN/60$  Hz and integer multiples (where  $t$  is the number of gear teeth). Often the overtone frequencies are significant. See Chapter 69. In fan noise, the fundamental blade-passing frequency  $nN/60$  (where  $n$  is the number of fan blades) and integer multiples are important noise sources. See Chapter 71.

Further machine noise examples could be quoted. Since these frequencies just mentioned are mainly proportional to machine rotational speed, a change of speed or load will usually immediately indicate whether a frequency component is related to a rotational source or not. A good example of this fact is diesel engine noise. Figure 7a shows the time history and power spectrum of the cylinder pressure of a six-cylinder direct injection engine,<sup>6</sup> measured by Seybert. Ripples in the time history are thought to be caused by a resonance effect in the gas above the piston producing a broad peak in the frequency spectrum in the region of 3 to 5 kHz. See Fig. 7b. That this resonance frequency is related to a gas resonance and not to the rotational speed can clearly be demonstrated. If the engine speed is changed, the frequency is almost unchanged (for constant load); although if the load is increased (at constant speed) the frequency increases. On further investigation the resonance frequency was found to be proportional to the square root of the absolute temperature of the gas (the gas temperature increases with load) and thus as the load increases, so does the resonance frequency.

Frequency analysis can sometimes be used with advantage to reveal information about noise or vibration sources and/or paths by carefully changing the source or the path in some controlled way. The following discussion gives some examples for an air conditioner and an airplane.

### 5.1 Change of Excitation Frequency

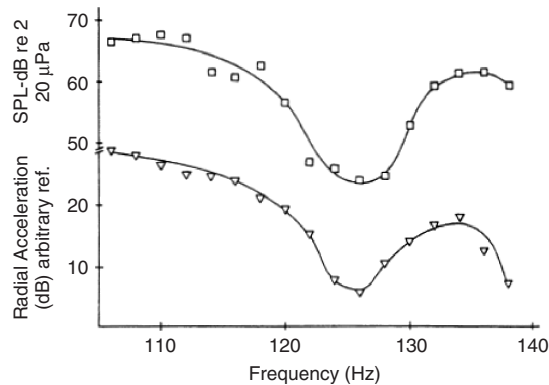
As already discussed, information on sources of noise and resonances in a diesel engine can be obtained when the load (and speed) are changed. In some cases (e.g., electrical machines) changing speed is difficult. In the case of the noise from an air conditioner, mechanical resonances in the system can be important.<sup>7</sup> These can be examined by exciting the air conditioner structure at different frequencies with an electromechanical shaker. However, this means changing the mechanical system in an unknown way. The approach finally adopted in Ref. 7 was to drive the air conditioner electric motors with an alternating current (ac) that could be varied from 50 to 70 Hz from a variable-speed direct current (dc) motor-AC generator set. Since the noise problem was caused by pure-tone magnetic force



**Figure 7** (a) Diesel engine cylinder combustion pressures vs. crank angle for three diesel engine load conditions at 2400 rpm and (b) combustion pressure spectra at 2400 rpm.  $P_a$ . (From Ref. 6.) Note: Pressure of 1 psi  $\equiv 6.89 \times 10^3 P_a$ .

excitation at twice line (mains) frequency, this was monitored with a microphone at the same time as the motor acceleration. Figure 8 shows the results. This experiment showed that the motor mounts were too stiff. Reducing the stiffness eliminated the pure-tone noise problem. Hague<sup>8</sup> has shown how this technique can be improved further in air-handling systems by using an electric motor in which rotational speed, line frequency, and torque magnitude (both steady and fluctuating) can be varied independently.

In the case just discussed with the air conditioner, it was shown that the transmission path was through the motor mount (which was too stiff). In cases where airborne and structure-borne noise are both known to be problems and the source is known (an engine), the dominant path can sometimes be determined quantitatively by cutting one or more of



**Figure 8** Sound pressure level and motor acceleration of condenser fan. (From Ref. 7.)

the paths or by modifying the paths in a known way. Examples include engine noise problems and airborne and structure-borne transmission in cars, farm tractors, and airplanes.

## 5.2 Path Blocking

One example is shown here of the evaluation of the structure-borne path of engine noise transmission by detachment of the engine from the fuselage in ground tests.<sup>9</sup> Figure 9 shows the A-weighted sound pressure levels of the cabin noise with and without the engine connected to the fuselage. When the engine was detached, it was moved forward about 5 cm to prevent any mechanical connections. The overall reduction of 3 dB suggests that the contributions of airborne and

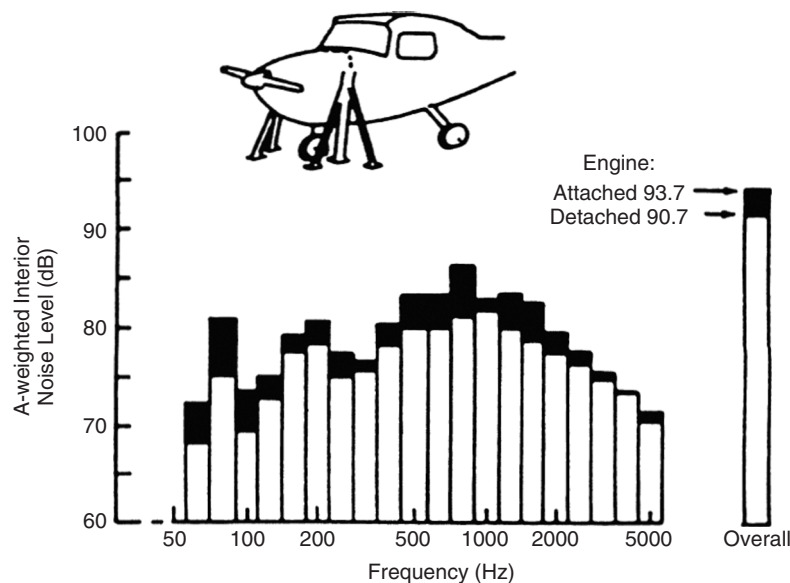
structure-borne noise to the cabin noise are about equal for this situation. There is a variation in the structural noise contribution with frequency, however, and at some frequencies the structure-borne contribution is seen to exceed the airborne contribution. McGary has presented a method of evaluating airborne and structure-borne paths in airplane structures.<sup>10</sup>

Airborne paths can be reduced or “blocked” by the addition of lead sheets or mass-loaded vinyl sheets of 5 to 10 kg/m<sup>2</sup>. Figure 10, for example, shows areas of the cabin walls of airplanes that were covered to reduce the airborne transmission.<sup>11</sup>

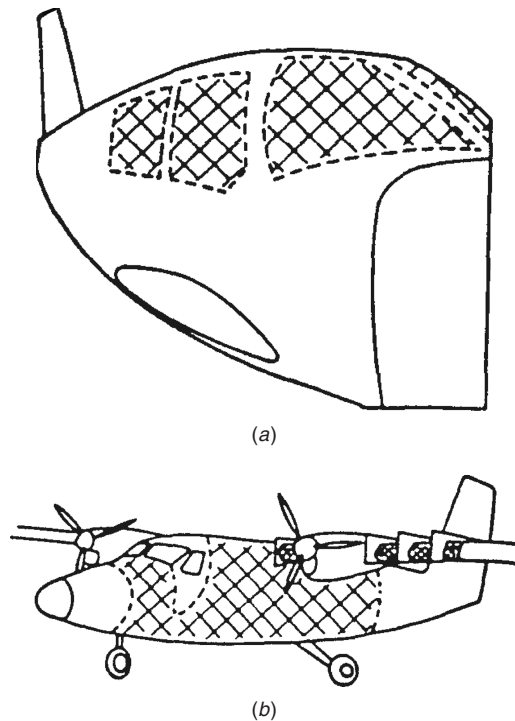
The spectrum of the noise in the cabin of a light twin-engine airplane is shown in Fig. 11. Discrete frequency tones associated with the blade passage frequency and harmonics are evident with the first two being dominant. The broadband noise at about 70 dB is associated with boundary layer noise. The tone at about 670 Hz can be related to the engine turbine speed and suggests the presence of engine-generated structure-borne noise.<sup>12</sup>

## 6 OTHER CONVENTIONAL METHODS OF NOISE SOURCE IDENTIFICATION

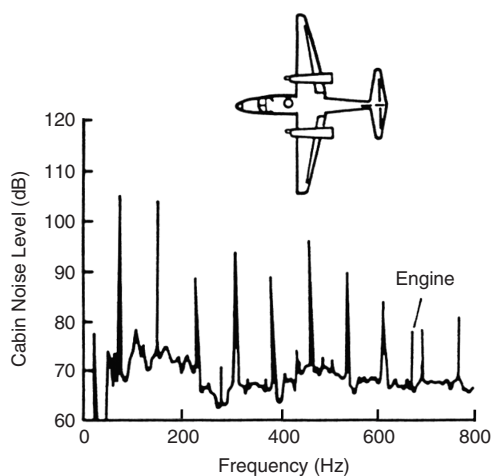
*Acoustical ducts* have been successfully used by Thien<sup>13</sup> as an alternative to the selective wrapping approach (see Fig. 12). One end of the duct is carefully attached to the part of the machine under examination by a “soundproof” elastic connection. Nakamura and Nakano have also used a similar approach to identify noise sources on an engine.<sup>14</sup> Thien has claimed that accurate repeatable results can be obtained using this method.<sup>13</sup> However, one should note various difficulties. Sealing the duct to the machine may be difficult. The surroundings should be



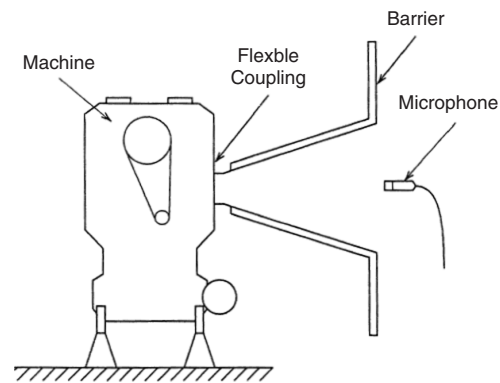
**Figure 9** Determination of structure-borne engine noise by engine detachment. (From Ref. 9.)



**Figure 10** Surfaces of airplane walls covered to aid in identifying importance of airborne and structure-borne paths. [From Ref. 11, based on figures from V. L. Metcalf and W. H. Mayes, Structure Borne Contribution to Interior Noise of Propeller Aircraft, *SAE Trans.*, Sect. 3, Vol. 92, 1983, pp. 3.69–3.74 (also SAE Paper 830735), and S. K. Jha and J. J. Catherines, Interior Noise Studies for General Aviation Types of Aircraft, Part II: Laboratory Studies, *J. Sound Vib.*, Vol. 58, No. 3, 1978, pp. 391–406, with permission.]



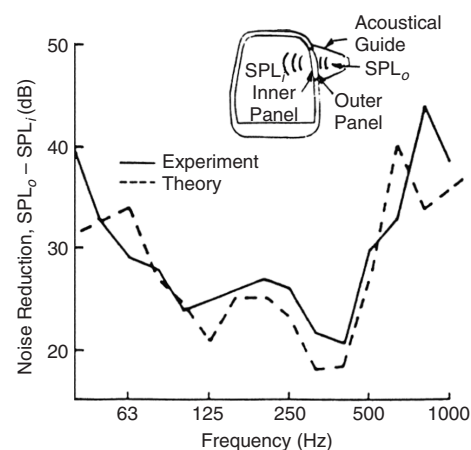
**Figure 11** Spectrum of cabin noise in flight of twin engine airplane. (From Ref. 12.)



**Figure 12** Acoustical duct used to identify sources.

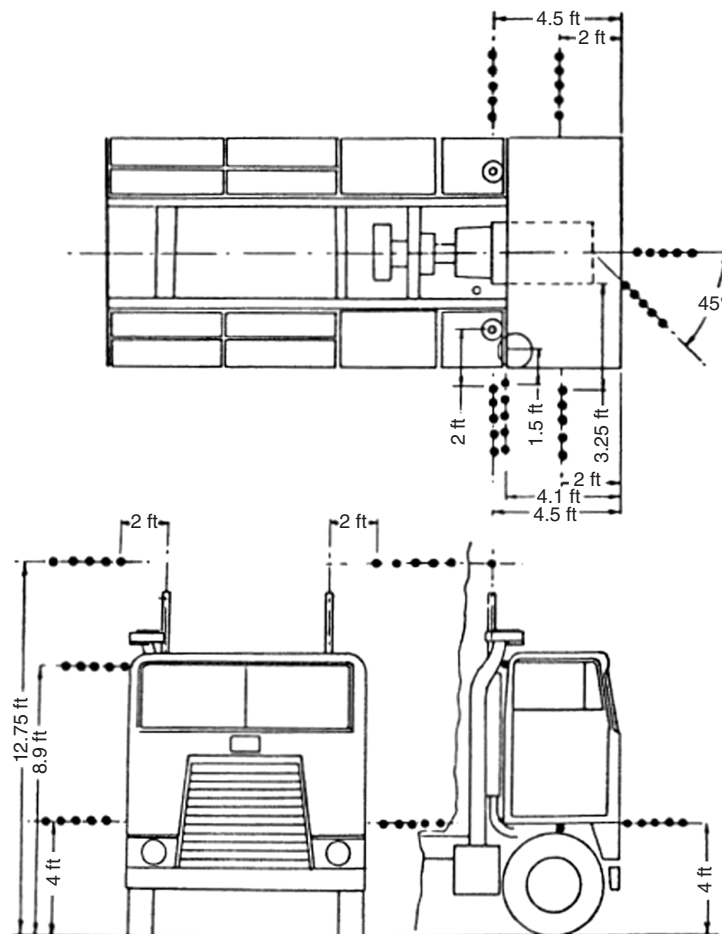
made as anechoic as possible to prevent contamination from any reverberant field. Theoretically the duct may alter the acoustic radiation from the machine part examined except for the frequency region much above coincidence. Fortunately this frequency region is normally the most important one with heavy machinery, and since in this region radiation is mainly perpendicular to the surface, it may be little affected in practice.

Acoustical ducts or guides have also been used to investigate paths of noise. Figure 13 shows an example where airborne noise was directed onto the cabin wall of a light airplane. The noise reduction through the wall of the airplane was measured and compared with theory. Note that the noise reduction here is defined to be the difference between the outside sound pressure level,  $SPL_o$  and the inside sound pressure level,  $SPL_i$ . The agreement between the experimental



**Figure 13** Investigation of airborne noise path through cabin wall of light airplane using acoustical guide or duct. (Reprinted from Ref. 15, Copyright 1980, with permission from Elsevier.)





**Figure 14** Microphone positions used in near-field noise measurements on a truck. Note: Distances are given in feet. 1 ft = 0.3048 m (From Ref. 16.)

results and the theoretical model theory was excellent at frequencies below about 250 Hz.<sup>15</sup>

*Near-field measurements* are very often used in an attempt to identify major noise sources on machines. This approach must be used with extreme care. If a microphone is placed in the acoustic near field where  $kr$  is small ( $k$  is the wavenumber  $= 2\pi$  frequency  $f \div$  wavespeed  $c$ , and  $r$  is the source to microphone distance), then the sound intensity is not proportional to sound pressure squared, and this approach gives misleading results. This is particularly true at low frequency. The acoustic near field is reactive: The sound pressure is almost completely out-of-phase with the acoustic particle velocity.

Thus, this near-field approach is unsuitable for use on relatively "small" machines such as engines. However, for "large" machines such as vehicles with several major sources including an engine cooling fan, exhaust, or inlet, the near-field approach has proved useful.<sup>16</sup> In this case where the machine is large, of characteristic

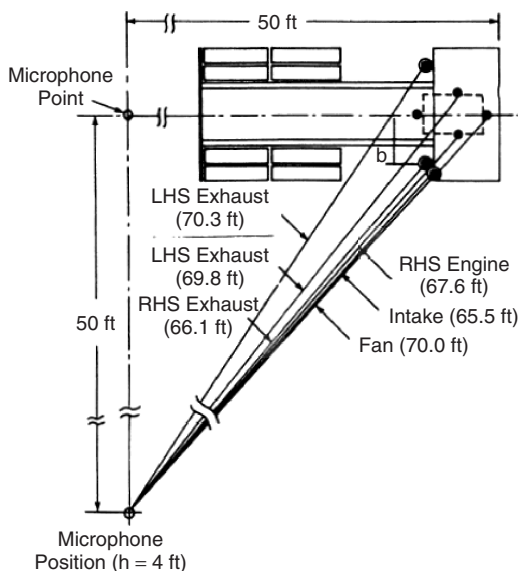
dimension  $l$  (length or width), it is possible to position the microphone so that it is in both the near geometric field, where  $r/l$  is small, and the far acoustic field, where  $kr$  is reasonably large (except at low frequency). In this case the microphone can be placed relatively close to each major noise source. Now the sound intensity is proportional to the square of the sound pressure, and the well-known inverse square law applies. Besides the acoustic near-field effect already mentioned, there are two other potential problems with this approach: (i) source directivity and the need to use more than one microphone to describe a large noise source and (ii) contamination of microphone sound signals placed near individual sources by sound from other stronger sources. Unfortunately, *contamination* cannot be reduced by placing the microphones closer to the sources because then the acoustic near field is stronger. However, *contamination* from other strong sources can be allowed for by empirical correction using the inverse square law and the distance to the contaminating source.

Despite the various potential problems with the near-field method, it has been used quite successfully to identify the major noise sources on a large diesel engine truck.<sup>16</sup> By placing microphones near each major noise source (Fig. 14) and then extrapolating to a position 50 ft (14.5 m) from the truck (Fig. 15), good agreement could be obtained with separate *selective operation* and *selective wrapping* drive-by measurements (Fig. 16). Averaging over five positions near each source and correcting for contaminating sources gave quite close agreement (Fig. 17).

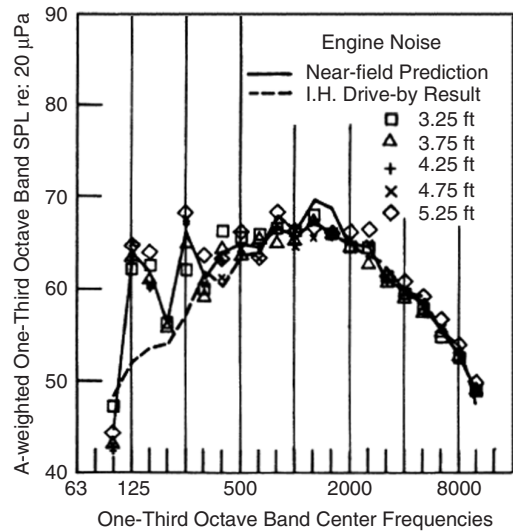
*Surface velocity* measurements have been used by several investigators to try to determine dominant sources of noise on engines and other machines. The sound power  $W_{\text{rad}}$  radiated by a vibrating surface of area  $S$  is given by

$$W_{\text{rad}} = \rho c S \langle v^2 \rangle \sigma_{\text{rad}} \quad (1)$$

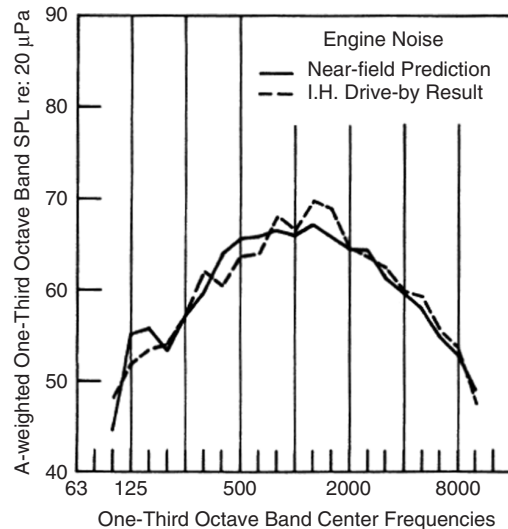
where  $\rho c$  is the characteristic impedance of air,  $\langle v^2 \rangle$  is the space-average of the mean-square normal surface velocity, and  $\sigma_{\text{rad}}$  is the radiation efficiency. Chan and Anderton<sup>17</sup> have used this approach. By measuring the sound power and the space-averaged mean-square velocity on several diesel engines, they calculated the radiation efficiency  $\sigma_{\text{rad}}$ . They concluded that above 400 Hz,  $\sigma_{\text{rad}}$  is approximately 1 for most diesel engines. There is a scatter of  $\pm 6$  dB in their results, although this is less for individual engines. Since  $\sigma_{\text{rad}}$  is difficult to calculate theoretically for structures of



**Figure 15** Position (in feet) of truck (in Fig. 14) in drive-by test when truck engine reached its governed speed of 2100 rpm in sixth gear.<sup>16</sup> Extrapolations to 50 ft (14.5 m) measurement location shown. (LHS = left-hand side, RHS = right-hand side. Distances are given in feet. Note: 1 ft = 0.3048 m).



**Figure 16** Near-field noise measurements (shown in Figs. 14 and 15) extrapolated to 50 ft (14.5 m) for comparisons with drive-by noise source identification procedure based on SAE J366a test. The near-field distances are given in feet. (From Ref. 16.)



**Figure 17** Engine noise at 50 ft (14.5 m) predicted from near-field measurements (see Fig. 16) after corrections are made to eliminate the contribution from the exhaust system noise, compared with the drive-by result. (From Ref. 16.)

complicated geometry such as a diesel engine, the assumption that  $\sigma_{\text{rad}} = 1$  can thus give an approximate idea of the sound power radiated by each component.

*Mapping* of the sound pressure level around a machine has been shown<sup>18</sup> to be a useful simple

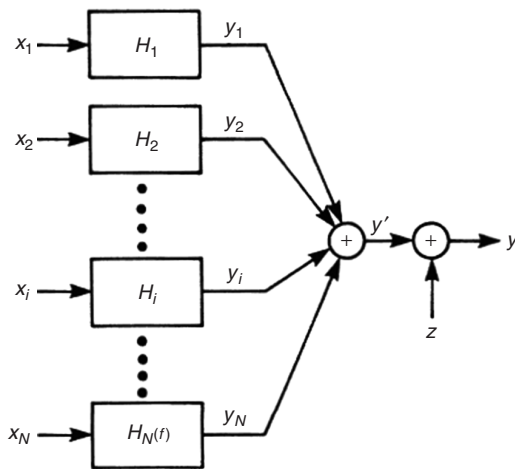
procedure to identify major noise sources. For sources radiating hemispherically, it is easy to show that the floor area within a certain level contour is proportional to the sound power output of the machine. This method is graphic and probably more useful to identify the noisiest machines in a workshop than the noisiest parts on the same machine, because of the contamination problems between different sources in the latter case. Reverberation in a workshop will affect and distort the lower sound pressure level contours.

## 7 USE OF CORRELATION AND COHERENCE AND TECHNIQUES TO IDENTIFY NOISE SOURCES AND PATHS

*Correlation and coherence* techniques in noise control date back over 50 years to the work of Goff<sup>19</sup> who first used the correlation technique to identify noise sources. Although correlation has often been used in other applications, it has not been widely used in noise source identification. One exception is the work of Kumar and Srivastava, who reported some success with this technique in identifying noise sources on diesel engines.<sup>20</sup> Since the ear acts as a frequency analyzer, the corresponding approach in the frequency domain (coherence) instead of the time domain is usually preferable. Crocker and Hamilton have reviewed the use of the coherence technique in modeling diesel engine noise.<sup>21</sup> Such a coherence model can also be used, in principle, to give some information about noise sources on an engine. Figure 18 shows an idealized model of a multiple-input, single-output system. It can be shown<sup>22</sup> that the autospectrum of the output noise  $S_{yy}$  is given by

$$S_{yy} = \sum_{i=1}^N \sum_{j=1}^N S_{ij} H_i H_j^* + S_{zz} \quad (2)$$

where  $N$  is the number of inputs,  $S_{ij}$  are cross-spectral densities between inputs,  $H_i$  and  $H_j$  are frequency



**Figure 18** Multiple-input, single-output system with uncorrelated noise  $z(t)$  in output.

responses, and  $S_{zz}$  is the autospectral density of any uncorrelated noise  $z$  present at the output. Note that the asterisk represents complex conjugate and that the  $S$  and  $H$  terms are frequency dependent.

If there are  $N$  inputs, then there will be  $N$  equations:

$$S_{iy} = \sum_{j=1}^N H_j S_{ij}, \quad i = 1, 2, 3, \dots, N \quad (3)$$

The frequency responses  $H_1, H_2, H_3, \dots, H_N$  can be found by solving the set of  $N$  equations (3).

Several researchers have used the coherence approach to model diesel engine noise.<sup>21-24</sup> This approach appears to give useful information on a naturally aspirated diesel engine, which is combustion-noise dominated and where the  $N$  inputs  $x_1, \dots, x_N$ , are the cylinder pressures measured by pressure transducers in each cylinder. In this case  $H_i$ , the frequency response (transfer function) between the  $i$ th cylinder and the far-field microphone can be calculated. Provided proper frequency averaging is performed, the difficulty of high coherence between the cylinder pressures can be overcome because the phasing between the cylinder pressures is exactly known.<sup>25</sup> In this case the quantity  $S_{ii}|H_i|^2$  may be regarded as the far-field output noise contributed by the  $i$ th cylinder. This may be useful noise source information for the engine designer. Hayes et al.<sup>26</sup> in further research have extended this coherence approach to try to separate combustion noise from piston-impact noise in a running diesel engine.

Wang and Crocker showed that the multiple coherence approach could be used successfully to separate the noise from sources in an idealized experiment such as one involving three loudspeakers, even if the source signals were quite coherent.<sup>27,28</sup> However, when a similar procedure was used on the more complicated case of a truck, which was modeled as a six-input system [fan, engine, exhaust(s), inlet, transmission], the method gave disappointing results and the simpler near-field method appeared better.<sup>16,27</sup> The partial coherence approach was also used in the idealized experiment and the truck experiments. It is believed that contamination between input signals and other computational difficulties may have been responsible for the failure of the coherence method in identifying truck noise sources.

## 8 USE OF SOUND INTENSITY FOR NOISE AND VIBRATION SOURCE AND PATH IDENTIFICATION

Studies have shown that sound intensity measurements are quicker and more accurate than the selective wrapping approach in identifying and measuring the strength of noise sources.<sup>3</sup> The sound intensity  $I$  is the net rate of flow of acoustic energy per unit area. The intensity  $I_r$  in the  $r$  direction is

$$I_r = \langle pu_r \rangle \quad (4)$$

where  $p$  is the instantaneous sound pressure,  $u_r$  is the instantaneous acoustic particle velocity in the  $r$  direction, and the angle brackets denote a time average. The sound power  $W$  radiated by a source can be obtained by integrating the component of the intensity  $I_n$  normal to any surface enclosing the source:

$$W = \int I_n dS. \quad (5)$$

The sound pressure  $p$  and particle velocity are normally determined with two closely spaced microphones (1 and 2) and the surface  $S$  is a surface enclosing the source. Chung first used this technique with the surface of a diesel engine subdivided into  $N = 98$  radiating areas.<sup>29</sup> It took about 2 min to determine the surface-average sound intensity radiated from each of the 98 areas. The engine was source identified in less than a day, which involved much less time than the selective wrapping technique. Since the intensity measurements were made only 20 mm above the engine surfaces, an anechoic or semianechoic room was unnecessary. Many other researchers have used similar sound intensity approaches to identify noise sources since then, as is discussed in more detail in Chapter 45.

## 9 TRANSFER PATH AND NUMERICAL ACOUSTICS

Recently, methods have been extended and adapted in a variety of ways to produce improved approaches for noise and vibration source and path identification.<sup>54–75</sup> One example is the so-called transfer path analysis (TPA) approach<sup>69</sup> and variations of it, which is to some extent based on an elaborated version of the earlier coherence approach to source and path modeling as was outlined in Section 7.<sup>21–29</sup>

Transfer path analysis is a procedure based on measurements and has been developed to allow tracing the flow of vibration and acoustic energy from sources, through a set of structure- and airborne pathways, to a given receiver location. In cases where multiple partially correlated sources exist, it is usually necessary to use airborne source quantification techniques as well as vibration source quantification techniques.<sup>69</sup>

In the TPA approach, the vector contribution of each path of energy from the source to the receiver is evaluated, so that the components along each path, which need modification, can be identified. The measurements are normally time consuming since several hundred frequency response functions (FRFs) may need to be acquired. The measurements are also difficult to perform because of the limited space available for transducers. In addition, large amounts of data are generated requiring careful data storage and management.

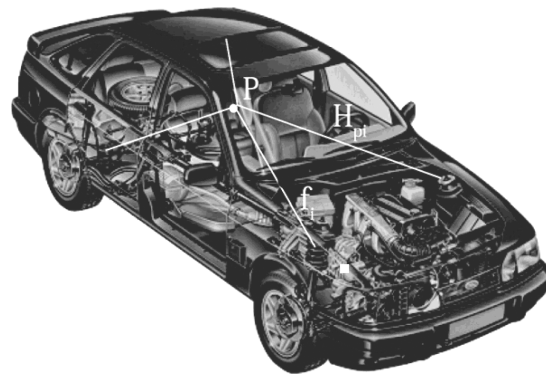
In complicated structures, which involve many sub-assemblies such as are found in complex machines, automobiles, buses, aircraft, and ships, the sound and vibration energy reaching a point will have been caused by some sound and vibration sources situated

close to and others further away from that particular location. TPA is used to assess the structure- and airborne energy paths between excitation source(s) and receiver location(s). For example, structure-borne energy from sources in an automobile is transmitted into the passenger cabin by several different paths, including the engine mounts, the exhaust system connection points, the drive shaft, and the wheel suspension system. Airborne contributions from sources, including the tires, the intake and exhaust systems, regions of separated airflow, and the like are also important. Some transfer paths may result in standing waves in the cabin and produce noise problems at some locations but not at others.

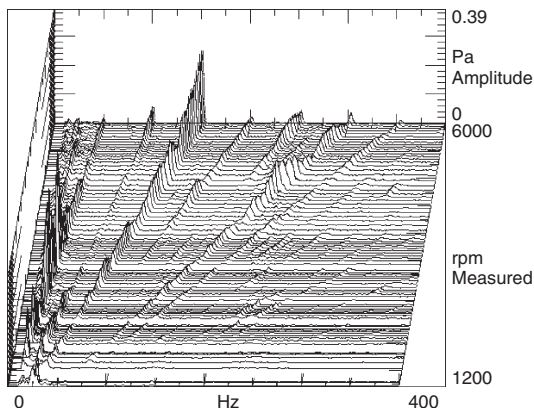
Figure 19 illustrates noise and vibration sources in an automobile.<sup>69</sup>  $P$  is an observation point. Three source locations are shown; one is a source of volume velocity  $Q_i$  and the other two are vibration sources caused by force inputs,  $f_i$ . A transfer function  $H_{pi}$  between a source  $i$  and the observation point  $P$  is shown.

In the case of the booming noise problem, the receiver sound can be measured in the car during engine runup by microphones located at the same position as the occupants' ears. An example of a measurement of the sound pressure amplitude as a function of frequency, made in a car during the idle runup of its 24-valve, 6-cylinder engine, is shown in Fig. 20. Clear (and annoying) booming effects are evident in the 1.5-engine order with a boom between 3000 and 4000 rpm, and another high-frequency boom around 5000 rpm (Fig. 21). In the third order there is a boom around 5000 rpm. The 0.5-engine order seems to be very important, although in practice it does not significantly affect acoustical comfort. The TPA approach can be used to study the sources and paths of such booming noise on more detail.<sup>69</sup>

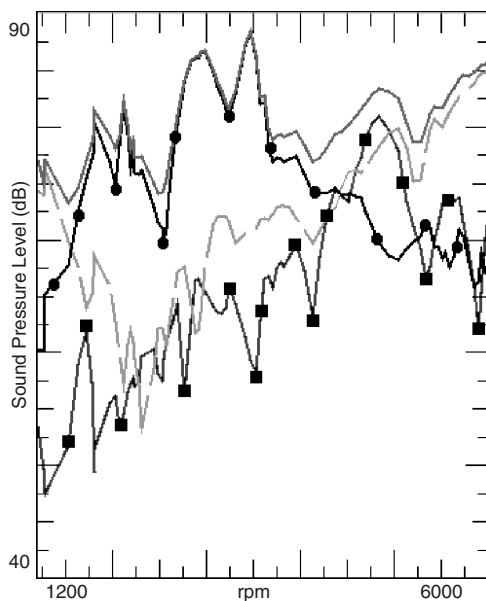
In transfer path analysis, the receiver and sources are normally considered to consist of two different subsystems. In structure-borne transfer path analysis, the two subsystems are assumed to be connected by several quite stiff connections—called the transfer paths.



**Figure 19** Airborne and structure-borne transfer paths in a vehicle. (From Ref. 69.)



**Figure 20** Waterfall diagram of sound pressure amplitude as a function of frequency at the driver's ear as the engine speed is changed from 1200 to 6000 rpm. (From Ref. 69.)



**Figure 21** Order sections. Overall level —; 0.5<sup>th</sup> order —●—; 1.5<sup>th</sup> order - - -; 3<sup>rd</sup> order —■—. (From Ref. 69.)

The primary transfer paths to be analyzed include paths through elements such as the engine support mounts, the transmission shaft supports, gearbox mounts, sub-frame mounts, and exhaust system connections. Secondary transfer paths will exist as well passing through the shock absorber and gear shift mounts. In airborne transfer path analysis, the transfer paths include the engine intake and exhaust pipes and the vibrating panels in the car interior. TPA requires knowledge of the frequency response functions between the receiver and

the inputs (forces or volume velocities) applied at the different source locations, and combines them with inputs (forces or volume velocities) that are active at these locations during vehicle operation. The receiver sound pressure level (or acceleration level, if appropriate) during operating conditions is then calculated from the summation of individual path contributions.<sup>69</sup>

Vibration and acoustical transfer functions are usually measured using either hammer or shaker excitation techniques. The acoustical transfer functions (from input volume velocity to output sound pressure) are normally measured using volume velocity source excitation techniques. The operational inputs (forces or volume velocities) are determined from (1) experimental data, (2) from analytical models, or (3) from indirect measurements. Three data sets are needed: (1) operating data (forces, volume velocities, accelerations, sound pressures), (2) frequency response functions [acoustical frequency response functions (FRFs) and/or accelerance FRFs], and (3) complex dynamic stiffness data for the mounts. Accelerance is defined as the output acceleration spectrum divided by the input force spectrum.<sup>69</sup>

The operating data are often acquired at more locations than there are channels available in the measurement system. To preserve phase information between channels, it is important to perform all measurements in relation to one reference measurement channel. For applications such as an operating automobile engine, a suitable reference signal can be obtained from an accelerometer mounted on the engine. For steady-state applications, cross-power measurements must be made with respect to the single reference channel. For non-stationary applications, the referenced measurements are processed to extract a set of selected order sections as functions of engine rpm. Source-receiver transfer functions are required for all transfer paths. At the receiver side of all of the transfer paths (often referred to as body-side transfer paths) either hammer impact or shaker excitation is normally used to measure the corresponding accelerance frequency response function. A volume velocity source can be used to measure the acoustical frequency response functions.

The vibration frequency response functions (between force and sound pressure) can either be measured in a direct way using hammer or shaker excitation or in a reciprocal way using a volume velocity source. These FRFs are measured best when the source side is disconnected from the receiver side of the transfer path. Measuring the body-side FRFs is a critical element in transfer path analysis. In practice there is usually little physical space between the engine and engine mount in which to locate the force transducers. In principle, the engine should be removed while the other side of the engine transfer path system is analyzed. A common approach is to remove the engine to gain access to the body side of the mount directly and to use a hammer or shaker to excite the system directly. In the same way, ideally, the suspension should be removed when measuring body-side FRFs that are related to road noise.<sup>69</sup>



The operating forces are usually estimated by indirect techniques, rather than direct measurements. Two alternative approaches are often used: the *complex stiffness method* and *matrix inversion*. For some transfer paths, the complex dynamic stiffness method is recommended. For others, because the mount stiffness data are not available, or the differential operating displacement over the connection is small, or because the connection is quite rigid, other approaches must be used.

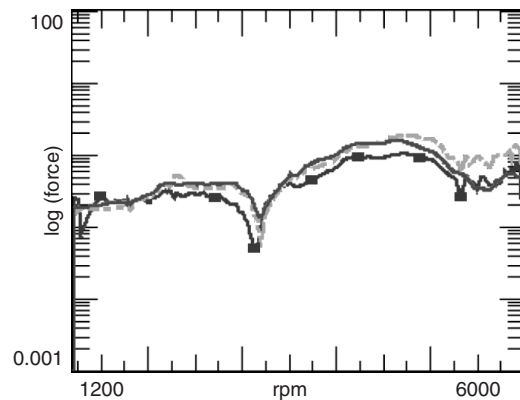
For transfer paths where the source side is connected to the receiver by mounts, the operating forces can be determined from knowledge of the complex frequency-dependent dynamic stiffness of the mounts and by determining the differential displacement over the mount during operation. The displacements are usually derived from acceleration measurements.

The complex dynamic mount stiffnesses should be determined as complex data functions of frequency. These can be assumed to be positive: either in tension or in compression. The mount characteristics can be expressed in terms of force–displacement, force–velocity, or force–acceleration. When evaluating the dynamic stiffness of mounts, it is important to preload them so that they function near to the actual operating conditions.

For transfer paths comprised of rigid connections, or where the mount stiffness is very large relative to the body impedance, inducing even a small relative displacement over the mount is not possible. In such cases, a technique based upon inversion of a measured accelerance matrix between structural responses on the receiver side due to force excitation at all transfer paths can be used. This accelerance matrix must be measured when the source is disconnected from the receiver. This matrix is then combined with measurements of the structural vibration at the receiver side to obtain force estimates. The use of singular value decomposition methods helps to minimize numerical problems in the matrix inversion.<sup>69</sup>

When applying the accelerance matrix inversion method, receiver-side vibrations usually must be measured in three directions in operating conditions. To obtain a unique solution for the operational forces, the number of responses ( $m$ ) should at least be equal to the number of input forces to be estimated ( $n$ ). However, more response measurements can be taken at the receiver side ( $m > n$ ), since the measurement locations are not restricted to the transfer path locations. The TPA approach is crucially dependent on good estimates of the input forces, volume velocities, and transfer paths. Figure 22 shows how different methods can be used to estimate input forces.<sup>69</sup> The agreement between the three methods is seen to be better for low than high engine speeds.

Airborne transfer paths are normally quantified by their input volume velocities. These volume velocities are usually estimated from indirect techniques, in a similar way to the input forces. Three techniques are available: (1) point-to-point surface sampling, (2) sound intensity measurements, and (3) matrix



**Figure 22** Comparison of operational forces at a car body. 1: +Z path, third order. Measured force via force transducer —■—; force estimated via complex dynamic stiffness method - - -; force estimated via matrix inversion method —■— (From Ref. 69.)

inversion. This first method is used to determine contributions from vibrating panels. The second can be used to determine the airborne contributions from an engine. A typical application of matrix inversion is to quantify the intake and exhaust noise.<sup>69</sup>

## 10 INVERSE NUMERICAL ANALYSIS APPROACH FOR SOURCE IDENTIFICATION

Other studies, which are similar to the TPA approach, have shown that numerical acoustics techniques can be used for source identification.<sup>70–75</sup> The approach described here is usually called inverse numerical analysis (INA) and is similar to the acoustical holography method described in Chapter 50. In TPA, the main concern is determining the exciting forces (e.g., the forces supplied by an engine through the engine mounts), while with INA the main concern is to reconstruct the surface vibration of an acoustic source. So, fundamentally, the objectives of TPA and INA are different.

The main difference between TPA and INA lies in the determination of the transfer functions,  $H$ . In TPA, these are usually obtained by experiment (e.g., the actual sources are turned off or disconnected, and a shaker is used in place of each vibration source in a sequential fashion). In INA, each transfer function,  $H$ , is defined as the ratio of the sound pressure at a point in the near field of the source to the vibration velocity at a point on the surface of the source; the acoustical transfer vector (ATV) is simply a row of these transfer functions between a given point in the near field and each surface point; ATM is a matrix in which each row is the ATV for each field point. Because the number of surface points can be in the thousands, the transfer functions are usually obtained from a boundary element model (BEM) model (although, in principle, transfer functions can be measured either directly or using reciprocity). Thus, INA is a model-based method

in which a BEM model is used to obtain the transfer functions.<sup>76</sup>

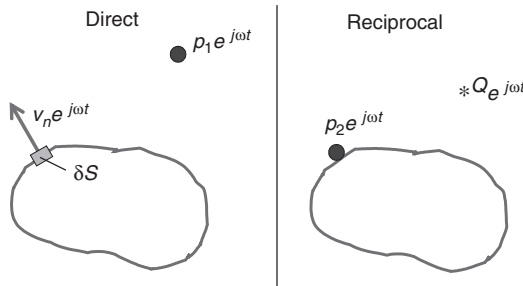
What is common to both methods is that they both require an inversion of a matrix of transfer functions. With TPA there are normally more equations than unknowns, so the system is overdetermined; with INA there are more unknowns than equations, so the system is underdetermined.

The starting point for the INA approach is the acoustical transfer vector (ATV). ATVs can be used in two different ways. First, ATVs can be used to conduct contribution analyses that can assess which parts of a machine act as the predominant noise sources. For example, the sound power contribution and radiation efficiency of different parts of an engine can be calculated if the distribution of the normal velocity on the surface is known. Additionally, ATVs can be used to reliably reconstruct the vibration on a machine surface. This procedure utilizes measured sound pressures along with ATVs to reconstruct the surface velocity.

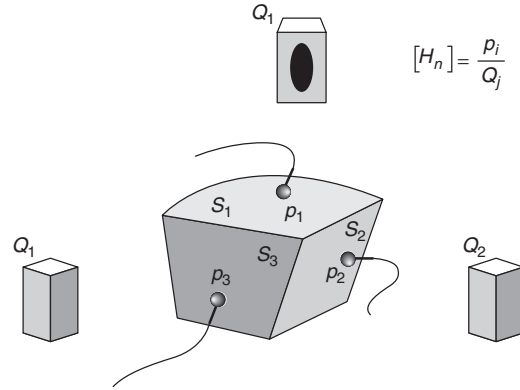
Fahy demonstrated that ATVs can be measured, and perhaps ATVs can best be understood using the concept of acoustical reciprocity, which he has explained.<sup>71</sup> Figure 23 illustrates this concept by comparing a direct and corresponding reciprocal case. For the situation shown in Fig. 23,

$$\frac{p_1}{v_n \delta S} = \frac{p_2}{Q} \quad (6)$$

where  $p_1$  and  $p_2$  are sound pressures,  $v_n$  is the normal velocity on the surface,  $\delta S$  is a differential area, and  $Q$  is the volume velocity of a point source. The right hand or the corresponding left hand side of Eq. (6) is a single element of an ATV. Thus, the row vector obtained by finding this ratio at each point or node on a radiating surface is the fully populated ATV at a given frequency. It follows that another ATV will be required for each sound pressure measurement location in the sound field. It should be apparent that ATVs can be measured most readily using the reciprocal approach (Fig. 23) since it is easier to traverse a microphone over the surface of a machine rather than some known sound source. Figure 24 shows how such measurements can be realized in practice.<sup>69</sup>



**Figure 23** Schematic showing the principle of acoustical reciprocity. (From Ref. 70.)



**Figure 24** Measurement of inverse transfer functions using the reciprocal approach. (From Ref. 69.)

If an appropriate numerical model can be produced, ATVs are more easily calculated than measured and really do not require any knowledge about the source except for the geometry and the location of any sound-absorbing materials that may be present. As mentioned previously, in principle, several different numerical methods could be used to calculate ATVs, although the BEM has generally been the method of choice. Because the number of surface points can be in the thousands, the transfer functions are usually obtained from a BEM model (although these transfer functions can be measured either directly or by using reciprocity). The sound pressure at a field point ( $p_f$ ) can be related to any surface vibration ( $v_n$ ) via

$$p_f = [H_{fn}] \{v_n\} \quad (7)$$

Here the acoustical transfer vector  $[H_{fn}]$  represents a row of transfer functions  $H_{fn}$ . For multiple field points, Eq. (7) can be written in matrix form as

$$\{p_f\} = [H_{fij}] \{v_n\} \quad (8)$$

where  $H_{fij}$  are elements of the acoustical transfer matrix,  $[H_{fij}]$  or ATM. The ATM is a collection of ATVs for different points in the field.

Inverse numerical acoustics (INA)<sup>70-75</sup> is the process of solving Eq. (8) in the reverse direction. The sound pressures at the field points ( $p_f$ ) are the known quantities, whereas the surface vibrations ( $v_n$ ) are the unknowns. In most cases, there are far more unknown vibrations than there are known or measured sound pressures. Thus, the problem could be classified as an underdetermined problem. Once the vibration on the surface is reconstructed, the characteristics of the vibrating source can be examined.

## REFERENCES

1. C. E. Ebbing and T. H. Hodgson, Diagnostic Tests for Locating Noise Sources, *Noise Control Eng.*, Vol. 3, 1974, pp. 30-46.

2. M. C. McGary and M. J. Crocker, Surface Intensity Measurements on a Diesel Engine, *Noise Control Eng.*, Vol. 16, No. 1, 1981, pp. 26–36.
3. T. E. Reinhart and M. J. Crocker, Source Identification on a Diesel Engine Using Acoustic Intensity Measurements, *Noise Control Eng.*, Vol. 18, No. 3, 1982, pp. 84–92.
4. R. L. Staadt, Truck Noise Control, in *Reduction of Machinery Noise*, rev. ed., Short Course Proc., Purdue University, Dec. 1975, pp. 158–190.
5. R. A. Collacott, The Identification of the Source of Machine Noises Contained within a Multiple-Source Environment, *Appl. Acoust.*, Vol. 9, No. 3, 1976, pp. 225–238.
6. A. F. Seybert, Estimation of Frequency Response in Acoustical Systems with Particular Application to Diesel Engine Noise, Ph.D. Thesis, Purdue University, Herrick Laboratories Report HL 76-3, Dec. 1975.
7. A. F. Seybert, M. J. Crocker, James W. Moore, and Steven R. Jones, Reducing the Noise of a Residential Air Conditioner, *Noise Control Eng.*, Vol. 1, No. 2, 1973, pp. 79–85.
8. J. M. Hague, Dynamic Vibration Exciter of Torsional Axial, and Radial Modes from Modified D.C. Motor, Paper No. 962 presented at ASHRAE, Semi-Annual Meeting, Chicago, IL, Feb. 13–17, 1977.
9. J. F. Unruh, et al., Engine Induced Structural-Borne Noise in a General Aviation Aircraft, NASA CR-159099, 1979.
10. M. C. McGary and W. H. Mayes, A New Measurement Method for Separating Airborne and Structureborne Aircraft Interior Noise, *Noise Control Eng.*, Vol. 20, No. 1, 1983, pp. 21–30.
11. J. S. Mixon and J. F. Wilby, Interior Noise, in *Aeroacoustics of Flight Vehicles: Theory and Practice*, Vol. 2: *Noise Control*, H. H. Hubbard, Ed., NASA Reference Publication 1258, August 1991, Chapter 16.
12. J. F. Wilby, and E. G. Wilby, In-Flight Acoustic Measurements on a Light Twin-Engine Turbo Prop Airplane, NASA CR-178004, 1984.
13. G. E. Thien, The Use of Specially Designed Covers and Shields to Reduce Diesel Engine Noise, SAE Paper 730244, 1973.
14. M. Nakamura and D. R. M. Nakano, Exterior Engine Noise Characterization Using an Acoustic Tube to Measure Volume Velocity Distribution, *Proceedings of the Institution of Mechanical Engineers, Part C: J. Mech. Eng. Sci.*, Vol. 217, No. 2, 2003, pp. 199–206.
15. R. Vailaitis, Transmission through Stiffened Panels, *J. Sound Vib.*, Vol. 70, No. 3, 1980, pp. 413–426.
16. M. J. Crocker and J. W. Sullivan, Measurement of Truck and Vehicle Noise, SAE Paper 780387 1978; see also SAE Transactions.
17. C. M. P. Chan and D. Anderton, Correlation between Engine Block Surface Vibration and Radiated Noise of In-Line Diesel Engines, *Noise Control Eng.*, Vol. 2, No. 1, p. 16, 1974.
18. P. Francois, Isolation et Revêtements, *Les Carte Wveaux Sonores*, Jan.–Feb. 1966, pp. 5–17.
19. K. W. Goff, The Application of Correlation Techniques to Source Acoustical Measurements, *J. Acoust. Soc. Am.*, Vol. 27, No. 2, 1955, pp. 336–346.
20. S. Kumar and N. S. Srivastava, Investigation of Noise Due to Structural Vibrations Using a Cross-Correlation Technique, *J. Acoust. Soc. Am.*, Vol. 57, No. 4, 1975, pp. 769–772.
21. M. J. Crocker and J. F. Hamilton, Modeling of Diesel Engine Noise Using Coherence, SAE Paper 790362, 1979.
22. J. Y. Chung, M. J. Crocker, and J. F. Hamilton, Measurement of Frequency Responses and the Multiple Coherence Function of the Noise Generation System of a Diesel Engine, *J. Acoust. Soc. Am.*, Vol. 58, No. 3, 1975, pp. 635–642.
23. A. F. Seybert and M. J. Crocker, The Use of Coherence Techniques to Predict the Effect of Engine Operating Parameters on Noise, *Trans. ASME, J. Eng. Ind.*, Vol. 97B, 1976, p. 13.
24. A. F. Seybert and M. J. Crocker, Recent Applications of Coherence Function Techniques in Diagnosis and Prediction of Noise, *Proc. INTER-NOISE 76*, 1976, pp. 7–12.
25. A. F. Seybert and M. J. Crocker, The Effect of Input Cross-Spectra on the Estimation of Frequency Response Functions in Certain Multiple-Input Systems, *Arch. Acoust.*, Vol. 3, No. 3, 1978, pp. 3–23.
26. P. A. Hayes, A. F. Seybert, and J. F. Hamilton, A Coherence Model for Piston-Impact Generated Noise, SAE Paper 790274.
27. M. E. Wang, The Application of Coherence Function Techniques for Noise Source Identification, Ph.D. Thesis, Purdue University, 1978.
28. M. E. Wang and M. J. Crocker, Recent Applications of Coherence Techniques for Noise Source Identification, *Proc. INTER-NOISE 78*, 1978, pp. 375–382.
29. J. Y. Chung, J. Pope, and D. A. Feldmaier, Application of Acoustic Intensity Measurement to Engine Noise Evaluation, SAE Paper 790502, 1979.
30. J. I. Huertas, J. C. Parra Duque, J. P. Posada Zuluaga, and D. F. Parra Mariño, Identification of Annoying Noises in Vehicles, Society of Automotive Engineers, Warrendale, PA, SAE Noise and Vibration Conference and Exposition, 2003.
31. H. Uchida and K. Ueda, Detection of Transient Noise of Car Interior Using Non-stationary Signal Analysis, Society of Automotive Engineers, Warrendale, PA, SAE International Congress and Exposition, 1998.
32. N. W. Alt, N. Wiehagen, and M. W. Schlitzer, Interior Noise Simulation for Improved Vehicle Sound, Society of Automotive Engineers, Warrendale, PA, SAE Noise and Vibration Conference and Exposition, 2001.
33. G. Eisele, K. Wolff, N. Alt, and Michel Hüser, Application of Vehicle Interior Noise Simulation (VINS) for NVH Analysis of a Passenger Car, Society of Automotive Engineers, Warrendale, PA, Noise and Vibration Conference and Exhibition, 2005.
34. G. Koners, Panel Noise Contribution Analysis: An Experimental Method for Determining the Noise Contributions of Panels to an Interior Noise, Society of Automotive Engineers, Warrendale, PA, SAE Noise and Vibration Conference and Exposition, 2003.
35. J. F. Unruh, P. D. Till, and T. J. Farwell, Interior Noise Source/Path Identification Technology, Society of Automotive Engineers, Warrendale, PA, SAE General Aviation Technology Conference and Exposition, 2000.
36. C.-K. Chae, B.-K. Bae, K.-J. Kim, J.-H. Park and N.-C. Choe, Feasibility Study on Indirect Identification of Transmission Forces through Rubber Bushing in Vehicle Suspension System by Using Vibration Signals Measured on Links, *Vehicle System Dynamics*, Vol. 33, No. 5, May 2000, pp. 327–349.



37. M. Browne and R. Pawlowski, Statistical Identification and Analysis of Vehicle Noise Transfer Paths, Society of Automotive Engineers, Warrendale, PA, SAE Noise and Vibration Conference and Exhibition, 2005.
38. D. Wang, G. M. Goetchius, and T. Onsay, Validation of a SEA Model for a Minivan: Use of Ideal Air- and Structure-Borne Sources, Society of Automotive Engineers, Warrendale, PA, SAE Noise and Vibration Conference and Exposition, 1999.
39. A. Rust and I. Edlinger, Active Path Tracking. A Rapid Method for the Identification of Structure Borne Noise Paths in Vehicle Chassis, Society of Automotive Engineers, Warrendale, PA, SAE Noise and Vibration Conference and Exposition, 2001.
40. R. Bocksch, G. Schneider, J. A. Moore, and I. Ver, Empirical Noise Model for Power Train Noise in a Passenger Vehicle, Society of Automotive Engineers, Warrendale, PA, SAE Noise and Vibration Conference and Exposition, 1999.
41. J. A. Steel, Study of Engine Noise Transmission Using Statistical Energy Analysis, *Proc. Instit. Mech. Eng., Part D: J. Automobile Eng.*, Vol. 212, No. 3, 1998, pp. 205–213.
42. S. Goossens, T. Osawa, and A. Iwama, Quantification of Intake System Noise Using an Experimental Source-Transfer-Receiver Model, Society of Automotive Engineers, Warrendale, PA, SAE Noise and Vibration Conference and Exposition, 1999.
43. N. W. Alt, J. Nehl, S. Heuer, and M. W. Schlitzer, Prediction of Combustion Process Induced Vehicle Interior Noise, Society of Automotive Engineers, Warrendale, PA, SAE Noise and Vibration Conference and Exposition, 2003.
44. S. Goossens, T. Osawa, and A. Iwama, Quantification of Intake System Noise Using an Experimental Source-Transfer-Receiver Model, Society of Automotive Engineers, Warrendale, PA, SAE Noise and Vibration Conference and Exposition, 1999.
45. P. Diemer, M. G. Hueser, K. Govindswamy, and T. D'Anna, Aspects of Powerplant Integration with Emphasis on Mount and Bracket Optimization, Society of Automotive Engineers, Warrendale, PA, SAE Noise and Vibration Conference and Exposition, 2003.
46. G. J. Kim, K. R. Holland, and N. Lalor, Identification of the Airborne Component of Tyre-Induced Vehicle Interior Noise, *Appl. Acoust.*, Vol. 51, No. 2, June 1997, pp. 141–156.
47. M. Constant, J. Leyssens, F. Penne, and R. Freymann, Tire and Car Contribution and Interaction to Low Frequency Interior Noise, Society of Automotive Engineers, Warrendale, PA, SAE Noise and Vibration Conference and Exposition, 2001.
48. J. J. Christensen, J. Hald, J. Mørkholt, A. Schuhmacher, and C. Blaabjerg, A Review of Array Techniques for Noise Source Location, Society of Automotive Engineers, Warrendale, PA, SAE Noise and Vibration Conference and Exposition, 2003.
49. R. Martins, M. Gonçalves Pinto, C. Magno Mendonça, and A. Ribeiro Morais, Pass by Noise Analysis in a Commercial Vehicle Homologation, Society of Automotive Engineers, Warrendale, PA, 12th SAE Brazil Congress and Exposition, 2003.
50. K. Genuit, S. Guidati, and R. Sottek, Progresses in Pass-by Simulation Techniques, Society of Automotive Engineers, Warrendale, PA, Noise and Vibration Conference and Exhibition, 2005.
51. S. F. Wu, N. E. Rayess, and N.-M. Shiau, Visualizing Sound Radiation from a Vehicle Front End Using the Hels Method, *J. Sound Vib.*, Vol. 248, No. 5, Dec. 13, 2001, pp. 963–974.
52. A. Frid, Quick and Practical Experimental Method for Separating Wheel and Track Contributions to Rolling Noise, *J. Sound Vib.*, Vol. 231, No. 3, Mar. 2000, pp. 619–629.
53. F. G. de Beer and J. W. Verheij, Experimental Determination of Pass-by Noise Contributions from the Bogies and Superstructure of a Freight Wagon, *J. Sound and Vib.*, Vol. 231, No. 3, 30 March 2000, pp. 639–652.
54. D. De Vis, W. Hendricx, and P. J. G. van der Linden, Development and Integration of an Advanced Unified Approach to Structure Borne Noise Analysis, Second International Conference on Vehicle Comfort, ATA, 1992.
55. W. Hendricx and D. Vandenbroeck, Suspension Analysis in View of Road Noise Optimization, Proc. of the 1993 Noise and Vibration Conference, SAE P-264, Traverse City, 1993, pp. 647–652.
56. T. C. Lim and G. C. Steyer, System Dynamics Simulation Based on Structural Modification Analysis Using Response Techniques, Proc. Tenth International Modal Analysis Conference, San Diego (A), Feb. 3–7, 1992, pp. 1153–1158.
57. P. Mas, P. Sas, and K. Wyckaert, Indirect Force Identification Based upon Impedance Matrix Inversion: A Study on Statistical and Deterministical Accuracy, Nineteenth ISMA Conference, Leuven, September 12–14, 1994.
58. D. Otte, Development and Evaluation of Singular Value Methodologies for Studying Multivariate Noise & Vibration Problems, Ph.D. Dissertation, KU Leuven, 1994.
59. D. Otte, in *The Use of SVD for the Study of Multivariate Noise & Vibration Problems, SVD and Signal Processing III: Algorithms, Architectures and Applications*, M. Moonen and B. De Moor, Eds., Elsevier Science, 1995, pp. 357–366, Amsterdam, Netherlands.
60. D. Otte, P. Van de Ponsseele, and J. Leuridan, Operating Deflection Shapes in Multisource Environments, Proc. 8th IMAC, Kissimmee, FL 1990, pp. 413–421.
61. D. Otte, J. Leuridan, H. Grangier, and R. Aquilina, Prediction of the Dynamics of Structural Assemblies Using Measured FRF Data: Some Improved Data Enhancement Techniques, Proc. Ninth International Modal Analysis Conference, Florence, 1991, pp. 909–918.
62. J. M. Starkey and G. L. Merrill, On the Ill Conditioned Nature of Indirect Force Measurement Techniques, *Anal. Exper. Modal Anal.*, Vol. 4, No. 3, 1989.
63. P. J. G. van der Linden and J. K. Fun, Using Mechanical-Acoustical Reciprocity for Diagnosis of Structure-Borne Sound in Vehicles, Proc. 1993 Noise and Vibration Conference, SAE Paper 931340, Traverse City, May 10–13, 1993, pp. 625–630.
64. J. W. Verheij, Experimental Procedures for Quantifying Sound Paths to the Interior of Road Vehicles, Proc. of the Second International Conference on Vehicle Comfort, Bologna, October 14–16, 1992.
65. J. Verheij, Multipath Sound Transfer from Resiliently Mounted Shipboard Machinery, Ph.D. Dissertation, 1986, Netherlands.
66. K. Wyckaert and W. Hendricx, Transmission Path Analysis in View of Active Cancellation of Road Induced Noise in Vehicles, Third International Congress

- on Air- and Structure-Borne Sound and Vibration, Montreal, June 13–15, 1994.
67. K. Wyckaert and H. Van der Auweraer, Operational Analysis, Transfer Path Analysis, Modal Analysis: Tools to Understand Road Noise Problems in Cars, SAE Noise & Vibration Conference, Traverse City, 1995, pp. 139–143.
68. P. J. G. van der Linden and P. Varet, Experimental Determination of Low Frequency Noise Contributions of Interior Vehicle Body Panels in Normal Operation, SAE Paper 960194, Detroit, February 26–29, 1996, pp. 61–66.
69. LMS, Transfer Path Analysis—The Qualification and Quantification of Vibro-acoustic Transfer Paths, see <http://www.lmsintl.com/downloads/cases>.
70. M. Tournour, L. Cremers, and P. Guisset, Inverse Numerical Acoustics Based on Acoustic Transfer Vectors, 7th International Congress on Sound and Vibration, Garmisch, Partenkirchen, Germany, 2000, pp. 2069–2076.
71. F. J. Fahy, The Vibro-Acoustic Reciprocity Principle and Applications to Noise Control, *Acustica*, Vol. 81, 1995, pp. 544–558.
72. W. A. Veronesi and J. D. Maynard, Digital Holographic Reconstruction of Sources with Arbitrarily Shaped Surfaces, *J. Acoust. Soc. Am.*, Vol. 85, 1989, pp. 588–598.
73. M. R. Bai, Application of BEM-based Acoustic Holography to Radiation Analysis of Sound Sources with Arbitrarily Shaped Geometries, *J. Acoust. Soc. Am.*, Vol. 92, 1992, pp. 533–549.
74. B. K. Kim and J. G. Ih, On the Reconstruction of the Vibro-Acoustic Field Over the Surface Enclosing an Interior Space using the Boundary Element Method, *J. Acoust. Soc. Am.*, Vol. 100, 1996, pp. 3003–3015.
75. A. F. Seybert and F. Martinus, Forward and Inverse Numerical Acoustics for NVH Applications, 9th International Congress on Sound and Vibration, P714–1, Orlando, FL, July 8–11, 2002.
76. A. F. Seybert, Personal Communication, November 13, 2006.

# CHAPTER 56

---

## USE OF ENCLOSURES

**Jorge P. Arenas**  
Institute of Acoustics  
Universidad Austral de Chile  
Campus Miraflores  
Valdivia, Chile

**Malcolm J. Crocker**  
Department of Mechanical Engineering  
Auburn University  
Auburn, Alabama

### 1 INTRODUCTION

Acoustical enclosures are used wherever containment or encapsulation of the source or receiver is a good, cost-effective, feasible solution. An enclosure corresponds to a noise control measure in the path. Often the main task is to keep the sound energy inside the enclosure and dissipate it by means of sound absorption. In some cases such as with personnel booths or automobile or aircraft cabins, the main task is to keep the noise outside and to absorb as much sound energy as possible that does penetrate the enclosure walls and come inside. Enclosures can be classified in five main types: (1) large loose-fitting enclosures in which complete machines are contained, (2) small enclosures used to enclose small machines or parts of large machines, (3) close-fitting enclosures that follow the contours of a machine or a part, (4) wrapping or lagging materials often used to wrap pipes, ducts, or other systems, and (5) large booths or room-sized enclosures and cabins in which personnel or vehicle passengers are contained.

The performance of enclosures can be defined in three main ways<sup>1</sup>: (1) *noise reduction (NR)*, (2) *transmission loss (TL)*, or equivalently the *sound reduction index*, and (3) *insertion loss (IL)*. Enclosures can either be complete or partial (in which some walls are removed for convenience or accessibility). Penetrations are also often necessary for machine maintenance or to provide access during manufacture or for cooling.

The physical behavior and the efficiency of an enclosure depend mainly on: (1) the transmission loss of the walls of the enclosure, (2) its volume and necessary openings (access for passing materials in and out, ventilation and cooling, inspection windows, etc.), and (3) the sound energy absorbed inside the enclosure walls that are lined with sound-absorbing materials.

### 2 REVERBERANT SOUND FIELD MODEL FOR ENCLOSURES

In the energy model for an enclosure it is assumed that the reverberant sound field produced within the enclosure is added to the direct sound field produced

by the sound source being enclosed. The sum of the two sound fields gives the total sound field within the enclosure, which is responsible for the sound radiated by the enclosure walls.

If the smallest distance  $\ell$  between the machine surface and the enclosure walls is greater than a wavelength  $\lambda$  ( $\ell > \lambda$ ), for the lowest frequency of the noise spectrum of the machine (noise source), then the enclosure can be considered large enough to assume that the sound field within the enclosure is diffuse (the sound energy is uniformly distributed within the enclosure). Another criterion<sup>2</sup> used to assume the diffuse sound field condition requires the largest dimension of the interior volume of the enclosure to be less than  $\lambda/10$ .

Therefore, according to classical theory, the reverberant sound pressure level within the enclosure,  $L_{prev}$ , is given by<sup>3,4</sup>

$$L_{prev} = L_W + 10 \log T - 10 \log V + 14 \quad (1)$$

where  $L_W$  is the sound power level of the source,  $T$  is the reverberation time within the enclosure in seconds, and  $V$  is the internal volume of the enclosure in cubic metres. Then, the reverberant sound intensity incident on the internal enclosure walls can be estimated from

$$I_i = \frac{\langle p^2 \rangle_{rev}}{4\rho c} \quad (2)$$

where  $\langle p^2 \rangle_{rev}$  is the reverberant mean-square sound pressure (space-time average) within the enclosure,  $\rho$  is the density of the medium (air) within the enclosure, and  $c$  is the speed of sound.

### 3 MACHINE ENCLOSURE IN FREE FIELD

The sound field immediately outside an enclosure will consist of two components: (1) sound radiated due to the internal reverberant sound field and (2) sound radiated due to the direct sound field of the machine noise source. The fraction of sound energy that is incident on the interior of the enclosure wall that is transmitted depends on its transmission coefficient.

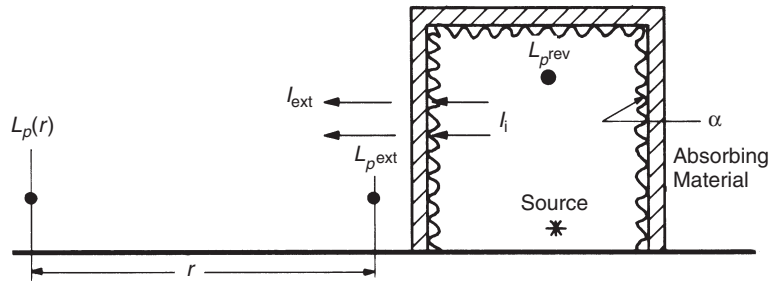


Figure 1 Acoustical enclosure placed in free field.

The transmission coefficient  $\tau$  of a wall may be defined as

$$\tau = \frac{\text{sound intensity transmitted by wall}}{\text{sound intensity incident on wall}} \quad (3)$$

and this coefficient  $\tau$  is related to the transmission loss (TL) (or sound reduction index) by

$$TL = 10 \log \frac{1}{\tau} \quad (4)$$

(See Chapter 54 for a definition and discussion of the transmission loss.)

If the enclosure is located in a free field, as shown in Fig. 1, the sound pressure level immediately outside the enclosure is<sup>3,4</sup>

$$L_{p,ext} = L_{p,rev} - TL - 6 \quad (5)$$

Therefore, the enclosure with its noise source inside can be considered to be an equivalent sound source placed in free-field conditions. Now, if the floor is hard and highly reflective, the sound pressure level at a distance  $r$  from an enclosure wall can be estimated by

$$L_p(r) = L_{p,ext} + 10 \log S - 10 \log(2\pi r^2) \quad (6)$$

where  $S$  is the total outer surface area of the enclosure walls.

#### 4 SIMPLE ENCLOSURE DESIGN ASSUMING DIFFUSE REVERBERANT SOUND FIELDS

If the sound fields are assumed to be reverberant both inside and outside a completely sealed enclosure (typical of a machine enclosure in a machine shop), then the noise reduction NR is given by

$$NR = L_{p1} - L_{p2} = TL + 10 \log \frac{A_2}{S_e} \quad (7)$$

where  $L_{p1}$  and  $L_{p2}$  are the reverberant sound pressure levels inside and outside the enclosure,  $A_2 = S_2 \bar{\alpha}_2$  is the *absorption area* in square metres of the receiving space where  $\bar{\alpha}_2$  is the surface average absorption coefficient of the absorption material in the receiving space averaged over the area  $S_2$ , and  $S_e$  is the enclosure surface area in square metres. (See Chapter 57 for definitions and further discussion of absorption area  $A$  and Chapter 54 for a definition and discussion of transmission loss.)

##### 4.1 Personnel Booth or Enclosure in a Reverberant Sound Field

Equation (7) can be used to design a personnel booth or enclosure in which the noise source is external and the reason for the enclosure is to reduce the sound pressure level inside (see Fig. 2). If the enclosure is located in a factory building in which the reverberant level is  $L_{p1}$ , then the enclosure wall TL and interior

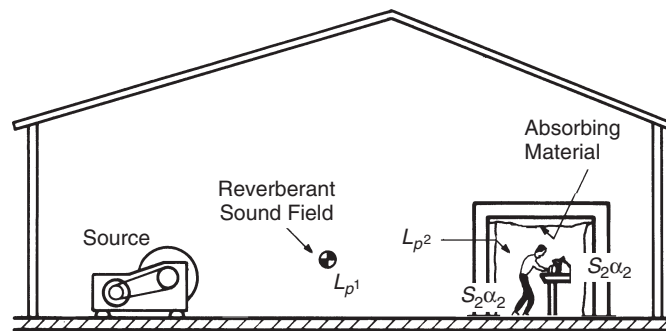


Figure 2 Personnel enclosure placed in a reverberant sound field.

absorption area  $A_2$  can be chosen to achieve a required value for the internal sound pressure level  $L_{p2}$ . In the case that the surface area  $S_2$  of the internal absorbing material  $S_2 = S_e$ , the enclosure surface area, then Eq. (7) simplifies to

$$NR = TL + 10 \log \bar{\alpha}_2 \quad (8)$$

The NR achieved is seen to be less than the TL in general. When  $\bar{\alpha}_2$ , the average absorption coefficient of the absorbing material in the receiving space approaches 1, then NR approaches TL (as expected), although when  $\bar{\alpha}_2$  approaches 0, then the theory fails.

**Example 1** Consider that the reverberant level in the assembly area of a manufacturing shop is 85 dB in the 1600-Hz one-third octave band. It is required to provide values of TL and  $\bar{\alpha}$  to achieve an interior level inside a personnel enclosure less than 60 dB. Assuming that  $S_2 = S_e$ , then if TL is chosen as 30 dB and  $\bar{\alpha} = 0.2$ ,  $NR = 30 + 10 \log 0.2 = 30 - 7 = 23$  dB, and  $L_{p2} = 62$  dB. Now, if  $\bar{\alpha}$  is increased to 0.4, then  $NR = 30 + 10 \log 0.4 = 30 - 4 = 26$  dB and  $L_{p2} = 59$  dB, meeting the requirement. Since TL varies with frequency [see Eq. (11)], this calculation would have to be repeated for each one-third octave band center frequency of interest. In addition, at low frequency, some improvement can be achieved by using a thicker layer of sound-absorbing lining material.

#### 4.2 Machine Enclosure in a Reverberant Space

When an enclosure is designed to contain a noise source (see Fig. 3), it operates by reflecting the sound back toward the source, causing an increase in the sound pressure level inside the enclosure. From energy considerations the insertion loss is zero if there is no sound absorption inside. The effect is an increase in the sound pressure at the inner walls of the enclosure compared with the sound pressure resulting from the direct field of the source alone. The buildup of sound energy inside the enclosure, can be reduced by placing sound-absorbing material on the walls inside the enclosure. It is also useful to place sound-absorbing materials inside personnel noise protection booths for similar reasons.

The internal surfaces of an enclosure are usually lined with glass or mineral fiber or an open-cell polyurethane foam blanket. However, the selection of the proper sound-absorbing material and its containment will depend on the characteristics of each noise source. Sound absorption material also requires special protection from contamination by oil or water, which weakens its sound absorption properties. If the noise source enclosed is a machine that uses a combustible liquid, or gas, then the material should also be fire resistant. Of course, since the sound absorption coefficient of linings is generally highest at high frequencies, the high frequency components of any noise source will suffer the highest attenuation.

The effect of inadequate sound absorption in enclosures is very noticeable. Table 1 shows the reduction in performance of an ideal enclosure with varying degrees of internal sound absorption.<sup>4</sup> The first column of Table 1 shows the fraction of internal surface area that is treated. The sound power of the source is assumed to be constant and unaffected by the enclosure.

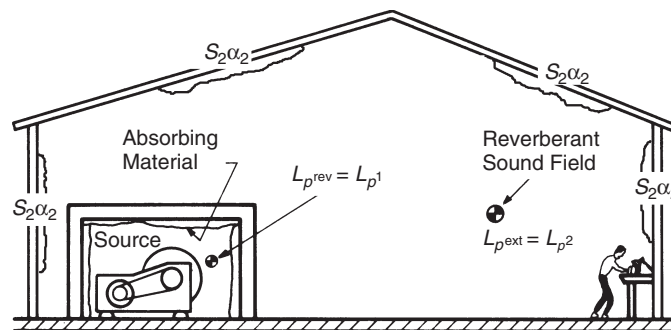
For an enclosure that is installed around a source with a considerable amount of absorbing material used inside to prevent any interior reverberant sound energy buildup, then from energy considerations

$$IL \cong TL$$

if the receiving space is quite absorbent and if IL and TL are averaged over wide frequency bands (e.g., at least one octave). If insufficient sound-absorbing material is put inside the enclosure, the

**Table 1 Reduction in Noise Reduction Performance of Enclosure as Function of Percentage of Internal Surface Covered with Sound Absorptive Material**

Percent Sound Absorbent (%)	Change in NR (dB)
10	-10
20	-7
30	-5
50	-3
70	-1.5



**Figure 3** Machine enclosure placed in a reverberant environment.

sound pressure level will continue to increase inside the enclosure because of multiple reflections, and the enclosure effectiveness will be reduced. From energy considerations it is obvious that if there is no sound absorption inside ( $\bar{\alpha} = 0$ ), the enclosure will be ineffective, and its insertion loss will be zero.

An estimate of the insertion loss for the general case  $0 < \bar{\alpha} < 1$  can be obtained by assuming that the sound field inside the enclosure is diffuse and reverberant and that the interior surface of the enclosure is lined with absorbing material of surface-averaged absorption coefficient  $\bar{\alpha}$ . Let us assume that (1) the average absorption coefficient in the room containing the noise source is not greater than 0.3, (2) the noise source does not provide direct mechanical excitation to the enclosure walls, and (3) the noise source volume is less than about 0.3 to 0.4 of the enclosure volume, then we may show that the insertion loss of a loose-fitting enclosure made to contain a noise source situated in a reverberant space is<sup>5</sup>

$$IL = L_{p1} - L_{p2} = TL + 10 \log \frac{A_e}{S_e} \quad (9)$$

where  $L_{p1}$  is the reverberant level in the room containing the noise source (with no enclosure),  $L_{p2}$  is the reverberant level at the same location (with the enclosure),  $A_e$  is the absorption area inside the enclosure  $S_i \bar{\alpha}_i$ , and  $\bar{\alpha}_i$  is the surface average absorption coefficient of this material. If the surface area of the enclosure  $S_e = S_i$ , the area of the interior absorbing material, then Eq. (9) simplifies to

$$IL = TL + 10 \log \bar{\alpha}_i \quad (10)$$

We see that normally the insertion loss of an enclosure containing a noise source is less than the TL. If  $\bar{\alpha}_i$ , the average absorption coefficient of the internal absorbing material approaches 1, the IL approaches TL (as expected), although when  $\bar{\alpha}$  approaches 0, then this theory fails.

**Example 2** Consider that the sound pressure level  $L_{p1}$  in a reverberant woodworking shop caused by a wood-planing machine in the 1600-Hz one-third-octave band in 90 dB. Then what values of TL and  $\bar{\alpha}$  should be chosen to guarantee that the reverberant level will be less than 60 dB? Assuming that  $S_i = S_e$ , then if TL is chosen to be 40 dB and  $\bar{\alpha} = 0.1$ ,  $IL = 40 + 10 \log 0.1 = 40 - 10 = 30$  dB and  $L_{p2} = 60$  dB. Now, if  $\bar{\alpha}$  is increased to 0.2, then  $IL = 40 + 10 \log 0.2 = 40 - 7 = 33$  dB and  $L_{p2} = 57$  dB, thus meeting the requirement. As in Example 1, we can observe that since TL varies with frequency  $f$  [see Eq. (11)], this calculation should be repeated at each frequency of interest. At low frequencies, since large values of TL and  $\bar{\alpha}$  are difficult to achieve, it may not be easy to obtain large values of IL.

Thus the TL can be used as an approximate guide to the IL of a sealed enclosure only when allowance is made for the sound absorption inside the enclosure. The transmission loss of an enclosure is usually mostly governed by the mass/unit area  $\rho_s$  of the

enclosure walls (except in the coincidence-frequency region). The reason for this is that when the stiffness and damping of the enclosure walls are unimportant, the response is dominated by inertia of the walls  $\rho_s(2\pi f)$  where  $f$  is the frequency in hertz.

The transmission loss of an enclosure wall for sound arriving from all angles is approximately

$$TL = 20 \log(\rho_s f) - C \quad (11)$$

where  $\rho_s$  is the surface density (mass/unit area) of the enclosure walls and  $C = 47$  if the units of  $\rho_s$  are kg/m<sup>2</sup> and  $C = 34$  if the units are lb/ft<sup>2</sup>. Equation (11) is known as the *field-incidence mass law*. The transmission loss of a wall [given by Eq. (11)] theoretically increases by 6 dB for each doubling of frequency or for each doubling of the mass/unit area of the wall.

Where the enclosure surface is made of several different materials (e.g., concrete or metal walls and glass), then the average transmission loss  $TL_{ave}$  of the composite wall is given by

$$TL_{ave} = 10 \log \frac{1}{\bar{\tau}} \quad (12)$$

where the average transmission coefficient  $\bar{\tau}$  is

$$\bar{\tau} = \frac{S_1 \tau_1 + S_2 \tau_2 + \cdots + S_n \tau_n}{S_1 + S_2 + \cdots + S_n}, \quad (13)$$

where  $\tau_i$  is the transmission coefficient of the  $i$ th wall element and  $S_i$  is the surface area of the  $i$ th wall element (m<sup>2</sup>).

## 5. OTHER MODELS FOR ENCLOSURES

In general, it is difficult to predict the insertion loss of an enclosure with a high degree of accuracy. This is because both the sound field inside and outside the enclosure cannot always be modeled using simple approaches. The models discussed so far are valid for large enclosures where resonances do not arise. However, in the design of enclosures at least two types of enclosure resonances have to be taken into account: (1) structural resonances in the panels that make up the enclosure and (2) standing-wave resonances in the air gap between the machine and the enclosure. At each of these resonance frequencies the insertion loss due to the enclosure is significantly reduced and in some instances can become negative, meaning that the machine with the enclosure may radiate more noise than without the enclosure. Therefore, the enclosure should be designed so that the resonance frequencies of its constituent panels are not in the frequency range where high insertion loss is required.

If the sound source being enclosed radiates predominantly low-frequency noise, then the enclosure panels should have high resonance natural frequencies, that is, the enclosure should be stiff and not massive. These requirements are very different from those needed for good performance of a single-leaf partition at frequencies below the critical frequency. To achieve a high

insertion loss in the stiffness controlled region, benefit can be gained by employing small panel areas, large panel aspect ratios, clamped edge conditions, and materials having a high bending stiffness.<sup>6</sup>

On the other hand, a high-frequency sound source requires the use of an enclosure with panels having low natural frequencies, implying the need for a massive enclosure. Additionally, the panels of the enclosure should be well damped. This would increase IL, in particular for frequencies near and above the critical frequency and at the first panel resonance.

In addition, mechanical connections between the sound source and the walls of the enclosure, air gap leaks, structure-borne sound due to flanking transmission, vibrations, and the individual radiation efficiency of the walls of the enclosure will reduce the IL in different frequency ranges.

For a sealed enclosure without mechanical connections between the source and the enclosure walls, the problem can be divided in three frequency ranges: (1) the low-frequency range, where the insertion loss is frequency independent and corresponds to frequencies below air gap or panel resonances, (2) the intermediate-frequency range, where the insertion loss is controlled by panel and/or air gap resonances that do not overlap so that statistical methods are not applicable, and (3) the high-frequency range, where high modal densities exist, consequently, statistical energy methods can be used for modeling. The insertion loss in the intermediate frequency region fluctuates widely with frequency and position and thus is very difficult to analyze by theoretical methods.<sup>2,7</sup>

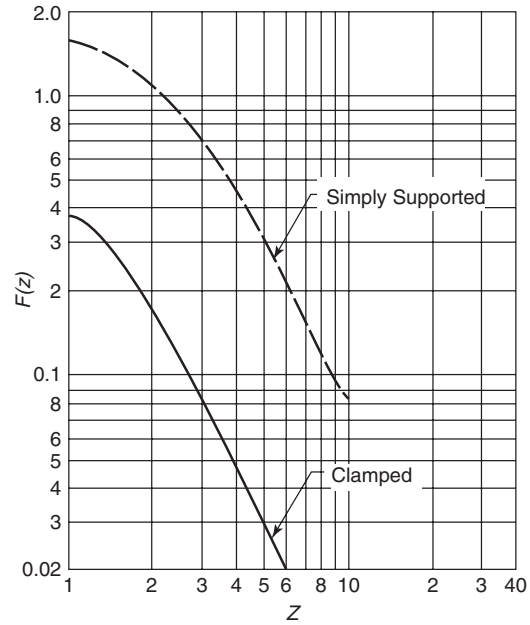
For a sealed, unlined, small rectangular acoustical enclosure, made of  $n$  separate, homogeneous, and isotropic panels, and where the sound field inside can be assumed as diffuse and reverberant, the insertion loss at very low frequencies is controlled by the volume compliance of the enclosure walls. Then the low-frequency insertion loss can be estimated by<sup>2,8</sup>

$$IL = 20 \log \left[ 1 + \frac{VEh^3}{12 \times 10^{-3}(1 - \nu^2)\rho c^2} \times \sum_{i=1}^6 \frac{1}{S_i^3 F(z_i)} \right] \quad (14)$$

where  $V$  is the internal enclosure volume,  $E$  is the Young's modulus of the wall panels,  $h$  is the thickness of the wall panels,  $\nu$  is the Poisson's ratio of the wall panels,  $S_i$  is the surface area of the  $i$ th wall panel,  $z_i$  is the aspect ratio (longest/smallest edge dimension) of the  $i$ th wall panel, and  $F(z)$  is a function given by Lyon and plotted in Fig. 4, for both clamped and simply-supported edges.<sup>8</sup> Equation (14) is valid for frequencies below the first mechanical resonance of the enclosure wall panels.

If the enclosure is a cube made of clamped panels of edge length  $a$ , Eq. (14) simplifies to

$$IL = 20 \log \left[ 1 + 41 \left( \frac{h}{a} \right)^3 \frac{E}{\rho c^2} \right] \quad (15)$$



**Figure 4** Panel volume compliance function  $F(z)$  plotted vs. the aspect ratio  $z$  for clamped and simply supported edges.<sup>8</sup> (Reproduced with permission of American Institute of Physics.)

For a large, lined, unsealed, machine-mounted acoustical enclosure, made of  $N$  separate, homogeneous, and isotropic panels, and where the sound field inside can be assumed as diffuse and reverberant, the insertion loss at high frequencies can be calculated using a statistical energy analysis model presented by Ver.<sup>2,9</sup> The insertion loss can be written as (adapting the notation of reference<sup>10</sup>)

$$IL = 10 \log \frac{\sum_{i=1}^7 S_{ai}}{S_{a2} + S_{a7} + S_{a8} + \frac{W_{SB}}{W_0} \sum_{i=1}^7 S_{ai}} \quad (16)$$

where  $W_0$  is the sound power radiated by the unenclosed machine and the other terms in Eq. (16) are defined in Table 2.

In the equations in Table 2,  $S_w$  is the total interior wall surface area,  $\alpha_w$  is the average energy absorption coefficient of the walls,  $S_{wi}$  is the surface area of the  $i$ th wall,  $TL_{wi}$  is the sound transmission loss of the  $i$ th wall,  $S_i \alpha_i$  is the total absorption area in the interior of the enclosure in excess of the wall absorption (i.e., the machine body itself),  $S_{sk}$  is the face area of the  $k$ th silencer opening (assumed completely absorbent),  $m$  is the attenuation constant for air absorption,  $V$  is the volume of the free interior space,  $S_{Gj}$  is the area of the  $j$ th leak or opening,  $TL_{Gj}$  is the sound transmission loss of the  $j$ th leak or opening,  $\Delta L_k$  is the sound

**Table 2** Definition of Terms Used in Eq. (16)

Physical Meaning	Term	Equation <sup>a</sup>
Power dissipation by the wall absorption	$S_{\alpha 1}$	$S_w \alpha_w$
Power loss due to sound radiation of walls	$S_{\alpha 2}$	$\sum_i S_{wi} 10^{-TL_{wi}/10}$
Power dissipation in walls through damping	$S_{\alpha 3}$	$S_w D$
Power dissipation by sound-absorbing surfaces in addition to the walls	$S_{\alpha 4}$	$S_j \alpha_j$
Sound power loss due to silencers	$S_{\alpha 5}$	$\sum_k S_{sk}$
Sound absorption in air	$S_{\alpha 6}$	$mV$
Sound transmission to the exterior through gaps and openings	$S_{\alpha 7}$	$\sum_j S_{Gj} 10^{-TL_{Gj}/10}$
Sound power transmitted through silencers	$S_{\alpha 8}$	$\sum_k S_{sk} 10^{-\Delta L_k}$
Sound power transmitted through structure-borne paths	$W_{SB}$	$\sum_{i=1}^n F_i^2 \left( \frac{\rho}{\rho_s^2 c} + \frac{\rho c \sigma}{2.3 \rho_s^2 c_L h \omega \eta} \right)$
Force transmitted by the $i$ th attachment point	$F_i$	$\frac{u_i}{ 1/2.3 \rho_s^2 c_L h + j\omega/s }$

<sup>a</sup>Definition of each term in the equations is given in the text.

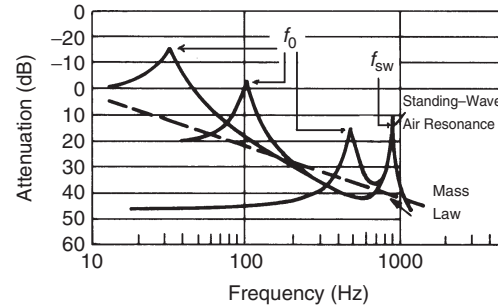
attenuation through the  $k$ th silencer opening,  $\rho$  is the air density,  $\rho_s$  is the wall panel surface density,  $c$  is the speed of sound,  $\sigma$  is the radiation efficiency,  $c_L$  is the speed of longitudinal waves in the wall panel material,  $h$  is the wall panel thickness,  $\omega = 2\pi f$ ,  $\eta$  is the loss factor of the wall panel,  $u_i$  is the vibration velocity of the machine at the  $i$ th attachment point,  $n$  is the total number of point attachments between the machine and the enclosure wall,  $j = \sqrt{-1}$ ,  $s$  is the dynamic stiffness of the resilient mount connecting the wall to the machine ( $s = \infty$  for rigid point connections), and  $D$  is a dimensionless term given by

$$D = \left( \frac{4\pi\sqrt{12}\rho c^3\sigma}{c_L h \rho_s \omega^2} \right) \left( \frac{\rho_s \omega \eta}{\rho_s \omega \eta + 2\rho c \sigma} \right) \quad (17)$$

From an examination of Eq. (16) it can be observed that for a properly designed enclosure the sound energy flows through gaps, openings, air intakes, and exhaust silencers, and structure-borne paths must be controlled so that their contributions to the sound radiation are small compared with the sound radiation from the walls. If these sound energy paths are fully controlled, then the sound energy dissipation is achieved by the total absorption area inside the enclosure  $A_e = S_w \alpha_w + S_j \alpha_j$ . Then if  $TL_{wi} = TL$  and  $S_w = S_e$ , Eq. (16) simplifies to Eq. (9).

## 6 CLOSE-FITTING ENCLOSURES

If the noise source occupies no more than about one-third of the volume of a sealed enclosure, then the theory described by Eqs. (16) and (17) can be used. However, in many cases when machines are enclosed it is necessary to locate the enclosure walls close to the machine surfaces, so that the resulting air gap is small. Such enclosures are termed close-fitting enclosures. In such cases the sound field inside the enclosure is neither reverberant nor diffuse, and the theory discussed at the beginning of this chapter can be used to calculate a first approximation of the insertion loss of an enclosure.

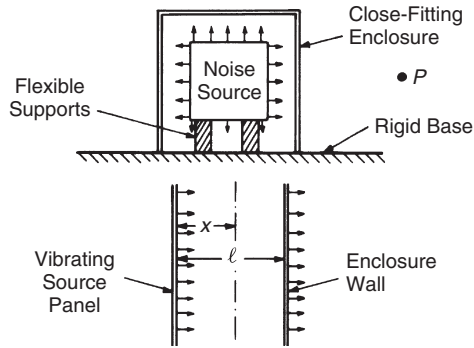


**Figure 5** Close-fitting enclosure attenuation in sound pressure level for different values of panel stiffness. The resonance frequency  $f_0$  is increased by increasing stiffness.

There are several effects that occur with close-fitting enclosures. First, if the noise source has a low internal impedance, then in principle the close-fitting enclosure can “load” the source so that it produces less sound power. However, in most machinery noise problems, the internal impedance of the source is high enough to make this effect negligible. Second, and more importantly, reductions in the IL occur at certain frequencies (when the enclosure becomes “transparent”). These frequencies  $f_0$  and  $f_{sw}$  are shown in Fig. 5. When an enclosure is close fitting, then to a first approximation the sound waves approach the enclosure walls at normal incidence instead of random incidence. When the air gap is small, then a resonant condition at frequency  $f_0$  occurs where the enclosure wall mass is opposed by the wall and air gap stiffness. This resonance frequency can be increased by increasing the stiffness, as seen in Fig. 5. In addition, standing-wave resonances can occur in the air gap at frequencies  $f_{sw}$ . These resonances can be suppressed by the placement of sound-absorbing material in the air gap.<sup>11,12</sup>

Jackson has produced simple theoretical models for close-fitting enclosures that assume a uniform air





**Figure 6** Simplified one-dimensional model for a close-fitting enclosure.

gap.<sup>11,12</sup> He modeled the source enclosure problem in terms of two parallel infinite panels separated by an air gap, as shown in Fig. 6. One panel is assumed to be vibrating and to be the noise source, and the second panel is assumed to be an enclosure panel. Then, the enclosure performance is specified in terms of the relative vibration levels of the two panels. Later, Junger considered both the source panel and enclosure panel to be of finite area.<sup>13</sup> He assumed that the source panel vibrates as a uniform piston and the enclosure panel vibrates as a simply supported plate excited by a uniform sound pressure field. Comparisons of the Jackson, Junger, and Ver models have been presented by Tweed and Tree.<sup>14</sup>

Fahy has presented details of an enclosure prediction model based upon a one-dimensional model similar to that of Jackson.<sup>15</sup> It is assumed that the enclosure panel is a uniform, nonflexible partition of mass per unit area  $\rho_s$ , and it is mounted upon viscously damped, elastic suspensions, having stiffness and damping coefficients

per unit area  $s$  and  $r$ , respectively. The insertion loss of the enclosure in this one-dimensional case is

$$IL = 10 \log \left\{ \left[ \cos k\ell - \frac{(\omega\rho_s - s/\omega) \sin k\ell}{\rho c} \right]^2 + \sin^2 k\ell \left( 1 + \frac{r}{\rho c} \right)^2 \right\} \quad (18)$$

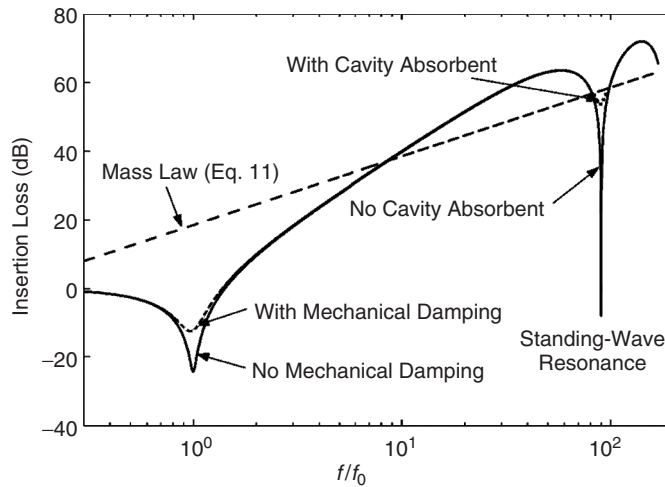
where  $k = \omega/c$  is the wavenumber, and  $\ell$  is the separation distance between the source and enclosure panel.

From an examination of Eq. (18) it is clear that the insertion loss will be zero at frequencies when the cavity width  $\ell$  is equal to an integer number of half-wavelengths and the panel enclosure velocity equals the source surface velocity. The insertion loss will also have a minimum value at the frequency  $\omega_0$ <sup>15</sup>

$$\omega_0^2 \approx \frac{\rho c^2}{\rho_s \ell} + \frac{s}{\rho_s} \quad (19)$$

where  $\omega_0 = 2\pi f_0$ . Figure 7 shows a generalized theoretical insertion loss performance of a close-fitting enclosure, according to Eq. (18).

Other theoretical models to predict the acoustical performance of close-fitting enclosures have been reported in the literature.<sup>16,17</sup> However, in practice, the real source panel exhibits forced vibrations in a number of modes and the air gap varies with real enclosures, and these simple theoretical models and some later ones can only be used to give some guidance of the insertion loss to be expected in practice. Finite element and boundary element approaches can be used to make insertion loss predictions for close-fitting enclosures with complicated geometries and for the intermediate frequency region.<sup>18</sup>



**Figure 7** Theoretical close-fitting enclosure insertion loss performance.

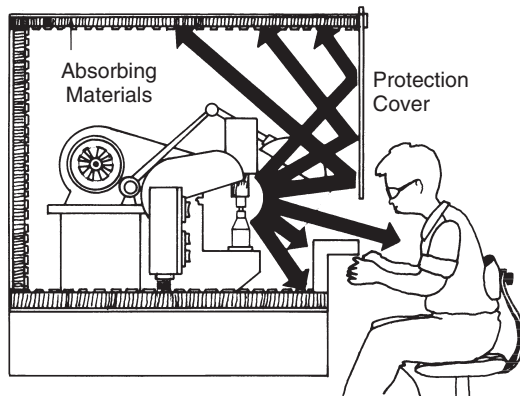


Figure 8 Partial enclosure.

## 7 PARTIAL ENCLOSURES

When easy and continuous access to parts of a machine is necessary or the working process of the machinery or the safety or maintenance requirements do not allow a full enclosure, a partial enclosure is usually used to reduce the radiated noise.<sup>19</sup> Figure 8 shows an example of a partial enclosure used in machinery noise control. The noise reduction produced by a partial enclosure will depend upon the particular geometry. Most of the time, the available attenuation will be limited by diffractive scattering and mechanical connections between the partial enclosure and the vibrating machine. It is recommended that partial enclosures be fully lined with sound absorption material. As a general rule, the enclosure walls of a partial enclosure should have a transmission loss of at least 20 dB. The maximum sound power reduction that can be achieved for such an enclosure is about 10 dB. However, in some cases, the noise levels radiated may be reduced more. Table 3 shows the effectiveness of partial enclosures, where the values are based on the assumption that the noise source radiates uniformly in all directions and that the partial enclosure that surrounds the source is fully lined with sound-absorptive material.<sup>20</sup>

## 8 PRACTICAL DETAILS

Most equations presented in this chapter will give good estimates for the actual performance of an enclosure. However, some guidelines should be followed in practice to avoid degradation of the effectiveness of

an enclosure. In addition, when designing an enclosure, care should be taken so that production costs and time, operational cost-effectiveness, and the efficiency of operation of the machine or equipment being enclosed are not adversely affected.

Most enclosures will require some form of ventilation through openings. Such necessary permanent openings must be treated with some form of silencing to avoid substantially degrading the performance of the enclosure. For a good design, it is required that the acoustical performance of access silencing will match the performance of the enclosure walls. The usual techniques employed to control the sound propagation in ducts can be used for the design of silencers (see Chapter 112).

When ventilation for heat removal is required but the heat load is not large, then natural ventilation with silenced air inlets low down close to the floor and silenced outlets at a greater height, well above the floor, will be adequate. If forced ventilation is needed to avoid excessive heat build up in the enclosure, then the approximate amount of airflow needed can be determined by<sup>4</sup>

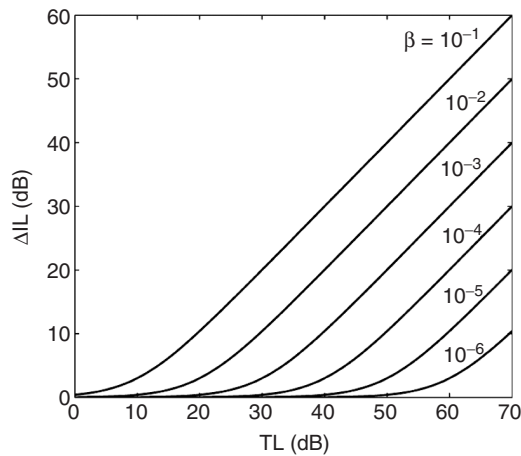
$$\rho C_p V = \frac{H}{\Delta T} \quad (20)$$

where  $V$  is the volume flow rate of the cooling air required ( $\text{m}^3/\text{s}$ ),  $H$  is the heat input to the enclosure (W),  $\Delta T$  is the temperature differential between the external ambient and the maximum permissible internal temperature of the enclosure ( $^{\circ}\text{C}$ ),  $\rho$  is the air density ( $\text{kg}/\text{m}^3$ ), and  $C_p$  is the specific heat of the air ( $\text{m}^2\text{C}^{-1}/\text{s}^2$ ). When high-volume flow rates of air are required, the noise output of the fan that provides the forced ventilation should be considered very carefully, since this noise source can degrade the performance of the enclosure. In general, large slowly rotating fans are always preferred to small high-speed fans since fan noise increases with the fifth power of the blade tip speed.

The effectiveness of an enclosure can be very much reduced by the presence of leaks (air gaps). These usually occur around removable panels or where ducts or pipes enter an enclosure to provide electrical and cooling air services and the like. If holes or leaks occur in the enclosure walls (e.g., cracks around doors or around the base of a cover) and if the TL of the holes is assumed to be 0 dB (as is customary), then the reduction in insertion loss as a function of the TL of the enclosure walls, with the leak ratio factor  $\beta$  as the parameter is given by Fig. 9.<sup>2</sup> The leak ratio factor  $\beta$  is defined as the ratio of the total face area of the leaks and gaps to the surface area (one side) of the enclosure walls. If the penetrations in the enclosure walls are lined with absorbing materials as shown in Fig. 10, then the degradation in the enclosure IL is much less significant. Results from both a statistical energy model and experimental work for a steel box, representing a cabin enclosure, are presented in Figs. 11 and 12.<sup>7</sup> Here the attenuation is defined as the difference in space-averaged sound pressure levels

Table 3 Effectiveness of a Partial Enclosure

Sound Energy Enclosed and Absorbed (%)	Maximum Achievable Noise Reduction (dB)
50	3
75	6
90	10
95	13
98	17
99	20



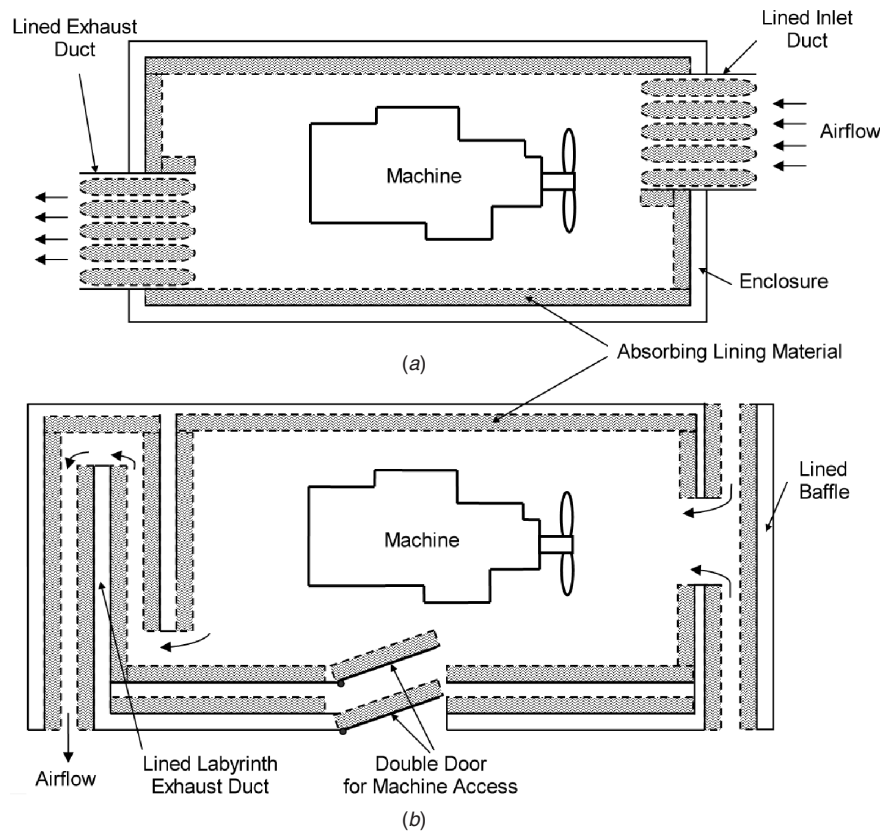
**Figure 9** Decrease of enclosure insertion loss,  $\Delta IL$ , as a function of the wall sound transmission loss  $TL$  with the leak ratio factor  $\beta$  as parameter.

outside and inside the enclosure. It can be observed how a circular aperture in one panel affects the

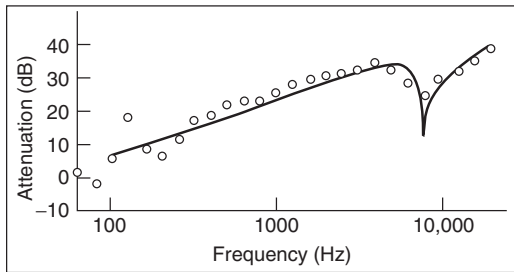
attenuation in the middle- and high-frequency range. Some studies indicate that leaks not only degrade the noise reduction but also can introduce resonances when the leak ratio factor is not very large.<sup>21</sup>

It is necessary to provide sufficient vibration isolation to reduce the radiation of noise from the surface on which the machinery is mounted, particularly if low-frequency noise is the main problem. Therefore, it is advisable to mount the machine and/or the enclosure itself on vibration isolators that reduce the transmission of energy to the floor slab. In doing so, control of both the airborne and the structure-borne sound transmission paths between the source and receiver will be provided. Great care is necessary to ensure that the machine will be stable and its operation will not be affected adversely. Insertion of flexible (resilient) connectors between the machine and conduit, cables, piping, or ductwork connected to it must be provided to act as vibration breaks.

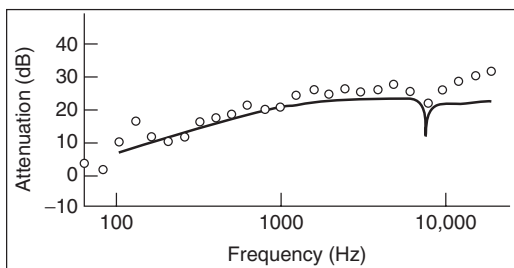
In addition, proper breaking of any paths that permit noise to "leak" through openings in the enclosure must be provided. Then all joints, seams, and penetrations of enclosures should be sealed using a procedure such as packing the leaks with mineral wool, which are



**Figure 10** Enclosures with penetrations (for cooling) lined with absorbing materials: (a) lined ducts and (b) lined baffles with double-door access provided to interior of machine.



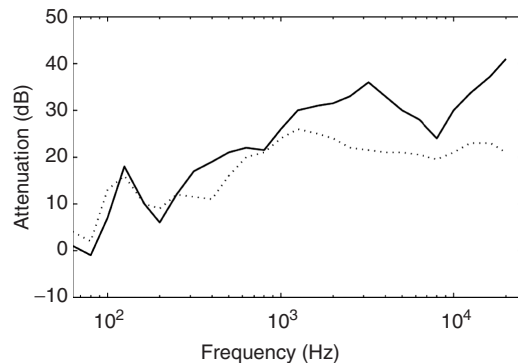
**Figure 11** Attenuation of a sealed box containing  $1.2 \text{ m}^2$  of absorbing material: —, predicted and  $\circ$ , measured.



**Figure 12** Attenuation of a box with a circular aperture (diameter of 0.035 m) in one panel. Box contains  $1.2 \text{ m}^2$  of absorbing material: —, predicted and  $\circ$ , measured.

closed by cover plates and mastic sealant.<sup>4</sup> Figure 13 shows the difference in experimental results between the attenuation of an idealized cab enclosure with the leaks between panels unsealed and sealed with clay.<sup>22</sup>

Any access doors to the enclosure must be fitted tightly and gasketed. Locking handles should be

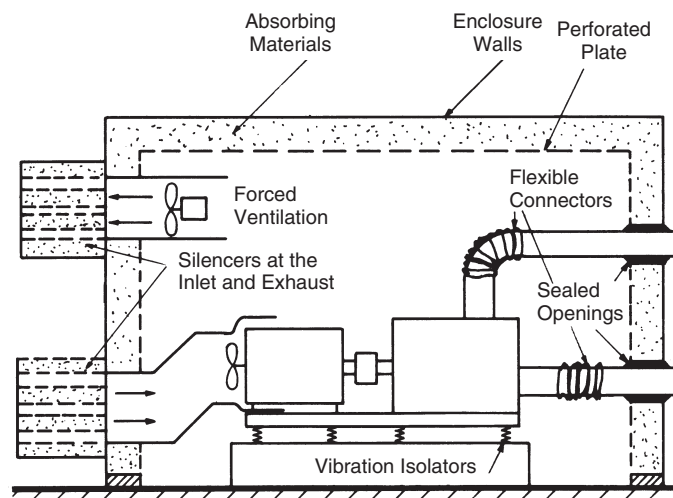


**Figure 13** Experimentally measured attenuation of a cabin model enclosure: —, joints sealed and - - - -, joints unsealed.

provided that draw all such doors tightly to the gasketed surfaces so as to provide airtight seals. Inspection windows should be double glazed and the glass thicknesses and pane separations should be chosen carefully to avoid degradation by structural/air gap resonances. Placing porous absorbing material in the reveals between the two frames supporting the glass panes can improve the transmission loss of a double-glazed inspection window. Figure 14 shows an enclosure in which some basic noise control techniques have been applied. Information about cost, construction details, and performance of several enclosures can be found in the manufacturers' literature and in some books.<sup>23</sup>

## REFERENCES

1. M. J. Crocker and F. M. Kessler, *Noise and Noise Control*, Vol. II, CRC Press, Boca Raton, FL, 1982.



**Figure 14** Basic elements of an acoustical enclosure used for machinery noise control.

2. I. L. Ver, Enclosures and Wrappings, in *Noise and Vibration Control Engineering: Principles and Applications*, (L. L. Beranek and I. L. Ver, Eds.), Wiley, New York, 1992.
3. T. J. Schultz, Wrapping, Enclosures, and Duct Linings, in *Noise and Vibration Control*, (L. L. Beranek Ed.), McGraw-Hill, New York, 1971.
4. D. A. Bies and C. H. Hansen, *Engineering Noise Control*, Unwin Hyman, London, 1988.
5. I. Sharland, *Woods Practical Guide to Noise Control*, Woods of Colchester Limited, Waterlow and Sons, London, 1972.
6. S. N. Hillarby and D. J. Oldham, The Use of Small Enclosures to Combat Low Frequency Noise Sources, *Acoust. Lett.* Vol. 6, No. 9, 1983, pp. 124–127.
7. V. Cole, M. J. Crocker, and P. K. Raju, Theoretical and Experimental Studies of the Noise Reduction of an Idealized Cabin Enclosure, *Noise Control Eng. J.*, Vol. 20, No. 3, 1983, pp. 122–133.
8. R. H. Lyon, Noise Reduction of Rectangular Enclosures with One Flexible Wall, *J. Acoust. Soc. Am.*, Vol. 35, No. 11, 1963, pp. 1791–1797.
9. I. L. Ver, Reduction of Noise by Acoustic Enclosures, Proc. of the ASME Design Engineering Technical Conference, Vol. 1, Cincinnati, OH, 1973, pp. 192–219.
10. T. A. Osman, Design Charts for the Selection of Acoustical Enclosures for Diesel Engine Generator Sets, *Proc. Instit. Mech. Eng.*, Series A, Vol. 217, No. 3, 2003, pp. 329–336.
11. R. S. Jackson, The Performance of Acoustic Hoods at Low Frequencies, *Acustica*, Vol. 12, 1962, pp. 139–152.
12. R. S. Jackson, Some Aspects of the Performance of Acoustic Hoods, *J. Sound Vib.*, Vol. 3, No. 1, 1966, pp. 82–94.
13. M. C. Junger, Sound Transmission through an Elastic Enclosure Acoustically Closely Coupled to a Noise Source, ASME Paper No. 70-WA/DE-12, American Society of Mechanical Engineers, New York, 1970.
14. L. W. Tweed and D. R. Tree, Three Methods for Predicting the Insertion Loss of Close Fitting Acoustical Enclosures, *Noise Control Eng.*, Vol. 10, No. 2, 1978, pp. 74–79.
15. F. J. Fahy, *Sound and Structural Vibration*, Academic, London, 1985.
16. K. P. Byrne, H. M. Fischer, and H. V. Fuchs, Sealed, Close-Fitting, Machine-Mounted Acoustic Enclosures with Predictable Performance, *Noise Control Eng. J.*, Vol. 31, No. 1, 1988, pp. 7–15.
17. D. J. Oldham and S. N. Hillarby, The Acoustical Performance of Small Close Fitting Enclosures, Part 1: Theoretical Models and Part 2: Experimental Investigation, *J. Sound Vib.*, Vol. 50, No. 2, 1991, pp. 261–300.
18. P. Agahi, U. P. Singh, and J. O. Hetherington, Numerical Prediction of the Insertion Loss for Small Rectangular Enclosures, *Noise Control Eng. J.*, Vol. 47, No. 6, 1999, pp. 201–208.
19. R. J. Alfredson and B. C. Seow, Performance of Three Sided Enclosures, *Appl. Acous.*, Vol. 9, No. 1, 1976, pp. 45–55.
20. C. G. Gordon and R. S. Jones, Control of Machinery Noise, in *Handbook of Acoustical Measurements and Noise Control*, C. M. Harris, Ed., 3rd ed., Acoustical Society of America, New York, 1998.
21. J. B. Moreland, Low Frequency Noise Reduction of Acoustic Enclosures, *Noise Control Eng. J.*, Vol. 23, No. 3, 1984, pp. 140–149.
22. M. J. Crocker, A. R. Patil, and J. P. Arenas, Theoretical and Experimental Studies on the Acoustical Design of Vehicle Cabs—A Review of Truck Noise Sources and Cab Design Using Statistical Energy Analysis, in *Designing for Quietness*, M. L. Munjal, Ed., Solid Mechanics and Its Applications Book Series, Vol. 102, Kluwer Academic, Dordrecht, 2002, pp. 47–66.
23. R. K. Miller and W. V. Montone, *Handbook of Acoustical Enclosures and Barriers*, Fairmont Press, Atlanta, 1977.

# CHAPTER 57

## USE OF SOUND-ABSORBING MATERIALS

**Malcolm J. Crocker**  
Department of Mechanical Engineering  
Auburn University  
Auburn, Alabama

**Jorge P. Arenas**  
Institute of Acoustics  
Universidad Austral de Chile  
Campus Miraflores  
Valdivia, Chile

### 1 INTRODUCTION

Sound-absorbing materials absorb most of the sound energy striking them and reflect very little. Therefore, sound-absorbing materials have been found to be very useful in the control of noise. They are used in a variety of locations: close to sources of noise (e.g., close to sources in electric motors), in various paths, (e.g., above barriers), and sometimes close to a receiver (e.g., inside earmuffs).

Although all materials do absorb some incident sound, the term *acoustical material* has been primarily applied to those materials that have been produced for the specific purpose of providing high values of sound absorption. The major uses of acoustical materials are almost invariably found to include the reduction of reverberant sound pressure levels and, consequently, the reduction of reverberation time in enclosures (rooms).

Since about 1965, the use and variety of available specialized acoustical materials has greatly increased. This has been due mainly to both increased technology and public awareness and concern about noise in everyday life. In turn, this has led many public bodies and commercial public service operations to realize the benefits of providing good acoustical conditions for their clients. The architect and acoustical engineer now have a wide choice of sound-absorbing materials that not only provide the desired acoustical properties but also offer an extremely wide variety of colors, shapes, sizes, light reflectivities, fire ratings, and methods of attachment. In addition to these qualities, users should consider the costs of purchase, installation, and upkeep.

### 2 SOUND ABSORPTION COEFFICIENT

When sound waves strike a boundary separating two media, some of the incident energy is reflected from the surface and the remaining energy is transmitted into the second medium. Some of this energy is eventually converted by various processes into heat energy and is said to have been absorbed by that medium. The fraction of the incident energy absorbed is termed the absorption coefficient  $\alpha(f)$ , which is a function of

frequency and defined as

$$\alpha(f) = \frac{\text{sound intensity absorbed}}{\text{sound intensity incident}} \quad (1)$$

The absorption coefficient theoretically ranges from zero to unity. In practice, values of  $\alpha > 1.0$  are sometimes measured. This anomaly is due to the measurement procedures adopted to measure large-scale building materials.

One sabin is defined as the sound absorption of one square metre of a perfectly absorbing surface, such as an open window. The sound absorption of a wall or some other surface is the area of the surface, in square metres, multiplied by the absorption coefficient.

### 3 NOISE REDUCTION COEFFICIENT

Another parameter often of interest in assessing the performance of an acoustical absorber is the single number known as the noise reduction coefficient (NRC). The NRC of a sound-absorbing material is given by the average of the measured absorption coefficients for the 250-, 500-, 1,000-, and 2,000-Hz octave bands rounded off to the nearest multiple of 0.05. This NRC value is often useful in the determination of the applicability of a material to a particular situation. However, where low or very high frequencies are involved, it is usually better to consider sound absorption coefficients instead of NRC data (see also Chapter 54).

### 4 ABSORBERS

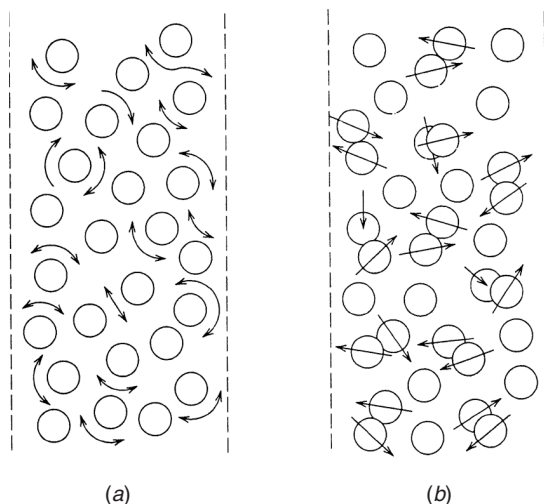
A wide range of sound-absorbing materials exist that provide absorption properties dependent upon frequency, composition, thickness, surface finish, and method of mounting. They can be divided into several major classifications. Materials that have a high value of  $\alpha$  are usually porous and fibrous. Fibrous materials include those made from natural or artificial fibers including glass fibers. Porous materials made from open-celled polyurethane are also widely used.

#### 4.1 Porous Fibrous Sound Absorbers

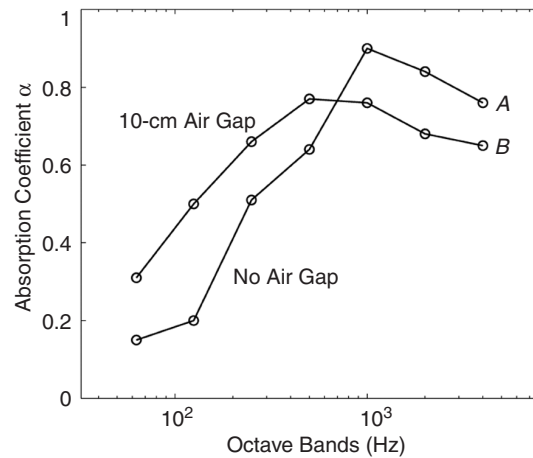
Porous materials are characterized by the fact that the nature of their surfaces is such that sound energy is

able to enter the materials by a multitude of small holes or openings. They consist of a series of tunnel-like pores and openings formed by interstices in material fibers or by foamed products. (Usually, within limitations, the more open and connecting these passages are, the larger the values of the sound-absorbing efficiency of the material.) If, on the other hand, the pores and penetrations are small and not joined together, then the material becomes substantially less efficient as a sound absorber. Included in this broad category of porous absorbers are fibrous blankets, hair felt, wood-wool, acoustical plaster, a variety of spray-on products, and certain types of acoustical tiles.

When a porous material is exposed to incident sound waves, the air molecules at the surface of the material and within the pores of the material are forced to vibrate and in the process lose energy. This is caused by the conversion of sound energy into heat due to thermal and viscous losses of air molecules at the walls of the interior pores and tunnels in the sound-absorbing material. At low frequencies these changes are isothermal, while at high frequencies they are adiabatic. In fibrous materials, much of the energy can also be absorbed by scattering from the fibers and by the vibration caused in the individual fibers. The fibers of the material rub together under the influence of the sound waves and lose energy due to work done by the frictional forces. Figure 1 shows the two main mechanisms by which the sound is absorbed in materials. For this reason high values of absorption coefficient in excess of 0.95 can be observed. Depending upon how  $\alpha$  is determined experimentally, values in excess of unity can also be measured just how this happens will be discussed later. The values of  $\alpha$  observed are usually strongly dependent upon (a) frequency, (b) thickness,



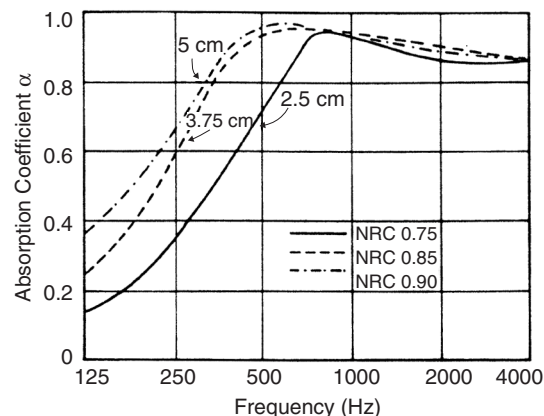
**Figure 1** Two main mechanisms believed to exist in sound-absorbing materials: (a) viscous losses in air channels and (b) mechanical friction caused by fibers rubbing together.



**Figure 2** Typical absorption coefficient vs. octave band frequency characteristics for a 25-mm-thick fibrous absorbing material. Curve A is for the material laid directly on a rigid backing, while curve B shows the effect of introducing a 10-cm air gap.

and (c) method of mounting. These should always be considered in the choice of a particular material.

Figure 2 shows typical sound absorption characteristics for a blanket-type fibrous porous material placed (Fig. 2a) against a hard wall, and (Fig. 2b) with a 10-cm airspace between the material and the wall. In both cases the absorption properties are substantially better at high frequencies than low. When the same material is backed by an airspace, the low-frequency absorption is improved without significantly changing the high-frequency characteristics. Figure 3 shows the effect of increasing the thickness of the material on a solid backing. Again, increased low-frequency absorption is observed for increased thickness.



**Figure 3** Sound absorption coefficient  $\alpha$  and noise reduction coefficient (NRC) for typical fiberglass foamboard.



An additional effect to consider is that of surface treatment since most materials will become discolored or dirty after prolonged exposure for several years and may require cleaning or refinishing. Because the surface pores must be open to incident sound for the porous material to function, it is essential that they should not be blocked with paint or any other surface-coating treatment. The effects of brush painting porous materials are usually more severe than spray painting; however, the usual effect is to lower the absorption coefficient to about 50% of its unpainted value particularly at high frequencies. In addition, the absorption peak is shifted downward in frequency as observed by Price and Mulholland.<sup>1</sup> As more coats of paint are applied, the paint membrane becomes more dense and more pores are sealed, the result of which is to shift the absorption peak even lower in frequency and magnitude.

It is useful now to describe briefly the physical parameters used to account for the sound-absorbing and attenuating properties of porous materials. These include flow resistivity, porosity, volume coefficients of elasticity of both air and the skeleton, structural form factor (tortuosity), and specific acoustic impedance. These will now be described separately.

**4.1.1 Flow Resistivity  $R$**  This accounts for the resistance offered to airflow through the medium. It is defined in the metre-kilogram-second (mks) system as

$$R = \frac{\Delta p}{U} \frac{1}{t} \quad (2)$$

where  $R$  is the flow resistivity (mks rayls/m),  $\Delta p$  is the differential sound pressure created across a sample of thickness  $t$ , measured in the direction of airflow ( $\text{N/m}^2$ ),  $U$  is the mean steady flow velocity (m/s), and  $t$  is the thickness of the porous material sample (m).

Typical values for porous fibrous materials vary from  $4 \times 10^3$  to  $4 \times 10^4$  mks rayls/m for a density range of 16 to 160  $\text{kg/m}^3$ . Generally speaking, if the flow resistivity  $R$  becomes very large, then most of the incident sound falling on the material will be reflected, while if  $R$  is too small, then the material will offer only very slight viscous losses to sound passing through it, and so it will provide only little sound absorption or attenuation. Although the absorption is proportional to thickness, it is generally found that for a given flow resistivity value  $R$ , the optimum thickness of material is approximately given by  $t = 100/\sqrt{R}$ .

**4.1.2 Porosity  $\epsilon$**  The porosity of a porous material is defined as the ratio of the void space within the material to its total displacement volume as

$$\epsilon = \frac{V_a}{V_m} \quad (3)$$

where  $V_a$  is the volume of air in the void space in the sample and  $V_m$  is the total volume of the sample. It has to be noticed that the void space is only that

accessible to sound waves. For a material composed of solid fibers the porosity can be estimated from

$$\epsilon = 1 - \frac{M_s}{V_s \rho_F} \quad (4)$$

where  $M_s$  is the total mass of sample (kg),  $V_s$  is the total volume of sample ( $\text{m}^3$ ), and  $\rho_F$  is the density of fibers ( $\text{kg/m}^3$ ). Typical values of porosity for acceptable acoustical materials are greater than 0.85.

**4.1.3 Volume Coefficient of Elasticity of Air  $K$**  This is the bulk modulus of air defined from

$$\Delta p = -K \frac{\Delta V}{V} \quad (5)$$

where  $\Delta p$  is the change in pressure required to alter the volume  $V$  by an increment  $\Delta V$  ( $\text{N/m}^2$ ),  $\Delta V$  is the incremental change in volume ( $\text{m}^3$ ), and  $K$  is the volume coefficient of elasticity ( $\text{N/m}^2$ ).

**4.1.4 Volume Coefficient of Elasticity of the Skeleton  $Q$**  This is defined in a similar way to the bulk modulus, which is the change in thickness of a sample sandwiched between two plates as the force applied on them is increased, that is,

$$\delta F = -Q \frac{\delta t}{t} S \quad (6)$$

where  $\delta F$  is the incremental force applied to the sample (N),  $\delta t$  is the incremental change in thickness of the sample (m),  $t$  is the original thickness (m),  $Q$  is the volume coefficient of elasticity of the skeleton ( $\text{N/m}^2$ ), and  $S$  is the sample area ( $\text{m}^2$ ).

**4.1.5 Structural Form Factor  $k_s$**  It is found that in addition to the flow resistance, the composition of the inner structure of the pores also affects the acoustical behavior of porous materials. This is because the orientation of the pores relative to the incident sound field has an effect on the sound propagation. This has been dealt with by Zwicker and Kosten<sup>2</sup> and treated as an effective increase in the density of the air in the void space of the material. Beranek<sup>3</sup> reports that flexible blankets have structure factors between 1 and 1.2, while rigid tiles have values between 1 and 3. He also shows that for homogeneous materials made of fibers with interconnecting pores the relationship between the porosity  $\epsilon$  and structure factor  $k_s$  is  $k_s \approx 5.5 - 4.5\epsilon$ . In the technical literature it is possible to find the self-explanatory term *tortuosity* instead of structural form factor. For most fibrous materials the structural form factor is approximately unity.

**4.1.6 Specific Acoustic Impedance  $z_0$**  This is defined as the ratio of the sound pressure  $p$  to particle velocity  $u$  at the surface of the material, for a sample of infinite depth, when plane sound waves strike the



surface at normal incidence. This is a complex quantity and it is defined mathematically as

$$z_0 = \frac{p}{u} = \rho c(r_n + jx_n) \quad (7)$$

where  $r_n$  is the normal specific acoustic resistance,  $x_n$  is the normal specific acoustic reactance,  $\rho c$  is the characteristic impedance of air (415 mks rays), and  $j = \sqrt{-1}$ .

It is useful to look briefly at some of the interesting relationships that exist between the specific impedance and the absorption coefficient under certain circumstances. For example, if a porous material is composed so that  $r_n \gg 1$  and  $r_n \gg x_n$ , the absorption coefficient  $\alpha_\theta$  for a sound wave striking a surface at angle  $\theta$  to the normal is given by

$$\alpha_\theta = \frac{4r_n \cos \theta}{(1 + r_n \cos \theta)^2} \quad (8)$$

Furthermore, for a diffuse sound field, the random incidence absorption coefficient  $\alpha$  is given by<sup>4</sup>

$$\alpha = \frac{8}{r_n} \left[ 1 + \frac{1}{1 + r_n} - \frac{2}{r_n} \ln(1 + r_n) \right] \quad (9)$$

If  $r_n > 100$  (materials with small absorption coefficients), this equation can be substantially simplified to  $\alpha = 8/r_n$ .

The use of the complex acoustic impedance, rather than absorption coefficient, allows a much more rigorous treatment of low-frequency room reverberation time analysis. Although often considerably more complex than the classical theory, this approach does predict more accurate values of reverberation times in rooms containing uneven distribution of absorption material, even if either pair of opposite walls are highly absorbing or if opposite walls are composed of one very soft and one very hard wall.<sup>4</sup>

Beranek shows<sup>3,5</sup> that the specific acoustic impedance of a rigid tile can be written in terms of the previously defined fundamental parameters as

$$z_0 = \left[ \rho \frac{k_s K}{\varepsilon} \left( 1 - j \frac{R}{\rho k_s \omega} \right) \right]^{1/2} \quad (10)$$

where  $\rho$  is the density of air ( $\text{kg/m}^3$ ) and  $\omega$  is the angular frequency (rads/).

It can therefore be seen from Eqs. (7), (9), and (10) that the absorption coefficient is proportional to the porosity and flow resistance of the material (provided  $r_n > 100$  and  $r_n \gg x_n$ ), and is inversely proportional to the density and structure factor. For soft blankets, the expressions for the acoustic impedance become very much more complex and the reader is directed to Refs. 2, 3, and 5 for a much more complete analysis.

The basic theory used to model the sound propagation within porous absorbents assumes that the

absorber frame is rigid and the waves only propagate in the air pores. This is the typical case when the porous absorber is attached to a wall or resting on a floor that constrains the motion of the absorber frame. Neglecting the effect of the structural form factor, it can be shown that plane waves in such a material are only possible if the wavenumber is given by<sup>6</sup>

$$k_p = k \sqrt{1 + j \frac{R\varepsilon}{\omega\rho}} \quad (11)$$

where  $k$  is the free-field wavenumber in air ( $\text{m}^{-1}$ ) and  $\rho$  is the density of air ( $\text{kg/m}^3$ ). In addition, the wave impedance of plane waves is

$$z_0 = \frac{\rho c k_p}{\varepsilon k} \quad (12)$$

In another method of analysis a fibrous medium is considered to be composed of an array of parallel elastic fibers in which a scattering of incident sound waves takes place resulting in conversion to viscous and thermal waves by scattering at the boundaries. This approach was first used by Rayleigh<sup>7</sup> and has since been refined by several researchers. Attenborough and Walker included effects of multiple scattering in the theory<sup>8</sup> that is able to give good predictions of the impedance of porous fibrous materials. However, even more refined phenomenological models have been presented in recent years.<sup>9</sup>

On the other hand, very useful empirical expressions to predict both the propagation wavenumber and characteristic impedance of a porous absorbent have been developed by Delany and Bazley.<sup>10</sup> The expressions as functions of frequency  $f$  and flow resistivity  $R$  are

$$k_p = k(1 + 0.0978X^{-0.7} - j0.189X^{-0.595}) \quad (13)$$

and

$$z_0 = \rho c(1 + 0.0571X^{-0.754} - j0.087X^{-0.732}) \quad (14)$$

where  $X = \rho f/R$ . Equations (13) and (14) are valid for  $0.01 < X < 1.0$ ,  $10^3 \leq R \leq 5 \times 10^4$ , and  $\varepsilon \approx 1$ .

Additional improvements to the Delany and Bazley empirical model have been presented by other authors.<sup>11,12</sup> If the frame of the sound absorber is not constrained (elastic-framed material), a more complete "poroelastic" model of sound propagation can be developed using the Biot theory.<sup>13</sup> In addition, both guidelines and charts for designing absorptive devices using several layers of absorbing materials have been presented.<sup>14,15</sup>

## 4.2. Panel or Membrane Absorbers

When a sound source is turned on in a room, a complex pattern of room modes is set up, each having its own

characteristic frequency. These room modes are able, in turn, to couple acoustically with structures in the room, or even the boundaries of the room, in such a way that acoustic power can be fed from the room modes to other structural modes in, for example, a panel hung in the room.

A simply supported plate or panel can only vibrate at certain allowed natural frequencies  $f_{m,n}$  and these are given by

$$f_{m,n} = 0.453c_L h \left[ \left( \frac{m}{l_x} \right)^2 + \left( \frac{n}{l_y} \right)^2 \right] \quad (15)$$

where  $f_{m,n}$  is the characteristic modal frequency,  $m$  and  $n$  are integers (1, 2, 3, ...),  $c_L$  is the longitudinal wave speed in the plate material (m/s),  $h$  is the thickness of the plate (m), and  $l_x$  and  $l_y$  are the dimensions of the plate (m).

If  $m = n = 1$ , then this gives the first allowable mode of vibration along with its fundamental natural frequency  $f_{1,1}$ . The above equation is valid only for plates with simply supported edges. For a plate with clamped edges the fundamental mode occurs at approximately twice the frequency calculated from Eq. (15). Thus a room mode, at or close to the fundamental frequency of a plate hung in the room, will excite the plate fundamental mode. In this way the plate will be in a resonant condition and therefore have a relatively large vibration amplitude. In turn, this will cause the plate to dissipate some of its energy through damping and radiation. Therefore, the plate can act as an absorber having maximum absorption characteristics at its fundamental frequency (and higher order modes), which will depend upon the geometry of the plate and its damping characteristics. In all practical cases this effect takes place at low frequencies, usually in the range 40 to 300 Hz. Particular care has to be taken, therefore, that any panels that may be hung in a room to improve reflection or diffusion are not designed in such a manner that they act as good low-frequency absorbers and have a detrimental effect on the acoustics of the space.

If a panel is hung in front of a hard wall at a small distance from it, then the airspace acts as a compliant element (spring) giving rise to a resonant system comprised of the panel's lumped mass and the air compliance. The resonance frequency  $f_r$  (Hz) of the system is

$$f_r \approx \frac{59.5}{\sqrt{Md}} \quad (16)$$

where  $M$  is the mass surface density ( $\text{kg/m}^2$ ), and  $d$  is the airspace depth (m).

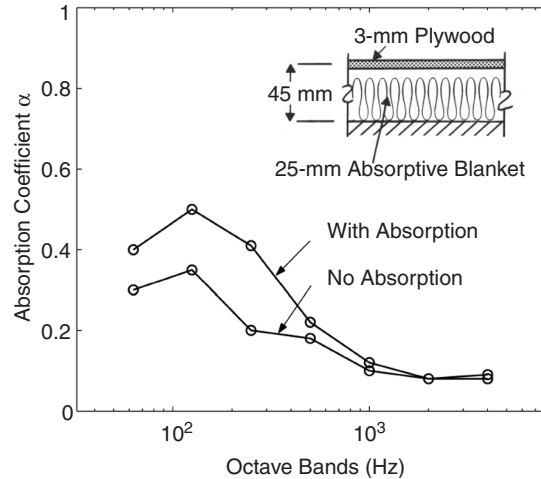
Hence, a thin panel of  $4 \text{ kg/m}^2$  weight placed a distance of 25 mm from a rigid wall will have a resonance frequency of 188 Hz. As in the case of a simply supported panel, a spaced panel absorbs energy through its internal viscous damping.<sup>16,17</sup> Since its vibration amplitude is largest at resonance, its sound-absorption is maximum at this frequency. Usually this

absorption can be both further increased in magnitude and extended in its effective frequency range (i.e., giving a broader resonance peak) by including a porous sound-absorbing material, such as a fiberglass blanket, in the airspace contained by the panel. This effectively introduces damping into the resonant system.

Figure 4 shows the effect of introducing a 25-mm-thick fibrous blanket into the 45-mm airspace contained by a 3-mm plywood sheet. The change is quite significant at low frequencies in the region of the resonance peak where both the magnitude and width of the peak are increased. On the other hand, there is little effect at high frequencies.

Membrane absorbers are one of the most common bass absorbers used in small rooms. In addition, their nonperforated surfaces are durable and can be painted with no effect on their acoustical properties. It is important that this type of sound absorber be recognized as such in the design of an auditorium. Failure to do so, or to underestimate its effect, will lead to excessive low-frequency absorption, and the room will have a relatively short reverberation time. The room will then be considered to be acoustically unbalanced and will lack warmth. Typical panel absorbers found in auditoriums include gypsum board partitions, wood paneling, windows, wood floors, suspended ceilings, ceiling reflectors, and wood platforms.

Porous materials also possess better low-frequency absorption properties when spaced away from their solid backing (see Fig. 2) and behave in a manner similar to the above solid panel absorbers. When the airspace equals one-quarter wavelength, maximum absorption will occur, while when this distance is a one-half wavelength, minimum absorption will be realized. This is due to the fact that maximum air particle velocity occurs at one-quarter wavelength from



**Figure 4** Effect on the sound absorption coefficient  $\alpha$  of placing a 25-mm-thick sound-absorptive blanket in the airspace (45-mm deep) behind a flexible 3-mm plywood panel.

the wall and hence provides the maximum airflow through the porous material. This, in turn, provides increased absorption at that frequency. Such an effect can be useful in considering the performance of curtains or drapes hanging in an auditorium. A similar effect is observed for hanging or suspended acoustical ceilings.<sup>18</sup>

To achieve well-balanced low-frequency absorption, a selection of different size and thickness spaced panels can be used and indeed have been used successfully in many auditoriums. Combinations of resonant panels have also been suggested.<sup>19</sup>

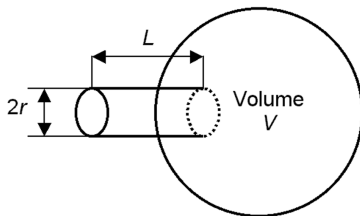
### 4.3 Helmholtz Resonator Absorbers

A Helmholtz resonator, in its simplest form, consists of an acoustical cavity contained by rigid walls and connected to the exterior by a small opening called the neck, as shown in Fig. 5. Incident sound causes air molecules to vibrate back and forth in the neck section of the resonator like a vibrating mass while the air in the cavity behaves like a spring. As shown in the previous section, such an acoustical mass-spring system has a particular frequency at which it becomes resonant. At this frequency, energy losses in the system due to frictional and viscous forces acting on the air molecules in and close to the neck become maximum, and so the absorption characteristics also peak at that frequency. Usually there will be only a very small amount of damping in the system, and hence the resonance peak is usually very sharp and narrow, falling off very quickly on each side of the resonance frequency. This effect can be observed easily if we blow across the top of the neck of a bottle, we hear a pure tone developed rather than a broad resonance.

If the neck is circular in cross section and if we neglect boundary layer effects, the undamped resonance frequency  $f_r$  is given by

$$f_r = \frac{c}{2\pi} \sqrt{\frac{S}{(L + 1.7r)V}} \quad (17)$$

where  $S$  is the area of the neck ( $\text{m}^2$ ),  $L$  is the length of neck (m),  $r$  is the radius of neck (m),  $V$  is the cavity volume ( $\text{m}^3$ ), and  $c$  is the speed of sound (m/s). The factor  $(L + 1.7r)$  in Eq. (17) gives the effective length

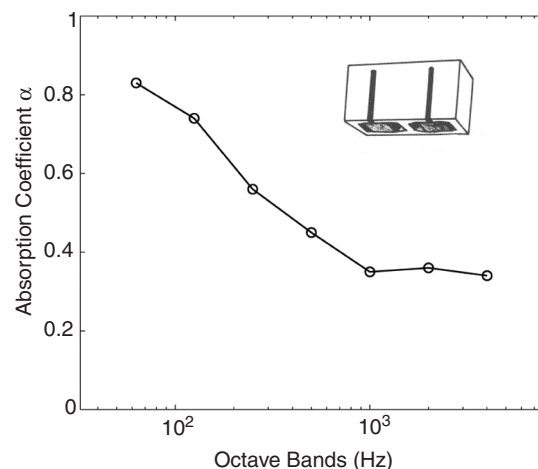


**Figure 5** A Helmholtz resonator consists of a neck of length  $L$  and cross-sectional area  $S$ , and backed by a closed volume  $V$ .

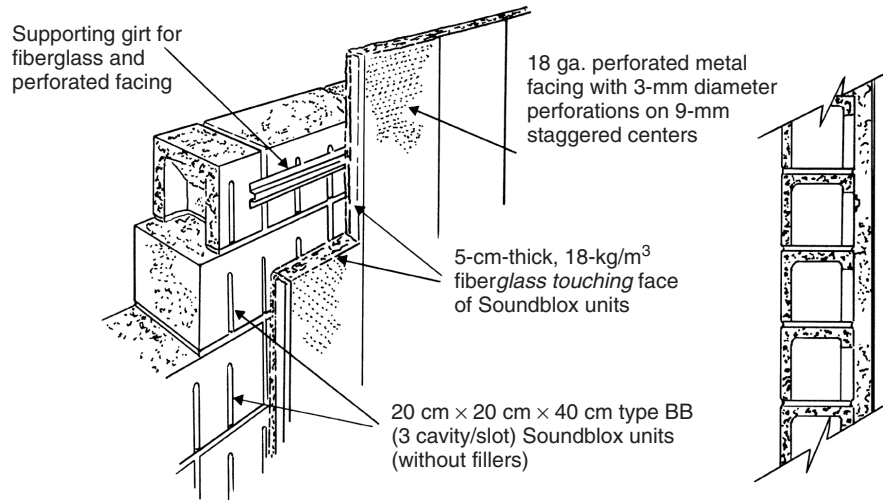
of the baffled neck. The factor  $1.7r$  is sometimes called the *end correction*.

Although Helmholtz-type resonators can be built to be effective at any frequency, their size is such that they are used mainly for low frequencies in the region 20 to 400 Hz. Because of their sharp resonance peaks, undamped resonator absorbers have particularly selective absorption characteristics. Therefore, they are used primarily in situations where a particularly long reverberation time is observed at one frequency. This frequency may correspond to a well-excited low-frequency room mode, and an undamped resonator absorber may be used to reduce this effect without changing the reverberation at other, even nearby, frequencies. They are also used in noise control applications where good low-frequency sound absorption is required at a particular frequency. In this respect special Helmholtz resonators, constructed from hollow concrete blocks with an aperture or slit in their faces, are used in transformer rooms and electrical power stations to absorb the strong 120-Hz noise produced therein.

This concept is well known and such a resonator was used hundreds of years ago in some churches built in Europe. Some damping may be introduced into such resonators by adding porous material either in the neck region or to a lesser extent in the cavity. The effect of increased damping is to decrease the absorption value at resonance but considerably to broaden the absorption curve over a wider frequency range. Figure 6 shows measured absorption coefficients for slotted concrete blocks filled with porous material. It can be seen that they offer especially good low-frequency absorption characteristics. In addition, they can be faced with a thin blanket of porous material and covered with perforated metal sheeting, as shown in Fig. 7, to improve their high-frequency absorption with only little effect on their low-frequency performance.



**Figure 6** Sound absorption coefficient vs. frequency for a slotted 20-cm concrete block filled with an incombustible fibrous material.



**Figure 7** Slotted concrete blocks faced with fiberglass and covered with a perforated metal provide good low- and high-frequency absorption characteristics.

It is useful to note that there is a limit to the absorption any given undamped resonator of this type can provide. According to Zwicker and Kosten<sup>2</sup> the maximum absorption possible,  $A_{\max}$  sabins, is given by

$$A_{\max} = 1.717 \left( \frac{c}{f_r} \right)^2 \quad (18)$$

where  $c$  is the speed of sound (m/s) and  $f_r$  is the resonance frequency (Hz). Therefore, if  $f_r = 150$  Hz, for example, then we cannot expect to realize more than  $A_{\max} = 8.5$  sabins per unit. Equation (18) also shows that as the resonance frequency becomes lower, more absorption can be obtained from the resonator.

In certain circumstances, the performance of a Helmholtz-type resonator can be drastically influenced by the effect of its surrounding space. This is particularly found in the case for such resonators mounted in a highly absorbing plane, when interference can take place between the sound radiated from the resonator and reflected from the absorbing plane. In such circumstances special care has to be taken.

**4.3.1 Perforated Panel Absorbers** As described above, single Helmholtz resonators have very selective absorption characteristics and are often expensive to construct and install. In addition, their main application lies at low frequencies. Perforated panels offer an extension to the single resonator absorber and provide a number of functional and economic advantages.

When spaced away from a solid backing, a perforated panel is effectively made up of a large number of individual Helmholtz resonators, each consisting of a “neck,” constituted by the perforation of the panel, and a shared air volume formed by the

total volume of air enclosed by the panel and its backing. The perforations are usually holes or slots and, as with the single resonator, porous material may be included in the airspace to introduce damping into the system. Perforated panels are mechanically durable and can be designed to provide good broadband sound absorption. The addition of a porous blanket into the airspace tends to lower the magnitude of the absorption maximum but, depending on the resistance of the material, generally broadens the effective range of the absorber.<sup>20</sup> At low frequencies the perforations become somewhat acoustically transparent because of diffraction, and so the absorbing properties of the porous blanket remain almost unchanged. This is not so at high frequencies at which a reduction in the porous material absorption characteristics is observed.

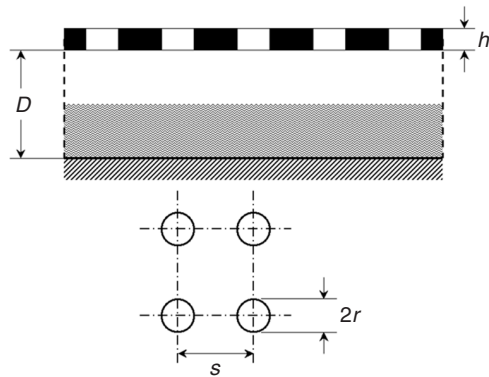
The resonance frequency  $f_r$  for a panel perforated with holes and spaced from a rigid wall may be calculated from

$$f_r = \frac{c}{2\pi} \sqrt{\frac{P}{Dh'}} \quad (19)$$

where  $c$  is the speed of sound (m/s),  $D$  is the distance from wall (m),  $h'$  is the thickness of the panel with the end correction (m),  $r$  is the radius of hole or perforation (m), and  $P$  is the open area ratio (or perforation ratio). For a panel made up of holes of radius  $r$  metres and spaced  $s$  metres apart, the open area ratio  $P$  is given by  $\pi(r/s)^2$  (see Fig. 8).

A full expression for  $h'$  in Eq. (19) that takes into account the boundary layer effect is given by<sup>21</sup>

$$h' = h + 2\delta r + \left[ \frac{8\nu}{\omega} \left( 1 + \frac{h}{2r} \right) \right]^{1/2} \quad (20)$$



**Figure 8** Geometry for a typical perforated panel absorber.

where  $h$  is the thickness of panel (m),  $\omega$  is the angular frequency (rad/s),  $\nu$  is the kinematic viscosity of air ( $15 \times 10^{-6} \text{ m}^2/\text{s}$ ), and  $\delta$  is the end correction factor. For panel hole sizes not too small we can write  $h' \approx h + 2\delta r$ . To a first approximation the end correction factor can be assumed to be 0.85, as we did in the previous section for a single hole. However, more accurate results that include the effects of the mutual interaction between the perforations have been predicted. Table 1 presents some of these results.

We can see that the resonance frequency increases with the open area ratio (i.e., the number of holes per unit area) and is inversely proportional to the thickness of the panel and its distance from the solid backing.

**Example 1** A perforated panel with a 10% open area ( $P = 0.10$ ) and thickness 6 mm is installed 15 cm in front of a solid wall. Assuming that the holes are not too small and if we neglect the end effect and put  $h' = h + 2\delta r = 6 \text{ mm}$  and  $D = 15 \text{ cm}$ , then the resonance frequency  $f_r = 560 \text{ Hz}$ . If the percentage open area is only 1% ( $P = 0.01$ ), then in the same situation,  $f_r = 177 \text{ Hz}$ .

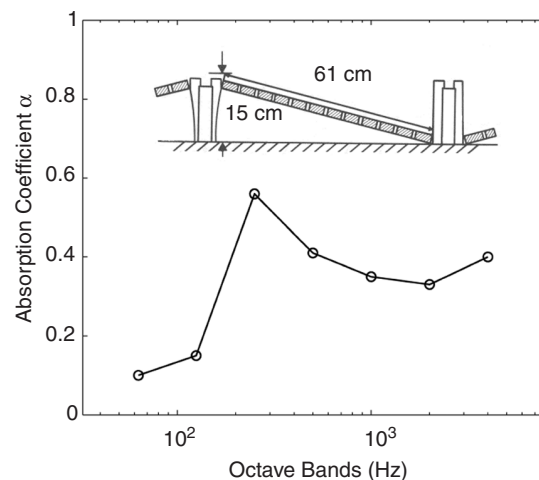
In practical situations, air spaces up to 30 cm can be used with open areas ranging from 1 to 30% and thicknesses from 3 to 25 mm. These particular restrictions would allow a resonance frequency range of 60 to 4600 Hz. Many perforated panels and boards

are commercially available and are readily used for perforated absorbers. These include: hardboards, plastic sheets, wood and plywood panels, and a variety of plane and corrugated metal facings. Some perforated sheets are available that consist of a number of different size perforations on one sheet. This can be useful to give broader absorption characteristics.

Recently, microperforated panels have been developed, which means that the diameter of the perforations is very small (less than a millimetre). In this case, the diameter is comparable to the thickness of the boundary layer, resulting in high viscous losses as air passes through the perforations and, consequently, achieving absorption without using a porous material.<sup>22–24</sup> Some commercial microperforated panels take advantage of this fact, allowing the construction of a transparent absorbent device similar to a double glazing unit. However, obtaining broadband sound absorption using microperforated panels is difficult and requires the use of multiple layers, increasing the depth and cost of the device.

Another technique commonly used to achieve broader absorption characteristics is to use a variable, often wedge-shaped, airspace behind the perforated panel,<sup>25</sup> as shown in Fig. 9. One of the commercial types of perforated absorber has been referenced in the literature as the “Kulihat.”<sup>26</sup> This is a conical absorber consisting of two or three perforated aluminum sectors held together by steel clips. The interior of the Kulihat is lined with mineral wool.

It is common practice to install a thin (1 to 2 mil) plastic sheet behind the perforated panel to cover and protect the porous absorbing material, as shown in Fig. 10. As long as this sheet is thin, its effect is usually only observed at high frequencies where the

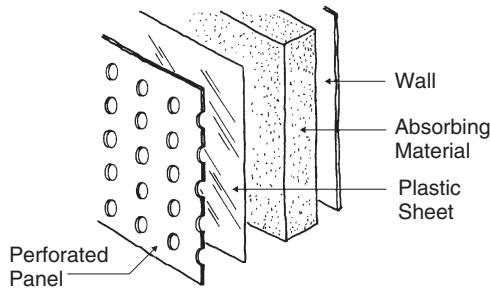


**Figure 9** Variable airspace perforated panels give broader absorption characteristics than those with a constant air depth. Here the panel is 16 mm thick and has holes of 9.5 mm in diameter spaced 3.5 cm on center.

**Table 1** Different Formulas for the End Correction Factor

$\delta$	Notes
0.85	Single hole in a baffle
$0.8(1 - 1.4\sqrt{P})$	For $P < 0.16$
$0.8(1 - 1.47\sqrt{P} + 0.47\sqrt{P^3})$	Includes $P = 1$
$0.85(1 - 1.25\sqrt{P})$	Square apertures; for $P < 0.16$
$-\ln[\sin(\pi P/2)]/\pi$	Slotted plate; in Eq. (20) $\nu = 0$ and $r = \text{width of slots}$





**Figure 10** Porous absorbing material protected by a thin plastic sheet behind the perforated panel.

effective absorption can be reduced by approximately 10% of its value with no covering sheet present.

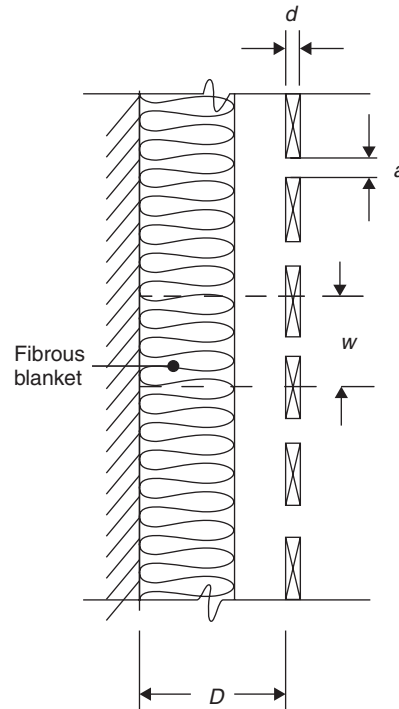
**4.3.2 Slit Absorbers** Another type of perforated resonator is the slit or slat absorber. These are made up of wooden battens fixed fairly close together and spaced at some distance from a solid backing. Porous material is usually introduced into the air cavity (see Fig. 11). This type of resonator is fairly popular architecturally since it can be constructed in many ways, offering a wide range of design alternatives. Equation (19) does not hold for slat absorbers since the perforations are very long. For a detailed discussion of the properties of such absorbers, the reader is advised to consult Refs. 27 and 28. The principle of the slit resonator is, however, the same as for a general Helmholtz resonator. The resonance frequency  $f_r$  (Hz) is given by the solution to the following equation:

$$f_r = \frac{c}{2\pi} \sqrt{\frac{a}{S}} \left\{ d + \frac{2a}{\pi} \left[ 1.12 + \ln \left( \frac{c}{\pi a f_r} \right) \right] \right\}^{-1/2} \quad (21)$$

where  $c$  is the speed of sound (m/s),  $a$  is the slit width (m),  $d$  is the slit depth (m), and  $S$  is the cross-sectional area (m<sup>2</sup>) of space behind slats formed by each slat (i.e., slat width  $W \times$  air space  $D$ ).

A typical acoustical design procedure would be to choose a resonance frequency  $f_r$  and a slat of width  $W$  and thickness  $d$  and then determine the required value of air space from  $S = W \times D$  for a chosen value of slit width  $a$ .

**Example 2** Let us suppose that we want  $f_r = 200$  Hz and that the resonator should be constructed of slats measuring  $25 \times 84$  mm. Therefore, we have  $W = 84$  mm and  $d = 25$  mm. Since the slit width should be approximately 10 to 20% the width of the slat, let us try a slat spacing (i.e., slit width) of 8 mm. Then, all the known values in Eq. (21) are  $f_r = 200$  Hz,  $W = 0.084$  m,  $d = 0.025$  m,  $a = 0.008$  m, and  $c = 334$  m/s. Equation (21) can be rewritten by multiplying and dividing both sides of the equation by  $\sqrt{S}$  and  $f_r$ , respectively. Then,  $S$  can be obtained by squaring both sides of the resulting equation. Replacing the known



**Figure 11** Slat type of resonator absorber (normally the mineral wool is placed immediately behind the slots).

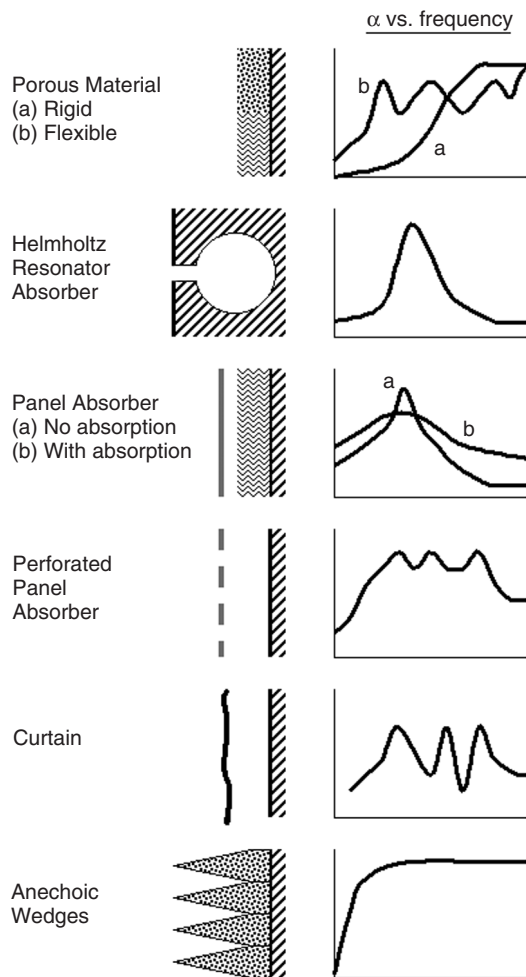
values gives  $S = 0.01\text{m}^2$  and since  $W = 0.084$  m, we require  $D = 0.13$  m.

We see, therefore, that for the above example of a slit resonator, an air space of 13 cm is required to provide a resonance frequency of 200 Hz. If the calculation is repeated for a 100-Hz resonance frequency, it is found that an air space of some 48 cm is required.

Figure 12 shows a comparison of typical sound absorption curves for most of the absorbers discussed above.

#### 4.4 Suspended Absorbers

This class of sound absorbers is known by several names including *suspended absorbers*, *functional absorbers*, and *space absorbers*. They generally refer to sound-absorbing objects and surfaces that can be easily suspended, either as single units or as a group of single units within a room. They are particularly useful in rooms in which it is difficult to find enough surface area to attach conventional acoustical-absorbing materials either through simple lack of available space or interference from other objects or mechanical services such as ducts and pipes, in the ceiling space (see Fig. 13). It is relatively easy and inexpensive to install them, without interference to existing equipment. For this reason they are often used in noisy industrial installations such as assembly rooms or machine shops.

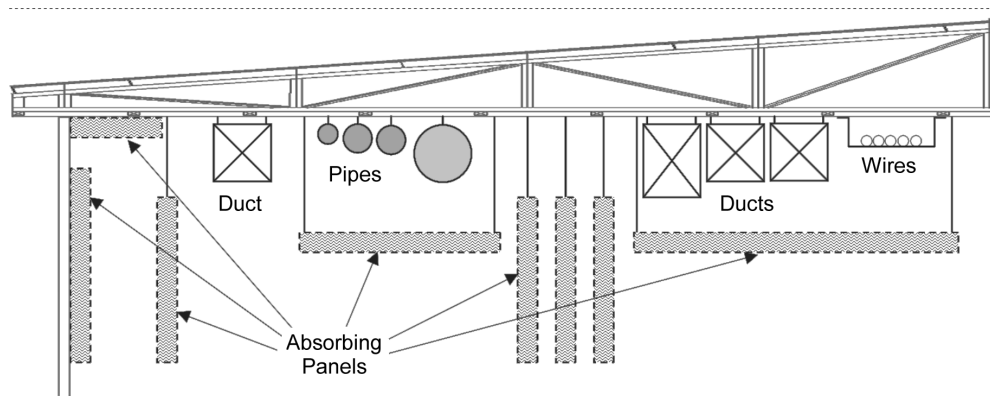


**Figure 12** Comparison of acoustical behavior for typical sound absorbers.

Functional absorbers are usually made from highly absorbing materials in the form of a variety of three-dimensional shapes, such as spheres, cones, double cones, cubes, and panels. These are usually filled with a porous absorbing material. Since sound waves fall on all their surfaces and because of diffraction, they are able to yield high values of effective absorption coefficients. It is, however, more usual to describe their absorption characteristics in terms of their total absorption in sabins per unit, as a function of octave band frequencies, rather than to assign an absorption coefficient to their surfaces. One also finds that when a group of functional absorbers are installed, the total absorption realized from the group depends upon the spacing between the individual units to a certain extent. Once a certain optimum spacing has been reached the effective absorption per unit does not increase.<sup>29,30</sup>

#### 4.5 Acoustical Spray-on Materials

These consist of a range of materials formed from mineral or synthetic organic fibers mixed with a binding agent to hold the fibrous content together in a porous manner and also to act as an adhesive. During the spraying application, the fibrous material is mixed with a binding agent and water to produce a soft lightweight material of coarse surface texture with high sound-absorbing characteristics. Due to the nature of the binding agent used, the material may be easily applied directly to a wide number of surface types including wood, concrete, metal lath, steel, and galvanized metal. When sprayed onto a solid backing, this type of spray-on material usually exhibits good mid- and high-frequency absorption and when applied to, for example, metal lath with an airspace behind it, the material then also exhibits good low-frequency absorption. As would be expected from previous discussions of porous absorbers (in Section 4.1), the absorption values increase with greater depth of application, especially at low frequencies. Spray-on depths of up to 5 cm are fairly common.



**Figure 13** Sound-absorbing material placed on the walls and under the roof and suspended as panels in a factory building.

The absorption characteristics of such materials are very much dependent upon the amount and type of binding agent used and the way it is mixed during the spray-on process. If too much binder is used, then the material becomes too hard and therefore a poor absorber, while on the other hand, if too little binder is employed, the material will be prone to disintegration; and, since it will have a very low flow resistance, it will also not be a good absorber.<sup>18</sup> Some products use two binders. One is impregnated into the fibrous material during manufacture, while the other is in liquid form and included during application. The fibrous material (containing its own adhesive) and the liquid adhesive are applied simultaneously to the surface using a special nozzle. The material is particularly resistant to disintegration or shrinkage and, furthermore, is fire resistant and possesses excellent thermal insulation properties.

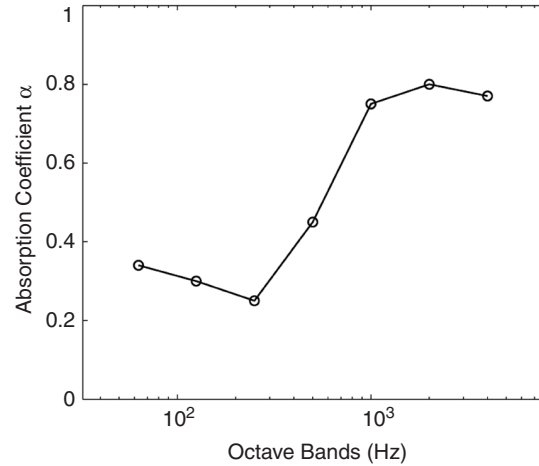
If visually acceptable, spray-on materials of this type can be successfully used as good broadband absorbing materials in a variety of architectural spaces including schools, gymnasiums, auditoriums, shopping centers, pools, sports stadiums, and in a variety of industrial applications such as machine shops and power plants. Disadvantages generally include the difficulty to clean and redecorate the material, although some manufacturers claim that their product can be spray painted without loss of acoustical performance. Such claims should be supported by data before proceeding to paint such a surface.

#### 4.6 Acoustical Plaster

This term has been applied to a number of combinations of vermiculite and binder agents such as gypsum or lime. They are usually applied either to a plaster base or to concrete and must have a solid backing. Because of this, acoustical plasters have poor low-frequency absorption characteristics (also due to the thickness of application, which rarely exceeds 13 mm). This can be slightly improved by application to metal lath. The material may be applied by a hand trowel or by machine. However, the latter tends to compact the material and give lower absorption characteristics. The surface of acoustical plasters can be sprayed with water-thinned emulsion paint without any significant loss of absorption, although brushed oil-based paints should never be used. Figure 14 shows typical sound absorption characteristics for a 13-mm-thick hand trowel applied acoustical plaster taken from a variety of published manufacturer's data.<sup>18</sup>

### 5 MEASUREMENT OF ABSORPTION COEFFICIENTS

Although some approximate values for absorption coefficients and resonance frequency characteristics can be estimated from the geometry, flow resistance, porosity, and other physical factors, it is clearly necessary to have actual measured values of absorption coefficients for a variety of materials and different constructions. There are two standardized methods to measure the sound absorption coefficient: using a



**Figure 14** Sound absorption coefficient  $\alpha$  of a 13-mm-thick acoustical plaster.

reverberant room and using an impedance tube. These methods will be described in the following sections.

#### 5.1 Using Reverberant Rooms

Since the reverberation time of a room depends upon the absorption present within it, this gives us a method to measure the absorption coefficient of a chosen material by observing the change in the reverberation time of the room caused by the introduction of the specimen. This method is particularly useful since large specimens of absorbing material can be measured that can be built and mounted in the same manner as they will be used in a real building. Therefore, these measurements should be more representative than those made on small samples.

If the reverberation time of a large, empty, and highly reverberant room is  $T_1$  seconds and the sound field is completely diffuse, introduction of a sample of absorbing material of surface  $S$  will change the reverberation time to  $T_2$  seconds at the same frequency. If we assume that the room temperature and humidity have remained unchanged throughout the measurements, the change in the total effective absorption  $\Delta A$  (difference between the total absorption area of room and sample and total absorption area with empty walls) is given by

$$\Delta A = \frac{55.3V}{c} \left( \frac{1}{T_2} - \frac{1}{T_1} \right) \quad (22)$$

where  $V$  is the room volume ( $\text{m}^3$ ) and  $c$  is the speed of sound ( $\text{m/s}$ ).

Since that change in total absorption area is due to the sample of area  $S$  and effective absorption coefficient  $\bar{\alpha}$  covering a wall surface, the effective absorption coefficient of the sample can be estimated



by the following equation:

$$\bar{\alpha} = \frac{55.3V}{Sc} \left( \frac{1}{T_2} - \frac{S_T - S}{S_T T_1} \right) \quad (23)$$

where  $S_T$  ( $\text{m}^2$ ) is the total area of all surfaces in the room including the area of the material under test. It must be realized that the values obtained for  $\bar{\alpha}$  are not a true measure of the energy absorption coefficient of the material for random incidence sound falling on the sample since many of the factors such as size and location of the sample influence the values obtained. We only really obtain a measure of the influence that the sample had on reverberation time of the test room.

In some circumstances it could be argued that the Sabine reverberation equation does not give accurate results and that perhaps some other formula such as the Eyring equation should be used. However, values of absorption coefficients listed by all manufacturers and testing laboratories are Sabine values calculated from Eq. (23). Provided the test room has a large volume and long reverberation time, and the test sound field is diffuse, the values obtained are usually fairly accurate. Nevertheless, despite the fact that measurements made in different reverberation rooms on the same absorbing sample often yield different values of absorption coefficient, the results of such tests have been used successfully by architectural acousticians in many situations.

A reverberation test room should have a large volume and long reverberation time to increase the acoustical modal density and decrease spatial variance in the sound field. To improve diffuseness, stationary or rotating vanes should be used. Since the effective absorption coefficient of a material depends to some extent upon its area,<sup>31</sup> due to diffraction at its edges, it is necessary for the test sample to be sufficiently large so that diffraction effects are minimized.

The American Society for Testing and Materials (ASTM) has set a standard for such measurements.<sup>32</sup> This standard covers the acoustical performance of the testing reverberant room and the sample size and mounting and governs the method for measuring the reverberation times. The room volume  $V$  should be greater than  $4\lambda^2$ , where  $\lambda$  is the longest wavelength used in the test. In addition, the smallest dimension of the room should exceed  $2\lambda$  and the ratio of the largest to the smallest dimension should be less than 2 : 1. This therefore requires rooms to have volumes in excess of 10,000  $\text{ft}^3$  (283  $\text{m}^3$ ) in order to operate at 100 Hz.

The ASTM standard also specifies that the average absorption coefficient of the empty room at all test frequencies should not exceed 0.06, including the effect of air absorption. This requirement, together with the above volume restrictions, guarantees that the reverberation time of the whole usable frequency range (125 to 4000 Hz, octave bands) should be greater than 3.6 s, assuming a 2400- $\text{ft}^2$  (223  $\text{m}^2$ ) surface area. One-third octave bands of white or pink noise are used to create the sound field in the room, and the slope of the resultant sound pressure level decay curve

should be measured over a decay range of not less than 30 dB, starting from at least 5 dB down from the beginning of the decay. The test sample should be not less than 48  $\text{ft}^2$  (4.5  $\text{m}^2$ ), although sample areas of 72  $\text{ft}^2$  (6.7  $\text{m}^2$ ) are recommended. The measured absorption coefficients should be rounded off to the nearest multiple of 0.01, while the NRC (average of 250 to 2000 Hz) should be rounded to a NRC of 0.05.

The International Organization for standardization (ISO) also has set a testing standard for reverberation room absorption testing.<sup>33</sup> The size of the testing chamber is again governed by the lowest test frequency desired, but in order to measure down to 100 Hz the room should be in excess of 225  $\text{m}^3$  (7945  $\text{ft}^3$ ) and also satisfy  $V > L^3/6.8$ , where  $L$  is the greatest diagonal length of the room. The sample size is restricted to rectangular plane samples of area from 10 to 12  $\text{m}^2$  (i.e., 108 to 130  $\text{ft}^2$ ). Strips of materials are to be avoided, and the ratio of sample length to breadth must be not less than 0.7. The reverberation times of the test room itself must exceed 5 s at 125, 250, and 500 Hz, 4.5 s at 1000 Hz, 3.5 s at 2000 Hz, and 2 s at 4000 Hz. Either one-third or one-half octave bands of white noise may be used and warble tones may also be used, provided the frequency of deviation from the tone is  $\pm 10\%$  for  $\leq 500$  Hz and  $\pm 50$  Hz for  $\geq 500$  Hz—the modulation frequency being set at 6 Hz. The use of stationary or rotating vane diffusers is again recommended.

Tables of absorption coefficients are published for a variety of acoustical materials in which numerous mounting systems are employed. Sound absorption coefficients and corresponding values of NRC of some common sound-absorbing materials and construction materials are shown in Table 2. More extensive tables of sound absorption coefficients of materials can be found in the literature. The book by Trevor Cox provides a good review on sound-absorbing materials.<sup>34</sup> The tables are very often made up after receiving absorption results from a number of independent testing laboratories for the same sample of material. It is found that even when all of the requirements of either the ISO or ASTM standards are met, quite large differences can still be observed between the values obtained for the absorption coefficients measured in different laboratories for the same sample.<sup>35</sup> These differences can be due to variations in the diffuseness of the testing rooms and to human error and bias in measuring the reverberation times.

## 5.2 Using Impedance Tubes

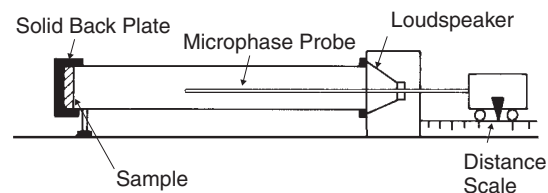
The standing wave or impedance tube provides a convenient laboratory method of measuring both the complex acoustic impedance and acoustic absorption coefficient of small samples for sound waves normally incident upon their surfaces.<sup>36,37</sup> Because of the sample size restrictions, this method is only useful for porous materials and some resonant perforated absorbers. It cannot be used for resonant panels or large slit resonators since their absorption characteristics depend upon the size of the sample.

**Table 2 Sound Absorption Coefficient  $\alpha(f)$  and Corresponding NRC of Common Materials**

Material	Frequency (Hz)						NRC
	125	250	500	1000	2000	4000	
Fibrous glass (typically 64 kg/m <sup>3</sup> ) hard backing							
25 mm thick	0.07	0.23	0.48	0.83	0.88	0.80	0.61
50 mm thick	0.20	0.55	0.89	0.97	0.83	0.79	0.81
10 cm thick	0.39	0.91	0.99	0.97	0.94	0.89	0.95
Polyurethane foam (open cell)							
6 mm thick	0.05	0.07	0.10	0.20	0.45	0.81	0.21
12 mm thick	0.05	0.12	0.25	0.57	0.89	0.98	0.46
25 mm thick	0.14	0.30	0.63	0.91	0.98	0.91	0.71
50 mm thick	0.35	0.51	0.82	0.98	0.97	0.95	0.82
Hair felt							
12 mm thick	0.05	0.07	0.29	0.63	0.83	0.87	0.46
25 mm thick	0.06	0.31	0.80	0.88	0.87	0.87	0.72
Brick							
Unglazed	0.03	0.03	0.03	0.04	0.04	0.05	0.04
Painted	0.01	0.01	0.02	0.02	0.02	0.02	0.02
Concrete block, painted	0.01	0.05	0.06	0.07	0.09	0.03	0.07
Concrete	0.01	0.01	0.02	0.02	0.02	0.02	0.02
Wood	0.15	0.11	0.10	0.07	0.06	0.07	0.09
Glass	0.35	0.25	0.18	0.12	0.08	0.04	0.16
Gypsum board	0.29	0.10	0.05	0.04	0.07	0.09	0.07
Plywood, 10 mm	0.28	0.22	0.17	0.09	0.10	0.11	0.15
Soundblox concrete block							
Type A (slotted), 15 cm (6 in.)	0.62	0.84	0.36	0.43	0.27	0.50	0.48
Type B, 15 cm (6 in.)	0.31	0.97	0.56	0.47	0.51	0.53	0.63
Spray-acoustical (on gypsum wall board)	0.15	0.47	0.88	0.92	0.87	0.88	0.79
Acoustical plaster (25 mm thick)	0.25	0.45	0.78	0.92	0.89	0.87	0.76
Carpet							
On foam rubber	0.08	0.24	0.57	0.69	0.71	0.73	0.55
On concrete	0.02	0.06	0.14	0.37	0.60	0.66	0.29

The sample material is placed in front of a heavy rigid termination at one end of a rigid walled tube (see Fig. 15), while a loudspeaker is mounted on the tube axis at the other end. The loudspeaker is fed with pure-tone signals (at one-third octave center frequencies) and this then radiates plane waves down the tube toward the sample; as long as the diameter of the tube is small compared with the sound wavelength, transverse modes cannot be set up within the tube. The plane waves are then partially reflected by the sample and travel back along the tube toward the loudspeaker. This results in a longitudinal interference pattern consisting of standing waves set up within the tube. A microphone connected to an extension probe tube is moved along the axis to measure the variation in sound pressure within the standing-wave tube. From measurements of the ratio of maximum to minimum sound pressure within the tube, the absorption coefficient of the sample, at normal incidence, can be calculated.

The *standing-wave ratio*,  $n$ , is defined as the ratio of maximum to minimum sound pressures within the



**Figure 15** Standing-wave apparatus used to determine both the normal incidence absorption coefficient and complex impedance of a sample of material placed at the end of the tube.

tube. Thus, the normal incidence absorption coefficient is given by

$$\alpha = \frac{4n}{(n+1)^2} \quad (24)$$

It is found that the normal incidence absorption coefficient values measured in an impedance tube

are generally lower than the random incidence values obtained from the reverberation room method. At low frequencies the difference is only slight, while at high frequencies the tube values are generally 50% lower than those measured in a room.

To ensure plane waves, and therefore no transverse waves in the tube, the length of the tube shall exceed  $\lambda/4$  and the diameter of the tube shall not exceed  $0.58\lambda$ . Hence a 4-in. (10-cm) diameter, 3-ft (91-cm) long tube would have a useful range of 90 to 1800 Hz. To make measurements over the range of 90 to 6000 Hz, two different size tubes are required, a smaller one for high frequencies and a larger one for low frequencies.

In addition, by measuring the distance between the sample and the first standing-wave minimum sound pressure, then the complex acoustic impedance of the specimen can also be calculated. The relationship between the statistical absorption coefficient and complex impedance has been discussed in the literature.<sup>38</sup>

More recently a technique to measure the complete spectrum of both the sound absorption coefficient and complex acoustic impedance has been developed and standardized.<sup>39,40</sup> This technique, usually called the *two-microphone method*, allows one to obtain rapidly the data by using a broadband sound source in a shortened tube. The tube has a number of fixed microphones (see Fig. 16), and the transfer function between two microphone positions is measured using a signal analyzer. Thus, the complex pressure reflection coefficient as a function of frequency is obtained as

$$R = \frac{H_{12} - e^{-jk\delta}}{e^{jk\delta} - H_{12}} e^{j2kz} \quad (25)$$

where  $H_{12}$  is the transfer function between microphone position 1 and 2,  $\delta$  is the microphone spacing,  $z$  is the distance shown in Fig. 16, and  $k$  is the free-field wavenumber. Then, the sound absorption coefficient is obtained as  $\alpha = 1 - |R|^2$ .

Equation (25) shows that the reflection coefficient cannot be determined at discrete frequency points for which the microphone spacing is almost equal to an integer multiple of  $\lambda/2$ . Therefore, the microphone spacing must be chosen such that  $\delta \leq \lambda/2$ . For a given microphone spacing, the measurement of sound absorption coefficients will be valid for frequencies for which  $0.05c/\delta < f < 0.45c/\delta$ . In addition, a careful calibration is required for the measured transfer function. One of the ways of doing it is the microphone switching procedure, which prevents the error due to phase mismatch and gain factor between the two measurement channels.<sup>40</sup>

## 6 APPLICATIONS

The main applications of sound absorbent materials in noise control are<sup>41</sup>: (1) incorporation in noise control enclosures, covers, and wrappings to reduce reverberant buildup of sound and hence increase insertion loss (see Chapter 56), (2) incorporation in flow ducts to attenuate sound from fans and flow control devices (see Chapter 112), (3) application to the surfaces of rooms to control reflected sound (e.g., to reduce steady-state sound pressure levels in reverberant fields), (4) in vehicles (walls, engine compartments, engine exhaust, see Chapter 94), (5) in lightweight walls and ceilings of buildings, and (6) on traffic noise barriers to suppress reflections between the side of the vehicle and the barrier or to increase barrier performance by the presence of absorbent on and around the top of the barrier (see Chapter 58).

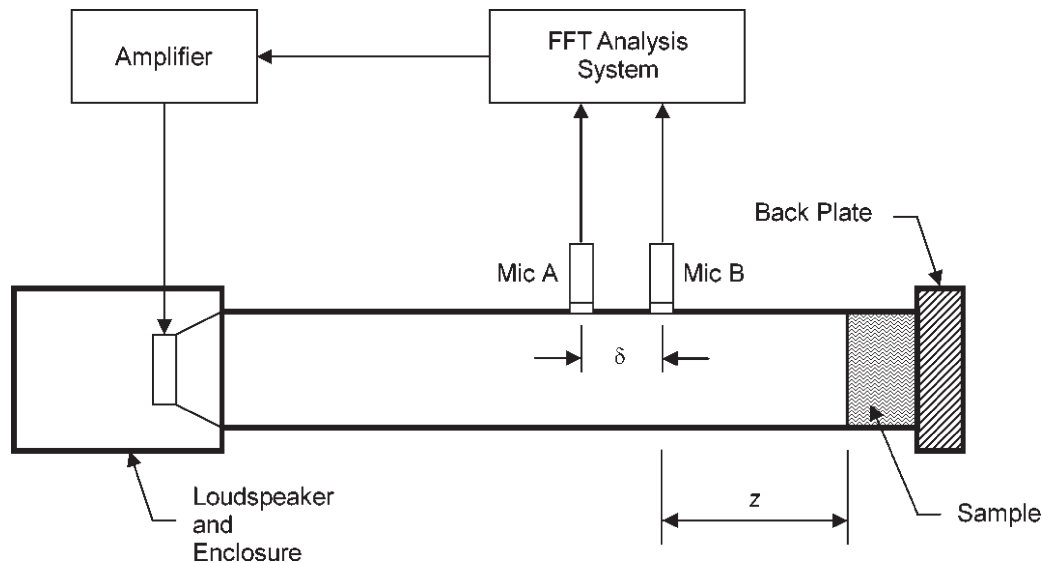


Figure 16 Experimental setup for the two-microphone method.

However, sound-absorbing materials are most commonly used to optimize the reverberation time in rooms and to reduce the sound pressure level in reverberant fields. These applications will now be described separately.

### 6.1 Optimization of the Reverberation Time

When sound is introduced into a room, the reverberant field level will increase until the sound energy input is just equal to the sound energy absorption. If the sound source is abruptly turned off, the reverberant field will decay at a rate determined by the rate of sound energy absorption.

As mentioned before, the reverberation time of a room depends upon the absorption present within it. In addition, the reverberation time has become recognized as the most important single parameter used to describe the acoustical performance of auditoriums. Changes in the total absorption can be made by modifying the values of areas and sound absorption coefficients of the room surfaces. Therefore, it is possible to change the values of reverberation time to provide players and listeners with a high degree of intelligibility throughout the room and optimum sound enrichment.

In a room, to understand speech fully, each component of the speech must be heard by the listener. If the room has a long reverberation time, then the speech components overlap and a loss of intelligibility results. Similarly, for music enjoyment and appreciation, a certain amount of reverberation is required to obtain the quality and blend of the music. It is, however, much more difficult to describe the acoustical qualities of a room used for music since many are subjective and therefore cannot be described in measurable physical quantities. Optimum reverberation time is not only required for good subjective reception but also for an efficient performance.

Optimum values of the reverberation time for various uses of a room may be calculated approximately by<sup>42</sup>

$$T_R = K(0.0118V^{1/3} + 0.1070) \quad (26)$$

where  $T_R$  is the reverberation time (s),  $V$  is the room volume ( $\text{m}^3$ ), and  $K$  is a constant that takes the following values according to the proposed use: For speech  $K = 4$ , for orchestra  $K = 5$ , and for choirs and rock bands  $K = 6$ . It has been suggested that, at frequencies in the 250-Hz octave band and lower frequencies, an increase is needed over the value calculated by Eq. (26), ranging from 40% at 250 Hz to 100% at 63 Hz. Other authors have suggested optimum  $T_R$  for rooms for various purposes.<sup>3,4</sup>

However, achieving the optimum reverberation time for a room may not necessarily lead to good speech intelligibility or music appreciation. It is essential to adhere strictly to the other design rules for shape, volume, and time of arrival of early reflections.<sup>43,44</sup>

**Example 3** Consider an auditorium of dimensions  $9 \text{ m} \times 20 \text{ m} \times 3.5 \text{ m}$ , with an average Sabine absorption coefficient  $\bar{\alpha} = 0.9$  for the whole room surface at 4000 Hz. Then the total surface area of the room is calculated as  $S = 2(20 \times 3.5 + 9 \times 3.5 + 9 \times 20) = 563 \text{ m}^2$  and its volume is  $V = 630 \text{ m}^3$ . Assuming that there is a uniform distribution of absorption throughout the room, the reverberation time can be obtained as given by Sabine  $T_R = 0.161V/(S\bar{\alpha}) = (0.161 \times 630)/(563 \times 0.9) = 0.2 \text{ s}$ . Now substituting the value of room volume in Eq. (26), and considering  $K = 4$  for using the room for speech, we obtain  $T_R = 0.2 \text{ s}$ . Therefore, the total absorption of such a room is optimum for its use as an auditorium, at least at 4000 Hz. This calculation may be repeated at each frequency for which absorption coefficient data are available.

### 6.2 Reduction of the Sound Pressure Level in Reverberant Fields

When a machine is operated inside a building, the machine operator usually receives most sound through a direct path, while people situated at greater distances receive sound mostly through reflections. In the case of machinery used in reverberant spaces such as factory buildings, the reduction in sound pressure level  $L_p$  in the reverberant field caused by the addition of sound-absorbing material, placed on the walls or under the roof (see Fig. 13), can be estimated for a source of sound power level  $L_W$  from the so-called room equation:

$$L_p = L_W + 10 \log \left( \frac{D}{4\pi r^2} + \frac{4}{R} \right) \quad (27)$$

where the room constant  $R = S\bar{\alpha}/(1 - \bar{\alpha})$ ,  $\bar{\alpha}$  is the surface average absorption coefficient of the walls,  $D$  is the source directivity, and  $r$  is the distance in metres from the source. The surface average absorption coefficient  $\bar{\alpha}$  may be estimated from

$$\bar{\alpha} = \frac{S_1\alpha_1 + S_2\alpha_2 + S_3\alpha_3 + \dots}{S_1 + S_2 + S_3 + \dots} \quad (28)$$

where  $S_1, S_2, S_3, \dots$  are the surface areas of material with absorption coefficients  $\alpha_1, \alpha_2, \alpha_3, \dots$ , respectively. For the suspended absorbing panels shown in Fig. 13, both sides of the panel are normally included in the surface area calculation.

If the sound absorption is increased, then from Eq. (27) the change in sound pressure level  $\Delta L$  in the reverberant space (beyond the critical distance  $r_c$ ) is

$$\Delta L = L_{p1} - L_{p2} = 10 \log \frac{R_2}{R_1} \quad (29)$$

If  $\bar{\alpha} \ll 1$ , then the reduction in sound pressure level (sometimes called *the noise reduction*) is given by

$$\Delta L \approx 10 \log \frac{S_2\bar{\alpha}_2}{S_1\bar{\alpha}_1} \quad (30)$$

where  $S_2$  is the total surface area of the room walls, floor, and ceiling and any suspended sound-absorbing material,  $\bar{\alpha}_2$  is the average sound absorption coefficient of these surfaces after the addition of sound-absorbing material, and  $S_1$  and  $\bar{\alpha}_1$  are the area and the average sound absorption coefficient before the addition of the material.

**Example 4** A machine source operates in a building of dimensions  $30 \text{ m} \times 30 \text{ m}$  with a height of  $10 \text{ m}$ . Suppose the average absorption coefficient is  $\bar{\alpha} = 0.02$  at  $1000 \text{ Hz}$ . What would be the noise reduction in the reverberant field if  $100$  sound-absorbing panels with dimensions  $1 \text{ m} \times 2 \text{ m}$  each with an absorption coefficient of  $\alpha = 0.8$  at  $1000 \text{ Hz}$  were suspended from the ceiling (assume both sides absorb sound)? The room surface area  $= 2(900) + 4(300) = 3000 \text{ m}^2$ , therefore  $R_1 = (3000 \times 0.02)/0.98 = 60/0.98 = 61.2$  sabins ( $\text{m}^2$ ). The new average absorption coefficient  $\bar{\alpha}_2 = (3000 \times 0.02 + 200 \times 2 \times 0.8)/3400 = 0.11$ . The new room constant is  $(3400 \times 0.11)/0.89 = 420$  sabins ( $\text{m}^2$ ). Thus from Eq. (29) the predicted noise reduction  $\Delta L = 10 \log(420/61.2) = 8.3 \text{ dB}$ . This calculation may be repeated at each frequency for which absorption coefficient data are available. It is normal to assume that about  $10 \text{ dB}$  is the practical limit for the noise reduction that can be achieved by adding sound-absorbing material in industrial situations.

## 7 ADDITIONAL CONSIDERATIONS

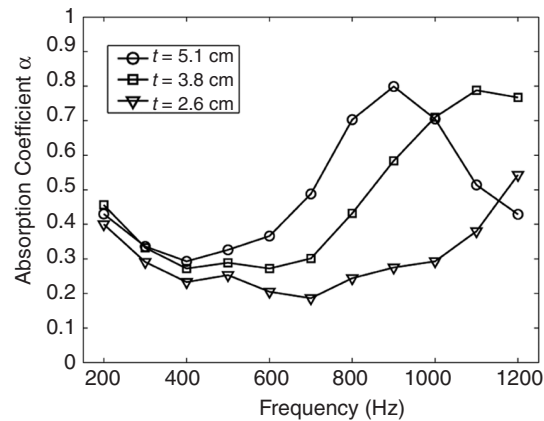
For each application of sound absorptive materials, not only the sound absorption coefficient (or NRC) has to be taken into account for the particular design. Specifications require that the material also be rated for flame spread and fire endurance, usually by use of a standardized test. In addition, consideration of dimensional stability, light reflectance, appearance, weight, maintenance, cleanliness, and cost is required in practice.<sup>30</sup> Most of these considerations are undertaken by the manufacturer.

To prevent the absorptive material from getting contaminated, a splash barrier should be applied over the absorptive lining. This should be a very light material such as one-mil plastic film (see Section 4.3.1). The surface of the absorptive layer may be retained for mechanical strength with expanded metal, perforated sheet metal, hardware cloth, or wire mesh. However, the retaining material should have at least  $25\%$  open area.<sup>45</sup>

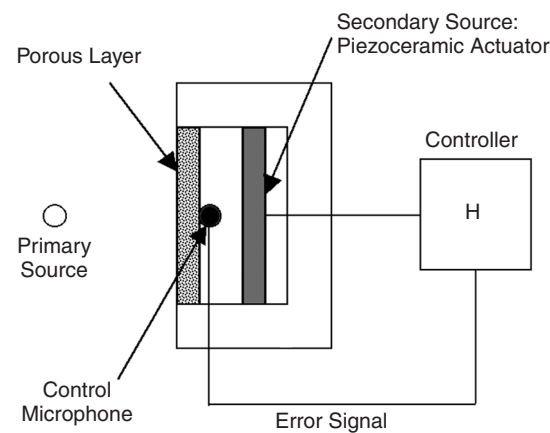
In certain applications (e.g., in the use of absorbing materials in mufflers for ventilation systems) it could be necessary to employ less porous materials such as ceramic absorbers, which have the advantages of much better durability, mechanical strength, and refractory properties. Particular care has to be taken with the use of synthetic mineral wools since they are irritants. These materials could cause long-term health effects for those working in the manufacture of these products.<sup>46</sup> On the other hand, the use of recycled materials to make absorbers has recently been investigated, showing some promising results, in

particular, for granulated mixes of waste foam<sup>47</sup> and small granules of discarded rubber from tires.<sup>48</sup>

The sound-absorbing properties of porous road pavements have been studied by Crocker and Li<sup>49</sup> to reduce interstate highway noise of automobiles. To evaluate the effect of different thicknesses, slabs were manufactured in the laboratory. The slabs consisted of a  $6.35\text{-mm}$  dense graded Superpave mix with a fine  $9.5\text{-mm}$  open graded fine core (OGFC) placed on top. Three different thickness layers were used ( $2.6$ ,  $3.8$ , and  $5.1 \text{ cm}$ ). Figure 17 shows the experimental results of absorption coefficient of OGFC samples measured using the technique described in Section 5.2. It can be observed that the thickness of the porous surface has a large effect on the sharpness of the peaks. Generally, the thicker the porous surface the lower is the peak frequency. With thicker porous surfaces the peaks generally also become broader and the peak absorption



**Figure 17** Sound absorption coefficient of a slab of dense graded Superpave mix with a fine open graded fine core of different thicknesses ( $t$ ) placed on top.



**Figure 18** Hybrid passive/active absorber cell.

is somewhat reduced. For the 5.1-cm sample, the peak frequency is about 900 Hz, which coincides with the noise generated by automobiles in interstate travel. In addition, the sound absorption peak is fairly broad, so it is attractive to use such a porous surface to reduce noise.

More recently, the use of active noise control (see Chapter 63) has been combined with passive control to develop hybrid absorbers. Active control technologies appear to be the only way to attenuate the low-frequency noise components. Therefore, a hybrid passive/active absorber can absorb the incident sound over a wide frequency range. Figure 18 shows the principle of such a device, which combines passive absorbent properties of a porous layer and active control at its rear face, and where the controller can be implemented using digital techniques.<sup>50,51</sup> The use of a piezoelectric actuator as a secondary source and wire meshes as porous material has allowed the design of thin active liners, composed of several juxtaposed cells of absorbers, to be used in the reduction of noise in flow ducts.<sup>51</sup> On the other hand, the combination of active and passive control using microperforated panels has given promising results to be applied in absorbers systems.<sup>52</sup>

## REFERENCES

1. A. J. Price and K. A. Mulholland, The Effect of Surface Treatment on Sound Absorbing Materials, *Appl. Acoust.*, Vol. 1, 1968, pp. 67–72.
2. C. Zwikker and C. W. Kosten, *Sound Absorbing Materials*, Elsevier, Amsterdam, 1949.
3. L. L. Beranek, *Noise and Vibration Control*, McGraw-Hill, New York, 1971.
4. L. E. Kinsler and A. R. Frey, *Fundamentals of Acoustics*, Wiley, New York, 1962.
5. L. L. Beranek, Acoustical Properties of Homogeneous Isotropic Rigid Tiles and Flexible Blankets, *J. Acoust. Soc. Am.*, Vol. 19, 1947, pp. 556–568.
6. D. G. Crighton, A. P. Dowling, J. E. Ffowcs Williams, M. Heckl, and F. G. Leppington, *Modern Methods in Analytical Acoustics*, Springer, London, 1992.
7. J. W. Strutt (Lord Rayleigh), *The Theory of Sound*, Dover, New York, 1945.
8. K. Attenborough and L. A. Walker, Scattering Theory for Sound Absorption in Fibrous Media, *J. Acoust. Soc. Am.*, Vol. 49, 1971, pp. 1331–1338.
9. J. F. Allard, *Propagation of Sound in Porous Media: Modeling Sound Absorbing Materials*, Elsevier Applied Science, London, 1993.
10. M. E. Delany and F. N. Bazley, Acoustical Properties of Fibrous Materials, *Appl. Acoust.*, Vol. 3, 1970, pp. 105–116.
11. J. F. Allard and Y. Champoux, New Empirical Equation for Sound Propagation in Rigid Frame Fibrous Materials, *J. Acoust. Soc. Am.*, Vol. 91, 1992, pp. 3346–3353.
12. F. P. Mechel, *Formulas of Acoustics*, Springer, 2002.
13. M. A. Biot, Theory of Propagation of Elastic Waves in a Fluid-Saturated Porous Solid, *J. Acoust. Soc. Am.*, Vol. 28, 1956, pp. 168–191.
14. F. Simon and J. Pfretzschner, Guidelines for the Acoustic Design of Absorptive Devices, *Noise Vib. Worldwide*, Vol. 35, 2004, pp. 12–21.
15. F. P. Mechel, Design Charts for Sound Absorber Layers, *J. Acoust. Soc. Am.*, Vol. 83, 1988, pp. 1002–1013.
16. R. D. Ford and M. A. McCormick, Panel Sound Absorbers, *J. Sound Vib.*, Vol. 10, 1969, pp. 411–423.
17. F. P. Mechel, Panel Absorber, *J. Sound Vib.*, Vol. 248, 2001, pp. 43–70.
18. M. J. Crocker and A. J. Price, *Noise and Noise Control*, Vol. I, CRC Press, Cleveland, 1975.
19. E. C. H. Becker, The Multiple Panel Sound Absorber, *J. Acoust. Soc. Am.*, Vol. 26, 1954, pp. 798–803.
20. U. Ingard, Perforated Facing and Sound Absorption, *J. Acoust. Soc. Am.*, Vol. 26, 1954, pp. 151–154.
21. A. W. Guess, Result of Impedance Tube Measurements on the Acoustic Resistance and Reactance, *J. Sound Vib.*, Vol. 40, 1975, pp. 119–137.
22. D. Y. Maa, Microperforated-Panel Wideband Absorbers, *Noise Control Eng. J.*, Vol. 29, 1984, pp. 77–84.
23. D. Y. Maa, Potential of Microperforated Panel Absorber, *J. Acoust. Soc. Am.*, Vol. 104, 1998, pp. 2861–2866.
24. T. Dupont, G. Pavic, and B. Laulagnet, Acoustic Properties of Lightweight Micro-perforated Plate Systems, *Acust. Acta Acust.* Vol. 89, 2003, pp. 201–212.
25. V. L. Jordan, The Application of Helmholtz Resonators to Sound Absorbing Structures, *J. Acoust. Soc. Am.*, Vol. 19, 1947, pp. 972–981.
26. K. B. Ginn, *Architectural Acoustics*, Brüel & Kjaer, Naerum, 1978.
27. J. M. A. Smith and C. W. Kosten, Sound Absorption by Slit Resonators, *Acustica*, Vol. 1, 1951, pp. 114–122.
28. U. R. Kristiansen and T. E. Vigran, On the Design of Resonant Absorbers Using a Slotted Plate, *Appl. Acoust.*, Vol. 43, 1994, pp. 39–48.
29. R. K. Cook and P. Chrazanowski, Absorption by Sound Absorbent Spheres, *J. Acoust. Soc. Am.*, Vol. 21, 1949, pp. 167–170.
30. R. Moulder, Sound-Absorptive Materials, in *Handbook of Acoustical Measurements and Noise Control*, 3<sup>rd</sup> ed., C. H. Harris, Ed., Acoustical Society of America, New York, 1998.
31. T. D. Northwood, M. T. Grisaru, and M. A. Medcof, Absorption of Sound by a Strip of Absorptive Material in a Diffuse Sound Field, *J. Acoust. Soc. Am.*, Vol. 31, 1959, pp. 595–599.
32. American Society for Testing and Materials, ASTM C423: Test Method for Sound Absorption and Sound Absorption Coefficients by the Reverberation Room Method, 1984.
33. International Standards Organization, ISO 354: Acoustics—Measurement of Sound Absorption in a Reverberation Room, 1985.
34. T. J. Cox and P. D'Antonio, *Acoustic Absorbers and Diffusers: Theory, Design, and Application*, Spon Press, London, 2004.
35. M. Koyasu, Investigations into the Precision Measurement of Sound Absorption Coefficients in a Reverberation Room, Proc. 6th Int. Congr. on Acoustics, Tokyo, Paper E-5-8, pE189, 1968.
36. American Society for Testing and Materials, ASTM C384: Test Method for Impedance and Absorption of Acoustical Materials by the Impedance Tube Method, 1985.
37. International Standards Organization, ISO 10534-2: Acoustics—Determination of Sound Absorption Coefficient and Impedance in Impedance Tubes, Part 1: Method Using Standing Wave Ratio, 1998.

38. W. Davern, Impedance Chart for Designing Sound Absorber Systems, *J. Sound Vib.*, Vol. 6, 1967, pp. 396–405.
39. American Society for Testing and Materials, ASTM E1050: Test Method for Impedance and Absorption of Acoustical Materials Using a Tube, Two Microphones and a Digital Frequency Analysis System, 1986.
40. International Standards Organization, ISO 10534-2: Acoustics—Determination of Sound Absorption Coefficient and Impedance in Impedance Tubes, Part 2: Transfer-Function Method, 1998.
41. F. J. Fahy and J. G. Walker, *Fundamentals of Noise and Vibration*, E&FN Spon, London, 1998.
42. R. W. B. Stephens and A. E. Bate, *Wave Motion and Sound*, Edward Arnold, London, 1950.
43. L. L. Beranek, *Concert and Opera Halls—How They Sound*, Acoustical Society of America, New York, 1996.
44. M. Barron, *Auditorium Acoustics and Architectural Design*, E&FN Spon, London, 1993.
45. D. P. Driscoll and L. H. Royster, Noise Control Engineering, in *The Noise Manual*, 5th ed., American Industrial Hygiene Association, Fairfax, VA, 2000.
46. National Institute of Occupational Safety and Health, NIOSH Publication 77–152: Criteria for a Recommended Standard: Occupational Exposure to Fibrous Glass, 1977.
47. M. J. Swift, P. Bris, and K. V. Horoshenkov, Acoustic Absorption in Re-cycled Rubber Granulates, *Appl. Acoust.*, Vol. 57, 1999, pp. 203–212.
48. J. Pfretzschner, Rubber Crumb as Granular Absorptive Acoustic Material, Forum Acusticum, Sevilla, Paper MAT-01-005-IP, 2002.
49. M. J. Crocker and Z. Li, Measurements of Tyre/Road Noise and of Acoustical Properties of Porous Road Surfaces, in *Proceedings of Ingeacous 2004*, Univ. Austral of Chile, Valdivia, 2004.
50. M. Furstoss, D. Thenail, and M. A. Galland, Surface Impedance Control for Sound Absorption: Direct and Hybrid Passive/Active Strategies, *J. Sound Vib.* Vol. 203, 1997, pp. 219–236.
51. M. A. Galland, B. Mazeaud, and N. Sellen, Hybrid Passive/Active Absorbers for Flow Ducts, *Appl. Acoust.*, Vol. 66, 2005, pp. 691–708.
52. P. Cobo, J. Pfretzschner, M. Cuesta, and D. K. Anthony, Hybrid Passive-Active Absorption Using Microperforated Panels, *J. Acoust. Soc. Am.*, Vol. 116, 2004, pp. 2118–2125.

# CHAPTER 58

## USE OF BARRIERS

Jorge P. Arenas  
Institute of Acoustics  
Universidad Austral de Chile  
Campus Miraflores  
Valdivia, Chile

### 1. INTRODUCTION

A barrier is a device designed to reflect most of the sound energy incident back toward the source of sound. The use of barriers to control noise problems is an example of a practical application of a complicated physical theory: the theory of diffraction, a physical phenomenon that corresponds to the nonspecular reflection or scattering of sound waves by an object or boundary. Most of the theories of diffraction were originally formulated for optics, but they find many applications in acoustics. Several models and design charts have been partly developed from these theories.

In particular, noise barriers are a commonly used measure to reduce the high levels of environmental noise produced by the traffic on highways. For their proper use, aspects of design, economics, materials, construction details, aesthetic, and durability must be considered to ensure good performance. The fundamentals of the diffraction at the edge of a thin semi-infinite, acoustically opaque plane barrier may be considered as the basis for all subsequent applications. Barriers are used both indoors and outdoors in some applications.

### 2 BASIC THEORY

#### 2.1 Insertion Loss of Barriers

Since the pioneering works on barrier diffraction of Sommerfeld, Macdonald,<sup>1</sup> and others, several

models to predict the acoustics of barriers have been developed. Design charts of Fehr,<sup>2</sup> Maekawa,<sup>3</sup> and Rathe<sup>4</sup> plus the physical and geometrical theories have made possible the development of some equations and convenient algorithms to predict the attenuation of simple barriers. The key work of Kurze and Anderson<sup>5</sup> simplified the task of calculating the attenuation by the use of geometrical parameters, such as Fresnel number.

As in the diffraction of light waves, when the sound reaches a listener by an indirect path over a barrier, there is a shadow zone and a bright zone, as shown in Fig. 1. However, the diffracted wave coming from the top edge of the barrier affects a small transition region close to the shadow zone by interfering with the direct wave.<sup>6</sup>

In 1957 Keller proposed the geometric theory of diffraction (GTD) for barriers, which has been employed in the formulation of many different physical problems.<sup>7</sup> Basically, he stated that from the set of diffracted sound rays from the barrier edge, the ray that reaches the reception point corresponds to the ray that satisfies Fermat's principle.

This geometrical theory of diffraction leads to relatively simple formulas, which combine the practicability of Kirchhoff's approximations with the greater accuracy of the Sommerfeld-type solutions and can be generalized to treat diffraction by three-dimensional

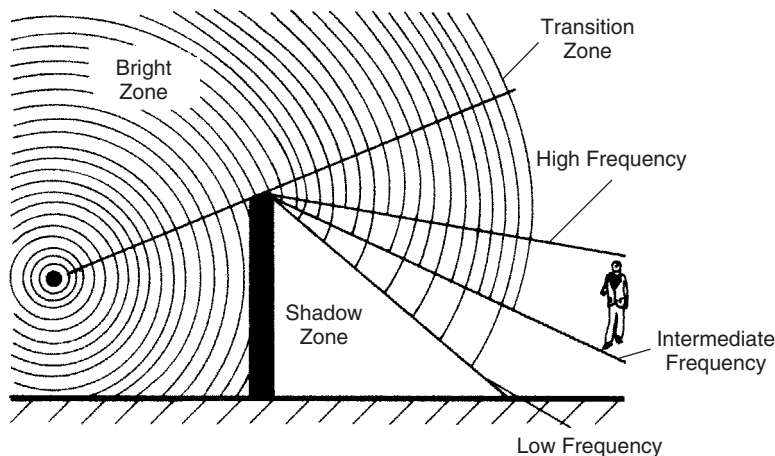


Figure 1 Diffraction by a rigid barrier.



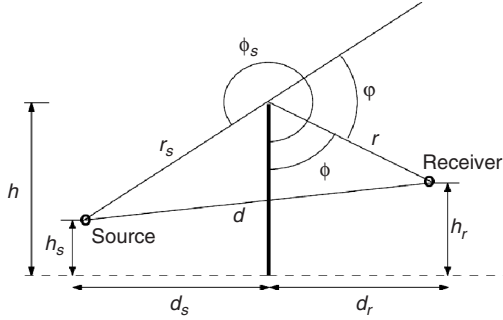


Figure 2 Geometry used in the theory of diffraction.

objects of any smooth shape.<sup>8</sup> The geometrical situation is sketched in Fig. 2. For an infinite extended and very thin semiplane, and assuming no reflections on the ground, the diffracted sound pressure amplitude is

$$\Psi = \frac{-1}{2\sqrt{2\pi k}} \frac{Q(\phi, \phi_s)}{\sqrt{rr_s(r+r_s)}} \exp \left\{ i \left( k[r+r_s] + \frac{\pi}{4} \right) \right\} \quad (1)$$

where  $r_s$  is the distance between the source and the top of the plane,  $r$  is the distance between the top of the plane and the reception point,  $k$  is the free-field wave number, and

$$Q(\phi, \phi_s) = \frac{1}{\cos \frac{1}{2}(\phi + \phi_s)} + \frac{1}{\cos \frac{1}{2}(\phi - \phi_s)} \quad (2)$$

The function  $Q(\phi, \phi_s)$  implies that the edge of the plane radiates sound as a directional sound source. Equation (1) must include the term  $1/\sqrt{2\pi k}$  to describe in a correct way the directivity of the diffracting edge when it is considered as a secondary source (frequency dependent). The sum in Eq. (2) corresponds to contributions from the source and its image due to reflection at the barrier. In addition, from Eq. (1) it is observed that for a fixed value of  $r_s$ , which satisfies the condition  $kr_s > 1$ , the amplitude of the sound wave is proportional to  $1/\sqrt{r}$  for points located close to the diffracting edge. This implies cylindrical divergence and thus a decay of 3 dB per doubling of distance.

On the other hand, for points far away from the edge, the amplitude will be proportional to  $1/r$ , that is, spherical divergence. Therefore, the sound pressure level will decay 6 dB per doubling the distance. This important fact can also be obtained from the asymptotic analysis of the physical solution obtained by Macdonald.<sup>1</sup> To obtain the insertion loss (IL) from Keller's theory, the ratio between Eq. (1) and the sound pressure amplitude for a spherical wave propagating with free-field conditions has to be found. The attenuation in decibels from Keller's theory is given by

$$IL_K = -10 \log \left[ \frac{d^2}{8k\pi rr_s(r+r_s)} |Q(\phi, \phi_s)|^2 \right] \quad (3)$$

where  $d$  is the straight line distance between the source and the reception point (see Fig. 2).

Certainly, from a practical point of view, most of the applications of the physical and geometrical theory had been difficult to use due to the complexity of the analysis, which does not permit fast calculation for design purposes. Because of this, several algorithms, charts, and plots have been developed from time to time. One of the most well-known simplifications was proposed by Redfearn in 1940.<sup>9</sup> A design chart was presented where the graphical relationship between the attenuation and the parameter  $h/\lambda$  can be read. The parameter  $h$  corresponds to the "effective height" of the barrier and  $\lambda$  is the wavelength of the incident sound wave. The parameter  $h/\lambda$  is usually known as the Redfearn parameter and it can be shown that

$$\frac{h}{\lambda} = \frac{rr_s}{\lambda d} \sin \phi \quad (4)$$

Since a rigorous solution of the diffraction problems involve several parameters in its formulation, it is clear that the approximations using the Redfearn chart could involve large errors.

In 1971 Kurze and Anderson reported a seminal study that presented one algorithm widely used today.<sup>5</sup> This algorithm was obtained by comparing the experimental results of Rathe<sup>4</sup> and Redfearn<sup>9</sup> and the geometric theory of diffraction. Their final equation can be derived from the Redfearn parameter. In fact, considering Eqs. (1) and (2) and the geometrical relationships between  $\phi$ ,  $\phi_s$ , and  $\varphi$ , the insertion loss (the difference of the sound pressure levels at the receiving point with and without the screen present), can be expressed as

$$IL_K = 10 \log \left[ 8\pi^2 \frac{h}{\lambda} \tan \left( \frac{\varphi}{2} \right) \right] - 10 \log \frac{d}{r+r_s} - 20 \log \left[ 1 + \frac{\sin(\varphi/2)}{\sin(\phi + \varphi/2)} \right] \quad (5)$$

where

$$\varphi = \arccos \frac{d_s d_r + h h_r - h^2}{\sqrt{[d_r^2 + (h - h_r)^2][d_s^2 + h^2]}} \quad (6)$$

and

$$\phi = \arcsin \frac{d_r}{\sqrt{d_r^2 + (h - h_r)^2}} \quad (7)$$

according to the geometry shown in Fig. 2.

For  $\varphi > \pi/4$ , the first term of Eq. (5) gives a good approximation to the results of Rathe. The second term is very small for perpendicular incidence  $\phi_s = 3\pi/2$ , and it could be very large for close positions of the source and receiver to the screen. The third term is small for small angles of diffraction, but it has to be considered when the receiver or the source is close to the barrier. Maekawa<sup>3</sup> presented a chart based on the physical theory of diffraction and also

numerous experimental results. His chart gave values of attenuation versus the dimensionless Fresnel number defined as

$$N = \pm \frac{2}{\lambda} \delta = \pm \frac{2}{\lambda} (r_s + r - d) \quad (8)$$

where  $\delta$  is called the path length difference. The  $\pm$  is used to indicate the corresponding zone, such that  $N$  is positive in the shadow zone and negative in the bright zone.

Now, the Fresnel number, in terms of the geometry shown in Fig. 2, can be calculated as

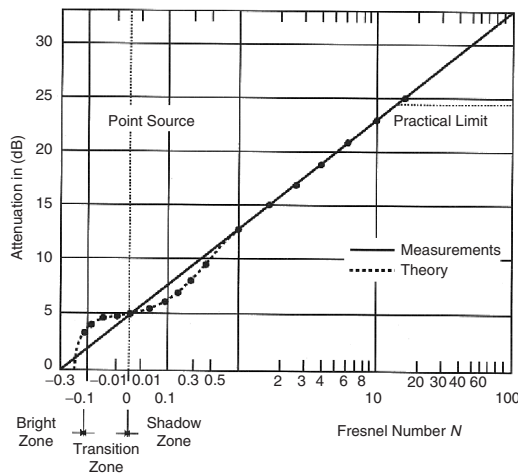
$$N = \sqrt{d_s^2 + h^2} + \sqrt{d_r^2 + (h - h_r)^2} - \sqrt{h_r^2 + (d_s + d_r)^2} \quad (9)$$

For values of  $N > 1$ , Maekawa's result for insertion loss can be approximated by  $13 + 10 \log N$ . When  $\varphi \ll 1$  and  $d \rightarrow r + r_s$ , the insertion loss can be approximated by  $5 + 10 \log 4\pi N$ .

However, to find a more reliable expression for attenuation, Kurze and Anderson<sup>5</sup> modified the results of the last expression and obtain an analytical-empirical equation known as the Kurze-Anderson algorithm given by

$$IL_{KA} = 5 + 20 \log \frac{\sqrt{2\pi N}}{\tanh \sqrt{2\pi N}} \quad (10)$$

Equation (10) gives good results in practice for  $N > 0$  and it shows good agreement with the experimental results obtained by Maekawa,<sup>3</sup> for values of attenuation up to 24 dB (see Fig. 3). Equation (10) has been the starting point to define most of the barrier design algorithms used today to mitigate the impact of noise from highways.



**Figure 3** Attenuation of the sound from a point source by a rigid screen as a function of Fresnel number.

## 2.2 Transmission Loss of Barriers

Barriers are a form of partial enclosure (they do not completely enclose the source or receiver) to reduce the direct sound field radiated in one direction only. The barrier edges diffract the sound waves, but some waves can pass through the barrier according to the sound transmission laws. All the theories of diffraction have been developed assuming that the transmission loss of the barrier material is sufficiently large that transmission through the barrier can be ignored. Obviously, the heavier the barrier material, or the higher the frequency, the greater the transmission loss for sound going through the barrier.

A generally applicable acoustical requirement for a barrier material is to limit the component of sound passing through it to 10 dB less than the predicted noise level due to sound diffracted over the barrier. Evidently, this is not a governing criterion for concrete or masonry, but can be important for light aluminum, timber, and for glazing panels. In addition, this may be an important consideration when designing "windows" in very tall barriers.

In a study on barriers used indoors, Warnock compared the transmitted sound through a barrier with the diffracted sound over the barrier.<sup>10</sup> He found that the transmitted sound is negligible if the surface density of a single screen satisfies the criterion  $\rho_s = 3\sqrt{\delta}$  kg/m<sup>2</sup>. The minimum acceptable value of  $\rho_s$  corresponds to the transmission loss at 1000 Hz being 6 dB higher than the theoretical diffraction loss. A formula for calculating the minimum required surface density for a barrier is<sup>11</sup>

$$\rho_s = 3 \times 10^{(A-10/14)} \text{ kg/m}^2 \quad (11)$$

where  $A$  is the A-weighted potential attenuation of the barrier in decibels when used outdoors.

As a general rule, when the barrier surface density  $\rho_s$  exceeds 20 kg/m<sup>2</sup>, the transmitted sound through the barrier can be ignored, and then the diffraction sets the limit on the noise reduction that may be achieved.

According to the discussion above, when butting or overlapping components assemble a noise barrier, it is important that the joints be well sealed to prevent leakage. As an indication, it is common for timber barriers to be manufactured from 19-mm-thick material. As indicated by the mass law, this provides a sound reduction index of 20 dB if joints are tight, which is quite sufficient for barriers designed to provide an attenuation of 10 dB. In some countries, the legislation requires a sample of barrier to be tested in accordance with the local standard for sound insulation of partitions in buildings.

## 3 USE OF BARRIERS INDOOR

Single-screen barriers are widely used in open-plan offices (or landscaped offices) to separate individual workplaces to improve acoustical and visual privacy. The basic elements of these barriers are freestanding screens (partial-height partitions or panels). However,

when placing a sound barrier in a room, the reverberant sound field and reflections from other surfaces cannot be ignored.

The diffraction of the sound waves around the barrier boundaries alters the effective directivity of the source [see Eq. (2)]. For a barrier placed in a rectangular room, if the receiver is in the shadow zone of the barrier and the sound power radiated by the source is not affected by insertion of the barrier, the approximate insertion loss can be calculated by<sup>12</sup>

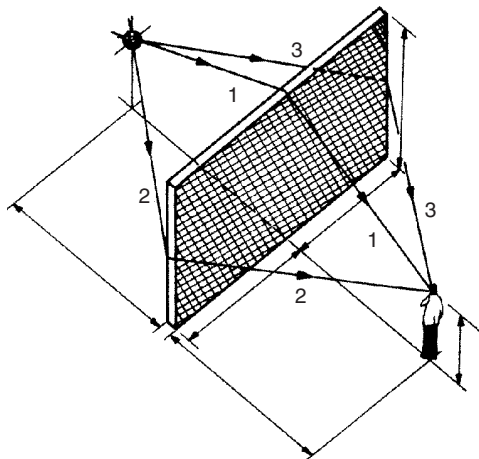
$$IL = 10 \log \left( \frac{\frac{Q_\theta}{4\pi r^2} + \frac{4}{S_0 \alpha_0}}{\frac{Q_B}{4\pi r^2} + \frac{4\Gamma_1 \Gamma_2}{S(1 - \Gamma_1 \Gamma_2)}} \right) \quad (12)$$

where  $Q_\theta$  is the source directivity factor,  $S_0 \alpha_0$  is the room absorption for the original room before placing the barrier,  $S_0$  is the total room surface area,  $\alpha_0$  is the mean room Sabine absorption coefficient,  $S$  is the open area between the barrier perimeter and the room walls and ceiling,

$$Q_B = Q_\theta \sum_{i=1}^n \left( \frac{1}{3 + 10N_i} \right) \quad (13)$$

is the effective directivity,  $n$  is the number of edges of the barrier (e.g.,  $n = 3$  for a freestanding barrier, see Fig. 4), and  $\Gamma_1$  and  $\Gamma_2$  are dimensionless numbers related to the room absorption on the source side ( $S_1 \alpha_1$ ) and the receiver side ( $S_2 \alpha_2$ ) of the barrier, respectively, as well as the open area, and given by

$$\Gamma_1 = \frac{S}{S + S_1 \alpha_1} \quad \text{and} \quad \Gamma_2 = \frac{S}{S + S_2 \alpha_2} \quad (14)$$



**Figure 4** Freestanding barrier used indoors and the three diffraction paths.

Therefore,  $S_1 + S_2 = S_0$  + (area of two sides of the barrier) and  $\alpha_1$  and  $\alpha_2$  are the mean Sabine absorption coefficients associated with areas  $S_1$  and  $S_2$ , respectively.

It has to be noticed that when the barrier is located in a highly reverberant field the IL tends to zero, which means that the barriers are ineffective in highly reverberant environments. Consequently, in this case the barrier should be treated with sound-absorbing material, increasing the overall sound absorption of the room.

The approximation for the effective directivity given in Eq. (13) is based on Tadge's result.<sup>13</sup> In deriving Eq. (12) the interference between the sound waves has been neglected, so Eq. (12) predicts the insertion loss accurately when octave-band analysis is used. However, the effects of the reflections in the floor and the ceiling are not taken into account. This effect will be discussed later. In general, the ceiling in an open-plan office must be highly sound absorptive to ensure maximum performance of a barrier. This is particularly important at those frequencies significant for determining speech intelligibility (500 to 4000 Hz).

A more general model for calculating the insertion loss of a single-screen barrier in the presence of a floor and a ceiling has been presented by Wang and Bradley.<sup>14</sup> Their model was developed using the image source technique.

Recently, a new International Organization for Standardization standard has been published on the guidelines for noise control in offices and workrooms by means of acoustical screens.<sup>15</sup> The standard specifies the acoustical and operational requirements to be agreed upon between the supplier or manufacturer and the user of acoustical screens. In addition, the standard is applicable to (1) freestanding acoustical screens for offices, service areas, exhibition areas, and similar rooms, (2) acoustical screens integrated in the furniture of such rooms, (3) portable and removable acoustical screens for workshops, and (4) fixed room partitions with more than 10% of the connecting area open and acoustically untreated.

#### 4 USE OF BARRIERS OUTDOORS

The use of barriers outdoors to control the noise from highways is surely the most well-known application of barriers. While noise barriers do not eliminate all highway traffic noise, they do reduce it substantially and improve the quality of life for people who live adjacent to busy highways. Noise barriers include walls, fences, earth berms, dense plantings, buildings, or combinations of them that interrupt the line-of-sight between source and observer. It appears that construction of barriers is the main alternative used for the reduction of noise, although quiet road surfaces, insulation of properties, or use of tunnels have also been used for this purpose.

The theory discussed so far has been established for point or coherent line sources. However, the sound radiated from a highway is composed for several incoherent moving sources (vehicles of different

types). It has been shown<sup>6</sup> that when a noise source approximates to an incoherent line source (stream of traffic), then the insertion loss is about 5 dB lower than the one calculated for a point source. From field results it has also been observed that earth berms (mounds of earth) produce about 3 dB more attenuation than walls of the same height. Then, predicted barrier attenuation values will always be approximations.

Attenuation other than resulting from wave divergence is called excess attenuation. Noise reduction due to a barrier is considered as a reduction to be added to other reductions due to such effects as spherical spreading, attenuation by absorption in the air, wind and temperature gradients, presence of grass and trees, and the like. Therefore, it is common to refer to the excess attenuation by a barrier instead of insertion loss of barriers.

#### 4.1 Finite Barrier

If a barrier is finite in length (as the barriers used indoors), flanking (noise traveling around the ends of the barrier) will reduce the attenuation. In highway applications, it is recommended that the minimum angle of view that should be screened to avoid flanking is 160°. This means that to effectively reduce the noise coming around its ends, a barrier should be at least eight times as long as the distance from the home or receiver to the barrier.

For a barrier finite in length, parallel to a highway, and located between the highway and the observer, as shown in Fig. 5, the approximate A-weighted attenuation in decibels is given by<sup>16</sup>

$$A = 10 \log \left( \frac{1}{\beta_2 - \beta_1} \int_{\beta_1}^{\beta_2} 10^{A(\beta)/10} d\beta \right) \quad (15)$$

where  $\beta$  is the angular position of the source from a perpendicular drawn from the observer to the highway,  $A(\beta)$  is a function given by:

1. For  $N_{\max} \cos \beta \leq -0.1916 - 0.0635b^*$ ,

$$A(\beta) = 0 \quad (16a)$$

2. For  $-0.1916 - 0.0635b^* < N_{\max} \cos \beta \leq 0$ ,

$$A(\beta) = 5(1 + 0.6b^*) + 20 \log \frac{\sqrt{-2\pi N_{\max} \cos \beta}}{\tan \sqrt{-2\pi N_{\max} \cos \beta}} \quad (16b)$$

3. For  $0 < N_{\max} \cos \beta < 5.03$ ,

$$A(\beta) = 5(1 + 0.6b^*) + 20 \log \frac{\sqrt{2\pi N_{\max} \cos \beta}}{\tan \sqrt{2\pi N_{\max} \cos \beta}} \quad (16c)$$

4. For  $N_{\max} \cos \beta \geq 5.03$ ,

$$A(\beta) = 20(1 + 0.15b^*) \quad (16d)$$

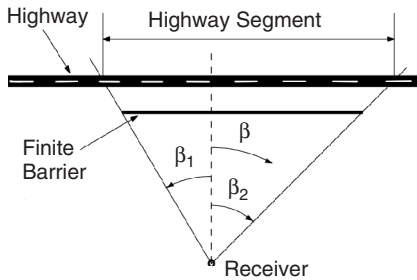
$N_{\max}$  is the Fresnel number when the source-to-observer path is perpendicular to the barrier, and  $b^*$  is the berm correction (0 for a freestanding wall or 1 for an earth berm). Thus, for an infinite barrier,  $\beta_1 = -\pi/2$  and  $\beta_2 = \pi/2$ .

The noise attenuation of a finite barrier calculated by Eq. (15) includes just the segment of incoherent source line that the receiver cannot see. Then, the contribution to the total noise of the segments not covered by the barrier should be estimated accordingly.<sup>17</sup>

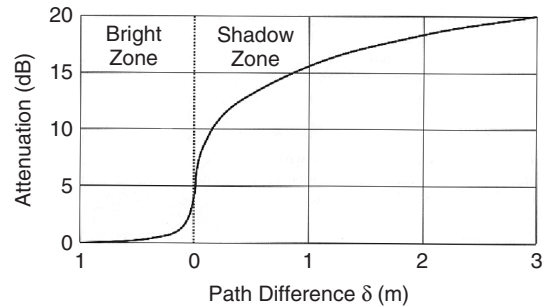
It is possible to calculate Eq. (15) for each frequency band. However, to save time, an effective radiating frequency of 550 Hz is, in general, used as representative of a normalized A-weighted noise spectrum for traffic over 50 km/h.<sup>18,19</sup> Then, the Fresnel number can be evaluated as  $N = 3.21 \times \delta$ . Under this assumption, the A-weighted barrier attenuation in decibels for an infinite freestanding wall, as a function of  $\delta$ , is shown in Fig. 6.<sup>17</sup>

#### 4.2 Nonparallel Barrier

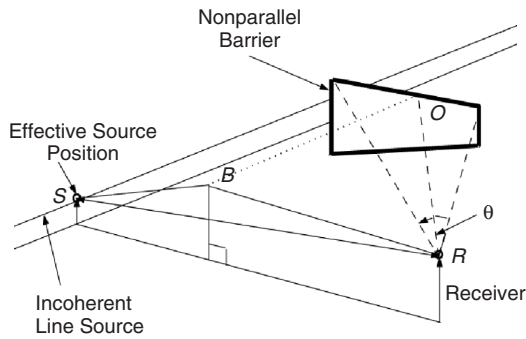
For evaluating the attenuation of a barrier not parallel to an incoherent source line, it is necessary to determine



**Figure 5** Top view of the finite barrier parallel to a highway.



**Figure 6** A-weighted attenuation for traffic noise as a function of path difference.



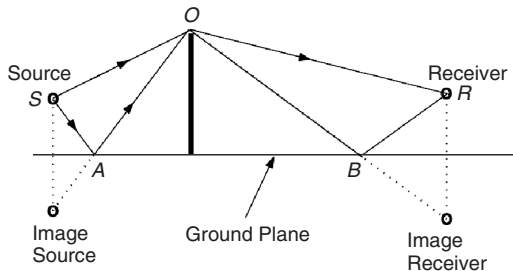
**Figure 7** Geometry for a barrier that is not parallel to the source line.

the equivalent path length difference ( $\delta$ ) that gives the effective source position.<sup>20</sup> The geometry is shown in Fig. 7. First, a line bisecting the angle  $\theta$  is drawn from the receiver point to the top edge of the barrier (point  $O$ ). Then, a line is drawn from point  $O$  parallel to the source line to meet the vertical plane (i.e., normal to the road surface), which passes through the receiver point  $R$  and the effective source position  $S$  at  $B$ .

Finally, the equivalent path difference is calculated as  $\delta = SB + BR - SR$ . The attenuation is then calculated for this equivalent  $\delta$ .

### 4.3 Reflections on the Ground

When considering the reflections of sound on the ground, extra propagation paths are created that can result in increased sound pressure at the receiver. The geometry showing reflection on an acoustically hard ground for an infinite barrier is shown in Fig. 8. Application of the image source method indicates that a total of four diffraction paths must be considered:  $SOR$ ,  $SAOBR$ ,  $SAOR$ , and  $SOBR$ . Therefore, the attenuation and expected sound pressure level at the receiver has to be calculated for each of the four paths. Then, the four expected sound pressure levels are combined logarithmically to obtain the sound level with the barrier. The process is repeated for the pressure case without the barrier (which has just two paths) to calculate the combined level at the receiver before placing the barrier. Then, the insertion loss is determined as usual. If the



**Figure 8** Image method for reflections on the ground.

barrier is finite, eight separate paths should be considered since the diffraction around the ends involves only one ground reflection.

Usually, the ground is somewhat absorptive. Therefore, the amplitude of each reflected path has to be reduced by multiplying its amplitude by the pressure reflection coefficient of the ground.<sup>17,21-24</sup>

Other reflections can affect the performance of a barrier, in particular when dealing with parallel barriers. This is the case when barriers are constructed on both sides of a road or when the road is depressed with vertical retaining walls. To overcome this problem of multiple reflections and insertion loss degradation, it is possible to:

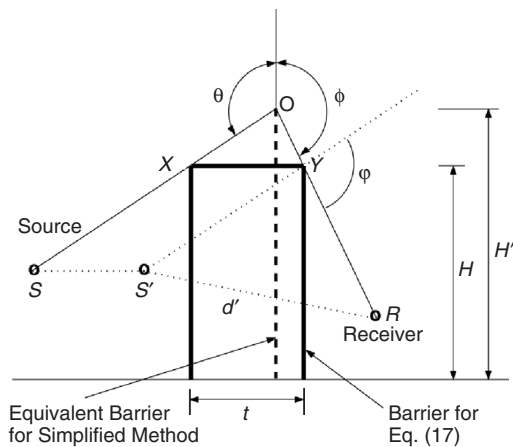
1. Increase the height of the barriers.
2. Use barriers with sound-absorbing surfaces facing the traffic [a noise reduction coefficient (NRC) greater than 0.65 is recommended].
3. Simply tilt the barriers outward (a tilt of  $5^\circ$  to  $15^\circ$  is usually recommended).

### 4.4 Thick Barrier

A barrier cannot always be treated as a very thin screen. An existing building can interrupt the line-of-sight between the source and a receiver acting as a thick barrier when its thickness is greater than the wavelength of the incident sound wave. Double diffraction at the two edges of a thick barrier may increase the attenuation. A simplified method to calculate the attenuation of a thick barrier is shown in Fig. 9. It is necessary to transform the thick barrier, of height  $H$ , into an equivalent thin barrier of height  $H'$ , and then to calculate its attenuation using the usual equations.

A more accurate method has been proposed.<sup>25</sup> The effect of the double diffraction is to add an additional term to the attenuation due to a thin barrier. In Fig. 9 the line  $S'Y$  is parallel to the line  $SX$ . The attenuation of the thick barrier is

$$A = A_0 + K \log \frac{2\pi t}{\lambda} \quad (17)$$



**Figure 9** Geometry for evaluating the attenuation of a thick barrier.



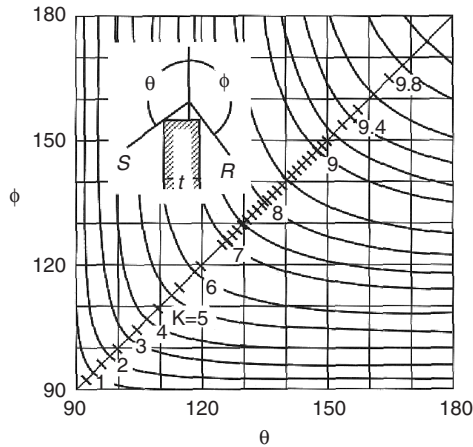


Figure 10 Thick barrier correction factor  $K$  for Eq. (17).

where  $A_0$  is the attenuation of a thin barrier for which  $\delta = S'Y + YR - d'$  (see Fig. 9),  $t$  is the barrier thickness, and  $K$  is a coefficient that can be estimated using Fig. 10.

#### 4.5 Double Barrier

In some cases inclusion of a second barrier placed parallel to and behind the first is used to seek additional attenuation or because of design requirements, as in the case of emergency access and maintenance. Figure 11 shows a double barrier. It can be observed that the edge of the barrier closer to the source will become a secondary line source for the second barrier.

A method to calculate the effective attenuation of the double barrier has been presented by Foss,<sup>26</sup> and this method has been implemented in the traffic noise model of the Federal Highway Administration (FHWA).<sup>17</sup> The effective attenuation is calculated by

$$A = F + J - \left\{ 6 \exp\left(\frac{-2W}{T}\right) + 1.3 \left[ \exp\left(\frac{-35W}{T} - 1\right) \right] \right\} \times \left[ 1 - \exp\left(\frac{-J}{2}\right) \right] \quad (18)$$

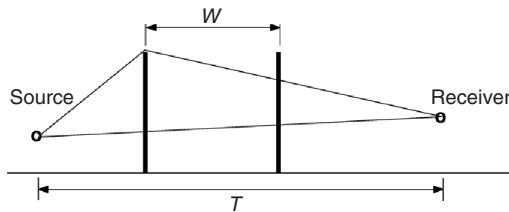


Figure 11 Double-barrier geometry.

where the parameters are defined in Fig. 11, and  $F$  and  $J$  are calculated according to the Foss double-barrier algorithm. First, the attenuation is calculated for each barrier alone, ignoring the other.  $F$  is the higher of the two attenuations, and its associated barrier is designated as the "best" barrier. Then, depending on which is closer, either the source or the receiver is moved to the top of the best barrier. A modified barrier geometry is then drawn from the top of the best barrier over the other barrier to actual source or receiver. The attenuation for this modified geometry is  $J$ . Then, the effective attenuation is calculated using Eq. (18).

The screening effect in the sound propagation outdoors has been included in an ISO standard.<sup>27</sup> This standard includes equations for both single and double diffraction and a correction factor for meteorological effects to predict the equivalent continuous A-weighted sound pressure levels. On the other hand, the in situ determination of the insertion loss of outdoor noise barriers is also described by an ISO standard.<sup>28</sup>

#### 4.6 Additional Improvements

In certain applications it may be necessary to enhance the attenuation provided by a single barrier without increasing its height. One example of this would be the need to increase a barrier's effectiveness without further reducing the view for residents living alongside a road that would be caused by use of a higher barrier. All the studies show that the use of some kind of element over the top of the barrier or the modification of its profile will change the original diffracted sound field.<sup>29</sup> In some cases this alternative can produce a significant improvement of the attenuation.

Theoretical and experimental studies on diffracting-edge modifications include T- and Y-shaped barriers,<sup>30-32</sup> multiple-edge barriers,<sup>33</sup> and tubular caps and interference devices placed on top of barriers.<sup>34-36</sup> Full-scale tests of the acoustical performance of new designs of traffic noise barriers have been reported by Watts et al.<sup>37</sup>

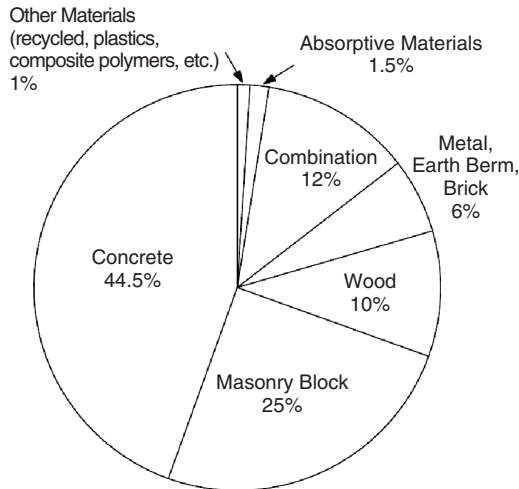
Other options to improve the performance of a barrier are the use of modular forms of absorbing barriers,<sup>38</sup> absorbent edges,<sup>39</sup> and by developing random profiles of different heights and widths, depending on the acoustic wavelength that has to be taken into account.<sup>40</sup>

However, these alternatives are still under research and, sometimes, it is difficult to compare the results between different studies since the barrier heights, source position, receiver position, and ground conditions are all different.

#### 5 DESIGN ASPECTS

In the design of a barrier all of the relevant environmental, engineering, and safety requirements have to be considered. In addition to mitigate the impact of a highway, a barrier will become part of the landscape and neighborhoods. Therefore, some consideration has to be taken to assure a positive public reaction.

Both acoustical and landscape issues, to give guidance on good practice and design aspects, have been discussed widely in the technical literature.<sup>41,42</sup>



**Figure 12** Types of material used to construct barriers in the United States (until 1998).

### 5.1 Materials and Costs

A good design has to take into account that a barrier should require minimal maintenance other than cleaning or repair of damage for many years. Therefore, attention should be paid to the selection of materials used in the construction of barriers, in particular, for areas subject to extreme weather conditions. Noise barriers can be constructed from earth, concrete, masonry, wood, metal, plastic, and other materials or combination of materials. A report showed that until 1998 most barriers built in the United States have been made from concrete or masonry block, range from 3 to 5 m in height, and slightly more than 1% have been constructed with absorptive materials.<sup>43</sup> Figure 12 presents a comparison of the types of material used to construct barriers in the United States.

Evidently, concrete or masonry walls require little or no maintenance during the service life, but transparent sections need frequent cleaning and might well need replacing after some time. The durability of sound-absorbing materials for highway noise barriers has been discussed by some authors.<sup>44</sup>

Often it is necessary to provide access from the protected side for maintenance purposes and for pedestrians or cyclists, which render a barrier vulnerable to vandalism. In addition, it may be advisable to avoid the use of flammable materials in some fire-risk areas and, in general, it may be appropriate to install fire-breaks to limit the spread of fire.<sup>45</sup> When plants are selected for use in conjunction with a barrier, they should generally be of hardy species (native plantings are preferable) that require a low level of maintenance.

A designer should seek detailed information for a specific project to estimate the cost of barrier construction and maintenance. This is particularly

important when cost effectiveness is a must for positive decision on the construction of a barrier, since in some countries governmental agencies and individual homeowners sometimes share the costs of noise barriers.

A broad indication of the relative costs, for a selection of typical forms of construction at a standard height of 3 m, is shown in Table 1.

Some additional aspects of the design of a barrier that need to be considered are the force caused by wind, aerodynamic forces caused by passing vehicles, the possibility of impact by errant vehicles, earthquakes, noise leaking through any gaps between elements or at the supports, and the effect of snow being thrown against the face of the barrier by clearing equipment.

### 5.2 Human Response

The public, increasingly well-informed about the problem of excessive noise, is taking actions on the development of new transport infrastructure projects and improvement to existing infrastructure.

Most of the residents near a barrier seem to feel that highway noise barriers effectively reduce traffic noise and that the benefits of barriers far outweigh the disadvantages of barriers. Some studies have shown that public reaction to highway noise barriers appears to be positive.<sup>46</sup> However, specific reactions vary widely. Residents adjacent to barriers have reported that conversations in households are easier, sleeping conditions are better, the environment is more relaxing, windows are opened more often, and yards are used more in the summer. In addition, residents perceived indirect benefits, such as increased privacy, cleaner air, improved views, a sense of ruralness, and healthier lawns. Negative reactions from residents have included a restriction of view, a feeling of confinement, a loss of air circulation, a loss of sunlight and lighting, and poor maintenance of the barrier.

On the other hand, motorists have sometimes complained of a loss of view or scenic vistas and a feeling of being "walled in" when traveling adjacent to barriers. High barriers substantially conceal the view of existing landmarks from the road, but they also conceal visual clutter, which might otherwise distract the attention of drivers. It is recommended that the appearance of barriers should be designed to avoid monotony. Surveys of drivers in Holland have indicated that a view that is unchanging for 30 s is monotonous.<sup>42</sup> This suggests that changes in design of barrier face every 800 m are desirable for long barriers adjacent to a high-speed road.

Noise barriers should reflect the character of their surroundings or the local neighborhood as much as possible to be acceptable to local residents. It is always recommended to preserve aesthetic views and scenic vistas. The visual character of noise barriers in relationship to their environmental setting should be carefully considered. For example, a tall barrier near a one-story, single-family, detached residential area can have a negative visual effect. In general, it is recommended to locate a noise barrier approximately

**Table 1 Construction and Maintenance Cost of Different Barriers**

Barrier Type	Assumed Features of Design	Factors of Maintenance	Relative Cost of Construction	Relative Cost of Maintenance
Earth mound	Agricultural land price, landscape planting excluded Local source of fill assumed	Grass cutting, planting maintenance	Very low	Fairly low
Timber screen	Designed in accordance with current standards	Inspection/repair, periodic treatment	Low	Low
Concrete screen	Precast pier, beams, and panels	Inspection/repair, periodic cleaning	Fairly low	Very low
Brickwork/masonry wall	Standard facing brick	Inspection/repair, periodic cleaning/repainting	Moderate	Very low
Plastic/planted system	Plastic building "blocks" (planters)	Inspection/repair, periodic cleaning, planting maintenance, irrigation	Moderate	Moderate
Metal panels	Plastic-coated metal panels with steel supports	Inspection/repair, repainting/treatment  Tighten bolts, check earthing	Moderate	Fairly low
Absorbent panels	Perforated (absorbent) metal panels with rockwool infill	Inspection/repair, periodic cleaning	Moderate	Fairly low
Transparent panels	Steel piers, etched glass panels	Inspection/repair, regular cleaning/treatment	Fairly high	Fairly high
Crib wall (concrete or timber)	Proprietary system or purpose designed High labor costs, agricultural land price	Inspection/repair	Very high	Low

Source: Adapted from Ref. 41.

four times its height from residences and to provide landscaping near the barrier to avoid visual dominance and reduce visual impact.<sup>46</sup>

### 5.3 Computational Aid

There are a number of commercially available software programs to help in designing barriers. Most programs are designed to predict the noise levels produced by sources such as factories, industrial facilities, highways, railways, and the like. Their use is widely accepted in environmental impact studies when the solution of problems of high geometrical complexity is required.

The programs are, in general, able to compute the sound pressure level contours, insertion loss contours, and level difference contours. Some of these programs implement governmental approved models to predict traffic noise as well as more specialized enhancements. Then, problems involving diffraction by building rows, trees zone, parallel-barrier degradation for barriers, or retaining walls that flank a roadway are possible to solve. Some of the programs can make work much easier in that they incorporate vehicle noise emission databases. The results predicted by these programs agree quite well with experimental results since the

**Table 2 Partial List of Noise Prediction Software**

Software Product Name	Developed by	Location	Website
ArcAkus	Akusti	Finland	www.akusti.com
CADNA	Datakustik	Germany	www.datakustik.de
ENM	RTA Technology	Australia	www.rtagroup.com.au
IMMI	Wölfel	Germany	www.woelfel.de
LIMA	Stapelfeldt	Germany	www.stapelfeldt.de
MITHRA	01 dB	France	www.01 dB.com
NoiseMap	WS Atkins N&V	United Kingdom	www.noisemap2000.com
SoundPlan	Braunstein + Berndt	Germany	www.soundplan.com
TNM	FHWA	United States	www.mctrans.ce.ufl.edu



models have been calibrated to field measurements. Several such programs are listed in Table 2.

## REFERENCES

1. H. M. MacDonald, A Class of Diffraction Problems, *Proc. Lond. Math. Soc.*, Vol. 14, 1915, pp. 410–427.
2. R. O. Fehr, The Reduction of Industrial Machine Noise, Proc. 2nd Ann. Nat. Noise Abatement Symposium, Chicago, 1951, pp. 93–103.
3. Z. Maekawa, Noise Reduction by Screens, *Appl. Acoust.*, Vol. 1, 1968, pp. 157–173.
4. E. J. Rathe, Note on Two Common Problems of Sound Propagation, *J. Sound Vib.*, Vol. 10, 1969, pp. 472–479.
5. U. J. Kurze and G. S. Anderson, Sound Attenuation by Barriers, *Appl. Acoust.*, Vol. 4, 1971, pp. 35–53.
6. U. J. Kurze and L. L. Beranek, Sound Propagation Outdoors, in *Noise and Vibration Control*, L. L. Beranek, Ed., McGraw-Hill, New York, 1971, Chapter 7.
7. J. B. Keller, The Geometrical Theory of Diffraction, *J. Opt. Soc. Am.*, Vol. 52, 1962, pp. 116–130.
8. U. J. Kurze, Noise Reduction by Barriers, *J. Acoust. Soc. Am.*, Vol. 55, 1940, pp. 504–518.
9. R. S. Redfearn, Some Acoustical Source-Observer Problems, *Phil. Mag. J. Sci.*, Vol. 30, 1940, pp. 223–236.
10. A. C. C. Warnock, Acoustical Effects of Screens in Landscaped Offices, *Canadian Building Digest*, Vol. 164, National Research Council of Canada, 1974.
11. Department of Transport, Noise Barriers—Standards and Materials, Technical Memorandum H14/76, Department of Transport, London, 1976.
12. J. Moreland and R. Minto, An Example of In-Plant Noise Reduction with an Acoustical Barrier, *Appl. Acoust.*, Vol. 9, 1976, pp. 205–214.
13. R. B. Tatge, Barrier-Wall Attenuation with a Finite-Sized Source, *J. Acoust. Soc. Am.*, Vol. 53, 1973, pp. 1317–1319.
14. C. Wang and J. S. Bradley, A Mathematical Model for a Single Screen Barrier in Open-Plan Office, *Appl. Acoust.*, Vol. 63, 2002, pp. 849–866.
15. ISO 17624, Acoustics—Guidelines for Noise Control in Offices and Workrooms by Means of Acoustical Screens, 2004.
16. T. M. Barry and J. Reagan, FHWA Highway Traffic Noise Prediction Model, Report No. FHWA-RD-77-108, Federal Highway Administration, Washington, DC, 1978.
17. C. W. Menge, C. F. Rossano, G. S. Anderson, and C. J. Bajdek, FHWA Traffic Noise Model—Technical Manual, Report No. FHWA-PD-96-010, Federal Highway Administration, Washington, DC, 1998.
18. J. Pfretzschner, F. Simon, C. de la Colina, and A. Moreno, A Rating Index for Estimating Insertion Loss of Noise Barriers under Traffic Noise Conditions, *Acustica*, Vol. 82, 1996, pp. 504–508.
19. F. Simon, J. Pfretzschner, C. de la Colina, and A. Moreno, Ground Influence on the Definition of Single Rating Index for Noise Barrier Protection, *J. Acoust. Soc. Am.*, Vol. 104, 1998, pp. 232–236.
20. Department of Transport and Welsh Office, Calculation of Road Traffic Noise, HMSO, London, 1988.
21. D. A. Bies, Acoustical properties of Porous Materials, in *Noise and Vibration Control*, L. L. Beranek, ed., McGraw-Hill, New York, 1971, Chapter 10.
22. T. F. W. Embleton, J. E. Piercy, and G. A. Daigle, Effective Flow Resistivity of Ground Surfaces Determined by Acoustical Measurements, *J. Acoust. Soc. Am.*, Vol. 74, 1983, pp. 1239–1244.
23. C. I. Chessell, Propagation of Noise along a Finite Impedance Boundary, *J. Acoust. Soc. Am.*, Vol. 62, 1977, pp. 825–834.
24. B. A. DeJong, A. Moerkerken, and J. D. van der Toorn, Propagation of Sound over Grassland and over an Earth Barrier, *J. Sound Vib.*, Vol. 86, 1983, pp. 23–46.
25. K. Fujiwara, Y. Ando, and Z. Maekawa, Noise Control by Barriers—Part 1: Noise Reduction by a Thick Barrier, *Appl. Acoust.*, Vol. 10, 1977, pp. 147–159.
26. R. N. Foss, Noise Barrier Screen Measurements: Double-Barriers, Research Program Report 24.3, Washington State Highway Commission, Olympia, WA, 1976.
27. ISO 9613-2, Acoustics—Attenuation of Sound During Propagation Outdoors, Part 2: General Method of Calculation 1996.
28. ISO 10847, Acoustics—In-situ Determination of Insertion Loss of Outdoor Noise Barriers of All Types, 1997.
29. J. P. Arenas and A. M. Monsalve, Modification of the Diffracted Sound Field by Some Noise Barrier Edge Design, *Int. J. Acoust. Vib.*, Vol. 6, 2001, pp. 76–82.
30. D. C. Hothersall, D. H. Crombie, and S. N. Chandler-Wilde, The Performance of T-Profile and Associated Noise Barriers, *Appl. Acoust.*, Vol. 32, 1991, pp. 269–287.
31. D. N. May and M. M. Osman, The Performance of Sound Absorptive, Reflective and T-Profile Noise Barriers in Toronto, *J. Sound Vib.*, Vol. 71, 1980, pp. 67–71.
32. R. J. Alfredson and X. Du, Special Shapes and Treatment for Noise Barriers, Proceedings of Internoise 95, Newport Beach, CA, 1995, pp. 381–384.
33. D. H. Crombie, D. C. Hothersall and S. N. Chandler-Wilde, Multiple-Edge Noise Barriers, *Appl. Acoust.*, Vol. 44, 1995, pp. 353–367.
34. K. Fujiwara and N. Furuta, Sound Shielding Efficiency of a Barrier with a Cylinder at the Edge, *Noise Control Eng. J.*, Vol. 37, 1991, pp. 5–11.
35. K. Iida, Y. Kondoh, and Y. Okado, Research on a Device for Reducing Noise, in *Transport Research Record*, Vol. 983, National Research Council, Washington, DC, 1984, pp. 51–54.
36. M. Möser and R. Volz, Improvement of Sound Barriers Using Headpieces with Finite Acoustic Impedance, *J. Acoust. Soc. Am.*, Vol. 106, 1999, pp. 3049–3060.
37. G. R. Watts, D. H. Crombie, and D. C. Hothersall, Acoustic Performance of New Designs of Traffic Noise Barriers: Full Scale Tests, *J. Sound Vib.*, Vol. 177, 1994, pp. 289–305.
38. F. J. Fahy, D. G. Ramble, J. G. Walker, and M. Sigiura, Development of a Novel Modular Form of Sound Absorbent Facing for Traffic Noise Barriers, *Appl. Acoust.*, Vol. 44, 1995, pp. 39–51.
39. A. D. Rawlins, Diffraction of Sound by a Rigid Screen with a Soft or Perfectly Absorbing Edge, *J. Sound Vib.*, Vol. 45, 1976, pp. 53–67.
40. S. S. T. Ho, I. J. Busch-Vishniac, and D. T. Blackstock, Noise Reduction by a Barrier Having a Random Edge Profile, *J. Acoust. Soc. Am.*, Vol. 101, Pt. 1, 1997, pp. 2669–2676.

41. B. Kotzen and C. English, *Environmental Noise Barriers—A Guide to Their Acoustic and Visual Design*, E&FN Spon, London, 1999.
42. Highways Agency, Design Guide for Environmental Barriers, in *Design Manual for Roads and Bridges, Part 1*, HA65/94, London, 1994, Chapter 10, Section 5.
43. U.S. Department of Transportation, Highway Traffic Noise Barrier Construction Trends, Federal Highway Administration, Office of Natural Environment, Noise Team, Washington, DC, 2000.
44. A. Behar and D. N. May, Durability of Sound Absorbing Materials for Highway Noise Barriers, *J. Sound Vib.*, Vol. 71, 1980, pp. 33–54.
45. Highways Agency, Environmental Barriers: Technical Requirements, in *Design Manual for Roads and Bridges, Part 2*, HA66/95, London, 1995, Chapter 10, Section 5.
46. U.S. Department of Transportation, Keeping the Noise Down: Highway Traffic Noise Barriers, Publication No FHWA-EP-01-004, Federal Highway Administration, Washington, DC, 2001.

# CHAPTER 59

## USE OF VIBRATION ISOLATION\*

Eric E. Ungar  
Acentech Incorporated  
Cambridge, Massachusetts

### 1 INTRODUCTION

Vibration isolation concerns the use of comparatively resilient elements—called vibration isolators—for the purpose of reducing the vibratory forces or motions that are transmitted from one structure or mechanical component to another. Practical vibration isolators usually consist of springs, of elastomeric elements, or of combinations of these. The primary purpose of isolators is to attenuate the transmission of vibrations, whereas the main purpose of dampers is the dissipation of mechanical energy.

Vibration isolation generally is employed (1) to protect a sensitive item of equipment from vibrations of a structure to which it is attached or (2) to reduce the vibrations that are induced in a structure by a machine that is attached to it. Reduction of structural vibrations may be desirable for reasons of structural integrity, human comfort, and control of noise radiated from structures, among others.

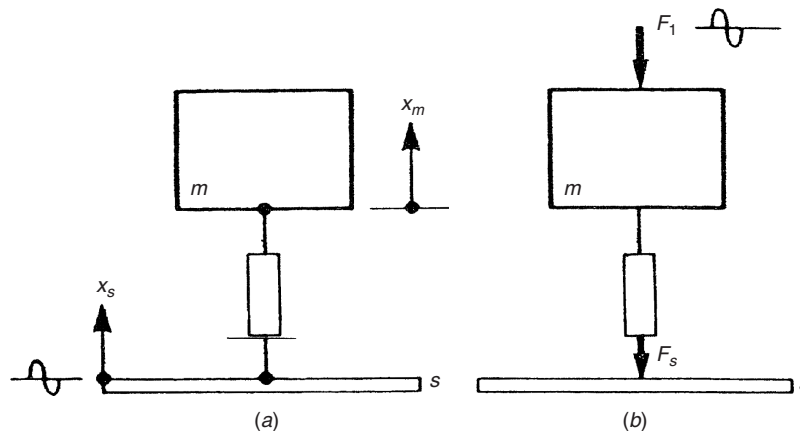
Simple models based on systems with a single degree of freedom are useful for establishing some fundamental relations. Extensions of these models can account for the nonrigidity of supports and isolated items, as well as for reaction effects on vibration sources. More complex models apply to the isolation

of masses that can rotate as well as translate and to two-stage isolation that can provide greater attenuation than single-stage isolation systems.

### 2 BASIC MODEL

Many aspects of vibration isolation can be understood on the basis of a simple model consisting of a mass that is connected to a support via an isolator, as shown in Fig. 1. In Fig. 1a the mass  $m$  represents a sensitive item that is to be protected from vibrational motion of the support  $S$ ; in Fig. 1b the support  $S$  is to be protected from a force that acts on it due to the vibrational force  $F_1$  that acts on the mass  $m$  of a machine. In this basic model the mass can move only in translation along a straight line (in the vertical direction of the figure) and the isolator is taken to be a linear massless spring. The restoring force produced by such a spring is proportional to its deflection.

The *transmissibility* represents the fraction of the applied excitation that is transmitted to the part that is to be protected. In the case that corresponds to Fig. 1a, the concern is the transmitted motion, and the corresponding *motion transmissibility* is defined as  $T_{\text{motion}} = X_m/X_s$ , where  $X_m$  and  $X_s$  denote, respectively, the amplitudes of the motions of the mass and of the support. In the case that corresponds to Fig. 1b the *force transmissibility* is defined as  $T_{\text{force}} = F_s/F_1$ , where  $F_s$  and  $F_1$  denote, respectively, the amplitudes of the force that acts on the support and the force that acts on the mass. If the support in the



**Figure 1** Basic system consisting of mass connected to support via an isolator (a) excited by support motion (b) excited by force acting on mass.

second case is immobile, then the two transmissibilities are given by the same expression.\* For the case where the isolator is undamped (i.e., where it dissipates no energy), this expression is

$$T = \frac{1}{|(f/f_n)^2 - 1|} \quad (1)$$

where the subscripts on  $T$  have been discarded. The symbol  $f$  denotes the excitation frequency and  $f_n$  denotes the natural frequency the isolator-mass system.

The natural frequency obeys

$$f_n = \frac{1}{2\pi} \sqrt{\frac{k}{m}} = \frac{1}{2\pi} \sqrt{\frac{g}{X_{st}}} \approx \frac{15.76}{\sqrt{X_{st}(\text{mm})}} \approx \frac{3.13}{\sqrt{X_{st}(\text{in.})}} \quad (2)$$

where  $k$  denotes the stiffness or *spring constant* of the isolator (the ratio of the force applied to the isolator to its deflection),  $g$  represents the acceleration of gravity, and  $X_{st}$  represents the *static deflection* of the isolator—that is, its deflection due to the weight of mass  $m$ .

For the more general situation where the isolator incorporates damping characterized by the loss factor.†  $\eta$  the transmissibility obeys

$$T = \sqrt{\frac{1 + \eta^2}{[(f/f_n)^2 - 1]^2 + \eta^2}} \quad (3)$$

If the damping is viscous—that is, if the isolator produces a retarding force proportional to the velocity (with a constant of proportionality  $c$ , called the viscous damping coefficient)—then the loss factor is  $\eta = 2\pi f c / k = 2\zeta(f/f_n)$ . Here  $\zeta = c/c_c$  denotes the so-called damping ratio, where  $c_c$  is the critical viscous damping coefficient.‡

Figure 2 shows how the transmissibility  $T$  varies with the frequency ratio  $f/f_n$  for several values of the loss factor and several values of the damping ratio. In all cases  $T$  is greater than 1 for frequency ratios less than  $\sqrt{2}$ —thus, at such low-frequency ratios the items that are to be protected are subjected to greater forces or motions than they would experience without any isolation. Protection of these items, corresponding to transmissibility values of less than unity, results only in the *isolation region*—that is, at frequency ratios that exceed  $\sqrt{2}$ —and greater protection (smaller transmissibility) is obtained at higher frequency ratios. Thus, to obtain good isolation in the presence of a disturbance at a given excitation frequency  $f$  one needs to make the natural frequency  $f_n$  much smaller than  $f$ .

\*Equality of the force and motion transmissibilities is a consequence of the reciprocity principle and holds between any two points of any mathematically linear system, including systems consisting of many masses, springs, and dampers.

†See Chapter 60 for definition and discussion of loss factor.

‡See Chapter 60 for information on measures of damping and their interrelation.

The effect of damping on transmissibility is also evident in Fig. 2. In the isolation region (i.e., where  $f/f_n > \sqrt{2}$ ) greater damping results in greater transmissibility (and thus in poorer isolation). However, this deleterious effect is significant only in the presence of considerable viscous damping; it is insignificant in the presence of even rather high damping that is characterized by frequency-independent loss factors. Because the damping of most practical conventional isolators is relatively small and characterized by frequency-independent loss factors, their performance in the isolation range is not significantly affected by damping and the transmissibility may be approximated by Eq. (1), which reduces to as  $T \approx (f_n/f)^2$  for large frequency ratios.

However, damping does have a significant effect on the transmissibility at and near resonance, where the excitation frequency matches the natural frequency. As Fig. 2 shows, greater damping results in reduced transmissibility in this frequency region. Therefore, greater damping often is desirable for isolating systems in which the excitation frequency can pass through resonance, for example, as a machine comes up to speed or coasts down.

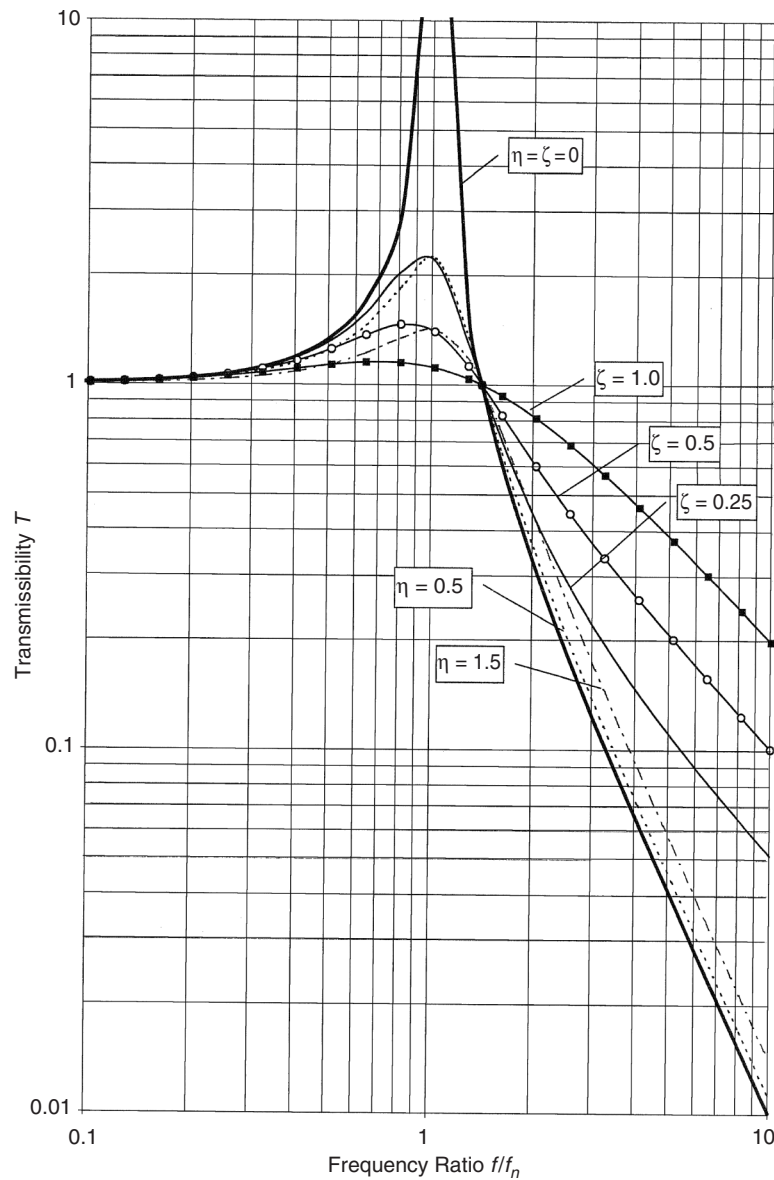
To obtain the smallest transmissibility, one needs to make the frequency ratio  $f/f_n$  as large as possible. For given driving frequencies  $f$  this implies that one should make the natural frequency as small as one can—usually by choosing the smallest practical isolator stiffness  $k$ . The mass  $m$  generally is given. However, to reduce the natural frequency, one may consider adding an *inertia base* (a massive support) to the mass  $m$  so as to increase the total effective mass. But the loads that practical isolators can support are limited, so that addition of an inertia base may necessitate the use of a stiffer isolation arrangement, resulting in negation of at least some of the natural frequency reduction expected from the increased mass. Nevertheless, an added inertia base generally serves to reduce the vibrational excursions of an isolated item due to forces that act on it directly.

The *isolation I* is defined by  $I = 1 - T$ . Better isolation performance corresponds to greater values of  $I$  but to smaller values of transmissibility  $T$ . The isolation indicates the fraction of the disturbing force or motion that does not reach the item that is to be protected, whereas the transmissibility indicates the fraction of the disturbance that is transmitted to the protected item. Isolation is often expressed in percent. For example, a transmissibility of 0.0085 corresponds to an isolation of 0.9915 or of 99.15%.

## 2.1 Limitations of Basic Models and of Transmissibility; Isolation Effectiveness

The basic models assume the mass and support to be rigid, the isolator to be massless and mathematically linear (i.e., is, to deflect in proportion to the applied force), and all motions to occur along a straight line.

In cases where the isolator mass is small compared to the masses of the support and the isolated item, and where the frequencies of concern are low enough so



**Figure 2** Transmissibility as function of ratio of forcing frequency to natural frequency of system consisting of mass supported on isolator modeled as damped spring, for various amounts of viscous damping (constant damping ratio  $\zeta$ ) and structural damping (constant loss factor  $\eta$ ).

that no significant wave effects occur in the isolator,\* an isolator does in effect act nearly as if it had no

mass. Although the force–deflection curves for some isolators, such as those made of rubber, typically are not straight lines—implying that the isolator is nonlinear—the isolator may in fact act linearly in the presence of small excursions. In that case its stiffness

\*At frequencies at which standing-wave resonances occur in the isolator, the isolation performance may be considerably degraded. It usually is useful to relegate the domain where such resonances can occur to high frequencies (beyond the range of frequencies of concern) by selecting isolators with

small dimensions and of configurations and materials with high wave speeds.

may be taken as the slope of its force–deflection curve at the average deflection. However, a correction may be required for some isolators that incorporate elastomeric materials, in which the dynamic stiffness may differ significantly from the quasi-static stiffness obtained from the slope of the force–deflection curve. The effects of nonrigid isolated items and of motions that are not just along a straight line are addressed in later sections of this chapter.

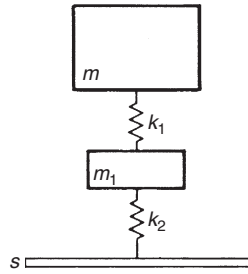
The transmissibility, being the ratio of the transmitted force or motion to the exciting force or motion, does not account for changes in the excitation force or motion that may occur when a more flexible isolator is used. With a more flexible isolator the excitation is less restricted and may increase, defeating some of the isolation improvement one would expect from use of a more flexible isolator. In situations where the excitation can change significantly, depending on the resistance it encounters, the *isolation effectiveness*  $E$  is a better measure of isolation performance than the transmissibility. The isolation effectiveness is defined as

$$E = |V_{Rr}/V_R| = |F_{Rr}/F_R| \quad (4)$$

where  $V_{Rr}$  and  $F_{Rr}$ , respectively, denote the velocity and the force experienced by the isolated item if the isolator is replaced by a rigid connection (i.e., if no vibration isolator is used) and where  $V_R$  and  $F_R$  represent these quantities for the situation where the isolator is in place. The velocity ratio definition of  $E$  applies for the motion transmission case of Fig. 1a; the force ratio definition applies for the force transmission case of Fig. 1b.

### 3 TWO-STAGE ISOLATION

Two-stage isolation systems, as shown schematically in Fig. 3, can provide considerably greater high-frequency isolation than can the single-stage arrangement of Fig. 1. Unlike in the basic system of Fig. 1, where the mass  $m$  is connected to the supporting structure via a single isolator, in a two-stage system the mass  $m$  is connected to the supporting structure via two isolators (indicated as springs in Fig. 3) and an intermediate mass  $m_1$ .



**Figure 3** Schematic diagram of two-stage isolation system.

The system of Fig. 3 has two natural frequencies  $f_n$  given by

$$(f_n/f_1)^2 = C \pm \sqrt{C^2 - R^2} \\ 2C = R^2 + 1 + k_1/k_2 \quad R = f_2/f_1 \quad (5)$$

Here

$$f_1 = \frac{1}{2}\pi\sqrt{m(1/k_1 + 1/k_2)} \quad (6)$$

denotes the natural frequency of the system consisting of the mass  $m$  supported on the two springs in mechanical series, in the absence of the intermediate mass, and

$$f_2 = \frac{1}{2}\pi\sqrt{(k_1 + k_2)/m_1} \quad (7)$$

represents the natural frequency of the mass  $m_1$  between the two springs for the situation where the mass  $m$  is held completely immobile. The symbols  $k_1$  and  $k_2$  represent the stiffnesses of the two springs, as shown in Fig. 3. The higher natural frequency  $f_n$ , which one obtains if one uses the plus sign before the square root in the first of Eq. (5), always is greater than the larger of  $f_1$  and  $f_2$ . The lower natural frequency, obtained if one uses the minus sign in the aforementioned equation, always is smaller than the smaller of  $f_1$  and  $f_2$ .

The (force and motion) transmissibility  $T$  of a two-stage system like that of Fig. 3 in the absence of damping\* obeys

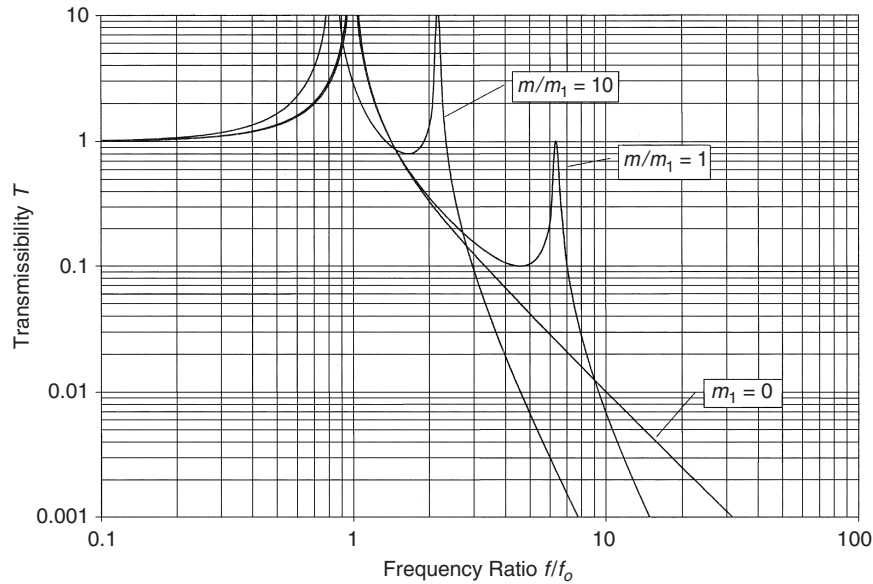
$$R^2/T = (f/f_1)^4 - [R^2 + k_1/k_2 + 1](f/f_1)^2 + R^2 \quad (8)$$

where  $f$  represents the excitation frequency and  $R$  is defined in Eq. (5). At high excitation frequencies the transmissibility obeys  $T \approx (f_1 f_2 / f^2)^2$  and thus varies as  $1/f^4$ , implying very good isolation performance in this frequency range. However, this good performance occurs only at frequencies that are above the higher of the two natural frequencies of the system, so that it is desirable to make this natural frequency as small as possible. Because this higher natural frequency in practice often is  $f_2$ , which depends on the intermediate mass  $m_1$ , one generally should use the largest practical intermediate mass.

Figure 4 illustrates the aforementioned fact. One may observe that with a smaller intermediate mass (i.e., with a larger ratio of the primary mass  $m$  to the intermediate mass  $m_1$ ), the rapid decrease of transmissibility with increasing frequency occurs at higher frequencies.

Where several items need to be isolated, it often is advantageous to support these on a common massive platform (sometimes called a “subbase” or “raft”), to isolate each item from the platform, and to isolate the platform from the supporting structure. In such

\*The damping present in most practical isolation systems has relatively little effect on isolation performance. A more complicated expression applies in the presence of considerable damping.

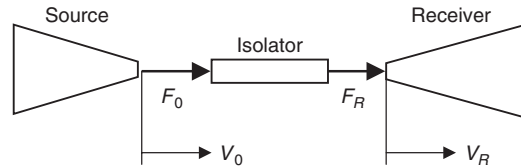


**Figure 4** Transmissibility of two-stage system of Fig. 3, with  $k_1 = k_2$ , for two ratios of primary to intermediate mass. The  $m_1 = 0$  curve corresponds to a single-stage system.

an arrangement, the platform acts as a relatively large intermediate mass for isolation of each of the equipment items, resulting in efficient two-stage isolation performance with a comparatively small total weight penalty. The platform should be designed so that it exhibits no resonances of its own in the frequency range of concern. If such resonances cannot be avoided, the platform structure should be highly damped.

#### 4 GENERAL SYSTEMS WITH ONE DEGREE OF FREEDOM

One may generalize the diagrams of Fig. 1 in terms of the diagram of Fig. 5, which shows a vibration source  $S$  connected to a "receiver" (an item or structure to be protected)  $R$  via an isolator. All motions and forces are assumed to act along the same line. Rather than representing the receiver as a rigid mass or an immovable support, one may consider a receiver whose velocity is proportional to the applied force (at each frequency). The ratio of the complex velocity\*  $V_R$  of the receiver to the complex applied force  $F_R$  is defined as the receiver mobility  $M_R = V_R/F_R$ . The receiver mobility  $M_R$  is a frequency-dependent complex quantity that may be evaluated by applying a force at the receiver driving



**Figure 5** General source connected to general receiver via an isolator.

point and measuring the magnitude and phase of the resulting velocity at that point.

Most vibration sources vibrate with lesser excursions if they act on stiffer structures and thus generate greater forces.<sup>†</sup> This behavior in its simplest terms is represented by a *general linear source* whose complex velocity  $V_0$  is related to its complex force  $F_0$  as  $V_0 = V_{\text{free}} - M_S F_0$ , where  $M_S = V_{\text{free}}/F_{\text{blocked}}$  is a complex quantity, called the *source mobility*.  $V_{\text{free}}$  represents the (frequency-dependent) complex velocity with which the source vibrates if it generates zero force.  $F_{\text{blocked}}$  denotes the frequency-dependent complex force that the source produces if it is blocked,

\*The complex velocity or velocity *phasor* contains magnitude and phase information. If  $V = V_r + jV_i$ , where  $j = \sqrt{-1}$ , then the magnitude of the velocity is given by  $|V| = \sqrt{V_r^2 + V_i^2}$  and the phase is given by  $\phi = \arctan(V_i/V_r)$ . Corresponding expressions apply for the complex force.

<sup>†</sup>For example, a flexible sheet-metal mounting foot of an appliance or the armature of a small electrodynamic shaker may vibrate with considerable excursions if it is not connected to any structure, but tends to vibrate with lesser excursions if it is connected to structures or masses. The excursions will be less with connections to items with greater resistance to motion.

so that its velocity is zero. These quantities, and thus the source mobility, may be determined from measurements on a given source.

The mobility of a massless isolator\* is defined as  $M_I = (V_0 - V_R)/F_R$  in terms of the complex velocity difference across the isolator and the force applied to it, as indicated in Fig. 5. (With an isolator of zero mass, the forces on the two sides of the isolator are the same,  $F_0 = F_R$ .) The frequency-dependent mobility of a given isolator may readily be determined by measurement. The effectiveness obtained with an isolator whose mass is negligible obeys

$$E = \left| 1 + \frac{M_I}{M_S + M_R} \right| \quad (9)$$

In the special case where the source velocity remains unchanged, no matter how much force the source generates,  $E = 1/T_{\text{motion}}$ . In the special case where the source force output is constant, no matter what the source velocity is,  $E = 1/T_{\text{force}}$ . The effectiveness obtained with an isolator that has finite mass (i.e., if isolator mass effects are significant) is discussed in Refs. 1 and 2.

## 5 ISOLATION OF THREE-DIMENSIONAL MASSES

Unlike the basic model of Fig. 1, where the mass is constrained to move only along a line without rotating and where the system has only one natural frequency, an actual rigid mass can translate along three axes and rotate about three axes. An elastically supported rigid mass thus has six natural frequencies; a nonrigid mass has additional ones associated with its deformations. Obtaining good isolation here generally requires that all of the natural frequencies fall considerably below the excitation frequencies of concern. Analytical

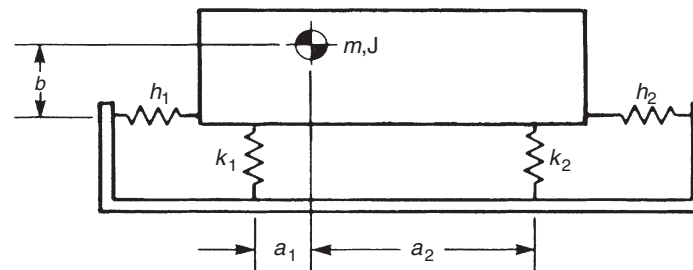
expressions for the natural frequencies and responses of general rigid masses on general resilient supports are available<sup>†</sup> but are complex and provide little practical design guidance; their application generally requires repeated trial-and-error computation. The following paragraphs deal with special cases that provide some insight and design guidance.

### 5.1 Two-Dimensional (Planar) Coupled Rotational and Translational Vibrations

Figure 6 is a schematic diagram showing a mass that is supported on two isolators and restrained horizontally by two collinear isolators, with all isolators represented as springs. This diagram is a two-dimensional idealization of a three-dimensional mass that moves only parallel to a plane (the plane of the paper).<sup>‡</sup> The horizontal isolators shown in the figure may represent the stiffnesses of actual horizontally acting isolators or the stiffnesses in the horizontal direction of the supporting isolators, or a combination of the two.

In general, an up-and-down force applied at the center of gravity of the mass produces both an up-and-down displacement of the center of gravity and a rotational vibration of the mass, the latter resulting from the moment due to the isolator forces. Similarly, an oscillatory torque acting about the center of gravity produces both rotational and translational motions. The rotational and translational vibrations then are said to be coupled.

To obtain effective isolation, one needs to select the system parameters so that the system's greatest natural frequency falls as far as possible below the excitation frequency range. In the following discussion the isolators are considered to be undamped linear springs. The effect of practical amounts of damping generally is negligible for excitation frequencies that lie well above the greatest natural frequency.



**Figure 6** Mass  $m$  with polar moment of inertia  $J$  supported on two vertically and two collinear horizontally acting isolators.

\*The mobility of an isolator is the velocity analog to its compliance (the reciprocal of the stiffness). The mobility is equal to the velocity difference across the isolator, divided by the applied force; the compliance is equal to the compression of the isolator (the displacement difference across it), divided by the applied force. The complex mobility accounts for damping of the isolator, as well as for its stiffness.

<sup>†</sup>For example, See Ref. 3.

<sup>‡</sup>Such planar motions occur for excitations that act at the center of gravity and parallel to the plane and for arrays of isolators whose stiffnesses are distributed so that a force acting in the plane of the center of gravity induces no rotation out of the plane. The isolators indicated in Fig. 6 may be considered as representing the resultant stiffnesses of the isolator arrays.



## 5.2 Systems with Zero Horizontal Stiffness

In absence of finite horizontal stiffnesses and horizontal force components, the center of gravity of the mass of Fig.6 moves only in the vertical direction. The natural frequency  $f_v$  corresponding to vibration in the vertical direction without rotation—the so-called uncoupled vertical translational natural frequency—is given by

$$2\pi f_v = \sqrt{\frac{k_1 + k_2}{m}} \quad (10)$$

where  $k_1$  and  $k_2$  represent the spring constants of the vertically acting isolators and  $m$  denotes the mass. The natural frequency  $f_r$  corresponding to rotational vibrations without displacement of the center of gravity—the so-called uncoupled rotational frequency—is given by

$$2\pi f_r = \sqrt{(k_1 a_1^2 + k_2 a_2^2)/J} \quad (11)$$

where  $a_1$  and  $a_2$  are the horizontal distances from the vertically acting isolators to the center of gravity, as shown in Fig. 6, and where  $J$  denotes the mass' polar moment of inertia about an axis through the center of gravity and perpendicular to the plane of the paper. The uncoupled rotational natural frequency  $f_r$  may be greater or smaller than the uncoupled vertical translational natural frequency  $f_v$ .

The two natural frequencies of the system generally differ from the aforementioned uncoupled natural frequencies and are given by the two values obtained from the following relation (one for the plus and one for the minus sign preceding the square root):

$$\begin{aligned} f_n^2 &= f_a^2 \pm \sqrt{f_a^4 + f_v^2 f_r^2 U} \\ f_a^2 &= \frac{f_v^2 + f_r^2}{2} \\ U &= \frac{(a_1 + a_2)^2}{(1/k_1 + 1/k_2)(k_1 a_1^2 + k_2 a_2^2)} \end{aligned} \quad (12)$$

The larger of these two “coupled” natural frequencies is greater than both  $f_v$  and  $f_r$ ; the smaller of the two coupled natural frequencies is smaller than both  $f_v$  and  $f_r$ .

To provide good isolation in the general case, one needs to select the isolators and their locations so that the larger coupled natural frequency falls considerably below the excitation frequencies of concern. It often is most convenient to select the isolator stiffnesses and locations so that the forces produced by the isolators when the mass is deflected vertically without rotation produce zero net torque about the center of gravity. This may be accomplished by selecting the isolation system so that all vertically acting isolators have the same static deflection due to the weight they support

statically.\* In this case vertical forces that act at the center of gravity or vertical motions of the support produce no rotational or “rocking” motions, and the natural frequencies of the system are the uncoupled natural frequencies discussed at the beginning of this section.

## 5.3 Systems with Finite Horizontal Stiffness

If the horizontally acting stiffnesses shown in Fig.6 are not negligible, then the system has three natural frequencies. For the case where the vertically acting isolators are selected and positioned so that they have the same static deflection, as discussed above, the vertical translational motion and the rotational motion are uncoupled and the natural frequency for vertical vibration is the aforementioned  $f_v$ . The other two natural frequencies, relating to coupled in-plane rotation and horizontal translation then are given by

$$(f_n/f_v)^2 = N \pm \sqrt{N^2 - PW} \quad (13)$$

where

$$\begin{aligned} 2N &= P \left( 1 + \frac{b^2}{r^2} \right) + W \\ P &= \frac{h_1 + h_2}{k_1 + k_2} \quad W = \frac{k_1 a_1^2 + k_2 a_2^2}{r^2(k_1 + k_2)} \end{aligned} \quad (14)$$

The dimensions  $a_1, a_2$ , and  $b$  are indicated in the figure,  $h_1$  and  $h_2$  denote the horizontal stiffnesses, and  $r = \sqrt{J/m}$  represents the radius of gyration of the mass about an axis through its center of gravity and perpendicular to the plane of the paper. For a rectangular mass of uniform density with height and length  $H$  and  $L$ ,  $r = \sqrt{(H^2 + L^2)/12}$ .

## 6 PRACTICAL ISOLATORS

A great many different isolators of numerous sizes and load capacities are available commercially. Details typically may be found in suppliers' catalogs.

Most isolators incorporate metallic and/or elastomeric resilient elements. Metallic resilient elements most often are in the form of coil springs but may also be in the form of leaf springs, rings, or Belleville washers, among others. Coil springs of metal predominantly are used in compression because their use in tension tends to require end supports that induce stress concentrations and result in reduced fatigue life. Many coil spring isolator assemblies make use of parallel and/or series arrangements of springs in suitable housings and may include damping devices (such as viscoelastic elements, wire mesh sleeves, or other friction devices), snubbers to limit excursions due to large disturbances such as earthquakes, and in-series elastomeric pads

\*It is assumed that the isolators are linear—that is, that each isolator's deflection is proportional to the force that acts on it. If the isolators are selected so that they have the same unloaded height, as well as the same static deflection, then the isolated mass will be level in its equilibrium position.

for enhanced damping and high-frequency isolation. Springs need to be selected to be laterally stable. Spring systems in housing need to be installed with care to avoid binding between the housing elements and between these and the springs.

Some commercial metallic isolators that do not employ conventional coil springs make use of pads or woven assemblies of wire mesh to provide both resilience and damping. Others use arrangements of coils or loops of wire rope to serve as a damped spring.

Many commercially available isolators employ elements of elastomeric materials (e.g., rubber or neoprene) that are bonded to support plates or sleeves that incorporate convenient means for fastening of these isolators to other components. The isolators may be configured so that the elastomeric elements work in shear, in compression, in torsion, or in a combination of these. There are also available a variety of elastomeric gaskets, grommets, sleeves, and washers, which are intended to be used in conjunction with conventional bolts or similar fasteners.

Pads of elastomeric material or of such other resilient materials as cork, felt, fiberglass, or metal mesh are often used as isolators by themselves. Such pads often are convenient and relatively inexpensive. Their areas can be selected to support the required loads and their thicknesses can be chosen to provide the desired resilience within practical limits.

In the selection of pads of a solid elastomeric material (in contrast to pads made of foamed material or of material with ribs or voids), one needs to take into account that such a pad's stiffness depends not only on its area and thickness but also on its shape and constraints. Because elastomeric materials are nearly incompressible, a pad of such a material exhibits greater stiffness if bulging of its edges is restricted to a greater degree. The *shape factor* of a pad is defined as the ratio of its loaded area to the total area that is free to bulge. The greater the shape factor, the greater the pad's stiffness. The stiffness is also affected by how easily the loaded surfaces of a pad can slip relative to the adjacent surfaces; the more this slipping is restrained, the greater is the stiffness of the pad. Isolation pads are often supplied with their top and bottom load-carrying surfaces bonded to thin metal plates or the like, not only to eliminate stiffness uncertainties associated with uncontrolled slippage but also to reduce creeping of the material out of the loaded areas.

To avoid the complications associated with the shape factor in the selection of elastomeric pads, commercial isolation pad configurations are available that incorporate a multitude of closely spaced openings into which the material can bulge, thus providing practically the same shape factor for any pad area. Arrays of holes, ribs, dimples, or the like typically serve this purpose. If stacks of such pads are used, metal sheets or the like generally are placed between adjacent load-carrying surfaces to avoid having protrusions on one pad extending into openings of an adjacent one.

Pneumatic or *air-spring* isolators obtain their resilience primarily from the compressibility of confined volumes of air. They may take the form of air-filled cylinders or rings of rubber or plastic, or they may consist essentially of pistons in rigid air-filled cylinders. Highly resilient air springs are available that can support large loads and provide natural frequencies as low as 1 to 2 Hz. Such isolation performance generally cannot readily be obtained with any of the aforementioned isolation arrangements that employ only solid materials. Piston-type air springs usually provide isolation primarily in the vertical direction and often need to be supplemented with other devices to enhance isolation in the horizontal direction. Some commercial air-spring systems can be obtained with leveling controls that keep an isolated platform in a given static position as the load on the platform changes or moves about.

The stiffness of a piston-type air spring is proportional to  $pA^2/V$ , where  $p$  denotes the absolute pressure of the air in the cylinder,  $A$  the piston surface area, and  $V$  the cylinder volume. The product  $(p - p_a)A$ , where  $p_a$  denotes the ambient air pressure, is equal to the load carried atop the piston. Thus, the pressure  $p$  may be adjusted to support a given load. If  $p$  is much greater than  $p_a$ , the stiffness of the air spring is proportional to the load, and the natural frequency one obtains with the air spring is independent of the load. This makes air springs particularly useful for applications in which the loads are variable or not fully predictable. The spring stiffness may be made small by use of a large volume; this is often achieved by means of auxiliary tanks that communicate with the cylinder via piping. In some instances flow restrictions are included in this piping to provide damping.

Pendulum arrangements often are convenient for isolation of vibrations in the horizontal directions. The natural frequency of a pendulum of length  $L$  is given by

$$f_n = \frac{1}{2\pi} \sqrt{\frac{g}{L}} \approx \frac{15.76}{\sqrt{L(\text{mm})}} \approx \frac{3.13}{\sqrt{L(\text{in.})}} \quad (15)$$

where  $g$  denotes the acceleration of gravity. Some commercial isolation systems combine pendulum elements for horizontal isolation with spring elements for vertical isolation.

Systems in which spring action is provided by magnetic or electrostatic means also have been investigated and used for some special applications, as have other systems where levitation is provided by streams or thin films of fluids. Active isolation systems recently have attracted considerable attention. Such systems in essence are dynamic control systems in which the vibration of the item that is to be protected is sensed by a suitable transducer whose appropriately processed output is used to drive an actuator so as to reduce the item's vibrations. Active systems require an external source of energy and tend to be rather complex, but they can provide better isolation than passive systems (i.e., systems that do not require an external source

of energy), notably in the presence of disturbances at very low frequencies.

## REFERENCES

1. E. E. Ungar, Vibration Isolation, 11 in *Noise and Vibration Control Engineering*, L. L. Beranek and I. L. Ver, Eds., Wiley, New York, 1992, Chapter 11.
2. E. E. Ungar and C. W. Dietrich, High-Frequency Vibration Isolation, *J. Sound Vib.*, Vol. **4**, 1966, pp. 223–241.
3. H. Himmelblau, Jr., and S. Rubin, Vibration of a Resiliently Supported Rigid Body, in *Shock and*

*Vibration Handbook*, 4th ed., C. M. Harris, Ed., McGraw-Hill, New York, 1995, Chapter 3.

## BIBLIOGRAPHY

- D. J. Mead, *Passive Vibration Control*, Wiley, Chichester, 1998.
- E. I. Rivin, *Passive Vibration Isolation*, American Society of Mechanical Engineers, New York, 2003.
- W. T. Thomson, *Theory of Vibration with Applications*, 2nd ed., Prentice-Hall, Englewood Cliffs, NJ, 1981.

# CHAPTER 60

## DAMPING OF STRUCTURES AND USE OF DAMPING MATERIALS\*

Eric E. Ungar  
Acentech Incorporated  
Cambridge, Massachusetts

### 1 INTRODUCTION

*Damping*—the dissipation of energy in a vibration—has a significant effect only on vibrational motion in which energy loss plays a major role. Increased damping increases the rate of decay of free (i.e., unforced) vibrations and reduces the amplitudes of steady vibrations at resonances, including vibrations due to random excitation. Damping reduces the rate of buildup of vibrations at resonances and limits the amplitudes of “self-excited” vibrations—that is, of vibrations in which a vibrating structure accepts energy from a steady source, such as flow of a fluid. Damping also increases the rate of decay of freely propagating waves and limits the buildup of forced wave motions. Furthermore, damping reduces the response of structures to sound and the transmission of sound through structures at frequencies above their coincidence frequencies.

Increased damping tends to result in the reduction of vibratory stresses and thus in increased fatigue life. It also leads to the reduction of noise associated with impacts, as well as to reduced transmission of energy in waves propagating along a structure. Damping increases the impedances of structures at their resonances and thus at these resonances may improve the effectiveness of vibration isolation.

Devices and materials that enhance the damping of structures are widely used in automobiles, ships, aerospace vehicles, and in industrial and consumer equipment. In many applications, *damping materials*—materials that can dissipate relatively large amounts of energy (typically plastics and elastomers)—are combined judiciously with conventional structural elements.

### 2 DAMPING MECHANISMS

Anything that results in loss of mechanical energy from a vibrating structure contributes to the damping of that structure. This includes friction between components, interaction of a structural component with adjacent fluids (including sound radiation into these fluids, which may play an important role in structures that are immersed in liquids), electromagnetic effects, transmission of energy to contiguous structures, and *mechanical hysteresis*—dissipation (conversion into

heat) of energy within the materials of the structure. This chapter focuses primarily on the damping of structures due to the energy dissipation in materials and in combinations of materials.

### 3 MEASURES AND MEASUREMENT OF DAMPING

The damping of a structure may be determined from the rates of the decay of vibrations of its modes, from the behavior of its structural modes<sup>†</sup> at and near their resonances, from direct measurement of energy loss in steady-state vibration, or from evaluation of the spatial rate of decay of freely propagating waves.

The dynamic behavior of a structural mode may be considered conveniently in terms of a simple mass–spring–damper system that has the same natural frequency as the mode and a representative *modal mass*  $m$  and a *modal stiffness*  $k$ . Because the assumption of *viscous damping*—that is, of dampers that provide a retarding force that is proportional to the velocity of the mass—leads to easily solved linear differential equations for the system motions, viscously damped systems have been studied extensively. Even though viscous damping is encountered relatively rarely in practice, results obtained for viscously damped systems provide some useful insights.

In a spring–mass–damper system with viscous damping the amplitude in a freely decaying motion varies with time  $t$  as  $e^{-\zeta\omega_n t}$ , where  $\omega_n = \sqrt{k/m}$  represents the undamped radian natural frequency of the system. The damping ratio  $\zeta = c/c_c$  relates the viscous damping coefficient  $c$  (the constant of proportionality of the retarding force to the velocity) to the so-called critical damping coefficient<sup>‡</sup>  $c_c = 2\sqrt{km} = 2m\omega_n$ . One may determine the damping ratio from the magnitudes of successive relative maxima in the record<sup>§</sup> of a freely decaying vibration by use of

\*This chapter is essentially a distillation of Ref. 1, where more details may be found.

<sup>†</sup>In general, different modes of a structure may exhibit different amounts of damping.

<sup>‡</sup>If a system with a viscous damping coefficient  $c$  that is smaller than the critical damping coefficient is displaced from equilibrium and released, it oscillates about its equilibrium position with decreasing amplitude. If a system with a viscous damping coefficient that is greater than the critical damping coefficient is similarly displaced and released, it drifts toward its equilibrium position without oscillating past it.

<sup>§</sup>The record may be of any quantity proportional to the displacement, velocity, or acceleration.

the relation

$$\zeta = \frac{\delta}{2\pi} = \frac{1}{2\pi N} \ln \frac{X_i}{X_{i+N}} \quad (1)$$

where  $X_i$  denotes the magnitude of a given maximum and  $X_{i+N}$  denotes the magnitude of the  $N$ th maximum after the given one. The symbol  $\delta$  represents a time-honored measure of damping, called the *logarithmic decrement*.

One may also evaluate the damping of a mode (or of the mass–spring–damper system that represents it) by subjecting it to sinusoidal forcing of constant amplitude  $F$  and observing its steady-state responses. The amplification at a given excitation frequency  $\omega$  is defined as the ratio of the displacement amplitude  $X(\omega)$  at that frequency to the quasi-static displacement amplitude  $X_{st}$  (the displacement amplitude for  $\omega \approx 0$ ). The amplification at resonance,  $Q$ , is defined as  $Q = X(\omega_n)/X_{st}$ , corresponding to the situation where the forcing frequency  $\omega$  is equal to the natural frequency  $\omega_n$ . In the presence of viscous damping,  $Q$  is related to the damping ratio by  $\zeta = \frac{1}{2}Q$ . One also may evaluate the damping from the relative bandwidth

$$b = (\omega_2 - \omega_1)/\omega_n = 1/Q \quad (2)$$

where  $\omega_1$  and  $\omega_2$  denote the two *half-power-point frequencies*—that is, the two excitation frequencies ( $\omega_1 < \omega_n$  and  $\omega_2 > \omega_n$ ) at which the amplification is equal to  $Q/\sqrt{2}$ . This equation is exact for the case of viscous damping, but it is also often used to quantify the damping in other situations.

The foregoing paragraphs deal with the special case of viscous damping. In the general case it is advantageous to use measures of damping that are based on energy considerations. One such measure is the damping capacity  $\psi$ , which is defined as the ratio of the energy  $D$  that is dissipated per cycle in a steady vibration to the time-average total energy  $W$  present in the vibrating system. (In lightly damped systems the total energy varies little with time and may be taken as constant for all practical purposes.) The most widely used measure of damping, the loss factor  $\eta$ , is defined analogously to the damping capacity, but in terms of the energy dissipated per radian:

$$\eta = \psi/2\pi = D/2\pi W \quad (3)$$

If the damping is small, the loss factor may be related to an equivalent viscous damping ratio via  $\eta \approx 2\zeta$ —in other words, a viscously damped system with damping ratio  $\zeta$  here dissipates essentially the same fractional amount of energy per cycle as a system with nonviscous damping that is characterized by a loss factor  $\eta$ .

The loss factor of a system that is vibrating in the steady state may be determined from direct measurement of the average energy that is dissipated per unit time, which is equal to the average energy

that is supplied to the system per unit time. The latter may be evaluated from measurement of the force and velocity at the point(s) where the system is driven. The energy stored in the system may be determined from its mass and mean-square velocity.

In analyzing the response of a system to sinusoidal excitation, it often is convenient to use complex or “phasor” notation. In terms of this notation the time-dependent variation of a variable  $x(t) = X \cos(\omega t + \phi)$  is expressed as  $x(t) = \text{Re}[\bar{X}e^{j\omega t}]$ , where  $j = \sqrt{-1}$  and  $\bar{X} = X_r + jX_i$  is a complex quantity consisting of real and imaginary components. This complex quantity contains information about both the magnitude (amplitude) and the phase  $\phi$  of the variable. If one uses phasor notation, one may represent the stiffness and damping of a system together in terms of a complex stiffness

$$\bar{k} = k + jk_i = k(1 + j\eta) \quad (4)$$

where  $\eta = k_i/k$  corresponds to the previously discussed loss factor.\*

One may represent the frequency-dependent behavior of realistic systems by taking the loss factor to vary with frequency to correspond to empirically measured data. The damping of metals and some other widely used structural materials often can be described by a loss factor that is practically independent of frequency, at least in limited frequency ranges of practical interest. A frequency-dependent loss factor also may be used to represent various mathematical damping models. For example, to a viscously damped system there corresponds the loss factor  $\eta = c\omega/k$ , which is proportional to frequency.

The various measures of damping are interrelated as follows:  $\eta = \psi/2\pi = k_i/k$  holds in general and at all frequencies, but  $\eta = 1/Q$  holds only at resonance. For small damping of any type,  $\eta \approx b$ . For viscous damping,  $\eta = 2\zeta = b = \delta/\pi \approx \Delta_\lambda/13.6$ . The symbol  $\Delta_\lambda$  represents the spatial decay rate (in decibels per wavelength), defined as the reduction of vibration level† per wavelength in freely propagating waves.

#### 4 DAMPING BEHAVIOR OF MATERIALS

The dynamic behavior of a material can be described most readily in terms of its complex modulus of elasticity, which may be determined from measurement of

\*One may also determine the damping of a mode from a plot of the imaginary versus the real part of the mobility, obtained from measurements over a range of frequencies that includes the resonance. (Mobility is defined as the ratio of the velocity phasor to the phasor of the exciting force.) The aforementioned plot is in the shape of a circle whose diameter is equal to  $Q = 1/\eta = 1/2\zeta$ . Commercial software for experimental modal analysis often uses this approach for evaluation of damping.

†The vibration level  $L$  of a vibration variable  $x(t)$  is defined in analogy to the sound pressure level in acoustics as  $L = 10 \log_{10}[x^2(t)/x_{\text{ref}}^2]$ , where  $x_{\text{ref}}$  represents an arbitrary constant reference value in the same units as the time-dependent variable.

the complex stiffness of a material sample. In analogy to the complex stiffness, as in Eq. (4), the complex modulus of elasticity is defined as

$$\bar{E} = E + jE_i = E(1 + j\beta) \quad (5)$$

The real part,  $E$ , is associated with strain energy storage and corresponds to the well-known modulus of strength of materials and elasticity theory; the imaginary part,  $E_i$ , is called the *loss modulus* and is associated with energy dissipation. The loss factor related to the modulus of elasticity obeys  $\beta = E_i/E$ . Completely analogous definitions apply for the shear modulus. For most materials of engineering interest the loss factor associated with the modulus of elasticity is for all practical purposes equal to the loss factor associated with the shear modulus.\*

The loss factor of a material in general may vary with frequency, temperature, strain amplitude, steady loading present in conjunction with a vibration, and previous cyclic loading. In most metals, the damping is relatively independent of frequency, of temperatures that are well below the melting point, and of strain amplitudes that are considerably below those at which structural fatigue tends to be a significant concern. Thus, for many applications the loss factor of a metal may be taken as essentially constant. On the other hand, the loss factors of plastics and rubbery materials generally vary markedly with frequency and temperature, as discussed below, but often are relatively independent of strain amplitude up to strains of the order of unity.

Figure 1 indicates typical ranges of the loss factors reported for materials at small strains, near room temperature, and at audio and lower frequencies. The range indicated for plastics and rubbers is large because it encompasses many materials and because the properties of individual materials of this type may vary considerably with frequency and temperature. On the whole, the loss factors of high-strength materials, particularly of metals, tend to be much smaller than those of plastics and rubbers, which are of lower strength.

Plastics and rubbers are called *viscoelastic materials* because they exhibit both energy dissipative (viscous) and energy storage (elastic) behaviors. The storage and loss moduli, as well as the loss factors, of these materials typically vary considerably with frequency and temperature. At the conditions at which these materials are used most often, their shear moduli are very nearly equal to one-third of the corresponding moduli of elasticity, and the loss factors in shear are very nearly equal to those in tension and compression. The properties of a sample of a given material are strongly dependent on the sample's composition and processing (e.g., on its chemical constituents and their molecular weight distribution and

cross-linking, and on its filler and plasticizer content), so that nominally similar samples may exhibit significantly different dynamic properties. The effects of preloading and strain amplitude on polymeric materials are discussed in Ref. 2.

Figure 2 illustrates how the (real) shear modulus and loss factor of a typical plastic material consisting of a single polymer varies with frequency and temperature.<sup>†</sup> At a given frequency, the modulus is relatively small at low temperatures and small at high temperatures, whereas the loss factor is relatively small at both low and at high temperatures and tends to exhibit a maximum in the region where the modulus changes most rapidly with temperature. At low temperatures the material is said to be in the glassy region because it tends to be hard and brittle; at high temperatures it is said to be in the rubbery region. The dividing point between these two regimes occurs at the so-called *glass transition temperature*, at which the rate of change of the modulus with temperature is greatest.

The material properties change with increases in frequency at constant temperature somewhat like they do with decreases in temperature at constant frequency. At a given temperature the modulus is relatively small at low frequencies and increases with increasing frequency, whereas the loss factor is relatively small at both low and high frequencies, with a maximum at intermediate frequencies. It has been observed that a given change in temperature has the same effect on the modulus and loss factor as does an appropriate shift in frequency. This *temperature-frequency equivalence* makes it possible to represent the behavior of many viscoelastic materials in terms of single curves for the modulus and loss factor as functions of a *reduced frequency*  $f_R = f\alpha_T$ , where  $f$  denotes the actual frequency and  $\alpha_T$  is a *shift factor* that depends on the temperature. This shift factor may be given via an equation or separate plot, or—most conveniently—via a nomogram that is superposed on the data plot as shown in Fig. 3. (Use of this nomogram is illustrated in the figure.) Plots of this type have come into wide use and have become standardized. Shift factor relations are discussed in Ref. 2 and 3.

Table 1 presents some key parameter values for several commercial viscoelastic materials intended for high-damping applications.<sup>‡</sup> The data in the table are useful for preliminary material comparison and selection for specific applications. In general it is advisable to select specific materials on the basis of complete data for the candidate materials. Such data

\*Approximate equality of the loss factors implies that the imaginary part of Poisson's ratio is negligible.

<sup>†</sup>The dynamic behavior of a material consisting of more than one polymer tends to be a blend of the behaviors of its components. The plots corresponding to Fig. 2 then exhibit more complex curvatures, and the loss factor curves may exhibit more than one peak.

<sup>‡</sup>Suppliers often change the designations of their materials. Some of the listed materials may be available with different designations, some may no longer be available.

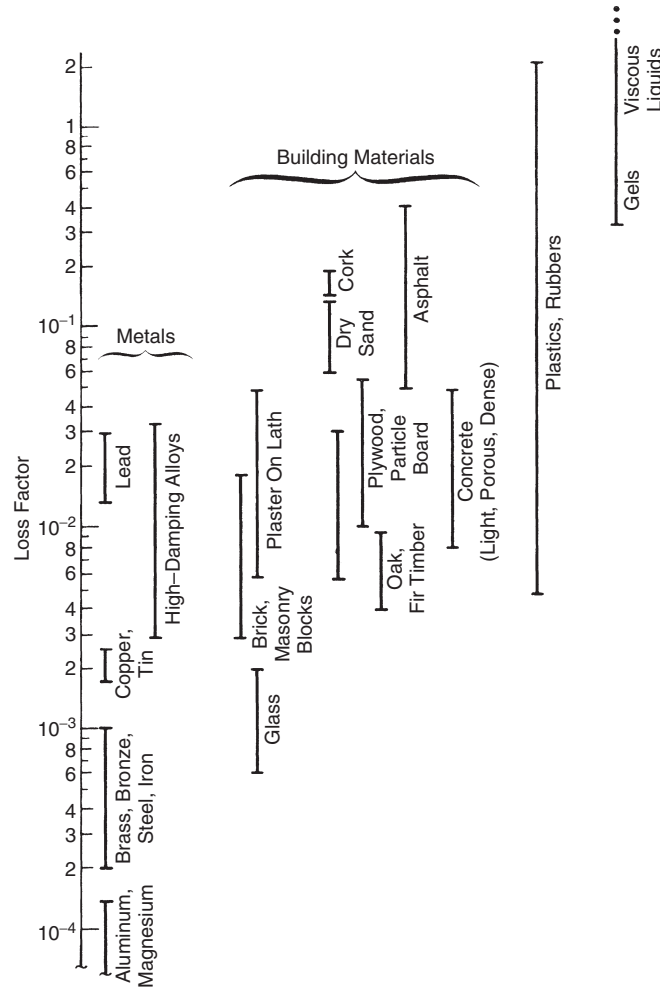


Figure 1 Typical ranges of material loss factors at small strains and audio frequencies, near room temperature.

typically are available from knowledgeable material suppliers.

## 5 DAMPING OF STRUCTURES WITH VISCOELASTIC COMPONENTS

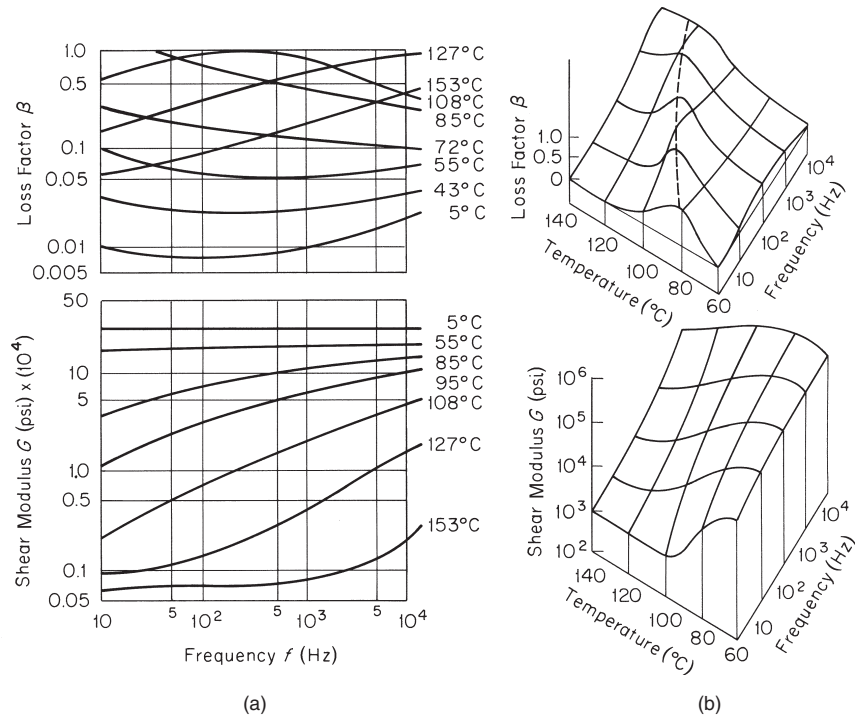
Because most structural materials are strong and have little damping, whereas most viscoelastic materials have considerable damping and relatively little strength, configurations are of interest that combine the strength of the former and the damping of the latter types of materials.

The loss factor  $\eta_{\text{comb}}$  of any multicomponent structure that vibrates in a manner in which all components deflect essentially in phase obeys  $\eta_{\text{comb}} = \sum \eta_i W_i / W_{\text{tot}}$ , where  $\eta_i$  denotes the loss factor of the  $i$ th component,  $W_i$  denotes the energy stored in that component, and  $W_{\text{tot}}$  denotes the total energy stored in all of the components. The sum extends over all of the components. The general equation reduces to

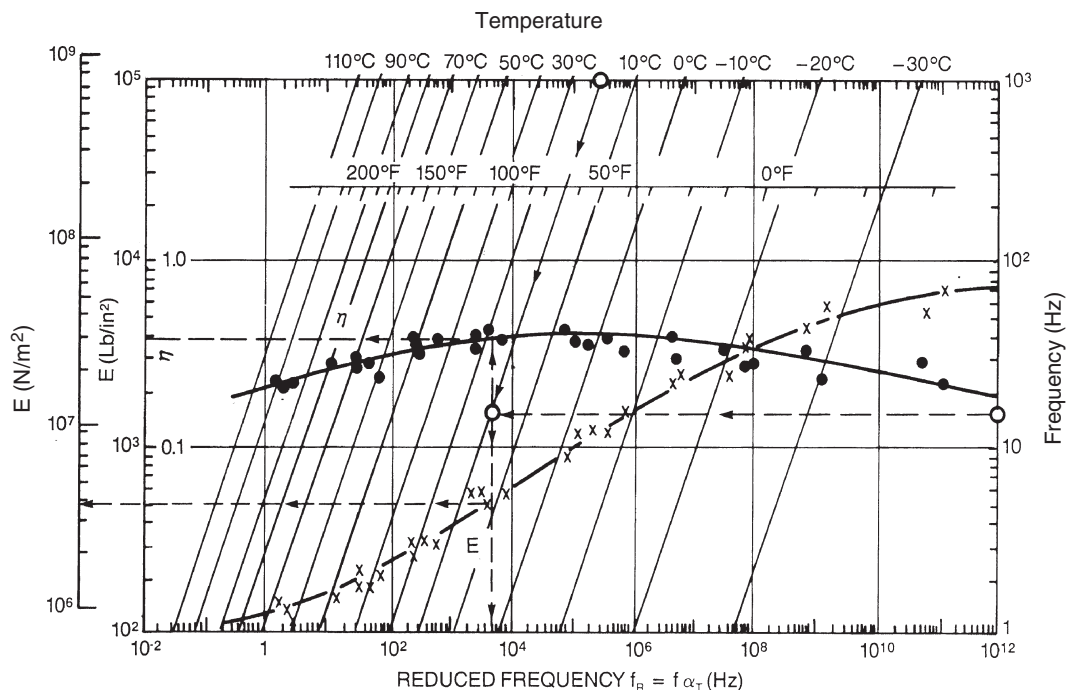
$\eta_{\text{comb}} = \eta_a W_a / W_{\text{tot}}$  if the structure includes only one component, identified by the subscript  $a$ , that has nonzero damping. This equation indicates that (1) the loss factor of the composite cannot be greater than the loss factor of the component with finite damping, and (2) if the composite is to have a considerable loss factor, not only does the loss factor  $\eta_a$  of the damped component have to be large, but that component also has to share in the total energy to a considerable extent.

### 5.1 Beams with Single Viscoelastic Components

In the bending of uniform beams with cross sections of the types illustrated by Fig. 4, where an insert or adhered layer of a viscoelastic material is added to a primary structure that has little inherent damping, energy dissipation is associated primarily with extension and compression of the viscoelastic elements. If



**Figure 2** Dependence of shear modulus and loss factor of a polyester plastic on frequency and temperature: (a) functions of frequency at constant temperatures and (b) three-dimensional plots on temperature log-frequency axes.



**Figure 3** Reduced frequency plot of modulus of elasticity  $E$  and loss factor  $\beta$  of a silicone potting compound. Points indicate measured data to which curves were fitted. Nomograph facilitates determination of reduced frequency  $f_R$  for given frequency and temperature as illustrated by dashed lines. For  $f = 15$  Hz and  $T = 20^\circ\text{C}$  one finds  $f_R = 5 \times 10^3$  Hz,  $E = 3.8 \times 10^6$  N/m<sup>2</sup>,  $\beta = 0.36$ .



**Table 1 Key Properties of Some Commercial Damping Materials<sup>a</sup>**

Material	$\beta_{\max}$	Temperature (°F) for $\beta_{\max}$ at			Elastic Moduli (1000 psi)			
		10 Hz	100 Hz	1000 Hz	$E_{\max}$	$E_{\min}$	$E_{\text{trans}}$	$E_{i,\max}$
Blachford Aquaplas	0.5	50	82	125	1,600	30	220	110
Barry Controls H-326	0.8	-40	-25	-10	600	3	42	34
Dow Corning Sylgard 188	0.6	60	80	110	22	0.3	2.6	1.5
EAR C-1002	1.9	23	55	90	300	0.2	7.7	15
EAR C-2003	1.0	45	70	100	800	0.6	22	22
Lord LD-400	0.7	60	80	125	3,000	3.3	100	70
Soundcoat DYAD 601	1.0	15	50	75	300	0.15	6.7	6.7
Soundcoat DYAD 606	1.0	70	100	130	300	0.12	6	6
Soundcoat DYAD 609	1.0	125	150	185	200	0.6	11	11
Soundcoat N	1.5	15	30	70	300	0.07	4.6	6.9
2M ISD-110	1.7	80	115	150	30	0.03	1	1.7
3M ISD-112	1.2	10	40	80	130	0.08	3.2	3.9
3M ISD-113	1.1	-45	-20	15	150	0.3	0.21	0.23
3M 468	0.8	15	50	85	140	0.03	2	1.6
3M ISD-830	1.0	-75	-50	-20	200	0.15	5.5	5.5
GE SMRD	0.9	50	80	125	300	5	39	35

<sup>a</sup>Tabulated values are approximate, taken from curves in Ref. 2.

$\beta_{\max}$  = Maximum loss factor of material.

Temperatures (°F) at which maximum loss factor occurs at the indicated frequencies may be converted to °C by use of the formula °C = (5/9) (°F - 32).

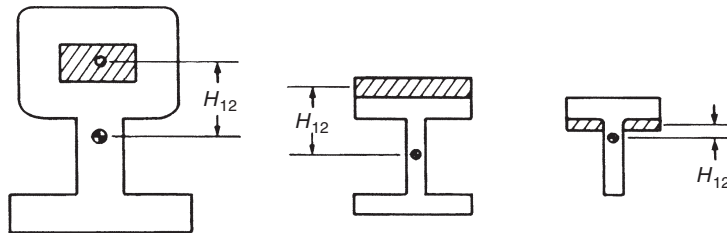
To obtain elastic moduli in N/m<sup>2</sup> multiply tabulated values by  $7 \times 10^6$ . Shear modulus values are one third of elastic modulus values.

$E_{\max}$  = Maximum value of real modulus of elasticity, applies at low temperatures and/or high frequencies.

$E_{\min}$  = Minimum value of real modulus of elasticity, applies at high temperatures and/or low frequencies.

$E_{\text{trans}}$  = Value of real modulus of elasticity in region where maximum loss factor occurs.

$E_{i,\max}$  = Value of imaginary modulus of elasticity in region where maximum loss factor occurs.



**Figure 4** Cross sections of beams with viscoelastic inserts or added layers. Viscoelastic material is shown shaded, structural material unshaded.  $H_{12}$  represents distance between neutral axes of components.

no slippage occurs at the interfaces and if the deformation shape of the beam is sinusoidal,\* then the loss factor contribution  $\eta$  of the viscoelastic element<sup>†</sup> is related to the loss factor  $\beta_2$  of the viscoelastic material

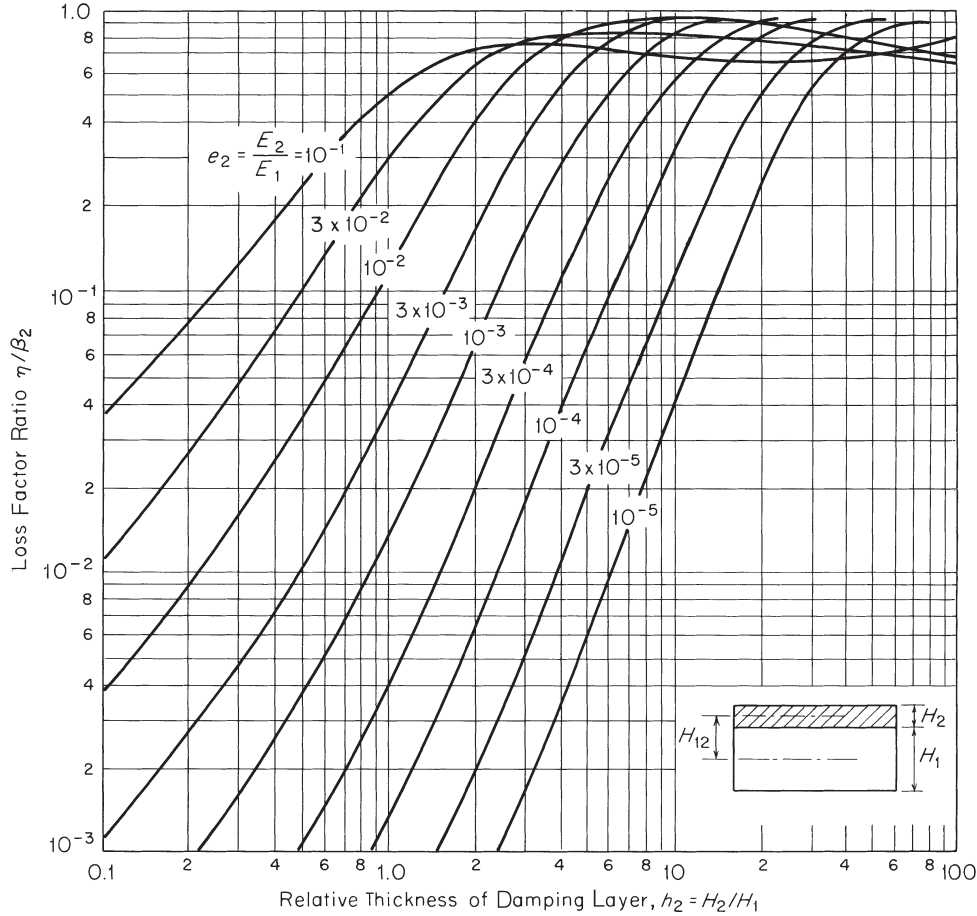
by

$$\eta = \beta_2 \left[ 1 + \frac{k^2(1 + \beta_2^2) + (r_1/H_{12})^2\gamma}{k[1 + (r_2/H_{12})^2\gamma]} \right]^{-1} \approx \frac{\beta_2 E_2 I_T}{E_1 I_1} \quad (6)$$

where  $\gamma = (1 + k)^2 + (\beta_2 k)^2$  and  $H_{12}$  denotes the distance between the neutral axes of the elastic and viscoelastic components, as indicated in Fig. 4. Here and subsequently the subscript 1 refers to the structural (undamped) component and subscript 2 to the viscoelastic component. Also,  $k = K_2/K_1$ , where  $K_n = E_n A_n$  denotes the extensional stiffness of component  $n$ , expressed in terms of its (real) modulus of elasticity  $E_n$  and cross-sectional area  $A_n$ . The radius of gyration of the area  $A_n$  is represented by  $r_n =$

\*The equations presented here also hold approximately if the deformation shape is not sinusoidal. They hold well for the higher modes of a beam, regardless of the end conditions, because the deformation shape associated with such a mode is essentially sinusoidal, except near the ends.

<sup>†</sup>The loss factor contribution of the viscoelastic element is equal to the loss factor of the composite beam if the loss factor of the other element is negligible.



**Figure 5** Dependence of loss factor  $\eta$  of plate with adhered viscoelastic layer on relative thickness and relative modulus of layer, for material loss factor  $\beta_2^2 \ll 1$ .

$\sqrt{I_n/A_n}$ , with  $I_n$  denoting the centroidal moment of inertia of that area.

The last, more approximate, form of equation (6) pertains to the often-encountered case where the structural component's extensional stiffness is much greater than that of the viscoelastic component, with  $I_T = I_2 + H_{12}^2 A_2$  and  $E_2 I_T \ll E_1 I_1$ . Note that the dominant viscoelastic material property is the product  $\beta_2 E_2$ , which is the loss modulus (the imaginary part of the complex modulus) of the material. Thus, an efficient damping material here needs to have both a large loss factor and a large modulus of elasticity.

## 5.2 Plates with Viscoelastic Coatings

A strip of a plate with a viscoelastic coating may be considered as a special case of a beam with a single viscoelastic component, where the beam and the viscoelastic element have rectangular cross

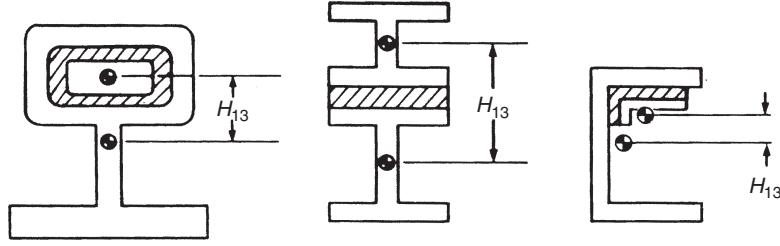
sections (see insert of Fig. 5).<sup>\*</sup> Then Eq. (6) and the foregoing relations apply with  $r_n = H_n/\sqrt{I_2}$  and  $H_{12} = (H_1 + H_2)/2$ , where  $H_n$  denotes the thickness of the component identified by the subscript, with subscripts 1 and 2 referring to the elastic and the viscoelastic layers, respectively. A plot of  $\eta/\beta_2$  for the often-encountered situation where  $\beta_2^2 \ll 1$  appears in Fig. 5.

For small relative thicknesses  $h_2 = H_2/H_1$ —that is, where the curves of Fig. 5 are nearly straight—the loss factor of a coated plate obeys

$$\eta \approx \frac{\beta_2 E_2}{E_1} h_2 (3 + 6h_2 + 4h_2^2) \approx 3 \frac{\beta_2 E_2}{E_1} \frac{H_2}{H_1} \quad (7)$$

and is essentially proportional to the thickness  $H_2$  of the viscoelastic layer. For very large relative

<sup>\*</sup>A viscoelastic layer without a “constraining layer” atop it is often called a *free* or *unconstrained* damping treatment.



**Figure 6** Cross sections of composite beams consisting of two structural components (unshaded) joined via a viscoelastic component (shaded).  $H_{13}$  denotes distance between neutral axes of structural components.

thicknesses, the loss factor of a coated plate approaches that of the viscoelastic coating layer itself. Because the loss factor of a coated plate is proportional to the loss modulus (the product  $\beta_2 E_2$ ) of the damping material, an effective damping material needs to have both a high loss factor and a large modulus of elasticity.

If two viscoelastic layers are applied to a plate, one layer on each side, and if the extensional stiffness of each is considerably less than that of the structural layer (i.e., if  $E_2 H_2 \ll E_1 H_1$ ), then the loss factor of the coated plate may be taken as the sum of the loss factors contributed by the individual layers, with each layer's contribution calculated as if the other layer were absent. A more complex relation applies in the case where the layers have large relative extensional stiffnesses; in this case the total damping contribution is less than the sum of the separately calculated contributions.

### 5.3 Three-Component Beams with Viscoelastic Interlayers

Figure 6 illustrates the cross sections of some beams, each consisting of two structural (nonviscoelastic) components interconnected via a relatively thin viscoelastic component. As uniform beams of this type vibrate in bending, energy dissipation occurs predominantly due to shear in the viscoelastic components.

The damping behavior of such a beam vibrating in bending with an essentially sinusoidal deflection shape may be described with the aid of a *structural parameter*  $Y$  and a *shear parameter*  $X$ , defined by

$$\frac{1}{Y} = \frac{E_1 I_1 + E_3 I_3}{H_{13}^2} S \quad X = \left( \frac{\lambda}{2\pi} \right)^2 \frac{G_2 b}{H_2} S \quad (8)$$

Here  $S = 1/E_1 A_1 + 1/E_3 A_3$ . Subscripts 1 and 3 refer to the structural components and 2 refers to the viscoelastic component.  $E_n$ ,  $A_n$ , and  $I_n$  represent, respectively, the modulus of elasticity, cross-sectional area, and cross-sectional moment of inertia (about its own centroid) of component  $n$ .  $H_{13}$  denotes the distance between the neutral axes of the two structural components (as indicated in Fig. 6) and  $G_2$  denotes the shear modulus (real part) of the viscoelastic material.  $H_2$  denotes the average thickness of the viscoelastic

layer and  $b$  represents the length of that layer's trace in the plane of the cross section of the beam.

The term  $\lambda$  denotes the bending wavelength, which for a spatially sinusoidal beam deflection obeys  $(\lambda/2\pi)^2 = \sqrt{B/\mu}/\omega$ , where  $B$  represents the magnitude of the (complex) flexural rigidity and  $\mu$  the mass per unit length of the composite beam. The complex flexural rigidity of a three-component beam obeys

$$\bar{B} = (E_1 I_1 + E_3 I_3) \left( 1 + \frac{\bar{X} Y}{1 + \bar{X}} \right)$$

where  $\bar{X} = X(1 + j\beta_2)$ .

The shear parameter is a measure of how well the viscoelastic component couples the flexural motions of the two structural components. For small values of  $X$ ,  $B$  is equal to the sum of the flexural rigidities of the two structural components—that is, to the flexural rigidity that the beam would exhibit if the two components were not interconnected. For large values of  $X$ , on the other hand,  $B$  is equal to  $1 + Y$  times the foregoing value and corresponds to the flexural rigidity the beam would exhibit if the two structural components were rigidly interconnected.

The structural parameter  $Y$  depends only on the geometry and on the moduli of elasticity of the two structural components, whereas the shear parameter  $X$  depends also on the properties of the viscoelastic component and on the wavelength of the beam deflection.

A plot of the loss factor  $\eta$  of a composite beam for given values of  $Y$  and of  $\beta_2$  versus the shear parameter  $X$  has the shape of an inverted parabola, as shown in Fig. 7. Each such plot exhibits a maximum loss factor

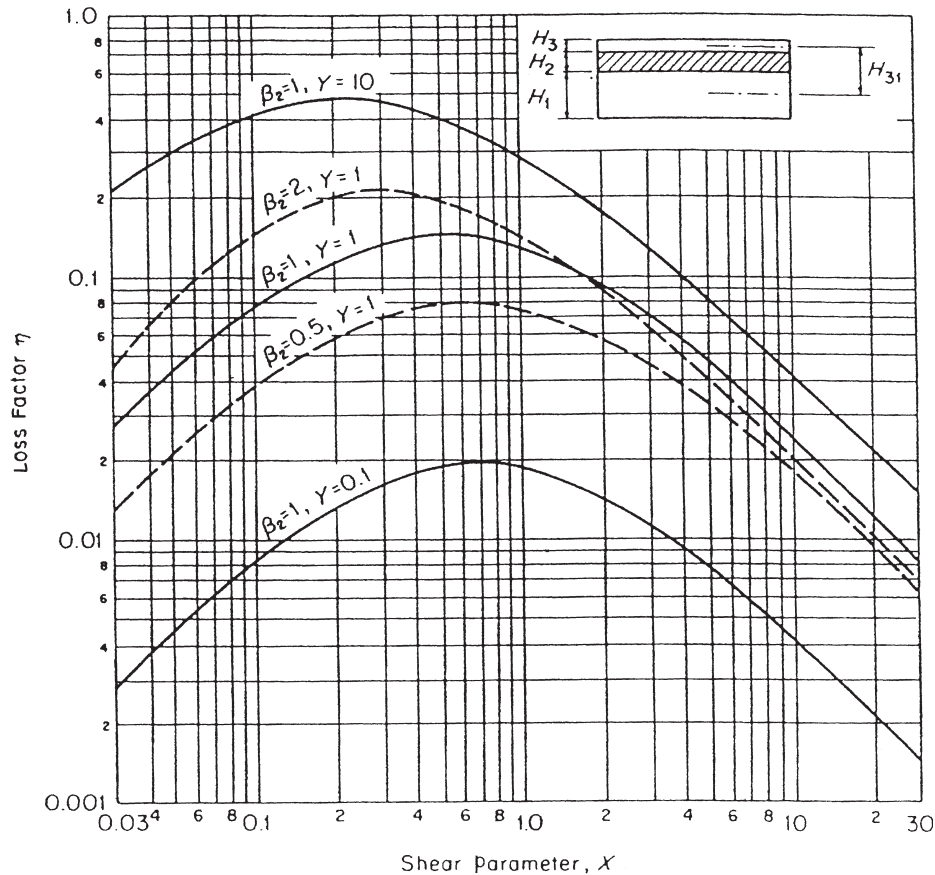
$$\eta_{\max} = \frac{\beta_2 Y}{2 + Y + 2/X_{\text{opt}}} \quad (9)$$

at an optimum value of  $X$ , which obeys

$$X_{\text{opt}} = [(1 + Y)(1 + \beta_2^2)]^{-1/2} \quad (10)$$

The equation

$$\frac{\eta}{\eta_{\max}} = \frac{2(1 + N)R}{1 + 2NR + R^2} \quad (11)$$



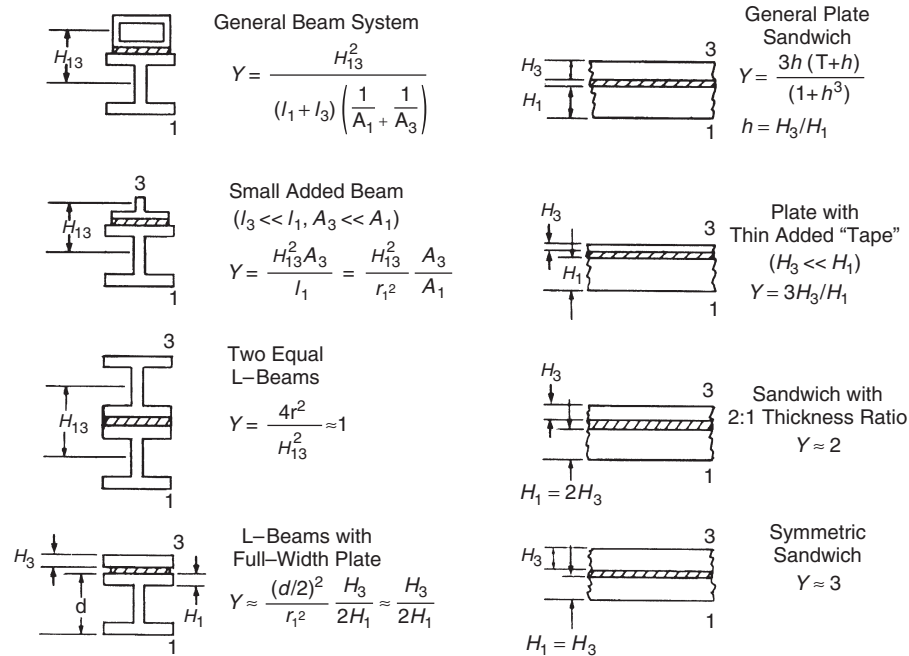
**Figure 7** Dependence of loss factor  $\eta$  of three-component structures with various structural parameters  $Y$  and damping material loss factors  $\beta_2$  on the shear parameter  $X$ .

where  $R = X/X_{\text{opt}}$  and  $N = (1 + Y/2)X_{\text{opt}}$ , indicates the dependence of the loss factor on  $X$ ,  $Y$ , and  $\beta_2$  and may be used to calculate the loss factor of a given three-component beam at a given frequency. It also is useful for determining how close a given beam's damping comes to the maximum that can be achieved with a given configuration and viscoelastic material.

If one knows the properties of the viscoelastic material under the conditions of interest and the bending wavelength  $\lambda$  of concern, one may readily determine  $X$  from its definition, Eq. (6). Otherwise, one needs to determine  $X$  from a process that takes account of the dependence of  $\lambda$  on  $B$  and of the dependence of  $B$  on  $X$ . A suitable approach consists of an iterative process that consists of (1) calculation of  $X_{\text{opt}}$ , (2) evaluation of the corresponding value of  $B$ , (3) calculation of the resulting value of  $\lambda$ , (4) using this value of  $\lambda$  to determine a new value of  $X$ , and (5) repeating these steps, beginning with the newly determined value of  $X$ , until the final and the initial values of  $X$  match to the desired degree. This process usually converges rapidly.

**5.3.1 Design Considerations** The maximum loss factor  $\eta_{\text{max}}$  that can be achieved in a composite beam by use of a damping material with a given loss factor  $\beta_2$  increases monotonically with the structural parameter  $Y$ . Thus, to obtain a highly damped beam, one should select a configuration with as large a structural parameter as practical. Figure 8 presents the expressions for the structural parameters for some typical composite beam configurations.\* Once one has selected  $Y$  and a damping material, one should make the expected loss factor equal to the greatest possible value,  $\eta_{\text{max}}$ . Since the maximum loss factor occurs at the optimum shear parameter  $X_{\text{opt}}$ , the value of which can readily be determined from  $Y$  and  $\beta_2$ , one should adjust the value of  $X$  at the frequency of interest so that it equals the calculated value of  $X_{\text{opt}}$ . For

\*Greater values of  $Y$  than those shown may be obtained by insertion of a shear-stiff, extensionally soft *spacer* layer (e.g., of a honeycomb material) between the viscoelastic element and one or both structural elements. This has the effect of increasing  $H_{13}$ .



**Figure 8** Expressions for structural parameter  $Y$  for various three-component beam and plate configurations with both structural components of the same material and with thin viscoelastic components (shown cross-hatched).  $I_n$  = centroidal moment of inertia of cross-sectional area  $A_n$  of component  $n$ ;  $r_n$  = radius of gyration of  $A_n$ ;  $H_{13}$  = distance between neutral axes of structural components.

a given composite beam configuration and damping material (at a given frequency and temperature), all parameters that appear in the expression for  $X$  then are established, except for the damping material thickness  $b$ . Thus, one should choose the value of  $b$  that makes  $X$  equal to  $X_{\text{opt}}$ . If this thickness turns out to be impractically small, then one needs to consider an alternative damping material with a greater shear modulus; if the thickness turns out to be too great, one needs to consider use of a damping material with a smaller shear modulus.

#### 5.4 Plates with Viscoelastic Interlayers

A strip of a plate consisting of a viscoelastic layer between two structural layers\* may be considered as a special case of three-component beams. All equations and considerations discussed for three-component beams apply here also. Here, however, the expressions for the structural and shear parameters reduce to

$$X = \left( \frac{\lambda}{2\pi} \right)^2 \frac{G_2}{H_2} S \quad \frac{1}{Y} = \frac{E_1 H_1^3 + E_3 H_3^3}{12 H_{13}^2} S$$

$$S = \frac{1}{E_1 H_1} + \frac{1}{E_3 H_3} \quad (12)$$

\*A viscoelastic layer between two structural layers is often called a *constrained layer damping treatment*.

#### 5.5 Extensional versus Shear Damping

The damping of beams with single viscoelastic components and of plates with unconstrained viscoelastic layers results primarily due to extension/compression in the viscoelastic material and is independent of the deflection wavelength. On the other hand, the damping of three-component beams and of plates with constrained viscoelastic layers is primarily due to shear in the viscoelastic components and depends markedly on the deflection wavelength. Thus, wavelength considerations need not be taken into account in the design of damping arrangements that depend on extension/compression, but wavelength (and related frequency) considerations are of crucial importance in the design of arrangements that depend on shear. As a result, extensional damping treatments require little design effort and arbitrarily added damping layers are likely to result in some damping benefit. However, shear damping treatments generally need to be designed and arbitrarily assembled arrangements of this type may exhibit very little damping.

Energy dissipation in an extensional damping configuration occurs predominantly at the antinodes of a vibrating structure, whereas energy dissipation in shear damping configurations occurs predominantly at the nodes. Thus, little damping reduction may be expected if viscoelastic material is removed near the nodes of an extensional damping configuration or near the antinodes of a shear damping configuration.

Shear damping treatments clearly are more complex than extensional treatments, but they have some advantages, even though their high-damping performance is limited to their design frequency and temperature range. Shear damping treatments permit one in practice to obtain greater damping in the design range, particularly for heavy structures. Such treatments also generally enable one to achieve a given amount of damping of light structures in the design range with a lesser weight penalty. Finally, because the viscoelastic material in a shear damping configuration can be fully encapsulated, such configurations are useful where interaction of this material with the environment may be a concern.

## REFERENCES

1. E. E. Ungar, Structural Damping, in *Noise and Vibration Control Engineering*, L. L. Beranek and I. L. Ver, Eds., Wiley, New York, 1992, Chapter 12.
2. A. D. Nashif, D. I. G. Jones, and J. P. Henderson, *Vibration Damping*, Wiley, New York 1985.
3. D. I. G. Jones, *Handbook of Viscoelastic Vibration Damping*, Wiley, Chichester, 2001.
4. D. J. Mead, *Passive Vibration Control*, Wiley, Chichester, 1998.

# CHAPTER 61

## DYNAMIC VIBRATION ABSORBERS

Leif Kari

The Marcus Wallenberg Laboratory for Sound and Vibration Research  
KTH—The Royal Institute of Technology  
Stockholm, Sweden

### 1 INTRODUCTION

Dynamic vibration absorbers (DVA)—also known as antivibrators, vibration neutralizers, and dynamic, tuned, shock, and vibration absorbers or dampers—are auxiliary mechanical systems attached to vibrating systems, whereby the motion of the (primary) vibration systems is reduced. They consist, in their simplest form, of a mass connected to the primary system by a spring and/or a damping element, such as a viscous, hysteric, or friction element. Since their first patent<sup>1</sup> at the beginning of the twentieth century with a prehistory of reducing ship rolling motion at the end of the nineteenth century, they have been extensively used for various engineering applications: To reduce wind-induced vibration in power transmission lines, towers, and skyscrapers, to reduce earthquake-induced bridge and building vibration, and to reduce pedestrian-induced walking bridges vibration. They are, moreover, applied to improve machine tool precision and to reduce helicopter rotor vibration and engine vibration in high-performance automotive racing cars and in light aircraft.

### 2 SINGLE-DEGREE-OF-FREEDOM SYSTEM

To analyze a single-degree-of-freedom (SDOF) DVA attached to a SDOF primary vibration system appears at a first sight as a rather trivial problem. However, its solution provides general and useful information on vibration absorber efficiency while determining the optimum parameters. In fact, many multi-degrees-of-freedom (MDOF) and continuous systems are condensable into SDOF systems close to their natural frequencies. Moreover, the properties of rotational SDOF DVAs and rotational primary vibration systems are directly attained from their rectilinear analogies by replacing displacement with angle, mass with moment-of-inertia, and force with moment.

#### 2.1 Undamped DVA

Consider the undamped DVA in Fig. 1, consisting of a rigid body of mass  $m$  and an idealized spring of stiffness  $k$ , attached to a primary vibration system of mass  $M$  and stiffness  $K$ . A steady-state, harmonic force

$$Q(t) = \text{Re}(Q_0 f^\alpha e^{i\Omega t}), \quad (1)$$

excites the primary system, where  $t$ ,  $\Omega$ , and  $i$  are time, angular frequency, and the imaginary unit  $\sqrt{-1}$ , respectively,  $f = \Omega/\Omega_0$ , and the constant  $Q_0$  is force

magnitude at frequency  $\Omega = \Omega_0 (f = 1)$ , where the natural frequency of the primary system

$$\Omega_0 = \sqrt{\frac{K}{M}} \quad (2)$$

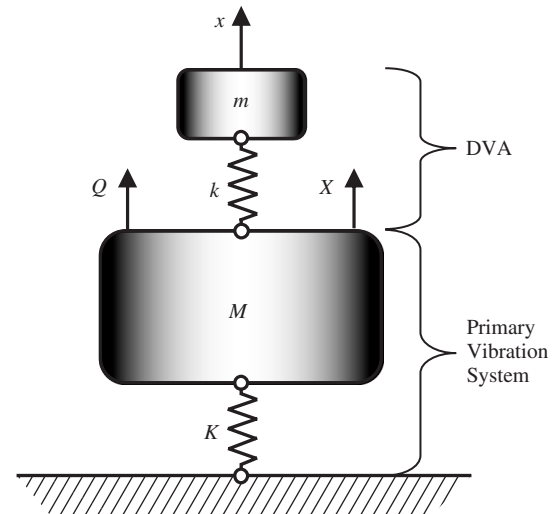
when considered as a separate SDOF system, and, finally,  $\alpha$  is an exponent. This exponent approximates the frequency dependence of the real force and is normally  $-2 \leq \alpha \leq 2$ , depending on the nature of the force and whether the real forcing system operates in the post- or preresonance mode. The most common values are either  $\alpha = 0$  or  $2$ , where the former represents a flat force spectrum, while the latter a force spectrum proportional to the frequency squared—approximating an inertia reaction to a rotating, unbalanced mass with a frequency-independent eccentricity.

The coupled equations of motion for the primary vibration system and DVA are

$$M \frac{d^2 X}{dt^2} + KX + k(X - x) = Q(t) \quad (3)$$

and

$$m \frac{d^2 x}{dt^2} + k(x - X) = 0 \quad (4)$$



**Figure 1** Undamped DVA attached to a primary vibration system.



respectively. The steady-state responses are

$$X(t) = \text{Re}(\hat{X}e^{i\Omega t}) \quad (5)$$

and

$$x(t) = \text{Re}(\hat{x}e^{i\Omega t}) \quad (6)$$

with the normalized solutions

$$\frac{\hat{X}}{X_{st}} = \frac{f^\alpha(f_0^2 - f^2)}{(1 - f^2)(f_0^2 - f^2) - \mu f_0^2 f^2} \quad (7)$$

and

$$\frac{\hat{x}}{X_{st}} = \frac{f^\alpha f_0^2}{(1 - f^2)(f_0^2 - f^2) - \mu f_0^2 f^2} \quad (8)$$

where  $X_{st} = Q_0/K$ , the relative absorber mass  $\mu = m/M$ , the tuning  $f_0 = \omega_0/\Omega_0$ , and the natural frequency of DVA

$$\omega_0 = \sqrt{\frac{k}{m}} \quad (9)$$

when considered as a separate SDOF system.

The normalized displacement  $|\hat{X}/X_{st}f^\alpha|$  versus normalized frequency  $f$  at  $f_0 = 0.75$  and  $1.00$  is shown in Fig. 2 for a primary vibration system connected to an undamped DVA with a relative mass of  $\mu = \frac{1}{10}$ . In addition, the result for a primary system without a DVA is shown for comparison. Clearly, the primary vibration system without a DVA has only one resonance at the normalized frequencies  $f = 1$ , while exhibiting two resonances, when connected to a DVA, at

$$f_{1,2} = \sqrt{\frac{1 + f_0^2(1 + \mu)}{2} \mp \sqrt{\left[\frac{1 + f_0^2(1 + \mu)}{2}\right]^2 - f_0^2}} \quad (10)$$

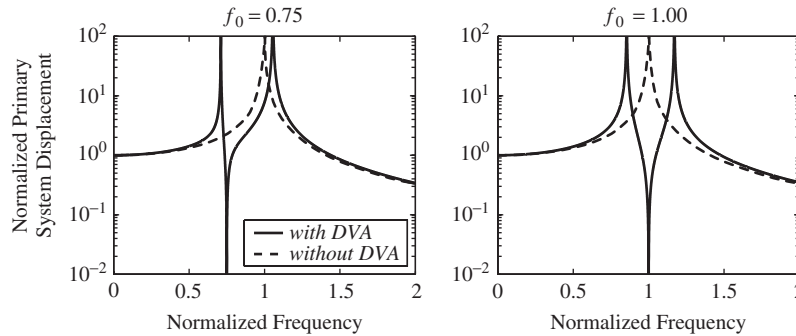
corresponding to the locations of the poles of Eqs. (7) and (8), and reading  $f_{1,2} = 0.71, 1.06$  ( $f_0 = 0.75$ ) and  $f_{1,2} = 0.85, 1.17$  ( $f_0 = 1.00$ ) for the studied systems in Fig. 2. Moreover, the system with a DVA has an antiresonance at  $f = f_0$ , corresponding to the location of the zero of Eqs. (7) and (8). Indeed, the displacement of the primary system vanishes at this frequency while the corresponding DVA displacement is finite, given by Eq. (8) to read

$$\frac{\hat{x}}{X_{st}f^\alpha} \Big|_{f=f_0} = -\frac{1}{\mu f_0^2} \quad (11)$$

Consequently, an undamped DVA attached to a primary vibration system results in the most favorable reduction of the primary system displacement at  $f = f_0$ . The DVA should therefore be tuned to meet  $f_0 = f$ . However, this condition is in practice difficult to fulfill. In fact, the excitation frequency  $\Omega$  may change while the realized DVA parameters may be different from their theoretical values, resulting in  $f_0 \neq f$ . Those disturbances may result in a poor vibration reduction, as the frequency bandwidth for effective primary system vibration reduction is rather narrow, see Fig. 2. From a physical point of view, the primary system displacement reduction arises from the DVA blocking force, transmitted via the connected spring while the DVA mass moves. No energy dissipation is present as no damping mechanism is involved.

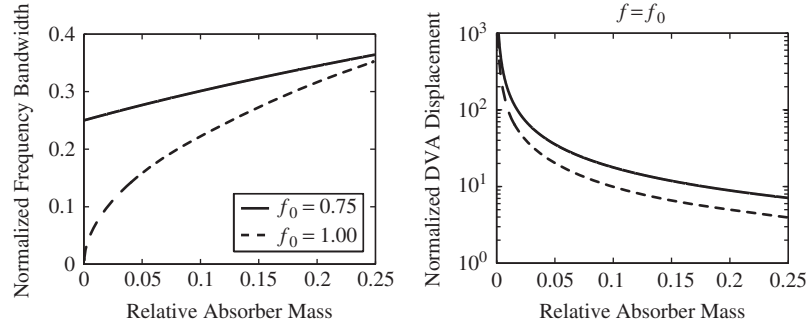
**Effect of Mass** The bandwidth for possible primary system displacement reduction is determined from the frequency points  $f_-$  and  $f_+$  where the relative normalized displacement  $|\hat{X}/X_{st}f^\alpha|$  curve, with DVA, in Fig. 2 crosses the corresponding curve, without DVA. These frequency points are

$$f_{-,+} = \sqrt{\frac{2 + f_0^2(2 + \mu)}{4} \mp \sqrt{\left[\frac{2 + f_0^2(2 + \mu)}{4}\right]^2 - f_0^2}} \quad (12)$$



**Figure 2** Normalized displacement  $|\hat{X}/X_{st}f^\alpha|$  vs. normalized frequency  $f$  for a primary vibration system connected to an undamped DVA (solid) and unconnected (dashed). Relative mass  $\mu = \frac{1}{10}$ .





**Figure 3** (Left) Normalized frequency bandwidth  $f_+ - f_-$  vs. relative mass  $\mu$ . (Right) Normalized displacement  $|\hat{x}/X_{st}f^\alpha|$  vs. relative mass  $\mu$  at  $f = f_0$ . Undamped DVA.

The normalized frequency bandwidth  $f_+ - f_-$  versus relative mass  $\mu$  at  $f_0 = 0.75$  and  $1.00$  is shown in Fig. 3 for a primary vibration system connected to an undamped DVA. Also shown is the normalized DVA displacement  $|\hat{x}/X_{st}f^\alpha|$  versus relative mass  $\mu$  at  $f = f_0$ , using Eq. (11). Note that the DVD displacement is very large at a small relative mass. Clearly, the effective bandwidth increases while the normalized DVA displacement decreases with increased relative mass. However, the main idea of applying a DVA to a real vibrating structure is to use a small relative mass, usually  $\mu \leq \frac{1}{10}$ , whereas substantially heavier DVA masses—as given by theoretical considerations—call for other vibration reduction procedures, including structural design modifications.

## 2.2 Viscously Damped DVA

Damped DVAs are applied to allow for energy dissipation, thereby motivating the term *absorber*. These realistic absorbers furthermore reduce their sensitivities to parameter variations from optimal values and reduce the primary system motions at the resonance frequencies  $f_1$  and  $f_2$ , while increasing their effective bandwidth, as compared to their undamped examples. Consider the viscously damped DVA in Fig. 4, being identical to the system in Fig. 1, however, added with a viscous damping element, having a viscous coefficient of  $c$ , between the masses.

Consequently, the coupled equations of motion for the primary vibration system and DVA are

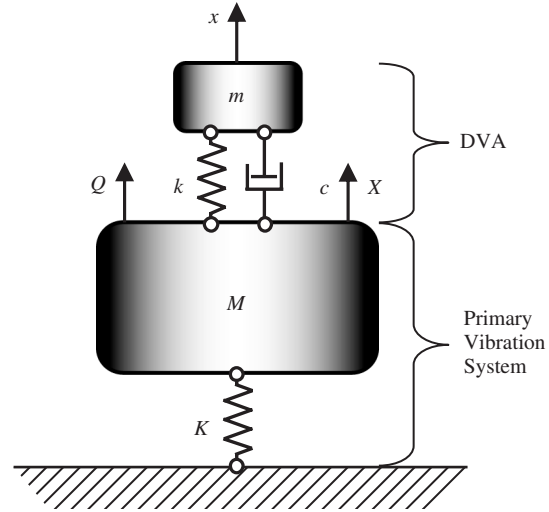
$$M \frac{d^2 X}{dt^2} + KX + c \left( \frac{dX}{dt} - \frac{dx}{dt} \right) + k(X - x) = Q(t) \quad (13)$$

and

$$m \frac{d^2 x}{dt^2} + c \left( \frac{dx}{dt} - \frac{dX}{dt} \right) + k(x - X) = 0 \quad (14)$$

respectively, with the normalized solutions

$$\frac{\hat{X}}{X_{st}} = f^\alpha \frac{(f_0^2 - f^2) + i\chi f}{[(1 - f^2)(f_0^2 - f^2) - \mu f_0^2 f^2 + i\chi f(1 - f^2 - \mu f^2)]} \quad (15)$$



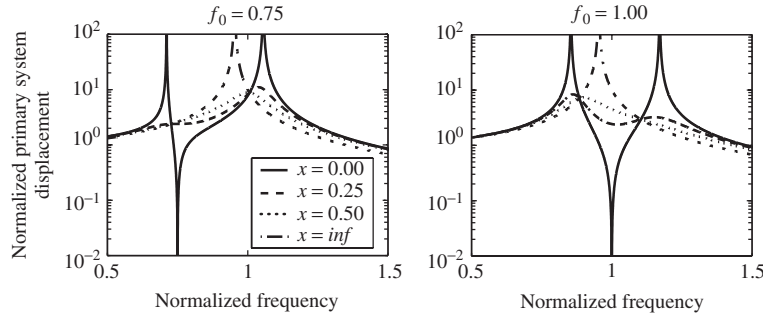
**Figure 4** Viscously damped DVA attached to a primary vibration system.

and

$$\frac{\hat{x}}{X_{st}} = f^\alpha \frac{f_0^2 + i\chi f}{[(1 - f^2)(f_0^2 - f^2) - \mu f_0^2 f^2 + i\chi f(1 - f^2 - \mu f^2)]} \quad (16)$$

following the same procedure as in Section 2.1, where  $\chi$  is the damping ratio  $\chi = c/\Omega_0 m$ .

The normalized displacement  $|\hat{X}/X_{st}f^\alpha|$  versus normalized frequency  $f$  at  $f_0 = 0.75$  and  $1.00$  is shown in Fig. 5 for a primary vibration system connected to the viscously damped DVA, with a relative mass of  $\mu = \frac{1}{10}$  and damping ratios of  $\chi = 0, 0.25, 0.50$ , and  $\infty$ . Clearly, the finitely damped DVA displays a smoother frequency characteristic than the corresponding undamped ( $\chi = 0$ ) example; thus, avoiding excess displacements at resonances while broadening the effective frequency bandwidth.



**Figure 5** Normalized displacement  $|\hat{X}/X_{st} f^\alpha|$  vs. normalized frequency  $f$  for a primary vibration system connected to a viscously damped DVA. Relative mass  $\mu = \frac{1}{10}$  and damping ratios  $\chi = 0, 0.25, 0.50$ , and  $\infty$ .

The infinitely damped ( $\chi = \infty$ ) example behaves as a SDOF with a mass of  $M + m$  standing on the spring of stiffness  $K$ , while displaying an undamped resonance at the normalized frequency  $f_\infty = 1/\sqrt{1 + \mu}$ , reading  $f_\infty = 0.95$  for the studied systems in Fig. 5. Not surprising, as the infinitely viscous damper rigidly connects the masses. Moreover, all curves in Fig. 5 pass through two fixed points, regardless of damping, at the invariant frequencies:

$$f_{A,B} = \sqrt{\frac{1 + f_0^2(1 + \mu)}{2 + \mu}} \mp \sqrt{\left[ \frac{1 + f_0^2(1 + \mu)}{2 + \mu} \right]^2 - \frac{2f_0^2}{2 + \mu}} \quad (17)$$

reading  $f_{A,B} = 0.73, 1.01$  ( $f_0 = 0.75$ ) and  $f_{A,B} = 0.88, 1.10$  ( $f_0 = 1.00$ ) for the studied systems.

The optimal parameter values are determined by a procedure originally developed by Den Hartog<sup>2</sup> while using the properties of the fixed points at the frequencies given by Eq. (17). This fixed-point method is considered highly accurate as a design method for viscously damped DVA.<sup>3</sup> The main idea is to derive the optimal tuning  $f_0^{\text{opt}}$  from the requirement of equal displacement magnitudes at the fixed points  $|\hat{X}(f_A)| = |\hat{X}(f_B)|$ , while the optimal damping ratio  $\chi^{\text{opt}}$  is determined from the requirement of vanishing slopes at the fixed points  $d|\hat{X}(f_A, \chi_A^{\text{opt}})|/df = 0$  and  $d|\hat{X}(f_B, \chi_B^{\text{opt}})|/df = 0$ , where the optimal damping ratio governs from its mean squares  $\chi^{\text{opt}} = \sqrt{[(\chi_A^{\text{opt}})^2 + (\chi_B^{\text{opt}})^2]/2}$ . The optimal parameter values are shown in Table 1 in terms of the relative mass  $\mu$  and excitation force exponent  $\alpha$ .

The normalized displacement  $|\hat{X}/X_{st}|$  versus normalized frequency  $f$ , for a force excitation exponent of  $\alpha = 0$  and 2, is shown in Fig. 6 for a primary vibration system connected to an optimally damped viscous DVA with a relative mass of  $\mu = \frac{1}{10}$ . The optimal parameters read  $f_0^{\text{opt}} = 0.91$ ,  $\chi^{\text{opt}} = 0.34$  ( $\alpha =$

**Table 1** Optimal Parameter Values for a Damped DVA

$\alpha$	$f_{A,B}$	$f_0^{\text{opt}}$	$\chi^{\text{opt}}$	$\eta^{\text{opt}}$
0	$\sqrt{\frac{1 \mp \sqrt{\frac{\mu}{2 + \mu}}}{1 + \mu}}$	$\frac{1}{1 + \mu}$	$\sqrt{\frac{3\mu}{2(1 + \mu)^3}}$	$\sqrt{\frac{\mu(3 + 2\mu)}{2 + \mu}}$
2	$\sqrt{\frac{1 \mp \sqrt{\frac{\mu}{2(1 + \mu)}}}{1 + \frac{\mu}{2}}}$	$\sqrt{\frac{1}{1 + \mu}}$	$\sqrt{\frac{3\mu}{(2 + \mu)(1 + \mu)}}$	$\frac{\sqrt{3\mu(2 + 3\mu)}}{2 + \mu}$

Source: From Ref. 4.

0) and  $f_0^{\text{opt}} = 0.95$ ,  $\chi^{\text{opt}} = 0.36$  ( $\alpha = 2$ ). In addition, the results for a primary system with an undamped DVA and without a DVA are shown for comparison. Clearly, the optimally damped DVA displays a flat frequency characteristic while avoiding the displacement peaks at the resonance for the corresponding undamped example. The effective frequency bandwidth is therefore increased.

### 2.3 Hysteretic Damped DVA

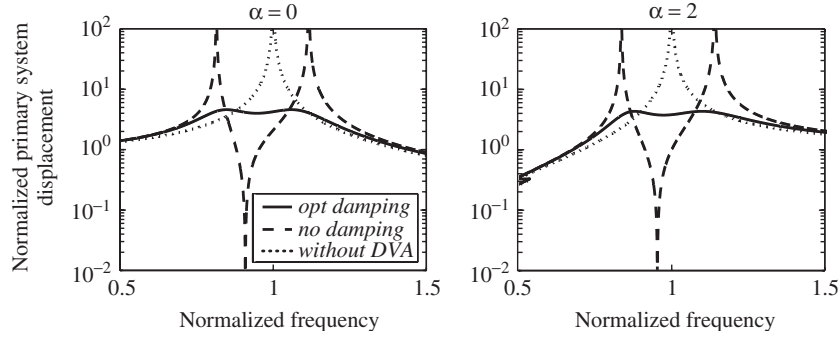
The energy dissipation in many engineering damping materials, such as rubber and plastics, are preferably expressed by a hysteretic damping model with a spring stiffness of  $k(1 + i\eta)$ , where  $\eta$  is a loss factor, normally considered as frequency independent. Consider the hysteretic damped DVA in Fig. 7, being identical to the system in Fig. 1, but with a complex valued stiffness.

Accordingly, the coupled equations of motion for the primary vibration system and DVA are

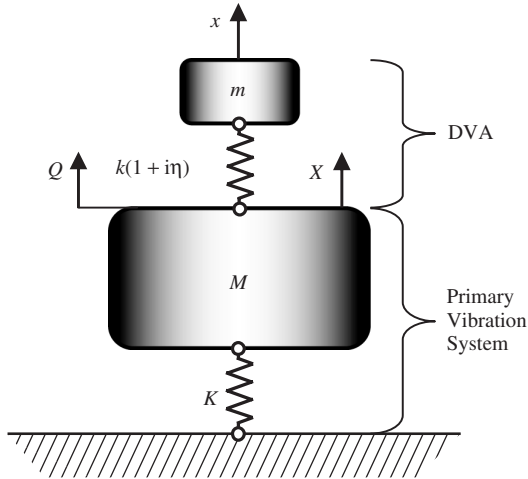
$$M \frac{d^2 X}{dt^2} + KX + k(1 + i\eta)(X - x) = Q(t) \quad (18)$$

and

$$m \frac{d^2 x}{dt^2} + k(1 + i\eta)(x - X) = 0 \quad (19)$$



**Figure 6** Normalized displacement  $|\hat{X}/X_{st}|$  vs. normalized frequency  $f$  for a primary vibration system connected to an optimally damped viscous DVA. Relative mass  $\mu = \frac{1}{10}$ , optimal tuning and optimal damping ratio.



**Figure 7** Hysteretic damped DVA attached to a primary vibration system.

respectively, with the normalized solutions

$$\frac{\hat{X}}{X_{st}} = f^\alpha \frac{(f_0^2 - f^2) + i\eta f_0^2}{[(1 - f^2)(f_0^2 - f^2) - \mu f_0^2 f^2 + i\eta f_0^2(1 - f^2 - \mu f^2)]} \quad (20)$$

and

$$\frac{\hat{x}}{X_{st}} = f^\alpha \frac{f_0^2 + i\eta f_0^2}{[(1 - f^2)(f_0^2 - f^2) - \mu f_0^2 f^2 + i\eta f_0^2(1 - f^2 - \mu f^2)]} \quad (21)$$

following the same procedure as in Sections 2.1 and 2.2.

The procedure of optimizing the parameters to a hysterically damped DVA is almost identical to that of a viscous damped DVA in Section 2.2, with

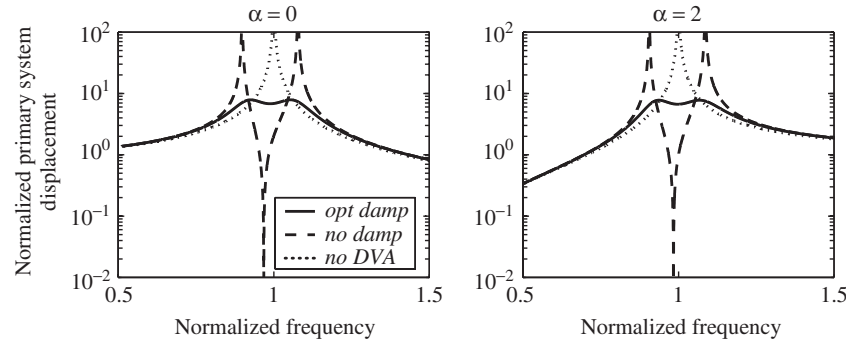
optimal parameter values shown in Table 1.<sup>4</sup> The normalized displacement  $|\hat{X}/X_{st}|$  versus normalized frequency  $f$ , for a force excitation exponent of  $\alpha = 0$  and 2, is shown in Fig. 8 for a primary vibration system connected to an optimally damped hysteretic DVA with a relative mass of  $\mu = \frac{1}{30}$ . The optimal parameters read  $f_0^{\text{opt}} = 0.97$ ,  $\eta^{\text{opt}} = 0.22$  ( $\alpha = 0$ ) and  $f_0^{\text{opt}} = 0.98$ ,  $\eta^{\text{opt}} = 0.23$  ( $\alpha = 2$ ). The results for a primary system with an undamped DVA, and without a DVA are shown for comparison. Obviously, the results are similar to that of a viscous damped DVA, displaying a smooth frequency characteristic over a broad frequency range, including the two undamped resonances.

## 2.4 Damped DVA and Primary Vibration System

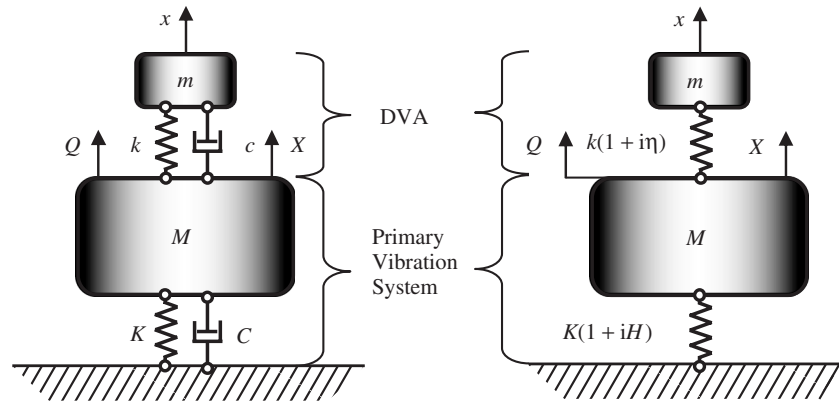
Consider the systems in Fig. 9, consisting of damped DVAs attached to damped primary vibration systems, displaying a damping mechanism of either viscous or hysteretic type. The determination of the primary system and DVA responses is straightforward, following the examples in Sections 2.1 to 2.3, resulting in slightly more involved expressions.<sup>4-7</sup> However, the Den Hartog method of fixed points for parameter optimization is not exactly applicable, as those points are missing for these systems, thus, calling for approximate or numerical methods. Fortunately, the optimal parameter values are close to those in Sections 2.3 and 2.4 for lightly damped primary systems (compared to the damping of DVAs). Moreover, DVAs are primary intended for undamped and lightly damped systems, whereas substantially more damped primary systems generally require other vibration suppression measures.

## 3 MULTI-DEGREES-OF-FREEDOM SYSTEM

The SDOF DVAs and primary vibration systems treated hitherto are readily extended into MDOF arrangements, either by allowing for a MDOF DVA, shown in Fig. 10, or for a MDOF primary vibration systems or for both being of MDOF, the former shown



**Figure 8** Normalized displacement  $|\dot{X}/X_{st}|$  vs. normalized frequency  $f$  for a primary vibration system connected to an optimally damped hysteretic DVA. Relative mass  $\mu = \frac{1}{30}$ , optimal tuning and optimal loss factor.



**Figure 9** Damped DVA and primary vibration system. Viscous (*left*) and hysteretic (*right*).

to the left in Fig. 11, while the latter to the right. Multi-mass/spring DVAs are applied for a number of various reasons: to distribute their action on the primary vibration system, to reduce the individual damper mass and size, and to enlarge their effective bandwidth (as compared to the mono-mass/spring DVA), to mention just a few examples.<sup>4</sup> However, attention to ensure that the added mass displacements are not excessively large is needed.

The design scheme for simple mass–spring DVAs, developed in Section 2, is successfully applied for MDOF primary vibration systems with well-separated natural frequencies, such as beams.<sup>4–7</sup> This procedure is not suggested for primary systems with a dense spectrum of natural frequencies, such as hipped plates and shells.

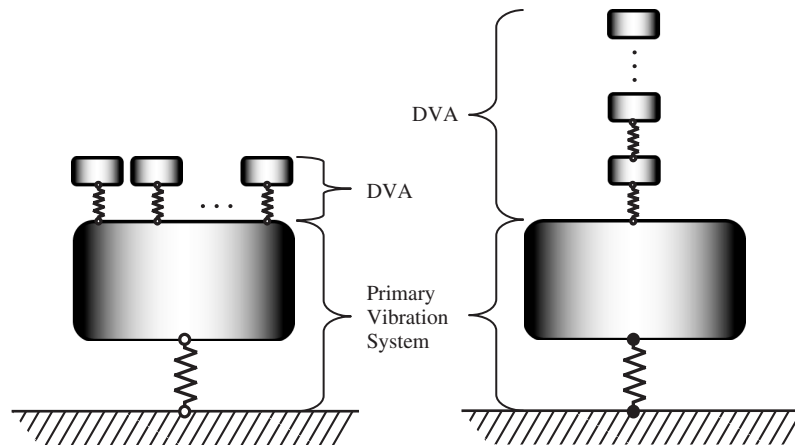
A fruitful method to reduce the vibrations of an MDOF primary vibration system is to use a single MDOF DVA, which is simultaneously effective at several resonance frequencies, such as a plate or beam DVA of infinitely many DOF, shown to the right in Fig. 11.

#### 4 DESIGN CONSIDERATIONS

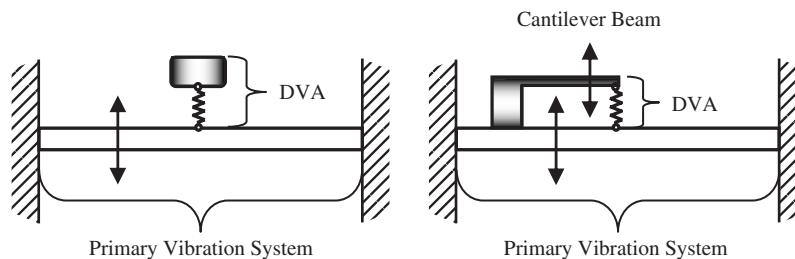
Unlike other vibration reduction procedures, DVAs are possible to specify and design not only at the drawing and construction stage of the primary vibrating system but also during its operational phase, in this manner suppressing unwanted and maybe unexpected vibrations. Moreover, the application of DVAs is considered as a fairly economical method to reduce vibrations.

There is a great variety of DVA and primary system designs. The undamped mass–spring DVA is the simplest configuration. However, this narrow-band tuned DVA is in practical application of little use as the excitations frequency generally varies and the realized damping and stiffness commonly differ from their optimal values. In practice, damped DVAs are used to enlarge the effective frequency range, while introducing an energy dissipation mechanism. Occasionally, detachable DVA masses of various weights are employed for fine tuning. Multi-mass/spring DVAs are also applicable.

Steel and rubber springs are often employed in DVAs. Hydraulic, pneumatic, and magnetic dampers,



**Figure 10** MDOF DVA attached to a SDOF primary vibration system. Parallel (*left*) and series (*right*) connection.



**Figure 11** SDOF DVA (mass-spring-damper) (*left*) and MDOF DVA (cantilever beam-spring) (*right*) attached to a MDOF primary vibration system (clamped beam or plate).

wired steel ropes, and polymer elements, such as from rubber and plastic, are frequently applied as the energy dissipation component of the DVA. The employed damping models are of a viscous, hysteretic, and, in some cases, of a Coulomb friction type. From the designer's point of view, the optimal loss factor required in Table 1 for a typical relative mass exceeds the realistic loss factor for many engineering materials showing hysteretic damping, including natural rubber. As a result, the relative mass must be decreased, in this way limiting the required loss factor to a realistic level. However, the maximum displacement of the DVA is then increased.

The design procedure outlined in this chapter is also applicable for multiharmonic excitation of the primary vibrating system. A damped DVA is then used for each excitation frequency. Continuous DVA structures, such as beams and plates, are also applicable while being simultaneously effective at several frequencies.

## 5 EXCURSION

Although harmonic forces are the most common primary vibration system excitation, other signals may exist, such as transients, random, and periodic

impulses. Their solutions are somewhat different from those given in this chapter.<sup>4</sup> Likewise, there are other types of DVAs: pendulum, nonlinear, liquid, and granular-material-filled DVAs, to mention just a few examples. The interested reader is referred to textbooks on DVAs.<sup>4-8</sup>

Recently, active DVAs are applied, generally providing more effective vibration suppression than their inactive counterparts, however, to the cost of higher complexity and larger outlays. Smart materials are also applied to DVAs, including piezoelectric, electro-, and magnetorheological materials. A survey on recent progress of passive, adaptive, and active DVAs is presented by Sun et al.<sup>9</sup>

## REFERENCES

1. H. Frahm, Device for Damping Vibrations of Bodies, U.S. Patent 989,958, 1909.
2. J. P. Den Hartog, *Mechanical Vibrations*, Dover, New York, 1985.
3. O. Nishihara and T. Asami, Closed-Form Solutions to the Exact Optimizations of Dynamic Vibration Absorbers (Minimizations of the Maximum Amplitude Magnification Factors), *J. Vib. Acoust.*, Vol. 124, 2002, pp. 576-582.

4. B. G. Korenev and L. M. Reznikov, *Dynamic Vibration Absorbers: Theory and Technical Applications*, Wiley, New York, 1993.
5. A. D. Nashif, D. I. G. Jones, and J. P. Henderson, *Vibration Damping*, Wiley, New York, 1985.
6. D. J. Mead, *Passive Vibration Control*, Wiley, New York, 1998.
7. J. C. Snowdon, *Vibration and Shock in Damped Mechanical Systems*, Wiley, New York, 1968.
8. J. B. Hunt, *Dynamic Vibration Absorbers*, Mechanical Engineering Publications, London, 1979.
9. J. Q. Sun, M. R. Jolly, and M. A. Norris, Passive, Adaptive and Active Tuned Vibration Absorbers—A Survey, *J. Mech. Design*, Vol. 117, 1995, pp. 234–242.

# CHAPTER 62

## ROTOR BALANCING AND UNBALANCE-CAUSED VIBRATION

Maurice L. Adams, Jr.

Department of Mechanical and Aerospace Engineering  
The Case School of Engineering  
Case Western Reserve University  
Cleveland, Ohio

### 1 INTRODUCTION

A rotor is said to be unbalanced if its *mass axis* does not coincide with its axis of rotation. A *mass axis* is the locus of the distributed *mass-center* along the rotor length. Rotor balancing is the most important and frequently addressed day-to-day operation in achieving smooth running rotating machinery. It starts with the basic machine design process coupled with the construction details of the rotor, including shop rotor balancing of new and repaired rotors using a *balancing machine*. For some machinery types and applications, this is all that may ever be required. However, in-service rebalancing of some machinery types is periodically needed to reduce their residual unbalance-driven vibration to within acceptable levels, being guided by an experienced-based criterion. There is a sharp distinction between *shop balancing* a rotor in a balancing machine and *in-service field balancing* a rotor in an assembled machine. When shop balancing a new or just repaired rotor, the bare exposed rotor is mounted in a balancing machine and balance correction weights may be placed at any of the balance correction axial planes designed into the rotor. Conversely, in-service rotor balancing usually dictates that balance correction weights can be added only at balance correction planes that are readily accessible while the rotor is installed in an operational machine.

### 2 NEED FOR ROTOR BALANCING

The mass axis does not exactly coincide with the axis of rotation of a rotor because of manufacturing inaccuracies and accumulated in-service balance degradation effects. The mass axis is the locus of the distributed mass center along the rotor length as illustrated in Fig. 1. Rotor balancing to achieve smooth operation of rotating machinery is necessary in most cases. It starts with the basic machine design process coupled with the construction details of the rotor, including shop rotor balancing of new and repaired rotors using a balancing machine. Figure 2 typifies two in-service machine vibration records where rebalancing will be necessary. Figure 3 shows a typical experienced-based guideline for vibration level assessment to determine if rebalancing is needed.

That the subject of rotor balancing warrants its own book was rectified by Rieger,<sup>1</sup> which is the most

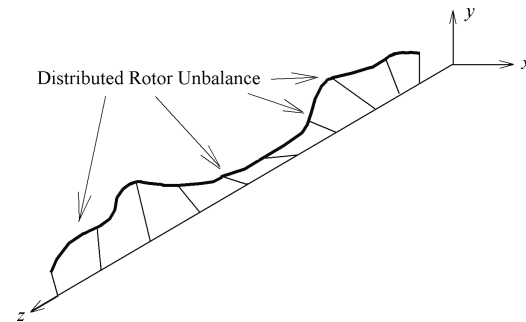


Figure 1 Isometric view of a general rotor unbalance axial distribution.

complete and comprehensive treatise on the subject to date. In addition to fundamental theory and application details for different balancing methods and balancing machines, Ref. 1 also provides a historical perspective on rotor balancing and a summary of balancing specifications for the different classes of machines. Thus, it provides coverage of the field both as needed by the designer/builder of rotating machinery as well as the in-service user/maintainer of rotating machinery. If one is just beginning to study rotor balancing, it is helpful to delineate between so-called *static unbalance* and *dynamic unbalance* as well as distinguish between so-called *rigid rotors* and *flexible rotors*. Due to some ever-present residual rotor mass unbalance, the largest vibration component is usually at the rotating-speed frequency. Figure 3 is a typical example guideline for assessment of operating machines, not a purchase specification acceptance standard.

### 3 STATIC UNBALANCE – SINGLE-PLANE BALANCE CORRECTIONS

The simplest rotor unbalance condition is characterized by the rotor mass center being eccentric to the rotor's geometric spin axis. This is called *static unbalance*. A static unbalance can be likened to an unbalance mass ( $m_s$ ) at some nonzero radius ( $r_s$ ) superimposed (in the radial plane of the rotor's mass center) upon an otherwise perfectly balanced rotor, as illustrated in Fig. 4. Such a concentrated static unbalance clearly acts on the rotor like an equivalent synchronous co-rotational force ( $F_u = m_s r_s \omega^2$ ) that is fixed in the rotor

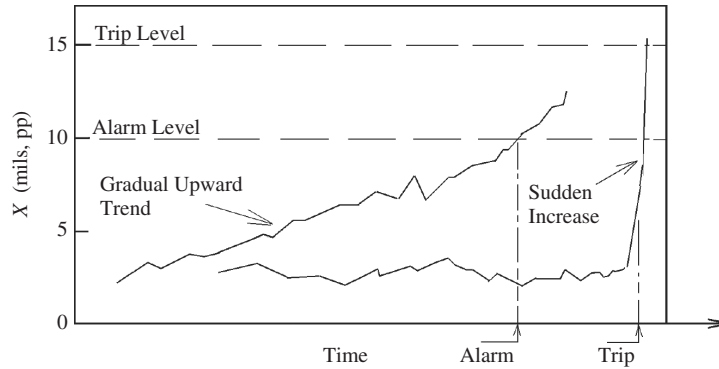


Figure 2 Trending unbalance vibration over time.

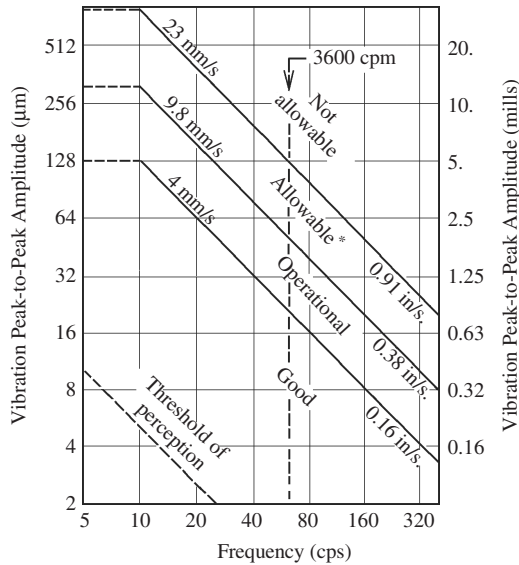


Figure 3 Bearing cap operating vibration displacement guideline. Allowable: operating zone only for short periods.

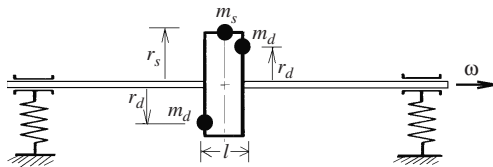


Figure 4 Combination of static and dynamic rotor disk unbalance.

(Fig. 5). Thus, a purely static unbalance on a simple rotor configuration as in Fig. 4 can theoretically be corrected by a single balance correction weight with the same magnitude ( $m_s r_s$ ) and in the same radial plane as the initial static unbalance, but positioned  $180^\circ$  from the initial unbalance.

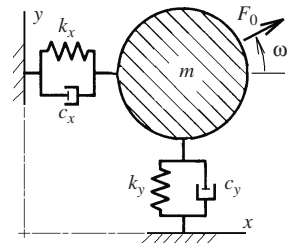


Figure 5 Model representation of an unbalance force upon the rotor.

That is, static unbalance is theoretically correctable by adding a balance correction mass in a *single plane*, specifically, in the plane of the unbalance. A quite common example of single-plane balancing is automotive tire-wheel units that are relatively narrow axially compared to their diameter and are thus approximated as a single-plane mass distribution rotor. The reason for spinning the tire-wheel unit in the tire shop balancing machine is to produce a sufficiently large measurement of the static unbalance force, not to perform a true dynamic balance (see next section). Furthermore, the reason the competent tire shop mechanic places half the weight correction on the outside rim and half on the inside rim (both at same angle) is so that the added static-balance correction weights do not produce a dynamic unbalance. There are many other examples where single-plane balancing produces an adequate state of rotor balance quality.

The two equations of motion for this model with the shown rotating excitation force are easily derived from  $F = ma$  to obtain the following:

$$m\ddot{x} + c_x\dot{x} + k_x x = F_0 \cos \omega t$$

$$m\ddot{y} + c_y\dot{y} + k_y y = F_0 \sin \omega t$$

#### 4 DYNAMIC UNBALANCE – RIGID-ROTOR TWO-PLANE BALANCE CORRECTION

*Dynamic unbalance* refers to rotor unbalance that acts like an equivalent radial co-rotational moment fixed



in the rotor. Referring again to Fig. 4 and using its nomenclature, the equivalent co-rotational moment of a concentrated dynamic unbalance has magnitude  $M_d = m_d r_d l \omega^2$ . If rotor flexibility is not a significant factor to unbalance vibration response, then the *rigid-rotor* assumption can be invoked. Then the total dynamic unbalance of a rotor is theoretically correctable by adding two equal-magnitude ( $m_c r_c$ ) corrections (separated by  $180^\circ$ ), one at each of two planes axially separated by  $l_c$  (where  $m_c r_c l_c = m_d r_d l$ ). The two  $m_c r_c$  corrections are positioned in the plane of the initial dynamic unbalance, but  $180^\circ$  out of phase with the initial dynamic unbalance. The initial dynamic unbalance is thereby theoretically negated since the co-rotational moment produced by the two correction masses has the magnitude  $m_d r_d l \omega^2$  of the initial dynamic unbalance, but  $180^\circ$  out of angular position with the co-rotational moment produced by the initial dynamic unbalance. Since a static unbalance can be negated by two in-phase correction weights appropriately placed in the same two planes as the dynamic unbalance correction masses, it is clear that a complete rotor balance (static + dynamic) of a "rigid" rotor can be accomplished by adding correction masses in only two planes. Since a general state of rotor unbalance is a combination of both static and dynamic unbalance, the correction weights at different axial locations will generally be neither at the same angular position but separated exactly by a  $180^\circ$  in their relative angular positions.

The defining property for so-called rigid rotors is that rotor flexibility is not a significant factor to unbalance vibration response. Therefore, the *two-plane* balance procedure for a rigid rotor can be performed at a speed lower than the operating speed of the rotor. In practical terms, this means the rotor may be balanced using vibration or dynamic force measurements at balancing spin speeds substantially lower than the rotor's in-service operating speed.

## 5 UNBALANCED FLEXIBLE ROTORS — MULTIPLANE BALANCE CORRECTIONS

A *flexible rotor* can be defined as being any rotor that cannot be effectively balanced throughout its speed range by placing suitable correction weights in two separate planes along its length. Synonymous with this definition is that a so-called flexible rotor has an operating speed range that closely approaches or encompasses one or more bending critical speeds whose rotor flexural bending contributes significantly to the corresponding critical speed mode shape(s) and unbalance vibration responses. Table 1 provides an introductory composite description of the increased rotor dynamic complexity produced when rotor flexibility is significant to unbalance vibration characteristics.

In contrast to a rigid rotor, adequate balancing of a flexible rotor often requires placement of correction weights in more than two separate planes along the rotor length. The adequate number of balancing planes and their optimum locations along the rotor are dictated by the mode shape(s) of the critical speed(s) that

significantly affect the rotor's unbalance vibration response. The first three flexure mode shapes of a uniform simply supported beam are illustrated in Fig. 6 and provide some insight into proper axial locations for balance correction weights in balancing flexible rotors. That is, for a rotor with critical speed mode shapes similar to those in Fig. 6, a mid-span balance plane clearly has maximum effectiveness on the first mode. Similarly, the  $\frac{1}{4}$  and  $\frac{3}{4}$  span locations have maximum effectiveness on the second mode, and the  $\frac{1}{6}$ ,  $\frac{1}{2}$ , and  $\frac{5}{6}$  span locations have maximum effectiveness on the third mode.


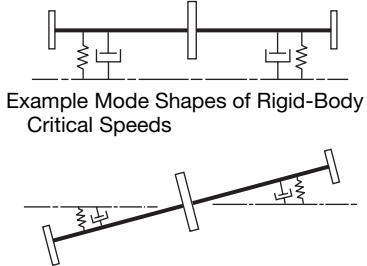
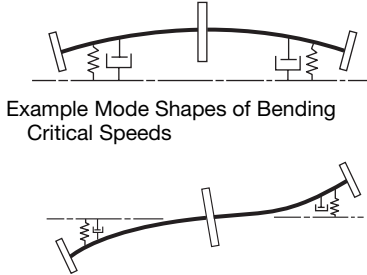
A flexible rotor is also definable as one with a dynamic bending shape that changes with rotational speed, and this speed-dependent dynamic bending may alter the state of balance. Ideally, a flexible rotor should therefore be balanced at full in-service rotational speed and at speeds near critical speeds within or near the operating speed range. This point is clearly demonstrated by an example from Ref. 2 illustrated in Fig. 7, which shows a uniform shaft in stiff bearings unbalanced by a single mass attached at the axial center of the shaft. Figure 7 also illustrates that the shaft has been rebalanced consistent with the low-speed rigid-rotor approach by adding a correction weight at each end of the shaft. As long as the shaft speed is significantly below its first bending critical speed, it will remain essentially straight and thus will remain in balance. But as its rotational speed approaches its first bending critical speed, it vibrates as illustrated in Fig. 8 (illustrated vibration deflection grossly exaggerated).

As is clear from Fig. 8, at speeds near its first bending critical speed the shaft illustrated in Fig. 7 has its initial unbalance and both unbalance correction weights acting in collaboration to excite the first bending critical speed. If this experiment were performed, one would find that the vibration near the first bending critical speed would be worse (higher) with the two low-speed-balancing correction weights attached than without. In this simple example, the initial unbalance is known to be concentrated at the mid-span location and thus it is a trivial case. In a general case with manufacturing and assembly tolerances, the unbalance is of an unknown distribution along the rotor, such as that illustrated in Fig. 1.

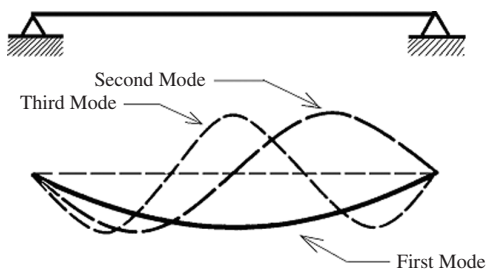
Balancing a dynamically flexible rotor is a considerably more involved process than low-speed two-plane balancing of rigid rotors. Each type of flexible rotor has its own preferred number and location of balance planes. Many multistage machines require a component balance of each impeller or bladed disk assembly before mounting and only then balancing the fully assembled rotor, for example, aircraft gas turbine jet engines.

Some flexible rotors can be adequately well balanced like a rigid rotor, that is, on a low-speed balancing machine with correction masses placed in only two planes along the rotor length. Such a rotor is characterized by having most of its unbalance concentrated at a known axial region of the rotor, for example, large double suction power plant centrifugal fans. There are

**Table 1 Three Elementary Rotor Lateral Vibration Complexity Categories**

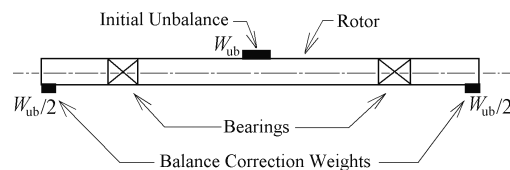
#	System Category	Design Considerations
1	Maximum speed below 80% of lowest critical speed 	Two-plane low-speed rigid-body balancing is all that is required. No elaborate analyses required.
2	Maximum speed is near lowest critical speed or above 1 or 2 critical speeds, but bearings are sufficiently soft that critical-speed modes are rigid-body like. 	Must calculate critical speed(s) to avoid continuous operation at or near a critical speed. Recommend analysis prediction of vibration amplitudes at critical speeds versus amount of available damping. Should also check for self-excited instability rotor vibration. Two-plane low-speed rigid-body balancing is adequate because rotor dynamic flexibility is not significant.
3	Maximum speed near or above one or more critical speeds and rotor flexing is a significant part of critical-speed mode shapes. 	Same recommendations as category 2, except that it will likely be necessary to perform multiplane rotor balancing at speeds up to the maximum operational speed because of the importance of bending critical speeds

Note: Rotor dynamic complexity increases with number.



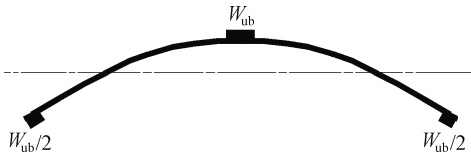
**Figure 6** First three planar mode shapes for a simply supported uniform beam.

a number of competing methods for balancing flexible rotors, the two most recognized being the *modal method* and the *influence coefficient method* (ICM).



**Figure 7** Simple uniform diameter flexible rotor.

Both of these assume that the rotor dynamic system is linear. Significant nonlinearity can be tolerated, but it will likely increase the number of balancing iterations needed to achieve the required quality of rotor balance. The *modal method* requires detailed modal information (mode shapes) for all the critical speeds that significantly influence the rotor's unbalance vibration characteristics over its entire speed range. To the



**Figure 8** Vibration mode shape of a first bending critical speed.

extent that critical-speed modal characteristics are a function of radial bearing dynamic characteristics, the bearings in a modal balancing machine need to match the dynamic characteristics of the actual machine's bearings, and this is often not practical. Thus, although the modal method is considered in some circles to be theoretically a more effective approach than the ICM for balancing flexible rotors, in practice the ICM is used in most applications, being less complicated and more practical than the modal method. The strong preference for the ICM is particularly true for in-service rebalancing of rotors in assembled machines, where a correction is often limited to one plane.

## 6 INFLUENCE COEFFICIENT METHOD

The ICM does not require critical-speed mode shapes, but approximate mode shapes can be helpful in the design process to prescribe where balance planes and unbalance vibration measurements are best located. However, after a rotor is installed in its machine, accessible planes for rebalancing are often limited to locations near the axial ends of the rotor, for example, at a coupling. Thus, all the potential benefits of multiplane rotor balancing are only of academic interest to the person in the power plant who must implement a "balance shot" during a short outage of a machine. A general summary of the ICM fashioned after Ref. 2 is presented here. Free software (disk) for general-purpose ICM balancing is available in Ref. 3 and includes several balancing examples using that software. Utilizing the basic dynamic linearity assumption, the rotor vibration response can be given as the superposition or sum of individual vibration responses from an unbalance at each of the selected balance planes, as expressed in the following equation:

$$V_j = \sum_{k=1}^{N_p} A_{jk} U_k \quad j = 1, 2, \dots, N_m$$

$$k = 1, 2, \dots, N_p \quad (1)$$

where  $N_m$  = number of independent vibration observations = number of locations  $\times$  number of speeds

$N_p$  = number of balance planes

$V_j$  = vibration response from  $j$ th measurement  $\equiv \mathbf{V}_j e^{i(\omega t - \theta_j)}$  (complex)

$U_k$  = unbalance at  $k$ th balance correction plane  $\equiv \mathbf{U}_k e^{i(\omega t + \phi_k)}$  (complex)

$A_{jk}$  = influence coefficient  $N_m \times N_p$  array  $\equiv \mathbf{A}_{jk} e^{i\alpha_{jk}}$  (complex)

Since the ICM is based only on the assumption of linear dynamic characteristics, nonplanar modes are automatically accommodated.

Vibration measurements need not be taken at the same locations as the balance correction planes. Also, any and all of the three commonly used vibration sensor types may be used, that is, accelerometer, velocity pickup, and proximity probe (displacement). Furthermore, vibration measurements may be made on adequately responsive nonrotating parts of the machine (e.g., bearing caps). For in-service rebalancing of machines with displacement probes installed (typically mounted on the bearings targeting the shaft), the rotor vibration relative to the bearing(s) may be used provided the shaft target mechanical and electrical runout are known and correctly subtracted from the total probe signals.<sup>3</sup>

The influence coefficients are experimentally obtained by measuring the incremental change in each of the measured vibration responses to a *trial mass* individually placed at each balance correction plane. With the influence coefficients known, balance corrections for each correction plane can be computed. After the correction masses ( $W_j, j = 1, 2, \dots, N_p$ ) are installed, the residual rotor vibration for all the specified observations (locations and speeds) are expressible as follows, where  $V_j^{(0)}$  are the measured vibration responses before adding the balance correction masses:

$$V_j = V_j^{(0)} + A_{jk} W_k \quad (2)$$

If the number of observations ( $N_m \geq N_p$ ) is equal to the number of balance correction planes ( $N_m = N_p$ ), then the influence coefficient array  $A_{jk}$  yields a square matrix that is presumably nonsingular by virtue of making  $N_m$  linearly independent vibration measurement observations. Using Eq. (2), unbalance vibration at the observation locations and speeds can then theoretically be made zero by using balance corrections given by the following equation:

$$\{W\} = -[A]^{-1}\{V^{(0)}\} \quad (3)$$

It is widely suggested that better balancing often results if the number of observations exceeds the number of correction planes, that is,  $N_m > N_p$ . Since it is then mathematically impossible to make all the observed vibrations go to zero, the approach generally taken is to base the balance correction masses on minimizing the sum of the squares of the residual observed vibrations.

What the ICM can theoretically achieve is best understood by considering the following. If the system were perfectly linear and the vibration observation measurements were made with zero error, then for the case of  $N_m = N_p$ , the observed vibrations (at location-speed combinations) are all made zero by the correction masses. Similarly, for the case of  $N_m > N_p$ , the sum of the squares of the residual observed vibrations can be minimized. However, there

is no mathematical statement for unbalance vibration amplitudes at any other location–speed combinations. By choosing balance speeds near all important critical speeds and at maximum operating speed, and balance planes where actual unbalance is greatest, as well as choosing vibration measurement points that are not close to critical speed mode-shape nodal points, smooth running over the full speed range is routinely achievable.

## 7 IN-SERVICE SINGLE-PLANE BALANCE “SHOT”

The most common day-to-day type of rotor balancing is the in-service balance shot, especially in power plants, process plants, and machine tool spindles. In these rotor balancing efforts, the machine is in-service and unbalance-caused vibration had increased (perhaps gradually) above allowable maximum amplitude levels (see Figs. 2 and 3). Typically, a balance correction weight is placed at a single plane which is readily accessible on a fully assembled machine. In power plants and process plants it is essential that the balancing shot can be accomplished as quickly as possible so the machine can be returned to operation (e.g., during a short weekend machine outage).

The objective of such single-plane in-service balance shots is to reduce the steady-state machine maximum vibration amplitudes. That is, it is not intended, nor is it feasible, that such single-plane balance shot provide the high degree of rotor balance quality that is achievable when the removed bare rotor is factory balanced in a precision balancing machine.

A caveat is appropriate to mention at this point. Reference 3 shows that a balance shot placed at a readily accessible rotor location may reduce the measured vibration levels, but may not appreciably reduce rotor vibration levels at machine internal locations where vibration measurements cannot be obtained and where balance weights cannot be placed. Thus, the small internal radial clearances between rotating and nonrotating components at mid-span locations (e.g., at turbine and compressor blade tips and pump sealing wear rings) may not benefit from such a balance shot, as Fig. 8 clearly demonstrates.

Applying the ICM to a single-plane balance shot can be illustrated on a polar phasor vector plot of the steady-state once-per-revolution (synchronous) vibration. Plant rotor balancing personnel often use such a polar plot to graph the amount and angular location of the balance correction weight. This is illustrated in Fig. 9 and is appropriate for any system of units and vibration measure (i.e., displacement, velocity, or acceleration). All boldface letters denote complex-valued phasor vectors. It is assumed that the trial weight ( $U_T$ , used to balance calibrate the system) is first removed before attaching the correct weight ( $U_c$ ) that theoretically brings the measured vibration to zero:

$$x = X \cos(\omega t + \theta) \quad \text{measured synchronous vibration signal}$$

$\omega$  = rotor angular velocity (rad/s) CCW,

$\theta$  = phase angle

$e^{i\theta} = \cos \theta + i \sin \theta$ ,     $\text{Re} \rightarrow$  real axis,

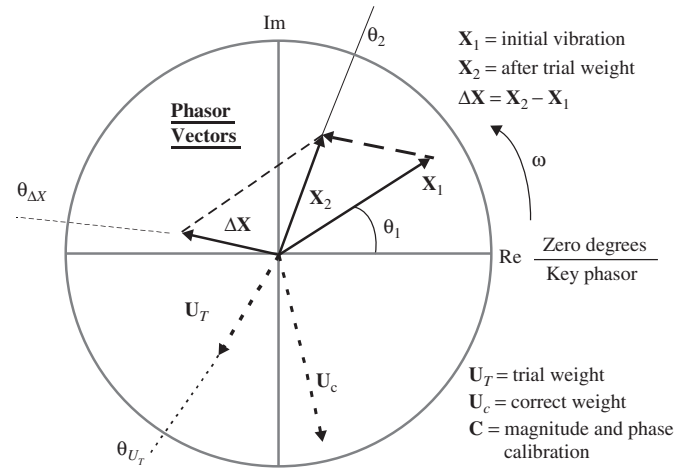
$\text{Im} \rightarrow$  imaginary axis,     $i = \sqrt{-1}$

## 8 CONTINUOUS AUTOMATIC IN-SERVICE ROTOR BALANCING

No comprehensive discussion on rotor balancing would be complete without mentioning automated real-time continuous rotor balancing systems. Figure 10 shows a cut-away view of an automatic balancing system. The rotor-mounted portion houses two equally unbalanced counterweight/stepping-motor rotors, separately indexed in  $5^\circ$  (or less) increments relative to the rotor. Power and control are through magnetic couplers.

Conventional rotor-mounted automatic balancing devices are designed to minimize residual rotor mass unbalance so that the rotor vibration level is maintained within a given application's requirements. Precision machine tool spindles, especially for grinding, are a major application for such devices since successful high-volume high-precision grinding requires continual automatic adjustment of balance correction weights on the rotating assembly as grinding wheel material is removed. The conventional devices available for such automated balancing are configured to change the correction weight magnitude and angular location based on many successive incremental moves that reduce the monitored vibration (usually measured with an accelerometer attached to the spindle housing). However, such conventional systems do not “know” the magnitude or angular location of the continuously changed correction weight nor are they able to execute a “command” to perform a specified incremental change to the correction weight.

Automatic balancing systems, such as shown in Fig. 10, have significantly advanced the field of automatic rotor balancing by tracking the magnitude and angular location of the instantaneous balance correction. The author has recently designed and constructed a new flexible-rotor test rig (Fig. 11) that is configured with two of such automatic rotor balancing devices. The software supplied with these two matched devices executes real-time two-plane automatic rotor balancing, with the controlling algorithm based on the influence coefficient method. The software also permits manual control of counterweight placement and magnitude [through a host PC (personal computer) controller]. That feature plays prominently in current ongoing model-based monitoring and diagnostics research in the author's laboratory.<sup>4</sup> That is, by being able to impose a known incremental change to the state of unbalance (i.e., active probing of the dynamical system), a continuous real-time comparison can be made between how the actual machine incrementally responds and how an observer model tracking the machine's vibration responds.



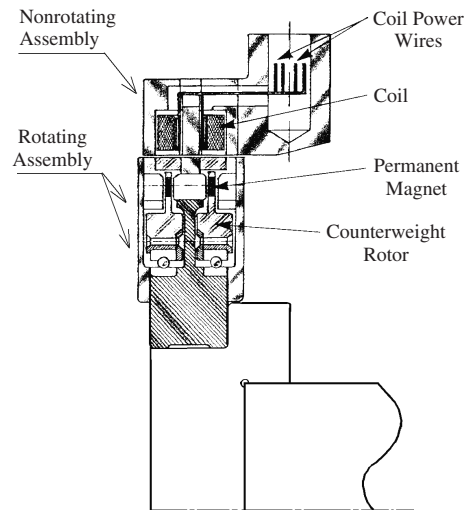
"Key phasor" is a fixed point on the shaft

$U_T$  and  $\Delta X$  are locked together in phase angle and magnitude proportion

$$\Delta X = C U_T \therefore C = \frac{\Delta X}{U_T} = \frac{\Delta X e^{i\theta_{\Delta X}}}{U_T e^{i\theta_{U_T}}} = \frac{\Delta X}{U_T} e^{i(\theta_{\Delta X} - \theta_{U_T})}, \theta_{U_T} - \theta_{\Delta X} = \text{constant}$$

$$\text{Zero vibration condition} \quad X_1 + C U_c = 0 \therefore U_c = -\frac{X_1}{C} = \frac{-X_1 e^{i\theta_1}}{C e^{i(\theta_{\Delta X} - \theta_{U_T})}} = \frac{-X_1}{C} e^{i(\theta_1 - \theta_{\Delta X} + \theta_{U_T})}$$

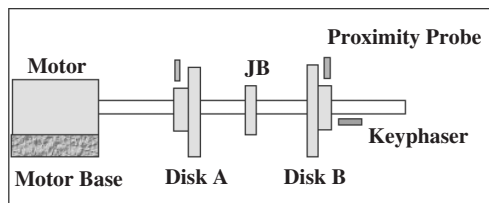
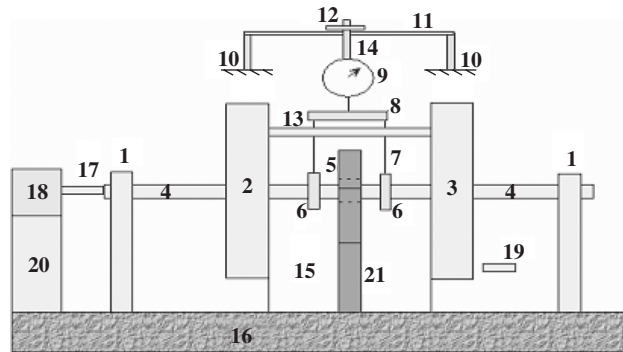
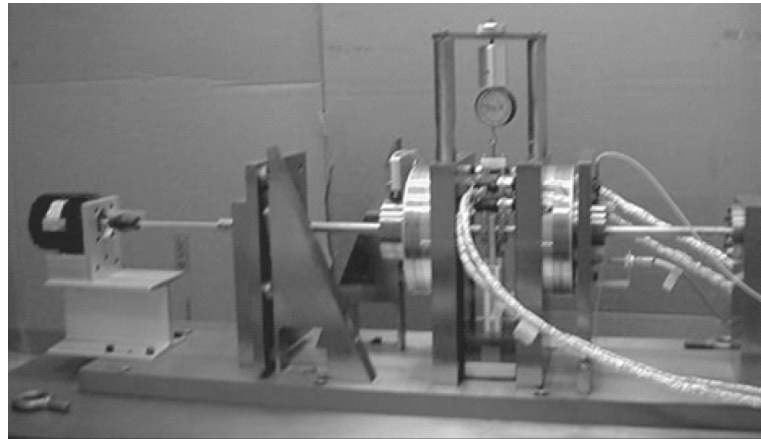
**Figure 9** Polar phasor vector plot of a single-plane balance correction.



**Figure 10** Automatic rotor mass balancer. (Courtesy of Lord Corporation.)

The author believes this new type of real-time automatic balancing system can be a quite cost-effective method for minimizing rotor vibration levels on flexible-rotor machines that currently necessitate considerable compromises between various important critical speeds and operating speeds that each are somewhat unique as to optimum balance correction weight placements. Many

large steam turbo-generator configurations now in service would benefit considerably from such a system, reducing the time required for rebalancing after a major scheduled outage by allowing the balance corrections to be made "on the fly" as the unit is slowly rolled up to synchronous operating speed, and likewise when the unit is taken off line as it coasts down to turning gear speed.



- |                            |                              |
|----------------------------|------------------------------|
| 1. End bearing             | 11. Beam                     |
| 2. Drive end balancer      | 12. Threaded knob            |
| 3. Out board balancer      | 13. Oil retaining lid        |
| 4. Shaft                   | 14. Threaded rod             |
| 5. Journal bearing         | 15. Transparent oil tank     |
| 6. Load support            | 16. Table                    |
| 7. Pivoted rods            | 17. Quill shaft              |
| 8. Balance beam            | 18. DC motor                 |
| 9. Load measurement device | 19. Key phasor probe         |
| 10. Columns                | 20. Motor support base       |
|                            | 21. Journal bearing pedestal |

**Figure 11** Flexible-rotor test facility with automatic balancers. (Courtesy of Case Western Reserve University, Cleveland, Ohio.)

## REFERENCES

1. N. F. Rieger, *Balancing of Rigid and Flexible Rotors*, The Shock and Vibration Information Center, Book No. SVM-12, U.S. Department of Defense, Washington, DC, 1986.
2. D. P. Fleming, Balancing of Flexible Rotors, Invited lecture Handout for Graduate Course in Rotating Machinery Vibration, Case Western Reserve University, Cleveland, OH, 1989.
3. M. L. Adams, *Rotating Machinery Vibration—From Analysis to Troubleshooting*, Marcel Dekker, New York, 2001.
4. K. A. Loparo, and M. L. Adams, *Development of Machinery Monitoring and Diagnostics Methods Based on Nonlinear Vibration Characteristics*, Proc., 52nd Meeting, Society for Machinery Failure Prevention, Virginia Beach, VA, March, 1998.

# CHAPTER 63

## ACTIVE NOISE CONTROL

Stephen J. Elliott  
Institute of Sound and Vibration Research  
University of Southampton  
Southampton, United Kingdom

### 1 INTRODUCTION

Active noise control is a method of reducing sound by destructive interference between the fields of the original, *primary*, source and a number of controllable, *secondary*, sources. The number of secondary sources required depends on the complexity of the sound field. For plane waves propagating in a duct, a single secondary source can be used to reflect the primary wave, or two sources can be used to absorb it. In free space, the number of secondary sources required to control a compact primary source increases as the square of the distance of the secondary source away from the primary source. In an enclosure the number of secondary sources required for control of the sound field depends upon the acoustical modal overlap and at higher frequencies increases as the cube of the frequency. Current industrial applications include the control of sound in ventilation and exhaust ducts, the control of sound in propeller aircraft, and active headsets.

### 2 CONTROL OF WAVE TRANSMISSION

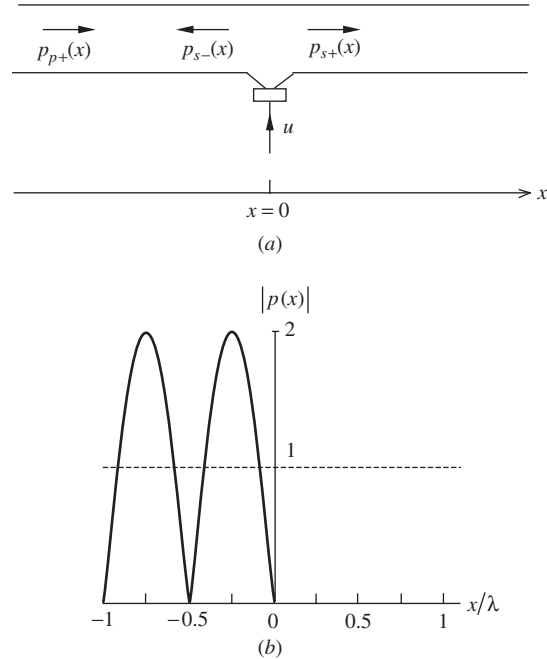
In this section, we consider the active control of sound that is transmitted as plane propagating waves in a uniform duct.<sup>1,2</sup> For sufficiently low frequency excitation only *plane waves* of sound can propagate in such a duct. In that case the waves have a uniform pressure distribution across any section of the duct and obey the one-dimensional wave equation. The fundamental approaches to active wave control can be illustrated using this simple example, but some of the complications involved in controlling higher order modes in ducts are also briefly discussed at the end of the section.

#### 2.1 Sound Cancellation

To begin with, it will be assumed that an incident harmonic sound wave, traveling in the positive- $x$  direction along a duct, is controlled by a single acoustic secondary source such as a loudspeaker mounted in the wall of the duct, as illustrated in Fig. 1a. The duct is assumed to be infinite in length, to have rigid walls, and to have a uniform cross section. The complex pressure of the incident primary wave is expressed as

$$p_{p+}(x) = Ae^{-jkx} \quad \text{for all } x \quad (1)$$

where the subscript  $p+$  denotes the primary wave traveling in a positive- $x$  direction, or *downstream*. An acoustic source, such as a loudspeaker driven at the same frequency as that of the incident wave, will produce acoustic waves traveling both in the



**Figure 1** (a) Active control of plane sound waves in an infinite duct using a single secondary source. (b) Amplitude of the pressure distribution in an infinite duct after a single secondary source, at  $x = 0$ , has been adjusted to cancel an incident plane wave of unit amplitude travelling in the positive  $x$  direction.

downstream direction and in the *upstream* or negative- $x$  direction, whose complex pressures can be written as

$$p_{s+}(x) = Be^{-jkx} \quad \text{for } x > 0, \quad (2a)$$

$$p_{s-}(x) = Be^{+jkx} \quad \text{for } x < 0 \quad (2b)$$

where the secondary source has been assumed to be at the position corresponding to  $x = 0$ , and  $B$  is a complex amplitude that is linearly dependent on the electrical input to the secondary source  $u$  in Fig. 1a. If this electrical input is adjusted in amplitude and phase so that  $B = -A$ , the total downstream pressure will be

$$p_{p+}(x) + p_{s+}(x) = 0, \quad \text{for } x > 0 \quad (3)$$

indicating that the pressure will be perfectly canceled at all points downstream of the secondary source. This



suggests that a practical way in which the control input could be adapted is by monitoring the tonal pressure at any point downstream of the secondary source and adjusting the amplitude and phase of the control input until this pressure is zero. The practicalities of such adaptive feedforward controllers are described by Elliott.<sup>2</sup> However, we are mainly interested here in the physical consequences of such a control strategy, and so we calculate the total pressure to the left, on the upstream side of the secondary source, which in general will be

$$p_{p+}(x) + p_{s-}(x) = Ae^{-jkx} + Be^{+jkx} \quad x < 0 \quad (4)$$

If the secondary source is adjusted to cancel the pressure on the downstream side, then  $B = -A$ , and the pressure on the upstream side becomes

$$p_{p+}(x) + p_{s-}(x) = -2jA \sin kx \quad x < 0 \quad (5)$$

since  $e^{jkl} - e^{-jkl} = 2j \sin kl$ . Thus a perfect acoustic *standing wave* is generated by interference between the positive-going primary wave and the negative-going wave generated by the secondary source. Notice that this standing wave has nodes of pressure at the position of the secondary source,  $x = 0$ , and at  $x = -\lambda/2$ ,  $x = -\lambda$ , and so on, where  $\lambda$  is the acoustic wavelength, and that when  $x = -\lambda/4$ ,  $x = -3\lambda/4$ , and so on, its amplitude is exactly twice the amplitude of the incident primary wave. The distribution of the pressure amplitude in the duct under these circumstances is shown in Fig. 1b.

In canceling the pressure downstream of the secondary source, the pressure at the secondary source location has been driven to zero by the effect of the active control system. The secondary source thus acts to create a pressure-release boundary condition as far as the incident wave is concerned and effectively *reflects* this wave back up the duct with equal amplitude and inverted phase, which gives rise to the standing wave observed in Fig. 1b. The acoustic power generated by a loudspeaker is equal to the time-averaged product of its volume velocity and the acoustic pressure on the cone surface. The fact that the acoustic pressure at the secondary source location is zero means that the secondary source can generate no acoustic power when operating to cancel the incident wave, and it acts as a purely reactive element. It is also possible to use an active control system to *absorb* the whole of the incident primary wave, instead of reflecting it back upstream, but such a strategy requires a pair of secondary sources.<sup>1,3</sup>

## 2.2 Control of Multiple Modes

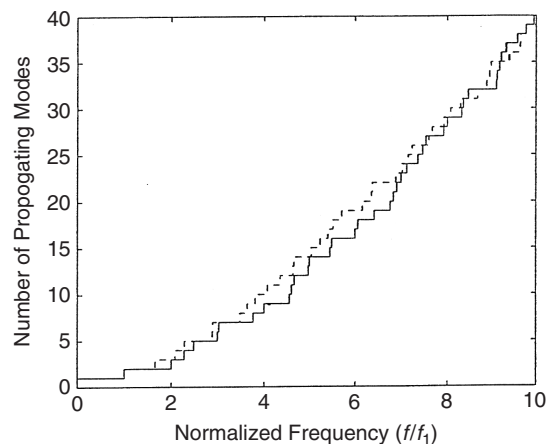
As the excitation frequency is increased, and the acoustic wavelength becomes comparable with the dimensions of the duct cross section, it becomes possible for more than just plane acoustic waves to propagate in the duct. The other types of acoustic field that can propagate in the duct have pressure distributions that are not uniform across the cross section of the duct and are referred to as higher order

modes. For a rectangular duct with a height  $L_y$ , which is greater than its depth  $L_z$ , the first higher order mode can propagate in the duct when it is excited above its first cuton frequency (also known as cutoff frequency) given by

$$f_1 = \frac{c_0}{2L_y} \quad (6)$$

If two identical secondary sources are used, one on either side of the duct, that are driven at the same amplitude, a plane wave will be produced when they are driven in phase; when they are driven out of phase, they will only excite the higher order mode. These two secondary sources can thus be used to excite any combination of amplitudes of these two modes and so could be used to actively control both modes. In general, it will require  $N$  secondary sources to control  $N$  modes, provided the combination of secondary sources is able to independently excite each of these modes.

Although it is, in principle, possible to actively control higher order modes using multiple secondary sources, there are several additional problems that are not encountered in the active control of plane acoustic waves, as discussed in more detail by, for example, Zander and Hansen.<sup>4</sup> There is an increasing interest in the active control of higher order acoustic modes in short ducts because of the potential application in controlling the fan tones radiated from the inlet of aircraft engines, particularly as the aircraft is coming in to land. It should be noted, however, that the number of higher order modes that are able to propagate in a duct increases significantly with the excitation frequency, as illustrated in Fig. 2 for both a rectangular and a circular duct. The number of propagating modes is proportional to the square of the excitation frequency when it is well above the lowest cuton frequency. If



**Figure 2** Number of acoustic modes that can propagate in a rectangular duct (solid line) or a circular duct (dashed line) as a function of excitation frequency, which has been normalized by the lowest cuton frequency of the duct,  $f_1$ .



a significant amount of energy is being transmitted in each of these modes, then an active control system with a very large number of channels would be required to attenuate the overall pressure level at high frequencies. However, if it is only required to reduce the sound radiating at particular angles from the end of the duct, such as that which causes significant sound on the ground from an aeroengine inlet duct, this could be achieved by controlling a much smaller number of modes. It is possible to detect the amplitude of these modes using an axial array of sensors placed inside the duct.<sup>5</sup>

### 3 CONTROL OF SOUND RADIATION IN THE FREE FIELD

In the previous section, we saw that waves traveling in one direction could be either reflected using a single secondary source or absorbed using a pair of secondary sources. In this section we consider the active control of disturbances propagating as waves in three dimensions. The physical interpretation is clearest if we initially restrict ourselves to the control of waves propagating only away from the sources, that is, in infinite systems with no reflections. The waves propagating in such three-dimensional systems cannot be perfectly canceled unless the secondary source is physically collocated with the primary source. Significant reductions in wave amplitude can, however, still be achieved if the separation between primary and secondary sources is not too great compared with a wavelength. The total acoustic power radiated by the combination of sources provides a convenient way of quantifying the space-average or *global* effect of various control strategies. In this section we will introduce the idea of minimizing such a global measure of performance by adjusting the secondary source strengths, rather than arranging for the secondary sources to cancel the primary field perfectly.

In a mechanical system, the power supplied by a mechanical point force is equal to the time-averaged product of the force multiplied by the resultant velocity, but we must be more careful with acoustic sources since the force is a distributed quantity, determined by the acoustic pressure, and an acoustic source can also have a nonuniform distribution of velocity. However, if we assume that the source is vibrating with equal amplitude in all directions, such as a pulsating sphere, and that this sphere is small compared with the acoustic wavelength, so that the pressure on its surface is reasonably uniform, its power output can be simply calculated by taking the time-average product of the acoustic pressure at the surface and the volume velocity of the source.<sup>1</sup> The volume velocity  $q$  is equal to the radial surface velocity multiplied by the surface area. Such an acoustic source is known as a monopole. A practical example of such an acoustic source might be the end of an engine's exhaust pipe radiating sound at low frequencies, which could be the primary source in an active control system.

The relation between the complex acoustic pressure at a distance  $r$  from an acoustic monopole source

operating at a single frequency may be expressed as

$$p(r) = Z(r)q \quad (7)$$

where  $q$  is the complex volume velocity of the monopole source and  $Z(r)$  is the complex acoustic transfer impedance. In an infinite medium with no acoustic reflections, that is, a free field, the acoustical transfer impedance is given by

$$Z(r) = \frac{\omega^2 \rho_0}{4\pi c_0} \left( \frac{je^{-jkr}}{kr} \right) \quad (8)$$

where  $\rho_0$  and  $c_0$  are the density and the speed of sound in the medium, and  $k$  is the acoustic wavenumber that is equal to  $\omega/c_0$  or  $2\pi/\lambda$ , where  $\lambda$  is the acoustic wavelength.

The time-average acoustic power generated by a monopole source is thus equal to

$$\Pi = \frac{1}{2} \text{Re}\{p^*(0)q\} \quad (9)$$

Using Eq. (7), this can be written as

$$\Pi = \frac{1}{2} |q|^2 \text{Re}\{Z(0)\} \quad (10)$$

where  $\text{Re}\{Z(0)\}$  is the real part of the acoustical input impedance, which in a free field is given from Eq. (8) by

$$\text{Re}\{Z(0)\} = \frac{\omega^2 \rho_0}{4\pi c_0} \quad (11)$$

If an array of monopole sources is present, whose complex volume velocities are represented by the vector

$$\mathbf{q} = [q_1, q_2 \cdots q_N]^T \quad (12)$$

which generate complex pressures at each of these sources, represented by the elements of the vector

$$\mathbf{p} = [p_1, p_2 \cdots p_N]^T \quad (13)$$

then the total power radiated by the array of monopoles can be written as

$$\Pi = \frac{1}{2} \text{Re}\{\mathbf{p}^H \mathbf{q}\} \quad (14)$$

where the superscript H denotes the Hermitian or complex-conjugate transpose.

The pressure at each of the source positions depends on the volume velocity of each of the sources in a way that can be represented in matrix form as

$$\mathbf{p} = \mathbf{Z}_p \mathbf{q} \quad (15)$$

where  $\mathbf{Z}$  is the matrix of input and transfer acoustic impedances between the sources, which is symmetric since the system is assumed to be reciprocal.

The total radiated power can now be written as

$$\Pi = \frac{1}{2} \text{Re}[\mathbf{q}^H \mathbf{Z}^H \mathbf{q}] = \frac{1}{2} \mathbf{q}^H \mathbf{R} \mathbf{q} \quad (16)$$

where  $\mathbf{R} = \text{Re}\{\mathbf{Z}\}$ .

The vectors of source strengths and pressures can now be partitioned into those due to primary sources,  $\mathbf{q}_p$  and  $\mathbf{p}_p$ , and those due to secondary sources,  $\mathbf{q}_s$  and  $\mathbf{p}_s$ ,<sup>2</sup> so that

$$\begin{bmatrix} \mathbf{p}_p \\ \mathbf{p}_s \end{bmatrix} = \begin{bmatrix} \mathbf{Z}_{pp} & \mathbf{Z}_{ps} \\ \mathbf{Z}_{sp} & \mathbf{Z}_{ss} \end{bmatrix} \begin{bmatrix} \mathbf{q}_p \\ \mathbf{q}_s \end{bmatrix} \quad (17)$$

If we similarly partition the matrix  $\mathbf{R}$  as

$$\mathbf{R} = \text{Re} \begin{bmatrix} \mathbf{Z}_{pp} & \mathbf{Z}_{ps} \\ \mathbf{Z}_{sp} & \mathbf{Z}_{ss} \end{bmatrix} = \begin{bmatrix} \mathbf{R}_{pp} & \mathbf{R}_{ps} \\ \mathbf{R}_{sp} & \mathbf{R}_{ss} \end{bmatrix} \quad (18)$$

then the total radiated power can be written as

$$\Pi = \frac{1}{2} (\mathbf{q}_s^H \mathbf{R}_{ss} \mathbf{q}_s + \mathbf{q}_s^H \mathbf{R}_{sp} \mathbf{q}_p + \mathbf{q}_p^H \mathbf{R}_{sp}^T \mathbf{q}_s + \mathbf{q}_p^H \mathbf{R}_{pp} \mathbf{q}_p) \quad (19)$$

where  $\mathbf{R}_{ps} = \mathbf{R}_{sp}^T$ , because of reciprocity.

Equation (19) is of Hermitian quadratic form, as described by Nelson and Elliott,<sup>1</sup> so that the power is a quadratic function of the real and imaginary parts of each element of the vector  $\mathbf{q}_s$ . This quadratic function must always have a minimum rather than a maximum associated with it, since otherwise for very large secondary sources, the total radiated power would become negative, which would correspond to the impossible situation of an array of sources absorbing power from the otherwise passive medium. It is shown by Nelson and Elliott<sup>1</sup> that the minimum possible value of power is given by a unique set of secondary sources provided the matrix  $\mathbf{R}_{ss}$  is positive definite, and that this optimum set of secondary sources is given by

$$\mathbf{q}_{s,\text{opt}} = -\mathbf{R}_{ss}^{-1} \mathbf{R}_{sp} \mathbf{q}_p \quad (20)$$

The positive definiteness of  $\mathbf{R}_{ss}$  is guaranteed on physical grounds in this case since the power supplied by the secondary forces acting alone is equal to  $\mathbf{q}_s^H \mathbf{R}_{ss} \mathbf{q}_s$ , which must be positive for all  $\mathbf{q}_s$ , provided they are not collocated. The minimum value of the total power that results from this optimum set of secondary sources is given by

$$\Pi_{\min} = \frac{1}{2} \mathbf{q}_p^H [\mathbf{R}_{pp} - \mathbf{R}_{sp}^T \mathbf{R}_{ss}^{-1} \mathbf{R}_{sp}] \mathbf{q}_p \quad (21)$$

Each of the elements in the matrix  $\mathbf{Z}$  in Eq. (17) can be calculated by using Eq. (8), using the geometric arrangement of the primary and secondary forces to compute the distance between each of them. The maximum possible attenuation of the input power for this geometric arrangement of primary and secondary sources can thus be calculated by taking the ratio of the power before control, given by Eq. (19) with  $\mathbf{q}_s$  set to zero, and after control, Eq. (21).

The maximum attenuation in input power has been calculated for the arrangements of primary and secondary sources shown in Fig. 3a, in which a single primary source is controlled by one, two, four, or eight secondary sources each uniformly spaced at a distance  $d$  from the primary source. The results of such a calculation are shown in Fig. 3b, in which the attenuation for an optimally adjusted set of secondary sources is plotted against the separation distance normalized by the acoustic wavelength. A practical arrangement corresponding to this model problem may be the use of an array of loudspeakers used as secondary sources placed round the end of an engine's exhaust pipe in the open air.

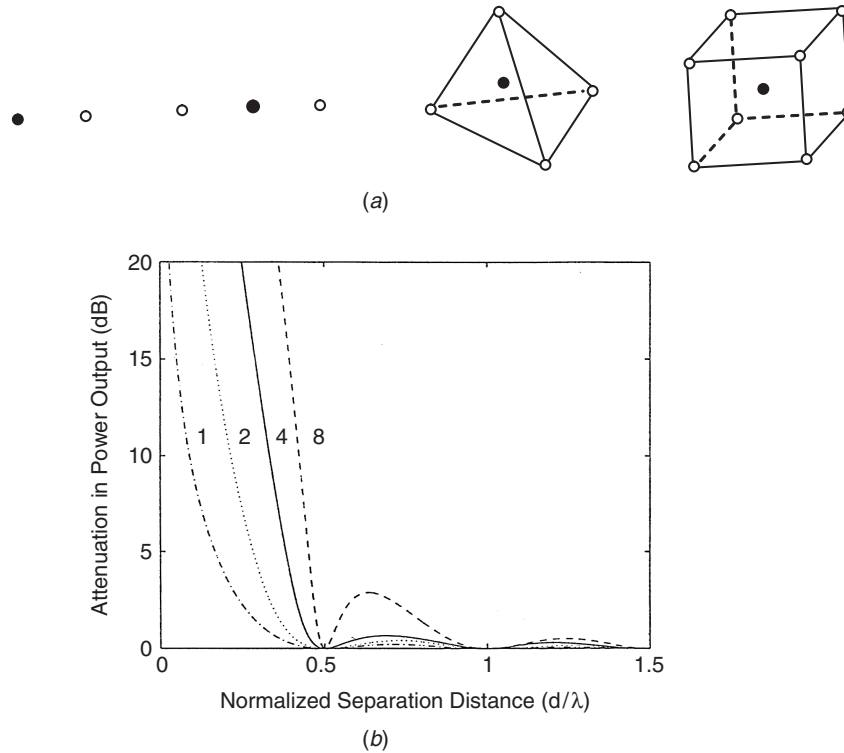
When the separation distance is small compared with the acoustic wavelength, the attenuation achieved in radiated power for a single secondary source is large. The decrease of attenuation as the normalized separation distance increases is rapid, however. With a larger number of secondary sources attenuation can be achieved for greater separation distances. The general trend is that the number of secondary sources required to achieve a given attenuation increases as the *square* of the normalized separation distance  $d/\lambda$ . The maximum separation distance allowable between each of the multiple secondary sources to achieve 10-dB attenuation in total power output is about half a wavelength.

With a single layer of acoustic monopoles, all at equal distances from the primary source, the power output of the primary source can be reduced by reflecting the outward-going wave back toward the primary source. It can be shown that the power output of all the secondary sources is identically zero when controlling a single primary source,<sup>6</sup> emphasizing their entirely reactive role; this case is thus directly analogous to the one-dimensional case whose pressure distribution is shown in Fig. 1b. It is also possible to use a double layer of acoustic monopoles, at unequal distances from the primary source, to *absorb* the waves radiated by the primary source. When operating in this manner, the pairs of monopole sources can be shown to be synthesizing a single point monopole/dipole source,<sup>1</sup> which is sometimes called a tripole.<sup>7</sup>

In practical applications, the sum of the squared pressures measured at microphones around the source array can be used as a measure of the radiated sound power. Multichannel control systems can be implemented to adjust the real and imaginary parts of the secondary source strengths to minimize this cost function, as described by Nelson and Elliott<sup>1</sup> and in more detail by Kuo and Morgan<sup>8</sup> and Elliott.<sup>2</sup>

#### 4 CONTROL OF ENERGY IN ENCLOSED SOUND FIELDS

One measure of the overall or *global* response of a finite system is the energy stored within it. In this section we discuss the active minimization of the acoustical energy in an enclosure. The energy stored in a system and the power supplied to it are related by the dissipation or damping in the system, since under steady-state conditions the power supplied to a system must increase its stored energy until the power lost



**Figure 3** (a) Arrangement of primary (solid sphere) and secondary acoustic monopole sources (open spheres) in free space, used in the calculation of the attenuation of total power output. Each of the secondary sources is positioned a distance of  $d$  from the primary source. (b) Attenuation in the total acoustic power radiated into free space by a primary monopole source when optimally controlled by one (---), two (....), four (—), or eight (-.-) secondary monopole sources, as a function of the distance from the primary to the secondary sources,  $d$ , normalized by the acoustic wavelength.

through dissipation is the same as the power supplied by the sources. We would thus expect that if an active control system were adjusted to minimize the total power supplied to a system, the energy stored by the system would also be minimized. This turns out to be true in the majority of cases of practical interest, and although the minimization of total input power and total stored energy does give slightly different analytical results,<sup>2</sup> the differences are generally of academic interest rather than practical importance.

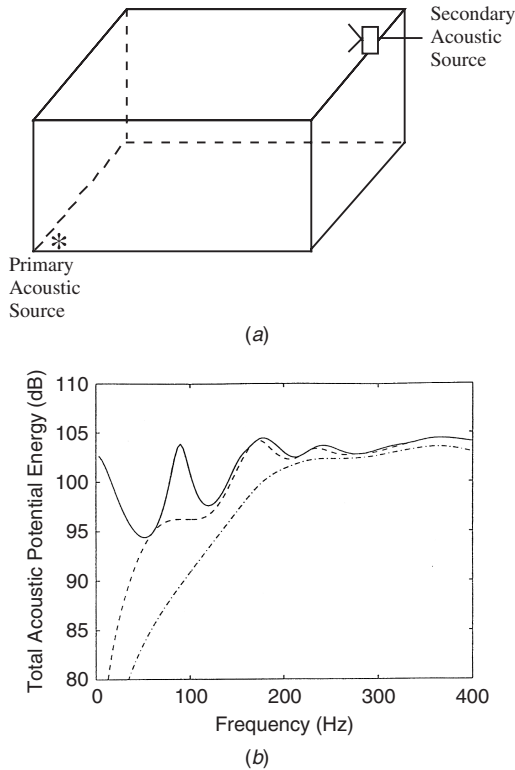
#### 4.1 Control of Acoustic Energy in an Enclosure

The total acoustic potential energy,  $E_p$ , provides a convenient cost function for evaluating the effect of global active control of sound in an enclosure. Because of the assumed orthonormality of the acoustic modes,  $E_p$  is proportional to the sum of the squared mode amplitudes, and these mode amplitudes can be expressed in terms of the linear superposition of the contributions from the primary and secondary sources. Thus the total acoustic potential energy is a Hermitian quadratic function of the complex strengths of the secondary acoustic sources, which can be

minimized in exactly the same way as described in Section 3.

The result of simulation of minimizing the total acoustic potential energy in an enclosure of dimensions  $1.9 \times 1.1 \times 1.0$  m, as shown in Fig. 4a, is illustrated in Fig. 4b. The acoustic modes have an assumed damping ratio of 10%, which is fairly typical for a reasonably well damped acoustical enclosure such as a car interior at low frequencies. The acoustic mode shapes in a rigid-walled rectangular enclosure are proportional to the product of three cosine functions in the three coordinates. The lowest order mode, with all  $n$ 's set to zero, has a uniform mode amplitude throughout the enclosure and corresponds to a uniform compression or expansion of the air at all points. The mode with the next highest natural frequency corresponds to fitting a half wavelength into the longest dimension of the enclosure. This first axial mode has a natural frequency of about 90 Hz for the enclosure shown in Fig. 4a, which is similar in size to the interior of a small car.

Figure 4b shows the total acoustic potential energy in the enclosure when driven only by the primary source placed in one corner of the enclosure and when the total acoustic potential energy is minimized by



**Figure 4** (a) Physical arrangement for the simulation of the active control of tonal sound in a rectangular enclosure, which is about the size of a car interior, excited by a primary acoustic source in one corner and a secondary acoustic source in the opposite corner. (b) Total acoustic potential energy in the enclosure when driven by the primary acoustic source alone at discrete frequencies (solid line) and when the total potential energy has been minimized using either the single secondary source shown in (a), optimally adjusted at each excitation frequency (dashed line), or seven secondary acoustic sources placed in all the corners of the enclosure not occupied by the primary source (dash-dot line).

a single secondary acoustic source in the opposite corner (broken line) or by seven secondary acoustic sources positioned at each of the corners of the enclosure not occupied by the primary source (dash-dot line). Considerable attenuations in the total acoustic potential energy are achieved with a single secondary source below about 20 Hz, where only the zeroth-order acoustic mode is significantly excited and for excitation frequencies close to the natural frequency of the first longitudinal mode at about 90 Hz.

The response of the system does not, however, show clear modal behavior for excitation frequencies above about 150 Hz, and very little attenuation can be achieved with a single secondary source above this frequency. This is because the spacing of the natural frequencies of the acoustic modes in a three-dimensional

enclosure becomes smaller with higher mode order. Even introducing seven secondary sources into the enclosure does not allow global control to be achieved at frequencies above about 250 Hz in this case.

The amplitude of an individual mode of a physical system could be completely controlled using a single secondary source, provided it was not placed on a nodal line. In controlling this mode, however, the secondary source will tend to increase the excitation of other modes of the system. The minimization of total energy generally involves a balance between canceling the dominant modes and not overly exciting the other, residual, modes of the system. This balance is automatically maintained when the total energy in the system is minimized. The attenuation obtained in the energy at any one excitation frequency will generally depend on the number of modes that contribute substantially to the response.

#### 4.2 Effect of the Modal Overlap

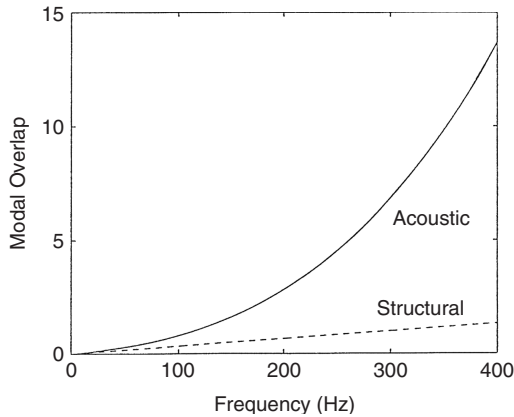
The number of modes that are significantly excited in a system at any one excitation frequency can be quantified by a dimensionless parameter known as the *modal overlap*,  $M(\omega)$ . This is defined to be the average number of modes whose natural frequencies fall within the half-power bandwidth of any one mode at a given excitation frequency  $\omega$ .  $M(\omega)$  is equal to the product of the modal density (average number of modal natural frequencies per hertz) and the modal bandwidth (in hertz), and both of these quantities can be calculated for the structural modes in a panel and the acoustic modes in the enclosure used in the simulations above.

For a three-dimensional rectangular enclosure, an approximate expression for the acoustic modal overlap can be calculated from that for the modal densities<sup>1</sup> as

$$M(\omega) = \frac{2\zeta\omega L}{\pi c_0} + \frac{\zeta\omega^2 S}{\pi c_0^2} + \frac{\zeta\omega^3 V}{\pi^2 c_0^3} \quad (22)$$

where  $L$  is the sum of the linear dimensions of the enclosure,  $S$  is its total surface area,  $V$  is the volume of the enclosure,  $\zeta$  is the damping ratio, and  $c_0$  is the speed of sound. At high frequencies the acoustic modal overlap increases as the cube of the excitation frequency. The modal overlap calculated for the acoustic modes in the enclosure shown in Fig. 4a is plotted in Fig. 5. In this case the modal overlap is less than unity for excitation frequencies below about 150 Hz, which was the limit of global control with one source in Fig. 4b, and is under seven for excitation frequencies below about 250 Hz, which was the limit of global control with seven sources in Fig. 4b.

The modal overlap can thus be seen to be a useful method of characterizing the complexity of the modal structure in a system at a given excitation frequency. It can also be used as a very approximate guide to the number of secondary sources required to achieve a given level of global control, that is, a given reduction in energy level in a system. The difference between the variation of modal overlap with frequency of a panel, shown dashed in Fig. 5, and of an acoustically excited enclosure, helps to explain the significant difference in



**Figure 5** Modal overlap,  $M(\omega)$ , for the structural modes on a plate and for the acoustic modes in the enclosure used for the simulations shown in Fig. 4b (solid line).

the physical limitations of active control in these two cases.

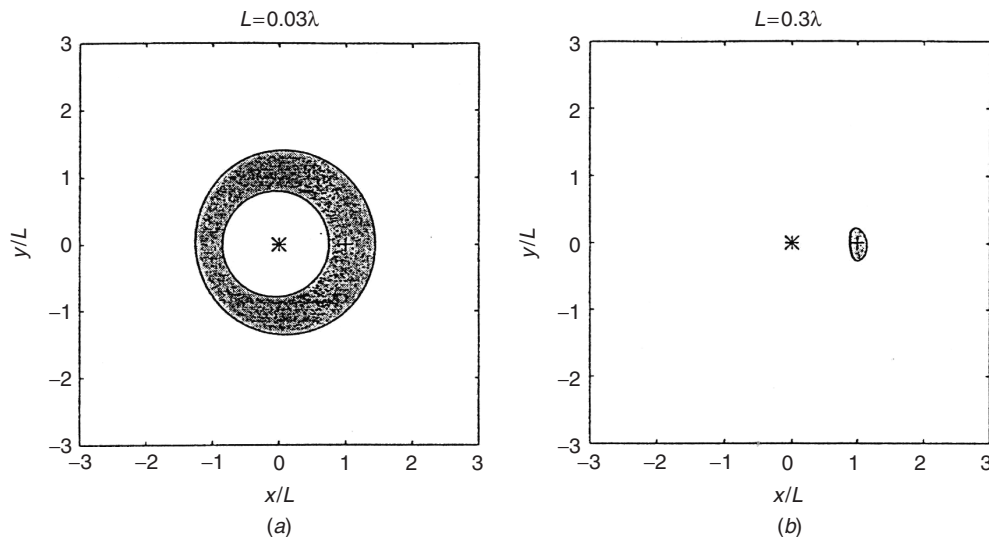
The total acoustic potential energy in an enclosure is proportional to the volume integral of the mean-square pressure. In a practical active control system, the total potential energy can be estimated using the sum of the squared outputs of a number of pressure microphones. The number of microphones required to obtain an accurate estimate of the total acoustic potential energy is proportional to the number of substantially excited acoustic modes within the enclosure and thus increases sharply at higher excitation frequencies.

## 5 LOCAL CONTROL OF SOUND

Apart from minimizing a global cost function, such as radiated power or total energy, an active control system can also be designed to minimize the local response of a system. The physical effect of such a local control system will be illustrated in this section by considering the cancellation of the pressure at a point in a room.

### 5.1 Cancellation of Pressure in a Large Room

Cross sections through the acoustical zones of quiet, generated by canceling the pressure at a point in a large three-dimensional space, are shown in Fig. 6. The sound field in the room is assumed to be diffuse, which occurs when the excitation frequency is such that the modal overlap in Eq. (22) is well above unity. In this case, when the distance from the secondary source to the cancellation point is very small compared with the acoustic wavelength, the zone of quiet forms a *shell* around the secondary source, as indicated by the shaded area in the two-dimensional cross section shown in Fig. 6a. If the pressure is canceled in the near field of an acoustic monopole source, the secondary field will only be equal and opposite to the primary field at distances from the secondary source that are about the same as the distance to the cancellation point, thus generating a shell of cancellation. At higher frequencies, when the distance from the secondary source to the cancellation point is not small compared with the wavelength, then the zone of quiet does not form a complete shell round the secondary source but is now concentrated in a sphere centered on the cancellation point, whose diameter is about  $\lambda/10$ ,<sup>9</sup> as shown in Fig. 6b.



**Figure 6** Cross section of the spatial extent of the acoustical "zone of quiet" generated by canceling the pressure at  $x = L$  in a three-dimensional free field using a point monopole acoustic secondary source at the origin of the coordinate system for (a)  $L = 0.03\lambda$  and (b)  $L = 0.3\lambda$ , where  $\lambda$  is the acoustic wavelength. The shaded area line corresponds to a 10-dB attenuation in the diffuse primary field.

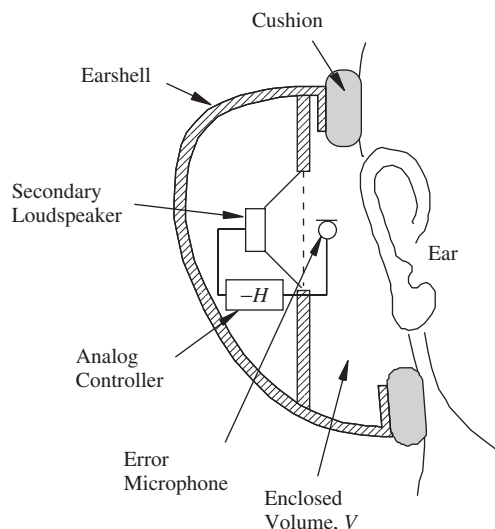
The advantage of a local control system is that the secondary source does not have to drive very hard to achieve control because it is very well coupled to the pressure at the cancellation point. Thus local zones of quiet can often be generated without greatly affecting the overall energy in the system. Local active control systems also have the advantage that, because the secondary actuator and the error sensor are close together, there is relatively little delay between them, which can improve the performance of both feedforward and feedback control systems. One of the earliest designs for a local active control system was proposed by Olsen and May,<sup>10</sup> who suggested that a loudspeaker on the back of a seat could be used to generate a zone of quiet round the head of a passenger in a car or an aircraft. Olson and May<sup>10</sup> had the idea of using a feedback control system to practically implement such an arrangement, although in the 1950s most of the design effort had to be spent in reducing the phase lag in the audio amplifier to ensure stability of the feedback loop. More recent investigations of such systems<sup>11</sup> have demonstrated the trade-off in such a system between good acoustic performance and robust stability of the feedback loop.

The upper frequency of control in such a system will be fundamentally determined by the acoustical considerations outlined above, and the extent of the listener's head movements. Zones of quiet of a useful size can be achieved in practice up to several hundred hertz. The obvious extension to such a local control system would be to arrange for the loudspeakers to move with the ears, as in an active headset. Under these conditions the entrance of the ear canal is kept very close to the position of the loudspeaker, and the fundamental acoustical limitations discussed above can generally be avoided up to a frequency of about 1 kHz. The main features of an active headset are illustrated in Fig. 7, in which an analog feedback controller is used to control the low-frequency pressure at a microphone located close to the ear. A well-designed headset will have good sound attenuation at high frequencies, and the low-frequency enhancement in the attenuation by the active system complements this passive performance at higher frequencies.

## 6 CONCLUSIONS

The physical principles of active sound control are most easily illustrated by the one-dimensional problem of plane waves propagating in a duct. A single secondary source can be used to reflect an incident primary plane wave and a pair of secondary sources can be used to absorb an incident plane wave. At higher frequencies, multiple waves can propagate in the duct and multiple actuators then need to be used to control the transmission of acoustic energy.

An electrical controller is required to drive the secondary acoustic source, and this can either take the form of a feedback controller or an adaptive feedforward controller if prior information about the primary field is available.<sup>2</sup> Although the principles of active noise control have been known since the 1930s<sup>12</sup> and significant advances were made in the 1950s,<sup>10,13</sup>



**Figure 7** Active headset in which the sound inside the headset is detected by the microphone and typically fed back via an analog controller to the loudspeaker to reduce the low-frequency sound pressure level.

it was not until the development of economical digital signal processing (DSP) devices in the 1980s that large-scale problems were practical. Apart from active headsets, current applications include the active control of sound in ducts, inside propeller aircraft,<sup>14</sup> and inside cars.<sup>15</sup>

The problem of spatial matching becomes more severe when secondary acoustic sources are used to attenuate the sound power output of a primary source in a three-dimensional space. If the sources are in the free field, a single monopole secondary source must be spaced within about one tenth of an acoustic wavelength of a monopole primary source if reductions of 10 dB are to be achieved in sound power output. If multiple secondary sources are used, the number of secondary sources necessary to obtain a given level of performance increases with the square of their distance from the primary source.

When the primary source drives an enclosed sound field, a number of different active control strategies may be used. These strategies can be illustrated most easily by returning to the one-dimensional field in a duct as discussed by Elliott,<sup>2</sup> which is closed at the two ends by the primary and secondary sources. Canceling the pressure in front of the secondary source effectively changes the end condition in the duct from open to closed; resonances are still apparent but are shifted in frequency. Driving the secondary source so as to absorb the incident sound wave suppresses these resonances. However, the most effective strategy for reducing the stored energy in the enclosure is to drive the secondary source so as to minimize the total power input to the duct from both the primary and secondary sources. This strategy maintains the sound field in an

antiresonant condition at each frequency and is almost equivalent to minimizing the total acoustic potential energy in the enclosure, giving significant reductions in the stored energy at each of the resonant frequencies.

The number of modes of a three-dimensional enclosure that are significantly excited at a given driving frequency well above the first natural frequency increases with the cube of that frequency, and a single secondary source is not sufficient to control such a sound field above the first resonance frequency. Multiple secondary sources can be used to achieve control in this case, provided there are at least as many secondary sources as significantly excited acoustic modes. By using an array of microphones, a practical approximation to the total acoustic potential energy can be measured in an enclosure, which can be used to automatically adjust the amplitude and phase of the multiple secondary sources to minimize this quantity.

Such a control system with 16 loudspeakers and 32 microphones was used in the original demonstration of the control of propeller noise in a passenger aircraft.<sup>16</sup> Commercial systems are now available for this purpose, although more recent systems use electromagnetic shakers attached to the fuselage as actuators instead of loudspeakers, which can control the vibration in the passenger cabin as well as the noise.<sup>14,17</sup>

Finally, the possibility of operating an active control system at higher frequencies is considered, by controlling only the local sound field around a person's head instead of the global sound field throughout an enclosure. It is shown that such a strategy can generate a zone of quiet that forms a shell round the secondary source at low frequencies. At high frequencies the quiet zone reduces, on average, to a sphere centred on the cancellation microphone, whose diameter is one tenth of an acoustic wavelength. Unless this zone of quiet can always be maintained close to the ear, as in the case of an active headset, degradation due to the natural movement of a listener's head will restrict the frequency range of a headrest system using such local active control to frequencies below a few hundred hertz.

Active control techniques are thus seen to complement conventional passive control methods since they are most effective at low frequencies. Current applications are mainly in the aerospace field, where the reduced weight of an active system for low-frequency noise control, compared with a passive one, is worth the additional cost and complexity of an electronic system.

## REFERENCES

1. P. A. Nelson and S. J. Elliott, *Active Control of Sound*, Academic, London, 1992.
2. S. J. Elliott, *Signal Processing for Active Control*, Academic London, 2001.
3. M. A. Swinbanks, The Active Control of Sound Propagating in Long Ducts, *J. Sound Vib.*, Vol. 27, 1973, pp. 411–436.
4. A. C. Zander and C. H. Hansen, Active Control of Higher-Order Acoustic Modes in Ducts, *J. Acoust. Soc. Am.*, Vol. 92, 1992, pp. 244–257.
5. P. Joseph, P. A. Nelson, and M. J. Fisher, Active Control of Fan Tones Radiated from Turbofan Engines. I: External Error Sensors, and, II: In-duct Error Sensors, *J. Acoust. Soc. Am.*, Vol. 106, 1999, pp. 766–778 and 779–786.
6. S. J. Elliott, P. Joseph, P. A. Nelson, and M. E. Johnson, Power Output Minimisation and Power Absorption in the Active Control of Sound, *J. Acoust. Soc. of Am.*, Vol. 90, 1991, pp. 2501–2512.
7. M. J. M. Jessel, Sur les absorbeurs actifs, 6th International Conference on Acoustics, Tokyo, Paper F-5-6, 82, 1968.
8. S. M. Kuo and D. R. Morgan, *Active Noise Control Systems, Algorithms and DSP Implementations*, Wiley, New York, 1996.
9. S. J. Elliott, P. Joseph, A. J. Bullmore, and P. A. Nelson, Active Cancellation at a Point in a Pure Tone Diffuse Field, *J. Sound Vib.*, Vol. 120, 1988, pp. 183–189.
10. H. F. Olsen and E. G. May, Electronic Sound Absorber, *J. Acoust. Soc. Am.*, Vol. 25, 1953, pp. 1130–1136.
11. B. Rafaely, S. J. Elliott, and J. Garcia-Bonito, Broad-band Performance of an Active Headrest, *J. Acoust. Soc. Am.*, Vol. 102, 1999, pp. 787–793.
12. P. Lueg, Process of Silencing Sound Oscillations, U.S. Patent, No. 2,043,416, 1936.
13. W. B. Conover, Fighting Noise with Noise, *Noise Control*, Vol. 2, 1956, pp. 78–82.
14. C. F. Ross and M. R. J. Purver, Active Cabin Noise Control, *ACTIVE 97*, Technical University of Budapest, Budapest, Hungary, 1997, pp. xxxix–xlvi.
15. H. Sano et al., Active Control System for Low-Frequency Noise Combined with an Audio System, *IEEE Trans. Speech Audio Process*, Vol. 9, No. 7, 2001, pp. 755–761.
16. S. J. Elliott, P. A. Nelson, I. M. Stothers, and C. C. Boucher, In-flight Experiments on the Active Control of Propeller-Induced Cabin Noise, *J. Sound Vib.*, Vol. 140, 1990, pp. 219–238.
17. C. R. Fuller, Experiments on Reduction of Aircraft Interior Noise Using Active Control of Fuselage Vibration, *J. Acoust. Soc. Am.*, Vol. 78, No. S1, 1985, pp. S88.



# CHAPTER 64

## ACTIVE VIBRATION CONTROL

Christopher Fuller

Department of Mechanical Engineering  
Virginia Polytechnic Institute and State University  
Blacksburg, Virginia

### 1 INTRODUCTION

Passive vibration control methods work well at high frequencies or in a narrow frequency range but often have the disadvantage of added weight and poor low-frequency performance. Active vibration control has demonstrated the potential to solve many of these problems. Although the potential of active vibration control has been well known for many years, recent advances in fast digital signal processing computer chips have made these systems realizable.

In active vibration control secondary vibration inputs are applied to the structure to modify its response in a desired manner. The major components of an active vibration control system are the plant, actuators, sensors, and a controller. The plant represents the physical system to be controlled. Error sensors are needed to measure the system response while control actuators provide the necessary inputs to the plant to modify its response. The controller implements the chosen control algorithm to ensure that the controlled (or closed-loop) system behaves as required. The closed-loop system consists of the open-loop (uncontrolled) system dynamics combined with the dynamics of the controller and thus behaves in a modified form. Examples of practical active vibration control systems include active engine supports in vehicles and active vibration isolation systems for propeller aircraft.

### 2 CONTROL ACTUATORS

The arrangement of an active control system is usually based upon the physics of the system to be controlled and thus, as illustrated below, is often application dependent.<sup>1</sup> There are many texts on active control of vibration, mainly focused on the control theory. The text by Meirovitch<sup>2</sup> provides an excellent theoretical basis while the text of Fuller et al.<sup>3</sup> describes in detail both feedforward and feedback control theory, actuators and sensors, as well as many relevant applications. Chapter 63 also discusses the related area of active noise control. It should be noted that active control is not a panacea for every vibration problem, and its application should be chosen with care depending upon a number of important characteristics such as the temporal nature of the disturbance, the spatial nature of the noise field, and the dynamic characteristics of the disturbance.<sup>4</sup>

Actuators are used to introduce control forces into the plant to modify its behavior, and their design/selection (in conjunction with the sensors) is

often the most important step in an active noise control project. Actuators can take various forms that are dependent upon system requirements such as the required control authority (amount of control force, moment, strain, or displacement), power frequency response, and physical constraints such as size, mounting requirements, and so on. Actuators are generally classified into two main categories: *fully active* actuators that apply a secondary vibrational response to the structure (i.e., can add energy to the structure) and *semiactive* actuators that are passive elements and can be used to adaptively adjust the mechanical properties of the system (i.e., do not add energy to the structure).

### 2.1 Electrodynamic Actuators

Electrodynamic actuators or shakers consist of a moving wire coil mounted inside a permanent magnet. As they are readily available and their behavior is relatively well understood (see Ref. 5 and Chapters 5 and 37), electrodynamic shakers are presently the most common control input as a fully active device. They are usually installed by either attaching directly to the structure by a stinger or placing in series or parallel with passive mounts, as in the case of active isolation (see Section 5). While electrodynamic actuators have the advantage of relatively large control displacement, they are usually bulky and require some form of support structure. However, there are many applications at low frequencies in which their use is more than adequate. Electrodynamic actuators are usually modeled in terms of control inputs as point forces, and they are thus “spectrally white” in terms of the spatial wavenumber response of the excited structure.

Typical structural components encountered in practice can often be simply represented as beams or plates. The transverse vibration displacement  $w$  of a simply supported thin plate excited by a point force  $F e^{i\omega t}$  is described by<sup>6</sup>

$$w(x, y, t) = \frac{-4F}{M} \sum_{m=1}^{\infty} \sum_{n=1}^{\infty} \frac{\sin(m\pi x_f/L_x) \sin(n\pi y_f/L_y) \sin(m\pi x/L_x) \sin(n\pi y/L_y) e^{i\omega t}}{\omega^2 - \omega_{mn}^2 + i2\zeta_{mn}\omega\omega_{mn}} \quad (1)$$

where the force is located at  $(x_f, y_f)$ ,  $\omega_{mn}$  is the natural frequency of the  $(m, n)$ th mode, and  $M$  is the total mass of the plate. In Eq. (1),  $L_x$  and  $L_y$  are the transverse dimensions of the plate,  $x$  and  $y$



are axial coordinates,  $\omega$  is the frequency of excitation, and  $\zeta_n$  is the modal damping ratio. Response of other more complex systems to point forces can be found in well-known texts such as Ref. 6.

## 2.2 Piezoelectric Actuators

As discussed in Ref. 7, piezoelectric transducers consist of material that expands or contracts when an electric field is applied over it. By applying an oscillating voltage to the piezoelectric element, its strain can be made to oscillate the same frequency as the input. Three major types of piezoelectric material are readily available: (1) a ceramic form such as PZT (lead zirconate titanate), which has relatively high control strain but is brittle; (2) a polyvinyl form such as a PVDF [polyvinylidene difluoride], which is flexible but has less control strain for the same configuration; and (3) a piezoelectric rubber, which is useful for underwater applications. Piezoelectric material is configured in the two main forms of *stack* and *wafer*, as shown in Fig. 1. Piezoelectric stacks are configured so that when a voltage is applied across the electrodes, the stack usefully expands in its long or 3–3 axis.<sup>7</sup> Stack arrangements such as Fig. 1 are thus suitable for actuators in vibration isolation in the two

configurations of parallel and series shown in Figs. 1a and 1b.

For a given applied voltage  $V$  the net static displacement  $\delta$  of the piezoelectric ceramic actuator shown in the parallel configuration of Fig. 1a can be calculated from

$$\delta = \frac{d_{33}V + F/K_a}{1 + K/K_a} \quad (2)$$

where  $d_{33}$  is the strain constant of the piezoelectric material in the 3–3 axis,<sup>7</sup>  $K$  is the external spring stiffness,  $K_a$  is the actuator stiffness ( $K_a = E_a A_a / L_a$ , where  $L_a$ ,  $A_a$ , and  $E_a$  are the actuator length, cross-sectional area, and Young's modulus, respectively);  $F$  is the external load force. Note Eq. (2) can be used as the basis of an approximate dynamic analysis, as discussed in Ref. 3. The significant advantage of the piezoelectric stack is that it can provide high force; however, its displacement is limited (relative to electrodynamic actuators), which, as discussed later, implies that its use is primarily in series-active isolation implementations.

The other common form of piezoelectric actuator is the wafer arrangement shown in Fig. 1c. In this form the transducer usefully strains in its thin transverse axis

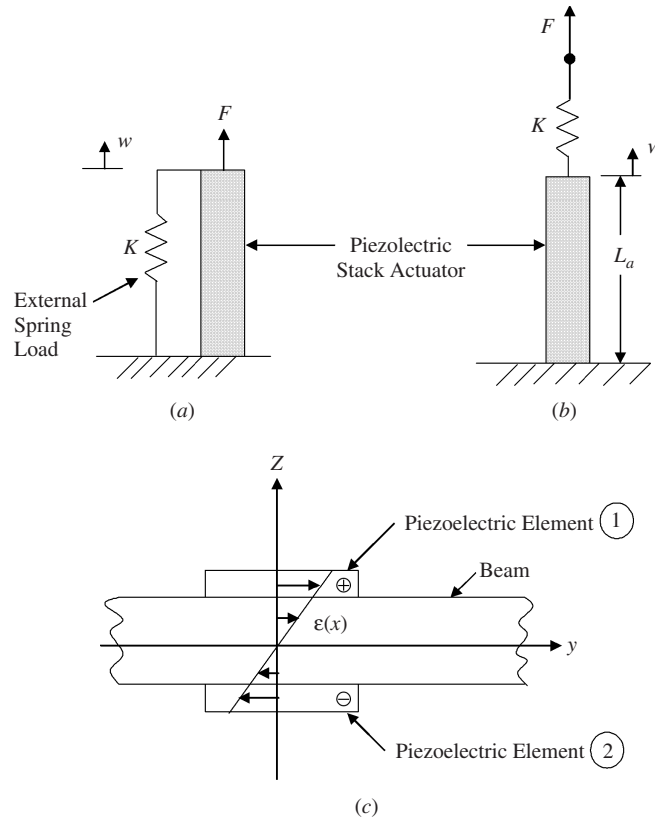


Figure 1 Piezoelectric actuator configurations: (a) stack in parallel, (b) stack in series, and (c) collocated wafer.

(3–1 or 3–2) when a voltage is applied across the electrodes. The wafer is usually bonded or embedded directly into the structure and actuates the structure by applying surface or interior strains. Figure 1c shows piezoelectric elements arranged to create pure bending. In this configuration the elements are wired 180° out of phase so that as one element expands, the other contracts. As discussed in Ref. 8, the surface-mounted collocated actuator with a perfect bonding layer (which is a good approximation if the glue layer is thin) effectively applies a line moment to the structure at the boundaries of the actuator.

For a two-dimensional patch system in spherical bending of a plate, the effective moments  $m_x, m_y$  of the actuator are given by<sup>9</sup>

$$m_x = m_y = \frac{-E_p(1 + \nu_{pe})}{3(1 - \nu_p)} \frac{2P'h^2\epsilon_{pe}}{(1 - \nu_p - (1 + \nu_{pe})P')} \quad (3)$$

where

$$P' = P \frac{1 - \nu_p^2}{1 - \nu_{pe}^2} \quad (4)$$

In Eqs. (3) and (4)  $\nu_{pe}$  and  $\nu_p$  are the Poisson's ratio of the piezoelectric and the plate material, respectively, while  $E_b$  and  $E_{pe}$  are the Young's elastic modulus of the beam material and piezoelectric element, respectively, while  $h$  is the half thickness of the beam,  $t$  is thickness of the piezoelectric element,  $V$  is the applied Voltage, and  $d_{31}$  is the piezoelectric transverse strain constant. The constant  $P$  can be found in Ref. 9. More information of piezoelectric elements and their properties as well as definitions of important terms can be found in Ref. 7. Excitation of plate and beam structures with piezoelectric patches is discussed in Refs. 9 and 10, respectively. Piezoelectric actuators can be used either in a semiactive or a fully active form.

### 2.3 Advanced Actuators

The desire for an optimum actuator has stimulated development of new materials and configurations. The requirements, depending upon application, are typically high force and/or displacement, large bandwidth of operation, lower power consumption, and ease of use.

*Shape memory alloy* (SMA) shows much potential for high-force actuation at direct current (dc) to very low frequencies. The mechanism by which SMA fibers or films exhibit their characteristic shape memory effect can be described very basically as follows: An object in the low-temperature martensitic condition, when plastically deformed and the external stresses removed, will regain its original (memory) shape when heated. The process is the result of a martensitic phase transformation taking place during heating. When SMA is heated through its transformation temperature, the elastic modulus of the material changes dramatically, and if the material is initially stretched, it will shrink back to its original size. If the SMA is constrained during this procedure, very high

restoring forces are generated. More information on SMA can be found in Ref. 11.

The SMA systems are usually configured by embedding the material in a structure in a similar manner to layups of composite structures. It can be activated in a steady-state manner, applying steady-state in-plane forces that can be used to tune the resonant frequencies or change the mode shapes of the system (i.e., as semiactive actuator).<sup>12</sup> Over a very limited frequency range it can be used as an oscillating control input (i.e., a fully active actuator) by positioning the SMA off the central axis of the structure and driving with an oscillating voltage.<sup>12</sup> The advantage of the SMA is the extremely high force and deflection that it can provide at very low frequencies. Disadvantages are high power consumption, a need for heat dissipation, and a limited frequency response, which depends entirely upon the cooling rate. Use of SMA in the control of transient vibration of a cantilevered beam as well as sound radiation control is discussed in Ref. 12.

*Magnetorestrictive* materials also show much possibility as advanced fully active actuators in that they fill the performance gap between low-force, high-displacement electromagnetic actuators and high-force, low-displacement piezoelectric devices. A typical actuator using the material Terfenol-D and approximately 11 cm in length and 5 cm in diameter can produce forces in excess of 450 N over a frequency range of 0 to 2.5 kHz.<sup>13</sup> However, the power requirements tend to be somewhat higher than electrodynamic and piezoelectric devices.

*Electrorheological (ER) fluids* are suspensions of highly polarized fine particles dispersed in insulating oil.<sup>14</sup> The viscosity and the elasticity of the ER fluid can be changed several orders of magnitudes when an electric field is applied to the medium. The ER fluid can thus be embedded in structural systems and used as a "semiactive" actuator to tune the system's properties such as damping and stiffness by varying the voltage applied to the ER fluid.<sup>15</sup>

### 3 ERROR SENSORS

Error sensors are employed to measure the motion of the system to be controlled. This information either is used directly as the variable(s) to be minimized or is used to calculate a related state for the system to be controlled. Sensors come in three main forms: point sensors, arrays of point sensors, and distributed sensors. Choice of the particular configuration is dependent upon the system variable to be controlled, as discussed below.

#### 3.1 Accelerometers, Force Transducers, and Impedance Heads

Accelerometers are commonly used as error sensors due to the ease of use and reliability of performance. Their implementation and behavior is discussed in more detail in Chapter 37. When attached to a vibrating structure, they can provide estimates of the time-varying acceleration (as well as velocity and displacement with signal processing) at the

point of attachment. Due to their small size, at low frequencies accelerometers provide a point sampling of the structural motion and thus are “spectrally white” in wavenumber response. Thus an individual accelerometer will equally sense all structural wavenumber or modally weighted contributions. Use of an accelerometer output as an error signal will result in direct control of the structural motion at that point.

Force transducers can also be used as error sensors, particularly in applications such as active isolation, where they may be placed in series with passive isolation. Minimization of the force transducer output will result in zero dynamic force being applied to the receiving structure. The point input impedance of a structure, such as at a disturbance location, can be estimated using an impedance head that consists of a collocated accelerometer and force transducer. The output of the impedance head can then be used as a narrow-band error sensor variable to minimize the real part of the structural input impedance and thus disturbance input power flow into the structure.

Choice of one of the above transducers as an error sensor is dependent upon the form of application. This will be illustrated in the later example applications.

### 3.2 Arrays of Point Sensors

Usually it is more effective to use accelerometers as error sensors in an array configuration whose output signal is processed to provide some global or distributed state associated with the system.

The *kinetic energy* of a thin vibrating system can be minimized by using a distributed array of accelerometers positioned over the required controlled domain. An estimate proportional to out-of-plane kinetic energy of the structure is given by

$$E = \sum_{i=1}^N |\dot{w}_i|^2 \quad (5)$$

where  $N$  is the total number of accelerometers and  $\dot{w}$  is the out-of-plane velocity obtained by integrating the acceleration signal. The variable  $E$  can be minimized, or if an  $N$ -channel controller is available, each accelerometer can be used as an individual control channel. The required number and spacing of accelerometers are determined by the Nyquist sampling criterion applied in the spatial domain: Two accelerometers must be spaced within at least a half-wavelength of the highest mode required to be observed and controlled. Alternatively, the accelerometers can be appropriately distributed throughout the surface whose global motion is to be controlled. Use of a lower number of accelerometers (relative to the number of actuators) often leads to large minimization at their locations but increased levels of vibration at other locations. This effect is termed control spillover. In general, to ensure controllability, a system state or mode has to be individually observed.

*Wavenumber* components of structural motion can be obtained using arrays of equispaced accelerometers

arranged along a coordinate axis. The spatial one-dimensional Fourier transform can be approximated using a discrete Fourier transform such as<sup>3</sup>

$$\hat{W}(k) = \sum_{n=1}^K w_m(x_n) e^{ikx_n} \Delta x \quad (6)$$

where  $w_m(x_n)$  is the measured out-of-plane complex displacement at position  $x_n$ . In Eq. (6) there are  $N$  measurement points equally spaced at a distance  $\Delta x$ . Note Eq. (6) can also be expanded into a time-space transform if necessary and extended to two dimensions. The output of Eq. (6) can be used to provide an error signal. Minimization of spectral components  $W(k)$  then will provide control of selected wavenumber values. For example, in a finite structure vibrating at a single frequency, the wavenumber components will be discrete and associated with particular modes or waves traveling in the positive or negative directions. In many situations it is appropriate to control these components directly.

*Modal decomposition* of the structural motion is also a useful processing technique. To achieve this, an array of accelerometers is used to measure out-of-plane motion at a number of points. Thus, knowing the structural mode shapes and using a pseudoinverse technique, the modal amplitudes can be estimated from<sup>16</sup>

$$[A] = ([L]^T [L]^{-1}) [L]^T [w_{me}] \quad (7)$$

where  $[A]$  is a vector of  $m$  unknown modal amplitudes and  $[w_{me}]$  is a vector of  $n$  measured displacements at  $(x_n, y_n)$ . In Eq. (7)  $[L]$  is an  $n \times m$  matrix associated with the mode shapes  $\Psi$  of the system defined as

$$[L] = \begin{bmatrix} \Psi_1(x_1, y_1) & \Psi_2(x_1, y_1) & \cdots & \Psi_m(x_1, y_1) \\ \vdots & & \ddots & \\ \Psi_1(x_n, y_n) & & & \end{bmatrix} \quad (8)$$

Equation (7) can also be readily modified to decompose narrow-band traveling-wave fields into individual wave components and can be implemented for broadband random disturbances, as outlined in the work of Gibbs et al.<sup>17</sup> Equation (10) can thus provide indirect error information of a global nature associated with each mode. Minimization of a modal estimate will ensure that a particular mode is globally controlled in a vibrating structure. This is of use when particular modes are more important than others in a control strategy.

*Kalman filtering* techniques are used extensively in linear quadratic (LQ) control problems,<sup>3</sup> where all the internal state variables of the system to be controlled must be known. Arrays of accelerometers can be used in conjunction with Kalman filtering to determine the states of the systems. When all the states are not measurable, they have to be estimated

using a mathematical model of the dynamic system and measurements of the output is the optimal estimator that minimizes the variance of the estimation error.<sup>18</sup>

Power flow can be estimated from an array of accelerometers mounted on the structure. For the simplest case of traveling bending waves on a thin beam, the net narrow-band bending power flow can be calculated by using two measurement points and finite difference theory as described in Ref. 19:

$$P(\omega) = \frac{2EI k_f^2}{\Delta x \omega^3} \text{Im}(S_{21}) \quad (9)$$

In Eq. (9)  $k_f$  is the flexural wavenumber at frequency  $\omega$ ,<sup>6</sup>  $\Delta x$  is the spacing of the two acceleration measurement points, and  $S_{21}$  is the cross spectrum between the output of the two accelerometers. Use of Eq. (9) as an error signal will thus result in minimization of net power flow in the structure in the vector direction of the alignment of the accelerometers. Extension of Eq. (9) to include near fields is also discussed in Ref. 19 (see also Chapter 16). As discussed above, it is also possible to decompose the motion of the structure into wave component amplitudes using a pseudoinverse technique. The power flow associated with each direction of propagation or wave type can be then estimated and used as an error signal. Using approaches such as these, it is possible to actively control termination impedances of beams.<sup>20</sup>

### 3.3 Distributed Piezoelectric Sensors

Piezoelectric material, when strained from its free state, also creates a charge.<sup>7</sup> Thus, when configured properly, piezoelectric material with attached electrodes to collect the charge can be used as an error sensor(s). The most common arrangement is to bond the piezoelectric material to one side of the surface of the structure whose motion is to be sensed. If the piezoelectric material is very thin, then it can be assumed that its presence has no effect on the motion of the structure. For a two-dimensional structure covered with a finite layer of piezoelectric material the charge output  $q(t)$  of the sensor (in rectangular coordinates) can be calculated from the following<sup>21</sup>:

$$\begin{aligned} q(t) = (h_p + h_s) \int \int_S \Gamma(x, y) \\ \times \left[ \epsilon_{31} \frac{\partial^2 w}{\partial x^2} + \epsilon_{32} \frac{\partial^2 w}{\partial y^2} \right. \\ \left. + 2\epsilon_{33} \frac{\partial^2 w}{\partial x \partial y} \right] dx dy \quad (10) \end{aligned}$$

where  $w(x, y)$  is the plate out-of-plane response,  $\Gamma(x, y)$  is the sensor shape function,  $h_p$  and  $h_s$  are the thickness of the plate and sensor, and  $\epsilon_{31}$ ,  $\epsilon_{32}$ , and  $\epsilon_{33}$  are the piezoelectric stress-charge coefficients where the subscripts 1, 2, 3, refer to the  $z$ ,  $x$ , and  $y$  directions of a three-dimensional coordinate system.<sup>7</sup> In effect, the piezoelectric material integrates the surface strain

of the structure over its area  $S$  (i.e., in the 1–2 plane) and thus provides continuous distributed sensing. The actual voltage output of the piezoelectric material is dependent upon the electrical circuitry used to measure the piezoelectric output. Shaped piezoelectric sensors are surface-mounted sensors that are of specified finite size and shape. Particular motions or modal components of the vibrating structure can be observed by cutting the piezoelectric material into a specialized shape. The charge output of an example rectangular piezoelectric strip mounted on a simply supported plate so that it extends completely over the plate in the  $x$  direction but is narrow in the  $y$  direction, is given by<sup>22</sup>

$$\begin{aligned} q(t) = K \sum_{m=1}^{\infty} \sum_{n=1}^{\infty} \frac{L_x L_y}{nm\pi^2} [\cos(m\pi) - 1] \\ \times \left[ \cos\left(\frac{m\pi d}{L_x}\right) - \cos\left(\frac{n\pi c}{L_y}\right) \right] \quad (11) \end{aligned}$$

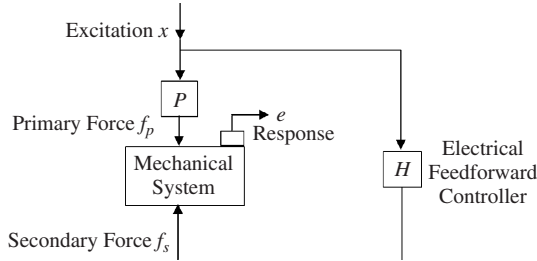
where  $L_x$ ,  $L_y$  is the dimension of the plate in the  $x$ ,  $y$  directions,  $K$  is a constant that modifies the charge output due to the external electrical load impedance,  $m$  and  $n$  are modal orders, and  $d$  and  $c$  are the vertical locations of the sensor boundaries in the  $y$  direction. Note Eq. (11) shows that for all even modes in the  $x$  direction ( $m = 2, 4, 6, \dots$ ) the sensor output is zero. Thus the sensor acts as a spatial wavenumber or modal filter only observing odd modes in the  $x$  direction. Positioning and sizing of the piezoelectric strip can be adjusted to observe required modal or wavenumber components.

To observe individual particular modes of motion, the piezoelectric strip can be cut into a shape corresponding to a system characteristic function or mode shape.<sup>21</sup> Thus, shaped sensors can provide a time-domain estimate of modal amplitudes of structural response, with minimal signal processing, in contrast to the previous method using arrays of accelerometers. However, once the sensor is shaped, its estimate is fixed, whereas the output of the accelerometer array can be manipulated by signal processing to observe various modes or waves.

The most commonly used piezoelectric sensing material is PVDF. It can easily be cut or etched into particular shapes. It is readily attached to the surface with double-sided tape or other means. Care must be taken to attach leads to the bottom of the element, and when the shaped sensor has phase changes throughout its segment each segment output should be wired together with the correct relative polarity to give the required sensor output. Note that matched shape piezoelectric material can be located on each side of a structure and the outputs either summed or differenced to selectively observe in-plane or bending motion, respectively.

## 4 CONTROL APPROACHES

The function of the controller is to process the error information received from the error sensors to calculate



**Figure 2** Simple feedforward control arrangement.

control signals so as to cause the controlled or closed-loop system to behave in a required manner. Control approaches can be divided into two main categories: *feedforward* and *feedback* approaches, as discussed by Fuller et al.<sup>3</sup>

In general, feedforward control has found application when the designer has direct access to information about the disturbance signal to the system. On the other hand, feedback control has primarily been applied when the disturbance cannot be directly observed. In this case the control signals are obtained from the sensor(s) whose output is affected by both disturbance source and the control actuator(s). Chapter 63 also has relevant material on the active control paradigms discussed here.

#### 4.1 Feedforward Control

Figure 2 presents a simple, illustrative arrangement of single-channel feedforward control; in this particular case the object is to minimize the vibration of a mechanical system at the error sensor,  $e$ . The most common form of electrical feedforward controller  $H$  is an adaptive finite impulse response (FIR) filter whose coefficients are updated by a control algorithm to drive the error signal to a minimum.

A critically important aspect of the feedforward approach is obtaining a reference or training signal that provides a coherent estimate of the disturbance signal and is “fed forward” through the adaptive filter to provide the control signal. The most commonly used update equation for dynamic systems is the time-domain Filtered X version of the Widrow-Hoff least-mean-squared (LMS) algorithm written in single-channel form as<sup>23</sup>

$$w^i(n+1) = w^i(n) - 2\mu e(n)f(n) \quad (12)$$

where  $w^i(n)$  is the  $i$ th coefficient of the adaptive filter at time  $n$ ,  $\mu$  is a convergence parameter, and  $e(n)$  is the error signal at time  $n$ . The filtered reference signal  $f(n)$  is given by

$$f(n) = \sum_{j=1}^P c^j x(n-j) \quad (13)$$

where  $c^j$ ,  $j = 1, 2, \dots, P$ , are the weights of a fixed FIR digital filter that models the plant dynamics from

the actuator signal to the error signal and  $x(n)$  is the reference signal taken directly from the disturbance. Equation (13) essentially accounts for the delay between the control system input and the error sensor output. The adaption of Eq. (12) also assumes no feedback of control signal to the reference signal. The fixed FIR filter is usually constructed before switching on the controller or with a low-level probe signal, as described in Refs. 3 and 4. In essence the Filtered X LMS algorithm is a gradient descent technique that finds the minimum of a quadratic cost function defined as the squared modulus of the error signal.

The choice of the filter format is dependent upon the noise disturbance. For a narrow-band signal it is necessary to use only two filter coefficients. Control of broadband signals require a larger filter in terms of coefficients, and causality aspects associated with relative delay through the control path become more important.<sup>3</sup> The Filtered X algorithm can be readily extended to a multichannel configuration, as discussed in more detail in Ref. 24.

Note that the use of a reference signal estimate from the disturbance implies that the system will respond only to information coherent with the reference signal. The system will thus appear open loop to all other disturbances uncorrelated with the error signal. The maximum achievable attenuation of the power of the error signal for a single-input, single-output feedforward control arrangement can be calculated from<sup>3,4</sup>

$$\Delta \text{dB} = -10 \log(1 - \gamma_{de}^2) \quad (14)$$

where  $\gamma_{de}^2$  is the coherence between the disturbance and the error signals. If there is control signal feedback on the reference signals, then the feedback can be compensated for as described in Ref. 25.

Similar to the feedback control, it can be demonstrated that closed-loop systems under feedforward control have new eigenvalues and eigenfunctions<sup>26</sup> and that, for narrow-band disturbances, feedforward and feedback approaches are essentially equivalent.<sup>3</sup> Due to convergence time requirements (the adaptive filter has to search for the minimum of the error surface), the feedforward algorithm does not presently work well with transients applied to nonmodeled systems but is suitable for pure tones or steady-state broadband signals. As the control filter is adaptive and “learns” the system by minimizing a cost function, it is not necessary to have an accurate model of the open-loop system behavior from the control actuator to the error sensor. For a single-channel time-domain controller applied at a single frequency, it is only required to estimate the fixed transfer function between the control input and error sensor within an accuracy of  $\pm 90^\circ$  to ensure controller convergence.

The behavior of feedforward controlled systems can also be analyzed using linear quadratic optimal control theory. For the system of Fig. 2 a quadratic cost function is constructed by squaring the modulus of the error signal (or summing the squared modulus of the error signals). The optimal control input is found

by setting the gradient of the cost function to zero (i.e., at the minimum).

For a system with  $L$  error sensor the quadratic cost function is formed by summing the squared modulus of the error signals,

$$J = \sum_{l=1}^L |e_l|^2 \quad (15)$$

The optimal control inputs to minimize the cost function are found by setting the gradient of the cost function to zero, as described by Nelson and Elliott.<sup>27</sup> For a multiple-input, multiple-output arrangement the optimal vector  $q_{s0}$  of control inputs to minimize the cost function is specified by

$$q_{s0} = A^{-1} Z^H w_p \quad (16)$$

where  $Z$  is a matrix of complex transfer impedances relating the control force inputs to the response at the error sensors, the matrix  $A = Z^H Z$  and  $w_p$  is the noise or primary complex field at the error sensors. More details on how to use Eq. (16) as well as calculating the minimum of the cost function can be found in Ref. 27. The above analysis is for a single-frequency, steady-state excitation and represents the maximum achievable performance. For random signals, the actual control performance will depend upon whether the control filters are physically realizable and other related issues, as described in Ref. 4.

## 4.2 Feedback Control

Figure 3 presents a typical arrangement of single-channel feedback control of motion of a general mechanical system. In this arrangement the control signal is derived from a sensor on the structure and is then “fed back” through a controller (or compensator) to provide a control input. The optimal controller is derived to perform a specified control task. Hence, generally speaking, for feedback control the system changes its dynamic characteristics for all disturbances applied to it, in contrast to the feedforward approach discussed previously.

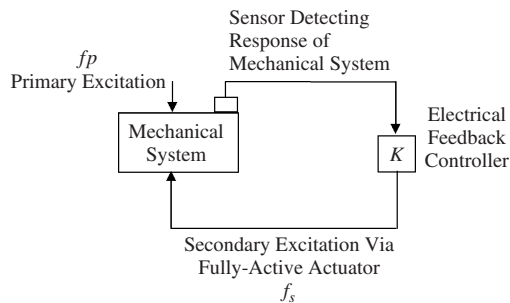


Figure 3 Simple feedback control arrangement.

The open-loop equation of motion of a single-degree-of-freedom system excited by a disturbance force  $f_p(t)$  can be written in the form<sup>3</sup>

$$m\ddot{w}(t) + c\dot{w}(t) + kw(t) = f_p(t) \quad (17)$$

where  $m$ ,  $c$ , and  $k$  are the system mass, damping, and stiffness, respectively. For the mechanical system in Fig. 3 this may correspond to the response of one mode.

Extensions to distributed systems are described in Refs. 2 and 3. The open-loop transfer function (i.e., the ratio of the response to the disturbance) of this system can be evaluated using the Laplace transform<sup>3</sup> and is given by

$$G(s) = \frac{W(s)}{F_p(s)} = \frac{1}{ms^2 + cs + k} \quad (18)$$

We now apply a secondary control force to the structure by feeding back a signal taken from the response of the system through a compensator with a transfer function  $K$  to drive the force  $f_s(t)$ . The closed-loop transfer function of the system with stiffness control, for example, is now given by

$$\frac{W(s)}{F_p(s)} = \frac{G(s)}{1 + G(s)K(s)} = \frac{1}{ms^2 + cs(K + k)s} \quad (19)$$

where  $s$  is the Laplace variable and  $K$  is the compensator gain or transfer function. Note that the closed-loop system effectively has a new effective stiffness  $(K + k)$  and thus new poles.

For transient control the objective is often to increase the damping of the system. In this case the closed-loop poles are moved further into the left  $s$ -plane by varying the compensator gain  $K$ . However, an important aspect of feedback control is stability, which can be determined by inspection of the position of the closed-loop poles as described in Ref. 28. Too much compensator gain  $K$ , for example, can lead to an unstable control system. Often, in practice, the stability is assessed from input–output measurements made on the system before control. The Nyquist stability criterion is then applied to check if the system is stable, as described in Ref. 27. The outcome is that the closed-loop system is stable only if the polar plot of the open-loop frequency response function does not enclose the point  $(-1, 0)$  in the complex Laplace plane  $s$ . Different forms of the compensator  $K$  to the simple example discussed above, can be chosen, depending upon the required control performance, and these are discussed in Ref. 3.

If it is possible to achieve a stable feedback system, then the error signal power is approximately reduced by an amount proportional to the loop gain,<sup>4</sup> and the attenuation is given by

$$\Delta \text{dB} = -10 \log \left| \frac{1}{1 + GK} \right|^2 \quad (20)$$

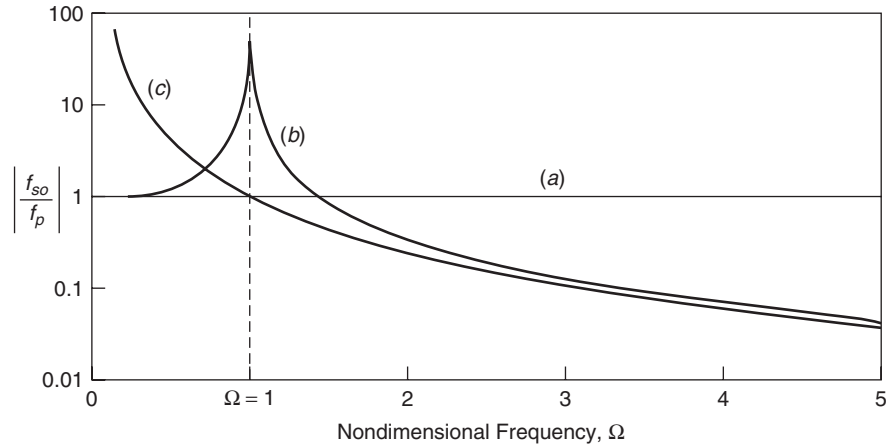


Figure 4 Control force required for (a) direct, (b) opposed, and (c) parallel active vibration isolation systems.<sup>29</sup>

In Eq. (20),  $G(s)$  is the transfer function through the plant and  $K(s)$  is the transfer function through the compensator.

In general, to calculate the optimal controller  $K$ , it is required to have an accurate model of the system to be controlled. This can be done through calculations such as finite element methods or more usually through estimates using system identification approaches as described in Ref. 3. Although multiple-input, multiple-output feedback control have a larger implementation requirement than feedforward control, it ensures that the system is controllable for all forms of linear noise disturbances if a realizable controller can be defined.

Extension of feedback control to multiple-input, multiple-output arrangements can be achieved using state space methods as outlined in Refs. 28 and 3. Other important factors affecting the performance and stability of feedback controllers are reviewed in Ref. 4.

## 5 EXAMPLE APPLICATIONS OF ACTIVE VIBRATION CONTROL

The following examples illustrate some of the wide diversity of present applications of active vibration control. Other implementations of active vibration control are discussed in Ref. 3.

### 5.1 Active Isolation of Vibration

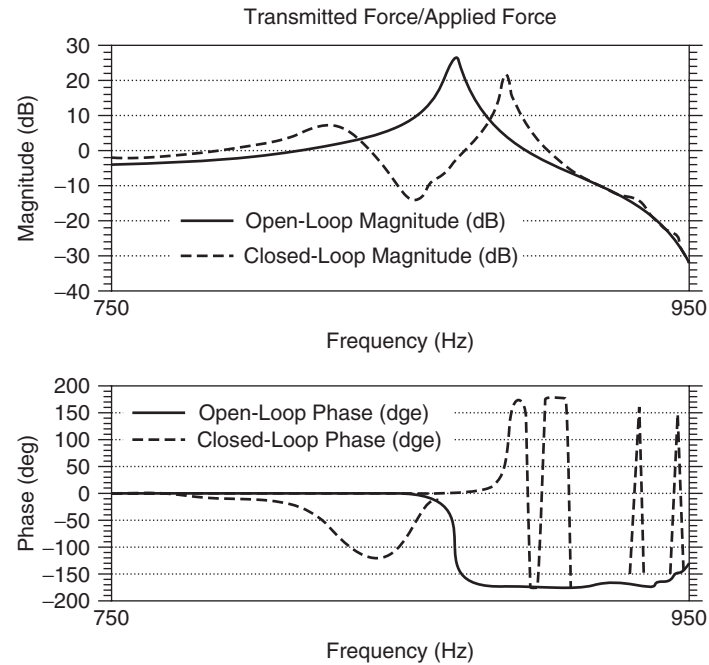
A classic approach to reducing unwanted machinery noise and vibration is to control these disturbances at transmission bottle necks (e.g., the machinery mount). Active vibration isolation has been studied by a number of authors, as summarized in Ref. 3, and a few representative examples will be presented here.

There are four possible configurations for active isolation: The two most common are *series*, in which the actuator opposes the load path, and *parallel*, where the active force is applied in parallel with the load path. As discussed by Scribner et al.,<sup>29</sup> if the actuator

is placed in parallel, it must overcome the stiffness of the passive mount, and the actuator deflection requirements are relatively larger. If the actuator is in series, then while the deflection requirements are lower than the parallel implementation, the actuator must carry the load and, as will be seen below, the force requirements are resonance are higher. Two other, less common implementations are when the active force is directly applied to the exciting system and when the active or secondary force is applied directly to the receiving structure at the mount location. This latter implementation is termed opposed. Both of these latter implementations have the disadvantage of requiring some form of inertial exciter (e.g., an electrodynamic shaker that is provided with a mass against which it can react).

Figure 4 presents the magnitude of the ratio of the secondary control force  $f_{s0}$  to the primary disturbance force  $f_p$  required for a “parallel” and “opposed” implementation calculated by Nelson et al.<sup>30</sup> for a lumped-parameter single-degree-of-freedom mass–spring system. The nondimensional frequency  $\Omega = \omega/\omega_n$ , where  $\omega_n$  is the natural frequency of the mass–spring system on a rigid base. Also shown is the relatively trivial case of when the control force is directly applied to the exciting mass and thus exactly equals the disturbance magnitude to drive the motion to zero. The results of the opposed case are similar in trend to the series implementation, which is discussed in much more detail in Ref. 31. The results show that at resonance the force requirements of the opposed system are much larger while below resonance the converse is true. Well above resonance the force requirements of both arrangements are similar. For control systems designed to operate near the plant resonance, the above characteristics usually imply that electrodynamic actuators (i.e., relatively large deflection, lower force) are used for the parallel implementation while piezoelectric ceramic actuators (i.e., relatively larger force, low deflection) are used for the series arrangement.





**Figure 5** Performance of a series active vibration isolation system.<sup>29</sup>

Scribner et al. have theoretically and experimentally studied the use of piezoelectric ceramic actuators in a “series” implementation of active isolation using a classical feedback approach<sup>29</sup> focused upon sinusoidal disturbances. Figure 5 presents typical values of open-loop and closed-loop behavior of the ratio of transmitted to applied force versus frequency. In this example the compensator natural frequency was set to 877 Hz and a large enhancement in transmitted force is observed near this design frequency. However, in the frequency range of  $825 \leq f \leq 850$  Hz, high attenuation in the transmitted force is achieved. Scribner et al.<sup>29</sup> also demonstrated how the controller could be implemented in a self-tuning implementation so as to track a disturbance frequency, even through structural resonance.

Nelson et al.<sup>3,30</sup> have also analytically and experimentally investigated narrow-band isolation of the vibration of a rigid raft from a flexible receiving structure using multiple active isolators configured in the parallel arrangement. In this case the active inputs were provided by four electromagnetic coil actuators used in conjunction with a multichannel adaptive LMS feedforward control approach. The error signals were taken from either four accelerometers located adjacent to the mount points or eight accelerometers distributed over the surface of the receiving structure. The results demonstrate that the use of eight accelerometers was more effective than four in attenuating the total energy of the receiving structure over much of the frequency range. This behavior illustrates the advantage in feedforward control of using more sensors than actuators; a

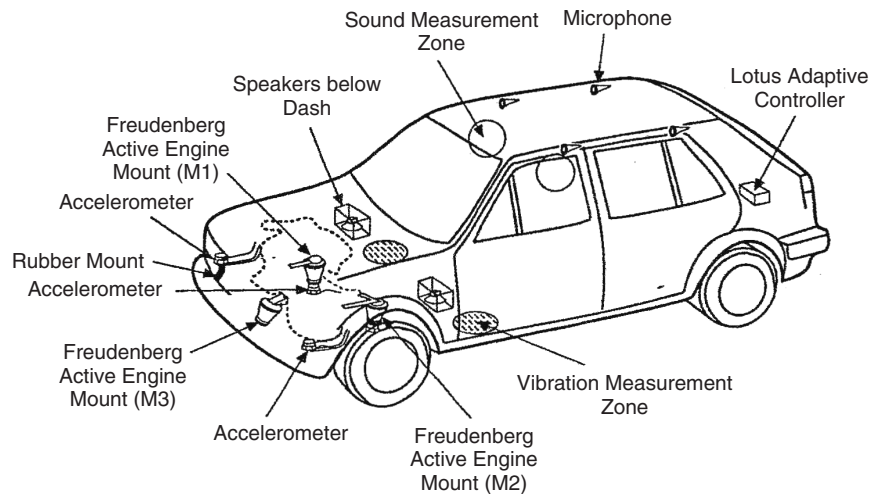
“square” feedforward control system with equal number of actuators and sensors will always try to drive the response to zero at the error sensors, and for high modal densities this can lead to “control spillover” or an increase in the response away from the error sensors. It is thus often beneficial to use more error sensors than actuators when global reduction is required. The results presented in Ref. 3 also show that the passive isolation (i.e., no active control) produced an increase in the receiving structure vibration at some of its resonance frequencies. This characteristic illustrates the importance of the receiving structure dynamics on the isolation performance.

Figure 6 shows a set of active isolation mounts fitted between the engine and frame of a Volkswagen Golf GTI. The system was developed and tested by Lotus Engineering.<sup>32</sup> A feedforward controller was used to minimize the sum of the squared vibration amplitudes measured at four accelerometers. A reference signal was generated by the engine tachometer. Figure 7 shows the measured reduction in the “second-order” vibration levels due to the active engine isolation mounts as a function of engine speed without control (solid line) and with control (dashed line). Significant reduction has been clearly achieved.

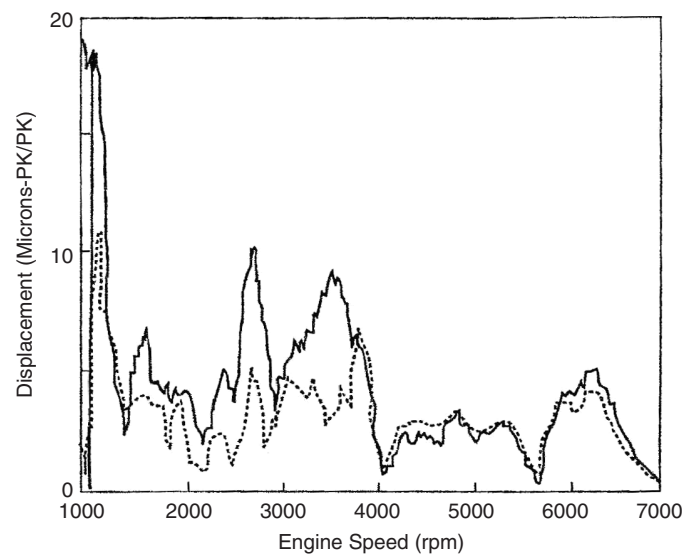
## 5.2 Distributed Active Vibration Control of Plates

The control of vibration of distributed structural elements such as plates is also an important problem. Figure 8 is an experimental arrangement used

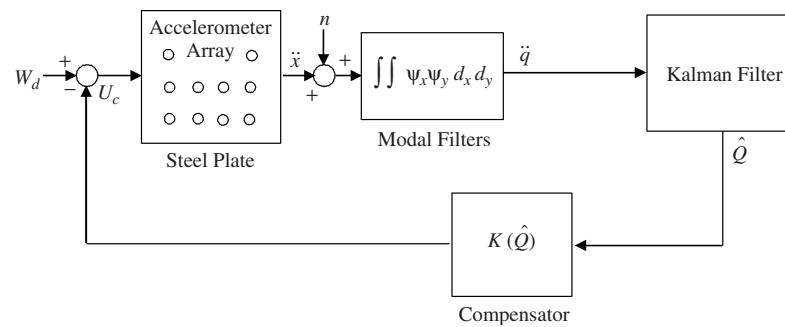




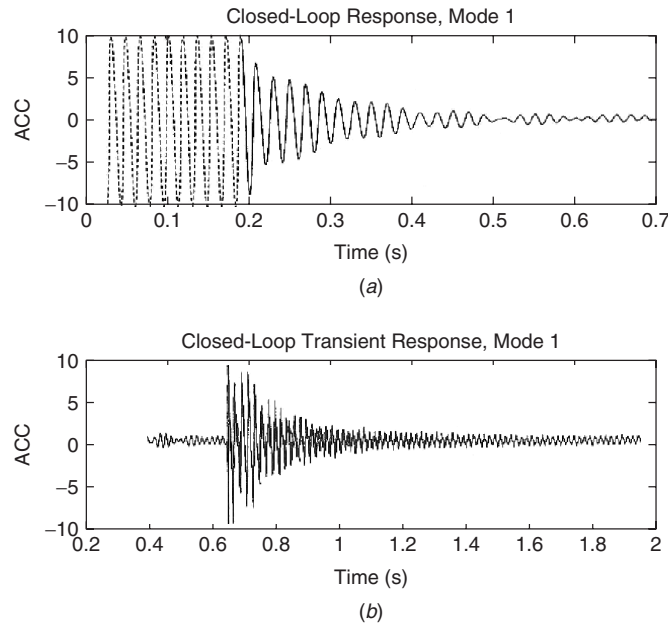
**Figure 6** Active isolation mounts installed in a Volkswagen Golf GTI.<sup>32</sup>



**Figure 7** Measured attenuation of vibration due to active engine mounts of the system of Fig. 6.<sup>32</sup>



**Figure 8** Linear quadratic Gaussian (LQG) feedback control system for active reduction of plate vibrations.<sup>33</sup>



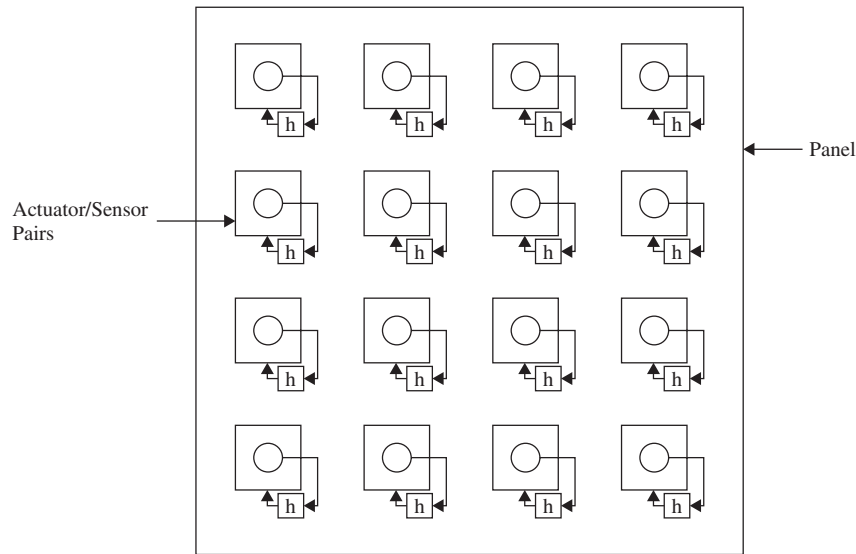
**Figure 9** Closed-loop response of the system of Fig. 10 for mode 1 with (a) narrow-band steady disturbance and (b) transient disturbance at  $t = 0.65$  s.<sup>33</sup>

by Rubenstein et al.<sup>33</sup> to implement linear quadratic Gaussian state space feedback control<sup>3</sup> of the vibration of a simply supported plate. The response of the system is sensed using an array of 12 accelerometers of the plate. The output of the accelerometers is passed through modal filters to obtain modal amplitudes and then through a Kalman filter to obtain the states of the system. The optimal controller  $K(\hat{Q})$  can be obtained using a Riccati equation solution of the state space feedback control arrangement.<sup>3</sup> In this experiment the steel panel was 0.6 by 0.5 m and 3 mm thick. The disturbance and control were implemented by electrodynamic shakers. Figure 9a shows a typical closed-loop response for mode 1 when the disturbance is narrowband, continuous excitation, while Fig. 9b gives closed-loop response to a transient disturbance applied at near  $t = 0.65$  s. In both cases high modal attenuation of the disturbance is achieved. Thus state space feedback methods show much potential for distributed active vibration control a wide range of input disturbances. Note that state space feedback control implies complete control of specified states of the system as opposed to feedforward control, which usually controls a direct output of the plant at the error sensors (displacement, velocity, etc.). Thus global control of the system is guaranteed if all the dominant states are observed and controlled with no control spillover. This is often difficult to achieve in practical systems. As discussed previously, the state space approach also guarantees control of the system to a wide range of disturbances without requiring access to a reference signal.

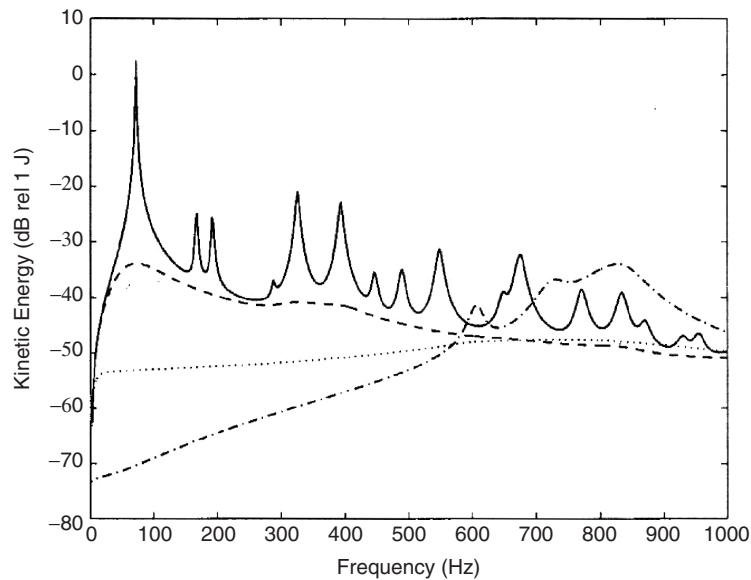
Although state space approaches can achieve high performance, it is often achieved with a certain degree of complexity. Elliott et al.<sup>34</sup> have developed an alternative approach that uses arrays of independent feedback loops with collocated actuators and sensors. Figure 10 shows such an approach applied to the global reduction of vibration of a panel.

Since the actuator and sensors in the system of Fig. 10 are collocated, the feedback control approach is minimum phase, and thus each loop is theoretically independently stable. However, since all the feedback loops are coupled by the distributed dynamics of the panel (i.e., the control input of one loop will be sensed by the feedback sensors of the other loops), the control system will likely be unstable with a general feedback compensator design. To overcome this problem Elliott et al.<sup>34</sup> have restricted the compensator design to paradigms that do not add energy to the structure (each feedback gain is limited to positive sign). Under this limitation it can be proved that the multiple independent feedback loops are stable and in effect represent semiactive approaches.

Figure 11 shows example predicted results where 16 independent feedback loops with feedback gains of 10 (dashed line), 100 (dotted line), and 1000 (dot-dashed line). The vertical axis is the calculated total kinetic energy of the plate, and the feedback loops employ point force actuators and velocity sensors. The disturbance to the panel is an acoustic plane wave. The uncontrolled vibration is shown as a solid line. As the gain is increased, the resonances of the panel response are increasingly damped as one would expect



**Figure 10** Multiple independent feedback loops used to control the global vibration of a panel.<sup>34</sup>



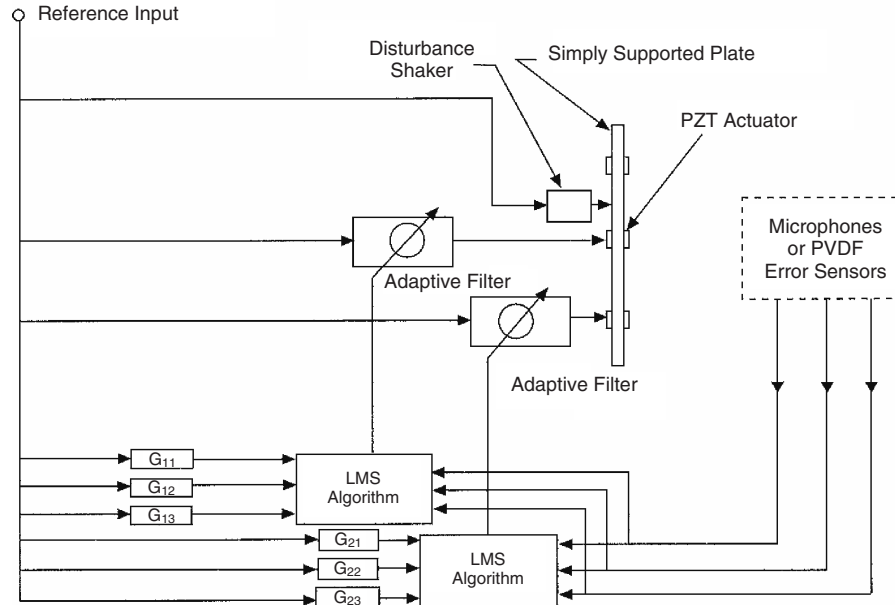
**Figure 11** Performance of multiple independent feedback loops used to control the global vibration of a panel.<sup>34</sup>

with a velocity feedback paradigm. Note that if the gains are increased too much, then control spillover appears above 600 Hz due to additional modes with short wavelengths due to the panel being pinned at the feedback sensor locations. For moderate gains, the results of Fig. 11 demonstrate that multiple uncoupled collocated feedback loops can provide high global attenuation of vibration. Since the system is uncoupled, it is possible to implement the feedback loops in analog

form, and thus the physical control system hardware requirements and complexity are small.

### 5.3 Active Structural Acoustical Control

Vibrating structures often radiate or transmit unwanted sound. An effective technique to control the structural sound radiation is to apply control inputs directly to the structure while minimizing the radiated sound or components of structural motion associated with

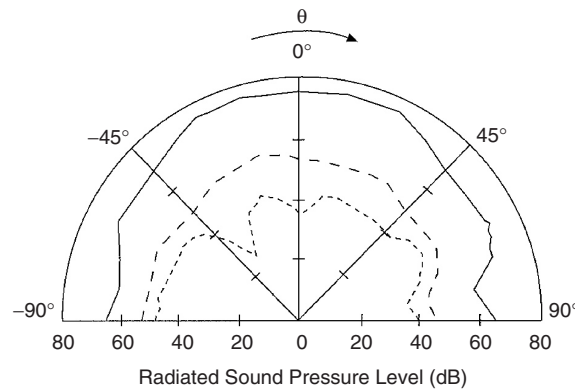


**Figure 12** Experimental arrangement and control block diagram for active reduction of sound radiation from a plate (ASAC).<sup>22</sup>

the sound radiation.<sup>3,35</sup> The technique called active structural acoustical control (ASAC) thus falls in the class of general active vibration control techniques. Figure 12 shows an experimental arrangement in which the sound radiation from a simply supported plate is to be minimized.<sup>22</sup> The noise disturbance is provided by a point force shaker attached to the plate and driven by a pure tone. The control inputs are multiple collocated piezoelectric ceramic actuators bonded to the plate surface and wired to produce pure bending. The error sensors are either microphones in the radiated far field or shaped PVDF sensors attached to one side of the

plate. The shaped PVDF sensors are rectangular strips positioned on the plate as discussed in Section 3.3, so as to observe only the odd-odd modes (the efficient modal radiators at low frequencies). The control arrangement is the multichannel feedforward implementation of the Filtered X algorithm discussed previously. The reference signal is taken from the noise input signal generator and is filtered as outlined in Eq. (17) before it is used in the LMS update equation, as described in Section 4.1.

Figure 13 presents results at 349 Hz, which is near the (3, 1) resonant frequency of the plate. The dotted



**Figure 13** Active structural acoustical control performance for the system of Fig. 12: —, uncontrolled; - - -, controlled with PVDF structural error sensors; and . . . controlled with far-field error microphones;  $f = 349$  Hz.<sup>22</sup>

line for a case where three piezoelectric ceramic actuators are used in conjunction with three error microphones in the radiated far field, and it is apparent that global attenuations of approximately 25 dB are achieved. The dashed line is a similar case except that now two piezoceramic actuators are used in conjunction with two PVDF strips arranged in the  $x$  and  $y$  direction on the plate, as outlined in Section 3.3. The results again demonstrate good global control of approximately 20 dB in the radiated sound pressure levels. These results and others discussed in Ref. 3 demonstrate the potential of using ASAC to reduce radiated sound. For the ASAC technique there are two main mechanisms of control.<sup>16</sup> *Modal suppression* corresponds to a direct reduction of the dominantly radiated modes or a fall in the plate wavenumber spectrum. *Modal restructuring* corresponds to the residual plate response having a lower overall radiation efficiency while its total magnitude of response is reduced only slightly or may even increase. This second case corresponds to attenuation of only supersonic components of the plate wavenumber spectrum while subsonic, nonradiating components are left unaffected. Thus the ASAC technique takes maximum advantage of the natural structural-acoustical coupling behavior to reduce the dimensionality of the controller. The technique has been successfully applied to the control of interior noise in aircraft and the reduction of transformer radiated noise as discussed in Refs. 3 and 4.

Active structural acoustical control systems have been successfully applied to propeller aircraft. Ultra Electronics has developed and marketed a system (called ATVA by Ultra) consisting of an array of electrodynamic actuators attached to the aircraft fuselage.<sup>36</sup> The actuators are used in conjunction with a feedforward controller to minimize the sum of the squares of the amplitudes of the pressure signals from an array of microphones located in the aircraft trim.<sup>36</sup> Reference signals were generated from the propeller shaft piper signals. When installed in a De Havilland Dash 8 aircraft, the ASAC system gives global reductions of the cabin sound field for the first four propeller tones. Measured attenuations range from around 10 dB at the propeller fundamental tone to 3 dB at the third harmonic.

From a system point of view, when multiple integrated actuators and sensors such as piezoelectric devices are used in conjunction with a non-model-based, adaptive controller, the application (such as ASAC discussed above) can be seen to be closely related to the field of *smart*, *adaptive* or *intelligent* structures (see Ref. 37 for a review of this field). Developments in the field of smart structures are likely to be used in advanced active vibration control and ASAC because of the inherent compactness, light weight, and adaptability of this class of systems.

## REFERENCES

1. L. L. Beranek, *Noise and Vibration Control*, INCE, Washington, DC, 1988.
2. L. Meirovitch, *Dynamics and Control of Structures*, Wiley, New York, 1990.
3. C. R. Fuller, S. J. Elliott, and P. A. Nelson, *Active Control of Vibration*, Academic, London, 1996.
4. C. R. Fuller and A. H. Von Flotow, Active Control of Sound and Vibration, *IEEE Control Systems Mag.*, December, 1995, pp. 9–19.
5. Ling Dynamic Systems, *User Manual*, Ling Dynamic Systems, Herts, England, 1973.
6. L. Cremer, M. Heckl, and E. E. Ungar, *Structural-Borne Sound*, Springer, Berlin, 1988.
7. A. J. Moulson and J. M. Herbert, *Electroceramics: Materials, Properties, Applications*, Chapman and Hall, London, 1990.
8. E. F. Crawley and J. de Luis, Use of Piezoelectric Actuators as Elements of Intelligent Structures, *AIAA J.*, Vol. 25, No. 10, 1989, pp. 1373–1385.
9. E. K. Dimitriadis, C. R. Fuller, and C. A. Rogers, Piezoelectric Actuators for Distributed Vibration Excitation of Thin Plates, *J. Vib. Acoust.*, Vol. 113, 1991, pp. 100–107.
10. R. L. Clark, C. R. Fuller, and A. L. Wicks, Characterization of Multiple Piezoceramic Actuators for Structural Excitation, *J. Acoust. Soc. Am.*, Vol. 90, No. 1, 1991, pp. 346–357.
11. C. M. Jackson, H. J. Wagner, and R. J. Wasilewski, 55-Nitinol-The Alloy with a Memory: Its Physical Metallurgy, Properties and Applications, NASA-SP-5110, Washington, DC, 1972.
12. C. A. Rogers, Active Vibration and Structural Acoustic Control of Shape Memory Alloy Hybrid Composites: Experimental Results, *Proceedings of International Congress on Recent Developments in Air- And Structure-Borne Sound and Vibration*, Auburn University, AL, 1990, pp. 695–707.
13. C. G. Miller, High Force, High Strain, Wide Bandwidth Linear Actuators Using the Magnetostrictive Material Terfenol-D, in *Proceedings of Recent Advances in Active Control of Sound and Vibration*, C. A. Rogers and C. R. Fuller Eds. (supplement), Technomic, Lancaster, PA, 1991.
14. J. E. Stangroom, Electrorheological Fluids, *J. Phys. Tech.*, Vol. 14, 1983, pp. 290–296.
15. M. V. Gandhi and B. S. Thompson, Dynamically-Tunable Smart Composite Featuring Electro-rheological Fluids, *Proceeding of the SPIE Conference on Fiber Optic Smart Structures and Skins II*, Boston, MA, 1989, pp. 294–304.
16. C. R. Fuller, C. H. Hansen, and S. D. Snyder, Active Control of Sound Radiation from a Vibrating Rectangular Panel by Sound Sources and Vibration Inputs: An Experimental Comparison, *J. Sound Vib.*, Vol. 145, No. 2, 1991, pp. 195–215.
17. G. P. Gibbs, C. R. Fuller, and R. J. Silcox, Active Control of Flexural and Extensional Power Flow in Beams Using Real Time Wave Vector Sensors, *Proceedings of the 2nd Conference on Recent Advances in Active Control of Sound and Vibration*, Technomic, Lancaster, PA, 1993, pp. 909–925.
18. K. J. Astrom and B. Wittenmark, *Computer Controlled Systems*, Prentice-Hall, Englewood Cliffs, NJ, 1984.
19. J. M. Downing and K. P. Shepherd, Power Flow in Beams Using a 5-Accelerometer Probe, *Proceedings of Noise-Con 88*, Purdue University, IN, 1988, pp. 335–340.
20. J. Scheuren, Active Control of Bending Waves in Beams, *Proceedings of Inter-Noise 85*, Munich, 1985, pp. 591–595.

21. C. K. Lee, W.W. Chiang, and T. C. O'Sullivan, Piezoelectric Modal Sensors and Actuators Achieving Critical Damping on a Cantilever Plate, *AIAA Paper*, No. 89-1390, 1989.
22. R. L. Clark and C. R. Fuller, Modal Sensing of Efficient Radiators with PVDF Distributed Sensors in Active Structural Acoustic Approaches, *J. Acoust. Soc. Am.*, Vol. 91, No. 6, 1992, pp. 3321-3329.
23. B. Widrow and S. D. Stearns, *Adaptive Signal Processing*, Prentice-Hall, Englewood Cliffs, NJ, 1985.
24. S. J. Elliott, I. M. Stothers, and P. A. Nelson, A Multiple Error LMS Algorithm and Its Application to the Active Control of Sound and Vibration, *IEEE Trans. Acoust., Speech and Signal Process.*, ASSP-35, 1987, pp. 1423-1434.
25. S. J. Elliott, *Signal Processing for Active Control*, Academic, London, 2001.
26. R. A. Burdisso and C. R. Fuller, Theory of Feedforward Controlled Systems Eigenproperties, *J. Sound Vib.*, Vol. 153, No. 3, 1992, pp. 437-451.
27. P. A. Nelson and S. J. Elliott, *Active Control of Sound*, Academic, London, 1992.
28. W. L. Brogan, *Modern Control Theory*, Prentice-Hall, Englewood Cliffs, NJ, 1982.
29. K. B. Scribner, L. A. Siervers, and A. H. von Flotow, Active Narrow Band Vibration Isolation of Machinery Noise From Resonant Substructures, *J. Sound Vib.*, Vol. 167, No. 1, 1993, pp. 17-40.
30. P. A. Nelson, M. D. Jenkins, and S. J. Elliott, Active Isolation of Periodic Vibrations, *Proceedings of Noise-Con 87*, Penn State University, State College, PA, 1987, pp. 425-430.
31. A. H. von Flotow, An Expository Overview of Active Control of Machinery Mounts, *Proceedings of the 27th Conference on Decision and Control*, Austin, TX, 1988.
32. A. M. McDonald, S. J. Elliott, and M. A. Stokes, Active Noise and Vibration Control Within an Automobile, *Proceedings of the International Symposium on Active Control of Sound and Vibration*, Acoustical Society of Japan, Tokyo, 1991, pp. 147-156.
33. S. Rubenstein, W. R. Saunders, G. K. Ellis, H. H. Robertshaw, and W. T. Baumann, Demonstration of a LQG Vibration Controller for a Simply Supported Plate, in *Proceedings of Recent Advances in Active Control of Sound and Vibration*, C. A. Rogers and C. R. Fuller, Eds., Technomic, Lancaster, PA, 1991, pp. 618-630.
34. S. J. Elliott, P. Gardonio, T. C. Sors, and M. J. Brennan, Active Vibroacoustic Control with Multiple Feedback Loops, *J. Acoust. Soc. Am.*, Vol. 111, No. 2, 2002, pp. 908-915.
35. C. R. Fuller, Analysis of Active Control of Sound Radiation from Elastic Plates by Force Inputs, *Proceedings of Inter-Noise 88*, Avignon, France, 1988, pp. 1061-1064.
36. C. F. Ross and M. R. J. Purver, Active Cabin Noise Control, *Proceedings of Active 97*, Budapest, Hungary, 1997.
37. B. K. Wada, J. L. Fanon, and E. F. Crawley, Adaptive Structures, *Mech. Eng.*, November, 1990, pp. 41-46.

# CHAPTER 65

## MICROELECTROMECHANICAL SYSTEMS (MEMS) SENSORS FOR NOISE AND VIBRATION APPLICATIONS

James J. Allen

MEMS Devices and Reliability Physics  
Sandia National Laboratories  
Albuquerque, New Mexico

### 1 INTRODUCTION

The use of microelectromechanical systems (MEMS) enables the fabrication of very small devices of overall size up to 1 to 2 mm and feature size as small as a micron. This capability enables sensors to be constructed with multiple axes, types, or arrays of sensors in the same package that enhance the ranges of applications for the sensors. However, issues of scale (size) impact the performance of a MEMS device that may necessitate the on-chip integration of microelectronics with the MEMS device, or special consideration to the method of signal transduction. MEMS are becoming more frequently used in noise and vibration problems and as miniature physical sensors for such applications as accelerometers, gyroscopes, pressure sensors, and microphones.

### 2 MICROELECTROMECHANICAL SYSTEM FABRICATION METHODS

#### 2.1 Fabrication Processes

Microelectromechanical system fabrication has its roots in the microelectronics infrastructure. These fabrication techniques frequently involve a sequence of deposition, patterning, and etching to form a piece of material of a particular shape. This type of fabrication sequence is typically repeated a number of times in a microelectronic or MEMS fabrication technology. Figure 1 is a schematic illustration of this sequence.

The workhorse technique for defining the pattern for a material layer is lithography (either contact or optical). The lithography process uses a mask that contains an optically opaque pattern that is to be transferred to the material, and a thin photosensitive material (photoresist) that is applied on top of the material to be patterned (Fig. 1*b*). Contact lithography brings the mask into close proximity or contact with the photoresist and illuminated with a source to which the photoresist is sensitive. The illumination causes a chemical change in the photoresist that allows the photoresist to be developed and the pattern defined in the photoresist layer (Fig. 1*c*). For contact lithography the features on the mask are the same size as the features to be patterned in the photoresist. Optical lithography can pattern finer features through the use of an optical system allowing the patterns on the mask to be reduced in size and imaged on the photoresist.

Optical lithography is the method used in most high-resolution applications.

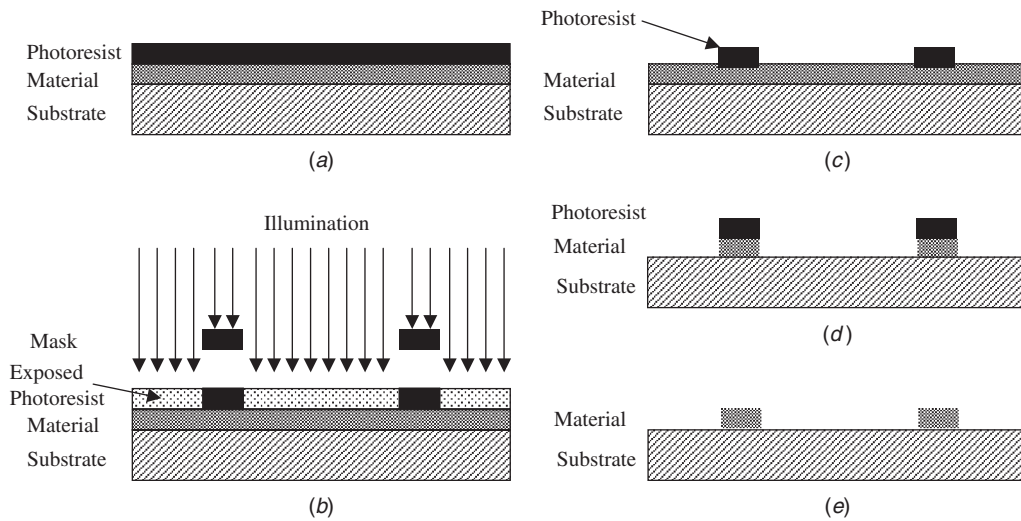
The underlying material can be etched using the patterned photoresist layer as a shield or mask to define the pattern in the material (Fig. 1*d*). There are a variety of etching processes that can etch the material isotropically or anisotropically depending on the material to be etched and etching process (wet chemical etch, plasma etch) utilized. Figure 2 illustrates anisotropic and isotropic etching of silicon materials. All of the instances shown in Figure 2 utilize a mask that is used to define an opening for the etchant to be exposed to the underlying material. An anisotropic etch can be performed on single-crystal silicon material with a wet chemical etch of potassium hydroxide (KOH). KOH etches 100 times faster in the (100) crystal direction than the (111) crystal direction. Patterned silicon dioxide, which KOH minimally etches, can be used as an etch mask for these type of etches. Very directional etches can be achieved with techniques such as this. Alternatively, an anisotropic etch of a material (Fig. 2*c*) can be achieved with dry plasma etches, which etch straight through the mask opening with near vertical sidewalls. An example of an isotropic etch is shown in Fig. 2*b*, which illustrates hydrofluoric (HF) acid isotropic etching of silicon dioxide through a masked opening.

These few paragraphs provide a brief flavor of the type of fabrication techniques involved in MEMS fabrication. The chemistry involved in the etching as well as the design and operation of the equipment of various fabrication steps are quite complex. More detailed information may be found in Refs. 1 and 2.

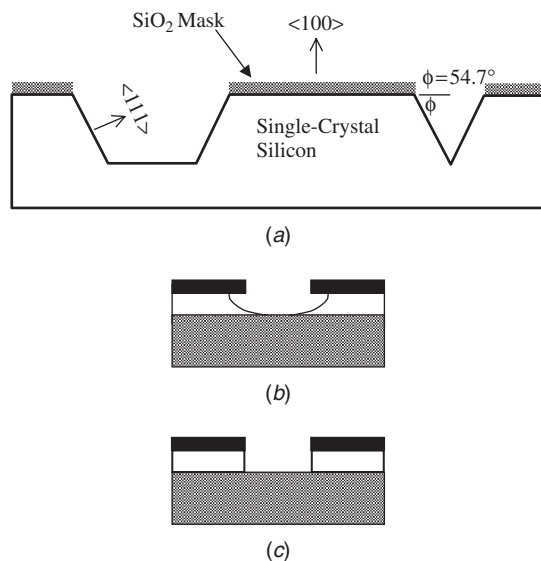
#### 2.2 Microelectromechanical System Fabrication Technologies

There are three dominant MEMS fabrication technologies (Fig. 3) that have been developed during the past three decades. A fabrication technology is a combination of a set of underlying deposition, patterning, and etching processes that are combined to form a technology capable of fabricating MEMS devices.

- Bulk micromachining
- Sacrificial surface micromachining
- LIGA (lithography, Galvanofarming, abforming)



**Figure 1** Pattern and Etch of a material deposited on a substrate. (a) Deposit a layer of material on a substrate and apply a thin layer photoresist. (b) Expose photoresist with a mask to define the pattern. (c) Develop and remove the exposed photoresist. (d) Etch material using the photoresist as a mask. (e) Strip photoresist.



**Figure 2** Anisotropic and isotropic etches of silicon-based materials. (a) Anisotropic etch of single-crystal silicon. (b) Isotropic HF wet etch of silicon dioxide layer. (c) Anisotropic plasma etch of a silicon layer.

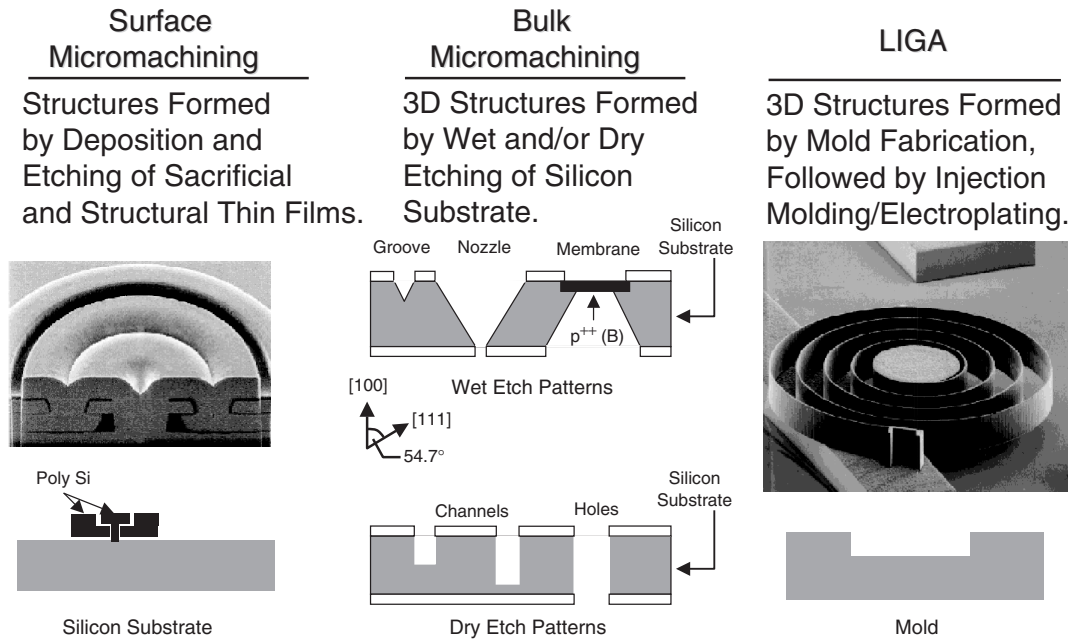
Each of these technologies is philosophically different in approach, but they each employ lithography to pattern the material with micron-size critical dimensions. Lithography is a technique that has been highly refined by the microelectronics industry to define micron and submicron features. Bulk micromachining and sacrificial surface micromachining are

most frequently silicon based and are generally very synergistic to the microelectronics industry since they tend to use the same materials and tool set.

Bulk micromachining utilizes wet<sup>3</sup> or dry plasma etch<sup>4</sup> processes to produce an isotropic or anisotropic etch profile in a material. Bulk micromachining can create large MEMS structures (10s of microns to a millimetre thick), which can be used for applications such as inertial sensing or fluid flow channels. Diaphragms useful in pressure sensors can be made by selective doping of the material, which affects the etch rate and selectivity. Commercial devices using bulk micromachining have been available since the 1970s. These applications include pressure sensors, inertial sensors, and ink-jet nozzles.

The concept of sacrificial surface micromachining (SSM) originated as far back as 1956,<sup>5</sup> but the first demonstration of an SSM fabrication technology<sup>6</sup> suitable for MEMS devices was accomplished in 1983. The fabrication processes used in SSM is a direct outgrowth of the microelectronic industry. This synergy provides a path toward the integration of electronics with MEMS structures that enable control and sensing functions in MEMS devices. SSM utilizes alternating layers of a structural material and a sacrificial material. A widely used material set for SSM is polycrystalline silicon and silicon dioxide for the structural and sacrificial material, respectively. SSM technologies can include as many as five layers of structural and sacrificial material that can be interconnected. SSM technology is generally limited to individual film thicknesses of 2 to 6  $\mu\text{m}$  with an overall device thickness of <15  $\mu\text{m}$ . Since the multiple layers can be connected during fabrication, the resulting devices are assembled as they are fabricated, thus relieving a very difficult task that gives





**Figure 3** Dominant MEMS fabrication technologies. (Courtesy Sandia National Laboratories.)

SSM technology a large advantage for applications involving large arrays of devices. SMM technology has had several commercial successes in the last decade, which include optical mirror arrays<sup>7</sup> and inertial sensors.<sup>8</sup> Both of these applications include integrated microelectronics for sensing and control functions.

The LIGA technology was demonstrated in the 1986.<sup>9</sup> This technology can fabricate devices with small critical dimension and high aspect ratio (i.e., thickness/width) with electroplated metallic materials. The metallic LIGA parts can be used directly or as a die for an injection molding process to produce plastic parts. This gives this technology the advantage in applications requiring a broader set of materials. LIGA technology has been used to fabricate piece parts such as springs, gears, and fluidic channels. Many applications require the LIGA piece parts to be assembled to perform their function. However, assembly of devices at the microscale is quite challenging, due to the large surface forces that exist at that scale.

Sacrificial surface micromachining and bulk micromachining are the MEMS fabrication technologies most relevant to production of noise and vibration sensors. However, each of these fabrication technologies has advantages and disadvantages relevant to the production of noise and vibration sensors as shown in Table 1.

### 2.3 Integration of MEMS and Electronics (IMEMS)

Of the three MEMS fabrication technologies previously discussed, surface micromachining is the most amenable to integration with electronics to form an

**Table 1 Comparison of Bulk Micromachining and Sacrificial Surface Micromachining**

Bulk Micromachining	Sacrificial Surface Micromachining
<b>Advantages</b>	
Large seismic masses (high aspect ratio etches)	Volume production Low cost in volume production
Lower cost fabrication facilities	On-chip integration of electronics Complex electrode structures and interconnection
<b>Disadvantages</b>	
Package level integration of electronics	Thin layers (limited seismic mass)
Device complexity limited	High-cost fabrication facilities

IMEMS process. There are several challenges to the development of an IMEMS process:

- **Large Vertical Topologies** Microelectronic fabrication requires planar substrates due to the use of precision photolithographic processes. Surface micromachine topologies can exceed 10  $\mu\text{m}$  due to the thickness of the various layers.
- **High-Temperature Anneals** Mitigation of the residual stress of the surface micromachine structural layers can require extended period time at high temperature (such as several hours

at 1100°C for polysilicon). This would have adverse effects due to the thermal budget of microelectronics that is limited due to dopant diffusion and metallization.

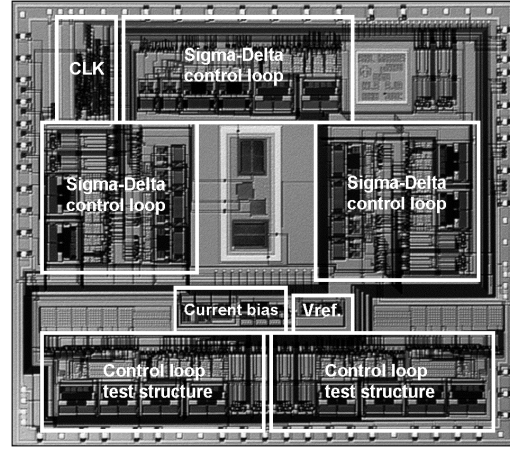
There are three strategies for the development of an IMEMS process.<sup>10</sup>

- *Microelectronics First* This approach overcomes the planarity restraint imposed by the photolithographic processes by building the microelectronics before the nonplanar micromechanical devices. The need for extended high-temperature anneals is mitigated by the selection of low-temperature anneal MEMS materials (e.g., aluminum, amorphous diamond) and/or selection of the high-temperature microelectronic metallization (e.g., tungsten instead of aluminum), which make the MEMS and microelectronic processing compatible. An example of this approach includes an all-tungsten complementary metal–oxide–semiconductors (CMOS) process that was developed by researchers at Berkeley Sensor and Actuator Center.<sup>11</sup>
- *Interleave the Microelectronics and MEMS Fabrication* This approach may be the most economical for large-scale manufacturing since it optimizes and combines the manufacturing processes for MEMS and microelectronics. However, this requires extensive changes to the overall manufacturing flow to accommodate the changes in the microelectronic device or the MEMS device. Analog Devices has developed and marketed an accelerometer and gyroscope that illustrates the viability and commercial potential of the interleaving integration approach.<sup>12</sup>
- *MEMS Fabrication First* This approach fabricates, anneals, and planarizes the micromechanical device area before the microelectronic devices are fabricated, which eliminates the topology and thermal processing constraints. The MEMS devices are built in a trench that is then refilled with oxide, planarized, and sealed to form the starting wafer for the CMOS processing. Figure 4 is an example of a three-axis accelerometer fabricated in the MEMS fabrication first approach.

### 3 SCALING ISSUES

Microelectromechanical Systems technology has allowed the design and engineering of systems that can be 1000 times smaller than previously achieved. At these large changes in scale, our macroworld intuition of the relevant physics may be erroneous. Our engineering intuition at the microscale may be change due to:

- Physical phenomena scale at different rates that changes their relative importance



**Figure 4** Multiaxis accelerometer fabricated in the MEMS first IMEMS process. (Courtesy Sandia National Laboratories.)

- Entering different physics regimes at a particular scale

To evaluate the impact of scaling, we will consider an isomorphic scaling of the system geometry (i.e., all dimensions scaled equally). A dimension of length  $X_0$  can be scaled to a smaller dimension  $X_s$  by a scale factor,  $S$  [Eq. (1)]. Since we are studying the effect of scale reduction,  $0 < S \leq 1$ . The scaling of area and volume may be considered in a similar manner:

$$X_s = SX_0 \quad (1)$$

Two fundamental parameters describing a mechanical system are the mass and stiffness. Since the mass is simply the product of volume and density, the mass scales as  $S^3$  (i.e., the mass is decreasing with the cube of the scale factor):

$$M_s = \rho S^3 V_0 = S^3 M_0 \quad (2)$$

The stiffness describes the ability of a mechanical system to resist applied forces. Stiffness,  $K$ , is the ratio of the force applied to the resulting deflection. Equation (3) shows the proportionality relationship between beam bending stiffness and Young's modulus of the material, beam width, and thickness. Isomorphic geometric scaling shows that the bending stiffness,  $K_{\text{bending}}$ , reduces proportionally with the size scale:

$$K_{\text{bending}} \propto \frac{Ewt^3}{L^3} \propto S \quad (3)$$

Since the mass and stiffness of a system are changing at significantly different rates, the system dynamics will be affected. For example, the natural frequency of a one-degree-of-freedom mechanical system is defined as the square root of the stiffness divided by the mass [Eq. (4)]. The scaling parameters

for mass and stiffness that have been developed above have been inserted to show that as a system reduces in scale,  $S$  the natural frequency scales, by  $1/S$ . This means the natural frequency increases for system scale reductions. The effect is due to the stiffness decreasing more slowly than the mass for a reduction in size:

$$f_n = \frac{1}{2\pi} \sqrt{\frac{K}{M}} \propto \sqrt{\frac{K}{M}} \propto \sqrt{\frac{S}{S^3}} \propto \frac{1}{S} \quad (4)$$

It has been noted that MEMS-scale devices are more rugged in mechanical shock and vibration environments than their macroworld counterparts. MEMS inertial sensors have been shown to survive shock environments of tens of thousands of  $g$ 's.<sup>13</sup> However, the scaling of natural frequency also reduces the mechanical sensitivity of the device, which motivates the use of IMEMS technology to increase the electrical sensitivity and reduce parasitics, which degrade performance.

Ratios such as the area-to-volume ratio are significant in many engineering fields, especially fluid dynamics and heat transfer. The area-volume ratio scales as the inverse of  $S$  [Eq. (5)]. Therefore, as systems are reduced to the MEMS scale, the area-volume ratio increases; this implies that physical phenomena sensitive to the area-volume ratio will change from our heuristic macroworld expectations. For example, heat transfer at the microscale occurs very rapidly. This scaling of the area-volume ratio makes surface forces and surface tension significant at the microscale:

$$A_s/V_s = 1/S(A_o/V_o) \quad (5)$$

*Brownian noise*, also called *thermal noise* or *Johnson noise* for electrical systems, is a low-level noise present in both electrical and mechanical systems. This noise source becomes significant for MEMS devices due to small size.<sup>14</sup> This thermal noise is present everywhere in our environment and is due to such things as the vibrations of atoms in the materials from which a device is made and the environment in which the device operates. Thermal noise is a function of temperature of these materials. The mechanisms that couple these thermal vibrations to the mechanical or electrical device of interest are the energy dissipation mechanisms (i.e., damping for mechanical devices, resistance for electrical devices). As a device is reduced in size, these thermal noises or vibrations become significant for MEMS-scale sensors. The total noise equivalent acceleration (TNEA) due to thermal noise of an inertial sensor is given by Eq. (6). TNEA is the minimum acceleration that can be sensed:

$$\text{TNEA} = \sqrt{\frac{4K_B T \omega_n}{QM}} \quad (\text{m/s}^2 \sqrt{\text{Hz}}) \quad (6)$$

where  $T$  = temperature (Kelvin)

$K_B$  = Boltzmann constant ( $1.38 \times 10^{-23}$  J/K)

$\omega_n$  = natural frequency

$Q$  = quality factor

$M$  = mass

## 4 SIGNAL TRANSDUCTION METHODS

### 4.1 Piezoresistance

The piezoresistive effect was first discovered by Lord Kelvin in 1856, which led to the use of metal and foil strain gauges that have been used for many years. The piezoresistive effect is a change in electrical resistance of a material due to applied mechanical strain. The discovery of the piezoresistive effect in silicon<sup>15</sup> in 1954 had significant impact in the development of MEMS for the following reasons.

- Integration with MEMS devices and microelectronics is possible due to material compatibility.
- Integration of the piezoresistive material and the MEMS device allow good transmission of strain without hysteresis or creep.
- The piezoresistive effect in silicon is over an order of magnitude greater than metals.
- MEMS fabrication processes allow good matching of resistors utilized in the Wheatstone bridge sensing circuits.

As a result of these advantages, piezoresistive sensing has been used as a transduction method for MEMS pressure and inertial sensors for many years. Piezoresistance transduction does not require on-chip electronics, which allows for lower cost, however, piezoresistive sensing may be limited by the Johnson noise of the resistors.

### 4.2 Capacitance Sensing

Electrostatic capacitance sensing is a frequently used transduction method for MEMS devices since capacitors with small electrode spacing may be readily made and integrated into the device. Matched capacitors can be readily made with MEMS fabrication technology, which enables differential sensing. Differential capacitors can be fabricated in such a manner that the two capacitors have the near equal capacitance in the unperturbed position, and change by equal and opposite amounts as the structure is deflected. The differential capacitor structure enables differential sensing that can cancel many adverse or common-mode effects to first order. Changing two capacitors by the same amount is a common-mode effect to which a differential capacitor structure does not respond.

The size of the capacitors utilized in MEMS devices are small, generally a fraction of a picofarad. The variation of the nominal capacitance that is to be sensed to provide the dynamic signal of interest is in the femtofarad range or less. There are also undesirable stray capacitances called *parasitic capacitances* that can interfere with capacitance sensing electronics. The parasitic capacitances will increase the overall electrical time constant of the device and limit the frequency at which it can be electrically charged and discharged, which will have an adverse effect on the sensor interface. Therefore, capacitive sensing typically required an integrated MEMS and electronics process where the electronics is on the same substrate

adjacent to the MEMS device. This will minimize the parasitic capacitances and increase the device sensitivity. Capacitance transduction is frequently used for high-resolution MEMS sensing.

## 5 MEMS PHYSICAL SENSORS

Since 1980 the MEMS field has made dramatic progress. MEMS fabrication processes have matured, enabling increased commercialization of MEMS applications that include optical mirror arrays for displays, inertial sensors, and DNA (deoxyribonucleic acid) analysis systems. This section will discuss the implementation of MEMS physical sensors such as accelerometers, gyroscope, pressure, and noise sensors. The use of MEMS noise and vibration sensors can provide significant advantages that include:

- Low-cost large-volume production
- Multiple devices within the same package
- Improved time response of the system
- Sensor arrays that may be used for directionality or intensity measurements

### 5.1 Microelectromechanical Systems Accelerometers

Microelectromechanical Systems accelerometers have found applications ranging from measurement and control to inertial navigation. MEMS implementations of accelerometers have found a large commercial market in automotive airbag deployment systems.<sup>8</sup> The basic components of an accelerometer consist of the inertial mass, suspension, and sensing element (Fig. 5). The inertial mass suspension will deflect under acceleration. The sensing element will measure the relative deflection,  $Z$ , of the inertial mass and accelerometer case. The transduction can be accomplished by a number of means, but the most common for MEMS devices are piezoresistive and capacitance:

$$M\ddot{Z} + C\dot{Z} + KZ = M\ddot{y} \quad (7)$$

The mechanical sensitivity of an accelerometer,  $S_M$ , is the relationship between the relative deflection

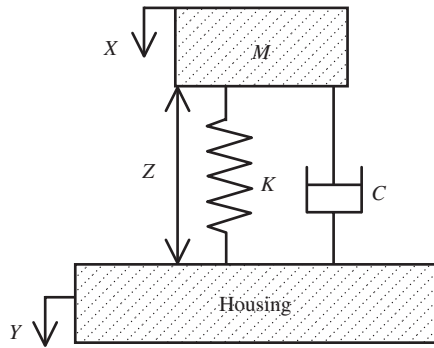


Figure 5 Schematic illustration of an accelerometer.

of the inertial mass and case,  $Z$ , and the input acceleration,  $\ddot{Y}$ . Since the operating range of the accelerometer is at low frequency, where  $\omega \approx 0$ , an acceleration input to the system may be approximated by a constant acceleration balanced by the suspension [Eq. (8)]. Hence the mechanical sensitivity,  $S_M$ , of an accelerometer is shown in Eq. (9). Figure 4 is an example of a capacitance-sensed accelerometer fabricated in the MEMS first IMEMS process:

$$KZ = M\ddot{Y} \quad (8)$$

$$S_M = \frac{M}{K} = \frac{1}{\omega_n^2} \quad (9)$$

### 5.2 Microelectromechanical Systems Gyroscopes

A gyroscope is an instrument for measuring angular rate (i.e., the rate an object turns). A vibratory gyroscope has been the principal approach for implementation in MEMS technology. Vibratory gyroscopes are based on *Coriolis acceleration*, which is acceleration produced due to the changing direction in space of the velocity of the body relative to the moving system.

For example, consider a mass  $M$  moving along a radial path on a platform rotating with angular velocity  $\Omega$ , shown in Fig. 6. The tangential velocity,  $V_t$ , increases as the mass moves further from the center of rotation [Eq. (10)]. For the mass to move outward (i.e.,  $r$  increases) on a radii relative to the platform the tangential velocity will need to increase:

$$V_t = \Omega r \quad (10)$$

The rate of increase of the tangential speed caused by the radial velocity,  $V_r$ , in a rotating system is *Coriolis acceleration*,  $a_{\text{Coriolis}}$ . An additional component of Coriolis acceleration arises from the changing direction of the radial velocity, which yields the following expression for Coriolis acceleration:

$$A_{\text{coriolis}} = 2\Omega \times V_r \quad (11)$$

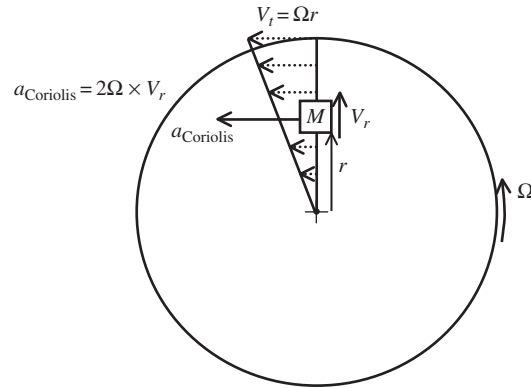


Figure 6 Illustration of Coriolis acceleration.

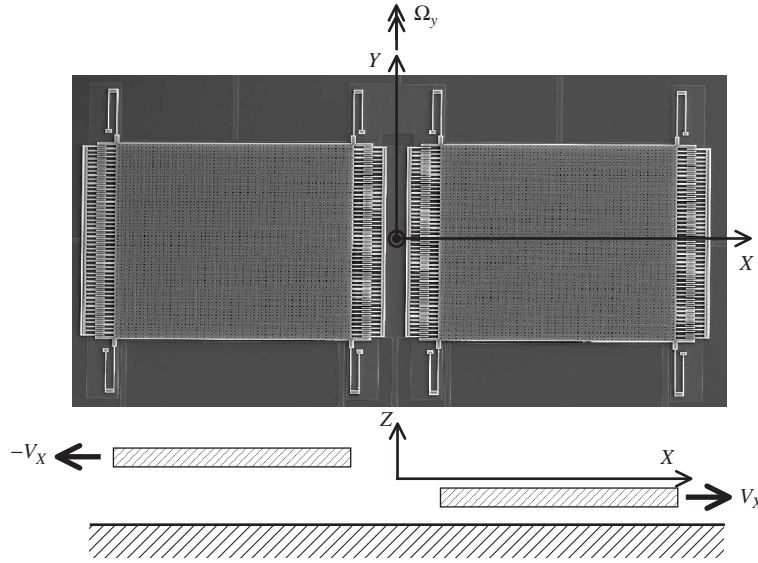


Figure 7 Tuning Fork Gyro (TFG) Schematic.

A vibratory gyroscope is comprised of a resonator that will oscillate a body along one axis and measure the orthogonal movement or force on the body due to Coriolis acceleration. The detection of Coriolis acceleration is the basis of a vibratory gyroscope.

Figure 7 is a schematic of a type of vibratory gyroscope known as a tuning fork gyroscope (TFG) that is being driven along the  $x$  axis, the rotation rate to be measured,  $\Omega$ , is along the  $z$  axis, and the Coriolis acceleration response is sensed along the  $y$  axis. Equations (12) and (13) are the equations of motion (force balance) for the body in the drive and sense axes, respectively. These are a system of coupled second-order equations that are coupled via the Coriolis acceleration terms. The physical mechanism for a vibratory gyroscope is the transfer of energy from one resonator axis to another via the Coriolis acceleration coupling. The suspension for this device can have a unique natural frequency,  $\omega_x$ ,  $\omega_y$ , and a unique damping ratio for  $\zeta_x$ ,  $\zeta_y$  each axis [Eq. (14)]. Frequently,  $\omega_y$  is designed to be slightly less than  $\omega_x$ , which will provide a modest mechanical gain without significant bandwidth or phase shift reductions.

The gyroscope will require the mass to be driven in the  $x$  axis a force,  $F_x$ , which is generated by electrostatics. The drive amplitude is very accurately controlled by an automatic gain control feedback loop since any variation will directly contribute to sensor error. Because the oscillatory drive portion of the gyroscope [Eq. (12)] is fixed to a high degree of accuracy by the gain control loop, Eq. (13) governs the dynamics of the gyroscope response. Since the Coriolis term input to Eq. (13) is a *modulated* signal, the gyroscope output will need to be *demodulated* to extract the rotation rate signal.

Erroneous signals (*quadrature error*), which contaminate the Coriolis signal, can be generated by dynamic force imbalances (stiffness, mass, electrostatic) in the vibrating structure. Quadrature errors can be minimized by error cancellation or synchronous detection methods to extract the Coriolis signal:

$$\ddot{x} + 2\zeta_x\omega_x\dot{x} + \omega_x^2x = \frac{1}{M}F_x - 2\Omega\dot{y} \quad (12)$$

$$\ddot{y} + 2\zeta_y\omega_y\dot{y} + \omega_y^2y = 2\Omega\dot{x} \quad (13)$$

$$\omega_y = \sqrt{\frac{K_y}{M}}\omega_x = \sqrt{\frac{K_x}{M}} \quad (14)$$

The first silicon integrated micromachined vibratory gyroscope was described by O'Connor and Shupe in 1981.<sup>16</sup> In the ensuing years, development of a MEMS gyroscope was spurred by the lure of a low-cost, mass-producible instrument. The configuration that has been employed both for macroscale and MEMS vibratory gyroscopes is the *tuning fork gyro* (TFG) (Fig. 7). The TFG consists of two plates that are driven in an antiphase manner (i.e., both plates move outward and inward relative to the center axis). The rotational field will cause the plates to move perpendicular to the substrate in opposite directions. This configuration enables differential sensing that will allow common-mode signals such as external accelerations to be rejected. The use of two masses vibrating in antiphase also causes momenta to cancel locally and make the gyroscope less sensitive to mounting. The two masses may have coupled or separate suspensions. Two MEMS TFGs have been successfully developed for commercial applications by Draper

Laboratories<sup>17,18</sup> and Analog Device.<sup>19</sup> Both of these gyroscopes have achieved resolutions in the low tens of degrees per hour range. The applications for a gyroscope such as this include tactical grade navigation, platform stabilization, automobile skid control, and stabilization.

The development of a MEMS spinning mass gyroscope was initially inhibited due to the lack of low friction bearings and the significant stiction and adhesion forces at the microscale. However, promising research on the development of an electrostatic levitated spinning mass MEMS gyroscope is proceeding.<sup>20,21</sup> This is an ambitious approach due to the necessity of closed-loop control to stabilize the levitation, in addition to driving the spinning mass and sensing its deflections due to precession. This approach is currently in the research stages with no MEMS spinning mass gyroscope commercial products available.

### 5.3. Microelectromechanical Systems Pressure and Noise Sensors

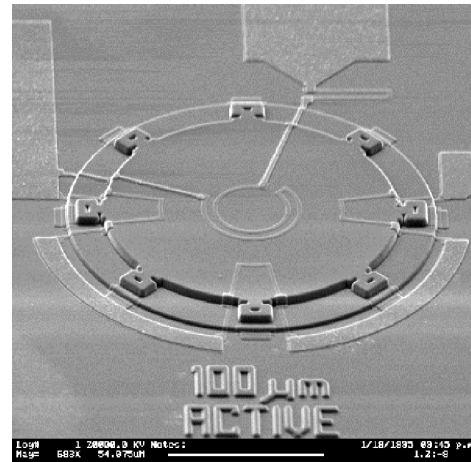
Most pressure sensors for greater than atmospheric pressure utilize a deformable diaphragm between a reference cavity containing a known pressure or a vented cavity, for absolute or relative pressure measurements, respectively. The deflection of the diaphragm is the measure of pressure that can be sensed by capacitive or piezoresistive means. The pressure sensor may measure absolute pressure, which has a vacuum or a reference pressure on one side of the diaphragm. Alternatively, a gauge pressure or differential pressure sensor would have one side of the diaphragm vented to atmosphere or to another pressure that would be a reference for the measurement.

Pressure sensors may be fabricated with bulk micromachining methods to form the cavity and diaphragm. The shape of bulk micromachined cavities are restricted by crystal orientation if anisotropic etching is used. The shape of surface micromachined pressure sensors are not restricted since they are photolithographically defined. Figure 8 shows a surface micromachined pressure sensor<sup>22</sup> which has a 2- $\mu\text{m}$ -thick diaphragm, 200- $\mu\text{m}$  diameter that is piezoresistively transduced.

A microphone is a dynamic pressure sensor where frequency response and mechanical sensitivity are important. The acoustic resistance and squeeze film damping between the diaphragm and stationary cavity typically minimize the effectiveness of a MEMS pressure sensor as a microphone. The design of the pressure sensor is typically modified through the use of perforated stationary plates<sup>23</sup> and venting into a larger cavity to produce a microphone with a flat frequency response over a broad frequency range. Piezoresistive<sup>24</sup> and piezoelectric<sup>25</sup> MEMS microphones have been reported as well as MEMS hydrophones.<sup>26</sup>

## 6 CONCLUDING REMARKS

The MEMS industry is thriving and growing rapidly largely due to the diversity of applications in which



**Figure 8** Surface micromachined pressure sensor.<sup>22</sup> (Courtesy Sandia National Laboratories.)

MEMS devices provide a solution. For example, today's automobiles have a number of MEMS sensors, which include accelerometers, gyroscopes, pressure sensors, wheel speed sensors, and oil condition sensors.<sup>27</sup> MEMS devices can produce unique capabilities for noise and vibration applications due to their small size, which will minimize the mass loading effect during measurement and the use of multiple sensors or arrays in one package that will enable unique measurement and diagnostic features.

## ACKNOWLEDGMENTS

The author is with Sandia National Laboratories and would like to acknowledge his colleagues at the Microsystem, Science and Components Center whose work is included here. Sandia National Laboratories is a multiprogram laboratory operated by the Sandia Corporation, a Lockheed Martin Company, for the U.S. Department of Energy under contract DE-AC04-94AL8500.

## REFERENCES

1. M. Gad-el-Hak, MEMS Fabrication, in *The MEMS Handbook*, CRC Press, Boca Raton, FL, 2002, Chapter 16.
2. J. J. Allen, *Microelectromechanical System Design*, CRC Press, Boca Raton, FL, 2005.
3. G. T. A. Kovacs, N. I. Maluf, and K. E. Petersen, Bulk Micromachining of Silicon, *Proc. of IEEE*, Vol. 86, No. 8, Aug. 1998, pp. 1536–1551.
4. U.S. Patent 5,501,893, Method of Anisotropically Etching Silicon, F. Laermer and A. Schlp, Robert Bosch GmbH, issued March 26, 1996.
5. U.S. Patent 2,749,598, Method of Preparing Electrostatic Shutter Mosaics, filed Feb. 1, 1952, issued June 12, 1956.
6. R. T. Howe and R. S. Muller, Polycrystalline Silicon Micromechanical Beams, *J. Electrochem. Soc.: Solid-State Sci. Techn.*, Vol. 130, No. 6, June, 1983, pp. 1420–1423.

7. Texas Instrument DLP™ technology, <http://www.ti.com/>.
8. Analog Devices IMEMS technology, <http://www.analog.com/>.
9. E. W. Becker, W. Ehrfeld, P. Hagmann, A. Maner, and D. Muchmeyer, Fabrication of Microstructures with High Aspect Ratios and Great Structural Heights by Synchrotron Radiation Lithography, Galvanoforming, and Plastic Molding (LIGA Process), *Microelectron. Eng.*, Vol. 4, 1986, p. 35.
10. R. Howe, Polysilicon Integrated Microsystems: Technologies and Applications, *Proc. Transducers*, Vol. 95, 1995, pp. 43–46.
11. W. Yun, R. Howe, and P. Gray, Surface Micromachined, Digitally Force Balanced Accelerometer with Integrated CMOS Detection Circuitry, *Proc. IEEE Solid-State Sensor and Actuator Workshop '92*, 1992, p. 126.
12. K. H. Chau and R. E. Sulouff, Technology for the High-Volume Manufacturing of Integrated Surface-Micromachined Accelerometer Products, *Microelectron. J.*, Vol. 29, 1998, pp. 579–586.
13. A. Lawrence, *Modern Inertial Technology*, Springer, New York, 1998.
14. T. B. Gabrielson, Mechanical-Thermal Noise in Micromachined Acoustic and Vibration Sensors, *IEEE Trans. Elec. Dev.*, Vol. 40, No. 5, May 1993, pp. 903–909.
15. C. S. Smith, Piezoresistive Effect in Germanium and Silicon, *Phys. Rev.*, Vol. 4, April, 1954, pp. 42–49.
16. J. M. O'Connor and D. M. Shupe, Vibrating Beam Rotation Sensor, U.S. Patent 4,381,672, issued May 3, 1983.
17. B. Greiff, T. Boxenhorn, T. King, and L. Niles, Silicon Monolithic Gyroscope, *Transducers '91, Digest Tech. Papers*, 1991, pp. 966–969.
18. A. Kourepenis, J. Borenstein, J. Connelly, R. Elliott, P. Ward, and M. Weinberg, IEEE 1998 Position Location and Navigation Symposium, PLANS 98, 1998, pp. 1–8.
19. J. A. Green, S. J. Silverman, J. F. Chang, and S. R. Lewis, Single-Chip Surface Micromachined Integrated Gyroscope with 50°/h Allan Deviation, *IEEE J. Solid-State Circuits*, Vol. 37, No. 12, Dec. 2002, pp. 1860–1866.
20. C. Shearwood, C. B. Williams, P. H. Mellor, R. B. Yates, M. R. J. Gibbs, and A. D. Mattingley, Levitation of a Micromachined Rotor for Application in a Rotating Gyroscope, *Electron. Lett.*, Vol. 31, No. 21, 1995, pp. 1845–1846.
21. C. Shearwood, K. Y. Ho, C. B. Williams, and H. Gong, Development of a Levitated Micromotor for Application as a Gyroscope, *Sensors Actuators*, Vol. 83, 2000, pp. 85–92.
22. W. P. Eaton, J. H. Smith, D. J. Monk, G. O'Brian, and T. F. Miller, Comparison of Bulk and Surface Micromachined Pressure Sensors, *Proc. SPIE*, Vol. 3514, Sept. 1998, pp. 431–438.
23. J. Bergqvist, F. Rudolf, J. Maisano, F. Parodi, and M. Rossi, A Silicon Condenser Microphone with a Highly Perforated Backplate, *Transducers '91*, 1991, pp. 266–269.
24. R. Schellin, M. Strecker, U. Nothelfer, and G. Schuster, Low Pressure Acoustic Sensors for Airborne Sound with Piezoresistive Monocrystalline Silicon and Electrochemically Etched Diaphragms, *Sensors Actuators A*, Vol. 46–47, 1995, pp. 156–160.
25. R. P. Pied, E. S. Kim, D. H. Hong, and R. S. Muller, Piezoelectric Microphone with On-Chip CMOS Circuits, *JMEMS*, Vol. 2, No. 3, Sept. 1993, pp. 111–120.
26. J. Bernstein, M. Weinberg, E. McLaughlin, J. Powers, and F. Tito, Advanced Micromachined Condenser Hydrophone, IEEE Solid State Sensor and Actuator Workshop, Hilton Head '94, 1994, pp. 73–77.
27. D. Forman, Automotive Applications, *smalltimes*, Vol. 3, No. 3, May/June 2003, pp. 42–43.

## BIBLIOGRAPHY

- J. Bardeen and W. H. Brattain, The Transistor, A Semi-Conductor Triode, *Phys. Rev.*, Vol. 74, 1948, pp. 130–231.
- R. P. Feynman, There's Plenty of Room at the Bottom, *Eng. Sci.* (California Institute of Technology), February 1960, pp. 22–36. Also *JMEMS*, Vol. 1, No. 1, March 1992.
- J. S. Kilby, Miniaturized Electronic Circuits, U.S. Patent 3,138,743, filed February 6, 1959.
- Kulite Semiconductor, <http://www.kulite.com/>.
- H. C. Nathanson, W. E. Newell, R. A. Wickstrom, J. R. Davis, The Resonant Gate Transistor, *IEEE Trans. Electron Devices*, Vol. ED-14, 1967, pp. 117–133.
- R. N. Noyce, Semiconductor Device and Lead Structure, U.S. Patent 2,918,877, filed July 30, 1959.
- K. E. Petersen, Silicon as a Mechanical Material, *Proc IEEE*, Vol. 70, No. 5, May 1982, pp. 420–457.
- W. Shockley, A Unipolar Field-Effect Transistor, *Proc. IRE*, Vol. 40, 1952, p. 1365.
- J. H. Smith, J. R. Ellis, S. Montague, and J. J. Allen, Critical Issues for the Application of Integrated MEMS/CMOS Technologies to Inertial Measurement Units, *Proc. SPIE*, Vol. 3046, 1997, pp. 242–247.



# CHAPTER 66

## DESIGN OF LOW-NOISE MACHINERY

**Michael Bockhoff**

**Ingénierie Bruit et Vibrations**

**Centre Technique des Industries Mécaniques (CETIM)**

**Senlis, France**

### 1 INTRODUCTION

This chapter presents a systematic approach aimed at integrating noise control aspects into the design process of entirely new machines or of machines to be redesigned partially. The main task of a designer of machines is to find solutions and to set up means that ensure the principal functions expected of the new machine. Generally, the choices and technical possibilities are limited by a group of additional requirements relative to cost, user friendliness, pollution, noise, and the like, which are difficult to reconcile; in particular, the function of low noise emission is not always compatible with parameters such as low cost, lightweight, and compactness.

Low-noise design is an important feature in many types of machinery, such as industrial machinery and equipment for the protection of operators, transportation systems, machinery used outdoors to reduce annoyance in residential neighborhoods, mechanical and ventilation equipment in buildings, household appliances, and car equipment to improve the comfort of passengers.

To meet the requirements of low-noise design in such a broad range of applications, the designer needs a general approach to machinery noise problems. Therefore, methodology for low-noise design needs to cover acoustical analysis and evaluation of the whole machine, its components, and underlying mechanical principles. It also must include rules and recommendations for noise reduction applicable at the different stages of the design process. Designers of machinery must be able to evaluate different possible design solutions with respect to noise criteria and to select the most appropriate one.

### 2 DESIGN PROCESS AND NOISE CONTROL

#### 2.1 Background

During the last 50 years general design methodologies have been set up, especially in Germany, and improved continuously.<sup>1–4</sup> A review is presented in Ref. 5. More recent works include also computer-assisted approaches.<sup>6,7</sup> Noise control of machinery is presented in most textbooks dealing with technical acoustics and vibrations.<sup>8–11</sup> The methodical link between both noise control and design has been developed more recently, mainly in Europe.<sup>12–18</sup> Some of these authors (together with the author of this chapter) have participated—in the frame of the International Organization for Standardization (ISO)—in an elaboration of a technical report on this matter.<sup>19</sup> Some

dedicated software has also become available: The EQUIP+ system was initially developed as prototype software within the scope of a European Brite-Euram project EQUIP.<sup>20</sup> The current version is the result of further development by TNO TPD, Netherlands. It consists of an information system and a noise path modeler for visualizing and quantifying the noise situation of machinery. The PRONS system (Product Noise Synthesiser) has similar features; issued from another European research project,<sup>21</sup> it is marketed by Head Acoustics GmbH, Germany.

Most of the acoustical concepts and methods used in this chapter are mentioned without any further theoretical development because they are already presented in detail in other chapters: for example, measurement techniques in Part V (especially Chapters 43 to 50), modeling techniques in Chapters 7, 8, and 17, and methods for noise and vibration control in Parts VI and VII.

#### 2.2 Concept of Low-Noise Design

Modern design procedures, used today by mechanical engineers, proceed in well-defined steps. Starting from a level of low knowledge about the future object, the following stages integrate successively the needed information and become more and more specific.

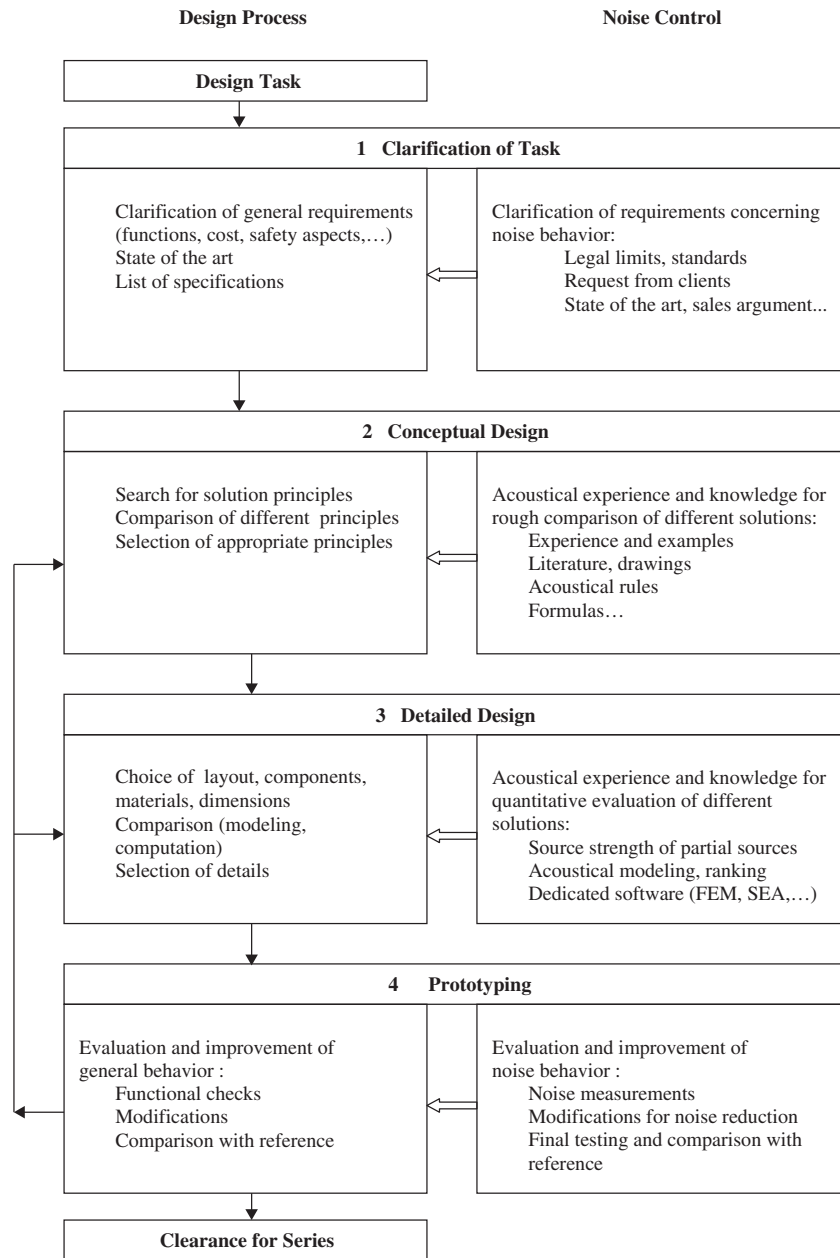
The concept of low-noise design of machinery is based on the same approach, but in addition it integrates at each step of the process the appropriate noise control aspects. Figure 1 shows a complete four-step scheme (according to Ref. 19) where the left column represents the general design process and the right column the needed inputs of acoustical knowledge at each step.

**Clarification of Task** At this stage the functional, economical, and safety requirements for the future product have to be listed, including noise specifications. Depending on the specific design task, these specifications will make reference to

- Legislation
- State of the art
- Requests from clients
- Products of competitors
- Sales arguments, and so forth

**Conceptual Design** Here potential solution principles have to be compared and the most appropriate ones selected. Knowledge on the final product is still limited; nevertheless, first statements on noise





**Figure 1** Stages of the design procedure.

behavior can be made by comparison to existing products, literature, former experience, and the like.

**Detailed Design** Next, the general layout of the machine, basic materials, and individual components are defined. At this point it becomes easier to make reasonable estimates for the expected noise emission and to compare different design options.

**Prototyping** Once the first prototype is built, noise and vibration measurements allow checking the overall behavior. In general, the results will not yet comply with the specifications and design improvements are needed. At this stage it becomes necessary to quantify major noise sources and sound paths. A priority list of noise control measures has to be set up that can potentially be implemented to reduce the noise emission.

### 3 CLARIFICATION OF TASK

To set up noise specifications for the future product, it is necessary to define first the noise emission quantities and corresponding measurement procedures (standardized or not) to be used and noise emission values serving as design targets.

Typical quantities are, for example:

- A-weighted sound power level  $L_{WA}$  according to ISO 3744 series
- A-weighted emission sound pressure level  $L_{pA}$  at the workstation according to ISO 11200 series
- Sound pressure spectra in one-third-octave bands at selected measurement points
- Psychoacoustic parameters such as loudness, roughness, sharpness, and the like

The targets can be defined, for example, with the help of:

- Legal limits existing for specific products
- Limits required by clients
- State of the art
- Company-specific requirements, and the like

### 4 CONCEPTUAL DESIGN

In general the determination of absolute noise values (e.g., by using rough empirical formulas) is difficult and only a ranking of solution principles can be achieved. Sometimes the differences between principles can be estimated from acoustical rules. Since in any design solution each functional system is linked to a physical operation principle, both have to be considered for the choice of a design concept.

**Basic Rule** The mode of operation with the lowest speed and changes in speed (acceleration) will generally provide the best acoustical solution. That applies to the motion of solid parts as well as to liquid and airflow.

It can be concluded that in the following ranking of dynamic principles an increasing improvement should be expected with the later solutions:

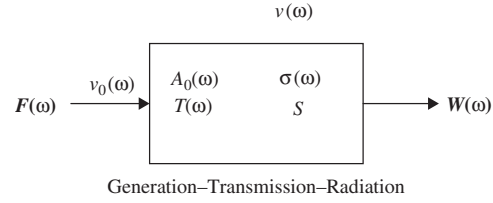
- Shock or impact
- Oscillating motion (back and fourth)
- Continuous translation or rotation

## 5 DETAILED DESIGN

### 5.1 Acoustical Modeling

To prepare a quantitative estimate of the noise emission of the future product, it is useful to set up an acoustical model, which distinguishes between the different types of noise and visualizes its global noise behavior. The basic model, which illustrates the principle, is shown in Fig. 2.

Here it is assumed that the noise generation mechanism (NGM) is a simple force  $F(\omega)$ . The machine is



**Figure 2** Basic acoustical model of a machine.  $F(\omega)$ , excitation force;  $v_0(\omega)$ , input velocity;  $v(\omega)$ , surface-averaged mean velocity;  $A_0(\omega) = v_0(\omega)/F(\omega)$ , input mobility;  $T(\omega) = v(\omega)/v_0(\omega)$ , transfer function;  $\sigma(\omega)$ , radiation efficiency;  $S$ , machine surface;  $W(\omega)$ , radiated sound power;  $\omega = 2\pi f$ , angular frequency.

characterized by an input mobility  $A_0(\omega)$  and a transfer function  $T(\omega)$ ; its response is given by the input velocity  $v_0(\omega)$  and by the resulting vibration velocity, averaged over the surface  $S$ ,  $v(\omega)$ . The radiation behavior is controlled by the radiation factor  $\sigma(\omega)$ , which, together with the surface  $S$ , determines  $W(\omega)$ . It is then possible to express the radiated sound power  $W(\omega)$  as a function of  $F(\omega)$  by the following equation:

$$W(\omega) = \rho c \sigma(\omega) S T^2(\omega) A_0^2(\omega) F^2(\omega) \quad (1)$$

or

$$W(\omega) = \rho c(\omega) S A_T^2(\omega) F^2(\omega)$$

with

$$A_T(\omega) = T(\omega) A_0(\omega) \quad (\text{transfer mobility})$$

In logarithmic form this becomes

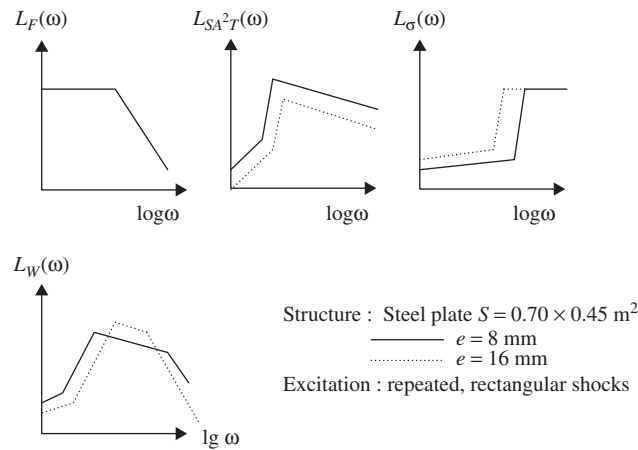
$$L_W(\omega) = L_F(\omega) + L_{SA_T^2}(\omega) + L_\sigma(\omega) \quad (1a)$$

The mechanical excitation of a structure can be considered to be *force controlled* when the load due to the structure has no significant influence on the force. This is the case when the input mobility of the structure is negligible compared with the internal mobility of the source component. (Examples: heavy, massive steel structures such as combustion engines, gear boxes, etc., excited by small components.)

The other limiting case is the *vibration controlled* excitation, which is observed when the input mobility of the structure is much higher than the internal mobility of the source. (Examples: lightweight structures such as platelike covers, panels of enclosures, etc., excited by heavy machinery parts.) In that case the radiated sound power can be calculated by a slightly modified equation:

$$W(\omega) = \rho c \sigma(\omega) S T^2(\omega) v_0^2(\omega) \quad (2)$$

The representation in Eq. (1a) of the sound power level  $L_W(\omega)$  as a sum of three terms that reflect different physical mechanisms can be very helpful for understanding the acoustical chain and the possibilities of noise reduction. Figure 3 shows a graphic



**Figure 3** Graphic illustration of Eq. (1a). The resulting sound power level is the sum of partial levels representing contributions of generation, transmission, and radiation.

illustration of Eq. (1a): The “machine” structure is a simply supported steel plate and the excitation is given by repeated (rectangular) shocks. The plotted spectra have been strongly simplified.  $L_F(\omega)$ , for example, which in reality is a line spectrum, has been replaced by its envelope, approximated by two straight lines. To show how this representation can reveal typical (antagonistic) trends in noise reduction, the curves are plotted for two values of plate thickness  $e$  but unchanged excitation. It is seen that in some frequency bands increased thickness reduces noise radiation, but in others (due to a higher radiation coefficient) noise radiation is even stronger.

In practice, calculations may be much more complex than suggested by Eq. (1) or (2) because real excitations are generally more complex (not simple, pointlike forces or vibrations, oriented in a direction perpendicular to the surface but combinations of forces and torque or situations where both, force and vibration, have to be considered, etc.). Nevertheless, Eqs. (1) and (2) show at least the general trend and point out already the parameters on which noise control actions could be taken.

The first step for setting up an acoustical model is to divide the machine in active and passive components:

- Active components are characterized by the presence of one or more noise generation mechanisms (NGM) (such as impact, unbalance, pressure fluctuations, turbulence).
- Passive components do not generate noise; they only transmit noise to other machine parts or radiate it to the outside.

In the next step NGMs and active components, divided into structure-borne, liquid-borne, and airborne types, should be detailed and located. Then the transmission paths of all contributions have to be analyzed. Finally, the potential radiating surfaces have to be identified.

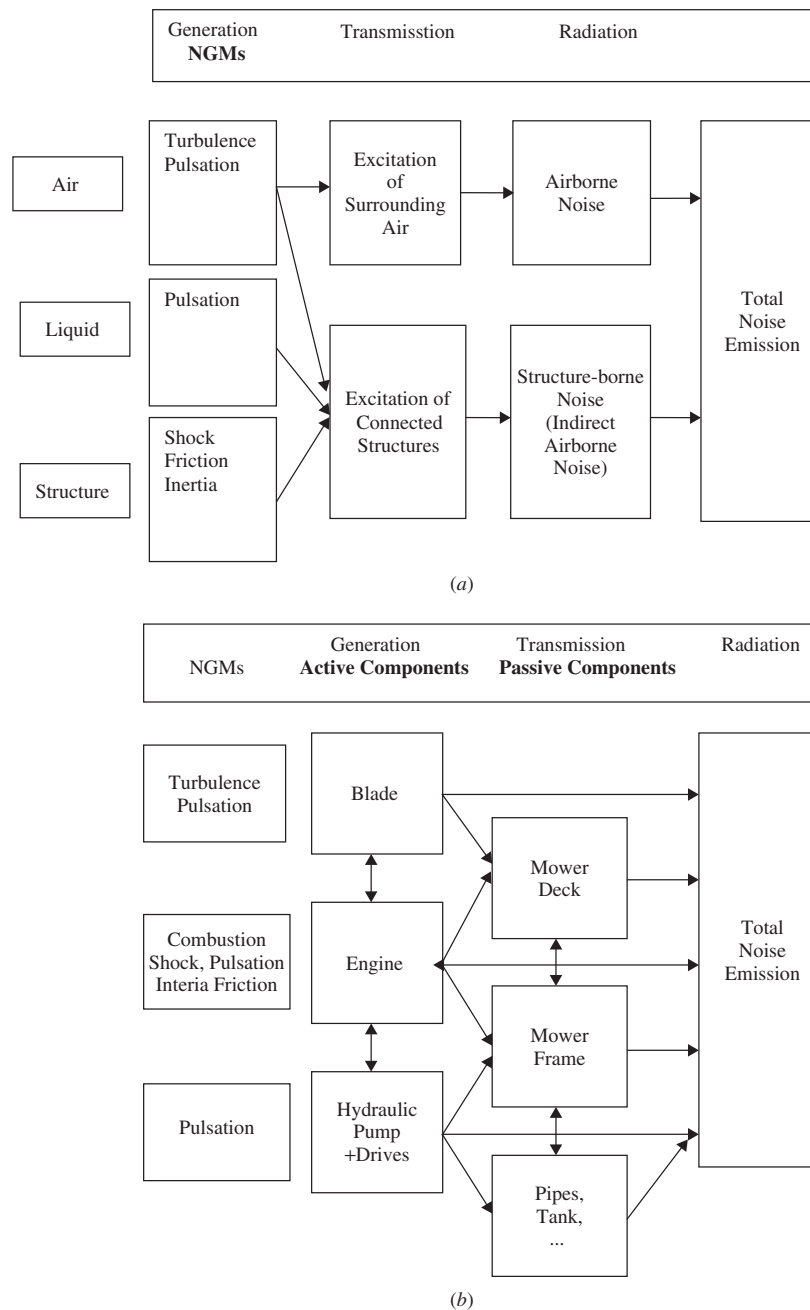
To avoid confusions, two domains have to be distinguished when describing the causal chain of noise generation: When acoustical mechanisms are analyzed, the causal chain is presented in terms of generation–transmission–radiation. When the physically involved machinery components are considered, the chain is presented in terms of source–path–surface. This representation is generally the more convenient for the designer. The graphic representations of these two domains are different. Figure 4 shows both for the example of a lawnmower.

The building of a visual model of the machine is an important step in the characterization of the noise situation, even if designers often would prefer to establish directly a more sophisticated calculation model. Therefore, the central module of the EQUIP+ software, mentioned in Section 2.1, is a *noise path modeler*. This software allows to set up rather quickly a component-based model by selecting noise relevant components, a receiver, and appropriate links. As an illustration, Fig. 5 presents the noise path model obtained for a diesel unit, which can be considered as a zoom-in on one of the main components (the “engine”) of the lawnmower model shown in Fig. 4. (Except lawnmowers are usually powered by gasoline engines and actual enclosures are generally very partial ones.)

Sometimes an even more detailed description of the machine may be needed. For example, if the radiation from the enclosure is dominant, it is necessary to distinguish between contributions from different walls and from openings. Generally, these improvements will be introduced only after a first ranking of contributions.

## 5.2 Ranking

To identify the dominant contributions to the overall noise, a ranking has to be made within each of the three steps of the chain (generation–transmission–radiation)



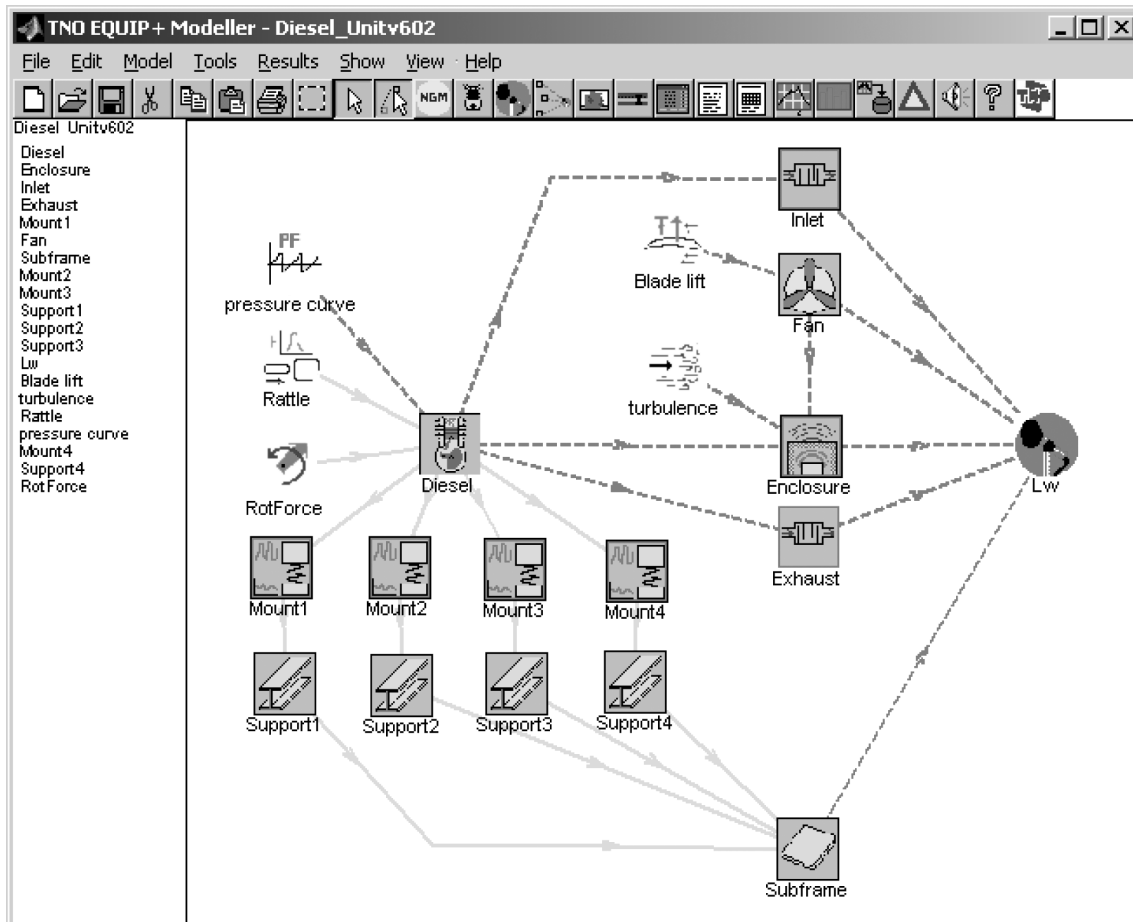
**Figure 4** Acoustical models of a ride-on lawnmower. (a) NGM-based model and (b) component-based model.

and for each noise type (structure-borne, liquid-borne, and airborne). If no particular information from similar products or former design solutions is available, the ranking will remain rough and qualitative, and conclusions have to be confirmed later during the prototype stage. Improvements of the prediction need

detailed input data and computation tools such as finite element models (FEM), SEA, or analytical models.

### 5.3 Rules for Noise Control

Once the dominant sources with their transmission paths and radiation areas are identified, improved



**Figure 5** Noise path model of a diesel unit, built with EQUIP+ software. (Courtesy TNO Delft, The Netherlands.) Square icons, components; circular icons, noise generation mechanisms (NGMs). Full arrows, structure-borne noise paths; dotted arrows, airborne noise paths.

design solutions can be elaborated. It is recommended to consider, first, the active components and, second, the passive components (transmission paths and radiation). Among the sources, of course, the dominant contributions have to be controlled first. Tables 1 to 3 present general design rules for the control of generation, transmission, and radiation of noise.

## 6 PROTOTYPING

### 6.1 General

The purpose of actions undertaken in this stage is to obtain compliance with target values such as legal or contractual limits, company targets (product improvement), or the state of the art (comparison with competitors). The procedure is generally an iterative one with the following steps:

#### Measurements

- Overall check: When compliance with the design tasks is achieved, the acoustical part of

prototyping is finished, otherwise the procedure continues.

- Detailed measurements (research of predominant sources and transmission paths)

#### Evaluation

- Ranking of sources
- Planning of noise control measures (priority list)

#### Modification

- According to priority list

### 6.2 Measurements

**6.2.1 Overall Check** Target values are very often single numbers that can be measured rather easily according to standardized test codes or other simple procedures defined in advance (A-weighted sound power level  $L_{WA}$ , A-weighted emission sound pressure level  $L_{pA}$  at the workstation or at specific positions, etc.).

**Table 1 Design Rules to Control Noise Generation**

Noise Type	NGM	Generation
		Design Rules
Airborne	Turbulence	Avoid obstacles in the flow and flow over cavities (generation of pure tones) Smooth flow profile Minimize flow velocity (increase diameter of ducts) Reduce pressure drops along the flow For jets, improve outlet geometry (minimize velocity changes across the jet) For nozzles, replace single hole outlet by multiple holes of smaller diameter (shift of dominant noise to nonaudible frequencies) For fans, minimize tip speed and increase clearance between rotor and casing
	Pulsation	Avoid obstacles near rotating blades of fans, turbines, etc. (generation of tonal noise) Smooth pressure pulsation (i.e., lower amplitude of pulses, increase rise time of pulses)
	Shock	Slow down pressure–time variation when releasing pressurized gas In supersonic flows reduce flow velocity
Liquid borne	Turbulence, pulsation, shock	Same rules as for airborne noise
	Cavitation	Avoid that static pressure along the flow drops below vapor pressure Smooth flow profile of pumps and valves Keep suction line short Place pump outlet higher than inlet Use a flow resistance in the outlet (creates a counterpressure) Reduce flow speed
Structure borne	Impact	Reduce the mass of impacting body Increase the fixed mass Avoid loose parts and play
	Tooth meshing	Use helical gears Increase the number of teeth Improve tooth profile quality Use plastics for low load
	Rolling	Increase flexibility in the contact area Use precision roller bearings Reduce tolerances in housing Use proper lubrication Keep rolling surfaces smooth
	Inertia	Optimize steadiness of motion (no accelerated masses) Reduce inertia forces by proper balancing
	Friction	Reduce friction by appropriate choice of materials Reduce friction by lubrication
	Electromagnetic fields	Optimize shape of poles in electric motors Optimize number and position of slots in electric motors For transformers reduce magnetostriction by selection of proper core material

In practice, problems may nevertheless occur in the choice of the test site:

- When the machine cannot be mounted in an acoustical test room—This generally is the case with big machines or when auxiliary equipment is needed (driving unit, fluids, etc.).
- When the nominal operating conditions cannot be achieved easily (e.g., lack of material or insufficient power).

If noise measurements are to be made at arbitrary industrial locations, preliminary tests are necessary to qualify the test environment (background noise, reverberation). Commonly used procedures are based on

outdoor measurements (no reverberation), measurements during night (no background noise) or measurements at the customer's site (auxiliary equipment). If no particular (standardized) test code is prescribed, the choice of the measurement method and appropriate instrumentation have to take into account the nature of expected noise.

**6.2.2 Detailed Measurements** When the overall check has revealed unacceptable high noise levels, more detailed measurements are needed to understand the noise generation mechanisms and to define noise control measures. As shown in Fig. 6, the analysis should be focused on the basic elements used in the design stage, but in a different order of the steps.

**Table 2 Design Rules to Control Noise Transmission**

		Transmission
Noise Type	Noise Reduction Technique	Design Rules
Airborne	Enclosure	Use isolating panels lined inside with an absorbing material Minimize leaks Use silencers for functional openings (ventilation, rotating shafts, pipes, transport of material and parts) Avoid rigid connections between machine and enclosure
	Screen	Use isolating panels lined on the source side by an absorbing material Screens may be used when only a limited area has to be protected (workplace)
	Silencer	For broadband noise (medium and high frequencies) use absorption-type silencers For narrow-band noise (low and medium frequencies) use reactive-type silencers For compressed air discharge use pneumatic expansion silencers
Liquid borne		Use hoses instead of rigid pipes For broadband noise use accumulators For narrow-band noise use side-branch-type silencers
Structure borne	Isolation	For low frequencies use elements or layers that are more resilient than source and receiver For high frequencies add a heavy foundation between source and receiver
	Damping	Add damping only when the initial damping is low Apply damping near the source Use damping layers on thin plates only Damping of transmission can only be expected above the frequency of first bending mode

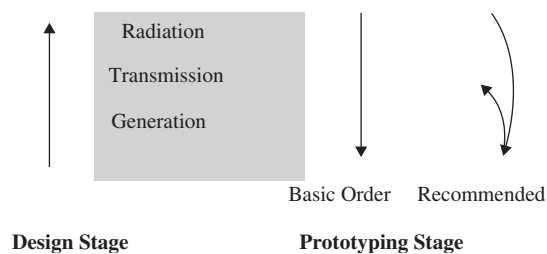
**Table 3 Design Rules to Control Noise Radiation**

		Radiation
Noise Type		Design Rules
Airborne		Optimize radiation directivity by placing the radiating openings in remote areas Fit the radiating openings with silencers or screens
Structure borne		Reduce the surface of radiating parts [see Eqs. (1) and (2)] Reduce radiation efficiency (decrease the thickness of plates or use perforated plates)

At this stage there is no more need for standardized methods but for some intuition! It is recommended to start with simple techniques and to increase complexity only if necessary. In the simple case of one dominating sound source and a small number of transmission paths and radiating parts, qualitative information may be sufficient to decide on the measures to be taken. In most cases however, it will be necessary to obtain quantitative information as well (i.e., the source strengths, transfer functions of transmission paths, radiation factors, etc.).

Typical escalation in complexity may be:

- Listening to noise (subjective impression, identification of tonal noise sources, etc.)

**Figure 6** Order of steps in the design and prototyping stages.

- Measurement of sound pressure levels in one or several points (noise mapping)
  - Linear or A-weighted levels
  - Spectra ( $\frac{1}{1}$ - or  $\frac{1}{3}$ -octave bands, narrow bands)
- Measurement of sound intensity levels for sound power determination on components
- Measurement of vibration levels
- Time records
- Analysis of combined quantities (impedance or mobility, coherence)

To limit the amount of work involved, it is useful to clearly define the purpose of each measurement step,

minimizing the amount of information where possible. For example, the use of one-third-octave spectra is often sufficient and practical.

**Analysis of Noise Radiation** As a first step it is recommended to start from the initial procedure (overall check) and to increase the resolution of analysis only at the basic measurement points:

**In the Frequency Domain** The measurement of some spectra already allows for detecting the frequency range(s) that are governing the overall noise level and on which noise reduction has to be focused. If the underlying physical principles of the machinery and of its components are known, the analysis of one spectrum may be sufficient to identify predominant internal sources. For example pure tones at characteristic frequencies of bearings, gears, pumps, fans, electric motors, and the like. Broadband noise due to flow or discharge of gases in valves and nozzles.

**In the Time Domain** When the noise emission is not stationary, it may be helpful to record sound pressure or other quantities as a time signal. This can be done for the overall level, a particular frequency band or for the whole spectrum ("waterfall"). Knowledge of the time history can give further insight into the NGMs and the involved components (impacts, sequences of different operations, etc).

In the next step it is useful to increase *spatial* resolution of analysis to get an idea of directivity and first information on transmission paths from the source to the boundaries of the machinery. A rough mapping of the global sound pressure levels around the machinery is carried out to determine areas of strongest emission. More thorough measurements, preferably made in the moderate near-field of the source (0.1 to 0.5 m), allow to identify radiating parts (openings, vibrating panels, noisy components...).

A powerful approach is given by sound intensity techniques, which allow precise information to be obtained even in the very near field of the source (0.05 to 0.20 m). These techniques include:

- Mapping of sound intensity levels (normal components)
- Determination of partial sound power radiated by specific areas of machine envelope
- Vector plots in different planes

An alternative technique is given by vibrational velocity measurements. This is recommended when:

- The acoustical environment is disturbed by strong or fluctuating background noise.
- Sources of aerodynamic noise are present in the machine. Then vibrational velocity measurements combined with airborne sound measurements allow to separate the different contributions from structure and air to the combined radiation.

**Identification of Sound Sources** If the noise radiation analysis has not yet allowed the identification of the predominant noise sources, several other techniques, summarized from Ref. 19 in Table 4, can be applied; they will supply mainly qualitative information. Quantification of vibroacoustic energy produced by the components may also be achieved by using structural intensity techniques according to Chapter 16.

**Analysis of Transmission Paths** It is necessary to distinguish between transmission of airborne, fluid-borne, and structure-borne noise. Propagation of *air-borne* noise is mainly observed:

- From inside to outside of casings, enclosures, and the like
- Through ducts (lined or not)
- Directly from a component to the machine environment.

All these paths are generally easy to detect and to characterize since input and output parameters can be measured by rather simple methods (sound pressure and/or sound power levels). When it is difficult to separate airborne and structure-borne contributions from a component, it may be recommended to use an artificial source, producing only airborne noise, instead of the machine component.

*Fluid-borne* noise propagation through pipes may be radiated directly by the piping but—since radiation efficiency of pipes is rather poor—the main problem is very often the structure-borne noise produced in connected structures (especially in lightweight structures such as thin plates). Measurements inside the fluid need special transducers and the interpretation of results is frequently complicated by strong standing waves.

The transmission paths of *structure-borne* noise are the most difficult to quantify since the input of structure-borne noise energy from a component to the machine structure is generally not known (it depends on both the source and the reception structure). Various isolation and/or damping techniques can be applied to the presumed transmission paths. When the radiated total sound pressure is measured before and after this operation, the difference illustrates the importance of the transmission path. These techniques are suitable only for the evaluation of major sound paths. In the case of unchanged results, it may be difficult to decide whether blocking was insufficient or if the considered sound path was not predominant.

### 6.3 Evaluation

The evaluation of the identified noise sources proceeds in three steps:

- Listing of all partial sound sources and their noise data (spectra of sound pressure, vibrational velocity, sound power, time records, etc.)
- Listing of corresponding transmission paths; rough estimation of partial energy transfers



**Table 4 Techniques for the Identification of Partial Noise Sources**

No.	Source Identification Technique	Pros	Cons
1	<b>Switching off partial noise sources:</b> The sound pressure as a function of frequency or time is measured on a normally running machine. Then measurements are made on the machine operated with one of the components switched off. The difference between both configurations shows the contribution of the switched-off partial noise source.	Simple instrumentation Arbitrary surroundings are allowed	Sometimes it is not possible to switch off the most relevant components. Even if it is possible, operating conditions of the machine may be altered.
2	<b>Shielding of partial noise sources:</b> Same approach as 1, but instead of switching off the particular component, only its noise emission is reduced. A partial airborne source, for example, may be shielded by an improvised enclosure. A partial structure-borne source may be isolated from the machine structure by improvised resilient elements.	Simple instrumentation Arbitrary surroundings are allowed	Needs changes at the machine.
3	<b>Variation of operational parameters:</b> Speed or load of the machine are varied and the radiated sound pressure is measured as a function of frequency or time.	Simple instrumentation Identification of partial sources is generally easier than in the case of constant operating condition Arbitrary surroundings are allowed	Variation is not always possible. Needs additional devices for the control of variation.
4	<b>Signature analysis:</b> On rotating machinery acceleration is measured at a point on the machine surface and synchronized with the signal of the rotating shaft. The analysis is carried out with special software.	Very suitable method to distinguish internal sources from the response of the machine structure	Special transducers and software are needed.
5	<b>Correlation and coherence methods:</b> The contribution of a partial source to the radiated total sound pressure is determined by analyzing the correlation between the total noise and a reference signal taken from the partial source.	No changes at the machine	Instrumentation is quite expensive. Sometimes it is difficult to get good reference signals.

- Ranking of contributions to the overall noise level

The planning of noise control measures should be guided by two main recommendations:

- Start with the predominant source, but do not forget that the sum of the remaining partial noise sources will limit all expected noise reduction! Therefore, it will generally be sufficient to reduce the noise level of a dominant component to approximately 5 dB below the residual level of the remaining partial noise sources. Further reduction of the dominant partial noise has only minor effects on the total noise.
- When there are several partial noise sources of approximately equal strength, the noise control measures must be applied to all these sources.

A noise reduction limited to selected individual noise sources will only have a marginal effect on the overall noise level.

## 6.4 Modification

The aim of this stage is to reduce individual contributions to the overall noise in the order of priority established in the evaluation stage. Since each contribution has been analyzed in terms of internal source, transmission path, and radiating part, in principle all these elements can be modified by noise control measures.

For some individual contributions the existing data may prove to be insufficient so that it is necessary to study more in depth mechanisms of excitation, transmission, and radiation (subbalance) before taking action on all three links of the noise generation chain.

In general, noise control measures are most effective when implemented close to the internal source. In

principle, the resulting order of priority should be that of the design stage, that is:

1. Internal source
2. Transmission through the structure
3. Radiating machinery parts

Since in practice the chosen strategy will not only depend on technical arguments but also on economical considerations, this order of priority may, of course, be modified.

Especially the size of the final product series will determine, for example, whether noise control measures are taken at the source (option to be considered in the case of big series) or if techniques based on enclosures are more suitable (small series or single machines). After each product improvement the priority list of major noise problems (see Section 6.3) must be updated to reflect the noise control measures taken.

## REFERENCES

1. G. Pahl and W. Beitz, *Konstruktionslehre—Methoden und Anwendung*, 3rd ed., Springer, Berlin, 1993. Also available in English: G. Pahl, W. Beitz, and K. Wallace, Eds., *Engineering Design*, 2nd ed., Springer, New York, 1996.
2. R. Koller, *Konstruktionslehre für den Maschinenbau. Grundlagen des methodischen Konstruierens*, 2nd ed., Springer, Berlin, 1985.
3. G. W. Rodenacker, *Methodisches Konstruieren. Grundlagen, Methodik, praktische Beispiele*, 4th ed., Springer, Berlin, 1991.
4. S. J. De Boer, *Decision Methods and Techniques in Methodical Engineering Design*, Academisch Boeken Centrum, De Lier, 1989.
5. S. Finger and J. R. Dixon, A Review of Research in Mechanical Engineering Design, *Res. Eng. Design*, Vol. 1, No. 1/2, 1989, pp. 51–67 and 121–137.
6. T. Takala, *Theoretical Framework for Computer Innovative Design*, North Holland, Helsinki, 1987.
7. L. A. Johnson, Designing by Functions, *Design Studies*, Vol. 12, No. 1, 1991, pp. 51–57.
8. E. J. Richards, Noise from Industrial Machines, in *Noise and Vibration*, R. G. White and J. G. Walker, Eds., Ellis Horwood, Chichester, England, 1982, pp. 497–606.
9. R. H. Lyon, *Machinery Noise and Diagnostics*, Butterworths, Boston, 1987.
10. L. L. Beranek and I. L. Ver, Eds., *Noise and Vibration Control Engineering*, Wiley, New York, 1992.
11. M. J. Crocker, Ed., *Handbook of Acoustics*, Wiley, New York, 1998.
12. U. J. Kurze and P. Dietz, *Lärmarm Konstruieren XIII—Schalltechnische Regeln und Konstruktionsmethodik*, Wirtschaftsverlag NW, Bremerhaven, 1985.
13. F. G. Kollmann, *Maschinenakustik*, Springer, Berlin, 1993.
14. M. Dittrich, M. Bockhoff, D. Haje, and U. Trautmann, A Knowledge-Based System for Low Noise Design, Proceedings Euronoise '95, Lyon, 1995.
15. W. Schirmer (Hrsg.), *Technischer Lärmschutz*, 2nd ed., Springer, Berlin, 2006.
16. D. Haje, *Lärmarm Konstruieren XVII—Entwicklung eines Informationssystems zur Konstruktion lärmarmen Produkte*, Wirtschaftsverlag NW, Bremerhaven, 1997.
17. P. Dietz and F. Gummersbach, *Lärmarm Konstruieren XVIII—Systematische Zusammenstellung maschinenakustischer Konstruktionsbeispiele*, Wirtschaftsverlag NW, Bremerhaven, 2000.
18. G. H. Koopmann and J. B. Fahline, *Designing Quiet Structures*, Academic, London, 1997.
19. ISO TR 11688, Acoustics—Recommended Practice for the Design of Low-Noise Machinery and Equipment, Part 1: Planning, Part 2: Introduction into Physics of Low-Noise Design, ISO, Geneva, 1995 and 1997.
20. M. Dittrich, D. Haje, M. Bockhoff, and U. Trautmann, Work Methodology for the Development of Quiet Products, BRITE-EURAM II, Project No. 5983 'EQUIP' (1993–1996), Final Technical Report, TNO Institute of Applied Physics, Delft, The Netherlands, 1997.
21. Noise Abatement Using Concurrent Component—Product Optimisation, GROWTH Program, Project No. GRD1–1999–10785 'NABUCCO' (2000–2002); Project leader: Cetim, Senlis, France.

# CHAPTER 67

## PSYCHOACOUSTICS AND PRODUCT SOUND QUALITY

Malcolm J. Crocker

Department of Mechanical Engineering  
Auburn University  
Auburn, Alabama

### 1 INTRODUCTION

Throughout the twentieth century, engineers have used increasingly sophisticated experimental and theoretical approaches to reduce the noise of machines, vehicles, aircraft, and the like. Since the mid-1980s it has become apparent to manufacturers that it is insufficient simply to reduce overall noise levels. In most cases the noise of vehicles, appliances, and the like has been sufficiently suppressed so that it no longer poses a hearing loss hazard after extended exposure or interferes with speech, sleep, and other activities of occupants. Other properties of the noise, in addition to its overall sound pressure level, such as loudness, frequency content, tonal components, impulsiveness, and level fluctuations may determine whether the quality of the noise is acceptable or not in particular circumstances. Product sound quality studies have been made on household appliances, air-conditioning systems, and high-speed trains, for example, although most attention has been paid to interior vehicle noise.

### 2 BACKGROUND

In the late 1980s engineers began to realize that it is insufficient to pursue the one-dimensional goal of reducing the sound pressure level of the noise of a manufactured product. Attention began to be paid to the time structure and frequency content of noise in addition to its level. The noise output of the product and the auditory events it produces was recognized as being a multidimensional phenomenon. The term *sound quality* was coined.<sup>1</sup>

More recently the term *sound quality* has become linked with the idea of *product quality* and specifically with a class of manufactured products, and the concept of *product sound quality* has been conceived. The discipline of *product sound engineering* has come into existence. Product sound quality may be defined as follows. *Product sound quality is a descriptor of the adequacy (or compatibility) of the sound associated with a particular product.* Product sound quality results from human judgments performed with reference to the desired features of the product, which are apparent to the users in their cognitive, utilization, and emotional situations.<sup>1</sup>

Since the mid-1930s, filters have been used as a simple approach to obtain a quantitative measure that approximates the loudness of sounds. The A-weighting filter has been used extensively for such purposes.

Although it has proved extraordinarily useful, it is an insufficient measure of loudness since it has been derived from loudness judgments of moderately low-level pure-tone sounds at different frequencies, and it does not make allowance for the bandwidth and duration of the different sounds. Noises with the same A-weighted sound pressure level can, of course, sound quite different. If the sound pressure level is high, broadband, impulsive, and/or of a short duration, then use of A-weighting can be inaccurate and even sometimes quite inappropriate.

The majority of studies of sound quality have concentrated on the interior noise of vehicles, and most of the practical examples given in this chapter will be assumed to apply to this problem. It should be realized, however, that much of the discussion that follows may also be applied to other commercial machinery products and domestic appliances.

The goal of most modern sound quality studies is to try to quantify the sound quality of a particular product so that this can be used as a baseline for improving the sound quality of the existing product such as a particular vehicle model. The baseline can also be used for comparisons with the sound quality of other competing products. There are several ways with which quantification of sound quality can be undertaken: (1) exposing subjects to the product's noise under controlled conditions and having subjects evaluate different noise properties and/or rank and then quantify the rankings, (2) recording the product's noise using an artificial head and then asking subjects to evaluate the noise in controlled audiometric conditions with the use of earphones and/or dual loudspeakers in a special room, (3) recording the product noise binaurally with an artificial head and then presenting the noise to listeners with and without electronic modification of the noise to evaluate possible product sound quality improvements, and (4) recording the product noise binaurally with an artificial head and then evaluating the principal sound quality properties of the sound signature using purely electronic means.

This chapter first reviews psychoacoustics aspects of noise, which are important in sound quality evaluations. Then, procedures are outlined for evaluating sound quality using human subjects together with the design of different ways to rank or scale sound quality evaluations. Then, binaural recording of the product noise with an artificial head and playback to subjects

with and without electronic modification and some case histories of various sound quality investigations are described. Finally, evaluating the principal sound quality properties of the sound signature using purely electronic means is reviewed.

### 3 PSYCHOACOUSTICS

For any study of the sound quality of a product to be successful, it is important to have a good understanding of psychoacoustics. Psychoacoustics concerns the human auditory response to sound. To make psychoacoustics of most use in engineering studies, it is desirable to quantify human judgments of various properties of the sound that are most related to its quality. The sound must be presented to the listeners in a carefully controlled manner. Sounds are usually played to listeners either in the real-life situation such as in a moving automobile, or after suitable recording through two loudspeakers, or preferably via two earphones when the listeners are situated in a quiet audiometric room. Fastl has written useful reviews concerning the psychoacoustics needed to have a good understanding of sound quality.<sup>2,3</sup> Several reference books are helpful in obtaining a good understanding of the fundamentals of psychological and physiological acoustics.<sup>4-14</sup>

#### 3.1 Hearing Envelope

Figure 1 presents the auditory field for an average, normal young person who has not suffered any hearing loss or damage. The lower curve represents the hearing threshold, that is, the quietest audible sound at any frequency. The upper curve represents the discomfort threshold, that is, the sound pressure level at any frequency at which there is a sensation of discomfort and even pain in the ears. See also Fig. 1 in Chapter 21 and subsequent discussion there concerning discomfort and pain thresholds.

Speech is mainly in the frequency range of about 250 to 6000 Hz and at sound pressure levels between about 30 to 80 dB at 1 to 2 m (depending upon

frequency). Of course, the sound pressure level of speech can approach 90 dB at about 0.2 to 0.3 m from someone if they are shouting loudly. The sound of vowels is mostly in the low-frequency range from about 250 to 1000 Hz, while the sound of consonants is mainly in the higher frequency range of about 1000 to 6000 Hz. Music is spread over a somewhat greater frequency range and a greater dynamic range than speech. See Chapters 1 and 32. (The dynamic range represents the difference in levels between the lowest and highest sound pressure levels experienced.) See Chapter 35.

#### 3.2 Loudness and Equal Loudness Contours

Sounds discerned to be louder than others are generally judged to be more annoying and less acceptable and thus of poorer sound quality. It must be noted that the human hearing mechanism does not judge different frequency sounds of the same sound pressure level to be equally loud.

Figure 2 shows equal loudness contours. The contours join the sound pressure levels of pure-tone sounds at different frequencies that listeners judge to be equally loud. Each curve is labeled with a number in *phons*, which is the value of each curve's sound pressure level at 1000 Hz. This is because such curves have been obtained by playing pure tones (normally of 1-s duration) at different frequencies to the listeners through earphones and asking them to adjust their sound pressure levels until they appear equally as loud as 1000-Hz pure tones played at the given sound pressure levels.

Figure 17 in Chapter 1 shows the A-weighting filter. This filter has approximately the same shape, except at very low frequency, as a smoothed version of the inverse of the 40-phon curve. Sound pressure level measurements obtained by prefiltering with the A-weighting filter have been used very often since the 1930s to give a single number approximation of human loudness. However, phon curves of higher levels are much flatter than the 40-phon curve and are not represented so well by the A-weighted sound pressure level. Also the A-weighting filter, although conveniently simple to use, has been derived from comparisons of pure-tone sounds at different frequencies. Thus it does not properly take into account the loudness of broadband sounds at different frequencies and the masking effect that these sounds have on each other. Another problem with A-weighting is that it does not allow for the fact that loudness increases with the bandwidth of the noise and also with the duration of the noise event for very short impulsive-type sounds of duration less than about 200 ms.

The concept of the critical band is of fundamental importance in psychoacoustics. It is of concern in studies of loudness, pitch, hearing thresholds, annoyance, speech intelligibility, masking and fatigue caused by noise, phase perception, and even the pleasantness of music. Figure 3 shows the loudness level of bands of filtered white noise centered at 1000 Hz as a function of bandwidth for the different constant sound pressure

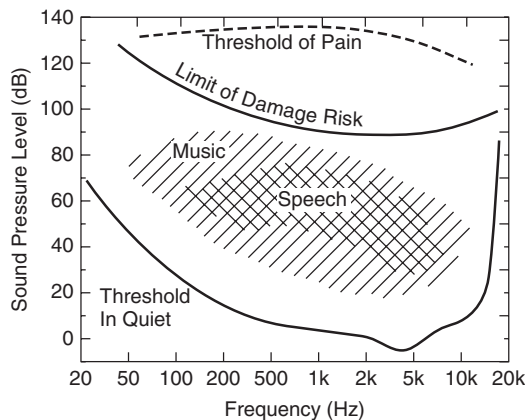
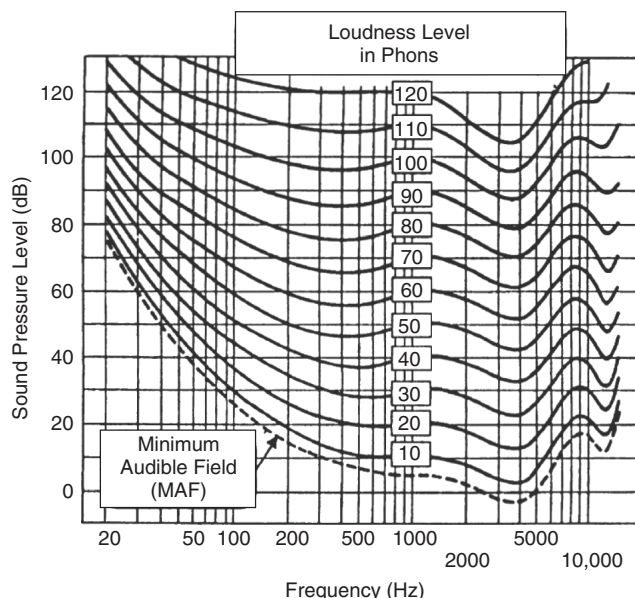
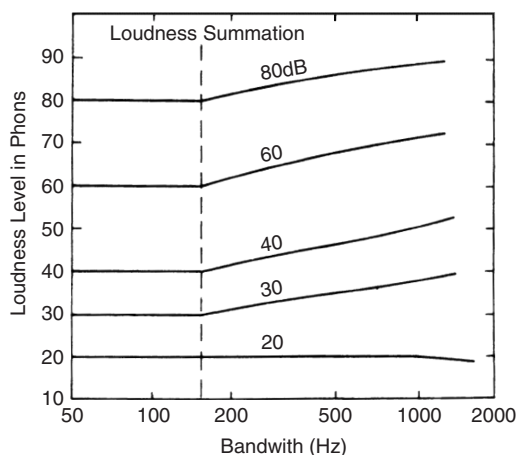


Figure 1 Human auditory field envelope.



**Figure 2** Equal loudness contours. The contours join the sound pressure levels of different frequency pure tones that are judged to be equally loud. The numbers on each contour are the loudness levels in phons.



**Figure 3** Loudness level in phons of a band of filtered white noise centered at 1000 Hz as a function of its bandwidth. The overall sound pressure level of each band of noise was held constant as its bandwidth was increased, and this level is shown on each curve. The dashed line indicates that the bandwidth at which the loudness starts to increase is about the same at all of the levels tested, except for the lowest level for which no increase in loudness occurs. (From Ref. 15; used with permission.)

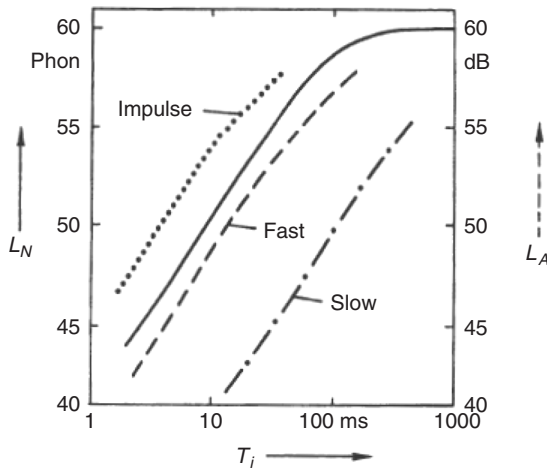
levels shown on each curve. The curves were obtained by a matching procedure in which listeners equated the loudness of a 1000-Hz pure tone with bands of noise

of increasing bandwidth. The level at which the pure tone was judged to be equal in loudness to the band of noise is shown as the ordinate. Thus the curves do not represent equal loudness contours, but rather they show how the loudness of the band of noise centered at 1000 Hz changes as a function of bandwidth. The loudness of a sound does not change until its bandwidth exceeds the so-called critical bandwidth. The critical bandwidth at 1000 Hz is about 160 Hz. (Notice that, except for sounds of very low level of about 20 phons, for which loudness is almost independent of bandwidth, the critical bandwidth is almost independent of level and that the slopes of the loudness curves are very similar for sounds of different levels.) (See Chapter 91 in the *Handbook of Acoustics*.<sup>15a</sup>) Critical bands are discussed further in Section 3.4 of this chapter.

The solid line in Fig. 4 shows that sounds of very short duration are judged to be very quiet and to become louder as their duration is increased. However, once the duration has reached about 100 to 200 ms, then the loudness level reaches an asymptotic value. Also shown by broken lines in Fig. 4 are A-weighted sound pressure levels recorded by a sound level meter using the “impulse,” “fast,” and “slow” settings. It is observed that the A-weighted sound pressure level measured by the fast setting on the sound level meter is closest of the three settings to the loudness level of the sounds.

### 3.3 Masking

The masking phenomenon is well known to most people. A loud sound at one frequency can cause



**Figure 4** Dependence of loudness level  $L_N$  (left ordinate) on duration  $T_i$  of 1-kHz tone impulses of constant sound pressure level compared with measurements of A-weighted sound pressure level  $L_A$  (right ordinate) using the time constants "impulse," "fast," or "slow."<sup>2</sup>

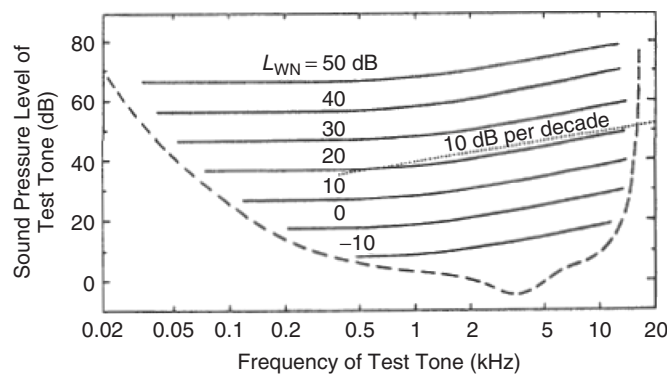
another quieter sound at the same frequency or a sound close in frequency to become inaudible. This effect is known as *masking*. Broadband sounds can have an even more complicated masking effect and can mask louder sounds over a much wider frequency range than narrow-band sounds. These effects are important in human assessment of product sound quality. Noise that contains pure tones is generally annoying and unpleasant. In the case of automobile interior noise, engine and exhaust system noise consists mostly of fundamental pure tones together with integer multiples and broadband engine combustion noise. Similarly cooling fan noise consists of pure tones and broadband aerodynamic fan noise. In the case of automobiles, exhaust and cooling fan noise have some strong pure-tone components. Wind noise and tire noise are mostly

broadband in nature and can mask some of the engine, exhaust, and cooling fan noise, particularly at high vehicle speed.

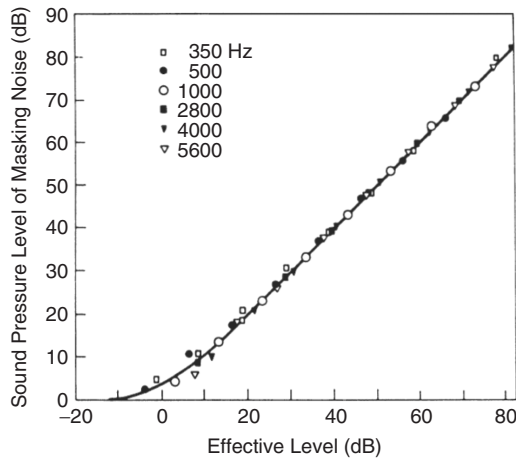
Figure 5 shows the masking effect of broadband white noise. The solid lines represent the sound pressure level of a pure test tone (given in the ordinate) that can just be heard when the masking sound is white noise at the level shown on each curve. For example, it is seen that white noise at 40 dB masks pure tones at about 55 dB at 100 Hz, 60 dB at 1000 Hz, and 65 dB at 5000 Hz.

The masking of noise has been studied extensively for more than 70 years. The curves in Fig. 5<sup>2,4</sup> are very similar to those of much earlier research work by Fletcher and Munson in 1950 but are shown here since they have been extended to lower and higher frequencies than these earlier published results.<sup>9</sup> One interesting fact is that the curves shown in Fig. 5 are all almost parallel and are separated by about 10-dB intervals, which is also the interval between the masker levels. This suggests that the masking of noise is almost independent of level at any given frequency. This fact was also established by Fletcher and Munson in 1950 as is shown in Fig. 6.<sup>16</sup> Here the amount of masking is defined to be the upward shift in decibels in the baseline hearing threshold caused by the masking noise.<sup>9</sup> Figure 5 shows that once the masker has reached a sufficient level to become effective, the amount of masking attained is a linear function of the masker level. This means, for instance, that a 10-dB increase in the masker level causes a 10-dB increase in the masked threshold of the signal being masked. It was found that this effect is independent of the frequency of the tone being masked and applies both to the masking of pure tones and speech.<sup>9,16</sup>

Figure 7 shows the masking effect of a narrow-band noise of bandwidth 160 Hz centered at 1000 Hz. The curves in Fig. 7 join the sound pressure levels of test tones that are just masked by the 1000-Hz narrow-band noise at the sound pressure level shown on each curve. It is observed that the curves are symmetric around 1000 Hz for low levels of the narrow-band noise, while



**Figure 5** Contours joining sound pressure levels of pure tones at different frequencies that are masked by white noise at the spectral density level  $L_{WN}$  shown on each contour.<sup>2,4</sup>



**Figure 6** Masking of tones by noise at different frequencies and sound pressure levels.<sup>16</sup> Reprinted with permission from *J. Acoust. Soc. Am.*, 1950, Vol. 22, pp. 6–13, American Institute of Physics.

for high levels, the curves become asymmetric. It is seen that high levels of the narrow band of noise mask high-frequency tones much better than low-frequency tones. Figures 5 and 7 show that using either white noise or narrow-band noise it is more difficult to mask low-frequency than high-frequency sounds. This fact is of some importance in evaluating the sound quality of a product since it is of no use to reduce or change the noise in one frequency range if it is masked by the noise at another frequency.

There are other masking effects that are not normally as important for sound quality evaluations as the frequency effects discussed so far but still need

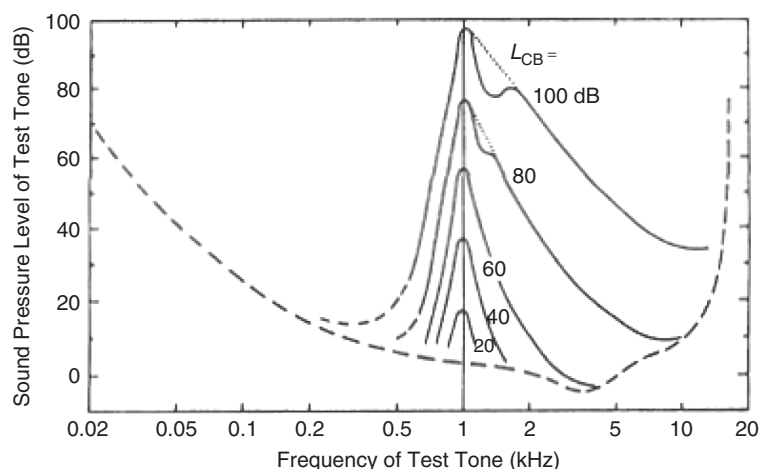
to be described.<sup>1–14</sup> When a masking noise stops, the human hearing system is unable to hear the primary sound signal immediately. This effect is known as postmasking (and is sometimes also known as forward masking.) The time it takes for the primary sound to be heard (normally called the delay time,  $t_d$ ) depends both upon the sound pressure level of the masking noise and its duration. Figure 8 shows how the primary sound is affected by different sound pressure levels of the masking noise. Also shown in Fig. 8 are dashed lines that correspond to an exponential decay in level with a time constant  $\tau$  of 10 ms. It is observed that the human hearing mechanism decay is not exponential, but rather that it is nonlinear and that the decay process is complete after a decay time of about 200 ms. This fact is of practical importance since some vehicle and machinery noise is quite impulsive in character such as caused by diesel engines, automobile door closings, brake squeal, warning signals, or impacts that may mask the sounds of speech or other wanted sounds.

Figure 9 shows how sounds are affected by different durations of the masking noise. Figure 9 presents the level of a just-audible 2-kHz test tone  $L_T$  as a function of delay time.

### 3.4 Critical Bands

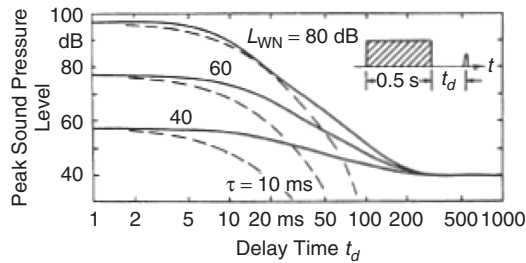
Another important factor is the way that the ear analyzes the frequency of sounds. The critical band concept already discussed in Section 3.2 is important here as well. It appears that the human hearing mechanism analyzes sound like a group of parallel frequency filters. Figure 10 shows the bandwidth of these filters as a function of their center frequency. These filters are often called *critical bands* and the bandwidth each possesses is known as its *critical bandwidth*.

As a band of noise of a constant sound pressure level increases in bandwidth, its loudness does not increase until the critical bandwidth is exceeded, after



**Figure 7** Masking effect of a narrow-band noise of bandwidth 160 Hz centered at 1000 Hz. The contours join sound pressure levels of pure tones that are just masked by the 1000-Hz narrow-band noise at the sound pressure level shown on each contour.<sup>2,4</sup>

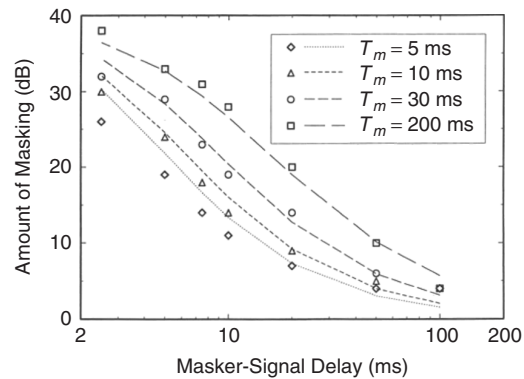




**Figure 8** Postmasking at different masker sound pressure levels.<sup>2</sup>

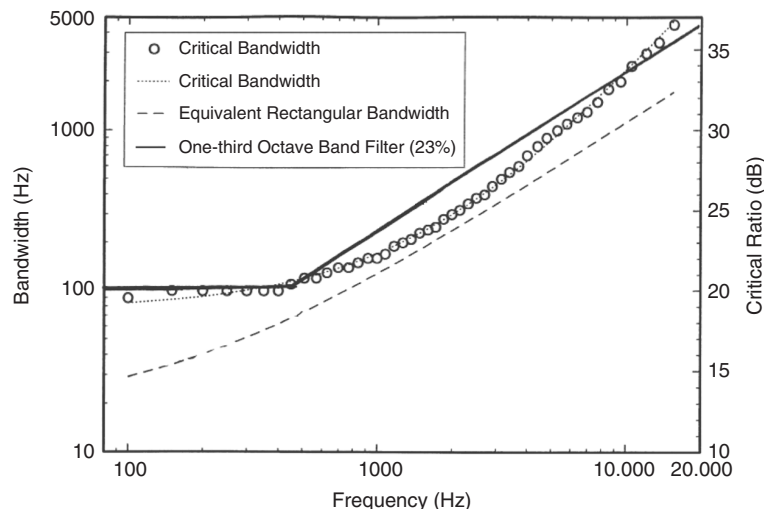
which the loudness continually increases. Thus the critical band may be considered to be that bandwidth at which subjective responses abruptly change.<sup>11</sup> It is observed that up to 500 Hz the critical bandwidth is about 100 Hz and is independent of frequency, while above that frequency it is about 21% of the center frequency and is thus almost the same as one-third octave band filters, which have a bandwidth of 23% of the center frequency shown by the solid line. (See Chapter 1.) This fact is also of practical importance in sound quality considerations since it explains some of the masking phenomena observed.

The *critical ratio* shown in Fig. 10 originates from the early work of Fletcher and Munson in 1937.<sup>11</sup> They conducted studies on the masking effects of wide-band noise on pure tones at different frequencies. They concluded that a pure tone is only masked by a narrow critical band of frequencies surrounding the tone, and that the power (mean-square sound pressure) in this band is equal to the power (mean-square sound pressure) in the



**Figure 9** Postmasking of 5-ms, 2-kHz tones preceded by bursts of uniform masking noise are plotted as a function of the delay between masker and signal offsets. The parameter is masker duration  $T_m$  as indicated. The symbols are data from Zwicker.<sup>17</sup> Reprinted with permission from *J. Acoust. Soc. Am.*, 1984, Vol. 75, pp. 219–223, American Institute of Physics.

tone.<sup>11</sup> From these assumptions the critical band can easily be calculated. From these assumptions, the critical bandwidth (in hertz) is defined to be the ratio of the sound pressure level of the tone to sound pressure level in a 1-Hz band (i.e., the spectral density) of the masking noise. This ratio is called the critical ratio to distinguish it from the directly measured critical band.<sup>11</sup> A good correspondence can be obtained between the critical band and the critical ratio by multiplying the critical ratio by a factor of 2.5. The critical ratio is given in decibels in Fig. 10 and is shown by the broken line.



**Figure 10** Critical bandwidth, critical ratio, and equivalent rectangular bandwidth as a function of frequency. (○) Critical bandwidth from Zwicker<sup>18</sup> is compared to the equivalent rectangular bandwidths according to a cochlear map function (---) (dashed line). (Based in part on Ref. 19.)



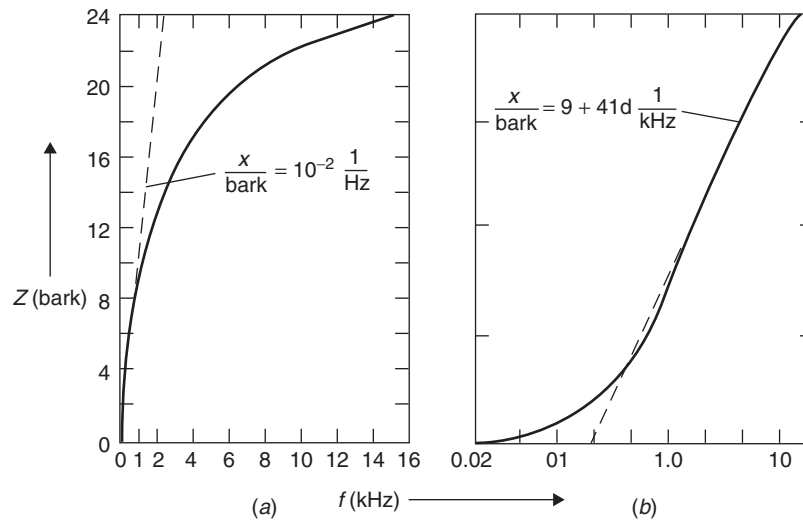


Figure 11 Relations between bark scale and frequency scale.<sup>2,4</sup>

### 3.5 Frequency (Bark)

It is well known from music that humans do not hear the frequency of sound on a linear scale. A piano keyboard is a good example. For each doubling of frequency (known as an octave), the same distance is moved along the keyboard in a logarithmic fashion. If the critical bands are placed next to each other, the bark scale is produced. The unit *bark* was chosen to honor Barkhausen. Figure 11 illustrates the relationship between the bark ( $Z$ ) as the ordinate and the frequency as the abscissa; on the left (Fig. 11a), frequency is given using a linear scale, and on the right (Fig. 11b) the frequency is given with a logarithmic scale. Also shown in Fig. 11 are useful fits for calculating bark from frequency. At low frequency a linear fit is useful (Fig. 11a), while at high frequency a logarithmic fit is more suitable. (Fig. 11b).

One advantage of the bark scale is that, when the masking patterns of narrow-band noises are plotted against the bark scale, their shapes are largely independent of the center frequency, except at very low

frequency. (See Fig. 12.) Care should be taken to note that the ear does not hear sounds at a fixed number of fixed center frequencies as might be suspected from Fig 12. Rather at any frequency  $f_m$  considered, the average ear has a given bandwidth.

### 3.6 Zwicker Loudness

The loudness of sounds was discussed in Section 3.2 where it was shown that A-weighted sound pressure level measurements underestimate the loudness of broadband noise. (See Fig. 3.) Methods to evaluate the loudness of broadband noise based on multiband frequency analysis have been devised by Stevens,<sup>20</sup> Kryter,<sup>14</sup> and Zwicker.<sup>21</sup> The Stevens' method was originally based on octave band analysis, but Kryter's and Zwicker's methods are based on one-third octave band analysis. Kryter's method has been standardized for aircraft certification noise measurements, while Zwicker's method has been standardized internationally and is most normally used to evaluate the

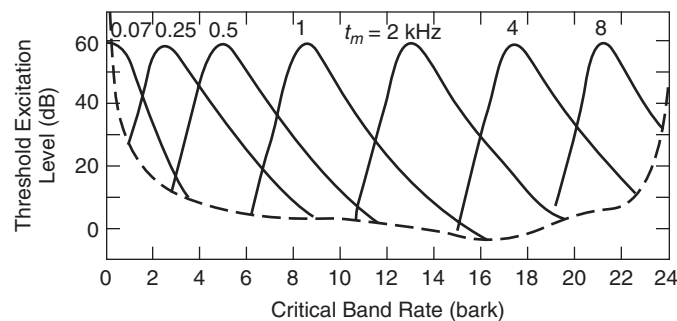


Figure 12 Masking patterns<sup>2,4</sup> of narrow-band noises centered at different frequencies  $f_m$ .

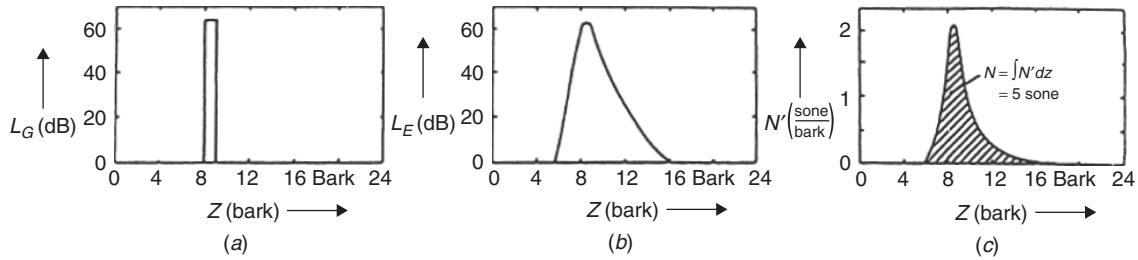


Figure 13 Schematic illustration of Zwicker's loudness model.<sup>2-4</sup>

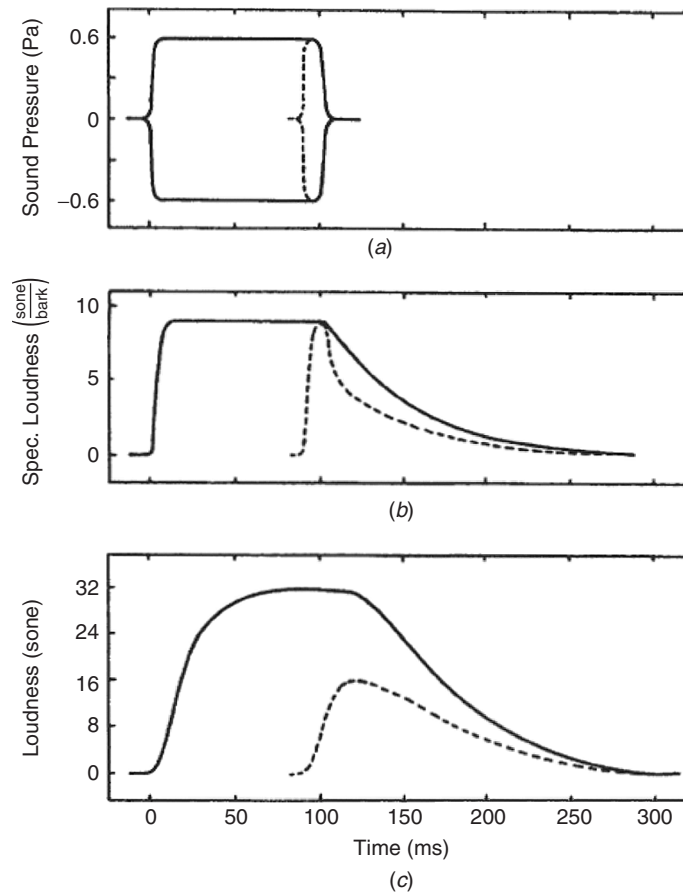


Figure 14 Illustration of temporal effects in loudness processing.<sup>2,4</sup>

loudness of many common sound sources including speech, music, machinery, and vehicles.

The procedure to evaluate loudness using Zwicker's method is shown in Fig. 13. Figure 13a shows a narrow band centered at 1000 Hz, which corresponds to 8.5 bark. Figure 13b shows the narrow band of noise at 1000 Hz, including masking effects caused by spectral broadening in the cochlea due to inner

ear mechanics. Figure 13c shows the specific loudness/critical band rate pattern (sone/bark), known as the *Zwicker diagram*. The transition from the masking pattern in Fig. 13b to the loudness pattern in Fig. 13c can be considered to be obtained by simply taking the square root of the sound pressure or the fourth root of the sound intensity. The shaded area in Fig. 13c is directly proportional to the perceived loudness.

While Fig. 13 illustrates the spectral process of obtaining the perceived loudness of a sound by the Zwicker method, Fig. 14 shows the process including temporal effects. Figure 14a shows two impulses in the time domain, one with a broken line of 10-ms duration and the other with a solid line of 100-ms duration. As discussed earlier in connection with Fig. 3, very short duration pulses of noise are perceived to be quieter than longer ones up to a duration of about 100 to 200 ms. Figure 14 is constructed by assuming that the hearing mechanism behaves like a parallel bank of 24 critical band filters. Figure 14b represents the processing of the loudness in each of the 24 channels of an empirical *loudness meter* used to model the hearing mechanism. Finally, Fig. 14c shows the time dependence of the total loudness summed up over all 24 channels of the empirical loudness meter. Figure 14b shows that the short 10-ms tone burst decays much more rapidly than the 100-ms tone burst. The results shown in Figs. 13 and 14 are important in evaluating the sound quality of machinery that has impulsive noise components, such as diesel engines and machines in which impacts occur.

### 3.7 Loudness Adaptation

The term *loudness adaptation* refers to the apparent decrease in loudness that occurs when a subject is presented with a sound signal for a long period of time. The effect has been studied extensively by presenting tones for an extended period of time to one ear and then allowing the subject to adjust the level of a second comparison tone of the same frequency to the other ear. Such experiments have demonstrated

that loudness adaptation of as much as 30 dB can be observed for very quiet sounds below 30 dB and much less for louder sounds of the order of 70 dB. However, other research has shown that loudness adaptation is reduced or even absent when binaural interactions are minimized. Recent research has shown that loudness adaptation is quite complicated. It varies from person to person. More adaptation occurs for very quiet sounds of about 30 dB and for high-frequency tones than for low-frequency tones or noise.<sup>9</sup> This phenomenon is obviously of interest to those concerned with sounds such as interior vehicle noise, that people experience over an extended period.

### 3.8 Empirical Loudness Meter

Figure 15 shows a block diagram of an empirical Zwicker-type dynamic loudness meter (DLM) that includes the spectral and temporal loudness processing portrayed in Figs. 13 and 14.<sup>3</sup> First, the *spectral processing* (1 and 2) shown in Fig. 14 using the critical band filter bank concept, *upward spread of masking* (7), and *spectral summation* (8) are illustrated. Second, the *temporal processing* discussed in relation to Fig. 14 is observed as shown in the blocks marked *envelope extraction*, *postmasking*, and *temporal integration* (see steps 3, 6, and 9.) Lastly and of most importance is step 5 (labeled *loudness transformation*), which represents the fact that the loudness is assumed to be proportional to the square root of the sound pressure (or the fourth root of the sound intensity. (See Fig. 13c.)

One advantage of the DLM discussed and shown in Fig. 15 is that, by suitable modification of the DLM

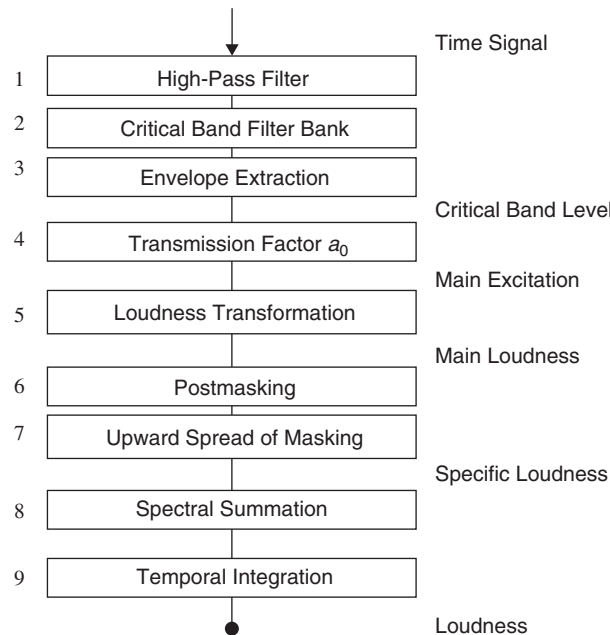
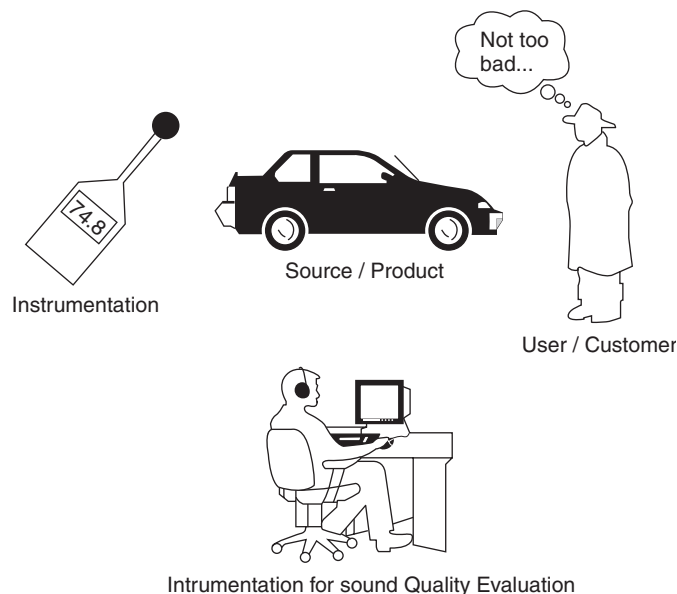


Figure 15 Block diagram of the dynamic loudness model (DLM).<sup>72</sup>



**Figure 16** Sound quality evaluation by humans (*right*), standard instrumentation (*left*), and instrumentation for sound quality evaluation (*bottom*).<sup>27</sup>

loudness transformation (step 5), the loudness perception of both normal hearing and hearing impaired subjects can be simulated.<sup>3</sup> This fact is important since the aging population in industrialized countries has suffered varying degrees of hearing impairment that should be allowed for in sound quality simulations. Some fraction of the younger population may have suffered mild to moderate hearing loss because of exposure to intense noise during recreational or leisure time activities.<sup>3</sup>

#### 4 SOUND QUALITY EVALUATION

Whenever we listen to the sound of a mechanical product, we form an opinion about its sound quality. (See the right side of Fig. 16.) Our reactions may be, to some extent, unconscious and our opinions influenced by visual impressions, other cues and expectations, and by previous experience.

While a single measurement of the A-weighted sound pressure level may be an adequate measure of the product for regulatory purposes (see the left side of Fig. 16), more elaborate approaches and measures are required for sound quality evaluations. (See the bottom of Fig 16.) Such sophisticated procedures for sound quality assessments and use of dedicated instrumentation have the advantage that (1) experiments can be carefully controlled and standardized so that they can be repeated by others, (2) different attributes of the product's sound signature can be properly evaluated, and (3) the product's sound signature information and measured results can be used to modify and/or redesign its sound signature as necessary.

Subjective evaluation of the sound quality of a product is normally found by exposing a panel of

listeners, or a jury, to the sound of the product and then asking them to make individual subjective responses on an appropriate scale, which are then averaged. Such evaluations usually consist first of the measurement and recording of the sound of the product. This is followed by the subjective ratings of the jury of the original recording and then of a suitably processed recording of the sound (either monaural or binaural). For example, by editing out a particular tone or part of the spectrum, it is possible to determine whether or not the edited version of the sound improves the perceived sound quality of the product. If the sound quality is improved by such changes, then engineering modifications can be sought to accomplish the new sound signature by quieting and/or appropriately modifying the responsible noise source(s).

Various psychoacoustic metrics such as loudness, noisiness, sharpness, and fluctuation strength have been developed to assist in predicting sound quality. Some researchers such as Lyon believe that these psychoacoustic metrics, although useful in scaling certain features of the sound of a product, still need further development to predict the acceptability of the sound quality of a product. Consequently, Lyon suggests that emphasis should currently be concentrated on the determination of sound quality through the assessment of subjective jury evaluations.<sup>22-25</sup>

Otto et al.<sup>26</sup> and Fastl<sup>3</sup> have discussed the use of jury tests to evaluate the sound quality of products, in particular automobiles. There are several different types of jury tests that have been used for many years to evaluate the sounds of different products, such as loudspeakers, electric clocks, and other appliances. In recent years these jury tests have been adapted for

use in evaluating the sound quality of automobiles. A jury test means that the test is conducted using a group of individuals instead of just one. There are a large number of jury tests in use in sound quality evaluations. We will concentrate here on some of the most common tests.<sup>3,26</sup>

#### 4.1 Paired Comparison Tests

Paired comparison tests involve the presentation of two sounds to each human subject. The subjects are then asked to give relative judgments on the sounds of each pair.<sup>26</sup> Various relative sound evaluations can be made. Three of these will be described here. First, in a *detection task* the subject is asked to decide which of the two sounds contains the signal to be detected. This type of test is useful to determine detection thresholds of a sound signature, for example, if a discrete frequency (tone) is buried in broadband noise. Second, an *evaluation task* involves the subject evaluating which pair of sounds possesses more or less of a certain attribute such as loudness, annoyance, pleasantness, and the like. Lastly, a *similarity task* requires the subject to decide which of the pairs of sounds are most similar to each other. This type of task can be used, together with multidimensional analysis and clustering studies, to determine which properties of a sound signature are important and/or unimportant in forming reliable judgments of the sound quality of a product.<sup>26</sup>

#### 4.2 Random-Access Ranking Procedure

In the random-access ranking procedure, the subject is asked to rank order  $N$  sounds from 1 to  $N$ , where  $N$  is the number of sounds.<sup>26</sup> This is one of the simplest sound quality evaluation procedures. It largely avoids the biasing that some of the other procedures may produce. Although the sounds are presented in an initial sequence, the subject is allowed to access each sound as many times as desired by clicking an icon, such as the loudspeaker icon in Fig. 17, and eventually to form a final judgment. To avoid too much complexity in the task, the number of sounds to be compared and ranked is normally kept to be less than five or six.<sup>3,26</sup> The freedom of the subject to choose the sounds in some random fashion and thus eliminate the influence of the person conducting the test makes this procedure preferred by many testing organizations. It does have the disadvantage, however, that since there is no scale obtained in the final result, that the sounds cannot be correlated with any objective sound quality attributes in the final analysis.<sup>26</sup>

#### 4.3 Semantic Differential Procedure

While the paired comparison test only considers one attribute, the semantic differential procedure considers many different attributes of a sound. The subject is asked to evaluate a sound signature using a number of bipolar pairs of adjectives as shown in Fig. 18. The two adjectives are normally antonyms and lie at the two ends of a scale with several gradations. Usually,

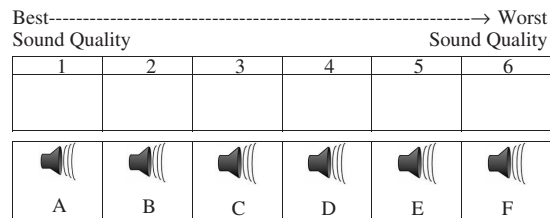


Figure 17 Example for ranking of the sound quality by the method random access.

Adjective Scales	
Loud	Soft
Deep	Shrill
Frightening	Not Frightening
Pleasant	Unpleasant
Dangerous	Safe
Hard	Soft
Calm	Exciting
Bright	Dark
Weak	Powerful
Busy	Tranquil
Conspicuous	Inconspicuous
Slow	Fast
Distinct	Vague
Weak	Strong
Tense	Relaxed
Pleasing	Unpleasing

Figure 18 Semantic differential scale.<sup>72</sup>

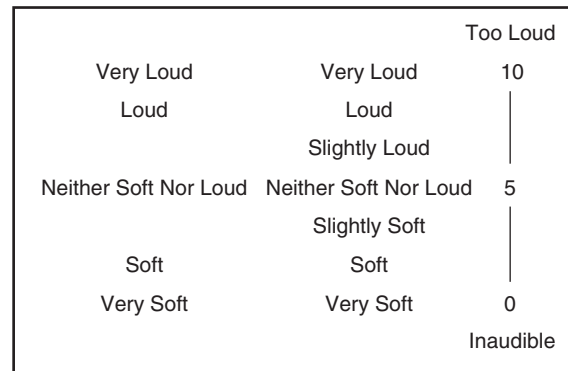
five, seven, or nine gradations are used between each adjective pair.<sup>3,8</sup>

#### 4.4 Category Scaling

Category scaling is often used when one attribute such as loudness needs to be evaluated.<sup>26</sup> Figure 19 shows a 5-step scale on the left and also a 7-step scale in the middle. In the middle of Fig. 19, the 7-step scale is further subdivided into 10 or more subcategories on the right, if a finer loudness evaluation is desired.<sup>3</sup>

#### 4.5 Magnitude Estimation

In the magnitude estimation procedure, two sounds are compared.<sup>3,26</sup> One of the sounds, A, is fixed and normally termed the anchor sound. The magnitude of the second test sound, B, must be decided by the subject. Usually loudness is chosen as the attribute to be considered, but another attribute such as annoyance can be chosen instead. The anchor sound, A, is usually given a value such as 100, and the subject is asked to evaluate the test sound and to give it a relative ranking greater or smaller than the anchor sound. The advantage of this procedure is that there is no ceiling fixed for the test sound.

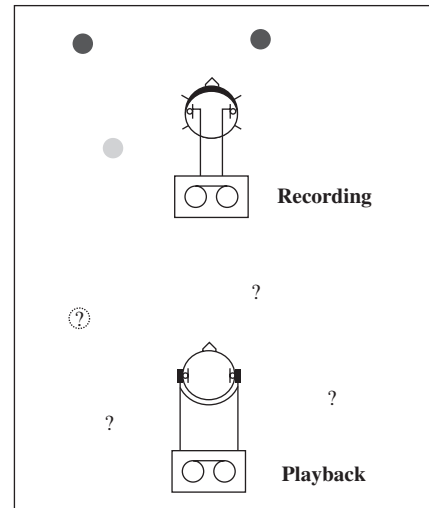


**Figure 19** Category scaling with five categories (left), seven categories (*middle*), and 10 subcategories (right).

## 5 RECORDING AND PLAYBACK

Recording of the product sound to be evaluated is often undertaken for later evaluation and product sound quality improvement. It is important to note that, for proper reproduction of product sound signatures, binaural recordings should be made. Most researchers emphasize the fact that single-channel recordings are normally inadequate, and binaural recordings are preferred for sound quality evaluations. Great care must be taken with such sound recordings so that distortion is avoided and that the reproduction of the sounds presented to the subjects is as faithful as possible to the original. For this purpose, microphones are sometimes located in both ear canals of a human subject and/or at both the eardrum positions of an artificial head. In playback, care must be taken to maintain the proper magnitude and phase difference between the two channels. Since the head, pinna, ear canal, and torso geometries and properties vary from person to person, dummy heads can only be made to represent statistically averaged geometries and properties of people. Several different dummy heads are available commercially, and they are made to meet standards such as International Electrotechnical Commission (IEC) 959, in which basic human characteristics are defined. Figure 20 illustrates the fact that during playback the subject must be able to sense that the sound source is in the same physical location as during the initial recording.<sup>27</sup>

For very low frequency product sound signatures, multichannel recordings may become necessary. At very low frequency, the sound is sensed by the human body as vibration as well as sound sensed by the ears. In cases where significant low-frequency components are present in the sound signature, some attempts have been made to give a realistic feeling for these components by the use of additional bass loudspeakers or woofers.<sup>27</sup> Some commercially available software tools allow for multichannel recordings not only of the binaural sound recordings, but of engine revolution/minute (rpm), vehicle speed, air temperature, and the like.



**Figure 20** Principle of binaural recording (*top*) and playback (*bottom*). In ideal conditions the different auditory events in the recording situation (*top*, filled circles) are perceived in the playback situation at exactly the same locations (*bottom*, open circles). Under nonideal circumstances different aspects might result in localization errors.<sup>27</sup>

It is normal procedure to convert the sound signals acquired from analog to digital form and then to store them on digital tape or more commonly directly onto a computer hard drive. These signals can then be played back to subjects through loudspeakers or earphones. Earphones are generally recognized as providing a more realistic representation of the original product sound. Recorded signals can also be analyzed, processed, and modified and then played back to subjects in modified form to try to determine the properties and qualities of the product sound signature that makes the sound more acceptable and pleasant for subjects. Many attempts have also been made to



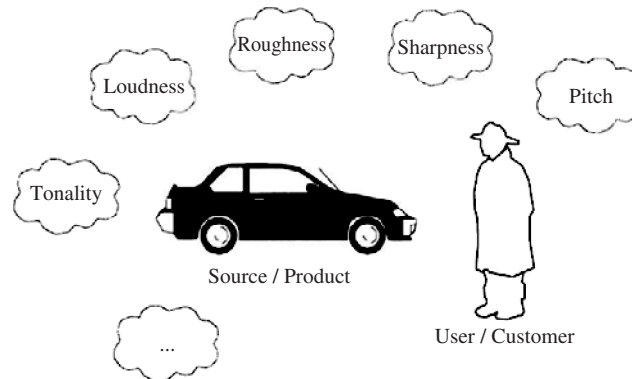


Figure 21 Pool of psychoacoustic quantities.<sup>27</sup>

analyze the recorded sounds and then, without the use of human subjects, to try to identify the most important properties of the sounds that contribute to sound quality.

Although A-, B-, and C-weightings give some initial impressions of the loudness and frequency content of a sound, are simple to use and are well known, they are generally recognized as being inadequate for sound quality research.<sup>27</sup> As already discussed, sound pressure level, loudness, frequency content, level fluctuation, pure-tone components, and impulsiveness are known to be important attributes of the quality of sound.

Auditory events can be broken down arbitrarily into a set of main categories. Figure 21 illustrates some of the psychoacoustical properties of sound that are known to affect sound quality. Of these, loudness, roughness, and sharpness are thought to be some of the most important properties in the case of automobile sound. Unfortunately, the quantitative calculation of most of these sound quality properties has not been internationally agreed upon, with the exception of Zwicker loudness.<sup>2,3</sup>

In most sound quality work, a target sound is chosen for the product. Efforts are then made to design and modify the product to achieve the target sound. See Fig. 22. Editing of the sound using filtering and other techniques, use of subjective sound quality evaluations, and suitable changes are made to the physical characteristics of the source in an attempt to achieve the target sound as shown in Fig 23.

Hardware and software have been developed to try to evaluate and calculate some sound quality attributes only by the use of signal processing of the sound signature of the product. Some specific hardware systems for sound quality calculations exist. It is possible, however, simply to operate some other commercially available software systems on most standard personal computers.<sup>27</sup> Both closed and open software systems exist. Some *stand-alone* systems, which are commercially available, include fixed procedures for the calculation of the sound quality properties, such as loudness, roughness, sharpness, and the like, and

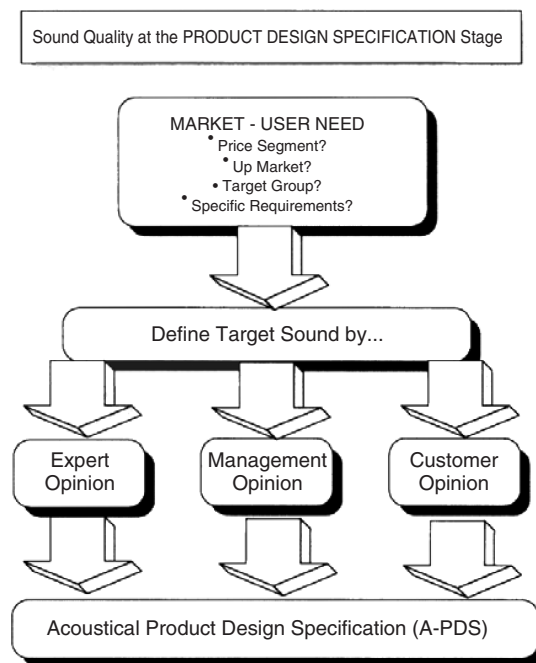
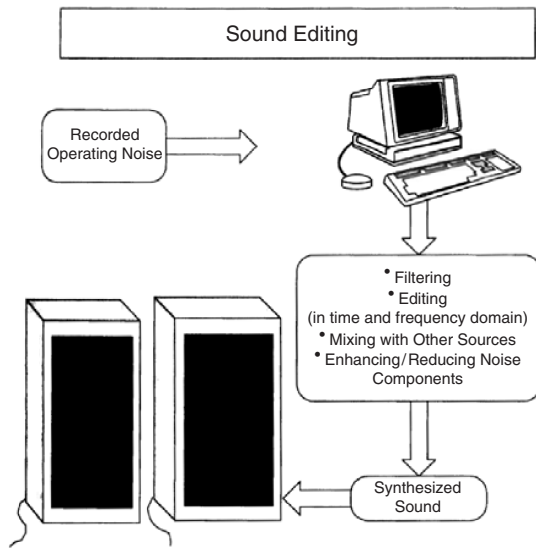


Figure 22 Target setting for sound quality.<sup>28</sup>

that do not allow these calculation procedures to be changed. Other systems are classified as *semiopen* and allow some formulas to be imported for calculations of some of these quantities. There are also systems, classified as *completely open*, that allow all of the calculation procedures for these properties to be imported. So far international organizations have only agreed upon the loudness property calculation.

Instrumentation and software for sound quality evaluation is still under continuous development. Some companies and institutes involved in sound quality research use their own software and methods



**Figure 23** Simulation of “preferred sound” by editing the recorded operating noise.<sup>28</sup>

to calculate sound quality. Others use commercially available software.

## 6 FURTHER PSYCHOACOUSTIC QUALITIES

### 6.1 Sharpness

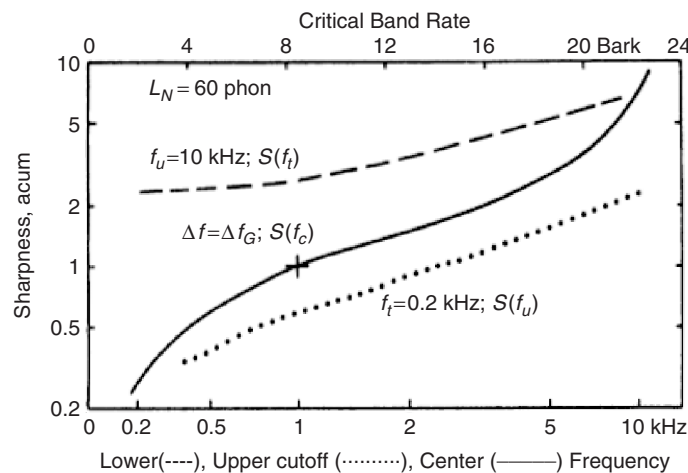
If the sound of a product has the right amount of *sharpness*, it can sound powerful; but if it has too much sharpness, it can sound harsh and unpleasant. As the word suggests, *sharpness* is a measure of the high-frequency content of sound. If one sound signal has more high-frequency content than another, it is said to have more *sharpness* than the other.

Figure 24 gives an indication of the dependence of sharpness on frequency content; the solid line represents the sharpness of narrow bands of noise with bandwidths of 1 bark.<sup>2,3</sup> The perceived sharpness is seen to increase as the band center frequency is increased. The broken line in the upper part of the figure shows the sharpness of high-pass filtered noise as a function of cutoff frequency, while the dotted curve presents the perceived sharpness of low-pass filtered noise as the cutoff frequency is changed. As shown by the upper broken curve, when the cutoff frequency of the high-pass filtered sound is decreased, the sound has reduced sharpness and sounds less harsh. This has implications for the sound quality of products. If some low-frequency sound is added to a harsh sounding product, the resulting sound will normally sound less harsh.<sup>7</sup> Of course, the loudness level of the resulting product sound will increase as well to some extent, but that may be acceptable if the product's loudness level is not very high at the outset. As the dotted curve shows, when the cutoff frequency of low-pass filtered noise is increased, it sounds sharper and it will, of course, also sound louder.

Figure 25 shows a model for sharpness. In Fig. 25a, the spectral distribution of a narrow-band noise (solid line), a broadband noise (broken line and dashed area), and a high-pass filtered noise (dotted line and cross-hatched area) are shown. The sharpness model corresponds to Fig. 13. In Fig 25b, the arrows indicate the center of gravity of the loudness patterns.<sup>2,3</sup> The higher frequencies are perceived to have more sharpness and are boosted by a weighing function,  $g$ .

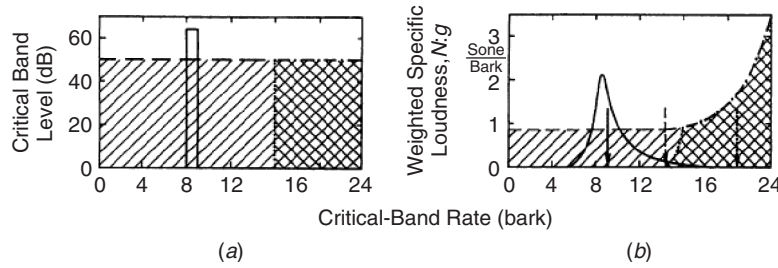
### 6.2 Fluctuation Strength

Another important psychoacoustic attribute is fluctuation strength. Sound that has a strong time-dependent fluctuation in sound pressure level,  $L_T$ , is more annoying than sound that has a steady sound pressure level. Experiments show that the fluctuation strength,



**Figure 24** Sharpness of narrow-band noise (solid), high pass noise (dashed), and low-pass noise (dotted).<sup>2</sup>





**Figure 25** Model of sharpness for narrow-band noise (solid), broadband noise (dashed), and high-pass noise (cross hatched).<sup>2,3</sup>

$F$ , possesses a bandpass character and has a maximum value for sounds with a modulation frequency of about 4 Hz. This fact is true for both amplitude and frequency-modulated sounds.<sup>2,3</sup> The fluctuation strength depends upon the modulation depth,  $\Delta L$ , and sound pressure level  $L_T$ . If the modulation depth is less than 3 dB, the fluctuation strength is zero. The fluctuation strength increases approximately linearly for greater values of  $L_T$ . For a level increase of about 40 dB, the fluctuation strength increases by a factor of 3. More details of fluctuation strength estimation are given by Zwicker and Fastl in Ref. 2 and 4.

One formula used to calculate the fluctuation strength,  $F$ , is given in Fig. 26. The hatched areas within the thin solid lines represent the time-dependent variation of the sound pressure level of the sound. The thick solid line represents the time-dependent masking pattern. Because of postmasking effects, the ear is unable to hear the sound properly in the very “quiet” valleys. So far no universal agreement has been obtained on this or any other formula for the calculation of fluctuation strength.

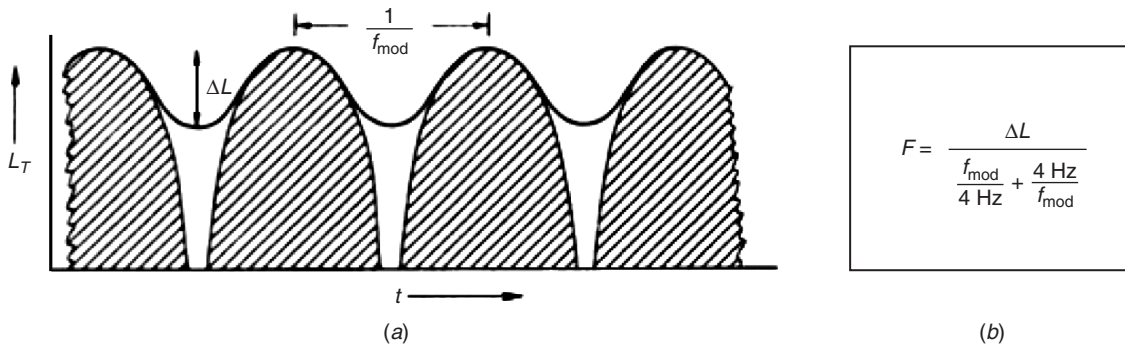
### 6.3 Roughness

If the modulation time period  $1/f_{\text{mod}}$  becomes very small, and the modulation frequency is more than about 20 Hz, the fluctuating strength is termed *roughness* as is shown in Fig. 27. The roughness of a sound

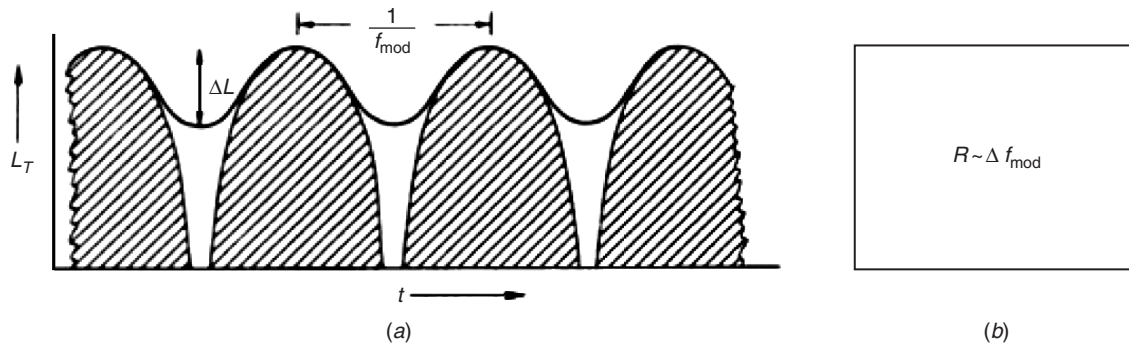
is found to be a maximum when the modulation frequency is about 70 Hz. This is true for both narrow-band and broadband sounds. Roughness depends upon the modulation depth,  $\Delta L$ , and sound pressure level  $L_T$ . An approximate relationship for roughness,  $R$ , is also given in this figure. For a level increase of 40 dB, the roughness increases by a factor of about 3. The roughness also increases with the sound pressure level  $L_T$ . More details about roughness calculations are given by Zwicker and Fastl in Refs. 2 and 4.

## 7 EXPERIMENTAL AND SYNTHESIS RESULTS

Further work continues on sound quality research using jury evaluations and electronic modification, synthesis, and evaluation of sound product signals.<sup>26,29-74</sup> A considerable amount of research on this subject has been conducted in Germany.<sup>1-3,27-37</sup> Most of this research work has concentrated on interior vehicle sound quality. Researchers in many other countries have also conducted research on vehicle sound quality<sup>38-62</sup> or on the sound quality of vehicle components, such as exhaust systems,<sup>41</sup> transmissions,<sup>42,43</sup> doors,<sup>44</sup> and on specific attributes of vehicle sound quality. Some others have conducted sound quality studies on off-road vehicles<sup>62</sup> and electric vehicles,<sup>63</sup> appliances, or industrial and other equipment,<sup>64-67</sup> telephones,<sup>68</sup> and vacuum cleaners.<sup>69</sup> Other researchers have concentrated



**Figure 26** Model for fluctuation strength.<sup>2-4</sup> (a) Envelope of amplitude-modulated sound (hatched) with corresponding temporal masking pattern (solid) and (b) basic formula for fluctuation strength  $F$ .



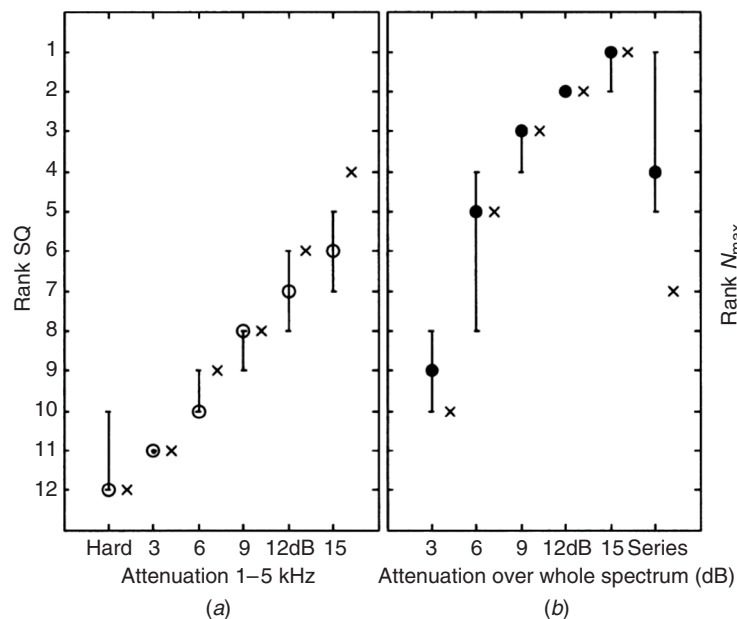
**Figure 27** Model of roughness.<sup>2-4</sup> (a) Envelope of amplitude-modulated sound (hatched) with corresponding temporal masking pattern (solid) and (b) basic relationship for roughness  $R$ .

on external vehicle sound quality.<sup>46-48</sup> Some other researchers have studied specific attributes of sound quality, including rumbling and booming.<sup>52-61</sup>

### 7.1 Results of Jury Tests

Figure 28 shows results of sound quality evaluations on a diesel engine.<sup>3</sup> The engine studied can be run in a “hard” setting as in Fig 28a or “normal” setting as in Fig 28b. In the hard setting the engine is more fuel efficient but makes more noise and this noise sounds “harder” and more unpleasant. Figure 28a shows sound quality rank assessments made with the engine running first in its hard setting. The subjects

were asked to evaluate the engine noise as the high-frequency part of the sound spectrum (1 to 5 kHz) was reduced in 3-dB steps up to an attenuation of 15 dB. The circles represent the sound quality ranks assigned to the sounds by the human subjects. The crosses represent predictions of the maximum loudness  $N_{max}$  made using a software calculation. The ranking 1 represents the best sound quality and quietest sound and 12 represents the worst sound quality and loudest sound. The motor with the unfiltered hard setting received the poorest sound quality (SQ) rankings of 12. Figure 28b shows the improvement in the sound quality and loudness rankings for the same



**Figure 28** Improvement of the sound quality of a *diesel* motor with “hard” motor adjustment and simulated absorptive measures that cause different amounts of attenuation. Circles denote subjective human subject sound quality estimates. Crosses mark loudness predicted from acoustical measurements.<sup>3</sup>

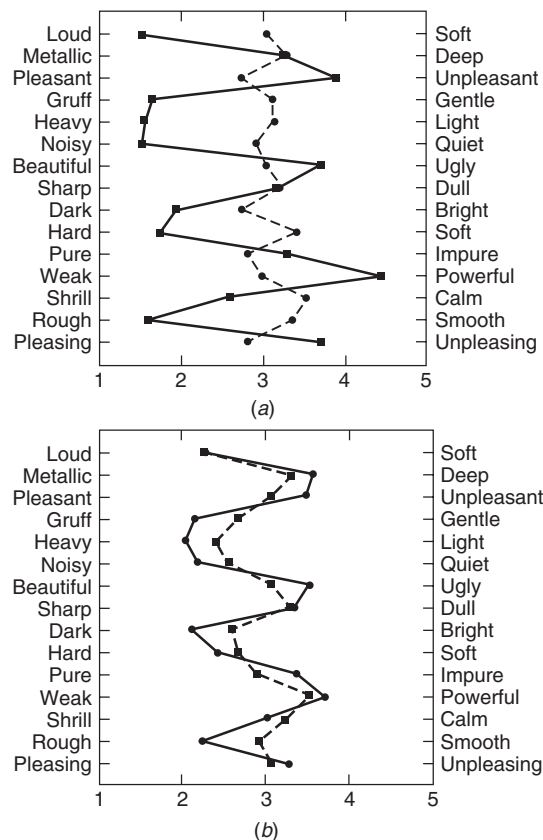
diesel motor running in its normal setting as different amounts of attenuation were used over the whole frequency range. The electronic attenuations of the sounds were made to simulate the motor sound, which would be heard with different amounts of attenuation achieved by engine enclosure and/or use of sound absorption treatment.

It is observed that in Fig. 28a after the sound was attenuated by 15 dB from 1 to 5 kHz, a sound quality ranking of only 7 was achieved, although the loudness  $N_{\max}$  was 4. The sound quality is poorer than the unattenuated normal "series" motor in Fig. 28b, in which the sound quality is 4 and the loudness is 7. It is seen that there is a general agreement in the trends of sound quality SQ and loudness  $N_{\max}$  rankings with increasing attenuation in Figs. 28a and 28b. Exceptions to the good agreement, however, exist for cases of (1) the sound quality and  $N_{\max}$  for the 15-dB attenuated sound in Fig. 28a and (2) the normal series motor in Fig. 28b. This demonstrates the fact that although loudness is a very important component, it is not always an adequate or completely reliable indicator of sound quality.<sup>2,3</sup>

Figure 29 shows the results of semantic differential jury evaluations made at the Sound and Vibration Research Laboratories at Auburn University on the interior sound of four automobiles. The four vehicles studied included a 2003 Jaguar S-type luxury car, a 2005 Acura sports sedan, a 1988 Porsche 911 Carrera sports car, and a 2005 sports utility vehicle (SUV). The vehicles were driven in steady cruise conditions at 63 km/h, and the interior noise in each vehicle was recorded binaurally directly onto the hard drive of a laptop computer using a dummy head, which was located in the passenger seat position. The A-weighted sound pressure levels were measured in each vehicle with a precision sound level meter. The recorded vehicle sound signatures were played back over two loudspeakers at the same A-weighted sound pressure level as recorded in the vehicles as illustrated in Fig. 23. Figure 29a shows the mean of the 27 subject evaluations of the Porsche sports car and the Jaguar luxury car. Figure 29b shows the mean evaluations of the SUV and Acura sports sedan car. The subjects listened to the vehicle recordings in a randomized order and were not informed which four vehicle recordings were being presented to them during the test. It can be seen that the sports car is rated much more noisy, rough, ugly, dull, and powerful than the luxury car. The SUV and sports sedan car received surprisingly similar mean evaluations from the subjects. Both of these cars were only about one year old.

## 7.2 Meaning of Sound

The majority of sound quality metrics can be divided into those that quantify some physical aspect of the sound (e.g., pressure level, frequency content) and those that try to quantify some physical effect taking place in the ear (e.g., impression of loudness, tone, etc.). In the first case, we assume that a particular physical measure of the sound is always going to produce



**Figure 29** Semantic differential evaluations for interior car sounds cruising at 63 km/h of a sports car, luxury sedan, SUV, and an economy sports sedan: (a) Porsche sports car, ■ — ■, and Jaguar, • - - •, and (b) Acura, ■ — ■, and SUV, • - - •.

a particular physical effect, and in the second case we assume that a particular physical effect is always going to produce a particular cognitive response. This model allows us to replace a human subject with a calculation system for some metrics once knowledge of the cognitive reactions is established. This approach has the obvious weakness that the assumptions are invariant as the following case demonstrates.

Figure 30 shows the results of the response of German and Japanese subjects to the sound of a bell.<sup>72</sup> The sound signal was perceived as being safe and pleasant by the German group and dangerous by the Japanese group. This was thought to be because most Japanese subjects associated the sound as a warning of the approach of a fire engine, while the subjects in the German group mostly associated the sound with church bells.

Recent research conducted to examine how the perceived meaning of a sound affects the judgment of sound quality has been carried out using an algorithm designed by Fastl and co-workers to remove the subjects' ability to identify a sound. The research

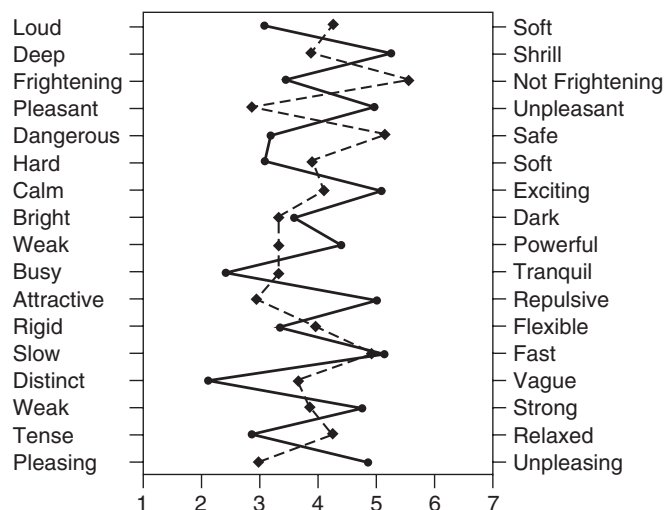


Figure 30 Evaluations of the sound of a bell by Japanese, —●— and German - -◆- - subjects.<sup>73</sup>

work assumes that discrepancies will exist between subjective judgments of identifiable and nonidentifiable sounds that have the same objective metric values. It also suggests that these differences will be due to the perceived meaning of the sound.<sup>70-72</sup> Fastl and others have now tried to remove the identifiability of the sounds by reversing them in the time domain and by other means.<sup>70-72</sup> Such signal time reversal can preserve the frequency content of the sound but largely remove its identification cues.

### 7.3 Other Differences Biasing Evaluations

Kuwani et al. have also reported semantic differential evaluations of the noise in passenger cars made by different groups of subjects.<sup>73</sup> Fourteen pairs of adjectives were used in the evaluations. The adjective pairs were presented in random order to the subjects. The subjects came from 21 countries. The interior cabin sounds of 5 kinds of accelerating noise were used as stimuli. The sounds were presented to people using earphones in a "soundproof" room. There were 21 female and 36 male subjects between the ages of 13 and 69. Comparisons were made between male and female subjects, between younger and older subjects (below and above the age of 39), and between U.S. and European subjects in the evaluations of the sound. In general, the younger subjects and the male subjects tended to evaluate the sounds close to the average of the whole group of 39 subjects, while the older and female subjects exhibited evaluations that were somewhat different. Figure 31 shows the different results for the American and European subjects. In this particular test there were 17 Americans and 18 Europeans. Both groups found stimulus 2 as unpleasant and stimulus 4 as being more acceptable.

However, the Americans found stimulus 2 more ugly, harsh, loud, unpleasant, strident, and rough than the Europeans.

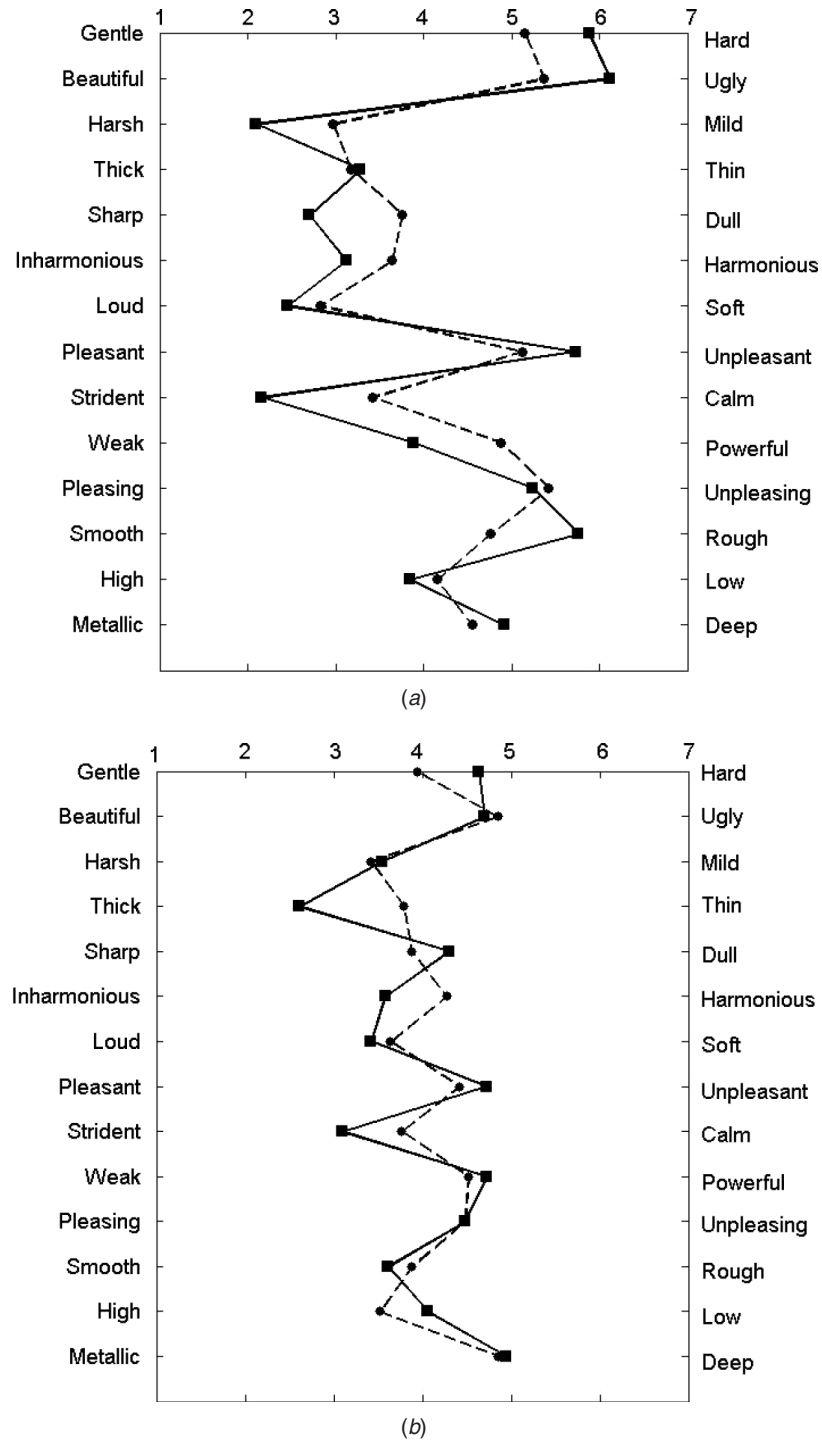
### 7.4 Results of Sound Synthesis Tests

Some researchers have conducted a considerable amount of research on two additional sound quality indicators, commonly called *booming* and *rumbling*. No international agreement has been reached on rumbling and booming indices. However, a proposal has been published for a booming index.<sup>53</sup>

Lee has described the results of some psychoacoustic experiments on the rumbling sound index for cars.<sup>54</sup> The index he used is based on several previous studies involving subjective evaluations of the sounds of vehicles. The conclusions of these studies showed that the rumbling sound quality can be related mostly to three qualities: the principal rumble component, loudness, and roughness. Based on this previous experimental work, a large number of synthetic interior sounds with different rumbling components were constructed electronically. Figure 32 shows a synthetic sound wave with a rumbling character. Figure 32a displays the time history of the amplitude-modulated wave formed by three half-order components used for the production of the rumbling sound. Figure 32b shows the spectrum of this amplitude-modulated wave. Finally Fig. 32c shows the principal component of the amplitude-modulated wave.

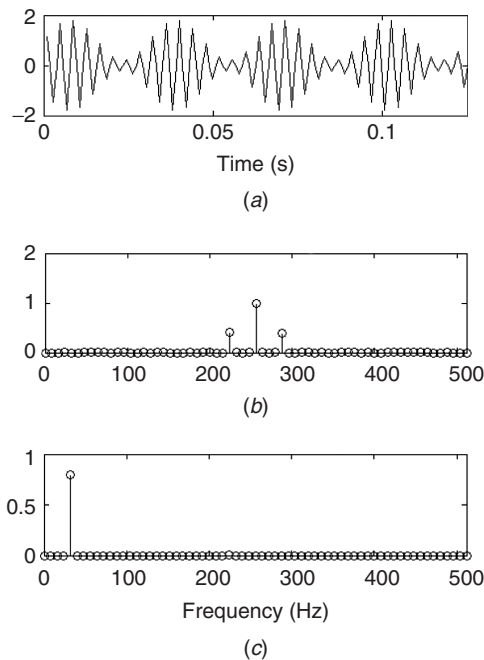
Figure 33 shows waterfall analysis of the interior sound of a passenger car as a function of engine rpm. Figure 33a shows the interior basic sound without the rumbling sound added, and Fig. 33b shows the modified sound with the rumbling sound added.

Altogether 240 different rumbling sounds were produced by varying the rumbling amplitude and the



**Figure 31** (a) U.S. (squares) and European (circles) of stimulus vehicle 2 and (b) U.S. (squares) and European (circles) evaluations of stimulus vehicle 4.



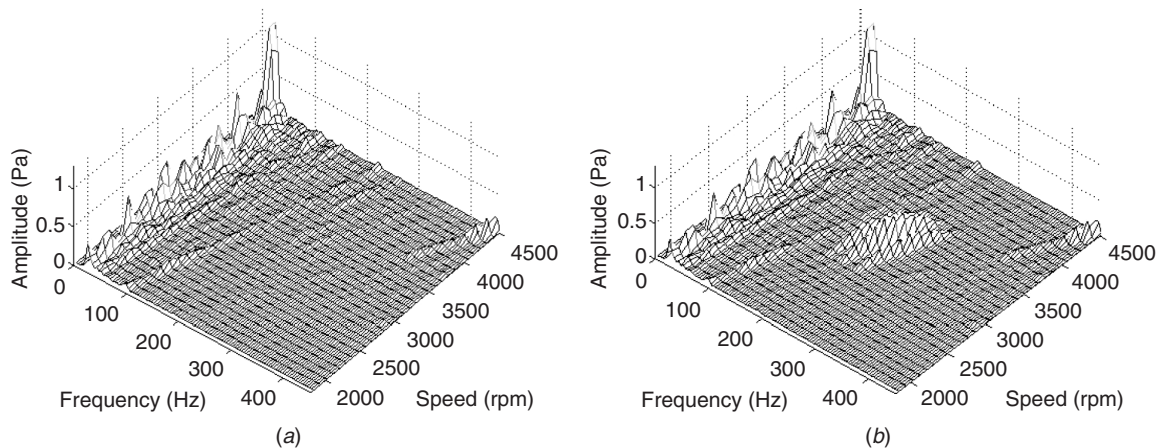


**Figure 32** Synthetic sound waves with rumbling sound quality: (a) amplitude-modulated wave formed by three half-order components used for the production of a rumbling sound, (b) spectrum of the amplitude-modulated wave, and (c) principal component of the amplitude-modulated wave.<sup>54</sup>

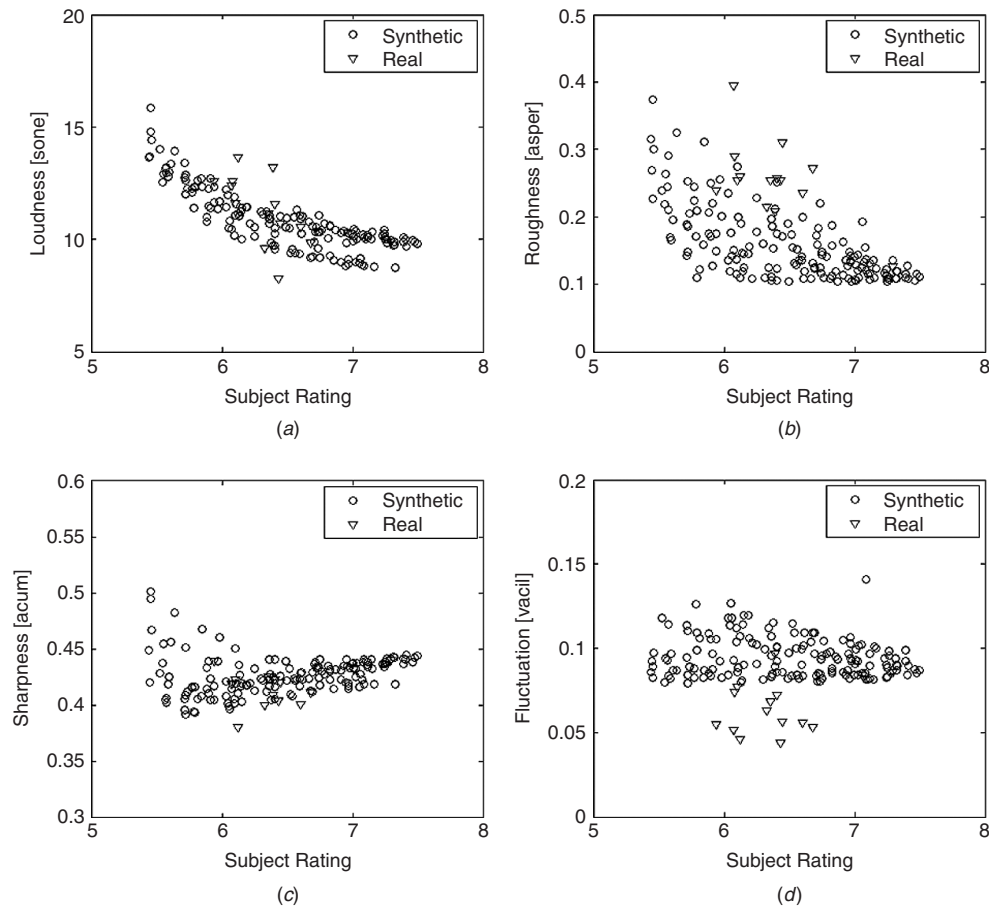
rumbling frequency as in Fig. 32. These rumbling sounds were then added to the basic vehicle sound to create 240 synthetic interior sounds for evaluation by the human subjects.

Before the 240 synthetic sounds were evaluated, 84 non-rumbling-like sounds were removed, and the interior sounds of 14 mass-produced passenger cars were added to the group, making a total of 170 interior sounds for evaluation by the subjects. The sounds were evaluated also using four sound quality units: loudness, sharpness, fluctuation strength, and roughness. The units of sharpness  $S$  (acum), fluctuation strength  $F$  (vacil), and roughness  $R$  (asper) are discussed by Fastl in Ref. 3 and further details and their definitions are given by Zwicker and Fastl in Ref. 4.

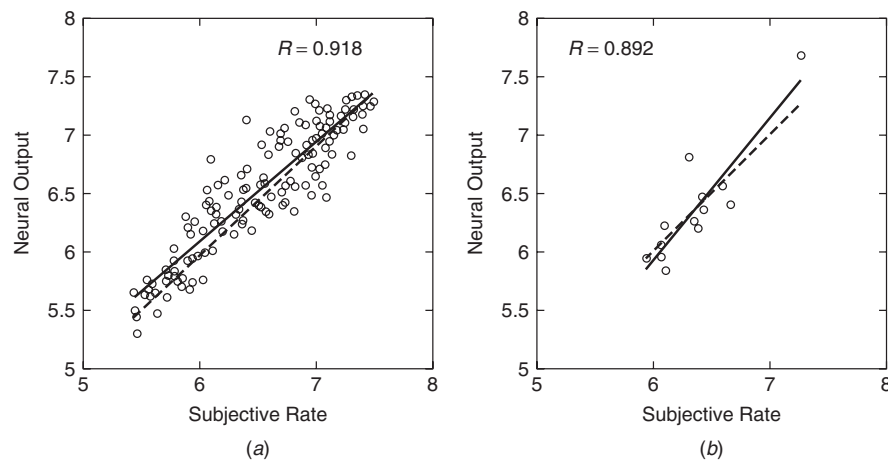
Figure 34 presents sound metrics for the 170 passenger car interior rumbling sounds. Figure 34a shows the loudness for the sound signals, evaluated using Zwicker's method, plotted against the subjective ranking of the sounds. The loudest sound has a value of about 17 sones and an average subjective ranking of about 5.5. The results of Fig. 34a indicate that the subjective ranking is equal approximately to the inverse of the loudness. Figure 34b displays the roughness of the 170 interior sounds calculated using Bismarck's model, plotted against their subjective rankings. The roughness is related to the amplitude modulation and frequency modulation as explained in Section 6.3 and Fig. 27. The maximum roughness is about 0.4 asper at a subjective ranking of 5.5. The relationship between the subjective ranking and roughness is not very clear. Figure 34c shows the sharpness for the 170 interior sounds, calculated using Aures' model. The maximum sharpness is seen to be about 0.5 acum at a subjective ranking of about 5.5. However, for most of the sounds, the sharpness is about 0.45 acum, and there is no clear relationship between the subjective ranking and the sharpness. Finally Fig. 34d shows the fluctuation strength for the 170 interior sounds calculated using Fastl's model. The fluctuation strength is described in Section 6.2 and Fig. 26, where the fluctuation strength is shown to be related to the amplitude modulation and frequency modulation in the region of 4 Hz. In Fig. 34d the



**Figure 33** Waterfall analysis for interior sound of a passenger car: (a) base sound and (b) modified sound with rumbling sound quality.<sup>54</sup>



**Figure 34** Sound metrics for the 170 interior sounds: (a) loudness for the signal filtered by 150 to 500 Hz frequency band filter using Zwicker's method, (b) sharpness for the 170 interior sounds of passenger cars using Bismarck's model, (c) roughness for the 170 interior sounds of passenger cars using Aures' model, and (d) fluctuation strength for the 170 interior sounds of passenger cars using Fastl's model.<sup>54</sup>



**Figure 35** (a) Correlation between the output of ANN and the averaged subjective rates for the 156 synthetic interior sounds and (b) correlation between the output of ANN and the averaged subjective rates for the 14 interior sounds of passenger cars.<sup>54</sup>  $R$  is the correlation coefficient.

fluctuation strength has a mean value of about 0.1 vacil, and there is no clear relationship seen between the human perception of rumbling sounds and the fluctuation strength.

Lee used the loudness and the principal rumble component of the 156 synthetic sounds to train a multiple layer artificial neural network (ANN).<sup>54</sup> The estimated subjective rates from the ANN are compared with subjective rankings in Fig. 35a. Figure 35a shows the correlation between the output of the ANN and the averaged subjective rates for the 156 synthetic interior sounds. Their correlation is 91.8%. Figure 35b shows the correlation between the output of ANN for the estimated rates and the averaged subjective rates for the 14 interior sounds of passenger cars. The correlation was found to be 89.2%.

The result of this research suggests that a rumbling sound index, such as the one suggested by Lee, can be devised to evaluate the subjective ranking of the rumbling sound quality of automobiles without the use of human subjects.<sup>54</sup>

The sound quality of different commercial products obviously cannot be evaluated with the same sound quality index. The rumbling index devised by Lee should not be used, for example, with a dentist drill or hair dryer. For such cases the annoyance estimator (PA) proposed by Fastl based on loudness, sharpness, and fluctuating strength would be more appropriate.<sup>54</sup>

## REFERENCES

1. J. Blauert and U. Jekosch, Sound-Quality Evaluation—A Multi-Layered Problem, *Acta Acust. (Stuttgart)*, Vol. 83, No. 5, Sept–Oct. 1997, pp. 747–753.
2. H. Fastl, Psychoacoustics of Sound-Quality Evaluation, *Acta Acust. (Stuttgart)*, Vol. 83, No. 5, Sept–Oct. 1997, pp. 754–764.
3. H. Fastl, Psychoacoustics and Sound Quality, in *Communication Acoustics*, J. Blauert, Ed., Springer, Berlin, 2005, Chapter 6.
4. E. Zwicker and H. Fastl, *Psychoacoustics. Facts and Models*, 2nd ed., Springer, Berlin-Heidelberg-New York, 1999.
5. B. C. J. Moore, *An Introduction to the Psychology of Hearing*, Academic, London, 1997.
6. R. D. Luce, *Sound & Hearing—A Conceptual Introduction*, Lawrence Erlbaum Associates, Hillsdale, NJ, 1993.
7. J. G. Neuhoff, Ed., *Ecological Psychoacoustics*, Elsevier, Academic, London, 2004.
8. J. D. Durrant and J. H. Lovring, *Bases of Hearing Science*, 3rd ed., Williams & Wilkins, Baltimore, MD, 1995.
9. S. A. Gelfand, *Hearing—An Introduction to Psychological and Physiological Acoustics*, 3rd ed., Marcel Dekker, New York, 1998.
10. B. C. J. Moore, Ed., *Hearing*, Academic, San Diego, CA, 1995.
11. J. V. Tobias, Ed., *Foundations of Modern Auditory Theory*, Vol. I, Academic, New York, 1970.
12. M. Martin and I. Summers, *Dictionary of Hearing*, Whurr, London, 1999.
13. E. D. Schubert, Ed., *Psychological Acoustics, Benchmark Papers in Acoustics*, Vol. 13, Dowden Hutchinson and Ross, Stroudsburg, PA, 1979.
14. K. D. Kryter, *The Effects of Noise on Man*, Academic, Orlando, FL, 1985.
15. R. Feldtkeller and E. Zwicker, *Das Ohr als Nachrichtenempfänger*, S. Hirzel, Stuttgart, 1956, p. 82.
- 15a. M. J. Crocker, Ed., *Handbook of Acoustics*, Wiley, 1998.
16. J. E. Hawkins and S. S. Stevens, The Masking of Pure Tones and of Speech by White Noise, *J. Acoust. Soc. Am.*, Vol. 22, 1950, pp. 6–13.
17. E. Zwicker, Dependence of Post-masking on Masker Duration and Its Relation to Temporal Effect in Loudness, *J. Acoust. Soc. Am.*, Vol. 75, 1984, pp. 219–223.
18. E. Zwicker, Subdivision of the Audible Frequency Range into Critical Bands (Frequenzgruppen), *J. Acoust. Soc. Am.*, Vol. 33, 1961, p. 248.
19. S. Buus, Auditory Masking, in *Encyclopedia of Acoustics*, M. J. Crocker, Ed., Wiley, New York, 1997, Chapter 115.
20. S. S. Stevens, The Measurement of Loudness, *J. Acoust. Soc. Am.*, Vol. 27, 1955, pp. 815–829.
21. E. Zwicker, Ein Verfahren zur Berechnung der Lautstärke, *Akustica*, Vol. 10, 1960, pp. 304–308.
22. R. H. Lyon, *Designing for Product Sound Quality*, Marcel Dekker, New York, 2000.
23. R. H. Lyon, Product Sound Quality, *J. Sound Vib.*, March 2003, pp. 18–22.
24. R. H. Lyon, “Product Sound Quality—From Design to Perception, *Internoise Proc.*, 2004.
25. M. Meilgaard, G. Civille, B.T. Carr, *Sensory Evaluation Techniques*, 3rd ed., CRC Press, Boca Raton, FL, 1999.
26. N. Otto, S. Amman, C. Eaton, and S. Lake, Guidelines for Jury Evaluations of Automotive Sounds, SAE Noise and Vibration Conference and Exposition, Society of Automotive Engineers, Warrendale, PA, 1999.
27. M. Bodden, Instrumentation for Sound Quality Evaluation, *Acta Acust. (Stuttgart)*, Vol. 83, No. 5, Sept–Oct. 1997, pp. 775–783.
28. W. Keiper, Sound Quality Evaluation in the Product Cycle, *Acta Acust. (Stuttgart)*, Vol. 83, No. 5, Sept–Oct. 1997, pp. 784–788.
29. R. Bisping, Car Interior Sound Quality: Experimental Analysis by Synthesis, *Acta Acust. (Stuttgart)*, Vol. 83, No. 5, Sept–Oct. 1997, pp. 813–818.
30. H. Van der Auweraer, K. Wyckaert, and W. Hendricx, From Sound Quality to the Engineering of Solutions for NVH Problems: Case Studies, *Acta Acust. (Stuttgart)*, Vol. 83, No. 5, Sept–Oct. 1997, pp. 796–804.
31. R. Guski, Psychological Methods for Evaluating Sound Quality and Assessing Acoustic Information, *Acta Acust. (Stuttgart)*, Vol. 83, No. 5, Sept–Oct. 1997, pp. 765–774.
32. U. Widmann, Three Application Examples for Sound Quality Design Using Psychoacoustic Tools, *Acta Acust. (Stuttgart)*, Vol. 83, No. 5, Sept–Oct. 1997, pp. 819–826.
33. K. Genuit, Background and Practical Examples of Sound Design, *Acta Acust. (Stuttgart)*, Vol. 83, No. 5, Sept–Oct. 1997, pp. 805–812.
34. C. V. Beidl and W. Stucklschwaiger, Application of the AVL-Annoyance Index for Engine Noise Quality



- Development, *Acta Acust. (Stuttgart)*, Vol. 83, No. 5, Sept–Oct. 1997, pp. 789–795.
35. H. Fastl, Sound Measurements Based on Features of the Human Hearing System, *J. Acoust. Soc. Japan (E)* (English translation of *Nippon Onkyo Gakkaishi*), Vol. 21, No. 6, Nov. 2000, pp. 333–336.
36. A. Miskiewicz, Psychoacoustics in the Automotive Industry, *Acta Acust.*, Vol. 85, 1999, pp. 646–649.
37. M. Pflueger and W. Stueckelschwaiger, Sound and Vibration Quality Map for Commercial Vehicles, SAE Noise and Vibration Conference and Exposition, Society of Automotive Engineers, Warrendale, PA, 2001.
38. M. Adams and P. van de Ponsele, Sound Quality Equivalent Modeling for Virtual Car Sound Synthesis, SAE Noise and Vibration Conference and Exhibition, Society of Automotive Engineers, Warrendale, PA, 2001.
39. N. Sato and Y. Miura, Study on Exterior Idling Sound Quality Evaluation Method for Diesel Engine Trucks, SAE Noise and Vibration Conference and Exhibition, Society of Automotive Engineers, Warrendale, PA, 1999.
40. L. Lamotte and B. Beguet, Quantification of Sound Quality for Engine in Stationary and Run-Up Conditions, SAE Noise and Vibration Conference and Exposition, Society of Automotive Engineers, Warrendale, PA, 1999.
41. M.-R. Lee, M. McCarthy, M. Romzek, T. Frei, and Y.-J. Bemman, Exhaust System Design for Sound Quality, SAE Noise and Vibration Conference and Exposition, Society of Automotive Engineers, Warrendale, PA, 2003.
42. B. Brassow and M. Clapper, Powertrain Sound Quality Development of the Ford GT, Noise and Vibration Conference and Exhibition, Society of Automotive Engineers, Warrendale, PA, 2005.
43. S.-Y. Hwang, K.-T. Kang, B.-S. Lim, and Y.-S. Lim, Noise Reduction and Sound Quality Improvement of Valve Train in V6 Gasoline Engine, SAE World Congress, Society of Automotive Engineers, Warrendale, PA, 2005.
44. A. Petniunas, N. C. Otto, S. Amman, and R. Simpson, Door System Design for Improved Closure Sound Quality, SAE Noise and Vibration Conference and Exposition, Society of Automotive Engineers, Warrendale, PA, 1999.
45. D. Scholl and M. Blommer, Wavelet-Based Modification of Impulsive Sound Character and Application to Diesel Sound Quality, Warrendale, PA, Noise and Vibration Conference and Exhibition, Society of Automotive Engineers, 2005.
46. T. Hashimoto, Sound Quality Approach on Vehicle Interior and Exterior Noise—Quantification of Frequency Related Attributes and Impulsiveness, *J. Acoust. Soc. Japan (E)* (English translation of *Nippon Onkyo Gakkaishi*), Vol. 21, No. 6, Nov. 2000, pp. 337–340.
47. D. Vastfjall, M.-A. Gulbol, M. Kleiner, and T. Garling, Affective Evaluations of and Reactions to Exterior and Interior Vehicle Auditory Quality, *J. Sound Vib.*, Vol. 255, No. 3, Aug. 15, 2002, pp. 501–518.
48. T. Ishiyama and T. Hashimoto, Impact of Sound Quality on Annoyance Caused by Road Traffic Noise: An Influence of Frequency Spectra on Annoyance, *JSAE Rev.*, Vol. 21, No. 2, Apr. 2000, pp. 225–230.
49. L. Zhang, A Sensory Approach to Develop Product Sound Quality Criterion, SAE Noise and Vibration Conference and Exposition, Society of Automotive Engineers, Warrendale, PA, 1999.
50. K. Noumura and J. Yoshida, Perception Modeling and Quantification of Sound Quality in Cabin, SAE Noise and Vibration Conference and Exposition, Society of Automotive Engineers, Warrendale, PA, 2003.
51. T. Mori, A. Takaoka, and M. Maunder, Achieving a Vehicle Level Sound Quality Target by a Cascade to System Level Noise and Vibration Targets, Noise and Vibration Conference and Exhibition, Society of Automotive Engineers, Warrendale, PA, 2005.
52. S.-K. Lee, B.-S. Kim, H.-C. Chae, D.-C. Park, and S.-G. Jung, Sound Quality Analysis of a Passenger Car Based on Rumbling Index, Noise and Vibration Conference and Exhibition, Society of Automotive Engineers, Warrendale, PA, 2005.
53. S. K. Lee and H. C. Chae, The Application of Artificial Neural Networks to the Characterization of Interior Noise Booming In Passenger Cars, *Proceedings Instn Mech. Engrs, Part D, J. Automobile Engineering*, London, 2004, 218.
54. S.-K. Lee, Improvement of Sound Quality in a Hyundai New Vehicle Based on Sound Quality Index, Proceedings of the Twelfth International Congress on Sound and Vibration, Lisbon, Portugal, July 11–14, 2005.
55. K. Tsuge, K. Kanamaru, T. Kido, and N. Masuda, A Study of Noise in Vehicle Passenger Compartment during Acceleration, The SAE 1998 World Congress and Exhibition, Detroit, MI, 1998, SAE980965.
56. T. Wakita, Y. Kozawa, K. Samada, G. Sugimoto, and T. Ogasawara, Objective Rating of Rumbling in Vehicle Passenger Compartment During Acceleration, Proceedings of the 1998 SAE Noise and Vibration Conference, Traverse City, MI, 1998, SAE981155.
57. M. Ishihama, Y. Sakai, I. Katano, and K. Nakamura, Effect of Basic Design Parameters of Automotive Engines on Their Sound Characteristics, Proceedings of the 2003 SAE Noise and Vibration Conference, Traverse City, MI, 2003, SAE2003-01-1507.
58. S. Matsuyama and S. Maruyama, Booming Noise Analysis Method Based on Acoustic Excitation Test, The SAE 1998 World Congress and Exhibition, Detroit, MI, 1998, SAE980588.
59. S. K. Lee, H. C. Chae, D. C. Park, and S. G. Jung, Sound Quality Index Development for the Booming Noise of Automotive Sound Using Artificial Neural Network Information Theory, Sound Quality Symposium 2002, Dearborn, MI, 2002, CD N0.5.
60. S.-H. Shin, J.-G. Ih, U.-S. Byun, and K.-T. Kang, Sound Quality Evaluation of Booming Noise in Passenger Cars, Proceedings of the 32nd International Congress and Exposition on Noise Control Engineering, Seogwipo, Korea, August 25–28, 2003.
61. S.-K. Lee, H.-C. Chae, D.-C. Park, and S.-G. Jung, Rumbling Noise Index for Sound Quality Analysis of a Passenger Car Using Artificial Neural Network, Proceedings of the 32nd International Congress and Exposition on Noise Control Engineering, Seogwipo, Korea, August 25–28, 2003.
62. P. Cho and A. Karavadi, Sound Quality Target Development Process for Agricultural and Construction

- Machinery, SAE International Off-Highway and Powerplant Congress and Exposition, Society of Automotive Engineers, Warrendale, PA, 1999.
63. N. C. Otto, R. Simpson, and J. Wiederhold, Electric Vehicle Sound Quality, SAE Noise and Vibration Conference and Exposition, Society of Automotive Engineers, Warrendale, PA, 1999.
  64. N. D. Porter and B.F. Berry, A Study of Standard Methods for Measuring the Sound Quality of Industrial Products: Final Report, NPL Report CIRA (EXT) 021, National Physical Laboratory, Teddington, Middlesex, UK, 1997.
  65. C. L. Fog and T. H. Pederson, Introduction to Product Sound Quality, Nordic Acoustical Meeting, 1998.
  66. C. L. Fog, Use of Product Optimisation Tools, Proceedings of the Sixth International Congress on Sound and Vibration, ICSV6, Copenhagen, Denmark, 1999.
  67. C. L. Fog, Product Sound as an Important Part of Product Design, *Internoise Proceedings*, 2001.
  68. S. Moller and A. Raake, Telephone Speech Quality Prediction: Towards Network Planning and Monitoring Models for Modern Network Scenarios, *Speech Commun.*, Vol. 38, Nos. 1–2, Sept. 2002, pp. 47–75.
  69. U. Benko, J. Petrovic, D. Juricic, J. Tavcar, J. Rejec, and A. Stefanovska, Fault Diagnosis of a Vacuum Cleaner Motor by Means of Sound Analysis, *J. Sound Vib.*, Vol. 276, Nos. 3–5, Sept. 22, 2004, pp. 781–806.
  70. H. Fastl, Neutralising the Meaning of Sound for Sound Quality Evaluations, *Internoise Proceedings*, 2001.
  71. W. Ellermeier, A. Zeitler, and H. Fastl, Predicting Annoyance Judgments from Psychoacoustic Metrics: Identifiable Versus Neutralized Sounds, *Internoise Proceedings*, 2004.
  72. H. Fastl, Keynote Lecture on Sound Quality Evaluations, Proceedings of the Thirteenth International Congress on Sound and Vibration, ICSV13, Vienna, Austria, 2006.
  73. S. Kuwani et al., in *Contributions to Psychological Acoustics*, A. Schick and M. Klatte, Eds., Oldenburg Symposium on Psychological Acoustics, University of Oldenburg, Germany, 1997, pp. 115–128.
  74. S. Kuwano, S. Namba, T. Hato, M. Matui, K. Miura and H. Imai, Psychological Evaluation of Noise in Passenger Cars: Analysis in Different Group of Subjects in Nationality, Age and Gender, in *Contributions to Psychological Acoustics*, A. Schick, Ed., Oldenburg Symposium on Psychological Acoustics, University of Oldenburg, Germany, 1993, pp. 521–536.

## **PART VII**

---

# **INDUSTRIAL AND MACHINE ELEMENT NOISE AND VIBRATION SOURCES – PREDICTION AND CONTROL**

# CHAPTER 68

## MACHINERY NOISE AND VIBRATION SOURCES

Malcolm J. Crocker

Department of Mechanical Engineering  
Auburn University  
Auburn, Alabama

### 1 INTRODUCTION

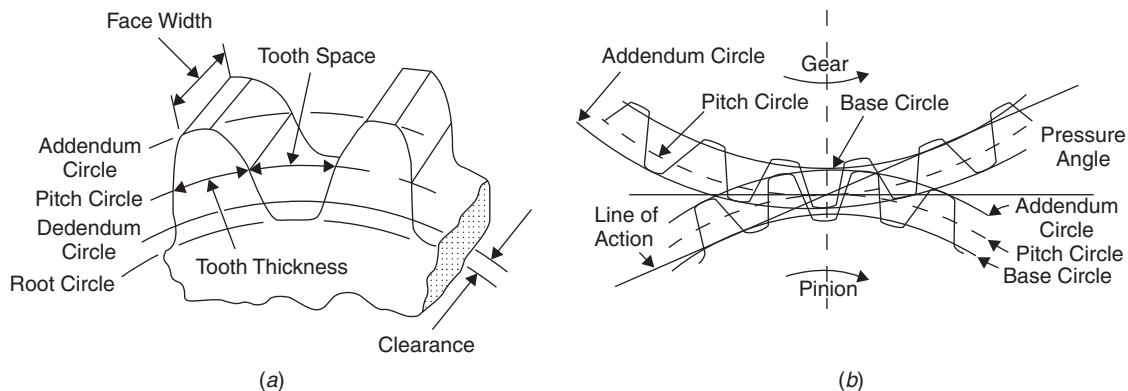
Many different machine components are used in appliances, vehicles, aircraft, and industry. Some machine components including bearings, gears, fans, burners, cutters, and valves are used in machines built from several of these components such as pumps, compressors, electric motors, and internal combustion (IC) engines. It is impossible to discuss every type of machine and machine component here; so the discussion is mainly concentrated on common machine components and machines. These machine components and machines do work, transfer energy, or convert one form of energy into another. In these processes some undesirable vibration and acoustical energy or noise is produced as an unwanted by-product. It is the purpose of this chapter to review briefly the functioning of these machine components and machines, noise and vibration generation mechanisms, and methods of control. In addition, this chapter also serves as an introduction to the chapters in Part VII of this book in which the noise and vibration of these machine components and machines are discussed in much more detail. Several other books, book chapters, and articles also discuss machinery noise mechanisms and noise and vibration sources in more detail than is possible here.<sup>1-15</sup>

### 2 GEARS

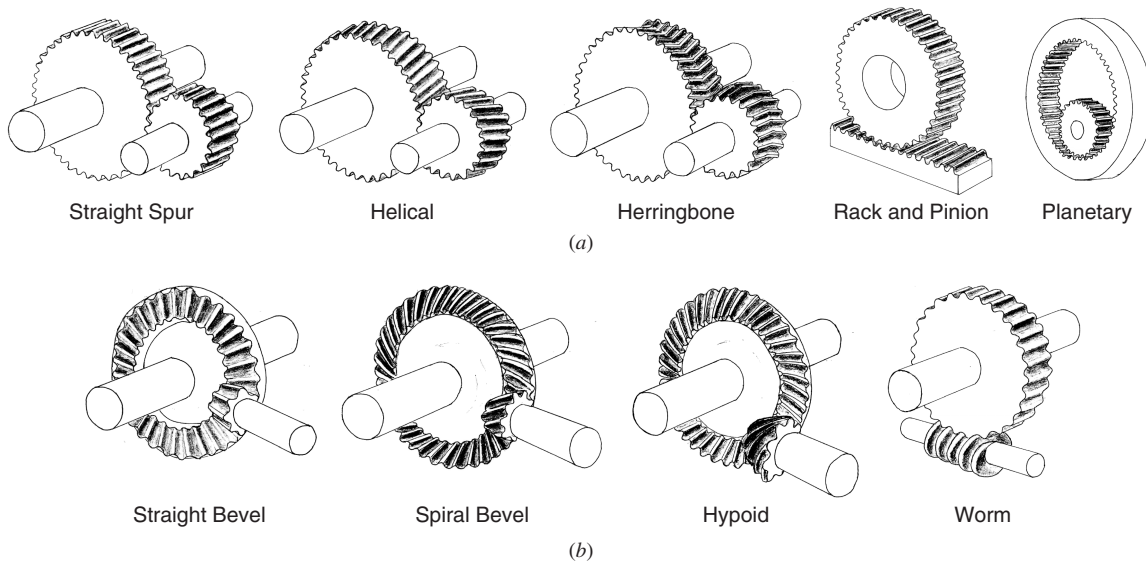
Chapter 69 provides a detailed discussion of the sources of noise and vibration in the main types

of gears in common use. Chapter 88 also contains some information on the noise of gearboxes and transmissions used in vehicles. Most modern gear teeth have an involute profile, although some have circular-arc profiles.<sup>1,2</sup> Figure 1a shows some of the terms used with involute gears and Fig. 1b shows two parallel-axis spur-type gears meshing together.

There are several different types of gears in common use, as shown in Fig. 2. They are of two main classes, either having (1) parallel axes (spur, helical) or (2) nonparallel axes (straight bevel, spiral bevel, hypoid). Spur gears and straight bevel gears are usually the noisiest, while helical spiral bevel gears are usually the quietest in their respective classes. This is because the load between gear wheel teeth is transferred more gradually with helical and spiral-bevel gears and rather more abruptly with spur and straight-bevel gears. Gear noise can arise from a variety of causes. As the gear teeth mesh, a pulsating force occurs at the gear tooth meshing frequency  $f_m$  and its harmonics. Harmonics are present because the pulsating force on the gear teeth is not purely sinusoidal. The strength of the harmonics depends on the force pulse shape and also on other impulsive forces caused by tooth deformation, production machinery errors, bearing misalignment, pinion wheel deformation, and so on. At high speeds, air or lubricating fluids can be expelled from between the meshing teeth at supersonic speeds and can even become the dominant source of noise. At low speed and load the sound pressure level produced by a gear increases by about 3 dB for a doubling of load, while



**Figure 1** Terms used with gears: (a) involute gear, (b) meshing of two parallel-axis spur gears. (Based in part on figures in Refs. 1, 2, and 3.)



**Figure 2** The main types of gear in use: (a) parallel axis (straight spur, helical, herringbone, rack and pinion, and planetary); (b) nonparallel axis (straight bevel, spiral bevel, hypoid, and worm.)

at higher speeds and loads the sound pressure level increases by about 6 dB for a doubling of speed or load.<sup>16</sup>

The noise of a gear set is quite dependent on the quality of manufacture and the tolerances achieved. Theoretical and experimental studies have been made that attempt to relate gear surface deformation and profiles to noise.<sup>17-19</sup> Precision gear sets can now be manufactured,<sup>20</sup> which make very low noise levels, although the cost is higher. In some cases, where low noise levels are required, it is more cost effective to choose a gear set of moderate cost and to vibration isolate the pinion and gear bearings, apply damping to the gear housing, and, if necessary, completely enclose it. With gears used to transmit only small loads (e.g., those in electric clocks), very low noise levels can be achieved by the use of soft plastic gears (which reduce the gear tooth force impulses) and by other means.<sup>21</sup> Manufacturing deficiencies can result in variations in pitch and profile from tooth to tooth and eccentricity of the gear wheel, which causes increased noise and vibration.<sup>1-4,16</sup> There would, however, be some noise generated even if the gears were without any imperfections. The frequency of this noise (and vibration) would only occur at the gear meshing frequency  $f_m$  and its harmonics:

$$f_m = \frac{N_p n_p}{60} \text{ Hz} \quad (1)$$

where  $N_p$  is the number of pinion teeth and  $n_p$  is the pinion speed in revolutions/minute (rpm). Noise and vibration measurements have also been used to produce a gear noise and vibration rating index in an

attempt to avoid the necessity for using a jury test for this purpose.<sup>22</sup>

### 3 BEARINGS

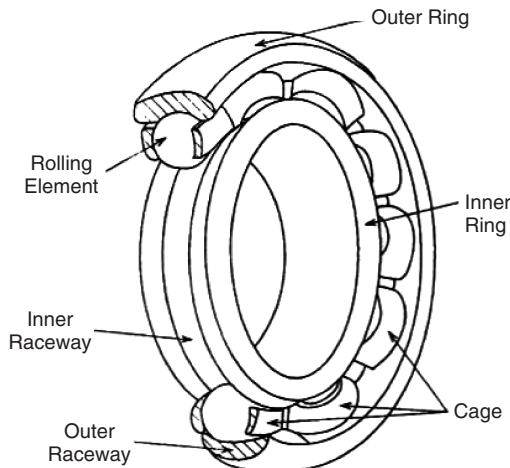
There are two main types of bearings: (1) rolling contact and (2) sliding contact.<sup>6,7</sup> Rolling contact bearings are more commonly used, but sliding contact bearings are usually quieter than rolling contact bearings, if properly manufactured, installed, and maintained. Proper lubrication is essential for both rolling and sliding contact bearings. Chapter 70 presents a detailed review of the noise of bearings.

*Rolling contact bearings* consist of the rolling elements contained between the *inner* and *outer raceways*. The rolling elements are normally kept from touching each other by a *cage*. The rolling elements may be spherical, cylindrical, tapered, or barrel-shaped.<sup>6</sup> Figure 3 shows a bearing with spherical rolling elements. The noise made by a rolling contact bearing is normally caused by vibration from two main sources: (1) rotation of bearing elements and (2) resonances in the elements, raceways, or cage. Table 1 in Chapter 70 provides formulas for the calculation of the main harmonic frequencies signifying rolling bearing defects. Reference 3 has likewise identified discrete frequencies (and their harmonics) that are related to bearing geometry and rotational speed. The fundamental frequency is the shaft rotational frequency  $f_s$ :

$$f_s = N/60 \text{ Hz} \quad (2)$$

where  $N$  is shaft rotational speed in rpm.

The other frequencies are related to the shaft frequency  $f_s$  by factors that depend on the roller



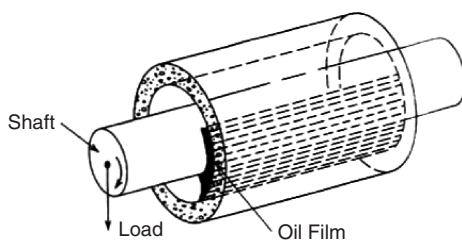
**Figure 3** Bearing with spherical rolling elements.

diameter, the pitch diameter of the bearing, the contact angle between the roller element and the raceway, and the number of rolling elements. Manufacturing imperfections and misalignment cause bearing noise. This noise can be increased further by wear.

Even a perfect bearing will make noise when loaded.<sup>2</sup> If a rolling bearing is manufactured to a higher grade of precision (smaller tolerance), then it normally becomes quieter (and more expensive). (Classes of tolerance are specified in ISO Standard 492–1986. Methods to test bearings for noise and vibration are given in ANSI/AFBMA Standard 13–1970. The (American) Military Specification MIL-B-17913D defines permissible vibration limits for bearings.)

*Sliding contact bearings* can be divided into three main types: (1) journal, (2) thrust, and (3) guide. Journal bearings are cylindrical in shape and allow rotation (see Fig. 4). Thrust bearings are used to prevent motion along a shaft axis, while guide bearings are normally used for motion of a part in one direction without rotation (e.g., a piston sliding in a cylinder of an internal combustion engine).

When shaft rotation occurs with a journal bearing, the shaft rides on a film of lubricant. Under some conditions, however, this film can break down, causing metal-to-metal contact and consequently wear, noise,



**Figure 4** Sliding contact bearing.

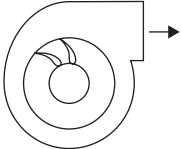
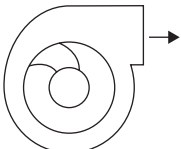
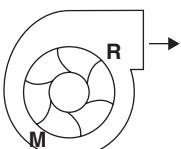
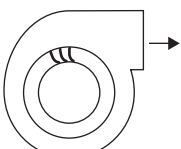
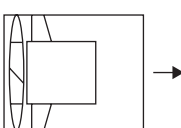
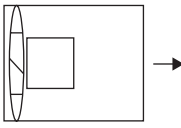
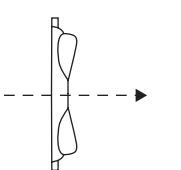
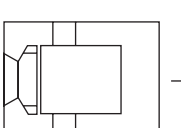
and vibration. A well-known instability condition called *oil whirl* can occur causing noise at a frequency of about half of the shaft rotational speed. This is because the average speed of the lubricant film is about half of the shaft speed. Oil-whirl noise can be magnified if a shaft resonance frequency occurs near to half the shaft rotational speed. To minimize sliding bearing noise, proper attention should be paid to lubricant viscosity, pressure, alignment, and structural stiffness. Proper installation of bearings is important to achieve low vibration and noise.<sup>23</sup> Increased bearing noise and vibration are an indication of wear and/or misalignment, and, if correctly analyzed, these can be indicative of potential bearing failure.<sup>24,25</sup> Active control of special magnetic bearings for a fan has been undertaken in an attempt to set the fan blades into vibration so that they become a secondary out-of-phase sound source to cancel the primary fan noise. Noise reductions of up to 4 dB have been reported.<sup>26</sup> Chapter 70 contains more detailed discussion on bearing noise. Further discussion can also be found in Refs. 2, 3, 6, and 7.

#### 4 FANS AND BLOWERS

Fans and blowers are used in appliances, in buildings, in air distribution systems for heating and cooling, and in industry for a variety of purposes. Fan noise, its generation, and control are discussed in detail in Chapter 71. There are two main types of fan designs: axial and centrifugal (see Fig. 5). The first three centrifugal fan types—airfoil, backward-curved, and radial—are mostly used in industrial applications. The airfoil fan is the most efficient but it is only suitable for clean-air industrial applications because dust and other particles can adhere to the fan blades and cause malfunctioning. The forward-curved fan is usually made of lightweight low-cost materials and is generally the least efficient. The radial fan is the noisiest and least efficient, but is useful for dirty or corrosive gas flows. Axial fans have the disadvantage that the discharged air rotates, unless downstream or upstream guide vanes (stators) are installed; these fans are mainly used in low- or medium-pressure air-conditioning systems. The vaneaxial fan is the most efficient axial type and can generate high pressures. The propeller type is the least expensive of the axial type. It has the lowest efficiency and is normally limited to low-pressure, high-volumetric flow applications.

The primary purpose of a fan is to move a required volumetric flow rate of air against a given back pressure with maximum efficiency and low cost and noise. There may be additional requirements such as high resistance to abrasion, ability to transport dusty air, ease of manufacture, maintenance and repair, and noise restrictions.

Fan noise has pure-tone and broadband frequency components. See Table 1 in Chapter 71. Although the mathematical theory of fan noise is well developed, it is beyond the scope of this chapter, and physical explanations are presented instead. Each time a blade passes a point in space or a solid-body obstruction, an impulsive force fluctuation is experienced by the

Fan Type	Description	Design Details
<b>Centrifugal Type Fans</b>		
<b>Airfoil</b>	Uses 10 to 16 airfoil shape blades; has highest efficiency of all centrifugal types; used where horsepower savings will be important; can be used on low-, medium-, and high-pressure systems.	
<b>Backward inclined backward curved</b>	Uses 10 to 16 blades; used for similar applications as airfoil fan; gas flow should be clean but need not be as clean as gas flow with airfoil fans.	
<b>Industrial (radial)</b>	Uses 6 to 10 blades of either radial (R) or modified radial (M) type; has lowest efficiency of centrifugal types; used mainly in industrial applications where gas is hot and dirty.	
<b>Forward Curved</b>	Uses 24 to 64 blades; construction is usually low-cost and lightweight; efficiency is lower than airfoil or backward curved fans; usually operates at lowest speed and is smallest of centrifugal types; used in low-pressure heating, ventilating, and air-conditioning (HVAC) systems.	
<b>Vaneaxial</b>	Uses 3 to 16 blades; high efficiency airfoil blades may be fixed or adjustable; used in low-, medium-, and high-pressure systems in HVAC and other industrial applications.	
<b>Axial-Type Fans</b>		
<b>Tubeaxial</b>	Uses 4 to 8 blades; usually more efficient than propeller type below and can operate at a higher pressure; does not use guide vanes as does vaneaxial type; used in low-, and medium-pressure systems in HVAC and other applications.	
<b>Propeller Type</b>	Uses 2 to 8 blades usually in a circular ring or orifice plate; efficiency low, this type usually limited to low-pressure, high volume flow applications such as exhaust or artice fans.	
<b>Tubular Centrifugal</b>	The fan wheel is usually similar in design to that of the airfoil or backward-curved type used in centrifugal fans since the air is discharged radially and must turn 90° in the guide vane section, its efficiency is lower than similar centrifugal fans; normally used in low-pressure HVAC return air systems.	

**Figure 5** Main types of fans with descriptions of their use and design.

fluid or solid body at the point. If a fan has  $n$  blades and the rotational speed is  $N$  rpm, then the number of impulses experienced per second  $f_B$  is

$$f_B = \frac{nN}{60} \text{ Hz} \quad (3)$$

The frequency  $f_B$  is known as the *blade-passing frequency* or often the *blade frequency* for short. Since the time history of the impulsive force on the fluid or solid body obstruction at the point will not be completely sinusoidal, harmonics will appear. The strength of the harmonics is affected by upstream or downstream solid-body flow obstructions.

The noise generated by a fan depends primarily on its design features, geometrical dimensions, and operating speed and load. Both broadband and pure-tone fan noise normally increase with increasing fan speed  $N$ . The frequency of the pure-tone noise generated by a fan increases with fan speed  $N$  as shown by Eq. (3). Structural resonances can also be excited. These resonance frequencies are largely independent of fan speed. If the fan is operated at off-design conditions, its noise can also be higher than normal. If the fan is operated at reduced volumetric flow rates, the A-weighted sound pressure level can be as much as 15 dB higher than normal because of fan surge and rotating fan stall. Fan sound power level data are normally provided by manufacturers in eight octave bands from 63 to 8000 Hz. Table 2 and the associated text in Chapter 71 provide an empirical method for predicting the noise of axial and centrifugal fans.

It is difficult to reduce fan noise by changing fan design parameters since such changes may adversely affect fan performance as well. Most fan noise reduction is achieved by proper use of well-known passive control methods. If noise is of major concern and the fan has been properly installed, it will probably be necessary to install intake and discharge sound attenuators (with flexible vibration breaks at attachment points to duct systems, if present). It is also possible to provide further noise attenuation by the use of ducting, elbows, and plenum chambers lined with sound-absorbing material. Care must be taken that significant noise is not generated in this ductwork. Chapter 110 describes the prediction and control of the noise and vibration in ducted heating, ventilation, and air-conditioning systems, and Chapter 111 discusses the aerodynamic sound generated in low-speed flow ducts.

Considerable efforts continue to be made to reduce fan noise since fans are used in most computers, electric motors, household appliances, vehicles, trucks, and many other items of machinery. Numerous studies have been conducted on the noise control of fans.<sup>26-41</sup> Both passive<sup>26-35</sup> and active<sup>36-40</sup> noise control methods continue to be studied. Experimental and theoretical studies have been made to aid in machinery noise reduction and noise predictions. Sound quality studies have also been conducted on the acceptability of fan noise.<sup>41</sup>

## 5 ELECTRIC MOTORS AND ELECTRICAL EQUIPMENT

Examples of electrical equipment that cause noise and vibration include motors, generators, and alternators,<sup>5,13</sup> transformers, relays, solenoids, and circuit breakers. Electric motors are used widely in appliances, vehicles, and industry in a variety of types and sizes. They may be commutated, synchronous, or induction types. Electrical energy is converted into mechanical energy, and in the process some heat is produced. Fans are often provided to remove the heat and are the main sources of noise in electric motors. Because of the requirement for most motors that they should operate in either direction of rotation, they are usually provided with axial or tubular centrifugal fans, which can be quite noisy. The sources of noise and vibration in electrical equipment are mostly aerodynamic, mechanical, and electromagnetic in nature. They are summarized in Table 1. Electric motors and the noise they generate are discussed in detail in Chapter 72.

Electric motor noise is normally controlled by passive means (use of enclosures, sound-absorbing materials, vibration isolation, etc.) The pure-tone vibration and noise produced at twice line frequency and multiples can also be reduced by active control methods, although active control of electrical equipment so far has received limited attention. One exception is the active control of the vibration and noise of large electrical transformers, which has been successfully reduced by active vibration control approaches.

## 6 PUMP AND PUMPING SYSTEM NOISE

Chapter 73 presents a detailed review of the noise of pumps and pumping systems. Pumps are used to transport liquids and suspensions of solid particles in hydraulic systems. The noise generated in such systems is produced not only by the pump but also by the driving motor (usually an electric motor with its cooling fan). The noise and vibration created is

**Table 1 Main Sources of Noise in Electric Motors**

Mechanical	Excessive bearing clearance
	Nonround bearings
	Rotor unbalance
	Rotor eccentricity
	Crooked shaft
	Brush and brush holder vibration
	Misalignment
	Loose laminations
Electromagnetic	Magnetostriction
	Torque pulsations
	Air gap eccentricity
	Air gap permeance variation
	Dissymmetry
	Sparking or arcing
Aerodynamic	Fan blade-passing frequency
	Turbulence
	Noise due to airflow path restrictions



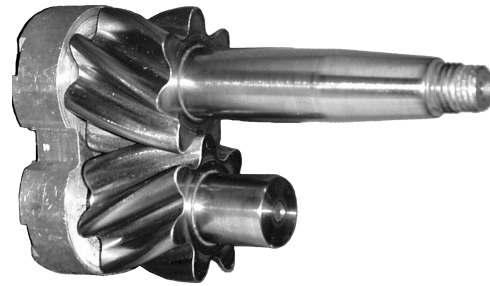
carried throughout the hydraulic system as fluid-borne noise and mechanically by the pipe system itself as structure-borne noise.<sup>42,43</sup>

There are three main types of pumps: (1) positive displacement, (2) kinetic (i.e., dynamic), and (3) special effect. Some of the main pump designs are illustrated in Fig. 1 of Chapter 73 and are similar in many ways to compressors used to pump or transport gases as described in the next section of this chapter and in Chapter 74. Positive-displacement pumps work by periodically adding energy to the fluid by one or more elements moving within a cylinder or pump case. In a similar way to positive displacement compressors, positive displacement pumps can be further subdivided into reciprocating and rotary types. The operation of a pump causes mechanical forces resulting in vibration, and even more important, pressure pulsations in the fluid, both of which cause noise. Rotary pumps can be divided into two main types: those possessing single rotors and those with multiple rotor elements. There are many different types of single- and multiple-type pumps including vane, gear, lobe, and screw types as shown in Fig. 1 of Chapter 73.

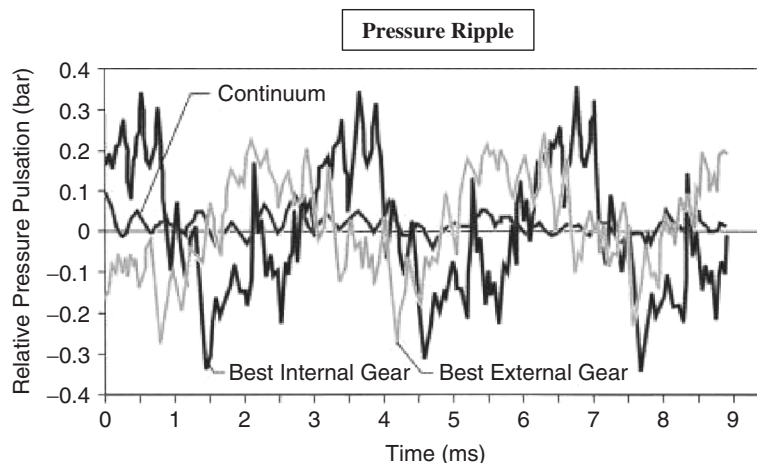
The main sources of noise in reciprocating pumps include: (1) flow and pressure pulsations sometimes called “ripple,” turbulent and separated flows, and vortex formation in the fluid, and (2) unbalanced mechanical forces, inlet and discharge valve impacts, and piston slap. The main sources of noise in rotary pumps depend upon the pump design and include (1) fluid pressure pulsations, turbulence, and vortices and (2) mechanical forces resulting from impacts between the teeth of gear pumps, the sliding of the vanes of vane pumps, and friction forces created in screw types of pumps. Gear pumps are noisy since they trap and compress the working fluid between the gear teeth and expel it perpendicular to the axes of revolution. They can operate at pressures of 150 bars

or more. Screw pumps are generally much quieter and move the fluid in a direction parallel to the screw axis but are limited to lower pressures, usually less than about 40 bars.

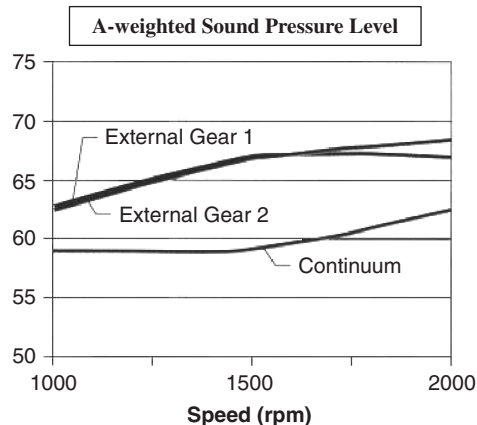
Various designs of pump have been produced to reduce ripple.<sup>43</sup> One novel design has gear/screw elements that makes it a cross between a gear and screw pump. (See Fig. 6.) The two contrarotating elements tend to balance internal forces and torques thus reducing vibration and noise. It is claimed that this type of pump, termed a Continuum<sup>®</sup> pump, virtually eliminates the trapping of fluid between gear teeth by using special helical gears, which results in much less pressure ripple and pump noise. The pump can operate at speeds up to 5000 rpm and pressures as high as 240 bars. Figure 7 shows the pressure pulsations (ripples) for two different designs of gear pump and the Continuum<sup>®</sup> pump when they were all operated at



**Figure 6** Continuum<sup>®</sup> continuous-contact pumps feature helical gears that do not trap fluid as they rotate, as is the case with conventional gear pumps. This minimizes pressure ripple and gives high efficiency and quiet operation at speeds to 5000 rpm.<sup>43</sup>



**Figure 7** Laboratory tests that show reduced pulsation pressure (ripple) for the continuous-contact Continuum<sup>®</sup> pump compared with similar gear pumps. The pulsation tests were conducted at 100 bars, 1500 rpm, and with pressure sampling at 100 kHz.<sup>43</sup>



**Figure 8** Laboratory measurements of the noise of two external gear pumps and the Continuum<sup>®</sup> pump. The measurements were made when all of the pumps were running at 1500 rpm. The pressure produced by all the pumps in the noise test was 150 bars.<sup>43</sup>

1500 rpm and a pressure of 100 bars. It is seen that these continuous-contact pumps exhibit a much smaller magnitude of ripple. Figure 8 presents the A-weighted sound pressure levels measured using the ISO 4412 method for two gear pumps and the continuous-contact pump when they were tested under similar operating conditions. The overall A-weighted sound pressure level of the continuous-contact pump does appear to be of the order of 5 to 8 dB lower than the noise levels of the two other pumps and supports the idea that the pressure ripple is a major source of noise in most pump types.

The flow and pressure ripple effects can also be reduced by the use of dampers or accumulators and/or by very careful and precise manufacturing and grinding of the parts of the pump. Dampers can be similar to muffler expansion chambers in design or have special design features including flexible membrane parts to absorb the pressure pulsations. Efforts continue to be made to reduce pump ripple<sup>44</sup> and cavitation,<sup>45,46</sup> which can cause serious damage to pumps and hydraulic systems. Different methods are used to improve pump design<sup>47-49</sup> and also for diagnostics and health maintenance of pumps and hydraulic systems.<sup>50,51</sup> Precision grinding of parts does add cost and this must be considered in choosing a pump system.

## 7 COMPRESSOR NOISE

Compressors can be considered to be pumps for gases. Although there are some differences in construction details between compressors and pumps, their principles of operation, however, are essentially the same. (See Chapter 74.) Since gases normally have much lower densities than liquids, it is possible to operate compressors at much higher speeds than pumps. However, gases have lower viscosities than most liquids

and so leakage with compressors is more of a problem than with pumps. Thus, this requires tighter manufacturing tolerances in the moving parts of compressors. Due to the low viscosity of gases and their compression, the temperature of the working medium and of the machine itself increases during compression. As a consequence, when the pressure ratio from after to before compression is more than about five, additional cooling is needed for the compressor and lubrication system. This makes compressors more complicated, as regards maintenance and servicing than pumps used for liquids. In general compressors are more expensive to operate than pumps.

Compressors are used for many different applications, and there are a large number of quite different designs. Rather like pumps, there are two basic types of compressor: (1) positive-displacement compressors including reciprocating piston, and rotary types and (2) dynamic compressors including axial and centrifugal types. Like pumps, there are a few special-effect compressor types as well. Positive-displacement compressors operate by increasing the pressure of the gas by reducing its volume in a compression chamber through work applied to the compressor mechanism. Dynamic compressors, on the other hand, work on the principle of using bladed impellers on continuously flowing gas to increase its kinetic energy, which is eventually converted into potential energy and gas of higher pressure.

Very large numbers of small positive-displacement compressors have been mass produced around the world for use in household refrigerators and domestic and automobile air-conditioning systems. Considerable efforts, which are driven in part by market forces, have been expended to produce quieter small positive-displacement compressors. Positive-displacement compressors can be characterized by the location of the motor: (1) External-drive (open-type) compressors have a shaft or other moving part extending through the casing and are driven by an external power source, thus requiring a shaft seal or equivalent rubbing contact between fixed and moving parts; (2) hermetic compressors have the compressor and motor enclosed in the same housing shell without an external shaft or shaft seal and the motor operates in the compressed gas; and (3) semi-hermetic refrigerant compressors have the compressor directly coupled to an electric motor and contained within a gas-tight bolted casing. Positive-displacement compressor mechanisms can be further subdivided into (a) reciprocating types: piston, diaphragm, or membrane, and (b) rotary types: rolling piston, rotary vane, single-screw, twin-screw, scroll and, trochoidal (lobe).

The noise generated by the piston type of compressor depends upon several factors, the most important being the reciprocating frequency and integer multiples, number of pistons, valve dynamics, and acoustical and structural resonances. The noise produced by the rotary types depends upon rotational frequency and multiples, numbers of rotating elements, flow capacity, and other flow factors. The

noise generated by centrifugal and axial compressors also depends upon rotational frequency, that is, the number of rotating compressor blade elements. Flow speed and volume flow rate, however, are also important factors. Such dynamic compressors are used in aircraft jet engines and large commercial electricity generating plants. Chapter 74 describes some design, operational noise, and vibration features of several categories of dynamic compressors in use and also gives some examples of how noise and vibration problems have been overcome in practice.

## 8 CONTROL VALVES

Control valves are used in industrial plants to control the rate of fluid flow by creating a pressure drop across the valve. The flow is first accelerated by this process and then the kinetic energy is converted into thermal energy or heat through turbulence and/or shock waves. In the process a small fraction of the energy is converted into acoustical energy and thus noise. The aerodynamic noise generated by control valves, regulators, and orifices is a major noise source in piping systems. In some cases exterior noise levels as high as 130 dB can be produced. In addition, in liquid flow systems, hydrodynamic noise (which is mostly due to cavitation) is of some importance. However, in most industrial situations, with high-speed gas flows, the aerodynamic noise is dominant.<sup>52</sup> The main noise-generating mechanisms include turbulent mixing, turbulence interaction with boundaries, cavitation in liquids, shock waves, interaction of turbulence with shocks, cavity resonances, flow separation, vortex shedding, "whistling," and resonant mechanical vibration of valve components.<sup>53,54</sup> Figure 9 presents a simplified view of a control valve and some of the noise sources.<sup>54</sup> See Chapter 75 for an extensive discussion on this subject. Comprehensive reviews of control valve noise have also been given by Reethof.<sup>53,54</sup> Seebold has reviewed control valve noise sources and approaches for noise control.<sup>55</sup>

The major noise-generating processes can be divided into two regimes: *subsonic*, consisting mostly

of turbulence–boundary interaction noise, and *supersonic*, consisting mainly of broadband shock noise. Although the flow is confined by the piping, the turbulent mixing noise is similar to the noise of a free jet discussed in Chapters 9 and 89 and is essentially quadrupole in nature. The shocks are caused by abruptly expanded flow after the valve, when it is operating above the critical pressure ratio. The shock noise has two main parts: screech and broadband noise. The screech is discrete in nature and is caused by a feedback mechanism and is not often encountered with valves and regulators. The broadband shock noise is common, however, and has been shown to be mostly independent of flow velocity and to be a function of the pressure ratio across the valve. Valve noise can be reduced by several approaches including design of valves with multiple streams, arranging for the pressure drop to occur through several stages, and using absorptive silencers, thicker pipe walls, and pipe lagging. Multiple stream valve designs and absorptive silencers are effective at reducing noise. Absorptive silencers can produce noise reductions of as much as 15 to 30 dB. However, such silencers can become plugged by solid particles and moisture can be a problem in the silencer material so that effectiveness is lost. Chapter 75 deals in detail with noise-generating mechanisms and the prediction and control of control valve noise. Several other authors have also given helpful reviews of valve and piping system noise, and the reader is referred to these as well for more detailed discussions.<sup>15,52–55</sup>

## 9 HYDRAULIC SYSTEM NOISE

Chapter 76 deals with high-pressure hydraulic fluid power systems using positive-displacement pumps. The diameter of pipes used in such systems is usually quite small (of the order of 10 to 50 mm). The flow is normally single phase with negligible gas bubble and solid particle content. The usual operating pressures are of the order of 100 to 300 bars. There are systems, however, which operate at pressures of up to 500 or even 650 bars. Hydraulic systems often produce very high noise levels that can limit the range of

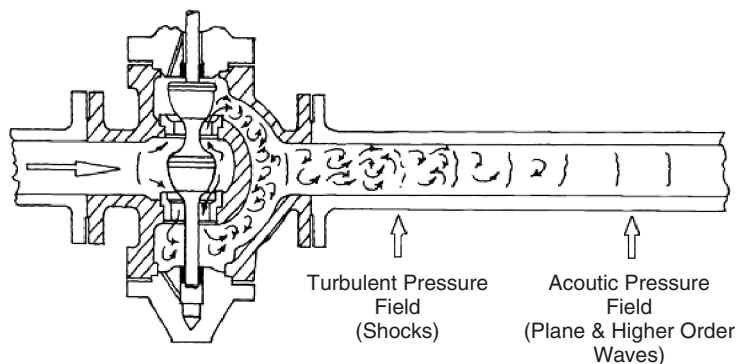


Figure 9 Schematic representation of control valve noise generation and propagation.<sup>54</sup>

applications of fluid power systems. Potential high-level noise problems can result in the choice of an alternative means of power transmission in cases where low-noise systems are required.

As discussed in Chapter 76, hydraulic system noise sources may be categorized as follows: (1) *Airborne noise* originates from the vibration of components, piping, and housings and is transmitted directly through the air. (2) *Structure-borne noise* is caused by the mechanical operation of pumps and motors and is transmitted from pumps directly through mounts, drive shafts, and pipes. Structure-borne noise can also arise from the pressure “ripple” in the hydraulic system. (3) *Fluid-borne noise* is caused primarily by unsteady flow from the pumps and motors but can also be caused by valve instability, cavitation, and/or turbulence. Fluid-borne noise can be transmitted considerable distances through pipework with little attenuation. Figure 10 gives an illustration of (a) structure-borne noise and (b) fluid-borne noise (commonly called ripples) created by a multipiston axial-flow pump.

The main sources of noise in a hydraulic system are usually the pumps and motors. Valves are also important noise generators. See Chapter 75 for further discussion on valve noise. Positive-displacement pumps are mainly used in fluid power applications. The most common types are piston pumps, gear pumps, and vane pumps. See Chapter 73 for more detailed discussion on pump noise. Positive-displacement pumps produce a steady fluid flow rate on which is superimposed

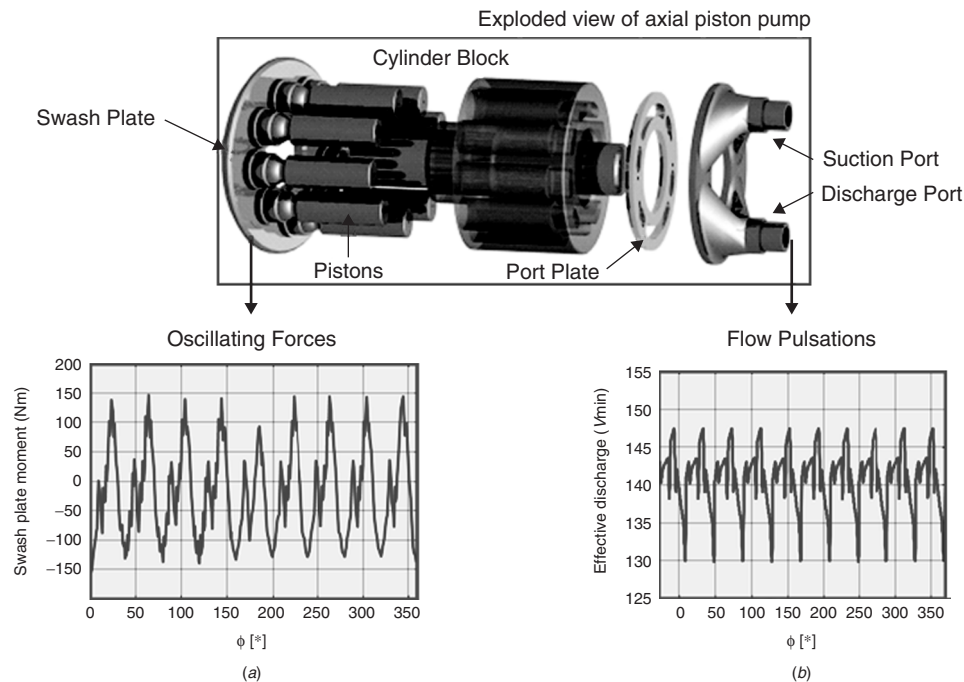
a flow fluctuation or ripple, which is caused by the cyclic nature of the pump operation. The flow ripple is also manifested as a pressure fluctuation or ripple. The magnitude of the flow ripple depends on the pump type and its operating conditions. See Chapter 76. Flow ripple normally occurs in both the suction and the discharge lines. Usually the discharge flow ripple is the most important noise source. Fluid-borne noise in the suction line may cause noise problems especially when it causes vibration and noise radiation from a large-surface reservoir.

There are several ways of reducing the noise of hydraulic systems as described in Chapter 76 and Ref. 9. These include (1) reduction of the pump or motor flow ripples,<sup>43</sup> (2) tuning of the circuit in order to avoid resonant conditions, (3) use of silencers or pulsation dampers, (4) using flexible hoses,<sup>42</sup> (5) vibration isolation,<sup>42</sup> and (6) use of enclosures or pipe cladding.

## 10 COMBUSTION NOISE

As described in Chapter 77, the phenomenon of thermoacoustically induced oscillations and combustion noise, or “roar,” in combustion systems is complicated and usually only qualitative explanations can be given. Various empirical methods have been developed to predict combustion noise. In practice, engineering solutions are mainly used to control combustion oscillations and noise.

Combustion systems consist of two main fuel and air delivery system components: (1) burner and



**Figure 10** Pump forces result as airborne noise (not shown) and (a) structure-borne noise through the piping system and (b) fluid-borne noise (flow and pressure fluctuations called ripples).

(2) combustor. The fuel injection component is usually called the burner. The element within which the heat release takes place is normally referred to as the combustor or furnace. The purpose of combustion systems is to add heat to an airstream. The main mechanisms that produce combustion noise are common to all combustion systems.

As described in Chapter 77, the purpose of the fuel burner is to mix and direct the flow of fuel and air to ensure rapid ignition and complete combustion within the furnace or combustor. The combustion of gaseous fuels takes place mainly in two ways: (1) when the gas and air are mixed before ignition, known as premix flames, and (2) when the gas and air are mixed after the fuel has been heated, known as diffusion flames.

The noise generated by the combustion can be considered to be either (1) combustion roar or (2) combustion-driven oscillations or thermoacoustic instabilities. The latter type of noise is observed when pressure oscillations are induced by heat release oscillations. Although thermoacoustic instabilities are closely related to flame instabilities, their instability criteria are different. The main focus of Chapter 77 is on thermoacoustic instabilities since they can produce higher sound pressure levels than combustion roar and since they also have a greater potential for structural damage. It should be noted that some researchers further subdivide combustion noise into four categories.<sup>56,57</sup> Figure 11 shows two types of flame. Type 1 flames tend to be relatively quiet and type 2 flames tend to be relatively noisy. It has been found by several researchers that if sufficient swirl is introduced into the flow that flames change from type 1 to type 2.<sup>56-59</sup>

There are two main passive noise control measures available: (1) reducing the combustion-induced sources and (2) use of traditional noise control approaches including use of absorptive mufflers,

acoustical resonators, enclosures for the burner, furnace, or boiler or other units to which they are attached. Active approaches to control thermoacoustic oscillations have also been attempted as described in Chapter 77.

## 11 METAL CUTTING

Many industrial processes involve cutting metals. Metal-cutting processes can either be *continuous* or *impulsive* in character. Examples of continuous processes include sawing, drilling, milling, and grinding. Additional continuous cutting processes use of water jets, for cutting steel plates up to 300-mm thickness and plasma and laser cutting techniques. Examples of impulsive processes include punching, piercing, and shearing. Chapter 78 discusses noise sources due to *continuous* metal-cutting processes and to *impulsive* impact/shearing processes. The chapter also covers basic theory for the noise emission caused in the cutting of metals. In addition various noise control approaches (such as use of enclosures, damping materials, sound absorption materials, barriers, and vibration isolation) to reduce metal-cutting noise are presented. Chapter 78 reviews numerical methods to predict metal-cutting noise and vibration as well.

As described in Chapter 78 the following noise sources can be observed in continuous metal-cutting processes: (1) aerodynamic noise usually caused by vortex shedding from a spinning tool such as from the teeth of a high-speed rotating saw, (2) noise caused by vibrations of the cutting tool, (3) noise due to structural vibration and radiation from the cutting tool and the workpiece such as regenerative chatter, and (4) noise due to material fracture in which energy is built up until it is released at fracture as acoustic emission.

The noise level radiated by continuous cutting processes depends on the feed rate of the workpiece,

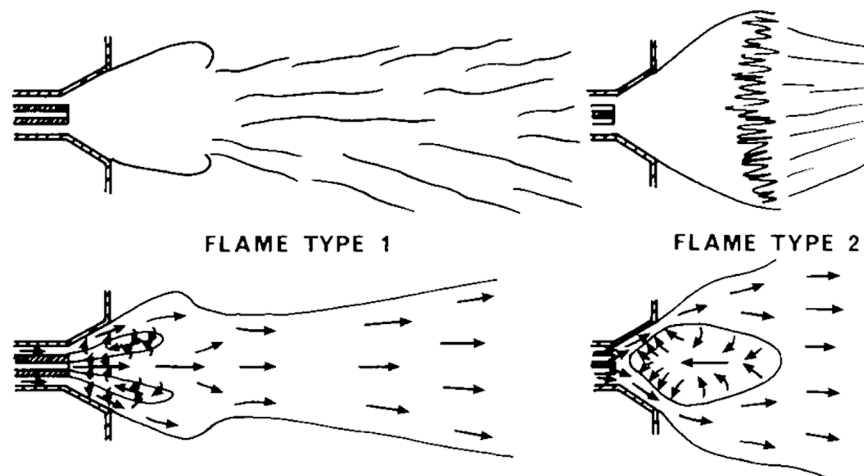


Figure 11 Flame types in burners incorporating swirl.<sup>57</sup>

the depth of cut, the resonance frequencies of the cutting tool and the workpiece, the geometry of the cutting tool and the workpiece, and the radiation efficiencies of the resonant modes of vibration. In impulsive cutting processes such as stamping, forging, punching, piercing, and shearing, impulsive forces are involved. The noise generated by these operations includes acceleration noise, ringing noise, noise due to fracture of the feedstock material (cutting noise), and other machinery noise sources. Acceleration noise is generated by the impact between the cutting blade and the feedstock, causing the air around to be compressed due to the rapid surface deformations. This noise is usually low frequency in nature and is normally much less than the ringing noise caused by flexural vibrations.

Ringing noise is generated from vibrations of the feedstock and machine structure including the machine foundations; it usually makes a significant contribution to the overall noise generated during the metal-cutting process. The magnitude of the ringing noise depends on the radiation efficiency, and spatial averaged mean-square normal vibration velocity of the surface and its area, the air density, and speed of sound in air. In some cases, the ringing noise can be effectively reduced by the judicious use of damping materials. Richards et al. have published extensive discussions on acceleration noise and ringing noise.<sup>60,61</sup> Chapter 78 also provides more details. Ringing noise can be reduced by mechanical clamping of the workpiece as shown, for example in Fig. 12. The blade-radiated noise is also reduced because the saw blade is "buried" beneath the work table for much of the time, and the operator is shielded from its noise. Acoustical shielding such as this is particularly effective for the high-frequency saw blade noise.

Large numbers of circular saws are used all over the world to cut metal, stone, and wood. They are an effective but very noisy form of cutting tool. Many different passive methods have been used to reduce the noise of circular saws. These range from source, path, to receiver approaches. The most effective approach is to control the saw noise at the source. One approach reported by Bobeczko involves minimizing the kerf (tooth width), slotting the blade body and adding collars to stiffen and damp the blade vibration, see Figs. 13 and 14.<sup>62</sup> Figure 14 shows that an A-weighted noise reduction of 19 dB was achieved in this particular case. This particular type of blade was used extensively over seven years without mechanical problems.<sup>62</sup> To avoid problems, however, it should be made by a skilled machinist.<sup>62</sup>

It is believed that the blade shown in Fig. 13 is substantially quieter than similar blades, because (1) the natural modes of vibration have been changed, (2) the slots allow some cancellation of sound radiated from the front and back of the blade, and (3) the added collars and plugged stress release holes add some stiffness and damping, thus reducing the blade vibration and consequent sound radiation. Research continues on reducing metal cutting noise.<sup>63-70</sup>

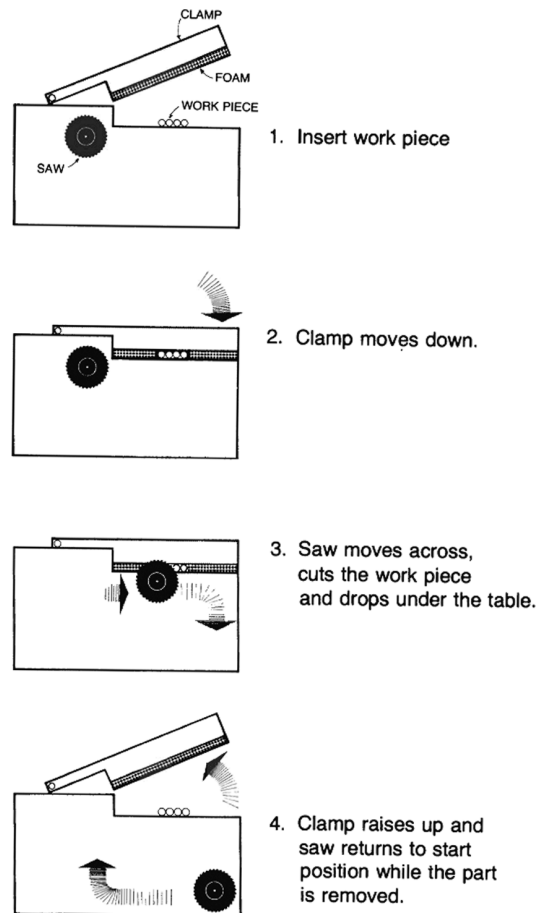


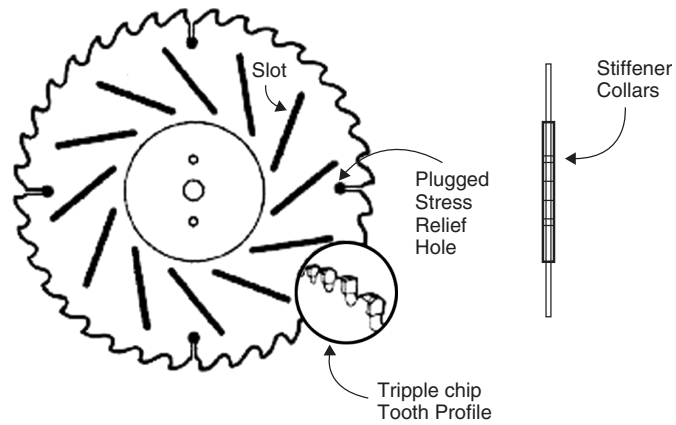
Figure 12 Saw blade noise control.<sup>62</sup>

## 12 WOODWORKING NOISE

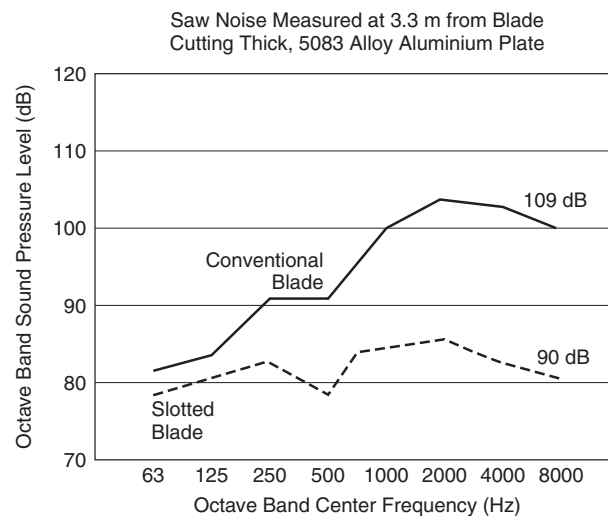
Woodworking machinery includes a wide variety of equipment, ranging from off-road forest equipment to simple circular saws, band saws, and jig saws used in industrial and residential workshops. Extremely high noise levels produced by these woodworking machines during both operating and machine idle conditions pose a severe threat to the hearing of the operators of such machinery. See Chapter 79.

Many industrial woodworking machinery noise sources result from the use of cutters and saw blades. Cutters are widely used in the woodworking industry on machines such as planers, molders, cutters, routers, and the like to smooth and shape wood. Most cutters have several rows of knives that protrude above the cutter body, which is normally cylindrical. In many cases the machining process involves a peripheral milling in which each knife removes a "chip," leaving a relatively smooth surface. The smoothness of the cut depends on the machine feeds and speeds used. Most cutters have straight knives (aligned parallel to





**Figure 13** Slotted saw blade.<sup>62</sup>



**Figure 14** Octave band noise levels of saw blades. Overall A-weighted levels also shown 109 dB — conventional blade, 90 dB — slotted blade.<sup>62</sup>



**Figure 15** (a) Use of complete panel enclosure for molder noise and (b) use of mass-loaded vinyl "curtains" to control rip saw noise.<sup>71</sup>

the cutter rotational axis). This design of cutter is used because it is easy to manufacture and sharpen as needed. Although this design of cutter is effective in working the wood, it is inherently noisy.

The compression of the air, which is caused when cutters rotate near to a stationary surface, results in a siren-type noise mechanism. This mechanism is very efficient in generating sound. This noise is pure tone in nature and occurs at the knife blade passage frequency. As discussed in Chapter 79, the rotating cutter A-weighted noise level increases with cutter rpm and also increases with decreasing distance (clearance) between the knives and the stationary surfaces. The A-weighted noise level produced by rotating cutters during idle also increases with increasing length of the cutter.

Complete durable panel enclosures such as those illustrated in Fig. 15a can have an A-weighted insertion loss of as much as 20 dB, provided considerable care is taken to seal the enclosure wherever it is possible and feasible. The enclosure shown in Fig. 15a was built to house a wood molder and is provided with a viewing window and an entry door to provide access to the tool inside. An additional barrier/guard at the wood output location is provided to accommodate varying sizes of wood parts being molded.<sup>71</sup> The insertion loss is limited in practice by the need for the penetration provided for the workpiece. Figure 20 in Chapter 54 shows another similar example of a woodworking machine enclosure for a band saw. The A-weighted insertion loss of mass-loaded vinyl barrier quilted blankets (commonly called "curtains"), as shown in Fig. 15b, is typically only about 5 to 7 dB. However, the assembly of the curtain system is relatively simple and the cost of the mass-loaded curtain system shown in Fig. 15b, is less than that of the complete enclosure shown in Fig. 15a. Curtains, however, are not as durable as panel enclosures and normally must be replaced periodically.

### 13 NOISE CONTROL OF INDUSTRIAL PRODUCTION MACHINERY

Chapter 80 discusses noise in production areas of manufacturing plants. Production machinery and equipment that generate intense noise include machines that operate with impacts such as forging hammers,<sup>72,73</sup> cold headers, stamping presses, riveters, jolting tables, some machine tools, and impact-generating assembly stations. With the exception of forging plants, in which forging hammers are the dominating source of noise, noise sources in manufacturing plants can be typically classified in order of intensity/annoyance as: (1) *compressed air* (leakages, air exhaust, air blowing nozzles), (2) *in-plant material handling systems*, and (3) *production and auxiliary machinery and equipment*. The two basic noise reduction techniques are (1) use of acoustical enclosures, which are expensive to build and maintain, may reduce efficiency of the enclosed equipment, and are not always feasible, and (2) noise reduction at the source, which is effective but often requires a research and development effort. Chapter 55 describes different methods of identifying sources of noise and vibration in machinery.

Chapters 54 and 56 to 62 describe the main methods of passive noise and vibration control. Chapters 63 and 64 describe methods of active noise and vibration control and Chapter 66 discusses ideas of how machines can be designed to be quiet, right from the inception. Reference 74 contains a large number of case histories of successful noise reduction projects carried out in industry.

### 14 MACHINE TOOL NOISE, VIBRATION, AND CHATTER

Chapter 81 discusses the problem in the manufacturing industry of the chatter-induced vibration in machine tools during machining. Such problems occur, for example, in turning, milling, boring, and grinding. Chatter is very undesirable. Not only does it create noise but the vibration that it produces also results in an uneven cut and undesirable cut quality. The vibration of machine tools may be divided into three different classes: (1) free or transient vibrations of machine tools excited by other machines or engagement of the cutting tool and the like, (2) forced vibrations usually associated with periodic forces within the machine tool, for example, unbalanced rotating masses, and (3) self-excited chatter that may be explained by a number of mechanisms. These mechanisms include, among others, the regenerative effect, the mode coupling effect, the random excitation of the natural frequencies of the machine tool caused by the plastic deformation of the workpiece material, and/or friction between the tool and the cut material. Vibration in machine tools affects the quality of machining, particularly the surface finish. Furthermore, machine tool life can be correlated with the vibration and noise levels produced. Machine tool chatter may be reduced by selective passive or active modification of the dynamic stiffness of the tooling structure and/or by the control of cutting data and its use to maintain stable cutting. Forced unbalance vibration in rotating tooling structures may be reduced by passive balancing or active online balancing.

The vibration of machine tools may be divided into three different classes: free or transient vibration, forced vibration, and self-excited chatter or vibration. Free or transient vibrations of machine tools may be excited by other machines in its environment via the machine tool base or/and by rapid movements of machine tables, engagement of the cutting tool, and the like. The forced vibrations are usually associated with periodic forces within the machine tool, for example, unbalanced rotating masses, or the intermittent tooth pass frequency excitation in milling. This type of vibration may also be excited by other machines in the environment of the machine tool via its base.

Machine tool vibrations during machining operations are usually denoted *self-excited chatter* or *tool vibration*. Depending on the driving force of tool vibration, the vibration is generally divided into one of two categories: regenerative chatter (secondary chatter) and nonregenerative chatter (primary chatter). See Refs. 75 to 77 for examples. Extensive research has been carried out on the mechanisms that control the induction



of vibrations in the cutting process. The majority of this research has involved the dynamic modeling of cutting dynamics focusing on analytical or numerical models. Usually, the purpose of this work is to produce dynamic models for the prediction of cutting data that ensure stable cutting and maximize the material removal rate. Active control has also been investigated for turning and boring operations.<sup>78,79</sup>

## 15 SOUND POWER LEVEL PREDICTIONS FOR INDUSTRIAL MACHINERY

Chapter 82 discusses procedures for calculating the sound power level of industrial machinery. In the European Community (EEC) it is required to determine the sound power level of some items of machinery and to provide a label on the machine giving this information. The measured or calculated sound power levels (given in Chapter 82) can be used for predicting the sound pressure levels in a space or developing purchase specifications for new equipment.

With any project, acoustical data measured and calculated in accordance with recognized standards should be obtained. Many manufacturers provide sound power levels or measured sound pressure levels at 1 m from their equipment, and some offer special low-noise options. If manufacturer's data are unavailable, efforts should be made to measure a similar unit in operation. If this is not practical, then the material in Chapter 82 can be used.

Most of the equations presented in this chapter are based on measured data and tend to be conservative, usually predicting somewhat higher sound pressure levels than are measured in the field. Due to recent efforts at reducing equipment noise, sound pressure levels for some equipment may be significantly (10 dB) quieter than the levels calculated in this chapter.

Some equipment consists of several different sound-producing components such as motors, pumps, blowers, and the like. The sound power levels for each component should be determined and then combined (using correct decibel addition) to get the total sound power levels.

## 16 INTERNAL COMBUSTION ENGINES

The internal combustion engine is a major source of noise in transportation and industrial use. The intake and exhaust noise can be effectively silenced. However, the noise radiated by engine surfaces is more difficult to control. In gasoline engines, a fuel-air mixture is compressed to about one-eighth to one-tenth of its original volume and ignited by a spark plug. In diesel engines air is compressed to about one-sixteenth to one-twentieth of its original volume and liquid fuel is injected in the form of a spray; then spontaneous ignition and combustion occurs. Because the rate of pressure rise is initially more abrupt with a diesel engine than with a gasoline engine, diesel engines tend to be noisier than gasoline engines. The noise of diesel engines has consequently received more attention from both manufacturers and researchers. The

noise of internal combustion engines is discussed in detail in Chapter 84.

The noise of engines can be divided into two main parts: combustion noise and mechanical noise. The combustion noise is caused mostly by the rapid pressure rise caused by ignition, and the mechanical noise is caused by a number of mechanisms, with perhaps piston slap being one of the most important, particularly in diesel engines. The noise radiated from the engine structure has been found to be almost independent of load, although dependent on cylinder volume and even more dependent on engine speed.<sup>80</sup> Priede has given a good review of internal combustion engine noise with an emphasis on diesel engine noise.<sup>81</sup> Reference 14 also includes detailed discussion on various aspects of engine noise.

## REFERENCES

1. L. H. Bell and D. H. Bell, *Industrial Noise Control*, 2nd ed., Marcel Dekker, New York, 1994.
2. C. M. Harris, Ed., *Handbook of Acoustical Measurement, and Noise Control*, 3rd ed., McGraw-Hill, New York 1991.
3. J. E. Shahan and G. Kamperman, Machine Element Noise, in *Handbook of Industrial Noise*, Industrial Press, 1976, Chapter 8.
4. J. D. Smith, *Gear Noise and Vibration*, 2nd ed., rev. and expanded, Marcel Dekker, New York, 2003.
5. P. L. Timar, Ed., *Noise and Vibration of Electric Machines*, Elsevier, Amsterdam, 1989.
6. P. Eschmann, L. Hasbargen, and K. Weigand, *Ball and Roller Bearings: Theory, Design, and Application*, Wiley, Chichester, 1985.
7. W. B. Rowe, *Hydrostatic and Hybrid Bearings Designs*, Butterworths, London, 1983.
8. D. D. Fuller, *Theory and Practice of Lubrication for Engineers*, 2nd ed., Wiley, Chichester, 1984.
9. S. Skaistis, *Noise Control of Hydraulic Machinery*, Marcel Dekker, New York, 1988.
10. G. Wilson, *Noise Control*, Prentice Hall, 1989, new edition, reprinted by Kreiger, New York, 2000.
11. M. P. Norton, *Fundamentals of Noise and Vibration Analysis for Engineers*, Cambridge University Press, Cambridge, 1989.
12. I. L. Ver and L. L. Beranek, Eds., *Noise and Vibration Control Engineering*, Wiley, New York, 2001.
13. J. F. Gieras, C. Wang, and J. C. Lai, *Noise of Polyphase Electric Motors*, Taylor and Francis, New York, 2006.
14. R. Hickling and M. M. Kamal, Eds., *Engine Noise, Excitation, Vibration and Radiation*, Plenum, New York, 1982.
15. W. F. Blake, *Mechanics of Fluid-Induced Sound and Vibration*, Academic, New York, 1986.
16. L. D. Mitchell, Gear Noise: The Purchaser's and the Manufacturer's Views. Noise and Vibration Control Engineering, *Proceedings of the Purdue Noise Control Conference*, M. J. Crocker, Ed., Purdue University, July 1971, pp. 95–106.
17. N. Amini, Gear Surface Machining for Noise Suppression, Ph.D Thesis, Chalmers University, Sweden, 1999, No. 1498, pp. 1–70.
18. Q. Lian and R. Dafoe, Using Advanced Theory, Geometry Modification, Manufacturing Realization to Localize Bearing Contact and Reduce Cylindrical Gear Noise, *VDI Bericht*, 2005, No. 19041, pp. 73–90.

19. Y. Chen and A. Ishibashi, Investigation of the Noise and Vibration of Planetary Gear Drives, *Gear Tech.*, Vol. 23, No. 1, 2006, pp. 48–55.
20. D. Palmer, Unique Gear Grinding Process Offers Low Noise and High Precision, *Eureka*, January 2005, pp. 13–14.
21. W. M. Viebrock and M. J. Crocker, Noise Reduction of a Consumer Electric Clock, *Sound Vib.*, Vol. 7, No. 3, 1973, pp. 22–26.
22. G. Wesley Blankenship and R. Singh, New Rating Indices for Gear Noise Based on Vibro-acoustic Measurements, *Noise Control Eng. J.*, Vol. 38, No. 2, 1992, pp. 81–92.
23. T. Zandbergen and G. van Nijen, Less Noise and Vibration by Proper Rolling Bearing Accuracy Design and Installation, *Shock Vib. Digest*, Vol. 32, No. 1, 2000, p. 40.
24. Extraction of Failure Characteristics of Roller Element Bearing Based on Wavelet Transform Under Strong Noise, *J. Harbin Inst. Tech. (New Series)*, Vol. 12, No. 2, 2005, pp. 169–172.
25. R. H. Lyon, *Machinery Noise and Diagnostics*, Butterworths, Boston, 1987.
26. G. E. Piper, J. M. Watkins and O. G. Thorp, Active Control of Axial-flow Fan Noise Using Magnetic Bearings, *J. Vib. Control*, Vol. 11, No. 9, 2005, pp. 1221–1232.
27. L. Huang and J. Wang, Acoustic Analysis of a Computer Cooling Fan, *J. Acoust. Soc. Am.*, Vol. 118, 2005, p. 2190.
28. L. Huang, Characterizing Computer Cooling Fan Noise, *J. Acoust. Soc. Am.*, Vol. 114, 2003, p. 3189.
29. L. Huang, Z. P. Zou, and L. Xu, Prediction of Computer Cooling Fan Noise Using a 3D Unsteady Flow Solver, *Noise-Con Proc.*, 2003, p. 84.
30. M. J. J. Nijhof, Y. H. Wijnant, A. de Boer, and W. M. Beltman, Optimizing Circular Side-Resonators to Reduce Computer Fan Noise, *Noise-Con Proc.*, 2004, p. 815.
31. J. W. Laage, P. Mahendra, P. J. Melzer, M. G. Olsen, J. Adin Mann, D. Yarbough, and C. Yu, Measurement Tools for Studying Fan Noise, *Noise-Con Proc.*, 2004, p. 593.
32. H. Shin, S. Lee, and K. B. Kim, The Axial Fan Noise Simulation by the FreeWake Method and Acoustic Analogy, *Noise-Con Proc.*, 2002, p. 2515.
33. W.-H. Jeon, D.-J. Lee, and H. Rhee, An Application of the Acoustic Similarity Law to the Numerical Analysis of Centrifugal Fan Noise, *Noise-Con Proc.*, 2002, p. 154.
34. M. S. Bobeczko, Condenser Fan Noise Reduction Solutions, *Noise-Con Proc.*, 2000, p. 133.
35. M. Langford, R. Burdisso, and W. Ng, An Overview of Flow Control for Fan Noise Reduction, *Noise-Con Proc.*, 2005, p. 289.
36. O. Jiricek and P. Konicek, Active Attenuation of Fan Noise in an Air-Conditioning Duct, *J. Acoust. Soc. Am.*, Vol. 103, 1998, p. 2836.
37. K. L. Gee and S. D. Sommerfeldt, Multi-channel Active Control of Axial Cooling Fan Noise, *Noise-Con Proc.*, 2002, p. 880.
38. K. Homma, C. Fuller, and K. Xiuting Man, Broadband Active-Passive Control of Small Axial Fan Noise Emission, *Noise-Con Proc.*, 2003, p. 410.
39. K. L. Gee and S. D. Sommerfeldt, Application of Theoretical Modeling to Multichannel Active Control of Cooling Fan Noise, *J. Acoust. Soc. Am.*, Vol. 115, 2004, p. 228.
40. J. Wang, L. Huang, and L. Cheng, A Study of Active Tonal Noise Control for a Small Axial Flow Fan, *J. Acoust. Soc. Am.*, Vol. 117, 2005, p. 734.
41. G. Minorikawa, H. Irikado, and T. Ito, Study on Sound Quality Evaluation of Fan Noise, *Noise-Con Proc.*, 2005, p. 36.
42. R. J. Becker, Noise Control in Hydraulic Equipment, *Noise-Con Proc.*, 1979, pp. 307–310.
43. Personal communication with Cesare Angeloni, 9 February 2006; see also website: [www.settimaafm.com](http://www.settimaafm.com) for further information on Continuum® pumps produced by Settima Meccanica s.r.l.
44. A. M. Harrison and K. A. Edge, Reduction of Axial Piston Pump Pressure Ripple, *Proc. Instit. Mech. Eng., Part I: J. Syst. Control Eng.*, Vol. 214, No. 1, 2000, pp. 53–63.
45. M. Čudina, Detection of Cavitation Phenomenon in a Centrifugal Pump Using Audible Sound, *Mech. Syst. Signal Proc.*, Vol. 17, No. 6, November 2003, pp. 1335–1347.
46. S. Al-Hashmi, F. Gu, Y. Li, A. D. Bail, T. Fen, and K. Lui, Cavitation Detection of a Centrifugal Pump Using Instantaneous Angular Speed, Proceedings of the 7th Biennial Conference on Engineering Systems Design and Analysis—2004, Manchester, UK, Vol. 3, pp. 185–190.
47. A. Johansson and J. O. Palmberg, Design Aspects for Noise Reduction in Fluid Power Systems, Proceedings of the Tenth International Congress on Sound and Vibration, July 7–10 2003, Stockholm, Sweden, pp. 3975–3982.
48. O. A. Mohamed, J. Charley, and G. Caignaert, Vibro-acoustical Analysis of Flow in Pipe System, *Am. Soc. Mech. Eng., Appl. Mech. Div.*, Vol. 253, No. 2, Proceedings of the 5th International Symposium on Fluid-Structure Interaction, Aeroelasticity, Flow-Induced Vibration and Noise, Vol. 2: Part B, 2002, pp. 881–888.
49. E. Carletti and I. Vecchi, Acoustical Control of External Pump Gear Noise by Intensity Measuring Techniques, *Noise Control Eng. J.*, Vol. 35, No. 2, 1990, pp. 53–59.
50. J. L. Parrondo, S. Velarde, J. Pistono, and R. Ballesteros, Diagnosis Based on Condition Monitoring of Fluid-Dynamic Abnormal Performance of Centrifugal Pumps, Proceedings of the 23rd International Conference on Noise and Vibration Engineering, ISMA, 1998, pp. 309–316.
51. Y. Gao, Q. Zhang, and X. Kong, Wavelet-based Pressure Analysis for Hydraulic Pump Health Diagnosis, *Trans. Am. Soc. Agric. Eng.*, Vol. 46, No. 4, July/August 2003, pp. 969–976.
52. K. M. Ng, Control Valve Noise, *ISA Trans.*, Vol. 33, 1994, pp. 275–286.
53. G. Reethof, Turbulence-Generated Noise in Pipe Flow, *Ann. Rev. Fluid Mech.*, 1978, pp. 333–367.
54. G. Reethof, Control Valve and Regulator Noise Generation, Propagation, and Reduction, *Noise Control Eng. J.*, Vol. 9, No. 2, 1977, pp. 74–85.
55. J. G. Seebold, Control Valve Noise, *Noise Control Eng. J.*, Vol. 24, No. 1, 1985, pp. 6–12.
56. A. A. Putnam, Combustion Noise in Industrial Burners, *Noise Control Eng. J.*, Vol. 7, No. 1, 1976, pp. 24–34.

57. A. Cabelli et al., Control of Noise from an Industrial Burner, *Noise Control Eng. J.*, Vol. 29, No. 2, 1987, pp. 38–44.
58. A. Putnam, *Combustion Driven Oscillation in Industry*, American Elsevier, 1971.
59. W. Leuckel and N. Fricker, The Characteristics of Swirl Stabilized Natural Gas Flames. Part 1: Different Flame Types and Their Relation to Flow and Mixing Patterns, *J. Inst. Fuel*, Vol. 49, 1976, pp. 103–112.
60. J. E. Richards, M. E. Westcott, and R. K. Jeyapalan, On the Prediction of Impact Noise, I: Acceleration Noise, *J. Sound Vib.*, Vol. 62, No. 4, 1979, pp. 547–575.
61. J. E. Richards, M. E. Westcott, and R. K. Jeyapalan, On the Prediction of Impact Noise, II: Ringing Noise, *J. Sound Vib.*, Vol. 65, No. (3), 1979, pp. 419–453.
62. M. Bobezko, Quieter Metal Cutting Methods and Machinery, *Noise Con Proc.*, 1979, pp. 163–169.
63. H. Trabelsi and E. Kannatey-Asibu, Tool Wear and Sound Radiation in Metal Cutting, in Production Engineering Division (Publication) PED, Vol. 45, Modeling of Machine Tools: Accuracy, Dynamics, and Control, Winter Annual Meeting of the American Society of Mechanical Engineers, Nov. 25–30 1990, Dallas, TX, 1990, pp. 121–131.
64. Y. Wu et al., Experimental Study of Cutting Noise Dynamics, in American Society of Mechanical Engineers, Design Engineering Division (Publication) DE, Vol. 36, Machinery Dynamics and Element Vibrations, 13th Biennial Conference on Mechanical Vibration and Noise presented at the 1991 ASME Design Technical Conferences, Sept. 22–25 1991, Miami, FL, 1991, pp. 313–318.
65. C. C. Ling, C. Cheng, J. S. Chen, and I. E. Morse, Experimental Investigation of Damping Effects on a Single Point Cutting Process, in American Society of Mechanical Engineers, Manufacturing Engineering Division, MED, Vol. 2–1, Manufacturing Science and Engineering, Proceedings of the 1995 ASME International Mechanical Engineering Congress and Exposition. Part 1 (of 2), Nov. 12–17 1995, San Francisco, CA, 1995, pp. 149–164.
66. A. Bahrami and H. M. Williamson, Effect of Blade Profile on Sheet Metal Shear Noise, Proceedings of the 1997 National Conference on Noise Control Engineering, NOISE-CON. Part 2, University Park, PA, June 15–17 1997, pp. 471–476.
67. M. A. Burgess, H. M. Williamson, and S. Kanapathipillai, Noise Reduction for Friction Saws, *Acoust. Austral.*, Vol. 26, No. 1, Apr. 1998, pp. 9–12.
68. A. Bahrami, H. M. Williamson, and J. C. S. Lai, “Control of Shear Cutting Noise: Effect of Blade Profile, *Appl. Acoust.*, Vol. 54, No. 1, May 1998, pp. 45–58.
69. J. C. S. Lai, C. Speakman and H. M. Williamson, Control of shear cutting noise: Effectiveness of Passive Control Measures, *Noise Vib. Worldwide*, Vol. 33, No. 7, July 2002, pp. 6–12.
70. A. Bahrami, J. C. S. Lai, and H. Williamson, Noise from Shear Cutting of Sheet Metal, in Proceedings of the Tenth International Congress on Sound and Vibration, Proceedings of the Tenth International Congress on Sound and Vibration, Stockholm, Sweden, July 7–10, 2003, pp. 4069–4076.
71. D. S. Cmar, Noise Control in the Woodworking Industry, September 2005. See the website: <http://www.phaseto.com/Noise%20Control%20in%20Woodworking%20Industry.htm>.
72. N. D. Stewart, J. A. Daggerhart, and J. R. Bailey, Experimental Study of Punch Press Noise, *J. Acoust. Soc. Am.*, Vol. 65, No. 6, 1974.
73. O. A. Shinaishin, Punch Press Noise, A Program for Analysis and Reduction, *J. Acoust. Soc. Am.*, Vol. 52, 1972, p. 156.
74. P. Jensen, C. R. Jockel, and L. Miller, *Industrial Noise Control Manual* (rev. ed.), NIOSH, December 1978, DHEW NIOSH Publication No. 79–117, PDF copy is available free of charge at the website: <http://www.cdc.gov/niosh/pdfs/79-117-a.pdf>.
75. H-Y Lai, Nonlinear Adaptive Modeling for Machining Chatter Identification and Monitoring, Vol. 7, Presented at the ASME Design Technology Conference—11th Biennial Conference on Mechanical Vibration and Noise., Boston, MA, 1987, pp. 181–187.
76. M. Shiraishi, K. Yamanaka, and H. Fujita, Optimal Control of Chatter in Turning, *Int. J. Machine Tools Manuf.*, Vol. 31, No. 1, 1991, pp. 31–43.
77. J. Pan and C-Y Su, Modeling and Chatter Suppression with Ultra-precision in Dynamic Turning Metal Cutting Process, Proceedings of the ASME Design Engineering Technical Conference, Vol. 6 B, 18th Biennial Conference on Mechanical Vibration and Noise, Pittsburgh, PA, Sept. 9–12 2001, pp. 1125–1132.
78. L. Andren, L. Hakansson, and I. Claesson, Active Control of Machine Tool Vibrations in External Turning Operations, *Proc. Instit. Mech. Eng., Part B: J. Eng. Manuf.*, Vol. 217, No. 6, 2003, pp. 869–872.
79. L. Andren, L. Hakansson, and I. Claesson, Performance Evaluation of Active Vibration Control of Boring Operations Using Different Active Boring Bars, Proceedings of the Tenth International Congress on Sound and Vibration, Stockholm, Sweden, July 7–10 2003, pp. 3749–3756.
80. R. G. White and J. G. Walker, (Eds.), *Noise and Vibration*, Ellis Horwood Publishers, John Wiley and Sons, New York, 1982.
81. T. Priede, in L. L. Beranek and I. L. Ver, Eds., *Noise and Vibration Control Engineering*, Wiley, New York, 1992, Chapter 19.

# CHAPTER 69

## GEAR NOISE AND VIBRATION PREDICTION AND CONTROL METHODS

Donald R. Houser

Gear Dynamics and Gear Noise Research Laboratory  
The Ohio State University  
Columbus, Ohio

### 1 INTRODUCTION

Gears are used in numerous applications where mechanical power is transmitted. If even an infinitesimal fraction of the transmitted power is converted to noise, gears can emit annoying and sometimes harmful sounds. The noise of gears in automobiles and other consumer products such as appliances, printers, and toys may be objectionable to the listener. The gear noise may actually exceed legal requirements and/or cause hearing damage in higher power products such as aircraft, ships, and industrial machines.

Two types of gear noise exist: whine and rattle. Gear whine is a periodic sound characterized by tones at the gear mesh frequency and its harmonics (integer multiples of mesh frequency). Gear rattle is an impulsive sound that occurs in lightly loaded gears that are externally excited by an oscillating torque. In practice, gear whine is usually more important than gear rattle, but gear rattle is sometimes of concern. The analysis of gear noise and its predominant frequencies are of considerable importance in the understanding of the gear vibration and noise generation process.

### 2 VIBRATION AND NOISE ENERGY FLOW

Figure 1 shows a typical gear arrangement of a modestly complex gearbox in which both displacement and force excitations occur at each gear mesh. The forces created at the mesh then excite the gear blanks and support shafting, both in the torsional and lateral directions. The resulting shaft dynamics then cause forces to be transmitted through the bearings to the housing, with the housing's vibrating panels radiating noise to the surroundings. Dynamic forces might also be transmitted either through the housing mounts or along the connecting shafts to other noise radiating surfaces. Figure 2 shows the energy flow in schematic form. This figure may be used by analysts to identify the steps in developing models to predict noise and vibration and by experimentalists to identify transducer locations along the gear noise and vibration paths.

### 3 GEAR NOISE AND VIBRATION IDENTIFICATION – THE FREQUENCY SPECTRUM

Gear whine is characterized by a periodic sound that has major components at the gear mesh frequency and

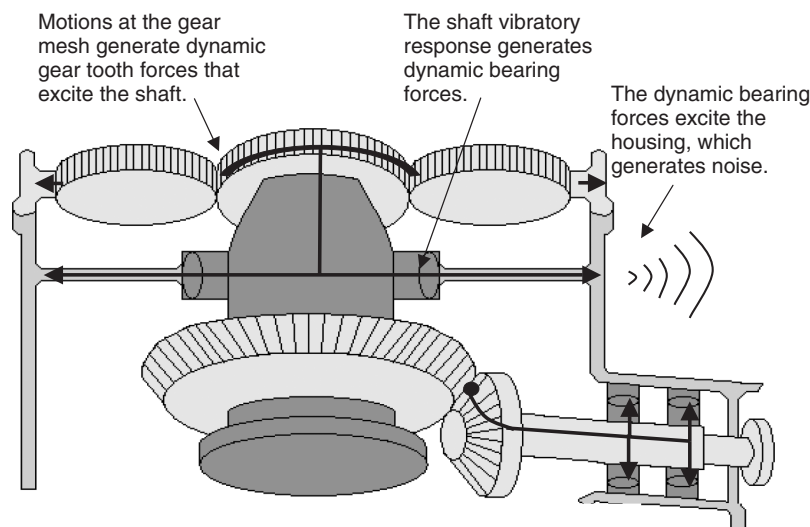
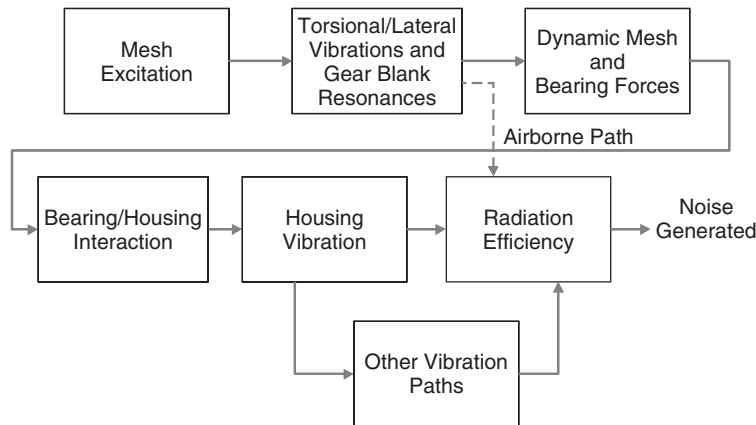


Figure 1 Multimesh gear train schematic.



**Figure 2** Gear noise energy flow diagram.

its harmonics. The mesh frequency may be calculated using the equation:

$$f_m = Nf_s$$

where  $N$  is the number of gear teeth and  $f_s$  is shaft frequency in hertz. A 25-tooth gear rotating at 1200 rpm has a mesh frequency of  $f_m = 25 \times 1200/60 = 500$  Hz. The mesh frequency computation for planetary gears is a bit more complex and depends upon the gear configuration.

The excitation of gear whine noise is periodic but is seldom sinusoidal. Therefore, gear whine noise will also occur at harmonics of mesh frequency. Modulations due to tooth spacing errors, eccentricities, and torsional vibrations may create sidebands that are spaced at shaft frequency intervals on either side of mesh frequency and its harmonics. These frequencies are identified on the frequency spectrum of Fig. 3.

Gear rattle, on the other hand, is difficult to identify from a frequency spectrum. The repeated impacts that occur from the loss of gear contact only increase

broadband noise that shows up as a rising of the noise floor of the spectrum.

#### 4 GEAR WHINE EXCITATION

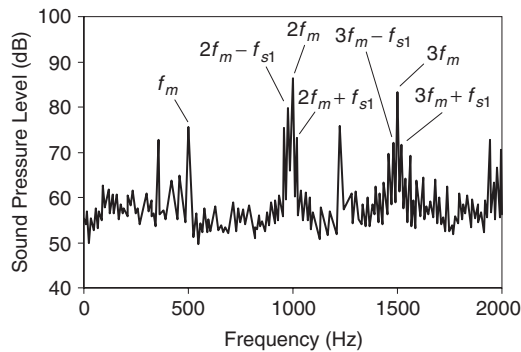
A survey of the literature has identified the following quantities that have been identified as excitations of gear whine noise<sup>1</sup>:

1. *Transmission Error (TE)* Defined as the deviation from perfect motion transfer of gears. Transmission error may be attributed either to profile deviations from perfect involutes (conjugate shapes) or to gear deflections that result from the transmitted load. The equation for angular transmission error, when referenced to the pinion, is

$$TE = \theta_p - m_g \theta_g$$

where  $\theta_p$  and  $\theta_g$  are the angular rotations of the pinion and gear, respectively, and  $m_g$  is the gear ratio. Transmission error may be expressed in linear units by multiplying the angular value by the pinion base radius.<sup>2-4</sup>

2. *Mesh Stiffness Variation* The change in tooth stiffness that occurs when the lengths of lines of contact change as the number of tooth pairs in contact change. These stiffness variations result in a time-varying parametric excitation of the torsional dynamic system. The deflection portion of transmission error results from mesh stiffness changes.<sup>5</sup>
3. *Axial Shuttling Force* A time-varying force at the bearings due to the centroid of the mesh force axially shifting back and forth along the tooth face width.<sup>6</sup>
4. *Friction Force* Results from the relative sliding that occurs in gear tooth meshing. As with axial shuttling, statics may be applied



**Figure 3** Frequency spectrum for a gear pair having a 25-tooth pinion rotating at 1200 rpm.

to obtain time-varying bearing forces resulting from friction.<sup>6,7</sup>

5. *Lubricant and/or Air Entrapment* In high-speed gearing, the air and lubricant in the root clearance and backlash regions must find an exit path. This may result in high velocities of pulsating fluid motion that can result in mesh frequency whistles.

Transmission error and mesh stiffness variation are closely related to one another and have historically been considered the primary gear noise excitations.<sup>5,8-11</sup> At light loads, transmission error is definitely the major cause of gear whine. However, at higher loads, low transmission error gears often still have significant gear noise, thus giving credence to load-dependent sources such as friction and shuttling. Since gear noise is generated from forces passing through the bearings and then exciting the housing, a more general gear excitation would be to calculate the net time-varying force that excites the bearings.<sup>12</sup>

#### 4.1 Gear Geometry Used in Predicting Gear Noise Excitations

Parallel axis, involute spur gearing will be discussed in this section, but the concepts presented may be extended to all types of gearing. The involute tooth shape is by far the most common tooth form in use today. The involute form is generated by unwrapping a string from the base circle (radii  $r_b$  and  $R_b$ , respectively) of each gear. In involute gears, the tooth contact force acts on a line tangent to the respective base circles of each gear as shown in Figure 4. Fig. 5 shows an expanded view of the line of contact in relation to a tooth of one of the mating pair. Here,  $Z$  is the length of the line of contact, which, for the driving gear tooth, begins at the start of the active profile (SAP) and extends to the tip of the tooth. As the gears rotate, the meshing begins with two pairs of teeth in contact and transitions to a single-tooth pair in contact in the central region of the tooth. Both the lowest point of single-tooth contact (LPSTC) and the highest point of single tooth contact (HPSTC) are designated on the figure. Contact ratio, the average number of tooth pairs in contact, is the ratio of the total length of contact,  $Z$ , to the base pitch,  $p_b$  (spacing of teeth along the base circle). The length of the contact may be calculated by

$$Z = \sqrt{r_o^2 - (r_p \cos \Phi)^2} + \sqrt{R_o^2 - (R_p \cos \Phi)^2} - C \sin \Phi$$

where  $r_o$  and  $R_o$  are the outside radii and  $r_p$  and  $R_p$  are the operating pitch radii of the respective gears,  $C$  is the center distance, and  $\Phi$  is the pressure angle.<sup>13</sup> A contact ratio of 1.4 means that two pairs of teeth are in contact 40% of the time and that one pair of teeth are in contact 60% of the time. When two tooth pairs are in contact, the mesh stiffness is about twice that of when one pair of teeth is in contact.

Figure 6 shows, for a perfect involute gear pair, the effect of stiffness change on the transmission error, first

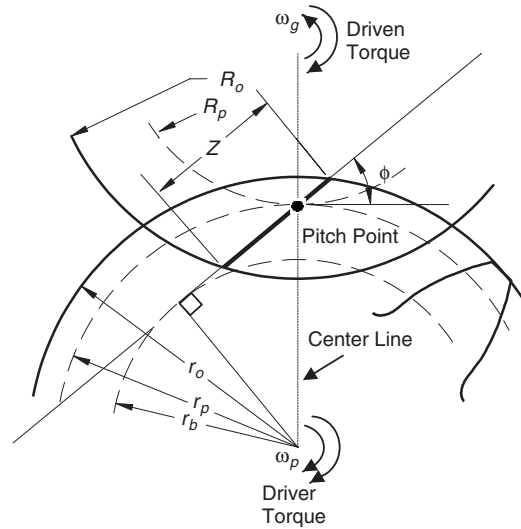


Figure 4 Gear contact line and the geometry associated with computing the contact ratio of a gear pair.

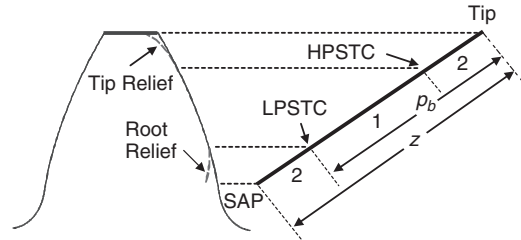


Figure 5 Line of contact nomenclature (numbers along the line indicate number of tooth pairs in contact).

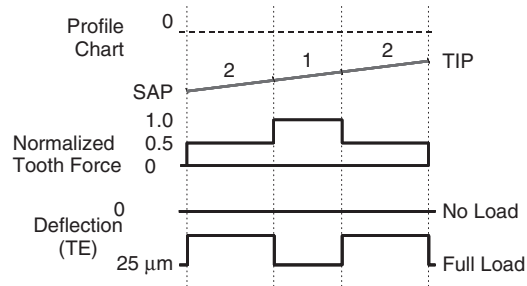


Figure 6 Transmission error and stiffness change for a perfect involute spur gear pair.

when the gears are under no load and then when they are fully loaded. Note that the gears run ideally with zero transmission error at no load. When the gears are loaded, the mesh deflection, which is a measure of transmission error, changes in a stepwise fashion as the number of tooth pairs in contact changes from one to two. A 3-module, fully loaded gear pair would have a deflection value in the order of 25  $\mu\text{m}$ , so a

typical transmission error in this situation would have a peak-to-peak value of 12.5  $\mu\text{m}$ . Also shown in this figure is the force carried by a single tooth as it rotates through the mesh. The step changes in tooth force are undesirable from a dynamics perspective.

#### 4.2 Minimizing Transmission Error – Effect of Profile Modifications

Transmission error in spur gears is minimized by removing material from the tip and root regions of the mating teeth such that the material removed compensates for the motion errors due to the change in stiffness. Assuming the tooth stiffness is linear with load, removing material linearly from each end of the tooth will achieve this cancellation (material removal is called tip relief or root relief, depending upon the region of the material removal). Figure 7 shows the tip relief starting at the highest point of single-tooth contact and progressing to the tip of the tooth. Root relief also varies linearly, and extends from the LPSTC to the SAP. The amplitude of the relief is equal to the single-tooth pair mesh deflection. The upper portion of Fig. 6 shows a straight-line profile chart for the perfect involute gear. The profile chart of Fig. 7 shows the linear shape of the profile modification along the tooth height. Figure 7 also shows that the transitions in tooth force are much more gradual, thus reducing the dynamic loads on the gear teeth. It should be noted that tip and root relief work well at minimizing the transmission error (TE) at the “design” load, but there will still be significant transmission error at other loads.

#### 4.3 Effects of Load and Contact Ratio on Transmission Error

A popular approach to achieving gear designs that have lower transmission error is to increase the contact ratio of the gear pair, thus reducing the mesh stiffness

variation. This is done by either increasing the tooth height or by using helical gears. The total contact ratio of helical gearing is expressed as the sum of the profile contact ratio and the axial or face contact ratio:

$$m_t = m_p + m_f = Z/p_b + F/p_x$$

where  $Z$  and  $p_b$  were defined previously,  $F$  is the face width, and  $p_x$  is the axial pitch.<sup>13</sup>

A set of geometries (Table 1) used in an experimental noise study by Drago et al.<sup>14</sup> will be used to show the effect of contact ratio on transmission error. Optimal profile and lead modifications have been applied to these gear pairs, and they have then been simulated<sup>15,16</sup> to determine the effect of load on transmission error. The results for each case are shown in Fig. 8. Here, for the perfect involute spur gear pair, the transmission error increases linearly with load (the line is distorted due to the log scale on the y axis). The spur gear pair with profile modifications has increased TE at light loads and a minimum TE at the design load. If low transmission error is desired at no load, the gears must have a perfect involute over at least one base pitch of rotation. One means of achieving this is to use gears with a contact ratio greater than 2.0 and apply the relief at the highest and lowest points of double-tooth contact, respectively. A typical TE plot for a high profile contact ratio set is shown as case C in Fig. 8.

Figure 8 shows that the helical gears, which have circular profile and lead modifications, have lower transmission error than the spur gears, and, as helix angle and, hence, contact ratio is increased, the transmission error continues to be reduced. The following guidelines, based on increasing contact ratio, for reducing gear noise and vibration are:

- Increase tooth height (longer cutting tool, lower pressure angle) so that  $Z$  increases.

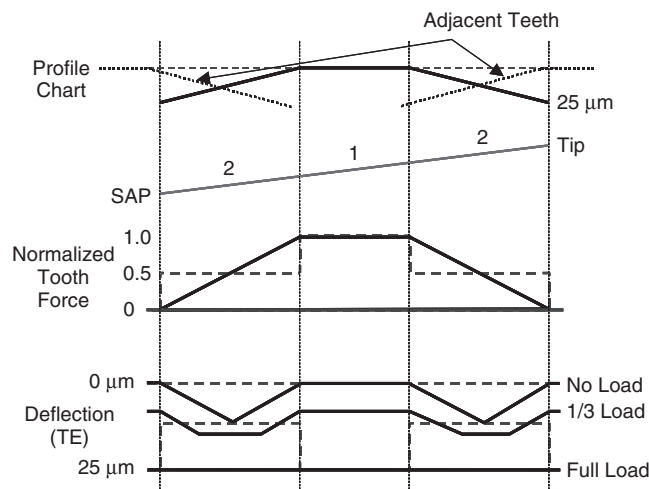
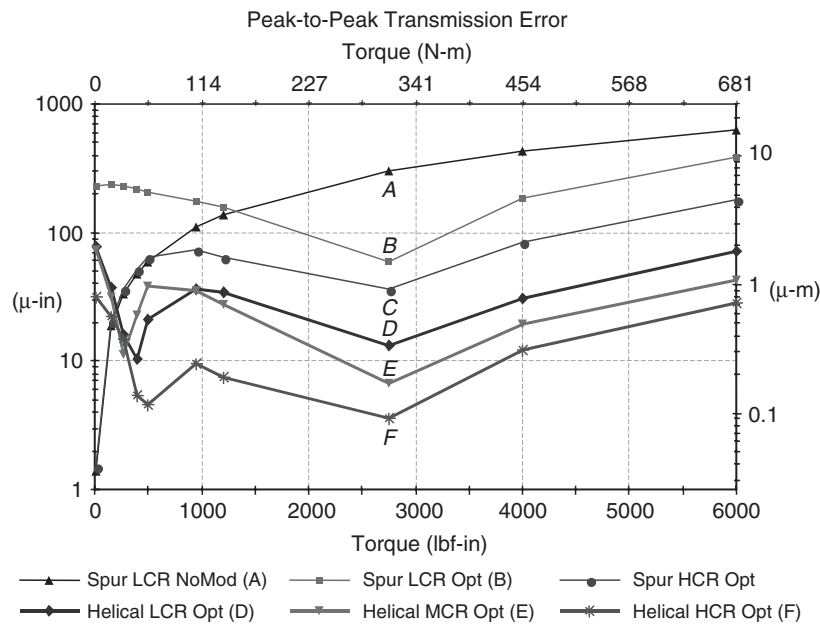


Figure 7 Transmission error and stiffness change for a modified spur gear pair.



**Table 1** Design Data for the Gears Whose Data Is Plotted in Fig. 8

	Pinion	Gear	Pinion	Gear	Pinion	Gear	Pinion	Gear	Pinion	Gear
	<i>A, B</i>		<i>C</i>		<i>D</i>		<i>E</i>		<i>F</i>	
	Spur LCR		Spur HCR		Helical LCR		Helical MCR		Helical HCR	
Module (mm)	3.18		3.18		2.95		2.78		2.59	
Pressure angle (degrees)	25		20		23.5		22.2		16.5	
Helix angle (degrees)	0		0		21.5		28.9		35.3	
Profile contact ratio	1.43		2.10		1.37		1.37		2.12	
Axial (face) contact ratio	0.00		0.00		1.25		1.76		2.25	
Total contact ratio	1.43		2.10		2.63		3.13		4.37	
Tip modification (mm)	A:	B:	0.016		0.013		0.010		0.013	
	NoMod	0.019								
Total lead crown (mm)	—		—		0.005		0.010		0.008	

**Figure 8** Effect of contact ratio on the transmission error of different modified gear tooth pairs.

- Increase helix angle to decrease  $p_x$ .
- Increase face width (least practical in most cases).

However, the gear designer faces practical limits in each of these. For instance, tip thickness and root clearance constraints limit the tooth height, increased helix angle causes larger axial forces that cause bearing design difficulties ( $35^\circ$  is a rough upper limit), and wide face widths result in larger deflections and load sharing difficulties. Another rule often quoted is that one should design to either an integer profile contact ratio or an integer face contact ratio, since either of these will provide reasonably constant mesh stiffness as the gears rotate. This concept works well when one is using perfect involutes, but if one is using tip

relief or lead crown on the teeth, it can be shown that the benefits of designing for integer contact ratios are reduced.

#### 4.4 Other Gearing Types

The tooth profiles of most other gear types, such as spiral bevel, hypoid, and worm gears, are tied much more closely to their manufacturing process than are the profiles of involute spur and helical gears. Nonetheless, the excitations of these gears are similar to those of parallel axis gearing, with transmission error and mesh stiffness still being the major quantities to be concerned with.<sup>17</sup> Again, tip relief and lead crown are used to compensate for stiffness variation, but now these terms are often described in terms of nonconjugate tooth curvature mismatch.



#### 4.5 Other Excitations

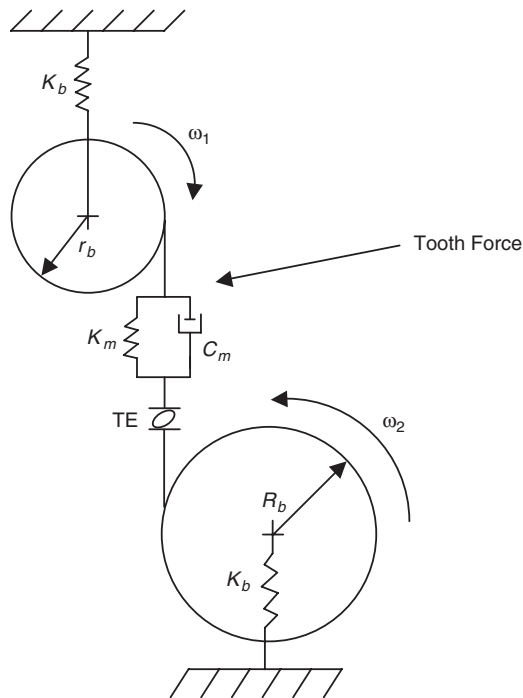
As mentioned earlier, the time-varying forces due to friction and the change in location and direction of the net force on the gear may also provide a substantial force excitation, particularly when one has already minimized forces due to transmission error and mesh stiffness variation. These force variations are quite easily computed for parallel axis gearing and may also be evaluated for the other gear types. An example of a general force metric that includes each of these excitations is presented by Houser and Harianto.<sup>12</sup>

### 5 NOISE PATH ANALYSIS/DYNAMICS

The remainder of the solution of gear noise and vibration problems involves reducing the effects of the noise/vibration path to the receiver. Classical vibration modeling and modal analysis approaches that are discussed in other chapters of this handbook are often appropriate. However, one should be aware that the gear mesh frequency might be in the 2- to 10-kHz region where the modal densities of housing panels may be extremely high. In these cases, statistical energy analysis has been used for gear path analysis.<sup>18</sup>

#### 5.1 Torsional/Lateral Dynamic Modeling

The first stage in the dynamic analysis of mating gears is to evaluate the torsional/lateral dynamics of the gear shaft system. The simplest acceptable model for evaluating gear dynamics is depicted in



**Figure 9** Simple spring-mass model for gear dynamics prediction.

Fig. 9.<sup>19</sup> Here, the gears are represented by both mass and rotary inertia, and the spring connecting the inertias at their respective base radii is called the gear mesh stiffness. This stiffness results from the sum of the tooth mesh deflections that result from Hertzian contact deflections, bending and shear deflections of the gear teeth, and the rotation and translation of the gear tooth base relative to the gear body. Each of these deflection components is of the same order of magnitude. A good estimate of the stiffness of a single tooth pair is  $14 \times 10^9$  N/m per metre of face width. Since the stiffness of a rolling-element bearing is of the same order of magnitude as the mesh stiffness, one finds that there may be significant coupling between the gear translation and gear rotation. The two primary excitations of this model are time-varying mesh stiffness variation and the displacement input resulting from transmission error (depicted by a cam in the figure). More degrees of freedom must be added to the model if the forces due to friction (at a right angle to the line of action) or shuttling are to be included. When operating gears such that the mesh frequency resonance is excited, there is the likelihood of loss of tooth contact, and in these situations it is necessary to include a backlash nonlinearity in the model.<sup>20</sup>

#### 5.2 Housing Dynamics

After obtaining the forces at the bearings due to the gear excitations, the response of the housing to these forces is required. A simple asymptotic modeling procedure for performing such an analysis is shown in Fig. 10. Depending on the assumptions that are made, this model can range from being extremely simple to extremely complex.

An idler gearbox that has three gears and a total of six bearings has been used as an example for applying a simple version of this model.<sup>21</sup> The average bearing force is used to excite a single panel of the housing, and the predicted mesh frequency noise level is shown in Fig. 11, as is the measured noise level. The asymptotic shapes of the measured and predicted responses are quite similar with the noise level of each plot having a low-frequency asymptote that increases with frequency at about 40 to 45 dB/decade. Data from other gearing applications have shown this slope to typically range from 30 dB per decade to 45 dB per decade.<sup>22</sup> The noise level flattens or starts dropping above a frequency that normally corresponds to the major mesh torsional resonance.

If a speed sweep of the gearbox reveals gearbox resonances, then classical approaches must be used to identify the mode shapes of the subject resonances and then one must either attempt to shift the subject resonance out of the operating speed range or apply damping to reduce the resonant amplitude. The shaft bending and torsional resonances, which are often difficult to measure, will always be evident. For reference, the main torsional natural frequency of a steel gear pair is in the 2- to 8 -kHz frequency region, and shaft lateral vibration natural frequencies are typically lower than the main torsional natural frequency.

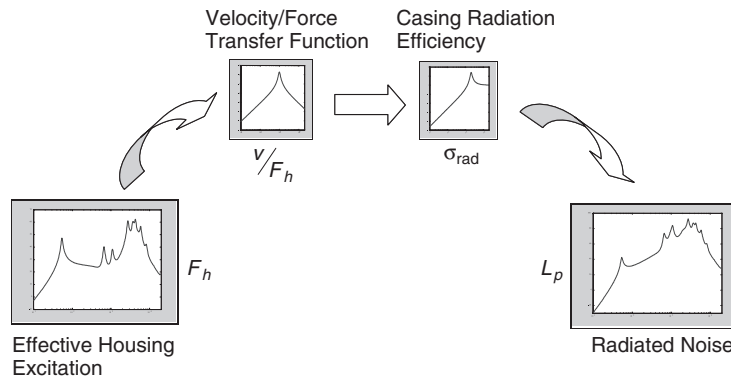


Figure 10 Noise prediction modeling procedure.

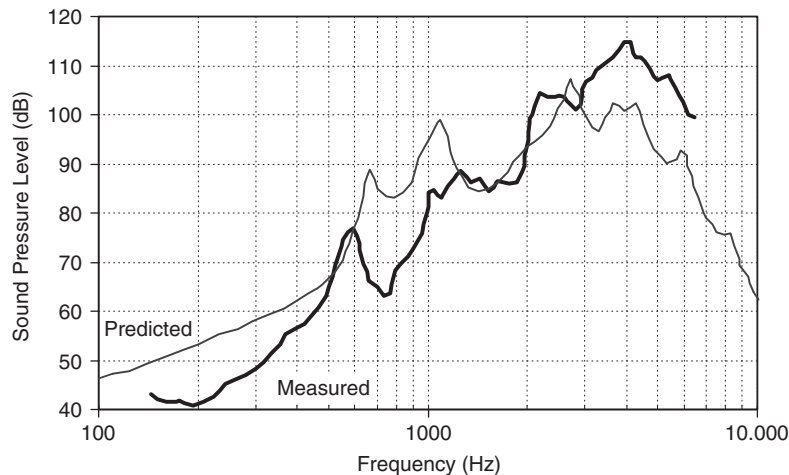


Figure 11 Mesh frequency order trace for an idler gear train.

## 6 GEAR RATTLE

Gear rattle is a lightly loaded phenomenon that is usually excited by time-varying torques in the drive system. Rattle is common in drive trains driven by an internal combustion engine where the prime excitation is at the engine firing frequency. Rattle results from the gear teeth losing contact so that they float in the backlash region and then come back into contact with repeated impacts. Although these repeated impacts have periodicity at the excitation frequency, one only hears the ringing impact response typical of the gears and their structural supports. The frequency spectrum of gear rattle usually shows an increase in broadband noise in the 1- to 5-kHz frequency region. The reduction of rattle may be achieved by minimizing backlash, but this is dangerous since manufacturing errors may result in tight mesh operation that could cause a significant increase in gear whine. Other approaches to minimizing rattle use system dynamics solutions such as providing a

backlash zone in the clutch or altering the system's mass-spring dynamics.<sup>20</sup>

## 7 TROUBLESHOOTING

Most gear noise problems show up after a product is in production, and the gear noise solution becomes a troubleshooting issue. Listed below are some of the steps that should be taken to achieve a viable solution for such problems:

- Identify whether the noise is a whine problem, a rattle problem, or some other type of sound. This is normally done by simply listening to the gears but may require observation of the frequency spectrum of the noise. If a gear whine problem is identified, the next steps are recommended.
- Identify the fundamental frequencies of the whine noise from the noise frequency spectrum. If the noise is at mesh frequency or any of

its harmonics, proceed to the next steps. If the noise is at a ghost frequency, a noninteger multiple of mesh frequency that still increases with speed, one must look for slight undulations of the tooth surface that are the result of the manufacturing process.<sup>24,25</sup> Solutions to ghost noise problems are usually achieved by altering some aspect of the gear machining process. Severe sidebanding is an indication of high torsional vibrations and/or a large eccentricity in one of the gears.

- Perform speed sweep measurements to determine if a resonance is causing the problem. Typically a waterfall plot or a color speed–frequency map is used for this purpose; however, this author finds that plotting the amplitude of individual harmonics of mesh frequency versus speed or frequency (called order plots) is particularly useful. Resonant problems have a wide range of solutions, but simply reducing the mesh excitation is an approach that should not be overlooked.

**Table 2 Effects of Different Gear Design and Manufacturing Parameters on Gear Noise**

	Direction to Reduce Noise	Noise Reduction (dB)	Comments
Number of teeth	Decrease	0–6	Lowers mesh frequency.
Contact ratio	Increase	0–20	Requires accurate lead and profile modifications.
Helix angle	Increase	0–20	Machining errors have less effect with helical gears. Little improvement above about 35°.
Surface finish	Reduce	0–7	Depends on initial finish — reduces friction excitation.
Profile modification		4–8	Good for all types of gears.
Lapping		0–10	Very effective for hypoid gears.
Pressure angle	Reduce	0–3	Reduces tooth stiffness, reduces eccentricity effect, and increases contact ratio.
Face width	Increase		Increases contact ratio for helical gears; reduces deflections.

**Table 3 Effects of Other Factors on Gear Noise**

Load	Noise typically increases with load.
Power	Noise typically goes up with power.
Speed	Noise increases at 30 to 45 dB/dec beneath torsional natural frequency. Resonances will affect response.
Module	Debatable, since decreasing causes increase in contact ratio, but increases the number of teeth.
Tooth height	Increases profile contact ratio, thus reduces noise but tip thickness provides a limit.
Contact line length	Was once felt to be important to keep constant but not that important for modified gears.
Recess action	Is favored due to lubrication considerations and the reduction in entering contact sliding.
Roll angle	Avoid contact at low roll angles, 8°–10° preferred.
Backlash	Little effect on gear whine, important for rattle.
Misalignment	If contact ratio reduces, noise increases. Use lead crown to minimize its effect.
Spacing errors	Little effect on mesh frequency noise, but for quiet gears, will affect the noise floor at all other frequencies.
Profile errors	S-shaped and concave shapes are bad.
Pressure angle error	Can considerably increase noise.
Lead crown	Compensates for misalignment; reduces noise of helical gears; can be effective with high contact ratio spur gears; should not be overdone.
Lubricant viscosity	Increasing tends to reduce friction and hence reduces noise.
Split path drives	Tend to be quieter, can phase gears; compactness tends to yield quieter drives.
Planetary gears	Special case of split path drive. Proper phasing is helpful, but shafts need concentricity and float.
Materials	Usually, gear load capacity determines material; effects are not as great as claimed.
Damping	Effective for reducing amplitudes at resonances; has been applied to reduce the effect of gear blank resonances; may improve rattle properties.
Bearing type	Plain bearings reduce noise relative to rolling-element bearings; preload can affect noise levels.
Housing mounts	Can reduce flanking noise path.
Tuned absorbers	Have been effective where resonances exist.

- If comparing results with predictions of excitations, it may be particularly useful to experimentally determine the effect of load on noise.
- At each torque, obtain the contact pattern using bluing or other type of dye that will wear off as the gears roll through mesh. If the pattern is near the edge of the teeth, this is an indication of severe shaft or gear tooth misalignment. Such misalignment reduces the effective contact ratio of the gear pair. The pattern that is observed always has an area that is greater than that of an individual tooth pair in mesh due to the thickness of the dye and the fact that the pattern is the sum of the patterns of all of the teeth that have meshed with the measured tooth.
- Obtain gear profile and lead measurements for use in ascertaining manufacturing difficulties.
- Using measured profiles and leads, perform simulations to predict TE and other excitations.
- Look into modifying the profile and lead modifications to minimize the noise, being sure to provide adequate lead crown to compensate for misalignment. However, one should be aware that manufacturing variations might provide a large amount of statistical variation in the noise levels, so robust designs that have a low sensitivity to manufacturing errors are desirable.<sup>26</sup>
- When all else fails, the gears may need to be redesigned with higher contact ratios or the sound path from the gearbox to the listener must be altered. The latter approach would include adding isolators to the mounts of the gearbox or going to the extreme solution of adding a cover over the gearbox.

## 8 GEAR DESIGN SUMMARY FOR MINIMUM NOISE AND VIBRATION

Anytime general statements are made about how much a given design change will reduce noise, an appreciation for the noise level prior to making changes is required. It is easier to reduce the noise of a poorly designed and manufactured gear set than one in which noise was considered from the beginning. Nonetheless, Table 2 provides a summary of some observations that have been made by many investigators that indicates some of the gains that might be achieved by altering transmission designs.<sup>27,28</sup> Beware!! The many reductions that are possible in the table are not additive in nature. Also, changing one design quantity inevitably changes other quantities, so it is difficult to determine the effects of individual changes. Table 3 briefly discusses the effects of other schemes that may be applied to reduce gear noise.

## REFERENCES

1. D. R. Houser, Gear Noise Sources and Their Prediction Using Mathematical Models, In *Gear Design Manufacturing and Inspection Manual*, Society of Automotive Engineers, Warrendale, PA, 1990, pp. 213–222.
2. R. W. Gregory, S. L. Harris, R. G. Munro, and Dynamic Behavior of Spur Gears, *Proc. I. Mech. E*, No. 8, April, 1953, pp. 207–226.
3. W. D. Mark, *Gear Noise Excitation*, Plenum, New York, 1982, pp. 55–93.
4. D. B. Welbourn, Fundamental Knowledge of Gear Noise—A Survey, *Proc. Noise and Vibration of Engines and Transmissions, I. Mech. Eng. Aut. Div.*, July 1979, pp. 9–14.
5. G. Niemann and J. Baethge, Transmission Error, Tooth Stiffness and Noise of Spur and Helical Gears—Part 1, Vol. 112 (Drehwegfehler, Zahnfederharte und Gerausch bei Stirnrädern), VDIZ, 1970.
6. J. Börner and D. R. Houser, Influence of Friction and Bending Moments on Gear Noise Excitations, SAE Noise and Vibration Conference and Exhibition, Paper 961816, Vol. 105 No. 6, 1996, pp. 1669–1676.
7. M. Vaishya and D. R. Houser, Modeling and Measurement of Sliding Friction for Gear Analysis, AGMA Fall Technical Meeting, Paper 99FTMS1, 1999.
8. D. R. Houser, F. B. Oswald, M. J. Valco, R. J. Drago, and J. W. Lenski, Comparison of Transmission Error Predictions with Noise Measurements for Several Spur and Helical Gears, *Proc. 30th AIAA/ASME/SAE/ASEE Joint Propulsion Conference*, 1994.
9. A. Kubo, T. Nonaka, N. Kato, S. Kato, and T. Ohmori Representative Form Accuracy of Gear Tooth Flanks on the Prediction of Vibration and Noise of Power Transmissions, *Trans. JSME*, Vol. 56, No. 532, pp. 238–243, AGMA Fall Technical Meeting, Paper 92FTM9, 1992.
10. R. E. Smith, The Relationship of Measured Gear Noise to Measured Gear Transmission Errors, AGMA Fall Technical Meeting, Paper 87FTM6, 1987.
11. J. D. Smith, *Gears and Their Vibration*, Macmillan, New York, 1983.
12. D. R. Houser and J. Harianto, The Effect of Micro-Geometry and Load on Helical Gear Noise Excitations, SAE Noise and Vibration Conference and Exhibition, Paper 2005-01-2295, 2005.
13. D. W. Dudley, *Handbook of Practical Gear Design*, McGraw Hill, New York, 1962.
14. R. Drago, J. Lenski, R. Spencer, M. Valco, and F. B. Oswald, The Relative Noise Levels of Parallel Axis Gear Sets with Various Contact Ratios and Gear Tooth Forms, AGMA Fall Technical Meeting, Paper 93FTM11, 1993.
15. T. F. Conry and A. Seireg, A Mathematical Programming Technique for the Evaluation of Load Distribution and Optimal Modifications for Gear Systems, *J. Eng. Ind., Trans. ASME*, Vol. 95, No. 4, November 1973, pp. 1115–1123.
16. D. R. Houser and J. Harianto, *Load Distribution Program Reference Manual*, GearLab, The Ohio State University, Columbus, OH, 2002.
17. A. Kubo, I. Tarutani, C. Gosselin, T. Nonaka, N. Aoyama, and Z. Wang, A Computer Based Approach for Evaluation of Operating Performances of Bevel and Hypoid Gears, *JSME Int. J.*, Vol. 40, No. 4, 1997, pp. 749–758.
18. L. K. H. Lu, W. B. Rockwood, P. C. Werner, and R. G. Dejong, An Integrated Gear System Dynamics Analysis over a Broad Frequency Range, *Shock and Vibration Bull.*, 55, Part 3, Shock and Vibration Information Center, 1985, pp. 1–11.

19. H. N. Özguven and D. R. Houser, Mathematical Models used in Gear Dynamics—A Review, *J. Sound Vib.*, Vol. 121, No. 3, Mar. 1988, pp. 383–411.
20. A. Kahraman and R. Singh, Interactions between Time-Varying Mesh Stiffness and Clearance Nonlinearity in a Gear System, *J. Sound Vib.*, Vol. 146, 1991, pp. 135–156.
21. V. Kartik and D. R. Houser, An Investigation of Shaft Dynamic Effects on Gear Vibration and Noise Excitations, SAE Transaction, *J. Passenger Car Mech. Syst.*, Paper 2003-01-1491, 2003.
22. M. Colabawala, J. Sorenson, and D. R. Houser, An Experimental Procedure for Characterization of Gear Whine Noise in a Variety of Applications, SAE Noise and Vibration Conference and Exhibition, Paper 2003-01-1488, 2003.
23. R. Singh, Dynamic Design of Powertrains for Reduced Vibro-Impacts, *Optimum Dynamic Design*, 1997, pp. 305–317.
24. D. R. Houser and P. Biggert, Gear Ghost Noise—A Case History Using Single Flank Transmission Error Measurements, Proc. NOISECON 91, Tarrytown, NY, 1991, pp. 95–102.
25. W. D. Mark, Contributions to the Vibratory Excitation of Gear Systems from Periodic Undulation on Tooth Running Surfaces, *J. Acoust. Soc. Am.*, Vol. 91, No. 1, 1992, pp. 166–186.
26. D. R. Houser and J. Harianto, Design Robustness and Its Effect on Transmission Error and Other Design Parameters, The International Conference on Mechanical Transmission, 2001; also in *Gear Tech. Mag.*, *J. Gear Manufact.*, March/April 2003, pp. 18–25.
27. D. R. Houser, Gear Noise, in *Dudley's Gear Handbook*, D. Townsend, Ed., McGraw Hill, New York; 1992, Chapter 14.
28. L. D. Mitchell, Gear Noise: The Purchaser's and the Manufacturer's View, Proc. of the Purdue Noise Control Conference, 1971, pp. 95–106.

# CHAPTER 70

## TYPES OF BEARINGS AND MEANS OF NOISE AND VIBRATION PREDICTION AND CONTROL

George Zusman  
IMI Sensors Division  
PCB Piezotronics  
Depew, New York

### 1 INTRODUCTION

Bearings are needed whenever one part of machine slides against another and can be classified as providing sliding or rolling contact. A sliding bearing typically uses a lubricant to reduce friction between sliding surfaces. A shaft and bushing bearing is known as a journal bearing. Bearings that provide sliding contact fall into three general classes: radial bearings that support shafts, thrust bearings that support axial loads on rotating shafts, and linear bearings that support parts in a straight line. Radial bearings are also called sleeve bearings. Rolling-contact bearings are often referred to as antifriction bearings.

Most vibration prediction and control techniques for bearings are based on signature and spectrum analysis. The root-mean-square (rms), shock pulse, kurtosis, high-frequency resonance technique, and eddy current direct displacement measurements are the main methods of bearing diagnostics.

#### 1.1 Use of Rolling Bearings and Construction of Bearing Assemblies

Thrust bearings take radial (axial) forces acting on the rotor and fix its radial (axial) position with respect to the machine body. The bearing assembly usually consists of two bearings:

- Fixed and floating
- Two bearings fixed only in one axial direction (two-sided fixing)

**Fixed Bearing** The fixed bearing takes up the radial load and the axial load simultaneously in two directions. The cylindrical roller bearings with one flange-less ring may be used in a fixed support together with another (thrust) bearing that takes up the axial loads; in this case the thrust bearing is installed in the housing with a radial clearance.

**Floating Bearing** The floating bearing takes up only a radial load and makes it possible for the shaft and housing to make relative displacement with respect to each other. The axial displacement is performed either in the bearing proper (cylindrical roller bearings) or when the bearing ring is clearance fitted with the mating part.

**Two-Sided Fixing** For two-sided fixing, use is made of radial ball bearings and roller bearings that take up axial loads at least in one direction.

**Internal Clearance in Bearings** The clearance in a bearing is a value of displacement of one bearing ring with respect to the other in a radial direction (radial clearance) or axial direction (axial clearance).

The following types of clearances are distinguished in a rolling bearing:

- Prior to assembly—initial clearance
- After assembly
- Clearance in operation conditions—working clear

**Lifetime of Rolling Bearings** The life of a rolling bearing is understood as the number of revolutions (or hours of operation at constant rotational frequency) that the bearing may perform before fatigue failure indications appear on its parts.

In practice, the life span of the same type bearings exhibits wide variations even in the totally coinciding operating conditions. When selecting rolling bearings, two specific parameters are used in addition to other parameters: dynamic load capacity and rated life or basic dynamic load rating ( $L_{10}$ ).

The service life of a bearing is understood as a time period within which the given bearing preserves serviceability under specified production conditions. The limit fatigue load ( $P_u$ ) is understood as such a load on the bearing that in ideal operating conditions does not ever cause fatigue failure.

#### 1.2 Causes of Bearing Failure

The first group of causes is incomplete scope of testing of restored bearings and rejected batches of *mala fide* manufacturers (manufacturing defects): The serious incoming inspection of bearings performed by a number of enterprises has shown that depending on the batch the bearings may contain up to 90% of defective pieces, though looking perfect at first glance.

The other group of reasons of bearing failure lies in defects of assembly and operation:

- Violation of lubrication conditions (quantity and quality), violation of maintenance conditions (40%)

- Wrong assembly, installation, and adjustment (30%)
- Wrong usage (off-design operating modes), high loads (pressure in radial and/or axial directions) and vibration (20%)
- Operation wear (abrasive or fatigue) and contamination (10%)

This distribution depends on the field of application of a rolling bearing. In transport vehicles the main reason of failure is fatigue. In the petrochemical industry the main cause is wrong assembly, installation, and lubrication. In the pulp and paper industry it is poor lubrication and contamination. The character of damage of rolling bearings depends on the cause of damage: By investigating a damaged bearing it is possible to determine the cause of defects and take measures to prevent systematic repetition of such defects in the future.

**Fatigue** The cause of fatigue lies in alternating transverse stresses developed in subsurface layers of raceways that cause cracks propagating toward the surface. When rolling over the cracks of rolling elements, spalling of material particles takes place. Spalling (rubbing) is developed under edge stresses and wear products brought together with lubricant.

The incubation period (until fatigue damage features appear) depends on the rotational frequency of the bearing, load, lubrication effectiveness, and cleanliness of the lubricant material. Fatigue spalling of rolling bearing elements (in normal operating conditions) develops rather slowly and is accompanied with the increase of noise and vibration of bearings, which permits detection of the damage and replacement of the bearing prior to its full destruction.

### 1.3 Inspection of Bearings

The purpose of bearing inspection is to detect the following (see Fig. 1):

- Disagreement of the temperature, oil level, and other parameters to be tested to the norms and standards
- Unusual noise, sounds, or vibration
- Spills or leaks of technical liquids (oils, lubricants) around the bearings
- Discontinuities or cracks of bearing body

**Temperature Monitoring** Increased (as compared with the normative value) temperature is evidence of abnormal operation of the bearing assembly and causes degradation of lubricant. It is necessary to register and analyze possible reasons. Prolonged operation at temperatures over 125°C causes essential reduction of the service life of a rolling bearing.

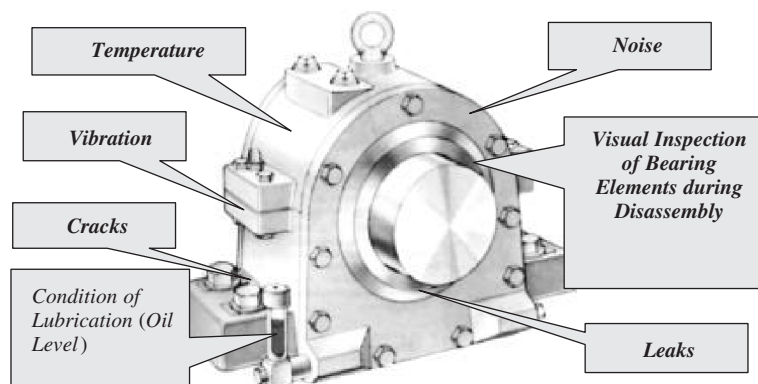
**Noise Monitoring (Organoleptic)** When in good condition, the bearing generates uniform, soft, humming (the so-called rustling) noise. Rattling, whistling, squeaking, or metallic (and other unusual sounds) noise is evidence of an abnormal state of the rolling bearing. The defects causing noise in bearings are irreversible and demand replacement of the bearing.

**Visual Observation** Seals protect the bearing assembly from dirt and keep lubricant inside the bearing assembly. Insufficient lubricant, change of color or darkening when contaminated, change of consistency, and the like are all factors that may cause fast deterioration of the bearing.

#### Visual Inspection of Bearings after Disassembly

For visual inspection a small mirror and a probe with a rounded end is used. The purpose of inspection is to detect local defects: burrs, dents, scratches, pits, cracks, mirror-polished spots, or change of metal colors (temper colors).

**Vibration Monitoring** Practically all defects emerging during manufacture, assembly, and operation of the rolling bearing (as a part of a machine) exert an influence on the vibration parameters. As defects are developing, macro and microgeometry of bearings



**Figure 1** Parameters and defects found during inspection of bearings.

undergoes changes, friction force properties, and loading conditions change. Nonlinearity and anisotropy of the vibration signal appears; the ratio between the random component and the periodic component of the vibration signal changes; shock pulses emerge to excite a broadband vibration of the bearing assembly; a low-frequency vibration appears. Various strategies and approaches are used for monitoring the parameters of vibration of rolling bearings.

#### 1.4 Main Methods of Diagnostics of Rolling Bearings

To ensure high reliability of diagnostics of the technical condition of bearings and to prevent their premature failure, it is necessary to perform complex research based on incoming inspection of the quality of bearings to be mounted, works on vibration adjustment, outgoing inspection (postrepair check) of the quality of restored machines, periodic monitoring of the temperature, vibration, and noise character, and visual observation of the state of the machine during operation. These measures make it possible to ensure a feedback that greatly enhances the nonfailure operating time and reliability of the machine.

The essential part of these works is vibration monitoring. Two groups of methods are widely adopted for the determination of the technical condition of rolling bearings and detection of defects.

The first group is based on separation and analysis of discrete components on certain frequencies of excited oscillations in the bearing. The diagnostic features are frequency components of the spectrum and characteristics of signal pulse shape associated with the characteristic frequencies of the bearings (see Tables 1 and 2): the pulse peak value (harmonic amplitude), the ratio of the pulse (harmonic) energy to the noise level, and the amplitudes of spectrum components at the pulse repetition frequency (harmonic). For analysis of these parameters use is made of vibration signal spectra in the range of 5 to  $10f_i$ , spectra of amplitude-modulated envelopes of narrow-band high-frequency components of the vibration signal in the range of 5 to 20 kHz, vibration forms.

The second group of methods is based on diagnostics of the technical condition of the bearing as a whole: In case of loss of serviceability it is necessary first of all to determine the necessity for the bearing replacement (i.e., to determine its technical state). The cause of failure may be determined later, if required, in the course of visual inspection of the bearing. The condition of the bearing is evaluated by the degree of development of degradation processes. The following may serve as diagnostic parameters: characteristics of amplitude distribution, moment characteristics (dispersion, excess), correlation and regression variances, amplitude discriminants, various parameters with the use of peak factor, and comparison of various vibration parameters in various frequency bands. During analysis of the latter, use is made of the rms values of vibration accelerations in the range of 15 to 40 kHz, the peak value and the rms values of vibration accelerations in the range of 1 to 10 kHz, and some others.

The best results are obtained in case of simultaneous use of all these methods. Several approaches (strategies) to the diagnostics of rolling bearings are used depending on the hours worked and design peculiarities of the machine.

1. Diagnostics in the process of operation of a rotor machine with coaxial shafts with initially installed defect-free bearings (practically all pumps, fans, etc.). It is possible to diagnose the condition of such machines with the use of minimum diagnostic methods: methods of the first and second groups are used, mainly frequency analysis of the vibration high-frequency envelope, parameters with the use of the peak factor, and comparison of various parameters of vibration in various frequency bands. In this case it is possible to perform the measurement "only one time."
2. Diagnostics in the process of operation of a rotor machine with mechanical transmission and initially installed defect-free bearings in the absence of defects during the machine assembly. Since the number of various contacting friction surfaces may be quite great (transmission elements, bearing elements) and the kinematics of transmission (bearing operating conditions) vary essentially as compared with the kinematics of a multishaft system with coaxial shafts, usually monitoring is used, or use of additional methods of analysis and parameters (e.g., cepstrum for transmission).
3. Diagnostics in the process of operation of a multishaft rotor machine with mechanical transmission for a wide range of defects with the possibility of obtaining a short-term prognosis of the technical condition of the machine. Presence of various contacting friction surfaces (bearing elements, transmission elements), integral kinematics of the multishaft rotor system with coaxial shafts and transmissions, influence of skew, violation of rigidity (deformations) and slackening, and shaft defects—all these require performance of a full-scale monitoring with the use of a detailed frequency analysis (spectra, spectrum envelopes, orbits, cepstrum, phase analysis, etc.).

When installing a new bearing, the probability of using a defective part should be minimized. It may be achieved by using items of known manufacturers and/or by incoming inspection of bearings. Compliance of levels of rms values of vibration velocity and vibration acceleration for definite frequency bands is checked during the incoming inspection at test benches to the requirements of specifications for rolling bearings with the aim to determine the class of the bearing as per the noise produced. Frequency analysis helps clarify the diagnosis.

To ensure long-term operation, outgoing inspection of machine assemblies containing rolling-element



bearings is performed after manufacture or repair. Tests (and primary running in of friction pairs in case of necessity) are performed on driven units with various values of rotational frequency and/or load. These procedures may be combined with operations on vibration adjustment: balancing in own bearings, adjustments, and the like. When performing the tests, the whole range of vibration analysis methods is used.

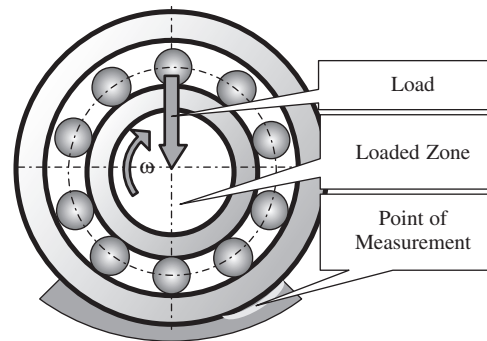
As the defect develops, passing various phases in the chain: cause—incipient defect—developed defect—developed defect with secondary damage features, the properties of the combination of forces that excite vibration undergo certain changes. To detect defects of assembly of bearings (in absence of outgoing inspection), a frequency analysis of high-frequency vibration is used. This high-frequency vibration appears as a result of modulation of friction forces. The contour characteristics are taken. Simultaneously, the difficulty of rotation of the shaft in the bearing is evaluated; the temperature of the bearing (support) is measured; the organoleptic analysis of the bearing acoustic noise is carried out.

For monitoring the defects of wear of the rolling and retainer surfaces in the course of development of the defect, a frequency analysis of high-frequency vibration of fixed elements and the bearing assembly housing is used. This vibration appears as a result of modulation of friction forces until the developed defect phase is reached. At the developed defect phase (particularly with secondary damage features), if a machine is going to be operated further, the main type of inspection becomes the vibration frequency analysis in the range with the upper boundary,  $5$  to  $10f_i$  (or  $50f_r$ , or in the range of  $10$  to  $2500$  Hz) and simultaneous visual analysis of the signal shape.

### 1.5 Vibration Test Points

During machine vibration (condition) checking, the general rule to be followed is the following: Measurements should be performed on rigid elements of the structure in the point as close to the critical assembly as possible; the number of mating surfaces along the path of propagation of the signal should be minimal. By measuring the radial vibration, the sensor (if possible) should be located so that its measuring axis crosses the rotation axis in three main orthogonal directions with respect to the axis. It is necessary to take into account a number of peculiarities of the rolling bearings that can introduce essential corrections into the general approach. When testing the condition (vibration) of the rolling bearing proper, the optimum measuring point may be on the part that directly contacts the bearing (usually on the housing) in the area of the loaded zone of the bearing, from the side of rolling elements entry into the load zone; see Fig. 2.

The sensor fastening method should ensure obtaining the upper boundary of the frequency band when getting the spectrum and vibration shapes to  $5$  to  $10f_i$  (usually up to  $2500$  Hz for the rotor rotational frequency of  $50$  Hz) while obtaining the spectrum envelope up to  $25$  kHz with the ultrasonic analysis up to  $40$  kHz.



**Figure 2** Optimum point of measurement of high-frequency vibration (ultrasonic oscillations) during monitoring.

With the periodic monitoring, maximum use is made of the fastening methods with the use of magnets, probes, and special connections. More rarely used is fastening with the stud with the help of glue, mastic (wax), or adhesive plate. With continuous monitoring only threaded connections are used.

When performing measurements with the help of a magnet or probe, the surface in the measuring point zone is cleaned of old paint and dirt. The surface in the place of contact (for the magnet) should be smooth; the area should be not less than  $0.5 \text{ cm}^2$ . To improve the acoustic contact and reduce the cavity-resonator quality, it is recommended to apply some plastic grease or low-viscosity oil on the surface to be measured.

When carrying out measurements with the help of a probe (indicator point), the latter should be reliably pressed to the surface to be measured; the measurement axis should be perpendicular to the surface of the machine; deviations for more than  $10^\circ$  are inadmissible. The recommended pressing force is  $10$  to  $15 \text{ N}$ .

For reliable use of the frequency analysis the following requirements should be met:

- The upper boundary of the vibration spectrum analysis frequency band should be selected not less than  $50f_i$  or  $5$  to  $10f_i$ .
- Higher harmonics of the rotor rotation frequency should be absent in the filter pass band for separation of high-frequency vibration envelope (or other toothed harmonics); there should be no high resonator quality fields (coupled with the method of fastening or properties of the machine), and the mean vibration level in the band should be comparable with the level of noise in the low and medium frequencies and should exceed the level of intrinsic noise of the device by not less than  $15$  to  $20 \text{ dB}$ .

In the process of monitoring, it is very important to perform the series of measurements strictly in the same measuring point.

Taking into consideration the above-mentioned facts, two main approaches are used in selecting the place of measurement:

1. An approach oriented on identification of the technical condition of the rolling bearing proper and measurement (sometimes "one-time") of the parameters of the high-frequency vibration (frequency analysis of the envelope).
2. An approach oriented on identification of the technical condition of the rolling bearing proper and the machine as a whole and (periodic) measurement of the parameters of vibration in the whole frequency range (frequency analysis of vibration in the band up to 5 to 10  $f_i$  and the high-frequency vibration envelope frequency analysis).

For each of the approaches there are own peculiarities (rules) for the selection of measuring points.

1. When the high-frequency vibroacoustic signal propagates in metal, it attenuates. Nevertheless, the attenuation is small over linear sections with the length of less than 0.4 m. Thus, with the overall size of the bearing housing less than 0.8 m, sufficient rigidity of the housing, bearing rotational frequency of less than 5 Hz, and quite sufficient spacing between the adjacent bearings, the measurements may be performed practically in any of the points.
2. With small size of gear case in which the bearings are located (e.g., most cradle-mounted pumps, small gear cases), the influence of

vibration of adjacent bearings in measuring points 7 and 8, and sometimes in the measuring points in the direction of bearing radius may be quite great, and it is not recommended to perform measurements in these points.

### 1.6 Types of Defects of Rolling Bearings and Their Generalized Diagnostic Features

Emergence of defects in rolling bearings causes the appearance of frequency components in the vibroacoustic signal, as presented in Table 1.

The expressions presented in Table 1 determine only the frequencies of the main harmonics (pulses) emerging in the vibroacoustic signal with various defects in the rolling-element bearings. Additionally, vibration on higher harmonics of these frequencies emerges, as well as vibration on a great number of combinational frequencies components (cumulative, differential) of the main frequency components. The levels of vibration of frequency components are determined by the type and degree of maturity of the defect, the properties of the loads, the condition of lubrication, the transmission characteristics of the bearing assemblies, and other reasons. The number of combinations of combinational frequencies may be so great that manual analysis becomes next to impossible to perform.

If the inner ring of the rolling bearing is fixed and the outer ring is rotational (e.g., wheel pairs), then the cage rotational frequency ( $f_{cg}$ ) in the formulas of Table 1 should be changed by the frequency ( $f_r - f_{cg}$ ). If the inner ring of the rolling bearing rotates and the outer ring is fixed (e.g., midshaft bearing in aviation engines), then the rotor rotational frequency ( $f_r$ ) in the formulas of Table 1 should be changed by

**Table 1 Formula for Calculation of Frequencies of Main Operational Failures of Bearing Parts**

No.	Designation	Formula	
		For Fine Calculation	For Approximate Calculation (95%) with $\alpha = 0^\circ$
1.	$f_{cg}$ Cage rotational frequency	$f_{cg} = \frac{1}{2} f_r \left( 1 - \frac{d_{rol}}{d_{cg}} \cos \alpha \right)$	$f_{cg} \gg 0.4 f_r$
2.	$f_o$ Frequency of tumbling of rolling elements over the outer race	$f_o = \frac{1}{2} f_r Z_{rol} \left( 1 - \frac{d_{rol}}{d_{cg}} \cos \alpha \right)$	$f_o \gg 0.4 Z_{rol} f_r$
3.	$f_i$ Frequency of tumbling of rolling elements over the inner race	$f_i = \frac{1}{2} f_r Z_{rol} \left( 1 + \frac{d_{rol}}{d_{cg}} \cos \alpha \right)$	$f_i \gg 0.6 Z_{rol} f_r$
4.	$f_{rol}$ Rotational frequency of rolling elements	$f_{rol} = \frac{d_{cg}}{2d_{rol}} f_r \left[ 1 - \left( \frac{d_{rol}}{d_{cg}} \right)^2 (\cos \alpha)^2 \right]$	
5.	$f_r$ Rotor rotational frequency (inner ring)		
	$\alpha$ Angle of contact between rolling elements and raceways		
	$Z_{rol}$ Number of rolling elements in the bearing		
	$d_{cg}$ Diameter of rolling bearing cage (pitch circle, circumference passing through the centers of rolling elements)		
	$d_{rol}$ Diameter of rolling elements in the bearing		

the differential frequency ( $f_{r1} - f_{r2}$ ) (frequencies of rotation of rotors  $f_{r1}$  and  $f_{r2}$ ), while the cage rotational frequency should be changed by the sum frequency ( $f_{r2} + f_{cg}$ ). It should be added that the analysis of integral or peak levels of vibration is mainly used for such machines in specially selected frequency bands.

### 1.7 Peculiarities of Diagnostics of Rolling Bearings by the Shape of Vibration Signal: Recommendations on Clarification of the Results of Diagnostics

The shape of the signal changes drastically as the defects of the rolling bearing develop: The ratio between the periodic harmonic and random components of the vibration signal changes, shock pulses appear (in a number of cases they appear periodically), the signal may become asymmetric, and vividly pronounced modulation appears. The visual analysis of the shape of the signal may be an essential complement to the results of the frequency analysis. The diagnostic features may be difficult for formalization, but the reproducibility is quite high. The shape of the signal usually becomes asymmetric in case of emergence of cracks or damage of bearing elements. When a vividly expressed local defect appears on one of the rings, shock pulses may appear in the shape of the signal with the periodicity of the rolling elements tumbling over the local defect. In case of severe wear of the bearing, the vibration signal modulation is vividly observed.

One of the most important peculiarities that help diagnose rolling bearings is emergence of vibrations on frequencies not multiple to the rotor rotational frequency. Nevertheless, in case of the appearance of a number of defects associated with the wear of the inner ring, nonhomogeneous radial fit, slippage, violations of rigidity, deformations of the support system, skewing, backlash, coupling defects, and vibrations appear on the rotor rotational frequency and its harmonics.

For localization and identification of these defects it is necessary to have comprehensive information on the condition of all assemblies of the machine. It is necessary to perform a joint analysis of the results of monitoring in all measuring points with due account of the machine operating modes, to study spatial distribution of vibration, to carry out the phase analysis, and the like.

If changes of the vibration state of several bearing assemblies arranged on one shaft axis are detected, very often these are not defects of several bearings, but severe defects of only one bearing. Such defects may appear as a result of the emergence of additional dynamic loads on the bearings adjacent to connection couplings, for instance, in case of skewing and problems with the coupling.

Very often vibration measurements testify of a change in the technical condition of the assembly, but the results of inspection do not allow reliable identification of the defect. The reason for the change of vibration may be the change in the operating mode of the machine, the change in the operating conditions, and influence of adjacent machines installed in the same premise with the machine undergoing diagnosis.

During analysis of machine vibration, it is required to observe several parameters simultaneously. For instance, the changes may take place only in the signal spectrum or in the envelope spectrum, or the pulses may be observed only on time realizations with the duration of 4 to 8 s, and so forth. This indicates the starting stage in the development of the bearing defect, lubrication defects, or appearance of hydraulic shocks. It is necessary to perform repeated measurements; if the results of measurements coincide, it is required to monitor the development of the defect within several days until the monitoring data (change of the machine vibration state) allows one to identify the defect.

In addition to the recommendations given in this chapter, the user may take into account the general recommendations presented in other chapters.

## 2 DIAGNOSTICS OF ASSEMBLIES WITH SLIDING BEARINGS AND SEALS

A sliding bearing could be represented as a part of the shaft called the journal, center shaft, and the like, which rotates inside a space limited by the bearing shell. The liquid lubricant (sometimes gas, magnetic field) prevents boundary friction of metal surfaces of bearing parts during its normal operation. The same lubricant, by interacting with the rotating shaft due to friction forces, forms the so-called oil wedge that forces it to float along the dynamic balance curve—the higher the curve, the greater is its rotational frequency.

Some works (see, e.g., Refs. 1 to 14) are dedicated to the methods of vibroacoustic diagnostics of sliding bearings as compared with rolling-element bearings, though they are also weak points in many machines and mechanisms, for instance, in ship diesel engines, in turbo generators, in various types of pumps, compressors, turbines, and the like. This may be explained by a number of reasons. One of them, evidently, is that the sliding bearing possesses weaker vibration activity as compared with other assemblies of the machine; therefore, one has to deal with minute vibroacoustic signals of the bearing proper, which are lost against the background of “noise”—signals produced by other elements of the machine when the measurements are performed by built-in sensors. Another reason is the difficulty of diagnosing the avalanche-like process of degradation of easily melted coatings of sliding bearing shells.

Certainly, not every defect of the sliding bearing is shown in the vibroacoustic signal that accompanies the work of the bearing. Nevertheless, such important defects from the point of view of reliability and safety of operation of machines equipped with sliding bearings as nonuniformity of clearances, play, rubbing-in/jamming, chipping, or melting of shells are well pronounced and vividly seen in the vibration signal; these can be used as diagnostic features. Consider the main defects and their possible features.

### 2.1 Irregularities of Clearances in Sliding Bearing (Seal)

In ideally designed and manufactured machines of the rotor type, the same distribution of clearances in each

bearing along the shaft axis is realized during operation in the nominal mode. Practically, the difference of clearances is checked with the removed upper cap of the bearing by direct measurements of side clearances between the shaft and the lower half of the bearing shell along its length, then the vertical clearances between the shaft and the upper half of the bearing shell are checked for equal values; also the vertical clearance change is evaluated during floating of the shaft journal in the working mode. Naturally, during assembly the out-of-roundness of the shaft journal is checked, as well as the condition of its working surface.

What are the reasons of appearance of such a defect? The main reason of appearance of irregular clearances is nondesign transverse load on the shaft, most probably coupled with the skew of the bearing axis relative to the shaft axis or misalignment of the axes of the shafts.

What is the influence of this additional cross load on the vibration signal? One of the characteristic diagnostic features is the deviation of the shaft center from the designed position on the dynamic balance curve in the given rotation-load mode.

In the frequency range it means enrichment of the spectral representation with reverse frequency harmonics. It should be noted that if this spectrum were obtained for the electric machine, then the increased level of the second harmonic of the reverse frequency with respect to the first harmonic would testify of a possible defect of the electromagnetic system (see Chapter 78).

Usually it is considered<sup>4</sup> that in the presence of a pure disbalance, that is, in the absence of other defects, including axis misalignments of various types, the shaft rotational frequency component predominates in the vibration spectrum. The experience shows that even when the rotational frequency harmonics have great amplitudes in the rotor machine vibration spectrum, it may happen that they are initiated exactly by the great disbalance and not by other reasons associated with the condition of the bearings or shafts. Therefore, as usual, it is helpful to attract additional information for clarification of the diagnosis.

When facing a situation like the above during vibration analysis, it would be good to study other possible causes of the emergence of components multiple to the rotational frequency. Thus, for instance, it may be out-of-roundness of the shaft journal (faced-like journal) that may generate the second, third, or even higher harmonic of the rotational frequency depending on the number of these "faces," as well as play of the shaft journal.

If the first defect is, more likely than not, intrinsic (apparently, only in exceptional cases it may be expected to appear and develop in the process of operation of the machine) and should be excluded with correct assembly of the equipment, the second defect may be a consequence of the development of the shaft crack (such cracks often appear near the thrust surfaces in places of concentration of loads). The vibration spectrum in this case shows an essential level of the

second harmonic of the rotational frequency. This is one of the indicative features. Much more informative is the feature obtained with slow rotation of the shaft, called "slow roll data." The high level of the second harmonic in this case is determined only by the play of the journal (naturally with the absence of ovality in it), since the response to the dynamic action is negligible due to the very low magnitude of this action at such low shaft speeds.

## 2.2 Abnormal Clearance Values (Looseness and Gripping): Brushing

Increased or reduced clearances in the bearings and seals emerging as a result of poor assembly or degradation of the technical condition of the machine during operation are not so bad by themselves as by the consequences of their impact on the machine behavior. The most important of such secondary defects in terms of service life and reliability of machine operation is brushing of rotating parts against fixed parts. Brushing of the journal against the sliding bearing shell, brushing of the shaft against the elements of labyrinth packing of the lubrication system, brushing of the impeller against the elements of the stator, and the like manifest themselves by appearance of shock pulses both in the radial and in the tangential directions (friction pulses), as well as by temporary change of rigidity, which is reflected quite naturally in the characteristics of the vibration process. The development of degradation phenomena causes local heating, disruption of continuity of oil (gas) film and boundary friction, rubbing, burrs and deformation of contacting surface, and the like.

The main types of movement of the shaft journal in the presence of *increased clearance* in the bearing, as considered in detail experimentally and theoretically in Ref. 2, may be normal when the balanced shaft rotates inside the bearing without boundary contact and defective, as listed below:

1. Constant contact of the shaft with the bearing (with insufficient lubrication—retrograde precession with continuous slippage in the direction of rotation, i.e., "breaking-in"; with flooded lubrication—direct precession with the rotational velocity, i.e., "slipping").
2. Periodic striking of the shaft against the shell (in this case precession may be direct or retrograde).
3. In case of horizontal position of a heavy shaft pressed by gravity to the lower part of the bearing, swinging of the shaft end appears as in a pendulum with the length equal to the value of the clearance measured along the lower arc of the bearing clearance.

Since the task of this publication does not include detailed description of all possible dynamic phenomena characteristic to such a state of the machine, we shall consider here only the events of shaft rotation

causing brushing, while some other defective states will be discussed in the following section.

The presence of play (clearance fit) of the bearing shell with quite considerable influence from the side of the shaft (e.g., due to its imbalance) may also cause strikes and hence brushing. The presence of tight fit (tight clearance) all over the circumference of the shell or seal may be easily determined during assembly either by hard turning of the shaft or by fast overheating of the bearing after the start. Therefore, we shall not discuss here the vibrodiagnostic features of this defect (more so, this defect is not likely to develop in the process of operation). What concerns partially tight clearance, its manifestations are similar to what has been described above, though there are some specific differences.

The most important feature of manifestation of these two bearing parameter deviations is brushing, as mentioned above. A transparent model of influence of this defect on the dynamics of the shaft is described in Ref. 5.

Thus, if part of the shaft rotation period is characterized by contact (or weakening of interaction) between the rotating and fixed parts of the machine, then the effective rigidity of the assembly changes for this time period. In the first case the "norm—touching" increases for some time, in the second case the "norm—play" decreases for some time. Correspondingly, the mean rigidity value for this period slightly changes, which causes change of the own frequency of the assembly, as is known, proportionally to the square root of the rigidity value.

Such change of system parameters within the course of one cycle (or sometimes over a longer period) associated with greater (in amplitude) radial and tangential pulses brings about the appearance of nonlinear oscillations causing the following. In addition to the proper frequency of the assembly, if the rotational frequency exceeds 2, 3, or 4 times the modified proper frequency, then self-excited oscillations appear on the corresponding subharmonic. In this case, apparently, self-adjustment of rigidity and damping parameters of the assembly is performed within a certain range and, correspondingly, adjustment of the proper frequency so that the range of "harmful" rotation speeds exciting strong subharmonic oscillations becomes wider than the band of the resonance curve unmodified by the defect. If the shaft rotation speed is increased, then the value of the self-excitation frequency at a certain moment jumps over to the next least ratio ( $\frac{1}{3}$ , e.g., after  $\frac{1}{2}$ ), and so on.

What concerns oscillations on the rotational frequency, due to nonlinear conversion of the torsional oscillations into radial, the amplitude of the first harmonic (1X) may grow with not so intensive brushing; but due to considerable damping with a severe defect, it falls down (though in this case the vibration of the housing may grow considerably). The maximum rise on the Bode diagram will be higher (in revolutions) for the tight clearance (i.e., for the norm—touching version) and lower for the looseness case (i.e., for the norm—play version) due to modification of the proper

frequency value. As always, for nonlinear oscillations the Bode diagrams differ greatly for rising and for lowering down of the revolutions.

The vibration spectrum may contain not only the rotational frequency and its subharmonic, but also their multiples; this is explained by the pulse influence of the defect.

When measuring relative vibrodisplacements of assemblies with such defects, it is useful to evaluate the position of the shaft center in the clearance (since its anomalous displacement is one of the main reasons of brushing) and the shape and swing of the orbit,<sup>5</sup> unambiguously shows the moments when the clearance between the shaft and the shell is taken up in the different modes.

With this defect, the position of the shaft center may sharply change both in the stationary modes and in the speeding-up and running-down modes. The spectral composition, orbit shape, and direction of precession of each frequency component may be evaluated by full vibration spectra.

In Refs. 8 and 13 it is shown that if rub occupies the whole perimeter of the shell or seal the orbit is a circumference, and the precession is retrograde, on the modified proper frequency. Thus, in the presence of brushing some of the following features may be manifest in relative vibration<sup>5,13</sup>:

- Change of vibration on the rotational frequency 1X
- Abnormal shape of the orbit
- Subharmonic vibration
- Components with retrograde precession
- Harmonics in the spectrum
- Changes in the mean position of the shaft, and some others

Since the phenomena taking place in the presence of such defects in the machine are essentially nonlinear, then the minutest changes in the assembly operating conditions cause considerable changes of oscillation characteristics. Therefore, when making a decision it is recommended to consider all the above-mentioned characteristics together, as a set.

When measuring vibration on the housing with the help of accelerometers, the above-mentioned characteristic features are not obtainable, but other features are manifested. Amplitude spikes corresponding to the moment of defect flicker in the contact zone appear in the region of one of the proper frequencies of the machine and the resonance frequency of the sensor. Since they create the modulation of these frequency components of great depth, the spectral characteristics of the amplitude envelope are a sensitive feature of the defect. An additional characteristic feature in this case is the appearance of frequency modulation of excitation frequencies (but not resonance frequencies!), since the pulse tangential forces emerging during boundary friction create a modulation of the torque that disrupts smooth rotation of the shaft. The spectral components

of the amplitude and frequency modulation are used as diagnostic features of brushing and burring.

The amplitude modulation manifests itself in a wide range of frequencies; its depth is the greatest in the vicinity of the resonance frequencies of the assembly or the measuring device. As a rule, the frequency modulation, by the rotational frequency and its harmonics, also manifests itself in the vicinity of the main excitation frequencies (blade, impeller, toothed, etc.). (It should be noted that this parameter is most sensitive in the case when the torsional oscillations of the shaft are measured directly.)

There is one more informative parameter of the vibration process that is sensitive to the process of touching and burring at the initial stage. It is kurtosis of the frequency curve of instantaneous vibration values in a wide or narrow informative frequency band. As a typical example it is possible to state experimental data<sup>8</sup> obtained during diagnostic testing of a water centrifugal turbopump. Burring of sliding bearing shell (using water lubrication) was simulated in the process of testing. Shaft touching the bearing shell, which caused burring of shaft surfaces, was stimulated by interrupting the supply of lubricant. Starting from this moment the process was developing increasingly. The swing of kurtosis change  $\Delta u$  of the vibroacoustic signal was particularly great in the vicinity of proper frequency of the assembly at the initial moment of defect development. Its mean value also grows fast at the early stage of assembly degradation. Then upon reaching the maximum value, it even starts decreasing. Such behavior of the given features is generally characteristic of the defects whose development is associated with appearance and increase of the number of pulses in the vibration signal. They are very effective for early diagnostics.

Since the development of this defect is difficult to predict, the features may vary widely in the process of operation of the machine; this makes it necessary to compare large quantities of information in order to obtain a reliable and thorough diagnosis.

### 2.3 Defects of Shell Surfaces

In practice, it sometimes becomes necessary to deal with shell surface defects appearing as a result of errors during assembly or wrong operation (chipping, melting out of babbit, etc.). The features of this defect are similar to the features of irregularities of clearances in the bearing. Some difference is due to a greater number of harmonics of the rotor rotational frequency as a result of considerable change of the signal shape. There is a characteristic feature stable to the mode change. It is based on a greater diagnostic value that the information on the phase relationships between the rotational frequency harmonic characteristics for this defect acquires, particularly the information on different vibration signals. For example, when conducting research of the features of bearing shell chipping, the Lissajous figures (very sensitive exactly to phase information) for the signals of relative vibration built up for the first harmonic of vertical vibration and third harmonic of horizontal vibration have changed shape and

acquired a characteristic form only in the presence of a defect independent of the load, rotational mode, and construction characteristics of the bearing.

### 2.4 Self-Exciting Oscillations on an Oil Wedge

**Mechanism of Excitation of Oscillations** In certain conditions very intensive low-frequency vibrations appear in the rotor-type aggregates, these vibrations being nonmultiple to the rotor rotational frequency. In most cases it is associated with the loss of dynamic stability of the rotor rotation emerging when the circulation forces of the oil film and/or aerodynamic circulation forces exceed the damping forces. This phenomenon is characteristic of the bearings having cylindrical or elliptical reboring of the shell and is frequent for high-speed aggregates with light rotors, aggregates with vertical rotor rotational axis, machines with low load on the bearings or with relatively long (with great contact area) thrust portion of the bearing. Loss of dynamic stability is induced by the reduction of load (i.e., unloading) of the bearing, increase of lubricant viscosity, problems with the bypass or overflow grooves, increase of clearances in the bearing, skewing of the shell axis with respect to the rotor (journal) axis, unbalanced relief steam force, and the like. It should be noted that though the discussion here is for the sliding bearings, these phenomena in principle are attributable to all assemblies consisting of two cylinders, one in the other, separated with lubricant and rotating relative to each other.

The main reason for the dynamic instability of rotors in sliding bearings is the behavior of the lubricant rotating in a narrow clearance between the shell and the rotor, an important characteristic of which is the relative mean rotational velocity. If the shaft is not sufficiently loaded for some reason, the shaft center is located near the bearing cross-sectional center. While picking up rotation speed and approaching the stability threshold, the shaft comes closer to the bearing walls as a result of orbit precessing (the dynamic eccentricity grows, while the static one remains close to zero). It means that the rigidity of the bearing changes, hence the stability threshold also changes. When the latter becomes equal to the rotation speed, oscillations of the limit cycle on this new proper frequency appear; they correspond to the given rigidity. In Ref. 9 it is shown that a feedback appears between the rotor oscillations, its revolutions, and threshold. Thus, at any constant speed above the threshold, the increase of the orbit swing increases the rigidity and displaces the threshold up, this causing the decrease of oscillations that, in their turn, immediately influence the rigidity. The threshold is reduced, the oscillations start rising again, and the whole process is repeated, maintaining a definite oscillation swing. With the rotation speed increase, the proper frequency and the threshold grow, gradually remaining subsynchronous, and the oscillations being governed by the same mechanism are gradually increasing in amplitude, while their frequency (changing proper frequency) follows the

changes of the rotor rotational frequency also in a subsynchronous manner.

Though the oscillations in the bearing may not exceed the clearance value, the shaft experiences considerable flexing impact, and this causes secondary defects of the type of rotor touching stator; this makes the modes of self-excited oscillations on the oil wedge very destructive and dangerous.

**Oil Whirl and Oil Whip** The experience of operating aggregates equipped with flexible rotors shows that reduction of stability and appearance of highly intensive resonance oscillations on the oil film are more characteristic of rotors with the working rotational frequency exceeding the first critical rotational frequency of the rotor, but less than the double first critical rotational frequency. In most cases the oil whirl is associated with an essential unloading of the bearing.

The oil whirl causes intensive vibration at the frequency,  $0.3$  to  $0.48 f_r$ . This vibration is determined by the direct precession of the shaft in the bearing under the action of the lubricant, which can be determined both by the filtered orbits and by the full spectra.

The influence of the oil whirl on the shape of the trajectory of the shaft journal movement in the bearing is that, depending on the ratio between the synchronous component and the subsynchronous component, it is

close to circle, or it has also an inner loop rotating in opposition to the rotor rotation.

As distinct from the oil whirl, appearance of such self-excited oscillations as of the type of oil whip happens in rotors with working rotational frequencies two and more times exceeding their first critical frequency and requires the supply of external energy to feed the whirl. It is associated, for instance, with the influence of vibration or load. The oil whip also causes intensive vibration of the sliding bearing on the frequency close to the first critical frequency of rotation of the rotor, only as distinct from the first case it does not readjust itself following the changing rotational frequency, but remains practically independent of the revolutions.

Since considerable oscillation amplitudes with unstable shaft oscillations may cause touching, it is possible to avoid the manifestations of such destructive defects by using a number of constructive methods:

- With two longitudinal grooves
- With three longitudinal grooves
- With lemon-shaped boring
- Geometric center of pad
- With displaced shells
- With mobile shell pads
- With oil pockets

**Table 2** Manifestation of Defects of Sliding Bearings in Full Spectra and Orbits

Type of Defect	Relative Frequency	Direction of precession		Notes
		Direct	Retrograde	
Partial rub	$1 \times$	+	+	Components $1 \times$ and $2 \times$ behave as in the case of unidirectional radial load: the amplitude of the reverse component grows, and that of the forward component goes down with the development of touching.
	$2 \times$	+	+	
	$\frac{1}{2} \times, \frac{1}{3} \times, \dots$	+	+	
Full annual rub by rotation angle	$1 \times$	+	—	Depending on dry friction between the rotor and the seal, its yield characteristic, attenuation, and imbalance values, the system may display either a forced response with predominance of the direct component $1X$ or a resonance response with predominance of the retrograde component.
	Proper frequency of pair: rotor seal	—	+	
Oil whirl	$\lambda X$	+	—	Dominating direct orbit with the inner loop (combination of the whirl component and component $1X$ ). In the full spectrum it is revealed as subharmonic direct component.
	$\lambda = 0.3, \dots, 0.49$			
Oil whip	Fundamental rotor frequency	+	+	Dominating direct orbit with the inner loop (combination of the whip component and component $1X$ ). In the full spectrum it is revealed as subharmonic direct component. Usually small retrograde components of $1X$ and subharmonics are present due to anisotropy of support rigidity.
Whirl breakaway	$\lambda X$	+	—	The whirl breakaway may be distinguished from self-excitation on the oil wedge by its disappearance while the flow through the compressor increases. The full spectrum resembles greatly the spectrum of the oil whirl.
	$\lambda = 0.1, \dots, 0.8$			

The most effective version is the version with hydrostatic bearings, since constant maintenance of high pressure of oil allows starting the machine without the usual shortcomings and does not require large clearances due to more stable position of the shaft in the machine clearances; besides, it helps prevent the possibility of self-excited oscillations.

In conclusion, let us present some of the described relationships and their manifestations in Table 2, which is adapted from Refs. 8 to 14.

## REFERENCES

1. L. Ya. Banakh, F. M. Dimenttberg, and N. V. Zvinogradsky, About Origination of Parametric Resonance in Horizontally Located Shaft with Weight Having Radial Clearance Bearing, News, Academy of Sciences of the USSR, OTN, *Mech. Machine Eng.*, No. 6, 1961.
2. L. Ya. Banakh, Some Phenomena Emerging during Movement of Shaft in Bearing with Clearance, *Mashinovedenie*, No. 1, 1965, pp. 70–77.
3. B. T. Runov, Ed., *Vibration in Steam Turbine Aggregates*, Energoizdat, Moscow, 1981.
4. E. A. Don and V. P. Osolovski, *Misalignment of Bearings in Turbine Aggregates*, Energoatomizdat, Moscow, 1994.
5. D. E. Bently with Charles T. Hatch, in *Fundamentals of Rotating Machinery Diagnostics*, Bob Grissom, Ed., Bently Pressurized Bearing Press, 2002.
6. D. E. Bently, and A. Muszynska, Role of Circumferential in Stability of Fluid-Handling Machine Rotors, Proceedings of the Fifth Workshop on Rotordynamics Instability Problems in High Performance Turbomachinery, Texas A&M University, College Station, Texas, NASA CP 3026, 1988, pp. 415–430.
7. D. Southwick, Using Full Spectrum Plots, *Orbit*, Vol. 15, No. 2, Part 2, June, 1994, pp. 11–15.
8. A. Muszynska, Stability of Whirl and Whip in Rotor/Bearing Systems, *J. Sound Vib.*, Vol. 127, No. 1, 17–21, 1988, pp. 129–136.
9. M. D. Genkin and A. G. Sokolova, *Vibroacoustic Diagnostics of Machines and Mechanisms*, Mashinostroenie, Moscow, 1987.
10. P. Goldman and A. Muszynska, Application of Full Spectrum to Rotating Machinery Diagnostics, *Orbit*, Vol. 20, No. 1, First Quarter, 1999, pp. 17–21.
11. T. A. Harris, *Rolling Element Bearing Analysis*, Wiley, New York, 1991.
12. J. J. Yu, D. E. Bently, P. Goldman, K. P. Dayton, and B. G. Van Slyke, Rolling Element Bearing Defect Detection and Diagnostics Using Displacement Transducers, *ASME J. Eng. Gas Turbines Power*, Vol. 124, 2002, pp. 517–527.
13. J. J. Yu, P. Goldman, D. E. Bently, and A. Muszynska, Rotor/Seal Experimental and Analytical Study on Full Annular Rub, *ASME J. Eng. Gas Turbines Power*, Vol. 124, 2002, pp. 340–350.
14. J. J. Yu, P. Goldman, D. E. Bently, and J. S. Jacob, The Effect of a Pressurized Mid-Span Gas Seal on Fluid-Induced Rotor Instability, *Int. J. Acoust. Vib.*, Vol. 7, 2002, pp. 21–26.



# CHAPTER 71

## CENTRIFUGAL AND AXIAL FAN NOISE PREDICTION AND CONTROL

Gerald C. Lauchle  
Graduate Program in Acoustics  
Pennsylvania State University  
University Park, Pennsylvania

### 1 INTRODUCTION

*Axial-flow fans* are air-moving devices that draw air into a rotating blade row—called a *rotor*—in a direction that is parallel to the axis of blade rotation. The expelled air is also directed axially, but there may be some rotational velocity components in the discharge. This is called *swirl*. *Centrifugal fans*, also called *centrifugal blowers*, draw air into the rotor, or *impeller*, axially, and then by design, turn the flow 90° and expel it radially.

Fan noise control does not usually involve modifying the fan itself because such noise control modifications almost always result in a degradation of the aerodynamic performance of the fan. Engineers are foremost concerned with the volumetric flow rate and pressure rise required for an application. Noise is a secondary factor, the control of which is usually performed on the propagation path and surrounding structures.

### 2 AIR-MOVING DEVICES

This chapter is concerned with the predicting and controlling of sound radiation from axial-flow fans and centrifugal blowers that operate at subsonic Mach numbers, based on the rotor tip speed. This sound radiation is considered as noise, noise that is due predominantly to aerodynamic sources. Fan and blower noise is a class of flow-induced noise. Detailed descriptions of the fundamentals of flow-induced noise are given in Chapter 9. Attenuation of fan noise in ducting systems is covered in Chapter 111, while Chapters 89, 90, and 91 deal with the aeroacoustics of high-speed jet and rotor noise.

Here we introduce various methods that may be used to estimate fan and blower noise emissions. For completeness, we will define relevant fluid flow concepts as required for the sound generation processes. From the outset it must be made clear that flow-induced noise generation for even the simplest of flows is a very complicated process that involves unsteady flow, stochastic turbulent flow, fluid–structure interactions, and acoustic wave propagation. Exact formulations are not generally possible, so we rely upon empirical models and simplified theory to describe the radiated sound pressure or sound power from fans and blowers of various complexities.

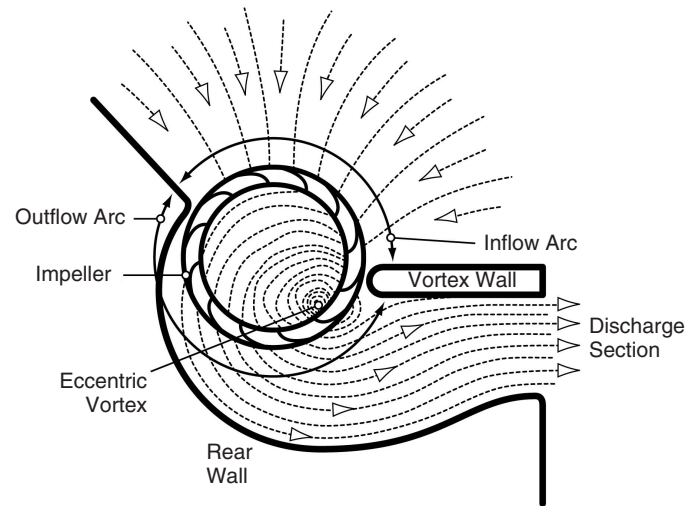
The most common types of small, subsonic air-moving devices are *centrifugal blowers*, *axial-flow*

*fans*, *plenum fans*, *cross-flow fans*, and *laminar-flow fans*. The laminar-flow fan moves air by the action of viscous drag on rotating disks rather than by lift created on rotating blade rows. The noise is obviously very low from these devices because there is no unsteady flow or turbulence, but their efficiency is not particularly high either. The reader is referred to Schlutt and Dowling<sup>1</sup> for a description and aerodynamic performance of such devices.

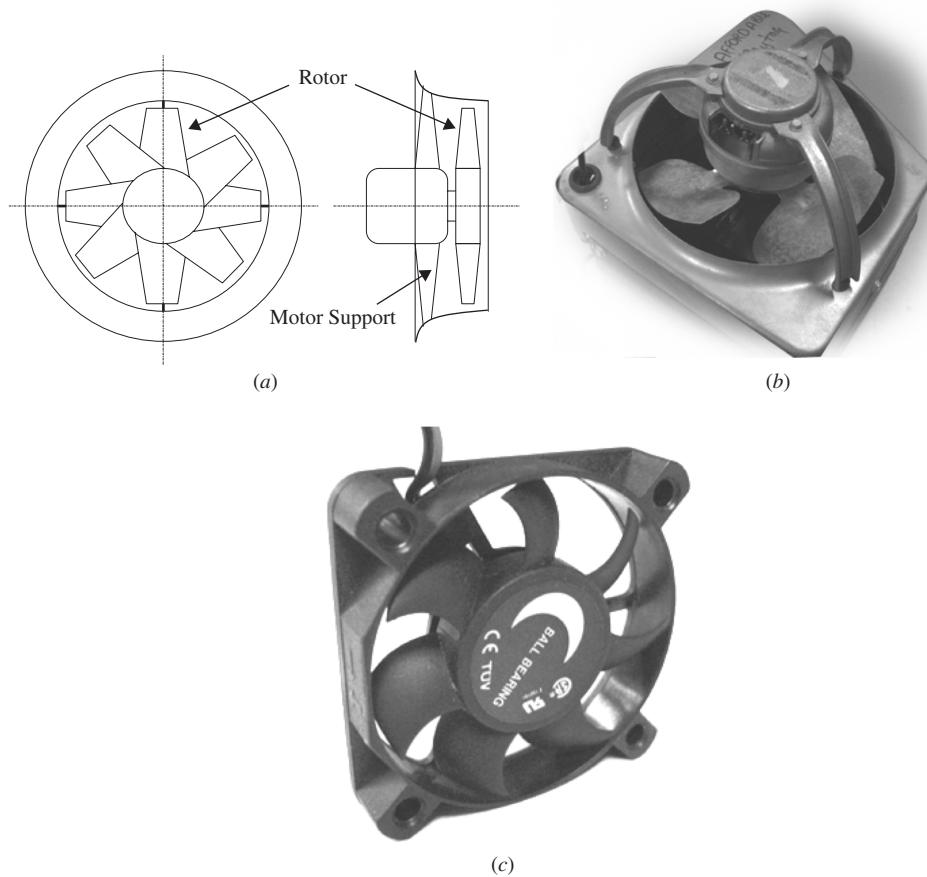
On a similar note, the acoustics of cross-flow fans—or *tangential fans*—is not very well documented. Cross-flow fans are widely used for air conditioners, air curtains, car ventilators, and household heaters. They have a drumlike impeller that is usually very long in comparison to the diameter. Figure 1 shows a schematic<sup>2</sup> of the flow field in such devices. The field is characterized by the double passage of air through the impeller blades and by the formation of a vortex within the impeller. Design goals for the cross-flow fan are centered about the position and strength of this vortex, which greatly affects performance and efficiency. Because the impeller length can be varied almost at will to produce the desired volume flow rate, the impeller speed is kept low. This low speed makes cross flow-fans inherently quiet. This type of air-moving device has thus not received much attention from the noise control engineering community, although Koo<sup>3</sup> describes an experimental study of the effect of casing design on noise. We will not consider further the cross-flow fan in this chapter.

Typical axial-flow fans used for ventilating and cooling purposes are shown in Fig. 2. Axial-flow fans can be configured with or without guide vanes, and they can be operated either in or out of ducts. The fans of Fig. 2 are seen to be encased in short cylindrical ducts. Regardless of the duct length, this feature identifies such a fan as a *tubeaxial* fan.

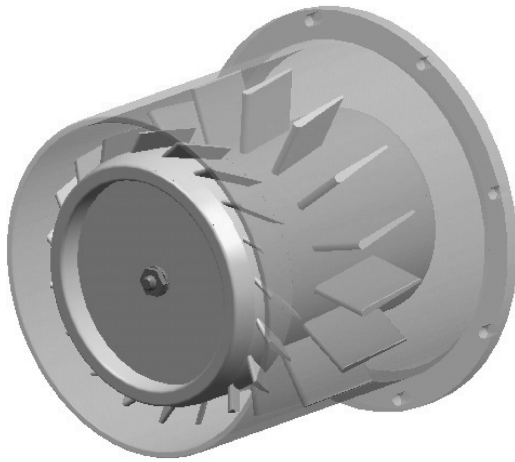
A *vaneaxial* fan is similar to the tubeaxial except that the duct is long enough to support inlet and/or outlet guide vanes, as illustrated in Fig. 3. The guide vanes are aerodynamically designed to improve the flow in the vicinity of the rotating blades, to take the swirl out of the downstream flow, and to generally improve the performance and efficiency of the fan. The energy that would be in the swirl is effectively converted to static pressure rise by downstream guide vanes. When no aerodynamically shaped guide vanes



**Figure 1** Schematic of the flow field in a cross-flow fan.



**Figure 2** (a) Schematic and (b, c) photographs of typical axial-flow fans.



**Figure 3** Schematic of a vaneaxial fan.

are used and the fan is operated in the open air, it is called a *propeller* fan, as illustrated in Fig. 4.

Centrifugal fans are composed of an impeller that operates within a volute housing, or *scroll*. The impeller blades may be canted in the forward, backward, or radial directions. Figure 5 illustrates the forward-curved impeller configuration. Air enters the impeller axially where the lift created by the rotating blades turns the flow  $90^\circ$ , directing it along the walls of the volute and eventually discharging it through the exit duct. Forward-curved blades direct the air into the scroll with a velocity greater than the tip speed of the impeller. These types of fans operate at relatively low speeds for a given pressure rise and airflow requirement. The low speed does not

usually imply low noise, however, because the blades support highly separated flow that leads to broadband turbulence noise.

Backward-curved impeller blades discharge air that has a relative velocity less than the tip speed. For a given airflow and pressure rise requirement, this type of fan operates at a higher wheel speed than does the forward-curved device, but because the aerodynamics are better, it is usually a quieter blower.

Radial blowers are rarely used for ventilation or cooling. They are used to move dust and particles. The speed of the air leaving the radial blades is essentially equal to the tip speed of the impeller. The pressure rise remains quite constant over varying volumetric flow rates. Because of intense pressure pulses that are created as radial blades pass by the tongue of the discharge, such fans are prone to producing annoying tones.

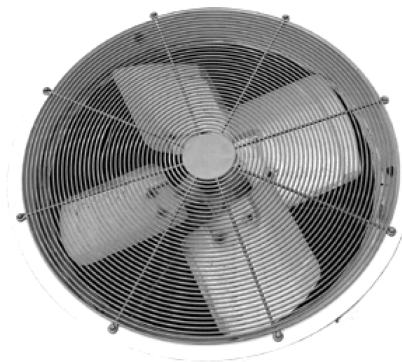
Air may enter on one or both sides of the impeller of a centrifugal blower leading to the distinction of *single-inlet* or *double-inlet* configurations, respectively. The single-inlet blower has one impeller wheel, while the double inlet typically has two impellers tied to the shaft of a common motor located between them.

*Mixed-flow* blowers usually have radial discharge blades along with a set of inlet blades that are aerodynamically shaped to improve the turning of the flow from an axial direction to the circumferential direction.

*Plenum* fans are backward-curved impellers that are mounted in rectangular plenums. They are used in many air-moving applications including room circulation, duct flow, roof and wall exhaust, and cooling of electronic components in cabinets. Figure 6 shows a typical motorized plenum fan. An axisymmetric inlet guide ring helps direct the inlet air axially into the

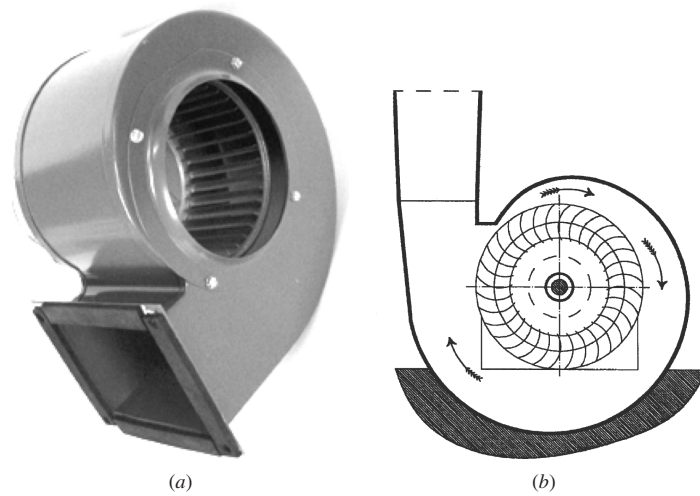


(a)

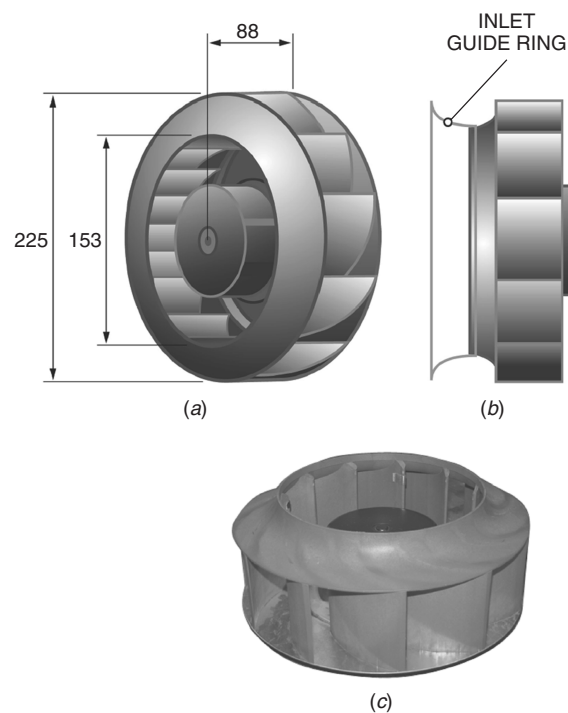


(b)

**Figure 4** Photographs of propeller fans.



**Figure 5** Schematic and photograph of a forward-curved centrifugal blower.



**Figure 6** Photograph and schematic of a typical backward-curved plenum fan.

core of the fan. The air is turned by the suction of the rotating blades and discharges tangentially in all directions; there is no scroll casing surrounding the rotor. In the absence of a scroll and cutoff, these fans produce little discrete-frequency noise. Acoustic emissions are broadband, apparently due to inlet turbulence, blade

passage turbulence, and trailing-edge noise-generating mechanisms.<sup>4</sup>

### 3 AIR-MOVING DEVICE PERFORMANCE

By way of nomenclature, the following definitions are used in this chapter:

$B$	number of rotor blades
$N$	rotor speed (rev/s, rps)
$\Omega$	rotor speed (rad/s)
$D$ ( $2R$ )	diameter of rotor (m)
$D_h$	hub diameter (m)
$Q$	volumetric flow rate ( $m^3/s$ )
$\Delta P$	static pressure rise (Pa)
$u_{tip}$	tip speed of rotor (m/s)
$\phi$	flow coefficient
$\Psi$	static pressure coefficient
BPF	blade pass frequency (Hz)
$U_\infty$	flow velocity through fan (m/s)
$\rho_0$	air density ( $kg/m^3$ )
$\eta_s$	static efficiency
$\Pi$	input shaft power in kilowatts (kW)
SHP	input shaft power in horsepower

$$\Psi = \frac{\Delta P}{\frac{1}{2} \rho_0 u_{tip}^2} = \frac{2 \Delta P}{\rho_0 \pi^2 D^2 N^2} \quad (3)$$

$$\eta_s = \frac{Q \Delta P}{\Pi} \quad (4)$$

$$BPF = NB \quad (5)$$

Air-moving device performance can be determined using the Air Movement and Control Association (AMCA) Standard 210.<sup>5</sup> Such performance is indicated by a *fan performance (head-flow) curve* as shown in Fig. 7. The performance curve depends on fan speed. The *system resistance curve* is based on the losses in the system where the fan is to do work. The energy equation is used to get this curve; that is why it is quadratic in  $Q$ . Where the two curves cross is called the *operating point*. It is noted that plots of pressure coefficient versus flow coefficient results in a single curve for the same fan operating over different conditions. The fan performance curve will change significantly when the device is operated at altitude (e.g., fans in aircraft). Figure 8 shows the effect.

#### 4 GENERAL FEATURES OF NOISE RADIATION FROM AIR-MOVING DEVICES

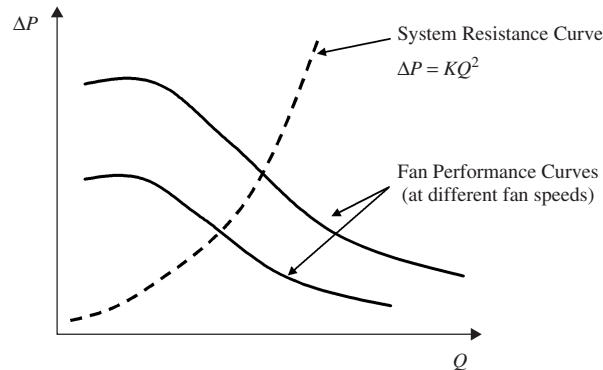
Various mechanisms cause noise from fans as summarized in Fig. 9. One of the more important causes

Interrelationships include:

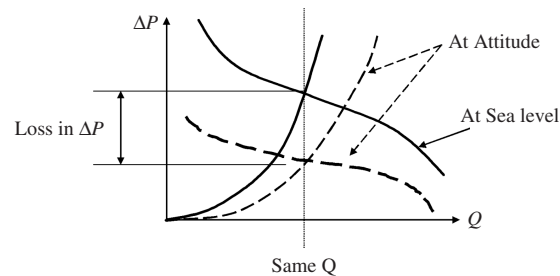
$$u_{tip} = \pi N D \quad (1)$$

$$\phi = \frac{U_\infty}{u_{tip}} \quad (2a)$$

$$\phi = \frac{(\pi D^2/4) U_\infty}{(\pi D^2/4) u_{tip}} = \frac{4Q}{\pi^2 D^3 N} \quad (2b)$$



**Figure 7** Sketch of fan performance curves and a system resistance curve. The intersection of these curves defines the operating point.



**Figure 8** Fan performance and system resistance curves change when the fan is operated at different altitudes.

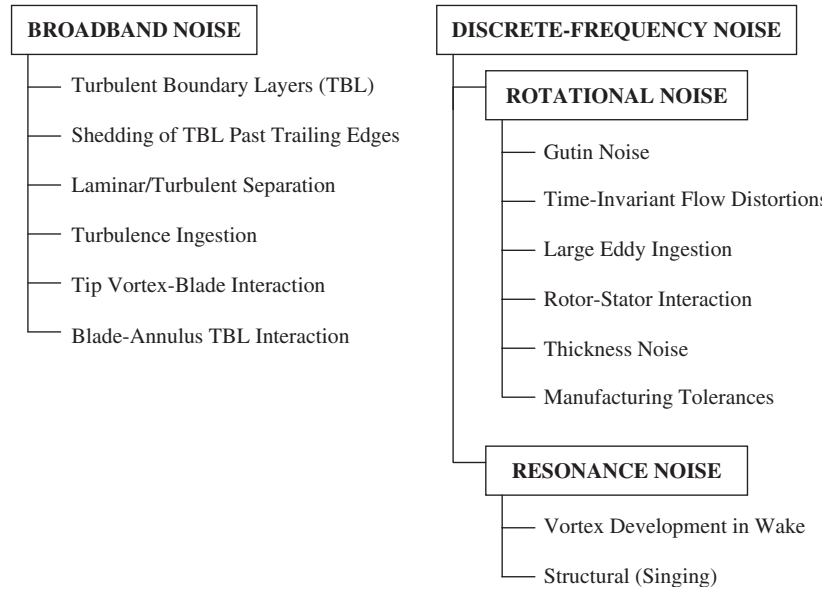


Figure 9 Mechanisms of fan noise generation.

of discrete-frequency noise is the passage of rotating blades past fixed obstructions. The obstructions cause time-invariant flow distortions that each blade responds to as it goes by it. The response is in the form of periodic changes in blade lift and drag due to local changes in blade relative velocity and angle of attack. For equally spaced blades the noise is radiated at harmonics of the blade pass frequency (BPF).

Basic flow noise theory shows that dynamically changing forces—blade lift and drag in this case—result in dipole sound radiation. Modeling of this type of noise is therefore confined to modeling the periodic force fluctuations. In the case of the acoustic wavelength being larger than say the fan diameter, the dipole radiation is *compact* and is easily computed from the force fluctuation, for example,

$$P(r, \omega) = \frac{i\omega \cos \beta}{4\pi r c_0} F(\omega) = \frac{ik_0 \cos \beta}{4\pi r} F(\omega) \quad (6)$$

where  $P(r, \omega)$  is the Fourier transform of the radiated sound pressure at radian frequency  $\omega$  due to force  $F$ ,  $c_0$  is sound speed,  $k_0 = \omega/c_0$ , and  $\beta$  is the angle measured from the direction of the force to the field point  $r$ . The *power spectrum* of the sound pressure is computed from Eq. (6) according to

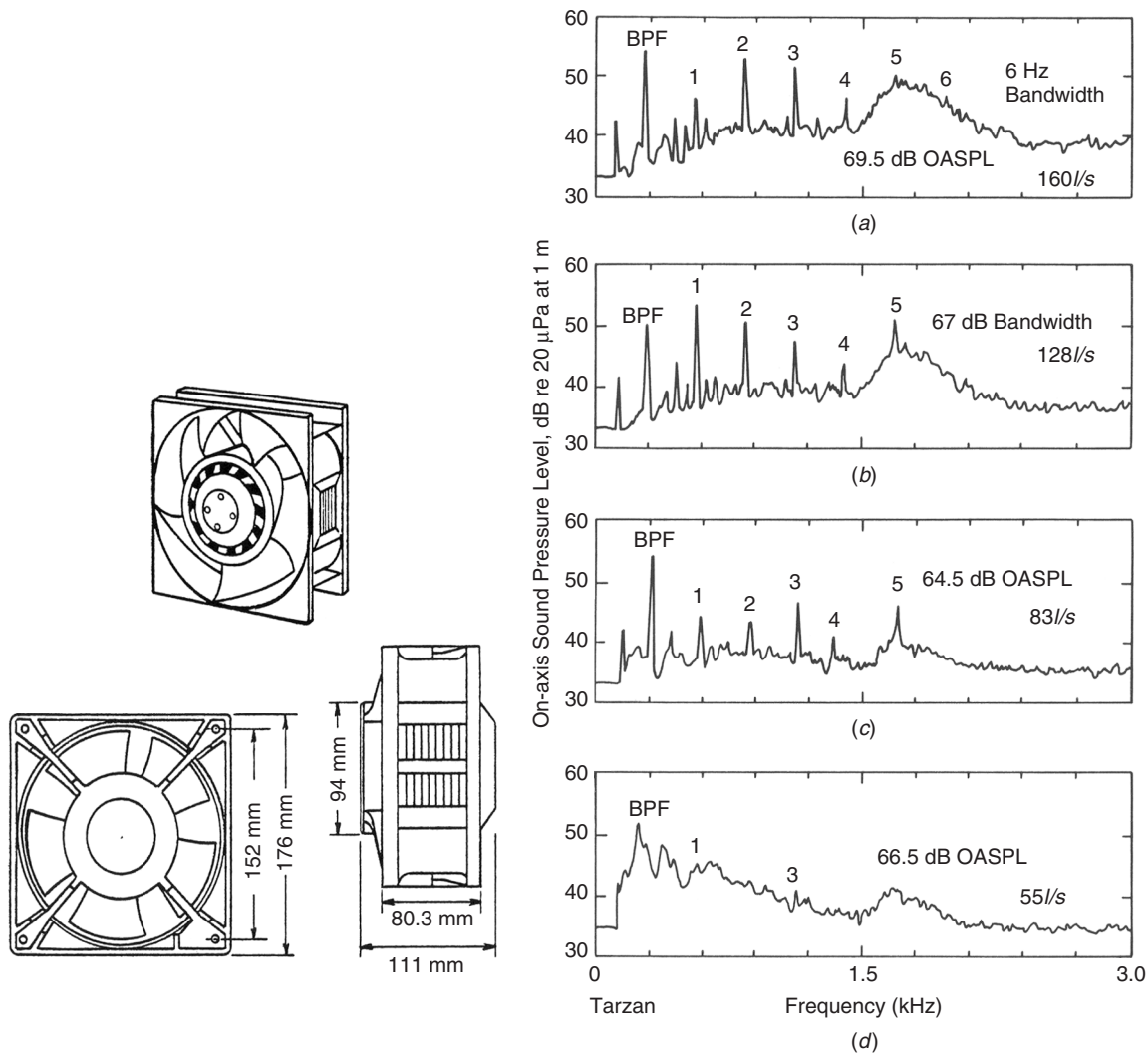
$$\begin{aligned} \Phi_{\text{rad}}(\omega) &= \frac{\langle P^*(r, \omega') P(r, \omega) \rangle}{\delta(\omega - \omega')} \\ &= \frac{k_0^2 \cos^2 \beta}{16\pi^2 r^2} \Phi_f(\omega) \end{aligned} \quad (7)$$

where  $\Phi_f(\omega)$  is the power spectrum of the force fluctuations. Chapter 42 provides details on spectrum analysis.

The delta function appearing in Eq. (7) is a reminder that individual frequency components of a power spectrum are statistically independent of each other. Note also that the delta function has units of  $\omega^{-1}$  (s) and the units of  $P(r, \omega)$  are  $\mu\text{Pa s}$ . The spectrum therefore has units of  $\mu\text{Pa}^2 \text{ s}$  or  $\mu\text{Pa}^2/\text{Hz}$  when cyclic frequency ( $f = \omega/2\pi$ ) in hertz is used. It is not our intent to oversimplify this analysis! It can be simple as indicated, but at higher frequencies, where the wavelength of sound becomes smaller than the characteristic fan dimension, the radiation is much more complicated. This is the condition of *noncompact* radiation and must be treated as special cases for each given mechanisms.

The loading on a fan has a considerable influence on the radiated noise spectrum. Figure 10 shows a sequence of measured spectra on a small computer cooling fan, each for a different operating condition. Spectrum (a) is for the free delivery condition, and the spectrum is rich in harmonic tones with a fundamental at the blade pass frequency. Overtones are labeled 1, 2, ... As the loading on the fan is increased (indicated by lower flow rates), the rotor blades begin to stall and a great deal of turbulence and vorticity is created. These are broadband noise mechanisms and the broadband noise masks the discrete-frequency radiation.

Interaction tones occur when fixed obstructions are placed in the fan inlet or outlet. Figure 11 illustrates this situation. The wake from the obstruction contains a velocity defect. As each blade in the rotor passes through this wake velocity defect, a dynamic change



**Figure 10** Sound pressure spectra measured by Fitzgerald and Lauchle<sup>6</sup> on a Rotron Tarzan fan. The volumetric flow rate through the fan is decreasing from (a) through (d).

in the blade force occurs, and dipole radiation is set up at the frequency of the blade pass. In the example shown, a cylinder spans the fan inlet; thus, each blade passes through the cylinder wake twice per revolution. A strong second harmonic of the BPF is thus created. As seen on the graph, the level of the second harmonic (first overtone) is larger than the fundamental. These levels diminish rapidly as the obstruction is moved away from the fan. The results indicate that fan installation must be carefully performed to avoid obstructions that lead to time-invariant flow distortions that then lead to tonal noise production.

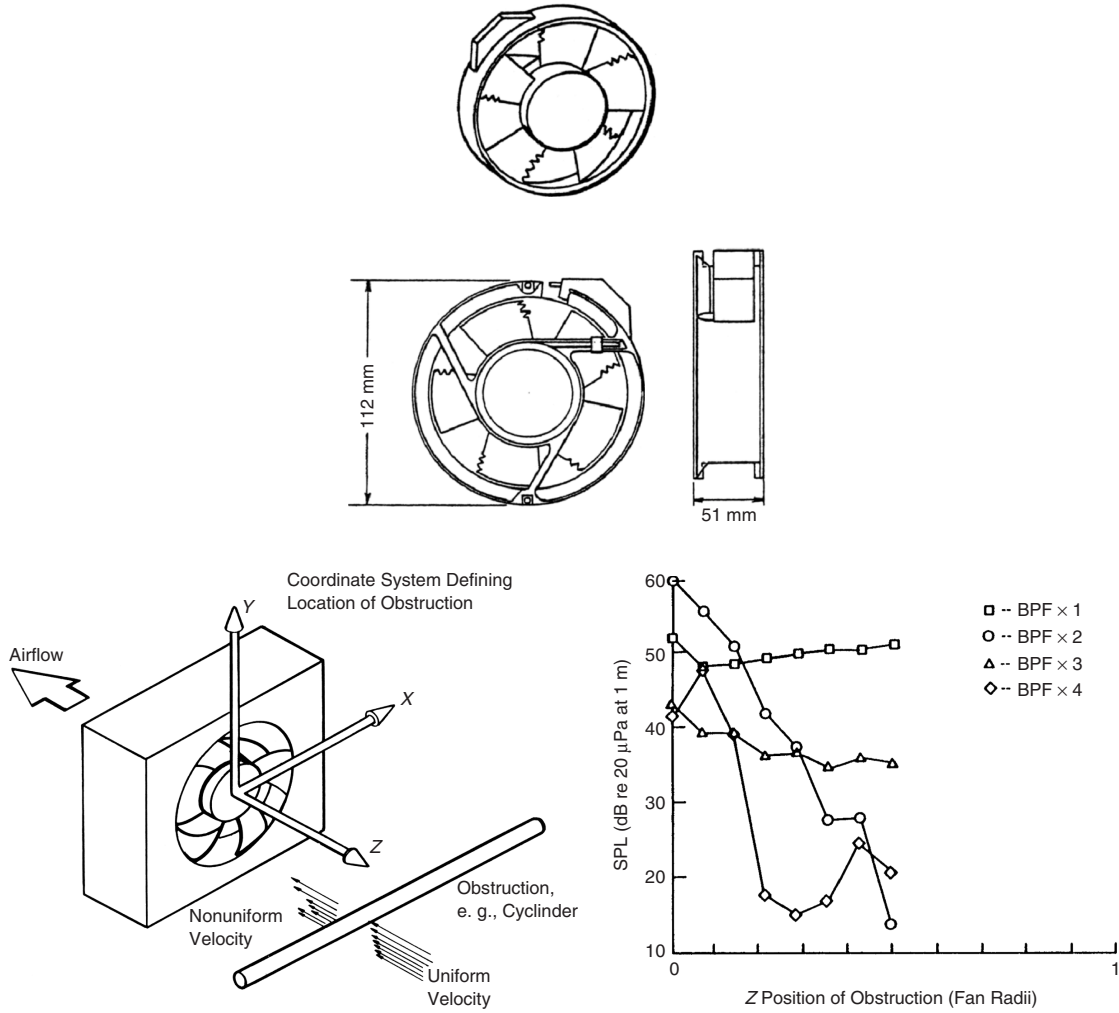
Figure 12 shows the variation of spectral character of the radiated sound power from a forward-curved centrifugal blower operating at constant speed but

under different static pressure conditions. For this blower, the best static efficiency point is at 1.22 in. of  $H_2O$  (304 Pa). It is interesting to note that the noise is predominantly broadband for this condition, low in level, and free of blade pass frequency tones. Blade pass frequency tones appear for off-design operating conditions, which is typical of forward-curved centrifugal blowers.

## 5 EMPIRICAL NOISE PREDICTION FOR AXIAL AND CENTRIFUGAL FANS

Fan noise prediction can be performed using simple empirical formulations, or if time, expertise, and resources exist, from detailed analysis, computational fluid mechanics, and computational aeroacoustic





**Figure 11** Experiments by Washburn and Lauchle<sup>7</sup> show that the sound radiation at the harmonics of the BPF are strongly affected by the location of a fixed obstruction placed in the fan inlet.

codes. In this chapter, we provide relatively simple methods of predicting the tonal and broadband noise components of axial and centrifugal fans. The empirical approach is basically adopted, although for some of the fan noise mechanisms, supplemental analytical formulations are included. In most empirical methods the overall noise level is estimated, while in others the spectrum can be determined. In regard to the former, an acoustic quantity called the *specific sound power level* was defined by Madison<sup>8</sup> to be

$$H(\phi) = \frac{W}{\Delta P^2 Q} \quad (8)$$

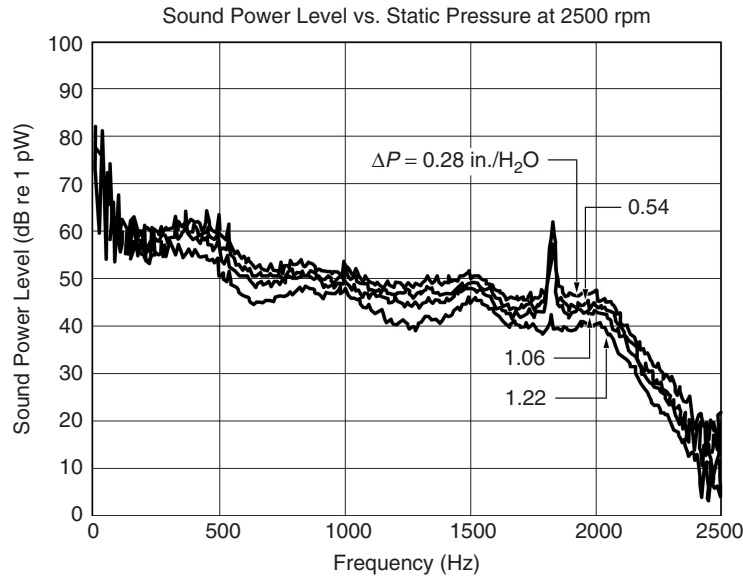
where  $W$  is the overall *sound power* in watts. Consider the variation of  $W$  with physical parameters under the

condition of constant  $H$ ,  $\phi$ , and  $\Psi$ :

$$\begin{aligned} W &= H(\phi) \Delta P^2 Q \\ &= H(\phi) \frac{\pi^4 \Psi^2 \rho_0^2 D^4 N^4}{4} \frac{\phi \pi^2 D^3 N}{4} \\ &= \frac{\pi^6 \Psi^2 \rho_0^2 \phi H(\phi)}{16} (D^7 N^5) \sim D^7 N^5 \\ &\sim D^2 u_{\text{tip}}^5 \end{aligned} \quad (9)$$

because  $u_{\text{tip}} = \pi N D$ . The overall sound power at a constant point of operation increases as the square of the fan diameter and the fifth power of the rotor tip speed. For a well-designed quiet fan, the static efficiency of the fan will peak in the same range of  $Q$





**Figure 12** Noise spectra measured on a forward-curved centrifugal blower, where the static pressure rise is the variable.

where the specific sound power level is at its lowest. Equation (8) is perhaps one of the simplest empirical fan noise formulas to be found. It predicts the *trends* in overall sound power with fan speed and fan diameter. It does not distinguish fan type, but it *does* have its usefulness in noise control engineering.

**Example** Consider a fan of diameter 0.3 m operating at 3400 rpm. Equation (9) can be used to find either a new diameter or new operating speed that affects a 10-dB noise reduction while maintaining the same flow and pressure coefficient. The equation states that  $W = D^7 N^5$ . At constant rpm, we have

$$\begin{aligned} \frac{W_1}{W} &= \frac{D_1^7 N_1^5}{D^7 N^5} \Rightarrow 10 \log_{10} \left( \frac{D_1}{D} \right)^7 \\ &= -10 \Rightarrow D_1 = 0.72 D \end{aligned}$$

At constant diameter, we have

$$\begin{aligned} \frac{W_1}{W} &= \frac{D_1^7 N_1^5}{D^7 N^5} \Rightarrow 10 \log_{10} \left( \frac{N_1}{N} \right)^5 \\ &= -10 \Rightarrow N_1 = 0.63 N \end{aligned}$$

Thus, we could change the diameter to 0.22 m or change the fan speed to 2142 rpm to obtain a 10-dB overall noise reduction while maintaining the same value of  $\phi$  and  $\Psi$ , which are nondimensional. The performance of the fan will suffer because of the noise reduction changes imposed. Equations (2b) and (3) indicate that at constant speed, the flow rate is proportional to  $D^3$  and the pressure rise

to  $D^2$ . The new flow would be  $Q_1 = 0.37 Q$  and the new pressure rise would be  $\Delta P_1 = 0.52 \Delta P$ . At constant diameter, these new values are  $Q_1 = 0.63 Q$  and  $\Delta P_1 = 0.40 \Delta P$ . One needs to decide from the application whether these decreases in performance can be justified. If flow rate is more important than pressure rise, then one might choose to lower the fan speed to obtain the 10-dB noise reduction, rather than the diameter.

### 5.1 Sound Power Spectrum of the Noise

Based on the research of Graham and Hoover<sup>9</sup> and others, Table 1 gives specific sound power levels in several octave bands for a variety of fans. These levels are given in decibels with the reference quantities:  $W_{\text{ref}} = 10^{-12} W$ ,  $Q_{\text{ref}} = 1 \text{ m}^3/\text{s}$ , and  $\Delta P_{\text{ref}} = 1 \text{ kPa}$ . We use the first of Eq. (9) to predict the octave-band sound power spectrum ( $L_W$  vs. octave band center frequency) of a given fan operating at nonreference values of  $Q$  and  $\Delta P$ . Simply add  $10 \log_{10} Q + 20 \log_{10} \Delta P$  to the tabulated levels. In the octave band where the BPF [Eq. (5)] lies, add to that level the increment given in the last column of the table. The sound powers computed by this approach include both fan inlet and fan outlet noise. Subtract 3 dB from the octave band levels if either inlet or outlet noise alone is desired.

## 6 OTHER EMPIRICAL METHODS FOR BROADBAND FAN NOISE PREDICTION

Although the specific sound power level method is widely used to make engineering estimates of the sound power radiated by typical commercial fans, there are other methods found in the fan noise literature that include additional details of the fan performance or geometry. We begin with one of the earliest.

**Table 1 Specific Sound Power Levels in Eight Lowest Octave Bands for a Variety of Axial and Centrifugal Fans**

Fan Type	Rotor Diameter (m)	Octave Band Center Frequency (Hz)								Add for BPF
		63	125	250	500	1000	2000	4000	8000	
Backward-curved centrifugal	>0.75	85	85	84	79	75	68	64	62	3
	<0.75	90	90	88	84	79	73	69	64	3
Forward-curved centrifugal	All	98	98	88	81	81	76	71	66	2
Low-pressure radial	>1.0	101	92	88	84	82	77	74	71	7
996 ≤ ΔP ≤ 2490	<1.0	112	104	98	88	87	84	79	76	7
Midpressure radial	>1.0	103	99	90	87	83	78	74	71	8
2490 ≤ ΔP ≤ 4982	<1.0	113	108	96	93	91	86	82	79	8
High-pressure radial	>1.0	106	103	98	93	91	89	86	83	8
4982 ≤ ΔP ≤ 14,945	<1.0	116	112	104	99	99	97	94	91	8
Vaneaxial										
0.3 ≤ D <sub>h</sub> /D ≤ 0.4	All	94	88	88	93	92	90	83	79	6
0.4 ≤ D <sub>h</sub> /D ≤ 0.6	All	94	88	91	88	86	81	75	73	6
0.6 ≤ D <sub>h</sub> /D ≤ 0.8	All	98	97	96	96	94	92	88	85	6
Tubeaxial	>1.0	96	91	92	94	92	91	84	82	7
	<1.0	93	92	94	98	97	96	88	85	7
Propeller	All	93	96	103	101	100	97	91	87	5

### 6.1 Centrifugal Blower Sound Power–Shaft Power Correlation

Realizing that acoustic efficiency ( $\eta$ ) is sound power divided by the mechanical power that drives the source, Beranek et al.<sup>10</sup> developed empirical noise formulations based on shaft horsepower of the fan. The sound power radiation from a wide class of blowers (where  $\eta = 10^{-6}$ ) operating in the ducts of building ventilation systems formed the foundation of this investigation. The authors measured the sound power spectrum from 14 different blowers operating in several different systems. The overall sound power measured in these experiments correlated to

$$L_W = 90 + 10 \log_{10} \text{SHP re } 10^{-12} \text{ W} \quad (10)$$

where SHP is the shaft power of the blower in horsepower. The measured data for the group of fans used in this study yield a spread of about  $\pm 4$  dB about the line computed from Eq. (10). The octave band sound power spectrum was found to slope off with increasing frequency at a rate of 5 dB per octave. The level of the first band, centered at 20 Hz, is 1 dB below the overall level predicted by Eq. (10).

### 6.2 Power Spectrum of Forward-Curved Centrifugal Blower Noise

Maling<sup>11</sup> expanded the empirical relation of Beranek et al.<sup>10</sup> to include the effects of diameter, blower width, blower speed, pressure rise, volumetric flow rate, flow coefficient, and Mach number. He arrived at empirical formulas for the narrow-band radiated sound power spectra based on measurements from a set of three groupings of geometrically similar forward-curved centrifugal blowers. All of the blowers had 28 blades. The widths and diameters varied from group to

group, but the width-to-diameter ratio remained fixed at 0.5. Maling defines the following nondimensional parameters:

$$\theta = E / \rho_0 c_0^3 D^2 \quad (E = \text{sound power/Hz})$$

$$M = \pi D N / c_0 \quad (\text{rotor tip speed Mach number})$$

$$\phi = 4Q / \pi^2 D^3 N \quad (\text{flow coefficient})$$

$$s = f / N \quad (\text{frequency parameter})$$

$$\text{Re} = \pi N D^2 / \nu \quad (\text{Reynolds number based on } u_{\text{tip}})$$

where  $\rho_0$  = density of air ( $\text{kg/m}^3$ ), and  $\nu$  = kinematic viscosity of air ( $\text{m}^2/\text{s}$ ). He also suggests that  $\theta = F(M, \phi, s)$ , so that the overall sound power is

$$W = \int_0^\infty E(f) df = \rho_0 c_0^3 D^2 F(M, \phi) \quad (11)$$

The experiments were performed in a special duct facility designed for the purpose. Maling's measurements of the blower sound power at different Mach numbers helped to define a new  $\theta$  function given by  $\theta = M^3 g(s, \phi)$ . The sound power spectral relations become

$$\begin{aligned} E &= \rho_0 c_0^2 D^3 M^3 g(s, \phi) \\ &= \rho_0 c_0^2 D^3 M^3 g_0(s) h(\phi) \end{aligned} \quad (12)$$

It was shown that the dependence on  $\phi$  is quite weak, and  $h(\phi) \simeq 1$ . Collectively, the measured data appear to correlate to within  $\pm 4$  dB of

$$g_0(s) = (f/N)^{-2.67} \quad (13)$$

The final empirical result for the sound power spectrum (per hertz) radiated by small forward-curved centrifugal blowers is

$$E = \rho_0 c_0^2 D^3 M^3 (f/N)^{-2.67} \quad (14)$$

From this relationship, the overall mean-square sound pressure scales like  $p^2 \sim D^{0.4} u_{\text{tip}}^{5.67}$ .

### 6.3 Axial Fan Broadband Noise Prediction

While the Beranek et al.<sup>10</sup> and Maling<sup>11</sup> methods help to predict broadband noise from centrifugal fans, Wright<sup>12</sup> addressed the broadband noise of axial fans. He measured the sound power from a variety of fans and correlated the data to the important flow and geometrical parameters. Considered are rotor-only propeller fans (R), fans with a rotor and outlet guide vanes (R-O), and fans with both inlet and outlet guide vanes straddling the rotor (I-R-O). Wright found that the measured power levels correlate well with a newly introduced *peak velocity* parameter. This velocity is the maximum surface velocity that exists on the rotor blades. It depends strongly on fan loading as indicated by the following expression:

$$V_p = K u_{\text{tip}} \left( \sqrt{1 + \phi^2} + \frac{\Psi b}{4C\eta_s} \right) \quad (15)$$

where  $C$  is the blade chord at the tip, and  $b$  the blade spacing. The factor  $K$  is related to the flow through the fan according to

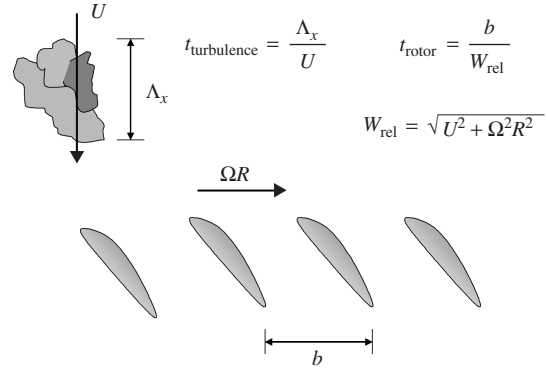
$$\begin{aligned} K &= 1 + 1.64|\hat{Q}|^{3/2} \quad \hat{Q} < 0 \\ &= 1 + 0.5|\hat{Q}|^{3/2} \quad \hat{Q} > 0 \end{aligned} \quad (16)$$

where  $\hat{Q} = (Q - Q_d)/|Q_s - Q_d|$ . Here, subscript  $d$  stands for *design* value and subscript  $s$  indicates the *stall* value. Empirical formulas that predict overall sound power, within  $\pm 3$  dB of measured data, for each of the three types of fans are

$$\begin{aligned} L_w &= 53.4 \log_{10} V_p - 25.7 \quad \text{I-R-O} \\ &= 50.9 \log_{10} V_p - 28.1 \quad \text{R-O} \\ &= 38.2 \log_{10} V_p - 6.1 \quad \text{R} \end{aligned} \quad (17)$$

### 6.4 Turbulence Ingestion Noise

Turbulence ingestion noise results when turbulence is ingested into either axial-flow or centrifugal fans; it is a low-frequency, broadband noise. This noise is due to the turbulence interacting with the rotor blade leading edges causing unsteady lift, which results in direct dipole sound radiation according to Eq. (6). Figure 13 shows a schematic of the situation. Two time scales exist, one associated with the turbulence and the other associated with the rotor. When  $t_{\text{turbulence}} \ll t_{\text{rotor}}$ , or



**Figure 13** Interaction of free-stream turbulence of axial length scale  $\Lambda_x$  interacting with a rotor blade row moving at circumferential velocity  $\Omega R$ .

when  $\Lambda_x \ll b$  (because  $W_{\text{rel}} \simeq U$ ), the unsteady rotor force spectrum is broadband with a continuous roll-off as the frequency increases. When these time scales become comparable, meaning that the turbulence scale becomes equal to or greater than the blade spacing, blade-to-blade correlation exists in the rotor force distribution. In other words, more than one blade interacts with a given turbulent eddy at a given instant. Then, broad humps, centered about the harmonics of the BPF appear in the unsteady rotor force and radiated noise spectrum. The large eddies behave like quasi-time-invariant inflow distortions. Such flows are common in fans operating near boundaries and behind grids, such as automotive engine cooling fans; for example, see Mani,<sup>13</sup> Mellin,<sup>14</sup> and Mugridge.<sup>15</sup> The theory for predicting fan rotor unsteady force spectra and noise due to turbulence ingestion is complicated and beyond the scope of this chapter. Please see Blake<sup>16</sup> and Howe<sup>17</sup> for the theoretical approaches.

## 7 DISCRETE-FREQUENCY FAN NOISE PREDICTION

### 7.1 Tonal Noise from Blowers

Blade pass frequency tones occur in centrifugal blowers, particularly when they are operated off-design. The major source of these tones is the interaction of the impeller blade trailing edges with the cutoff. Neise<sup>18</sup> used a spectral decomposition technique to separate a fan-radiated noise spectrum into independent functions that are multiplied together. One function depends on Helmholtz number  $D/\lambda$  and describes the acoustics of the system in which the fan is operated. The second is the fan aerodynamic source function that depends on Strouhal number and describes the aerodynamically induced sound generated by the fan. The Strouhal number defined by Neise is

$$\text{St} = \frac{f D}{u_{\text{tip}}} \frac{\pi}{B}$$

**Table 2 Aerodynamic Source Function of Eq. (18) Measured and Compiled by Neise<sup>18</sup> for Three Different Centrifugal Blowers Radiating Sound at the Indicated Harmonics of the BPF<sup>a</sup>**

Strouhal Number $St = \frac{\pi f D}{B u_{tip}}$	Aerodynamic Source Function $20 \log_{10} F(St) \text{ (dB)}$
1	143.0
2	136.5
3	133.5
4	132.5
5	131.0
6	129.0

<sup>a</sup> The uncertainty in these data is  $\pm 2$  dB

It is seen to equal 1, 2, 3, ... at each of the respective harmonics of the blade pass frequency. The aerodynamic source function, tabulated in Table 2, is given by

$$F(St) = \frac{p(St)/p_0}{M^\alpha R e^\beta} \quad (18)$$

with constants  $\alpha \approx 2.1$ ,  $\beta \approx 0.2$ , and  $p_0 = 20 \mu\text{Pa}$ . The parameters of this equation are the same as those preceding Eq. (11). The mean-square sound pressure radiated at the harmonics of the blade pass frequency follow  $\overline{p^2}(St) = u_{tip}^{6.2} D^{0.4}$ , which shows a lesser dependence on diameter than the Madison law<sup>8</sup> but agrees well with the Maling<sup>11</sup> results.

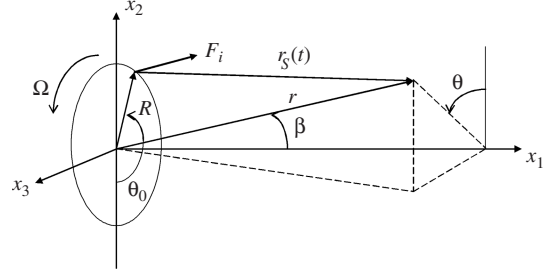
## 7.2 Theory of Interaction Noise in Axial Fans

Detailed derivations of the discrete-frequency components observed in the unsteady force and radiated noise spectrum of axial-flow devices may be found in many different research studies; Blake<sup>16</sup> provides a complete summary of these. Interaction noise theory assumes that a rotor is exposed to a time-invariant, spatially nonuniform inflow velocity field. The essence of the theory is the development of a Green's function that describes the field at  $\mathbf{x}$  due to a simple rotating source (or force) at  $\mathbf{y}$ :

$$G(\mathbf{x}; \mathbf{y}, \omega') = \sum_{n=-\infty}^{\infty} \frac{e^{ik_0 r}}{4\pi r} J_n(k_0 R \sin \beta) \times e^{in(\theta - \theta_0 - \pi/2)} \delta(\omega' - \omega + n\Omega) \quad (19)$$

Figure 14 provides a definition of the symbols used in this function, and  $J_n$  is the Bessel function of the first kind and order  $n$ . If the rotating source at radius  $R$  is a time-periodic source of frequency  $\omega_0$ , then the radiated sound pressure spectrum is given by

$$\Phi_{\text{rad}}(\omega) = \frac{1}{16\pi^2 r^2} \sum_{n=0}^{\infty} \Phi_d(\omega_0 \pm n\Omega) \times \left| J_n \left( \frac{\omega_0 \pm n\Omega}{c_0} \right) R \sin \beta \right|^2 \times \delta(\omega - \omega_0 \pm n\Omega) \quad (20)$$



**Figure 14** Definition of variables used for analyzing the radiation from a rotating force  $F_i$  or acoustic source at radius  $R$ .

where  $\Phi_d(\omega)$  is the *discrete* pressure spectrum of the source. This, for example, may be due to the impulsive loading at each radial position of a blade that periodically intersects the wake of a fixed obstruction like an upstream guide vane. Even though the source is periodic at  $\omega_0$ , the field contains an infinite number of sideband frequencies at integer multiples of the source rotation rate  $\Omega$ . These are a result of Doppler effects. The term in Eq. (20) that contains the Bessel function is called the *Bessel envelope*. It is a curve that envelopes the magnitudes of all of the tones in the radiation spectrum. These discrete tones are  $\omega_n = \omega_0 \pm n\Omega$ . Note that the Bessel envelope changes shape with the value of the observation angle  $\beta$ .

Now if the rotating source (or force) has a nondiscrete *continuous* spectrum  $\Phi_c(\omega)$ , then the radiated noise spectrum is simply

$$\Phi_{\text{rad}}(\omega) = \frac{\Phi_c(\omega)}{16\pi^2 r^2} \quad (21)$$

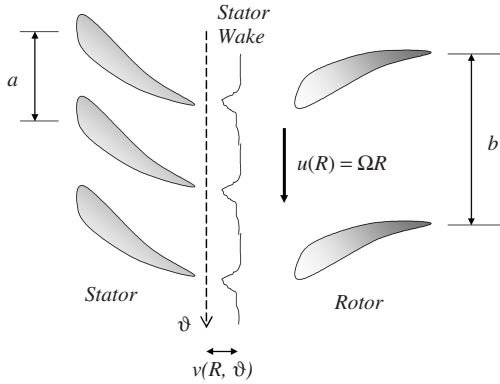
A broadband rotating source is unaffected by Doppler effects and its sound spectrum is proportional to the source spectrum. This is the situation for radiation from rotor trailing edges, blade surface turbulent boundary layers, and localized blade flow separation zones.

*Rotor-stator interactions* cause many tones to appear in the spectrum of fans with inlet and/or outlet guide vanes. Figure 15 describes the problem. The radiated sound pressure Fourier component is composed of the contributions from many modal pressure patterns:

$$P(\mathbf{x}, \omega) = \sum_{m=-\infty}^{\infty} \sum_{w=-\infty}^{\infty} P_{w,m}(\mathbf{x}, \omega) \quad (22)$$

where

$$P_{w,m}(\mathbf{x}, \omega) = -\frac{iB}{4\pi r} \left( f_{1,w} k_0 \cos \beta + \frac{mB - w}{0.7R_t} f_{\theta,w} \right) \times J_{mB-w}(0.7k_0 R_t \sin \beta) \times e^{i[k_0 r + (mB-w)(\theta - \pi/2)]} \delta(\omega - mB\Omega) \quad (23)$$



**Figure 15** Rotor–stator interaction noise occurs when the wakes of a fixed-blade row interact with the rotating blade row.

Equation (7) can be used to express the radiation spectrum based on these Fourier components.

The modal sums of Eq. (22) are over the harmonics of the BPF and over the harmonics of the circumferential wavenumber distribution of the stator wake perturbation. For a given blade section of chord length  $C$ , canted at the angle  $\gamma$  from the axial direction, the axial and circumferential lift per wake harmonic are given, respectively, by

$$f_{1,w} = \int_{R_h}^{R_t} L'_w \left( \frac{C}{R}, \frac{wC}{R} \right) \cos \gamma e^{i w \vartheta_w} dR \quad (24)$$

$$f_{\vartheta,w} = \int_{R_h}^{R_t} L'_w \left( \frac{C}{R}, \frac{wC}{R} \right) \sin \gamma e^{i w \vartheta_w} dR \quad (25)$$

The forces to be integrated represent *unsteady lift* and *unsteady drag* per unit span. They depend on the radial ( $1/R$ ) and circumferential ( $w/R$ ) wavenumbers as used in the two-dimensional Sears function<sup>19</sup>:

$$L'_w \left( \frac{C}{R}, \frac{wC}{R} \right) = \pi \rho C |V(R, w)| u(R) S_{2D} \left( \frac{C}{R}, \frac{wC}{R} \right) \quad (26)$$

where  $|V(R, w)|$  is the magnitude of the circumferential wavenumber spectrum of the spatially nonuniform and time-invariant rotor inflow velocity profile. The two-dimensional Sears function is

$$S_{2D}(x, y) = S_e(x) \frac{1 + 3.2\sqrt{x}}{1 + 2.4y^2 + 3.2\sqrt{x}} \quad (27)$$

where

$$S_e(x) = \frac{2}{\pi x [H_0^{(1)}(x) + i H_1^{(1)}(x)]} \quad (27a)$$

is the one-dimensional Sears function, and  $H_n^{(1)}(x) = J_n(x) + i Y_n(x)$  is the Hankel function of the first kind.

The wavenumber spectrum is determined from the measured or predicted rotor inflow field. Computational tools exist to predict the wake profile from upstream stator blade rows. Or, measurements can be performed with standard techniques such as laser-Doppler velocimetry, particle imaging, or scanned five-hole pressure probes. See Chiu et al.<sup>20</sup> for an example of the experimental approach. Essentially, the radially dependent circumferential variation of mean velocity in the wake of the stator is broken into Fourier components:

$$V(R, w) = \frac{1}{2\pi} \int_0^{2\pi} v(R, \vartheta) e^{-i w \vartheta} d\vartheta \quad (28)$$

$$v(R, \vartheta) = \sum_{w=-\infty}^{\infty} V(R, w) e^{i w \vartheta}$$

Examination of the modal pressure given by Eq. (23) reveals the following:

1.  $\delta(\omega - mB\Omega) \Rightarrow$  sound is produced only at  $\omega = mB\Omega$ , the frequencies of radiation are multiples of the blade pass frequency.
2.  $J_0 > J_n \Rightarrow n = mB - w = 0$  results in the highest magnitude modal pressure. The strongest axial forces and sound are produced when  $w = mB$ .

**Example** Consider a rotor–stator interaction where there are  $B$  rotor blades and  $V$  stator vanes. This relation means that when  $nV = mB$  (where  $n$  and  $m$  are integers) there will be large axial forces. For example, if  $B = 3$ , and  $V = 4$ , we find  $4B = 3V = 12$  is the lowest combination of integers that makes the equality. Since  $m = 4$ , the fourth harmonic of the BPF will radiate substantial sound. It can also be shown that for *minimum radiation* at the fundamental BPF, choose rotor–stator combinations such that

$$V_{\min} + \frac{V_{\min}}{B} = V_{\max} - \frac{V_{\max}}{B} \quad (28a)$$

If  $B = 4$ , Eq. (28a) suggests that the best number of stator vanes would be 3 or 5.

3. When  $mB - w = 0$ , the tangential forces contribute nothing to the modal pressure.
4. However, when  $w = mB \pm 1$ , the tangential (side) forces will be large. For rotor–stator interactions, large side forces exist when  $nV = mB \pm 1$ . For the case of  $B = 3$  and  $V = 4$ , the side force (and vibration) will be large at the BPF.
5. When  $w = 0$ , the inflow is *steady* and *uniform*. The resulting noise, called *Gutin* noise, is from

the *steady-state thrust* of the rotor.<sup>21</sup> Gutin noise is discrete at harmonics of the shaft rate, and it is important only when  $M_{\text{tip}} = u_{\text{tip}}/c_0 \rightarrow 1$ .

6. In the time domain, the delta function returns to  $e^{-imB\Omega t}$ . Couple this with  $e^{i(mB-w)\theta}$  to get  $e^{-i(mB\Omega t - mB\theta + w\theta)}$ . On a constant phase trajectory (wavefront)  $n\theta \equiv mB\theta - w\theta = mB\Omega t$  from which  $d\theta/dt = mB\Omega/n$ . This angular velocity of the phase trajectory implies that the mode  $n$  is "spinning." There will be some higher-order spinning modes that have modal tip speeds greater than the sonic velocity,  $\theta R_t \geq c_0$ . These pressure components will propagate to great distances.

### 7.3 Other Sources of Tonal Noise in Fans

*Thickness* noise, like Gutin noise, is a high Mach number source of sound that is not normally encountered in low-speed fans. It is a monopole (volume) source caused by the dynamical displacement of fluid as a blade of nontrivial thickness cuts through it. Thickness noise is one source of helicopter rotor noise.

In the complex fields of fluid-structure and fluid-acoustic interactions, a situation called *locking-in* is defined when one unsteady characteristic of a process reinforces a similar characteristic in another process (and vice versa) such that a feedback loop forms causing the common characteristic of both processes to be amplified. Several examples of lock-in are covered in Howe<sup>17</sup> and in Lucas et al.<sup>22</sup> and some of them occur in fans.

Mechanical resonances of fan rotor blades, vanes, and other components can be excited by fluid flow. These events may produce additional fan noise tones. One common lock-in phenomenon for fan blades is *singing*. This happens when the frequency of a resonant flexural mode of blade vibration matches the frequency of vortex shedding from that blade. The acoustic tone generated is not situated at any particular harmonic of the shaft rate frequency, but it is at the mechanical resonance frequency of the vibratory mode.

A more complex form of lock-in that can occur in low-speed fans is called *laminar boundary layer-wake interaction*. Qualitatively speaking, periodic shear layer velocity perturbations, due to Tollmein-Schlichting waves and hairpin vortices, occur during transition from laminar-to-turbulent boundary layer flow on rotor blades when the Reynolds number based on chord length is in the approximate range  $10^5 < UC/\nu < 10^6$ , where  $U$  is the velocity at the leading edge of the blade. If the frequency of these periodic shear layer instabilities matches the frequency of vortex shedding, then a hydrodynamic lock-in phenomenon takes place. This causes the periodicity in the wake of the blade to be amplified. If these vortex frequencies happen to be near a harmonic of the BPF, then significant increases in the sound at this frequency will occur. Turbomachinery designers try to design rotor and stator blades that operate at

chord Reynolds numbers in excess of a million. That assures that the boundary layers are turbulent and free of organized vortex structures that can lead to lock-in problems. It further assures that the performance of the fan does not become unstable under certain flow conditions within the operating envelope. This instability problem has been encountered with small, subsonic cooling fans in the range of  $Q$  corresponding to the peak in static efficiency.<sup>23</sup>

## 8 NOISE CONTROL FOR FANS AND BLOWERS

The specific sound power levels given in Table 1 are based on fans operating at or very near their peak (static) efficiency point. As previously mentioned, minimum noise from a well-designed fan occurs when it is operated in this range. The notable exception is for small cooling fans that may be unstable in this range. Therefore, one must be cautious in attempting to lower noise by adjusting fan speed or size based on Eqs. (8) and (9). This was demonstrated by the example following those equations.

Caution must also be exercised when modifying an already well-designed fan for noise control purposes. Some noise reduction may be achieved, but more than likely, the fan performance will be degraded along the way. Nevertheless, over the many decades of fan design and fan noise research, there have been some successes at lowering fan noise through component redesign or modification without serious degradation of performance. A few of those methods are highlighted.

Embleton<sup>24</sup> studied various methods to reduce centrifugal blower noise, particularly noise radiating at the BPF:

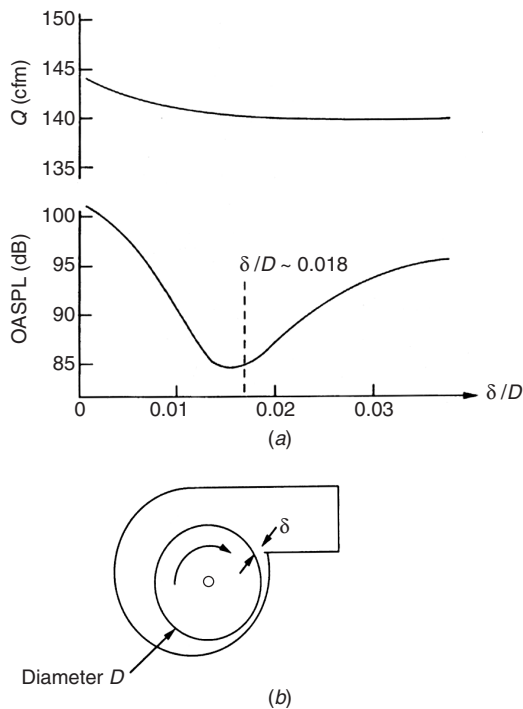
1. Increasing the impeller-to-cutoff distance lowered BPF noise. Figure 16 shows that there is an optimum distance of approximately  $0.018D$  that should exist between the impeller trailing edge and the volute cutoff for minimum noise.

2. Increasing the radius of the cutoff tends to reduce the impulsive pressure created by the rotating blades; thus, the practice is a proven noise reducer.

3. Skewing or spiraling the impeller blades relative to the cutoff is a relatively expensive manufacturing option that can significantly reduce BPF noise. The technique is also used in laying out knife patterns on the cutterheads of planers and joiners used in the woodworking industry.

4. Staggering the blade rows in double-row impellers can also help to reduce BPF noise.

5. Mismatching the acoustic impedance of a fan inlet (and outlet) from that of the connecting ductwork is a passive means of attenuating fan noise (see also Chapter 57). For an axial fan, this can easily be accomplished by placing relatively short sections of lined pipe up and downstream of the fan. The sound-absorbing material that makes up the liner attaches to the inside of the pipe. Choose a liner that has a protective covering so that particulates of the absorbing material are not swept away by the airflow. Because the fan is a dipole source, be sure that the length of

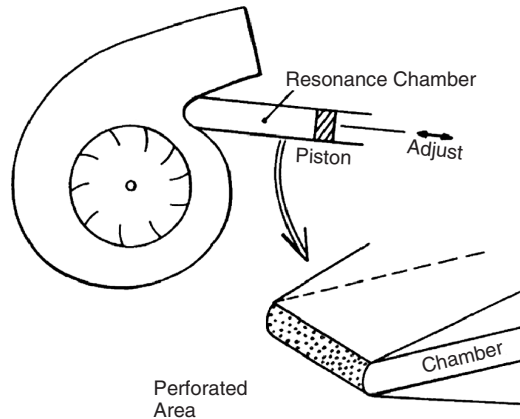


**Figure 16** Effect of cutoff distance on overall sound pressure level, OASPL, and on volumetric flow rate,  $Q$ , of centrifugal blower. (From Embleton.<sup>24</sup>)  $\text{ft}^3/\text{min}$  (cfm)  $= 0.472 \times 10^{-3} \text{ m}^3/\text{s}$ .

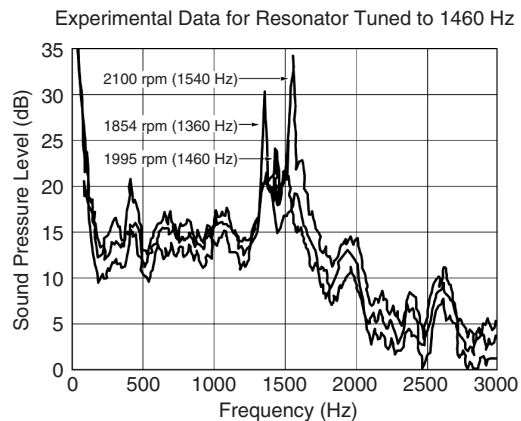
the lined sections of pipe are not an integer multiple of a half wavelength of sound at the BPF, or at other frequencies of concern.<sup>25</sup> In the case of blowers, a dissipative muffler can be added at both inlet and outlet. Such mufflers that do not affect the airflow are commercially available.

6. Use tuned resonators for controlling tones. A tuned resonator for a blower might consist of a cavity mounted behind the cutoff. Screen or perforated plate separates the cavity from the moving air in the cutoff region. For axial fans, the cavity can be integrated into the hub. The cavity is designed to have rigid walls and to be a one-quarter wavelength ( $\lambda/4$ ) long at the BPF. This wavelength is  $\lambda = c_0/\text{BPF}$ . The application of this method to a centrifugal blower was demonstrated by Neise and Koopmann.<sup>26</sup> Figure 17 shows a sketch of a cutoff-mounted resonator. Figure 18 shows acoustic data measured by the author on the same blower of Fig. 12 with a one-quarter wavelength resonator installed in the cutoff.

7. Unequal rotor and/or stator blade spacing is a technique that shifts the high-level sound energy that is in the few harmonics of the BPF to the many more harmonics of the shaft rate frequency. It generally does not change the overall sound power because the original sound energy is simply redistributed into different (and many more) frequency bands. The sound



**Figure 17** Sketch of a quarter wavelength resonator for blower BPF noise control.



**Figure 18** Sound pressure level spectra measured for a forward-curved centrifugal blower at different speeds. A cavity resonator is mounted in the cutoff of the volute. When the length of the cavity corresponds to the one-quarter wavelength at the frequency of the BPF, tonal noise reduction is observed. The frequencies in parentheses are the BPF's for the noted rotor speed.

pressure spectrum has fewer high-level tones and many more lower-level tones. The spectrum is essentially "whitened." Arranging the rotor and stator blades in a circumferential unequal pattern is a *sound quality control* technique rather than a noise control technique.

Mellin and Sovran<sup>27</sup> provide tables of blade spacing for optimum suppression of the strongest blade rate harmonic, based on the number of blades and whether or not the configuration is dynamically balanced. For a given circumferential pattern of rotor and stator blades, strong interaction occurs because of the cumulative effect of one discontinuity passing by all of the others set up by the stationary blade row. Frederick and Lauchle<sup>28</sup> show that this is a cross-correlation function  $R_{AW}(\Delta\theta)$  that is formed between



the rotor circumferential blade pattern and the stator circumferential vane pattern. Fourier transforming the cross-correlation function yields a cross spectrum  $S_{AW}(m)$  for the orders of shaft rate that will dominate the noise spectrum. In particular,

$$R_{AW}(\Delta\theta) = \frac{1}{2\pi} \int_0^{2\pi} W(\theta)A(\theta + \Delta\theta) d\theta \quad (29)$$

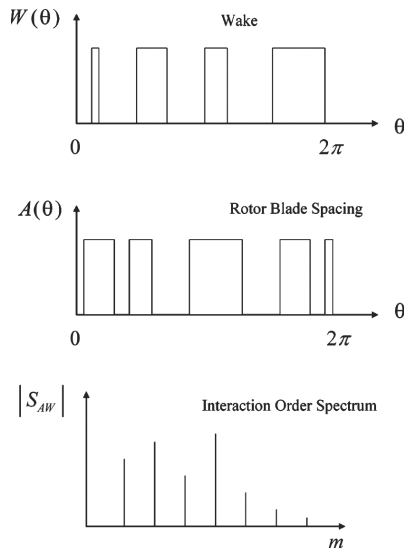
$$S_{AW}(m) = \int_0^{2\pi} R_{AW}(\Delta\theta)e^{-im\Delta\theta} d\Delta\theta \quad (30)$$

Figure 19 shows an example wake and rotor spacing pattern along with the resulting interaction spectrum. The method yields the frequencies and relative magnitudes of the radiation tones that will be generated from unequal blade spacing. Practical examples of the method may be found in Frederick and Lauchle<sup>28</sup> and in Brungart and Lauchle.<sup>29</sup> The technique can also be used to design acoustically pleasing tire tread patterns.

8. Trailing-edge modifications can reduce broadband noise. The acoustic pressure spectrum of trailing-edge noise is proportional to the product of the spectrum of the local wall pressure fluctuations that occur near the trailing edge and to the spanwise correlation length of these pressure fluctuations. The correlation length is the average (statistically speaking) distance over which a pressure-producing eddy remains correlated with itself. Typically, this length is some fraction of the turbulent boundary layer thickness at the

trailing edge. The largest correlation lengths—and noise—occur when the flow leaves the surface at right angles to the span, as it does, say in plenum impellers (Fig. 6). Roughening the trailing edge with applied sandpaper decorrelates the pressure fluctuations but raises the level of the local wall pressures; thus, such a measure is not usually effective in reducing overall noise. Serration of the trailing edge, on the other hand, does little to the local wall pressure fluctuations, but it can reduce the correlation lengths. Howe<sup>17</sup> analyzes the noise reduction due to serrations of sinusoidal shape and of sawtooth shape. The sawtooth pattern yields larger noise reductions than the sinusoidal edge pattern. When a sawtooth serration of peak-to-peak amplitude  $2h$  and period  $\lambda_{\text{edge}}$  is added to a blade trailing edge, Howe shows that the attenuation in decibels is  $10 \log_{10}[1 + (4h/\lambda_{\text{edge}})^2]$ . The angle that the sawtooth makes with the free-stream velocity vector should be less than  $45^\circ$  and  $h = \delta$  for effective noise reduction, where  $\delta$  is the boundary layer thickness at the trailing edge. Choosing  $h/\lambda_{\text{edge}} = 1$  results in 12.3 dB trailing-edge noise reduction.

9. Active control is a technique that has shown some success in reducing tonal noise from fans. Two approaches are possible: create antisound from a speaker, or an array of speakers, placed near the fan,<sup>30–32</sup> or create antiferce with a mechanical shaker that is presumed to cancel the unsteady aerodynamic forces created by the fan.<sup>33</sup> Both approaches utilize the feedforward, filtered-x, least-mean-square adaptive noise control algorithm<sup>34</sup> that requires a fan blade rotational sensor, like a tachometer. Both approaches are effective in reducing the lower-order blade pass frequency tonal noise. Sound pressure level reduction of the BPF noise has been shown to be as high as 22 dB, while global sound power reductions of up to 14 dB have been demonstrated. Reduction of broadband fan noise by active means is still in a developmental stage.



**Figure 19** In analyzing the tones that are created in an unequally spaced rotor–stator combination, the positions of the rotor blades and interacting stator wakes are plotted circumferentially as unit step functions. The interaction order spectrum is the cross spectrum between these two circumferential patterns. It shows those multiples of the shaft rate frequency where tones will occur in the fan noise spectrum.

## REFERENCES

1. M. G. Schlutt and D. R. Dowling, Volume Flow-Rate Measurements and Scaling Laws for a Transverse-Inlet Multiple-Disk Fan, *Trans. ASME J. Fluids Eng.*, Vol. 118, 1996, pp. 857–860.
2. A. Toffolo, A. Lazzaretto, and A. D. Martegani, Cross-Flow Fan Design Guidelines for Multi-objective Performance Optimization, *Proc. Inst. Mech. Eng., Power and Energy*, Vol. 218A, 2004, pp. 33–42.
3. H.-M. Koo, An Experimental Study of the Noise and Performance of Cross-Flow Fans in Room Air Conditioning Systems, *Noise Control Eng. J.*, Vol. 48, 2000, pp. 41–47.
4. G. C. Lauchle, Effect of Inlet Turbulators on Backward-Curved Impeller Noise, *Proceedings of 2nd International INCE Fan Noise Symposium*, A. Guedel, Ed., CETIM, Senlis, France, 2003.
5. *Laboratory Methods of Testing Fans for Ratings*, Air Movement and Control Association, Standard 210, Arlington Heights, IL.



6. J. M. Fitzgerald and G. C. Lauchle, Reduction of Discrete Frequency Noise in Small, Subsonic Axial-Flow Fans, *J. Acoust. Soc. Am.*, Vol. 76, 1984, pp. 158–166.
7. K. B. Washburn and G. C. Lauchle, Inlet Flow Conditions and Tonal Sound Radiation from a Subsonic Fan, *Noise Control Eng. J.*, Vol. 31, 1988, pp. 101–110.
8. R. Madison, *Fan Engineering (Handbook)*, 8th ed., Buffalo Forge Company, Buffalo, NY, 1983.
9. J. B. Graham and R. M. Hoover, Fan Noise, in *Handbook of Acoustical Measurements and Noise Control*, 3rd ed., C. M. Harris, Ed., McGraw-Hill, New York, 1991, Chapter 41.
10. L. L. Beranek, G. W. Kamperman, and C. H. Allen, Noise of Centrifugal Fans, *J. Acoust. Soc. Am.*, Vol. 27, 1955, pp. 217–219.
11. G. C. Maling, Jr., Dimensional Analysis of Blower Noise, *J. Acoust. Soc. Am.*, Vol. 35, 1963, pp. 1556–1564.
12. T. Wright, A Velocity Parameter for the Correlation of Axial Fan Noise, *Noise Control Eng. J.*, Vol. 19, 1982, pp. 17–25.
13. R. Mani, Noise Due to Interaction of Inlet Turbulence with Isolated Stators and Rotors, *J. Sound Vib.*, Vol. 17, 1971, pp. 251–260.
14. R. C. Mellin, Selection of Minimum Noise Fans for Given Pumping Requirement, *Noise Control Eng. J.*, Vol. 4, 1975, pp. 35–45.
15. B. D. Mugridge, The Noise of Cooling Fans Used in Heavy Automotive Vehicles, *J. Sound Vib.*, Vol. 44, 1976, pp. 349–367.
16. W. K. Blake, *Mechanics of Flow-Induced Sound and Vibration*, Vols. I and II, Academic, New York, 1986.
17. M. S. Howe, *Acoustics of Fluid-Structure Interactions*, Cambridge University Press, Cambridge, UK, 1998.
18. W. Neise, Application of Similarity Laws to the Blade Passage Sound of Centrifugal Fans, *J. Sound Vib.*, Vol. 43, 1975, pp. 61–75.
19. W. R. Sears, Some Aspects of Non-stationary Airfoil Theory and Its Practical Application, *J. Aeron. Sci.*, Vol. 8, 1941, pp. 104–108.
20. W.-S. Chiu, G. C. Lauchle, and D. E. Thompson, Subsonic Axial Flow Fan Noise and Unsteady Rotor Force, *J. Acoust. Soc. Am.*, Vol. 85, 1989, pp. 641–647.
21. P. M. Morse and K. U. Ingard, *Theoretical Acoustics*, McGraw-Hill, New York, 1968, pp. 738–747.
22. M. J. Lucas, R. A. Noreen, L. C. Sutherland, J. E. Cole III, and M. C. Junger, *Handbook of the Acoustic Characteristics of Turbomachinery Cavities*, ASME Press, New York, 1997.
23. G. C. Maling, Jr., and A. L. Boggess, Jr., Ventilating Systems for Small Equipment, in *Handbook of Acoustical Measurements and Noise Control*, 3rd ed., C. M. Harris, Ed., McGraw-Hill, New York, 1991, Chapter 44, p. 44.8.
24. T. F. W. Embleton, Experimental Study of Noise Reduction in Centrifugal Blowers, *J. Acoust. Soc. Am.*, Vol. 35, 1963, pp. 700–705.
25. P. K. Baade, Effects of Acoustic Loading on Axial Flow Fan Noise Generation, *Noise Control Eng. J.*, Vol. 8, 1977, pp. 5–15.
26. W. Neise and G. H. Koopmann, Reduction of Centrifugal Fan Noise by Use of Resonators, *J. Sound Vib.*, Vol. 73, 1980, pp. 297–308.
27. R. C. Mellin and G. Sovran, Controlling the Tonal Characteristics of the Aerodynamic Noise Generated by Fan Rotors, *Trans. ASME J. Basic Eng.*, Vol. 92D, 1970, pp. 143–154.
28. D. M. Frederick and G. C. Lauchle, Aerodynamically-induced Noise in an Automotive Alternator, *Noise Control Eng. J.*, Vol. 43, 1995, pp. 29–37.
29. T. A. Brungart and G. C. Lauchle, Modifications of a Handheld Vacuum Cleaner for Noise Control, *Noise Control Eng. J.*, Vol. 49, 2001, pp. 73–78.
30. G. H. Koopmann, W. Neise, and W. Chen, Active Noise Control to Reduce the Blade Tone Noise of Centrifugal Fans, *Trans. ASME J. Vib. Acoust. Stress Relia. Des.*, Vol. 110, 1988, pp. 377–383.
31. D. A. Quinlan, Application of Active Control to Axial Flow Fans, *Noise Control Eng. J.*, Vol. 39, 1992, pp. 95–101.
32. K. L. Gee and S. D. Sommerfeldt, A Compact Active Control Implementation for Axial Cooling Fan Noise, *Noise Control Eng. J.*, Vol. 51, 2003, pp. 325–334.
33. G. C. Lauchle, J. R. MacGillivray, and D. C. Swanson, Active Control of Axial-Flow Cooling Fan Noise, *J. Acoust. Soc. Am.*, Vol. 101, 1997, pp. 341–349.
34. P. A. Nelson and S. J. Elliott, *Active Control of Sound*, Academic, San Diego, CA, 1992.

# CHAPTER 72

## TYPES OF ELECTRIC MOTORS AND NOISE AND VIBRATION PREDICTION AND CONTROL METHODS

George Zusman  
IMI Sensors Division  
PCB Piezotronics  
Depew, New York

### 1 INTRODUCTION

Electric motors, or machines, are used to convert electrical energy into mechanical energy and may be subdivided into asynchronous, synchronous, and direct current (dc) machines. The sources of noise and vibration in electric machines are the following: electromagnetic forces, bearings, aerodynamic forces, imbalance, and rubbing. Electromagnetic forces are active in the air gap between the stator and the rotor and are characterized by rotating or pulsating power waves. In most types of electric machines, the magnetic vibration is in the range of 100 to 4000 Hz. The intensity of the vibration and noise in bearings is determined by the quality of manufacture, the accuracy of machining of the bearing seats, and the vibroacoustic properties of the end brackets.

Noise based on aerodynamic forces depends on the construction of the fan and ventilation channels of the machine. Mechanical imbalance of rotors may excite an appreciable amount of vibration, particularly in high-speed machines. The rubbing of brushes against the commutator or contact rings is predominantly a high-frequency source of noise. Vibration and noise prediction and control methods of electromagnetic origin are based on the diagnostics of electrical motor defects using spectrum analysis of the vibration signals.

### 2 OSCILLATORY FORCES OF ELECTROMAGNETIC ORIGIN

The vibration of electromagnetic origin in electric machines may have several different components. They are mainly concerned with electrodynamic, electromagnetic, and magnetostrictive oscillatory forces.

The electromagnetic forces acting in the defect-free electric machine have radial direction and angular symmetry. Therefore, in the defect-free machine the sum of electromagnetic forces acting on the rotor is equal to zero. The stator is affected by the electromagnetic forces that tend to deform it, the spatial shape of these forces being a circular wave characterized by a number of waves  $r$  appearing on the circumference of the stator. The value  $r$  is called the order of stator oscillations. The mechanical rigidity of the stator grows fast with the growth of the oscillations order; therefore, during analysis of vibrations only deformations on low orders are taken into consideration.<sup>1</sup>

The greatest oscillations of the stator of a defect-free alternating current (ac) machine excited by electromagnetic forces from the main magnetic field wave happen in electric machines with alternating current with one pair of poles  $p = 1$ . In such machines the stator deformation is of second order  $r = 2$ , and the body oscillation amplitude on the doubled feed voltage frequency is about 10 mm/s. In case of asymmetric clearance, first-order oscillatory forces appear, and the vibration of the machine may grow sharply.

The electrodynamic forces in the electric machine are arbitrarily called electrodynamic since the windings are in the slots and the magnetic field does not cross the conductors with current. Actually, the windings of the stator and rotor create their own electromagnetic fields in the machine clearance rotating with one speed and shifted in the circle with respect to one another for a certain displacement angle  $\theta$ . These fields tend to compensate one another to create a working moment of the machine. Naturally, in a defect-free machine, the mechanical forces act not on the conductors but on the teeth of the rotor (stator).

However, for the magnetic saturation of the tooth zone the oscillatory forces start acting directly on the windings, which sharply decreases their reliability and service life. In real electric machines both the current in the rotor (armature) or stator windings and the electromagnetic field created by them contain not one but many harmonic components of various frequencies and amplitudes. Many of these components appear or essentially change in the presence of defects in the electromagnetic system of the electric machine.

In a defect-free electric machine supplied with ideal-shaped voltage, the additional variable components of the magnetic field and current appear due to:

- Discrete distribution of windings in several slots causing a nonsmooth shape of the magnetomotive force created by the windings
- Irregularities of the air gap due to the presence of teeth or apparent poles in the active armature bringing about the appearance of magnetic conductance components  $\Lambda$  (as per the circular coordinate  $v$ )

With the appearance of defects in the electromagnetic system of the electric machine the number of components of the oscillatory forces of electromagnetic nature may grow due to:

- Asymmetry of the air gap, partially the static eccentricity of the gap caused by the displacement of the stator axis with respect to the rotor rotation axis, or the dynamic eccentricity of the gap caused by displacement of the rotor geometric axis with respect to its rotation axis
- Magnetic saturation of separate tooth zones of the rotor (armature) or stator
- Defects either in the windings of the rotor or stator, or their active armatures causing asymmetry of magnetic fields
- Appearance of armature current pulsations in the dc machine due to defects in the brush-commutator assembly or armature windings, as well as pulsations of the field current in dc machines or synchronous ac machines

The causes of changing of parameters of the electromagnetic field in the air gap and other parts of electric machines (in addition to the above-mentioned defects) may be looseness of active armature packets, defects of end windings, asymmetry, or nonlinear distortions of the electric machine supply voltage.<sup>2</sup>

The analysis of oscillatory forces and vibrations of electromagnetic origin emerging in the electromagnetic system of an electric machine, as a rule, make it possible to detect possible defects in the machine or distortions in the electric line supply voltage. Vibration diagnostics pays more attention to the pulsating moments that change greatly with appearance of defects that to the radial electromagnetic forces calculated in the process of machine designing and controlled within the framework of its postmanufacture outgoing inspection. This approach to electric machine vibration diagnostics offers certain advantages compared with machine diagnostics performed by spectral components of the consumed current.<sup>2,3</sup>

### 3 VIBRATION DIAGNOSTICS OF ASYNCHRONOUS ELECTRIC MOTORS

In asynchronous electric motors the number of various-frequency vibration components of electromagnetic nature is much more than in synchronous electric machines or dc machines. This is explained by a small value of the air gap  $\delta$  and slippage of the rotor with respect to the rotating magnetic field of the stator. The magnetic field of the asynchronous electric motor is characterized by two main frequencies, namely the supply voltage angular frequency  $\omega_1$  and the magnetic field main spatial wave rotational frequency  $\Omega_1$  determined by the circular velocity of motion of this wave  $\Omega_1 = \omega_1/p$ , where  $p$  is the number of pole pairs.

Rotor rotation is characterized by a somewhat lower frequency  $\omega_{rt} = \Omega_1(1 - S) = \omega_1/p(1 - S)$ , where  $S$  is the rotor slippage, which is usually within the range of  $0.01 < S < 0.05$ . With the growth of load

in the asynchronous electric motor, the rotor slippage frequency and the current induced in it change, while the amplitude of the main magnetic field remains practically the same. The value of the clearance in an asynchronous electric motor depends on its size and the number of pole pairs, diminishing from the value of 2 mm in two-pole machines with power over 500 kW to 0.2 mm in multipolar machines of low power.<sup>4</sup>

The "toothedness" of the stator leads to the fact that the magnetomotive force of the stator in addition to the main harmonic with a frequency of the supply mains voltage contains a number of higher harmonics, and the magnetomotive force induced in the rotor, in addition to the main harmonic has a number of higher harmonics determined by the toothedness of the rotor. The harmonics of the magnetomotive force of the rotor and stator create corresponding magnetic field components in the clearance; these components, in their turn, are sources of electromagnetic radial oscillatory forces. The same components of the magnetic field, by interacting with the currents existing in the stator and rotor windings, create tangential electrodynamic constant and oscillatory forces (moments of forces). The peculiarity of the action of the oscillatory forces is their wave character. In defect-free asynchronous electric motors, by integrating over the surface of the rotor, the oscillatory forces (radial and tangential) are reduced, while the overall oscillatory forces acting on the rotor are equal to zero. The same holds true for the tangential electrodynamic forces acting on the stator. The low-order electromagnetic radial oscillatory forces tend to flex the stator, which can be represented in the form of a thick-walled cylindrical casing, by creating a wave of radial oscillations of doubled frequency and doubled spatial order.

The number of components of asynchronous electric motor vibration excited by radial electromagnetic forces is large even in the absence of defects in the machine and on the condition that it is fed from the mains with an ideal voltage. At the same time, the main contribution to vibration of defect-free asynchronous electric motors is made by several electromagnetic components with frequencies equal to the double supply voltage frequency and toothed frequencies. These vibration components are usually controlled at the design development stage and during outgoing inspection (after manufacture or major overhaul) of vibration characteristics of the machine.<sup>1</sup> These vibration components are noticed in machines having defects in the electromagnetic system and, first of all, in machines with asymmetry of the air gap; namely its fixed (static eccentricity) and rotating (dynamic eccentricity) asymmetry. Only in the last few years has it become possible to take account of possible changes of vibration of asynchronous electric motors due to pulsating oscillatory forces and moments appearing when the asynchronous electric motor is supplied with an asymmetric or nonsinusoidal voltage.<sup>2</sup> It is associated first of all with the use of static frequency converters of the supply voltage used in drives with variable speed control.

Many such converters do not ensure high-quality voltage signal at the output, thus increasing vibration of the asynchronous electric motor.

The vibration spectrum of the electromagnetic system of an asynchronous electric motor is in fact richer with the presence of various defects in it and is saturated with a great number of weak components excited first of all by tangential electrodynamic forces. The spectrum analysis of the components of asynchronous electric motor vibration makes it possible to detect and identify a large group of defects of the electromagnetic system. Radial components of vibration of an asynchronous electric motor stator may change greatly with the appearance of defects, particularly in case of eccentricities of the air gap. These changes happen first of all due to the reduction of the spatial order of oscillations on frequency  $2\omega_1$  and toothed frequencies, as well as due to the appearance of electromagnetic forces with a frequency equal to the rotor rotation. These forces act between the rotor and stator and prevent essential reduction of asynchronous electric motor vibration achieved by balancing the rotor in proper supports.<sup>1,2</sup>

In asynchronous electric motors operating often in the start mode, the strongest tooth component of vibration is usually the component with a frequency of  $\omega_{z2} = \omega_z + 2\omega_1$ , and for stable operation in one selected mode dominating tooth vibration frequency is  $\omega_z - 2\omega_1$ .

Taking into consideration that the mechanical resistance of the stator and the body of the asynchronous electric motor represented by a thick-walled cylindrical casing on high frequencies is much less, the toothed components of vibration may be very essential and determine to a large extent the vibration, particularly the air noise of the asynchronous electric motor.

To reduce the toothed components of the asynchronous electric motor vibration the slots are beveled. Usually beveling of slots is done on the rotor for one slot section, which helps reduce magnetic components of vibration of the motor three to five times.<sup>1</sup> The description of the electromagnetic vibration components in an asynchronous electric motor is coupled with the evaluation of the influence of defects, first of all, the asymmetry of the air gap, on the radial vibration of the machine.

In technical specifications for certain types of asynchronous electric motors, the limit values of admissible eccentricities of both types of the first spatial order are usually of the order of 10%, though in practice any type of eccentricity may reach magnitudes of the order of 50% and even higher, mainly due to the wear of bearings or the deformation of the stator as a result of errors when rigidly fastening the asynchronous electric motor to the foundation.

Due to static eccentricity in the clearance, additional components of the magnetic field appear with frequency  $\omega_1$ , including those having a lower spatial order. Due to dynamic eccentricity, there appear magnetic field components with frequencies  $\omega_1 \pm k\omega_{\pi}$ .

With static eccentricity, the maximum contribution to radial vibration is introduced by electromagnetic

forces of the first order with frequency  $2\omega_1$ , the amplitude of which in the first approximation is equal to the following:

$$F_{1st} \approx \frac{\varepsilon_{1st}}{2p\mu_0} B_0^2 \ell_{\pi} R_{\pi} \quad (1)$$

where  $\varepsilon_{1st}$  = relative eccentricity of the gap

$B_0$  = amplitude of flux density in a defect-free asynchronous electric motor

$\ell_{\pi}$  = length of the active portion of the rotor

$R_{\pi}$  = radius of the rotor

$p$  = number of poles

The amplitude of the excited frequency  $2\omega_1$  of vibration of the test points on the end brackets or the body of the asynchronous electric motor is determined by the rigidity of the rotor and bearings (first critical frequency of the rotor), as well as by the rigidity of the end bracket and fastening assemblies used to secure the machine to the foundation. With great eccentricities of the gap ( $\varepsilon > 0.1$ ) this vibration component may determine the low-frequency vibration of the asynchronous electric motor.

With dynamic eccentricity of the gap, the frequency of one of the components of radial electromagnetic forces determined by the interaction between the main and auxiliary waves of the magnetic field coincides with the rotor rotational frequency. The vibration excited by these forces may be less than the vibration of an asynchronous electric motor of frequency  $2\omega_1$ , since the mechanical resistance of the oscillatory system rotor-stator of frequency  $2\omega_1$  may be much less than frequency  $\omega_{\pi}$ . Nevertheless, it is exactly this component of electromagnetic force that determines the limit of reduction of asynchronous electric motor vibration at the rotational frequency in the process of balancing of the rotor on proper supports.

In addition to radial oscillatory forces of frequency  $\omega_{\pi}$ , the dynamic eccentricity of the gap is a cause of radial components at oscillatory forces and vibration on frequencies of  $2\omega_1 \pm \omega_{\pi}$  and essentially weaker components with frequencies of  $2\omega_1 \pm k\omega_{\pi}$ ,  $k > 1$ .

The static eccentricity of the clearance may cause growth of toothed components of radial vibration of an asynchronous electric motor differing from the main toothed component by a frequency of  $\pm 2\omega_j$ , while the dynamic eccentricity may cause growth of toothed components of vibration differing by a frequency of  $\pm j\omega_{\pi}$ . It should be noted that greater changes of vibration of toothed frequencies with the eccentricity of the clearance may be caused by pulsating moments created by electrodynamic forces.

The next task of description of vibration is the determination of tangential oscillatory forces and pulsating moments in defect-free asynchronous electric motors operating from supply voltage mains with asymmetry and nonlinear distortions of the supply voltage.

The pulsating moment with frequency  $2\omega_1$  depends not only on the amplitude of the field components and the current of forward and reverse succession, but also

on the difference of the corresponding initial phases of the field and current.

With electric asymmetry of the rotor winding (squirrel's cage), current additionally appears with a frequency  $s\omega_1$  of having a direction of rotation opposite to that of the rotor.

It is quite difficult to calculate the pulsating moment of frequency  $2s\omega_1$ , and in case of the rupture of the rods in the squirrel's cage it may be evaluated only approximately.

As a rule, the frequency  $2s\omega_1$  is quite low, that is, it may cause angular modulation of the rotational frequency of the asynchronous electric motor with a deviation of the rotational frequency quite sufficient for practical diagnostics. In the vibration spectrum of the asynchronous electric motor all harmonic components have side harmonics differing from the central frequency  $\omega_r$  by values  $2s\omega_1$ .

The dynamic eccentricity of the air gap causes of a variable component of clearance conductivity with frequency  $\omega_r$  and considerably lower (in amplitude) conductivity components with frequencies  $k\omega_r$ , where  $k = 1, 2$ .

Interaction of additional components of the flux density of the stator with the main wave of the rotor line current load and additional components of the rotor current with the main induction wave in the clearance causes tangential forces. However, integrated over the surface of the rotor they do not contribute greatly to the pulsating moment of an asynchronous electric motor of frequency  $\omega_r$ .<sup>1</sup>

All rotor current components take part in creating the magnetic field of the rotor, in which there are field components determined by the variable conductivity of the air gap with dynamic eccentricity. New components have frequencies  $\omega_1 \pm \omega_r \pm \omega_r$ , though their amplitude is essentially lower. They induce current in the stator winding, which interacts with the main line current load of the rotor creating tangential electrodynamic forces at frequencies  $\omega_1$  and  $2\omega_r$ . The pulsating moments acting on frequency  $2\omega_r$  in an asynchronous electric motor with dynamic eccentricity of the clearance are not usually enough to significantly change the low-frequency vibration of the motor; nevertheless, they exert considerable influence on the selection of diagnostic parameters.

In two-pole asynchronous electric motors the modulation frequency of the magnetic field waves during dynamic eccentricity coincides with the frequency of the pulsating moment appearing as a result of electric asymmetry of the rotor; nevertheless, in multipole asynchronous electric motors ( $p > 1$ ) these frequencies vary, which makes it possible to distinguish between two types of defects causing angular modulation of rotor rotational frequency by different frequencies  $2s\omega_1$  and  $2ks\omega_1/p$ .

The static eccentricity of the clearance in an asynchronous electric motor results in current changes or one of the sections of the stator winding nearest to the point with minimal clearance: it is equivalent to presenting an "additional" single-phase winding in stator. An analogous effect has caused short-circuited

turns in the winding or in the active stator armature, as well as incorrect connection of winding sections.

Since the symmetry axis (in radial direction) of the static eccentricity of the clearance may not coincide with the axis of one of the stator windings, the "additional" stator winding partially performs the function of an additional pole in the asynchronous electric motor, which may result in new vibration components characteristic of an asynchronous electric motor with the number of pole pairs equal to  $p \pm 1$ . The parameters of these vibration components may also be used as indicators of static eccentricity of the clearance; though these parameters have no unambiguous connection to the defect value.

With static eccentricity of the clearance, saturation of the toothed zone of the stator and/or rotor is also possible. This zone is fixed with respect to the stator and has a reverse circular speed of rotation  $\omega_r$  relative to the rotor. Nonlinear limitations of the main wave of the magnetic field result in the "additional" stator harmonics, in addition to the field with frequency  $\omega_1$ , creating component fields with the frequencies  $(2k + 1)\omega_1$ ,  $k = 1, 2, 3, \dots$ , rotating in different directions. As in the case of static eccentricity without saturation of the toothed zone, a feedback current appears in the rotor and with frequencies  $(2k + 1)\omega_1$ ; this current interacts with the stator main field, creating pulsating moments with frequencies  $2(k + 1)\omega_1$ . The diagnostic aspects of greatest interest are vibration components of electromagnetic origin with frequencies  $4\omega_1$  and  $8\omega_1$ , which are practically absent in defect-free asynchronous electric motors.

The diagnostic features of defects may be divided into two main groups. Referred to the first group are features associated with the change of low-frequency vibration of the asynchronous electric motor starting with the frequency of  $\omega_r/2$  and finishing with frequencies of  $12\omega_1$ . The distinguishing peculiarity of this group of features is their independence of the number of teeth in rotor and stator. The second group of features is coupled with the changes in the teeth components of vibration of an asynchronous electric motor; it is more sensitive to the emergence and growth of defects; nevertheless, it requires the presence of information about the number of teeth in the rotor ( $Z_r$ ) and the stator ( $Z_{st}$ ).

Some types of defects, the diagnostic features of which are coupled with the appearance of amplitude or frequency modulation of vibration components of electromagnetic origin in an asynchronous electric motor, may be detected and identified by a one-time measurement of vibration. It should be taken into account that many vibration components with frequencies that are in multiple to the rotor rotational frequency may be of mechanical and electromagnetic origin, and their modulation may refer only to one of the components.

All diagnostic features of main defects of an asynchronous electric motor and violations of the normal supply conditions are presented in Table 1. The table presents the values of frequencies of low-frequency vibration components, the amplitude of which changes

**Table 1** Frequencies of Vibration Components Corresponding Defects of Asynchronous Electric Motors and Their Supply Voltage<sup>a</sup>

Ref. No.	Designation of Defect	Growth of Low-Frequency Vibration	Growth of High-Frequency Vibration	Notes
1	Defects of stator windings	$2f_1$ (R, T)	$kf_{Z_{rt}} \pm 2f_1$	
2	Defects of rotor windings (squirrel's cage)	$kf_{rt} \pm 2k_1Sf_1$ (R, T)	$kf_{Z_{rt}} \pm 2k_1Sf_1Z_{rt}$	
3	Static eccentricity of clearance	$2f_1$ (R, T)	$kf_{Z_{rt}} \pm 2f_1$	
4	Static eccentricity	$2f_1$ (R, T)	$kf_{Z_{rt}} \pm 2k_1f_1$ , $k_1 \geq 2$	
5	Dynamic eccentricity of clearance	$2(k+1)f_1$ (R, T) $f_{rt}$ (R) $2f_{rt}$ (T) $2f_1 \pm f_{rt}$ (R)	$kf_{Z_{rt}} \pm k_1f_{rt}$ , $kf_{Z_{st}}$	
6	Dynamic eccentricity with saturation of teeth	$kf_{rt} \pm 2k_1f_1S/p$ (R,T)	$kf_{Z_{rt}} \pm k_1f_{rt}$ , $k_1 \geq 3$	
7	Asymmetry of supply voltage	$2f_1 \pm k_1f_{rt}$ (R) $2kf_1 \pm k_1f_{rt}$ (T) $2f_1$ (T)	$kf_{Z_{st}} \pm k_1f_{rt}$ , —	With all asynchronous motors
8	Nonlinear distortions of voltage	$6kf_1$ (R, T)	$kf_{Z_{rt}} \pm 4k_1f_1$	With all asynchronous motors

<sup>a</sup> Where  $f_1$  = frequency of supply voltage, Hz  
 $f_{rt}$  = frequency of rotor rotation, Hz  
 $f_{Z_{rt}} = f_{rt}Z_{rt}$  or  $f_{Z_{rt}} = f_{rt}Z_{rt} \pm 2f_1$  = toothed frequencies of the rotor, Hz  
 $f_{Z_{st}} = f_{rt}Z_{st}$  = toothed frequency of the stator, Hz  
 $Z_{rt}$  = number of rotor teeth  
 $Z_{st}$  = number of stator teeth  
 $S$  = rotor slippage  
 $k, k_1$  = integers  
 $R, T$  = radial and tangential directions of vibration excitation

(grows) with appearance (growth) of defects. Also shown in the table are the frequencies of vibration of toothed components, the structure of which changes both with the appearance of the above-mentioned defects and with deviation of the rotor/stator surface shape from the correct shape (ovality, "facedness," etc.). For the purpose of uniformity of presentation of tables with diagnostic defect features for various types of machines and equipments, the frequencies are given in linear units of  $f$  (hertz).

In making diagnostic measurements of low-frequency vibrations of asynchronous electric motors, particular attention should be paid to the selection of the place and direction of vibration measurement, since one portion of vibration components is excited by radial forces and the other portion by pulsating moments. The optimum may be for the measurements to be performed in two planes, in which the rotational supports of the asynchronous electric motor are located and in two directions (radial and tangential). The measurement points are selected, as a rule, on the body of the asynchronous electric motor at a distance from the point of its fastening to the foundation. For practical diagnostics it is sometimes sufficient to perform one vibration measurement in one direction for asynchronous electric motors of small size and two measurements for motors of

great size. To align the diagnostic and monitoring measurements, it is preferred to perform them on the body (end brackets) of the asynchronous electric motor in the horizontal direction with displacement with respect to the rotor rotational axis.

To effectively detect defects it is necessary to measure vibration spectra of the asynchronous electric motor with high-frequency resolution. Thus, in the frequency range up to triple the rotor rotational frequency, the spectrum bandwidth should be not more than  $f_1/400p$ , where  $f_1$  is the supply voltage frequency in hertz. In the frequency band from  $2f_1$  to  $13f_1$ , the spectrum bandwidth should not exceed  $f_1/100$  Hz, and in the vibration toothed zone, not more than  $f_1/5p$ .

#### 4 VIBRATION DIAGNOSTICS OF SYNCHRONOUS MACHINES

Synchronous machines may be used as generators of ac voltage or as motors, particularly in high-power drives. The possibilities of diagnostics of the technical condition of synchronous machines by the vibration signal are somewhat narrower than the vibration diagnostics of asynchronous electric motors, but they are wider than the possibilities of diagnostics by the current or electromagnetic field.

The synchronous machine stator field, just like in an asynchronous electric motor, is created by the power winding distributed along the slots of the stator active armature. The peculiarity of the stator and the rotor of large-size synchronous machines is the use of direct gas or water cooling systems. The design solutions used for this purpose exert an essential influence on the operation and vibration of these machines.

The rotor of a synchronous machine may be defined, in particular in slow-speed machines or hydrogenerators, or have a distributed excitation winding (in slots). In the first case, the sinusoidal shape of the excitation field is provided by the shape of the poles (irregular air gap between the pole and the stator), and in the second case it is ensured by the distribution of the excitation winding in the slots of the rotor. Active armatures of the rotor and stator are made of laminated steel, but in the rotor armature the steel sheets have no insulation coating, just like in the stator core. In the rotors of explicit-pole machines with power over 100 kW, a short-circuited winding is installed, which is the analog of a squirrel's cage in the asynchronous electric motor.

The rods of a squirrel's cage are placed in the slots on the poles of a synchronous machine and are interconnected over the end surfaces with current conducting plates. If a synchronous machine works in the motor mode, the squirrel's cage is used as a starting winding. If a synchronous machine works in the generator mode, the squirrel's cage performs the function of a damper that reduces the high-frequency components of the field and output voltage. In implicit-pole machines, this winding may be absent, and its function may be performed by the active rotor armature, which is most often made of a single forging of special steel.

The starting (damping) winding of the synchronous machine influences essentially the process of formation of oscillatory forces of electromagnetic origin. All harmonics of the magnetic field in the clearance having a circular rotational frequency  $\Omega_i$ , differing from the rotor rotational frequency  $\omega_{\pi} = \omega_1/p$ , excite current in the damper winding and/or rotor armature. This current compensates the corresponding harmonics of the magnetic field in the clearance and reduces the radial oscillatory forces excited by these harmonics. At the same time the current in the damper winding (armature), by interacting with the main wave of the stator magnetic field, excites essential tangential oscillatory forces that may result in great (by amplitude) pulsating moments acting on the stator and rotor of the synchronous machine.

Defects of electromagnetic origin exerting an influence on the vibration of motors and generators include defects of rotor windings (excitation and damper), static eccentricity of the air gap, stator winding defects, and excitation current source defects. In addition to the above-mentioned defects, vibration of synchronous machines is influenced by the asymmetry and nonlinear distortions of the supply voltage. The radial oscillatory forces of electromagnetic origin and the vibration excited by them in defect-free synchronous machines are determined in the same way as in asynchronous electric motors.

When determining the frequencies of high-frequency components of vibration and evaluating their amplitudes in explicit-pole and implicit-pole machines, it is necessary to take into account a number of peculiarities of these machines. In explicit-pole synchronous machines, in addition to the toothed vibration components, there are also high-frequency components presented that are determined by the higher harmonics of the stator magnetomotive force appearing due to the discreteness of its windings and the higher harmonics of the clearance conductivity due to its irregularity determined by the shape of the poles.

The amplitudes of higher harmonics of the stator magnetomotive force are a  $k_{st}pq$  times lower than the amplitudes of the main magnetomotive force harmonic, where  $p$  is number of poles,  $q$  is the number of stator slots per pole and phase, and  $k_{st}$  is the number of the harmonic. The number of these magnetomotive force harmonics is equal to  $\omega_1$  while the spatial order is  $r = (6q' + 1)p$ , where  $q' = \pm 1; \pm 2; \pm 3; \dots$ <sup>1</sup>

The amplitudes of higher harmonics of the clearance conductivity determined by the shape of the poles is  $3j_{\pi}$  times less than the mean value of the clearance conductivity; their frequencies are equal to  $2j_{\pi}\omega_1$  and the spatial orders are  $r = 2j_{\pi}p$ . Thus, the magnetic field in the clearance of an explicit-pole synchronous machine has a harmonic row of flux density components with frequencies  $(2j_{\pi} \pm 1)\omega_1$  and spatial orders  $2pj_{\pi} \pm (6q' + 1)p$ . The interaction of these components with the main wave of flux density brings about radial oscillatory forces between the stator and the rotor.

The components differing from the toothed vibration frequency of  $\pm k2\omega_1$  may contribute greatly into the vibration of electromagnetic origin of explicit-pole synchronous machines<sup>1</sup> due to the low spatial order of the oscillatory forces.

The peculiarities of the toothed components of vibration of defect-free synchronous machines excited by radial sources due to the "toothedness" of the poles are determined by the distance between the teeth and the inner surface of the stator, as well as the angular distances between the teeth of one, and adjacent poles are not being strictly equal. Therefore, the vibration components determined by the 'toothedness' of the rotor of a synchronous machine have amplitude and angular modulation, that is, they have a great number of side components with frequencies  $k\omega_{\pi}Z_{\pi} \pm k_1\omega_{\pi}$ , where  $k_1 = 1, 2, 3, \dots, k_2 = 1, 2, 3, \dots$ <sup>2</sup> When determining the frequency of toothed vibration governed by the toothedness of the poles, there is a great probability of an error since the rated number of teeth may differ from  $2pZ_n$ , where  $Z_n$  is the number of teeth at the pole of the synchronous machine.

As a rule, the full number of slots (teeth) at the poles of a synchronous machine is close to the number of stator slots; therefore, certain vibration components due to the toothedness of the rotor and stator may coincide. It should be noted that the harmonics of clearance conductivity due to the toothedness of the rotor are smaller than the analogous harmonics due to the irregularities of the clearance between the poles and

the stator; therefore, the vibration components of the synchronous machine determined by the toothedness of the rotor are essentially less. As a consequence, when calculating the vibration of the synchronous machine, these components are usually not taken into account. At the same time, they may carry an essential diagnostic information value.

In implicit-pole defect-free synchronous machines the number of high-frequency components of vibration of electromagnetic origin is less than in explicit-pole synchronous machines and asynchronous electric motors. Most often the strongest high-frequency components of vibration in implicit-pole synchronous machines are determined by the interaction of the higher harmonics of the stator magnetomotive force with the toothed harmonics of the rotor conductivity. The reason is that the higher harmonics of the stator magnetomotive force have a spatial order  $r = (6q' + 1)p$  where  $q' = \pm 1, \pm 2, \pm 3, \dots$ , while the number of rotor slots is usually presented by the value  $Z_{\text{r}} = 6q''p$  where  $q'' = 2, 3, 4, \dots$ ; here the excitation winding occupies two thirds of possible rotor slots, which makes it possible to reduce to zero the higher spatial harmonics of the exciting field with the order multiple to three. The other harmonics of the exciting field, except the fifth, make up less than 1% of the main harmonic. Very often in the rotors of implicit-pole synchronous machines the slots free of windings are not machined, that is, the rotor has  $2p$  "great" teeth, while the radial oscillatory forces of the order of toothedness of the rotor acquire amplitude modulation due to these teeth. For such rotors, during calculation of the frequency of toothed vibration it is necessary to take into account the specified value  $Z_{\text{r}} = 3Z'_{\text{r}}/2$  where  $Z'_{\text{r}}$  is the real number of rotor slots as specified in the technical documentation.

The next task of describing the vibration of defect-free synchronous machines is the determination of the pulsating moments and tangential vibration of the machine when it is fed from the supply mains with asymmetric voltage and distorted voltage shape.

With asymmetry of supply voltage in explicit-pole machines and implicit-pole synchronous machines, the current in the stator and the magnetic field in the clearance, same as in asynchronous electric motors, represents a sum of direct and reverse sequences having frequency  $\omega_1$ .

The current component of the reverse sequence in the stator interacts with the main wave of the excitation field creating tangential electrodynamic forces. The stator reverse sequence magnetic field component interacts analogously with the rotor excitation current. Since the spatial orders of the waves of the field and current are the same, the tangential forces (integrating over the surface of the rotor and stator of the synchronous machine) create a pulsating moment of forces with frequency  $2\omega_1$ . This moment excites tangential vibration of rotor and stator armature in the synchronous machine. In large synchronous machines the stator armature is usually resiliently (in tangential direction) suspended to the machine housing; therefore, in such machines the vibration of the housing on

frequency  $2\omega_1$  may vary within a small range in case of asymmetry of supply voltage.

With nonlinear distortions of the supply voltage, just as in case of asynchronous electric motors, currents are induced in the rotor armature and in the damper windings of the synchronous machines. These currents are determined by the frequency and direction of rotation of the higher harmonics of the stator magnetomotive force. Correspondingly, the induced currents, by interacting with the variable component of the magnetic field, excite tangential electrodynamic forces and pulsating moments with frequencies  $6q'\omega_1$ .

In implicit-pole synchronous machines the pulsating moments appearing due to nonlinear distortions of the voltage may be calculated in the same way as for asynchronous electric motors. It should be noted that the values of currents  $I_{6q'-1}$  and  $I_{6q'+1}$  with equal distortions in the synchronous machine may be less, and for evaluation of the pulsating moments, they should be better determined experimentally.

In explicit-pole synchronous machines with equal initial phases of the supply voltage higher harmonics, there are pulsating moments with frequencies  $6q'\omega_1$ .<sup>2</sup> In large synchronous machines with resilient suspension of the stator armature in the housing of the machine, the vibration of the housing at frequencies  $6q'\omega_1$  with maximum admissible nonlinear distortions of the supply voltage may be considerably lower than the vibration excited by the electromagnetic forces at other frequencies.

The vibration of the synchronous machine depends essentially on the quality of the excitation voltage in accordance with an addition to the constant component may be present in harmonic components of various frequencies. The variety of means of forming the excitation voltages does not allow thorough determination of the spectrum composition of the excitation current; therefore, in practice it should be determined experimentally by measuring its spectrum. For this purpose, it is best to use a hook-on meter and those facilities for analysis of electric signals used for analysis of vibration signals.

Very often rectifiers are used for feeding the excitation windings of synchronous machines. In the absence of defects in the rectifier, the output of the rectifier in addition to the constant component may have additional harmonic components with frequencies  $6k\omega_1$  where  $k = 1, 2, 3, \dots$ , where  $\omega_1$  is the frequency of the supply voltage. Depending on the electric circuit of the rectifier, tolerances for its characteristics and possible defects, the output voltage may contain harmonic components with frequencies  $2k\omega_1, 3k\omega_1$  and other frequencies.<sup>6</sup> Variable voltage components may also appear at the output of the rectifier in the presence of asymmetry or nonlinear distortions of the supply voltage in the electric mains used to supply voltage to the rectifier.

The variable components of the synchronous machine excitation current give rise to components of the excitation magnetic field of the same frequency. In turn, these excitation field components induce currents with the same frequencies in the damper winding and



the active steel of the rotor. The variable components of the excitation field interact with the main wave of the stator current; the variable components of the current in the damper windings (steel) of the rotor interact with the main wave of the magnetic field and thus create tangential electrodynamic forces of zero spatial order and, as a result, pulsating moments acting on the rotor and stator in opposite directions. The frequencies of the pulsating moments coincide with the frequencies of the corresponding variable components of the excitation current.

The amplitude of the pulsating moment effective in the synchronous machine having a frequency equal to the corresponding excitation current component is proportional in first approximation, to the load moment of the synchronous machine. The ratio of the variable component is proportional to the constant component of the excitation current. As a rule, the variable components of the excitation current do not exceed a value of 1 to 2% of the constant component and do not exert a great influence on the electromagnetic vibration of the synchronous machine. At the same time, in diagnostic tasks it is necessary to take into account even the synchronous machine vibration components associated with nonlinear distortions of the excitation voltage.

When determining the technical condition of the synchronous machine, it is necessary to evaluate the state of the brush-commutator assembly. Its defects, as a rule, cause pulsations of resistance of the electric excitation circuit and, as a result, pulsations of the excitation current. But, as distinct from the pulsations caused by the defects of the rectifier, these pulsations represent a sum of harmonic components with frequencies  $k\omega_{\pi}$ . This permits separation of the indications of defects of the brush-commutator assembly from those of the rectifier as a result of analyzing the synchronous machine excitation current spectrum. It is more difficult to detect defects of the brush-commutator assembly using the vibration spectra of the synchronous machine, since it is difficult to separate their indications from the indication of mechanical defects of the rotor or connecting couplings.

For the synchronous machine electromagnetic system most defects are associated with the excitation windings and static eccentricity of the clearance. The defects associated with the excitation windings are manifested in the change of the excitation field shape. These changes are greatest in the multipole synchronous machines in which, in the presence of winding defects (or change of the shape of poles in explicit-pole synchronous machines), the excitation field becomes asymmetric in the radial plane with respect to the axis. As a result, an additional radial electromagnetic force rotating with the frequency  $\omega_{\pi}$  appears, as well as the pulsating moment with the frequency  $2\omega_{\pi}$ .

The next (in amplitude) radial oscillatory forces, as in the case of asynchronous electric motors with dynamic eccentricity of the clearance, have frequencies  $2\omega_1 \pm k\omega_{\pi}$ . They are a consequence of the amplitude modulation of the radial forces excited by the main wave of the magnetic field, in the vibration test point on the body of the machine.

In addition to the above-mentioned peculiarities of influence of the asymmetric excitation field on the vibration of the synchronous machine, it is possible to additionally note the growth of the pulsating moments acting in the machine having frequencies  $k\omega_1$  and an amplitude modulation of toothed components determined by the toothedness of the stator, characterized by frequencies  $k\omega_{\pi}$ .

At an early stage of defect development, various indication features may be used for detecting defects in the form of a static eccentricity of the clearance and defects of stator windings for various types of synchronous machines. Thus, in large synchronous machines with resiliently suspended stator armatures, it is better to detect these defects by the tangential growth of stator vibration at a frequency of  $2\omega_1$ . The same defects in implicit-pole synchronous machines may be detected by the growth of toothed components of vibration and side components with frequencies  $k_1\omega_{Z_{st}} \pm k_2\omega_1$ .

Most difficult is the detection of clearance eccentricity in explicit-pole synchronous machines in which even in the absence of defects there are noticeable vibration components with frequencies  $k_1\omega_{Z_{st}} \pm k_2\omega_1$ . The toothed components determined by the toothedness of the rotor are also difficult to identify and separate from the toothed components determined by the toothedness of the stator. Therefore, it is possible to indirectly identify defects by the growth of the side component of vibration with frequencies  $k_1\omega_{Z_{st}} \pm k_2\omega_1$  with  $k_2 > 2$ , and if it is possible to separate groups of toothed components determined by the toothedness of the rotor with frequencies  $k_1\omega_{Z_{st}} \pm 2k_2\omega_1 \pm k_3\omega_{\pi}$ , in which  $k_1$  and  $k_3 = 1, 2, 3, \dots$ , and  $k_2 = 0$  or  $1$ , then by the growth of the side components with  $k_2 = 1$ .

The diagnostic features of the main defects in explicit-pole synchronous machines are summarized in Table 2, and those of implicit-pole synchronous machines in Table 3. The tables present frequencies (in linear units) of those vibration components in the synchronous machine for which the amplitude grows with the appearance and growth of the specified defects.

In making diagnostic measurements of low-frequency vibration of synchronous machines particular attention should be paid to the selection of the location and direction of measurement of vibration since with appearance of many defects the tangential vibration grows predominantly, this vibration being excited by the pulsating moments. The optimum test points for measurements in large synchronous machines with resilient suspension of the stator are points on the stator core with the direction of measurement tangential to the core. In other synchronous machines it is recommended to perform the measurements on the housing of the machine, just like in asynchronous electric motors.

## 5 VIBRODIAGNOSTICS OF DIRECT CURRENT (dc) MACHINES

Direct current machines may be used both as generators and as motors particularly with variable-speed

**Table 2 Frequencies of Vibration Components Corresponding Defects in Explicit-Pole Synchronous Machines and Supply Voltages<sup>a</sup>**

Ref. No.	Designation of Defect	Growth of Low-Frequency Vibration	Growth of High-Frequency Vibration	Notes
1	Defects of stator windings	$2f_1$ (R, T)	—	
2	Defects of rotor windings	$f_{rt}; 2kf_1 \pm f_{rt}$ (R)	$k_1 f_{Z_{st}} \pm k_2 f_{rt}$	$k \neq 3, 6, 9, \dots$
3	Static eccentricity of clearance	$2f_1; 2kf_1$ (R, T)	$k_1 f_{Z_{st}} \pm 2k_2 f_1$	$k \neq 3, 6, 9, \dots$
4	Static eccentricity with saturation of teeth	Predominantly	$k_1 f_{Z_{st}} \pm 2k_2 f_1$	$k_2 \geq 3$
5	Defects of excitation voltage source	$4f_1$ (R, T) $3kf_1$ (T)	$k_1 f_{Z_{rt}} \pm 2k_2 f_1$ —	Measure excitation current spectrum
6	Asymmetry of supply voltage	$2f_1$ (T)	—	With all synchronous machines
7	Nonlinear distortions of voltage	$6kf_1$ (R,T)	—	With all synchronous machines
8	Defects of starting shorted winding	$kf_{rt} \pm 2Sf_1$ (R,T)	—	In asynchronous electric motor mode

<sup>a</sup> See footnote to Table 1 for definitions.

**Table 3 Frequencies of Vibration Components Corresponding Defects in Implicit-Pole Synchronous Machines and Supply Voltages<sup>a</sup>**

Ref. No.	Designation of Defect	Growth of Low-Frequency Vibration	Growth of High-Frequency Vibration	Notes
1	Defects of stator windings	$2f_1$ (R, T)	—	
2	Defects of rotor windings	$f_{rt}; 2kf_1 \pm f_{rt}$ (R)	$k_1 f_{Z_{rt}} \pm k_2 f_{rt}$	$k \neq 3, 6, 9, \dots$
3	Static eccentricity of clearance	$2f_1$ (R, T)	$k_1 f_{Z_{rt}} \pm 2k_2 f_1$	$k_2 = 1; 2$
4	Static eccentricity with saturation of teeth	Predominantly	$k_1 f_{Z_{rt}} \pm 2k_2 f_1$	$k_2 > 2$
5	Defects of excitation voltage source	$4f_1$ (R, T) $3kf_1$ (T)	—	Measure excitation current spectrum
6	Asymmetry of supply voltage	$2f_1$ (T)	—	With all synchronous machines
7	Nonlinear distortions of supply voltage	$6kf_1$ (R,T)	—	With all synchronous machines
8	Defects of starting shorted winding	$kf_{rt} \pm 2Sf_1$ (R,T)	—	In asynchronous electric motor mode

<sup>a</sup> See footnote to Table 1 for definitions.

drives. A large starting moment of dc machines is the main reason of using them in transport vehicles as traction motors.

The main design peculiarity determining the vibration of electromagnetic origin in dc machines is a large value of the air gap between the armature and the pole piece, which sometimes reaches a value of 10 to 15 mm in high-power dc machines. The life-time and overhaul period of operation of dc machines is less than that of asynchronous electric motors or synchronous machines first of all due to large currents in the armature and accelerated wear of the brush-commutator assembly. Hence, the task of monitoring the technical condition and performing diagnostics of dc machines is the greatest out of all types of electric machines.

In recent years regulated static rectifiers are more widely used for feeding and adjusting the rotational frequency of dc machines, which makes it more difficult to solve the task of monitoring the technical condition of the machine both by the parameters of armature and excitation current, and by vibration, due to pulsations of the supply voltage.

The possibilities of vibration diagnostics on dc machines are not good due to lack of spectral composition of electromagnetic vibration. Therefore, it is recommended to complement the vibration diagnostics of the dc machines with diagnostics using armature current spectrum, and for the case of independent excitation, by using excitation current. The effectiveness of vibration diagnostics of dc machines increases in cases where there is a possibility

of comparing vibration of the machine with two different loads (resistance) in operating modes.

The low-frequency vibration of electromagnetic origin in the dc machines is determined, as in ac machines, by three main causes, namely, the peculiarities of the design, the defects, and the presence of pulsations of the dc supply voltage mains.<sup>1</sup> Since the electromagnetic field of dc machines does not rotate, there are no intensive vibration components with frequency  $2p\omega_n$  determined by rotation of the excitation field. As a result, the main contribution to vibration of electromagnetic origin in defect-free dc machines is made by the toothed components determined by the toothedness of the armature.

Out of the forces of electromagnetic origin acting on the housing of the defect-free dc machine are predominantly radial oscillatory forces of the toothed frequency and its upper harmonics, which may be presented by the components applied to the edges of the pole pieces. The reaction forces act on the armature; and the sum of all components of the reaction forces applied to the armature in a defect-free dc machine is equal to zero.

The value of each of these components at the frequency  $\omega_z$  equals as follows<sup>1</sup>:

$$F_{r,\omega_z} = B_0^2(k_c - 1)\ell b/2\pi\mu_0\alpha \quad (2)$$

where  $B_0$  = mean flux density value in the clearance

$k_c$  = Carter (air gap) coefficient

$\ell, b$  = length and width, respectively, of the pole arc

$\alpha$  = number of slots over the length of a pole arc

$\mu_0$  = magnetic permeability of air

With half-integer value  $\alpha = q' + \frac{1}{2}$ , where  $q'$  is the number of the forces acting on the opposite ends of the pole, pieces are in-phase and are summed up, and with an integer value  $\alpha = q'$  a bending moment acts on the pole. The order of oscillations of the frame under the action of these forces and moments is determined by the phase states between the forces acting on the adjacent poles.

Generally, the accuracy of the manufacture and the assembly of a dc machine is such that, depending on the value of the loading moment, the symmetry axes of the magnetic field under the poles are displaced, while the widths of the polar arc over the magnetic field change within a short range, but sufficiently to change the spatial order of the oscillatory forces and vibration. To reduce the value of these forces and to smooth down the boundaries of transition from some forms of oscillations to others, beveling of the slots of the armature for one slot division and/or beveling of the pole edges is performed. The vibration of a defect-free dc machine with beveled slots at the toothed frequencies may be evaluated by assuming the action of two opposing radial forces with a value  $F_{r,\omega_z}/kp$  where  $k = 1, 2, 3, \dots$ , on the frame in the opposite points that excite ring oscillations of the second order  $p = 2$ .

When the dc machine works under load, the magnetic field in the clearance changes its shape, increasing in the direction of one edge of the pole piece.<sup>6</sup> Correspondingly, the oscillatory force acts predominantly on one edge of the pole piece and grows in value by up to two times with full load of the dc machine. While doing so, the spatial shape of the oscillatory forces has a zero order, and the vibration excited by these forces in a defect-free dc machine changes only within a limited range. Nevertheless, even with small static eccentricity of the clearance, the toothed vibration of the machine may grow substantially since oscillatory forces of the first spatial order appear; for these forces the mechanical compliance of the frame with the poles is many times more than for the forces of the zero and higher orders.

In addition to the radial forces of the toothed frequency the poles and the armature of the dc machine are acted upon by tangential forces. Thus, the edge of each pole (and armature) is acted upon by the tangential force determined by the following expression:

$$F_{t,\omega_z} = 2B_0^2(k_c - 1)\ell\delta/\pi\mu_0 \quad (3)$$

where  $\delta$  is the value of the clearance.

At idle revolutions, the tangential forces acting on the two edges of one pole are antiphase, and the total pulsating moment in the dc machine at the toothed frequency is close to zero. Nevertheless, under load the force acting on one edge of the pole grows while the force acting on the other edge reduces, and this may bring about the growth of a pulsating moment and vibration in the dc machine.

The vibration of defect-free dc machines changes greatly when fed from a static rectifier with pulsations of the output voltage. The spectral composition of these pulsations depends essentially on the characteristics of the static rectifier. Many up-to-date static rectifiers contain low-frequency filters used to smooth the rectified voltage of the ac mains, and regulation of the output voltage in them is performed by pulse width regulators with high (usually several kilohertz) switching frequency and subsequent filtration of the output voltage. But since many machines continue to use simple thyristor regulators with considerable pulsations of the output voltage, it is necessary first of all to control the spectrum composition of the armature current (excitation) and secondly to evaluate its influence on the vibration of a dc machine.

In most regulated rectifiers, the frequency of pulsations of the output voltage is a multiple of frequency of the ac voltage  $\omega_1$  in the supply mains, and the main harmonics of the armature current belong to the harmonic series  $k\omega_1$  where  $k = 1, 2, 3, \dots$ ; here the harmonics maximal in amplitude may have frequencies  $2k\omega_1, 3k\omega_1, 6k\omega_1$ , and others. In this connection, the vibration diagnostics of a dc machine should be performed at such rotational frequencies with which the harmonic series of the vibration components with frequencies  $k_1\omega_n$  and  $k_2\omega_1$  are well separated in the frequency band. The optimal rotational

frequencies may be considered such that frequencies  $k\omega_{\pi}$  and  $\omega_1$  where  $k$  is the whole number of  $\omega_1/\omega_{\pi}$ , differ by 5 to 10%.

The vibration of the dc machine is affected by defects of the brush-commutator assemblies, armature windings (additional poles), the static eccentricity of the clearance (skewing of the poles), loose pole fastenings, and defects of excitation windings. Defects of the brush-commutator assembly occur most often. They are manifested in the form of nonuniform wear of the brushes and the commutator and the protrusion of separate insulation gaskets between the bars or rupture of bars (commutator lugs). Nonuniform wear of the brushes and/or commutator rupture most often cause problems in the process of commutation of the current of the armature, predominantly with one of the brushes in one of the commutator zones limited by the number of bars. Absence of contact between the brush and one of the commutator bars or rupture of a bar or a section of the winding leads to redistribution of current in the armature winding; the current is connected through balancing connections on the brush pairs remaining intact. With partial load of a dc machine there may be no impairment of the process of commutation, but a pulsating moment with frequency  $2p\omega_{\pi}$  starts acting in the machine. This moment tends to cause growth of tangential vibration of the machine at frequencies of  $2kp\omega_{\pi}$ .

In the case of skewing of auxiliary poles, as well as in the case of appearance of short-circuited turns in the windings of the auxiliary poles or in the excitation of windings, the current commutation conditions may be impaired in the brush zone of the defective pair of poles. The variable components of the armature current with commutator frequencies  $k\omega_v = kZ_v\omega_{\pi}$  where  $Z_v$  is the number of commutator bars that start to grow, and hence there appears vibration of the dc machine at the commutator frequencies. In most dc machines, as the supply voltage increases, the number of commutator bars is several times greater than the number of teeth in the armature; this makes it possible to separate the higher harmonics of the armature current and dc machine vibration into toothed and commutator components.

The growth of commutator components of the dc machine vibration, particularly under load, is one of the main diagnostic features of defects in the brush-commutator assembly and the auxiliary poles, but identification of the defects by these features is difficult. For preliminary identification of a defect it is possible to use the properties of the side components of vibration on commutator frequencies. Thus, if there are no side frequencies, the most probable reason of commutation violation is a defect in the poles or their windings. If the side components of vibration are present and differ from the commutator frequency by frequencies  $k\omega_{\pi}$ , then mechanical defects, for instance, rupture of the commutator or wear of the brushes (commutator) are most possible, and if side components are present differing by frequencies  $2kp\omega_{\pi}$ , then defects of the commutator bars or armature winding are most probable.

The possibilities of identification of dc machine defects and in a number of cases of increasing

the sensitivity of the diagnostic features to incipient defects may be expanded by conducting parallel measurements and analysis of the armature current spectra. In the most general case, the armature current may contain harmonic component series with frequencies  $kf_{\pi}$ ,  $2kpf_{\pi}$ ,  $kf_{Z_v}$ , and  $kf_{Z_e}$  and, depending on presence of various defects in the electromagnetic system of the dc machine, with side components differing by frequencies  $\pm kf_{\pi}$ ,  $\pm 2kpf_{\pi}$ , and  $\pm kf_{Z_v}$ .

In real conditions, there may be many more harmonic components of various frequencies in the spectrum of the armature current due to variable loads in the dc electric drive and from the other machines coupled to the dc motor. This makes it possible to obtain additional diagnostic information on the operation and state of the coupled machines.

In certain cases it is possible to measure and compare current spectra in the slip rings of different pole pairs of the dc machine. This makes it possible to determine in which machine/pole pair there are defects detectable by vibration or armature current, and sometimes to specify the value of the defect.

The features of the main defects in dc machines during their diagnostics by vibration spectra and/or armature current are summarized in Table 4. The table presents frequencies of those vibration components and armature current components that grow as a result of emergence and growth of the said defects.

For monitoring vibration during dc machine diagnostics, it is better to select the test points on its housing in the plane of fastening of the end brackets. As in diagnostics of asynchronous electric motors, it is recommended to perform vibration diagnostics of large-size machines by measuring the vibration at two points near both end brackets. In low-power machines (less than 50 to 100 kW) it is possible to measure vibration in one point, predominantly from the side of the commutator where high-frequency commutator vibration may appear, this vibration being not only electromagnetic in nature but also of mechanical origin.

The direction of measurement of vibration should not be radial to the axis of rotation of the armature since in this case the results of measurements may change little with the appearance of pulsating moments at low and medium frequencies in the machine. It is best of all to prepare the place for fastening the measuring transducer so that it has equal sensitivity to the radial and tangential vibration and much lower (two to three times) sensitivity to the axial vibration of the machine housing.

When selecting the diagnostic model, preference should be given to group models, which use measurements of vibration spectra of the housing and armature current of dc machines in two operating modes, if possible, with a strongly varying load. For diagnostics of machines operating continuously in one mode of operation it is possible to use "historical" diagnostic models by accumulating the data of periodic changes (statistics) within the first year of operation with intervals not exceeding one month and introducing corrections into the model after each maintenance service of the machine.

**Table 4** Frequencies of Vibration Components and Armature Current Corresponding to Defects in dc Machines and Pulsations of Supply Voltage<sup>a</sup>

Ref. No.	Designation of Defect	Growth of Vibration Harmonics	Growth of Current Harmonics	Notes
1	Static eccentricity of clearance, skewing of poles	$f_{Z_{arm}}; f_{Z_v}$ (R, T)	$f_{Z_{arm}}; f_{Z_v}$	Growth of vibration when changing load modes
2	Defects of armature windings, rupture of commutator bars	$2pf_{Z_{arm}}$ (T) $kf_{Z_v} \pm 2pf_{rt}$ (R, T) $kf_{Z_{arm}} \pm 2pf_{rt}$ (R, T) $kf_{Z_v} \pm 2pf_{rt}$ (R, T)	$2pf_{rt}$ $kf_{Z_{arm}} \pm 2pf_{rt}$	
3	Defects of excitation windings	$kf_{Z_v}$ (R, T)	$kf_{Z_v}$	Growth when changing load modes
4	Defects of commutation	$kf_{Z_v}$ (R, T)	$kf_{Z_v}$	
5	Wear of commutator brushes, rupture of commutator	$k_1f_{Z_v} \pm k_2f_{rt}$ (R, T)	$k_1f_{Z_v} \pm k_2f_{rt}$	
6	Pulsations of supply voltage	$kf_1$ (R, T)	$kf_1$	

<sup>a</sup> Where  $f_1$  = frequency of the supply mains of the rectifier, Hz  
 $f_{rt}$  = armature rotational frequency, Hz  
 $f_{Z_{arm}} = f_{rt}Z_{arm}$  is the toothed frequency, Hz  
 $Z_{arm}$  = number of armature slots  
 $f_{Z_v} = f_{rt}Z_v$  commutator frequency, Hz  
 $Z_v$  = number of commutator bars  
 $k = 1, 2, 3, \dots; k_2 = 1, 2, 3, \dots$  are integers

## REFERENCES

1. I. G. Shybov, *Noise and Vibration of Electric Machines*, Energy, Leningrad, 1974.
2. A. A. Alexandrov, A. V. Barkov, N. A. Barkova, and V. A. Shafransky, *Vibration and Vibrodiagnostics of Ship Electrical Equipment*, Sudostroenie, Leningrad, 1986.
3. A. V. Barkov, N. A. Barkova, Yu. A. Azovtsev, *Monitoring and Diagnostics of Rotor Machines by Vibration*, Gosudarstvennyi Morskoy Technicheskiy Universitet, St. Petersburg, 2000.
4. Kh. E. Zaidel, V. V. Kogen-Dalin, V. V. Krymov et al., *Electrical Engineering*, 3rd ed., Vysshaya Shkola, Moscow, 1985.
5. O. D. Goldberg, Yu. S. Gurin, and I. S. Sviridenko, *Design of Electric Machines*, Vysshaya Shkola, Moscow, 1984.
6. A. I. Voldek, *Electric Machines*, 3rd ed., Energy, Leningrad, 1976.
7. N. P. Ermolin, and I. P. Zherikhin, *Reliability of Electric Machines*, Energy, Leningrad, 1976.
8. L. G. Mamikonyants and Yu. M. Elkin, Eds., *Detection of Defects in Hydrogenerators*, Energoatomizdat, Moscow, 1985.
9. R. Miller and M. R. Miller, *Electrical Motors*, Wiley, Indianapolis, 2004.
10. H. A. Hamid and G. B. Kliman, Eds., *Handbook of Electrical Motors*, Marcel, 2004.

# CHAPTER 73

## PUMPS AND PUMPING SYSTEM NOISE AND VIBRATION PREDICTION AND CONTROL

Mirko Čudina

Laboratory for Pumps, Compressors and Technical Acoustics  
Faculty of Mechanical Engineering  
University of Ljubljana  
Ljubljana, Slovenia

### 1 INTRODUCTION

Hydraulic pumps are used for transporting chilled, hot, and condenser water or any other liquid in hydraulic systems. They are also used for transporting suspensions of liquid and solid particles from one location to another through pipes or closed/opened channels and passages. Common applications include use in processing plants, hydraulic fluid power, clean water supply, ships, and the like. Operation of a pump creates pressure pulsations, vibration, and noise, which can be spread by pipes (structure-borne noise) and by liquid (fluid-borne noise) far away from the pump itself, emitting noise (from pipes) around the whole pumping system. Noise generated by the pump depends on its type and size, on its power, and on the operating conditions (speed and load). Noise of the pumping system depends on its geometry and type and number of the built-in fittings and armatures. Noise and vibration of a hydraulic system can be controlled by proper selection or redesigning of the pump and/or pumping system and by optimizing of the operating conditions [for operating near the best efficiency point (BEP) and without cavitation]. Tuning of the operating frequency with regard to the resonance frequencies of the pumping system, and by proper balancing of all rotating masses, and the like is important.

### 2 TYPES OF PUMPS

Pumps are classified according to the principle of adding energy to the fluid into three main groups: kinetic, positive-displacement, and special-effect pumps (Fig. 1):

*Kinetic pumps*, in which energy is continuously added to the pumped liquid within the pump first by increasing the fluid velocity and then toward the end of the pump by increasing the delivery pressure, are subdivided into centrifugal or radial-flow, diagonal or mixed-flow, and axial-flow or propeller pumps (Fig. 1a). Centrifugal pumps are further divided into single and multistage pumps, with a volute collector or a multiple vane diffuser, with a straight vane or a Francis vane impeller, and with a fully open, a semiopen, and a fully closed impeller. Kinetic pumps are non-self-priming pumps but are the most widely used due to their high efficiency and reliable operation.

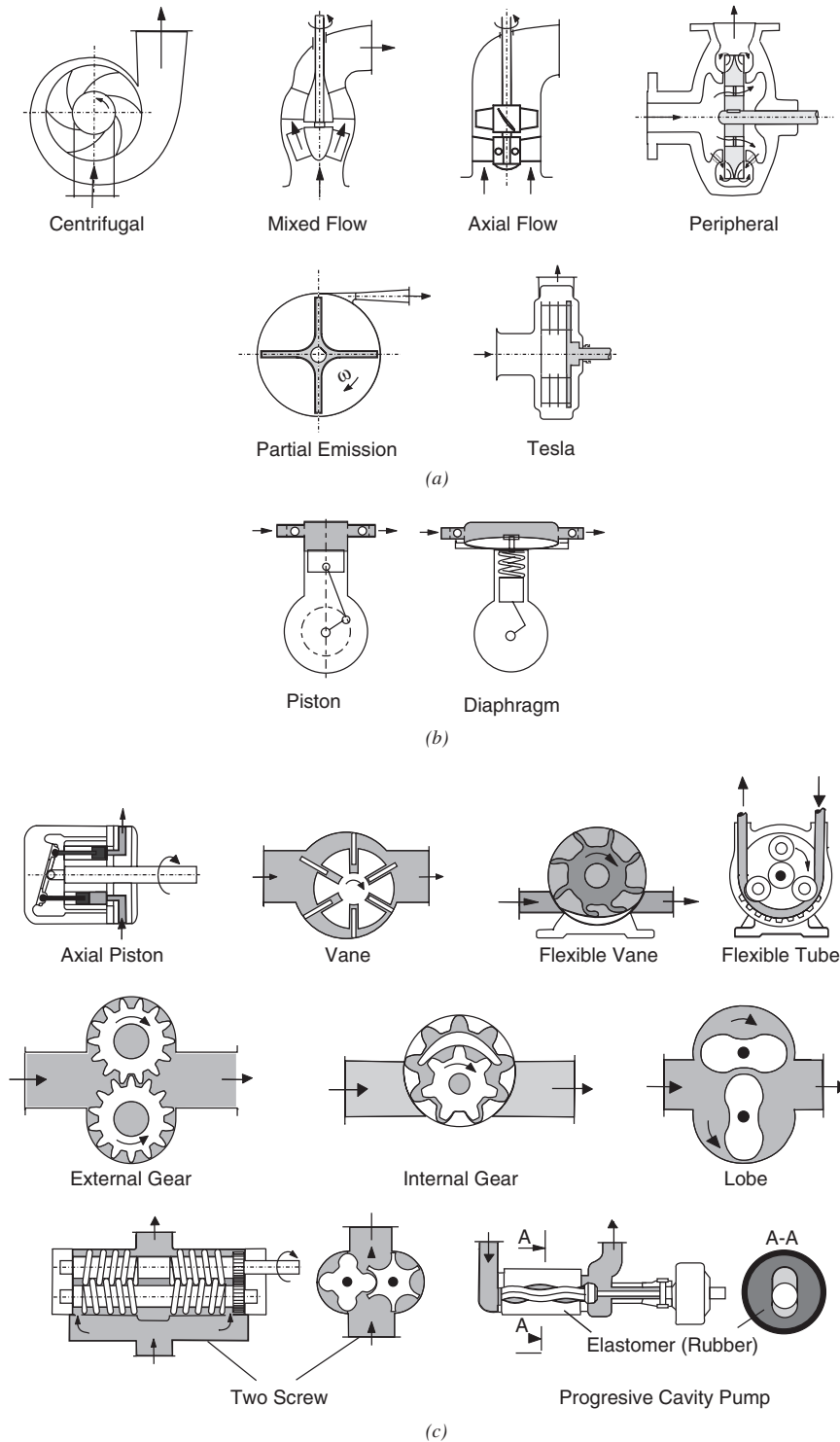
*Special-effect kinetic pumps* are in the form of peripheral (called also regenerative, turbulence, turbine, and vortex) pumps, partial-emission (called also

straight-radial-vane high-speed single-stage, vertical, paddle wheel according to Barske<sup>1</sup>) pumps, and Tesla (called also disk and viscous shear) pumps (Fig. 1a). The peripheral pumps have many radial vanes mounted on the periphery of the disk that rotate within an annular chamber. Liquid within the casing is separated by rotating vanes into many particular elements (vortices) with a high level of recirculation. The partial emission pumps consist of an open or semiopen radial (90°) vane centrifugal impeller, which rotates with very high speed (15,000 to 30,000 rpm, and up to 120,000 rpm) in circular casing with a single emission point to a conical diffusion section. Partial emission pumps are used to relatively higher heads and lower capacities. The Tesla pumps have two or more rotating parallel disks in which a viscous drag is created. They must rotate very fast, usually above 10,000 rpm, in order for the viscous drag to generate the forces to move the liquid.

*Positive-displacement pumps*, in which energy is periodically added by application of force to one or more movable working elements (piston, gear, vane, screw etc.) in a cylinder or appropriate casing, are divided, according to the nature of movement of the pressure-producing members, into reciprocating and rotary pumps.

*Reciprocating pumps* are further divided into piston, plunger, and diaphragm pumps (Fig. 1b) with one or more cylinders. They are self-priming pumps and are used for high pressure and low capacity. The piston(s) or plunger(s) or diaphragm are driven through slider-crank mechanisms and a crankshaft from an external source; therefore, they have a pulsating discharge. The flow rate is varied by changing either the rotating speed or the stroke length. Reciprocating pumps need one-way suction as well as discharge check valves separating the discharge from the suction side of the pump. These valves may be in the form of a plate, wing or flapper, ball, plug, and slurry.<sup>2</sup>

*Rotary pumps* are divided into pumps with a single-rotor and multiple rotors. The single-rotor rotary pumps are further divided into vane (blade, bucket, roller or slipper, or flexible impeller vane), flexible tube or peristaltic, screw (single screw and single screw with eccentric or progressive cavity) pumps. The pumps with multiple rotors are circumferential piston (axial and radial), gear (external and internal), lobe or Root's, and screw (two to five screw) (Fig. 1c). Rotary pumps are also self-priming, but they do not



**Figure 1** Types of pumps: (a) kinetic pumps, (b) reciprocating pumps, and (c) rotary pumps.

need valves or a crankshaft, therefore, they are relatively small and due to relative high efficiency are appropriate for pumping of liquids with high viscosities at medium pressures and capacities. Depending on the type, rotary pumps produce relatively small flows and pressure pulsations, so that the generated noise is much lower than with reciprocating pumps. This is also due to appropriate radial and axial clearances between the rotating elements and the casing that prevent mechanical contact and also due to utilization of a fluid film between the teeth at the gear or screw pumps, and between vanes and casing at vane rotary pumps, which reduces the impact and sliding effects. In spite of this, generated noise can be considerable, especially at the higher discharge pressures.

*Special-effect pumps*, in which energy is added by application of special physical principles, such as exchanging of the impulse or momentum in jet pumps (ejector or injector with water or vapor jet), by lifting power in air lift pumps, by pressure pulsation in hydraulic rams, or by applying Biot–Savart’s law in electromagnetic pumps, are rarely used and therefore beyond the scope of this section.

### 3 HYDRAULIC AND MECHANICAL SOURCES OF NOISE

Noise generated by a hydraulic pumping system consists of the noise generated by the pump itself, by the driving motor, usually a fan-cooled electric motor, which is beyond the scope of this section, and that generated by the pumping system, and is mainly hydrodynamic and partially mechanical in origin. Both types of noise origins are transmitted throughout the system over the fluid and/or structure as structure-borne sound before exciting the surrounding air and reaching us as noise. A pump as the prime mover is only part of a pumping system; therefore, we have to distinguish between the noise generated by the pump and the pumping system.

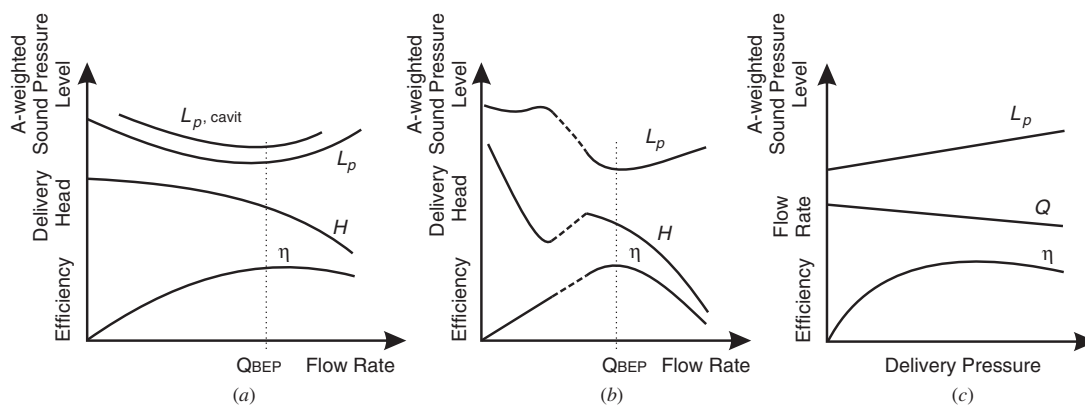
Noise generated by a pump depends on the pump type, on its geometry (size and form), and on the operating conditions (speed and load). The main sources

of noise in kinetic pumps are interaction between the impeller blade and the volute tongue or diffuser vanes in centrifugal pumps, and between the impeller blade and guide vanes in axial-flow pumps, so called blade passage frequency (BPF), followed by pressure fluctuations caused by turbulence, flow friction, flow separation, and vortices in the radial and axial clearances, especially between the open or semiopen rotor and the adjacent stationary part of the casing.

Major sources of internal noise in *reciprocating pumps* are piston-induced pulsation, piston mechanical reactions, and impacts in inlet and discharge valves, which are exerted by the up and down motion of a piston or plunger. Intermittent liquid flow and fluctuating dynamic forces and machinery imbalance of the reciprocating and rotating internal parts (pistons, crankshaft, etc.) are then sources of intensive noise. Additional sources of noise in reciprocating pumps are turbulence, flow friction, vortex formation from separated flow around obstructions, piston slap in a form of impact excitation, which is a result of the clearance between the piston and cylinder wall and the high pressure that pushes on the top of the piston during compression strokes.

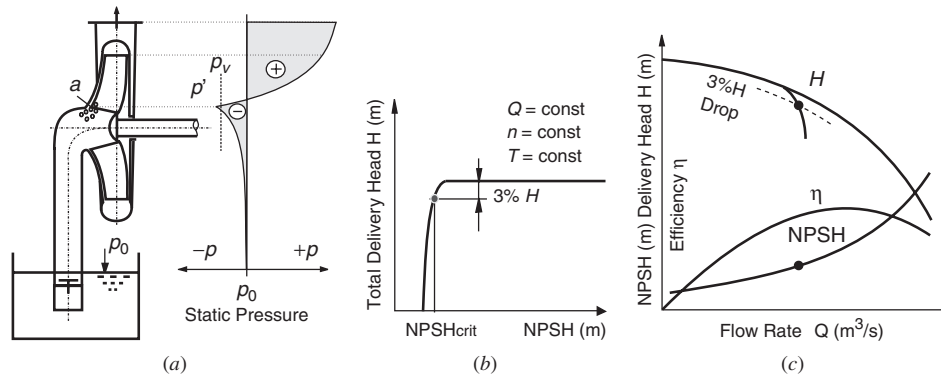
Major sources of noise in *rotary pumps* are impact between teeth in gear pumps, friction between screws at the screw pumps, and sliding of the vanes on the casing in vane rotary pumps. When the cavities between the gear teeth are not filled completely by the incoming liquid, the resulting vortices in voids generate a distinct noise, similar in nature to flow separation in centrifugal pumps during recirculation. Additional sources of noise are turbulence and flow friction in compression spaces.

The magnitude and frequency of the noise vary from pump to pump and are dependent on the magnitude of the pump head being generated and the amount by which pump flow at off-design operation deviates from ideal flow at the design or best efficiency point (BEP). The last is especially important with the kinetic pumps producing minimum noise at BEP. At off-design operation, the emitted noise generated by kinetic pumps steadily increases toward a zero flow rate and toward free delivery (Fig. 2). At higher flow



**Figure 2** Performance and noise characteristics of (a) a centrifugal pump, (b) axial-flow pumps, and (c) positive-displacement pumps.





**Figure 3** Cavitation in centrifugal pumps: (a) pressure within pump, (b) NPSH determination according to Ref. 3, and (c) NPSH determination according to Ref. 4.

rate ( $Q > Q_{BEP}$ ) this is due to laminar and turbulent boundary layer vortex shedding caused by higher flow velocity and turbulence, and at lower flow rate ( $Q < Q_{BEP}$ ) it is due to flow separation at the impeller blades and diffuser or guide vanes, and internal recirculation in the impeller eye and impeller discharge (Fig. 4).

Another factor that increases noise of a pump is pump instability, which may be caused by cavitation and, in kinetic pumps, by the appearance of stall and surge. Cavitation in kinetic pumps can occur within the entire operating regime, whereas stall and surge can only occur at partial flow rate. Cavitation can occur without stall and surge, and vice versa. Cavitation in kinetic pumps occurs more easily at higher flow rates ( $Q > Q_{BEP}$ ) due to the increased flow velocity and pressure drop.

*Cavitation in pumps* occurs when the absolute static pressure at some point within a pump or pumping system falls below the saturated vapor pressure of the fluid at the prevailing temperature conditions; the fluid starts to flash and vaporization occurs. Vaporization of the flowing fluid is connected with the onset of bubbles. The bubbles are caught up by the flowing liquid and collapse within the pump (valve or piping system) when they reach a region of higher pressure, where they condense. This process is accompanied by a violent collapse or implosion of the bubbles and a tremendous increase in pressure, which has the character of water hammer blows. The process of cavitation and bombardment of the pump surface by the bursting bubbles causes three different, undesirable effects: (a) deterioration of the hydraulic performance of the pump (total delivery head, capacity and efficiency), (b) possible pitting and material erosion in the vicinity of the collapsing bubbles, and (c) vibration of the pump walls excited by the pressure and flow pulsations and resultant undesirable (crackling or hissing) noise.

Cavitation in kinetic pumps (centrifugal, mixed flow, and axial) appears first at the point of minimum static pressure. In centrifugal pumps cavitation appear first in the region of the highest flow velocity, which is

usually on the inlet edges of impeller blades (see point *a* in Fig. 3a), or when the local static pressure  $p'$  falls below the vapor pressure  $p_v$  corresponding to the local temperature of the pumping liquid,  $p' < p_v$ . The bubbles so originated collapse in close proximity to impeller walls acting like impulses (impact waves) to the metal itself and eroding it. By development of the cavitation, the bubbles are spread upstream toward the suction nozzle and suction pipe, and downstream toward impeller blades, shrouds, guide vanes, and volute casing.

Cavitation in rotary pumps appears first in the suction pipe before the entry of fluid in the pump, as well as in gaps between the teeth and casing in gear pumps or the rotating elements and casing of any rotary pumps. In reciprocating pumps cavitation appears in the cylinder, at the beginning of the suction stroke and in the suction pipe. However, the cavitation damage in positive-displacement pumps is not as severe or loud as in centrifugal pumps due to lower speed at which they operate and the higher vapor pressure of the fluid usually pumped.

Since the implosion of the bubbles appears randomly and chaotically, turbulent noise occurs over a wide frequency spectrum or at a specific frequency, so that the onset of cavitation can cause a change either in the total noise level or just in a particular frequency band. Figure 2a shows emitted noise level for a centrifugal pump without ( $L_p$ ) and with cavitation ( $L_{p,cav}$ ). The curve representing the A-weighted noise level with cavitation is approximately 3 dB higher than that without cavitation. In some cases the A-weighted noise level is due to cavitation up to 10 dB higher. To avoid cavitation process in a pump the static pressure  $p'$  in Fig. 3a has to be greater than the vapor pressure  $p_v$  of liquid at that temperature.

Cavitation is associated with insufficient suction head of the pump. Therefore, the beginning of cavitation within kinetic pumps can be obtained by determination of the net positive suction head (NPSH). The NPSH required ( $NPSH_r$ ) value is a head that is required above the liquid vapor pressure at the place of the lowest static pressure, for example, point *a* in

Fig. 3a, in order to prevent the inception of cavitation and safe and reliable operation of pump. The difference between the actual pressure of the liquid available and the vapor pressure of that liquid is called the net positive suction head available (NPSH<sub>a</sub>). When the NPSH<sub>a</sub> is equal to or greater than the NPSH<sub>r</sub>, the pump will not cavitate, and when the NPSH<sub>a</sub> is less than that required by the pump, cavitation occurs.

The NPSH required is determined by a test in which the total head is measured at a constant speed, flow rate, and test water temperature, under varying NPSH conditions. Lowering the NPSH value to the point where the available NPSH is insufficient causes a cavitation sufficient to degrade the performance of the pump and the total delivery head deteriorates (Fig. 3b). The exact value of NPSH required for a centrifugal pump is determined by a 3% drop in the total delivery head (Fig. 3b) and represents the required or critical value at which cavitation is fully developed.<sup>3</sup> An alternative procedure is to establish a constant NPSH available and then vary the pump flow by means of a discharge control valve until a 3% drop in the pump total delivery head is observed (Fig. 3c).<sup>4</sup> The methods need a special test standard according to ISO 3555 standard,<sup>5</sup> and a set of measurement results to determine the NPSH required value at different flow rate. At the centrifugal pumps NPSH required value decreases by decreasing the flow rate, that is, by decreasing flow velocity (see Fig. 3c). At the mixed-flow pumps NPSH required value increases at off-design operation, so toward partial flow rate as well as toward free delivery. At the axial-flow pumps NPSH required value increases at off-design operation much more steeply as by the mixed-flow pumps.

Instead of the ISO 3555 standard the sound pressure level of a discrete frequency tone, or a group of discrete-frequency tones, in audible range (between 20 and 20,000 Hz) can also be used for determination of the NPSH required or critical value as well as to detect the incipient of the cavitation process and its development. Experiments have shown that the maximum discrete-frequency tone (or group of discrete-frequency tones) corresponds to the 3% drop in the total delivery head. The discrete-frequency tone(s) with maximal changes can be at BPF/2 (Fig. 5a)<sup>5,6</sup> or at any other frequency.<sup>7</sup> The differences in the level of the discrete-frequency tone before the incipient of cavitation and after it was fully developed can be great enough (between 10 and 20 dB at a distance of 0.5 or 1 m, and up to 40 dB and more with microphone position in a near field) that it could also be used for control cavitation in the pump, by means of initiating an alarm, shutdown, or control signal via an electrical control system.<sup>5-9</sup>

*Stall and surge* appear in kinetic pumps at partial flow rates. In suction and discharge areas of the impeller, internal recirculation first appears and then rotating stalls and surge causing additional hydraulic noise. The internal recirculation and rotating stall (A and B in Fig. 4) start at approximately 80% of the design flow. When the flow rate is reduced further, a sudden decrease in static pressure occurs within the

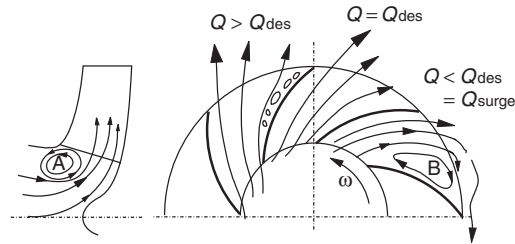


Figure 4 Flow distribution in impeller of centrifugal pump at design and off-design operation.

rotating stalls and the stalls spread over the entire suction and discharge cross sections. When stall cells A and B in the suction and discharge side of the impeller merge, a surge phenomenon occurs causing an unstable pump characteristic. When a surge appears, a pump is not able to sustain the static pressure difference between the discharge and the suction sides of the pump. Water surges back through the pump impeller and its discharge pressure is momentarily reduced. The flow rate and pressure fluctuations at the surge cause an intense vibration and additional turbulent noise.

*Noise in the piping system* is a result of both the mechanical vibration excited by pump and piping system components as well as by the liquid motion in the pump and piping system. Mechanical noise sources are vibrating components or surfaces, such as pistons, unbalanced rotating elements, and vibrating pump housing, which is transmitted to the inlet and outlet pipe to which it is connected (even through a flexible connection), producing vibrations of pipe walls and acoustic pressure fluctuations in adjacent media. Due to its cylindrical and usually curved form, piping generates a (single and/or two-dimensional) cylindrical noise. In addition to the frequencies associated with the pump and flow, pipes also vibrate at their own natural or resonant frequencies. Liquid or hydraulic noise sources are the result of friction, turbulent flow, and vortex formation in high-velocity flow and pulsating flow. With positive-displacement pumps, pressure fluctuation due to flowing liquid is noticeable when repeating momentum impulses are imparted to the fluid, and partially also with centrifugal pumps due to the action of the impeller blades against the volute tongue.

The amount of vibration and noise transmitted through the housing and pipework depends on the rotational speed of the pump, operating pressure and capacity, flowing fluid properties (velocity, density, viscosity, temperature), the material and geometry of the housing and pipework, suction and pressure reservoirs, elbows, Y- and T- branches, restrictions, block and control valves, wall thickness, supporting and hanging elements of the piping system, and so on.

Another factor that causes intense noise from a piping system is instability caused by cavitation, water hammer, and system resonances:

*Cavitation within piping system*, with the danger of pitting and material erosion, is a result of pressure drops, usually with partially closed control valves, when the critical flow rate is reached or due to high flow velocity (for cold water above 7 m/s).

*Water hammer* is a result of transient pressure impact when a suddenly closed control valve abruptly interrupts steady flow in a pumping system, for example. The sudden interruption of flow results in an extremely sharp pressure rise at the point of interruption; the entire distribution system is then shock excited into vibration. Water hammer is a more serious problem in this type of installation when long pipelines are involved and when a motor-driven pump stops delivering water almost instantaneously.

#### 4 SOURCES OF VIBRATION IN HYDRAULIC SYSTEMS

There are different sources of vibration within hydraulic system, but the main source is the pump built-in. The vibration generated within the pump can be transmitted to the pumping system, and vice versa, especially if they are coupled rigidly or mounted on a rigid basement or wall, without elastic elements, directly.

*Vibration generated by a pump* has mechanical and hydraulic origins and depends on the pump type, on its manufacture (first of all balancing of rotating masses), assembling and wearing, and on operating conditions (operating point). Mechanical sources of vibration are mechanical imbalance of the rotating or reciprocating masses, due to poor balancing or careless assembly. The vibrations of a kinetic pump are strongly dependent on the shaft vibration. Shaft vibration and its failures are strongly influenced by the torsional resonances of the system, which are the angular natural frequencies of the system caused by dynamic forces of mechanical and hydraulic origin. Additional sources of mechanical vibration are rotational subsynchronous [at  $n/2$ ,  $n$  is the rotational speed in revolutions per second (rps)], synchronous (at  $n$ ), and super synchronous (at  $2n$ ,  $3n$ , etc.) resonance (foreign particles in the rotor, damaged impellers, contortion, due to deposits, corrosion, galled parts, and abrasion), rubbing, excessive wearing, bushing, excessive bore clearance of sleeve bearings or loose fits on the shaft or housing in the case of ball bearings causing poor support of the rotor; impacts, nonconstant friction (e.g., stick-slip, chatter), mechanical interactions, magnetic effects and so on.

Hydraulic sources of vibration are pressure pulsations, turbulent liquid flow, suction recirculation, stall and surge, blade passing frequency, hydraulic imbalance due to uneven flow distribution before the impeller and in all blade passages, misalignment or other leakage clearances, unsteady fluid flow (e.g., turbulence, vortex shedding), increased axial and radial hydraulic forces in the volute casing of a centrifugal pump at off-design operation; pump manufacturer casting/or machining defects, wear, oil-whirl, cavitation, and so on.

#### 5 SOURCES OF VIBRATION AND NOISE IN PUMP COUPLING AND SUPPORTING ELEMENTS

A major source of externally induced vibration and noise is misalignment between the pump and its driver, which depend on the coupling used. There are two primary groups of coupling: rigid and flexible. Rigid couplings are used for direct coupling and for precise alignment, whereas the flexible couplings are used for accommodating a set amount of misalignment (angular, axial, and radial or parallel) between the driving and driven shaft, and also radial and axial loads on the motor bearings. Rigid couplings are in sleeve-type or flange-type and are used when the pump impeller is mounted directly on the motor shaft (monobloc pumps). Flexible couplings may be mechanically flexible and "material flexible." The mechanically flexible couplings are in gear or grid form, which need lubrication. The material-flexible couplings have a flexible element in steel, rubber, elastomer, or plastic material and do not need lubrication. They are in the form of metal disk or disk pack or in the form of contoured diaphragm, or as an elastomer in compression or shear type with rubber jaws on driving and driven shafts corresponding to the number of cogs belt or a central spider on the flexible element with several radial segments.

There are also special types of couplings to transmit power with independent input and output shaft that allow desired adjustments of load speeds. Such couplings are the eddy-current slip couplings and fluid couplings (in hydrokinetic, hydrodynamic, hydroviscous, or hydrostatic form) using fluid (natural or synthetic oil).

A second source of externally induced vibration and noise at a pump are supporting bearings, with which it is equipped. The hydraulically and mechanically produced noise and other failings of the pump rotating and moving elements are transmitted over the bearings to the pump housing and as structural noise throughout the pumping system. Most pumps are equipped with external bearings in a classical three-bearing arrangement, journal or sleeve type (with hydrodynamic fluid film), antifriction (rollers, tapered rollers, or bearings in single or multiple rows), and magnetic bearings. At normal operation of a journal bearing the shaft forms a liquid film of the lubrication oil completely separates it from the bearing. The antifriction bearings operate with a very low coefficient of friction associated with rolling motion as distinct from sliding motion. To minimize the heat generated by sliding friction, antifriction bearings require oil or grease lubrication. The magnetic bearings are free from contact within the bearings, therefore they produce the lowest mechanical noise among all type of bearings, follow the journal or sleeve and antifriction bearings, which are the noisiest.

Vibration problems and noise in a pump increase when a failure in the bearings and/or coupling misalignment occurs. Bearing failure may be caused by water or product contamination in the bearing housing or by highly unbalanced radial loads, which can result

from operating at or near shutoff. Nonconstant friction forces usually are caused by poor lubrication, at low shaft speed or low fluid viscosity in journal bearings, when the strength of the liquid film is insufficient to support the load on the bearing and the shaft rubbing the bearing, or by unfavorable combinations of sliding interface materials, geometric arrangements, and sliding velocities. Damage of the rolling bearings causes vibrations at the integer number of rotational frequency, whereas the oil whirl in hydrodynamic bearings causes vibrations at a fraction of rotational speed. Poor lubrication and defects in the rolling elements or races in antifriction bearings exhibit very high frequency resonance and noise of about 20 kHz.

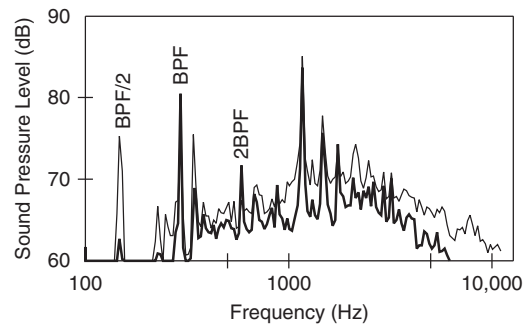
## 6 SOUND SPECTRA OF PUMPS AND PIPING SYSTEMS

Pumps and piping systems generate broadband or turbulent noise spectra with pronounced discrete frequency or pure tones. The broadband noise is a result of different forms of hydraulic noise, caused by turbulence and the effects of flow instability already discussed. The broadband noise is usually secondary in magnitude and related to poor pump design or applications, and on the intensity of turbulence, appearance of cavitation, or water hammer. Impact and roughness in bearings also produce broadband noise.

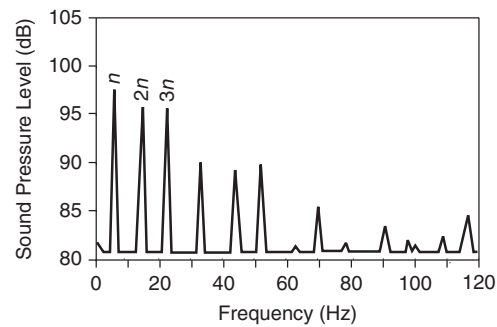
Discrete-frequency tones in the noise spectrum of a pump are provoked by interaction of the moving elements with nearby stationary or moving objects and appear at the rotational frequency  $f_1 = n$  ( $n$  is the number of revolutions or strokes per second) and at the frequency  $f_2 = inz_f$  ( $z_f$  is the number of impeller blades in the kinetic pumps or the number of compression or intermittent operation of piston or plunger or diaphragm in reciprocating pumps, or the number of pumping events per rotation at rotary pumps, for example, number of teeth, vanes, lobes and the like, and  $i$  is the harmonic number (1, 2, 3, ...), also called blade passage frequency (BPF) with kinetic pumps. In many cases, the first three harmonics of the  $f_1$  and  $f_2$  are predominant (see Fig. 5). Figure 5a shows the noise spectrum of a centrifugal pump without (thick curve) and with cavitation (thin curve).

With *reciprocating pumps* the impact source of noise is abrupt, therefore the noise spectrum contains major pronounced discrete-frequency tones typically dominated by fundamental frequencies and their higher (prominent 3 to 10 or more) harmonics. The fundamental frequency is defined by the number of strokes per second, whereas the amplitudes of the particular discrete-frequency tones depend on the stroke length. Figure 5b portrays the spectrum of a three-plunger pump with three pronounced spikes among them; the third represents the plunger frequency. Discrete frequency tones in a reciprocating pump may also be due to failures and damage of the piston ring and internal check valves.

With *rotary pumps*, discrete-frequency tones are provoked by fluctuating flow caused by teeth, vanes, screw and lobes, unbalanced rotating parts, misaligned parts, fluctuations in the load, failures and damage of



(a)



(b)

**Figure 5** Noise spectra with tonal and turbulent noise: (a) for kinetic pump and (b) for piston pump.

displacement elements, impact between teeth at gear pumps, and so on.

*Noise spectra of piping systems* are usually also broadband in nature with pronounced discrete frequency tones. The broadband noise is a result of piping vibrations occurring by flow-induced pulsations in the piping system. Noise in pipe fittings such as dampers, elbows, and branch takeoffs and obstructions is also generally broadband and limited to a frequency range between 500 and 8000 Hz. Instability in the piping system, such as cavitation, flashing, and water hammer, also causes mostly broadband noise. The discrete-frequency tones in the piping system are a result of incoming noise produced by an operating pump, especially in the case of positive-displacement pumps and due to excited piping resonances. Among them only the first two resonance orders is worth examining: the first-order resonance or fundamental frequency and the second-order resonance or second harmonic. The resonant frequency depends on the distance between supporting places (the longer the distance, the lower the mode of vibration or resonances), and on the type of hanger or supporting elements.

## 7 EFFECTS OF PUMP TYPE, GEOMETRY, PRESSURE, SPEED, SIZE, AND MATERIALS

The magnitude and frequency of noise generated by a pump depend on the pump type, on its material,

geometry (size and form), and on the operating conditions (speed and load), that is, on the operation point on its characteristic curve. In general, total noise level increases by increasing the rotational speed and dimension, but the effect of load depends on the operating characteristics of the pump. With kinetic pumps, the flow rate can be changed from zero to the maximum flow rate or free delivery, with BEP in between. The noise characteristic depends on the operation point and has a minimum usually at the BEP (Fig. 2a, b). At off-design operation, noise level increases toward a zero flow rate and toward free delivery. With kinetic pumps with unstable characteristics, maximum noise level can appear at the surge point, which usually appears at a flow rate between 30 and 60% of the BEP for centrifugal pumps, and between 70 and 80% of the BEP for axial-flow pumps. According to Lips,<sup>10</sup> by increasing pump power from 1 to 1000 kW, the sound power level increases by 40 dB (from 70 to 110 dB) for centrifugal pumps, and by 30 dB (from 80 to 110 dB) for axial-flow pumps.

With positive-displacement pumps, the flow characteristic is almost independent of load; the flow rate is nearly constant at different delivery pressures; therefore, the total noise level depends on the pump type and dimension (size or working volume), speed, and delivery pressure. Effect of the pump operating pressure, working volume and power consumption on the emitted sound power level is presented in Table 1.<sup>10,11</sup>

Pump noise depends also on the material from which the pump was fabricated. Pumps fabricated from a rubber polyvinyl chloride (PVC), elastomer, composite, lead and coated steel housing, impeller, piston or screw by rubber, or Teflon (due to low friction also by glass, enamel, etc.) generate less noise than those fabricated from steel, cast or alloy steel, cast iron, and similar rigid material.

## 8 PREDICTION OF NOISE AND VIBRATION GENERATED BY PUMPS AND PIPING SYSTEMS

Noise and vibration generated by a pump and pumping system is difficult to predict due to numerous generating mechanisms that are changed by changing of the operation conditions. The total emitted noise consists of the pump noise and the piping system noise, both of them having fluid-borne and the structure-borne origins.

Equations for calculation of the A-weighted sound power levels in dependence on the power pump are given in Table 2 for different types of pumps.<sup>12,13</sup> These equations are valid for a limited range of the power consumption within which the measurements were done, and by taking into account a certain degree of uncertainty, which is given in each equation.

Noise emission from piping systems having characteristics of a line source depends on the structure-borne noise generated in the piping and armature and on the

**Table 1 Increase in A-weighted Sound Power Level of Pump by Increasing Operating Pressure, Working Volume, and Pump Power**

Pump	Axial Piston Pump	Gear Pumps	Vane Rotary Pumps
Increasing of operating pressure from 20 to 300 bars	Up to 20 dB	Up to 10 dB	Up to 4 dB
Increasing of pump working volume from 5 to 250 m <sup>3</sup>	Up to 30 dB	Up to 22 dB	Up to 4 dB
Increasing of pump power from 1 to 125 kW (see also Table 2)	Up to 25 dB (from 73 to 98 dB)	Up to 8 dB (from 76 to 84 dB) with outer teeth, and up to 20 dB (from 65 to 85 dB) with inner teeth	Up to 20 dB (from 72 to 92 dB)

**Table 2 Prediction of the A-weighted Sound Power Level Generated by Different Pumps**

Type of Pump	A-weighted Sound Power Level, ( $P$ in kW, $P_{ref} = 1$ kW) in dB	Valid for Power Consumption $P$
Centrifugal pumps (single stage)	$L_{WA} = 71 + 13.5 \log P \pm 7.5$	$4 \text{ kW} \leq P \leq 2,000 \text{ kW}$
Centrifugal pumps (multistage)	$L_{WA} = 83.5 + 8.5 \log P \pm 7.5$	$4 \text{ kW} \leq P \leq 20,000 \text{ kW}$
Axial-flow pumps	$L_{WA} = 78.5 + 10 \log P \pm 10$ at $Q_{BEP}$ $L_{WA} = 21.5 + 10 \log P + 57Q/Q_{BEP} \pm 8$	$10 \text{ kW} \leq P \leq 1,300 \text{ kW}$ $0.77 \leq Q/Q_{BEP} \leq 1.25$
Multipiston pumps (inline)	$L_{WA} = 78 + 10 \log P \pm 6$	$1 \text{ kW} \leq P \leq 1,000 \text{ kW}$
Diaphragm pumps	$L_{WA} = 78 + 9 \log P \pm 6$	$1 \text{ kW} \leq P \leq 100 \text{ kW}$
Screw pumps	$L_{WA} = 78 + 11 \log P \pm 6$	$1 \text{ kW} \leq P \leq 100 \text{ kW}$
Gear pumps	$L_{WA} = 78 + 11 \log P \pm 3$	$1 \text{ kW} \leq P \leq 100 \text{ kW}$
Lobe pumps	$L_{WA} = 84 + 11 \log P \pm 5$	$1 \text{ kW} \leq P \leq 10 \text{ kW}$

fluid-borne noise generated by moving fluid in the piping system. Both of them depend on the type, size, and rotating speed of the pump built in the hydraulic system, on the pumping fluid characteristics and its velocity, temperature, and suspended rigid and gas particles in, then on, the dimension (length, diameter, and wall roughness), configuration and material of the piping system, and on the armatures built-in and their coupling to the pipe, as well as on the support of the pumping system and distances between fixings, and so on. Due to the complexity of the pumping system, only formulas for prediction of the total emitted noise from its particular components, excited by structure-borne noise or by fluid-borne noise, within the flowing fluid, pipe, and armature, or from the piping to the surrounding air are on disposal.

For prediction of the A-weighted sound power level of a straight piping to surrounding air excited by structure-borne noise the next formula can be used:<sup>10</sup>

$$L_{WA} = 10 \log(\overline{v^2}/v_0) + 10 \log(S/S_0) + 10 \log \sigma \quad \text{dB} \quad (1)$$

where  $\overline{v^2}$  is the mean-squared vibration velocity measured on the piping wall (in  $\text{m}^2/\text{s}^2$ ),  $v_0$  is the reference velocity (1 m/s),  $S$  is the outer cross section of the pipeline ( $\pi D^2/4$ ) (in  $\text{m}^2$ ),  $S_0$  is the reference surface 1  $\text{m}^2$ , and  $\sigma$  is the frequency-dependent radiation ratio, which can be estimated for a case without any pronounced discrete-frequency tones by next formula:

$$\sigma(f) \approx \frac{1}{1 + [c/(4Df)]} \quad (2)$$

where  $c$  is the speed of sound in the air around the pipeline (in m/s),  $f$  is the central frequency of the frequency band observed (in Hz), and  $D$  is the pipe outer diameter (in m).

For prediction of the internal A-weighted sound power level of the noise generated by the flow within straight pipeline with constant cross section, the next formula can be used:

$$L_{WA} = K + 10 \log(w/w_0) + 10 \log(S/S_0) + 10 \log(p/p_0) - \log(L/L_0) \quad \text{dB} \quad (3)$$

where  $K = 8 - 0.16w$ ,  $w$  is the flow velocity within pipe (in m/s),  $w_0 = 1$  m/s,  $S$  is the internal cross section of the pipe (in  $\text{m}^2$ ),  $p$  is the sound pressure in fluid (in Pa),  $p_0 = 10^5$  Pa,  $L$  is the pipe length (in m), and  $L_0 = 1.4$  m.

This fluid-borne noise is heard outside the pipe but reduced for transmission loss in the pipe wall. The transmission loss depends on the material and geometry of the piping and can be calculated by<sup>10,14</sup>

$$R_R = 9 + 10 \log \frac{\rho_w c_w s_w}{\rho_F c_F D_i} \quad \text{dB} \quad (4)$$

where  $\rho_w$  is the density of the pipe wall,  $\rho_F$  is the density of the flowing fluid,  $c_w$  is the speed of sound in the wall of the pipeline,  $c_F$  is the speed of sound in flowing fluid (in  $\text{kg}/\text{m}^3$ ),  $s_w$  is the pipe wall thickness, and  $D_i$  is the internal diameter of the pipe.

An additional reduction in transmitted sound energy by fluid-filled circular pipeline wall can be expected, for a pipe diameter nearly equal to the wavelength, at the next (resonant) frequencies:

$$f_{D,n} = \kappa_n c_F / (\pi D_i) \quad \text{and} \quad f_R = c_L / (\pi D_i) \quad (5)$$

where  $n = 1, 2, 3, \dots, 6$ ,  $\kappa_n = 2D_i/\lambda_F$ ,  $\lambda_F$  is the wavelength in the flowing fluid.

*Vibration of the hydraulic system* also cannot be predicted by a common formula since there is a lot of excited forces and modes of vibration depending on the pump (its type, size, and speed) and on the piping system and its dimension and configuration. Therefore, there are only formulas for prediction of vibration for particular hydraulic system components, such as driving shaft of the pump, piping, and some armatures. Vibration energy from the pumping system is important below 100 Hz when resonances can cause large structural displacements and corresponding high stresses.

Vibration of drive shaft is a result of two independent forms of vibration, translational due to oscillation about its ideal "at rest" centerline and torsion due to the twisting of the shaft about the centerline. If the driving shaft is designed with torsion frequency well outside any exciting frequencies and so outside the torsion natural frequency, for more than 50% as usual case is, then torsion vibration of the shaft is not problematic. The translational vibration can be problematic especially in the case of a higher degree of unbalance. The lowest natural frequency due to translational vibration can be calculated for the drive shaft with circular cross section by

$$f_1 = \frac{\gamma_1^2 D}{8\pi L^2} \sqrt{\frac{E}{\rho}} \quad (6)$$

where  $f_1$  is the first-order shaft resonance (in Hz),  $\gamma_1$  is the coefficient of bending resonance,  $D$  is the diameter of the shaft (in mm),  $L$  is the effective length of the shaft (between both the driving and the driven ends) (in mm),  $E$  is the modulus of elasticity (in Pa), and  $\rho$  is the density of the shaft (in  $\text{kg}/\text{m}^3$ ). According to Karasik and McGuire,<sup>1</sup> the average bearing housing vibration velocity for pumps with running speed between 1500 and 4500 rpm increases with pump speed to about the 0.33 power of the speed ratio. Usual vibration velocities are between 0.7 and 4.4, and up to 10 mm/s root mean squared (rms). Pumps with bearing housing vibration velocity below 2 mm/s rms are good, between 2 and 4 mm/s are acceptable, between 4 and 5.5 mm/s are poor, between 5.5 and 9 mm/s are schedule for repair, and above 9 mm/s rms has to be shutdown immediately.

Vibrations of the piping system occur in three most important natural modes of free vibration: compression, bending, and radial. Each of these modes occurs only at particular discrete frequencies, called resonant frequencies, which depend on the stiffness and the mass of the piping. The bending and radial modes are the most important since the pipe wall motion is perpendicular to the length of the pipe. The bending mode resonant frequencies for a straight piping system of uniform diameter and physical properties can be calculated by

$$f_n = \frac{\gamma_n^2}{2\pi L^2} \sqrt{\frac{EIg}{G}} \quad (7)$$

where  $f_n$  is the resonance frequency (in Hz),  $\gamma_n$  is the coefficient of bending resonance,  $L$  is the length of pipe between supports (in m),  $E$  is the modulus of elasticity (in Pa),  $I$  is the moment of inertia (in m<sup>4</sup>),  $g$  is the acceleration due to gravity (9.81 m/s<sup>2</sup>), and  $G$  is the weight (including fluid) per unit length (in N/m). Values for  $\gamma_n$  depend on the boundary conditions describing how the pipe is supported at the end of a pipe section (simply, anchored, or combination), and the order of the mode. For fundamental resonance its values are for a simply support 3.14, for anchored support is 4.73, and for combined support 3.93, and so on.<sup>15</sup>

Within a piping system there are also acoustic resonances caused by the running pump producing pressure pulsations. The natural acoustic resonant frequencies of a straight, uniform length of pipe open or closed at both ends can be calculated by

$$f_n = nc/2L \quad (8)$$

where  $n$  is the resonance order ( $n = 1, 2, 3, \dots$ ),  $c$  is the wave propagation speed of fluid, and  $L$  is the length of the column of fluid between discontinuities where a reflection is anticipated.

## 9 NOISE CONTROL OF PUMPING SYSTEMS

Noise control of a hydraulic pumping system can be made at the source, transmission path, and at the receivers (listener). At the source, noise can be controlled by changing the pump operating condition or by modifying the basic pumping system design (by redesigning or changing the connection of assembled parts, by including different kind of dampers and silencers between the pump and piping system, etc.). On the transmission path, noise can be controlled by interrupting the path between the pumping system and listener, for example, by enclosing the pump and piping system or by erecting barriers between the pumping system and listener. At the receiver, noise can be reduced by physically enclosing the listener or by use of personal protecting equipment. Noise control by using barriers and by protecting the listener is beyond the scope of this section.

A hydraulic pumping system consists of a pump and piping system; therefore, we have to distinguish

between the noise control of the pump and pumping system. There are different methods for noise reduction. The most powerful is changing the operating point of the pump. The *operating point of the pump* can be changed by changing the rotational speed and load with kinetic and rotary pumps or by changing number and length of strokes with reciprocating pumps. The lower the rotational speed and number and length of strokes, the lower the noise and vice versa; however, the load should always be at or close to the BEP. With proper operating point and design, we also have to avoid the onset of cavitation in the pump. The operation point depends also on the pumping system characteristic or resistance curve, which depends on many parameters, such as dimension, configuration, and armature built-in. Therefore, modification of particular components or dimensions of a pumping system can change the operation point and is frequently an effective tool for noise reduction, although it can sometimes be also ineffective.

Noise control of a pump can be achieved by a reduction of rotating frequency, by modification or elimination of causes of hydrodynamic and mechanically generated noise. With kinetic pumps it can be achieved by changing the number and form of the impeller blades and diffuser or guide vanes. With centrifugal pumps, noise can be effectively reduced by changing (increasing) the radial clearance between impeller diameter and volute tongues or diffuser vanes (preferably 5 to 10% of impeller diameter); that is, by reducing the effect of BPF. The radial clearance can be increased by turning the impeller outer diameter or by grinding (reducing) the volute tongue, but in this case we must take into account that volumetric efficiency (and also the total efficiency and total delivery head) decreases. With positive-displacement pumps, noise can be reduced by increasing the number of pistons or plungers (preferably an odd number, nine at the most) to reduce pulsation of the delivery flow and pressure differences in the discharge vessel, by the exact closure of the inner valves at reciprocating pumps, by optimization of the number and form of rotating elements (teeth, screws, vanes, lobes), radial and axial clearances between rotating elements and casing, and by modification of the interaction of the components, which strike each other to produce the impact at rotary pumps.

The noise of positive-displacement pumps can also be reduced by modification of impact surfaces and time of impact (e.g., by using conical or ball valves instead of a plate type of inner valve plug), by replacing stiff, rigid materials with resilient materials (durable polymers and plastics instead of steel valves) at reciprocating pumps, by helical or spiral gear sets instead of spur or bevel gears, by finer pitches and shorter teeth, by improving gear lubrication, by introducing a soft material (such as lead, rubber, or plastic) in gear pumps and by using roller instead of plate types of vanes in vane rotary pumps.

The noise of a pump can be further reduced by use of journal-type instead of antifriction bearings, by replacement or adjustment of worn, loose, or



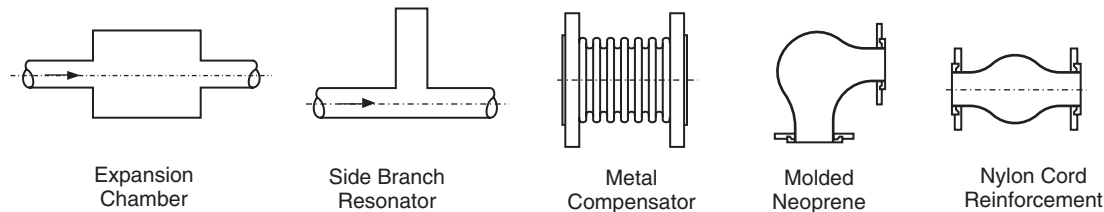


Figure 6 Methods for reduction of pressure pulsation in piping.

unbalanced parts of pump, by changing of the size, stiffness, or weight to change the resonance frequency, by flexible shaft couplings and mounts, by resilient flooring, by belts instead of gears for drives, by rubber or plastic bumpers or cushions (pads), by different pump models or types to permit operation at reduced speeds, and so on.

Noise generated by a pump is radiated to the surrounding air through the vibrations of the pump case, the pipe wall, or other structures to which the pump system is coupled by liquid or mechanical attachment. Therefore, pump noise can be reduced by enclosures, built in-line silencers or dampers, isolation mounts between the pump and the reservoir, by avoiding in-line mounting, and so on. The use of enclosures around a pump or piping system has the highest transmission loss, when its area density is high and is not mechanically tied to the vibrating surfaces of the pump. A total enclosure around a pump must have openings to prevent overheating, formation of explosive mixtures, and access for maintenance of the pump. Treating the interior of the enclosure with sound-absorbing material reduces the apparent source strength by preventing reverberant buildups in the enclosure.

*Noise control of a piping system* can be achieved by redesigning the piping system and/or by modification or interruption of the transmission path in the piping system, that is, from the pump to the radiating surfaces (piping). Redesigning the piping system is based on changing the size, form, and material of piping, by changing the form, number, and position of the built-in valves, T and Y approaches, dampers and silencers, and the supporting elements. Interruption of the transmission path can be achieved by reducing pressure pulsation in the pump's suction and discharge piping, by changing structural or natural frequencies of vibrating piping system, by built-in intake and exhaust damping elements, such as flexible sections in pipe runs (short lengths of flexible hose near the pump inlet and discharge), by the addition of damping to structural elements, for example, fabric sections in ducts with viscoelastic damping materials in the form of pipe lagging and wrapping materials, jackets made from absorptive materials of a heavy, solid, impervious skin of plaster, cement, metal, or mass-loaded vinyl, sacks of sand, thermal foil, mineral or fiber wool, and metal covers.

Reduction of *pressure pulsation* can be achieved by installing flexible connectors, by use of mufflers and dampers or expansion chambers, by acoustic filters or pulsation dampers (filled with liquid or air),

and by side-branch accumulators or tuned resonators (a closed-end tube attached to the main pipe), by the use of flexible couplings or compensators in the piping systems (rubber or metal compensators, flexible PVC, molded rubber, two layers of ribbed neoprene, fiberglass, nylon cord reinforcement, or a combination of these) and so on (see Fig. 6).

*Structural vibrations* or natural frequencies and their higher harmonics can be reduced or modified by dynamically balancing all rotating and oscillating components of the pump. To avoid shaft torsion vibration and resonances, the fundamental exciting frequencies must be at 50% below or above the natural frequency, and passing through the natural frequency range has to be as quick as possible. Structural vibrations can also be reduced by detuning, which implies changing either the driving frequency of the pump or the natural frequency of the piping system. These can be achieved by an increase of the stiffness or rigidity and weight of a radiating surface, that is, by changing the stiffness-to-weight ratio, or by raising or lowering natural frequencies by using dynamic absorbers or vibration isolators, that is, by attachment of a passive mass to a vibrating element or system with a resilient component, for example, a rubber, steel spring, pads, or slabs of resilient materials under the base plate (Fig. 7), by decoupling between a heavy, airtight outer coating and the vibrating pipe wall, or by mechanical isolation of the pumping system from the structure with vibration isolators (resilient pipe hangers and supports), by increasing the piping resonance frequencies above the highest machine frequency (by more than 50%), by avoiding rotational speeds that match or excite the natural or resonance frequencies of the translational vibration of the drive shaft, and by shifting the natural frequency to a higher frequency where human hearing is weaker and sound is more easily attenuated. Resilient elements may be inserted anywhere along the transmission path, but they are usually most effective near the source or near radiating surfaces.

The *noise of control valves* and radiation from the pipework can be reduced by lagging or burying of piping and valves, fitting multihole orifice plates in the line downstream from the valve to split the required pressure drop into several stages (each stage preferably having less than critical pressure drop), fitting in-line silencers downstream and possibly upstream of the valve in conjunction with lagging of the piping between valve and silencer, and fitting a low-noise control valve.



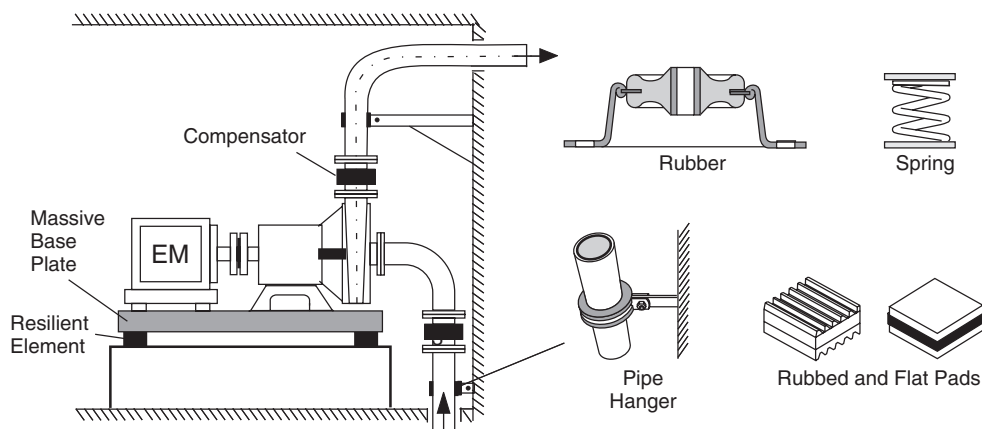


Figure 7 Methods for reduction of structural vibrations.

*Cavitation in pumps* can be controlled by raising the NPSH available value or the net inlet static pressure in the pump, which must be above the vapor pressure. The NPSH required can also be provided by replacing the existing pump or impeller with one that can operate with the existing NPSH, by a small axial-flow booster pump placed ahead of the first-stage impeller (driving on the lower rotation speed), by an inducer used as a first cascade of the whole inducer-centrifugal-impeller wheel, by lowering the liquid temperature, reducing the impeller speed, increasing the suction pipe diameter, decreasing the suction losses, simplifying the suction piping layout, injecting a small quantity of air into pump suction, which reduce also the cavitation curve, and so on.

*Cavitation in the pumping system* can be controlled by keeping pressure above the vapor pressure of the fluid being pumped, by reducing pressure pulsation, by burying the pipeline, by employment of adequate valve size, by reducing flow velocities without obstructions, by degasifying the fluid, by including cage-type valve trim for globe valves that moves the primary fluid restriction away from the valve plug seat line, and by two or more valves in series, each taking a portion of the total desired pressure reduction and so by preventing dropping pressure within the valve below the vapor pressure of the fluid, and so forth. Effect of cavitation can be prevented by using heavy-walled piping (which is subject to damage) and by furnishing hardened materials to increase resistance to cavitation. Cavitation noise can be reduced by applying acoustical insulation on the valve and associated piping, by installing the valve in an enclosure, and the like.

*Water hammer* in pump discharge lines can be reduced by starting a pump against a closed gate valve and then opening the valve slowly afterward, by stopping the pump after the valve has been fully closed (this method fails when a unit is stopped suddenly by control or power failure), by shutting the gate valve slowly, by increasing the size of the discharge line and lowering the flow velocity, by employing a

special protective valve (which opens wide quickly with the drop of pressure that is part of a water hammer cycle, and then closes slowly to throttle the resulting back flow), by further employment of air-charged surge tanks or shock-absorbing air chambers near the control valve, by lengthening the stopping time using a flywheel on the unit in a high-head installations, and so on.

## REFERENCES

1. I. J. Karassik, and T. McGuire, *Centrifugal Pumps*, 2nd ed., Pergamon Press, New York, 1997.
2. I. J. Karassik, J. P. Messina, P. Cooper, and C. C. Heald, *Pump Handbook*, 3rd ed., McGraw-Hill, New York, 2001.
3. ISO 3555, Centrifugal, Mixed Flow and Axial Pumps—Code for Acceptance Tests—Class B, 1977.
4. *Hydraulic Institute Standards for Centrifugal, Rotary & Reciprocating Pumps*, 14th ed., Hydraulic Institute, Cleveland, Ohio, 1983.
5. M. Čudina, Detection of Cavitation Phenomenon in a Centrifugal Pump Using Audible Sound, *Mech. Syst. Signal Proc.*, Vol. 17, No. 6, 2003, pp. 1335–1347.
6. M. Čudina, Noise as an Indicator of Cavitation in a Centrifugal Pump, *Acoust. Phys.*, Vol. 49, No. 4, 2003, pp. 463–474.
7. M. Čudina and J. Prezelj, Use of Audible Sound for Determination of the NPSH in Centrifugal Pumps, Proceedings of the 14th International Seminar on Hydropower Plants, Vienna, Nov. 22–24, 2006.
8. M. Čudina, *Technical Acoustics*, Faculty of Mechanical Engineering, University of Ljubljana, Ljubljana, Slovenia, 2001.
9. M. Čudina, Use of Audible Sound for Cavitation Measurement in Centrifugal Pumps, Patent No. SI 21010 A2, Office of Republic of Slovenia for Intellectual Property, Ljubljana, Slovenia, 2003.
10. W. Lips, *Stromungsakustik in Theorie und Praxis*, 2. Auflage, Expert Verlag, Akademie Esslingen, 1997.
11. H. M. Nafz, Einfluss von Bauart, Betriebsbedingungen und Messanordnung auf die Ermittlung des Geräuschemissionswertes von Hydraulikpumpen, Ph.D. Dissertation, Fakultät Fertigungstechnik der Universität

- Stuttgart, Institut für Werkzeugmaschinen der Universität Stuttgart, 1989.
12. VDI-Richtlinien 3743, Blatt 1, Emissionskennwerte technischer Schallquellen: Pumpen, Kreiselpumpen, 1982.
  13. VDI-Richtlinien 3743, Blatt 2, Emissionskennwerte technischer Schallquellen: Pumpen, Verdrängerpumpen, 1989.
  14. W. Schirmer, Technischer Lärmschutz. Grundlagen und praktische Massnahmen an Maschinen und Lärm in Arbeitsstätten zum Schutz des Menschen vor Lärm und Schwingungen, VDI Verlag, Düsseldorf, 1996.
  15. R. L. Sanks, G. Tchobanoglous, D. Newton, B. E. Bossermann II, and G. M. Jones, *Pumping Station Design*, Butterworth, Boston 1989.
- BIBLIOGRAPHY**
- L. Bachus and A. Custodio, *Know and Understand Centrifugal Pumps*, Elsevier Advanced Technology, Oxford, New York, 2003.
- R. S. Beebe, *Predictive Maintenance of Pumps Using Condition Monitoring*, Elsevier Advanced Technology, Oxford, New York, Tokyo, 2004.
- D. A. Bies and C. H. Hansen, *Engineering Noise Control, Theory and Practice*, 2nd ed., Department of Mechanical Engineering, University of Adelaide, Australia, E&FN Spon, London, 1997.
- H. P. Bloch and A. R. Budris, *Pump User's Handbook: Life Extension*, Fairmont Press, Lilburn, GA, 2004.
- P. N. Cheremisinoff, and P. P. Cheremisinoff, *Industrial Noise Control Handbook*, Ann Arbor Science, Collingwood, MI, 1977.
- W. J.: Coad, Centrifugal Pumps: Construction and Application, *Heating/Piping/Air Conditioning*, Sept. 1981, pp. 124–129.
- M. Čudina, Noise as an Indicator of Cavitation and Instability in Centrifugal Pumps, *J. Mech. Eng.*, Vol. 45, No. 4, 1999, pp. 134–146.
- J. W. Dufour and W. E. Nelson, *Centrifugal Pump Source book*, McGraw-Hill, New York 1993, p. 258.
- L. M. Evans, Control of Vibration and Noise from Centrifugal Pumps, *Noise Control*, Jan. 1958, p. 28.
- G. Gaignaert, Ed., *Pump Noise and Vibrations*, 1st International Symposium, Clamart (France), CETIM, 1993.
- E. Grist, *Cavitation and the Centrifugal Pump: A Guide for Pump Users*, Taylor & Francis, Philadelphia, 1999.
- Guide Acoustique des Installations de Pompage*, CETIM, 1997.
- J. F. Gülich, *Kreiselpumpen. Ein Handbuch für Entwicklung und Betrieb*, Springer, Berlin, 1999.
- C. M. Harris, *Handbook of Noise Control*, 2nd ed., McGraw-Hill, New York, 1979.
- P. A. Kamis, Techniques for Reducing Noise in Industrial Hydraulic Systems, *Pollution Eng.*, Vol. 7, No. 5, 1975, pp. 46–49.
- H. Kinno and J. F. Kennedy, Waterhammer Charts for Centrifugal Pump Systems, *Proc. ASCE, J. Hydraulics Div.*, May 1965.
- S. C. Li, *Cavitation of Hydraulic Machinery*, Imperial College Press, London, 2000.
- R. H. Lyon, *Machinery Noise and Diagnostics*, Butterworth, Boston, 1987.
- J. Matley, Fluid Movers: Pumps, Compressors, Fans and Blowers, *Chem. Eng.* McGraw-Hill, New York, 1979.
- N. Mayerson, Sources of Noise in Power Plant Centrifugal Pumps with Considerations for Noise Reduction, *Noise Control Eng.*, Vol. 2, No. 2, 1974, p. 74.
- L. Nelik, *Centrifugal and Rotary Pumps, Fundamentals with Applications*, CRC Press Boca Raton, FL, 1999.
- B. Nesbitt, Ed., *Guide to European Pumps & Pumping: The Practical Reference Book on Pumps and Pumping with Comprehensive Buyers Guide to European Manufacturers and Suppliers*, Professional Engineering Publishing, Bury St. Edmunds and London, 2000.
- B. Neumann, *The Interaction between Geometry and Performance of a Centrifugal Pump*, Mechanical Engineering Publications, London, 1991.
- G. Paresch and O. Moniz, *Practical Centrifugal Pumps: Design, Operation and Maintenance*, Elsevier, Amsterdam, 2005.
- C. R. Spareks and J. C. Wachel, Pulsation in Centrifugal Pump and Piping Systems, *Hydrocarbon Proc.*, July 1977, p. 183.
- G. Vetter, *Leckfreie Pumpen, Verdichter und Vakuumpumpen*, Vulkan, Essen, 1998.
- K. W. Wang, *Handbook of Air Conditioning and Refrigeration*, McGraw-Hill, New York 1993.
- R. G. White and J. G. Walker, *Noise and Vibration*, Wiley, Ellis Horwood, New York, 1982.
- C. Wilkins, NPSH and Pump Selection: Two Practical Examples, *Heating/Piping/Air Conditioning*, Oct. 1988, pp. 55–58.
- H. W. Wojda, First Aid for Hydraulic System Noises, *Pollution Eng.* April 1975, p. 38.

# CHAPTER 74

## NOISE OF COMPRESSORS

Malcolm J. Crocker

Department of Mechanical Engineering  
Auburn University  
Auburn, Alabama

### 1 INTRODUCTION

Compressors are used widely throughout the world in household appliances, air-conditioning systems, vehicles, and industry. Compressors are also used in health-care applications to provide air for dentists' drills and for breathing apparatus in hospitals. It is clear that control of noise and vibration is crucial in these applications. Various compressors are used for these applications, and there are a large number of quite different designs. The compressor design adopted for each application depends upon several factors, including the gas or working fluid that must be compressed and the discharge pressure and flow rates that need to be achieved. There are two basic types of compressors: (1) positive-displacement compressors including reciprocating piston and rotary types and (2) dynamic compressors including axial and centrifugal types. Positive-displacement compressors can be further subdivided by the location of the motor: (1) external-drive (open-type) compressors have a shaft or other moving part extending through the casing and are driven by an external power source, thus requiring a shaft seal or equivalent rubbing contact between fixed and moving parts, (2) hermetic compressors have the compressor and motor enclosed in the same housing shell without an external shaft or shaft seals and the motor operates in the compressed gas, and (3) semihermetic refrigerant compressors have the compressor directly coupled to an electric motor and contained within a gas-tight bolted casing and the motor operates in the compressed gas.

### 2 BACKGROUND

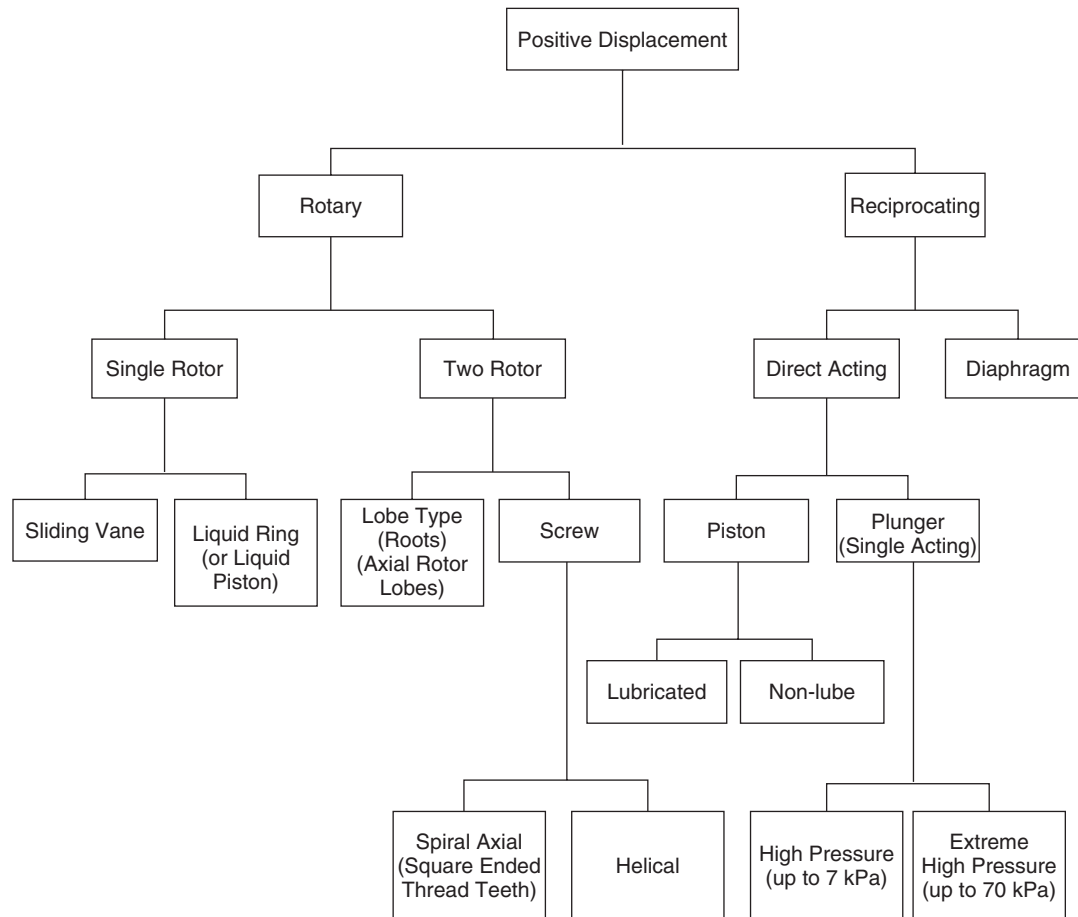
The noise generated by the piston type of compressor depends upon several factors, the most important being the reciprocating piston frequency and integer multiples, number of pistons, valve dynamics, and acoustical and structural resonances. The noise produced by the rotary types depends upon rotational frequency and multiples, numbers of rotating elements, flow capacity, and other flow factors. The noise generated by centrifugal and axial compressors also depends upon rotational frequency; the number of rotating compressor blade elements, flow speed, and volume flow rate, however, are also important factors. This chapter describes some design and operational features of several categories of commercially available gas compressors, noise and vibration sources and paths, and some examples of how noise and vibration problems have been overcome in practice.

Compressors can be considered to be pumps for gases. (See Chapter 73 on pumps.) Although there are some differences in construction details between compressors and pumps, their principles of operation are essentially the same. Since gases normally have much lower densities than liquids, it is possible to operate compressors at much higher speeds than pumps. However, gases have lower viscosities than most liquids, so leakage with compressors is more of a problem than with pumps. Thus, this requires tighter manufacturing tolerances in the moving parts of compressors. The mechanical action of the compressor causes the gas volume to decrease and a considerable amount of work done on the gas usually is turned into heat. There is a necessity to cool the gas sufficiently; otherwise overheating can occur resulting in excessive wear and compressor failure. To achieve large pressure rises, compression can be done in successive stages, with cooling applied between the stages. Compressors are usually classified as either of two basic types: (1) positive-displacement or (2) dynamic machine types.

Positive-displacement compressors increase the pressure of the gas by reducing its volume in a compression chamber through work applied to the compressor mechanism. Positive displacement compressor mechanisms can be further subdivided into: (1) reciprocating types: piston, diaphragm, or membrane and (2) rotary types: rolling piston, rotary vane, single-screw, twin-screw, scroll, and throchoidal (lobe.) Figure 1 presents a schematic of the main types of positive-displacement compressors. Dynamic compressors increase the pressure of the gas by a continuous transfer of angular momentum from the rotating machine components to the gas. This process is followed by the conversion of this momentum into a pressure rise. Dynamic compressors can be divided into (1) centrifugal, (2) axial, and (3) ejector types. Figure 2 provides a schematic of the main types of dynamic compressors.

### 3 COMPARISON OF PERFORMANCE AND CAPABILITIES OF VARIOUS COMPRESSOR TYPES

Positive-displacement compressors are normally used for small volumetric flow rate capacity requirements such as in household refrigerators or room air conditioners. For higher flow rate capacities, valve and seal leakage, mechanical friction, and flow effects quickly decrease the efficiency of positive-displacement compressors.



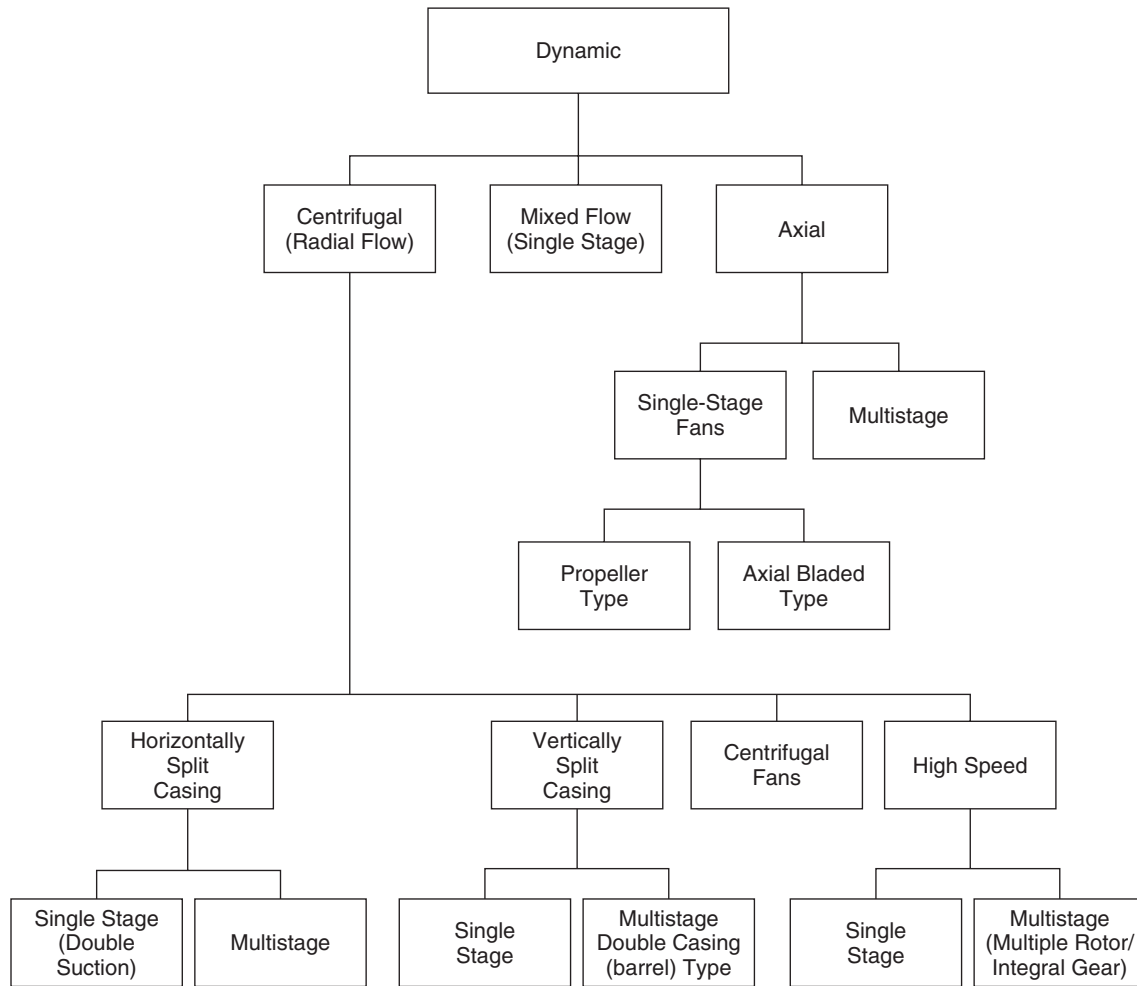
**Figure 1** Schematic showing types of positive-displacement compressors.<sup>1</sup>

Centrifugal compressors generally have higher efficiencies than positive-displacement types and can provide higher volumetric flow rates. Centrifugal compressors are unsuitable for small flow rate capacities. The sealing surface is large for a centrifugal compressor compared to the compressor element, and the rotating impeller surface area. However, as the compressor size is increased, to achieve higher flow rate capacities the sealing surface losses increase much more slowly than the impeller area, which leads to improved overall efficiencies.

Axial compressors achieve the highest overall efficiencies when high flow rate capacities are required. The mechanical and fluid mechanics losses are small for axial compressors and efficiencies can be as high as 90% or more. Axial compressors also have the highest flow rate capacities for a given volumetric size. Axial compressors can thus be made compact and lightweight, which explains why they are favored for use in aircraft jet engines. Continual design improvements over the years have resulted in higher efficiencies.

Dynamic compressors create the increase in discharge pressure by adding kinetic energy to a continuously moving fluid flow. The fluid streamlines through the rotating blades of an axial compressor are gently curved with a fairly large radius. The streamlines in a centrifugal compressor, however, are extremely curved and undergo considerable changes in radius and cross-sectional flow area, resulting in subsequent area reduction. For that reason, the centrifugal compressor can achieve a much greater pressure ratio per stage than an axial-flow compressor; but an axial-flow compressor can achieve a much greater volume flow rate than a centrifugal compressor for the same frontal area. An axial-flow compressor behaves almost like a variable pressure ratio, constant flow rate machine, while a centrifugal compressor behaves almost like a constant pressure ratio, variable flow rate machine.

Table 1 presents a comparison of some of the advantages and disadvantages of different compressor designs.



**Figure 2** Schematic showing types of dynamic compressors.<sup>1</sup>

**Table 1 Advantages and Disadvantages of Different Compressor Designs**

Type	Advantages	Disadvantages
Positive displacement	Pressure ratio capability affected by gas properties	Limited capacity
Centrifugal	Good efficiencies at low specific speeds Wide operating range Low maintenance High reliability	High weight-to-capacity ratio Unstable at low flow Moderate efficiency
Axial	High efficiency High-speed capability Higher flow for given size	Low-pressure ratio per stage Narrow flow range Fragile and expensive blading
Ejector	Simple design Inexpensive No moving parts High-pressure ratio	Low efficiency Requires high-pressure source

Source: From Ref. 2.

#### 4 POSITIVE-DISPLACEMENT COMPRESSORS

This section provides brief descriptions and simplified diagrams of the main operating features of commonly used positive-displacement compressors. For more extensive construction and operating details, and the advantages and disadvantages of each compressor type, the reader is referred to specialized books on compressor design and operation.<sup>1-8</sup>

##### 4.1 Reciprocating Piston Compressors

The reciprocating compressor was the first type designed for mass production. It still sees service in a wide variety of industrial and household applications, and it remains the most versatile compressor design. It can operate economically to produce very small pressure changes in the deep vacuum range up to very high pressures of the order of 150,000 to 450,000 kPa, for example, in a chemical polyethylene plant service. Figure 3 shows the principle of operation of a reciprocating piston compressor.

The operation of a reciprocating piston compressor is in many ways similar to that of an internal combustion engine, although the design of such small compressors is simpler. Small reciprocating compressors are the units often chosen for operation in household refrigerators and heat pumps. The mechanical system of a typical small refrigerator reciprocating compressor is comprised of an electric motor driving a reciprocating piston axially in a cylinder to change the gas volume. Two thin metal "reed" valves are provided. As the piston moves to compress the working gas during the compression stroke, the suction valve closes and the discharge valve opens. After the piston has reached top dead center, and it begins the suction stroke, the suction valve opens and the discharge valve closes.

##### 4.2 Diaphragm Compressors

Diaphragm compressors, such as shown in Fig. 4, are a form of piston compressor. The diaphragm separates

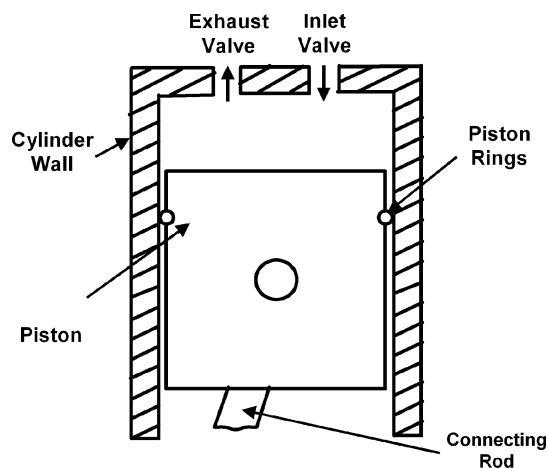


Figure 3 Reciprocating piston compressor.

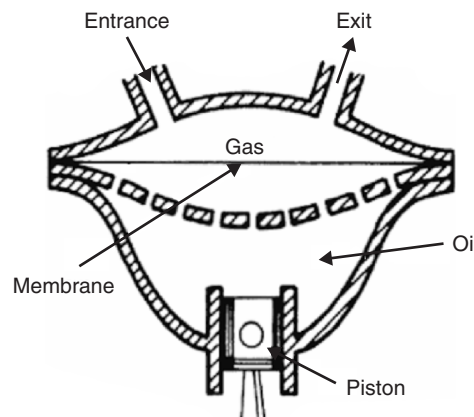


Figure 4 Vibrating diaphragm compressor.<sup>8</sup>

the gas undergoing compression on one side from the hydraulic working fluid on the other side. A piston is provided to force the hydraulic fluid upward; it is commonly driven by an electric motor via a connecting rod, which is eccentrically connected to the motor drive shaft. As the piston moves up, it displaces the incompressible hydraulic fluid upward making the diaphragm move up also. The membrane is sandwiched between two perforated metal plates that allow hydraulic fluid to flow through the perforations in the lower plate and gas to flow through the perforations in the upper plate. When the piston is at top dead center, the diaphragm is pressed hard against the underside of the top plate by the hydraulic fluid and the discharge valve has already opened but is ready to start closing. On the piston down stroke, the diaphragm is drawn downward, thus allowing the intake valve to open and a fresh charge of gas to enter above the diaphragm ready to be compressed on the next upward stroke of the piston.

Diaphragm compressors are often used where very low flow rates of the order of 0.03 to 3.0 m<sup>3</sup>/minute and pressures of the order of  $10 \times 10^6$  to  $500 \times 10^6$  Pa, are needed, or where it is necessary to keep the gas or corrosive fluid to be compressed out of contact with the piston and its lubricating oil. One example is where oxygen is being compressed. In such cases, contact between oxygen and the piston's lubricating oil could be dangerous. In some cases, such as with oxygen compression, soapy water is used instead of oil as the hydraulic working fluid to lessen the chance of hazardous contact between the oxygen gas and flammable oil. For higher flow rates of 3.0 m<sup>3</sup>/min and above, the diaphragm compressor has limited application since use of a larger stroke of the diaphragm is needed, which can lead to diaphragm fatigue and eventual failure. For larger flow rates, either reciprocating piston compressors or rotary compressors are normally used.

##### 4.3 Screw Compressors

Screw compressors are formed by the intermeshing action of two helical rotors. See Fig. 5. The rotors

are comprised of two types: male and female. The male rotors have convex lobes and the female rotors have convex flutes. The gas to be compressed enters through the inlet port and is trapped by the rotors, which continually reduce the volume available to the gas until it is expelled through the discharge port. A typical screw compressor has four lobes on the male rotor and six flutes on the female rotor. In such an arrangement the compressor has six compression cycles during each revolution of the female rotor, which is operated at two thirds of the male rotor speed. Screw compressors are normally chosen for flow capacity rates greater than those delivered efficiently by reciprocating compressors, but less than those delivered efficiently by centrifugal compressors. In this mid-flow rate range, centrifugal compressors tend to be large and thus very heavy and are normally less efficient than screw compressors in this range.

Screw compressors have the advantages that they are (1) lighter and more compact than reciprocating compressors, (2) do not have reciprocating masses requiring expensive vibration isolation, and (3) the rotors can be operated in a dry condition without the need for oil lubrication. Their main disadvantages include the fact that they have rapid rotor wear when operated in a dry state and that they are inherently very noisy. Oil is sometimes used as a lubricant to reduce wear and the use of water as a lubricant is under development.

#### 4.4 Lobe or "Roots" Compressors

Figure 6 shows one of the oldest and simplest designs of compressor, known as a straight lobe or "roots" compressor. This type of compressor normally employs two identical cast-iron rotors. Each rotor has a figure eight shape with two rounded lobes. As the rotors turn they sweep the gas into a constant volume between the rotors and the compressor case wall. Compression takes place as the discharge port becomes uncovered. Initially backflow occurs from

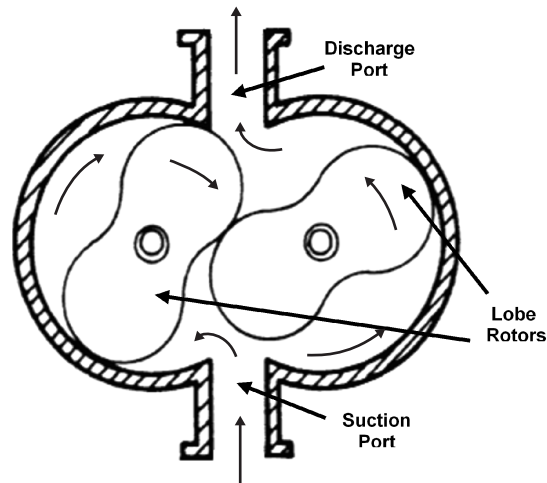


Figure 6 Lobe or roots compressor.<sup>8</sup>

the discharge line into the casing cavity, until the cavity pressure reaches the compressed gas pressure. The gas flow then reverses direction, and further rotation of the rotors causes increasing gas pressure with a reducing gas volume as the gas is then swept into the discharge line. Lobe or roots compressors have the advantage of being low cost and needing low maintenance. They have the disadvantage that they (1) are less efficient than screw or centrifugal compressors, (2) only achieve low pressure increases, and (3) are inherently noisy because of the high-frequency flow reversal that occurs at the discharge port.

#### 4.5 Sliding Vane Compressors

The sliding vane compressor consists of a rotor mounted in an eccentric casing. Nonmetallic sliding vanes are fitted to the rotor in slots as shown in Fig. 7. The vanes are held in contact with the casing by centrifugal force. In Fig. 7 the gas is taken in from the suction inlet on the left side and discharged through the port to the right. The gas is trapped and sucked into volumes that increase with vane rotation up to top dead center.

The trapped gas is then compressed as the trapped gas volume continually decreases after top dead center. There are no inlet and discharge valves. The times at which the inlet and discharge ports are open are determined by the time when the vanes are located over the ports. The inlet port is designed to admit gas until the gas "pocket" between the two vanes is largest. The port closes when the second vane of that pocket passes the inlet port. The gas pocket volume is decreased when the vanes have passed the top dead center and compression of the gas continues until the discharge port is opened when the leading vane of the pocket passes over the discharge port opening. The discharge port closes when the second valve passes the end of the port.

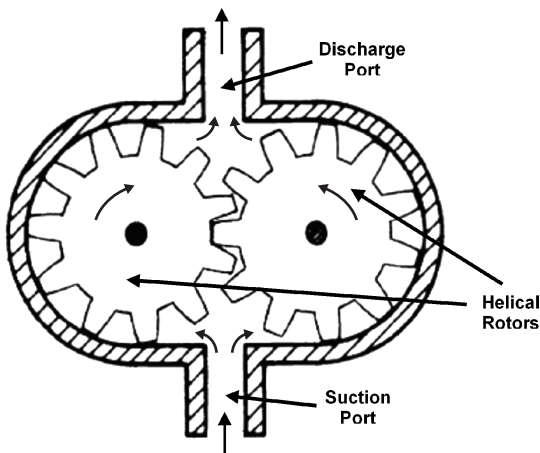


Figure 5 Screw compressor.<sup>8</sup>



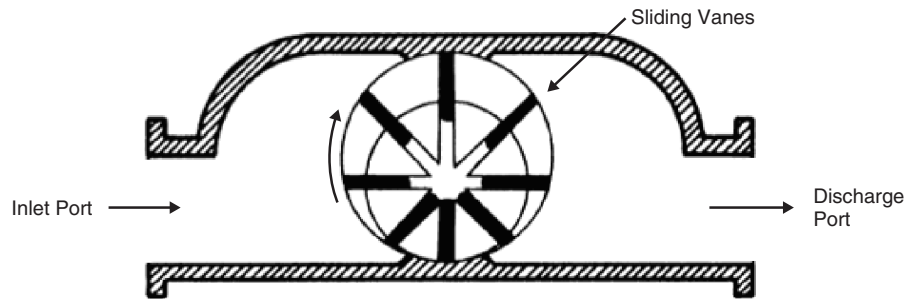


Figure 7 Sliding vane compressor.<sup>8</sup>

#### 4.6 Rolling Piston Compressors

Rolling piston rotary compressors are widely used because they are small in size, lightweight, and efficient. Small rolling piston rotary compressors are often driven by electric motors. The rolling piston is contained in a cylinder, and the piston is connected to a crankshaft eccentrically mounted to the drive shaft of the motor. See Fig. 8. The stator of the electric motor is normally fixed to the interior of a hermetic shell. A spring-mounted sliding vane is provided. As the piston rotates inside the cylinder, the volume of gas trapped ahead of the piston—between the piston, cylinder, and vane—is reduced and the gas is expelled through the discharge. Simultaneously, gas is sucked into the increasing volume following the piston. After the piston has passed top dead center and the inlet (at the left side of Fig. 8), the volume of trapped gas ahead of the piston is decreased again as the piston moves further toward the discharge valve and the compression cycle is repeated.

#### 4.7 Orbital Compressors

High-efficiency and high-performance refrigeration and air-conditioning systems are in great demand. So-called orbital compressors have many good characteristics such as high efficiency, good reliability, and low noise and vibration. A common type of orbital

compressor, is the scroll compressor which uses two interlocking, spiral-shaped scroll members to compress refrigerant vapor.<sup>9,10</sup> Such compressors are now in common use in residential and industrial buildings for air-conditioning and heat-pump applications and also for automotive air conditioners. They have high efficiency and low noise but have poor performance if operated at low suction pressures and they need good lubrication. Scroll compressors normally have a pair of matched interlocking parts, one of which is held fixed and the other made to perform an orbital path. Contact between the two scrolls happens along the flanks of the scrolls, and in the process a pocket of gas is trapped and progressively reduced in volume during the rotary motion until it is expelled through the discharge port. Most scroll compressors are hermetically sealed inside a shell casing. Another type of orbital compressor is the so-called trochoidal type. The well-known Wankel design has a three-sided epitrochoidal piston with a two-envelope cylinder casing.<sup>9,10</sup>

### 5 DYNAMIC COMPRESSORS

Centrifugal and axial compressors are used when high gas flow rates are required. They can be made to be of low weight and generally have higher efficiencies than positive-displacement types. Their operational principles are very similar to fans. See Chapter 71 for discussion of fan types, principles of operation, and noise generation mechanisms.

#### 5.1 Centrifugal Compressors

Centrifugal compressors are widely used in large buildings, offices, factories, and industrial plants that require large central air-conditioning and cooling systems.<sup>1-6</sup> Such centrifugal compressors eliminate the need for valves. The number of parts with sliding contact and close clearances are reduced, compared with positive-displacement types. Thus maintenance costs are reduced, although operating costs may be increased due to their somewhat lower efficiency than comparable positive-displacement compressors. They are smaller and lighter in weight, and generally have lower original equipment and installation costs than equivalent reciprocating types. The noise and vibration characteristics are quite different, however,

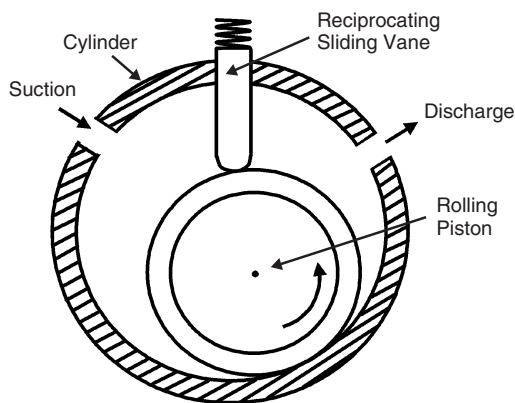


Figure 8 Rolling cylinder compressor.



due to the higher speed and the lack of out-of-balance machine parts. The main components of a centrifugal compressor include (1) an inlet guide vane, (2) an impeller, (3) a diffuser, and (4) a volute.

## 5.2 Axial Compressors

Axial and centrifugal compressors are competitive for volume flow rates from about 25 to 90 m<sup>3</sup>/s, but when volume flow rates higher than about 60 m<sup>3</sup>/s are needed, axial-flow compressors are normally used instead of centrifugal-flow machines.<sup>3</sup> This is because they are more efficient, smaller in size and weight, and require lower installation costs. They have several disadvantages, however, including generally more complex control systems, a narrower range of available flow rates, and surge and ingestion protection requirements. They also produce higher noise levels than centrifugal types, thus requiring more extensive acoustical treatment. Currently, axial compressors have their greatest use in aircraft and air transportation systems.

## 5.3 Ejector Compressors

The ejector compressor is the simplest form of dynamic compressor.<sup>1,4</sup> It has no moving parts and is thus low cost. It is inexpensive, but has a low efficiency, however, and thus sees use mostly for vacuum applications. It requires a high-pressure source and transfers the momentum of the high-pressure jet stream to the low-pressure process gas.

## 6 NOISE CONTROL OF POSITIVE-DISPLACEMENT COMPRESSORS

It is normal to classify noise problems in terms of the source-path-receiver framework. In the case of compressors, it is not always so easy to make a distinct division between sources and paths. With positive-displacement compressors, the main noise source is the time-varying pressure pulsations created between the suction (inlet) and discharge manifolds of the compressor. This fluctuating pressure forces the compressor casing and any connecting structures into vibration, which consequently results in sound radiation. Many compressors have housing shell structures, and it is normal to vibration isolate the compressor casing from the compressor shell housing, which itself may or may not be completely hermetically sealed. Suction and discharge piping must be provided, and care must be taken to reduce vibration transmission paths from the casing to the shell housing through this piping. It is not possible to completely eliminate the vibration transmission through the compressor vibration isolation system, and the piping and the gas between the casing and housing also provides another path for sound energy transmission to the shell.

### 6.1 Compressor Valves

Positive-displacement compressors must be provided with valves to allow the transfer of the low- and high-pressure gas to and from the compressor. There are two

main types of valves: (1) demand valves and (2) gate valves.

**6.1.1 Demand Valves** Demand valves are designed to open only when the compressor pressure conditions require them to do so. In the case of the discharge valve, this is when the cylinder pressure exceeds the discharge manifold pressure, and in the case of the suction valve, when the cylinder pressure is less than the suction manifold pressure. Demand valves are normally provided with spring mechanisms to ensure that the valves stay closed during the required parts of the compression cycle process. The spring force can be produced by the bending force in the case of reed valves or by the provision of a coil or another type of spring in the case of some plate or poppet valves. Unfortunately, such valves tend to flutter, which introduces additional pressure modulations onto the already time-varying compressor pressure fluctuations. Such flutter-induced fluid pressure modulations result in additional compressor noise. Valve flutter is thus normally suppressed where possible to reduce this noise but also to try to prevent valve vibration and the possibility of valve fatigue and failure during service.

Valve flutter is a feedback mechanism and there are two main types. First, when the valve opens, it happens in an impulsive manner so that its natural frequencies of vibration are excited and the fluttering process is initiated. The flutter frequency is usually close to the natural frequency of the valve. The second mechanism is related to the Bernoulli effect. A negative pressure may be created in the discharge valve seat, which causes a delay in its opening.<sup>11-13</sup> When opening does occur, the valve can overshoot its equilibrium position and shut again before discharge is complete, and the cycle can be repeated. Structural damping of the valve motion has been found to have only limited effectiveness in reducing flutter. Flutter can, however, be reduced and sometimes almost eliminated by use of a motion limiter. However, the valve will hit the limiter and thus cause impact noise. When the valve closes again, it also causes impact noise as it hits the valve seat. Some attempts have been made to reduce motion limiter and valve seat impact noise by using soft materials. But success in using soft materials is limited because of the need to ensure sufficient material durability and proper sealing after valve closure.

**6.1.2 Gate Valves** Gate valves open and close during certain parts of the compressor cycle. They are used on rotary vane, screw, and scroll compressors. Gate valves have the advantage that reeds or plate valves are not needed, and so the flutter problems of demand valves are avoided. But gate valves are less efficient than demand valves since their opening and closing cannot easily be adjusted for different suction and discharge pressure requirements. Also gate valves suffer from their own noise problems. The fluctuating pressure caused by the opening and closing of the valves is periodic but not purely simple harmonic, so that in addition to a fundamental frequency, harmonics

are created. In addition, the sudden pressure increase at the opening of the discharge valve excites the natural frequencies of the discharge manifold gas. A similar situation exists at the suction valve with the suction manifold.

## 6.2 Manifold Mufflers

To try to reduce periodic pressure fluctuations from the discharge and suction valves propagating along the piping, discharge and suction mufflers are normally used. The simplest compressor muffler works as a Helmholtz resonator. For example, in the case of the discharge valve, a flow-through Helmholtz resonator design is sometimes used for the discharge muffler. In this case, the volume of the discharge manifold gas, which is located directly after the discharge valve, acts as the resonator spring. The neck of the Helmholtz resonator is usually formed by the short pipe or passage that opens into a second volume, known as the decoupling volume, which in turn empties into the discharge pipe.<sup>11–13</sup> Simple suction mufflers can also be designed using Helmholtz resonator principles. In the case of a hermetically sealed compressor, the manifold volume in front of the suction valve can be made to act as the volume spring. The resonator neck can be formed by the narrow passage or short pipe that connects to the suction gas in the volume between the hermetic shell and the compressor casing.

The behavior of a flow-through Helmholtz muffler is similar to a forced mass–spring–damper system (see Fig. 10 in Chapter 1 or Fig. 4 in Chapter 54). The Helmholtz muffler behaves like a low-pass filter. Well below its natural frequency, the muffler is transparent to sound waves passing through. At and near its natural frequency, it actually amplifies the sound. At frequencies above the square root of two times its natural frequency, it attenuates the sound transmitted. More complicated mufflers can be built with a cascade of pass-through Helmholtz muffler systems. In such a cascaded system, the gas volumes will act as the springs and the connecting pipes as the Helmholtz resonator necks. The volumes and necks can be adjusted to have different natural frequencies. Side-branch Helmholtz mufflers can also be used, which attenuate sound at their natural frequencies. If the connecting pipes and the gas volumes used become long in terms of wavelengths (i.e., at high frequency), then the pipes should no longer be assumed to act as noncompressible masslike elements, and the volumes as simple springs.<sup>11–13</sup> The attenuation characteristics of such muffler systems need to be analyzed with numerical approaches such as finite element or boundary element methods.

## 6.3 Gas Chamber Pressure Pulsations

As discussed, gas chamber pressure pulsations will occur at the *forcing frequencies* created by the compressor pumping frequencies and harmonic multiples. Gas volumes will have their own *natural frequencies*. If the forcing frequencies coincide with the natural frequencies, then resonance occurs. It is desirable to try to

avoid resonance conditions since gas resonances will excite the casing and shell (if present) into vibration. It must be remembered that the gas volume natural frequencies are temperature dependent. So that after the compressor has “warmed up,” the frequencies will change and they may also change as the valves open and close and other volumes become interconnected. The volume and temperature of the gas above the piston in the case of reciprocating compressors also change with time, thus causing the natural frequencies to vary with time. So it is not always possible to avoid gas resonance and coincidence with structural resonance for all compressor operating speeds and pressure conditions.<sup>13</sup> Unless the volumes are simple axisymmetrical shapes, their natural frequencies and mode shape characteristics need to be analyzed with numerical approaches such as finite element or boundary element methods. See Chapters 7 and 8.

## 6.4 Casing, Piping, and Shell Vibration and Sound Radiation

For the purposes of the discussion here, the compressor casing is defined as the structure containing the piston or rotating compressor elements but excluding the piping and external shell housing. Because of geometrical complexities, the casing and shell natural frequencies and mode shapes have to be calculated with three-dimensional finite element models (FEM). The natural frequencies of small reciprocating compressor casings are usually quite high, on the order of 2000 Hz and higher.<sup>11–13</sup> Shell natural frequencies are usually somewhat lower, on the order of 1200 Hz and above, since the shells are usually made of thinner metal and are larger in size than the casings. The sound radiation from the shell can be calculated using the boundary element method (BEM), provided the normal surface velocity distribution has been calculated using FEM, or it has been measured experimentally. If viscous damping materials are used to reduce shell vibration at the elevated shell temperature, and consequently to reduce the sound radiation as well, the materials selected must be chosen to have the maximum damping value at the compressor shell operating temperature.

The suction and discharge piping is connected to the compressor casing, and in the case of hermetic compressors it is usually soldered to the shell. It can act as a direct short-circuit transmission path for vibration from the compressor casing to the shell housing. Some attempts have been made to vibration isolate the piping from the casing and/or shell by the use of flexible materials. Unfortunately, such materials are not compatible with the working fluid and/or oil and are not durable enough. The tubing is usually bent, and since it is slender it has a large number of natural frequencies in the range from about 100 to 5000 Hz. Some attempts have been made to reduce vibration transmission along the tubes by damping them with wire spring, which is wound around the tubes. It is thought that this system provides vibration damping by impacts between the wire and tubes.<sup>14</sup>

## 7 CASE HISTORIES OF NOISE CONTROL OF POSITIVE-DISPLACEMENT COMPRESSORS

### 7.1 Noise Control of Small Reciprocating Piston Compressors

Webb was one of the first to write about noise control of small reciprocating piston refrigeration compressors in 1957.<sup>15</sup> Since then many other authors have discussed their noise and vibration sources and methods of noise control.<sup>16–35</sup> All of the main sources of noise in a small reciprocating compressor originate from the compression process. The sources include: (1) gas flow pulsations through the inlet and discharge valves and pipes, (2) gas flow fluctuations in the shell cavity, which excite the cavity and shell modes, (3) turbulent eddy formation in the shell cavity and inlet and exhaust pipes, (4) vibrations caused by the mechanical system rotation of the drive shaft and out-of-balance reciprocating motion of the piston and connecting rod, and (5) impulsive motion of the valves and impacts they cause. Electric motors are the normal power sources. In refrigeration compressors, noise and vibration are transmitted from the sources in four main ways: (1) a low-pressure refrigerant gas path, (2) a high-pressure discharge tube path, (3) external and internal suspension system paths, and (4) lubricating oil path. All four paths contribute directly or indirectly to the compressor shell vibration response and result in shell sound radiation,

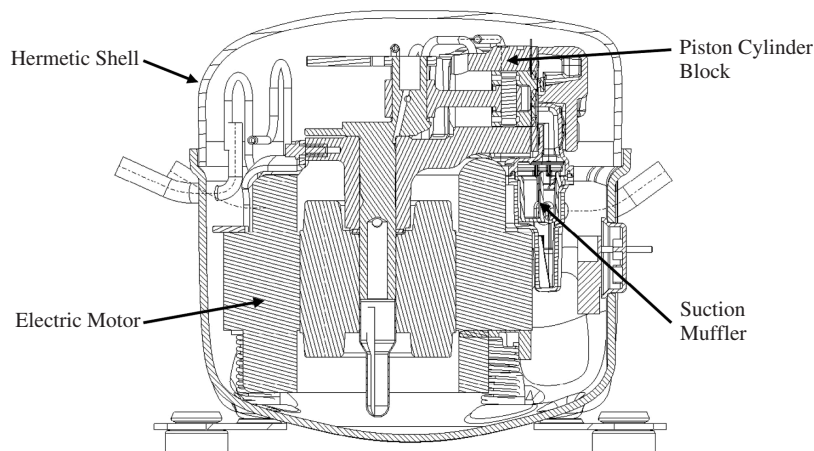
Figure 9 gives a detailed cut-away drawing of a typical reciprocating piston compressor. With such a reciprocating piston system, impulsive noise is created by mechanical impacts caused by rapid closure of the suction and discharge valves. In addition, since the fit of the piston in its cylinder is not perfect, and a small amount of clearance must be provided, the gas forces on it caused by compression make it “rock” from side to side resulting in impacts known as “piston slap.” This is another potential source of radiated noise. Blow-by noise caused by gas escaping

through the piston/cylinder clearance can sometimes also be important. Although steady nonturbulent flow, in principle, does not cause the creation of sound waves, fluctuating flow does, and impulsive flow changes caused by the rapid opening and closing of the suction and discharge valves is responsible for the creation of sound waves that propagate throughout the inlet and discharge pipe work. The mechanical system is normally hermetically sealed in a compressor shell. Such compressors are expected to have a long operating life of at least 10 years.

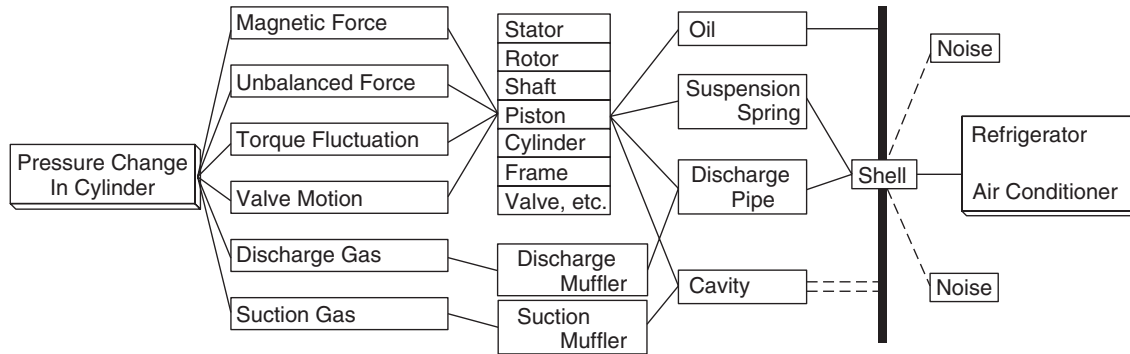
Figure 10 presents a schematic of the main noise and vibration sources in a reciprocating piston compressor used in household refrigerators, air conditioners, and heat pumps. In many such compressors, the noise and vibration sources are strongly correlated (interrelated), and it is difficult to separate them.<sup>15–17</sup> In a typical household refrigerator, besides the airborne noise radiated from the compressor shell, airborne noise is also produced by the cooling fan, flow-induced noise of the refrigerator, and structure-borne noise caused by all of these sources, which is then radiated as airborne noise by the refrigerator itself. Thus, to study the compressor noise experimentally, it is necessary to remove the compressor from the refrigerator and mount it in a load stand that provides the compressor with the correct refrigerant and pressure conditions. The load stand noise sources are separated from the compressor noise stand in well-designed experiments.<sup>15–17</sup>

**7.1.1 Vibration and Noise Measurements on Reciprocating Piston Compressors** Figure 11 shows an example of the setup for vibration and noise measurements conducted on a small reciprocating piston compressor.<sup>34</sup>

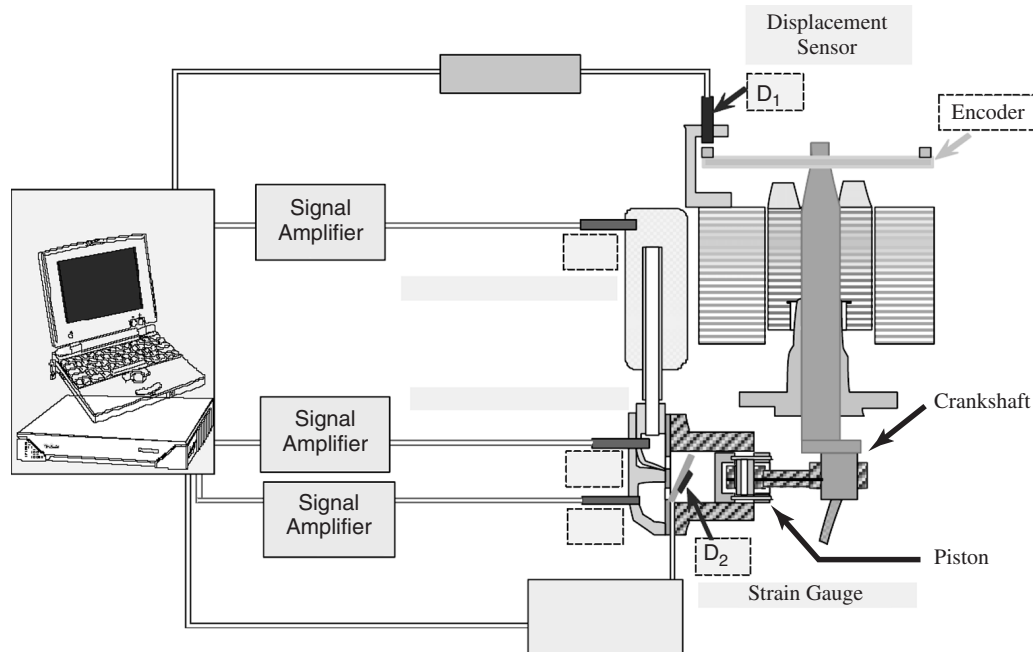
Figure 12 presents measured time-history results obtained with the setup in Fig. 11. It is observed that there is no obvious close correlation between the compressor body vibration ( $V_1$ ) and the low-frequency



**Figure 9** Vertical cut through a typical oscillating piston refrigerator compressor.<sup>33</sup>



**Figure 10** Schematic noise generation mechanisms in a reciprocating piston compressor driven by an electric motor.<sup>17</sup>



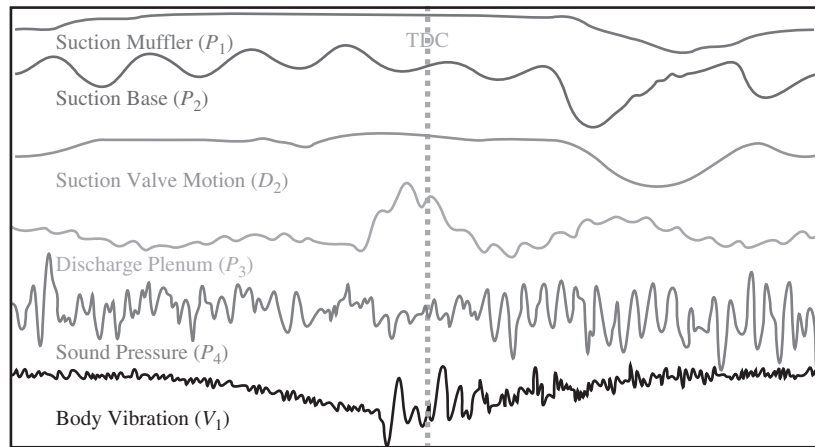
**Figure 11** Measurements of the suction and discharge pressure fluctuations and valve motion on a reciprocating compressor;  $D_1$  encoder gap measurement with displacement gauge using shaft signal;  $D_2$  strain gauge measurement of suction reed valve to give valve motion.<sup>34</sup>

sound pressure (noise) ( $P_4$ ). The compressor working fluid has a discrete-frequency component of 240 Hz in the discharge pressure and of 480 Hz in the suction pressure. In such a compressor, modification of the fluid path volumes and pipe diameters to ensure that none of these frequency components match with the shell cavity volume natural frequency normally helps to reduce the low-frequency compressor noise in the range of 25 to 1000 Hz. The fundamental acoustic natural frequency of the cavity depends on its temperature of operation and will always be excited momentarily if the excitation frequency passes through

this natural frequency during compressor startup and/or shutdown.

### 7.1.2 Improved Design of Suction Muffler

Other methods of noise control include improved suction muffler design. Figure 9 shows a section through a typical refrigerator compressor.<sup>33</sup> In this design, the compressor pump unit consists of a piston–cylinder block that is mounted on top of an electric motor. The compressor pump–motor unit is enclosed in a 3-mm-thick hermetic steel shell, which together with the suction and discharge lines connects



**Figure 12** Experimental results for compressor discharge pressures, valve suction motion and body vibrations, and sound pressure;  $P_1$  suction muffler inlet pressure,  $P_2$  suction outlet base pressure, and  $P_3$  cylinder head (discharge plenum) pressure.<sup>34</sup>

the unit with the appliance.<sup>33</sup> The suction chamber and its muffler can be seen at the top right of Fig. 9.

A cut-through view of the muffler is given in Fig. 13a and of a BEM model of it in Fig. 13b. When the compressor was operated under appliance conditions, it was observed that the sound power increased in the 800-Hz, 3.2-kHz, and 4-kHz one-third octave bands. Separate experiments on the compressor showed that the dominating source of noise in these bands is caused by the suction valve.<sup>33</sup> Pressure pulsations near to the inlet of the suction valve were thought to excite cavity modes. The lowest cavity modal resonance frequencies are at about 620 Hz and 720 Hz, and they have associated sound pressure distributions that are favorable at exciting deformed (breathing) modes of the hermetic shell. Unfortunately, these shell vibrations have rather high radiation efficiencies. These cavity resonances were assumed to be responsible for the relatively high sound power levels particularly in the 630 Hz and 800 Hz one-third octave bands.

Two other resonance frequencies were found to be very important with this compressor. These are the shell vibration natural frequencies of 2970 and 3330 Hz. These presumably are responsible for the high sound power levels in the 3.2-kHz one-third octave band seen in Fig. 15. The original suction muffler used in this compressor possesses two chambers connected in series by the inlet and the flow guide tube. See Figs. 13a and 13b. Figure 13c shows a schematic diagram of the model that was used to analyze the insertion loss of the suction muffler system.

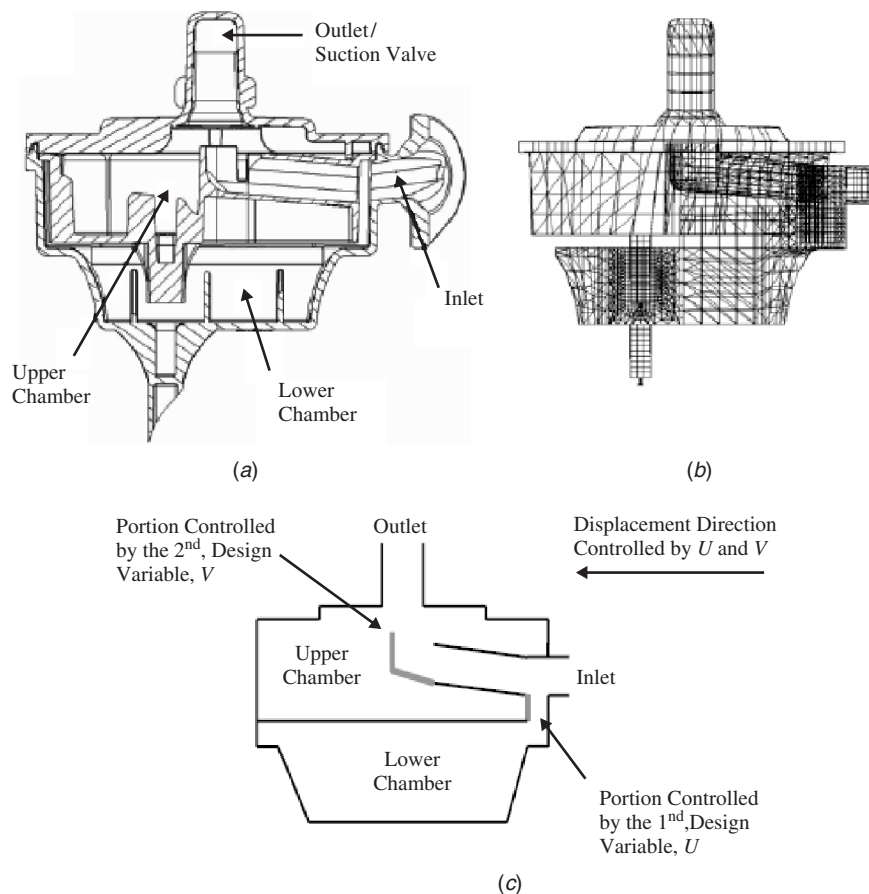
The insertion losses (IL) measured and predicted using a BEM model are shown in Fig. 14a. It is observed that there is very good agreement up to a frequency of almost 2000 Hz. Above that frequency, the prediction is not so accurate, presumably because the BEM mesh size used was not small enough. The BEM program used to predict the IL was run changing

two variables  $U$  and  $V$  (see Fig. 13c). By increasing the slit between the inlet suction tube and the flow guide tube from 2.4 to 4.8 mm and moving the bent portion of the flow guide tube 1.4 mm in the direction of the arrow (see Fig. 13c) BEM predictions showed that the muffler insertion loss was improved. This is shown in the predictions in Fig. 14b. Finally Fig. 15 presents the measured sound power levels radiated before and after these design changes were incorporated in the real muffler and compressor. The sound power radiated at the four resonances 620 Hz, 720 Hz, 2970 Hz, and 3300 Hz is reduced. The sound power level of the unit was measured in both standard operating conditions as specified by the suction and discharge pressures (suction 0.6 bar and discharge 7.7 bar) and in the appliance operating conditions (suction 1.1 bar and discharge 6.0 bar) for the cooling medium (R600a).

From Fig. 14b, the BEM calculations predicted a reduction in noise of 9 dB at 3.2 kHz. The sound power measurements in Fig. 15, however, show a reduction of 13 dB at that frequency. Subsequent measurements revealed an even greater reduction of 23 dB.

**7.1.3 Reed Valve Vibration and Noise** The compression process in reciprocating compressors is controlled by suction and discharge valves. These are very often constructed as cantilever beams that impact the valve stops and seats and thus may be excited at their own natural frequencies. An oscillating discharge valve, for example, may cause a 130-N to 180-N oscillating force on the piston and a resulting vibration of the compressor structure.

In one case, the reduction of the noise of a reciprocating compressor was achieved by modification of the piston cylinder head and valves.<sup>35</sup> Figure 16a shows a schematic of a standard compressor cylinder head, piston, and valves before modification, and Fig. 16b



**Figure 13** (a) Suction muffler cut-through drawing, (b) boundary element model (BEM)<sup>33</sup> and (c) diagram of original muffler; gray thick lines show which structural items were modified geometrically.<sup>33</sup>

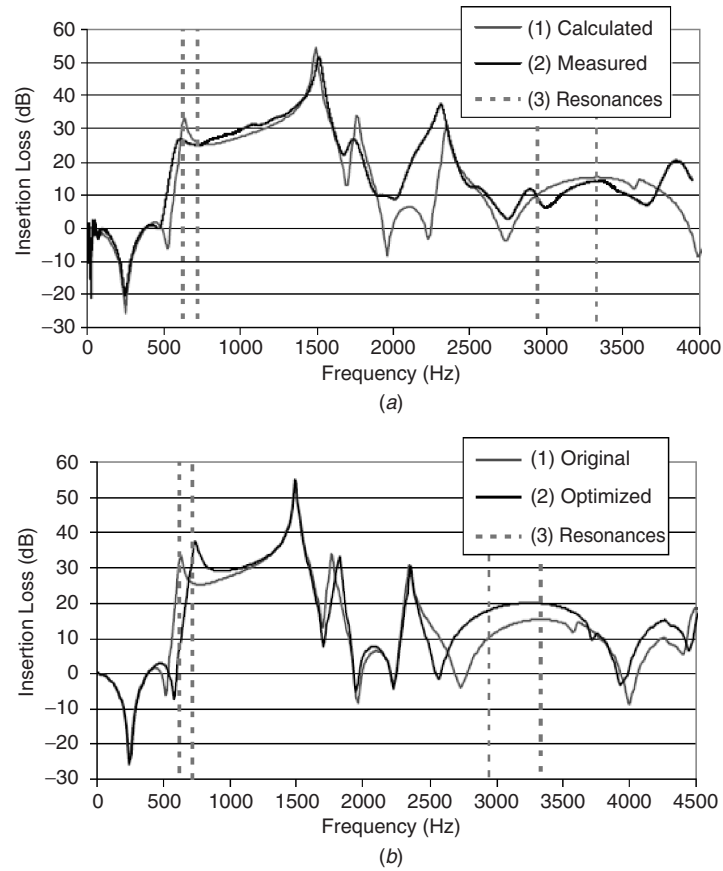
shows the same compressor parts after modification. The modified compressor had a Mota-compressor-clearance tap (MCCT) piston and suction valve as shown. The MCCT piston is seen to have a small “tap” attached to its upper surface that is made to fit into the discharge port when the piston reaches top dead center of its stroke. With the use of the tap the new piston assembly reduces the clearance volume when the piston is at top dead center, and this prevents back flow occurring during the suction stage, thus permitting the use of thinner suction and discharge “reed” valves. Use of the thinner reed valves changes the suction and discharge process and reduces the valve impact excitation and resulting compressor vibration response. It was found that these changes produced reductions of 3 dB in both the suction and discharge space-averaged externally radiated A-weighted sound pressure levels.

**7.1.4 Shell Vibration** The hermetic compressor shell is a closed shell usually consisting of a cylindrical part of circular or nearly elliptical cross section with domed heads at each end. The end heads usually have

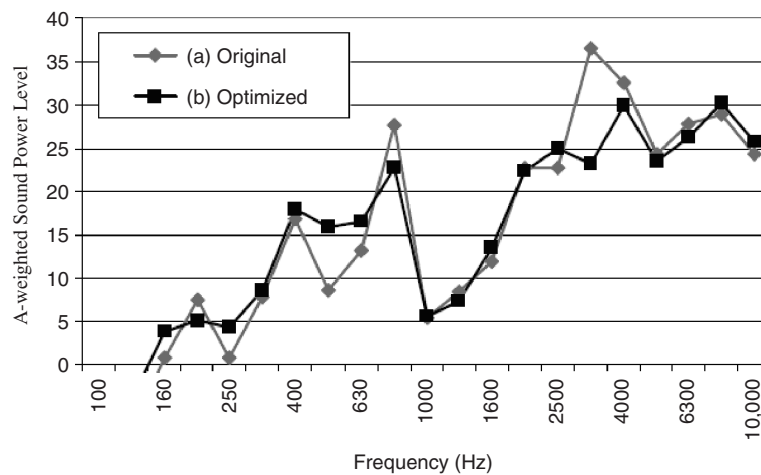
more bending resistance than the cylindrical sides since they have curvature in two directions, and as such the cylindrical sides normally make the major contribution to the sound radiation.

The noise radiated by the compressor of a household refrigerator is mostly contributed by the noise radiated by the compressor shell. Many attempts have been made to study and understand compressor shell radiation from small compressors.<sup>31</sup> There are three noise paths to the shell in an operating hermetic compressor: (1) forces are transmitted to the shell by the bracket springs used for the mounting of the compressor inside the shell (structure path), (2) suction and discharge tubing for the Freon or other working gas in the cavities in between the compressor and internal surface of the shell (gas path), and (3) the oil pool at the bottom of the shell (liquid path).

The importance of each transmission path to the shell was investigated by Holm<sup>36</sup> who found that the relative strength of each path depends on the compressor operating conditions. The gas path predominates when the compressor first starts

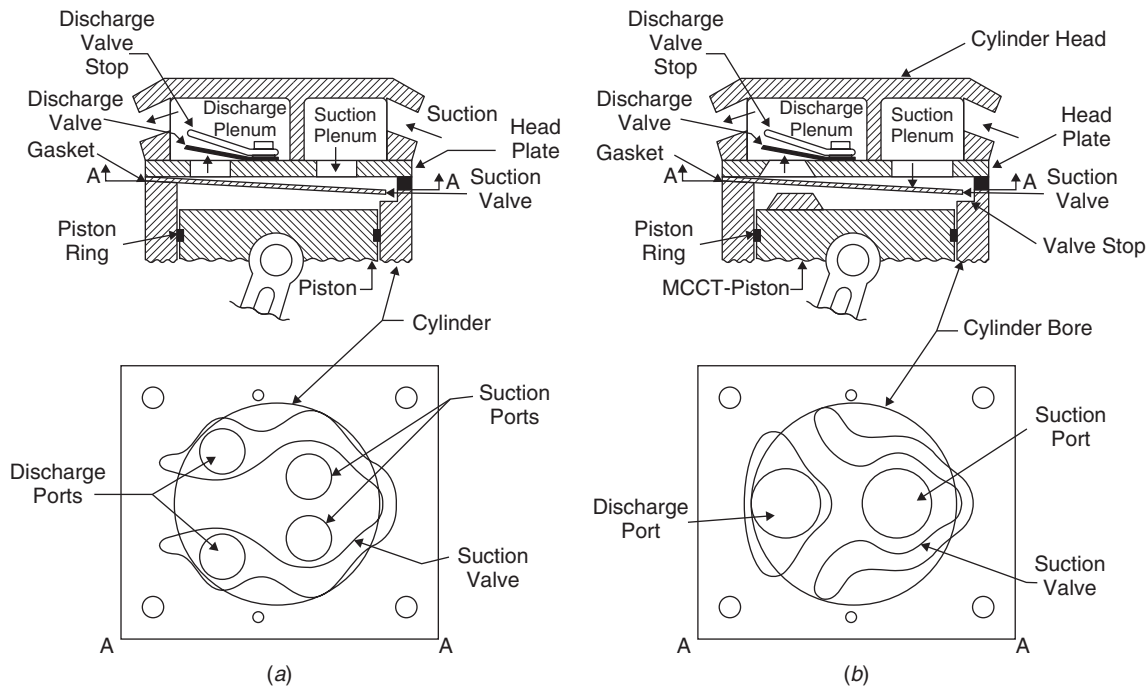


**Figure 14** (a) Calculated and measured insertion loss of original muffler (1) calculated and (2) measured, together with (3) resonance frequencies.<sup>33</sup> (b) Calculated insertion loss of (1) original, (2) optimized muffler together with (3) resonance frequencies.<sup>33</sup>



**Figure 15** Measured sound power level of compressor at appliance operating conditions with (a) standard muffler and (b) optimized muffler. Averaged A-weighted spectrum of five compressors.<sup>33</sup>





**Figure 16** Hermetic reciprocating refrigeration compressor. (a) Side view (top) and plan view (bottom) of original compressor. (b) Side view (top) and plan view (bottom) after modification of compressor.<sup>35</sup>

and the suction pressure is 200 kPa to 400 kPa higher than normal. When the initial pressure has reduced to the normal operating pressure, the gas path noise transmission reduces the compressor sound by approximately 15 dB. The noise transmission through the oil path is much less effective when it contains Freon or working fluid bubbles. When the oil contains bubbles, the noise transmission can be reduced by as much as 24 dB compared to the condition when it contains no bubbles. Special chemical additives that initiate bubble formation in the oil can be used to weaken the oil transmission path and reduce noise.

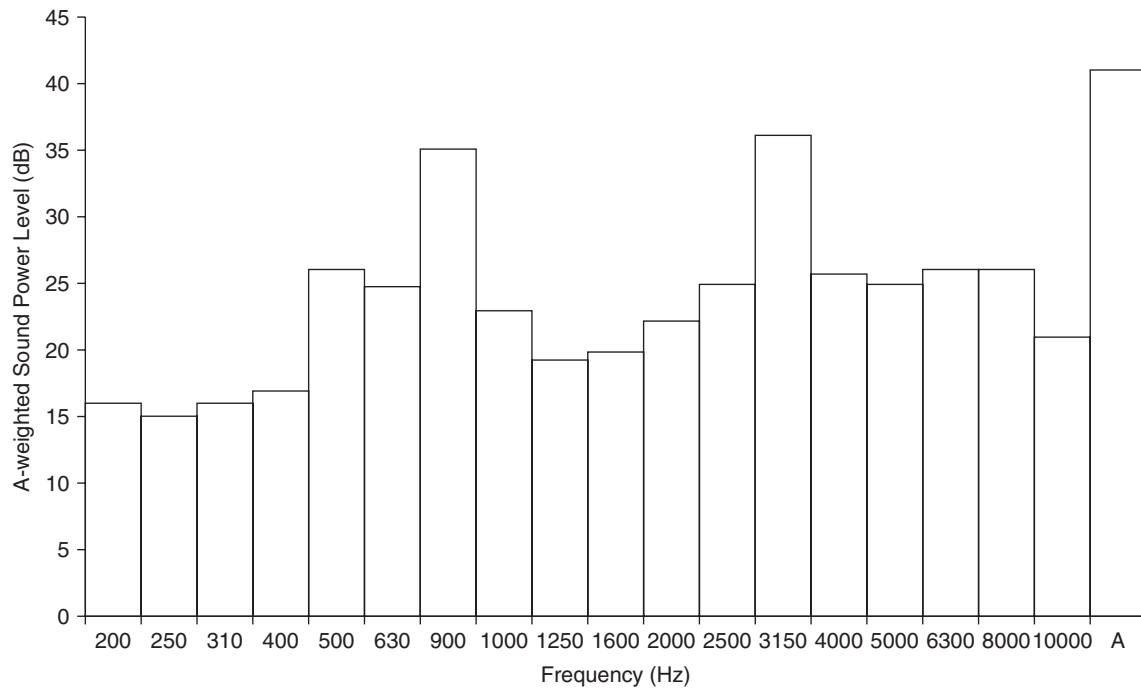
In one small refrigerator compressor, modal analysis tests, sound intensity contour plots, and sound power frequency spectra were measured in an attempt to identify sources and paths of vibration/noise energy transmission.<sup>31</sup> Figure 17 shows that the sound power radiated was dominant in two one-third octave bands at 800 and 3150 Hz. Further investigation with excitation by a calibrated impact hammer and use of modal analysis software revealed that two modes of vibration at 2810 and 3080 Hz were responsible for the intense sound generated in the 3150-Hz one-third octave frequency band. The modal analysis contour plots and the mode shapes (see Fig. 18) show that for this compressor the intense sound in the 3150-Hz one-third octave band is radiated predominantly by the 2810- and 3080-Hz modes from the bottom of the compressor shell. The intense noise radiated in the 800-Hz one-third octave was found

to be related to forces fed through the compressor spring mounts to the shell resulting in shell sound radiation.<sup>31</sup>

Research has also been conducted on compressor shell vibration using theoretical models. Most small compressor shells have a cylindrical shape, of either circular or elliptical cross section with doomed end caps or plates at each end of the cylinder. The shell modes of vibration can be grouped into three main classes: (1) *cylindrical modes* in which large deflections of the cylindrical part of the shell occur, but the end plates remain essentially undeflected, (2) *top-bottom modes* in which large deflections of the end plates occur leaving the cylindrical part largely unaffected, and (3) *mixed modes* in which both the cylindrical and end plates undergo deflections simultaneously. Cossalter et al. studied the vibration response of a shell system to the main excitation forces (a) by the discharge pipe force and (b) by the spring suspension forces.<sup>24</sup> They showed that, with the elliptical cylinder shell studied, for the same force amplitude, the discharge pipe force excites more modes and with the seventh mode having a natural frequency of 2676 Hz with the greatest vibration amplitude.

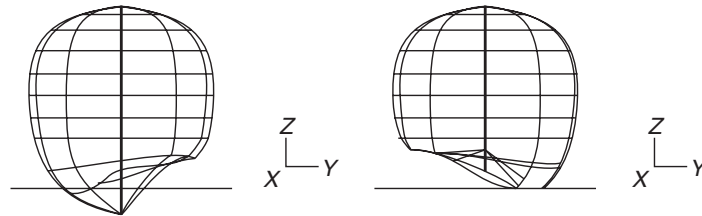
To reduce shell vibration and noise, compressor shells very often are made much thicker than is



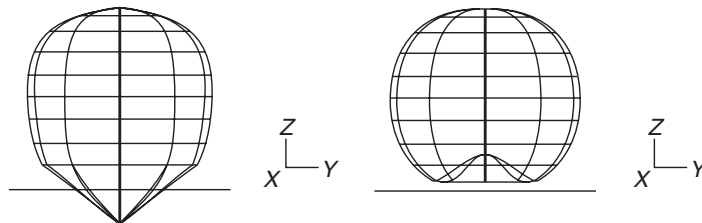


**Figure 17** A-weighted sound power level frequency spectrum.<sup>31</sup>

Mode # : 2  
 Frequency : 2810 Hz  
 Damping : 118.33 m %



Mode # : 3  
 Frequency : 3030 Hz  
 Damping : 65.87 m %



**Figure 18** Natural frequencies and the corresponding natural modes of the compressor shell.<sup>31</sup>

necessary for the mechanical strength requirements of the system. This means that high-capacity presses and more expensive progressive tooling are required, and the cost of the compressor is correspondingly increased. Using a different number of spring support systems, moving the location of the spring supports relative to the discharge pipe location, ensuring that the compressor shell natural frequencies are not close to any internal forcing frequencies, and increasing the shell damping can also all be effective in reducing the compressor shell radiated noise without the need to increase the shell thickness.

## 7.2 Noise Control of Rotary Compressors

As discussed before, there are many types of rotary compressors in use. Some noise control work has been conducted on such types.<sup>35,37–42</sup> It is not possible to discuss the noise sources and methods of control on all of these types. Some case histories of noise control on rolling piston and scroll compressors are described here. Wang et al. have conducted noise control studies on a rotary compressor enclosed in a hermetic shell.<sup>43</sup>

Figure 19 shows the compressor disassembled for modal testing. Figure 19c shows the complete compressor with one shell end cap removed. Figure 19a shows the shell with the rotor and cylinder only, while Fig. 19b shows the shell with the stator. Modal analysis and finite element analysis were carried out in parallel. The experiments were conducted first with the completely disassembled unit and then with the unit built-up step by step in order to understand the complicated dynamics of the complete compressor-shell structure. In this compressor, the stator and cylinder block are welded at three points to the shell. This makes the shell stiffer but allows vibrations of the cylinder assembly to be transmitted directly to the shell. It was found that the shell has its first structural natural frequency at about 600 Hz. Table 2 gives a comparison of the first five shell natural frequencies of the shell on its own calculated by (1) finite element (FE) analysis and (2) measured by the modal analysis tests.

When the rotor and cylinder block were attached, the natural frequencies of the shell were changed. The measured mode shapes and natural frequencies

**Table 2 Comparison of Natural Frequencies of Compressor Shell Predicted by Finite Element (FE) Method with Those Measured**

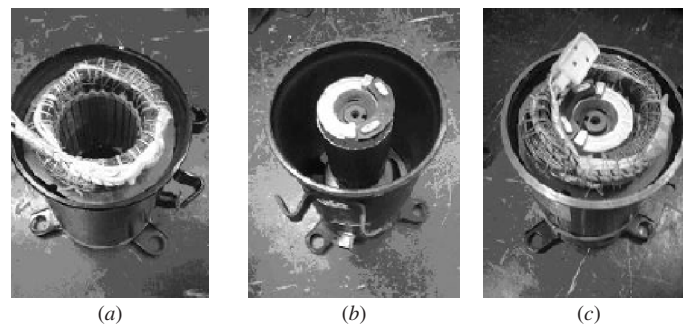
Mode number	1st	2nd	3rd	4th	5th
FE analysis (Hz)	616	1712	2465	2813	3153
Modal test (Hz)	635	1742	2464	2731	3132
Error (%)	3.0	1.8	0	2.9	0.7

Source: From Ref. 43.

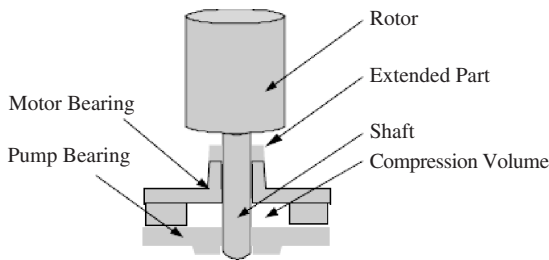
agree qualitatively with those predicted. The measured natural frequencies are mostly within a bound of  $\pm 3\%$  of the predicted values. The differences are presumably caused by inexact knowledge of the boundary conditions and imprecise geometrical descriptions used in the FE analysis. The attachment of the stator to the shell at the three interior shell weld points stiffens the shell and raises the natural frequencies considerably.<sup>43</sup>

Wang et al. also studied the complete built-up compressor system using both FE analysis and modal testing.<sup>43</sup> The conclusion was that two main compressor resonances occurred. In the 1.5-kHz region, vibration of the cylinder block system excited the shell in a rigid body mode, while in the 3.5-kHz frequency region, the cylinder block vibration excited the shell in an elastic bending mode. Modal testing gave a frequency of 3368 Hz for the latter elastic mode, while FE modeling predicted a frequency of 3512 Hz for this mode. It was concluded that, for the elastic bending mode in the 3500-Hz region, the nodal points were close to the weld points. It was thought that most of the vibration energy was transferred to the shell from the cylinder assembly at these weld locations. The rotation of the rotor is supported by the motor and pump bearings and it was believed that these are the main sources of excitation for the shell vibration in the 3500-Hz frequency region. To reduce the excitation, the hub length of the motor bearing was increased to try to make the shaft rotation more stable.<sup>43</sup> See the extended part shown in Fig. 20.

The bearing modification reduced the compressor noise not only in the 3500-Hz frequency range but in



**Figure 19** Modal test models: (a) shell with rotor and cylinder, (b) shell with stator, and (c) full model.<sup>43</sup>



**Figure 20** Schematic diagram of rotor and cylinder block and modification of the rotor bearing.<sup>43</sup>

the 1500-Hz range as well. See Fig. 21. Note that the sound pressure level results in Fig. 21 have been A-weighted to give an approximate idea of the loudness of different frequency regions of the noise.

**7.2.1 Rolling Piston Compressors** In a rolling piston compressor, the interaction between the suction and discharge pressure pulsations, mechanical forces, reciprocating motion of the sliding vane, roller motion, roller driving forces, and electromagnetic forces in the electric motor is very complicated. Refrigerant gas pulsations take place on both the low- and high-pressure sides of the rolling piston system. During the compressor operation, the rolling piston and sliding vane divide the gas into variable volume suction chamber and discharge gas chamber volumes. (See Fig. 8.) The suction chamber is asymmetric in shape and during operation, flow reversal occurs resulting in intense pressure fluctuations and turbulence, although the suction pressure fluctuations are reduced to some extent by the external accumulator. The suction port acts somewhat as a throttle. In addition, the discharge gas pulsations can excite the different cavity volumes inside the shell and also the fluctuating magnetic field and the resulting fluctuating electric motor torque result in forces transmitted to the hermetic compressor shell. It is difficult to model the forced vibration and noise system as a whole. Experimental approaches to reduce vibration and noise radiation are normally used.

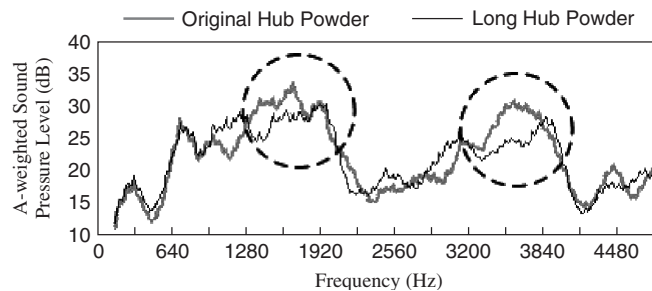
In one study, the vibration magnitudes were mapped over the shell surface.<sup>44</sup> High levels of vibration at different frequencies were recorded on the

shell above and below the electric motor stator, on the accumulator strap, and near to the wire welds and suction line. Three main methods of reducing the compressor vibration and noise were applied successfully: (1) a vibration damper consisting of wire loops wound around the compressor housing near to the regions of maximum vibration magnitude resulted in an A-weighted sound pressure level reduction of 2.5 dB, (2) modification of the suction inlet passageway to provide a smoother inlet passage, a narrow smaller cross-section passage to act as a diffuser throat and a more symmetric inlet passage in the cylinder sidewall to connect with the cylinder suction volume produced a drop in the A-weighted sound pressure level radiated of about 2.0 dB, and (3) a redesigned rotor and crankshaft thrust bearing made of low-friction polyamide material gave a further A-weighted sound pressure level reduction of about 2.0 dB. See Fig. 22.

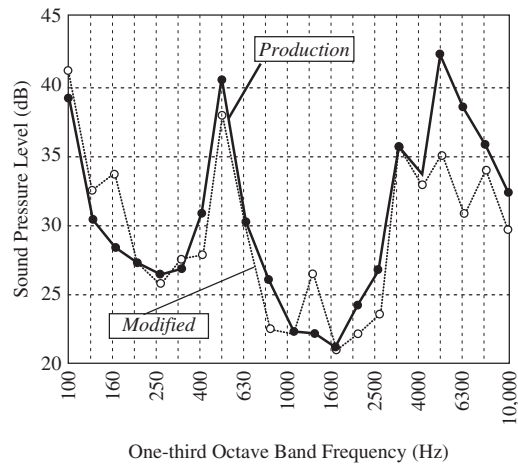
Larger household refrigerators continue to be in demand by consumers. Such refrigerators require larger compressors that tend to be more noisy. Although a single rotor rolling piston rotary compressor can be produced to have more cooling capacity and be more efficient than an equivalent reciprocating compressor, it can suffer more from vibration and noise problems. To reduce vibration and noise a twin-rotor rolling piston compressor was developed. This compressor is about twice as big and has twice the weight of a single-rotor rolling piston compressor, and it has twice the cooling capacity. This twin rotor compressor has about one-third of the compression torque and only about one-fifth of the vibration amplitude of an equivalent cooling capacity single-rotor compressor.<sup>39</sup>

Figure 23 compares the spectra of the sound pressure levels produced by single- and twin-mechanism rolling piston rotary compressors.<sup>39</sup> It is observed that for the larger 480-liter capacity refrigerator, the twin-rotor design is about 7 dB quieter than the same capacity single-rotor design. The lower noise is particularly evident at high frequency above about 1000 Hz.

**7.2.2 Scroll Compressors** The noise characteristics of a scroll compressor vary considerably with load. Measurements must be conducted under real load conditions to investigate the operating noise characteristics of the compressor. It is difficult to carry out noise source identification under load conditions.



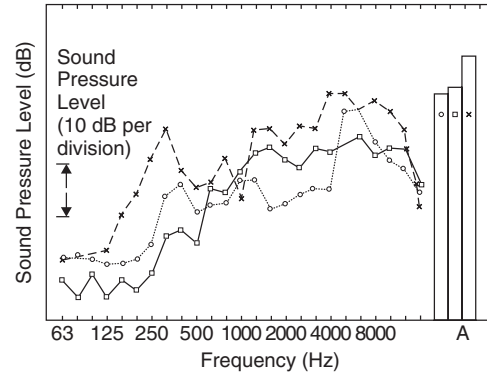
**Figure 21** A-weighted sound pressure levels before and after modifications to the compressor.<sup>43</sup>



**Figure 22** Effect of the use of the modified thrust bearing on the compressor noise.<sup>44</sup>

Figure 24 shows a typical test setup for noise identification studies on a high-pressure scroll compressor by Zhao et al.<sup>45</sup>

In another study by Kim and Lee, identification of noise sources on a scroll compressor and redesign of its structure were performed.<sup>42</sup> An array of 15 microphones was used to identify the noise sources on the

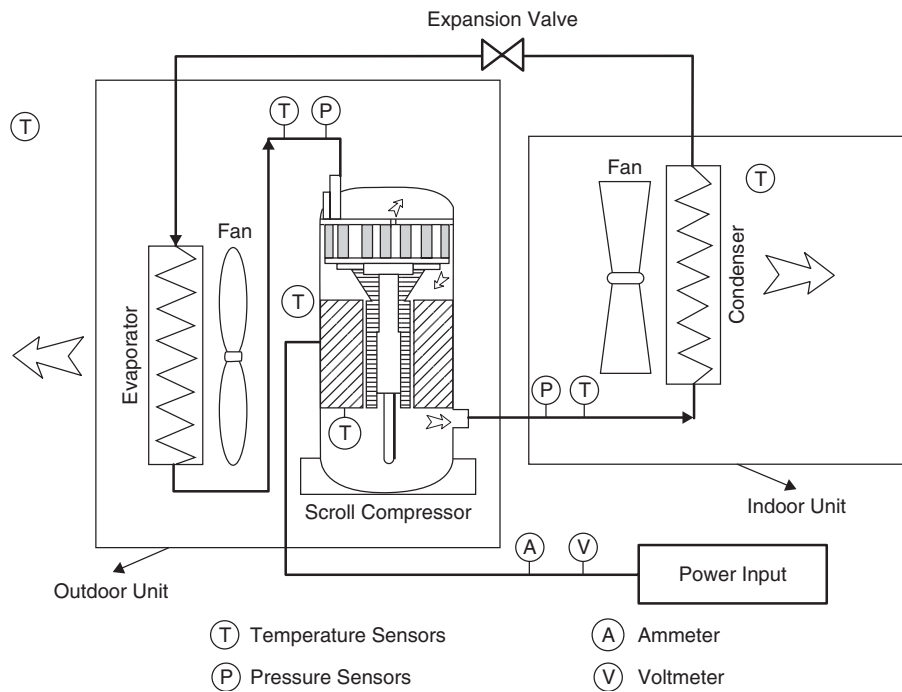


Key

- x Single-mechanism rotary compressor for 480-liter refrigerator
- o Twin-mechanism rotary compressor for 480-liter refrigerator
- Single-mechanism rotary compressor for 350-liter refrigerator

**Figure 23** Compressor noise. The sound pressure level was measured at 30 cm from the compressor shell with the compressor operating on a 50-Hz supply.<sup>39</sup>

compressor. Since the noise generated depends considerably on the load, the noise source identification was conducted under load. It was found that the noise was predominant in the 1600-Hz and 2500-Hz one-third octave frequency bands. Structural resonances of the upper frame and fixed scroll were found to be at

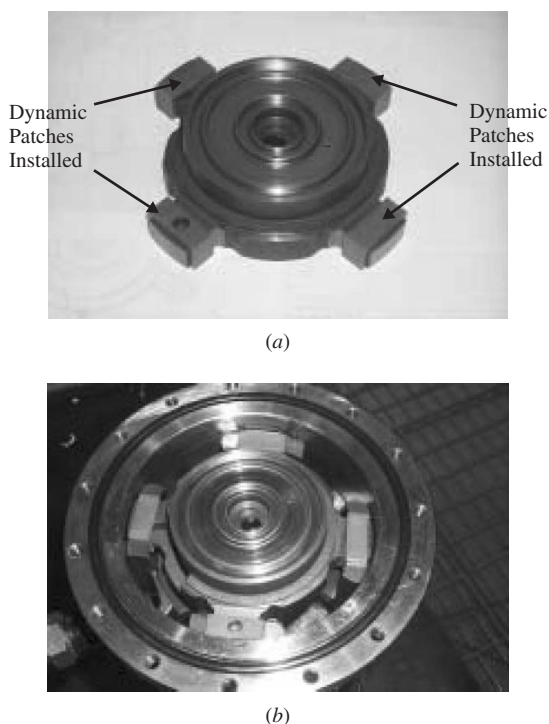


**Figure 24** Test system for tests on a scroll compressor.<sup>45</sup>

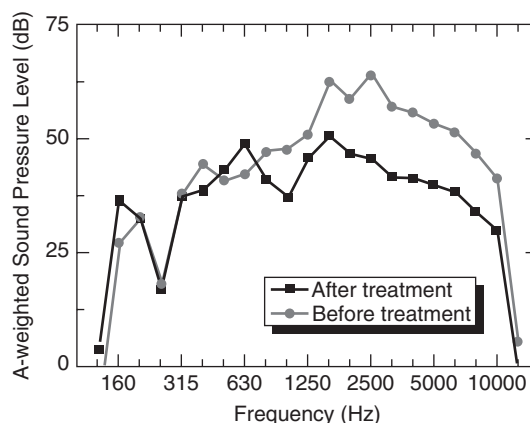
1458-Hz and 1478-Hz, respectively. It was observed from holograph measurements that the 1600-Hz one-third octave band noise is related to impacts between the fixed scroll and the upper frame, while the noise in the 2500-Hz one-third octave band is related to the sound radiated from the upper chamber.<sup>42</sup>

For the reduction of the impact noise, damping material that had good characteristics at high operating temperatures was used. The thickness of the material chosen was 1 mm, as shown in Fig. 25. The material was applied to the upper frame. As a result, the A-weighted sound pressure level was reduced from 68.1 dB, when the original fixed scroll was used, to 56.2 dB when the modified fixed scroll was used, as seen in Fig. 26. By inserting a 0.5-mm-thick copper sheet between the interchamber and the upper frame, the transmission of impact energy was reduced and this resulted in a further 3.3-dB reduction.

As a result, an A-weighted sound pressure level reduction of about 12 dB was achieved by the use of damping material. Further modifications of the upper chamber and the fixed scroll were not put into practice because of manufacturing difficulties. The sound pressure level of this compressor was higher than usual because of the use of a compressor type in which the internal components can be changed easily. The overall noise level reduction achieved by the use of the damping material on its own was about 12 dB.



**Figure 25** Damping material used for impact noise reduction on a scroll compressor.<sup>42</sup>



**Figure 26** Comparison of A-weighted sound pressure level before and after treatment.<sup>42</sup>

## 8 CASE HISTORIES OF THE NOISE CONTROL OF DYNAMIC COMPRESSORS

### 8.1 Noise Control of Centrifugal Compressors<sup>43,46-48</sup>

Jeon and Lee<sup>48</sup> have studied the possibility of reducing the noise of a high-speed centrifugal compressor designed to operate nominally at 14,500 rpm in a turbochiller. This type of compressor-chiller unit is typical of those used to cool large buildings. The chiller uses R134a as the refrigerant. See Fig. 27a. The rotational speed (rps) in cycles/second (Hz) is thus  $14,500/60$  or about 258 Hz. The impeller has 11 long blades and 11 short splitter blades, making a total of 22 blades (see Fig 27b). The inlet guide vane has 7 blades and the diffuser has 13 blades. The main noise sources were found to be related to the blade passing frequency (BPF) of the impeller and to the aerodynamic interaction of the impeller and the diffuser and impeller and inlet guide vane (IGV). The dominant noise occurs at the 22 BPF of the impeller, nominally at  $14,500 \times 22/60$ , or about 5317 Hz. See Fig. 28. Sound is also generated at frequencies of  $\text{rps} \times 11$ ,  $\text{rps} \times 22$ ,  $\text{rps} \times 33$ , and  $\text{rps} \times 44$ . With such centrifugal compressors, the high-frequency sound is normally generated at the elbow and radiated from the duct there. The low-frequency sound generated propagates into the duct, excites the condenser wall, and is reradiated as noise by the wall. In this case history, both sound-absorbing material and a redesigned elbow were used to reduce the noise.

The rotating impeller is normally the main source of noise in such compressors. The noise is also caused by interactions between the impeller and the inlet guide vanes and between the impeller and the diffuser. The identification and location of the main noise sources on this compressor were investigated by the use of sound intensity using an intensity probe and by vibration measurements using an accelerometer. The sound pressure levels were measured near to the condenser and near to the evaporator. The sound

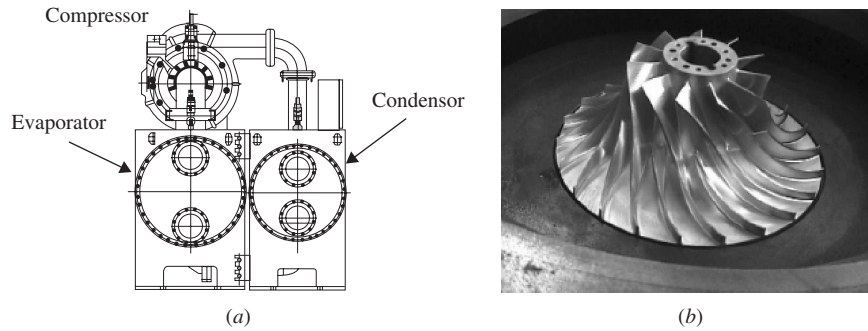


Figure 27 (a) Turbocooler unit and (b) impeller used in the compressor. <sup>48</sup>

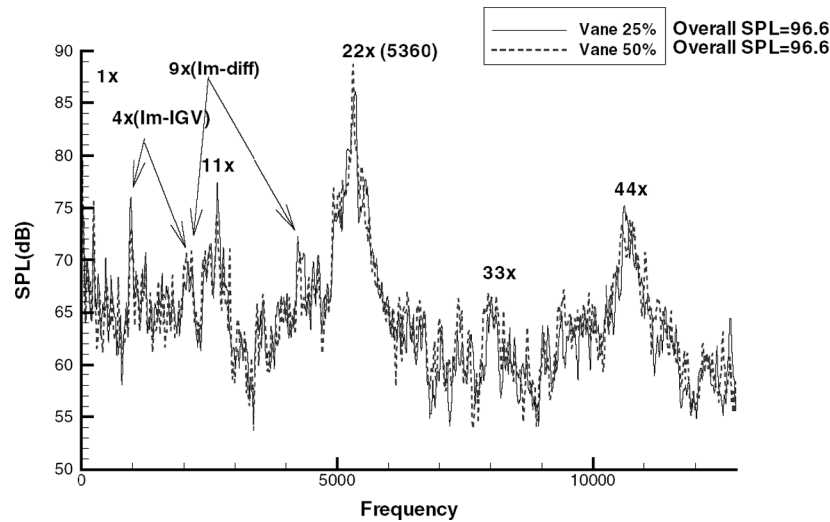


Figure 28 Measured acoustic signal of centrifugal chiller.

pressure level was found to be 10 dB higher near the condenser than near the evaporator. The sound pressure level was then measured at 1.5 m from the side of the condenser.

Figure 28 shows the measured spectrum of the sound pressure level at 1.5 m from the condenser. It is seen that the spectrum is dominated by the BPF peak at 22 times the rps, or about 5360 Hz. This frequency is shown in Fig. 28 as 22x (5360). The second harmonic of the BPF is also quite strong and is indicated in Fig. 28 by 44x. The other PBF caused just by the 11 compressor blades is shown as 11x together with its third harmonic shown as 33x. The interaction peaks of the impeller-guide vane and the impeller-diffuser are shown in Fig. 28 as 4x (Im-IGV) and 9x(Im-diff), respectively. Figure 29 shows spectra of the acceleration magnitude measured on the volute, elbow duct, and condenser wall.

It is seen that the acceleration is the highest on the elbow duct, while that on the volute is the lowest.

The acceleration magnitude on the condenser wall is intermediate. The levels are particularly high at the BPF of about 5360 Hz and the second harmonic at about 10,720 Hz. The accelerations measured on the elbow duct, condenser wall, and volute at the BPF were 83.2, 19.9, and 14.9 m/s<sup>2</sup>. Assuming that the radiation frequencies are similar for the three components and remembering that the sound power radiated is related to surface space-averaged velocity squared, the elbow duct can be assumed to be a very strong noise-radiating surface.

To test these assumptions, the turbocooler was completely lagged in sound-absorbing material and a drop of about 9 dB overall was observed. See Fig. 30. The drop in sound pressure level at the BPF was 11.7 dB. Then to attempt to determine the importance of the noise radiated by the elbow duct, the sound-absorbing material was removed from this area. The overall level was increased from 83 to 87 dB, although



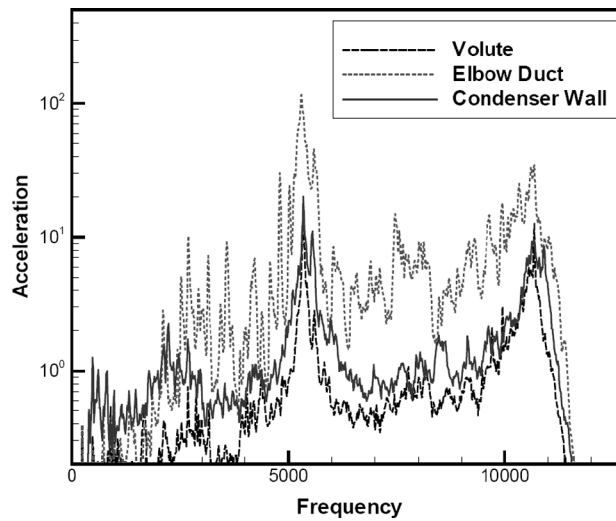


Figure 29 Measured acceleration.

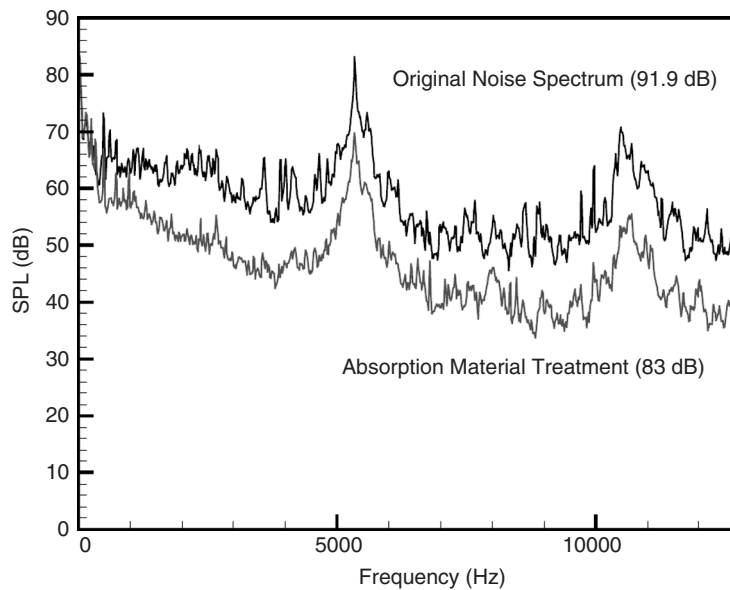


Figure 30 Effect of sound-absorbing material.<sup>8</sup>

it should be noted that the elbow duct area is relatively small.

When the sound-absorbing lagging was removed from the condenser wall, but not from the elbow duct, the overall sound pressure level was also increased from 83 to 87 dB, despite the fact that the area of the condenser walls is about 50 times that of the elbow duct. Several analytical studies have been also performed to try to predict compressor noise radiation from centrifugal compressors.<sup>7</sup>

## 9 NOISE CONTROL IN COMPRESSOR INSTALLATIONS

Mobile compressors are used on building sites, highway construction, and for other similar purposes. They are normally enclosed to reduce noise, but interior heat rejection and buildup requires the use of a cooling fan, which causes additional noise problems. Chapter 54 includes a case history on mobile compressor noise reduction.

The control of the noise of large industrial compressors poses a different problem from that of mobile compressors and small household compressors, which are mainly of the positive displacement design. Since there are very many different compressor designs of various capacities and uses, each noise problem in most cases is unique to the particular application. In many cases, noise control of the compressor must be accomplished during or after its installation in service. In such cases, well-established passive noise control approaches are used. Such approaches are discussed in Chapter 54. These approaches are also described well in several books.

Slow-speed industrial reciprocating compressors are generally much quieter than other large industrial types. The A-weighted sound pressure level at 1 m is usually in the range of 85 to 95 dB. Since manufacturers' data are often difficult to obtain, in many cases, it may be necessary to make noise measurements near to the compressor in question before trying to apply passive noise and vibration control approaches. The passive noise control measures usually applied to compressors include the use of (1) enclosures, (2) sound-absorbing materials, (3) mufflers/silencers applied upstream and downstream, (4) vibration isolation, and (5) barriers. See Chapter 54.

If the compressor is driven by an electric motor or internal combustion engine motor, then the motor may produce more noise than the compressor itself. In such a case it is often necessary to enclose both the compressor and the motor. As a compressor becomes larger, its surface area increases more slowly than its volume, and natural heat rejection from its surface area is normally insufficient. The related enclosure interior heat buildup increases, and so use of a forced-draft system to ensure adequate cooling is essential. If both the compressor and its power source (motor) are enclosed, it is normal to enclose each separately and to ensure that a greater positive pressure is maintained in the motor enclosure than in the compressor enclosure. This positive pressure difference is important if gases other than air are being compressed and prevents the possibility of gases reaching the motor that could cause corrosion, or in the case of combustible gases, even an explosion.

Most such large industrial compressors have much greater flow rates than smaller household types and in the case of large dynamic centrifugal and axial compressors, they have much higher flow velocities as well. In the case of large reciprocating compressors, pressure pulsations that occur in the compression chambers result in sound waves transmitted into inlet and exhaust compressor ductwork. It is common practice to incorporate either absorbent or reactive silencers/mufflers upstream and downstream of the compressor to reduce inlet and exhaust noise.

## 10 CONCLUDING DISCUSSION

Work on reducing the noise and vibration continues. Papers may be found in several different journals and conference proceedings. It is impossible to review

all of these in detail in this short chapter. The proceedings of the International Compressor Engineering Conferences held biannually at Purdue University are a good source of papers on recent work on compressor noise and vibration.<sup>49–80</sup> For instance, in the 2004 and 2006 proceedings papers can be found on the noise of reciprocating compressors,<sup>49–51,60,61</sup> the noise of rotary compressors and the increasingly popular scroll compressor,<sup>52–57</sup> muffler design,<sup>58–61</sup> sound quality,<sup>62,63</sup> compressor vibration,<sup>64–70</sup> and a variety of other compressor noise and vibration research topics.<sup>71–80</sup>

## REFERENCES

1. H. P. Bloch et al., *Compressors and Expanders: Selection and Application for the Process Industry*, Dekker, New York, 1982.
2. M. T. Gresh, *Compressor Performance: Aerodynamics for the User*, Butterworth-Heinemann, Boston, 2001.
3. R. H. Aungier, *Axial-Flow Compressors: A Strategy for Aerodynamic Design and Analysis*, ASME Press, New York, 2003.
4. N. P. Cheremisinoff and P. N. Cheremisinoff, *Compressors and Fans*, Prentice Hall, Englewood Cliffs, NJ, 1992.
5. A. E. Nisenfeld, *Centrifugal Compressors: Principles of Operation and Control*, Instrument Society of America, Research Triangle Park, NC, 1982.
6. P. Pichot, *Compressor Application Engineering*, Book Division, Gulf Pub., Houston, 1986.
7. A. H. Middleton, Noise from Industrial Plant, Chapter 17 in *Noise and Vibration*, Ellis Horwood, Halstead Press, Wiley, New York, 1982.
8. S. N. Y. Gerges and J. P. Arenas, *Fundamentos y Control del Ruido e Vibraciones*, N. R. Editora, Florianopolis, S. C., Brazil, 2004.
9. F. C. McQuiston, J. D. Parker, and J. D. Spitler, *Heating, Ventilating, and Air Conditioning: Analysis and Design*, 5th ed., Wiley, New York, 2000.
10. ASHRAE *Guide and Data Book*, ASHRAE, 1975.
11. W. Soedel, *Mechanics, Simulation and Design of Compressor Valves, Gas Passages and Pulsation Mufflers (Short Course Text)*, Purdue University, Ray W. Herrick Laboratories, West Lafayette, IN., 1992.
12. J. F. Hamilton, *Measurements and Control of Compressor Noise (Short Course Text)*, Purdue University, Ray W. Herrick Laboratories, West Lafayette, IN., 1988.
13. W. Soedel, *Sound and Vibrations of Compressors*, CRC/Dekker, Boca Raton, FL, 2007.
14. S. Wang and J. Park, Noise Reduction Mechanisms of a Spring Wound LDT for a Reciprocating Compressor, Paper 928 in Proceedings of the Thirteenth International Congress on Sound and Vibration (ICSV13), July 2–6, 2006, Vienna, Austria.
15. H. E. Webb, Compressor, Household Refrigerator, and Air-Conditioner Noise, in *Handbook of Noise Control*, C. M. Harris, Ed., McGraw-Hill, New York, 1957, Chapter 28.
16. N. Ishii, K. Imaichi, N. Kagoroku, and K. Imasu, Vibration of a Small Reciprocating Compressor, ASME Paper, No. 75-DET-44, 1975.
17. K. Tojo, S. Machida, S. Saegusa, T. Hirata, M. Sudo, and S. Tagawa, Noise Reduction of Refrigerator Compressors, Purdue Res. Found., 1980, pp. 235–242.



18. F. Saito, S. Maeda, N. Okubo, and T. Uetsuji, Noise Reduction of Hermetic Compressor by Improvement on Its Shell Shape, *Purdue Res. Found.*, 1980, pp. 228–234. I. Lafayette, Indiana, USA.
19. D. E. Montgomery, R. L. West, and R. A. Burdisso, Acoustic Radiation Prediction of a Compressor Housing from Three-Dimensional Experimental Spatial Dynamics Modeling, *Appl. Acoust.*, Vol. 47, No. 2, Feb. 1996, pp. 165–185.
20. C. Ozturk, Experimental Investigation on the Cycle Nature of Pressure Time History in the Compression Chamber of a Domestic Refrigeration Compressor, ICASSP, IEEE International Conference on Acoustics, Speech and Signal Processing—Proceedings, Vol. 6, 2000, pp. 3874–3877.
21. B.-S. Yang, W.-W. Hwang, D.-J. Kim, and A. C. Tan, Condition Classification of Small Reciprocating Compressor for Refrigerators Using Artificial Neural Networks and Support Vector Machines, *Mech. Syst. Signal Proc.*, Vol. 19, No. 2, March, 2005, pp. 371–390.
22. N. Tsujiuchi, T. Koizumi, S. Usui, and K. Tsukiori, Vibration and Noise Reduction of Household Refrigerator Using Modal Component Synthesis Technique, Proceedings of the 1990 International Compressor Engineering Conference, 1990, p. 917. Purdue University, West Lafayette, Indiana.
23. R. J. Comparin, Vibration Isolation for Noise Control in Residential HVAC Systems—A Case Study, Proceedings—National Conference on Noise Control Engineering, Progress in Noise Control for Industry, 1994, pp. 661–666. Purdue University, West Lafayette, Indiana.
24. V. Cossalter, A. Doria, P. Gardonio, and F. Giusto, Dynamic Response and Noise Emission of a Reciprocating Compressor Shell, *Proc. SPIE—Int. Soc. Opt. Eng.*, Vol. 1923, Pt. 2, 1993, pp. 1347–1352.
25. N. Gupta, R. J. Bernhard, and J.F. Hamilton, Prediction of the Transient Start-up and Shut-down Vibrations of a Reciprocating Compressor, ASME Paper, 85-DET-168, 1985.
26. A. T. Herfat, Gas Pulsation Noise Analysis of Reciprocating Compressors Using Four Poles Method (FPM), Proceedings of the Eleventh International Congress on Sound and Vibration, 2004, pp. 2065–2072.
27. A. T. Herfat, Acoustical Analysis of Reciprocating Compressors Using Four Poles (Parameters) Method (FPM), Proceedings of the Eleventh International Congress on Sound and Vibration, 2004, pp. 879–886. Lisbon, Portugal.
28. N. Dreiman and K. Herrick, Noise Control of Fractional Horse Power Hermetic Reciprocating Compressor, Proceedings of the Sixth International Congress on Sound and Vibration, 1999, pp. 2441–2448. Lyngby, Denmark.
29. S.-K. Lee, K.-R. Rho, H.-C. Kim, and B.-H. An, Condition Monitoring System for the Reciprocating Compressor, Proceedings of the 32nd International Congress and Exposition on Noise Control Engineering, 2003, pp. 4648–4655. Jeju, Korea.
30. N. Dreiman, Noise Reduction of Fractional Horse Power Reciprocating Compressor, Proceedings of the Tenth International Congress on Sound and Vibration, 2003, pp. 3967–3974. Stockholm, Sweden.
31. H. Erol, The Noise Source Identification of a Reciprocating Refrigeration Compressor, Proceedings of the Sixth International Congress on Sound and Vibration, 1999, pp. 2427–2434. Lyngby, Denmark.
32. J. Tian and X. Li, Noise Control for an Air-Conditioner, Proceedings of the 2001 International Congress and Exhibition on Noise Control Engineering, 2001. The Hague, The Netherlands.
33. C. Svendsen and H. Møller, Acoustic Optimization of Suction Mufflers in Reciprocating Hermetic Compressors, *Proceedings of the Twelfth International Congress on Sound and Vibration*, 2005. Lisbon, Portugal.
34. M. C. Yoon, H. Seomoon, K. O. Ryu, and S. W. Park, Experimental and Analytical Approach to Reduce Low Frequency Noise and Vibration of Reciprocating Compressor for Refrigerator, Proceedings of the 32nd International Congress and Exposition on Noise Control Engineering, 2003, pp. 3965–3970. Jeju, Korea.
35. M. C. C. Tsao, Theoretical and Experimental Analysis of the Noise of a Hermetic Reciprocating Refrigeration Compressor, *Compendium—Deutsche Gesellschaft fuer Mineraloelwissenschaft und Kohlechemie*, 1978, pp. 281–288.
36. R. D. Holm, Hermetic Compressor Noise-I, Transmission Paths and Shell Resonances, Westinghouse Research Report 68-ID7—MECNO-R1, Pittsburgh, July 17, 1968.
37. T. Uetsuji, T. Koyama, N. Okubo, T. Ono, and K. Imaichi, Noise Reduction of Rolling Piston Type Rotary Compressor for Household Refrigerator and Freezer, Proceedings of the Purdue Compressor Technology Conference, 1984, pp. 251–258. Purdue University, West Lafayette, Indiana.
38. H.-J. Kim and Y. M. Cho, Noise Source Identification in a Rotary Compressor: A Multidisciplinary Synergetic Approach, *J. Acoust. Soc. Am.*, Vol. 110, No. 2, 2001, pp. 887–893.
39. M. Sakai and H. Maeyama, Twin-Mechanism Rotary Compressor for Large-Capacity Refrigerators, *Mitsubishi Electric Advance*, Vol. 70, Mar. 1995, pp. 14–16.
40. H. Zhou, K. Naoya, and N. Mii, Measurement of Vibration Intensity on the Cylindrical Casing of Compressor, *Proc.—Int. Conf. Noise Control Eng.*, Vol. 1, 1995, p. 677.
41. J. Iizuka, N. Kitano, S. Ito, and S. Otake, Improvement of Scroll Compressor for Vehicle Air Conditioning Systems, *SAE Special Publications*, Vol. 1239, *Automotive Climate Control Design Elements*, 1997, 970113, pp. 55–70.
42. C.-H. Kim and S.-I. Lee, Noise Source Identification and Control of a Scroll Compressor, Proceedings of the 32nd International Congress and Exposition on Noise Control Engineering, 2003, pp. 1414–1420. Jeju, Korea.
43. S. Wang, J. Park, I. Hwang, and B. Kwon, Noise Generation of the Rotary Compressors from the Shell Vibration, Proceedings of the 32nd International Congress and Exposition on Noise Control Engineering, 2003, pp. 921–928. Jeju, Korea.
44. J. Tantari, Experiments on a Screw Compressor Source Properties, Proceedings of the 2001 International Congress and Exhibition on Noise Control Engineering, 2001. The Hague, The Netherlands.
- N. Dreiman, Noise Control of Hermetic Rotary Compressor, Proceedings of the Seventh International Congress on Sound and Vibration, 2000, pp. 643–650. Garmisch Partenkirchen, Germany.
45. Y. Zhao, L. Li, H. Wu, P. Shu, and J. Shen, Research on the Reliability of a Scroll Compressor in a Heat

- Pump System, *Proc. Instit. Mech. Eng., Part A: J. Power Energy*, Vol. 218, No. 6, September, 2004, pp. 429–435.
46. H. Sun, H. Shin, and S. Lee, Analysis and Optimization of Aerodynamic Noise in a Centrifugal Compressor, *J. Sound Vib.*, June 2005.
  47. H. Sun and S. Lee, Low Noise Design of Centrifugal Compressor Impeller, Proceedings of the 32nd International Congress and Exposition on Noise Control Engineering, 2003, pp. 1375–1380.
  48. W.-H. Jeon and J. Lee, A Study on the Noise Reduction Method of a Centrifugal Compressor, Proceedings of the 2001 International Congress and Exhibition on Noise Control Engineering, 2001. The Hague, The Netherlands.
  49. W. Ruixiang, L. Hongqi, L. Junming, and W. Yezheng, Study on Reciprocating Compressors with Soft Suction Structures and Discharge Structures, Paper C7-1, Proceedings of the International Compressor Engineering Conference at Purdue, July 16–19, 2002.
  50. J. Ventimiglia, G. Cerrato-Jay, and D. Lowery, Hybrid Experimental and Analytical Approach to Reduce Low Frequency Noise and Vibration of a Large Reciprocating Compressor, Paper C14-2, Proceedings of the International Compressor Engineering Conference at Purdue, July 16–19, 2002.
  51. V. Medica, B. Pavkovic, and B. Smoljan, The Analysis of Shaft Breaks on Electric Motors Coupled with Reciprocating Compressors, Paper C134, Proceedings of the International Compressor Engineering Conference at Purdue, July 12–15, 2004.
  52. M. Yanagisawa, T. Uematsu, S. Hiodoshi, M. Saito, and S. Era, Noise Reduction Technology for Inverter Controlled Scroll Compressors, Paper C18-5, Proceedings of the International Compressor Engineering Conference at Purdue, July 16–19, 2002.
  53. T. Toyama, Y. Nishikawa, Y. Yoshida, S. Hiodoshi, and Y. Shibamoto, Reduction of Noise and Over-Compression Loss by Scroll Compressor with Modified Discharge Check Valve, Paper C20-4, Proceedings of the International Compressor Engineering Conference at Purdue, July 16–19, 2002.
  54. M. K. Kiem, Y. K. Kim, D. Lee, S. Choi, and B. Lee, Noise Characteristics of a Check Valve Installed in R22 and R410A Scroll Compressors, Paper C20-1, Proceedings of the International Compressor Engineering Conference at Purdue, July 16–19, 2002.
  55. M. Mézache, Dynamic Response of a Floating Valve: A New Shutdown Solution for Scroll Compressors, Paper C22-5, Proceedings of the International Compressor Engineering Conference at Purdue, July 16–19, 2002.
  56. H. Bukac, Self-Excited Vibration in a Radially and Axially Compliant Scroll Compressor, Paper C041, Proceedings of the International Compressor Engineering Conference at Purdue, July 12–15, 2004.
  57. S. Wang, J. Park, I. Hwang, and B. Kwon, Sound Reduction of Rotary Compressor Using Topology Optimization, Paper C14-4, Proceedings of the International Compressor Engineering Conference at Purdue, July 16–19, 2002.
  58. J.-H. Lee, K. H. An, and I. S. Lee, Design of the Suction Muffler of a Reciprocating Compressor, Paper C11-5, Proceedings of the International Compressor Engineering Conference at Purdue, July 16–19, 2002.
  59. L. Chen and Z. Huang, Analysis of Acoustic Characteristics of the Muffler on Rotary Compressor, Paper C015, Proceedings of the International Compressor Engineering Conference at Purdue, July 12–15, 2004.
  60. C. Svendsen, Acoustics of Suction Mufflers in Reciprocating Hermetic Compressors, Paper C029, Proceedings of the International Compressor Engineering Conference at Purdue, July 12–15, 2004.
  61. B.-H. Kim, S.-T. Lee, and S.-W. Park, Design of the Suction Muffler of a Reciprocating Compressor Using DOE (Theoretical and Experimental Approach), Paper C053, Proceedings of the International Compressor Engineering Conference at Purdue, July 12–15, 2004.
  62. E. Baars, A. Lenzi, and R. A. S. Nunes, Sound Quality of Hermetic Compressors and Refrigerators, Paper C11-3, Proceedings of the International Compressor Engineering Conference at Purdue, July 16–19, 2002.
  63. G. Cerrato-Jay and D. Lowery, Investigation of a High Frequency Sound Quality Concern in a Refrigerator and Resulting Compressor Design Study, Paper C14-1, Proceedings of the International Compressor Engineering Conference at Purdue, July 16–19, 2002.
  64. J. Ling, The Digital Simulation of the Vibration of Compressor and Pipe System, Paper C16-3, Proceedings of the International Compressor Engineering Conference at Purdue, July 16–19, 2002.
  65. A. T. Herfat, Experimental Study of Vibration Transmissibility Using Characterization of Compressor Mounting Grommets, Dynamic Stiffness. Part I. Frequency Response Technique Development, Analytical, Paper C17-1, Proceedings of the International Compressor Engineering Conference at Purdue, July 16–19, 2002.
  66. A. T. Herfat and G. A. Williamson, Experimental Study of Vibration Transmissibility Using Characterization of Compressor Mounting Grommets, Dynamic Stiffness. Part II. Experimental Analysis and Measurements, Paper C17-2, Proceedings of the International Compressor Engineering Conference at Purdue, July 16–19, 2002.
  67. J. Chen and D. Draper, Random Vibration Fatigue Tests to Prove Integrity of Cantilevered Attachments on Compressor Shells, Paper C17-3, Proceedings of the International Compressor Engineering Conference at Purdue, July 16–19, 2002.
  68. L. Gavric and M. Dapras, Sound Power of Hermetic Compressors Using Vibration Measurements, Paper C16-1, Proceedings of the International Compressor Engineering Conference at Purdue, July 16–19, 2002.
  69. M. Della Libera, A. Pezzutto, M. Lamantia and G. Buligan, Simulation of a Virtual Compressor's Vibration, Paper C075, Proceedings of the International Compressor Engineering Conference at Purdue, July 12–15, 2004.
  70. W. Zhou and F. Gant, Compressor Rigid-Body Vibration Measurement, Paper C138, Proceedings of the International Compressor Engineering Conference at Purdue, July 12–15, 2004.
  71. S. E. Marshall, Reducing Compressor Noise While Considering System Interactions, Paper C11-2, Proceedings of the International Compressor Engineering Conference at Purdue, July 16–19, 2002.
  72. W. C. Fu, Sound Reduction for Copeland Midsize Semihermetic Compressors Using Experimental Methods, Paper C001, Proceedings of the International Compressor Engineering Conference at Purdue, July 12–15, 2004.

73. M. Della Libera, C. Gnesutta, A. Pezzutto, and G. Buligan, Sensitive Dependence from the Cylinder Head Position on the Compressor's Noise Emission—A Numerical Analysis, Paper C074, Proceedings of the International Compressor Engineering Conference at Purdue, July 12–15, 2004.
  74. S. Wang, J. Kang, J. Park, and C. Kim, Design Optimization of a Compressor Loop Pipe using Response Surface Method, Paper C088, Proceedings of the International Compressor Engineering Conference at Purdue, July 12–15, 2004.
  75. A. R. da Silva, A. Lenzi, and E. Baars, Controlling the Noise Radiation of Hermetic Compressors by Means of Minimization of Power Flow through Discharge Pipes Using Genetic Algorithms, Paper C096, Proceedings of the International Compressor Engineering Conference at Purdue, July 12–15, 2004.
  76. H. Bukac, Instantaneous Frequency: Another Tool of Source of Noise Identification, Paper C040, Proceedings of the International Compressor Engineering Conference at Purdue, July 12–15, 2004.
  77. K. Morimoto, Y. Kataoka, T. Uekawa and H. Kamishida, Noise Reduction of Swing Compressors with Concentrated Winding Motors, Paper C051, Proceedings of the International Compressor Engineering Conference at Purdue, July 12–15, 2004.
  78. M. Silveira, Noise and Vibration Reduction in Compressors for Commercial Applications, Paper C065, Proceedings of the International Compressor Engineering Conference at Purdue, July 12–15, 2004.
  76. J. Park, S. Wang, J. Kang, and D. Kwon, Boundary Element Analysis of the Muffler for the Noise Reduction of the Compressors, Paper C089, Proceedings of the International Compressor Engineering Conference at Purdue, July 12–15, 2004.
  80. F. A. Ribas, Jr, and C. J. Deschamps, Friction Factor under Transient Flow Condition, Paper C097, Proceedings of the International Compressor Engineering Conference at Purdue, July 12–15, 2004.
- BIBLIOGRAPHY**
- Y. M. Cho, Noise Source and Transmission Path Identification via State-Space System Identification, *Control Eng. Practice*, Vol. 5, No. 9, Sept. 1997, pp. 1243–1251.
  - N. Dreiman, Noise Control of Hermetic Rotary Compressor, Proceedings of the Seventh International Congress on Sound and Vibration, 2000, pp. 643–650. Garmisch Partenkirchen, Germany.
  - Y. Ebita, M. Mikami, N. Kojima, and B.-H. Ahn, Measurement and Analysis of Vibration Energy Flow on Compressor Casings, *Proceedings of the 32nd International Congress and Exposition on Noise Control Engineering*, 2003, pp. 4250–4256. Jeju, Korea.
  - H. Erol and A. Gürdoğan, On the Noise and Vibration Characteristics of a Reciprocating Compressor: Effects of Size and Profile of Discharge Port, *Proc. 15th Int. Compressor Eng. Con.*, Vol. 2, 2000, pp. 677–683.
  - H. Erol and M. Ünal, On the Noise and Vibration Characteristics of a Reciprocating Compressor with Two Different Type of Cylinder Heads: Conventional Head and a New Design Head, *Proc. 7th Int. Cong. Sound Vib.*, Vol. 2, 2000, pp. 651–658.
  - H. Erol, T. Durakbaşı and H. T. Belek, Dynamic Modeling and Measurements on a Reciprocating Hermetic Compressor, *Proc. 13th Int. Compressor Eng. Conference*, Vol. 1, 1996, pp. 199–204.
  - L. Gavric, Characterization of Acoustic Radiation of Hermetic Reciprocating Compressor Using Vibration Measurements. Inter-noise 2000, Nice, France.
  - L. Gavric, and A. Badie-Cassegnat, Measurement of Gas Pulsations in Discharge and Suction Lines of Refrigerant Compressors, Purdue Compressor Conference, 2000. Purdue University, West Lafayette, Indiana.
  - T. Loyau, Identification of Mechanical Forces Generated by an Air Compressor by Using Neural Networks, Proceedings of the Tenth International Congress on Sound and Vibration, 2003, pp. 1881–1888.
  - Y.-C. Ma and O.-K. Min, Pressure Calculation in a Compressor Cylinder by a Modified New Helmholtz Modeling, *J. Sound Vib.*, Vol. 243, No. 5, June 21, 2001, pp. 775–796.
  - D. Norfield, Noise Vibration and Harshness on Motors Driving Blowers, Compressors and Pumps, Electrical Insulation Conference and Electrical Manufacturing and Coil Winding Conference and Exhibition, 2003, pp. 343–346.
  - P. Potočnik, E. Govekar, J. Gradišek, P. Mužič, I. Grabec, and A. Strmec, Acoustic Based Fault Detection System for the Industrial Production of Compressors, Proceedings of the Tenth International Congress on Sound and Vibration, 2003, pp. 1371–1378. Stockholm, Sweden.
  - Y. V. Siva Prasad, C. Padmanabhan, and N. Ganesa, Acoustic Radiation from Compressor Shells, *Int. J. Acoust. Vib.*, Vol. 9, No. 2, June 2004, pp. 81–86.
  - S. Steffenato, M. Marcer, and P. Olalla Ayllon, Correlation between Refrigerator Noise and Compressor Vibrations. Development of a New Measurement Method for Compressor Vibrations, Proceedings of the Sixth International Congress on Sound and Vibration, 1999, pp. 2223–2230. Lyngby, Denmark.
  - H. Sun and S. Lee, Numerical Prediction of Centrifugal Compressor Noise, *J. Sound Vib.*, Vol. 269, Nos. 1–2, Jan. 6, 2004, pp. 421–430.

# CHAPTER 75

## VALVE-INDUCED NOISE: ITS CAUSE AND ABATEMENT

Hans D. Baumann  
Palm Beach, Florida

Mats Åbom  
The Marcus Wallenberg Laboratory for Sound and Vibration Research  
KTH—The Royal Institute of Technology  
Stockholm, Sweden

### 1 INTRODUCTION

On-off valves operating generally at low fluid velocities usually pose no noise problems. However, control valves that are widely employed in industrial applications and that are used to reduce pressure can be the source of significant sound pressure levels, exceeding in some cases 130 dB at the exterior of a steel pipe. One has to distinguish among different noise-producing mechanisms to take corrective measures, if needed. These are, in order of importance: aerodynamic noise caused by high gas velocities; cavitating, and to a lesser extent, turbulent liquid flow; noise caused by resonant vibration of valve components; and, finally, “whistling” sound caused by resonant coupling of sound waves with gas flow.

While unwanted noise is a source of annoyance, it can also have legal and safety consequences. For example, the Occupational Safety and Health Administration (OSHA) regulations limit the 8-h A-weighted sound pressure level exposure for workers to 90 dB. On the other hand, a continuous A-weighted sound pressure level exposure at 1 m from an uninsulated pipe of about 130 dB can cause structural pipe failures<sup>1</sup> and therefore can have dire consequences. It is for all of these reasons that the use of a reliable and reasonable noise prediction method is a must in the evaluation of proposed valve purchases to avoid problems after installation.

### 2 FUNDAMENTAL CONSIDERATIONS

All control valves basically control the rate of flow and through this mechanism the downstream pressure, temperature, or liquid level in a tank, to name a few. In order to do so, a valve must have a higher inlet pressure than the downstream pressure. This *potential energy* is then converted first into an acceleration of the fluid or into *kinetic energy* and finally through turbulence or shock waves in heat, or *thermal energy*. This kinetic energy can produce sound power ( $W_a$ ) as a byproduct.

The amount of sound power is typically a small fraction of the *mechanical power*,  $W_m$ , that is converted into heat:

$$W_m = mU^2/2 \quad (\text{W}) \quad (1)$$

where  $m$  = mass flow (kg/s), and  $U$  = jet velocity (m/s). The acoustic power is given now by the mechanical power multiplied by an *acoustical efficiency factor*,  $\eta$ , making

$$W_a = \eta W_m \quad (\text{W}) \quad (2)$$

This equation works both for noise produced by liquid turbulence as well as for aerodynamically produced noise. The acoustical efficiency factor for turbulent liquids<sup>2</sup> is given by  $(U/c_l) \times 10^{-4}$ , while  $\eta$  for aerodynamic noise<sup>3</sup> at sonic velocity (Mach 1) is also given by  $(U/c_g) \times 10^{-4}$ , where  $c_l$  is the speed of sound in liquids and  $c_g$  is the speed of sound in gases in metres per second.

In some valve types only a fraction of the internally generated sound power escapes into the downstream pipe. An  $r_w$  coefficient<sup>3</sup> describes this fraction. For globe valves  $r_w$  is assumed to be 0.25. While the resultant numbers seem small, in practice pipe internal sound power nevertheless can reach magnitudes of more than 10 kW. Fortunately for us, most valves are installed in a piping system where most of the sound power is reflected by the pipe wall. The difference in sound pressure level between the interior and the exterior of the pipe is called the transmission loss (TL). Typical values of transmission losses range between 40 and 60 dB.

Finally, there is a decrease in the observed sound pressure level between the pipe exterior and the distance to the observer (typically 1 m). Here the distance correction is equivalent to  $10 \log_{10}[(h + D_0/2)/D_0/2]$ , where  $h$  is the distance between pipe wall and observer and  $D_0$  is the outside diameter of the pipe.

### 3 AERODYNAMICALLY PRODUCED SOUND

This is the most common type of acoustic annoyance in industrial plants. Fortunately, reliable prediction techniques are now available through the International Electrical Commission (IEC) Standard 60534-8-3. This standard<sup>3</sup> is based on the original work by Lighthill<sup>4</sup> covering free jet noise and further modified by Baumann<sup>5</sup> to account for the behavior of confined jets, the effects of pressure recovery, and

**Table 1 Typical  $F_d$  Values of Control Valves. Full Size Trim**

Valve Types	Flow Direction	Max. $C_1/d^2$	$F_N$	$F_d$ @% of Rated Flow Capacity ( $C_1$ )					
				10	20	40	60	80	100
Globe, parabolic plug	To open	13	0.28	0.10	0.15	0.25	0.31	0.39	0.46
Globe, 3 V-port plug	To open	10	0.44	0.29	0.40	0.42	0.43	0.45	0.48
Globe, 4 V-port cage	Either <sup>a</sup>	10	0.38	0.25	0.35	0.36	0.37	0.39	0.41
Globe, 6 V-port cage	Either <sup>a</sup>	10	0.26	0.17	0.23	0.24	0.26	0.28	0.30
Globe, 60-hole drilled cage	Either <sup>a</sup>	8	0.14	0.40	0.29	0.20	0.17	0.14	0.13
Globe, 120-hole drilled cage	Either <sup>a</sup>	6.5	0.09	0.29	0.20	0.14	0.12	0.10	0.09
Butterfly, swing-through, to 70°	Either	32	0.34	0.26	0.34	0.42	0.50	0.53	0.57
Butterfly, fluted vane, to 70°	Either	26	0.13	0.08	0.10	0.15	0.20	0.24	0.30
Eccentric rotary plug valve	Either	13	0.26	0.12	0.18	0.22	0.30	0.36	0.42
Segmented V-ball valve	Either	21	0.67	0.60	0.65	0.70	0.75	0.78	0.80

<sup>a</sup> Limited  $P_1 - P_2$  in flow toward center,  $d$  = valve size in inches, and  $F_N$  = valve-specific noise parameter, defined by the author as the  $F_d$  at a flow capacity ( $C_v$ ) equivalent to  $6.5d^2$ . Depending upon pipe size, a lower  $F_N$  means less external noise due to higher pipe wall attenuation. Courtesy ISA.

the influence of jet diameter on the peak frequency, which in turn determines the magnitude of the transmission loss. This method has been improved (the last revision dates from the year 2000) and gives prediction accuracies for the A-weighted sound pressure level typically within a range of  $\pm 3$  dB. This assumes, of course, that all service conditions are known and that valve type specific sizing parameters such  $F_L$  and  $F_d$  (see Table 1) are known. The  $F_L$  factor is used to calculate the exact gas or liquid velocity in the restricted jet diameter portion of the valve. This velocity in turn then determines the amount of mechanical power that is converted into heat, and, second, the type of noise-producing mechanism for gases such as dipole (predominant when the jet interacts with wall surfaces of the valve) or quadrupole (free jet turbulence). The IEC method assumes from Baumann<sup>6</sup> that both dipole and quadrupole sources are of equal magnitude at a jet velocity of Mach 1. Here the acoustical efficiency  $\eta$  is assumed to decrease from  $10^{-4}$  at a rate proportional to  $U^{3.6}$ . Shock cells predominate at supersonic velocities, which can exist downstream of the valve's orifice; here the acoustical efficiency increases proportional to  $M^{6.6}$  to finally reach a maximum<sup>7</sup> at  $1 \times 10^{-3}$  at a Mach number of 1.4. The  $F_d$  factor is equally important since it determines the size of the jet emanating from one or more valve orifices. This in turn defines the peak frequency  $f_p$  (Hz) of the sound pressure level inside the pipe, where

$$f_p = 0.2 \times U / (F_d d) \quad (3)$$

where  $d$  = the apparent orifice diameter (in metres) as calculated from the total flow area. For low noise valve trims consisting of cages with multiple drilled holes (see Fig. 6),  $F_d = 1/N_0^{0.5}$ , where  $N_0$  defines the number of equally sized holes. For example, a trim having 100 identical passages in parallel for the fluid to pass through has an  $F_d$  of 0.1. As a general rule,

valves having a high  $F_L$  number but a low  $F_d$  factor are less noisy (see Table 1).

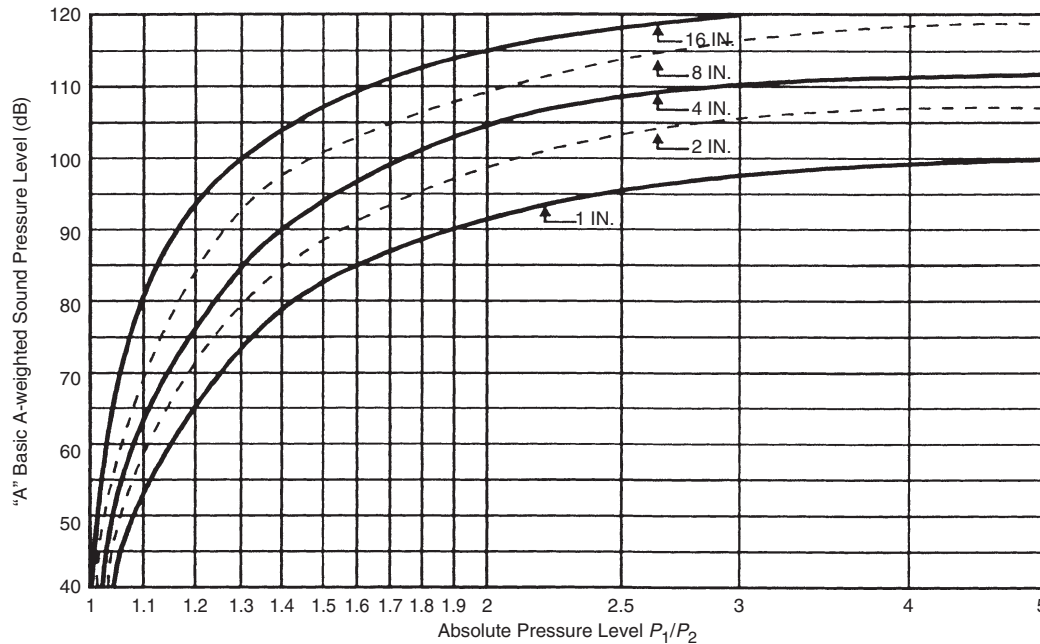
The reader may sense that modern noise prediction techniques are quite complex and really require a programmed computer. It is for this reason that we do not want to reproduce the whole prediction schema but like to offer instead a simplified graphical method (courtesy of The International Society of Measurement and Control, ISA) as shown in Fig. 1. While not as accurate as a computerized method, this graph nevertheless will give an idea whether a given valve will likely exceed a given noise limit.

Here is how to use this method: First, find the  $P_1/P_2$  ratio, that is, the absolute inlet pressure divided by the absolute outlet pressure. Next read up to the given valve size and obtain the corresponding "basic sound pressure level"  $A$  from the scale on the left. The next step is to correct for the actual inlet pressure. This is given by  $B = 12 \log(P_1/667)$  where the pressure is in kilopascals. Finally, add  $C$ , a correction for the pipe wall if it is other than Schedule 40. Here  $C = +1.4$  for Schedule 20, 0 for Schedule 40,  $-3.5$  for Schedule 80, and  $-7$  for Schedule 160. The total sound level now is the sum of  $A + B + C$ . Subtract another 3 dB in case of steam.

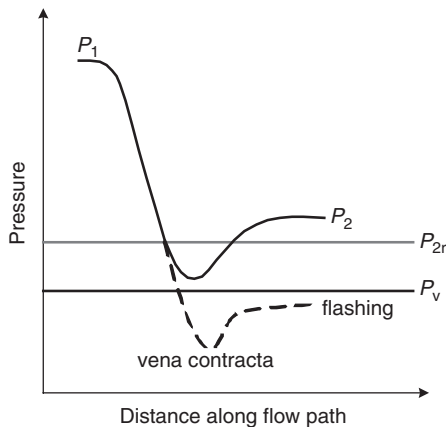
**Example** An 80-mm (3-in.) globe valve with parabolic plug is reducing steam pressure from 3600 to 2118 kPa; the pipe Schedule is 80. Going to Fig. 1, we do not find a 3-in. valve. However, we can extrapolate between the lines and find the  $A$  factor to be 98 dB for the pressure ratio of 1.7. Factor  $B$  calculates as  $12 \log(3600/667) = 8.8$  dB. Finally we add  $-3.5$  dB for Schedule 80 and we subtract 3 dB for steam. This results in a total A-weighted sound pressure level of 100.8 dB at 1 m from the pipe wall. Using the computerized IEC equations gives an A-weighted sound pressure level of 103 dB.

#### 4 HYDRODYNAMIC SOUND

For cases with a "incompressible" medium (liquids) the Mach number is normally very small, and it can



**Figure 1** Basic aerodynamic A-weighted sound pressure level in decibels for conventional control valves at approximately 70% of rated flow capacity, at 667-kPa inlet pressure and schedule 40 downstream pipe, measured 1 m from the downstream pipe wall. (Courtesy ISA.)

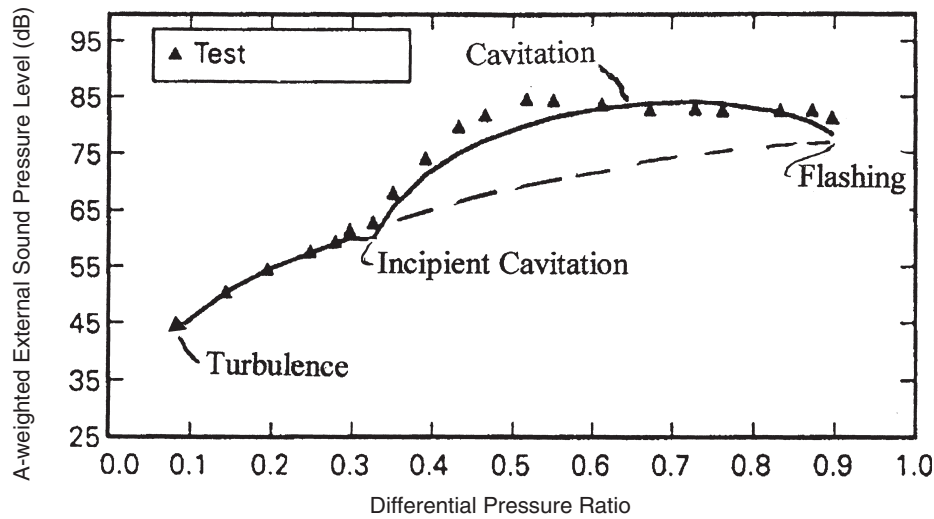


**Figure 2** Principal behavior of cavitation in a valve,  $P_1$  and  $P_2$  denote upstream and downstream static pressure, respectively. When the minimum static pressure is less than a certain critical value ( $P_{2r}$ ) cavitation starts. When the downstream pressure  $P_2$  is less than the vapor pressure  $P_v$ , a phenomenon called “flashing” can occur. In this case a liquid-gas mixture approaches the vena contracta and partial vaporization of the liquid occurs during acceleration of the flow.

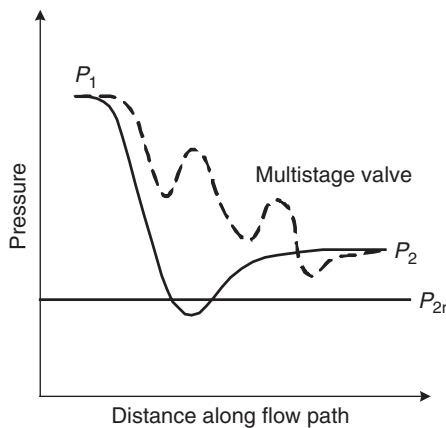
for cavitation, that is, the creation of vapor-filled bubbles that then implode. The rapid collapse of the bubbles can create very high local pressure peaks with levels up to  $10^{10}$  Pa that can result in mechanical damage.<sup>8</sup> When the flow is accelerated toward the vena contracta of a valve, the speed increases and the static pressure drops, in accordance with Bernoulli’s equation; see Fig. 2. Cavitation starts when the local static downstream pressure reaches a certain critical limit  $P_{2r}$ , the value of which depends on the temperature and the amount of solved gas in the liquid. The minimum value for the critical pressure is the vapor pressure of the liquid  $P_v$ . The IEC Standard 60543-8-4<sup>9</sup> introduces an incipient cavitation pressure ratio  $(P_1 - P_2)/P_1$  at which cavitation commences; it is called  $X_{fz}$ . Typical values for  $X_{fz}$  are given by the valve manufacturer. Values range from 0.2 for large valves to 0.35 for small valves.

The principal behavior of cavitation noise<sup>10</sup> can be illustrated by Fig. 3. At  $(P_1 - P_2)/P_1 < X_{fz}$  the emitted sound increases due to a process of fluid-induced turbulence. Above this pressure ratio cavitation commences quite rapidly and then reaches a maximum. The sound pressure level thereafter decreases again as more vapor is produced and then reaches a point that corresponds to the continuing slope of the turbulent noise. At this stage we have “flashing,” that is, the vapor bubbles no longer collapse. One should also realize that valves operating in the laminar flow regime do not experience

be expected that the monopole type of mechanism will dominate.<sup>2</sup> In liquids there is also the possibility



**Figure 3** Test data taken for 25-mm globe valve with a parabolic plug, flow to open. Calculated values are represented by solid line. The flow coefficient and other data are: Valve sizing coefficient  $2.16 \times 10^{-4} \text{ m}^2$  ( $C_v = 9 \text{ gal/min (lb/in}^2\text{)}^{0.5}$ ). Jet diameter = 0.0285 m,  $F_L = 0.9$ ,  $F_d = 0.38$ ,  $X_{fz} = 0.32$ .  $P_1 = 1000 \text{ kPa}$ .



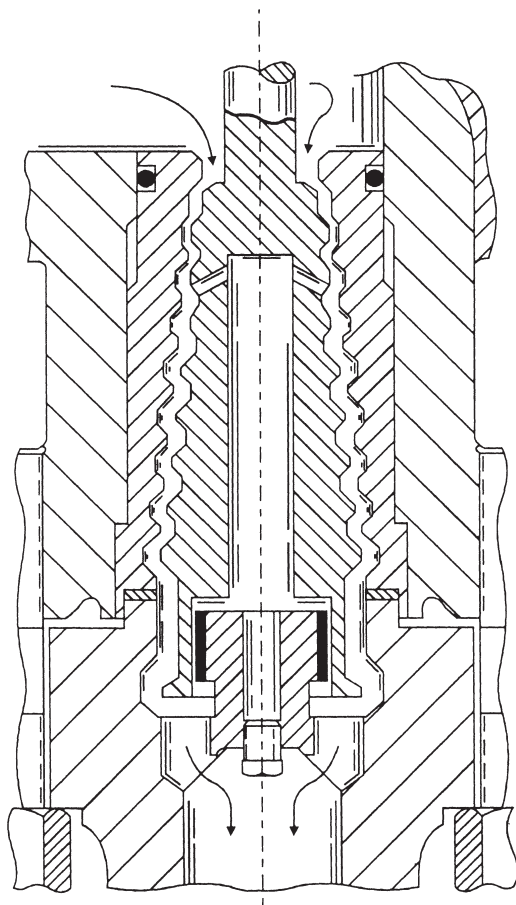
**Figure 4** Use of multistage arrangement to create a certain pressure drop without reaching the critical cavitation pressure in the system, see also Fig. 5.

cavitation. A good way to avoid cavitation in large valves is to use a special valve trim having multiple throttling stages as shown in Figs. 4 and 5.

Prediction of cavitation noise is even more complex than that of aerodynamic noise, and the reader is referred to IEC Standard 60543-8-4 or to Ref. 9. One should note that, in contrast to aerodynamic noise, for water the point of maximum sound transmission through the pipe wall is at the ring frequency of the pipe ( $f_r$ ), where, for steel pipes  $f_r = 5000/3.14D_i$  (Hz) and  $D_i$  = the inside diameter of the pipe (m).

## 5 MECHANICAL NOISE

This normally originates from the valve plug and is mainly a problem in liquid-filled systems and especially if there is a gas–fluid mixture involved. The cause is periodic flow separation creating fluctuating fluid forces, which excite structural vibrations in the valve plug + stem, for example, bending modes. A particularly dangerous situation arises when a periodic flow phenomenon around the valve plug, characterized by a Strouhal frequency  $f_{St}$ , is close to a structural eigenfrequency  $f_{Mek}$ , where  $f_{Mek} = 0.16 \times (\text{spring rate of the valve stem/mass of valve plug})^{0.5}$ . This can create a self-sustained oscillator, which means that the two phenomena form a positive feedback loop, where energy from the mean flow is fed into the structural eigenfrequency. A growing oscillation at a dominating frequency will then be created, limited in amplitude only by losses or nonlinear effects.<sup>11,12</sup> This type of phenomenon is normally referred to as valve screech and can create very high vibration amplitudes with risk for mechanical failure as well as high emitted noise levels. Screech can also be created by interaction between an acoustical mode in the pipe system and a structural valve mode. Also for this case, the energy feeding the structural and acoustical modes is taken from the mean flow via the fluid forces acting on the valve plug. To eliminate valve screech, there exist two main alternatives: (i) to disturb or reduce the amplitude of the periodic flow phenomenon at the valve plug (sometimes a reversal in flow direction will help) and (ii) to damp or move the mechanical eigenfrequency (reduce the weight of the plug, or, increase the stem stiffness



**Figure 5** Single-flow area, multistep valve plug. This low-noise trim uses 11 throttling steps with a single, annular flow area. Note, areas gradually enlarge to accommodate changes in gas density due to lowering of pressure. Benefits are lower throttling velocities.

by shortening its length or increasing its diameter). Concerning the first alternative, typical methods are based on decreasing the pressure drop across the valve or using geometrical modifications to reduce flow instabilities.

## 6 WHISTLING

Another powerful sound source also related to the creation of a self-sustained oscillator is whistling.<sup>11,12</sup> This can occur when a periodic flow phenomenon forms a positive feedback loop with an acoustic eigenfrequency. Two possibilities exist, either at a low-frequency plane wave mode, corresponding to a multiple of half a wave length in a pipe branch, or the cutoff frequency for a higher order mode over a pipe cross section.<sup>12,13</sup> The first case normally corresponds

to low-frequency tones (up to a few hundred hertz) while the nonaxial case typically correspond to the kilohertz range.<sup>13</sup> Presently, there are no simple methods to predict with certainty the existence or the level of fluid-driven self-sustained oscillators. Fortunately, this is a rather rare phenomenon.

## 7 MEASUREMENT OF VALVE NOISE

For gas-filled systems most of the generated sound will be emitted on the downstream side of the valve.<sup>7</sup> For liquid-filled systems there is typically a more uniform distribution and the sound tends to radiate equally in all directions, that is, around 50% of the power is radiated from the valve body and 25% is radiated up- and downstream.<sup>2</sup> Normally, valve noise measurements are based on the international standard<sup>14</sup> IEC 60534-8-1. Testing is done by placing the valve into an anechoic chamber to isolate the valve from ambient noises. Negligible downstream reflections are required; so a reflection-free termination must be used. Basic measurements consist of measuring the A-weighted sound pressure level 1 m downstream from the valve outlet and 1 m perpendicular from the pipe wall. Radiated sound power can be calculated by taking into account the transmission loss of the pipe wall.

## 8 ANALYSIS OF PIPE SYSTEMS

The standard approach for an acoustic analysis of a complete pipe system is to use power-based methods, that is, each source is treated separately, and the resulting acoustic power from several sources is simply obtained by addition. The sound power in a pipe is assumed to propagate along the system where it is attenuated by natural damping at the walls and radiation or by dissipative silencers. This power-based approach is valid for broadband sources and for frequencies well above the plane wave range. A useful guideline for an acoustic power-based analysis of noise in pipes is the VDI 3733.<sup>15</sup> For the plane wave range strong standing-wave effects and coupling between acoustic sources can be expected, which will change the acoustic power output. For this low-frequency range, power-based methods should not be used; instead more detailed analysis methods based on acoustic two-ports is more appropriate; see Chapter 85 in this handbook.

In the power-based methods the effect of multiple reflections is normally neglected. Such reflections can lead to an increase in the sound power level inside a pipe and thereby to an increase in the radiated level and are therefore important to include. A recent treatment of the problem that offers a new formalism based on two-ports for acoustic power flow, is the work of Åbom and Gijrath.<sup>16</sup> The new formalism has the advantage of having the same structure as the existing two-port formalism for the plane wave range. This means that existing codes for two-port plane wave analysis easily can be modified and used for a power-based analysis that takes multiple reflections into account.



## 9 NOISE REDUCTION METHODS

Noise reduction measures can either be applied at the valve itself or along the transmission path; both of these alternatives will be discussed below.

### 9.1 Reduction at the Valve

Here the discussion will focus on the steady-state noise associated with control valves. From a thermodynamic point of view a control valve converts pressure energy into heat to control the mass flow. The heat conversion normally takes place via turbulent flow losses with associated noise generation. Of course, it is possible to design control valves where the heat production is created via laminar flow losses, but that is quite impractical. Standard valve designs are based on turbulent dissipation and for such valves the generated noise is proportional to orifice velocity to the 3.6th power.<sup>6</sup>

The first alternative is to use so-called single-flow path, multistage valve trims where a desired pressure drop is split into a number of steps. Assuming an unchanged jet area and  $N$  equal steps that act as independent sources, the individual pressure drop per stage and its corresponding velocity is lower, producing less total sound power ( $\sim N^{2.6}$ ) compared to the single-step arrangement.

For instance, with three steps the reduction in sound power will be around 12 dB. Unfortunately, for gases, the area of each stage has to be expanded to accommodate the density changes. This then negates a good part of the above noise reduction. An example of a multistage pressure reduction trim is shown in Fig. 5.

Noise reduction for a given valve can also be achieved by a series of carefully designed downstream throttling plates as described for instance by Hynes.<sup>17</sup> Here the pressure drop across an inherently noisy valve is reduced by up to 90% and instead shifted to the multistep and (high-frequency producing) multihole plates. As a result, an overall A-weighted noise level reduction of up to 25 dB can be achieved.

The second alternative is the so-called single-stage multiple-flow path valve trims, where the outlet jet is split into a number of smaller jets. This procedure will lead to a substantial increase in the peak frequency ( $f_p$ ), which in turn increases the pipe's transmission loss. Here  $f_p = 0.2U/d_H$  (Hz), where  $d_H$  is the hydraulic diameter (m) of the jet (or each of multiple jets).<sup>3</sup>

For high frequencies in the mass-damped region of the pipe, the increase in transmission loss is proportional to 6 dB per octave. Thus, reducing the size of an orifice by a factor of 10 (hence increasing the peak frequency by 10) can reduce the external A-weighted sound pressure level by 20 dB. No wonder that this is by far the most popular method of reducing valve noise; see Fig. 6. Care should be taken not to place adjoining orifices too close to each other in order to avoid jet

interaction. This will create combined larger jet diameters and therefore negate the desired peak frequency increase.

It is also possible to combine both alternatives and design multipath and multistage valve trims as shown in Fig. 7. Some of these trims operate at peak frequencies of up to 50 kHz. The question then is why is there any concern for noise, since the human ear cannot hear above 20 kHz?

Well, the reason is the sound pressure level inside the pipe decreases from the peak frequency level at a rate of about 6 dB per octave ( $20 \log f$ ). Thus, there is still a substantial amount of sound escaping at the point of the lowest transmission loss (the first coincidence or cut-on frequency  $f_{c1}$  for gases<sup>3,6</sup>). For example, let's assume  $f_{c1} = 8000$  Hz and  $f_p = 50,000$  Hz. The sound pressure level at the peak frequency is assumed to be 146 dB. The pipe internal sound pressure level at  $f_{c1}$  will now be  $146 - 20 \log (f_p/f_{c1}) = 130$  dB. Assuming a pipe transmission loss of 46 dB gives an external sound pressure of  $130 - 46 = 84$  dB outside of the pipe wall. If this valve would have had a standard trim operating at a peak frequency close to  $f_{c1}$ , the external sound level would have been  $146 - 46 = 100$  dB.

A more modern low-noise trim is shown in Fig. 8. Here we have multiple inlet orifices separated by a resonant settling chamber and then followed by additional multiple outlet ports (total outlet area adjusted for lower downstream density). The inlet ports are well rounded and have the general shape of a venturi, thus deliberately creating supersonic jets with lower, or terminal, acoustic efficiency due to shock-cell interaction. Here more than 90% of the pressure energy is converted within the inlet orifice alone. The last, multiple exit stages are on purpose not streamlined and therefore operate at relatively low velocity (below Mach 1) and essentially at the less efficient quadrupole mechanism. This is believed to be the first low-noise valve trim taking advantage of the latest acoustic theories. Thus, it offers noise reductions of about 30 dB over conventional trims while being very compact.

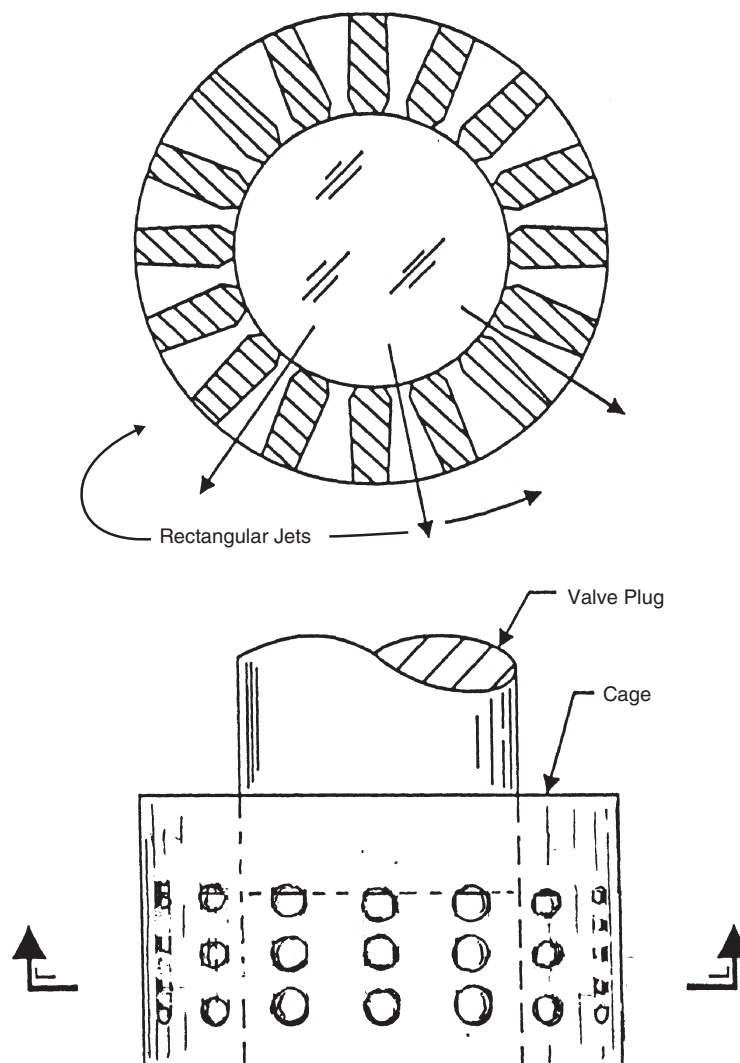
## 10 VALVE NOISE REDUCTION GUIDELINES

Here are some guidelines on how to handle anticipated noise problems with valves. These are applicable for both liquids and gases. The listing is in order of severity.

### Source Treatment

- Specify a valve trim that has a low-pressure recovery (high  $F_L$  factor); this will reduce jet velocity. Typical noise savings 5 dB.\*

\*A single-stage cage or plug is limited to a pressure ratio ( $P_1/P_2$ ) of about 4:1 unless a multistage trim (nested cage) is used.



**Figure 6** Multiorifice cage trim. Single-step but multiple flow passages characterize this cage trim. Benefits are higher internal peak sound frequencies and resultant increase in pipe transmission losses. Hence lower external noise.

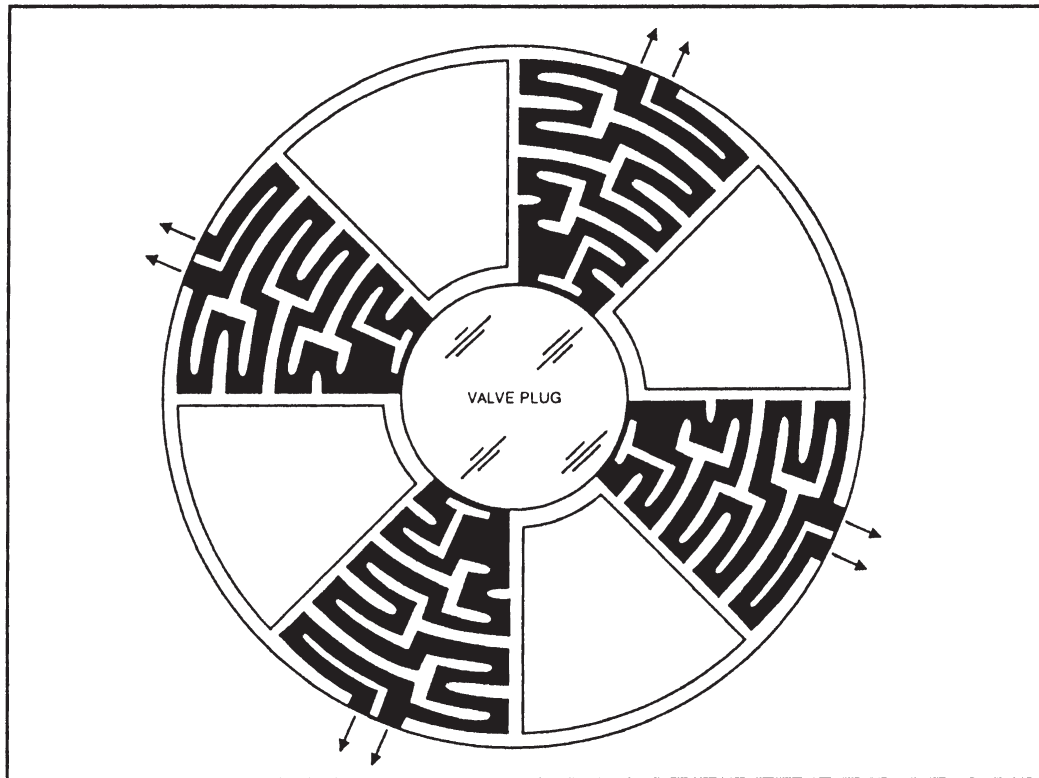
- Use a multistep trim. Typical noise reduction 10 dB.
- Specify a multiported cage or valve plug.<sup>11</sup> Noise reduction about 15 dB.
- Consider a combined multiported and multistep trim\* Noise savings typically 25 dB.
- Combination of low-noise trim and multiported plate (or plates) installed in downstream pipe. Noise reduction up to 30 dB.

#### Path Treatment

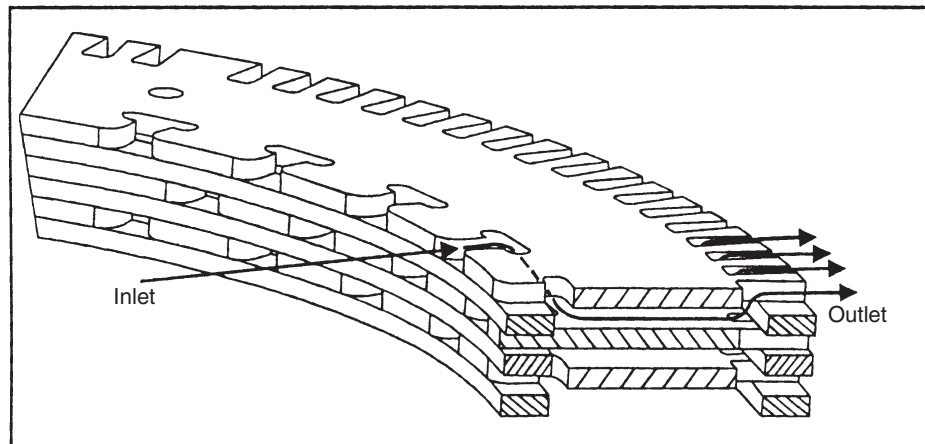
- Acoustic (or thermal) lagging<sup>†</sup> Reduces noise typically by 20 dB.
- Silencer downstream (gas only). Noise reduction up to 15 dB.
- Silencer upstream and downstream (gas only). Noise reduction typically 30 dB.

\*Check for gas velocity in the valve outlet port if  $P_1/P_2$  ratio is high. Outlet velocity should not exceed 0.2 Mach.

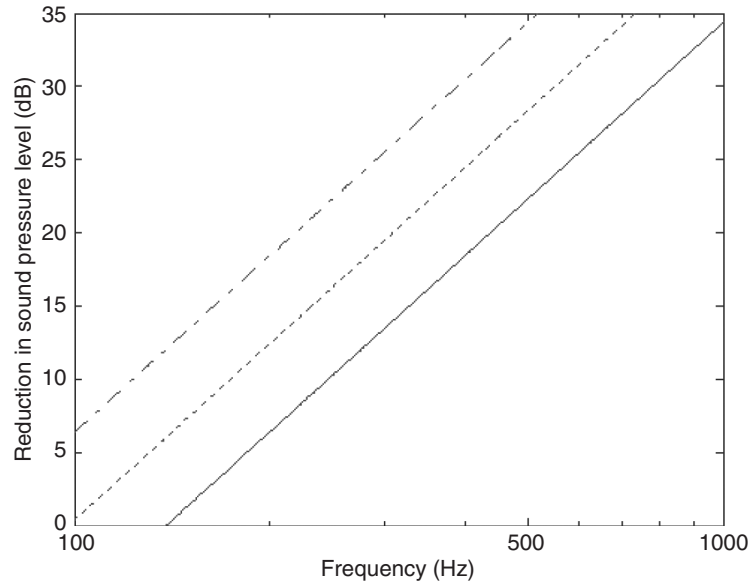
<sup>†</sup>It is preferable to reduce at least a portion of the generated sound pressure level within the source. Remember, source (valve) sound pressure levels above 110 dB can lead to mechanical failures due to associated high vibration levels.



**Figure 7** Labyrinth-type cage insert featuring a combination of multistep and multipath grooved flow channels for reduced velocity and increased frequency benefits.



**Figure 8** Two-stage, multipath, low-noise trim fabricated from identical stampings. Inlet passages are streamlined to create supersonic jets under high-pressure ratios while outlet areas have more abrupt passages with increased cross sections for subsonic velocities. Both passage sets are separated by a settling chamber. (Courtesy Fisher Controls International.)



**Figure 9** Reduction in sound pressure level caused by acoustical lagging based on Eq. (6) using a 0.5-mm steel sheet: - - -  $h = 0.20$  m; - . . -  $h = 0.10$  m; —  $h = 0.05$  m. Note higher values than 35 dB are not reached with single layers.

## 11 REDUCTION ALONG THE PATH

Besides noise from valves, also noise created by a high-speed ( $>40$  m/s for gases) turbulent flow in a pipe must be considered. However, in practice, pipe noise will only exceed valve noise at gas velocities at the valve's outlet exceeding 0.3 Mach for standard trims and 0.2 Mach for low noise trims.<sup>18</sup> The internal sound power (dB re 1 pW) created by the turbulent boundary layer in a straight pipe is according to VDI 3733<sup>15</sup> given by

$$L_{W+}(f) = 20 - 0.16U + 10 \log_{10}(A \times P \times U^6) - 25 \log_{10} \frac{NT}{N_0 T_0} - 15 \log_{10} \frac{\gamma}{1.4} - 15.5 \log_{10} \frac{f}{U} \quad (4)$$

where  $A$  is the cross-sectional area of the pipe (in  $\text{m}^2$ ),  $P$  is the static pressure (in Pa) normalized with the reference pressure 100 kPa,  $U$  is the flow speed (in m/s),  $N$  is the gas constant ( $N_0 = 287$  J/kg K),  $T$  is the absolute temperature ( $T_0 = 273$  K),  $\gamma$  is the specific heat ratio, and  $f$  is the octave band midfrequency (in Hz). The formula is valid in the range  $12.5 \leq f/U \leq 800$ .

In addition, bends and regions with flow separation, for example, area expansions, can represent important sources of flow-induced noise. To avoid excessive flow separation and noise generation expansions (from

the valve outlet to the pipe) should be in the form of conical sections with an angle not exceeding  $15^\circ$ , except where gas exit velocities at the valve outlet exceed Mach 0.3. Bends should also be separated from the outlet jet ( $> 5D_j$ ) of a valve to avoid a strong excitation of wall vibrations and sound radiation. It can also be noted that bends will have a higher sound transmission than a straight pipe section of the same diameter and wall thickness due to mode conversion.

For a given internal sound power in a pipe the radiated sound depends on the sound reduction index of the pipe wall. A representative value<sup>19,20</sup> for the sound reduction index in the midfrequency range between  $f_{c1}$  (the 1st coincidence frequency) and  $f_r$  (the ring frequency), where maximum transmission occurs, is given by

$$R'_W = 10 + \log_{10} \frac{\rho_w c_L t_w}{\rho_f c_f D_i} \quad (5)$$

where  $D_i$  is the inner diameter,  $\rho_w$  is the density of the wall material,  $\rho_f$  is the density of the fluid,  $t_w$  the thickness of the wall,  $c_f$  is the speed of sound in the fluid, and  $c_L$  is the longitudinal wave speed in the wall. From this equation it follows that an increase of the wall thickness with a factor 2 will reduce the radiated sound pressure level by 3 dB. The IEC procedure predicts a larger influence of the wall thickness with an increase up to 6 dB per doubling of wall thickness. It

follows that changing the wall thickness is not a very efficient way of reducing the radiated sound. Instead so-called acoustic lagging is preferable when large reductions ( $>10$  dB) are needed.<sup>21–23</sup> This basic idea is similar to a vibration isolation and aims at shielding the original pipe with a structure that has a reduced vibration level. This is done first by wrapping the pipe with a porous material (mineral wool) and covering this with a limp and impervious top sheet. The porous material provides sound absorption together with the enclosed air stiffness and damping. The damping is important to reduce the effect of acoustic modes between the pipe wall and the top sheet. The porous material used should have a high flow resistivity ( $> 20$  Rayl/cm) and a low modulus of elasticity ( $E < 0.15$  MN/m<sup>2</sup>).

Assuming that the top sheet is mass controlled the reduction in the radiated sound pressure level, for frequencies above the fundamental mass-spring resonance, will be<sup>15</sup>

$$\Delta L_p \approx \frac{40}{1 + 0.12/D_0} \log_{10} \left( \frac{f}{2.2f_0} \right)^2 \quad f > f_0 \quad (6)$$

where  $f$  is the frequency (Hz),  $f_0$  is the mass-spring resonance frequency (Hz), and  $D_0$  is the outer diameter (m) of the pipe (without lagging). The mass-spring resonance can be calculated from

$$f_0 = 60 \sqrt{\frac{m_t'' + m_p''}{m_t' m_p' h}} \quad (\text{Hz}) \quad (7)$$

where  $m''$  is the surface mass (kg/m<sup>2</sup>), the superscript  $t$  denotes the top sheet and  $p$  the pipe, and  $h$  is the thickness (m) of the porous (air-filled) layer. Equation (6) has been plotted in Fig. 9, assuming pipe walls that are much heavier than the top sheet and with diameters  $> 0.12$  m. In practice, using a single-walled lagging a maximum reduction of 30 to 35 dB can be reached. Higher values can be reached in particular in the high-frequency range by using double-walled designs.

In gas-filled systems silencers can also be used to reduce radiated noise from the downstream side of a valve and also at its upstream side, since a good portion of the sound power generated at the valve's interior will escape upstream (typically 10 dB less the downstream). This is especially prevalent for "line-of-sight" valves such as butterfly or ball valves. It is then important that the silencer is positioned as close as possible to the valve or the upstream end of a pipe from which radiation is to be reduced. There are two basic types of silencers: reflective and dissipative, see also Chapter 85. Reflective silencers create a reflection of waves by an impedance mismatch, for example, by an area change or a side-branch resonator. The reflective silencer type is primarily intended for the plane wave range and is efficient for stopping single tones. Dissipative silencers are based on dissipation

of acoustic energy into heat via porous materials such as fiberglass or steel wool. These silencers are best suited for broadband sources and for the mid- or high- frequency range, which means that dissipative silencers are best suited for reducing valve noise.

## REFERENCES

1. V. A. Carucci and R. T. Mueller, ASME Paper 82-WA/PVP-8, Acoustically Induced Piping Vibration in High Capacity Pressure Reducing Systems, 1982.
2. H. D. Baumann and G. W. Page, A Method to Predict Sound Levels from Hydrodynamic Sources Associated with Flow through Throttling Devices, *Noise Control Eng. J.*, Vol. 43, No. 5, 1995, pp. 145–158.
3. IEC Standard 60534-8-3, Control Valve Aerodynamic Noise Prediction Method, International Electrical Commission, Geneva, Switzerland, 2000.
4. M. J. Lighthill, On Sound Generated a Aerodynamically. I. General Theory, *Proc. Roy. Soc.*, Vol. A211, 1952, pp. 564–587.
5. H. D. Baumann, On the Prediction of Aerodynamically Created Sound Pressure Level of Control Valves, ASME Paper WA/FE-28, 1970.
6. H. D. Baumann, A Method for Predicting Aerodynamic Valve Noise Based on Modified Free Jet Noise Theories, ASME Paper 87-WA/NCA-7 28, 1987.
7. G. C. Chow and G. Reethof, Paper A Study of Valve Noise Generation: Processes for Compressible Fluids, ASME 80-WA/NC-15, 1980.
8. R. T. Knapp, Recent Investigations of the Mechanics of Cavitation and Cavitation Damage, *ASME*, Vol. 77, 1955, pp. 1045–1054.
9. IEC Standard 60534-8-4, Prediction of Noise Generated by Hydraulic Fluids, International Electrical Commission, Geneva, Switzerland, 2000.
10. H. D. Baumann and G. Kiesbauer, Valve Noise, *Noise Control Eng. J.*, Vol. 52, No. 2, 2004, pp. 49–55.
11. W. K. Blake, *Mechanics of Flow-Induced Sound and Vibration*, Vol. 1, Academic Press, New York, 1986.
12. U. Ingard, Valve Noise and Vibration, Report No. 40, prepared for Värmeforsk, Sweden, 1977.
13. G. Reethof, Control Valve Reduction and Regulator Noise Generation, Propagation and Reduction, *Noise Control Eng. J.*, Vol. 9, No. 2, 1977, pp. 74–85.
14. IEC Standard 60534-8-1, Laboratory Measurement of Noise Generated by Aerodynamic Flow through Control Valves, International Electrical Commission, Geneva, Switzerland, 1990.
15. VDI 3733, Noise at Pipes, *Verein Deutscher Ingenieure*, July 1996.
16. H. Gijrath and M. Åbom, A Matrix Formalism for Fluid-Borne Sound in Pipe Systems, *Proc. ASME 5:t Int. Symp. New Orleans Nov-02*, NCA 33356, 2002.
17. K. M. Hynes, The Development of a Low-Noise Constant Area Throttling Device, *ISA Trans.*, Vol. 10, No. 4, 1971, pp. 416–421.
18. H. D. Baumann, Predicting Valve Noise at High Exit Velocities, *INTECH*, Feb. -97, 1997, pp. 56–59.
19. L. Cremer, Theorie der Schalldämmung zylindrischer Schalen, *Acustica* Vol. 5, 1955, pp. 245–256.

20. M. Heckl, Experimentelle Untersuchungen zur Schalldämmung von Zylindern, *Acustica*, Vol. 8, 1958, pp. 259–265.
21. E. Hale and B. A. Kugler, The Acoustic Performance of Pipe Wrapping Systems, ASME Paper 75, WA/Pet-2, 1975.
22. W. H. Bruggeman and L. L. Faulkner, Acoustic Transmission of Pipe Wrapping Systems, ASME Paper 75, WA/Pwr-7, 1975.
23. ISO Standard 15665, Acoustic Insulation for Pipes, Valves and Flanges, 2003.

# CHAPTER 76

## HYDRAULIC SYSTEM NOISE PREDICTION AND CONTROL

Nigel Johnston

Department of Mechanical Engineering  
University of Bath  
Bath, United Kingdom

### 1 INTRODUCTION

This chapter focuses on high pressure hydraulic fluid power systems using positive displacement pumps. In such systems line diameters are generally relatively small (typically 10 to 50 mm). The flow is generally considered to be single phase (quantities of gas bubbles or solid particles are negligible), and pressures are typically up to 100 to 300 bars. These systems have a reputation for often producing unacceptably high levels of noise. This problem can limit the range of applications of fluid power and often causes the system designer to favor other means of power transmission. However, there are several measures that can be taken for noise reduction.

*Airborne noise* originates from vibrations of components, pipeworks, and housing. This vibration or *structure-borne noise* may be caused directly by the mechanical action of pumps and motors and can be transmitted from pumps through mounts, driveshafts, and pipes. Structure-borne noise may also arise from system pressure ripple or *fluid-borne noise*. Fluid-borne noise is caused primarily by unsteady flow from pumps and motors but sometimes from valve instability, cavitation, or turbulence. Fluid-borne noise can be transmitted long distances through pipework.

### 2 POSITIVE DISPLACEMENT PUMP FLOW RIPPLE AND NOISE

The prime sources of noise in a hydraulic circuit are usually the pumps and motors, although valves are also important noise generators.<sup>1-4</sup> In addition, prime movers can be noisy; diesel engines produce high noise and vibration levels, and electric motors generally have fan cooling systems that produce noise.

Pumps for fluid power applications are generally positive displacement devices. The most common types are piston pumps, gear pumps, and vane pumps, and there are several variations for each type.<sup>5</sup> The following discussion also applies to hydraulic motors, which work in a similar way to pumps.

Positive displacement pumps tend not to produce an absolutely steady flow rate. Instead, the flow consists of a mean value on which is superimposed a flow ripple. The magnitude of the flow ripple is dependent upon the pump type and operating conditions but usually has a peak-to-peak amplitude of between 1 and 10% of the mean flow rate. Pump flow ripple tends to have a periodic waveform due to the cyclic nature

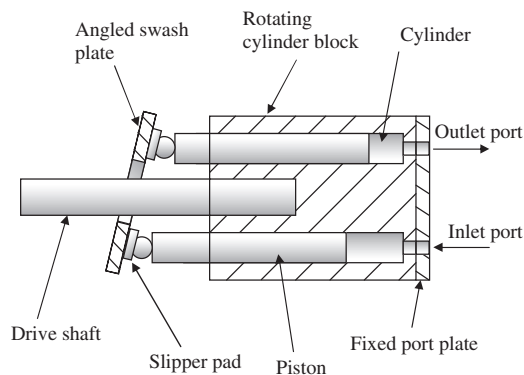
of a pump's operation, and different classes of pump have different characteristic flow ripple waveforms. This flow ripple interacts with the characteristics of the connected circuit to produce a pressure ripple. There are methods available for measuring pump flow ripple and fluid-borne noise characteristics. See, for example, Ref. 6 and 7.

Flow ripple occurs in both the suction and the discharge lines. Normally, the discharge flow ripple is most important in terms of noise. However, fluid-borne noise in the suction line may cause noise problems especially when it causes vibration of the reservoir. The large surface area of the reservoir may act as a "loudspeaker."

### 2.1 Flow Ripple from an Axial Piston Pump

Axial piston pumps are commonly used in high-performance applications as they can have variable capacity and can operate at very high pressures. A simplified cross section of an axial piston pump is shown in Fig. 1. A rotating cylinder block is attached to the shaft, and an angled swash plate causes the pistons to reciprocate. At the other end of the cylinders is a fixed port plate to provide communication between the cylinders and the inlet and outlet ports.

Consider first of all the flow that is produced by an idealized single cylinder. The piston moves sinusoidally, and the port plate is arranged so that the cylinder communicates with either the suction or



**Figure 1** Simplified cross section of an axial piston pump.

discharge port, depending on the direction of motion of the piston. First, we will assume that the cylinder switches from one port to the other at exactly top dead center (TDC) and bottom dead center (BDC), and ignore fluid compressibility. The flow from the cylinder into the discharge will be equivalent to half a sinusoid as shown in Fig. 2. This is termed the *kinematic* component as it is determined purely from geometric considerations.

In reality, however, as the piston passes BDC and the discharge port opens to the cylinder, the difference between the high-pressure discharge and the low pressure in the cylinder causes a reverse flow into the cylinder until the pressure equalizes. This can take the form of a sharp spike as shown in Fig. 2. The amplitude of this spike is pressure dependent and it can be quite large. Fluid inertia in the port plate can cause oscillations after the spike as shown in the figure. A similar effect will occur in reverse as the cylinder passes TDC and opens to the inlet port.

The total flow ripple from a multicylinder pump is the sum of individual cylinder flows. Usually, the main feature of the flow ripple is the flow spike due to fluid compression, which can lead to severe system noise. This repeats itself for each cylinder; a nine-cylinder pump will have nine spikes per revolution. The magnitude of the flow ripple from axial piston pumps is strongly dependent on the design of the pump, in particular the port plate geometry. Fig. 3 shows some measured flow ripples for a piston pump<sup>5</sup> (the plots are offset vertically for clarity). The compression pulse is clearly apparent and its magnitude is roughly proportional to pressure.

The flow ripple can be reduced by use of carefully designed relief grooves in the port plate as shown in Fig. 4. These have the effect of slowing down the compression of the fluid in the cylinders and making the reverse flow spike less severe, as Fig. 5 shows. Most pumps of this type make use of this feature.

Retardation of the opening of the port plate can also reduce the flow ripple. In this way, the piston motion can be used to precompress the fluid in the cylinder to the delivery pressure before the delivery port opens. This can be very effective as shown in Fig. 5, but

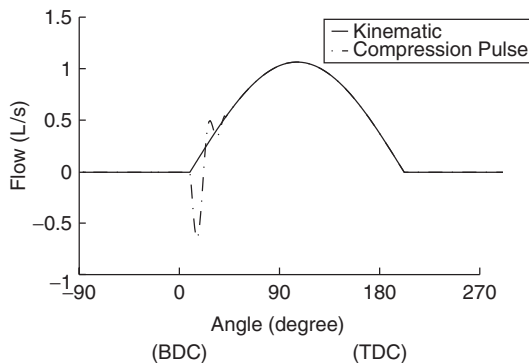


Figure 2 Flow from a single cylinder.

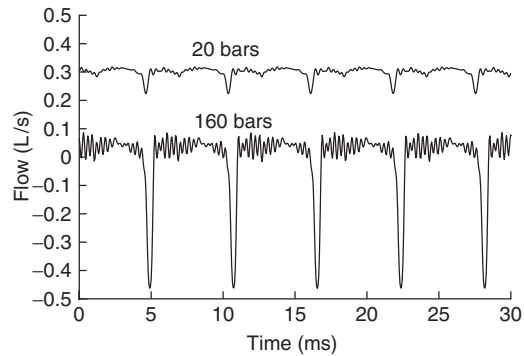


Figure 3 Measured piston pump flow ripple.

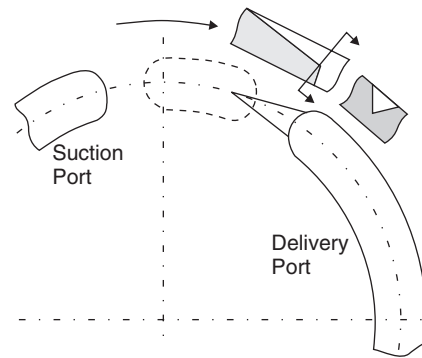


Figure 4 Axial piston pump relief grooves.

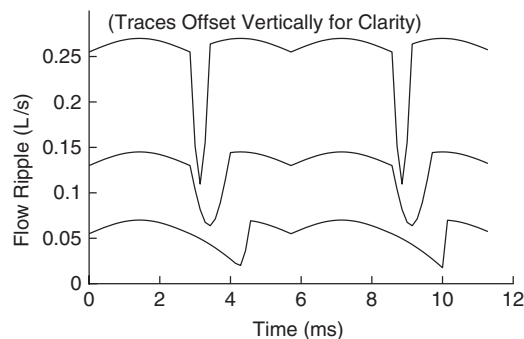


Figure 5 Typical flow ripples for different port plate configurations.

the optimum delay depends on the load pressure, swash setting, and fluid properties. Most pumps have a combination of relief grooves and retarded ports. Adjustable delays have been tried, but this can be very complicated to implement successfully.

The fundamental frequency is equal to the *pumping* frequency, that is, the speed of the pump (in revolutions/second) times the number of pistons, gear teeth, or other pumping elements. A typical plot of the flow

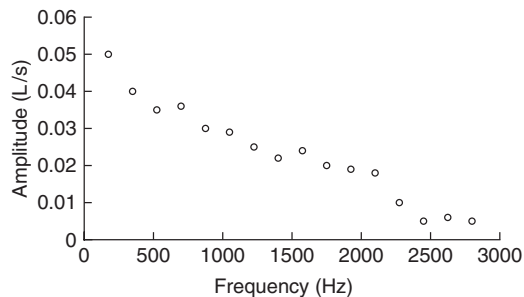


ripple harmonic amplitudes for an axial piston pump is shown in Fig. 6. The “spiky” nature of the flow ripple waveform is manifested in a large number of strong harmonics over a broad frequency range.

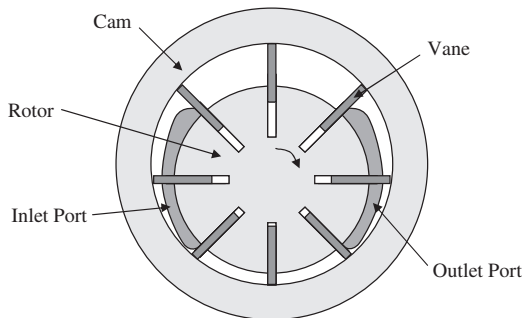
## 2.2 Flow Ripple from Vane Pumps

Vane pumps incorporate a slotted rotor and a eccentric or oval cam ring. Flat metal vanes slide in the rotor slots and bear against the cam ring as shown in Fig. 7.

The flow ripple from vane pumps has similar features to that from axial piston pumps. The flow ripple depends on the shape of the cam ring, but



**Figure 6** Typical piston pump flow ripple spectrum.



**Figure 7** Simplified diagram of a vane pump.

generally the dominant component is produced by fluid compression as a vane passes the start of the delivery port. This can be made more gradual by the use of relief grooves. The magnitude of the flow ripple tends to be increased if cavitation or air release occurs because of increased fluid compression. Hydraulic power-assisted steering systems often use engine-driven vane pumps with integral flow and pressure control valves, in which the excess flow is bypassed internally through a valve from the pump delivery back to the intake. Cavitation or air release can occur in the bypass valve, resulting in gas bubbles being recirculated through the pump.

## 2.3 Flow Ripple from Gear Pumps

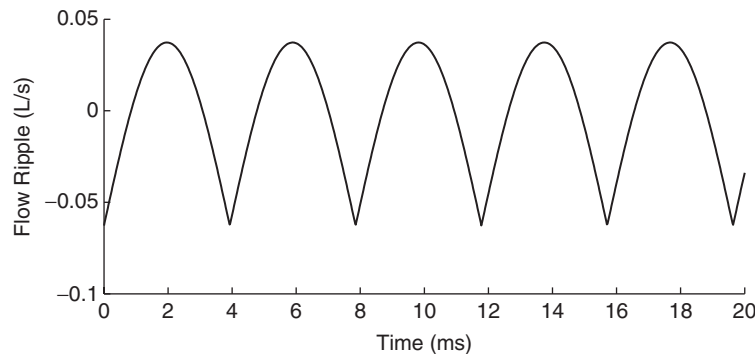
External gear pumps consist of two meshing gears in a housing. Fluid is pumped via the gaps between the gear teeth. The idealized form of the source flow ripple from an external gear pump is shown in Fig. 8. It is due to the changing geometry of the meshing of the gears as they rotate. It is generally assumed to be independent of pressure. Fluid compression, although it does take place between the inlet and outlet ports, normally tends to be less sudden as it is spread over a large angle of gear rotation and is therefore not as significant as for axial piston pumps.

The spectrum of this flow ripple consists of a very strong fundamental component and rapidly diminishing higher harmonics, as shown in Fig. 9. This can result in a quite different audible tone to that of a piston or vane pump.

Several attempts to produce low noise external gear pumps have been made, such as using helical gears or multiple, phased gears, or by reducing the gear backlash. However, these all incur a cost penalty.

## 2.4 Reduction of Pump Flow Ripple

The noise problem is tackled at its true source by reducing the flow ripple of the pump or motor. However, this cannot normally be controlled by the user except by changing the operating conditions. Reducing pressure can help but is generally not practical.



**Figure 8** Ideal gear pump flow ripple.

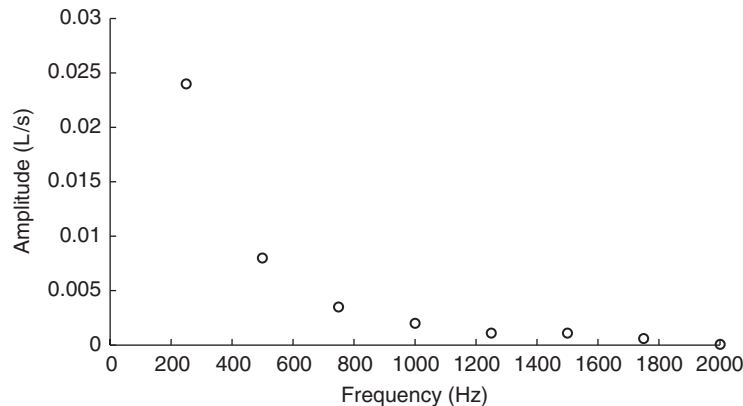


Figure 9 Typical gear pump flow ripple spectrum.

Air bubbles in the fluid can increase the fluid compressibility and hence increase pump flow ripple. Good reservoir design and suction line design can minimize air bubbles and air release.

Cavitation is the formation of bubbles of vapor that occurs in regions where the pressure falls to the vapor pressure of the liquid (the vapor pressure is typically about 100 to 1000 Pa absolute). Cavitation can increase pump noise, as well as being highly damaging. The cavitation can be directly audible either as a hissing or a harsh rattle. Additionally, cavitation releases air bubbles in the fluid. Cavitation can be avoided by good inlet line design or the use of a boost pump if necessary.

Selection of a different pump with less flow ripple may be a solution to a noise problem. Cost must, of course, be taken into account. Classes of pumps that generally produce low flow ripple include internal gear pumps and screw pumps. Screw pumps are used in submarines precisely because of their low noise, but rarely used elsewhere because of their cost. Pumps with high-flow ripple include external gear pumps and axial piston pumps. Generally, there are several other criteria that also need to be considered, and it is rarely possible to select a particular class of pump purely on the basis of its noise characteristics. Also, different pumps of the same class can produce radically different fluid-borne noise levels (Table 1).

### 3 VALVE NOISE

Valves can cause noise in a number of ways:

- Cavitation, air release, and turbulence

- Chatter or instability
- Water hammer

#### 3.1 Cavitation, Air Release, and Turbulence Noise

Cavitation frequently occurs in valves where it causes a distinct high-frequency hissing noise. The random nature of the bubbles causes a broadband spectrum. Flow and pressure control valves contain variable orifices to control the fluid flow. An orifice acts to restrict the flow causing a high-velocity jet. Bernoulli's equation states that the sum of static pressure and dynamic pressure is constant (if losses and gravity are neglected). The dynamic pressure is proportional to the square of the fluid velocity. In a high-velocity jet the dynamic pressure is high and hence the static pressure is low. Most of the dynamic pressure is dissipated through turbulence and viscous losses downstream of the orifice, but some may be converted back to static pressure when the jet slows down. This means that the pressure in the valve can be less than the downstream pressure. Also intense turbulence can occur around the jet, causing localized, unsteady low-pressure regions. Cavitation can occur if the localized pressure falls to the vapor pressure. Air release may also occur.

Some valve types are more prone to cavitation and turbulence noise than others. Laminar flow valves have been designed that avoid turbulence; however, the flow characteristics of these tend to be strongly dependent on the fluid viscosity and hence on temperature.

Cavitation is strongly influenced by the back pressure downstream of the valve. Often cavitation noise can be reduced by increasing the back pressure. One way of achieving this is to use two valves in series. Unfortunately, increasing the back pressure can sometimes have the converse effect of worsening cavitation noise, as cavitation noise tends to reach a peak at a certain back pressure and falls for lower or higher pressures.<sup>8</sup>

Table 1 Comparative Noise Levels of Typical Pumps

Noisiest	Axial piston pumps
.	External gear pumps
.	Vane pumps
.	Internal gear pumps
Quietest	Screw pumps

### 3.2 Valve Instability

Some valves can generate self-excited oscillations, which results in a squealing or whistling sound, sometimes very loud. This is an inherent feature of the valve and may be due to a combination of low damping, positive feedback, jet oscillation, and resonance. It tends to be highly dependent on pressure, flow, and temperature and sometimes comes and goes for no apparent reason. In some cases it can be eliminated easily by small changes in valve position or conditions, but in other cases it is more tenacious and may be avoided only by use of a different component.

### 3.3 Water Hammer

Water hammer<sup>9</sup> is a common name for hydraulic shocks or surges that usually occur when a valve is suddenly opened or closed. When a valve is closed the fluid is decelerated suddenly, causing a pressure rise at the inlet and fall at the outlet due to the momentum of the fluid. This results in a pressure wave that travels at the speed of sound through the pipelines (the speed of sound in hydraulic fluid is typically 1000 to 1400 m/s, considerably higher than in air). The wave is reflected when it reaches a valve, pump, reservoir, or other change. Cavitation can occur if a low-pressure wave is formed. Water hammer can cause severe transient vibration and “banging”. As well as causing noise, it can be damaging to the system. Water hammer is best avoided by preventing sudden valve closures. In severe cases shock alleviators such as accumulators can be used.

## 4 TUNING OF THE CIRCUIT TO AVOID RESONANT CONDITIONS

It may be helpful to understand the behavior of pressure waves as they travel in a hydraulic circuit. Consider a simple system consisting of a pump, a pipe, and a restrictor valve. The pump produces a flow ripple that consists of a broad spectrum of harmonic components. We shall examine what happens to one

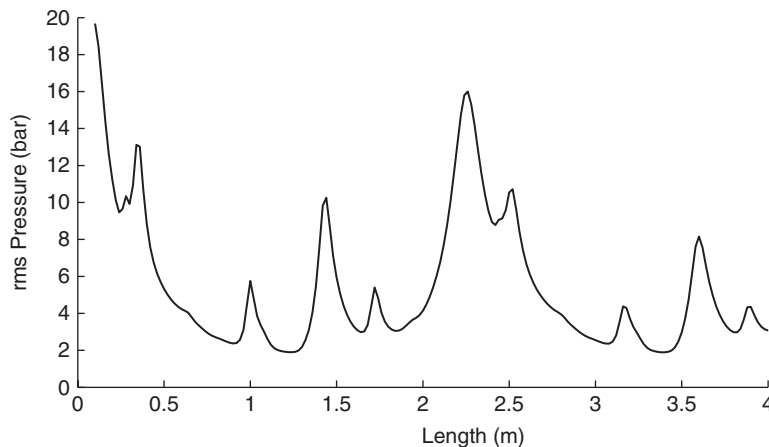
single harmonic (i.e., a pure sinewave) of this flow ripple.

The sinusoidal flow ripple harmonic produces a pressure wave that travels along the pipe at the speed of sound. When the wave reaches the other end of the pipe, it is reflected and travels back to the pump. It is reflected again at the pump, where it combines with the original wave. It may combine so as to reinforce the original wave, in which case high-pressure ripple levels can build up. This is a resonant condition. Alternatively, it may combine so as to partially cancel out the original wave, resulting in much lower pressure ripple levels. This is an antiresonant condition. Whether resonance, antiresonance, or something in between occurs depends on the length of the pipe and the frequency.

For the simple pump–pipe–restrictor system, the length of pipe has a great effect upon the pressure ripple levels. This also applies to more complicated systems. Thus by judicious system design, it may be possible to cause a significant reduction in the pressure ripple levels. However, for this to be done in a rational manner, detailed knowledge of the relationships between the circuit configuration and fluid-borne noise is required. For all but the most trivial of systems this relationship is not simple.

For example, Fig. 10 shows a graph of the simulated root-mean-square (rms) pressure ripple at the pump exit in a typical hydrostatic transmission consisting of a piston pump, a length of flexible hose, a length of rigid pipe, and a motor for a range of different rigid pipe lengths. Only the pressure ripple pump flow ripple is considered in this simulation; the motor is modeled as a passive termination. It can be seen that there is a very large variation in the simulated pressure ripple levels, and resonant peaks are apparent.

Some specialist software packages are available for prediction of fluid-borne noise levels.<sup>10,11</sup> These can aid the designer in determining what circuit dimensions



**Figure 10** Example of simulated pressure ripple magnitude in a hydrostatic transmission versus pipe length.

will cause resonance, so that steps can be taken to avoid these conditions. Alternatively, trial-and-error can be used. Tuning of the system is most likely to be effective when the speed of the pump is fixed, as it is difficult to avoid resonances if the harmonic frequencies are varying.

## 5 FLUID-BORNE NOISE SILENCERS OR PULSATION DAMPERS

A wide range of proprietary fluid-borne noise silencers (attenuators, pulsation dampers) is available. These, when used correctly, can be extremely effective in reducing the fluid-borne noise in a circuit, reductions of 20 to 40 dB (10:1 to 100:1) being typical. Specialized silencers tend to be expensive, and may be bulky and heavy, requiring robust supports. They normally are only suitable for situations in which the fluid-borne noise level is very critical and where cost, size, and weight are less important, such as in naval vessels. However, other common hydraulic circuit components such as accumulators and flexible hoses may be effective as fluid-borne noise silencers and provide a low-cost solution.

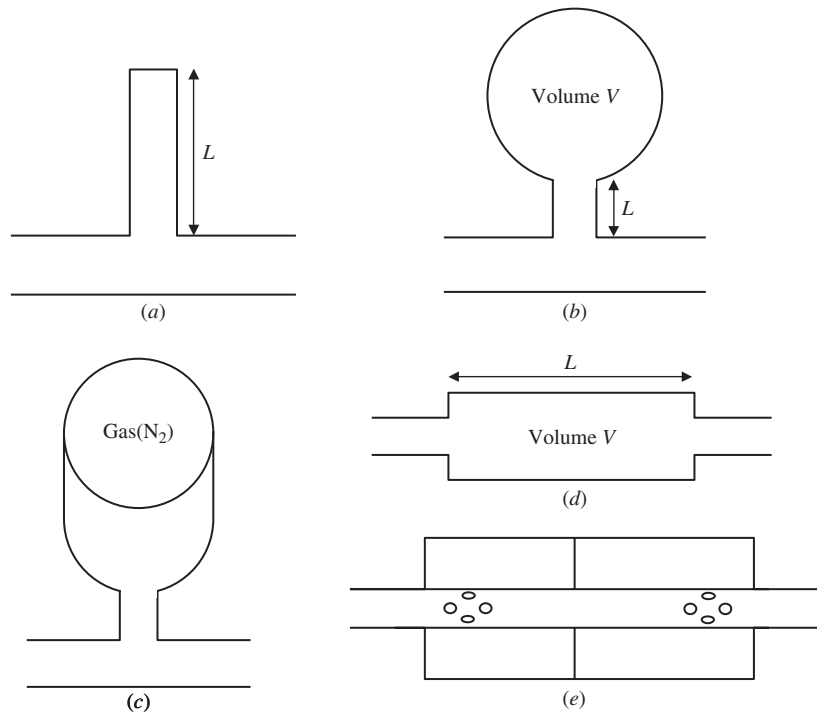
Figure 11 shows some common silencers and Fig. 12 shows their attenuation characteristics. This is described by the *transmission loss*, which is the ratio of the input fluid-borne sound power to the output fluid-borne sound power under controlled conditions, normally expressed in decibels.

The side branch and Helmholtz resonators (Fig. 11a and 11b) are tuned devices and only provide good attenuation over narrow bands, which limits their range of applications. Both are effective at their resonant frequencies at which they have a low entry impedance. Side branch resonators are sometimes known as quarter wavelength resonators, as the lowest frequency at which this happens is when the resonator length is a quarter of the wavelength, that is,

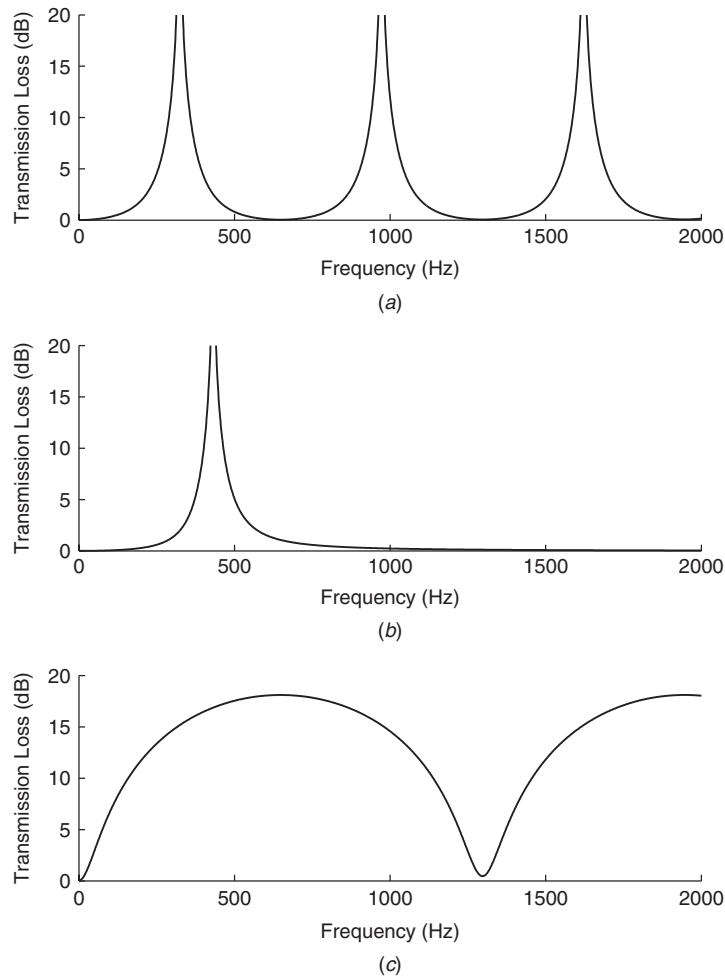
$$f = \frac{c}{4L} \text{ Hz}$$

where  $c = \sqrt{B/\rho}$ , is the speed of sound in the fluid (in m/s),  $B$  is the effective bulk modulus of the fluid (in N/m<sup>2</sup>),  $\rho$  is the fluid density in (kg/m<sup>3</sup>), and  $L$  is the tube length. Attenuation bands also exist at odd integer multiples of this frequency (i.e.,  $3c/4L$ ,  $5c/4L$ , etc.), as shown in Fig. 12a. These can be used to attenuate several harmonics produced by a pump or motor, but it is not possible to attenuate a complete harmonic series; it can be tuned to the first, third, and other odd harmonics but not simultaneously to the even harmonics.

The speed of sound is typically about 1000 to 1400 m/s, but it depends on pressure and temperature and can be considerably reduced by air bubbles or by flexible tube walls. For this reason it can be difficult to tune such a device accurately. Care should be



**Figure 11** Some fluid-borne noise silencers: (a) Side branch; (b) Helmholtz resonator, (c) accumulator, (d) expansion chamber, and (e) typical double chamber silencer.



**Figure 12** Silencer performance characteristics: (a) Side-branch resonator,  $L = 1$  m,  $C = 1330$  m/s; (b) Helmholtz damper,  $V = 0.5$  L,  $A = 1\text{ cm}^2$ ,  $L = 5$  cm; (c) expansion chamber,  $L = 0.5$  m, area ratio = 16.

taken to avoid trapped air; for example, it should be positioned pointing downward to allow bubbles to escape by buoyancy. If flexible hose is used for the side-branch resonator, allowance must be made for the compliance of the hose, which can reduce the effective bulk modulus by a factor of between 2 (for a stiff, high-pressure hose) and 10 (for a lower pressure textile-braided hose). In addition, the higher frequency attenuation bands may not be uniformly spaced in frequency because of the complex hose behavior.

A Helmholtz resonator has a single resonant frequency given by

$$f = \frac{c}{2\pi} \sqrt{\frac{A}{VL}} \quad \text{Hz}$$

where  $A$  is the cross-sectional area of the neck (in  $\text{m}^2$ ),  $V$  is the volume of the chamber (in  $\text{m}^3$ ), and  $L$  is

the length of the neck. The attenuation characteristics are shown in Fig. 12b. The liquid volume acts as a capacitor or spring, and the fluid in the neck as an inductor or mass. Similar considerations apply as for side-branch resonators.

The accumulator (Fig. 11c) behaves in a similar way to the Helmholtz damper. Because of the low stiffness of the gas, it generally has quite a low resonant frequency, and this depends strongly on pressure as the gas volume and stiffness changes. Standard accumulators are not particularly effective as high-frequency attenuators, although special types are available for this purpose. One silencer design based on the accumulator principle utilizes a tubular diaphragm through which the hydraulic fluid flows, with pressurized gas in an annular chamber surrounding the diaphragm. Because the neck of the accumulator is eliminated from this design, it can be very effective as a silencer. However,

the gas precharge pressure is critical, and it may not be effective or reliable in applications where the hydraulic pressure varies greatly. It will also require more regular maintenance than a simple expansion chamber.

The expansion chamber (Fig. 11*d*) consists of an in-line chamber (usually cylindrical) with a larger diameter than the connected pipes. It has the attenuation characteristics shown in Fig. 12*c*. It has a broadband behavior, apart from narrow bands of poor attenuation at frequencies given by

$$f = \frac{c}{2L} \text{ Hz}$$

where  $L$  is the chamber length. The peak transmission loss (TL) is given approximately by<sup>1,9</sup>

$$TL_{\text{MAX}} = 20 \log_{10}(r) - 6 \text{ dB}$$

where  $r$  is the ratio of expansion chamber cross-sectional area to line cross-sectional area.

Expansion chambers are ineffective at very low frequencies. The lowest cutoff frequency, below which the transmission loss is less than 3 dB, is given approximately by

$$f_0 = \frac{c}{\pi L r} = \frac{Ac}{\pi V} \text{ Hz}$$

where  $A$  is the line cross-sectional area and  $V$  the expansion chamber volume. Thus, for good low-frequency attenuation a large volume chamber is needed.

Commercial silencers as shown in Fig. 11*e* tend to be combinations of expansion chambers, side-branch resonators, Helmholtz dampers and orifices, and can be very effective over a broad frequency range, typically providing broadband attenuation of 30 dB or more. However, they can be bulky and expensive, particularly if they are to be effective at low frequencies.

## 6 FLEXIBLE HOSE

Flexible hose is often a convenient and cost-effective way of attenuating or isolating both fluid-borne and structure-borne noise. A suitable length of flexible hose should be fitted close to the noise source to reduce noise and vibration in the rest of the system.<sup>1-3</sup> In providing mechanical isolation for a pump, it is essential to use flexible hoses for both suction and delivery. Depending on the relative importance of quietness and other factors such as cost and compactness, hose lengths are likely to vary from about 1 m to around 3 m.

If the pipework can be firmly clamped to a support of high impedance at the point where it is connected to the hose, this will improve the isolation.

While flexible hose is very effective at isolating structure-borne noise, it is not always so effective for reducing fluid-borne noise. Typical measured fluid-borne noise transmission loss characteristics of 1 m lengths of several common hose types are shown in Fig. 13. The nylon-braided hose provides a useful level of attenuation over a broad frequency range. This hose was designed for a power-assisted steering application and is limited to pressures below about 80 bars. The single steel-braided, double steel-braided, and four-spiral steel hoses, which have much higher pressure

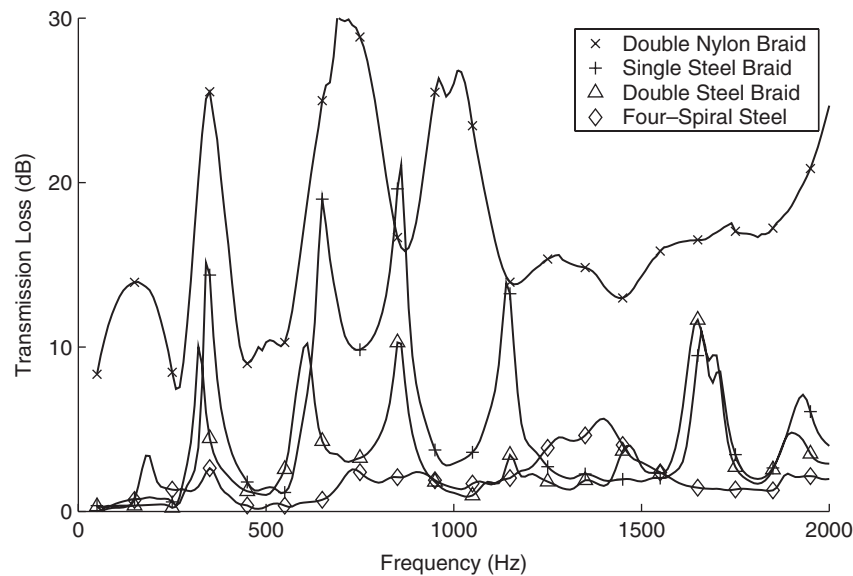


Figure 13 Typical fluid-borne transmission loss characteristics of 1 m of flexible hose.

ratings, have poor transmission loss characteristics except in narrow frequency bands. The transmission loss is especially poor at low frequency.

The nylon-braided hose is far more expandable and compliant than the steel-reinforced hoses. It is this expandability, along with the inherent damping of the rubber and reinforcement, that provides fluid-borne noise reduction. High-pressure steel-reinforced hoses do not provide much attenuation, and hose may not be very effective for reducing fluid-borne noise produced by a high-pressure pump. However, the hose will still provide useful structure-borne noise isolation.

For fluid-borne noise attenuation, generally speaking the more hose the better. However, it is possible to use too much hose because:

- Hose is expensive compared with rigid pipe, and long lengths may not be cost effective.
- For a given level of fluid-borne noise, the more flexible walls of hose will radiate more airborne noise per metre length than an equivalent steel pipe.

### 6.1 Tuner Inserts for Hoses

In hydraulic power-assisted steering systems, flexible hoses are used as the main noise attenuation device. Highly compliant textile-braided hoses are generally used, as these provide good vibration isolation and noise reduction and the pressures are usually relatively low ( $<100$  bars). To improve the fluid-borne noise attenuation further, tubular “tuner” inserts are often fitted inside the hose as shown in Fig. 14. These usually consist of a flexible metal or plastic tube attached inside one end of the hose and provide a form of tuned attenuator. The plastic tubes may be perforated to improve the performance. Sometimes restrictors and sleeves are used in conjunction with the tubular insert. Tuner inserts can provide excellent attenuation at low cost but need to be “tuned” carefully to the system.<sup>12,13</sup> To be effective these devices rely on compliant hoses and are likely to be less effective in higher pressure systems because stiffer hoses are needed.

## 7 VIBRATION ISOLATION

Isolating the mechanical vibration of a pump from the foundation on which it is mounted is achieved using

flexible mounts. There are two basic types of arrangement: The pump and driving motor can be mounted separately and connected by sufficiently flexible couplings, or they can be rigidly connected together and the combined unit can be flexibly mounted. The former method is not usually recommended. Misalignment is inevitable and, even with flexible couplings, this can put loads on the bearings of the pump and motor, which are undesirable and may themselves generate vibration. The only circumstance in which separate mounting should be considered is when transmission of the pump vibration to the motor causes unacceptable radiation of noise from the much larger surface area of the latter. Even then, an acoustic enclosure or cladding may be the best answer.

Normally, the pump is connected to its driving motor either by a bell housing or by having both the pump and the motor on a common base. The surface area of a base should be as small as possible to minimize airborne noise radiation; the base should be as rigid as possible, and in the case of both the base and the bell housing it is an advantage to choose materials and construction to give some damping, for example, by using cast iron or by using a bolted or riveted construction. Thin rubber gaskets can be helpful on a bell housing. The worst type of base would be a flat plate, which would act as an effective sounding board.

Even with a combined mounting arrangement, care needs to be taken in the selection and fitting of a suitable shaft coupling between pump and motor. This should incorporate a resilient material, but the torsional stiffness should not be such as to allow torsional resonances in the operating range. Accurate alignment is desirable.

Because of their small surface area, pipes are not usually strong sources of airborne noise, but problems tend to occur when pipes are mounted incorrectly. A pipe attached rigidly to a metal surface can produce a very effective loudspeaker! Flexible plastic or rubber mounts should be used, as their resilience reduces the transmission of vibration from the pipe and also damps out resonances in the pipe. The mounts should be located at stiff points in the supporting structure, and not in the middle of panels.

## 8 ACOUSTIC ENCLOSURES AND CLADDING

Enclosure of a hydraulic system<sup>1-4</sup> within a sound barrier can be a very effective means of noise

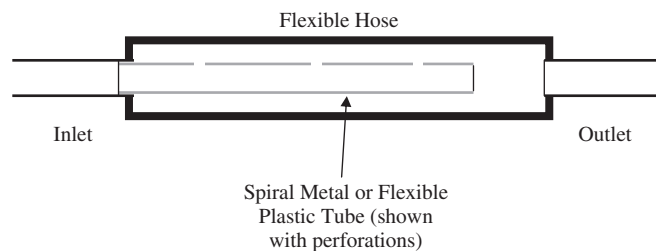


Figure 14 Hose with tuner insert.



reduction. It may be feasible to enclose the "power pack" (pump, prime mover, reservoir, and ancillary components) within a chamber, but it is rarely possible to enclose the complete hydraulic system. Often this is sufficient as the power pack may be the prime source of airborne noise. However, pipes are very effective conductors of fluid-borne noise, and structure-borne noise and it may not be practicable to enclose these and the rest of the circuit. Flexible hose is usually necessary to provide isolation in both supply and return lines.

Great care must be taken when enclosing the power pack to prevent overheating. In particular, a free airflow path must be provided for electric motor cooling. Baffled ducts are needed to limit the escape of noise through the vents. Apart from the vents, the enclosure must be well sealed as small gaps can seriously impair the performance of the enclosure. Easy access must be included to facilitate regular maintenance.

It is very important that the hydraulic components or other vibrating parts do not touch the acoustic enclosure, as the enclosure will act as a sounding board and make the problem worse. Particular care should be taken where pipes enter or leave the enclosure.

## 9 CONCLUSIONS

Noise in hydraulic systems is a broad and complex subject. The noise level of a system is dependent on the complex interaction of a large number of components. Pump flow ripple causes fluid-borne noise that then causes structure-borne and airborne noise. There are several established methods for reducing noise, and with some care significant improvements can be made with little or no increase in cost.

## REFERENCES

1. S. Skaistis, *Noise Control of Hydraulic Machinery*, Dekker, New York, 1988.
2. BHRA (British Hydro-Mechanical Research Association), *Quieter Fluid Power Handbook*, Cranfield, UK, 1980.
3. British Fluid Power Association, *Guidelines to the Design of Quieter Hydraulic Fluid Power Systems*, 1986.
4. *Guide Acoustique des Installations de Pompage*, CETIM, 1997.
5. F. D. Norvelle, *Fluid Power Technology*, West, 1995.
6. ISO Standard 10767-1, Hydraulic Fluid Power—Determination of Pressure Ripple Levels Generated in Systems and Components. Part 1. Precision Method for Pumps, 1996.
7. ISO Standard 10767-2, Hydraulic Fluid Power—Determination of Pressure Ripple Levels Generated in Systems and Components. Part 2. Simplified Method for Pumps, 1999.
8. R. A. Heron, The Control of Cavitation in Valves, 7th Int. Fluid Power Symposium, Bath, England, 1986.
9. E. B. Wylie and V. L. Streeter, *Fluid Transients*, Prentice Hall, Englewood Cliffs, NJ, 1993.
10. D. N. Johnston and K. A. Edge, Simulation of the Pressure Ripple Characteristics of Hydraulic Circuits, *Proc IMechE*, part C, Vol. 203, 1989, pp. 119–127.
11. J. E. Drew, D. K. Longmore, and D. N. Johnston, The Systematic Design of Low Noise Power Steering Systems, 4th Scandinavian Fluid Power Conference, Tampere, Finland, Sept. 1995.
12. J. E. Drew, D. K. Longmore, and D. N. Johnston, Theoretical Analysis of Pressure and Flow Ripple in Flexible Hoses Containing Tuners, *Proc IMechE* Vol. 212, Pt I, 1998, pp. 405–422.
13. M. C. Hastings and C. Chen, Analysis of Tuning Cables for Reduction of Fluid-borne Noise in Automotive Power Steering Hydraulic Lines, Trans. SAE, Paper 931295, 1995.



# CHAPTER 77

## FURNACE AND BURNER NOISE CONTROL

**Robert A. Putnam**  
Environmental Engineering Acoustics  
Siemens Power Generation, Inc.  
Orlando, Florida

**Werner Krebs**  
Siemens AG  
Mülheim an der Ruhr, Germany

**Stanley S. Sattinger**  
Advanced Fossil Energy Systems  
Siemens Power Generation  
Pittsburgh, Pennsylvania

### 1 INTRODUCTION

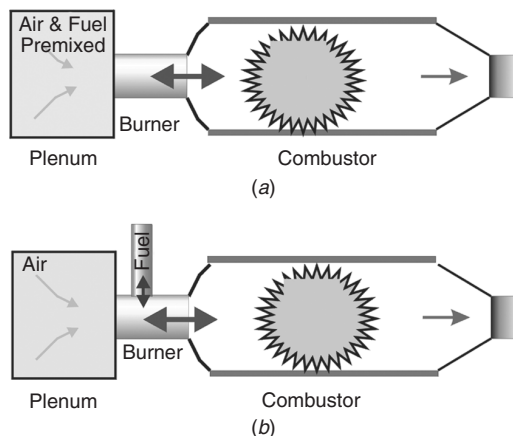
A combustion system is composed of a burner in which fuel is added to the air or pure oxygen stream and a combustor or furnace that encloses the reaction zone. In furnaces and burner systems, heat chemically stored in the fuel is released, providing an increase in temperature of the working medium ranging from 1000 K up to 3000 K. The temperature increase depends on the fuel enthalpy.

Furnace and burner applications range from domestic heating units to power generation central station boilers to gas turbine engines and use solid, liquid, and gaseous fuels. Due to their high heat release density, furnace and burner applications are prone to combustion instabilities. The principles of combustion noise in industrial and power systems using gas and liquid fuels apply generally to all types of combustion systems. The phenomenon of thermoacoustically induced oscillations in combustion systems is complicated and usually only qualitative explanations can be given. Various prediction methods have been developed in the past decade. Technical solutions are available to damp and control combustion oscillations.

### 2 OVERVIEW OF COMBUSTION SYSTEMS

Combustion systems consist of fuel and air delivery systems, a burner, and a combustor. The fuel injection element is typically referred to as the burner. The element within which heat release takes place is typically referred to as the combustor or furnace. The elements of a simplified premix combustion system are shown in Fig. 1.

The purpose of combustion systems is to add heat to an airstream. The power density of combustion systems ranges from approximately 100 kW/m<sup>3</sup> in atmospheric systems to 100 MW/m<sup>3</sup> in modern stationary gas turbines operating at pressurized conditions and as



**Figure 1** Main elements of premix combustion systems for (a) an ideal premix system and (b) a technical premix system.

high as 500 MW/m<sup>3</sup> in jet engines operating at pressures up to 40 bars. The main mechanisms for combustion noise are common to all combustion systems.

The purpose of a fuel burner is to mix and direct the flow of fuel and air to ensure rapid ignition and complete combustion within the furnace or combustor. The combustion of gaseous fuels takes place in two ways: (1) when the gas and air are mixed before ignition, as in a Bunsen burner, referred to as premix flames (Fig. 1 depicts both ideally premixed and technically premixed cases) and (2) when the gas and air are mixed after the fuel has been heated, referred to as diffusion flames.<sup>1</sup>

In diffusion mode the fuel and oxidizer enter the reaction zone separately and diffuse through it. Combustion takes place at stoichiometric conditions

and is typically stable and high in temperature, causing high levels of oxides of nitrogen emissions ( $\text{NO}_x$ ). Premix mode is characterized by lower combustion temperatures, permitting  $\text{NO}_x$  emissions as low as 9 ppm for pressurized gaseous combustion and below 2 ppm for atmospheric gaseous combustion. Premix systems utilizing liquid fuel have first to evaporate the liquid droplets, then to mix them with the air prior to combustion.<sup>2</sup> Solid fuels such as coal can only be burned in diffusion mode with combustion taking place on the surface or in the core of the solid particle, requiring other measures for  $\text{NO}_x$  abatement.

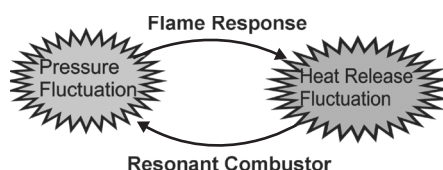
Flame stabilization or anchoring consists of an equilibrium condition established between the heat release rate or reaction rate of the reacting species and the flow velocity. This equilibrium is maintained by providing flow recirculation zones and/or piloting, which provides a small region of high temperature at which reaction of main flow can be anchored. In case of low turbulent flow the heat transfer by conduction and radiation toward the cooled walls also affects this equilibrium.

Swirl, imparted by the burner, is commonly used to augment flame stabilization by forming large reverse flow zones with resultant increased mixing rates. In premix burners the flow velocity must be high enough to avoid flashback into the burner but not so high as to cause blowoff at the burner outlet, extinguishing the flame.<sup>3,4</sup>

Noise generated by the combustion process can generally be characterized as one of two types: (1) combustion roar and (2) combustion-driven oscillations or thermoacoustic instabilities. The latter type of noise is observed when pressure oscillations are induced by heat release oscillations. The term thermoacoustic reflects the strong relationship between heat release oscillations and pressure oscillations that can establish a feedback cycle as shown in Fig. 2.<sup>5,6</sup> Although thermoacoustic instability is closely connected to flame stabilization, their instability criteria are different. In this chapter the main focus is on thermoacoustic instability owing to its higher sound pressure levels and greater potential for structural damage.

### 3 TYPES OF COMBUSTION SYSTEMS

*Premix burners* are used for many natural-draft and forced-draft applications where accurately controlled conditions must be maintained. Natural-draft premix burners use fuel spuds (jet orifices) and injectors to aspirate the air into a mixing volume that forms a



**Figure 2** Simplified feedback cycle that generates thermoacoustic combustion instability.

portion of the burner. An adjustable shutter may be included for the control of the air flow rate in an aspirated-air burner. Alternately, premix burners for use with forced air may aspirate the fuel gas.

*Nozzle-mix burners* mix the air and gas within the furnace or combustor downstream of the burner itself. Jets of fuel gas and/or air produce turbulence that sustains the mixing process. Some nozzle-mix burners employ rotating spiders to increase turbulence.

*Diffusion-flame burners* are not commonly employed as primary burners for furnaces and combustors. In modern low-emissions combustors, diffusion flames serve only as pilot flames using in the range of 3 to 15% of the total fuel flow to initiate and/or sustain ignition of the primary burner flames.

The general category of *oil-fired burners* may include all liquid-fueled burners. Any differences in the nature of noise emissions from oil-fired burners relative to gas-fired burners probably arise either from the presence of two distinct flame regions within oil-fired burners, the primary and secondary flame, or from the inherently different fuel nozzle arrangements. The primary flame is where the lighter fractions of oil are heated to ignition temperature and is also the source of heating for the secondary flame, where the heavier fractions are burned. Some liquid fuels require additional preheating, and as for all fuels the maximum temperature must be carefully controlled to avoid excessive flame instability.

Low  $\text{NO}_x$  emissions can be achieved in oil-fired burners by adding water to the flame, either via separated water spray or by a water-fuel emulsion. Due to the evaporation heat and the high heat capacity of the evaporated water molecules, the combustion peak temperatures are lowered, and  $\text{NO}_x$  emissions are significantly reduced. However, the evaporation of water also represents a volume source that in resonance with the combustion chamber may amplify combustion oscillations considerably.

As a general rule, high-frequency (1 kHz and higher) sound emissions from oil fuel combustion tend to be higher than for gas fuel. At low frequencies (approximately 150 Hz and below, including infrasonic frequencies), oil fuel combustion tends to generate lower overall sound pressure levels. At all other midfrequencies, there is essentially no difference. Thus, audible airborne A-weighted sound pressure level from gas firing is expected to be quieter, whereas overall unweighted or C-weighted sound pressure level from oil firing may be expected to be quieter. Such differences, however, are seldom more than 2 to 5 dB.

*Pulse combustors* are combustion-driven, non-steady-flow devices in which the fuel is reacted intermittently. With inherently high-energy conversion efficiencies on gas or liquid fuel, these devices are being applied in a variety of commercial uses, including gas turbine combustors.<sup>7</sup> Their inherently high noise levels, however, limit their use somewhat.

### 4 PHENOMENOLOGICAL DESCRIPTION OF COMBUSTION NOISE

The noise spectrum for combustion roar has a broadband "haystack" form similar to, but flatter than, that of noise

from a jet. There is a spectral peak frequency, which, for open turbulent flames, increases with the mean velocity and decreases with increasing diameter and fuel mass fraction.<sup>8</sup> The basic noise source is the turbulent motion of the flame front. Levels of combustion roar are heavily dependent on the levels of turbulence in the flame.<sup>5</sup> Typical efficiencies of conversion from chemical energy input of a burner to combustion roar sound power emission are in the range  $10^{-8}$  to  $10^{-5}$ . While combustion system enclosures typically attenuate this sound radiation, components of the combustion roar spectrum may be amplified at the natural frequencies of these enclosures, thus modifying the spectrum shape and increasing energy conversion efficiency.

Combustion-driven oscillations are characterized by a feedback cycle that converts chemical energy to oscillation energy as shown in Fig. 2 at an efficiency on the order of  $10^{-4}$ . In general, a fluctuating flame produces a periodic but nonsinusoidal wave output of energy. Thermoacoustic oscillations in the form of dynamic pressure resonances will cause furnace or combustor liner vibrations that can only be tolerated within certain limits. Maximum permissible pressures will be unique to each design and typically will be a function of frequency. Excessive heat transfer to surfaces can produce structural softening or weakening and when combined with excessive pressure oscillations can yield disastrous consequences.

Pressure oscillations in the combustion chamber induce volume flow oscillations at the burner exit, which in turn cause fluctuations in the flow of reacting species toward the flame front, resulting in heat release oscillations. In nonideal premixed systems this pulsating flow of reactants couples with fluctuations in fuel concentration generated at the mixing location due to the unequal acoustical impedances of the air and fuel supply systems. It may be said that the air supply is acoustically soft (compliant) due to small pressure losses, whereas the fuel supply is acoustically

hard (stiff), characterized by a high-pressure drop. In liquid-fuel injection systems the fuel supply is considered incompressible.

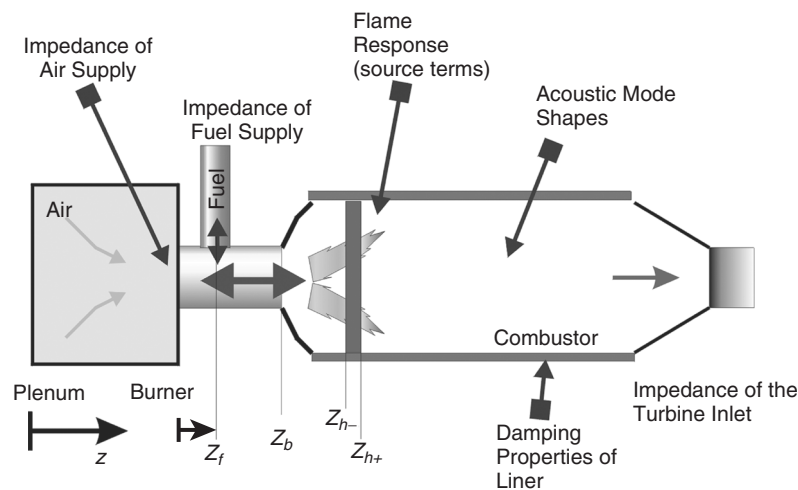
The combustion instability criterion follows Lord Rayleigh<sup>9</sup>: In the absence of acoustic damping, a positive correlation of the pressure fluctuations  $p'$  and the heat release fluctuations  $q'$  results in combustion instabilities. The mathematical formulation of this criterion is the Rayleigh criterion:

$$R_{g,\text{norm}} = \frac{\int_t^{t+T_{\text{per}}} \int_{V_{\text{Hz}}} p'(\mathbf{r}, t) q'(\mathbf{r}, t) d\mathbf{r} dt}{\overline{pq} V_{\text{Hz}} T_{\text{per}}} > 0 \quad (1)$$

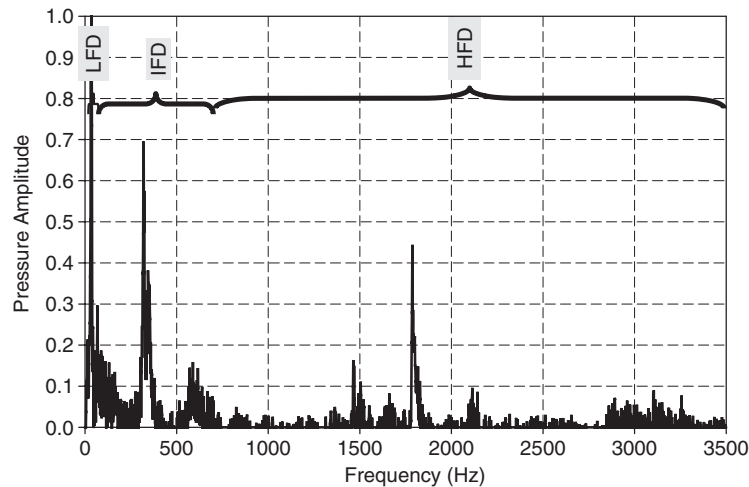
where  $\mathbf{r}$  is the position vector,  $t$  denotes time,  $p'$  and  $q'$  denote the steady components of pressure and heat release,  $V_{\text{Hz}}$  denotes the combustor volume, and  $T_{\text{per}}$  denotes the time period of the oscillation.

The combustion-driven oscillation feedback cycle is complicated by the interaction of the influence parameters shown in Fig. 3. A typical spectrum depicting the spikes due to pressure oscillations induced by thermoacoustic instabilities is shown in Fig. 4.

The acoustic waves at low and intermediate frequencies have long wavelengths compared to the transverse dimensions of the combustion system, and they propagate through all of the adjoining components. The dimensions and acoustic properties of the burner plenum impact the impedance of the burner exit, affecting the magnitude of pressure-induced volume flow fluctuations. The acoustic properties of the fuel lines determine the magnitude of fuel flow fluctuations at the fuel nozzles. The acoustic geometry of the combustor determines the shapes of the acoustic modes, which are also influenced by the acoustic boundary conditions at the combustor exit. The central player in the feedback cycle is the flame.



**Figure 3** Thermoacoustically relevant influence parameters of the feedback cycle.



**Figure 4** Typical spectrum of thermoacoustically induced pressure oscillations.

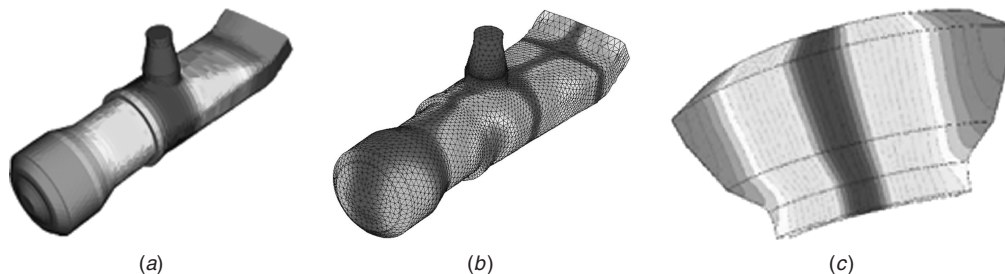
The spectra of thermoacoustically induced pressure oscillations may be divided into low-, intermediate-, and high-frequency regions. For example, in gas turbine practice these regions are approximately: 4 to 70 Hz, low-frequency dynamics (LFD); 70 to 700 Hz, intermediate-frequency dynamics (IFD); and 700 to 4000 Hz, high-frequency dynamics (HFD). In the gas turbine combustor spectrum of Fig. 4, the IFD and HFD regions exhibit typically pronounced frequency peaks, although the HFD region includes more broadband excitation in addition.

Low-frequency dynamics are caused by periodic flame extinction, which is the result of poor flame stabilization. The flame reactions are quenched in the first part of the oscillation period and are then reignited during the second part. The feedback cycle involving total quenching of the flame is characterized by long time constants, and, hence, only low frequencies are excited. The frequencies are so low that the corresponding mode shape is a bulk mode in which all pressure fluctuations have the same phase. This instability is suppressed by either decreasing the flow

velocity or increasing the size of the recirculation zone, providing low-velocity regions for flame stabilization.

Intermediate-frequency dynamics are characterized by standing waves in which fluid elements oscillate with different phase angles. Mode shapes may, for example, be first-order or second-order axial modes for can-type combustors in gas turbines as shown in Figure 5. In annular combustors, azimuthal mode shapes are excited as shown in Figure 5c.<sup>10</sup> The feedback cycle between pressure and heat release oscillations for IFD is characterized by time constants in the range of 3 to 6 ms.

High-frequency dynamics are excited by a feedback cycle involving very small time constants (below 0.5 ms). In general, a large number of mixed mode shapes featuring axial, azimuthal, and radial dependence fit into combustors of all types at this frequency range as shown in Fig. 5b. Different modes excited in parallel result in a more broadband spectrum. Not much is known about the excitation mechanism due to the small time scales, which cannot be resolved with current measurement technologies. Future work using modern fast data acquisition systems allowing



**Figure 5** Mode shapes for the different types of frequency ranges: (a) axial Mode, 300 Hz, (b) combined mode, 1700 Hz, and (c) annular combustor, second azimuthal mode, 200 Hz.

higher time resolution will provide more insight into these phenomena. However, since the performance of damping systems increases with frequency, HFD has been suppressed successfully by using dampers such as Helmholtz resonators.

## 5 THEORETICAL DESCRIPTION OF COMBUSTION OSCILLATIONS

Combustion instabilities are described by nearly the same equations for the propagation of the acoustic pressure and acoustic velocity as outlined in Part I of this handbook. Differences are due to the source term representing the heat release fluctuations. Assuming only small perturbation, the linearized transport equations for acoustic pressure and velocity are then formulated as<sup>4</sup>

$$\frac{\partial \mathbf{u}'}{\partial t} + (\mathbf{u}' \cdot \nabla) \mathbf{u}' + \mathbf{u}' \nabla \mathbf{u}' = -\frac{1}{\rho} \nabla p' \quad (2)$$

$$\frac{\partial p'}{\partial t} + \mathbf{u}' \cdot \nabla p' + \mathbf{u}' \cdot \nabla \bar{p} + \gamma(\bar{p} \nabla \cdot \mathbf{u}') + \gamma(p' \nabla \cdot \mathbf{u}') = (\gamma - 1)q' \quad (3)$$

Neglecting the impact of mean flow the equations are simplified to be

$$\frac{\partial^2 p'}{\partial t^2} - c^2 \nabla^2 p' = (\gamma - 1) \frac{\partial q'}{\partial t} \quad (4)$$

$$\frac{\partial \mathbf{u}'}{\partial t} = -\frac{1}{\rho} \nabla p' \quad (5)$$

## 6 PREDICTION METHODS

A number of different methods for solving thermoacoustic problems have been developed. Table 1 lists a

selection of solution methods sorted according to the type of equation and the corresponding assumptions to which they refer. In column 4 comments relating to treatment of boundary conditions and the flame are given. Most modern design tools cover the low-Mach-number and the low-amplitude range, where the linear acoustic assumptions are valid. Details of treatments of nonlinear phenomena are limited to special considerations as published by Dowling<sup>11</sup> and Culick<sup>12</sup> or the nonlinear phenomena are addressed using more powerful computing methods.<sup>4,13,14</sup>

An elegant method to determine the thermoacoustic stability is the Galerkin method.<sup>12,15,21</sup> Here the spatial dependencies of the acoustic properties are represented by mode shape functions (see Fig. 5), determined by solving the Helmholtz equation, while the time dependence of the amplitude function of the instability is obtained by solving ordinary differential equations. Since the transverse dimensions of many combustion systems are small with respect to the wavelength of the instability, solution methods have been developed treating one-dimensional propagating waves at LFD and IFD frequencies.

In general, the acoustic properties of different components are represented by transfer functions relating downstream to upstream acoustic properties. Large networks of a number of components can be created, requiring a large matrix solution. These methods have been widely developed and are already used for thermoacoustic design of modern combustion systems.<sup>17–20</sup>

Efforts have been made to link the heat release oscillations due to acoustic forcing and equivalence ratio fluctuations to the pressure oscillations.<sup>4,22–29</sup> Heat release fluctuations may also be amplified by coherent flow structures, which are generally periodic

**Table 1 Literature Survey of Different Solution Methods**

Group	Assumption	Name of Method	References	Comments
1	No assumption	Direct numerical simulation (DES) or large eddy simulation (LES)	4, 13, and 14	Very time consuming; special treatment for the flame; special treatment of acoustic boundaries
2	Nonviscous flow	Nonlinear solution	11 and 12	Limited to special cases
3	Low amplitudes, linear limit	Three-dimensional Galerkin method	12, 15, and 16	Careful treatment of the acoustic jump conditions
4	Low-frequency limit one-dimensional propagating waves	One-dimensional transfer function networks	17–20	
			18	Very universal functionality, however-restricted to 1D geometry
			19	

in nature.<sup>30</sup> Although the flame–vortex interaction is the subject of several recent publications,<sup>31–34</sup> knowledge of the impact of design parameters on this amplification factor is limited.

## 7 PASSIVE MEANS FOR NOISE CONTROL

In general, there are two fundamental means of passive noise control available to burner designers: (1) reducing the combustion-induced source terms and (2) increasing the acoustical damping.

### 7.1 Reducing Noise Sources: Changing the Time lag; Fuel Staging Concepts

The most relevant parameters expressing the dynamic property of the flame are the injection time lag  $\tau_i$  and burner time lag  $\tau_b$ . They directly control the phase relation between heat release oscillations and pressure oscillations. The burner timelag  $\tau_b$ , which expresses the time a fluid element needs to flow from the burner outlet to the flame front, can be altered by changing the burner exit geometry. A cylinder mounted on the exit of the burner can be used to locate the heat release zone further downstream.<sup>35</sup> Another option is to change the swirl momentum flux of the burner exit flow. Reducing swirl generally leads to a longer flame with a wider heat release distribution. Increasing the swirl momentum flux shortens the heat release zone. Other means of changing the flame location are to modify the fuel concentration profile at the burner exit of partially premixed operating systems and/or to use cooling air across the flame tube to impact flame stabilization.

Care must be taken here because the success of the modifications depends on the interaction with the acoustic environment, which will differ from case to case. Care must also be taken if fuel compositions are changed since they will have an impact on fuel–air mixing and hence on the fuel concentration profile. In addition, the laminar burning velocity may change, altering the location of the heat release zone.

Richards and Janus<sup>36</sup> point out the impact of changing the injection time lag  $\tau_i$  on dynamics by moving the fuel injection position. More flexibility is obtained if the fuel can be injected at different locations characterized by different time lags  $\tau_i$ . Then operational flexibility is achieved by changing the fuel split between stages at different operating conditions.<sup>36,37</sup> If the combustion system provides flexibility to do so, the flame response can be changed by changing the fuel–air ratio, which determines directly the density jump condition in the heat release zone.<sup>38</sup> Another way to directly affect the flame response is to change the burner size<sup>39</sup> and/or burner exit velocity. Both changes will lead to a different size of the heat release distribution. Generally, a more widespread heat release distribution yields a lower excitation of pronounced frequencies.

In blast-furnace stoves featuring diffusion-type gas burner with acoustically soft air and/or fuel supplies, the fuel injection may be located at a pressure node of the combustion chamber to suppress combustion-driven oscillations.<sup>5</sup> In addition, the length of the fuel

supply line can be modified to detune the system. This is consistent with other approaches applied to more complex gas-fired combustion systems such as gas turbines. Experiments involving tuning of the fuel line impedance have succeeded in suppressing pressure fluctuations.<sup>40</sup> Fuel line impedance adjustments may be even more promising if the fuel lines have low impedances as in syngas combustion systems. The impact of coherent structures may be reduced by increasing the turbulence level,<sup>30</sup> but doing so may also increase turbulence-induced combustion roar. Flame stabilization and hence dynamic flame response may also be affected by the heat transfer to an environment changing in temperature.<sup>41</sup> That is the reason for different stability behavior of the burner during startup of the heater.

### 7.2 Resonators for Noise Control

Acoustic resonators can provide effective means for increasing the damping of selected modes. These devices may either be add-ons to existing apparatus or designed-in features of new equipment. In principle these devices resemble either simple Helmholtz resonators or quarter-wave tubes:

- A simple Helmholtz resonator is shown in Fig. 6. A small cavity is acoustically connected to the combustion chamber or furnace through an orifice.<sup>42</sup> The fluid inertia of air or combustion gases residing in the orifice oscillates against the volumetric compliance of the small cavity at a well-defined natural frequency given by

$$f_0 = \frac{c}{2\pi} \sqrt{\frac{S}{V(\ell + \Delta\ell)}} \quad (6)$$

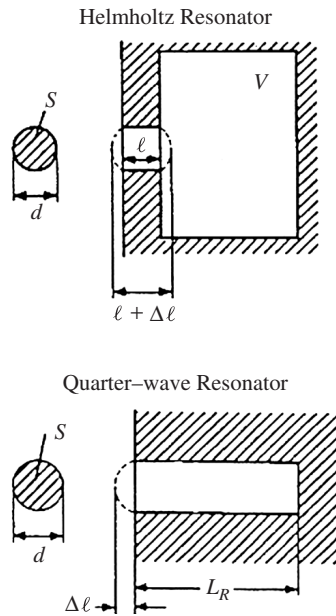
- A quarter-wave tube is also shown in Fig. 6, in which an elongated cavity length provides the fluid inertia in lieu of an orifice. The natural frequency of the quarter-wave resonator is given by

$$f_0 = c/4(L_R + \Delta\ell) \quad (7)$$

In the above formulas,  $\Delta\ell$  is a length correction to account for the acoustic mass addition at the resonator opening. At low-pressure amplitudes it may be estimated as 0.85 times the diameter for a two-sided opening. A flow-through resonator configuration may also be employed, but the calculations are more involved.<sup>43</sup>

The increment of damping added by a single resonator will be in proportion to its acoustic conductance at the frequency of the pressure waves and to the square of the pressure magnitude (normalized to a spatial peak value of unity) at the resonator's location. When the frequency of the pressure wave matches the tuned natural frequency of the resonator, its conductance reaches a maximum value. If a resonator or an array of resonators is to be used to suppress combustion instabilities through increased





**Figure 6** Simple Helmholtz resonator and a quarter-wave resonator tube.

damping of a targeted acoustic mode, each resonator must be: (a) located near a pressure antinode of the mode, (b) sized to provide adequate conductance, and (c) tuned to achieve the closest attainable match with the natural frequency of the mode. Obviously, if the temperature of the gas in the plenum changes under various operating conditions the effective frequency

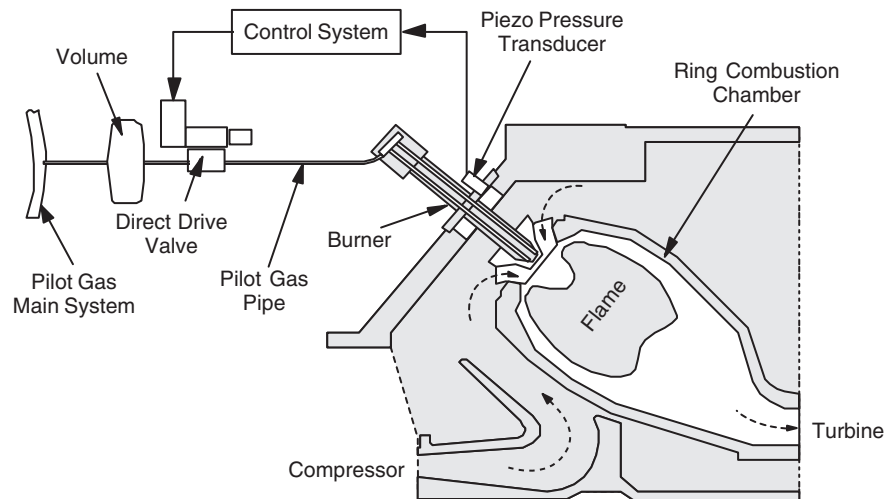
of these devices will be altered. Further, the proper location of any such resonator is critical.

## 8 ACTIVE MEANS FOR NOISE CONTROL

Another option to suppress thermoacoustic oscillations is the application of active means,<sup>44</sup> which use feedback control with or without adaptive features to suppress thermoacoustic instabilities. It is best explained referring to Fig. 7, showing an implementation of the method in a commercially operated gas turbine.

Signals from a transducer that senses pressure fluctuation or heat release in the combustion zone are processed by a controller, amplified, and transmitted as command signals to an actuator that suppresses the self-excitation process. An overview of different sensors applied to active combustion control has been published by Docquier and Candel.<sup>46</sup> The active measures modulate flows in either the fuel supply system or the air or exhaust gas stream. Modulation of the air or exhaust gas stream is limited to small combustion systems and/or low-pressure systems. Modulation of the fuel flow rate, on the other hand, is advantageous in most combustion systems because of the moderate volume flow rates that must be modulated. In systems such as blast-furnace stoves, where the volume flows of air and fuel are nearly equal, the fuel flow modulation will not hold an advantage.

The modulation of the air, exhaust gas, or fuel flow rate must occur at the frequency of the thermoacoustic instabilities, which can exceed 1000 Hz, posing a performance challenge in the selection of the actuator. Optimization of both the actuator phase and amplitude is key to control performance, as the flow rate oscillation must produce a change in the heat release rate that is exactly opposite to the heat



**Figure 7** Active instability control system installed in a commercial gas turbine. (Reprinted Courtesy of Siemens.)

release caused by the self-excitation process. The actuator thus counteracts the combustion oscillations and the resultant pressure oscillations. Recently, adaptive controllers have been developed in which the controller algorithm changes according to excited frequencies and operating conditions.<sup>47</sup> Still challenging for active control are systems in which the multiple frequencies are excited or in which the frequencies of the excited modes are not constant. In general, the feasibility and efficacy of active noise control methods are inversely proportional to frequency.

Active operation point control, on the other hand, is related to systems that use control strategies in low-frequency range (1 to 100 Hz). Here, the injection of fuel is regulated to maintain certain flame parameters like the equivalence ratio in a prescribed range of values.

## 9 NOISE CONTROL ENGINEERING SOLUTIONS

All noise control solutions deal with one or a combination of the source, path, or receiver. The general topic of noise control engineering here includes all of the means to attenuate the unwanted noise along the path from the source to the receiver. The preceding sections dealing with changing the time lag of the flame, fuel staging concepts, and resonators all address attenuation at the source of the noise. Any measures undertaken to control the level of the noise at the receiver are dealt with in other chapters of this handbook. Passive attenuation along the path of the noise consists of external controls: mufflers, insulation and lagging, enclosures or burner internal absorption, all of which are also addressed in other sections of this handbook.

**Mufflers** These include passive absorptive attenuators made up of parallel splitter baffles or reactive-type mufflers. Absorptive baffles or duct wall liners will typically utilize porous acoustically absorbent materials enclosed, as effectively as possible, within blankets or pillows of acoustically porous materials as a means of retaining the absorbent fill over the life of the unit. In small residential or commercial installations, such silencers may involve low flow velocities and only moderate temperatures (a few hundred degrees Celsius). However, large industrial facilities such as gas turbines will involve high-velocity, highly turbulent flow, at temperatures in excess of 600°C, necessitating specialized designs by experienced vendors and fabricators.

For installations using exhaust gas catalysts of any type for the control of air pollutant emissions, it is important to carefully evaluate the use of absorptive muffler silencers upstream of any such catalyst. The gas passages for such catalysts tend to be small enough that there is a potential for clogging of the passages due to out-migration of fine particles from any acoustically absorptive material installed upstream. However well wrapped the absorptive elements are, a certain amount of material loss is inevitable, with a buildup of lintlike material likely at the catalyst. Commercial manufacturers of industrial mufflers have

developed reactive nonabsorptive muffler designs to overcome the problem of catalyst clogging. Resonators in the burner chamber itself are addressed in the preceding section, but other reactive-type resonators may be installed at any point along the exhaust gas stream.

**Enclosures** The designer must decide whether to apply acoustical enclosures or acoustical barriers to the burner, the furnace, or the boiler unit to which they attach, or to the appropriate auxiliary component. A peculiarity of combustion noise from large units, especially industrial gas turbines, is their capability of generating significant low-frequency sound emissions, associated, for instance, with combustion oscillations, that may be particularly difficult to attenuate. Furthermore, the very nature of gas turbine operations tends to create low-frequency sound energy that is generated neither by nor within the combustor, nor is it due to combustion-driven oscillations, but rather is generated in the turbulent exhaust gas stream itself. The economies of low-frequency noise attenuation seldom favor modifications to the burner or combustion system, despite the sometimes considerable investment in structures and hardware often necessary for the attenuation of low-frequency sound energy.

Various combustion noise reduction strategies are available to the designer, as with other noise control engineering measures. Simply separating the sensitive receivers from the source, or vice versa, is self-evident. Replacement of noisy equipment with more modern, low-noise designs, continually being developed by manufacturers, will often prove to be the most cost-effective solution.

## REFERENCES

1. R. H. Perry and C. H. Chilton, Eds., *Chemical Engineers' Handbook*, McGraw-Hill, New York, 1973, pp. 9-25-9-27.
2. A. Lefebvre, *Gas Turbine Combustion*, McGraw-Hill, New York, 1983.
3. J. Chomiak, *Combustion: A Study in Theory, Fact and Application*, *Energy and Engineering Science Series*, Gordon and Breach Science, New York, 1990.
4. T. Poinsot and D. Veynante, *Theoretical and Numerical Combustion*, R. T. Edwards, Philadelphia, PA, 2001.
5. A. A. Putnam, Combustion Noise in Industrial Burners, *Noise Control Eng. J.*, **7**, No. 1, 1976, pp. 24-34.
6. F. E. C. Culick, Combustion Instabilities in Propulsion Systems, *Unsteady Combustion*, F. E. C. Culick, M. V. Heiter, J. H. Whitelaw, Eds., Kluwer Academic Publications, London, 1966, pp. 173-176.
7. J. A. C. Kentfield, *Non-steady, One-Dimensional, Internal, Compressible Flows Theory and Application*, Oxford University Press, New York, 1993, Chapter 8.
8. Stephenson and Hassan (1977).
9. Lord Rayleigh, The Explanation of Certain Acoustical Phenomena, *Roy. Instit. Proc.*, Vol. 3, 1878, pp. 536-542.
10. G. Walz, W. Krebs, S. Hoffmann, and H. Judith, Detailed Analysis of the Acoustic Mode Shapes of an Annular Combustion Chamber, *ASME J. Eng. Gas Turbines Power*, Vol. 124, 2002, p. 3.



11. A. P. Dowling, Nonlinear Self-Excited Oscillations of a Ducted Flame, *J. Fluid Mech.*, Vol. 346, 1997, pp. 271–290.
12. F. E. C. Culick, Combustion Instabilities in Propulsion Systems, in *Unsteady Combustion*, F. E. C. Culick, M. V. Heitor, and J. H. Whitelaw, Eds., Kluwer Academic, London, 1996, pp. 173–243.
13. Y. Huang, H. Sung, S.-Y. Hsieh, and V. Yang, Large Eddy Simulation of Combustion Dynamics of Lean Premixed Swirl-Stabilized Combustor, *J. Propulsion Power*, Vol. 19, 2003, pp. 782–794.
14. S. Menon and W. Jou, Large Eddy Simulations of Combustion Instability in an Axisymmetric Ramjet, *Combustion Sci. Tech.*, Vol. 75, 1991, pp. 53–72.
15. B. Zinn and M. Lores, Application of the Galerkin Method in the Solution of Non-linear Axial Combustion Instability Problems in Liquid Rockets, *CST*, Vol. 4, 1972, pp. 269–278.
16. S. Bethke, U. Wever, and W. Krebs, Stability of Gas Turbine Combustion Chamber, AIAA Paper No. 2005–2831, Monterey, CA, May 23–25, 2005.
17. S. Hubbard and A. P. Dowling, Acoustic Instabilities in Premix Burners, AIAA 98–2272, Toulouse, France, 1998.
18. U. Krüger, J. Hüren, S. Hoffmann, W. Krebs, P. Flohr, and D. Bohn, Prediction and Measurement of Thermoacoustic Improvements in Gas Turbines with Annular Combustion Systems, *ASME J. Eng. Gas Turbines Power*, Vol. 123, 2001, p. 557.
19. B. Schuermans and W. Polifke, Modelling Transfer Matrices of Premixed Flames and Comparison with Experimental Results, ASME Paper 99-GT-132, 1999.
20. G. C. Hsiao, R. P. Pandalai, H. S. Hura, and H. C. Mongia, Combustion Dynamic Modeling for Gas Turbine Engines, AIAA Paper 98–3380, Seattle, WA, 1998.
21. W. Krebs, G. Walz, and S. Hoffmann, Thermoacoustic Analysis of Annular Combustors, AIAA Paper 99–1971, 1999.
22. A. P. Dowling, A Kinematic Model of a Ducted Flame, *J. Fluid Mech.*, Vol. 394, 1999, pp. 51–72.
23. W. Polifke, A. Poncet, C. O. Paschereit, and K. Döbbeling, Reconstruction of Acoustic Transfer Matrices by Stationary Computational Fluid Dynamics, *J. Sound Vib.*, Vol. 245, 2001, pp. 485–510.
24. W. Krebs, P. Flohr, B. Prade, and S. Hoffmann, Thermoacoustic Stability Chart for High Intense Gas Turbine Combustion Systems, *Combustion, Sci. Tech.*, Vol. 174, 2002, pp. 99–128.
25. T. Lieuwen and B. T. Zinn, The Role of Equivalence Ratio Oscillations in Driving Combustion Instabilities in Low NO<sub>x</sub> Gas Turbines, 27th Symposium (Int.) on Combustion, Boulder, CO, August 2–7, 1998, pp. 1809–1816.
26. T. Lieuwen, Modeling Premixed Combustion-Acoustic Wave Interactions: A Review, *J. Propulsion Power*, Vol. 19, 2003, pp. 765–781.
27. M. Fleiß, A. Annaswamy, Z. A. Ghoneim, and A. Ghoniem, Response of a Laminar Premixed Flame to Flow Oscillations: A Kinematic Model and Thermoacoustic Instability Results, *Combustion Flame*, Vol. 106, 1996, pp. 487–510.
28. D. Bohn, G. Deutsch, and U. Krüger, Numerical Prediction of the Dynamic Behavior of Turbulent Diffusion Flames, ASME Paper 96-GT-133, 1996.
29. S. Ducruix, T. Schuller, D. Durox, and S. Candel, Combustion Dynamics and Instabilities: Elementary Coupling and Driving Mechanisms, *J. Propulsion Power*, Vol. 19, 2003, pp. 723–734.
30. C. M. Coats, Coherent Structures in Combustion, *Prog. Energy Combustion Sci.*, Vol. 22, 1996, pp. 427–509.
31. P. H. Renard, S. Candel, J. C. Rolon, and D. Thevenin, Dynamics of Flame/Vortex Interactions, *Prog. Energy Combustion Sci.*, Vol. 26, 2000, 225–283.
32. C. J. Mueller, J. F. Discroll, M. C. Drake, D. L. Reuss, and M. E. Rosalik, Vorticity Generation and Attenuation as Vortices Convect through a Premixed Flame, *Combustion Flame*, Vol. 112, 1998, pp. 342–359.
33. T. Mantela and J. M. Samaniego, Fundamental Mechanisms in Premixed Turbulent Flame Propagation via Flame-Vortex Interactions, *Combustion Flame*, Vol. 118, 1999, pp. 537–583.
34. H. Büchner, M. Lohrmann, N. Zarzalis, W. Krebs, Flame Transfer Function Characteristics of Swirl Flames for Gas Turbine Applications, ASME Paper GT-2003-38113, 2003.
35. B. Prade, U. Gruschka, H. Hermsmeyer, S. Hoffmann, W. Krebs, and U. Schmitz, V64.3A Gas Turbine Natural Gas Burner Development, ASME Paper GT-2002-30106, 2002.
36. G. Richards and M. C. Janus, Characterisation of Oscillation During Premix Gas Turbine Combustion, ASME Paper 97-GT-244, 1997.
37. T. Scarinci, and J. L. Halpin, Industrial Trent Combustor—Combustion Noise Characteristics, *Trans. ASME, J. Eng. Gas Turbines Power*, Vol. 122, 2000, pp. 280–286.
38. M. Elsari and A. Cummings, Combustion Oscillations in Gas Field Appliances: Eigenfrequencies and Stability Regimes, *Appl. Acoust.*, Vol. 64, 2003, pp. 565–580.
39. P. K. Baade, Design Criteria and Models for Preventing Combustion Oscillations, *ASHRAE Trans.*, Vol. 84, 1978, p. 449.
40. G. Richards and D. Straub, Control of Combustion Dynamics Using Fuel System Impedance, ASME Paper GT2003-38521, 2003.
41. K. R. A. M. Schreel, E. L. van den Tillaart, R. W. M. Janssen, and L. P. H. de Goey, The Effect of Heat Transfer on Acoustics in Burner Stabilized Flat Flames, Proc. 3rd European Conference on Small Burner Technology and Heating Equipment, 2003, pp. 145–151.
42. E. Laudien, R. Pongratz, R. Pierro, and D. Preclik, Experimental Procedures Aiding the Design of Acoustic Cavities, in *Liquid Rocket Engine Combustion Instability*, Vol. 169, Progress in Astronautics and Aeronautics, AIAA, Washington, DC, 1995.
43. V. Bellucci, C. Paschereit, P. Flohr, and F. Magni, On the Use of Helmholtz Resonators for Damping Acoustic Pulsations in Industrial Gas Turbines, ASME Paper 2001-GT-0039, 2001.
44. K. R. McManus, T. Poinso, and S. M. Candel, A Review of Active Control of Combustion Instabilities, *Prog. Energy Combust. Sci.*, Vol. 19, 1993, pp. 1–29.
45. J. R. Seume, N. Vortmeyer, W. Krause, J. Hermann, C. C. Hantschk, P. Zangl, S. Gleis, D. Vortmeyer, and A. Orthmann, “Application of Active Combustion Instability Control to a Heavy Duty Gas Turbines, ASME Paper No. 97-AA-119, 1997.

- 46. N. Docquier and S. Candel, Combustion Control and Sensors: A Review, *Progr. Energy Combustion Sci.*, Vol. 28, 2002, pp. 107–150.
- 47. C. E. Johnson, Y. Neumeier, and B. T. Zinn, Online Identification Approach for Adaptive Control of Combustion Instabilities, 35th AIAA Joint Propulsion Conference, Paper 99–2125, Los Angeles, CA, 1999.

#### BIBLIOGRAPHY

L. Crocco, and S. L. Cheng, *Theory of Combustion Instability in Liquid Propellant Rocket Motors*, Agardograph No. 8, Butterworths, London, 1956.

- R. D. Giammar and A. A. Putnam, Combustion Roar of Premix Burners, Singly and in Pairs, *Combustion Flame*, Vol. 18, 1972, pp. 435–438.
- W. Krebs, G. Walz, P. Flohr, and S. Hoffmann, Modal Analysis of Annular Combustors: Effect of the Burner Impedance, ASME Paper 2001-GT-0042, Amsterdam, 2001.
- S. S. Sattinger, Y. Neumeier, A. Nabi, B. T. Zinn, D. J. Amos, and D. D. Darling, Sub-scale Demonstration of the Active Feedback Control of Gas-Turbine Combustion Instabilities, *ASME J. Eng. Gas Turbines Power*, Vol. 122, 2000, pp. 262–268.

# CHAPTER 78

## METAL-CUTTING MACHINERY NOISE AND VIBRATION PREDICTION AND CONTROL

Joseph C. S. Lai

Acoustics & Vibration Unit

School of Aerospace, Civil and Mechanical Engineering

University of New South Wales at the Australian Defence Force Academy  
Canberra, Australia

### 1 INTRODUCTION

Many workers all over the world suffer significant hearing loss as well as psychological and physical stress as a result of exposure to high levels of industrial noise. Many industrial processes involve cutting metal products such as sawing, milling, grinding, punching, piercing, and shearing. As a result of operation processes, the noise from metal-cutting machines can be continuous, such as in saws, drills, lathes, and milling machines or impulsive such as in punch presses.

In this chapter, noise sources due to a continuous metal-cutting process and to an impact/shearing process are discussed. The basic theory of acoustic noise emission due to cutting metal products is introduced. Various noise control options (such as damping, sound absorption, barriers, and vibration isolation) for metal-cutting noise are examined using specific examples. Finally, modern numerical methods for prediction of noise and vibration are described.

### 2 CONTINUOUS METAL-CUTTING PROCESSES

Metal-cutting machines that fall into this category include saws, drills, lathes, and milling machines. Modern lathes and milling machines are generally not considered as occupational noise problems because an operator of these machines is rarely subjected to an overall A-weighted sound pressure level exceeding 85 dB. In particular, for most milling machines, both the cutting tool and the workpiece (product) are completely enclosed for containing liquid coolants and for safety. These enclosures provide substantial noise reduction. In general, the following noise sources can be distinguished: aerodynamic noise, noise due to vibrations of cutting tool, noise due to vibrations of workpiece, noise due to impact/interactions between the cutting tool and the workpiece, and noise due to material fracture. The radiated noise level is highly dependent on the feed rate of the workpiece, the depth of cut, the resonance frequencies of the cutting tool and the workpiece, the geometry of the cutting tool and the workpiece, and the radiation efficiencies at the resonance modes. Noise due to impact and material fracture will be treated in Section 3 on impact cutting processes.

### 2.1 Aerodynamic Noise Source

Aerodynamic noise in cutting tools is generated due to the vortex shedding off a spinning tool, such as the teeth in a high-speed rotating saw, producing a whistling noise. If the vortex shedding frequency coincides with the blade natural frequency, the noise radiated can be significantly amplified. It has been found by Bies<sup>1</sup> that the radiated noise for an idling circular saw is characterized by dipoles and the radiated sound power, proportional to the tooth area, increases with the rotational speed to a fifth power. Consequently, it is not unusual that the aerodynamic noise radiated from an idling circular saw at high speeds exceeds an A-weighted sound pressure level of 100 dB.<sup>2</sup> The strong aerodynamic noise source in an idling circular saw has been attributed by Martin and Bies<sup>2</sup> to the interaction of the vortex shed by an upstream tooth with the leading edge of the following downstream tooth. Hence this noise is dependent on the tooth geometry.

Various control options to minimize the aerodynamic noise (as applied to a circular saw) are available. By reducing the interactions between vortices and teeth using a variable pitch instead of a fixed pitch, a noise reduction of about 20 dB is possible. Saw blades made of high-damping alloys have been used to reduce blade vibrations at resonance and hence the radiated noise. It has been shown that a noise reduction up to between 10 and 20 dB could be achieved over a range of the peripheral velocity from 30 to 60 m/s.<sup>3</sup> Generally, applications of damping disks to saw blades might provide noise reduction up to 10 dB.

### 2.2 Noise due to Structural Vibrations

Noise due to structural vibrations include noise due to vibrations of the cutting tool, to the workpiece, and to the interactions between the two. In terms of reducing the noise due to vibrations of the cutting tool, for example, in the case of a circular saw, the structural resonance frequencies could be shifted away from the vortex shedding frequency by designing blades with different hole patterns, widened gullets and irregular pitch<sup>4</sup> or novel tooth design.<sup>5</sup> In terms of reducing the noise due to vibrations of the workpiece, appropriate clamping and application of damping plates to the workpiece has been found to be useful.

The interactions between the cutting tool and the workpiece might cause instability. In most machining operations such as milling and turning, the cutting forces are highly dependent on the geometry of the cutting tool, the workpiece feed rate, the spindle speed, and the depth of cut. Under certain combinations of these parameters, self-excited instability, known as regenerative chatter, occurs.<sup>6,7</sup> As a result of regenerative chatter, not only is the quality of the surface finish degraded and the wear of the cutting tool accelerated, but the radiated noise could be also significantly increased. Regenerative chatter and hence noise due to the interactions between the cutting tool and the workpiece could be significantly reduced by proper selection of the spindle speed, spindle speed variation, and the geometry of the cutting tool,<sup>6,7</sup> as well as active control.<sup>8</sup>

Other control options for machining operations include partially enclosing the cutting area, applying sound-absorbing materials to reflective surfaces, and better vibration isolation of the machine structure.

### 3 IMPACT METAL-CUTTING PROCESSES

Impact cutting operations typically consist of an initial impact where energy is built up until the material is fractured, accompanied by acoustic emission. The noise and vibration may be transmitted via the machinery and/or via the metal stock. In addition, material handling sometimes produce significant impact noise, such as when metal sheet products are stacked or moved on roller conveyors. As some of the available noise control options such as damping, enclosure, cutting tool geometry are, in principle, applicable for both continuous and impact metal-cutting processes, they will be discussed here in greater details using an impact shear cutting machine as an example.

#### 3.1 Theoretical Considerations

In the classic study of Richards et al.<sup>9</sup> noise sources of some 43 different machines or processes are listed. In most metal-cutting processes such as sawing, planing, stamping, forging, punching, piercing, and shearing, impulsive forces are involved, and numerous studies have been conducted to study noise sources and noise transmission paths for these operations.<sup>9–17</sup> Generally, the noise arising from these operations include acceleration noise, ringing noise, noise due to fracture of the feedstock material (cutting noise), and other machinery noise.

Acceleration noise<sup>9</sup> is primarily generated by the impact between the cutting blade and the feedstock and the air around it is compressed due to rapid surface deformations. This noise normally occurs at low frequencies<sup>18</sup> and is usually small compared with the ringing noise caused by flexural vibrations.<sup>19,20</sup>

Ringing noise is generated from vibrations of the feedstock and machine structure including machine foundations<sup>9,12</sup> and is usually a significant contributor to the overall noise radiated during metal-cutting operations. The magnitude of the ringing noise is dependent on the radiation efficiency, spatial averaged

mean-squared normal surface vibrational velocity, the surface area, the density of air, and the speed of sound in air.<sup>9,12</sup>

Noise due to fracture of feedstock material (cutting noise) is dependent on material properties and could be a dominant noise source especially in presses.<sup>21–24</sup> Other machinery noise in metal-cutting machinery includes exhaust, operations of clutches, fans, and compressors.

According to Richards,<sup>13</sup> the total energy in an impact cutting process is composed of the work done on the product, the work transferred to the ground or foundation, the energy dissipated as heat through structural damping, and the energy radiated as noise. It has been derived by Richards<sup>13</sup> using this energy accountancy concept that the equivalent A-weighted continuous noise level  $L_{Aeq}$  is related to the time ( $t$ ) history of the induced force  $f(t)$  by

$$L_{Aeq} = 10 \log_{10} \sum |f'(t)|_{\max}^2 + C = L_{f'} + C \quad (1)$$

Here  $|f'(t)|_{\max}$  is the amplitude of the local maximum of the first derivative of the induced force, and  $C$  is a constant dependent on the physical properties of the machine structure and the feedstock material. Equation (1) has also been derived by Evensen<sup>25</sup> using the Helmholtz integral concept. In deriving Eq. (1), it has been assumed that the dominant radiated noise is due to structural vibration; and that the structure is linear and is only excited at the point of cutting with no backlash noises.

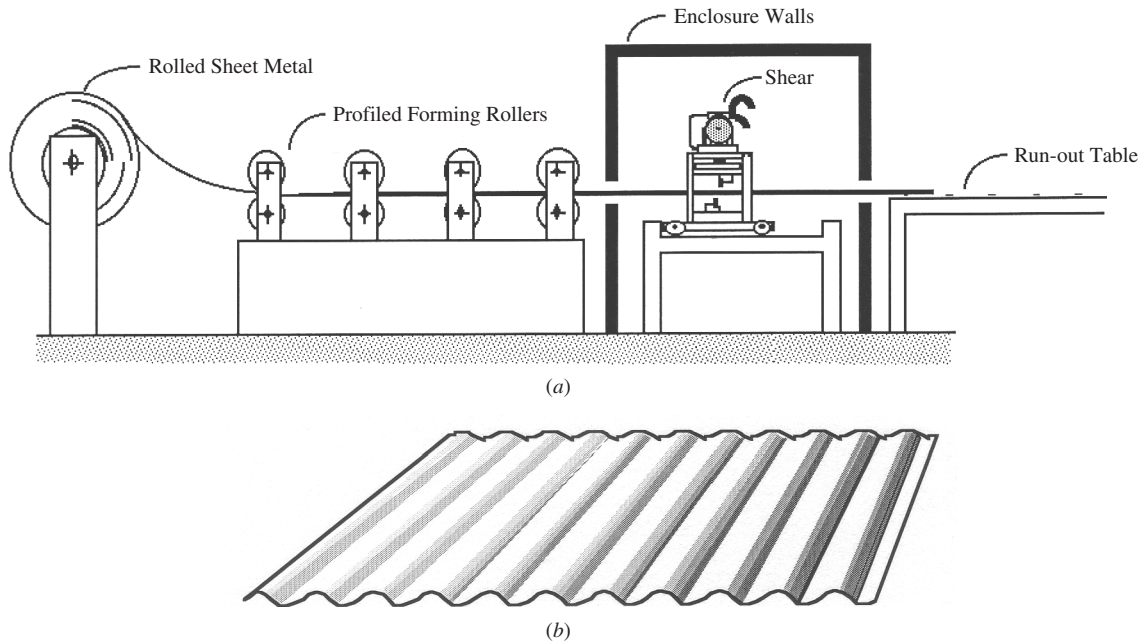
There are two significant implications in Eq. (1): (i) if the induced-force time history is known, then the radiated A-weighted sound pressure level can be predicted; and (ii) if the maximum rate of change of the induced force,  $[f'(t)]_{\max}$ , can be reduced, then  $L_{Aeq}$  will be reduced.

Results obtained for a 200-kN punch press,<sup>26</sup> a 80-kN punch press,<sup>27</sup> and a roll former shear<sup>28,29</sup> for a range of operating conditions, materials, material thickness, and tooling parameters (such as clearance and blade profile) support the linear relationship between  $L_{Aeq}$  and  $L_{f'}$  as given in Eq. (1), but the slope  $m$  as indicated in Eq. (2) may not be 1. It has been shown numerically<sup>28,29</sup> that this might be attributed to the creation of different force sources (backlash forces produced at bearing impacts) at different locations of the machine structure with different magnitudes and phases.

$$L_{Aeq} = mL_{f'} + C \quad (2)$$

#### 3.2 Noise Control Methods

To illustrate the effectiveness of various noise control methods in treating different noise sources, a roll former machine commonly used in sheet metal industries is used as an example here. As shown in Fig. 1a, the flat sheet metal is first uncoiled and passed through a series of rollers to form the finished product profile (Fig. 1b), which is then cut to length in a continuous process using a shear moving with the product.



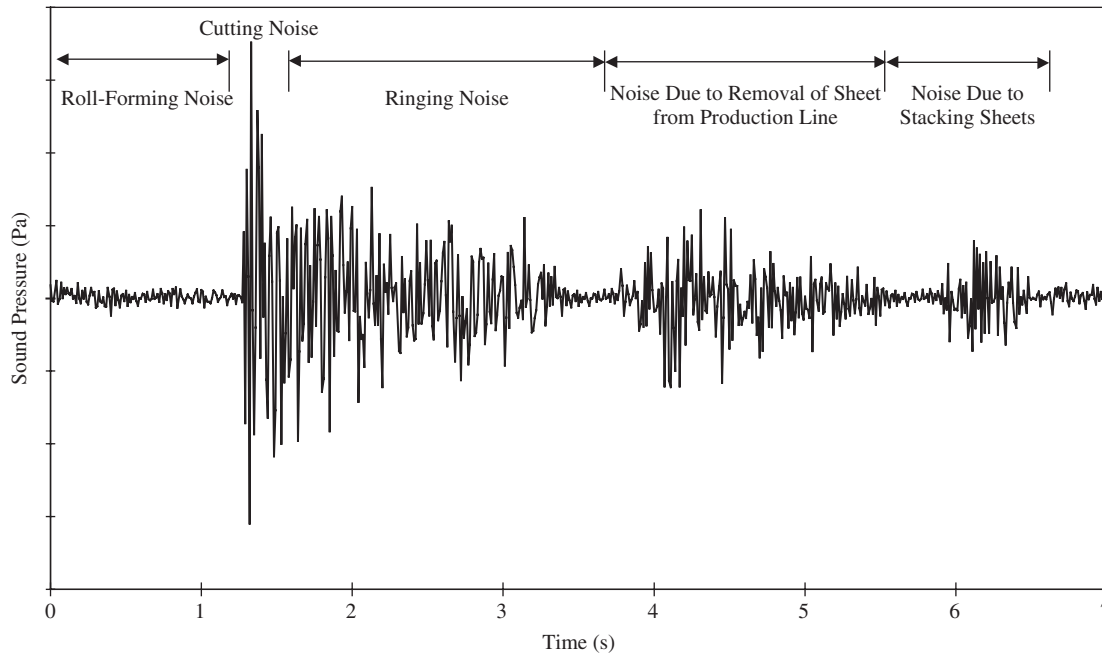
**Figure 1** (a) Schematic diagram of a typical roll-forming production line. (b) Sheet product with a sinusoidal profile. (Reprinted from Ref. 35, with permission of Elsevier.)

The profiled sheet then has to be removed either by an operator or an automatic stacker from the production line and stacked on a pile ready for delivery. These sheet metal products, which come in a variety of profiles, thicknesses and surface coating, are used extensively for roofing, walling, and fencing of industrial and domestic buildings. The lower and the upper blades of the shear are profiled to approximately match the profile of the product. The lower blade is fixed and the upper blade is moved vertically by a driver actuated either mechanically, pneumatically, or hydraulically. The noise radiated at various stages of the operation of a roll former production line can be identified from the noise signature shown in Fig. 2. These include the noise due to roll forming a flat metal sheet into a profiled sheet, cutting the sheet to required length, removing the sheet from the production line and dropping the sheet onto a stack. It can be seen that high impulsive noise levels are produced by the cutting action (fracturing the metal) and the resulting impact-induced vibration of the product and the surrounding structure ("ringing" noise). The noise due to removal of the product from the production line and stacking the product may be reduced by changing the operator's work practice or by installing an automatic stacking machine.<sup>30</sup>

**3.2.1 Control at the Source by Changing Tooling Parameters** With the somewhat rare exception of noisy auxiliary equipment, the primary noise excitation in a metal-cutting machine is usually the initial contact between the cutting tool (blade)

and the metal feedstock. Hence, it is important to consider tooling parameters such as blade profile, clearance, and operating speeds to minimize the impact-induced vibrations without compromising the quality of the product. If the initial impact by the blade on the product is reduced, then the ringing noise due to vibration of the product and the machine structure may also be reduced. Considerable research has been carried out into the effects of tooling parameters on radiated noise from punching or piercing machines. It has been shown by Sahlin,<sup>24</sup> Koss,<sup>21,22</sup> and Shinaishin<sup>31</sup> that the major noise source during blanking is fracture of the work material. Shinaishin's experiments achieved a reduction of 12 dB in radiated noise by applying shear to the punch. Burrows<sup>26</sup> and Evensen<sup>25</sup> have experimentally investigated tooling effects such as blade clearances and shearing effect on the radiated noise of a punch press and have achieved a reduction of an overall A-weighted sound pressure level up to 10 dB for specific operations.

The linear relationship between  $L_{Aeq}$  and  $L_{f'}$  suggests that the radiated noise could be reduced by reducing the magnitude of  $L_{f'}$  (i.e., the maximum rate of change of the induced force) or the constant term  $C$  in Eq. (2). For a given machine,  $C$  is determined by physical factors such as the structural response, bulkiness, radiation efficiency, and structural loss factors.  $L_{f'}$  may be reduced by changing the tooling parameters such as the cutting speed, clearance, and the blade angle. For the roll former shear, it has been found<sup>28,29,32</sup> that increasing the blade angle, decreasing



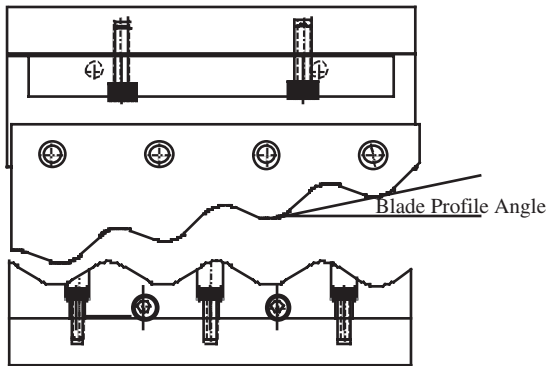
**Figure 2** Typical sound pressure trace during the operation of a roll former shear.

the clearance, and decreasing the cutting speed reduces  $L_{f'}$ . By designing a shear such that the fracturing process is prolonged,  $[f'(t)]_{\max}$  may be significantly reduced. This can be achieved by installing the upper blade at an angle to the lower blade as shown in Fig. 3 to allow progressive shearing across the sheet. By increasing the blade angle (i.e., softening the cutting process), the slope of the induced force term in Eq. (2) is reduced. As shown in Fig. 4, a reduction of 22 dB in the maximum A-weighted sound pressure level ( $L_{A\max}$ ) was obtained by increasing the blade angle from  $0^\circ$  to  $4^\circ$  in cutting zinc/aluminum alloy coated steel sheets with an approximately sinusoidal profile as in Fig. 1b. For comparisons, results documented by Bahrami<sup>29</sup> indicate a noise reduction of 2 to 5 dB by reducing the clearance and the cutting speed. For all blade angles tested except  $0^\circ$ , Fig. 4 shows that  $L_{A\max}$  is significantly increased by even a small misalignment of 3 mm along the blade direction. However, for  $0^\circ$  blade angle, there is a reduction of 10 dB in  $L_{A\max}$  because as a result of the small misalignment, not all the points on the blade are in contact with the sheet simultaneously during the shearing operation so that the rate of change of the induced force is reduced. Hence, a new blade set was designed with a constant blade angle of  $2^\circ$ , which corresponds to the maximum stroke of the existing machine. The original blade set consists of an upper blade with a stretched profile and pivoted so that the blade angle varies roughly from  $0^\circ$  to  $3^\circ$  along the blade.<sup>32</sup> As shown in Fig. 5, a reduction of 6 dB in over 3 s has been achieved with this new set of blades cutting

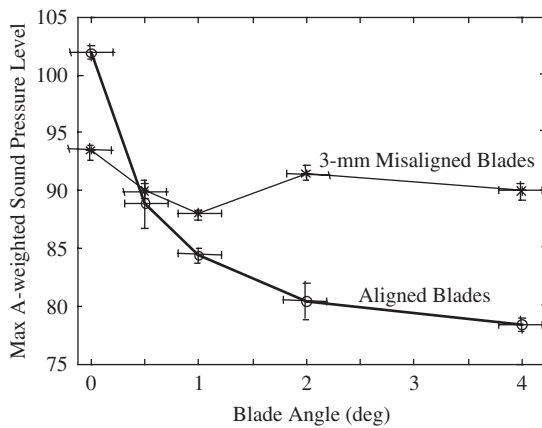
850 mm  $\times$  4000 mm  $\times$  0.45 mm profiled steel sheets in an industrial operating environment compared with the old blade. This result indicates that a profile blade with a constant angle is more effective in reducing the shear cutting noise than a profiled blade with varying blade angle along the blade. This is because if the shearing angle changes during the cutting process, the impact due to the blade movement would cause a greater shock in the product and the shear structure and consequently higher noise level. A constant shearing angle during cutting, as implemented in the new blade not only would reduce the cutting force but also would reduce the maximum rate of change of the induced force, hence lowering noise level according to Eq. (2).

### 3.2.2 Control of the Noise Transmission Path

**Treatment of Airborne Noise** The purpose of a noise abatement enclosure is to reduce the noise level outside the enclosure by containing and absorbing noise radiated from the enclosed noise source through airborne paths. The magnitude of the noise reduction depends on a number of factors such as the mechanical properties of the enclosure walls, the vibration isolation of the noise source from the outside of the enclosure, and the size of openings or gaps in the enclosure walls. Practical aspects for the design of enclosures have been given by Crocker and Kessler.<sup>33</sup> The basic construction of noise enclosure wall panels normally consists of two components: a noise barrier to provide resistance to transmission of sound and an absorptive inner lining to reduce reflection of sound within the enclosure. It is normally



**Figure 3** Sinusoidal blade assembly. (Reprinted from Ref. 32, with permission of Elsevier.)

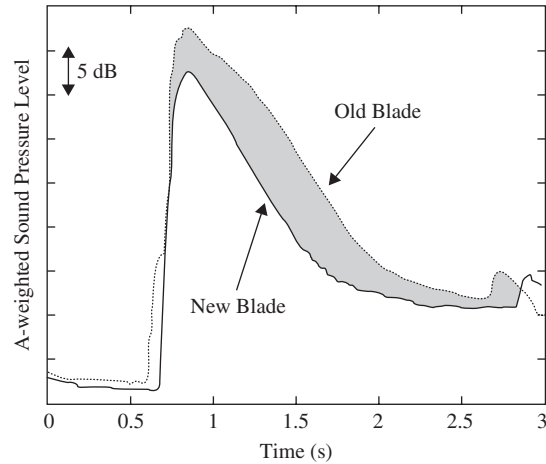


**Figure 4** Effect of shearing blade angle and its misalignment on radiated noise in profiled blade sets. (Reprinted from Ref. 32, with permission of Elsevier.)

necessary to provide doors, windows, ventilation, and other openings. However, a plain opening, which covers 1% of the area of the panel, will reduce the transmission loss to approximately 20 dB.<sup>34</sup> It is, therefore, important that when openings cannot be avoided, they should, where possible, open through a long, narrow duct lined with absorptive material.

It is both costly and impractical to enclose the whole roll-forming production line. This is because the production line is often longer than 20 m, the operator requires access to the machine to remove and stack the product once it is cut, and there are a number of points in the process that require continuous observation and frequent operator intervention.

Three different enclosures were designed and tested, details of which are given in Ref. 35. The walls of the enclosure consist of at least two layers of noise barrier materials (such as steel, particleboard, hardboard) and one or two layers of absorption materials (such as rock wool or fiberglass). The sheet

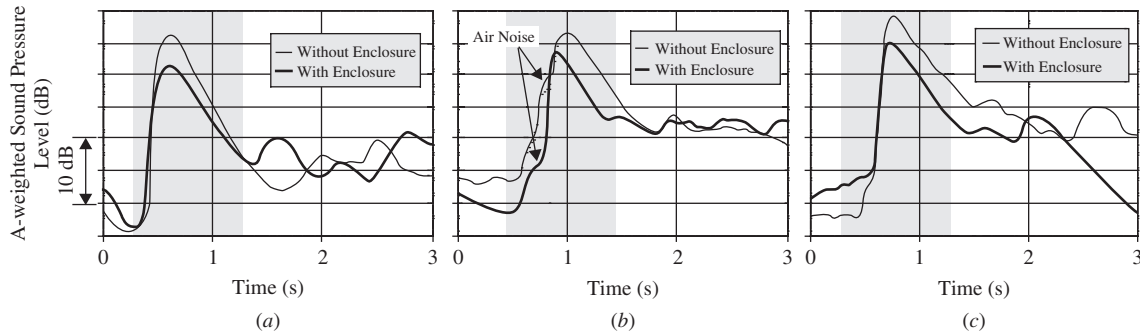


**Figure 5** Comparison of the sound pressure level during cutting with an old blade and a new blade. (Reprinted from Ref. 32, with permission of Elsevier.)

product is fed through an inlet opening approximately 100 mm × 1000 mm and a similar sized opening at the exit, as shown in Fig. 1a. The estimated reduction provided by the three enclosures A, B, and C in Fig. 6 against airborne noise is 12, 17, and 19 dB, respectively, which agree well with measurements using an airborne noise source.<sup>35</sup> It should be noted that the shears enclosed by the three enclosures had different actuating mechanisms. For the shear with enclosure A, it was operated pneumatically. The shear with enclosure B was operated mechanically using a flywheel while the shear with enclosure C was operated hydraulically.

Typical noise traces from each noise enclosure at the operator's position are given in Fig. 6. The time period indicated by the shaded area in Fig. 6 represents the noise due to cutting. By calculating the equivalent continuous sound pressure level ( $L_{eq}$ ) for the cutting period from 10 tests, it has been found that the noise reduction provided by the enclosures at the operator's position appears to be limited to 4 to 5 dB, independent of the variety of enclosure construction and shear configurations. As this reduction is substantially lower than the minimum of 12 dB estimated for enclosure A, some noise must be escaping from the enclosures through some structure-borne paths. Thus if only the shear is enclosed, the performance of an enclosure is virtually independent of the enclosure panel design. It is clear that unless the structure-borne noise is reduced, the use of expensive materials and complex construction will not give a corresponding increase in the performance of the noise enclosure.

**Treatment of Structure-Borne Noise** The enclosures are effective in reducing the direct airborne noise resulting from the blade impacting the product, but



**Figure 6** Comparison of A-weighted sound pressure level at the operator's position with and without enclosures: (a) enclosure A, (b) enclosure B, and (c) enclosure C. (Reprinted from Ref. 35, with permission of Elsevier.)

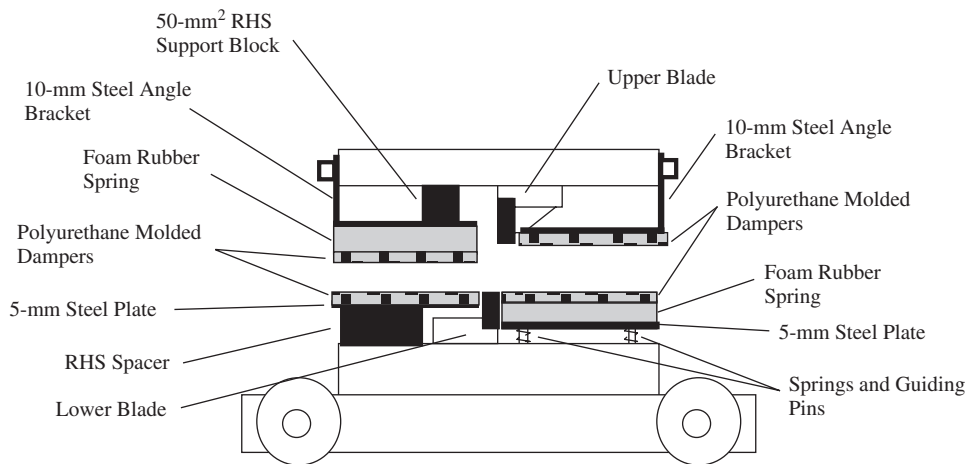
the resulting ringing noise caused by the sheet vibrations due to the blade impact is only slightly reduced because most of the product surface is outside the noise enclosure. To reduce the vibrations transmitted to the sheet from the impact of the shear blades during the cutting action, a damping system was designed to clamp the sheet prior to and just after the cutting of the sheet.

As shown in Fig. 7, the polyurethane dampers were manufactured from a number of damper segments each consisting of a single corrugation. The angle bracket for the upper inlet side damper was fixed in place and the clamping action was achieved by using a large foam rubber spring. The angle bracket for the upper exit side damper was fixed in place, and the damping segments were individually spaced to match the rake of the upper blade. The lower exit side damper was placed on a sprung base with small guiding pins sliding into the lower blade bolster. Where foam springs were used, the foam rubber was glued to the metal base plates and the polyurethane dampers were glued to the

foam rubber using a two-part epoxy glue. The hardness was set to 40 durometer hardness as this was found to be more effective than the harder material. Figure 8 shows that a noise reduction of over 5 dB has been achieved by the sheet dampers at the operator position. The performance cost of the three enclosures ranges from US\$2000/ dB to US\$3500/ dB compared with US\$500/ dB for sheet dampers.

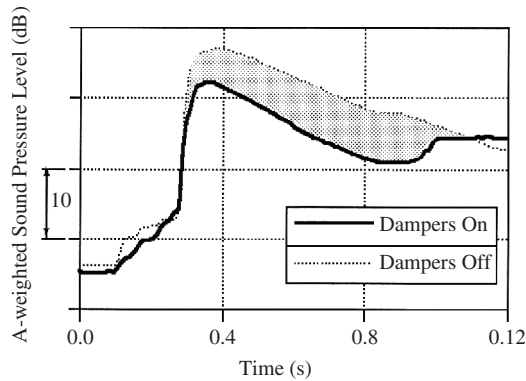
#### **Another Example of Noise Control of Metal-Cutting Machine**

Another example of a metal-cutting machine is a 120-tonne expanded-metal press.<sup>36</sup> Expanded-metal mesh such as that shown in Fig. 9 is manufactured from flat metal plate feedstock in a range of thickness, sizes, styles, and materials. They are used in a wide variety of applications such as sun screens, machinery safety guards, facades, fences, security door grilles, and floors. Similar to the roll-former shear, treatment of the noise source could be applied by changing tooling parameters such as blade profile, clearance, and operating speed. It has been found that when the operating speed was reduced by



**Figure 7** Schematic diagram of sheet dampers.





**Figure 8** Comparison of the sound pressure level during cutting with and without sheet dampers.

45%,  $L_{Aeq}$  was reduced by 6 dB.<sup>10</sup> To treat the airborne transmission path, a partial enclosure was built around the entry and exit sides of the press. A full enclosure was not practical because of the large size of the press and the need to allow the feedstock to enter and the product to leave from the machine. A noise reduction of between 2 and 7 dB was achieved by this partial enclosure depending on the measurement locations and the length of the unprocessed feedstock plate.<sup>37</sup> The feedstock plate on the entry side of the press is the source of structure-borne noise and its vibrations could be reduced by applying mechanical and electromagnetic clamps to the feedstock as shown in Fig. 10. A noise reduction of up to 11 dB was achieved.<sup>38</sup>

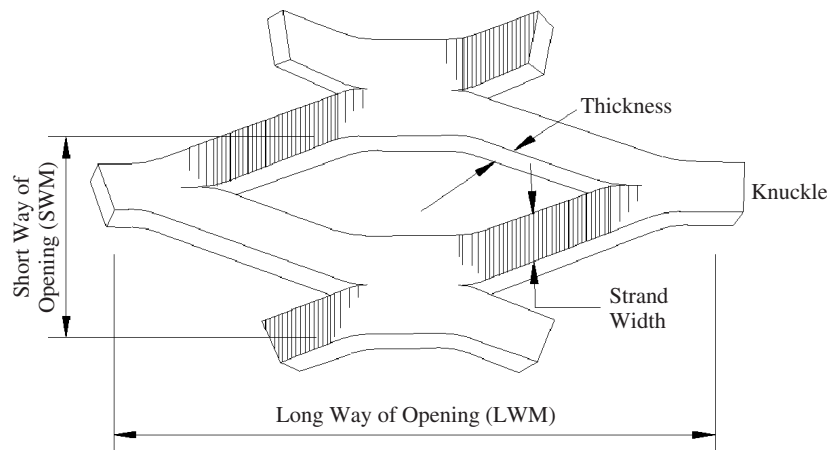
#### 4 NOISE AND VIBRATION PREDICTION

There have been numerous studies into the prediction of metal-cutting machinery noise.<sup>9–17,39</sup> Equation (2) is one means of estimating the noise radiation for

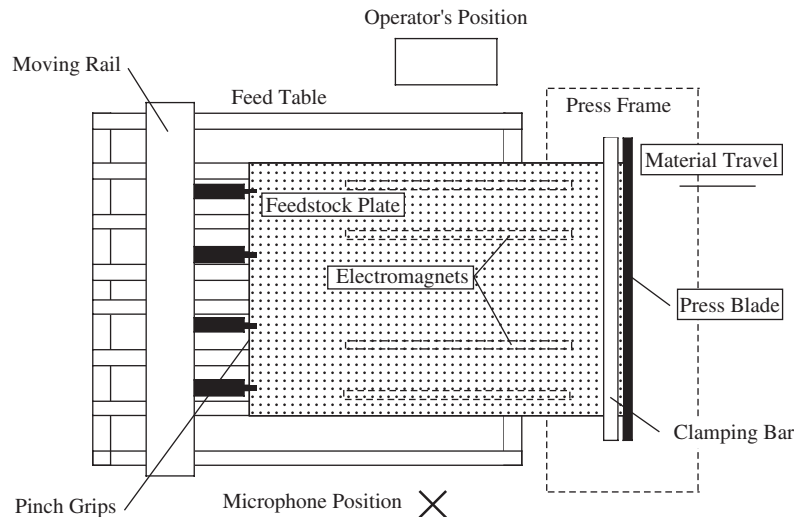
noise due to impact if the induced-force time history is known. Modern techniques of noise prediction generally employ finite element/boundary element modeling.<sup>28,39,40</sup> An interesting technique for reducing experimental measurements over a wide range of operating conditions is to use dimensional analysis traditionally employed in the field of fluid mechanics.<sup>41</sup> In the study of the expanded-metal press, it was postulated that the sound pressure  $p$  is a function of the feedstock thickness  $h$ , feedstock length  $a$ , feedstock bending stiffness  $D$ , the feedstock density  $\rho$ , and press speed expressed in strokes per second (sps). By using the Buckingham  $\pi$  theorem,<sup>41</sup> three nondimensional groups have been found:  $h/a$ ,  $p/(h^2 \times \text{sps}^2 \times \rho)$ , and  $ph^3/D$ .<sup>10,42</sup> Data<sup>10,42</sup> obtained for five different press operating speeds and three different feedstock thicknesses of mild steel indicate that these data collapse onto a single line on a log-log plot with the independent variables being two nondimensional groups:  $p/(h^2 \times \text{sps}^2 \times \rho)$  and  $(h/a)^{[1.36+0.102(h/h_{ref})]}$ . This relationship allows the radiated noise level from the expanded-metal press to be estimated to within 2 dB.

#### 5 SUMMARY

In this chapter, major noise sources in metal-cutting machinery that involve both continuous and impulsive cutting forces have been described. Broadly, they can be classified as aerodynamic noise, noise due to vibrations of the cutting tool, noise due to vibrations of the workpiece, and noise due to the interactions and/or impact between the cutting tool and the workpiece, and noise due to material fracture. These noise sources have been discussed with reference to metal-cutting machines, such as saws, lathes, milling machines, and impact cutting machines. Noise control strategies by treating the noise source, the noise transmission paths for both airborne noise and structure-borne noise have been demonstrated for these machines. These noise control options include the application of damping,



**Figure 9** An expanded metal mesh.



**Figure 10** Application of mechanical and electromagnetic clamps to reduce feedstock noise radiation.

installation of enclosures, and the change of tooling parameters such as tool geometry, clearance, feed rate, and depth of cut. In general, an effective noise control strategy would normally involve a combination of all these methods.

## REFERENCES

1. D. A. Bies, Circular Saw Aerodynamic Noise, *J. Sound Vib.*, Vol. 154, No. 3, 1992, pp. 495–513.
2. B. T. Martin and D. A. Bies, On Aerodynamic Noise Generation from Vortex Shedding in Rotating Blades, *J. Sound Vib.*, Vol. 155, No. 2, 1992, pp. 317–324.
3. N. Hattori, S. Kondo, K. Ando, S. Kitayama, and K. Momose, Suppression of the Whistling Noise in Circular Saws Using Commercially-Available Damping Metal, *Holz als Roh- und Werkstoff*, Vol. 59, 2001, pp. 394–398.
4. M. Spruit, M. Rao, J. Holt, L. Boyer, A. Barnard, and W. Dayton, Table Saw Noise Control, *J. Sound Vib.*, Vol. 2004, pp. 20–25.
5. K. Yanagimoto, C. D. Mote, and R. Ichimiya, Reduction of Vortex Shedding Noise in Idling Circular Saws Using Self-Jets of Air through Saw Teeth, *J. Sound Vib.*, Vol. 188, No. 5, 1995, pp. 745–752.
6. R. P. H. Faassen, N. van de Wouw, J. A. J. Oosterling, and H. Nijmeijer, Prediction of Regenerative Chatter by Modelling and Analysis of High-Speed Milling, *Int. J. Machine Tools Manufact.*, Vol. 43, 2003, pp. 1437–1446.
7. S. Y. Liang, R. L. Hecker, and R. G. Landers, Machining Process Monitoring and Control: The State-of-the-Art, *J. Manufact. Sci. and Eng.*, Vol. 126, 2004, pp. 297–310.
8. N. D. Sims and Y. Zhang, Active Damping for Chatter Reduction in High Speed Machining, AMAS Workshop on Smart Materials and Structures SMART'03, Jadwisin, 2003, pp. 195–212.
9. J. E. Richards, M. E. Westcott, and R. K. Jeyapalan, On the Prediction of Impact Noise. I: Acceleration Noise, *J. Sound Vib.*, Vol. 62, No. 4, 1979, pp. 547–575.
10. D. Eager and H. Williamson, 'Literature Review of Impact Noise Reduction in the Sheet Metal Industry, *Acoust. Australia*, Vol. 24, Vol. 1, 1996, pp. 17–23.
11. D. Eager, Acoustic Analysis of an Expanded-Metal Press, Ph. D. Dissertation, University of New South Wales, Australia, 1999.
12. J. E. Richards, M. E. Westcott, and R. K. Jeyapalan, On the Prediction of Impact Noise. II: Ringing Noise, *J. Sound Vib.*, Vol. 65, No. 3, 1979, pp. 419–453.
13. J. E. Richards, On the Prediction of Impact Noise. III: Energy Accountancy in Industrial Machines, *J. Sound Vib.*, Vol. 76, No. 2, 1981, pp. 187–232.
14. J. M. Cushieri and J. E. Richards, On the Prediction of Impact Noise. IV: Estimation of Noise Energy Radiated by Impact Excitation of a Structure, *J. Sound Vib.*, Vol. 86, No. 3, 1983, pp. 319–342.
15. J. E. Richards, On the Prediction of Impact Noise, V: The Noise from Drop Hammers, *J. Sound Vib.*, Vol. 62, No. 4, 1983, pp. 547–575.
16. J. E. Richards, A. Lenzi, and J. M. Cushieri, On the Prediction of Impact Noise, VI: Distribution of Acceleration Noise with Frequency with Application to Bottle Impacts, *J. Sound Vib.*, Vol. 90, No. 1, 1983, pp. 59–80.
17. J. E. Richards and A. Lenzi, On the Prediction of Impact Noise, VII: The Structural Damping of Machinery, *J. Sound Vib.*, Vol. 97, No. 4, 1984, pp. 549–586.
18. H. A. Evenson, C. W. Frame, and C. J. Crout, Experiments in Forge Hammer Noise Control, International Conference on Forging Noise Control, Atlanta, 1976, pp. 1–73.
19. M. M. Sadek and S. A. Tobias, Research on Noise Generated in Impact Forming Machines at the University of Birmingham, 1971–1976, *Proc. Instit. Mech. Eng.*, Vol. 180, No. 38, 1977, pp. 895–906.
20. H. G. Trengrouse and F. K. Bannister, Noise Due to Air Ejection from Clashing Surfaces of an Impact Forming Machine, *J. Vib. Acoust., Trans. ASME*, Vol. 73-DET-62, 1973, pp.

21. L. L. Koss and R. J. Alfredson, Identification of Transient Sound Sources on a Punch Press, *J. Sound Vib.*, Vol. 34, No. 1, 1974, pp. 11–33.
22. L. L. Koss, Punch Press Load-Radiation Characteristics, *Noise Control Eng. J.*, Vol. 8, 1977, pp. 33–39.
23. O. A. Sinaishin, On Punch Press Diagnostics and Noise Control, *Inter-noise 72*, Washington, DC, 1972, pp. 243–248.
24. S. Sahlin and R. Langhe, Origins of Punch Press and Air Nozzle Noise, *Noise Control Eng. J.*, Vol. 3, 1974, pp. 4–9.
25. H. A. Evenson, A Fundamental Relationship between Force Waveform and the Sound Radiated from a Power Press During Blanking or Piercing, *J. Sound Vib.*, Vol. 68, No. 3, 1980, pp. 451–463.
26. J. M. Burrows, The Influence of Tooling Parameters on Punch Press Noise, M.Sc. Dissertation, University of Southampton, 1979.
27. R. B. Coleman, Identification and Control of Noise Sources on a Manual Punch Press, M.Sc. Dissertation, North Carolina State University, 1981.
28. A. Bahrami, J. C. S. Lai, and H. Williamson, Noise from Shear Cutting of Sheet Metal, Tenth Int. Cong. on Sound & Vibration (ICSV10), Adelaide, Australia, 2003, pp. 4069–4076.
29. A. Bahrami, Effects of Tooling Parameters on Noise Radiated from Shear Cutting of Sheet Metal, Ph.D., University of New South Wales, 1999.
30. M. Burgess, H. Williamson, and C. Speakman, Retrofit Noise Reduction Techniques for the Control of Impact Noise in the Sheet Metal Industry, University of New South Wales, Acoustics and Vibration Centre, Report 9703, 1997.
31. O. A. Shinaishin, Impact Induced Industrial Noise, *Noise Control Eng. J.*, Vol. 2, No. 1, 1974, pp. 30–36.
32. A. Bahrami, H. Williamson, and J. C. S. Lai, Control of Shear Cutting Noise: Effect of Blade Profile, *Appl. Acoust.*, Vol. 54, No. 1, 1998, pp. 45–58.
33. M. J. Crocker and F. M. Kessler, *Noise and Noise Control*, Vol. II, CRC Press, Boca Raton, FL, 1982.
34. C. M. Harris, *Handbook of Acoustical Measurement and Noise Control*, 3rd ed., McGraw-Hill, New York, 1991.
35. J. C. S. Lai, C. Speakman, and H. Williamson, Control of Shear Cutting Noise—Effectiveness of Enclosures, *Appl. Acoust.*, Vol. 58, 1999, pp. 69–84.
36. D. Eager, H. Williamson, J. C. S. Lai, and M. J. Harrap, Noise Source Parameters for an Expanded Metal Press, *Inter-noise 94*, Yokohama, Japan, 1994, pp. 737–740.
37. C. Speakman, D. Eager, H. Williamson, and J. C. S. Lai, Effectiveness of Partial Enclosure Panels for an Expanded Metal Press—A Case Study, University of New South Wales, Acoustics and Vibration Centre, Report 9622, 1994.
38. C. Speakman, D. Eager, H. Williamson, and J. C. S. Lai, Retrofit Noise Reduction Techniques Applied to an Expanded Metal Press—A Case Study, University of New South Wales, Acoustics and Vibration Centre, Report 9414, 1994.
39. J. E. Richards and G. J. Stimpson, On the Prediction of Impact Noise: Part IX, The Noise from Punch Press, *J. Sound Vib.*, Vol. 103, No. 1, 1985, pp. 43–81.
40. Y. W. Lam and D. C. Hodgson, The Prediction of Ringing Noise of a Drop Hammer in a Rectangular Enclosure, *J. Acoust. Soc. Am.*, Vol. 93, No. 2, 1993, pp. 875–884.
41. A. K. Al-Sabeeh, Finite Element Utilization in the Acoustical Improvement of Structure-Borne Noise of Large Industrial Machines, Ph.D. Dissertation, North Carolina State University, Raleigh, NC, 1983.
42. F. M. White, *Fluid Mechanics*, McGraw-Hill, New York, 2003, p. 880.

# CHAPTER 79

## WOODWORKING MACHINERY NOISE

**Knud Skovgaard Nielsen**  
AkustikNet  
Broenshoej, Denmark

**John S. Stewart**  
Department of Mechanical and Aerospace Engineering  
North Carolina State University  
Raleigh, North Carolina

### 1 INTRODUCTION

Woodworking machinery, in the broad sense, includes a wide range of equipment, ranging from off-road equipment used to harvest and transport logs to simple jig saws used in home hobby shops. In the United States, woodworking factories have typically been among the most frequently cited industrial operations by the Occupational Safety and Health Administration (OSHA) for excessive employee exposure to noise. This is due in part to the extremely high noise levels produced by these machines during both operating and machine idle conditions, as well as the relative lack of automation in many segments of the woodworking industry.

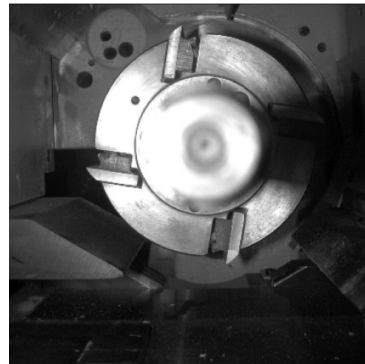
Noise produced by woodworking-related machinery results from a variety of general noise sources (motors, gears, hydraulic systems, conveyors, etc.), in addition to noise produced by sources that are unique to woodworking. In some cases, unique solutions need to be sought for noise problems that occur in industrial woodworking operations such as sawmills, planer mills, molding plants, window/door plants, furniture and cabinet plants, wood flooring manufacturing plants, and the like. Many industrial woodworking machinery noise sources result from the use of cutters and saw blades. Although a variety of other sources are associated with the machines that utilize these tools, many woodworking machinery noise problems can be resolved by dealing with the noise produced as a result of the use of cutters and saw blades.

### 2 NOISE PRODUCED BY MACHINES UTILIZING CUTTERS

Cutters are used throughout the woodworking industry on machines such as planers, molders, panel machines with cutters, routers, and the like to smooth and shape wood products. A typical industrial machine utilizing cutters incorporates feed rolls and holddown bars to transport the workpiece by the cutter (in some cases the cutter is moved by the workpiece). The typical cutter has several rows of knives that protrude above the cutter body (which is typically cylindrical). The machining process is typically a peripheral milling process in which each knife removes a “chip,” leaving a relatively smooth surface (depending on the machine feeds and speeds). Traditionally, cutters have incorporated straight

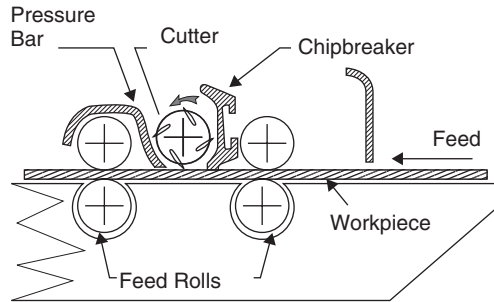


**Figure 1** Cutting area of typical industrial moulder machine.

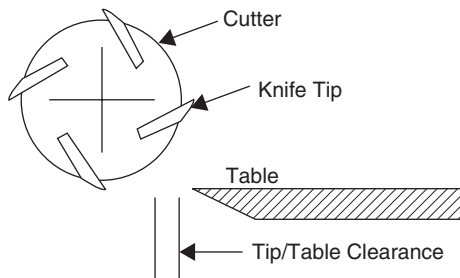


**Figure 2** Typical straight knife cutter mounted on moulder spindle.

knives (aligned parallel to the cutter rotational axis), primarily due to ease of manufacture and maintenance (sharpening) issues. This design is quite effective in removing wood material, however, it is inherently noisy. A typical industrial molder and standard straight knife cutter mounted on the molder spindle are shown in Fig. 1 and 2.



**Figure 3** Typical planer cross section showing cutter, hold-down bars, feed rolls, and workpiece.

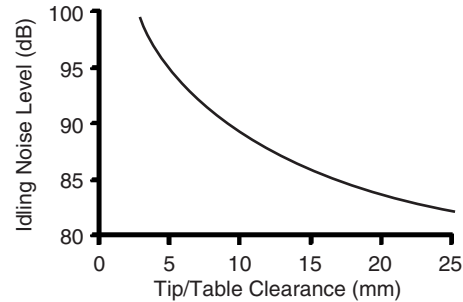


**Figure 4** Illustration of straight knife cutter located near stationary surface (table).

## 2.1 Noise Generation Mechanisms for Machines Utilizing Cutters

A cross section of a typical industrial planer (surfacer) is shown in Fig. 3. During idle (when the machine is not cutting wood), the rotating cutter “disturbs” the surrounding air and, for straight knife designs, actually entrains air in the gullet (chip clearance) area similar to the action of a centrifugal fan. Cutters rotating in open space produce turbulence-type noise that is usually broadband in nature (similar to air-handling noise in duct systems). Cutters used in woodworking, however, usually operate in close proximity to the workpiece and stationary surfaces (tables, pressure bars, etc.) used to hold and stabilize the workpiece (as shown in Fig. 3).

The air compression caused by cutter rotation near a stationary surface results in a siren-type noise mechanism, which is an extremely efficient mechanism for sound radiation. This noise is pure tone in nature, dominated by noise occurring at the knife passage frequency [number of knives ( $n$ )  $\times$  revolutions per minute (rpm)/60 Hz]. The rotating cutter noise increases with rpm and is strongly dependent on the clearances between the cutter knives and the stationary surfaces, as shown in Fig. 4, and increases in the range of 12 dB to 16 dB for a doubling of rpm.<sup>1</sup> The noise level produced by rotating cutters during idle also increases with increasing cutter length at approximately 3 dB per doubling of head length. The increase in noise level with decreasing distance (clearance) between the

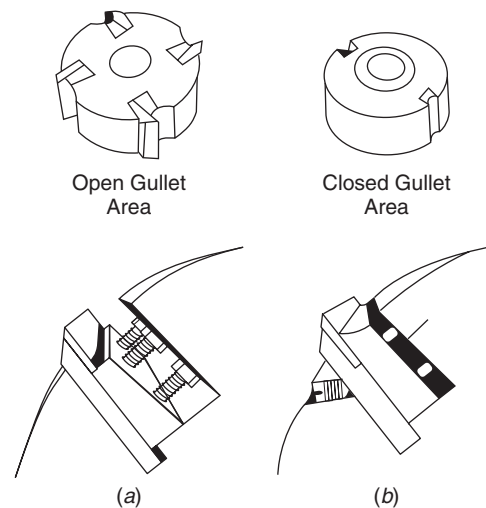


**Figure 5** Effect of cutter-stationary surface (lip) clearance on idling noise for typical straight knife cutter.

knives and stationary surfaces (table, lip, etc.) is shown in Fig. 5.

The noise during idle for machines equipped with cutters also increases with increased height of the knives above the cutter body and increased open area of the gullet. Figure 6 shows the gullet area for two cutters—one with a closed gullet area (*a*) and the other with a more open gullet area (*b*).<sup>2,3</sup>

During cutting, an additional noise source usually becomes the dominant source.<sup>4,5</sup> This noise source is the vibration of the wood workpiece (board), which is excited to vibrate by the periodic impact of the cutter knives (occurring at the knife passage frequency). These impacts cause a structural vibration response of the workpiece primarily at the knife passage frequency and multiples (harmonics) of this frequency. Due to the relatively large amount of damping



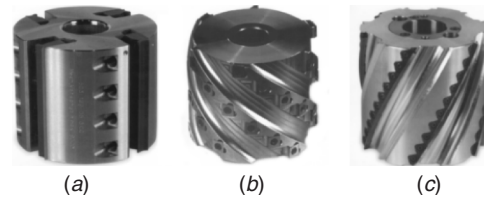
**Figure 6** Illustration of (a) open and (b) closed gullet areas.<sup>2,3</sup>

present in wood materials, noise produced by resonant vibration response of the workpiece is not usually an issue. The amplitude of the resulting vibration (and noise) depends on several factors, including (a) the magnitude of the impact force (governed by knife sharpness, cutter rpm, wood properties, hardness, damping, etc.), (b) the workpiece geometry, which governs the efficiency of sound radiation, (c) the cutter design and operating conditions, which governs the vibration excitation response characteristics and frequencies, and (d) the details of the workpiece support/holddown system, which governs the propagation of vibration along the workpiece length, the vibration mode shapes, external damping, and the like.

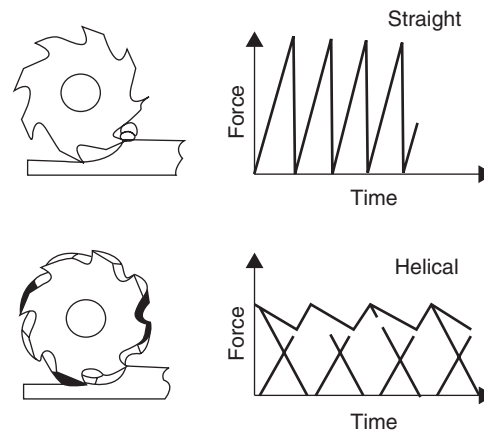
One of the more important determinants with regard to noise generation during cutting is the workpiece geometry. The workpiece width is strongly related to cutter power consumption (energy input) and also governs the radiation efficiency of the workpiece (narrow workpieces do not radiate low to midrange frequencies as efficiently as wider workpieces). The increase in noise level with workpiece width has been shown to be approximately 6 dB per doubling of width for straight knife-type cutters. The workpiece thickness also affects the vibration response of the workpiece and is responsible for the considerable reduction of noise generation as workpiece thickness increases (beyond about 50 mm thickness). The effect of workpiece length on employee exposure is somewhat more complicated since the vibrational energy provided by cutter impacts is distributed along the workpiece length. Although the total sound power produced by workpieces of different length is nearly constant, localized noise levels (at operator locations) may be substantially different for different workpiece lengths.<sup>6</sup> Unless vibration suppression techniques<sup>6</sup> (pressure bars, rubber tire feed rolls, etc.) capable of reducing the propagation of vibration are employed, this vibration occurs over the entire length of the workpiece while it is engaged in the cutter. This has important implications with regard to the use of acoustical enclosures for noise reduction for machines equipped with cutters processing relatively long workpieces; since the length of any enclosure (and/or acoustical tunneling system) must be nearly twice the length of the workpiece to contain the entire noise source within the enclosure at all times.

## 2.2 Noise Reduction Techniques for Machines Utilizing Cutters

**2.2.1 Noise Control at the Source for Machines Utilizing Cutters** The most direct approach to noise reduction for machines employing cutters is cutter redesign. A large variety of cutter designs is available, however, the acoustical performance (as well as operational and maintenance characteristics) varies considerably. It is important to consider the overall capabilities of a cutter when selecting alternative designs, including allowable feed rates and depths of cut, power consumption, surface quality, tool wear/breakage, and maintenance. From an acoustical standpoint, a continuous (tightly wound) helical design



**Figure 7** (a) Standard straight knife, (b) stagger tooth, and (c) helical cutters commonly used on industrial planers and moulders. (Courtesy of Weinig Group; [www.weinigusa.com](http://www.weinigusa.com).)

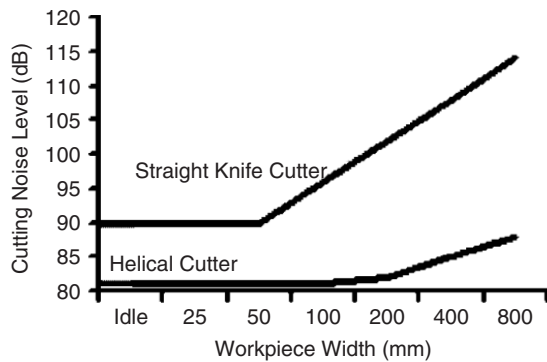


**Figure 8** Smoothing of force-time history for helical vs. straight knife cutter.<sup>5</sup>

(with as many rows of knives as practical) has been shown to be the most effective for reducing both idling and cutting noise.<sup>5</sup> During idle, the helical design does not compress air as each knife passes by a stationary surface, and instead moves air in an axial direction. During cutting, the combination of a tightly wound helical knife geometry and a relatively large number of knife rows provides nearly continuous contact between the knives and the workpiece, which effectively smooths out the force input that drastically reduces workpiece vibration. Typical straight knife, stagger tooth, and helical-type cutters are shown in Fig. 7. Stagger tooth cutters are widely used in woodworking applications. Although these cutters provide less noise reduction than the true helical design, they typically have maintenance-related advantages. When using helical or shear cutters, it is important to ensure that the axial forces push the workpiece toward the machine guide.

The cutter geometry controls the nature of the vibration excitation of the workpiece, which is directly related to the noise generated. Figure 8 illustrates the cutter force-time history for straight knife and helical cutters.



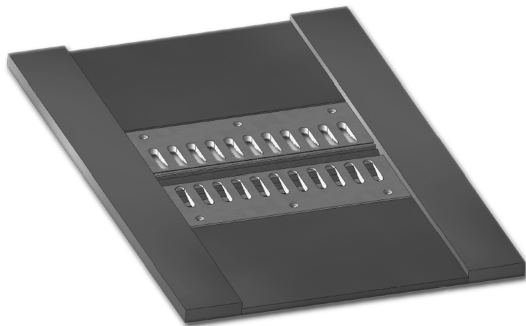


**Figure 9** Effect of workpiece width ( $w$ ) on cutting noise caused by workpiece vibration for helical vs. straight knife cutter.<sup>5</sup>

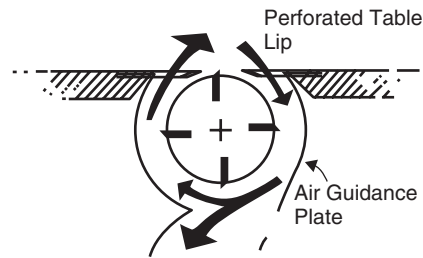
The width of the workpiece is one of the primary workpiece-related determinants of the resulting noise levels. The effect of workpiece width on noise level close to the operator location (1 m) for a typical planer/surfacers is shown in Fig. 9.<sup>5</sup>

In some cases noise reduction during idle alone is sufficient to reduce operator exposure to acceptable levels (without dealing with cutting noise). Reductions in idling noise can be accomplished by increasing the knife tip/stationary surface clearance (as shown in Fig. 5), reducing the knife tip projection and open gullet area (as shown in Fig. 6), and altering the geometry of stationary surfaces close to the cutter<sup>7</sup>; such as slotted tables and air guides (shown in Figs. 10 and 11), which help reduce air compression as the cutter knife rotates. These techniques are capable of reducing idling noise levels for machines equipped with cutters by as much as 6 dB, depending on tip speed and stationary surface location.

Machine design changes can also significantly reduce noise. Although most planers, molders, and the like are designed so that cutters operate at fixed peripheral speed, a reduction in peripheral speed of the cutter, when practical, can result in significant reductions in



**Figure 10** Slotted table for reducing idling noise on cutter equipped machines.<sup>7</sup>



**Figure 11** Slotted table with airflow guides for reducing idling noise on cutter-equipped machines.<sup>7</sup>

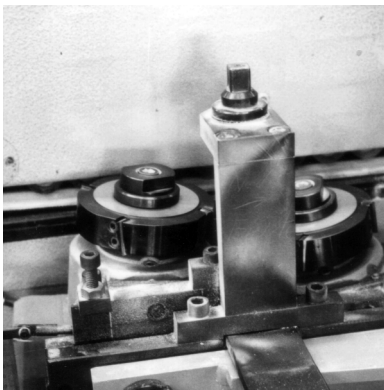
both idle and cutting noise. In some instances, a large-diameter cutter operating at a lower rpm (as opposed to a smaller diameter cutter with the same number of knife rows) can also provide a significant noise reduction due to the lower frequency knife impact and the resulting reduction in sound generation efficiency of the workpiece (in this case, the feed per tooth of the milling process would be increased).

Modification of feed rates and rpm are practical noise control alternatives for some machines, such as industrial router machines. These machines range in size from small machines, such as simple pin routers, to large CNC machines that have multiple tables and spindles. The large CNC machines often utilize router cutters (bits) to cut parts from sheet material. The noise levels produced by these operations can be quite high, however, the primary noise source in many cases is vibration of the tool, chuck, and/or spindle rotor system, as opposed to workpiece vibration. For high-speed machines cutting hard materials, the cutting action can excite resonant tool vibration that can produce an intense whistling noise. This resonant noise is quite sensitive to the operational feeds and speeds (which controls the tooth passage frequency) and the tool geometry and chucking details (which controls the resonant frequencies and overall system damping). Noise reduction in these cases can often be accomplished through adjustments in feed rate and or spindle rpm, changes in tool diameter, and/or number of teeth and alternative tool chucking systems that introduce damping at the tool-chuck interface. In cases where vibration of the spindle bearing system is the dominant noise source, it is common for noise levels to be high during idle and actually be lower during cutting due to the damping provided by the workpiece. Noise reduction in this case may require rework of the spindle/bearing system and/or improved balancing procedures.

Machine design changes involving the nature of contact between the cutter and workpiece and the support of the workpiece can also reduce noise. In some cases, it may be possible to convert from perpendicular cutting to parallel cutting by changing from horizontal spindles to vertical spindles [a cutter impacting the workpiece in the weak (perpendicular) direction normally produces more noise than for the parallel case]. Figures 12 and 13<sup>8</sup> show a double-end tenoner



**Figure 12** Double-end tenoner machine with horizontal spindles.<sup>8</sup>



**Figure 13** Double-end tenoner machine with vertical spindles.<sup>8</sup>

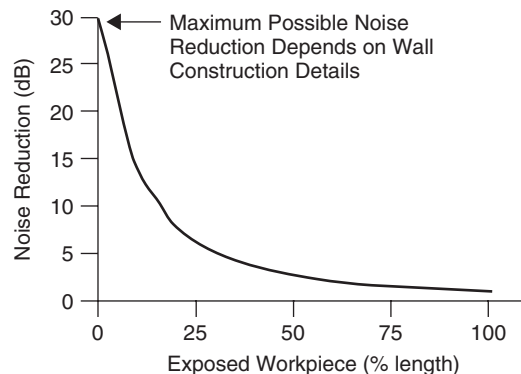
machine in which the cutting action has been converted from perpendicular to parallel to the workpiece by changing from horizontal to vertical spindles. This approach can reduce cutting noise by as much as 10 dB. Adding workpiece supports near the cutter impact area has also been shown to reduce noise. In general, machine design changes such as those described here should be done in cooperation with the machine manufacturer.

**2.2.2 Noise Control in the Path for Machines Utilizing Cutters** The use of acoustical enclosures is widespread in the woodworking industry. However, due to the radiation of noise from the entire workpiece while it is engaged in the cutter, many enclosures do not actually enclose the main noise source during operation (much of the vibrating workpiece is outside the enclosure at any given time). The performance

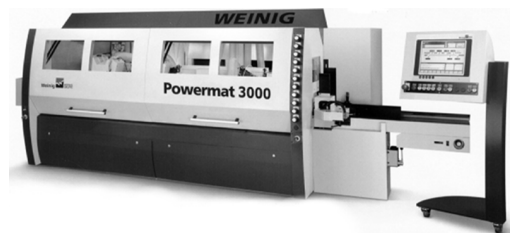
of these enclosures can be improved by using special feed roll and holddown designs, however, such modifications are best left to the machine manufacturer. The use of properly designed, removable acoustical tunnels can also be of benefit when used in conjunction with machine enclosures. In addition to the loss in performance due to the exposed vibrating workpiece, excessive and/or unsealed openings also render acoustical enclosures ineffective. The adverse effect of the exposed vibrating workpiece (which occurs when the workpiece is engaged in the cutter) on acoustical performance is shown in Fig. 14. In the case where an enclosure is designed to enclose only the cutter area, the exposed vibrating workpiece is nearly 100% of the length of the workpiece and there is essentially no reduction in the noise produced by the workpiece vibration. An enclosure that encloses 25% of the vibrating workpiece length is capable of producing only a 6-dB reduction in far-field noise, regardless of enclosure wall construction or how well the openings in the walls are sealed.

Safety/acoustical enclosures are often provided by equipment manufacturers. These enclosures are typically close-fitting units that are often attached directly to the machine frame, as shown in Fig. 15.

While these enclosures are excellent safety enclosures, the noise reduction capability during operation



**Figure 14** Approximate loss in enclosure effectiveness due to exposed vibrating workpiece.



**Figure 15** Safety/acoustical enclosure integrated into machine design. (Courtesy of Weinig Group; [www.weinigusa.com](http://www.weinigusa.com).)



is often limited by the relatively short length of the enclosure, which results in exposed vibrating workpiece noise. If these enclosures are not properly isolated from the machine, vibration can also be transmitted into the enclosure, which is, in turn, radiated as sound, further reducing the enclosure effectiveness. Large free-standing enclosures are by far the most effective, however, this type of enclosure is best suited for conveyor-fed machinery. In all cases involving cutters, the length of the workpiece must be taken into consideration in the enclosure design. Free-standing enclosures of proper length, or when used in conjunction with properly designed workpiece tunnels, can reduce operating noise levels near the machine (due to workpiece vibration) by more than 30 dB. For high-speed planers, this results in a reduction in noise level near the machine from the 115-dB range to below 85 dB. Enclosures of this type can be prefabricated metal construction (with sound-absorbing and damping materials) or conventional plywood/studwall construction (double wall with multiple sheets of plywood and appropriate sound-absorbing materials).

### 3 NOISE PRODUCED BY MACHINES UTILIZING CIRCULAR SAW BLADES

Sawing is one of the most common woodworking operations. The main types of sawing operations are circular sawing and band sawing. Circular and band sawing operations exhibit some similarity in that noise is produced by aerodynamic sources involving the tooth and gullet area of the blade during idle as well as structural vibration noise that is produced by blade and workpiece-related sources. Although large band saws (of the type used in sawmills) can produce intense noise, circular saws are responsible for the great majority of employee overexposures found in the woodworking industry and are the focus of this section. The circular saw blades under consideration here are primarily of the carbide-tipped design operating at relatively high peripheral speed (greater than 50 m/s) and are commonly found on cutoff/trim saws, single- and multiple-blade rip saws, and panel saws. Large-diameter cutoff saw blades found in primary breakdown operations (sawmills), which typically operate at lower peripheral speeds and are often equipped with operator booths, are not considered in this discussion. A typical industrial cutoff saw machine and circular saw blade used in furniture manufacturing are shown in Figs. 16 and 17, respectively.

#### 3.1 Noise Generation Mechanisms for Machines Utilizing Circular Saw Blades

A great deal of effort has gone into research relating to understanding noise generation mechanisms and reducing the noise produced by circular saws.<sup>9-14</sup> Although this chapter is concerned primarily with techniques for circular saw noise reduction, as opposed to noise source mechanism theory, it is necessary to review some basic noise source theory as it pertains to noise control techniques. Circular sawing noise can be grouped into three distinct source categories. These sources, although inter-related, are generally accepted to be aerodynamically

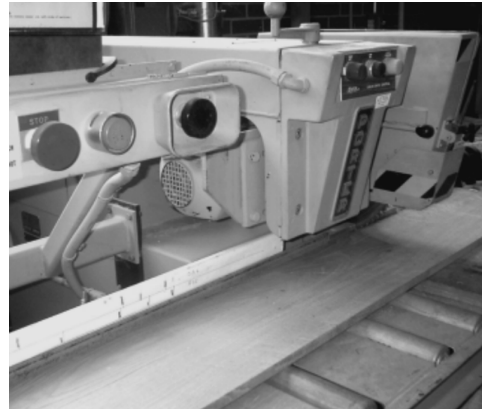


Figure 16 Typical industrial cutoff saw machine.

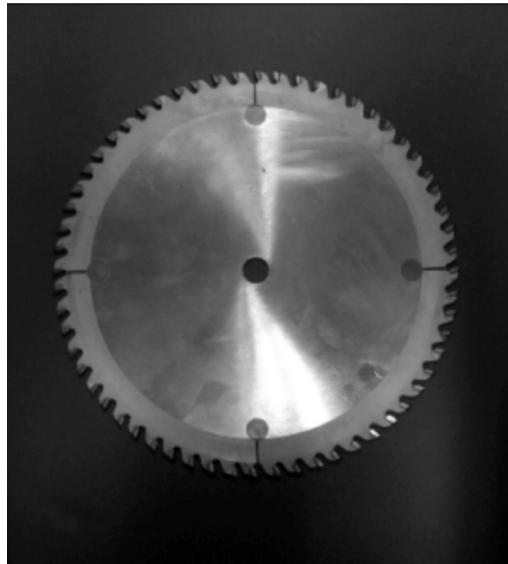
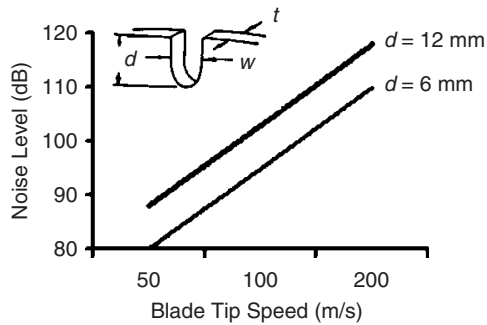


Figure 17 Typical saw blade for cutoff saw machine (450-mm diameter).

produced noise, blade vibration produced noise, and workpiece vibration produced noise.

**3.1.1 Aerodynamic Noise** The research devoted to aerodynamic noise of circular saw blades has largely consisted of studies of airflow disturbances created by rotating rigid disks with various types of openings (gullets) cut into the periphery. It is usually assumed (a) that aerodynamic noise created by a rotating disk is essentially unaffected by any blade vibration that may be present and (b) that aerodynamic noise results primarily from gullets cut into the periphery (since a smooth disk without gullets or teeth creates relatively little aerodynamic noise). Most researchers agree that the aerodynamic source mechanism involves fluctuating forces set up near the blade periphery.



**Figure 18** Effect of tip speed and gullet depth ( $d$ ) on aerodynamic noise generation for circular saw blades.<sup>9</sup>

However, relatively little agreement among researchers has been achieved as to details of how this fluctuating force is created or how details of disk geometry and disk opening (gullet) geometry affect the nature of the noise produced. Based on experimental studies,<sup>9</sup> the following observations have been made concerning aerodynamic noise.

1. Aerodynamic noise depends strongly on tip speed and exhibits an approximate velocity to the 5.5 to 6.0 power relationship. This results in a 15- to 18-dB increase in aerodynamic noise level per doubling of tip speed, as shown in Fig. 18.
2. Noise levels depend on details of gullet geometry and saw blade plate thickness. The gullet depth also has a direct effect on noise level, as shown in Fig. 18. The effect of gullet width depends on the gullet width to plate thickness ratio, which has been shown to affect both the magnitude and frequency characteristics of aerodynamic noise. The size (area) of open (gullet) area alone is not a reliable predictor of aerodynamic noise; and details of gullet and tooth geometry (that might affect air disturbances in a nonturbulent flow field) do not have a significant effect on aerodynamic turbulence noise levels for the types of blades and tip speeds under consideration.
3. As with many aerodynamic noise sources, the frequency distribution of circular saw blade aerodynamic noise can be broadband or exhibit a relatively narrow-band character, depending on source mechanism details. This has caused a great deal of confusion with respect to source identification since both blade vibration noise and aerodynamic noise (in some cases) can be pure tone in nature.

**3.1.2 Blade Vibration Noise** Blade vibration noise results from two distinct sources: resonant blade vibration response, which may occur during idle (excited by aerodynamic or other forces) or cutting (excited by tooth impact forces), and forced blade

vibration response, which is caused by tooth impact that occurs only during cutting.

Resonant blade vibration noise has received the most attention and spawned the greatest number of blade design changes. Part of this attention has been due to the blade stability issues associated with resonant vibration, which has a direct affect on blade performance and minimizing saw kerf. The vibration characteristics of circular plates are such that for typical saw blades, many natural (resonant) frequencies are located within the audible frequency range. In addition, thin, center-clamped steel plates have relatively little damping, which results in an ideal situation for resonant structural vibration sound generation. Since the vibration amplitude at resonance is (theoretically) controlled only by damping, the resonant vibration noise produced by circular saw blades can be extremely intense, sometimes resulting in the so-called whistling saw blade.<sup>12,15</sup> Most researchers agree that resonant blade excitation during idle can be excited by aerodynamic forces acting near the blade periphery (smooth disks rarely exhibit resonant response when idling), however, it has also been reported that this resonant response can be excited in some cases by excessive blade run-out and/or blade unbalance.<sup>16</sup> The mechanism of sound generation for vibrating structures is well known, and the acoustic power radiated depends on the surface area, the magnitude of vibration, and the acoustical efficiency (which depends primarily on frequency and surface area). The damping present in the saw blade and blade support system also dramatically affect the resulting vibration amplitude and resulting noise generation.

The whistling blade represents an extremely interesting and difficult to predict physical phenomenon. A whistling blade during idle produces an intense pure tone noise resulting from blade resonant vibration. The whistling noise may take several seconds to develop (after the blade is up to speed) and may drift in and out of the whistling condition while rotating at constant rpm. The blade often continues to vibrate after rotation has stopped, producing an audible "ringing" sound. The whistling sound, which is pure-tone in nature, is the result of an excitation force (aerodynamic, etc.) providing energy in the frequency range where at least one strong, easily excited, blade resonant frequency exists. In the case of a typical (lightly damped) saw blade, this can result in extremely high level pure tone noise usually occurring at one of the blade resonant frequencies, which is acoustically efficient (usually several thousand hertz). The whistling blade has been the source of much confusion since, by definition, this type of resonant response is unstable and is the result of a delicate "balance" of conditions. The whistling sound may develop for a given blade on a particular machine and not develop for the same blade on an apparently identical machine. Furthermore, the whistling phenomena may or may not develop for the same blade run on the same machine at different times. Modifications to the blade such as retensioning, minor changes in the contact between the support collars and the blade, the introduction of acoustically

reflective surfaces near the blade, and making very minor changes in rpm can cause tremendous changes in the noise level for a whistling blade or result in the complete elimination of whistling. Attempts to quantify noise levels and noise reductions for inherently unstable whistling saw blades have been unsuccessful.

During cutting, blade resonances may also be excited due to tooth impact. Tooth impact excitation produces broadband vibrational energy as well as energy at the tooth passage frequency and harmonics (multiples) of the tooth passage frequency. Resonant response during cutting may involve one or more resonant frequencies. Figure 19<sup>10</sup> shows one of the many natural frequency (resonant) modal patterns (nodal lines are shown in white) for a circular saw blade. Figure 20 shows the typical effect on noise level due to resonant blade vibration provided by conventional saw collars during cutting.

Forced-blade vibration noise is analogous to a loudspeaker (as compared to blade resonant response, which is analogous to a tuning fork). The acoustic output depends primarily on the input excitation (tooth

impact magnitude and frequency), radiating surface geometry and properties (which govern the resulting vibration velocity), and the acoustic coupling between the blade and the surrounding air. The forced vibration occurring at nonresonant frequencies is not as sensitive to damping as is the resonant case. For this reason, techniques that are quite effective in reducing resonant vibration noise may have relatively little effect on forced-blade vibration noise. Forced-blade vibration noise is characterized by strong frequency peaks at the tooth passage frequency and harmonics. For blades having nonstraight tooth designs, such as alternating top bevels on the top face of the teeth, the base frequency becomes the lowest periodic event frequency (the alternate top bevel spectrum also contains energy at one half the tooth passage frequency and harmonics).

**3.1.3 Workpiece Vibration Noise** This source primarily involves forced vibration of the workpiece. Since wood-based materials usually have relatively high damping, resonant workpiece response is not usually a noise-related issue. The forced workpiece response is typically of concern only for gang ripping applications involving multiple blades. In these cases, the noise generation mechanisms for the workpiece are similar to those discussed for cutters.

### 3.2 Noise Reduction Techniques for Machines Utilizing Circular Saw Blades

The primary saw-blade-related noise sources for wood-working machinery involve circular saw blades and band saw blades. Since most band saw noise problems involve large machines typically used in sawmilling operations where employee booths and free-standing acoustical enclosures are routinely utilized, the focus here is on circular saw blades.

The avenues available for reducing noise from circular sawing machines fall into two distinct categories: noise control at the source (through blade and blade support system modifications) and path controls, which involves the use of acoustically treated guards, shields, enclosures, and the like.

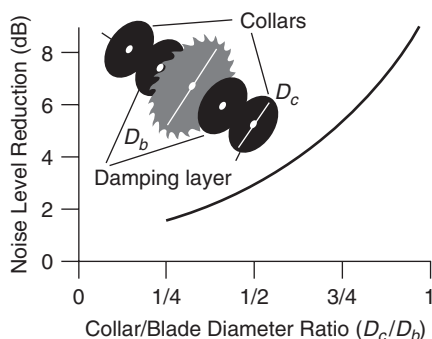
#### 3.2.1 Noise Control at the Source for Machines Utilizing Circular Saw Blades

##### *Reduction of Aerodynamic Noise at the Source*

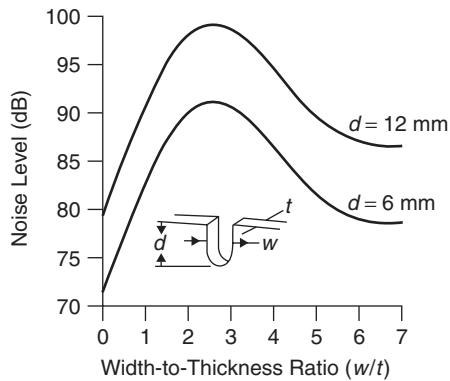
Aerodynamic noise for circular saw blades is highly dependent on tip speed and gullet depth, as shown in Fig. 18. The effect of reducing tip speed on noise level is approximately 15 dB per halving of tip speed, and the effect of reducing gullet depth is approximately 8 dB per halving of gullet depth. While adjusting these parameters can be extremely useful in reducing noise, the reduction of tip speed and/or gullet depth often necessitates the use of more teeth to avoid excessive feed per tooth conditions and/or overloading of gullets. Aerodynamic noise can also be reduced through careful selection of gullet geometry, as shown in Fig. 21.<sup>9</sup> This figure shows the importance of the gullet width to plate thickness ratio in aerodynamic noise generation. Noise level reductions of as much as 10 dB can be achieved in some instances by adjusting this ratio. In general, ratios



**Figure 19** Resonant vibration modal pattern for a circular saw blade (1004 Hz excitation).<sup>10</sup>



**Figure 20** Effect of collar diameter on resonant blade noise generation produced by circular saw blades during cutting.<sup>16</sup>

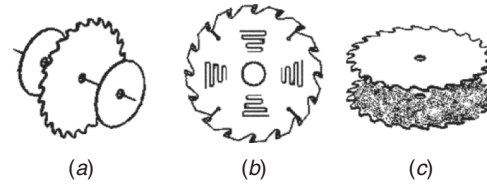


**Figure 21** Effect of gullet width-to-plate thickness ratio ( $w/t$ ) on aerodynamic noise level.<sup>10</sup>

in the 1.5 to 3.5 range cause intense noise in a narrow frequency band and should be avoided.

**Reduction of Blade Vibration Noise at the Source** The primary cause of resonant blade response during both idle and cutting is the extremely low damping present in typical saw blades and blade support systems. A number of “low-noise” saw blades are currently on the market; however, these designs are mostly effective in reducing resonant blade vibration noise during idle. These designs include the use of laser cut slots (with and without damping material) and plugs (usually used in conjunction with expansion slots) to introduce damping.<sup>17,18</sup> Although the laser cut slots and plugged expansion slots cause localized “disruption” of vibrational wave propagation for certain vibrational modes, the primary noise-reducing mechanism is the damping introduced by relative motion (scrubbing), which occurs in laser slots and plugged holes (similar to the friction damping mechanism provided by riveted joints).

The most notable advance in the reduction of circular saw noise for carbide-tipped blades is the laminated blade design,<sup>19</sup> commercialized in the early 1970s. This design utilizes the principle of constrained layer damping by “bonding” two thin plates together to form the body of the blade. This design is by far the most effective means developed to date for introducing sufficient damping into the saw body to significantly reduce both blade resonant vibration during idle and blade vibration noise during cutting. There are, however, some drawbacks to this approach, including more demanding maintenance procedures. An alternative, but usually less effective, means of introducing constrained layer damping involves the use of collars (concave ground plates clamped to the blade), however, the diameter of these collars must be at least 50% of the blade diameter to be effective in resonant blade noise reductions (this depends on the particular blade resonant vibrational mode shapes, which, in turn, depends on blade design and blade internal stresses). Several free layer damping systems are also on the



**Figure 22** Techniques for reducing resonant blade vibration noise: (a) blade collars, (b) slot/plugs, and (c) laminated saw body.

market; consisting of a foil tape that is adhered to the blade. These systems are less effective than constrained layer damping systems and are susceptible to damage under some industrial operational conditions.

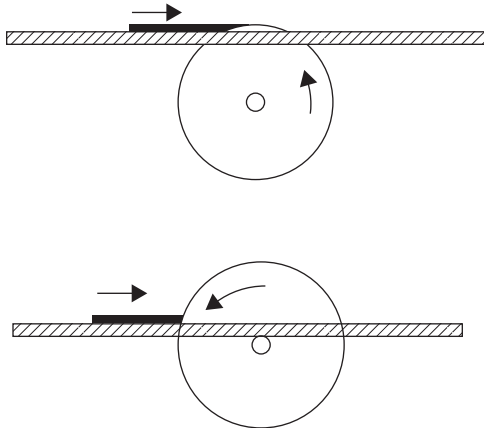
Figure 22 shows several of the techniques currently in use in industry to reduce resonant blade vibration. While all of these techniques are capable of preventing the whistling situation during idle, only the laminated blade has been found to provide reliable large-scale reduction of resonant blade vibration noise during cutting.

Forced-blade vibration noise is heavily dependent on tip speed, tooth number, tooth width (kerf), tooth cutting angles (clearance, rake, top bevel, etc.), tooth sharpness, and damping (especially when a tooth passage frequency (or harmonic) is closely aligned with a resonant frequency). In general, forced blade vibration noise levels are reduced by reducing tip speed, increasing tooth number, reducing plate thickness (kerf), employing shear cutting angles (alternate top bevel, etc.), and utilizing sharp blades. Aside from the highly effective laminated blade construction discussed above, typical damping treatments usually provide only minor reduction of forced-blade vibration-produced noise.

Noise control through improved blade design (improved gullet geometry and blade damping systems) is in widespread use for cross-cutting operations, and noise level reductions of 5 dB to 10 dB during both idle and cutting are commonplace. These techniques have been less successful for rip sawing applications due to restrictions on gullet geometry and problems involving blade heating due to friction.

Both resonant and forced-blade vibration noise can be reduced by the use of properly designed blade guides. For some sawmill operations, guides utilizing a liquid film between the guide and the rotating blade are often standard machine equipment. Other guide systems are available that incorporate air-bearing systems, magnetic force systems, and the like; however, these systems are application sensitive and are not in widespread use.

**Reduction of Forced-Workpiece Vibration Noise at the Source** Reduction of forced-workpiece vibration (also caused by tooth impact) is a difficult issue and has received far less attention than blade aerodynamic noise and blade vibration noise. Fortunately, most circular sawing machines used in woodworking employ one or two relatively thin saw blades that do not result in the high-amplitude workpiece vibration (for wood-based products) as is the



**Figure 23** Illustration of correct (*upper*) and incorrect (*lower*) saw blade position.<sup>2,3</sup>

case for cutters. In the case of a relatively wide workpiece acted on by several circular saw blades spaced a relatively small distance apart, the vibration response closely resembles the response that occurs for a cutter contacting the entire width of the workpiece. Unfortunately, there are relatively few practical and effective source controls for workpiece vibration noise, aside from improved workpiece holddown systems, the use of thinner kerf saw blades, and the use of acoustical enclosures covering the vibrating workpiece.

The use of proper cutting practices can also help reduce workpiece vibration and noise. As discussed for cutters, structural vibration is much easier to produce in the weak (perpendicular) plane. Figure 23 shows the correct (*upper*) and incorrect (*lower*) saw blade position relative to the workpiece. In the correct position, more teeth are in contact with the workpiece at any given time than in the incorrect position; and the cutting force is almost parallel to the workpiece.

**3.2.2 Noise Control in the Path for Machines Utilizing Circular Saw Blades** The use of acoustical enclosures for circular sawing operations is primarily found on conveyor-fed multiblade trim saws and gang rip saws, where minimal operator interaction with the machine is required and a free-standing enclosure can be used. As is the case for cutter-related enclosures, it is important to consider the vibrating workpiece noise source when considering an acoustical enclosure. The adverse effect of an exposed vibrating workpiece and unsealed openings is similar to the case for cutter-related enclosures.

Figure 24 shows a free-standing enclosure for a multiblade trim saw used in sawmill operations. In this case, the saw blades and the entire workpiece are contained within the enclosure, so that all sawing-related noise sources are enclosed. Typical noise level reductions for this application are 10 dB to 15 dB; resulting in noise levels at the operator location in the 85 dB range during both idle and cutting. Enclosure construction of this type can be the



**Figure 24** Commercially available trim saw enclosure.

commercially available metal construction as shown in Fig. 24 (with sound-absorbing and damping material) or conventional plywood/studwall construction.

The use of acoustical treatments in guards located near saw blades has received some attention and has been successful in achieving relatively small noise reductions [usually in the 2-dB to 4-dB range] in aerodynamic and resonant blade vibration noise in some applications. These methods are highly dependent on the details of the application and the results are typically unpredictable.

#### 4 AUXILIARY EQUIPMENT

In addition to cutter- and saw blade-related sources, several other noise sources are often found in woodworking operations. The most important source is related to the operation of chip and dust extraction systems.

##### 4.1 Chip and Dust Extraction System Noise

Due to the fact that dust collection systems are in operation almost continuously during the workday, reduction of noise from the chip and dust extraction system should be pursued even if the noise emission is lower than the noise emission from the wood-processing machines. Operators often find the low-frequency noise from chips and dust extraction annoying even when the wood-processing machines determine their daily noise exposure. Noise control alternatives for chip and dust extraction systems include<sup>21</sup>:

- Using well-balanced fans with low-noise emission
- Using extraction hoods and ducts with smooth-walled interiors
- Installing sound-insulating outer walls
- Using a large radius where ductwork bends ( $1.5 \times$  diameter or more)
- Minimizing air leakage
- Avoiding abrupt changes of airflow direction
- Avoiding excessively high extraction velocity
- Installing silencers
- Reducing conveying velocity



- Avoiding the squeezing of chips between the interior walls of the extraction system and moving parts

Pneumatic noise sources (air blow-off nozzles, etc.) are often used to assist in chip and dust collection. Reduction of this noise usually involves changes in nozzle design, nozzle orientation, and the use of silencers. These noise control techniques are covered elsewhere in this handbook.

## 5 FORESTRY MACHINERY

Forestry machinery includes a variety of handheld tools and mobile machines. The special cases of portable handheld machines and mobile wood chippers are addressed below.

### 5.1 Portable Handheld Machines

Reduction of internal combustion engine noise is an important noise control measure for portable handheld machines since chain saws, trimmers, and brush cutters normally run without sawing or cutting for considerable time periods. Since internal combustion engines emit more noise than electric engines, electrically powered chain saws, trimmers, and the like, should be used wherever possible.

When buying new machines, low-noise machines should be specified. For portable handheld machines, ISO/TR 22520<sup>21</sup> may be used for comparing the noise emission data for the actual machine with noise emission data collected worldwide for different makes of machines. The noise emission data for chain saws and for trimmers and brush cutters are presented separately in ISO/TR 22520 for three different regions of the world (Europe, United States/Canada, and Australia).

### 5.2 Mobile Wood Chippers

Mobile wood chippers are commonly used in processing trees, and the noise levels can be as high as 120 dB at the operator's position. The cutting device is usually a flywheel equipped with cutting blades running in the 1000-rpm range. The cutting process is typically performed in two stages, both of which cause sound generation: (a) the primary cut where the cutting blade contacts the free piece of wood and moves it toward a fixed counter knife and (b) the final cut when the workpiece contacts the counter knife.

Experiments<sup>22</sup> have shown that a noise level reduction in the range of 10 dB may be achieved by proper adjustment of the position of the counter knife and the in-feed rolls. This essentially combines the double cut into a single cut, which stabilizes the workpiece during the final cut, thereby reducing noise. The noise emission may be further reduced by partial enclosures and absorbing linings in the in-feed area.<sup>23</sup>

## 6 NOISE EMISSION DATA

Noise emission data should be available for use in the buying and selling of woodworking machinery and equipment. Therefore, there is a need for standardized methods for the determination and declaration of such emission data. A number of basic acoustic standards for

determination of sound pressure levels and sound power levels are available. To obtain reproducible test results allowing comparison of noise emission from different makes of a family of machines, the noise emission must be tested using identical operating conditions.

### 6.1 ISO Standards for Woodworking Machines

International Organization for Standardization (ISO) 7960 (together with international standards describing acoustic measurement procedures and data reporting) prescribes standardized operating conditions for 19 types of woodworking machines that are widely used in the woodworking industry.

ISO 7960 covers airborne noise emitted by machine tools and operating conditions for woodworking machines.

### 6.2 ISO Standards for Forestry Machinery

ISO 7182 covers noise measurement at the operator's position of airborne noise emitted by chain saws.

ISO 7917 covers noise measurement at the operator's position of airborne noise emitted by brush saws.

ISO 9207 covers noise emission of manually portable chain saws with internal combustion engines and determination of sound power levels (engineering method, grade 2).

ISO 10884 covers manually portable brush cutters and grass trimmers with internal combustion engines and determination of sound power levels (engineering method, grade 2).

ISO DIS 22868 covers portable handheld forestry machines with internal combustion engines and determination of A-weighted sound pressure levels (at the operator's ear) and sound power levels (engineering method, grade 2).

(Revision of ISO 7182:1984, ISO 7917:1987, ISO 9207:1995, and of ISO 10884:1995)

### 6.3 Comparison of Noise Emission Data for Families of Machine

Comparison of noise emission data for families of machinery has mainly been organized at a national level. For chain saws, trimmers, and brush cutters, noise emission data have been collected worldwide. Noise emission data for Europe, United States/Canada, and Australia can be found in ISO/TR 22520:2005, which covers A-weighted sound pressure levels at the operator's station for portable handheld forestry machines (comparative data, 2002). An ongoing European project is aimed at establishing similar data for sawing machines and planing machines.

## 7 CONCLUDING REMARKS

A great deal of information and technology is available for the practical reduction of woodworking machinery noise. Unfortunately, as a recent survey in Germany<sup>24</sup> illustrated, many effective noise reduction technologies are not gaining widespread acceptance. This illustrates the need for continuing dissemination of knowledge

focusing on low-noise machine designs, tooling, and operating principles.

Many of the difficulties involved in reducing wood-working machinery noise could be overcome through the more widespread use of automation. During the past decade, the application of computer-controlled machines and robots along with the automation of production lines has provided new opportunities for the successful use of noise-reducing enclosures. The implementation of new production technology and automation is expected to continue to contribute to a decreased noise exposure in woodworking industries in the future.

Several websites<sup>25–28</sup> are included in the references that provide information on low-noise tooling and machining practices for woodworking.

## REFERENCES

1. T. F. Brooks and J. R. Bailey, Mechanisms of Aerodynamic Noise Generation in Idling Woodworking Machines, ASME, New York, Publication 75-DET-47, September 1975.
2. *Noise from Woodworking Machines*, SMS Handbook 507, SIS, Stockholm, 1984 (in Swedish).
3. P. Lykkeberg, Noise Control in the Woodworking Industry, Videncenter for Arbejdsmiljø, Copenhagen, 1999 (in Danish) ([www.arbejdsmiljobutikken.dk](http://www.arbejdsmiljobutikken.dk)).
4. J. S. Stewart and F. D. Hart, Analysis and Control of Industrial Wood Planer Noise, *Sound Vib. Mag.*, March, 1972, pp. 24–27.
5. J. S. Stewart and F. D. Hart, Control of Industrial Wood Planer Noise through Improved Cutterhead Design, *Noise Control Eng. J.*, Vol. 7, No. 1, 1976, pp. 4–9.
6. J. S. Stewart and F. D. Hart, Workpiece Vibration Control in Wood Planers, ASME, New York, Publication 73-DET-79, June 1973.
7. E. Christiansen, E. von Gertten, H. J. Moelstrand, and K. S. Nielsen, Reduction of Noise Emission from Woodworking Machinery, Reports F1–F8 of the Danish Technological Institute, Taastrup, 1977/1978 (in Swedish).
8. K. S. Nielsen, Design of Low Noise Machines; State of the Art Report, Danish Acoustical Institute (DELTA Acoustics & Vibration), Report 106, 1983 (in Danish) ([www.delta.dk](http://www.delta.dk)).
9. J. S. Stewart, An Investigation of the Aerodynamic Noise Generation Mechanism of Circular Saw Blades, *Noise Control Eng. J.*, Vol. 11, No. 1, 1978, pp. 5–11.
10. W. F. Reiter and R. F. Keltie, On the Nature of Idling Noise of Circular Saw Blades, *J. Sound Vib.*, Vol. 44, No. 4, February 1976, pp. 531–543.
11. D. A. Bies, Circular Saw Aerodynamic Noise, *J. Sound Vib.*, Vol. 154, No. 3, May 1992, pp. 495–573.
12. D. S. Dugdale, Discrete Frequency Noise from Free Running Circular Saws, *Journal of Sound and Vibration*, Vol. 10, 2, September 1969, pp. 296–304.
13. C. D. Mote, Jr. and W. H. Zhu, Aerodynamic Far Field Noise in Idling Circular Sawblades, *J. Vib., Acoust., Stress, Reliability Design*, Vol. 106, No. 3, July, 1984, pp. 441–446.
14. H. S. Cho and C. D. Mote, Jr., On the Aerodynamic Noise Source in Circular Saws, *J. Acoust. Soc. Am.*, Vol. 65, 1979, pp. 662–671.
15. C. D. Mote, Jr. and M. C. Leu, Whistling Instability in Idling Circular Saws, *J. Dynamic Syst., Measurement Control, Trans ASME*, Vol. 102, No. 2, June, 1980, pp. 114–122.
16. J. S. Stewart and F. D. Hart, Noise Control Technology Demonstration for the Furniture Industry, Proceedings of Noise-Con '81, Institute of Noise Control Engineering, North Carolina State University, Raleigh, NC, June 1981.
17. A. Trochidis, Vibration Damping of Circular Saws, *Acustica*, Vol. 69, 1989, pp. 270–275.
18. K. A. Broughton, Practical Assessment of the Damping Effects of Laser Cut Circular Saw Blades, Euro-Noise Proceedings, Book 2, pp. 521–532, Imperial College, London, 14–18, September 1992.
19. Gomex Company, Orchard Road, Finedon, Wellingborough, Northants, NN95JF, UK ([www.gomex.co.uk](http://www.gomex.co.uk)).
20. EN 12779, Safety of Woodworking Machines, Chip and Dust Extraction Systems with Fixed Installations; Safety Related Performances and Safety Requirements.
21. ISO/TR 22520:2005, Portable Hand-Held Forestry Machines; A-Weighted Emission Sound Pressure Levels at the Operator's Station, 2002.
22. M. Klausner, Noise Reduction at Mobile Wood-Chipping Machines, *InterNoise, Prague, Czech Republic*, 2004.
23. B. B. Jessen and M. W. Grove, Reduction of Noise Emission from Mobile Wood Chippers, Danish Acoustical Institute (DELTA Acoustics & Vibration), Report 129, 1986 (in Danish) ([www.delta.dk](http://www.delta.dk)).
24. J. H. Maue and R. Hertwig, Low-Noise Circular Saw Blades, CFA/DAGA, 2004.
25. [www.safetyline.wa.gov.au](http://www.safetyline.wa.gov.au).
26. [www.hse.gov.uk](http://www.hse.gov.uk).
27. [www.cdc.gov/niosh](http://www.cdc.gov/niosh).
28. [www.woodworkingtips.com](http://www.woodworkingtips.com).

## BIBLIOGRAPHY

- D. A. Bies, Circular Saw Noise Generation and Control, Tenth International Congress on Acoustics, Satellite Symposium: Engineering for Noise Control, Adelaide, Australia, 1980.
- N. Curle, The Influence of Solid Boundaries upon Aerodynamic Sound, *Proc. Roy. Soc. A.*, Vol. 231, 1955, p. 505.
- F. Heydt, The Origin of Noise from Multi-side Moulding Machines for Woodworking, University of Stuttgart, 1980 (in German).
- F. Heydt and H. J. Schwartz, Noise Emission and Noise Control Measures for Woodworking Machines Forschungsbericht Nr. 150 BAuA, Dortmund, 1976 (in German) ([www.baua.de](http://www.baua.de)).
- F. Heydt and H. J. Schwartz, Noise Emission and Noise Control Measures for Moulding Machines, Forschungsbericht Nr. 171 BAuA, Dortmund, 1978 (in German) ([www.baua.de](http://www.baua.de)).
- F. Koenigsberger and A. Sabberwal, An Investigation into the Cutting Force Pulsations During Milling Operations, *Int. J. Machine Tool Design Res.*, Vol. 1, 1961, pp. 15–33.
- E. Stephenson and D. Plank, *Circular Saws*, Thomas Robinson, Rochdale, England, 1972.
- M. Zockel, D. A. Bies, and S. G. Page, Solutions for Noise Reduction on Circular Saws, Noise-Con 79, Purdue University, West Lafayette, IN.



# CHAPTER 80

## NOISE ABATEMENT OF INDUSTRIAL PRODUCTION EQUIPMENT

Evgeny Rivin  
Wayne State University  
Detroit, Michigan

### 1 INTRODUCTION

Maintaining acceptable noise levels inside production areas of manufacturing plants (on the “shop floor”) is important both for productivity and morale of the shop floor employees. With the exception of forging plants in which forging hammers are the dominating source of noise, noise sources in manufacturing plants can be typically classified in order of intensity/annoyance as<sup>1</sup>: (1) *compressed air* (leakages, air exhaust, air-blowing nozzles), (2) *in-plant material handling system*, and (3) *production and auxiliary machinery and equipment*. Production machinery and equipment that generate objectionable noise levels include machines that operate with impacts such as forging hammers, cold headers, stamping presses, riveters, jolting tables; some machine tools; and impact-generating assembly stations. Two basic abatement techniques are (1) acoustical enclosures, which are expensive to build and maintain, may reduce efficiency of the enclosed equipment, and are not always feasible, and (2) noise reduction at the source, which is effective but often requires a research and development effort. Research and development in plant noise reduction in the United States has diminished since the 1970s and early 1980s due to a more lax enforcement of noise level regulations. All the sound pressure levels given in this chapter are A-weighted.

### 2 COMPRESSED AIR SYSTEM

The flow/jet noise generated by a simple nozzle (Fig. 1), is caused by pressure and velocity fluctuations (turbulence) in mixing of the air jet with stationary ambient air, with sound intensity proportional to the eighth power of jet velocity. *Leakages* can generate intense noise levels (up to 105 dB) and economic losses up to \$1000 per leak per year. The preferred abatement method is maintenance.

Treatments of *air exhaust* noise should satisfy two contradictory requirements: noise reduction and low flow resistance (back pressure). These can be simultaneously satisfied by channeling the exhaust air away from the operator(s) position(s) by hoses/ducts. Another widely used technique is exhaust mufflers selected by noise levels, back pressure, size, and cost. Basic types of exhaust mufflers are shown in Fig 1: multiple jet, dividing the airstream into several jets with less turbulence and 5-dB to 10-dB noise reduction; restrictive diffusers, in which air passes through a fiber mesh or through a porous plug, thus reducing the effective jet velocity and providing a more significant noise reduction, up to 20 to 25 dB, but at the price of a two to three times higher back pressure; and air shroud in which mixing with the ambient air is achieved by its “entraining” along the large outside surface, thus providing for ~10-dB noise

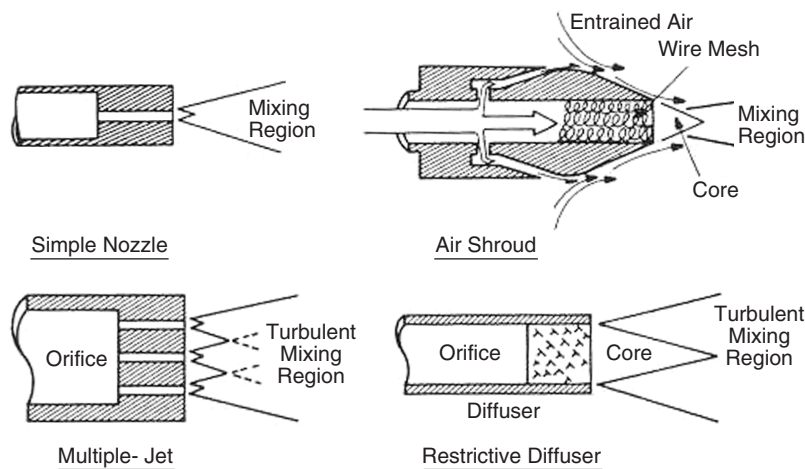


Figure 1 Typical in-plant compressed air nozzles.<sup>2</sup>

level reduction with low back pressure but resulting in a relatively large and expensive device.

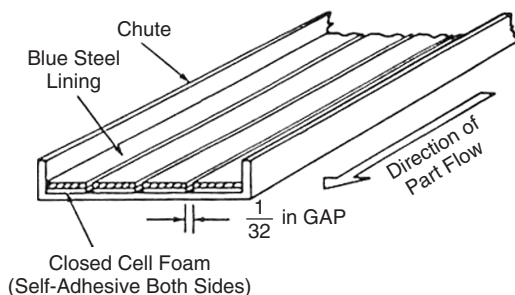
*Blow-off nozzles* are intense noise generators (up to 110 dB) due to the turbulent mixing of the air jet with the ambient air and, additionally, due to impingement of the jet on the solid target. Also, they consume significant amounts of compressed air per the required blowing force (thrust). "Quiet" nozzles combine noise reduction with delivery of the required force. The most effective technique is synchronization of nozzle usage with the actual needs, thus reducing the noise exposure and saving on air consumption. Multijet nozzles deliver the same magnitudes of concentrated thrust versus air consumption as the simple nozzles, but with noise level reductions of 5 dB to 10 dB; air shroud nozzles provide the same total thrust versus air consumption and noise level reductions of 5 dB to 10 dB, while delivering less concentrated thrust (e.g., for cleaning purposes); restrictive diffusers reduce noise levels by 15 to 20 dB but require two to three times greater air consumption.<sup>2</sup>

### 3 IN-PLANT MATERIAL HANDLING SYSTEM

It includes chutes, containers, vibratory feeders, towed trailers, and the like, generating up to 100-dB to 110-dB noise levels. A great variety of the devices requires diverse treatments with some generic underlying concepts.<sup>1</sup>

*Chutes* for parts and scrap are the most widely used devices, such as gravity sliding chutes (mostly, impact-generated noise), rolling chutes (part-rolling noise), vibration-assisted chutes (structure ringing noise).

In *gravity sliding chutes* noise (up to 100 to 105 dB) is generated by ringing of the chute itself and of the dropping parts/scrap pieces. Some noise reduction can be achieved by reducing the drop height. Often noise levels radiated from the chute and from the parts/scrap are commensurate, thus a damping treatment of the chute structure without influencing the part noise radiation (a frequently used technique) is effective only for stiff parts. If the part ringing is important (e.g., sheet metal stampings), an A-weighted level reduction of only about 3 dB reduction can be achieved. Abatement of both sources can be achieved by making the impact surface compliant by assembling it from thin narrow steel strips attached to the chute structure using



**Figure 2** Low-noise gravity action sliding chute.<sup>1</sup>

self-adhesive foam strips (Fig. 2).<sup>1</sup> In this design, the dropping part has an extended contact area with the compliant chute surface and thus prolonged impact duration, which greatly reduces its ringing. Noise level reductions of 15 dB to 25 dB have been recorded.<sup>1</sup>

*Gravity rolling chutes* are used for transporting round parts, for example, wheel rim preforms, between workstations. The overall ringing is excited by part drop impacts, irregularities of the part shape and the chute rolling surface, scratching the chute walls by the "wobbling" rolling parts, and by co-impacting between the parts. Effective antinoise means are, accordingly, wire mesh drop cushions, wire grid protected rubber lining of the rolling surface and of the walls, and rubber flap curtains preventing direct co-impacting between the subsequent rolling parts. Reduction of the equivalent noise level from 107 to 89 dB after these treatments had been recorded.<sup>1</sup>

*Vibration-assisted chutes* are excited by attached pneumatic ball vibrators generating rotating circular vibration vectors. This results in reduction of effective friction between the chute and the sliding part, thus allowing small inclination angles of the chutes. The noise is generated mostly by ringing of the chute structure excited by higher harmonics of the vibratory force, with vibrators oversized due to low efficiency of friction reduction by the rotating vibration vector. The situation can be improved by attaching the vibrator to the chute as shown in Fig. 3a<sup>3</sup> by anisotropic elastomeric gaskets. Such installation has a high natural frequency  $f_c$  in the compression (high stiffness) direction of the gaskets and a low natural frequency  $f_s$  in the shear (low stiffness) direction of the gaskets. Thus, vibrations with the rotational frequency  $f_r$  of the vibrator are transmitted to the chute structure without attenuation in the compression direction and with significant attenuation in the shear direction (Fig. 3b). This transforms the circular vibration vector into a narrow elliptical vector, which can be inclined to the chute surface by an appropriate positioning of the bracket. The optimal inclination angle,  $\sim 45^\circ$  (which can be adjusted while in place), results in about 10 times reduction of part transporting time along the chute; thus smaller vibrators and/or lower air pressure can be used, with the corresponding noise reduction and significant savings of compressed air. In addition, the elastomeric gaskets provide isolation of the high-frequency vibration harmonics (e.g., the second-harmonic  $2f_r$  in Fig. 3b) from the chute structure. A 23-dB noise level reduction (from 106 dB to 83 dB) has been recorded.<sup>3</sup>

#### 3.1 Containers

Parts/scrap pieces conveyed along the chutes are usually further transported in containers. Parts, especially massive, generate noise levels in excess of 100 dB (ringing part and ringing container structure when the part hits its wall), usually decreasing while the container fills up. Large numbers of containers are used in manufacturing plants, but only a few working stations are associated with the container-generated noise. Accordingly, treating/"quieting" all the containers is useless and very expensive. The potentially

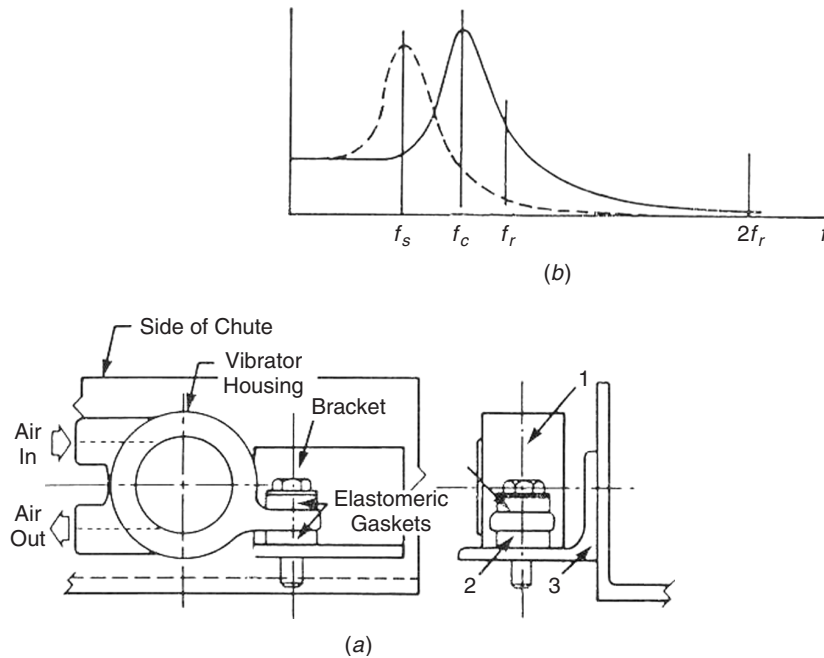


Figure 3 (a) Vibration force vector transformer and (b) its transmissibility plots.<sup>3</sup>

noisy workstations should be equipped with noise-reducing means not obstructing the operation. Filling an empty container with perishable foam (e.g., soap foam) reduces noise levels by  $\sim 5$  dB. Pressing rubber-coated rollers externally to the container wall results in an A-weighted noise level reduction of about 6 dB.<sup>1</sup> The pressing action is activated by the weight of the container when it is placed into its workstation.

### 3.2 Towed Trailers

In many plants empty and loaded containers are conveyed by trains of up to five to six towed trailers driven at speeds up to 10 mph (16 km/h). Wheel excitations from floor unevenness induce intense structural vibrations with accelerations exceeding 1 g, causing noise and a secondary rattling of containers. Friction reduction by vibration also causes horizontal movements/impacting of containers. Noise levels up to 115 dB were recorded, together with fast deterioration of bearings, king pins, and other joints caused by dynamic loading. Since loads on trailers vary significantly (empty trailer—trailer loaded with empty containers—trailer loaded with full containers—stationary trailer loaded with stacked-up full containers in storage mode), a spring suspension with linear load-deflection characteristics is either too stiff for lightly loaded condition or has an excessive deflection for the loaded condition, preventing assembling of the train. Also, an expensive redesign of the trailers inventory is required.

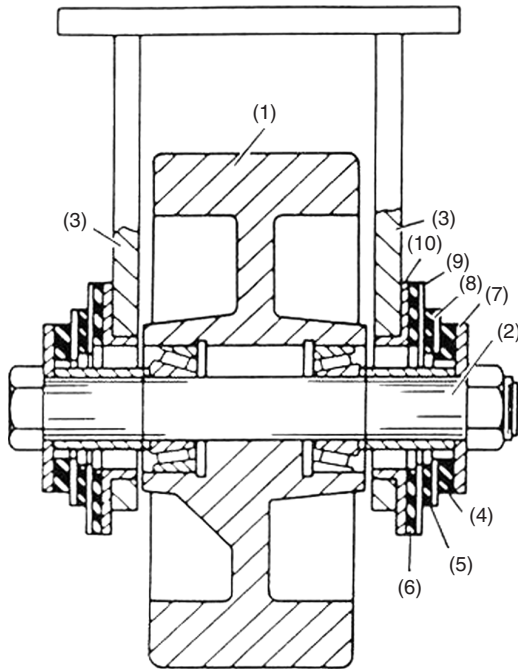
Rubber-metal *shear disk* suspension (Fig. 4)<sup>1</sup> having nonlinear hardening characteristic and nearly

constant natural frequency  $\sim 5$  Hz of the trailer regardless of its loading resulted in about 16-dB reduction of equivalent noise levels combined with small ( $\sim 15$  mm) height difference between empty and fully loaded trailer,  $\sim 15$  times reduction of impact accelerations and, consequently, 10 times greater periods between repairs. In Fig. 4, axle 2 of wheel 1 is connected to frame 3 via two “shear disks” comprising rubber-in-shear layers 4, 5, 6 sandwiched between metal plates 7, 8, 9, 10. At low trailer loads all rubber layers are deforming (connected in series) thus having low stiffness. At an increased load, the softest rubber disk 4 contacts the axle, and stiffness is increasing; at even greater load, the next rubber disk 5 contacts the axle; and in storage mode all disks contact the axle thus preventing their overstressing.

### 3.3 Vibratory Feeder Bowls<sup>3</sup>

These “solid-state” devices are widely used in manufacturing, especially assembly, operations, but high noise levels up to and sometimes exceeding 105 dB prevent even wider use. The principal noise sources are ringing of the bowl in the 250- to 500-Hz range excited by high-frequency harmonics of the driving vibratory torque; ringing in the 2- to 8-kHz range excited by impacts from conveyed parts moving in a “tossed up” regime; and noise radiation in the 2- to 16-kHz range from diffuser-shaped bowl cavity. The corresponding preferred noise abatement techniques can be applied individually or combined.

External damping treatment of the bowl and of the nonworking surfaces of the part track and the exit ramp

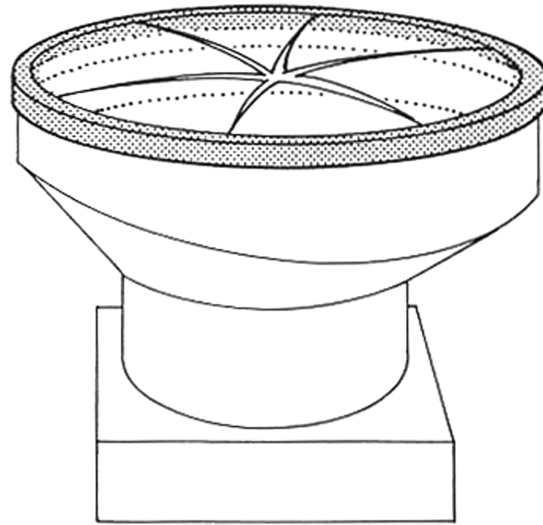


**Figure 4** Castor wheel with shear disk suspension.<sup>1</sup>

achieves ~10-dB reduction. Instead, the bowl can be made from a nonringing plastic (e.g., polyurethane). Coating the working track surface with a high-friction and low-impact velocity restitution coefficient material (e.g., polyurethane) reduces noise by about 8 dB and accelerates uphill vibration-stimulated conveyance, up to 40% for solid parts (less for thin-walled parts). Screening the radiated noise by a “see through, load through, reach through” segmented acoustical cover made from a transparent high-damping polyvinyl chloride (PVC) material (Fig. 5) with segments prevented from sagging by thin spring steel strips provides a noise level reduction up to 12 dB. Combinations of these technique reduce the noise level by 15 dB to 20 dB.

#### 4 PRODUCTION MACHINERY

Both stationary and handheld production machinery becomes a dominating factor in the noise environment after compressed air and material handling systems are treated. Total acoustical enclosures for stationary machinery, in addition to high initial costs, reduce productivity of the machine by 3 to 5%, generate substantial maintenance expenses (up to 15 to 20% of the initial costs annually), create inconveniences for machine operators, and may become a problem for management if enclosures are used by employees as nonacoustical shelters. Two cost-effective noise abatement techniques are selection of best models/units, especially for handheld machines, and engineering treatments based on studies of noise-generating mechanisms.



**Figure 5** Segmented acoustical lid for vibratory feeder.<sup>3</sup>

#### 4.1 Handheld Machines

Since many models of handheld machines for a given purpose are commercially available, selection of the best units can be very effective. Similar machines of different designs may vary substantially in sound pressure level, performance, and energy consumption. Often, a quieter machine has better performance characteristics and/or lower energy consumption, thus making the selection a very cost-effective exercise. This was confirmed by comparative testing of various models of handheld compressed-air-driven grinders, whose noise levels differed within the 12-dB range and air consumption varied within a 2:1 range. Noise levels of different design pile drivers vary by as much as 43 dB.<sup>4</sup> Selection testing of handheld machines requires low-noise load simulators, for example, eddy-current or magnetic power brakes for machines with rotating tools, and using nonringing workpiece simulators for percussion machines.

In airplane factories, noise from riveting produces short-duration, high-amplitude sounds with high-level components at frequencies where the human ear is most sensitive. Control of the impulsive sound of riveting without affecting production was achieved by applying constrained-layer damping pads to the skin of an aluminum panel being riveted<sup>5</sup> (treatment similar to silencing treatment of containers described above). A pad is held against a panel by a vacuum pressure of about 90 kPa. The time-averaged A-weighted sound pressure level at a position representative of the ear of the operator of a riveting hammer was reduced by about 5.5 dB.

#### 5 NOISE SOURCES AND THEIR TREATMENT FOR STATIONARY IN-PLANT MACHINERY

The selection process is not always effective for stationary machines since the machine noise is usually

specified at idle condition, without loading by the working process, and a quieter machine at idle is not necessarily the quietest one in production. Stamping press noise level specifications (without a die) call for 84 dB, while the part-producing presses are characterized by averaged (equivalent) noise levels up to 90 dB to 95 dB, with peak levels up to 105 dB to 110 dB. Testing of the machine under load is not a solution since the test results depend on the tool (die) design, workpiece material and design, and the like. Accordingly, it is important to perform testing in a simulated environment wherein unified loading conditions are used for different machine models.

Figure 6 shows a load simulator for punch presses<sup>6</sup> that is placed on the press bolster instead of the die for noise testing. Disk (Belleville) springs (2) can be preloaded by calibrated or instrumented bolts (1) to the specified load. When the press ram on its way down is touching the head (6), it unloads the bolts (1) from springs-induced load. The ram travel for fully unloading the springs is equal to the small initial deformation of the bolts. Both the load magnitude and duration of the unloading process are adjustable by changing the preload and by changing length and cross section of the bolts (1). Thus, the load pulse applied to the ram and to the press structure is very short, similar to the load pulse during the breakthrough event in the punching operation, and can be adjusted according to the test standard/specification.

### 5.1 Impact Machinery

The most intensive noise emitters in manufacturing plants are machines generating impact forces for performing productive work. The most numerous impact-generating machines are metal-forming machines, although some other types of machinery (such as jolting tables in foundries) have similar noise-generating mechanisms, which can be treated by the same techniques as metal-forming machines. Metal-forming machines represent the most productive metal-working equipment. Also, in many cases

the workpieces produced by these machines are characterized by significantly better material properties. This includes forging machines for complex three-dimensional shaping of material as well as sheet metal stamping (forming and punch) presses, much more numerous than the forging machines. The noisiest group—forging machines—include “drop” or “anvil” and “counterblow” hammers, and “screw” and “crank” forging presses. The noisiest mechanical forging crank presses are embodied as horizontal cold-heading machines. Hydraulic presses are substantially more expensive but less noisy.

### 5.2 Stamping Presses

Noise sources in *stamping presses* can be distinguished as “idling” sources, such as gear noise, air noise, impacts in clearances of revolute joints and gibbs (guideways), impacts of the stripper plate against the upper die and keepers (Fig. 7), “knock-out bars” in cold-forming presses, and process noise. All impact interactions excite structural modes of the press frame, thus adding ringing of the structure to the impact noise. The process noise in sheet-metal forming presses has a relatively low intensity, mostly due to ringing of the metal sheet during loading into and unloading from the die. On the other hand, the breakthrough event in punching presses is characterized by a short intense force pulse that excites numerous structural modes of the press. A significant reduction of the press noise is possible only by addressing both groups of sources.<sup>6,7</sup>

Noise of the breakthrough event can be reduced by optimizing velocity of the punch in the moment of impact (by adjusting the die setting), by tuning the clearance between the punch and the die, or by a proper die alignment. Optimization of these parameters can reduce the peak noise level by 5 dB to 10 dB. Shearing/slanting of the die and/or punch staggering extends the duration of the force pulse and has a substantial effect in a broad frequency range. However,

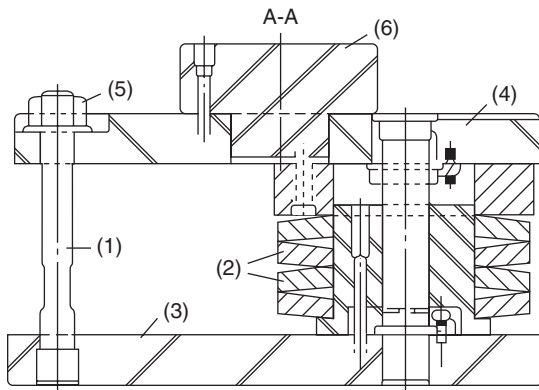


Figure 6 Punch breakthrough load simulator.<sup>6</sup>

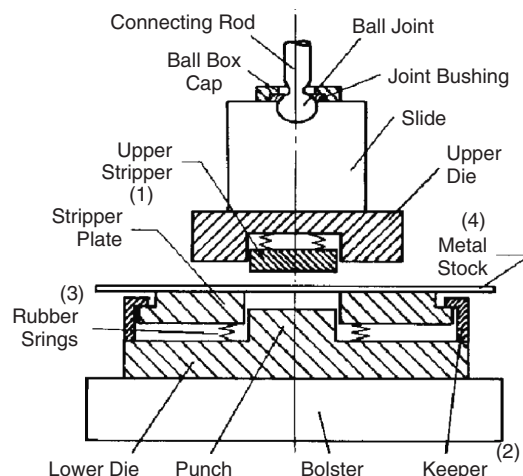


Figure 7 Stamping die system of a punch press.<sup>6</sup>



it increases initial and maintenance (sharpening) die costs. In some cases it can adversely affect the part quality.<sup>6</sup> Hydraulic shock absorbers<sup>8</sup> arrest the abrupt load release after the punch breakthrough resulting in 2-dB to 6-dB peak noise level reduction. The absorber has to be readjusted for the die changeover; may require an oil-cooling device; increases press power consumption by 4 to 15%; and is expensive. In the presses driven by servo-controlled motors and ball screws, a controlled change of the breakthrough load pulse may result in 3-dB to 5-dB noise level reduction.<sup>9</sup>

The most important noise sources besides the breakthrough event are hard impacts in auxiliary systems of the presses (stripper, keeper, knock-out bars) and in structural clearances. Since impact-generated contact pressures in these mechanisms are very high (up to ~6 MPa), solid rubber cushioning pads (allowed contact pressure from impact load 0.5 to 1.0 MPa) cannot be used. Thin-layered rubber-metal laminates easily tolerate contact pressures above 50 to 60 MPa<sup>7,10</sup> and can be used as durable impact cushions. Use of the rubber-metal laminated cushions for the slide-connecting rod ball joints and for keeper joints resulted in an A-weighted sound pressure level reduction of 2 dB to 2.5 dB for each treated joint.<sup>7</sup> A similar reduction had been achieved by using the stripper plate made from a wear-resistant plastic (UHMW polyethylene) reinforced by a steel frame, instead of the solid steel plate.<sup>6</sup>

The structural ringing can be reduced by using more powerful (overrated) presses to perform relatively low-force stamping operations and by applying damping treatments to the frame. Both approaches are expensive ones for a relatively modest noise reduction (~3 dB). Obviously, the above-listed source treatments also result in a reduction of the structural ringing.

Noise in the vicinity of stamping presses can be significantly reduced by installation of the press on properly selected vibration-isolating mounts. Such installation is especially important if the press is surrounded by an acoustical enclosure. Vibration isolation of a majority of machines in a shop reduces the overall noise level in the shop; see Section 5.4.

### 5.3 Drop Hammers and Forging Presses

The maximum work capacity for drop hammers is determined by the mass of the dropping ram (tub) and by the height from which it is dropped, and is measured by the maximum energy of one blow  $W_{\max}$  in newton-metres or joules, and for presses by the maximum force  $F_{\max}$  in newtons. A hammer and a screw press are equivalent as production machines if the  $W_{\max}$  of the hammer in newton-metres and  $F_{\max}$  of the press in kilonewtons are related as 3.5:1; a hammer and

a crank press are equivalent if  $W_{\max}:F_{\max} = 2.5:1$ ; and the equivalence ratio between the maximum forces of a crank press  $F_{\max c}$  and a screw press  $F_{\max s}$  is  $F_{\max c}:F_{\max s} = 1:0.75$ .<sup>11</sup> Thus, a crank press with  $F_{\max} = 10,000 \text{ kN} = 10 \text{ MN} \approx 1000 \text{ ton}$  is equivalent from the forging point of view to a drop hammer with  $W_{\max} = 25,000 \text{ N} \cdot \text{m} = 25 \text{ kJ}$ . A crude but useful approximation for "fast" A-weighted sound level of forging machines at 1 m ( $L_{A1}$ ) and 7 m ( $L_{A7}$ ) from the machine as a function of the machine capacity are shown in Table 1, where  $W_{\max}$  is in kilonewton-metres, and  $F_{\max}$  is in meganewtons.

Considering the above equivalencies, drop hammers are exhibiting the highest sound levels and the slowest decay with the distance, followed by screw presses and crank presses. For the latter, the noise levels are only weakly correlated with their size. The "true" peak sound emanated by forging hammers is ~20 dB higher than the "fast" levels listed in Table 1.<sup>11</sup>

The sound intensity is increasing with each blow until the workpiece (billet) is completely forged, and the most intense sound pulse is generated by die-to-die impact. This most intensive impact is used to describe the noise emission of forging hammers. The major noise-generating mechanisms are<sup>11</sup>:

- Sudden deceleration of co-impacting bodies (dies) with the radiated pressure pulse depending on strength (magnitude) and duration of the blow pulse (Table 2).<sup>12</sup>
- Transverse expansion of billet and dies during the blow, with the generated sound pressure level depending on the blow intensity, billet/die cross section, and transverse stiffness.
- Structural ringing of the hammer at its natural modes, which intensifies by up to 10 to 15 dB if the blow is off-center.
- Air expulsion from between the dies prior to the impact produces shock waves whose pressure levels depend on impact velocity and die design; not a significant noise source outside of low-frequency range (<100 Hz).
- Vibration of the ground excited by the pulselike blows and contributing to the noise radiation; its

**Table 1 Noise Levels of Forging Machines**

	Drop Hammer	Screw Press	Crank Press
$L_{A1}$	$0.10W_{\max} + 112$	$1.1F_{\max} + 99$	107
$L_{A7}$	$0.10W_{\max} + 106$	$1.1F_{\max} + 92$	99

Source: From Ref. 11.

**Table 2 Impact Pulse Parameters for Forging Hammers**

Tup + upper die mass, $m$ , t	1	2	3	5	5.5	10	15	20
Pulse duration, $\tau_{p1}$ , $10^{-3}$ s	1.0	1.26	1.44	1.69	1.75	2.07	2.45	2.64
Pulse magnitude, $P_0$ , kN	1,930	2,830	3,700	5,130	5,500	7,500	10,900	12,400

Source: From Ref. 12.

role in the overall noise level is increasing with increasing distance from the hammer, besides being itself a major vibratory annoyance.

Noise and vibration generated by forging hammers are objectionable both for the operators and for the surrounding communities. The few practical noise abatement techniques addressing both of these constituents are increasing the frame mass of a hammer for a given blow strength (e.g., by using overrated hammers), improving die design to produce a desired workpiece with less intense blows, and introducing controllable hammers allowing fine tuning of the blow strength to the billet size and condition.<sup>11</sup>

While the hammer operators are somewhat protected by individual ear protectors, the greatest objections to forging hammers' noise and vibration are from residents of the areas surrounding the forging shop and from users of precision and other vibration-sensitive equipment. The noise levels at the "property boundary" of forging shops are 90 to 100 dB,<sup>11</sup> far exceeding the norms for residential areas. Ground-transmitted vibration is even more objectionable, especially in winter time in cold areas, when the frozen soil is a much better vibration transmitter. Vibrations from forging hammers may blur microscope images and cause shaking of office equipment at as far as 300 m from the shop, with much worse effects on frosty days. Transmission of noise and vibration outside the shop can be reduced by acoustical treatment of walls (and ceilings) and by vibration isolation of hammers.

Usually hammer is being installed on a massive foundation block supported by compliant steel springs or rubber isolators. The maximum amplitude of force transmitted to the ground  $P_{g \max}$  relative to blow force magnitude  $P_0$  (Table 2) is<sup>12</sup>

$$\frac{P_{g \max}}{P_0} \cong 6.9 \sqrt{\frac{m_3 m_4^2}{[(m_3 + m_4)(m_1 + m_2 + m_3)] \times (m_1 + m_2 + m_3 + m_4)}} \tau_{p1} f_{vz} \quad (1)$$

where  $m_1$  is mass of dropping tup + upper die,  $m_2$  = mass of anvil,  $m_3 = m'_3 + m''_3$  is mass of frame  $m'_3$  attached to foundation block  $m''_3$ ,  $m_4$  = mass of foundation box,  $\tau_{p1}$  is blow pulse duration (Table 2),  $f_{vz}$  is vertical natural frequency of hammer + foundation on vibration isolators.

Equation (1) describes the effectiveness of the vibration isolation system. It shows that for the short pulse excitation the transmitted force ( $P_{g \max}$ ) is proportional to the natural frequency of the isolation system (for isolation of steady, e.g., sinusoidal, vibrations the transmitted force is proportional to the second power of the natural frequency). However, in the latter case the transmitted vibration is of the same frequency as the excitation, while for the pulse excitation a less hazardous low frequency (equal to  $f_{vz}$ ) is transmitted. The isolation effectiveness does not directly depend on stiffness of the auxiliary isolation system between the anvil and the hammer frame (usually belting, oak boards, etc.).

Damping in isolators improves effectiveness of the isolation system, thus  $f_{vz}$  can be increased (thus allowing to use a smaller and less expensive foundation block) by increasing damping (log decrement  $\delta$  of the isolation system) if the following isolation criterion  $\Phi_{fh}$  is kept constant,

$$\Phi_{fh} = \frac{f_{vz}}{\delta^{0.25}} \quad (2)$$

Increasing damping in both main and anvil isolators from  $\delta = 0.3$  to 1.25 allows to increase the natural frequency of the vibration isolation system by a factor of  $\sim 1.5$ , from  $f_{vz} = 2 - 6$  Hz to  $f_{vz} = 3 - 9$  Hz without reducing isolation effectiveness.

Other pulse-generating machines are jolting tables in foundries, impact-testing machines, and the like. Usually, these machines are smaller than hammers and require less operator supervision (e.g., automatic cycling) and often are used with rigid or flexible (PVC strips) enclosures. Protection of the surrounding area is provided by vibration isolation conceptually similar to that of forging hammers above.

Hydraulic forging presses and large punch presses generate significantly lower noise levels since the ram motion and, thus, structural vibrations can be controlled by the electrohydraulic system.<sup>13</sup> While the overall noise levels in the vicinity of a hydraulic forging press are still significant, the main sources of the noise are not necessarily the forging force pulse related, but are due to compressed air systems, material handling systems, and ancillary devices. These sources can be treated by the techniques described above. For example, noise sources for the hydraulic forging press for artillery shells<sup>14</sup> (the overall level 110 dB) are impacts of shells moving along the gravity chute (95 dB), pneumatic controls on shell-handling robotic arms (110 dB), air jets for blowing out the shell (110 dB), and hydraulic pumps and electric motors (85 to 88 dB).

While there are few forging hammers in industry and usually not more than two or three in one plant, cold headers are widely used for making standard fasteners and relatively small mass-produced mechanical parts. Usually dozens of cold headers are placed in one shop resulting in sound pressure levels of 90 dB to 102 dB and sound power of 99 dB to 115 dB.<sup>15</sup> Techniques for noise reduction in the source include reduction of acceleration/deceleration of the ram, damping enhancement of the structure (frame), damping enhancement of the ejection rocker arm and the flywheel, tightening clearances between the crankshaft and the connecting rod to reduce rattling during reversals, and vibration isolation. These techniques are not widely adopted by the machine manufacturers. However, practically all models of cold headers can be supplied with the full enclosures that, if properly maintained, can provide 9- to 13-dB noise level reduction.

Noise radiation from the shop floor as well as disruption of operation of precision production and measuring equipment can be reduced by mounting cold headers on vibration isolators having high vertical



(compression) stiffness and low horizontal stiffness (in the working pulse direction), thus attenuating the pulse transmission to the floor. The recommended horizontal natural frequency for high-force/low-speed machines is  $f_x \leq 7$  to 9 Hz. It is desirable to assure decoupling horizontal/rocking and vertical modes in the vibration isolation system<sup>12</sup> to reduce vibration excitation in the vertical direction where the floor stiffness is relatively low.

#### 5.4 Metal-Cutting Machine Tools

Most modern machine tools use coolant fluids at high pressures. Because of this, they usually have hermetic enclosures around the working area, which provide a noise abatement effect. There are sometimes objectionable noise levels from machine tools using milling cutters due to the impact character of cutting. A noticeable noise reduction can be achieved by using milling cutters with nonuniform pitch of their cutting edges, used for reduction of chatter vibrations.<sup>16</sup>

The important noise source is radiation from the floor due to high-frequency vibration transmitted from the machine tool. Installation of a majority of machine tools on vibration isolators was shown to result in 2-dB to 3-dB noise level reduction in the shop and noise level reduction in the most annoying frequency range of 2000 Hz to 3000 Hz by 4 dB to 5 dB.<sup>12</sup>

#### REFERENCES

1. E. I. Rivin, Cost Effective Noise Abatement of In-Plant Equipment, *Noise Control Eng. J.*, Nov.-Dec., 1983, pp. 103-117.
2. B. Huang and E. I. Rivin, Noise and Air Consumption of Blow-Off Nozzles, *J. Sound Vib.*, Vol. 109, No. 7, 1985, pp. 26-63.
3. E. I. Rivin, Noise Abatement of Vibration-Stimulated Material Handling Equipment, *Noise Control Eng. J.*, May-June, 1980, pp. 132-142.
4. H. S. Gill, Control of Impact Pile Driving Noise and Study of Alternative Techniques, *Noise Control Eng. J.*, No. 2, 1983, pp. 76-83.
5. M. Amram and G. E. Brooks, Noise Control in Airplane Manufacturing, *Noise Control Eng. J.*, Vol. 44, No. 4, 1996, pp. 193-199.
6. E. I. Rivin and S. Shmutter, Metal Stamping Presses Noise Investigation and Abatement, SAE Tech. Paper 800495, 1980.
7. E. I. Rivin, A Laminated Material for Impact Noise Abatement and Its Applications, *Noise Control Eng. J.*, Vol. 38, No. 3, 1992, pp. 127-131.
8. C. Bramberger, Noise Reduction at Punch Presses by Means of Shock Absorber, Proceedings of Noise-Con 79 Conference, 1979, Purdue University, West Lafayette, IN.
9. M. Otsu, C. Yamagata, and K. Osakada, Reduction of Blanking Noise by Controlling Press Motion, *Annals CIRP*, Vol. 52 No. 1, 2003, pp. 245-248.
10. E. I. Rivin, *Stiffness and Damping in Mechanical Design*, Marcel Dekker, New York, 1999.
11. H. A., Evensen, C. W. Frame, and C. J. Crout, Experiments in Forge Hammer Noise Control, Proceedings of the International Conference on Forging Noise Control, 1977, October 26-28, Atlanta, GA.
12. E. I. Rivin, *Passive Vibration Isolation*, ASME Press, 2003.
13. M. I. Korytko, Damping High Pressure Low-Flow Energy Instantaneously, *Hydraulics and Pneumatics*, April, 1978, pp. 55-67.
14. R. W. Heymann, Noise Control of Various Activities Associated with Forging, Proceedings of the International Conference on Forging Noise Control, 1977, October 26-28, Atlanta, GA.
15. J. R. Jacques, Noise in Cold-Heading Industry, *Noise Control Eng. J.*, Jul.-Aug., 1986, pp. 20-29.
16. E. Budak, Improving Productivity and Part Quality in Milling of Titanium Based Impellers by Chatter Suppression and Force Control, *Annals CIRP*, Vol. 49, No. 1, 2000, pp. 31-34.

# CHAPTER 81

## MACHINE TOOL NOISE, VIBRATION, AND CHATTER PREDICTION AND CONTROL

Lars Håkansson, Sven Johansson, and Ingvar Claesson

Department of Signal Processing  
Blekinge Institute of Technology  
Ronneby, Sweden

### 1 INTRODUCTION

A frequent problem in the manufacturing industry today is the vibrations or chatter induced in machine tools during machining; for example, in turning, milling, boring, and grinding. The vibration of machine tools may be divided into three different classes: (1) free or transient vibrations of machine tools excited by other machines or engagement of the cutting tool, (2) forced vibrations usually associated with periodic forces within the machine tool, for example, unbalanced rotating masses, and (3) self-excited chatter that may be explained by a number of mechanisms. These mechanisms include, among others, the regenerative effect, the mode coupling effect, the random excitation of the natural frequencies of the machine tool caused by the plastic deformation of the workpiece material, and/or friction between the tool and the cut material. Vibrations in machine tools affect the result of machining, particularly the surface finish. Furthermore, machine tool life can be correlated with the degree of vibration and acoustic noise introduced. Machine tool chatter may be reduced by selective passive or active modification of the dynamic stiffness of the tooling structure and/or by the control of cutting data to maintain stable cutting. Forced unbalance vibration in rotating tooling structures may be reduced by passive balancing or active online balancing.

### 2 MACHINE TOOL CHATTER AND VIBRATION

In machine tools the chain—tool, tool holder system, machine structure, and workpiece—forms complicated dynamic systems.<sup>1–4</sup> The vibration of machine tools may be divided into three different classes: free or transient vibration, forced vibration, and self-excited chatter or vibration.<sup>1–4</sup> Free or transient vibrations of machine tools may be excited by other machines in the environment via the machine tool base or/and by rapid movements of machine tables, engagement of the cutting tool, and the like. The forced vibrations are usually associated with periodic forces within the machine tool, for example, unbalanced rotating masses, the intermittent tooth pass excitation in milling. This type of vibration may also be excited by other machines in the environment of the machine tool via its base.

Machine tool vibrations during machining operations are usually termed *self-excited chatter* or *tool*

*vibration*. Depending on the driving force of tool vibration, the vibration is generally divided into one of two categories: regenerative chatter (secondary chatter) and nonregenerative chatter (primary chatter).<sup>1–3,5–8</sup> Extensive research has been carried out on the mechanisms that control the induction of vibrations in the cutting process. The majority of this research has been carried out on dynamic modeling of cutting dynamics focusing on the analytical or a numerical model. Usually, the purpose of these works is dynamic models that enables to predict cutting data that enables stable cutting and maximize the material removal rate.<sup>1,2,4,9–11</sup>

### 2.1 Chatter Mechanisms and Properties

The two most widely used theories explaining self-excited chatter are the regenerative effect and the mode coupling effect. These theories are generally explained based on the dynamic interaction of the cutting process and the machine tool structure, that is, the basic cause of chatter.<sup>1–3,12</sup> Self-excited chatter and two of its energy-providing mechanisms, the regenerative effect and the mode coupling effect, are usually described as follows: During cutting, a force  $F_r(t)$  is generated between the tool and the workpiece; see Fig. 1.

The cutting force will strain the structure elastically and may cause a relative displacement of the tool and

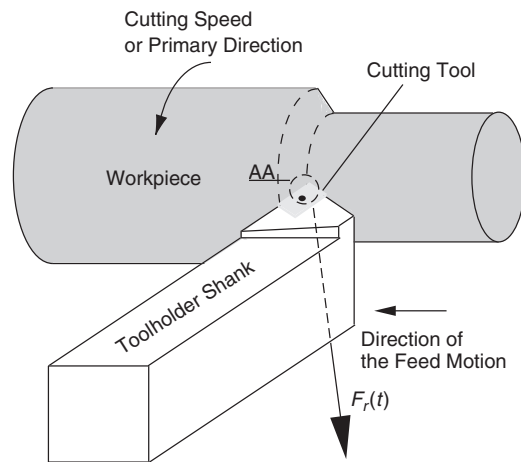
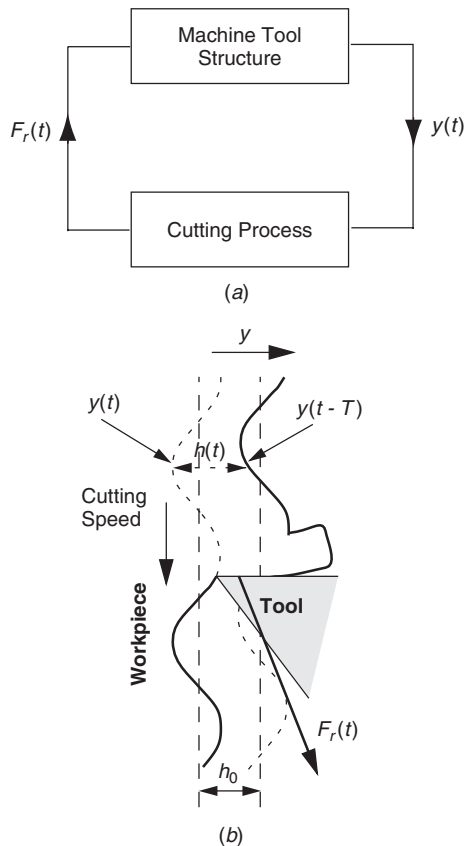


Figure 1 External longitudinal turning.



**Figure 2** (a) Simplified block diagram of the closed-loop cutting-process structural system and (b) the principle for cutting tool regenerative chatter.<sup>3</sup>

the workpiece, which alters the tool and workpiece engagement. This, in turn, indicates a feedback system relation between the cutting force  $F_r(t)$  and the relative displacement of the tool and the workpiece; see Fig. 2a. This justifies a possibility for the initial vibration to be self-sustaining (unstable) and increase, with the machine oscillating in one of its natural modes of vibration. Basically, the closed-loop cutting process structural system is considered unstable if a mechanism exists for transferring energy into the structure to maintain vibration.<sup>1-3,12</sup> The regenerative effect is considered to be the dominant mechanism of instability and chatter.<sup>1-3,12</sup> It may occur when successive passes of the cutting tool overlap, that is, when the tool at any instant is removing an undulation on the workpiece surface that was cut on the previous pass of the tool or revolution of the workpiece. This is illustrated in Fig. 2b where  $h_0$  is the intended chip thickness,  $h(t)$  is the actual chip thickness at time  $t$ ,  $y(t)$  is the displacement of the tool in the  $y$  direction at time  $t$ , and  $y(t - T)$  is the displacement of the tool in the  $y$  direction at previous pass of the tool or revolution of the workpiece.

Depending on the phase between these waves on the workpiece surface, the force variation and excitation energy may increase after successive passes of the tool and the vibration will build up.<sup>1-4,12</sup> The limit of stability as a function of frequency—a stability chart—may be produced from

$$1 = -G_{yr}(f)[k_1(1 - \mu_c e^{-j2\pi f T}) + k_2 2\pi / \Omega j 2\pi f]$$

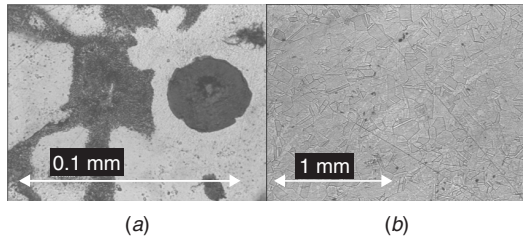
where  $G_{yr}(f)$  is the cross receptance between the cutting force  $F_r(t)$  and the tool response  $y(t)$  (m/N),  $k_1$  is the cutting stiffness coefficient (N/m),  $\mu_c$  is the overlap factor,  $k_2$  is a constant (N/m),  $\Omega$  is turning the rotational speed of the workpiece (rad/s), and  $f$  is frequency (Hz).<sup>3</sup>

On the other hand, the mode coupling effect may occur when successive passes of the tool do not overlap and when the eigenmodes of the machine-tool system are closely matched. The mode coupling chatter exists if vibration in the primary cutting direction generates vibration in the feed direction and vice versa. This results in an elliptic tool tip motion in the primary direction-feed direction plane, where the part of the elliptic motion in direction of the primary direction produces a greater average depth of cut as compared to the part of the elliptic motion where the tool tip has a motion in the reverse primary direction. This results in a net input of energy to the machine-tool system.<sup>1-3,12</sup>

The mode coupling effect is in the set of primary chatter mechanisms. The set of primary chatter mechanisms also includes random excitation of the machine tools eigenfrequencies due to plastic deformation of workpiece material and/or friction between the tool and the cut material, the tendency of the cutting force excitation to change with the cutting speed, the dynamic effects of the geometry of the cutting tool on the cutting process, and so forth.<sup>1,10,11,13,14</sup>

In this context it should, however, be observed that machine-tool chatter frequently exhibits stochastic properties.<sup>10-14</sup> This may be explained by the fact that the mechanical properties of materials, such as chemical composition, inhomogeneity, microstructure, and hardening, generally have spatial stochastic variations.<sup>15</sup> As a consequence of the stochastic variation of the mechanical properties, the deformation properties of the material will also show random variations.<sup>13</sup> In Fig. 3 photos of the material structure of two different work materials, one cast iron and one stainless steel, are shown.

This in turn will introduce a broadband excitation of the machine tool.<sup>10,11,13</sup> Generally, machine-tool systems are classified as narrow-band systems.<sup>4,10,11,13,16,17</sup> The chatter or tool vibration is usually related to a low-order bending mode of, for example, the tool holder shank in external turning, the boring bar in internal turning, and spindle-cutter assembly in milling.<sup>10,11,13,16,17</sup> Frequently, the tool holder responses during continuous unstable machining have nonlinear properties.<sup>10,11,13,14,18</sup> Boring bar vibration, for instance, usually has spectra containing harmonics of the dominating resonance frequency as well



**Figure 3** Structure of (a) SS 0727-02 or AISI 80-55-06 (magnification 1000 $\times$ ). (b) SS 2343-02 or AISI 316 (magnification 50 $\times$ ).<sup>13</sup>

as non-Gaussian probability density.<sup>10,11</sup> Occasionally, these properties may also be observed in tool holder shank vibration in external turning which, however, usually is Gaussian distributed.<sup>13,18</sup> For constant cutting data, tool holder shank vibrations in external turning are generally described well by second-order weakly stationary random processes, while boring bar vibrations usually exhibit nonstationary stochastic behavior.<sup>10,11,13</sup> Low-frequency revolution-dependent workpiece motion due to residual rotor mass unbalance in the spindle–chuck–workpiece system may influence the motion of the tool holder via the relative dynamic motion between the cutting tool and workpiece. As a result, the motion of a tool holder is influenced by force modulation<sup>10</sup> and thus exhibits cyclostationary properties.<sup>19</sup> In milling, both the tooth pass frequency and the residual rotor mass unbalance in the spindle–cutter assembly may also influence the tool holder response during machining.<sup>14,16,17</sup>

### 3 METHODS OF VIBRATION AND CHATTER CONTROL

Generally, the tooling structure—the interface between the cutting tool or insert and the machine tool—is the weakest link in a machining system.<sup>20</sup> In many cases, the tooling structure is the bottleneck concerning the achievable accuracy imposed by static deflections and the cutting regimes as well as the surface finish due to forced and self-excited vibrations. For instance, long-overhang cantilever tooling is frequently the critical part of the tooling structure. In the case of tooling based on steel bars the upper limit for stable machining with a reasonable machining regime is generally considered to be  $L/D = 4$ , where  $L/D$  = bar overhang/bar diameter.<sup>20–22</sup> But in more demanding applications, such as internal threading and grooving, vibrations may start at an overhang between two and three times the bar diameter.<sup>22</sup>

Basically, all methods for improving the tooling structure concern modifications of the tooling structure's dynamic stiffness and/or balancing of rotating parts of the tooling structure.<sup>18,20–28</sup> All the elements and joints in the chain from the tool or insert to toolholder–clamping—machine or toolholder—spindle interface have been addressed with the purpose of enhancing the chatter resistance of machine tools. The

trend of continuously increasing requirements on speed and accuracy has also turned the focus toward the balancing of tool holders for rotating tools.<sup>20</sup>

Methods for reduction of vibration and chatter comprise the increase of the damping and/or stiffness of insert or tool attachment systems, the reduction of the toolholder stiffness to enable the tool to retract out of the workpiece when the dynamic cutting force increases, the increase of the dynamic stiffness of toolholder shanks by means of passive or active control methods, the reduction of the stiffness of the toolholder shank while increasing the damping of the clamping, the improvement of the dynamic stiffness of the interface between tool and clamping device, the improvement of the dynamic stiffness of the tool clamping devices/spindle connection, the active and passive balancing of toolholders for rotating tools, and the like.<sup>20</sup>

#### 3.1 Control Strategies

Two main directions have evolved for the control of machine tool chatter: one concerns the selective modification of the dynamic stiffness of the tooling structure<sup>18,20–28</sup>; the other concerns the control of cutting data to maintain stable cutting, that is, to avoid cutting data resulting in chatter or to continuously vary cutting data in a structured manner to avoid chatter.<sup>20,29,30</sup>

In the reduction of forced unbalance vibration in rotating tooling structures two basic balancing concepts are passive balancing systems, both offline and online (self-balancing), and active online balancing using sensors and actuating devices on the rotating component.<sup>20</sup>

#### 3.2 Passive Control

Generally, increased dynamic stiffness is associated with passive vibration control. However, successful application of turning toolholders, boring bars, and face milling cutter with selectively reduced static stiffness in the primary direction have been achieved for enhanced chatter resistance.<sup>1,20,31</sup> This will enable the tool or tools to retract out of the workpiece—reducing the effective chip area—when the dynamic cutting force increases.<sup>1,20</sup>

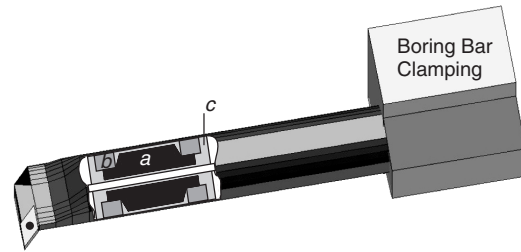
The improvement of the chatter resistance of tooling structures usually involves a static stiffness reduction simultaneous with an increased damping of the tooling structure, that is, an enhancement of the dynamic stiffness and stability.<sup>1,20,22,32,33</sup> This method has, for instance, been utilized successfully in clamping devices for drilling, in a tool clamping for external longitudinal turning in the direction normal to the workpiece, in grinding wheels, in boring bar clamping devices, and the like.<sup>20,32,33</sup>

The long-overhang cantilever tooling is frequently the critical part of the tooling structure, and several passive techniques have been implemented within the boundaries of these cantilever structures. These passive methods are well-known to enhance the dynamic stiffness and stability (chatter resistance) of long cutting tools and, thus, enables the allowable overhang

to be increased.<sup>20,22,23</sup> A common way of increasing the dynamic stiffness of cantilever tooling is by making them in high Young's modulus nonductile materials such as sintered tungsten carbide and machinable sintered tungsten.<sup>20,22,23</sup> Solid bars made of both these materials allow stable cutting with ratios  $L/D < 7$ .<sup>20,22</sup> The dynamic stiffness of cantilever tooling may be further increased at the cost of reduced static stiffness by, for example, implementing a tungsten carbide rod inside a tube-formed boring bar.<sup>20</sup> The boring bar design with an internal tungsten carbide rod can cut chatter free at a depth of 15 to 30% greater than a solid carbide bar of the same diameter at  $L/D = 6.5$ .<sup>20</sup>

At present, the most common approach to enhancing the dynamic stability of long cantilever tooling is the application of an widely used method for vibration suppression; the passive tuned vibration absorbers (TVA).<sup>20,22,23</sup> In the literature the tuned vibration absorbers are also refereed to as tuned mass dampers (TMD) or dynamic vibration absorbers (DVA). A TVA is usually implemented in a tube form, for example, boring bar at the tool end. A cylindrical damper body may, for example, be coupled to the bar via rubber rings at each end of the cylindrical damper body with damper oil in between the rubber rings<sup>20,22,23</sup>; see Fig. 4. The placement of the tuned vibration damper at the tool end enables the greatest control force into the fundamental bending modes.<sup>34</sup> The absorber is tuned to a given frequency range by adjusting the weight of the reactive mass and the stiffness and damping properties of the elastic element. The vibration absorbers are tuned either to a tonal or a broadband application.

Steel boring bars with TVAs allow stable cutting with ratios  $L/D < 10$ .<sup>22,23</sup> The performance of TVA boring bars may be improved further by making the root segment of the bar closest to the clamping of



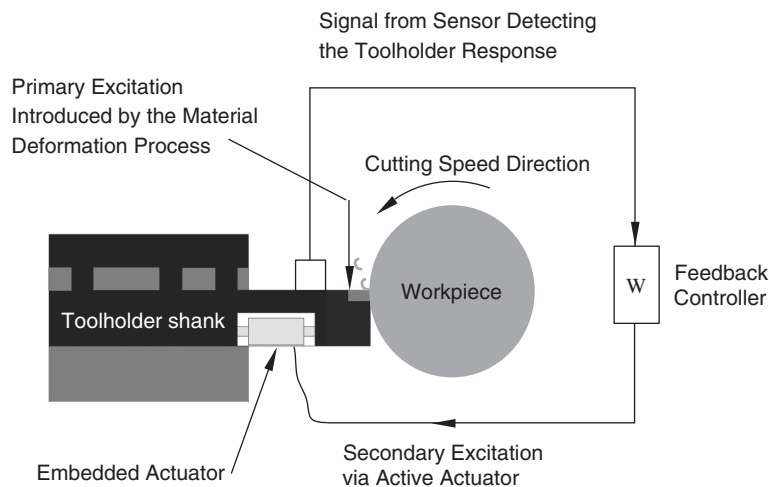
**Figure 4** Passive damped boring bar.<sup>20,22,23</sup> (a) Heavy tuning body. (b) Rubber ring. (c) Damper oil.

high Young's modulus materials such as sintered tungsten carbide and machinable sintered tungsten.<sup>20,22,23</sup> Carbide-reinforced TVA boring bars enable stable cutting with ratios  $L/D < 15$ .<sup>20,22,23</sup>

### 3.3 Active Control of Chatter – A Promising New Development

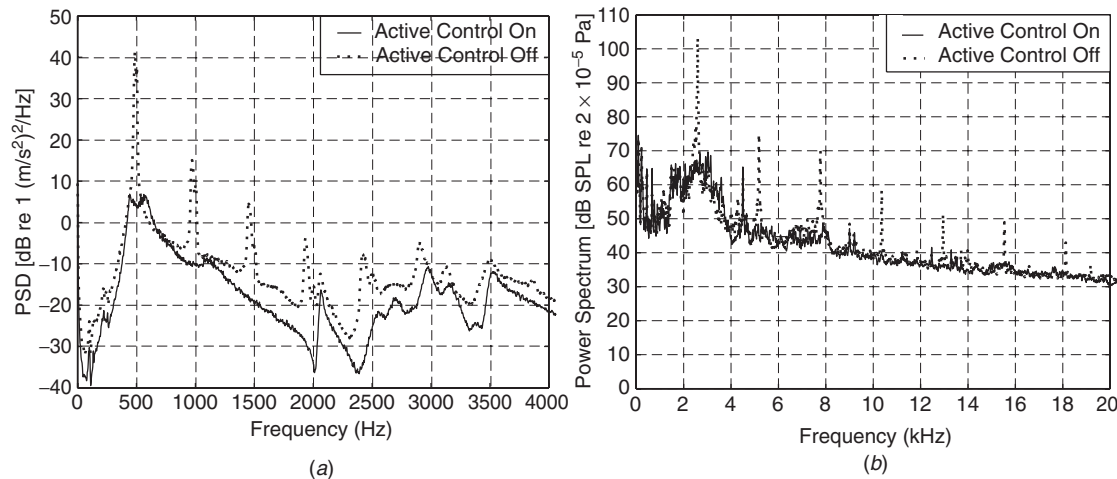
Active vibration control of machine–tool vibration comprises a number of different methods for introducing the control force into fundamental bending modes of toolholder shanks; it also includes different controller approaches. As the original excitation of the tool vibrations—the chip formation process—cannot be directly observed, the control methods are all based on feedback control.<sup>18,24–28</sup> Figure 5 shows a machine–tool feedback control system.

One of the approaches concerns the adaptive active control of tool vibration using embedded and integrated actuators adjacent to the clamping below the centerline of holder shanks for external turning and boring bars controlled by the feedback filtered-x LMS algorithm.<sup>24,25</sup> Figure 6 shows control results



**Figure 5** Machine–tool feedback control system.





**Figure 6** (a) Power spectral density (PSD) of boring bar vibrations with and without feedback filtered-x LMS control. Cutting speed  $v = 80$  m/min, cutting depth  $a = 1.5$  mm, feed rate  $s = 0.3$  mm/rev, DNMG 150608-SL, grade 7015. (b) Power spectrum of the absolute-calibrated sound pressure level excited by tool vibration in external longitudinal turning with and without feedback filtered-x LMS control. Cutting speed  $v = 80$  m/min, cutting depth  $a = 0.9$  mm, feed rate  $s = 0.23$  mm/rev, DNMG 150608-SL, grade 7015.

for a toolholder shank and a boring bar produced using this method.

Another method for active control of boring bar vibration involves LQ control<sup>35</sup> and piezoelectric inertial-mass actuators mounted at the tool end.<sup>26</sup> Also, a control approach based on active clamping and the feedback filtered-x LMS algorithm for boring bars has been developed. The active clamping consists of two actuator pairs: one pair for the introduction of the control force in the cutting speed direction and one pair for the introduction of the control force in the cutting depth direction.<sup>26</sup> An active spindle unit for the control of tool vibration in milling has recently been developed.<sup>28</sup> Two actuator pairs introduce secondary vibrations into two orthogonal radial directions into the spindle.<sup>28</sup> The actuators are steered by an LQG controller<sup>35</sup> fed with strain gauge signals that senses the bending motion in the spindle-cutter assembly.<sup>28</sup>

### 3.4 Cutting Data Control

Cutting data, feed rate, and cutting speed may also be controlled to maintain stable cutting. Control can, for example, be carried out on the basis of estimates of the damping ratio of a relevant natural frequency of the joint dynamics of the cutting process and of the machine tool structure using an ARMA model with recursively estimated parameters.<sup>29</sup> Other approaches including continuous variation of the cutting speed to maintain stable cutting have also been suggested. The amplitude and frequency of a sinusoidal spindle speed variation may be controlled with respect to minimum energy input by the cutting process based on knowledge of the spindle speed and the chatter frequency.<sup>30</sup>

### REFERENCES

1. S. A. Tobias, *Machine-Tool Vibration*, Blackie & Son, Glasgow, Scotland, 1965.
2. F. Koenigsberger and J. Tlustý, *Machine Tool Structures*, Vol. 1, Pergamon, Oxford, England, 1970.
3. G. Boothroyd and W. A. Knight, *Fundamentals of Machining and Machine Tools*, 2nd ed., Marcel Dekker, New York, 1989.
4. Y. Altintas, *Manufacturing Automation, Metal Cutting Mechanics, Machine Tool Vibrations, and CNC Design*, Cambridge University Press, Cambridge, UK, 2000.
5. H. E. Merritt, Theory of Self-Excited Machine-Tool Chatter, Contribution to Machine-Tool Chatter, Research—1, *J. Eng. Ind., Trans. ASME*, Vol. 87, 1965, pp. 447–454.
6. S. Kato and E. Marui, On the Cause of Regenerative Chatter Due to Workpiece Deflection, *J. Eng. Ind.*, Vol. 96, 1974, pp. 179–186.
7. M. K. Khraisheh, C. Pezeshki, and A. E. Bayoumi, Time Series Based Analysis for Primary Chatter in Metal Cutting, *J. Sound Vib.*, Vol. 180, No. 1, 1995, pp. 67–87.
8. M. N. Hamdan and A. E. Bayoumi, An Approach to Study the Effects of Tool Geometry on the Primary Chatter Vibration in Orthogonal Cutting, *J. Sound Vib.*, Vol. 128, No. 3, 1989, pp. 451–469.
9. J. Tlustý, Analysis of the State of Research in Cutting Dynamics, *Annals CIRP*, Vol. 27, 1978, pp. 583–589.
10. L. Andrén, L. Håkansson, A. Brandt, and I. Claesson, Identification of Dynamic Properties of Boring Bar Vibrations in a Continuous Boring Operation, *J. Mech. Syst. & Signal Proc.*, Vol. 18, No. 4, 2004, pp. 869–901.
11. L. Andre'n, L. Håkansson, A. Brandt, and I. Claesson, Identification of Motion of Cutting Tool Vibration in a Continuous Boring Operation—Correlation to Structural Properties, *J. Mech. Syst. Signal Proc.*, Vol. 18, No. 4, 2004, pp. 903–927.

12. D. B. Welbourn and J. D. Smith, *Machine-Tool Dynamics, An Introduction*, Cambridge University Press, Cambridge, UK, 1970.
13. P.-O. H. Sturesson, L. Håkansson, and I. Claesson, Identification of the Statistical Properties of the Cutting Tool Vibration in a Continuous Turning Operation—Correlation to Structural Properties, *J. Mech. Syst. Signal Proc.*, Vol. 11, No. 3, 1997, pp. 459–489.
14. T. Insperger, G. Stépán, P. V. Bayly, and B. P. Mann, Multiple Chatter Frequencies in Milling Processes, *J. Sound Vib.*, Vol. 262, 2003, pp. 333–345.
15. D. R. Askeland, *The Science and Engineering of Materials*, 2nd ed., Chapman & Hall, London, 1990.
16. S. Engin and Y. Altintas, Mechanics and Dynamics of General Milling Cutters. Part I: Helical End Mills, *Int. J. Machine Tools Manuf.*, Vol. 41, 2001, pp. 2195–2212.
17. S. Engin and Y. Altintas, Mechanics and Dynamics of General Milling Cutters. Part II: Inserted Cutters, *Int. J. Machine Tools Manuf.*, Vol. 41, 2001, pp. 2213–2231.
18. I. Claesson and L. Håkansson, Adaptive Active Control of Machine-Tool Vibration in a Lathe, *IJAV—Int. J. Acoust. Vib.*, Vol. 3, No. 4, 1998, pp. 155–162.
19. A. Brandt, L. Håkansson, and I. Claesson, Cyclostationary Analysis of Boring Bar Vibrations, International Modal Analysis Conference-XXI, Dearborn, MI, 2004, pp. 313–319.
20. E. I. Rivin, Tooling Structure: Interface between Cutting Edge and Machine Tool,” *Annals CIRP*, Vol. 49, No. 2, 2000, pp. 591–634.
21. Sandvik, *Modern Metal Cutting—A Practical Handbook*, AB Sandvik Coromant, Sandviken, Sweden, 1994.
22. N. A. Ruud, R. Karlson, K. Sørby, and C. Richt, Minimizing Vibration Tendencies in Machining, Technical Article at: <http://www.coromant.sandvik.com>, 2005.
23. <http://www.teeness.no>, 2005.
24. L. Andrén, L. Håkansson, and I. Claesson, Active Control of Machine Tool Vibration in External Turning Operations, Proceedings of the Institution of Mechanical Engineers, Part B, *J. Eng. Manuf.*, Vol. 217, No. B6, 2003, pp. 869–872.
25. L. Andrén, L. Håkansson, and I. Claesson, Performance Evaluation of Active Vibration Control of Boring Operations Using Different Active Boring Bars, Proc. of the Tenth International Congress on Sound and Vibration, ICSV10, Stockholm, Sweden, 2003.
26. S. G. Tewani, K. E. Rouch, and B. L. Walcott, A Study of Cutting Process Stability of a Boring Bar with Active Dynamic Absorber, *Int. J. Machine Tools Manuf.*, Vol. 35, No. 1, 1995, pp. 91–108.
27. D. R. Browning, I. Golioto, and N. B. Thompson, Active Chatter Control System for Long-Overhang Boring Bars,” *Proc. SPIE*, Vol. 3044, 1997, pp. 270–280.
28. J. L. Dohner, J. P. Lauffer, T. D. Hinnerichs, N. Shankar, M. Regelbrugge, C.-M. Kwan, R. Xu, B. Winterbauer, and K. Bridger, Mitigation of Chatter Instabilities in Milling by Active Structural Control, *J. Sound Vib.*, Vol. 269, 2004, pp. 197–211.
29. C. M. Nicolescu, On-line Identification and Control of Dynamic Characteristics of Slender Workpieces in Turning, *J. Mat. Proc. Tech.*, Vol. 58, 1996, pp. 374–378.
30. E. Al-Regib, J. Ni, and S.-H. Lee, Programming Spindle Speed Variation for Machine Tool Chatter Suppression, *Int. J. Machine Tools Manuf.*, Vol. 43, No. 12, 2003, pp. 1229–1240.
31. E. I. Rivin and H. L. Kang, Enhancement of Dynamic Stability of Cantilever Tooling Structures, *J. Machine Tools Manuf.*, Vol. 32, No. 4, 1992, pp. 539–562.
32. E. I. Rivin and H. L. Kang, Improvement of Machining Conditions for Slender Parts by Tuned Dynamic Stiffness, *J. Machine Tools Manuf.*, Vol. 29, No. 3, 1989, pp. 361–376.
33. J. Peters, Contribution of CIRP Research to Industrial Problem in Grinding, *Annals of CIRP*, Vol. 33/2, 1984, pp. 451–468.
34. M. J. Brennan and J. Dayou, Global Control of Vibration Using a Tunable Vibration Neutralizer, *J. Sound Vib.*, Vol. 232, No. 3, 2000, pp. 585–600.
35. K. J. Åström and B. Wittenmark, *Computer Controlled Systems, Theory and Design*, 3rd ed., Prentice Hall, Englewood Cliffs, NJ, 1997.



# CHAPTER 82

## SOUND POWER LEVEL PREDICTIONS FOR INDUSTRIAL MACHINERY

Robert D. Bruce  
CSTI Acoustics  
Houston, Texas

Charles T. Moritz  
Blachford, Inc.  
West Chicago, Illinois

Arno S. Bommer  
CSTI Acoustics  
Houston, Texas

### 1 INTRODUCTION\*

The sound power level is the measure of the sound power radiated by a sound source expressed in a logarithmic scale relative to  $10^{-12}$  W with a unit of decibels. Procedures for calculating the sound power level of industrial machinery are presented in this chapter. The calculated sound power levels can be used for modeling the sound pressure levels in a space or developing purchase specifications for new equipment.

With any project, acoustical data measured and calculated in accordance with recognized standards should be obtained. Many manufacturers provide sound power levels or measured sound pressure levels at 1 m from their equipment, and some offer special low-noise options. If manufacturer's data is unavailable, efforts should be made to measure a similar unit in operation. If this is not practical, then the material in this chapter can be used.

Most of the equations presented in this chapter are based on measured data and tend to be conservative, usually predicting somewhat higher sound pressure levels than are measured in the field. Due to recent efforts at reducing equipment noise, sound pressure levels for some equipment may be significantly (10 dB) quieter than the levels calculated in this chapter.

Some equipment consists of several different sound-producing components such as motors, pumps, blowers, and the like. The sound power levels for each component should be determined and then combined (using correct decibel addition) to get the total sound power levels.

\*Much of this material was published earlier as Chapter 86 of Volume 2 of *Encyclopedia of Acoustics*, John Wiley & Sons, Inc. 1997, which utilized formulas from several references, especially Ref. 1. In this chapter, some formulas have been modified to use metric units and to give the A-weighted sound power level directly from the equipment parameters.

### 2 POWER SOURCES

#### 2.1 Boilers<sup>1</sup>

**Main Steam Boilers** Main steam boilers of a power plant radiate igniter, flow, and combustion noise from their surfaces. The A-weighted sound power level for main steam boilers (between 125 and 800 MWe) can be calculated using Eq. (1) where MWe is the electrical generating rating of the unit. The unweighted octave band sound power levels can be obtained by subtracting the values shown in Table 1.

$$L_W = 72 + 15 \log \text{MWe} \quad \text{dB} \quad (1)$$

**Auxiliary Boilers** The noise produced by auxiliary boilers is often due primarily to the blower and the burner, not the walls of the boiler. An estimate of the A-weighted sound power level for auxiliary boilers between 0.5 and 20 MW can be calculated using Eq. (2). The unweighted octave band sound power levels can be obtained by subtracting the values shown in Table 1. For boilers rated in other units, 1 MW = 102 bhp = 1600 kg steam/h.

$$L_W = 94 + 4 \log \text{MW} \quad \text{dB} \quad (2)$$

#### 2.2 Electric Motors

**Motors under 750 kW<sup>2</sup>** Totally enclosed fan-cooled (TEFC) motors are the most common type of electric motors. They are generally cylindrical in shape with a fan at one end, the output shaft at the other end, and fins along the body. The A-weighted sound power level for TEFC motors can be calculated using the following equations:

$$\begin{aligned} < 40 \text{ kW} : L_W = 16 + 17 \log \text{kW} \\ &+ 15 \log \text{rpm} + 10 \log S \quad \text{dB} \quad (3) \end{aligned}$$

$$\begin{aligned} \geq 40 \text{ kW} : L_W = 27 + 10 \log \text{kW} \\ &+ 15 \log \text{rpm} + 10 \log S \quad \text{dB} \quad (4) \end{aligned}$$

**Table 1 Octave Band Sound Power Level Adjustments**

Source	31.5	63	125	250	500	1000	2000	4000	8000
Main steam boiler	-8	-7	-2	4	5	7	9	9	9
Auxiliary boiler	-3	-3	-2	0	3	6	9	12	15
TEFC motors under 750 kW	13	13	10	8	5	5	6	11	19
Drip-proof motors under 750 kW	5	5	3	3	2	5	8	14	23
Gas turbine casing	8	5	3	2	2	2	2	2	2
Gas turbine exhaust	8	4	2	2	3	5	7	11	17
Gas turbine intake	19	18	17	17	14	8	3	3	6
Reciprocating engines (<600 rpm)	8	8	2	1	3	5	8	14	24
Reciprocating engines (600–1500 rpm)	11	6	4	5	4	4	6	10	16
Reciprocating engines w/blower (600–1500 rpm)	21	15	17	13	2	3	9	14	25
Reciprocating engines (> 1500 rpm)	20	12	5	5	6	4	5	11	18
Reciprocating engine turbocharged air inlet	1	8	10	10	9	6	5	6	14
Reciprocating engine exhaust	-7	-3	-9	-5	3	7	13	23	31
Steam turbines	6	2	1	4	5	5	7	8	12
Steam turbine generator units	-3	-9	-7	-2	2	6	9	17	23
Transformers	3	-3	-5	0	0	6	11	16	23
Centrifugal air compressor casing	8	8	9	11	11	9	5	6	10
Centrifugal air compressor air inlet	18	16	14	10	8	6	5	10	16
Rotary and reciprocating air compressors	9	13	8	9	11	8	3	6	13
Feed pumps (1–9 MW)	7	1	3	4	5	6	7	8	12
Feed pumps (9.5–18 MW)	18	12	14	10	4	4	6	18	22
Centrifugal fan <sup>a</sup>	11	9	7	8	9	9	13	17	24
Centrifugal fan casing <sup>a</sup>	3	6	7	11	16	18	22	26	33
Axial-flow fans <sup>a</sup>	8	7	6	5	5	5	7	11	12
Propeller fans <sup>a</sup>	12	12	9	2	4	5	8	14	16
Gas recirculation fan casing	-2	-5	-8	-5	6	8	13	15	19
Generators	7	4	3	3	3	5	7	10	15
Gears	13	10	7	7	7	7	7	7	7
Motor-driven pumps	11	10	9	7	7	4	7	11	17
Cooling towers (full speed)	-1	-4	-4	-1	2	6	9	12	20
Cooling towers (half speed)	4	1	1	5	5	6	6	9	15
Chillers with reciprocating compressor	—	19	11	7	1	4	9	14	—
Centrifugal chillers, internal geared	—	8	5	6	7	8	5	8	—
Centrifugal chillers, direct drive	—	8	6	7	3	4	7	12	—
Centrifugal chillers, > 1000 tons	—	11	11	8	8	4	6	13	—
Chillers with rotary-screw compressor	20	14	10	-2	1	5	10	15	17
Diesel-powered, mobile equipment	—	6	1	-2	3	5	8	14	20

<sup>a</sup> Equations (29)–(32) are for the unweighted sound power levels. Subtracting the values in this table will yield the unweighted octave band sound power levels. After making the adjustments described in the text for the blade passage frequency [calculated in Equation (28)], the A-weighted sound power level can be calculated.

where kW is the nameplate motor rating (1 kW = 1.34 hp), rpm is the speed at which the motor is operating, and  $S$  is the conformal surface area (in square metres) at 1 m from the motor (see the Appendix to this chapter for the equation for the conformal surface area). For TEFC motors between 300 and 750 kW, use the value 300 kW in Eq. (4). The unweighted octave band sound power levels can be obtained by subtracting the values shown in Table 1.

For drip-proof motors, the A-weighted sound power level can be calculated using the following equations:

$$\begin{aligned} <40 \text{ kW: } L_W = 8 + 17 \log \text{ kW} \\ + 15 \log \text{ rpm} + 10 \log S \text{ dB (5)} \end{aligned}$$

$$\begin{aligned} \geq 40 \text{ kW: } L_W = 19 + 10 \log \text{ kW} \\ + 15 \log \text{ rpm} + 10 \log S \text{ dB (6)} \end{aligned}$$

For drip-proof motors between 300 and 750 kW, use the value 300 kW in Eq. (6).

The unweighted octave band sound power levels can be obtained by subtracting the values shown in Table 1.

**Motors between 750 and 4000 kW<sup>1</sup>** The sound power level for large drip-proof electric motors (between 750 and 4000 kW) can be estimated by using Table 2.

### 2.3 Gas Turbines<sup>2</sup>

Manufacturers of gas turbines often have sound power level data for the exhaust and inlet. Obtaining accurate casing data can be difficult due to contributions from the inlet, exhaust, or other equipment. The A-weighted sound power level for gas turbines can be estimated using Eqs. (7) to (9). The unweighted octave band sound power level for each of these sources can be obtained by subtracting the values shown in

**Table 2 Octave Band and A-Weighted Sound Power Levels for Drip-Proof Electric Motors (750–4000 kW)**

Speed (rpm)	31.5	63	125	250	500	1000	2000	4000	8000	A
1800 or 3600	94	96	98	98	98	98	98	95	88	104
1200	88	90	92	93	93	93	98	88	81	101
900	88	90	92	93	93	96	96	88	81	101
<720	88	90	92	93	93	98	92	83	75	100
250 or 400 (vertical)	86	87	88	88	88	98	88	78	68	99

Table 1.

$$\text{Casing : } L_W = 118 + 5 \log MW \quad \text{dB} \quad (7)$$

$$\text{Exhaust : } L_W = 129 + 10 \log MW \quad \text{dB} \quad (8)$$

$$\text{Intake : } L_W = 127 + 15 \log MW \quad \text{dB} \quad (9)$$

## 2.4 Reciprocating Engines<sup>2</sup>

The major noise sources of natural-gas and diesel reciprocating engines are the engine casing, exhaust noise, radiator (fan) noise [see Eq. (32)], and for turbocharged engines, the air inlet. The sound power levels for each component must be determined. The component levels can then be added together (correct decibel addition) to determine the total sound power levels.

**Engine Casing Noise** The A-weighted sound power level for engine casing noise can be calculated using Eq. (10) where kW is the full-load rating of the engine, and *A*, *B*, *C*, and *D* are correction factors obtained from Table 3. The octave band sound power levels can be obtained by subtracting the values shown in Table 1.

$$L_W = 90 + 10 \log kW + A + B + C + D \quad \text{dB} \quad (10)$$

**Air Inlet** For all naturally aspirated engines and for turbocharged engines under about 340 kW, the casing-noise calculation includes the air inlet noise. For turbocharged engines above 340 kW, the A-weighted

sound power level of the air inlet can be calculated using Eq. (11) where  $d_{\text{inl}}$  is the length of the inlet ducting in metres. The unweighted octave band sound power levels can be obtained by subtracting the values shown in Table 1.

$$L_W = 92 + 5 \log kW - (d_{\text{inl}}/1.8) \quad \text{dB} \quad (11)$$

**Engine Exhaust** The A-weighted sound power level for the unmuffled exhaust can be calculated using Eq. (12) where *T* is a turbocharger correction term (*T* = 6 if the engine has a turbocharger, *T* = 0 if there is no turbocharger) and  $d_{\text{exh}}$  is the length of the exhaust pipe in metres. The unweighted octave band sound power levels can be obtained by subtracting the values shown in Table 1.

$$L_W = 108 + 10 \log kW - T - (d_{\text{exh}}/1.2) \quad \text{dB} \quad (12)$$

## 2.5 Steam Turbines<sup>1</sup>

Manufacturers of steam turbines often have sound pressure level measurements, but the levels may not have been measured in accordance with a recognized standard. The A-weighted sound power level for steam turbines can be estimated using Eq. (13), and the unweighted octave band sound power levels can be obtained by subtracting the values shown in Table 1.

$$L_W = 88 + 4 \log kW \quad \text{dB} \quad (13)$$

**Table 3 Sound Power Level Correction Terms for Casing Noise of Reciprocating Engines**

Correction Term	Qualifying Condition	dB
<i>A</i>	Less than 600 rpm	−5
	600–1500 rpm	−1
	Over 1500 rpm	2
<i>B</i>	Diesel and/or natural gas fuel	0
	Natural gas only (with small amount of "pilot oil")	−3
<i>C</i>	In-line cylinders	0
	V-type or radial cylinders	−1
	Unducted air inlet to unmuffled roots blower	5
<i>D</i>	All other types of inlets (with or without turbocharger)	0

## 2.6 Steam Turbine–Generator Units<sup>1</sup>

The A-weighted sound power level for main steam turbine–generator units (between 200 and 1100 MWe) can be calculated using

$$L_W = 101 + 4 \log \text{MWe} \quad \text{dB} \quad (14)$$

The unweighted octave band sound power levels can be obtained by subtracting the values shown in Table 1. Equation (14) takes into account sound contributions from the high- and low-pressure turbines, generators, and shaft-driven exciters. Noisy couplings and steam control valves can cause higher sound power levels than those predicted with this equation.

## 2.7 Transformers<sup>1</sup>

Noise from the body of the transformer is made up of tones at the even harmonics of the line frequency. In the United States, where the line frequency is 60 Hz, the harmonics are 120, 240, 360, 480, ... Hz with the 120-Hz tone usually being the dominant sound. When additional cooling of the transformer is needed, noise from the cooling fans can become the dominant noise source. Lower fan speeds and optimal blade shapes have helped make newer fans much quieter, which is particularly helpful in noise-sensitive applications.

The National Electrical Manufacturers Association (NEMA) sound pressure level rating is the A-weighted sound pressure level 1 ft from the transformer and can be estimated from the following formulas:

### Standard transformer:

$$\text{NEMA sound rating} = 55 + 12 \log \text{MVA} \quad \text{dB} \quad (15)$$

### Quieted transformer:

$$\text{NEMA sound rating} = 45 + 12 \log \text{MVA} \quad \text{dB} \quad (16)$$

where MVA is the voltage–ampere rating of the transformer in MVA. These equations are valid for transformers between 20 and 450 MVA. The A-weighted sound power level can be calculated using

$$L_W = \text{NEMA sound rating} + 10 \log S \quad \text{dB} \quad (17)$$

where  $S$  is the surface area of the four side walls in square metres. The term  $10 \log S$  may be estimated from the MVA rating by using

$$10 \log S = 14 + 2.5 \log \text{MVA} \quad \text{dB} \quad (18)$$

Unweighted octave band sound power and pressure levels can be obtained by subtracting the appropriate octave band correction factors shown in Table 1.

## 3 DRIVEN EQUIPMENT

### 3.1 Air Compressors

**Centrifugal Compressors<sup>1,3</sup>** The frequency band of maximum sound power from the casing or discharge piping for large centrifugal compressors can be calculated based on the impeller tip speed,  $U$ , in metres per second ( $30 < U < 230$ ):

$$f_p = 4.1U \quad (19)$$

The octave band sound power level in that frequency band can be calculated using Eq. (20) where  $m$  is the surface weight of the casing or pipe wall in kilograms per square metre and  $f$  is the octave band center frequency.

$$L_W = 20 \log \text{kW} + 50 \log U - 17 \log (mf) - 1.5 \text{ dB} \quad (20)$$

The adjacent octave bands above and below  $f_p$  roll off at a rate of 3 dB/octave. The A-weighted sound power level can be calculated from the octave band values.

If the tip speed is not known, the A-weighted sound power level for the casing noise of centrifugal compressors between 1100 and 3700 kW can be calculated using Eq. (21), and the unweighted octave band sound power levels can be obtained by subtracting the values shown in Table 1.

$$L_W = 77 + 10 \log \text{kW} \quad \text{dB} \quad (21)$$

The A-weighted sound power level for the unmuffled air inlet of centrifugal compressors can be calculated using Eq. (22), and the unweighted octave band sound power levels can be obtained by subtracting the values shown in Table 1.

$$L_W = 80 + 10 \log \text{kW} \quad \text{dB} \quad (22)$$

**Reciprocating Compressors<sup>3</sup>** For reciprocating compressors, the fundamental frequency is calculated from the number of cylinders ( $B$ ) and the speed as follows:

$$f_p = B \text{ rpm}/60 \quad (23)$$

The octave band sound power level in the frequency band containing  $f_p$  that is radiated from the casing or discharge piping for large reciprocating compressors can be calculated using Eq. (24) where  $m$  is the surface weight of the casing or pipe wall in kilograms per square metre and  $f$  is the octave band center frequency:

$$L_W = 150 + 10 \log \text{kW} - 17 \log (mf) \quad (24)$$

This equation assumes that the sound power is radiated from 15 m of discharge piping. The adjacent octave bands above and below  $f_p$  roll off at a rate of 3 dB/octave. The A-weighted sound power level can be calculated from the octave band values.

**Rotary and Reciprocating Air Compressors<sup>1</sup>**

Equation (25) presents an alternative method for calculating the A-weighted sound power level of reciprocating air compressors based on just the kW rating. This equation can also be used with rotary compressors and includes the noise of partially muffled air inlets. The unweighted octave band sound power levels can be obtained by subtracting the values shown in Table 1.

$$L_W = 88 + 10 \log \text{ kW} \quad \text{dB} \quad (25)$$

**3.2 Boiler and Reactor Feed Pumps<sup>1</sup>**

The A-weighted sound power level for large boiler and reactor feed pumps driven by motors or steam turbines can be estimated by Eqs. (26) and (27), and the unweighted octave band sound power levels can be obtained by subtracting the values shown in Table 1.

$$1\text{--}9 \text{ MW} : \quad L_W = 83 + 7 \log \text{ kW} \quad \text{dB} \quad (26)$$

$$9.5\text{--}18 \text{ MW} : \quad L_W = -32 + 36 \log \text{ kW} \quad \text{dB} \quad (27)$$

**3.3 Fans**

Fan noise is produced primarily by airflow around the blades. Manufacturer's fan data is highly recommended due to significant variations in fan noise levels. The levels presented in this section assume a static efficiency of 95 to 100%. Sound pressure levels increase about 1 dB for every 3% reduction in the static efficiency from 99%.

**Blade Passage Frequency Calculation<sup>1</sup>** The blade passage frequency (BPF) for fans is calculated as follows:

$$\text{BPF} = (\text{fan rpm} \times \text{No. of blades})/60 \quad (28)$$

**Centrifugal-Type Fans with Airfoil or Backward-Curved Blades<sup>1</sup>** The unweighted sound power level of the inlet noise of forced-draft fans with inlet control vanes or the discharge noise of induced-draft fans can be calculated using

$$L_W = 10 + 10 \log Q + 20 \log \delta P \quad \text{dB} \quad (29)$$

where  $Q$  is the airflow in cubic metres per minute and  $\delta P$  is the pressure drop across the fan in pascals (newtons per square metre). The octave band sound power levels can be obtained by subtracting the values shown in Table 1 and by making the following corrections for the blade passage frequency [Eq. (28)]:

- For forced-draft fans used in high-pressure applications, add 5 dB in the octave band containing the BPF.
- For induced-draft fans, add 10 dB in the bands containing the BPF and its harmonic (twice the BPF).

The A-weighted sound power level can be calculated from the octave band values after making all of the corrections.

If there is ducting on the inlet to the fan, the unweighted sound power level of the uninsulated fan casing may be calculated using

$$L_W = 1 + 10 \log Q + 20 \log \delta P \quad \text{dB} \quad (30)$$

The octave band sound power levels can be obtained by subtracting the values shown in Table 1 and by adding 5 dB in the octave band containing the BPF [Eq. (28)] for high-pressure applications.

The noise generated at the uninsulated fan breaching (discharge ductwork) is approximately 6 dB lower than that generated by the uninsulated fan housing. The frequency spectrum is similar to that for the uninsulated fan housing. The A-weighted sound power level can be calculated from the octave band values.

**Axial-Flow Fans<sup>1</sup>** The unweighted sound power level of the inlet noise of forced-draft fans or the discharge noise of induced-draft fans can be calculated using

$$L_W = 21 + 10 \log Q + 20 \log \delta P \quad \text{dB} \quad (31)$$

The octave band sound power levels can be obtained by subtracting the values shown in Table 1 and by adding 6 dB in the octave band containing the BPF. The A-weighted sound power level can be calculated from the octave band values.

For vaneaxial fans, inlet guide vanes cause much higher blade passage noise than outlet guide vanes. These modifications will change the A-weighted sound power level.

**Propeller Fans<sup>3</sup>** The unweighted sound power level of the inlet or outlet of a propeller fan with a diameter of 3.5 m or less can be calculated using

$$L_W = 60 + 10 \log Q + 20 \log \delta P \quad \text{dB} \quad (32)$$

The octave band sound power levels can be obtained by subtracting the values shown in Table 1 and by adding 5 dB in the octave band containing the BPF. The A-weighted sound power level can be calculated from the octave band values.

**Gas Recirculation Fan Casing<sup>1</sup>** The A-weighted casing sound power level for centrifugal fans used for gas recirculation service (1300 to 4100 kW) can be calculated using Eq. (33), and the unweighted octave band sound power levels can be obtained by subtracting the values shown in Table 1.

$$L_W = 1 + 10 \log Q + 20 \log \delta P \quad \text{dB} \quad (33)$$

### 3.4 Gears<sup>2</sup>

The following equation provides an estimate of the A-weighted sound power levels based on studies of gearboxes rated from 200 to 17,500 kW:

$$L_W = 86 + 3 \log \text{ rpm} + 4 \log \text{ kW} + 10 \log S \quad \text{dB} \quad (34)$$

where  $L_W$  is the A-weighted sound power level, rpm is the speed of the slower gear shaft, kW is the power transmitted through the gearbox, and  $S$  is the conformal surface area (in square metres) at 1 m from the gearbox (see the Appendix to this chapter for the equation for the conformal surface area).

The un-weighted octave band sound power levels can be obtained by subtracting the values shown in Table 1. The actual levels in the octave bands containing the gear-meshing and gear-ringing frequencies may differ from these estimates.

### 3.5 Generators<sup>3</sup>

The A-weighted sound power level for generators (not including the driver noise) can be calculated from Eq. (35), and the unweighted octave band sound power levels can be obtained by subtracting the values shown in Table 1.

$$L_W = 80 + 10 \log \text{ MW} + 6.6 \log \text{ rpm} \quad \text{dB} \quad (35)$$

### 3.6 Pumps<sup>2</sup>

The A-weighted sound power level for motor-driven pumps under 2000 kW can be calculated using Table 4. In this table, kW is the nameplate motor rating and  $S$  is the conformal surface area (in square metres) at 1 m from the pump (see the Appendix to this chapter for the equation for the conformal surface area). The unweighted octave band sound power levels can be obtained by subtracting the values shown in Table 1. These equations are based on sound pressure level measurements at 1 m from the pump and therefore include some sound contributions from the driver and suction and discharge piping. For high-pressure applications, the level in the band that contains the blade passage frequency and its second harmonic may be 5 to 10 dB higher than the calculated levels.

## 4 VALVE AND PIPING NOISE

The sound pressure level produced by gas control valves is dependent on whether the flow through the valve is subcritical or supercritical (choked-valve

condition). For subcritical flow, the valve noise is due to turbulent mixing and turbulence–boundary interaction. For supercritical flow, the valve noise is due primarily to broadband shock noise.

Most valve manufacturers, such as Fisher or Masoneilan, have semiempirical models to predict the sound pressure level at a position 1 m downstream of the valve and 1 m out from the piping. These models are expected to predict the A-weighted sound pressure level to within 5 dB of the actual level. For situations when the manufacturer cannot provide data or as an alternative, Ng<sup>4</sup> provides a control valve calculation procedure. All of these methods assume some number of straight piping sections downstream of the valve. The presence of a tee, mitered bend, or an elbow near the valve discharge can significantly increase the sound pressure level from quiet trim valves.

Turbulence generated in piping can also be a significant source of noise. CONCAWE<sup>5,6</sup> and Norton<sup>7</sup> have published procedures by which flow-induced sound power levels can be predicted. These procedures require a fairly detailed knowledge of the flow conditions and piping and are beyond the scope of this chapter. In general these procedures are expected to predict the A-weighted sound pressure level to within 3 dB.

## 5 INDUSTRY-SPECIFIC EQUIPMENT

### 5.1 Air Conditioning for Buildings

#### Cooling Towers<sup>1</sup>

**Mechanical-Draft Cooling Towers** The A-weighted sound power level of mechanical-draft propeller-type cooling towers can be calculated using

$$\text{Full speed : } L_W = 86 + 10 \log \text{ kW} \quad \text{dB} \quad (36)$$

$$\text{Half speed : } L_W = 83 + 10 \log \text{ kW} \quad \text{dB} \quad (37)$$

where kW is the full-speed power rating of the fan. The octave band sound power levels can be obtained by subtracting the values shown in Table 1. When calculating sound pressure levels at distances greater than 10 to 20 m from the tower, the values shown in Table 5 should be added to these values to account for directional effects.

**Natural-Draft (No Fans) Cooling Towers** The A-weighted sound power level of the rim, located at the base, and the discharge, located at the top, of large natural-draft cooling towers is presented in Table 6. Since the low-frequency noise levels of the water flow

**Table 4 Overall Sound Power Level of Motor-Driven Pumps**

Operating Speed (rpm)	For Motor Ratings under 75 kW	For Motor Ratings above 75 kW
450–900	$68 + 10 \log \text{ kW} + 10 \log S$	$79 + 3 \log \text{ kW} + 10 \log S$
1000–1500	$70 + 10 \log \text{ kW} + 10 \log S$	$81 + 3 \log \text{ kW} + 10 \log S$
1600–1800	$75 + 10 \log \text{ kW} + 10 \log S$	$86 + 3 \log \text{ kW} + 10 \log S$
3000–3600	$72 + 10 \log \text{ kW} + 10 \log S$	$83 + 3 \log \text{ kW} + 10 \log S$

**Table 5 Octave Band and A-Weighted Sound Power Level Adjustments for Directional Effects of Cooling Towers**

Source	31.5	63	125	250	500	1000	2000	4000	8000	A
Mechanical draft, air inlet side	0	0	0	1	2	2	2	3	3	2
Mechanical draft, enclosed side	-3	-3	-3	-3	-3	-3	-4	-5	-6	-4
Mechanical draft, top	3	3	3	3	3	4	4	3	3	3

**Table 6 Octave Band and A-Weighted Sound Power Levels for Natural Draft Cooling Towers**

Source	125	250	500	1000	2000	4000	8000	A
Base rim noise	105	104	106	108	110	112	110	117
Discharge noise	100	99	101	103	105	107	105	112

are not significant, sound power levels are not listed for the 31.5- and 63-Hz octave bands.

**Packaged Chillers with Compressors** The noise from packaged chillers is due primarily to the compressor, not the drive motor, and can be calculated as a function of heat removal (in kW) and the conformal surface area,  $S$  (in square metres) at 1 m from the unit (see the Appendix to this chapter for the equation for the conformal surface area). One ton of cooling capacity is equal to 3.52 kW of heat removal.

**Packaged Chillers with Reciprocating Compressors<sup>8</sup>** For units with reciprocating compressors, the A-weighted sound power level can be calculated with Eq. (38), and the unweighted octave band sound power levels can be obtained by subtracting the values shown in Table 1. The standard error of this equation is estimated to be 5 dB.

$$L_W = 66 + 9 \log \text{ kW} + 10 \log S \quad \text{dB} \quad (38)$$

**Packaged Chillers with Centrifugal Compressors<sup>8</sup>** For units with centrifugal compressors, the A-weighted sound power level can be calculated from Eq. (39), and the unweighted octave band sound power levels can be obtained by subtracting the values shown in Table 1.

$$L_W = 54 + 11 \log \text{ kW} + 10 \log S \quad \text{dB} \quad (39)$$

The standard error of this equation is estimated to be 4 dB. For larger units with built-up assemblies, use the conformal area of the compressor section only.

**Packaged Chillers with Rotary-Screw Compressors<sup>2</sup>** For rotary-screw compressors between 350 and 1000 kW of heat removal operating at approximately 3600 rpm, the A-weighted sound power level is given by Eq. (40), and the unweighted octave band sound power levels can be obtained by subtracting the values shown in Table 1.

$$L_W = 90 + 10 \log S \quad \text{dB} \quad (40)$$

## 5.2 Construction Equipment: Diesel-Powered, Mobile Equipment<sup>1</sup>

The A-weighted sound power level for diesel-powered, mobile equipment such as crawler tractors, dozers, tractor shovels, front-end loaders, backhoes, graders, mobile cranes, and trucks can be calculated using

$$L_W = 94 + 10 \log \text{ kW} \quad \text{dB} \quad (41)$$

where  $L_W$  is the A-weighted sound power level and kW is the power rating of the engine. This equation is for turbocharged or naturally aspirated engines with conventional exhaust mufflers. In the typical application, the sound pressure level will average about 4 dB lower than the calculated level since the engine is frequently not operated in the maximum power condition. The unweighted octave band sound power levels can be obtained by subtracting the values shown in Table 1.

## 6 OIL FIELD EQUIPMENT

Increased governmental noise regulations and concerns about drilling in environmentally sensitive locations have created a need for drilling rig sound pressure level analyses. Representative sound power level data for a standard degasser, drawworks, mud pump, and top drive are presented in Table 7. Some manufacturers offer special noise control options that can provide a reduction of 5 dB to 10 dB from the values provided in Table 7. The sound power for the degasser is typical for a unit rated at 227 m<sup>3</sup>/h and includes the contribution from the drive motor. The sound power levels for the mud pump and drawworks do not include the drive motors.

## 7 REGULATIONS

Some governments regulate the sound pressure level or sound power level of different items of machinery. In the United States, no industrial equipment items are regulated at this time.

### 7.1 European Union Regulations

The European Union published the limits on sound power level as shown in Table 8.<sup>9</sup> The reported A-weighted sound power level shall be rounded to



**Table 7 Octave Band and A-Weighted Sound Power Levels for Oil Field Equipment**

Source	31.5	63	125	250	500	1000	2000	4000	8000	A
1200-kW triplex mud pump	102	104	108	105	104	99	93	86	83	105
Mud reconditioning degasser	78	83	82	87	94	94	95	88	81	99
Drawworks	96	104	109	112	112	108	105	102	96	113
Top drive	98	97	100	110	105	100	100	96	82	108

**Table 8 Limits by the European Union on the Permissible Sound Power Level of Industrial Equipment**

Type of Equipment	Net Installed Power $P$ (in kW), Electrical Power <sup>a</sup> $P_{el}$ in kW, Mass of Appliance $m$ in kg, Cutting Width $L$ in cm	Permissible A-weighted Sound Power Level in dB re 1 pW	
		Stage I, from 3 Jan. 2002	Stage II, from 3 Jan. 2006
Compaction machines (vibrating rollers, vibratory plates, vibratory rammers)	$P \leq 8$	108	105
	$8 < P \leq 70$	109	106
	$P > 70$	$89 + 11 \log P$	$86 + 11 \log P$
Tracked dozers, tracked loaders, tracked excavators-loaders	$P \leq 55$	106	103
	$P > 55$	$87 + 11 \log P$	$84 + 11 \log P$
Wheeled dozers, wheeled loaders, wheeled excavator-loaders, dumpers, graders, loader-type landfill compactors, combustion engine-driven counterbalanced lift trucks, mobile cranes, compaction machines (nonvibrating rollers), paver-finishers, hydraulic power packs	$P \leq 55$	104	101
	$P > 55$	$85 + 11 \log P$	$82 + 11 \log P$
Excavators, builders' hoists for the transport of goods, construction winches, motor hoes	$P \leq 15$	96	93
	$P > 15$	$83 + 11 \log P$	$80 + 11 \log P$
Handheld concrete-breakers and picks	$m \leq 15$	107	105
	$15 < m < 30$	$94 + 11 \log m$	$92 + 11 \log m$
	$m \geq 30$	$96 + 11 \log m$	$94 + 11 \log m$
Tower cranes		$98 + \log P$	$96 + \log P$
Welding and power generators	$P_{el} \leq 2$	$97 + \log P_{el}$	$95 + \log P_{el}$
	$2 < P_{el} < 10$	$98 + \log P_{el}$	$96 + \log P_{el}$
	$P_{el} \geq 10$	$97 + \log P_{el}$	$95 + \log P_{el}$
Compressors	$P \leq 15$	99	97
	$P > 15$	$97 + 2 \log P$	$95 + 2 \log P$
Lawnmowers, lawn trimmers, lawn edge trimmers	$L \leq 50$	96	94 <sup>b</sup>
	$50 < L \leq 70$	100	98
	$70 < L \leq 120$	100	98 <sup>b</sup>
	$L > 120$	105	103 <sup>b</sup>

<sup>a</sup>  $P_{el}$  for welding generators: conventional welding current multiplied by the conventional load voltage for the lowest values of the duty factor given by the manufacturer.

$P_{el}$  for power generators: prime power according to ISO 8528-1:1993, point 13.3.2.

<sup>b</sup> Indicative figures only. Definitive figures will depend on amendment of the Directive following the report required in Article 20(3). In the absence of any such amendment, the figures for stage I will continue to apply for stage II.

the nearest whole number (less than 0.5, use lower number; greater than or equal to 0.5 use higher number).

## 7.2 Corporate Requirements

Many corporations require vendors to supply measured acoustical data when providing equipment for new

projects. Often, the A-weighted sound pressure level at 1 m from the equipment outline is limited, such as a maximum sound pressure level of 85 dB. Such a noise specification often results in overestimations of the noise levels in the area of the equipment since the noise levels vary and are actually below the maximum level at many locations around the equipment. Assuming

that the maximum sound pressure level exists at all locations around the equipment may result in sound power level estimates that are higher than actual.

A better specification would be to require the vendor to provide the A-weighted and octave band sound power levels for the equipment. Meeting this specification requires that the vendor measure the sound pressure level at numerous locations around the equipment, and as a result, the sound power level that is calculated from these measurements will more accurately represent the expected sound power in the field.

## 8 SUMMARY

This chapter has presented procedures for calculating the sound power level of industrial machinery. The reader is encouraged to require vendors to provide sound power level data for their machinery. If all buyers were to require sound power data, then vendors will develop the means to provide it.

## APPENDIX: CALCULATION OF CONFORMAL SURFACE AREA

A conformal surface is a hypothetical surface located a distance  $d$  from the nearest point on the envelope of the reference box around the equipment. It is different from a rectangular surface because a conformal surface has rounded comers. For large surfaces, the difference in area between a rectangular surface and a conformal surface is typically small ( $10 \log S < 1$  dB); however, for small surfaces the difference in areas can be significant ( $10 \log S > 2$  dB). The area of a conformal surface can be calculated from

$$S = LW + 2H(L + W) + \pi d[L + W + 2(H + d)] \quad (42)$$

where  $L$  is the length,  $W$  is the width, and  $H$  is the height of the reference box and  $d$  is the sound-measurement distance from the reference box.

For example, a noise source 1 m wide, 3 m long, and 2 m high will have a conformal surface area of 50.4 m<sup>2</sup>

for a 1-m measurement distance. If the energy average A-weighted sound pressure level around the box were 85 dB, the A-weighted sound power level would be 102 dB.

## REFERENCES

1. L. N. Miller, E. W. Wood, R. M. Hoover, A. R. Thompson, and S. L. Patterson, *Electric Power Plant Environmental Noise Guide*, rev. ed., Edison Electric Institute, Washington, DC, 1984, Chapter 4.
2. *Noise and Vibration Control for Mechanical Equipment*, Manual TM5-805-4/AFM 88-37/NAVFAC DM-3.10, manual prepared by Bolt, Beranek, and Newman for the Joint Department of the Army, Air Force, and Navy, Washington, DC, 1980, Chapter 7.
3. D. A. Bies and C. H. Hansen, *Engineering Noise Control*, Spon Press, London, 2003, Chapter 11.
4. K. W. Ng, *Control Valve Aerodynamic Noise Generation and Prediction*, Proceedings of NOISEXPO, 1980, Acoustical Publications, Bay Village, OH, 1980, pp. 49–54.
5. J. N. Pinder, The Study of Noise from Steel Pipelines, CONCAWE Report No. 84/55, 1984, Brussels, Belgium.
6. P. H. M. Corbet and P. J. van de Loo, Experimental Verification of the ISVR Pipe Noise Model, CONCAWE Report No. 84/64, 1984, Brussels, Belgium.
7. M. P. Norton and A. Pruiti, Universal Prediction Schemes for Estimating Flow-Induced Industrial Pipeline Noise and Vibration, *Appl. Acoust.*, Vol. 33, 1991, pp. 313–336.
8. ASHRAE, Sound and Vibration Control, in *HVAC Applications*, American Society of Heating, Refrigerating and Air-Conditioning Engineers, Atlanta, 1991, Chapter 42.
9. Directive 2000/14/EC of the European Parliament and of the Council of 8 May 2000 on the Approximation of the Laws of the Member States Relating to the Noise Emission in the Environment by Equipment Use Outdoors, Article 12, pp. 6–8, 2000.

## **PART VIII**

---

# **TRANSPORTATION NOISE AND VIBRATION – SOURCES, PREDICTION, AND CONTROL**

# CHAPTER 83

## INTRODUCTION TO TRANSPORTATION NOISE AND VIBRATION SOURCES

Malcolm J. Crocker  
Department of Mechanical Engineering  
Auburn University  
Auburn, Alabama

### 1 INTRODUCTION

The numbers of vehicles and aircraft used in road, rail, and civilian air transportation continues to increase worldwide. Road traffic noise is really a greater problem than aircraft noise in most countries since it affects many more people. The noise of railroad and rapid transit vehicles is also a problem for people living near to rail lines. Noise and vibration sources in road and rail vehicles and aircraft affect not only the occupants but nontravelers as well. Major sources consist of (1) those related to the power plants and (2) those non-power-plant sources generated by the vehicle or aircraft motion. Most rail and rapid transit vehicles have power plant noise and vibration sources that are similar to road vehicles. With rail and rapid transit vehicles, however, tires are mostly replaced with metal wheels, and the wheel-rail interaction becomes a major source of noise and vibration. Brake, gearbox, and transmission noise and vibration are additional problems in road and rail vehicles. In the case of aircraft and helicopters, similar power plant and motion-related sources exist. Some small aircraft are powered by internal combustion engines. Nowadays many general aviation and all medium-size airliners and helicopters are powered by turboprop

power plants. Aircraft propeller and helicopter rotors are major noise sources that are difficult to control. All large civilian aircraft are now powered by jet engines in which the high-speed exhaust and turbomachinery are significant noise sources.

### 2 NOISE EMISSION IN GENERAL

In cars, trucks, and buses, major power plant noise sources include gasoline and diesel engines, cooling fans, gearboxes and transmissions, and inlet and exhaust systems. Other major sources include tire/road interaction noise and vibration and aerodynamic noise caused by flow over the vehicles.<sup>1</sup> (See Fig. 1.)

Chapters 84 to 93, in Part VIII of this handbook, discuss vehicle and aircraft noise and vibration sources in considerable detail. Although vehicle noise and vibration have been reduced over the years, traffic noise remains a problem because of the continuing increase in the numbers of vehicles. In addition, most evidence suggests that the exterior noise of most new cars, except in first gear, is dominated in normal operation by *rolling noise* (defined here as tire/road interaction noise together with aerodynamic noise), which becomes increasingly important at high speed and exceeds *power train noise* (defined here as engine,

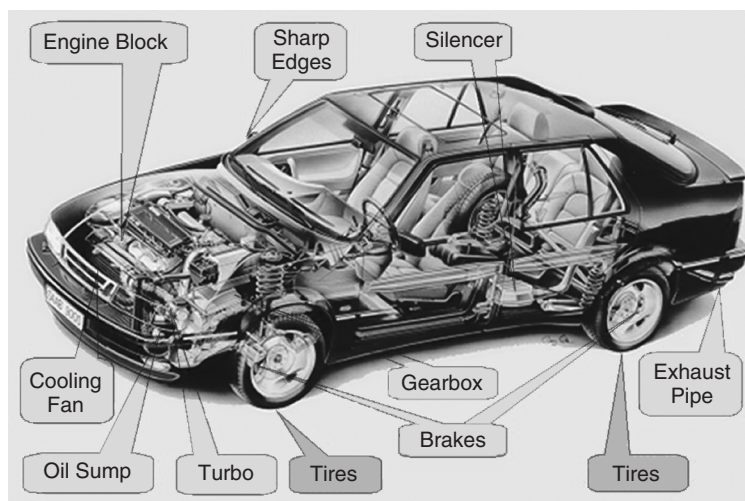


Figure 1 Location of sources of power plant, tire, and wind noise on an automobile.<sup>1</sup>

**Table 1 Comparison of Rolling and Power Train A-weighted Sound Pressure Levels**

Road Speed (km/h)	Vehicle Class	Rolling Noise (dB)	Power Train Noise (dB)	Total Noise (dB)
20	Heavy <sup>a</sup>	61	78	78
	Light	58	64	65
80	Heavy <sup>a</sup>	79	85	86
	Light	76	74	78

<sup>a</sup> Heavy vehicles are defined as having an unloaded mass of greater than 1525 kg.

Source: From Nelson.<sup>2</sup>

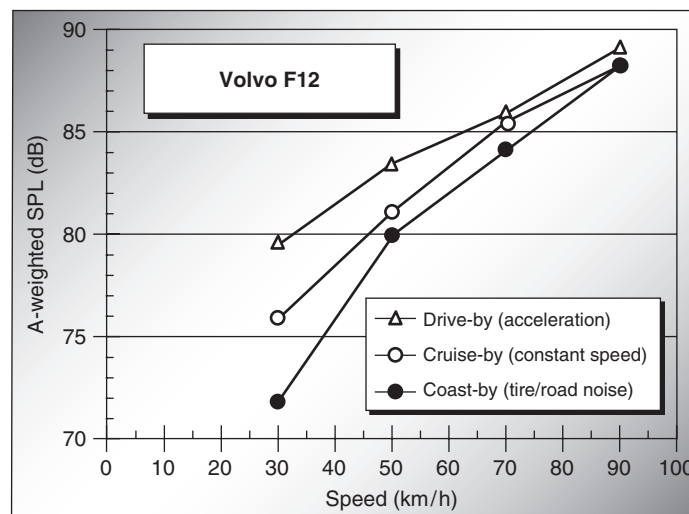
air inlet, exhaust, cooling system, and transmission). See Table 1 and the detailed review of vehicle noise by Nelson, who concludes that rolling noise has a negligible effect on the noise produced by heavy vehicles at low speed, but at speeds above 20 km/h for cars and 80 km/h for heavy vehicles, rolling noise contributes significantly to the overall noise level.<sup>2</sup> At speeds above 60 km/h for cars, rolling noise becomes the dominant noise source.<sup>2</sup>

Figure 1 of Chapter 86 shows that there is little difference between the exterior noise generated by (1) a modern car at steady speeds (in the top three gears) and (2) the car operating in a coast-by condition at the same steady speeds without the power plant in operation. This suggests that tire noise together with aerodynamic noise are the dominant sources for most normal operations of such a modern car at steady highway speeds. Trucks are dominated by power train noise at low speeds, but at higher speeds above about 80 km/h, exterior truck noise is mostly dominated by tire/road noise and aerodynamic noise. (See Fig. 2, which shows that above 70 to 80 km/h there is little difference between the

exterior noise of the truck whether it is accelerating, cruising at a steady speed, or coasting by with the power plant turned off.<sup>1</sup> Again this suggests that above 70 to 80 km/h this truck's exterior noise is dominated by tire/road noise and aerodynamic noise.) At high speeds above about 130 km/h, vehicle noise starts to become dominated by aerodynamic flow noise.<sup>1</sup> Due to different noise standards for vehicles in different countries and regions, and the condition of the vehicles, the speed at which tire noise starts to dominate may be higher than indicated above. The data here are for modern European vehicles in new condition. For example, in the United States the truck power plants are generally noisier than in Europe. One interesting approach to predict vehicle pass-by noise involves the use of the reciprocity technique.<sup>3</sup>

Although the latest passenger jets with their bypass turbofan engines are significantly quieter than the first generation of jet airliners, which used pure turbojet engines, the noise of passenger jet aircraft remains a serious problem, particularly near airports. The noisiest pure jet passenger aircraft have been or will soon be retired in most countries. Airport noise, however, is likely to remain a difficult problem since in many countries the frequency of aircraft operations continues to increase and because of the public opposition to noise voiced by some citizens living near airports. This opposition has prevented runway extensions to some airports and the development of some new airports entirely because of environmental concerns.

Additional aspects of vehicle, rail, and aircraft noise sources and control including engines, muffler design, tires, brakes, propellers, gearbox and transmissions, aerodynamic, jet, propeller, and helicopter rotor noise are discussed in Part VIII of this handbook. Part IX is mainly concerned with the interior noise and vibration of road vehicles, off-road vehicles, ships, and aircraft,



**Figure 2** Exterior noise of a Volvo F12 truck under different driving conditions.<sup>1</sup>

which are experienced by passengers or operators. Noise regulations and limits for vehicle noise that apply to new highway vehicles sold in the United States, Canada, the European Union, Japan, and other countries are described by Chapter 120 and Chapter 71 in Ref. 3. Chapter 120 also describes test procedures used to measure vehicle noise. Part XI of this book deals with community and environmental noise sources, many of which are transportation related. Chapter 121 reviews rail system environmental noise prediction and control methods. Chapter 123 describes ground-borne vibration from roads and rail systems, Chapter 125 discusses aircraft and airport noise, and Chapter 126 describes off-road vehicle noise in the community.

### 3 INTERNAL COMBUSTION ENGINE NOISE

Although hybrid vehicles, which partially use relatively quiet electric motors, are increasing in use the internal combustion engine (ICE) remains a major source of noise in transportation and industry. ICE intake and exhaust noise can be effectively silenced. (See Chapter 85 in this book.) The noise radiated by vibrating engine surfaces, however, is more difficult to control. In gasoline engines a fuel–air mixture is compressed to about one-eighth to one-tenth of its original volume and ignited by a spark. In diesel engines air is compressed to about one-sixteenth to one-twentieth of its original volume, liquid fuel is injected in the form of a spray, then spontaneous ignition and combustion occurs. Because the rate of cylinder pressure rise is initially more abrupt with a diesel engine than with a gasoline engine, diesel engines tend to be noisier than gasoline engines. The noise of ICE diesel engines has consequently received the most attention from both manufacturers and researchers. The noise of engines can be divided into two main parts: combustion noise and mechanical noise. The combustion noise is caused mostly by the rapid pressure rise created by ignition, and the mechanical noise is caused by a number of mechanisms with perhaps piston slap being one of the most important, particularly in diesel engines. Chapter 84 reviews internal combustion engine noise in detail.

The noise radiated from the engine structure has been found to be almost independent of load, although it is dependent on cylinder volume and even more dependent on engine speed. Measurements of engine noise over a wide range of cylinder capacities have suggested that the A-weighted sound pressure level of engine noise increases by about 17 dB for a 10-fold increase in cylinder capacity.<sup>4</sup> A-weighted engine noise levels have been found to increase at an even greater rate with speed than with capacity (at least at twice the rate) with about 35 dB for a 10-fold increase in speed. Engine noise can be reduced by attention to details of construction. In particular, stiffer engine structures have been shown to reduce radiated noise. Partial add-on shields and complete enclosures have been demonstrated to reduce the A-weighted noise level of a diesel engine of the order of 3 to 10 dB.

Although engine noise may be separated into two main parts—combustion noise and mechanical noise—there is some interaction between the two noise sources. The mechanical noise may be considered to be the noise produced by an engine that is motored without the burning of fuel. Piston slap occurs as the piston travels up toward top dead center and is one of the mechanical sources that results in engine structural vibration and radiated noise. But piston slap is not strictly an independent mechanical process since the process is affected by the extra forces on the piston generated by the combustion process. The opening and closing of the inlet and exhaust valves, the forces on the bearings caused by the system rotation, and the out of balance of the engine system are other mechanical vibration sources that result in noise. The mechanical forces are repeated each time the crankshaft rotates, and, if the engine is multicylinder, then the number of force repetitions per revolution is multiplied by the number of cylinders. Theoretically, this behavior gives rise to forces at a discrete frequency,  $f$ , which is related to  $R$ , the number of engine revolutions/minute (rpm), and  $N$ , the number of cylinders:

$$f = NR/60 \text{ Hz} \quad (1)$$

Since the mechanical forces are not purely sinusoidal in nature, harmonic distortion occurs. Thus, mechanical forces occur at integer multiples of  $f$  given by the frequencies  $f_n = nf$ , where  $n$  is an integer, 1, 2, 3, 4, . . . . Assuming that the engine behaves as a linear system, these mechanical forces result in forced vibration and mechanical noise at these discrete frequencies. Combustion noise is likewise partly periodic in nature, and this part is related to the engine rpm because it occurs each time a cylinder fires. This periodic combustion noise frequency,  $f_p$ , is different for a two-stroke from a four-stroke engine and is, of course, related to the number of cylinders,  $N$ , multiplied by the number of firing strokes each makes per revolution,  $m$ .

Some of the low-frequency combustion noise is periodic and coherent from cylinder to cylinder. Some of the combustion noise is not periodic because it is caused by the unsteady burning of the fuel–air mixture. This burning is not exactly the same from cycle to cycle of the engine revolution, and so combustion noise, particularly at the higher frequencies, is random in nature. Research continues on understanding engine noise sources and how the noise energy is transmitted to the exterior and interior of vehicles.<sup>5,6</sup>

### 4 INTAKE AND EXHAUST NOISE AND MUFFLER DESIGN

Ducted sources are found in many different mechanical systems. Common ducted-source systems include engines and mufflers (also known as silencers), fans, and air-moving devices (including flow ducts and fluid machines and associated piping). Silencers (also known as mufflers) are used as well on some other machines including compressors, pumps, and air-conditioning systems. In these systems, the source is

the active component and the load is the path, which consists of elements such as mufflers, ducts, and end terminations. The acoustical performance of the system depends on the source–load interactions. System models based on electrical analogies have been found useful in predicting the acoustical performance of systems. Various methods exist for determining the internal impedance of ducted sources. The acoustical performance of a system with a muffler as a path element is usually best described in terms of the muffler insertion loss and the sound pressure radiated from the outlet of the system. Chapter 85 provides a detailed review of the performance of muffler systems. Chapter 14 in the *Handbook of Acoustics* also discusses muffler design and its interaction with the source and load.

There are two main types of mufflers that are fitted to the intake (inlet) and exhaust (outlet) pipes of machinery ductwork. Reactive mufflers function by reflecting sound back to the source and also to some extent by interacting with the source and thereby modifying the source's sound generation. Absorptive silencers on the other hand reduce the sound waves by the use of sound-absorbing material packed into the silencer. The exhaust and intake noise of internal combustion engines is so intense that they need to be “muffled” or “silenced.” Internal combustion engine pressure pulsations are very intense and nonlinear effects should be included. Exhaust gas is very hot and flows rapidly through the exhaust system. The gas stream has a temperature gradient along the exhaust system, and the gas pressure pulsations are of sufficiently high amplitude that they may be regarded almost as shock waves. Some of these conditions violate normal acoustical assumptions. Modeling of an engine exhaust system in the time domain has been attempted by some researchers to account for the nonlinear effects. But such have proved to be challenging. Most modeling techniques have used the transmission matrix approach in the frequency domain and have been found to be sufficiently effective.

The acoustical performance of a ducted-source system depends on the impedances of the source and load and the four-pole parameters of the path. This complete description of the system performance is termed *insertion loss* (IL). The insertion loss is the difference between the sound pressure levels measured at the same reference point (from the termination) without and with the path element, such as a muffler, in place. See Fig. 3a.

Another useful description of the path element is given by the *transmission loss* (TL). The transmission loss is the logarithmic ratio of the incident to transmitted sound powers  $S_i I_i / S_t I_t$ . See Fig. 3b.

The *noise reduction* (NR) is another descriptor used to measure the effect of the path element and is given by the difference in the measured sound pressure levels upstream and downstream of the path element (such as the muffler), respectively. See Fig. 3c.

The insertion loss is the most useful description for the user since it gives the net performance of the path element (muffler) and includes the interaction

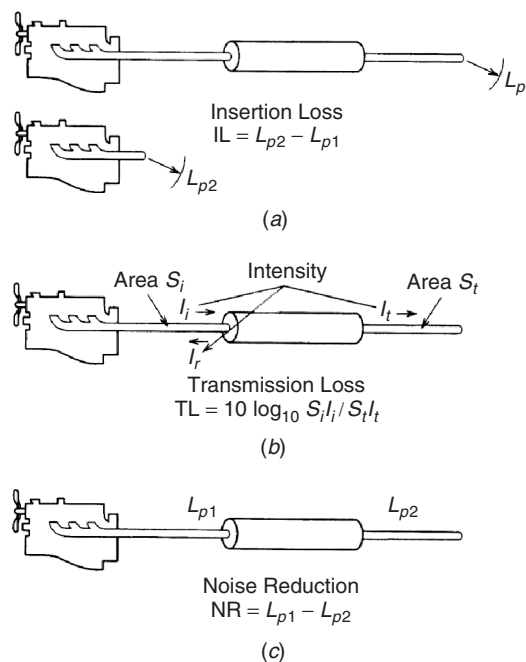


Figure 3 Definitions of muffler performance.

of the source and termination impedances with the muffler element. It can be shown that the insertion loss depends on the source impedance. It is easier to measure insertion loss than to predict it because the characteristics of most sources are not known.

The transmission loss is easier to predict than to measure. The transmission loss is defined so that it depends only on the path geometry and not on the source and termination impedances.

The transmission loss is a very useful quantity for the acoustical design of a muffler system path geometry. However, it is difficult to measure since it requires two transducers to separate the incident and transmitted intensities. The description of the system performance in terms of the noise reduction requires knowledge of both the path element and of the termination.

Figure 3 shows various acoustical performance descriptors used for ducted-source systems. It should be noted that similar system terminology to that described here and shown in Fig. 3 is commonly used for the acoustical performance of enclosures and partition walls in buildings. (See Chapters 58 and 122.) The terminology used for the acoustical performance of barriers is also similar, although the additional descriptor “attenuation” is also introduced for barriers. Note that with barriers the insertion loss descriptor can have a slightly different meaning. (See Chapter 5.)

Chapter 85 contains an extensive review of muffler and silencer modeling and design. Chapter 14 in the *Handbook of Acoustics* also gives a brief review of



modeling of ducted-source systems with emphasis on muffler design. Work on muffler design and modeling continues with approaches varying from completely experimental to mostly theoretical.<sup>7-11</sup>

## 5 TIRE/ROAD NOISE SOURCE MECHANISMS

In most developed and developing countries, vehicle traffic is the main contributor to community noise. Aircraft noise is a lesser problem since it mostly affects small areas of urban communities that are located near to major airports. The substantial increase in road vehicle traffic in Europe, North America, Japan, and other countries suggests that road vehicle traffic will continue to be the dominant source of community noise into the foreseeable future. Legislative pressures brought to bear on vehicle manufacturers, particularly in Europe and Japan, have resulted in lower power unit noise output of modern vehicles. Tire/road interaction noise, caused by the interaction of rolling tires with the road surface, has become the predominant noise source on new passenger cars when operated over a wide range of constant speeds, with the exception of the first gear. When operated at motorway speeds, the situation is similar for heavy trucks and again tire road noise is found to be dominant.

As discussed in Chapter 86, one European study suggests that, for normal traffic flows and vehicle mixes on urban roads, about 60% of traffic noise sound power output is due to tire/road interaction noise. On motorways at high speed this increases to about 80%. Both exterior power plant noise (the noise from the engine, gearbox/transmission, and exhaust system) and tire/road noise are strongly speed dependent. Measurements show that exterior tire/road noise increases logarithmically with speed (about 10 dB for each doubling of speed). Since an increase of 10 dB represents an approximate doubling of subjective loudness, the tire/road noise of a vehicle traveling at 40 km/h sounds about twice as loud as one at 20 km/h; and at 80 km/h, the noise will sound about four times as loud. Studies have shown that there are many possible mechanisms responsible for tire/road interaction noise generation. Although there is general agreement on the mechanisms, there is still some disagreement on their relative importance. The noise generation mechanisms may be grouped into two main types: (1) vibrational (impact and adhesion) and (2) aerodynamic (air displacement).

There are five main methods of measuring tire noise. These methods include (1) close proximity CPX (trailer), (2) cruise-by, (3) statistical pass-by, (4) drum, and (5) sound intensity. Figure 4 shows tire noise being measured by a CPX trailer built at Auburn University.<sup>12</sup>

Figure 5 shows A-weighted sound pressure levels measured with the Auburn CPX trailer. Note that the A-weighted spectrum peaks between 800 to 1000 Hz, and the peak increases slightly in magnitude and frequency as the vehicle speed is increased. Knowledge of tire/road aerodynamic and vibration noise generation mechanisms suggests several approaches, which



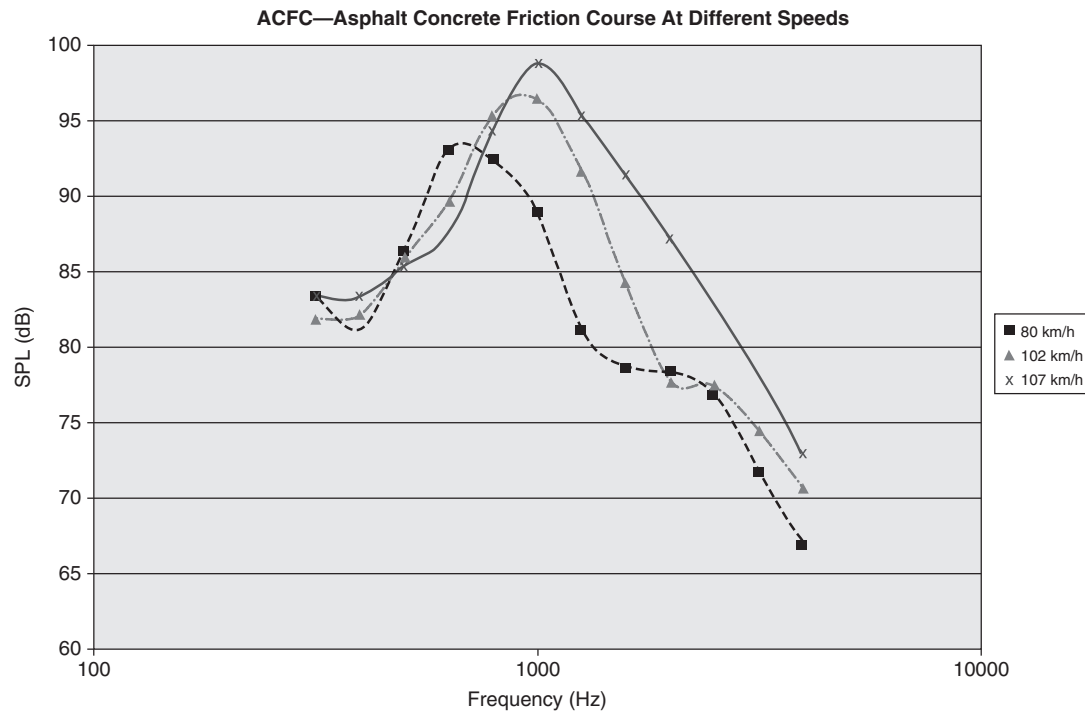
**Figure 4** View of finished CPX trailer built at Auburn University.<sup>12</sup>

if used properly can be used to help suppress tire/road noise. See Chapter 86.

Perhaps the most hopeful, lower cost, approach to suppress tire/road noise is the use of porous road surface mixes.<sup>12</sup> Porous roads, with up to 20 to 30% or more of air void volume, are being used increasingly in many countries. They can provide A-weighted sound pressure level reductions of up to 5 to 7 dB, drain rain water, and reduce splash-up behind vehicles as well. If the porous road can be designed to have maximum absorption at a frequency between 800 and 1000 Hz, it can be most effective in reducing tire/road interaction noise. Tire/road interaction noise generation and measurement are discussed in detail in Chapter 86. Much research continues into understanding the origins of tire/road noise.<sup>13-18</sup>

## 6 AERODYNAMIC NOISE SOURCES ON VEHICLES

The interaction of the flow around a vehicle with the vehicle body structure gives rise to sound generation and noise problems both inside and outside the vehicle. Turbulent boundary layer fluctuations on the vehicle exterior can result in sound generation. The pressure fluctuations also cause structural vibration, which in turn results in sound radiated both to the exterior and to the vehicle interior. Abrupt changes in the vehicle geometry result in regions of separated flow that considerably increase the turbulent boundary layer fluctuations. Poorly designed or leaking door seals result in aspiration (venting) of the seals, which allows direct communication of the turbulent boundary layer pressure fluctuations into the vehicle interior. Appendages on a vehicle, such as external rear-view mirrors and radio antennas also create additional turbulence and noise. The body structure vibrations are also increased in intensity by the separated flow regions. Although turbulent flow around vehicles is the main cause of aerodynamic noise, it should be noted that even laminar flow can indirectly induce noise. For example, the flow pressure regions created by laminar flow can distort body panels, such as the hood (bonnet), and incite vibration.



**Figure 5** A-weighted sound pressure level one-third octave band tire/road noise measurements made with a CPX trailer built at Auburn University.

At vehicle speeds above about 130 km/h the vehicle flow-generated noise exceeds the tire noise and increases with speed to the sixth power. Because of the complicated turbulent and separated flow interactions with the vehicle body, it is difficult to predict accurately the aerodynamic sound generated by a vehicle and its radiation to the vehicle interior and exterior. Vehicle designers often have to resort to empiricism and/or full-scale vehicle tests in wind tunnels for measurements of vehicle interior and exterior aerodynamic flow generation and interior noise predictions. See Chapter 87 for a detailed discussion on aerodynamic noise generation by vehicles. Statistical energy analysis and computational fluid dynamics have also been utilized to predict interior wind noise on vehicles.<sup>19</sup>

## 7 GEARBOX NOISE AND VIBRATION

Transmissions and gearbox systems are used in cars, trucks, and buses to transmit the mechanical power produced by the engine to the wheels. Similar transmission systems are used in propeller aircraft to transmit power to the propeller(s) from the engine(s) or turbine(s). Transmission gearboxes are also used in some railroad systems and ships. Some modern high-speed rail vehicles, however, are beginning to use motive power systems (electric motors) mounted directly onto the axles of each rail vehicle, resulting in quieter operation and reduced noise problems.

The gearbox can be the source of vibration and radiated noise and should be suitably soft mounted to the vehicle structure, wherever possible. Shaft misalignment problems must be avoided, however, with the mounting system chosen. The principal components of a gearbox are comprised of gear trains, bearings, and transmission shafts.

Unless substantial bearing wear and/or damage have occurred, gear meshing noise and vibration are normally the predominant sources in a gearbox. The vibration and noise produced depend upon gear contact ratios, gear profiles, manufacturing tolerances, load and speed, and gear meshing frequencies. Different gear surface profiles and gear types produce different levels of noise and vibration. In general, smaller gear tolerances result in smoother gear operation but require increased manufacturing costs.

Gearboxes are often fitted with enclosures to reduce noise radiation, since the use of a low-cost gearbox combined with an enclosure may be less expensive than the use of a high-performance gear system and gearbox without an enclosure. Gearbox enclosures, however, can result in reduced accessibility and additional maintenance difficulties. A better approach, where possible, is to try to utilize a lower noise and vibration gear system so that a gearbox enclosure is unnecessary. Chapter 88 deals with gearbox noise and vibration. Chapter 69 specifically addresses gear noise and vibration prediction and control methods.

## 8 JET ENGINE NOISE GENERATION

The introduction of commercial passenger jet aircraft in the 1950s brought increasing complaints from people living near airports. Not only were the jet engines noisier than corresponding piston engines on airliners, since they were more powerful, but the noise was more disturbing because it had a higher frequency content than piston engines. This was most evident during the 1950s and 1960s when pure turbojet engines were in wide use in civilian jet airliners. Pure jet engines are still in use on some supersonic aircraft and in particular on high-speed military aircraft.

A pure turbojet engine takes in air through the inlet, adds fuel, which is then burnt, resulting in an expanded gas flow and an accelerated very high speed exhaust jet flow. The whole compression, combustion, and expansion process results in the thrust produced by the engine. The kinetic energy in the exhaust is nonrecoverable and can be considered as lost energy. Since the 1970s, turbofan (or bypass) jet engines have come into increasing use on commercial passenger airliners. Turbofan engines have a large compressor fan at the front of the engine, almost like a ducted propeller. A large fraction of the air, after passing through the fan stage, bypasses the rest of the engine and then is mixed with the high-speed jet exhaust before leaving the engine tail pipe. This results in an engine that has a much lower exhaust velocity than for the case of a pure jet engine. The thrust can still be maintained if a larger amount of air is processed through the turbofan engine than with the pure turbojet engine (in which no air is bypassed around the combustion chamber and turbine engine components). The efficiency of the turbofan engine is greater than that of a pure turbojet engine, however, since less kinetic energy is lost in the exhaust jet flow.

A simplified calculation clearly shows the advantage of a turbofan engine over a turbojet engine. For instance, if a turbofan engine processes twice as much air as a turbojet engine, but only accelerates the air half as much, the kinetic energy lost will be reduced by half ( $1 - 2 \times \frac{1}{4}$ ), while the engine thrust is maintained. If the engine processes four times as much air, but accelerates the air only one quarter as much, the kinetic energy lost will be reduced by three quarters ( $1 - 4 \times \frac{1}{16}$ ) and the engine thrust is still maintained. In each successive case described, the engine will become more efficient as the lost kinetic energy is reduced. Fortunately, as originally shown by Lighthill, there is an even more dramatic reduction in the sound power produced since in a jet exhaust flow the sound power produced is proportional to the exhaust velocity to the eighth power.<sup>20-22</sup> A halving in exhaust velocity then, theoretically, can give a reduction of  $2^8$  in exhaust sound power and mean square sound pressure, and in sound power level and sound pressure level of about  $80 \log_{10} (2)$  or about 24 dB. But, of course, if the mass flow is twice as much, then the reduction in sound power and in the mean square pressure is about  $2^7$ , or a reduction in sound power level and sound pressure level of about 21 dB.

The major noise sources for a modern turbofan engine are discussed in detail in Chapter 89. Chapter 9 is devoted to a review of the theory of aerodynamic noise and in particular jet noise generation. The relative sound pressure levels generated by each engine component depend on the engine mechanical design and power setting. During takeoff, the fan and jet noise are both important sources with the exhaust noise usually dominant. During landing approach, the fan noise usually dominates since the engine power setting and thus jet exhaust velocity are reduced. Noise from other components such as the compressor, combustion chamber, and turbine is generally less than that from the fan and the jet. The noise radiated from the inlet includes contributions from both the fan and compressor but is primarily dominated by the fan. Downstream radiated noise is dominated by the fan and jet, but there can also be significant contributions from the combustor and turbine, whose contributions are very much dependent on each engine design.

Reliable jet engine noise prediction methods are difficult to develop since they depend on accurate prediction of the unsteady flow field in and around the engine. Methods for reducing jet engine noise include modifying the unsteady flow field, redirecting the sound generated, absorbing the sound using acoustical treatments, and/or combinations of all three. See Chapter 89 for a fuller discussion.

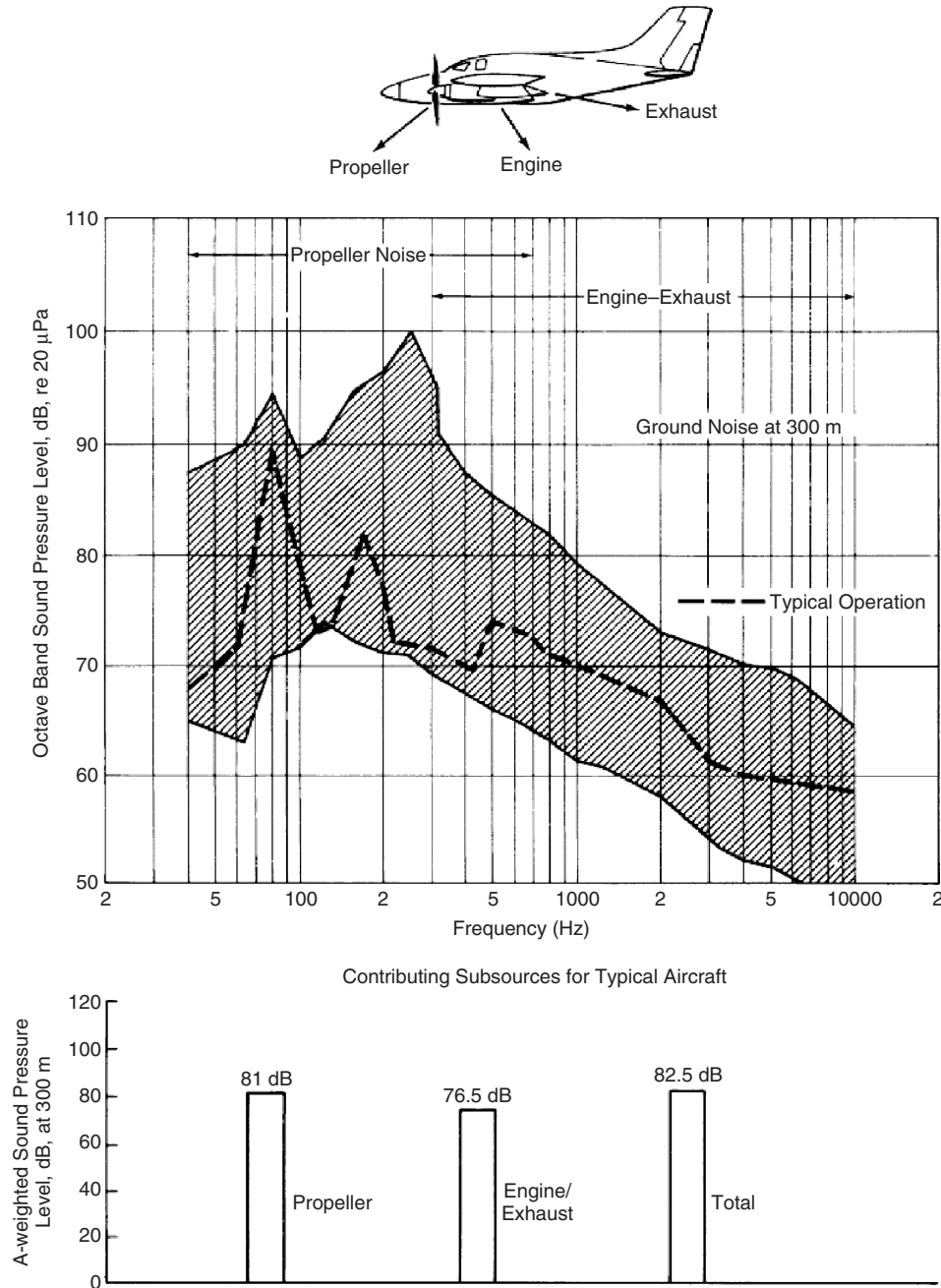
## 9 AIRCRAFT PROPELLER NOISE

As described in Chapter 90, propellers are used on small general aviation aircraft as well as small to medium size passenger airliners. (see Fig. 6.) In small general aviation aircraft, propellers operate with a fixed-blade pitch. In larger general aviation and commuter aircraft, they operate with adjustable pitch to improve aircraft takeoff and flight performance. Smaller aircraft have two-blade propellers while larger aircraft have three or more blades. The propeller operation gives rise to blade thrust and drag forces.

For a single propeller, tones are generated, which are harmonics of the blade passage frequency (BPF). This phenomenon occurs even for the case of tones generated by blade-turbulence interaction, which is caused by turbulent eddies in the airflow approaching the propeller. The BPF is the product of the shaft frequency and the blade number.

Theoretically, the BPF is a discrete frequency,  $f_{BPF}$ , which is related to the number of blades,  $N$ , and the engine rpm,  $R$ , and is given by  $f_{BPF} = NR/60$  Hz. Since the thrust and drag forces are not purely sinusoidal in nature, harmonic distortion occurs as in the case of the noise generated by fans, diesel engines, pumps, compressors, and the like. Thus, blade passing harmonic tones occur at frequencies  $f_{BPFn}$  given by  $f_{BPFn} = nNR/60$  Hz, where  $n$  is an integer, 1, 2, 3, 4, ...

Prediction of propeller noise is complicated. Accurate noise predictions require methods that include the influence of the flow field in which the propeller operates. Predictions may be made both in the time domain and the frequency domain. Noise reduction approaches



**Figure 6** Noise levels and spectra of general aviation aircraft.<sup>23</sup>

are normally based both on experimental tests and theoretical predictions. See Chapter 90 for a more complete discussion.

The spectrum of the propeller noise has both discrete and continuous components. The discrete frequency components are called tones. The continuous

component of the spectrum is called broadband noise. There are three main kinds of propeller noise sources. These are (1) thickness (monopole-like), (2) loading (dipole-like), and (3) nonlinear (quadrupole-like) noise sources. All three of these source types can be steady or unsteady in nature. The loading dipole axis exists

along the local normal to the propeller plane surface. For the first few harmonics of a low-speed propeller, the simple Gutin formula<sup>2</sup> gives the noise level in terms of the net thrust and torque. Unsteady sources can be further classified as periodic, aperiodic, or random. Steady and periodic sources produce tonal noise while random sources produce broadband noise.

Quadrupole sources are normally only important when the flow over the propeller airfoil is transonic or supersonic. Quadrupole sources are not important noise generators for conventional propellers, but they can be important in the generation of the noise of highly loaded high-speed propellers such as propfans. (See Chapters 9 and 10 for more detailed discussions on aerodynamic noise and nonlinear acoustics.)

## 10 HELICOPTER ROTOR NOISE

The generation of helicopter rotor noise is very complicated. Chapter 91 provides an in-depth discussion about its causes. Sources of helicopter noise include (1) main rotor, (2) tail rotor, (3) the engines, and (4) the drive train components. The dominant noise contributors are the main rotor and the tail rotor. Engine noise is normally less important, although for large helicopters engine noise can be dominant at take-off. Rotor noise including main rotor and tail rotor noise can be classified as (1) discrete-frequency rotational noise, (2) broadband noise, and/or (3) impulsive noise (also of discrete-frequency character).

Helicopter rotor noise is comprised of *thickness noise* (the noise generated from the periodic volume displacement of the rotating blades) and *loading noise* (caused by the rotating lift and drag forces). Thickness noise is more important in the low-frequency range of the rotor-noise spectrum (at the blade passage frequency and first few harmonics). It also contains mid- and high-frequency components since it is of an impulsive nature). At low rotational speeds and for low blade loading, the thickness noise line spectrum can be exceeded by the *broadband noise* components. Broadband noise is a result of turbulent inflow conditions, blade/wake interferences, and blade self-noise ("airframe noise").

Of great importance are *impulsive-type noise sources*, resulting in the familiar "bang, bang, bang" sound. There are two main kinds: high-speed (HS) impulsive noise and blade-vortex interaction (BVI) impulsive noise. Tail rotor noise has similar characteristics to the main rotor noise. The flow around the tail rotor is the sum of the interacting flows generated by the wakes of the main rotor, the fuselage, the rotor hub, as well as the engine exhaust and empennage flows in addition to its own wake. For most helicopters, the tail rotor noise dominates at moderate speed straight flight conditions and during climb. Practical *rotor noise reduction measures* include passive reduction of high-speed impulsive noise, reduction of tail rotor noise, and active reduction of blade-vortex interaction. (See Chapter 91 for a more detailed discussion of helicopter rotor noise.) Lowson has provided an in-depth review on helicopter noise.<sup>24</sup>

## 11 BRAKE NOISE PREDICTION AND CONTROL

Brake noise has been recognized as a problem since the mid-1930s. Research was initially conducted on drum brakes, but recent work has concentrated on disk brakes since they are now widely used on cars and trucks. The disk is bolted to the wheel and axle and thus rotates at the same speed as the wheel. The brake caliper does not rotate and is fixed to the vehicle. Hydraulic oil pressure forces the brake pads onto the disk, thus applying braking forces that reduce the speed of the vehicle.

As is discussed in Chapter 92, from a dynamics point of view a braking system can be represented as two dynamic systems connected by a friction interface. The normal force between the two systems results from the hydraulic pressure and is related to the friction force. The combination of the friction interface and the dynamic systems makes it difficult to understand and reduce brake noise. Brake noise usually involves a dynamic instability of the braking system.

There are three overlapping "stability" parameters of (1) friction, (2) pressure, and (3) temperature. If the brake operates in the unstable area, changes in the parameters have little or no effect, and the brake is likely to generate noise. Such conditions may be caused by excessively low or high temperatures, which cause changes in the characteristics of the friction material. The "stable" area may be regarded to represent a well-designed brake in which the system only moves into the "unstable" region when extreme changes in the system parameters occur. Brake noise and vibration phenomena can be placed into three main categories: (1) judder, (2) groan, and (3) squeal.

*Judder* occurs at a frequency less than about 10 Hz and is related to the wheel rotation rpm or a multiple of it. It is a *forced* vibration caused by nonuniformity of the disk, and the vibration is of such a low frequency that it is normally sensed rather than heard. There are two types of judder: cold and hot judder. Cold judder is commonly caused by the brake pad rubbing on the disk during periods when the brakes are not applied. Hot judder is associated with braking at high speeds or excessive braking when large amounts of heat can be generated causing transient thermal deformations of the disk.

*Groan* occurs at a frequency of about 100 Hz. It usually happens at low speed and is the most common unstable brake vibration phenomenon. It is particularly noticeable in cars and/or heavy trucks coming to a stop or moving along slowly and then gently braking. It is thought to be caused by the stick-slip behavior of the brake pads on the disk surface and because the friction coefficient varies with brake pad velocity.

*Squeal* normally occurs above 1 kHz. Brake squeal is an unstable vibration caused by a geometric instability. It can be divided into two main categories: (1) low-frequency squeal (1 to 4 kHz), diametrical nodal spacing in the disk, and (2) high-frequency squeal (>4 kHz). See Chapter 92 for a more detailed discussion of brake noise. References 25 to 30 describe recent research on brake noise.

## 12 WHEEL–RAIL INTERACTION NOISE

Noise produced by wheel–rail interaction continues to be of concern in railway operations. Many studies have been conducted on wheel–rail interaction noise. Most of the studies have involved various measurement approaches.<sup>31–40</sup> Main wheel–rail sources include (1) rolling noise, which is caused by small-scale vertical profile irregularities (roughness) of wheel and rail, (2) impact noise caused by discrete discontinuities of the profile such as wheel flats, rail joints, or welds, and (3) squeal noise that occurs in curves. In each case, the noise is produced by vibrations of the wheels and track. The dynamic properties of the wheel and track have an affect on the sound radiation. Control measures for rolling noise include reduced surface roughness, wheel shape optimization and added wheel passive damping treatments, increased rail support stiffness, or use of local wheel–rail shielding. The use of trackside noise barriers is becoming common for railways. Barriers are discussed in Chapter 58. For squeal noise, mitigation measures include friction control by lubrication or friction modifiers. Chapter 93 discusses causes of wheel–rail noise and methods for its control.

A train running on straight unjointed track produces rolling noise. This is a broadband, random noise radiated by wheel and track vibration over the range of about 100 to 5000 Hz. The overall radiated sound pressure level increases at about 9 dB per doubling of train speed. This represents almost a doubling of subjective loudness for a doubling of speed. Rolling noise is induced by small vertical profile irregularities of the wheel and rail running surfaces. This is often referred to as roughness, although the wavelength range is between about 5 and 250 mm, which is greater than the range normally considered for microroughness. Wheel and rail roughness may be considered incoherent and their noise spectra simply added. The roughness causes a relative displacement between the wheel and rail and makes the wheel and rail vibrate and radiate noise. See Chapter 93 for a complete discussion on wheel–rail interaction noise.

## REFERENCES

1. U. Sandberg and J. A. Ejsmont, *Tyre/Road Noise Reference Book*, Informex, SE-59040 Kisa, Sweden, 2002, www.informex.info.
2. P. Nelson, Controlling Vehicle Noise—A General Review, *Acoust. Bull.*, Vol. 1, No. 5, 1992, pp. 33–57.
3. S. Maruyama, J. Aoki, and M. Furuyama, Source: Application of a Reciprocity Technique for Measurement of Acoustic Transfer Functions to the Prediction of Road Vehicle Pass-by Noise, *JSAE Rev.*, Vol. 18, No. 3, 1997, pp. 277–282.
4. L. L. Beranek and I. L. Ver, Eds., *Noise and Vibration Control Engineering*, Wiley, New York, 1988.
5. J. A. Steel, Study of Engine Noise Transmission Using Statistical Energy Analysis, *Proc. Institution Mech. Eng., Part D: J. Automobile Eng.*, Vol. 212, No. 3, 1998, pp. 205–213.
6. J.-H. Lee, S.-H. Hwang, J.-S. Lim, D.-C. Jeon, and Y.-S. Cho, A New Knock-Detection Method Using Cylinder Pressure, Block Vibration and Sound Pressure Signals from a SI Engine, SAE International Spring Fuels and Lubricants Meeting and Exposition, Society of Automotive Engineers, Warrendale, PA, 1998.
7. I. J. Lee, A. Selamet, and N. T. Huff, Acoustic Characteristics of Coupled Dissipative and Reactive Silencers, SAE Noise and Vibration Conference and Exposition, Society of Automotive Engineers, Warrendale, PA, 2003.
8. J.A. Steel, G. Fraser, and P. Sendall, A Study of Exhaust Noise in a Motor Vehicle Using Statistical Energy Analysis, *Proc. Institution Mech. Eng. Part D, J. Automobile Eng.*, Vol. 214, No. D1, 2000, pp. 75–83.
9. F. H. Kunz, Semi-Empirical Model for Flow Noise Prediction on Intake and Exhaust Systems, SAE Noise and Vibration Conference and Exposition, Society of Automotive Engineers, Warrendale, PA, 1999.
10. S. Goossens, T. Osawa, and A. Iwama, Quantification of Intake System Noise Using an Experimental Source-Transfer-Receiver Model, SAE Noise and Vibration Conference and Exposition, Society of Automotive Engineers, Warrendale, PA, 1999.
11. N. Møller and S. Gade, Operational Modal Analysis on a Passenger Car Exhaust System, Congresso 2002 SAE Brasil—11th International Mobility Technology Congress and Exhibition, Society of Automotive Engineers, Warrendale, PA, 2002.
12. M. J. Crocker, D. Hansen, and Z. Li, Measurement of the Acoustical and Mechanical Properties of Porous Road Surfaces and Tire/Road Noise, *TRB J.*, No. 1891, 2004, pp. 16–22.
13. G. J. Kim, K. R. Holland, and N. Lalor, Identification of the Airborne Component of Tyre-induced Vehicle Interior Noise, *Appl. Acoust.*, Vol. 51, No. 2, 1997, pp. 141–156.
14. J. Perisse, A Study of Radial Vibrations of a Rolling Tyre for Tyre-Road Noise Characterization, *Mech. Syst. Signal Proc.*, Vol. 16, No. 6, 2002, pp. 1043–1058.
15. D. Boulahbal, J. D. Britton, M. Muthukrishnan, F. Gauterin, and Y. Shanshal, High Frequency Tire Vibration for SEA Model Partitioning, Noise and Vibration Conference and Exhibition, Society of Automotive Engineers, Warrendale, PA, 2005.
16. P. R. Donavan and B. Rymer, Assessment of Highway Pavements for Tire/Road Noise Generation, SAE Noise and Vibration Conference and Exposition, Society of Automotive Engineers, Warrendale, PA, 2003.
17. M. Constant, J. Leyssens, F. Penne, and R. Freymann, Tire and Car Contribution and Interaction to Low Frequency Interior Noise, SAE Noise and Vibration Conference and Exposition, Society of Automotive Engineers, Warrendale, PA, 2001.
18. E.-U. Saemann, C. Ropers, J. Morkholt, and A. Omrani, Identification of Tire Vibrations, SAE Noise and Vibration Conference and Exposition, Society of Automotive Engineers, Warrendale, PA, 2003.
19. P. G. Bremner and M. Zhu, Recent Progress Using SEA and CFD to Predict Interior Wind Noise, SAE Noise and Vibration Conference and Exposition, Society of Automotive Engineers, Warrendale, PA, 2003.
20. M. J. Lighthill, On Sound Generated Aerodynamically. I. General Theory, *Proc. Roy. Soc. A*, Vol. 211, 1952, pp. 564–587.
21. M. J. Lighthill, On Sound Generated Aerodynamically. II. Turbulence as a Source of Sound, *Proc. Roy. Soc. A*, Vol. 222, 1954, pp. 1–32.

22. A. Powell, Aerodynamic and Jet Noise, in *The Encyclopedia of Acoustics*, Vol. 1, Wiley, New York, 1997, Chapter 28.
23. Wyle Laboratories, Transportation Noise and Noise from Equipment Powered by Internal Combustion Engines, EPA Report No. NTID 300.13, 1971.
24. M. V. Lowson, Progress Towards Quieter Civil Helicopters, *Aeronaut. J.*, Vol. 96, No. 9, 56, 1992, pp. 209–223.
25. K. A. Cunefare and R. Rye, Investigation of Disc Brake Squeal via Sound Intensity and Laser Vibrometry, SAE Noise and Vibration Conference and Exposition, Society of Automotive Engineers, Warrendale, PA, 2001.
26. S.-W. Kung, V. C. Saligrama, and M. A. Riehle, Modal Participation Analysis for Identifying Brake Squeal Mechanism, 18th Annual Brake Colloquium and Engineering Display, Society of Automotive Engineers, Warrendale, PA, 2000.
27. H. Lee and R. Singh, Sound Radiation from a Disk Brake Rotor Using a Semi-Analytical Method, SAE Noise and Vibration Conference and Exposition, Society of Automotive Engineers, Warrendale, PA, 2003.
28. E. Gesch, M. Tan, and C. Riedel, Brake Squeal Suppression through Structural Design Modifications, Noise and Vibration Conference and Exhibition, Society of Automotive Engineers, Warrendale, PA, 2005.
29. M. Bettella, M. F. Harrison, and R. S. Sharp, Investigation of Automotive Creep Groan Noise with a Distributed-Source Excitation Technique, *J. Sound Vib.*, Vol. 255, No. 3, 2002, pp. 531–547.
30. J. Charley, G. Bodoville, and G. Degallaix, Analysis of Braking Noise and Vibration Measurements by Time-Frequency Approaches, *Proc. Instit. Mech. Eng., Part C: J. Mech. Eng. Sci.*, Vol. 215, No. 12, 2001, pp. 1381–1400.
31. D. J. Thompson and P. J. Remington, Effects of Transverse Profile on the Excitation of Wheel/Rail Noise, *J. Sound Vib.*, Vol. 231, No. 3, 2000, pp. 537–548.
32. C. Dine and P. Fodiman, New Experimental Methods for an Improved Characterisation of the Noise Emission Levels of Railway Systems, *J. Sound Vib.*, Vol. 231, No. 3, 2000, pp. 631–638.
33. A. Frid, Quick and Practical Experimental Method for Separating Wheel and Track Contributions to Rolling Noise, *J. Sound Vib.*, Vol. 231, No. 3, 2000, pp. 619–629.
34. D. H. Koo, J. C. Kim, W. H. Yoo, and T. W. Park, An Experimental Study of the Effect of Low-Noise Wheels in Reducing Noise and Vibration, *Transport. Res. Part D: Transport Environ.*, Vol. 7, No. 6, 2002, pp. 429–439.
35. M. G. Dittrich and M. H. A. Janssens, Improved Measurement Methods for Railway Rolling Noise, *J. Sound Vib.*, Vol. 231, No. 3, 2000, pp. 595–609.
36. H. Sakamoto, K. Hirakawa, and Y. Toya, Sound and Vibration of Railroad Wheel, *Proceedings of the 1996 ASME/IEEE Joint Railroad Conference* (Cat. No.96CH35947), 1996, pp. 75–81.
37. F. G. de Beer and J. W. Verheij, Experimental Determination of Pass-by Noise Contributions from the Bogies and Superstructure of a Freight Wagon, *J. Sound Vib.*, Vol. 231, No. 3, 2000, pp. 639–652.
38. M. Kalivoda, M. Kudrna, and G. Presle, Application of MetaRail Railway Noise Measurement Methodology: Comparison of Three Track Systems, *J. Sound Vib.*, Vol. 267, No. 3, 2003, pp. 701–707.
39. A. E. J. Hardy, Measurement and Assessment of Noise within Passenger Trains, *J. Sound Vib.*, Vol. 231, No. 3, 2000, pp. 819–829.
40. M. G. Dittrich and M. H. A. Janssens, Improved Measurement Methods for Railway Rolling Noise, *J. Sound Vib.*, Vol. 231, No. 3, 2000, pp. 595–609.



# CHAPTER 84

## INTERNAL COMBUSTION ENGINE NOISE PREDICTION AND CONTROL – DIESEL AND GASOLINE ENGINES

Thomas E. Reinhart  
Engine Design Section  
Southwest Research Institute  
San Antonio, Texas

### 1 INTRODUCTION

Internal combustion engines designed to operate on gasoline or diesel fuel (or their substitutes) have different combustion systems that lead to significantly different noise characteristics. Gasoline engines use spark ignition to control the combustion process, while diesel cycle engines use compression ignition. The forces generated inside internal combustion engines cause vibration of the engine structure, leading to radiated noise. Important forcing functions include cylinder pressure, piston slap, and impact excitations, which are generated as clearances open and close. Engines with timing gears have backlash rattle, and most timing drives experience meshing frequency forces. Engine accessories often produce tonal noise that contributes to the overall engine noise. Which forcing function dominates the noise of an engine depends on the engine design, combustion system, and operating condition. The relative importance of different forcing functions varies as a function of speed and load.

The noise of internal combustion engines can be predicted using information about the size, speed, and combustion process. Noise levels of all engine types increase with bore size and operating speed. However, a number of techniques are available to control engine noise, so all engines of a given size, speed, and combustion process will not have identical noise levels. Noise control techniques include changes to the combustion process, to the engine structure, and to internal and external components such as pistons and valve covers. Engine or vehicle-mounted enclosures are often used to limit noise radiation.

### 2 BASIC CHARACTERISTICS OF DIESEL AND GASOLINE ENGINES

Many books have been devoted to the design of diesel and gasoline engines. In this chapter, we will only consider characteristics relevant to noise generation. Diesel and gasoline engines share many similarities. They all have pistons, cylinders, connecting rods, crankshafts, blocks, heads, valve or porting systems, and so forth. These components often look similar between gasoline and diesel engines, but diesel components tend to be designed to withstand higher loads. The primary distinction between gasoline and

diesel engines lies in the combustion process and how fuel is delivered to and burnt in the cylinder.

Gasoline engines, along with many alternate fueled engines, use the Otto cycle, with spark ignition. Spark ignition (SI) engines create a mixture of air and fuel in the cylinder and ignite it with a spark plug. The air–fuel mixture starts burning at the spark plug, and the flame front propagates across the cylinder until all the fuel has been burned. It is critical that the unburned air and fuel not spontaneously ignite. This autoignition in an SI engine is called *knock*. It causes a step increase in cylinder pressure, which produces the characteristic “pinging” or “knocking” noise. Significant levels of knock are highly destructive to an SI engine since the engine components are not designed to withstand the huge forces and high temperatures created by knock.

Compression ratios and peak cylinder pressures are limited in SI engines by the need to avoid knock. The fuel is also developed to help avoid knock. The familiar octane ratings are a measure of the ability of fuel to resist autoignition. A higher octane rating allows the engine designer to use higher compression ratios and cylinder pressures without fear of knock, which can improve both power and efficiency.<sup>1</sup>

Diesel engines are also known as compression ignition (CI) engines. They rely precisely on the type of combustion that SI engines try to avoid: autoignition. In a diesel engine, the air–fuel mixture is compressed until ignition occurs spontaneously. As a result, diesel engines tend to have much higher compression ratios, peak cylinder pressures, and rates of pressure rise than SI engines. Diesel engines are designed to withstand the higher forces produced by the compression ignition process. Diesel fuel is designed to promote autoignition, and this characteristic is measured and reported as the cetane value. A fuel with higher cetane will ignite more easily.

The different combustion methods used in SI and CI engines go a long way toward explaining the noise and vibration disadvantages that diesel engines face compared to gasoline engines. The forces from cylinder pressure and the high-frequency excitation from rates of pressure rise are much higher in CI engines. Rapid pressure rise involves significant high-frequency energy content, which manifests itself in the typical diesel knocking sound. Heavier moving parts, required to survive the higher forces in a diesel,

also contribute to the higher noise and vibration levels of diesels. The high compression ratios of diesels cause large fluctuations of crankshaft speed (torsional vibration). Torsional vibration produces torque reactions that are transmitted to the engine mounts, making it more difficult to achieve good vibration isolation with diesel engines.

### 3 DIRECT INJECTION VERSUS INDIRECT INJECTION

Many small SI engines still use carburetion to mix air and fuel before introducing it into the cylinder for combustion, but most larger SI and all CI engines use some form of fuel injection. However, SI and CI injection systems are quite different. CI (diesel) engines typically inject fuel at very high pressures. On modern diesels, injection pressures of 1400 to over 2000 bar are common. Modern gasoline port injection systems, on the other hand, work at pressures of 3 to 6 bar. Even direct injection gasoline systems generally use pressures of under 100 bar. Creating and controlling the extremely high pressures used in diesel fuel systems makes the systems themselves potentially significant noise sources.

All diesel engines use some form of fuel injection. Indirect injection (IDI) used to be very common in small and medium size diesels, while larger engines tended to use direct injection (DI). Recently, the trend is toward direct injection for all but the smallest diesel engines. An important advantage of IDI is lower combustion noise. This is because the effect of forcing air and fuel through the passage between the prechamber and main cylinder reduces rates of pressure rise in the cylinder. However, the prechamber produces pumping losses that have the effect of reducing fuel economy by 10 to 15%. The better fuel economy of DI engines has driven the trend toward DI in smaller diesels.<sup>2,3</sup>

### 4 PREDICTING NOISE FROM ENGINE SIZE, SPEED, AND COMBUSTION SYSTEM

Engine noise is widely known to vary with engine size, speed, and combustion system. The empirical relationships among these have been described in several published works. For example, in 1970, Anderton et al. evaluated a large sample of diesel engines and concluded that sound pressure level was proportional to speed to the third power for naturally aspirated engines and speed to the fourth power for turbocharged engines. For both engine types, noise was proportional to bore to the fifth power.<sup>4</sup> In the mid-1970s, two papers were published that included empirical equations to predict the overall average 1-m noise level for several types of engines.<sup>5,6</sup> These equations also covered high-speed IDI diesels and gasoline engines.

In 2004 a new paper was published by one of the original authors of Ref. 5 providing updated empirical equations based on more recent engine noise tests.<sup>7</sup> The average A-weighted sound pressure level in

decibels, measured 1m from the engine, for an engine running at full load is given by:

$$30 \log(N) + 50 \log(B) - 106$$

(for NA DI diesels) (1)

$$25 \log(N) + 50 \log(B) - 86$$

(for turbocharged diesels) (2)

$$36 \log(N) + 50 \log(B) - 133$$

(for IDI diesels) (3)

$$50 \log(N) + 30 \log(B) + 40 \log(S) - 223.5$$

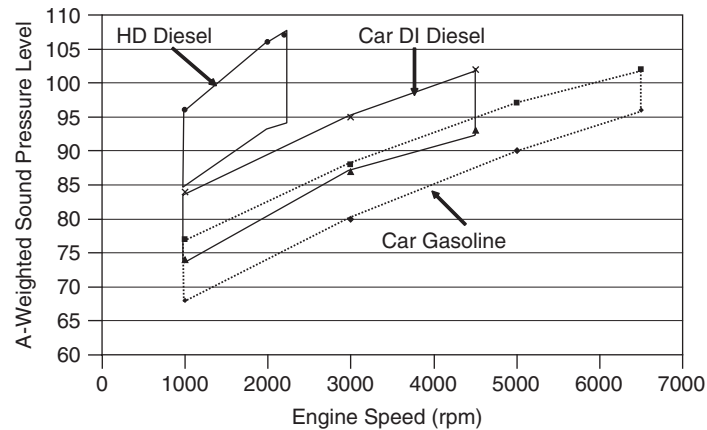
(for gasoline) (4)

where  $N$  = speed in rpm,  $B$  = bore in mm, and  $S$  = stroke in mm, NA refers to natural aspiration, and base 10 logarithms are used.

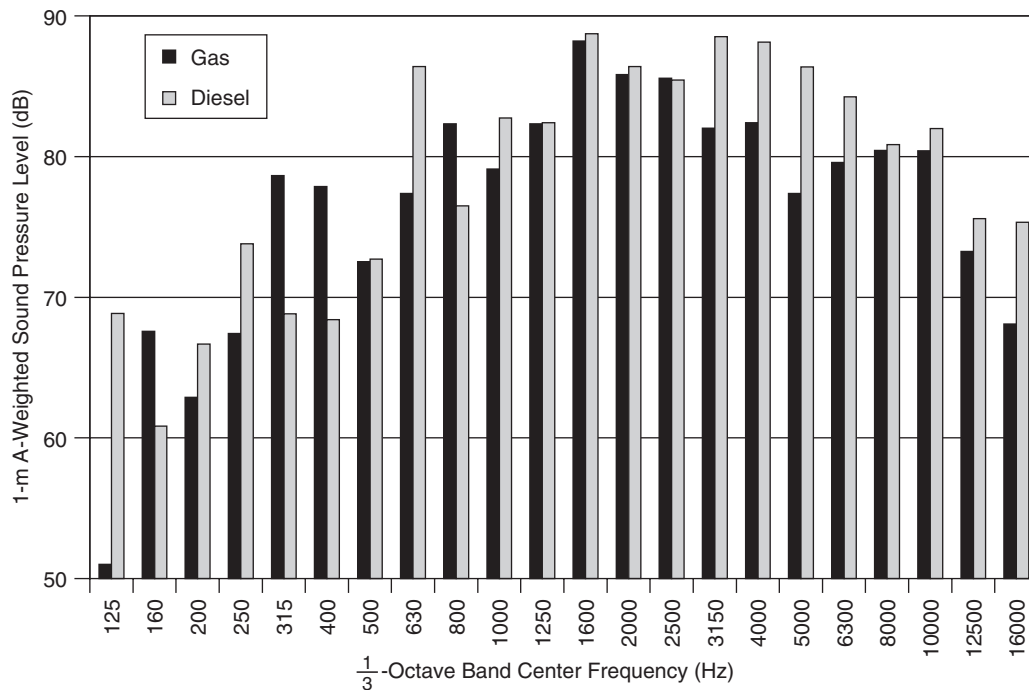
A recent study of heavy-duty (HD) diesel engines failed to support the empirical equations from the above references, or indeed any clean relationship between noise, speed, and engine size.<sup>8</sup> This study found that changes in emissions regulations have caused a new forcing function, gear train rattle, to become the dominant noise forcing function in many HD diesel engines. For certain HD diesel engines, gear train design parameters proved to be a much more reliable indicator of noise than bore and speed.<sup>8</sup>

One interesting observation is that most engines make about the same amount of noise at their maximum speed and load. As Fig. 1<sup>9</sup> shows, from small gasoline car engines to large, heavy-duty truck diesels, average 1-m A-weighted sound pressure levels at rated speed and load are often in the 95 dB to 105 dB range. Larger engines tend to have a lower maximum speed than small engines, and inherently loud diesel engines have a lower maximum speed than quieter gasoline engines. The net result is that many engines have similar noise levels at maximum speed and load, although noise levels compared at a given speed can vary by up to 30 dB.

Figure 2 shows typical sound pressure spectra for two engines operating at maximum speed and load. One engine is a small four-cylinder gasoline car engine, while the other is a heavy-duty truck V-8 turbocharged DI diesel. The overall noise levels for the two engines are not very different, but some differences in the sound pressure spectra can be observed. There is no clear pattern below 1250 Hz. In one band, the diesel is higher, while the gasoline engine is higher in the next band. From 1250 to 2500 Hz, the two engines are nearly identical. The diesel is louder in frequencies above 2500 Hz. This high-frequency content is due to combustion, gear train, and fuel system excitations and is responsible for the relatively poor sound quality of the diesel. Even though overall levels at maximum speed and load are similar, the gasoline engine is about 20 dB quieter than the diesel at idle.<sup>10</sup>



**Figure 1** Typical full-load sound pressure levels of engines, measured 1 m from the engine.<sup>9</sup>

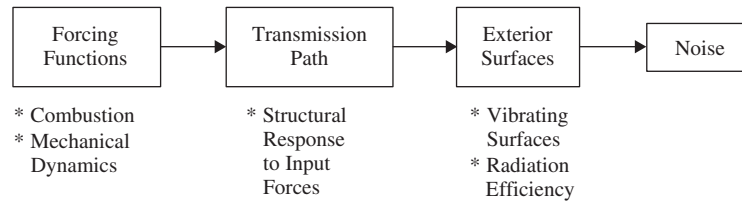


**Figure 2** Sound pressure level spectra of a small four-cylinder gasoline car engine and a V-8 turbocharged DI heavy-duty diesel truck engine at maximum speed and load.<sup>10</sup>

## 5 NOISE GENERATION MODEL

Figure 3 shows a model in block diagram form for engine noise generation that applies to both gasoline and diesel engines. Large forces are generated inside an engine, and these forces are applied to the internal structure. The applied forces are typically divided into two categories: combustion forces (cylinder pressure) and mechanical forces (all other forcing functions).

These forces produce vibration in the structure, and the vibration is transmitted to external components that can radiate sound. The design of the structure determines how much vibration is transmitted to the external components for a given amount of force input. The design of the external components determines how much of the vibration transmitted through the structure is transformed into radiated noise. There are



**Figure 3** Block diagram model of engine noise generation.

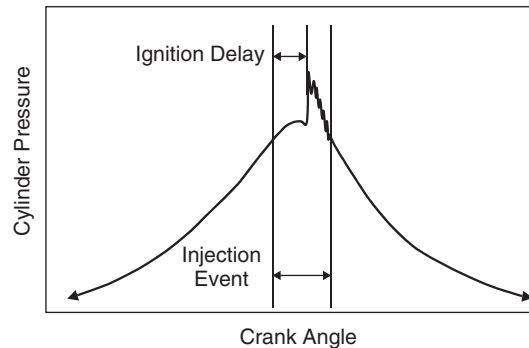
opportunities for the designer to intervene at each stage of the noise generation process. Design changes can be made to reduce the input forces, or to make the structure less responsive to given input forces, or to make the external components radiate less noise for a given structural vibration input.

## 6 COMBUSTION NOISE

Combustion can be a dominant noise source in both SI and CI engines. The distinction between combustion and mechanical noise seems clear, but in practice separating the two can be difficult. Combustion excites the engine structure through rapid changes in cylinder pressure. The direct excitation of the engine structure (piston and cylinder head) by cylinder pressure is normally referred to as *combustion noise*. However, cylinder pressure is directly or indirectly responsible for many mechanical noises in the engine. For example, cylinder pressure can drive bearing impacts and piston slap. Cylinder pressure also leads to crankshaft speed fluctuations, which can cause gear train rattle or timing chain slap. If changes are made to the engine that result in a reduction of peak cylinder pressure or in the rate of pressure rise, it can be difficult to determine whether the observed noise reduction is because of a reduction in direct combustion noise or because of a change in some mechanical noise source(s), which are driven by cylinder pressure.<sup>8</sup>

Figure 4 shows a typical cylinder pressure trace for a diesel engine, while Fig. 5 shows typical cylinder pressure frequency spectra for gasoline and diesel engines. The diesel cylinder pressure trace in Fig. 4 is similar to that of a gasoline engine experiencing knock. In a diesel, cylinder pressure increases smoothly up past the beginning of injection. Once injection begins, the fuel evaporates, heats up, and finally reaches the conditions where autoignition is possible. When autoignition occurs, virtually all the fuel injected in the cylinder up to the point of ignition burns explosively, causing a very rapid rise in cylinder pressure. This explosive onset of combustion is often referred to as *premixed combustion*.

The step increase in cylinder pressure produced by premixed combustion causes the broadband increase in cylinder pressure spectrum of the diesel, shown in Fig. 5. Since the combustion is not perfectly symmetric, the pressure then oscillates at the natural frequencies of the air volume trapped in the cylinder, as can be seen in Fig. 4 at the point just after the cylinder pressure spike. Often, more than one



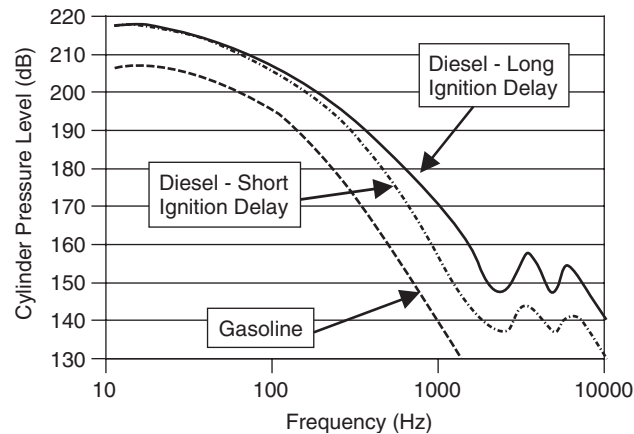
**Figure 4** Typical cylinder pressure trace of a diesel engine at low boost pressure.

resonance frequency can be seen in a spectrum of cylinder pressure because the first few modes of the gas trapped in the cylinder can all be excited (see the high-frequency peaks in Fig. 5).

The frequency content of the cylinder pressure is crucial to determining the level of combustion noise. If the cylinder pressure trace is smooth, there will be very high amplitudes of low-frequency excitation to the engine structure but little high-frequency content. If premixed combustion (or knock in an SI engine) causes a step increase in cylinder pressure, there will be much more high-frequency excitation of the engine structure. The frequency spectrum of the cylinder pressure trace is therefore a useful predictor of combustion noise. In fact, combustion noise meters were developed in the 1980s to take advantage of this effect. The transfer function between the cylinder pressure spectrum and the engine-radiated noise spectrum was determined for a number of engines, averaged, and built into a meter.<sup>11</sup> The combustion noise meter allows performance development engineers to predict the effect of combustion system changes on overall engine noise. The predictions of a combustion noise meter are valid only as long as the transfer function used by the meter is a reasonably accurate representation of the engine being tested.

## 7 REDUCING COMBUSTION NOISE

In all engines, combustion noise is controlled by the rate of heat release (combustion), which determines the rate of rise in cylinder pressure. In gasoline engines, heat release is controlled by factors such as:



**Figure 5** Typical cylinder pressure level spectra of diesel and gasoline engines. Gasoline engines have lower levels at low frequency because of lower peak cylinder pressure. The peaks in the high-frequency spectra of diesels reflect combustion chamber resonances excited by premixed combustion.

- Ignition (spark) timing
- Spark plug location
- Number of spark plugs
- Swirl and tumble of the air–fuel mixture

Retarding ignition toward top dead center (TDC) reduces combustion noise significantly, at a cost in performance. A centrally located spark plug will produce more rapid combustion than one located near the side of the combustion chamber. Two spark plugs fired together speed combustion compared to a single plug. Higher swirl and tumble of the air–fuel mixture speeds combustion. Swirl and tumble are controlled by a number of factors, including port design, valve lift, valve timing, and combustion chamber shape (squish).

In diesel engines, the rate of heat release is also controlled by a number of factors, including:

- Injection timing
- Boost pressure
- Compression ratio
- Intake manifold temperature
- Injection characteristics
- Fuel cetane

Retarding injection timing reduces combustion noise, unless the start of combustion is pushed after TDC. Increasing boost pressure causes the fuel to evaporate and mix more quickly, shortening the ignition delay and thus reducing combustion noise. In fact, at boost pressures above about 0.7 bar, combustion noise often becomes insignificant. Higher compression ratios and higher intake manifold temperatures also have the effect of shortening ignition delay and reducing combustion noise. Injection characteristics such as pilot injection and rate shaping can have a dramatic effect on combustion noise, by reducing the amount of fuel

injected during the ignition delay. In some DI diesel engines, the use of pilot injection can reduce overall noise under low-speed and light-load conditions by 5 dB or more, with a dramatic improvement in sound quality. Higher cetane fuel reduces ignition delay. European diesel fuel has typical cetane values of 50 to 52, compared to American fuel at about 42. In engines where combustion noise controls the overall noise level, the use of higher cetane fuel will reduce overall noise by 1 to 2 dB and improve sound quality.

## 8 CONNECTIONS BETWEEN COMBUSTION NOISE, PERFORMANCE, EMISSIONS, AND FUEL ECONOMY

As with many systems, the most straightforward ways of reducing noise also tend to degrade the system performance. There is considerable competition between competing priorities in engine development, and combustion noise is a typical example.

With spark ignition engines, many efforts to improve emissions and fuel economy result in more rapid combustion. This, in turn, leads to higher rates of cylinder pressure rise and more high-frequency content in the cylinder pressure spectrum. For example, features such as high turbulence in the combustion chamber or twin spark plugs are ways of improving emissions or performance at the expense of combustion noise. Noise and vibration compromises frequently need to be made when developing a new combustion system.

In compression ignition engines, the situation is even more difficult. The compression ignition combustion method at the heart of the diesel by its nature causes substantial combustion noise. Historically, it has been difficult to significantly reduce combustion noise without large performance or emissions penalties. However, new fuel systems and electronic controls have opened the door to much improved trade-offs in recent years. The ability to provide several

separate injection events with precise control of quantity and timing has allowed much better trade-offs between noise, emissions, and performance. Many modern diesels combine high power density, good fuel economy, relatively low emissions, and low combustion noise in a way that was simply not possible 10 to 15 years ago, and there appears to be considerable scope for further improvement in the future.

## 9 MECHANICAL NOISE SOURCES

Many mechanical noises in an engine are caused by the clearances that must exist to allow the engine to function. Most clearance-driven noise sources produce broadband, impact-like inputs to the engine structure. For example, piston slap is caused by the piston moving laterally or rocking in the cylinder and impacting against the cylinder wall. Connecting rod and crankshaft bearings produce impact excitations as the components move through the available clearance. Valve train components produce impacts as they move through their clearances and as valves close against their seats. Engines with gear-driven components may suffer gear rattle impacts, driven by the cyclic torques applied to some of the components such as the crankshaft, camshaft, and fuel system.

Other mechanical noise sources in an engine are periodic in nature. An oil pump will produce pressure fluctuations at a frequency determined by the number of gear teeth or lobes in the pump, combined with the pump's drive ratio. Gear and chain drives can produce pure tone noise at the tooth or sprocket meshing frequency. Alternators, power steering pumps, and other engine-mounted accessories can produce significant pure-tone noise.

Identifying pure-tone engine noise sources is often relatively straightforward. The frequency of the measured noise at a certain speed can be compared to calculations of potential source frequencies. Identifying the sources of impact noise can be much more difficult. By nature, impact noise is broadband, so frequency analysis is of limited help. Measuring when the impacts occur as a function of crank angle may provide guidance. Introducing modified parts designed to magnify or eliminate particular clearances can also be used to identify the source of impact excitations. For example, Teflon-padded pistons can be used to determine the amount of noise generated by piston slap.

## 10 REDUCING MECHANICAL NOISE

There is extensive literature that describes efforts to reduce mechanical noise. Piston slap has perhaps received the most attention. Analytical models have been created to model and predict the relative motion between the piston and bore.<sup>12–14</sup> Piston slap modeling software is sold by companies such as AVL, FEV, and Ricardo. These models can be modified to explore a wide range of potential design alternatives, such as changes in clearance, piston pin location, or piston mass. However, it must be noted that piston slap is a complex and sometimes nonlinear phenomenon with many variables, so a model that can accurately simulate it must also be complex.

Piston slap reduction efforts have focused on the effects of these and other variables:

- Piston skirt profile, both top to bottom and around the circumference
- Bore distortion
- Piston pin offset
- Piston coatings to reduce friction or to allow a tighter fit
- Piston inserts to control thermal expansion
- Piston skirt stiffness

A tight-fitting piston provides less opportunity for slap. Reducing bore distortion, controlling thermal expansion, modifying the skirt profile, and using coatings are all means of allowing a tighter fit without risking scuffing and engine seizure. Piston pin offsets have been demonstrated to help reduce piston slap noise by changing the way pistons rotate while crossing the bore. Getting the relatively soft and light piston skirt to impact on the cylinder wall first provides less excitation than having the piston top land impact first.

Both experimental and analytical work has been done on the effects of crankshaft and connecting rod bearing clearances and oil film characteristics.<sup>15,16</sup> The analytical work is made complex by the nonlinear nature of oil film behavior. To model crankshaft, oil film, and bearing behavior, commercial software packages are available from companies such as AVL and Ricardo.

Valve train noise is a significant problem in many engines. Hydraulic valve lifters are often used to eliminate the lash in valve trains and thus reduce noise. Careful tuning of cam profiles to eliminate force spikes in the valve train can reduce noise. Minimizing “jerk,” the derivative of acceleration, is an important tool for reducing valve train noise. Several software packages are available that can be used to model valve train dynamics.

Noise reduction of accessories such as oil pumps, power steering pumps, alternators, air-conditioning compressors, and the like is often important. It is also important that accessories be mounted to the engine in a way that avoids mounting bracket resonances being excited by important forcing functions such as engine firing frequency. Designers often try to design accessory mounting brackets to achieve a mounted natural frequency above firing frequency at maximum speed.

## 11 REDUCING STRUCTURAL RESPONSE TO FORCE INPUTS

The engine structure should be designed to produce a minimum of vibration response to known or suspected force inputs. High stiffness is normally used to improve the forced response of the engine structure. An ideal structure would incorporate impedance mismatches to minimize the response of the structure. Impedance mismatches are step changes in stiffness. For example, an engine block could be designed to be very stiff at the location where crankshaft forces

are transmitted through the main bearings, but soft between the main bearing area and the oil pan flange, and stiff again at the oil pan flange. These transitions in stiffness would make it difficult for forces applied at the main bearings to produce vibration at the oil pan flange.

In practice, most structural parts of engines are castings or forgings, which makes it very difficult to achieve large changes in stiffness. Therefore, while efforts to reduce the structural response can provide significant benefits, there are limits to the improvements that can be achieved within weight and cost limitations. In practice, the noise reductions achieved by optimizing the structure are often modest, and they can be easily outweighed by changes in forcing functions.

Finite element models are frequently used to help design engine structures in a way that minimizes vibration response to forces applied.<sup>17</sup> Measured or calculated forces are applied to a model of the structure, and the response at important locations is calculated. The models can be used to test a variety of design alternatives much more quickly than can be done by building and testing hardware.

Smaller engines often radiate a significant amount of noise from the first few modes of the engine or power train, such as the first bending and torsional vibration modes. Finite element models can be used to ensure that important modes occur above the frequency range of primary excitations such as engine firing. Larger engines often radiate significant energy from local modes of the structure, such as panel modes of the engine block. Again, modeling can be used to cost effectively modify the structure to push these modes up beyond the range of strong forcing functions.

## 12 NOISE RADIATION FROM EXTERIOR SURFACES

Exterior surfaces include both covers, such as the oil pan and valve covers, and structural portions of the engine, such as the block and cylinder heads. A number of options are available to reduce radiated noise, such as stiffening of exterior surfaces, reducing the stiffness of surfaces, adding damping treatments, or isolating the connection between the structure and covers.

Most engineers intuitively believe that adding stiffness is bound to be a good way to reduce noise. Unfortunately, this is not always the case. Adding stiffness can sometimes cause a substantial noise *increase*. A number of factors must be understood in order to determine whether stiffening is a good idea.

Consider the oil pan of a heavy-duty diesel engine as an example. In many engines, the oil pan is not a structural member, allowing the designer a great deal of freedom in choosing the stiffness of the pan. One consideration is the frequency content of the vibration at the pan rail of the engine block, which forms the input excitation to the oil pan. If the pan rail vibration is primarily at low frequencies, it makes sense to stiffen the pan so that the first resonance frequency is above the primary input vibration frequencies. On the other hand, if there is a lot of high-frequency

input, stiffening the pan will have less, or even a negative, benefit. The second consideration is A-weighting. In many cases, noise targets are set using A-weighted levels, which discounts low-frequency noise and emphasizes noise in the 1- to 4- kHz range. Increasing the stiffness of the pan pushes resonances up into the range where A-weighted levels will be higher.

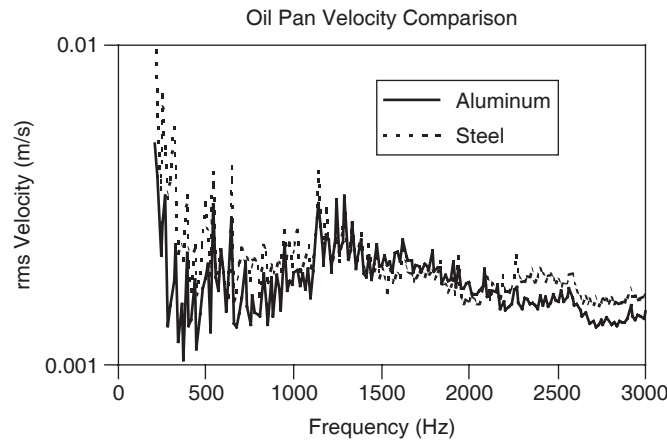
The final design consideration is radiation efficiency. Radiation efficiency is a measure of how much of the vibration in a surface is translated into radiated sound. If the wavelength of sound in air is long compared to the mode shape of the oil pan, radiation efficiency is low. Radiation efficiency peaks when the wavelength of sound in air matches the wavelength of the pan's mode shape, and this is called the critical frequency. Radiation efficiency remains high when the wavelength of sound in air is shorter than the mode shape's wavelength. Reducing radiation efficiency of a given mode shape requires lowering the natural frequency of the mode. Another way to look at radiation efficiency is to say that for a given frequency, the more complex mode shapes will generally have lower radiation efficiency. Closed-form solutions are available to calculate the radiation efficiency of simple geometries such as flat plates, but the complex shapes of real engine components usually require numerical solutions.<sup>18</sup>

Figure 6 shows a comparison of mean square surface velocity for two different oil pans on a heavy-duty diesel engine. The cast-aluminum oil pan is much stiffer than the stamped steel oil pan, and its natural frequencies are higher. As a result, the aluminum pan enjoys somewhat lower surface velocities over most of the frequency range, even though the input vibration at the pan rail is the same for the two engines.

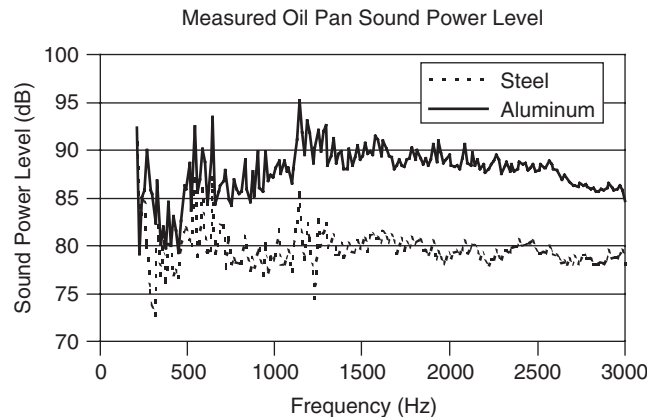
As Fig. 7 shows, however, the aluminum pan's modest advantage in surface velocity does not translate into a noise advantage. In fact, the aluminum pan is about 10 dB louder at many frequencies. This difference is due entirely to higher radiation efficiency of the stiffer aluminum oil pan. The stamped steel pan enjoys a 7-dB lower overall A-weighted sound power than the much stiffer cast-aluminum pan.

In general, large covers with large, flat areas can benefit most from low stiffness. This is especially apparent with the heavy-duty diesel oil pan example. In this case, every factor works in favor of a less stiff design: first, there is a lot of high-frequency vibration at the pan rail, making it impossible to stiffen the pan so that natural frequencies are above the input frequency. Second, A-weighting favors low-frequency noise. Third, it is easy to achieve low natural frequencies of the pan and thus low radiation efficiencies, given the large, flat surfaces of a heavy-duty diesel oil pan. Smaller covers, on the other hand, may not achieve a noise advantage through low stiffness. Smaller, more complex shapes are inherently stiffer. It may not be possible to achieve the low stiffness required to get low radiation efficiency without sacrificing mechanical integrity of a small cover. However, small covers can often be stiffened





**Figure 6** Comparison of mean square surface velocity for a stiff cast-aluminum oil pan and a relatively flexible stamped steel pan on the same heavy-duty diesel engine.



**Figure 7** Comparison of radiated sound power level for a stiff cast-aluminum oil pan and a relatively flexible stamped steel pan on the same heavy-duty diesel engine.

to the point where the first resonance is beyond the frequency range of significant excitation. In many cases, it is not obvious whether increasing or reducing stiffness is a better noise reduction path. Design alternatives can be explored in hardware or by using noise radiation models, which will be described in Section 14.

Adding damping is another option for reducing noise of engine covers. Cast-aluminum and stamped steel covers tend to be highly resonant and lightly damped, so they may amplify the vibration fed into them from the engine structure. Constrained layer steel is widely used to add damping in oil pans, valve covers, and other engine components of both gasoline and diesel engines. Damping treatments are available for cast-aluminum components as well.

Covers can also be isolated from the engine structure to reduce noise. Isolation normally takes

the form of a soft gasket and grommets to avoid any metal-to-metal contact with the structure. The isolation system can be designed with a relatively low natural frequency, limited by the need to control the position of the component and to avoid leaks. Vibration reduction is greatest if there is a large impedance mismatch, so isolation systems work best between a stiff structure and a stiff cover. Isolated covers are common on both SI and CI engines.

### 13 NOISE SHIELDS AND ENCLOSURES

Shields and enclosures can be viewed as engineering Band-Aids. If the effort to reduce forcing functions, improve the structure, and improve covers does not achieve the required noise reduction, an engineer can always cover the problem up with a shield or enclosure. These components are normally isolated from the engine structure to prevent vibration transmission to

their surfaces. High damping and low stiffness are usually chosen to minimize noise radiation. Enclosures are typically mounted directly on the engine, while shields may be mounted on other nearby structures.

Shields and enclosures are not a noise reduction panacea. They tend to be expensive and heavy and can be very difficult to package in an engine installation. Even small gaps or holes will allow a significant amount of noise to escape, but enclosures must allow for plumbing, wiring, tool clearance, cooling airflow, and other openings. Once all the required openings are put into a shield, the noise reduction performance may be quite modest.

#### 14 MODELING ENGINE NOISE GENERATION

Many noise sources have been successfully modeled, but engines have proven to be a very difficult source to model with a reasonable degree of accuracy. There are a number of reasons for this:

- The forcing functions can be difficult or impossible to simulate or measure experimentally.
- Both forcing functions and engine dynamics are often nonlinear and thus difficult to model.
- Many forces are transmitted through nonlinear oil films.
- It is not always clear where forces are applied to the structure, or which forces are important enough that they must be considered.
- The structure and covers are complex, offering multiple transmission paths.
- The many bolted joints of an engine create damping that is difficult to model accurately.

These difficulties apply just to calculating vibration velocities on the external surfaces of the engine. The task of calculating radiated noise remains.

A great deal of academic and industrial research has focused on modeling the noise generation of engines. As a result, a number of commercial software packages are available to deal with various aspects of the problem. First come models to predict the airflow and combustion behavior of the engine. This information is required in order to predict cylinder pressure, which is the driving force behind many engine noise forcing functions. Once cylinder pressure is known or predicted, other forcing functions must be modeled. Some models deal only with predicting the behavior of the crank train, and the resulting forces transmitted through the main bearings and oil films to the engine block. Other programs model the dynamics of valve trains or pistons, predicting the resulting force inputs. Elastohydrodynamic models of oil film behavior are an important element of these modeling programs, both to get the dynamics of the components right and to predict the forces put into the engine structure.

Once the forces being applied to the engine structure are understood, the next task is to model the structural response. This is normally done using widely

available finite element models. The models created for stress analysis are usually not appropriate for noise modeling because the large size of stress models leads to unacceptable run times for a dynamic analysis. A relatively coarse model of the engine structure is required. The known or predicted forcing functions are applied, and the dynamic response of the engine structure is calculated. The result is a velocity spectrum for each node in the model.

The final step is to predict the radiated noise, based on the velocities of the external surfaces. In doing this, radiation efficiency is directly or indirectly calculated. The most common approach is to create a boundary element model of the external surface. The velocities are entered as inputs, and overall sound power or sound pressure at specific locations can be calculated.

Boundary element models require considerable computational resources. There is a strong trade-off between model resolution (and thus the maximum frequency that can be accurately predicted) and run time. Other approaches may be considered. First, Rayleigh integral programs can predict overall radiated sound power with far less computational resources, but they cannot deal with calculating pressure at a point in space, or with noise in an enclosed space.<sup>18</sup> Second, statistical energy analysis (SEA) can be used in situations where the modal density is high enough to allow individual modes and resonances to be ignored. This suggests that SEA is only valid at relatively high frequencies, but the lower frequency limit is a matter of debate.<sup>19,20</sup> Alternative methods are also under development.<sup>21</sup>

A successful engine noise modeling effort is far from a plug-and-chug operation. It is easy to get a model to give the right answer for the wrong reasons. As a result, many experimental and analytical validation steps are required to show that each step of the modeling process is giving an accurate result, and that the assumptions made in the model are valid. Close cooperation between engineers doing the experimental and modeling work is essential. Only when models have been fully validated can they be used with any confidence to explore design alternatives.

#### REFERENCES

1. J. Haywood, *Internal Combustion Engine Fundamentals*, McGraw-Hill, New York, 1988.
2. *Bosch Automotive Handbook*, 6th ed., Robert Bosch, Stuttgart, Germany, 2004.
3. *Diesel Engine Management*, 3rd ed., Robert Bosch, Stuttgart, Germany, 2004.
4. D. Anderton, E. C. Grover, N. Lalor, and T. Priede, Origins of Reciprocating Engine Noise—Its Characteristics, Prediction, and Control, ASME Paper 70-WA/DGP-3, New York, American Society of Mechanical Engineers, 1970.
5. D. Anderton and J. M. Baker, Influence of Operating Cycle on Noise of Diesel Engines, SAE Paper 730241, Society of Automotive Engineers, Warrendale, PA, 1975.

6. B. Challen and M. Croker, The Effect of Combustion System on Engine Noise, SAE Paper 750798, Society of Automotive Engineers, Warrendale, PA, 1975.
7. D. Anderton, Basic Origins of Automotive Engine Noise, Lecture E2 of Engine Noise and Vibration Control Course, University of Southampton, Southampton, UK, 2004.
8. A. Zhao and T. Reinhart, The Influence of Diesel Engine Architecture on Noise Levels, SAE Paper 1999-01-1747, Society of Automotive Engineers, Warrendale, PA, 1999.
9. Data on gasoline and small diesel engines provided by AVL List, Graz, Austria, 2004. HD diesel engine data from the author's collection.
10. Data provided by Roush Industries, Inc., Livonia, MI, 2005.
11. M. F. Russell and R. Haworth, Combustion Noise from High Speed Direct Injection Diesel Engines, SAE Paper 850973, Society of Automotive Engineers, Warrendale, PA, 1985.
12. T. Nakada, A. Yamamoto, and T. Abe, A Numerical Approach for Piston Secondary Motion Analysis and Its Application to the Piston Related Noise, SAE Paper 972043, Society of Automotive Engineers, Warrendale, PA, 1997.
13. J. de Luca, N. Lalor, and S. Gerges, Piston Slap Assessment Model, SAE Paper 982942, Society of Automotive Engineers, Warrendale, PA, 1998.
14. R. Künzel, M. Werkmann, and M. Tunsch, Piston Related Noise with Diesel Engines—Parameters of Influence and Optimization, SAE Paper 2001-01-3335, Society of Automotive Engineers, Warrendale, PA, 2001.
15. J. Raub, J. Jones, P. Kley, and M. Rebbert, Analytical Investigation of Crankshaft Dynamics as a Virtual Engine Module, SAE Paper 1999-01-1750, Society of Automotive Engineers Warrendale, PA, 1999.
16. K. Yamashita et al., Prediction Technique for Vibration of Power-Plant with Elastic Crankshaft System, SAE Paper 2001-01-1420, Society of Automotive Engineers Warrendale, PA, 2001.
17. P. Hayes and C. Quantz, Determining Vibration, Radiation Efficiency, and Noise Characteristics of Structural Designs Using Analytical Techniques, SAE Paper 820440, Society of Automotive Engineer Warrendale, PA, 1982.
18. A. Seybert, D. Hamilton, and P. Hayes, Prediction of Radiated Noise from Engine Components Using the BEM and the Rayleigh Integral, SAE paper 971954, Society of Automotive Engineers Warrendale, PA, 1997.
19. G. Stimpson and N. Lalor, Noise Prediction and Reduction Techniques for Light Engine Covers, Proc. International Symposium on Automotive Technology and Automation (ISATA), Florence, Italy, May 1987.
20. N. Lalor, The Practical Implementation of SEA, Proc. International Union of Theoretical and Applied Mechanics (IUTAM) Conference on Statistical Energy Analysis, University of Southampton, Southampton, UK, July 1997.
21. F. Gerard et al., Numerical Modeling of Engine Noise Radiation through the Use of Acoustic Transfer Vectors—A Case Study, SAE Paper 2001-01-1514, Society of Automotive Engineers, Warrendale, PA, 2001.

# CHAPTER 85

## EXHAUST AND INTAKE NOISE AND ACOUSTICAL DESIGN OF MUFFLERS AND SILENCERS

Hans Bodén and Ragnar Glav

The Marcus Wallenberg Laboratory for Sound and Vibration Research  
Department of Aeronautical and Vehicle Engineering  
KTH—The Royal Institute of Technology  
Stockholm, Sweden

### 1 INTRODUCTION

A muffler or silencer is a device used in a flow duct to prevent sound from reaching the openings of the duct and radiating as far-field noise. Reactive silencers reflect sound back toward the source, while absorptive silencers attenuate sound using absorbing material. Mufflers and silencers are necessary components used in the design of any exhaust or intake system for internal combustion engines. No car or truck can pass the standard noise tests required by legislation or compete on the market without their use. There are three basic requirements for a modern exhaust system: compact outer geometry, sufficient attenuation, and low pressure drop.

Different acoustical design and analysis techniques to predict the acoustical performance of internal combustion engine exhaust and intake systems have been in use for many years. These theories and techniques can be used also for other applications, such as compressors and pumps and to some extent also for air-conditioning and ventilation systems. Techniques are not yet available for the prediction of the acoustical performance of modern intake systems made from plastic material with nonrigid walls.

### 2 TYPES OF MUFFLERS

Two different physical principles are used for sound reduction in mufflers. Sound can be attenuated by the use of sound-absorbing materials in which sound energy is converted into heat mainly by viscous processes. Typical sound-absorbing materials used are rock wool, glass wool, and plastic foams. To force the exhaust flow through the absorbing material would create a large pressure drop so the material is usually placed concentrically around the main exhaust pipe; see Fig. 1. To protect the absorbing material and prevent it from being swept away by the flow, a perforated pipe is usually inserted between the main pipe and the absorbing material. Sometimes a thin layer of steel wool is included for additional protection. In some cases the outer chamber containing the absorbing material is flattened because of space limitations in fitting the muffler under a car; see Fig. 2.

The other physical principle used is reflection of sound, which is caused by area changes or use of

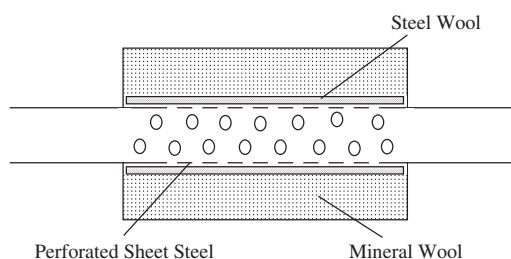


Figure 1 Typical exhaust system absorption muffler.<sup>1</sup>

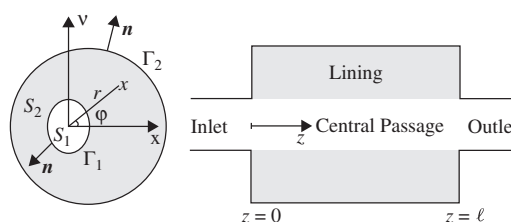


Figure 2 Absorption muffler of flat oval type.<sup>1</sup>

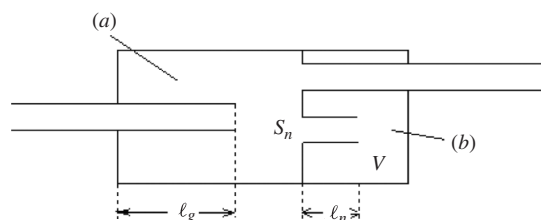
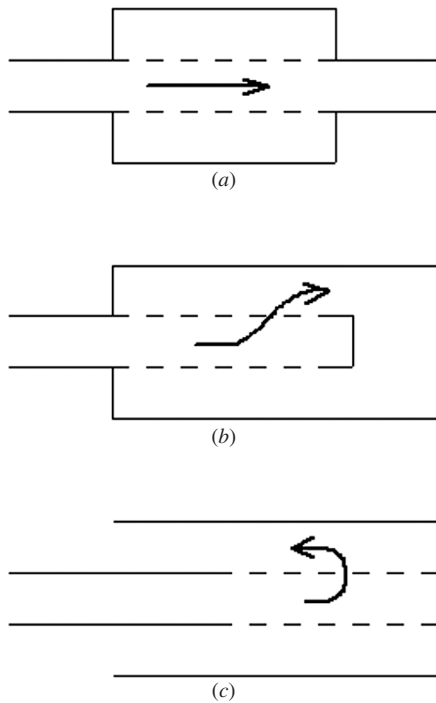


Figure 3 Different types of resonators in a typical reactive automobile silencer: (a)  $\lambda/4$  resonator and (b) Helmholtz resonator.<sup>1</sup>

different kinds of acoustical resonators; see Fig. 3. These types of mufflers are called reactive. If the acoustic energy is reflected back toward the source, then the question is what happens with it once it



**Figure 4** Different types of perforated muffler elements having both reactive and resistive character: (a) through flow, (b) cross flow, and (c) reverse flow.<sup>1</sup>

reaches the source. It could of course be that the source is more or less reflection free, but this is not usually the case. If multiple reflections in between the source and the reactive muffler occur, the sound pressure level should build up in this region and cause an increase further downstream too. The answer to this apparent paradox is that a reactive muffler when properly used causes a mismatch in the acoustic properties of the exhaust system and the source to actually reduce the acoustic energy generated by the source.

There are also cases where resistive and reactive properties are combined in the same muffler element. All reactive muffler elements do, in fact, cause some loss of acoustic energy in addition to reflecting a significant part of the acoustic energy back toward the source. The losses can be increased, for instance, by reducing the hole size of perforates, especially if the flow is forced through the perforates. Figure 4 shows some typical perforate muffler elements, where especially the cross-flow and reverse-flow type have a significant resistive as well as reactive character.

### 3 DEFINITIONS OF MUFFLER PERFORMANCE

To assess the success of a new muffler design, there is a need for measures to quantify the sound reduction obtained. There are at least three such measures in

common use: transmission loss, insertion loss, and noise reduction.

The transmission loss (TL) is defined as the ratio between the sound power incident to the muffler ( $W_i$ ) and the transmitted sound power ( $W_t$ ) for the case that there is a reflection-free termination on the downstream side

$$TL = 10 \log(W_i / W_t) \quad (1)$$

This makes it difficult to measure transmission loss since an ideal reflection-free termination is difficult to build, especially if measurements are to be made with flow. There are measurement techniques<sup>2,3</sup> that can be used to determine transmission loss by using multiple pressure transducers upstream and downstream of the test object. It is also necessary to make two sets of measurements either by using two acoustic sources, one downstream and one upstream of the test object, or by using two different downstream acoustic loads. The advantage of using transmission loss is, on the other hand, that it only depends on the properties of the muffler itself. It does not depend on the acoustic properties of the upstream source or the downstream load. Transmission loss can, therefore, also be calculated if the acoustic properties of the muffler is known without having to consider the source or load characteristics. Since the transmitted sound power can never be larger than the incident, the transmission loss must always be positive. A high transmission loss value tells us that the muffler has the capacity to give a large sound reduction at this frequency. It will not tell us how big the reduction will be since this depends on the source and load properties.

Insertion loss (IL) is defined as the difference in sound pressure level at some measurement point in the pipe or outside the opening when comparing the muffler element under test to a reference system:

$$IL = 20 \log(\tilde{p}_m / \tilde{p}_r) \quad (2)$$

where  $\tilde{p}_m$  is the root-mean-square (rms) value of the sound pressure for the muffler under test, and  $\tilde{p}_r$  is the rms value of the sound pressure for the reference system. It is common that the reference system is a straight pipe with the same length as the muffler element under test, but it could also be a baseline muffler design against which new designs are tested. Insertion loss is obviously easy to measure, as it only requires a sound pressure level measurement at the chosen position for the two muffler systems. It does, however, depend on both upstream acoustic source characteristics and downstream acoustic load characteristics. Insertion loss is, therefore, difficult to calculate since especially the source characteristics are difficult to obtain. Methods for determining source data will be further discussed in Section 6. Insertion loss has the advantage that it is easy to interpret. A positive value means that the muffler element under test is better than the reference system while a negative value means that it is worse.

Sound reduction (SR) is defined as the difference in sound pressure level between one point upstream of the muffler and one point downstream:

$$SR = 20 \log(\tilde{p}_u / \tilde{p}_d) \quad (3)$$

where  $\tilde{p}_u$  is the rms value sound pressure upstream of the muffler, and  $\tilde{p}_d$  is the rms value of the sound pressure downstream of the muffler. Just as insertion loss, sound reduction is easy to measure but difficult to calculate since it depends on source and load properties. The interpretation is less clear compared to transmission loss and insertion loss. It does tell us the difference in sound pressure level over the muffler for the test case, but the result may depend heavily on where the measurement positions are placed.

#### 4 THEORETICAL DESIGN APPROACHES

Development of computer programs for acoustical design and analysis of flow ducts can be said to have started in the 1970s, although some codes were certainly in existence earlier. The low-frequency region is usually most important for Internal Combustion (IC) engine applications. This means that a one-dimensional or plane-wave approach is sufficient for the main exhaust and intake pipes. Most of the codes developed have used the so-called transfer matrix method,<sup>4-8</sup> which is described in Section 4.1. This is a linear frequency-domain method that means that any nonlinearity in the sound propagation caused by high sound pressure levels is neglected. Local nonlinearity at, for instance, perforates can, however, be handled at least approximately. The assumption of linear sound propagation has experimentally been shown to be reasonably good.<sup>9,10</sup> There are other analytical linear frequency-domain methods like the mobility matrix formulation<sup>11</sup> and the scattering matrix formulation,<sup>7,12</sup> which have advantages for arbitrarily branched systems. Numerical methods such as the finite elements method (FEM)<sup>6</sup> can also be used to solve the linear equations. They are especially useful for mufflers with complicated geometry and large cross-sectional area where the plane-wave propagation is no longer sufficient to describe the sound propagation in the frequency range of interest, but do increase the complexity of the calculations significantly. FEM should, therefore, only be considered as complement to the analytical methods for cases where they fail. Nonlinear time-domain techniques such as the method of characteristics or computational fluid dynamics (CFD) techniques<sup>6,13</sup> have also been suggested. They are usually linked to a nonlinear model of the gas exchange process of the engine and are not really adapted for modeling muffler components even though some interesting attempts have been made. There are commercial codes available for simulating the engine gas exchange process that are in use by the automotive industry. They are an interesting alternative for obtaining information about the engine as an acoustic source, which will be further discussed in Section 6.

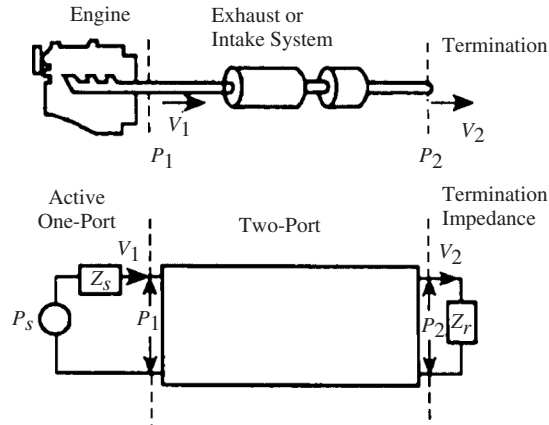


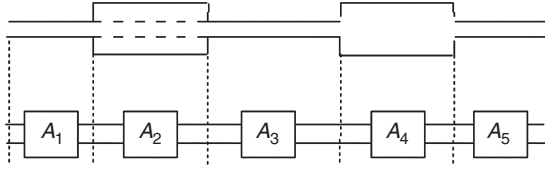
Figure 5 IC engine equipped with muffler and its acoustical representation.

##### 4.1 Transfer Matrix Method

The transfer matrix method is an effective way for the analysis of sound propagation inside a duct network, especially if most of the acoustical elements are connected in cascade. The exhaust system of an internal combustion engine does in many cases have this kind of transmission line character. The method, which is often referred to as the four-pole method, was originally developed for the theory of electric circuits. To get a complete model accurate for analysis and design of exhaust systems, we must also take the influence of the sound source and the termination of the system into account. That is the sound generation and acoustic reflection characteristics of the engine as an acoustic source and the sound reflection and radiation characteristics of the termination. Using the assumptions of linearity and plane waves, the actual physical system with engine, exhaust system, and outlet can be described by a sound source, transmission line, and acoustic load; see Fig. 5.

The source is fully determined by the source strength  $P_s$  and the source impedance  $Z_s$ , which reveals how the source reacts to an arbitrary outer load such as an exhaust system. The load is described by a termination impedance. The source data and load data will be discussed further in Sections 6 and 7.

Three basic assumptions concerning the sound field inside the transmission line are made in the transfer matrix method. First, the field is assumed to be linear, that is, the sound pressure is typically less than one percent of the static pressure. This allows the analysis to be carried out in the frequency domain, and transfer function formulations can be used to describe the physical relationships. The assumption of linearity does not, however, mean that no nonlinear acoustic phenomena inside the system can be modeled. Some local nonlinear problems can, for example, be solved in the frequency domain by iteration techniques. The second assumption requires that the system within the black box is passive, that is, no



**Figure 6** Exhaust system modeled with the transfer matrix method.<sup>1</sup>

internal sources of sound are allowed. Finally, only the fundamental acoustic mode, the plane wave, is allowed to propagate at the inlet and outlet sections of the system. Provided the above-mentioned assumptions are valid, there exists a complex  $2 \times 2$  matrix  $\mathbf{T}$ , one for each frequency, that completely describes the sound transmission within the system:

$$\begin{bmatrix} \hat{P}_1 \\ \hat{V}_1 \end{bmatrix} = \begin{bmatrix} t_{11} & t_{12} \\ t_{21} & t_{22} \end{bmatrix} \begin{bmatrix} \hat{P}_2 \\ \hat{V}_2 \end{bmatrix} \quad (4)$$

where  $\hat{P}_1$  and  $\hat{P}_2$  are the temporal Fourier transforms of the sound pressures, and  $\hat{V}_1$  and  $\hat{V}_2$  are the temporal Fourier transforms of the volume velocity at the inlet and the outlet, respectively. The major advantage with the transfer matrix method is the simplicity with which the transfer matrix for the total system is generated from a combination of subsystems, each described by its own transfer matrix; see Fig. 6.

The transfer matrix for a number of elements  $A_1, A_2, \dots, A_N$  connected in cascade is obtained from repeated matrix multiplication:

$$\mathbf{T} = \prod_{j=1}^N \mathbf{A}_j \quad (5)$$

This is a procedure that for long transmission lines is much more effective than solving a large system of equations, as will be the alternative if the mobility matrix formulation is used.

The division of the total system into more easily analyzed subsystems can be done in many different ways as long as the coupling sections between the elements fulfill two conditions. First, there must be continuity in sound pressure and volume velocity. This is achieved by choosing a suitable formulation of the transfer matrix, where the effects of discontinuities are included within the described element. Second, the coupling sections must not allow any higher order modes to propagate. This condition implies that the allowed frequency range for the classical transfer matrix method has an upper limit that coincides with the cut-on frequency for the first higher order mode in the coupling section. With modal decomposition the number of modes can easily be extended by increasing the dimension of the transfer matrix and accordingly the frequency range.<sup>14</sup> Once the division of the system into acoustical elements has been done, the final task is to generate the total transfer matrix. This is done

in analogy with the theory of electric circuits, that is, by regarding the system as a network of cascade- or parallel-coupled elements. In exhaust systems, most of the elements are usually connected in cascade, and the transfer matrix formulation is, therefore, especially powerful for this application.

## 5 MODELING OF MUFFLER ELEMENTS

### 5.1 Straight Ducts

A typical automobile exhaust system consists of two or three silencers connected by ordinary sheet steel pipes. These are usually straight or slightly curved with circular constant cross section (diameter typically around 50 mm) and wall thickness of 1 to 1.5 mm. A truck system typically has pipes with 100-mm to 150-mm diameter. To be able to use the transfer matrix or scattering matrix method, only plane waves should propagate in the pipes. The expression for the cutoff frequency of the first higher order mode in a circular cross section pipe is given by

$$f^c = \frac{1.841c}{\pi d} \quad (6)$$

where  $c$  is the speed of sound and  $d$  is the duct diameter. The cutoff frequency for a typical automotive system would, therefore, be above 4 kHz and for a truck system it would be above 1.3 kHz at room temperature. In the exhaust systems the temperatures will be higher, which means that the speed of sound and the cutoff frequency will increase. For the typical curvatures and diameters, the influence of the bends may be neglected in the frequency range of interest: 30 to 2000 Hz.<sup>15</sup>

The solution for the sound pressure and volume velocity can in the frequency domain be written as

$$\hat{p} = \hat{p}_+ \exp(-ik_+z) + \hat{p}_- \exp(ik_-z) \quad (7)$$

$$\hat{V} = \frac{S}{\rho_0 c'} \{ \hat{p}_+ \exp(-ik_+z) - \hat{p}_- \exp(ik_-z) \} \quad (8)$$

where  $\hat{p}_+$  and  $\hat{p}_-$  are the wave amplitudes,  $z$  is the coordinate in the propagation direction,  $S$  is the cross-sectional area,  $k_+$  and  $k_-$  are the complex wavenumbers representing downstream and upstream propagating waves,<sup>16,17</sup> respectively,

$$k_+ = k \frac{K_0}{1 + MK_0} \quad (9)$$

$$k_- = k \frac{K_0}{1 - MK_0} \quad (10)$$

where  $K_0$  is given by

$$K_0 = 1 + \frac{1+i}{s\sqrt{2}} \left( 1 + \frac{\gamma-1}{\sigma} \right) \quad (11)$$



and  $\gamma$  is the specific heat coefficient ratio,  $\sigma = \sqrt{\mu C_p / \kappa}$  is the Prandtl number,  $s = (d/2)\sqrt{\rho_0 \omega / \mu}$  is the shear wavenumber,  $\mu$  is the shear viscosity coefficient,  $\kappa$  is the thermal conductivity coefficient,  $C_p$  is the specific heat coefficient for constant pressure,  $\rho_0$  is the density, and  $d$  is the duct diameter. These expressions include the effect of viscous and thermal boundary layer losses and losses due to turbulence. Equations (9) to (11) are valid for large  $s$  and small  $M$ , typically  $M < 0.3$  and  $s > 40$ . Howe<sup>18</sup> has presented a theory with wider application range but yielding more complicated expressions.

Following the notation of Section 4.1 denoting the inlet or source side 1 and the outlet side 2, the transfer matrix is given by

$$\begin{aligned} t_{11} &= \frac{1}{2} \{ \exp(ik_+\ell) + \exp(-ik_-\ell) \} \\ t_{12} &= \frac{\rho_0 c}{2S} \{ \exp(ik_+\ell) - \exp(-ik_-\ell) \} \\ t_{21} &= \frac{S}{2\rho_0 c} \{ \exp(ik_+\ell) - \exp(-ik_-\ell) \} \\ t_{22} &= \frac{1}{2} \{ \exp(ik_+\ell) + \exp(-ik_-\ell) \} \end{aligned} \quad (12)$$

In the long pipes between the different silencers there may be temperature gradients. This problem can be solved by dividing the pipe into a number of elements, each with a constant but different temperature, and thus obtain the desired temperature gradient.<sup>19</sup>

## 5.2 Dissipative Muffler Elements

A typical dissipative exhaust system muffler is shown in Fig. 1. The most simple approach that can be used for this kind of muffler is that the walls are locally reacting, that is, each point in the wall acts as if it were completely isolated from the rest of the wall.<sup>20</sup> This is often a good assumption in the case of walls covered with porous material, but it is an approximation. The alternative is to use an extended reaction model where sound propagation in the liner is considered. The locally reacting wall is characterized by a locally reacting impedance,  $Z_w$ . The linear, nonviscous, adiabatic sound field within a duct with locally reacting walls can be found from the wave equation by adding a source term.<sup>20</sup> This term is really originating from the equation of continuity, where it accounts for the volume velocity through the walls. It should be noted that this approach is really one-dimensional and the wave is thus still plane, as discussed above. The solution in the frequency domain may be expressed in a way similar to the solution in (7) and (8), but with different wavenumbers:

$$\begin{aligned} k_{\pm} &= \pm \frac{i}{1 - M^2} \left\{ ikM + \frac{\rho_0 c M}{2Z_w S} \right. \\ &\quad \left. \mp \sqrt{\left( \frac{\rho_0 c M}{2Z_w S} \right)^2 + \frac{ik\rho_0 c}{Z_w S} - k^2} \right\} \end{aligned} \quad (13)$$

The upper sign represents the downstream wave and the lower sign represents the upstream wave.

In a conventional dissipative automobile silencer (Fig. 1), the porous material is covered by perforated sheet steel. Thus  $Z_w$  really consists of two impedances, the porous material  $Z_a$  and the perforated shielding  $Z_p$ . The acoustic effect of the perforations can, however, be neglected if the porosity, that is, the percentage open area, is higher than around 20%. This is often true if the perforated pipe was included just to guide the flow and keep the absorbing material in place and not to have any acoustic effect. For the description of the porous material the model according to Zwikker and Kosten<sup>21</sup> can be used. An extensive description of different models for the acoustical properties of porous materials is given in Ref. 22. In the Zwikker–Kosten model the effects of the porous material on acoustic motion are included in the equations of motion and conservation of mass through three parameters. The first is called porosity,  $\Omega$ , and accounts for the obvious fact that a specific volume is no longer completely occupied by the fluid; there is also a solid structure. The fluid within the porous material can only propagate along certain paths, which means that the reaction of some fluid particle to a pressure gradient not necessarily needs to be in the direction of the gradient. Provided these paths are randomly oriented, that is, the absorber is isotropic, this effect is described by the structure factor,  $\chi$ . Finally, the increased friction within the fluid due to the solid structure is considered by the flow resistivity  $\phi$ . The following impedance as seen from the duct toward the lining can be deduced,

$$Z_a = -i\rho_e c_e (\omega h / c_e) \quad (14)$$

where  $h$  is the thickness of the lining,  $\rho_e$  is the effective density, and  $c_e$  is the effective speed of sound. These are given by

$$\rho_e = \rho_0 \left( \frac{\chi}{\Omega} - \frac{i\phi}{\omega\rho_0} \right) \quad (15)$$

$$c_e = \frac{1}{\sqrt{\rho_e \kappa_p \Omega}} \quad (16)$$

In this expression  $\kappa_p$  is the compressibility for the porous material, which for low frequencies behaves more or less isothermally due to the heat conduction between solid and fluid. At higher frequencies the acoustic motion is very fast, no heat conduction can appear, and the motion is adiabatic. These assumptions are verified experimentally,<sup>23</sup> and usually the true compressibility lies somewhere between  $\kappa_T$  and  $\kappa_s$ .

## 5.3 Perforated Muffler Elements

Perforated tubes are commonly found in automotive mufflers. Two basic configuration examples are shown in Fig. 7. In a commercial muffler the configuration

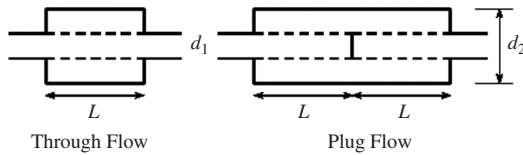


Figure 7 Basic muffler configurations.



Figure 8 Examples of commercial perforated mufflers.

is usually much more complicated, as illustrated in Figs. 8 and 9.

Perforates can be used to confine the mean flow in order to reduce the back-pressure to the engine and the flow generated noise inside the muffler, such as in the through-flow configuration. Ideally, perforates are then acoustically transparent and permit acoustic coupling to an outer cavity acting as a muffler. Perforates can also be used to create losses when the flow is forced through the perforates, such as for the plug flow configuration. Being able to theoretically model these mufflers enables car manufacturers to optimize their performance and increase their efficiency in attenuating engine noise. Therefore, there has been

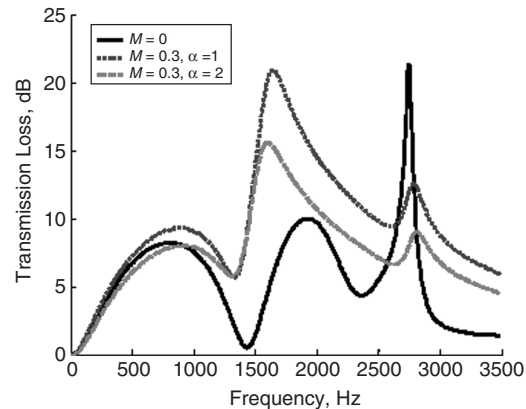


Figure 9 Effect of coupling condition and Mach number on the transmission loss of the through-flow muffler.<sup>35</sup>

a lot of interest to model the acoustics of two ducts coupled through a perforated plate or tube. Generally, the modeling techniques can be divided into two main groups, the distributed parameter approach and the discrete or segmentation approach.

In the distributed approach, the perforated tube is seen as a continuous object, and the local pressure difference over the tube is related to the normal particle velocity via surface-averaged wall impedance. The main challenge facing this approach is the decoupling of the equations on each side of the perforate. Using this approach results in closed-form expressions for the acoustic transmission, and therefore the calculations are very fast. Sullivan and Crocker<sup>24</sup> presented the first analysis of this approach. They only considered through-flow concentric resonators with the flow confined in the main duct. They did not have the decoupling problem because the flow inside the cavity was assumed to be zero. Therefore, their model cannot be applied to situations with cross flow. Moreover, it does not work for nonrigid boundary conditions at the side plates of the muffler, for example, extended inlet and outlet configurations.

Later, Jayaraman and Yam<sup>25</sup> introduced a decoupling approach based on a mathematical assumption that requires the mean flow Mach number to be equal on both sides of the perforate. This is considered a major disadvantage because this case is hardly found in practice. The two Mach numbers are in inverse proportion to the cross-sectional area of the two ducts, which are usually different. Rao and Munjal<sup>26</sup> presented a method to overcome this problem with a generalized decoupling analysis that allows for different flow Mach numbers in the two pipes. They used the same equations as Sullivan and Crocker.<sup>24</sup> They also extended the method to be able to handle any boundary conditions at the muffler end plates. Peat<sup>27</sup> pointed out that their decoupling conditions are only satisfied for the two simple cases of  $M_1 = M_2 = 0$  or  $M_1 = M_2$ . He was unable to find analytical expressions that fully satisfy the generalized approach and hence resorted to

a numerical decoupling solution. Munjal et al.<sup>28</sup> presented a first attempt to use the numerical decoupling technique, but they reported problems of numerical instabilities close to the peaks of the transmission loss. Peat<sup>27</sup> derived more general equations than all previous models by allowing the Mach number and impedance to vary along the length of the perforate. This generalization contains some of the properties and advantages of the segmentation approach. He only made calculations using constant parameters. Numerical decoupling overcomes the modeling deficiencies of the analytical techniques, introducing an additional cost in terms of computing time as it requires solving an eigenvalue problem. Dokumaci<sup>29</sup> developed a new approach for numerical implementation of the distributed parameter method based on the so-called Matrizant theory. This approach is comparable to Peat's numerical decoupling method in that an eigenvalue problem has to be solved; however, it is able to correctly handle a mean flow velocity gradient that was earlier a shortcoming of the distributed parameter methods. Dokumaci criticized Peat's method pointing out that a gradient term appears to be missing in the governing equations, and that he neglected the mean flow variation in some terms that might be of the same order as the retained terms. There was a published correspondence on this issue.<sup>30</sup>

Finally, Dokumaci<sup>29</sup> concludes that "the distributed parameter theory of plane wave propagation in a perforated pipe provides a more satisfactory setting than the segmentation method for the analysis of the effects of axially varying quantities such as the mean flow velocity." But later, Dokumaci<sup>31</sup> himself stated that "the discrete approach is computationally simpler and more versatile than the more commonly known distributed parameter method."

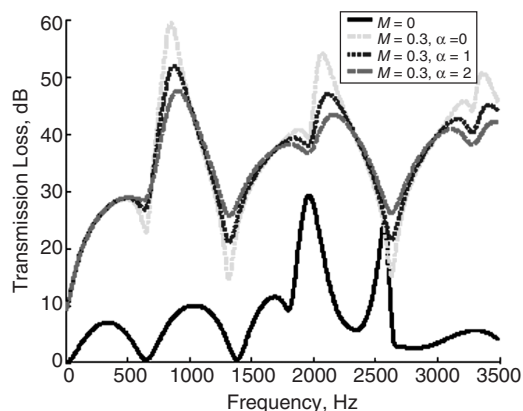
The discrete or segmentation approach was first developed by Sullivan.<sup>32,33</sup> In this approach, the coupling of the perforate is divided into several discrete coupling points with straight hard pipes in between. Each segment consists of two straight hard pipes and a coupling branch. The total  $4 \times 4$  transmission matrix of the perforated element is found from successive multiplication of the transmission matrices of each segment. Kergomard et al.<sup>34</sup> used this concept and presented, for the case of two waveguides communicating via single holes, a model for wave transmission in a periodic system. Dokumaci<sup>31</sup> presented another discrete approach based on the scattering matrix formulation. He discussed several possibilities for modeling the connecting branch. He proposed a continuous viscothermal pipe model, a continuous isentropic pipe model with end corrections, and a lumped impedance model (as in Sullivan). The conclusion was that the lumped-element model is the most appropriate for this problem. He sometimes added a correction to the segment length so that his results match Sullivan experiments. It was unclear how he determined this end correction and on what basis he includes it or not.

The distributed approach is mainly convenient for relatively simple perforated mufflers. There are, however, many complicated muffler configurations in

which perforations are used in nonstandard ways. The discrete approach is more convenient to analyze advanced muffler systems because of numerical simplicity and flexibility. It is also straightforward to model gradients in mean flow and temperature using this approach, and as demonstrated in<sup>33</sup> arbitrary complex perforated systems can be also handled. One main difference between the distributed and discrete approaches is the definition of the coupling conditions over the perforate. In the distributed approach, continuity of acoustic momentum is usually imposed, whereas in the discrete approach, continuity of acoustic energy is usually assumed. Recently, Aurégan and Leroux<sup>35</sup> presented an experimental investigation of the accuracy of these coupling conditions with flow. They demonstrated that neither continuity of momentum nor energy seems to be strictly valid. Aurégan and Leroux suggested that the coupling condition should be something in between conservation of energy and conservation of momentum. The sensitivity of the results to the assumption of the coupling condition was investigated by Elnady<sup>36</sup> using a generalized segmentation model based on Sullivan's approach. This general model is able to use any specified coupling condition based on a single parameter,  $\alpha$ , which has the value of 1 for continuity of energy, 2 for continuity of momentum, or can be assigned any value in between. The sensitivity of the transmission loss results were compared for the simple muffler configurations shown in Figs. 7 and the results are shown in Figs. 9 and 10.

The effect of flow on the transmission loss caused by the increased resistance when the flow is forced through the perforates can be clearly seen in Fig. 10. It can also be seen that the choice of coupling condition is of importance for these simple mufflers. A complicated multichamber muffler was also analyzed in Ref. 36. See Fig. 11.

A comparison between measured and predicted transmission loss at 0.15 Mach is shown in Fig. 12. A reasonable agreement between measured and predicted results is obtained. It can also be seen that the



**Figure 10** Effect of coupling condition and Mach number on the transmission loss of the plug flow muffler.<sup>35</sup>

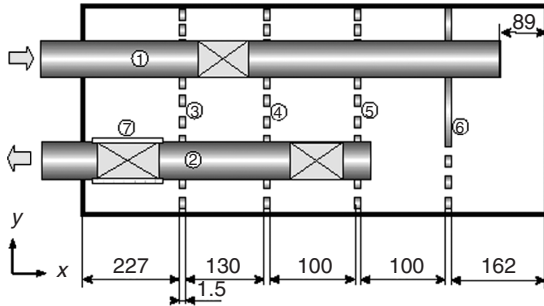


Figure 11 Sketch of complex perforated muffler analyzed.<sup>35</sup>

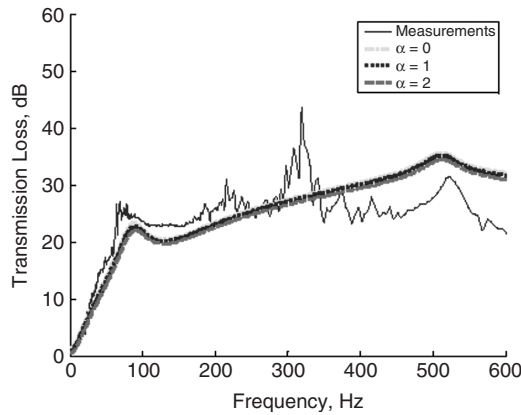


Figure 12 Comparison between measured and calculated transmission loss at  $M = 0.15$  for complex perforated muffler analyzed.<sup>35</sup>

choice of coupling condition is much less important in this case. The reason is probably that a number of other parameters besides the losses caused by flow through the perforates are important for the complex muffler. These losses are, however, very important for obtaining the high transmission loss over the wide frequency band seen in Fig. 12.

#### 5.4 Expansion Chambers

The dimensions of a typical exhaust expansion chamber usually makes it necessary to consider the effects of propagating higher modes for an analysis in the usual frequency range of interest, 30 to 2000 Hz. Since typical expansion chambers are quite short, the losses due to viscosity and heat conduction can be neglected along with the flow-acoustic interaction, which may occur especially at the inlet and outlet regions. The convection can also be neglected for typical Mach numbers even if it is accounted for in one of the models discussed below. A simple analytical approach, such as mode matching,<sup>37</sup> can often be used for ducts of cross-sectional shape and boundary conditions for

which the solutions to the wave equation form a complete set of eigenfunctions. These functions are usually very complicated, and accordingly the method is most suited for cases where the eigenfunctions are orthogonal. This analysis is carried out for ducts of circular cross section, and cylindrical coordinates  $(r, \phi, z)$  are chosen in which the boundary condition of nonflexible walls are easily formulated. As an extension to Eq. (7) the three-dimensional solution to the wave equation can be written as a mode sum:

$$\hat{p} = \sum_n \{ \hat{p}_n^+(r, \phi) \exp(-ik_n^+ z) + \hat{p}_n^-(r, \phi) \exp(ik_n^- z) \} \quad (17)$$

where  $\hat{p}_n^+$  and  $\hat{p}_n^-$  are the eigenfunctions for the duct cross section, and  $k_n^+$  along with  $k_n^-$  are the longitudinal wavenumbers for each mode as determined by the boundary conditions, where  $n = 0$  generates the usual plane wave. Two different types of chambers, flush-mounted inlet and outlet and concentric inlet and outlet will be discussed below.

**5.4.1 Eccentric Inlet and Outlet** This configuration of a circular expansion chamber (Fig. 13) with the inlet and outlet mounted in plane with the end walls but otherwise arbitrarily has been treated by Ih and Lee<sup>38</sup> using the assumptions above, although including the convective effect of mean flow. The influence of higher order modes in the inlet and outlet ducts is completely neglected in their analysis, that is, only the end corrections toward the chamber are included. The approach is similar to that of a duct with one closed nonflexible end and the other driven by a plane piston. To match the field inside the chamber with the incident, reflected and transmitted plane waves, it is averaged over the inlet and outlet cross-section areas.

**5.4.2 Extended Inlet and Outlet** Another common type of expansion chamber (Fig. 14) is with extended inlet and/or outlet, forming a annular  $\lambda/4$  resonator with the end plates.

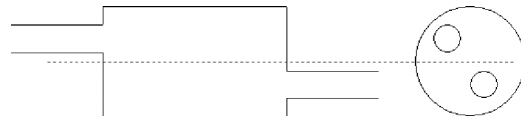


Figure 13 Expansion chamber with flush-mounted eccentric inlet and outlet.

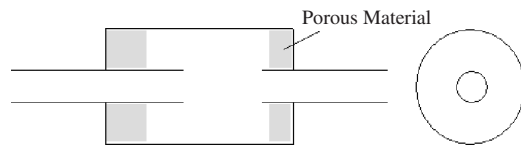


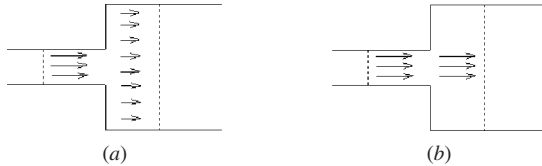
Figure 14 Expansion chamber with concentric extended inlet and outlet.

To simplify the analysis the inlet and outlet are assumed to be mounted concentrically, and further all effects of mean flow are neglected. This analysis using the mode-matching technique is explained in detail by Åbom.<sup>39</sup> It should be noted that higher modes are included not only in the main chamber but also in the  $\lambda/4$  resonator region and in the inlet and outlet ducts, although only plane waves are assumed to be incident on the chamber in these ducts. The number of analyzed modes is prescribed for the main chamber and the number of modes in the other regions, required for accurate analysis, is then given by the so-called edge condition.<sup>38</sup>

### 5.5 Area Discontinuity Muffler Elements

The analysis of sound propagation through sudden changes in the cross-section area of a flow duct is complicated in the case of superimposed mean flow. This is due to the interaction between the mean flow field and the acoustic field in these regions. From the theoretical point of view, the problem is that the actual mean flow velocity profile near the expansion or the contraction is too complicated to allow any exact analytical approach, at least so far.

However, by assuming a simpler velocity profile, the problem has still been treated in a number of references.<sup>14,40,41</sup> The original assumption, made by Ronneberger,<sup>40</sup> is that the distance over which the mean flow is expanded or contracted is negligible compared to the acoustic wave length. This assumption is also adopted by Alfredson and Davies<sup>42</sup> and will be used here, as it enables the transmission properties of the area discontinuity to be formulated (Fig. 15). Another assumption, introduced by Cummings<sup>41</sup> is that the velocity profile reacts more slowly to the change in area. For a typical expansion chamber this means that the mean flow “jet” entering the chamber is not assumed to expand in the short distance between inlet and outlet of the chamber. The analysis using both these assumptions is one-dimensional and valid for quasi-steady conditions, including the irreversible losses due to turbulence in the conservation of energy. A three-dimensional more rigorous and extensive analysis has been presented by Nilsson and Brander<sup>14</sup> imposing a strict Kutta condition at the area discontinuity. In this theory the hydrodynamic modes, which are excited at the sudden expansion but further downstream turned into turbulence, are included. For exhaust systems, where



**Figure 15** Mean flow velocity profile of an area expansion and control volume for quasi-stationary analysis according to (a) Ronneberger<sup>40</sup> and (b) Cummings.<sup>41</sup>

the Mach numbers typically are less than 0.1 and the analysis is restricted to rather low frequencies, it has been found that the differences between the different formulations are small. The simple analysis of Alfredson and Davies is quite accurate for this application, although the acoustic near-field effects have to be included. In the following analysis these effects are added as indicated by Davies<sup>43</sup> and Lambert and Steinbrueck<sup>44</sup> using Karal's end correction.<sup>45</sup> The usual silencer element where the inlet or outlet are extended into the larger duct is also modeled. The analysis includes both positive and negative mean flow, and application to an intake system is therefore also possible.

**5.5.1 Area Contraction** The transfer matrix expression given below was derived following the assumptions indicated above and regarding the acoustic wave as a one-dimensional quasi-stationary perturbation of the mean flow and further assuming adiabatic contraction and positive isentropic flow. This means that losses caused by flow separation at the flow contraction has been neglected. This is an approximation but is usually justified. The following transfer matrix  $C$  is obtained over the control volume given in Fig. 15:

$$\begin{aligned} t_{11} &= 1 - \frac{M_1 \rho_0 c}{z S_1 (1 - M_1^2)} \\ t_{12} &= \rho_0 c \frac{(S_1/S_2 - S_2/S_1) M_1 - \rho_0 c M_1^2 / z S_2}{S_2 (1 - M_1^2)} \\ &\quad + m_{12} \frac{1 - \rho_0 M_1}{z S_1 (1 - M_1^2)} \\ t_{21} &= \frac{1}{z (1 - M_1^2)} \\ t_{22} &= \frac{1 - (M_1^2 + \rho_0 c M_1 / z S_1) (S_1/S_2)^2}{1 - M_1^2} \\ &\quad + \frac{m_{12}}{z (1 - M_1^2)} \end{aligned} \quad (18)$$

where  $m_{12} = i \omega \rho_0 \Delta_e / \pi a^2$  and index 1 is for the inlet side and index 2 for the outlet side. The boundary condition of a nonflexible end wall is in the case of extended outlet replaced by an impedance condition given by  $\lambda/4$  resonator of length equal to the distance between the outlet opening and the end wall  $\ell$ :

$$Z = -i \rho_0 c \cot\{k(\ell + \Delta_e)\} \quad (19)$$

To estimate the effects of the acoustic near field at the area discontinuity, we use the end correction according to Karal, which is deduced in the case of no mean flow for a contraction, or expansion, in a circular duct. For the extended outlet/inlet case, this correction will be slightly too large, although sufficiently accurate for this application according to



Davies.<sup>7</sup> The correction acts as an extra length added to the smaller duct. The end correction  $\Delta_e$  is given as

$$\Delta_e = 8H(\alpha)a/3\pi \quad (20)$$

with

$$H(\alpha) \approx 0.875(1 - \alpha)(1.371 - \alpha) \quad 0.5 \leq \alpha \leq 1.0$$

$$H(\alpha) \approx 1 - 1.238\alpha \quad 0 \leq \alpha \leq 0.5$$

and  $\alpha$  as the ratio of the duct diameters (smaller/larger).

As there are only plane waves propagating, we have in Eq. (18) made the following definition:

$$z = Z/|S_1 - S_2| \quad (21)$$

For intake systems where the mean flow is in the opposite direction to the sound propagation, there will be turbulent losses at an acoustic contraction, and the problem is similar to that of an exhaust system area expansion, which is treated in the next section. To obtain the desired four-pole, we only have to change the sign of the volume velocity and invert the transfer matrix for an expansion with positive mean flow.

**5.5.2 Area Expansion** In the case of an area expansion, we have to consider the irreversible turbulent losses that occur at the discontinuity due to the expanding mean flow. Including a corresponding change in entropy, the following transfer matrix is obtained:

$$\begin{aligned} t_{11} &= \frac{1 + \{\gamma(1 - S_1/S_2)^2 - 1\}M_1^2}{\det} \\ &\quad + m_{12} \frac{1 + \gamma(M_1 S_1/S_2)^2}{z \det} \\ t_{12} &= \frac{2\rho_0 c M_1 (S_1/S_2 - 1)}{S_2 \det} \\ &\quad + m_{12} \{1 + (M_1^2 S_1/S_2)(1 - 2S_1/S_2) \\ &\quad + 2\rho_0 c M_1 S_1/S_2^2 z\}/\det \\ t_{21} &= \frac{1 + \gamma(M_1 S_1/S_2)^2}{z \det} \\ t_{22} &= \{1 + M_1^2 S_1(1 - 2S_1/S_2)/S_2 \\ &\quad + 2\rho_0 c M_1 S_1/z S_2^2\}/\det \end{aligned} \quad (22)$$

where

$$\begin{aligned} \det &= 1 + M_1^2 \{\gamma - 1 + (\gamma - 1)(S_1/S_2)^2 \\ &\quad + (1 - 2\gamma)S_1/S_2\} + 2\rho_0 c M_1/S_2 z \end{aligned}$$

As above, for the intake system application with negative mean flow, the transfer matrix can be obtained from the transfer matrix for a contraction with positive

mean flow. Due to reciprocity, which is known to be valid in the case of no irreversible losses, no inversion is necessary, and the desired transfer matrix is obtained from Eq. (18) by simply shifting notations 1 and 2.

## 5.6 Horn Muffler Elements

A smooth expansion or contraction in a flow duct, that is, a horn is often used to decrease the pressure drop in an exhaust system. Neglecting losses, mean flow, and higher modes and further considering the walls of the horn to be nonflexible, the wave equation can be integrated to yield Webster's horn equation.<sup>46</sup> Simple analytical solutions to this equation only exist for a few types of horns, where the cross-section area (or radius) is some simple function of the length coordinate,  $S = S(z)$ . A typical example is the exponential horn where  $S = S_0 \exp(mz)$ , where  $m$  is called the flare constant. Another example, which we will refer to later, is the conical horn where the radius of the circular cross section is linearly dependent on the length coordinate,  $r = a_0 + k_0 z$ . To allow for an arbitrarily varying cross section, the approach used above for temperature gradients can be applied. The horn is divided into a number,  $N$ , of short "ordinary pipes" connected in cascade and continuity in pressure, and volume flow is assumed. Thus, this formulation extends the analysis to, in an approximate manner, include also mean flow and losses. Although this method has been successful in other applications as well, see, for instance Åbom,<sup>47</sup> no formal proof has been found for the convergence.

It should finally be mentioned that Doak and Davies<sup>48</sup> have presented an analysis of sound propagation in horns including the effects of mean flow. They also suggest that their solution replaces the straight pipe solution used above in order to reduce the number of segments,  $N$ .

## 5.7 Resonators

Traditionally, resonator silencers were mostly used for IC engines running at constant speed. The increasing demand for silencers with low pressure drop but still sufficient low-frequency attenuation has, however, made resonators more frequently used in automobile exhaust systems, especially in combination with dissipative silencers. The resonator silencer is very efficient regarding maximum attenuation versus pressure drop. The major disadvantages are the rather narrow frequency bands for which this attenuation occurs and the sensibility to variations in temperature. There may also be flow-acoustic interaction that causes the resonator to "sing." The acoustical concept of the resonator and, in fact, of all reactive silencers is to create a discontinuity in impedance along the flow duct, which causes a reflection of the propagating wave. For resonators this is achieved at the frequencies where the resonator mounted in the duct wall has zero impedance, neglecting losses, as seen from the flow duct, that is, at resonance. The following analysis is restricted to applications where the orifice of the resonator, which sometimes is called the mouth, and the diameter of the flow duct are small compared to the wavelength. The pressure is, therefore, uniform at the orifice and equal

to the upstream and downstream values, thus indicating a lumped description. The transfer matrix for this element of no extension along the transmission line is easily formulated:

$$\begin{aligned} t_{11} &= 1 \\ t_{12} &= 0 \\ t_{21} &= S_r/Z_r \\ t_{22} &= 1 \end{aligned} \quad (23)$$

where  $Z_r$  is the impedance of the resonator as seen from the flow duct and  $S$  is the area of the resonator mouth. Three different resonators are now described. Due to the restriction mentioned above and the fact that resonators mainly are silencers for tonal low-frequency noise, the models used in these sections are only valid in the low-frequency region, where the fundamental tone and the first harmonics are present.

**5.7.1 Helmholtz Resonator** The Helmholtz resonator is the most common type of resonator due to its geometrical compactness. This really means that it is possible to design a quite small Helmholtz resonator with a low-resonance frequency. It should be noted, however, that the efficiency of the resonator is related to the size, and rigorous design is necessary.

The Helmholtz resonator is the acoustical counterpart to the mechanical mass-spring system where the fluid in the neck is equivalent to the mass and the fluid in the cavity is equivalent to the spring. This lumped description is, of course, only valid as long as the wavelength is large compared to the dimensions of cavity and neck. Assuming the motion to be adiabatic, the impedance for the Helmholtz resonator can be written as

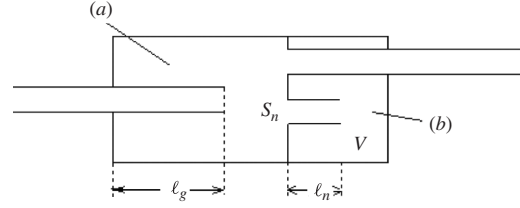
$$\begin{aligned} Z_{hr} &= R_{tu} + R_v + i\omega\rho_0(\ell_n + \Delta_i + \Delta_o) \\ &\quad - i\rho_0c^2 S_n/\omega V \end{aligned} \quad (24)$$

where  $\ell_n$  and  $S_n$  are the length and cross-section area of the neck, respectively; see Fig. 16;  $\Delta_i$ , and  $\Delta_o$  are the end corrections due to the inner and outer near field as given by<sup>46</sup>

$$\Delta_i + \Delta_o = 0.85a(1 + \varepsilon) \quad (25)$$

where  $\varepsilon$  is given by the following relations:

$$\begin{aligned} \varepsilon &= 1 - \frac{V_f}{fd_p} \leq \frac{0.24a}{d_p} \\ \varepsilon &= \left(1 + 0.3\frac{d_p}{a}\right) \\ &\quad \times \exp\left(\frac{0.24a/d_p - V_f/fd_p}{0.25 + d_p/2}\right) \\ &\quad - 0.3\frac{d_p}{a} \quad \frac{V_f}{fd_p} > \frac{0.24a}{d_p} \end{aligned}$$



**Figure 16** Different types of resonators within a typical reactive automobile silencer: (a)  $\lambda/4$  resonator and (b) Helmholtz resonator.

where  $V_f$  is the friction velocity and equals  $V_0\sqrt{\psi/2}$  for a fully developed turbulent flow.  $V$  is the volume of the cavity and finally  $R_{tu}$  and  $R_v$  are the turbulent and viscous losses at the mouth assuming a circular cross section. Obviously, maximum attenuation is obtained for  $\omega = c\sqrt{S_n/V(\ell_n + \Delta_i + \Delta_o)}$ . The amount of attenuation is related to the losses, which determines how resonant the system is.

**5.7.2  $\lambda/4$  Resonator** The closed-pipe or  $\lambda/4$  resonator is also a frequently used resonator silencer in exhaust systems, especially in combination with other elements such as expansions and contractions; see Fig. 16. The resonant behavior is generated by the incident wave reflected at the closed end of the resonator. The efficiency of all resonators is, besides the mouth geometry, also dependent on the stiffness of the walls. This is a difficult problem due to the wave motion of the walls. In this simple model only the end wall is allowed to be flexible, introducing a frequency-independent reflection coefficient,  $\Re$ . Restricting the analysis to the plane-wave region and further adopting the flexible end wall boundary condition  $\Re = \hat{p}_-/\hat{p}_+$  gives

$$Z_{sr} = \rho_0c \frac{\exp(ik\ell) + \Re \exp(-ik\ell)}{\exp(ik\ell) - \Re \exp(-ik\ell)} \quad (26)$$

where  $\ell$  is the sum of the geometrical length  $\ell_g$  of the resonator, and the end correction, which for a resonator mounted flush in the wall of a duct is given by  $\Delta_i$  in Eq. (25). As the end correction is related to the geometry of the orifice, which is small compared to the length for a typical  $\lambda/4$  resonator, it can usually be neglected.  $k$  is the wavenumber. The viscothermal and turbulent losses at the mouth can be included as for the Helmholtz resonator. As seen from Eq. (26) the  $\lambda/4$  resonator will decrease the amplitude of the fundamental tone,  $f_0 = c/4\ell$  and every even harmonic,  $(2n+1)f_0$  where  $n = 1, 2, \dots$ , as long as no higher modes are propagating in the resonator pipe.

**5.7.3 Conical Resonator** The conical resonator (Fig. 17) is similar to the  $\lambda/4$  resonator but has the advantage that it also attenuates the odd harmonics. Even though a conical silencer was patented already in 1935,<sup>49</sup> it has not been used a lot probably due to its



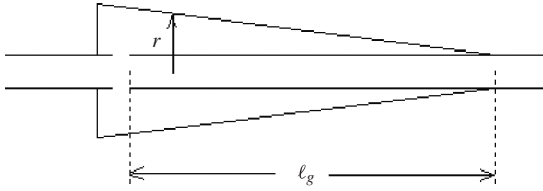


Figure 17 Conical side branch resonator.

rather bulky geometry. The acoustical properties can be estimated from Webster's horn equation, which for a linear cone, see Section 5.6, has a simple analytical solution:

$$\hat{p} = [\hat{p}_+ \exp(-ikz) + \hat{p}_- \exp(ikz)] / \sqrt{S_r} \quad (27)$$

where  $S_r$  is the inlet area/mouth of the conical side branch. The impedance of the conical resonator is given by

$$Z_{cr} = \frac{i\rho_0 c}{\cot(k\ell) - 1/k\ell} \quad (28)$$

where  $\ell$  as before is the acoustical length, that is, the sum of the geometrical length, see Fig. 12, and the end correction for the cone. For a long and narrow cone it is probably an accurate assumption to use the end correction obtained for the  $\lambda/4$  resonator.

## 5.8 After-Treatment Devices

Modern diesel engine exhaust systems often have after-treatment devices including both catalytic converters and diesel particulate traps. See Fig. 18.

**5.8.1 Catalytic Converters** Automobile catalytic converters became standard on cars in both the United States and Europe during the 1990s. The key

element in a typical automobile catalytic converter is the honeycomb structure in which the oxidation or reduction of the exhaust gases takes place. It consists of a large amount of parallel capillary pipes coated with aluminum oxide and a catalyst (e.g., platinum). A number of models normally expressed in the form of a two-port have been presented for the acoustics of such devices. One of the first attempts to present an acoustical model was made by Glav et al.<sup>50</sup> The model is based on an ad hoc combination of a classical formula for damping in narrow pipes with no flow with a model for flow-induced damping. A number of improved models have been presented, and for practical applications the most useful are perhaps the works of Dokumaci.<sup>16,51</sup> In Ref. 16 he showed that the equations for sound propagation in a thermoviscous fluid, simplified in the manner of the Zwikker and Kosten theory,<sup>21</sup> could be solved exactly for a circular pipe with plug flow. This result was used to analyze the sound propagation in catalytic converters. However, the cross section of the narrow pipes in a catalytic converter is close to quadratic. Therefore, in a later paper<sup>51</sup> Dokumaci extended the model to rectangular cross sections by expanding the solution in terms of a double Fourier sine series. The effect of strong axial temperature gradients at the inlet has been treated by Peat,<sup>52,53</sup> and the results show a marked effect on the attenuation and noticeable effect on the phase speed. The effect of temperature gradients dominates over the effect of flow convection at low shear wavenumbers.

The transfer matrix of a catalytic converter (CC) can be split into three different parts, the inlet cross section (IN), the narrow pipes with hard impermeable walls, and the outlet cross section (OUT):

$$T_{CC} = T_{IN} T_P T_{OUT} \quad (29)$$

The IN and OUT sections represent coupling two-ports, which are needed since pressure and volume

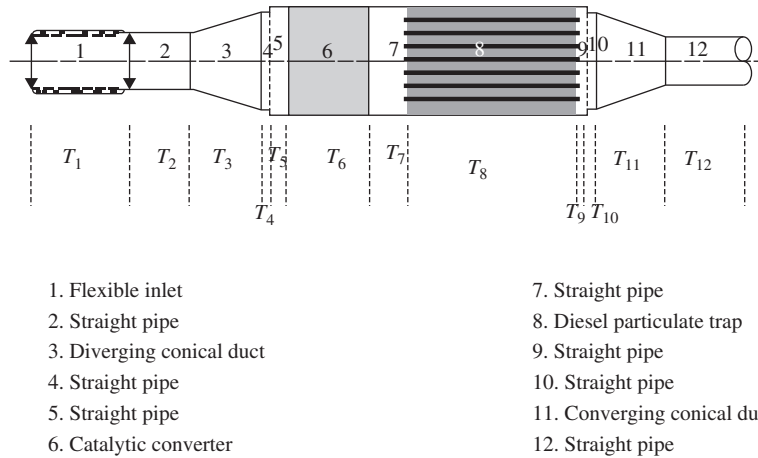


Figure 18 Sketch of a modern diesel engine after-treatment device containing both catalytic converter and diesel particulate filter.

velocity are not continuous at a sudden area change with flow. The two-port for the narrow pipe section is obtained using the model proposed by Dukomaci.<sup>16</sup> The IN and OUT two-ports are obtained by applying the principle of conservation of energy and momentum, respectively. Since the Mach number in the CC section is very small, in practice ( $<0.05$ ), these relations can be derived assuming an incompressible mean flow. The resulting two-ports are given in Ref. 54.

A point that can be made concerning the previous publications on CCs is that a large focus is put on the effect of mean flow on the damping. However, in typical exhaust systems the Mach number in the main pipe is normally less than 0.3. Then since the area expansion ratio into the CC section is typically of the order of 10, the Mach number into a CC is normally less than 0.03. This implies that the mean flow effects in practice are quite small and can be neglected. In addition since the cross-sectional shape of the CCs channels is quadratic the wave damping of a circular section with the same hydraulic diameter should be a good approximation. Therefore, as an alternative to the Dukomaci model, the two-port for the narrow pipe section can be calculated using the classical Kirchhoff solution for narrow pipes.<sup>55</sup> This implies

$$T_P = \begin{bmatrix} \cos(k_p L_p) & (i Z_p / N) \sin(k_p L_p) / Z_p \\ i N \sin(k_p L_p) / Z_p & \cos(k_p L_p) \end{bmatrix} \quad (30)$$

where  $k_p = \omega / c_p$  is the wavenumber,  $L_p$  is the length of the CC section,  $Z_p = \rho_p c_p / S$ , and  $N$  is the number of channels; the density and speed of sound are calculated based on the Kirchhoff solution for each narrow pipe:

$$\rho_p = \frac{\rho_0}{1 - F(s)} \quad (31)$$

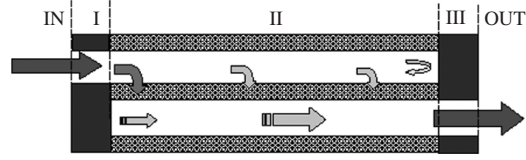
$$c_p = c_0 \frac{\sqrt{1 - F(s)}}{\sqrt{1 - (\gamma - 1)F(s)}} \quad (32)$$

where  $c_0$  is the adiabatic speed of sound,  $\sigma = \sqrt{\mu C_p / \kappa}$  is the Prandtl number,  $\kappa$  is the thermal conductivity coefficient,  $C_p$  is the specific heat coefficient for constant pressure, and

$$F(s) = \frac{2}{s\sqrt{-j}} \frac{J_1(s\sqrt{-j})}{J_0(s\sqrt{-j})} \quad (33)$$

where  $J$  is the Bessel function of the first type. To obtain an equivalent radius for the Kirchhoff model, the hydraulic radius has been used. For square narrow pipes  $\rho_p$  and  $c_p$  can be calculated according to Stinson.<sup>56</sup> Comparing the results with the previous values using the hydraulic diameter gives a difference less than 2%.

**5.8.2 Diesel Particulate Filters** The first acoustical model for diesel particulate filters was the one-dimensional model presented by Allam and Åbom.<sup>55</sup>



**Figure 19** Cross section of a unit cell in a DPF split into five sections — each described by an acoustical two-port. Note the filter section (II) is actually an acoustical four-port but can be reduced to a two-port due to the hard walls in sections I and III.

This model has been improved<sup>52,56</sup> using an extended version of the model proposed by Dukomaci for catalytic converters.<sup>16</sup> A brief summary of the models is given below. A cell in a diesel particulate filter (DPF) is shown in Fig. 19, which illustrates how the flow and acoustic waves are forced through the porous walls. As seen from this figure, the filter can be split into five sections: the inlet cross section (IN), a short narrow pipe with hard impermeable walls (I), the filter section consisting of narrow pipes with porous walls (II), a short narrow pipe with hard impermeable walls (III), and the outlet cross section (OUT). In the plane-wave range these sections can be described via two-port transfer matrices ( $T$ ). The resulting transfer matrix for a filter unit is then simply given by

$$T_{\text{DPF}} = T_{\text{IN}} T_I T_{\text{II}} T_{\text{III}} T_{\text{OUT}} \quad (34)$$

The IN and OUT sections represent coupling two-ports associated with a sudden area change and are obtained by applying the principle of conservation of energy and momentum.<sup>54</sup> At room temperature this model must be modified since then there is turbulent channel flow in a part of the narrow channels. This creates a quadratic pressure drop that can be expressed as an equivalent acoustic resistance at the IN and OUT sections. This resistance can be represented as a lumped two-port element. Regarding sections I to III, they can either be represented using the one-dimensional model of Allam<sup>54</sup> and Keefe<sup>57</sup> or the model from Allam<sup>54</sup> and Allam and Åbom,<sup>57,58</sup> which fully includes the viscothermal effects.

## 6 SOURCE DATA

As mentioned in Section 4.3 information about the properties of the engine as an acoustic source and the exhaust tailpipe opening as an acoustic load is needed for predicting the sound radiated from the exhaust. For predicting the insertion loss, the reflection properties of the source in the form of the source impedance is needed. In the following sections it is explained how source data can be obtained from experiments or from simulations using gas exchange codes. In some cases source data is not available, and some authors have suggested estimates based on experience from practical design of exhaust systems. Callow and Peat,<sup>59</sup> for example, suggested the frequency-independent source

impedance  $Z_S = \rho_0 c \exp(i\pi/4)$ , as a good estimate when source data information is not available.

In the review papers<sup>5,60,61</sup> on the subject, source models applicable for different types of sources are discussed. For internal combustion engines it is usually sufficient to consider one-dimensional models for the sound propagation in the main exhaust pipes. The main question is whether a linear time-invariant source model can be used or if time variance and nonlinearity must be considered.

### 6.1 Linear Time-Invariant One-Port Source Models

If there is only one degree of freedom at the interface between a linear source and the system, a one-port source models can be used. For in-duct fluid-borne sound sources, this corresponds to cases where there is a plane wave state in the connected duct.

In the frequency domain an acoustical one-port can be completely described by a source strength ( $p^s$  or  $q^s$ ) and a normalized source impedance ( $\zeta_s$ ):

$$p = p^s - Z_0 \zeta_s q \quad (35)$$

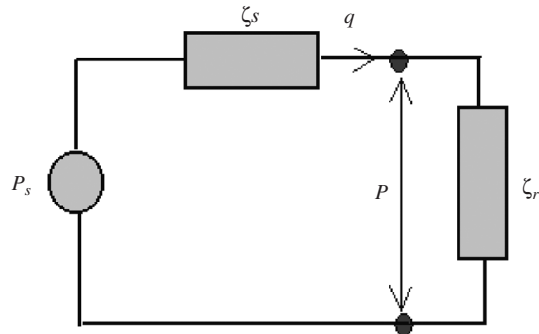
where  $p^s$  is the source pressure,  $p$  and  $q$  are acoustic pressure and volume velocity, respectively, and  $Z_0$  is the characteristic impedance of the fluid. The volume velocity  $q$  is defined positive in the outward direction from the source, and all quantities are referred to a reference cross section. Describing the exhaust or intake system as a passive (i.e., source-free) linear and time-invariant duct system, the following relationship will also apply:

$$p = Z_0 \zeta_r q \quad (36)$$

where  $\zeta_r$  is the normalized receiver or load impedance. The interaction between source and receiver is normally represented as an equivalent circuit as in Fig. 20.

### 6.2 Experimental Methods for Determining Acoustical One-Port Source Data

The measurement methods can be divided into direct or external source methods and indirect or multi-load

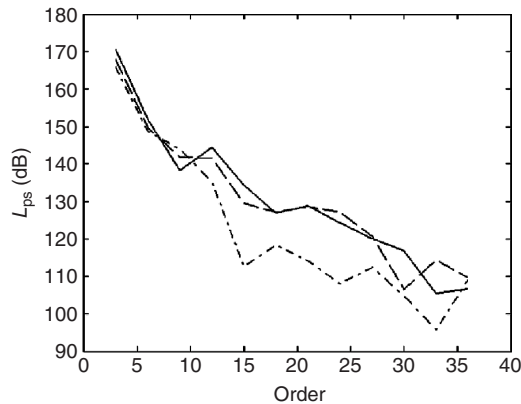


**Figure 20** Representation of a fluid-borne sound one-port source as an equivalent circuit.

methods. The *direct* methods are two-step methods. First the passive source data is determined by exciting the source from an external source. The same type of methods used to measure the acoustic impedances or mobilities of passive systems can be used. In the second step the external source is turned off, and the source strength is determined by making a measurement when a known receiver load is applied to the source. One problem with this method is that in the first step when the external source is used only, the signal from this source and not the signal from the source under test must be picked up by the transducers. The problem can in principle be solved by increasing the level of the external source. This has been attempted for IC engines<sup>62,63</sup> but did not succeed completely, and good results could not be obtained in the low-frequency region, where the engine produced the highest sound pressure levels. Another possibility is to use a reference signal correlated with the sound field from the external source, for example, an electrical signal exciting a loudspeaker, but not correlated with the sound field from the machine under test and by signal processing methods extracting the signal from the external source. Still sometimes it is difficult to find an external source that produces sufficiently high sound pressure levels. There may also be practical problems in mounting the external source in, for example, hot and “hostile” environments. This makes the indirect methods attractive for IC engine applications.

When using the *indirect* methods, the two unknowns—the source strength and the source impedance or mobility—are determined via a *multiload* procedure, that is, by applying known loads and measuring the sound pressure or the vibration velocity at the source receiver interface. Since there are two unknowns, two loads should be sufficient, which leads to the *two-load* method.<sup>64,65</sup> If more than two loads are used, an overdetermined problem is obtained, which can be useful for improving the measurement results<sup>66,67</sup> and for checking if the source behaves as a linear system.<sup>68,69</sup> The two-load method applied to fluid-borne sound sources requires that it is possible to make complex pressure measurements, which means that a reference signal unaffected by acoustic load variations and related to the sound generating mechanism of the source is needed. For fluid machines with a periodic mode of operation the normal solution is to try to obtain a trig signal for each period. This procedure can catch the harmonic part of the spectrum generated by the machine but not the broadband part. It can also be noted that a trig signal always can be used to remove flow noise disturbances from measured pressure signals. An alternative method for flow noise suppression is to create a “noise-free” acoustic reference signal, by using one or several microphones with turbulence screens. Figure 21 shows an example of results from measurements on a six-cylinder truck diesel engine.

For situations where no suitable source reference is available, alternative methods have been developed where the autospectra of the pressures are measured



**Figure 21** Effect of load variation on source strength, 1800 rpm, 100% load—full line; 50% load—dashed line; 25% load—dash-dot line.

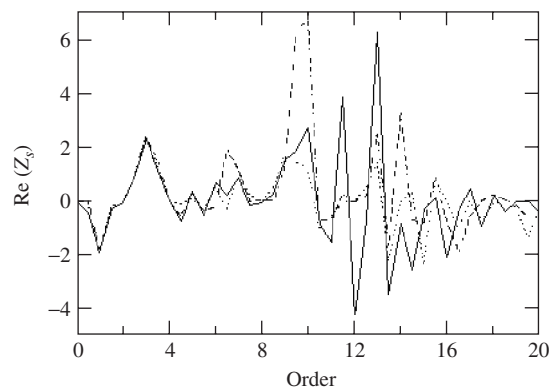
instead of the complex pressures. The first such method was the *three-load* method.<sup>70</sup> By taking the squared magnitude of Eq. (36) one gets, after substituting,  $q = p/Z_0\zeta_l$ , a real-valued equation with three unknowns, that is,  $G^s = |p^s|^2$  and the real and imaginary parts of  $\zeta_s$ ,  $[\text{Re}(\zeta_s)$  and  $\text{Im}(\zeta_s)]$ . To determine the unknowns, one therefore needs to make measurements using three different loads. The resulting system of equations is nonlinear and can have more than one real-valued solution. This method is quite impractical to use and has also been reported to give large measurement errors. In the *four-load* method<sup>71</sup> a fourth measurement is used to eliminate the nonlinear term containing  $|\zeta_s|^2$ . This method has also been reported to give large measurement errors. Bodén<sup>72</sup> showed that the four-load method can be formulated as a linear system of equations, if the nonlinear term is interpreted as an independent unknown. By analyzing this formulation, it was concluded that the main reason for the previously reported measurement errors is the choice of loads. A new improved method for analyzing the same experimental data used for the four-load method was also presented.<sup>72</sup> This method is based on a direct numerical fit of the data to the nonlinear model using least-squares methods. A comparison between the results obtained when applying the different measurement methods described above to various sources was also made. Based on this comparison it was concluded that (when it is possible to use them) the direct methods give the best results. A further improvement of the technique of Bodén<sup>72</sup> has been presented by Jang and Ih.<sup>73</sup>

### 6.3 Linear Time-Varying Source Models

When determining the passive acoustic data, that is, the source impedance of a fluid machine, it is assumed that it does not change with time. If the machine in action is studied, it is observed that pistons, valves, or fan blades move. One can, therefore, in principle

expect that even the passive acoustic properties should be time varying. In mathematical terms this means that the source is described by linear differential equations with time-varying coefficients. The time variation in the coefficients is normally caused by the periodic motion of the machine and will therefore be periodic. Using such a model for the machine, the problem can be solved either in the time domain or in the frequency domain. In the so-called Helmholtz resonator model, which has mainly been used for compressors,<sup>74,75</sup> a set of linear differential equations with time-varying coefficients is derived and solved in the time domain by a Runge–Kutta method. A frequency-domain linear time-varying source model was developed by Wang<sup>76,77</sup> for an internal combustion engine inlet system. By assuming that the variables and the coefficients have a periodic time dependence, so that they can be expanded in Fourier series, a frequency-domain model for the source can be deduced. Here the source strength is replaced by a vector containing the data for each frequency component, and the source impedance is replaced by a matrix that also describes the coupling between different frequency components that can occur at the source.

Bodén<sup>66</sup> and Bodén and Albertson<sup>78</sup> have presented measurement methods for determining the source data for such a model. The methods used are similar to the *multiload* methods used for time-invariant one-port sources. No major advantage of using these methods for applications on IC engines have, however, been found. The measurement methods have been applied to data from measurements on a compressor<sup>66</sup> and on the exhaust side of a truck diesel engine. Earlier measurements using the two-load method have indicated possible nonlinear engine source characteristics. Figure 22 shows the real part of the measured normalized source impedance for the truck engine. As can be noted the real part of the source impedance is negative for many frequencies, which is not physically correct for a linear source model. This could be an indication of nonlinear source behavior. Peat and Ih<sup>79</sup> have, however, shown that time variation



**Figure 22** Real part of normalized source impedance. Engine speed 1200 rpm; three different engine loads.

alone can cause negative resistance values if a time-varying source is analyzed, assuming that it is time invariant.

#### 6.4 Nonlinear Source Models

Many fluid machines such as compressors and IC engines are high-level acoustic sources. The validity of modeling them as linear time-invariant systems may, therefore, indeed be questioned. As discussed in the previous section, assuming a linear time-invariant source model when experimentally determining the source data frequently gives unphysical negative source resistance values. This has been interpreted as the effect of time variance and nonlinearity. The alternative is, of course, to use nonlinear models to describe the complete system; see, for example, Jones.<sup>81</sup> Most works in this field have started from first principles, that is, the equations describing the conservation of energy, momentum, and mass in a fluid. To simplify the problem somewhat, lumped source models and one-dimensional sound propagation have normally been assumed. The resulting equations are solved in the time domain using the method of characteristics or finite difference methods. The disadvantage of using these methods, compared to the linear frequency-domain methods, is that they are more complicated and time consuming to use, and they cannot treat all the complicated geometries found in, for example, automobile silencers.

#### 6.5 Linearity Tests

When using experimental methods to determine the source data of linear multiports, described in the previous sections, it is of interest to get a check of to what degree the source under test deviates from linearity and time invariance. For the one-port source a linearity test for direct methods has been proposed by Lavrentjev et al.<sup>68</sup> Further linearity tests for indirect or multiload methods were proposed by Bodén and Albertsson.<sup>69</sup> The idea behind the tests is to verify that the source data ( $p^s$ ,  $Z_s$ ) are unchanged under acoustic load variations.

#### 6.6 Hybrid Linear/Nonlinear Source Models

The hybrid linear/nonlinear methods, where a nonlinear time-domain model is used for the source and a linear frequency-domain model is used for the receiving system, was first introduced for in-duct sources in Singh and Soedel<sup>75</sup> and Elson and Soedel.<sup>81</sup> They used a frequency-domain iterative method to perform the coupling between the time-domain solution for the source and the frequency-domain description of the rest of the system. The same technique was also suggested by Jones<sup>78</sup> for application to IC engine exhaust systems and tested by Bodén<sup>66</sup> for a modified compressor with unstable results. The problem seems to be the chosen coupling technique, even though acceptable results were obtained.<sup>75,81</sup> The harmonic balance technique is an alternative frequency-domain technique with better convergence properties. It has been used for microwave circuits in forced

oscillations and was adapted for modeling the self-sustained oscillations of woodwind instruments by Gilbert et al.<sup>82</sup>

The hybrid methods can be divided into a number of main groups. One group is the iterative techniques, which can be further subdivided into frequency-domain iterative techniques<sup>75,81,83</sup> and time-domain iterative techniques,<sup>84</sup> depending on which domain the convergence check and the coupling is performed. Another group is the convolution techniques where the frequency-domain impedance boundary condition is transformed into the time domain. The impedance boundary condition is given by

$$P(\omega) = Z(\omega)Q(\omega) \quad (37)$$

where  $P(\omega)$  is the pressure at the boundary,  $Z(\omega)$  is the impedance and  $Q(\omega)$  is the flow velocity at the boundary. This equation can be transformed into the time domain giving

$$p(t) = \int_0^t z(t - \tau)q(\tau) d\tau \quad (38)$$

where  $z(t - \tau)$  is the impulse response of the system with frequency response  $Z(\omega)$ . The convolution can be solved numerically, which can be rather time consuming. It has also been reported that the impulse response convolution technique can give unstable results. An alternative is to reformulate the boundary condition using the reflection coefficient  $R$ . The boundary condition is then given by

$$p^-(\omega) = R(\omega)p^+(\omega) \quad (39)$$

where  $p^+(\omega)$  and  $p^-(\omega)$  are the amplitude of the incident and reflected pressure waves at the boundary. The corresponding time-domain expression is given by

$$p^-(t) = \int_0^t r(t - \tau)p^+(\tau) d\tau \quad (40)$$

where  $r(t)$  is the reflection function of the system with reflection coefficient  $R(\omega)$ . The reflection function seems to give more stable results. A reflection function convolution technique was used by Gazengel et al.,<sup>85</sup> as well as a number of other authors in musical acoustics, for time-domain simulation of single-reed wind instruments. An impulse response convolution technique was suggested in Gupta and Munjal<sup>84</sup> in conjunction with iteration. In some works on IC engine exhaust and inlet systems convolution using the reflection function<sup>86,87</sup> or scattering matrix<sup>88,89</sup> has been used. In these studies nonlinear wave propagation calculated using the method of characteristics, in the exhaust pipe upstream of the linear system boundary or even in between mufflers is an important part of the model.

## 7 LOAD DATA

The passive termination of the flow duct is, in general, more simple to model compared to the source, and at least in the case of negligible mean flow accurate theoretical models exists for the most common geometries. The effects of mean flow on flow duct terminations have been studied, both theoretically and experimentally, in a number of works. Due to the complexity of including an unstable vortex sheet, some discrepancies between the different works are found. Neglecting all effects of viscosity and heat conduction, the free-space termination has been rigorously treated by Levine and Schwinger in their classical work from 1948.<sup>90</sup> A good empirical fit to their results for the reflection coefficient  $\Re$  is obtained from<sup>91</sup>

$$\Re = -\Re_0 \exp(-ik2a\zeta) \quad (41)$$

where  $a$  is the tailpipe radius;  $\Re_0$  and  $\zeta$  are given by the following expressions;

$$\zeta = 0.6133 - 0.1168(ka)^2 \quad ka \leq 0.5$$

$$\zeta = 0.6393 - 0.1104 ka \quad 0.5 \leq ka \leq 2.0$$

$$\Re_0 = 1 + 0.01336 ka - 0.59079(ka)^2 + 0.33576(ka)^3 - 0.06432(ka)^4 \quad ka \leq 1.5$$

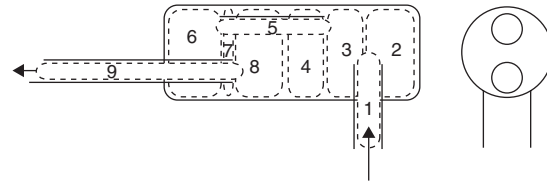
The load impedance may now be expressed as

$$Z_L = \rho_0 c \frac{1 + \Re}{1 - \Re} \quad (42)$$

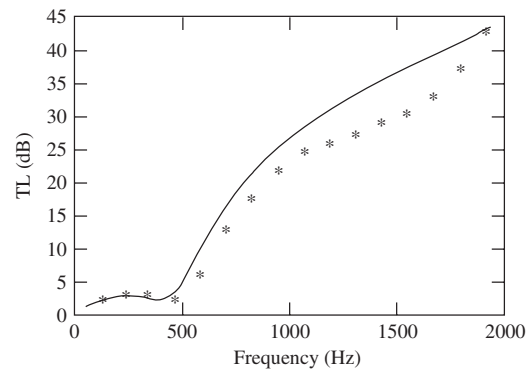
A theoretical solution for sound radiation from a pipe with flow has been given by Munt.<sup>89,90</sup>

## 8 AN APPLICATION

To illustrate the applicability of the linear frequency-domain analysis of a silencer for a small two-stroke IC engine with varying displacement is presented below. This analysis constitutes one step in the design of an improved silencer for a portable rock drill machine. Due to the complexity of the engine, it was not possible to obtain any reliable acoustic source data, and the analysis is restricted to transmission loss. This



**Figure 23** Geometry and acoustical elements of the reactive rock drill silencer.



**Figure 24** Calculated and measured (\*) transmission loss for the rock drill silencer.

may seem as a major drawback, but the guidance given by this analysis is still useful in many practical design applications. As all measurements were made at room temperature and pressure (using a loudspeaker source), so are the simulations. The Mach number is at typical running conditions less than 0.05, and therefore all mean flow effects are neglected. The silencer is divided into acoustical elements as shown in Fig. 23 and specified in Table 1.

From these elements connected in cascade from inlet to outlet (elements 1 to 9), the transfer matrix and the corresponding transmission loss for the silencer have been generated. The transmission loss has also been measured using the two-microphone method and

**Table 1** Type and Data for Elements Used to Model the Two-Stroke IC Engine Silencer<sup>a</sup>

Element Number	Type	Data (cm, cm <sup>2</sup> )	Comments
1	Straight pipe	$\ell = 3.5 + 1.1, * S = 5.6$	*End correction from (71)
2	$\lambda/4$ resonator	$\ell = 3.6, S_r = 18.2, \Re = 1$	No yielding walls
3	Straight pipe	$\ell = 1.7, S = 18.2$	
4	$\lambda/4$ resonator	$\ell = 1.7, S_r = 15.7, \Re = 1$	
5	Straight pipe	$\ell = 4.6 + 2 \times 0.4, * S = 2.5$	*End corrections from (71)
6	$\lambda/4$ resonator	$\ell = 3.4, S_r = 15.7, \Re = 1$	
7	Straight pipe	$\ell = 0.6, S = 18.2$	
8	$\lambda/4$ resonator	$\ell = 2.5, S_r = 15.7, \Re = 1$	
9	Straight pipe	$\ell = 10.6 + 0.4, * S = 2.5$	*End correction from (71)

<sup>a</sup> The length given for each element is the actual geometrical length, i.e., no end corrections apart from those specified are added



comparison between theory and experiments is thus possible.

As seen from Fig. 24 the agreement between calculated and measured transmission loss is reasonably good. The discrepancies that occur for higher frequencies are most likely due to near-field effects, which as seen from Table 1 either have been neglected or estimated from a similar geometry. Especially the effects in the region between elements 5 to 9, where the "flow" is reversed, are difficult to estimate. As the inlet and outlet to this region, that is, elements 5 and 9, are located eccentrically and on "opposite sides," the geometry is well suited to excite the first higher order mode of the main cross section, and increased accuracy thus requires three-dimensional analysis. Nevertheless, the simulation is still useful revealing the poor attenuation below 500 Hz, which, regarding the character of the exhaust noise emitted from most IC engines, shows that this prototype needs to be improved.

## REFERENCES

1. R. Glav, On Acoustical Modelling of Silencers, Doctoral thesis, KTH, Stockholm, Sweden, 1994.
2. A. G. Doige, M. L. Munjal, and H. S. Alves, An Improved Experimental Method for Determining Transfer Matrices of Pipeline Elements with Flow, *NOISE-CON 88*, 1977, pp. 481–485.
3. M. Åbom, Measurement of the Scattering-Matrix of Acoustical Two-Ports, *Mech. Syst. Signal Proc.* Vol. 5, No. 2, 1991, pp. 89–104.
4. M. J. Crocker, Internal Combustion Engine Exhaust Muffling, *NOISE-CON 77*, 1977, pp. 331–358.
5. M. G. Prasad and M. J. Crocker, *Handbook of Acoustics*, Wiley, New York, 1998, Chapter 14.
6. M. L. Munjal, *Acoustics of Ducts and Mufflers*, Wiley, New York, 1987.
7. P. O. A. L. Davies, Practical Flow Duct Acoustics, *J. Sound Vib.*, Vol. 124, 1988, pp. 91–115.
8. L. J. Eriksson, P. T. Thawani, and R. H. Hoops, Acoustical Design and Evaluation of Silencers, *J. Sound Vib.*, July, 1983, pp. 20–27.
9. M. P. Sacks and D. L. Allen, Effects of High-Intensity Sound on Muffler Element Performance, *J. Acoust. Soc. Am.*, Vol. 52, 1972, pp. 725–731.
10. P. O. A. L. Davies and E. A. A. Yaseen, High Intensity Sound Propagation in Flow Ducts, *J. Sound Vib.*, Vol. 114, 1987, pp. 153–157.
11. A. Frid, Fluid Vibration in Piping Systems—A Structural Mechanics Approach. I. Theory, *J. Sound Vib.*, Vol. 133, 1989, pp. 423–438.
12. W. Eversman, A Systematic Procedure for the Analysis of Multiply Branched Acoustic Transmission Lines, *ASME J. Vib. Acoust. Stress Reliability*, Vol. 109, 1987, pp. 168–177.
13. A. D. Jones and G. L. Brown, Determination of Two-Stroke Engine Exhaust Noise by the Method of Characteristics, *J. Sound Vib.*, Vol. 82, 1982, pp. 305–327.
14. B. Nilsson and O. Brander, The Propagation of Sound in Cylindrical Ducts with Mean Flow and Bulk-reacting Lining, Part I–IV, *IMA J. App. Math.*, Vols. 26 and 27, 1980 and 1981.
15. D. Firth and F. J. Fahy, Acoustic Characteristics of Circular Bends in Pipes, *J. Sound Vib.*, Vol. 97, 1984, pp. 287–303.
16. E. Dokumaci, Sound Transmission in Narrow Pipes with Superimposed Uniform Mean Flow and Acoustic Modeling of Automobile Catalytic Converters, *J. Sound Vib.*, Vol. 182, 1995, pp. 799–808.
17. E. Dokumaci, A Note on Transmission of Sound in a Wide Pipe with Mean Flow and Viscothermal Attenuation, *J. Sound Vib.*, Vol. 208, No. 4, 1997, pp. 653–655.
18. M. S. Howe, The Damping of Sound by Wall Turbulent Shear Layers, *J. Acoust. Soc. Am.*, Vol. 98, No. 3, 1995, pp. 1723–1730.
19. K. S. Peat, 1988 The Transfer Matrix of a Uniform Duct with a Linear Temperature Gradient, *J. Sound Vib.*, Vol. 123, 1988, pp. 43–53.
20. P. M. Morse and K. U. Ingard, *Theoretical Acoustics*, McGraw-Hill, New York, 1968.
21. C. Zwikker and C. W. Kosten, *Sound Absorbing Materials*, Elsevier, Amsterdam, 1949.
22. L. L. Beranek, Acoustical Properties of Homogeneous, Isotropic Rigid Tiles and Flexible Blankets, *J. Acoust. Soc. Am.*, Vol. 19, 1947, p. 556.
23. U. Ingard and H. Ising, Acoustic Nonlinearity of an Orifice, *J. Acoust. Soc. Am.*, Vol. 42, 1967, pp. 6–17.
24. J. Sullivan and M. J. Crocker, Analysis of Concentric-Tube Resonators Having Unpartitioned Cavities, *J. Acoust. Soc. Am.*, Vol. 64, 1978, pp. 207–215.
25. K. Jayaraman and K. Yam, Decoupling Approach to Modelling Perforated Tube Muffler Components, *J. Acoust. Soc. Am.*, Vol. 69, 1981, pp. 390–396.
26. N. Rao and M. Munjal, A Generalized Decoupling Method for Analyzing Perforated Element Mufflers, Proceedings of the 1984 Nelson Acoustics Conference, Madison, Wisconsin, 1984.
27. K. S. Peat, A Numerical Decoupling Analysis of Perforated Pipe Silencer Elements, *J. Sound Vib.*, Vol. 123, 1988, pp. 199–212.
28. M. Munjal, N. Rao, and A. Sahasrabudhe, Aeroacoustic Analysis of Perforated Muffler Components, *J. Sound Vib.*, Vol. 114, 1987, pp. 173–188.
29. E. Dokumaci, Matrizant Approach to Acoustic Analysis of Perforated Multiple Pipe Mufflers Carrying Mean Flow, *J. Sound Vib.*, Vol. 191, 1996, pp. 505–518.
30. K. Peat, Comments on Matrizant Approach to Acoustic Analysis of Perforated Multiple Pipe Mufflers Carrying Mean Flow, *J. Sound Vib.*, Vol. 191, 1996, pp. 606–611.
31. E. Dokumaci, A Discrete Approach for Analysis of Sound Transmission in Pipes Coupled with Compact Communicating Devices, *J. Sound Vib.*, Vol. 239, 1996, pp. 679–693.
32. J. W. Sullivan, A Method for Modeling Perforated Tube Muffler Components. I. Theory, *J. Acoust. Soc. Am.*, Vol. 66, 1979, pp. 779–788.
33. J. W. Sullivan, A Method for Modeling Perforated Tube Muffler Components. II. Applications, *J. Acoust. Soc. Am.*, Vol. 66, 1979, pp. 779–788.
34. J. Kergomard, A. Khettabi, and X. Mouton, Propagation of Acoustic Waves in Two Waveguides Coupled by Perforations. I. Theory, *Acta Acoust.*, Vol. 2 1994, pp. 1–16.
35. Y. Aurégan and M. Leroux, Failures in the Discrete Models for Flow Duct with Perforations: An Experimental Investigation, *J. Sound Vib.*, Vol. 265, 2003, pp. 109–121.



36. T. Elnady, Modelling and Characterization of Perforates in Lined Ducts and Mufflers, Ph.D. Thesis, Department of Aeronautical and Vehicle Engineering, KTH, Stockholm, Sweden, 2004.
37. R. Mittra and S. W. Lee, *Analytical Techniques in the Theory of Guided Waves*, MacMillan, New York, 1971.
38. J.-G. Ih and B.-H. Lee, Analysis of Higher-Order Mode Effects in the Circular Expansion Chamber with Mean Flow, *J. Acoust. Soc. Am.*, Vol. 77, 1985, pp. 1377–1388.
39. M. Åbom, Derivation of Four-Pole Parameters Including Higher Order Mode Effects for Expansion Chamber Mufflers with Extended Inlet and Outlet, *J. Sound Vib.*, Vol. 137, 1990, pp. 403–418.
40. D. Ronneberger, Experimentelle Untersuchungen zum akustischen Reflexionsfaktor von unstenigen Querschnitts nderungen in einem luftdurchströmten Rohr, *Acustica*, Vol. 19, 1967/68, pp. 222–235.
41. A. Cummings, Sound Transmission at Sudden Area Expansions in Circular Ducts, with Superimposed Mean Flow, *J. Sound Vib.*, Vol. 38, 1975, pp. 149–155.
42. R. J. Alfredson and P. O. A. L. Davies, Performance of Exhaust Silencer Components, *J. Sound Vib.*, Vol. 15, 1971, pp. 175–196.
43. P. O. A. L. Davies, Practical Flow Duct Acoustics, *J. Sound Vib.*, Vol. 124, 1988, pp. 91–115.
44. R. F. Lambert and E. A. Steinbrueck, Acoustic Synthesis of a Flow Duct Area Discontinuity, *J. Acoust. Soc. Am.*, Vol. 67, 1980, pp. 59–65.
45. F. Karal, The Analogous Acoustical Impedance for Discontinuities and Constrictions of Circular Cross Section, *J. Acoust. Soc. Am.*, Vol. 25, 1953, pp. 327–334.
46. A. D. Pierce, *Acoustics, An Introduction to Its Physical Principles and Applications*, McGraw-Hill, New York, 1981.
47. M. Åbom, An Analytical Model for Reactive Silencers Based on Bragg-Scattering, *J. Sound Vib.*, Vol. 112, 1987, pp. 384–388.
48. P. O. A. L. Davies and P. E. Doak, Spherical Wave Propagation in a Conical Pipe with Mean Flow, *J. Sound Vib.*, Vol. 137, 1990, pp. 343–346.
49. R. B. Bourne, U.S. Patent Office, Patent no. 2.017.744, Sound Attenuating Device, 1934.
50. R. Glav, H. Bodén, and M. Åbom, An Acoustic Model for Automobile Catalytic Converters, *Proceedings, Inter-Noise 88*, 1988, pp. 1261–1266.
51. E. Dokumaci, On Transmission of Sound in Circular and Rectangular Narrow Pipes with Superimposed Mean Flow, *J. Sound Vib.*, Vol. 210, No. 3, 1998, pp. 375–389.
52. K. Peat, Convected Acoustic Wave Motion along a Capillary Duct with an Axial Temperature Gradient, *J. Sound Vib.*, Vol. 203, No. 5, 1997, pp. 855–866.
53. K. Peat and R. Kirby, Acoustic Wave Motion along a Narrow Cylindrical Duct in the Presence of an Axial Mean Flow and Temperature Gradient, *J. Acoust. Soc. Am.*, Vol. 107, No. 4, 2000, pp. 1859–1867.
54. S. Allam, Acoustic Modelling and Testing of Advanced Exhaust System Components for Automotive Engines, Ph.D. Thesis, Department of Aeronautical and Vehicle Engineering, KTH, Stockholm, Sweden, 2004.
55. D. H. Keefe, Acoustical Wave Propagation in Cylindrical Ducts: Transmission Line Parameter Approximations for Isothermal and Nonisothermal Boundary Conditions, *J. Acoust. Soc. Am.*, Vol. 75, No. 1, 1984, pp. 58–62.
56. M. R. Stinson, The Propagation of Plane Sound Waves in Narrow and Wide Circular Tubes, and Generalization to Uniform Tubes of Arbitrary Cross-Sectional Shape, *J. Acoust. Soc. Am.*, Vol. 82, No. 2, 1991, pp. 550–558.
57. S. Allam and M. Åbom, 2002 On Acoustic Modeling and Testing of Diesel Particulate Filters, *Proceeding of Inter-Noise conference*, Dearborn, MI, paper number 250., 2002.
58. S. Allam and M. Åbom, On Transmission of Sound in Diesel Particulate Filters (DPFs), *Proceedings of the 10th International Congress on Sound and Vibration*, Stockholm, Sweden, 2003.
59. G. D. Callow and K. S. Peat, Insertion Loss of Engine Intake and Exhaust Silencers, *IMEchE C19/88*, 1998, pp. 39–46.
60. H. Bodén and M. Åbom, 1995 Modelling of Fluid Machines as Sources of Sound in Duct and Pipe Systems, *Acta Acoust.*, Vol. 3, 1995, pp. 549–560.
61. H. Bodén, Keynote paper: Characterisation of Fluid-Borne and Structure-Borne Sound Sources, *Proceedings of the 9th International Congress on Sound and Vibration*, Orlando, FL, 2002.
62. D. F. Ross and M. J. Crocker, Measurement of the Acoustic internal Impedance of an Internal Combustion Engine, *J. Acoust. Soc. Am.*, Vol. 74, 1983, pp. 18–27.
63. M. G. Prasad and M. J. Crocker, 1981 Insertion Loss Studies on Models of Automotive Exhaust Systems, *J. Acoust. Soc. Am.*, Vol. 70, 1981, pp. 1339–1344.
64. D. P. Egolf and R. G. Leonard, Experimental Scheme for Analyzing the Dynamic Behaviour of Electro-Acoustic Transducers, *J. Acoust. Soc. Am.*, Vol. 62, 1977, pp. 1013–1023.
65. M. L. Kathuriya and M. L. Munjal, Experimental Evaluation of the Aeroacoustic Characteristics of a Source of Pulsating Gas Flow, *J. Acoust. Soc. Am.*, Vol. 65, 1979, pp. 240–248.
66. H. Bodén, The Multiple Load Method for Measuring the Source Characteristics of Time-Variant Sources, *J. Sound Vib.*, Vol. 148, 1991, pp. 437–453.
67. H. Bodén, Error Analysis for the Two-Load Method, *J. Sound Vib.*, Vol. 126, 1988, pp. 173–177.
68. J. Lavrentjev, H. Bodén, and M. Åbom, A Linearity Test for Acoustic One-Port Sources, *J. Sound Vib.*, Vol. 155, 1992, pp. 534–539.
69. H. Bodén and F. Albertson, 2000 Linearity Tests for Induct Acoustic One-Port Sources, *J. Sound Vib.*, Vol. 237, No. 1, 2000, pp. 45–65.
70. H. S. Alves and A. G. Doige, A Three-Load Method for Noise Source Characterization in Ducts, *Proceedings of NOISE-CON 87*, 1987, pp. 329–334.
71. M. G. Prasad, A Four-Load Method for Evaluation of Acoustical Source Impedance in a Duct, *J. Sound Vib.*, Vol. 114, 1987, pp. 347–356.
72. H. Bodén, On Multi-load Methods for Determination of the Source Data of Acoustic One-Port Sources, *J. Sound Vib.*, Vol. 180, 1995, pp. 725–743.
73. S.-H. Jang and J.-G. Ih, Refined Multiload Method for Measuring Acoustical Source Characteristics of an Intake or Exhaust System, *J. Acoust. Soc. Am.*, Vol. 107, 2000, pp. 3217–3225.
74. B. R. C. Mutyala and W. Soedel, A Mathematical Model of Helmholtz Resonator Type Gas Oscillation Discharges of Two-Stroke Cycle Engines, *J. Sound Vib.*, Vol. 44, 1976, pp. 479–491.

75. R. Singh and W. Soedel, Mathematical Modeling of Multicylinder Compressor Discharge System Interactions, *J. Sound Vib.*, Vol. 63, 1979, pp. 124–143.
76. W. M. Wang, Matrix Formulation in Acoustic Analysis of Mechanically Driven Fluid Systems, *J. Acoust. Soc. Am.*, Vol. 41, 1967, pp. 1418–1423.
77. W. M. Wang, Acoustical Analysis of a Multicylinder Engine Air Induction System, *J. Acoust. Soc. Am.*, Vol. 42, 1967, pp. 1244–1249.
78. H. Bodén and F. Albertson, Application of the Multiple Load Method for Non-Linear Sources, in Seventh International Congress on Sound and Vibration, 4–7 July 2000, Garmisch-Partenkirchen, Germany, 2000.
79. K. S. Peat and J.-G. Ih, An Analytical Investigation of the Indirect Measurement Method of Estimating the Acoustic Impedance of a Time-Varying Source, *J. Sound Vib.*, Vol. 244, No. 5, 2001, pp. 821–835.
80. A. D. Jones, 1984 12–31. Modelling the Exhaust Noise Radiated from Reciprocating Internal Combustion Engines—A Literature Review, *Noise Control Eng.*, Vol. 23, 1984, pp. 12–31.
81. J. P. Elson and W. Soedel, 1974 Simulation of the Interaction of Compressor Valves with Long Discharge Lines, *J. Sound Vib.*, Vol. 34, No. 2, 1974, pp. 211–220.
82. J. Gilbert, J. Kergomard, and E. Nagoya, Calculation of the Steady State Oscillations of a Clarinet Using the Harmonic Balance Technique, *J. Acoust. Soc. Am.*, Vol. 86, 1989, pp. 35–41.
83. F. Albertsson and J. Gilbert, 2001 Harmonic Balance Methods Used for Calculating the Steady State Oscillations of a Simple One Cylinder Cold Engine, *J. Sound Vib.*, Vol. 241, No. 4, 2001, pp. 541–565.
84. V. H. Gupta and M. L. Munjal, On Numerical Prediction of the Acoustic Source Characteristics of an Engine Exhaust System, *J. Acoust. Soc. Am.*, Vol. 92, 1992, pp. 2716–2725.
85. B. Gazengel, J. Gilbert, and N. Amir, Time Domain Simulation of Single Reed Wind Instruments. From the Measured Input Impedance to the Synthesis Signal. Where Are the Traps? *Acta Acust.* Vol. 3, 1995, pp. 445–472.
86. P. O. A. L. Davies and M. F. Harrison, Hybrid Systems for IC Engine Breathing Noise Synthesis, *Proc. Inst. Acoust.*, Vol. 15, 1993, pp. 369–374.
87. M. F. Harrison, Time and Frequency Domain Modelling of Vehicle Intake and Exhaust Systems, Ph.D. Thesis, I.S.V.R., University of Southampton, 1994.
88. J. M. Desantes, A. J. Torregrosa, and A. Broatch, Hybrid Linear/Nonlinear Method for Exhaust Noise Prediction, SAE Paper-950545, 1995.
89. F. Payri, J. M. Desantes, and A. J. Torregrosa, Acoustic Boundary Condition for Unsteady One-Dimensional Flow Calculations, *J. Sound Vib.*, Vol. 188, No. 1, 1995, pp. 85–110.
90. H. Levine and J. Schwinger, On the Radiation of Sound from an Unflanged Circular Pipe. *Phys. Rev.*, Vol. 73, 1948, pp. 383–406.
91. R. M. Munt, The Interaction of Sound with a Subsonic Jet Issuing from a Semi-infinite Cylindrical Pipe, *J. Fluid Mech.*, Vol. 83, 1977, pp. 609–640.
92. R. M. Munt, Acoustic Transmission Properties of A Jet Pipe with Subsonic Jet Flow: I. The Cold Jet Reflection Coefficient, *J. Sound Vib.*, Vol. 142, 1990, pp. 413–436.

# CHAPTER 86

## TIRE/ROAD NOISE – GENERATION, MEASUREMENT, AND ABATEMENT

Ulf Sandberg  
Department of Applied Acoustics  
Chalmers University of Technology  
Gothenberg, Sweden

Jerzy A. Ejsmont  
Mechanical Engineering Faculty  
Technical University of Gdansk  
Gdansk, Poland

### 1 INTRODUCTION

The term *tire/road noise* denotes the noise emitted from a rolling tire as a result of the interaction between the tire and the road surface. In this chapter, only noise emitted outside the vehicle is considered; that is, *exterior tire/road noise*. In principle, not only the tire may radiate this type of noise; most notably structure-borne sound may spread to the rim and parts of the vehicle body and radiate from there, possibly also from part of the road surface, but radiation from the tire itself dominates.

A number of terms are used to describe this type of noise. For example, Americans currently tend to prefer *pavement–tire noise* or *tire–pavement noise*, and Germans tend to prefer *rolling noise* (*Rollgeräusch*). However, in this chapter the term *tire/road noise* is used since this was the term used in 1979 at an international conference and workshop where a particular working group addressed the terminology issue.<sup>1</sup>

Exterior tire/road noise is one of the major environmental problems of modern society and one that is not stabilized or “under control.” Most other environmental problems where there are schemes, such as the Kyoto Protocol, intend to result in lowering or at least a status quo of future pollutions. Indications of the growing noise problem are social surveys and records of complaints to authorities. The substantial growth in traffic, especially in Europe and China, is another factor that suggests an increasing tire/road noise problem.

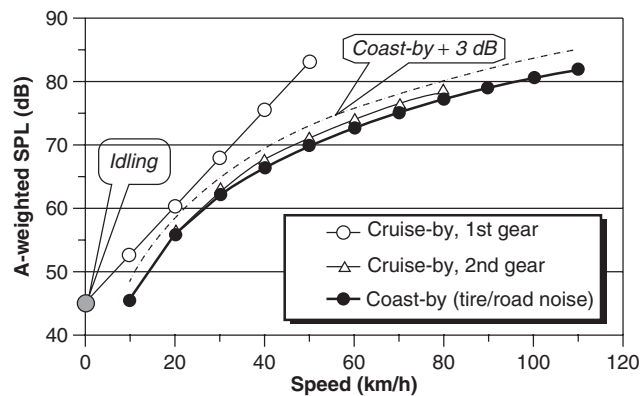
### 2 SIGNIFICANCE OF TIRE/ROAD NOISE EMISSION

Vehicle noise is composed mainly of tire/road noise and noise from the powering of the vehicle, what is here called *power unit noise*. Power unit noise, often also called *propulsion noise*, is composed of noise from the engine and all its accessories, the exhaust system and the transmission. Both tire/road and power unit noise have strong relationships with vehicle speed. Tire/road noise levels generally increase approximately logarithmically with speed (Fig. 1), which means that

on a logarithmic speed scale, noise levels increase linearly with speed. Power unit noise depends on a number of vehicle operating factors, most notably the gear selection and the engine speed, and its relation with vehicle speed is much more complicated than that of tire/road noise. At high speeds it follows almost the same noise–speed curve as tire/road noise, but at lower speeds it levels out at close to or somewhat above that of idling.

To simplify things very much, one can say that at low speeds power unit noise dominates while at high speeds tire/road noise dominates, and there is a certain *crossover speed* where the contributions are about the same. Figure 1 shows a rather typical example of vehicle noise from a modern car at various (but constant) speeds. Measuring conditions were similar to that of the International Organization for Standardization (ISO) 362<sup>2</sup> and ISO 13325.<sup>2</sup> Tire/road noise alone is represented by the curve labeled Coast-by. If one has two (incoherent) noise sources that are equally strong, the overall level will be 3 dB higher than the level for the single source, and one can then say that the power unit noise level equals tire/road noise level when the overall curve is 3 dB higher than tire/road noise. If it is less than 3 dB higher, tire/road noise will dominate. From Fig. 1 it follows that tire/road noise dominates over power unit noise for all speeds and gears except when driving in first gear. In practice, it means that at constant-speed driving tire/road noise always dominates.

Figure 1 is valid for only one passenger car, albeit rather typical for modern European, American, and Japanese cars. A more representative and general case, also including heavy vehicles, is shown in Fig. 2, which is based on data from the German model MOBILEV.<sup>3</sup> The two parts of the figure show the contribution of tire/road noise to overall vehicle noise in an urban street and in a motorway situation. Since the figure is based on a model that has been developed from a huge amount of measurements, one may consider the results as representative of vehicles having “average” acoustic characteristics for north and middle European locations.



**Figure 1** A-weighted vehicle sound pressure level SPL at constant speeds (cruise-by), as well as tire/road noise (coast-by) for a Volvo S40 (2000) in new condition. Cruise-by includes power unit and tire/road noise. Cruise-by levels for gears 3, 4, and 5 are very close to the coast-by curve and are therefore not shown. (From *Tyre/Road Noise Reference Book*.<sup>4</sup>)

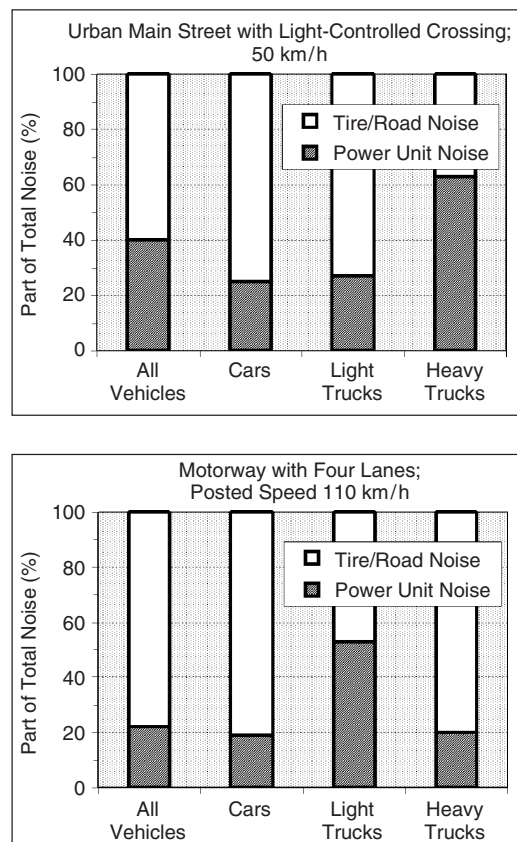
The data in Fig. 2 may also be representative of Japanese conditions since Japan and Europe have equally stringent vehicle noise emission regulations. For North America and Australia, however, there are no corresponding data, but the authors' experience is that the heavy vehicles have noisier power units there; thus resulting in decreasing proportions of tire/road noise in these regions relative to the case shown in Fig. 2. In developing countries or in countries in transition, one may expect still higher power unit noise emissions leading to lower tire/road noise contributions.

### 3 TIRE/ROAD NOISE GENERATION

The generation mechanisms of tire/road noise have been explored since the 1970s. All this research has resulted in identification of an extremely complicated mix of mechanisms and related phenomena, all of which have been demonstrated to have some influence. The most influential mechanisms are listed in Table 1, which is the result of the authors' judgments based on the current status of research. There is generally no disagreement among most experts on the existence of these mechanisms and phenomena. However, the experts tend to dispute the relative importance of them.

There are some phenomena closely related to the generation mechanisms that influence the noise emitted to the roadside but that cannot be regarded as generation mechanisms. These are also included in the table, under Amplification or Reduction Mechanisms. Some of these are active immediately at the source, such as the pipe resonances, while others are active during propagation from the source to the far field, such as the horn effect and the sound absorption effect.

Tire/road noise generation mechanisms can be divided into two main groups according to the media in which they occur and their effects. One group is directly related to mechanical *vibrations* of the tire and are structure borne, as shown in Fig. 3. The other group is related to *aerodynamic* phenomena and are airborne and are pictured in Fig. 4. In the latter figure,



**Figure 2** Share of total vehicle noise that comes from the tire/road interaction (white part of bars). The top figure is for an urban main street at a light-controlled intersection, posted speed 50 km/h, whereas the bottom figure is for a motorway with four lanes, posted speed 110 km/h, traffic volume (AADT) 50000. Data from a German study.<sup>3</sup> (From *Tyre/Road Noise Reference Book*.<sup>4</sup>)

Table 1 Generation and Amplification Mechanisms of Tire/Road Noise

GENERATION MECHANISMS	
<b>Structure Borne</b>	
<b>Impact mechanism</b> (mostly radial vibrations)	<p><b>Tread impact:</b> Impact of tire tread blocks or other pattern elements on road surfaces, causing radial and to some extent also tangential vibrations in the tire tread and belt, spreading to the sidewalls</p> <p><b>Texture impact:</b> Impact of road surface texture on the tire tread, also causing radial and to some extent also tangential vibrations in the tire tread and belt, spreading to the sidewalls</p> <p><b>Running deflection</b> of tire tread at leading and trailing edges, giving tire belt/carcass vibrations</p>
<b>Adhesion mechanism</b> (mostly tangential vibrations)	<p><b>Stick/slip</b> tread element motions relative to the road surface, causing tangential tire vibrations, also called “scrubbing”</p> <p>Rubber-to-road <b>stick/snap</b> (adhesive effect); giving either tangential or radial vibrations</p>
<b>Aerodynamical (airborne)</b>	
<b>Air displacement mechanisms</b>	<p><b>Air turbulence:</b> turbulence around tire due to the tire displacing air when rolling on the road, and air dragged around by the spinning tire–rim</p> <p><b>Air pumping:</b> air displaced into/out of cavities in or between tire tread and road surface, without necessarily being in resonance</p>
AMPLIFICATION OR REDUCTION MECHANISMS	
<b>Pipe resonances</b>	Air displacement in grooves (“pipes”) in the tire tread pattern amplified by resonances, so-called $\lambda/2$ resonators
<b>Helmholtz resonances</b>	Air displacement into/out of connected air cavities in the tire tread pattern and the road surface amplified by resonances
<b>Horn effect</b>	The curved volume between the tire leading and trailing edges and the road surface constitute something similar to an exponential horn used to amplify sound
<b>Acoustical impedance effect</b>	Communicating voids in porous surfaces act like sound-absorbing material, affecting source strength
<b>Mechanical impedance effect</b>	Same, but affecting sound propagation to a far-field receiver
	The road surface gives more or less reaction to tire block impacts depending on dynamic tire/road stiffness proportions
	Some tire vibrations may be transferred to the road surface, possibly radiating as sound (speculation)
<b>Tire resonance</b>	<p>Belt resonances (mechanical resonances in the belt)</p> <p>Torus cavity resonance (resonance in the air column of the tire)</p>

also the *amplification* or *reduction* phenomena have been included since they are mostly (but not entirely) related to the aerodynamic mechanisms. These two figures are taken from the *Tyre/Road Noise Reference Book*.<sup>4</sup>

The various generation and amplification/reduction mechanisms are active or effective in different frequency ranges. There is no simple answer to the question of which mechanism is the most important, since their relative contributions vary for different tires, roads, and operating conditions. It must be stressed that for traffic noise impact considerations, not only generation mechanisms, but also the propagation of the sound from the source to the recipient is of great importance. More details on frequency ranges for the mechanisms and the relations between them are found in Ref. 4 or as further reading in various reports.<sup>5–7</sup>

#### 4 MODELING OF TIRE/ROAD NOISE

Several research institutes, universities, and R&D departments of tire and road manufacturers are developing models intended to describe and quantify the basic tire/road interaction mechanisms that lead to the

generation of noise. Probably, since it is more “handy” to work with car tires, these studies have so far mainly focused on passenger car tires. However, the noise generated by truck tires is often dominant and is expected to become increasingly important in the future, therefore requiring more emphasis on truck tire noise modeling in the near future.

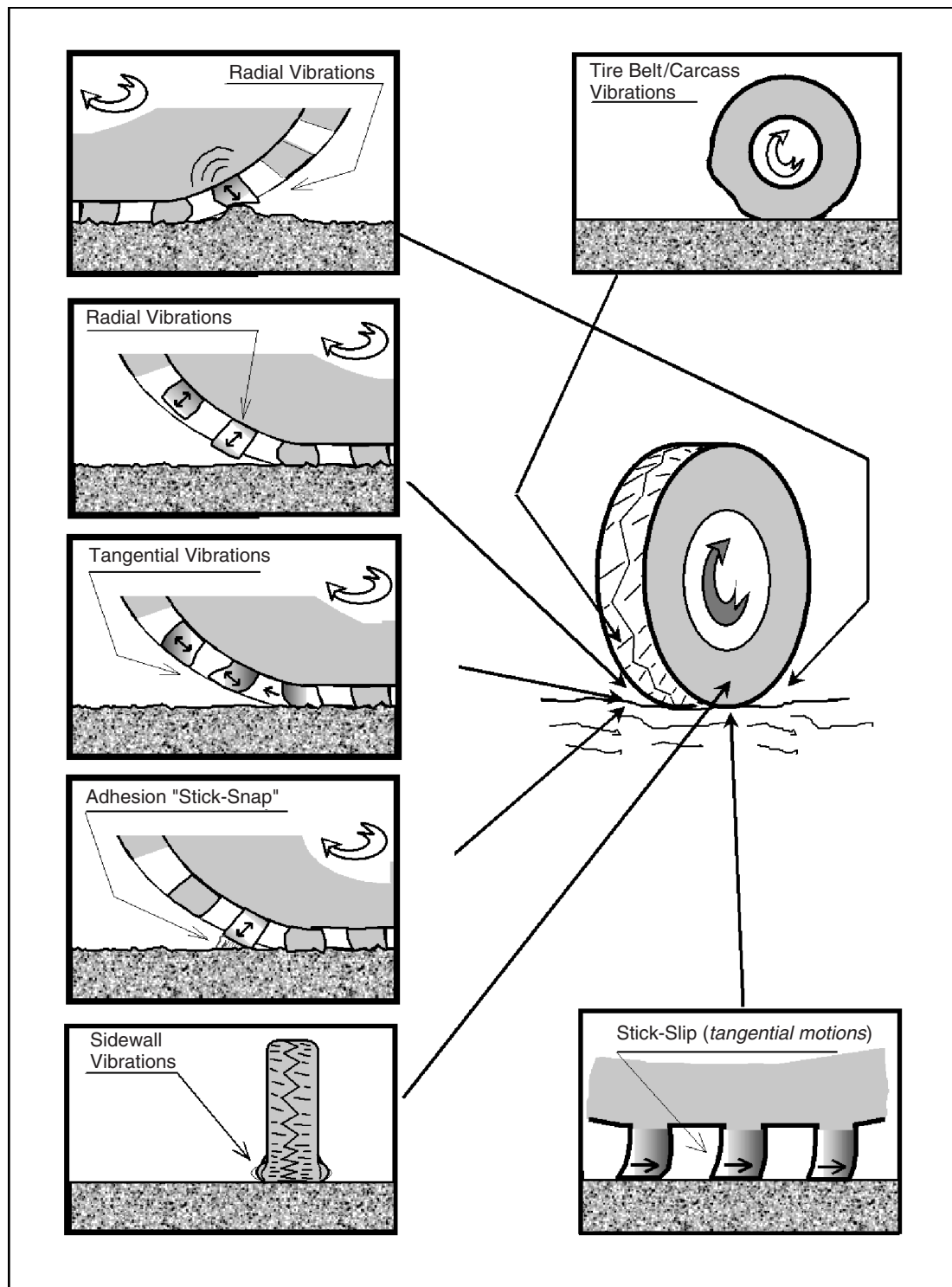
The most frequently referenced model is probably the one produced at Chalmers University of Technology, Department of Applied Acoustics, Sweden. The structure of this model is shown in Fig. 5 as an illustration of all components needed in advanced modeling.

To review the various models, which in general are very advanced and complicated physical tools, in the limited space of this chapter is impossible. Instead, some references to models and modeling work are listed in the References.<sup>6,8–23</sup> (this list is by no means complete, and we apologize for those not listed).

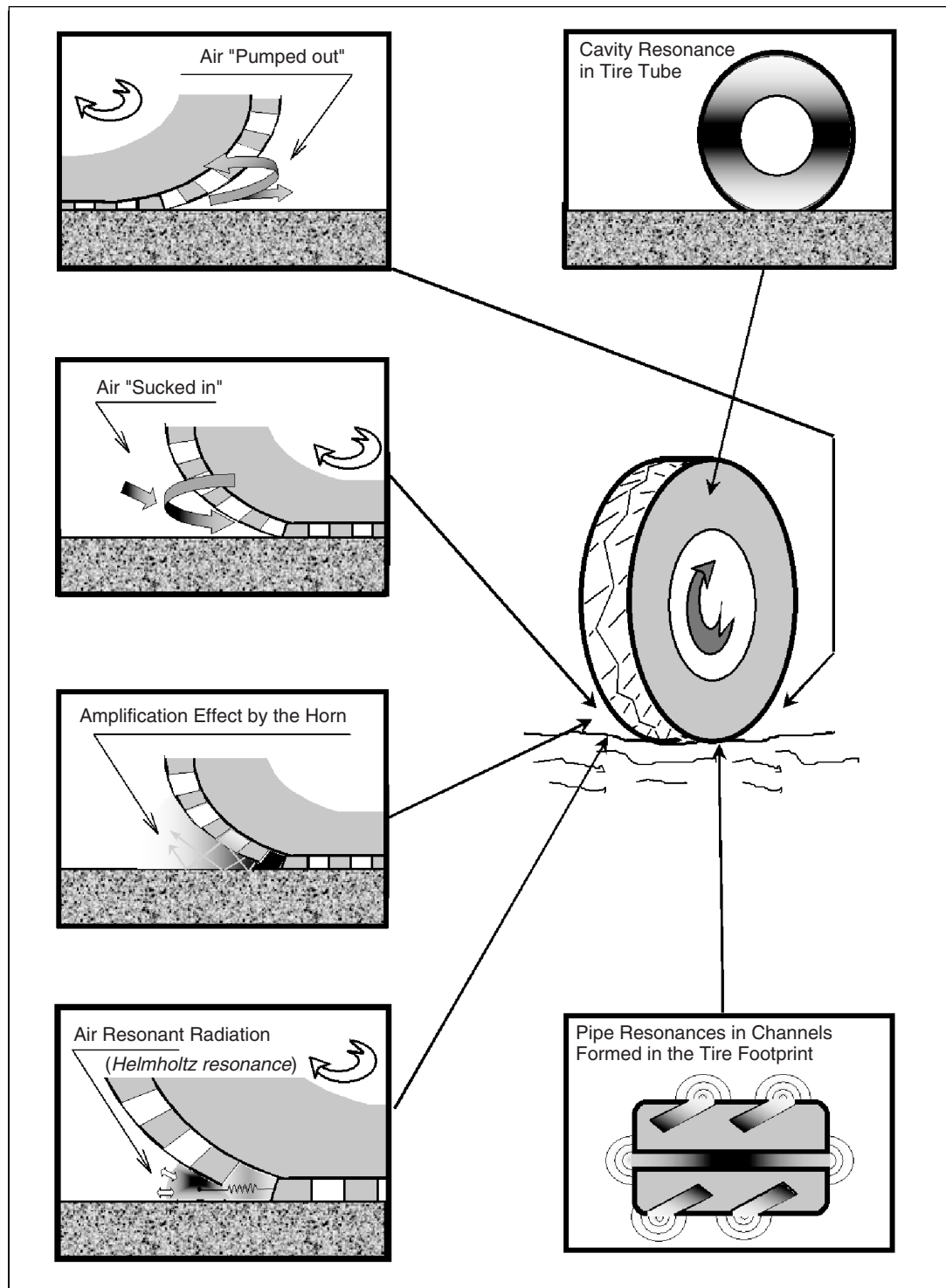
#### 5 MEASUREMENT METHODS

##### 5.1 Methods Mainly for the Study of Tires

A method developed for testing tires is specified in ISO 13325.<sup>2</sup> This specifies the so-called *coast-by method*

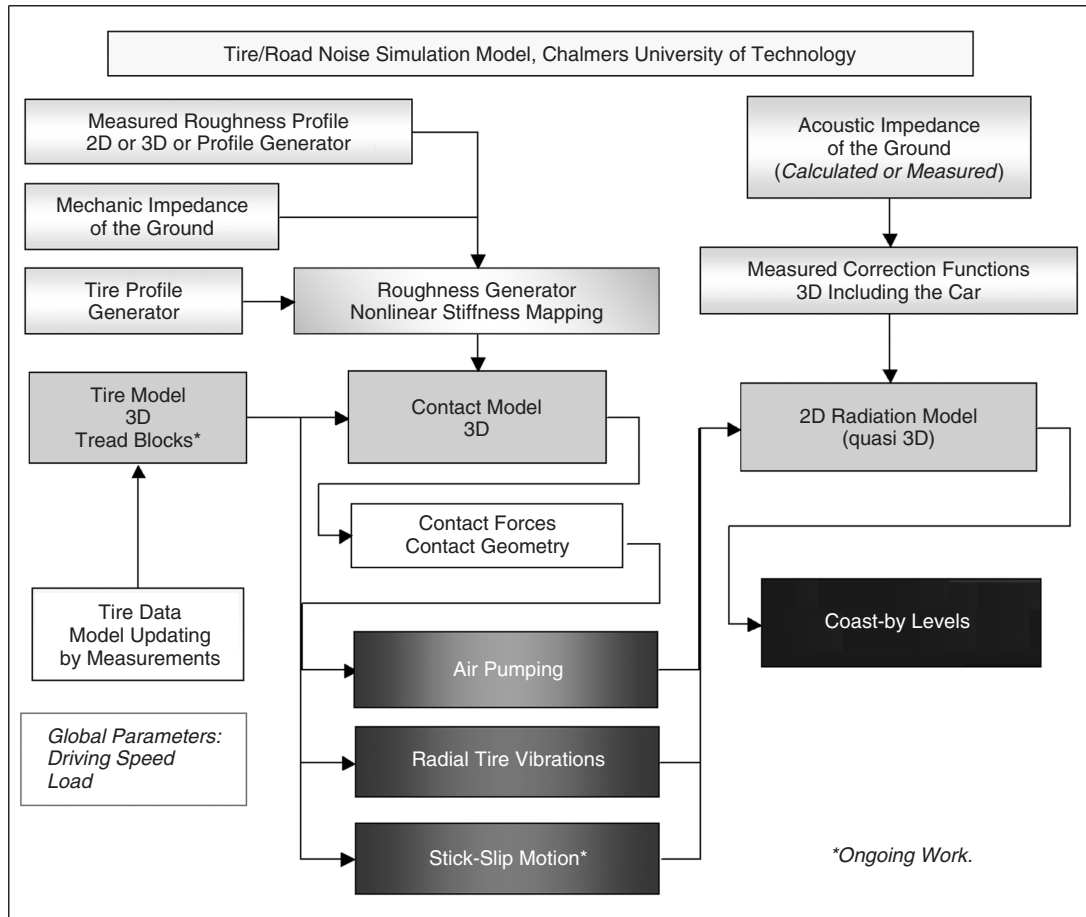


**Figure 3** Vibration-related mechanisms of tire/road noise generation (tread impact and adhesion). (From the *Tyre/Road Noise Reference Book*.<sup>4</sup>)



**Figure 4** Aerodynamically related generation (air displacement) and amplification mechanisms of tire/road noise. (From the *Tyre/Road Noise Reference Book*.<sup>4</sup>)





**Figure 5** Tire/road noise simulation model developed at Chalmers University, Sweden. (Picture used with permission.)

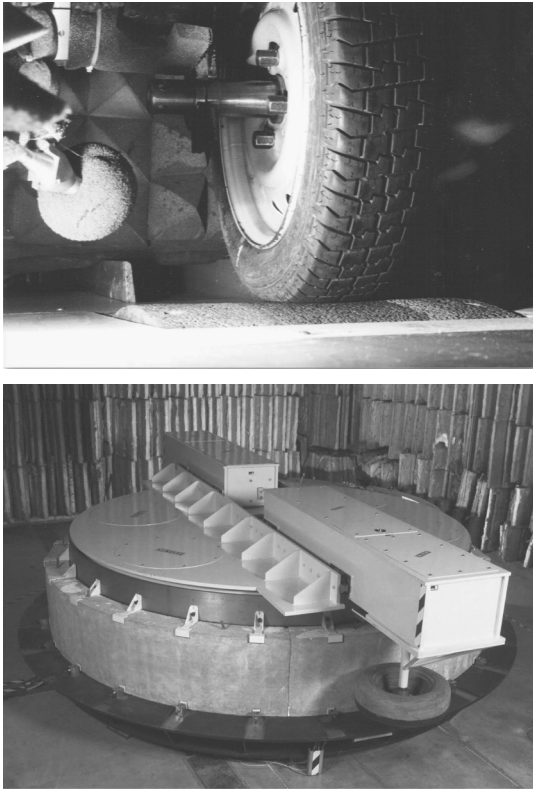
for measuring tire/road noise; that is, a test vehicle is coasted past the microphone location with the engine switched-off. There is a microphone on each side of the vehicle (which often is simplified to only one side) at a 7.5-m distance from the center of the vehicle path and at 1.2 m above surface level. The illustration in Fig. 7 is applicable also to this method, although ideally one should measure on both sides of the test vehicle.

Laboratory drum facilities are often preferred for noise studies of tires; in cases where drum surfaces easily can be exchanged, the drums may also be used for pavement studies. In particular, drums are useful during the development phases of tires. In general, the test tire rolls on the rotating drum; but there are cases also when the drum is fixed and the tire is driven around the drum. Two such very different drum facilities are shown in Fig. 6. Furthermore, the test tire may be rotated either on the outer side of the drum or on its inner side. There is no standard method for drum measurements, but the setup of microphones in the close-proximity (CPX) method described in the next section is frequently

used. The two major concerns about the laboratory drum method are (1) representative drum surface and (2) drum curvature.

Earlier, drum facilities used a drum surface that was either just the plain steel surface or a sandpaper-like surface called "safety walk." Such surfaces give noise emissions that are totally unrepresentative of actual roads. Nowadays, many facilities use surfaces that are made as replicas of actual pavements by use of molding techniques. In principle, one may have several such pavement replicas that can fairly rapidly be exchanged on the drum.

Studies of drum curvature influence on noise emission have indicated rather small or moderate effects. For car tires it seems that drum diameters down to 1.5 m are acceptable, for truck tires one would prefer at least 2.5 m.<sup>24</sup> In the United States most drum facilities use 3-m drums (10-ft diameter) in order to approximate the road geometry. Nevertheless, even meeting such requirements, there is little doubt that the curvature will influence noise to some degree,<sup>25</sup>



**Figure 6** Laboratory drum facilities at the Technical University of Gdansk (TUG) in Poland<sup>4</sup> (top) and at the Institute for Safe, Quiet and Durable Highways (SQDH) in the United States (bottom). Only the top part of the TUG drum is visible above the floor. (Pictures used with permission.)

although it may be neglected in many cases in relation to other measurement errors.

## 5.2 Methods Mainly for the Study of Pavements

An ISO standard for measurement of pavement influence on traffic noise (ISO 11819-1)<sup>2</sup> was published in 1997. It is called the *Statistical Pass-by (SPB) method* and relies on a roadside measurement on a statistical selection of cars and heavy vehicles passing by the microphone (a minimum of 80 vehicles of each category). The measurements are processed in regression analysis of noise versus vehicle speed, from which an index called the Statistical Pass-By Index (SPBI) is determined, which is the characteristic vehicle sound pressure level for the particular pavement at a chosen reference speed. This method satisfies the type testing need above and is currently widely used. A revision with the aim to improve certain details in the method is underway. Figure 7 illustrates the SPB method.

To satisfy the needs of conformity of production (COP) tests and general surveys, work is underway in the ISO to standardize a measuring method for tire/road noise called the *close-proximity (CPX) method*, which was previously called “the trailer method.” Close proximity refers to the principle of the method that means that microphones (in this case two microphones) are positioned close to a test tire that is rolling over the pavement test section. Four test tires of different design have been defined in previous drafts, but this will be reduced to two tires in future drafts. The test tire is usually mounted on a trailer that is towed by a car or van, but the test tire may also be one of the normal four tires of a van or car. A committee draft, ISO/CD 11819-2, was accepted in 2000, and a new ISO draft is underway in which the CPX method is utilized for measurements comparing the noise characteristics of pavements. The CPX method is already widely used, essentially in Europe and the United States, but it is agreed within the ISO that it cannot replace the SPB method as the major method for classification of pavements; it is intended just for surveys and for tests of conformity of production. Figure 8 shows one example of a vehicle designed for CPX measurements according to the preliminary method worked out within the ISO. Many more devices are shown in the *Tyre/Road Noise Reference Book*.<sup>4</sup>

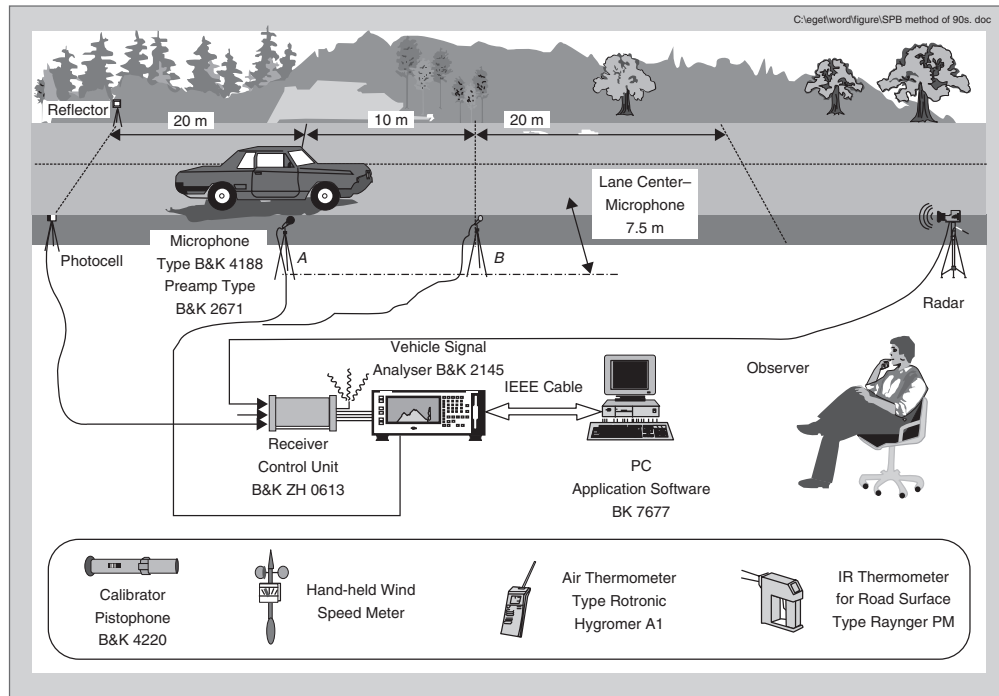
Measurements with the CPX method according to the ISO work are based on measurement of the sound pressure levels in the microphones. In United States, however, it is preferred by some to use an intensity probe (this also uses two microphones) and measure sound intensity rather than sound pressure.<sup>26,27</sup> Sound intensity measurement is described in Chapter 45 of this handbook.

Sound intensity measurement has some advantages over sound pressure measurements, but there are also disadvantages, limitations, and problems. The setups used in the United States are usually similar to the example in Fig. 9. U.S. researchers have obtained excellent correlations between the sound intensity CPX measurements and cruise-by measurements on a test vehicle with similar tires.<sup>27</sup> Researchers are arguing about the pros and cons, but when this is written the sound intensity method is being developed into a possible national standard in the United States, whereas it has been rejected in Europe and on the international level due to its shortcomings.

The work to standardize the SPB and CPX methods has been and is being performed within ISO/TC 43/SC 1/WG 33, while the European Union (EU) project SILVIA further studied these methods and also provided detailed guidance on their use.<sup>28</sup>

The ISO 13325<sup>2</sup> standard is sometimes also used for comparison of pavements. A variation of this is the so-called controlled pass-by (CPB) method, mostly practiced in France, in which a few special test vehicles and test tires are used as the measuring objects running at constant speed past the microphone on the pavements to be tested.

Many “low-noise” road pavements have significant sound absorption characteristics. ISO/TC 43/SC 1/WG



**Figure 7** Typical setup for the SPB method, used at VTI. Recently the 2145 has been replaced with a B&K pulse system.<sup>4</sup>



**Figure 8** Example of trailer used for measurements with the CPX method. This trailer is from the Technical University of Gdansk in Poland. For characterization of pavements, the method requires the use of two or four reference tires, which are used one at a time.<sup>4</sup>

38 is responsible for carrying out work on this, that is, for measurement of absorption characteristics in situ. One that is already worked out, ISO 13472-1,<sup>2</sup> is a free-field method, measuring a surface of a few square metres, with special signals emitted by a loudspeaker above the road and with microphone(s) picking up the signal for further advanced processing. Another method is being worked out with the intention to arrive at an in situ method with a better low-absorption resolution, utilizing a tube method, which measures the

absorption of a relatively small spot. These methods are mainly used for research and development so far.

Comparisons of the methods have been made.<sup>4,28</sup> An international experiment to test the CPX method and compare several of the trailers in use today was conducted in the summer of 1998 in Europe.<sup>29</sup> In general, measurements conducted with the different methods may have a good correlation to each other if they are properly performed according to standards and



**Figure 9** Typical setup for the sound intensity method.<sup>26,27</sup> (Picture used with permission.)

“good practice.” On the other hand, if such concerns are not observed, correlation may be very poor.

## 6 LEGAL AND OTHER REQUIREMENTS

The only legal requirements with regard to noise from tires is Directive 2001/43/EC<sup>30</sup> of the European Union, amending Council Directive 92/23/EEC relating to tires for motor vehicles and their trailers and to their fitting. The directive requires new tires to meet the limits indicated in Table 2, which are illustrated for car tires in Fig. 10. The measuring method is the coast-by method similar to ISO 13325,<sup>2</sup> using a reference surface according to ISO 10844.<sup>2</sup> All measured and limit values are normalized to 80 km/h for cars and vans and for trucks to 70 km/h.

**Table 2** Noise Emission Limits for New Tires in the EU<sup>a</sup> Expressed as A-weighted Sound Pressure Levels

Type of Tire, Section Width (mm)	Limit Value (dB)	Limits after First Tightening	Limits after Second Tightening
<b>For cars (C1)</b>			
≤145	72	71	70
>145 ≤ 165	73	72	71
>165 ≤ 185	74	73	72
>185 ≤ 215	75	74	74
>215	76	75	75
<b>Light trucks (C2)</b>			
Normal	75		
Snow	77		
Special	78		
<b>Heavy trucks (C3)</b>			
Normal	76		
Snow	78		
Special	79		

<sup>a</sup> Note that the values in the third and fourth columns are only indicative for tightenings in 2007–2009. Refer to the directive<sup>30</sup> for details. Final values will be decided after further studies have been made by the commission.

For car tires (class C1), the limits depend on tire section width; see Table 2. Reinforced tires are allowed *one* extra decibel and “special” tires (e.g., for off-road use) are allowed *two* extra decibels. For van or light truck tires (class C2), as well as for heavy truck tires (class C3), the limits do not depend on tire width but rather on the use of the tires: *normal*, *winter*, and *special*. Special tires are, for example, tires for use on trucks partly driven off-road, for example, trucks carrying building construction material, like gravel.

The broken lines in Fig. 10 show the *nominal* limit values, identical to those of Table 2. However, the measuring method requires that measured values be truncated, meaning that decimals are deleted. Furthermore, measured values shall be reduced by 1 dB. In practice, these two rules mean that a measured level of 75.9 will become 74 dB when a comparison with limits is to be made. It means that the effective limit in relation to what one measures is 1.9 dB higher than the nominal limit. The actual limits are therefore indicated in Fig. 10 as solid lines. Also shown in this figure are recently measured values, one point per tire. These data were measured in 2000–2004 by various organizations in Germany, Austria, Norway, and the Netherlands.<sup>31–35</sup>

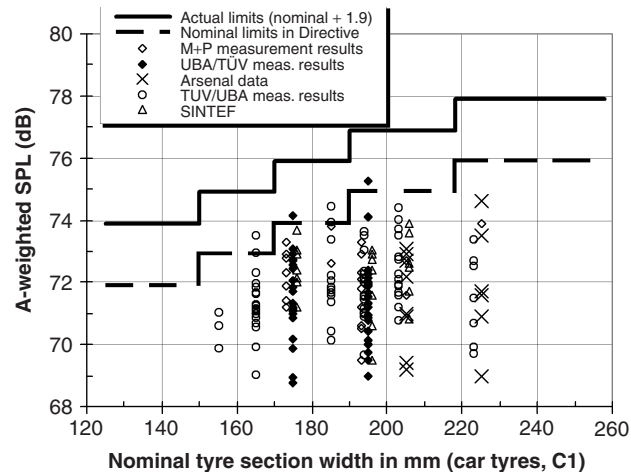
Figure 10 shows that the limits are substantially above the actually measured noise levels of current tires. Therefore, they are considered by all researchers to have no significant effect. Nevertheless, the EU Council of Ministers in the autumn of 2004 rejected a proposal to bring the limits down to levels where they would eliminate some tires.

In Japan, having no limits on tire noise, it has been considered to introduce the same limits as in Europe. However, a simulation study showed that the limit values are so high that they would not affect the Japanese traffic noise levels in any significant way. The EU limits were then rejected.<sup>36</sup>

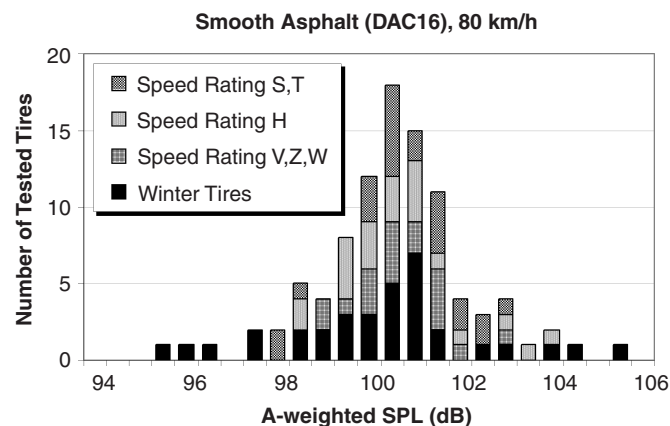
## 7 INFLUENCE OF TIRES

Figure 10 already gives a rough idea of how much noise levels between different tires differ, namely 6 dB in this selection. Data for a wider selection of car tires is presented in Fig. 11. This indicates a range of 10 dB between the best and the worst tire in a sample of nearly 100 tires of approximately similar sizes (the tires were all new or newly retreaded and available in tire shops). For truck tires, a study indicated a range of 10 dB between the best and the worst of 20 tires of similar size, measured on a surface that had similarities with an ISO surface, and 8 dB on another smooth surface.<sup>37</sup> Figure 10 indicates a difference between the worst and the best truck tires of 8 dB.

If one includes a large number of tires, one may get a range of about 10 dB, but when limiting the number to (say) less than 10, it is common to get a range of only 3 to 4 dB. In many cases, studies also concentrate on fairly similar tires. In addition to the ranges quoted above, one shall keep in mind that other variables like tire width and state of wear also affect noise levels and will increase the range further. When taking all such



**Figure 10** Tire noise limits of European Directive 2001/43/EC,<sup>30</sup> as well as recently measured noise levels for tires. Car tires are in the top half (163 tires) and truck tires are in the bottom half (30 tires). (Data used with permission.)

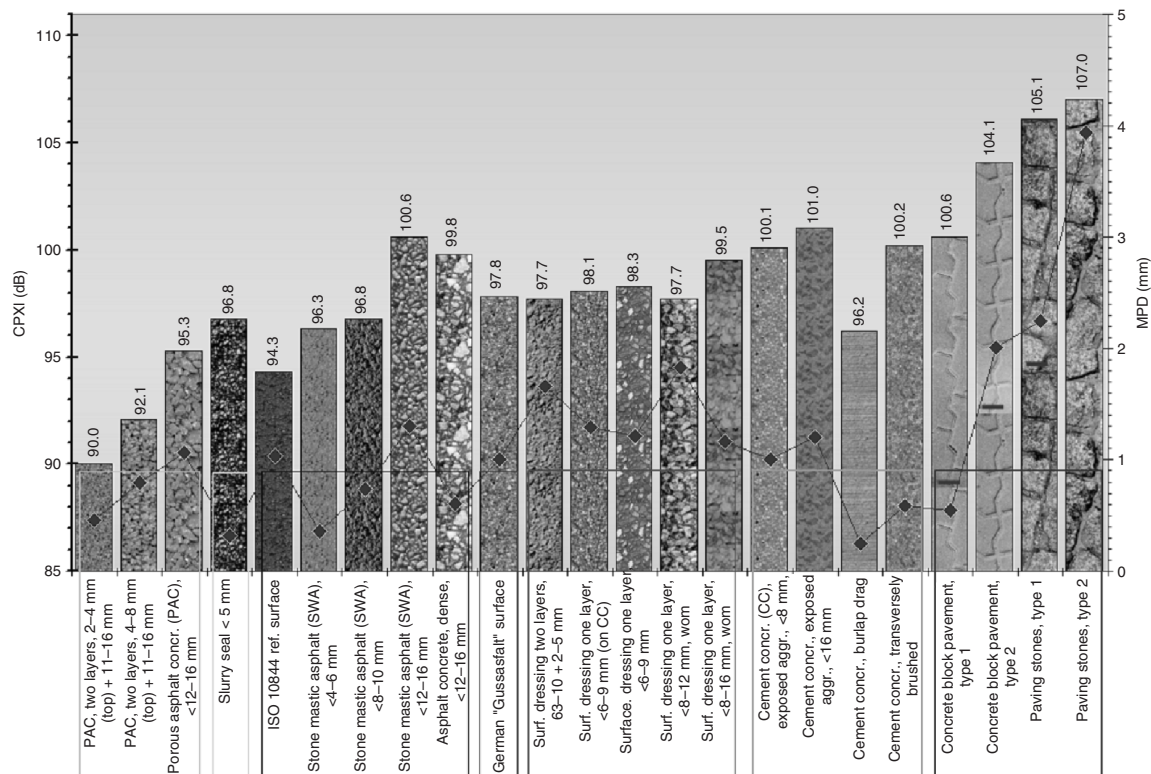


**Figure 11** Distribution of noise levels for a test sample of almost 100 tires.<sup>4</sup> Measurement at 80 km/h with the CPX method on a dense asphalt concrete with a maximum aggregate size of 16 mm. The speed rating of the summer tires is indicated.

effects into account, it seems that the range for tires is approximately as large as for pavements.

In countries where people change from the normal summer to winter or to M + S tires in wintertime, most people expect that this leads to higher noise levels. The main reason is the “more aggressive” tire tread that winter tires need to have in order to carry away or penetrate slush and snow. The all-season tires are in an intermediate situation, with somewhat higher air–rubber ratio in the tread pattern. However, Fig. 11 shows that the winter tires are no longer noisier than the summer tires, except for a few types. The quietest tires are found in the winter group, and not even the average level is higher than for summer tires. If one would fit studs into the tread pattern, which is common

in Sweden, Norway, Finland, Iceland, Canada, and parts of Russia and United States, studs are generally increasing the noise emission by about 3 to 6 dB. It will then be possible to find certain studded winter tires that are less noisy than normal summer tires! The reasons are believed to be that winter tires generally have softer rubber compound than the summer tires and that their tread patterns are crossed by narrow sipes, giving a lamellae-like pattern—all making the tread block impact and footprint movements smoother. The tread patterns are also much more elaborate than in earlier times, not the least with the intention to reduce noise emission, and especially interior noise. However, traction tires that are intended for off-road operations usually have a hard tread compound that,



**Figure 12** Tire/road noise level on various pavements, expressed as the CPXI measured with the CPX method, in this case using the TUG trailer of Fig. 8 at 80 km/h. Also indicated is the texture of each surface, expressed as mean profile depth (MPD) (see ISO 13473-1) and indicated by diamonds connected by solid lines.<sup>4</sup>

in combination with very distinctive block pattern, usually makes them noisy.

## 8 INFLUENCE OF PAVEMENTS

Large differences in tire/road noise emission have been measured on various pavements. See, for example, Fig. 12, which shows a range of 17 dB between the most "quiet" and the most "noisy" surfaces that have been measured. In Fig. 12 noise levels are expressed as levels of CPXI (close-proximity index) according to ISO/DIS 11819-2, measured with the TUG trailer.<sup>4</sup> The CPXI is simply an average value of noise levels measured for the four reference tires provisionally used in this method. It seems to be an incredibly large range, but then one should not forget that the endpoints are indeed extreme surfaces. If one would limit the surface types to such that are safe surfaces for more general use, the range shrinks to 9 to 11 dB. The surfaces that are on the quiet side will probably also become less efficient after some wear, and the most noisy surfaces among the remaining would probably not be considered in a noise-sensitive situation.

The type of Portland cement concrete (PCC) surfaces widely used on U.S. high-volume roads, which are generally textured with transverse tines,

are not included in the sample of Fig. 12. However, comparing with measurements made in the United States,<sup>37</sup> the authors estimate that such pavements would fall in the range 101 to 104 on the scale of Fig. 12.

Figure 12 also indicates the texture of each surface represented by the mean profile depth (MPD) as measured with the ISO 13473-1<sup>2</sup> method. The diamonds connected with a line are the texture values, which relate to the scale on the right. The MPD has been found to be a good measure of surface texture for describing influence on wet friction and is increasingly used to characterize pavements. Note also that each bar contains a photo of its texture (common scale). It appears that the relation between the CPXI and MPD is far from clear; one can imagine a relation only when the surfaces are very rough.

In France, one can find a very comprehensive database on national pavement influence on tire/road noise; although there is one also in Germany. The French database is updated periodically and its most recent version is presented in Fig. 13. This version has been processed by the authors from data obtained from F. Besnard at SETRA.<sup>39</sup> The figure shows a compilation of a great number of measurements on



**Table 3 Factors or Parameters Having a Major Influence on Tire/Road Noise**

Speed of the vehicle	25 dB (increase from 30 to 130 km/h)
Pavement (incl. extremes)	17 dB (from the best porous asphalts to the worst stone setts)
Pavement (conventional)	11 dB (if stone setts are excluded)
Truck tire type (conventional, one size)	10 dB (same size; a couple of decibels more if different sizes are considered)
Car tire type (conventional)	10 dB (including width range 145–255 mm)
Car tire type (conventional)	8 dB (same width)
Studs in tire (relative to no studs)	8 dB (for new studs at low speeds; less at higher speeds)
Load and inflation	5 dB (for $\pm 25\%$ variation around nominal recommended values)
Road condition (wet/dry)	5 dB (increase in heavy rain; light rain gives lower influence)
Temperature	4 dB (over range 0–40°C; mostly decreasing noise with increasing temperature)
Torque on the wheel (normal driving)	3 dB (over range 0–3 m/s <sup>2</sup> ; increasing noise with increasing acceleration)

Source: From Sandberg and Ejsmont.<sup>4</sup>

French roads on various sites in different conditions using the SPB method (ISO 11819-1).

Each group or column of data represents one major pavement category, and each point in it represents a measured pavement within this category. The individual points show the range of measured values for that particular pavement type, and the horizontal bar in the middle of each noise level distribution shows the arithmetic mean of all points. The noise differences appear to be 10 dB over the range of pavements if averages within each group are considered and 15 dB if individual values are considered. For the truck traffic, these ranges shrink to 5 and 10 dB, respectively.

## 9 OTHER PARAMETER INFLUENCE

The major factors or parameters that influence tire/road noise are listed in Table 3. The authors have attempted to list them in terms of their relative influence. Note that this is just a rough estimation since each factor is very much dependent on a number of conditions.

No other single factor has such a prominent influence on tire/road noise as speed. It is well known that the noise relationship with vehicle speed very closely follows the ideal relation:

$$L = A + B \log(V)$$

where  $L$  is the sound pressure level (SPL) in decibels,  $V$  is the speed in kilometres/hour, and  $A, B$  are speed coefficients (constants). The curve for coast-by in Fig. 1 is a good example of this. If this curve would be fitted into a diagram where speed scale is logarithmic instead of linear, the noise–speed curve will be essentially a straight line. However, on top of this basic relation, there is often a “fine structure”, at least if the pavement is smooth and the tire has a nonrandomized pattern.

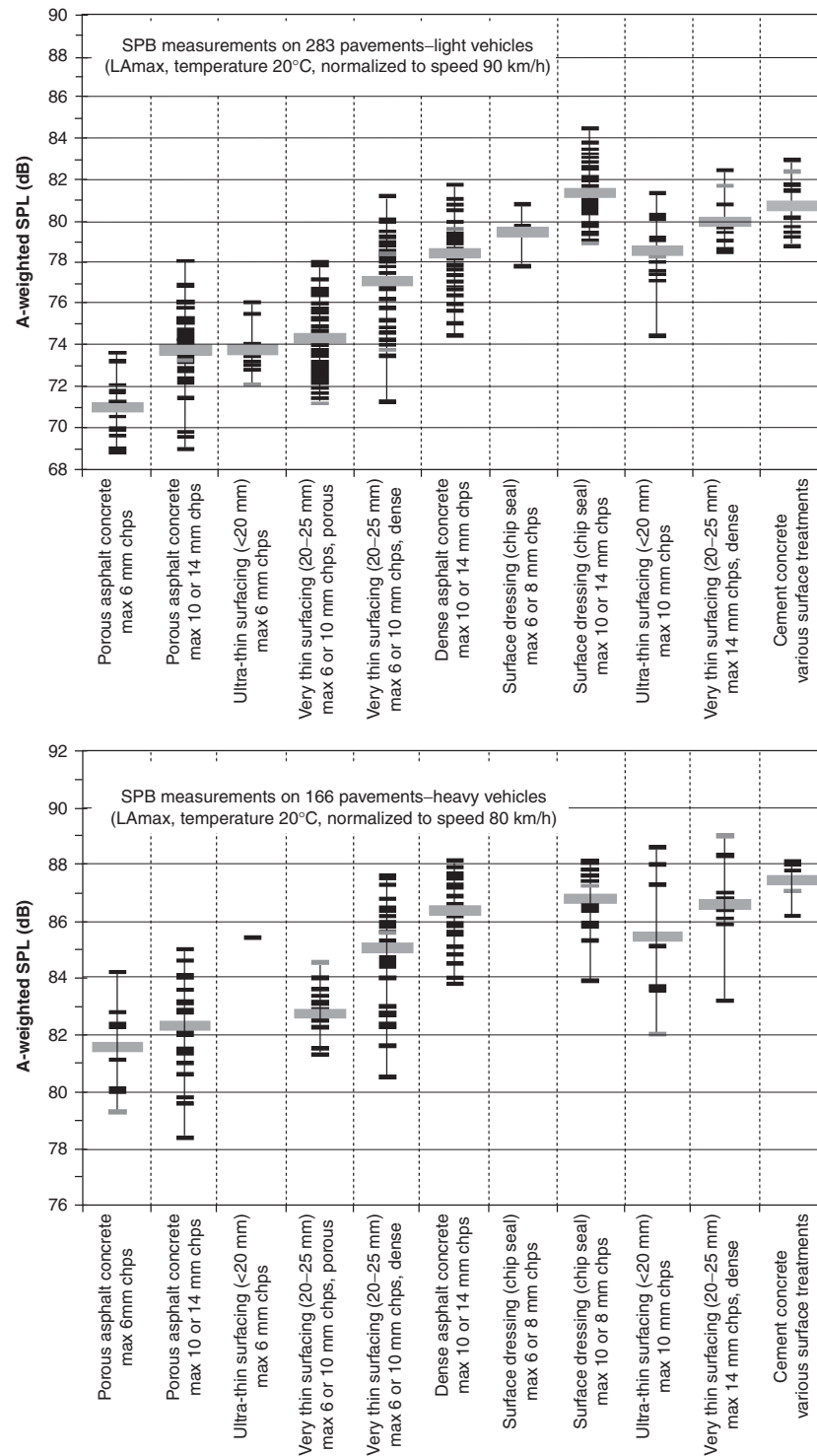
## 10 COMMON SPECTRAL FEATURES AND THE “MULTICOINCIDENCE PEAK”

Frequency spectra may have very different shapes depending on the particular tire–pavement combination. However, Fig. 14 is an attempt to show some

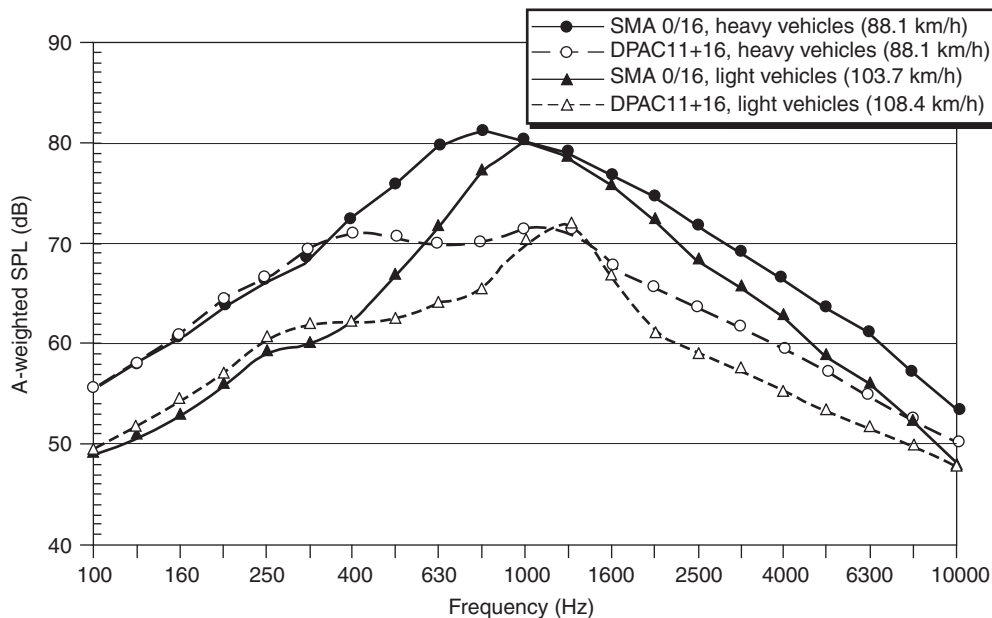
common features. The figure contains spectra from a great number of cars and trucks cruising past the wayside microphone (7.5 m distance, 1.2 m height) and captured when the A-weighted level is at its maximum. The spectra are averages for each vehicle group collected by means of the SPB method. Spectra for two pavement types are shown: one stone mastic asphalt (SMA, maximum 16 mm chippings) having a “medium rough” texture, and one double-layer porous asphalt (DPAC, maximum 11 mm chippings in the top layer and 16 mm in the bottom layer, total thickness 80 mm). The SMA is the dominating type of pavement on Swedish highways, and the DPAC is a state-of-the-art noise-reducing pavement. Due to the averaging for all vehicles, the spectra are smoother than they would be for individual vehicles cruising by. There is also a small contribution of power unit noise at frequencies outside the range of 600 to 1200 Hz for trucks. If a more rough-textured surface would be tested, the levels at frequencies below about 800 Hz would increase significantly, while the levels above about 1000 Hz would decrease somewhat. If a smoother surface would be tested, the contrary effects would be recorded.

In Fig. 14 it can be seen that the light vehicles display a rather pronounced peak around 1000 Hz. Tire manufacturers nowadays employ very advanced methods to make sure that tread patterns are properly randomized, in order to avoid tonal components. It follows that tire/road noise spectra should show broadband characteristics. However, typical A-weighted frequency spectra often have a shape that contains a pronounced peak at around 800 to 1250 Hz; see Fig. 14 for an average fleet of cars but also Fig. 15, which is for individual tires. The measurements in Fig. 15 were made with the CPX method on a laboratory drum covered with a replica of an ISO 10844 surface. However, similar results were obtained on other fairly smooth surfaces and for CPX measurements made on trafficked roads. Narrow-band spectra do not reveal any special features in this case, so it is justified to say that randomization has been successful. However, one cannot really say that the 50 spectra are of broadband character, having one or two third-octave bands at 800 to 1250 Hz dominating the emission.

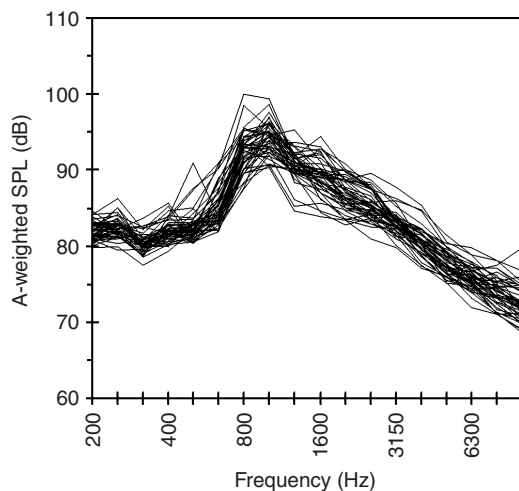




**Figure 13** Comparison of A-weighted sound pressure levels measured in France with the SPB method on a great number of different pavements, classified into 11 categories.<sup>39</sup> The figure is based on data collected over many years. The top half contains data relevant to traffic by light vehicles (cars); the bottom half data is relevant to traffic by heavy trucks. Note: chps = chippings.



**Figure 14** Third-octave band spectra for an average of about 100 heavy vehicles and about 150 light vehicles traveling at constant speed on two different pavements (see text); measured 2003 in Sweden with the SPB method.



**Figure 15** A-weighted third-octave band spectra obtained for 50 different car tires running on a drum with an ISO replica road surface at a speed of 90 km/h.<sup>40</sup>

The reason for this peak is the unfortunate coincidence of several generation, amplification, and propagation mechanisms, several of which happen to have prominent features around 1000 Hz; the so-called multi-coincidence peak.<sup>40</sup> These mechanisms are further identified and discussed in the reference. In addition, the peak corresponds with the frequency bands where the human hearing is sensitive.

## 11 LOW NOISE SOLUTIONS: TIRES

Figures 10 and 11 indicate that there are tires that are much quieter than the majority of tires. Some of them might be designated low-noise tires.<sup>4</sup> The quietest tire in Fig. 10 is, for example, 8 dB less “noisy” than what the EU Directive allows. Evidently, there is a substantial potential for improvements just by selection of the quietest tires.

Low-noise solutions for tires may be sought in the principles applied to modern winter tires: soft rubber compounds, the extensive use of narrow sipes, not too wide tires. As far as possible one should attempt to reduce the multi-coincidence peak since this dominates the A-weighted overall level totally. Further, it is essential to design the tread in a way that optimizes the impact of tread elements on the pavement, by suitable directions and angles of the tread elements. Grooves that can create pipe resonances shall be designed for maximum “ventilation,” and they should not have a constant width or a well-defined length.<sup>41</sup>

The major tire development centers work on noise reduction for their tires, mainly because of requirements for interior noise and mainly due to pressure from the vehicle manufacturers. Some of this extensive work also has a positive influence on exterior noise.

Projects for development of quieter tires conducted and reported openly are not many. An example is a planned EU project SILENCE, which will have as one of its many activities related to road and rail traffic noise a work package aimed at development of a quieter tire. A second example is the recently



**Figure 16** Prototype for a composite wheel. Note the slots in the tread band, which are providing ventilation to the grooves in the tread band.<sup>4</sup>

completed German Silent Traffic research program.<sup>42</sup> However, no document on this matter seems to be available in English. Another example is a project run by the authors in which prototypes for a so-called composite wheel are developed in cooperation with its inventor H. E. Hansson.<sup>43</sup> One such prototype is seen in Fig. 16. The same principle was reported already in 1990 to give very low noise emission,<sup>44</sup> although the version of Fig. 16 has serious problems with frequencies generated by the periodic spoke impact. When this was written, Michelin had just launched its new “revolutionary” TWEEL construction,<sup>45</sup> which is a combined tire and wheel resembling the one in Fig. 16.

Another innovative design tested recently is the porous tread tire. This tire uses the carcass of a conventional tire but has a tread that is not cut into grooves, blocks, and other elements but is composed of rubber granules a few millimetres in size that are bound together with polyurethane and then form into a porous band.<sup>46</sup> See Fig. 17. This porous tread tire had, when this was written, been tested only partly, but current results indicate a noise emission that on both smooth- and rough-textured pavements was substantially lower than any pneumatic tire, including slick tires. Rolling resistance was comparable to the conventional tire, but wet skid resistance was poorer, the latter probably due to the use on nonoptimized rubber compounds (the rubber granules were produced from old scrap tires of various qualities).<sup>46</sup>

## 12 LOW-NOISE SOLUTIONS: PAVEMENTS

A number of low-noise solutions for pavements have been proposed of which some are already implemented. The following is a list of such solutions:

**Porous Pavements** Asphalt or concrete pavements designed with a high proportion of air voids give a porous structure that absorbs some of the sound during



**Figure 17** Two prototypes of the porous tread tire, produced by B. Kalman (VTI, Sweden) and A. R. Williams (UK, formerly at Dunlop Tyres).

its propagation and also reduces the aerodynamically related mechanisms at the source. The most effective design seems to be the double-layer porous asphalt, in which a top layer has rather small chippings to create a smooth surface to roll on and a bottom layer has much larger chippings, which will provide effective escape channels for water and air. The void content should exceed 20% in order to be effective. Total pavement thickness is usually 45 to 90 mm. Porous asphalt has a potential for reduction of vehicle noise (including tire/road noise) by 5 to 8 dB in new condition but the problem is the durability. Clogging of the porosities quickly reduces the acoustic durability and ravelling (loss of chippings) limit the technical durability in situations where substantial tangential tire/road forces occur. Modifying the binder with, for example, rubber may improve the performance in certain ways.

The DPAC pavement in Fig. 14 is an example of a very favorable one and shows the spectral effects achieved in such a case. The reductions are basically caused by a combination of (1) reduced air pumping due to excellent drainage, (2) reduced horn effect due to the lower horn surface being acoustically transparent, and (3) sound absorption during propagation to the receiver.

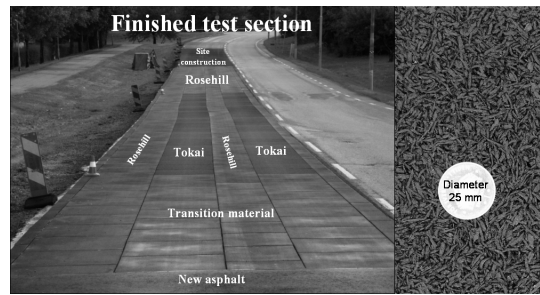
Porous asphalt pavements are rather widely applied already. For example, approximately 70% of the Dutch national highways are covered with porous asphalt, aiming at 100%. Most major expressways in Japan have porous asphalt as a wearing course. Recently, the use of porous asphalt has increased rapidly in large Japanese cities.

**Optimized Texture** In this case the megatexture is kept at a minimum and the macrotexture is aimed at providing drainage by using as small chippings as is consistent with requirements for appropriate wet skid resistance. The chippings may be rather small but they should provide a high degree of macrotexture in the texture wavelength range of 2 to 6 mm.<sup>4</sup>

Examples of such surfaces are surface dressings with dominating chipping sizes in the range of 2 to 6 mm. One proprietary surface dressing that is claimed to be suitable for low-noise solutions is the Italgrip pavement. Thin surfacings are usually thinner versions of dense asphalt concrete or stone mastic asphalt (SMA), which are easier to roll in order to obtain a flat top surface with plenty of voids in between. They usually provide some noise reduction, in general, based on texture optimization principles, since they are often based on rather small maximum chipping sizes and attempt to obtain an open structure. Thin surfacings have a potential for at least 4 dB of noise reduction compared to a dense asphalt or SMA with a maximum aggregate size of 16 mm.

**Grinding; Exposing the Aggregate** These are special treatments often applied to cement concrete pavements. Without special treatment, such pavements tend to have too low macrotexture, and to improve skid resistance increases in drainage are desirable. The old way of achieving this (still widely used in the United States but abandoned in Europe) is to provide laterally orientated grooves, so-called tining. Tining usually creates excessive tire/road noise; if the spacing is not properly randomized, it may even cause tonal noise components that are subjectively very objectionable and have given concrete pavements a bad reputation. A somewhat better way, with regard to traffic noise emission is to give the tines or grooves a longitudinal orientation. An alternative way to provide a suitable macrotexture is to grind the surface by a machine, so-called diamond grinding, which creates longitudinal narrow grooves but also a smooth surface. Another alternative way is to expose the aggregate, which is a technique to remove, during the cement curing process, the sand in the pavement surface, which then exposes the aggregate (the chippings). If the chippings thus exposed are small and closely packed together, such a pavement may get noise characteristics almost as good as the best (dense) asphalt pavements, which is also the case for the diamond ground pavements.

**Asphalt Rubber Pavements** In Arizona, to a smaller extent also in California and Texas, substantial amounts of very small rubber granules have been mixed into the binder of a pavement somewhat similar to an SMA, however, with much higher binder content than used in conventional mixes (up to 10% by weight). The term used in Arizona is asphalt rubber friction course (ARFC). ARFC pavements have a dense structure that somewhat resembles a texture-optimized surface and are also somewhat softer than conventional asphalt pavements and thus provide a softer impact between tire tread and pavement chippings. The authors believe that these properties combined contribute to the low-noise emission. According to recent measurements conducted both in the United States and Europe, the ARFC pavements in Arizona are almost as quiet as the European porous pavements<sup>48</sup> despite their generally somewhat denser structure.



**Figure 18** Overview of test section with three types of poroelastic pavement (Rosehill, Tokai, Site construction), laid 2004 in Stockholm, Sweden, with a closeup view of the Rosehill surface texture on the right.<sup>49</sup>

**Poroelastic Pavements** A poroelastic pavement is one that combines the porous structure with a soft aggregate. This is accomplished by adding substantial proportions of rubber particles into the mix. The most extreme pavement of this type is one that contains rubber particles bound with polyurethane and just minor additions of friction-increasing material such as sand or metal fibers. Such pavements often have a void content (by volume) of 30 to 40%. Sound reduction is achieved due to the porosity (see above) but also due to the softer impact between tire and pavement particles. Figure 18 shows an example of a field experiment with such pavements that took place in Stockholm in 2004. Measurements on three poroelastic pavement types showed tire/road noise reductions of 10 to 12 dB for normal tires and 13 to 15 dB for studded tires.<sup>49</sup> For a vehicle cruising by with the engine on, corresponding reductions were 6 to 8 dB. The Rosehill and Tokai types (see Fig.18) were prefabricated panels, the “site construction” was laid on-site with a small asphalt laying machine. Layer thickness was 30 mm. Similar field experiments with poroelastic pavements took place in Japan in 2002 and 2003 (but were interrupted in 2004).<sup>50</sup> This technique is not yet ready for full-scale application; further research is underway in Japan and Sweden.

**Acknowledgments** A number of illustrations and some data appearing in this chapter have been obtained from colleagues in other countries to whom the authors are grateful for their willingness to share their experience and results. It is acknowledged that the primary affiliation of the first author is the Swedish Road and Transport Research Institute (VTI), although this particular work was made within his secondary affiliation (Chalmers Institute of Technology).

## REFERENCES

1. Anon., Proc. of the International Tire Noise Conference 1979, STU Information No. 168–1980, NUTEK, Stockholm, Sweden (out of print, but the authors may provide excerpts).
2. A great number of ISO standards are mentioned in the text. The reader is recommended to visit the

- ISO website, [www.iso.org](http://www.iso.org), to identify the particular standard. Use the "Extended search" option offered there, type in the number of the ISO standard, and the particular standard title should appear.
3. H. Steven, Personal communication in 2001 with H. Steven, TÜV Nord Mobilität, Germany, but data are partly presented in H. Steven, Minderungspotenziale beim Strassenverkehrslärm, *Zeitschrift fuer Laermbekämpfung*, Vol. 48, No. 3, 2001 (in German).
  4. U. Sandberg and J. A. Ejsmont, *Tyre/Road Noise Reference Book*, Informex, SE-59040 Kisa, Sweden, 2002, ([www.informex.info](http://www.informex.info)).
  5. R. J. Bernhard and R. L. Wayson, An Introduction to Tire/Pavement Noise, Report No. SQDH 2005-1, The Institute for Safe, Quiet, and Durable Highways (SQDH), Purdue University, IN, 2005.
  6. J. S. Bolton and Y. J. Kim, Visualization of Tire Vibration and Sound Radiation and Modeling of Tire Vibration with an Emphasis on Wave Propagation, Final Research Report No. SQDH 2003-4, The Institute for Safe, Quiet, and Durable Highways (SQDH), Purdue University, IN, 2003.
  7. R. J. Bernhard and U. Sandberg, Tire-Pavement Noise: Where Does It Come From? *TR News*, September–October, 2005.
  8. M. Heckl and W. Kropp, A Two Dimensional Acoustic Rolling Model for Describing the Contribution of Tyre Vibrations to Rolling Noise, *J. Tech. Acoust.*, Vol. 1, No. 1, 1994.
  9. K. Larsson, *Modelling of Dynamic Contact—Exemplified on the Tyre/Road Interaction*, Report F 02-02, (Ph.D. thesis), Department of Applied Acoustics, Chalmers University of Technology, Gothenburg, Sweden, 2002.
  10. F. Wullens, Excitation of Tyre Vibrations Due to Tyre/Road Interaction, Ph.D. Thesis, Report F 04-03, Department of Applied Acoustics, Chalmers University of Technology, Gothenburg, Sweden, 2004.
  11. P. Andersson and K. Larsson, Validation of a High Frequency Three-Dimensional Tyre Model, *Acta Acust. United with Acust.*, Vol. 91, 2005, pp. 121–131.
  12. P. Guisnet and F. Augusztinovicz, TINO Noise Emission: Analysis and Prediction Models, Paper 99.06, First International Colloquium on Vehicle Tyre Road Interaction—May 28th, 1999, Rome, Italy (printed by the University of Rome, Faculty of Engineering).
  13. P. Guisnet, W. Hendrickx, and C. McCulloch, Tyre Noise Models, Analysis and Prediction, Paper presented at the ISATA Conference 2000, Dublin, Ireland.
  14. T. G. Clapp, A. C. Eberhardt, and C. T. Kelley, Development and Validation of a Method for Approximating Road Surface Texture-Induced Contact Pressure in Tire-Pavement Interaction, *Tire Sci. Tech. (TSTCA)*, Vol. 16, No. 1, January–March 1988, pp. 2–17.
  15. K. J. Plotkin and E. Stusnick, A Unified Set of Models for Tire/Road Noise Generation, Wyle Research Report WR 81-26, July 1981, Wyle Laboratories, Arlington, VA (also EPA Report No. 550/9-82-345, U.S. Environmental Protection Agency, Washington, DC).
  16. A. C. Eberhardt, Development of a Transient Response Model for Tire/Pavement Interaction," Proc. of Inter-Noise 84, Honolulu, Hawaii, 1984, pp. 77–82.
  17. E. Gerretsen, E. D. Schoen, F. J. M. van der Eerden, and E. Mulder, Relevant Parameters for Low-Noise Tyre Designs—An Optimisation Study, TNO Report HAG-RPT-010163, TNO-TPD, Sound and Vibration Division, Delft, the Netherlands, 2002.
  18. F. de Roo and E. Gerretsen, TRIAS—Tyre Road Interaction Acoustic Simulation Model, Proc. of Inter-Noise 2000, Nice, France, 2000.
  19. A. Kuijpers, Tyre/Road Noise Modelling: The Road from a Tyre's Point-of-View, Report No. M + P.MVW. 01.8.1, M + P Raadgevende ingenieurs bv., Netherlands 2001. May be downloaded from <http://www.silentroads.nl>.
  20. A. Kuijpers, Further Analysis of the Sperenberg Data—Towards a Better Understanding of the Processes Influencing Tyre/Road Noise, Report No. M + P.MVM.99.3.1, M + P Raadgevende ingenieurs bv., Netherlands, 2001. May be downloaded at <http://www.silentroads.nl>.
  21. A. Kuijpers, Tyre/Road Noise Models in the Last Two Decades: A Critical Evaluation, Paper presented at Inter-Noise 2001, the Hague, the Netherlands, M + P Raadgevende ingenieurs bv., Netherlands, 2001. May be downloaded from <http://www.silentroads.nl>.
  22. A. P. Dowling, R. A. G. Graf, and W. R. Graham, A Mathematical Model of Tyre-Road Interaction Noise, European Conference on Vehicle Noise and Vibration 2002, IMech E Conference Transactions, 2002, pp. 133–143.
  23. R. J. Pinnington and A. R. Briscoe, A Wave Model for a Pneumatic Tyre Belt, *J. Sound Vib.*, Vol. 253, No. 5, 2002, pp. 969–987.
  24. U. Sandberg and J. A. Ejsmont, Review of Comparative Studies of Tyre/Road Noise Measurements on Drums and Roads, VTI report 265A, Swedish National Road and Transport Research Institute, Linköping, Sweden, 1983.
  25. L. G. Hartleip and T. J. Roggenkamp, Case Study—Experimental Determination of Airborne and Structure-borne Road Noise Spectral Content on Passenger Vehicles, SAE Paper 2005-01-2522, Society of Automotive Engineers International, Warrendale, PA, 2005.
  26. P. R. Donovan and B. Rymer, Assessment of Highway Pavements for Tyre/Road Noise Generation, SAE paper 2003-01-1536, Society of Automotive Engineers International, Warrendale, PA, 2003.
  27. P. R. Donovan and B. Rymer, Quantification of Tyre/Pavement Noise: Application of the Sound Intensity Method, Proc. of Inter-Noise 2004, Prague, Czech Republic, 2004.
  28. EU project SILVIA—Sustainable Road Surfaces for Traffic Noise Control, 2005. Check the project website <http://www.trl.co.uk/silvia/> for reports about classification of road surfaces and measuring methods.
  29. H. Steven, D. Küppers, G. J. van Blokland, M. H. van Houten, and R. van Loon, International Validation Test for the "Close Proximity Method" (CPX), CD-ROM from M + P Raadgevende ingenieurs bv, Bruistensingel 232, NL-5232 AD 's-Hertogenbosch, the Netherlands, 2000.
  30. EU Commission, Directive 2001/43/EC of the European Parliament and of the Council of 27 June 2001 Amending Council Directive 92/23/EEC Relating to Tyres for Motor Vehicles and Their Trailers and to Their Fitting, *Official J.*, 4 August 2001.

31. W. Reithmaier and T. Salzinger, Determination of the State-of-the-Art Concerning Rolling Noise, Rolling-Resistance and Safety Properties of Modern Passenger Car Tyres, Research report 201 54 112, TÜV Automotive, Tire-/Wheel-Test-Center, Munich, Germany, 2002.
32. M. S. Roovers, Tyre/Road Noise Measurements for Passenger Cars According to EU Directive 2001/43, Report dated January 16th, M + P Noise and Vibration Consultants, the Netherlands, 2003.
33. R. Stenschke and P. Vietzke, Tyre/Road Noise Emissions, Rolling Resistance and Wet Braking Behaviour of Modern Tyres for Heavy-Duty Vehicles (State of the Art), Proc. of Inter-Noise 2001, the Hague, the Netherlands, 2001.
34. M. Haider, K. Fallast, and G. Strohmayer, Definition und Erarbeitung eines Systems zur Förderung lärmarmer KFZ-Reifen, Variante 2, bezogen auf Österreichische Fahrbahndecken und lärmindernde Fahrbahndecken auf dem letzten Stand der Technologie, Endbericht Proj. Nr. FFF 806231-SP/TU, Proj. Nr. Arsenal: 2.05.00127.1.0, Arsenal, Vienna, Austria, 2004.
35. T. Berge and A. Ustad, Støymålinger på bildekk i henhold til EU-direktiv 2001/43/EC, Foreløpige måleresultater fra 2003 og 2004, SINTEF Rapport STF90 A04083, SINTEF IKT, Trondheim, Norway, 2005.
36. Y. Oshino, Personal communication with Y. Oshino, Japan Automobile Research Institute, Tsukuba, Japan, 2004.
37. U. Sandberg, Survey of Noise Emission from Truck Tires, Proc. of Inter-Noise 91, Sydney, Australia, 1991.
38. D. A. Kuemmel, R. C. Sontag, J. A. Crovetto, Y. Becker, J. R. Jaekel, and A. Satanovsky, Noise and Texture on PCC Pavements. Results of a Multi-State Study. Final Report, Report No. WI/SPR-08-99, Marquette University, Milwaukee, WI, 2000. Download at: [http://www.trc.marquette.edu/noise&texture/noise\\_and\\_texture\\_final\\_report\\_6-2000.pdf](http://www.trc.marquette.edu/noise&texture/noise_and_texture_final_report_6-2000.pdf).
39. F. Besnard, Personal communication with F. Besnard, SETRA, Bagneux, France, 2005. Although these data have not been published earlier, a former version (lacking the newest data) was published in 2001 in the following reference: Influence de la couche de roulement de la chaussée sur le bruit du trafic routier, Comité Français des Techniques Routières, Note d'information No. 4, June 2001.
40. U. Sandberg, The Multi-Coincidence Peak around 1000 Hz in Tyre/Road Noise Spectra, Proc. of Euro-Noise 2003, Naples, Italy, 2003.
41. U. Sandberg, A Closer Look at the Tread Groove Resonance in Tyre/Road Noise, Proc. of the 18th Intern. Conf. on Acoustics (ICA 2004), Kyoto, Japan, 2004.
42. B. Krieger and H. Schmidt, German Joint Project Leiser Straßenverkehr (Silent Traffic), Exposé of the First Research Results, Paper N478, Proc. of Inter-Noise 2003, Jeju, Korea, 2003.
43. U. Sandberg, J. A. Ejsmont, W. Kropp, and K. Larsson, Low Noise Tires—A Cooperation Project in Northern Europe, Paper N494, Proc. of Inter-Noise 2003, Jeju, Korea, 2003.
44. U. Sandberg and J. A. Ejsmont, Tire/Road Noise from an Experimental Composite Wheel, Proceedings of the International Tire/Road Noise Conference (INTROC 90) 8–10 August 1990, Gothenburg, STU Information No. 794–1990, NUTEK, Stockholm (available from the authors).
45. Michelin Tires (USA) presented the TWEEL at the North American International Auto Show (NAIAS) in Detroit, January 9, 2005.
46. U. Sandberg, The Porous Tread Tire—The Quietest Pneumatic Tire Measured So Far?, Proc. of Inter-Noise 2005, Rio de Janeiro, Brazil, 2005.
47. B. Andersen and H. Bendtsen, Experiences with Thin Noise Reducing Pavements, Proc. of Forum Acusticum 2004, Budapest, Hungary, 2004.
48. P. Donavan, J. Reyff, and L. Scofield, Reduction of Traffic and Tire/Pavement Noise: Initial Results of the Arizona Quiet Pavement Program, Proc. of Inter-Noise 2005, Rio de Janeiro, Brazil, 2005.
49. U. Sandberg and B. Kalman, The Poroelastic Road Surface—Results of an Experiment in Stockholm, Proc. of Forum Acusticum 2004, Budapest, Hungary, 2004.
50. T. Fujiwara, S. Meiarashi, Y. Namikawa, and M. Hasebe, Noise Reduction Effect of Porous Elastic Road Surface and Drainage Asphalt Pavement, TRB paper 05-0451, presented at the TRB Annual Meeting 2005, Transportation Research Board, Washington, DC, 2005.

# CHAPTER 87

## AERODYNAMIC SOUND SOURCES IN VEHICLES – PREDICTION AND CONTROL

Syed R. Ahmed

German Aerospace Research Establishment  
Braunschweig, Germany

### 1 INTRODUCTION

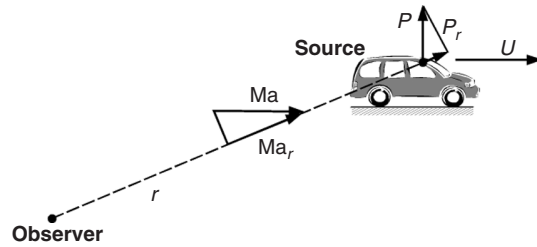
In the unsteady flow around a moving vehicle, aerodynamic sound is generated at (a) abrupt changes in body geometry, (b) gaps in the body structure, (c) leaking or pliable seals, (d) appendages, and (e) interior heating, ventilation, and air-conditioning equipment (HVAC). Separated flow regions with fluctuating pressure exist at (a), (b), (d), and (e) and cause the radiation of sound. Leaking or vibrating seals and the flow from heating and air-conditioning systems also create interior noise. Structural vibration caused by the flow radiates sound into the air enclosed in the vehicle and to the surroundings.

Aerodynamic sound becomes significant at vehicle speeds above 130 km/h and increases approximately with the sixth power of speed. At speeds of 70 km/h and above, the aerodynamic sound becomes dominant in the frequency range of 330 to 900 Hz and remains so at higher speeds. At lower speeds, the tire/road interaction sound dominates in the vehicle interior. Interior sound affects the passengers' comfort level and has become the main focus for aeroacoustic optimization of vehicles.

The prediction and control of sound needs an interdisciplinary approach since fluid mechanics, structural mechanics, sound generation, propagation, and its structure-borne transmission are linked together. The exterior sound radiated and transmitted into the vehicle interior is a product of these coupled nonlinear mechanisms. Computational fluid dynamics (CFD) and computational aeroacoustic (CAA) methods addressing this problem are under development. Sophisticated testing techniques and experimental facilities are currently industrial tools widely used for the analysis and control of aerodynamic sound in vehicles.

### 2 IDEALIZED CONCEPTS OF SOUND SOURCES

Any sound source can be viewed as comprised of a distribution of (a) mass flow (monopole), (b) fluctuating pressure (dipole), and (c) fluctuating viscous force (quadrupole) sound sources. A monopole source is created by an unsteady volumetric addition or subtraction such as by the exhaust pipe or intake of a piston engine. It can also be generated by volumetric addition to the interior of a car through a leaking door seal. A dipole source is created by unsteady pressures acting on a rigid surface. A von Karman vortex impinging on a rigid body panel is such an example. A quadrupole



**Figure 1** Sound pressure sensed by an observer from a moving sound source.

source develops due to a collision of two fluid elements as in a turbulent shear layer, creating fluctuating viscous forces in the flow.

For an observer on the ground (Fig. 1), a moving sound source produces a sound pressure  $p_a$  at location  $x$  and time  $t$ , given by

$$4\pi p_a(x, t) = \frac{\partial}{\partial t} \iint_S \left[ \frac{\rho v_n}{r(1 - Ma_r)} \right]_{\text{ret}} dS + \frac{1}{c} \frac{\partial}{\partial t} \iint_S \left[ \frac{P_r}{r(1 - Ma_r)} \right]_{\text{ret}} dS + \frac{1}{c^2} \frac{\partial^2}{\partial t^2} \iiint_V \left[ \frac{T_{rr}}{r(1 - Ma_r)} \right]_{\text{ret}} dV \quad (1)$$

where  $p_a$  = magnitude of air pressure fluctuation

$\rho$  = air density

$v_n$  = velocity normal to body surface

$r$  = distance between observer and a point on body surface

$Ma_r = U_r/c$ ; Mach number of (body) velocity component  $U_r$  in direction of observer

$dS$  = element of body surface  $S$

$c$  = speed of sound

$P_r$  = component of pressure in direction of observer

$T_{rr}$  = Lighthill tensor<sup>1</sup> (fluctuating viscous-stress tensor)

$U$  = body velocity

$dV$  = element of flow field volume  $V$

The integrals on the right-hand side (rhs) of Eq. (1) are the monopole, dipole, and quadrupole source terms, respectively, which are to be evaluated at the



“retarded” time (subscript “ret”). This is the time  $t$  at which the sound signal is perceived by the observer minus the time needed for the signal to travel the distance between the body and the observer when the signal was emitted. The expression in Eq. (1) is usually known as the *acoustical analogy* associated with the name of Ffowcs Williams and Hawkins<sup>1</sup> (FWH analogy).

### 3 MONOPOLE, DIPOLE, AND QUADRUPOLE SOUND SOURCES AND THEIR DEPENDENCE ON SPEED, MACH NUMBER, AND FREQUENCY

The sound power (in watts) relationship of the individual sound sources is, after Chanaud and Muster,<sup>2</sup>

$$P_M \sim S_n^2 \text{Ma} \frac{Q^2}{(UL^2)^2} \rho U^3 L^2 \quad (2)$$

$$P_D \sim S_n^2 \text{Ma}^3 \frac{F^2}{(\rho U^2 L^2)^2} \rho U^3 L^2 \quad (3)$$

$$P_Q \sim S_n^4 \text{Ma}^5 \frac{T_{rr}^2}{(\rho U^2 L^3)^2} \rho U^3 L^2 \quad (4)$$

where  $P_M$ ,  $P_D$ ,  $P_Q$  = sound power of monopole, dipole, and quadrupole, respectively

$S_n = fL/U$  (Strouhal number)

$\text{Ma} = U/c$  (Mach number)

$Q$  = fluctuating volumetric flow rate

$F$  = fluctuating force (due to fluctuating pressure)

$f$  = frequency

$L$  = characteristic body length

From Eqs. (2), (3), and (4), an estimation of the relative importance of the sound sources can be made. With regard to *speed*, the sound power of the sources varies as

$$P_M : P_D : P_Q :: U^4 : U^6 : U^8 \quad (5)$$

With respect to *Mach number*, the ordering is

$$P_M : P_D : P_Q :: \text{Ma} : \text{Ma}^3 : \text{Ma}^5 \quad (6)$$

With regard to *frequency* the dependence is

$$P_M : P_D : P_Q :: f^2 : f^2 : f^4 \quad (7)$$

The efficiency of sound generation of a source depends upon the degree to which the fluctuations of mass (monopole), pressure (dipole), or viscous stresses (quadrupole) induce partially compressible fluctuations in the flow, which are then radiated to an observer as sound.

Experimental investigations of total sound radiated exterior to an automobile are indicative of monopole behavior for speeds below 120 km/h and dipole above it. The low Mach number speed range of ground vehicles

makes the quadrupole contribution insignificant, as seen from Eq. (6).

Since mass flow fluctuations are related to the overall size of the body, the monopole contribution to the frequency ( $f = U/L$ ) for a body of 4 m length, moving at 140 km/h, would be in the range of 10 Hz. The length scale of the various separated flow regions on the body, which are the sources of the fluctuating pressures, is much smaller, say about  $0.01L$ , then the dipole contribution, which lies in the frequency range of about 1000 Hz. The quadrupole sound, which is intrinsically related to pressure fluctuations but scaled to eddy size, is important at the highest frequencies.

### 4 LOCATIONS OF AERODYNAMIC SOUND SOURCES ON VEHICLE BODY

The overriding consideration for ground vehicle body shape is dictated by the requirements of utility rather than aerodynamics or aeroacoustics. As noted in the introduction, at various locations on the vehicle body small or extensive flow separation regions exist with fluctuating pressure as shown in Fig. 2.

Type (a) locations (Fig. 2) are, for example, hood front edge, windshield base, windshield/front door transition (A-pillar), around recessed window panes, wheel wells, and the body underside. Multiple and extensive separated regions may be present between rear window and trunk lid (notch-back), and at the base of fast-back or hatch-back vehicles.

Type (b) locations (Fig. 2) are at structure gaps such as around doors, rain gutters, hood/windshield base, trunk lid, and the like. Type (c) locations (Fig. 2) are around doors, windows, trunk lid, sunroof, and the like. Type (d) locations (Fig. 2) are at external rear-view mirrors, windshield wipers, radio antenna, sunroof, popup head lamps, and the like. Type (e) locations are in the ducting and venting circuit of high-volume air-conditioning equipment.

### 5 FLOW DETAILS AND ACOUSTICS OF SOME TYPICAL VEHICLE BODY SOUND SOURCES

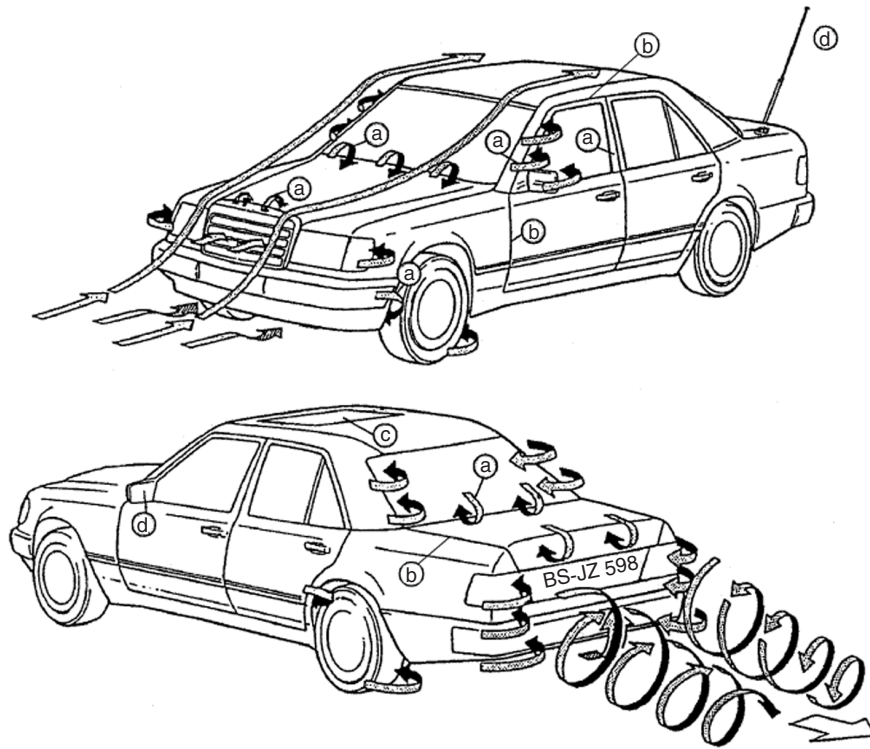
#### 5.1 Flow at a Step Discontinuity

A backward- and forward-facing step can be present at a window pane and elsewhere. A backward facing step creates a pocket of separated flow, where the entrapped flow recirculates causing pressure fluctuations that increase dramatically in the vicinity of the flow attachment point as seen in the variation of the pressure coefficient  $C_p$  (Fig. 3).<sup>3</sup>

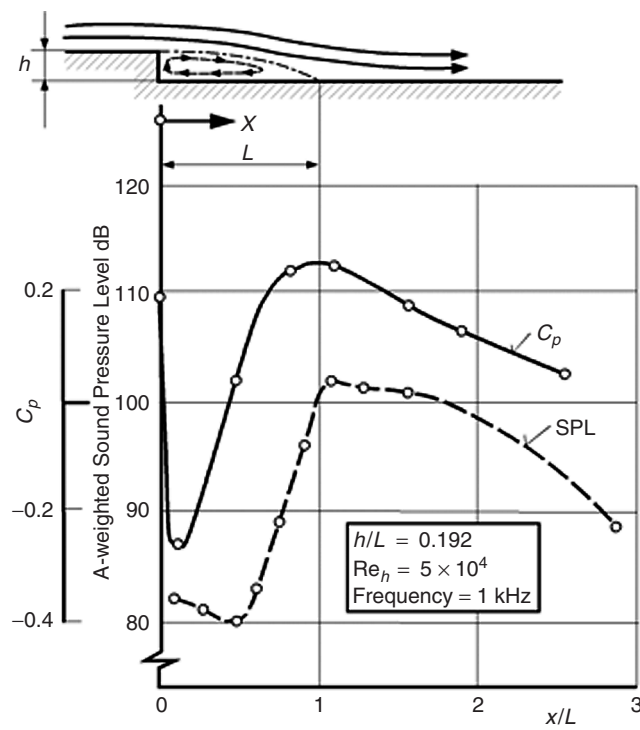
The effect of the flow disturbance can persist along distances over 50 times the step depth. The sound pressure level (SPL), for example, for 1 kHz frequency, may rise 20 dB above the level upstream of the step. Experimental results on a forward-facing step indicate a reduction of 4 to 5 dB for increasing the edge radius–step height ratio from 0 to 0.3, especially in the high-frequency range of 4 to 20 kHz (see Section 5.2).

#### 5.2 Flow in a Cavity

Due to functional requirements, at various locations on the vehicle body gaps exist with a cavity underneath. The cavity air communicates with the external flow. Door,



**Figure 2** Some locations of sound sources on an automobile body.



**Figure 3** Flow details and acoustics of a step discontinuity.<sup>3</sup>

hood, and trunk lid slits, hood rear-edge/windshield base, rain gutters, open sunroof/window, and vehicle interior, are such examples. Flow of air over narrow cavities may produce high-frequency sound containing single or multiple discrete tones and in openings backed by a large volume, a low-frequency “wind throb.”

The boundary layer flow coming off the cavity upstream edge changes into a shear layer over the cavity mouth. This layer is inherently unstable and can oscillate. Its impingement on the cavity downstream-edge produces sound. Additionally, the fluctuating cross flow in the cavity mouth may produce sound. The downstream disturbances travel upstream, are enhanced at the cavity upstream edge and feed the shear layer oscillation. Rockwell and Naudascher<sup>4</sup> categorized the oscillations as (a) fluid-dynamic, (b) fluid-resonant, and (c) fluid-elastic resonant. Type (a) oscillations occur due to instability of the shear layer. Resonant waves in the cavity air, by themselves or coupled to other phenomena, lead to type (b) oscillations. Fluid-elastic resonance oscillations [type (c)] are generated when the cavity air resonance is coupled to vibrations of the cavity surface. The intensity of the radiated sound depends upon how well the frequency of type (a) oscillation matches with that of resonance of type (b) and/or type (d) oscillation. A detailed discussion of cavity-flow oscillation mechanisms is given by J. Milbank.<sup>5</sup>

Rossiter<sup>6</sup> found different modes occurring in fluid-resonant cavity oscillations. All predominant frequencies of cavity sound were found to lie close to the frequency bands of these modes. Work of Koch<sup>7</sup> and others<sup>8,9</sup> confirms this finding. Using Rossiter's semiempirical equation

$$\frac{K}{2\pi} = \text{Ma} \frac{c}{c_0} \frac{j - \gamma_R}{\frac{1}{K_R} + \text{Ma}} \quad (8)$$

where  $K = \omega L / c_0$  (dimensionless frequency)

$L$  = streamwise cavity length

$\omega = 2\pi f$  (circular frequency)

$c, c_0$  = local and ambient speed of sound

$j = 1, 2, 3, \dots$  (mode number)

$\gamma_R$  = phase shift of acoustic scattering at cavity downstream edge

$K_R$  = ratio of convective speed of the shear layer vortices to free stream velocity

the frequency of the modes can be estimated. Rossiter used the values 0.25 and 0.61 to 0.66 for  $\gamma_R$  and  $K_R$ , respectively.

For a cavity of  $L = 0.5$  cm on a vehicle moving at 72 km/h, using Eq. (8) with  $c = c_0 = 340$  m/s and  $K_R = 0.61$ , the resonance frequency for mode number 1 is about 1.8 kHz. As the human ear is very sensitive to frequencies around 1 to 5 kHz, this sound inside the vehicle can be very annoying. Door slits, uncovered holes, rain gutters, and the like etc. are thus sources of high-frequency sound.

At high speeds, the outer flow can induce sufficient forces on the door<sup>3</sup> to deform or pull out the door

panels, causing leakage past the sealing or, if the flow is fluctuating, induce a similar response of the sealing, even if no leakage occurs. The flow mechanisms in the door slit, which can produce sound inside the vehicle, have been explained by Callister and George.<sup>10</sup>

Defective sealings and other sound leaking areas can be detected by placing an ultrasound emitter inside the vehicle and traversing the suspected outside area with a hand-held ultrasound receiver. The intensity of the received signal is a measure of the severity of the defect. Also a survey with a stethoscope inside the vehicle during wind tunnel or road tests is a simple means to detect air leaks.

Ethembaouglu<sup>11</sup> examined the sound attenuation by various geometries of the cavity downstream edge. A gradual slant or an elliptical edge was the most effective configuration.

Wheel wells are another location where a complex cavity flow is generated, which is mainly a source of external sound. Wind tunnel results for a full-scale vehicle (with stationary wheels) show sound with one-third octave center frequencies between 3150 and 6300 Hz close to the vehicle.<sup>3</sup>

Badger and Jones<sup>12</sup> modeled the “wind throb” due to an open window or sun roof and found the frequency of the oscillation is given by

$$f = \frac{c}{2\pi} \frac{\sqrt[4]{A}}{\sqrt{0.96V}} \quad (9)$$

with  $A$  the area of the opening and  $V$  the volume of the enclosure. For  $A = 0.06$  m<sup>2</sup> and  $V = 3$  m<sup>3</sup>, the oscillation frequency is about 16 Hz.

Since the natural frequency of the human head and eyes lies in the range of 15 to 20 Hz, this can be a source of serious discomfort and fatigue. Increasing the value of  $A$  raises the frequency at which the throb can occur and thus avoid it when the cruising speed remains the same.

### 5.3 A-Pillar Flow

The A-pillar flow is one of the most often investigated subjects both theoretically and experimentally. The airflow coming off laterally from the windshield separates as a sheath at the A-pillar and curls up into a conical vortex, much like the flow observed over a delta wing at incidence. The SPL values along a line aligned with vehicle motion and across the vortex, show a large increase in the vicinity of the flow reattachment on the side window pane—a location close to the driver's ear. The window glass pane being a poor sound insulator, the importance of this sound source is evident. The high SPL levels generated by the conical vortex are a consequence of its strong vorticity content. Due to safety considerations, the outside rear-view mirror is placed in the region of A-pillar flow, enhancing the sound generating flow on the window pane. Measures to inhibit the sound aim at matching the geometry of the A-pillar and the rear-view mirror to lower the vortex intensity of the flow.

The A-pillar curvature is an important parameter influencing the sound intensity. Large radii pillars are less sensitive to yaw-flow modulation of the interior sound. Sound modulation is an irritant, which lowers the comfort feeling inside the vehicle.<sup>13</sup>

#### 5.4 Flow around Exterior Rear-View Mirror

The exterior rear-view mirror is an essential item to ensure driving safety and is placed in the viewing area of the driver, which is near the A-pillar vortex where high velocities exist. The mirror body may generate a closed bubble type of wake with recirculating flow inside or vortex shedding off its rim, depending upon minute geometry details. This flow may be partially or fully embedded in the A-pillar flow, creating a complex unsteady flow impinging on the side window. Wind tunnel results with a real car show an A-weighted SPL increase of 4 to 6 dB by a mirror over a one-third octave band of 1 to 10 kHz, inside the car. Small grooves and gaps in the rear-view mirror assembly are often sources of tonal sound. Tiny surface protuberances at suitable locations of mirror body help break up the periodic tone-generating flow.<sup>5,13</sup>

The mirror body and attachment need a detailed matching with the local vehicle geometry. The goal thereby is to inhibit the pressure fluctuations, divert the flow away from or below the lower edge of the window pane and away from the driver's ear as well as decrease its vertical extent.<sup>3</sup>

#### 5.5 Windshield Wipers

Windshield wipers whether in use or stationary are exposed to high velocities and the arm and wiper blade can generate significant amount of interior sound. Measures to reduce the sound focus on yaw-flow optimized geometry of the wiper arm and deflection of the airflow to above the wiper with an upward twist of the hood rear edge or placing the wiper below the edge to shield it from the airflow when stationary. Experimental results quoted in Helfer<sup>13</sup> report a significant decrease in the SPL inside the vehicle over the frequency range of 1 to 10 kHz due to such measures.

#### 5.6 Roof Racks

Roof racks are a common feature on SUVs and RVs and tonal sound from the rack crossbars can be a source of annoyance. The crossbars are exposed to the flow over the vehicle roof, and the periodic shedding of von Karman vortices from them produces a dipole-type tonal sound of a discrete frequency. With speeds above 70 km/h, this sound is readily heard inside the vehicle. A way out is the choice of a nonsymmetric cross section of the crossbar, which can significantly reduce the strength of the shed vortices without compromising the structural integrity needed for carrying the payload.<sup>14</sup>

#### 5.7 Radio Antenna

The mechanism of “whistling” tones produced by a radio antenna is due to vortex shedding as mentioned for the roof rack. The use of a nonsymmetric cross section is unsuitable here as it affects the reception quality. The vortex shedding is actually three dimensional as depicted in Fig. 4.<sup>3</sup> At one point the vortices are shed off the top (case A), and some distance away they are shed at the bottom (case B). Between these shedding nodes, there is an oscillating flow that moves along the axis of the cylinder. Since these flow mechanisms excite vibration of the thin and long antenna, the fluid dynamics and structural dynamics are coupled in the sound generation.

This tonal sound can be transmitted structure borne into the vehicle interior. A vibration absorbing fixture or tilted attachment of the antenna to the vehicle may reduce the sound to some extent but affects the radio reception. A helical strake of thin wire on the antenna rod can break up the intensity of the vortex shedding and sharply reduce the decibel level of the interior sound. Experimental results on a real car<sup>3</sup> have shown an SPL reduction of about 15 dB at the original whistling frequency for a straked antenna.

#### 5.8 Underbody Flow

Almost all vehicles have strongly structured undersides as exhaust pipes, mufflers, wheel axles, wheel cavities,

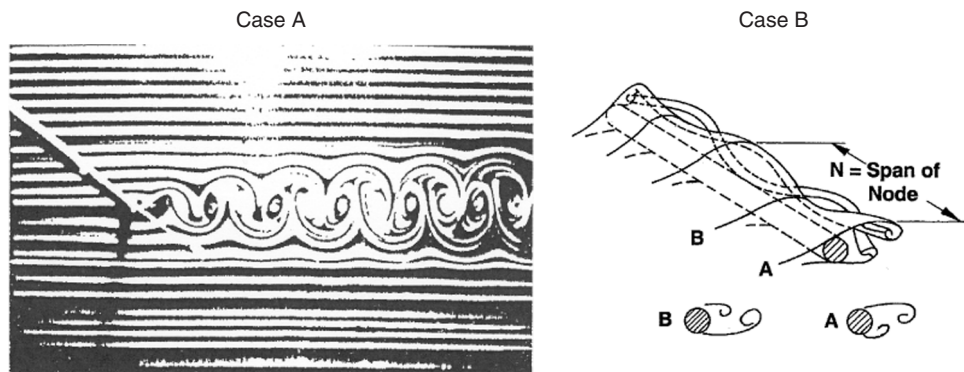


Figure 4 Vortex shedding off a long thin cylinder.<sup>3</sup>

and the like, are arranged on this surface. Most of the car engines are mounted in the front and the underside here is left open to improve the engine cooling. The air drawn in by the cooling fan in the engine compartment produces a complex turbulent flow that is fed into the gap flow between the underside and the road. This air flow interacts with the rough understructure and with the faster moving airflow along the sides. Since the vehicle body is elastically mounted on the wheels, its movement and road unevenness creates a time-varying ground clearance that translates into a time-dependent flow on the undersurface affecting also the global flow around the vehicle. The fluctuating pressures on the underbody are, due to its large plan form area, important for interior sound. The contribution is primarily of the low-frequency content. As is well known, the low-frequency sound is more difficult to insulate with floor carpeting. Wind tunnel results on a full-scale car with blocked underside flow show a typical reduction of about 2 to 5 dB at the driver's ear location<sup>3</sup> in the A-weighted SPL for the one-third octave band of 50 to 150 Hz.

### 5.9 Rear-End Flow

At the rear end, all the characteristics of the upstream flow merge to form a complex time-dependent wake where viscosity effects dominate. Basically the wake coming off the blunt base is a time-dependent structure, containing low-frequency circulating regions with axes lateral and parallel to the vehicle base in an elliptical bubble (hatch-back vehicles) or longitudinal high-intensity vortices coming off the base slant of fast-back vehicles with a small wake bubble in the middle.<sup>3</sup> The impinging of the fluctuating wake flow on the trunk lid and vehicle base is a source of interior sound. The large extent of the wake region leads essentially to low-frequency sound, which can be transmitted to the rear car interior. This can be readily observed with a slightly open trunk lid during driving. Reduction of vehicle drag through wake management in this area has often a beneficial effect on the sound generated.

## 6 SOURCES OF SOUND IN HVAC EQUIPMENT

A variety of components of the HVAC equipment contribute to the interior sound of the vehicle, which can be structure borne or aeroacoustic sound. HVAC sound is mainly of concern in the vehicle interior. It affects the comfort level, induces fatigue, and may, through distraction, lower the driving safety.

Components that generate aeroacoustic sound are the air ducts and vents, blower and the manifold. Sudden area changes, sharp bends, and other separation-prone details in the ducting lead to pockets of separated flow that are then the sound sources. Structure-borne sound is due to step motors, evaporator and heater, and the control unit. Details of the internal flow in these accessories as well as their mounting and location need to be examined in detail to inhibit their sound contributions.<sup>3</sup>

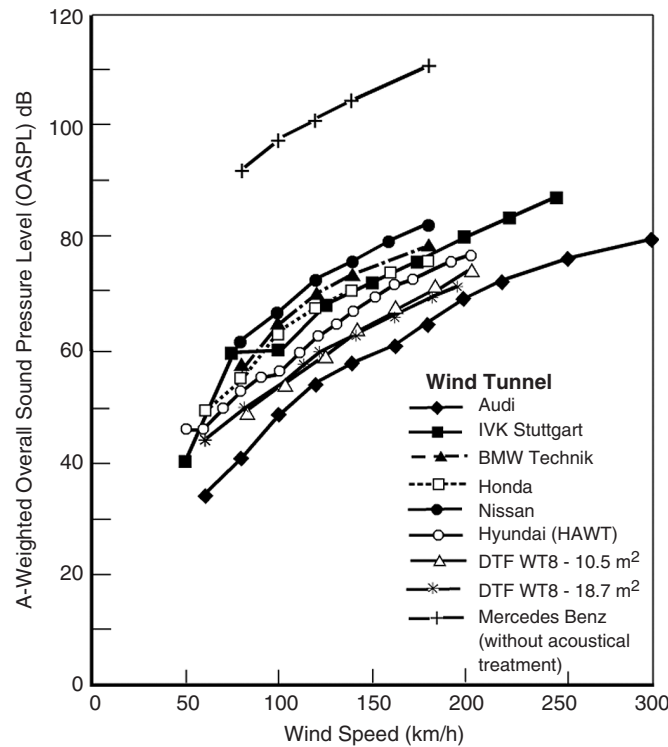
## 7 TEST FACILITIES FOR ROAD VEHICLE AEROACOUSTICS AND SOME ILLUSTRATIVE RESULTS

Aeroacoustic optimization of ground vehicles is mostly done in wind tunnels and to some extent with road tests. The tests are preferably performed at full scale, due to lack of a similarity law for sound such as exists for drag. Additionally, minute configuration details, which can be decisive sound sources, often cannot be duplicated on subscale models. The main advantage of wind tunnels is the controlled test conditions and the high accuracy of test techniques that ensure reproducible results. However, simulation of some real life situations like side winds, unbounded surrounding air, and the like are difficult or impossible to realize in a wind tunnel. Road tests are then the answer, but these are fraught with many uncertainties due to changing weather conditions and pavement qualities that are uncontrollable. This makes repeatability of the tests very difficult, and meaningful results can be obtained only from averaging a number of carefully selected test runs under consideration of the monitored weather conditions.

### 7.1 Aeroacoustic Wind Tunnels<sup>3</sup>

Automotive wind tunnels are normally equipped with either a  $\frac{3}{4}$ -open, slotted, or closed test section. The  $\frac{3}{4}$ -open jet closed-circuit configuration seems to be the preferred choice among European,<sup>3,13</sup> Japanese,<sup>15,16</sup> and newer tunnels in the United States.<sup>17</sup> The open test section allows ease of access as well as efficient sound absorption of the plenum chamber where out-of-flow and far-field measurements can be made. However, the development of a shear layer around the jet and its impingement on the collector are sources of sound and flow oscillations (see Section 5.2) that can contaminate the sound measurements. As evident from Eq. (5), the sound power is strongly dependent on the vehicle speed. This means that during wind tunnel tests, the wind speed has to be maintained very precisely. Consequently, sound measurements are difficult to perform during road tests. The correct location of appendages on the body is also of prime importance as otherwise they may be exposed to a different velocity field.<sup>13</sup>

Aeroacoustic tests in the wind tunnel place stringent demands on the "background" SPLs in the test section. The purpose of the acoustical experiments is to simulate sound sources in the open atmosphere. The requirement is then that the background SPL in the empty test section should be significantly lower than level with the test object installed. An A-weighted SPL difference of about 10 dB over the frequency range of 50 to 8000 Hz is accepted as sufficient in the industrial practice. Another requirement is that the sound reflected by the tunnel walls should not contaminate the sound emitted by the test object. Ideally in such "anechoic" tunnels, the SPL decays at distances  $r$  larger than the wavelength  $\lambda$ , as  $1/r$ . This relationship—also called the *inverse square law*—governs the sound decay in the open atmosphere. Some details of



**Figure 5** Background out-of-flow sound pressure levels of some aeroacoustic full-scale automotive wind tunnels.<sup>3,13,15–17</sup>

the background sound suppression measures are available in the literature cited in Refs. 3 and 13.

A feeling for the out-of-flow background SPLs of some modern full-scale aeroacoustic automotive wind tunnels is gained from Fig. 5. The comparison of newer tunnels with the older Mercedes Benz (MB) tunnel (which is without an acoustical treatment) shows the improvement in the acoustics of the newer designs. The Audi tunnel in Germany achieves a decrease of almost 50 dB (A-weighted overall sound pressure level, OASPL) compared to the MB tunnel. The Hyundai and Ford DTF tunnels show values about 40 and 45 dB lower than the MB tunnel. The General Motors tunnel in the United States is about 10 dB quieter than MB tunnel; similar figures for DNW in Netherlands are about 15 dB, for Porsche slotted-wall tunnel in Germany and Volvo tunnel in Sweden, about 12.5 dB. The Volkswagen (acoustically untreated) tunnel is on par with the MB facility.

## 7.2 Some Aeroacoustic Measurement Techniques

A comprehensive overview of aeroacoustic measurement techniques used in ground vehicle work is available in Callister and George<sup>10</sup> and Ahmed.<sup>3</sup> Basically there are three different types of measurements

performed: (a) inside the vehicle, (b) outside the vehicle but inside the tunnel airflow, and (c) outside the vehicle and tunnel airflow. Each of these requires a different instrumentation and procedure.

**7.2.1 Microphone Location** Placing the data acquisition microphones outside the airflow increases the distance between the sound source and the data acquisition point reducing the *signal-to-background-sound* ratio. Also the sound signal, in an open-jet wind tunnel, has to cross the shear layer of the jet to reach the microphone. A refraction correction has then to be applied to the sound signal.<sup>18</sup>

Microphone placement inside the flow with supports makes them producers of sound besides the scattering effects on the sound to be measured. Hydrodynamic pressure fluctuations around the microphone body enhance the signal. Commercially available “nose cones,” slipped over the microphone head, alleviate the problem but are of little help when yaw flow conditions are encountered.

**7.2.2 Acoustical Mirror** This device, developed originally for aeronautical applications<sup>19</sup> has found its way in a number of automotive tunnels. It is a convenient and robust system to directly identify the location and spatial distribution of the sound intensity of sound sources and is suitable for out-of-flow operation in open-jet wind tunnels.

Figure 6 illustrates the basic principle of this device. The concave mirror on the left is a segment of the ellipsoid of revolution indicated by the dashed line. The two focal points are the locations of a signal acquiring microphone and the sound source, respectively. Sound waves emitted by the source are focused on the microphone by reflection at the mirror, thereby greatly enhancing the signal sensed by the microphone. Since the measured SPL is directly related to the sound intensity of the source, the sound intensity distribution in a plane normal to the mirror axis can be surveyed by moving the mirror parallel to such a plane. Tests have shown that an elliptical mirror provides a better amplification than a spherical or a parabolic mirror.

For an efficient reflection of the sound waves, the wavelength  $\lambda$  of the oncoming sound waves should be small compared to the mirror diameter  $D$ , ( $\lambda \ll D$ ). The frequency range of interest in automobile aeroacoustics is from about 50 to 8000 Hz. With  $\lambda = c/f$  and  $c = 340$  m/s, the corresponding wavelengths turn out to be 6.8 and 0.042 m. To capture the lowest frequencies, the mirror diameter becomes very large.

The amplification of the sound signal of a point source is shown in the inset of Fig. 6. The base width of this curve is a measure of the spatial resolution of the sound signal by the mirror. For the half width  $w$  the relationship is<sup>19</sup>

$$w \approx 0.54\lambda \left( \frac{S}{D} \right) \quad (10)$$

with  $S$  as the distance between the mirror base and the source. Choosing a value for  $S$  of 4 m, which is a

typical distance in a full-scale automotive wind tunnel test, and  $D = 2.16$  m, one obtains for the half width

$$w \approx \lambda \quad (11)$$

The spatial resolution of a mirror of this diameter varies linearly with  $\lambda$  and would improve with higher values of the frequency. A mirror of this diameter is unwieldy, and smaller size mirrors are used in the industrial practice.

An example of exterior sound measurement on a real car with an acoustical mirror is presented in Fig. 7.<sup>13</sup> The tests were conducted in a wind tunnel at a wind speed of about 140 km/h with the mirror placed 4 m away from the car. The OASPL results for the lower frequency range (0.5 to 4 kHz) show the front tire area and the trunk-mounted antenna as the major producers of sound. For the higher frequencies (4 to 9.5 kHz), the hood front, tires, rear-view mirror, and A-pillar area are the main sound contributors.

**7.2.3 Spatial Transformation of Sound Fields (STSF)** The STSF technique enables the evaluation of the spatial sound field with near-field acoustical holography. The principle of this Fourier-transform-based technique is to measure the cross-correlated spectra of an array of “scan” microphones, which are traversed in a plane close to the vehicle (inset in Fig. 8<sup>13</sup>), and one or more fixed “reference” microphones.<sup>13,20</sup> The cross-correlated spectra are determined for each scan-reference microphone combination as well as for reference microphones among themselves. Using Helmholtz’s integral

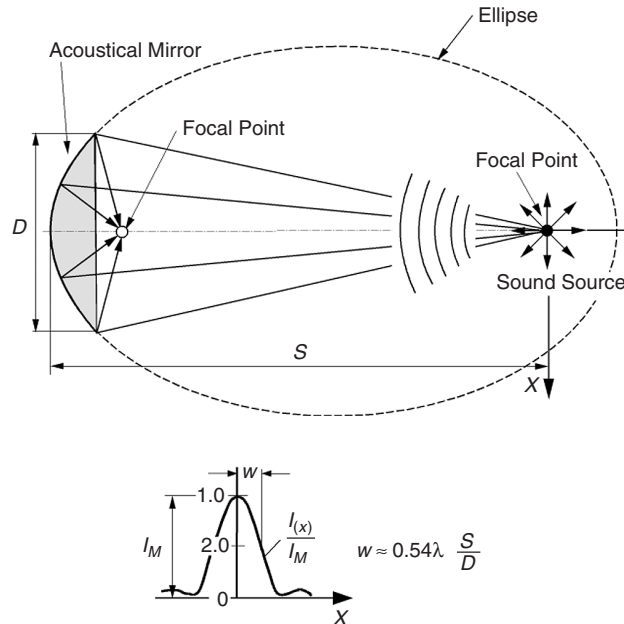


Figure 6 Working principle of the acoustical mirror.



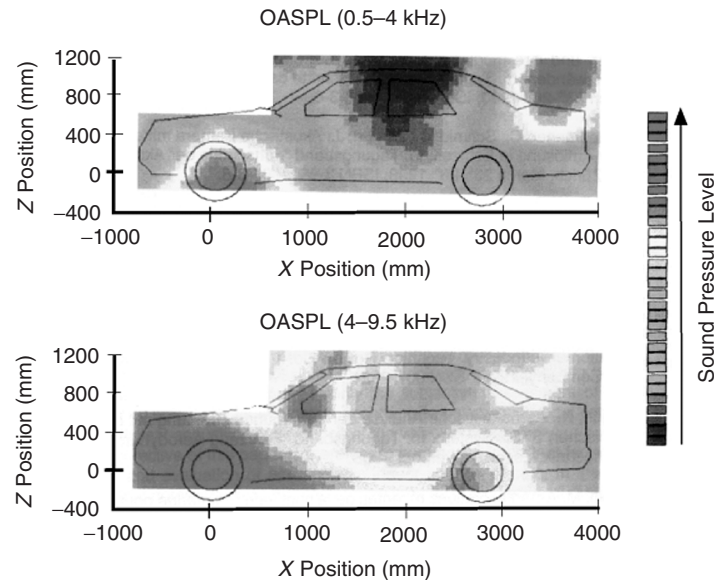


Figure 7 Measured sound pressure level map of a production car obtained with an acoustical mirror.<sup>13</sup>

relationship,<sup>20</sup> this data is used to determine SPL and sound intensity in other near- and far-field locations. The cross-correlation process eliminates mostly the self-induced signals of the array microphones through averaging so that the array microphones can be placed in the airflow. The location of the reference microphones is critical to the success of this approach, and exposure of these microphones to the airflow is to be avoided.

A result of this technique is shown in Fig. 8. The top right sound map shows some spurious sound sources in the rear-view mirror wake, when the traverse plane was too close to the vehicle surface. The elimination of microphone self-sound for this distance is incomplete. The lower maps, obtained at larger distances from the body are free of this error, exhibit somewhat lower SPLs.

**7.2.4 Artificial Head Device** The artificial head is a replica of the human head with microphones installed in the ear cavities. It is used for the *subjective* assessment of the spatial sound field in the vehicle interior. By hearing the recorded sound with headphones, a more realistic relative ranking of a set of different sample recordings can be obtained.<sup>21</sup>

**7.2.5 Structure-Borne Sound Transmission** To help identify sources of interior sound, the transmission paths of structure-borne sound need to be investigated. Often piezoelectric accelerometers are attached to the critical body parts to evaluate their vibration intensity and correlate with sound measurements inside the vehicle. The mass of the accelerometer has to be small so as not to alter the vibration characteristics of the part studied.<sup>13</sup>

A nonintrusive method for the purpose is the laser Doppler vibrometry.<sup>22</sup> It is based on the principle of reflection of a laser beam from a vibrating body surface. The difference in the frequency of the incident and reflected beam is a measure of the vibration intensity at the point of reflection. This technique allows a rapid scan of vibration-prone surfaces.

## 8 PROBLEMS AND PROSPECTS OF COMPUTING SOUND GENERATION BY ROAD VEHICLES<sup>3</sup>

An analysis of airflow-induced sound involves, as mentioned in the introduction, the study of the unsteady flow field and flow-induced structural vibrations. This poses a formidable challenge to a purely theoretical approach. Ignoring the nonlinear coupling between the two, CFD and CAA may, in principle, be used to directly compute the sound generation and its propagation.

The flow around ground vehicles is for all practical purposes fully turbulent with Reynolds numbers (Re) around 7 to 8 million. It is adequately described by the unsteady Navier–Stokes (NS) equations. An overview of the CFD approaches to compute the ground vehicle flow was given by Ahmed.<sup>23</sup> The goal is to obtain the unsteady pressure distribution on the vehicle body or at least in areas of interest. The aeroacoustic part uses the fluctuating pressures, in a following step, to predict the sound with the help of some form of acoustical analogy such as given in Section 2.

Some problems that arise with a purely CFD-based sound analysis have been discussed by Hardin.<sup>24</sup> In brief these are:

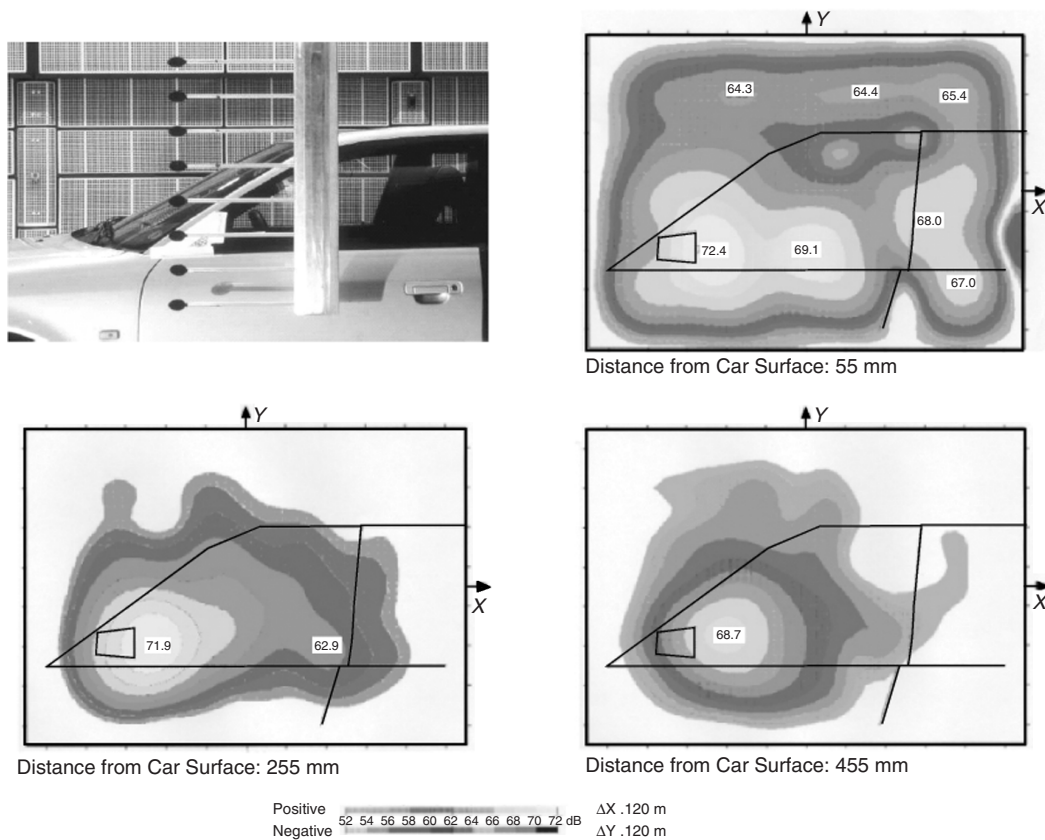


Figure 8 STSF scan-microphones and sound field map results.<sup>13</sup>

- The magnitude of the fluctuating pressures is of the order of  $10^{-2}$  to  $10^{-5}$  of the mean pressure. To capture such small values, the demands on accuracy become extreme.
- Numerical schemes affect amplitude “dissipation” and phase shift through “dispersion” in the propagating waves. High-frequency acoustic waves may thus be distorted.
- In CFD, grids are made dense in regions of interest and sparse elsewhere. For example, capturing the flow details in and around small cavities requires extreme fine grids. Such nonuniform grids can strongly distort the wave propagation.
- For exterior problems, the propagation domain is unbounded. A computation can be performed only over a finite domain. This raises the question of what boundary conditions are to be specified at the finite domain boundaries.
- The introduction of the time dimension dramatically increases the computational expense.

## 8.1 Some Computational Approaches

**8.1.1 Lattice-Boltzmann Method (LBM)** The method is of interest for vehicle aeroacoustics and offers an alternative to the conventional NS-equations-based CFD approaches. The principle underlying the method is briefly, as follows:

The movement of air is approximated as the movement of discrete air “particles” on a grid (lattice). Thus instead of the  $10^{24}$  real-valued degrees of freedom of air molecules, a finite number of the degrees of freedom is allowed. As discussed by Rothmann and Zeleski,<sup>25</sup> the description of the motion need not be so detailed, yet it gives—in macroscopic sense—realistic fluid mechanic simulations.

The particles of the fictitious fluid move on a fixed lattice. Initially, the particles, each of unit mass, are located at the nodes of the lattice and possess equal velocities oriented along the lattice spokes. During a computation step, the particles hop to the next node, collide with other particles arriving at the same node and scatter along the lattice spokes according to a set of prescribed “collision rules.” The collisions cause the velocity and direction of movement of the particles to change, but neither the total number of

particles nor the vector sum of their velocities is changed. This means that the mass and momentum is conserved. Ensemble averages of the particle dynamic behavior lead asymptotically to the incompressible NS equations. Since the collision rules are framed to conserve mass, momentum, and energy of a particle ensemble after each computation step, the code mimics unsteady flow.

The time accurate computation of the unsteady aerodynamics makes the LBM method attractive for the computation of aeroacoustics using, for example, the unsteady pressure as input to the acoustical analogy-based codes. A commercial version of the LBM method, the PowerFLOW code, was used by Uchida and Okumura<sup>26</sup> to compute the sound generation on the front side window of a detailed vehicle model (Fig. 9). The simulation, done for a vehicle speed of 100 km/h on a 16-processor Origin 2000 workstation required 47 h of computer time.

Figure 9 gives an overview of the numerical model, the locations of the microphones on the window during the wind tunnel test, and a comparison of the computations with experiment. In general, the theoretical results show a higher SPL at the low and vice versa at high frequencies than the experiment. This example demonstrates the possibilities that may be available in future with more refinements of the code and denser grids.

For details of boundary element method (BEM) applications to sound radiation by a vibrating body, a cavity or the performance of mufflers, reference could be made to Seybert and Wu.<sup>27</sup>

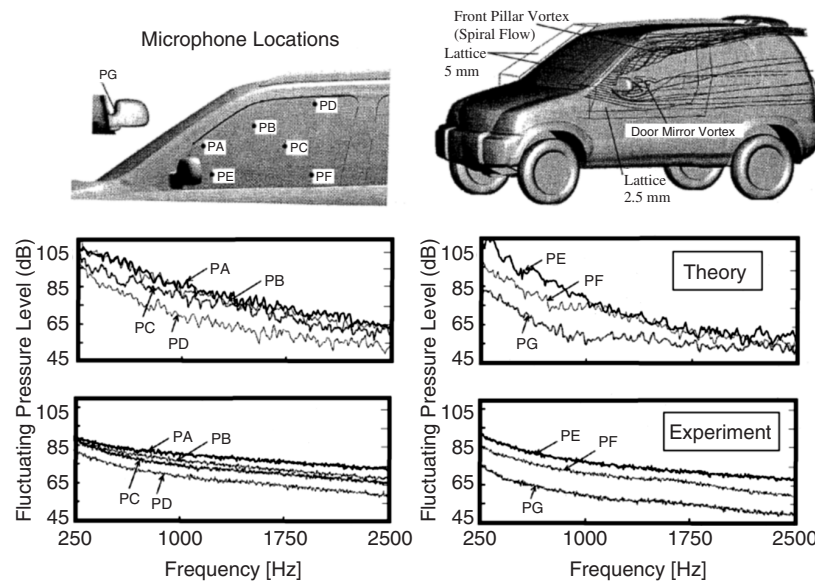
**8.1.2 CAA Methods** The CAA approach uses computational techniques to calculate all aspects of sound generation and propagation directly from the NS

equations.<sup>28</sup> Despite recent advances in prediction of sound with CAA, work of direct interest to vehicles is currently limited to simple basic geometries.

The low Mach number laminar boundary layer flow over a vehicle door cavity with a lip was investigated by Loh and Lin (see Ref. 28). They studied the influence of boundary layer thickness on the resonance modes, their frequency, and maximum SPL. Their results show the existence of more than three resonance modes (see Section 5.2) for both the thin and thick boundary layers. In both cases, the maximum SPL at a point above the cavity was due to the third mode. Kurbatski and Tam (see Ref. 28) (also considering a laminar flow over the same cavity) state that if the boundary layer becomes thick beyond a critical value, no tone is emitted.

**8.1.3 Non-CFD Methods** A number of sound estimation methods have been proposed in the literature based on *measured* fluctuating pressures at critical locations on the body and using this to predict the exterior or interior sound generation in a vehicle. The advantage of these methods is the inclusion of the structure–vibration contribution to the sound in the measured values.

Using the measured fluctuating pressure at various outside locations on the front side-window of a car, Haruna, Kamimoto, and Okamoto<sup>29</sup> isolate sound “sources” on the window pane by plotting pressure isobars for various frequencies. Each of these sound sources is accorded with a *correlation area*, which is obtained by observing the correlation behavior of the fluctuating pressure at the source and at points in the neighborhood. The contour passing through points with the highest correlation factor is the correlation area for the source. The source sound intensity  $I$  at a



**Figure 9** Sound generation on the front side window of a vehicle. Results of a computation with PowerFLOW code.<sup>26</sup>

distance  $r$ , radiated from  $n$  sources is given by

$$I = \frac{1}{(4\pi)^2 \rho c^3} \left( \frac{\cos \Theta}{r} \right)^2 \sum_{i=1}^n (p_a f S_c)^2 \quad (12)$$

where  $\Theta$  = angle between the surface normal at the source and  $r$   
 $S_c$  = the correlation area.

Defining a standard intensity  $I_0$  as

$$I_0 = \frac{1}{(4\pi)^2 \rho c^3} \left( \frac{\cos \Theta_0}{r_0} \right)^2 (p_{a0} f_0 S_{c0})^2 \quad (13)$$

where  $\Theta_0 = 0^\circ$

$$p_{a0} = 2 \times 10^{-5} \text{ (Pa)}$$

$$f_0 = 1 \text{ kHz}$$

$$S_{c0} = 1 \text{ m}^2$$

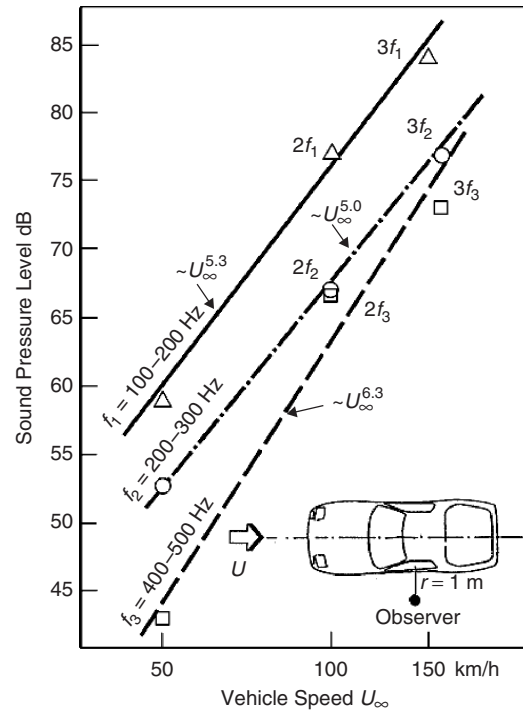
$$r_0 = 1 \text{ m}$$

The SPL value is obtained as

$$\text{SPL} = 10 \log_{10} \frac{I}{I_0} \quad (14)$$

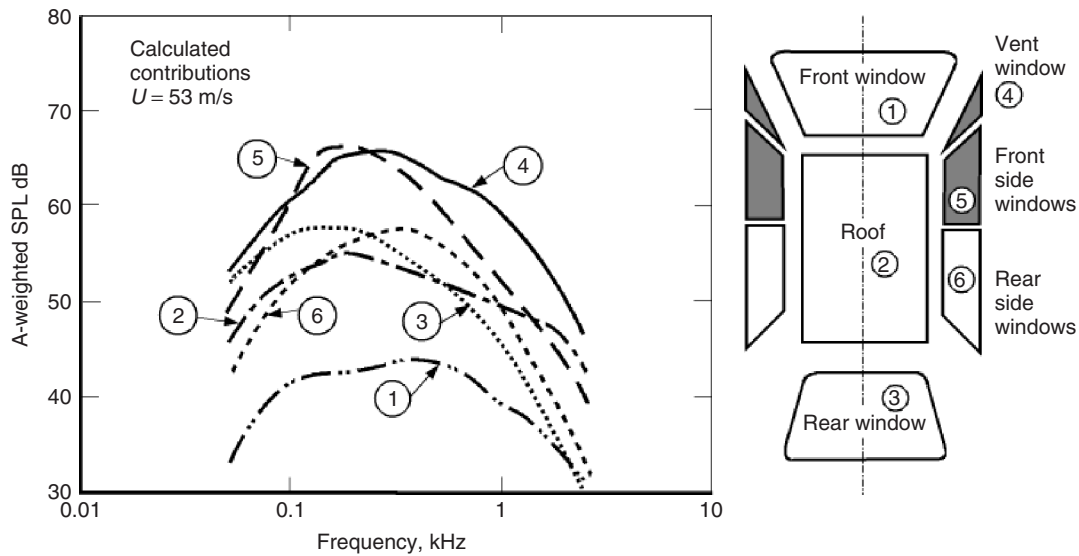
A result of this method is shown in Fig. 10 for the distance of 1 m for three different sets of frequencies over the speed range of 50 to 150 km/h. The SPL increases with the vehicle speed depending upon the frequency considered. For the lower frequencies (100 to 200 Hz) the exponent is 5.3, for the higher frequencies, it is 6.3.

An estimation method for the car interior sound has been developed by Dobrzynski.<sup>30</sup> The method uses the *measured* external fluctuating pressure and pressure



**Figure 10** Estimated SPL from measured fluctuating pressure at side window of an automobile.<sup>29</sup>

field correlation lengths to evaluate the SPL inside the car. The model simulates the pressure by a distribution



**Figure 11** Estimated A-weighted sound pressure level contributions from different areas of the automobile body at driver's ear level.<sup>30</sup>

of point forces acting on a homogenous panel. The forces produce bending waves in the panel that radiate acoustic energy. The obtained relationship states: The power of the sound generated is proportional to the root-mean-square (rms) value of the fluctuating force. The fluctuating force is the product of the pressure and a correlation area, which is an area in which the pressure fluctuations are in phase.

The intensity of surface pressure fluctuations (rms value) and correlation area are determined from experiment as a function of the frequency. The power of the radiated sound from any panel can then be obtained by adding the contributions of the correlation areas. To apply the method in a practical application, first all those locations on a vehicle body are identified that contribute significantly to the pressure fluctuations and evaluate there the fluctuating pressure intensity and the correlation quantities.

Figure 11 shows the estimated contributions from different areas of a fast-back-type full-scale car. The location considered is the driver's left ear of a right-hand drive car. As seen, the major contribution comes from the front vent and side window, which are engulfed in the A-pillar flow. The large area of the roof, which experiences low-intensity pressure fluctuations, is a comparatively weak contributor to the interior sound. The car rear, with a large flow separation, generates low-frequency sound perceived in the vehicle interior. The windshield turns out to be the lowest sound contributor of all the areas considered.

## REFERENCES

1. J. E. Ffowcs Williams and D. L. Hawkins, Sound Generation by Turbulence and Surfaces in Arbitrary Motion, *Phil. Trans. Roy. Soc., A*, Vol. 264, No. 1151, 1969, pp. 321–342.
2. R. C. Chanaud and D. Muster, Aerodynamic Noise from Motor Vehicles, *J. Acoust. Soc. Am.*, Vol. 58, No. 1, July 1975, pp. 31–38.
3. S. R. Ahmed, Eighth International Congress on Sound and Vibration, Tutorial on Automobile Aeroacoustics, Hong Kong, China, 2–6 July, 2001.
4. D. Rockwell and E. Naudascher, Review—Self-Sustaining Oscillations of Flow Past Cavities, *Trans. ASME, J. Fluids Eng.*, Vol. 100, June 1978, pp. 152–165.
5. J. Milbank, *Tonal Wind Noise Design Guide*, Report No. WTR 16–10–04, Vehicle and Industrial Aerodynamics Group, RMIT University, Melbourne, Australia, 2004.
6. J. E. Rossiter, Wind Tunnel Experiments on the Flow over Rectangular Cavities at Subsonic and Transonic Speeds, Aeronautical Research Council Reports and Memorandum No. 3438, London, 1966.
7. W. Koch, Acoustic Resonances in Rectangular Open Cavities, *AIAA J.*, Vol. 43, No. 11, November 2005, pp. 2342–2349.
8. L. East, Aerodynamically Induced Resonance in Rectangular Cavities, *J. Sound Vib.*, Vol. 3, No. 3, 1966, pp. 277–287.
9. C. Tam, The Acoustic Modes of a Two-Dimensional Rectangular Cavity, *J. Sound Vib.*, Vol. 49, No. 3, 1976, pp. 353–364.
10. J. R. Callister and A. R. George, *Topics on Wind Noise—Automobile Wind Noise and Its Measurement (Part II)*, SAE SP-1457, Society of Automotive Engineers, Warrendale, PA, 1999.
11. S. Ethembaoglu, *On the Fluctuating Flow Characteristics in the Vicinity of Gate Slots*, Division of Hydraulic Engineering, University of Trondheim, Norwegian Institute of Technology, Trondheim, Norway, June 1973.
12. W. K., Badger, and C. M. Jones, Aerodynamic Windthrob in Passenger Cars, Paper No. 840 A, *SAE Automobile Week*, March 1964.
13. M. Helfer, Kraftfahrzeug-Aeroakustik, in *Aerodynamik des Automobils*, W-H. Hucho, Ed., GWV Fachverlage, Wiesbaden, Germany (in German), 2005.
14. M. Lee, J. Lee, and D. Kim, Reduction of Aeolian Noise from Roof Rack Crossbars Using Asymmetric Cross-Section Geometry, SAE Paper No. 2002-01-1275, SAE SP-1667, Society of Automotive Engineers, Warrendale, PA, March 2002.
15. N. Ogata, N. Iida, and Y. Fujii, Nissan's Low-Noise Full-Scale Wind Tunnel, SAE Paper No. 870250, Society of Automotive Engineers, Warrendale, PA, 1987.
16. M-S. Kim, J-H. Lee, J-D. Lee, and J-H. Chang, Hyundai Full Scale Aero-acoustic Wind Tunnel, SAE Paper No. 2001-01-0629, SAE SP-1600, Society of Automotive Engineers, Warrendale PA, March 2001.
17. J. Walter, E. Duell, B. Martindale, S. Arnette, and P. A. Nagle, The Driveability Test Facility Wind Tunnel No. 8, SAE Paper No. 2002-01-0252, SAE SP-1667, Society of Automotive Engineers, Warrendale PA, March 2002.
18. R. K. Amiet, Corrections of Open Jet Wind Tunnel Measurements for Shear Layer Refraction, AIAA Paper No. AIAA-93-1711, 1996.
19. F. R. Grosche, H. Stiewitt, and B. Binder, Acoustic Wind Tunnel Measurement with a Highly Directional Microphone, *AIAA J.*, Vol. 15, No. 11, Nov. 1997, pp. 1590–1596.
20. J. Hald, *Use of Spatial Transformation of Sound Fields (STSF) Techniques in the Automotive Industry*, Technical Review No. 1–1995, Brüel & Kjær, Nærum, Denmark, 1995.
21. N. C. Otto, and B. J. Feng, Wind Noise Sound Quality, SAE Paper No. 951369, Society of Automotive Engineers, Warrendale PA, 1995.
22. M. M. Marchi, A. Petniunas, and D. E. Everstine, Measurement of Aeroacoustically Induced Door Glass Vibrations Using a Laser Vibrometer, SAE Paper 951331, Society of Automotive Engineers, Warrendale PA, 1995.
23. S. R. Ahmed, Computational Fluid Dynamics, in *Aerodynamics of Road Vehicles*, W-H. Hucho, Ed., SAE, Warrendale, PA, 1998.
24. J. C. Hardin, VKI Lecture Series 1996-04, Computational Approaches to Computational Aeroacoustics, in *Applied Aeroacoustics: Prediction Methods*, Rhode-St. Genese, Brussels, Belgium, 1996.
25. D. H. Rothmann and S. Zaleski, *Lattice Gas Cellular Automata*, Cambridge University Press, Cambridge, England, 1997.
26. K. Uchida, and K. Okumura, Aerodynamic Noise Simulation Based on Lattice Boltzmann Method, in *Vehicle Aerodynamics and Wind Noise*, SAE SP-1441, SAE, Warrendale, PA, 1999.
27. A. F. Seybert and T. W. Wu, Acoustic Modeling—Boundary Element Methods, in *Handbook of Acoustics*, M. J. Crocker, Ed., McGraw-Hill, 1955.

28. J. C. Hardin, D. Huff, and C. Tam, Eds., Third Computational Aeroacoustics (CAA) Workshop on Benchmark Problems, NASA/CP-2000-209790, Glenn Research Center, Cleveland, OH, August 2000.
29. S. Haruna, I. Kamimoto, and S. Okamoto, Estimation Method for Automobile Aerodynamic Noise, SAE Paper No. 920205, Society of Automotive Engineers, Warrendale, PA, 1992.
30. W. Dobrzynski, DFVLR Forschungsbericht DFVLR-FB83-28, *Zur Bedeutung von Strömungswechseldrucken für den Innenlärm von Personenkraftfahrzeugen*, DLR, Köln, Germany (in German), 1983.

# CHAPTER 88

## TRANSMISSION AND GEARBOX NOISE AND VIBRATION PREDICTION AND CONTROL

Jiri Tuma

Faculty of Mechanical Engineering  
Department of Control Systems and Instrumentation  
VSB—Technical University of Ostrava  
Ostrava, Czech Republic

### 1 INTRODUCTION

Except for severe bearing defects or extreme structure–resonance amplification, gears are the main sources of high-frequency vibration and noise, even in newly built transmission and gearbox systems. The gearbox overall noise level is usually no more than 5 dB above the noise level associated with the meshing gears. There are two possible solutions for reducing the noise of a transmission unit. Introducing an enclosure to reduce noise radiation is the easiest but creates maintenance difficulties. A more sophisticated and efficient solution involves tackling noise problem at the source. This requires improvements in gear design and manufacturing and results in the greatest reduction of noise. Vehicle transmission units are operated at many different loads and speeds. In designing low-noise transmission and gearbox systems, it is necessary to assess the noise and vibration sources and be aware of measurement methods, test procedures, and methods of diagnostics. Analysis tools for gearbox inspection are based on the frequency- and time-domain methods, including envelope and average tooth mesh analysis. To reduce noise radiated by transmission and gearbox systems, it is important to understand the effect of load, gear contact ratio, and tooth surface modification on noise and vibration.

### 2 DESCRIPTION OF TYPICAL VEHICLE GEARBOX AND TRANSMISSION SYSTEM

A typical two-stage car transmission unit arrangement with five forward manual gears and one reverse gear is shown in Fig. 1. It transmits power from the engine to the drive wheels, and it varies the amount of torque. There are actually two sets of gears in the drive train: the transmission and the differential. The transmission allows the gear ratio to be adjusted, and the differential lets the drive wheels turn at different speeds. The differential pinion, driven by the secondary shaft, turns the ring gear, which acts like a single-speed transmission reducing revolutions/minute (rpm) and increasing torque by a set ratio. Figure 2 shows two gear trains under load with the others free running.

Two single-gear trains transferring power from the input shaft to an additional countershaft divide up all the basic gears of the truck transmission unit. The gearbox output power is transferred to the axles via

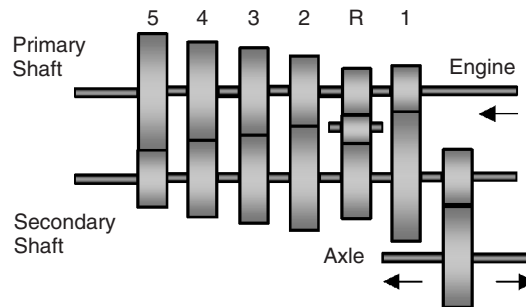


Figure 1 Kinematic scheme of the car gearbox.

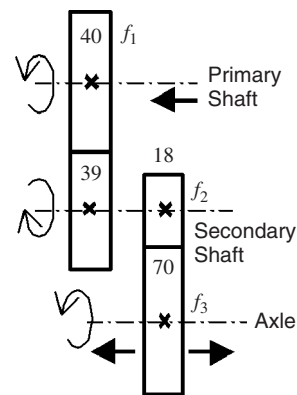


Figure 2 Fourth-gear train under load.

a drop gearbox working either at a fix gear ratio or at two gear ratios in the case that the drop gearbox is a planetary gearbox.

### 3 SOURCES OF GEARBOX NOISE AND VIBRATION

Gearbox noise is tonal. It means the noise frequency spectrum consists of sinusoidal components at discrete frequencies with low-level random background noise. The frequency that is the product of the gear rotational speed in hertz and the number of teeth are referred to as the base tooth-meshing frequency. A simple gear



train (a pair of meshing gears extended optionally by idler gears) is characterized by only one tooth-meshing frequency. All the basic spectrum components are usually broken down into a combination of the following effects:

- Low harmonics of the shaft speed originating from unbalance, misalignments, a bent shaft, and resulting in low-frequency vibration, therefore without influence on the gearbox noise level.
- Harmonics of the base tooth-meshing frequency and their sidebands due to the modulation effects, which are very audible; the noise and vibration of the geared axis systems is originating from parametric self-excitation due to the time variation of tooth-contact stiffness in the mesh cycle, the inaccuracy of gears in mesh, and nonuniform load and rotational speed.
- Ghost (or strange) components due to the errors in the teeth of the index wheel of the gear-cutting machine, especially gear-grinding machines employing the continuous shift grinding method that results in high-frequency noise due to the large number of the index wheel teeth; these ghost components obviously disappear after running.
- Components originating from faults in rolling-element bearings usually of the low-level noise except for severe bearing defects as the cracking or pitting of the inner or outer race or of the rolling element itself.

The frequency of the components, which are associated with the meshing gears, is an integer multiple of the shaft rotational frequency. There are subharmonic components as well. These components are excited at the half of the teeth resonant frequency in high-speed units (thousands of rpm) due to the nonlinearity of tooth stiffness. Other subharmonics originate from the rate at which the same two gear

teeth mesh together<sup>1</sup> (hunting tooth frequency). All these spectrum components are designated as orders of the shaft rotational frequency.

#### 4 PASS-BY VEHICLE NOISE TESTS AND SIMULATIONS

The pass-by noise test requires the vehicle to be driven through a test site at full acceleration according to the International Organization for Standardization (ISO) 362:1994 Acoustic-Measurement of Noise Emitted by Accelerating Road Vehicles—Engineering Methods standard or the appropriate U.S. standards, namely the Society of Automotive Engineers (SAE) J-1470, SAE J-366, and SAE J-986. The A-weighted peak noise level at time constant FAST, measured in the decibel scale at a distance of 7.5 m (ISO) or 15 m (SAE) from the center of the test track. To analyze contributions of each individual simple gear train to the overall noise level, it is preferable to measure the time history of acoustic pressure and engine rpm during the pass-by test, as shown in Fig. 3. In contrast to a measurement with a stationary vehicle, during a pass-by noise test, the effect of the relative speed of the noise source and microphones is translated into the Doppler phenomenon and causes a positive (approaching) or negative (receding) frequency shift (typically from 2 to 5%) in the signals received by the microphones. As the Doppler frequency shift can lead to considerable errors for order tracking using a narrow-band pass filter, the noise source relative velocity to the stationary microphone must be evaluated using the instantaneous position and velocity of the vehicle on the test track.

Both these quantities can be either measured employing a radar system or estimated on the base of the engine rpm and the transmission unit gear ratio, including a mathematical model of the tire slip as a function of the longitudinal and normal force acting on the tire by the road surface.<sup>2</sup>

A noise multispectrum can be used as the input data for order tracking controlled by the frequency of receiving sound waves. A more suitable technique can

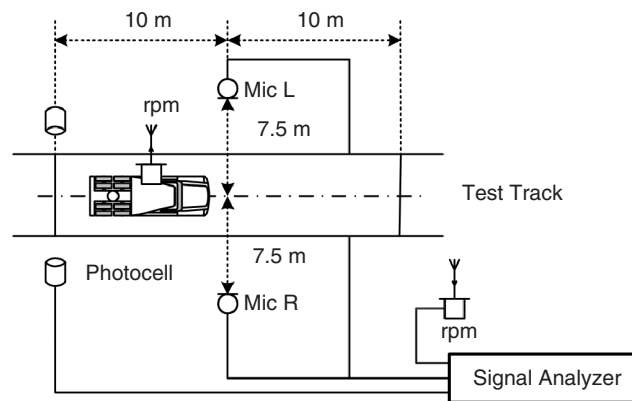


Figure 3 Pass-by vehicle noise measurements.

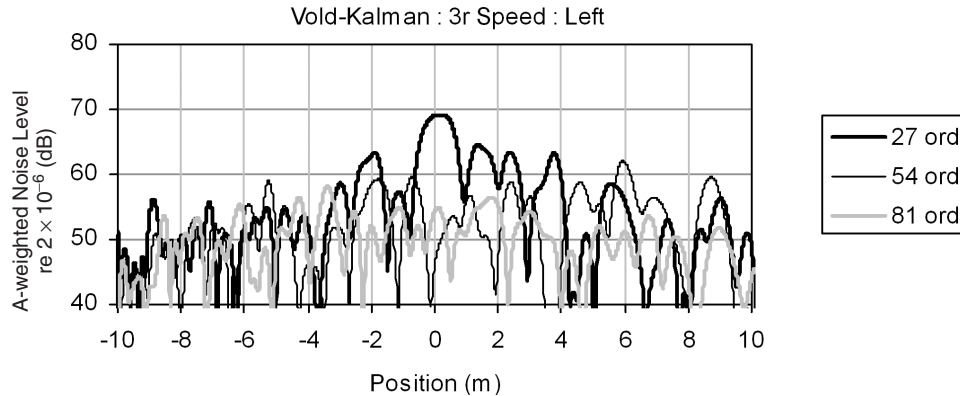


Figure 4 A-weighted noise level of the 27-tooth gear vs. vehicle position on test track.

be based on the Vold–Kalman order-tracking filter.<sup>3</sup> An example dealing with the noise level of the first three harmonic components, which are excited by the 27-tooth gear, as a function of the vehicle position on the test track, is shown in Fig. 4. The filter bandwidth is required to be equal to 0.1 order of the engine rotational speed to reach the high selectivity of the noise signal analysis. The bandwidth of the bandpass filter in percentage to the basic frequency is equal to  $0.1/27 \times 100\% = 0.37\%$ , while the bandwidth for the second-harmonic component is equal to half of 0.37%, that is, equal to 0.18%. Both of the bandwidths are very narrow in comparison to the extreme value of the frequency shift due to the Doppler effect, which is equal to 1% for trucks.

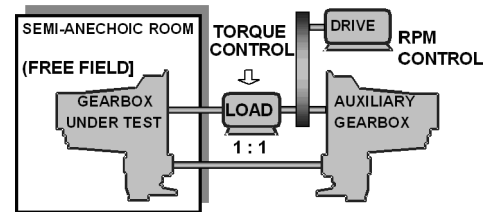
## 5 TEST STANDS

The operating conditions of gears can be simulated using test stands to drive the gearbox in a similar way as during the pass-by noise test. Two possible solutions of the test stand arrangements are shown in Fig. 5.

In contrast to the open-loop test stand, the back-to-back test rig configuration saves drive energy. The torque to be transmitted by the gearbox is induced by a planetary gearbox. The gearbox under testing is enclosed in a semianechoic room. The quality of the semianechoic room is of great importance for the reliability of the results. The reverberation time should be less than is required in the frequency range at least from 200 Hz to 3 kHz. The input shaft speed is slowly increased from a minimal to maximal rpm, while the gearbox is under a load corresponding to full vehicle “acceleration”. To simulate the gearbox operational condition during deceleration, the noise test continues slowly decreasing from a maximal to minimal rpm.

Noise is usually measured by microphones located by the side of the gearbox under testing at the certain distance. One or two microphones can carry out measurements. Accelerometers attached on the surface of the gearbox housing near the shaft bearings can extend information about the noise sources. A tacho probe, generating a string of pulses, is usually employed to measure the gearbox primary shaft rotational speed.

### Back-to-back test rig



### Open loop test stand

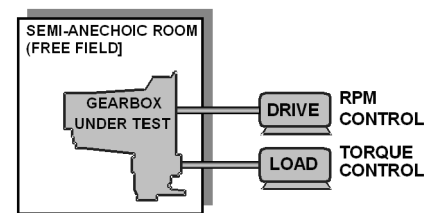


Figure 5 Test stand arrangements.

## 6 FREQUENCY-DOMAIN ANALYSIS

The basic tool for signal processing in diagnostics is the Fourier transform (FT) of signals. The base frequency of all the exciting forces is related to the gearbox shaft rotation frequency. The gearbox is tested during steady-state rotation or run-up/coast-down. Clear information about the origin of extensive vibrations cannot be given by a single-frequency spectrum. Extensive vibration is excited when the tooth-meshing frequency or its harmonics meet the structural resonance frequency of the gearbox structure. It should be mentioned that any driven unit does not rotate at a purely constant speed, but its speed slowly varies around an average value. Spectrum components of the diagnostic signal result from the simultaneous, amplitude and phase modulation of the so-called carrying harmonic components that correspond to the excitation at a purely steady-state rotation. An amplitude modulation

of harmonic signals arises from the nonuniform periodic load, while a phase modulation is due to nonuniform rotational speed. Rotational speed variations at fixed signal-sampling frequency cause the smearing of the dominating components in the frequency spectra.

An analysis of signals from machines running in cyclic fashion is preferred in terms of order spectra rather than frequency spectra. The order spectra are evaluated using the Fourier transform of time records that are measured in dimensionless revolutions rather than seconds, and the corresponding spectrum components are associated with dimensionless orders rather than frequency in hertz. This technique is called order analysis or tracking analysis, as the rotation frequency is being tracked and used for analysis. The resolution of the order spectrum is equal to the reciprocal value of the revolution number per record, which is an input data vector of the length, equal to a power of 2, for the fast Fourier transform (FFT).

The signal-noise ratio is improved by averaging in both the frequency and time domains. Signal

resampling to the fix sample number per revolution is employed to eliminate the phase modulation effect at a tacho pulse frequency.

An example of gearbox noise spectra in decibels (Hanning time window and acoustic weighting of the A-type) during the runup test under load is shown in Fig. 6. The input shaft rotational speed was slowly increased from 1800 to 3500 rpm. As the rotational speed is increased roughly proportionally to the elapsed time, the three-dimensional spectral map illustrates how the various harmonics fall along radial lines and can thus be separated from the constant-frequency components due to excessive amplification by a structural resonance. The three-dimensional plot of noise order spectra in the form of a spectral map with the rotational speed in RPM as the third axis is shown in Fig. 7. Acoustical weighting of the A-type and the rectangular time window are employed. The constant-frequency components show up on hyperbolic curves in the number of rotations—harmonic order plane. The example in Fig. 7 corresponds to the gearbox described

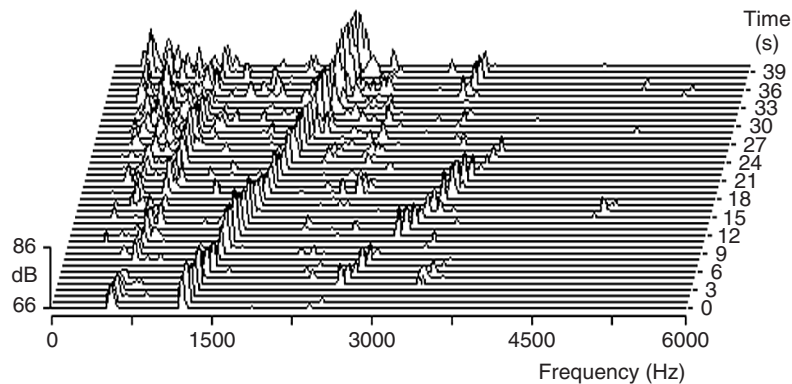


Figure 6 Running noise autospectra in rms (waterfall).

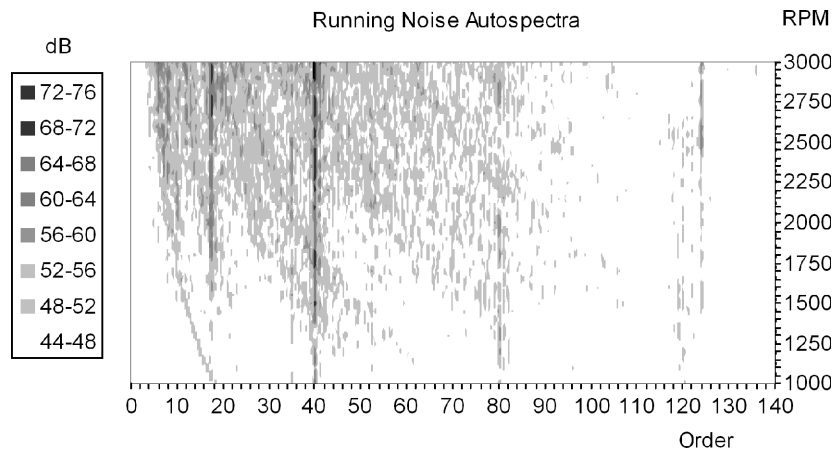


Figure 7 Running noise autospectra in rms (spectral map).

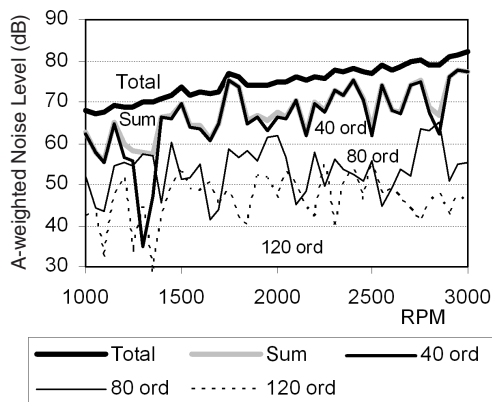
by Figs. 1 and 2. The 40th harmonic, or in other words the 40th order of the input shaft rotational speed as the 40-tooth tooth-meshing frequency, dominates running autospectra in Fig. 7. The first five harmonics of the tooth-meshing frequency are usually sufficient to set up the frequency range for measurements.

The dependence of the overall noise level in decibels and the levels of the 40-tooth gear tooth-meshing frequency harmonics on the input shaft rotational speed is shown in Fig. 8. The curve in this diagram, designated by Sum, is a sum of the power contributions of the 40, 80, and 120 order components resulting in a noise level excited only by the pair of the 40-tooth and 39-tooth gears. As the pass-by vehicle noise test is based on the determination of the maximum of the overall noise level, the maximum of the gearbox overall noise level (Total) and the maximum of the noise level of each individual gear pairs can be chosen as a gear quality criterion. Because of the low tooth-meshing frequency of the 18-tooth gear, the maximum of the overall noise level exceeds the maximum of the 40-tooth gear noise level only by 2 dB. Almost only the meshing-gear pair contributes significantly to the overall gearbox noise level at its maximum.

Gearbox shafts are running coherently, therefore, it is possible to use the above-mentioned order analysis technique. On the other hand, the orders of noncoherently running systems, for instance, a gearbox during gearshift, with close or crossing orders can be extracted by the Vold-Kalman order tracking. The standard method based on the Fourier transform enables only speed-limited order tracking, while the Vold-Kalman order-tracking filtering is without slew rate limitation.<sup>3</sup>

## 7 TIME-DOMAIN ANALYSIS BASED ON SYNCHRONOUS AVERAGING

To study the excitation at each gear mesh cycle, the time-domain analysis based on synchronous time-domain averaging is more suitable than the frequency-domain analysis. This technique is also known as a



**Figure 8** Overall A-weighted noise level (total) and level of the 40th, 80th, and 120th harmonic components vs. input.

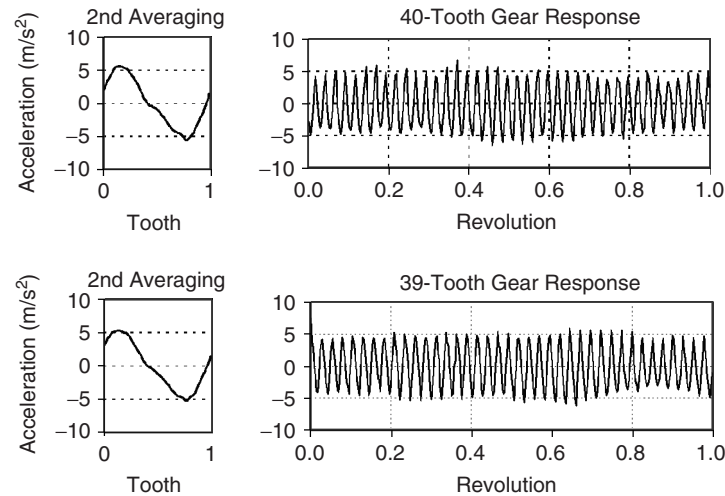
signal enhancement, which has been treated by many authors, for example, McFadden<sup>4</sup> and Angelo.<sup>5</sup> This technique can be regarded as a “magnifying glass” (Angelo), whereby one can “focus” on the shaft to be examined. Noise and vibration signals are sampled using a tracking technique in such a way that the length of the time record is equal to the time interval of a gear revolution. Time records are triggered synchronously with a shaft rotation, and all the records contain the same number of samples (equal to a power of 2). The time-domain averaging of the samples on the same position in all the records results in a comb filtering with center frequencies coinciding with the integer multiples of the rotational frequency. The frequency response function of synchronous averaging is discussed in the Chapter 46.

Averaging in the time domain results in the reduction of the root mean square (rms) of an uncorrelated random signal, which is an obvious part of measured signals, that is, proportional to the reciprocal of the square root of the average number. For instance, if the averaging number equals to 100, then the rms of random signals is reduced by 20 dB. The responses of the gears, whose rotational frequency is a fractional multiple of the trigger frequency, and rolling bearings (fractional order of the rotational speed) are considerably attenuated as well. Except for timing gears, an ideal set of gears for even wear on each tooth does not have a tooth number with a common factor other than unity, which results in the mentioned fractional multiple.

## 8 AVERAGE TOOTH MESH AND ENVELOPE ANALYSIS

The averaged time records corresponding to a gear rotation are corrupted by modulation signals, which are in correlation with gear geometry errors or varying gear load. The modulation signals give rise to sidebands around the carrying components with a frequency that is corresponding to the harmonics of the tooth-meshing frequency. If all the spectrum components, except harmonics of the tooth-meshing frequency, are removed, then the purely periodic tooth-mesh waveform without the modulation effects is obtained. In view of this, the shape of this function may be illustrated by only one period corresponding to the time interval of one circular pitch rotation. In this way filtered signals (second averaging) are called average tooth-mesh signals.<sup>6</sup> The average tooth-mesh acceleration measured on the gearbox housing close to the shaft bearing is proportional to the dynamic forces acting between the teeth in mesh.

An example of the gearbox acceleration signal averaging in the time domain is shown in Fig. 9. This figure contains the individual gear responses produced by each gear in mesh of the 40-tooth and 39-tooth gear pair under load (see Fig. 2). The response of the 40-tooth gear corresponds to the result of averaging, while the response of the 39-tooth gear is necessary to separate from the response of the 18-tooth gear (see Fig. 10) rotating at the same speed. Both these gears on the gearbox secondary shaft are under load.



**Figure 9** Acceleration responses of the 40- and 39-tooth gear train, envelopes, and averaged tooth-mesh signals.

An efficient way to separate both the responses is the transformation of the time record into the frequency domain using FFT. After putting some spectrum components to zero (the 18 order harmonics with their sidebands), the “frequency” signal is transformed back to the time domain using an inverse FFT; see Fig. 10.

It can be noticed that both the average tooth-mesh signals corresponding to meshing gears have the same shape. This fact follows from Newton’s third law. To assess a uniformity of tooth meshing during a complete gear rotation, an envelope analysis can be employed. The theory of analytic signals and the

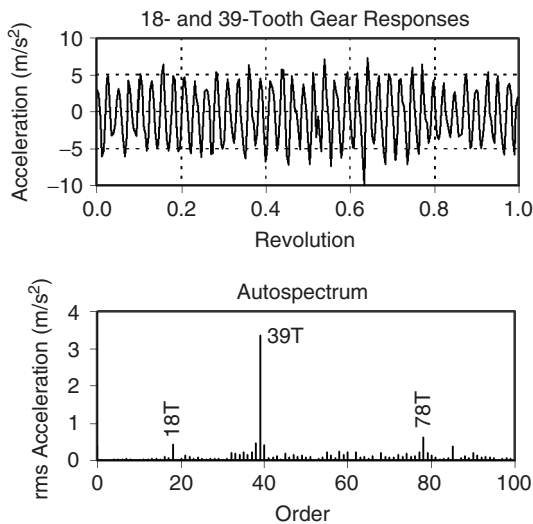
Hilbert transform is a tool for envelope detecting. In contrast to the similarity of the averaged tooth-mesh signals, the envelopes of signals generated by meshing gears may differ from each other.

## 9 CEPSTRUM ANALYSIS

Analytical tools for gearbox noise and vibration can be extended by exploitation of cepstra to discover the periodicity in the frequency spectrum. The cepstrum can be considered as a spectrum of a logarithmic spectrum. The details are discussed in the Chapter 48. Comparison of both these functions is shown in Fig. 11. The spectrum frequency axis is replaced in the cepstrum by a querecence in time units. The cepstrum is sensitive to the components spaced in the frequency spectrum by a small difference. The cepstrum tooth-meshing components are situated at the very beginning of the querecence axis as its frequency belongs to the middle frequency range. The cepstrum is a useful tool in fault diagnostics of rolling bearings that are an obvious part of the transmission unit.

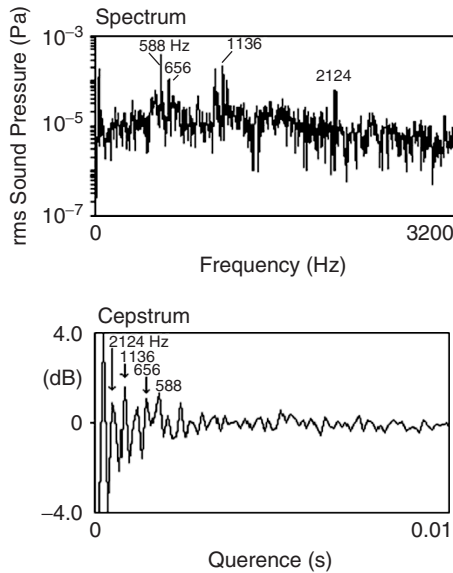
## 10 TRANSMISSION ERROR MEASUREMENTS

Noise and vibration problems in gearing are mainly concerned with the smoothness of the drive. The parameter employed to measure smoothness is the transmission error<sup>7</sup> (TE). This parameter can be expressed as a linear displacement at a base circle radius defined by the difference of the output gear’s position from where it would be if the gear teeth were perfect and infinitely stiff. Many references have attested to the fact that a major goal in reducing gear noise is to reduce the transmission error of a gear set. Experiments<sup>8</sup> show that decreasing TE by 10 dB results in decreasing the A-weighted sound pressure level by 7 dB.



**Figure 10** Time response of the main-shaft gears and its FFT spectrum.





**Figure 11** Spectrum and corresponding cepstrum.

The basic equation for TE of a simple gear set is given as

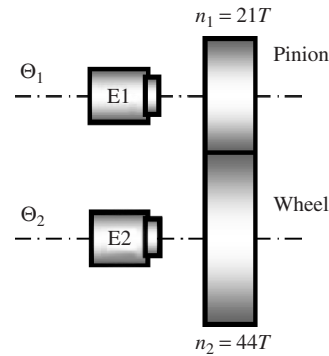
$$TE(m) = \left( \Theta_2 - \frac{n_1}{n_2} \Theta_1 \right) r_2 \quad (1)$$

where  $n_1, n_2$  are teeth numbers of pinion and wheel, respectively,  $\Theta_1, \Theta_2$  are angles of rotation of the mentioned gears, and  $r_2$  is a wheel radius.

Transmission error results not only from manufacturing inaccuracies, such as profile errors, tooth pitch errors, and run-out, but also from a bad design. The pure tooth involute deflects under load due to the finite mesh stiffness caused by tooth deflection. A gear case and shaft system deflects due to load as well. While running under load, one of the very important parameters, tooth contact stiffness, is varying, which excites the parametric vibration and consequently noise.

There are many possible approaches to measuring TE, but, as Smith points out,<sup>9</sup> in practice, measurements based on the use of encoders dominate. The sketch of the gear set consisting of the 21- and 44-tooth gears under test and attached incremental rotary encoders, designated by E1 and E2, is shown in Fig. 12. Both the encoders generate a string of pulses. As a consequence of Shannon's sampling theorem, a few pulses must be recorded during each mesh cycle. It means that the number of pulses produced per encoder revolution must be a multiple of the tooth number. If five harmonics of tooth-meshing frequency are required, then the number of pulses per gear revolution must be at least 10 times greater than the number of teeth. The encoder generating 500 pulses per revolution seems to be an optimum.

There are two approaches on how to process the pulse signals. The first one is based on the



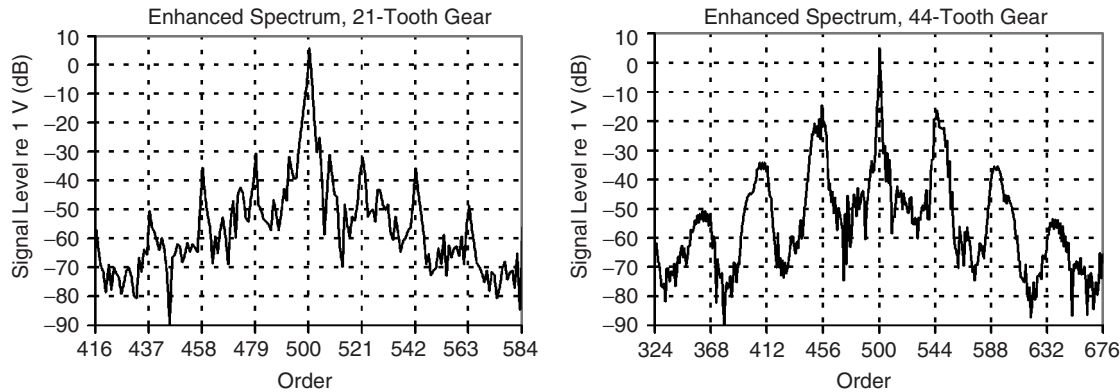
**Figure 12** TE measurement arrangement.

measurement of the time interval between adjacent pulses using the high-frequency pulse generator (e.g., up to 1 GHz in the Rotec signal analyzer) and the counter, which is triggered by the encoder output signals. The instantaneous angular velocity is primary information for TE evaluation and needs integration. Henriksson and Pärssinen present an example of this measurement.<sup>10</sup> The second method is based on the phase demodulation of the sampled pulse signals, which is described below. This method gives as primary information the instantaneous rotation angle and is especially suitable for the FFT analyzers.<sup>11</sup>

A perfectly uniform rotation of gear produces an encoder signal having in its frequency spectrum a single component at the frequency that is a multiple of the gear rotational frequency. The phase of this carrying component is a linear function of time. As the phase is the argument of the cosine function, it can be associated with the gear rotation angle. The nonuniform rotation results in small variation of the rotation angle around the mentioned linear function of time. In this case the basic frequency of the pulse signal is modulated, which gives rise to sidebands around the carrying component in the frequency spectrum.

The phase modulation signal is a part of the phase of an analytical signal that is evaluated using the Hilbert transform technique. The complex analytical signal is compounded from the real part, which is the sampled pulse signal, and the imaginary part, which is the mentioned Hilbert transform of the signal real part. As the angle of the complex values ranges from  $-\pi$  to  $+\pi$ , the phase of the analytical signal (as the time function) contains jumps by reaching the value of  $-\pi$  or  $+\pi$  radians. The true phase can be obtained by the so-called unwrapping phase. The unwrapping algorithm is based on the fact that the absolute value of the difference between two consecutive samples of the phase is less than  $\pi$ . The described algorithm is called phase demodulation.

The Hilbert transform can be evaluated by using either FFT or a digital filter (Hilbert transformer). Before evaluating FFT, it is recommended to resample the measured signal according to the gear rotational



**Figure 13** Frequency spectrum of phase-modulated signal generated by the E1 and E2 encoders.

frequency in such a way that the length of resampled time record equals to a power of 2, namely to at least 2048 samples per gear revolution for the 500-pulse encoder. The pulse signal order spectrum for the 2048-sample record ranges to the value of 800 orders. There is a space for  $\pm 300$  sideband components around the carrying component of 500 orders.

The gear speed variation at the tooth-meshing frequency results in the phase modulation of the impulse signal base frequency. As noted above the phase-modulated signal contains sideband components around the carrying component situated in Fig. 13 at  $500 \pm 21k$  order for the 21-tooth pinion and at  $500 \pm 44k$  order for the 44-tooth wheel, where  $k = 1, 2, \dots$ . Take notice of the fact that the dominating components in both the sideband families exceed the background noise level at least by 20 dB or even more. Both the spectra were evaluated from time signals that are a result of the synchronized averaging of 100 revolutions of gears under testing.

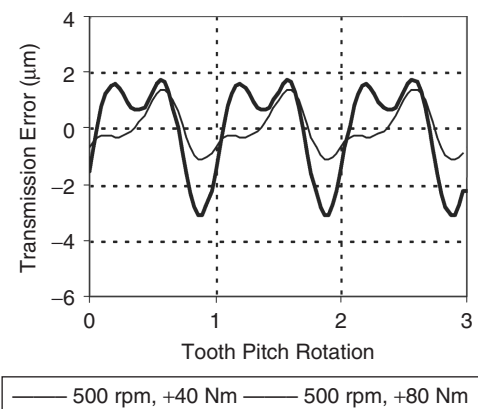
Phase demodulation of the averaged pulse signals results in the phase variation during a rotation of both the meshing gears. As in the case of the average tooth-mesh of the vibration signal, both the phase variation signal can be averaged again to obtain an averaged representative for angular vibration during the gear tooth pitch rotation. Angle variations can be easily transformed into arc length variations.

The arc length difference is not a final step for evaluation TE. As both the encoder signals are recorded separately, the true phase delay between these signals is to be detected. This problem can be solved thanks to the fact that the average tooth mesh responses, for example, in acceleration of some point on the gear case, to dynamic forces acting between meshing teeth are theoretically the same. Therefore, both the encoder pulse signals are sampled together with the acceleration signal. A two-stage averaging of the twice-measured acceleration signal gives average tooth-mesh responses that are delayed against each other. The lag for the maximum correlation gives the value of relative delay.

Transmission error is given as the difference between the angular vibration signals in the arc length produced by the meshing gears. The result for three times repeating tooth pitch rotations and two levels of loading is shown in Fig. 14.

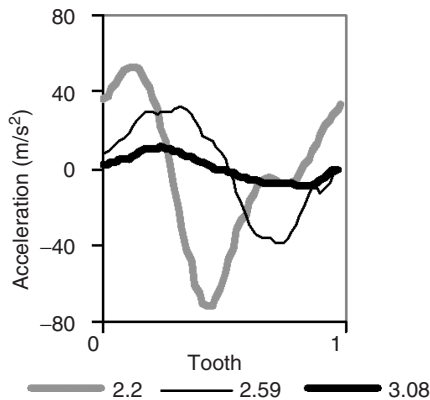
#### 11 EFFECT OF GEARBOX DESIGN PARAMETERS, GEAR QUALITY, AND OPERATION CONDITIONS

The averaged tooth-mesh signals are contact ratio sensitive. It is well known that contact ratio (simply, though not quite accurately stated, contact ratio is the average number of teeth in contact during a mesh cycle) is one of the most important parameters determining gear tooth excitation and thus noise level. Three examples of the average tooth-mesh signals, shown in Fig. 15, deal with helical gears under load differing in profile contact ratio ( $\epsilon_\alpha$ ) while overlap ratio [face contact ratio ( $\epsilon_\beta$ )] is approximately equal to 1.0. Total contact ratio ( $\epsilon_\gamma$ ) is indicated by the diagram legend. The value of the profile contact ratio,



**Figure 14** Transmission error against rotation angle in tooth pitch rotation.



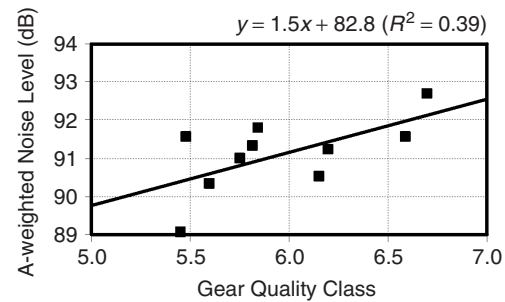


**Figure 15** Effect of contact ratio on the average tooth-mesh acceleration signal.

which is less than 2.0, is called low contact ratio (LCR) gearing while the gearing with this parameter equal to 2.0 or more is designated as high contact ratio (HCR). The integer value for the profile contact ratio and the overlap ratio result in considerable reduction of gearbox vibration and noise. It can be estimated that introducing the HCR toothing results in reducing the noise level of gearboxes with LCR toothing by approximately 6 dB. Experiments<sup>8</sup> show that the transmission A-weighted sound pressure level decreases at approximately 10 dB per 1.0 increase (4.0 through 5.0) in contact ratio.

Evaluation of the averaged tooth-mesh signal is an effective method for verifying contact ratio, detecting a regular error in tooth profile geometry and improving toothing by modification of tooth profile and load, while the envelope of acceleration signal during a complete revolution is important only for quality control.

The gear tooth quality is given by the permissible maximum values of individual variations. Individual variations are those variations from their nominal values, which are exhibited by the various parameters of the gear teeth, such as pitch, profile shape, base diameters, pressure angle, tooth traces, and helix angle. It is known that a gear could be absolutely perfect referring to these variations and yet be very noisy in the conditions of meshing. We can find in the tolerance data a few microns and have many times more deformations due to the loading. In reverse some low-noise gears are imperfect. An example of the effect of the gear tooth quality on the noise level emitted is shown in Fig. 16. However, it can be estimated that an improvement by class 1 of DIN 3961 quality results in a noise level reduction of approximately 1.5 dB. The data were taken from measurements on a truck gearbox with gears finished by grinding. Gear quality class is a weighted quantity that is influenced mainly by the variations in the tooth profile (tooth trace form or angle). The more significant difference in noise levels can be identified when comparing

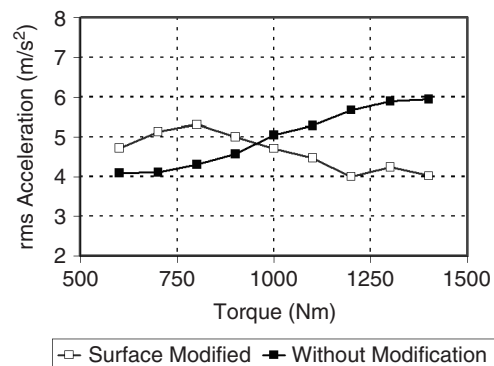


**Figure 16** Effect of mean gear quality on the A-weighted noise level in at 1 m.

the tested gears, which are finished by grinding or hobbing. The gearbox noise level correlates with the gear geometry deviations if the gearbox structure is stiff enough.

The research work on noise reduction employed different methods to identify the dynamic properties and to discover the dynamically “weak” parts of gearbox structures. Using ribs increases stiffness of the gearbox housing structure. In reality, the effect of these improvements, which are limited by the given gearbox structure, on the overall noise level is of small significance. However, they are important because after introducing these improvements the noise level of newly built units varies in correlation with errors of gear geometry. The most efficient improvement can be reached when the noise problem is controlled at its very source, which is the tooth contact of meshing gears.

An example of the effect of gearbox load on the rms value of gearbox acceleration is shown in Fig. 17. The gearbox design input torque is equal to 1200 Nm. To prevent the increase of vibration and consequently the noise level due to the teeth and gearbox structure deformation, the modification of the tooth profile and lead by crowning across the face and tapering of the lead is introduced.<sup>12,13</sup> Comparison



**Figure 17** Effect of load on rms acceleration.

of the modified toothing with the toothing, which is without modification, shows that the gear pair with the modified surface meshes more smoothly at nominal loading than the gears without modification. This design improvement can result in reducing the noise level by 3 dB.

## 12 TRANSMISSION FAULT DIAGNOSIS

Fault diagnosis is a topic discussed in Chapter 48. As stated above, the recorded signals depend on the operating condition given by rotational speed and load. To demonstrate the effect of load on the vibration signal, the response to the pitting on the tooth surface is shown in Fig. 18. The vibration signal of the loaded gears results only from time-varying tooth contact stiffness and overlaps the deviations in gear geometry or the local tooth defect.

It is well known that the vibration and noise level during the gearbox life test are maintained at a relatively stable level up to the moment when gear tooth fatigue crack<sup>14</sup> starts as a very quickly developing process finishing with gear damage during a few minutes.

Continuous even wear of teeth results in increasing the higher harmonics of the tooth-meshing component.<sup>15</sup> More details on the diagnosis of the gear faults are given in Taylor's handbook.<sup>1</sup>

**Acknowledgment** The author is grateful to Prof. V. Moravec, the head of the team for developing the HCR gearing at the company TATRA at the beginning of 1990s, for his help and valuable comments dealing with gear design and accuracy.

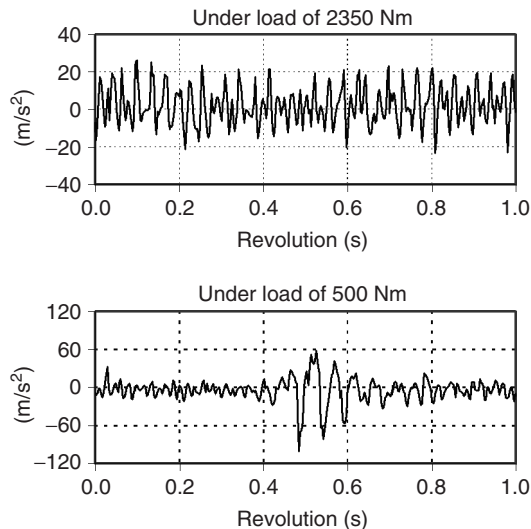


Figure 18 Tooth meshing of pitted gears.

## REFERENCES

1. J. I. Taylor, *The Gear Analysis Handbook*, Vibration Consultants, Tampa Bay, FL, 2000.
2. J. Tuma, Dopplerisation in Vehicle External Noise Measurements, in Proceedings of Eleventh International Congress on Sound and Vibration (ICSV11), St. Petersburg, July 5–8, 2004, pp. 151–158.
3. H. Vold and J. Leuridan, High Resolution Order Tracking at Extreme Slew Rates, Using Kalman Tracking Filter, SAE Paper 931288, Society of Automotive Engineers, Warrendale, PA, 1993.
4. P. D. McFadden, Detecting Fatigue Cracks in Gears by Amplitude and Phase Demodulation of the Meshing Vibration, *ASME J. Vib. Acoustic. Stress Rel. Des.*, Vol. 108, April 1986, pp. 165–170.
5. M. Angelo, Vibration Monitoring of Machines, *Brüel & Kjaer Tech. Rev.*, No. 1, 1987.
6. J. Tuma, R. Kubena, and V. Nykl, Assessment of Gear Quality Considering the Time Domain Analysis of Noise and Vibration Signals, in Proceedings of 1994 Gear International Conference, Newcastle, September 1994, pp. 463–468.
7. D. B. Welbourn, Fundamental Knowledge of Gear Noise—A Survey, in *Proc. Noise Vib. Eng. Trans.*, I Mech E, Vol. 14, 1979, pp. 9–14.
8. Ch-H. Chung, G. Steyer, T. Abe, M. Clapper, and Ch. Shah, Gear Noise Reduction through Transmission Error Control and Gear Blank Dynamic Tuning, SAE Paper 1999-01-1766, Society of Automotive Engineers, Warrendale, PA, 1999.
9. D. J. Smith, *Gear Noise and Vibration*, Marcel Dekker, New York and Basel, 1999.
10. M. Henriksson and M. Pärssinen, Comparison of Gear Noise and Dynamic Transmission Error Measurements, in Proceedings of Tenth International Congress on Sound and Vibration (ICSV10), Stockholm, July 7–10, 2003, pp. 4005–4012.
11. J. Tuma, Phase Demodulation of Impulse Signals in Machine Shaft Angular Vibration Measurements, in Proceedings of Tenth International Congress on Sound and Vibration (ICSV10), Stockholm, July 7–10, 2003, pp. 5005–5012.
12. Z. Dejl and V. Moravec, Modification of Spur Involute Gearing, in The Eleventh World Congress on Mechanism and Machine Science, Tianjin, China, April 1–4, 2004, pp. 782–786.
13. Z. Dejl and V. Moravec, Load Capacity of Non-standard Involute Gearing in Surface Contact, in The JSME International Conference on Motion and Power Transmissions, Fukuoka, Japan, November 15–17, 2001, pp. 279–283.
14. C. D. Begg, C. S. Byington, and P. M. Kenneth, Dynamic Simulation of Mechanical Fault Transition, in Proceedings of the 54th Meeting of the Society for Machinery Failure Prevention Technology, Virginia Beach, VA, May 1–4, 2000, pp. 203–212.
15. T. Elnady, Effect of Machine Defects on Its Radiated Noise. In Proceedings of Tenth International Congress on Sound and Vibration (ICSV10), Stockholm, July 7–10, 2003, pp. 4021–4028.

# CHAPTER 89

## JET ENGINE NOISE GENERATION, PREDICTION, AND CONTROL

Dennis L. Huff and Edmane Envia  
NASA Glenn Research Center  
Cleveland, Ohio

### 1 INTRODUCTION

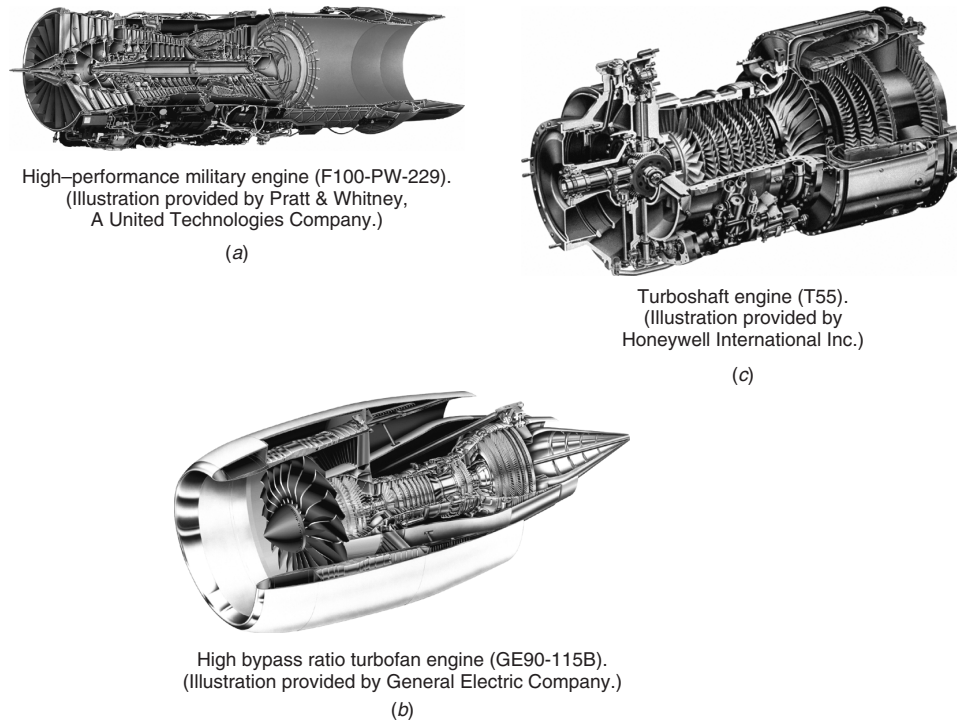
A jet engine is an air-breathing propulsion system that provides thrust for aircraft propulsion. Air is drawn into the engine through an inlet, is compressed through a fan and multiple compressor stages, heated through a combustor, expanded through multiple turbine stages, and exhausted from the engine nozzle. Collectively, these components produce the engine's propulsive force (i.e., thrust). Unfortunately, they also generate noise due to the conversion of a portion of the energy of the flow fluctuations into sound. The character of sound produced depends on the particular engine component. The fan, compressors, and turbines generate tones and broadband noise due to the unsteady flow impinging on both rotating and stationary blades. The combustor and jets produce broadband noise due to turbulent fluctuations in the flow field. In general, noise increases as the velocity of the flow through the engine increases. Reliable noise prediction methods are difficult to develop since they depend on accurate prediction of the unsteady flow field in and around the engine. Strategies for mitigating engine noise include modifying the unsteady flow field, redirecting the sound propagation, absorbing the sound using acoustical treatment, or combinations of all three.

### 2 BACKGROUND

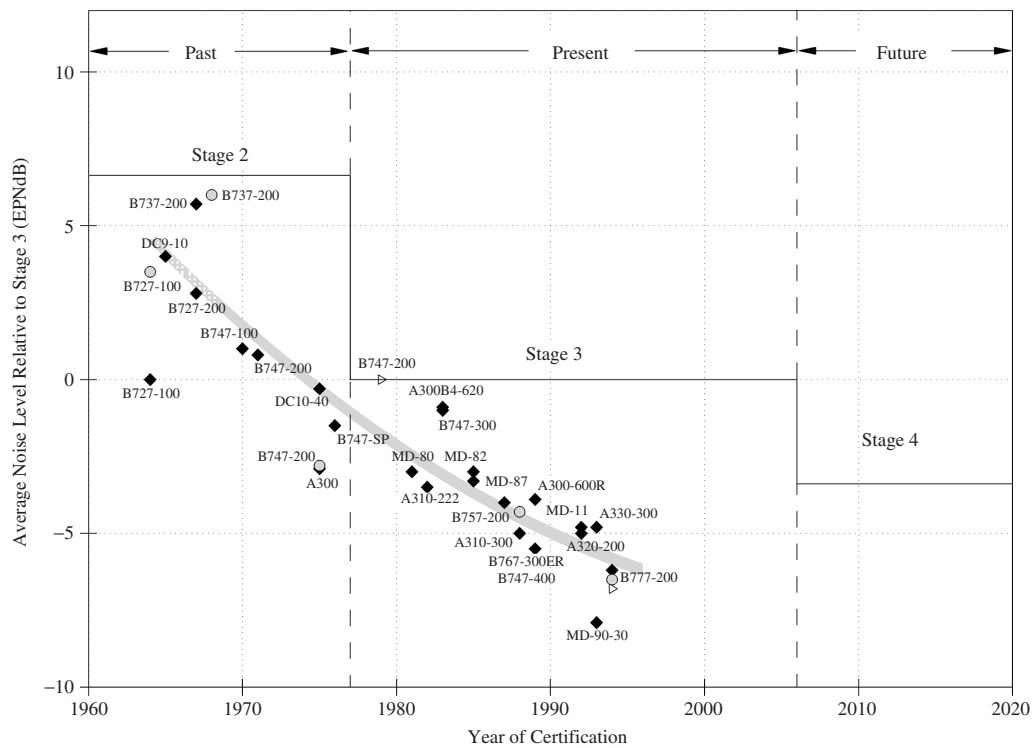
Aircraft noise has been a problem near airports for many years. It is a quality-of-life issue that impacts millions of people around the world. Solving this problem has been the principal goal of noise reduction research that began when commercial jet travel became a reality. While progress has been made in reducing both airframe and engine noise, historically, most of the aircraft noise reduction efforts have concentrated on the engines. This was most evident during the 1950s and 1960s when turbojet engines were in wide use. This type of engine produces high-velocity hot exhaust jets during takeoff, generating a great deal of noise. While there are fewer commercial aircraft flying today with turbojet engines, supersonic aircraft, including high-performance military aircraft, use engines with similar exhaust flow characteristics. The Pratt & Whitney F100-PW-229, pictured in Fig. 1a, is an example of an engine that powers the F-15 and F-16 fighter jets. The turbofan engine was developed for subsonic transports, which in addition to better fuel efficiency also helped mitigate engine noise by reducing the jet exhaust velocity. These engines

were introduced in the late 1960s and power most of the commercial fleet today. Over the years, the bypass ratio (i.e., the ratio of the mass flow through the fan bypass duct to the mass flow through the engine core) has increased to values approaching 9 for modern turbofans such as the General Electric GE-90 engine (Fig. 1b). The benefits to noise reduction for high bypass ratio (HBPR) engines are derived from lowering the core jet velocity and temperature and lowering the tip speed and pressure ratio of the fan, both of which are the consequences of the increase in bypass ratio. The HBPR engines are typically very large in diameter and can produce over 100,000 lb of thrust for the largest engines. A third type of engine flying today is the turboshaft, which is mainly used to power turboprop aircraft and helicopters. An example of this type of engine is shown in Fig. 1c, which is a schematic of the Honeywell T55 engine that powers the CH-47 Chinook helicopter. Since the noise from the propellers or helicopter rotors is usually dominant for turboshaft engines, less attention has been paid to these engines insofar as community noise considerations are concerned. This chapter will concentrate mostly on turbofan engine noise and will highlight common methods for their noise prediction and reduction.

Over the years, aircraft noise reduction research has led to significant progress as indicated in Fig. 2, where noise levels from a few representative aircraft-engine combinations are shown using their noise levels in EPNdB (effective perceived noise level in decibels) as a function of the approximate year they entered service. While some of the noise reduction is due to design changes for engine and aircraft, most of the reduction comes from cycle changes to the engine such as the introduction of higher bypass ratio turbofan engines. Commercial aircraft use the EPNdB noise metric and distinguish takeoff and approach conditions. The three main certification points are takeoff (also called "sideline"), takeoff with cutback, and approach (see Chapter 125 for more information on aircraft noise metrics). The certified noise levels are regulated by organizations such as the Federal Aviation Administration (FAA) in the United States and are recommended by members of the International Civil Aviation Organization (ICAO) to provide international standards. Takeoff noise levels are usually dominated by the engine, while approach levels consist of sources from both the airframe and engine. In fact, some aircraft are dominated by airframe noise sources such



**Figure 1** Various aircraft engine types.



**Figure 2** Evolution of aircraft noise reduction.

as landing gear, flaps, and slats during approach. For more information on these noise sources, see Chapter 9. Military aircraft are not included in Fig. 2 since they are exempt from certification. However, there has been increased sensitivity by the general public to noise from these aircraft near air bases over the past few years. General aviation aircraft and rotorcraft are also not included in Fig. 2. In addition to EPNdB, other metrics such as A-weighted sound pressure levels for low-altitude flyovers are used.

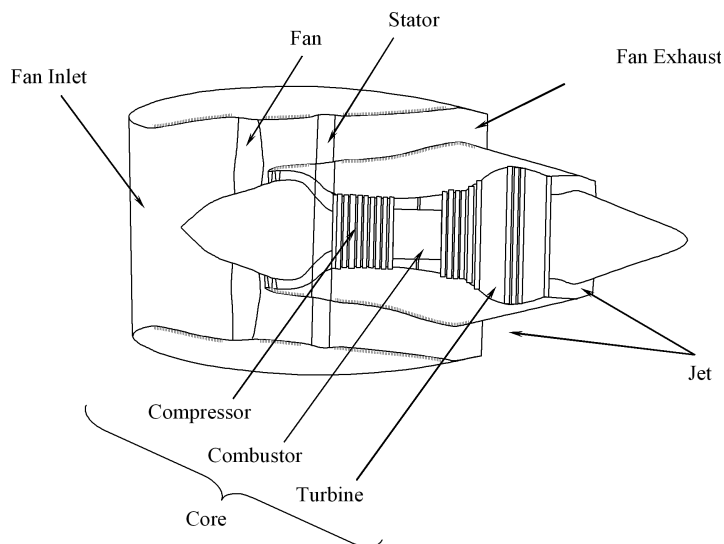
Aircraft engine noise is primarily an aerodynamic source and is not produced by structural vibration. However, there are some cases, particularly for propeller-driven aircraft, where structural vibrations from the engines couple with the aircraft structural and acoustic modes in the cabin and cause high levels of interior noise. This distinction has given rise to the term *aeroacoustics* when describing aerodynamically generated noise. Engine noise is caused by the interaction of flow field's coherent and random fluctuations (i.e., turbulence) with the solid surfaces inside the engine producing tonal and broadband components of noise, respectively. Noise can also be produced by fluctuations in the flow field that radiate sound (such as jet noise). For more information on the fluid mechanics associated with aerodynamic noise, see Chapter 9.

### 3 ENGINE NOISE SOURCES

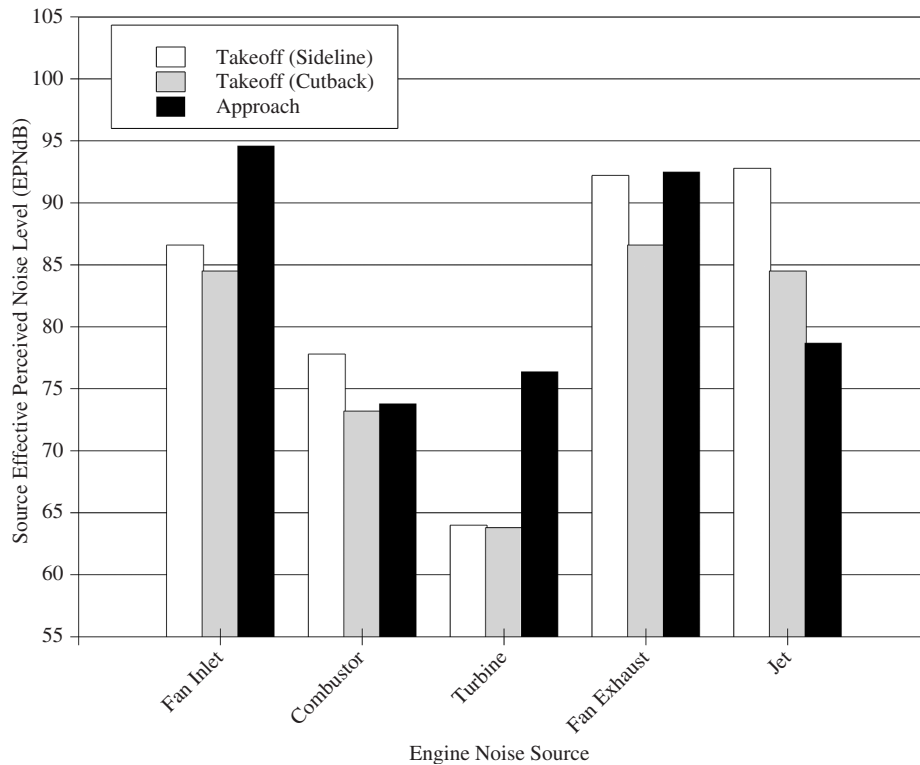
The major noise sources for a modern turbofan engine are shown in Fig. 3. The relative sound pressure levels from each component depend on the engine architecture and power setting. At takeoff condition, the fan and jet noise usually dominate. For approach condition, the fan usually dominates since the jet velocity is reduced. Noise from other components such as the compressor, combustor, and turbine is generally less than that from the fan and the jet. This is why most

of the noise reduction research over the past 25 years has emphasized fan and jet noise reduction. The noise radiated from the inlet includes contributions from both the fan and compressor but is primarily dominated by the fan. Aft-radiated noise is dominated by the fan and jet, but there can also be significant contributions from the combustor and turbine, which are highly dependent on the particular engine. The noise levels shown in Fig. 4 represent an average from engines that were available in 1992 that powered a medium-sized twin-engine aircraft such as the Boeing 757 or 767 (nominally 400,000 lb takeoff gross weight with 60,000 lb thrust from each engine). Engine component noise levels are also available for other aircraft types such as small business jets, small twin-engine aircraft such as the Boeing 737, and large four-engine aircraft such as the Boeing 747.<sup>1</sup>

Typical radiation patterns (called source directivities) from various engine noise sources are shown in Fig. 5. Source directivity depends on the engine architecture, power setting, and noise source. Directivity can be used as a criterion to select only those engine noise sources that contribute to the community noise metrics. For example, tones from the turbomachinery can be analyzed using modal decomposition and expressed in terms of their cutoff ratio. The cutoff ratio is a measure of how well a mode can propagate inside the engine duct. Highly cut-on modes tend to radiate along the axis of the engine (both upstream and downstream) and do not impact the community since they are directed away from the ground and attenuate through the atmosphere. On the other hand, modes that are just cut-on propagate  $90^\circ$  from the engine axis, and acoustical treatment in the nacelle is most effective since the sound waves propagate directly into the liner. Modes that propagate from  $30^\circ$  to  $60^\circ$  from the forward engine axis are the most difficult to control. The



**Figure 3** Dominant turbofan engine noise sources.



**Figure 4** Typical engine effective perceived noise levels. It should be noted that the locations for the microphones are not the same for all three certification points.

use of modal analysis to characterize turbomachinery tones was pioneered by Tyler and Sofrin<sup>2</sup> and is still used today to understand engine noise sources.

#### 4 NOISE REDUCTION STRATEGIES

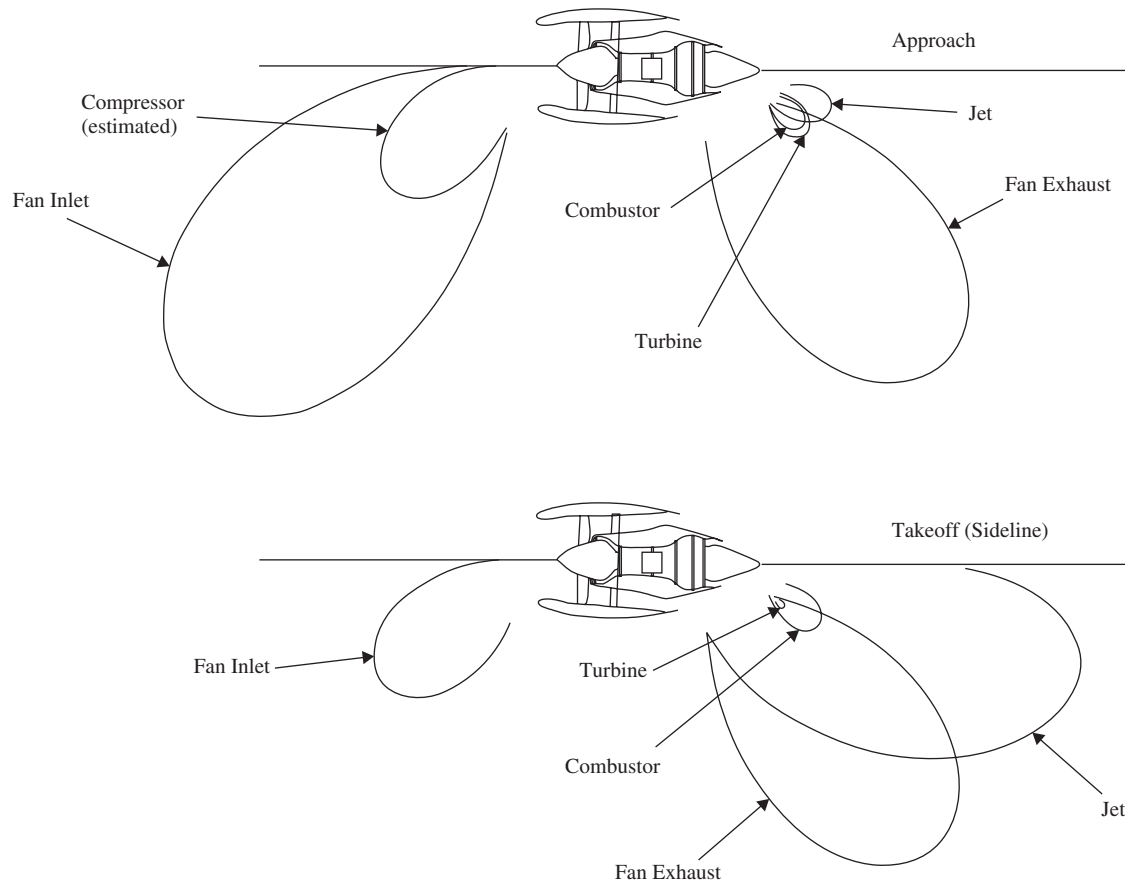
Most of the engine noise reduction advances have come from changing the engine cycle and incorporating low-noise technologies. During the 1960s and 1970s, low-noise design guidelines were developed that include eliminating inlet guide vanes in front of the fan, incorporating acoustical liners in the fan duct and the core, increasing the spacing between rotors and stators, using lobed mixers on the exhaust, and developing “wide-chord” fans with lower tip speeds. Many of these advances have dual benefits for reducing noise and increasing the propulsive efficiency. Some of the techniques that have been developed over the past 25 years are highlighted for each engine component below.

##### 4.1 Fan Noise

Fan noise research requires simulation of conditions representative of the engine operating during takeoff and approach. Static tests use an inflow control device<sup>3</sup> (ICD), which resembles a large mesh golf ball that is usually much larger than the diameter of the fan and

is mounted on the inlet. It was discovered during the 1970s that running a fan without flow conditioning caused large-scale turbulence and ground vortices to be ingested into the fan producing extraneous fan noise in the process. The purpose of the ICD is to break up the turbulence into small eddies that decay rapidly to levels representative of atmospheric turbulence entering the engine in forward flight. Unfortunately, many good noise reduction ideas tested before this discovery were prematurely discarded because of contaminated data. An alternate approach is to run the fan in a wind tunnel with appropriately low levels of free-stream turbulence to simulate the forward flight conditions. If the wind tunnel is large enough, angle of attack simulations can also be done to make sure inflow distortions into the fan are not a major noise source.

Since it is difficult to extract the fan noise from engine spectra that contain other sources, most of the research on fan noise is done in fan rigs where the fan source can be isolated. Results from decades of tests have shown that fan tip speed and pressure ratio control the overall fan noise levels. For subsonic tip speeds, the interaction of fan wakes with the stators is the dominant source. This dependence has been demonstrated in recent *source diagnostic tests* at Boeing and the NASA Glenn Research Center.<sup>4,5</sup> Methods



**Figure 5** Typical noise radiation from turbofan engines.

for reducing this noise at the source include decreasing the fan tip speed, reducing the fan pressure ratio, increasing the fan/stator spacing,<sup>6</sup> sweeping and leaning the stators to reduce tones,<sup>7,8</sup> selecting favorable fan blade–stator vane ratios to reduce the tones,<sup>6</sup> and reducing the number of stators to reduce the broadband noise.<sup>4,5</sup> For supersonic fan tip speeds, the self-noise generated by the fan becomes an important contributor, especially for inlet-radiated noise. With the exception of multiple pure-tone (MPT) noise, less is known about the source mechanisms associated with the rotor self-noise since noise measurements are typically dominated by rotor–stator interaction source. Special experiments have been done to help isolate this source,<sup>4,5</sup> but no noise reduction strategies have been successful beyond tip speed and pressure ratio changes, both of which affect fan aerodynamic loading.

Multiple pure tones, or “buzzsaw” noise, is associated with the rotor operating at supersonic tip speeds. This source is due to small blade-to-blade geometric differences (e.g., stagger angle) that cause the shocks on each blade to have a unique propagation characteristic upstream of the fan. Depending on the particular

fan, tones at multiples of the shaft order frequencies can be heard in the far field as the aircraft approaches an observer. Noise reduction methods for this source include rearranging the fan blades on the fan disk to modify the frequency content, using tighter manufacturing tolerances to minimize blade-to-blade differences, optimizing acoustical treatment in the inlet to absorb these tones, or using blade sweep to reduce the strength of the blade shocks and capture the associated normal shocks inside the fan blade passages.

Another fan noise source is the interaction of inflow distortions or inlet surface boundary layers with the fan. This source is believed to be secondary for well-designed nacelles where inflow distortions and boundary layers are minimized for performance and operability reasons. Depending on the diffusion downstream of the inlet throat and the tip clearance between the fan case and the fan tip, the boundary layer on the inlet may not interact with enough of the fan blade span to be a major noise source.

Acoustical treatment is used in turbofan engines primarily to reduce turbomachinery noise from the fan, compressor, or turbine. Since the liners need to



endure harsh environments (high temperature, cyclic weather conditions including ice and jet fuel by-products), materials are limited and often not optimal for maximum noise reduction. Liners usually consist of a face sheet with porosity to provide desired resistance without significantly increasing the skin friction. Sometimes a fine wire mesh is used in place of the porous face sheet. The face sheet covers cavities that are sized to provide the desired impedance over a range of frequencies for noise attenuation. Metal honeycomb is a common structure for the cavities. In some applications, multiple layers of liners are used that are designed to different peak attenuation frequencies to provide a wider bandwidth of suppression. Single, double, and sometimes triple degrees of freedom liners are used in modern engines. Cost and weight are also factors considered for liner selection. It is most common to use acoustical liners in the fan inlet and the bypass duct downstream of the fan on both the nacelle and the core cowl. The design of a liner starts with determining the "hard-wall" (no acoustical treatment) spectra and choosing a frequency range where attenuation is needed. It is best to use a perceived noise level (PNL) weighting (Chapter 125), which usually targets 2 to 4 kHz. Recent improvements in manufacturing methods have helped minimize the splices associated with the circumferential segments that make up the liner. The splices cause a spatial discontinuity of the acoustic impedance that could cause the fan noise to increase. Reducing the number of splices and circumferential extent of the splice increases the effectiveness of the liners. Higher bypass ratio engines have shorter inlets and nacelles to minimize aerodynamic drag, which compromise the available treatment area. So even though higher bypass ratio engines are quieter at the source, acoustical treatment can be less effective due to less treatment area.

To overcome the problem, several alternate methods have been developed recently such as scarf inlets and active noise control. Scarf inlets resemble a sugar scoop in that the lower lip extends further upstream than that at the top of the inlet. This redirects the inlet-radiated fan noise away from the ground. Acoustical treatment is used to absorb the acoustic rays that impact the sound pressure levels on the ground. While this idea was first developed in the 1970s, only recently modern computational fluid dynamic (CFD) methods have provided improved aerodynamic prediction methods to help make scarf inlets more practical. Boeing has developed a scarf inlet that integrates acoustical treatment to optimize the inlet for lower noise.<sup>9</sup> Despite these advances, scarf inlets have not yet entered service.

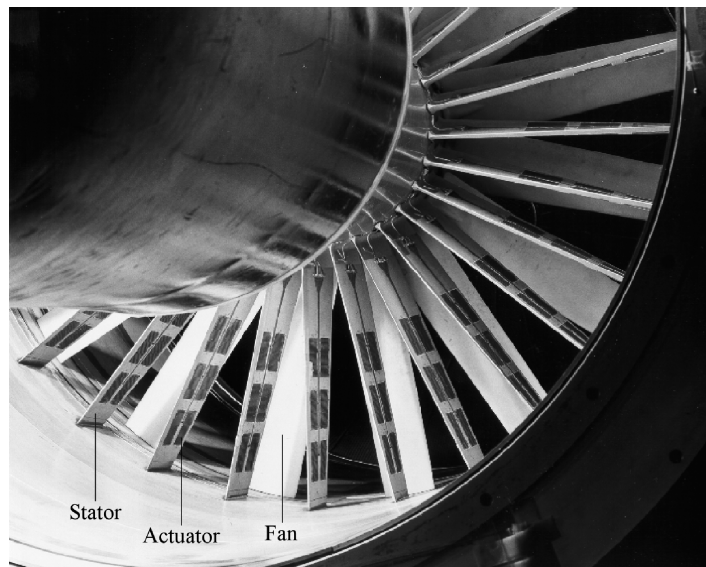
Active noise control is still in its infancy for turbofan applications. While this technique has been successful in mitigating noise in simple configurations, such as plane waves in a ventilation duct, its application to reduce turbofan noise has proven to be very challenging. This is primarily because of the complexity of the noise source, which typically consists of many circumferential and radial modes for even a

single tone. Nonetheless, over the past 10 years, active noise control research has made significant strides (in idealized configurations), progressing from single frequency/mode cancellation to multiple frequency/mode cancellation involving both the inlet- and aft-radiated fan noise. A typical active noise control system consists of ring(s) of actuators to provide the cancellation source, a set of error microphones to monitor the cancellation level, and a control algorithm to provide real-time optimization of the noise cancellation. (A summary of active noise control systems is included in Chapter 63). The source actuators have been placed in various locations of the inlet and aft fan duct and sometimes imbedded in the acoustical treatment. One test,<sup>10</sup> performed by BBN and NASA, used actuators embedded in the stators to provide more control over the radial spinning modes (Fig. 6). However, the number of error microphones and source actuators needed to reduce a complex fan noise source (especially at higher frequencies) is too large for practical applications. In addition, the actuators need to be robust, produce high-amplitude sound output, and be effective over a range of frequencies. Creative ways to reduce the system requirements and cost are needed to make active noise control feasible for aircraft engines. Another strategy for active noise control is to integrate it with the acoustic treatment to make the liners more effective. An example of this hybrid active/passive approach has been developed by Northrop Grumman.<sup>11</sup> A summary of active noise control research for fans can be found in an article by Envia.<sup>12</sup>

## 4.2 Jet Noise

Jet noise reduction research is also typically done in model-scale rig tests. This noise source is distributed along the jet plume and is responsible for the low-frequency rumble that can be heard as the aircraft is flying away from an observer. Since most of the jet noise is generated external to the engine, noise reduction methods are difficult to implement. It is important to simulate forward flight effects when evaluating jet noise reduction concepts since the strengths of the shear layers from the exhaust nozzles vary with forward flight speed.<sup>13</sup> Generally, there is less jet noise in flight compared to the static condition. Reduction methods that work well for static tests often have a reduced benefit when forward flight simulations are included. Many engine noise tests are done on static test stands, which require corrections for jet noise using either model-scale data that includes forward flight or correlations based on previous experience. This raises the level of uncertainty and sometimes leads to incorrect jet noise assessments. Another major consideration is running the jets at realistic temperatures. Cold jets display different characteristics in the noise spectra than hot jets,<sup>14</sup> and noise reduction concepts need to work for a range of operating conditions.

The major parameter controlling jet noise is the exhaust velocity gradient. The common rule of thumb holds that the jet noise varies with the velocity raised to the eighth power for jets with subsonic flows. This was first derived by Lighthill.<sup>15</sup> For a single-flow, round jet



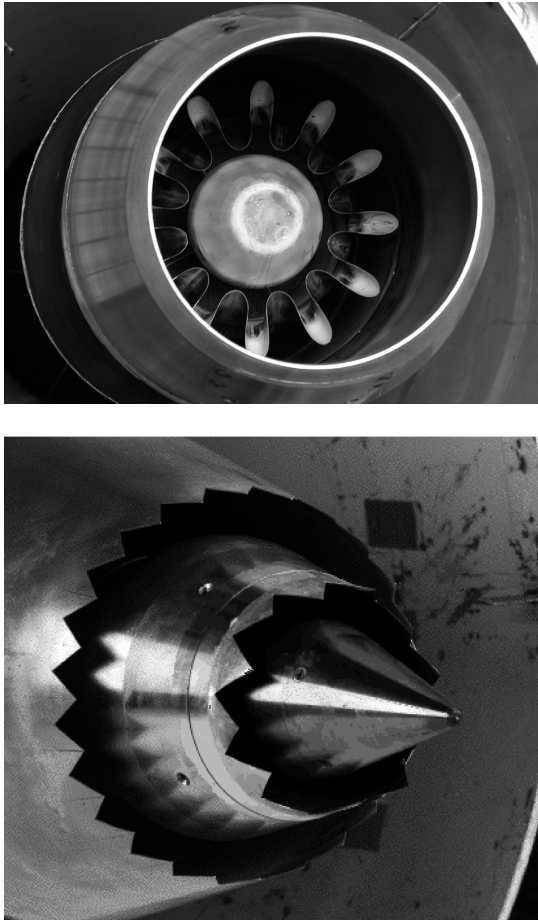
**Figure 6** Active noise control for fan noise reduction.

with subsonic exhaust velocities, the jet noise spectra consist of broadband noise with a peak frequency that scales with the Strouhal number ( $fD/U$ , where  $f$  is the frequency,  $D$  is the jet diameter, and  $U$  is the fully expanded jet velocity). The most common and effective way to reduce jet noise is to simply reduce the exhaust velocity. For higher bypass ratio turbofans, the core stream velocity is reduced as more energy is extracted from the turbine. This reduces the relative velocity between the core and the bypass streams and between the fully mixed jet and the ambient air.

There are two basic types of exhausts on turbofans: internally mixed, where the core flow mixes with the bypass flow inside the nacelle, and separate flow nozzles, where the flows mix downstream of the nacelle exit plane. Lobed mixers are used for internally mixed engines to provide both noise reduction and performance benefits. They resemble cookie cutters located at the core nozzle exit (Fig. 7). The purpose is to mix the flow streams in a way that lowers the peak velocity exiting the engine without introducing additional turbulence that causes high-frequency noise. It also provides a favorable static pressure and temperature profile at the exit that can improve the engine thrust. Many experiments have been carried out that investigate different mixer designs by varying the penetration of the lobe into the bypass and core flows, the number of lobes, and the shape of the lobes. CFD methods are now able to aid the design of complex nonaxisymmetric mixers. While the performance assessments are fairly reliable, the link to noise generation and propagation is still a research topic. The optimum mixer design is dependent on the engine configuration and operating parameters. It is difficult to derive general noise reduction design guidelines other than being careful not to mix the flow

so aggressively that high-frequency noise generation penalty negates the low-frequency noise reduction benefit. In some applications, acoustical treatment is added to help absorb the high-frequency noise if it is generated inside the engine. Generally speaking, mixer designs with good aerodynamic performance (i.e., mixing with low losses) are also good acoustical designs.

Separate flow nozzles are common on larger engines. Until recently, there were no noise suppression methods implemented on engines for reducing the jet noise from these exhaust systems. In 1996, NASA worked with several U.S. companies to investigate the use of tabs and chevrons to mix the core and bypass flow streams for jet noise reduction. Chevrons, which resemble a sawtooth pattern on the trailing edge of the nozzle (Fig. 7), were found to reduce the jet effective perceived noise level by about 3 EPNdB without significant thrust loss. The success of all engine noise reduction methods is based on the amount of noise reduction that can be achieved without significant thrust loss. Similar to the internal mixers, the key is providing just enough mixing of the flow streams to impact the turbulence in the jet without increasing the high-frequency mixing noise. The penetration of the chevrons into the core and bypass flow is small but sufficient enough to generate streamwise vorticity into the shear layer, which reduces the velocity gradients in the plume. Over the past few years, chevrons have been introduced on new engines such as General Electric's CF34-10. Proceedings from a jet noise workshop sponsored by the AeroAcoustics Research Consortium (AARC) provide a good overview of recent progress in jet noise control and prediction.<sup>16</sup>



**Figure 7** Lobed mixer (top) and chevron nozzle (bottom) are two practical methods for jet noise reduction.

#### 4.3 Compressor Noise

There has not been much research done on compressor noise for many years. If it is a problem, it is usually identified as tones radiating from the inlet. These tones are easily identified using narrowband spectra in the far field, knowing the shaft rotational speed and the number of rotor blades in the compressor stages (blade passing frequency = number of blades  $\times$  shaft rpm/60). For compressors, rotor–stator interaction is the dominant noise source, especially due to the close rotor–stator coupling that may excite the potential field interaction between the adjacent blade rows in addition to the viscous wake interaction. The interactions are also more complex than those of the fan since multiple stages are involved. The blade passing frequencies and higher harmonics associated with each blade row create many tones in the spectra. Fortunately, transmission losses across the rotors and stators block the radiated noise from the stages deeper in the engine core. Attention is usually given to the first one or two

stages that do not get this benefit. The blade–vane ratio and tip speeds are carefully chosen to take advantage of cutoff using the theory of Tyler and Sofrin.<sup>2</sup> Another strategy is to select blade and vane numbers that produce counterrotating circumferential modes that are more efficiently blocked by upstream blade rows (the acoustic waves tend to hit the blades broadside and reflect rather than being transmitted through the blade row).

#### 4.4 Combustor Noise

In modern turbofan engines, combustion noise is usually the lowest priority for noise reduction. Most of the research that was done in the 1970s is still used today to understand this source and provide design guidelines. Combustion noise propagates through the turbine stages and peaks at downstream angles centered around  $120^\circ$  from the inlet axis and has a broadband character that peaks anywhere from 400 to 600 Hz. It is sometimes hard to distinguish this source from the jet noise. Combustion noise is usually most apparent at low engine power settings such as idle. As the engine speed increases, the combustion noise becomes masked by the jet noise. Cross-correlation techniques using unsteady pressure measurements in the combustor, turbine exit, and far field have been used with limited success to identify this source. Examples of combustion noise reduction methods include increasing the number of fuel nozzles in the burners, decreasing the fuel–air ratio, decreasing the burner pressure, and decreasing the flow through the combustor.<sup>17</sup>

#### 4.5 Turbine Noise

The character of turbine noise is similar to that of compressor noise in that it is mostly tones radiating from the multiple stages of the turbomachinery. The tones radiate aft through the shear layer between the core and bypass streams. This causes the tones to scatter into adjacent frequency bands and appear as haystacks when measured in the far field. Since there can be many tones, even with narrow-band analysis this source may appear as broadband noise. It is also difficult to distinguish aft-radiated fan noise from turbine noise. A common diagnostic technique is to use acoustical treatment in the tail-cone near the turbine exit and compare the spectra with the total spectra from the engine over a range of speeds. Turbine noise reduction concepts are challenging since the engine cores need to be compact to reduce engine weight, making less room available for conventional noise reduction approaches. Modern turbofans use fewer stages in both the compressor and turbine components with increased aerodynamic loading on the blades, which can increase the noise. Common noise reduction concepts include selecting the blade numbers and rotational speeds for cutoff or increased transmission loss<sup>18</sup> and using acoustical treatment. Engines that can run the turbines at higher rotational speeds benefit from placing the tones at frequencies that are high enough to be less annoying.

## 5 ENGINE NOISE PREDICTION METHODS

To predict the noise from an engine, one must predict the noise from its constituent components, namely fan, jet, compressor, combustor, and turbine. Once the noise levels from individual components are predicted, they can be combined to develop a system-level noise prediction for the engine. The current state of the art in the engine system noise prediction capability is exemplified by the Aircraft Noise Prediction Program (ANOPP code)<sup>19</sup> which actually includes provisions for both the engine and airframe. In its current form, the engine noise modules in ANOPP are empirically based owing to the complexity of the sources involved, but eventually it is hoped that those modules would be replaced by more sophisticated physics-based prediction capabilities. In the following sections an overview of the methodologies being used (or developed) for predicting noise from the various engine sources are discussed.

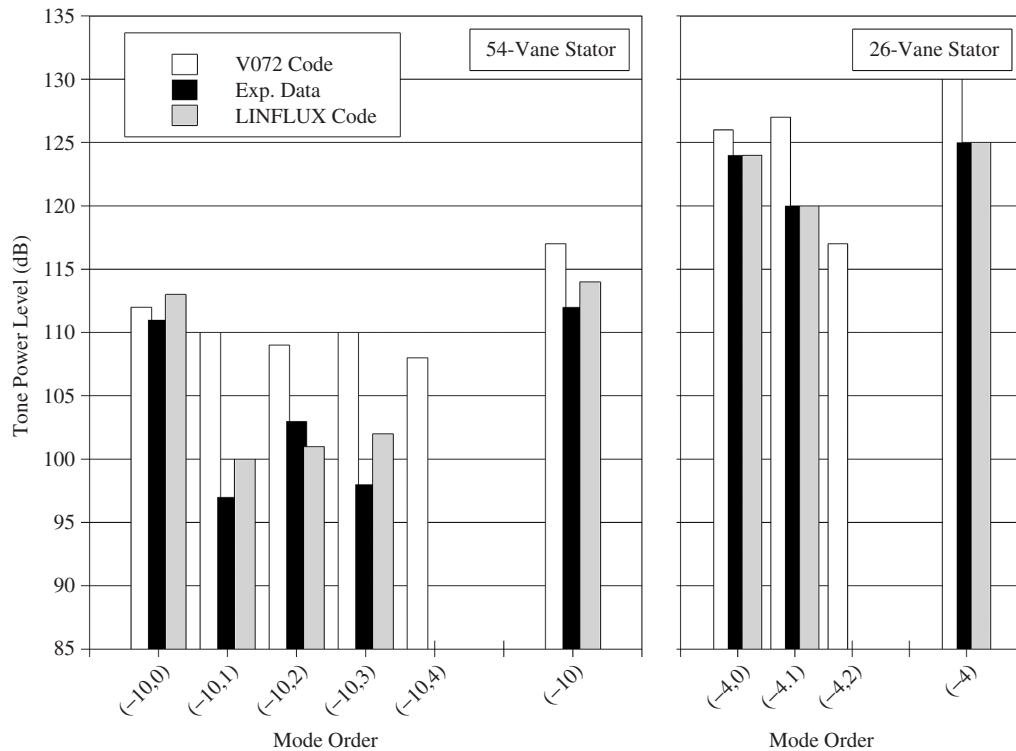
### 5.1 Fan Noise

Fan noise prediction methods can be grouped into three broad categories: empirical, analytical, and computational. In the first category methods, of which Heidmann's<sup>20</sup> is a good example, experimental data are used to construct correlations between appropriate fan noise metrics and operating parameters. Typically, the chosen noise metric is the EPNdB and the operating parameter is either the fan tip speed or its pressure ratio. The correlations are often constructed for overall fan noise levels, but improved results might be obtained by developing separate correlations for each of the contributing mechanisms of fan noise (see earlier discussion). While it takes experience and skill to discern the appropriate correlation relationships, once constructed these methods are easiest to use. The main shortcoming of the empirical methods is that their applicability is limited by the range of data used to construct the correlations. As a result, they cannot be reliably used to predict noise when the fan design and/or operating conditions lie outside of the envelope of the databases used to construct the correlations. These methods are widely used, principally as part of system-level prediction codes for engine design evaluation studies.

As the name suggests, the methods in the second category are analytical in nature, relying on first principles as well as phenomenological considerations of the noise generation and propagation processes. Most of the methods in this category are based on the acoustic analogy theory developed by Lighthill.<sup>15</sup> In the acoustic analogy theory, the aerodynamic and acoustic aspects of the problem are treated separately. Mathematically, this is done by a rearrangement of the exact equations of the motion so that a linear wave equation is obtained whose left-hand side describes the propagation of sound and its right-hand side represents a "known" aerodynamic source that generates the sound. The aerodynamic source is to be measured, computed, or otherwise modeled independently. The solution to the wave equation is given formally in terms of integrals that describe convolution of the source distribution and propagation characteristics. Depending on the

level of approximations involved in the description of the fan geometry and/or flow conditions, the solution can be expressed either in closed form or may require the use of quadrature schemes to evaluate the solution integrals. The overall fidelity of these methods is predicated on the level of approximations used to describe the source(s), the fan geometry, and flow conditions. Many examples of analytical methods exist, among them that developed by Ventres et al.<sup>21</sup> It should be noted that when very simple descriptions of fan geometry and flow conditions are used (i.e., flat-plate blades and uniform background flow), the aerodynamic and acoustic aspects of the problem can be combined into a single problem and solved simultaneously. Examples of such methods include one developed by Hanson.<sup>22</sup> The analytical fan noise prediction methods can often be used to predict the trends, but they cannot be reliably used to predict the absolute levels correctly. A good example of a fan noise prediction code in this category is called V072,<sup>23</sup> which is used to predict tone levels produced as a result of the interaction between the fan wakes and fan exit guide vanes. Another class of methods in this category use Kirchhoff formula to compute the radiation of sound away from the source region once the appropriate information (usually acoustic pressure and velocity perturbations) are given in sufficient details over a surface enclosing the source region.

The third category of fan noise prediction methods encompasses those approaches that, like the analytical methods, start with the equations of motion but make little or no approximations regarding the fan geometry or flow field. The resulting coupled system of unsteady flow equations, therefore, retain their complexity and can only be solved numerically through the use of appropriate computational algorithms. These methods, generically called computational aeroacoustics (CAA) methods,<sup>24</sup> include linearized frequency-domain methods (e.g., LINFLUX<sup>25</sup>) on the one end of the modeling spectrum and nonlinear time-domain methods (e.g., BASS Code<sup>26</sup>) on the other. If, in addition to sound, the flow turbulence is also to be predicted, the computational complexity grows significantly. Depending on the range of turbulence scales to be computed directly, the calculation is referred to as unsteady Reynolds averaged Navier–Stokes (URANS), large eddy simulation (LES), or direct numerical simulation (DNS). The latter approach can be used to compute the unsteady flow down to the smallest turbulence eddy sizes where viscosity converts the kinetic energy to heat. While the application of LES and DNS methods for predicting noise from realistic fan configurations is still years away, with recent advances in computer hardware and computational algorithms, the CAA methods that compute only the sound field (like LINFLUX) are beginning to take their place in the "tool box" of fan noise prediction methods. Figure 8 shows a comparison of the predicted and measured modal acoustic power levels for two different stators. The V072 code predicts the change in the total power from one stator to the



**Figure 8** Example of fan tone noise prediction capability. Results shown are for rotor–stator interaction noise at a simulated approach condition.

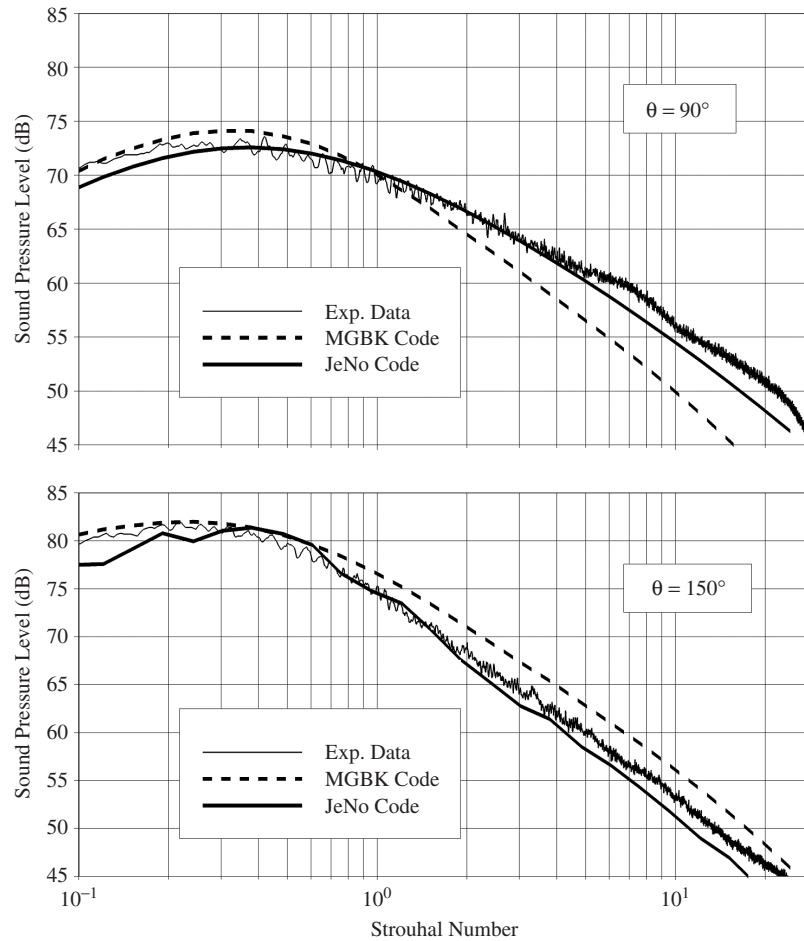
other accurately but fails to predict the modal distribution correctly. The LINFLUX code, on the other hand, predicts both the trends and absolute levels rather well.

## 5.2 Jet Noise

Jet noise prediction methods can also be grouped into the same three categories as those for fan noise. The empirical methods, such as the SAE,<sup>27</sup> StoneJet,<sup>28</sup> and Fisher and Morfey,<sup>29</sup> rely on correlations between the noise level (typically third-octave sound power level) and such jet parameters as the nozzle diameter, exhaust velocity, and exhaust temperature. Correlations are typically developed for round single-stream cold jets, so more complicated jet configurations (e.g., hot, multiple-stream, nonaxisymmetric, nonconcentric, etc.) are represented by a round jet with equivalent velocity, temperature, and diameter. Methods like the SAE<sup>27</sup> make no distinction between the various noise-producing regions of the jet, while others (like StoneJet<sup>28</sup>) divide the flow field into regions with different source characteristics. Due to the differences in the principal mechanisms involved, there are separate correlations for subsonic and supersonic jets. As in the case of fans, the empirical jet noise prediction methods are widely used as design evaluation tools.

Most widely used analytically based jet noise prediction methods are based on a variant of the

acoustic analogy theory due to Lilley,<sup>30,31</sup> which accounts for sound refraction and other effects due to nonuniformities in the background flow (assumed to be parallel and transversely sheared) as part of the wave operator. A notable exception is the JET3D code,<sup>32</sup> which uses Lighthill's original theory. As in the case of the fan, the aerodynamic source of jet noise must be calculated separately. This is usually done through the use of CFD, which provides both the background flow through which sound propagates, the source strength distribution in the form of intensities, and integral time and length and scales of turbulence. The most widely known example of these methods is the MGB code, which is named after its original developers Mani, Gliebe, and Balsa.<sup>33</sup> Over the years, it has been shown that the approximations employed in the MGB code are too restrictive, and, as a result, a number of improved jet noise codes have been developed. These include the JeNo code,<sup>34</sup> the Tam model,<sup>35</sup> and the Morris model.<sup>36</sup> The distinction among these codes lies in subtle, but important, differences in the modeling and interpretation of the aerodynamic sound source. When high-fidelity CFD is used to model the source, often reasonably accurate predictions are obtained using these methods. As an example, measured and predicted spectra for a single-flow subsonic round jet at two far-field angles (relative to the engine inlet



**Figure 9** Example of jet noise level prediction capability. Results shown are for a single-flow, subsonic jet (Mach number  $M = 0.9$ .)

axis) are shown in Fig. 9. The predictions include those from the JeNo code as well as a variant of the MGB code called MGBK.<sup>37</sup> The level of agreement between jet noise predictions and experimental data varies for more complex nozzle designs and is a current research topic. These methods generally apply when the jet exit velocity is subsonic relative to the ambient speed of sound. The methods for calculating noise from supersonic jets<sup>38</sup> have not yet been developed to the same level of fidelity and utility as the ones for subsonic jets.

Over the past decade, significant progress has been made in applying CAA to jet noise prediction and, as in the case of fans, less is modeled a priori and more is computed directly. A host of methods<sup>39</sup> including URANS, LES, and DNS have been used to compute the jet noise directly from the first principles. Of course, it will be some time before the CAA methods can routinely be used for design work. To put the scale of the challenge in perspective, the landmark

DNS simulation by Freund<sup>40</sup> required a massively parallel computer running several months to compute the unsteady field for a jet at the Reynolds number of  $Re = 3500$ . By contrast, a realistic jet from a turbofan engine at takeoff has a Reynolds number closer to  $10^7$ . Since the computational complexity (as measured by the number of grid points) is thought to be proportional to  $Re^{9/2}$ , much more powerful (and cost effective) computers are needed for CAA to become a practical design tool. For now, CAA is principally a diagnostic tool to investigate the myriad of subtle physical processes that contribute to jet noise.

### 5.3 Core Noise (Compressor, Combustor, and Turbine)

Unlike the fan and jet components, the prediction tools for core noise are mostly empirical and are based on work that was done in the 1970s. This is mainly a reflection of the fact that for modern turbofans the

dominant sources are the fan and jet, and so they have historically received most of the development work. The most widely used tools today for predicting core noise are a collection of correlations for predicting compressor, combustor, and turbine noise.<sup>17,20,41–43</sup> The correlations are used to fit experimental spectra in regions where the particular component is thought to dominate. Since the overall core levels are below the fan and jet noise, only portions of the spectra can be matched, which makes this procedure difficult especially as the noise levels from other sources are similar and there are no distinguishing characteristics in the spectra. Source diagnostic tests are used to help isolate the sources and are the basis for many of the correlations available today. With the progress that has been made in developing noise reduction technologies for the fan and jet components, the core noise is beginning to receive more attention as the next obstacle to be tackled for designing quiet aircraft engines. It is likely that within the next decade, analytical as well as computational tools will be developed to help improve the core noise prediction capability.

## 6 FURTHER READING

For more information on aircraft and engine noise, there are a few excellent references available. One is the book by Smith<sup>44</sup> published by the Cambridge University Press that provides a comprehensive overview of aircraft noise. Another is a technical report originally published by NASA in 1991 that has since been published by Springer.<sup>45</sup> In this report, each noise source is explained in detail, and a comprehensive list of references is also provided at the end of each chapter.

## REFERENCES

- H. A. Kumasaka, M. M. Martinez, and D. S. Weir, Definition of 1992 Technology Aircraft Noise Levels and the Methodology for Assessing Airplane Noise Impact of Component Noise Reduction Concepts, NASA CR-198298, June 1996.
- J. M. Tyler and T. G. Sofrin, Axial Flow Compressor Studies, *SAE Trans.*, Vol. 70, 1962, pp. 1248–1249.
- D. Chestnutt, Ed., Flight Effects of Fan Noise, NASA CP-2242, 1982.
- U. W. Ganz, P. D. Joppa, T. J. Patten, and D. F. Scharpf, Boeing 18-Inch Fan Rig Broadband Noise Test, NASA CR-1998-208704, 1998.
- R. P. Woodward, C. E. Hughes, R. J. Jeracki, and C. J. Miller, Fan Noise Source Diagnostic Test—Far-field Acoustic Results, AIAA Paper 2002-2427, 8th AIAA/CEAS Aeroacoustics Conference, Breckenridge, Colorado, 2002.
- P. R. Gliebe and R. A. Kantola, Effects of Vane/Blade Ratio and Spacing on Fan Noise, NASA CR-174664, Vol. I—Final Technical Report, Vol. II—Data Supplement, NASA CR-174665, 1983.
- R. P. Woodward, D. M. Elliott, C. E. Hughes, and J. J. Berton, Benefits of Swept and Leaned Stators for Fan Noise Reduction, AIAA Paper 99-0479, 1999.
- E. Envia and M. Nallasamy, Design Selection and Analysis of a Swept and Leaned Stator Concept, *J. Sound Vib.*, Vol. 228, No. 4, December 1999, pp. 649–678.
- R. P. Dougherty, Nacelle Acoustic Design by Ray Tracing in Three Dimensions, AIAA Paper 96-1773, 1996.
- A. R. D. Curtis, Active Control of Fan Noise by Vane Actuators, NASA/CR-1999-209156, 1999.
- C. A. Parente, N. Arcas, B. E. Walker, A. S. Hersh, and E. J. Rice, E.J., Hybrid Active/Passive Jet Engine Noise Suppression System, NASA/CR-1999-208875, 1999.
- E. Envia, Fan Noise Reduction: An Overview, *Int. J. Aeroacoust.*, Vol. 1, No. 1, January 2001, pp. 43–64.
- C. L. Morfey and B. J. Tester, Noise Measurements in a Free Jet Flight Simulation Facility: Shear Layer Refraction and Facility-to-Flight Corrections, *J. Sound Vib.*, Vol. 54, No. 1, 1977, pp. 83–106.
- C. L. Morfey, V. M. Szewczyk, and B. J. Tester, New Scaling Laws for Hot and Cold Jets Based on a Geometrical Acoustics Model, *J. Sound Vib.*, Vol. 61, No. 2, 1978, pp. 255–292.
- M. J. Lighthill, On Sound Generated Aerodynamically. I. General Theory, *Proc. Roy. Soc. London*, Ser. A, Vol. 211, No. 1107, March 20, 1952, pp. 564–587.
- D. L. Huff, Ed., Proceedings of the Jet Noise Workshop, NASA/CP-2001-211152, 2001.
- D. C. Mathews, N. F. Rekos, and R. T. Nagel, Combustion Noise Investigation, DOT/FAA Report Number FAA-RD-77-3, February 1977.
- S. P. Lavin, P. Y. Ho, and R. Chamberlin, Measurement and Prediction of Energy Efficient Engine Noise, AIAA-84-2284, October 1984.
- W. E. Zorunski, “Aircraft Noise Prediction Program Theoretical Manual”, NASA TM 83199, February 1982.
- M. F. Heidmann, Interim Prediction Method for Fan and Compressor Source Noise, NASA TM X-71763, 1975.
- C. S. Ventres, M. A. Theobald, and W. D. Mark, Turbofan Noise Generation, NASA CR-167951, Vol. 1—Analysis, NASA CR-167952, Vol. 2—Computer Programs, 1982.
- D. B. Hanson, Acoustic Reflection and Transmission of Rotors and Stators Including Mode and Frequency Scattering, AIAA Paper 97-1610, 3rd AIAA/CEAS Aeroacoustics Conference, Atlanta, Georgia, 1997.
- H. D. Meyer and E. Envia, *Aeroacoustic Analysis of Turbofan Noise Generation*, NASA-CR 4715, March 1996.
- E. Envia, A. G. Wilson, and D. L. Huff, Fan Noise: A Challenge to CAA, *Int. J. Comput. Fluid Dynam.*, Vol. 18, No. 6, August 2004, pp. 471–480.
- J. M. Verdon, *Linearized Unsteady Aerodynamic Analysis of the Acoustic Response of Wake/Blade-Row Interaction*, NASA/CR-2001-210713, 2001.
- M. Nallasamy, R. Hixon, and S. Sawyer, Computed Linear/Nonlinear Acoustic Response of a Cascade for Single/Multi Frequency Excitation, AIAA Paper 2004-2998, 10th AIAA/CEAS Aeroacoustics Conference, Manchester, UK, 2004.
- A-21 Aircraft Noise Measurement Committee, Gas Turbine Coaxial Exhaust Flow Noise Prediction, AIR1905, SAE, December 1985.
- J. R. Stone, Interim Prediction Method for Jet Noise, NASA TMX 71618, 1974.
- M. J. Fisher and C. L. Morfey, Jet Noise, in *Aerodynamic Noise*, AGARD-LS-80, NATO, pp. 3.1–3.23, 1977.
- G. M. Lilley, On the Noise from Jets, in *Noise Mechanisms*, CP-131, AGARD, pp. 13.1–13.12, 1974.
- R. Mani, The Influence of Jet Flow on Jet Noise. Part 1. The Noise of Unheated Jets, *J. Fluid Mech.*, Vol. 73, No. 4, 1976, pp. 753–778.



32. C. Hunter and R. Thomas, Development of a Jet Noise Prediction Method for Installed Jet Configurations, AIAA-2003-3169, 9th AIAA/CEAS Aeroacoustics Conference and Exhibit, Hilton Head, South Carolina, 2003.
33. R. Mani, P. R. Gliebe, and T. F. Balsa, High Velocity Jet Noise Source Location and Reduction, Federal Aviation Administration, Task 2 Report, FAA-RD-76-79-II, May 1978.
34. A. Khavaran and J. Bridges, Modeling of Turbulence Generated Noise in Jets, AIAA Paper 2004-2983, 10th AIAA/CEAS Aeroacoustics Conference, Manchester, UK, 2004.
35. C. K. W. Tam and L. Auriault, Jet Mixing Noise from Fine-Scale Turbulence, *AIAA J.*, Vol. 37, No. 2, 1999, pp. 145–153.
36. P. J. Morris and F. Farassat, Acoustic Analogy and Alternative Theories for Jet Noise Prediction, *AIAA J.*, Vol. 40, No. 7, 2002, pp. 671–680.
37. A. Khavaran, Role of Anisotropy in Turbulent Mixing Noise, *AIAA J.*, Vol. 37, No. 7, July 1999, pp. 832–841.
38. J. E. Ffowcs-Williams, The Noise from Turbulence Convected at High Speed, *Proc. Roy. Soc., A*, Vol. 255, 1963, pp. 469–503.
39. C. Baily and C. Bogey, Contribution of Computational Aeroacoustics to Jet Noise Research and Prediction, *Int. J. Computat. Fluid Dynam.*, Vol. 18, No. 6, August 2004, pp. 481–491.
40. J. B. Freund, Noise Sources in a Low Reynolds Number Turbulent Jet at Mach 0.9, *J. Fluid Mech.* Vol. 438, 2001, pp. 277–305.
41. E. A. Krejsa, Interim Prediction Method for Turbine Noise, NASA TMX 73566, 1976.
42. S. B. Kazin and R. K. Matta, Turbine Noise Generation, Reduction, and Prediction, *Aeroacoustics: Fan Noise and Control; Duct Acoustics; Rotor Noise*, Vol. 44 of *Progress in Astronautics and Aeronautics*, I. R. Schwartz, Ed., American Institute of Aeronautics and Astronautics, pp. 109–138, 1976.
43. R. G. Huff, B. J. Clark, and R. G. Dorsch, Interim Prediction Method for Low Frequency Core Engine Noise, NASA TMX 71627, 1974.
44. M. J. T. Smith, *Aircraft Noise*, Cambridge University Press, Cambridge, UK, 1989.
45. H. H. Hubbard, Ed., *Aeroacoustics of Flight Vehicles: Theory and Practice*, Acoustical Society of America, Melville, NY, 1994.

# CHAPTER 90

## AIRCRAFT PROPELLER NOISE – SOURCES, PREDICTION, AND CONTROL

**F. Bruce Metzger**  
Metzger Technology Services  
Simsbury, Connecticut

**F. Farassat**  
NASA Langley Research Center  
Hampton, Virginia

### 1 INTRODUCTION

A thorough understanding of propeller noise requires knowledge of sources, propeller noise measurements, propeller noise prediction methodology, and methods of control. Since the study and control of propeller noise has been the subject of research since the early 1900s, there is an extensive body of literature on the subject that allows the reader to thoroughly investigate all aspects of propeller noise, its prediction, measurement, and reduction.

Prediction of propeller noise is fairly complicated but is tractable analytically if computerized methods are used. Even personal computers can be used to produce accurate and almost instant predictions for most general aviation and commuter aircraft propellers. It should be noted, however, that accurate predictions of noise require methodology that addresses the influence of the flow field in which the propeller operates. Predictions may be made both in the time domain and the frequency domain. Noise reduction methods can be based both on experimental tests and theoretical predictions. The contribution of piston engine noise (particularly at lower propeller rotational speeds) makes a substantial addition to aircraft flyover noise.

### 2 DESCRIPTION OF PROPELLERS, THEIR INSTALLATION, AND THE CHARACTER OF NOISE PRODUCED

Propellers are open rotors. In smaller general aviation and ultralite aircraft they operate with fixed pitch. In larger general aviation and commuter aircraft they operate with adjustable blade pitch to improve aircraft performance. Smaller aircraft have two-blade propellers, while larger aircraft have three to as many as eight blades. Also, advanced propellers have used the counterrotation concept with two blade rows on the same axis of rotation. The front and rear blade rows, with sometimes different blade numbers, operate in opposite direction of rotation.

Most propellers are mounted on the nose of the aircraft or on the nose of nacelles on the aircraft wings. There are only a few pusher installations due to blade structural problems and noise associated with

interaction with disturbances created by the fuselage, wing, or tail surfaces.

Propeller noise can be described as mostly tone like. Tones produced by an aircraft during a flyover are primarily associated with the production of propeller thrust and torque forces (called loading noise) and the volume of the blades (called thickness noise). At high subsonic or supersonic operating conditions, the blades also produce tone noise due to nonlinear effects. However, this mechanism is not significant for the conventional propellers used in general aviation and commuter applications. Counterrotation propellers produce tone noise due to the interaction of the two blade rows. Under static conditions the ingestion of atmospheric turbulence and ground vortices or vortices originating on the aircraft also causes tonelike noise. This disappears as the aircraft accelerates for takeoff. There is also a broadband noise component of propeller noise due to interaction of the blades with turbulence from atmosphere or from the wake of any upstream aircraft structure with the blade leading or trailing edges.

### 3 PROPELLER NOISE SOURCES

The spectrum of the propeller noise has both discrete and continuous components. The discrete components are called tones. The continuous component of the spectrum is called the broadband noise. In this chapter the classification of propeller noise sources will be based on the mathematical model of the acoustical analogy,<sup>1</sup> which is used universally in the propeller industry. There are three kinds of propeller noise sources. These are the thickness, the loading, and the nonlinear or quadrupole sources. These sources generate the thickness, loading, and quadrupole noise. The thickness and loading sources are blade surface sources while the quadrupole sources are volume sources in the vicinity of the blades. All these three sources can be steady or unsteady from the point of view of an observer sitting on the blade surface. The unsteadiness can be further classified as periodic and aperiodic or random. As a general rule, steady and periodic sources produce tone noise while random sources produce broadband noise. It is important to remember that the most important source of broadband noise for propellers is the random loading source. Furthermore,

for general aviation and commuter aircraft propellers, the thickness and loading sources are the most important sources of noise generation.

The thickness noise is generated by the blade volume, which causes the displacement of the air (i.e., pushing the air out near the leading edge and sucking the air in near the trailing edge) as a propeller blade rotates. The thickness noise source is also said to be of monopole type. The monopole strength per unit area is the density of the undisturbed air times the local normal velocity of the blade surface. The thickness noise source is a strong function of the propeller helical tip speed, but it also depends on the spanwise distribution of blade airfoil shape, blade chord, and blade thickness (particularly near the blade tip). This source is, in general, steady or periodic (e.g., when the aircraft forward velocity vector is not parallel with the propeller axis). There is no experimental evidence of broadband noise generation by random thickness sources (which exist when the blade surfaces have random vibration), although this is a theoretical possibility. Therefore, for all practical purposes, the thickness sources of a propeller generate only tones. The directivity of the thickness noise peaks in or near the plane of the propeller disk.

Loading noise sources depend on blade surface pressure. Loading noise source is said to be of the dipole type. The dipole strength per unit surface area is the local blade surface pressure, and the dipole axis is along the local normal to the surface. Blade surface pressure generates the propeller thrust and torque. For the first few harmonics of a low-speed propeller, the Gutin formula<sup>2</sup> gives the noise level in terms of the net thrust and torque. In general, it can be shown mathematically that the loading noise of a propeller at moderate or high tip speeds cannot be related to its net thrust and the torque. Nevertheless, the Gutin model is a useful mental picture. From this simple point of view, the loading noise is said to be generated by the thrust and torque.

The steady and periodic loading sources produce tones. Steady loading sources from the blade steady surface pressure produce the useful thrust and torque. The periodic loading sources are generated by periodic surface pressure fluctuations. These are caused by any phenomenon that is periodic, for example, by the nonuniform inflow into a propeller at an angle of attack during the climb and descent. Counterrotation propellers experience unsteady loading due to the aerodynamic interaction of the front and rear blade rows. Random pressure fluctuations on the propeller blades are produced by the ingestion of atmospheric turbulence or vortices that originate on the ground or on the fuselage. One must be careful in interpretation of the noise generation process when turbulence is ingested into the propeller disk. Hanson<sup>3</sup> has shown that when turbulent eddies are sucked into a static propeller, they are stretched to such an extent that the blades intersect each eddy for many revolutions at the same region of blade surface. Such a phenomenon produces periodic surface pressure fluctuations that generate tonelike noise. For a propeller in forward flight, the atmospheric turbulent eddies do not have enough time to stretch

considerably and, thus, blade-turbulence interaction is a very inefficient phenomenon in producing tonelike noise.

In general, spatially random pressure fluctuations on the blade surface produce broadband noise. Turbulent eddies, which pass completely through the propeller disk in a time scale much shorter than the period of the revolution, and intersect the blades at random locations, produce broadband noise. The directivity of the loading noise peaks out of the propeller disk. Note that the thickness and the loading noise of a propeller at an observer position are not, in general, in phase. This means that there is a possibility of partial or even full cancellation of thickness and loading noise at some points in space. Hanson<sup>4</sup> showed that at some points in space, sweeping the blades also has a favorable effect in reduction of the peak values of both the thickness and loading noise. This idea can be used in the reduction of the level of radiation in the direction of peak directivity.

For piston engine-driven aircraft Dobrzynski has reported<sup>5</sup> that additional propeller tone noise is generated by nonuniform torque transmitted to the propeller due to impulses generated by the engine firing. Such impulses generate both unsteady thickness and unsteady loading noise.

Quadrupole sources are important when the flow over the propeller airfoil is transonic or supersonic. The quadrupole or nonlinear noise then should be added to the thickness and loading noise. Note again that thickness, loading, and nonlinear noise are not, in general, in phase. The quadrupole source strength per unit volume is basically the Reynolds stress. For propeller noise prediction, one should only be concerned with the steady sources. Fortunately, Hanson and Fink<sup>6</sup> have shown that the quadrupole sources are not significant noise generators for conventional propellers but could be important in generation of the noise of highly loaded high-speed propellers such as propfans.

For a single propeller, the tones are harmonics of the blade passage frequency (BPF). This is so even for the tones generated by blade-turbulence interaction. The BPF is the product of the shaft frequency and the blade number. For counterrotation propellers, the number of blades on the front propeller may be different from that on the rear propeller so there will be two different BPFs. As in the case of single propellers, the tones will be the harmonics of the BPFs as well as additional tones called interaction tones.<sup>7</sup>

#### 4 PROPELLER NOISE MEASUREMENTS

Propeller noise measurements are made (1) under static conditions, (2) with ground-mounted microphones as an aircraft flies overhead, (3) on the surface of an aircraft, and (4) in wind tunnels to simulate flight under controlled conditions. Propeller noise measurements are also made within the cabin of an aircraft to address passenger comfort, but this is beyond the scope of this chapter as it is influenced by interaction of the propeller noise with structural response of the fuselage and with cabin volume resonances.

In the past, many experimental research programs were conducted where the noise of a propeller was

measured while the propeller, or the aircraft on which the propeller was mounted, was stationary. At that time it was not recognized that the noise sources dominating the static propeller were different than those that dominated a propeller in flight. Under static conditions the ingestion of atmospheric turbulence or ground or fuselage vortices caused tonelike narrow-band random noise to be a dominant mechanism so the levels measured could not be related to that which occurred during an aircraft flyover. The reader is cautioned to use static measurements only as an indication of noise under static conditions.

Ground-level measurements of propellers during aircraft flyovers are important not only for research programs but also for noise certification and evaluation of the impact of propeller aircraft noise on the environment. For research programs, microphones should be mounted flush with the ground surface since microphones mounted above the ground produce results that are influenced by the constructive and destructive interference of the sound propagating directly from the aircraft to the microphone and the sound propagating from the aircraft that is reflected from the ground to the microphone. Note that, when comparing flyover measurements with noise predictions, propagation effects must be considered. Also, recent research has shown that the engine on propeller-driven airplanes is a significant noise source. Intermittent combustion engines commonly found on general aviation aircraft are known to produce tones that may occur at the same frequencies as propeller noise, so this must be considered in any research program. Also, shielding and scattering effects from the aircraft fuselage and wings may influence the noise reaching the ground.<sup>8</sup> Measurements of propeller noise are also made on the surface of multiengine aircraft to provide information for design of fuselage treatment to reduce cabin noise. These measurements are made with microphones mounted flush with the fuselage surface.

Measurements of propeller noise are made at full and model scale in wind tunnels. In some cases acoustically treated tunnels are used where the microphones are placed in the tunnel flow. Therefore, microphone configurations that minimize self-noise caused by interaction with the tunnel flow are needed to allow the accurate sensing of the propeller noise. In other cases an open jet tunnel is used for measurements. Here, an anechoic chamber surrounds the open jet and microphones are placed outside the jet in still air. This eliminates the problem of interaction between the microphone and the tunnel flow but introduces the requirement to correct the data for the passage of the propeller noise through the shear layer surrounding the open jet. The advantage of tunnel testing is that operating conditions can be precisely controlled, and there are no flight safety concerns that exist in aircraft flyover tests.

## 5 PROPELLER NOISE PROPAGATION EFFECTS

In this chapter the effects of propagation from the propeller source to the point where it is heard or measured are briefly discussed. A more extensive

discussion of these effects can be found in Ref. 9 and elsewhere in this book.

### 5.1 Doppler Frequency Shift

This is the upward shift in frequency observed as a sound source approaches a stationary listener to a lowering of frequency after the sound source passes by. For propeller aircraft flyover noise where the source is dominated by tones, this effect must be addressed in any accurate prediction procedure. For propeller noise heard or measured where both the propeller and listener or measurement equipment is traveling at the same speed, there is no Doppler frequency shift. In acoustical wind tunnels where the propeller and measuring equipment are stationary, there is no Doppler frequency shift even though the propeller is experiencing the wind tunnel airflow. It should also be noted that additional Doppler frequency shift can also occur during aircraft flyover tests if significant wind conditions exist. This, of course, would not occur during aircraft noise certification flights where low wind speed is a requirement.

### 5.2 Atmospheric Refraction Effects

As sound from an aircraft in flight propagates to the ground, refraction occurs due to the change in temperature and pressure that occurs naturally in the atmosphere. Refraction also occurs as propeller noise propagates through the fuselage boundary layer to a measurement location on an aircraft.

### 5.3 Scattering and Shielding by Wing and Fuselage

With a wing-mounted propeller the noise reaching the fuselage can be affected by the presence of the fuselage or wing. At higher frequencies the fuselage acts like an infinite plate when receiving normal incidence sound and produces perfect pressure doubling (an increase of 6 dB compared with the level that would occur if the fuselage were not there). At nonnormal incidence the sound is scattered and measured levels are less. As the measuring point on the fuselage is moved toward the opposite side of the aircraft from the propeller, shielding further reduces noise. This is an area in need of further research. Some recent works on this problem are reported by Dunn and Tinetti.<sup>8</sup>

### 5.4 Atmospheric Absorption

As sound propagates through the atmosphere, there is a reduction in level due to absorption. This is in excess of the reduction in level that occurs due to normal spherical spreading (6 dB per doubling of distance from the source). In general, noise at high frequencies is absorbed more as it propagates. Procedures to calculate this effect as a function of temperature and relative humidity of the atmosphere are available, but the effects are small unless the aircraft noise propagates to the ground from a high altitude.

### 5.5 Ground Reflection Effects

For noise certification of propeller-driven airplanes the measuring microphone is sometimes mounted

above the ground. Therefore, the sound from the airplane propagates directly to the microphone and also propagates to the ground and is reflected to the microphone. The direct and reflected sound travels in two path lengths so it is combined at the microphone with constructive and destructive interference. If the noise of the flyover is to be predicted accurately, the effect must be included in the prediction procedure.

### 5.6 Excess Ground Attenuation

When the sound of a propeller propagates laterally while the aircraft is on or near the ground, it has been found that the noise level is less than that found when the aircraft flies overhead even though all effects of propagation have been considered. Wing and fuselage shielding may explain some of this effect, but other effects may occur that are not understood analytically. One possibility is that noise propagating near the ground from the aircraft to the measuring station is being absorbed by the ground cover.

## 6 PREDICTION METHODS AND COMPARISON WITH MEASUREMENTS

Since 1919 attempts have been made to predict the noise of propellers. Morfey,<sup>10</sup> Farassat and Succi,<sup>11</sup> and Metzger<sup>12</sup> provide references for this work. Early work was hampered by a lack of computers for processing the complex calculations of theoretical formulations. Also, these early efforts were hampered by limitations in experimental equipment for measuring noise. Some progress was made in the time period up to the early 1950s, and the advent of computers at that time led to the development of methods that addressed a significant portion of the propeller noise generation process. Between the 1950s and early 1970s some progress was made in refining the prediction methods. Empirical methods were also developed in this time period that provided an indication of the effects on noise of some operating and geometric parameters without having to use computer calculations.

Since the early 1970s there has been a renewed interest in propeller noise prediction. This has been driven by the need to design propellers for general aviation and commuter aircraft to meet international noise certification limits, to evaluate environmental impact of aircraft noise around airports and in national parks, and as the basis for controlling propeller aircraft cabin noise. Both empirical and theoretical methods were developed in this time period. The empirical methods were generally refinements of earlier methods, but some also used regression analysis of propeller aircraft databases to define improvements. In the 1980s the need to control the noise of the propfan high-power advanced high cruise speed turboprop inspired the development of new methodology. Most of the recent theoretical methods have been based on the acoustical analogy proposed by Lighthill in 1952.<sup>13</sup> Also, computational aeroacoustic methods based on the Euler equation have been developed.<sup>14</sup> Prediction methodology in the time domain is discussed in this chapter's Farassat references. Prediction methodology

in the frequency domain is discussed in this chapter's Hanson references. Prediction methodologies by both authors have reached a stage in development where predictions compare quite well with measurements.

Prediction of propeller noise is fairly complex but is tractable analytically if computerized methods are used. Even personal computers can be used to produce almost instant predictions for most propellers. It should be noted, however, that accurate predictions of noise require detailed analysis of the influence of the effect of the flow field in which the propeller operates. Also, it has been established that engine noise is a contributor to aircraft flyover noise (particularly at lower propeller rotational speeds). Some methodology is available to address this noise source, but it is less well developed than propeller noise methodology.

### 6.1 Empirical Methods

Prediction of propeller noise has occupied researchers for decades. Complex theoretically based methods do exist that have been extensively refined for use in optimizing propeller designs. There is, however, a need for a simple empirically based method for preliminary design studies.

In May 1977 an empirically based graphical procedure for predicting sound pressure levels produced on the ground by propeller-driven airplanes in flight was published in the Society of Automotive Engineers (SAE) Aerospace Information Report 1407.<sup>15</sup> Over the years, as additional sets of sound pressure level data for propeller-driven airplanes became available, the procedure was refined. The refined procedure was developed over a period of several years by the SAE Aircraft Noise Committee with the intent to publish it as an Aerospace Recommended Practice (ARP).<sup>16</sup>

Comparisons of flyover measurements and the ARP empirical predictions, in some cases, show good agreement. For example, comparison with the data of Dobrzynski and Gehlhar<sup>17</sup> showed remarkably good agreement. These flyover tests used propellers with two to six blades with the diameter reduced by 5% for each increase in blade number. Figure 1 shows the comparison of the the Dobrzynski measurements and the ARP predictions. ARP empirical predictions in the figure are surprisingly good for the two-, three-, and four- blade propellers, but predictions for the five- and six- blade propellers show noticeable disagreement with the measurements. This is probably due to the presence of engine noise in the flyover noise data, which is not addressed in the ARP prediction procedure. Other studies using more refined methods that include the ability to predict engine noise support this opinion.

Since the ARP method does not address the effect on noise of blade planform, airfoil thickness, and airfoil shape, the agreement between prediction and measurement shown in Fig. 1 may not be the norm. The agreement shown in the figure does indicate that the ARP is satisfactory for preliminary design studies. However, the reader is cautioned that propeller thrust is not a parameter used in the ARP so the influence, on thrust, of changing horsepower cannot be assessed.

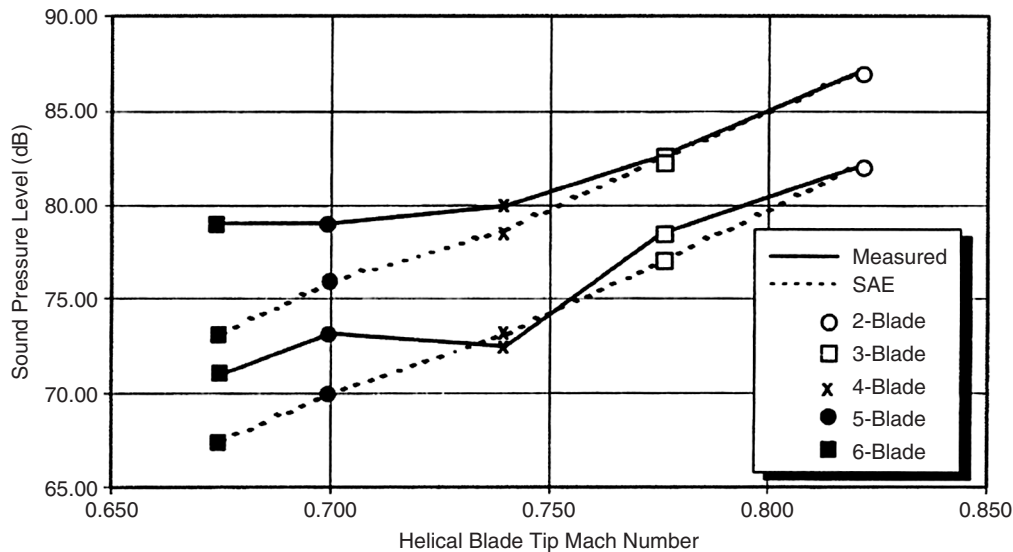


Figure 1 Measured and ARP-predicted effect of blade number on flyover noise level.

## 6.2 Theoretical Time-Domain Methods

Time-domain (TD) methods are of more recent origin than the frequency-domain (FD) methods. There are two reasons for the surge in interest in TD methods since the early seventies. First, the development of high-speed digital computers has made it possible to seek a numerical solution to the propeller acoustics in TD. Second, advances in generalized function theory have helped both in formulating the governing wave equation of acoustics of rotating blades and solving this equation. The most significant development in this area was the publication of a study by Ffowcs Williams and Hawkins<sup>1</sup> in 1969 based on Lighthill's acoustical analogy. These authors derived the Ffowcs Williams and Hawkins (FW-H) equation, which is a generalization of Lighthill's jet noise equation.<sup>13</sup> The FW-H equation is a linear wave equation in terms of the density perturbations in the air with three inhomogeneous source terms known as the thickness, loading, and quadrupole sources. We have already discussed the classification of propeller noise sources in Section 3.

There are many equivalent solutions of the FW-H equation in TD.<sup>18</sup> In general, time-domain methods require the detailed propeller geometry, kinematics, and the steady and unsteady blade surface pressures from aerodynamic codes. For a propeller in forward flight, the most important cause of the unsteady blade surface pressure is the nonuniform inflow into the propeller caused either by the flow field of the intake system or the nonaxial flow into the propeller disk. The calculation of the unsteady blade loads is difficult and time consuming on a computer. However, such calculations are becoming available and should result in more accurate prediction of propeller noise in TD.

A more recent advance in TD noise prediction is the realization that to include the most important nonlinear effects one should use the FW-H equation applied to a penetrable data surface that encloses the propeller blades.<sup>19</sup> In the conventional application of the FW-H equation, the blade surface itself that does not allow fluid penetration is the data surface. This use of the FW-H equation with penetrable (or permeable) data surface appears to be the ideal method for the prediction of high-speed propeller noise.

Time-domain methods complement frequency-domain methods in understanding propeller noise generation. Technically, both methods require the same amount of information for noise prediction. In specific cases, one may be able to accept approximations to blade geometry and loading. In general, it is prudent to use as little approximations of the input data as possible to ensure the quality of the predicted data. In the development of propeller noise prediction codes, one should pay much attention to devising efficient algorithms for number crunching. It is, therefore, highly recommended that one use existing propeller noise prediction codes or do a thorough study of the propeller noise literature before embarking on code development.

**6.2.1 Farassat** Two formulations of Farassat are used in the propeller noise prediction code ASSPIN (Advanced Subsonic and Supersonic Propeller Induced Noise).<sup>20</sup> This code includes only the thickness and loading source terms of the FW-H equation. The propeller blades are divided into panels each of which radiates independently to the observer. The observer can be stationary with respect to the ground or be moving with the aircraft. The selection of the formulations is based on the following criteria. For

panels traveling at subsonic speed, formulation 1A<sup>21</sup> is used exclusively for noise prediction. For panels traveling at transonic or supersonic speeds, the Mach number in radiation direction  $M_r$  is calculated first at emission time or times. If the Doppler factor  $|1 - M_r| > 0.05$  at all the emission times, formulation 1A is used to predict the noise generated by the panel. Otherwise, formulation 3<sup>22</sup> is used. Thus, for panels traveling at transonic or supersonic speeds, ASSPIN uses both formulations 1A and 3 depending on the size of the Doppler factor at the emission times of the panel. ASSPIN has also been used for counterrotation propeller noise prediction.

References 22 and 23 present results of TD noise prediction for two supersonic propellers (propfan) and comparison with measured data. The comparisons are generally good to excellent, particularly in the region of maximum noise radiation. Further comparisons of TD predicted and measured high-speed propeller noise for nonaxial inflow are presented in Ref. 24. In an accompanying study in the same journal, Hanson has presented similar calculations in FD with favorable agreement with TD results under almost identical geometric, kinematic, and aerodynamic input data as used in the TD predictions.

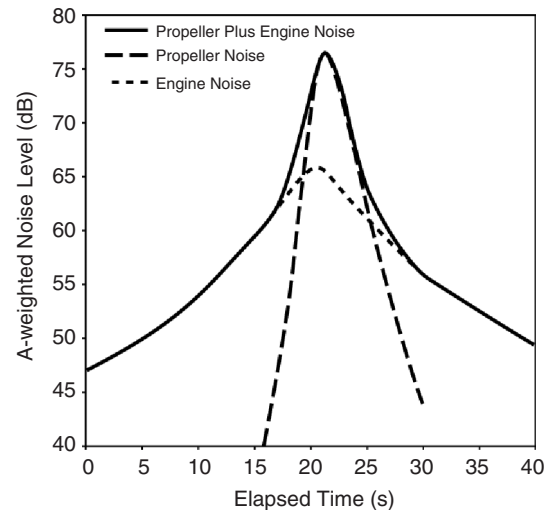
Farassat now advocates the use the FW-H equation with penetrable data surface for high-speed propellers and propfans. Since the flight speed of the aircraft is subsonic, only formulation 1A is used on the penetrable data surface in this case. An unsteady aerodynamic code supplies the input data. The computation time and complexity is considerably reduced compared to the use of ASSPIN.

Formulation 1A is used in the National Aeronautics and Space Administration (NASA) comprehensive aircraft noise prediction code, and the helicopter rotor noise prediction code WOPWOP. All NASA codes use this highly efficient formulation using exact blade geometry and kinematics. These codes are run on a desktop computer.

**6.2.2 Dobrzynski** Dobrzynski<sup>25</sup> developed a method that allows the prediction of A-weighted noise level as a function of time for flyovers of general aviation aircraft. The contribution of both engine and propeller noise as measured by a microphone at ground level is predicted. The starting point for development of this method was predictions of the noise of 11 general aviation aircraft using a time-domain method based on Farassat's solution of the FW-H equation. These results were calibrated relative to actual flyover measurements of the 11 aircraft.

The method predicts noise as a function of propeller blade number, propeller diameter, propeller revolutions/minute (rpm), propeller power absorbed, and flight altitude. The most significant parameter is the propeller tip helical Mach number. This is the square root of the sum of the propeller rotational tip speed squared and the flight speed squared with the resulting value divided by the speed of sound.

A unique feature of Dobrzynski's method is the ability to include engine noise. This is a function



**Figure 2** Propeller and engine noise contributions to flyover A-weighted noise level.

of operating engine power and rpm as compared with maximum engine power and rpm. The separation of propeller and engine contributions deduced from flyover noise measurements and modeled in Ref. 25 is shown in Fig. 2. Engine noise generally dominates the flyover noise of a piston engine powered general aviation aircraft at times before and after the flyover of the aircraft. The propeller noise shows a sharper peak in amplitude near the time when the aircraft is directly overhead. This propeller noise peak dominates the peak flyover noise of most general aviation aircraft. As aircraft flyover noise is reduced by optimizing propeller design, the total aircraft noise is more influenced by engine noise. It is possible that an engine muffler may be required at some point to achieve significant reductions in general aviation aircraft noise.

Dobrzynski's report shows remarkably good agreement between predictions and measured flyover time history as well as maximum A-weighted flyover noise levels for most of the general aviation aircraft considered. The most significant discrepancy was found for an aircraft with very short engine exhaust pipes leading from each cylinder and exiting the aircraft just below the wing/fuselage. The lack of any muffling of the exhaust and the presence of reflecting surfaces at the point where the exhaust flow exits the aircraft is believed to cause a significant noise level compared to more typical aircraft.

### 6.3 Theoretical Frequency-Domain Methods

Hanson<sup>4,6,7,26–35</sup> has been one of the prime developers of the frequency-domain methodology for propeller noise prediction. The reader interested in a single summary of this approach should review Ref. 9. His extensive work since the 1980s has been the basis for design of both single rotation and counterrotation propfans and general aviation/commuter propellers.



His work has been the basis for several propeller noise prediction methods. The first is the Unified Aeroacoustic Analysis for High-Speed Turboprop Aerodynamics and Noise.<sup>36</sup> His work was also the basis of two other methods, the Propeller Acoustical Change Estimation (PACE) Model<sup>37</sup> and the General Aviation Integrated Noise (GAIN)<sup>38</sup> Method, for predicting the noise of conventional single-rotation propellers used on general aviation and commuter aircraft. These methods are discussed below.

### 6.3.1 Propeller Acoustical Change Estimation

**Model** PACE<sup>36</sup> is a theoretical frequency-domain method. Its purpose is to provide a user-friendly tool for estimating propeller noise based on propeller geometry, operational information, and propeller installation information. It utilizes code from two previously developed propeller noise prediction programs: NASA's WOBBLE prediction code<sup>38</sup> and the Federal Aviation Administration's (FAA's) V/STOL propeller noise prediction program.<sup>39–42</sup> These computer prediction codes were modified and integrated along with a graphical user interface to produce PACE. The result of this effort is a PC-based program that can be used without the need for an in-depth understanding of aeroacoustics.

The PACE model has some limitations. First, the model does not include the effects on noise of nonuniform inflow generated by the nose of the aircraft in tractor installations or the disturbances of the wing and other aircraft surfaces on flow into pusher propellers. Nonuniform inflow can produce higher noise levels than uniform inflow, so PACE may produce lower predictions than actual noise levels. Second, the noise levels produced by the PACE model include only propeller noise and exclude other noise sources such as engine noise. As propeller rpm is reduced, the aircraft's engine may become a more significant contribution to the total aircraft noise. Third, the model does not include the noise created by interactions of ground vortices or atmospheric turbulence with the propeller. This would result in predicted noise levels less than actual noise levels at flight speeds below 35 kt (particularly at static conditions). Finally, the PACE model does not include a method for predicting nonlinear effects that occur when the propeller speed nears sonic conditions. Under conditions where the combination of flight and rotational Mach numbers approaches the speed of sound, the predicted noise levels will be less than the actual noise levels.

### 6.3.2 General Aviation Integrated Noise (GAIN)

**Method** The GAIN computer program was developed in a NASA/FAA/industry funded program to predict the flyover noise of general aviation aircraft. It was completed in August 2001 and will be available to the public in August 2006. It is PC based and includes the capability to predict propeller performance and noise and intermittent combustion piston engine noise. It is a fairly complete user-friendly method. The following discussion on the various modules of the GAIN code are based on information from the users manual.<sup>38</sup>

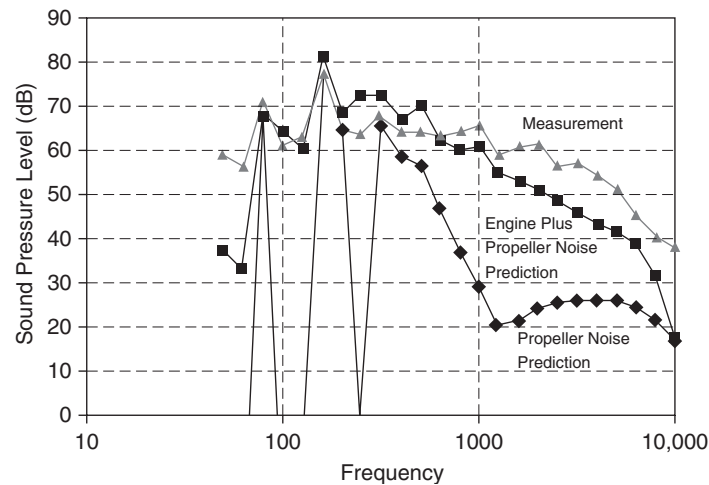
The performance module of GAIN is designed to predict propeller blade loading and overall performance at normal operating conditions. The code can be used for either fixed-pitch or constant-speed (variable-pitch) propellers. It contains airfoil data for Clark-Y, NACA 4-digit, and NACA 16-series airfoils and is capable of calculating unsteady lift coefficients due to angular inflow to the propeller and/or installation flow fields. The code can be run for an isolated propeller, a propeller at an inflow angle in either the pitch or yaw direction, or a propeller in an aircraft flow field. The user can select between seven built-in aircraft flow fields or provide a separate file containing aircraft flow field data.

Thickness and loading tone noise predictions are made by use of a program based on the frequency-domain approach of Hanson.<sup>39</sup> The theory utilizes the thickness and loading terms of the FW-H equation for a uniformly moving medium. The analysis incorporates the influence of angular inflow, due to aircraft angle of attack (pitch and yaw) or due to the aircraft installation flow field. In the presence of angular inflow, both the monopole and dipole source distributions are unsteady in the propeller reference frame, due to varying blade section relative speed.

Propeller quadrupole tone noise predictions in GAIN are based on the time-domain approach of Brentner.<sup>43</sup> The theory utilizes the quadrupole term of the FW-H equation and requires numerical evaluation of source integrals over a volume surrounding the propeller blade. After calculation of the time-domain pressure field, a Fourier transform is used to extract the frequency components of the radiation field. Quadrupole effects are typically fairly small for general aviation propellers so a number of approximations in the quadrupole source modeling have been made in GAIN. The quadrupole module is included in the GAIN program to provide the user with an option for assessing the importance of quadrupole source effects, for situations where they might become important (such as cases involving high subsonic relative Mach numbers near the tip of the propeller blade).

The broadband noise source that is modeled in GAIN is the interaction of the boundary layer turbulence with the trailing edge of the propeller blade. The code is based on the analysis of Amiet and Schlenger<sup>44,45</sup> in which the boundary layer turbulence is assumed to produce a "frozen" pressure field that convects past the trailing edge. The frozen pressure field of the boundary layer turbulence is represented by an empirical model. Linear acoustics theory is used to calculate the sound radiated by the interaction of this frozen pressure field with the trailing edge. Additional information on this can be found in Ref. 9.

The engine on an aircraft produces noise that may be significant in aircraft flyover measurements. GAIN provides aircraft intermittent combustion (piston) engine tone and broadband noise predictions. The approach is an empirical method based on interpolation of a database of experimental measurements of engine noise spectra. The user can select one of three



**Figure 3** Measured and PACE-predicted one-third octave band spectra of aircraft flyover noise level.

engine options: Lycoming O-320 D1D, Lycoming O-360 A-series, or Lycoming O-320 D1D with Cessna 172 Standard Muffler. Additional information can be found in Ref. 25, 46, and 47. After execution of the noise source modules, the GAIN postprocessor module applies noise propagation effects (Doppler factors, spherical spreading, atmospheric attenuation, and ground reflection) to each noise source.

Validation studies have shown that the GAIN predictions agree quite well with high-quality flyover noise measurements. Figure 3 shows the agreement for measurements of a typical general aviation aircraft. The one-third octave band spectra are those that occur when the highest A-weighted noise level occurs. The importance of engine noise in accurate prediction of aircraft flyover noise can be seen in Fig. 3. It can be seen that the tones that are indicated by three spikes in the spectrum below 500 Hz are in reasonable agreement with the measured peak in the spectrum. However, above 500 Hz, the agreement between the propeller alone prediction and the measurement becomes greater with increasing frequency. If the engine noise prediction is added to the propeller noise prediction, it can be seen that the agreement with the measured spectrum is quite good. The corresponding overall noise level and the A-weighted noise level for the measured and predicted spectra are also in good agreement. This good agreement has been found in many other comparisons of GAIN predictions with general aviation propeller aircraft flyover measurements.

#### 6.4 Computational Fluid Dynamics–Based Computational Aeroacoustic Method

Because of the advances in computational fluid dynamics (CFD) and availability of powerful digital computers, the calculation of propeller noise in the near field is now feasible by this method, which is now known as the CFD-based computational aeroacoustic (CAA) method. Such a methodology is based on very

sophisticated turbomachinery codes. This approach is computer intensive. One of the chief advantages of this method is the capturing of the nonlinear effects that can be important for highly loaded high-speed propellers operating in asymmetric flow fields. However, it must be emphasized that the accuracy of most unsteady turbomachinery codes deteriorate with distance from the propeller. Therefore, the best one can hope for is the accurate prediction of unsteady surface pressure on the fuselage that is the cause of aircraft cabin noise. Lim et al.<sup>14</sup> have demonstrated that near-field noise can be accurately predicted using this approach. Since the other time-domain and frequency-domain methods described in this chapter produce quite accurate results and are much less computer intensive, computational aeroacoustic methods are not often used for conventional propeller noise studies. However, for high-speed propeller noise prediction, coupling this method in the near field to the FW-H equation with penetrable data surface for radiation calculation appears to be an ideal and highly accurate method of noise prediction.

#### 7 METHODS OF CONTROLLING PROPELLER NOISE

The major objective in controlling propeller flyover noise is to meet the level required for certification. Propeller noise is the natural result of the production of the thrust required to permit an aircraft to fly. Both experimental and analytical studies have been conducted for many years to establish methods to reduce propeller noise while maintaining the thrust required for aircraft flight. The most beneficial elements of noise reduction are: reduce propeller rpm, reduce propeller diameter, increase the number of blades, reduce the blade width, thin the blade airfoils particularly near the tip, and use a round or elliptical blade tip rather than a square tip. Other elements of noise reduction are: blade planform

sweep and unequal circumferential blade spacing. Further discussion of propeller noise reduction technology can be found in Ref. 9 and 48.

It should be noted that there are penalties for reducing rpm to reduce noise. For a given engine reducing rpm reduces power. If power is maintained at the lower rpm by using a larger engine, there will be a cost and weight impact.

The reduction of propeller and propfan noise at high-speed cruise was the subject of considerable research in the 1980s. Blade sweep was found to be beneficial in reducing cruise noise reaching the fuselage.<sup>4</sup> Reductions of about 5 dB were found in tests comparing noise produced by unswept and swept blade propellers.

Noise of counterrotation propellers consisting of two blade rows rotating in opposite direction has been addressed by Hanson. He showed that, in addition to the noise sources of single-row propellers, noise due to acoustic and aerodynamic interference must be included in predictions of counterrotation propellers.

Experimental programs have been conducted over the years in attempting to find the propeller modifications that reduce noise. However, the benefits of changes in configuration were difficult to quantify because of the cost of building and testing a sufficient number of propellers with systematic variations in configuration. For example, the experimental program conducted by Dobrzynski and Gelhar<sup>17</sup> where the number of blades was incrementally increased from two to six used propellers that did not have systematic differences. As the number of blades increased by one, the diameter was reduced by 5%. However, blade geometry for the different propellers was not changed in a consistent manner due to cost constraints in the program. Figure 1, based on information from Ref. 17, confirms that increasing blade number while reducing diameter reduces noise. With this set of data it was also shown that increasing the number of blades to more than four did not further reduce the measured noise. However, the predicted noise continued to be reduced as number of blades was increased. This was attributed to a level of engine noise, which prevented the reduction in propeller noise to be observed.

The cost and complexity of the test programs such as that described above can now be overcome by use of computer-based noise predictions. Even though the strategy for reducing propeller noise involves complex trade-offs, these can now be addressed with user-friendly PC-based computer programs with remarkably accurate results.

Reference 49 summarizes a systematic analytical study to determine the noise reduction potential of increasing the number of blades. This study made use of the PC-based PACE method described elsewhere in this chapter. The reference for this study was a two-blade variable-pitch propeller. The effect on noise of (1) increasing the number of blades to three and four, (2) reducing the blade width as the number of blades was increased, and (3) reducing diameter was evaluated. The study addressed the fact that reducing the diameter of a propeller at a given rpm increases slipstream velocity. This increase in velocity increases

aircraft drag. This increase in drag was calculated for each diameter studied to keep aircraft performance constant. All of the blade geometric characteristics used in the study were based on a single generalized configuration contained in PACE. The propellers with the highest blade width that met the required thrust were identified. These configurations are the most likely to meet structural requirements.

The results of the study showed that increasing the blade number from two to three and reducing diameter by 9% (while reducing blade width) reduced the A-weighted noise level by about 13 dB. Increasing the blade number to four was found to be unacceptable as the required thrust could not be achieved. It should be noted that the noise reductions predicted do not include the influence of engine noise because the PACE program does not include engine noise. Reducing the blade airfoil thickness near the blade tip and rounding the square tip reference blade was found to reduce noise in some cases by less than 2 dB. It should be noted that the effect of the interaction of the propeller with the flow field induced by the nose of the airplane is not included in PACE. This interaction has been found to be important in studies using the GAIN program described elsewhere in this chapter. Also, the added tone noise caused by torque impulses generated by engine firing are not a part of PACE so could not be included.

It should be emphasized that the structural acceptability of the configurations of the above study were not established, so it is not likely that the full A-weighted noise level reduction of 13 dB can be achieved in a production configuration. Furthermore, as propeller noise is reduced, the noise of a typical piston engine will become more significant in the total peak aircraft flyover noise, thus limiting the noise reduction that can be achieved. Repeating the above study using the GAIN code (which includes the flow field effects and the engine noise contribution) and establishing the structural limits for promising configuration changes would provide practical guidance for reducing general aviation aircraft flyover noise.

## REFERENCES

1. J. Ffowcs Williams and D. Hawkins, Sound Generation by Turbulence and Surfaces in Arbitrary Motion, *Philos. Trans. Roy. Soc. London*, Ser. A, vol. 264, no. 1151, May 8, 1969, pp. 321–342.
2. L. Gutin, On the Sound Field of a Rotating Propeller, NACA TM 1195, 1948.
3. D. Hanson, Spectrum of Rotor Noise Caused by Atmospheric Turbulence, *J. Acoust. Soc. Am.*, Vol. 56, No. 1, July 1974, pp. 110–126.
4. D. Hanson, Influence of Propeller Design Parameters on Far-Field Harmonic Noise in Forward Flight, *AIAA J.*, Vol. 18, No. 11, November 1980, pp. 1313–1319.
5. W. Dobrzynski and B. Gehlhar, The Noise from Piston Engine Driven Propellers on General Aviation Airplanes, AIAA/CEAS 97, Paper No. 1997–1708, Atlanta, May 12–14, 1997.
6. D. Hanson and M. Fink, The Importance of Quadrupole Sources in Prediction of Transonic Tip Speed Propeller Noise, *J. Sound Vib.*, Vol. 62, No. 1, 1979, pp. 19–38.

7. D. Hanson and C. McColgan, Noise of Counter-rotation Propellers with Nonsynchronous Rotors, *AIAA J. Aircraft*, Vol. 22, No. 12, December 1985, pp. 1097–1099.
8. M. Dunn and A. Tinetti, Aeroacoustic Scattering Via Equivalent Source Method, *J. AIAA*, 2004-2937, 2004.
9. B. Magliozzi et al., Propeller and Propfan Noise, in *Aeroacoustics of Flight Vehicles: Theory and Practice, Vol. 1, Noise Sources*, H. H. Hubbard, Ed., NASA Reference Publication 1258, Vol. 1, WRDC Technical Report 90–3052, pp. 1–64, August 1991.
10. C. Morfey, Rotating Blades and Aerodynamic Sound, *J. Sound Vib.*, Vol. 28, No. 3, 1973, pp. 587–617.
11. F. Farassat and G. Succi, A Review of Propeller Discrete Frequency Noise Prediction Technology with Emphasis on Two Current Methods for Time Domain Calculations, *J. Sound Vib.*, Vol. 71, August 1980, pp. 399–419.
12. F. Metzger, A Review of Propeller Noise Prediction Methodology 1919–1994, NASA Contractor Report 198156, June 1995.
13. M. Lighthill, On Sound Generated Aerodynamically—I. General Theory, *Proc. Roy. Soc. (London) A*, Vol. 211, 1952, pp. 564–587.
14. T. Lim et al., A Technique for the Prediction of Propeller Induced Acoustic Loads on Aircraft Structures, AIAA 93–4340, 15th AIAA Aeroacoustics Conference, Long Beach, CA, October 1993.
15. Society of Automotive Engineers, Aerospace Information Report 1407, May 1977.
16. Society of Automotive Engineers, Aerospace Recommended Practice, 4th Draft, March 1994.
17. W. Dobrzynski and B. Gehlhar, Propeller Blade Number: A Parameter for Flyover Noise Reduction? International Noise and Vibration Control Conference in St. Petersburg, Russia, May 31–June 3, 1993.
18. F. Farassat, Linear Acoustic Formulas for Calculation of Rotating Blade Noise, *AIAA J.*, Vol. 19, No. 9, September 1981, pp. 1122–1130.
19. K. Brentner and F. Farassat, An Analytical Comparison of the Acoustic Analogy and Kirchhoff Formulation for Moving Surfaces, *AIAA J.*, Vol. 36, No. 8, 1998, 1379–1386.
20. M. Dunn and G. Tarkenton, Computational Methods in the Prediction of Advanced Subsonic and Supersonic Propeller Induced Noise—ASSPIN Users' Manual, NASA Contractor Report 4434, April 1992.
21. K. Brentner, Prediction of Helicopter Rotor Discrete Frequency Noise, NASA TM-87721, 1986.
22. F. Farassat et al., Advanced Turboprop Noise Prediction Based on Recent Theoretical Results, *J. Sound Vib.*, Vol. 119, No. 1, 1987, pp. 53–79.
23. M. Dunn and F. Farassat, High Speed Propeller Noise Prediction—A Multidisciplinary Approach, *AIAA J.*, Vol. 30, No. 7, July 1992, pp. 1716–1723.
24. F. Farassat et al., Advanced Propeller Noise Prediction in the Time Domain, *AIAA J. (Technical Note)*, Vol. 30, No. 9, September 1992, pp. 2337–2340.
25. W. Dobrzynski, Determination of Emission Values for Noise Emission Calculation at General Aviation Airports (in German), Report DLR-IB 129-94/17, German Aerospace Center, Sept. 1994.
26. D. Hanson, Helicoidal Surface Theory for Harmonic Noise of Propellers in the Far Field, *AIAA J.*, Vol. 18, No. 10, October 1980, p. 1213.
27. D. Hanson, Compressible Helicoidal Surface Theory for Propeller Aerodynamics and Noise, *AIAA J.*, Vol. 21, No. 6, June 1983, p. 881.
28. D. Hanson, Shielding of Prop-Fan Cabin Noise by the Fuselage Boundary Layer, *J. Sound and Vib.*, Vol. 92, No. 4, 1984, pp. 591–598.
29. D. Hanson, Near-Field Frequency-Domain Theory for Propeller Noise, *AIAA J.*, Vol. 23, No. 4, April 1985, p. 4.
30. D. Hanson, Noise of Counter-Rotation Propellers, *AIAA J. Aircraft*, Vol. 22, No. 7, July 1985, pp. 609–617.
31. D. Hanson, Propeller Noise Caused by Blade Tip Radial Forces, AIAA-86-1892, AIAA 10th Aeroacoustics Conference, Seattle, WA, July 1986.
32. D. Hanson, Near Field Noise Theory for Propellers with Angular Inflow, DGLR/AIAA-92-02-049, DGLR/AIAA 14th Aeroacoustics Conference, Aachen, Germany, May 1992.
33. D. Hanson, Unified Aeroacoustics Analysis for High Speed Turboprop Aerodynamics and Noise, NASA Contractor Report 4329, March 1991.
34. D. Hanson, Direct Frequency Domain Calculation of Open Rotor Noise, *AIAA J. Aircraft*, Vol. 30, No. 9, Technical Notes, 1992, p. 2334.
35. D. Hanson and D. Parzych, Theory for Noise of Propellers in Angular Inflow with Parametric Studies and Experimental Verification, NASA Contractor Report 4499, March 1993.
36. R. Menthe, C. McColgan, and R. Ladden, Unified Aeroacoustic Analysis for High Speed Turboprop Aerodynamics and Noise; Vol. IV—Computer User's Manual for UAAP Turboprop Aeroacoustic Code, NASA Contractor Report 185194, May 1991.
37. Metzger Technology Services, Propeller Acoustical Change Estimation (PACE) Model, User's Manual—Version 2.0, U.S. Department of Transportation, Federal Aviation Administration, May 2000.
38. E. Kerschen and B. Magliozzi, Users Manual for AGATE Propeller and Engine Noise Prediction Computer Program, Integrated Design & Manufacture Work Package, AGATE Integrated Propulsion Systems Design & Analysis Tool, Aug. 31, 2001.
39. D. Hanson and D. Parzych, Theory for Noise of Propellers in Angular Inflow with Parametric Studies and Experimental Verification NASA Contractor Report 4499, March 1993.
40. B. Magliozzi, V/STOL Rotary Propulsion Systems Noise Prediction and Reduction, Vol. I—Identification of Sources, Noise Generating Mechanisms, Noise Reduction Mechanisms, and Prediction Methodology; Vol. II—Graphical Prediction Methods; Vol. III—Computer Program User's Manual, Report Number FAA-RD-76–49 III, May 1976.
41. B. Magliozzi, V/STOL Rotary Propulsion Systems Noise Prediction Model Update and Evaluation, Report Number FAA-RD-79-107, December 1979.
42. B. Magliozzi, V/STOL Rotary Propulsion Systems Noise Prediction Model, Ground Reflection Effects and Propeller Thickness Noise, Report Number FAA-EE-82-15, August 1982.
43. K. Brentner, An Efficient and Robust Method for Predicting Helicopter Rotor High-Speed Impulsive Noise, *J. Sound Vib.*, Vol. 203, No. 1, 1997, pp. 87–100.
44. R. Amiet, Noise Due to Turbulent Flow Past a Trailing Edge, *J. Sound Vib.*, Vol. 47, No. 3, 1976, pp. 1076–1082.

45. R. Schlinker and R. Amiet, Helicopter Rotor Trailing Edge Noise, NASA CR-3470, 1981.
46. H. Patrick, Engine Noise Prediction Algorithm, AGATE Acoustics Work Task 3.7.2; AGATE Acoustics Work Meeting, ERAU, Daytona Beach, February 1999.
47. H. Patrick, Extending the IC Exhaust Noise Database, AGATE Acoustics Work Task 3.7.2 1999 Final Report, 1999.
48. F. Metzger, An Assessment of Propeller Aircraft Noise Reduction Technology, NASA Contractor Report 198237, August 1995.
49. Metzger Technology Services, Analytical Investigation of Acoustical Effects of Increase in Propeller Blade Count on Certification Noise, Contractor Report to the FAA Office of Environment and Energy, April 2001.

# CHAPTER 91

## HELICOPTER ROTOR NOISE: GENERATION, PREDICTION, AND CONTROL

Hanno H. Heller and Jianping Yin

German Aerospace Center (DLR)

Institute of Aerodynamics and Flow Technologies (Technical Acoustics)  
Braunschweig, Germany

### 1 INTRODUCTION

Helicopters are highly versatile flight vehicles. They can fly straight ahead, land and take off vertically, and even fly sideward and backward. Their most distinctive capability is that of hovering. Almost no other aircraft can do all that in a controlled manner (the vectored thrust Harrier is a notable exception in the fixed-wing realm). These singular “talents” are made possible by the helicopter’s unique lifting and propulsion systems (including its tail-rotor-related antitorque system), but are, however, accompanied by very complex aeroacoustical phenomena on the rotors with inherent and equally complex noise generation and radiation mechanisms. Although rotor noise usually dominates, there are helicopters where engine noise could prevail.

To appreciate the complexities of rotor aeroacoustics, this chapter starts with a discussion of *rotor kinematics*, followed by an elaboration on *rotor source characteristics* with emphasis on impulsive types (high-speed impulsive and blade–vortex interaction impulsive noise). The subsequent section deals with *theoretical aspects of rotor noise prediction* featuring Lighthill’s acoustical analogy, integral formulations [such as Ffowcs Williams and Hawkins (FW-H) and Kirchhoff formulations], and computational aeroacoustics (CAA) methods. The chapter concludes with description of *rotor noise reduction measures*, specifically active reduction of blade–vortex interaction noise, passive reduction of high-speed impulsive noise, and reduction of tail rotor noise.

### 2 ROTOR KINEMATICS

Unlike on fixed-wing aircraft, the entire lift (upward pushing force to raise the helicopter’s mass) as well as the propulsive thrust is solely generated by the main rotor utilizing a highly complex blade control system. A helicopter main rotor can be considered a “rotating wing.” Under conditions of forward flight, the tip of that rotating wing (i.e., the rotor blade tip) experiences high speeds on the “advancing side” of the rotor azimuth due to the combination of the rotor rotational speed (e.g., 220 m/s at the tip) and the flight speed (e.g., 50 to 80 m/s), as can be seen in Fig. 1. Since these two speeds simply *added* together, the blade tip at and around the azimuthal angle of  $\psi = 90^\circ$  sees “incoming flow” speeds between, say, 270 and 300 m/s. A fraction of a second later, that same tip

on the “retreating side” of the rotor azimuth (i.e., near  $\psi = 270^\circ$ ) is exposed to lower flow speeds, of, say, between 140 and 170 m/s, because now the flight speed is *subtracted* from the tip speed.

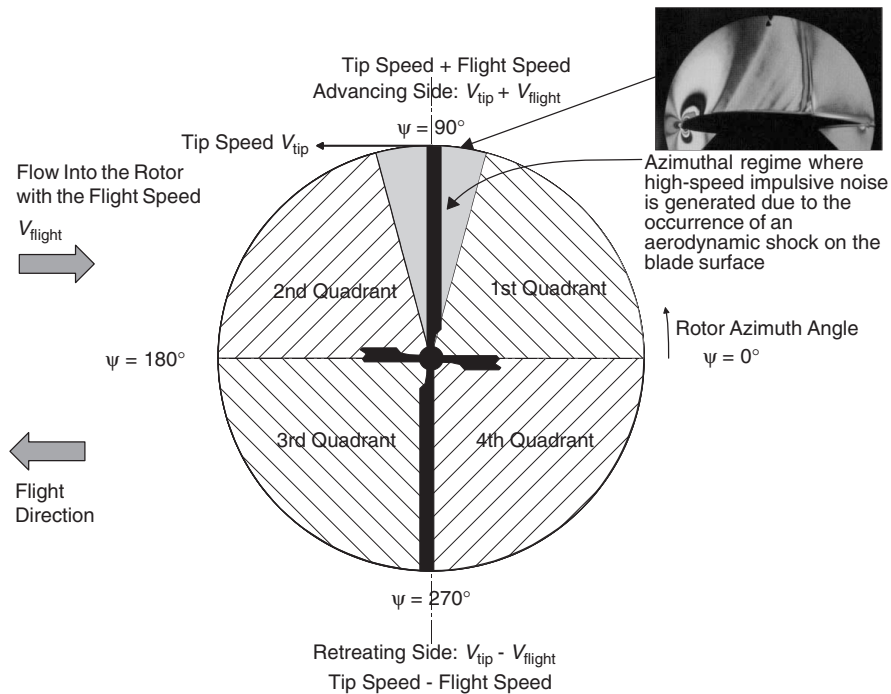
If the blade pitch (i.e., the geometrical angle of a blade with respect to the rotor plane) stayed the same, then the lift, which the rotating wing provides, would vary dramatically during a rotor revolution. The helicopter would tend to wobble around. The technical answer is to control that flow angle of attack in such a way as to attain low values on the advancing side and higher ones on the retreating side, with smoothly varying values in between.

This is achieved by controlling the kinematic motions of the rotor blade. While spinning around, a rotor blade executes *flapping motions* (vertical to the rotor plane), *pitching motions* (about the blade axis), and *lead-lag motions* (in the rotor plane). For these three motions bearings or hinges at the blade root are required. These are mechanically quite involved. Many of the heavier helicopters feature bearings and thus articulated rotors. For light- and medium-weight helicopters, some manufacturers employ flexible hinges (semirigid rotors), thus taking advantage of elastic elements at the blade roots and the thereby possible “natural” flapping (and other) motions of the blades, depending on the equilibrium of the acting forces: lift, weight, centrifugal, and other accelerating forces.

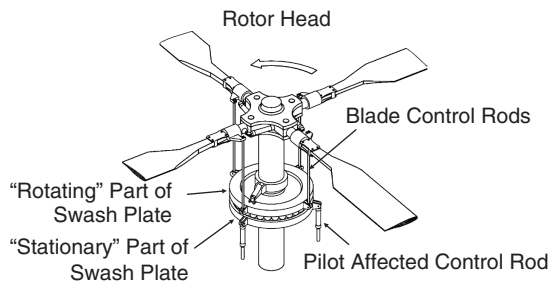
On the *advancing* side, the elastic blade tends to move upward. This induces a vertical flow speed component such that the effective flow angle of attack is slightly reduced, causing a reduction in the lift—which is the desired effect. On the *retreating* side, the enormous centrifugal forces (some 20 tons!) pulling outward on the blade tips reduce the local coning angle, which increases the effective flow angle of attack, resulting in higher lift—which, again, is the desired effect. In this way, the lift across the rotor plane remains, inherently so to speak, fairly uniform.

To attain forward speed, the blade pitch must be actively increased on the rear arc (i.e., near  $\psi = 0^\circ$ ) and decreased on the forward arc (i.e., near  $\psi = 180^\circ$ ). This way, more lift is generated at the rear and less at the front, thus pushing the nose of the helicopter down; the rotor now blows air slightly backward and downward thus driving the helicopter forward.

To actually affect the blade pitch, the pilot through his control inputs changes the tilt of the swash plate on the rotor hub (Fig. 2). A typical swash plate may



**Figure 1** Aerodynamics and acoustics of rotor during high-speed straight level flight.



**Figure 2** Main rotor head kinematics.

consist of a lower *stationary* portion whose motions are mirrored by the upper *rotating* portion, which in turn is linked to the leading edge of each blade. Thus, by acting on the swash plate, the pilot is able to control the pitch of the blades as they rotate. A swash-plate tilt with respect to the rotor shaft results in up and down motions of the blade control rods. The blade pitch then follows these sinusoidal control rod motions, affecting the blade lift and, thus, the blade flapping motions (with a certain phase delay depending on the blade stiffness), up during one half of the rotation, down during the other. This way, the pitch of the rotor blade could be lower in the forward arc and higher in the rear arc to result in forward flight. The opposite would be the case for a backward flight. Likewise, sideward flights to the left or the right could

be controlled by appropriately changing the tilt of the swash plate. Pushing the entire swash-plate assembly up or down (rather than tilting it) would simply cause a simultaneous pitch change of all blades by the same amount across the rotor plane, resulting in an upward or downward flight without any horizontal movement.

The tail rotor—while preventing the helicopter to turn in the opposite rotational direction of the main rotor—is also instrumental for position control in sideward flights, turns, and the like. Most importantly, the tail rotor counteracts the moment of the main rotor. The thrust of the tail rotor is adjusted such that it exactly compensates that main rotor push, thus allowing the helicopter to fly straight ahead. A tail rotor experiences “dramatic” inflow changes similar to those occurring on the main rotor in that its forward-moving blade tip “sees” high speeds and the backward-moving blade lower speeds. The tail rotor also operates in the shed aerodynamic wake of the upstream main rotor and also in the wakes of the main rotor hub and of the fuselage. The flow conditions near and around a helicopter tail rotor are extremely complex. Therefore prediction of tail rotor aerodynamics and noise is likewise an extremely complex problem, which presents a major issue for designers.

### 3 ROTOR NOISE GENERATION

Sources of helicopter noise are its main rotor, its tail rotor, the engines, and the drivetrain components. The dominant noise contributors though are the main rotor and the tail rotor since they operate in the



**Table 1** Classification of Rotor Noise

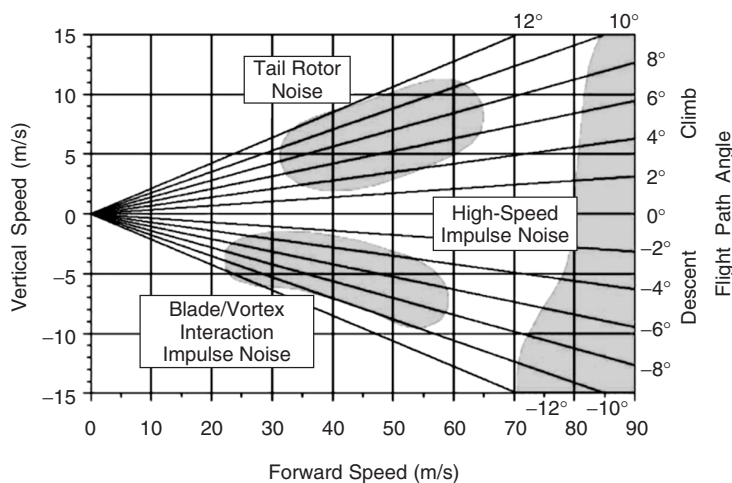
Physical Mechanism	Acoustic Source Type	Spectral Character	Rotor-Specific Noise Type
Volume displacement Nonlinear effects (predominantly at high blade tip Mach numbers)	Thickness noise Noise from periodic shock separation	Discrete frequency Discrete frequency	Impulsive noise HS impulsive noise
Rotating blade forces	Deterministic loading noise	Discrete frequency	Rotational noise
Blade–vortex interaction (BVI) (predominantly at moderate speed descent)	Deterministic loading noise	Discrete frequency	BVI impulsive noise
Turbulent inflow, blade–wake interference, flow separation	Nondeterministic loading noise	Stochastic	Broadband noise
Main rotor wake–tail rotor interaction (specifically main rotor tip vortex–tail rotor interaction)	Deterministic loading noise	Contains discrete frequency and stochastic components	“Periodic” broadband noise

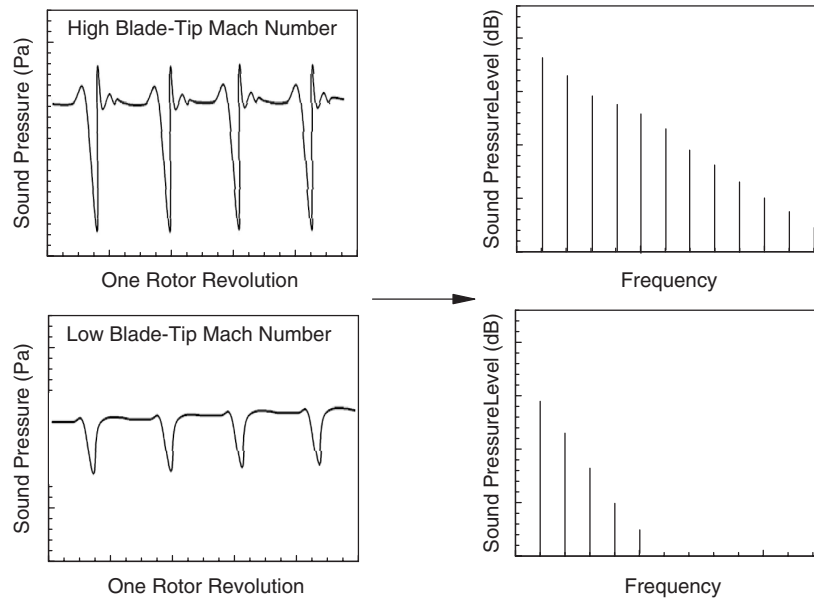
free atmosphere and thus radiate noise unobstructedly into the surroundings. Engine noise often plays a lesser role, although for large helicopters engine noise could dominate at takeoff. Rotor noise including main rotor and tail rotor noise can be classified into discrete-frequency rotational noise, broadband noise, and impulsive noise (also of discrete-frequency character), as shown in Table 1.

Accordingly, rotational noise comprises *thickness noise* (i.e., noise generated from the periodic volume displacement by the rotating blades) and *loading noise* (rotating lift and drag forces). The former is more important in the low-frequency range of the rotor noise spectrum (i.e., at the blade passage frequency and first few harmonics, but it contains mid-, and

high-frequency components too, being of impulsive-type nature). At low rotational speeds and for low blade loading, the thickness noise line spectrum can be exceeded by the *broadband noise* components. Broadband noise is a result of turbulent inflow conditions, blade/wake interferences, or even blade self-noise (“airframe noise”).<sup>1–6</sup>

Of greater importance are *impulsive-type noise sources*, resulting in the familiar “bang, bang, bang” sound. Of these, there are two kinds: High-speed (HS) impulsive noise and blade–vortex interaction (BVI) impulsive noise. As shown in Fig. 3 (flight envelope: climb–descent rate vs. flight speed diagram), the former appears predominantly at high flight speeds, independent of the climb or descent rate, while the

**Figure 3** Helicopter operational flight envelope.



**Figure 4** Pressure amplitude time history signatures and corresponding sound pressure level spectra for high and low tip speeds.

latter occurs predominantly during moderate speed descent. Tail rotor noise has almost all characteristics of main rotor noise. The flow around the tail rotor is the sum of the interacting flows generated by the wakes of the main rotor, the fuselage, the rotor hub, as well as the engine exhaust and empennage flows in addition to its own wake. It is known for most helicopters that tail rotor noise dominates at moderate speed straight flight conditions and during climb, though. Tail rotor noise broadband component are of low levels and need not actually be considered. As mentioned above, engine noise could dominate for some helicopter during takeoff as discussed in Refs. 7 and 8.

### 3.1 Main Rotor High-Speed (HS) Impulsive Rotor Noise

A rotor blade is not infinitely thin but has a finite thickness. Also, its chordwise surface profile is curved, probably more so on the upper surface than on the lower surface. As the air over the upper curved surface moves faster than over the slightly lesser (or not at all) curved lower surface, the *difference* in pressure (lower pressure on top, higher pressure on the bottom) provides the wanted upward suction, or lift.

For conditions of high-speed forward flight, this increase in speed on the upper curved surface may now result in the surface  $M_{AT}$  (advancing tip Mach number) to assume values *above* 1, even if the “local inflow Mach number” toward the blade was only 0.9. That is, that Mach number is slightly supersonic, however, only for the *very short* time span, when the blade moves through the “advancing side rotor azimuth” near

$\Psi \approx 90^\circ$ . When this occurs, an aerodynamic shock appears in the flow immediately above the upper blade surface. The supersonic flow above the blade surface suddenly—across a shock front—assumes subsonic values: upstream of the shock front local flow speeds are supersonic, behind the shock front they are subsonic with a sudden steep pressure rise. The sudden appearance (and disappearance) of such an aerodynamic shock on the blade causes an impulsive sound signal (Fig. 4). For a four-bladed rotor, for example, which spins around 5 times a second, 20 such impulses (“bangs”) per second would occur. The phenomenon is termed *high-speed (HS) impulsive rotor noise*.<sup>9–15</sup> HS noise is most strongly radiated into the forward arc, that is, the flight direction, and roughly along the rotor plane—not much above and not much below. Thus, HS noise is heard when a helicopter approaches from far away; once the helicopter is overhead, HS noise disappears and loading noise, and/or tail rotor noise, tends to dominate.

For lesser flight speeds, when advancing tip Mach numbers,  $M_{AT}$ , are lower (say below 0.85 or so) and in the absence of HS noise, loading noise and thickness noise take over acoustically. Loading noise has a maximum in a downward (and upward) direction. Hence, when the helicopter flies overhead, one hears its characteristic “thud/thud/thud” noise.

### 3.2 Main Rotor Blade–Vortex Interaction (BVI) Impulsive Noise

When a blade (a lifting surface) moves through the air, a strong vortex is shed from its tip. The vortex trail shed from the tip of a rotating blade assumes

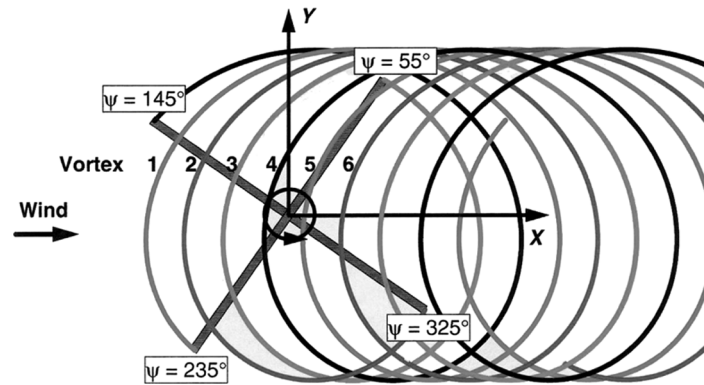


Figure 5 Epicyclical tip vortex trails and interaction of blades.

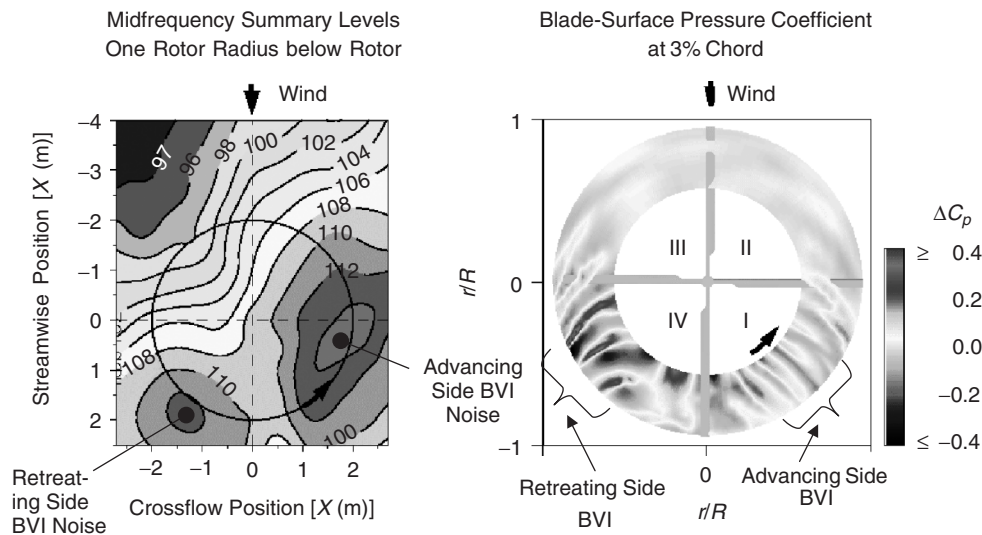


Figure 6 Blade-surface pressure coefficient patterns and resulting radiated acoustics one rotor radius below rotational plane (from DNW experiments) for conditions of strong blade–vortex interaction (BVI) employing a model B0105 main rotor.

an epicyclical pattern. A subsequent rotor blade may collide with such a vortex (Fig. 5), causing sudden local velocity changes, and, hence, local lift changes. Conditions for such collisions occur invariably during descent flights at moderate speeds (typically at flight speeds of 25 to 50 m/s and descent angles of  $5^\circ$  to  $8^\circ$ ). Under these circumstances, the vortex trails are sucked into the rotor plane to cause a sequence of multiple interactions, each time a blade hits a vortex trail. This phenomenon, BVI impulsive rotor noise, is discussed in Refs. 16–24. The intensity of BVI impulsive noise depends on the ratio of flight and descent speeds, that is, on the flight angle and the through-flow through the rotor plane, or, conversely, on the tip path plane angle and the advance ratio (ratio of flight and blade

tip speeds); it grows with thrust coefficient and blade tip Mach number.

From the kinematics of BVI (as illustrated in Fig. 6 from wind tunnel results on a model main rotor), it becomes evident that such strong interactions would occur in the first rotor quadrant (near  $\Psi \approx 45^\circ \pm 20^\circ$ ) on the advancing side, where a blade's leading edge would encounter the vortex trail in a parallel manner and, thus, over a fairly extended radial blade span, with the consequence of a very strong impulse. The same would be the case at the fourth rotor quadrant (near  $\Psi \approx 315^\circ \pm 20^\circ$ ) on the retreating side, where, again, the interaction would occur over an extended regime of the leading edge. In contrast, near the second quadrant ( $90^\circ < \Psi < 180^\circ$ ) and the third quadrant ( $180^\circ < \Psi < 270^\circ$ ), interactions would be a very localized event

over a very small extent of the blade leading edge, thus causing a very weak acoustical signal. Hence, one speaks about *advancing side BVI* and *retreating side BVI*.

Blade–vortex interaction noise differs in its acoustical directivity compared to HS noise. Wind tunnel research has shown that advancing side BVI radiates most strongly in a forward/downward direction (roughly  $45^\circ$  to  $60^\circ$  down from the rotor plane) while retreating side BVI exhibits its directivity peak in a downward/backward direction, again roughly  $45^\circ$  to  $60^\circ$  down from the rotor plane.

### 3.3 Tail Rotor Noise

Although the tail rotor operates in the strong wake of the main rotor (of particular importance being the interaction of the tail rotor with the tip vortices shed by the main rotor blades) and of the fuselage, certain aeroacoustical features are quite similar to those of the main rotor.

The main acoustical components are again thickness noise (especially on high-speed tail rotors) and loading noise. Furthermore, the combination of flight speed and tail rotor rotational tip speed may result in locally transonic inflow speeds, again causing the appearance of shocks and the associated acoustical events. Also, the impingement of the main rotor wake flow onto the tail rotor may cause blade–wake interactions with impulsive sounds to occur. The periodicity of this interaction noise may be one per main rotor revolution when the ratio of the rotor revolutions/minute (rpm) between main rotor and tail rotor is an integer number instead of one per tail rotor revolution for self-generated tail rotor BVI noise. Due to this source's largely forward/upstream directivity, it can often be detected well ahead of the approaching helicopter, although directivity details may depend on the relative position of the tail rotor and the main rotor. Tail-rotor-related thickness noise exhibits a directivity downward (and maybe upward), clearly detectable when the helicopter flies overhead. In general, though, tail rotor noise is heard under conditions of straight level flight or climb, that is, when the strong main rotor BVI noise components (occurring only under descent flight conditions) are inherently absent. For a helicopter in descent flight, the tail rotor noise would be drowned by the main rotor BVI noise. But as said, a tail rotor may also generate its own BVI noise.

In some light- to medium-weight helicopters the open tail rotor is replaced by a fan-in-fin or “fenestron.” Rotor stator interactions must then be considered along with sound wave scattering on the duct lips. Tail rotor noise is discussed in Refs. 25 to 27.

## 4 ROTOR NOISE PREDICTION

Several modern approaches have been developed to predict helicopter rotor noise, known under the designations *Lighthill's acoustical analogy* (aeroacoustical source terms), *integral formulations*, such as *Ffowcs Williams and Hawkings*, *FW-H*, as well as *Kirchhoff formulations* (as part of using aerodynamic field information hybrid methods), and *computational*

*aeroacoustics (CAA)* (use of aerodynamic methods for direct noise calculations). CAA methods are designed to accurately capture the unsteady flow and noise radiation, but, presently, solving acoustical problems involving “three-dimensional rotors” by means of CAA is still too expensive and impractical. Therefore, integral formulations, such as FW-H and Kirchhoff formulations, are still very useful for the purpose. A general schematic of alternative rotor noise prediction approaches appears in Fig. 7.

To predict rotor noise, say in terms of sound pressure time histories at an observer point, noise may be broken down into three source types occurring on a rotor, namely thickness noise, loading noise, and compressibility noise.

Hence, the acoustical analogy approach utilizes three corresponding aerodynamic source terms: the linear thickness noise term (with the characteristics of an aerodynamic monopole), the linear loading noise term (with the characteristics of an aerodynamic dipole), and the non linear compressibility noise term (with the characteristics of an aerodynamic quadrupole) as inputs into appropriate acoustical codes, such as the FW-H formulation,<sup>28,29</sup> which in turn is based on the classical Lighthill formulation of aerodynamic noise.<sup>30</sup>

The *monopole source term* can be computed solely from information on blade geometry and kinematics, the latter depending on rotor operational conditions. The *dipole source term* can be determined in several ways. One approach is based on inviscid potential flow methods, such as *lifting line* or *lifting surface theory*, or *unsteady panel methods* based on singularity theory to yield, respectively, high-resolution unsteady blade loadings or high-resolution unsteady blade pressures. Another approach to determine the acoustic dipole source term is based on solutions of *Euler equations*, which, again, provide high-resolution blade pressure information. The characteristics of the inviscid potential flow methods are as follows:

- In *lifting line theory* (see Ref. 31) the lift is considered to be generated by a single (“bound”) vortex filament at the blade quarter chord along the blade span. Pressure equalization at the blade root and tip generates root and tip vortices. Blade rotation and forward motion cause these “wake” vortices to follow a complicated epicyclic path to constitute the wake. Often this vortex wake is taken as time invariant (“prescribed wake”), although it is presently fully recognized that a free wake model must be included into the lifting line code, as must the elastic properties of the blade, to arrive at better simulations. The output of the calculation is only the lift distribution over the blade span as input into the acoustical codes, without regard to the details of blade planform, tip shape, profile, and the like.
- If the lift variation over the chord is of importance, the *lifting surface method* (see Ref. 32) accounts for it with a distribution of lifting lines over the blade chord. The

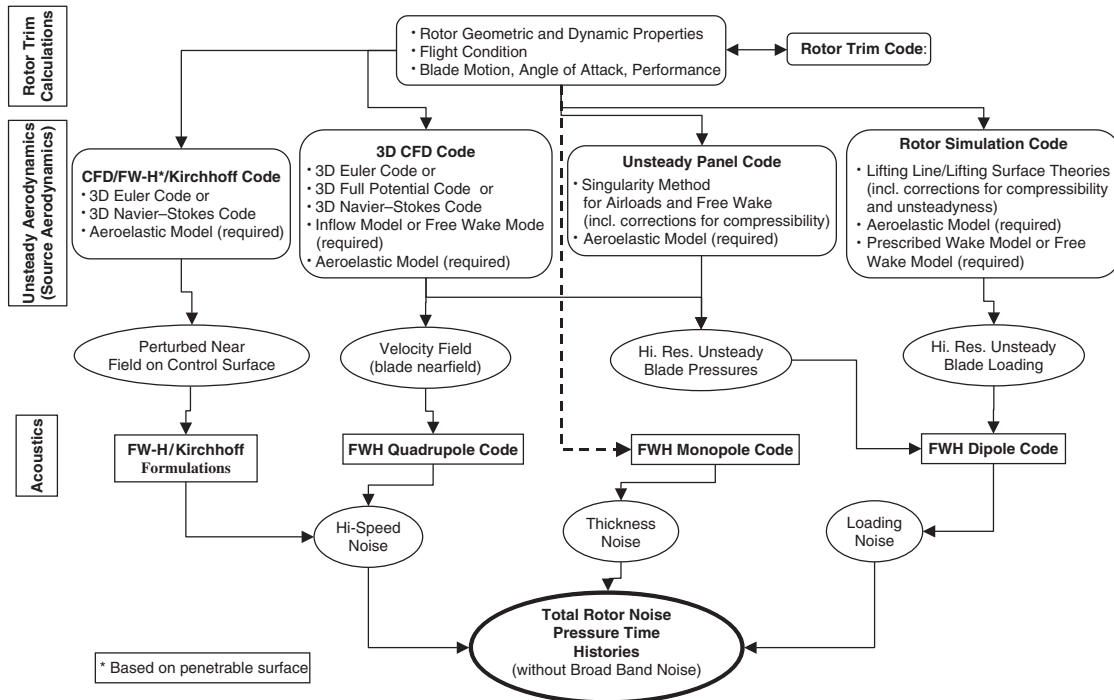


Figure 7 Helicopter rotor noise prediction schematic (alternative methods).

concept allows for both including or neglecting blade thickness as the distribution is spread over a blade chord. Thus, nonrectangular blade planforms with twist and blade tip modifications can be simulated and the ensuing pressure data be used as input into the acoustical codes.

- *Unsteady panel methods in combination with free wake model* (see Ref. 33) permit the modeling of the aerodynamics of the rotor and especially the aerodynamic interactions among the rotors.<sup>34</sup> In essence, all geometric parameters of a real blade (profile geometry, planform, twist, tip shape, etc.) can now be accounted for. The calculations yield the pressure and velocity distribution on the upper and lower blade surfaces. Accordingly, a more realistic simulation of blade geometry and, correspondingly, more detailed aerodynamic information is available as input for the acoustical codes.
- The alternative method to arrive at the dipole source term is to compute the acoustic near-field blade pressures by means of an *Euler solver*. Blade loading is evaluated by integrating the pressure over the surface grid of the blade used for the aerodynamic computations (see Ref. 35). This method inherently accounts for the blade's geometrical details.

Linearized potential flow methods to compute the dipole source term need only moderate computation

time and are well suited for application in prediction schemes of rotor noise for blade tip speeds well below those where major supersonic flow regions on the blade would appear, that is, at low to moderate forward speeds. Their inherent drawback is their inability to account for compressibility effects as needed to compute the *quadrupole source term*. At higher speeds, though, the quadrupole source term must be included, even if only in an approximated form, once supersonic flow regions and shocks near the blade tip appear during forward flight (see Ref. 36).

Treatment of such nonlinear effects is the domain of "field methods" such as *full potential* or *Euler methods*.<sup>37</sup> If the rotor is encompassed by a shock, the quadrupole field must be accurately evaluated through appropriate volume integration procedures. This, however, is a very involved process.

Here, the *combination of computational fluid dynamics (CFD) and Kirchhoff methods*<sup>38</sup> is to determine the near-field aerodynamics by means of full potential or Euler/Navier–Stokes equations, accounting for all nonlinear compressibility effects, which are then integrated onto the Kirchhoff surface. The Kirchhoff surface should completely surround the rotor at an appropriate distance. Starting from that surface around the nonlinear near field of the rotor, computation of the subsequent sound propagation into the far field requires only linear equations.

Hence, the Kirchhoff surface divides the flow region into an inner part where nonlinear effects prevail (and where the flow solution is obtained by solving the Euler equations) and an outer part where linear acoustic wave propagation prevails. This combination of the Euler and Kirchhoff methods provides better agreement of measurements and prediction than the direct computation of the acoustic far field solely by means of an Euler approach.

The combination of CFD and the FW-H formulation based on penetrable surface (P-FW-H)<sup>39,40</sup> represents a more appropriate and, in fact, more flexible technique to compute the acoustic radiation at high tip speeds for conditions of hover or level flight compared to the Euler–Kirchhoff approach. The reasons are:

- The Kirchhoff solution is very sensitive on the location of the integral surface because the Kirchhoff method requires placing the integral surface in the region where the flow is completely governed by a homogeneous linear wave equation.
- Current CFD simulation could only support information that is close to the source region, where nonlinear effects cannot be avoided. The error due to nonproper location of the Kirchhoff surface can be large, especially if the integral surface is positioned in the nonlinear region, even if in a slightly nonlinear region.
- P-FW-H has all the advantage embedded in the Kirchhoff formulation and is valid even if the integration surface is located in the nonlinear region and the region containing vorticity so that it is less sensitive to the placement of the integration surface.
- Input quantities are directly available from CFD codes, which is not the case for the Kirchhoff formulation.

In summary, then, (a) linearized inviscid potential flow methods in combination with the acoustical analogy approach and (b) analyses using Euler results in combination with acoustical analogy approaches are suitable for rotor noise predictions at low to moderate tip speeds. For high-tip-speed cases, including those where shock delocalization occurs, CFD and FW-H and Kirchhoff approaches may be better qualified. Here, the CFD-based computationally expensive flow-field calculations are confined to the near-field inside the FW-H and Kirchhoff surface where nonlinear effects prevail. Prediction of the far field sound pressure field can be realized with the FW-H and Kirchhoff surface integration.

Predicting the noise of a helicopter already in the design stage is thus a rather involved undertaking. While it might be possible to predict the noise from an isolated main rotor, already accounting for the realistic fuselage refraction effects adds another level of complexity. Even more complicated would be the computation of the interaction effects of main and tail rotor unsteady aerodynamics/acoustics to arrive

at a viable far-field noise prediction. Often empirical or semiempirical prediction schemes are employed, based, for example, on flyover noise measurements from which the noise for different specific flight conditions (takeoff, low-speed and high-speed level flight, and climb flight) are determined. From these the directivity pattern on a fictitious hemispherical surface around the helicopter (e.g., at a radius of 100 m) is derived. This “acoustical directivity hemisphere” is then “flown over the landscape,” to obtain a (fairly accurate) acoustical footprint for the helicopter under consideration. But already extrapolating these findings toward another helicopter is quite uncertain.

A rough indication of the noise of helicopters may be obtained from noise certification data, as published by the national aviation authorities. Here, albeit for very specific flight conditions, the overall, weighted noise levels are available. Such data can be—with limitations—also used for land-use planning purposes.

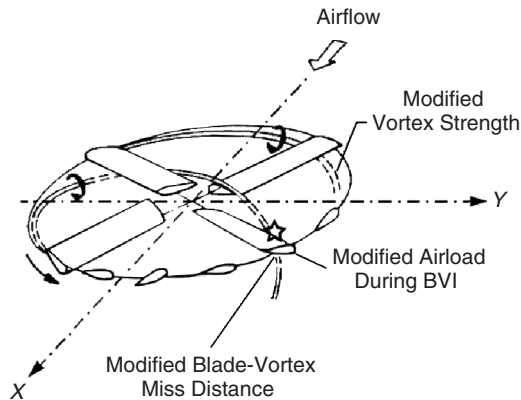
## 5 ROTOR NOISE REDUCTION

Reducing rotor noise really constitutes a balancing act. As in any noise control effort, different noise sources need to be “equalized” such that none dominates above the other. In the case of a helicopter, there would be a need to balance the relative noise levels of main rotor and tail rotor, including the interaction sources (and in some cases engine noise). Corresponding considerations are important in the design of a quiet helicopter. For a helicopter, of course, there is the added complication that different sources dominate at different flight conditions.

### 5.1 (Active) Noise Reduction of Main Rotor BVI Noise

Blade–vortex interaction noise intensity can be reduced in three ways: (1) by decreasing the vortex strength (the maximum velocity near the vortex core) as such, (2) by minimizing the intensity of the very interaction process, and (3) by increasing the distance the vortex passes the blade, that is, the “miss distance” (Fig. 8). All this can be achieved, for example, by appropriately controlling the blade pitch “at the right moment” during the rotor rotation either by blade pitch control through the *higher harmonic control*, or HHC, technique or by the “*individual blade control*, or IBC, technique. The difference is that for HHC, the (additional) control actuators act on the “stationary” portion of the swash plate thus causing the identical blade-pitch variation on all blades during any rotor revolution, while for IBC, the actuators are attached to the rotating portion of the swash-plate, such that the pitch motion of each blade during any rotor revolution can be controlled individually. Evidently, the latter method offers greater flexibility. The two kinds of blade control are illustrated in Fig. 9. Only the IBC technique will be discussed further.

The above-mentioned BVI impulsive noise minimization methods are based on the following techniques:



**Figure 8** Illustration of BVI noise reduction concept by means of blade higher harmonic control (HHC) or individual blade control (IBC).

1. The strength of a vortex as it separates from the blade tip is largely a function of the local tip speed and of the blade pitch. There is an optimum blade pitch that results in minimum vortex strength. If this "optimum" blade pitch could be attained just for the brief instant in time when that particular vortex is shed, which, one or two rotor revolutions later, interacts with a blade, then BVI noise should be less. Such, in fact, could be achieved by means of the IBC technique.

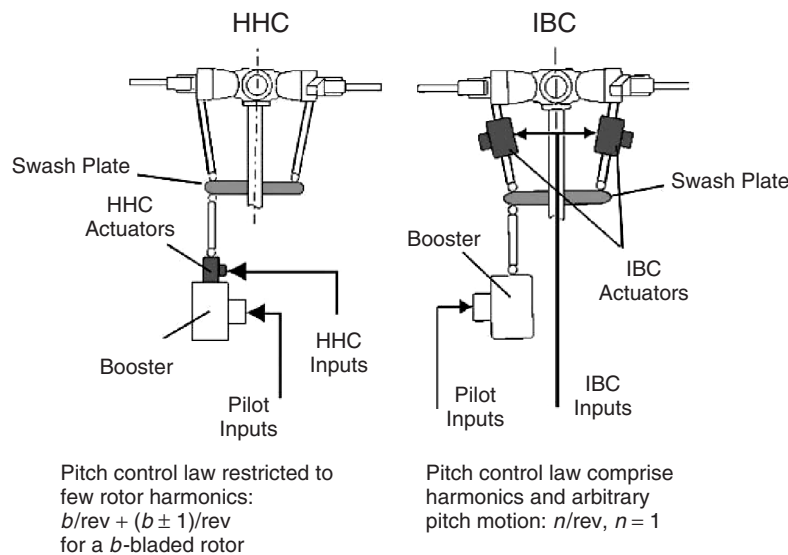
Normally, the blade pitch varies sinusoidally once per revolution (the cyclic pitch change). By means of the IBC technique, an additional

blade pitch variation of whatever waveform can be superimposed, so that the blade pitch, in addition to its sinusoidal cyclic pitch change, would experience changes of the desired kind (Fig. 10). Thus, the blade would locally change its pitch several times during a revolution rather than only once.

2. The very same technique can be utilized to effect the second of the above-cited noise reduction methods. If the blade pitch can be affected in any manner during each rotor revolution, one may also optimize its value for the same purposes during the very blade-vortex interaction process, that is, when the vortex comes into contact with a blade's leading edge, to thus minimize the local airload changes.
3. Finally, it should be possible to optimize the blade pitch during the vortex-shedding process as such so that the vortex, during the interaction process, passes the blade at some distance below or above, and not "square-on."\* Alternatively, it should be possible to slightly change the path of the tip during the encounter such that the blade passes above or below the vortex.

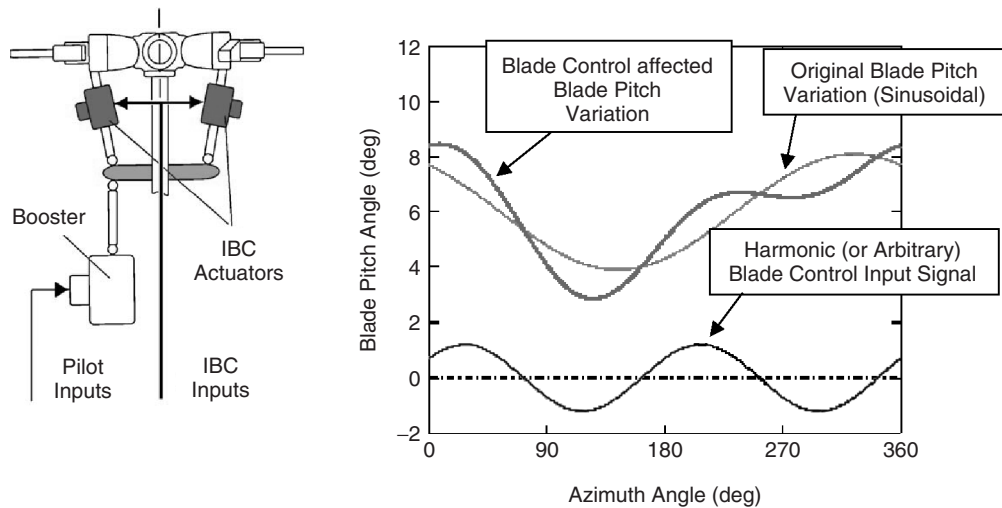
The basics of these blade control techniques have been developed in the German Dutch Wind

\*Actually, this is not quite correct since maximum BVI does not occur when the vortex cuts directly across the blade but at some, albeit very small, distance from it. But in any case, if the miss distance "vortex-to-blade" is made as large as possible, the interaction intensity is much reduced.

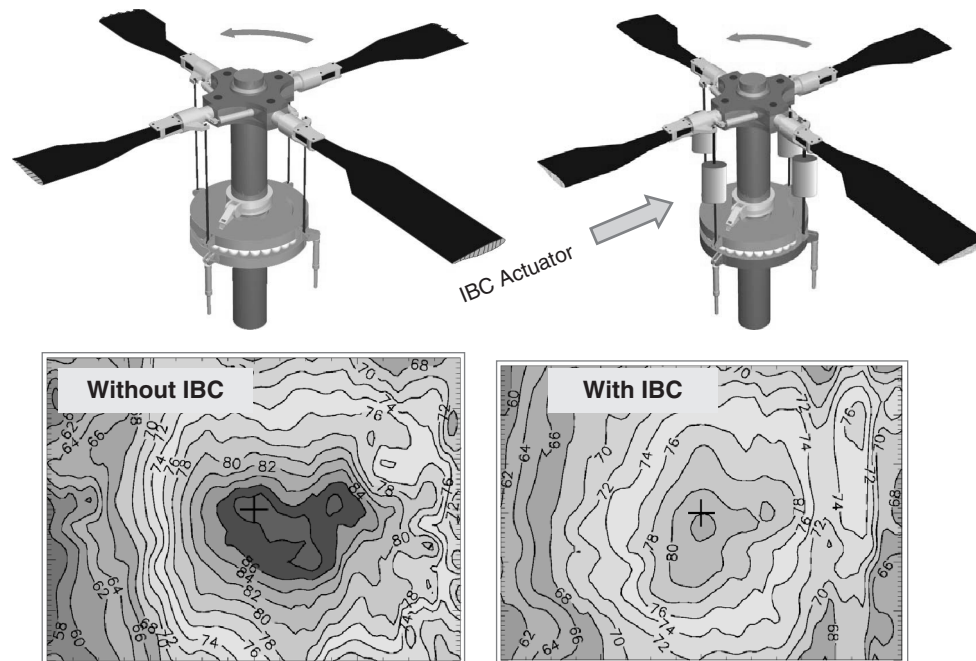


**Figure 9** Active blade root control concepts.





**Figure 10** Blade pitch angle variation during one rotor revolution when affected by an individual/arbitrary blade control input.



**Figure 11** Ground signature noise reduction employing IBC versus baseline case (from flyover noise tests).

Tunnel, DNW, and later validated in flight tests on a real helicopter, a EUROCOPTER BO105, in a cooperative effort. Here, the “flight-worthy” actuators were installed above the swash plate and controlled in such a way as to achieve maximum noise reduction. The tests were successful: compared to the condition without blade control, the very BVI impulsive noise

was reduced by some 6 dB, that is, reduced by 50% (Fig. 11).<sup>41</sup> IBC may also be favorably employed in reducing rotor blade vibrations. BVI noise reduction methods by the HHC technique are discussed in Refs. 42 to 44. A state-of-the-art survey on rotor noise reduction by means of harmonic or individual blade control appears in Ref. 45. BVI noise may, however,

also be passively reduced by means of appropriate shapes of the blade planform.<sup>46,47</sup>

The most beneficial possibility for rotor noise reduction lies in cutting back the rotational speeds and to thus reduce the tip speed, but such a measure has adverse effects on the rotor stability and power, and even on the gears, by requiring a larger torsional momentum and perhaps incurring a weight penalty. However, helicopters featuring variable rotational speeds are being developed for this purpose.

An interesting method to reduce BVI noise has been proposed in Ref. 48. Here it is stated that for a given descent angle the rotor tip path plane angle can be increased through a “negative acceleration” (= deceleration). For a deceleration of 0.1g a significant reduction in BVI noise was observed. This beneficial effect is caused by the blades no longer directly intersecting the vortex trails. Technically, this could be achieved by some sort of an additional drag device during descent. In that case, the tip path plane angle corresponds to one at smaller descent angles without drag device. Hence a “clever” combination of the variables *flight speed*, *descent angle*, *deceleration*, and (perhaps) *added drag* can lead to a significant (BVI) noise reduction.

## 5.2 (Passive) Main Rotor High-Speed Impulsive Noise Reduction

There is no way to actively reduce high-speed impulsive noise. The only route is via optimization of the blades’ geometry and airfoil shape. The point is to try to avoid the appearance of an aerodynamic shock above the surface of the blade tip area.

For one, it would be advantageous to make a blade near the tip as thin as possible. Obviously, there are structural limitations to such an approach, the more promising way being the reduction of the local flow speed into the rotor blade along the outer span. An appropriate backward sweep should have the desired beneficial aerodynamic effect in minimizing the strength of the aerodynamic shock. Now the local inflow velocity component toward the blade’s leading edge is distinctly reduced, thus also reducing the supersonic area on the blade. This way, the occurrence of an aerodynamic shock is largely avoided. Wind tunnel tests have proven this technique, which represents the current state of technology, as many of today’s helicopters feature main rotor airfoil shapes of such kind.

While such a rotor blade planform would be desirable to reduce the noise during high-speed forward flight, it might actually be worse under descent flight conditions when it comes to BVI. Here the alignment of the blade leading edge and the vortex trace, if parallel, would cause maximum BVI impulsive noise. So, the art of a blade designer is to make a blade that (1) fulfills the performance requirements while (2) being quiet under *all* flight conditions, that is, both under conditions of high-speed level flight and of moderate speed-landing approach.

## 5.3 Tail Rotor Noise Reduction

Of the several measures to reduce tail rotor noise, the following will be mentioned: (1) reduction of rotational speed and hence tip speed; (2) utilization of many blades rather than only two, such as on the “fenestron”/“ducted fan” solutions, where the blade passing frequency is increased (this means that the generated sound is attenuated more by distance because of its higher frequency content, although this effect is counteracted by the higher auditory sensitivity of the human ear at frequencies around and above 1 kHz; sometimes uneven blade spacing is used); (3) changing the tail rotor sense of rotation and variation of tail rotor position with respect to the main rotor will eventually change the characteristics of tail rotor and main rotor wake interaction, which may induce some noise reduction; (4) shrouding the tail rotor, which increases its performance and allows lesser rotational speeds, albeit at the cost of additional weight, or even (4) elimination of the tail rotor altogether; the latter has been realized in the medium-weight American helicopter Explorer. The technique is called NOTAR (for “NO TAIL Rotor”). The physics behind the NOTAR approach is based on the Coanda effect/boundary layer control along the length of the tail boom, combined with the use of a direct jet thruster at the end of the tail boom. Unfortunately, this technique can only be used on smaller helicopters, as the weight penalty for such a device providing the required quite substantial amount of tail thrust on even a medium-weight helicopter is prohibitive. The means to reduce helicopter noise by use of a quiet tail rotor are discussed in Ref. 25.

## 6 CURRENT DEVELOPMENTS

New design helicopters, undoubtedly, will feature advanced blade geometries and airfoil characteristic shapes, inherently generating less noise and vibrations. New blade control techniques are developed to minimize noise and vibration, probably not so much by technically elaborate individual blade control techniques, but by employing *local* blade control techniques, where the shape of a blade in the tip area as such is dynamically changed by employing advanced piezoelectric devices embedded in the very blade surface. This would eliminate the need for elaborate and heavy actuators on the hub. Such novel techniques could also avoid early flow separation during high-speed and maneuvering flights, reducing additional power requirements. Ultimately, the entire conventional control system within the rotating system (control at the blade root or on flaps in the outer blade region) might become replaced by such elegant, light, and mechanically much less involved local control systems that act where they are needed, that is, in the outboard regime of the blade.

## REFERENCES

1. T. F. Brooks and T. H. Hodgson, Trailing Edge Noise Prediction Using Measured Surface Pressures, *J. Sound Vib.*, Vol. 78, 1981, pp. 69–117.

2. T. F. Brooks and R. H. Schlinker, Progress in Rotor Broadband Noise Research, *VER-TICA*, Vol. 7, 1983, pp. 287–307.
3. T. F. Brooks, M. A. Marcolini, and D. S. Pope, Main Rotor Broadband Noise Study in the DNW, *J. Am. Helicopter Soc.*, Vol. 34, No. 2, 1989, pp. 3–12.
4. T. F. Brooks, D. S. Pope, and M. A. Marcolini, Airfoil Self Noise Prediction, NASA RP-1218, 1989.
5. S. Wagner, R. Bareiss, and G. Guidati, *Wind Turbine Noise*, Springer, Berlin, Heidelberg, 1996.
6. T. Brooks, Jr., and W. Humphreys, Flap Edge Aeroacoustic Measurements, AIAA/CEAS-2000-1975, 2000.
7. A. Damongeot, F. d'Ambra, and B. Masure, Towards a Better Understanding of Helicopter External Noise, Proc. 39th Annual Forum of the American Helicopter Society, St. Louis, MI, May, 1983, pp. 445–457.
8. R. Janakiram, M. J. Smith, and H. Tadghighi, Importance of Engine Noise as a Source of Helicopter External Noise, AIAA-89-1147, AIAA 12th Aeroacoustics Conference, San Antonio, TX, April, 1989.
9. F. H. Schmitz and D. A. Boxwell, In-flight Farfield Measurement of Helicopter Impulsive Noise, *J. Am. Helicopter Soc.*, Vol. 21, No. 4, 1976, pp. 2–16.
10. M. P. Isom, Acoustic Shock Waves Generated by a Transonic Helicopter Blade, Paper 63, 36th Annual National Forum of the American Helicopter Society, Washington, DC, May 13–14, 1980.
11. D. A. Boxwell, F. H. Schmitz, W. R. Spletstoesser, and K. J. Schultz, Model Helicopter Rotor High Speed Impulsive Noise—Measured Acoustics and Blade Pressures, NASA TM-85850 and USAVRADCOM Technical Report-83-A-14, 1983.
12. F. H. Schmitz and Y. H. Yu, Helicopter Impulsive Noise: Theoretical and Experimental Status, NASA TM-84390, 1983.
13. F. H. Schmitz, D. A. Boxwell, W. R. Spletstoesser, and K. J. Schultz, Model Rotor High Speed Impulsive Noise: Full Scale Comparisons and Parametric Variations, *VERTICA*, Vol. 8, No. 4, 1984, pp. 395–422.
14. J. Prieur, Calculation of Transonic Rotor Noise Using a Frequency Domain Formulation, 43rd AHS Forum Proc., St. Louis, MO, 18–20 May, 1987.
15. K. J. Schultz and W. R. Spletstoesser, Measured and Predicted Impulsive Noise Directivity Characteristics, Paper 1.2, 13th European Rotorcraft Forum, Arles, France, 1987.
16. D. R. Hoad, Helicopter Model Scale Results of Blade/Vortex Interaction Impulsive Noise as Affected by Tip Modifications, Paper 80-62, 36th Annual Forum, American Helicopter Society, Washington, DC, May 13–14, 1980.
17. Y. Nakamura, Prediction of Blade/Vortex Interaction Noise from Measured Blade Pressure, Paper 32, 7th European Rotorcraft and Powered Lift Aircraft Forum, Garmisch-Partenkirchen, 1981.
18. D. A. Boxwell and F. H. Schmitz, Full-Scale Measurements of Blade/Vortex Interaction Noise, *J. Am. Helicopter Soc.*, Vol. 27, 1982; also Preprint 8061, Proceedings 36th Annual Forum, American Helicopter Society, 1980.
19. A. R. George and S. B. Chang, Noise Due to Blade/Vortex Interactions, Paper No A-83-39, Proceedings 39th Annual Forum, American Helicopter Society, St. Louis, MO, 1983.
20. W. R. Spletstoesser, K. J. Schultz, D. A. Boxwell, and F. H. Schmitz, Helicopter Model Rotor-Blade/Vortex Interaction Impulsive Noise: Scalability and Parametric Variations, Paper No 18, 10th European Rotorcraft Forum, The Hague, The Netherlands, 1984, also NASA TM-86007.
21. W. R. Spletstoesser, K. J. Schultz, and R. Martin, Rotor Blade/Vortex Interaction Impulsive Noise Source Identification and Correlation with Rotor Wake Predictions, AIAA-87-2744, AIAA 11th Aeroacoustics Conference, Palo Alto, CA, 1987.
22. D. R. Hoad, Helicopter Blade/Vortex Interaction Location Scale Model Acoustic and Free Wake Analysis Results, NASA TP-2658, 1987.
23. R. M. Martin, W. R. Spletstoesser, J. W. Elliott, and K. K. J. Schultz, Advancing Side Directivity and Retreating Side Interactions of Model Rotor Blade/Vortex Interaction Noise, NASA TP 2784, AVSCOM TR 87-B3, 1998.
24. R. M. Martin, M. A. Marcolini, W. R. Spletstoesser, and K. J. Schultz, Wake Geometry Effects on Rotor Blade/Vortex Interaction Noise Directivity, NASA TP-3015, 1990.
25. J. W. Levertton, Reduction of Helicopter Noise by Use of a Quiet Tail Rotor, Paper No 24, 6th European Rotorcraft Forum, Bristol, UK, September 16–19, 1980.
26. J. Fitzgerald, and F. Kohlhepp, Research Investigation of Helicopter Main Rotor/Tail Rotor Interaction Noise, NASA CR-4143, 1988.
27. R. M. Martin, C. L. Burley, and J. W. Elliott, Acoustic Test of a Model Rotor and Tail Rotor—Results for the Isolated Rotors and Combined Configuration, NASA TM-101550, 1989.
28. J. E. Ffowcs Williams and D. L. Hawkings, Sound Generated by Turbulence and Surfaces in Arbitrary Motion, *Phil. Trans. Roy. Soc.*, Ser. A., Vol. 264, No. 1151, May 1969, pp. 321–342.
29. F. Farassat, Theory of Noise Generation from Moving Bodies with an Application to Helicopter Rotors, NASA TR R-451, December 1975.
30. M. J. Lighthill, On Sound Generated Aerodynamically, *Phil. Trans. Roy. Soc.*, Vol. 211, No. 1107, 1952, pp. 564–587.
31. B. Van der Wall, An Analytical Model of Unsteady Profile Aerodynamics and Its Application to a Rotor Simulation Program, 16th European Rotorcraft Forum, Amsterdam, Netherlands, September, 1989.
32. J. A. Lieser, D. Lohmann, and K. J. Schultz, Prediction of Rotor Aeroacoustics in Forward Flight by a Lifting Surface Method, 50th AHS Annual Forum Proc., Vol. 1, Washington, DC, May, 1993.
33. S. R. Ahmed and V. Vidjaja, Unsteady Panel Method Calculation of Pressure Distribution on BO 105 Model Rotor Blades and Validation with DNW Test Data, 50th AHS Annual Forum Proc., Vol. 2, Washington DC, May, 1993.
34. J. Yin and S. Ahmed, Helicopter Main-Rotor/Tail-Rotor Interaction, *J. Am. Helicopter soc.*, Vol. 45, No. 4, October, 2000, pp. 293–302.
35. K. Pahlke and J. Raddatz, 3D Euler Methods for Multibladed Rotors in Hover and Forward Flight, Paper No. C20, 19th European Rotorcraft Forum, Cernobbio, Italy, September, 1993.
36. Y. H. Yu, F. X. Caradonna, and F. H. Schmitz, The Influence of the Transonic Flow Field on High Speed Helicopter Impulsive Noise, Paper No. 58, 4th European Rotorcraft and Powered Lift Aircraft Forum, Stresa, Italy, September, 1978.

37. J. D. Baeder, Euler Solutions to Non-linear Acoustics of Non-lifting Hovering Rotor Blades, 16th European Rotorcraft Forum, Glasgow, September, 1990.
38. A. S. Lyrintzis, Review: The Use of Kirchhoff's Method in Computational Aeroacoustics, *J. Fluids Eng.*, Vol. 116, No. 4, 1994, pp. 665–676.
39. Di Francescantonio, A New Boundary Integral Formulation for the Prediction of Sound Radiation, *J. Sound and Vib.*, Vol. 202, No. 4, 1997, pp. 491–509.
40. K. S. Brentner and F. Farassat, An Analytical Comparison of the Acoustic Analogy and Kirchhoff Formulation for Moving Surfaces, *AIAA J.*, Vol. 36, No. 8, 1998, pp. 1379–1386.
41. W. R. Splettstoesser, K. J. Schultz, B. van der Wall, H. Buchholz, W. Gemblar, and G. Niesl, The Effect of Individual Blade Pitch Control on BVI Noise—Comparison of Flight Test and Simulation Results, Proceedings AC07, 24th European Rotorcraft Forum, Marseilles, France, 1998.
42. T. F. Brooks and E. R. Booth, The Effects of Higher Harmonic Control on Blade-Vortex Inter-Action Noise and Vibration, *J. Am. Helicopter Soc.*, Vol. 38, No. 3, 1993, pp. 45–55.
43. W. R. Splettstoesser, K. J. Schultz, R. Kube, T. F. Brooks, E. R. Booth, G. Niesl, and O. Streby, A Higher Harmonic Control Test in the DNW to Reduce Impulsive BVI Noise, *J. Am. Helicopter Soc.*, Vol. 39, No. 4, 1994, pp. 3–13.
44. W. R. Splettstoesser, R. Kube, W. Wagner, U. Seelhorst, A. Boutier, F. Micheli, E. Mercker, and K. Pengel, Key Results from a Higher Harmonic Control Aeroacoustic Rotor Test (HART), *J. Am. Helicopter Soc.*, Vol. 42, No. 1, 1997, pp. 58–78.
45. Y. H. Yu, B. Gmelin, W. R. Splettstoesser, J. J. Philippe, J. Prieur, and T. F. Brooks, Reduction of Helicopter Blade-Vortex Interaction Noise by Active Rotor Control Technology, *Prog. Aerospace Sci.*, Vol. 33, 1997.
46. T. F. Brooks, Studies of Blade-Vortex Interaction Noise Reduction by Rotor Blade Modification, Proceedings Noise-Con 93, Noise Control in Aeroacoustics, Williamsburg, VA, 1993.
47. J. Prieur and W. R. Splettstoesser, ERATO—An ONERA-DLR Cooperative Programme on Aeroacoustic Rotor Optimization, Proceedings, 25th European Rotorcraft Forum, Rome, Italy, 1999.
48. G. Gopalan, F. H. Schmitz, and B. W. C. Sim, Flight Path Management and Control Methodology to Reduce Helicopter Blade-Vortex (BVI) Noise, AHS Vertical Lift Aircraft Design Conference, San Francisco, CA, 2000.

# CHAPTER 92

## BRAKE NOISE PREDICTION AND CONTROL

**Michael. J. Brennan**  
Institute of Sound and Vibration Research  
University of Southampton  
Southampton, United Kingdom

**Kihong Shin**  
School of Mechanical Engineering  
Aandong National University  
Aandong, South Korea

### 1 INTRODUCTION

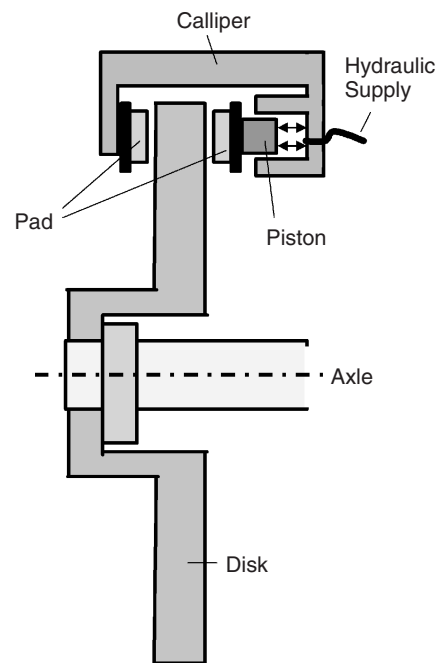
Brake noise remains a concern throughout the automotive industry despite efforts over a number of decades to reduce its occurrence. The earliest work was on drum brakes but, as disk brakes gradually came into widespread use on cars and trucks, the focus of research shifted to these, as they have a much greater propensity to generate noise. The focus of many recent studies is on disk brake noise, the way in which a disk brake system generates noise, and current methods to reduce the noise. Comprehensive treatments of the subject are available in the literature.

### 2 BRAKE NOISE – A FUGITIVE PROBLEM

Problems with brake noise were reported as long ago as the 1930s. Since then much research work has been conducted; the reader is referred to reviews by Crolla and Lang,<sup>1</sup> Ionnidis et al.,<sup>2</sup> and Kinkaid et al.<sup>3</sup> to gain an overview of the development of knowledge in this area.

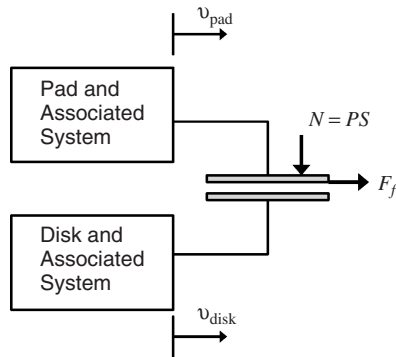
A schematic of a disk brake is shown in Fig. 1. The disk is bolted to the wheel and axle and thus rotates at the same speed as the wheel. The calliper does not rotate and is fixed to the vehicle. Hydraulic oil pressure forces the brake pads onto the disk, thus applying braking forces that reduce the speed of the vehicle.

From the dynamics point of view, a braking system can be represented schematically as shown in Fig. 2, which depicts two dynamic systems connected by a friction interface. The normal force  $N$  is a result of the hydraulic pressure  $P$  and is related to the friction force  $F_f$ . It is the combination of the friction interface and the dynamic systems that makes the understanding and elimination of brake noise so difficult. As described in the next section, brake noise usually involves a dynamic instability of the braking system. Of course, brake systems are not manufactured to be unstable (as they would never sell) but many of them are conditionally stable systems that drift in and out of instability depending on operating conditions. A diagram depicting this situation is shown in Fig. 3.<sup>4</sup> Because of this, brake noise has been described as being fugitive. Three overlapping “stability” parameters of friction, pressure,



**Figure 1** Schematic of a disk brake showing the disk, brake pads, and calliper. This type of brake has a floating calliper.

and temperature are depicted (although there could be more, such as humidity). Within the area, marked “unstable,” changes to the parameters have little or no effect, and the brake has a high propensity to generate noise. Within the “conditionally stable” areas the brake would generally be quiet unless the operating conditions caused the system to move into the unstable area. Such conditions may be excessive cold or heat and a consequential change in the characteristics of the friction material. The stable area may be regarded as a well-designed brake, where the system may only move into the unstable region if there are dramatic changes in the system parameters.



**Figure 2** Schematic showing a disk brake as two dynamic systems connected by a sliding interface of area  $S$ . The normal force  $N$  is a result of the pressure  $P$  and is related to the friction force  $F_f$ .

### 3 BRAKE NOISE CLASSIFICATION

Noise, vibration, and harshness (NVH) engineers classify brake noise and vibration using a variety of different words, such as *judder*, *groan*, *moan*, *hum*, *howl*, *squeal*, *squeak*, *sqelch*, *wire brush*, although none of these terms has a strict definition. In this chapter the types of vibrations/noise are grouped into three categories, which are chosen for distinct physical reasons.

**Judder (around 10 Hz or Less)** Judder occurs at the frequency of wheel rotation or a multiple of it. It is a *forced* vibration caused by non-uniformity of the disk and is generally felt rather than heard. There are two types of judder: cold and hot judder. Cold judder is commonly caused by the brake pad rubbing on the disk during periods when the brakes are not applied. Hot judder is associated with braking at high speeds or excessive braking when large amounts of heat can

be generated causing transient thermal deformations of the disk.

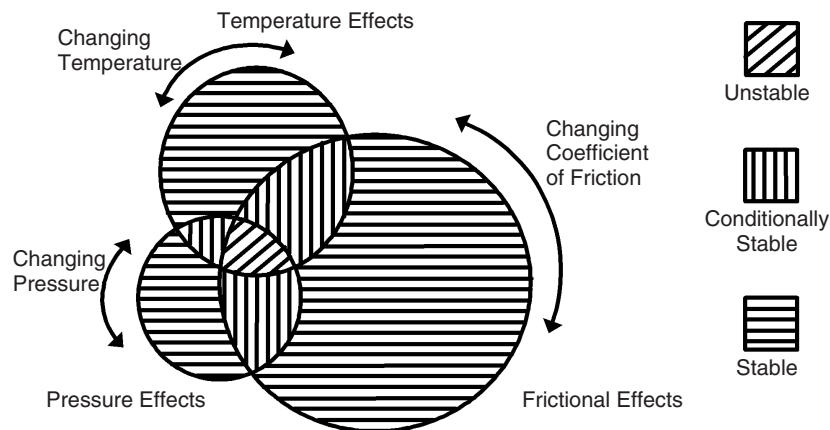
**Groan (around 100 Hz)** Groan occurs at low speeds and is the first of the unstable brake vibrations. It is particularly noticeable in heavy goods vehicles coming to a stop and in automatic cars edging forward in a queue of traffic. It is thought to be caused by stick-slip behavior of the brake pads at the disk surface and the velocity dependence of the friction coefficient. The velocity dependence is because the dynamic coefficient of friction is lower than the static coefficient of friction.

**Squeal (>1 kHz)** Brake squeal is an unstable vibration caused by a geometric instability rather than a negative coefficient of friction–velocity slope. It is split into two categories; low frequency squeal (1 to 4 kHz), where the length of a brake pad is less than the length of the diametrical nodal spacing in the disk, and high-frequency squeal (>4 kHz), where the length of a brake pad is greater than the diametrical nodal spacing in the disk. A hologram taken by Fieldhouse,<sup>5</sup> depicting the vibration of a squealing disk brake is shown in Fig. 4. The disk is rotating at 10 revolutions/minute (rpm), the squeal frequency is 10.75 kHz, and the nodal diameters are rotating about the center of the rotor at about 1344 Hz.

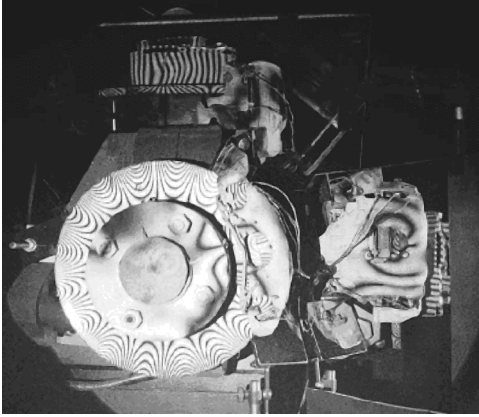
### 4 MECHANISMS OF NOISE GENERATION

Of the three categories of brake noise/vibration, judder is a forced vibration, and groan and squeal are unstable (self-excited) vibrations. Den Hartog<sup>6</sup> distinguishes between forced and self-excited vibration as follows:

*In a self-excited vibration the alternating force that sustains the motion is created or controlled by the motion itself; when the motion stops the alternating force disappears.*



**Figure 3** Diagram showing the way in which frictional, pressure, and temperature effects affect the stability of a disk brake system.



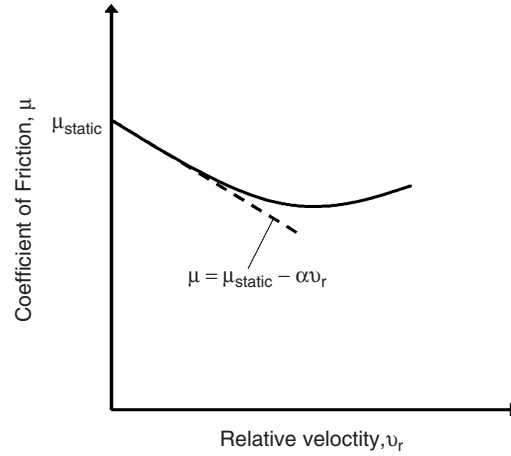
**Figure 4** Vibration of a squealing brake.<sup>4</sup> The disk is rotating at 10 rpm, the squeal frequency is 10.75 kHz, and the nodal diameters are rotating about the center of the rotor at about 1344 Hz.

*In a forced vibration the sustaining alternating force exists independently of the motion and persists even when the vibratory motion is stopped.*

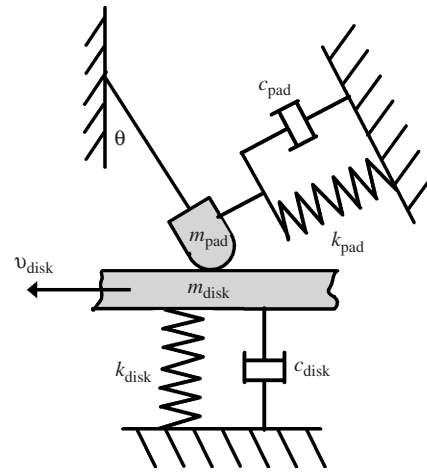
Several mechanisms that cause dynamic instabilities in braking systems have been suggested and are described below.

**Negative Friction–Velocity Slope** This characteristic is illustrated in Fig. 5. At low speeds the dynamic coefficient of friction  $\mu$  is related to the static coefficient of friction  $\mu_{\text{static}}$  by  $\mu = \mu_{\text{static}} - \alpha v_r$ , where  $\alpha$  is the gradient and  $v_r$  is the relative velocity between the pad and the disk. As mentioned above, this is thought to be the mechanism responsible for groan. In general, a viscous damping force is proportional to velocity. In a braking system with a low disk velocity, the action of the sliding interface is to act as a negative damper because the slope of the force–velocity graph is negative. Once the negative damping caused by the sliding interface exceeds the damping in either the brake or the pad system, self-excited vibration ensues, generating a noise.<sup>7</sup> The amplitude of vibration is determined by the nonlinearities in the system such as a positive force velocity slope at high velocities, as shown in Fig. 5. To determine the amplitude of vibration of an unstable system, a full nonlinear analysis needs to be conducted. Because this is computationally expensive, it is rarely done in practice.

**Sprag-Slip** This mechanism for brake squeal was first proposed by Spurr<sup>8</sup> and developed by Jarvis and Mills.<sup>9</sup> They showed that it is possible for unstable vibrations to occur even when the coefficient of friction is independent of relative velocity between the pad and the disk. A simple illustrative model of a brake-disk system that behaves in this way is shown in Fig. 6. In this example, vibrations occur due to the constrained



**Figure 5** Graph showing the relationship between the dynamic coefficient of friction and the relative velocity between the disk and a pad.



**Figure 6** Simple two-degrees-of-freedom model illustrating sprag-slip behavior.

interaction of the degrees of freedom in the system. If the sliding components are oriented with respect to each other such that the normal force increases as the components slide over each other, then an unstable vibration occurs. This is because an increase in the normal force causes the disk to move laterally, which results in a sudden reduction in normal force; the normal force then increases as before due to the sliding action and the cycle repeats, leading to a sprag-slip limit cycle. For the system shown in Fig. 6, the system is stable provided that  $\frac{1}{2}(\mu - \tan \theta) \sin 2\theta < c_{\text{pad}}/c_{\text{disk}}$ . In a disk brake system, the contact point between the piston and the brake pad backing plate changes slightly because of wear, dirt, thermal deformation, and the



like, which may help to explain the intermittent nature of brake squeal.

**Flutter** Flutter is an unstable vibration that results from an interaction between modes of vibration. This type of instability is possible even when the coefficient of friction is constant. North<sup>10</sup> was the first person to consider this mechanism as a cause of brake squeal.

The equation of motion of a brake system may be written as:

$$\mathbf{M}\ddot{\mathbf{x}} + \mathbf{C}\dot{\mathbf{x}} + \mathbf{K}\mathbf{x} = \mathbf{0} \quad (1)$$

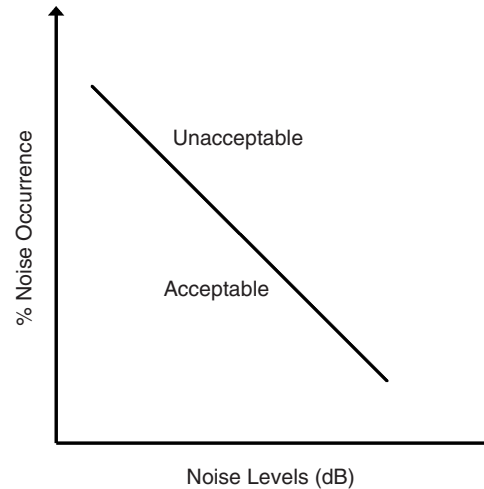
where  $\mathbf{M}$ ,  $\mathbf{C}$ , and  $\mathbf{K}$  are the mass, damping, and stiffness matrices of the brake system, respectively, and  $\ddot{\mathbf{x}}$ ,  $\dot{\mathbf{x}}$ , and  $\mathbf{x}$  are the acceleration, velocity, and displacement vectors, respectively. The stiffness matrix  $\mathbf{K}$  is given by

$$\mathbf{K} = \hat{\mathbf{K}} + \mathbf{K}_{\text{friction}} \quad (2)$$

where  $\hat{\mathbf{K}}$  is the system stiffness matrix, and  $\mathbf{K}_{\text{friction}}$  is the friction stiffness matrix that couples the normal and the tangential forces in the sliding interface and is *asymmetric*. This means that  $\mathbf{K}$  is not symmetric. The lack of symmetry in the stiffness matrix causes one or several modes of vibration to become unstable, which means that these modes have a negative damping ratio. Brake designers can currently check this out using finite element methods to model a brake system. An eigenvalue analysis of a model of a brake system can then be conducted and the real parts of the eigenvalues examined; if some of them are positive, then the system is potentially unstable at the natural frequencies associated with these eigenvalues. Ouyang<sup>11</sup> has also shown that in certain situations it is necessary to consider moving, rather than stationary, loads when conducting stability analysis.

## 5 METHODS TO ELIMINATE BRAKE NOISE

It is not possible for engineers to design a guaranteed noise-free brake using current knowledge and state-of-the-art techniques, although finite element analysis is frequently used to design braking systems, for example.<sup>12,13</sup> Consequently, brake systems undergo extensive testing to minimize the risk that they will be noisy when installed in a vehicle. Typically, braking systems will be installed in a special test rig so that they can be tested at a variety of different speeds, different hydraulic pressures, different directions of rotation, and so forth. All of these data are recorded along with temperature and noise generated by the brake. The data is then processed and plotted on a graph similar to that shown in Fig. 7, in which the percent occurrence of noise is plotted against the noise level in decibels. The noise level, and the duration of the noise that can be tolerated by drivers, can be estimated, so that a line can be drawn on the graph separating it into two regions: acceptable and unacceptable. Provided that no data point from the test



**Figure 7** Diagram showing the way in which data from a brake test would be plotted. If any data from the test is in the unacceptable region of the graph, then the brake system would fail the noise test.

is in the unacceptable region, then the brake is deemed to be acceptable from the point of view of noise.

Discussion of specific methods to eliminate brake noise follows.

**Judder** To eliminate judder, designers should ensure that (i) the off-brake running clearance between the disk and the pad is sufficient, by careful attention to the detailed design and tolerances, and (ii) there is careful attention paid to the thermal characteristics of the system.

**Groan** The approach to this problem is tackled in three ways. The first is to change the characteristics of the friction interface by changing the brake pad material. The second is to change the dynamic characteristics of the system by adjusting the modal properties of the system,<sup>14</sup> such that the natural frequencies of the dynamic systems on either side of the sliding interface are not in close proximity. The third method is to apply damping materials to the pad, such as shims or “insulators,”<sup>15</sup> or antiseize grease. These add viscoelastic damping to the system such that the inherent damping in the system is greater than the negative friction-induced damping and thus the brake system remains stable. It is possible, however, that in some circumstances this can make the situation worse rather than better.<sup>7</sup>

**Squeal** Brake squeal is perhaps the most annoying of all brake noise and is probably the most difficult noise problem to solve. The methods used to reduce groan are also used to reduce squeal. Additionally the disk may be smoothed using sandpaper, the pads may be chamfered at the edges and/or have slits machined in them. The center of pressure between the pistons and

the pad backing plate can also be adjusted by the use of shims. Brooks et al.<sup>16</sup> suggest that moving the center of pressure toward the leading edge of the brake pad can have a beneficial effect, reducing the propensity of a brake to squeal. It has also been shown by Baba et al.<sup>17</sup> that there is some benefit if the part of the disk that is attached to the wheel has variable wall thickness to disrupt the rotational symmetry.

## 6 SUMMARY

This chapter has described the various types of noise generated by a brake system. The fugitive nature of the problem has been highlighted, and the various mechanisms that cause brake noise have been discussed. Because of the difficulty in predicting brake noise, an experimental method used to test a brake system's propensity to generate noise has been described and the current "fixes" to brake noise problems have briefly been mentioned.

**Acknowledgment** The authors gratefully acknowledge the provision of Fig. 4. by Dr John Fieldhouse, the University of Huddersfield.

## REFERENCES

1. D. A. Crolla and A. M. Lang, Brake Noise and Vibration—The State of the Art, in *Vehicle Tribology*, Vol. 18, D. Dowson, C. M. Taylor, and M. Godet, Eds., in Tribology Series, Leeds, England, 1991, pp. 165–174.
2. P. Ioannidis, P. C. Brooks, D. C. Barton, and M. Nishiwaki, *Brake System Noise and Vibration—A Review*, Braking 2002, Professional Engineering Publications, Bury St. Edmunds, England, 2002, pp. 53–73.
3. N. M. Kinkaid, O. M. O'Reilly, and P. Papadopoulos, Review: Automotive Disc Brake Squeal, *J. Sound Vib.*, Vol. 267, 2003, pp. 105–166.
4. J. D. Fieldhouse and T. P. Newcomb, An Experimental Investigation into Disc Brake Noise, Institution of Mechanical Engineers paper C444/036, London, 1993.
5. J. D. Fieldhouse, private communication, 2004.
6. J. P. Den Hartog, *Mechanical Vibrations*, Dover, New York, 1984.
7. K. Shin, M. J. Brennan, J. E. Oh, and C. J. Harris, Analysis of Disc Brake Noise Using a Two-Degree-of-Freedom Model, *J. Sound Vib.*, Vol. 254, No. 5, 2002, pp. 837–848.
8. R. T. Spurr, A Theory of Brake Squeal, *Proc. Inst. Mech. Eng., Automotive Div.*, No. 1, 1961/62, pp. 33–52.
9. R. P. Jarvis and B. Mills, Vibrations Induced by Dry Friction, *Proc. Inst. Mech. Eng.*, Vol. 178, Pt. 1, No. 32, 1963/64, pp. 847–857.
10. M. R. North, Disc Brake Squeal, in *Braking of Automobile Vehicles*, Automotive Division of the Institution of Mechanical Engineers, Mechanical Engineering Publications, London, 1976, pp. 169–176.
11. H. Ouyang, Moving Loads and Car Disc Brake Squeal, *Noise Vib. Worldwide*, December 2003, pp. 7–15.
12. W. Nack, Brake Squeal Analysis by Finite Elements, SAE Paper, 199-01-1736, Society of Automotive Engineers, Warrendale, PA, 1999.
13. P. Blaschke, M. Tan, and A. Wang, On the Analysis of Brake Squeal Propensity Using Finite Element Method, SAE Paper, 200-01-2765, Society of Automotive Engineers, Warrendale, PA, 2000.
14. K. Brent Dunlap, M. A. Riehle, and R. E. Longhouse, An Investigative Overview of Automotive Disc Brake Noise, SAE Paper, 1999-01-0142, Society of Automotive Engineers, Warrendale, PA, 1999.
15. R. Singh, A. A. Sheikh, and M. J. Mitchell, Viscoelastic Damping to Control Disc Brake Squeal, *Sound Vib.*, October 1998, pp. 18–22.
16. P. C. Brooks, D. A. Crolla, A. M. Lang, and D. R. Shafer, Eigenvalue Sensitivity Analysis Applied to Disc Brake Squeal, in *Braking of Road Vehicles*, Institution of Mechanical Engineers, Mechanical Engineering Publications, Bury St. Edmunds, England, 1993, pp. 135–143.
17. H. Baba, T. Wada, and T. Takagi, Study on Reduction of Brake Squeal Caused by In-plane Vibration of Rotor, SAE Paper, 2001-01-3158, Society of Automotive Engineers, Warrendale, PA, 2001.

# CHAPTER 93

## WHEEL–RAIL INTERACTION NOISE PREDICTION AND ITS CONTROL

David J. Thompson

Institute of Sound and Vibration Research  
University of Southampton  
Southampton, United Kingdom

### 1 INTRODUCTION

Noise produced by wheel–rail interaction is a major concern in railway operations. Prediction methods for this noise using engineering models are available. A distinction must be made between (1) rolling noise, which is caused by small-scale vertical profile irregularities (roughness) of wheel and rail, (2) impact noise caused by discrete discontinuities of the profile such as wheel flats, rail joints, or welds, and (3) squeal noise occurring in curves. In each case, the noise is produced by vibrations of the wheels and track. The role of the dynamic properties of the wheel and track, along with the factors that affect sound radiation, needs to be considered. Control measures for rolling noise can be sought in reduced surface roughness, wheel shape optimization and added damping, rail support stiffness, or local shielding. The use of track-side noise barriers, which are becoming common for railways, is discussed in Chapter 58. For squeal noise, mitigation measures include friction control by lubrication or friction modifiers.

### 2 ROLLING NOISE

#### 2.1 Overview of Rolling Noise

A train running on straight unjointed track produces rolling noise.<sup>1</sup> This is a broadband, random noise radiated by wheel and track vibration over the range of at least 100 to 5000 Hz. Its overall sound pressure level increases at a rate of roughly  $30 \log_{10}(V)$  where  $V$  is the train speed.

Rolling noise is induced by small vertical profile irregularities of the wheel and rail running surfaces. This is often referred to as roughness, although the wavelength range is between about 5 and 250 mm,

which is longer than the range normally considered for microroughness. The corresponding amplitudes are much less than a micron at short wavelengths, increasing to tens of microns at longer wavelengths. Wheel and rail roughness may be considered incoherent and their spectra simply added.<sup>2</sup>

In Fig. 1 a flowchart is given of the mechanisms involved in the excitation of rolling noise. This is the basis of theoretical models.<sup>3–5</sup> The roughness causes a relative displacement between the wheel and rail.<sup>6</sup> Depending on their respective point mobilities,  $Y_w$  and  $Y_r$ , the wheel and rail are caused to vibrate. Local elasticity between them results in a third mobility,  $Y_c$ , corresponding to the contact spring. The vibration velocity amplitude of the wheel and rail,  $v_w$  and  $v_r$ , at frequency  $\omega = 2\pi f$  due to a roughness amplitude  $r$  is given by

$$v_w = \frac{-i\omega r Y_w}{Y_r + Y_w + Y_c} \quad (1)$$

$$v_r = \frac{i\omega r Y_r}{Y_r + Y_w + Y_c} \quad (2)$$

where roughness of wavelength  $\lambda$  excites frequencies

$$f = V/\lambda \quad (3)$$

where  $V$  is the train speed. In practice, coupling is present in other coordinate directions as well as vertical, leading to more complex matrix equations,<sup>6</sup> but the excitation remains vertical roughness. Typical vertical mobilities of the wheel, track, and contact

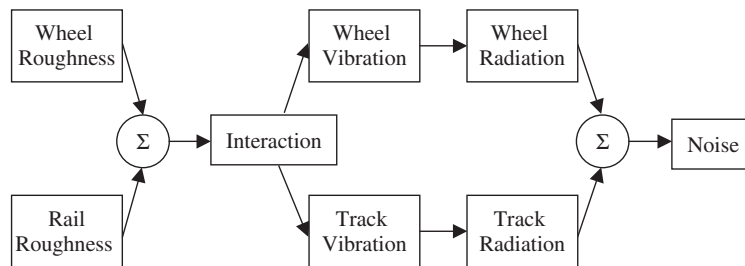
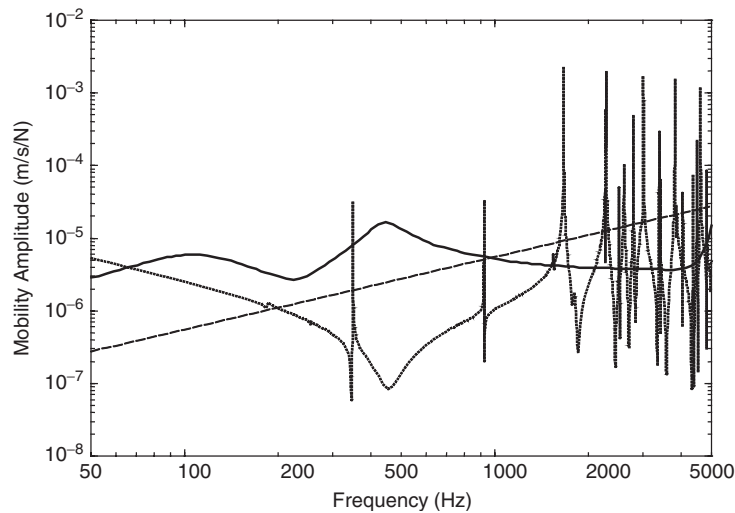


Figure 1 Schematic flowchart of the wheel–rail rolling noise model.



**Figure 2** Typical mobilities at the wheel-rail contact in the vertical direction. . . . ., wheel; —, track; — —, contact spring.

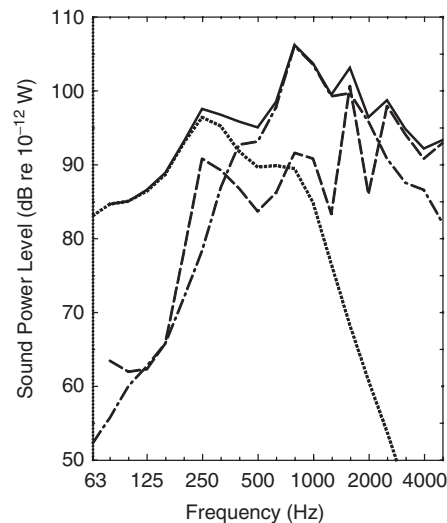
spring are shown in Fig. 2. From this it can be seen that the track has the highest mobility for frequencies between about 100 and 1000 Hz. At these frequencies the rail vibration at the contact point is approximately equal to the amplitude of the roughness; see Eq. (2).

Figure 3 shows typical predicted contributions to rolling noise of the vibrations of the wheels, rails, and sleepers (cross ties). In the present example the wheel and track have similar contributions to the overall noise, with the track contributing slightly more than the wheel.

If the roughness or train speed changes, the levels of all components in a given frequency band increase at the same rate, so that the relative importance of each component in a given band remains the same. However, as train speed increases, the relative importance of higher frequencies increases, so that the balance of wheel and track in the overall noise level changes.

## 2.2 Roughness and Contact Filtering

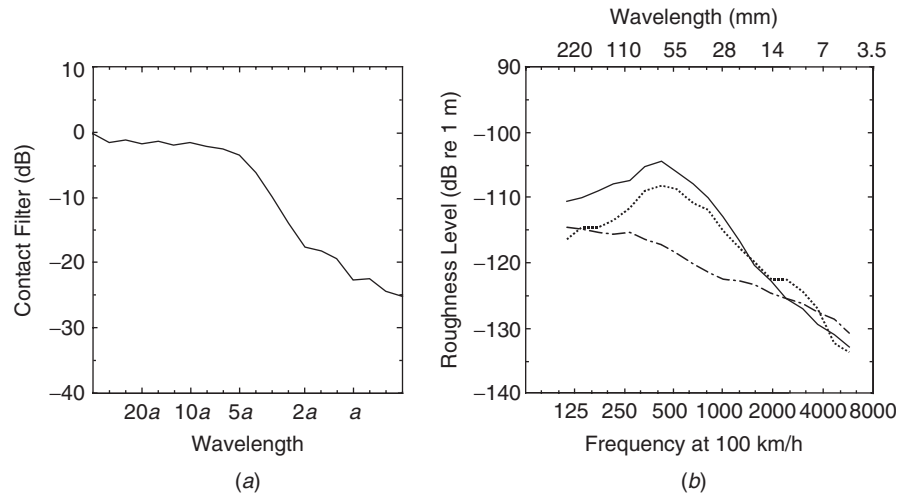
The wheel-rail contact exists over an area approximately 10 to 15 mm in length and width. These dimensions depend weakly on the wheel diameter and load.<sup>7</sup> Wavelengths that are similar to, or short in comparison with this, are attenuated in their excitation of the wheel-rail system. This is expressed as a filter effect,<sup>8,9</sup> as shown in Fig. 4a. Typical roughness spectra are shown in Fig. 4b. These can be seen to fall in amplitude toward shorter wavelengths (higher frequencies). To use these spectra for other speeds, the one-third octave band spectra can be simply shifted to the right or left according to Eq. (3). As speed increases and the spectrum is shifted to the right, the excitation at high frequencies increases more than that at low frequencies, leading to changes in the balance of wheel and track components of the sound radiation.



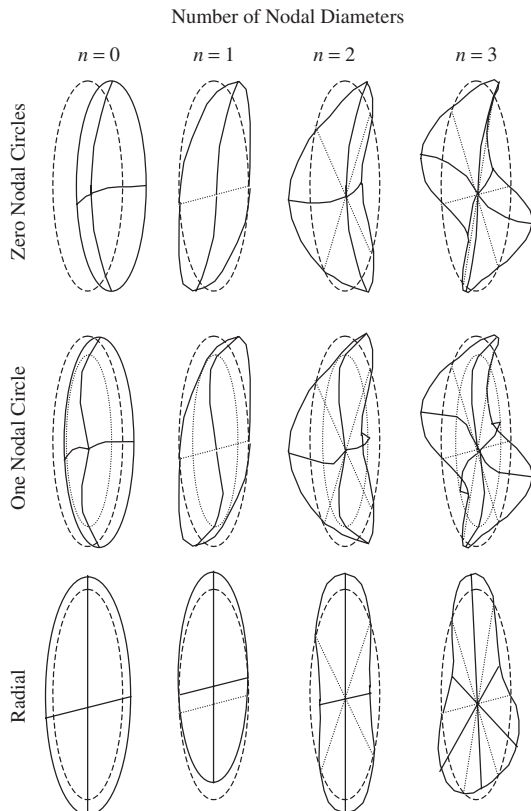
**Figure 3** Typical predicted contributions in one-third octave bands from the wheel, rail, and sleepers to the wheel-rail rolling sound power level from the passage of a single wheel along the track at 100 km/h. —, total (overall A-weighted level 110.9 dB); — —, wheel (overall A-weighted level 105.2 dB); . . . . ., sleepers (overall A-weighted level 96.1 dB); — · —, rail (overall A-weighted level 109.4 dB).

## 2.3 Wheel Modes

A railway wheel is a lightly damped resonant structure, and it is therefore instructive to consider its modes of vibration.<sup>10</sup> Some of the modes of a wheel are shown schematically in Fig. 5. Each mode can be



**Figure 4** (a) Typical contact filter effect. The roughness wavelength is normalized to the contact patch semiaxis length, *a*. (b) Typical one-third octave wheel roughness spectra: —, disk brakes with supplementary cast-iron block brakes; — — —, cast-iron block tread brakes; — · — ·, disk brakes.



**Figure 5** Schematic view of modes of vibration of a railway wheel (isometric view): —, deformed shape; — — —, undeformed shape; . . . . ., node lines.

characterized by the number of nodal diameters and nodal circles. Typically, the axial modes with no nodal circles occur from around 200 Hz upward, whereas those with one nodal circle occur above about 1.5 kHz. Radial modes also occur above about 2 kHz.

Since rolling noise is excited by vertical roughness, modes with a large radial component are of greatest importance. These are the one-nodal-circle and radial modes. The one-nodal-circle modes contain significant radial motion due to coupling as a result of the asymmetry of the wheel cross section. Similarly, the radial modes contain considerable axial motion. Modes with zero or one nodal diameters experience considerable coupling with the motion of the axle and are consequently more heavily damped than modes with two or more nodal diameters.

The modes of importance in rolling noise, the radial and one-nodal-circle modes with two or more nodal diameters, usually occur at frequencies above 1.5 kHz and correspond to the part of the frequency range in which the wheel component of noise is greatest, as seen in Fig. 3. They can be seen as the sharp peaks in the point mobility shown in Fig. 2.

## 2.4 Track Vibration and Decay Rates

A railway track is effectively an infinite waveguide, and therefore its vibration is characterized not by natural modes but by propagating waves.<sup>11,12</sup> The frequency response of the track is seen from Fig. 2 to be much flatter than that of the wheel. At low frequencies, the support structure, consisting of ballast, sleepers, and usually a resilient rail pad beneath the rail, prevents the propagation of waves. In this frequency region the sleepers are strongly coupled to the rails. Above a few hundred hertz, free waves propagate in the rails as bending or torsional waves.

Above about 1 kHz, cross-sectional deformation of the rail occurs and additional wave types occur as a result.

The periodic, or quasi-periodic, support of the rails at the sleepers is only significant at frequencies where the rail half-wavelengths are an integer fraction of the sleeper spacing, the so-called pinned-pinned frequencies. Here standing-wave patterns are formed with nodes at the sleepers. The most important such frequency is at about 1 kHz in the vertical direction for a sleeper spacing of 0.6 m. These are not included in the curve in Fig. 2, which represents a continuously supported rail. Their influence is greater for stiff pads than for soft pads and is much smaller for lateral vibration than for the vertical direction. The pinned-pinned behavior does not have a large influence on the noise radiation except through its effect on roughness growth.

The rail vibration determined by Eq. (1) corresponds to the contact point. As waves are transmitted along the rail, a large section of rail can vibrate due to the excitation of each wheel. This is limited by the damping of the track, measured in terms of the decay rate with distance, as discussed further in Section 3.5.

## 2.5 Sound Radiation

The sound radiation from the wheel and rail can be determined in terms of sound power  $W$  simply by using the standard expression

$$W = \rho c S \sigma \langle v^2 \rangle \quad (4)$$

where  $\rho c$  is the acoustic impedance of air,  $S$  is the surface area of the radiating body (both sides), and  $\langle v^2 \rangle$  is the spatially averaged mean-square normal velocity. For the rail  $W$  represents the power per unit length and  $S$  the perimeter length. The parameter  $\sigma$  is the radiation efficiency (or ratio) and can be evaluated by analytical or numerical models. At high frequency  $\sigma \rightarrow 1$ , whereas at low frequency it is considerably less than 1 depending on the dimensions of the wheel

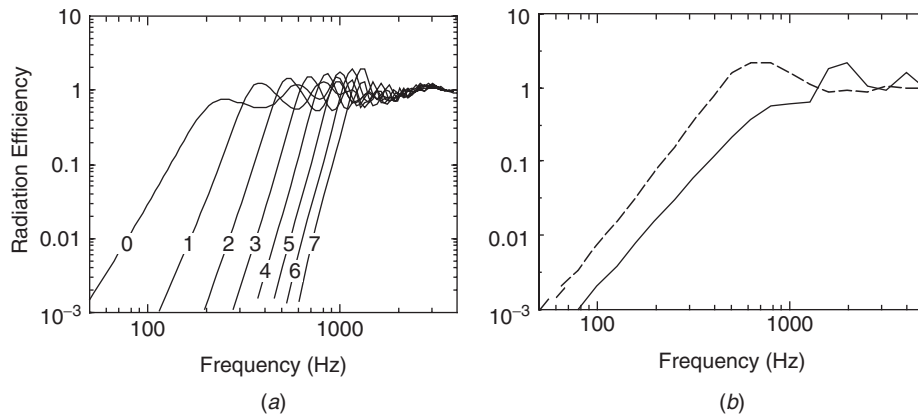
or rail and the mode shape. Figure 6 shows radiation efficiencies of a wheel in various modes of vibration<sup>13</sup> and of a rail vibrating vertically or laterally.<sup>14</sup> This infinite (two-dimensional) model of rail radiation gives good results at frequencies above about 250 Hz, but at low frequencies the decay of vibration along the length of the rail is quite rapid and the source becomes more like a point source. Corrections to the calculation using the two-dimensional model can be applied for this.<sup>14</sup> The directivity of sound radiation from wheels and rails is not particularly strong and can be approximated by simple monopole or dipole directivities, particularly if only the average sound pressure during the passage of a train is required.

## 2.6 Measurement Methods for Railway Noise

The international measurement standard for exterior noise from trains<sup>15</sup> has long been considered to provide inadequate control of the measurement situation. It prescribes a measurement position at 25 m from the track and 3.5 m above rail head level. Its greatest inadequacy lies in the potentially quite large variability that can arise due to the surface roughness of wheel and rail, and to a lesser extent the variability due to track construction. This standard is being revised to include a specification of a rail roughness limit. If the rail roughness is below this limiting spectrum, it is anticipated that the results should be relatively insensitive to the actual rail roughness (although they will not be completely unaffected by it) due to the presence of the wheel roughness, which is generally greater than the rail roughness limit.

In parallel, efforts have been made to develop measurement standards in connection with the introduction of vehicle noise emission limits as part of the European Community Technical Specifications for Interoperability.<sup>16</sup> These differ in the details of the roughness limit and the specifications for the track at the test site.

For the measurement of rail and wheel roughness, several different measurement systems have been



**Figure 6** Radiation efficiencies (ratios) (a) of a wheel in axial modes with 0 nodal circles (number of nodal diameters indicated), (b) of an infinite rail vibrating vertically (—) or laterally (---), calculated using boundary element models.

developed.<sup>17,18</sup> Various comparisons have been made between the results measured by different systems,<sup>2,19</sup> but the case remains that the results obtained depend on the measurement system used and the way in which the data are analyzed, so that great care is needed.

### 3 REDUCING ROLLING NOISE

#### 3.1 Introduction

According to the flowchart in Fig. 1, reductions of rolling noise can be sought by reducing the input (the combined surface roughness), modifying the response and radiation of the wheels and track, or by introducing shielding to reduce sound transmission.<sup>20</sup> If the combined roughness is reduced, the whole noise output is reduced in proportion; for other changes the overall reduction depends on the relative importance of the wheel and track and on any interaction between them. Moreover, combinations of measures are not wholly additive in their effect.

#### 3.2 Reducing Roughness

Vehicles that are braked by cast-iron blocks acting on the wheel tread are common in Europe. These develop a corrugation pattern on the wheel running surface that yields higher rolling noise levels. Replacement by disk-braked stock can yield reductions of typically 10 dB,<sup>21</sup> and, as most modern passenger stock is disk-braked, this has led to considerable reductions in noise over the last two decades. Alternative, for example, composite, brake block materials can also be used in the tread brake system to similar effect. Indeed, North American freight stock is usually tread-braked using composite blocks. However, other problems such as wheel heating have to be overcome before these can be introduced on a like-for-like basis.

Rail roughness develops at some locations into a near periodic corrugation. Considerable understanding of the mechanism of its development has been produced in recent years,<sup>22</sup> involving track dynamic behavior as well as metallurgy. Strong antiresonances of the track system such as the pinned-pinned mode can induce high dynamic forces enhancing corrugation formation. Nevertheless the case remains that the usual remedy is grinding of the rail head using special grinding trains. The use of such grinding trains has other advantages in terms of maintaining rail transverse profiles and removing cracks and other surface damage before they develop into rail failures.

#### 3.3 Wheel Damping and Shape

It might appear that the light damping of a wheel (see Fig. 2) makes it an ideal candidate for added damping treatment. However, the coupling with the track introduces considerable effective damping that must be exceeded if a damping treatment is to be effective against rolling noise. Thus, although the wheel itself has damping loss factors around  $10^{-4}$  to  $10^{-3}$ , the effective loss factor increases to around  $10^{-3}$  to  $10^{-2}$  when coupled to the rail.<sup>10</sup>

Additional wheel damping can be provided by constrained layer treatments or tuned absorber

systems.<sup>23,24</sup> In some situations overall reductions of over 6 dB have been obtained,<sup>25</sup> but in such situations the starting point is clearly one in which the wheel dominates in the sound radiation. Where the track is the dominant source initially, the overall reductions will be limited to only 1 or 2 dB unless simultaneous noise reduction of the track is applied.

It is also possible to reduce the wheel component of noise by optimizing its shape. A symmetrical web cross-sectional design is around 2 to 3 dB quieter than a curved web cross section due to reduction of the coupling between radial and axial motion. A thicker web is also beneficial, due to the increase in modal frequencies. This means that less modes are excited in the frequency range below the cutoff of the contact filter. Similarly, a reduction in diameter increases the modal frequencies while also reducing the radiating area. In one study, a combination of these features (with an 18% reduction in diameter) led to predicted reductions in wheel noise of over 10 dB.<sup>26</sup> Very small wheels are used in some specialist low-floor freight wagons and have been found to have wheel components of noise of up to 20 dB less than more usual standard designs. However, the smaller diameter leads to a slightly shorter contact patch, and consequently to a lessening of the contact patch filter effect and a small increase in noise from the rail.<sup>27</sup>

Resilient wheels can also lead to a reduction in the noise from the wheel, due to isolation of the wheel tread from the remainder of the wheel, and increased damping, but this too can lead to an increase in noise from the rail.<sup>28</sup>

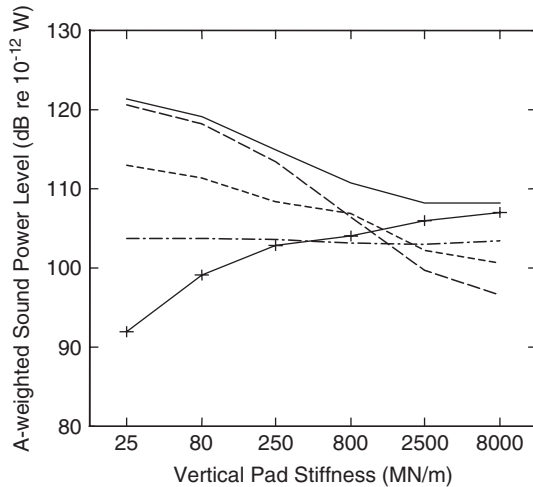
#### 3.4 Rail Pad Stiffness and Rail Damping

The stiffness of the pad inserted between the rail and the sleepers has a moderate effect on the input mobility of the rail but a much greater effect on the decay of rail vibration with distance and the coupling between the rails and sleepers.<sup>29</sup> The effect is summarized in Fig. 7. This shows that as the pad stiffness is reduced, the rail becomes progressively decoupled from the sleepers, leading to reduced sleeper noise, but the rail vibrates over a greater distance due to its reduced decay rate, giving greater rail noise. The wheel noise is virtually independent of these changes. An optimum can be envisaged where the overall noise has a minimum. However, this corresponds to a rather stiff pad. In fact the modern trend in track design is toward the use of softer pads to minimize track component damage due to high impact loads and also to reduce the likelihood of rail corrugation. Therefore, there is a need to increase the track decay rates without increasing the rail pad stiffness.

The results of Fig. 7 do not take account of the nonlinear stiffening of the rail pads under train loads, particularly prevalent for softer pads, which tends to reduce the slope of the dependence of noise on pad stiffness.<sup>30</sup> Rail pad properties also change over time.

In an attempt to increase the rail decay rates, several rail damper systems have been developed in recent years.<sup>31,32</sup> The most successful of these depend on

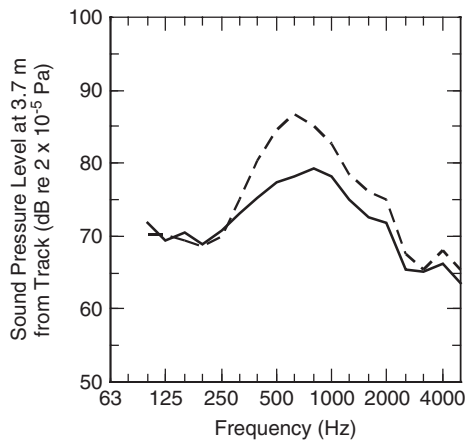




**Figure 7** Predicted dependence of rolling noise on rail pad stiffness: —, total track noise; — — —, rail vertical; . . . ., rail lateral; + + +, sleepers; — · — ·, wheel.

using a damped mass–spring system added to the rail. The maximum damping effect is produced at the tuning frequency of the system, but due to the use of high damping materials, considerable damping is achieved over a broad frequency range.

An example of the effect of using such dampers is given in Fig. 8.<sup>32</sup> Here the noise from the track has been reduced by about 6 dB. The actual reduction achievable depends on the pad stiffness—for tracks with stiff pads the reductions are unlikely to exceed 2 to 3 dB.



**Figure 8** Measured effect of applying silent track rail dampers on one-third octave band sound pressure spectrum at 3.7 m from the track, train speed 100 km/h, low noise wheels: —, with absorbers (overall A-weighted level 85.1 dB); — — —, reference track (overall A-weighted level 90.5 dB).

### 3.5 Local Shielding

As an alternative to the various structural measures mentioned above, or to complement them, it is possible to use a combination of low barriers close to the rail and vehicle-mounted shields. The success of such a system relies on ensuring that any gap through which direct sound can be radiated is minimized. Effective experimental configurations have been shown to demonstrate reductions of 10 dB.<sup>33</sup> In other cases, where the loading gauge and track structure gauge requirements prevented the barrier and shields from overlapping one another, reductions of less than 3 dB have been found.<sup>34</sup>

### 4 IMPACT NOISE

Impact noise is generated when the wheel rolls over a discrete discontinuity in the rail surface, for instance, at rail joints, welds, or points and crossings.<sup>35</sup> Additionally, discontinuities can occur on the wheel surface, for example, “wheel flats” due to sliding of the wheel during braking in imperfect adhesion conditions.

Noise is generated by a similar mechanism to that applying for rolling noise, a vertical relative displacement input between the wheel and rail. The relative contributions of wheel and track vibration to the noise radiation follow the same pattern as for rolling noise. However, since large discrete inputs are involved, the nonlinearity of the contact spring becomes important and in extreme cases the wheel–rail contact force can become zero.<sup>36,37</sup> Very large dynamic forces occur on reestablishment of contact (impact).

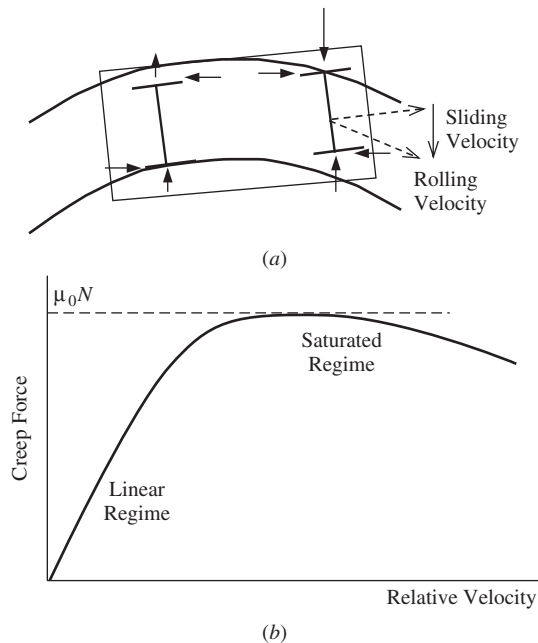
Although the same mitigation measures can be used as for rolling noise, the most effective is adequate maintenance. Good wheel slide protection can prevent the formation of wheel flats. Monitoring systems can be used to detect wheel flats and to recall those vehicles for wheel reprofiling provided they are properly installed. Similarly, good maintenance of rail joints and straightening of rail welds is important for minimizing impact noise. The use of swing nose crossings can eliminate gaps at high-speed crossings to reduce impacts and hence noise.

### 5 WHEEL SQUEAL

#### 5.1 Mechanisms

When a railway vehicle traverses a sharp curve, the front axle of each bogie (truck) tends to run in flange contact on the outer rail and with a significant angle of attack, see Fig. 9a. The rear wheelset runs in flange contact at the inner rail at low speed, but its angle of attack is much less than the leading axle.

As a result of the large angle of attack at the leading wheelset, the leading inner wheel experiences a considerable lateral sliding velocity in addition to the forward velocity of the vehicle; that is, in order to traverse the curve it must slide sideways as well as roll forward. This induces a frictional (or creep) force. In common with many dry friction phenomena (see also Chapter 92), this leads to dynamic instability since at large sliding velocities the frictional force falls with



**Figure 9** Excitation of squeal noise (a) attitude of typical two-axle bogie in a sharp curve showing forces acting on each wheel and (b) typical rolling friction characteristic.

increasing sliding velocity; see Fig. 9b. This can be seen as introducing a negative damping to the system. At large amplitudes the motion becomes a stick-slip type of oscillation. The vibration usually corresponds to one of the modes of vibration of the wheel, and a squealing noise is produced with a strongly tonal character.

The wheel modes of relevance to squeal noise are those with a large lateral component at the wheel-rail contact point and a small radial component. Thus the zero-nodal-circle modes (see Fig. 5) are usually excited in curve squeal. Although the rail also vibrates at the squeal frequency, the noise radiation is dominated by the wheel.

Models for squeal noise due to the above mechanism have been developed by Rudd,<sup>38</sup> Fingberg,<sup>39</sup> Heckl,<sup>40</sup> and de Beer.<sup>41</sup> In addition to the above mechanism, squeal noise is also generated at the flange contact with the outer rail.<sup>42</sup> This generally produces a higher frequency, more intermittent noise, often in the frequency region above 5 kHz, although it can also occur at lower frequencies. Other forms of curving noise occur, for example, due to low-frequency stick-slip in the longitudinal direction involving torsional modes of the wheelset. Names such as "graunching" and "judder" describe some of these lower frequency phenomena. Further research is needed into these various phenomena. The discussion in the following section is limited to the squeal noise generated by lateral slip at the rail head.

## 5.2 Reduction of Curve Squeal

Since squeal noise involves a dynamic instability, the addition of a small amount of damping to the wheel can often eliminate the excitation and produce noise reductions of tens of decibels. As well as the damping systems described in Section 3.3, ring dampers have been found to be effective.<sup>43,44</sup> Resilient wheels also increase the damping sufficiently to reduce the instance of squeal noise.<sup>45</sup>

Rail damping has also been applied and found to reduce curve squeal, although it is not clear according to the mechanism described above how this is achieved. Such a measure is attractive as it only needs to be applied at the locations where problems occur.

Other solutions are based on modifying the friction behavior. Squeal noise is less prevalent in wet weather and so water sprays have been used effectively. Lubrication using grease is also commonly used, although this is normally only applied to the gauge face of the rail, not to the running surface where it would compromise braking performance. This, therefore, does not modify directly the friction behavior at the leading inner wheel. Instead, it modifies the attitude of the bogie in the curve.

Friction modifiers have been introduced in recent years that can also be applied to the rail head.<sup>46</sup> Rather than reduce the overall friction level, these aim to reduce the "negative friction" characteristics, introducing instead a positive slope of the friction curve and eliminating the instability.

## 6 CONCLUSION

Theoretical models for rolling noise are well developed and can be used to design intrinsically quieter wheels and tracks. Models for impact noise and curve squeal are also quite well developed, although many aspects remain to be solved. Further information about reducing rolling noise, in particular, and railway noise, in general, can be found in chapters of various books.<sup>47–50</sup>

## REFERENCES

1. P. J. Remington, Wheel/Rail Noise, Part IV: Rolling Noise, *J. Sound Vib.*, Vol. 46, 1976, pp. 419–436.
2. D. J. Thompson, On the Relationship between Wheel and Rail Surface Roughness and Rolling Noise, *J. Sound Vib.*, Vol. 193, 1996, pp. 149–160.
3. D. J. Thompson, B. Hemsworth, and N. Vincent, Experimental Validation of the TWINS Prediction Program for Rolling Noise, Part 1: Description of the Model and Method, *J. Sound Vib.*, Vol. 193, 1996, pp. 123–135.
4. D. J. Thompson, P. Fodiman, and H. Mahé, Experimental Validation of the TWINS Prediction Program for Rolling Noise, Part 2: Results, *J. Sound Vib.*, Vol. 193, 1996, pp. 137–147.
5. D. J. Thompson and C. J. C. Jones, A Review of the Modelling of Wheel/Rail Noise Generation, *J. Sound Vib.*, Vol. 231, No. 3, 2000, pp. 519–536.
6. D. J. Thompson, Wheel-Rail Noise Generation, Part I: Introduction and Interaction Model, *J. Sound Vib.*, Vol. 161, 1993, pp. 387–400.

7. K. L. Johnson, *Contact Mechanics* Cambridge University Press, Cambridge, UK, 1985.
8. P. J. Remington and J. Webb, Estimation of Wheel/Rail Interaction Forces in the Contact Area Due to Roughness, *J. Sound Vib.*, Vol. 193, 1996, pp. 83–102.
9. D. J. Thompson, The Influence of the Contact Zone on the Excitation of Wheel/Rail Noise, *J. Sound Vib.*, Vol. 267, No. 3, 2003, pp. 523–535.
10. D. J. Thompson, Wheel-Rail Noise Generation, Part II: Wheel Vibration, *J. Sound Vib.*, Vol. 161, 1993, pp. 401–419.
11. D. J. Thompson, Wheel-Rail Noise Generation, Part III: Rail Vibration, *J. Sound Vib.*, Vol. 161, 1993, pp. 421–446.
12. D. J. Thompson and N. Vincent, Track Dynamic Behaviour at High Frequencies. Part 1: Theoretical Models and Laboratory Measurements, *Vehicle Syst. Dynamics Suppl.*, Vol. 24, 1995, pp. 86–99.
13. D. J. Thompson and C. J. C. Jones, Sound Radiation from a Vibrating Railway Wheel, *J. Sound Vib.*, Vol. 253, 2002, pp. 401–419.
14. D. J. Thompson, C. J. C. Jones, and N. Turner, Investigation into the Validity of Two-Dimensional Models for Sound Radiation from Waves in Rails, *J. Acoust. Soc. Am.*, Vol. 113, 2003, pp. 1965–1974.
15. ISO 3095-1975 Railway Applications—Acoustics—Measurement of Noise by Railbound Vehicles, International Organization for Standardization, Geneva, Switzerland, 1975.
16. Commission Decision 2002/735/EC Concerning the Technical Specification for Interoperability (TSI) Relating to the Rolling Stock Subsystem of the Trans-European High-Speed Rail System, *Official J. European Comm.*, 12.9.2002 L245/402-506, 2002.
17. G. Hölzl, M. Redmann, and P. Holm, Development of a Highly Sensitive Rail Surface Measuring Device as Contribution to Further Noise Reduction on the Railway (in German), *Eisenbahn Technische Rundschau*, Vol. 39, 1990, pp. 685–689.
18. S. L. Grassie, M. Saxon, and J. D. Smith, Measurement of Longitudinal Rail Irregularities and Criteria for Acceptable Grinding, *J. Sound Vib.*, Vol. 227, 1999, pp. 949–964.
19. E. Verheijen, Ed., *Proceedings of the Workshop Roughness Measurements*, Utrecht, The Netherlands, 1999.
20. N. Vincent, Rolling Noise Control at Source: State-of-the-Art Survey, *J. Sound Vib.*, Vol. 231, 2000, pp. 865–876.
21. B. Hemsworth, Recent Developments in Wheel/Rail Noise Research, *J. Sound Vib.*, Vol. 66, 1979, pp. 297–310.
22. J. C. O. Nielsen, R. Lundén, A. Johansson, and T. Vernerström, Train-Track Interaction and Mechanisms of Irregular Wear on Wheel and Rail Surfaces, *Vehicle Syst. Dynamics*, Vol. 40, 2003, pp. 3–54.
23. C. J. C. Jones, D. J. Thompson, A. Frid, and M. O. Wallentin, Design of a Railway Wheel with Acoustically Improved Cross-Section and Constrained Layer Damping, *Internoise 2000*, Vol. 2, Nice, France, 28–30 August 2000, pp. 673–678.
24. P. Bouvet, N. Vincent, A. Coblenz, and F. Demilly, Rolling Noise from Freight Railway Traffic: Reduction of Wheel Radiation by Means of Tuned Absorbers, *Proc. Internoise Nice, France, 2000*.
25. G. Hölzl, A Quiet Railway by Noise-Optimised Wheels (in German), *ZEV + DET Glas. Ann.*, Vol. 118, No. 1, 1994, pp. 20–23.
26. P. E. Gautier, N. Vincent, D. J. Thompson, and G. Hölzl, Railway Wheel Optimization, *Proceedings of InterNoise 93*, Leuven, Belgium, 1993, p. 1455–1458.
27. D. J. Thompson and C. J. C. Jones, A Study of the Use of Vehicles with Small Wheels for Determining the Component of Noise from the Track, *Proceedings of IOA Spring Conference*, Salford, UK, March, 2002.
28. C. J. C. Jones and D. J. Thompson, Rolling Noise Generated by Wheels with Viscoelastic Layers, *J. Sound Vib.*, Vol. 231, 2000, pp. 779–790.
29. N. Vincent, P. Bouvet, D. J. Thompson, and P. E. Gautier, Theoretical Optimization of Track Components to Reduce Rolling Noise, *J. Sound Vib.*, Vol. 193, 1996, pp. 161–171.
30. D. J. Thompson, C. J. C. Jones, T. X. Wu, and G. de France, The Influence of the Nonlinear Stiffness Behaviour of Railpads on the Track Component of Rolling Noise, *Proceedings of the Institution of Mechanical Engineers, Part F, J. Rail Rapid Transit*, Vol. 213, 1999, pp. 233–241.
31. P. Fodiman, Line Test Validation of Low Noise Railway Components, *Proceedings of World Congress on Railway Research*, Colorado Springs, CO, June 1996, pp. 497–502.
32. D. J. Thompson, C. J. C. Jones, and D. Farrington, The Development of a Rail Damping Device for Reducing Noise from Railway Track, *Internoise 2000*, Vol. 2, Nice, France, 28–30 August 2000, pp. 685–690.
33. R. R. K. Jones, Bogie Shrouds and Low Barriers Could Significantly Reduce Wheel/Rail Noise, *Railway Gazette Int.*, July 1994, pp. 459–462.
34. R. Jones, M. Beier, R. J. Diehl, C. Jones, M. Maderboeck, C. Middleton, and J. Verheij, Vehicle-Mounted Shields and Low Trackside Barriers for Railway Noise Control in a European Context, *Internoise 2000*, Nice, France, August 2000.
35. I. L. Vér, C. S. Ventres, and M. M. Myles, Wheel/Rail Noise, Part II: Impact Noise Generation by Wheel and Rail Discontinuities, *J. Sound Vib.*, Vol. 46, 1976, pp. 395–417.
36. T. X. Wu and D. J. Thompson, A Hybrid Model for the Noise Generation Due to Railway Wheel Flats, *J. Sound Vib.*, Vol. 251, 2002, pp. 115–139.
37. T. X. Wu and D. J. Thompson, On the Impact Noise Generation Due to a Wheel Passing Over Rail Joints, *J. Sound Vib.*, Vol. 267, 2003, pp. 485–496.
38. M. J. Rudd, Wheel/Rail Noise, Part III: Wheel Squeal, *J. Sound and Vib.*, Vol. 46, 1976, pp. 381–394.
39. U. Fingberg, A Model of Wheel-Rail Squealing Noise, *J. Sound Vib.*, Vol. 143, 1990, pp. 365–377.
40. M. A. Heckl, Curve Squeal of Train Wheels, Part 2: Which Wheel Modes Are Prone to Squeal? *J. Sound and Vib.*, Vol. 229, 2000, pp. 695–707.
41. F. G. de Beer, M. H. A. Janssens, and P. P. Kooijman, Squeal of Rail Bound Vehicles Influenced by Lateral Contact Position, *J. Sound Vib.* Vol. 267, 2003, pp. 497–507.
42. A. Monk-Steel and D. Thompson, Models for Railway Curve Squeal Noise, 7th Int. Conf. Recent Advances in Structural Dynamics, Southampton, England, July 2003.
43. I. Lopez, J. Vinolas, J. Busturia, and A. Castanares, Railway Wheel Ring Dampers, *Proc. Internoise 2000*, Nice, France, 2000.

44. P. Wetta and F. Demilly, Reduction of Wheel Squeal Noise Generated on Curves or During Braking, 11th Int. Wheelset Congress, Paris, June 1995, pp. 301–306.
45. P. J. Remington, Wheel/Rail Squeal and Impact Noise: What Do We Know? What Don't We Know? Where Do We Go from Here? *J. Sound Vib.*, Vol. 116, 1987, pp. 339–353.
46. D. T. Eadie, M. Santoro, and W. Powell, Local Control of Noise and Vibration with Keltrack Friction Modifier and Protector Trackside Application: An Integrated Solution, *J. Sound Vib.*, Vol. 267, 2003, pp. 761–772.
47. V. V. Krylov, Ed., *Noise and Vibration from High Speed Trains*, Thomas Telford, London, 2001.
48. P. M. Nelson, Ed., *Transportation noise reference book*, Butterworth, London, 1987.
49. F. J. Fahy and J. G. Walker, Eds., *Advanced Applications of Noise and Vibration*, E&FN Spon, London, 2004.
50. J. T. Nelson, Ed., *Wheel/Rail Noise Control Manual*, TCRP Report 23, Transportation Research Board, Washington, DC, 1997.

## **PART IX**

---

# **INTERIOR TRANSPORTATION NOISE AND VIBRATION SOURCES - PREDICTION AND CONTROL**

# CHAPTER 94

## INTRODUCTION TO INTERIOR TRANSPORTATION NOISE AND VIBRATION SOURCES

Malcolm J. Crocker

Department of Mechanical Engineering  
Auburn University  
Auburn, Alabama

### 1 INTRODUCTION

Noise and vibration are important considerations for the comfort of operators and passengers in surface transportation vehicles, off-road vehicles, aircraft, and ships. Noise and vibration energy is transmitted from the sources to the passenger, operator and crew by airborne and structure-borne paths. The amount of noise and vibration energy reaching people depends upon the strength of the individual sources and the effectiveness of structural paths. The strength of the individual sources and of the paths varies from vehicle to vehicle and depends on vehicle operating conditions including power plant settings, speed, and also upon the frequency range considered. For many types of vehicles, aircraft, and ships, the dominant path for low-frequency noise (below about 400 to 500 Hz) is structure borne. In most cases, in the mid- to high-frequency range, airborne paths from the noise sources to occupied spaces tend to dominate. The relationship between airborne and structure-borne paths also varies from vehicle to vehicle and is somewhat different for aircraft and ships, since the flow noise caused by the turbulent boundary layer fluctuations is a more important source of excitation than with the other vehicle types. Interior noise level criteria depend upon the vehicle type and the occupied space considered. For passengers, speech communication and privacy are the main concerns, while for truck, railroad vehicle, and ship engine room operators and crew, hearing protection and speech communication remain as important issues.

### 2 INTERIOR ROAD VEHICLE NOISE AND VIBRATION

The interior noise in the occupied spaces of automobiles, buses, and trucks is mainly caused by the engine, exhaust, transmission, power train, tire/road interaction, and wind/structure interaction. Many of the same noise and vibration problems exist in rail, off-road vehicles, and passenger ships as in surface transportation vehicles. Airborne and structure-borne paths from noise and vibration sources are also of concern with these other vehicles and means of transportation. Some of the discussion in Section 2 of this chapter is also relevant to these other types of vehicle. With automobiles, trucks, and buses, structure-borne

noise usually tends to be dominant below about 400 to 500 Hz, while airborne noise from tire/road interaction and airflow/structure interaction (wind noise) tends to dominate in the mid- and high-frequency ranges.

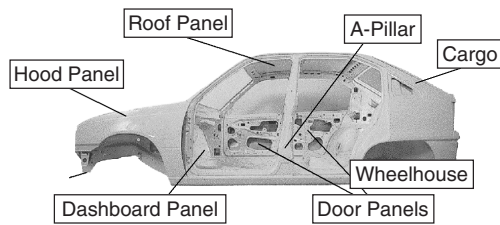
Chapter 95 describes the relative contributions from different noise and vibration sources and paths to the vehicle interior. Interior noise levels depend also upon vehicle operating conditions and in particular on speed. During acceleration, engine noise tends to dominate; while during cruise conditions, above about 80 km/h, tire noise becomes the major contributor, and at higher speeds above about 120 km/h, wind noise becomes dominant. Improper sealing around vehicle doors, windows, dashboards, windshields, and the like causes excessive external turbulent pressure fluctuations from airflow over the vehicle (wind noise) to be transmitted to the vehicle interior. This is known as aspiration, as discussed in Chapter 95. Some luxury vehicles have multiple door seals to accomplish effective sealing to reduce the transmission of these external turbulent pressure fluctuations to the occupied interior.

To reduce airborne and structure-borne noise reaching the vehicle's occupants, various well-known techniques are often used, including (1) increasing structural damping, (2) improving the transmission loss of body panels and windows, (3) increasing the use of sound-absorbing materials in the engine, passenger, and luggage compartments, and (4) vibration isolation of mechanical components. Hirabayashi et al. have described how all four of these techniques are used in the automotive industry to reduce noise and vibration in vehicles.<sup>1</sup> Rao has provided a useful review of the use of vibration damping materials in automobiles and commercial aircraft.<sup>2</sup> Polce et al. have also presented a detailed study on improvements in cabin noise obtained by using damping treatments.<sup>3</sup> Add-on constrained layer, spray-on, and integral damping materials are often used. Table 1 lists various locations on a typical automobile, such as illustrated in Fig. 1, where these are often used.

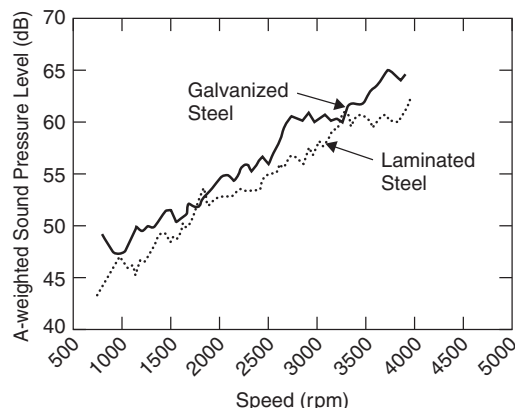
Damping materials are generally more effective at reducing structure-borne vibration (particularly panel resonances) rather than at reducing the airborne sound transmitted through panels. Of the damping approaches, spray-on damping material is easiest to

**Table 1 Automotive Applications<sup>1</sup>**

Engines and Power Trains	Body Structures	Brakes and Accessories
Oil pans	Dash panels	Brake insulators
Valve covers	Door panels	Backing plates
Engine covers	Floor panels	Brake covers
Push rod covers	Wheelhouses	Steering brackets
Transmission covers	Cargo bays	Door latches
Timing belt covers	Roof panels	Window motors
Transfer case covers	Upper cowl	Exhaust shields

**Figure 1** Locations in a typical automobile where damping treatments are often applied.<sup>2</sup>

apply, but constrained damping layers comprised of a viscoelastic layer constrained by a thin surface layer normally provide higher damping for the same weight or less weight through shearing action in the viscoelastic layer. The oil pan (or sump) of an engine can be responsible for radiating 50% of the sound power of an engine.<sup>2,4</sup> Figure 2 shows the A-weighted interior sound pressure level in a vehicle at the driver's ear position with: (a) a regular galvanized steel oil pan and (b) with the oil pan replaced by a high damping laminated steel oil pan.<sup>2</sup> The A-weighted sound pressure levels were obtained during a stationary

**Figure 2** A-weighted sound pressure levels obtained during a stationary engine runup tests for two different oil pans with increasing engine rpm.<sup>2</sup>

engine run up test with increasing engine revolutions per minute (rpm). Figure 2 shows that reductions in the A-weighted interior noise level of about 5 dB were obtained with the laminated steel oil pan.

Water-based spray-on damping materials are also used in automobile manufacture. Their advantage is that they can be sprayed robotically on areas such as floor panels and other locations that are hard to reach (such as wheel housings).<sup>2</sup> Thicknesses of between 1 and 3 mm are normally used. The disadvantage of the use of such materials is that they require costly spray and robotic equipment.<sup>2</sup> It is believed that the use of body and floor panel damping is effective mostly at reducing structure-borne interior automobile noise in the 100- to 500-Hz range. Although increased damping normally has disappointing results in increasing sound insulation, spray-on damping materials do also add *mass*, which can also reduce airborne sound transmission through areas such as floor panels.

The use of laminated glass to reduce automobile interior noise continues to increase.<sup>5</sup> Figure 7 in Chapter 95 shows the effect of using laminated glass in reducing wind noise and tire/road noise. The reduction in airborne noise by the use of the laminated glass is probably caused by the material impedance mismatch, which results in sound reflection at each interface layer; while the reduction in structure-borne noise is likely caused mostly by the increase in vibration damping produced by use of the laminated glass. At some frequencies the damping loss factor for the laminated glass is twice that of the standard tempered glass. The increased damping can reduce sound transmission in the coincidence frequency region.

The use of laminated vibration-damped steel (LVDS) is now being studied for its capability in reducing airborne and structure-borne noise reaching the passenger compartment from the engine and power train components. See an example of an LVDS dash panel in Fig. 3. The advantage of LVDS is that no add-on damping treatment is needed. Improvements in sound quality and speech interference level through the use of LVDS must be considered in light of cost and other factors.

In the automotive industry, materials used to enclose a noise source (such as the engine) or the passengers (the cabin enclosure) are usually termed *barrier* materials. Such barrier materials are required





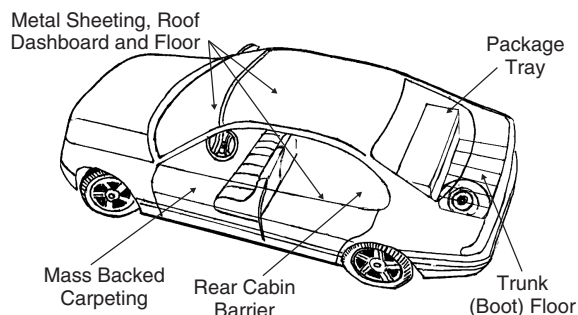
**Figure 3** Dashboard panel made of laminated vibration damped steel.<sup>2</sup>

to reduce airborne sound reaching the cabin from noise sources, including the engine, fan, exhaust system, tires, and wind. Below the coincidence frequency region, the sound transmission loss (TL) of such materials is mostly dominated by the mass/unit area ( $m$ ) of a partition (see Chapters 54 and 56). For single-layer partitions this means that TL increases by 6 dB for each doubling of frequency or by 6 dB at a given frequency if  $m$  is doubled. Multilayer partitions, particularly with intervening air gaps between layers, can achieve TL results quite a lot better than mass law would predict, and the TL for such panels can be more like 12 dB/octave rather than 6 dB/octave. Great care must be taken to avoid air leaks for high

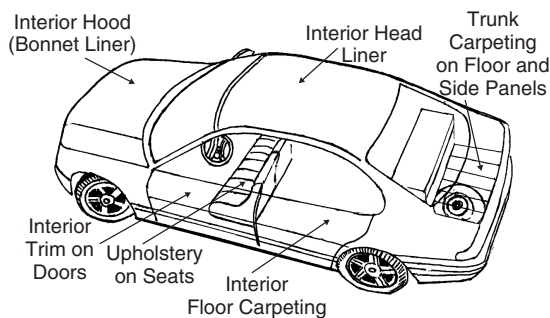
values of TL to be achieved in practice. Figure 4 shows locations where barrier materials are often applied in an automobile.

Once airborne and structure-borne sound has penetrated into the cabin, the sound can be absorbed effectively by the use of sound-absorbing material. See Chapters 54 and 57. Generally, thicker sound-absorbing materials are better than thinner ones, and a material works best if its thickness approaches one-quarter wavelength of the sound. This thickness can only be approached at quite high frequency in an automobile. Figure 5 shows locations where sound-absorbing materials are often applied.

A variety of theoretical methods, such as statistical energy analysis, finite element analysis, boundary element analysis, and computer-aided engineering methods are used to predict sound and vibration energy transmission from exterior sources to the vehicle interior as described in many publications.<sup>6-31</sup> Because of complicated structural geometries, analytical approaches must often be supplemented with laboratory noise testing in anechoic rooms, wind tunnels, and actual tests with real full-scale vehicles on dedicated test tracks. Chapter 95 discusses noise sources and paths, methods of modeling, and noise reduction approaches in more detail. With automobiles and trucks, it is insufficient to simply reduce noise reaching the passenger compartment. Passengers expect different types of vehicles such as passenger cars, sports



**Figure 4** Typical locations in an automobile where “barrier” materials are utilized.



**Figure 5** Typical locations in an automobile where sound-absorbing materials are utilized.

cars, sport utility vehicles, luxury cars, and light trucks to have distinctive sounds. In some cases, manufacturers' brand names are often associated with a particular vehicle sound, and it is important not just to reduce interior noise but also to consider the quality of the sound. See Chapter 67 for more detailed discussion on sound quality.

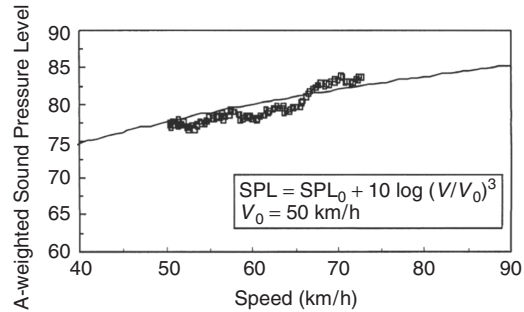
### 3 NOISE OF RAILROAD CAR AND RAPID TRANSIT SYSTEM VEHICLES

The main concern in the design of railroad passenger cars and rapid transit system (RTS) vehicles is the provision of a comfortable noise environment for the passengers. A balance must be achieved between acoustical privacy and speech interference. Passengers want the sound pressure level to be low enough so that they can carry on conversations and use cell (mobile) telephones easily. On the other hand, they do not want the level to be so low that their conversations can be overheard by other passengers nearby. The noise environment in railroad car and RTS vehicles is caused by a variety of sources that depend mostly upon the power plant setting and vehicle speed. At low speed, interior noise is caused mainly by the power plant and air-conditioning systems. Wind noise is normally unimportant for slow or medium-speed RTS vehicles, but it can become the dominant noise source with railroad systems when they are operated at very high speeds. The balance between acoustical privacy and speech interference changes with speed and it is difficult to optimize this balance without the use of artificial masking noise during low speed or stationary operations of the vehicles. Various power plants are used to propel the railroad and RTS vehicles, and in some high-speed railroad vehicle designs several sets of traction motors are used to drive each passenger car, instead of just the locomotive, or individual electric motors are employed to drive the vehicle wheels directly. Wheel-rail noise becomes important at medium and high speeds and depends upon rail roughness and wheel wear.<sup>32-34</sup>

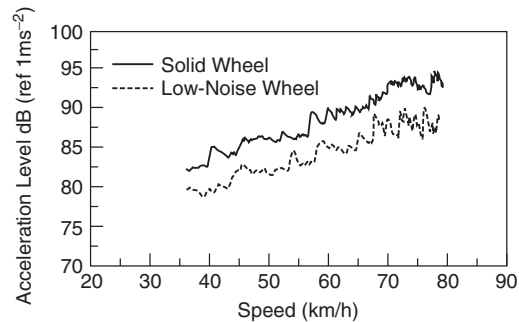
Soft rubber wheel suspensions have been used on some rapid transit systems (e.g., Mexico City) in an attempt to reduce noise. Rubber or elastomeric damping blocks have also been built into the wheel systems of some other passenger railcars and crew locomotives.<sup>35</sup> If damping blocks and damping rims are implemented, they should be properly tested to demonstrate that they can be used safely in service.

Figure 6 shows the A-weighted interior noise level at moderate speeds for one particular railcar.<sup>35</sup> It is observed that the A-weighted sound pressure level increases at a rate of 9 to 10 dB for each doubling of speed in the range of measurements shown. Subjectively, this amounts to approximately a doubling of linear loudness (in sones) for a doubling of train speed. It should be emphasized, however, that this result may be somewhat different for other railcar designs.

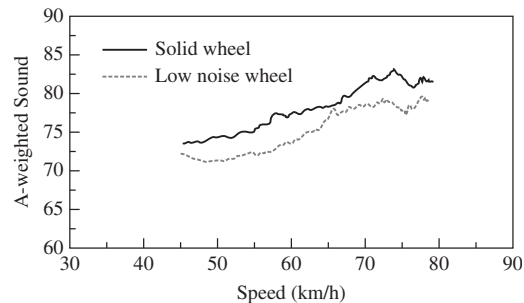
Figure 7 shows acceleration levels measured on the railcar floor with conventional solid wheels and



**Figure 6** Sound pressure level as a function of train speed.<sup>35</sup>



**Figure 7** Comparison of floor vibrations for solid wheel and low-noise wheel.<sup>35</sup>



**Figure 8** Comparison of interior noises for solid wheel and low-noise wheel.<sup>35</sup>

low-noise wheels. Figure 8 shows a comparison of the interior A-weighted sound pressure level of the same railcar as in Fig. 6 with conventional wheels and with the low noise wheels. Figure 8 demonstrates that in this particular railcar, at the speeds shown, the wheel/rail interaction noise is very important. This study shows that there is not complete correspondence between the reduction in the floor acceleration level and the reduction in interior sound pressure level, achieved by the use of low noise wheels. This indicates

the presence of other noise sources, such as power plant, wind noise, and air-conditioning noise.

As is described in Chapter 96, it is normal practice to set target noise level goals for passenger comfort and to specify maximum power plant and air-conditioning system source sound powers from equipment manufacturers and suppliers in order to achieve the noise targets. Target A-weighted equivalent interior sound pressure levels of between 65 and 70 dB are commonly chosen. To achieve such target noise levels, the vehicle structure must also be carefully designed from the start so that the noise and vibration paths sufficiently attenuate the power plant, wheel/rail, wind, and air-conditioning noise reaching the passenger compartments. The contribution to the internal noise caused by wheel/rail interaction can be predicted from knowledge of the roughness of the rails. It is important for the rail roughness levels to be defined at the beginning of the acoustical design process. Both airborne and structure-borne paths must be considered. Cabin wall airborne sound transmission properties, structural damping, and interior sound absorption all affect the transmission of sound and vibration and the resulting sound pressure level in the cabin interior. Accurate prediction of the interior cabin noise can only be made with a knowledge of all of the external and internal cabin noise and vibration sources and paths.

Chapter 96 discusses noise sources and noise level targets in high-speed railroad cars. Chapter 97 describes target noise levels in rapid transit system cars and the acoustical design processes commonly used to achieve them. There is extensive literature on noise and vibration sources and paths in rail vehicles.<sup>36–44</sup> Squeal noise is a problem experienced on curved tracks.<sup>39,42</sup>

#### 4 INTERIOR NOISE AND VIBRATION OF OFF-ROAD VEHICLES

Off-road vehicles are used for a variety of tasks including earth moving, road, railway and airport construction, and use on building sites and in agriculture, as described in Chapter 98. The vehicles are provided either with wheels or tracks for propulsion. Cabs are used to protect the operator from rollover and other operational hazards, from the weather, and from noise and vibration. One of the main concerns with these vehicles is to provide a safe acoustical environment for the operator inside the cab. To achieve this, the time-averaged A-weighted equivalent sound pressure level inside the operator cab should be no higher than about 75 dB. Since noise levels vary with time as vehicles undertake various activities such as earth moving or grading, noise measurement methods to record the sound pressure levels generated have been standardized internationally, which take account of this operational variability. A-weighted internal cab noise measurements are normally made with a single microphone in the presence of the operator. The microphone is oriented horizontally at the operator head height and pointed forward or in the direction in which the operator normally looks.

Interior noise levels depend upon the strength of the noise and vibration sources and paths including the power plant, exhaust, transmission, hydraulic systems, mounting systems, and wheel and/or track ground surface interactions. It is important to ensure that the sources are vibration isolated from the vehicle structure and that proper care is taken to achieve satisfactory operator sound isolation by providing a suitable transmission loss (sound reduction index) for the cab enclosure. Air leaks should be minimized if the cab noise level can only be achieved with windows closed. Structural damping and interior sound-absorbing material, if properly used in the design stage, can help achieve the necessary interior cab noise level design goals.

Analytical models, which are often employed in the design of off-road vehicle cabs, include statistical energy analysis, finite element analysis (FEA) and boundary element methods (BEM).<sup>46,47</sup> The track undercarriage can become a dominant noise source for tracked vehicles. Experimental confirmation that cabin noise goals have been achieved is necessary during prototype vehicle development and testing. The sound pressure level depends on vehicle operations including earth moving and other working cycles. Chapter 98 discusses the interior noise and vibration of off-road vehicles and methods to reduce the interior noise.

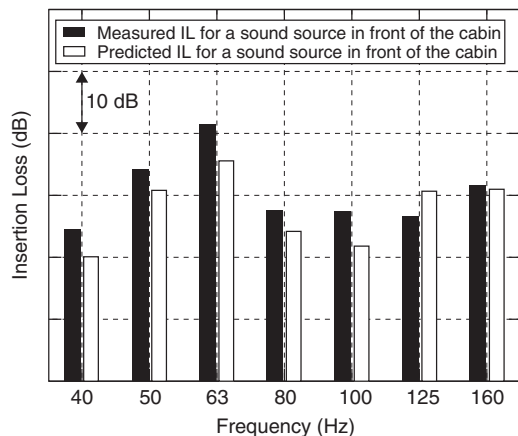
A-weighted sound pressure levels in off-road vehicle cabs have been measured to be as high as 107 dB. See Ref. 48. By proper passive noise control approaches, these levels can be reduced considerably as described in Chapter 98. Approaches vary from mostly experimental to almost completely theoretical.<sup>45–47</sup> Both structure-borne and airborne noise and vibration paths to the cab interior must be considered.<sup>46</sup> A quite sophisticated study of the noise transmitted into the operator cab of an agricultural machine using both scale models and theoretical FEA and BEM has been reported.<sup>46</sup> Figure 9 shows the operator cabin studied by Desmet et al. The scale model was used to obtain experimental results. Both FEA and BEM meshes were used for the cabin structure and acoustical space. A comparison between the measured and predicted sound insertion loss (IL) of the model cabin is shown in Fig. 10.

#### 5 AIRCRAFT CABIN PASSIVE NOISE AND VIBRATION CONTROL

As discussed in Chapter 99, low interior cabin noise is important for passenger and crew comfort. High cabin noise levels experienced in passenger jet aircraft in the 1960s and 1970s have now been considerably reduced by the use of turbofan engines instead of noisy pure jet engines. Obtaining satisfactory cabin noise environments, which satisfy both speech interference and speech privacy criteria, remains a difficult problem since there is a large variety of noise sources that become dominant during different aircraft operating conditions. As is the case with surface transportation vehicles, with aircraft there are many different noise sources that contribute to the acoustical environment inside aircraft cabins.



**Figure 9** Operator cabin of an agricultural harvester machine.<sup>46</sup>



**Figure 10** Measured and predicted agricultural cabin sound insertion loss.<sup>46</sup>

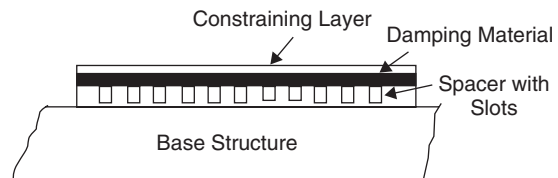
The dominant cabin noise sources are mainly those exterior to the aircraft cabin and include power plant noise and vibration and turbulent boundary layer excitation. The relative strength of the sources depends upon the aircraft operating conditions and flight speed. Internal cabin noise sources include air-conditioning systems, hydraulic systems, and electrical and mechanical equipment. These sources are mainly of concern with aircraft during ground operations

before takeoff. Power plant noise tends to be dominant at low flight speeds during takeoff and landing, while the noise generated by turbulent boundary layer excitation of the cabin walls is dominant at higher speeds, after takeoff and during subsequent climb, during landing descent, and in cruise conditions.

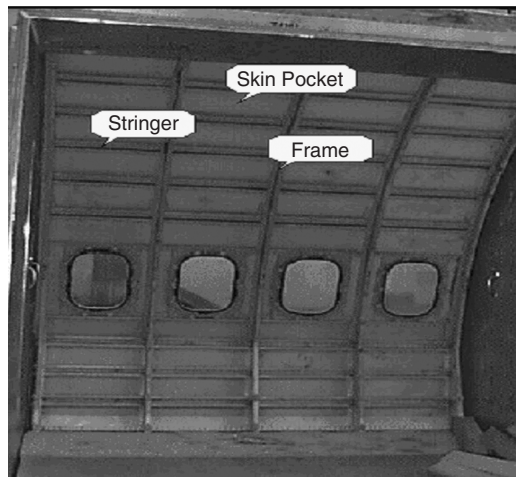
In the front of the cabin, turbulent boundary layer noise tends to peak at high frequency. While, in the middle to rear of the cabin, the boundary layer noise peaks at a much lower frequency. This is because the turbulent eddies in the thick boundary layer at the rear of the aircraft are larger than those in the thinner boundary layer at the front of the cabin. Jet noise is likewise more pronounced at the rear of the aircraft cabin for wing-mounted engines since jet noise is predominantly radiated downstream. See Chapters 83 and 89. For passenger aircraft with rear-mounted jet engines, the engine noise is mainly experienced at the rear part of the cabin. In cruise conditions, the noise from the engines is mostly structure borne and is caused by small out-of-balance forces created by minor aircraft engine manufacturing imperfections.

To reduce interior cabin noise caused by engine noise and boundary layer noise, it has been normal practice to make use of lightweight damping materials. In the case of propeller aircraft, passive dampers are sometimes used, which are tuned to the blade passing frequency and/or the second and third multiples and that are attached to the fuselage interior skin panels.

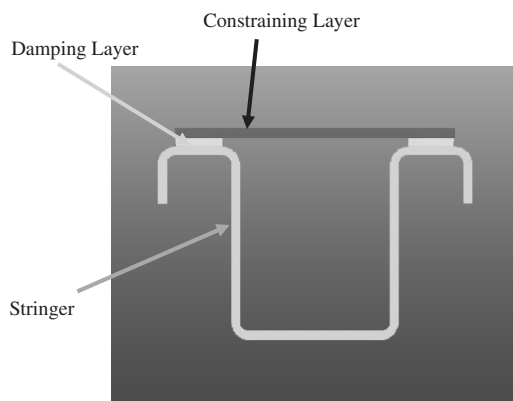
In the case of jet passenger aircraft, constrained layer dampers are normally used and are placed at the center of skin pockets between the stringers and ring frames. Figure 11 shows a typical “stacked” damper system, and Fig. 12 shows the skin pockets of a passenger jet aircraft where they are usually located. In most designs, a layer of viscoelastic damping material is constrained by a thin metal constraining layer of metal or Kevlar. A spacer is located between the base structure (airplane fuselage skin) to move the viscoelastic damping material as far as possible away from the neutral axis of the fuselage skin. The spacer is normally slotted to reduce its weight and minimize its bending stiffness. Ideally, the spacer should also have high shear stiffness. By this means, the shear distortion in the viscoelastic damping layer is magnified as the aircraft skin flexes in bending, and the damping effectiveness of the stacked damper is increased. Since the aircraft fuselage skin gets very cold at cruising altitude and the stacked damper is in close contact with the aircraft skin, special viscoelastic



**Figure 11** Stacked constrained layer damper system.<sup>2</sup>



**Figure 12** Interior of fuselage skin showing pockets between the stringers and ring frames.<sup>2</sup>



**Figure 13** Use of constrained layer damping with an aircraft stringer.<sup>2</sup>

material must be used that has a maximum damping loss factor at the skin temperature during normal cruise conditions.

Viscous constrained damping layers are often used on aircraft stringers. Figure 12 shows the location of stringers on an aircraft fuselage skin. Figure 13 shows how the damping material is constrained between an aircraft stringer and the fuselage skin, which in this case acts as the constraining layer. Damping layers are also often applied to ring frames. Since the ring frames are in contact with the cabin air, they are not as cold as the fuselage skin and the viscoelastic material used is normally selected to have a maximum damping loss factor closer to the normal cabin air temperature.

In some parts of the aircraft cabin, separated flow and shock waves can occur near abrupt changes in

the airplane geometry. For example, such geometric changes usually occur near the cockpit and can cause intense noise to be experienced nearby in the cabin. Cabin noise in propeller-driven aircraft poses a special problem, which is somewhat different from the interior noise of passenger jet aircraft. The interior noise from the power plants of propeller-driven aircraft is dominant over the entire flight regime, not just during takeoff and landing. Propeller noise occurs at the fundamental blade passage frequency and the first few integer multiples, and for wing-mounted engines this noise can be intense if the propellers pass close to the passenger cabin fuselage. The propeller noise, being predominantly low frequency, is difficult to control using passive methods. There is obviously a limit to the amount of mass, which can be added to reduce airborne sound transmission. Sound-absorbing materials are not very effective either at low frequency. The cabin noise levels can be reduced to some extent by the use of damping materials, which will also improve speech intelligibility. However, vibration transmitted from the engines to the airframe and thus resulting in cabin noise is also a matter of concern.<sup>49,50</sup>

## 6 ACTIVE CONTROL OF AIRCRAFT CABIN NOISE AND VIBRATION

Although passive noise source and path control methods have been improved considerably in recent years, in some cases aircraft cabin noise environments are still unsatisfactory. This is particularly true in the case of propeller-powered aircraft, and active control methods have been successfully employed to reduce the low-frequency cabin noise at the fundamental blade passing frequency and the first few multiples.

Active noise control systems are particularly successful in the low-frequency region in which the cabin sidewall sound transmission loss is poor and at which the blade passing frequency occurs. The active control is achieved by introducing multiple secondary sources in the cabin and the use of active headsets or "silent" seats. In the case of silent seats, small secondary sources are located in the top of the passenger seats in order to create a zone of "silence" near to the passenger's head. Structure-borne noise is also reduced on some aircraft by locating active 180° out-of-phase vibration sources near to aircraft engine mounts. Attenuation of broadband cabin noise is a more difficult task but can be undertaken provided sufficient numbers of secondary 180° out-of-phase noise sources are located inside the cabin. Since jet power plant noise has been successfully reduced in recent years, and in any case is minimal during cruise conditions, broadband turbulent boundary layer noise is becoming recognized as an increasing problem during cruise conditions. Active noise control of aircraft cabins is discussed in Chapter 100. Active control of the structure close to the engine can also be undertaken to reduce structure-borne noise reaching the passenger cabin.<sup>51</sup> See Chapter 64 for further discussion on active vibration control, and Chapter 63 for further discussion on active noise control.



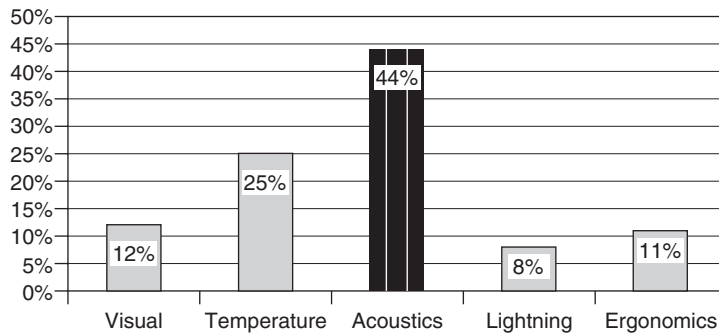


Figure 14 Percentage of passengers choosing various criteria needing improvement on a cruise ship.<sup>52</sup>

## 7 CONTROL OF SHIPBOARD CABIN NOISE AND VIBRATION

Many of the same noise problems exist in passenger ships as in surface transportation vehicles and aircraft. Airborne and structure-borne paths from noise and vibration sources can be of similar and sometimes of equal concern during different ship operations. The main sources include the power plant machinery and the propulsion units including screws and propellers.

Noise levels can be intense in the engine room compartments of ships, and consideration needs to be given to providing low enough sound pressure levels so that speech communication is possible and audible alarm signals can be heard. Crew comfort must also be considered in crew rest areas so that they can recuperate from the high noise levels experienced in engine rooms and other high-noise regions of ships. Noise levels in rest areas must be low enough so that the effects of noise on sleep and overall crew performance are minimized. Figure 14 shows that the acoustical environment on cruise ships often receives most complaints.<sup>52</sup>

Some A-weighted noise level criteria for crew rest areas are as low as 45 dB, while others permit levels as high as 60 dB in such areas. Noise levels in passenger spaces in ships are generally low enough that speech communication and sleep interference are not issues; providing passenger comfort is the predominant concern in this case. Acoustical prediction methods and the design of ships to achieve effective noise and vibration control are discussed in Chapter 101. Various studies have been made on the noise in ships.<sup>52–54</sup> Studies have been made using sound intensity to identify noise sources in ships. In one shipboard study the sound intensity field was measured close to a double cabin window to try to identify the source of ship cabin noise problems.<sup>53</sup>

## REFERENCES

1. T. Hirabayashi, D. J. McCaa, R. G. Rebandt, P. Rusch, and P. Saha, Automotive Noise and Vibration Control Treatments, *J. Sound Vib.*, April 1999, pp. 22–32.
2. M. D. Rao, Recent Applications of Viscoelastic Damping for Noise Control in Automobiles and

Commercial Airplanes, *J. Sound Vib.*, Vol. 262, No. 3, 1 May 2003, pp. 457–474.

3. C. T. Polce III, P. Saha, J. A. Groening, and R. Schappert, A Data Analysis Approach to Understand the Value of a Damping Treatment for Vehicle Interior Sound, SAE Noise and Vibration, Society of Automotive Engineers, Warrendale, PA.
4. T. E. Reinhart and M. J. Crocker, Source Identification on a Diesel Engine Using Acoustic Intensity Measurements, *Noise Control Eng.*, Vol. 18, No. 3, 1982, pp. 84–92.
5. R. A. Esposito and G. E. Freeman, *Glazing for Vehicle Interior Noise Reduction*, International Body Engineering Conference and Exhibition, Society of Automotive Engineers, Warrendale, PA, USA, 2002.
6. K. Misaji, H. Tada, T. Yamashita, M. Nakamura, H. Tanaka, S. Kokabu, and D. Morie, *Testing Uniqueness of a Hybrid SEA Modeling Solution for a Passenger Car*, SAE Noise and Vibration Conference and Exposition, Society of Automotive Engineers, Warrendale, PA, 2003.
7. C. R. Fredö, A Modification of the SEA Equations: A Proposal of How to Model Damped Car Body Systems with SEA, Noise and Vibration Conference and Exhibition, Society of Automotive Engineers, Warrendale, PA, 2005.
8. K. Nishikawa, K. Misaji, T. Yamazaki, and M. Kamata, SEA Model Building of Automotive Vehicle Body in White Using Experiment and FEM, SAE Noise and Vibration Conference and Exposition, Society of Automotive Engineers, Warrendale, PA, 2003.
9. A. Sol and F. Van Herpe, Numerical Prediction of a Whole Car Vibro-Acoustic Behavior at Low Frequencies, SAE Noise and Vibration Conference and Exposition, Society of Automotive Engineers, Warrendale, PA, 2001.
10. Q. Zhang, D. Wang, A. Parrett, and C. Wang, SEA in Vehicle Development Part II: Consistent SEA Modeling for Vehicle Noise Analysis, SAE Noise and Vibration Conference and Exposition, Society of Automotive Engineers, Warrendale, PA, 2003.
11. K. Misaji, H. Tada, T. Yamashita, M. Nakamura, H. Tanaka, S. Kokabu, and D. Morie, Development of a Hybrid SEA Modeling Scheme for a Passenger Car, SAE 2003 World Congress, Society of Automotive Engineers, Warrendale, PA, 2003.

12. J. A. Moore, R. Powell, and T. Bharj, Development of Condensed SEA Models of Passenger Vehicles, SAE Noise and Vibration Conference and Exposition, Society of Automotive Engineers, Warrendale, PA, 1999.
13. V. Cotonì, B. Gardner, P. Shorter, and S. Lane, Demonstration of Hybrid FE-SEA Analysis of Structure-Borne Noise in the Mid Frequency Range, Noise and Vibration Conference and Exhibition, Society of Automotive Engineers, Warrendale, PA, 2005.
14. W. Zhang, A. Wang, and N. Vlahopoulos, Validation of the EFEA Method through Correlation with Conventional FEA and SEA Results, SAE Noise and Vibration Conference and Exposition, Society of Automotive Engineers, Warrendale, PA, 2001.
15. A. C. Aubert, J. T. Long, R. E. Powell, and M. J. Moeller, SEA for Design: A Case Study, SAE Noise and Vibration Conference and Exposition, Society of Automotive Engineers, Warrendale, PA, 2003.
16. H. H. Yan and A. Parrett, A FEA Based Procedure to Perform Statistical Energy Analysis, SAE Noise and Vibration Conference and Exposition, Society of Automotive Engineers, Warrendale, PA, 2003.
17. A. Galasso, G. Montuori, S. De Rosa, and F. Franco, Vibroacoustic Analyses of Car Components by Experimental and Numerical Tools, SAE Noise and Vibration Conference and Exposition, Society of Automotive Engineers, Warrendale, PA, 2003.
18. L. Huang, R. Krishnan, T. Connelly, and J. D. Knittel, Development of a Luxury Vehicle Acoustic Package Using SEA Full Vehicle Model, SAE Noise and Vibration Conference and Exposition, Society of Automotive Engineers, Warrendale, PA, 2003.
19. A. Parrett, Q. Zhang, C. Wang, and H. He, SEA in Vehicle Development Part I: Balancing of Path Contribution for Multiple Operating Conditions, SAE Noise and Vibration Conference and Exposition, Society of Automotive Engineers, Warrendale, PA, 2003.
20. D. Wang, G. M. Goetchius, and T. Onsay, *Validation of a SEA Model for a Minivan: Use of Ideal Air- and Structure-Borne Sources*, Society of Automotive Engineers, SAE Noise and Vibration Conference and Exposition, Society of Automotive Engineers, Warrendale, PA, 1999.
21. W. Kozukue and I. Hagiwara, Development of Sound Pressure Level Integral Sensitivity and Its Application to Vehicle Interior Noise Reduction, *Eng. Comput. (Swansea, Wales)*, Vol. 13, No. 5, 1996, pp. 91–107.
22. N. W. Alt, N. Wiehagen, and M. W. Schlitzer, *Interior Noise Simulation for Improved Vehicle Sound*, SAE Noise and Vibration Conference and Exposition, Society of Automotive Engineers, Warrendale, PA, 2001.
23. G. Eisele, K. Wolff, N. Alt, and Michel Hüser, *Application of Vehicle Interior Noise Simulation (VINS) for NVH Analysis of a Passenger Car*, Noise and Vibration Conference and Exhibition, Society of Automotive Engineers, Warrendale, PA, 2005.
24. N. W. Alt, J. Nehl, S. Heuer, and M. W. Schlitzer, Prediction of Combustion Process Induced Vehicle Interior Noise, SAE Noise and Vibration Conference and Exposition, Society of Automotive Engineers, Warrendale, PA, 2003.
25. R. F. Nunes, A. Botteon, J. Jamaguiva, V. S. Mizutani, F. Gerab, D. Lima, and J. L. Mondoni, Cabin Interior Noise Acoustic Assessment under the Influence of Air Intake System: Simulation and Experimental Investigation, Congresso 2002 SAE Brasil ~ 11th International Mobility Technology Congress and Exhibition, Society of Automotive Engineers, Warrendale, PA, 2002.
26. A. R. Patil and M. J. Crocker, *Prediction and Optimization of Radiated Sound Power and Radiation Efficiency of Vibrating Structures Using FEM*, SAE 2000 World Congress, Society of Automotive Engineers, Warrendale, PA, 2000.
27. R. Bocksch, G. Schneider, J. A. Moore, and I. Ver, Empirical Noise Train Model for Power Train Noise in a Passenger Vehicle, SAE Noise and Vibration Conference and Exposition, Society of Automotive Engineers, Warrendale, PA, 1999.
28. M. Mealman, R. Unglenieks, and K. Naghshineh, A Method to Determine the Power Input Associated with Rain Excitation for SEA Models, SAE Noise and Vibration Conference and Exposition, Society of Automotive Engineers, Warrendale, PA, 2001.
29. R. Guedes Sampaio and P. J. P. Gonçalves, Investigation of Sub-System Contribution to a Pickup Truck Boom Noise Using a Hybrid Method Based on Noise Path Analysis to Simulate Interior Noise, 12th SAE Brazil Congress and Exposition, Society of Automotive Engineers, Warrendale, PA, 2003.
30. L. E. Schroeder, Feasibility of Using Acoustic Room Models and Measured Sound Power to Estimate Vehicle Interior Noise, SAE Noise and Vibration Conference and Exposition, Society of Automotive Engineers, Warrendale, PA, 2001.
31. M.-G. Kim, J.-S. Jo, J.-H. Sohn, and W.-S. Yoo, Reduction of Road Noise by the Investigation of Contributions of Vehicle Components, SAE Noise and Vibration Conference and Exposition, Society of Automotive Engineers, Warrendale, PA, 2003.
32. E. Verheijen, A Survey on Roughness Measurements, *J. Sound Vib.*, Vols. 293, No. 3–5, 13 June 2006, pp. 784–794.
33. R. J. Diehl and P. Holm, Roughness Measurements—Have the Necessities Changed? *J. Sound Vib.*, Vols. 293, No. 3–5, 13 June 2006, pp. 777–783.
34. A. E. J. Hardy, R. R. K. Jones, and S. Turner, The Influence of Real-World Rail Head Roughness on Railway Noise Prediction, *J. Sound Vib.*, Vol. 293, No. 3–5, 13 June 2006, pp. 965–974.
35. D. H. Koo, J. C. Kim, W. H. Yoo, and T. W. Park, An Experimental Study of the Effect of Low-Noise Wheels in Reducing Noise and Vibration, *Transport. Res. Part D: Transport Environ.*, Vol. 7, No. 6, November, 2002, pp. 429–439.
36. A. E. J. Hardy, Measurement and Assessment of Noise within Passenger Trains, *J. Sound Vib.*, Vol. 231, No. 3, March, 2000, pp. 819–829.
37. M. G. Dittrich and M. H. A. Janssens, Improved Measurement Methods for Railway Rolling Noise, *J. Sound Vib.*, Vol. 231, No. 3, 30 March 2000, pp. 595–609.
38. M. Kalivoda, M. Kudrna, and G. Presle, Application of MetaRail Railway Noise Measurement Methodology: Comparison of Three Track Systems, *J. Sound Vib.*, Vol. 267, No. 3, Oct. 23, 2003, pp. 701–707.
39. F. G. De Beer, M. H. A. Janssens, and P. P. Kooijman, Squeal Noise of Rail-Bound Vehicles Influenced by



- Lateral Contact Position, *J. Sound Vib.*, Vol. 267, No. 3, 2003, pp. 497–507.
40. D. J. Thompson and P. J. Remington, The Effects of Transverse Profile on the Excitation of Wheel/Rail Noise, *J. Sound Vib.*, Vol. 231, No. 3, 2000, pp. 537–548.
  41. P.-E. Gautier, A Review of Railway Noise Research and Results Since the 5th IWRN in Voss (Norway), *J. Sound Vib.*, Vol. 231, No. 3, 30 March 2000, pp. 477–489.
  42. N. Vincent, J. R. Koch, H. Chollet, and J. Y. Guerder, Curve Squeal of Urban Rolling Stock—Part 1: State of the Art and Field Measurements, *J. Sound Vib.*, Vol. 293, No. 3–5, 13 June 2006, pp. 691–700.
  43. C. Mellet, F. Létourneaux, F. Poisson, and C. Talotte, High Speed Train Noise Emission: Latest Investigation of the Aerodynamic/Rolling Noise Contribution, *J. Sound Vib.*, Vols. 293, No. 3–5, 13 June 2006, pp. 535–546.
  44. K. Nagakura, Localization of Aerodynamic Noise Sources of Shinkansen Trains, *J. Sound Vib.*, Vols. 293, No. 3–5, 13 June 2006, pp. 547–556.
  45. S. Wang and R. Bernhard, Energy Finite Element Method (EFEM) and Statistical Energy Analysis (SEA) of a Heavy Equipment Cab, SAE Noise and Vibration Conference and Exposition, Society of Automotive Engineers, Warrendale, PA, 1999.
  46. W. Desmet, B. Pluymers, and P. Sas, Vibro-acoustic Analysis Procedures for the Evaluation of the Sound Insulation Characteristics of Agricultural Machinery Cabins, *J. Sound Vib.*, Vol. 266, No. 3, 18 Sept. 2003, pp. 407–441.
  47. N. Tsujiuchi, T. Koizumi, I. Kubomoto, and E. Ishida, Structural Optimization of Tractor Frame for Noise and Vibration Reduction, SAE International Off-Highway and Powerplant Congress and Exposition, Society of Automotive Engineers, Warrendale, PA, 1999.
  48. M. Legris and P. Pouline, Noise Exposure Profile Among Heavy Equipment Operators, Associated Laborers, and Crane Operators, *AIHA J.*, Vol. 59, 1998, pp. 774–778.
  49. J. DePriest, Aircraft Engine Attachment and Vibration Control, SAE General Aviation Technology Conference and Exposition, Society of Automotive Engineers, Warrendale, PA, 2000.
  50. L. Choi Chow, P. Lempereur, and K. Mau, Aircraft Airframe Noise and Installation Effects—Research Studies, *Air & Space Europe*, Vol. 1, No. 3, May–June 1999, pp. 72–75.
  51. D. G. MacMartin, Collocated Structural Control for Reduction of Aircraft Cabin Noise, *J. Sound Vib.*, Vol. 190, No. 1, 15 February 1996, pp. 105–119.
  52. B. Goujard, A. Sakout, and V. Valeau, Acoustic Comfort on Board Ships: An Evaluation Based on a Questionnaire, *Appl. Acoust.*, Vol. 66, No. 9, Sept. 2005, pp. 1063–1073.
  53. S. Weyna, The application of Sound Intensity Technique in Research on Noise Abatement in Ships, *Appl. Acoust.*, Vol. 44, No. 4, 1995, pp. 341–351.
  54. H. Zheng, G. R. Liu, J. S. Tao, and K. Y. Lam, FEM/BEM Analysis of Diesel Piston-Slap Induced Ship Hull Vibration and Underwater Noise, *Appl. Acoust.*, Vol. 62, No. 4, April 2001, pp. 341–358.

# CHAPTER 95

## AUTOMOBILE, BUS, AND TRUCK INTERIOR NOISE AND VIBRATION PREDICTION AND CONTROL

**Robert J. Bernhard**  
School of Mechanical Engineering  
Purdue University  
West Lafayette, Indiana

**Mark Moeller**  
Spirit AeroSystems  
Wichita, Kansas

**Shaobo Young**  
Vehicle Design Research and Advanced Research and Innovation Center  
Ford Motor Company  
Dearborn, Michigan

### 1 INTRODUCTION

Interior noise in automobiles, buses, and trucks is caused primarily by the engine, exhaust, transmission, and driveline components (power train noise), tire/pavement interaction (road noise), and airflow around the vehicle (wind noise). From the source, vibration or sound energy is transferred by airborne or structure-borne paths to the passenger cabin interior. Generally speaking, structure-borne noise is the dominant component of vehicle interior total noise below 400 Hz, and airborne noise starts to become dominant above 400 Hz. For different applications, dominant noise sources or paths may be different. For example, power train noise is dominant during the accelerations of most vehicles; tire/road noise is the dominant noise source when a vehicle is cruising on a smooth road at about 80 km/h; and at high speeds of above 130 km/h, wind noise will surpass other noise sources and becomes the dominant noise source inside a vehicle. Testing and prediction are important to understand the cause of noise in the passenger cabin for a particular application and to optimize noise reduction methods. This chapter begins with a description of the primary sources of noise and vibration and how sound is transmitted to the passenger cabin of the vehicle. This discussion is followed by a summary of how test-based and computer-aided engineering (CAE) methods are applied to predict road noise, wind noise, and power train noise and to evaluate acoustic noise reduction solutions. The chapter closes with a summary of noise reduction methods currently used for automobile, bus, and truck applications.

### 2 VEHICLE NOISE SOURCES

#### 2.1 Road Noise

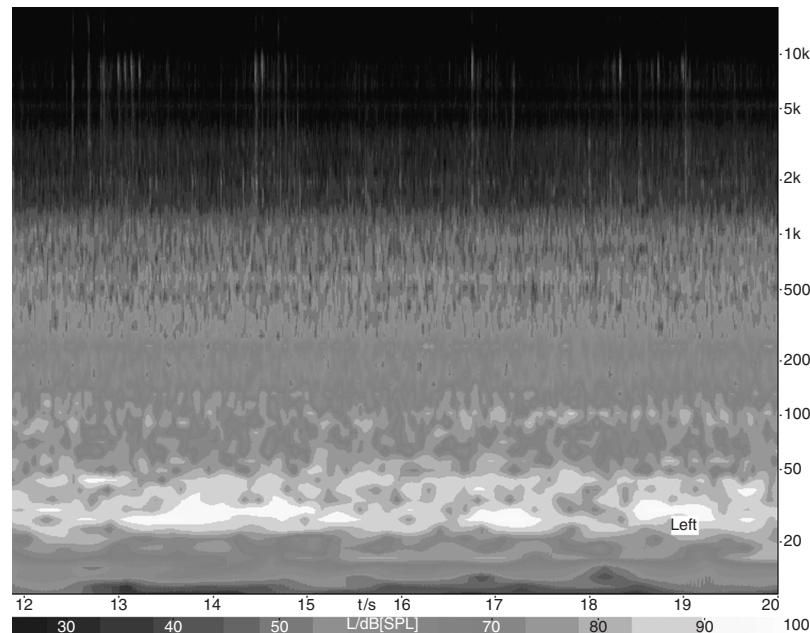
Road noise is generated by events that occur at the tire/pavement interface. The source mechanisms are

complex and change depending on speed and the pavement and tire combination.<sup>1,2</sup> Airborne sound radiation from the tread blocks and the sidewall of the tire can be a noise source for vehicles that do not have a well-sealed door and floor structure. Most of the time, road noise refers to structure-borne noise due to vibrations caused by vehicle tire/road surface impacts transmitted through the suspension mounts and that then excite the vehicle structure to generate low-frequency sound (<400 Hz). Tire/wheel imbalances can also introduce structure-borne road noise in the same fashion. Figure 1 shows a spectrogram of road noise of a typical vehicle. As can be seen in Fig. 1, the road noise of a typical vehicle is dominant at low frequencies (below 400 Hz). Tire ring noise (~260 Hz) can also be discerned with this vehicle.

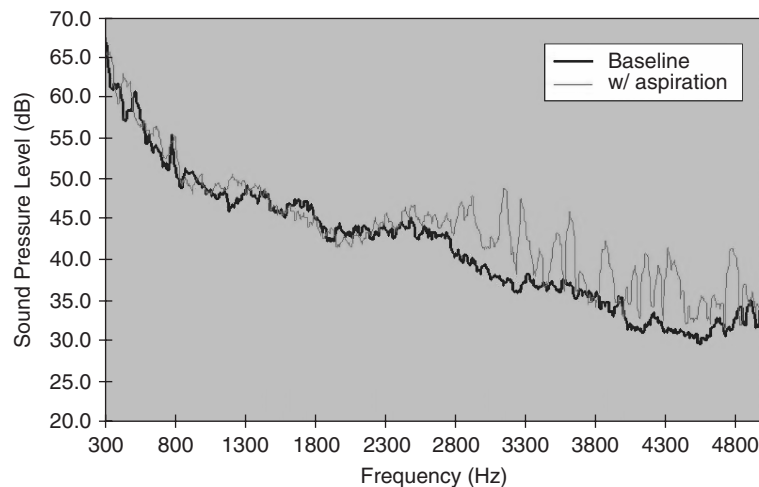
#### 2.2 Wind Noise

Wind noise is the dominant source of cabin noise at high vehicle speed (>130 km/h). As the noise treatments for engine noise and road noise become more and more efficient, wind noise starts to become a serious issue for all vehicle manufacturers. To study vehicle wind noise, vehicle manufacturers are using wind tunnels similar to the ones used in the aerospace industry. Some manufacturers even designed and built their own acoustically treated wind tunnels. Ford and Daimler Chrysler have recently invested in new quiet acoustical wind tunnel facilities for wind noise testing.<sup>3</sup> Comprehensive reviews of wind noise have been organized by George,<sup>4</sup> and George and Callister.<sup>5</sup>

The performance of vehicle door sealing systems is critical for the control of wind noise. At high speeds, the door on a vehicle tends to move outward due to the difference between the aerodynamic pressure outside



**Figure 1** Typical vehicle road noise spectrogram. (The x axis represents time in seconds, and the y axis represents frequency, Hz.)



**Figure 2** Wind noise level inside passenger compartment with and without aspiration.

the vehicle and that inside the cabin. If the door seal does not have enough ability to remain in tight contact with its mating surface, air can travel through the seal and cause aspiration. The loss of the seal material elasticity over time and the variation of the seal gap along the door perimeters can also cause aspiration to occur. From the dynamic performance point of view, if a seal takes a longer time to respond to its mating surface vibration, aspiration occurs. When aspiration

occurs, it is the most dominant source of wind noise in the passenger cabin. Figure 2 illustrates interior sound with and without aspiration.

Aspiration noise is a major wind noise concern, especially from the viewpoint of the passengers. Aspiration noise is usually broadband high-frequency noise; it is very directional and easily perceived by passengers inside a vehicle. Passengers may attribute aspiration noise to poor vehicle quality, whereas they will more

readily tolerate louder overall wind noise (other than aspiration), surmising that such noise has been caused by strong wind conditions outside the vehicle. To avoid aspiration noise situations, some vehicles have as many as three layers of seals. Low interior noise levels will not be achieved if aspiration occurs.

The next important source of wind noise is referred to as shape noise. A turbulent boundary layer is formed by the flow over a vehicle, with a large separated flow at the A-pillar, roof line, underbody, wheel wells, and rear of the vehicle. Aeroacoustic sound is generated by the turbulence in these separated flow regions. Aeroacoustic sound is treated as an acoustic source and transmitted into a vehicle's interior through a conventional noise transmission mechanism. Hydrodynamic pressure fields associated with these turbulent flows also load the surfaces of the vehicle. The hydrodynamic flow is treated as a dynamic pressure loading on the surface of the vehicle and causes the vehicle surface to vibrate and to generate structure-borne noise, which directly radiates into the vehicle interior.

### 2.3 Power Train Noise

Power train noise includes sound from all sources associated with generating and supplying power to move the vehicle, except the tires and brakes, which are covered separately. Power train sources include the engine, transmission, intake and exhaust system, and driveline. All of the power train components are both sound and vibration sources. The sound energy created by the vibration of the surfaces of these components and the aerodynamic loads within these components is radiated as airborne sound. The mechanical shaking forces and other vibration induced by the component are transmitted mechanically through the attachment points and structure-borne paths to the cabin.

For power train noise, all operating conditions are considered, including engine startup (cranking noise), idle conditions (stabilized warm idle), high-speed operation, and transient events such as engine runups [wide open throttle (WOT) or partial open throttle (POT) operation] and transmission shifts. The frequency range of interest for powertrain noise covers the entire range of human perception—approximately 20 to 20,000 Hz.

Figure 3 shows the engine noise of a typical vehicle measured in the passenger compartment when the vehicle is undergoing an engine runup in a WOT condition. Some discrete frequency lines are apparent in the engine WOT spectrogram. These lines represent sound spectrum peaks that are related to the engine speed or engine order changes during runup. These engine-order-related sounds dictate how an engine sounds during its operation. Many research studies have been focused on understanding how to design engine order sounds in order to create and enhance vehicle brand images.

## 3 NOISE AND VIBRATION PATHS

Noise and vibration transmission from the source to the interior of the vehicle are commonly referred to as either structure-borne or airborne paths. Structure-borne paths are characterized by direct mechanical

connections through the structure to the panels on the surface of the passenger cabin where the energy is radiated as sound to the interior acoustical space. Airborne noise paths refer to cases in which sound generated outside the passenger cabin is transmitted through the vehicle panels to the interior space.

### 3.1 Structure-Borne Noise

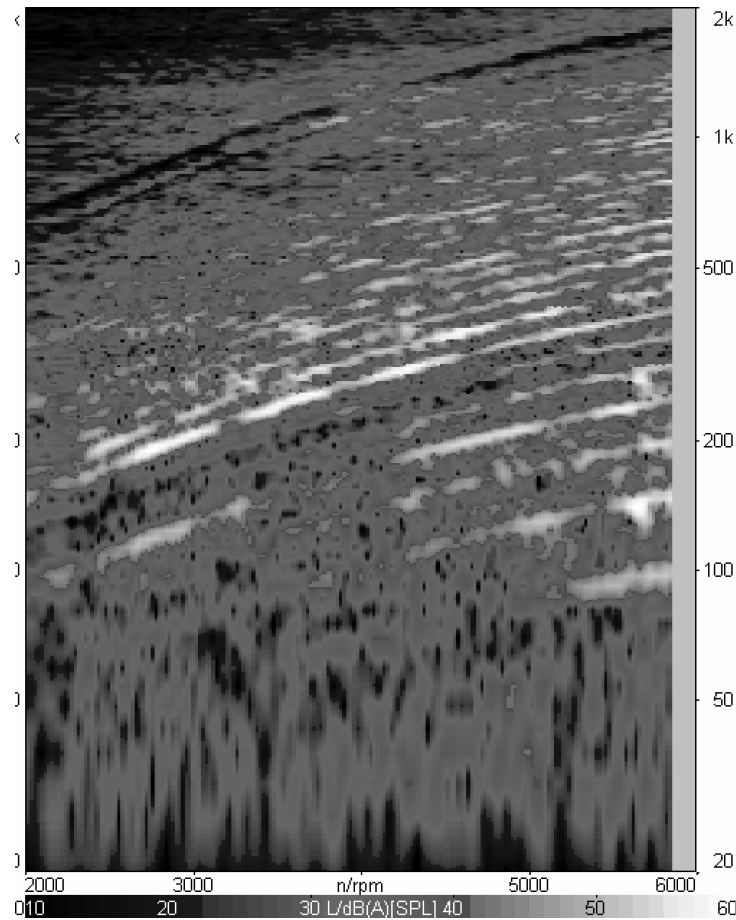
Low-frequency road noise is a classic example of structure-borne noise. The interaction of the tire patch and the pavement is the source. Vibration of the tire is transmitted to the wheel and to the spindle. From the spindle, the vibration energy is transmitted through various paths consisting of many different combinations of suspension components, chassis members, and body panels. For different vehicles or different operating conditions, the dominant path may be different. The dominant path usually includes well-coupled components that are resonant at an excitation frequency of importance. For unibody automobiles, structure-borne noise tends to dominate road noise from 300 to 500 Hz and might be important up to 800 Hz, depending on the source and the vehicle design. For a body on frame vehicle, the structure-borne noise may be dominant only up to 300 Hz depending on the performance of the isolation system between the body and frame.

Structure-borne paths are also responsible for low-frequency engine noise including engine boom noise (<100 Hz) and engine moan noise (100 to 200 Hz). The shaking forces of the engine are transmitted through the engine mounts and into the chassis and vehicle body. On some occasions, the dynamic forces of other power train components are well coupled structurally to the panels surrounding the passenger cabin and will radiate sound into the cabin. Problems occur when exhaust system hangers, high-volume air-conditioning (HVAC) piping, electrical system wiring harnesses, or similar structures are poorly designed and efficiently couple vibration energy directly to passenger cabin panels. Such problems are usually unanticipated and must be resolved at the prototype stage. The coupling between the power train component excitation and the vehicle cabin cavity is also a significant source of vehicle interior low-frequency boom noise (<50 Hz).

### 3.2 Airborne Noise

Airborne sound transmission in automobiles, trucks, and buses is similar to transmission loss behavior in buildings. For road noise, the sound generated at the tire propagates under the vehicle and is transmitted by airborne paths through the floor panels. Road noise also propagates around the body of the vehicle and is transmitted through windows and passenger cabin panels. Sometimes, road noise travels through the engine compartment or trunk and is transmitted through body panels into the passenger cabin. Airborne noise tends to dominate the high-frequency band of road noise. It starts to become important at frequencies from 300 to 800 Hz depending on the vehicle design.

The sound radiated by power train components is also transmitted by airborne paths to the passenger



**Figure 3** Typical vehicle interior engine noise with wide open throttle engine.

cabin. For example, sound from the engine, transmission, and intake manifold is transmitted through the dash panel. Sound from exhaust components is transmitted through floor panels.

Most wind noise is transmitted from the source to the cabin by airborne paths. Aspiration noise is generated directly in the cabin. Aeroacoustic sound is transmitted through glass and panels. Hydrodynamic loads cause sound radiation from the panels or glass that experience the dynamic pressure of the hydrodynamic loads.

#### 4 CABIN NOISE CRITERIA

There are many different events that affect the user's evaluation of the quality of automobiles, trucks, or buses. The automotive industry still depends heavily on subjective evaluation of either trained experts or jury testing with perspective customers. However, a great deal of recent attention has been paid to the development of objective measures of noise, and such metrics are becoming more prevalent. Cabin noise is a competitive quality characteristic of automobiles. Thus, thresholds

and criteria are largely company specific. Also, different objective measures are used for various events because they correlate better to customer preferences. A set of example events and criteria used include:

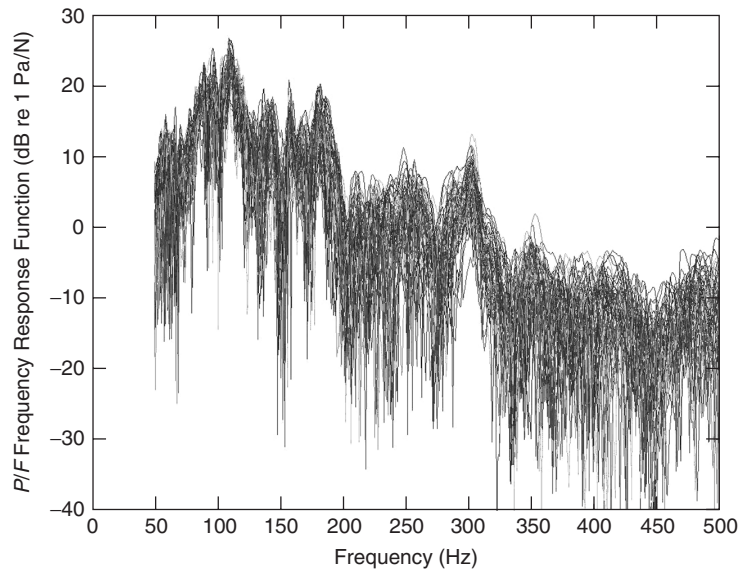
*Road noise:* Overall level, spectrum levels, speech intelligibility

*Wind Noise:* Overall level, spectrum levels, directionality, impulsiveness

*Power Train Noise:* Overall level, speech intelligibility, order tracking

It is still common to use A-weighted sound pressure level as an objective measure for some applications, particularly stationary events such as road and wind noise. The overall level is often decomposed into a frequency spectrum when diagnostic information is desired.

It is worthwhile to note that many large vehicle manufacturers are increasingly using psychological-acoustics terms to better correlate their vehicle quality



**Figure 4** Frequency response function between force excitation at the spindle and sound pressure at the driver's ear location for 98 nominally identical Isuzu Rodeo vehicles. (From Ref. 8. Reprinted with permission.)

to customer perceptions. In these types of studies, loudness, sharpness, roughness, and pitch variation are often used to describe the product performance. Many of the vehicle original equipment manufacturer (OEM) researchers are developing their own metrics for the purpose of product evaluations.

Comparison of sound pressure level is widely used to evaluate power train noise. However, sound quality metrics are increasingly used, especially for luxury vehicles. Based on human perception studies, targets for various engine harmonics are set so that an ideal overall sound signature of the power train is achieved to meet the vehicle's marketing image—for example, sporty, safe, reliable, and so forth.<sup>6,7</sup> Desired signatures can be achieved either through passive design changes, primarily through intake and exhaust system design, or by active means through sound cancellation and/or addition. To improve the sound quality of the power plant, unwanted power train noise—for example, gear whine—must be reduced in level sufficiently so that it is masked by the desired sound.

Speech interference indices are sometimes used to assess the ability of the customers in the vehicle to hold a conversation or listen to music during vehicle operation. Transient events, such as power train runups, require specialized metrics. Door slam, wiper noise, and road impact events are all important quality characteristics of automobiles and require specialized description to characterize a customer's evaluation of the vehicle.

## 5 PREDICTION METHODS

The purpose of testing and analysis is either to assess and understand the behavior of existing hardware,

particularly if noise performance goals are not met, or to optimize the design of future vehicles. One key issue for automobiles, trucks, and buses, and one that will be emphasized in this discussion because it is pervasive, is to accomplish these predictions in the presence of variation.<sup>8–10</sup> Typical variation is illustrated in Fig. 4. This type of variation occurs in all automotive vehicle applications and must be accounted for when implementing test or prediction.

Because automobiles, trucks, and buses are relatively complex, testing and prediction for NVH characteristics is a significant challenge with current tools. NVH stands for noise, vibration, and harshness. While the terms noise and vibration are familiar to most, harshness is a relatively specialized term that describes the perception of a vehicle product. Harshness describes the total sound and vibration a customer feels when he or she operates a vehicle. A harsh vehicle would be one that gives rise to a sensation of one with hard tires, which would give the impression of a harsh ride. A quality operating system (QOS) for test and prediction is critical for improving the performance of noise and vibration prediction process over time. A QOS is used to provide a historical basis for how well a process performed in the past to avoid repeating the same mistakes. The QOS should include formal validation exercises and ongoing performance checking of the tools used to make noise and vibration prediction assessments. The quality of the data should drive the decision-making process.

### 5.1 Test-Based Methods

A nonexhaustive list of test-based tools used in automotive applications includes:

Road test	Structural damping
Wind tunnel testing	Laser doppler vibrometer
Wide open throttle	Modal analysis
Idle test	Operating deflection shape
Acoustical holography	Transfer path analysis
Acoustic reciprocity	Shaker testing/hammer testing
Acoustic absorption	Point and transfer mobilities
Acoustic intensity	Static sealing
Sound power testing	Static stiffness
Reverberation room	Chassis dynamometer
Transmission suite	Power Train dynamometer
Noise reduction testing	Test-based SEA
Acoustic reciprocity	Pass-by testing
Laser holographic interferometry	

Many of these methods are discussed in other chapters. In this chapter, the focus of the discussion will be on the best practice for the most common methods applied to automobiles, trucks, and buses.

For test-based approaches, transfer function analysis is often coupled with a body panel contribution analysis. The panel motions are correlated with the forcing functions to determine which motions are contributing to sound in the passenger cabin interior. This is accomplished with either an array of accelerometers or with a scanning laser.

An experimental transfer path modeling approach is often used for predictive models and path identification since the source, path, and receiver are typically independent for this application.<sup>11–13</sup> Improvements are achieved either at the source or by reducing, or in some cases increasing, the magnitude of the transfer path.

Chassis roll testing is often used to simulate road events. Large-diameter rollers are used to make the surface appear as flat as possible. Both smooth surface rollers and replicate castings of rough road surfaces are used. This provides a controlled environment for road noise testing.

Because of the complexity of the vehicles involved and the variability in the vehicles, systematic and formal testing processes are important. There are two main strategies for testing: One factor at a time testing (OFT) and design of experiments (DoE). Both strategies are common. In either case it is necessary to design the experiment to resolve the effect of interest in the presence of the natural variation in the product. The testing should be conducted in a fashion that is robust to significant variation across the ensemble to be able to discriminate against the variation. One means of identifying sources of variation in test procedures is to do *component variance studies*.<sup>14,15</sup> Once measurement variation is reduced as much as practical, it is important to periodically check that the test process continues to conform to the measurement quality standard.

Proponents of the OFT approach chose this method to simplify the process of determining which factor is

responsible for the change in the response. However, this approach ignores interactions between factors whereby one factor may depend on the setting or value of another factor. The OFT approach is also not efficient. As each factor is studied in turn, data collected to study other factors is ignored. Each set of data supplies information on only one factor.

Experiment designs (e.g., factorial) provide an alternative to the OFT approach. These designs allow the study of interactions between factors. The structure of factorial designs allows all the data from the experiment to be used to study each factor, which results in a significant increase in efficiency over OFT. The interested reader is directed to references on experimental design.<sup>16,17</sup> Most of the experiment design literature discusses single-number response variables. However, the same data collection and analysis techniques documented in the literature can be applied spectral band by spectral band.<sup>18,19</sup>

## 5.2 CAE-Based Methods

The CAE-based tools used in automotive noise and vibration prediction include (not exhaustive):

Finite element analysis	Computational fluid dynamics
Finite difference techniques	Acoustic ray tracing
Boundary element analysis	Analytical solutions
Statistical energy analysis	Porous element FEM

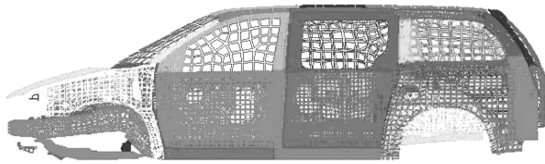
Most of these methods have been discussed in detail in other chapters. In this chapter the application of the most common methods for analysis of automobiles, trucks, and buses will be discussed.

When using analysis to assess program performance, it is important to understand how well the numerical model represents the hardware. Generally, this is accomplished by doing correlation studies. A corporate process controlled by a quality operating system is important to provide a historical perspective about analysis performance so every model does not require ongoing correlation. Important components of the quality operating system include capturing the performance of the models and charting the results at the end of the analysis effort. This allows statistical process control techniques to be applied to the analysis process to identify common and special case variation in the analysis process.

It is also possible to assess the ability of analysis to span the design space. This assessment is accomplished by comparing the predicted design sensitivities to those obtained from OFT or designed experiments. These data provide confidence that analytical results will provide meaningful data when used in optimization studies for configurations where correlation is not possible.

Finite element models (FEM) and Statistical energy analysis (SEA) are used most widely for noise and vibration prediction. The unique aspects of application of these methods to automotive applications will be discussed.





**Figure 5** Illustration of a vehicle FEM model (element size = 250,000).

**5.2.1 Finite Element Analysis** Noise and vibration prediction models of automotive vehicles for the frequency band of interest are generally large. The time and effort required for creating and exercising finite element analysis for noise and vibration prediction of vehicles is dominated by development and validation of body models, often with over 250,000 elements. (See Fig. 5.) Here, the quality operating system becomes vital for managing the data for highly detailed geometry, property values, plus the connectivity of the model parts. In general, the quality operating system should also be used to supervise the relationship between model building and analysis software, even when the codes are provided by the same vendor.

Because of the large number of elements in these finite element models, most analyses are limited to linear approximations of the body and other major structural components. Even so, the computational effort is large enough that model reduction is necessary.<sup>20,21</sup> Dynamic reduction and component mode synthesis,<sup>22</sup> as well as tools for reusing previous results when analyzing changes, are widely used for automotive applications. For example, modal superposition methods are widely used to reduce finite element models from several hundred thousand physical degrees of freedom (DOF) to a few thousand modal DOF for vehicle or body or a few dozen modal degrees of freedom for simple components such as control arms. Finite element models are discussed in Chapter 7.

Finite and boundary element models have also been developed to predict the performance of the composite acoustical material systems used for noise reduction in passenger cabins.<sup>23–26</sup> These models are used to predict wave propagation behavior in acoustical materials and the structural backing plates. The resulting model is either incorporated into the deterministic FEM method of the vehicle or noise reduction properties are derived to be incorporated into SEA models.

Vehicle level models are used to compute the response of the vehicle to sinusoidal or random inputs in the form of either applied loads or enforced displacements. These frequency responses are processed to evaluate performance. The quality operating system should be used to address how the bridge is built between CAE-based prediction and objectives that are based on true performance improvement.

**5.2.2 Statistical Energy Analysis** Application of SEA models in the automotive industry began in approximately 1986. Currently, this technology is in widespread use across the vehicle manufacturer and

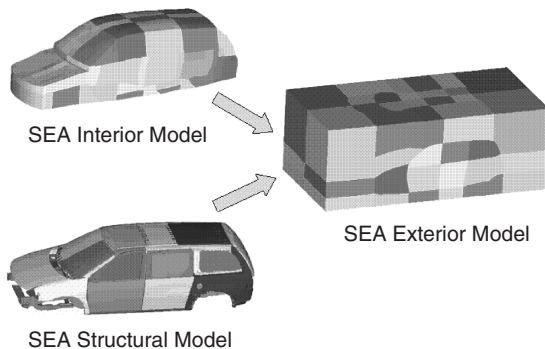
supplier base. Commercial codes with extensive pre-processing capabilities have been developed primarily for automotive applications. SEA technology is capable of both airborne and structure-borne modeling. The most extensive use of SEA is for modeling airborne noise transmission into the vehicle interior. A review of SEA modeling for automotive applications can be found in the references.<sup>27,28</sup>

The SEA models in use today tend to be full vehicle models. Having a full vehicle model allows for simulation of events such as four-tire airborne noise. It also allows for multievent optimization of the noise control treatments. As a result, the industry trend is to have a general full vehicle SEA model, which is modified to the particular properties of a vehicle, rather than a single-use model or partial model.

For an SEA model, the vehicle structure is idealized into mode groups along natural boundaries where possible. Body panels and the greenhouse glass are modeled as plate bending and inplane mode groups. The body structure, such as the pillars and the rocker panels, tend to be modeled as beams at low frequencies and transition to plates at higher frequencies. Subsystem boundaries tend to be at natural changes in impedance for the body structure. For example, joints would occur at the B-pillar or the front rail at the shocktower. The interior cabin space is often subdivided into several different acoustic mode groups. An SEA model describes how energy is transferred among different systems outside and inside a vehicle. A typical vehicle SEA model is composed of three parts: a vehicle interior model, vehicle structural model, and vehicle exterior model. For a steady-state SEA, the analytical solution requires simply that the input power must equal the output power for each acoustic or structural subsystem in each frequency band. Steady-state and transient SEA models are discussed in Chapter 17.

Transient SEA analysis at its most basic level simply includes time-dependent terms in the power flow balance equations. Although this may not at first seem to significantly add to the complexity of the solution, in actuality, the adoption of a numerical method is required for a transient solution. In this numerical method, each time step is solved as a function of the energy in each subsystem during the previous time step and of the change in energy with respect to time. So a solution technique that is purely analytical and closed form for a steady-state solution needs to use a numerical approach when a transient solution is calculated.

Statistical energy analysis models have been successfully applied to airborne noise reduction events. These events include engine noise reduction, induction noise, tire noise reduction, and interior noise due to exhaust noise. SEA modeling for wind noise is actively being pursued as well.<sup>31</sup> Transient SEA for modeling vehicle transient sound phenomenon has been developed for modeling impact sound events such as door slams.<sup>29</sup> SEA for structure-borne events is not being as actively pursued at this time. The analyst community



**Figure 6** Typical SEA models (including vehicle interior, structural, and exterior models).

tends to use deterministic methods such as the finite element method for structure-borne events.

Figure 6 shows the SEA models for a sports utility vehicle. The complete vehicle model includes separate SEA models for interior, structure, and exterior. There are two distinct ways to represent the sound package in current SEA models. One way is to explicitly model the sound package layout (pure CAE modeling). This is accomplished by representing the substrate as a plate bending subsystem and modeling the acoustic modes in the interstitial air in the fiber/foam material as an isothermal acoustic space. The carpet/barrier is modeled as either a limp mass or a bending subsystem with appropriate properties.<sup>30,31</sup> The alternative modeling scheme is to use test/analysis data for the layout and import the consolidated properties as a transmission loss into the SEA model (CAE/test hybrid method). Data for the structure-borne noise reduction is also provided for coupling the plate vibration to the acoustic space. The hybrid method often yields more reliable predictions at low frequencies where model densities of the SEA systems are low and less accurate. Both pure CAE and CAE test techniques are in active use.

Statistical energy analysis models have been subject to rigorous validation.<sup>32–35</sup> These model validations include:

1. Component impedance comparison (modal density)
2. Component testing (e.g., barrier TL measurements)
3. Damping measurements
4. Acoustic intensity scans
5. Response plot comparisons
6. Thermogram comparisons (test based—analytical)
7. Doe sensitivity assessment
8. Source determination
9. Hardware prove out—response comparisons

The SEA models have been shown to span the design space. Validations by both One Factor at a Time and designed experiment have been reported in the literature.<sup>30,35</sup>

## 6 NOISE REDUCTION

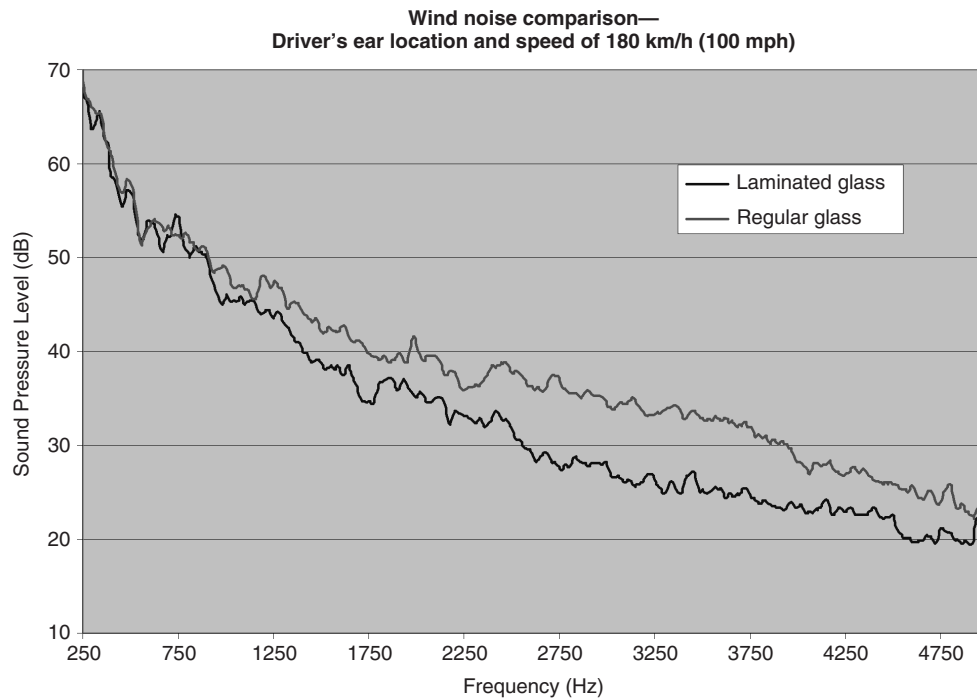
Noise reduction strategies in automobiles, trucks, and buses include a large menu of potential solutions depending on the source, path, and application. In most cases, vehicles are sensitive to weight and cost and solutions must be highly efficient.

Noise reduction typically starts at the source. Suppliers of components usually face challenging specifications for noise. Most components, such as engines, motors, and tires, are becoming quieter while maintaining or improving performance and price.

The challenge of the vehicle manufacturer is usually to control the paths. The airborne paths are usually treated by closing up openings (i.e., with seals), adding mass to panels and windows, and adding sound absorption inside the passenger cabin. Structure-borne noise is treated by optimizing the mount (e.g., using isolators, impedance mismatch), damping of resonant systems, or building in vibration breaks. A few particular examples of noise reduction strategy applied to automobiles will be discussed.

A large proportion of the airborne noise in automobiles occurs in the front of the vehicle. Road noise, power train noise, exhaust noise, intake noise, front-end accessory drive noise, and wind noise are all transmitted through the dash panel, front floor panels, and windscreen glass. There are two main strategies for achieving noise reduction. The classical technique is to provide a mass backed isolation material over sheet metal surfaces to increase mass and improve transmission loss. Recently, similar noise reductions have been achieved with significantly reduced weight by eliminating the mass backed decoupling layer on the dash panel and significantly increasing the interior acoustic absorption. Another important strategy is minimizing the number of penetrations from the engine compartment to the interior. These penetrations include accelerator cable, brake, steering column, several heating ventilation and air-conditioning system penetrations, engine computer, and electrical cabling. Some vehicles have been designed to keep the number of penetrations to as few as 8. Less well designed vehicles can have as many as 18 penetrations through the dash panel. Managing the sealing of these penetrations and their associated noise control treatments is critical. The most important frequency range is in the critical speech intelligibility frequencies from 800 Hz to 4 kHz.

Other strategies for noise reduction include dash doublers, pillar sealers, damping materials in doors, door panels, and greenhouse glass. In a luxury car, the sealing systems/isolators are effective enough that the dominant acoustic path is the windscreen glass. In this case further noise reduction can be achieved by using laminated glass for the side windows as well as for the windshield and backlight glass. Laminated glass, due to its high internal damping, radiates



**Figure 7** Wind noise in vehicle interior when laminated side windows are used.

much less sound when it vibrates. The multilayer structure of laminated glass also eliminates or shifts the coincidence frequency region of 2 to 3 kHz (the value for monolithic glass) and therefore yields a much better sound insulation performance. Figure 7 illustrates a typical wind noise performance improvement achieved by the use of laminated glass.

Interior acoustic absorption plays a significant role in noise reduction. There are several surfaces available for application of noise control treatments including the headliner, the seats, and the floor treatment.<sup>36,37</sup>

For road noise, the noise reduction strategies in order of consideration are:

1. Optimizing point mobilities either using isolators or by structural design to minimize force transmission
2. Damping materials to minimize panel vibration
3. Sound insulation to block airborne noise paths
4. Tire geometry and properties to reduce source noise
5. Selective increases of the stiffness of body components

In general, body-on-frame vehicles are quieter than unibody vehicles because of an extra level of isolation (frame-to-cab isolation). However, some body-on-frame vehicles have poor performance in the low-frequency range because of flat body panels and minimal sound packages.

## 7 CONCLUSIONS

Automobile, bus, and truck NVH data show a trend of continuous improvement. New vehicles have been quieter than the models they have replaced. New tools and processes are being developed to meet these aggressive NVH targets.

Computer-aided engineering tools are being widely used across the manufacturing base to support automobile, bus, and truck noise issues. However, application of these techniques to automobiles, trucks, and buses is challenging. To be fully integrated into the design process, these techniques must account for the natural variation across the ensemble. And to effectively use these tools, a quality operating system must be implemented to continually learn from experience and achieve systematic improvement of both the modeling process and the resulting product.

**Acknowledgments** The authors would like to gratefully acknowledge the contributions of Scott Bergeon at LMS, and Robert S. Thomas and Poyu Tsou from the Ford Motor Company.

## REFERENCES

1. U. Sandberg and J. A. Ejsmont, *Tyre/Road Noise Reference Book*, Informex, SE-59040 Kisa, Sweden, 2002.
2. P. R. Donovan and B. Rymer, Assessment of Highway Pavements for Tire/Road Noise Generation, Proceedings of the 2003 SAE Noise and Vibration Conference, SAE Paper 2003-01-1536, SAE International, Detroit, MI, 2003.

3. J. Walter, E. Duell, B. Martindale, S. Arnette, P. A. Nagle, W. Gulker, S. Wallis, and J. Williams, The Driveability Test Facility Wind Tunnel No. 8, SAE 2002 World Congress, SAE Paper 2001-01-0252, SAE International, Detroit, MI, 2002.
4. A. R. George, Ed., *Automobile Wind Noise and Its Measurement*, SAE Special Publication SP-1184, SAE International, Detroit, MI, 1996.
5. A. R. George and J. R. Callister, Ed., *Topics in Wind Noise and Its Measurement Part II*, SAE Special Publication SP-1457, SAE International, Detroit, MI, March, 1999.
6. U. Linder and A. Mueller, Sounddesign—the BMW Inline Six-Cylinder Engine in 9. Different Vehicle Applications. Proceedings of the 2001 SAE Noise and Vibration Conference, SAE Paper 2001-01-1428, SAE International, Detroit, MI, 2001.
7. N. Terazawa, T. Wakita, H. Nakagawa, and T. Uno, A New Method of Engine Sound Design for Car Interior Noise Using a Psychoacoustic Index, SAE Paper 2004-01-0406, 2004 World Congress, Detroit MI, March, 2004.
8. M. S. Kompella and R. J. Bernhard, Measurement of the Statistical Variation of Structural-Acoustic Characteristics of Automotive Vehicles, *Noise Control Eng. J.*, Vol. 44, No. 2, pp. 93–99.
9. J. A. Cafeo, S. Doggett, D. A. Feldmaier, R. V. Lust, D. J. Nefske, and S. H. Sung, A Design of Experiments Approach to Quantifying Test to Test Variability for a Modal Test, Proceedings of the 15th International Modal Analysis Conference, Orlando, FL, 1997.
10. B. Gardhagen and J. Plunt, Variation of Vehicle NVH Properties Due to Component Eigenfrequency Shifting—Basic Limits of Predictability, Proceedings of the 1995 SAE Noise and Vibration Conference, SAE paper 951302, SAE International, Detroit, MI, May 1995.
11. M. S. Kompella and R. J. Bernhard, Techniques for Prediction of the Statistical Variation of Multiple-Input-Multiple-Output System Response, *Noise Control Eng. J.*, Vol. 45, No. 3, 1997, pp. 133–142.
12. M. Stebbins, J. R. Blough, and D. L. Brown, Measuring and Including the Effects of Moments and Rotations on Automobile Bodies for the Accurate Modeling of Transmitted Forces, Proceedings of the 14th International Modal Analysis Conference, Dearborn, MI, 1996.
13. J. Park, P. Gu, J. Juan, A. Ni, and J. Van Loon, Operational Spindle Load Estimation Methodology for Road NVH Applications, Proceedings of the 2001 SAE Noise and Vibration Conference, SAE Paper 2001-01-1606, SAE International, Detroit, MI, 2001.
14. R. D. Moen, T. W. Nolan, and L. P. Provost, *Improving Quality Through Planned Experimentation*, Appendix 8A, Calculation of Variance Components, McGraw Hill, New York, 1991.
15. M. Kriss, T. Mouch, and R. S. Thomas, Variance Components Analysis to Improve Automotive Body System NVH Measurement Quality, Proceedings of the 15th International Modal Analysis Conference, Orlando, FL, January 1997.
16. G. E. P. Box, W. G. Hunter, and J. S. Hunter, *Statistics for Experimenters*, Wiley, New York, 1978.
17. R. D. Moen, T. W. Nolan, and L. P. Provost, *Improving Quality through Planned Experimentation*, McGraw-Hill, New York, 1991.
18. T. Dyer, T. W. Nolan, W. Shapton, and R. S. Thomas, The Analysis of Frequency Domain Data from Designed Experiments, Proceedings of the 1995 SAE Noise and Vibration Conference, SAE Paper 951274, SAE International, Detroit, MI, 1995.
19. R. S. Thomas, J. Pan, M. J. Moeller, and T. Nolan, Improving SEA Models Using Quality Technology, *Noise Control Eng. J.*, Vol. 45, 1997, pp. 27–34.
20. N. Atalla and R. J. Bernhard, Review of Numerical Solutions for Low Frequency Structural-Acoustic Problems, *Appl. Acoust.*, Vol. 43, 1994, pp. 271–294.
21. D. J. Nefske, J. A. Wolf, and L. J. Howell, Structural-Acoustic Finite Element Analysis of the Automobile Passenger Compartment—A Review of Current Practice, *J. Sound Vib.*, Vol. 80, No. 2, 1982, pp. 247–266.
22. R. R. Craig, Jr., *Structural Dynamics: An Introduction to Computer Methods*, Wiley, New York, 1981.
23. Y. J. Kang and J. S. Bolton, Finite Element Modeling of Isotropic Elastic Porous Materials Coupled with Acoustical Finite Elements, *J. Acoust. Soc. Am.*, Vol. 98, No. 1, 1995, pp. 635–643.
24. C. Y. R. Cheng, A. F. Seybert, and T. W. Wu, A Multidomain Boundary Element Solution for Silencer and Muffler Performance Prediction, *J. Sound Vib.*, Vol. 151, No. 1, 1991, pp. 119–129.
25. J. Lee, D. J. Thompson, H. H. Yoo, and J. M. Lee, Vibration Analysis of a Vehicle Body and Suspension System Using a Substructure Synthesis Method, *Int. J. Vehicle Design*, Vol. 24, No. 4, 2000, pp. 360–371.
26. S. W. Kang, J. M. Lee, and S. H. Kim, Structural-Acoustic Coupling Analysis on Vehicle Passenger Compartment with the Roof, Air-gap, and Trim Boundary, *ASME J. Vib. Acoust.*, Vol. 112, No. 3, 2000, pp. 196–202.
27. M. J. Moeller and R. E. Powell, Review of Statistical Energy Analysis (SEA) Applied to the Automotive Industry 1985–1997, *Proc. Noise-Con. 98*, Ypsilanti, MI, 1998.
28. C. Vicari, F. Sini, G. Nerop, and G. Orefice, The Application of SEA Models to Improve the Acoustic Comfort inside the Vehicle, *Proc. INTER-NOISE 2004*, Prague, Czech Republic, 2004.
29. C. Musser and S. Young, Application of Transient SEA for Vehicle Door Closure Sound Quality, Proceedings of the 2005 SAE Noise and Vibration Conference, SAE Paper SAE-2005-01-2433, SAE International, Detroit, MI, 2005.
30. J. Pan, B. Semeniuk, J. Ahlquist, and D. Caprioli, Optimal Sound Package Design Using Statistical Energy Analysis, Proceedings of the 2003 SAE Noise and Vibration Conference, SAE Paper 2003-01-1544, SAE International, Detroit, MI, 2003.
31. T. Connelly and J. Guan, Sound Package Design for a Convertible Using Statistical Energy Analysis, Proceedings of the 2001 SAE Noise and Vibration Conference, SAE Paper 2001-01-1623, SAE International, Detroit, MI, 2001.
32. R. G. DeJong, T. S. Bharj, and J. J. Lee, Vehicle Wind Noise Analysis Using an SEA Model with Measured Source Levels, Proceedings of the 2003 SAE Noise and Vibration Conference, SAE Paper 2001-01-1629, SAE International, Detroit, MI, 2001.
33. J. Pan, R. S. Thomas, and M. J. Moeller, Verifying Vehicle SEA Model Predictions for Airborne Noise

- Transmission Using Designed Experiments, *Proc. INTER-NOISE 1996*, Liverpool, UK, April 1996.
34. M. J. Moeller, J. Pan, and R. G. DeJong, A Novel Approach to Statistical Energy Analysis Model Validation, Proceedings of the 1995 SAE Noise and Vibration Conference, Traverse City, MI, May 1995.
35. M. J. Moeller, R. S. Thomas, and R. E. Powell, An Assessment of SEA Model Quality, Proceedings of the 2003 SAE Noise and Vibration Conference, SAE Paper 2001-01-1624, SAE International, Detroit, MI, 2001.
36. N. Koybayashi and H. Tachibana, A SEA-Based Optimizing Approach for Sound Package Design, Proceedings of the 2003 SAE Noise and Vibration Conference, SAE Paper 2003-01-1556, SAE International, Detroit, MI, 2003.
37. M. Sanderson, G. Ebbitt, P. Deacon, S. Wang, and R. Woodcock, Performance of Perforated Leather Seats: SEA Predictions and Validation, *Proc. INTER-NOISE 2002*, Dearborn, MI, August, 2002.

# CHAPTER 96

## NOISE MANAGEMENT OF RAILCAR INTERIOR NOISE

Glenn H. Frommer  
Mass Transit Railway Corporation  
Kowloon Bay  
Kowloon, Hong Kong

### 1 INTRODUCTION

With increasing rail services worldwide and passenger expectations for improved privacy and mobile telephones, noise inside railway cars is becoming an increasingly significant concern. This development presents a challenging task for the noise control engineer. Balancing the technical and commercial skills obtained from a wide variety of noise control applications is necessary for a cost-effective achievement of this requirement.

Well-tried methodologies to manage and achieve noise and vibration specification for railcars are now available. The use of such methodologies requires that the noise control engineer is completely knowledgeable about all relevant prediction and control techniques for noise and vibration control. These approaches can be used wherever commercial specifications for noise and vibration requirements are identified.

### 2 STANDARDS FOR NOISE CONTROL IN RAILCARS

While some minor changes to the final noise environment can be made once the vehicle is completed, it is not possible to reach the high levels of performance required for satisfactory speech intelligibility and privacy if the interior noise performance is not incorporated at the outset of the vehicle design. It is necessary to survey passenger expectations, consult possible levels of achievement with manufacturers, and agree on a set of practicable standards with the owner/operator before launching into the noise and vibration design.

For example, in Hong Kong, the Mass Transit Railway Corporation (MTRC) system regularly notes that about 7% of its passengers use a mobile telephone at any one time, and this is expected to increase with the widening use of third-generation (3G) mobile phone technology. For best speech intelligibility, it has been found that the A-weighted sound pressure level inside a railway car should not exceed 79 dB when traveling in a tunnel and 70 dB at top speed on open track. The reverberation time should also be kept short, between 0.6 and 1.0 s.

The specification used by the MTRC is given in Table 1<sup>1</sup> and has since become a standard for railway passenger car service in the Asia-Pacific region. These requirements were based primarily on English. However, further research has shown that speech intelligibility requirements are not very different for Cantonese and

Mandarin but should be checked for other languages.<sup>2</sup> At standstill the noise from the air-conditioning and ventilation system as well and the door opening and closing should be considered, as these could impact intelligibility and provoke an emergency evacuation.

Table 1 specifies target/acceptance A-weighted sound pressure levels with target levels slightly more restrictive than the acceptance levels. Experience with commercially driven noise and vibration design development has shown some safety factor should be included into the design process. Here the target/acceptance level provides that degree of design safety. In essence, the differences are a contractual means to incorporate imprecision and inaccuracy of the modeling and performance.

#### 2.1 Safety Criticality

A noise control engineer tasked with establishing, delivering, and controlling the internal noise environment of a railway car must be able to work very closely with designers, consultants, manufacturers, and contract engineers. The noise control engineer must become familiar with the contractual requirements for

**Table 1 Internal A-weighted Sound Level Specifications – Airport Express Train**

Specification	Condition	Target/ Acceptance
	Test Method	
External top speed 135 km/h, braking and acceleration	ISO 3095	80/83 dB (135 km/h)
External 0 km/h – 7.5 m	ISO 3095	70/72 dB
Internal top speed – free field	ISO 3381	65/70 dB (135 km/h)
Internal top speed – tunnel	ISO 3381	74/79 dB (135 km/h)
Internal stand still	ISO 3381	60/65 dB
Door opening and closing	ISO 3095 and 3381	65/70 dB
T60 (125 Hz)	ISO 3382	1 s $\pm$ 0.2 s
T60 (250–4 kHz)	ISO 3382	0.4 s $\pm$ 0.2 s
RASTI		0.55 (minimum)

the rolling stock and, in particular, the requirements for the reliability, availability, maintainability, and safety (RAMS) of the vehicle fleet. These four factors are critical to safe operations of a railway, and there can be no compromise on passenger safety. There will be many and possibly significant changes to the vehicle design throughout the manufacturing process, and the noise control engineer must have his or her own consistent means of achieving the agreed upon internal noise specification.

## 2.2 Developing the Specification

There are essentially two methods of meeting the noise and vibration specification. The first requires the owner/operator to prescribe all steps and all specifications in detail. The advantage of this method is that the manufacturer can accurately price the work taking advantage of standard designs and components in a straightforward design and build contract. However, given that the new design of the rolling stock will probably change to meet RAMS requirements, this procedure has a high element of risk.

The second method is to prescribe noise and vibration performance contractually, including general outlines of the plans, submissions, and achievements that the manufacturer must provide during the continuing design and manufacture of the rolling stock. The owner/operator may perceive the above contract strategy as a means to gain confidence that the noise requirement would be met. On the other hand the manufacturer may perceive the contract strategy as a means to minimize and control the risks of not meeting the client's specification. A mature owner/operator would take advantage of both the confidence building and the risk control of the latter method and develop a commercially beneficial partnership. Care, however, must be taken to allocate the proper type of resources to the process and overall management regardless of the method chosen. The remainder of this chapter will follow the latter contractual methodology.

## 2.3 External Noise

It is an *a priori* assumption that the achievement and control of the specified internal noise values for the rolling stock are commensurate with maintaining a minimum external noise emission of the vehicle. In a typical rolling stock contract the maximum external noise levels at standstill and at maximum speed are specified as are the internal levels at both standstill and top speed. Recent changes in the International Organization for Standardization (ISO) standards for noise measurement of railcars reflect the need to standardize the roughness of the wheel-rail interface.<sup>3</sup>

Experience has concluded that a robust design philosophy is one where the external A-weighted sound pressure level emissions for all electrical and mechanical equipment shall be about 10 dB below that for the wheel and rail noise at top vehicle speed and during braking and acceleration. In addition the wheel and rail profiles and hardness as well as the track and primary vehicle bogie stiffness should be optimized and maintained for a minimum wear scenario.<sup>4</sup> This is

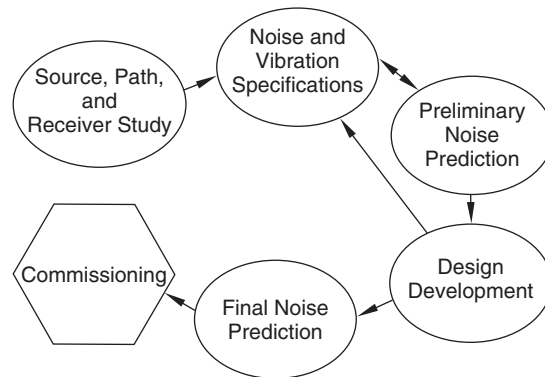


Figure 1 Noise assurance plan.

far from trivial and is outside the scope of this chapter. The reader is referred to descriptions of rolling noise simulations in the literature, for example, TWINS.<sup>15</sup>

## 3 NOISE ASSURANCE PLAN

The conceptual heart of the methodology is the noise assurance plan (NAP). Shown diagrammatically in Fig. 1, a requirement for the NAP is specified within the contract documents with the particular specification. The NAP contains six main stages: source-path-receiver study, noise and vibration specification, preliminary noise prediction, design development, final noise prediction, and commissioning.

### 3.1 Noise Management Plan (NMP)

The contractual arrangements for rolling stock will have particular stages connected to payments, and the noise control engineer must devise and implement a strategy for achieving the specified performance through a noise management plan. The management of the noise control must be structured to fit the overall contractual deliverables for the rolling stock while allowing the manufacturer the flexibility to design an acceptable low-noise vehicle. Thought must also be given as to level of manpower resources needed to achieve the desired noise performance as well as training other members of the design team.

A possible NMP, included as Table 2, shows how a proposed set of tasks can be grouped into particular rolling stock stages that can fit into an overall contractual program requirement for design, manufacturing, and commissioning. The tasking can also be used to determine the skills and remuneration for specialist subconsultants undertaking this work for the client or manufacturer. The task number and title shown in Table 2 allow a unique definition to fit into an overall contract program while permitting a description and verification of a deliverable for payment.

### 3.2 Source Pathway Receiver Considerations

In the first stage of the rolling stock contract, the manufacturer will propose and agree on the basic



**Table 2 Noise Management Plan (NMP)**

Rolling Stock Contract Stage		Task Number	Task Title
Number	Title		
1	Source, Path, Receiver Study	1	Preparation of Project and Noise Plan
		2	Conceptual Low-Noise Design
		3	Noise Source Study
2	Noise and Vibration Specification	4	Car Body Study
		5	Preliminary Prediction of Reverberation Time
		6	Preliminary Subsupplier Specifications
3	Preliminary Noise Prediction	7	Preliminary Noise Prediction
		8	Progress Meetings
		9	Documentation
4	Design Development	10	Systematic Low-Noise Design
		11	Preparation of Final Subsupplier Specifications
		12	Testing of Bogie and Car Body
5	Final Noise Prediction	13	Final Noise Prediction
		14	Documentation
		15	Progress Meetings
6	Commissioning	16	Inspection, Test, and Approval of Components
		17	Assembly Test
		18	Progress Meetings
		19	Documentation
		20	Predelivery Factory Test
		21	Documentation
		22	Commissioning
		23	Documentation

design, methodologies, and plans, stating how they will achieve the required level of RAMS. The noise control engineer must similarly require an NMP stating how the noise and vibration specifications will be met. Experience indicates that excessive detail is not overly beneficial at this juncture. The focus must be forming a team with a high level of practical experience. However, it is necessary that there is sufficient contractual authority and control given to noise control engineering to ensure that the final result will be achieved. With weight, performance, design, and power considerations, a firm but flexible hand is needed.

Once the detailed NMP is agreed upon, attention can then be focused on the achievement of the specification. A source–pathway–receiver study focuses on the various noise and vibration sources that exist within the rolling stock, as shown in Fig. 2. There are both airborne sources and structure-borne sources. Examples of the airborne noise are noise from the wheel–rail interface transmitted through the floor, walls, and roof and noise from the ventilation system. Examples of structure-borne noise are the reradiated noise through the vehicle floor, walls, and roof from the bogie and vibrating or rotating mechanical equipment and air turbulence from a pantograph reradiated through the roof and walls.

The emissions of each of the sources identified in Fig. 2 must be specified, controlled through prototype testing, subsystems testing, and during the final commissioning phase. General guidance on noise sources and pathways is given below.

### 3.3 Noise and Vibration Specification

From an understanding of the impact on the passengers, the source–path–receiver study implies values for the noise and vibration sources and transmission reduction and radiation values (Table 2, task 3). Together with a car body study and a preliminary prediction of reverberation time, this initial assumption results in a set of preliminary assumptions for the noise and vibration specification of the electrical and mechanical components of the vehicle. A listing of possible sources and pathways is given in Table 3.

### 3.4 Noise and Vibration Specification

Specifications for the main equipment should include sound pressure and or sound power levels as well as vibration levels in three dimensions. It is also essential to identify how the data will be tested

**Table 3 Noise Specification**

<b>Main Equipment</b>
Traction motor
Variable voltage, variable frequency (VVVF) inverter
Static inverter
Driving gear with gear coupling
Bogies
Gangway
Bodyside doors
Air-conditioning unit
Compressed air supply and brake system
<b>Sound Transmission Loss, Transfer, and Radiation</b>
<b>Index</b>
Floor
Lower sidewall
Sidewalls in driver's cab
Sidewall between windows
Windows
Entrance doors
Sidewall above the windows
Roof
Bellow

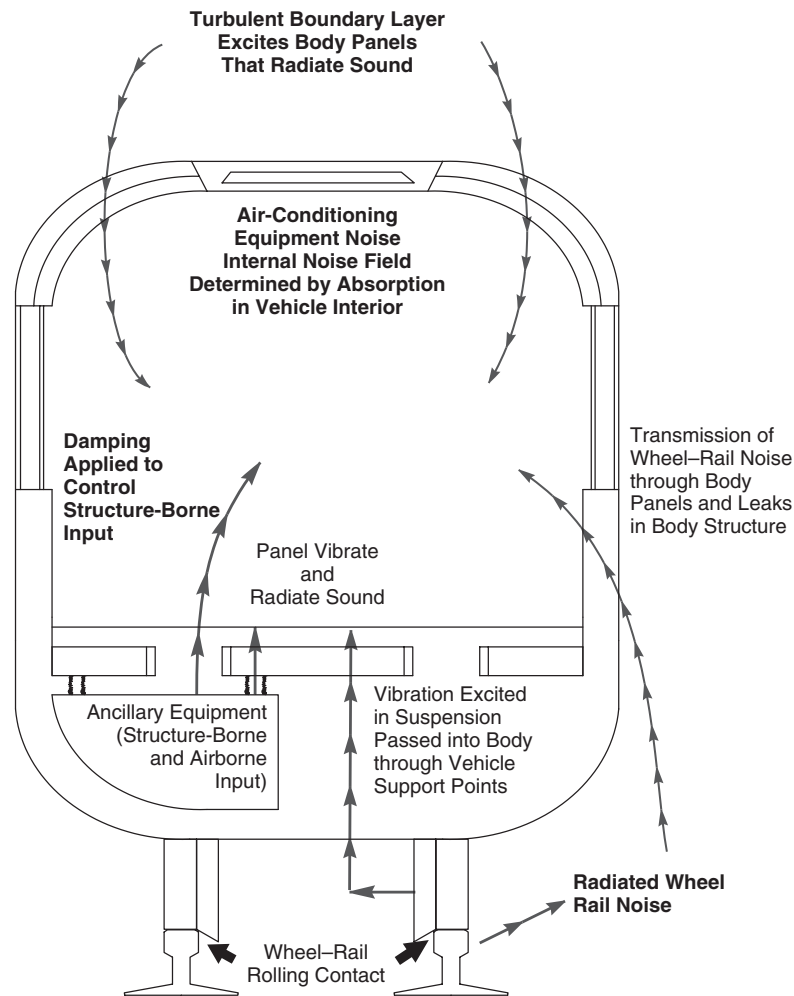


Figure 2 Source-path-receiver study.

and analyzed (A-weighted, octave, or one-third-octave values), the relevant international norms and standards to be used, and who will be testing the equipment (approved laboratory, consultant, or manufacturer and their qualifications). Experience has shown that the specification should be written in two parts, a general specification detailing the standards and measurements methods and the particular specifications detailing the acceptance criteria. Note that this is a preliminary set of subsupplier specifications based on a number of design assumptions that must be confirmed and closed out in the further design development.

### 3.5 Preliminary Noise Prediction

A preliminary noise prediction will be concluded from the noise and vibration specification with the help of a predictive model (Table 2, task 7). Model use will be discussed in more detail below. At this time it is

most informative to provide noise level predictions along the length of the vehicle, as the owner/operator may allow noise levels directly over the bogey area to be slightly higher than noise levels in the middle of the car. The preliminary prediction not only indicates how successful the design will be at achieving the specification but will also indicate the critical design challenges to be faced in the systematic low-noise design task.

### 3.6 Design Development

The next stage in achieving the internal noise level will require that the contractor or his or her specialist consultant participates in the design development of the vehicle. As noted above, there may be significant discussions on the design of components to meet RAMS requirements and in particular a low-weight fire performance. Designs of the floor, walls,

and roof as well as electrical and mechanical subsystems and air-conditioning and ventilation systems may be redesigned. The noise control engineer must ensure that the materials to be used and their installation will meet the agreed performance. It is strongly recommended that a tracking mechanism for sources, materials, drawings, and installation methods be established at an early time in the design development process and audited at regular intervals during the design and manufacturing process.

### 3.7 Final Noise Prediction

Once the detailed design has been completed and Table 2, task 4, is approved, the finalized noise and vibration specification allows the manufacturer to purchase the specified equipment and material. However, throughout the manufacturing and subsupplier phase, the noise control engineer must ensure that the installations are correct and the subsystems function as required. Vigilance regarding design and specification changes in this stage through the engineer's instructions must also be weighed. As noted above, there is a need to track and audit the key subsystems, and the engineer may require tests for key elements of the vehicle; for example, the floating floor and silencers on the traction motor and the air-conditioning units (Table 2, tasks 16 and 17). The noise control engineer should be available to accept design changes during the tests and provide a proper paper trail. With confidence now at a high level, the commissioning tests should show compliance with the internal noise specification for the vehicle.

The noise control engineer must consider how to best present the results and estimations to higher management for decisions. Information will be presented both to the design team responsible for RAMS and perhaps to more senior management if decisions must be taken impacting cost, program, or future maintenance. The author has found the use of simple bar charts and graphs to be most helpful. Additionally, noise simulations are exceptionally useful. These employ internally recorded noise levels from vehicles that have been mixed to a sound quality that will mimic the pertinent predictions. While the use of complicated and detailed sound quality has not been used in this area previously, there is no doubt a possible benefit for the noise control engineer to exploit this technique.

A word of caution is, however, necessary. These simulations and predictions will typically be played in executive offices or meeting rooms and as a result may not give the psychologically relevant results that the noise control engineer may prefer. Forethought is needed to prepare the simulations accordingly.

### 3.8 Commissioning

The resources used in tracking individual components and the testing of subassemblies assure that the final product will generally achieve the specifications. While the intention is that there are no surprises at this point, there can be some surprises. Experience has taught that the assembly of the air-conditioning unit may present some unwanted structure-borne noise

issues, and a mismatch of the rotational frequency of the ventilation fans could create a low-frequency resonance experienced throughout the vehicle. The engineer should allow some additional resources for this last stage.

## 4 GENERAL DESIGN GUIDANCE

### 4.1 Mathematical Models

The prediction of the internal noise in a railway car will depend on many different forms of mathematical modeling. There are an increasing number of analytical models to predict internal noise within railway cars: Finite element modeling (FEM), boundary elements modeling (BEM), and statistical energy analysis (SEA) (see Chapters 7, 8, and 17). Rolling noise is predicted by TWINS and modeling of pantograph noise can be undertaken with computation fluid dynamic (CFD) modeling (see Chapter 7). Given the number of airborne and structure-borne sources, the modeling is difficult and imprecise, incorporating a number of assumptions, for example, coupling factors and damping. This raises doubt as to the robustness and veracity of any one approach.

Considering the complexity of the overall design, it is this author's experience that it is best to keep the models as simple as possible and use base modeling on measurable and controllable parameters. As a result those models based on the measurement of sound power and vibration levels of airborne and structure-borne sources, sound reduction, and radiation values in existing railway cars combined with spread-sheet transparency of results tend to give a more robust prediction than more theoretical approaches.<sup>6</sup> However, the use of the more analytical methods to examine and optimize subsystem performance is advisable and cost effective. SEA is particularly helpful in prioritizing noise control efforts for maximum cost-effectiveness but is not suitable for the prediction of overall absolute noise levels.<sup>7</sup>

### 4.2 Validation

For railcars that are of newer design, the choice of model will be a critical one. One way of examining the robustness and sensitivity is to require validation of all modeling and or procedures within the tendering phase or in the stage 1 deliverable of the NAP (Table 2, task 2). Generally, the models should be able to predict the internal A-weighted sound pressure levels at any position within the vehicle to  $\pm 2$  dB with all external and internal conditions prescribed. The engineer must note that a validation requires a comparison between known and controllable inputs and measured outputs, for example, noise levels along the car. No "tuning" of the model should be allowed once the physical parameters of the railway car are input. Typically, a validation is proven on a previous project. There is much confusion with modelers with the erroneous assumption that verification is the same as a validation.<sup>8</sup>

### 4.3 Noise Sources

As detailed above, achievement of a low level of internal noise in railway cars will depend on the control

and mitigation of airborne and structure-borne noise sources with full cognizance of the RAMS requirement for the vehicle. Once the RAMS targets and the means to meet the targets are agreed, there should remain significant flexibility allowing the noise control engineer to meet his or her goal.

There are three major speed regimes regarding external noise generation:

- From 5 to approximately 50 km/h, the propulsion noise will dominate and will increase by approximately 10 log(vehicle speed).
- From 50 to approximately 220 km/h, the main noise source will be the wheel-rail interface with noise for disk-braked vehicles increasing roughly as 25 log(vehicle speed).
- Above 220 km/h, air turbulence will be the dominant source and will increase as 80 log(vehicle speed).<sup>9</sup>

For most intercity and mass-transit trains, the dominant airborne noise source will be the wheel-rail interface or rolling noise.

Within the bogie there are essentially two levels of vibration control: a primary and a secondary suspension. It is the secondary suspension that provides the ride quality of the vehicle while the primary suspension controls the car body motion. Both suspensions will effect the transmission of vibration from the wheel-rail interface and the propulsion system into the vehicle through the center pin, as will any further connection of the bogie to the vehicle frame, antiroll bars, and horizontal dampers.

An essential element of the control of the wheel-rail or rolling noise is to ensure that the tread surface of the wheel and the contact patch on the rail is as smooth as practically possible. For the rail this can be achieved by regular grinding and for the wheel by regular turning and lubrication of the wheel flange. The regularity of grinding and wheel turning is dependent on the operational characteristics and economics of the system. Rail maintenance models are normally used to predict the optimal maintenance conditions.<sup>10</sup>

It is best to employ disk brakes rather than tread brakes to maintain the smoothest wheel tread. Tread brakes can cause wheel flats and roughen the running surface of the wheel. The increased wheel roughness gives an increased mechanism to excite the natural modes of the wheel and exacerbate rail vibration. Wheel profiles and to some extent rail profiles can be designed to minimize airborne noise emissions. However, the rail industry tends to be conservative, and the use of unusual designs will take some time for acceptance.

The second important factor is the use of continuously welded rail. Rails with fish plates or bolted connections between rails will cause the well-known clickity-clack noise that could defeat even the best low-noise railway car design.

Another area of focus is the propulsion system consisting of the traction motor, gearbox, and the coupling. Most common traction motors rely on air cooling for controlling the motor temperature.

Excessively high temperatures will cause bearing and insulation failure and possibly an underfloor fire. Typically near the exit of the motor, the fan will draw cool air in over the internal structures of the motor and exhaust the hot air. This can be very noisy and contain pure tones if the fan is not designed correctly. The better fan designs include variably spaced blades where attention has been placed on the blade edge design. A good design can essentially remove all pure tones from the fan noise spectrum, and attention to individual blades design can provide an additional 3 dB to 5 dB attenuation in the A-weighted noise level.

Nonetheless, the noise from the traction motor is generally very high, and additional silencing is needed both on the inlet and exit of the traction motor. The design of the silencing is difficult since it must provide an A-weighted noise level attenuation of 10 dB to 15 dB, while not significantly increasing the pressure drop through the motor, and be easily demountable for thorough maintenance. An increased pressure drop will cause increased heating exacerbating bearing wear. It has been found best to work with the traction motor manufacturer, establishing a test facility where sound power from the motor can be readily measured and combine this with the possibility for building and testing various silencer designs. Silencing material can either be fiberglass, mineral wool, or sintered aluminum with the choice of the material dependent on the cost and application. Maintenance aspects must also be considered.<sup>4</sup>

The gearbox is another key noise source. The use of FEM for gearbox design can be very beneficial in determining the thickness of the material and optimizing the gearbox weight. The design of the gearbox should ensure that there are no gear meshing frequencies close to any of the natural frequencies for the gearbox itself. If there are, the pure tones from the natural gear meshing frequency will be emitted as airborne noise and could enter the vehicle.

The design of the air-conditioning and or heating systems will depend on the requirement for passenger fresh air. A general rule is to supply of the order of 3 litres/second/passenger. It is also suggested that the issue of thermal comfort is considered in the overall design of the railway vehicle. Generally, fresh air is taken in through the bulkheads and through the overhead vents in the air-conditioning or ventilation system. Heating is supplied in the foot panels. However, fresh air inlets will be a noise source particularly in tunnels. The fresh air channels in the car bulkheads must be designed with the appropriate mitigation and packaged with mineral wool or fiberglass.

A vehicle may have two air-conditioning or ventilation units on opposite ends of the vehicle roof, incorporating the use of vehicle return air and blending this with a fresh air source. The units are self-contained consisting of exhaust and evaporator fans, a compressor, coolant storage, and heat exchanger. The units feed into a set of ducts such that both units supply the middle of the vehicle while only one unit supplies each end. The airflow through the ducts and the ventilation outlets must also be noise controlled as must the break-out noise from the

underside of the unit and ducts. There is also a challenge to control of the vibration and reradiation of noise from the compressor and fans. Caution must again be exercised in that noise attenuation does not prohibit adequate airflow to passengers. There are not a large number of air-conditioner manufacturers that include noise and vibration requirements into their performance specification and as such the noise control engineer has a huge task to ensure compliance to the noise and vibration specification. Note that there are other environmental restrictions in place regarding the choice of coolant and use of additives to transformer oils.

#### 4.4 Sound transmission

Given the air and structure-borne sources noted above, achievement of a controlled and low internal noise level will depend on the success in implementing a “box within a box” construction philosophy. Well-known from isolation treatments and aircraft and ships, the internal environment within the railway car must be as mechanically independent from the outside structure as practical. However, the need to provide safe, cost-effective, light-weight structures while safely including all of the electrical and mechanical services is demanding. There is a need to balance the sound transmission and the sound radiation capabilities of the surfaces.

The sound transmission through the vehicle floor, doors, windows, roofing, and bellows between vehicles are key elements. As noted above analytical models can assist in the design of the floor. However, attention is needed to provide a design that is safe for fire protection as well as mechanically coherent. Typical sound transmission control (STC) values for flooring for low values of internal noise will be in the upper 40 to low 50 dB. This is typically a double-walled construction with plywood internal flooring placed on rubber blocks supported by steel or aluminum profiles with beams—a floating floor. The design of the floating floor will depend on the chosen elastic material and floor design. Weight must be minimized. The rubber used must have fire retarding properties as well as the preferred elastic properties to ensure a proper overall high value of sound transmission class. There will also be many cables and possibly hydraulic piping through or directly attached to the underside of the floor. All attachments shall be elastic wherever possible to avoid the transmission of vibrations along the vehicle. Care must be taken to ensure that resonances are well damped.

The design of the internal walls of the vehicle is likewise important. Where possible this should be a double-wall construction. However, due to the structural and mechanical requirements on the walls, some walls are made with a honeycomb core, similar to marine bulkheads. The detailed connection between the flooring and the wall including the connections between the seats, the wall, and the floor is likewise critical.

Window construction is typically double-walled windows. These can have asymmetrically thick glass and possibly contain a rare gas to increase the noise transmission loss. Detailed care in the connection of the window to the wall is essential to avoid

any openings and to minimize vibration transmission between the walls and windows.

The doors must be designed to compromise the conflicting requirements between mechanical requirement to withstand forces from passenger movement and the flexibility for high noise reduction. Sliding or plug doors can be used for a low-noise design, but the future maintenance will be much less for the plugged doors. Doors tend to be a single-leaf construction, and the use of handles within the doors for maintenance access further increases noise transmission. Another critical factor is the rubber trim between doors and the vehicle body. Gaps will provide a source for airborne noise to enter the car and will become worn more quickly with sliding doors.

The design of the driver's cab also deserves special mention. The client should include additional noise control criteria in the cab referring to occupational health and safety requirements. In addition to all of the noise sources noted above, there is an additional noise source through the windscreen and possibly through a separate ventilation or air-conditioning system. Some adjustments may need to be made on-site in a mock-up to examine the placement and connection of the installed equipment.

#### 4.5 Reverberation Control

In predicting the internal noise of the vehicle, it is also necessary to treat adequately the surfaces for a controlled reverberation time while at the same time ensuring these surfaces are maintainable without fire loading or excessive cost. For example, the simulations accurately represent the effects of sound absorption on the vehicle ceiling and the effect of cushioned seats. There are a number of standard software packages available, and they will all display similar trends. However, given the fact that the reverberation times are 1 s and below and that there are many reflecting services within the vehicle, modeling should be applied cautiously.

#### 4.6 Fabrication

A value engineering process is normally undertaken to optimize the design and manufacturing process as the final component of the detailed design prior to fabrication. This may present challenges to the low-noise design, and the noise control engineer must ensure that the tracking process established earlier is sufficiently robust to maintain the essential elements of the low-noise design. This refers to the materials, their performance, the installation, and their fixation.

The author has found it most useful to incorporate testing on subsystem prototypes and one of the prototype vehicles at an early stage in fabrication. This needs to be specified within the NMP, usually in stage 3. The testing uses a large shaker to provide vibrations to the steering pin of the bogey and loudspeakers to provide airborne noise. Typically, the internal noise levels of the vehicle will be checked along with vibrations of surfaces. Sound intensity measurements will be required to measure the sound transmission and determine the sound radiation of some surfaces.

#### 4.7 Commissioning and Maintenance

The final stage of the NAP is the commissioning tests. These tests will identify the noise levels within the cab and throughout the railway cars. It is essential that the surface of the wheels and the rails are prepared accordingly to provide the appropriate running surfaces. It is normal to include descriptions for the wheel and track within the specifications for the rolling stock should testing be undertaken by the manufacturer. As a final deliverable, the manufacturer or owner/operator should establish fleet averages and variations for the different car types.

The internal noise of the vehicle will change as the railway ages. A railway car can be operated for 30 years and with upgrading 40 years. A railway operator will normally have a planned rolling stock maintenance regime with different types of maintenance undertaken at regular intervals. A best practice is to maintain the noise control measures as well, allowing only a small degradation of the internal noise levels. The degradation of internal noise levels will mostly depend on the state of the ventilation and air-conditioning system and the rubber trim around the doors and possibly windows. The exhaust or ventilation fans could be operating at slightly different speeds and gaps could be forming in the rubber trim. It is best practice to monitor the internal noise levels regularly and schedule maintenance accordingly.

Given the attention and care to internal noise performance throughout the vehicle lifetime, the railway operator can look forward to a cost-effective operation with satisfied regular customers.

#### REFERENCES

1. G. H. Frommer, The Acoustical Design and Delivery of the Airport Railway Rolling Stock, in ICSV6, Hong Kong, 1999, pp. 1383–1388.
2. L. Kiang, Comparison of Speech Intelligibility between English and Chinese, *J. Acoust. Soc. Am.*, Vol. 103, 1998, pp. 1213–1216.
3. ISO/NP 3095, Acoustics—Measurement of Noise Emitted by Railbound Vehicles, 2005.
4. G. H. Frommer and A. Budge-Reid, An Investigation into Optimum Design of Trackform, SDVNC Proceedings, Hong Kong, D. M. Zhu and J. M. Ko, Eds., 1995, pp. 406–412.
5. D. J. Thompson, Theory of Generation of Wheel/ Rail Rolling Noise, in *Noise and Vibration from High-Speed Trains*, V. V. Krylov, Ed., Thomas Telford, London, 2001.
6. ODS “TRAINNOISE,” see website: <http://www.odegaard.dk/>.
7. B. Stegemann, Development and Validation of a Vibroacoustic Model of a Metro Rail Car Using Statistical Energy Analysis (SEA), MScEng Thesis, Report E02-05, Chalmers University of Technology, Göteborg, Sweden, December 2002.
8. D. E. Post and V. G. Lawrence, Computational Science Demands a New Paradigm, *Phys. Today*, January 2005, pp. 35–41.
9. J. J. A. Van Leeuwen, Generic Prediction Models for Environmental Railway Noise, in *Noise and Vibration from High-Speed Trains*, V. V. Krylov, Ed., Thomas Telford, London, 2001.
10. P. J. Remington, Wheel and Rail Excitation from Roughness, in *Noise and Vibration from High-Speed Trains*, V. V. Krylov, ed., Thomas Telford, London, 2001.
11. P. Nelson, *Transportation Noise Reference Handbook*, Butterworth-Heinemann, Cambridge, UK, 1987.

# CHAPTER 97

## INTERIOR NOISE IN RAILWAY VEHICLES – PREDICTION AND CONTROL

Henrik W. Thrane  
Ødegaard & Danneskiold-Samsøe  
Copenhagen, Denmark

### 1 INTRODUCTION

The interior noise level in a railway vehicle is one of the key parameters for the comfort of the passengers. It is therefore important to apply the principles of low noise early on in the design, both to ensure that the desired noise level is achieved and to minimize the cost of low-noise design. A large number of noise sources and paths, both airborne and structure borne, are present in modern railway vehicles. The contribution from the structure-borne paths is normally dominant in the low-frequency range, while the contribution of the airborne paths usually dominates in the middle and high frequencies. The acoustical strength of the noise sources can be controlled by means of specifications. The overall acoustical design is often optimized by applying prediction models based mainly on a statistical energy analysis approach. Optimization of the transmission of structure-borne noise from the equipment to the car body is usually made using finite element modeling techniques. The contribution from aeroacoustic sources is a special topic mainly of relevance for high-speed vehicles and is not the main concern in the control of noise in rapid transit railway vehicles.

### 2 ACOUSTIC DESIGN PROCESS

The acoustical design process, from the conceptual design of the vehicle through to the production stage, consists of a number of separate tasks, as described in detail below. The acoustical design process also involves noise management in the form of a noise assurance plan describing the process, responsibilities, and methods of corrective action as covered in Chapter 96.

#### 2.1 Noise Specifications

The basis for the whole design process is naturally the target internal noise level. Today the noise levels in the public spaces of the vehicle normally fall below legal or official limits. Consequently, the desired noise levels, when developing a new train type, can be set according to the train manufacturers estimate of which noise levels meet present-day standards. More often a client, for example, an operator, prepares the noise specifications.

Legal limits or limits set forward by trade unions may apply when considering the noise exposure of the driver. With the exception of the noise problems related to the driver's cab of diesel locomotives,

driver's cab noise issues are more a matter of providing a proper working environment for intellectual work than of preventing hearing damage.

When measuring the noise level, it is preferable to use the equivalent continuous A-weighted sound pressure level,  $L_{pAeqT}$ , (averaged over typically 5 to 10 s) rather than the maximum noise level,  $L_{pAFmax}$  or  $L_{pASmax}$  (maximum level during short time). The continuous level gives a much more statistically stable result than the second where a single event will determine the noise level. The latter is not a good descriptor of the overall noise level in the train.

It is not fully certain whether the A-weighted sound pressure level provides a good correlation to the sound quality experienced by the passengers.<sup>1</sup> Dedicated specification of sound quality parameters is not yet standard and is normally limited to expressions like "rattling noise must not be present."

In addition to the above parameters, limits for the presence of pure tones and impulses are often specified, typically as a level penalty based on rules originating from evaluation of annoyance caused by pure tones and impulses in the environment. The internal noise specification should include a description of the roughness of the rails as function of wavelength in the range 0.01 to 0.2 m at the test site for the noise measurements. If this is not the case, the roughness levels have to be defined at the onset of the acoustical design.

Over the years a trend toward demanding still lower levels has been observed. Very low noise levels affect the mass and cost of the vehicle, so the question regarding reasonable noise levels should be raised. An optimum acoustical comfort is supposedly achieved when the variations in the noise level during a journey is kept small, as stated in Ref. 2. This means that the difference between standstill noise levels and driving noise levels should be reduced. Likewise the very low noise levels found in trains designed for a speed of, for example, 180 km/h but running at 100 km/h when used in local traffic, result in reduced comfort due to lack of privacy and to information-carrying background noise (passenger conversation or use of cellular phones). A possible solution could be to utilize the public address (PA) system or the high-volume air-conditioning (HVAC) system to provide masking noise. A noise level that provides a reasonable compromise between privacy and speech interference is generally considered to be the optimum noise level.



**Table 1 Checklist for Tender Documents**

Cause	Effect
Low floor designs	Insufficient height for floor construction
Low floor height/big wheel diameter	Insufficient height for floor construction
External/internal dimension ratio	Insufficient width for wall construction
Low weight	Need for double constructions with sufficient building height
Layout	Low-noise area above major noise sources
Layout	Acoustically weak components located close to noise sources
Design, internal	No separation between noisy and low-noise areas
Design, internal	Restrictions in use of absorbing panels
Design, external	Restrictions in use of skirts
Material selection	Restrictions in use of optimal acoustical materials
Aluminum profiles for car body	Low mass-to-sound-transmission ratio
Seat selection	Insufficient sound absorption
Fire requirements	Restrictions in use of optimal acoustical materials
Vandalism protection	Restrictions in use of optimal acoustical constructions, e.g., seats
Choice of equipment	Client specification of noisy components, e.g., self-ventilated motors, piston compressors

It seems that an A-weighted noise level of 65 to 68 dB should be the target.

With the currently used layout of trains with no or very few internal doors, a significant jump in the specified noise level is not possible (e.g., for a compartment adjacent to a vestibule and the vestibule). The reason being, even with highly absorbing interiors, only a limited lengthwise attenuation of the noise level of the order of 1 to 2 dB per metre is possible. This fact can result in the specified level in the compartment determining the acceptable level in the vestibule. The consequence could be a requirement to install thicker, heavier, and more expensive external doors.

One solution to this problem, which is even more severe in the intercommunication gangway area, is to install internal doors or to accept that the noise level in the passenger area close to the vestibule or gangway is higher than in the rest of the compartment.

## 2.2 Equipment Specifications

The internal noise levels are determined by a great number of factors, including the airborne and structure-borne noise source strength of the equipment used on the train. Therefore equipment specifications have to be prepared to set targets for the noise and vibration design by subsuppliers. The task of setting limits for the allowable contribution for each type of equipment is difficult and has to be based on a proper balance between the different equipment, using information of source strength for state-of-the-art equipment. For further discussions of handling equipment specifications see Chapter 96.

## 2.3 Conflicting Requirements

As an interaction is present, the acoustical requirement should not be separated from other requirements of the train: reliability, availability, maintainability, and safety (RAMS). For example, when setting a floor height above head of rail and a wheel diameter, the allowable construction height of the floor has also been defined. The allowable space for the floor has a major

impact on the noise properties of the whole car, a fact that sometimes is not recognized. A related problem is found in the articulation area of low floor trams where the restricted space most often hinders use of the more efficient double-wall construction, thereby resulting in an insufficient sound transmission loss of the construction. These space restrictions inherently lead to a conflict relative to the mass of the vehicle, as lack of space calls for heavier constructions. Table 1 summarizes some of the conflicts that should be examined at the tendering phase, and then followed by corrective action as needed.

## 3 PREDICTIONS OF INTERNAL NOISE

When predicting internal noise, it is necessary to describe both the airborne and the structure-borne source properties, as opposed to external noise problems where only the airborne noise is considered. Two types of propagation paths thus exist, which are treated separately. For example, a separation into convenient subpaths could yield:

- Sound power of source to sound pressure outside the train, for example, a window
- Transmission through the window
- Radiated sound power from inside of window to noise level in train

The structure-borne path is usually treated in a similar way using several subpaths. Unlike the airborne noise, the structure-borne noise is considered independent of the external acoustical environment (e.g., running in a tunnel).

## 4 PREDICTION METHODS

A number of analytic tools are available for the prediction of the internal noise level: statistical energy analysis (SEA), boundary element modeling (BEM), and finite element modeling (FEM). An analytic model of a complete railway vehicle becomes extremely large

in number of subsystems or elements. The resulting complexity makes it difficult to maintain the necessary overview.<sup>3</sup> Furthermore, a great number of details are not defined at the outset, indicating that use of BEM or FEM models cannot be justified. For SEA models, a violation of the assumption of weakly coupled structures cannot be avoided, especially when using the SEA model for external and internal air volumes. Therefore, use of semiempirical tools seems to be advantageous for modeling of complete cars. SEA and FEM models are, however, considered to be extremely helpful to optimize subsystems.

Semiempirical tools work by dividing the car into sections along the car body and into levels in the vertical direction. This results in several elements, one or more at each section and level. For the airborne noise, the sound pressure level on the outer side of each element is determined based on the geometry of the car body and the position of the individual noise sources. The contribution to the internal noise level from each element is determined from the sound pressure level over the element and the airborne noise transmission loss. Likewise the structure-borne noise level of each element is calculated on the basis of the propagation loss of the car body structure and the coupling loss from, for example, the car body sidewall to the interior trim. The structure-borne radiated noise from each element is then calculated based on the structure-borne vibration level of the element and the radiation index of the element. The total sound power radiated to the inside of the car is found by a summation of the airborne and structure-borne contributions from all elements. The resulting sound pressure level distribution can then be calculated using a dedicated room acoustic ray-tracing/image source modeling program as, for example, discussed in Ref. 4. This kind of modeling is said to be semiempirical because it is based on classical vibroacoustic calculations, subsequently verified and adjusted by means of measurements.

In the case of early concept studies or quick checks of the airborne noise contribution from critical elements close to the source, a rough estimation can be made using the difference of the A-weighted total level for the source strength and the weighted sound transmission loss for the element in question. For the detailed studies the modeling is normally done using octave bands. In the opinion of this author the statistical uncertainty of the underlying data does not justify a modeling in, for example, one-third octave bands.

## 5 SOURCES

Data on the airborne and structure-borne source strength of the noise sources is needed as input to the model. Suppliers are sometimes able to provide the airborne noise source strength, but data on structure-borne noise is rarely available. This implies that the source strength has to be based on experience with similar constructions using data from a databank or using values from handbooks. The true source strength of the structure-borne sources, that is, the

power injected into the receiving structure, is quite difficult to establish.<sup>5</sup> Therefore, the more simple approach of just using the free velocity level,  $L_v$ , of the mounting brackets as the descriptor is very often applied beneficially. The velocity level is used, since the sound pressure level is proportional to the velocity level. It is also possible to use the excitation forces as a descriptor, but this asks for a very complicated setup if the force shall be measured directly. A more complete description of the properties of the equipment in question is obtained when the complex mobility of the mounting brackets is known.

Table 2 gives an overview of the major sources and their relative importance. Diesel engines are included since these are used in both suburban trains and modern low-floor trams. Diesel engines can be mounted both as underfloor units and as roof-mounted units using a diesel-electric propulsion system.

As a rule of thumb, the velocity level of the structure-borne noise sources decreases with frequency while the level of the airborne noise sources generally peaks in the middle frequency range. Taking the airborne and structure-borne properties of the vehicle structure into account, the net result is that the contribution from structure-borne noise to the A-weighted noise level dominates in the frequency range up to 200 to 400 Hz. In the remainder of the frequency range the airborne noise is normally dominating.

### 5.1 Discussion of Major Sources

**Wheel–Rail Contact** The roughness of the rail and the wheel excite the wheel and rail, causing airborne and structure-borne noise. The structure-borne noise propagates to the car body through the bogie structure while the airborne noise from the wheels and the rails propagates around and along the vehicle. The source strength is proportional to the combined roughness,<sup>6</sup> indicating that the combined roughness should be minimized. For well-maintained systems the rail controls the roughness at the longer wavelengths while the wheels dominate at the shorter wavelengths.

In addition to the combined roughness the source strength depends on a number of factors, such as wheel type, train speed, stiffness, and loss factor of rail pads and sleeper type, and can be calculated using prediction tools such as TWINS. The impact of train speed on the airborne source strength,  $L_v$ , is calculated as  $30 \log(v/v_{\text{ref}})$  where  $v$  is the speed and  $v_{\text{ref}}$  is a reference speed.

The frequency content shifts somewhat toward higher frequencies at increasing speeds as the higher modes of the wheel will be excited. When predicting internal noise of suburban trains and trams, this effect is normally disregarded due to its limited influence.

**Bogie Connections to Car Body** In addition to the source strength of the wheel–rail contact, the structure-borne input to the car body is influenced by the bogie design and the flexibility of the resilient element used for connecting the various elements to the bogie frame and car body. At each connecting point between the bogie and car body, three translational and

**Table 2 Overview of Sources and Their Importance to the Internal Noise**

Source	Airborne Source	Structure-Borne Source	See Chapter
Wheel–Rail contact	+++	+++	93
Bogie connections to car body		+++	
Traction motor, self-ventilated	+++	+++	72
Traction motor, liquid cooled	+	+++	72
Cooling units for liquid-cooled motors	+++	+	71
Traction gear	++	+++	69, 88
Axle gear	++	+++	69, 88
Diesel engines	+++	+++	84
Turbo gear for diesel engines	+++	++	69, 88
Diesel engine intake	++		85
Diesel engine exhaust	++	+	85
Diesel engine cooling units	++	+	71
Traction inverter	+	++	
Transformers	+	++	
Braking system	+	++	92
HVAC unit, driver's cab	+++	+	111
HVAC unit, passenger saloon	+++	+	111
Auxiliary inverter	+	+	
Hydraulic equipment	+	+++	76
Air compressor	+	+	74
Brake resistors	+	++	
Warning horns, whistles	++	+	

three rotational components are present. A simplified approach is needed to enable a feasible description of the source strength that must also include the influence of multiple connections.

For engineering purposes the cross-coupling contributions are ignored, and a conservative estimation of the source strength per octave band is obtained by an energy summation of the maximum translational component independent of direction of the different connections in the octave band in question. The effect of train speed on the structure-borne source strength,  $L_v$ , is calculated using  $25 \log(v/v_{\text{ref}})$ .

**Traction Motors** Electrical traction motors are normally of the asynchronous type. There are two major noise generation mechanisms, a mechanical source due to bearing and magnetic forces and an aerodynamic source caused by the cooling air. For liquid-cooled motors this latter source is moved from the motor to the cooling unit.

Independent of motor cooling scheme, the mechanical noise dominates at lower speeds as the restricted switching frequency of the semiconductors controlling the motor speed and power results in a nonsinusoidal current being supplied to the motor. The motor torque fluctuates with frequencies related to the pulse pattern used.

The typical controlling scheme results in a torque that pulsates with a fixed frequency between approximately 600 and 800 Hz at low train speeds. At intermediate speeds the frequency of the pulsating torque changes with train speed, often in a quite complicated way, with a frequency span often between 600 and 1000 Hz. At higher train speeds a block-type pulse pattern is used, reducing the level of the pulsating torque.

This means the pure tone problems can be found at speeds up to 50% of maximum speed.

The presence of pulsation torque at low speeds aggravates the pure-tone problem as the masking from the broadband wheel–rail noise is missing. The magnitude of the pulsating torque in the motor air gap is considerable; a value corresponding to 30% of the nominal torque is quite normal creating a high structure-borne noise level at frequencies where structural resonance problems can hardly be avoided.

Some remedial actions are, however, at hand:

- The pulse frequencies can be changed to avoid a resonance condition.
- At lower train speeds with fixed pulse frequency, dynamic absorbers can be applied, thereby decreasing the mobility of the structure.
- Structural changes and use of soft resilient mountings, possibly combined with blocking masses, can reduce the transmission of structure-borne noise to the car body.

For self-ventilated motors the fan noise follows a 50 to 55 log speed dependence. The source strength is normally rather high, as the fan has to work for both driving directions, which means that a noisy radial straight blade design is applied. Absorption-type silencers have been used on traction motors to reduce airborne A-weighted noise levels by as much as 10 dB to 13 dB without reducing the airflow or causing a significant increase in motor temperature.

For vehicles with a single-floor construction both the airborne and structure-borne contribution from the motors has significant impact on the internal noise,

whereas structure-borne noise has the greatest impact where double-floor construction is used.

**Cooling Units** The noise from roof cooling units is a key element in the external noise. It is important to place such units away from openings connecting the outside of the vehicle to the interior, for example, the exhaust air openings for the HVAC system. Sufficient space, 50 to 100mm, should be left between the underside of the unit and the roof of the train to avoid coupling through the cavity. Proper balancing of the fans can reduce structure-borne noise problems.

**Gearbox** The main problem with gears is the structure-borne noise. The main transmission is normally through the torque reaction arm connected to the bogie frame. The transmission of structure-borne noise can be reduced by using soft rubber bushings (Shore A < 50°) in combination with a low mobility of the source and receiving structure. Due to lack of masking from other sources, natural frequencies of the supporting structure being excited by the tooth mesh forces at low to middle speed of the vehicles should be avoided. The source strength of gears follows a 25 log speed dependence and a 10 to 15 log power dependence.

**Diesel Engines** Diesel engines are particularly troublesome as both the airborne and structure-borne source strength is high. During both idling and acceleration, masking noise from other sources is absent. Consequently, a highly efficient mounting, most likely double elastic, is needed in combination with a high sound transmission loss of the car body structure adjacent to the engine. For roof-mounted engines, an enclosure closed toward the roof reduces the problems of airborne noise, provided adequate cavity height is observed. It is the experience of the author that, provided the Shore hardness is below 50°, a mounting system using rubber mounts can be very efficient. The source strength of diesel engines follows a 20 to 25 log speed dependence and a 4 to 6 log power dependence.

**Traction Inverter and Transformers** Besides noise from fans, which affect the external noise, the main problem here is pure-tone excitation (as discussed for the traction motor). A well-designed resilient mounting can minimize the contribution from this equipment.

**Heating, Ventilation, and Air-Conditioning Units** HVAC units are sources of both airborne and structure-borne noise. Structure-borne noise problems are more pronounced when using reciprocating piston-type compressors. The excitation originates from the unbalanced forces and moments of the compressor and from the pressure pulsations in the cooling circuit. When a reciprocating compressor is used, a well-designed resilient mounting of the complete unit can reduce the structure-borne noise sufficiently. With adequate space between the unit and the neighboring car body structure as described above, the remaining airborne noise

problem originates from the fresh air supply fan(s). For high air exchange rates the A-weighted sound power level of the fan can be up to 85 to 90 dB. The traditional solution is to introduce a baffle-type absorbing silencer between the fans and the first air outlets. An active solution has not yet been implemented in trains. The silencer can often have a length of 1 to 1.5 m, which indicates that the air duct concept has to take the silencer into account. Likewise the return air ducts should be designed with absorption in order to avoid break-out noise from the mixing chamber. Another problem of HVAC systems are the duct connections between the outside and interior of the train for fresh air intake and exhaust air outlet. It is necessary to ensure that these openings will not degrade the sound transmission loss of the train element in question. The aforementioned silencers will often help achieve the necessary sound transmission loss.

**Hydraulic Equipment** Hydraulic systems incorporating an engine-mounted pump and hydraulic motors for driving fans and generators are sometimes used on diesel and diesel/electric trains. The structure-borne source strength caused by pressure pulsations of these systems is very high, and severe pure-tone noise problems can be present. These systems should always be equipped with in-line silencers of the reactive type in order to reduce the level of the pressure pulsations. Furthermore, resilient mounting of the high-pressure pipes is necessary. Blocking masses are quite often necessary as the source mobility of the pipes is high.

**Brake Resistors and High-Power Cables** Brake resistors and high-power cables can be a source of structure-borne noise with the excitation mechanism due to magnetic forces and frequencies similar to those described for traction motors. Bundling of the cables minimizes the external field and can reduce the source strength. As the brake resistor structure normally is quite lightweight, a resilient mounting of the unit and/or use of blocking masses at the mounting positions can be helpful.

## 5.2 Typical Source Strength

Figure 1 shows typical source strengths of some of the sources discussed above. The levels stated are for low-noise equipment normalized to a train speed of 130 km/h. The structure-borne properties shown are the level at the interface to the car body.

## 6 PATH

### 6.1 Airborne Noise

**Exterior Sound Field around Car** The sound pressure level outside the car is attenuated as the distance to the sources increase due to geometrical spreading and diffraction. Figure 2 shows the calculated A-weighted sound pressure level at the outer surface of a typical car running in free field using a typical source spectrum

**Sound Transmission Loss of Car Body and Elements** The highest sound pressure level is normally found under the train adjacent to the bogies,

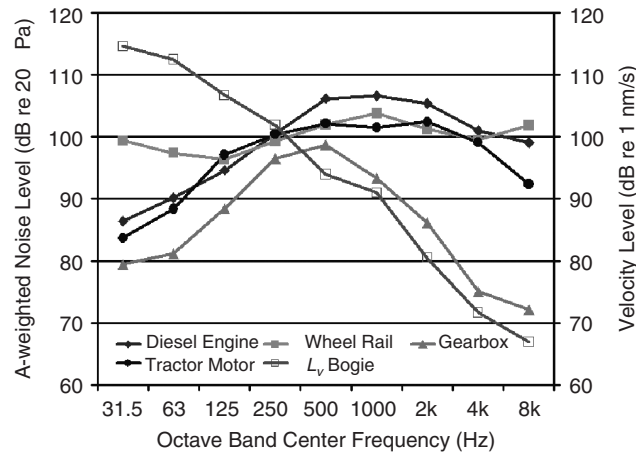


Figure 1 Typical source strengths at 130 km/h.

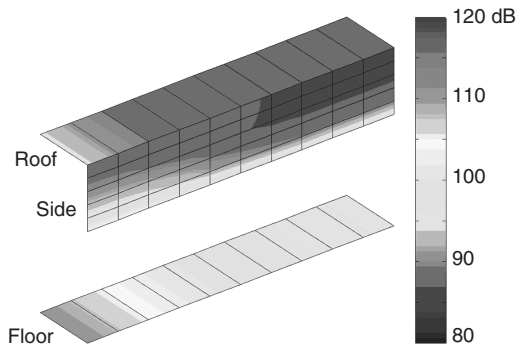


Figure 2 A-weighted sound pressure level around the car body.

indicating a need for a high sound transmission loss. Because of the desirable low mass design, a double construction is required. The double-wall resonance frequency should be as low as possible (50 to 100 Hz), which means the cavity height should be a minimum of 50 to 60 mm to match the surface mass of typical floor constructions. Car bodies made of extruded aluminum profiles present a special problem, as the sound transmission loss of the double-wall profiles is lower than expected per the mass law in the middle-frequency range. The low sound transmission loss is caused by an acoustical unfavorable mass/bending stiffness ratio resulting in a low coincidence frequency. A sufficient cavity height is therefore particularly important. The cavity should be completely filled with highly efficient absorption material such as mineral wool or fiberglass in order to achieve the maximum sound transmission loss in the middle- to high-frequency range.

Rigid connections between the inner floor and the car body will reduce the sound transmission loss above the double-wall resonance. A floating floor, that is,

resilient support of the upper floor, can result in 5 to 15 dB higher sound transmission loss. The resilient supports can be either point supports or line supports. The line support principle can offer better results, as the local mobility differences are greater than what can be achieved with point supports.

Sandwich panels are becoming increasingly popular as this construction offers low mass and high bending stiffness. If a foam-type core material with a fairly low shear modulus (<20 MPa) is used, a favorable combination of high static stiffness and a sound transmission loss similar to a single panel of the same mass can be obtained.<sup>7</sup>

Double-glazing windows should be asymmetric, and double lip seals should be used for doors.

**Typical Sound Transmissions Losses** Examples of sound transmissions losses for constructions used in trains are shown in Table 3.

Figure 3 shows the sound transmission loss plotted against octave band center frequency for some typical floor constructions.

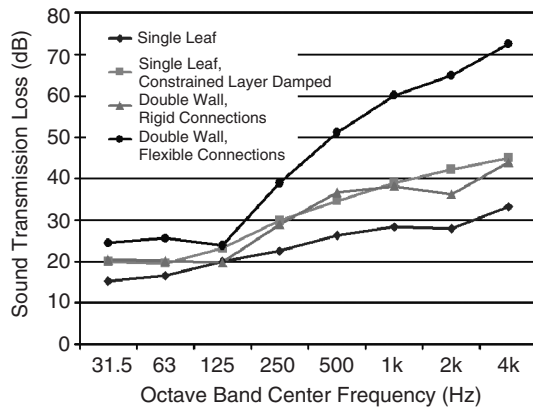
## 6.2 Structure-Borne Noise

**Receiver Properties** Reducing the mobility of the mounting position on the car body especially when a resilient element is present between the source and receiver can reduce the transmission of structure-borne noise to the car body. A reasonable target for the mobility level, in the frequency range of 30 to 1600 Hz, is  $-100$  to  $-90$  dB re 1 m/Ns for underfloor-mounted equipment and  $-90$  to  $-80$  dB for roof-mounted equipment. The expected mobility levels can be calculated using FEM.

**Damping of the Car Body** Traditional sprayable damping compounds in 3 to 5 mm thickness are used to increase the mechanical losses of steel car bodies. This measure has also been applied to aluminum car bodies, but due to the much higher bending stiffness

**Table 3** Examples of A-weighted Sound Transmission Losses

Item	A-weighted Sound Transmission Loss, $R_w$ (dB)
Floor, single-leaf plywood, 15 mm with floor cover	28
Floor, single-leaf plywood, 15 mm with steel constrained layer damping and floor cover	39
Floor, double wall, 1.25-mm steel, 30-mm cavity with rigid fixed 15-mm plywood with floor cover	37
Floor, double wall, 1.25-mm steel, 45-mm cavity with resilient supported 15-mm plywood with floor cover	49
Floor, 40-mm closed aluminum profile with rigid fixed 15-mm plywood	35
Floor, double wall, 70-mm closed aluminum profile, 35-mm cavity with resilient supported 15-mm foam sandwich	42
Floor, double wall, 60-mm closed aluminum profile, 55-mm cavity with resilient supported 20-mm foam sandwich	44
Sidewalls	37–49
Double-glazed window	33
Roof	50
Entrance door	34–38
Single-leaf bellow	26
Double-leaf bellow	42

**Figure 3** Sound transmission loss for typical floor constructions.

the damping is only efficient above 400 to 500 Hz, that is, above the frequency range where the structure-borne noise normally has an influence.

In cases where space restrictions hinder the use of floating floors, an improvement of the structure-borne noise properties can be achieved by applying constrained layer damping to the car body structure at the point of excitation and the surrounding area. Normal floor plates of plywood have sufficient bending stiffness to work as the constraining layer.

**Typical Propagation Losses** For a rough estimation, the typical structure-borne propagation losses in the range of 63 to 500 Hz are of the order of 5 dB/m in the vertical direction and 1 to 3 dB/m in the lengthwise direction. The actual losses will depend on the specifics

of the car body structure and can be determined using SEA calculations combined with measurements.

**Typical Structure-Borne Sound Transmission Losses and Radiation Ratios** The structure-borne sound transmission loss,  $TL_v$ , describes the difference between the vibration level on the outer skin of the car body and the vibration level on the interior surface. Resilient mounting of the inner panel as used for, for example, floating floors increases the structure-borne transmission loss. Resilient mounting of lightweight panels on a significantly heavier structure such as the car body side should be used with caution to avoid the risk of increased vibration levels on the inner panel.

The  $TL_v$  of, for example floating floors is controlled partly by the transmission through the resilient supports and partly by airborne excitation via the cavity.<sup>8</sup> This means that the properties of the resilient support are less critical with a small cavity height and vice versa.

Measured radiation ratios are considerably higher than those found by the classical Maidanik method.<sup>9</sup> Since the majority of the surfaces radiating structure-borne noise to the interior are part of a double construction, the radiation ratio differs probably because of the forced wave excitation from the acoustical field in the cavity.

## 7 RECEIVER

The receiver is the passenger area or the driver's cab. Besides using internal doors to separate noisy areas such as entrances and gangways from the rest of the passenger area, it is very beneficial to maximize the amount of absorption. Increasing the absorption decreases the sound pressure level and the reverberation time and improves the privacy and RASTI figures. Absorption can also help reduce standing-wave problems. Cushion seats with cloth cover can provide large absorption areas if the specific flow resistance of the

cloth is of the order of 1 to 3 times  $\rho_{\text{air}}c$ , and the cushion material has good absorption properties. Materials with these properties that also meet strict fire requirements are available. The ceiling can also provide a high absorption area when the specific flow resistance is approximately 2 times  $\rho_{\text{air}}c$ . This can be achieved with a thin permeable sheet, thus avoiding any risk of contamination by fibers.

## 8 VALIDATION

The acoustical model of the vehicle will be based on a number of assumptions and simplifications. To validate the acoustical model before the train is running on the track, a number of measurements should be carried out. Performing these validation measurements allows for corrective action at as early a stage as possible.

1. One must verify that the equipment has met specifications.
2. One must verify that the car body elements have the calculated properties.
3. One must verify that the complete car has the modeled properties.

Testing of equipment follows relevant International Organization for Standardization (ISO) standards and procedures as defined in the equipment specifications. Testing of important car body elements, such as floor, sidewall, windows, and intercommunication gangways should follow ISO 140 procedures. The sample size for floors can be as little as 1.5 m<sup>2</sup> for initial investigations. For final measurements the sample size should follow the ISO recommendation, that is, 10 m<sup>2</sup> in order to obtain reliably low frequency results. The measurement results shall include the airborne sound transmission loss, the radiation ratio, and the structure-borne sound transmission loss. For testing of the airborne noise properties of the car, the interior of the car is used as sending room and the transmitted sound power through the element under investigation is measured using intensity. Practical experience shows that shielding of the other surfaces improves the accuracy of the measurement. The structure-borne properties are investigated using an electrodynamic shaker as source while the radiated noise to the interior of the car is measured using the intensity technique. Again shielding improves the accuracy. This method can also be used to measure the global pressure/force or pressure/velocity transfer function. However, this method is rather time consuming if you need the transmission properties from several connection points in three directions. Using a type 1 reciprocity technique<sup>10</sup> the pressure/velocity transfer function can be readily determined for all connections and directions by

measuring the free velocity at the uncoupled connection points when exciting the interior with an omnidirectional sound source of known volume velocity strength.

## 9 VERIFICATION

Testing methods and procedures for commissioning measurements are defined in ISO 3381 for internal noise.<sup>11</sup> This standard has recently been revised. The revised standard offers more well-defined test conditions, enabling repeatable and comparable results. The revised standard prescribes that the surface roughness of the rails at the test site must be measured and under a certain limit.

## REFERENCES

1. P. Wahlström, Sound Quality Criteria for Railway Vehicles, Proceedings, Sixth International Congress on Sound and Vibration, Copenhagen, Denmark, 5–8 July 1999, pp. 3113–3118.
2. M. Shafiquzzaman Khan, Determination of Sound Quality in Swedish Passenger Trains, Proc. Internoise 2001, 2001.
3. B. Stegemann, Development and Validation of a Vibroacoustic Model of a Metro Rail Car Using Statistical Energy Analysis (SEA), Chalmers University of Technology, Göteborg, Sweden, Report E 02–05, 2002.
4. Odeon, <http://helmholtz.oersted.dtu.dk/~odeon/>.
5. M. Ohlrich, Structure-Borne Sound Sources and Their Power Transfer, Proc. Internoise 2001, 2001.
6. P. Dings and M. Dittich, Roughness on Dutch Railway Wheels and Rails, *J. Sound Vib.*, Vol. 193, No. 1, 1996, pp. 103–112.
7. A. C. Nilsson, Wave Propagation and Sound Transmission through Sandwich Plates, *J. Sound Vib.*, Vol. 138, No. 1, 1990, pp. 73–94.
8. M. Berg, Prediction of Sound Insulation of Double Walls Using SEA, TRITA-FKT 2002:24, KTH, Stockholm, 2002.
9. F. Fahy, *Sound and Structural Vibration*, Academic, London, 1985.
10. T. Ten Wolde, J. W. Verheij, and H. F. Steenhoek, Reciprocity Method for the Measurement of Mechano-acoustical Transfer Functions, *J. Sound Vib.*, Vol. 42, No. 1, 1975, pp. 49–55.
11. EN ISO 3381:2005, Railway Applications—Acoustics—Measurements of Noise inside Railbound Vehicles, ISO, Geneva, Switzerland, August 2005.
12. M. Wollström, On Vibration Characteristics of Floating Floors, Licentiate thesis, TRITA-FKT 2000:31, KTH, Stockholm, 2000.
13. P. M. Nelson, Ed., *Transportation Noise Reference Book*, Butterworth, London, 1987.
14. V. V. Krylov, *Noise and Vibration from High-Speed Trains*, Thomas Telford, London 2001, Chapters 1, 2, 4, and 6.



# CHAPTER 98

## NOISE AND VIBRATION IN OFF-ROAD VEHICLE INTERIORS – PREDICTION AND CONTROL

**Nickolay Ivanov**

Department of Environmental Engineering  
Baltic State Technical University  
St. Petersburg, Russia

**David Copley**

Sound and Cooling Research  
Caterpillar, Inc.  
Peoria, Illinois

### 1 INTRODUCTION

Off-road vehicles are self-propelled machines used largely for infrastructure development and maintenance or agricultural applications. Common uses for such vehicles include earth moving, automobile and railway construction, communication networks, airport and building construction, various kinds of repair and maintenance, and farming. Modern off-road vehicles can be self-contained vehicles or machines attached to tracked or wheeled industrial tractors. The following are some of the uses of these off-road vehicles: (1) preparation of agricultural or building sites, (2) earth moving, (3) road laying, and (4) as cranes. Common machine types that perform these functions include tractors, tracked bulldozers, graders, loaders, cranes, vibratory compactors, excavators, and other types of track/crawler or wheeled vehicles.

Most off-road machines are equipped with cabs that provide safety and comfort for operators. The A-weighted sound pressure levels inside cabs during machine operation are usually in the range of 65 to 85 dB. The interior noise level depends on a number of factors. Among the most significant factors are the operation of the machine and various vibroacoustical properties such as the efficiency of the cab vibration isolation, cab wall sound transmission loss, structural damping, interior sound absorption, and the features and locations of the dominant noise sources. Interior noise reduction is effective if two main problems are solved: first, if the dominant noise source and path contributions to the cab noise are well understood and, second, if optimal noise reduction methods are used.

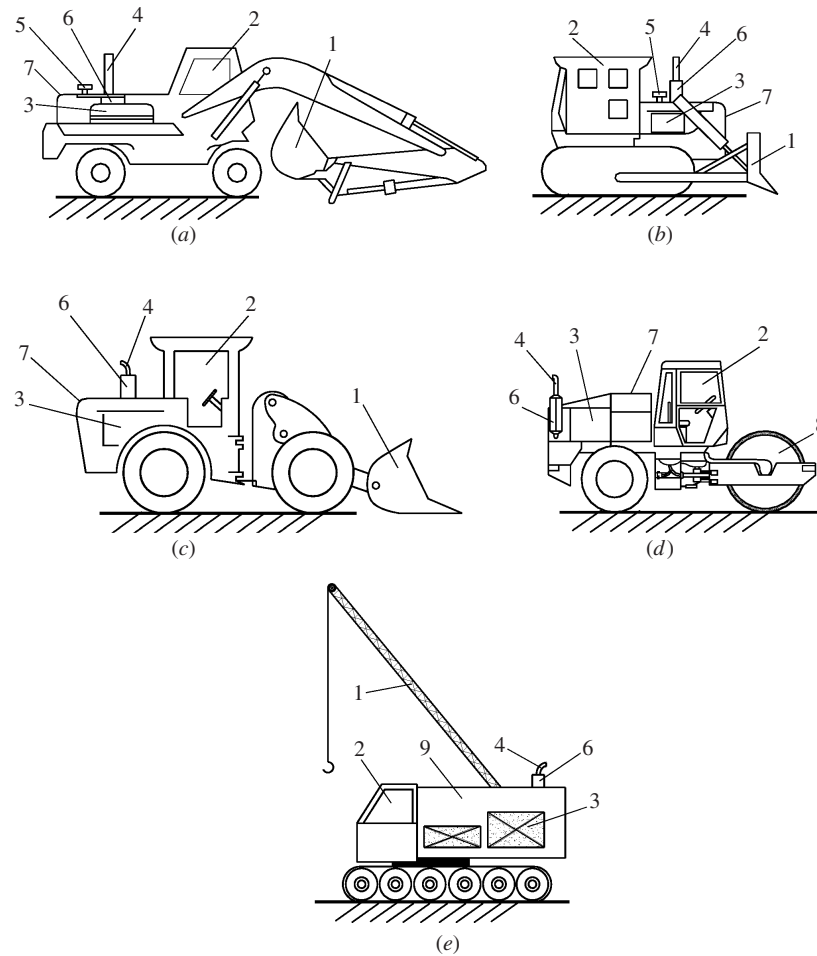
### 2 TYPICAL CONSTRUCTION DETAILS AND MAIN NOISE SOURCES OF OFF-ROAD VEHICLES

Off-road vehicles are usually powered by a diesel internal combustion engine (ICE) coupled with a mechanical drive. The internal combustion engine may be located within a hooded enclosure (Figs.1a–d) or in a diesel compartment (Fig.1e). Some off-road vehicles

such as cranes may have an electrical drive, where the diesel engine powers an electric generator that in turn powers the machine implement. Most off-road vehicles (graders, loaders, excavators, tracked dozers, etc.) are equipped with specific attachments (buckets, blades, etc.) that, as a rule, do not emit significant noise during operation cycles. The primary noise sources for such machines are typically the ICE body (mechanical noise source), the exhaust, and intake of the ICE (air dynamical noise sources). The internal combustion engine cooling system fan is an aerodynamic noise source in off-road machines, and transmission elements are mechanical noise sources. Hydraulics pumps and lines are fluid-borne or fluid-structural noise sources. If a vehicle attachment is characterized by significant emission of noise and vibration (such as a vibratory compactor), these attachments usually become the dominant noise source. In general, a track undercarriage is a dominant noise source of a tracked off-road vehicle during dynamic operating cycles.

The shock interaction of two or more objects, friction of interacting surfaces, aerodynamic turbulence of airflows, forced oscillations of solid bodies, influence of variable magnetic forces, and pressure pulsations in hydraulic systems may each be significant contributors to cab noise. Considering the causes and characteristics, noise sources in off-road vehicles may be divided into the four following classes: mechanical, aerodynamic, hydraulic, and electromagnetic.

Table 1 contains typical sound power level spectra of primary noise sources of off-road vehicles.<sup>1</sup> It is shown that noise emitted by the ICE exhaust and intake systems is characterized by distinct low-frequency components; noise emitted by the ICE body has high-frequency characteristics, and the other noise sources have mid- to high-frequency characteristics. Table 1 also presents A-weighted sound power levels varying from 85 dB to 105 dB for several types of off-road machines. It is shown that the ICE body and vibrating attachments are the noisiest sources, while the ICE intake is the quietest source for most types of off-road machines.



**Figure 1** Examples of off-road vehicles: (a) excavator, (b) tracked dozer, (c) loader, (d) vibratory compactor, and (e) crane (engine compartment type): (1) machine attachment (bucket, dozer, crane boom, etc.), (2) cab, (3) internal combustion engine, (4) ICE exhaust pipe, (5) ICE intake, (6) muffler, (7) ICE enclosure, (8) vibration active attachment (vibrating roller), and (9) diesel compartment.

**Table 1** Average Sound Power Level Spectra of Typical Noise Sources of Off-Road Vehicles

No.	Type of Noise Source	Sound Power Levels (dB) in Octave Frequency Bands (Hz)								A-weighted Sound Power Level (dB)
		63	125	250	500	1000	2000	4000	8000	
1	ICE body	90	100	96	98	100	100	98	95	105
2	ICE exhaust system (with presence of a muffler)	95	105	100	90	90	87	85	80	95
3	ICE intake	82	92	86	80	80	80	75	73	85
4	ICE cooling fan	85	95	100	97	95	92	87	82	100
5	Vibrating roller	100	102	96	104	101	90	83	72	105
6	Track	75	78	85	83	82	85	78	69	90
7	Hydraulic pump	78	80	86	92	92	85	80	76	95

### 3 OFF-ROAD VEHICLE INTERIOR NOISE MEASUREMENT PROCEDURE

Two international standards are most often employed to measure noise at the operator station for a large majority of off-highway vehicles.<sup>2,3</sup> Other standards for measuring operator noise have been developed for specific machine types (e.g., agricultural machines), but their approach is similar to the procedures in Refs. 2 and 3.

The operator is in the driving position during measurements. The microphone is oriented horizontally, pointing in the direction in which a person occupying the operator's seat would normally look. The microphone is located  $200 \pm 20$  mm from the medium plane to the side of the operator's head where the time-averaged A-weighted sound pressure level is highest.

Measurements can be made for stationary and dynamic conditions. The time-averaged A-weighted sound pressure level, in decibels, is determined either by using Eq. (1) or by using digital integration sound level meters:

$$L_{p_{Aeq}T} = 10 \log \left[ \frac{1}{T} \int_0^T \frac{p_A^2(t)}{p_0^2(t)} dt \right] \text{ dB} \quad (1)$$

where  $T$  = measurement period

$p_A(t)$  = instantaneous A-weighted sound pressure of the sound signal, Pa

$p_0(t)$  = reference sound pressure  
( $p_0 = 2 \times 10^{-5}$  Pa)

Measurements are taken with the doors and windows closed and the ventilating system(s) running. The minimum number of measurements at each microphone position is three. It is necessary to have two of the readings be within 1 dB of each other. If this condition is not satisfied, additional readings are taken to meet the requirement. The reported value of the time-averaged A-weighted sound pressure level will be the arithmetic mean of the two highest values that are within a 1-dB range of each other.

Other measurement techniques (e.g., sound intensity) are also suitable for scientific and detailed studies of these kinds of vehicles.<sup>4-6</sup>

### 4 OFF-ROAD INTERIOR NOISE LIMITS

Off-road interior noise limits are settled by each country considering domestic legislation and may have obligatory or recommendation status. Table 2 contains permissible levels at operator position of off-road vehicles accepted by several countries.

At the same time, low interior noise as well as sound quality can play a significant role in product differentiation and commercial success. Thus, interior noise levels are being driven lower by market pressures and competition.

### 5 INTERIOR NOISE CHARACTERISTICS

Characteristic spectra of interior noise of two off-road vehicles are presented in the Fig. 2. Experimental investigations show that off-road vehicle interior noise is characterized by dominant contributions of low-frequency

**Table 2 Off-Road Interior Noise Level Limits**

Country	Interior A-weighted Sound Pressure Level Limit (dB)
United States	85
Japan	73
European Union countries	85
Russia	80

components. In contrast, the major contributions to exterior noise (e.g., noise emitted by the ICE body, vibrating roller, etc.) are characterized by higher frequency content.<sup>1,7</sup> This suggests that cabs of off-road machines, as a rule, have relatively high sound isolation.

All off-road vehicles may be conventionally divided onto three groups considering dominant interior noise contributions:

Group I is characterized by dominant noise emitted by the ICE.

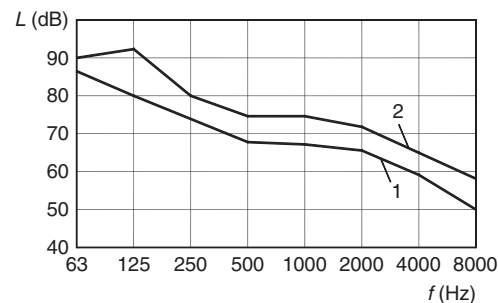
Group II is characterized by dominant noise emitted by vibration-active attachment and lower contribution emitted by internal combustion engine.

Group III is characterized by similar noise contributions emitted by the ICE and by an undercarriage drive.

Average interior levels of wheel and tracked off-road vehicles and vibratory compactors with enclosures adjoined to cabs are presented in the Table 3.

Separating the vehicle cab from the engine compartment by an air gap can yield additional A-weighted sound pressure level reduction of 3 to 5 dB. Interior noise in wheel and tracked vehicles in static conditions is 1 to 3 dB lower than in dynamic conditions and is in the range of 70 to 75 dB. A vibratory compactor's interior A-weighted sound pressure level measured during dynamic conditions is about 10 dB higher than static conditions and is dominated by the ICE and the vibrating roller drum.

Interior noise depends significantly on the operating conditions. Reducing the engine speed is one way to provide lower noise emissions of off-road vehicles.



**Figure 2** Average characteristic sound pressure level spectrum of interior noise in some off-road vehicles for specific conditions of work: (1) vehicles without vibration active attachments (e.g., excavators, loaders, tracked dozers, graders) and (2) vehicles with vibration active attachments (e.g., vibratory compactor).

**Table 3 Interior Noise in Diesel-Powered Off-Road Vehicles During Typical Operating Conditions**

Vehicle Group	Vehicle Type	Interior A-weighted Sound Pressure Levels for Various Work Conditions (dB)	
		Stationary Condition	Dynamic Condition
I	Wheel excavators, loaders, graders	70–75	71–77
II	Self-propelled vibratory compactors	73–76	80–86
III	Tracked dozers	70–75	72–78

Such measures may reduce the interior A-weighted sound pressure level by 2 dB to 3 dB.

Interior noise levels also depend on the year of vehicle production. Around 25 to 30 years ago the interior A-weighted sound pressure level in most off-road vehicles was about 90 dB to 95 dB.

## 6 PREDICTION OF AIRBORNE NOISE IN CABS

An example of predicting airborne sound contribution in a tracked dozer cab is presented below. The calculation scheme of the noise generation processes inside a tracked dozer cab is shown in Fig. 3. The following noise sources are considered in the calculation scheme: the ICE body located in engine compartment, exhaust and intake pipes located outside and above the enclosure, and the crawler undercarriage.

There are several dominant noise propagation paths into the cab: from the engine compartment through the partition, through the enclosure panels, and then through the cab elements (excluding the cab floor and the partition), from the exhaust stack and intake port through cab elements, through the undercarriage, and then through the cab floor and other panels.

Sound pressure levels are predicted in octave bands, and the A-weighted sound pressure level is estimated using the A-weighting filter correction of a sound level meter.

The primary assumptions of the prediction method include the following statements<sup>1</sup>: The sound field in the cab is quasi-diffuse, the sound sources are incoherent, and the sound pressure at the receiving point is determined by the energy summation principle. The cutoff frequency (frequency where the field is regarded as quasi-diffuse) for the aforementioned

assumptions is estimated by Eq. (2):

$$f_{\text{dif}} = \frac{200}{\sqrt[3]{V}} \text{ Hz} \quad (2)$$

where  $V$  is the cab volume (in  $\text{m}^3$ ).

An analytical description of the primary noise source contributions into the off-road vehicle interior sound field is presented below. The noise contribution from the diesel engine that propagates into the cab through the partition, located between the engine compartment and the cab (e.g., a firewall), is determined by the Eq. (3):

$$L_{\text{eng\_part}}^{\text{int}} = L_W^{\text{enc}} + 10 \log \left( \frac{\chi_{\text{enc}}}{S_{\text{enc\_total}}} + \frac{4\psi_{\text{enc}}}{B_{\text{enc}}} \right) + 10 \log \frac{S_{\text{part}}}{\sum_{i=1}^n S_{\text{enc}_i}} - \bar{S}_{\text{part}} - 10 \log A_{\text{cab}} + 6 \text{ dB} \quad (3)$$

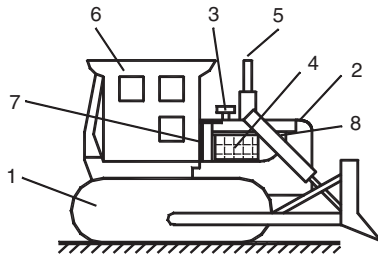
where  $L_W^{\text{enc}}$  = total sound power emitted within the enclosure, dB

$\chi_{\text{enc}}$  = coefficient of the effect of the near sound field of the enclosure (Fig. 4)<sup>1</sup>

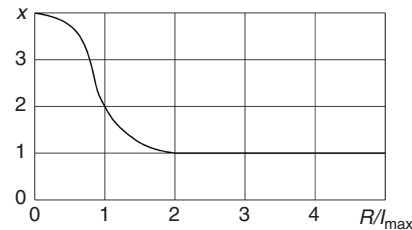
$\psi_{\text{enc}}$  = coefficient of the sound field diffusivity violation under the enclosure (Fig. 5)<sup>1</sup>

$S_{\text{enc\_total}}$  = total area of the enclosure panels,  $\text{m}^2$

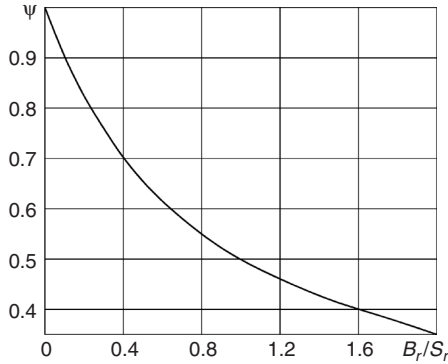
$B_{\text{enc}}$  = enclosure constant,  $\text{m}^2$ , which is estimated as follows:



**Figure 3** Scheme of main noise contributions considered in the prediction model of the airborne noise emitted by a tracked dozer: (1) crawler undercarriage, (2) enclosure, (3) intake, (4) engine, (5) exhaust, (6) cab, (7) partition, and (8) engine compartment.



**Figure 4** Diagram of the  $\chi$ -coefficient estimation depending on the ratio of the distance  $R$  and the maximum linear dimension of the noise source  $l_{\text{max}}$ .



**Figure 5** Dependence of the coefficient  $\psi$  of the sound field diffusivity violation in a closed room on the ratio of the room constant ( $A_r$ ) to the room area ( $S_r$ ).

$$B_{\text{enc}} = \frac{A_{\text{enc}}}{1 - \bar{\alpha}_{\text{enc}}}$$

where  $A_{\text{enc}}$  = equivalent enclosure sound absorption,  $\text{m}^2$ , estimated by the following equation:  $A_{\text{enc}} = \bar{\alpha}_{\text{enc}} S_{\text{enc\_total}}$

$\bar{\alpha}_{\text{enc}}$  = average coefficient of sound absorption of the enclosure

$\sum_{i=1}^n S_{\text{enc}_i}$  = area of the enclosure panels, where sound propagates into the environment,  $\text{m}^2$

$S_{\text{enc}_i}$  = area of the  $i$ th panel of the engine enclosure where sound propagates into the environment,  $\text{m}^2$

$n$  = number of panels where sound propagates into the environment

$\bar{S}\bar{I}_{\text{part}}$  = average sound isolation of the partition, dB

$S_{\text{part}}$  = area of the partition located between the diesel compartment and the cab,  $\text{m}^2$

$A_{\text{cab}}$  = equivalent cab sound absorption,  $\text{m}^2$ , estimated by the following equation:

$$A_{\text{cab}} = \bar{\alpha}_{\text{cab}} S_{\text{cab}}$$

$\bar{\alpha}_{\text{cab}}$  = average coefficient of sound absorption of the cab

$S_{\text{cab}}$  = total area of cab shielding elements (glass, floor, walls, ceiling, etc.),  $\text{m}^2$

Measured sound absorption coefficients of cabs and enclosures are presented in the Table 4. Magnitudes of  $L_{W_{\text{exh}}}^{\text{enc}}$  and  $\bar{S}\bar{I}_{\text{part}}$  may be determined by theoretical predictions or from experiments.<sup>1,7</sup>

The exhaust contribution to the interior noise is estimated by the Eq. (4):

$$L_{\text{exh}}^{\text{int}} = L_{W_{\text{exh}}} - 20 \log \frac{R_{\text{exh}}}{r} - 10 \log \frac{\sum_{i=1}^m S_{\text{cab}_i}}{\sum_{i=1}^m S_{\text{cab}_i} \times 10^{-0.1(S\bar{I}_{\text{cab}_i} + t_{\text{dif}_i}^{\text{cab}})}} + 10 \log \frac{\sum_{i=1}^m S_{\text{cab}_i}}{A_{\text{cab}}} + \text{DI}_{\text{exh}} - x + 6 \quad (4)$$

where  $L_{W_{\text{exh}}}$  = sound power level generated by the exhaust (to be predicted or measured), dB

$R_{\text{exh}}$  = distance between the exhaust pipe end and the nearest panel of the cab, m

$r$  = distance from the exhaust pipe end to the microphone position where exhaust noise was measured, m

$S_{\text{cab}_i}$  = area of the  $i$ th cab panel through which noise penetrates into the cab,  $\text{m}^2$

$n$  = number of cab panels where sound penetrates into the cab

$S\bar{I}_{\text{cab}_i}$  =  $i$ th cab panel sound isolation, dB

$t_{\text{dif}_i}^{\text{cab}}$  =  $i$ th cab panel sound isolation

correction (depends on location of the panel relatively the exhaust pipe), dB,  $t_{\text{dif}_i}^{\text{cab}} = 5$  dB for the ceiling and the side panels of the cab,  $t_{\text{dif}_i}^{\text{cab}} = 8$  dB for the back panel

$\text{DI}_{\text{exh}}$  = exhaust directivity index, dB

$x$  = radiation correction, which depends on the spatial angle of sound radiation,  $x = 10 \log \Omega$ , where  $\Omega$  is the noise source spatial angle of sound radiation, in other words,  $x = 5$  dB, for  $\Omega = \pi$  ("1/4 space" radiation),  $x = 8$  dB, for  $\Omega = 2\pi$  ("half-space" radiation),  $x = 11$  dB, for  $\Omega = 4\pi$  ("full-space" radiation)

$A_{\text{cab}}$  = as already defined in Eq. (3)

**Table 4** Magnitudes of Average Coefficients of Sound Absorption of Close Volumes

Descriptor	Octave Frequency Bands Magnitudes of Average Sound Absorption Coefficients							
	63	125	250	500	1000	2000	4000	8000
$\alpha_{\text{cab}}$	0,09	0,15	0,18	0,25	0,25	0,25	0,25	0,28
$\alpha_{\text{enc}}$	0,08	0,12	0,16	0,2	0,26	0,3	0,3	0,35

The undercarriage contribution to the interior sound field of an off-road vehicle propagating through a cab floor is determined by the Eq. (5):

$$L_{\text{undercar\_floor}}^{\text{int}} = L_{W_{\text{undercar}}} - 10 \log \frac{R_{\text{undercar}}}{r} - \overline{SI}_{\text{floor}} + 10 \log \frac{S_{\text{floor}}}{A_{\text{cab}}} + 1 \quad \text{dB} \quad (5)$$

where  $L_{W_{\text{undercar}}}$  = sound power emitted by the undercarriage, dB

$R_{\text{undercar}}$  = average distance from the undercarriage to the floor

$\overline{SI}_{\text{floor}}$  = average sound isolation of the floor  
 $r$  = distance where undercarriage noise is measured, m, ( $r = 1$  m)

$S_{\text{floor}}$  = floor area, m<sup>2</sup>

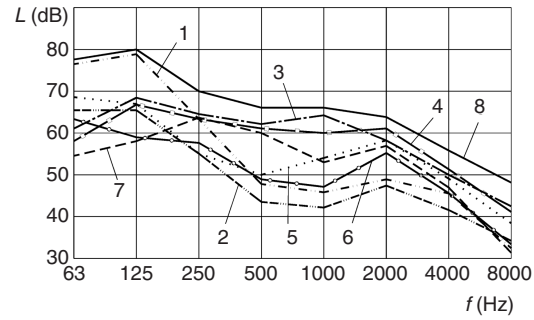
Other contributions, such as intake noise ( $L_{\text{int\_pipe}}^{\text{int}}$ ), noise propagating through the enclosure underneath opening considering ground reflection ( $L_{\text{open}}^{\text{int}}$ ), undercarriage noise propagating through the cab walls ( $L_{\text{undercar\_walls}}^{\text{int}}$ ), and noise emitted by the engine that is transmitted through the enclosure and cab panels ( $L_{\text{eng\_encl}}^{\text{int}}$ ) are each determined in a manner similar to the components already considered. The total spectrum of the off-road interior noise is estimated by Eq. (6):

$$L_{\text{airborne}}^{\text{int}} = 10 \log (10^{0.1 L_{\text{int\_pipe}}^{\text{int}}} + 10^{0.1 L_{\text{open}}^{\text{int}}} + 10^{0.1 L_{\text{eng\_enc}}^{\text{int}}} + 10^{0.1 L_{\text{eng\_part}}^{\text{int}}} + 10^{0.1 L_{\text{undercar\_floor}}^{\text{int}}} + 10^{0.1 L_{\text{undercar\_walls}}^{\text{int}}} + 10^{0.1 L_{\text{exh}}^{\text{int}}}) \quad \text{dB} \quad (6)$$

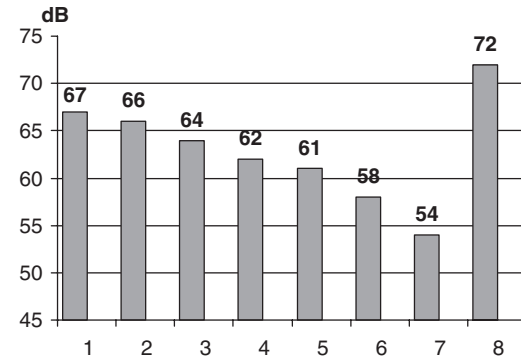
Examples of interior noise in a tracked dozer cab is presented in Figs. 6 and 7. It follows from analysis of Fig. 7 that the dominant noise components propagate into the cab by the first and second pathways (from engine compartment through the partition between the cab and diesel compartment and from engine compartment through the enclosure underneath opening). This suggests that the most effective noise reduction would be achieved by increasing the sound isolation of the partition and from decreasing the opening underneath the enclosure. The next step would be to enhance the ICE exhaust muffler's efficiency. The predicted results also help determine the magnitude of the required noise reduction level for each component to achieve certain interior sound field goals.

This prediction method allows one to solve at least two important tasks:

- Theoretically predict interior sound field parameters of an off-road vehicle at the design stage
- Separate noise source contributions into interior sound field for already produced vehicle



**Figure 6** Example of theoretically predicted interior noise spectrum of a tracked dozer: (1) exhaust noise contribution, (2) intake noise contribution, (3) diesel noise contribution propagating through the partition between the engine compartment and the cab, (4) diesel noise propagating through enclosure underneath opening, (5) diesel compartment noise propagating through the enclosure panels, (6) undercarriage noise contribution propagating through the cab panels, (7) undercarriage noise contribution propagating through the cab floor, and (8) total airborne interior sound field of a tracked dozer.



**Figure 7** Example of predicted separate A-weighted sound pressure levels emitted by a tracked dozer noise sources propagating into a cab by the following paths: (1) from diesel compartment through the partition between the cab and diesel compartment, (2) from diesel compartment through the enclosure underneath opening, (3) from exhaust, (4) from the undercarriage through the cab floor, (5) from the diesel compartment through the enclosure panels, (6) from the undercarriage through the cab panels (except cab floor), (7) from intake, and (8) total airborne interior sound field.

## 7 DETERMINATION OF STRUCTURE-BORNE SOUND CONTRIBUTION

The internal combustion engine (ICE) and attachments with intrinsic vibration or shock emissions are the main sources of structure-borne sound in off-road vehicles. Vibration is transmitted through the base of the vibration source onto the vehicle frame and then propagates through the cab base to shielding elements of the cab. Vibration attenuation may be



achieved in bearing junctions if vibration isolation is used. Vibration also may be reduced during vibration transmission through the frame or shielding elements of the cab. Separation of structure-borne and airborne sound is an important step of interior noise reduction. Structure-borne sound in the cab may be separated from the airborne sound by means of analytical or numerical methods.<sup>8,9</sup>

Finite element method (FEM) is one of most widely used numerical methods for prediction of interior structure-borne sound. Vibration velocity levels emitted by cab surfaces are initial input data for FEM prediction. Cab elements such as the air volume, rubber seals for cab windows, and hard edges are represented by sets of elements. An FEM model of a cab is presented in Fig. 8. Various commercial software tools for FEM analysis are available. FEM has several significant restrictions, which often result in it being applied only to the low-frequency range (up to 200 to 250 Hz) for typical cab models. Estimation is carried out per particular fixed frequencies while interior noise characteristics are often determined in octave frequency bands. Results of structure-borne sound prediction in a cab of a vibratory compactor and their comparison with experimental data are represented in Fig. 9.

Until recently, most components in off-road vehicles were hard mounted to frames or to each other. For recent designs, it may be stated that structure-borne sound reduction in most modern off-road vehicles (graders, excavators, loaders, etc.) has not been as critical as airborne reduction. This is because effective means of vibration isolation for internal combustion engines and cabs and effective vibration damping materials (with high loss factor) have become widely used in these vehicles, replacing older hard-mount junctions.

Contributions from structure-borne sound is comparable to airborne sound contribution in cabs only in the low-frequency range (usually 31.5 to 63 Hz), or in other words near the natural frequency of the internal combustion engine crankshaft (most internal combustion engines speeds are in the range of 1500 to 3000 rpm, or in other words, 25 to 50 Hz).

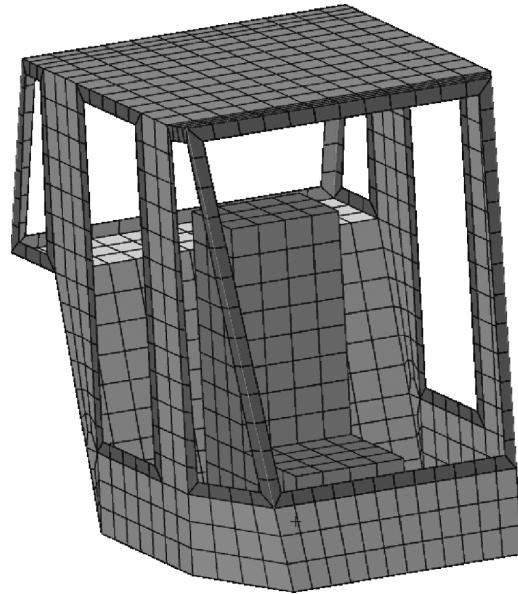


Figure 8 FEM model of a cab.

Structure-borne sound contribution is more significant for vehicles with an active attachment. In this case dominant vibration is found at frequencies close to a natural frequency of the vibrating attachment but some structure-borne contribution in higher frequencies (up to 200 to 250 Hz) is also considered.

For higher frequency analysis, beyond the typical frequency range of finite element analysis (FEA), statistical energy analysis (SEA) is often used to model off-road vehicle cabs. Instead of discretizing the cab geometry into small elements as with FEA, the SEA approach assumes the cab parts are larger, primitive structures such as plates, cylinders, beams, and acoustical volumes. SEA is used for both structure-borne and airborne situations. A simple cab model is shown in Fig 10.

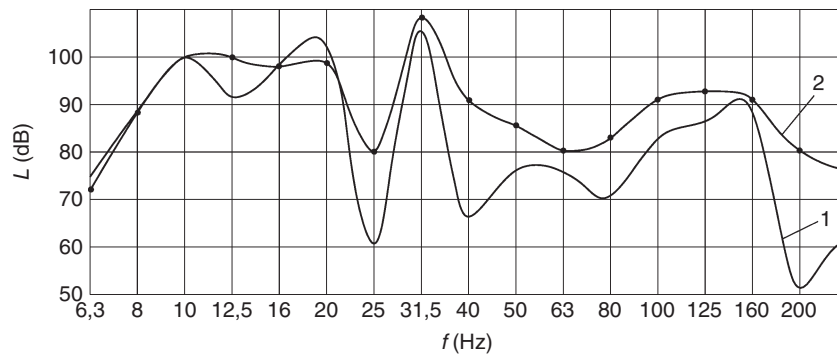
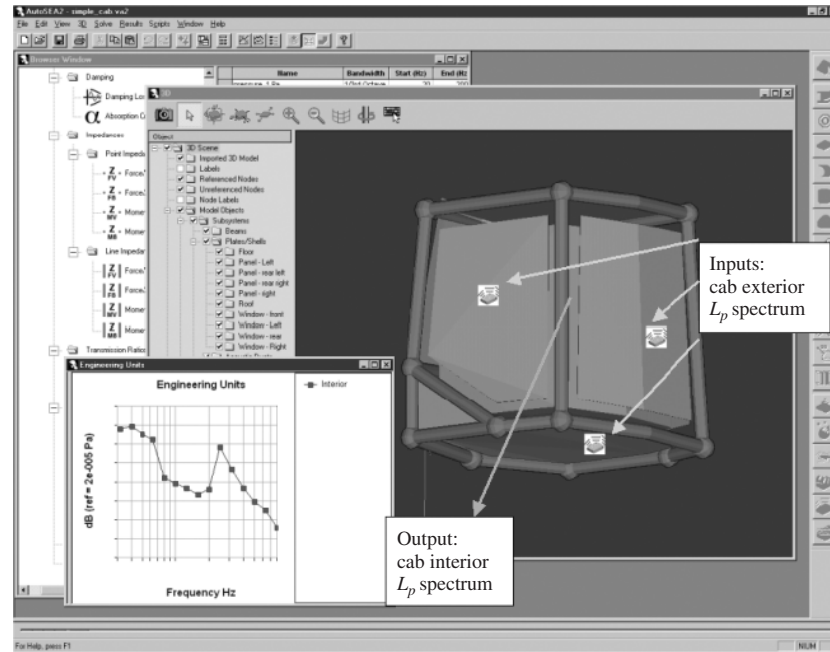
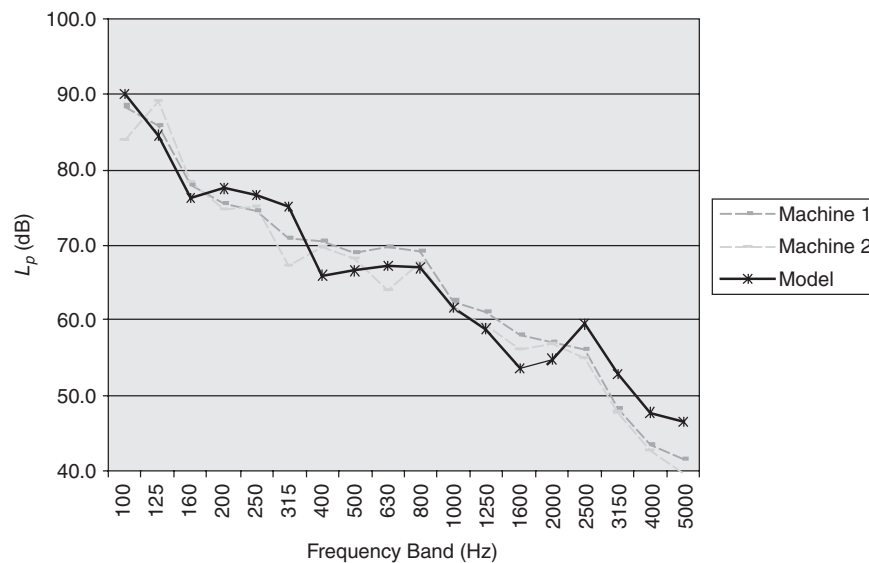


Figure 9 Sound pressure levels inside a vibratory compactor cab for a condition when vibrating roll is active: (1) predicted results and (2) experimental data.





**Figure 10** Simple SEA model of a cab. In this model the front window, door, and floor are single plate elements, which represent the flexural wave fields excited but an external pressure field.



**Figure 11** Example results showing comparison of sound pressure level between SEA and measurement.

Figure 11 compares predicted spectrum from a SEA cab model compared to measured spectra from two identical machines. The solid line is the model prediction and the two dashed lines are from two different machines of the same type. This spectrum

is the sound level as predicted and measured in a cab of construction machine running at static, high idle.

Statistical energy analysis does not yield exact, deterministic results such as FEA. Rather, it produces spatially averaged, and band-averaged results. Run

times for a typical cab SEA model are on the order of 1 or 2 min, as opposed to hours for typical FEA models. Because SEA models work well for high-frequency prediction, they are a convenient tool for assessing acoustical trim options, such as materials for headliners or optimal thickness of a floormat decoupler. Also, because SEA models are typically less costly to build and validate than FEA models, SEA is often used to assess design trade-offs in the early concept phase before the design is too constrained.

## 8 NOISE REDUCTION IN CABS

### 8.1 Classification of Interior Noise Reduction Methods and Means

All interior noise reduction methods and means may be divided onto three main groups considering the following features: source of noise excitation; transmissibility; and response.<sup>1,9–11</sup>

*Source of excitation:* Reducing the intensity of the exterior sound fields around a cab and decreasing the sound field emitted by noise sources inside a cab is accomplished by reducing the noise sources, by increasing of a distance between the cab and the noise source, by applying local baffles between the noise source and a cab, by installing mufflers, and by other means to lessen the source strengths or path contributions to the cab interior field.

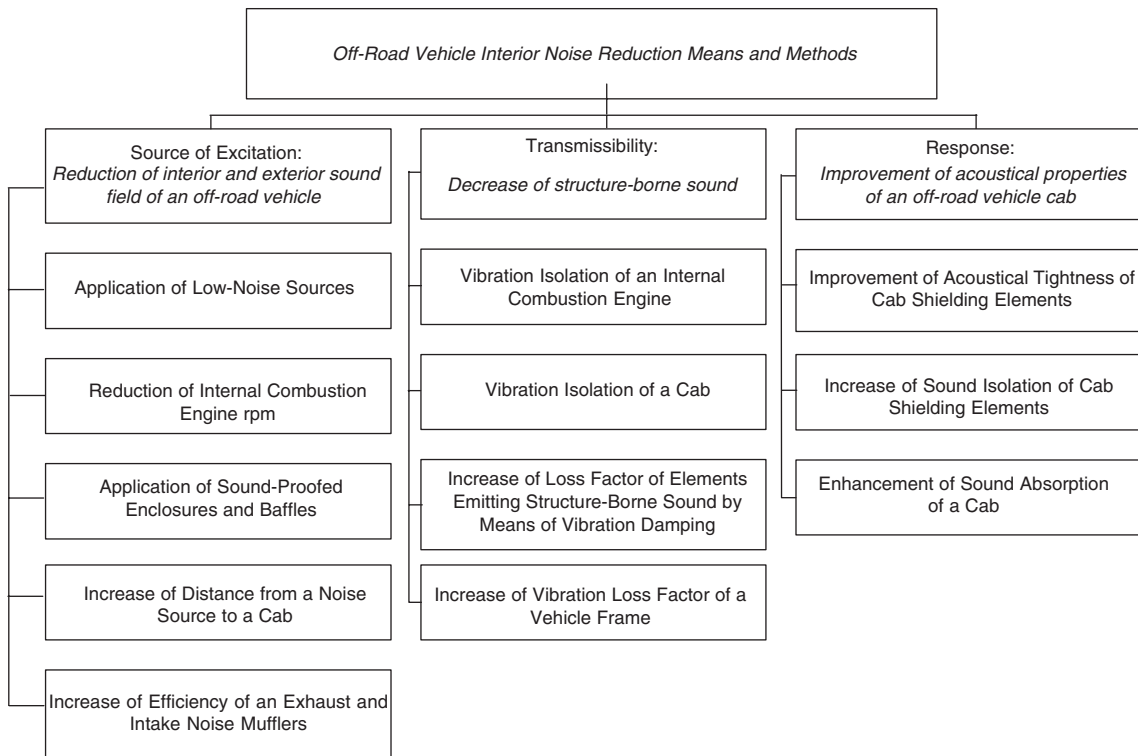
*Transmissibility:* Structure-borne sound reduction is obtained by vibration isolation of a cab and/or the vibration source, by increasing the loss factor of cab elements emitting structure-borne sound, and by increasing of loss factor of vehicle frame constructions.

*Response:* Sound isolation of cab elements, sound absorption of inner cab volume, and acoustical tightness of a cab (preventing sound propagation through elements with lower sound isolation, openings, other leaks) are the main acoustical characteristics of a cab. Acoustical tightness of a cab may be improved with the use of baffles, tightening, and sealing of nonclosed elements, openings, and apertures. In particular, careful attention must be made to any penetrations into the cab (e.g., electrical wirings, hoses, linkages, brake lines, etc.) and any cab elements that open and shut (doors, windows). If a cab is not well sealed the effects of other noise control measures may be compromised.

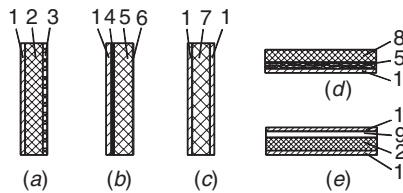
A detailed classification of interior noise reduction methods is presented in Fig.12.

### 8.2 Sound Isolation and Sound Absorption

One-layer, two- or three-layer, and multilayer structures are used for sound isolation of off-road vehicles. Most simple examples of a one-layer cab shielding elements are glass panels. If other conditions are not changed sound isolation increases when surface mass is increased and when number of layers is increased.



**Figure 12** Classification of off-road vehicle interior noise reduction means and methods.



**Figure 13** Examples of multilayer structures used for off-road cab shielding: (a, b) cab wall, (c) partition, (d, e) cab floor, (1) steel sheet, (2) soft sound absorptive porous material, (3) soft material (e.g. perforated vinilite), (4) damping coating, (5) fibered sound absorption material, (6) finishing material, (7) foam plastic, (8) rubber, and (9) intermediate air gap.

The last phenomenon is due to sound transmission through layers characterized by different impedance. It is well known that resonance phenomena in one-layer structures significantly decrease sound isolation. Application of multilayer structures increases sound isolation of a shielding element and may influence sound absorption and damping of a structure if some layers have good sound absorption or provide reliable vibration damping.

High sound isolation is found in three-layer structures with an intermediate connecting layer. Some examples of sound-proofed multilayer elements of off-road vehicles are presented in the Fig. 13. Table 5 contains average magnitudes of sound isolation of shielding elements of an off-road vehicle cab obtained from experiments.<sup>1</sup>

Usually shielding elements of an off-road vehicle cab have rather high sound isolation of about 25 to 40 dB in the frequency range of 500 to 8000 Hz. At the same time sound isolation of cab floor in the medium and high-frequency range is by 10 to 15 dB lower than sound isolation of other metal panels at a particular frequency. This may be explained by insufficient acoustical tightness of a cab floor or the presence of some flanking path. The data shown in Figs. 6 and 7 show that the dominant noise contributions propagate into the cab through a partition located between the diesel compartment and the cab. Thus, increasing the sound isolation of this partition is the next step toward more effective interior noise reduction.

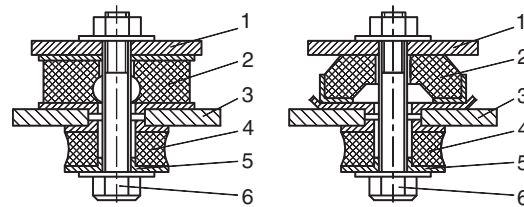
The average sound absorption coefficient ( $\bar{\alpha}_{cab}$ ) is a characteristic of sound absorptive properties of a cab. Higher  $\bar{\alpha}_{cab}$  yields lower reflected sound energy and

consequently lower interior noise. Sound absorption in a cab is obtained by adding sound absorptive materials, usually in the form of soft porous materials that are located at the cab ceiling (headliner) and on side or rear cab panels. The average sound absorption coefficient depends not only on the acoustical treatment of cab panels but also on sound absorptive characteristics of the driver seat and driver's clothing. An example of an average sound absorption coefficient spectrum from an off-road vehicle cab is represented in the Table 4. The values reach 0.1 to 0.2 in the low-frequency range and 0.2 to 0.3 in the medium and high frequencies. This means that some potential for further interior noise reduction of the A-weighted sound pressure level (by 1 dB to 1.5 dB) exists and may be obtained by using acoustical treatment with sound absorption in the medium- and high-frequency range of 0.35 to 0.45. Further increasing the average sound absorption of a cab is almost impossible for most off-road vehicles due to construction features of an off-road vehicle cab (e.g., most cabs have a high percentage of glass).

### 8.3 Vibration Isolation and Vibration Damping

Double vibration isolation is widely used in off-road vehicles. Vibration isolators are mounted under the internal combustion engine and under the cab, as a rule. Combined vibration isolators made from rubber and metal are used (Fig. 14).

Vibration isolation efficiency is determined by the value of the static displacement of a vibration-isolated object located on vibration isolators and by correlation of the frequency of forced oscillations ( $f_f$ ) and the natural frequency ( $f_n$ ). Higher static displacement provides more significant effect on vibration isolation. The vibration effect (VE) for low-frequency range



**Figure 14** Examples of vibration isolators of off-road vehicle cabs: (1) cab bracket, (2) main rubber element, (3) bracket, (4) additional rubber element, (5) fixing element, and (6) fastening bolt.

**Table 5** Average Magnitudes of Sound Isolation of Shielding Elements of an Off-Road Vehicle Cab

Type of Shielding Element of a Cab	Sound Isolation (dB) in Octave Frequency Bands (Hz)							
	63	125	250	500	1000	2000	4000	8000
One-layer glass	13	18	25	28	32	29	32	38
Multilayer metal element	18	23	27	31	35	33	36	40
Three-layer partition between diesel compartment and a cab	15	21	24	26	27	30	30	35
Multilayer floor	14	18	21	21	20	23	26	30

of  $(2 \div 5) \frac{f_f}{f_n}$  may be estimated by the following equation:

$$VE = 40 \log \frac{f_f}{f_n} \text{ dB} \quad (7)$$

where  $f_f$  is the frequency of forced oscillations.

The frequency of forced oscillations of an internal combustion engine crankshaft may be determined by Eq. (8):

$$f_f = \frac{n}{60} \text{ Hz} \quad (8)$$

where  $n$  is number of cycles, in revolutions/minute (rpm).

The natural frequency of a vibration-isolated object depends on the static displacement by Eq. (9):

$$f_n = \frac{5}{\sqrt{x}} \text{ Hz} \quad (9)$$

where  $x$ , in centimetres, is the static displacement of a vibration-isolated object (the difference between positions of vibration isolators in the vertical axis before and after the force application).

In most cases the frequency of technological vibration (forced frequency) during operating conditions is very close to the natural frequency of the vehicles and may cause significant resonances. This feature often determines the application of rubber vibration isolators for off-road vibration reduction that are characterized by substantial stiffness and by a high vibration loss factor. Vibration loss factor ( $\eta$ ) in rubber vibration isolators may reach values  $\eta = 0.2$  to  $0.4$  providing reasonable attenuation in resonance conditions.

Vibration damping is used to reduce structure-borne noise excited in plane metal shielding elements of a cab (e.g. sheet metal panels). Vibration damping coverings are characterized by high internal friction. The damping covering is usually in 1.5 to 2 time thicker than a treated metal sheet. Sandwich constructions are used in some cases when surface friction between two metal constructions is applied and as a partition between the diesel compartment and a cab in off-road vehicles. An additional effect of noise reduction is obtained due to

the lowering of structure-borne sound and the reduction of resonance effects in metal panels.

## REFERENCES

1. M. J. Crocker and N. I. Ivanov, Eds., *Noise and Vibration Control in Vehicles*, Politechnica, St. Petersburg, 1993.
2. ISO 6394:1998(E), Acoustics—Measurement at the Operator's Position of Noise Emitted by Earth-Moving Machinery—Stationary test conditions, International Organization for Standardization, Geneva, Switzerland, 1998.
3. ISO 6396: 1992 (E), Acoustics—Measurement at the Operator's Position of Noise Emitted by Earth-Moving Machinery—Dynamic Test Conditions, International Organization for Standardization, Geneva, Switzerland, 1992.
4. E. Carletti and I. Veechi, Intensity Vector Measurements Outside and Inside Cabs of Earth-Moving Machines, *Noise Control Eng. J.*, Vol. 37, No. 3, 1989, pp. 109–114.
5. M. J. Crocker, Ed., *Encyclopedia of Acoustics*, Wiley, New York 1997.
6. C. Harris, Ed., *Handbook of Acoustical Measurements and Noise Control*, Acoustical Society of America, New York, 1998.
7. N. Ivanov, D. Copley, and D. Kuklin, Practical Use of Noise Source Contribution Prediction Methods for Effective Noise Control in Construction Machines, Proceedings of the Tenth International Congress on Sound and Vibration, 7–10 July 2003, Stockholm, Sweden, pp. 2981–2988.
8. P. E. Boileau and S. Rakheja, Vibration Attenuation Performance of Suspension Seats for Off-Road Forestry Vehicles, *Int. J. Ind. Ergonomics*, Vol. 5, No. 3, 1990, pp. 275–291.
9. P. Donati, Survey of Technical Preventive Measures to Reduce Whole-Body Vibration Effects When Designing Mobile Machinery, *J. Sound Vib.*, Vol. 253, No. 1, 2002, pp. 169–183.
10. L. L. Beranek and I. L. Ver, Eds., *Noise and Vibration Control Engineering: Principles and Applications*, Wiley, New York, 1992.
11. G. Brambilla, E. Carletti, and F. Pedrielli, Perspective of the Sound Quality Approach Applied to Noise Control in Earth Moving Machines, *Int. J. Acoust. Vib.*, Vol. 6, No. 2, 2001, pp. 90–96.

# CHAPTER 99

## AIRCRAFT CABIN NOISE AND VIBRATION PREDICTION AND PASSIVE CONTROL

John F. Wilby  
Wilby Associates  
Calabasas, California

### 1 INTRODUCTION

Aircraft cabin noise can be generated by a variety of sound and vibration sources and transmitted into the cabin by airborne and structure-borne paths. The sources may be inside or outside the fuselage and, depending on the type of airplane, can include engines, propellers, turbulent boundary layer, air-conditioning systems, and propulsion system gearboxes. The main airborne noise transmission path is through the sidewall of the cabin and can involve resonant and nonresonant components. Structure-borne paths are usually associated with vibration excitation at different locations on the airframe. Potential sound and vibration sources, and their transmission paths, are described in this chapter, and methods of identifying the contributions from the different sources and paths are discussed. Passive control of cabin noise levels can be achieved by reduction of the source or by attenuation during transmission; various methods for achieving passive noise control are identified. Finally, analytical methods for the modeling of noise transmission into an airplane cabin, including modal methods, statistical energy analysis, and numerical methods, are discussed. Active control of aircraft cabin noise is discussed in Chapter 100.

### 2 NOISE AND VIBRATION SOURCES

Several sources contribute to cabin interior noise and vibration levels.<sup>1,2</sup> The sources may be external (engines, propeller, turbulent boundary layer) or internal (air-conditioning system, gearbox, etc.) to the fuselage. Typical exterior noise sources are shown schematically in Fig. 1 for two aircraft configurations. Contributions from propeller and engine noise sources are often determined by near-field characteristics that differ from the far-field characteristics of interest to community noise. A complete description of the exterior fluctuating pressure fields for use in the prediction of interior sound pressure levels involves pressure spectra and cross spectra and the spatial distribution over the excitation surface.

#### 2.1 Boundary Layer Fluctuating Pressures

The turbulent boundary layer pressure field on the exterior of the fuselage is the main source of broadband noise in the cabins of many fixed-wing airplanes.<sup>1,3,4</sup> The turbulent boundary layer is attached over most of the fuselage, but there may be some regions of separated flow in the neighborhood of protrusions and

around the cockpit. Even for subsonic cruise, there may be some areas of supersonic flow with shock waves, particularly above the cockpit. Interior noise generated by the external turbulent boundary layer is usually important in the mid and upper frequency ranges, as is indicated in Fig. 2, which shows interior sound pressure levels measured in a business jet airplane at three Mach numbers.

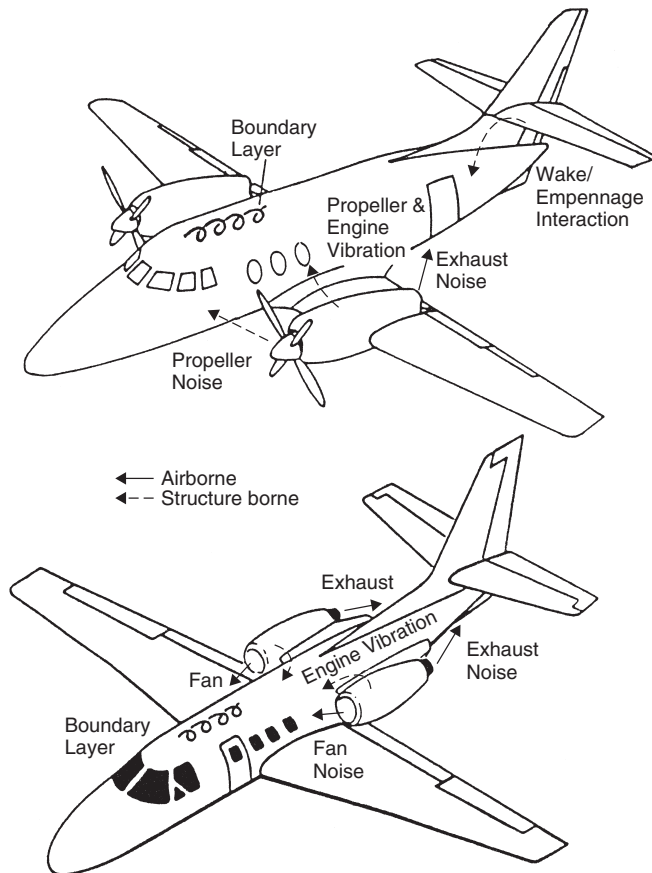
Separated flow and shock waves cause sound pressure levels at low frequencies to increase relative to those for attached boundary layers.<sup>5</sup> Wind tunnel and flight measurements have been used to develop semiempirical representations for attached and separated turbulent boundary layer pressure fields that can be used in noise transmission models.<sup>1,5,6</sup> Interior noise levels are influenced by aerodynamic coincidence, which occurs when the convection speed in the turbulent boundary layer matches the flexural wave speed in the fuselage panels.<sup>2</sup>

#### 2.2 Propeller Noise

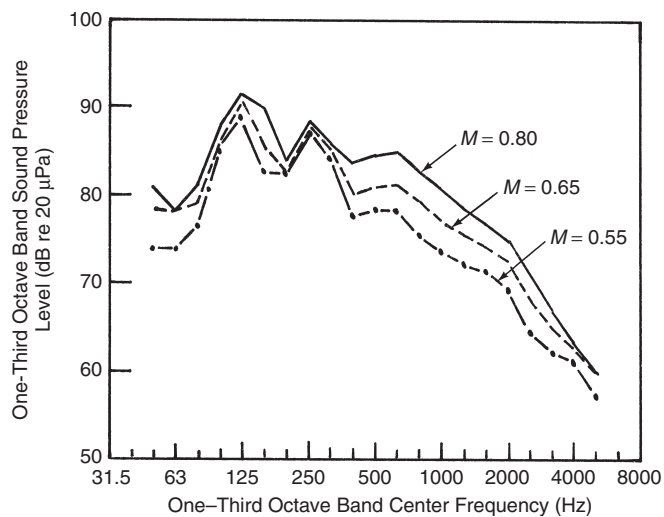
Propeller noise spectra (see Chapter 90) are dominated by discrete frequency components at the propeller blade passage frequency,  $f_b$ , and harmonics thereof.<sup>7,8</sup> The blade passage frequency is given by  $f_b = B\Omega/60$  Hz, where  $\Omega$  is the rotational speed in revolutions/minute [rpm] of the propeller and  $B$  is the number of blades. A typical sound pressure spectrum measured in the untreated cabin of an airplane with two wing-mounted turboprop engines is shown in Fig. 3. The broadband noise inside many propeller-driven airplanes is dominated by the turbulent boundary layer rather than the propeller, particularly at higher flight speeds.<sup>7</sup>

Propeller location is a significant factor in determining propeller noise levels in the cabin because of strong directivity characteristics. Airplanes with a single tractor propeller mounted in the nose of the airplane usually have relatively low levels of propeller noise in the cabin, whereas multiengine airplanes with engines mounted on the wing have high cabin sound pressure levels in the vicinity of the plane of rotation of the propeller. Pusher propellers that are mounted aft of the cabin operate in a disturbed flow field and propeller noise radiates forward, impinging on the airplane fuselage.

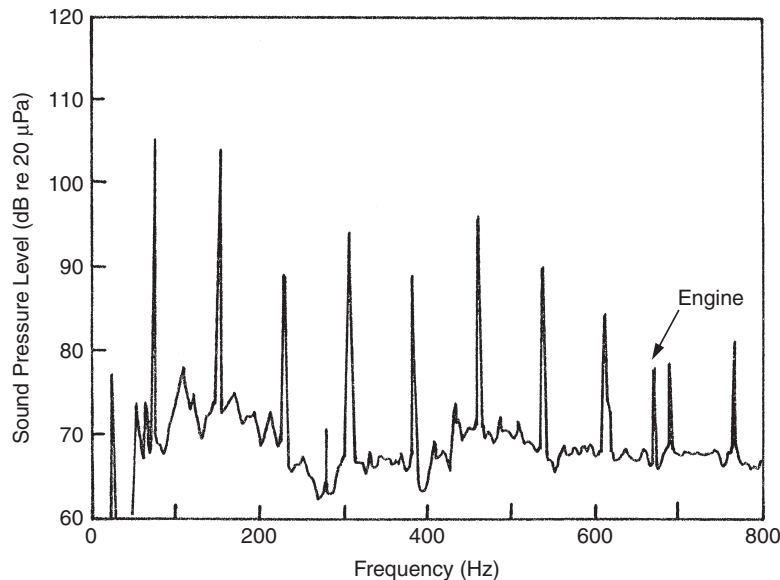
In the neighborhood of the plane of rotation of the propeller, where the distance between the fuselage and the propeller tip is small relative to the acoustic wavelength, the fuselage is in the acoustic near



**Figure 1** Sources and transmission paths of aircraft interior noise. (Reprinted with permission from SAE Paper 820961 © 1982 SAE International.)



**Figure 2** Sound pressure levels in business jet airplane at different flight Mach numbers. (Reprinted with permission from SAE Paper 820961 © 1982 SAE International.)



**Figure 3** Narrow-band interior noise spectrum for propeller-driven airplane with untreated cabin. (Reprinted with permission from SAE Paper 850876 © 1985 SAE International.)

field or aerodynamic potential field of the propeller, with the source moving with the propeller blade.<sup>5,9</sup> Elsewhere, the fuselage is in the acoustic far field. Beats will occur in multiengine airplanes if propellers are not synchronized. Also, pressure cancellation and augmentation due to phase differences between propellers can result in rapid spatial variations in interior sound pressure level.

### 2.3 Jet Noise

Airborne transmission of jet noise is associated mainly with aircraft with wing-mounted engines. It affects cabin regions aft of the engine exhaust and is generally limited to low frequencies.<sup>3</sup> Jet noise levels (see Chapter 89) are determined by the relative velocity between the exhaust and the surrounding air and decrease as the airplane accelerates during takeoff and climb. Jet noise spectra are broadband and peak at different frequencies for different locations in the near field.<sup>5</sup> The spectra can be normalized in terms of a nondimensional frequency using jet nozzle diameter,  $D$ , and jet velocity,  $U_j$ , as the normalizing parameters, and the pressure cross spectrum can be represented by a simple formulation for use in analytical models.<sup>5</sup>

### 2.4 Engine Fan Noise

Fan noise from a turbofan engine can be transmitted into the fuselage interior, particularly at locations forward of the engine inlet, but the contribution to cabin sound pressure levels is significant only at low flight speeds such as takeoff and initial climb.<sup>3,10</sup> Fan noise is associated with the blade passage frequency of the fan and with multiple pure tones (or buzz-saw)

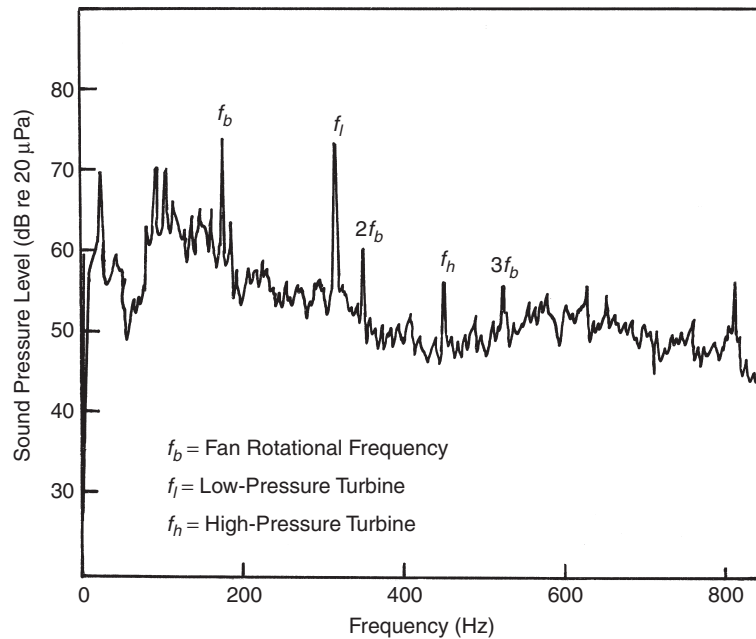
created by shock waves generated in the supersonic flow region of the fan blades. The fundamental frequency of multiple pure tones is  $f_{mpt} = \Omega/60$  Hz, but the fundamental and lower order harmonics are below the inlet duct cutoff frequency and do not radiate from the inlet.

### 2.5 Engine Vibration

Out-of-balance forces from reciprocating and jet engines excite the mounting structure with resultant sound radiation into the fuselage interior. This is especially true when jet engines are mounted on the rear of the fuselage, as they are closely coupled to the fuselage structure<sup>11</sup> but may also be true in the case of wing-mounted engines even though the mounting structure is more massive.<sup>2</sup> Turbofan out-of-balance forces are usually dominated by the fundamental component that occurs at the rotational frequency of the fan, compressor, or turbine. Figure 4 shows a narrow-band sound pressure spectrum measured in the cabin of a business jet airplane with two turbofan engines mounted on the rear of the fuselage.

Discrete frequency components are observed at the rotational frequencies of the fan,  $f_b$ , low-pressure turbine,  $f_l$ , and high-pressure turbine,  $f_h$ , plus harmonics of the fan and low-pressure turbine. The sound pressure levels are sensitive to small changes in engine balance and the airplane structure, with the result that they vary markedly from airplane to airplane and are difficult to predict. Vibration-induced noise from reciprocating engines can occur in general aviation airplanes at the same discrete frequencies as the propeller blade passage frequency and its harmonics.<sup>12,13</sup>





**Figure 4** Narrow-band interior noise spectrum for business jet airplane. (Reprinted with permission from SAE Paper 820961 © 1982 SAE International.)

## 2.6 Reciprocating Engine Noise

The exhaust outlets of reciprocating engines on small general aviation aircraft can be close to the airplane cabin. The fundamental frequency for a single cylinder is  $f_c = \Omega/120$  Hz, and the fundamental frequency for the total exhaust is  $f_e = N_c \Omega/60$  Hz, where  $N_c$  is the number of cylinders. The magnitude of the noise level depends on the design of the exhaust system and the effectiveness of any muffler.

## 2.7 Wake-Structure Interaction

Interaction between a propeller wake and the wing or horizontal stabilizer structure downstream of the propeller can cause vibration that is transmitted to the airplane cabin and radiated as sound.<sup>1,2</sup> The components of wake-induced noise will be at the same frequencies as the components of propeller noise.

## 2.8 Helicopter Rotors and Gears

Helicopter main and tail rotors (see Chapter 91) contribute to helicopter interior noise levels.<sup>14</sup> Since discrete frequency noise from rotors is radiated mainly in directions close to the plane of rotation, the tail rotor may make a greater contribution to cabin noise levels than does the main rotor. Several factors determine the relative magnitudes of main and tail rotor noise in the cabin, including the distance of tips of main and tail rotors from the cabin, the directivity of rotor noise fields, and attenuation characteristics of the cabin sidewall.

The gearbox of a helicopter is a major source of cabin noise.<sup>1,14</sup> It is usually mounted close to the cabin, with strong airborne and structure-borne transmission paths into the cabin. Gear noise (see Chapters 69 and 88) occurs at the teeth-meshing frequencies and harmonics thereof.

## 2.9 Internal Noise Sources

Noise sources inside an aircraft include air-conditioning systems, hydraulic systems, pressure relief valves, vents and drains, and electrical and mechanical equipment. Noise sources in an air-conditioning system include the air cycle machine, fans, valves and orifices in the ducts, separated flow in duct bends, and high-velocity flow through air grilles.<sup>15</sup> Noise sources in a hydraulic system include pumps and valves.

## 3 TRANSMISSION PATHS

Transmission paths from source to cabin interior can be classified as either airborne or structure borne (Fig. 1). A flow diagram can be constructed to show the different paths.<sup>1</sup>

### 3.1 Airborne Paths

Airborne noise is associated with noise transmission from an acoustic or aerodynamic pressure field through a structure into the cabin. The transmitting structure could be the fuselage sidewall, when the noise source is external to the fuselage, the floor of the cabin when the noise source is in an underfloor compartment, or the cabin wall of a helicopter when the noise source is

inside the fuselage shell but outside the cabin. Critical airborne noise transmission paths occur where the noise control treatments are compromised.<sup>16</sup>

Airborne noise transmission can have two components—resonant and nonresonant transmission. Nonresonant transmission is the mass-law transmission that is familiar in architectural acoustics and can be important for an acoustic source. Resonant transmission is the dominant airborne transmission path associated with turbulent boundary layer excitation and with acoustic excitation at frequencies above coincidence. Acoustic coincidence occurs when the speed of sound in air equals the flexural wave speed in the structure.

Fuselage structures respond differently to turbulent boundary layer excitation and acoustic excitation.<sup>1,2,4,17</sup> Acoustic excitation is highly correlated over large distances and can excite large regions of the structure including frames and stringers.<sup>17</sup> In contrast, turbulent boundary layer excitation is uncorrelated over large distances, particularly in the circumferential direction, and fuselage response shows little correlation between adjacent panels.<sup>17</sup> Similarly, noise transmission characteristics are different for the two types of excitation.

### 3.2 Structure-Borne Paths

Structure-borne noise is associated with vibrational energy that is transmitted through the structure from external sources and then radiated into the cabin as sound. Sources that generate structure-borne noise include out-of-balance forces in the engine,<sup>2,11,12</sup> propeller wake interacting with the wing or tail surfaces, air cycle machines<sup>15</sup> or hydraulic pumps beneath the cabin floor, and gearboxes mounted outside the cabin of a helicopter.<sup>14</sup> The spectrum in Fig. 3 contains a structure-borne component, at a frequency of 669 Hz, associated with engine turbine out-of-balance forces. This component was transmitted through the engine mounts and wing structure to the fuselage. In the case of mechanical excitation, the vibration power transmitted from the source to the aircraft structure is a function of the point impedances of the source and structure at the excitation location, as well as the magnitude of the excitation force.<sup>1</sup>

### 3.3 Cabin Cavity

Although not often considered as part of the airborne or structure-borne transmission paths, the acoustical characteristics of the cabin cavity do play a role. Analytically, acoustical modes of a cabin are important in the prediction of cabin noise levels. However, there are few reports in the literature regarding actual measurements of the acoustical characteristics of a furnished aircraft cabin. Occasionally, evidence of standing waves has been found, but those events were typically associated with unfurnished or partly furnished cabins.<sup>1,7</sup> For example, it was speculated that acoustic resonances influenced the poor repeatability of cabin noise levels in an unfurnished propeller-driven general aviation airplane, where the noise spectrum was dominated by discrete frequency components.<sup>7</sup>

Sound absorption provided by cabin furnishings is sufficient, in most cases, to damp out acoustic resonances. Analysis has indicated that a sound absorption coefficient greater than 0.2 is sufficient to suppress acoustic modes in a cabin.<sup>1</sup>

## 4 SOURCE/PATH IDENTIFICATION

Identification of noise sources or transmission paths can be performed by experiment, analysis, or a combination of both.<sup>18</sup> It is often found that no single approach is adequate—a combination of a number of methods may be necessary.

### 4.1 Source Identification

**Frequency Identification** When sources have well-defined frequency components that are distinct from those of other sources, components in the narrow-band spectra (see Chapter 46) of cabin noise can be used as source identifiers. Such is the case for propeller noise and noise due to engine out-of-balance forces (Figs. 3 and 4). However, spectral analysis cannot distinguish between contributions from different sources operating at precisely the same frequency.

**Correlation** The separation of jet noise and turbulent boundary layer contributions to the fluctuating pressures measured on the exterior of an airplane is difficult because both contributions are broadband. However, the two contributions to the exterior pressure field can be separated by the use of cross-spectrum or correlation techniques.<sup>10</sup> Correlation techniques cannot be used with sinusoidal signals because the signals are always fully coherent. However, partial coherence techniques have been successful when there are two discrete frequency sources with very close, but not identical, frequencies.<sup>19</sup>

**Source Modification** Source modification involves changing the operating conditions of one or more noise sources and measuring the resulting changes in cabin sound pressure levels.<sup>1,20</sup> However, it should be recognized that changes to the operating condition might change the contributions from other sources. For example, propellers of a twin-engine airplane can be operated at slightly different rotational speeds. The advantage of the method is that the contributions from the two propellers can be identified without a significant change in air speed.<sup>7</sup> The disadvantage is that the method eliminates destructive or constructive interference between sound pressures from the two sources that might occur in normal operation. Alternatively, engine power can be varied and the aircraft allowed to climb or descend through specified values of altitude and speed to determine engine noise contributions.<sup>20</sup>

**Source Elimination** The effect of eliminating a noise source is similar to that of source modification, and the advantages and disadvantages are also similar. For example, all engines can be set to flight idle and the airplane placed in a shallow dive to measure turbulent boundary layer noise.<sup>8,12,20</sup> The disadvantages of this

method are that the airflow over the airplane may change, and cruise flight speed will not be maintained. In a second example, internal equipment, such as the environmental control system, can be turned off and cabin noise levels measured.<sup>20</sup>

#### 4.2 Path Identification

Path identification is critical to the optimum implementation of noise control measures. However, direct measurement of structure-borne noise is difficult because it requires, in part, measurement of power flow in flexural, longitudinal, and torsional waves. Consequently, other approaches have been used. Path identification methods are often experimental in nature, but the supplemental use of analytical methods can be useful.<sup>1</sup>

**Source Simulation** Ground tests can be performed using sound (loudspeaker) or vibration (shaker) sources or an actual propeller to simulate the in-flight source.<sup>1,21</sup> The sound source can be placed in an enclosure so that the area of exposure on the fuselage can be limited to a window or other small region of interest.<sup>1</sup> Alternatively, an array of loudspeakers with phase control can be used.<sup>22</sup> Shakers can be placed at engine mounts or other locations.

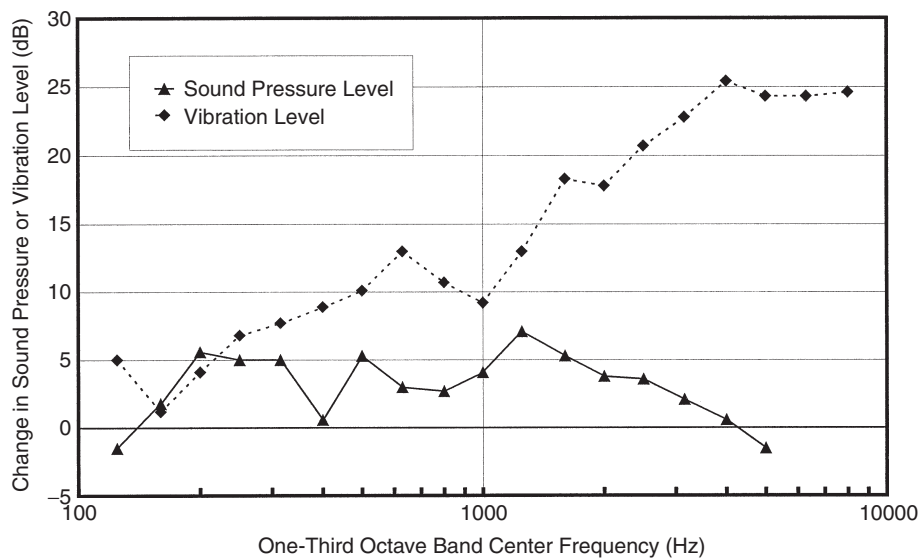
**Acoustical Enclosure** An enclosure can be used in the cabin to limit the area of sound radiation and investigate noise transmission paths. The enclosure should be constructed to minimize sound transmission through the walls and to prevent reverberant buildup inside.

**Path Interruption** The path interruption method usually requires tests on a stationary airplane on the

ground or in the laboratory.<sup>1,13</sup> The assumption is made that the results obtained from the ground tests are still valid in flight. For a propeller-driven airplane with a single engine, the engine can be mounted on supports and operated when it is connected and disconnected to the fuselage.<sup>13</sup> In the case of propeller wake interaction with the airplane wing, the wing can be detached from the fuselage structure or enclosed in a sleeve that isolates the wing structure from the fluctuating pressures in the propeller wake.<sup>1</sup>

**Path Modification** Changes in a transmission path may alter the transmitted noise sufficiently to infer the importance of that path. The method assumes that airborne and structure-borne noise components are statistically independent, which may not be true when discrete frequency components are involved. A common technique in path modification is the use of heavy mass-loaded vinyl sheets to cover cabin surfaces of interest.<sup>1,20</sup> It is possible that sound pressure levels might increase at some frequencies because of a decrease in sound absorption in the cabin or blockage of a transmission path to the exterior.

For structure-borne noise transmission from an engine, the standard isolation mounts for the engine can be replaced with solid metal blocks and the tests repeated.<sup>12</sup> Figure 5 shows the results from a test on a single-engine, propeller-driven airplane.<sup>12</sup> Sound pressure levels were measured in the airplane cabin and vibration levels were measured on the airplane structure near to the engine mounts. When the engine isolation mounts were replaced with hard mounts, the structure-borne vibration increased by up to 25 dB, but the cabin sound pressures increased by a maximum of only 7 dB. The results imply that the



**Figure 5** Change in cabin sound pressure level and structural vibration level when engine isolation mounts are replaced with solid metal blocks on a single-engine propeller-driven airplane.<sup>12</sup>

cabin sound pressure levels are controlled by structure-borne vibration transmission only in the frequency range below about 400 Hz.

**Transfer Function Methods** The transfer function method is applied in three steps.<sup>1</sup> First, the transfer function between the source of interest and cabin noise levels is obtained. Second, the source level under flight conditions is measured. Third, the product of transfer function and flight source level is calculated to obtain an estimate of interior noise level in flight due to that source. The first step is usually performed in a nonoperational environment when no other sources are present. The accuracy of the third step depends on the validity of the assumption that the imposition of flight loads does not change the transfer function.

In the case of structure-borne engine noise, a transfer function relating structural acceleration at the engine mount to cabin interior sound pressure levels is measured during ground tests.<sup>12</sup> That transfer function is then applied to in-flight measurements of vibration to estimate the contribution to cabin sound pressure levels. The transfer function method can also be used to estimate the cabin noise components associated with wing vibration induced by propeller wake impingement. Shakers are used to induce vibration into the wing structure while sound pressure levels are measured in the cabin. Then, wing vibration is measured in flight. If measurement of the transfer function is not feasible, it may be possible to use the principle of reciprocity, which can be applied to acoustical or mechanical sources.<sup>1</sup>

**Intensity** Sound intensity methods (see Chapter 45) can be used to determine the relative importance of noise transmission paths.<sup>1,18,20</sup> The surfaces of interest in the cabin (sidewall, floor, ceiling, windows, etc.) are divided into small areas. The intensity probe is then traversed over each subarea to determine the sound power transmitted through that subarea.

**Acoustical Holography** Near-field acoustical holography (see Chapter 50), in conjunction with boundary element methods, can be used to investigate fuselage vibration and interior sound fields.<sup>1</sup> The method has been applied, for example, in a turboprop airplane to the blade passage frequency and its first two harmonics.<sup>23</sup>

## 5 PASSIVE NOISE CONTROL

A successful passive noise control program often has to address several noise sources and transmission paths. A balanced noise control treatment would consider all combinations of sources and paths such that all contribute approximately equally. Reducing the noise from one source to a level well below the contributions for the other sources would not be cost or weight effective. A successful noise reduction program often requires a combination of test and analysis.<sup>18</sup>

### 5.1 Reduction at Source

#### Reduction of Propeller Near-Field Noise Levels

Cabin noise levels can be reduced by increasing the

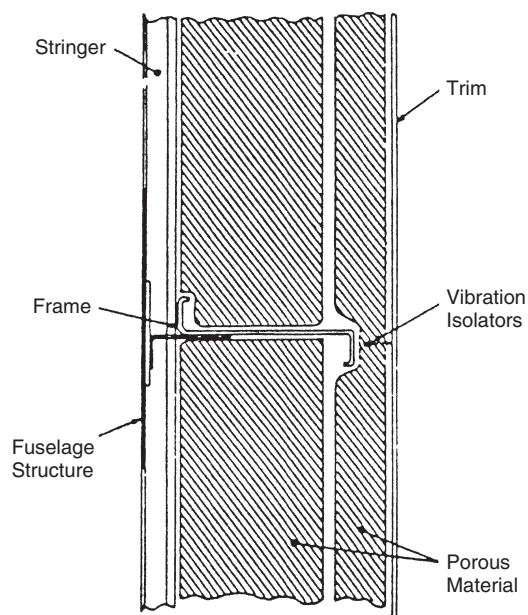
clearance between the propeller tip and the fuselage and decreasing the propeller tip Mach number.<sup>24</sup> This could require an increase in the number of propeller blades or relocation of the engines further outboard. Direction of rotation may be a factor in determining interior sound pressure levels; a solution would require that propellers on opposite sides of the fuselage rotate in opposite directions.<sup>24</sup>

**Engine Balancing** The out-of-balance forces imposed by turbofan engines can be reduced by improving the balancing of the rotors, particularly the fan as it is the most massive of the rotors.<sup>25</sup>

### 5.2 Reduction in Transmission

The most effective way to reduce noise transmission is to modify the transmission path as close as possible to the source, for example, at the mounts of an engine or air cycle machine. In principle, this is true for both airborne and structure-borne transmission, but it is more difficult to achieve in the airborne case because the noise sources are usually distributed over a large surface area, whereas sources of structure-borne noise tend to be local and well defined.

**Sidewall** Cabin sidewalls are generally constructed from multiple layers of porous material. A simple sidewall is depicted in Fig. 6 where porous material is placed between the fuselage frames and over the frames.<sup>1,16</sup> The porous material typically consists of glass fiber blankets with a density of about 7 kg/m<sup>3</sup>. This is a compromise between weight and



**Figure 6** Cross section through typical cabin sidewall treatment. (Reprinted with permission from SAE Paper 820961 © 1982 SAE International.)

transmission loss. Heavier blankets could be used if additional transmission loss is required. The blankets are contained in impervious bags to prevent moisture retention. A sheet of heavy, limp material can be placed between layers of the porous material to increase sound transmission loss. A trim panel is attached to the frames to cover the porous material. The attachment should be by means of vibration isolation mounts, to prevent structure-borne paths that would short out the acoustical insulation.<sup>16</sup> Sound transmission through a cabin window can be reduced by increasing the thickness of the window pane.<sup>18</sup>

**Sound Absorption** Sound absorption is provided in the cabin by the carpet and seats. Additional sound absorption may be obtained by treatment of the ceiling and bottom of the stowage bins. Sound absorption material is often required in the neighborhood of entry doors and in galleys.<sup>16</sup>

**Damping Material** Damping material (see also Chapter 60), often in the form of constrained layer damping tape with a viscoelastic adhesive and an aluminum foil backing layer, has been used to reduce airplane interior noise.<sup>16,26</sup> Usually, damping material is applied to fuselage skin panels where it is effective mainly at frequencies above the panel fundamental frequency, but the effectiveness might be extended to lower frequencies by application of damping material to frames and stringers.<sup>27,28</sup> Damping material can also be applied to trim and floor panels.<sup>20,29</sup>

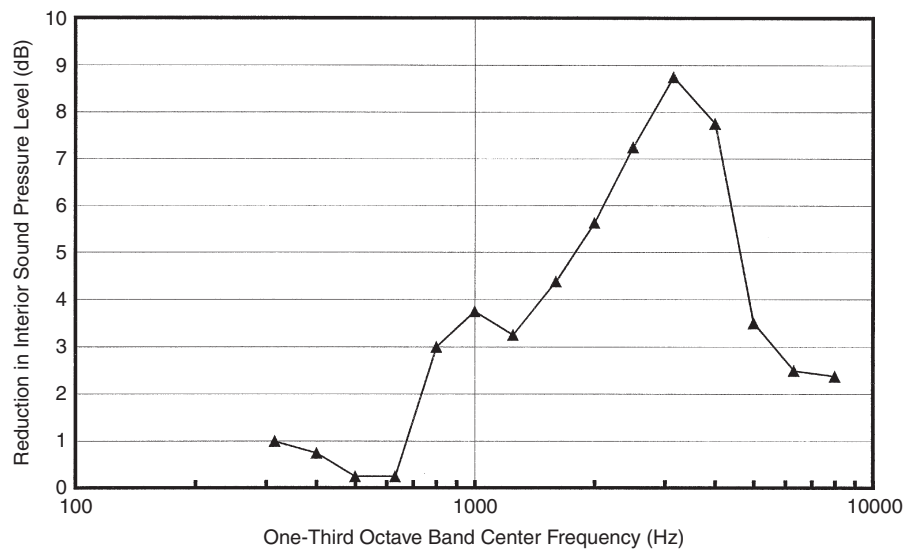
Optimized damping tape treatments cover about 80% of the panel area.<sup>26,29</sup> However, the effectiveness can be increased by the use of a spacer between the structure and the viscoelastic layer, and the area covered can be reduced.<sup>18</sup> Damping materials should

be selected for the operating temperatures of the structure being treated.

Figure 7 shows the reduction in cabin noise obtained by the use of damping tape on an airplane pressurized fuselage excited by a turbulent boundary layer.<sup>26</sup> In this case, all cabin furnishings, including sidewall insulation, had been removed. The damping tape was applied to about 80% of the panel area. In addition to the increased damping, the tape also increased the mass of the fuselage panels by about 10%. Significant noise reductions occur only in the frequency range of 1000 to 4000 Hz, which is the frequency range of the lower order modes of the individual panels of the pressurized fuselage and the frequency range in which there is good coupling between the excitation and the structure (known as aerodynamic coincidence).

**Isolated Shell** A self-supporting isolated interior shell can be constructed to reduce structure-borne noise transmission.<sup>25,30</sup> The interior shell is mounted on vibration isolators placed on the floor, or on frames near to the floor, where the vibration levels are low. The number of attachment points should be kept to a minimum and the isolators designed for maximum effectiveness.

**Dynamic Absorbers and Tuned Dampers** These resonant devices (see Chapter 61) can be used to reduce interior noise levels of aircraft where the excitation is discrete frequency.<sup>2</sup> Dynamic absorbers are effective only in a narrow frequency band and are used mainly in cases where the propeller or engine rotational speed is essentially constant over much of the flight regime. A tuned damper can have a greater effective bandwidth, but at the expense of less attenuation.<sup>31</sup> When more than one frequency is to be attenuated, sufficient damping



**Figure 7** Effect of damping tape on sound pressure level in an unfurnished pressurized fuselage exposed to turbulent boundary layer excitation.<sup>26</sup>

has to be introduced to broaden the attenuation peak, or different absorbers have to be designed for each frequency of interest. Dynamic absorbers or tuned dampers have been installed at the attachment location of rear-mounted turbofan engines,<sup>11</sup> on fuselage frames to reduce the propeller noise transmission,<sup>31–33</sup> or on trim panels in the cabin.<sup>32,33</sup>

**Engine Mounts** Passive engine mounts are usually proprietary designs of viscoelastic material or metal, and represent a compromise between static and dynamic stiffness. The static stiffness has to be sufficient to withstand the static loads imposed by engine weight and thrust without shorting out, while the dynamic stiffness has to be low enough that the vibration is not transmitted into the fuselage structure (see Chapter 59). The effectiveness of the mounts can be increased by increasing the input impedance of the airplane structure.

**Propeller Synchronphasing** Adjustment of relative phase angles among the propellers, often referred to as “synchronphasing,” can reduce cabin sound pressure levels.<sup>1,24,32</sup> The potential for noise reduction appears to be greater for four-engine aircraft than for two-engine aircraft because there are more possibilities for cancellation.

**Mufflers and Suppressors** Noise transmission can be attenuated by the use of mufflers (see also Chapter 85) in reciprocating engine exhausts, air cycle machine ducts, and drain and vent systems. Pulsation dampers or surge suppressors can be installed to attenuate hydraulic pump noise. Sound-attenuating material can be placed in the return air grilles of the environmental control system.<sup>20</sup>

**Acoustic Leaks** It is critical that all acoustic leaks be identified and eliminated because leaks severely degrade the performance of noise control treatments.

## 6 ANALYTICAL METHODS

Several different approaches can be applied to the analytical modeling of airborne and structure-borne noise transmission into airplanes. The choice of a particular method is often determined by the frequency range of interest because it determines, to some extent, the computational requirements and the validity of the assumptions in the model. The main methods used are closed-form modal approaches, power balance methods, statistical energy analysis, and numerical methods.

### 6.1 Modal Methods

The modal approach is based on modal representations of the fuselage structure and interior cavity.<sup>34</sup> The approach can be combined with the power balance method<sup>35</sup> or the traveling-wave approach.<sup>36</sup> At high frequencies, the power balance approach merges into statistical energy analysis. The fuselage structure can be modeled as a simple cylinder or as a cylinder with an integral floor.<sup>37</sup> At low frequencies, stiffeners can be represented as discrete elements or “smeared” over the fuselage panels to give effective orthotropic panels. At high frequencies, the influence of the stiffeners

can be neglected and the structure divided into a number of substructures. The cabin volume can be modeled as a closed-form modal representation, or finite difference numerical methods can be used.<sup>37,38</sup> Sound transmission through the cabin sidewall can be modeled separately using the transfer impedance method of architectural acoustics or as an integral part of the sound transmission model.<sup>37</sup>

### 6.2 Statistical Energy Analysis

Statistical energy analysis (SEA) methods (see Chapter 17) can be used when there is a sufficient number of modes (say three or more) in any given frequency band of interest, usually a one-third octave band.<sup>1,5</sup> SEA has been applied to the transmission of jet noise, turbulent boundary layer noise, engine vibration, and propeller noise into an airplane fuselage, with the understanding that there will be an increased variance in the results at low frequencies where there are few modes. In order to mitigate the scarcity of modes, the size of the subsystems in an SEA model should not be too small.<sup>16,39,40</sup>

Statistical energy analysis assumes resonant response of a structure or cavity. This is adequate for aerodynamic excitation such as a turbulent boundary layer, but in the case of acoustic excitation, the nonresonant or mass-law path has to be included.<sup>1</sup> In the case of aircraft with long cabins, the cabin can be divided into several sections, using physical bulkheads where possible.<sup>16,39</sup>

### 6.3 Numerical Methods

Numerical methods (see Chapter 7) generally involve finite element methods (FEM) and boundary element methods (BEM). Most applications to aircraft cabin noise involve FEM-FEM coupled analyses where finite element methods are used to model both the aircraft structure (including the multilayer sidewall) and the cabin cavity. However, boundary elements can be used to model the acoustic radiation into the cabin in FEM-BEM analyses.<sup>41</sup> Numerical methods are usually restricted to low frequencies so that the model does not become excessively large or require too much detail. Consequently, the methods are used mainly to analyze airborne and structure-borne transmission of propeller noise and engine vibration.

It is possible to model the entire cabin of a small aircraft, but models for larger aircraft are usually restricted to a section of the cabin.<sup>9,21,40</sup> Reductions in model size can be achieved using symmetry of the fuselage to model only one half. In that case, the computations are performed first for symmetrical modes and then repeated for antisymmetrical modes. The model should include some representation of structures adjacent to the cabin.<sup>40</sup>

## REFERENCES

1. J. S. Mixson and J. F. Wilby, Interior Noise, in *Aeroacoustics of Flight Vehicles: Theory and Practice*, Vol. 2, *Noise Control*, H. H. Hubbard, Ed., NASA Reference Publication 1258, NASA, Washington, DC, August 1991, Chapter 16.

2. J. F. Wilby, Aircraft Interior Noise, *J. Sound Vib.*, Vol. 190, 1996, pp. 545–564.
3. W. V. Bhat, Flight Test Measurement of Exterior Turbulent Boundary Layer Pressure Fluctuations on Boeing Model 737 Airplane, *J. Sound Vib.*, Vol. 14, 1971, pp. 439–457.
4. G. P. Mathur, B. Tran, and M. Simpson, MD-90 Cabin Noise Diagnostics Ground and Flight Tests, AIAA Paper AIAA-99-1834, 1999.
5. J. F. Wilby, Vibration of Structures Induced by Sound, in *Harris' Shock and Vibration Handbook*, 5th ed., C. M. Harris and A. G. Piersol, Eds., McGraw-Hill, New York, 2002, Chapter 29, Part III.
6. W. F. Blake, *Mechanisms of Fluid-Induced Sound and Vibration*, Academic, New York, 1986.
7. J. F. Wilby and E. G. Wilby, Measurements of Propeller Noise in a Light Turboprop Airplane, *J. Aircraft*, Vol. 26, 1989, pp. 40–47.
8. M. S. Ewing, M. A. Kirk, and J. D. Swearingen, Beech 1900D Flight Test to Characterize Propeller Noise on the Fuselage Exterior, AIAA Paper AIAA-2001-2110, 2001.
9. P. Goransson, Finite Element Calculations of the Interior Noise of the Saab 340 Aircraft, SAE Paper 891081, 1989.
10. W. V. Bhat, Use of Correlation Technique for Estimating In-Flight Noise Radiated by Wing-Mounted Jet Engines on a Fuselage, *J. Sound Vib.*, Vol. 17, 1971, pp. 349–355.
11. J. van Dyke, Jr., J. Schendel, C. Gunderson, and M. Ballard, Cabin Noise Reduction in the DC-9, AIAA Paper 67-401, 1967.
12. R. E. Hayden, B. S. Murray, and M. A. Theobald, A Study of Interior Noise Levels, Noise Sources and Transmission Paths in Light Aircraft, NASA CR-172152, 1983.
13. J. F. Unruh and D. C. Scheidt, Engine Induced Structural-Borne Noise in General Aviation Aircraft, *SAE Trans.*, Vol. 88, 1980, pp. 2171–2184.
14. J. F. Wilby and J. I. Smullin, Interior Noise of STOL Aircraft and Helicopters, *Noise Control Eng.*, Vol. 12, 1979, pp. 100–110.
15. R. L. Cohen, Experimental Resolution of Air-Conditioning Pack Tones on a Commercial Jet Airplane, AIAA Paper AIAA-99-1836, 1999.
16. R. B. Tate and E. K. O. Langhout, Aircraft Noise Control Practices Related to Ground Transport Vehicles, SAE Paper 810853, 1981.
17. J. F. Wilby and F. L. Gloyna, Vibration Measurements of an Airplane Fuselage Structure II, Jet Noise Excitation, *J. Sound Vib.*, Vol. 23, 1972, pp. 467–486.
18. W. V. Bhat, T. A. Hirt, and G. G. Hadford, Process of Designing Add-on Treatment for Reducing Aircraft Passenger Cabin Noise, AIAA Paper AIAA-98-2342, 1998.
19. B. N. Tran and M. A. Simpson, The Use of Partial Coherence Techniques for Identifying Noise Transmission Paths on the MDC UHB Demonstrator Aircraft, AIAA Paper AIAA-90-3968, 1990.
20. T. N. Christenson and T. J. Ferguson, Experimental Localization of Noise Entry Points into an Aircraft Cabin, AIAA Paper AIAA-99-1835, 1999.
21. C. I. Florentin and L. C. Chow, Propeller Driven Aircraft Cabin Noise Reduction, AIAA Paper CEAS/AIAA-95-046, 1995.
22. M. A. Simpson, M. R. Cannon, P. L. Burge, and R. P. Boyd, Interior Noise Control Ground Test Studies for Advanced Turboprop Aircraft Applications, NASA CR-181819, 1989.
23. E. G. Williams et al., Interior Near-Field Acoustical Holography in Flight, *J. Acoust. Soc. Am.*, Vol. 108, 2000, pp. 1451–1463.
24. F. B. Metzger, Strategies for Aircraft Interior Noise Reduction in Existing and Future Propeller Aircraft, SAE Paper 810560, 1981.
25. C. I. Holmer, Approach to Interior Noise Control, Part II: Self-Supporting Damped Interior Shell, *J. Aircraft*, Vol. 22, 1985, pp. 729–733.
26. W. V. Bhat and J. F. Wilby, Interior Noise Radiated by an Airplane Fuselage Subjected to Turbulent Boundary Layer Excitation and Evaluation of Noise Reduction Treatments, *J. Sound Vib.*, Vol. 17, 1971, pp. 449–464.
27. M. A. Simpson, P. M. Druez, A. J. Kimbrough, M. P. Brock, P. L. Burge, G. P. Mathur, M. R. Cannon, and B. N. Tran, UHB Demonstrator Interior Noise Control Flight Tests and Analysis, NASA-CR-181897, 1989.
28. G. SenGupta, Reduction of Low Frequency Cabin Noise during Cruise Condition by Stringer and Frame Damping, *AIAA J.*, Vol. 17, 1979, pp. 229–236.
29. C. I. Holmer, Approach to Interior Noise Control, Part I: Damped Trim Panels, *J. Aircraft*, Vol. 22, 1985, pp. 618–623.
30. R. Navaneethan and R. L. Howes, Effect of an Isolated Shell on Interior Noise Levels in a Turboprop Aircraft, SAE Paper 891083, 1989.
31. W. G. Halvorsen and U. Emborg, Interior Noise Control of the SAAB 340 Aircraft, SAE Paper 891080, 1989.
32. E. H. Waterman, D. Kaptein, and S. L. Sarin, Fokker's Activities in Cabin Noise Control for Propeller Aircraft, SAE Paper 830736, 1983.
33. H. J. Hackstein, I. U. Borchers, K. Renger, and L. Schauwecker, Interior Noise and Exterior Noise of the Dornier 328, AIAA Paper AIAA-95-045, 1995.
34. J. A. Cockburn and A. C. Jolly, Structural-Acoustic Response, Noise Transmission Losses and Interior Noise Levels of an Aircraft Fuselage Excited by Random Pressure Fields, AFFDL-TR-68-2, 1968.
35. D. C. Rennison, J. F. Wilby, and E. G. Wilby, Prediction of the Interior Noise Levels of High-Speed Propeller-Driven Aircraft, AIAA Paper 80-0998, 1980.
36. J. D. Revell, F. J. Balena, and L. R. Koval, Analysis of Interior Noise-Control Treatments for High-Speed Propeller-Driven Aircraft, *J. Aircraft*, Vol. 19, 1982, pp. 31–38.
37. L. D. Pope, E. G. Wilby, and J. F. Wilby, Propeller Aircraft Interior Noise Model, Part I, Analytical Model, *J. Sound Vib.*, Vol. 118, 1987, pp. 449–467.
38. L. D. Pope, On the Prediction of Propeller Tone Sound Levels and Gradients in an Airplane Cabin, *J. Acoust. Soc. Am.*, Vol. 88, 1990, pp. 2755–2765.
39. J. S. A. Lin, Airplane Interior Noise Modeling Using Statistical Energy Analysis Approach, AIAA Paper AIAA-99-1903, 1999.
40. A. E. Landmann, H. F. Tillema, and G. R. MacGregor, Application of Analysis Techniques for Low Frequency Interior Noise and Vibration of Commercial Aircraft, NASA CR-189555, 1992.
41. J. P. G. Coyette, Finite Element and Boundary Element Models for Predicting the Vibro-Acoustic Behaviour of Multi-Layered Structures, AIAA Paper CEAS/AIAA-95-100, 1995.



# CHAPTER 100

## AIRCRAFT CABIN NOISE AND VIBRATION PREDICTION AND ACTIVE CONTROL

Sven Johansson, Lars Håkansson, and Ingvar Claesson

Department of Signal Processing  
Blekinge Institute of Technology  
Ronneby, Sweden

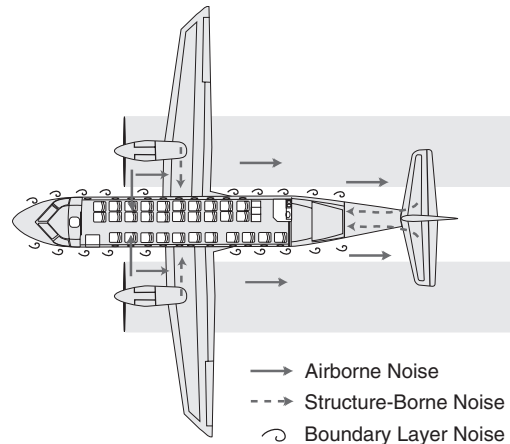
### 1 INTRODUCTION

Low interior noise is important to passenger and crew comfort in aircraft. High noise levels are disturbing, tiring, and reduce the ability to converse with passengers in adjacent seats. The noise levels should not be intrusive and should not have discernible discrete tones, beats, or pulsations. The cabin noise is mainly created by the aircraft's propulsion system and turbulent boundary layer pressure fluctuations, which excite the fuselage and produce fuselage vibrations, resulting in the creation of the cabin sound field. The degree to which noise may be reduced in an aircraft at low frequency is determined primarily by the stiffness and weight of the structure of the fuselage. A general problem is that the noise transmission loss of the fuselage structure is rather small in the low-frequency range. One method of reducing cabin noise in this frequency range is to adopt active control techniques. These techniques are based on introducing secondary sources for controlling the interior cabin sound field or the structural fuselage vibrations. The latter technique reduces the sound radiation into the cabin. The active control systems for reducing tonal cabin noise are generally based on either active noise control or active structural acoustic control. One may attenuate broadband cabin noise with the aid of active headsets or silent seats.

### 2 CABIN NOISE AND VIBRATION SOURCES

Both internal and external sources cause noise and vibration in an aircraft.<sup>1–5</sup> One internal noise source is the air-conditioning system; the most predominant sources, however, are external. There are several external sources of noise and vibration in an aircraft: engines, propellers, jet engine fans, the boundary layer, and the like. Each source has its own characteristics and transmission paths into the cabin, for example, airborne paths and/or the structure-borne paths.<sup>1–3</sup> Figure 1 illustrates the sources of noise and vibration in an aircraft and their transmission paths into the cabin.

The main source of cabin noise in turboprop aircraft is the airborne noise produced by the propellers.<sup>1,2</sup> The propeller blades pass the fuselage, thereby producing periodic pressure fluctuations on the external of the fuselage; this in turn causes vibrations in the internal cabin walls and an excitation of the interior cabin sound field. The structural vibration modes coupled to the interior acoustic modes result in a transfer of energy from the fuselage outside into the cabin.<sup>6,7</sup> Cabin

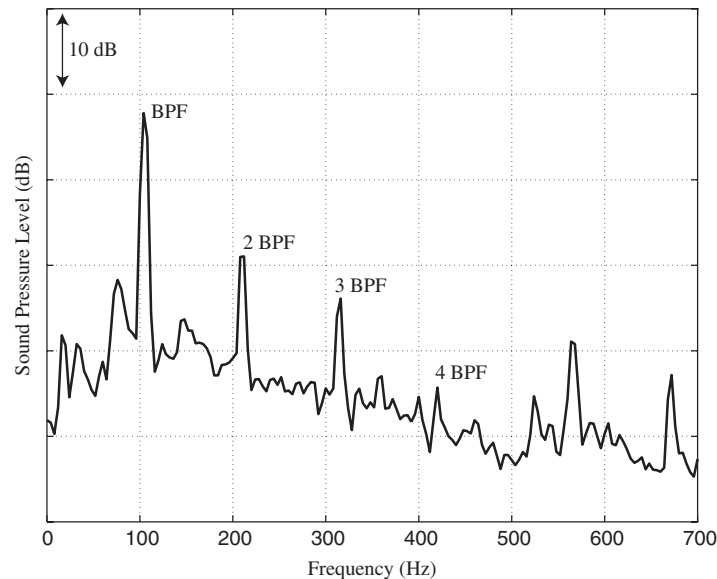


**Figure 1** Sources of noise and vibration in an aircraft and their transmission paths.<sup>3</sup>

noise in turboprop aircraft usually takes the form of tonal noise related to the fundamental blade passage frequency (BPF). The dominant frequency components are generally in the frequency range of 60 to 400 Hz; the blade passage frequency and two or three of its harmonics predominate.<sup>1,2</sup> Figure 2 shows a typical spectrum of the cabin noise level in a turboprop aircraft during cruise flight. Generally, aircraft are equipped with a synchronization unit to synchronize the rotational speed of the propellers. Any difference in the rotational speed leads to unpleasant acoustical beating.<sup>1</sup>

For high wings and tail aircraft designs with small propeller tip clearance, the transmission paths of the propeller noise are dominated by the airborne path between the propeller and the fuselage.<sup>3,8</sup> For aircraft with low wings and tail, the turbulent airstream behind the propeller is also a significant excitation factor. The airstream excites the wing and tail structure, causing complex transmission paths of propeller-induced noise into the cabin. In jet aircraft, airborne transmission of noise is generally associated with aircraft with wing-mounted engines; in this type of aircraft, the broadband jet noise affects cabin regions aft of the engine exhaust, particularly when the engines are mounted close to the fuselage.<sup>2,5</sup>

Imbalances in rotating parts of an aircraft propulsion system excite vibration of the fuselage via the



**Figure 2** Sound pressure level spectrum for typical cabin noise in a turboprop aircraft.

engine-supporting structure, and the fuselage structural vibration radiates noise into the cabin; such noise is called *structure-borne noise*.<sup>1,2</sup> In the case of turboprop propulsion systems, the gearbox normally excites the structure and produces gear whine at frequencies on the order of hundreds of hertz,<sup>1</sup> and propeller imbalance produces vibrations from 15 to 20 Hz.<sup>1</sup> In jet aircraft with tail-mounted engines, the principal structure-borne noise excitation source is the two spools of each jet engine; these normally run between 100 and 500 Hz.<sup>1,2,5</sup>

Boundary layer noise, or wind noise, is audible in all aircraft.<sup>1,2,5</sup> During flight, the interaction between the surrounding air and fuselage wall induces turbulence pressure fluctuations that act on the external fuselage along the length of the aircraft; this in turn radiates noise into the cabin. Particularly high levels of boundary layer noise are created at any point on the outer fuselage where the shape of the skin changes abruptly, for example, antenna fairings. Boundary layer noise is highly dependent upon the flight speed and is of a random broadband nature, the majority of its energy being above approximately 400 Hz.<sup>1,2</sup> With decreasing levels of propulsion-induced cabin noise, the boundary layer noise becomes increasingly apparent.<sup>2</sup>

### 3 ACTIVE CONTROL OF NOISE

#### 3.1 Noise Control Introduction

Cabin noise in aircraft is often difficult to attenuate adequately by means of passive noise control approaches due to weight restrictions.<sup>1,3,4</sup> A common passive method is to increase the dynamic stiffness of the fuselage by using passive-tuned vibration dampers.<sup>1,7–9</sup> This method is based on the principle

that passive-tuned dampers attached to the fuselage structure absorb vibration energy at the resonance frequency, thereby reducing noise transmission into the cabin.<sup>4,8</sup> The dampers are tuned to reduce vibrations at a specific frequency, for example, the BPF for cruise flight, and are unable to track frequency variations. Generally, the first few harmonics of the BPF may be significant, and to reduce several harmonics a large number of dampers tuned for different frequencies must be used; this adds significantly to the weight of the aircraft.<sup>4</sup> Furthermore, the engines may be run at different speeds in different parts of the flight cycle. In contrast to the passive dampers, the active control system is usually synchronized with the engines and is able to track variations in noise; attenuation is maintained throughout the flight cycle, including cruise, climb, and descent.<sup>4,8</sup> If the controller is synchronized with both engines, the acoustical beating that appears as the engines become unsynchronized is also controlled. Even with many secondary sources, the active control system adds less weight to the aircraft than does a normal set of passive-tuned dampers.<sup>8</sup>

#### 3.2 Active Control

The basic principle of active control is to introduce secondary sources for controlling either the sound field or the structure radiating the noise.<sup>6,7,10,11</sup> If a few, well-defined transmission paths of noise into the cabin are established, it is possible to act directly on the transmission paths to reduce noise transmission.<sup>5,6,8,12–15</sup> On the other hand, if the transmission paths are complex or unknown, the noise is controlled after its transmission into the cabin by using loudspeakers mounted in the trim.<sup>4,8,10,12–15</sup> Strategically located

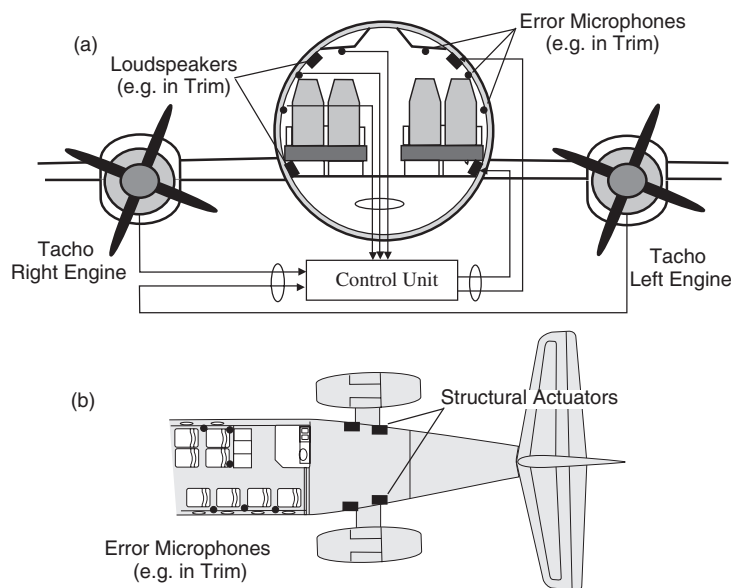
error sensors are used to allow continuous adaptation of the control system driving the control sources.<sup>10,16</sup> The error sensors are usually composed of microphones mounted in the trim that observe the cabin sound field. The objective of the active control system is to minimize the sound pressure in the error microphones.<sup>10,16</sup> One commonly used objective is to minimize the squared sound pressures measured in the error microphones. Figure 3a shows an illustration of an active noise control system synchronized with both engines. In situations where the aim is to reduce the sound radiation from the fuselage, the loudspeakers are replaced with structural actuators controlling the fuselage vibrations<sup>6,8,14</sup>; see Fig 3b.

The sound field in the cabin, or in an enclosure, can be viewed as the superposition of the acoustic modes.<sup>6,7,10</sup> Each mode is related to a resonance frequency of the enclosure, and the mode shape describes the spatial pattern of pressure, maximum and minimum, that is, antinodes and nodes. Active control of the disturbing acoustic modes is achieved by introducing loudspeakers. The purpose of the loudspeakers is to produce independent modal responses that are of equal amplitude and opposite phase to each of the corresponding uncontrolled disturbing acoustic modes.<sup>10</sup> Normally, at low frequencies a few modes dominate the sound field; these modes are usually well separated. Controlling noise fields characterized by separate modes results in large volumes of noise attenuation, so-called global control. The objective with global control of enclosed sound fields is to reduce the total acoustical potential energy in the enclosure.<sup>10</sup> In fact, it turns out that such a strategy has the effect of leveling out the

spatial variation of the pressure level in the enclosure since dominant acoustic modes are suppressed.

At higher frequencies, the distance in frequency between two adjacent modes becomes smaller and smaller and many modes contribute to the sound field.<sup>10</sup> The modal density increases and the individual modes will be indistinguishable. As the frequency increases, the sound field is changed from modal type to be considered diffuse with high modal overlap.<sup>10</sup> Since the modal density and modal overlap are high, global control is not possible at these frequencies; however, local active noise control is possible under such circumstances.<sup>10</sup> Global reduction is possible only if the secondary source is placed very close to the primary noise source.<sup>10</sup> This is not possible in the aircraft applications. Local control is based on the strategy to achieve local areas of reduced noise, for example, a localized zone of "quiet" around the head of a seated passenger. The zones with reduced noise will be found close to the control microphones, and the size of the quiet zones are highly dependent on the frequency: The size of the zone decreases with increasing frequency.<sup>10</sup> Accordingly, local control requires that the control microphones be located in the vicinity of the passengers' head positions, for example, on the headrests instead of the trim. The local control of sound fields is used in the silent seat application where each seat is equipped with individual loudspeakers and microphones in the headrest.<sup>10,12</sup>

Structural actuators may also be applied as secondary sources in active control of acoustical noise in aircraft.<sup>6,8</sup> This method is used when there are some dominant noise transmission paths into the cabin.



**Figure 3** Active control of aircraft interior noise: (a) active noise control system in a turboprop aircraft, and (b) active structural/acoustical control in a jet aircraft.

The structural aircraft fuselage vibrations produced by the propulsion system and pressure fluctuations from the propellers acting on the external fuselage generally excite the interior cabin sound field. The purpose of applying structural actuators is to apply control forces to the fuselage, thereby controlling the structural modes of the fuselage associated with significant sound radiation into the cabin.<sup>10</sup>

The structural actuators are located in the dominant noise transmission paths to reduce the sound transmission through the structure.<sup>5,8,10</sup> The disadvantage of this approach is that any noise reaching the cabin via other transmission paths cannot be controlled. Such noise is controlled inside the cabin. The active structural/acoustical controlled approach reduces the dominant acoustically coupled structural modes, which normally results in global noise attenuation.<sup>6</sup> A comparison between the active noise control approach and the active structural/acoustical control approach usually shows that fewer secondary structural actuators than loudspeakers are used for a global control of the interior cabin sound field.<sup>6,12</sup>

The error sensors are again microphones to adapt the control system. Thus, where the aim is to reduce the sound pressure level, it is recommended to use error microphones, which observe the interior sound field, rather than error accelerometer sensors, which observe structural fuselage vibrations.<sup>6</sup> The minimization of vibrations at selected points, that is, the accelerometer positions, does not necessarily guarantee the reduction of sound radiated into the cabin. In fact, minimizing local vibrations often leads to an increased sound pressure level.<sup>6</sup> One disadvantage of the active structural/acoustical control approach is that even though the noise level is reduced, the structural vibrations can sometimes increase.<sup>6</sup>

The active control of acoustic and structural modes may influence nondisturbing modes.<sup>6,10</sup> Modal density increases with increasing frequency, and a higher modal overlap is obtained. As a consequence, the influence of control source excitation of nondisturbing modes also increases. This control spillover reduces the effect of the active control system.<sup>6,10</sup> The modal overlap<sup>6,10</sup> for acoustic modes increases rapidly with frequency and is roughly proportional to  $f^3$ , while the modal overlap for the flexural structural modes demonstrates a less pronounced increase with frequency, approximately proportional to  $f$ . Structural control enables global control of the sound field at higher frequencies than may be achieved with control of the acoustic modes.<sup>6,10</sup> High modal overlap and control of the acoustic modes result in local control around the error microphones.<sup>10</sup>

### 3.3 Active Control Strategies

The active control strategy used to attenuate cabin noise in aircraft depends primarily on the type of propulsion system, transmission paths, aircraft design, and noise characteristics. In commercial aircraft, one of two different kinds of large-scale (multichannel) active control strategies is normally used today to control tonal cabin noise. Both strategies are of adaptive

feedforward type and use error microphones to observe the controlled sound field. The ANC (active noise control) system uses loudspeakers as secondary sources while the ATVA (active tuned vibration absorber) system uses inertial mass actuators as structural secondary sources.<sup>4,5,8,14,15</sup> The principle of ATVA is similar to that of the ASAC (active structural/acoustical control) approach described in the relevant literature.<sup>6</sup> In recent years, active headsets have been introduced in the first- and business-class cabins of wide-bodied jets.<sup>12</sup> The headsets are directed toward the control of broadband noise found on wide-bodied jet aircraft. These headsets are based on feedback control and normally rely on analog control.<sup>7,10,17</sup>

**Global Control Approaches** ANC has proved effective and will continue to be the favored option on turboprop aircraft with complicated and/or multiple noise transmission paths into the cabin. Examples of such aircraft are the Saab 340 and Saab 2000.<sup>4</sup> The Saab 340 was the first commercially available aircraft in the world in which ANC was used; the first aircraft was delivered in the spring of 1994. The first Saab 2000 was delivered later the same year.<sup>18</sup>

A low wing and, in particular, low tail (directly acted on by the propeller backwash) combined with a low tip clearance result in a variety of noise paths; methods that act directly on these paths are thus both problematic and expensive.<sup>4,8</sup> On the other hand, ATVA is used commercially on both turboprop and jet aircraft. The ATVA approach is used on the turboprop aircraft in the Bombardier Q series Dash-8.<sup>8,14</sup> These aircraft have high wings and tail and a small propeller tip clearance. Here, the predominant transmission path consists of the direct action of the propeller wash on the fuselage in and around the plane of the propellers. The ATVA approach has also been successfully applied to jet aircraft. In jet aircraft, out-of-balance forces from the engine shafts excite the fuselage via the engine mounts and pylons (the predominant transmission paths) thereby causing vibration-induced noise within the aircraft cabin.<sup>5,12–15</sup> The active control performance for different control strategies are presented in Table 1.

**Local Control Approaches** In recent years, active headsets—normally integrated into the passenger entertainment system—have been introduced into the first- and business-class cabins of wide-bodied jets.<sup>12</sup> Also, quiet seats creating a localized zone of noise attenuation around the passenger head by using active digital feedback control have been developed for wide-bodied jet aircraft.<sup>12,14</sup> Both active headsets and quiet seats alleviate the problem of broadband noise on wide-bodied jet aircraft, a noise that is less dominated by the tones found in turboprops and jet aircraft with tail-mounted engines.

### 3.4 Multichannel Adaptive Feedforward Control

To obtain a significant global noise reduction in a large cavity such as that found in aircraft cabins, a large

**Table 1 Active Control System Performance in Turboprop and Jet Aircraft**<sup>3,8,14,15</sup>

	A-weighted Sound Pressure Level			
	Active Control OFF (dB)	Active Control ON (dB)	Attenuation (dB)	Active Control Strategy
<b>Turboprop Aircraft</b>				
SAAB 340	89	80	9	ANC
SAAB 2000	82	76	6	ANC
Beech1900D	95	89	6	
King Air 90	90	80	10	ANC
King Air 200	85	78	7	ANC, optional ATVA
King Air 300	88	80	8	ANC
King Air 350	90	80	10	ANC
Twin Commander	92	85	7	ANC
Q Dash 8-300	87	76	11	ATVA
<b>Jet Aircraft</b>				
Challenger	72	70	2	ATVA
Fokker F-28	88	81	7	ATVA
Cessna Citation II	85	79	6	ATVA
DC-9/MD-80.			10–15 <sup>a</sup>	ATVA
UltraQuiet seat			10	ANC
Active headsets			20, <sup>a</sup> 100–200 Hz	ANC

<sup>a</sup>Unweighted sound pressure level.

number of control sources and error sensors are generally needed.<sup>10</sup> For a twin-engined aircraft, the control system and the algorithm must also be able to handle two synchronization signals, one from each engine, to control individually the noise from the two sources.<sup>8,10</sup> The reference signals to the feedforward controller, which are generated from the synchronization signals, contain the same frequencies as the noise components to be suppressed, for example, the BPF and its harmonics. With reference signals generated in this manner the control becomes selective.<sup>7,11,16</sup> It is possible to determine which of the harmonics are to be controlled and which are not.

The control algorithm is the part of the total control system that takes up the major part of the processor capacity; it is thus extremely important to use an algorithm with low computational complexity. The capacity of an adaptive control system to handle tonal components that are close in frequency is dependent on the structure of the controller, that is, how the multiple frequencies are processed.<sup>11</sup> The controllers are generally based on either a single-filter structure or a parallel-filter structure using several filters.<sup>11</sup> The single-filter structure is based on a composite reference signal containing all frequencies to be controlled. For tonal components that are close in frequency, a long FIR filter is required; this results in slow convergence of the adaptive algorithm.<sup>11</sup> For the parallel-filter structure, each frequency component is individually processed. This results in shorter filters and thus improved convergence performance.<sup>11</sup> Where possible, the parallel structure rather than the single-filter structure should thus be used to achieve efficient and robust control of frequencies that are close together. An example of

such a sound field is the beating sound produced by propellers rotating at slightly different speeds.

The well-known time-domain filtered-x least mean squares (FXLMS) algorithm<sup>7,11,16</sup> may be generalized to multichannel control applications comprising the  $R$  single-frequency reference signals  $x_r(n)$ ,  $r \in \{1, \dots, R\}$ ,  $L$  control source signals  $y_l(n)$ ,  $l \in \{1, \dots, L\}$ , and  $M$  error sensor signals  $e_m(n)$ ,  $m \in \{1, \dots, M\}$ . Figure 4 shows a block diagram illustrating the feedforward control system based on parallel-filter structure and the multichannel FXLMS algorithm.

The leaky FXLMS algorithm is, however, usually used to steer the adaptive filter coefficients when solving practical control problems.<sup>11,16</sup> Based on  $RL$  adaptive FIR filters and  $ML$  FIR filter control path estimates, the time-domain multichannel leaky FXLMS algorithm is given by<sup>11,16</sup>

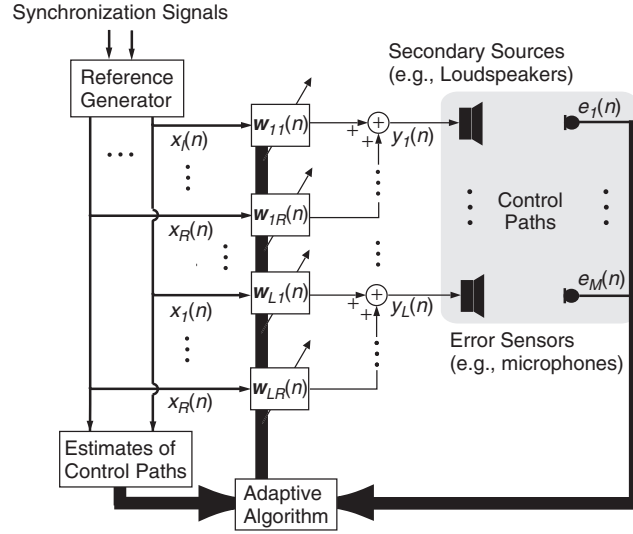
$$\begin{aligned} \mathbf{y}(n) &= \mathbf{X}^T(n) \mathbf{w}(n) \\ \mathbf{e}(n) &= \mathbf{d}(n) + \mathbf{y}_C(n) \\ \mathbf{w}(n+1) &= \gamma \mathbf{w}(n) - \mu \mathbf{X}_C^T(n) \mathbf{e}(n) \end{aligned} \quad (1)$$

where  $\mu$  is the adaptation step size and  $\gamma$  is a real positive leakage factor in the range  $0 < \gamma < 1$ ,  $\mathbf{y}(n)$  is the output signal vector from the controller containing the  $L$  secondary actuator signals, and

$$\mathbf{w}(n) = [\mathbf{w}_1^T(n) \quad \dots \quad \mathbf{w}_L^T(n)]^T$$

is the vector containing the coefficients of the  $RL$  adaptive FIR filters. Each vector

$$\begin{aligned} \mathbf{w}_l(n) &= [w_{l10}(n) \quad \dots \quad w_{l1J-1}(n) \\ &\quad w_{l20}(n) \quad \dots \quad w_{lRJ-1}(n)]^T \end{aligned}$$



**Figure 4** Feedforward active control system based on the multichannel Filtered-X LMS algorithm.

is composed of the coefficients of the adaptive FIR filters controlling the secondary source  $l$ . Also

$$\mathbf{d}(n) = [d_1(n) \quad \dots \quad d_M(n)]^T$$

is the vector containing noise to be controlled at the error sensors,

$$\mathbf{e}(n) = [e_1(n) \quad \dots \quad e_M(n)]^T$$

is the residual vector containing the  $M$  residual signals, and

$$\mathbf{y}_C(n) = [y_{C_1}(n) \quad \dots \quad y_{C_M}(n)]^T$$

is the control sound vector, that is,  $y_{C_m}(n)$  is the superposition of the contributions from the  $L$  secondary sources at error sensor  $m$ . The  $RLJ \times L$  reference signal matrix  $\mathbf{X}(n)$  is defined as

$$\mathbf{X}(n) = \text{diag}[\mathbf{x}(n) \quad \dots \quad \mathbf{x}(n)]$$

where

$$\mathbf{x}(n) = [\mathbf{x}_1^T(n) \quad \dots \quad \mathbf{x}_R^T(n)]^T$$

and

$$\mathbf{x}_r(n) = [x_r(n) \quad \dots \quad x_r(n - J + 1)]^T$$

denote FIR filter reference signal vectors. The length of the adaptive FIR filters is  $J$ .  $\mathbf{X}_{\hat{C}}(n)$  is the  $RLJ \times M$  filtered reference signal matrix, and the elements are produced by filtering the reference signals with FIR filter estimates of the physical paths between the secondary sources and the error sensors, that is, the control paths.

Differences between the estimate of the control paths and the true control paths influence both the stability properties and the convergence rate of the algorithm.<sup>11,16</sup> To ensure convergence of the mean coefficient vector  $E[\mathbf{w}(n)]$ , the step size  $\mu$  requires that  $0 < \mu < (2(\Re\{\lambda_{lrj}\} + \alpha)/|\lambda_{lrj} + \alpha|^2)_{\min}$ , where  $\Re\{\cdot\}$  denotes the real part.<sup>11,16</sup> Here,  $\lambda_{lrj}$  is an eigenvalue of the correlation matrix  $E[\mathbf{X}_{\hat{C}}(n)\mathbf{X}_{\hat{C}}^T(n)]$ ,  $\alpha$  is a real positive constant related to the leaky coefficient as  $\gamma = 1 - \mu\alpha$  and  $\mathbf{X}_C(n)$  is the filtered reference signal matrix produced by filtering the reference signals  $x_r(n)$  with the actual control paths. Generally, the correlation matrix is ill-conditioned and has a large eigenvalue spread<sup>16</sup>; this usually results in a slow convergence speed, particularly when long adaptive FIR filters are used in the algorithm. The problems of an ill-conditioned correlation matrix and high computational complexity can be reduced by using frequency-domain versions of the multichannel FXLMS algorithm.

An alternative approach to the multichannel FIR-based control system for controlling tonal noise, for example, propeller-induced noise, is a system based on either complex arithmetic or a frequency-domain algorithm.<sup>11,16,19</sup>

If each of the  $R$  complex reference signals,  $x_r(n)$ , may be separately controlled by an adaptive complex weight  $w_{rl}(n)$ , this results in the complex weight vector

$$\mathbf{w}_{rh}(n) = [w_{rh1}(n) \quad \dots \quad w_{rhL}(n)]^T$$

A low-complexity control algorithm based on the complex FXLMS algorithm for updating the weight can now be formulated in a matrix notation as<sup>11,19</sup>

$$\mathbf{w}_r(n+1) = \gamma \mathbf{w}_r(n) - x_r^*(n) \mathbf{M}_r \hat{\mathbf{C}}_r^H \mathbf{e}(n) \quad (2)$$

where the superscripts  $*$  and  $H$  denote the complex conjugate and conjugate-transpose, respectively, and  $\gamma$  is a real positive leakage factor.  $\hat{\mathbf{C}}_r$  is an  $M \times L$  matrix of estimated frequency responses  $\hat{C}_{rml}$  from the secondary source  $l$  to the error sensor  $m$ , and  $\mathbf{e}(n) = [e_1(n), \dots, e_M(n)]^T$ , that is, the real broadband error sensor signals. The  $L \times L$  matrix  $\mathbf{M}_r$  is a convergence factor matrix containing spatially normalized convergence factors.<sup>12,15,20</sup> This matrix affects convergence properties and system performance. Normalization is important for large multichannel applications where the acoustical coupling, that is, the magnitude of the frequency responses between different secondary sources and error sensors can vary.

The convergence factor matrix for the Newton-type algorithm is given by  $\mathbf{M}_r = \mu_0 [\rho_r \hat{\mathbf{C}}_r^H \hat{\mathbf{C}}_r]^{-1}$ , where  $\mu_0$  is the step size parameter,  $0 < \mu_0 < 1$ , and  $\rho_r$  denotes the mean power of the reference signal  $x_r(n)$ .<sup>16,19</sup> The signal power can be predetermined in the reference generator or estimated at run time, for example, by using the exponential average  $\hat{\rho}_r(n) = \varepsilon |x_r(n)|^2 + (1 - \varepsilon) \hat{\rho}_r(n-1)$ ,  $0 < \varepsilon < 1$ .<sup>11</sup> In practical applications, normalization is also important to compensate for variations in the mean power of the reference signal. In the Newton-type algorithm, all frequency responses in the control configuration are used in the update of every adaptive weight. In control applications comprising a large number of secondary sources and error sensors, it can be assumed that acoustical coupling decreases as the distance between the sources and sensors increases. This results in a diagonally dominant matrix  $\hat{\mathbf{C}}_r^H \hat{\mathbf{C}}_r \approx \text{diag}\{\hat{\mathbf{C}}_r^H \hat{\mathbf{C}}_r\}$ , which in turn leads to the actuator-normalized algorithm.<sup>19</sup> The convergence factor matrix for the algorithm—which is normalized for each actuator—is given by  $\mathbf{M}_r = \mu_0 [\rho_r \text{diag}\{\hat{\mathbf{C}}_r^H \hat{\mathbf{C}}_r\}]^{-1}$ ,  $0 < \mu_0 < 1/RL$ .<sup>19</sup> Since the frequency responses  $\hat{\mathbf{C}}_r$  are estimated before control takes place, quantities in the convergence factor matrix  $\mathbf{M}_r$  can be calculated before controlling,<sup>19</sup> thereby significantly reducing the calculation burden during run time.

The real controller output signals are generated according to  $\mathbf{y}(n) = \sum_{r=1}^R \text{Re}\{x_r(n) \mathbf{w}_r(n)\}$ , where  $\text{Re}\{\cdot\}$  denotes the real part. In the practical implementation only the real part of the product is evaluated. The complex LMS algorithm has properties that are superior to those of the FIR-based LMS algorithm when it comes to controlling harmonic sound fields with the aid of a multichannel control system. Some of the most interesting advantages include a simple controller structure, individually controlled harmonics, efficient algorithm normalization with high tracking performance, favorable implementation properties, and reduced calculation complexity.

### 3.5 Active Headsets and Quiet Seats

The feedforward control systems rely on the existence of some prior knowledge of the noise to be controlled.<sup>11,16</sup> This knowledge is provided by reference signals, for example, from the engines. The

feedback control systems do not rely on reference signals.<sup>11,16</sup> The basic principle acoustical feedback control is that the output signal of the error microphone is fed back to the control unit where it is processed and then used to drive the loudspeaker. The loudspeaker is located in the vicinity to the error sensor. The objective of the control system is principally to minimize the perceived sound pressure. Active headsets and quiet seats usually rely on feedback control.<sup>7,10,16</sup> Headsets are normally of the analog type; quiet seats use digital control.<sup>7,14,16</sup> Both active headsets and quiet seats deal with broadband noise.

The sound pressure under control,  $p_e(f)$ , is inside an active headset or on either side of the quiet seat headrest, and can be written as  $p_e(f) = p_d(f) / [1 + W(f)C(f)]$  where  $p_d(f)$  is the sound pressure inside the active headset or at the headrest without control,  $W(f)$  is the frequency function of the controller, and  $C(f)$  is the frequency function of the control path, that is, the transfer path comprising the loudspeaker, headset cavity, and error microphone. By allowing the loop gain  $|W(f)C(f)|$  to assume large values, the magnitude of the denominator becomes large, and the sound pressure under control is reduced. In practice, however, the performance of an active feedback control system is limited by closed-loop stability requirements, that is, the Nyquist stability criterion.<sup>7,16</sup> The electroacoustical response of the loudspeaker and the acoustical path from the loudspeaker to the microphone introduce time delay due to propagation time, and this will introduce increasing phase shift with frequency and thus limit the performance of the control system. The time delay can be reduced by bringing the error microphone closer to the loudspeaker. This in turn increases the operation bandwidth. Analog active noise control headsets typically produce an attenuation of about 20 dB at 100 to 200 Hz, which falls to zero below approximately 30 Hz and above approximately 1 kHz.<sup>17</sup> Active noise control headsets can also be used as ordinary stereo headphones in combination with external electronics, for example, portable CD players, the aircraft entertainment system, or radio communication system used by pilots.

### 4 OPTIMIZATION OF SECONDARY SOURCES, ERROR SENSOR LOCATION, AND PERFORMANCE PREDICTION

The optimum arrangement of the control sources and error sensors depends upon whether the objective is to minimize the noise globally or minimize the noise locally.<sup>16</sup> The control of an enclosed sound field requires spatial and temporal matching between the uncontrolled sound field and the sound field generated by the active noise control system.<sup>10,21</sup> Temporal matching is maintained by the adaptive controller system, while spatial matching depends on the placement of the secondary sources and the error sensors. For an active noise control system to be effective, the secondary sources must be able to drive the sound field at all the desired frequencies; it is also important that the error sensors are able to observe the



controlled sound field properly.<sup>10</sup> Accordingly, the secondary sources should be distributed in such a way that they couple effectively into the sound field, resulting in source positions close to the pressure maximum (antinodes) of the controlled acoustic modes. Similarly, the error microphones should also be distributed in such a way that their positions do not coincide with the pressure minimum (nodes) of the controlled acoustic modes.<sup>10</sup> Generally speaking, one must conclude that positioning sources and error sensors at, or close to, nodal surfaces should be avoided. In complex geometric enclosures, for example, aircraft cabins, identifying the nodal surfaces for the dominant acoustic modes is a complex task, making it difficult to position the secondary sources and error sensors.<sup>10,16</sup> Furthermore, the installation of the system is also limited by practical restrictions, for example, a loudspeaker requires a certain volume behind the speaker, a position can already be occupied by other cabin equipment, or the position is impractical for assembly and maintenance purposes. The loudspeakers and error microphones are often mounted in the interior trim of the aircraft, see Fig. 3. The objective of the control system is to minimize the sound pressure in the error microphones. In most practical applications it is not possible to place the error microphones exactly in the positions where the noise reduction is most desired, for example, in the headrests. For this reason, when one evaluates the performance of the active control system a set of *evaluation* microphones is placed in those positions where noise reduction is most desirable, for example, in positions near the ears of the passengers. These microphones are used for evaluation purposes only.<sup>4,22</sup> The purpose of the positioning of the secondary sources and error sensors is to determine a source and sensor configuration that will result in the desired noise reduction at the  $M_e$  *evaluation* microphones. Furthermore, it is important to find a robust configuration that leads to a significant reduction in all frequencies of interest; one must also find a configuration that leads to a significant reduction over a range of flight conditions rather than one that is useful for one flight condition only.<sup>4,10</sup> The source and sensor positioning procedure can be seen as a combinatorial optimization problem, that is, one selects the configuration  $\mathbf{s}$  consisting of  $L$  sources and  $M$  error sensors ( $L > M$ ) from all the  $L_c$  conceivable source positions and the  $M_c$  conceivable error sensor positions.<sup>16,19,22</sup> The total number of different system configurations possible is given by

$$N_{\text{tot}} = \binom{L_c}{L} \binom{M_c}{M} = \frac{L_c! M_c!}{(L_c - L)! L! (M_c - M)! M!} \quad (3)$$

where  $L_c!$  denotes the  $L_c$  factorial, that is,  $L_c(L_c - 1)(L_c - 2) \dots 1$ .<sup>16</sup> To compare the performance of different placements of the secondary sources and error sensors, it is necessary to assess the sound field at the *evaluation* microphones. The evaluation cost function, related to the frequency  $f$ , for a specific configuration  $\mathbf{s}$  chosen from the conceivable positions can be formed according to the sum

of the squared evaluation microphone output signals,  $J_{e,f}(\mathbf{s}) = \mathbf{e}_{e,f}^H(\mathbf{s}) \mathbf{e}_{e,f}(\mathbf{s})$ .<sup>16,19</sup> However, the cost function can be extended using other cost terms, for example, the maximum level of the loudspeaker input signals or the mean power consumption of the complete active noise control system. Here,  $\mathbf{e}_{e,f}(\mathbf{s}) = \mathbf{d}_{e,f} + \hat{\mathbf{F}}_{e,f}(\mathbf{s}) \mathbf{y}_{\text{opt},f}(\mathbf{s})$  where  $\mathbf{d}_{e,f} = [d_{e1,f}, \dots, d_{eM_e,f}]^T$  is a complex vector of the uncontrolled sound field at the evaluation points,  $\hat{\mathbf{F}}_{e,f}(\mathbf{s})$  forms an  $M_e \times L$  matrix of the frequency responses  $\hat{F}_{m_e,l,f}$  between the  $L$  chosen secondary sources and the  $M_e$  evaluation points, and  $\mathbf{y}_{\text{opt},f}(\mathbf{s}) = [y_{\text{opt}1,f}, \dots, y_{\text{opt}L,f}]^T$  is the optimal driving signals from the secondary sources given by  $\mathbf{y}_{\text{opt},f}(\mathbf{s}) = -[\hat{\mathbf{C}}_f^H(\mathbf{s}) \hat{\mathbf{C}}_f(\mathbf{s})]^{-1} \hat{\mathbf{C}}_f^H(\mathbf{s}) \mathbf{d}_f(\mathbf{s})$ . The optimal driving signals for configuration  $\mathbf{s}$  are obtained by minimizing the controlled sound field in the *error* sensors,  $\mathbf{e}_f(\mathbf{s}) = \mathbf{d}_f(\mathbf{s}) + \hat{\mathbf{C}}_f(\mathbf{s}) \mathbf{y}_f(\mathbf{s})$ , in least-squares sense.<sup>16</sup> Here,  $\mathbf{d}_f(\mathbf{s}) = [d_{1,f}, \dots, d_{M,f}]^T$  is a complex vector of the uncontrolled sound field at the error sensors, and  $\hat{\mathbf{C}}_f(\mathbf{s})$  denotes an  $M \times L$  matrix of the frequency responses  $\hat{C}_{m,l,f}$  between the chosen secondary sources and error sensors. The noise attenuation in decibels for a specific configuration at the frequency  $f$  can be assessed by  $10 \log_{10} [\mathbf{d}_{e,f}^H \mathbf{d}_{e,f} / \mathbf{e}_{e,f}^H(\mathbf{s}) \mathbf{e}_{e,f}(\mathbf{s})]$ .

Devising a practical system installation is a complex task that is often difficult and time consuming. As an example, let  $L_c = 20$ ,  $M_c = 30$ ,  $L = 8$ , and  $M = 16$  (possible configuration for small turboprop aircraft), resulting in  $N_{\text{tot}} \approx 1.8 \times 10^{13}$ . Assume that the time consumption for evaluating the performance for a single configuration is approximately 1 ms, a total of 570 years is required to evaluate all possible configurations. Accordingly, an exhaustive search over all conceivable configurations is *not* possible; some kind of optimization technique must thus be applied to establish a configuration of the secondary sources and error sensors in a reasonable period of time.<sup>4,16</sup> Depending on the aircraft type and size, the number of secondary sources and error sensors may vary, for example, a 50-seat Saab 2000 is equipped with 36 loudspeakers and 72 microphones, and the Q series Dash-8 has approximately 36 to 42 active tuned vibrations absorbers (ATVAs) and 71 to 80 microphones.<sup>4,12</sup>

The cost as a function of secondary source and error sensor positions is nonconvex; standard gradient search methods are thus of no use since the gradient algorithms are unable to escape from local minima in the nonconvex cost function.<sup>16</sup> A very simple approach to escape from local minima is random search; one selects at random a number of source and sensor configurations and hopes that a configuration with satisfactory noise attenuation will be found among these. This principle of selecting a configuration often results in unsatisfactory noise attenuation due to the limited number of configurations that can be evaluated in a reasonable period of time. A more sophisticated search algorithm must be applied to obtain higher noise reduction in a systematic manner. Powerful optimization methods for finding a suitable configuration in a reasonable time are the genetic search (GS) algorithms and the

simulated annealing (SA) algorithms.<sup>16,19</sup> One advantage of these algorithms is the ability to escape from local minima in a nonconvex cost function. Both methods are inspired by nature: GS algorithms are based on the biological mechanisms of Darwin's theory of evolution,<sup>20,23</sup> and SA algorithms are based on the fixation of the atoms in a substance during the annealing process, that is, the temperature is gradually reduced to obtain a low-energy, atomic arrangement.<sup>24,25</sup> The SA algorithm is based on the Metropolis sampler.<sup>26</sup> It follows a number of iteration steps; these are briefly described below.<sup>16,19</sup>

The first step is to select at random an initial configuration  $\mathbf{s}_i$  from the conceivable secondary source and error sensor positions; for each new iteration select a new configuration  $\mathbf{s}_j$ . If  $J_{e,f}(\mathbf{s}_j) \leq J_{e,f}(\mathbf{s}_i)$  accept  $\mathbf{s}_j$  as the new configuration ( $\mathbf{s}_i = \mathbf{s}_j$ ), or if  $J_{e,f}(\mathbf{s}_j) > J_{e,f}(\mathbf{s}_i)$ , accept  $\mathbf{s}_j$  as the new configuration with the probability  $P(\mathbf{s}_i, \mathbf{s}_j) = \exp([J_{e,f}(\mathbf{s}_i) - J_{e,f}(\mathbf{s}_j)]/T)$ , where  $T$  is a pseudotemperature. The algorithm will accept a configuration with a higher value on the cost function in accordance with a probability function; this in turn allows one to escape from local minima in the cost function. However, the probability of escaping from local minima decreases during the search process. The above iteration steps are performed for  $N$  iterations using a fixed pseudotemperature  $T_n$ ; the best configuration is subsequently stored. The temperature is then updated and further  $N$  iterations are performed. The temperature is updated according to  $T_{n+1} = \alpha T_n$ ,  $n \in \{0, 1, \dots, N_a - 1\}$ , where the temperature is reduced by the cooling factor  $\alpha$ , ( $0 < \alpha < 1$ ), and where  $T_0$  is the initial temperature. The search is terminated after  $N_a$  iterations, and the best configuration is then found among the stored configurations. New configurations are obtained by exchanging one or more loudspeakers and error microphones in the configuration. The exchange can take place at random or following some predetermined procedure. Optimization is carried out using different methods, for example, optimizing the sources first and then the sensors, or optimizing the sensors first, followed by the sources.<sup>16,19,22</sup> By combining these methods, the source and sensor locations can be optimized alternately or simultaneously. However, experience shows that certain combined methods are preferable.<sup>19</sup>

## REFERENCES

1. A. von Flotow and M. Mercadal, The Measurement of Noise and Vibration Transmitted into Aircraft Cabins, *J. Sound Vib.*, 1995, pp. 16–19.
2. J. F. Wilby, Aircraft Interior Noise, *J. Sound Vib.*, Vol. 190, No. 3, 1996, pp. 545–564.
3. C. F. Ross and M. R. J. Purver, Active Cabin Noise Control, *Proc. Active 97*, 1997, pp. XXXIX–XLVI.
4. U. Emborg, Cabin Noise Control in the Saab 2000 High-Speed Turboprop Aircraft, *Proc. of ISMA23*, 1998, pp. 13–25.
5. K. J. Harrison, Quest for the Quieter Cabin, *Aviation International News*, January 2003.
6. C. R. Fuller, S. J. Elliott, and P. A. Nelson, *Active Control of Vibration*, Academic, London, 1996.
7. C. H. Hansen and S. D. Snyder, *Active Control of Noise and Vibration*, E & FN Spon, London, 1997.
8. C. F. Ross, A Comparison of Techniques for the Active Control of Noise and Vibration in Aircraft, *Proc. of ISMA23*, 1998, pp. 831–835.
9. J. Q. Sun, M. R. Jolly, and M. A. Norris, Passive, Adaptive and Active Tuned Vibration Absorbers—A Survey, *Trans. ASME*, Vol. 117, 1995, pp. 234–242.
10. P. A. Nelson and S. J. Elliott, *Active Control of Sound*, Academic, London, 1992.
11. S. M. Kuo and D. R. Morgan, *Active Noise Control Systems*, Wiley, New York, 1996.
12. C. F. Ross, Active Noise Control in Aircraft, *Proc. of 6th Inter. Cong. on Sound and Vibration*, 1999, pp. 1653–1658.
13. M. A. Simpson, T. M. Luong, C. R. Fuller, and J. D. Jones, Full-Scale Demonstration Tests of Cabin Noise Reduction Using Active Vibration Control, *J. Aircraft*, Vol. 28, No. 3, 1991, pp. 208–215.
14. <http://www.ultraquiet.com> (2005).
15. <http://www.lordmpd.com> (2005).
16. S. J. Elliott, *Signal Processing for Active Control*, Academic, London, 2001.
17. L. Håkansson, S. Johansson, M. Dahl, P. Sjösten, and I. Claesson, Noise Canceling Headsets for Speech Communication, in *CRC Press Handbook on Noise Reduction in Speech Applications*, G. M. Davis, Ed., CRC Press, Boca Raton, FL, 2002, pp. 305–327.
18. U. Emborg, Saab AB, Personal communication, 1998.
19. P. Sjösten, S. Johansson, P. Persson, and I. Claesson, Considerations on Large Applications of Active Noise Control, Part I, Theory, *Acta Acoust.*, Vol. 89, No. 5, 2003, pp. 822–833.
20. T. Martin and A. Roure, Active Noise Control of Acoustic Sources Using Spherical Harmonics Expansion and a Genetic Algorithm, Simulation and Experiment, *J. Sound Vib.*, Vol. 212, No. 3, 1998, pp. 511–523.
21. S. J. Elliott, P. A. Nelson, I. M. Stothers, and C. C. Boucher, In-flight Experiments on the Active Control of Propeller-Induced Cabin Noise, *J. Sound Vib.*, Vol. 140, No. 2, 1990, pp. 219–238.
22. P. Sjösten, S. Johansson, P. Persson, and I. Claesson, Considerations on Large Applications of Active Noise Control. Part II. Experimental Results, *Acta Acoust.*, Vol. 89, No. 5, 2003, pp. 834–843.
23. K. S. Tang, K. F. Man, S. Kwong, and Q. He, Genetic Algorithms and Their Applications, *IEEE Signal Proc. Mag.*, 1996, pp. 22–37.
24. E. Aarts and J. Korst, *Simulated Annealing and Boltzmann Machines*, Wiley, New York, 1989.
25. S. Kirkpatrick and C. D. Gelatt, Jr., and M. P. Vecchi, Optimization by Simulated Annealing, *Science*, Vol. 220, 1983, pp. 671–680.
26. G. Winkler, *Image Analysis, Random Fields and Dynamic Monte Carlo Methods*, Springer, New York, 1995.

# CHAPTER 101

## NOISE PREDICTION AND PREVENTION ON SHIPS

**Raymond Fischer**  
Noise Control Engineering, Inc.  
Billerica, Massachusetts

**Robert D. Collier**  
Thayer School of Engineering  
Dartmouth College  
Hanover, New Hampshire

### 1 INTRODUCTION

Ship noise prediction, reduction, and control are important factors in the performance of underwater acoustical systems and in the habitability of the vessel for the crew and passengers. Mammals can also be affected by a ship's radiated signature. One of the principal objectives of this chapter is to provide engineering procedures for estimating the source–transmission path–receiver acoustical relationships applicable to ships. For any vessel the major sources are the propulsion machinery and propulsors. The airborne and structure-borne transmission paths are equally important due to the low damping loss factors in typical ship constructions. The received level in the compartment or the ocean depends on how the vibrations of local structure couple to the adjacent fluid. Criteria, specification development, design guidance, and abatement techniques are provided to assist the engineer in achieving an optimal system.

### 2 CRITERIA

Ship noise as it relates to human factors is a critical issue in ship design and operations. For 1999, the hearing compensation claims paid to veterans totaled \$291.7 million, and for 2004 this number increased to \$633.8 million. U.S. Navy and Marine Corps payments were \$63.5 million in 1999 and \$158.4 million in 2004. This exponentially increasing toll on human hearing and medical cost is preventable by bringing together the work of the engineering, safety, and medical communities.<sup>1,2</sup>

International, national, and local criteria exist for habitability noise, habitability vibration, and underwater radiated noise. Quoting from the International Maritime Organization (IMO) Resolution A.468 (XII) code for noise levels on ships,<sup>3</sup> page 7 these criteria are intended to:

- Provide for safe working conditions by giving consideration to the need for speech communication and for hearing audible alarms. . .
- Provide the seafarer with an acceptable degree of comfort in rest, recreation and other spaces

and also provide conditions for recuperation from the effects of exposure to high noise levels.

The third purpose of habitability noise criterion is to protect or reduce noise-induced hearing loss. This code also addresses intermittent noise in addition to steady-state noise. High noise levels are expected to adversely impact speech intelligibility, sleep, and overall performance.

Per IMO, crew berths have an A-weighted noise criterion of 60 dB. The most stringent A-weighted cabin requirement typically invoked is as low as 45 dB. The U.S. Coast Guard<sup>3a</sup> has noise requirements published in NVIC 12–82 (1982). Other regulatory guidelines exist for American Bureau of Shipping<sup>4</sup>—including ship and off-shore crews and passengers, Det Norske Veritas Comfort Class Rules,<sup>4a</sup> and Lloyd's Register Provisional Rules—Passenger and Crew Accommodation and Comfort<sup>4b</sup> (where noise and vibration limits are addressed).

The latest available Navy airborne noise criteria (OPNAVINST 9640.1A Shipboard Habitability Design Criteria Manual, 1996<sup>4c</sup>) are given by the noise category designations defined below:

- *Category A:* Spaces where direct speech communication must be understood with minimal error and without need for repetition. Acceptable noise level is based on a talker–listener distance of either 3 or 12 ft. Category A-3 A-weighted limit 70 dB—applies when extreme talker-to-listener distance is less than 6 ft. Category A-12 A-weighted limit 60 dB—applies when the extreme talker-to-listener distance is 6 ft or greater.
- *Category B:* Spaces where comfort of personnel in their quarters is the primary consideration and communication considerations secondary—A-weighted limit 70 dB.
- *Category C:* Spaces where it is essential to maintain especially quiet conditions—A-weighted limit 65 dB.

- *Category D:* High-noise-level areas where voice communication is not important, ear protection is not provided, and prevention of hearing loss is the primary consideration—A-weighted limit 84 dB.
- *Category E:* High-noise-level areas where voice communication is at short distances and there is high vocal effort and where amplified speech and telephones are normally available—A-weighted limit 80 dB.

Other criterion addresses the far-field airborne signature of vessels to minimize impact on communities. This is especially true for ferries and harbor tugs. Underwater noise criteria are being developed to minimize the potential disturbance of ship noise on mammals—both with respect to their hearing and habitat.<sup>5,6</sup>

There is a stringent underwater radiated criterion for vessels conducting fisheries research.<sup>7</sup> For these noise critical ships it may be necessary to invoke noise and vibration limits on machinery. Various machinery vibration acceptance criteria also exist.<sup>8,9</sup>

### 3 SPECIFICATION DEVELOPMENT

New or rehabilitated vessels should have a comprehensive acoustical section as part of the ship's specification. This specification should define the acoustical limits versus ship operational conditions, methods to be invoked for quality assurance and verification methods. The International Organization for Standardization (ISO) has developed standard ship measurement procedures.<sup>10,11</sup> The limits—for both habitability and hearing conservation—may vary with the ship's operational conditions and should consider length of operation at that condition, for example, station keeping with the thrusters at full or partial power. The specification should define the extent of any noise control program (see Section 4). Verification testing, operating conditions, witnesses, and reporting requirements should be delineated.

To minimize confusion, avoid the mixed use of performance specifications and treatment (hardware) specifications. If the designer/builder is responsible for the acoustical environment, do not specify treatment approaches, other than minimum accepted treatments, if necessary. If treatments and noise control approaches are specified, do not impose a noise limit to be achieved. Often it will be beneficial to have a separate noise goal for heating, ventilation, air-conditioning (HVAC) equipment (dockside operation) and underway operation. As a minimum the HVAC noise goals should be 5 dB below the criterion when underway.

### 4 ACOUSTICAL CONTROL PLAN

The most successfully designed quiet ships have instituted a control plan. To the extent possible, the plan should define the owner's, designer's, and builder's roles and that of any acoustical subcontractor. The plan needs to address and provide information on administrative, management, and construction functions and

program schedules for integration of noise into the overall design. It should cover the planned acoustical goals, prediction methods, noise control treatment selection and optimization, review of drawings incorporating those designs, factory equipment testing, treatment construction inspections, and verification testing during dockside and underway trials.

### 5 ACOUSTICAL MODELING

Acoustical modeling for either habitability or radiated noise needs to account for:

- Source noise and vibration levels for critical equipment
- Noise transmitted over airborne, structure-borne, and secondary structure-borne paths (the later results from airborne noise impinging on the structure, which then transmits the noise along the structural path)—see Figure 1
- Noise radiating from the structure forming the compartment of interest
- Room acoustical characteristic of the receiver compartment (see Section 9.4)

For ships with powerful sources, varied construction materials, low damping, and distributed sources and receivers, this can be a formidable task. Diesels and propellers can produce high levels at low frequencies, thus octave band analyses between 31.5 and 8000 Hz are typically required to derive an accurate A-weighted noise level. Thus dozens of sources and hundreds of paths need to be accounted for on most vessels.

Comprehensive acoustical modeling documents are *Fundamentals of Ship Acoustics*<sup>12</sup> and *Design Guide for Shipboard Airborne Noise Control*<sup>13</sup> and its *Supplement*,<sup>14</sup> all available from the Society of Naval Architects and Marine Engineers (SNAME). Empirical methods tracing the “source–path–receiver” have

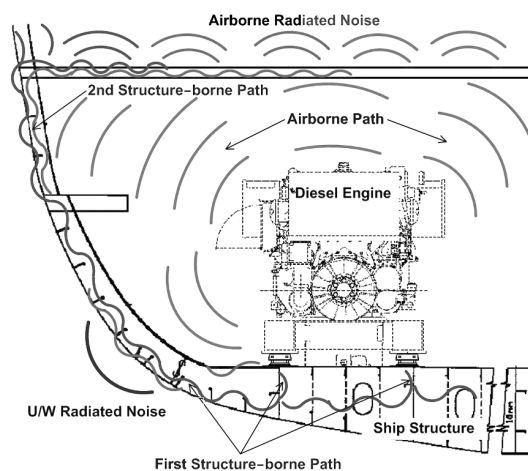


Figure 1 Source/path acoustical model.

been developed, but these are laborious and prone to error.<sup>13–15</sup> The following sections provide a general review of this technique. With the advent of statistical energy analysis (SEA) an accurate accounting of the flow of energy can be made with three-dimensional acoustical models. These models significantly improve the accuracy over empirical methods. A hybrid SEA model whose algorithms consider the acoustical impact of many factors that are specific for ships—water loading of surfaces, finite sizes and orientation of mechanical sources in small compartments, hydrodynamic sources like propellers, thrusters, splash noise (for high-speed ships), the ship's HVAC noise, and on-deck sources—currently exist.<sup>16,17</sup> With the advent of these types of programs and their quick turn-around time, trade-off studies and treatment optimization can be facilitated.

## 6 RADIATED NOISE

### 6.1 General Characteristics

In naval operations the noise radiated by a ship is a dominant source of information, that is, signal, for underwater sonar systems. Radiated noise from ships can be an important contributor to ocean ambient noise, as discussed in Chapter 48 of Ref. 18, and as a factor in oceanographic research and geophysical exploration and cruise ships operating in environmentally sensitive areas. Engineering estimates for noise predictions of specific classes of ship machinery are given in this chapter based on weight, power, and foundation types.

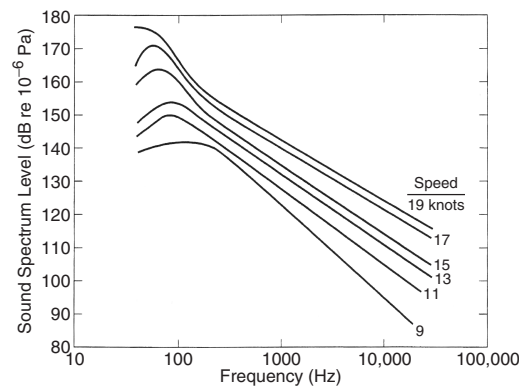
A singularly important text is *Mechanics of Underwater Noise*,<sup>19</sup> which provides detailed information on both mechanical and hydrodynamical noise sources and radiation. Chapter 41 of Ref. 18 summarizes the physics of sound radiation from ship structures and illustrates the basic mechanisms with simple mathematical models. The effects of fluid loading on acoustic radiation of plates and cylindrical structures are described in Chapter 6. In addition, detailed descriptions of hydroacoustical noise sources, including propellers, cavitation, vortex shedding, and turbulent boundary layer flow-induced noise are covered in Chapter 45 of Ref. 18. These chapters provide valuable information directly related to the sources and characteristics of ship noise.

The five principal groups of radiated noise sources are (1) machinery vibration caused by propulsion

machinery and ships' services and auxiliary machinery, including steam, water, and hydraulic piping systems; (2) propellers, jets, and other forms of in-water propulsion; (3) acoustical noise within compartments below the waterline; (4) hydroacoustical noise generated external to the hull by flow interaction with appendages, cavities, and other discontinuities, and (5) fluid connected openings in the hull. A summary of these noise sources and their radiated noise characteristics is discussed in Ref. 20, from which Table 1 gives representative source levels as a function of frequency for a range of surface ships. The data for ships operating between 10 and 20 knots illustrate the dominance of low-frequency noise.

The speed/power dependence of the radiated underwater noise of surface ships is further illustrated by the measurements plotted in Fig. 2.<sup>19</sup> The 9-knot noise spectrum is governed by machinery sources while the significant increase in low-frequency noise as speed is increased is due to both propulsion machinery and the inception and development of propeller cavitation noise. The latter source of radiated noise is dealt with in Section 7. Ross<sup>19</sup> provides estimation formulas for broadband underwater source levels,  $L_s$ , as a function of size or displacement tonnage and speed or power, for example,

$$L_s = 134 + 60 \log[U_a/(10 \text{ knots})] + 9 \log T_D \quad (1)$$



**Figure 2** Radiated underwater noise levels of passenger ship *Astrid*, U.S. Office of Scientific R&D, published 1960.<sup>19</sup> (From Ref. 18, Chapter 46, Fig. 1.)

**Table 1** Representative Ship-Radiated Underwater Noise Levels Measured at 1 m from Center of Hull Side

Ship Class	Source Underwater Sound Pressure Levels re 1 $\mu$ Pa 1-Hz Bands (dB)						
	0.1 kHz	0.3 kHz	1.0 kHz	3.0 kHz	5.0 kHz	10.0 kHz	25.0 kHz
Freighter, 10 knots	152	142	131	121	117	111	103
Passenger, 15 knots	162	152	141	131	127	121	113
Battleship, 20 knots	176	166	155	145	141	135	127
Cruiser, 20 knots	169	159	148	138	134	128	120
Destroyer, 20 knots	163	153	142	132	128	122	114

Source: From Ref. 18, Chapter 46.

where  $U_a$  is ship speed in knots and  $T_D$  is displacement tonnage. Ross states that this formula is applicable for frequencies above 100 Hz and ships weighing under 30,000 tons. The acoustical efficiencies of ships have been found to range from 0.3 to 5 W of acoustic power for ship mechanical propulsion power of 1 MW; Ross suggests acoustical conversion efficiencies of  $1 \times 10^{-6}$  for machinery sources and  $1.5 \times 10^{-6}$  for cavitating propellers.

## 6.2 Noise Spectra

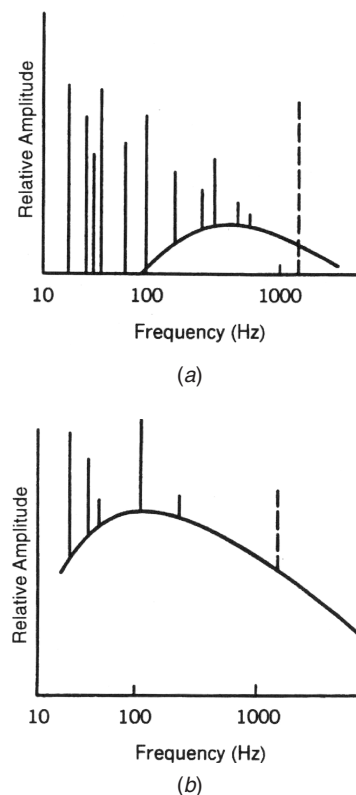
Noise spectra are generally classified in two types: (a) broadband noise having a continuous spectrum such as that associated with cavitation and (b) tonal noise containing discrete frequency or line components related to machinery, gears, propeller blade passage rate, and modulation of broadband noise. In addition to steady-state noise, ship noise is also characterized by transient and intermittent noise caused by impacts, loose equipment or rudders, or unsteady flow that have particular spectral properties. Ship noise is generally a combination of continuous and tonal noise covering the audio spectrum and is usually concentrated in the low-frequency region. Figure 3 shows a diagrammatic comparison of two radiated noise spectra in which auxiliary machinery tonal noise governs the low-speed condition, and propulsion system speed-related frequencies are superimposed on broadband propeller cavitation noise at high speeds. Figure 4 gives an overview of the frequency range of the major sources of radiated noise and shows that the majority of machinery sources produce noise from 10 to 1000 Hz, and significant sources such as cavitation and turbine lines may extend into the 10-kHz region and above.<sup>21</sup>

## 6.3 Machinery Noise

The principal mechanisms that generate vibratory forces involve mechanical unbalance, electromagnetic force fluctuations, impact, friction, and pressure fluctuations. The classes of machinery that produce noise may be categorized according to their functions, such as (a) propulsion machinery (diesel engines, steam turbines, gas turbines, main motors, reduction gears, etc.) and (b) auxiliary machinery (pumps, compressors, generators, air-conditioning equipment, hydraulic control systems, etc.).

Figure 5 is a schematic view of the machinery components of a diesel-electric propulsion system and their associated noise sources, which are described as follows:

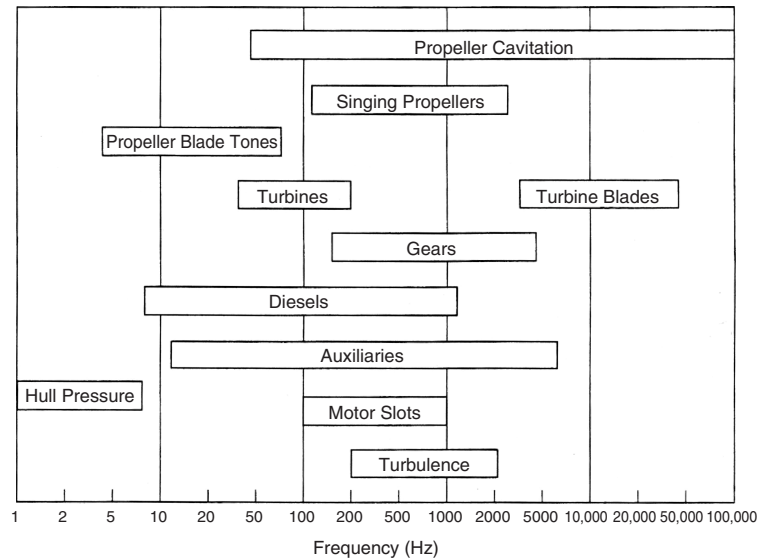
1. Piston slap, which is a dominant noise mechanism of diesel engines and is caused by the impact of a piston against the cylinder wall, results in a spectrum made up of a large family of harmonically spaced tonals.
2. Mechanical imbalances of the generator and auxiliary machinery result in fluctuating forces and moments that are proportional to the square of the angular speed. Since the force is proportional to vibration velocity, the radiated power



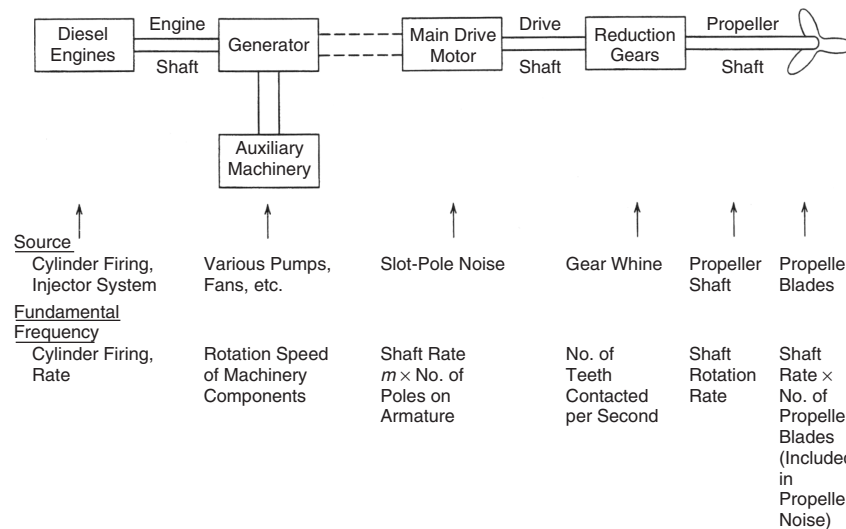
**Figure 3** Diagrammatic spectra of submarine underwater noise at (a) low and (b) high speeds.<sup>20</sup> (From Ref. 18, Chapter 46, Fig. 2.)

increases as the fourth power of rotational speed.

3. Electromagnetic force fluctuations of the main drive motor are related to changes in the flux density, which are a function of the number of poles and result in low-frequency line spectra.
4. Reduction gear noise is dominated by gear tooth impacts and results in tones at multiples of the tooth contact frequency. Helical gears are significantly quieter than spur gears.
5. Propeller noise, which is discussed in Section 7, consists of two major components: (a) direct radiation from the propeller blades and (b) low-frequency hull vibration modes induced by hydrodynamic fluctuating forces acting on the blades and transmitted through the propeller shaft and thrust bearings to the hull. The hull response is thus related to the shaft rpm revolutions/minute and the number of propeller blades. The modes of hull vibration and resulting sound radiation are discussed in Chapter 41 of Ref. 18.



**Figure 4** Frequency ranges of noise radiated by ship noise sources.<sup>21</sup> (From Ref. 18, Chapter 46, Fig. 3.)



**Figure 5** Machinery components and noise sources on a diesel-electric ship.<sup>20</sup> (From Ref. 18, Chapter 46, Fig. 4.)

#### 6.4 Machinery Vibration Levels

The prediction of radiated noise from machinery sources is based on the traditional noise model, which involves vibration levels measured on the feet of machinery sources, transmission path dynamics including vibration isolation and foundation transfer functions, and hull vibration and radiation. The role of foundation structural mobilities is a critical part of this system and directly determines the vibration levels of the source machinery, as discussed in Chapter 71 of Ref. 18. The purpose of this section is to

provide engineering estimates for machinery vibration levels, based on an extensive database, as an input to structural design and noise radiation calculations developed for SNAME.<sup>13,14</sup>

The source level algorithms are provided for engineering guidance. Reliable measured data should be used when available. Also, the parametric dependencies of the prediction algorithms can be used to scale from measured data for similar classes of machinery. It should be noted that the source vibration levels assume that the machine is mounted on



low-frequency vibration isolation mounts. Thus the effect of rigid mounting is to decrease machinery source vibration levels due to the increased constraining effect of the foundation relative to that of resilient mounts.

Table 2 gives source vibration velocity levels in decibels relative to  $10^{-6}$  cm/s as a function of octave bands for two types of gas turbines and for representative classes of electric motors. Table 3 gives formulas for overall machinery source vibration levels expressed as baseline vibration velocity in decibels relative to  $10^{-6}$  cm/s. The machinery parameters

include  $w$  = gross weight in kilograms,  $kW$  = rated power in kilowatts, and actual and rated rpm. The types of machinery include diesels, generators, pumps, and reduction gears. For each type, adjustments to the overall levels are given in Table 4 to obtain estimates of vibration levels for the designated octave bands. Alternative prediction procedures may be found in other handbooks.<sup>15,22-24</sup>

### 6.5 Structural Vibration Transfer Functions

The effects of the transmission of vibratory energy (structure-borne noise) along and through different structural paths are expressed as transfer functions that

**Table 2 Baseline Octave Band Vibration Levels Measured on Feet of Machinery Sources**

Machinery Type	Baseline Vibration Levels, $L_{VB}$ (dB re $10^{-6}$ cm/s)										
	Octave Band Center Frequency										
	16 Hz	31.5 Hz	63 Hz	125 Hz	250 Hz	500 Hz	1 kHz	2 kHz	4 kHz	8 kHz	16 kHz
Gas turbines											
Small high speed	80	85	95	100	100	90	110	100	100	95	95
Intermediate	110	104	106	103	98	93	86	80	73	67	57
Electric motors											
AC	102	96	90	84	78	72	66	60	54	48	42
AD	88	88	83	78	76	73	68	58	53	48	43

Source: From Ref. 18, Chapter 46.

**Table 3 Overall Vibration Levels of Machinery Sources<sup>a</sup>**

Machinery Class	Baseline Overall Vibration Levels of Machinery Source, $L_{VB}$ (dB re $10^{-6}$ cm/s)
Diesel	$-20 \log(w) + 20 \log(kW) + 30 \log\left(\frac{rpm}{rpm_0}\right) + 136$
Reduction gears	$64 + 10 \log(kW)$
Generator	$53 + 10 \log(kW) + 7 \log(rpm)$
Pumps	
Nonhydraulic	$65 + 10 \log(kW)$
Hydraulic	$63 + 10 \log(kW)$

<sup>a</sup>  $w$  = gross weight (kg),  $kW$  = rated power,  $rpm$  = given rotational speed,  $rpm_0$  = rated rotational speed. See Table 4 for octave band adjustments.

Source: From Ref. 18, Chapter 46.

**Table 4 Octave Band Adjustments to Overall Baseline Vibration Levels of Machinery Sources (Table 3)**

Machinery Type	Vibration Source Levels										
	Center Frequency										
	16 Hz	31.5 Hz	63 Hz	125 Hz	250 Hz	500 Hz	1 kHz	2 kHz	4 kHz	8 kHz	16 kHz
Diesel	0	-3	-4	-4	5	-6	-6	-10	-18	-29	-44
Reduct. Gears	0	-2	1	-11	-12	-3	1	-5	-16	-32	-38
Generator	0	3	8	5	-1	-5	-10	-15	-21	-27	-35
Pumps											
Nonhydraulic	10	10	12	19	11	9	4	-6	-8	-15	-25
Hydraulic	10	20	27	32	33	36	30	25	20	5	-10

Source: From Ref. 18, Chapter 46.

relate the input (machinery) and output (foundation or hull) vibration levels. In this section an empirical procedure is given for estimating transfer functions for different transmission paths. The U.S. Navy has published several design handbooks to guide structural designers.<sup>25–28</sup> It should be noted that state-of-the-art PC-based noise models can provide greatly refined and more accurate transfer function estimates for specified structural configurations, and the accompanying estimates should only be used for guidance. Furthermore, multiple vibration transmission paths must generally be considered for ship noise predictions.

**Vibration Isolation Mountings** The transfer function or transmission loss is expressed as the log ratio of vibration velocity above the mounts at the attachment to the machine subbase to that on the foundation structure below the mounting system. In this design guide, sources of vibration are divided into three weight classes: class I, less than 450 kg; class II, 450 kg to 4500 kg; and class III, over 4500 kg.

Table 5 gives representative transmission loss values for four types of mounting configurations: hard mounted (no vibration isolation), distributed isolation material (DIM), single-stage low-frequency isolation mounts, and two-stage isolation with intermediate rafts. The estimates are presented as average values for the designated octave bands. For the hard-mounted case lightweight machines can be expected to have a modest loss at low frequencies, while all classes of machinery have little or no loss above 250 Hz. The DIM installations are effective for lightweight machines above 250 Hz, but their performance decreases as the machinery weight increases.

The losses of low-frequency mounts closely follow theoretical predictions for lightweight machines, that is, 20 dB to 30 dB transmission loss over the given frequency range. However, as the weight of a machine increases relative to that of the foundation structure, the degree of isolation decreases, reflecting the overall impedance relationships. Two-stage mounting systems have been implemented extensively in ship designs and have proved to be highly effective, assuming potential airborne flanking paths are considered (see Section 9.5). Double-stage isolation mounts have been used successfully for diesel generators on at least eight fisheries research vessels built to the International Council for the Exploration of the Sea (ICES) radiated noise standards.<sup>7</sup>

## 6.6 Hull Vibration-Radiated Underwater Noise

The relationships between hull structural vibration levels and radiated noise are discussed in Chapter 6 of this handbook and Chapter 41 of Ref. 18. Assuming that the radiation efficiency  $\sigma_r$  is known, a first-order estimate of the sound radiated from hull plating can be calculated by<sup>13</sup>

$$L_s = L_v + 10 \log \sigma_r + 10 \log A_p + 10 \log n + 73 \quad (2)$$

where  $L_s$  is the equivalent source underwater sound pressure level at 1 m,  $L_v$  is the space average vibration velocity level of the hull plating,  $A_p$  is the area of a single hull plate in square metres and  $n$  is the number of radiating panels.

**Table 5 Representative Transmission Loss Values versus Octave Band Center Frequency for Ship Machine Mounting Arrangements (dB)**

Machinery Weight Class <sup>a</sup>	Transmission Loss, dB								
	Center Frequency								
	31.5 Hz	63 Hz	125 Hz	250 Hz	500 Hz	1000 Hz	2000 Hz	4000 Hz	8000 Hz
<i>Hand Mounted</i>									
I	13	10	8	5	3	2	1	0	0
II	9	7	5	3	1	0	0	0	0
III	5	3	2	1	0	0	0	0	0
<i>Distributed Isolation Material</i>									
I	0	1	5	9	12	15	15	15	15
II	0	0	1	3	5	8	9	10	10
III	0	0	1	2	3	3	4	5	8
<i>Low-Frequency Isolation Mounts</i>									
I	20	25	30	30	30	30	30	30	30
II	12	16	20	23	25	25	25	25	25
III	5	6	8	12	15	18	20	20	20
<i>Two-Stage Mounting System</i>									
I	25	33	40	45	50	50	50	50	50
II	22	30	35	40	45	48	50	50	50
III	20	25	30	30	35	45	50	50	50

<sup>a</sup> Machinery weight classes: class I, under 450 kg; class II, 450–4500 kg; class III, over 4500 kg. Values based on relatively rigid or high-impedance foundation structures.

Source: From Ref. 18, Chapter 46.

**Table 6 Hull Grazing Transmission Loss versus Frequency (dB)**

Octave Band Center Frequency (Hz)	Transmission Loss at Distance $r$ (dB re $r_0 = 1$ m)
250	$10 \log r/r_0$
500	$13 \log r/r_0$
1000	$17 \log r/r_0$
2000	$23 \log r/r_0$
4000	$27 \log r/r_0$
8000	$27 \log r/r_0$

Source: From Ref. 18, Chapter 46.

## 6.7 Hull Vibration Transmission

Hull vibration (calculated or measured) in the area of machinery foundation attachment locations (e.g., deep frames) is transmitted through the steel hull structure. Thus, larger areas of the hull may contribute to radiated noise. Also, the transmission of machinery excited hull vibration into sonar array structures can contribute to sonar self-noise (see Section 8). A useful guideline for broadband transmission loss in typical damped ship structures is 0.15 to 0.25 dB/m for cases of free-layer damping and 0.5 dB/m for structures, including wetted hulls, with constrained layer damping. Structural details are needed to establish frequency dependence.

## 6.8 Hull Grazing Sound Transmission Loss

Table 6 provides frequency-dependent expressions of propagation losses for sound traveling in the water along the length of the hull, which is grazing sound. The hull is considered to be an air-backed baffle, and the grazing sound transmission loss applies to a 1-m source level for far-field radiation. The theoretical basis for these estimates involves energy transmission through both the hull structure and the water path.

# 7 PROPELLER NOISE

## 7.1 General Characteristics

Propulsion propellers constitute a major source of underwater ship noise and, similar to fans, aircraft turboprops, helicopters, and other devices with rotating blades operating in nonuniform flow fields, are the subject of continuing noise control efforts. The interaction of blade forms and hydrodynamic flows and the resulting dynamic response of the blades and the associated acoustic radiation are complex phenomena that depend on a wide range of design and operational variables that do not lend themselves to simple models and noise predictions. Hydrodynamic noise sources are discussed in Chapter 45 of Ref. 18; in particular, Section 3 in that chapter provides the theoretical background for cavitation inception, development, and associated noise.

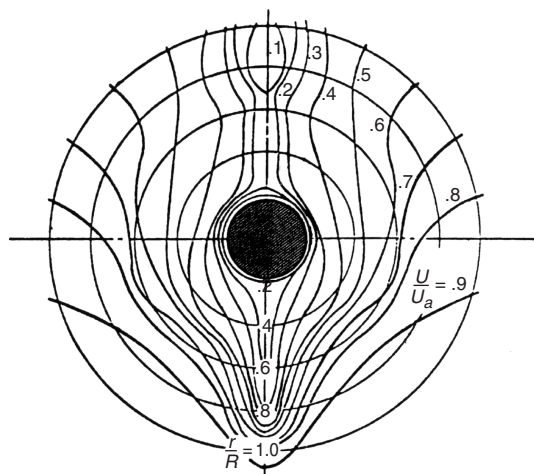
The guidelines for estimating propeller noise included in this chapter are based on the original work of Ross<sup>19</sup> and the more recent engineering analyses presented in the report of the Nordic cooperative

project.<sup>23</sup> Waterjet and bow thrusters are also important sources for both internal and external noise. Noise and vibration levels and design guidance for minimizing bow thruster noise is provided in Ref. 29. Marine propeller noise reduction has benefited from parallel aerodynamic acoustical studies, which are the subject of other chapters in this handbook. For example, significant reductions in both propeller and fan noise have been achieved through smoothing and control of inlet flows and the design of skewed blades.

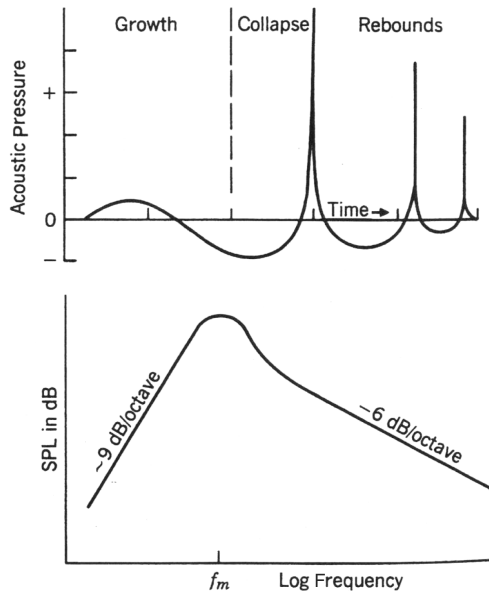
## 7.2 Propeller Noncavitating Underwater Noise

There are generally two to three components in the spectrum of a noncavitating propeller: (a) blade tonals related to propeller shaft speed and the number of blades; (b) propeller broadband noise related to blade vibratory response to turbulence ingestion and trailing-edge vortices; and/or (c) propeller singing due to coincidence of vortex shedding and blade resonant frequencies. Blade tonals and harmonics result from oscillating components of forces or propeller thrust variations caused by circumferential variations of the wake inflow velocity. Figure 6 illustrates, by use of equivalent velocity contours, the velocity variations in the plane of a single-propeller merchant ship. The flow speed varies from 10 to 90% of the forward speed of the propeller. These velocity differences cause large variations of the angle of attack and associated lift forces, which lead to significant fluctuations in thrust and torque during each revolution of the shaft and, in turn, to high-level, low-frequency hull vibration. Thus, the most important design consideration is the relationship between the harmonic structure of the wake and the number and blade form of the propellers.

The primary propeller design factors include diameter, shaft rpm, number of blades, expanded area ratio,



**Figure 6** Wake diagram for a single-screw merchant ship.<sup>19</sup> (From Ref. 18, Chapter 46, Fig. 5.)



**Figure 7** Cavitation pressure pulses from collapsing cavity and idealized spectrum of sound pressure level.<sup>19</sup> (From Ref. 18, Chapter 46, Fig. 6.)

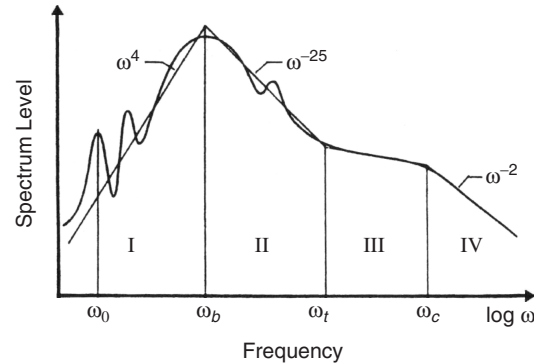
blade load distribution, skew distribution, blade tip-hull clearance, and the spatial and temporal characteristics of the inflow field (see Ref. 30).

### 7.3 Propeller Cavitation Noise

As stated above, a description of cavitation is provided in Chapter 45 of Ref. 18. There are four types of propeller cavitation: driving face, suction face, tip vortex, and hub vortex. The blade tip speed governs cavitation inception, as shown in Eq. (14) of that chapter. Broadband cavitation noise results from the growth and collapse of a sheet of bubbles occupying a volume on the individual blades. Figure 7 illustrates this process for a single cavitation bubble with the resultant idealized spectrum. The general noise spectrum of blade cavitation is shown in Fig. 8 and has four principal spectral regions:

- I. Low frequency: contains blade frequency  $\omega$  and harmonics; mean power level increases as  $\omega^4$ .
- II. Midfrequency: starts at bubble frequency  $\omega_b$ ; mean power level increases as  $\omega^{-5/2}$ .
- III. Intermediate frequency: transition region between regions II and IV.
- IV. High frequency: starts at bubble frequency  $\omega_c$ ; mean power level decreases as  $\omega^{-2}$ .

In regions I and II the fluctuations of the sheet cavitation volumes may be represented by a large bubble that acts as an acoustic monopole. In region



**Figure 8** General noise spectrum level of a cavitating propeller.<sup>23</sup> (From Ref. 18, Chapter 46, Fig. 7.)

IV, the power is caused by cavity collapse or by shock wave generation by nonlinear wave propagation. Region III contains a mixture of regions II and IV. Figure 9 is an example of a comparison between predicted and full-scale measured source levels for a 32,000-ton vessel.<sup>18,23</sup>

## 8 PLATFORM AND SONAR SELF-NOISE

### 8.1 General Characteristics

Conceptually, self-noise is that noise in a sonar system attributable to the presence of the platform, as illustrated in Fig. 10. In practice, sonar self-noise measurements always include the contribution of the ambient noise. The self-noise term in the sonar equation set forth in Chapter 49 of Ref. 18 is also all inclusive. Thus, sonar self-noise is really the total noise level of a sonar when there is no target present.

Two kinds of self-noise measurements are made: *platform noise* measurements are self-noise measurements made with omnidirectional hydrophones; *sonar self-noise* measurements are made at the output of the designated array. Platform noise is  $L_N$  in the sonar equation, while sonar self-noise  $L_e$  is the equivalent of  $L_N - N_{DI}$ , where  $N_{DI}$  is the measured array gain. It is important to measure the sonar self-noise directly because the array signal-to-noise gain depends upon the spatial properties of the noise field. The directivity index, which is based on isotropic noise, is a first-order approximation of the ability of an array to discriminate against noise, but it usually does not equal the actual array gain. In fact, coherent noise sources can appear as target signals on sonar displays.

In treating sonar self-noise, it is convenient to consider six dominant noise sources:

1. Ambient ocean noise
2. Local machinery sources
3. Remote machinery sources
4. Propeller noise
5. Local flow noise
6. Local cavitation and/or bubble sweepdown

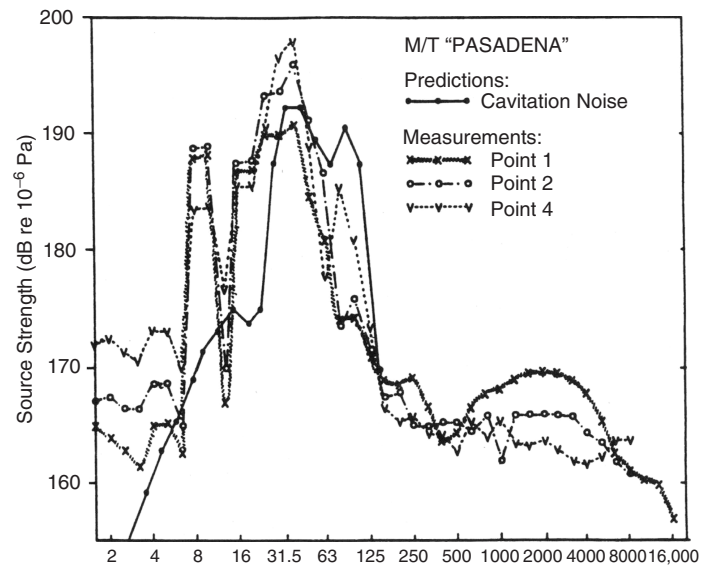


Figure 9 Comparison between predicted and measured noise levels.<sup>23</sup> (From Ref. 18, Chapter 46, Fig. 8.)

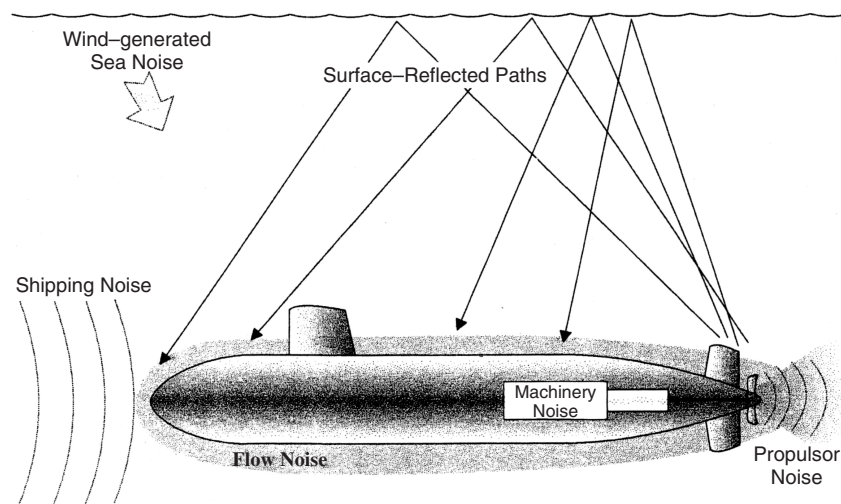
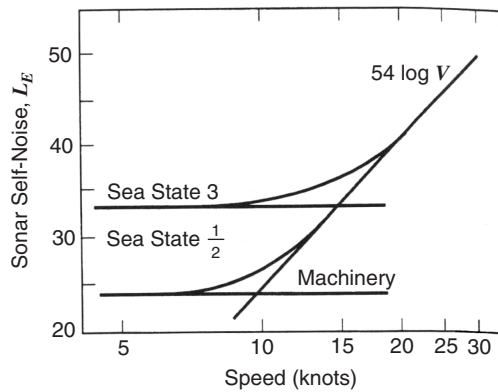


Figure 10 Primary sources of self-noise.<sup>21</sup> (From Ref. 18, Chapter 46, Fig. 9.)

Ambient noise is discussed in Chapter 47 of Ref. 18. It generally dominates only at slow speeds. Figure 11 illustrates how at low sea states (e.g., sea state  $\frac{1}{2}$ ) ambient noise may control sonar self-noise only at low ship speeds before other speed-dependent noise sources begin to dominate. At sea state 3, ambient noise controls sonar self-noise up to higher ship speeds.

At the other extreme, *local cavitation* on the sonar dome is generally a problem only at the highest speeds of surface ships. In moderate to high sea states,

bow wave splash is a significant noise source that extends along the line of the breaking bow wave. It is highly dependent on ship motion with respect to the seaway. Machinery can contribute noise into the sonar arrays by vibrational paths, and these sources may be significant over a wide speed range. Propeller noise may be transmitted to sonar arrays by hull vibration, hull grazing (see Table 6), and by surface-reflected paths. Small water area twin hull (SWATHs) may also have a "cross-hull" path. Each type of noise source has individual speed and power dependencies



**Figure 11** Speed-dependent self-noise as a function of sea state, relative sonar noise level vs. speed, knots.<sup>19</sup> (From Ref. 18, Chapter 46, Fig. 10.)

that contribute in varying degrees to the overall sonar self-noise level as a function of speed.

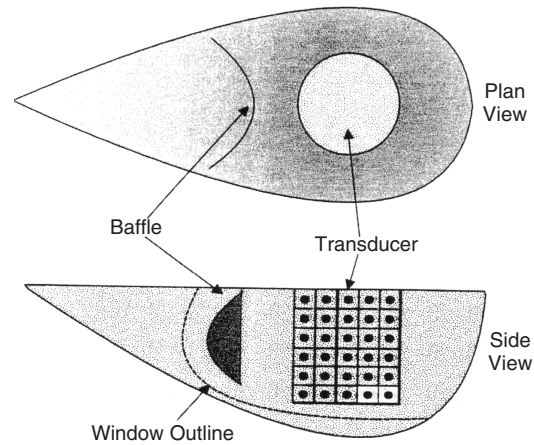
At higher speeds *local flow noise* is a dominant noise source. The mechanisms whereby turbulent boundary layer pressure fluctuations excite flush-mounted hydrophones, sonar domes, and structures local to the sonar are discussed in Chapter 45 of Ref. 18. The wavenumber of the convective turbulent excitation is much larger than that of the acoustical signal of the same frequency. It is thus possible to design hydrophones and arrays to discriminate against flow noise while maximizing signal gain.

The importance of remote machinery and propellers as contributors to self-noise is apparent when close correlations between radiated noise and sonar self-noise are recognized. The two principal paths are surface boundary reflection or scattering and hull vibration. Hull vibration is particularly important for low-frequency noise while the acoustical path surface ship sonar self-noise is often higher in shallow water than in deep water. Generally speaking, the reduction of radiated noise can also be important to improving sonar performance.

## 8.2 Dome Design

The term *dome* refers to a vaulted structure. It probably originated when rounded projections were first installed to protect protruding hydrophones. Today the term encompasses any structure housing arrays or hydrophones, whatever the shape, and sometimes even describes the supporting structure and array. Domes may now comprise the whole front portion of a submarine or the bulbous bow of a surface ship. They are either conformal domes (i.e., conforming to the general shape of the ship) or appendage domes (i.e., protruding into the water flow around the ship, as illustrated in Fig. 12).

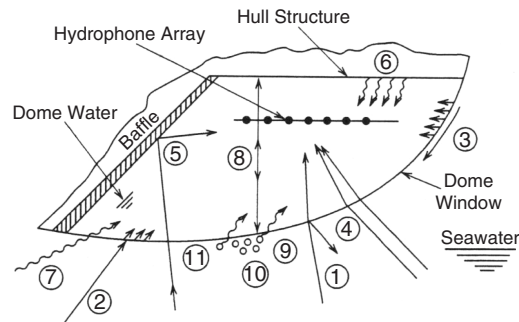
The structural and acoustical factors involved in dome design and ship installations are dealt with in Ref. 31 and illustrated in Fig. 13. The acoustical factors in dome design, which are numbered



**Figure 12** Sonar dome schematic. (From Ref. 18, Chapter 46, Fig. 11.)

in Fig. 13, are (1) transmission through material, (2) compressional and flexural coincidence angles, (3) flow excitation, (4) refraction, (5) internal reflection, (6) structure-borne noise, (7) waterborne noise, (8) reverberation, (9) cavitation, (10) bubbles, and (11) fouling.

When designing and installing sonar domes, the emphasis is on protecting the transducers, minimizing ship impact, and enhancing signal-to-noise ratio. The interposition of the dome, or window, reduces the signal level and, therefore, low-transmission-loss structures and materials are mandatory. At low frequencies, where large arrays and domes are required, the wavelengths are large and attenuation through the material is low. The thicker windows required for mechanical strength do not, therefore, cause unacceptable attenuation losses at these frequencies. Thus, design becomes a compromise between acoustic, hydrodynamic, and structural requirements and the location, size, operating frequency, and shape of the array.



**Figure 13** Acoustical considerations in dome design. (From Ref. 18, Chapter 46, Fig. 12.)

**Table 7 Hull-Mounted Sonar Array Baffle Diffraction Loss versus Frequency (dB)**

Type of Barrier/Baffle	Diffraction Loss (dB)					
	250 Hz	500 Hz	1000 Hz	2000 Hz	4000 Hz	8000 Hz
Water backed	0	0	0	5	5	5
Air backed	8	11	14	17	20	23

Source: From Ref. 18, Chapter 46.

The dome or window should be made of tough, hard-to-damage, material because hydroelastic excitation or flutter around a damaged portion can cause noise. It can also be excited by the flow of water past its surface and radiated to the hydrophone if it is constructed of an elastic material (e.g., steel or fiberglass). A highly damped, low-modulus material such as rubber reduces flow noise problems. But in every case, it is important to maintain both the fairness and smoothness of the dome and the adjacent hull surfaces. Step discontinuities must be avoided.

The fluid inside the dome may become warmer than the surrounding sea and, thus, may not have the same speed of sound as the external water. This results in refractions and focusing, which leads to degradation in beam former performance and gives erroneous bearings. Thus dome design should provide for flushing and replacement of the internal dome water.

The dome is usually equipped with baffles aft of the array to reduce the effect of ship machinery and propeller noise on the sonar array. However, these baffles can also mask targets in the stem sectors. Flat or curved surfaces inside the dome can reflect incoming signals, and nonreflecting surface materials may be needed to reduce the possibility of spurious signals appearing in the array output. Table 7 gives values for diffraction losses as a function of frequency for typical water and air-backed sonar baffles.

### 8.3 Flow-Induced Noise

Turbulence is generated along the hull of a ship as it passes through the water. The fluctuating pressures associated with a turbulent boundary layer radiate noise directly into the water (flow noise) and excite vibrations in ship structures because the mechanism of direct radiation of flow noise into the water is inefficient. Flow noise is usually not a significant source of ship noise. However, flow-induced noise transmitted through excitation and radiation of sonar domes and adjacent hull structures becomes a significant source of sonar self-noise at higher speeds. Chapter 5 of this handbook and Chapter 45 of Ref. 18 provide more detailed information on hydroacoustic noise and structure-fluid interactions.

The estimates of platform self-noise given below are sound pressure levels at individual element locations within sonar domes. For flow-induced noise, platform noise levels inside the sonar domes are estimated by adding the values given below to the baseline level,

$L_N$  (see Ref. 32):

$$L_N = 34 + 45 \log(V) - 20 \log(h) + 10 \log(A) \quad (3)$$

where  $V$  is ship speed in knots,  $h$  is the thickness of the sonar dome in centimetres, and  $A$  is the surface area of the sonar dome in square metres.

Octave Band Adjustments in Decibels (Add to  $L_N$ )

Center frequency (Hz)	31.5	63	125	250	500	1000	2000	4000	8000
Flow noise	39	28	19	16	13	10	7	4	1

## 9 INTERIOR COMPARTMENT NOISE

### 9.1 General Characteristics

The airborne noise levels in ships constitute a major area of ship acoustics. The high airborne noise levels of propulsion machinery and reduction gears in confined machinery spaces constitute a serious hearing and communication problem.

### 9.2 Airborne Sound Pressure Levels of Sources

The acoustic source levels of representative machinery noise sources in ships are expressed as sound power levels in octave bands with adjustments given in Table 8.<sup>13,14,32</sup> Additional sources, such as exhaust pipe vibration and wave impact noise are considered in the *Supplement*<sup>14</sup> to the original *SNAME Design Guide*.<sup>13</sup> The *Supplement*<sup>14</sup> also contains Excel spreadsheets that provide source noise and vibration levels for many marine sources, material absorption, and transmission loss values, as well as measured isolation mount performance characteristics.

1. Diesel engines intake, exhaust and casing radiation, baseline;

$$L_{WB} = 58 + \log(kW) \quad \text{dB re } 10^{-12} \text{ W} \quad (4)$$

2. Gas turbines, intermediate exhaust;

$$L_{WB} = 74 + \log(kW) \quad \text{dB re } 10^{-12} \text{ W} \quad (5)$$

Often machinery vendors only measure sound pressure levels at 1m and do not provide sound power levels (which would be independent of the acoustical



**Table 8 Machinery Noise: Source Sound Power Levels (dB re 10<sup>-12</sup> W) Octave Band Adjustments**

Machinery Class	Source Sound Power Levels (dB re 10 <sup>-12</sup> W)								
	31.5 Hz	63 Hz	125 Hz	250 Hz	500 Hz	1000 Hz	2000 Hz	4000 Hz	8000 Hz
<i>Equation (4)</i>									
Diesel engines									
Intake	21	21	27	28	26	24	20	13	4
Exhaust	44	40	46	42	34	30	24	14	6
Casing	4	6	15	18	17	15	11	4	0
<i>Equation (5)</i>									
Gas turbines									
Exhaust	22	22	22	22	22	20	16	14	4

Source: From Ref. 18, Chapter 46, Table 9.

room environment in which they are measured). For a finite size source, the following method can be used to convert from the vendor-supplied data at a set distance to sound power levels or to the sound pressure level for another distance from the source.

The estimated sound power level, for equipment with dimensions  $L$ ,  $B$ ,  $H$ , in metres, may be found in accordance with the formula (independent of frequency)<sup>14</sup>

$$L_W = L_p(r_0) + 10 \log[12r_0^2 + 4r_0(L + B + 2H) + 2H(L + B) + LB] \quad (6)$$

where  $L$  is the machinery length,  $B$  is the width ( $B < L$ ), and  $H$  is the height. In this formula,  $r_0$  is the average distance between the equipment surface and the point where the noise levels were measured and  $L_p$  is the sound pressure level measured at a distance  $r_0$ .

The direct field sound pressure level at some arbitrary distance  $r$  from the casing is equal to<sup>14,34</sup>

$$L_p(r) = L_p(r_0) - 20\xi(\varphi) \log\left(\frac{r}{r_0}\right) + 10 \log[Q] - 1 \text{ dB} \quad (7)$$

where  $L_p(r_0)$  is sound pressure level at distance  $r_0$  from the machinery casing,  $\xi(\varphi)$  is a function of the source shape and direction from the center of the source to the point of interest, and  $Q$  is the source directivity, and where  $Q = 1$  for a source in the middle of the room, and  $Q = 2$  for a source in a corner. Values of  $\xi(\varphi)$  range between 0.15 and 0.9. Its value also depends on the angle between the equipment's longitudinal axis and direction to the point of interest in the machinery room.<sup>14</sup>  $\xi(\varphi)$  is lowest for high values of  $L/\sqrt{(BH)}$ .

### 9.3 Acoustic Transmission Path

Noise control measures in ships are similar to those in other architectural acoustic applications. An extensive and broad base of materials technology has been

developed and applied by the U.S. Navy and industry to meet surface ship and submarine habitability and environmental requirements. This technology is largely available to nonmilitary ship designers. A general noise model is given in Fig. 14. In addition, statistical energy analysis noise models are available to support alternative designs for noise control treatment combinations.

Examples of available noise control technology are as follows:

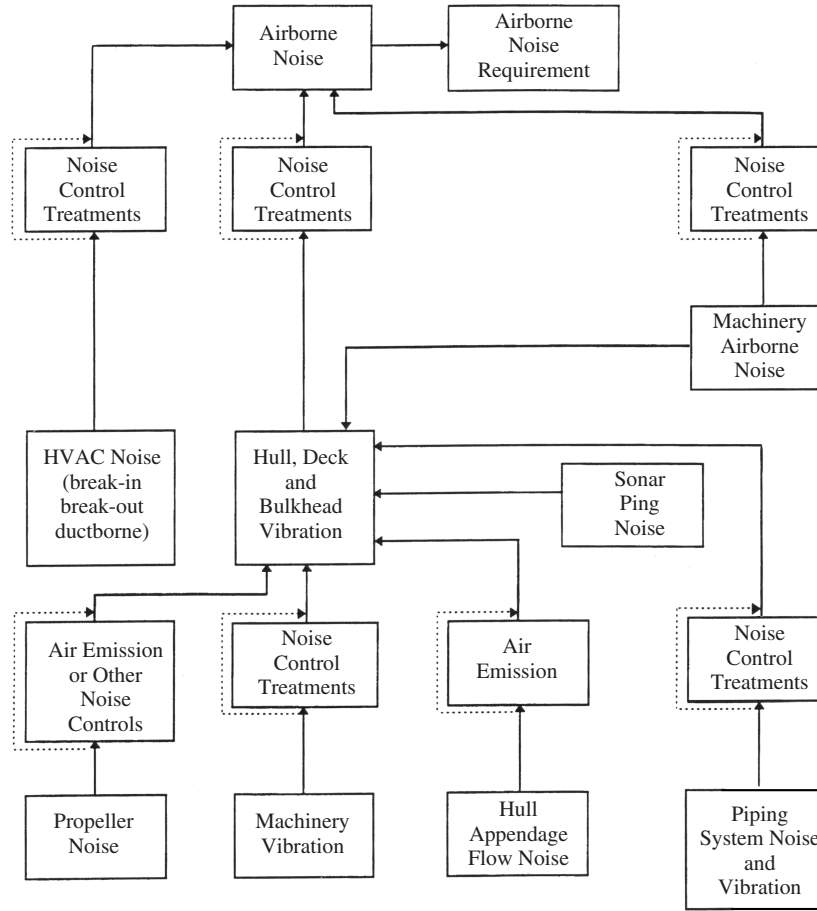
1. Internal high-transmission-loss "sandwich"-type composite treatments (e.g., fiberglass blanket/loaded vinyl septum/fiberglass blanket) or tuned double-wall constructions for reduction of airborne noise transmission through the hull or through partitions between compartments
2. Internal sound absorption materials for installation on bulkheads and overheads of ship compartments to reduce individual compartment noise levels
3. Vibration damping materials for application to internal ship structures to reduce transmission of structure-borne noise to interior compartments

Transmission loss data on a representative sample of commercial products that meet U.S. Navy requirements are given in Table 9.<sup>35</sup>

### 9.4 Acoustic Absorption Materials — Room Constants

There are two classes of acoustical materials for sound absorption applications in (1) "clean" spaces and (2) machinery and equipment spaces and a third class to supplement structural transmission loss of decks, bulkheads, and interior joiner work.

Type I treatments are simply designed to reduce the reverberant sound field by increasing the sound absorption characteristics of interior bulkheads and overheads. Typically, 50mm-thick fiberglass blankets with perforated facings are used for this purpose. Such treatments typically provide on the order of 5 dB noise reduction in the A-weighted noise.



**Figure 14** General noise model for ship systems airborne noise control. (From Ref. 18, Chapter 46, Fig. 13.)

Type II treatments are similar in function to type I treatments but generally consist of a 50-mm layer of fibrous glass material faced with an impervious fabric for protection and to reduce the risk of degradation in absorption characteristics due to oil and water contamination. However, the facing material generally degrades the absorption performance of the overall treatment.

Type III treatments are designed to supplement the transmission loss afforded by baseline structural decks and bulkheads and interior joiner work. Typically, these treatments incorporate relatively high density fiberglass installed as two separate blankets separated by a thin septum of lead-loaded or barium-sulfate-loaded vinyl. The outer, exposed layer of fibrous glass material can have either a perforated facing to maximize sound absorption or a thin facing impervious to oil and water. Table 10 provides data on ship acoustical materials.<sup>32</sup>

The relationship between the received sound pressure level in a compartment and the acoustic power

radiated into the compartment is determined by<sup>36</sup>

$$L_p = L_w - 10 \log([Q/(4\pi r^2) + (R/4)] \quad (8)$$

where  $L_p$  is the received sound pressure level in dB re 20  $\mu$ Pa,  $L_w$  is the acoustic power level in dB re 1 pW,  $Q$  is the directivity factor of the source,  $r$  is the distance from the source to the receiver in metres, and  $R$  is the room constant in square metres. The room constant depends on many factors, including<sup>37</sup>

$$R = S_{\text{total wall}} \left[ 10^{-(TL_{\text{wall}}/10)} + \left( \frac{4\pi\sqrt{12}\rho c^3\sigma}{c_L t \rho_s \omega^2} \right) \times \left( \frac{\rho_s \omega \eta}{\rho_s \omega \eta + 2\rho c \sigma} \right) \right] + \sum_i S_{gi} \alpha_{gi} + \sum_i S_{gi} 10^{-(TL_{gi}/10)} + \sum_i S_i \alpha_i \quad (9)$$

**Table 9 Transmission Loss for Representative Ship Structure and Materials<sup>a</sup>**

Material No.	Panel Description, Type, and Thickness	Transmission Loss (dB)						
		125 Hz	250 Hz	500 Hz	1000 Hz	2000 Hz	4000 Hz	STC
1	Bare aluminum bulkhead, $\frac{1}{4}$ in.	20	25	30	35	30	39	30
2	One layer, 2 in. MIL-A-23054	18	27	37	47	48	57	39
3	One layer, 2 in. MIL-A-23054 +1 lb/ft <sup>2</sup> lead vinyl	14	37	51	56	59	69	38
4	Two layers, 2 in. MIL-A-23054 +1 lb/ft <sup>2</sup> lead vinyl	23	44	57	65	68	75	38
5	One layer, 1 in. Mylar-faced fiberglass	17	23	33	44	45	59	35
6	One layer, 1 in. Mylar-faced fiberglass and W.R. 1 lb/ft <sup>2</sup> lead	21	34	49	60	63	75	40
7	Two layers, 1 in. Mylar-faced fiberglass and W.R. 1 lb/ft <sup>2</sup> lead	20	33	51	61	61	72	39
8	One layer, 2 in. Mylar-faced fiberglass	18	25	38	48	48	67	38
9	One layer, 2 in. Mylar-faced fiberglass and F.G.R. 1 lb/ft <sup>2</sup> LD	12	36	49	57	60	72	36
10	Two layers, 2 in. Mylar-faced fiberglass and F.G.R. 1 lb/ft <sup>2</sup> LD	17	38	54	57	60	78	41
11	Two layers, 2 in. Mylar-faced fiberglass (no septum)	16	33	47	56	55	73	40
12	One layer, 2 in. fiberglass with 14 oz/ft <sup>2</sup> lead face septum	14	35	45	57	58	67	38
13	Two layers, 2 in. fiberglass with 14 oz/ft <sup>2</sup> lead septum	17	38	52	58	55	65	41
14	Quilted blanket, two layers 1 in. fiberglass with lead septum	14	28	40	47	48	53	37

<sup>a</sup> Tests conducted in accordance with ASTM E90. 1 in. =  $2.54 \times 10^{-2}$  m, 1 oz/ft<sup>2</sup> = 0.306 kg/m<sup>2</sup>, 1 lb/ft<sup>2</sup> = 4.9 kg/m<sup>2</sup>.

Source: From Ref. 18, Chapter 46, Table 10.

**Table 10 Sound Absorption Coefficients for Representative Shipboard Materials**

Material Type	Thickness (in.)	Sound Absorption Coefficient					
		125 Hz	250 Hz	500 Hz	1000 Hz	2000 Hz	4000 Hz
Board	1.0	0.07	0.25	0.70	0.90	0.75	0.70
2.5 ± 0.5 lb/ft. <sup>2</sup>	1.5						
		0.15	0.45	0.90	0.90	0.80	0.75
Navy II	2.0	0.25	0.70	0.90	0.85	0.75	0.75
	0.5	0.04	0.10	0.20	0.40	0.45	0.55
	1.0	0.06	0.20	0.45	0.65	0.65	0.65
	2.0	0.15	0.40	0.75	0.75	0.75	0.70
	3.0	0.20	0.60	0.90	0.80	0.80	0.75
	4.0	0.25	0.65	0.95	0.85	0.85	0.80
Navy III	2.0	0.43	0.96	1.0	1.0	0.70	0.35

Source: From Ref. 18, Chapter 46, Table 11.

where the last term is the boundary surface room constant and the first term accounts for room compliance and wall transmission loss. This equation varies with frequency. The first term is insignificant above 250 Hz. The following definitions apply:

$S_{\text{totalwall}}$  is total area of all boundary surfaces in the compartment of interest.

$TL_{\text{wall}}$  is the average sound transmission loss of the compartment's boundary, including the structure and attachments such a joiner panels or insulation.

$\rho$  is the density of air, 1.21 kg/m<sup>3</sup>.

$\rho_s$  is the average mass per unit area of the boundary surface, kg/m<sup>2</sup>.

$\omega$  is  $2\pi f$ , where  $f$  is the octave band center frequency.

$\eta$  is the loss factor of a typical boundary surface, see the Design Guide<sup>13</sup> and Supplement<sup>14</sup> for values.

$\sigma$  is the average radiation efficiency of a typical panel (between frames).

$c_L$  is the longitudinal wave speed of the plate material, 5200 m/s in steel and aluminum.

$t$  is the plate thickness, m.

$S_g$  is the area of the  $i$ th gaps or openings (including duct terminals and door louvers), m<sup>2</sup>.

$TL_g$  is the transmission loss of the  $i$ th opening or gap (typically 0 to 5 dB); it can be computed

as  $TL_g = 20 \log\{(t + 1.6a_g)/(a_g\sqrt{2})\}$ , where  $a_g^*$  is the equivalent radius of the hole or gap and  $a_g < \lambda = (c/f)^\dagger$ ; for a large gap (greater than 10% of the wall) the composite transmission loss should be computed per Eq. 7–15 of the Design Guide,<sup>14</sup> and this value used in the computation of  $TL_{wall}$  and the term containing  $TL_g$  in Eq. (9) set to zero. To be conservative a  $TL_g$  value of zero can be used for gaps.

$\alpha_g$  is the absorption of the  $i$ th opening or gap (typically 0.5 to 0.99); for small holes this value can be computed as

$$\alpha_g = 10^{TL_g/10}$$

for a large gap,  $a_g > \lambda$  use a value,  $\alpha_g > 0.5$ .

$\alpha_i$  is the absorption coefficient of the  $i$ th room boundary surface.

$S_i$  is the surface area of the  $i$ th room boundary surface, ft<sup>2</sup> or m<sup>2</sup>

### 9.5 Airborne-to-Structure-Borne Paths

When there is isolation-mounted equipment, particularly double-stage mounts, the secondary structure-borne path can become important. Sound incident on the compartment's boundaries induces vibration in the structure. For bare exposed steel plating, secondary structure-borne vibration levels are computed for the frequency of interest as follows<sup>14</sup>:

$$L_{a2nd} = L_{pinc} + 10 \log \left[ \left( \frac{\sigma_{rad}}{8.4t^2(\sigma_{rad} + 3.0\eta t)} \right) \right] \quad (10)$$

In this formula,  $L_{a2nd}$  is the secondary structure-borne-induced vibration level,  $L_{pinc}$  is the incident sound pressure level near the center of the structure of interest in the machinery room,  $t$  is the thickness of the structure plate, (inch),  $\eta$  is the structure's loss factor, and  $\sigma_{rad}$  is the structure's radiation efficiency.

**Acknowledgments** The authors' wish to acknowledge the contributions of many colleagues to the database that underlies the information presented in this chapter. In particular, the selection and summarizing of this material has benefited from discussions with Dr. Donald Ross, author of the text *Mechanics of Underwater Noise*, and Daniel Nelson, of Bolt, Beranek and Newman, Inc., who originated a major part of the SNAME noise and vibration performance predictions for shipboard machinery systems.

\*For rectangular opening,  $a_g = (LW/\pi)^{0.5}$ , where  $L$  and  $W$  are the length and width, respectively; or  $a_g$  = the gap dimension for a small circumferential opening.

<sup>†</sup> $\lambda = 11$  m at 31.5 Hz, 5.4 m at 63 Hz, 2.7 m at 125 Hz, 1.4 m at 250 Hz, 0.7 m at 500 Hz, 0.34 m at 1000 Hz, 0.17 m at 2000 Hz, 0.085 m at 4000 Hz, and 0.04 m at 8000 Hz.

### REFERENCES

1. K. Yankaskas and S. Fast, CVN Flight Operations: Crossing the Aircraft/Ship Interface, *Naval Eng. J.*, Vol. 111, No. 3, May 1999, pp. 347–357.
2. K. Yankaskas and R. Fischer, X-Craft: An HSI Application, American Society of Naval Engineers Human Systems Integration Symposium, Arlington, VA, June 2005.
3. International Maritime Organization (IMO), Code on Noise Levels on Board Ships, IMO Resolution A.468 (XII), London, UK 1981.
- 3a. U. S. Coast Guard Navigation and Vessel Inspection Circular No. 12–82, Recommendations On Control of Excessive Noise, 2 June 1982.
4. American Bureau of Shipping, Guide for Crew Habitability on Ships, Dec. 2001; Guide for Crew Habitability on Off-Shore Installations, May 2002; and Guide for Passenger Comfort on Ships, Dec. 2001, American Bureau of Shipping, Houston TX.
- 4a. Det Norske Veritas, Rules for Classification of Ships, Vol. 3, Chapter 12, Jan. 2004, Norway.
- 4b. Lloyd's Register, Provisional Rules, Passenger and Crew Accommodation Comfort (Noise and Vibration), Feb 1999, London, UK.
- 4c. Department of the Navy, OPNAV Instruction 9640.1A, Shipboard Habitability Program, Sept. 1996.
5. National Research Council, *Ocean Noise and Marine Mammals*, National Academies Press, Washington, DC, 2003.
6. W. John Richardson, Charles Green Jr, Charles Malme, Denis Thomson, *Marine Mammals and Noise*, Academic Press, San Diego, CA, 1995.
7. International Council for the Exploration of the Sea (ICES), Underwater Noise of Research Vessels, Review and Recommendations, Report 209, Copenhagen, Denmark, 1995.
8. American National Standard ANSI S2.16–1997: Vibratory Noise Measurements and Acceptance Criteria of Shipboard Equipment, ANSI, Washington, DC, 1997.
9. International Organization for Standardization (ISO) 10816-1995: Mechanical Vibration—Evaluation of Machine Vibration, ISO, Geneva, Switzerland, 1995.
10. International Organization for Standardization (ISO) 2922-1975: Acoustic—Measurement of Noise Emitted by Vessels on Inland Water-Ways and Harbours, ISO, Geneva, Switzerland, 1975.
11. International Organization for Standardization (ISO) 29232-1975: Acoustic—Measurement of Noise on Board Vessels, ISO Geneva, Switzerland, 1975.
12. H. Loeser, *Fundamentals of Ship Acoustics*, Society of Naval Architects and Marine Engineers, Jersey City, NJ, 1999.
13. R. W. Fischer, C. B. Burroughs, and D. L. Nelson, Design Guide for Shipboard Airborne Noise Control, *SNAME Tech. Res. Bull.*, 1983, pp. 3–37.
14. R. Fischer and L. Boroditsky, *Supplement to Design Guide for Shipboard Airborne Noise Control*, Society of Naval Architects and Marine Engineers, Jersey City, NJ, 2000.
15. M. Heckl, Entwicklung von Methode zur Schallpegel-prognose für den Unterkunft—und Maschinenraumbereich von Schiffen, Bericht Nr. 193/1988, Technische Universität, Berlin, Hamburg, Germany, 1988.
16. R. Fischer, L. Boroditsky, W.-H. Joo, and J.-H. Park, Verification of a Hybrid Model for Shipboard Noise

- Predictions, InterNoise 03, Inst. of Noise Control Engineers, Korea, Aug., 2003.
17. R. Fischer, L. Boroditsky, and K. Yankaskas, Shipboard Noise Prediction Program—JERICHO, NoiseCon 03, Inst. of Noise Control Engineers (INCE), Cleveland, OH, June 23, 2003.
  18. M. J. Crocker, Ed., *Encyclopedia of Acoustics*, Wiley, New York, 1997.
  19. D. Ross, *Mechanics of Underwater Noise*, Peninsula Publishing, Los Altos, CA, 1987.
  20. R. J. Urick, *Principles of Underwater Sound for Supervisors*, McGraw-Hill, New York, 1967.
  21. D. Ross and R. D. Collier, *Mechanics of Underwater Noise*, Course Notes, Applied Technology Institute, Columbia, MD, 1985–94.
  22. *Noise Control Handbook*, British Ship Research Association, Naval Architecture Department, London, UK, February 1982.
  23. S. Nilsson and N. P. Tyvand, Eds., *Noise Sources in Ships: I Propellers, II Diesel Engines*, Nordic Cooperative Project: Structure Borne Sound in Ships from Propellers and Diesel Engines, Nordforsk, Norway, 1981.
  24. *Handbook for Shipboard Airborne Noise Control*, Bolt Beranek and Newman, Technical Publication 0730100, U.S. Coast Guard and U.S. Naval Ship Engineering Center, February 1974.
  25. *Design Handbook. Resilient Mounts*, U.S. Naval Sea Systems Command, NAVSEA 0900-LP-089-5010, 1977.
  26. *Design Handbook. Distributed Isolation Material*, U.S. Naval Sea Systems Command, NAVSEA S9078-AA HBK-OIO-DIM, 1982.
  27. *Design Handbook. Piper Hangers*; U.S. Naval Sea Systems Command, NAVSEA S9073-A2 HBK-OIO, undated.
  28. *Design Handbook of Vibration Damping*, Mare Island Naval Shipyard, Report No. 11–77, U.S. Naval Sea Systems Command, January 1979.
  29. R. Fischer, Bow Thruster Induced Noise and Vibration, MTS Dynamic Positioning Conference, Houston, TX, October 17–18, 2000.
  30. W. Blake, *Mechanics of Flow-Induced Sound and Vibration*, Academic, New York, 1986, Chapter 9 and 11.
  31. *Design Handbook for Sonar Installations*, U.S. Naval Underwater Systems Center, TD 6059, undated.
  32. *Design Data Sheet. Ship Damping and Special Acoustic Materials*, Bolt Beranek and Newman, DDS-636-1, 1980.
  33. D. L. Nelson, *Main Propulsion Gas Turbine Exhaust Noise*, Bolt Beranek and Newman, TM-339, Cambridge, MA, February 1977.
  34. L. Boroditsky and R. Fischer, Direct Acoustic Field of a Finite Size Source, InterNoise 04, Institute of Noise Control Engineers, Prague, Aug. 2004.
  35. R. D. Collier, *Noise Control Materials and Application*, Bolt Beranek and Newman, Cambridge, MA, Report No. 6637, 1987.
  36. L. Beranek, Ed., *Noise and Vibration Control*, McGraw-Hill, New York, 1971.
  37. I. Ver, Reduction of Noise by Acoustic Enclosures, in Isolation of Mechanical Vibration, Impact, and Noise, ASME Colloquium, ASME Design Engineering Technical Conference, Cincinnati, OH, 1973.

**PART X**

---

**NOISE AND VIBRATION  
CONTROL IN BUILDINGS**

# CHAPTER 102

## INTRODUCTION – PREDICTION AND CONTROL OF ACOUSTICAL ENVIRONMENTS IN BUILDING SPACES

Louis C. Sutherland  
27803 Longhill Drive  
Rancho Palos Verdes, California

### 1 INTRODUCTION

The prediction of the acoustical and vibration environments in buildings must take into account acoustic, vibration, and seismic sources and wind excitation. Descriptors are commonly used to assess the environment both inside and outside of buildings. Practical details are needed to make the engineering analyses of these noise and vibration environments.

In providing suitable acoustical environments in buildings, it is important to evaluate the sound fields inside the building spaces through prediction and measurement. The control of the sound fields is primarily achieved by the acoustical treatment of the room surfaces. The control of noise in commercial, industrial, and residential buildings from external noise sources such as traffic and internal sources such as heating, ventilation, and air-conditioning (HVAC) and plumbing systems is also a matter of concern. Such control measures include the reduction of noise transmission from these external sources through the building shell and the evaluation and control of noise at the source from internal equipment. The special low-frequency problems associated with noise and vibration from wind and seismic loads on buildings need also to be addressed in providing satisfactory noise environments inside these buildings.

### 2 SOUND FIELDS AND REVERBERATION IN BUILDING SPACES

Sound fields in building spaces are distinguished by their spatial and temporal variations. The spatial pattern of sound fields in a room varies with the ratio of characteristic room dimensions to sound wavelengths, with the distance from sound source to receiver, and with the room shape. When the ratio of characteristic room dimensions to sound wavelength is much less than 10, the sound field will tend to be characterized by deterministic (sinusoidal) spatial variation of sound pressure levels in discrete room modes. At higher frequencies (shorter wavelengths), the sound field is usually described in statistical terms and can contain many such room modes, each covering a narrow frequency range corresponding to the resonance bandwidth of the mode. Such a sound field is often described as diffuse and may have a fairly uniform spatial distribution of sound pressure

levels. However, this description may not apply for rooms that are long and narrow such as corridors or other similarly shaped rooms with one dominant dimension.

The sound field inside a room is a composite of the *direct sound* from interior sources or from sound transmitted into the room and the *reverberant field*. The latter is comprised of all the sound remaining in the room after the first reflections from room surfaces. This characterization is especially meaningful for rooms with an approximately diffuse sound field. The magnitude of the direct sound field relative to that of the reverberant field plays a vital role in assessing the suitability of the room for various applications, such as for speech or music presentations or for environmental noise control design in industrial spaces. For the former, emphasis is usually placed on maximizing the ratio of direct to reverberant sound while control of the reverberant sound may be more critical for industrial work spaces.

The temporal variation in speech sounds in a room depends on the room reverberation or *room echo*. Biblical admonitions in Exodus 26(7) to "... make curtains of goats hair to be covering upon the tabernacle" and the guidance by the Roman architect, Vitruvius to "... choose a site in which the voice may fall smoothly, and not be returned by reflection so as to convey an indistinct meaning"<sup>1</sup> are early examples of concern about acoustical treatment and reverberation in buildings well before room acoustics was understood. The first scientific study of room reverberation was carried out by Wallace Sabine in his pioneering study to correct the room acoustics of a lecture room at Harvard University.<sup>2</sup> By careful observations over 3 years of experiments on how the reverberation time in the room changed as the number of seat cushions were changed, Sabine was able to derive a basic relationship between the reverberation time, room volume, and the total acoustical absorption over the room surfaces. This relationship, known as the Sabine equation [Eq. (22) in Chapter 103] has been refined by alternate forms identified in Chapter 104 as the Norris–Eyring and the Millington–Sette equations for higher accuracy when the average sound absorption coefficient over the room surfaces is small ( $<0.4$ ). When the acoustical absorption treatment is very nonuniform over the room surfaces, or the room is very long or narrow (e.g., a non-Sabine room),<sup>2</sup> a further refinement is provided by



the Fitzroy or Fitzroy–Kuttruff equations described in Chapter 104. Nevertheless, the simple Sabine equation is often still used for approximate room acoustics evaluations. All of these expressions provide a measure of the room reverberation in terms of its reverberation time,  $RT_{60}$ , the time required for a sound that is suddenly turned off to decay by 60 dB.

One topic addressed briefly in this chapter is the spatial decay in the sound field in small office or conference rooms or in industrial spaces—all of which contain a large number of furnishings or machinery. Sound scattering by these objects causes the sound field from a single source to decay with distance in a manner not predicted by diffuse field theory [Eq. (6) in Chapter 104]. This anomalous decay with distance of the total sound field was found, empirically, by Schultz to have a decay rate of  $-3$  dB/double distance (DD) for a wide range of small furnished spaces.<sup>3</sup> In contrast, diffuse field theory dictates that the decay should be  $-6$  dB/DD close to the source and then reach a constant value in the reverberant field of the source. Similarly, Hodgson has found the decay in the total sound field in industrial halls to fall well below this asymptotically zero rate of decay far from a source as dictated by diffuse field theory (see Ref. 7 in Chapter 104).

Chapter 104 also briefly treats sound absorption in the air, which is important in large rooms at high frequencies, especially at high temperatures and low relative humidity. The end of the chapter reviews the important aspects of the design of various forms of porous acoustical absorbing materials best suited for high frequencies and flexible panel absorbers better suited for low frequencies.

### 3 NOISE RATINGS AND DESCRIPTORS FOR BUILDING AND OUTDOOR ACOUSTICAL ENVIRONMENTS

The various ratings and descriptors considered in Chapters 105 to 115 are used for a wide range of acoustical environment problems. These include establishing noise control design goals for internal building structure or equipment components, the exterior structural shell, or for land-use planning guidelines. They also include assessment of environmental impact or acceptability of both outdoor and indoor noise environments or assessment of the suitability of indoor acoustical environments for speech communication. More specifically, these chapters treat ratings and descriptors for:

- Acoustical performance of building components for laboratory or field measurements (Chapters 105 and 106)
- Acceptable noise environments in offices for activity involving speech privacy and speech communication requirements (Chapters 109 and 110)
- Building assemblies for building codes to achieve required sound isolation (Chapter 110)
- Rating or noise control design of building equipment and services such as HVAC (Chapters 111 and 113)

- Acceptable noise environments inside residences to avoid annoyance (Chapter 114)
- Acceptable noise environments inside industrial or commercial buildings to avoid annoyance (Chapter 115)
- Outdoor environments from any outdoor noise source or from specific noise sources such as highway traffic relative to annoyance criteria (Chapters 114 and 115)

The wide application of these descriptors makes in unavoidable that they be also applied in many other chapters in this handbook. For example, noise descriptors needed to assess industrial plant noise environments for hearing conservation concerns (see Chapter 36), apply some elements of descriptors utilized for evaluation of industrial or commercial noise environments.

All of the descriptors share one element in common—they incorporate some measure of the frequency content of the acoustical environment being evaluated. This may be through use of a frequency weighting, such as an A-weighting for measurement of an A-weighted sound pressure level by a sound level meter that incorporates an A-weighting frequency response in its measurement system. Alternatively, frequency content of a sound may be assessed by matching its octave band spectrum to a fixed set of octave band spectrum shape contours to define its noise rating—for example, a noise criterion (NC) value. A similar spectrum contour matching process is employed to establish a sound transmission class (STC) or impact isolation class (IIC) of the airborne or structure-borne sound transmission loss of a structural assembly measured by one-third octave band values of sound transmission loss.

One important refinement for such frequency-dependent descriptors is in the evaluation of speech privacy—an important measure of the suitability of an office space for productive work. In this case, the speech privacy index (SPI) is the sum of the frequency-dependent (A-weighted) noise reduction (NR) and the noise criterion (NC) rating. These and other forms of frequency-dependent descriptors are discussed in Chapter 109.

For time-varying (usually outdoor) noise environments, an energy average of the noise level is normally employed to provide a single number value, such as an A-weighted day–night average sound pressure level (DNL). This process provides a practical means of assessing acceptability of fluctuating noise environments over a fixed time period.

### 4 SOUND TRANSMISSION IN BUILDINGS

Sound transmission within a building occurs by transmission through the air in the spaces bounded by walls or roof/ceiling assemblies or by structural transmission through these assemblies. Chapter 105 provides an overview of theory and measurements of sound transmission in buildings based on the chapter author's years of experience with NRC in Canada in laboratory measurements of airborne and structure-borne sound transmission through building wall and

floor/ceiling assemblies. Chapter 105 is supported with a list of 69 references emphasizing measured data. (A periodically updated source for such sound transmission data is also provided by Ref. 4 in Chapter 105). Key elements treated in this chapter are briefly reviewed here.

#### 4.1 Airborne Sound Transmission

For the simplest case of a solid single-leaf wall with very low stiffness, the transmission of airborne sound through the wall roughly follows the so-called mass law. That is, the sound transmission loss increases in direct proportion to the surface mass of the wall and the frequency of the incident sound. Theoretically, doubling the surface mass or the frequency increases the wall sound transmission loss (STL) by 6 dB. While this simple mass law does, in fact, describe a general trend in STL for many constructions, there are many important deviations from this simple model. These include the dip in the mass law transmission loss at the so-called coincidence frequency of the wall, typically in the range of 2000 to 5000 Hz, where the trace wavelength of the incidence sound wave matches the structural bending wavelength of the wall. Other important deviations from the mass law occur, for double-leaf walls, at the mass–airspace–mass resonance frequency (generally below 200 Hz) of the double-leaf system and the simple acoustical resonance frequencies (typically in the range of 2000 to 3000 Hz) for the air gap between the wall leaves. The sound transmission loss of a composite wall must also consider the sound transmission loss of each of the fenestrations, such as windows and doors, combined with that of the basic wall.

#### 4.2 Structural or Impact Sound Transmission

Transmission of impact sound through a floor–ceiling assembly, quantified by a single number impact insulation class (IIC), is obtained from measurements using a standard impact source (tapping machine). It is strongly dependent on structural details of the assembly, including any floor covering. In this respect, a misleadingly high IIC rating can be obtained when carpeting is employed on the same floor driven by the tapping machine. While beneficial for reducing impact noise, such as heel clicks, the actual impact noise reduction may not be as high as indicated by the IIC rating. Measured IIC ratings are provided by many of the references in Chapter 105 and in Ref. 4 of this chapter.

An important factor to be considered in evaluating transmission of airborne and structure-borne sound through a structure is the occurrence of flanking transmission paths. These can short-circuit the intended transmission path to reduce its effectiveness.

### 5 PREDICTION AND CONTROL OF NOISE AND VIBRATION FROM BUILDING EQUIPMENT

The application of the various descriptors considered in Section 3 is especially important in evaluation of interior sources of noise and vibration in buildings and determination of methods for their control.

#### 5.1 Heating, Ventilation, and Air-Conditioning Systems

A dominant interior noise source in most buildings is the heating, ventilation, and air-conditioning equipment. Methods for noise assessment and control are reviewed in Chapters 110 and 111, in the references cited therein, and in many similar sources.<sup>5–7</sup> HVAC noise control cannot always invoke the classical *source–path–receiver* noise control model. In this case, the source cannot always be isolated to just one location. HVAC noise can arise from several sources: the circulation fan and its motor, the air-conditioning compressor and its motor, the aeroacoustic noise generated by turbulence in the ventilation duct system, and by turbulence-generated noise at the duct diffuser or outlet. Each of these sources are amenable to noise control measures by several methods. These include selection of low-noise fan designs, that is, fans that minimize the rate of change of momentum of the air through the fan blades, minimization of turbulence in the ducts by use of aerodynamically smooth turning vanes at duct elbows or by reducing discharge airflow rates at the outlet diffuser. An important factor in such aeroacoustic noise control measures is that for such sources, sound intensities can vary as the (turbulent) air velocity to the fourth to eighth power, depending on the aero-acoustic source mechanism. Thus, reduction of airflow velocities and minimization of turbulence in any part of the system is highly desirable.

For HVAC systems, the path most readily subject to noise control is the duct system where duct lining and duct geometry at junctions, corners, or at mixing boxes play a vital role. Vibration isolation of the moving components as well as the duct supports is also essential for good control of structurally transmitted HVAC system noise. At the diffuser or outlet, the path is really the receiving room, and appropriate sound absorption at the surfaces of the room, as discussed in Chapter 104, provide control of the reverberant sound from the HVAC diffusers.

#### 5.2 Noise Control of Other Interior Sources of Noise in Buildings

In addition to HVAC systems, other sources of building equipment noise can include steam turbines, transformers, elevators, and plumbing systems. Prediction and noise and vibration control methods for such building services equipment are treated in Chapter 113. For open plan offices, sound masking systems to help maintain a high speech privacy index are another source of interior noise in office buildings. The design and evaluation of such systems are treated in Chapter 109.

### 6 PREDICTION AND CONTROL OF NOISE IN SINGLE- AND MULTIFAMILY HOUSING AND IN COMMERCIAL AND PUBLIC BUILDINGS

The control of ambient noise inside single-family dwellings, other than from occupants, is treated in Chapter 114 primarily in terms of noise intrusion from outdoor sources such as highway traffic or aircraft.

Thus, the focus is on noise isolation provided by the exterior building shell. This necessarily also draws on the noise control and noise rating concepts considered earlier in this part.

For multifamily housing, in addition to noise control for these external sources, primary emphasis is normally placed on noise isolation between dwelling units—either units on the same floor separated by a part wall or one above the other separated by a floor-ceiling system. In this case, the noise source may be loud conversation or TV in one room adjacent to a bedroom of another dwelling, heel impacts on the floor above this bedroom, or annoying plumbing noise heard in an adjacent apartment. Litigation by angry apartment dwellers against the builder or developer of multifamily dwellings that have failed to incorporate adequate airborne or structure-borne noise isolation between dwellings is all too common. One of the causes of such problems is the systematic failure of developers, building designers, and building construction trades to recognize or appreciate the many airborne and structure-borne paths that building sounds can take between different parts of an apartment building. Remedial action to correct such shortcomings is invariably very expensive for all concerned—far more expensive than the initial cost of proper noise and vibration control design that is correctly executed. Laboratory test data and advanced analytical design methods, including statistical energy analysis (SEA) and finite element models (FEM) are available to support the design effort called for by the noise and vibration control problems addressed in this section.

The control of ambient noise inside commercial and industrial buildings is covered in Chapter 115 in terms of noise intrusion from outdoor sources such as traffic or aircraft, as in Chapter 114, and requirements for both noise isolation for exterior and interior walls and reverberation times for interior spaces for various uses. The focus is on specific design specifications covering these problems. Again, this draws on the noise control and noise rating concepts considered earlier.

## 7 ATYPICAL NOISE AND VIBRATION IN BUILDINGS

A few special problems in building noise and vibration are treated in the last three chapters in this part X.

### 7.1 Noise and Vibration Induced by Wind

As high-rise buildings with curtain walls and/or aerodynamically shaped surfaces become more common, wind-induced vibration of such buildings has become more significant. Dynamic (time-varying) wind loads on buildings, treated in Chapter 116, usually depend on the magnitude and fluctuating nature of the wind, its vertical profile (dependent on ground roughness, i.e., buildings, trees, etc.), and the type and shape of the structure being driven by the wind. The latter factors govern the aerodynamic forces attributable to the wind. Also involved may be the frequency of fluctuating forces induced by structural response to the wind and by vortex shedding or buffeting in the wake of the wind

incident on the structure. One classic example of such wind-induced dynamic loads is the catastrophic collapse of the 470-m-long Tacoma Narrows (suspension) Bridge near Tacoma, Washington, in November 1940. Sustained winds of only 16 to 19 m/s induced swaying vibration and finally catastrophic torsional oscillation of the deck at a frequency of 0.2 Hz.<sup>8</sup> The failure was finally attributed to aerodynamic instability as a self-excited vibration of the thin bridge deck. This deck acted much like an aircraft wing to generate sufficient lift and cause unstable torsional vibration, eventually resulting in the structural failure of the suspension system and the deck. Lessons learned from this unforeseen incident now include a requirement that such similar suspension bridges undergo model tests in a wind tunnel prior to construction. Similar tests or analyses are now common in the design of high-rise buildings.

More routine structural vibration responses to wind are considered in this chapter. These include the frequency spectrum of vortex shedding or wake buffeting forces on a structure and the gusts or random fluctuations in the velocity of wind incident on a building. For example, the peak frequency of the broad spectrum associated with vortex shedding from a cylinder-like structure is the Strouhal frequency approximately equal to about 0.1 to 0.2 times the ratio of wind speed to a characteristic dimension normal to the wind vector. When this peak in the vortex frequency spectrum is close to a resonance frequency of a structure, resonant wind-induced structural vibration may occur. Fluctuations in speed of horizontal wind also have a broad frequency spectrum extending up to about 0.2 Hz but with a peak at about 0.015 Hz,<sup>9</sup> well below resonance frequencies of buildings. However, annoying or uncomfortable wind-induced vibration of elastic building structures can occur from steady or fluctuating aerodynamic forces from the wind.<sup>10</sup> Such phenomena and other aspects of wind-induced building vibration are reviewed in Chapter 116.

### 7.2 Seismic-Induced Building Vibration

Continuing the concerns about vibration response of structures to dynamic loads, Chapter 117 considers seismic response and design of buildings to earthquakes. Related building design considerations include the frequency response of building vibration modes, their time-history response to dynamic loads, damping methods to minimize resonance response and dynamic loads, or responses of secondary building services such as plumbing and electrical services. Analytical modeling for such building responses can range from simple shock spectra analyses providing estimates of responses for mass-spring-damper models of building modes to complex finite element dynamic models capable of evaluating building vibration in great detail. A thorough overview of these approaches is provided in Chapter 117 with support by extensive references.

A critical element in the design of building for earthquakes is the establishment of a “design earthquake” spectra of ground acceleration, velocity, or displacement. These are frequently established on the basis of measured ground motion of actual earthquakes

in one location giving consideration to possible differences in soil conditions between the design and the measured sites. Support in evaluating the dynamic stress response of a structure to an earthquake could be provided by the classic relationship by Hunt.<sup>11</sup> This states that the maximum stress in a structure vibrating in one of its normal modes is proportional to what might be called its *structural Mach number*, the ratio of the maximum structural modal velocity to the longitudinal speed of sound in the structure.<sup>12</sup> The proportionality constant is the modulus of elasticity of the structure multiplied by a shape- and material-dependent factor varying from about 0.9 to 2. This relationship between structural stress and velocity helps explain the common use of a maximum structural velocity of the order of 0.05 m/s (2 in./s) as a damage threshold for structures exposed to surface mining blasts.<sup>13</sup>

### 7.3 Low-Frequency Noise in Buildings

The frequent use of low-cost, light-weight timber construction for multifamily structures and the proliferation of loud home hi-fi systems and other interior noise sources has aggravated problems in low-frequency noise environments in buildings. Test data and design methods to achieve high sound isolation in the frequency range from 400 down to 50 Hz or lower are often inadequate to eliminate the presence of annoying low-frequency noise indoors. The last chapter in Part X, Chapter 118, covers this problem, focusing on anomalies in low-frequency sound isolation measurements, the large spatial variation in sound pressure levels for discrete low-frequency room modes. It identifies practical design concepts and remedial correction measures that can be employed to minimize the problem.

### REFERENCES

1. F. V. Hunt, *Origins in Acoustics*, Yale University Press, New Haven, 1978.
2. E. A. Wetherill, Sabine's first experiment—Analysis of the acoustics of the Fogg Art Museum lecture room, in *Proceedings, Wallace Clement Sabine Centennial Symposium*, Acoustical Society of America Cambridge, MA, 1994, pp. 33–36.
3. T. J. Schultz, Relationship Between Sound Power Level and Sound Pressure Level in Dwellings and Offices, *ASHRAE Trans.*, Vol. 91, Pt 1, 1985.
4. Gypsum Association, Fire Resistance Design Manual—Sound Control, Gypsum Assoc., 810 First St. NE, Washington, DC, 2003.
5. R. M. Hoover and W. E. Blazier, Noise Control in Heating, Ventilating and Air-Conditioning Systems, in *Handbook of Acoustical Measurements and Noise Control*, C. M. Harris, Ed., McGraw-Hill, New York, 1991, pp. 42–1 to 42.31.
6. M. E. Schaffer, A Practical Guide for Noise and Vibration Control for HVAC Systems, *ASHRAE Trans.*, Vol. 97, Part 1, 1991, pp. 354–358.
7. M. E. Schaffer, Sound and Vibration Control, in *ASHRAE Handbook—HVAC Applications*, ASHRAE, Atlanta, GA, 2003, Chapter 47.
8. T. Irvine, The Tacoma Narrows Bridge Failure, Revision A, 1999. (See websites: [www.vibrationdata.com/Tacoma.htm](http://www.vibrationdata.com/Tacoma.htm) for a definitive description of the nature and cause of the bridge failure and [www.rwdi.com/aspx/pub/Misc/MiscPage.aspx?pg=116](http://www.rwdi.com/aspx/pub/Misc/MiscPage.aspx?pg=116) for graphic portions of the unique movie taken of the bridge collapse.)
9. I. van der Hoven, Power Spectrum of Horizontal Wind Speed in the Frequency Range of 0.0007 to 900 Cycles per Hour ( $2 \times 10^{-7}$  to 0.25 Hz), *J. Meteorol.*, Vol. 14, 1957, pp. 160–164.
10. W. A. Dalglish and D. W. Boyd, Wind on Buildings, in *Canadian Building Digest*, CBD-28, NRC Institute for Research in Construction, Ottawa, Ontario, Canada, 1962.
11. F. V. Hunt, Stress and Strain Limits on the Attainable Velocity in Mechanical Vibration, *J. Acoust. Soc. Am.*, Vol. 32, 1960, pp. 1123–1128.
12. L. C. Sutherland, R. Brown, and D. Goerner, Evaluation of Potential Damage to Unconventional Structures to Sonic Booms, HSD-TR-90-021, Human Systems Division, Air Force Systems Command, Brooks Air Force Base, TX, 1990.
13. D. E. Siskind, M. S. Stagg, J. W. Kupp, and C. H. Dowding, Structural Response and Damage Produced by Ground Vibration from Surface Mine Blasting, Bureau of Mines Report of Investigations, RI 8507, U.S. Dept. of the Interior, Washington, DC, 1980.

# CHAPTER 103

## ROOM ACOUSTICS

Colin H. Hansen  
School of Mechanical Engineering  
University of Adelaide  
Adelaide, South Australia, Australia

### 1 INTRODUCTION

The acoustics of rooms can be divided into low- and high-frequency regions. Sound in rooms is strongly affected by the reflective properties of the room surfaces. When the room surfaces are highly reflective, multiple reflections occur, and in the high-frequency range, a reverberant field will be established in addition to the direct field from the source. Thus, at any point in such a room, the overall sound pressure level is a function of the energy contained in the direct and reverberant fields.

At low frequencies, where the ratio of the wavelength to room dimension is greater than about 0.1 and where there are relatively few acoustic modes resonant in an octave band, the sound field may be described in terms of a superposition of sound fields corresponding to each normal mode in the frequency range of interest as well as modes immediately outside the frequency range of interest. However, the number of acoustical resonances in a room increases very rapidly as the frequency of excitation increases. Consequently, in the high-frequency range, the possible resonances become so numerous that they cannot be distinguished from one another. Thus, in terms of total energy density (but not sound pressure), the sound field in the regions away from the source (reverberant field) becomes relatively uniform. In this frequency range, the resulting sound field is essentially diffuse and may be described in statistical terms or in terms of average properties.

A room used for assembly and general living and in which one dimension does not exceed any other by more than a factor of 3 is generally referred to as a Sabine enclosure, named after the man who initiated investigation of the acoustical properties of such rooms. Rooms in which one dimension is much

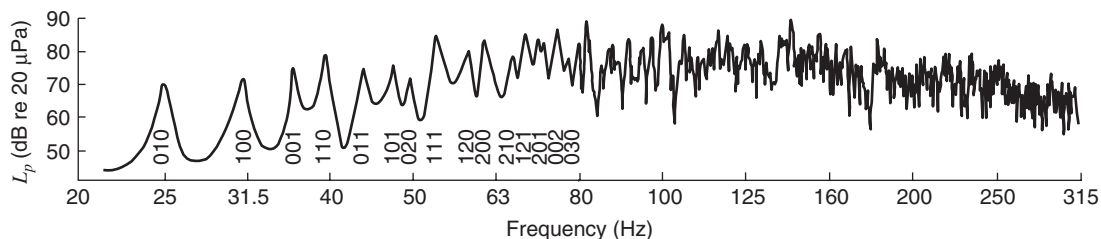
smaller than the other two are called flat rooms and are characteristic of many industrial facilities.

### 2 WAVE ACOUSTICS AND NORMAL MODES

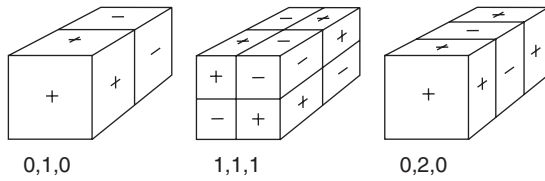
The following sections on room acoustics are by necessity brief. For more detailed discussions, including practical applications, textbooks on the subject should be consulted.<sup>1-4</sup>

In the low-frequency range, the sound field in an enclosure is dominated by standing waves at certain characteristic frequencies. Large spatial variations in the reverberant sound field are observed if the enclosure is excited with pure-tone sound, and the sound field in the enclosure is said to be dominated by resonant or modal response. This is illustrated in the low-frequency range of Fig. 1, which shows the sound pressure level measured at a microphone in the corner of the room as the room was excited by a loudspeaker in another corner. The electrical signal into the speaker was sinusoidal and was kept at a constant amplitude while the frequency was slowly increased. In this example, the room was a rectangular reverberation chamber with concrete walls having very low values of absorption coefficient. The room volume was 180 m<sup>3</sup> and the surface area was 200 m<sup>2</sup>. The mode numbers identified on the figure refer to the number of nodes (planes of sound pressure minima or theoretically zero sound pressure) in the standing-wave pattern along each of the Cartesian axes. Thus "0,1,0" refers to one planar node in the y direction (in the center of the room) and no nodes in the other two directions. Some mode shapes for a rectangular room are illustrated in Fig. 2.

When a source of sound in an enclosure is turned on, the resulting sound waves spread out in



**Figure 1** Measured sound pressure level frequency response of a 180-m<sup>3</sup> rectangular room. Below 80 Hz, room resonances are identified by mode numbers. Above about 80 Hz, peaks in the room response cannot be associated with room resonances identified by mode numbers.



**Figure 2** Some low-order mode shapes of a rectangular room. The plus and minus signs represent the phase of the sound pressures. Plus is 180° out of phase with minus.

all directions from the source. When the advancing sound waves reach the walls of the enclosure, they are reflected, generally with a small loss of energy, eventually resulting in waves traveling around the enclosure in all directions. If each path that a wave takes is traced around the enclosure, there will be certain paths of travel that repeat upon themselves to form normal modes of vibration, and at certain frequencies, waves traveling around such paths will arrive back at any point along the path in phase. Amplification of the wave disturbance will result and the normal mode will be resonant. When the frequency of the source equals one of the resonance frequencies of a normal mode, resonance occurs and the interior space of the enclosure responds strongly, being only limited by the absorption present in the enclosure. As waves traveling along the same path but in opposite directions produce standing waves, a normal mode may be characterized as a system of standing waves, which in turn is characterized by nodes and antinodes. Where the oppositely traveling waves arrive in pressure antiphase, pressure cancellation will occur, resulting in a pressure minimum called a node. Similarly, where the oppositely traveling waves arrive in pressure phase, pressure amplification will occur, resulting in a pressure maximum called an antinode.

In an enclosure at low frequencies, the number of resonance frequencies within a specified frequency range will be small. Thus, at low frequencies, the response of a room as a function of frequency and location will be quite irregular; that is, the spatial distribution in the reverberant field will be characterized by pressure nodes and antinodes.

A rectangular room provides a convenient model for understanding modal response and the placement of sound absorbents for sound control. However, it should be emphasized that modal response is by no means peculiar to rectangular or even regular-shaped rooms. Modal response characterizes enclosures of all shapes. Splayed, irregular, or odd numbers of walls will not prevent resonances and accompanying pressure nodes and antinodes in an enclosure constructed of reasonably reflective walls; nor will such peculiar construction necessarily result in a more uniform distribution in frequency of the resonances of an enclosure than may a rectangular room of appropriate dimensions. However, it is simpler to calculate the resonance frequencies and mode shapes for rectangular rooms.

For sound in a rectangular enclosure, the resonance frequency of the  $n$ th mode is given by<sup>1</sup>

$$f_n = \frac{c}{2} \sqrt{\left(\frac{n_x}{L_x}\right)^2 + \left(\frac{n_y}{L_y}\right)^2 + \left(\frac{n_z}{L_z}\right)^2} \quad (\text{Hz}) \quad (1)$$

In this equation the subscript  $n$  on the frequency variable  $f$  indicates that the particular solutions or “eigen”-frequencies of the equations describing the sound field in the room are functions of the particular mode numbers  $n_x$ ,  $n_y$ , and  $n_z$ , and  $c$  is the speed of sound in the room space. The sound pressure distribution for the  $n$ th mode can be shown to be

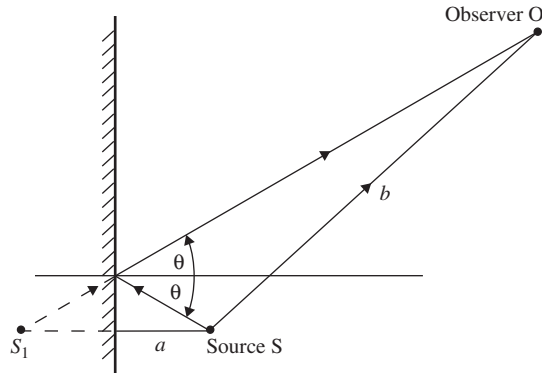
$$p_n = \bar{p}_n \cos\left(\frac{\pi n_x x}{L_x}\right) \cos\left(\frac{\pi n_y y}{L_y}\right) \cos\left(\frac{\pi n_z z}{L_z}\right) e^{j\omega t} \quad (2)$$

The mode numbers  $n_x$ ,  $n_y$ , and  $n_z$  take on all positive integer values including zero, and the bar over the  $p$  represents a modal amplitude (time and space invariant). There are three types of normal modes of vibration in a rectangular room, which have their analogs in enclosures of other shapes. They may readily be understood as follows:

1. Axial modes for which only one mode number is not zero, which correspond to wave travel back and forth parallel to an axis of the room
2. Tangential modes for which one mode number is zero, which correspond to waves traveling essentially parallel to two opposite walls of an enclosure while successively reflecting from the other four walls
3. Oblique modes for which no mode number is zero, which correspond to wave travel oblique to all room surfaces

### 3 GEOMETRIC ACOUSTICS AND SOUND FIELD MODELING

In the field of architectural acoustics, there are a number of commercially available software packages that are used for modeling the enclosed sound field for the purpose of predicting sound pressure level distributions and reverberation time. These packages are primarily based on ray tracing and geometric acoustics. As a convenience in the modeling process, specular reflection of sound from a surface is modeled by assuming an additional sound source being located as far behind the surface as the original source is in front, as illustrated in Fig. 3. When the reflecting surface absorbs some of the incident energy, the image source is made weaker by the appropriate amount. The ratio of absorbed energy to incident energy is referred to as the absorption coefficient of the surface and is related to the surface construction and covering material. In many instances in auditoria, sound is not reflected from the room surfaces specularly. It is scattered and the reflection is considered diffuse. In this case, the modeling software assumes a new source to be located on the reflecting surface and radiating energy in all directions



**Figure 3** Geometry illustrating reflection from a plane rigid surface.

so that the total radiated energy is the incident energy multiplied by  $(1 - \alpha)$ , where  $\alpha$  is the surface absorption coefficient. Computer modeling is discussed in more detail in manuals available from software vendors and textbooks.<sup>5</sup>

#### 4 BOUND BETWEEN LOW-FREQUENCY AND HIGH-FREQUENCY BEHAVIOR

There is a need for a quantitative definition for the crossover from the low-frequency range, where modal analysis is appropriate, to the high-frequency range, where statistical analysis is appropriate. Reference to Fig. 1 provides no clear indication of a possible bound from clearly distinguishable resonance peaks to where the individual resonance peaks cannot be separated. Rather, a continuum of gradual change is observed. However, it is possible to determine a bound analytically, but to understand the determination of the bound, called here the crossover frequency, three separate concepts are required: modal density, modal damping, and modal overlap.

##### 4.1 Modal Density

The number of modes,  $N$ , which may be excited in the frequency range from zero up to  $f$  is given by the following expression<sup>5</sup>:

$$N = \frac{4\pi f^3 V}{3c^3} + \frac{\pi f^2 S}{4c^2} + \frac{fL}{8c} \quad (3)$$

In Eq. (3),  $c$  is the speed of sound,  $V$  is the room volume,  $S$  is the room total surface area, and  $L$  is the total perimeter of the room. In a rectangular room the latter quantity is the sum of lengths of all edges. It has been shown that Eq. (3) has wider application than for rectangular rooms; to a good approximation it describes the number of modes in rooms of any shape.

For the purpose of estimating the number of modes that, on average, may be excited in a narrow frequency band, the derivative of Eq. (3), called the modal density, is useful. The expression for the modal density

is as follows:

$$\frac{dN}{df} = \frac{4\pi f^2 V}{c^3} + \frac{\pi f S}{2c^2} + \frac{L}{8c} \quad (4)$$

Equation (4) shows that the modal density increases with the square of the frequency, so that at high frequencies many modes will be excited by a narrow frequency band of noise. It is evident that at high frequencies the number of oblique modes [term 1 in Eq. (4)] will far exceed the number of tangential and axial modes, and to a good approximation at high frequencies the latter two mode types may be ignored.

##### 4.2 Modal Damping and Bandwidth

Referring to Fig. 1, a bandwidth,  $\Delta f$ , may be defined and associated with each mode, being the frequency range about resonance over which the sound pressure level is within 3 dB of the peak value at resonance. The lower and upper frequencies bounding a resonance and defined in this way are known as the half-power points and are easily isolated for the first few modes (see Fig. 1).

The bandwidth,  $\Delta f$ , is dependent upon the damping of the mode; the greater the modal damping, the larger will be the bandwidth. If the modes are not well separated, the bandwidth can be estimated from the modal damping, which in turn can be estimated from the room reverberation time,  $T_{60}$ , using<sup>1</sup>:

$$\Delta f = 2.20/T_{60} \quad (5)$$

where  $T_{60}$  is the time it takes for sound in the room to decay by 60 dB following cessation of the source of sound.

##### 4.3 Modal Overlap

Modal overlap,  $M$ , is calculated as the product of the average bandwidth given by Eq. (5), and the modal density given by Eq. (4). Thus,

$$M = \Delta f dN/df \quad (6)$$

The modal overlap is a measure of the extent to which the resonances of a reverberant field cover the range of all possible frequencies within a specified frequency range. The concept is illustrated for a hypothetical case of a low modal overlap of 0.6 in Fig. 4. In the figure, three resonant modes, their respective bandwidths, and the frequency range of the specified frequency band are indicated.

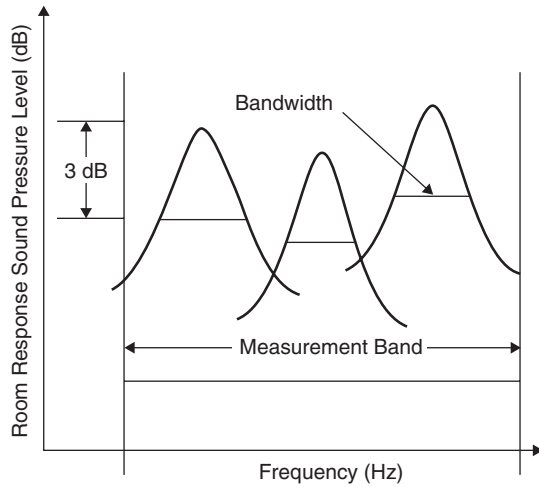
In Fig. 4, the measurement band is 100 Hz wide and the bandwidth of each mode (3 dB down from the peak response) is 20 Hz.

##### 4.4 Crossover Frequency

There are two criteria commonly used for determining the crossover frequency. The criterion that is chosen will depend upon whether room excitation with bands of noise or with pure tones is of interest.

If room excitation with one-third octave, or wider bands of noise, is to be considered, then the criterion





**Figure 4** Sound pressure level response of three modes in a specified frequency range with a modal overlap of 0.6.

for statistical (high-frequency) analysis is that there should be a minimum of between three and six modes resonant in the frequency band. The exact number required is dependent upon the modal damping and the desired accuracy of the results. More modes are necessary for low values of modal damping or if high accuracy is required. If room excitation with a pure tone or a very narrow band of noise is of concern, then the criterion for reliable statistical analysis is that the modal overlap should be greater than or equal to 3.<sup>6</sup>

## 5 HIGH FREQUENCIES, STATISTICAL ANALYSIS

At high frequencies the sound field in a reverberant space may be thought of as composed of plane waves traveling in all directions with equal probability. If the mean square pressure amplitude of any traveling plane wave is on average the same, independent of direction, then the sound field is said to be diffuse. In a reverberant space, the sound field is diffuse when the modal overlap is 3 or greater, in which case the sound field steady-state frequency response is essentially a random phenomenon.

In a diffuse (reverberant) field, sound propagation in all directions is equally likely, and consequently the sound intensity at any point in the field is zero. However, an effective intensity associated with power transmission in a specified direction can be defined, and this is the intensity incident on the walls of the room. According to Bies and Hansen,<sup>1</sup> this effective sound intensity  $I$  in any direction may be written in terms of the time-averaged energy density,  $\psi$ , as

$$I = \psi c / 4 \quad (7)$$

Bies and Hansen<sup>1</sup> derive the following expression for the time-averaged energy density in terms of the space-averaged mean square pressure,  $\langle p^2 \rangle$ , which holds for

one-, two-, and three-dimensional sound fields:

$$\psi = \langle p^2 \rangle / (\rho c^2) \quad (8)$$

where  $\rho$  is the density of the medium containing the sound field.

Substitution of Eq. (8) into Eq. (7) gives the following expression for the effective intensity in one direction a diffuse field:

$$I = \langle p^2 \rangle / (4 \rho c) \quad (9)$$

### 5.1 Steady-State Response

At any point in a room, the sound field is a combination of the direct field radiated by the source and the reverberant field.

The sound pressure squared due to the direct field at a point in the room at a distance  $r$  and in a direction  $(\theta, \phi)$ , in the far field of a source, may be written as<sup>1</sup>

$$\langle p^2 \rangle_D = W \rho c D_\theta / 4 \pi r^2 \quad (10)$$

The quantity  $D_\theta$  is the directivity factor of the source in direction  $(\theta, \phi)$ , and  $W$  is the sound power radiated by the source in watts.

Consider that the direct field must be once reflected to enter the reverberant field. The fraction of energy incident at the walls, which is reflected into the reverberant field is  $(1 - \bar{\alpha})$ , where  $\bar{\alpha}$  is the average surface absorption coefficient, representing the fraction of incident energy absorbed by the room boundaries. Using Eq. (9), and noting that the sound power incident on a surface is the area of the surface multiplied by the sound intensity, the sound pressure squared due to the reverberant field may be written as

$$\langle p^2 \rangle_R = 4 W \rho c (1 - \bar{\alpha}) / (S \bar{\alpha}) \quad (11)$$

The sound pressure level at any point due to the combined effect of the direct and reverberant sound fields is obtained by adding together Eqs. (10) and (11) and taking 10 log of both sides (as described in more detail in Chapter 2 and in Bies and Hansen<sup>1</sup>). Thus,

$$L_p = L_w + 10 \log_{10} \left( \frac{D_\theta}{4 \pi r^2} + \frac{4}{R} \right) + 10 \log_{10} \left( \frac{\rho c}{400} \right) \quad (12)$$

At 20°C, where  $\rho c = 414$  (in the International System of Units), there would be an error of approximately 0.1 dB if the last term in Eq. (12) is omitted. The sound pressure level,  $L_p$ , is referenced to 20  $\mu$ Pa and the sound power level,  $L_w$ , is referenced to  $10^{-12}$  W. Equation (12) has been written in terms of the room constant  $R$  where the room constant is

$$R = \frac{S \bar{\alpha}}{1 - \bar{\alpha}} \quad (13)$$

In common industrial spaces, which have lateral dimensions much greater than their height, Eq. (12) underpredicts reverberant field noise levels close to the

**Table 1 Sabine Absorption Coefficients for Some Commonly Used Materials**

	Octave Band Center Frequency (Hz)					
	125	250	500	1000	2000	4000
Concert hall audience, per person seated $S\bar{\alpha}$ (m <sup>2</sup> )	0.23	0.37	0.44	0.45	0.45	0.45
Audience, per person standing $S\bar{\alpha}$ (m <sup>2</sup> )	0.15	0.37	0.43	0.44	0.44	0.43
Fiber-glass or rockwool blanket						
16 kg/m <sup>3</sup> , 25 mm thick	0.12	0.28	0.55	0.71	0.74	0.83
16 kg/m <sup>3</sup> , 50 mm thick	0.17	0.45	0.80	0.89	0.97	0.94
16 kg/m <sup>3</sup> , 75 mm thick	0.30	0.69	0.94	1.0	1.0	1.0
16 kg/m <sup>3</sup> , 100 mm thick	0.43	0.86	1.0	1.0	1.0	1.0
24 kg/m <sup>3</sup> , 25 mm thick	0.11	0.32	0.56	0.77	0.89	0.91
24 kg/m <sup>3</sup> , 50 mm thick	0.27	0.54	0.94	1.0	1.0	1.0
24 kg/m <sup>3</sup> , 75 mm thick	0.28	0.79	1.0	1.0	1.0	1.0
24 kg/m <sup>3</sup> , 100 mm thick	0.46	1.0	1.0	1.0	1.0	1.0
48 kg/m <sup>3</sup> , 50 mm thick	0.3	0.8	1.0	1.0	1.0	1.0
48 kg/m <sup>3</sup> , 75 mm thick	0.43	0.97	1.0	1.0	1.0	1.0
48 kg/m <sup>3</sup> , 100 mm thick	0.65	1.0	1.0	1.0	1.0	1.0
60 kg/m <sup>3</sup> , 25 mm thick	0.18	0.24	0.68	0.85	1.0	1.0
60 kg/m <sup>3</sup> , 50 mm thick	0.25	0.83	1.0	1.0	1.0	1.0
Polyurethane foam, 27 kg/m <sup>3</sup> 15 mm thick	0.08	0.22	0.55	0.70	0.85	0.75
Wood floor on joists	0.15	0.11	0.10	0.07	0.06	0.07
Concrete, marble or terrazzo	0.01	0.01	0.01	0.02	0.02	0.02
Concrete block painted	0.01	0.05	0.06	0.07	0.09	0.08
Linoleum, asphalt, rubber or cork tile on concrete	0.02	0.03	0.03	0.03	0.03	0.02
Carpet, heavy, on concrete	0.02	0.06	0.14	0.37	0.60	0.65
Carpet, 6 mm thick, on underlay	0.03	0.09	0.20	0.54	0.70	0.72
Cork floor tiles (3–4 inch thick) — glued down	0.08	0.02	0.08	0.19	0.21	0.22
Hard surfaces (brick walls, plaster, hard floors, etc.)	0.02	0.02	0.03	0.03	0.04	0.05
Gypsum board on 50 × 100 mm studs	0.29	0.10	0.05	0.04	0.07	0.09
Plaster, gypsum or lime,						
Smooth finish; on brick,	0.013	0.015	0.02	0.03	0.04	0.05
On concrete block,	0.012	0.09	0.07	0.05	0.05	0.04
On lath	0.014	0.10	0.06	0.04	0.04	0.03
Solid timber door	0.14	0.10	0.06	0.08	0.10	0.10
13-mm mineral tile direct fixed to floor slab	0.10	0.25	0.70	0.85	0.70	0.60
13-mm mineral tile suspended 500 mm below ceiling	0.75	0.70	0.65	0.85	0.85	0.90
Glass, heavy plate	0.18	0.06	0.04	0.03	0.02	0.02
Ordinary window	0.35	0.25	0.18	0.12	0.07	0.04

noise source and overpredicts levels far away from the source.<sup>7</sup>

In cases where there are many sources, Eq. (12) may be written as

$$L_p = L_w + 10 \log_{10} \left( \sum_1^n \frac{d_i D_i}{4\pi r_i^2} + \frac{4}{R} \right) \quad (14)$$

In the above equation the weighting factor  $d_i$  and the directivity factor  $D_i$  for the  $i$ th source have been introduced. The weighting factor is calculated as  $d_i = W_i/W$  where  $W_i$  is the sound power of the  $i$ th source and  $W$  is the arithmetic sum of all sources, both in consistent units. The directivity factor  $D_i$  may be taken as 1 for a source raised up off the floor and 2 for a source on the floor. Alternatively, if the directional properties of the source are known, then this information may be used instead. The quantities  $r_i$  are the linear distances from the assumed acoustical centers of the several sources to the point of observation.

## 5.2 Transient Response

If sound is introduced into a room, the reverberant field level will increase until the rate of sound energy introduction is just equal to the rate of sound energy absorption. If the sound source is abruptly shut off, the reverberant field will decay at a rate determined by the rate of sound energy absorption. The time required for the reverberant field to decay by 60 dB, called the reverberation time, is the single most important parameter characterizing a room for its acoustical properties. For example, a long reverberation time may make the understanding of speech difficult but may be desirable for organ recitals.

As the reverberation time is directly related to the energy dissipation in a room, its measurement provides a means for the determination of the energy absorption properties of a room. Knowledge of the energy absorption properties of a room in turn allows estimation of the resulting steady-state sound pressure level in the reverberant field when sound of a given power level is introduced. The energy absorption properties

of materials placed in a reverberation chamber may be determined by measurement of the associated reverberation times of the chamber (see Chapter 104 for details of measurement procedures), with and without the material under test in the room. The Sabine absorption coefficient, which is assumed to be a property of the material under test, is determined in this way and standards<sup>8-10</sup> are available that provide guidance for conducting these tests (see also Chapter 104). Some typical values of Sabine absorption coefficient are listed in Table 1.

At high frequencies, the reverberant field may be described in terms of a simple differential equation, which represents a gross simplification of the physical process but nonetheless gives generally useful results.

Using Eq. (7), the relation that the rate of energy absorbed by a surface is the incident intensity multiplied by the surface area and the surface absorption coefficient, and the observation that the rate of change of the energy stored in a reverberant field equals the rate of supply,  $W_0$ , less the rate of energy absorbed,  $W_a$ , gives the following result:

$$W = Vd\psi/dt = W_0 - \psi Sc\bar{\alpha}/4 \quad (15)$$

Introducing the dummy variable:

$$X = (4W_0/Sc\bar{\alpha}) - \psi \quad (16)$$

and using Eq. (16) to rewrite Eq. (15), the following result is obtained:

$$\frac{1}{X} \frac{dX}{dt} = -\frac{Sc\bar{\alpha}}{4V} \quad (17)$$

Integration of the above equation gives

$$X = X_0 e^{-Sc\bar{\alpha}t/4V} \quad (18)$$

where  $X_0$  is the initial value.

Two cases will be considered. Suppose that initially, at time zero, the sound field is nil and a source of power,  $W_0$ , is suddenly turned on. The initial conditions are time  $t = 0$  and sound pressure  $\langle p^2 \rangle_0 = 0$ . Use of Eq. (8) and substitution of Eq. (16) into Eq. (18) gives the following expression for the resulting reverberant field at any later time  $t$ :

$$\langle p^2 \rangle = \frac{4W_0\rho c}{S\bar{\alpha}} (1 - e^{-Sc\bar{\alpha}t/4V}) \quad (19)$$

Alternatively, consider that a steady-state sound field has been established when the source of sound is suddenly shut off. In this case, the initial conditions are time  $t = 0$ , sound power  $W_0 = 0$ , and sound pressure  $\langle p^2 \rangle = \langle p_0^2 \rangle$ . Again, use of Eq. (8) and substitution of Eq. (16) into Eq. (18) gives, for the decaying reverberant field at some later time  $t$ :

$$\langle p^2 \rangle = \langle p_0^2 \rangle e^{-Sc\bar{\alpha}t/4V} \quad (20)$$

Taking logarithms to the base 10 of both sides of Eq. (20) gives the following:

$$L_{p0} - L_p = 1.086Sc\bar{\alpha}t/V \quad (21)$$

Equation (21) shows that the sound pressure level decays linearly with time and at a rate proportional to the Sabine absorption  $S\bar{\alpha}$ . It provides the basis for the measurement and the definition of the Sabine absorption coefficient  $\bar{\alpha}$ .

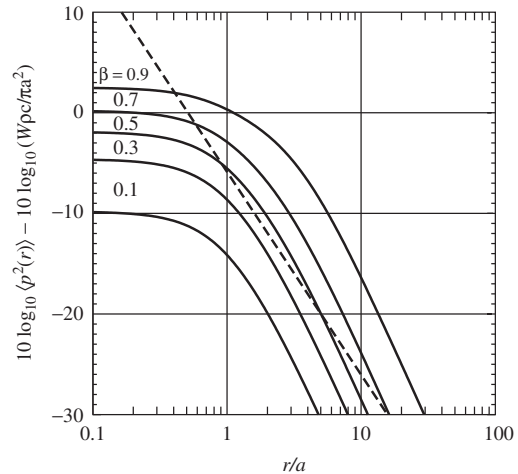
Sabine introduced the reverberation time,  $T_{60}$  (seconds), as the time required for the sound energy density level to decay by 60 dB from its initial value. He showed that the reverberation time,  $T_{60}$ , was related to the room volume,  $V$ , the total wall area including floor and ceiling,  $S$ , the speed of sound,  $c$ , and an absorption coefficient,  $\bar{\alpha}$ , which was characteristic of the room and generally a property of the bounding surfaces. Sabine's reverberation time equation, which follows from Eqs. (20) and (21) with  $L_{p0} - L_p = 60$ , may be written as follows:

$$T_{60} = \frac{55.25V}{Sc\bar{\alpha}} \quad (22)$$

Measurement of the reverberation time is discussed in Chapters 43 and 104. There is also special-purpose equipment and special functions on some general-purpose instrumentation to allow semiautomatic measurements.

## 6 FLAT ROOMS

Many factories are large laterally compared to their height, and for these the reverberant field will steadily decay as the distance from the sound source increases. In Chapter 7 of Bies and Hansen,<sup>1</sup> flat rooms with a



**Figure 5** Direct and reverberant sound fields in a flat room of height  $a$  with diffusely reflecting floor and ceiling as a function of the normalized distance from source to receiver. The reverberant field contribution is shown as a function of the energy reflection coefficient,  $\beta$ , assumed the same for floor and ceiling. The direct field is indicated by the dashed diagonal straight line.

range of different surface conditions as well as tunnels are discussed. Here, only flat rooms with diffusely reflecting surfaces are discussed as this is a good model for most factory situations where there is often pipework on the ceiling and machinery on the floor to scatter the incident sound. Determination of effective surface reflection coefficients generally requires an empirical approach. For noise control purposes, the proposed model is useful in spite of the difficulty in determining surface reflection coefficients, as it provides the basis for determining the effectiveness of the introduction of measures designed to reduce the floor and/or ceiling reflection coefficients. Based on the work of Kuttruff<sup>11</sup> and the analysis in Bies and Hansen,<sup>1</sup> the reverberant and direct sound fields in a flat room with a diffusely reflecting floor and ceiling may be represented as in Fig. 5, where the direct and reverberant fields are shown separately as a function of distance,  $r$  from the source for different values of surface reflection coefficient. The ordinate axis represents the sound pressure squared (either reverberant or direct), normalized with respect to the source sound power and the room height squared.

## REFERENCES

1. D. A. Bies and C. H. Hansen, *Engineering Noise Control: Theory and Practice*, Spon Press, London, 2003, Chapter 7.
2. A. Lawrence, *Architectural Acoustics*, Elsevier Science, Oxford, UK, 1970.
3. H. Kuttruff, *Room Acoustics*, 4th ed., Spon Press, London, 2000.
4. P. M. Morse and R. H. Bolt, Sound Waves in Rooms, *Rev. Mod. Phys.*, Vol. 16, 1944, pp. 65–150.
5. Z. Maekawa and P. Lord, *Environmental and Architectural Acoustics*, Spon Press, London, 1994.
6. M. R. Schroeder, Effect of Frequency and Space Averaging on the Transmission Responses of Multimode Media, *J. Acoust. Soc. Am.*, Vol. 46, 1969, pp. 277–283.
7. M. Hodgson, When Is Diffuse-Field Theory Accurate? Proceedings of the Wallace Clement Sabine Symposium, Cambridge, MA, 1994, pp. 157–160.
8. AS1045–1988. Acoustics: Measurement of Sound Absorption in a Reverberation Room, Standards Association of Australia, Sydney, Australia, 1988.
9. ASTM C423-99a, Standard Test Method for Sound Absorption and Sound Absorption Coefficients by the Reverberation Room Method, ASTM, Philadelphia, 1999.
10. ISO 354—1985, Acoustics: Measurement of Sound Absorption in a Reverberation Room, ISO, Geneva, Switzerland, 1985.
11. H. Kuttruff, Stationäre Schallausbreitung in Flachräumen, *Acustica*, Vol. 57, 1985, pp. 62–70.

# CHAPTER 104

## SOUND ABSORPTION IN ROOMS

Colin H. Hansen  
School of Mechanical Engineering  
University of Adelaide  
Adelaide, South Australia, Australia

### 1 INTRODUCTION

The sound absorption coefficient of a material is the fraction of the sound energy absorbed by the material compared with the sound energy incident. Sound in an enclosed space is strongly affected by the absorptive properties of the enclosing surfaces and any other objects in the room. Sound absorption in enclosures plays an important part in the determination of sound pressure levels resulting from the operation of interior and exterior sound sources of known sound power output, as well as in determining the amount of reverberation or “liveliness” of the enclosure, which is quantified in terms of its reverberation time. From knowledge of the sound absorption in an enclosure, obtained from estimations of the acoustical properties of the surfaces or from measurements of the reverberation time, one can calculate the effect of absorption on the sound pressure level, created by a sound source, in an enclosure. Relationships have been developed between sound absorption, acoustic impedance, and flow resistance for acoustically absorptive materials.

### 2 ENERGY ABSORPTION AT BOUNDARIES OF AN ENCLOSURE

The following sections on sound absorption in rooms are by necessity brief. For more detailed discussion, relevant books and standards should be consulted.<sup>1-4</sup>

Consider a diffuse sound field in an enclosure and suppose that a fraction of the incident energy is absorbed upon reflection at the enclosure boundaries. Let the average fraction of incident energy absorbed be  $\bar{\alpha}$ , called the Sabine absorption coefficient. Implicit in the use to which the Sabine absorption will be put is the assumption that this absorption coefficient is strictly a property that may be associated with the absorptive material. Whatever the material, this assumption is not strictly true; it is a useful approximation that makes tractable an otherwise very difficult problem. The concept of absorption coefficient follows from the assumption that the walls of an enclosure may be considered to be locally reactive and thus characterized by an impedance, which is a unique property exhibited by the wall at its surface and is independent of interaction between the incident sound and the wall anywhere else. The assumption is then explicit that the wall response to the incident sound depends solely on local properties and is independent of the response at other points on the surface.

The locally reactive assumption has proven very useful for architectural purposes but is apparently of very little use in predicting interior noise in aircraft and vehicles of various types. In the latter cases, the modes

of the enclosed space couple with modes in the walls, and energy stored in vibrating walls contributes very significantly to the resulting sound field. In such cases, the locally reactive concept is not even approximately true, and neither is the concept of Sabine absorption that follows from it.

### 3 AIR ABSORPTION

In addition to energy absorption on reflection, some energy is absorbed during propagation between reflections. Generally, propagation loss due to air absorption is negligible, but at high frequencies above 500 Hz, especially in large enclosures, it makes a significant contribution to the overall loss.

Air absorption may be taken into account as follows. As shown by Bies and Hansen,<sup>1</sup> the mean distance,  $\Lambda$ , traveled by a plane wave in an arbitrarily shaped enclosure between reflections, is called the mean free path and is given by

$$\Lambda = \frac{4V}{S} \quad (1)$$

where  $V$  is the room volume and  $S$  is the room surface area. Note that several other longer and more complex derivations have been published many years earlier by various authors. It will now be assumed that the fraction of propagating sound energy lost due to air absorption between reflections is linearly related to the mean free path. If the fraction lost is not greater than 0.4, then the error introduced by this approximation is less than 10% (0.5 dB).

At this point many authors write  $4m'V/S = \alpha_a$ , for the contribution due to air absorption, and they provide tables of values of the constant  $m'$  as a function of temperature and relative humidity. However, it is possible to use values of air absorption,  $m$ , in terms of decibels per 1000 m as tabulated in the International Organization for Standardization (ISO) standard, ISO 9613/1-1993. In a distance of one mean free path the attenuation of sound is

$$\frac{4mV}{S} 10^{-3} = -10 \log_{10} e^{-4m'V/S} \quad (2)$$

Let

$$4m'V/S = \alpha_a \quad (3)$$

Thus,

$$\alpha_a = 4mV/(S10^4 \log_{10} e) = 9.21 \times 10^{-4} mV/S \quad (4)$$

**Table 1 Attenuation due to Atmospheric Absorption**

Relative Humidity (%)	Temperature (°C)	<i>m</i> (dB per 1000 m)						
		63 Hz	125 Hz	250 Hz	500 Hz	1 kHz	2 kHz	4 kHz
25	15	0.2	0.6	1.3	2.4	5.9	19.3	66.9
	20	0.2	0.6	1.5	2.6	5.4	15.5	53.7
	25	0.2	0.6	1.6	3.1	5.6	13.5	43.6
	30	0.1	0.5	1.7	3.7	6.5	13.0	37.0
50	15	0.1	0.4	1.2	2.4	4.3	10.3	33.2
	20	0.1	0.4	1.2	2.8	5.0	10.0	28.1
	25	0.1	0.3	1.2	3.2	6.2	10.8	25.6
	30	0.1	0.3	1.1	3.4	7.4	12.8	25.4
75	15	0.1	0.3	1.0	2.4	4.5	8.7	23.7
	20	0.1	0.3	0.9	2.7	5.5	9.6	22.0
	25	0.1	0.2	0.9	2.8	6.5	11.5	22.4
	30	0.1	0.2	0.8	2.7	7.4	14.2	24.0

Sources: Calculated from Sutherland<sup>5</sup>; see also the relevant ISO standard.<sup>6</sup>

Using the above relation, the total mean absorption coefficient, including air absorption may be written as

$$\bar{\alpha} = \bar{\alpha}_{\text{wcf}} + 9.21 \times 10^{-4} m V / S \quad (5)$$

where  $\bar{\alpha}_{\text{wcf}}$  is the average surface absorption coefficient (walls, ceiling, and floor), representing the fraction of incident energy that is absorbed by the room boundaries. Some typical values of  $m$  are given in Table 1.

#### 4 SOUND PRESSURE LEVEL IN AN ENCLOSURE

At any point in a room or enclosure, the sound field is a combination of the direct field radiated by the source and the reverberant field. Thus, the total sound energy measured at a point in a room is the sum of the sound energy due to the direct field and that due to the reverberant field (see Chapter 103) and is

$$L_p = L_w + 10 \log_{10} \left( \frac{D_\theta}{4\pi r^2} + \frac{4}{R} \right) + 10 \log_{10} \left( \frac{\rho c}{400} \right) \quad (6)$$

In common industrial spaces, which have lateral dimensions much greater than their height, Eq. (6) underpredicts reverberant field noise levels close to the noise source and overpredicts levels far away from the source.<sup>7</sup> Equation (6) has been written in terms of the room constant  $R$  where the room constant is

$$R = \frac{S\bar{\alpha}}{1 - \alpha} \quad (7)$$

where values of Sabine absorption coefficients for areas  $S_i$  are known, perhaps by reference to a table of measured values. The mean Sabine absorption coefficient  $\bar{\alpha}$  is calculated as the area-weighted average as follows:

$$\bar{\alpha} = \sum_i^n \frac{S_i}{S} \bar{\alpha}_i \quad (8)$$

The quantity  $S_i \alpha_i$  has units of square feet or square metres, but in either case it has the name sabin. Here it will be called a metric sabin when it has the units of square metres. It is interesting to note that a seated audience in an auditorium has an absorption of about 0.45 metric sabins in the frequency range, 500 to 4000 Hz, 0.37 metric sabins at 250 Hz, and 0.23 metric sabins at 125 Hz.

The reduction in sound pressure level,  $L_p$ , in the reverberant field due to treatment with sound-absorbing material may be calculated using the following equation<sup>1</sup>:

$$\Delta L_p = 10 \log_{10} |R_f / R_i| \quad (9)$$

Here  $R_i$  is the initial value and  $R_f$  is the final value of the room constant after the addition of absorbent.

#### 5 EFFECT OF SOUND ABSORPTION ON REVERBERATION TIME

When sound is introduced into a room, the reverberant field level will increase until the sound energy introduction is just equal to the sound energy absorption. If the sound source is abruptly shut off, the reverberant field will decay at a rate determined by the rate of sound energy absorption. The time required for the reverberant field to decay by 60 dB is called the reverberation time and is the single most important parameter describing the acoustical properties of a room. The room absorption and reverberation time are related by the following equation, derived in Chapter 103:

$$T_{60} = \frac{55.3V}{Sc\bar{\alpha}} \quad (10)$$

The term,  $S\bar{\alpha}$ , is referred to as the equivalent absorption area,  $A$ , of a room and if the speed of sound,  $c$ , is set equal to 340 m/s<sup>2</sup>, Eq. (30) of Chapter 4, which is the well-known Sabine equation, is obtained. It is interesting to note that the effective Sabine absorption coefficient used to calculate reverberation times in

spaces such as typical concert halls or factories is not the same as that measured in a reverberation room,<sup>8,9</sup> which often leads to inaccuracies in predicted reverberation times. For this reason it is prudent to follow the advice given in the next section.

## 6 MEASUREMENT OF THE ROOM CONSTANT, $R$

Measurements of the room constant,  $R$ , given by Eq. (7), may be made using either a reference sound source or by measuring the reverberation time of the room in the frequency bands of interest.

### 6.1 Reference Sound Source Method

The reference sound source is placed at a number of positions chosen at random in the room to be investigated, and sound pressure levels are measured at a number of positions in the room for each source position. In each case, the measurement positions are chosen to be remote from the source, where the reverberant field of the room dominates the direct field of the source. The number of measurement positions for each source position and the total number of source positions used are usually dependent upon the irregularity of the measurements obtained. Generally, four or five source positions with four or five measurement positions for each source position are sufficient, giving a total number of measurements between 16 and 25. The room constant  $R$  for the room is then calculated using Eq. (6), excluding the direct field term, as measurements are made well away from the sound source, and rearranging the equation as follows:

$$R = 4 \times 10^{(L_w - L_p)/10} \quad (11)$$

In Eq. (11),  $L_p$  is the room average sound pressure level, measured away from the source and the enclosure walls. It is calculated using:

$$L_p = 10 \log_{10} \left[ \frac{1}{N} \sum_{i=1}^N 10^{(L_{pi}/10)} \right] \quad (\text{dB re } 20 \mu\text{Pa}) \quad (12)$$

In Eq. (11)  $L_w$  is the sound power level (dB re  $10^{-12}$  W) of the reference sound source, and in Eq. (12)  $N$  is the total number of measurements.

### 6.2 Reverberation Time Method

The second method is based upon a measurement of the room reverberation time. When measuring reverberation time in a room, the source of sound is usually a speaker driven by a random noise generator in series with a bandpass filter. When the sound is turned off, the room rate of decay is measured by using a sound level meter attached to a level recorder, which records the sound field in decibels as a function of time.

The reverberation time,  $T_{60}$ , in each frequency band is determined as the reciprocal sound pressure level decay rate obtained using the level recorder. The slope, generally measured as the best straight line fit to the recorded decay between 5 and 35 dB down from the

initial steady-state level, is used to determine the decay rate. Note that some instrumentation is capable of calculating reverberation times for all octave bands simultaneously without using a level recorder.

It is usual to employ several different microphone positions in the room, and to determine the reverberation times at each position. The value of  $T_{60}$  used in the subsequent calculations is then the average of all the values obtained for a given frequency band where Eq. (14) is used to obtain each average. Once found, the reverberation time,  $T_{60}$ , is used in Eq. (10), rearranged as follows, to calculate the room absorption. Thus,

$$S \bar{\alpha} = \frac{55.3V}{cT_{60}} \quad (\text{m}^2) \quad (13)$$

Note that when processing the data, average decay rates, not decay times, are needed! Thus, what is required is

$$\frac{1}{T_{60}} = \frac{1}{N} \sum_{i=1}^N \frac{1}{T_{60i}} \quad (14)$$

When observing reverberation decay curves (average sound pressure level versus time), it will be noted that for almost any room, two different slopes will be apparent. The steeper slope occurs for the initial 7 to 10 dB of decay, the exact number of decibels being dependent upon the physical characteristics of the room and contents. When this initial slope is extrapolated to a decay level of 60 dB, the corresponding time is referred to as the early decay time (EDT). The slope of the remainder of the decay curve, when extrapolated to 60 dB corresponds to what is commonly referred to as the reverberation time (RT). The ratio of EDT to RT as well as the absolute values of the two quantities are widely used in the design of architectural spaces. For more information see architectural acoustics books.<sup>3,10-13</sup>

## 7 MEASUREMENT OF THE SABINE ABSORPTION COEFFICIENT, $\bar{\alpha}$

Sabine absorption coefficients for materials are generally measured in a laboratory using a reverberant test chamber. Procedures and test chamber specifications are described in various standards.<sup>14-16</sup> The material to be tested is placed in a reverberant room and the reverberation time,  $T_{60}$ , is measured. The test material is removed and the reverberation time,  $T'_{60}$ , of the room containing no test material is measured next. Provided that the absorption of the reverberation room in the absence of the test material is dominated by the absorption of the walls, floor, and ceiling, the reverberation times are related to the test material absorption,  $S\bar{\alpha}$ , by the following equation [derived directly from Eq. (10)]:

$$S \bar{\alpha} = \frac{55.3V}{c} \left( \frac{1}{T_{60}} - \frac{S' - S}{S'T'_{60}} \right) \quad (\text{m}^2) \quad (15)$$

The quantity,  $S'$ , is the total area of all surfaces in the room, including the area of the material under test. Equation (15) is written with the implicit assumption that the surface area,  $S$ , of the test material is large



enough to measurably affect the reverberation time but not so large as to seriously affect the diffusivity of the sound field, which is basic to the measurement procedure. The standards recommend that  $S$  should be between 10 and 12 m<sup>2</sup> with a length-to-breadth ratio between 0.7 and 1.0.

In many cases, the absorption of a reverberation room is dominated by things other than the room walls, such as loudspeakers at low frequencies, stationary and rotating diffuser surfaces at low and midfrequencies, and air absorption at high frequencies. For this reason, the contribution of the room to the total absorption is often considered to be the same with and without the presence of the sample. In this case, the additional absorption due to the sample may be written as

$$S \bar{\alpha} = \frac{55.3V}{c} \left( \frac{1}{T_{60}} - \frac{1}{T'_{60}} \right) \quad (\text{m}^2) \quad (16)$$

Equation (16) is what appears in most current standards. Because the sample of absorbing material diffracts the sound field so that more energy falls on it than would fall on the same area of uncovered floor, it is possible to measure Sabine absorption coefficients that are in excess of 1.0, which does not make much sense as it implies that the material absorbs more sound than actually falls on it.

The measured value of the Sabine absorption coefficient is dependent upon the sample size, sample distribution, and the properties of the room in which it is measured. Because standards specify the room characteristics and sample size and distribution for measurement, similar results can be expected for the same material measured in different laboratories (although even under these conditions significant variations have been reported). However, these laboratory-measured values are used to calculate reverberation times and reverberant sound pressure levels in auditoria and factories that have quite different characteristics, which implies that under these circumstances, values of reverberation time,  $T_{60}$ , and reverberant field sound pressure level,  $L_p$ , calculated from measured Sabine absorption coefficients are approximate only. However, the errors in room constant calculations as a result of the errors in absorption coefficient measurements using Eq. (15) are much less than the errors that would be introduced using Eq. (11).

## 8 STATISTICAL ABSORPTION COEFFICIENT AND ITS DETERMINATION FROM MEASURED DATA

The statistical absorption coefficient differs from the Sabine coefficient in terms of how it is defined and measured. Whereas the Sabine absorption coefficient is measured in a reverberation room and defined in terms of a reverberation time, the statistical absorption coefficient is calculated for a material from measurements of the normal incidence absorption coefficient in an impedance tube. However, both coefficients are intended to describe the fraction of incident energy that the material absorbs in a randomly incident sound field each time there is a reflection.

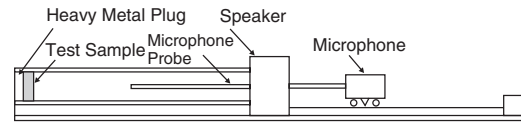


Figure 1 Equipment for impedance tube measurement.

The normal incidence absorption coefficient may be measured using an impedance tube, which can be constructed from any heavy-walled tube, as shown in Fig. 1. The older and simpler method uses a movable microphone that traverses the length of the tube to map the sound field in the tube for a single-frequency sound. This method is slow but easily implemented. A much quicker method makes use of two fixed microphones and a digital frequency analysis system. However, both methods are described in standards and texts.<sup>1,17,18</sup>

Implicit in the use of the impedance tube is the assumption that only plane waves propagate back and forth in the tube. This assumption puts upper and lower frequency bounds on the use of the impedance tube. Let  $d$  be the tube diameter if it is circular in cross section or the larger dimension if it is rectangular in cross section. Then the upper frequency limit (or cut-on frequency) is  $0.586c/d$  for circular cross-section tubes and  $0.5 c/d$  for rectangular tubes. Here,  $c$  is the speed of sound and the frequency limit is given in hertz. The low-frequency bound is given by the requirement that the length  $\ell$  of the tube should be greater than  $d + \frac{3}{4}c/f$  where  $f$  is the low-frequency bound in hertz.

When the material to be tested is in place and the resulting field within the impedance tube is explored, a series of maxima and minima will be observed. The maxima will be effectively constant in level, but the minima will increase in level as the distance from the surface of the test material is increased. For best results, it is recommended that successive minima be determined and extrapolated back to the surface of the sample by drawing a straight line joining the first two minima to the location corresponding to the surface of the sample on the plot of sound pressure level in decibels versus distance along the tube. The standing-wave ratio  $L_0$  is then determined as the difference between the maximum level  $L_{\max}$  and the extrapolated minimum level  $L_{\min}$ .

The normal impedance  $Z_N$  of the test material, used in the calculation of the statistical absorption coefficient, can be calculated using:

$$\begin{aligned} K_0 &= 10^{L_0/20} \\ M &= 0.5(K_0 + K_0^{-1}) \\ N &= 0.5(K_0 - K_0^{-1}) \\ \theta &= 360(2D_1/\lambda - \frac{1}{2}) \quad (\text{degrees}) \quad (17) \\ R &= (M - N \cos \theta)^{-1} \\ X &= RN \sin \theta \\ Z_N/(\rho c) &= R + jX = \xi e^{j\beta} \end{aligned}$$

where

$$\beta = \tan^{-1}(X/R)$$

$$\xi = \sqrt{R^2 + X^2} \quad (18)$$

The statistical absorption coefficient can then be calculated using:<sup>19</sup>

$$\alpha_{st} = \left( \frac{8 \cos \beta}{\xi} \right) \left\{ 1 - \left( \frac{\cos \beta}{\xi} \right) \right.$$

$$\times \ln(1 + 2\xi \cos \beta + \xi^2) + \left[ \frac{\cos(2\beta)}{\xi \sin \beta} \right]$$

$$\times \tan^{-1} \left( \frac{\xi \sin \beta}{1 + \xi \cos \beta} \right) \left. \right\} \quad (19)$$

## 9 STATISTICALLY BASED MODELS FOR REVERBERATION TIME CALCULATIONS

By treating the room response as a superposition of normal modes, Bies and Hansen<sup>1</sup> show how the following well-known reverberation time equation of Norris–Eyring may be derived:

$$T_{60} = -\frac{55.3V}{Sc \ln(1 - \bar{\alpha}_{st})} \quad (20)$$

This equation is often preferred to the Sabine equation by many who work in the field of architectural acoustics as some authors claim that it gives results that are closer to measured data.<sup>20</sup> However, Beranek and Hidaka<sup>21</sup> obtained good agreement between measured and predicted reverberation times in concert halls using the Sabine relation. Of course, if sound absorption coefficients measured in a reverberation chamber are to be used to predict reverberation times, then the Sabine equation must be used, as the Norris–Eyring equation is only valid if statistical absorption coefficients are used.

Note that air absorption must be included in  $\bar{\alpha}_{st}$  in a similar way as it is included in  $\bar{\alpha}$  [Eq. (5)]. It is worth careful note that Eq. (20) is a predictive scheme based upon a number of assumptions that cannot be proven, and consequently inversion of the equation to determine the statistical absorption coefficient  $\bar{\alpha}_{st}$  is not recommended.

With a further simplification, the famous equation of Sabine is obtained. When  $\bar{\alpha}_{st} < 0.4$ , an error of less than 0.5 dB is made by setting  $\bar{\alpha}_{st} \approx \log_e(1 - \bar{\alpha}_{st})$  in Eq. (20), and then by replacing  $\bar{\alpha}_{st}$  with  $\bar{\alpha}$ , Eq. (13) is obtained.

Alternatively, if in Eq. (20), the quantity,  $\bar{\alpha}_{st}$  is replaced by  $(1 - \beta_{st})$ , where  $\beta_{st}$  is the mean statistical reflection coefficient, the following equation of Millington and Sette is obtained:

$$T_{60} = -\frac{55.3V}{Sc \ln \beta_{st}} \quad (21)$$

The quantity  $\beta_{st}$  is interpreted as the area-weighted geometric mean of the random incidence energy reflection coefficients,  $\beta_i$ , for all of the room surfaces; that is,

$$\bar{\beta}_{st} = \prod_{i=1}^n \beta_i^{S_i/S} \quad (22)$$

The quantity  $\beta_i$  is related to the statistical absorption coefficient  $\alpha_i$  for surface  $i$  of area  $S_i$  by  $\beta_i = 1 - \alpha_i$ . It is of interest to note that although taken literally, Eq. (21) would suggest that an open window having no reflection would absorb all of the incident energy and there would be no reverberant field, the interpretation presented here suggests that an open window must be considered as only a part of the wall in which it is placed and the case of total absorption will never occur.

## 10 EMPIRICAL MODELS FOR REVERBERATION TIME CALCULATIONS

For calculating reverberation times in rooms for which the distribution of absorption was nonuniform (such as rooms with large amounts of absorption on the ceiling and floor and little on the walls), Fitzroy<sup>22</sup> proposed the following empirical equation:

$$T_{60} = \frac{0.16V}{S} \left[ \frac{-S_x}{\ln(1 - \bar{\alpha}_{x,st})} \right.$$

$$\left. + \frac{-S_y}{\ln(1 - \bar{\alpha}_{y,st})} + \frac{-S_z}{\ln(1 - \bar{\alpha}_{z,st})} \right] \quad (23)$$

where  $V$  is the room volume ( $m^3$ ),  $S_x$ ,  $S_y$ , and  $S_z$  are the total areas of two opposite parallel room surfaces ( $m^2$ ),  $\bar{\alpha}_{y,st}$ ,  $\bar{\alpha}_{y,st}$ , and  $\bar{\alpha}_{z,st}$  are the average statistical absorption coefficients of a pair of opposite room surfaces [see Eq. (8)] and  $S$  is the total room surface area.

Neubauer<sup>20</sup> presented a modified Fitzroy equation, which he called the Fitzroy–Kuttruff equation, that gave more reliable results than the original Fitzroy equation. In fact, this equation has been shown to be even more accurate than the Norris–Eyring equation for architectural spaces with nonuniform sound absorption. The Fitzroy–Kuttruff equation is as follows:

$$T_{60} = \left( \frac{0.32V}{S^2} \right) \left[ \frac{L_z(L_x + L_y)}{\bar{\alpha}_w} + \frac{L_x L_y}{\bar{\alpha}_{cf}} \right] \quad (24)$$

where  $L_x$ ,  $L_y$ , and  $L_z$  are the room dimensions (m) and

$$\bar{\alpha}_{cf} = -\ln(1 - \bar{\alpha}_{st}) + \left[ \frac{\beta_{cf}(\beta_{cf} - \bar{\beta}_{st})S_{cf}^2}{(\bar{\beta}_{st}S)^2} \right] \quad (25)$$

$$\bar{\alpha}_w = -\ln(1 - \bar{\alpha}_{st}) + \left[ \frac{\beta_w(\beta_w - \bar{\beta}_{st})S_w^2}{(\bar{\beta}_{st}S)^2} \right] \quad (26)$$

where  $\bar{\alpha}_{st}$  is the arithmetic mean over the six room surfaces of the surface-averaged statistical absorption coefficient,  $\beta = (1 - \alpha)$  is the reflection coefficient, the subscript  $w$  refers to the walls and the subscript  $cf$  refers to the ceiling and floor. Other empirical schemes are discussed elsewhere.<sup>23</sup>

Equations (10), (20), (21), (23), and (24) for reverberation time are all based on the assumption that the room dimensions satisfy the conditions for Sabine rooms (no one dimension greater than three times any of the other two) and that the absorption is reasonably well distributed over the room surfaces. However, in practice, this is not often the case and for rooms that do not meet this criterion, Kuttruff<sup>9</sup> has proposed that Eq. (10) be used except that  $\bar{\alpha}$  should be replaced with  $\alpha$  defined as follows:

$$\alpha = -\ln(1 - \bar{\alpha}_{st})[1 + 0.5\gamma^2 \ln(1 - \bar{\alpha}_{st})] + \frac{\sum_{i=1}^n \beta_i (\beta_i - 1 + \bar{\alpha}_{st}) S_i^2}{S^2 (1 - \bar{\alpha}_{st})^2} \quad (27)$$

In Eq. (27),  $n$  is the number of room surfaces (or part room surfaces if whole surfaces are subdivided),  $\bar{\alpha}_{st}$  is the statistical absorption coefficient, area averaged over all room surfaces [see Eq. (8)] and  $\beta_i$  is the statistical energy reflection coefficient of surface  $i$  of area  $S_i$ . The first term in Eq. (27) accounts for room dimensions that exceed the Sabine room criterion. The quantity  $\gamma^2$  is the variance of the distribution of path lengths between reflections divided by the square of the mean free path length. It has a value of about 0.4 provided that the room shape is not extreme. The second term in Eq. (27) accounts for nonuniform placement of sound absorption.

Neubauer<sup>24</sup> provided an alternative modified Fitzroy equation for flat and long rooms:

$$T_{60} = \left[ \frac{0.126 S_x}{\ln(1 - \bar{\alpha}_{st,x}) P_x} + \frac{0.126 S_y}{\ln(1 - \bar{\alpha}_{st,y}) P_y} + \frac{0.126 S_z}{\ln(1 - \bar{\alpha}_{st,z}) P_z} \right]^{1/2} \quad (28)$$

where  $P_x$  and  $P_y$  are the total perimeters for each of the two pairs of opposite walls and  $P_z$  is the total perimeter of the floor and ceiling. Similar definitions apply for  $S_x$ ,  $S_y$ , and  $S_z$  and also for  $\bar{\alpha}_x$ ,  $\bar{\alpha}_y$ , and  $\bar{\alpha}_z$ . Note that for a cubic room, Eq. (28) may be used with the exponent  $\frac{1}{2}$  replaced by  $\frac{1}{3}$ .

## 11 POROUS SOUND ABSORBERS

### 11.1 Flow Resistance

The flow resistance of a porous acoustic material can be measured as described in Appendix C of Bies and Hansen.<sup>1</sup> Once measured, the flow resistance can be used to calculate the normal impedance of a layer

of sound-absorbing material with a rigid backing or with a cavity backing. The effect of a limp impervious protective cover and/or a perforated steel cover can also be calculated. The normal impedance can be used together with Eq. (19) to calculate the statistical absorption for each case.

The relationships between porous material flow resistivity and the characteristic impedance,  $Z_m$ , and propagation constant,  $k_m$ , that have been generally accepted<sup>25,26</sup> and that are accurate in the flow resistivity range  $R_1 = 10^3$  to  $5 \times 10^4$  MKS rayls/m are as follows:

$$Z_m = \rho c [1 + 0.0571 X^{-0.754} - j 0.087 X^{-0.732}] \quad (29)$$

$$k_m = (\omega/c) [1 + 0.0978 X^{-0.700} - j 0.189 X^{-0.595}] \quad (30)$$

where

$$X = \rho f / R_1 \quad (31)$$

More accurate (and more complex) expressions that cover a wider frequency range are given in Appendix C of Bies and Hansen.<sup>1</sup>

The normal impedance for a rigidly backed porous material is

$$Z_N = -j Z_m / \tan(k_m \ell) \quad (32)$$

Substituting the result from Eq. (32) into Eqs. (17) and (18), and substituting the result for  $\beta$  and  $\xi$  into Eq. (19) allows the statistical absorption coefficient to be calculated. Evaluation of Eq. (19) for a range of frequencies and flow resistance values results in the curves shown in Fig. 2.

### 11.2 Porous Materials with a Backing Cavity

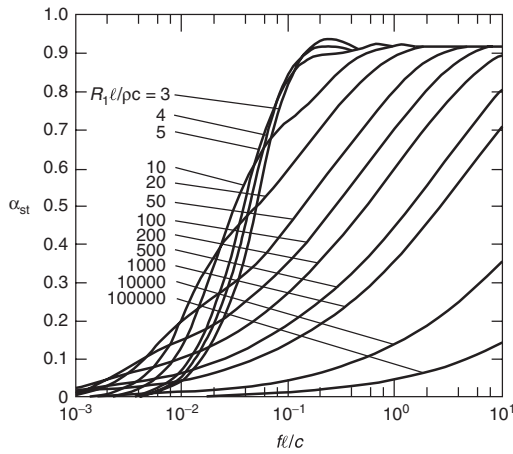
The performance of a porous blanket material can be improved by mounting it so that an air gap between the material and the hard backing wall is provided. The effect of the cavity can be determined by calculating the combined normal impedance due to the cavity and the sound-absorbing material and substituting the result into Eq. (19).

For a material of infinite depth, the normal impedance is equal to the characteristic impedance of Eq. (29). For a porous blanket of thickness,  $\ell$ , backed by a cavity of any depth,  $L$  (including  $L = 0$ ) with a rigid back, the normal impedance (in the absence of flow past the cavity) may be calculated using an electrical transmission line analogy and is given by<sup>27</sup>

$$Z_N = Z_m \frac{Z_L + j Z_m \tan(k_m \ell)}{Z_m + j Z_L \tan(k_m \ell)} \quad (33)$$

The specific normal impedance,  $Z_L$ , of a rigidly terminated, partitioned backing cavity is given by

$$Z_L = \frac{-j \rho c}{\tan(2\pi f L / c)} \quad (34)$$



**Figure 2** Calculated statistical absorption coefficient for a rigidly backed porous material in a reverberant field, as a function of a frequency parameter, for various indicated values of flow resistance. The quantity  $R_1$  is the flow resistivity of the porous material (MKS rays/m),  $\rho$  is the density of air ( $\text{kg/m}^3$ ),  $c$  is the speed of sound in air (m/s),  $f$  is the frequency (Hz) of the incident sound, and  $\ell$  is the porous material thickness (m).

and for a rigidly terminated, nonpartitioned backing cavity:

$$Z_L = \frac{-j\rho c \cos \theta}{\tan(2\pi fL/c)} \quad (35)$$

where  $\theta$  is the angle of incidence of the sound wave measured from the normal to the surface. A partitioned cavity is divided into compartments by partitions that permit propagation normal to the surface while inhibiting propagation parallel to the surface of the liner. The depth of each compartment is equal to the overall cavity depth.

### 11.3 Porous Liner Covered with a Limp Impervious Layer

In practice, it is often necessary to protect a porous liner from contamination by moisture, dust, oil, chemicals, and the like, which would render it useless. For this reason the material is often wrapped in a thin, limp, impervious blanket made of polyurethane, polyester, aluminum, or polyvinyl chloride (PVC). The effect of the introduction of a wrapping material is generally to improve the

low-frequency absorption at the expense of the high-frequency absorption. However, if the wrapping material is sufficiently thin (e.g., 20-mm-thick polyurethane), then the effect is not measurable. The effect can be determined by calculating the combined normal impedance due to the membrane and the sound-absorbing material and substituting the result into Eq. (19).

If the porous material is protected by a covering or by enclosing it in an impervious blanket of thickness  $h$  and mass per unit area,  $\sigma'$ , the effective specific normal impedance at the outer surface of the blanket,  $Z_{NB}$ , which can be used together with Eq. (19) to find the absorption coefficient of the construction, is as follows:

$$Z_{NB} = Z_N + j2\pi f\sigma' \quad (36)$$

where  $f$  is the frequency of the incident sound, tone, or center frequency of a narrow band of noise. Typical values for  $\sigma'$  and  $\sqrt{E/\rho}$  are included in Table 2 for commonly used covering materials.

Guidelines for the selection of suitable protective coverings are given by Andersson.<sup>28</sup>

### 11.4 Porous Liner Covered with a Perforated Sheet

When mechanical protection is needed for a porous liner, it may be covered using perforated wood, plastic, or metal panels. If the open area provided by the perforations is greater than about 20%, the expected absorption is entirely controlled by the properties of the porous liner, and the panel has no effect.

Alternatively, if the facing panel has an open area of less than 20%, the statistical absorption coefficient of the panel plus sound-absorbing material can be determined by calculating the specific normal impedance of the combined construction and using the result in Eq. (19). According to Bolt<sup>29</sup> the normal impedance is

$$Z_{NP} = Z_N + \frac{(100/P)\{j\rho c \tan[k\ell(1-M)] + R_a A\}}{1 + (100/j\omega m P)\{j\rho c \tan[k\ell(1-M)] + R_a A\}} \quad (37)$$

where  $Z_N$  is the normal specific acoustic impedance of the porous acoustic material with or without a cavity backing (and in the absence of flow),  $\ell$  is the effective length (see Chapter 9 of Bies and Hansen<sup>1</sup>) of each of the holes in the perforated sheet,  $\omega$  is the radian

**Table 2** Properties of Commonly Used Limp Impervious Wrappings for Protection of Porous Materials

Material	Density ( $\text{kg/m}^3$ )	Typical Thickness ( $\mu\text{m} = 10^{-6} \text{ m}$ )	$\sigma' (\text{kg/m}^2)^a$	$c_L \approx \sqrt{E/\rho} \text{ (m/s)}$
Polyethylene (LD)	930	6–35	0.0055–0.033	460
Polyurethane	900	6–35	0.005–0.033	1330
Aluminum	2700	2–12	0.0055–0.033	5150
PVC	1400	4–28	0.005–0.033	1310
Melinex (polyester)	1390	15–30	0.021–0.042	1600
Metalized polyester	1400	12	0.017	1600

<sup>a</sup>  $\sigma'$  and  $c_L$  are, respectively, the surface density and speed of sound in the wrapping material.

frequency,  $P$  is the percent open area of the holes,  $R_d$  is the acoustic resistance of each hole (see Chapter 9 of Bies and Hansen<sup>1</sup>),  $A$  is the area of each hole,  $M$  is the Mach number of the flow past the holes, and  $m$  is the mass per unit area of the perforated sheet.

The frequency,  $f_{\max}$ , of maximum absorption for a perforated panel (of open area less than 20%) is given approximately by the following transcendental equation, which can be solved by trial and error:

$$(2\pi f_{\max} L/c) \tan(2\pi f_{\max} L/c) = \frac{PL/100}{t + 0.85d(1 - 0.22d/q)} \quad (38)$$

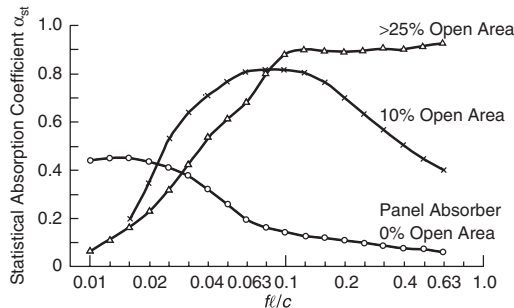
In Eq. (38),  $P$  is the percentage open area of the panel,  $L$  is the depth of the backing cavity including the porous material layer,  $t$  is the panel thickness,  $d$  is the diameter of the perforations, and  $q$  is the spacing between hole centers. If the porous material fills the entire cavity so that the thickness of the porous material is also  $L$ , then the speed of sound  $c$  should be replaced with  $0.85c$  to account for isothermal rather than adiabatic propagation of sound in the porous material at low frequencies. Measured data for a panel of 10% open area are presented in Fig. 3.

### 11.5 Porous Liner Covered with a Limp Impervious Layer and a Perforated Sheet

In this case, the impedance of the perforated sheet and impervious layer are both added to the normal impedance of the porous acoustic material so that:

$$Z_{NBP} = Z_N + \frac{(100/P)\{jPc \tan[k\ell(1-M)] + R_d A\}}{1 + (100/j\omega m P)\{j\rho c \tan[k\ell(1-M)] + R_d A\}} + j2\pi f\sigma' \quad (39)$$

where  $\sigma'$  is the mass per unit area of the impervious membrane. It is important that the impervious layer and the perforated sheet are separated, using something



**Figure 3** Effect of perforations on the sound absorption of a panel backed by a porous liner. The panel surface weight is  $2.5 \text{ kg/m}^2$  and its thickness is 3 mm. The porous liner is 50 mm thick and about  $5 \rho c$  flow resistance.

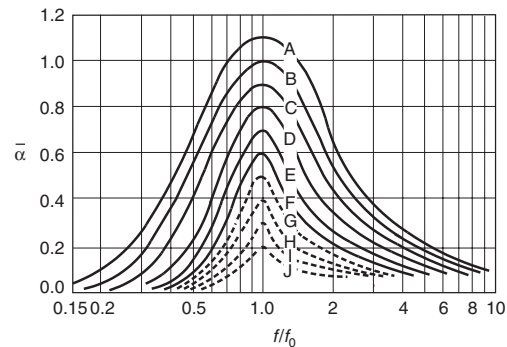
like a mesh spacer, otherwise the performance of the construction as an absorber will be severely degraded.

### 12 PANEL SOUND ABSORBERS

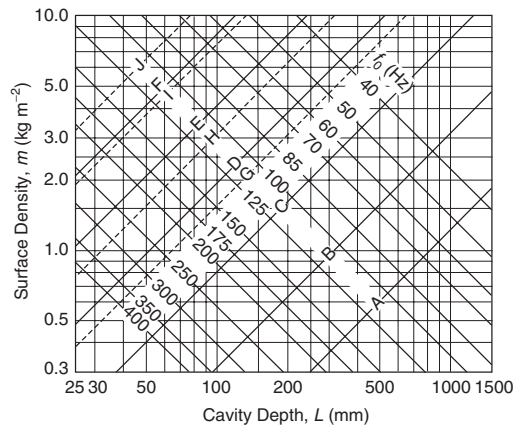
Porous liners are not very effective in achieving low-frequency absorption. When low-frequency absorption is required, panel absorbers are generally used. These consist of flexible panels mounted over an airspace, for example, on battens attached to a solid wall. Alternatively, such panels may be mounted on a suspended ceiling. In any case, to be effective the panels must couple with and be driven by the sound field. Acoustic energy is then dissipated by flexure of the panel. Additionally, if the backing airspace is filled with a porous material, energy is also dissipated in the porous material. Maximum absorption occurs at the first resonance of the coupled panel-cavity system.

It is customary to assign a Sabine absorption coefficient to a resonant panel absorber, although the basis for such assignment is clearly violated by the mode of response of the panel absorber; that is, the absorption is not dependent upon local properties of the panel but is dependent upon the response of the panel as a whole. Furthermore, as the panel absorber depends upon strong coupling with the sound field to be effective, the energy dissipated is very much dependent on the sound field and thus on the rest of the room in which the panel absorber is used. This latter fact makes prediction of the absorptive properties of panel absorbers difficult. A typical example of absorption coefficients for a panel absorber is shown in Fig. 3.

The following method for determining the Sabine absorption of panel absorbers is empirical<sup>30</sup> and is based upon data measured in auditoria and concert halls. The essence of the prediction scheme is contained in Figs. 4 and 5. First of all, the type of Sabine



**Figure 4** Sabine absorption coefficients for resonant plywood panels. The panel configurations corresponding to the curves labeled A–J may be identified using Fig. 5. Dashed curves (G–J) represent configurations with no absorptive material in the cavity behind the panel. Configurations A–F require a sound-absorbing blanket between the panel and backing wall. The blanket must not contact the panel and should be between 10 and 50 mm thick and consist of glass or mineral fiber with a flow resistance between 1000 and 2000 MKS rays. Panel supports should be at least 0.4 m apart.



**Figure 5** Design curves for resonant plywood panels to be used in conjunction with Figure 4. The quantity  $f_0$  is the frequency at which maximum sound absorption is required.

absorption curve desired is selected from curves A to J in Fig. 4. The solid curves are for configurations involving a blanket (25 mm thick and flow resistance between  $2 \rho c$  and  $5 \rho c$ ) in the air gap behind the panel, while the dashed curves are for no blanket. Next, the frequency  $f_0$ , which is the fundamental panel resonance frequency and the frequency at which maximum absorption is required, is determined, and Fig. 5 is entered for the chosen curve (A to J) and the desired frequency  $f_0$ . The required air gap (millimetres) behind the panel and the required panel surface density (kilograms per square metre) are read directly from the figure. The resonance frequency used in the preceding procedure is calculated using:

$$f_0 = \frac{1}{2\pi} \sqrt{\frac{\rho c^2}{mL}} \quad (40)$$

which does not take into account the panel rigidity or geometry. A more accurate equation for a plywood panel is<sup>31</sup>

$$f_0 = \frac{1}{2\pi} \sqrt{\frac{\rho c^2}{mL + 0.6L\sqrt{ab}}} \quad (41)$$

where  $m$  is the mass per unit area of the panel (kilograms per square metre),  $L$  is the depth of the backing cavity, and  $a, b$  are the panel dimensions. Thus, it is recommended that before using Fig. 5, the frequency of maximum desired absorption be multiplied by the ratio:

$$f_0 = \sqrt{\frac{m}{m + 0.6\sqrt{ab}}} \quad (42)$$

## REFERENCES

1. D. A. Bies and C. H. Hansen, *Engineering Noise Control: Theory and Practice*, Spon Press, London, 2003.
2. ISO 11690-3, Recommended Practice for the Conception of Workplaces—Part 3: Propagation of Sound and Prediction of Noise, 1997.
3. A. Lawrence, *Architectural Acoustics*, Elsevier Science, Oxford, UK, 1970.
4. H. Kuttruff, *Room Acoustics*, 4th ed., Spon Press London, 2000.
5. L. Sutherland, A Review of Experimental Data in Support of a Proposed New Method for Computing Atmospheric Absorption Losses, DOT-TST-75-87, 1979.
6. ISO 9613/1—1993, Acoustics—Attenuation of Sound During Propagation Outdoors. Part 1: Calculation of the Absorption of Sound by the Atmosphere, 1993.
7. M. Hodgson, When Is Diffuse-Field Theory Accurate?, Proc. of the Wallace Clement Sabine Symposium, Cambridge, MA, 1994, pp. 157–160.
8. M. Hodgson, Are Room Surface Absorption Coefficients Unique? Proc. of the Wallace Clement Sabine Symposium, Cambridge, MA, 1994, pp. 161–164.
9. H. Kuttruff, Sound Decay in Enclosures with Non-diffuse Sound Field, Proc. of the Wallace Clement Sabine Symposium, Cambridge, MA, 1994, pp. 85–88.
10. L. L. Beranek, *Music, Acoustics and Architecture*, Wiley, New York, 1962.
11. L. Cremer and H. A. Müller (English translation by T. J. Schultz), *Principles and Applications of Room Acoustics*, Vol. I, Applied Science, London and New York, 1982, Chapter 2.1.
12. M. D. Egan, *Architectural Acoustics*, McGraw Hill, New York, 1987.
13. R. Mackenzie, Ed., *Auditorium Acoustics*, Elsevier Applied Science, London, 1979.
14. AS1045—1988, Acoustics: Measurement of Sound Absorption in a Reverberation Room, 1988.
15. ASTM C423-99a, Standard Test Method for Sound Absorption and Sound Absorption Coefficients by the Reverberation Room Method, 1999.
16. ISO 354-1985, Acoustics: Measurement of Sound Absorption in a Reverberation Room, 1985.
17. ASTM C384-98, Standard Test Method for Impedance and Absorption of Acoustical Materials by the Impedance Tube Method, 1998.
18. ASTM E1050-98, Standard Test Method for Impedance and Absorption of Acoustical Materials Using a Tube, Two Microphones, and a Digital Frequency Analysis System, 1998.
19. P. M. Morse and R. H. Bolt, Sound Waves in Rooms, *Rev. Mod. Phys.*, Vol. 16, 1944, pp. 65–150.
20. R. O. Neubauer, Existing Reverberation Time Formulae—A Comparison with Computer Simulated Reverberation Times, Proceedings of the 8th International Congress on Sound and Vibration, Hong Kong, July, 2001, pp. 805–812.
21. L. L. Beranek and T. Hidaka, Sound Absorption in Concert Halls by Seats, Occupied and Unoccupied and by the Hall's Interior Surfaces, *J. Acoust. Soc. Am.*, Vol. 104, 1998, pp. 3169–3177.
22. D. Fitzroy, Reverberation Formula Which Seems to Be More Accurate with Nonuniform Distribution of Absorption, *J. Acoust. Soc. Am.*, Vol. 31, 1959, pp. 893–897.
23. EN 12354-6:2003, Building Acoustics—Estimation of Acoustic Performance of Buildings from the Performance of Elements—Part 6: Sound Absorption in Enclosed Spaces, 2003.

24. R. O. Neubauer, Estimation of Reverberation Times in Non-rectangular Rooms with Non-uniformly Distributed Absorption Using a Modified Fitzroy Equation, Proceedings of the 7th International Congress on Sound and Vibration, Garmisch-Partenkirchen, Germany, July, 2000, pp. 1709–1716.
25. M. E. Delany and E. N. Bazley, Acoustical Characteristics of Fibrous Absorbent Materials, Aero Report Ac 37, National Physical Laboratory, Teddington, UK, 1969.
26. M. E. Delany and E. N. Bazley, Acoustical Properties of Fibrous Absorbent Materials, *Appl. Acoust.*, Vol. 3, 1970, pp. 105–106.
27. P. C. Magnusson, *Transmission Lines and Wave Propagation*, Allyn and Bacon, Boston, 1965.
28. P. Andersson, Guidelines for Film Faced Absorbers, *Noise Vib. Control Worldwide*, January/February, 1981.
29. R. H. Bolt, On the Design of Perforated Facings for Acoustic Materials, *J. Acoust. Soc. Am.*, Vol. 19, 1947, pp. 917–921.
30. Hardwood Plywood Manufacturers' Association, Design Procedure for the Sound Absorption of Resonant Plywood Panels, Bolt, Beranek and Newman Inc., Report 925, 1962.
31. J. J. Sendra, *Computational Acoustics in Architecture*, WIT Press, Southampton, 1999.



# CHAPTER 105

## SOUND INSULATION – AIRBORNE AND IMPACT

Alfred C. C. Warnock  
National Research Council of Canada  
Ottawa, Ontario, Canada

### 1 INTRODUCTION

The control of airborne and impact sound transmission through common building elements is of considerable importance. Airborne sound originates from a source radiating sound waves into the air that then impinge on the surfaces of building elements. Examples are speech or music from a television or a loudspeaker. Impact sound is generated when some object strikes a surface of the building. The most common source of impact sound is footsteps, but there are others, such as furniture being moved and cleaning and other equipment that is operating directly on the surface of floors, stairs, and landings. Achieving good sound isolation in buildings demands careful consideration of all possible paths for sound and the junctions between walls and floors (flanking sound transmission); it is not enough to consider only the direct path through the common wall or floor. Airborne and flanking sound transmission can be estimated from theoretical considerations or determined from laboratory measurements.

### 2 AIRBORNE SOUND INSULATION

When sound strikes one surface of a wall, floor, or other building element, a very small fraction of the incident energy is radiated from the other side. The *sound transmission loss*\* (TL) is the ratio of the incident sound energy relative to the transmitted sound energy, expressed in decibels (dB).

Two-room methods for measuring sound insulation are specified in standards.<sup>1,2</sup> The test specimen is mounted between reverberant source room and receiving rooms so the only significant path for sound transmission is through the specimen; transmission along other paths is suppressed. Laboratory tests allow comparison among different elements and with requirements in certain building codes. Similar test methods are available to check the degree of sound isolation achieved in buildings.<sup>3,4</sup> To measure the airborne sound insulation of facade elements and facades special methods<sup>5,6</sup> are used.

Introduced in 1981,<sup>7</sup> sound intensity measurements to determine sound insulation have now been standardized,<sup>8,9</sup> but great care is needed to obtain accurate results. Differences at low frequencies have been found<sup>10,11</sup> between results from the standard two-room test procedures and those from intensity measurements.

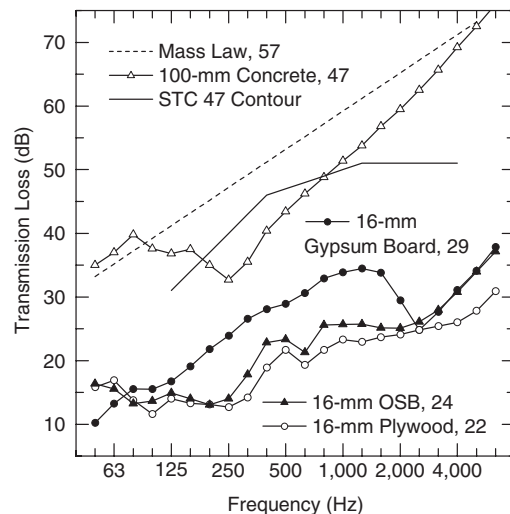
\*Sound transmission loss is also known as sound reduction index,  $R$ , in European and ISO standards.

### 2.1 Single-Leaf Building Elements

The transmission loss of a homogeneous, *limp*, non-porous plate for plane-wave incidence is commonly approximated by the *field incidence mass law*,<sup>12</sup>  $TL = 20 \log mf - 47$  dB, where  $m$  is the surface mass of the plate ( $\text{kg/m}^2$ ), and  $f$  is frequency (Hz).

Bending waves in panels with finite stiffness give rise to the *coincidence effect*.<sup>12</sup> At every frequency above a certain *critical frequency*,  $f_c$ , there is an angle of incidence for which the wavelength of the bending wave in the plate becomes equal to the wavelength of sound in air projected onto the plate; the waves coincide. Because of this effect, a region of relatively low sound insulation occurs in some frequency range in the curve of transmission loss. For example, the curve for gypsum board in Fig. 1 shows a coincidence dip with a minimum at 2500 Hz.

For a given material with thickness  $h$ , the product  $f_c h$  is a constant that depends only on its physical properties. Table 1 gives values of  $f_c h$  for common building materials. The resonance dip due to the coincidence effect usually begins about an octave



**Figure 1** Sound transmission through some common building materials: 100-mm concrete ( $233 \text{ kg/m}^2$ ), 16-mm plywood ( $7.5 \text{ kg/m}^2$ ), and 16-mm oriented strandboard ( $9 \text{ kg/m}^2$ ) on joists, and 16-mm gypsum board ( $11.3 \text{ kg/m}^2$ ). The dashed line represents mass law predictions for  $233 \text{ kg/m}^2$ . The numbers next to each curve are STC ratings.

**Table 1 Surface Mass for 1-mm Thicknesses and Constant  $f_c h$  for Some Common Building Materials**

Material	Surface Mass (kg/m <sup>2</sup> per mm)	$f_c h$ (Hz mm)
Aluminum	2.7	12,900
Concrete, dense poured	2.3	18,700
Hollow concrete block	1.1	20,900
Fir timber	0.55	8,900
Glass	2.5	15,200
Lead	11.0	55,000
Plexiglass or Lucite	1.15	30,800
Steel	7.7	12,700
Gypsum board	0.7	39,000
Oriented strand board <sup>a</sup>	0.6	15,000
Plywood <sup>a</sup>	0.5	16,000

<sup>a</sup> These materials are orthotropic and show very broad, shallow coincidence dips. The values given estimate the frequency at the middle of the dip.

below the critical frequency; its depth depends on damping of the panel.

## 2.2 Single-Number Ratings

The sound transmission spectra in Fig. 1 present more information than is convenient for use in building codes. Standard methods assign a single-number rating to such spectra by means of reference curves or weighted summation procedures. *Sound transmission class*<sup>13</sup> (STC) is calculated according to American Society for Testing and Materials (ASTM) E413. The *weighted sound reduction index*,<sup>14</sup>  $R_w$ , is the International Organization for Standardization (ISO) equivalent. Figure 1 shows the STC contour fitted to the data for the concrete slab. The differences between the data points below the contour and the contour value are deficiencies. The sum of the deficiencies must be no greater than 32 dB, and no deficiency can exceed 8 dB (the 8-dB rule). The ASTM reference contour extends from 125 to 4000 Hz; the ISO  $R_w$  contour has the same shape but extends from 100 to 3150 Hz. There is no 8-dB rule in ISO 717. The numerical values of the two ratings are usually very close.

Weighted summation methods have been developed in ISO 717<sup>14</sup> that take into account the higher importance of low frequencies in traffic noise and modern music systems. These methods produce corrections—spectrum adaptation terms—to be used in conjunction with the  $R_w$  rating. The proposed ratings are simply the change in A-weighted level for a pink noise signal and for a specific traffic noise spectrum that are supposed to pass through the specimen. The outdoor–indoor transmission class<sup>15</sup> (OITC), also gives a transportation noise rating; it uses a different frequency range and source spectrum from the corresponding ISO standard and can differ quite significantly.

## 2.3 Orthotropic and Corrugated Materials

Many common building materials are not isotropic; the bending stiffness varies for different directions

along the panels. Plywood and oriented strandboard are two such materials, and they show greatly broadened coincidence dips as a result (Fig. 1). In practice, there is little that can be done economically to change to properties of common materials. Corrugating a sheet of material or adding ribs to it increases the bending stiffness in one direction. This can result in significant reductions in sound insulation. For example, a flat sheet of 0.7-mm-thick steel has an STC of 26. Corrugating the metal in two different ways gave STC values of 22 and 25, in each case with reductions of around 10 dB at the coincidence dips. Methods for estimating sound transmission through such materials are given in Ref. 12 and 16.

## 2.4 Single-Leaf Poured Concrete

For common thicknesses of concrete slabs, the critical frequency usually lies in the range where single-number ratings are calculated (Fig. 1). Because the coincidence effect significantly reduces the transmission loss relative to the ideal mass law values, the STC and  $R_w$  ratings are less than might be expected from considering mass only. Transmission loss for a concrete slab depends on the energy losses in the system and so can vary quite widely. For monolithic slabs,  $R_w$  or STC is given approximately by<sup>17</sup>  $37.5 \log m - 42$ , where  $m$  is the mass per unit area of the slab (kg/m<sup>2</sup>). Inhomogeneous elements, such as floors and exterior masonry with large cavities, may provide lower sound insulation because of resonance effects.<sup>18</sup> Thus, simple concrete partitions provide STC ratings from about 45 to 58. The most effective way to significantly increase STC beyond 58 is to attach additional layers of gypsum board to form a multileaf partition as discussed below.

## 2.5 Single-Leaf Concrete Masonry Walls

Solid and hollow-core concrete blocks are manufactured in a variety of thicknesses, core sizes, aggregates, and densities. Representative values of STC for block walls can be calculated<sup>19</sup> from  $STC = 0.51 \times \text{block weight (kg)} + 38$ . (The dimensions of the block face are 190 × 390 mm.) The estimated values are only valid if the wall surfaces are properly sealed and the mortar joints well made.

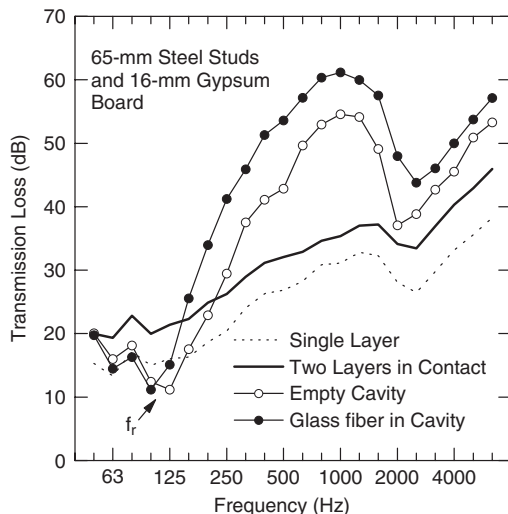
Porous blocks allow sound to leak through and reduce the transmission loss. The greater the porosity, the greater the improvement when the surfaces of the block are sealed (e.g., by latex block sealer, epoxy paint, or a skim coat of plaster). Improvements of 5 to 10 in STC are common. It is enough to apply the sealant on one face of the block only. A layer of gypsum board attached directly with screws or dabs of glue to the block surface is *not* an effective seal because it is still able to vibrate as a separate layer. Even when gypsum board on studs or resilient supports is to be used to finish a block or concrete wall, the wall should be sealed. Covering a crack or some other flaw with gypsum board does not eliminate the detrimental effects of the flaw.

## 2.6 Double-Leaf Building Elements

When high sound insulation is required with minimum weight, the best approach is to construct a wall consisting of two solid leaves with a cavity between them. Ideally, there should be no solid connections between the two leaves; these provide a path for sound and lower the transmission loss. When properly designed, a double-leaf construction provides greater sound insulation at the important frequencies than a single leaf of the same mass per unit area.

Typical methods for reducing vibration transmission between leaves include (1) separate rows of wood studs, (2) staggered wood studs on a common sole plate, (3) staggered wood studs with resilient metal channels on one side (to reduce transmission around the periphery), (4) a single row of wood studs or load-bearing steel studs with resilient metal channels on one or both sides, and (5) non-load-bearing steel studs (typically made from 0.5-mm sheet steel). In all cases, connections to panels, even when resilient, should be minimized; the closer the spacing of studs or resilient metal channels, the lower the sound reduction.<sup>20</sup>

Figure 2 shows the transmission loss through 16-mm gypsum board for four cases: (1) installed as a single sheet, (2) installed as two sheets screwed together as a single leaf, (3) installed as two sheets with a cavity between them, and (4) installed as two sheets with a cavity filled with glass fiber batts. This figure shows typical behavior for double-leaf walls with no solid connections. At the frequency marked  $f_r$  there is a dip in the transmission loss curve that reduces the sound insulation below that for the two



**Figure 2** Transmission loss of double-leaf and of single-leaf gypsum board walls. The 25 ga. (0.5 mm) steel studs in the double wall are  $38 \times 65$  mm deep. The sound-absorbing material is glass fiber with a thickness of 65 mm and a flow resistivity of  $3600 \text{ N s/m}^2$ .

sheets in contact—even below that for the single sheet. The transmission loss of the double-leaf wall becomes equal to that for two sheets in contact below the resonant frequency. Above the resonance, there are very significant improvements in transmission loss relative to the curve for the two sheets in contact.

The reduced transmission loss at  $f_r$  is caused by the mass–air–mass resonance; the enclosed air acts as a spring, the gypsum board leaves are the masses. For an air-filled cavity,  $f_r$  can be calculated from

$$f_r = \frac{1}{2\pi} \sqrt{\frac{\rho_0 c^2}{d M_{\text{eff}}}} \quad (1)$$

where  $\rho_0$  is the density of air ( $\text{kg/m}^3$ );  $c$  is the speed of sound in air ( $\text{m/s}$ );  $d$  is the distance between the inner surfaces ( $\text{m}$ );  $M_{\text{eff}}$  is the effective mass per unit area of the two layers given by  $M_{\text{eff}} = (1/m_1 + 1/m_2)^{-1}$ ; and  $m_1, m_2$  are the masses per unit area of the two layers ( $\text{kg/m}^2$ ). For a given total mass, this frequency has its minimum value when both masses are equal. Generally, the lower  $f_r$ , the higher the STC.

Another feature to notice in Fig. 2 is the prominent dip in the transmission loss curve around 2500 Hz due to the coincidence effect. Such dips are often significant in determining STC or  $R_w$ . If two sheets of gypsum board are used on each side, the dip is less deep because of damping due to friction between the sheets. When different materials having different critical frequencies are used on each face of the wall or floor, the coincidence dips are less prominent.

Placing sound-absorbing material in the cavity of double-leaf wall or floor gives greatly improved sound insulation<sup>21–23</sup>; STC ratings typically increase about 6 to 10 dB. Adding sound-absorbing material to the cavity lowers the frequency at which the mass–air–mass resonance occurs and leads to higher transmission loss values above  $f_r$ . As an approximate guide, when the wall cavity contains sound-absorbing material, multiply the frequency calculated from Eq. (1) by 0.7 to estimate the value of  $f_r$ . The sound-absorbing material also damps cross-cavity resonances. These occur at  $f_1 = c/2d$  and integer multiples of this frequency.

The more sound-absorbing material in the cavity, the higher the transmission loss, but increasing the thickness has less effect than the initial addition of the material. In a series of measurements on a floor with 235-mm-deep joists, the STC increased from 50 to 53 as the thickness of glass fiber in the cavity was increased from 65 to 240 mm.<sup>24</sup> The STC for the empty cavity was 43. Changing the type of commonly used sound-absorbing materials has little effect on STC in common wall and floor constructions.

Prediction of sound transmission through double-leaf walls has been attempted by many authors using different models of varying complexity. When the two panels in a double-leaf partition are completely isolated

from each other, the empirical approach in Ref. 25 can be used to estimate transmission loss as follows:

$$TL = \begin{cases} 20 \log[(m_1 + m_2)f] - 47 & f < 2f_r/3 \\ TL_1 + TL_2 + 20 \log fd - 29 & f_r < f < f_1 \\ TL_1 + TL_2 + 6 & f > f_1 \end{cases} \quad (2)$$

where  $TL_1, TL_2$  are the transmission losses for each leaf of the double wall measured or calculated separately. The expressions in Eq. (2) are slightly different from those in Ref. 25 and give an approximate way of dealing with the low-frequency resonances that often limit the sound insulation of lightweight double-panel walls.

Thus in a double-leaf partition, high sound insulation can be attained by (1) avoiding solid connections between the leaves, (2) selecting a high mass per unit area of the leaves, (3) selecting a deep cavity, and (4) filling the cavity with sound-absorbing material to ensure a low mass-air-mass resonance frequency. In practice, it is very difficult to construct a double-panel wall where the two panels are not connected in some way, and the sound reductions predicted by Eq. (2) are seldom achieved at high frequencies; there is often a solid connection around the edges of a partition for practical reasons.

## 2.7 Double-Leaf Gypsum Board Walls

Table 2 gives a few examples of measured STC values for walls constructed from wood or steel studs and fire-rated gypsum board.<sup>20</sup> The type of sound-absorbing material has only a small effect on the single-number rating.

When two sheets of gypsum board are joined using screws or dabs of glue, the bending stiffness of the double sheet is not significantly altered from that of a single sheet, and the critical frequency does not move

to a lower frequency where it might adversely affect the STC. Using two sheets is *not* the same as using a sheet twice as thick.

It is always detrimental to have shallow cavities within a wall or floor. For example, adding a single, solid, nonporous layer to one set of studs in the middle of a double-stud wall with sound-absorbing material in both stud cavities reduces the STC by about 3 to 4 dB.<sup>20</sup> A second layer added internally to the other set of studs decreases the sound insulation even more because of the small cavity in the middle of the wall.

For stud walls, even for a double-stud wall, the sound reduction is influenced by the spacing of the studs and resilient channels that support the gypsum board. Within practical limits, it is best if these are as far apart as possible. Thus a 610-mm spacing gives better results than 406-mm spacing. For double wood studs the increase in STC is about 2.<sup>20</sup>

## 2.8 Joist Floors

The same principles outlined above control sound transmission through double-leaf floors. To avoid having the floor and ceiling layers rigidly connected usually requires resilient supports for the ceiling or separate joists. It is relatively simple to get high STC ratings with joist construction because of the large cavity depth; resilient ceiling supports and sound-absorbing material are all that is needed.<sup>24,26</sup> If a concrete topping is used, STC ratings close to 70 can easily be attained. Just as in walls, small air cavities increase sound transmission, so resilient metal channels should *never* be used between layers of gypsum board in a floor or a wall.

## 2.9 Two-Leaf Masonry or Concrete Walls

Two-leaf masonry or concrete walls can, in principle, provide very high sound insulation.<sup>27</sup> The insulation attained is usually limited, however, by the practical difficulties of constructing two leaves that are structurally isolated. Depending on the height of a block wall, metal ties are required for structural reasons or to meet applicable building codes. Solid metal ties transmit sound energy from one leaf to the other, but ties designed to reduce sound transmission are available.

Also important is transmission of energy along the floor and ceiling, along walls abutting the periphery of the cavity wall, and through other parts of the structure. These *flanking paths* bypass the cavity wall and reduce its apparent sound insulation. Physical breaks in the floor, ceiling, and abutting walls are needed to reduce transmission along such paths. However, even if gaps are included in the design, during construction the airspace between leaves may become bridged by mortar droppings or rubble that will reduce the sound insulation. In practical installations careful design of the whole system, good supervision, and care during construction are needed for two-leaf block walls to achieve their potential.

**Table 2 Approximate STC Ratings for Walls with 16-mm Fire-Rated Gypsum Board (~11 kg/m<sup>2</sup>) on Both Faces<sup>a</sup>**

	1 1	1 2	2 2
38 × 89 mm wood studs, 406 mm oc, RC(610) <sup>b</sup>	46	53	59
Staggered 38 × 89 mm wood studs	47	52	56
Staggered 38 × 89 mm wood studs, RC(610) <sup>b</sup>	51	56	62
Two rows of 38 × 89 mm wood studs, 406 mm oc	58	62	67
90 mm steel studs, 25 gauge, 406 mm oc	49	52	56
90 mm steel studs, 25 gauge, 610 mm oc	49	54	57

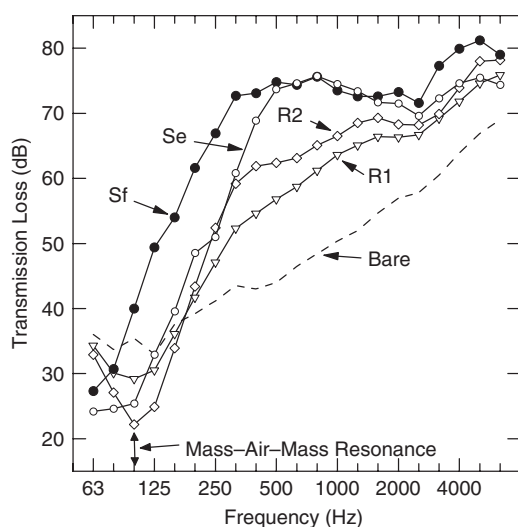
<sup>a</sup> (1|1, 1|2, 2|2 indicates the number of layers of gypsum board on each face. oc = on center = spacing between stud midplanes.) All walls are about 75% filled with glass fiber. Using 13-mm gypsum board reduces the STC by 1 to 2 dB.

<sup>b</sup> Resilient metal channels on one side, 610 mm oc.

## 2.10 Block or Concrete Walls with Added Gypsum Board

The sound insulation of a heavy wall is often improved by adding finishing layers of gypsum board, or something similar, supported independently on resilient mounts to form a cavity construction. Gypsum board is usually added on both sides of the wall, so the construction becomes a triple-leaf wall. Measurements on 190-mm-thick concrete block wall systems<sup>28</sup> showed the importance of avoiding small cavity depths that result in the mass–air–mass resonance being within or near the range used in calculating STC or  $R_w$ . Adding sound-absorbing material to the cavity clearly lowered the mass–air–mass resonance frequency. Adding gypsum board on both sides of the blocks caused the mass–air–mass resonance to be deeper than it was when the gypsum board was applied on just one side. When the cavity depth was only 13 mm, the STC was reduced by one point, but the detrimental effects on the sound insulation below 160 Hz were much more serious. These points are illustrated in Fig. 3. Table 3, based on this research, gives approximate expressions for estimating the improvement in STC rating, which results from the attachment of 13- or 16-mm fire-rated gypsum board to a concrete block wall.

Some concrete blocks are sufficiently porous that the cavity formed behind the gypsum board has an effective depth that is greater than the distance from the surface of the blocks to the rear face of the gypsum board; the air in the cavity penetrates the block.<sup>29</sup> This



**Figure 3** Sound transmission loss through a bare 190-mm concrete block wall (STC 50) and with 16-mm gypsum board attached on 13-mm resilient metal channels, glass fiber, and gypsum board on one side—R1 (STC 54), and on both sides—R2 (STC 49). Curve Se is for gypsum board and 65-mm steel studs on both sides with empty cavities (STC 57). Curve Sf is the same system as Se with 65-mm glass fiber in the cavities (STC 72).

**Table 3** Approximate Expressions for Estimating Change in STC,  $\Delta$ STC, When 16-mm Fire-Rated Gypsum Board ( $\sim 11 \text{ kg/m}^2$ ) Is Attached Resiliently to a Masonry Wall or Supported Independently in Front of It at a Distance  $d$  mm<sup>a</sup>

Cavity absorption	Finish on	$\Delta$ STC
Empty	One side	$0.11 \times d - 1.2$
Filled	Both sides	$0.14 \times d - 2.8$
Empty	One side	$0.12 \times d + 1.9$
Filled	Both sides	$0.44 \times d - 7.4$

<sup>a</sup>The gypsum board is applied on one or both sides, and the cavity is either empty or filled with fibrous absorber.

lowers the mass–air–mass resonance and increases sound insulation, but the blocks themselves do not provide the full sound insulation expected from their mass. If the blocks are sealed on one face to offset this, there is no longer an increase in effective cavity depth on the sealed side, but there still is on the unsealed side; overall there can be considerable benefit.

The detrimental effects of the mass–air–mass resonance can be counteracted by including Helmholtz resonators in the cavity of a double-leaf construction.<sup>30–32</sup> This may increase costs but the benefits can be substantial.

## 2.11 Doors

The sound insulation provided by a door depends not only on the type of door but also on installation details (including the door frame and gaskets around the perimeter). For well-sealed single doors approximate STC values are 20 (hollow core), 28 (solid core wood), and 30 (metal door). Since doors must be operable and therefore not too heavy, the sound insulation available from mass alone is limited. High insulation can be obtained, however, by the use of two doors. For best performance, the width of the airspace between the doors should be large or increased to form a vestibule whenever possible. Absorptive material in the airspace will improve sound insulation. For such double doors, the STC ranges from about 44 to 50 as their separation ranges from 70 to 230 mm. For good sound insulation, double doors must still be well sealed.

“Acoustical” doors—laboratory-tested—provide STC ratings from 35 to over 50. Installation is of critical importance in achieving high sound insulation. The rated performance will not be achieved unless the door frame is fitted into the wall to avoid cracks or hollows that could transmit sound, the gaskets are properly adjusted, and flanking transmission is avoided.

## 2.12 Windows

The STC rating of single sheets of glass is adversely affected by the coincidence effect; the critical frequency,  $f_c$ , for typical thicknesses of glass falls in the STC range. Some improvement can be obtained by using laminated glass—thin glass panes with an



intervening plastic layer. The use of two thin layers keeps the critical frequency fairly high and the plastic provides some damping. For single panes with thicknesses of 13 mm or less,  $STC$  (or  $R_w$ ) may be calculated from  $STC = 0.61t + 27.9$  for solid panes, or  $STC = 0.47t + 31.5$  for laminated panes, where  $t$  is the total thickness of the pane including the lamination (mm).

To obtain an improvement in  $STC$  by using double glazed windows requires a cavity depth of about 20 mm or more. An airspace smaller than 100 mm is inadvisable if a weighted sound reduction index of more than about 40 dB is sought. The  $STC$  for double sheets of glass with an airspace between can be estimated using  $STC = 12.4 + 10.8 \log(t) + 10.7 \log(d)$ , where  $t$  is the total glass thickness (mm) and  $d$  is the depth of the cavity (mm). Using panes of different thickness can reduce the influence of coincidence effect and increase sound insulation. Absorption added in the cavity by lining the perimeter (reveals head and sill if possible) gives most benefit at high frequencies. Further improvements can be made using resonant cavities around the perimeter.<sup>30,31</sup> More information on window glass can be found in Refs. 33 and 34.

Actual  $STC$  values obtained for commercial, operable window systems depend on effectiveness of the sealing systems, proper installation, and other details. With double windows it is even more important than with single windows to ensure proper sealing with resilient materials of high durability.

### 2.13 Outdoor Sound Penetration

The composite sound insulation of a building facade depends on the areas and transmission losses of the walls, windows, doors, roofs, and other elements. The sound fields incident on homes are different from those created for laboratory testing. It is best to use data collected or software created specifically to address this problem.<sup>35–37</sup>

### 2.14 Multielement Partitions, Apertures, and Leaks

The composite transmission coefficient of a multielement partition is given by the sum of terms  $\tau_i A_i / A_t$  for each component:  $A_i$  and  $\tau_i$  represent the area and transmission coefficient of the  $i$ th component of the partition, and  $A_t$  is the total area of the multielement partition. The transmission coefficient for each component may be calculated using  $\tau = 10^{-TL/10}$ . In theory, the transmission coefficient of an opening is approximately one. For many practical cases,  $\tau = 1$  is not a good approximation.<sup>38–40</sup>

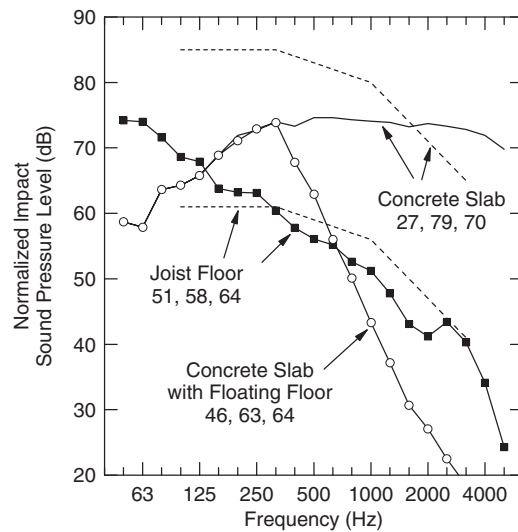
## 3 IMPACT SOUND INSULATION

### 3.1 Impact Sound Ratings

Impact sound is radiated from a floor into rooms below, but it also propagates horizontally, often causing significant annoyance. Impact sound transmission through floor systems is evaluated using a standard

tapping machine<sup>41–44</sup> incorporating five 500-g hammers. Normalized impact sound pressure levels are collected and a reference curve is used to calculate ratings: the impact insulation class<sup>45</sup> (IIC) and the weighted index<sup>46</sup>  $L_{n,w}$ . These are the ratings most frequently used in building codes, and the discussion here focuses primarily on the factors that reduce them. The rating curve is identical in each standard (see Fig. 4), but there are differences in the ratings. As in the case of airborne sound, the ASTM IIC procedure does not allow any unfavorable deviation to be greater than 8 dB, and the IIC rating, like  $STC$  and  $R_w$ , increases as the impact sound insulation improves. The  $L_{n,w}$  rating decreases as the impact sound insulation improves. The relationship between the two ratings is  $IIC = 110 - L_{n,w}$  if the 8-dB rule has not been invoked.

**Proposed New Rating** Since its inception, there has been considerable debate about the usefulness of ISO tapping machine data obtained on different types of floors.<sup>47–50</sup> The current version of ISO 717-2 suggests the use of a spectrum adaptation term,  $C_I$ , to deal with low-frequency noise typical of that generated below a lightweight joist floor. The actual rating suggested,  $L_{n,w} + C_I$ , is just the unweighted sum of the energy in the one-third octave bands from 50 or 100 to 2500 Hz minus 15 dB. This rating is expected to correlate better with subjective evaluation of the noise



**Figure 4** Examples of tapping machine levels. The concrete slab is 150 mm thick. The three numbers under each legend are IIC,  $L_{n,w}$ , and the sum of the energy from 50 to 2500 Hz – 15 dB. The fitted IIC contour is shown for the bare concrete slab and the joist floor. The joist floor comprises 19-mm oriented strandboard, sound-absorbing material, and two layers of 13-mm gypsum board suspended on resilient metal channels. The floating floor is 22-mm parquet on 4-mm cork.

below floors,<sup>51,52</sup> especially if the frequency range for the summation is extended down to 50 Hz.

**Ratings for Floor Coverings** The impact sound insulation of concrete floors is unsatisfactory unless improved by a soft floor covering or a floating floor. Often a designer needs to compare different floor coverings. This is virtually impossible when coverings are tested in different laboratories on different base floor structures. Standard methods<sup>53,54</sup> have been developed to facilitate these comparisons.

A floor covering placed on a concrete slab causes a reduction of impact sound pressure level  $\Delta L(f)$ , that is, to a large extent, independent of the concrete slab on which it has been measured. Therefore to get a rating for the floor covering only, the measured values of  $|\Delta L(f)|$  are added to a reference spectrum for a hypothetical reference floor.<sup>45,53</sup> The resulting curve is evaluated following the standard procedures<sup>45,46</sup> to get the rating for the combination. The improvement rating for the covering is the difference between the rating for the uncovered reference floor and that for the covered reference floor,  $\Delta IIC$  or  $\Delta L_w$  depending on which standard is being used. Note that these ratings are usually different because of the 8-dB rule in ASTM E989.<sup>46</sup> Note also that they do not apply when the floor covering is placed on a joist floor with a wood subfloor.

### 3.2 Concrete Floors

For a homogeneous reinforced concrete floor, doubling the thickness causes an improvement in impact sound insulation of about 10 dB. In practice the thickness of concrete floors only varies from about 150 to 250 mm. With no coverings or with hard finishes cemented directly to the floor, these floors are not satisfactory; the IIC ranges from about 25 to 35 and  $L_{n,w}$  from about 85 to about 75 (Fig. 4 gives an example for a 150-mm-thick slab).

Ceilings suspended under concrete slabs reduce impact and airborne sound transmission to an extent that depends on the cavity depth, cavity absorption, and method of support. Reductions in impact sound pressure levels measured under a 150-mm concrete are shown in Table 4 for four cases. The same improvements were measured for transmission loss in each case. In buildings, if flanking transmission in the walls is not controlled, these improvements may not be achieved.

**Soft Floor Coverings on Concrete Slabs** Soft floor coverings reduce the impact sound pressure level due to the standard tapping machine beginning at a resonant frequency,  $f_0$ , given by  $5.98 \times 10^{-3} (E/h)^{1/2}$  where  $E$  is the dynamic Young's modulus of the covering (N/m) and  $h$  is the thickness of the covering (m). Improvement in impact sound insulation above the frequency  $f_0$  is given approximately by  $\Delta L(f) = 40 \log(f/f_0)$  dB. Improvements in IIC range from about 5 to 10 for thin floor coverings to more than 50 dB for the combination of a soft underpad and a carpet.

**Floating Floors** When a hard floor finish is desired, the most practical means of obtaining high-impact sound insulation is to use a floating floor construction. A floating floor consists of a load-distributing slab resting on a resilient support on top of the structural floor. Floating slabs may consist of concrete (about 30 to 60 mm thick) or of gypsum, asphalt, or of wooden floor boards nailed to battens. The resilient support might be a layer of rock wool, glass fiber, foamed plastics, or the like. Instead of a continuous resilient layer, an array of resilient pads may be used and the cavity between the floating slab and the structural floor filled with soft sound-absorbing material. Special attention has to be paid to avoid solid connections between the floating slab and the

**Table 4 Reduction in Impact Sound Pressure Level due to Suspended Ceiling Systems.**

Case <sup>a</sup>	$\Delta IIC$	50	63	80	100	125	160	200	250	315	400	500
A	15	-8	-8	-8	-5	0	3	2	14	14	17	17
B	18	-5	-6	-3	-7	0	1	4	8	16	19	19
C	24	-8	-1	4	6	12	15	19	20	22	21	22
D	42	15	13	18	20	22	25	30	31	29	36	34
		630	800	1000	250	1600	2000	2500	3150	4000	5000	
A		11	16	16	12	14	15	14	15	16	16	
B		22	21	19	21	21	17	18	24	25	27	
C		23	21	19	18	20	20	22	25	26	28	
D		36	35	33	38	45	44	41	42	47	51	

<sup>a</sup>A: A single layer of 13-mm gypsum board on resilient channels below a ribbed concrete slab. The average air gap was 57 mm.  $\Delta IIC = 15$ .

B: Two layers of 16-mm gypsum board suspended using steel spring and neoprene hangers. The average air gap was 65 mm.  $\Delta IIC = 18$ .

C: Same as B but with 38 mm of rock fiber in the cavity.  $\Delta IIC = 25$ .

D: Two layers of 16-mm gypsum board suspended using steel spring and neoprene hangers. 90 mm of glass fiber in the cavity. The average air gap was 150 mm.  $\Delta IIC = 40$ .

The same improvements apply to transmission loss.



structural floor. Resilient strips, placed around all slab edges, are necessary to avoid reduction of the impact sound insulation, caused by sound transmission from the load-distributing slab to the walls. Some thin floating floors comprise resilient layers about 4 to 12 mm thick finished with a layer of hardwood, about 12 mm thick. These can give  $\Delta$  IIC values around 20<sup>55</sup> (Fig. 4).

A floating floor has a fundamental resonance frequency that is determined by the mass per unit area of the floating floor and the dynamic stiffness per unit area of the resilient support.<sup>56</sup> The latter consists of the dynamic stiffness per unit area of the material and that of the enclosed air,<sup>57</sup> which includes the effects of airflow resistivity.<sup>58,59</sup> Above the resonance frequency, an increase in  $\Delta L(f)$  of around 30 dB/decade in frequency is typical. As with other resonant systems, there can be a *decrease* in sound insulation around the resonance frequency. Procedures for estimating the reduction in impact sound pressure level resulting from the use of a floating floor are given in Ref. 60.

### 3.3 Joist and Truss Floors

The same factors that control airborne sound transmission are important in the control of impact sound through double-leaf floors. Ceilings should be supported resiliently to take advantage of the large cavity provided by the joists, and the cavity should have sound-absorbing material placed in it. Joist or truss floors are generally much lighter than solid concrete floors and, because of the lack of mass, transmit more impact sound at frequencies below 100 Hz, the limit for evaluating IIC and  $L_{n,w}$ . Figure 4 shows a typical impact spectrum for a joist floor, the ratings for which are determined primarily by the levels at low frequencies. In practice, these can only be reduced by increasing the total mass in the floor layers. Adding a resilient finish on the floor decreases high-frequency levels, but the ratings remain essentially unchanged.

The concrete slab in Fig. 4 is greatly improved at high frequencies when a light floating floor is added. Such floating floors placed on joist floors do *not* give the same improvement as on a concrete or other hard surface. In some lightweight joist systems the resilient layer gives no benefit.<sup>55</sup>

With lightweight joist floors, the IIC or  $L_{n,w}$  rating might meet all building code requirements, but occupants may still complain about low-frequency impact sound from walkers. For example, using a carpet will give high IIC or  $L_{n,w}$  ratings but provides little reduction in footstep noise at low frequencies.

A common practical solution for joist construction is to use a slab of concrete or gypsum concrete resting on a resilient layer. The weight of the concrete provides increased protection against low-frequency impacts. The resilient layer reduces high-frequency transmission but, if necessary, the final floor covering can be resilient to some degree. This kind of floating floor inherently provides high STC and IIC ratings and is also an effective means of controlling flanking transmission in the subfloor.

## 4 FLANKING TRANSMISSION

When sound transmission is measured in a laboratory, there is, in principle, negligible transmission of sound energy along paths other than the *direct* path through the specimen. In buildings, all surfaces in both rooms may interact with the common wall to increase the net sound transmission. Sound transmission along paths other than that through the common wall or floor is called *flanking transmission*. When sound isolation is measured in a building, the level in the receiving room includes all flanking sound from all surfaces and energy from sound leaks. The energy is usually ascribed to the common partition and the quantity calculated is called the *apparent sound reduction index* or *apparent transmission loss*.

Flanking transmission can often dominate the sound isolation to the point that improvements in the primary separating element have little or no effect on the composite sound isolation. Procedures for estimating sound isolation between rooms when flanking transmission is present have been proposed<sup>61,62</sup> and standardized<sup>17,60</sup> in Europe. These procedures are more suited to concrete construction than wood or steel frame construction. In framed construction, the layers of material are relatively light and flanking transmission can be very serious<sup>63–67</sup>; structure-borne transmission along the floor can be particularly detrimental. The use of a resiliently supported slab—40 mm or so of concrete—reduces the serious flanking that occurs when the subfloor is common to two adjacent apartments.

During the design of a building, all possible flanking paths must be considered and steps taken to minimize their effect. Otherwise, the net sound isolation can be *much less* than that expected from laboratory testing, and building code requirements may not be met. With good design of the junctions between walls and floors and the use of floating floors and resiliently supported wall and ceiling surfaces, flanking can be reduced so sound isolation ratings measured in the field are close to those obtained in the laboratory.

### 4.1 Acoustical Requirements in Building Codes

National building codes and standards usually contain requirements for sound insulation, aimed at meeting the demands of different functions of rooms and buildings (see Chapter 114). Often, requirements are stated in terms of laboratory measurements. This is an unsatisfactory approach. Flanking transmission can drastically reduce sound isolation between homes. For occupant satisfaction, it is better to assume that the intent of the code is to provide minimum *apparent* STC or IIC values and design accordingly to control flanking sound.

## 5 SOURCES OF INFORMATION ON SOUND TRANSMISSION

Many manufacturers provide collections of sound transmission data using their products. As well, other agencies have printed collections of information.<sup>68,69</sup> When comparing apparently identical structures among

such publications, it is important to be sure that all details are identical. Changes in mass, screw, or stud spacing or some other detail can have a large effect on the sound transmission.

## REFERENCES\*

- ISO 140-3, Acoustics—Measurement of Sound Insulation in Buildings and of Building Elements—Laboratory Measurements of Airborne Sound Insulation of Building Elements, 1995.
- ASTM E90, Standard Test Method for Laboratory Measurement of Airborne Sound Transmission Loss of Building Partitions, 2004.
- ISO 140-4, Acoustic—Measurement of Sound Insulation in Buildings and of Building Elements—Field Measurements of Airborne Sound Insulation Between Rooms, 1998.
- ASTM E336, Standard Test Method for Measurement of Airborne Sound Insulation in Buildings, 2005.
- ASTM E966, Standard Guide for Field Measurement of Airborne Sound Insulation of Building Facades and Facade Elements, 2004.
- ISO 140-5, Acoustics—Measurement of Sound Insulation in Buildings and of Building Elements—Field Measurement of Airborne Sound Insulation of Facade Elements and Facades, 1998.
- M. J. Crocker, P. K. Raju, and B. Forssen, Measurement of Transmission Loss of Panels by Direct Determination of Acoustic Intensity, *Noise Control Eng.*, Vol. 17, 1981, p. 6.
- ASTM E2249, Standard Test Method for Laboratory Measurement of Airborne Transmission Loss of Building Partitions and Elements Using Sound Intensity, 2002.
- ISO 15186-1, Acoustics—Measurement of Sound Insulation in Buildings and of Building Elements Using Sound Intensity—Part 1: Laboratory Conditions; Part 2: In-situ Conditions, 2000.
- R. E. Halliwell and A. C. C. Warnock, Sound Transmission Loss, Comparison of Conventional Techniques with Sound Intensity Techniques, *J. Acoust. Soc. Am.*, Vol. 77, 1985, pp. 2094–2103.
- J. C. S. Lai, M. A. Burgess, P. P. Narang, and K. Mikl, Transmission Loss Measurements: Comparisons between Sound Intensity and Conventional Methods, *InterNoise 91*, p. 1029.
- L. L. Beranek and I. L. Vér, *Noise and Vibration Control Engineering*, Wiley, New York, 1992, Chapter 9.
- ASTM E413, Classification for Rating Sound Insulation, 2004.
- ISO 717, Acoustics—Rating of Sound Insulation in Buildings and of Building Elements—Part 1: Airborne Sound Insulation, 1996.
- ASTM E1332, Classification for Determination of Outdoor-Indoor Transmission Class, 2003.
- D. A. Bies and C. H. Hansen, *Engineering Noise Control*, 3rd ed., Unwin Hyman, London, 2003.
- European Standard EN 12354-1, Estimation of Acoustic Performance of Buildings from the Performance of Elements. Part 1: Airborne Sound Insulation between Rooms.
- K. Gösele, Verringerung der Luftschalldämmung von Wänden durch Dickenresonanzen, *Bauphysik*, Vol. 12, 1990, pp. 187–191.
- A. C. C. Warnock, Controlling Sound Transmission through Concrete Block Walls, Construction Technology Update 13, IRC, NRCC, 1998.
- W. Loney, Effect of Cavity Absorption on the Sound Transmission Loss of Steel Stud Gypsum Wallboard Partitions, *J. Acoust. Soc. Am.*, Vol. 49, 1971, pp. 385.
- R. A. Novak, Sound Insulation of Lightweight Double Walls, *Appl. Acoust.*, Vol. 37, 1992, p. 281.
- P. P. Narang, Effect of Fiberglass Density and Flow Resistance on Sound Transmission Loss of Cavity Plasterboard Walls, *Noise Control Eng. J.*, Vol. 40, No. 3, 1993, p. 215.
- A. C. C. Warnock and J. A. Birta, Summary Report for Consortium on Fire Resistance and Sound Insulation of Floors: Sound Transmission Class and Impact Insulation Class Results, Report IR-766, IRC, NRCC, 1998; and Detailed Report for Consortium on Fire Resistance and Sound Insulation of Floors: Sound Transmission and Impact Insulation Data in 1/3 Octave Bands, Report IR-811, IRC, NRCC, 2000.
- B. H. Sharp, A Study of Techniques to Increase the Sound Insulation of Building Elements, U.S. Dept. of Housing and Urban Development, Washington DC NTIS PB 222 829/4; and Prediction Methods for the Sound Transmission of Building Elements, *Noise Control Eng. J.*, Vol. 11, 1978, p. 53.
- J. D. Quirt, A. C. C. Warnock, and J. A. Birta, Summary Report for the Consortium on Gypsum Board Walls: Sound Transmission Loss Results, Report IR693, IRC, NRCC, 1995.
- A. C. C. Warnock, Summary Report for Consortium on Fire Resistance and Sound Insulation of Floors: Sound Transmission and Impact Insulation Data, Report RR169, IRC, NRCC, 2005.
- A. C. C. Warnock, Sound Transmission Loss Measurements through 190 mm and 140 mm Blocks with Added Gypsum Board and through Cavity Block Walls, Report IR586, IRC, NRCC, 1990.
- A. C. C. Warnock, Sound Transmission through Concrete Blocks with Attached Drywall, *J. Acoust. Soc. Am.*, Vol. 90, 1991, pp. 1454–1463.
- A. C. C. Warnock, Sound Transmission through Two Kinds of Porous Concrete Blocks with Attached Drywall, *J. Acoust. Soc. Am.*, Vol. 92, 1992, pp. 1452–1460.
- J. Enger and T. E. Vigran, Transmission Loss of Double Partitions Containing Resonant Absorbers, *Proc. Inst. Acoust.*, Vol. 7, Part 2, 1985, p. 125.
- J. M. Mason and F. J. Fahy, The Use of Acoustically Tuned Resonators to Improve the Sound Transmission Loss of Double-Panel Partitions, *J. Sound. Vib.*, Vol. 124, No. 2, 1988, p. 367.
- A. C. C. Warnock, Sound Transmission through Slotted Concrete Blocks with Attached Gypsum Board, *J. Acoust. Soc. Am.*, Vol. 94, No. 5, 1993, p. 2713.
- J. D. Quirt, Sound Transmission through Windows. I. Single and Double Glazing, *J. Acoust. Soc. Am.*, Vol. 72, No. 3, 1982, p. 834.

\*IRC/NRCC reports are available from the Institute for Research in Construction, National Research Council of Canada, 1200 Montreal Road, Ottawa, ON K1A 0R6, Canada or directly from the Internet site at [http://irc.nrc-cnrc.gc.ca/pubs/index\\_e.html](http://irc.nrc-cnrc.gc.ca/pubs/index_e.html).

34. J. D. Quirt, Sound Transmission through Windows. II. Double and Triple Glazing, *J. Acoust. Soc. Am.*, Vol. 74, No. 2, 1983, p. 534.
35. J. S. Bradley and J. A. Birta, Laboratory Measurements of the Sound Insulation of Building Façade Elements, Report IR-818, IRC, NRCC, October 2000.
36. J. S. Bradley, K. Lay, and S. G. Norcross, Measurements of the Sound Insulation of a Wood Frame House Exposed to Aircraft Noise, Report IR-831, IRC, NRCC, March 2002.
37. J. S. Bradley, IBANA-Calc Validation Studies, Research Report (RR-125), IRC, NRCC, November 2002.
38. M. C. Gomperts and T. Kihlmann, The Sound Transmission Loss of Circular and Slit-Shaped Apertures in Walls, *Acustica*, Vol. 18, 1967, pp. 144–150.
39. G. P. S. Wilson and W. W. Soroka, Approximation to the Diffraction of Sound by a Circular Aperture in a Rigid Wall of Finite Thickness, *J. Acoust. Soc. Am.*, Vol. 37, 1965, pp. 286–297.
40. T. R. T. Nightingale and J. D. Quirt, Effect of Electrical Outlet Boxes on Sound Insulation of a Cavity Wall, *J. Acoust. Soc. Am.*, Vol. 104, No. 1, 1998, p. 266.
41. ISO 140-6, Acoustics—Measurement of Sound Insulation in Buildings and of Building Elements—Laboratory Measurements of Impact Sound Insulation of Floors, 1998.
42. ISO 140-7, Acoustics—Measurement of Sound Insulation in Buildings and of Building Elements—Field Measurement of Impact Sound Insulation of Floors, 1998.
43. ASTM E492, Standard Method of Laboratory Measurement of Impact Sound Transmission through Floor-Ceiling Assemblies Using the Tapping Machine, 2004.
44. ASTM E1007, Standard Test Method for Field Measurement of Tapping Machine Impact Sound Transmission through Floor-Ceiling Assemblies and Associated Support Structures, 2004.
45. ISO 717-2, Acoustics—Rating of Sound Insulation in Buildings and of Building Elements—Impact Sound Insulation, 1996.
46. ASTM E989, Classification for Determination of Impact Insulation Class (IIC), 2006.
47. T. Mariner and W. W. Hehmann, Impact Noise Rating of Various Floors, *J. Acoust. Soc. Am.*, Vol. 41, 1967, pp. 206–214.
48. R. Josse, How to Assess the Sound-Reducing Properties of Floors to Impact Noise (Footsteps), *Appl. Acoust.*, Vol. 5, 1972, pp. 15–20.
49. E. Gerretsen, A New System for Rating Impact Sound Insulation, *Appl. Acoust.*, Vol. 9, 1976, pp. 247–263.
50. K. Bodlund, Alternative Reference Curves for Evaluation of the Impact Sound Insulation between Dwellings, *J. Sound Vib.*, Vol. 102, 1985, pp. 381–402.
51. J.H. Rindel, On the Influence of Low Frequencies on the Annoyance of Noise from Neighbours, *InterNoise 2003*, p. 1500.
52. K. Hagberg, Ratings Adapted to Subjective Evaluation for Impact and Airborne Sound and Its Application in Building Regulations—A Literature Survey, Paper 5D.08.05, Proc 17th ICA, Rome, 2001.
53. ASTM E2179, Standard Test Method for Laboratory Measurement of the Effectiveness of Floor Coverings in Reducing Impact Sound Transmission through Concrete Floors, 2003.
54. ISO 140-8, Acoustics—Measurement of Sound Insulation in Buildings and of Building Elements—Laboratory Measurement of the Reduction of Transmitted Impact Noise by Floor Covering on a Standard Floor, 1997.
55. A. C. C. Warnock, Impact Sound Measurements on Floors Covered with Small Patches of Resilient Materials or Floating Assemblies, Report IR802, IRC, NRCC, 2001.
56. ISO 9052-1, Acoustics—Determination of Dynamic Stiffness—Materials Used under Floating Floors in Dwellings, 1989.
57. E. E. Ungar, Design of Floated Slabs to Avoid Stiffness of Entrapped Air, *Noise Con. Eng.*, Vol. 12, July–August, 1975, pp. 12–16.
58. ISO 9053, Acoustics—Material for Acoustical Applications—Determination of Airflow Resistance, 1991.
59. ASTM C522, Standard Test Method for Airflow Resistance of Acoustical Materials, 2003.
60. European Standard EN 12534-2, Estimation of Acoustic Performance of Buildings from the Performance of Elements. Part 2: Impact Sound Insulation between Rooms.
61. E. Gerretsen, Calculation of Sound Transmission between Dwellings by Partitions and Flanking Structures, *Appl. Acoust.*, Vol. 12, 1979, p. 413.
62. E. Gerretsen, Calculation of Airborne and Impact Sound Insulation between Dwellings, *Appl. Acoust.*, Vol. 19, 1986, p. 245.
63. J. D. Quirt, T. R. T. Nightingale, and R. E. Halliwell, Dealing with Flanking Transmission in Wood Framed Construction, *Canadian Acoust.*, Vol. 31, No. 3, 2003, p. 52.
64. T. R. T. Nightingale, R. E. Halliwell, and J. D. Quirt, Flanking Transmission in Multi-Family Dwellings. Phase II: Effects of Continuous Structural Elements at Wall/Floor Junctions, Research Report RR-103, IRC, NRCC, November 2002.
65. T. R. T. Nightingale, R. E. Halliwell, and J. D. Quirt, Vibration Response of Floors and the Effectiveness of Toppings to Control Flanking Transmission, *InterNoise 2002*.
66. R. E. Halliwell, J. D. Quirt, and T. R. T. Nightingale, Construction Details Affecting Flanking Transmission in Wood Framed Multifamily Dwellings, *InterNoise 2002*.
67. T. R. T. Nightingale and R. E. Halliwell, Flanking Transmission at Joints in Multi-Family Dwellings. Phase 1: Effects of Fire Stops at Floor/Wall Intersections, Report IR-754, IRC, NRCC, December 1997. <http://irc.nrc-cnrc.gc.ca/fulltext/ir-754>.
68. R. A. Hedeon, *NIOSH Compendium of Materials for Noise Control*, DHEW Publication No. 80-116. U.S. Department of Health, Education and Welfare, 4676 Columbia Parkway, Cincinnati, OH. 45226.
69. R. B. Dupree, *Catalog of STC and IIC Ratings for Wall and Floor/Ceiling Assemblies*, Office of Noise Control, California Department of Health Services, Berkeley, CA, 1981.

# CHAPTER 106

## RATINGS AND DESCRIPTORS FOR THE BUILT ACOUSTICAL ENVIRONMENT

Gregory C. Tocci  
Cavanaugh Tocci Associates, Inc.  
Sudbury, Massachusetts

### 1 INTRODUCTION

Sound in spaces, as well as the acoustical performance of materials or building elements, most often vary significantly with frequency. Easily measured, single-number quantities often do not fully characterize sound in spaces or the acoustical performance of materials. For this reason, *acoustical ratings* or *descriptors* have been developed that characterize in a single number two or more of the three fundamental characteristics of sound: (1) spectral content, (2) level, and (3) time-varying character. These are referred to as ratings or descriptors since many of them cannot be treated mathematically as simple logarithmic values such as sound pressure level or sound transmission loss. Nevertheless, ratings of all kinds have been developed and are most widely used in determining the suitability of sound in spaces or the relative performance of materials.

In speaking of sound in spaces, the term *built environment* has been used to denote that “spaces” as here considered, go beyond simple enclosed building spaces such as offices and classrooms, but are relevant to any place where sound as a signal or as a background needs to be tailored to suit the needs of a listener.

Generally, ratings for acoustical environments either set limits on background sound to achieve an acceptable venue or set requirements for audio signal levels to achieve acceptable functionality. In addition, architectural acoustical criteria set limits for sound transmission through building partition constructions, for example, outdoor sound transmitted indoors and indoor sound transmitted between rooms.

This chapter identifies descriptor and rating methods used in establishing acoustical criteria in buildings in the United States. (Descriptors and rating methods used in Europe are discussed in Chapter 114.) Many of these are defined in other chapters of this handbook; those that are, are only briefly described in this chapter.

The chapter begins with a description of common acoustical descriptors used to quantify sound in the environment. These include sound pressure level, speech interference level, equivalent sound level, and so forth. Many of these are discussed in more detail elsewhere, in particular in Chapter 34. Section 2 of this chapter discusses ratings used to quantify and characterize sound inside and outside of buildings. These include day–night average sound pressure level, noise criteria curves, and so forth. Section 3 discusses descriptors and ratings for the acoustical performance of materials and systems used in the construction

of buildings. These generally break down into two types of ratings. These are ratings used to quantify the ability of building materials to absorb sound and the ability of building materials and systems to resist the transmission of sound. Section 4 discusses descriptors used to assess the quality of sound in building spaces. The discussions draw heavily on standards and methods of the American National Standards Institute (ANSI) and American Society for Testing and Materials (ASTM).

### 2 GENERAL ACOUSTICAL DESCRIPTORS

#### 2.1 A-Weighted Sound Pressure Level

The human ear is sensitive to sound extending from approximately 20 to 20,000 Hz but is most sensitive to sound in the 500- to 4000-Hz frequency range. Above and below this frequency range, in which the ear is most sensitive, the ear is progressively less sensitive to sound. Since sound measurement instrumentation is typically more uniformly sensitive to sound over a considerably wider frequency range than human hearing, sound level meters use electronic filtering to reproduce the varying sensitivity of the ear to sound at different frequencies. Using this filtering, sound level meters indicate a sound level that is more representative of what the ear hears. This filtering is called A-weighting, and sound measured using A-weighted filtering is called A-weighted sound pressure level (abbreviation, AL; letter symbol,  $L_A$ ).

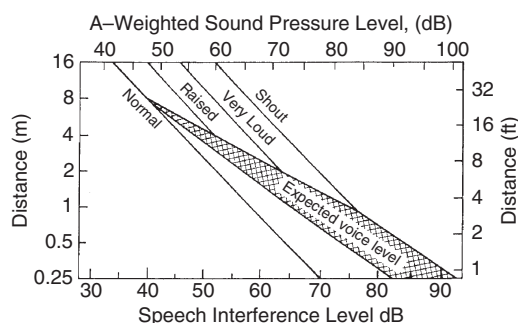
The A-weighted sound pressure level is often used to evaluate general human exposure to sound. The A-weighted sound pressure level is most widely used as it is a convenient single-number quantifier of sound over the audible frequency range (as discussed in Chapter 34). Originally, A-weighting was intended to represent the varying sensitivity of the ear to sound at sound pressure levels ranging between 40 and 60 dB. B- and C- weightings were intended to represent the varying sensitivity of the ear to sound over higher sound pressure level ranges. Both B- and C-weightings allow more low-frequency sound energy with C-weighting being nearly flat across the audible frequency range. However, B- and C-weightings are no longer widely used, with the exception that C-weighting is used by some agencies and researchers in assessing transient sound. Also, in the absence of spectral information (octave band sound pressure levels), the difference between A-weighted and C-weighted sound pressure levels can be used to indicate

the relative content of low-frequency energy in the sound spectrum.

## 2.2 Speech Interference Levels

The speech interference level (SIL) is the arithmetic average of the sound pressure level in octave bands centered at 500, 1000, 2000, and 4000 Hz.<sup>1</sup> SIL is also discussed in Section 7 of Chapter 34. Because the definitions and octave bands used in the past have changed, ANSI S3.14 recommends that the abbreviation SIL be followed by an indication of the octave bands used for computation, for example, SIL (0.5, 1, 2, 4). Figure 1 shows the relationship between speech interference level and vocal effort required at various distances to achieve just-reliable speech communication. The cross-hatch range indicates expectant voice level, that is, the natural inclination of speakers to raise their voices in the presence of high background sound pressure levels. The rate at which the voice is raised ranges between 3 dB and 6 dB for every 10-dB increase in the background A-weighted sound pressure level above 50 dB.

The SIL criteria presented in Fig. 1 are applicable to both indoor and outdoor environments and simply relate to speech communication, without any



**Figure 1** Talker-to-listener distances for just-reliable communication. The curves show maximum permissible talker-to-listener distances for just-reliable speech communication. The parameter on each curve indicates the relative voice level. Since a talker will raise his or her voice in noise, typically at the rate of 3–6 dB for every 10-dB increase in the A-weighted noise level above 50 dB, the expected voice level will increase with increasing noise level. The cross-hatched area shows the range of permissible talker-to-listener distances under these conditions. The lower bound of the cross-hatched area is for voice level being raised at the rate of 3 dB per 10-dB increase in noise level; the upper bound is for a rate of increase of 6 dB per 10-dB increase in noise level. Instructions for use: (1) Measure the A-weighted sound pressure level of the background noise using the slow response of the sound level meter. (2) Locate this sound pressure level on the upper abscissa. (3) A perpendicular dropped from this point will intersect several curves, indicating the maximum distance between the talker and listener for just-reliable speech communication for various levels of vocal effort.

accounting for other circumstances or activities in a space.<sup>2</sup> This figure also includes instructions for its use for determining minimum vocal effort and/or maximum distance to achieve just-reliable speech articulation (articulation index of 0.45) in the presence of broadband (flat spectrum) background noise. The method is not valid for (1) situations where the background sound spectrum departs significantly from being “flat,” (2) situations where the background or the signal sound levels vary significantly with time, (3) communications in highly reverberant environments, and (4) situations when speech is distorted.

## 2.3 Loudness Level

The loudness level (LL) is a single-number rating expressed in units of phons. It is described more fully in Chapters 34 and 119. The loudness level in phons is the level of a 1000-Hz reference tone with a loudness that appears to be equal to that of the spectrum being rated.<sup>3</sup> The loudness level of an octave band spectrum is obtained by a procedure described in ANSI S3.4–1980(R1986).<sup>4</sup> The procedure involves overlaying an octave band spectrum of sound to be rated on contours of approximate equal loudness and interpolating loudness index values for each octave band level of the spectrum. These loudness index values are then used with specified formulas to arrive at a single-number loudness level rating in phons. Phons are a logarithmic quantity. The corresponding linear quantity is sones where 1 sone is the loudness of a sound whose loudness level is 40 phons. A doubling of amplitude in sones corresponds to a factor of 10 increase in loudness level expressed in phons.

## 2.4 Equivalent Sound Pressure Level

As discussed in Chapters 34, 125, and 127, the equivalent sound pressure level (QL; symbol,  $L_{eq}$ ) is the energy average sound pressure level occurring at a particular location over a given time interval. The equivalent sound pressure level is also discussed in Section 9 of Chapter 34. Often, the ambient sound pressure level is monitored for 1-h intervals for environmental sound assessments. When appropriate, hourly equivalent sound pressure levels may be combined in order to determine the equivalent sound pressure level for a 24-h period, or equivalent sound pressure levels for shorter time intervals can be combined to determine the hourly equivalent sound pressure level. Most often, the equivalent sound pressure level is an A-weighted sound pressure level, and the  $L_{eq}$  symbol implies A-weighting. Some agency criteria incorporate the C-weighted equivalent sound pressure level, symbolized as  $L_{Ceq}$ .

## 2.5 Sound Exposure Level

The sound exposure level (SEL; symbols,  $L_{ET}$  or  $L_{AE}$ ) quantifies the total A-weighted sound energy integrated over a time interval for a given acoustical event. To simplify the units to decibels, the SEL of an event is described as the hypothetical equivalent sound pressure level enduring for a period of one second that would have the same amount of acoustic energy as the

specific transient event for which the SEL was measured. The SEL is used to quantify the sound energy associated with a transient event such as an aircraft over flight. Its practical use requires setting a measurement start and a finish time, but if the maximum sound pressure level occurring during an event is high enough in amplitude compared to levels before and after the event, defining precise start and finish times has little influence on the SEL value reached.

## 2.6 Single-Event Noise Exposure Level

The single-event noise exposure level (SENEL) is similar to the SEL except that it incorporates the integration of sound energy from and to defined points in time before and after a transient event. These points in time are defined as the moments during which the event sound pressure level rises above and falls below a specific sound pressure level threshold. For environmental sound analysis, a commonly used threshold is an A-weighted sound pressure level of 65 dB. This threshold is not set by any standard, but by measurement personnel seeking a clear point at which the sound pressure level associated with a transient event is sufficiently above the ambient so that lesser transients in the ambient do not trigger an SENEL event. The concept of SENEL has its roots in instrumentation developed to measure transient events from sources such as aircraft and trains.

In other chapters of this handbook, most particularly Chapters 34, 119, 125, and 127, A-weighting, speech interference level, loudness level, equivalent sound level, sound exposure level, and single-event noise exposure level are discussed. Certain of these do not have direct bearing on current criteria and standards but are sometimes used in data analysis. For example, the SEL and SENEL are sometimes used to determine the day–night exposure level at building sites produced by transient events such as trains or aircraft. In the 1960s, sound produced by building mechanical equipment was often expressed in sones (loudness level). Despite the current use since the 1970s of sound power level and sound pressure level at reference distances, sones are sometimes still used by certain manufacturers for quantifying sound produced by their equipment.

## 2.7 Percentile Sound Pressure Levels

Percentile sound levels ( $L_{XX\%}$ ) are A-weighted sound pressure levels exceeded an indicated (by the  $XX\%$  value) percent of a time interval. Percentile sound levels are also discussed in Section 11 of Chapter 34. Strictly speaking, the descriptor should also indicate the interval length, for example,  $L_{90}(1\text{ h})$ . The  $L_{90}(1\text{ h})$  is the A-weighted sound pressure level exceeded a total of 54 min out of a continuous 60-min interval. Accordingly, the  $L_{10}(20\text{ min})$  is the A-weighted sound pressure level exceeded 2 min out of a continuous 20-min interval.

The  $L_{10}$  is representative of intrusive sounds, sounds of short duration, but high level. The  $L_{90}$ , on the other hand, is representative of nearly the lowest levels of sound occurring during quiet interludes and is often referred to as the background or residual sound level.

The U.S. Federal Highway Administration (FHWA) has developed guidelines for evaluating the impact of highway noise for adoption by state highway agencies. These guidelines allow the alternative use of  $L_{10}$  or  $L_{eq}$  (one or the other, but not both) for assessing traffic sound levels and uses these descriptors to set guideline limits for traffic noise exposure at wayside areas according to various categories of land use.<sup>5</sup>

Some states and municipalities in the United States set environmental noise limits based on percentile sound level limits. For example, the Commonwealth of Massachusetts Department of Environmental Protection requires that sound generated by a commercial facility may not cause an ambient noise level that exceeds the preexisting background A-weighted sound pressure level ( $L_{90}$ ) without the facility operating by more than 10 dB.<sup>6</sup> The City of Cambridge, Massachusetts, requires that construction 10-percentile sound pressure levels  $L_{10}(20\text{ min})$  should not exceed 75 dB at the nearest residential property.<sup>7</sup>

## 3 RATINGS USED TO ASSESS THE ACCEPTABILITY OF AMBIENT SOUND

### 3.1 Day–Night Average Sound Level

The day–night average sound pressure level (DNL; symbol,  $L_{dn}$ ) is a 24-h average A-weighted sound pressure level where a 10-dB “penalty” is applied to sound occurring between the hours of 10:00 p.m. and 7:00 a.m. The 10-dB penalty accounts for the heightened sensitivity of a community to noise occurring at night. This descriptor is also discussed in Section 10 of Chapter 34. Day–night average sound pressure level has become the primary descriptor for general environmental sound in the United States and is often used to assess sound from transportation systems. Among agencies using the day–night average sound pressure level in their criteria and regulations are the U.S. Environmental Protection Agency (EPA),<sup>8</sup> the Federal Aviation Administration (FAA),<sup>9</sup> and the U.S. Department of Housing and Urban Development (HUD).<sup>10</sup>

The U.S. EPA has taken the lead among all federal agencies in unifying usage of environmental sound pressure level descriptors. The EPA has promoted the development of the day–night average sound pressure level but has not enacted regulations controlling general environmental noise. Instead, it has issued guidelines that identify yearly DNL “sufficient to protect public health and welfare from the effects of environmental noise.” Table 1 presents EPA’s suggested levels to protect public health and welfare. The EPA specifically cautions that these tabulated levels are not to be used as regulations by other agencies without addressing economic and other considerations associated with sound level restrictions. Of these levels, the most widely cited are a day–night average sound pressure level of 55 dB for outdoor residential areas and a day–night average sound pressure level of 45 dB for indoor residential spaces. Again, these are only to be used as levels with a margin of safety incorporated and not as EPA’s recommendations for agency limits.

**Table 1** Yearly DNL Values That Protect Public Health and Welfare with a Margin of Safety

Effect	Level	Area
Hearing	$L_{eq}(24) \leq 70$ dB	All areas (at the ear)
Outdoor activity interference and annoyance	$L_{dn} \leq 55$ dB	Outdoors in residential areas and farms and other outdoor areas where people spend widely varying amounts of time and other places in which quiet is a basis for use
	$L_{eq}(24) \leq 55$ dB	Outdoor areas where people spend limited amounts of time, such as school yards, playgrounds, etc.
Indoor activity interference and annoyance	$L_{dn} \leq 45$ dB	Indoor residential areas
	$L_{eq}(24) \leq 45$ dB	Other indoor areas with human activities such as schools, etc.

### 3.2 Community Noise Equivalent Level

The community noise equivalent level (CNEL) is similar to the DNL except that, in addition to the 10-dB penalty applied between the hours of 10:00 p.m. to 7:00 a.m., there is a 5-dB penalty applied to sound between the hours of 7:00 p.m. and 10:00 p.m. CNEL is defined in Chapter 34. Use of this descriptor seems to be declining nationally but is most commonly used in California standards, where it is allowed as an alternative environmental sound pressure level descriptor to the day–night average sound pressure level for assessing environmental sound transmission into building spaces.<sup>11</sup> It is also used to assess community noise, in particular, near airports (Chapter 125).

### 3.3 Noise Criterion Curves

Speech interference level and loudness level are not widely used to evaluate ambient sound in building acoustics. More widely used descriptors are noise criterion (NC) curves. The curves are designed to allow satisfactory speech intelligibility or acoustical comfort in enclosed spaces. They are based on extensive interviews of workers in various noise environments and simultaneously measured octave band noise levels.<sup>12</sup> Noise criterion curves are a simpler alternative to the evaluation of perceived loudness than the loudness level computation procedure. NC curves are also discussed in Section 8 of Chapter 34. Figure 2 contains the set of NC curves.<sup>13</sup> The NC curves are smoothed versions of the loudness level index curves. The NC value shown for each curve is the SIL (600 to 1200, 1200 to 2400, and 2400 to 4800 Hz), that is, in the “old” octave bands, for each curve. Beranek slightly redefined these curves for the preferred octave bands and listed them in tabular form. The definitions of fifth NC increment curves beginning with NC 15 are given in Table 2.<sup>14</sup>

Often, the NC rating of a spectrum is considered within a limited frequency range, such as 500 to 4000 Hz for speech intelligibility or 63 to 125 Hz for low-frequency “rumble”-type sound levels, typically associated with heating, ventilation, and air-conditioning (HVAC) systems.

It should also be noted that NC curves are generally used in evaluating continuous sound inside building spaces produced by mechanical systems or

**Table 2** NC Curve Definitions<sup>14</sup>

NC	Octave Band Frequencies in Hz								A
	63	125	250	500	1000	2000	4000	8000	
70	83	79	75	72	71	70	69	68	77
65	80	75	71	68	66	64	63	62	72
60	77	71	67	63	61	59	58	57	67
55	74	67	62	58	56	54	53	52	63
50	71	64	58	54	51	49	48	47	58
45	67	60	54	49	46	44	43	42	53
40	64	56	50	45	41	39	38	37	49
35	60	52	45	40	36	34	33	32	44
30	57	48	41	35	31	29	28	27	40
25	54	44	37	31	27	24	22	21	36
20	51	40	33	26	22	19	17	16	31
15	47	36	29	22	17	14	12	11	27

environmental sound transmitted into building spaces. Guidelines for assessing the acceptability of sound in buildings generally presume that the background sound does not have tonal or temporal characteristics that lend a distinctive feature to sound, such as transformer hum or fan blade passage tones. Using these criteria to evaluate tonal noise may not be appropriate as it may underestimate the interference of sound on occupant use of spaces.

In the United States background sound in building spaces produced by mechanical systems is not limited by any specific regulation or agency. Instead, the building design profession has, through various organizations, established design criteria for noise in architectural spaces. The two most commonly used criteria are the design guidelines for HVAC system noise in unoccupied spaces established by the American Society of Heating, Refrigerating, and Air-Conditioning Engineers (ASHRAE) and American National Standards Institute (ANSI) S12.2-1995 Criteria for Evaluating Room Noise. For most of the many years that ASHRAE has published recommended design criteria for spaces, it has expressed them as acceptable ranges of NC curves.

In the 1980s, ASHRAE introduced a new set of curves called room criterion (RC) curves, which are discussed below. On their first introduction, ASHRAE publications suggested that RC curves *could* be used



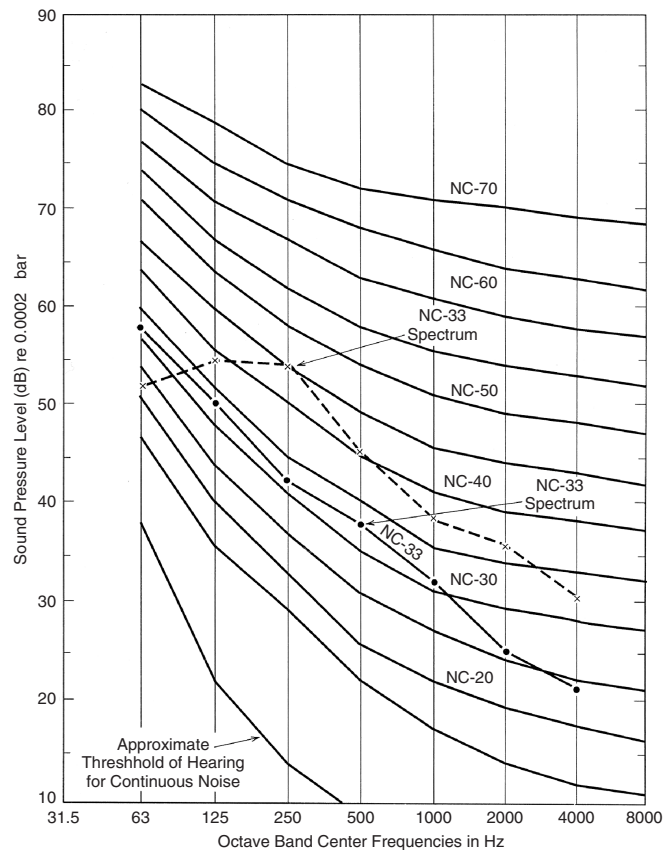


Figure 2 Noise criterion curves.

in lieu of NC curves. As the years progressed, the use of RC curves was cited as *preferred* to the use of NC curves. In the 2003 *ASHRAE Applications Handbook*<sup>15</sup> recommended ranges of background sound in building spaces are expressed *only* as ranges of RC(N) curves (p. 47.29). The 2003 *ASHRAE Applications Handbook* states (footnote b, Table 34, page 47.29), “When quality of sound in the space is important, specify criteria in terms of RC(N). If quality of sound in the space is of secondary concern, the criteria may be specified in terms of NC or NCB levels of similar magnitude.”

Although RC curves represent a better quality of background sound, NC curves are still in wider use at this time as they represent an acceptable compromise between economy and quality of background sound. As a result, the 2005 edition of the *ASHRAE Fundamentals Handbook*<sup>16</sup> presents several methods. These include A-weighting, NC, RC, RC Mark II, and NCB (balanced noise criteria) rating methods. The 2005 *ASHRAE Fundamentals Handbook* indicates (page 7.17) that the RC Mark II method is recommended by ASHRAE, presumably conditioned by the above-mentioned table

footnote b in the 2003 *ASHRAE Applications Handbook*. Table 3 presents the ASHRAE recommended design guidelines for HVAC system noise in unoccupied spaces. These are expressed in RC(N) levels. For use with NC curves, substituting NC levels equal to the RC levels shown is generally acceptable, subject to the cautionary footnote b in Table 3.

### 3.4 Room Criterion Curves

ASHRAE has adopted the use of room criterion (RC) curves for evaluating the background sound in building spaces produced by mechanical systems. These curves have undergone some refinements<sup>17</sup> and a new auxiliary descriptor, quality assessment index (QAI), has been added. The revised curves together with the QAI descriptor comprise what is now called the RC Mark II method. Unlike NC curves, RC curves are straight lines, as shown in Fig. 3. The Mark II RC curves differ slightly from the original curves in that they are flat below 31 Hz. These curves are used by superposing them on a measured octave band spectrum.

The RC value of the spectrum is determined through the following procedure:

**Table 3 Design Guidelines for HVAC-Related Background Sound in Rooms**

Room Types	RC(N) (QAI $\leq$ 5 dB) <sup>a,b</sup>
Residences, Apartments, Condominiums	25–35
Hotels/Motels	
Individual rooms or suites	25–35
Meeting/banquet rooms	25–35
Corridors, lobbies	35–45
Service/support areas	35–45
Office Buildings	
Executive and private offices	25–35
Conference rooms	25–35
Teleconference rooms	25 (max)
Open-plan offices	30–40
Corridors and lobbies	40–45
Hospitals and Clinics	
Private rooms	25–35
Wards	30–40
Operating rooms	25–35
Corridors and public areas	30–40
Performing Arts Spaces	
Drama theaters	25
Concert and recital halls <sup>c</sup>	
Music teaching studios	25
Music practice rooms	30–35
Laboratories (with Fume Hoods)	
Testing/research, minimal speech communication	45–55
Research, extensive telephone use, speech communication	40–50
Group teaching	35–45
Church, Mosque, Synagogue	
General assembly with critical music programs <sup>c</sup>	25–35
Schools <sup>d</sup>	
Classrooms	25–30
Large lecture rooms (without speech amplification)	25–30
Libraries	25
Courtrooms	30–40
Unamplified speech	25–35
Amplified speech	30–40
Indoor Stadiums, Gymnasiums	
Gymnasiums and natatoriums <sup>e</sup>	45–55
Large seating-capacity spaces with speech amplification	45–55

<sup>a</sup> Values and ranges are based on judgment and experience, not on quantitative evaluations of human reactions. They represent general limits of acceptability for typical building occupancies. Higher or lower values may be appropriate and should be based on a careful analysis of economics, space usage, and user needs.

<sup>b</sup> When quality of sound in the space is important, specify criteria in terms of RC(N). If quality of sound in the space is of secondary concern, the criteria may be specified in terms of NC or NCB levels of similar magnitude.

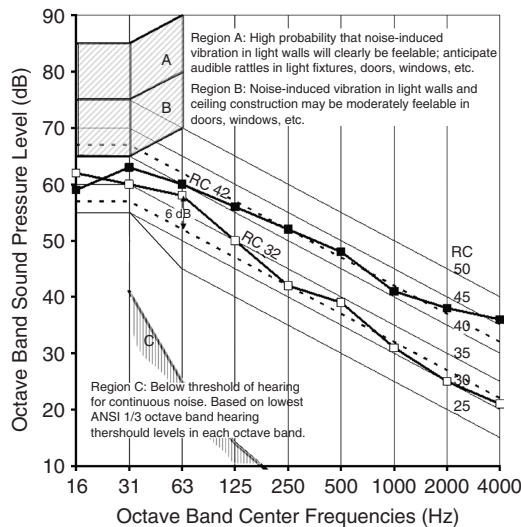
<sup>c</sup> An experienced acoustical consultant should be retained for guidance on acoustically critical spaces (below RC 30) and for all performing arts spaces.

<sup>d</sup> Some educators and others believe that HVAC-related sound criteria for schools, as in previous editions of this table, are too high and impede learning for affected groups of all ages. See ANSI *Standard* S12.60-2002 for classroom acoustics and a justification for lower sound criteria in schools. The HVAC component of total noise meets the background noise requirement of that standard if HVAC-related background sound  $\leq$  RC 25(N).

<sup>e</sup> RC or NC criteria for these spaces need only be selected for the desired speech and hearing conditions.

Source: Reprinted with permission from the 2005 ASHRAE *Applications Handbook*.<sup>16</sup>

1. Determine the midfrequency average level ( $L_{MF}$ ). This is the arithmetic average, to the nearest whole number, of the sound pressure levels in the 500-, 1000-, and 2000-Hz octave frequency bands. This is the RC rating associated with the room sound pressure level spectrum.
2. Draw a line having a  $-5$  dB/octave slope through the RC level at 1000 Hz determined from step 1.
3. Classify the subjective spectral balance of the room sound pressure level spectrum as follows:
  - a. *Neutral*. A spectrum classified as neutral is free of tonal quality and would be perceived as unobtrusive or bland. A neutral sound spectrum falls exactly along or close to a single RC contour. If the octave band data do not exceed the RC curve determined in step 2 by more



**Figure 3** Room criterion curves plus examples of RC 42(N) and RC 32(R) sound pressure level spectra.

than 5 dB at and below 500 Hz and do not exceed the RC curve by more than 3 dB at and above 1000 Hz, the spectrum is considered neutral, and the designator (N) is placed after the RC level.

- b. *Rumble.* A sound spectrum that is perceived to have a “rumbly” quality has an excess of low-frequency sound energy. A rumbly spectrum is characterized as one with octave band sound levels that exceed the RC curve determined in step 2 by more than 5 dB at and below 500 Hz. For such spectra the designator (R) is placed after the RC level.
- c. *Hiss.* A sound spectrum that is perceived to have a “hissy” quality has an excess of high-frequency energy. A hissy spectrum is characterized as one with octave band sound levels that exceed the RC curve determined in step 2 by more than 3 dB above 500 Hz. For such spectra, the designator (H) is placed after the RC level.
- d. *Acoustically Induced Perceptible Vibration.* The cross-hatched region of the RC curves in Fig. 3 indicates sound pressure levels in the 16- to 63-Hz octave bands at which perceptible vibration in building walls and ceilings can occur. These sound levels often produce rattles in cabinets, doors, pictures, lighting fixtures, and so forth. For spectra with levels that fall into this range, the designator (RV) is placed after the RC level.

Figure 3 also provides examples of two types of spectra. In one case, the spectrum follows along the RC 42 curve (i.e., the average of the sound pressures in the 500-, 1000-, and 2000-Hz octave bands is 42 dB).

In this spectrum, all of the octave band levels are within the prescribed limits, and is therefore designated an RC 42(N) spectrum. The spectrum labeled RC 32(R) is generally 10 dB lower than the RC 42(N) spectrum, except in the low frequencies where the 63-Hz octave band exceeds the RC 32 contour by 6 dB, thus constituting a low-frequency rumble component.

Once, having determined the RC rating and the spectral balance characteristic of a spectrum (i.e., neutral, rumbly, or hissy), the QAI can then be determined using the following three steps.

Step 1 is to determine the RC rating using the  $L_{MF}$  as previously discussed. For convenience, this curve should be plotted together with the spectrum or listed in a table as discussed below.

Step 2 is to calculate the energy-average spectral deviations in each of the three previously mentioned frequency regions. These are as follows:

$$\Delta LF = 10 \log \left( \frac{10^{\Delta L_{16}/10} + 10^{\Delta L_{31}/10} + 10^{\Delta L_{63}/10}}{3} \right)$$

$$\Delta MF = 10 \log \left( \frac{10^{\Delta L_{125}/10} + 10^{\Delta L_{250}/10} + 10^{\Delta L_{500}/10}}{3} \right)$$

$$\Delta HF = 10 \log \left( \frac{10^{\Delta L_{1000}/10} + 10^{\Delta L_{2000}/10} + 10^{\Delta L_{4000}/10}}{3} \right)$$

In the above relationships, the  $\Delta L_f$  values are the differences between the spectrum value and the RC curve value at that frequency.

Step 3 is to determine the quality assessment index (QAI). The QAI is the difference between the highest and lowest energy-average spectral deviations. If the QAI is less than or equal to 5 dB, then the spectrum is presumed to be neutral, that is, the spectrum exhibits proper balance between low-, mid-, and high-frequency ranges. Accordingly, the qualitative descriptor following the RC rating would be (N). If the QAI is greater than 5 dB, then the qualitative descriptor would be determined by the maximum energy-average spectral deviation and signified (LF), (MF), or (HF). If the spectrum exceeds the moderate or clearly noticeable criteria, the qualitative descriptors ( $LV_A$ ) or ( $LV_B$ ) would also be used. It is possible that two descriptors would be needed, that is, one of (N), (LF), (MF), or (HF) and one of ( $LV_A$ ) or ( $LV_B$ ).

Using the above three-step process, the QAI for the RC 32 spectrum of Fig. 3 has been computed in the worksheet presented in Table 4. The following is a brief explanation of the worksheet in Table 4.

Line 2 is the measured or calculated sound pressure level spectrum.

Line 3 is the  $L_{MF}$ , the arithmetic average of sound pressure levels at 500, 1000, and 2000 Hz and is also the RC Mark II rating of the spectrum.

**Table 4 RC Mark II Rating and QAI Worksheet**

Line	Column 1	2	3	4	5	6	7	8	9	10	11	12	13
		Octave Band Frequencies (Hz)											
1		16	31	63	125	250	500	1000	2000	4000	8000	16000	A
2	$L_p$	62	60	58	50	42	39	31	25	21	0	0	41
3	$L_{MF}$							32					
4	RC curve	57	57	52	47	42	37	32	27	22			
5			LF			MF			HF				
6	$\Delta L_f$	5	3	6	3	0	2	-1	-2	-1			
7	$\Delta LF, \Delta MF, \Delta HF$		4.8			1.8			-1.3				
8	QAI					6.1							
9	Quality Descriptor												
10													
11		1/1 Center Freq. (Hz)											
12		16	31	63	Max								
13	LFV <sub>A</sub>	75	75	80									
14	$L_p - LFV_B$	-13	-15	-22	-13								
15													
16		1/1 Center Freq. (Hz)											
17		16	31	63	Max								
18	LFV <sub>B</sub>	65	65	70									
19	$L_p - LFV_B$	-3	-5	-12	-3								

Line 4 is the corresponding neutral RC curve.

Line 5 includes the three band groupings in each three-band set.

Line 6 lists the arithmetic differences between the spectrum and the RC curve values in each frequency.

Line 7 includes the energy-average spectral deviation factors.

Line 8 is the arithmetic difference between the highest and lowest energy-average spectral deviation factors and is the QAI.

Line 13 is the clearly noticeable vibration criterion.

Line 14 is the arithmetic difference between the measured spectrum levels of line 2 and the clearly noticeable vibration criterion of line 13.

Line 18 is the moderately noticeable vibration criterion.

Line 19 is the arithmetic difference between the measured spectrum levels of line 2 and the clearly noticeable vibration criterion of line 18.

Table 5 presents a summary of the RC Mark II rating for the RC 32 spectrum shown in Fig. 3 and entered into Table 4. A copy of a Microsoft Excel spreadsheet to perform the RC Mark II computations for a given spectrum is available from the ASHRAE technical committee on sound and vibration (TC 2.6).

Having determined an RC Mark II rating, Blazier<sup>17</sup> provides a means to determine how a room occupant might respond to a given spectrum. Occupant subjective responses are indicated "acceptable," "marginal," and "objectionable." These responses presume that the RC rating (which is the  $L_{MF}$ ) is consistent with recommendations for such ratings on the basis of space use. The subjective responses are provided in Table 6.<sup>17</sup>

**Table 5 Summary of QAI Computation for RC 32 Spectrum of Figure 3**

RC Mark II Evaluation Summary	
RC neutral curve	32
A-weighted sound pressure level (dB)	41
LFVB or LFVA or neither?	0
<i>Energy-average spectral deviations</i>	
LF	4.8
MF	1.8
HF	-1.3
<i>Quality Assessment Index</i>	
QAI	6.1
Qualitative descriptor	LF
Spectrum RC Mark II Rating	<b>RC 32(LF)</b>

According to data in Table 5, the spectrum analyzed in Table 4 is neutral in character and has a QAI of 6.1. Since the spectrum predominates in the low-frequency range (LF) and the QAI is greater than 5 dB, the sound represented by the spectrum should be perceived as marginally acceptable as long as the RC 32 rating is appropriate for the space in which it occurs.

### 3.5 Balanced Noise Criterion Curves

Beranek<sup>18,19</sup> has drawn upon low-frequency hearing considerations to extend NC curves down to low frequencies. He has also sloped downward the high-frequency ends of the NC curves to reduce the subjectively hissy nature of sound spectra that conform to NC spectra shapes, thereby creating a "balanced" spectrum subjectively perceived as more uniform

**Table 6 Interpretation of RC Mark II Ratings Presuming Spectra Are Appropriate for Space Use<sup>17</sup>**

Sound Quality Descriptor	Subjective Perception	QAI	Occupant Response
(N) Neutral	Balanced, no one frequency range dominates	$QAI \leq 5 \text{ dB}$ ( $L_{16}, L_{31.5} \leq 65 \text{ dB}$ )	Acceptable
(LF) Rumble	Low-frequency range dominant (16–63 Hz)	$\leq 5 \text{ dB}$ ( $L_{16}, L_{31.5} > 65 \text{ dB}$ ) $5 \text{ dB} < QAI \leq 10 \text{ dB}$	Marginal Marginal
(LFV <sub>A</sub> ) Rumble, perceptible surface vibration	Low-frequency range dominant (16–63 Hz)	$QAI > 10 \text{ dB}$ $QAI \leq 5 \text{ dB}$ ( $L_{16}, L_{31.5} > 75 \text{ dB}$ )	Objectionable Marginal
(LFV <sub>B</sub> ) Rumble, perceptible surface vibration	Low-frequency range dominant (16–63 Hz)	$5 \text{ dB} < QAI \leq 10 \text{ dB}$ $QAI > 10 \text{ dB}$ $QAI \leq 5 \text{ dB}$ ( $L_{16}, L_{31.5} > 65 \text{ dB}$ )	Marginal Objectionable Marginal
(MF) Roar	Mid-frequency range dominant (125–500 Hz)	$5 \text{ dB} < QAI \leq 10 \text{ dB}$ $QAI > 10 \text{ dB}$ $5 \text{ dB} < QAI \leq 10 \text{ dB}$	Marginal Objectionable Marginal
(HF) Hiss	High-frequency range dominant (1000–4000 Hz)	$QAI > 10 \text{ dB}$ $5 \text{ dB} < QAI \leq 10 \text{ dB}$ $QAI > 10 \text{ dB}$	Objectionable Marginal Objectionable

and devoid of significant tonal content. A set of balanced noise criterion curves (NCBs) are presented in Fig. 4. NCB curves are also discussed in Section 8 of Chapter 34. As with RC curves, NCB curves are accompanied by a procedure for assessing the perceived balance of a sound spectrum, that is, whether or not a spectrum will be perceived as neutral, rumble, or hissy. This procedure is much like that used with the RC curves, including the use of designators (N), (R), (H), and (RV) following the BNC rating. Rules for assessing rumble and hissy qualities of sound spectra using NCB curves are as follows:

1. Determine the PSIL for the spectrum being evaluated. The PSIL is the arithmetic average of sound levels in the 500-, 1000-, 2000-, and 4000-Hz octave bands rounded to the nearest decibel, for example, XX. This spectrum would then be denoted an NCB-XX spectrum.
2. The spectrum will be perceived as rumble if any octave band sound pressure level at or below 1000 Hz is above the NCB-YY curve. YY is equal to the XX value in step 1 plus 3 dB.
3. The spectrum will be perceived as hissy if any octave band sound pressure level at frequencies above 500 Hz exceeds the NCB-ZZ curve. To determine the value ZZ, first determine the arithmetic average of sound pressure levels in the three octave bands 125 through 500 Hz. Then determine which NCB curve has this sound pressure level at 250 Hz. This is the NCB-ZZ curve.

Figure 4 also illustrates the evaluation of a spectrum using NCB curves. The example spectrum is the lower of the two spectra shown in Fig. 3 used to illustrate the use of RC curves. Note that using the NCB curves, this spectrum exhibits rumble characteristics in the 63-, 125-, and 500-Hz octave bands where octave band

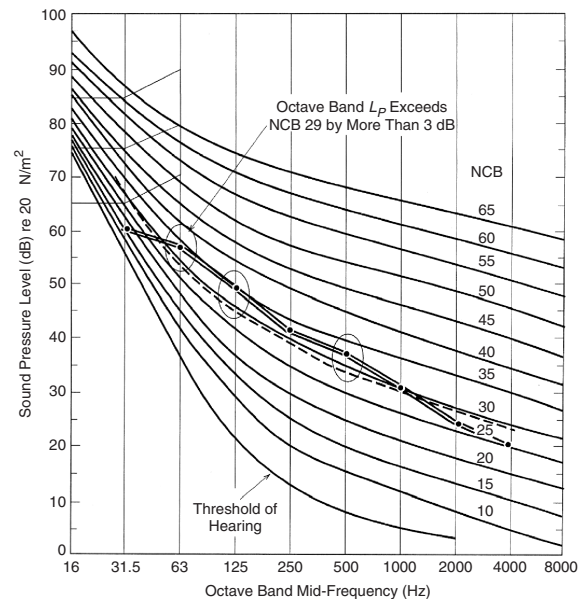
sound levels exceed the NCB 29 curve by more than 3 dB.

#### 4 DESCRIPTORS AND RATINGS FOR MATERIALS AND BUILDING CONSTRUCTIONS THAT AFFECT SOUND INSIDE BUILDING SPACES

##### 4.1 Sound Absorption Coefficient

The ability of a material to absorb sound is characterized by the sound absorption coefficient ( $\alpha$ ). This is the ratio of the amount of sound energy absorbed to the amount incident on the surface of a sound-absorbing material. Theoretically, this can range between 0 and 1.0. The higher the sound absorption coefficient the better the ability of the material to absorb sound. Normally, materials considered to be sound absorbing have sound absorption coefficients greater than or equal to 0.5 (i.e., 50%). Because sound-absorbing materials have differing sound absorption performances at different frequencies, sound absorption coefficients are generally determined via measurements and reported in octave band frequencies—generally 125, 250, 500, 1000, 2000, and 4000 Hz. Sound absorption coefficient can be measured in a reverberation chamber<sup>20</sup> or in an impedance tube using any one of a variety of specified mounting methods.<sup>21</sup> Mounting methods, especially clearance between the material and hard backing surface (reverberation room walls, floor, or ceiling) can affect the measured sound absorption coefficient significantly.

It should be noted that there are two different approaches to measuring sound absorption coefficient. The Sabine absorption coefficient is derived from the measurement of the decrease in reverberation time when an absorptive material is mounted in a reverberation chamber. A reverberation chamber is a large room built with hard, sound reflective surfaces. The reverberation time, as discussed below, is the time it takes



**Figure 4** Balanced noise criterion curves for occupied rooms. Octave-band sound pressure levels of the magnitudes indicated in regions A and B may induce audible rattles or feelable vibrations in lightweight partitions and ceiling constructions (e.g., thin plaster or gypsum board on metal framing) as follows: region A, clearly noticeable vibrations; region B, moderately noticeable vibrations. (From Ref. 13.)

for the sound pressure level in the room to decay by 60 dB. This technique for quantifying absorption coefficient is best applied to relative reflective materials, though in practice the method is widely used to evaluate sound absorption coefficient of materials over the full range of sound absorption coefficient. Using this method to evaluate sound absorption coefficient tends to overestimate  $\alpha$  for materials with relative high sound absorption coefficients.

The random incidence sound absorption coefficient, also referred to as the statistical absorption coefficient, is derived mathematically from measurements of sound absorption using an impedance tube. An impedance tube is a circular or rectangular tube with cross-sectional dimensions much smaller than the shortest wavelength to be measured. The length of the tube is longer than the first null determined by drawing the microphone probe away from the surface of the sound absorption material. A sound absorption material sample is placed at the closed end of the tube. A loudspeaker at the opposite end produces a pure tone that creates a standing wave. The distance of the standing-wave null from the surface of the material is used to calculate the normal absorption coefficient of the material. From this, the random sound absorption coefficient is computed.<sup>22</sup>

The Sabine and random sound absorption coefficients are similar in that both are defined for a reverberant sound field in which energy is uniformly incident on surfaces from all directions. Moreover, Sabine and random sound coefficients are virtually identical for

surfaces with sound absorption coefficients of 0.1 or lower, that is, for surfaces that are mostly reflective.

The Sabine and random sound absorption coefficients differ in that the Sabine absorption coefficient is determined through an experiment by which it is measured. The analysis of the experimental data uses the Sabine reverberation formula which has three presumptions. These are that the total sound absorption in the room is the sum of the absorptions of individual surfaces, all surfaces have nearly the same absorption coefficient, and the sound absorption coefficient is small. On the other hand, the random incidence absorption coefficient is predicted from the knowledge of the absorption coefficient for a particular direction of incidence.

Use of the random incidence absorption coefficient generally produces better results in large auditoria. This is since in large auditoria two Sabine formula assumptions are often not met. These are that all surfaces have about the same sound absorption and that all surface absorptions are small. Large auditoria most often have seating areas that are much more sound absorptive than other surfaces. (For more information, refer to Lam.<sup>22</sup>)

## 4.2 Noise Reduction Coefficient

To simplify comparison between sound-absorbing materials, a single-value descriptor called the noise reduction coefficient (NRC)<sup>20</sup> is used. It is the arithmetic average of the sound absorption coefficients at 250, 500, 1000, and 2000 Hz rounded to the nearest 0.05. Generally, for sound-absorbing materials, the

NRC falls between 0.55 and 0.95. Again, the higher the NRC, the higher the sound absorption performance of a material. Table 7 presents octave band sound absorption coefficients and the corresponding noise reduction coefficients for the common building materials listed.

Often, the sound absorption of building components, such as upholstered chairs in an auditorium or room sound absorption devices sold as units, are quantified in sabins, either metric (square metres) or English (square feet). This is the case for chairs, pews, and seated audience in Table 7. One sabin is an amount of room absorption equivalent to one square foot (or one square meter in metric units) of material having a sound absorption coefficient of 1.0.

### 4.3 Noise Reduction

The sound transmission loss (TL) of a material or building construction element is measured in a laboratory under specific conditions generally not typical of

how these materials or constructions are used in actual buildings.<sup>23</sup> The TL is related to the noise reduction (NR), which is the arithmetic difference between the one-third octave band sound pressure levels measured in the source and receiver rooms. In actual field conditions, which generally do not conform to minimum required laboratory conditions, the NR is measured and no attempt is made to adjust it to approximate the TL measured in a laboratory.<sup>24</sup> Instead, the NR is used and the sound transmission class (STC) rating method as described below is applied to the NR data.<sup>25</sup> The result as explained below is the noise insulation class (NIC) rating.

Noise reduction is influenced by mass, stiffness, and damping but also by the surface area size of the partition and the acoustical conditions of the source and receiver rooms. Noise reduction is not only related to the ability of a wall construction to resist the transmission of sound, but it is also related to the size

**Table 7 Sound Absorption Coefficients of General Building Materials and Furnishings**

Material	Sound Absorption Coefficient ( $\alpha$ )						NRC
	125 Hz	250 Hz	500 Hz	1000 Hz	2000 Hz	4000 Hz	
Brick, unglazed	0.03	0.03	0.03	0.04	0.05	0.07	0.05
Carpet, heavy, on concrete	0.02	0.06	0.14	0.37	0.60	0.65	0.45
Same, on 40-oz hairfelt or foam rubber	0.08	0.24	0.57	0.69	0.71	0.73	0.55
Concrete block, painted	0.10	0.05	0.06	0.07	0.09	0.08	0.05
Fabrics							
Light velour, 10 oz/yd <sup>2</sup> , hung straight, in contact with wall	0.03	0.04	0.11	0.17	0.24	0.35	0.15
Medium velour, 14 oz/yd <sup>2</sup> , draped to half area	0.07	0.31	0.49	0.75	0.70	0.60	0.55
Heavy velour, 18 oz/yd <sup>2</sup> , draped to half area	0.14	0.35	0.55	0.72	0.70	0.65	0.60
Floors							
Concrete or terrazzo	0.01	0.01	0.02	0.02	0.02	0.02	0.00
Linoleum, asphalt, rubber, or cork tile on concrete	0.02	0.03	0.03	0.03	0.03	0.02	0.05
Wood	0.15	0.11	0.10	0.07	0.06	0.07	0.10
Glass, large panes of heavy plate	0.18	0.05	0.04	0.03	0.02	0.02	0.05
Gypsum board, $\frac{1}{2}$ in. nailed to 2 × 4's 16 in. on center	0.29	0.10	0.05	0.04	0.07	0.09	0.05
Marble or glazed tile	0.01	0.01	0.01	0.01	0.02	0.02	0.00
Openings							
Stage, depending on furnishings				0.25–0.75			
Deep balcony, upholstered seats				0.50–1.00			
Grilles, ventilating				0.15–0.50			
Other surfaces							
Plaster, gypsum, or lime, smooth finish on tile or brick	0.13	0.15	0.02	0.03	0.04	0.05	0.05
Plaster, gypsum, or lime, rough finish on lath	0.02	0.03	0.04	0.05	0.04	0.03	0.05
Same, with smooth finish	0.02	0.02	0.03	0.04	0.04	0.03	0.05
Plywood paneling, in. thick	0.28	0.22	0.17	0.09	0.10	0.11	0.05
Water surface, as in a swimming pool	0.01	0.01	0.01	0.02	0.02	0.03	0.00
Air, sabins per 1000 ft <sup>3</sup>	—	—	—	—	2.30	7.20	—
Type of Seats/Audience	Absorption <sup>a</sup>						
	125 Hz	250 Hz	500 Hz	1000 Hz	2000 Hz	4000 Hz	
Audience, seated in upholstered seats, ft <sup>2</sup> of floor area	0.60	0.74	0.88	0.96	0.93	0.85	
Unoccupied cloth-covered upholstered seats, ft <sup>2</sup> of floor area	0.49	0.66	0.80	0.88	0.82	0.70	
Unoccupied leather-covered upholstered seats, ft <sup>2</sup> of floor area	0.44	0.54	0.60	0.62	0.58	0.50	
Wooden pews, occupied, ft <sup>2</sup> of floor area	0.57	0.61	0.75	0.86	0.91	0.86	
Chairs, metal, or wood seats, each, unoccupied	0.15	0.19	0.22	0.39	0.38	0.30	

<sup>a</sup>Values given are in sabins per square foot of seating area or per unit. (oz/yd<sup>2</sup> = 0.034 kg/m<sup>2</sup>; ft<sup>2</sup> = 0.0929 m<sup>2</sup>.)



of the transmitting wall and the reverberant character of the receiver room. Hence, a wall construction used in different circumstances may result in different noise reductions. Most importantly, noise reduction is significantly affected by the quality of construction, specifically with respect to sound leakage paths associated with gaps and penetrations in the construction, including the perimeter of doors and windows, electrical outlets, fixtures, ductwork, and so forth.

#### 4.4 Sound Transmission Loss

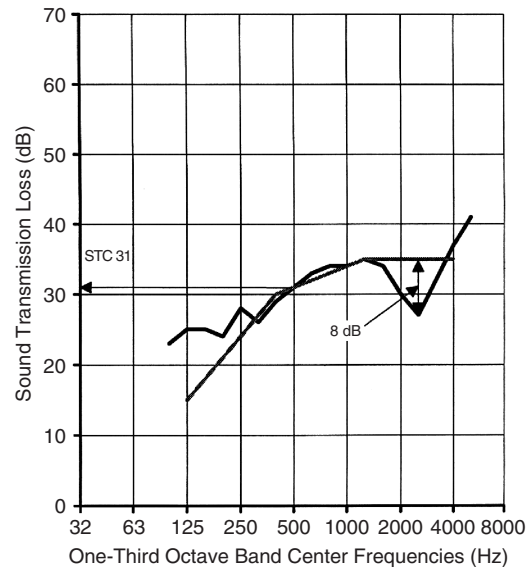
Sound transmission loss is 10 times the logarithm of the ratio between the sound energy incident on a material or sound isolation construction, divided by the sound energy transmitted through this material, and is expressed in decibels. Unlike noise reduction, sound transmission loss is measured in a laboratory according to standards established in ASTM E90.<sup>23</sup> The standard requires that sound transmission loss be measured in one-third octave frequency bands in a source room–receiver room test suite that complies with certain standards of sound isolation and room dimensions. The result of the test standard is a one-third octave band sound transmission loss spectrum extending from 100 (80 optionally) to 5000 Hz.

Unlike noise reduction, the TL is influenced only by mass, stiffness, and damping and how a construction is configured. Specifying the performance of a wall construction in terms of TL is more logical in that TL is only influenced by characteristics directly related to properties of the material or wall construction type.

#### 4.5 Sound Transmission Class Rating

Since TL is frequency dependent, it is generally reported in the one-third octave frequency bands between 125 and 4000 Hz. As a convenience, a single-number rating method has been developed that allows a single value to be ascribed to a transmission loss spectrum that is a set of 16 one-third octave band TL values. This rating is referred to as the sound transmission class (STC), which has been defined in ASTM E413.<sup>25</sup> This standard defines a procedure for determining the STC rating for a TL spectrum that involves fitting a specified contour to one-third octave band TL data.

The STC value was originally developed to approximate the performance of a material in reducing the transmission of intelligible speech sounds and other household sounds. The STC characterization of TL is useful for a quick comparison of materials, but it is not necessarily useful for assessing the performance of a material with respect to other nonspeech sounds such as music and transportation noise sources. For this purpose, it is necessary to consider octave or third octave band TL spectra with specific attention paid to sound in the low-frequency range, typically at frequencies below 500 Hz. The STC contour is shown in Fig. 5. Determining the STC for a partition construction and/or material involves fitting this contour



**Figure 5** A  $\frac{1}{4}$ -in. glass sound transmission loss and STC contour. (1 in. =  $2.54 \times 10^{-2}$  m.)

to the 16 one-third octave band TL values. This procedure involves raising or lowering the contour until the following two rules are met:

1. The contour may not be raised above the point at which the TL in any one-third octave band falls more than 8 dB below the contour.
2. The contour may not be raised above the point at which the total number of deficiencies is greater than 32.

A deficiency occurs when the TL data in any one-third octave band falls below the contour. For example, three deficiencies would be when the TL data in any one-third octave fall 3 dB below the contour, or when the data in three one-third octave bands fall 1 dB below the contour. Figure 5 further illustrates the meaning of a deficiency.

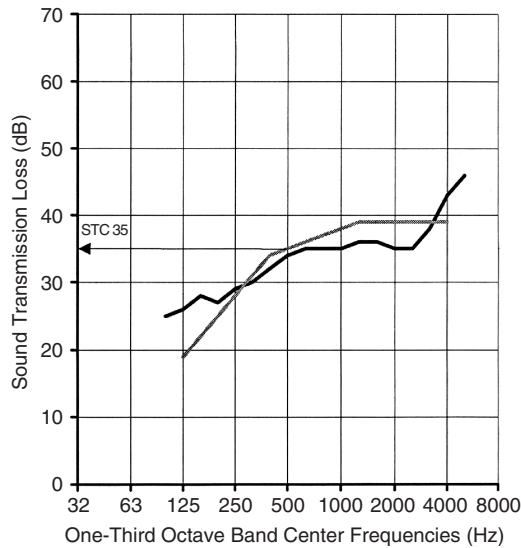
The STC rating from the contour fitting procedure is the TL value of the contour at 500 Hz. This is illustrated in Figs. 5 and 6.

In Fig. 5,  $\frac{1}{4}$ -in. monolithic glass is shown to have an STC rating of 31. In this example, the STC contour placement is constrained by the maximum allowed 8 dB deficiency at 2500 Hz (rule 1).

In Fig. 6, which shows TL data for  $\frac{1}{4}$ -in. laminated glass, the dip in the TL data, characteristic of  $\frac{1}{4}$ -in. monolithic glass, is removed by the damping interlayer. In the case of  $\frac{1}{4}$ -in. laminated glass, the STC contour placement is constrained by the maximum 32-dB deficiency requirement (rule 2).

#### 4.6 Field Sound Transmission Class Rating

The field sound transmission class (FSTC) rating is used for in situ wall and floor/ceiling sound isolation



**Figure 6** A  $\frac{1}{4}$ -in. laminated glass sound transmission loss and STC contour. (1 in. =  $2.54 \times 10^{-2}$  m.)

performance assessment.<sup>26</sup> The standard requires the measurement of sound transmission loss and includes a required procedure to show that the FSTC rating was not influenced by flanking of sound around the partition intended to be tested. Sound transmission class and FSTC ratings are intended by standard to be equivalent; however, practical experience indicates that FSTC ratings tend to be up to five rating points less than laboratory-measured STC ratings.

#### 4.7 Noise Isolation Class

The NIC rating is similar to the STC and FSTC. It differs in that the standard STC rating contour is applied to the one-third octave band noise reduction data measured in a field situation, rather than the transmission losses measured in the field.<sup>24</sup> No correction to the measured noise reduction data is made to account for partition size, receiving room absorption, or sound flanking. Like the STC and FSTC ratings, the field-measured NIC rating of a noise reduction spectrum is equal to the value of the contour crossing at 500 Hz. In the absence of sound flanking, the NIC is generally within five points of the laboratory STC rating for typical building partition constructions. The NIC rating is used to assess the sound isolation performance of in situ partition constructions, especially complicated ones that involve multiple sound transmission paths that are not suited for laboratory testing. There are no widely used standards using the NIC rating; however, the NIC rating is often used in lieu of STC and FSTC ratings.

#### 4.8 Normalized Noise Isolation Class

The normalized noise isolation class (NNIC) is the same as the NIC rating except the receiving room absorption is normalized to correspond to a 0.5-s reverberation time.<sup>24</sup>

#### 4.9 Outdoor-Indoor Transmission Class

The STC rating was developed to assess the sound isolation performance of partitions and materials with respect to speech and household sounds, that is, sounds produced by home appliances and entertainment equipment.<sup>27</sup> “Household sound” tends to be rich in mid- and high-frequency sound energy. However, environmental sound, typically associated with transportation systems and equipment, is rich in low- and mid-frequency sound energy. The outdoor-indoor transmission class (OITC) rating is a single-number rating that can be used for comparing the sound isolation performance of building facades and facade elements. The rating has been devised to quantify the ability of these to reduce the perceived loudness of ground and air transportation noise transmitted into buildings. This standard is contained in ASTM E1332-90 (R2003) Standard Classification for Determination of Outdoor-Indoor Transmission Class.<sup>28</sup>

The standard establishes a single-number rating, the OITC, by defining a standard spectrum of ground and air transportation noise. This spectrum is used with sound transmission loss data measured in a laboratory using the ASTM E90 method and a mathematical relationship given in the standard to calculate the OITC rating.

The OITC rating is similar to the STC rating in that it uses ASTM E90 TL data and uses these data to derive a single-number rating that increases with increasing sound isolation ability. It differs in that the OITC does not involve a contour fitting process but instead uses a standard spectrum and a mathematical relationship. The mathematical relationship is as follows:

$$\text{OITC} = 100.14 - 10 \log \sum_f 10^{(L_f - T L + A_f)/10} \text{ dB}$$

Table 8<sup>29</sup> presents a worksheet summarizing the method for calculating the OITC rating for  $\frac{1}{4}$ -in. glass. As indicated in Table 8, the OITC rating for  $\frac{1}{4}$ -in. glass is 29. Note that the TL in the 80-Hz band in the worksheet of Table 8 is not shown since it was not measured. The actual TL value in the 80-Hz band, were it included, would not affect the OITC rating indicated in this table.

#### 4.10 Impact Isolation

In residential buildings, quantifying the impact isolation of floor/ceiling constructions with respect to footfall is defined in ASTM E492-04<sup>30</sup> and ASTM E1007-04<sup>31</sup> for laboratory and field situations, respectively. Both standards involve placing a mechanical impacting device called a tapping machine on the floor of the construction to be tested and measuring resulting sound levels below.

The design and use of the tapping machine are described in ISO 140/6.<sup>32</sup> The result of the test is a one-third octave band impact sound pressure level in the room beneath the floor/ceiling construction being tested.

**Table 8 Worksheet for Calculating the OITC Rating of  $\frac{1}{4}$ -in. Glass**

Band Center Frequency (Hz) (1)	Reference Sound Spectrum (dB) (2)	A-Weighting Correction (dB) (3)	Column 2 plus Column 3 (dB) (4)	Specimen TL (dB) (5)	Column 4 minus Column 5 (dB) (6)	$10^{(\text{Column 6}/10)}$ (7)
80	103	-22.5	80.5			
100	102	-19.1	82.9	23	59.9	977,237
125	101	-16.1	84.9	25	59.9	977,237
160	98	-13.4	84.6	25	59.6	912,011
200	97	-10.9	86.1	24	62.1	1,621,810
250	95	-8.5	86.4	28	58.4	691,831
315	94	-6.6	87.4	26	61.4	1,380,384
400	93	-4.8	88.2	29	59.2	831,764
500	93	-3.2	89.8	31	58.8	758,578
630	91	-1.9	89.1	33	56.1	407,380
800	90	-0.8	89.2	34	55.2	331,131
1000	89	0.0	89.0	34	55.0	316,228
1250	89	0.6	89.6	35	54.6	288,403
1600	88	1.0	89.0	34	55.0	316,228
2000	88	1.2	89.2	30	59.2	831,764
2500	87	1.3	88.3	27	61.3	1,348,963
3150	85	1.2	86.2	32	54.2	263,027
4000	84	1.0	85.0	37	48.0	63,096
						12,317,071
						$10 \log \left( \sum \right) = 70.91$
						$\text{OITC} = 100.14 - 10 \log \left( \sum \right) = 29$

Source: From *Solutia Acoustical Glazing Design Guide*.<sup>29</sup>

#### 4.11 Impact Isolation Class

Similar to the STC, the impact isolation class (IIC)<sup>33</sup> rating is a single-number rating that facilitates the comparison of the impact sound isolation performance of floor/ceiling constructions. The IIC rating is determined by fitting a standard contour to the one-third octave band sound pressure level data measured in accordance with ASTM E 492.

#### 4.12 Field Impact Isolation Class

The field impact isolation class (FIIC) rating is the same as the IIC rating except it is used to rate the impact sound insulation performance of in situ floor/ceiling constructions and is used in conjunction with the ASTM E 1007<sup>31</sup> test method. The standard includes procedures for assessing flanking conditions.

### 5 DESCRIPTORS ASSESSING THE QUALITY OF SOUND INSIDE BUILDING SPACES

#### 5.1 Reverberation Time

The reverberation time ( $T_{60}$ ) is the time it takes for sound to decay by 60 dB. Reverberation time is controlled in interior building spaces to enhance speech intelligibility or enhance music quality. Generally, speech intelligibility benefits from a short reverberation time (typically 1 s) while orchestral concert and organ music benefit from long reverberation times (2 to 5 s). Figure 7 presents criteria for reverberation time in spaces according to use for music or speech and according to room volume.

There are four generally accepted methods for calculating the reverberation time. The first and probably most widely used is the *Sabine equation*. It is more appropriately used in moderately to highly reverberant spaces. The Sabine equation is as follows:

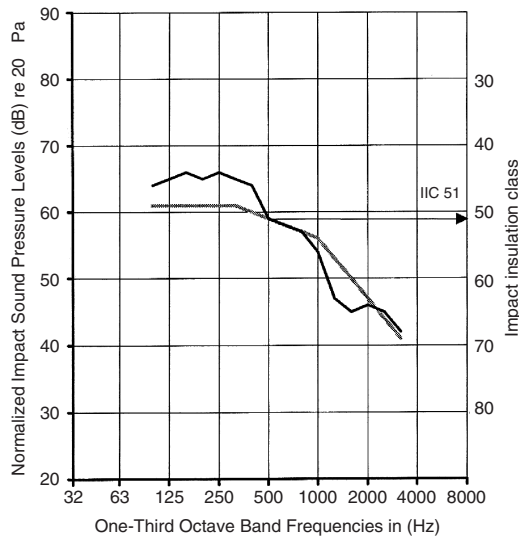
$$T_{60} = \frac{0.049V}{A} \quad (\text{English units})$$

The second method for determining room reverberation is the *Norris-Eyring equation*. It is most appropriately used in highly absorptive and large rooms. The Norris-Eyring equation is as follows:

$$T_{60} = \frac{0.049V}{(-S) \ln(1 - \alpha)} \quad (\text{English units})$$

The third method for determining room reverberation is the *Fitzroy equation*. It is used primarily for rooms where the absorption of parallel surfaces is approximately the same. The Fitzroy equation is as follows:

$$T_{60} = \frac{X}{S} \left( \frac{0.049V}{S \bar{\alpha}_x} \right) + \frac{Y}{S} \left( \frac{0.049V}{S \bar{\alpha}_x} \right) + \frac{Z}{S} \left( \frac{0.049V}{S \bar{\alpha}_x} \right) \quad (\text{English units})$$



**Figure 7** Typical impact sound pressure level spectrum and IIC contour.

In the above equations,  $V$  is room volume,  $S$  is room surface area,  $A$  is room absorption,  $\bar{\alpha}$  is average sound absorption coefficient (the  $x$ ,  $y$ , and  $z$  subscripts are the average sound absorption coefficients of walls normal to the  $x$ ,  $y$ , and  $z$  axes), and  $X$ ,  $Y$ , and  $Z$  are the surface areas of walls normal to the  $x$ ,  $y$ , and  $z$  axes. If units of volume, surface area, and absorption are metric, then the 0.049 constant in each equation should be 0.161.<sup>28</sup>

## 5.2 Room Constant

Room constant ( $R$ ) is defined as the ratio of room sound absorption to the quantity 1 minus the average room absorption coefficient. Using the above symbol definitions, the relationship is expressed as

$$R = \frac{A}{1 - \bar{\alpha}}$$

There are no criteria that make use of room constant; however, it can be useful in assessing the *critical distance*, defined as the distance from a source at which the reverberant field sound pressure level equals the directly radiated sound pressure level.

## 5.3 Articulation Index

The articulation index (AI) is a weighted proportion of a speech signal usable to convey information. The procedure<sup>35</sup> for estimating articulation index involves accounting for signal strength, background or masking noise, time-varying character of background noise, speech signal clipping, and reverberation. The estimation procedure is carried out in one-third or full octave frequency bands. The calculated articulation index is used to estimate percent of syllables, words, or sentences

understood correctly. This analysis can be used to assess both speech intelligibility or its inverse, speech privacy. AI is also described in Section 6 of Chapter 34.

## 5.4 Speech Transmission Index

The speech transmission index (STI) is similar to the articulation index. It differs in that the STI uses a modulation transfer function.<sup>36,37</sup> In its evaluation, it incorporates a procedure for expressing the loss in articulation produced by room reverberation as an equivalent background noise contribution, which can be added to the actual measured background noise level.<sup>38</sup>

## 5.5 Rapid Speech Transmission Index

The rapid speech transmission index (RaSTI) is similar to the STI, uses fewer modulation frequencies, and incorporates only speech and background sound levels in only two octave bands—500 and 2000 Hz. The RaSTI value is considered sufficiently accurate only if no nonlinearities in speech transmission exist and if the background sound pressure level is devoid of strong tonal components.

## REFERENCES

1. American National Standards Institute, Rating Noise with Respect to Speech Interference, S3.14–1977 (R1986).
2. C. M. Harris, Ed., *Handbook of Acoustical Measurements and Noise Control*, 3rd ed., McGraw-Hill, New York, 1991, p. 16.10.
3. C. M. Harris, Ed., *Handbook of Acoustical Measurements and Noise Control*, 3rd ed., McGraw-Hill, New York, 1991, p. 17.9.
4. American National Standards Institute, Procedure for the Computation of Loudness of Noise, S3.4–1980 (R1986).
5. Procedures for Abatement of Highway Traffic Noise and Construction Noise, in *Federal-Aid Program Manual*, U.S. Department of Transportation, Federal Highway Administration, Washington, DC, August 9, 1982, Vol. 7, Chapter 7, Section 3.
6. Massachusetts Department of Environmental Protection, Bureau of Waste Prevention-Air Quality, Supplemental Form for Survey of Noise Potential, BWP AQ SFP 03.
7. City of Cambridge, Massachusetts, Noise Ordinance, Ordinance No. 877, 1977.
8. Protective Noise Levels—Condensed Version of EPA Levels Documents, U.S. Environmental Protection Agency, Publication No. EPA 550/9–79–100, November 1978.
9. Noise Control and Compatibility Planning for Airports, U.S. Department of Transportation, Federal Aviation Administration, Advisory Circular AC 150/5020-1, August 5, 1983.
10. 24 CFR Part 51, U.S. Department of Housing and Urban Development, Environmental Criteria and Standards, 44 FR 40860, July 12, 1979; amended by 49 FR 880, January 6, 1984.
11. 2001 California Building Code, California Code of Regulations, Title 24, Part 2, Volume 1.
12. L. L. Beranek, Ed., *Noise and Vibration Control*, Institute of Noise Control Engineering, Ames, IA, 1988, p. 569.

13. L. L. Beranek, Ed., *Noise Reduction*, McGraw-Hill, New York, 1960, pp. 518–520.
14. L. L. Beranek, Ed., *Noise and Vibration Control*, McGraw-Hill, New York, 1971, p. 566.
15. ASHRAE, *2003 ASHRAE Applications Handbook*, American Society of Heating, Refrigeration, and Air-Conditioning Engineers, New York, 2003.
16. ASHRAE, *2005 ASHRAE Fundamentals Handbook*, American Society of Heating, Refrigerating, and Air-Conditioning Engineers, New York, 2005.
17. Warren E. Blazier, Jr., RC Mark II: A Refined Procedure for Rating the Noise of Heating, Ventilating, and Air-Conditioning (HVAC) Systems in Buildings, *Noise Control Eng. J.*, Vol. 45(b), Nov.–Dec. 1997.
18. L. L. Beranek, Application of NCB Noise Criterion Curves, *Noise Control Eng. J.*, Vol. 33, No. 2, 1989.
19. L. L. Beranek, Balanced Noise-Criterion (NCB) Curves, *J. Acoust. Soc. Am.*, Vol. 86, No. 2, 1989.
20. American Society for Testing and Materials, *Section 4—1991 Annual Book of ASTM Standards*, Standard Test Method Sound Absorption and Sound Absorption Coefficients by the Reverberation Room Method, C423–02a.
21. American Society for Testing and Materials, *Section 4—2006 Annual Book of ASTM Standards*, Standard Practices for Mounting Test Specimens during Sound Absorption Tests, E795–05.
22. Y. W. Lam, Sabine and Random Incidence Absorption Coefficients, in *Acoustics of Enclosed Spaces*, AEOF3/AEOF4, University of Salford, Salford, UK, [http://www.acoustics.salford.ac.uk/student\\_area/bsc3/room\\_acoustics/Measabs.pdf](http://www.acoustics.salford.ac.uk/student_area/bsc3/room_acoustics/Measabs.pdf).
23. American Society for Testing and Materials, *Section 4—2006 Annual Book of ASTM Standards*, Standard Test Method for Laboratory Measurement of Airborne Sound Transmission Loss of Building Partitions and Elements, E90–04, p. 907.
24. American Society for Testing and Materials, *Section 4—2006 Annual Book of ASTM Standards*, Standard Test Method for Measurement of Airborne Sound Attenuation between Rooms in Buildings, E336–05, p. 932.
25. American Society for Testing and Materials, *Section 4—2006 Annual Book of ASTM Standards*, Classification for Rating Sound Insulation, E413–04, p. 943.
26. American Society for Testing and Materials, *Section 4—2006 Annual Book of ASTM Standards*, Standard Test Method for Measurement of Airborne Sound Insulation between Rooms in Buildings, Annex A1. Measurement of Field Sound Transmission Loss, E336–05.
27. G. C. Tocci, A Comparison of STC and EWR for Rating Glazing Noise Reduction, *Sound Vib.*, October 1987, p. 32.
28. ASTM, ASTM E1332-90 (R2003), Standard Classification for Determination of Outdoor–Indoor Transmission Class.
29. *Solutia Acoustical Glazing Design Guide*, 3rd ed., 1995.
30. American Society for Testing and Materials, *Section 4—2006 Annual Book of ASTM Standards*, Standard Test Method for Laboratory Measurement of Impact Sound Transmission through Floor-Ceiling Assemblies Using the Tapping Machine, E492-04, p. 958.
31. American Society for Testing and Materials, *Section 4—2006 Annual Book of ASTM Standards*, Standard Test Method for Field Measurement of Tapping Machine Impact Sound Transmission through Floor-Ceiling Assemblies and Associated Support Structures, E1007-04, p. 1041.
32. International Standards Organization, Acoustics—Measurement of Sound Insulation in Buildings and of Building Elements: Part 6—Laboratory Measurements of Impact Sound Insulation of Floors, Standard 140/6.
33. ASTM, ASTM E989-06, Standard Classification for Determination of Impact Insulation Class (IIC).
34. K. A. Hoover, *An Appreciation of Acoustics*, Berklee School of Music, Boston, MA.
35. American National Standards Institute, Methods for the Calculation of the Articulation Index, ANSI S3.5–1969 (RI986).
36. T. Houtgast and H. J. M. Steeneken, A Review of the MTF Concept in Room Acoustics and Its Use for Estimating Speech Intelligibility in Auditor, *J. Acoust. Soc. Am.*, Vol. 77, No. 3, March 1985.
37. D. Davis and C. Davis, *Sound System Engineering*, 2nd ed., Howard W. Sams, Indianapolis, IN, 1987, p. 235.
38. C. M. Harris, Ed., *Handbook of Acoustical Measurements and Noise Control*, 3rd ed., McGraw-Hill, New York, 1991, p. 16.

# CHAPTER 107

## ISO RATINGS AND DESCRIPTORS FOR THE BUILT ACOUSTICAL ENVIRONMENT

Heinrich A. Metzen  
DataKustik  
Greifenberg, Germany

### 1 INTRODUCTION

In 1988, the European Building Products Directive moved to harmonize technical standards and guidelines, thus enabling the free trade of building materials and products throughout the member states of the European Community.<sup>1</sup> Protection against noise is one of the so-called essential requirements applying to construction works (both building and civil engineering works). Others are mechanical resistance and stability, safety in case of fire, energy economy and heat retention, safety in use, and hygienic, health, and environmental aspects. As far as sound insulation is concerned, the task was to draft new or to revise existing standards to cover all relevant technical aspects dealing with measurement, weighting, and calculation procedures for building products, elements, and buildings. Due to the Vienna Agreement in 1991 between the European Standardization Body (CEN) and the International Organization for Standardization (ISO), this huge task was heavily facilitated as existing ISO standards were allowed to be revised under CEN or ISO with a final parallel voting procedure. This concerned mainly the revision of the ISO 140- and ISO 717- series covering the measurement of sound insulation of building elements and of buildings and the procedures for weighting of spectral data resulting in single-number ratings. Furthermore, the sound-absorbing properties of building products are tested according to ISO 354 while a weighting procedure for specifying sound absorption by a single-number rating did not exist. Further acoustical properties related to building products that had to be covered are noise from water and wastewater supply systems, dynamic stiffness and airflow resistivity of acoustic materials, and survey test methods for airborne and impact sound insulation, besides the standard test methods in ISO 140.

### 2 AIRBORNE SOUND INSULATION

The revision of ISO 717-1 (1982 edition) originated from discussions in ISO about the suitability of the reference curve method for specifying performance with respect to outdoor noise. An ISO study group was set up that analyzed and listed the main points of criticism:

- The single-number ratings obtained by applying the ISO reference curve (e.g., the weighted sound reduction index  $R_w$ \*) are not sufficiently sensitive

to low frequencies, while the high frequencies cause a strong impact on the final result.

- The reference curve method is not suitable to express element or building performance for different noise spectra, such as road noise traffic with dominating low frequencies.
- This combines with the request to extend the frequency range by the third octaves 50 to 80 Hz and 4000 to 5000 Hz.
- Several European countries established national rules that qualification tests on site can or have to be performed in octave band widths. The new rating methods, therefore, had to include procedures for data in third octaves and in octaves.

Furthermore, the so-called 8-dB rule was a point of discussion. The first edition of ISO/R 717 (1968) stated that the average of unfavorable deviations should be not more than 2 dB, and that any one-third octave band value should be not more than 8 dB below the shifted reference curve. In ISO 717-1 (1982 edition) deviations of more than 8 dB had just to be stated without influencing the final rating.

The new edition (1996) of ISO 717-1<sup>2</sup> describes the procedures to calculate single-number ratings from measurement results in frequency bands of building elements and of buildings considering the former discussions. This includes:

- Single-number quantities for airborne sound insulation between rooms in buildings and of building elements, such as walls, floors, windows, and doors.
- Spectrum adaptation terms  $C$  and  $C_{tr}$  to correct the single-number ratings with respect to two different sound pressure level spectra, referring to an indoor (term  $C$ ) and a traffic noise spectrum (term  $C_{tr}$ ).
- Procedures to evaluate single-number ratings for measurement results in third octave (laboratory and field tests) and in octave bands (field tests only) in accordance with the ISO 140 series.

The single-number quantities obtained by the reference method can be combined with one of the spectrum adaptation terms as a sum to characterize the sound

\*Subscripts in this chapter have the following meanings:  $c$  = ceiling,  $e$  = element,  $f$  = flanking,  $n$  = normalized,  $s$  =

surface,  $T$  = reverberation time,  $w$  = weighted, and  $2m = 2$  metres.

**Table 1 Application of Single-Number Quantities for Airborne Sound Insulation in Conjunction with Spectrum Adaptation Terms (Examples)**

Objective	Examples
Specifying element performance	$R_w(C; C_{tr}) = 50 (-2; -7)$ dB $D_{n,f,w}(C; C_{tr}) = 45 (-1; -5)$ dB
Specifying building performance	$R'_w(C; C_{tr}) = 52 (-1; -6)$ dB or $D_{n,w}(C; C_{tr}) = 50 (-2; -5)$ dB or $D_{nT,w}(C; C_{tr}) = 53 (-1; -5)$ dB
Stating the minimum requirement between rooms (e.g., in building regulations)	$R_w \geq 53$ dB or $R'_w + C_{50-3150} \geq 53$ dB or $D_{nT,w} + C_{tr} \geq 45$ dB

insulating properties of building elements or the acoustical performance of buildings between rooms inside buildings or from the outside to the inside (Table 1).

The advantage of this solution is that the former reference method could be kept and test results applying

former editions of ISO 717-1 match still with the principal weighting procedure. On the other hand, the spectrum adaptation terms can be calculated from the measured spectrum without requiring a new test. As the spectrum adaptation terms are sensitive to deviations in single-frequency bands, the former 8-dB rule no longer applies. Meanwhile, several European countries have installed revised or new national building regulations making use of the new weighting procedures (Table 2). In several European countries additional national standards specifying classification schemes for increased sound insulation exist.<sup>3</sup>

The 1996 edition of ISO 717-1 has created a large diversity of descriptors used in the ISO member countries. As spectrum adaptation terms can be calculated also for the enlarged frequency range (downward to 50 Hz and/or upward to 5000 Hz), a maximum of eight spectrum adaptation terms result from one spectrum, for example, for the weighted sound reduction index  $R_w$ :

$$\begin{aligned}
 &R_w(C; C_{tr}; C_{100-5000}; C_{tr,100-5000}; C_{50-5000}; \\
 &C_{tr,50-5000}; C_{50-3150}; C_{tr,50-3150}) \\
 &= 50(-2; -7; -1; -7; -2; -8; -3; -8) \text{ dB}
 \end{aligned}$$

Legal requirements for sound insulation against outdoor noise differ even more than requirements for sound insulation inside buildings. In some countries

**Table 2 Airborne Sound Insulation Requirements in European Countries (as of 2004)<sup>a</sup>**

Country	Descriptor	Multistorey Buildings (dB)	Semidetached and Row Houses (dB)
Austria	$D_{nT,w}$	$\geq 55$	$\geq 60$
Belgium <sup>b</sup>	$D_{nT,w}$	$\geq 54$	$\geq 58$
Czech Republic	$R'_w$	$\geq 52$	$\geq 57$
Denmark	$R'_w$	$\geq 52^c$	$\geq 55$
Estonia	$R'_w$	$\geq 55$	$\geq 55$
Finland	$R'_w$	$\geq 55$	$\geq 55$
France	$D_{nT,w} + C$	$\geq 53$	$\geq 53$
Germany	$R'_w$	$\geq 53^c$	$\geq 57$
Hungary	$R'_w$	$\geq 52$	$\geq 57$
Iceland	$R'_w{}^c$	$\geq 52$	$\geq 55$
Latvia	$R'_w$	$\geq 54$	$\geq 54$
Lithuania	$D_{nT,w}$ or $R'_w$	$\geq 55$	$\geq 55$
Italy	$R'_w$	$\geq 50$	$\geq 50$
Netherlands	$I_{lu,k} (R'_w \approx 55 + I_{lu,k})$	$\geq 0$	$\geq 0$
Norway	$R'_w$	$\geq 55^d$	$\geq 55^d$
Poland	$R'_w + C$	$\geq 50^c$	$\geq 52$
Portugal	$D_{n,w}$	$\geq 50$	$\geq 50$
Russia	$I_b$	$\geq 50$	<sup>e</sup>
Slovakia	$R'_w$	$\geq 52$	$\geq 52$
Slovenia	$R'_w$	$\geq 52$	$\geq 52$
Spain <sup>b</sup>	$D_{nT,w} + C_{100-5000}$	$\geq 50$	$\geq 50$
Sweden	$R'_w + C_{50-3150}$	$\geq 53$	$\geq 53$
Switzerland	$D_{nT,w} + C$	$\geq 54$	$\geq 54$
United Kingdom	$D_{nT,w} + C_{tr}$	$\geq 45$	$\geq 45$

<sup>a</sup>See also Table 4 in Chapter 114.

<sup>b</sup>Proposed new requirements.

<sup>c</sup>For vertical direction the requirement is 1 dB higher.

<sup>d</sup>It is recommended that the same criteria are fulfilled by  $R'_w + C_{50-3150}$ .

<sup>e</sup>No requirements.



**Table 3 Single-Number Quantities of Airborne Sound Insulation of Building Elements**

Derived from One-Third Octave Band Values			
Single-Number Quantity	Term and Symbol	Defined in	Equation <sup>a</sup>
Weighted sound reduction index $R_w$	Sound reduction index $R$	ISO 140-3	$R = L_1 - L_2 + 10 \log \frac{S}{A}$
Weighted suspended-ceiling normalized level difference $D_{n,c,w}$	Suspended-ceiling normalized level difference $D_{n,c}$	ISO 140-9	$D_{n,c} = L_1 - L_2 + 10 \log \frac{A_0}{A}$
Weighted element-normalized level difference $D_{n,e,w}$	Element-normalized level difference $D_{n,e}$	ISO 140-10	$D_{n,e} = L_1 - L_2 + 10 \log \frac{A_0}{A}$
Weighted normalized flanking level difference $D_{n,f,w}$	Normalized flanking level difference $D_{n,f}$	ISO 10848-2	$D_{n,f} = L_1 - L_2 + 10 \log \frac{A_0}{A}$

<sup>a</sup>  $L_1$  = average sound pressure level in the sending room, in dB

$L_2$  = average sound pressure level in the receiving room, in dB

$S$  = area of the test specimen, in square metres (equals the test opening)

$A$  = equivalent sound absorption area in the receiving room, in square metres

$A_0$  = reference absorption area ( $A_0 = 10 \text{ m}^2$ )

the required sound insulation of facades is specified as a function of the outdoor noise level, perhaps with different day and night requirements. In a number of countries the indoor level  $L_{A,eq,24h}$  must meet a predefined limit. In some countries there are no general or national requirements but only local or district requirements. In addition, the methods for determination of the exterior noise exposure vary considerably. In total, the situation is even more complex than with indoor noise. In the mean time, the Technical Committee Room and Building Acoustics (TC-RBA) of the European Acoustical Association (EAA) has initiated a project to gather information on classification schemes and to give guidance on how to harmonize the use of concepts for sound insulation.

## 2.1 Descriptors for Element Performance and for Building Performance

The single-number ratings specifying element and building performance and the measured term according to the ISO 140 series and other measurement standards are listed in Tables 3 and 4. All element data is measured in test facilities with suppressed flanking transmission.

## 2.2 Weighting Procedure

The ISO weighting procedure applies to measurement results obtained in accordance with ISO 140-3, ISO 140-4, ISO 140-5, ISO 140-9, ISO 140-10, and ISO 10848-2 in the following frequency ranges:

- From 100 to 3150 Hz for one-third octave bands
- From 125 to 2000 Hz for octave bands (for field tests only)

The spectral data shall be given to an accuracy of 0.1 dB. The single-number rating in decibels is obtained by shifting the relevant reference curve in steps of 1 dB toward the measured curve until the sum of unfavorable deviations is as large as possible but not more than 32.0 dB (measurement in 16 one-third octave bands) or 10.0 dB (measurement in 5 octave bands). An unfavorable deviation at a particular frequency occurs when the result of measurements is less than the reference value. Only the unfavorable deviations are taken into account. The value of the reference curve at 500 Hz after having shifted the reference curve is the single-number rating  $R_w$ ,  $R'_w$ ,  $D_{n,w}$  or  $D_{nT,w}$  (see Tables 3 and 4). The reference curve in octave bands should be applied just with results of measurements in octave bands in the field (Fig. 1).

By the slightly different shape of the two reference curves, it is ensured that the difference among single-number ratings calculated from field measurements in third octave or in octave bands is  $\pm 1$  dB at the most.

## 2.3 Spectrum Adaptation Terms

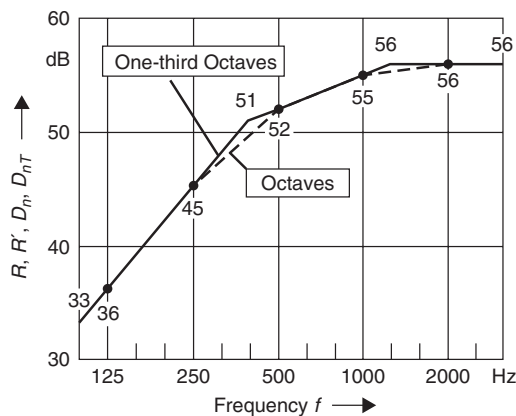
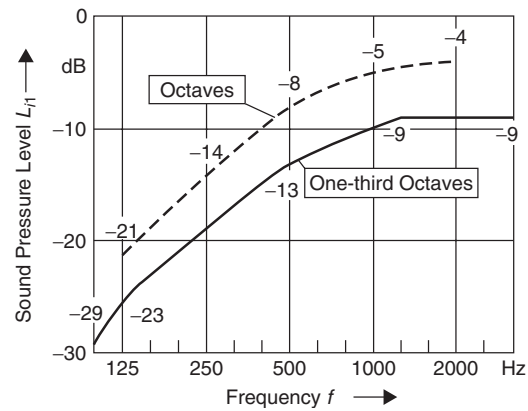
The specification of the spectrum adaptation terms  $C$  and  $C_{tr}$  is a normative requirement when stating the performance of building elements or of buildings according to ISO 717-1.<sup>2</sup> The spectrum adaptation terms for the enlarged frequency range  $C_{100-5000}$ ;  $C_{tr,100-5000}$ ;  $C_{50-5000}$ ;  $C_{tr,50-5000}$ ;  $C_{50-3150}$ ; and  $C_{tr,50-3150}$  may be given if available.

The spectrum adaptation term is a figure in decibels that has to be added to an ISO single-number rating (e.g.,  $R_w$  or  $D_{nT,w}$ ) to express element or building performance with respect to a sound pressure level spectrum. As the spectrum adaptation terms are sensitive to negative deviations in single bands from the

**Table 4** Single-Number Quantities of Airborne Sound Insulation in Buildings

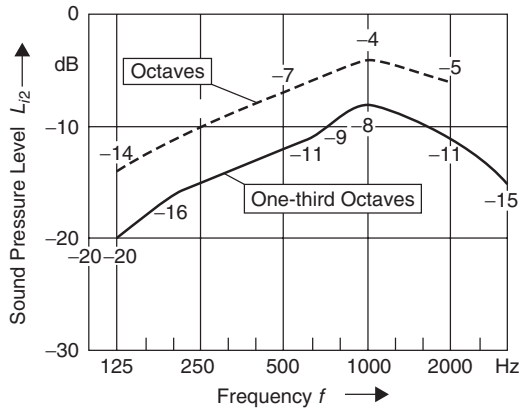
Derived from One-Third Octave or Octave Band Values			
Single-Number Quantity	Term and Symbol	Defined in	Equation <sup>a</sup>
Weighted apparent sound reduction index $R'_w$	Apparent sound reduction index $R'$	ISO 140-4	$R' = L_1 - L_2 + 10 \log \frac{S}{A}$
Weighted apparent sound reduction index $R'_{45^\circ, w}$	Apparent sound reduction index $R'_{45^\circ}$	ISO 140-5	$R'_{45^\circ} = L_{1,s} - L_2 + 10 \log \frac{S}{A} - 1.5 \text{ dB}$
Weighted apparent sound reduction index $R'_{tr, s, w}$	Apparent sound reduction index $R'_{tr, s}$	ISO 140-5	$R'_{tr, s} = L_{eq, 1, s} - L_{eq, 2} + 10 \log \frac{S}{A} - 3 \text{ dB}$
Weighted normalized level difference $D_{n, w}$	Normalized level difference $D_n$	ISO 140-4	$D_n = L_1 - L_2 - 10 \log \frac{A}{A_0}$
Weighted standardized level difference $D_{nT, w}$	Standardized level difference $D_{nT}$	ISO 140-4	$D_{nT} = L_1 - L_2 + 10 \log \frac{T}{T_0}$
Weighted standardized level difference, $D_{ls, 2m, nT, w}$ or $D_{tr, 2m, nT, w}$	Standardized level difference $D_{ls, 2m, nT}$ or $D_{tr, 2m, nT}$	ISO 140-5	$D_{2m, nT} = L_{1, 2m} - L_2 + 10 \log \frac{T}{T_0}$

- <sup>a</sup>  $L_1$  = average sound pressure level in the sending room, in dB  
 $L_2$  = average sound pressure level in the receiving room, in dB  
 $L_{1,s}$  = average sound pressure level on the surface of the test specimen, in dB  
 $L_{1,2m}$  = outdoor sound pressure level 2 m in front of the facade, in dB  
 $L_{eq, 1, s}$  = average value of the equivalent continuous sound pressure level on the surface of the test specimen including reflecting effects from the test specimen and facade, in dB  
 $L_{eq, 2}$  = average value of the equivalent continuous sound pressure level in the receiving room, in dB  
 $S$  = area of the test specimen, in square metres (equals the test opening)  
 $A$  = equivalent sound absorption area in the receiving room, in square metres  
 $A_0$  = reference absorption area ( $A_0 = 10^2$ )  
 $T$  = reverberation time in the receiving room, in s  
 $T_0$  = reference reverberation time ( $T_0 = 0.5$  s)

**Figure 1** Reference curves for airborne sound, in one-third octave and octave bands.**Figure 2** Sound pressure level spectra  $L_{f1}$  for spectrum adaptation term C (in one-third octave and octave bands).

shifted reference curve, they replace the former 8-dB rule. In ISO 717-1 two kinds of spectrum adaptation terms (in third octave and octave bands) referring to two sound pressure level spectra are introduced.

The spectrum adaptation term  $C$  is calculated from an A-weighted pink noise spectrum (Fig. 2) and the spectrum adaptation term  $C_{tr}$  from an A-weighted urban traffic noise spectrum (Fig. 3). The spectrum adaptation terms are defined as the difference between the calculated value  $X_{Aj}$  and the single-number rating



**Figure 3** Sound pressure level spectra  $L_{12}$  for spectrum adaptation term  $C_{tr}$  (in third octave and octave bands).

$X_w$  resulting from the reference curve procedure:

$$C_j = X_{Aj} - X_w \quad (\text{in dB})$$

with  $C_j$  = spectrum adaptation term for spectrum  $j$ , where

$j = 1$ , A-weighted pink noise

$j = 2$ , A-weighted urban traffic noise

$X_w$  = single-number rating from the reference curve procedure

$X_{Aj}$  = calculated value according to

$$X_{Aj} = -10 \log \sum 10^{(L_{ij}-X_i)/10} \quad (\text{in dB})$$

$i$  = index for third octaves 100 to 3150 Hz  
resp., octaves 125 to 2000 Hz

$L_{ij}$  = sound pressure levels at frequency  $i$  for the spectrum  $j$

$X_i$  = measured value in frequency band  $i$  ( $R_i$ ,  $R'_i$ ,  $D_{n,i}$ ,  $D_{nT,i}$ ), given to the nearest 0.1 dB

The spectra  $L_{i1}$  for A-weighted pink noise and  $L_{i2}$  for A-weighted urban traffic noise are normalized to an energy sum of 0 dB. The spectrum adaptation terms are calculated to 0.1 dB and rounded according to ISO 31-0.<sup>4</sup>

Table 5 shows a scheme for the calculation of the single-number rating according to the ISO-reference curve and the spectrum adaptation terms  $C$  and  $C_{tr}$  for the normative frequency range of 100 to 3150 Hz. The statement of result in this case is

$$R_w(C; C_{tr}) = 50(-1; -5) \text{ dB}$$

Both spectrum adaptation terms may be applied to additional types of noise. Table 6 lists a number of different noise sources to which the spectrum adaptation terms,  $C$  or  $C_{tr}$ , can be attached. If the A-weighted spectrum of a certain type of noise is known, it can be compared with the data in Figs. 2 and 3 to decide which spectrum adaptation term may apply to the present spectrum.

**Table 5** Calculation of Single-Number Quantity and Spectrum Adaptation Terms  $C$  and  $C_{tr}$  for Frequency Range 100–3150 Hz (according to ISO 717-1)

$f_i$ (Hz)	$R_i$ (dB)	Spectrum No. 1			Spectrum No. 2		
		$R$ Ref. (dB)	Shifted $R$ Ref. -2	Unfavorable Deviation	$L_{i1}$ (dB) for $C$ and $C$ , 50-3150	$L_{i2}$ (dB) for $C_{tr}$ and $C_{tr}$ , 50-3150	
					$L_{i1} - R_i$ (dB)	$L_{i2} - R_i$ (dB)	$10^{(L_{i2}-R_i)/10}$ ( $10^{-5}$ )
100	33.7	33	31	0	-29	-53.7	0.43
125	37.3	36	34	0	-26	-57.3	0.19
160	37.4	39	37	0	-23	-55.4	0.29
200	38.9	42	40	1.1	-21	-54.9	0.32
250	38	45	43	5	-19	-53	0.50
315	39.7	48	46	6.3	-17	-53.7	0.43
400	42.1	51	49	6.9	-15	-55.1	0.31
500	45.4	52	50	4.6	-13	-57.4	0.18
630	46.9	53	51	4.1	-12	-57.9	0.16
800	50.8	54	52	1.2	-11	-59.8	0.10
1000	54.3	55	53	0	-10	-62.3	0.06
1250	55.6	56	54	0	-9	-64.6	0.03
1600	56	56	54	0	-9	-66	0.03
2000	57.5	56	54	0	-9	-68.5	0.01
2500	58.7	56	54	0	-9	-71.7	0.01
3150	60.6	56	54	0	-9	-75.6	0.00
Sum ( $\leq 32$ ) =				29.2	Sum 100–3150 =	1.38	Sum 100–3150 =
Sum/16 =				1.8250	$X_{Aj} = -10 \log(\text{sum}) =$	48.6	$X_{Aj} =$
$R_w =$				50 dB	$C = X_{Aj} - R_w =$	-1.4	$C_{tr} = X_{Aj} - R_w =$
					$C =$	-1 dB	$C_{tr} =$
							-5 dB

**Table 6 Relevant Spectrum Adaptation Term for Different Types of Noise Source**

Type of Noise Source	Relevant Spectrum Adaptation Term
Living activities (talking, music, radio, TV)	$C$ (spectrum No.1)
Children playing	
Railway traffic at medium and high speed	
Highway road traffic >80 km/h	
Jet aircraft, short distance	
Factories emitting mainly medium- and high-frequency noise	$C_{tr}$ (spectrum No.2)
Urban road traffic	
Railway traffic at low speeds	
Aircraft, propeller driven	
Jet aircraft, large distance	
Disco music	
Factories emitting mainly low- and medium-frequency noise	

Additional procedures for the calculation of spectrum adaptation terms (based on different spectra  $L_{i1}$  and  $L_{i2}$ ) for the enlarged frequency range (50 to 3150 Hz, 100 to 5000 Hz, or 50 to 5000 Hz) are contained in an additional, informative annex of ISO 717-1.

## 2.4 Examples

From studies on a number of constructions, the following conclusions can be drawn:

- For monolithic walls and floors with increasing sound reduction index over frequency, the spectrum adaptation term  $C$  is in the range of  $-1$  to  $-2$  dB (Table 7). The value of  $C$  is governed by the low- and medium-frequency range. The spectrum adaptation term  $C_{tr}$  for monolithic exterior walls is about  $C_{tr} = -4$  dB. As the levels of spectrum  $L_{i2}$  at the low frequencies are higher than with spectrum  $L_{i1}$ , the term  $C_{tr}$  is much more dominated by the difference  $L_{i2} - R_i$  in the first third octaves.
- Double walls (such as heavy walls with wall linings or lightweight walls with metal or wooden studs) show spectrum adaptation terms  $C$  in the range of  $-2$  to  $-5$  dB. This is caused by the double-wall resonance frequency at low frequencies and—for lightweight elements—by the reduced insulation near the critical frequency in the high-frequency region. The spectrum adaptation term  $C_{tr}$  for double-wall constructions with resonance frequencies  $100 \text{ Hz} \leq f_0 \leq 160 \text{ Hz}$  can drop down to  $-8 \text{ dB} \leq C_{tr} \leq -12 \text{ dB}$  while for lower resonance frequencies ( $f_0 \leq 80 \text{ Hz}$ )  $C_{tr}$  tends to be more positive with a range of  $-6 \text{ dB} \leq C_{tr} \leq -8 \text{ dB}$ .
- Glazing constructions with air or argon as fill gases have a spectrum adaptation term  $C$  of  $-1$  to  $-2$  dB and a spectrum adaptation term  $C_{tr}$

of  $-3$  dB to  $-7$  dB (depending on gap width and thickness of panes).

## 3 IMPACT SOUND INSULATION

The ISO procedures for obtaining the single-number ratings for impact sound insulation have been thoroughly discussed in the revision of the former ISO 717-2 (1982 edition). The main points of criticism were:

- The shape of the ISO reference curve lacks the necessary influence on low-frequency impact noise while the high frequencies have too strong an influence on the final single-number rating.
- The single-number rating (weighted normalized impact sound pressure level) does not reflect the subjective disturbance of impact noise such as walking.
- The weighting procedure causes the subjective impact noise disturbance of heavy floors to be underrated, while lightweight timber floors with wooden joists without additional carpets or floating floors are overrated.

These problems are caused by the spectral characteristics of the impact noise source. The force spectrum of the standardized tapping machine is dominated by higher frequencies, which is not comparable with real impact noise sources (e.g., walking, moving of chairs/tables, children playing, etc.). Several new reference curves with different shapes have been discussed and assessed. Finally, it was decided keep the existing reference curve procedure to avoid confusion among users and to prevent malpractice, which possibly would occur with several single-number ratings characterizing the impact sound insulation of floors.

The new edition of ISO 717-2<sup>5</sup> describes the procedures to calculate single-number ratings from measurement results in frequency bands of building elements and of buildings. This includes:

- Single-number quantities for the impact sound insulation in buildings and of floors (ISO 140-6 and ISO 140-7).
- Single-number quantities for the impact sound reduction of carpets and floating floors from the results of measurements carried out in accordance with ISO 140-8.
- Procedures to evaluate single-number ratings for measurement results in third-octave (laboratory and field tests, ISO 140-6 and ISO 140-7) and in octave bands (field tests only, ISO 140-7).

With this approach, the single-number quantities obtained by the reference method (e.g., the weighted normalized impact sound pressure  $L_{n,w}$ ) is maintained as the prime rating quantity.

An informative annex introduces a spectrum adaptation term for impact noise by a walking person ( $C_i$ ,  $i = \text{impact}$ ). Several studies have shown that the unweighted (linear) impact level generated by the tapping machine is more representative of the A-weighted walking noise levels for all types of floor.<sup>6-9</sup>

**Table 7 Weighted Sound Reduction Index  $R_w$  and Spectrum Adaptation Terms  $C$  and  $C_{tr}$  of Typical Building Elements (Examples)**

No.	Element Type	Layer Description	$R_w$ ( $C$ ; $C_{tr}$ )
1	Monolithic wall	Aerated concrete 100 mm, plastered	39 (−1; −4) dB
2	Monolithic floor	Concrete 200 mm	58 (−1; −5) dB
3	Monolithic wall with wall lining	Aerated concrete 100 mm, plastered Mineral wool slab 50 mm (glued) Render 15 mm	51 (−2; −8) dB
4	Monolithic floor with floating floor	Concrete 160 mm Glass wool slab 13 mm Calcium-sulfate screed 40 mm	64 (−4; −11) dB
5	Timber floor with wooden joists (cross section 120 × 180 mm)	Wooden particle board 22 mm Mineral wool 27 mm Wooden particle board 22 mm Glass wool 100 mm (inside cavity) Gypsum board 12.5 mm (on wooden battens)	64 (−4; −11) dB
6	Lightweight double-wall (single metal studs 60 × 100 mm)	Gypsum board 12.5 mm Glass wool 100 mm (inside cavity) Gypsum board 12.5 mm	52 (−2; −7) dB
7	Lightweight double-wall (single wooden studs 38 × 89 mm)	Gypsum board 13 mm (on resilient furring channel) Glass wool 90 mm (inside cavity) Gypsum board 13 mm	48 (−5; −13) dB
8	Inclined roof (with wooden rafters)	Concrete tiles Glass wool 160 mm (between rafters) Gypsum board 12.5 mm (on wooden battens)	52 (−3; −9) dB
9	Metal facade	Corrugated metal sheet 0.88 mm Glass wool 100 mm Corrugated metal sheet 0.88 mm	36 (−2; −7) dB
10	Glazing	4-mm glass 12-mm air 6-mm glass	34 (−1; −4) dB
11	Window	Aluminum frame with center sealing at frame and interior rabbet sealing Glazing: 6-mm glass, 16-mm air, 4-mm glass	39 (−3; −6) dB

The intention of this spectrum adaptation term is to allow—in combination with the single-number rating according to the reference curve—a more correct weighting with respect to the excitation by walking persons. This rating is also more restrictive to single noise peaks and replaces thereby the 8-dB rule used in the former (1982) edition of ISO 717-2. Studies clearly indicate that the difference between the ISO single-number rating plus the spectrum adaptation term for impact noise ( $L_{n,w} + C_i$ ) and the A-weighted impact noise by a walking person  $L_A$  on several types of floors is more or less constant, at least for hard footwear.<sup>10</sup>

The single-number quantities are intended for rating the impact sound insulation of floors, bare floors, and of carpets or floor coverings and for the formulation of acoustical requirements in building codes. The specification of numerical values of the single-number quantities remains a national task (Table 8).

As for airborne sound insulation, several European countries have meanwhile revised their national building

regulations (Table 9). Furthermore, national classification schemes for increased sound insulation make use of the spectrum adaptation term for walking noise.<sup>3</sup>

### 3.1 Descriptors for Element Performance and for Building Performance

The single-number ratings specifying element and building performance with respect to impact sound insulation properties and the measured term according to the ISO 140 series and other measurement standards are listed in Tables 10 and 11. As with airborne sound insulation, all element data is measured in test facilities with suppressed flanking transmission.

### 3.2 Weighting Procedures

The ISO weighting procedure applies to measurement results made in accordance with ISO 140-6, -7 and ISO 10848-2 in the frequency ranges:

- From 100 Hz to 3150 Hz for one-third-octave bands

**Table 8 Application of Single-Number Quantities for Impact Sound Insulation in Conjunction with the Spectrum Adaptation Term for Walking Noise (Examples)**

Objective	Examples
Specifying element performance (floor)	$L_{n,w} = 52$ dB $L_{n,w} (C_i) = 52$ (2) dB
Specifying element performance (carpet or floating floor)	$\Delta L_w = 34$ dB $\Delta L_w (C_{i,\Delta}) = 34$ (−13) dB $\Delta L_{lin} = \Delta L_w + C_{i,\Delta} = 21$ dB
Specifying building performance	$L'_{n,w} = 53$ dB $L'_{nT,w} = 50$ dB
Stating the minimum requirement between rooms (e.g., in building regulations)	$L'_{n,w} \leq 53$ dB or $L'_{nT,w} \leq 53$ dB or $L'_{n,w} + C_i \leq 53$ dB $L'_{n,w} + C_{i,50-2500} \leq 56$ dB

- From 125 Hz to 2000 Hz for octave bands (for field tests only)

The spectral data shall be given to 0.1 dB. The single-number rating in decibels is obtained by shifting the

reference curve in steps of 1 dB toward the measured curve until the sum of unfavorable deviations is as large as possible but not more than 32.0 dB (measurement in 16 one-third octave bands) or 10.0 dB (measurement in 5 octave bands). An unfavorable deviation at a particular frequency occurs when the measurement results exceed the reference value. Only the unfavorable deviations shall be taken into account.

As with airborne sound insulation, two types of reference curve exist: one for data in one-third octave band and another for data in octave band width (Fig. 4). For the evaluation of data in one-third octave bandwidth, the single-number rating equals the value in decibels of the reference curve at 500 Hz, after having shifted the reference curve. Due to the different bandwidth, the single-number rating for the evaluation of data in octave band is the value in decibels of the reference curve at 500 Hz, after having shifted the reference curve, reduced by 5 dB.

The reference values for the octave bands are equivalent to the energetic sum of the reference values in one-third octave bands. The reference value for the octave band of 2000 Hz has been reduced to take care of the one-third octave band of 3150 Hz, which (for bare massive floors) may contribute considerably to the

**Table 9 Impact Sound Insulation Requirements in European Countries (as of 2004)<sup>a</sup>, see also Table 5 in Chapter 114)**

Country	Descriptor	Multistorey Buildings (dB)	Semidetached and Row Houses (dB)
Austria	$L'_{nT,w}$	$\leq 48$	$\leq 46$
Belgium <sup>b</sup>	$L'_{nT,w}$	$\leq 58$	$\leq 50$
Czech Republic	$L'_{n,w}$	$\leq 58$	$\leq 53$
Denmark	$L'_{n,w}$	$\leq 58$	$\leq 53$
Estonia	$L'_{n,w}$	$\leq 53$	$\leq 53$
Finland	$L'_{n,w}$	$\leq 53$	$\leq 53$
France	$L'_{nT,w}$	$\leq 58$	$\leq 58$
Germany	$L'_{n,w}$	$\leq 53$	$\leq 48$
Hungary	$L'_{n,w}$	$\leq 55$	$\leq 47$
Iceland	$L'_{n,w}$	$\leq 58$	$\leq 53$
Latvia	$L'_{n,w}$	$\leq 54$	$\leq 54$
Lithuania	$L'_{n,w}$	$\leq 53$	$\leq 53$
Italy	$L'_{n,w}$	$\leq 63$	$\leq 63$
Netherlands	$I_{co} (\approx L'_{n,w} - 49 \dots 56)$	$\geq 5$	$\geq 5$
Norway	$L'_{n,w}^c$	$\leq 53^c$	$\leq 53^c$
Poland	$L'_{n,w}$	$\leq 58$	$\leq 53$
Portugal	$L'_{n,w}$	$\leq 60$	$\leq 60$
Russia	$I_y (\approx L'_{n,w} + 7)$	$\leq 67$	— <sup>d</sup>
Slovakia	$L'_{n,w}$	$\leq 58$	$\leq 58$
Slovenia	$L'_{n,w}$	$\leq 58$	$\leq 58$
Spain <sup>b</sup>	$L'_{nT,w}$	$\leq 65$	$\leq 65$
Sweden	$L'_{n,w} + C_{i,50-2500}$	$\leq 56^e$	$\leq 56^e$
Switzerland	$L'_{nT,w} + C_i$	$\leq 50$	$\leq 50$
United Kingdom	$L'_{nT,w}$	$\leq 62$	None

<sup>a</sup>See also Table 5 in Chapter 114.

<sup>b</sup>Proposed new requirements.

<sup>c</sup>It is recommended that the same criteria are fulfilled by  $L'_{n,w} + C_{i,50-2500}$ .

<sup>d</sup>No requirements.

<sup>e</sup>The same criteria shall also be fulfilled by  $L'_{n,w}$ .

**Table 10** Single-Number Quantities of Impact Sound Insulation Properties of Floors and Floor Coverings

Derived from One-third Octave Band Values			
Single-Number Quantity	Term and Symbol	Defined in	Equation
Weighted normalized impact sound pressure level $L_{n,w}$	Normalized impact sound pressure level $L_n$	ISO 140-6	$L_n = L_i + 10 \log \frac{A}{A_0}$
Weighted reduction in impact sound pressure level $\Delta L_w$	Reduction in impact sound pressure level $\Delta L$	ISO 140-8	$\Delta L = L_{n,0} - L_n$
Weighted normalized flanking level difference $D_{n,f,w}$	Normalized flanking level difference $D_{n,f}$	ISO 10848-2	$L_{n,f} = L_f + 10 \log \frac{A}{A_0}$

**Table 11** Single-Number Quantities of Impact Sound Insulation between Rooms in Buildings

Derived from One-third Octave or Octave Band Values			
Single-Number Quantity	Term and Symbol	Defined in	Equation <sup>a</sup>
Weighted normalized impact sound pressure level $L'_{n,w}$	Normalized impact sound pressure level $L'_n$	ISO 140-7	$L'_n = L_i + 10 \log \frac{A}{A_0}$
Weighted standardized impact sound pressure level $L'_{nT,w}$	Standardized impact sound pressure level $L'_{nT}$	ISO 140-7	$L'_{nT} = L_i - 10 \log \frac{T}{T_0}$

$L_i$  = impact sound pressure level: average sound pressure level in the receiving room when the floor under test is excited by the tapping machine, in dB

$L_{n,0}$  = normalized impact sound pressure level of the heavy standard floor without the floor covering

$L_n$  = normalized impact sound pressure level of the heavy standard floor with the floor covering

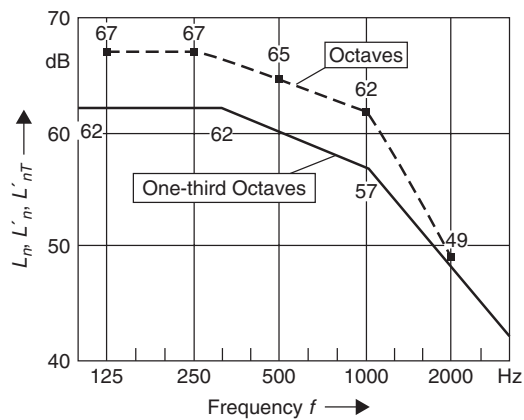
$L_f$  = flanking impact sound pressure level: average sound pressure level in the receiving room by the flanking transmission due to the test element when excited by the tapping machine, in dB

$A$  = equivalent sound absorption area in the receiving room, in m<sup>2</sup>

$A_0$  = reference absorption area ( $A_0 = 10$  m<sup>2</sup>)

$T$  = reverberation time in the receiving room, in seconds

$T_0$  = reference reverberation time ( $T_0 = 0.5$  s)

**Figure 4** Reference curves for impact sound, in one-third octave and in octave bands.

unfavorable deviations. This ensures that deviations between single-number ratings obtained from data in one-third octave or in octave bands differ  $\pm 1$  dB at the most.

The weighting procedure for the improvement of impact sound insulation by carpets or floatings floors is described by the reduction in impact sound pressure level  $\Delta L$ , measured in one-third octave bands on a heavy concrete floor of  $(140 \pm 20)$  mm thickness. The frequency-dependent reduction in impact sound pressure level  $\Delta L$  when tested on homogeneous concrete floors is independent of the normalized impact sound pressure level of the bare concrete floor  $L_{n,0}$ . However, as the weighted normalized impact sound pressure level of the floor with and without a floor covering depends to some extent on  $L_{n,0}$  a reference curve is required to obtain the same weighted reduction of impact sound pressure level  $\Delta L_w$  for the same floor covering on different types of bare floors being installed in laboratories. The weighted normalized impact sound pressure level  $L_{n,r,0,w}$  of the reference floor is 78 dB and represents the idealized spectrum of homogeneous concrete floor of 120 mm thickness. The weighted reduction in impact sound pressure level  $\Delta L_w$  is calculated from:

$$\begin{aligned} L_{n,r} &= L_{n,r,0} - \Delta L \\ \Delta L_w &= L_{n,w,r,0} - L_{n,w,r} = 78 \text{ dB} - L_{n,w,r} \text{ in dB} \end{aligned}$$



**Table 12 Normalized Impact Sound Pressure Level of the Reference Floor  $L_{n,r,0}$** 

$f$ (Hz)	100	125	160	200	250	315	400	500
$L_{n,r,0}$ (dB)	67	67.5	68	68.5	69	69.5	70	70.5
$f$ (Hz)	630	800	1000	1250	1600	2000	2500	3150
$L_{n,r,0}$ (dB)	71	71.5	72	72	72	72	72	72

where  $L_{n,r}$  = calculated normalized impact sound pressure level of the reference floor with the floor covering under test  
 $L_{n,r,0}$  = defined normalized impact sound pressure level of the reference floor (Table 12),  
 $\Delta L$  = reduction in impact sound pressure level measured in accordance with ISO 140-8  
 $L_{n,w,r}$  = calculated weighted normalized impact sound pressure level of the reference floor with the floor covering under test  
 $L_{n,r,0,w}$  = obtained from the spectrum  $L_{n,r,0}$  by applying the reference curve method

The reduction in impact sound pressure level  $\Delta L$  measured on a concrete floor slab as defined in ISO 140-8 and thus the single-number quantity  $L_w$  may only be used in conjunction with heavy floors (e.g., concrete, hollow concrete, hollow bricks). It is not appropriate for use on other types of constructions, especially with any kind of lightweight floors, such as timber floors with wooden joists.

In 1994, the ISO Working Group 22 was created to study the possibilities for setting up procedures to evaluate the improvement of impact sound insulation by carpets or floatings floors on lightweight floors, such as timber floor with wooden joists. This work resulted in the edition of ISO 140-11 specifying methods for measuring the acoustic properties of floor coverings installed on lightweight floors.<sup>11</sup> In addition, a modified tapping machine and a heavy impact source are introduced to assess the impact sound insulation of a floor covering against impact sources with strong components at low frequencies, such as human footsteps or children jumping. The procedures to obtain single-number ratings from these measurement results will be drafted by a CEN working group.

### 3.3 Spectrum Adaptation Term for Impact Noise

As the impact noise spectrum produced by the tapping machine does not quite represent the noise generated by walkings persons, a spectrum adaptation term for impact noise  $C_i$  is introduced in an informative annex of ISO 717-2.<sup>5</sup> In combination with the single-number rating obtained by applying the reference curve method, the new value allows a more correct weighting with respect to the excitation by a walking person. The spectrum adaptation term  $C_i$  can be calculated for the normal frequency range from 100 to 2500 Hz for one-third-octave bands (from 125 to 2000 Hz for octave bands) or for the extended frequency range from 50

to 3150 Hz for one-third-octave bands (from 63 to 2000 Hz for octave bands).

As with airborne sound insulation the spectrum adaptation term for impact noise  $C_i$  represents the difference of the A-weighted energetic sum  $X_A$  for common impact noise by a walking person in buildings and the single-number rating obtained from the ISO reference curve procedure:

$$C_i = X_A - L_{n,w} \quad (\text{in dB})$$

Because the A-weighted difference between the normalized impact sound pressure level and impact noise spectra is approximately constant above frequency, the sum of the ISO single-number rating plus the spectrum adaptation term  $C_i$  can be expressed by the energetic sum  $L_{n,ges}$  corrected by a constant value:

$$\begin{aligned} L_{n,w} + C_i &= 10 \log \sum 10^{(L_{n,i}-15)/10} \\ &= L_{n,ges} - 15 \text{ dB} \end{aligned}$$

The constant has been defined to result in a spectrum adaptation term for monolithic floors with floor coverings of about  $C_i = 0$  dB. Thus, there exists a linear relation between the weighted normalized impact sound pressure level and the spectrum adaptation term  $C_i$ :

$$C_i = L_{n,sum} - 15 - L_{n,w} \quad (\text{in dB})$$

or

$$C_i = L'_{n,sum} - 15 - L'_{n,w} \quad (\text{in dB})$$

or

$$C_i = L'_{nT,sum} - 15 - L'_{nT,w} \quad (\text{in dB})$$

The values of  $L_{n,ges}$ ,  $L'_{n,ges}$  or  $L_{nT,ges}$  are the energetic summation of the normalized, respectively, standardized impact sound pressure levels for  $n$  frequency bands, for example,

$$L_{n,sum} = 10 \log \sum_{i=1}^n 10^{L_{n,i}/10} \quad (\text{in dB})$$

The spectrum adaptation terms are calculated to 0.1 dB and rounded according to ISO 31-0.<sup>4</sup>

For floor coverings an additional spectrum adaptation term is required describing the improvement of impact sound insulation applying a flat (linear) weighting. This spectrum adaptation term is calculated from:

$$C_{i,\Delta} = C_{i,r,0} - C_{i,r} = -11 - C_{i,r} \quad (\text{in dB})$$

where  $C_{i,\Delta}$  = spectrum adaptation term for the reduction in impact sound pressure level applying a linear weighting

$C_{i,r}$  = spectrum adaptation term for the reference floor with the floor covering under test

$C_{i,r,0}$  = spectrum adaptation term for the reference floor ( $C_{i,r,0} = -11$  dB)

**Table 13** Calculation of Single-Number Quantities for a Bare Floor, Combined with a Floor Covering, and the Floor Covering Itself in Conjunction with the Respective Spectrum Adaptation Terms  $C_i$  for Frequency Range 100–3150 Hz according to ISO 717-2

$f_i$ (Hz)	Bare Floor				Bare Floor + Floor Covering				Floor Covering							
	$L_{ni}$ (dB)	$L_n$ Ref. (dB)	Shifted $L_n$ Ref. 17	Unfavor. Deviation (dB)	$L_{ni}$ (dB)	$L_n$ Ref. (dB)	Shifted $L_n$ Ref. −20	Unfavor. Deviation (dB)	$L_{ni}$ without (dB)	$L_{ni}$ with (dB)	Difference $\Delta L$ (dB)	$L_{n,r,0}$ Ref. Floor (dB)	$L_{n,r,0}$ $\Delta L$ (dB)	$L_n$ Ref. (dB)	Shifted $L_n$ Ref. −19	Unfavor. Deviation (dB)
100	65.5	62	79	0	56.2	62	42	14.2	65.5	56.2	9.3	67	57.7	62	43	14.7
125	66.5	62	79	0	50	62	42	8	66.5	50	16.5	67.5	51	62	43	8
160	67	62	79	0	47.4	62	42	5.4	67	47.4	19.6	68	48.4	62	43	5.4
200	67.4	62	79	0	43.6	62	42	1.6	67.4	43.6	23.8	68.5	44.7	62	43	1.7
250	67.8	62	79	0	39.1	62	42	0	67.8	39.1	28.7	69	40.3	62	43	0
315	68.2	62	79	0	36.4	62	42	0	68.2	36.4	31.8	69.5	37.7	62	43	0
400	68.6	61	78	0	33.2	61	41	0	68.6	33.2	35.4	70	34.6	61	42	0
500	69	60	77	0	31.7	60	40	0	69	31.7	37.3	70.5	33.2	60	41	0
630	69.3	59	76	0	31	59	39	0	69.3	31	38.3	71	32.7	59	40	0
800	69.6	58	75	0	29.6	58	38	0	69.6	29.6	40	71.5	31.5	58	39	0
1000	70	57	74	0	24.7	57	37	0	70	24.7	45.3	72	26.7	57	38	0
1250	70.3	54	71	0	23.5	54	34	0	70.3	23.5	46.8	72	25.2	54	35	0
1600	70.5	51	68	2.5	22.6	51	31	0	70.5	22.6	47.9	72	24.1	51	32	0
2000	70.7	48	65	5.7	24.3	48	28	0	70.7	24.3	46.4	72	25.6	48	29	0
2500	71	45	62	9	19.1	45	25	0	71	19.1	51.9	72	20.1	45	26	0
3150	71.2	42	59	12.2	14.3	42	22	0	71.2	14.3	56.9	72	15.1	42	23	0
$L_{n,sum} = 81.3$ dB			Sum = 29.4	$57.9$ dB			Sum = 29.2	Sum = 29.8								
			Sum/16 = 1.8375				Sum/16 = 1.8250	Sum/16 = 1.8625								
			$L_{n,w} = 77$ dB				$L_{n,w} = 40$ dB	$L_{n,w,r} = 41$								
								$\Delta L_w = L_{n,w,r,0} - L_{n,w,r} = 78$ dB								
								$L_{n, Sum} - 15$ dB – $L_{n,w,r} = 37$								
								$L_{n, Sum} - 15$ dB – $L_{n,w,r} = 3.20$								
								$C_r = 3$								
								$-11 - C_r = -14.2$								
								$C_i, \Delta = -4$ dB								

**Table 14** Weighted Impact Sound Pressure Level  $L_{n,w}$  and Spectrum Adaptation Term for Walking Noise  $C_i$  of Typical Floor Constructions (Examples)

No.	Element Type	Layer Description	$L_{n,w} (C_i)$
1	Monolithic floor	Concrete 200 mm	73 (−11) dB
2	Timber floor with wooden joists	Wooden plank 20 mm Joist, height 180 mm (filling: 50 mm sand) Gypsum board 12.5 mm	69 (0) dB
3	Monolithic floor with floating floor	Concrete 200 mm Glass wool 13 mm Calcium sulfate 40 mm	36 (1) dB
4	Timber floor with wooden joists with floating floor	Cement screed 40 mm Glass wool 250 mm Chipboard 22 mm Joist, height 240 mm (filling: glass wool 100 mm) Gypsum board 12.5 mm	52 (2) dB

**Table 15** Weighted Reduction in Impact Sound Pressure Level  $\Delta L_w$  and Spectrum Adaptation Term for Walking Noise  $C_{i,\Delta}$  of Floor Coverings (Examples)

No.	Element Type	Layer Description	$\Delta L_w (C_{i,\Delta})$
1	Dry floating floor	Chipboard 22 mm Rock wool 32 mm	26 (−13) dB
2	Cementitious floating floor	Calcium sulfate 40 mm Glass wool 13 mm	37 (−14) dB
3	Floor covering	PVC, 2 mm	15 (−10) dB

have a volume of at least 150 m<sup>3</sup>, while for new test rooms a minimum volume of 200 m<sup>3</sup> is recommended. Plane absorbers as test specimen shall have a test area between 10 and 12 m<sup>2</sup> with a rectangular shape and with a ratio of width to length between 0.7 and 1. Different standard mounting conditions for plane absorbers (direct, glued, suspended, hanging, plaster materials) or for discrete sound absorbers (e.g., absorber pads or baffles) are described in a normative annex of ISO 354.

Test results for the sound absorption coefficient  $\alpha_s$  in one-third octaves from 100 to 5000 Hz normally range from 0 to 1. However, absorption coefficients well above unity can result from the diffraction of sound at the specimen edges, which is proportional to the ratio of the perimeter and the area of the sample.<sup>13</sup>

#### 4.2 Practical Absorption Coefficient

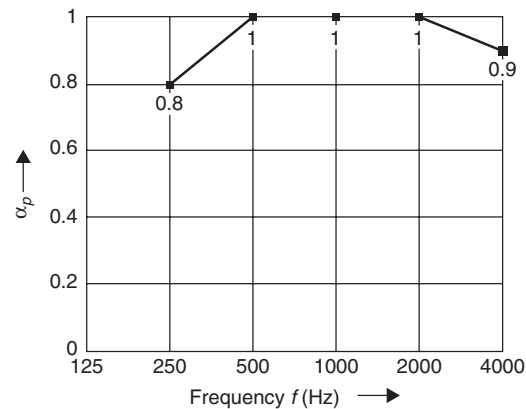
The *practical absorption coefficient*  $\alpha_p$  according to ISO 11654<sup>14</sup> is calculated by averaging arithmetically the sound absorption coefficients measured in third octave bands in each octave and rounding the result to the nearest 0.05 step.

$$\alpha_p = \frac{(\alpha_{i1} + \alpha_{i2} + \alpha_{i3})}{3}$$

Practical absorption coefficients  $\alpha_p > 1$  are maximized to  $\alpha_p = 1$ .

#### 4.3 Weighted Sound Absorption Coefficient

The single-number rating  $\alpha_w$  is obtained from the comparison of the  $\alpha_p$  spectrum with a reference

**Figure 5** Reference curve for sound absorption according to ISO 11654.

curve (Fig. 5). The reference curve is shifted in steps of 0.05 towards the measured value until the sum of the unfavorable deviations in the frequency range of 250–4000 Hz is less than or equal to 0.10. An unfavorable deviation occurs at a particular frequency when the measured value is less than the value of the reference curve. Only deviations in the unfavorable direction shall be counted. The weighted sound absorption  $\alpha_w$  is defined as the value of the shifted reference curve at 500 Hz.

The reference curve is lowered to 0.8 at 250 Hz to adapt the curve to the shape of conventional porous

absorbers. The decrease at 4000 Hz is due to the fact that mechanical typewriters with strong noise emission at high frequencies are nowadays less common in office rooms and absorbers for hygienic applications show often a decreasing sound-absorbing coefficient in this frequency range, both causing the higher frequencies to be less relevant when judging noise absorption characteristics.

#### 4.4 Shape Indicators

A shape indicator is used whenever the practical sound absorption coefficient  $\alpha_p$  at one or more frequencies exceeds the value of the shifted reference curve by 0.25 or more. Capital letters (in parentheses) indicate in such cases that an excess occurs in the low, medium, or high-frequency domain. An excess absorption at 250 Hz is marked by the indicator *L*, an excess at 500 or 1000 Hz by *M*, and an excess at 2000 or 4000 Hz by *H*. In general, a shape indicator means that the sound absorption coefficient at one or several frequencies is considerably higher than the values of the shifted reference curve. Negative deviations (values below the reference curve) are not considered as they are already maximized to 0.1 in the curve-shifting procedure.

#### 4.5 Examples

In Example 1 the calculation of the weighted sound absorption coefficient for a normal porous absorber with increasing sound absorption over frequency is

explained (Table 16). The reference curve is shifted in steps of 0.05 towards the measured value (i.e., downward) until the sum of the unfavorable deviations is equal or smaller 0.10. An unfavorable deviation occurs at 250 Hz and the result is  $\alpha_w = 0.60$ . No shape indicators are given as the differences between  $\alpha_p$ , and the values of the shifted reference curve is less than 0.25 at all center frequencies.

In Example 2, the shape indicator is calculated for a resonance absorber (Table 17). The unfavorable deviation is equal to that of example 1 and thus the same  $\alpha_w$  value is obtained. However, as the practical sound absorption coefficient of the absorber exceeds that of the shifted reference curve by more than 0.25 at 500 Hz, the mid-frequency (*M*) shape indicator is added resulting in the designation  $\alpha_w = 0.60(M)$ .

From studies on a number of practical absorber designs, the following conclusions can be drawn:

- For plane porous absorbers (e.g., mineral wool or open-cellular foams), the weighted sound absorption coefficient  $\alpha_w$  equals quite often the measured sound absorption coefficient  $\alpha$  at 500 Hz minus 0 to 0.10.
- The majority of plane porous absorbers receive the shape indicator *H* which means that the shifted reference curve is exceeded by more than 0.25 at 2000 or/and 4000 Hz. Hence, the absorber is more effective at these frequencies than indicated by the single-number rating  $\alpha_w$ .

**Table 16 Calculation Scheme for Example 1**

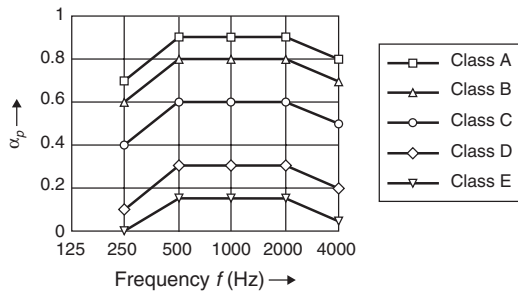
1	2	3	4	5	6	7
<i>f</i> (Hz)	$\alpha_p$	Ref. Curve	Shifted Ref. Steps 0.05 −0.40	Unfavorable Deviation	Difference Column 2– Column 4	Form Indicator If $\geq 0.25$
125	0.20					
250	0.35	0.8	0.40	0.05	−0.05	
500	0.70	1	0.60	0.00	0.10	
1000	0.65	1	0.60	0.00	0.05	
2000	0.60	1	0.60	0.00	0.00	
4000	0.55	0.9	0.50	0.00	0.05	
				Sum = 0.05 $\alpha_w = 0.60$		—

**Table 17 Calculation Scheme for Example 2**

1	2	3	4	5	6	7
<i>f</i> (Hz)	$\alpha_p$	Ref. Curve	Shifted Ref. Steps 0.05 −0.40	Unfavorable Deviation	Difference Column 2– Column 4	Form Indicator If $\geq 0.25$
125	0.20					
250	0.35	0.8	0.40	0.05	−0.05	
500	1.00	1	0.60	0.00	0.40	<i>M</i>
1000	0.65	1	0.60	0.00	0.05	
2000	0.60	1	0.60	0.00	0.00	
4000	0.55	0.9	0.50	0.00	0.05	
				Sum = 0.05 $\alpha_w = 0.60$		( <i>M</i> )

**Table 18 Sound Absorption Classes According to ISO 11654, Annex B**

Sound Absorption Class	$\alpha_w$
A	0.90; 0.95; 1.00
B	0.80; 0.85
C	0.60; 0.65; 0.70; 0.75
D	0.30; 0.35; 0.40; 0.45; 0.50; 0.55
E	0.25; 0.20; 0.15
Not classified	0.10; 0.05; 0.00

**Figure 6** Reference curves limiting the different sound absorption classes in ISO 11654.

- Resonance-type absorbers can receive various shape indicators depending on the individual characteristics of the frequency curve.
- Absorbers primarily used in office buildings at conventional wall distances receive no shape indicator when compared with the reference curve.

#### 4.6 Sound Absorption Classes

Depending on the value of the single-number rating,  $\alpha_w$ , absorbers can be grouped into classes (Table 18). These sound absorption classes intend to facilitate the selection of suitable absorbers for a specific applications by architects or building designers. National regulations can refer either to the weighted sound absorption coefficient or the sound absorption class.

#### REFERENCES

1. Council Directive 89/106/EEC of 21 December 1988 on the Approximation of Laws, Regulations, and Administrative Provisions of the Member States Relating to Construction Products, *Official Journal L 040*, 11/02/1989, pp. 0012–0026.
2. ISO 717-1 (1996-12), Acoustics—Rating of Sound Insulation in Buildings and of Building Elements—Part 1: Airborne Sound Insulation.
3. B. Rasmussen, Sound Insulation between Dwellings—Classification Schemes and Building Regulations in Europe, *Proc. Internoise 2004*, Prague.
4. ISO 31-0 (1992-08), Quantities and Units; Part 0: General Principles.
5. ISO 717-2 (1996-12), Acoustics—Rating of Sound Insulation in Buildings and of Building Elements—Part 2: Impact Sound Insulation.
6. W. Fasold, Untersuchungen über den Verlauf der Sollkurve für den Trittschallschutz im Wohnungsbau, *Acustica*, Vol. 15, 1965, pp. 271–284.
7. E. Gerretsen, A New System for Rating Impact Sound Insulation, *App. Acoust.* Vol. 9, 1976, pp. 247–263.
8. K. Bodlund, Rating of Impact Sound Insulation between Dwellings, *J. Sound Vib.*, Vol. 102, 1985, pp. 381–402.
9. D. Aubree and T.A. Carman, A Comparison of Methods for Rating the Insulation of Floors Against Impact Noise, CSTB/BRE Report, 1988.
10. P. Leistner, H. Schroeder, and B. Richter, Gehgeräusche bei Massiv- und Holzbalkendecken (Walking Noise on Heavy and Timber Floors, in German), *Bauphysik*, Vol. 25, 2003, pp. 187–196.
11. ISO 140-11 (05–2005), Acoustics—Measurement of Sound Insulation in Buildings and of Building Elements—Part 11: Laboratory Measurements of the Reduction of Transmitted Impact Sound By Floor Coverings on Lightweight Reference Floors.
12. ISO 354 (2003-05), Acoustics—Measurement of Sound Absorption in a Reverberation Room.
13. H. Kuttruff, *Room Acoustics*, 3rd ed., Elsevier Science, London, 1991.
14. ISO 11654 (1997-04), Acoustics—Sound Absorbers for use in Buildings—Rating of Sound Absorption.

# CHAPTER 108

## ACOUSTICS DESIGN IN OFFICE WORK SPACES AND OPEN-PLAN OFFICES

Carl J. Rosenberg  
Acentech Incorporated  
Cambridge, Massachusetts

### 1 INTRODUCTION

Acoustical considerations in offices relate to noise control of equipment, speech privacy, and freedom from distraction. These considerations have been shown to influence the productivity of office workers and can, therefore, have both an economic and psychological impact on the office environment. The understanding focus on office acoustics has paralleled the growth of architectural acoustics as a building science and the development of acoustical products. Tools are available for evaluating and enhancing the acoustical design of office work spaces.

Basic terms of reference have been developed for architectural acoustics in general and for analysis of office acoustics in particular. These include the A-weighted sound pressure level, sound transmission class (STC), noise criteria (NC) ratings, noise isolation class (NIC), noise reduction coefficient (NRC), and articulation index (AI; a measure of signal-to-noise ratio). These terms are used both to measure existing conditions and to predict the results of a new design. More recently, as acoustical analysis has addressed open plan office issues, newer terms and analysis tools related to speech intelligibility and privacy have been developed. Sound-masking systems have become an accepted component of acoustical design.

### 2 CURRENT ANALYTICAL FRAMEWORK

A seminal study by Cavanaugh et al. from 1962 added an important tool to the analytical acoustical arsenal.<sup>1</sup> It was found that the reduction of noise between offices did not alone correlate with acceptability or privacy. It was formulated that background sound, specifically steady-state sources such as fan noise from ventilation systems that did not vary or carry their own messages, were a significant factor in achieving acceptability to office workers for their privacy. Higher levels of background sound provided a speech-masking effect. Lower levels of background sound meant that intrusive noise was much more noticeable and annoying. The role of background sound was quantified, and privacy was correlated with signal-to-noise ratio, not with just noise reduction of construction. This relationship is stated as

$$\begin{aligned} \text{Speech privacy} &= \text{Noise reduction} \\ &+ \text{Background sound pressure levels} \end{aligned}$$

This is the framework for the current evaluation of office acoustics for both closed- and open-plan offices.

### 3 EFFECT OF ACOUSTICS ON HUMAN PRODUCTIVITY

Acoustics profoundly impacts human performance and has been objectively measured in office settings for its effect on productivity. In fact, numerous demonstrations of these impacts on office workers have been a concern for research scientists for decades, some work going back almost 80 years.<sup>2</sup> In addition to the focus on productivity, there is currently a strong concern for privacy. This has recently acquired much broader relevance due to a sensitivity to privacy as a civil right and the passage of numerous privacy protection laws by foreign countries (e.g., EU Directive 95.46) and at the federal level in the United States. For instance, with regard to an individual's health records, current legislation in United States requires that the transfer of health records, in whatever format, conform with requirements for privacy (e.g., the Health Insurance Portability and Accounting Act, HIPAA). This includes privacy for digital transfer of health records between providers of health care and presumably *aural* privacy as well. Similar concerns are entering the realm of potential legislation for the financial world also (e.g., the Gramm Leach Bliley Act, relating to privacy of financial transactions).

### 4 NOISE REDUCTION AND ACOUSTICAL FACTORS IN CLOSED OFFICES

Closed offices by definition have walls that extend at least to the ceiling plane and have a door. Ceiling heights can range from 2.5 m (just over 8 ft) up to 4 m (13 ft) and more. Noise sources within a closed office can be conversations on the telephone or conversations between workers and visitors in the same office. These sources become a distraction to the neighboring space.

The analysis of sound transfer between offices follows traditional procedures of source–path–receiver. The acoustical power of the source, the size of the room, and the finishes on the walls and ceiling will all determine the sound energy within the *source* room. Construction systems for the primary and secondary sound *paths* will determine how much sound energy is transmitted to a neighboring space. The primary sound path is the common wall that may or may not have a doorway or window as part of that path. The secondary sound paths include sound transfer through

the ceiling plenum, through gaps and leaks, through common ducts (both supply and return), through openings around pipes, and through exterior lightweight window systems or even through open windows. The background sound pressure level in the *receiver* room will determine the final signal-to-noise ratio and hence effect the resulting speech privacy. See Fig. 1.

**Common Wall** Existing standard literature in architectural acoustics provides guidelines for typical sound reduction performance of this primary sound path.<sup>3-8</sup> For example, wall constructions with STC 40 are usually thought to have modest to poor ability to block sound and hence provide poor speech privacy. Constructions with performance in the range of STC 50 are more typical of performance that is necessary for confidential speech privacy.

**Wall Constructions** For typical modern offices, the range of construction options is limited to just the number of layers of gypsum board on the wall, the type of stud framing, and whether or not there is insulation in the cavity of the wall. A single metal stud with a single layer of gypsum board on each side of the stud and no insulation in the cavity will have a performance in the range of STC 40. If the layers of gypsum board are doubled (i.e., two layers on each side), then the overall STC value will increase by about 5 STC points. There is negligible difference between the performance

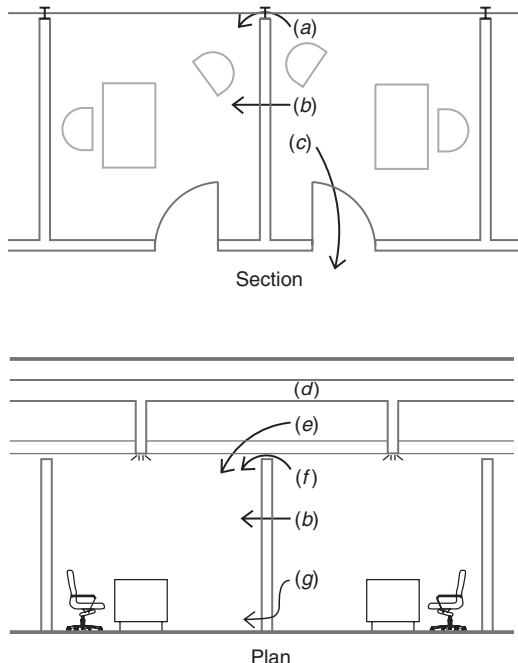
of the wall with gypsum board that is 12.5 mm ( $\frac{1}{2}$  in.) thick or 15.6 mm ( $\frac{5}{8}$  in.) thick. Insulation in the cavity of a wall with a single stud may provide an additional 3 to 5 STC points performance. Wood studs instead of metal studs provide a more rigid path for the transfer of sound and will degrade the performance by 3 to 5 STC points. Further improvements above STC 50 require the use of resilient channels or double-stud framing.<sup>3-8</sup>

**Ceiling Path** In modern lightweight buildings, walls often do not extend to the structure. In these cases, the path for sound through the ceiling plenum is the weakest sound path between offices. This sound path is rated by a ceiling attenuation class (CAC) that is analogous to an STC rating. The CAC value is measured in accordance with ASTM (American Society for Testing and Materials) standards and measures the sound transfer from one standard sized office through an acoustic tile ceiling, then into a standard plenum, and then back into the neighboring office again through an acoustic tile ceiling. Mineral fiber acoustic tiles typically have a rating of CAC 35 to 39. CAC values (or STC values for the same configuration) are provided with a 5-point range. In cases where there is a return-air grille in the ceiling so air can be exhausted through the plenum, or where there is a light fixture with openings, the field performance of the ceiling path will be significantly degraded.

**Ceiling Path — Noise Control Options** Glass fiber ceiling tiles have CAC values too low to be considered as an effective barrier of any kind. Sometimes offices need the high absorptive properties of a glass fiber ceiling (high NRC) and at the same time a high CAC performance. In this case, the suitable choice is a composite acoustic tile that combines high NRC with high STC, such as a layer of gypsum board or mineral fiber acoustic tile to which a finish layer of glass fiber has been surface mounted. Alternatively, it may be necessary to add a plenum barrier above the partition. This plenum barrier must be of a dense material (gypsum board or sheet lead) with an STC value that is sufficient to upgrade the CAC of the ceiling path so it is equal to the STC of the wall. The plenum barrier must also extend over the corridor wall of adjacent offices so as to prevent flanking around the ends of the plenum barrier.

**Gaps and Cracks** Openings in the wall will obviously degrade the acoustical performance since the STC rating for an opening is 0. Typical open gaps and cracks are the perimeter around an interconnecting door, gaps at window mullions, open doors to a common corridor, and pipe and duct penetrations that are not sealed airtight.

**Other Flanking Paths** Sound also travels between adjacent closed offices through lightweight building elements that are common to both rooms. In modern buildings, these flanking paths include lightweight strip windows, curtain walls, common floors, and exterior walls.



**Figure 1** Closed office sound paths: (a) continuous strip window, (b) through wall, (c) open doors, (d) interconnecting duct, (e) through plenum, (f) over partition, and (g) gaps at partition.



**Composite Constructions** In looking at the performance of a common wall between offices, or in evaluating multiple paths that include flanking paths and ceiling paths, often it is necessary to consider the composite effect of the wall elements. Doors and interior windows are notorious for their ability to degrade the acoustic performance of the composite wall. The overall noise reduction of a composite construction is dependent on (a) the performance or STC rating of the weakest path, (b) the STC rating of the primary wall construction, and (c) the area of the weaker path relative to the surface area of the primary construction.

**Field versus Laboratory Performance** As with any construction system, the actual in-field performance seldom approaches the theoretical or laboratory STC rating for the construction. This is due to flanking paths, field conditions, poor construction practices, and lack of caulking. Noise reduction is measured in the field by a noise isolation class (NIC). Typically, the NIC value will be 5 to 10 points less than the STC rating of a given construction.

**Demountable Walls** Some offices use so-called demountable walls that have the physical attributes of permanent walls, but the walls can be removed and relocated, thus providing a degree of flexibility that is not available with gypsum board walls and traditional stud construction. These walls extend only to the underside of a continuous ceiling, so the field NIC performance of the wall is usually quite a bit less than its laboratory STC rating.

**Background Sound Pressure Levels** The background sound pressure level has a strong impact on the degree of speech privacy that can be achieved in closed offices. If the ambient sound is very quiet, NC-30 or less, then even very good constructions can be inadequate to provide privacy. If the ambient is rather loud, NC-40 or above, then even very poor constructions can provide adequate normal privacy. Ambient sound can be contributed by traffic outside, by a central ventilation system, by unit ventilators or fan coil units in the office, or by an electronic sound-masking system.

Ambient noise can also be a source of distraction, as may be the case from exterior noise sources reflecting from adjacent buildings or reverberating from interior courtyards. In these cases, the open windows are often the controlling sound paths, and attention must be paid to the sound transmission from exterior sources through the building envelope. The problems can be exacerbated by U-shaped building configurations in urban environments.

**Measure of Privacy** As noted above, the relationship between privacy, noise reduction, and background sound pressure levels is indicated in the following relationship:

$$\begin{aligned} \text{Speech privacy} &= \text{noise reduction} \\ &+ \text{Background sound pressure levels} \end{aligned}$$

In one design approach, this general relationship has been transformed into a quantifiable formula:

$$\text{SPI} = \text{NR} + \text{NC}$$

where SPI = speech privacy index

NR = noise reduction, measured as an NIC rating.

NC = measured noise criteria rating

Source room levels are assumed to be normal voice level and normal office sizes. SPI values of 75 or above relate to *confidential* speech privacy, which is a condition where a listener is not able to understand speech from a neighboring office when a talker is using normal voice level. SPI values of 68 to 75 relate to *normal* speech privacy, where only occasional words would be intelligible. SPI values below 68 do not provide speech privacy.

## 5 NOISE REDUCTION AND ACOUSTICAL FACTORS IN OPEN-PLAN OFFICE

Open-plan offices are characterized by the absence of fixed walls, partitions that do not extend full height to the ceiling, and no doors. These layouts were developed first in the 1960s to provide flexibility in office arrangements, cost savings in office construction, and innovative patterns of work flow. Activities in open-plan offices include the full range of traditional office work activities. These may require (but seldom attain) confidential speech privacy between adjacent spaces or just freedom from distraction.

Although specific layouts may vary dramatically, open-plan offices are the predominant format for office layout today. The offices may have a traditional cubicle format or may be a new "team space" concept. The workstation may be surrounded by stand-alone screens, walls, office furniture, modular workstations, or no barrier whatsoever. Open-plan offices are considered to be less expensive and less costly to rearrange than closed offices. However, because workstations or cubicles do not have full-height partitions, lack of privacy and increased distraction make office workers less productive, as discussed earlier above. Acoustics is an extremely important aspect of open-plan office design and has been an issue of concern since the inception of open-plan office design.<sup>9,10</sup>

### 5.1 Privacy Metrics

**Articulation Index** Speech intelligibility and acoustics in open-plan offices can be rated in terms of articulation index (AI). (See Appendix.) AI is a frequency-weighted measure of the ratio between a signal (e.g., a talker in a classroom, a neighbor's voice, or some intrusive speech) and steady background noise (ambient noise from mechanical equipment, traffic, or electronic sound masking). The frequency ratings reflect the fact that certain octave bands are more important than others for their contribution to speech intelligibility. AI was originally developed to evaluate communication systems and has been widely applied to assess

conditions for speech intelligibility in rooms. AI values range from near 0 (very low signal and relatively high noise; poor intelligibility and good speech privacy) to 1.0 (very high signal and rather low noise, excellent communication and no speech privacy). When privacy is desired (e.g., in an office), it is necessary to have a low AI. When communication is desired (e.g., in classrooms or teleconference rooms), it is necessary to have a high AI so people can understand speech clearly.

**Speech Intelligibility Index** To some extent, AI is being replaced by the speech intelligibility index (SII) in acoustical standards for office acoustics. (See Appendix.) SII is still, like AI, a weighted-speech-to-noise-ratio. However, it is somewhat more complex to calculate than AI and includes revised frequency weightings and the masking effect of one frequency band on nearby frequency bands. Like AI, it has values that range between 0 and 1, but for the same conditions SII values are a little larger than AI values. An empirical relationship has been developed that allows one to approximate a correlation between AI and SII by two simple adjustment factors.<sup>11</sup>

**Privacy Index** Low AI numbers indicate a higher degree of privacy. Since this may be confusing to laypersons who want to focus on better privacy conditions, a new metric called privacy index (PI) has been developed. The privacy index is defined as

$$PI = (1 - AI) \times 100, \text{ presented as a \%}$$

where PI = privacy index

AI = articulation index

In this manner, *higher* PI numbers indicate more privacy; lower PI numbers mean less privacy. For example, an AI of 0.10 equals a privacy index of 90%.

**Confidential and Normal Privacy** General accepted practice today for design of open-plan offices refers to two levels of speech privacy. *Confidential privacy* is defined as a condition where there is no phrase intelligibility but some isolated word

intelligibility. *Normal privacy* allows modest amounts of intelligibility, but normal work patterns are usually not interrupted. These terms are codified in ASTM 1374 Standard Guide for Open Office Acoustics and Applicable ASTM Standards. (See Appendix.)

**Recommended Values** Average noise requirements for various office functions are shown in Table 1.

## 5.2 Analysis Tools

As with any acoustical analysis, open-plan office acoustics can be addressed in terms of the *source* (people talking), the *path* (direct line of sight, barrier effects, reflections) and *receiver* (location of listener in relation to the source and contribution of sound masking). Following is a discussion of factors that influence privacy in open-plan offices (Fig. 2).

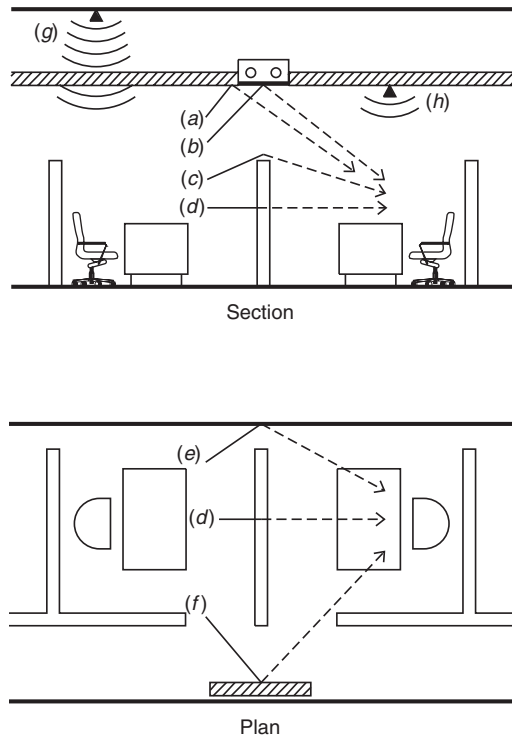
## 5.3 Source

**Level** Values for typical voice levels have been standardized in American National Standards Institute (ANSI) S3.5 Methods for the Calculation of Articulation Index. (See Appendix.) However, recent research has shown that the occupants of open-plan offices often speak at lower than normal levels, and this has to be taken into account in an analysis of open-plan acoustics. Speech levels in open-plan offices are typically 3 dB to 10 dB quieter than the typical levels from ANSI standards. This is probably due to the increased sense of exposure that talkers have. If a talker can hear others, that talker will sense that he or she can be heard by others. This naturally develops a sense of office etiquette that should be encouraged. It promotes lower voice levels in open areas and suggests to workers that they should relocate to closed offices when having more active (louder) discussions or when increased privacy is required or when using speaker phones.<sup>11,12</sup>

**Orientation** The human voice has directional characteristics. Noise levels behind a talker can be up to 10 decibels quieter than levels on axis with the direction of a person talking. However, since the orientation to which a person will be talking is seldom in only one

**Table 1 AI, SII, and PI for Open-Plan Offices**

AI Value	SII Value	Privacy Index	Criteria Definition	Noise Requirements
>0.65		<35%	Good communication	Necessary when communication is desirable (conference rooms, classrooms, auditoriums, etc.)
0.35		65%	Freedom from distraction	Reasonable work conditions not requiring heavy concentration or speech privacy; can hear and understand neighboring conversations
0.20	0.27	80%	Normal speech privacy	Only occasional intelligibility from a neighbor's conversation; work patterns not interrupted
<0.05	<0.10	>95%	Confidential speech privacy	Aware of neighbor's conversation, but it is not intelligible



**Figure 2** Open-plan office sound paths: (a) reflections off ceiling, (b) reflections off light fixtures, (c) diffraction over partial height barrier, (d) through barrier, (e) around end of barrier, (f) secondary reflections, (g) sound masking from loudspeakers above the ceiling, and (h) sound masking from direct-field emitters.

direction, and since an office often has reflecting surfaces in front of a talker, most models of acoustics in open-plan offices do not account for this factor.

**Office Layout and Size** The size of an office indirectly determines the distance from a source to the nearest barrier and thus effects the barrier effect and also the distance to the receiver. Space for an office is often the single most expensive element in the design, and there is strong pressure to reduce office cubicle size in many situations. A normal office might be in the range of 3 m × 3 m (10 ft × 10 ft) but some conditions can be as small as 2 m × 2 m (6.6 ft × 6.6 ft) or 2.5 m × 2.5 m (8.2 ft × 8.2 ft).

#### 5.4 Path

**Barrier Effect (Screen Height)** Partial height barriers or partitions are necessary to block direct sound transmission between workstations. If there is no barrier, the direct path will govern the sound transfer and, unless there are extraordinary distances between source and receiver, speech privacy will be unattainable. The barrier must be high enough and wide enough to interrupt the line of sight between

a source and a receiver. The height of the mouth of a talker and the ear of a listener is normally about 1.2 m (4 ft) above the floor. Hence, the first 1.2 m (4 ft) or so of barrier height do not help speech privacy at all, and barriers or partitions need to be significantly higher than this height so as to be able to block sound. This means a barrier must have a height of about 1.5 m (5 ft) as a minimum requirement for acoustical separation, and a height of 1.8 m (6 ft) typically for normal privacy. Above this height there are diminishing returns because of reflections off the ceiling and diffraction over the barrier.<sup>13</sup>

**Barrier Absorption** The absorption on the surface of a barrier does not have any direct effect on the sound transfer between the neighboring workstations except if there are secondary reflections off barriers on the other side of the cubicle. It is good practice to reduce these reflections, and even modest NRC values of 0.65 for the inside surface of a cubicle can be beneficial.

**Barrier Transmission Loss** The barrier should be able to block sound at least as well as the path for sound diffracting over the barrier, which means a minimum laboratory sound transmission class value of STC 20. This is more than adequate. Barriers or screens should extend to the floor or leave only a small opening at the bottom. There should be no open gaps between adjacent panels. Values higher than STC 20 are of no additional benefit.

**Barrier Location** A barrier is most effective if placed close to the source or receiver.

**Ceiling Absorption** The ceiling in an open-plan office is the most important surface to treat with highly efficient sound-absorbing material. The ceiling should have a noise reduction coefficient (NRC) of at least 0.90 or an articulation class (AC) of at least 180. These terms are described further below. A ceiling with absorption properties lower than these may make privacy less than acceptable. A ceiling with absorption properties higher than these can be of more benefit since it may help mitigate the adverse contribution of other less effective components. Therefore, glass-fiber ceiling panels, which typically have high absorption properties, are the preferred material for ceilings in open-plan offices. Regular mineral-fiber acoustical panels have typical NRC value of only about 0.55 to 0.65. Hard sound reflective materials such as exposed structure or gypsum board have NRC values less than 0.10 and will dramatically reduce privacy and raise annoying sound pressure levels in an office. Most ceiling tile manufacturers provide extensive data on the sound absorptive properties of their products and will have special products for use in open-plan spaces. Materials must also be selected for their ability to reflect light.

**NRC, SAA, and AC** The sound absorptive performance of acoustical ceilings can be determined in either of two ways. One process is the measure of

sound absorption coefficients in a reverberation chamber in accordance with ASTM C423. (See Appendix.) This determines the random incidence sound absorption coefficients ( $\alpha$ ) for the test material. From these data, manufacturers typically report the NRC. The NRC value is a good first approximation of the ability of a material to absorb sound in the human speech range. NRC is the average of coefficients of absorption for four mid-range frequencies (250 Hz, 500 Hz, 1000 Hz, and 2000 Hz), rounded to the nearest .05. NRC values range from 0 to 1.

$$\text{NRC} = \frac{\alpha_{250} + \alpha_{500} + \alpha_{1000} + \alpha_{2000}}{4}$$

(rounded to nearest 0.05)

Another term gaining increasing application is the sound absorption average (SAA). SAA is a single-number rating that is the average, rounded off to the nearest 0.01, of the sound absorption coefficients of a material for the 12 one-third octave bands from 200 through 2500 Hz. The SAA can be used in conjunction with NRC rating. (See Appendix.)

In an open-plan office, the actual effectiveness of the ceiling in determining noise reduction is related to its absorptive performance and the height of the barrier that separates two workstations and the distance between a talker and listener. Therefore, another term has been developed for a measure of the ceiling's contribution to noise reduction between typical (but specifically designated) workstations. This is the articulation class (AC), measured in an office mockup environment in accordance with ASTM E1111 and E1110. (See Appendix.) AC values range from about 150 to 220. The AC is the sum of the weighted sound attenuation numbers in a series of 15 test bands for a carefully specified office layout, barrier height, and ceiling height.

**Ceiling Height** The height of a ceiling also impacts its effectiveness in open-plan office acoustics. Typical ceiling heights might be in the range of 2.7 m (8.8 ft). Lower ceilings will have a noticeable adverse impact on privacy because sound reflected off the ceiling will be at a higher sound pressure level. This is due to the shorter sound path of the reflected sound energy, which increases the level of the disrupting signal, increases the signal-to-noise ratio, increases the AI, and therefore reduces the privacy index. The lower the ceiling, the more important the absorptive properties are for controlling reflections and providing speech privacy. Higher ceilings do not make a radical improvement, unless you go to significantly higher spaces with 5.4-m (18-ft) ceilings or above. Such very high ceilings of hard sound-reflecting materials will increase overall noise levels but may not degrade speech intelligibility.

**Wall Reflections** Reflections and diffraction around the ends of a partial-height partition also must be taken into account. In particular cases where such reflections are detrimental to the desired low AI, the

wall reflections should be eliminated. This can be done with the closure of a panel tight against the wall (hence eliminating the flanking path around the end of the panel altogether), or there should be additional sound-absorbing material at the offending sound-reflecting wall. This can be analyzed with a relatively simple ray diagram. To be effective in reducing sound energy from the offending reflecting surface, the additional material should have an NRC value of 0.80 or higher.

**Ceiling Reflections** Sometimes elements in the plane of the ceiling may degrade speech privacy because they reflect sound from one workstation to another. In particular, flat lens light fixtures act as acoustical mirrors and should be avoided, especially if the fixtures are aligned right over the partial-height wall.

**Office Layout** Office layout also affects speech privacy. Offices should be arranged so that entrances are offset, and direct line of sight or an open view through doorways from one workstation to another should be eliminated. Workstations should be 2.45 m by 3.0 m (8 ft to 10 ft) apart so voice levels are adequately reduced over distance (see Fig. 3).

**Floor** Carpet, whether thick or thin, is very helpful in an open-plan office because it reduces footfall noise, eliminates the sound of moving chairs, and cuts down on any reflected sound that bounces between spaces off hard floor surfaces. However, carpet is of very little direct benefit in actually absorbing sound in the office.

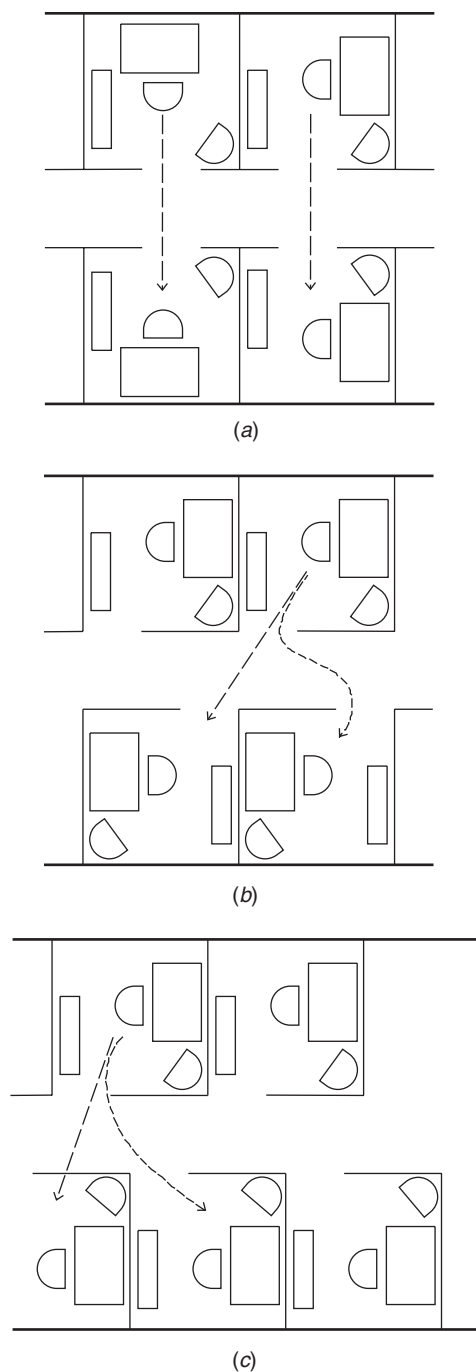
## 5.5 Receiver

Background sound can be generated by a ventilation system, by outdoor traffic noise (at least for offices closest to exterior windows), or by an electronic system. There are many advantages of an electronic system. It can provide a preferred sound pressure level and spectrum. It will not vary depending on the outside temperature or inside heat load. It can provide evenly distributed coverage throughout an office while a ventilation system may be too loud near diffusers and too quiet elsewhere.

In concept, an electronic sound-masking system comprises a noise generator, spectrum shaper with filters, amplifiers, and loudspeakers. Many systems use loudspeakers hidden above a suspended acoustic tile ceiling. The sound pressure level and spectrum for these plenum loudspeakers are then adjusted until the desired effect below the ceiling at the workstation is achieved. Other newer technologies use loudspeakers directly in the plane of the ceiling that do not need any spectrum adjustment.

## 6 SOUND-MASKING TECHNOLOGY AND DESIGN

**Masking Sound Spectrum** The character and level of background sound is perhaps the most important acoustical design consideration for an open-plan office. A modest level of background or ambient sound will cover, or mask, annoying intrusive sounds.



**Figure 3** Open-plan office layout configurations: (a) poor layout, (b) fair layout, and (c) better layout.

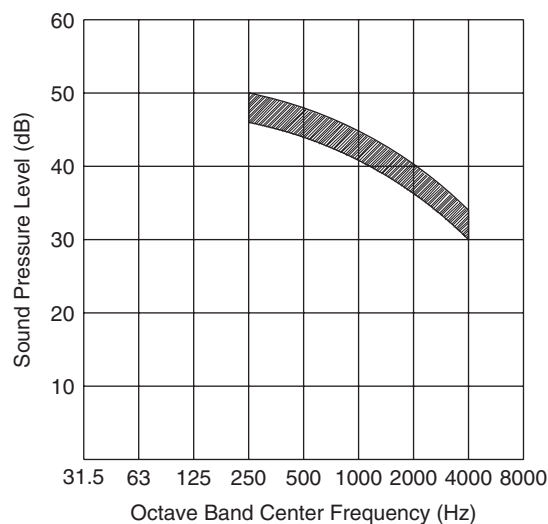
The masking sound must be pleasant and neutral with an even tonal spectrum (like the sound of a comfortable ventilation system) that drops off at the

high end of the frequency range. There should be no pure tones or annoying characteristics (like the humming sound of a fluorescent light ballast). A sample spectrum that is well accepted is shown in Fig. 4. There are variations on this spectrum that are also acceptable.<sup>14</sup>

**Masking Sound Pressure Levels** The sound should be evenly distributed throughout the office so the sound is no louder in some areas than others. In addition, the generally accepted practice is that the level should not vary in the open-plan area by more than 3 dB in any octave band. Masking sound should be loud enough to cover intrusive noises, but never loud enough to be distracting in itself. Many studies have concluded that the preferred range of A-weighted sound pressure levels is perhaps between 45 and 50 dB.<sup>10</sup> Conference rooms and private offices require lower levels of background sound for ease of communication within the room.

#### Use of HVAC Systems as Masking Sound Source

In theory, normal air-conditioning and ventilation systems could generate appropriate background noise to mask speech between offices or workstations. To do so, the ambient sound from the heating and ventilation system would have to be of the correct loudness, acceptable spectrum (frequency distributions), steady and constant throughout the day, and uniformly distributed spatially throughout the office. This is seldom the case. Heating, ventilating, and air-conditioning (HVAC) systems are not designed for this purpose. Many office buildings use variable volume air distribution, so noise from the HVAC system may be erratic and uneven in distribution, and it may change in level over time and season. Mechanical engineers usually design office mechanical systems to provide typical



**Figure 4** Desired spectrum and level for background sound (speech masking) in open-plan offices.

operating A-weighted sound pressure levels from 5 to 10 dB below the desired range for masking sound. Diffusers are placed for air distribution concerns, not for acoustics. All in all, the HVAC system cannot be relied upon to meet the speech-masking needs of offices.

**Electronic Sound-Masking Systems—Loudspeakers above Ceiling** Traditional sound-masking systems have used loudspeakers installed above the office ceiling, hidden above an accessible acoustic tile or panel. This type of system must have the ability to adjust the spectrum easily in order to provide the correct frequency distribution. The system must generate enough power to transfer adequate sound energy through the ceiling panel. And the system must be designed to assure even spatial uniformity for the occupied office space. Even a 3-dB variation from one workstation to another can have a dramatic effect on speech privacy. Without the benefit of even spatial distribution, a system may be either operated at a level that is so loud that it causes annoyance to many users, or conversely may be operated at a level that is so low that it does not provide good privacy throughout the office.

The design of these above-ceiling systems is made more difficult because of the sound attenuation characteristics of typical ceiling and plenum materials, openings for return-air trough diffusers and light fixtures, and reflections off structure or ductwork in the plenum. Theoretically, there are some measures that can be taken to mitigate the design problems, such as providing each loudspeaker with a volume control, using many more loudspeakers, and providing sound attenuating “boots” at each opening in the ceiling. Realistically, however, these measures are rarely employed because of the resulting costs.

**Electronic Sound-Masking Systems—Loudspeakers below Ceiling** New technology uses sound-masking emitters (loudspeakers) in the plane of the ceiling, so-called direct-field emitters that radiate sound directly into the occupied space below, rather than into the above-ceiling plenum. In this manner, the system may provide much better uniformity of masking sound throughout the open-plan office. The principal advantage of direct-field emitters is that there is no nonuniformity caused by HVAC openings in the ceiling or ventilation slots in lighting fixtures, or by building structure, fireproofing, and large ducts or other mechanical components in the plenum. Such anomalies no longer have any significant effect on the spatial distribution of masking sound in the office. The system designer can assure very uniform coverage simply by providing a well-defined and simple layout of masking loudspeakers, without a precise knowledge or consideration of above-ceiling building elements.

Another significant advantage of direct-field emitters is that these systems also assure that the frequency distribution of sound is optimum because there are no significant frequency-dependent acoustical attenuators between the loudspeakers and office occupants.

No spectrum adjustments are necessary in the field. To the user, this means that the system is able to provide effective masking at considerably lower sound pressure level and lower potential for annoyance, and that the acoustical effectiveness is maintained throughout the building.

Also, the direct-field emitters beneath the ceiling require lower power level than required for above-ceiling loudspeakers since they are radiating directly into the sound field, not into a plenum. However, the loudspeakers need to be quite omnidirectional except at the very highest frequencies.

Because of these acoustical advantages as well as economic factors, these systems are gaining increased acceptance in the marketplace. To be acceptable visually, however, the loudspeakers will either have to look like a ceiling acoustic tile or will have to be very inconspicuous.

**Electroacoustic Issues** Experience has found that having incoherent masking sound from multiple channels reduces the chance of localization or peaking due to phase interference or phase amplification. Some systems have up to four incoherent channels to avoid interference effects.

## 7 METHODS FOR CALCULATING ARTICULATION OR PRIVACY INDEX

Acousticians have been developing unified theories and programs to combine the different aspects of open-office acoustics into a reliable predictive methodology. The systems vary from simple worksheets to complex computer programs, and they have been developed to combine the effect of these variables and to assign an estimated AI value to a particular layout or range of materials. In this way, the influence of each parameter of the office design on the expected speech privacy in the office can be determined ahead of time. Pertinent variables include all the items noted above to varying degrees, such as the ceiling absorption, the height of partial height panels, and the workstation plan size are shown to be most important.<sup>9</sup> The success of any of these analysis tools depends on the correctness of the model and the accuracy of the assumptions on which it is based.

## 8 OFFICE MACHINERY

Other equipment in a typical office should also be identified and treated appropriately to reduce annoyance and distraction to nearby workers. This equipment includes copiers, telephones, collators, paging systems, and other sources that are distractions. Copiers are best located in a separate alcove or preferably in a separate room with a door, and with sound-absorptive materials close to the cooling fans, which are the predominant noise source.

## 9 FUTURE DEVELOPMENTS

Although open-plan schools have been found to be inappropriate for teaching environments, open-plan offices will undoubtedly remain an important part

of office layout and design. Acoustics is a major concern. Masking is a critical component of good privacy and freedom from distraction; its vital role for speech privacy and productivity has gained increasing recognition. We can expect to see greater use of easy-to-install sound-masking systems, perhaps brought right to the desk-top workstation, perhaps integrated directly into furniture systems.

#### APPENDIX STANDARDS RELATED TO PREDICTING, EVALUATING, AND MEASURING SPEECH INTELLIGIBILITY AND PRIVACY PARAMETERS USED IN ACOUSTICS DESIGN OF OFFICE WORK SPACES AND OPEN-PLAN OFFICES

ANSI (American National Standards Institute)	
S3.2	Method for Measurement of Monosyllabic Word Intelligibility
S3.5	Methods for the Calculation of Articulation Index
ASTM (American Society of Testing and Materials)	
E-90	Standard Method for Laboratory Measurement of Airborne Sound Transmission Loss of Building Partitions
E-1041	Guide for Measurement of Masking Sound in Open Offices
E 1110	Standard Classification for Determination of Articulation Class
E 1111	Standard Test Method for Measuring Interzone Attenuation of Ceiling Systems
E 1130	Standard Test Method for Objective Measurement of Speech Privacy in Open Offices Using Articulation Index
E 1179	Specification for Sound Sources Used for Testing Open Office Components and Systems
E 1374	Standard Guide for Open Office Acoustics and Applicable ASTM Standards
E 1375	Standard Test Method for Measuring the Interzone Attenuation of Furniture Panels Used as Acoustical Barriers

E 1376	Standard Test Method for Measuring the Interzone Attenuation of Sound Reflected by Wall Finishes and Furniture Panels
C 423	Standard Test Method for Sound Absorption and Sound Absorption Coefficients by the Reverberation Room Method
ISO (International Standards Organization)	
60268-16	Objective Rating of Speech Intelligibility by Speech Transmission Index
9921-01	Speech Interference Level and Communication Distances for Persons with Normal Hearing Capacity in Direct Communication (SIL method)

#### REFERENCES

1. W. J. Cavanaugh, W. R. Farrell, P. W. Hirtle, and B. G. Watters, Speech Privacy in Buildings, *J. Acoust. Soc. Am.*, Vol. 34, No. 4, 1962, pp. 425–492.
2. E. Thompson, *The Soundscape of Modernity: Architectural Acoustics and the Culture of Listening in America, 1900–1933*, M.I.T. Press, Cambridge, MA, 2002.
3. W. J. Cavanaugh and J. A. Wilkes, Eds., *Architectural Acoustics—Principles and Practice*, Wiley, New York, 1998.
4. J. P. Cowan, *Architectural Acoustics: Design Guide*, McGraw-Hill, New York 2000.
5. M. D. Egan, *Architectural Acoustics*, McGraw-Hill, New York, 1988.
6. M. Mehta, J. Johnson, and J. Rocafort, *Architectural Acoustics: Principles and Design*, Prentice Hall, New York, 1999.
7. Charles A. Salter, Associates, *Acoustics: Architecture-Engineering-the Environment*, William Stout, San Francisco, 1998.
8. Acoustics, in *Architectural Graphic Standards*, American Institute of Architects, 9th ed., Wiley, New York, 1998.
9. R. Pirm, Acoustical Variables in Open Planning, *J. Acoust. Soc. Am.*, Vol. 49, No. 5, May 1971.
10. A. C. C. Warnock, Studies of Acoustical Parameters in Open-Plan Offices, *J. Acoust. Soc. Am.*, Vol. 63, No. 3, March 1978.
11. J. S. Bradley, The Acoustical Design of Conventional Open Plan Offices, *Canadian Acoust.*, Vol. 27, No. 3, 2003.
12. J. S. Bradley and B. N. Gover, Describing Levels of Speech Privacy in Open-Plan Offices, Research Report, Institute for Research in Construction, National Research Council Canada, September 2003 (IRC-RR-138, B3144.8).
13. J. S. Bradley and C. Wang, Measurements of Sound Propagation between Mock-Up Workstations, Research



- Report, Institute for Research in Construction, National Research Council Canada, January 2001 (IRC-RR-145, B3205.3).
14. J. A. Veitch, J. S. Bradley, L. M. Legault, S. Norcross, and J. M. Svec, Masking Speech in Open-Plan Offices with Simulated Ventilation Noise: Noise Level and Spectral Composition Effects on Acoustic Satisfaction, Research Report, Institute for Research in Construction, National Research Council Canada (IRC-IR-846, April 2002).
- BIBLIOGRAPHY**
- N. R. French and J. C. Steinberg, Factors Governing the Intelligibility of Speech Sounds, *J. Acoust. Soc. Am. (JASA)*, Vol. 19, No. 1, 1947, pp. 90–99.
- C. J. G. Marquardt, J. A. Veitch, and K. E. Charles, Environmental Satisfaction with Open-Plan Office Furniture Design and Layout, Research Report, Institute for Research in Construction, National Research Council Canada, September 2002 (IRC-RR-106, B3205.14).
- M. Navai and J. A. Veitch, Acoustic Satisfaction in Open-Plan Offices: Review and Recommendations, Research Report, Institute for Research in Construction, National Research Council Canada, July 2004 (IRC-RR-151, B3205.17).
- PBS-C.1, Standard Method of Test, Method for the Direct Measurement of Speech-Privacy Potential (SPP) Based on Subjective Judgments (May 1975 Revision), and PBS-C.2, Standard Method of Test, Method for the Sufficient Verification of Speech-Privacy Potential (SPP) Based on Objective Measurements Including Methods for Rating of Functional Inter-zone Attenuation and NC-Background (May 1975 Revision), from GSA, Public Building Services.
- A. C. C. Warnock and W. Chu, Voice and Background Noise Levels Measured in Open Offices, IRC Report IR-837, January 2002.
- Charles M. Salter Associates, Case Studies of a Method for Predictive Speech Privacy in the Contemporary Workplace, Center for the Built Environment, University of California, Berkeley, January 2003.

# CHAPTER 109

## ACOUSTICAL GUIDELINES FOR BUILDING DESIGN AND NOISE CONTROL

**Chris Field**

Arup Acoustics San Francisco  
San Francisco, California

**Fergus Fricke**

Faculty of Architecture Design and Planning  
University of Sydney  
Sydney, New South Wales, Australia

### 1 INTRODUCTION

In the acoustical design of buildings, consideration must be given to the location, the user requirements, the primary function of the building, and the budget available. The acoustical requirements for buildings can vary greatly according to the intended use of the individual spaces that may include speech, music, sports, and art exhibitions. Compatibility with nonacoustical requirements such as structural integrity, building services, and ventilation standards is also essential.

Acoustical design and noise control guidelines are available for various buildings, including performance spaces, offices, dwellings, art galleries, sports halls, hospitals, churches, and conference facilities. To determine acoustic and noise control requirements, a methodical approach is required.

International sound isolation and room acoustic standards are available and appropriate acoustical treatments and sound insulating constructions should be utilized to meet these standards.

### 2 METHODOLOGY FOR DETERMINING ACOUSTIC AND NOISE CONTROL FOR BUILDINGS

When determining the acoustic and noise control requirements in the design of buildings, the following steps can be used to ensure all acoustic requirements and standards are dealt with:

1. Review the range of uses of the building.
2. Review the building location in relation to any adjacent noisy or noise-sensitive spaces.
3. Set the appropriate background noise level design target for the building.
4. Set the room acoustic requirements/qualities for the building. This includes compliance with the relevant building codes and standards.
5. Assess the proposed internal geometry for the building with the required shape to optimize acoustics.
6. Calculate the room acoustic requirements, including amount and placement of acoustic treatment necessary to meet design targets.

7. Calculate the required level of sound isolation of the building with respect to steps 2 and 3.

The following sections describe in detail the methodology required in each of the above steps. Calculations of building services noise levels should also be carried out to ensure the resultant levels are compatible with the background noise level targets. Calculation methodology for building services noise control is given in Chapter 111.

#### 2.1 Range of Uses of the Building

Ever increasing construction costs and limited financial budgets often mean that a particular building must cater for different uses. An example is the so-called multipurpose hall where the uses may include dramatic theater, symphonic music, amplified contemporary music, conferences, seminars, and trade shows. Each of these uses has its own set of acoustic requirements that often conflict.

Therefore, one of the first steps in the acoustic and noise control design of a building is to establish the range of uses of the building. By carrying out this assessment, conceptual acoustic design elements to fulfil the requirements of the building can be included from the beginning of the building design. These elements may include variable acoustic treatment systems, temporary acoustic shells, or the ability to increase or decrease the physical volume of the building to alter the acoustic characteristics.

#### 2.2 Review of Building Location

A review of the building location in relation to external noise sources, or the location of acoustically sensitive spaces relative to noise-generating spaces within a building, must be carried out.

For existing external noise sources, such as ground transport traffic or railway systems, a noise survey should be carried out to quantify the intrusive noise levels incident on the proposed building. These noise levels can be used as the basis for determining sound isolation requirements for the building facade.

For any proposed internal noise sources, such as equipment located in plant rooms, manufacturer's

noise data for the proposed plant should be obtained. These equipment sound pressure levels would be used as the basis for determining sound isolation requirements for separating constructions of walls or floors to prevent noise intrusion to the acoustically sensitive areas of the building.

### 2.3 Background Noise Level Targets in Buildings

Excessive background noise can create a distracting and annoying working environment, lead to poor concentration, and result in poor productivity. In performance spaces, it can impair the acoustic enjoyment of a performance. Note, however, a reasonable level of background noise, with an appropriate frequency spectrum shape, can enhance speech privacy in offices by masking intrusive noise from adjacent spaces.

The source of background noise in buildings is generally from building services such as plant, air-conditioning, and plumbing systems. Noise break-in from external sources, such as ground transport traffic or aircraft, through facade glazing, roofs, and ventilators can also be significant.

By the careful design of air-conditioning systems, plant rooms, and facade constructions, the background noise level can be controlled to meet commonly recommended criteria in the relevant spaces. These criteria are outlined in Section 3.3.

### 2.4 Determination of Criteria for Acoustical Quality and Reverberance Control

The calculation of reverberance in a space is important to determine the appropriateness of the space for its use. For example, should the reverberance in a space be too long, speech may be unintelligible or classical music may lack clarity. Conversely, should the reverberance be too short, speakers may have to strain their voices to reach the rear of the space and instrumental pieces may sound dead.

Multiple reflections are normally assessed in terms of the reverberation time, which is the time taken for the sound pressure level to decay by 60 dB after the source output ceases. The reverberation time of a space can be easily measured using appropriate instrumentation. Reverberation time criteria for various spaces are given in Section 3.2. In addition to reverberation time, there are many other parameters used to describe the acoustic quality of spaces. The design of musical performance spaces, for example, includes parameters to quantify the clarity of instrumental sound, warmth, ensemble, and listener envelopment. Barron<sup>1</sup> and Beranek<sup>2</sup> provide detailed information into the parameters used in the specialist acoustic design for performance spaces.

### 2.5 Sound Isolation Requirements

To achieve speech privacy ratings, and also to generally control noise intrusion to sensitive spaces, adequate sound isolation performance from the building facade and internal partitions must be achieved.

Design standards for residential buildings are well documented in various international codes, as discussed in Section 3.3. Recommended standards are also presented for other building types.

On-site construction of partitions is a critical consideration since sound isolating ratings ( $STC/R_w$ ) are based on laboratory tests under ideal conditions. This performance is rarely met on-site due to constraints on workmanship and noise flanking paths (see Chapter 115).

### 2.6 Review of Internal Building Geometry

The internal geometry of buildings has a significant effect on the acoustical quality of the space. Performance spaces such as concert halls, for example, rely on the shape and size of the stage enclosure and auditorium to project instrumental sound to the audience. Therefore, at the conceptual stage of the building design, suitable internal geometry should be defined to suit the use of the space. Guidelines for various building uses are given in Section 4.5.

### 2.7 Calculations to Determine Room Acoustic and Noise Control Requirements

Once the design targets and user requirements have been established, calculations to determine room acoustic and noise control requirements can be carried out. For room acoustics, there are several methods for predicting the reverberation time in a building.<sup>3</sup>

For calculation of sound isolation requirements, an equation based on the calculation of the reverberant sound field in an internal space can be used.<sup>3</sup> These methods are presented in Section 4.2.

## 3 ACOUSTICAL DESIGN CRITERIA AND REQUIREMENTS FOR BUILDING SPACES

### 3.1 Suitable Internal Background Noise Level Targets

British Standard 8233:1999<sup>4</sup> and Australian Standard 2107<sup>5</sup> provide reasonable guidance for design background noise levels for various types of occupancy. The limits apply to steady-state or quasi-steady-state sounds such as noise from air-conditioning systems and are given as overall A-weighted sound pressure level limits for many room types.

Noise criterion (NC) or NR curves are commonly used as an alternative or a complement to A-weighted sound pressure level values for the specification of services noise limits because they allow noise levels with a “balanced” frequency content to be achieved. NC curves were derived from interviews with users of buildings with various noise environments with noise measurements made in occupied rooms with building services systems operating normally. NC values are defined by a series of curves that give noise level limits in octave bands across the frequency range of human hearing. Chapter 106 provides details of NC curves and other noise criterion curves (NR, PNC, NCB) used for internal spaces.

The use of NC curves is recommended for the control of building services noise levels. For common building services noise spectra, the NC rating is

**Table 1 Examples of Recommended Target Noise Limits in Spaces**

Area	Recommended Internal Noise Level Targets
Concert halls	NC 15–20
Theaters	NC 20–25
Art galleries	NC 25–30
Sports halls	NC 40
Open-plan office/workstations	NC 40
Enclosed/private offices	NC 35
Conference/large meeting rooms	NC 30
Meeting rooms	NC 35
Video conference rooms	NC 25
Cafeterias	NC 45
Store/utility spaces	NC 45
Office break-out areas	NC 45
Undercover car parks	NC 60
Plant rooms (excluding chiller/generator)	NC 65
Lift motor rooms	NC 65

typically 5 dB below the equivalent A-weighted sound pressure level [e.g., a noise limit of NC 30 is approximately equivalent to an A-weighted sound pressure level of 35 dB].

Typical target noise limits for steady-state noise generated by building services and noise break-in from external sources have been determined by a combination of guidance from BS8233, AS 2107, and conditions in existing buildings. Table 1 outlines noise level targets for the various spaces to be achieved by all services running normally and together plus external noise break-in. Chapter 115 provides targets for other noise-sensitive spaces.

### 3.2 Room Acoustic Requirements

Guidance for suitable reverberation times for various types of spaces can be found in AS2107-2000,<sup>5</sup> BS8233-1999,<sup>4</sup> and Lawrence.<sup>6</sup> Table 2 presents

**Table 2 Examples of Recommended Mid-Frequency Reverberation Times for Various Spaces**

Space	Typical Mid-Frequency Reverberation Time (500–1000 Hz) in Seconds
Churches	2.5–5.0
Concert halls	1.5–2.3
Conference/meeting rooms	0.6–0.8
Sports halls	1.5–1.8
Multipurpose halls	0.9–1.6
Offices	0.4–0.9
Swimming pools (indoor)	1.3–3.0
Theaters	0.6–1.5
Art galleries	1.0–1.4
Open-plan office/workstations	0.6–0.8
Cafeterias	1.0–1.5

examples of typical mid-frequency reverberation time objectives for various spaces.

### 3.3 Sound Isolation Performance of Building Elements

The sound isolation performance of partitions is usually limited by flanking paths, penetrations, and air gaps in and around the partition rather than a weakness in the construction itself. Typical partition constructions and their ideal sound isolation performances are presented below. Information on other transmission paths, which weaken the acoustic performance of partitions, is also given to serve as guidance during the design process.

**3.3.1 Residences** National building codes specify minimum sound isolation requirements between various habitable spaces in dwellings. Several national building codes are currently being reviewed due to the general acknowledgment that the current codes do not provide satisfactory standards on internal sound isolation. For guidance, a general summary of suitable sound isolation ratings for control of internal noise within residential dwellings, using relevant information from German,<sup>7</sup> Australian,<sup>8</sup> and Nordic standards<sup>9,10</sup> is given in Table 3. Noise regulations in U.S. building codes vary greatly according to particular states and localities. Tocci<sup>11</sup> presents a general discussion of noise control in U.S. building codes.

**3.3.2 Performance Spaces and Recording Studios** The sound isolation requirements for performance spaces and recording studios are generally very high, due to the requirement to have very low background noise levels in these spaces. The requirements, however, are highly dependent on the desired quality of the space in relation to the available budget. To meet these generally high isolation standards, space planning is an important aspect of the design process.

In performance space buildings, sound lobbies with multiple door sets are used as buffers to external noise intrusion. Structural isolation of critical areas such as the auditorium is typically carried out. The building

**Table 3 Summary of International Guidance on Suitable Sound Isolation for Control of Internal Noise within Residential Dwellings**

Separating Construction	Airborne Sound Isolation Requirement (STC/ $R_w$ )	Impact Sound Isolation Requirement ( $L'n, w$ )
Floors between dwellings	54–58	46–53
Party walls between dwellings	53–58	46–53
Walls between dwellings and hallways/stairwells	52–58	48–58
Walls between dwellings and bathrooms/kitchens in adjacent dwellings	53–58	46–53

envelope is generally a high-density concrete or solid-block work construction.

In recording studios, the studio box is often structurally isolated using a “box-in-box” construction. Further guidance in the design of recording studios can be obtained from the *British Broadcasting Corporation Guide to Acoustic Practice*.<sup>12</sup>

**3.3.3 Office Buildings** Acoustic privacy in offices, or other spaces used for speech, is affected by several parameters, including:

- The level of intrusive speech in the originating space
- Background noise levels in the “receiving” areas
- Sound isolation provided by partitions or screens separating adjacent areas
- Sound absorption within the space

The higher the level of background noise in the receiving room the greater the speech privacy in that room. Conversely, lower background noise levels provide less speech privacy and require partitions with higher sound isolation to achieve the same level of privacy.

A balance must be struck between the level of background noise that can be accommodated without being disturbing to the occupants and the level of sound isolation that can be reasonably achieved by the partition. For example, conference rooms require a relatively low background noise level and, therefore, require partitions with a correspondingly high sound isolation. (Note that to achieve a 5-dB increase in the sound isolation of a partition generally requires a doubling of either the mass of the partition or a doubling of the cavity width). Chapter 115 presents a method of predicting the frequency-dependent transmission loss of partitions based on the partition surface density.

For general occupational noise resulting from speech, a convenient method to assess the level of isolation offered by a particular partition is to allocate each construction a *speech privacy rating*. Table 4 summarizes the different levels of speech privacy classification and their subjective meanings.

It is recommended that the following speech privacy ratings are set as targets in the following room types:

Private offices—Good to very good  
Open-plan offices—Fair to good  
Classrooms/dance studios—Fair  
Meeting/conference rooms—Very good  
Video conference room—Very good  
Theaters—Excellent

Note that it is not generally possible to achieve these ratings across partitions incorporating doors, due to the difficulty in providing adequate acoustic seals on a door without compromising its ease of use, or providing a lobbied “sound lock” arrangement. Careful planning of door locations is likely to result in more practical outcomes. Table 5 indicates the level of sound isolation of the separating partition and relative to the background noise level in order to achieve the specified speech privacy ratings given above.

**3.3.4 Typical Constructions for Controlling Noise** Typical partition constructions for achieving sound isolation ratings are given in Table 6. Further examples are given in Chapter 115. It should be noted that the  $STC/R_w$  ratings given are laboratory-measured ratings. It is common practice to reduce these laboratory ratings by 5 dB due to site installation constraints.

**3.3.5 Doors and Seals** Doors will limit the overall sound isolation of a partition since they are generally of much lighter construction than the partition, and they are difficult to effectively seal. While high-performance doors can be provided, it should be understood that they are likely to be heavy, more difficult to operate, and relatively expensive.

Depending on the arrangement of the door, and the relationship of the room to other adjacent spaces, a door with a sound isolation performance considerably less than the partition itself will be appropriate. One must be aware that some contradictions may appear between the acoustical objectives and the safety requirements (e.g., ease of exit preventing the use of an airlock, or fire proofing preventing the use of efficient sealing).

Table 7 gives typical door constructions required in the acoustically rated partitions.

**3.3.6 Other Transmission Paths Ceiling Voids** For partitions with a sound isolation rating greater than an  $R_w$  of 35, noise transfer via the ceiling void can limit the overall sound isolation of the partition. Ceiling void

**Table 4 Subjective Speech Privacy Ratings**

Speech Privacy Rating	Subjective Description	
	Normal Speech	Raised Voices
Poor	Intelligible	Clearly intelligible and possibly disturbing
Fair	Audible, could be intelligible if speaker and/or subject well known	Intelligible
Good	Audible but not intelligible	Audible, could be intelligible if speaker and/or subject well known
Very good	Just audible	Audible but not intelligible
Excellent	Inaudible	Just audible

**Table 5 Speech Privacy Ratings**

Normal Speech	Raised Voices	Continuous Listener Background Noise Level			$D_W + NC^a$	Speech Privacy Rating
		NC30 Room-to-Room Level Difference	NC35 Room-to-Room Weighted	NC40 Level Difference $D_W$		
Intelligible	Clearly intelligible and possibly disturbing	<35	<30	<25	<65	Poor
Audible. Could be intelligible if speaker and/or subject well known	Intelligible	35–40	30–35	25–30	65–70	Fair
Audible but not intelligible	Audible. Could be intelligible if speaker and/or subject well known	40–45	35–40	30–35	70–75	Good
Just audible Inaudible	Audible but not intelligible Just audible	45–55 >55	40–50 >50	35–45 >45	75–85 >85	Very good Excellent

<sup>a</sup>NC is defined in Section 4.2.**Table 6 Examples of Typical Sound Isolation Performance of Wall Constructions**

Sound Isolation Performance, STC/ $R_w$	Wall Buildup
35	<ul style="list-style-type: none"> <li>10.38-mm laminated glass</li> <li>1 × 13-mm plasterboard each side of a 64-mm metal stud (total width 90 mm)</li> <li>100-mm block work (low density 600–900 kg/m<sup>3</sup>)</li> </ul>
40	<ul style="list-style-type: none"> <li>1 × 13-mm plasterboard each side of a 64-mm metal stud with 50-mm absorptive quilt in cavity</li> <li>100-mm block work (low density 600–900 kg/m<sup>3</sup>) rendered 13 mm both sides</li> </ul>
45	<ul style="list-style-type: none"> <li>2 × 13-mm plasterboard each side of a 64-mm metal stud (total width 116 mm)</li> <li>112-mm fair faced brick (unplastered)</li> <li>140-mm medium-density block work (1400 kg/m<sup>3</sup>)</li> </ul>
50	<ul style="list-style-type: none"> <li>2 × 13-mm high-density plasterboard each side of 2 × 64-mm studs offset in 92-mm track with 50-mm absorptive quilt in cavity</li> </ul>

**Table 6 (continued)**

55	<ul style="list-style-type: none"> <li>224-mm fair faced brick (unplastered)</li> <li>190-mm medium-density block work (1900 kg/m<sup>3</sup>) plastered or rendered 13 mm on both side</li> <li>2 × 13-mm high-density plasterboard each side of staggered 64-mm studs in 92-mm width track with 50-mm absorptive quilt in cavity</li> </ul>
60	<ul style="list-style-type: none"> <li>112-mm fair faced brick each side of a 75-mm air gap, resiliently tied and plastered both sides</li> <li>2 × 16-mm high-density plasterboard, 2 × 64-mm separate studs, 2 × 16-mm high-density plasterboard with 100-mm absorptive quilt in cavity</li> </ul>

barriers, or full-height partitions, should therefore be used for all partitions with a performance requirement greater than  $R_w$  35. The barrier should comprise either mass-loaded vinyl with a minimum surface density of 8 kg/m<sup>2</sup> or one layer of plasterboard sealed airtight.

**Services Penetrations** Penetrations through the cavity barrier must be made good with further layers of plasterboard close-cut to the duct or pipe work or further overlapping layers of mass-loaded vinyl. Penetrations must be fully sealed with a polysulfide sealant (for plasterboard), or taped up (mass-loaded vinyl).

**Table 7 Examples of Typical Door Construction Requirements in Acoustically Rated Partitions to Corridors and Open-Plan Spaces**

Partition Sound Isolation Rating, $R_w$ /STC	Typical Corresponding Door Sound Isolation Rating, $R_w$ /STC	Typical Door Construction and Sealing Arrangement
35	15	Aluminum framed glazed door or hollow-core door with simple frame seals (e.g., self-adhesive)
35	20	32- to 35-mm solid-core door with simple frame seals, threshold close cut to carpet
40	25	35-mm solid-core door with frame seals
45	30	35- to 40-mm solid-core door with frame and threshold seals
50	35	40- to 45-mm solid core door, with high-performance rebated frame and threshold seals, possibly proprietary doorset
55	40	Proprietary acoustic doorset, 50–80 mm with double rebated seals
60	45	Proprietary acoustic doorset, 80 mm with double or triple seals

**Mechanical Services Ducts** Ducts between offices also have the potential to lower the effective sound isolation between spaces. Cross-talk attenuators may, therefore, be required in ductwork crossing high-performance partitions. The acoustic performance of the cross-talk attenuator should be sufficient to maintain the performance of the ceiling cavity barrier. Beware that attenuators may be proscribed by safety regulations when the duct network can be used for smoke exhaust purposes.

**Glazed Partitions** They are likely to limit the maximum level of privacy that can be achieved. The typical sound isolation performance of a single glazed partition (10.38-mm laminated glass) is around  $R_w$  35. Consequently, the level of privacy provided via these partitions will be relatively poor. Double-glazed systems may be used and can generally achieve  $R_w$  42 for a standard sealed system.

**Operable Partitions** They are likely to be the limiting factor for speech privacy in rooms where they are used. This is due mainly to the limitations of the perimeter seals of the demountable wall. The maximum sound isolation performance, of commercially available operable partitions, is claimed by the manufacturers to be  $R_w$  48 to 52—achieving this on-site is particularly challenging.

## 4 CALCULATIONS FOR ACOUSTIC AND NOISE CONTROL DESIGN

### 4.1 Acoustic Quality and Reverberation Time

**4.1.1 Prediction of Reverberation Time** Several methods have been developed to calculate the reverberation time of a space according to its physical characteristics. A comprehensive summary of the methods is given in Beranek.<sup>3</sup>

The most common equation used in engineering design is the one determined by Sabine. This equation has its limitations (see Beranek<sup>3</sup>) but gives an easy way of calculating the reverberation time of a space quickly. Sabine's equation is often used in the preliminary stages of a design. As the design of a space progresses, computer modeling techniques are used to obtain a more realistic prediction of

reverberation time (RT), which accounts for location of absorptive materials and unusual sound fields in spaces, both of which are not accounted for by Sabine's equation.

The form of Sabine's equation often used is as follows:

$$RT = \frac{0.161V}{A}$$

where  $V$  is the volume of the space ( $m^3$ ) and  $A$  is the total absorption in the space ( $m^2$  sabin):

$$A = \sum S_n \alpha_n$$

where  $S_n$  is the surface area of the material having an absorption coefficient of  $\alpha_n$ .

Absorption coefficients of common materials are presented in Table 8. Further information on absorption coefficients of various materials can be found in Bies and Hansen.<sup>13</sup>

**4.1.2 Shape of Space and Placement of Absorptive Material** Sabine's equation gives us an indication of the amount and type of material to be added to the internal surfaces of a space to control reverberance. In addition to providing enough material, the location of the material in the space is also important.

When considering the placement of acoustic absorption in the space, the following attributes of the space should be noted:

- The use of the space (classical music, speech, amplified music)
- The distance between the source and receiver
- The shape of the space

The design of the shape of the space is a very important aspect of acoustic design of auditoria and performance spaces and requires much greater detail than can be presented here. Barron<sup>1</sup> provides further guidance in this aspect of acoustic design.



**Table 8 Examples of Absorption Coefficients of Some Common Materials**

Material	Octave Band Center Frequency (Hz)					
	125	250	500	1000	2000	4000
Thick carpet on foam underlay	0.08	0.24	0.57	0.69	0.71	0.73
Concrete or terrazzo tile	0.01	0.01	0.01	0.01	0.02	0.02
Medium velour drapes	0.07	0.31	0.49	0.75	0.7	0.6
Glass window	0.35	0.25	0.02	0.12	0.07	0.04
Mineral wool 25 mm thick	0.18	0.24	0.68	0.85	1.00	1.00
Wood stage with void beneath	0.40	0.30	0.20	0.17	0.15	0.10
Water (surface of a pool)	0.01	0.01	0.01	0.02	0.02	0.03
Plaster on brick wall	0.01	0.10	0.06	0.04	0.04	0.03

## 4.2 Sound Isolation Calculations

When determining the transmission of sound through a partition, the important factors are:

- The transmission loss (TL) properties of the partition
- The area  $S$  of the partition exposed to the receiving space
- The volume  $V$  of the receiving space
- The reverberation time of the space

The reverberant level in the receiving space can be given by<sup>3</sup>

$$L_{pr} = L_{ws} + 10 \log S - TL - 10 \log V + 10 \log RT + 14 \text{ dB}$$

where  $L_{ws}$  is the sound power level in the source room or outside, and  $S$  is the exposed area of the partition to the receiving space.

This equation can be rearranged to determine the required transmission loss of the partition (TL) for a given reverberant background noise limit compatible with the use of the building, as given in Table 1. Chapter 115 also presents an equation to determine the outdoor-to-indoor transmission loss requirements for building facades.

## 5 ACOUSTIC DESIGN GUIDANCE FOR BUILDING CATEGORIES

This section presents general design guidelines for particular spaces. It should be noted that Chapter 109 deals with noise in offices and open-plan spaces, Chapter 113 deals with noise in mechanical equipment rooms, Chapter 114 deals with noise in single- and multifamily residences, and Chapter 115 deals with noise in commercial and public buildings.

### 5.1 Performance Spaces (Unamplified)

For unamplified classical music, strong early reflections of instrumental sound is necessary to project to the audience. The musicians themselves also need strong early reflections of sound to gain some feedback to their playing or a sense of ensemble. For this reason,

concert halls are usually designed with highly reflective surfaces located around and close to the stage, angled to provide strong early reflections of sound to the audience. In addition to being hard and reflective, surfaces are often made to be diffusive—hard surfaces with aggressive profiles to scatter sound in various directions rather than providing specular or focused reflections of sound. To prevent discrete late reflections of sound from more distant surfaces such as rear and side walls, which reduce the clarity of instrumental sound, acoustic absorption can also be used.

A modern technique in concert hall design involves the use of acoustic banners that can be unrolled or rolled up to fine-tune the reverberance of the space. The use of movable walls to increase the volume of the space has also been used to adjust the reverberation time of performance spaces. Note that such devices can seriously complicate compliance with the safety regulations in force.

### 5.2 Amplified Music

For modern amplified music performances in multipurpose venues, there is less reliance on the acoustic characteristics of the building. The ceiling should be absorptive and positioned at a greater height than for unamplified classical performance. Walls around the stage should be a balance of absorptive and diffusive panels to provide some sense of ensemble on stage but also prevent focused reflections of foldback sound toward the performers. Walls around the audience should be absorptive to prevent late reflections of loudspeaker sound from distant surfaces.

### 5.3 Meeting/Hospitality

If the space is to be used for presentations involving speech, the ceiling should be reflective above and in front of the speaker's head and positioned at low height to obtain useful reflections of sound toward the audience. Ceiling areas away from the speaker, for example, behind the speaker's head, should be absorptive. Side walls near the speaker should be reflective to obtain useful early reflections of sound to the audience and be movable to create a smaller enclosure around the speaker.

A classic scenario is the design of a company boardroom. In this case, the ceiling above the boardroom table should be made hard and reflective to provide early reflections of the speaker's voice to augment

direct sound reaching the listener. The floor and the remaining part of the ceiling should be absorptive to control reverberance in the room. The walls at seated head height should include a band of absorptive material (e.g., fabric panels) to prevent late reflections of sound from the speaker reaching the listener, which would impair the intelligibility of the speech.

#### 5.4 Worship

Modern houses of worship can be used for a wide range of functions in terms of acoustics, including amplified and unamplified speech and music. Even the genre of music played in churches can vary greatly from traditional unamplified choral music to modern amplified rock music. Houses of worship must, therefore, be designed with the same approach as a multipurpose space.

As a consequence, the following acoustic guidelines are provided for houses of worship:

- A reflective ceiling above the stage/pulpit to assist in projection of speech to the congregation
- Sound absorptive treatment to control reverberance to an appropriate mid-frequency reverberation time target for the uses of the space
- Sound absorptive treatment on the rear wall to prevent late reflections of loudspeaker sound
- Appropriately designed sound-isolating constructions (walls and doors) to prevent noise break-out to noise-sensitive receivers

#### 5.5 Industrial/Transport

For transportation and industrial buildings, the aim is to determine the amount and distribution of acoustic absorption likely to be required to control reverberance and to control background noise levels in occupied areas. Speech intelligibility of public address (PA) and emergency public address (EPA) systems is then dependent upon the placement of acoustic treatment and background noise levels.

In the interest of cost efficiency of such buildings, the key is to strike a balance between the PA and EPA system design (type, location, and orientation of the loudspeakers) and the use of acoustic treatment. The strategy is to use the minimum amount of acoustic treatment in optimum locations. For example, priority should be given to placement of acoustic treatment on surfaces likely to produce detrimental reflections of sound from loudspeakers or on curved surfaces likely to focus sound on areas occupied by people.

#### 5.6 Arenas/Stadiums

Partially enclosed arenas and stadiums pose a challenge in terms of acoustic design as, by nature, they include issues related to both fully enclosed spaces and open venues including:

- Aim to provide good speech intelligibility from the PA and EPA systems during sports commentary and emergency message broadcasts.

- Augment the acoustic quality of the sound system if music is required.
- Help provide a feeling of intimacy and excitement for athletes/performers and spectators—this has an important influence on the roof design and materials.
- Ensure that noise from stadium events does not affect surrounding noise-sensitive receivers.
- Ensure that noise from the surrounding area does not disturb athletes/performers inside the stadium/arena.

To provide good speech intelligibility from the sound system in a large volume of space, care is required to ensure that adequate coverage is provided and that, where necessary, provision is made for full-range sound reinforcement loudspeakers (for music) and appropriate delay lines. This is particularly important if the stadium system is to be used in conjunction with a touring system provided by high-profile performers.

Acoustic absorption should be considered in covered areas of the stadium/arena where late reflections of sound are likely to adversely affect speech intelligibility of loudspeaker sound. Such areas include the underside of the roof and rear walls of the venue.

Sources of noise break-out from stadium/arena events include crowd noise, PA announcements, amplified music, and mechanical services plant noise. Positioning of noise sources, such as plant and loudspeakers, away from noise-sensitive receivers is therefore critical. Consideration should be given to the selection of quiet plant and noise mitigation measures (which might include attenuators, screens, and enclosures). Adequate sound isolation performance of the venue facade and roof is also important.

#### 5.7 Critical Spaces

Acoustically critical spaces such as anechoic chambers and broadcast/recording studios require extensive acoustic mitigation to prevent disturbance to the operation of the space. Mitigation methods include structural isolation to prevent vibration and impact noise problems generated by activities and noise sources in surrounding areas. Box-in-box constructions are usually used.

Space planning should be carefully considered to ensure that noisy spaces (e.g., plant rooms) are located far away from the acoustically critical space they are servicing. Building services noise is usually a major consideration for such spaces and represent the baseline noise and vibration sources within these critical spaces. Care must be given to appropriate design of mechanical services fans, prevention of cross talk between adjacent spaces via ductwork, and plant room noise break-out to internal areas.

It should be noted that noise intrusion to broadcast/recording studios is a less significant issue than in the past due to modern close microphone techniques and the use of equalization/high-pass filtering to reduce the impact of low-frequency noise intrusion without significantly affecting the quality of the final output. Determination of appropriate design criteria suitable

for its use is the key to ensuring the successful operation of such a space.

## REFERENCES

1. M. Barron, *Auditorium Acoustics and Architectural Design*, E & FN Spon, London, 1993.
2. L. L. Beranek, *How They Sound—Concert and Opera Halls*, Acoustical Society of America, New York, 1996.
3. L. L. Beranek, Ed., *Noise and Vibration Control*, 2nd ed., Institute of Noise Control Engineering, Ames, IA, 1988.
4. BS8233:1999, Sound Isolation and Noise Reduction for Buildings, Code of Practice, British Standard.
5. AS2107:2000, Recommended Design Sound Levels and Reverberation Times for Building Interiors, Standards Australia.
6. A. B. Lawrence, *Architectural Acoustics*, Elsevier Science, New York, 1970.
7. DIN4109:1989, Sound Isolation in Buildings, Requirements and Testing.
8. Australian Building Codes Board, Building Code of Australia, 2004.
9. VDI4100 Noise Control in Housing—Criteria for Planning and Assessment.
10. Draft Nordic Standard INSTA 122:1997, Sound Classification of Dwellings.
11. G. C. Tocci, Noise Control in US Building Codes, in M. J. Crocker, Ed., *Encyclopedia of Acoustics*, Wiley, New York, 1997, pp. 1205–1218.
12. K. A. Rose, *British Broadcasting Corporation Guide to Acoustic Practice*, BBC Architectural and Civil Engineering Department, BBC, London, 1990.
13. D. A. Bies and C. H. Hansen, *Engineering Noise Control—Theory and Practice*, 2nd ed., E & FN Spon, London, 1996.

# CHAPTER 110

## NOISE SOURCES AND PROPAGATION IN DUCTED AIR DISTRIBUTION SYSTEMS

Howard F. Kingsbury  
State College, Pennsylvania

### 1 INTRODUCTION

This chapter deals with the generation, propagation, and control of noise in a ducted air distribution system. First, fan noise control is considered with reference to a simple system, with complications added later. The discussion refers to octave band noise generation and control. Included is discussion of both *natural attenuation*, that is, the noise reduction that occurs due to the transmission of sound through the duct walls, the division of noise due to duct branches, and the effect of duct fittings. Also treated are the effects of porous duct linings and packaged attenuation units (silencers). Consideration is also given to the conversion of sound power levels to sound pressure levels in the room served by the fan system. The methods and effects of varying the air volume delivered by the fan is discussed. Second, turbulent flow noise generation and control in the ducts are covered. The generation and control of *break-out noise*, that is, noise that is radiated through the duct wall, is discussed, as are the differences between round and rectangular duct in the control of this noise. The effects of volume control dampers located near outlets are included. Special consideration is given to roof-top units, where turbulent flow is a common cause of noise generation. Third, noise generation and control in the outlet devices are considered. Both constant-air-volume and variable-air-volume (VAV) types of terminals are

included, including so-called fan-powered terminals. Information on the sound generated by fans is given in Chapter 71.

### 2 FAN NOISE CONTROL IN DUCTED SYSTEMS

Understanding of noise control in a ducted air distribution system can best be developed by beginning with a simple system and then adding the complications. Figure 1 shows a ducted system reduced to its barest essentials. It is a constant-volume system, with a single fan running at constant speed, enclosed in a plenum, both supplying and returning the air from the room being served. Eliminated from this system are such accessories as heating or cooling coils, filters, and so on. Usually, the most critical part of the system is the room closest to the fan serving that system unless other rooms downstream require lower sound pressure levels.

The recommended noise control procedure is as follows, working in octave bands:

1. Determine the sound power output of the fan(s) that is emitted into the duct system.
2. Determine the so-called natural attenuation of the duct system. While doing so, determine if the sound generated by fittings and takeoffs

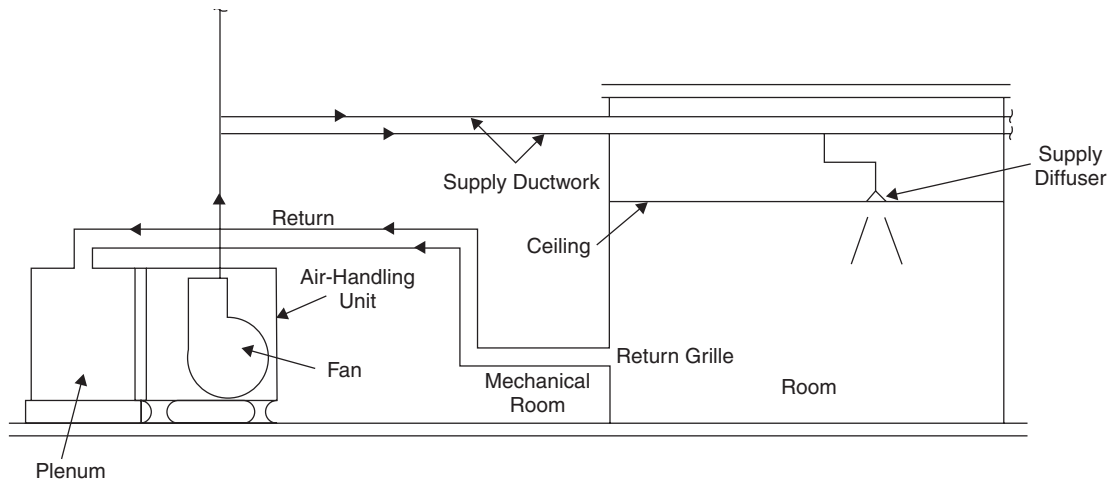


Figure 1 Ducted air distribution system.

**Table 1 Attenuation of Unlined Sheet Metal Ducts (dB/unit length) by Octave Band Center Frequency Attenuation (dB/m)**

	63 Hz	125 Hz	250 Hz	>250 Hz
Rectangular Duct Sizes <sup>a</sup>				
300 × 300 mm	1	0.6	0.3	0.2
600 × 600 mm	0.8	0.6	0.3	0.2
1200 × 1200 mm	0.45	0.3	0.2	0.06
Round Duct Sizes				
175–380 mm	0.09	0.09	0.09	0.2
380–750 mm	0.06	0.06	0.03	0.15
750–1500 mm	0.03	0.03	0.03	0.06

<sup>a</sup> If duct is externally insulated, double values.

Source: From Ref. 1, pp. 47.14 and 47.15. Used with permission.

may add to that being transmitted down the duct.

3. Convert from the sound power level at the outlet to the resulting sound pressure level in the space being served (so-called room factor or space effect) and compare it with the chosen sound pressure level criterion for that space.
4. Add any required sound attenuation measures to the system needed to meet the criterion in 3.
5. Determine if sound transmission through the duct wall (break-out noise) may be a problem and, if so, apply proper sound control procedures.
6. Repeat the entire procedure for the return side of the system.

In addition to these considerations of fan noise, note that the final sound pressure level in the room will be a combination of the noise from the fan and noise from the chosen outlet device(s), which will be discussed later.

## 2.1 Natural Attenuation

The first aspect of noise control in a duct distribution system is the so-called natural attenuation, which has four components. First, some sound is radiated through the duct wall, causing the duct wall to vibrate; this is sensed as a reduction of energy inside the duct (see Table 1). Round and flat oval ducts show less of this effect than rectangular ducts due to their shape. A

**Table 2 Division of Sound Power Level at Branch Takeoffs**

Ratio <sup>a</sup>	dB Reduction
1.0	0
0.5	3
0.25	6
0.10	10

<sup>a</sup> Ratio = branch duct/continuing duct area.

second mechanism is the division of energy between the main duct and the takeoffs. In the absence of specific information to the contrary, it is assumed the energy division is proportional to the ratio of the branch duct area to that of the main duct (see Table 2). A third common loss occurs at the end of the duct, where it enters the room. This is called end-reflection loss (some of the sound energy is reflected back into the duct system) and is most pronounced when there is a sudden transition from the duct to the room. Diffusers reduce this by an unknown amount. However, for diffusers that are round or square (or nearly so), the number in Table 3 will give reasonable results. The effect of high-aspect ratio diffusers, such as slot diffusers, is not known. Finally, a fourth component is the conversion from sound power in the duct system to the sound pressure in the room (the room factor noted above). For most practical rooms, the classical equation (Chapter 2), which assumes both a direct and reverberant field, does

**Table 3 Duct End Reflection Loss by Octave Band Center Frequency<sup>a</sup>**

Mean Duct (mm)	Reflection Loss (dB)				
	63 Hz	125 Hz	250 Hz	500 Hz	1000 Hz
150	18	12	8	4	1
250	14	9	5	1	0
500	9	5	1	0	0
1000	4	1	0	0	0

<sup>a</sup> If duct terminates in a diffuser, deduct 6 dB (63 Hz) and 4 dB (125 Hz) for duct sizes under 300 mm, 3 dB (63 Hz) for duct sizes over 300 mm. Do not apply to linear diffusers or diffusers tapped directly into primary ductwork.

Source: From Ref. 1, p. 42.16. Used with permission.

not apply. In a room having an acoustical ceiling and in which the ceiling height is significantly less than either of the horizontal dimensions, the Schultz equation should be used for this conversion.

## 2.2 Lined Duct Attenuation

In many systems additional attenuation is required. This may be obtained by lining the interior surfaces of the duct with sound-absorbing material or by use of packaged attenuators or both. Duct lining serves two purposes: It is a thermal insulant and a sound absorber. While 13-mm thickness may be sufficient for thermal reasons, for acoustical purposes the thickness should be a minimum of 25 mm, and 50 mm is often desirable. This is due to the minimal low-frequency attenuation provided by thin linings, and it is in the low-frequency region that most duct system noise control problems occur.

The acoustical characteristics of glass fiber duct lining in rectangular ducts have been rather extensively investigated; the same is not true for round ducts, and the data on their attenuation are primarily from manufacturers' determinations. Data for both rectangular and round ducts are shown in Table 4. The data in Table 4 should not be used for ducts with a lightweight metallic foil covering due to the limited transmission loss of such material.

## 2.3 Lined Rectangular Elbows

Elbows with turning vanes also provide worthwhile attenuation. Round elbows, lined or unlined, provide

relatively little attenuation, in general 5 dB or less. Table 5 provides typical values for rectangular elbows.

## 2.4 Passive Attenuators or Silencers

These items are available in a variety of sizes, shapes, and lengths. Dissipative silencers commonly contain fiberglass acoustical media; also available are reactive-type silencers that contain no acoustical fill but are composed of a series of tuned resonators that act as the sound-attenuating elements. Commonly available lengths of rectangular silencers are 0.9, 1.5, 2.1, and 3.1 m. The length of most circular cross-sectional silencers is a function of their diameter. In the selection of silencers, three interrelated factors must be considered: (1) insertion loss, (2) pressure drop, and (3) self-generated noise. The primary controlling element is the airflow velocity through the face area of the silencer. Increasing velocity increases both the pressure drop and the self-noise; it reduces the insertion loss slightly. Manufacturers' literature should be consulted for details on these items. A recognized test method for determining these properties is ASTM E477-06a,<sup>2</sup> which measures the insertion loss by the duct-to-reverberant-room method with and without airflow.

## 2.5 Active Sound Attenuation

Recent developments in computer technology have led to the development of phase-canceling systems having

**Table 4 Insertion Loss (dB/unit length) for Lined Rectangular and Round Ducts, with 25- or 50-mm Lining, by Octave Band Center Frequency Insertion Loss (dB/m)**

	63 Hz		125 Hz		250 Hz		500 Hz		1000 Hz		2000 Hz	
	25 mm	50 mm	25	50	25	50	25	50	25	50	25	50
Rectangular Duct Sizes												
150 × 150 mm	—	—	1.8	2.4	4.5	7.0	8.1	14.7	17.4	21.6	22.2	22.2
300 × 300 mm	—	—	1.2	1.5	3.2	4.8	5.7	10.5	12.0	15.0	12.3	12.3
600 × 600 mm	—	—	0.6	0.9	1.5	2.7	4.2	7.5	8.4	10.5	6.6	6.6
Round Duct, Diameter												
150 mm	1.1	1.7	1.8	2.4	2.8	4.1	4.6	6.5	6.5	6.5	5.7	5.7
300 mm	0.7	0.8	0.8	1.4	1.7	3.0	3.0	6.0	5.1	5.1	3.7	3.7
600 mm	0.2	0.8	0.8	1.4	1.7	3.0	3.0	6.0	5.1	5.1	3.7	3.7

Source: Ref. 1, pp. 47.15 and 47.16. Used with permission.

**Table 5 Insertion Loss for Lined, Square Elbows with Turning Vanes by Octave Band Center Frequency**

Duct Width <sup>a</sup> (mm)	Insertion Loss (dB)					
	63 Hz	125 Hz	250 Hz	500 Hz	1000 Hz	2000 Hz
125–250	0	0	1	2	3	4
260–510	0	1	2	3	4	6
520–1020	1	2	3	4	5	6
1030–2030	2	3	3	5	6	8

<sup>a</sup> Duct width is dimension in plane of the turn.

Source: Ref. 1, p. 42.15. Used with permission.

application to low-frequency noise in ducted systems. Both random noise and tones are accounted for, with an upper frequency limit of about 400 Hz and insertion losses typically of 20 to 30 dB.

## 2.6 Attenuation of Noise in Lined Plena

The noise reduction offered by lined fan plena, as shown in Fig. 2, should be taken into account. The following approximate expression, while somewhat dated, may be used to calculate the effects of such a lined plenum<sup>3</sup>:

$$\text{Attenuation} = 10 \log \left[ S_e \left( \frac{\cos \theta}{2\pi d^2} + \frac{1 - \alpha}{\alpha S_w} \right) \right]^{-1} \quad (1)$$

where  $\alpha$  is the absorption coefficient of lining at octave band center frequencies,  $S_e$  the plenum exit area in square metres,  $d$  the slant distance between entrance and exit in metres,  $S_w$  the plenum wall area in square metres, and  $\theta$  the angle of incidence at exit, that is, the angle that  $d$  makes with the normal to the exit. The results of this calculation are accurate to within a few decibels for frequencies where the wavelength is much less than the plenum dimensions. It is conservative at low frequencies. For a fuller treatment of the effect of plena, recently published Ref. 4 should be consulted. This covers the experimental determination of the plenum effect for low frequencies as well as high, differing sizes, the effect of different plenum linings, and locations of inlet and outlet. Unhoused fans, mounted on one wall, are being incorporated into plena, where the fan discharges into the plenum, from a bell-shaped inlet. This can result in considerably lower fan sound pressure levels, providing the plenum is large enough and has a sound-absorptive lining.

## 3 AIR TERMINAL DEVICES

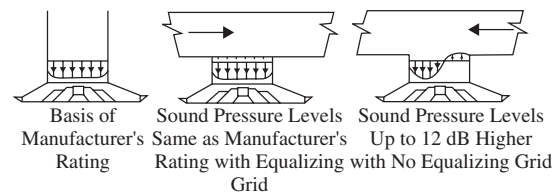
In most ducted systems, a device is placed at the end of the duct to deliver the air to the room. These are most commonly diffusers, grilles, or registers and may contain volume control devices. Since they radiate sound directly into the room, they must be selected to meet the room noise level criterion. For the most part, their noise emissions occur in the octave bands above 250 Hz. Manufacturers' literature should be consulted

for appropriate sound ratings. Care should be taken that the conditions for which the data are presented match the application at hand and any adjustments made as necessary. The noise radiated by a terminal device is dependent not only on the volume and velocity of the airflow through the element but also on the upstream flow conditions. Manufacturer's data are taken under essentially ideal flow conditions; poor flow conditions may add 10 to 15 dB to the catalog data. A variety of upstream airflow conditions and associated additional sound pressure levels are shown in Fig. 3. Frequently, flexible duct is used to connect the terminal device to the branch duct. The length of this flexible duct should be kept as short as possible to avoid additional flow noise, with 1 m being a suggested maximum. Misalignment of the flexible duct can cause increased sound pressure levels, as shown in Fig. 4.

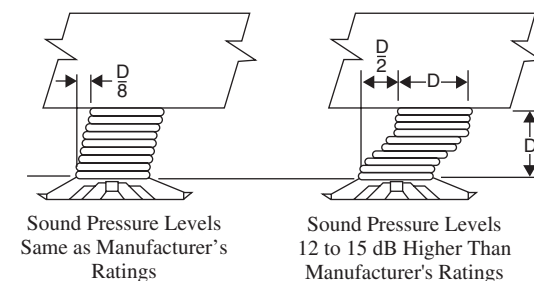
Volume control dampers may be another source of increased noise levels, typically if located close to the outlet. The noise they create is a function of the additional pressure drop they introduce into the system; the additional noise is 20 log of the ratio of the additional pressure drop to that of the diffuser itself. In acoustically critical spaces, volume control dampers should be located well back in the duct system (5 to 10 duct diameters from the outlet), with the lined duct between the damper and the outlet.

## 3.1 Variable-Air-Volume Systems

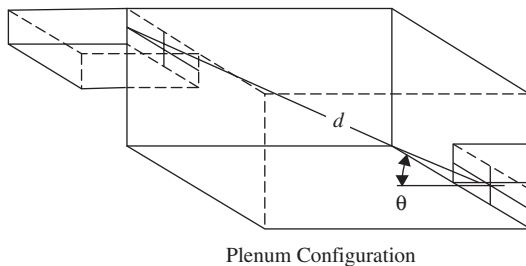
For energy conservation reasons, many current air-conditioning systems modulate the airflow to the conditioned space to match the required heating or



**Figure 3** Noise effect of poor diffuser flow condition. (From Ref. 1, p. 47.10. Used with permission.)



**Figure 4** Effect of proper and improper alignment of flexible duct connector. (From Ref. 1, p. 47.10. Used with permission.)



**Figure 2** Diagram of sound-absorbing plenum.



cooling load, as it varies throughout the day and year. These VAV systems have two distinguishing characteristics from the acoustical point of view: (1) a terminal device to modulate the airflow and (2) some method of varying the flow volume from the fan. Such modulation can cause two acoustical problems: (1) loss of privacy when the airflow is at the minimum, due to the lack of diffuser noise, and (2) excess low-frequency noise (rumble), depending on the method of varying the flow from the fan (see Section 3.4).

### 3.2 Variable-Air-Volume Terminals

In its simplest form, the terminal device consists of an automatically operating damper in a sheet metal box. It is commonly connected directly to the supply duct and with one or more outlets feeding diffusers. Noise is created by the damper as a function of the pressure drop across the damper. This noise can be radiated by two paths: (1) directly through the wall of the unit and (2) downstream through the connected duct(s). This noise is frequently controlled by a section of lined duct between the box and the outlet(s). A more difficult control case is presented when the outlet and VAV terminal are combined. In some situations, the casing-radiated sound must be controlled. In most cases, such terminal units are located over acoustical panel ceilings, which have limited sound transmission loss properties and may contain acoustically transparent areas such as return-air grilles and light fixtures. In general, VAV boxes that handle more than about  $0.8 \text{ m}^3/\text{s}$  should not be located over acoustical environments such as offices; they should be located over more noncritical spaces such as corridors, storage areas, or toilet rooms. In some cases, where such acoustically less sensitive spaces are not available and large box sizes must be used, it may be necessary to increase the transmission loss characteristics of the ceiling by incorporating a layer of 12.5-mm gypsum board between the unit and the acoustical ceiling or encasing the box with a 25-mm layer of glass fiber and 12.5-mm gypsum board.

### 3.3 Fan-Powered VAV Terminals

A special case is a VAV terminal that incorporates a fan to mix the air from the plenum above the ceiling with the primary air. These are called fan-powered terminals (FPTs) and are of two kinds: one in which the fan cycles on and off, as required, and a second in which the fan runs full time. Since the fan in the first goes on and off, the occupants are more aware of the control unit sound. The noise emitted by these units consists of both the noise radiated by the casing and the fan and that through the room air outlet. By reason of the fan contribution to the total direct radiated noise, units handling more than about  $0.8 \text{ m}^3/\text{s}$  commonly produce noise levels in the space below corresponding to a noise criteria (NC) rating of 40 or above and hence should not be located over spaces requiring a lower sound level. Some possible noise control measures for these units include, in addition to moving them to more remote locations, keeping them

at least 2 m from any open return grilles in the ceiling, installing sound attenuators if offered as an option by the manufacturer, or field fabricating lined elbows for installation on the induced air opening of the FPT. Consult manufacturers' literature for appropriate information on the noise levels produced by these units and how to determine the noise levels in the occupied space served by them. Data on these units are taken in accordance with the Air-Conditioning & Refrigerating Institute (ARI) Standard 880–98.<sup>5</sup> See Ref. 1 for estimation of the sound pressure level in the occupied space.

### 3.4 Fan Volume Control

As the airflow volume through the terminals varies to meet the required heating or cooling load, the volume of air produced by the fan must also vary. There are three basic methods of doing so: (1) use of inlet vanes on the fan, (2) motor speed controls, and (3) varying the pitch of the fan blades.

*Inlet vanes* are positioned at the inlet to the fan scroll and close down to reduce airflow. They add resistance to the system and, depending on the fan type, may cause significant additional low-frequency fan sound, which must be dealt with further downstream. Since resistance to flow is added, there is also energy usage inefficiency when the vanes are in their partially open position.

*Variable-speed controls* reduce the speed of the fan and thus the volume flow; they also reduce the fan noise generation. Variable-speed controls have a significant energy savings over inlet vanes; this should be taken into account in the selection process.

*Variable-pitch blades* are available for some axial-flow fans; this also results in quieter operation at reduced flow.

## 4 SOUND TRANSMISSION THROUGH DUCT WALLS

Sound radiated through duct walls may be a problem if not sufficiently attenuated before the duct passes over or through occupied space. This is most frequently a problem close to the fan room, where the noise in the duct may be composed of both that from the fan and that aerodynamically generated due to poor flow conditions. Typically, this noise is concentrated in the octave bands below 250 Hz and may extend down through the 31.5-Hz band. It is commonly called *break-out noise*, and its level is dependent on the noise level within the duct, the duct cross section, and the length of the duct in or over the occupied space. The transmission loss characteristics of rectangular, flat oval, and round ducts have been determined; representative values for round and rectangular ducts are shown in Table 6. The transmission loss of rectangular ducts does not vary significantly as a function of duct size or construction; the transmission loss of round ducts does vary as a function of the duct diameter and values for several typical diameters are included. Note that at low frequencies the transmission loss of round ducts is markedly higher than for rectangular ones. Using round ducts is an excellent

**Table 6** Transmission Loss<sub>out</sub> for Rectangular and Round Duct by Octave Band Center Frequency (Hz)

	63 Hz	125 Hz	250 Hz	500 Hz	1000 Hz	2000 Hz
Rectangular Sizes (300–1200 mm)	20	23	26	29	32	38
Round Duct Diameter (mm)						
200	>48	>65	>75	>72	56	56
350	>48	>53	55	33	34	35
650	>48	>53	36	32	32	28
800	>48	42	38	25	26	24

Source: Ref. 1, p. 42.23. Used with permission.

method of controlling low-frequency break-out noise. Since the noise is better contained, additional duct system attenuation may be needed downstream for appropriate control of room sound pressure levels. The transmission loss of flat oval duct is intermediate between rectangular and round duct, but due to the relatively large flat surfaces, it tends to follow the same characteristics as that of rectangular duct, that is, lower values at low frequencies.

## 5 TURBULENT AIRFLOW NOISE CONTROL

Although fans are usually the major source of noise in a duct system, aerodynamic noise may be generated at elbows, turns, takeoffs, silencers, and other duct elements. The generated noise levels depend on the element geometry as well as the airflow velocity. Since the intensity of flow-generated sound is proportional to between the fifth and sixth power of the local velocity in the duct, the best methods of control are to (1) keep the duct velocities as low as possible and (2) avoid closely spaced elements (turns, takeoffs) or abrupt changes in duct area that can contribute to turbulent flow. In general, if the flow velocities are below about 10 m/s and elements can be separated by about three

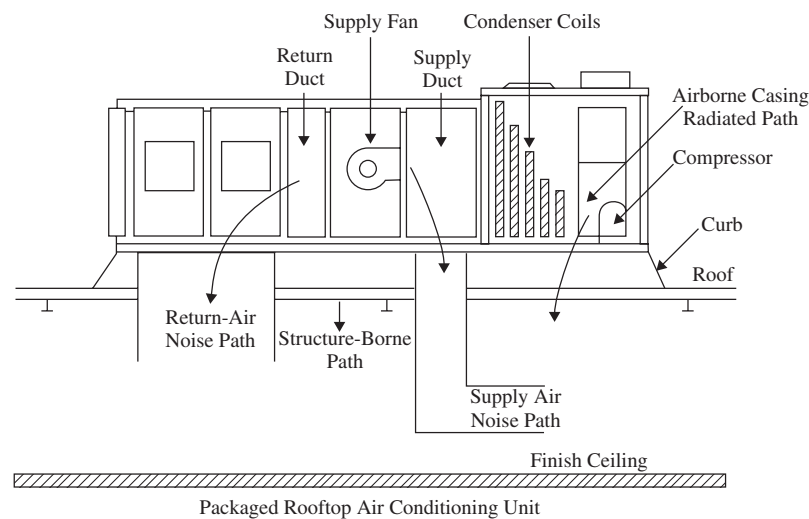
to five duct diameters, most aerodynamically induced noise control problems are minimized.

## 6 ROOFTOP UNITS

Rooftop units (packaged, factory-assembled units containing fans and associated heating and cooling equipment) pose important noise control problems. They are frequently mounted on curbs supported by lightweight roof structure directly above occupied space. Because of their proximity to the building interior, they should be located over acoustically noncritical spaces. The primary noise paths that need consideration, as shown in Fig. 5, are<sup>1</sup> (1) the casing-radiated noise, (2) the supply and return-air ducts, and (3) structure-borne noise.





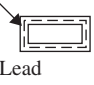
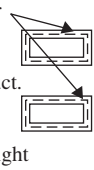
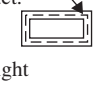
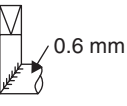
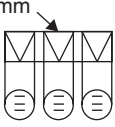
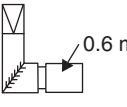
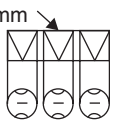
### 6.1 Casing-Radiated Noise

This noise is best controlled by making certain the roof structure inside the curb has adequate mass to block the sound being radiated by the fan casing and compressor, if included. This construction may consist of concrete or multiple layers of gypsum board. Sealing around the perimeter of the curb and around the supply and return duct penetrations is important. The supply and



**Figure 5** Noise paths in typical rooftop installations. (From Ref. 1, p. 47.6. Used with permission.)

**Table 7 Duct Break-out Insertion Loss: Potential Low-Frequency Improvement over Bare Duct Elbow**

Discharge Duct Configuration of Horizontal Supply Duct	Duct Break-out Transmission Loss at Low Frequencies (dB)			Side View	End View
	63 Hz	125 Hz	250 Hz		
Rectangular duct: no turning vanes (reference)	0.0	0.0	0.0		
Rectangular duct: two-dimensional turning vanes	0.0	0.5	1.0		
Rectangular duct: wrapped with foam and lead	4.0	3.0	4.5	See end view	
Rectangular duct: wrapped with glass fiber, one layer of gypsum board	4.0	7.0	5.5	See end view	
Rectangular duct: wrapped with glass fiber, two layers of gypsum board	7.5	8.5	9.0	See end view	
Rectangular to multiple drop: round mitered with turning vanes, three parallel round supply ducts	17.5	11.5	13.0		
Rectangular to multiple drop: round mitered elbow with turning vanes, three parallel round lined double-wall supply ducts	18.0	13.0	16.0		

Source: Ref. 1, p. 47.8. Used with permission.

return ducts are commonly directly above the ceiling of the occupied space, and often there is insufficient space for easy application of adequate noise control measures. On the supply side, low-frequency break-out noise is a common problem. Control methods consist of proper configuration of the fan outlet and ducts. A common problem is the duct elbow between the fan outlet and the horizontal duct above the ceiling. Round elbows and round duct are a very important way of controlling this noise. See Table 7.

## 6.2 Structure-Borne Noise

This noise is controlled by proper vibration isolation. Internal isolation of fans in units without compressor/condenser units will usually be sufficient if the isolators have adequate deflection; steel springs of 50 to 75 mm deflection are usually required. Several manufacturers can supply curbs with high deflection springs for such isolation.

An alternate noise control technique is to raise the unit above the roof on a structure (commonly called dunnage). In this configuration, the ducts can be run above the roof before entering the building, creating

the opportunity to include noise control measures before the ducts enter the building; casing-radiated noise through the bottom of the unit is also less difficult. If the unit contains compressor/condenser units, it is usually necessary to isolate the entire unit. Vibration transfer to a lightweight roof is avoided since the dunnage is usually supported from heavier roof-supporting structures.

## REFERENCES

1. ASHRAE, *Handbook, HVAC Applications*, ASHRAE, Atlanta, GA, 2003.
2. ASTM, *Standard Test Method for Measuring Acoustical and Airflow Performance of Duct Liner Materials and Prefabricated Silencers*, ASTM E477-06a, American Society for Testing and Materials, West Conshohocken, PA, 2007.
3. R. J. Wells, *Acoustical Plenum Chambers*, *Noise Control*, July, 1958.
4. The Aero-Acoustic Properties of Common HVAC Plena, Final Report RP-1026, ASHRAE, Atlanta, GA, 2000.
5. ARI, *Air Terminals*, ARI 880-98, Air-Conditioning and Refrigeration Institute, Arlington, VA, 1998.

# CHAPTER 111

## AERODYNAMIC SOUND GENERATION IN LOW SPEED FLOW DUCTS

**David J. Oldham**

Acoustics Research Unit  
School of Architecture and Building Engineering  
University of Liverpool  
Liverpool, United Kingdom

**David C. Waddington**

Acoustics Research Centre  
School of Computing, Science and Engineering  
University of Salford  
Greater Manchester, United Kingdom

### 1 INTRODUCTION

The interaction between the turbulent airflow and discontinuities in low-speed flow ducts, such as in ventilation systems, can result in the generation of noise as eddies are shed from duct irregularities or even the rough sides of the airways. In free space these turbulent eddies are relatively harmless as they are inefficient noise generators at the velocities encountered in ventilation systems. Efficient generation of noise occurs when the turbulence is shed from the object or discontinuity or when it impinges subsequently on an obstruction, and the corresponding velocity variations are converted into pressure fluctuations. Airflow noise increases as approximately the sixth power of flow velocity and is generally broadband. The spectrum of the noise produced will depend on the size of the obstacle or discontinuity and the maximum velocity. For typical fittings and flow velocities, the overall regenerated power level is likely to be in the region of 50 to 70 dB, but the levels vary with frequency. At considerable distances from the fan, airflow-generated noise from duct fittings can become the major noise problem. If the fittings are located near terminal devices, there may not be enough duct length available between the duct fitting and terminal device to provide sufficient attenuation of the flow-generated noise.

### 2 SOURCES OF NOISE IN FLOW DUCTS

Although extensive research on flow-generated noise has been carried out over the past 40 years, the emphasis has largely been on jet engine noise (see Chapter 9). The airflow speeds involved in this situation are generally close to the speed of sound and not applicable to the situation of ventilation systems where velocities between 10 and 30 ms<sup>-1</sup> are common. Relatively little is known about the situation of noise produced by turbulent flow in ventilation systems, which is complicated by the presence of resonances and flow instabilities.

In ventilation systems, turbulent mixing can occur in the absence of solid surfaces, for example, induction

airstream mixing and boundary layer turbulence. When the air leaves the duct, it enters a region of zero-flow velocity. The high-velocity gradients that exist at the interface of the moving and stationary media produce shear forces in the fluids, which generate turbulent mixing and noise. The noise sources are distributed spatially along and across the regions of mixing. Lighthill has proposed that a quadrupole represents a model of the acoustic source that dominates high-speed subsonic, turbulent air jets.<sup>1,2</sup>

Curle extended Lighthill's general theory of aerodynamic sound by incorporating the effect of solid boundaries upon the sound field.<sup>3</sup> These effects include reflection and diffraction of the sound waves at the solid boundaries and a resultant dipole field at the solid boundaries. When turbulent flow interacts with a solid surface, or when turbulence in the form of a wake is generated by a solid surface, changes occur in the momentum field around the spoiler that are time-dependent, require fluctuating forces, and these must in general exist on the solid surface. Any such forces may be resolved into *lift* and *drag* components, and the sound generated is represented by an acoustic dipole, the axis of which is aligned with that of the fluctuating force. If the dipole source distribution is random, the sound spectrum is of a broadband nature. A well-ordered distribution results in a discrete sound spectrum.

Gordon has demonstrated, by means of a simple yet elegant experiment, that the wideband noise resulting from the interaction of airflow with an in-duct flow spoiler increases as the sixth power of flow velocity.<sup>4,5</sup> This is consistent with the generally accepted view that most of the sound generation mechanisms in ventilation systems can be represented by the dipole character.

The analysis of noise generated by flow spoilers usually assumes that the spoilers are small compared to the wavelength of sound at the frequency in question to ensure that the flow field in the neighborhood of the spoiler may be treated as incompressible. Davies and Ffowcs-Williams have noted that when a sound source is confined within an infinitely long duct of diameter

small in comparison to a wavelength, the character of the problem changes from three dimensional to one dimensional.<sup>6</sup> This change affects both the acoustic impedance of the surroundings and the amount of sound power radiated by the source. At low frequencies, the dipole sources, when confined in a small-diameter duct, would have sound power outputs increasing as  $U^4$  rather than the familiar  $U^6$  characteristics of these sources in an infinite fluid. As the frequency of the sound source increases, the sound power radiated by the source in the duct approaches that in the free field.

### 3 APPROACHES TO THE PREDICTION OF AIRFLOW-GENERATED NOISE IN VENTILATION SYSTEMS

Empirical formulas for predicting the sound power level generated by in-duct components are generally based upon the assumption of a sixth-power law dependence of sound power on air velocity and involve an equation of the following form:

$$L_W = C + 10 \log A + 60 \log(U_c) \quad (1)$$

where  $L_W$  is the airflow-generated noise power level (dB),  $C$  is a constant, which varies with the fitting,  $A$  is the minimum flow area of the fitting ( $m^2$ ), and  $U_c$  is the maximum flow velocity in the fitting ( $ms^{-1}$ ). In Eq. (1) the logarithm of the velocity is multiplied by 60, which is the result of assuming a  $U^6$  dependence of sound power on flow velocity. Equation (1) illustrates the importance of limiting the velocity since a doubling of velocity results in an 18-dB increase in regenerated sound power.

The intensity of the noise generated from the airflow will be determined primarily by the magnitude of the velocity increase created by the obstruction and so forth. The spectrum of the noise produced will depend on the size of the obstacle or discontinuity and on the maximum velocity. In general, the spectrum is a function of a representative dimension of the obstruction or discontinuity  $d$ , and the maximum (or constricted) flow rate around the obstacle or through the discontinuity  $U_c$ .

Flow noise data can normally be "nondimensionalized" by expressing spectral data as a function of a Strouhal number,  $St$ , given by

$$St = f_c d / U_c \quad (2)$$

where  $f_c$  is the octave band center frequency.

The calculation of the Strouhal number is, in general, the starting point for predicting flow-generated noise. The ventilation system designer usually tries to predict flow-generated noise using procedures laid down in such publications as the American Society of Heating, Refrigerating and Air-Conditioning Engineers (ASHRAE) or the UK Chartered Institution of Building Services Engineers (CIBSE) guides.<sup>7,8</sup> The information contained in these publications has been drawn from the published work of a number of different investigators who worked on a limited range of in-duct components and a limited range of duct sizes.<sup>9,10</sup>

Application of their results to systems often having very different configurations from those on which the original measurements were made can produce dubious results. Attempts have been made to use the limited available data to develop more generalized prediction methods for various types of duct component.

### 4 PREDICTION OF AIRFLOW GENERATED NOISE IN VENTILATION SYSTEMS DUE TO IN-DUCT ELEMENTS

For in-duct elements such as bends, transition pieces, damper, and the like, the results of recent research have led to a prediction method based upon pressure loss characteristics. The effect of a discontinuity in a duct carrying airflow is to generate turbulence, some of which is converted into sound energy. The power required to generate the turbulence in the vicinity of the discontinuity is supplied by the system fan, and the work done by the fan in the region of a discontinuity is manifested as a loss of static pressure across the discontinuity. The larger the discontinuity, the greater is the pressure loss and the greater is the sound power radiated. The pressure loss characteristics of an in-duct element are usually expressed in terms of a pressure loss coefficient,  $C_L$ , given by

$$C_L = \Delta P / 0.5 \rho_0 U^2 \quad (3)$$

where  $\Delta P$  = static pressure loss due to the component

$U$  = velocity of air in unobstructed region of the duct

$\rho_0$  = density of air

The pressure-based prediction method is based upon a theory originally proposed by Nelson and Morfey.<sup>11</sup> The underlying assumption of this theory is that the sound power radiated by an in-duct spoiler is related to the total fluctuating drag force acting on the spoiler, which is a function of the turbulence intensity in the region of the spoiler. Since they were unable to determine the actual spectrum of the turbulence intensity in the vicinity of the spoiler, Nelson and Morfey made the further assumption that the fluctuating drag force is in direct proportion to the steady drag force. This assumption had originally been made by Gordon<sup>4,5</sup> and was later experimentally verified by Heller and Widnall.<sup>12</sup>

Nelson and Morfey collapsed their experimental data into a generalized spectrum to form the basis of a predictive technique by the empirical evaluation of the constant of proportionality between the fluctuating and steady drag forces as a function of Strouhal number. However, their curves were obtained from measurements made on simple strip spoilers for which the necessary parameters for determining the Strouhal number, a representative dimension and open-area ratio (which determined the constriction velocity in the region of the spoiler), could be established by simple inspection. In work on airflow-generated noise in ducts arising from the presence of inclined dampers and orifice plates, Oldham and Ukpoho extended the work

of Nelson and Morfey to other spoiler configurations.<sup>13</sup> They first rewrote the Nelson and Morfey equations in terms of the pressure loss coefficient, which is a parameter more commonly used in ventilation system design than the drag coefficient employed by Nelson and Morfey. They then proposed the use of simple empirical methods based upon measurement of the pressure loss coefficient to determine the open-area ratio and the characteristic dimension for more complex spoilers. The equations obtained resulting from these modifications are shown below.

For  $f_c < f_0$ ,

$$120 + 20 \log_{10} K(\text{St}) \\ = SWL_D - 10 \log_{10} [\rho_0 A \sigma^4 C_L^2 U_C^4 / 16 c_0] \quad (4)$$

For  $f_c > f_0$ ,

$$120 + 20 \log_{10} K(\text{St}) \\ = SWL_D - 10 \log_{10} [\rho_0 \pi A^2 (\text{St})^2 \sigma^4 C_L^2 U_C^6 / 24 c_0^3 d^2] \\ - 10 \log_{10} [1 + (3\pi c_0 / 4 \omega_c)(a + b) / A] \quad (5)$$

where  $K(\text{St})$  = Strouhal number dependent constant

$SWL_D$  = in-duct sound power level

$f_c$  = center frequency of the band of frequencies under consideration

$\omega_c$  = angular center frequency

$f_0$  = cut-on frequency of the duct

$c_0$  = speed of sound in air

$A$  = cross-sectional area of duct

$a$  = duct height

$b$  = duct width

The open area ratio is given by

$$\sigma = \frac{C_L^{1/2} - 1}{C_L - 1} \quad (6)$$

The maximum effective (constriction) velocity is given by

$$U_C = \frac{U}{\sigma} \quad (7)$$

The characteristic dimension is given by

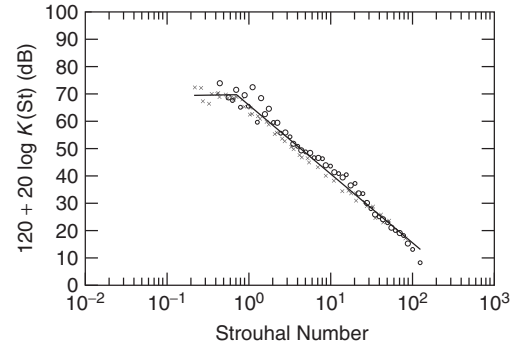
$$d = \frac{A(1 - \sigma)}{b} \quad (8)$$

The Strouhal number is given by:

$$\text{St} = \frac{f_c d}{U_C} \quad (9)$$

Note there are different expressions for noise regeneration below and above the duct cut-on frequency, which is the frequency above which complex acoustic modes are propagated in the duct.

Waddington and Oldham have recently applied Eqs. (4) to (9) to data measured on a number of in-duct

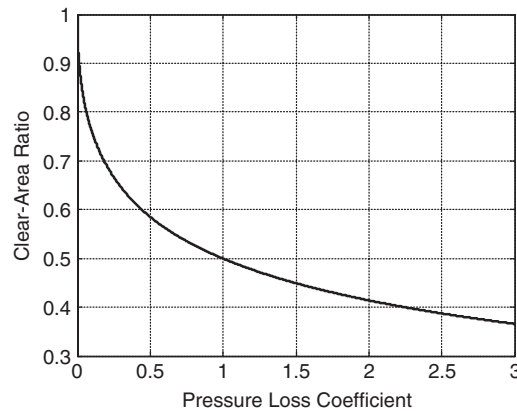


**Figure 1** Collapse of measured sound power level data as a function of Strouhal Number for mitred bends without vanes: (x) 0.4-m diameter, (o) 0.6-m diameter.

elements.<sup>14</sup> Figure 1 shows the collapse of measured data on the basis of the above equations for a range of component sizes and duct air velocities. It can be seen that individual spectra corresponding to different air velocities and component sizes collapse onto one single spectrum, and the best-fit curve through this data then forms the basis of a predictive design curve for this type of component. From knowledge of the pressure loss coefficient, duct dimensions, and air velocity one can calculate the sound power level for any chosen octave band center frequency. It is necessary to first obtain values for the clear-area ratio and the characteristic dimension  $d$ . As shown above, the clear-area ratio can be approximated by a simple function of the pressure loss coefficient, which is plotted in Fig. 2.

The procedure for determining the regenerated noise level for a given one-third octave band frequency is thus as follows:

1. Determine the clear-area ratio  $\sigma$ , from Eq. (6) or Fig. 2.



**Figure 2** Clear-area ratio as a function of pressure loss coefficient.

2. Calculate the constriction velocity  $U_c$  from Eq. (7).
3. Calculate the representative dimension  $d$  from Eq. (8).
4. Calculate the Strouhal number (St) corresponding to the chosen one-third octave band center frequency  $f_c$ ,  $d$  and  $U_c$  from Eq. (9).
5. Read off appropriate value of  $20 \log [K(\text{St})]$  from the best-fit curve in Fig. 1.
6. Insert values in Eq. (4) or Eq. (5) depending on whether the one-third octave band frequency  $f_c$  is below or above duct higher mode cut-on  $f_0$ .

### 5 PREDICTION OF AIRFLOW-GENERATED NOISE IN VENTILATION SYSTEMS AT TERMINAL DEVICES

As there is no opportunity to attenuate energy produced by terminal units such as grilles, diffusers, and induction units, before it reaches the room, flow noise generation at terminal units is of particular importance. Two main types of diffuser can be identified:

1. Circular ceiling diffusers supplied through circular ductwork with a neck area of  $A_N$  with or without plenum boxes.
2. Linear and rectangular grilles, registers, or slots fed from plenum boxes and having a free discharge area  $A_F$ .

For both types the radiated sound power level is given by the general equation:

$$L_w = \text{Constant} + 57 \log Q - 47 \log A \quad \text{dB} \quad (10)$$

where  $Q$  is the volume flow rate ( $\text{m}^3\text{s}^{-1}$ ) and  $A$  is the area ( $\text{m}^2$ ).

The form of this expression will apply for the overall total radiated sound power level or to the octave bands of the noise spectrum; however, the constant term will vary and can be determined experimentally. It can be seen that the radiated sound power level is very sensitive to changes of flow rate or grille area.

A typical value for the total radiated sound power level is given by<sup>15</sup>

$$L_{w\text{total}} = 32 + 57 \log Q - 47 \log A_F \quad \text{dB} \quad (11)$$

A similar expression relates the total radiated sound power level to neck flow rate:

$$L_{w\text{total}} = 32 + 60 \log V_N + 13 \log A_N \quad \text{dB} \quad (12)$$

where  $V_N$  is the neck (or maximum) flow velocity in metres/second.

Figure 3 illustrates general spectral distribution for circular diffusers, which can be applied directly to the overall sound power level. The Strouhal number is given by the product of frequency and neck diameter divided by the neck flow velocity. Octave band levels at frequencies higher and lower than the peak frequency can also be obtained approximately

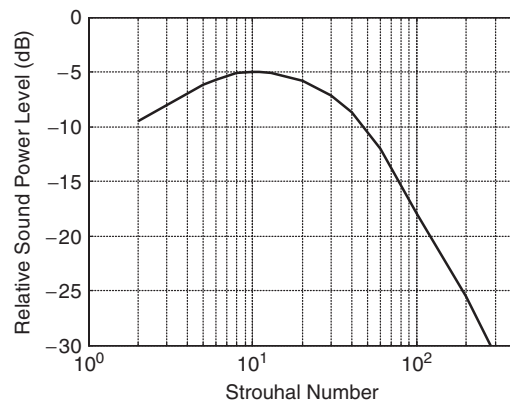


Figure 3 Generalized spectrum for diffuser.

by deducting 3 dB/octave at lower frequencies and deducting 5 dB/octave at higher frequencies.

When the duty of a diffuser is specified by the volume flow rate  $Q$  and the pressure drop  $\Delta P$ , the general equation becomes

$$L_{w\text{total}} = \text{Constant} + 10 \log Q + 26 \log \Delta P \quad \text{dB} \quad (13)$$

where  $\Delta P$  is the grille pressure drop in pascals. An alternative approach to the prediction of diffuser noise can be found in Berarek and Ver<sup>16</sup> and *Sound and Vibration Design and Analysis*.<sup>17</sup>

Ceiling diffusers designed to deflect the air horizontally, known as having a wide throw, will exhibit a greater pressure loss and generate more noise than those with a small or no throw, as illustrated in Fig. 4.

A control damper added to a grille or diffuser will increase the flow noise generated by a diffuser. A vortex shedding noise component will arise from the damper blades themselves, but more significantly there will also be the impact of the damper blade turbulence wake upon the grille or diffuser vanes. Manufacturers of grilles

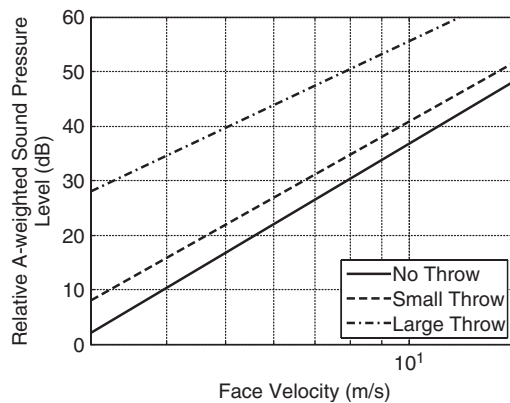


Figure 4 The effect of diffuser throw on sound power generated.



and diffusers usually supply data for the sound power level produced for their grille/damper assemblies, as a function of face velocity, volume flow rate or pressure drop across the unit. In the absence of such data an increase in the above-estimated sound power level of 5 dB can be assumed in each octave band for the addition of an integral damper vane set fully open. It can further be assumed that, for subsequent flow adjustment resulting in an increase in pressure drop across the damper, the overall sound power level will increase approximately according to the following equation:

$$\Delta L_{w\text{total}} = 33 \log(\Delta P / \Delta P_0) \text{ dB} \quad (14)$$

where  $\Delta P$  is the static pressure drop across the unit and  $\Delta P_0$  is the pressure drop for the same volume flow rate with damper vanes fully open.

## 6 DESIGNING FOR LOW FLOW-GENERATED NOISE

There are a number of simple principles for duct design that should be followed in order to avoid turbulence and the associated pressure loss and noise.<sup>18</sup> Flow-generated noise in duct fittings can be reduced by choosing geometries that minimize the generation of vortices and the interaction of the vortices with sharp edges. Some obstructions, such as dampers, are necessary, but multiple dampers are preferred to single dampers in a noise-sensitive system. Dampers should be fitted at least 1.5 to 2.0 m back from a duct termination in order to reduce damper noise escaping into occupied space.

The noise generated at bends can be reduced by the use of circular bends rather than mitered bends. Splitters or turning vanes can also be employed to enhance the airflow at bends. In critical situations, narrow chord and large radius bends are preferable.

Cross-sectional area changes where flow separation occurs should be avoided. The transition angle should be less than 10° to minimize the risk of flow detachment. In critical situations, if the available transition length is insufficient to obtain less than a 10° transition angle, a perforated plate can be employed to diffuse the flow evenly into the larger duct. The high-frequency noise generated by the perforated plate can be easily attenuated by duct lining downstream of the area change.

Flow-generated noise at branchings and takeoffs can be reduced by using duct fittings that provide a smooth flow and by avoiding a change of velocity pressure, especially the reduction of the velocity pressure, which is usually accompanied by flow separation. Cross and tee junctions where the volume flow in one branch is substantially smaller than the volume flow in the other branches should be avoided. A branch takeoff should be more than five duct diameters downstream of the main junction so that the turbulence generated in the main junction decays before it reaches the downstream branching.

It should be noted that there are other aspects of flow-generated noise that have not been covered in this brief chapter. Attenuators constitute a possible source of in-duct turbulence such that they not only reduce noise generated elsewhere in the system but

can also generate significant self-noise. Attenuator manufacturers, therefore, typically provide both static (no flow) and dynamic (with airflow) insertion loss data. It is also possible for the turbulent flow downstream of a discontinuity to excite the relatively thin walls of a duct into vibration and thus cause significant noise break out.

## REFERENCES

1. M. J. Lighthill, On Sound Generated Aerodynamically: 1, General Theory, *Proc. Roy. Soc. (London)*, Series A211, 1952, pp. 564–587.
2. M. J. Lighthill, On Sound Generated Aerodynamically: 11, Turbulence as a Source of Sound, *Proc. Roy. Soc. (London)*, Series A, 1953, pp. 1–32.
3. N. Curle, The Influence of Solid Boundaries upon Aerodynamic Sound, *Proc. Roy. Soc. (London)*, Series A231, 1955, pp. 505–514.
4. C. G. Gordon, Spoiler Generated Flow Noise. 1, Experiment, *J. Acoust. Soc. Am.*, Vol. 43, 1968, pp. 1041–1048.
5. C. G. Gordon, Spoiler Generated Flow Noise. 11, Results, *J. Acoust. Soc. Am.*, Vol. 45, 1969, pp. 214–223.
6. H. G. Davies and J. E. Ffowes-Williams, Aerodynamic Sound Generation in a Pipe, *J. Fluid Mech.*, Vol. 32, 1968, pp. 765–778.
7. Sound and Vibration Control, in *ASHRAE Handbook & Product Directory, Applications Volume*, American Society of Heating, Refrigerating, and Air-Conditioning Engineers, Atlanta, 1999, Chapter 46.
8. *Noise and Vibration Control for HVAC*, CIBSE Guide B5, Chartered Institution of Building Services Engineers, London, 2002.
9. W. W. Soroka, Experimental Study of High Velocity Air Discharge Noise from Some Ventilating Ducts and Elbows, *Appl. Acoust.*, Vol. 3, 1970, pp. 308–321.
10. U. Ingard, A. Oppenheim, and M. Hirschorn, Noise Generation in Ducts, ASHRAE Project Report 37, 1967.
11. P. A. Nelson and C. L. Morfey, Aerodynamic Sound Production in Low Speed Flow Ducts, *J. Sound Vib.*, Vol. 79, 1981, pp. 263–289.
12. H. H. Heller and S. E. Widnall, Sound Radiation from Rigid Flow Spoilers Correlated with Fluctuating Forces, *J. Acoust. Soc. Am.*, Vol. 47, 1970, pp. 924–936.
13. D. J. Oldham and A. U. Ukpofo, A Pressure-Based Technique for Predicting Regenerated Noise Levels in Ventilation Systems, *J. Sound Vib.*, Vol. 140, 1990, pp. 259–272.
14. D. C. Waddington and D. J. Oldham, Generalised Flow Noise Prediction Curves for Air Duct Elements, *J. Sound Vib.*, Vol. 222, 1999, pp. 163–169.
15. Noise Control in Building Services, Sound Research Laboratories, Colchester, 1988.
16. L. L. Beranek and I. Ver, Eds., *Noise and Vibration Control Engineering*, Wiley Interscience, Chichester, 1992.
17. Sound and Vibration Design and Analysis, National Environmental Balancing Bureau, Gaithersburg, MD, 1994.
18. M. A. Iqbal, T. K. Willson, and R. J. Thomas, *The Control of Noise in Ventilation Systems*, E&F N Spon, London, 1977.

# CHAPTER 112

## NOISE CONTROL FOR MECHANICAL AND VENTILATION SYSTEMS

Reginald H. Keith  
Hoover & Keith, Inc.  
Houston, Texas

### 1 INTRODUCTION

To evaluate the acoustical impact of mechanical equipment rooms, detailed knowledge of the acoustical emission levels of the mechanical equipment is required. The best source for these data is the equipment manufacture. However, in the initial design the specific manufacturer and equipment model may not be known. The information given in this chapter is suggested for initial design uses.

### 2 SOUND PRESSURE AND SOUND POWER LEVELS FOR TYPICAL EQUIPMENT

These data are presented in the form of octave band sound power levels (re  $10^{-12}$  W) or normalized octave band sound pressure levels. The normalized octave band sound pressure level data are representative of a distance at 1 m and a room constant of 75 m<sup>2</sup>.

#### 2.1 Chillers<sup>1,2</sup>

Chillers are used to provide cooling water for air-conditioning systems. The three principal types are (1) packaged chillers with reciprocating compressors, (2) packaged chillers with rotary-screw compressors, and (3) packaged chillers with centrifugal compressors. In addition, absorption machines, which are heat-operated refrigeration machines, are sometimes used to provide cooling water. Specific considerations for each classification are as follows:

**Packaged Chillers with Reciprocating Compressors** The overall sound power level can be expressed by

$$L_W = 82 + 8.5 \log(CC) \quad (1)$$

where CC is the rated cooling capacity in kilowatts. The specific octave band sound power levels are shown in Table 1.

**Packaged Chillers with Rotary-Screw Compressors** The octave band sound power levels representing near-maximum noise levels for the size range of 350 to 1000 kW cooling capacity, operating at or near 3600 rpm are shown in Table 2.

**Packaged Chillers with Centrifugal Compressors** Packaged chillers can be divided into three groups. A description of each group is given together with an equation to compute the overall sound power level (where CC is the cooling capacity in kilowatts). The values in Table 3 can be subtracted from the

**Table 1 Sound Power Levels for Packaged Chillers with Reciprocating Compressors**

Octave Frequency Band (Hz)	Sound Power Level (dB) Cooling Capacity (kW)		
	35–108	109–284	285–703
31	86	88	90
63	91	93	95
125	92	94	96
250	93	96	99
500	94	97	100
1000	93	96	99
2000	90	93	96
4000	86	89	92
8000	81	84	87
Overall	100	103	106
A-weighted	97	100	103

**Table 2 Sound Power Levels for Packaged Chillers with Rotary Screw Compressors**

Octave Frequency Band (Hz)	Sound Power Level (dB) 350–1055 kW Cooling Capacity	
31	78	
63	84	
125	88	
250	100	
500	97	
1000	93	
2000	88	
4000	83	
8000	81	
Overall	103	
A-weighted	98	

overall sound power level to obtain the octave band sound power level.

Group 1 is for internally geared, hermetically sealed centrifugal compressors rated at or under 3500 kW. The overall sound power level for the compressors in this group is given by

$$L_W = 78 + 9 \log(CC) \quad (2)$$

Group 2 is for direct-drive, hermetic compressors rated at or under 3500 kW. The overall sound power level for the compressors in this group is given by

$$L_W = 60 + 14 \log(CC) \quad (3)$$

**Table 3 Frequency Adjustments (in dB) for Three Groups of Centrifugal Refrigeration Compressors**

Octave Frequency Band (Hz)	Group 1 <sup>a</sup>	Group 2 <sup>b</sup>	Group 3 <sup>c</sup>
31	10	9	12
63	9	8	11
125	8	7	10
250	7	6	9
500	10	10	11
1000	8	10	6
2000	8	10	6
4000	12	14	11
8000	19	21	17
A-weighted	3	4	1

<sup>a</sup>Group 1: Internally geared hermetic, or if drive arrangement is not known, at and under 3500 kW.

<sup>b</sup>Group 2: Direct-drive hermetic, at and under 3500 kW.

<sup>c</sup>Group 3: All hermetic above 1000 tons (3500 kW).

Group 3 is for all hermetic compressors rated at or above 3500 kW. The overall sound power level for the compressors in this group is given by

$$L_W = 90 + 6 \log(CC) \quad (4)$$

**Absorption Machines** The sound of absorption machines is generally masked by other noises in a mechanical equipment room. The machine usually includes one or two small pumps; steam flow noise or steam valve noise may also be present. The overall sound power level is normally less than 100 dB and the A-weighted sound power level is less than 96 dB.

**Built-up Refrigeration Machines** The sound of packaged chillers, as presented in the preceding paragraphs, includes the sound of both the compressor and the drive unit. If a refrigeration system is built of separate pieces, then the noise level estimate should include the noise of each component making up the assembly. Compressor sound power levels should be taken from the packaged chiller data. Sound power level data for the drive units (motors, gears, steam turbines) should be taken from the appropriate tables in this chapter or obtained from the manufacturers.

## 2.2 Boilers<sup>1</sup>

The wide variety of blower assemblies, air and fuel inlet arrangements, burners, and combustion chambers provides such variability in the noise data that it is impossible to correlate noise with heating capacity. Sound power levels at the normalized 0.9-m distance may be as high for the smallest as for the largest units. The estimated sound power levels given in Table 4 are believed applicable for all boilers in the size range of 50 to 2000 boiler horsepower (1 bhp = 33,500 Btu/h or 9818 W). These sound power levels apply to the front of the boiler. Thus, when other distances are of concern, the distance should always be taken from the front surface of the boiler. Sound power levels are lower off the side and rear of the typical boiler.

**Table 4 Sound Power Levels for Boilers**

Octave Frequency Band (Hz)	Sound Power Level (dB) Heating Capacity	
	50–300 bhp (490–2950 kW)	301–2000 bhp (2951–20,000 kW)
31	99	102
63	99	102
125	98	101
250	96	99
500	93	96
1000	90	93
2000	87	90
4000	84	87
8000	81	84
Overall	105	108
A-weighted	96	99

## 2.3 Cooling Towers<sup>1,2</sup>

Four general types of cooling towers are sketched in Fig. 1: centrifugal-fan flow-through type, axial-flow blow-through type (with the fan or fans located on a side wall), induced-draft propeller type, and “underflow” forced-draft propeller type (with the fan located under the assembly).

**Sound Power Level of Propeller-Type Cooling Towers** The approximate overall sound power levels of propeller-type cooling towers are given by

$$L_W = 100 + 8 \log(\text{fan kW})$$

for overall  $L_W$ , under 75 kW (5)

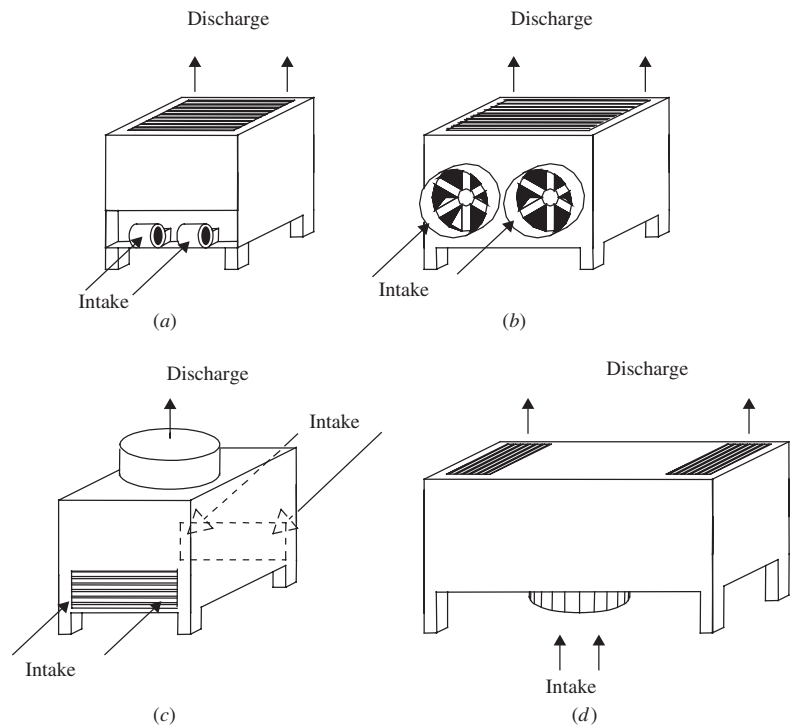
$$L_W = 96 + 10 \log(\text{fan kW})$$

for overall  $L_W$ , over 75 kW (6)

where fan kilowatt is the nameplate power rating of the motor that drives the fan. Octave band sound power levels can be obtained by subtracting the values of Table 5 from the overall  $L_W$  obtained by Eq. (5) or (6).

**Table 5 Frequency Adjustments (in dB) for Propeller-Type Cooling Towers**

Octave Frequency Band (Hz)	Value Subtracted from Overall PWL (dB)
31	8
63	5
125	5
250	8
500	11
1000	15
2000	18
4000	21
8000	29
A-weighted	9



**Figure 1** Principal types of cooling towers. (a) Centrifugal-fin blow-through type, (b) axial-flow blow-through type, (c) induced-draft propeller type, and (d) forced-draft propeller-type underflow.

**Sound Power Level of Centrifugal-Fan Cooling Towers** The approximate overall sound power levels of centrifugal-fan cooling towers are given by

$$L_W = 85 + 11 \log(\text{fan kW})$$

for overall  $L_W$ , under 60 kW (7)

$$L_W = 93 + 7 \log(\text{fan kW})$$

for overall  $L_W$ , over 60 kW (8)

where fan kilowatt is the nameplate power rating of the motor that drives the fan. When more than one fan or cooling tower is used, the fan power rating should be the total motor drive rating of all fans or towers. Octave band sound power levels can be obtained by subtracting the values of Table 6 from the overall  $L_W$  obtained by Eq. (7) or (8).

**Directionality of Cooling Towers** Cooling towers usually radiate different amounts of sound in different directions, and the directional adjustments of Table 7 should be made to the octave band sound power levels (PWLs). These corrections apply to the five principal directions from a cooling tower, that is, in a direction perpendicular to each of the four sides and to the top of the tower.

**Noise Reduction with Reduced Fan Speed** When it is practical to do so, the cooling tower

**Table 6** Frequency Adjustments (in dB) for Centrifugal-Fan Cooling Towers

Octave Frequency Band (Hz)	Value Subtracted from Overall PWL (dB)
31	6
63	6
125	8
250	10
500	11
1000	13
2000	12
4000	18
8000	25
A-weighted	7

fan can be reduced to half speed in order to reduce noise. Half speed produces approximately two-thirds cooling capacity and approximately 8- to 10-dB noise reduction in the octave bands that contain most of the fan-induced noise. For half-speed operation, the octave band  $L_p$  or  $L_W$  of full-speed cooling tower noise may be reduced by the following amounts, where  $f_B$  is the blade passage frequency and is calculated from the relation  $f_B = \text{number of fan blades} \times \text{shaft rpm}/60$ :

**Table 7 Corrections to Average SPLs for Directional Effects of Cooling Towers**

Octave Frequency Band (Hz)	31	63	125	250	500	1000	2000	4000	8000
<b>Centrifugal-fan blow-through type</b>									
Front (fan inlet)	+3	+3	+2	+3	+4	+3	+2	+2	+2
Side (enclosed)	0	0	0	-2	-3	-4	-5	-5	-5
Rear (enclosed)	0	0	-1	-2	-3	-4	-5	-6	-6
Top (discharge)	-3	-3	-2	0	+1	+2	+3	+4	+5
<b>Axial-flow blow-through type</b>									
Front (fan inlet)	+2	+2	+4	+6	+6	+5	+5	+5	+5
Side (enclosed)	+1	+1	+1	-2	-5	-5	-5	-5	-6
Rear (enclosed)	-3	-3	-4	-7	-7	-7	-8	-11	-8
Top (discharge)	-5	-5	-5	-5	-2	0	0	+2	+1
<b>Induced-draft propeller type</b>									
Front (air inlet)	0	0	0	+1	+2	+2	+2	+3	+3
Side (enclosed)	-3	-3	-3	-3	-3	-3	-4	-5	-6
Top (discharge)	+3	+3	+3	+3	+3	+4	+4	+3	+3
<b>Underflow forced-draft propeller type</b>									
Any side	-1	-1	-1	-2	-2	-3	-3	-4	-4
Top	+2	+2	+2	+3	+3	+4	+4	+5	+5

Octave Band that Contains	Noise Reduction due to Half Speed
$\frac{1}{8} f_B$	3 dB
$\frac{1}{4} f_B$	6 dB
$\frac{1}{2} f_B$	9 dB
$1 f_B$	9 dB
$2 f_B$	9 dB
$4 f_B$	6 dB
$8 f_B$	3 dB

If the blade passage frequency is not known, it may be assumed to fall in the 63-Hz band for propeller-type cooling towers and in the 250-Hz band for centrifugal cooling towers. Waterfall noise usually dominates in the upper octave bands, and it would not change significantly with reduced fan speed.

**Closed Confined Locations** Most of the preceding discussion assumes that cooling towers will be used in outdoor locations. If they are located inside enclosed mechanical equipment rooms or within courts formed by several solid walls, the sound patterns will be distorted. In such instances, the  $L_W$  of the tower (or appropriate portions of the total  $L_W$ ) can be placed in that setting, and the enclosed or partially enclosed space can be likened to a room having certain estimated amounts of reflecting and absorbing surfaces.

## 2.4 Pumps<sup>1,2</sup>

The overall normalized sound pressure levels for pumps are given in Table 8 and are representative of most pumps encountered in commercial situations. The pump power rating is taken as the nameplate power of the drive motor. Octave band sound pressure levels are obtained by subtracting the values of Table 9 from the overall sound pressure level of

**Table 8 Overall Sound Pressure Levels in dB at 1-m Distance for Pumps**

Speed Range (rpm)	Drive Motor Nameplate Power	
	Under 75 kW	Above 75 kW
3000–3600	71 + 10 log hp	85 + 3 log hp
1600–1800	74 + 10 log hp	88 + 3 log hp
1000–1500	69 + 10 log hp	83 + 3 log hp
450–900	67 + 10 log hp	81 + 3 log hp

Table 8. Pumps intended for high-pressure operation have small clearances between the blade tips and the cutoff edge and, as a result, may have higher noise peaks in the octave bands containing the impeller blade passage frequency and its first harmonic. These would usually fall in the 1000- and 2000-Hz octave bands.

**Table 9 Frequency Adjustments to Obtain Pump Octave Band and A-weighted SPLs at 1 m**

Octave Frequency Band (Hz)	Value Subtracted from Overall SPL (dB)
31	13
63	12
125	11
250	9
500	9
1000	6
2000	9
4000	13
8000	19
A-weighted	2

**Table 10 Specific Sound Power Levels  $K_W$  (in dB) and Blade Frequency Increment (in dB) for Fans of Various Types and Sizes for Use in Eq. (9)<sup>a</sup>**

Fan Type and Size	Octave Band Center Frequency (Hz)								BFI
	63	125	250	500	1000	2000	4000	8000	
Centrifugal airfoil, backward curved or inclined blade									
Over 760 mm	37	37	36	31	27	20	16	14	3
Under 760 mm	42	42	40	36	31	25	21	16	3
Centrifugal forward curved blade									
All sizes	50	50	40	33	33	28	23	18	2
Centrifugal radial blade									
Low pressure (1000 Pa–2500 Pa)									
Over 1-m diameter	53	44	40	36	34	29	26	23	7
Under 1-m diameter	64	56	50	40	39	36	31	28	7
Mid-pressure, (2500 Pa–5000 Pa)									
Over 1-m diameter	55	51	42	39	35	30	26	23	8
Under 1-m diameter	65	60	48	45	43	38	34	31	8
High pressure, (5000 Pa–15,000 Pa)									
Over 1-m diameter	58	55	50	45	43	41	38	35	8
Under 1-m diameter	68	64	56	51	51	49	46	43	8
Vaneaxial									
Hub ratio 0.3–0.4	46	40	40	45	44	42	35	31	6
Hub ratio 0.4–0.6	46	40	43	40	38	33	27	25	6
Hub ratio 0.6–0.8	56	49	48	48	46	44	40	37	6
Tubeaxial									
Over 1-m diameter	48	43	44	46	44	43	36	34	7
Under 1-m diameter	45	44	46	50	49	48	40	37	7
Propeller	45	48	55	53	52	49	43	39	5

<sup>a</sup>These values apply for either inlet or discharge noise.

## 2.5 Fans<sup>3,4</sup>

Manufacturers often furnish in-duct sound power level data of their fans on request. However, in early designs the specific model or manufacturer is not known. In these cases, the octave band sound power of a fan can be estimated by<sup>3,4</sup>

$$L_W = K_W + 10 \log Q + 20 \log P + \text{BFI} + C - 45 \quad (9)$$

where  $L_W$  is the total in-duct sound power level of the fan (inlet and outlet),  $K_W$  is the specific sound power level for the particular fan design (Table 10),  $Q$  is the volume flow rate in liters per second (L/s), and  $P$  is the static pressure produced by the fan in pascals (Pa). The blade frequency increment (BFI) is added to the octave band containing the blade passage frequency (i.e., rotational rate of the fan in cycles per second times the number of fan blades). The estimate given by this method assumes ideal inlet and outlet flow conditions and operation of the fan at its peak design condition. The sound emission level is quite critical to these conditions and increases significantly for deviations from ideal. Based on studies of noise and operational data from several fan manufacturers, Warren Blazier<sup>4</sup> suggests an additional correction to Eq. (9): Add 1 dB to the fan noise for each 3% efficiency below 95% of peak static efficiency for the particular fan operation. It is suggested that if the operating static efficiency is not known, 5 dB be added to the levels obtained from

Eq. (9). The operating static efficiency of a fan may be calculated by

$$\text{Static efficiency} = \frac{Q \times P}{1002 \times \text{BkW}} \quad (10)$$

where  $Q$  is air volume in liters per second,  $P$  is total static pressure in kilopascals, and BkW is the brake power in kilowatts. The ratio of calculated static efficiency to peak efficiency determines the correction factor  $C$ . For cursory design the maximum peak efficiency can be taken as 65% for centrifugal fans with forward curved blades, 80% for centrifugal fans with backward inclined blades, and 70% for vane axial fans.

The fan housing and its nearby connected ductwork radiate fan noise into the fan room. Because of the number of variables involved, there exists no simple analysis procedure for estimating the  $L_W$  of the noise radiated by the housing and ductwork. However, Table 11 offers a method to estimate this type of noise. These are simply deductions, in decibels, from the induct fan sound power levels.

## 2.6 Air Compressors<sup>1</sup>

The normalized sound pressure levels for air compressors commonly found in commercial buildings are given in Table 12.

## 2.7 Emergency Generators<sup>1</sup>

Emergency generators are typically driven by reciprocating engines or small gas turbines. As a general rule,

**Table 11 Octave Band Adjustments for Estimating the PWL of Noise Radiated by a Fan Housing and Its Nearby Connected Ductwork**

Octave Frequency Band (Hz)	Value Subtracted from In-Duct Fan PWL (dB)
31	—
63	0
125	0
250	5
500	10
1000	15
2000	20
4000	22
8000	25

**Table 12 Sound Pressure Levels in dB at 3-ft (0.9-m) Distance for Air Compressors**

Octave Frequency Band (Hz)	Sound Pressure Level (dB)		
	Air Compr. Power (kW)		
	0.75–1.5	2–6	7–50
31	82	87	92
63	81	84	87
125	81	84	87
250	80	83	86
500	83	86	89
1000	86	89	92
2000	86	89	92
4000	84	87	90
8000	81	84	87
Overall	93	96	99
A-weighted	91	94	97

the sound pressure level of the generator is not significant with respect to the driver. Typically, each engine type has three sound sources of interest: the engine casing, the air inlet, and the engine exhaust.

**Reciprocating Engines** The overall  $L_W$  radiated by the casing of a natural-gas or diesel reciprocating engine is given by

$$L_W = 93 + 10 \log(\text{rated kW}) + A + B + C + D \quad (11)$$

where  $L_W$  is the overall sound power level (dB), “rated kW” is the engine manufacturer’s continuous full-load rating for the engine, and  $A$ ,  $B$ ,  $C$ , and  $D$  are correction terms given in Table 13.

Octave band sound power levels for the casing can be obtained by subtracting Table 14 values from the overall  $L_W$  given by Eq. (11) together with any the modifications of Table 13.

Most large engines have turbochargers at their inlet to provide pressurized air into the engine for increased

**Table 13 Correction Terms Applied to Eq. (11) for Estimating Overall PWL of Casing Noise of Reciprocating Engine**

<b>Speed correction term A</b>	dB
Under 600 rpm	–5
600–1500 rpm	–2
Above 1500 rpm	0
<b>Fuel correction term B</b>	
Diesel fuel only	0
Diesel and natural gas	0
Natural gas only (including small amount of “pilot oil”)	–3
<b>Cylinder arrangement term C</b>	
In-line	0
V-type	–1
Radial	–1
<b>Air intake correction term D</b>	
Unducted air inlet to unmuffled roots blower	+3
Ducted air from outside the room or into muffled roots blower	0
All other inlets to engine (with or without turbocharger)	0

**Table 14 Frequency Adjustments in dB for Casing PWL of Reciprocating Engines**

Octave Frequency Band (Hz)	Value Subtracted from Overall PWL (dB)			
	Engine Speed under 600 rpm	Engine Speed 600–1500 rpm		Engine Speed over 1500 rpm
		Without Roots Blower	With Roots Blower	
31	12	14	22	22
63	12	9	16	14
125	6	7	18	7
250	5	8	14	7
500	7	7	3	8
1000	9	7	4	6
2000	12	9	10	7
4000	18	13	15	13
8000	28	19	26	20
A-weighted	4	3	1	2



**Table 15 Frequency Adjustments (in dB) for Turbocharger Air Inlet**

Octave Frequency Band (Hz)	Value Subtracted from Overall PWL (dB)
31	4
63	11
125	13
250	13
500	12
1000	9
2000	8
4000	9
8000	17
A-weighted	3

performance. Turbine configuration and noise output can vary appreciably, but an approximation of the  $L_W$  for the turbocharged inlet is given by

$$L_W = 95 + 5 \log(\text{rated kW}) - \frac{L}{1.8} \quad (12)$$

where  $L_W$  and “rated kW” are as previously defined, and  $L$  is the length, in metres, of a ducted inlet to the turbocharger. The octave band adjustments given in Table 15 are subtracted from the overall  $L_W$  of Eq. (12) to obtain the octave band sound power levels of turbocharged inlet noise.

The sound power level of the noise radiated from the unmuffled exhaust of an engine is given by

$$L_W = 120 + 10 \log(\text{rated kW}) - T - \frac{L}{1.2} \quad (13)$$

where  $T$  is the turbocharger correction term ( $T = 0$  dB for an engine without a turbocharger and  $T = 6$  dB for an engine with a turbocharger), and  $L$  is the length, in metres, of the exhaust pipe. The octave band sound power levels of unmuffled exhaust noise are obtained by subtracting the values of Table 16 from the overall

**Table 16 Frequency Adjustments (in dB) for Unmuffled Engine Exhaust PWL**

Octave Frequency Band (Hz)	Value Subtracted from Overall PWL (dB)
31	5
63	9
125	3
250	7
500	15
1000	19
2000	25
4000	35
8000	43
A-weighted	12

$L_W$  derived from Eq. (13). If the engine is equipped with an exhaust muffler, the final noise radiated from the end of the tailpipe is the  $L_W$  of the unmuffled exhaust minus the insertion loss of the muffler.

**Small Gas Turbine** As with reciprocating engines, the three principal sound sources of turbine engines are the engine casing, the air inlet, and the exhaust. All gas turbine manufacturers can provide sound power level estimates for each of these sources.

## 2.8 Electric Motors<sup>1</sup>

Electric motors used in commercial building are usually either a total enclosed fan-cooled (TEFC) motor or an open drip-proof motor (DRPR):

**TEFC Motors** The normalized unweighted sound pressure levels for TEFC motors follow approximately the following relationships:

$$L_p = 17 + 17 \log \text{ kW} + 15 \log \text{ rpm} \quad (14)$$

for power ratings under 37 kW, and

$$L_p = 28 + 10 \log \text{ kW} + 15 \log \text{ rpm} \quad (15)$$

for power ratings above 37 kW, where “kW” is the nameplate motor range and rpm (revolutions/minute) is the motor shaft speed. For motors above 300 kW, the calculated noise value for a 300-kW motor should be used. Equation (15) is not applicable to large commercial motors in the power range of 750 to 4000 kW. The octave band adjustments for TEFC motors are given in Table 17. Some TEFC motors produce strong tonal sounds in the 500-, 1000-, or 2000-Hz octave bands because of the cooling fan blade frequency. The octave band frequency adjustments of Table 17 allow for a moderate amount of these tones, but a small percentage of motors may still exceed these calculated levels by as much as 5 to 8 dB. When specified, motors that are quieter than these calculated values by 5 to 10 dB can be purchased.

**Table 17 Frequency Adjustments (in dB) for TEFC Electric Motors**

Octave Frequency Band (Hz)	Value Subtracted from Overall (dB)
31	14
63	14
125	11
250	9
500	6
1000	6
2000	7
4000	12
8000	20
A-weighted	1

**Table 18 Frequency Adjustments (in dB) for DRPR Electric Motors**

Octave Frequency Band (Hz)	Value Subtracted from Overall (dB)
31	9
63	9
125	7
250	7
500	6
1000	9
2000	12
4000	18
8000	27
A-weighted	4

**DRPR Motors** The normalized unweighted sound pressure levels for DRPR motors follow approximately the following relationships

$$L_p = 12 + 17 \log \text{kW} + 15 \log \text{rpm} \quad (16)$$

for power ratings under 37 kW, and

$$L_p = 23 + 10 \log \text{kW} + 15 \log \text{rpm} \quad (17)$$

for power ratings above 37 kW. For motors above 300 kW, the calculated noise value for a 300-kW motor should be used. The octave band adjustments for DRPR motors are given in Table 18.

## 2.9 Steam Turbines<sup>1</sup>

Steam turbines are sometimes used as primary or backup drivers for chillers, pumps, and air compressors. The noise levels of steam turbines are found generally to increase with increasing power rating, but it has not been possible to attribute any specific noise characteristics with speed or turbine blade passage frequency. Suggested normalized sound pressure

levels for steam turbines, with a power range of 370 to 11,000 kW, are given in Table 19.

## 2.10 Transformers<sup>1</sup>

Transformer manufacturers commonly provide an average A-weighted sound pressure level for their products. Typically, this is an average of the sound pressure levels, on a reference sound producing surface space at a distance of 0.3 m from the outline of the transformer. On the basis of field studies of many transformer installations, the sound power level in octave bands has been related to the average A-weighted sound pressure level and the area of the four side walls of the unit. This relationship is expressed by

$$L_W = \text{average } L_{pA} + 10 \log A + C + 10 \quad (18)$$

where  $A$  is the total surface of the four side walls of the transformer in the square metres and  $C$  is an octave band correction that has different values for different uses, as shown in Table 20. If the exact dimensions of the transformer are not known, an approximation will suffice. If in doubt, the area should be estimated on the high side. An error of 25% in area will produce a change of 1 dB in the sound power level. The most nearly applicable  $C$  value from Table 20 should be used. The  $C_1$  value assumes normal radiation of sound. The  $C_2$  value should be used in regular-shaped confined spaces where standing waves will likely occur, which typically may produce 6 dB higher sound pressure levels at the transformer harmonic frequencies of 120, 240, 360, 480, and 600 Hz (for 60-Hz line frequency; or other sound frequencies for other line frequencies). The  $C_3$  value is an approximation of the noise of a transformer that has grown noisier (by about 10 dB) during its lifetime. This happens occasionally when the laminations or tie bolts become loose, and the transformer begins to buzz or rattle. In a highly critical location, it would be wise to use this value. Field measurements have shown that transformers may actually have A-weighted sound pressure levels that range from a few decibels (2 or 3 dB) above to as much as 5 or 6 dB below the quoted

**Table 19 Normalized Sound Pressure Levels for Steam Turbines**

Octave Frequency Band (Hz)	Sound Pressure Level (dB)		
	Steam Turbine Power [hp (kW)]		
	500–1500 (373–1119)	1501–5000 (1120–3730)	5001–15,000 (3731–11,190)
31	86	88	90
63	91	93	95
125	91	93	95
250	88	90	92
500	85	87	89
1000	85	88	91
2000	87	91	95
4000	84	88	92
8000	76	81	86
Overall	97	99	102
A-weighted	92	95	99

**Table 20 Octave Band Corrections for Transformers**

Octave Frequency Band (Hz)	Octave Band Corrections (dB)		
	$C_1^a$	$C_2^b$	$C_3^c$
31	-11	-11	-11
63	-5	-2	-2
125	-3	+3	+3
250	-8	-2	+2
500	-8	-2	+2
1000	-14	-11	-4
2000	-19	-19	-9
4000	-24	-24	-14
8000	-31	-31	-21

<sup>a</sup> Use  $C_1$  for outdoor location or for indoor location in a large mechanical room (over 140 m<sup>3</sup>) containing many other pieces of mechanical equipment that serve as obstacles to diffuse sound and breakup standing waves.

<sup>b</sup> Use  $C_2$  for indoor locations in transformer vaults or small rooms (under 140 m<sup>3</sup>) with parallel walls and relatively few other large-size obstacles that can diffuse sound and breakup standing waves.

<sup>c</sup> Use  $C_3$  for any location where a serious noise problem would result if the transformer should become noisy following its installation and initial period of use

A-weighted sound pressure level. Quieted transformers that contain various forms of noise control treatments can be purchased at as much as 15 to 20 dB below normal A-weighted ratings.

### 3 PROPAGATION OF AIRBORNE NOISE FROM MECHANICAL EQUIPMENT ROOMS

The analysis of the impact of mechanical equipment, on surrounding spaces is relatively straightforward.<sup>5</sup> Once the sound pressure level within the mechanical equipment room has been established, the degree of transmission to adjacent spaces can be determined with knowledge of the transmission loss properties of the walls, floor, and ceiling of the mechanical room and the acoustical properties of the adjacent room.

#### 3.1 Transmission Loss of Mechanical Room Partitions

Transmission loss data for different partitions can be found in many publications. As a general rule this information is derived from laboratory measurements (e.g., ASTM E90-04).<sup>6</sup> However, due to measurement limitation, transmission loss data below 100 Hz is rarely reported. Large mechanical equipment will often produce significant acoustic energy below 100 Hz. Therefore, there is a need to obtain transmission loss performance below 100 Hz, or alternatively, estimate the low-frequency performance. Quite often a single-number rating, such as the sound transmission class (STC) is provided. However, most of these single-number classifications are heavily weighted toward the 500- to 2000-Hz frequency range. While this range is suitable for the evaluation of isolation for speech, some music, and most transportation noise sources,

it is not suitable for the evaluation of mechanical equipment noise sources. An alternative rating called the mechanical transmission class (MTC) may be used for rating partition transmission loss for mechanical equipment. The determination of the MTC is similar to the STC in that it uses the same reference curve and measured one-third octave band transmission loss data. The determination of the MTC rating differs from the determination of the STC rating in that:

1. No deficiencies are allowed in the 125- and 160-Hz one-third octave bands.
2. Moreover, if there are any surpluses above the STC contour in the 125- and 160-Hz one-third octave bands, the rating is increased by one-third of the sum of the surpluses.

Studies have indicated that, when the A-weighted sound pressure level within the mechanical equipment room is less than the sum of the MTC rating of the partition and the room criterion (RC) rating of the background sound within the adjacent room, the intrusive noise should be acceptable. MTC ratings are useful as a cursory evaluation technique. Final selection of partition types should be based on a more complete analysis (e.g., octave or one-third octave band analysis).

#### 3.2 Openings in Walls

An opening, such as a door, window, or louvered vent, in an exterior wall of a noisy room will allow noise to escape from that room and perhaps be disturbing to neighbors. The sound power of the sound that passes through the opening can be estimated from

$$L_W = L_p + 10 \log A \quad (19)$$

where  $L_p$  is the sound pressure level in the room at the location of the opening and  $A$  is the area, in square metres, of the opening. For normal openings (windows or vents) without ducted connections to the noise source, it may be assumed that the sound radiates freely in all directions in front of the opening.

### 4 VIBRATION ISOLATION OF MECHANICAL EQUIPMENT<sup>1</sup>

If mechanical equipment is not provided with proper vibration isolation, acoustic energy will be transmitted into the supporting structure resulting in unwanted vibration and structure-borne sound. The isolator types and isolation guidelines presented in this chapter are based on experience with successful installation of mechanical equipment in commercial buildings.

#### 4.1 Isolator Types and Transmissibility

A transmissibility curve is often used to indicate the general behavior of a vibration-isolated system. Transmissibility is roughly defined as the ratio of the force transmitted through the isolated system to the supporting structure to the driving force exerted by the piece of vibrating equipment. Strict interpretation

**Table 21 Suggested Schedule for Estimating Relative Vibration Isolation Effectiveness of a Mounting System**

Ratio of Driving Frequency of Source to Natural Frequency of Mount	Degree of Vibration Isolation
Below 1.4	Amplification
1.4–3	Negligible
3–6	Low
6–10	Fair
Above 10	High

of transmissibility data and isolation efficiencies, however, must be adjusted for real-life situations. Usually, floors that have large column spacing will have larger deflections than floors of shorter column spacing.

The *static deflection* (SD) of a mount is simply the difference between the free-standing height of the uncompressed, unloaded isolator and the height of the compressed isolator under its static load. This difference is easily measured in the field or estimated from the manufacturer's catalog data. For this reason it is often most beneficial to specify the static deflection for the vibration isolation system, taking into account the type of isolator, the linearity of the isolator system, and the rigidity of the structure of the equipment base and supporting structure.

Table 21 provides a suggested schedule for achieving various degrees of vibration isolation in normal construction. This table is based on the transmissibility curve but suggests operating ranges of the ratio of driving frequency to natural frequency ( $f_n$ ) as define by

$$f_n = 15.77 \sqrt{\frac{1}{SD}} \quad (20)$$

where SD is in millimetres.

The terms *low*, *fair*, and *high* are merely word descriptors, but they are more meaningful than such terms as 95 or 98% isolation efficiency, which are clearly erroneous if they do not take into account the mass and stiffness of the floor slab. Vibration control recommendations given in this chapter are based on the application of this table. Table 22 lists the principal types of vibration isolators used in the isolation of building mechanical equipment and their general range of applications:

**Steel Spring Isolators** Steel springs are used to support heavy equipment and to provide isolation for the typical low-frequency range of about 3 to 60 Hz (180- to 3600-rpm shaft speed). Steel springs have natural frequencies that fall in the range of about 1 Hz (for approximately 254-mm static deflection) to about 6 Hz (for approximately 6-mm static deflection). Springs can transmit high-frequency vibrational energy. For this reason springs are often used in series

with a neoprene, compressed glass fiber, or cork-pad-type isolator when used to support equipment directly over critical locations in a building. Unhoused “stable” steel springs have a diameter that is about 0.8 to 1.2 times their compressed height. They have a horizontal stiffness that is approximately equal to their vertical stiffness; therefore, they do not have a tendency to tilt sideways when a vertical load is applied.

**Neoprene-in-Shear Isolators** Neoprene is a long-lasting material that, when properly shaped, can provide good vibration isolation for the conditions shown in Table 22. The mount usually has an interior hollow space that is conically shaped. The total effect of the shaping is that for almost any direction of applied load, there is a shearing action on the cross section of neoprene. A solid block of neoprene in compression is not effective as a vibration isolator. Manufacturers' catalogs will show the upper limit of load-handling capability of neoprene-in-shear mounts. Two neoprene-in-shear mounts are sometimes constructed in series in the same supporting bracket to provide additional static deflection. This is the double-deflection mount referred to in Table 22.

**Compressed Glass Fiber** Blocks of compressed glass fiber serve as vibration isolators when properly loaded. The manufacturers have several different densities available for a range of loading conditions. Typically, a block is about 50 mm thick and has an area of about 60 to 130 cm<sup>2</sup>, but other dimensions are available. These blocks attenuate high-frequency structure-borne noise, and they are often used alone, at various spacings, to support floating concrete floor slabs. The manufacturer's data should be used to determine the density and area of a block required to achieve the desired static deflection. Unless otherwise indicated, a static deflection of about 5 to 10% of the uncompressed height is normal. With longtime use, the material may compress an additional 5 to 10% of its height. This gradual change in height must be kept in mind during the designing of floating floors to meet floor lines of structural slabs.

**Ribbed Neoprene Pads** Neoprene pads with ribbed or waffle pattern surfaces are effective as high-frequency isolators. In stacks of 2 to 4 layers, with each layer separated by a metal plate, they are also used for vibration isolation of low-power rotary equipment. The pads are usually about 6 to 10 mm thick, and they compress by about 20% of their height when loaded at about 140 to 350 kPa. Higher durometer pads may be loaded up to about 700 kPa. The pads are effective as isolators because the ribs provide some shearing action, and the spaces between the ribs allow lateral expansion as an axial load is applied. The manufacturer's literature should be used for proper selection of the material (load-deflection curves, durometer, surface area, height, etc.).

**Felt Pads** Felt strips or pads are effective for reducing structure-borne sound transmission in the mounting of piping and vibrating conduit. One or more

**Table 22 General Types of Applications of Vibration Isolators<sup>a</sup>**

Isolator Type	Typical Range of Static Deflection (mm)	Approx. Range of Natural Frequency (Hz)	Vibration Isolation Applications, Nonspecific			
			Noncritical Locations <sup>b</sup>		Critical Locations <sup>b</sup>	
			Rotary Equipment	Reciprocating Equip.	Rotary Equipment	Reciprocating Equip.
Steel spring <sup>c</sup>	6–250	6 to 1	Yes	Yes	Yes	Special <sup>d</sup>
Neoprene-in-shear, double deflection	6–13	6 to 4	Yes	Yes	Yes	No <sup>e</sup>
Neoprene-in-shear, single deflection	2.5–6	10 to 6	Yes	Yes	Yes	No <sup>e</sup>
Block of compressed glass fiber, 2-in. (50-mm) thickness <sup>f</sup>	0.5–4	20 to 8	Yes	No	Yes	No
Neoprene pad, rib or waffle pattern, 1–4 layers <sup>f</sup>	0.5–6	20 to 6	Yes	No	Yes	No
Felt or cork pads or strips	0.25–2.5	30 to 10	See text for applications and limitations.			
Air spring	—	10 to 1	See text for applications and limitations.			

<sup>a</sup>See text for additional information on isolator types and specific equipment installations.

<sup>b</sup>Critical locations are those that should have a noise level of NC 35 or lower and noncritical locations are those that can allow a noise level of NC 40 or higher.

<sup>c</sup>Always use pad-type isolator in series with spring to control high-frequency structure-borne noise in critical locations.

<sup>d</sup>Special design required for reciprocating equipment at critical locations, especially for low speeds.

<sup>e</sup>Not normally recommended for this application but can be adapted as special design.

<sup>f</sup>May be used alone for relatively high-speed rotary equipment or in series with steel springs in critical locations for reduction of high-frequency structure-borne noise. Not normally used alone for vibration isolation of reciprocating equipment.

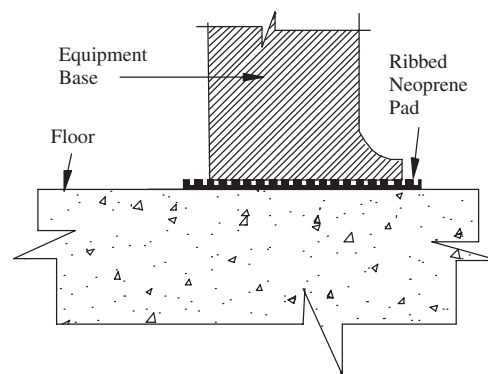
layers of 3- or 6-mm-thick strips should be wrapped around the pipe under the pipe clamps that attach the piping to building structures. Felt pads will compress under long-duration and high-load application and should not be used alone to vibration isolate heavy equipment.

**Air Springs** Air springs are the only practical vibration isolator for very low frequencies, down to about 1 Hz or even lower for special applications. An air mount consists of pressurized air enclosed in a resilient reinforced neoprene chamber. Since the air chamber is subject to slow leakage, a system of air mounts usually includes a pressure sensing system and external air supply. A group of air mounts can be arranged to maintain very precise leveling of a base by automatic adjustment of the pressure in the individual mounts. Specific design and operation data should be obtained from the manufacturer.

#### 4.2 Mounting Assembly Types

In this section, five basic mounting systems are described for the vibration isolation of equipment. These mounting systems are applied to specific types of equipment in Section 4.3.

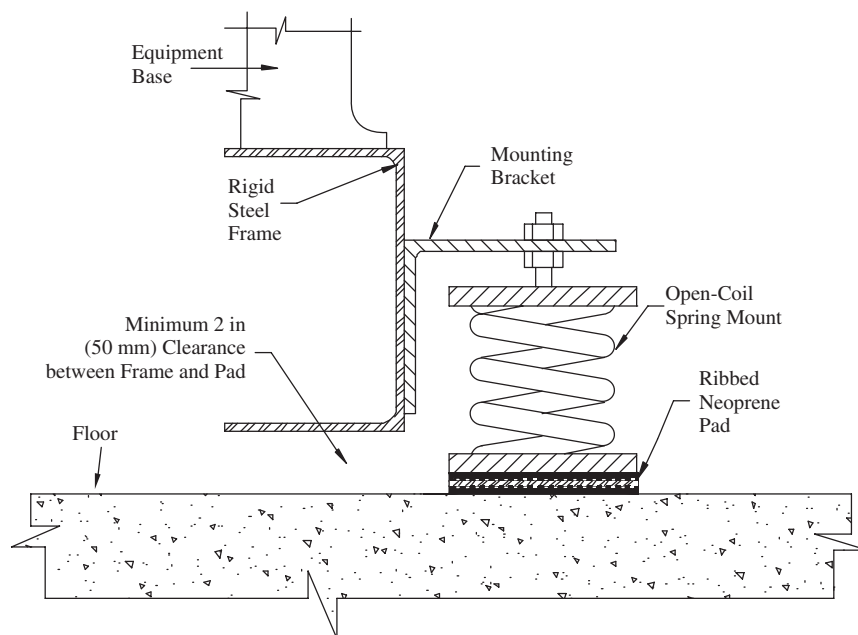
**Type I Mounting Assembly** The equipment should be mounted on an array of *pad mounts*. The pads may be of compressed glass fiber or of multiple layers of ribbed neoprene or waffle pattern neoprene of sufficient height and of proper stiffness to support



**Figure 2** Type I mounting assembly.

the load while meeting the required static deflection (see Fig. 2).

**Type II Mounting Assembly** The equipment or the assembly of equipment should be mounted on a steel frame that is stiff enough to allow the entire assembly to be supported on flexible point supports without fear of distortion of the frame or misalignment of the equipment. The frame should then be mounted on resilient mounts, steel springs, neoprene-in-shear mounts, or isolation pads, as the static deflection would require. If the equipment frame itself already has



**Figure 3** Type II mounting assembly with spring mount.

adequate stiffness, no additional framing is required, and the isolation mounts may be applied directly to the base to the equipment (see Fig. 3).

**Type III Mounting Assembly** This mount is the same as the type I mount in all respects except that the mounting brackets and the top of the steel springs should be located as high as practical on the concrete inertia block but not necessarily as high as the vertical center-of-gravity position of the assembly (Fig. 4). The steel springs can be recessed into pockets in the concrete block, but clearances around the springs should be large enough to assure no contact between any spring and any part of the mounted assembly. Provision must be made to allow positive visual inspection of the spring clearance. When this type of mounting is used for a pump, the concrete inertia block can be given a T-shape plan, and the pipes to and from the pump can be supported rigidly with the pump onto the wings of the T. In this way, the pipe elbows will not be placed under undue stress.

**Type IV Mounting Assembly** The specified equipment should be mounted rigidly on a concrete inertia block. The length and the width of the inertia block should be at least 30% greater than the length and width of the supported equipment. Mounting brackets for stable steel springs should be located off the sides of the inertia block at or near the height of the vertical center of gravity of the combined completely assembled equipment and concrete block. The clearance between the floor and the concrete inertia block shall be at least 100 mm, and provision should be

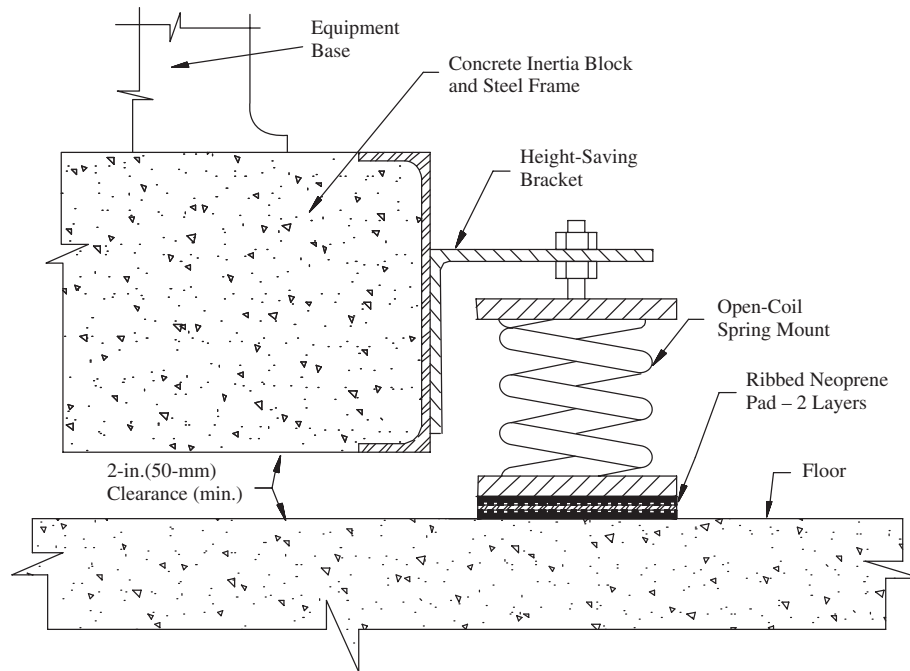
allowed to check this clearance at all points under the block. The inertia block adds stability to the equipment and reduces motion of the equipment (see Fig. 5).

**Type V Mounting Assembly** Large, low-speed propeller-type cooling towers located on roof decks of large buildings may produce serious vibration in the building if adequate vibration isolation is not provided. It is recommended that the entire cooling tower assembly be isolated on stable steel springs similar to the type III mount (see Fig. 4). An alternative is to only isolate the motor and fan only (see Fig. 6); however, this does not prevent water fall noise from entering the structure.

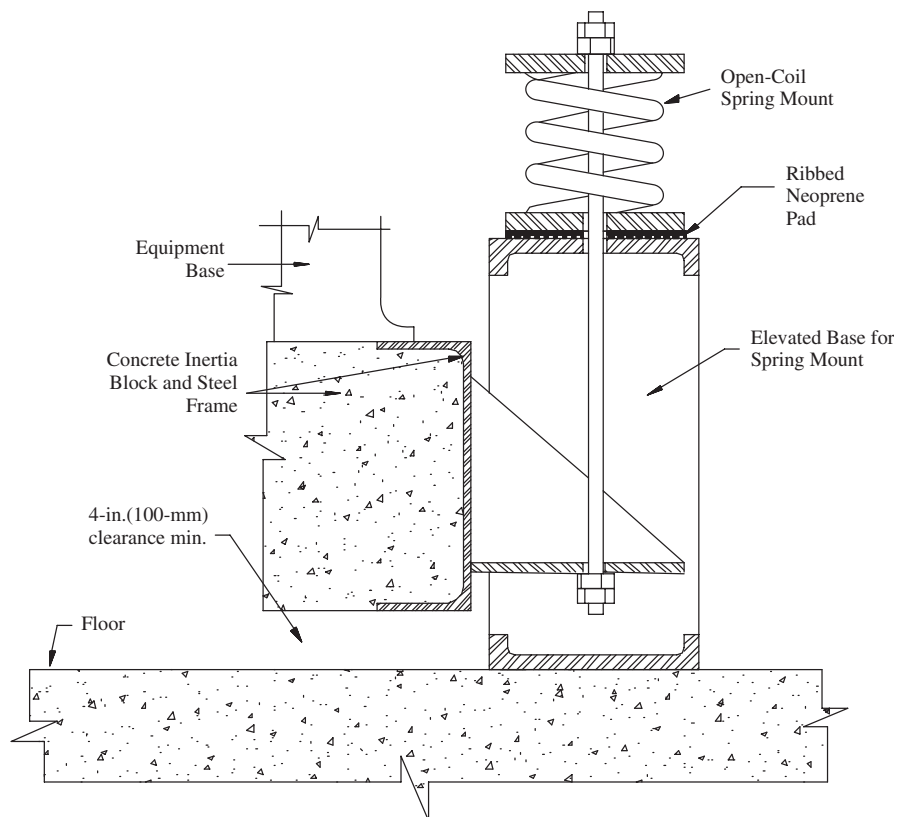
#### 4.3 Tables of Recommended Vibration Isolation Details

Tables 23 to 34 (Ref. 1) provide suggested vibration isolation for the most commonly found mechanical equipment in commercial buildings. A common format is used for all the tables that summarize the recommended vibration isolation details for the various types of equipment. Additional comments follow.

**Centrifugal and Axial-Flow Fans** Ducts should contain flexible connections at both the inlet and discharge of the fans, and all connections to the fan assembly should be clearly flexible. The entire assembly should bounce with little restraint when one jumps up and down on the unit. Large ducts (cross section area over 1.5 m<sup>2</sup>) that are located within about 10 m of the inlet or discharge of a large fan (over 15 kW) should be supported from the floor or ceiling with resilient mounts having a static deflection of at least 6 mm.



**Figure 4** Type III mounting assembly with spring mount.



**Figure 5** Type IV mounting assembly with spring mount.

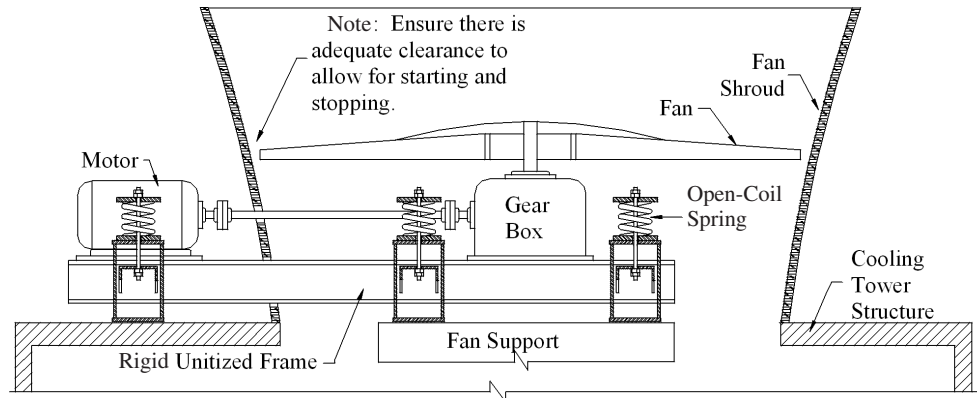


Figure 6 Type V mounting assembly with spring mount.

**Table 23 Recommended Vibration Isolation Mounting Details for Centrifugal and Axial-Flow Fans**

Equipment Conditions			Mounting Recommendations <sup>a</sup>				
Equipment Location	Power Range (kW)	Speed Range (rpm)	Column 1	Column 2	Column 3		
					9 m	12 m	15 m
On grade slab	Under 2.2	Under 600	Vibration isolation not required				
		600–1200					
		Over 1200					
	2.2–18	Under 600	II			25	
		600–1200	II			19	
		Over 1200	II			13	
	19–187	Under 600	II			38	
		600–1200	II			25	
		Over 1200	II			13	
On upper floor above noncritical area	Under 2.2	Under 600	II		25	38	50
		600–1200	II		13	19	25
		Over 1200	II		13	13	19
	2.2–18	Under 600	III	2	25	38	50
		600–1200	II		38	50	75
		Over 1200	II		25	38	50
	19–187	Under 600	III	2	50	75	100
		600–1200	III	2	38	50	75
		Over 1200	III	2	25	38	50
On upper floor above critical area	Under 2.2	Under 600	III	2	38	50	75
		600–1200	II		38	50	75
		Over 1200	II		25	38	50
	2.2–18	Under 600	III	3	50	75	100
		600–1200	III	2	38	50	75
		Over 1200	III	2	25	38	50
	19–187	Under 600	III	3	75	100	100
		600–1200	III	2	50	63	75
		Over 1200	III	2	25	38	50

<sup>a</sup>Column 1: Mounting type (see text).

Column 2: Minimum ratio of weight of inertia block to total weight of supported load. Applies only to mounting types III and IV.

Column 3: Minimum static deflection of stable steel springs (in mm) for indicated floor span (in m).



**Table 24 Recommended Vibration Isolation Mounting Details for Reciprocating Compressor Refrigeration Equipment Assembly (Including Motor, Gear, or Steam Turbine Drive Unit)**

Equipment Conditions			Mounting Recommendations <sup>a</sup>				
Equipment Location	Cooling Capacity (kW)	Speed Range (rpm)	Column 1	Column 2	Column 3		
					9 m	12 m	15 m
On grade slab	35–176	600–900	II			50	
		901–1200	II			38	
		1201–2400	II			25	
	180–616	600–900	III	2–3		50	
		901–1200	II			50	
		1201–2400	II			38	
On upper floor above noncritical area	35–176	600–900	III	2–3	50	75	100
		901–1200	III	2–3	38	50	75
		1201–2400	III	2–3	25	38	50
	180–616	600–900	III	3–4	75	100	125
		901–1200	III	3–4	50	75	100
		1201–2400	III	2–3	50	50	75
On upper floor above critical area	35–176	600–900	III	3–4	75	100	125
		901–1200	III	3–4	50	75	100
		1201–2400	III	2–3	50	50	75
	180–616	600–900	IV	4–6	75	100	125
		901–1200	III	3–5	50	75	100
		1201–2400	III	3–4	50	50	75

<sup>a</sup>Column 1: Mounting type (see text).

Column 2: Minimum ratio of weight of inertia block to total weight of supported load. Applies only to mounting types III and IV.

Column 3: Minimum static deflection of stable steel springs (in mm), for indicated floor span (in m)

**Table 25 Recommended Vibration Isolation Mounting Details for Rotary-Screw Compressor Refrigeration Equipment Assembly (Including Motor Drive Unit)**

Equipment Conditions			Mounting Recommendations <sup>a</sup>				
Equipment Location	Cooling Capacity (kW)	Speed Range (rpm)	Column 1	Column 2	Column 3		
					9 m	12 m	15 m
On grade slab	350–1760	2400–4800	II			25	
On upper floor above noncritical area	350–1760	2400–4800	II		25	38	50
On upper floor above critical area	350–1760	2400–4800	III	2–3	25	38	50

<sup>a</sup>Column 1: Mounting type (see text).

Column 2: Minimum ratio of weight of inertia block to total weight of supported load. Applies only to mounting types III and IV.

Column 3: Minimum static deflection of stable steel springs (in mm) for indicated floor span (in m)

**Reciprocating-Compressor Refrigeration Equipment** These recommendations apply also to the drive unit used with the reciprocating compressor. Pipe connections from this assembly to other equipment should contain flexible connections.

**Centrifugal-Compressor Refrigeration Equipment** The recommended vibration isolation details for this equipment include the drive unit and the condenser and evaporator tanks.

**Boilers** The recommended vibration isolation for boilers is shown on Table 28. This applies for boilers with integrally attached blowers. Table 24 should be followed for the support of blowers that are not directly mounted on the boiler. A flexible connection or a thermal expansion joint should be installed in the exhaust breaching between the boiler and the exhaust stack.

**Motor-Pump Assemblies** Electrical connections to the motors should be made with long “floppy”

**Table 26 Recommended Vibration Isolation Mounting Details for Centrifugal Compressor Refrigeration Equipment Assembly (Including Condenser and Chiller Tanks and Motor, Gear, or Steam Turbine Drive Unit)**

Equipment Conditions			Mounting Recommendations <sup>a</sup>				
Equipment Location	Cooling Capacity (kW)	Speed Range (rpm)	Column 1	Column 2	Column 3		
					9 m	12 m	15 m
On grade slab	350–1,760	Over 3,000	II			19	
	1,761–14,000	Over 3,000	II			25	
	Over 14,000	Over 3,000	II			38	
On upper floor above noncritical area	350–1,760	Over 3,000	II		25	38	50
	1,761–14,000	Over 3,000	II		38	50	75
	Over 14,000	Over 3,000	II		50	75	100
On upper floor above critical area	350–17,60	Over 3,000	II		50	75	100
	1,761–14,000	Over 3,000	II		25	38	50
	Over 14,000	Over 3,000	II		38	50	75

<sup>a</sup>Column 1: Mounting type (see text).

Column 2: Minimum ratio of weight of inertia block to total weight of supported load. Applies only to mounting types III and IV.

Column 3: Minimum static deflection of stable steel springs, (in mm) for indicated floor span (in m).

**Table 27 Recommended Vibration Isolation Mounting Details for Absorption-Type Refrigeration Equipment Assembly**

Equipment Conditions			Mounting Recommendations <sup>a</sup>			
Equipment Location	Cooling Capacity (kW)		Column 1	Column 2	Column 3	
					9 m	15 m
On grade slab	All sizes	I			6	
On upper floor above noncritical area	All sizes	II		13	19	25
On upper floor above critical area	All sizes	II		25	38	50

<sup>a</sup>Column 1: Mounting type (see text).

Column 2: Minimum ratio of weight of inertia block to total weight of supported load. Applies only to mounting types III and IV.

Column 3: Minimum static deflection of stable steel springs (in mm) for indicated floor span (in m)

**Table 28 Recommended Vibration Isolation Mounting Details for Boilers**

Equipment Conditions			Mounting Recommendations <sup>a</sup>			
Equipment Location	Cooling Capacity bhp (kW)		Column 1	Column 2	Column 3	
					9 m	15 m
On grade slab	All sizes			Vibration isolation not required		
On upper floor above noncritical area	Under 200 (Under 1962)	II		3	6	13
	200–1000 (1962–9810)	II		6	13	25
	Over 1000 (Over 9810)	II		6	13	25
On upper floor above critical area	Under 200 (Under 1962)	II		13	25	38
	200–1000(1962–9810)	II		25	38	50
	Over 1000 (Over 9810)	II		25	38	50

<sup>a</sup>Column 1: Mounting type (see text).

Column 2: Minimum ratio of weight of inertia block to total weight of supported load. Applies only to mounting types III and IV.

Column 3: Minimum static deflection of stable steel springs (in mm) for indicated floor span (in m).

**Table 29 Recommended Vibration Isolation Mounting Details for Propeller-Type Cooling Towers<sup>a</sup>**

Equipment Conditions			Mounting Recommendations <sup>b</sup>		
Equipment Location	Power Range (kW)	Speed Range (rpm)	Column 1	Column 3	Notes
On grade slab	All sizes	All speeds			Vibration isolation usually not required.
On upper floor above noncritical area	Under 19	150–300	V	100	Install on dunnage attached to building columns only.
		301–600	V	75	
		Over 600	V	75	
	19–112	150–300	V	150	Springs may be located under drive assembly or under entire tower base.
		301–600	V	100	
		Over 600	V	75	
	Over 112	150–300	V	200	
		301–600	V	125	
		Over 600	V	100	
On upper floor above critical area	Same as for location above noncritical area, except install several layers of ribbed or waffle pattern neoprene pads between tower base and building support structure.				

<sup>a</sup>Where several towers are placed at the same general location, the power range for total power of all towers should be used.

<sup>b</sup>Column 1: Mounting type (see text).

Column 2: Minimum ratio of weight of inertia block to total weight of supported load. Applies only to mounting types III and IV.

Column 3: Minimum static deflection of stable steel springs (in mm) for indicated floor span (in m)

**Table 30 Recommended Vibration Isolation Mounting Details for Centrifugal-Fan Cooling Towers<sup>a</sup>**

Equipment Conditions			Mounting Recommendations <sup>b</sup>				
Equipment Location	Cooling Capacity (kW)	Speed Range (rpm)	Column 1	Column 2	Column 3		
					9 m	12 m	15 m
On grade slab	All sizes	All speeds			Vibration isolation usually not required.		
On upper floor above noncritical area	Under 19	450–900	II		25	38	50
		901–1800	II		19	25	38
		Over 1800	II		19	25	38
	19–112	450–900	II		38	50	75
		901–1800	II		25	38	50
		Over 1800	II		19	25	38
	Over 112	450–900	II		50	75	100
		901–1800	II		38	50	75
		Over 1800	II		25	38	50
On upper floor above critical area	Under 19	450–900	II <sup>c</sup>		38	50	75
		901–1800	II <sup>c</sup>		25	38	50
		Over 1800	II <sup>c</sup>		19	25	38
	19–112	450–900	II <sup>c</sup>		50	75	100
		901–1800	II <sup>c</sup>		38	50	75
		Over 1800	II <sup>c</sup>		25	38	50
	Over 112	450–900	II <sup>c</sup>		75	100	125
		901–1800	II <sup>c</sup>		38	50	75
		Over 1800	II <sup>c</sup>		25	38	50

<sup>a</sup>Power is total of all fans at the same general location. Install on dunnage or on thick concrete roof slab.

<sup>b</sup>Column 1: Mounting type (see text).

Column 2: Minimum ratio of weight of inertia block to total weight of supported load. Applies only to mounting types III and IV.

Column 3: Minimum static deflection of stable steel springs (in mm) for indicated floor span (in m).

<sup>c</sup>Include ribbed or waffle pattern neoprene between tower and building.

**Table 31 Recommended Vibration Isolation Mounting Details for Motor-Pump Assemblies**

Equipment Conditions			Mounting Recommendations <sup>a</sup>				
Equipment Location	Power range (kW)	Speed Range (rpm)	Column 1	Column 2	Column 3		
					9 m	12 m	15 m
On grade slab	Under 15	450–900	Vibration isolation usually not required for acoustic purposes.				
		901–1800					
		Over 1800					
	15–75	450–900	III	2–3		38	
		901–1800	III	1–2		25	
		Over 1800	III	1–2		19	
	Over 75	450–900	III	2–3		50	
		901–1800	III	2–3		38	
		Over 1800	III	1–2		25	
On upper floor above noncritical area	Under 15	450–900	III	2–3	38	50	75
		901–1800	III	1–2	25	38	50
		Over 1800	III	1–2	19	25	38
	15–75	450–900	III	2–3	38	50	75
		901–1800	III	2–3	25	38	50
		Over 1800	III	1–2	25	38	50
	Over 75	450–900	III	3–4	50	75	100
		901–1800	III	2–3	38	50	75
		Over 1800	III	2–3	25	38	50
On upper floor above critical area	Under 15	450–900	III	3–4	38	50	75
		901–1800	III	2–3	25	38	50
		Over 1800	III	2–3	19	25	38
	15–75	450–900	III	3–4	50	75	100
		901–1800	III	2–3	38	50	75
		Over 1800	III	2–3	25	38	50
	Over 75	450–900	III	3–4	75	100	125
		901–1800	III	2–3	50	75	100
		Over 1800	III	2–3	38	50	75

<sup>a</sup>Column 1: Mounting type (see text).

Column 2: Minimum ratio of weight of inertia block to total weight of supported load. Applies only to mounting types III and IV.

Column 3: Minimum static deflection of stable steel springs (in mm) for indicated floor span (in m).

**Table 32 Recommended Vibration Isolation Mounting Details for Steam-Turbine-Driven Rotary Equipment, Such as Gear, Generator, or Gas Compressor<sup>a</sup>**

Equipment Conditions			Mounting Recommendations <sup>b</sup>				
Equipment Location	Power range (kW)	Speed Range (rpm)	Column 1	Column 2	Column 3		
					9 m	12 m	15 m
On grade slab	373–1119	Over 3000	II			13	
	1120–3730	Over 3000	II			19	
	Over 3730	Over 3000	II			25	
On upper floor above noncritical area	373–1119	Over 3000	II		25	38	50
	1120–3730	Over 3000	II		38	50	75
	Over 3730	Over 3000	II		50	75	100
On upper floor above critical area	373–1119	Over 3000	III	2–3	25	38	50
	1120–3730	Over 3000	III	2–3	38	50	75
	Over 3730	Over 3000	III	2–3	50	75	100

<sup>a</sup>Use Table 24 for reciprocating compressor driven by steam turbine. Use Table 26 for centrifugal compressor driven by steam turbine.<sup>b</sup>Column 1: Mounting type (see text).

Column 2: Minimum ratio of weight of inertia block to total weight of supported load. Applies only to mounting types III and IV.

Column 3: Minimum static deflection of stable steel springs (in mm) for indicated floor span (in m).

**Table 33 Recommended Vibration Mounting Details for Transformers**

Equipment Conditions		Mounting Recommendations <sup>a</sup>				
Equipment Location	Power Range (kVA)	Column 1	Column 2	Column 3		
				9 m	12 m	15 m
On grade slab	Under 10	I		3	3	3
	10–100	I		3	3	3
	Over 100	I		6	6	6
On upper floor above noncritical area	Under 10	I		3	6	6
	10–100	II		6	6	13
	Over 100	II		6	13	25
On upper floor above critical area	Under 10	II		6	13	19
	10–100	II		13	19	25
	Over 100	Air Spring		See footnote	See footnote	See footnote

<sup>a</sup>Column 1: Mounting type (see text).

Column 2: Minimum ratio of weight of inertia block to total weight of supported load. Applies only to mounting types III and IV.

Column 3: Minimum static deflection of stable steel springs (in mm) for indicated floor span (in m). For air springs the manufacturer should be consulted prior to selection.

**Table 34 Recommended Vibration Isolation Mounting Details for One- and Two-Cylinder Reciprocating-Type Air Compressors between 7.5 kW and 76 kW**

Equipment Conditions			Mounting Recommendations <sup>a</sup>				
Equipment Location	Power Range (kW)	Speed Range (rpm)	Column 1	Column 2	Column 3		
					9 m	12 m	15 m
On grade slab	Under 15	300–600	IV	4–8	100	100	100
		601–1200	IV	2–4	50	50	50
		Over 1200	IV	1–2	25	25	25
	15–75	300–600	IV	6–10	125	125	125
		601–1200	IV	3–6	75	75	75
		Over 1200	IV	2–3	38	38	38
On upper floor above noncritical area	Under 15	300–600	Not recommended for these conditions.				
		601–1200	IV	3–6	100	150	No <sup>b</sup>
		Over 1200	IV	2–3	50	100	No <sup>b</sup>
	15–75	300–600	Not recommended for these conditions.				
		601–1200	Not recommended for these conditions.				
		Over 1200	IV	3–6	75	125	No <sup>b</sup>
On upper floor above critical area	Under 15	300–600	Not recommended for these conditions.				
		601–1200	Not recommended for these conditions.				
		Over 1200	IV	3–6	100	150	No <sup>b</sup>
	15–75	All speeds	Not recommended for these conditions.				

<sup>a</sup>Column 1: Mounting type (see text).

Column 2: Minimum ratio of weight of inertia block to total weight of supported load. Applies only to mounting types III and IV.

Column 3: Minimum static deflection of stable steel springs (in mm) for indicated floor span (in m).

“No” means “Not recommended for these conditions.”

lengths of flexible armored cable, and piping should be resiliently supported. For most situations, a good isolation mounting of the piping will overcome the need for flexible connections in the pipe. An important function of the concrete inertia block (type II mounting) is its stabilizing effect against undue bouncing of the pump assembly at the instant of starting. This gives better longtime protection to the associated piping. These same recommendations may

be applied to other motor-driven rotary devices such as centrifugal-type air compressors and motor-generator sets in the power range up to a few hundred kilowatts.

**Steam Turbines** Table 32 provides a set of general isolation recommendations for steam-turbine-driven rotary equipment, such as gears, generators, or centrifugal-type gas compressors. The material given in Table 26 applies when a steam turbine is used to drive centrifugal-compressor refrigeration equipment.

The recommendations given in Table 24 apply when a steam turbine is used to drive reciprocating-compressor refrigeration equipment or reciprocating-type gas compressors.

**Gears** When a gear is involved in a drive system, vibration isolation should be provided in accordance with recommendations given for either the main power drive unit or the driven unit, whichever imposes the more stringent isolation conditions.

**Transformers** Power leads to and from the transformers should be as flexible as possible. In outdoor locations, earth-borne vibration to nearby neighbors is usually not a problem, so no vibration isolation is suggested. If vibration should become a problem, the transformer could be installed on neoprene or compressed glass fiber pads having 6-mm static deflection.

**Air Compressors** Recommended mounting details for centrifugal-type air compressors of less than 75 kW are the same as those given for motor-pump units in Table 31. The same recommendations would apply for small (under 8 kW) reciprocating-type air compressors. For reciprocating-type air compressor (with more than two cylinders) in the 8-kW to 37-kW range, the recommendations given in Table 24 apply for the particular conditions. For 8 kW to 80 kW, one- or two-cylinder, reciprocating-type air compressors, the recommendations of Table 34 apply. This equipment is a potentially serious source of low-frequency vibration in a building if it is not isolated. In fact, the compressor should not be located in certain parts of the building, even if it is vibration isolated. When these compressors are used, all piping should contain flexible connections, and the electrical connections should be made with flexible armored cable.

#### 4.4 Vibration Isolation: Miscellaneous

It is good practice to isolate all piping in the mechanical equipment room that is connected to vibrating equipment with resilient ceiling hangers or from floor-mounted resilient supports. As a general rule, the first three pipe supports nearest the vibrating equipment should have a static deflection of at least one-half the static deflection of the mounting system used with that equipment. Beyond the third pipe support, the static deflection can be reduced to 6 or 12 mm for the remainder of the pipe run in the mechanical equipment room. When a pipe passes through the mechanical equipment room wall, a minimum 25-mm clearance should be provided between the pipe and the hole in the wall. The pipe should be supported on either side of the hole, so that the pipe does not rest on the wall. The clearance space should then be stuffed with fibrous filler material and sealed with a nonhardening caulking compound at both wall surfaces. Vertical pipe chases through a building should not be located beside acoustically critical areas. If they are located beside critical areas, pipes should be resiliently mounted from the walls of the pipe chase for a distance of at least 3 m beyond each such area, using both low-frequency

and high-frequency isolation materials. Pipes to and from the cooling tower and the associated mechanical equipment room should be resiliently supported for their full length between the cooling tower and the associated mechanical equipment room. Steam pipes should be resiliently supported for their entire length of run inside the building. Resilient mounts should have a static deflection of at least 12 mm.

Whenever a steel spring isolator is used, it should be in series with a neoprene isolator. For ceiling hangers, a neoprene washer or grommet should also be included; and if the pipe hangers are near a very critical area, the hanger should be a combination hanger that contains both a steel spring and a neoprene-in-shear mount. During inspection, the hanger rods should be checked to ensure they are not touching the sides of the isolator housing and thereby shorting-out the spring.

To be at all effective, a flexible pipe connection should have a length that is approximately 6 to 10 times its diameter. Tie rods should not be used to bolt the two end flanges of a flexible connection together. Flexible connections are either of the bellows type or are made up of wire-reinforced neoprene piping, sometimes fitted with an exterior braided jacket to confine the neoprene.

When a mechanical equipment room is located directly over or near a critical area, it is usually desirable to isolate most of the "nonvibrating equipment" with a simple mount made up of one or two pads of neoprene or a 25- or 50-mm layer of compressed glass fiber. Heat exchangers, hot water heaters, water storage tanks, large ducts, and some large pipe stands may not themselves be noise sources, yet their pipes or their connections to vibrating sources transmit small amounts of vibrational energy that they then may transmit into the floor. A simple minimum isolation pad will usually prevent this noise transfer.

#### REFERENCES

1. *Noise and Vibration Control for Mechanical Equipment*, Army Manual TM 5-805-4, Headquarters Department of Army, The Air Force and Navy, Washington, DC, 1983.
2. ASHRAE, *HVAC Systems and Equipment*, American Society of Heating, Refrigerating and Air-Conditioning Engineers, Atlanta, GA, 2004.
3. J. B. Graham and R. M. Hoover, Fan Noise, in *The Handbook of Acoustical Measurements and Noise Control*, 3rd ed., C. M. Harris, Ed., Acoustical Society of America, Melville, NY, 1998.
4. W. E. Blazier, D. A. Towers, and N. P. Miller of Bolt Beranek and Newman Inc., Development of a Mechanical Equipment Noise-Control Permit Scheme for Model Building Code (draft, September 1977), prepared for U.S. Environmental Protection Agency (BBN Report 3566), 1977.
5. ASHRAE, *HVAC Applications*, American Society of Heating, Refrigerating and Air-Conditioning Engineers, Atlanta, GA, 2003.
6. ASTM, *Standard Test Method for Laboratory Measurement of Airborne Sound Transmission Loss of Building Partitions and Elements*, ASTM E90-04, American Society for Testing and Materials, West Conshohocken, PA, 2004.

# CHAPTER 113

## NOISE CONTROL IN U.S. BUILDING CODES

Gregory C. Tocci  
Cavanaugh Tocci Associates, Inc.  
Sudbury, Massachusetts

### 1 INTRODUCTION

The purpose of this chapter is to provide an overview of building codes in the United States. Building codes in Europe are covered in Chapter 114. These are covered separately as the origination and applicability of noise control provisions in U.S. building codes are different from those of Europe. Generally speaking, U.S. building codes are developed and promoted by private organizations and adopted by jurisdictions as determined by state law. Yet, not all jurisdictions have building codes or noise control provisions. A few larger cities have developed their own codes with provisions that differ from codes of their home states.

Nevertheless, building codes set standards of quality and uniformity for all aspects of building construction. Building codes have been in use since before the 1900s. Since the development of a comprehensive code covering all aspects of building construction exceeded the technical abilities of most cities, even large cities, several organizations were formed between 1920 and 1940 to serve the needs of building regulators in cities and towns. A large part of the work of these organizations was to develop model building codes that could be used by participating localities and states. Unlike Europe, where building codes have been developed and enforced by governmental agencies, building codes in the United States have been developed by organizations of building officials and adopted as law as appropriate by jurisdictions. At the close of the twentieth century, there were three main building code organizations that represented most U.S. jurisdictions. These were as follows:

- Building Officials and Code Administrators International (BOCA).
- International Conference of Building Officials (ICBO).
- Southern Building Code Congress International (SBCCI)

In the latter part of the 1990s, these three organizations merged to form the International Code Council (ICC). It was the objective of the ICC to assemble a new model code from portions of the BOCA, ICBO, and SBCCI model codes. In so doing, it has created separate model codes for buildings (architectural and structural), mechanical systems, plumbing systems, fire, and electrical. Noise provisions in the original three codes fit into the building (architectural and structural) codes. It was the decision of the ICC to adopt the BOCA provisions for noise in buildings

and omit adopting any of the existing provisions from both the ICBO and the SBCCI model codes. All three of the former model codes were discussed in detail in the *Encyclopedia of Acoustics*.<sup>1</sup>

The International Building Code (IBC), as with its predecessor codes, is available for adoption in whole or in part, and/or amended by jurisdictions. Most often, these jurisdictions are state legislatures, but sometimes they are county governments or smaller jurisdictions.

The federal government does not require states or localities to have building codes. Federal agencies use their own building codes or use the IBC for their own projects. The International Code Council is a private organization and has as its membership building code officials. The ICC serves its membership by producing bodies of code that are adopted by states and localities and administered by the membership. Hence, a large part of the activity of ICC is to educate its membership in code practices and enable them to make judgments regarding the conformance of building construction to code requirements.

There are many jurisdictions in the United States that do not have building codes. Others have their own building code, for example, New York City and Chicago. Each state determines whether it will adopt the building code on a statewide basis or leave it to the localities to make the decision whether or not to adopt a building code. The noise control provisions of the IBC are contained in Chapter 12 of the code as discussed below. Changes and additions to the IBC noise provisions adopted by California are discussed as examples of the wide latitude in changes that jurisdiction may take. However, it is unusual for jurisdictions to make changes or omit in whole noise control provisions of the IBC. For comparison, the noise control provisions of the New York City building code are also described later in this chapter.

### 2 TYPES OF NOISE LIMITS

Noise ordinances, regulations, criteria, and standards are promulgated by jurisdictions to serve the needs of those jurisdictions. Cities and towns publish noise ordinances that appear as part of their town regulations or in their zoning or planning bylaws. These regulations are usually *imission* type regulations in that they typically control environmental sound by limiting sound that a source may produce at a *receptor* location.

*Emission*-type limits set constraints on sound produced by a *source*. Emission limits are more prevalent among agencies setting standards for specific sound-source producing industries. Often, these are expressed using descriptors other than sound pressure

level; for example, sound power level is sometimes used.

Many federal agencies have noise regulations, but these are usually intended only to apply to sources and receptors affected by projects funded by those agencies and are not generally applicable to all projects or facilities. The U.S. Environmental Protection Agency (U.S. EPA) has not set general environmental sound pressure level limits but has identified sound pressure levels that protect public health and welfare with a margin of safety and has set limits on specific types of equipment such as trucks and air compressors.

U.S. building codes are intended to set standards to ensure construction quality. Most prevalent among these are lower limits on the sound isolation performance of sound-isolating constructions. The implication is that building codes tend to be imission-type standards. This is true of the IBC. However, as seen in the New York City building code, emission limits do also appear in some codes as well.

This chapter discusses noise limits that appear in the 2003 IBC model building code.<sup>2</sup> They are limits for which the local building official is obligated to judge as having or having not been met. The local building official is normally not obligated to evaluate conformance of building construction with noise limits that are not part of the building code. For example, a building official may not be explicitly required to evaluate the conformance of noise produced by a rooftop unit at nearby residential property in accordance with a municipal noise limit; however, he or she would have the authority to do so if judged to be prudent by that official.

### 3 NOISE REGULATION FORMAT

Noise regulations share several facets. These are as follows:

1. *Status.* Every standard states whether it is voluntary or obligatory, and, if it is obligatory, under what circumstances individuals or organizations must conform to the standard.
2. *Object.* Every standard is devised to limit sound exposure at a receiver or to limit sound emitted by a source.
3. *Scope.* Every standard will indicate the specific type of noise exposure and condition under which the ordinance is applicable.
4. *Limit.* Every standard expresses its limits either as numerical values for one or more noise descriptors or in some other specific way such as establishing hours of operation or in some subjective manner such as not allowing noise that constitutes an "annoyance."
5. *Evaluation.* Every standard should indicate the means by which conformance can be objectively established.

### 4 INTERNATIONAL BUILDING CODE (IBC)

The following is a detailed discussion of the noise control provisions of the IBC. The full code text

can be obtained from the International Code Council ([www.iccsafe.org](http://www.iccsafe.org)). The noise control provision for sound appears in Section 1207, Sound Transmission. Since the noise control provisions are part of the body of the IBC, its *status* is obligatory; that is, a state or locality that adopts the IBC must include this section on building noise control or pass specific legislation to remove or modify it.

The *object* of IBC Section 1207 is the receiver; that is, it seeks to limit noise at a receptor as opposed to controlling sound emitted by a source. The scope of the code is limited to the sound isolation performance of "all common interior walls, partitions, and floor/ceiling assemblies between adjacent dwelling units or between a dwelling unit and adjacent public areas..." Note that this section of the IBC only addresses sound transmission between dwelling units even though the code covers all types of building construction.

The *scope* of Section 1207 includes the airborne and impact sound isolation performance of constructions separating dwelling units. The airborne sound isolation performance *limit* is expressed as minimum party wall and floor/ceiling sound transmission class (STC) rating of 50, if such rating has been determined on the basis of sound transmission loss measured in a laboratory, or 45 if determined from noise reduction measured in the field. Similarly, the impact sound isolation performance *limit* is expressed as a minimum floor/ceiling impact isolation class (IIC) rating of 50, if such rating has been determined on the basis of impact sound pressure levels produced by an ISO tapping machine and measured in a laboratory, or 45 if determined from tapping machine sound pressure levels measured in the field.

The reference standards imply that the *evaluation* of a building assembly can be made by a building official by comparing proposed or constructed partition and floor/ceiling assemblies with lists of tested assemblies. It specifically references a publication dated 1944, which does not provide STC ratings; however, there are many agency and commercial publications that provide such information. Hence, the code does not explicitly require the involvement of an engineer or some other professional and does not require testing, but permits testing for unrated assemblies or where performance may be in question. Only American Society for Testing and Materials (ASTM) laboratory tests for sound transmission loss and impact isolation are cited. The corresponding ASTM field tests are not cited.

### 5 STATE ADOPTIONS OF IBC NOISE PROVISIONS

#### 5.1 California

States and other jurisdictions sometimes modify code limits and/or formats. This is true of acoustical provisions as well, although it is quite rare. The State of California has made modifications to the IBC on sound transmission by adding provisions to the IBC limits and adding new limits.

The California building code is contained in the California Code of Regulations, Title 24, Part 2,



Volume 1.<sup>3</sup> The California building code section on sound transmission is similar to the IBC section but differs in four ways. First, the California code provides more detail regarding the application of STC and IIC ratings. For example, it provides definitions and lists applicable standards. Second, it expands the application of residential limits to other residential-type spaces such as hotel guest rooms and other residential-type occupancies. Third, it is more specific about how and by whom field testing is to be conducted, and the types of sound isolation descriptors that should be measured. This includes specifying a minimum STC rating of 26 for corridor doors and minimum composite STC rating of 30 for corridor walls with doors. And fourth, it establishes a limit for sound inside residential spaces produced by exterior noise sources such as highway traffic and aircraft.

The California amendment on interior sound pressure level produced by exterior noise is expressed as a day–night average sound pressure level (DNL) not to exceed 45 dB. The standard permits the alternative use of the community noise exposure level (CNEL) and indicates that the interior CNEL sound pressure level must also not exceed 45 dB. The day–night average sound pressure level is the 24-h equivalent sound pressure level with a 10-dB penalty added to sound pressure levels occurring between 10 p.m. and 7 a.m. The community noise exposure level is similar in that it is a 24-h equivalent sound pressure level, but with a 5-dB penalty applied to sound pressure levels occurring between 6 p.m. and 10 p.m., and a 10-dB penalty applied to sound pressure levels occurring between 10 p.m. and 7 a.m. The California code expresses a preference for use of the DNL but permits the use of the CNEL.

A building official responsible for evaluating the conformance of a building with California code sound limits may do so by comparing wall and floor–ceiling assemblies with those assemblies listed in Appendix Chapter 12, Section 1208A.4.2. Or the official can request certification through field testing by an acoustician. The acoustician can judge conformance or nonconformance of a building construction to the code through the use of one or more of the following noise descriptors:

- Noise isolation class (NIC)
- Normalized noise isolation class (NNIC)
- Field impact insulation class (FIIC)
- Normalized A-weighted sound pressure level difference ( $D_n$ )

The NIC, NNIC, and FIIC are defined in ASTM standards. The  $D_n$  is described in Appendix Chapter 12, Section 1208A.4.2 of the California code.

The Appendix Chapter 12 evaluation of interior sound pressure levels requires an acoustical analysis to be conducted before construction if the DNL or the CNEL exceeds 60 dB. The standard also alternatively requires an evaluation report by an acoustician after construction is completed.

## 5.2 New York City

New York City has its own building code and does not reference the IBC or its predecessors; however, it is similar in its requirements to both the IBC and its predecessors. The first modern building code for the City of New York was enacted in 1938. It was replaced by a “new code” in 1968. The noise control provisions of the Building Code of the City of New York are contained in Title 27, Construction and Maintenance, Subchapter 27, Article 9, Noise Control in Multiple Dwellings.<sup>4</sup> The *object* of the city code Article 9 is the receiver. The *scope* of the code includes the sound isolation performance of party walls and floor–ceiling assemblies between dwelling units or between a dwelling units and adjacent public and utility areas.

The airborne sound isolation performance *limit* is a minimum party wall and floor–ceiling STC rating of 50, if such rating has been determined on the basis of sound transmission loss measured in a laboratory, or 48 if determined from noise reduction measured in the field. The code requires that the entrance door to dwelling units have an STC rating of not less than 35. Additionally, the code provides recommendations on the treatment of wall penetrations and the like to avoid compromising airborne sound isolation performance.

The impact sound isolation performance *limit* is expressed as a minimum floor–ceiling impact noise rating (INR) of 50, if such a rating has been determined on the basis of impact sound pressure levels produced by an ISO tapping machine and measured in a laboratory, or –2 if determined from tapping machine sound pressure levels measured in the field. Note that the INR is no longer used and is approximately as follows:

$$\text{INR} \cong \text{IIC} - 51$$

where the INR is the impact noise rating and IIC is the impact isolation class rating.

The reference standards imply that the *evaluation* of a building assembly can be made by a building official by comparing proposed or constructed partition and floor–ceiling assemblies with lists of tested assemblies.

The code also sets limits on sound produced by various building noise sources and provides guidelines for equipment vibration isolation. The only receptor limit provided is that sound produced by exterior building equipment transmitted to inside dwelling units must not exceed NC-35.

The code also limits the amount of sound that building mechanical equipment can produce. It sets limits on the sound power levels in mechanical spaces or shafts adjoining dwelling spaces and sound power produced by exterior mechanical equipment adjoining buildings. Both are expressed as sound power levels in octave bands 63 to 8000 Hz. In the case of exterior equipment located adjacent to other buildings, the permitted sound power levels are also given for various distances between source equipment and receptor buildings.

## 6 COMPARISON OF BUILDING CODES

Table 1 summarizes the provisions of the International Building Code, the California building code Section 1208 on sound transmission control, and the City of New York Subchapter 12, Article 9, on noise control. The provisions of all three codes are similar with respect to airborne sound isolation with some differences as noted.

## 7 GUIDE TO BUILDING NOISE CRITERIA

Conformance with building code requirements for sound isolation does not always ensure that the expectations of occupants of a building will be met. When providing assistance to an architect or owner of a new building, the acoustical consultant must recognize this and be vigilant in identifying those situations where occupants will expect greater building sound isolation performance. It is this author's experience that buildings in which sound isolation complaints have occurred have often had sound isolation characteristics that conform to minimum code requirements. Perhaps the most common instance of complaints is one where a family sells a single-family home in a quiet suburb and

moves to a more expensive condominium, many times in a more urban setting. Having been swayed by their perceived quality of the condominium's fit and finish, as well as the unit's cost, and having lived for many years in a single-family home, the reality of hearing sounds from adjacent units and/or mechanical equipment sound often becomes a source of disappointment and complaints. The acoustical consultant must guide the architect in avoiding this pitfall by providing recommended sound isolation performances that meet the likely expectations of future occupants while fitting within the reality of budget constraints.

Table 2 presents a guide for establishing sound isolation criteria for three categories of residential construction defined as minimally sensitive, moderately sensitive, and highly sensitive. These sensitivities are of persons occupying multiresidential buildings. Persons of minimal sensitivity in this context are those not expecting special qualities in building performance or do not anticipate intensive use of their living unit for activities requiring quiet, for example, studying or intently listening to quiet music. High ambient sound pressure levels produced by mechanical systems are typical of living units served by window air conditioners. High ambient

**Table 1 Summary of IBC, California Title 24 Code, and City of New York Section 1208.0 Provisions on Noise**

IBC	California	City of New York
<i>Title</i>		
Chapter 12 Interior Environment Section 1207 Sound Transmission	Appendix Chapter 12: Section 1208 & 1208A Sound Transmission Control	Building Code of the City of New York Title 27, Construction and Maintenance, Subchapter 27, Section 1208.0 Noise Control in Multiple Dwellings
<i>Status</i>		
Obligatory	Obligatory	Obligatory
<i>Object</i>		
Receiver	Receiver	Receiver and Source
<i>Scope</i>		
Interior walls, and floors between dwelling units	Interior walls, floors between dwelling units, exterior walls Interior sound pressure levels produced by exterior noise sources	Interior walls, floors between dwelling units, dwelling unit entry doors Interior and exterior building equipment
<i>Limits</i>		
STC $\geq 50$ (45 if field tested) IIC $\geq 50$ (45 if field tested)	STC $\geq 50$ (45 if field tested) IIC $\geq 50$ (45 if field tested) Corridor entrance doors and seals STC $\geq 26$	STC $\geq 50$ (48 if field tested) INR $\geq 0$ (IIC $\geq 51$ ) (IIC $\geq 49$ if field tested) Dwelling entry doors STC $\geq 35$ NC-35 max produced by mechanical equipment
	DNL or CNEL $\geq 45$ dB	Maximum sound power levels specified for mechanical equipment
<i>Evaluation</i>		
Comparison with listed assemblies	Comparison with listed assemblies and report by acoustical consultant (testing if assembly not listed)	Comparison with listed assemblies

sound pressure levels are common in buildings overlooking major highways and with windows providing low noise reduction because of lightweight glazing and/or because of poor window gaskets.

Persons of moderate sensitivity would expect good speech privacy and low enough ambient sound pressure levels to ensure uninterrupted intelligibility of spoken and television speech at moderate levels. Mechanical systems serving these units would require sound attenuation. In noisier urban areas, acoustical windows may be required to sufficiently control exterior sound transmission into living areas. Achieving the IIC ratings in Table 2 would require standard carpeting or fairly sophisticated hard-finished floor systems incorporating resilient underlayments.

Persons falling in the highly sensitive category would expect minimally audible airborne and impact sound transmission from adjacent units, good speech intelligibility for low-level signals, and an ability to play moderately loud music without disturbing neighbors. Even in quiet environs, acoustical windows may be required. Special attention must also be paid to controlling noise from mechanical systems serving these living units. Achieving the IIC rating indicated in Table 2 would require carpeting or floated hard-finished floors. Floated floors would be characterized as a concrete or other heavy construction isolated from the building structural floor by vibration isolation elements.

To achieve building floor–ceiling constructions that provide IIC ratings of 50 or higher generally requires special construction details including resilient floor underlayments (or floated floor constructions) and sound isolation ceilings. IIC ratings higher than 65 are generally easily obtained by using floor carpeting. As a compromise, condominium complexes sometimes create rules that permit hard-finished floors, providing they can achieve a minimum IIC rating of 50, if carpeting is used in unit walkways and halls, and if the total carpeting floor coverage is in a range of 40 to 70%.

Interior sound pressure levels produced by mechanical systems and indicated in Table 2 are consistent with the recommendations of the American Society

of Heating, Refrigerating, and Air-Conditioning Engineers (ASHRAE).<sup>5</sup> Tonal sound, such as that produced by transformers and other electrical equipment, may need to adhere to lower sound pressure level limits than indicated for mechanical systems. This is also true for transient sound, such as sound produced by elevators.

The suggested criteria for environmental sound in Table 2 apply to transportation sound, that is, sound produced by road traffic, aircraft, and railroads. The criteria may not be suitable for industrial noise or weapons firing sound, for example.

The information of Table 2 is to be used only as a general guide for setting criteria and should not be included in building project specifications without further consideration of project needs, feasibility, and local code requirements. The interpretation of sensitivity for categorizing residential occupancies must be done with care, and individual circumstances may influence categorizations.

## 8 SUMMARY

In the last 10 years much has changed in U.S. building codes. The three former code organizations—Building Officials and Code Administrators International (BOCA), International Conference of Building Officials (ICBO), and Southern Building Code Congress International (SBCCI)—have collaborated to form a new code organization—the International Code Council (ICC). The three model codes have been withdrawn from use and the new International Building Code (IBC) has been promoted by the three organizations. The IBC is generally comprised of the portions of each of the three former model codes. The IBC acoustical limits appear in Section 1207, Sound Transmission. This code section most closely matches that of the BOCA code on sound, except that the IBC code sets minimum STC and IIC ratings of 50, instead of 45, for party wall and floor–ceiling constructions of residential units in multiresidential buildings.

The ICC increase of STC and IIC rating limits from 45 to 50 has brought sound isolation performances up to general expectations in this author's experience.

**Table 2 Guidelines for Acoustical Criteria in Multiresidential Buildings**

Sound Isolation Type	Minimally Sensitive	Moderately Sensitive	Highly Sensitive
Party wall/floor sound isolation			
Wall and floor sound isolation (STC rating)	50	55	60 <sup>a</sup>
Floor impact sound isolation (IIC rating)	50	55	60 <sup>a</sup>
Mechanical equipment sound isolation (Criteria curve, NC, RC)			
Sleeping rooms	35	30	20
All other rooms	40	35	25
Exterior environmental sound isolation			
Exterior environmental sound pressure levels inside units (day–night average sound pressure level in dB)	45	35	25
Maximum exterior environmental A-weighted sound pressure level inside unit (measured with meter slow response)	65	55	45

<sup>a</sup>Higher values may at times be desired or required, but these represent the general limits of modern construction normally encountered in the United States, with the exception that the IIC rating of floor–ceiling constructions can be increased beyond what is shown if carpet is used on floors.

Market rate properties nevertheless generally require higher STC and IIC ratings on the order of 55 as suggested in Table 2 for moderate sensitivity to noise.

The IBC still lacks the exterior facade/fenestration limits of the California building code and of building codes of several European countries. Programs to establish compatible land-use zoning around airports and other noise-producing activities have been widely established. Nevertheless, economic and social pressures are still causing noise-sensitive building development to occur near major noise sources. Today, construction of residential subdivisions within a few feet of major highways and in areas affected by noise is still common. Oddly enough, sometimes the attraction of noisy sites for development is the source itself, that is, the convenience of being near a highway or an airport. Hence, the only way to protect the eventual building occupant is for jurisdictions to incorporate exterior facade/fenestration sound isolation provisions into their building codes.

#### ACKNOWLEDGMENTS

The author wishes to thank Brion G. Koning, Cavanaugh Tocci Associates, for his assistance in

gathering information for this chapter. Finally, the author thanks Solutia for its support in gathering U.S. building code information.

#### REFERENCES

1. M. J. Crocker, *Encyclopedia of Acoustics*, Wiley, New York, 1997.
2. 2003 International Building Code, Chapter 1207 Sound Transmission, International Code Council, Washington, DC, 2003, p. 241.
3. 2001 California Building Code, California Code of Regulations, Title 24, Part 2 (Volume 1), Sections 1208 and 1208A, Sound Transmission Control, pp. 1–331.
4. Building Code of the City of New York, Subchapter 12, Article 9, Noise Control in Multiple Dwellings, October 1, 2004, p. 289.
5. ASHRAE, Sound and Vibration Control, in *2003 ASHRAE HVAC Applications Handbook*, American Society of Heating, Refrigerating, and Air-Conditioning Engineers, Chapter 47, p. 47.26.

# CHAPTER 114

## SOUND INSULATION OF RESIDENTIAL HOUSING – BUILDING CODES AND CLASSIFICATION SCHEMES IN EUROPE

**Birgit Rasmussen**  
SBI, Danish Building Research Institute  
Hørsholm, Denmark

### 1 INTRODUCTION

Most countries in Europe have legal sound insulation requirements for dwellings. However, fulfillment of legal requirements does not ensure satisfactory conditions, and for this reason classification schemes have been introduced in several countries to meet the need to specify a higher level of acoustical comfort than prescribed by the legal requirements. It is important to observe that acoustical comfort for a person is related to the person both as a receiver of sound but also as a source of sound. It can be annoying to be exposed to noise from the neighbors, but it can be equally annoying to know that your activities can be heard by other people, implying lack of privacy or causing annoyance. The classification schemes define a number of classes, which are intended to reflect different levels of acoustical comfort. While requirements for sound insulation between dwellings have existed approximately 50 years in several countries, it is only during the last few decades that facade sound insulation requirements have become common in Europe. At the same time there is a focus on creating improved acoustical environments. The aim of current noise policy in Europe is to reduce the noise exposure of people in order to avoid adverse effects. Within building acoustics, the international (ISO) standards for laboratory and field measurements are implemented as European (EN) standards. A few years ago, EN standards for prediction of sound insulation in buildings were developed and subsequently published as ISO standards.

### 2 ACOUSTICAL COMFORT IN DWELLINGS

Acoustical comfort can be characterized as follows:

- Absence of unwanted sound
- Desired sounds having the right level and quality
- Opportunities for acoustical activities without being heard by or annoying other people

Poor sound insulation between dwellings can be a cause of conflicts and a cause of restraints of activities.<sup>1</sup>

To achieve acoustical comfort in a dwelling, certain requirements have to be fulfilled concerning:

- Airborne sound insulation
- Impact sound insulation
- Noise level from traffic and industry
- Noise from building services and equipment

It has often been claimed that people want good sound insulation but are not willing to pay extra to get it. In 1995 an investigation was made in Sweden to find the desired level of sound insulation of new dwellings.<sup>2</sup> In all, 2322 questionnaires were used for the analysis: 65% of the participating people lived in multistory housing, 20% in detached housing, 10% in terraced housing, and 5% in other kinds of housing. One of the main questions was about the willingness to pay a higher rent if the sound insulation of the apartment could be significantly improved. In summary it can be concluded that around 60% of the population were willing to pay on average a 10% higher rent if the sound insulation of the dwelling could be improved. On the other hand, if a dwelling is expensive and marketed as “luxury,” the occupants expect a proportional sound insulation.<sup>3</sup> Besides, there is in general an increasingly stronger request for comfort. Additional challenges are new lifestyle trends, such as bare floors, powerful home entertainment, and more flexible hours.

In spite of the fact that a dwelling is probably the biggest investment during most people’s lifetime, that much time is spent in the dwelling, and that acoustical comfort is very important to well-being, objective information about the acoustical conditions is rarely available, or it might happen that the concepts applied for quantification of the performance are not suitable. This is very unsatisfactory to prospective occupants of a dwelling, as acoustical quality is a “hidden” quality, which is not easily evaluated by other means. Fulfillment of legal requirements does not ensure satisfactory conditions, and for this reason classification schemes have been introduced in several countries to meet the need to specify a higher level of acoustical comfort than prescribed by the legal requirements. The classification schemes define a number of classes, which are intended to reflect different levels of acoustical comfort. Thus, it is, of course, important that concepts applied for evaluation of sound insulation correlate well with the subjective evaluation of the sound insulation experienced in practice. In Europe, concepts as

well as the level of requirements differ widely according to the results of a survey<sup>4</sup> carried out in 24 countries in 2004. Considerations on concepts are further elaborated in Ref. 5.

In Europe there is a focus on creating improved acoustical environments, see the Environmental Noise Directive (END)<sup>6</sup> and the strategy paper.<sup>7</sup> The aim of current noise policy is to reduce the noise exposure of people in order to avoid adverse effects. Therefore, the policy has to consider some general principles that exist both at a technical level and at a legal level. The *legal principles* are related to noise management, other environmental issues, and sustainability.

The *technical principles* refer to the management and reduction of noise emission and exposure and have a clear ranking:

1. To avoid and reduce noise at its source (noise that is not generated cannot lead to noise exposure)
2. To reduce noise in its propagation (measures as close to the source as possible should be preferred because such measures protect the highest number of people)
3. To reduce noise at the receiver (these measures should only be used if other measures are ineffective)

Following these principles, the European Union (EU) has developed a comprehensive policy on environmental noise that is based on the two fundamentals: emission-related legislation for controlling noise at its source and the Environmental Noise Directive<sup>6</sup> (END) with elements closely related to noise perception. The END<sup>6</sup> defines three key elements for future noise policy that constitute a standard approach to the management of environmental noise:

- Harmonized assessment of environmental noise
- Informing and consulting the public
- Appropriate actions

The basis for the *assessment of environmental noise* is strategic noise maps, which are to be established with common noise indicators and methods. On the basis of the assessment provided by the strategic noise maps, competent authorities must draw up *action plans* to reduce noise where it is necessary, to maintain environmental noise quality where it is good, and to protect quiet areas in agglomerations. The Directive does not set any limit value, nor does it prescribe the measures to be used in the action plans, which remain at the discretion of the competent authorities.

To have widespread *information to the public* about noise exposure, its effects, and the measures considered to address noise, the most appropriate information channels should be selected. Action plans should address priorities in areas of interest and

should be drawn up by the competent authorities in *consultation with the public*.

While the END<sup>6</sup> creates focus on the environments, including facades, there is no similar EU initiative concerning sound insulation between dwellings, although the above-mentioned three key elements (harmonization, information, actions) are applicable to this topic.

### 3 CONCEPTS FOR EVALUATION OF SOUND INSULATION

In the beginning of the twentieth century, it was realized that insufficient sound insulation could initiate conflicts between neighbors and reduce the well-being of the occupants, and thus the need for sound insulation requirements was recognized. The very first sound insulation requirements were qualitative; for example, "the building constructions shall be designed to provide sufficient sound insulation between dwellings according to the assessment made by the building commission" (example from municipal requirements in Denmark, 1936). In the middle of the twentieth century, the requirements became more specific but still were not quantified. Typically, they were comparative, for example, requiring "a sound insulation as good as a 1/1 brick wall or another construction providing at least the same sound insulation" (example from national requirements in Denmark, 1956). Later, more specific concepts appeared, for example,  $R_m$  being an arithmetic average of one-third octave values. It was only in the 1960s that several countries introduced quantified requirements referring to specific concepts and standards.

Now, at the beginning of the twenty-first century, more than 50 years after implementation of the first national sound insulation requirements in Europe, most countries in Europe have legal requirements, although the criteria and enforcement differ widely. In general, building regulations in Europe have been developed and enforced by governmental agencies. Within building acoustics, the ISO standards are implemented as European (EN) standards, and the majority of countries apply the field measurement methods described in ISO 140 parts 4, 5, 7 from 1998<sup>8</sup> and the rating methods in ISO 717 from 1996.<sup>9</sup> Due to the fact that ISO 717 offers a variety of concepts, several countries can keep concepts applied in the past and still refer to ISO 717, implying that the incentive to harmonization is insufficient.

The first international standard for rating of sound insulation of dwellings was ISO/R 717:1968,<sup>10</sup> which was based on extensive investigations (see Chapter 107) and supporting field measurements according to ISO/R 140:1960.<sup>11</sup> The maximum allowable unfavorable deviation from the reference curve was 8 dB. A revised ISO 717 consisting of three parts was published in 1982<sup>12</sup> and the series supported the ISO 140 series published in 1978.<sup>13</sup> The basic reference curves were the same as in ISO/R 717:1968,<sup>10</sup> but the 8-dB rule was removed. However, the 8-dB rule survived partly in the 1982 revision, in the sense that the maximum deviation must be indicated in the test report, if it exceeded 8 dB.

When the first legal sound insulation requirements appeared more than 50 years ago, the frequency range of 100 to 3150 Hz became the “traditional” frequency range for European building acoustical requirements, field tests, and laboratory tests. However, in countries with lightweight building practice, for example, Sweden and Norway, the need to include lower frequencies (<100 Hz) gradually became obvious.

Influenced by the French concepts  $R_{\text{rose}}$  and  $R_{\text{route}}$  and the increasing need in other countries for evaluation of traffic noise insulation and for including low frequencies (down to 50 Hz), ISO 717:1982 was revised thoroughly. The next (and most recent) version of ISO 717:1996<sup>9</sup> includes a range of spectrum adaptation terms for rating of sound insulation. As a consequence, the standard opens up the possibility to apply these adaptation terms for an extended frequency range down to 50 Hz by adding such terms when specifying the requirements for sound insulation. In parallel, ISO 140 was updated, the field parts being published in 1998; see Ref. 8. The ISO 140 standards and ISO 717 standards have also been published as European standards (EN ISO). An overview of the ISO 717 history is found in Table 1.

The current international concepts for evaluation of airborne and impact sound insulation are defined in ISO 717-1<sup>9</sup> and ISO 717-2,<sup>9</sup> respectively. In Table 2 an overview is found of the basic ISO 717 concepts (single-number quantities) and the spectrum adaptation terms intended for specification and test of:

- Airborne sound insulation between dwellings
- Airborne sound insulation for facades
- Impact sound insulation between dwellings

The spectrum adaptation terms have been introduced to take into account different spectra of noise sources:  $C$  and  $C_{\text{tr}}$  (corresponding to pink noise and road traffic noise, respectively) for airborne sound insulation (see Table 3) and  $C_1$  ( $L'_{n,w} + C_1 + 15$  corresponds to the energy sum) for impact sound insulation. The spectrum adaptation terms—colloquially named  $C$  corrections—may be calculated for the usual frequency range or for an enlarged frequency range including the one-third octave frequency bands 50, 63, and 80 Hz ( $C$ ,  $C_{\text{tr}}$ ,  $C_1$ ) and/or 4000 and 5000 Hz ( $C$  and  $C_{\text{tr}}$  only). The octave band measurement results may be used for rating field measurements. The  $C$  corrections are equipped with indices specifying the type of spectrum and the frequency range, if enlarged (see Table 2). The maximum unfavorable deviation shall no longer be indicated, even if it exceeds 8 dB. However, the  $C$  corrections are more restrictive to dips and peaks in the airborne and impact sound insulation curves, respectively, thereby to some extent substituting for the former 8-dB rule.

The single-number quantities and the spectrum adaptation terms are derived from one-third octave values (laboratory and field) or 1/1 octave values (field only) measured according to ISO 140.<sup>8</sup> The

different adaptation terms will enable one to take into account different types of noise spectra, without leaving the well-known reference curve system. Thus,  $C$ ,  $C_{\text{tr}}$ , and  $C_1$  have not been included directly in any single-number quantities but have been introduced as separate terms to be added. In Table 2 the “one-third octave” ISO 717 single-number field quantities, spectrum adaptation terms, and the total number of concepts are indicated.

A requirement may be expressed as the sum of a single-number quantity and a spectrum adaptation term or solely as the single-number quantity. Consider examples on statements of airborne and impact sound insulation requirements:

$$\begin{aligned} D_{nT,w} &\geq 55 \text{ dB} & L'_{nT,w} &\leq 50 \text{ dB} \\ D_{nT,w} + C &\geq 55 \text{ dB} & L'_{nT,w} + C_1 &\leq 50 \text{ dB} \\ D_{nT,w} + C_{50-3150} &\geq 55 \text{ dB} & L'_{nT,w} + C_{1,50-2500} &\leq 50 \text{ dB} \end{aligned}$$

In 2004 a survey describing the main sound insulation requirements between dwellings was carried out in 24 countries in Europe.<sup>5</sup> A comparison of requirements revealed considerable differences, not only in level of requirements but also in terms of descriptors used and the frequency range applied. In the lower part of Table 2—based on the 2004 survey<sup>5</sup>—information has been added about the number of concepts actually applied in Europe. Table 2 also indicates the number of countries applying spectrum adaptation terms (including low-frequency terms). The results of the European survey are described in Sections 4 and 5. In Section 6 are found the basic single-number quantities for field use, the terms they are derived from as well as equations, and references to definitions in the relevant standards. Building codes in the United States are covered in Chapter 113.

All ISO standards mentioned in this chapter are also EN standards and thus implemented in the CEN member countries. Although implemented in all CEN countries, ISO 717 field concepts are not necessarily applied in all national building regulations, for example, national concepts  $I_{w,k}$  and  $I_{co}$  are applied in the Netherlands; compare Section 4. Only products subject to free trade must apply concepts defined in the harmonized standards.

The above considerations concern concepts as defined in ISO 717. The United States and Canada use American Society for Testing and Materials (ASTM) standards, defining slightly different single-number quantities and no spectrum adaptation terms. For airborne sound the ASTM method differs in two main aspects: Frequency range of 125–4000 Hz and the 8-dB rule is included. The ASTM rating procedure for impact sound insulation is also similar to the ISO procedure, but again ASTM applies the 8-dB rule. For further information about the ASTM impact sound ratings, see Refs. 14 and 15. Japan has partly incorporated ISO standards in the Japanese standards, but they are seldom used in the field, see Ref. 16 for an overview of building acoustical standards in Japan.

**Table 1 Historic Overview of ISO 717 Standards with Indication of Main Characteristics**

1968	ISO/R 717 : 1968, <sup>10</sup> Rating of Sound Insulation for Dwellings	Field concepts: $I_a, I_i$ 8-dB rule
1982	ISO 717 : 1982, <sup>12</sup> Acoustics — Rating of Sound Insulation in Buildings and of Building Elements: Part 1: Airborne Sound Insulation in Buildings and of Interior Building Elements Part 2: Impact Sound Insulation Part 3: Airborne Sound Insulation of Facade Elements and Facades	Field and laboratory: $R_w, R'_{w,}$ etc. $L_{n,w}, L'_{n,w},$ etc. No 8-dB rule, but unfavorable deviations more than 8 dB shall be reported
1996	ISO 717 : 1996, <sup>9</sup> Acoustics — Rating of Sound Insulation in Buildings and of Building Elements: Part 1: Airborne Sound Insulation Part 2: Impact Sound Insulation	No reporting of deviations Several spectrum adaptation terms: $C, C_{tr}, C_l$ Various frequency ranges

**Table 2 Overview of ISO 717 Concepts for Evaluation of Sound Insulation in Buildings and Application in Europe**

	Airborne Sound Insulation between Rooms (ISO 717-1)	Airborne Sound Insulation of Facades (ISO 717-1)	Impact Sound Insulation between Rooms (ISO 717-2)
Basic concepts (single-number quantities)	$R'_w$ $D_{n,w}$ $D_{nT,w}$	$R'_w$ $D_{n,w}$ $D_{nT,w}$	$L'_{n,w}$ $L'_{nT,w}$
Spectrum adaptation terms (listed according to intended main applications, see Table 2)	None $C$ $C_{50-3150}$ $C_{100-5000}$ $C_{50-5000}$	None $C$ $C_{tr}$ $C_{50-3150}$ $C_{tr,50-3150}$ $C_{100-5000}$ $C_{tr,100-5000}$ $C_{50-5000}$ $C_{tr,50-5000}$	None $C_l$ $C_{l,50-2500}$
Total number of concepts	$3 \times 5 = 15$	$3 \times 9 = 27$	$2 \times 3 = 6$
Number of concepts applied — based on survey (cf. Ref. 4) in 24 countries in Europe	BC: 7 of 15 CS: 6 of 15 BC+CS in total: 9 of 15	Facades not fully included in survey	BC: 4 of 6 CS: 3 of 6 In total: 4 of 6
Number of countries (cf. Ref. 5) applying spectrum adaptation terms in a BC or a CS	BC: 5 (1 lf) of 24 countries CS: 9 (7 lf) of 9 schemes	Some countries apply spectrum adaptation terms in BCs	BC: 2 (1 lf) of 24 countries CS: 7 (6 lf) of 9 schemes

BC = Building Code (legal requirements); CS = Classification scheme; lf = low-frequency

**Table 3 Relevant Spectrum Adaptation Term for Different Types of Noise Sources**

Type of Noise Source	Relevant Spectrum Adaptation Term
Living activities (talking, music, radio, TV)	$C$
Children playing	(spectrum 1 <sup>b</sup> : A-weighted pink noise)
Railway traffic at medium and high speed <sup>a</sup>	
Highway road traffic > 80 km/h <sup>a</sup>	
Jet aircraft short distance	
Factories emitting mainly medium and high-frequency noise	
Urban road traffic	$C_{tr}$
Railway traffic at low speeds <sup>a</sup>	(spectrum 2 <sup>b</sup> : A-weighted urban traffic noise)
Aircraft propeller driven	
Jet aircraft large distance	
Disco music	
Factories emitting mainly low- and medium-frequency noise	

<sup>a</sup>In several European countries calculation models for highway road noise and railway noise exist, which define octave band levels; these could be used for comparison with spectra 1 and 2.

<sup>b</sup>The spectra 1 and 2 are defined in ISO 717-1.

Source: Table A.1 from ISO 717-1 : 1996.<sup>9</sup>



#### 4 BUILDING CODES IN EUROPE

Building codes include typically acoustical requirements concerning:

- Airborne sound insulation between dwellings
- Impact sound insulation between dwellings
- Facade sound insulation (or indoor noise levels from traffic and industry)
- Noise from building services and equipment

In addition, there may be other requirements. Examples are limits concerning vibration levels and reverberation time. This chapter mainly deals with the main requirements related to airborne and impact sound insulation. For facades only qualitative overview information is included.

To ensure that completed buildings fulfill the requirements, detailed designs may be carried out applying prediction methods, for example, EN 12354,<sup>17</sup> based on the performance of the building elements (direct transmission) and junctions (flanking transmission). The performance data may be determined by calculations (applying construction and material characteristics) or by laboratory measurements carried out according to ISO 140<sup>8</sup> (direct transmission) and ISO 10848<sup>18</sup> (flanking transmission). An overview of the principles of the prediction methods is found in Ref. 19.

The main requirements on airborne sound insulation between dwellings in the 24 European countries responding in the 2004 survey<sup>5</sup> are presented in Table 4. Similarly, the main requirements on impact sound insulation are presented in Table 5. In several countries the sound insulation requirements were originally based on the actual performance of traditional building constructions that were considered to offer a sufficient level of sound insulation; see Section 3. An exception is Austria, where the requirements<sup>20</sup> were based directly on a large survey in 1974<sup>21</sup>; the strictest requirements in the world are probably found in Austria.

The requirements in Tables 4 and 5 cannot be compared without being converted to the same concept. However, a correct conversion depends on the actual conditions for room dimensions, partition area, and other conditions and the conversion of values between different concepts is highly uncertain, especially when “low-frequency” spectrum adaptation terms—including  $C_{tr}$ —are involved. Based on previous experience, a rough conversion has been presented in Ref. 4, although the conditions for the conversion are no longer valid due to changes in building practice.

A comparison of requirements revealed considerable differences, not only in level of requirements but also in terms of descriptors used and the frequency range applied. Ten different concepts were applied for airborne and six for impact sound insulation requirements, not counting variants and additional recommendations. Significant differences are found when comparing sound insulation requirements in different countries:

Airborne Sound Insulation	Impact Sound Insulation
10 concepts + variants/recommendations	6 concepts + variants/recommendations
For multistory housing variation > 5 dB	For multistory housing variation > 15 dB
For terraced housing variation > 10 dB	For terraced housing variation > 15 dB
The strictest requirements are found in Austria	The strictest requirements are found in Austria

The total number of concepts applied is found in Table 2. The most recent version of the standard ISO 717<sup>9</sup> has contributed to the diversity by allowing different concepts and by introducing spectrum adaptation terms with different—extended—frequency ranges for the evaluation. In addition, national, special rules have been added in some countries to compensate for shortcomings or difficulties of field test procedures and conditions.

During the last decade low-frequency descriptors have been introduced in all five Nordic countries and in Lithuania. The low-frequency terms are included in the legal minimum requirements in Sweden (see Tables 4 and 5) and in the criteria for the higher, voluntary quality classes in classification schemes in all six countries, see Section 5.

In building acoustics, the frequency range has traditionally been 100 to 3150 Hz. However, a trend toward lightweight building constructions has increased the low-frequency problems, for example, due to neighbors’ music and footfall noise. Thus, a growing need to include the low-frequency sound insulation has been recognized. In general, there seems to be a trend toward increasing the requirements and including the spectrum adaptation terms in the concepts defining the airborne and impact sound insulation requirements, although the process is slow.

In 2003 the United Kingdom took a step in a different direction than other countries by introducing the spectrum adaptation term  $C_{tr}$  as a part of the required criterion for airborne sound insulation between dwellings in general, although  $C_{tr}$  is based on an average traffic noise spectrum and has a strong weight at low frequencies. The “ $C_{tr}$  spectrum” is intended for optimizing sound insulation against traffic and other sources with significant low-frequency contents, for example, disco music. The idea behind including  $C_{tr}$  for evaluation of sound insulation between dwellings is to take into account low frequencies without actually having to design for or test at low frequencies (assuming that if a construction gives good sound insulation down to 100 Hz, the sound insulation below 100 Hz is probably also good). The idea is interesting, but apart from the conference paper,<sup>22</sup> there seems to be no official reports or articles available justifying that this is a cost-effective and balanced way to meet the needs for increased sound insulation in an

**Table 4 Airborne Sound Insulation between Dwellings — Main Requirements in 24 European Countries<sup>a,b</sup>**

Country	Concept <sup>c</sup>	Multistory Housing	Terraced Housing
		Req. (dB)	Req. (dB)
Austria	$D_{nT,w}$	$\geq 55$	$\geq 60$
Belgium <sup>d</sup>	$D_{nT,w}$	$\geq 54$	$\geq 58$
Czech Rep.	$R'_w$	$\geq 52$	$\geq 57$
Denmark <sup>e</sup>	$R'_w$	$\geq 52^f$	$\geq 55$
Estonia	$R'_w$	$\geq 55$	$\geq 55$
Finland	$R'_w$	$\geq 55$	$\geq 55$
France	$D_{nT,w}+C$	$\geq 53$	$\geq 53$
Germany <sup>e</sup>	$R'_w$	$\geq 53^f$	$\geq 57$
Hungary	$R'_w$	$\geq 52$	$\geq 57$
Iceland	$R'_w^g$	$\geq 52^h$	$\geq 55$
Italy	$R'_w$	$\geq 50$	$\geq 50$
Latvia	$R'_w$	$\geq 54$	$\geq 54$
Lithuania	$D_{nT,w}$ or $R'_w$	$\geq 55$	$\geq 55$
Netherlands	$I_{lu,k}^i$	$\geq 0$	$\geq 0$
Norway	$R'_w$	$\geq 55^j$	$\geq 55^j$
Poland	$R'_w+C$	$\geq 50^f$	$\geq 52$
Portugal	$D_{n,w}$	$\geq 50$	$\geq 50$
Russia	$I_b^k$	$\geq 50$	$l$
Slovakia	$R'_w$	$\geq 52$	$\geq 52$
Slovenia	$R'_w$	$\geq 52$	$\geq 52$
Spain <sup>d</sup>	$D_{nT,w}+C_{100-5000}$	$\geq 50$	$\geq 50$
Sweden	$R'_w+C_{50-3150}$	$\geq 53$	$\geq 53$
Switzerland	$D_{nT,w}+C$	$\geq 52$	$\geq 55$
United Kingdom	$D_{nT,w}+C_{tr}$	$\geq 45$	$\geq 45$

<sup>a</sup>Data collected 2002–2006.<sup>b</sup>Overview information only. Detailed requirements to be found in the building codes.<sup>c</sup>There exists no generally applicable conversion between the different concepts, as the relations depend on the characteristics of the rooms and the constructions. Exact conversion can only be made in every specific case.<sup>d</sup>Belgium, Spain: Proposed new requirements, enforcement expected in 2007.<sup>e</sup>Revision of requirements expected in 2007.<sup>f</sup>Horizontal, requirement for vertical is 1 dB higher.<sup>g</sup>In addition to the rating procedure described in ISO 717, the Icelandic building regulations prescribe max 8 dB unfavorable deviation.<sup>h</sup>55 dB recommended.<sup>i</sup> $I_{lu,k} \approx R'_w - 55$  dB.<sup>j</sup>It is recommended that the same criteria are fulfilled by  $R'_w + C_{50-3150}$ .<sup>k</sup> $I_b = R'_w - 2$  dB.<sup>l</sup>No requirements. Probably the requirements for multistory housing are used.

optimized way. In 2004 Australia followed the United Kingdom by also introducing  $C_{tr}$  in the requirements for airborne sound insulation between dwellings, and in addition  $C_1$  for impact sound insulation requirements was introduced, see Ref. 23.

Typically, sound insulation requirements have originally, that is, more than 50 years ago, been based on the actual performance of traditional building constructions—which have been considered to offer a sufficient level of sound insulation—and since then

**Table 5 Impact Sound Insulation between Dwellings — Main Requirements in 24 European Countries<sup>a,b</sup>**

Country	Concept <sup>c</sup>	Multistory Housing	Terraced Housing
		Req. (dB)	Req. (dB)
Austria	$L'_{nT,w}$	$\leq 48$	$\leq 43$
Belgium <sup>d</sup>	$L'_{nT,w}$	$\leq 58^e$	$\leq 50$
Czech Rep.	$L'_{n,w}$	$\leq 58$	$\leq 53$
Denmark <sup>f</sup>	$L'_{n,w}$	$\leq 58$	$\leq 53$
Estonia	$L'_{n,w}$	$\leq 53$	$\leq 53$
Finland	$L'_{n,w}^g$	$\leq 53^g$	$\leq 53$
France	$L'_{nT,w}$	$\leq 58$	$\leq 58$
Germany <sup>f</sup>	$L'_{n,w}$	$\leq 53$	$\leq 48$
Hungary	$L'_{n,w}$	$\leq 55$	$\leq 47$
Iceland	$L'_{n,w}^h$	$\leq 58^i$	$\leq 53$
Italy	$L'_{n,w}$	$\leq 63$	$\leq 63$
Latvia	$L'_{n,w}$	$\leq 54$	$\leq 54$
Lithuania	$L'_{n,w}$	$\leq 53$	$\leq 53$
Netherlands	$I_{co}^j$	$\geq +5$	$\geq +5$
Norway	$L'_{n,w}^g$	$\leq 53^g$	$\leq 53^g$
Poland	$L'_{n,w}$	$\leq 58$	$\leq 53$
Portugal	$L'_{n,w}$	$\leq 60$	$\leq 60$
Russia	$I_y^k$	$\leq 67$	$l$
Slovakia	$L'_{n,w}$	$\leq 58$	$\leq 58$
Slovenia	$L'_{n,w}$	$\leq 58$	$\leq 58$
Spain <sup>d</sup>	$L'_{nT,w}$	$\leq 65$	$\leq 65$
Sweden	$L'_{n,w}+C_{1,50-2500}$	$\leq 56^m$	$\leq 56^m$
Switzerland	$L'_{nT,w}+C_1$	$\leq 53$	$\leq 50$
United Kingdom	$L'_{nT,w}$	$\leq 62$	None

<sup>a</sup>Data collected 2002–2006.<sup>b</sup>Overview information only. Detailed requirements to be found in the building codes.<sup>c</sup>There exists no generally applicable conversion between the different concepts, as the relations depend on the characteristics of the rooms and the constructions. Exact conversion can only be made in every specific case.<sup>d</sup>Belgium, Spain: Proposed new requirements, enforcement expected in 2007.<sup>e</sup>From any “nonbedrooms” outside the dwelling to a bedroom  $\leq 54$  dB is required.<sup>f</sup>Revision of requirements expected in 2007.<sup>g</sup>It is recommended that the same criteria are fulfilled by  $L'_{n,w} + C_{1,50-2500}$ .<sup>h</sup>In addition to the rating procedure described in ISO 717, the Icelandic building regulations prescribe max 8 dB unfavorable deviation.<sup>i</sup>53 dB recommended.<sup>j</sup> $I_{co} \approx 59 - (L'_{nT,w} + C)$  dB  $\approx 70 - L'_{nT,w}$  dB for bare concrete floors or  $I_{co} \approx 59 - L'_{nT,w}$  dB for other floors like wooden floors, floating floors, and floors with soft coverings.<sup>k</sup> $I_y = L'_{n,w} + 7$  dB.<sup>l</sup>No requirements. Probably the requirements for multistory housing are used.<sup>m</sup>The same criteria shall also be fulfilled by  $L'_{n,w}$ .

remained essentially unchanged in several countries, although neighbor noise levels and the demand for comfort have increased. There may be several reasons for being reluctant to change requirements, one of them being the fear of economic consequences, another

being the difficulties with update of guidelines without extensive experience. In spite of this, stricter requirements have been implemented or proposed in some countries during the last few years, but it is a very slow process for the above-mentioned reasons. However, sound classification schemes can partly compensate for lack of appropriate legal requirements and at the same time provide different quality levels; see Section 5.

Legal requirements concerning sound insulation against traffic noise differ even more than requirements for sound insulation between dwellings due to not only different concepts but also different principles. There is a variety of ways to express facade sound insulation requirements. Several countries specify the required sound insulation of facades as a function of the outdoor noise level (often in quite rough 5-dB steps), sometimes with different day and night requirements. Other countries require the indoor level  $L_{A,eq,24h}$  to be below a certain limit, and there may be additional maximum limits for "events." In addition, the methods for determination of the exterior noise exposure vary considerably. In some countries there are no general, national legal sound insulation requirements, but only local. In total, the situation is quite complex. On a European level the Environmental Noise Directive 2002/49/EC (often abbreviated END)<sup>2</sup> defines two main indicators,  $L_{den}$  and  $L_{night}$  for description of annoyance and sleep disturbance, respectively, to be introduced in EU member states and to be applied for mapping. Future criteria for facades might be expected to be expressed by these harmonized environmental noise indicators. Noise mapping and actions are required according to the time schedule in the END.<sup>2</sup> The main purpose is to reduce noise exposure to a more reasonable level outdoor as well as indoor. The primary goal is to reduce outdoor noise levels by reducing emission from vehicles (road, railway, air, construction equipment) and to increase facade sound insulation, where necessary to obtain satisfactory conditions for the inhabitants. The activities are described in several publications, see, for example, Ref. 7.

For years, there have been discussions about the sufficiency or insufficiency of the ISO tapping machine, and alternative sources, for example, rubber balls, have been proposed. However, it seems as if the main problem might be that the low-frequency energy actually produced by the tapping machine is ignored in

most countries.<sup>4</sup> Sweden is the only country applying  $C_{1,50-2500}$  for legal requirements; see also Table 5.

To gather information and share experience more systematically about sound insulation requirements, a working group, EAA TC-RBA WG4,<sup>24</sup> has been established under the European Acoustical Association (EAA), Technical Committee Room and Building Acoustics (TC-RBA) aiming at recommendations for harmonization of concepts applied for sound insulation requirements.

## 5 CLASSIFICATION SCHEMES IN EUROPE

Acoustical classification schemes exist in nine countries in Europe. France and Germany were the first countries to prepare and publish such schemes. An overview of European classification schemes is found in Table 6. The main criteria for airborne and impact sound insulation between dwellings are found in Tables 7 and 8. Criteria for sound insulation internally in dwellings are found in Tables 9 and 10. Facade sound insulation criteria are described in Ref. 25. The schemes include several other criteria concerning sound insulation and noise levels. For complete information, see the standards.<sup>26-34</sup>

For lightweight buildings it is important that low-frequency spectrum adaptation terms (down to 50 Hz) according to ISO 717<sup>9</sup> are included, implying a significantly improved correlation between subjective and objective sound insulation; see Ref. 35. The low-frequency descriptors have been introduced in all five Nordic countries and in Lithuania, but in no other countries. The low-frequency terms are included in the legal minimum requirements in Sweden and in the criteria for the higher, voluntary quality classes in the classification schemes in all six countries. The importance of including low frequencies for impact sound is also emphasized in Refs. 4, 14, 15, and 36. The Nordic schemes are based on a common Nordic draft,<sup>37</sup> following several investigations.<sup>38-40</sup> A list of all European schemes is found in Table 6.

The different classes in classification schemes are intended to reflect different levels of acoustical comfort. Taking into account also economical factors, different classes in the same scheme may apply different concepts as in the five Nordic countries and Lithuania.

**Table 6 Overview of European Schemes for Sound Classification of Dwellings**

Country	Class Denotations	Year of Implementation	Reference
Denmark (DK)	A/B/C/D	2001	DS 490 (2001) <sup>26</sup>
Finland (FIN)	A/B/C/D	2004	SFS 5907 (2004) <sup>27</sup>
Iceland (IS)	A/B/C/D	2003	IST 45 (2003) <sup>28</sup>
Norway (N)	A/B/C/D	1997/2005	NS 8175 (2005) <sup>29</sup>
Sweden (S)	A/B/C/D	1996/1998/2004	SS 25267 (2004) <sup>30</sup>
France (F)	QL/QLAC	1993/1995/2000	Guide Qualitel (2000) <sup>31</sup>
Germany (D)	I/II/III	1994	VDI 4100 (1994) <sup>32</sup>
Lithuania (LT)	A/B/C/D/E	2004	STR 2.01.07 (2003) <sup>33</sup>
Netherlands (NL)	1/2/3/4/5	1999	NEN 1070 (1999) <sup>34</sup>

**Table 7 Airborne Sound Insulation between Dwellings – Main Criteria in European Schemes for Sound Classification**

Class Criteria (dB) in DK, FIN, IS, N, S					
	DK	FIN	IS	N	S
A	$R'_w + C_{50-3150} \geq 63$	$R'_w + C_{50-3150} \geq 63$	$R'_w + C_{50-3150} \geq 63$	$R'_w + C_{50-5000} \geq 63$	$R'_w + C_{50-3150} \geq 61$
B	$R'_w + C_{50-3150} \geq 58$	$R'_w + C_{50-3150} \geq 58$	$R'_w + C_{50-3150} \geq 58$	$R'_w + C_{50-5000} \geq 58$	$R'_w + C_{50-3150} \geq 57$
C	$R'_w \geq 55$	$R'_w \geq 55$	$R'_w \geq 55^a$	$R'_w \geq 55^a$	$R'_w + C_{50-3150} \geq 53$
D	$R'_w \geq 50$	$R'_w \geq 49$	$R'_w \geq 50$	$R'_w \geq 50$	$R'_w \geq 49$
Class Criteria (dB) in F, D, LT, NL					
	F	D/Multistory <sup>b</sup>	D/Terraced	LT	NL
QLAC	$D_{nT,w} + C \geq 56$	III H: $R'_w \geq 59$ V: $R'_w \geq 60$	III $R'_w \geq 68$	A $R'_w + C_{50-3150} \geq 63$ or $D_{nT,w} + C_{50-3150} \geq 63$	1 $D_{nT,w} + C \geq 62$
QL	$D_{nT,w} + C \geq 53$	II H: $R'_w \geq 56$ V: $R'_w \geq 57$	II $R'_w \geq 63$	B $R'_w + C_{50-3150} \geq 58$ or $D_{nT,w} + C_{50-3150} \geq 58$	2 $D_{nT,w} + C \geq 57$
		I H: $R'_w \geq 53$ V: $R'_w \geq 54$	I $R'_w \geq 57$	C $R'_w$ or $D_{nT,w} \geq 55^a$	3 $D_{nT,w} + C \geq 52$
				D $R'_w$ or $D_{nT,w} \geq 52$	4 $D_{nT,w} + C \geq 47$
				E $R'_w$ or $D_{nT,w} \geq 48$	5 $D_{nT,w} + C \geq 42$

<sup>a</sup>Use of  $C_{50-3150/5000}$  is recommended also in class C.<sup>b</sup>H = horizontal; V = vertical.**Table 8 Impact Sound Insulation between Dwellings – Main Criteria in European Schemes for Sound Classification**

Class Criteria (dB) in DK, FIN, IS, N, S					
Class	DK	FIN	IS	N	S
A	$L'_{n,w} + C_{1,50-2500} \leq 43$	$L'_{n,w} \leq 43$ and $L'_{n,w} + C_{1,50-2500} \leq 43$	$L'_{n,w} \leq 43$ and $L'_{n,w} + C_{1,50-2500} \leq 43$	$L'_{n,w} \leq 43$ and $L'_{n,w} + C_{1,50-2500} \leq 43$	$L'_{n,w} \leq 48$ and $L'_{n,w} + C_{1,50-2500} \leq 48$
B	$L'_{n,w} + C_{1,50-2500} \leq 48$	$L'_{n,w} \leq 49$ and $L'_{n,w} + C_{1,50-2500} \leq 49$	$L'_{n,w} \leq 48$ and $L'_{n,w} + C_{1,50-2500} \leq 48$	$L'_{n,w} \leq 48$ and $L'_{n,w} + C_{1,50-2500} \leq 48$	$L'_{n,w} \leq 52$ and $L'_{n,w} + C_{1,50-2500} \leq 52$
C	$L'_{n,w} \leq 53$	$L'_{n,w} \leq 53^a$	$L'_{n,w} \leq 53^a$	$L'_{n,w} \leq 53^a$	$L'_{n,w} \leq 56$ $L'_{n,w} + C_{1,50-2500} \leq 56$
D	$L'_{n,w} \leq 58$	$L'_{n,w} \leq 63$	$L'_{n,w} \leq 58$	$L'_{n,w} \leq 58$	$L'_{n,w} \leq 60$
Class Criteria (dB) in F, D, LT, NL					
	F	D/Multistory	D/Terraced	LT	NL
QLAC	$L'_{n,w} \leq 52$	III $L'_{n,w} \leq 39$	III $L'_{n,w} \leq 34$	A $L'_{n,w} + C_{1,50-2500} \leq 43$	1 $L'_{nT,w} + C_1 \leq 43$
QL	$L'_{n,w} \leq 55$	II $L'_{n,w} \leq 46$	II $L'_{n,w} \leq 41$	B $L'_{n,w} + C_{1,50-2500} \leq 48$	2 $L'_{nT,w} + C_1 \leq 48$
		I $L'_{n,w} \leq 53$	I $L'_{n,w} \leq 48$	C $L'_{n,w} \leq 53^a$	3 $L'_{nT,w} + C_1 \leq 53$
				D $L'_{n,w} \leq 58$	4 $L'_{nT,w} + C_1 \leq 58$
				E $L'_{n,w} \leq 60$	5 $L'_{nT,w} + C_1 \leq 63$

<sup>a</sup>Use of  $C_{50-3150/5000}$  is recommended also in class C.

**Table 9 Airborne Sound Insulation Internally<sup>a</sup> in Dwellings – Criteria in European Sound Classification Schemes**

Class Criteria (dB) in DK, FIN, IS, N, S						
	DK	FIN		IS	N	S
A	None	$R'_w + C_{50-3150} \geq 48$		$R'_w + C_{50-3150} \geq 48$	$R'_w + C_{50-5000} \geq 48$	$D_{n,w} \geq 44$
B	None	$R'_w + C_{50-3150} \geq 43$		$R'_w + C_{50-3150} \geq 43$	$R'_w + C_{50-5000} \geq 43$	$D_{n,w} \geq 40$
C	None	None		None	None	None
D	None	None		None	None	None
Class Criteria (dB) in F, D, LT, NL						
	F	D/Multistory and Terraced <sup>b</sup>		LT	NL	
QLAC	None	III	H: $R'_w \geq 48$ V: $R'_w \geq 55$	A $R'_w + C_{50-3150} \geq 48$ or $D_{nT,w} + C_{50-3150} \geq 48$	1	$D_{nT,w} + C \geq 52$
QL	None	II	H: $R'_w \geq 48$ V: $R'_w \geq 55$	B $R'_w + C_{50-3150} \geq 44$ or $D_{nT,w} + C_{50-3150} \geq 44$	2	$D_{nT,w} + C \geq 42$
			I	H: $R'_w \geq 40$ V: $R'_w \geq 50$	C None	3
		D None		4	$D_{nT,w} + C \geq 22$	
		E None		5	$D_{nT,w} + C \geq 12$	

<sup>a</sup>Conditions vary. Typically at least one (sleeping) room shall fulfill the conditions.<sup>b</sup>H = horizontal; V = vertical.**Table 10 Impact Sound Insulation Internally<sup>a</sup> in Dwellings – Criteria in European Sound Classification Schemes**

Class Criteria (dB) in DK, FIN, IS, N, S						
Class	DK	FIN		IS	N	S
A	None	$L'_{n,w} \leq 58$ $L'_{n,w} + C_{1,50-2500} \leq 58$		$L'_{n,w} \leq 58$ $L'_{n,w} + C_{1,50-2500} \leq 58$	$L'_{n,w} \leq 58$ $L'_{n,w} + C_{1,50-2500} \leq 58$	$L'_{n,w} \leq 64$
B	None	$L'_{n,w} \leq 63$ $L'_{n,w} + C_{1,50-2500} \leq 63$		$L'_{n,w} \leq 63$ $L'_{n,w} + C_{1,50-2500} \leq 63$	$L'_{n,w} \leq 63$ $L'_{n,w} + C_{1,50-2500} \leq 63$	$L'_{n,w} \leq 68$
C	None	None		None	None	None
D	None	None		None	None	None
Class Criteria (dB) in F, D, LT, NL						
F		D/Multistory and Terraced		LT		NL
QLAC	None	III	$L'_{n,w} \leq 46$	A	$L'_{n,w} + C_{1,50-2500} \leq 53$	1 $L'_{nT,w} + C_1 \leq 53$
QL	None	II	$L'_{n,w} \leq 46$	B	$L'_{n,w} + C_{1,50-2500} \leq 58$	2 $L'_{nT,w} + C_1 \leq 63$
		I	$L'_{n,w} \leq 56$	C	None	3 $L'_{nT,w} + C_1 \leq 73$
				D	None	4 $L'_{nT,w} + C_1 \leq 83$
				E	None	5 $L'_{nT,w} + C_1 \leq 93$

<sup>a</sup>Conditions vary. Typically at least one (sleeping) room shall fulfill the conditions.

Concerning sound insulation against traffic noise, the schemes in Norway, Denmark, and Iceland specify maximum indoor level  $L_{A,eq,24h}$  20, 25, 30, and 35, and dB for classes A, B, C, and D (class C equals legal requirements). Sweden has slightly different criteria. The upper class seems to be quite strict and may not be realistic. The German schemes (and legislation) apply a different approach. The sound insulation of

the facade is specified as a function of the outdoor level, and classes I and II refer both to the same legal requirements, while class III specifies +5 dB higher sound insulation. Future criteria for facades might be expressed by the harmonized environmental noise indicators  $L_{den}$  and  $L_{night}$  for description of annoyance and sleep disturbance, respectively, see definitions in Ref. 2.

As an alternative or supplement to extensive classification schemes, some countries have defined a simple set of criteria for specification of increased acoustical comfort, for example, added in an Annex in the document describing the legal requirements. Such criteria are found in for example, Austria<sup>20</sup> and Germany.<sup>41</sup> The Austrian criteria<sup>20</sup> are described as improvements in decibels compared to the legal minimum requirements: (1) For airborne sound insulation between dwellings and for airborne sound insulation of facades, an improvement of 3 dB is defined; (2) for impact sound insulation between dwellings, an improvement of 5 dB is required; and (3) noise levels from technical installations shall be reduced by 5 dB.

Considering the classification schemes in Europe there are several discrepancies:

- Concepts used for description of sound insulation and noise criteria
- Number of quality classes and intervals between classes
- Use of low-frequency spectrum adaptation terms according to ISO 717:1996<sup>9</sup>
- Sound insulation internally in dwellings
- Common or separate quality levels for multi-story and terraced housing
- Balance between criteria for airborne and impact sound insulation
- Relation to legal requirements

The status of the classification schemes in relation to the legal requirements varies. In some countries the building code and the classification standard are incoherent. In other countries they are strongly “integrated,” implying that the building code refers to a specific class in the classification standard rather than describing the requirements. In Finland, Norway, Sweden, and Lithuania, class C equals the legal

**Table 11 Airborne Sound Insulation between Rooms – Definitions of Field Properties according to ISO 140-4**

Weighted Value	Equations <sup>a</sup> for 1/3 or 1/1 Octave Values	Explanations of Symbols
$R'_w$	(6) $R' = L_1 - L_2 + 10 \log(S/A)$ dB	$L_1$ is the average SPL in the source room.
$D_{n,w}$	(3) $D_n = L_1 - L_2 - 10 \log(A/A_0)$ dB	$L_2$ is the average SPL in the receiving room.
$D_{nT,w}$	(4) $D_{nT} = L_1 - L_2 + 10 \log(T/T_0)$ dB	$S$ is the area of the separating element. $A$ is the equivalent sound absorption area in the receiving room. $A_0$ is the reference absorption area, in square metres; $A_0 = 10 \text{ m}^2$ . $T$ is the reverberation time in the receiving room. $T_0$ is the reference reverberation time; for dwellings, $T_0 = 0.5 \text{ s}$ . $A = 0.16V/T$ , where $V$ is the room volume.

<sup>a</sup> Definitions and equation numbers refer to ISO 140-4:1998.<sup>8</sup>

**Table 12 Airborne Sound Insulation of Facades – Definitions of Field Properties according to ISO 140-5<sup>a</sup>**

Weighted Value	Equations <sup>a</sup> for 1/3 or 1/1 Octave Values	Explanations of Symbols <sup>b</sup>
$R'_{45^\circ,w}$	(3) $R'_{45^\circ} = L_{1,s} - L_2 + 10 \log(S/A) - 1.5$ dB	$L_{1,s}$ is the average SPL on the surface of the test specimen.
$R'_{tr,s,w}$	(4) $R'_{tr,s} = L_{eq,1,s} - L_{eq,2} + 10 \log(S/A) - 3$ dB	$L_2$ is the average SPL in the receiving room.
$D_{ls,2m,n,w}^c$	(7) $D_{2m,n} = L_{1,2m} - L_2 - 10 \log(A/A_0)$ dB	$L_{eq,1,s}$ is the average value of the equivalent continuous SPL on the surface of the test specimen including reflecting effects from the test.
$D_{ls,2m,nT,w}^a$	(6) $D_{2m,nT} = L_{1,2m} - L_2 + 10 \log(T/T_0)$ dB	$L_{eq,2}$ is the average value of the equivalent continuous sound pressure level in the receiving room $L_{1,2m}$ is the outdoor SPL 2 m in front of the façade. $S$ is the area of the test specimen, determined as given in annex A.

<sup>a</sup> Definitions and equation numbers refer to ISO 140-5:1998.<sup>8</sup>

<sup>b</sup> For explanation of  $A$ ,  $A_0$ ,  $T$ ,  $T_0$ ,  $A = 0.16V/T$ , see Table 11.

<sup>c</sup> ISO 140-5, Table 1, has an overview of different measurement methods corresponding to different sound sources (loudspeakers as well as road, railway, and air traffic). Guidelines for positioning of loudspeakers and outdoor microphones are also found in ISO 140-5. If traffic is applied as source, the “ls” in the index should be replaced by “tr”.

**Table 13 Impact Sound Insulation between Rooms – Definitions of Field Properties according to ISO 140-7**

Weighted Value	Equations <sup>a</sup> for 1/3 or 1/1 Octave Band	Explanations of Symbols <sup>b</sup>
$L'_{n,w}$	(2) $L'_n = L_i + 10 \log(A/A_0)$ dB	Impact sound pressure level, $L_i$ , is the average SPL in the receiving room when the floor under test is excited by the standardized impact source; it is expressed in decibels.
$L'_{nT,w}$	(3) $L'_{nT} = L_i - 10 \log(T/T_0)$ dB	

<sup>a</sup> Definitions and equation numbers refer to ISO 140-7:1998.<sup>8</sup>

<sup>b</sup> For explanation of  $A$ ,  $A_0$ ,  $T$ ,  $T_0$ ,  $A = 0.16V/T$ , see Table 11.

requirements, and classes A and B define higher levels of acoustical comfort. As a consequence, attention is drawn to the fact that the legislative requirements are minimum requirements, providing a possibility to voluntarily specify and design for a better acoustical quality.

## 6 FIELD MEASUREMENTS – CHECK OF COMPLIANCE WITH CRITERIA

A check for compliance with requirements may be made by carrying out field tests in the finished building. The equations to be applied, when testing sound insulation in buildings, are found in Tables 11, 12, and 13 for airborne sound insulation between dwellings, for facade sound insulation, and for impact sound insulation between dwellings, respectively. The evaluation concepts are found in the left columns in the tables. Names of properties and corresponding single-number quantities are described in Table 14.

The property to be measured in a specific situation is specified in the legal requirements or by the builder. The test results are to be compared with the limits, and the test methods are defined in the standards. Thus, it should be simple. However, in practice there are several precautions to take to ensure reliable sound insulation measurement results. Examples on questions and situations relate to among other things the shapes of the rooms, for example, irregular, long, narrow, staggered, partly divided, extremely complicated room geometry, big differences in room volume, and to microphone and source positions. Concerning facade sound insulation measurements, there are some additional questions about the type of source (traffic or loudspeaker). If a loudspeaker is used, which position should it be used in, how should it be arranged, and so forth.

Due to severe difficulties in the field, a whole set of guidelines have been made and published in ISO 140-14, which is to be applied in combination with ISO 140-4 and ISO 140-7. ISO 140-14 has five Annexes with guidelines aiming at more reliable measurements according to ISO 140-4 and ISO 140-7.

The extent of the guidelines indicates how important it is to choose concepts for building regulations that reduce the difficulties as much as possible, of course, also taking into account the importance

**Table 14 Names of Sound Insulation Field Properties Listed in Tables 11–13**

Term <sup>a</sup>	Symbol <sup>b</sup>	Definition
Apparent sound reduction index	$R'$	Table 11
Normalized level difference	$D_n$	Table 11
Standardized level difference	$D_{nT}$	Table 11
Apparent sound reduction index	$R'_{45^\circ}$	Table 12
Normalized level difference	$D_{2m,n}^c$	Table 12
Standardized level difference	$D_{2m,nT}^c$	Table 12
Normalized impact sound pressure level	$L'_n$	Table 13
Standardized impact sound pressure level	$L'_{nT}$	Table 13

<sup>a</sup> The corresponding single-number quantity has the same names with “Weighted” added in front of the term indicated; see also ISO 717.

<sup>b</sup> The corresponding single-number quantity has the same symbol with “w” added in the end of the index, see ISO 717.

<sup>c</sup> The index has a prefix “tr” or “ls” dependent on whether the sound source is traffic or a loudspeaker.

of correlation with subjective evaluation. Thus, it is important that the properties applied are well defined (i.e., all parts of the basic equation should exist) and that the results are reproducible, that is, the measurement uncertainty should be low, so it is easy to determine compliance with requirements. The goal for concepts must be a high correlation between prediction, measurement results, and subjective evaluation. This subject is further elaborated in Ref. 6.

## 7 SUMMARY

After approximately 50 years with almost no changes in building acoustical requirements in Europe, there is a trend toward stricter requirements, although the process is slow. During the last decade voluntary classification schemes describing different levels of acoustical comfort have been introduced in nine

countries in Europe, thus covering the need to define different quality levels.

A comparison between 24 European countries of the legal requirements for sound insulation between dwellings reveals significant differences concerning concepts as well as levels, and the requirements for facades differ even more. None of the voluntary classification schemes are identical.

The most recent version of standard ISO 717<sup>9</sup> has contributed to the diversity by allowing different concepts and by introducing spectrum adaptation terms with different—extended—frequency ranges toward lower and higher frequencies for the evaluation. In addition, national, special rules have been added in some countries to compensate for shortcomings or difficulties of field test procedures and conditions.

The findings do not reflect a harmonized Europe. In the future, efforts should be made to increase the harmonization of concepts (not necessarily levels), and the requirements for facades should be based on the harmonized environmental noise indicators  $L_{den}$  and  $L_{night}$  (see Ref. 2) for description of annoyance and sleep disturbance, respectively.

To gather information and share experiences more systematically about sound insulation requirements, a working group, EAA TC-RBA WG4,<sup>24</sup> has been established under the European Acoustical Association (EAA), Technical Committee Room and Building Acoustics (TC-RBA) aiming at recommendations for harmonization of concepts applied for sound insulation requirements.

More noise sources—including neighbors' activities—and an increased demand for high quality and comfort together with a trend toward lightweight constructions are contradictory and call for optimizing building design using acoustical prediction models; see Ref. 19.

The benefits of a harmonization include facilitating the exchange of information and experience and development of design tools. Based on the experience, legal requirements and classification criteria might be adjusted and optimized.

**Acknowledgments** The author is grateful to all the people who provided information about national sound insulation requirements and classification schemes. I hope that the data have been correctly understood and described. Any corrections or updates of information will be appreciated.

## REFERENCES

1. C. J. Grimwood, Effects of Environmental Noise on People at Home, BRE information paper IP 22/93, 1993.
2. S. Wibe, *Efterfrågan på tyst boende* (The Demand for Silent Dwellings), Anslagsrapport A4:1997, Byggnadsnämnden, Stockholm, Sweden, 1997.
3. W. E. Blazier and R. B. DuPree, Investigation of Low-Frequency Footfall Noise in Wood-Frame, Multifamily Building Construction, *J. Acoustic. Soc. Am.*, Vol. 96, No. 3, 1994, pp. 1521–1532.
4. B. Rasmussen, Sound Insulation between Dwellings—Classification Schemes and Building Regulations in Europe, InterNoise 2004, Prague, Paper ID 778, 2004.
5. B. Rasmussen and J. H. Rindel, Concepts for Evaluation of Sound Insulation of Dwellings—From Chaos to Consensus? Forum Acusticum 2005, Budapest, Hungary, Paper ID 7820, 2005.
6. European Directive 2002/49/EC of 25 June 2002 Relating to the Assessment and Management of Environmental Noise, Note: Often referred to as the Environmental Noise Directive or END, Europe—Environment—Noise Policy, <http://www.europa.eu.int/comm/environment/noise/home.htm>.
7. Research for a Quieter Europe in 2020, An updated strategy paper of the CALM network, European Commission, Research Directorate—General, 2004. [http://www.calm-network.com/index\\_preports.htm](http://www.calm-network.com/index_preports.htm).
8. ISO 140, Acoustics—Measurement of Sound Insulation in Buildings and of Building Elements:
  - Part 1: Requirements for Laboratory Test Facilities with Suppressed Flanking Transmission, 1998.
  - Part 1: AMD 1: Specific Requirements on the Frame of the Test: 2004.
  - Part 2: Determination, Verification and Application of Precision Data, 1991.
  - Part 3: Laboratory Measurements of Airborne Sound Insulation of Building Elements 1995.
  - Part 3: AMD 1: Installation Guidelines for Lightweight Twin Leaf Partitions, 2004.
  - Part 4: Field Measurements of Airborne Sound Insulation between Rooms, 1998.
  - Part 5: Field Measurements of Airborne Sound Insulation of Facade Elements and Facades, 1998.
  - Part 6: Laboratory Measurements of Impact Sound Insulation of Floors, 1998.
  - Part 7: Field Measurements of Impact Sound Insulation of Building Elements, 1998.
  - Part 8: Laboratory Measurements of the Reduction of Transmitted Impact Noise by Floor Coverings on a Heavyweight Standard Floor, 1997.
  - Part 9: Laboratory Measurements of Room-to-Room Airborne Sound Insulation of a Suspended Ceiling with a Plenum above, 1985.
  - Part 10: Laboratory Measurements of Room-to-Room Airborne Sound Insulation of a Suspended Ceiling with a Plenum above it, 1991.
  - Part 11: Laboratory Measurements of the Reduction of Transmitted Impact Noise by Floor Coverings on Lightweight Framed Standard Floor, 2005.
  - Part 12: Laboratory Measurements of Room-to-Room Airborne and Impact Sound Insulation of an Access Floor, 2000.
  - Part 13: Guidelines, ISO/TR 140-13:1997.
  - Part 14: Guidelines for Special Situations in the Field, 2004.
9. ISO 717, Acoustics—Rating of Sound Insulation in Buildings and of Building Elements
  - Part 1: Airborne Sound Insulation, 1996.
  - Part 2: Impact Sound Insulation, 1996.
10. ISO/R 717:1968, Rating of Sound Insulation for Dwellings.
11. ISO/R 140:1960, Field and Laboratory Measurements of Airborne and Impact Sound Transmission.
12. ISO 717, Acoustics—Rating of Sound Insulation in Buildings and of Building Elements:
  - Part 1: Airborne Sound Insulation in Buildings and of Interior Building Elements, 1982.
  - Part 2: Impact Sound Insulation, 1982.



- Part 3: Airborne Sound Insulation of Facade Elements and Facades, 1982.
13. ISO 140:1978, Acoustics—Measurement of Sound Insulation in Buildings and of Building Element, Parts I, II, III, IV, V, VI, VII, VIII; extended by part 9 in 1985 and part 10 in 1991 (Parts I–VIII revised 1991–1998, see Ref. 8).
  14. A. C. C. Warnock, Floor Research at NRC Canada, Conference in Building Acoustics, Acoustic Performance of Medium-Rise Timber Buildings, Dec. 3–4, Dublin, Ireland, 1998.
  15. A. C. C. Warnock, Impact Sound Ratings: ASTM versus ISO, InterNoise 2004, Prague, Paper ID 694, 2004.
  16. M. Koyasu, J. Yoshimura, and H. Tachibana, Building Acoustics Classifications for Sound Insulation in Japan, InterNoise 2004, Paper ID 773, 2004.
  17. EN 12354, Building Acoustics—Estimation of Acoustic Performance of Buildings from the Performance of Elements:  
Part 1: Airborne Sound Insulation between Rooms, 2000.  
Part 2: Impact Sound Insulation between Rooms, 2000.  
Part 3: Airborne Sound Insulation against Outdoor Sound, 2000.  
Part 4: Transmission of Indoor Sound to the Outside, 2000.  
Part 5: Sound Levels Due to Service Equipment in Buildings, prEN, 2004.  
Part 6: Sound Absorption in Enclosed Spaces, 2003.  
Note: Parts 1–4 have been published as ISO 15712 standards in 2004.
  18. ISO 10848, Acoustics—Laboratory Measurement of the Flanking Transmission of Airborne and Impact Noise between Adjoining Rooms:  
Part 1: Frame Document, 2005.  
Part 2: Application to Light Elements When the Junction Has a Small Influence, 2005.  
Part 3: Application to Light Elements When the Junction Has a Substantial Influence, 2005.  
Part 4: All Other Cases, ISO/CD 2004.
  19. E. Gerretsen, Development and Use of Prediction Models in Building Acoustics as in 12354, Forum Acusticum, Budapest, Hungary, Paper ID 2290, 2005.
  20. ÖNORM B 8115-2:2002–12–01, Schallschutz und Raumakustik im Hochbau. Teil 2: Anforderungen an den Schallschutz (Sound Insulation and Room Acoustics in Building Construction—Part 2: Requirements for Sound Insulation), 2002.
  21. F. Bruckmeyer and J. Lang, Richtlinien für die Anwendung wirtschaftlicher Schallschutzmassnahmen im Wohnungsbau als Vorbereitung für legislative Massnahmen (Guidelines for the Application of Economic Sound Insulation Measures in Residential Housing as a Preparation for Legislative Measures), Report No. 55, Research Institute for Housing, Building and Planning, Vienna, 1974.
  22. J. Seller, Airborne Sound Insulation Requirements in England from the 1950s to the Present, Forum Acusticum Budapest, Hungary, Paper ID 8760, 2005.
  23. M. J. Patterson, Recent Changes to the Sound Insulation Provisions of the Building Code of Australia, Professional Services, Australian Building Codes Board, Canberra, Australia, Acoustics Forum, 2004.
  24. EAA TC-RBA WG4, Sound Insulation Requirements and Sound classification—Harmonization of Concepts, European Acoustical Association (EAA), Technical Committee Room and Building Acoustics (TC-RBA); see <http://www.eaa-fenestra.org/TCs/RBA/Workgroups/WG4>.
  25. B. Rasmussen, Facade Sound Insulation Comfort Criteria in European Classification Schemes for Dwellings, EuroNoise 2006, Tampere, Finland, Paper ID 434, 2006.
  26. DS 490:2001, Lydklassifikation af boliger (Sound Classification of Dwellings), Denmark, 2001, under revision.
  27. SFS 5907:2004, Rakennusten Akustinen Luokitus, Finland, English version Acoustic Classification of Spaces in Buildings, July 2005.
  28. IST 45:2003, Acoustics—Classification of Dwellings, Iceland, 2003.
  29. NS 8175:2005, Lydforhold i bygninger, Lydklassifisering av ulike bygningstyper (Sound Conditions in Buildings—Sound Classes for Various Types of Buildings), Norway, 2005.
  30. SS 25267:2004, Byggakustik—Ljudklassning av utrymmen i byggnader—Bostäder (Acoustics—Sound Classification of Spaces in Buildings—Dwellings), Sweden, 2004.
  31. La méthode qualitel, Association Qualitel, France, 2000.
  32. VDI 4100:1994, Schallschutz von Wohnungen—Kriterium für Planung und Beurteilung, Germany, 1994.
  33. STR 2.01.07:2003, Dėl Statybos Techninio Reglamento Str 2.01.07:2003; Pastatu Vidaus Ir Isores Aplinkos Apsauga Nuo Triuksmo (Lithuanian Building Regulations. Protection Against Noise in Buildings), Patvirtinimo, Lithuania, 2003.
  34. NEN 1070:1999, Geluidwering in gebouwen—Specificatie en Beoordeling van de Kwaliteit (Noise Control in Buildings—Specification and Rating of Quality), The Netherlands, 1999.
  35. J. H. Rindel, On the Influence of Low Frequencies on the Annoyance of Noise from Neighbours, InterNoise Korea, 2003, PaperID N1038, 2003.
  36. K. Bodlund, Rating of Impact Sound Insulation between Dwellings, Technical Report SP-RAPP 1985–01. Includes the article: Alternative Reference Curves for Evaluation of the Impact Sound Insulation between Dwellings, *J. Sound Vib.*, Vol. 102, No. 3, 1985, pp. 381–402.
  37. INSTA 122, Sound Classification of Dwellings, Revised Final DP INSTA 122, Aug. 1998.
  38. K. Hagberg, Ljudkrav med stöd av ISO/DIS 717 (Acoustic Requirements Supported by ISO/DIS 717), NKB Committee and Work Reports 1996:02, Nordic Committee on Building Regulations, Helsinki, Finland, 1996.
  39. S. Hveem, A. Homb, K. Hagberg, and J. H. Rindel, Low-Frequency Footfall Noise in Multi-storey Timber Buildings, NKB Report 1996:12E, Nordic Committee on Building Regulations, Finland, 1996.
  40. B. Rasmussen, Implementation of the New ISO 717 Building Acoustic Rating Methods in Europe, NKB Report 1996:04E, Nordic Committee on Building Regulations, Finland, 1996.
  41. DIN 4109:1989, Schallschutz im Hochbau. Beiblatt 2. Hinweise für Planung und Ausführung. Vorschläge für einen erhöhten Schallschutz. Empfehlungen für den Schallschutz in eigenen Wohn- oder Arbeitsbereich (Sound Insulation in Buildings; Guidelines for Planning and Execution; Proposals for Increased Sound Insulation; Recommendations for Sound Insulation in Personal Living and Working Areas), 1989.

# CHAPTER 115

## NOISE IN COMMERCIAL AND PUBLIC BUILDINGS AND OFFICES – PREDICTION AND CONTROL

**Chris Field**

Arup Acoustics San Francisco  
San Francisco, California

**Fergus Fricke**

School of Architecture  
University of Sydney  
Sydney, New South Wales, Australia

### 1 INTRODUCTION

Commercial and public buildings such as offices, malls, stores, motels, hospitals, schools, universities, airport terminals, law courts, police stations, libraries, museums, and churches all have the potential to be seriously effected by noise. These buildings represent a very diverse group. Although some buildings may require special noise control considerations, for most of these buildings, it is possible to set down a general approach to noise control by considering noise criterion, noise sources (such as transportation and mechanical services), and noise control techniques. The most common techniques include consideration of transmission of sound through walls and floors, vibration isolation, and sound absorption in the rooms. A commonly used method of designing for noise in commercial and public buildings is given, based on tabulated data of planning noise criteria, interior sound sources, measurements or estimates of exterior noise, and the acoustical properties of materials and constructions. In some special buildings, such as concert halls, a more sophisticated approach to noise control must be used and noise issues considered at an early stage in the design.

### 2 GENERAL APPROACH TO NOISE CONTROL IN BUILDINGS

Noise control in commercial and public buildings usually involves consideration of the effect of sound transmission from interior and exterior sources and the reverberation of sound in occupied spaces, on speech privacy, speech intelligibility, and annoyance. In some cases, issues of concentration on tasks, sleep, and even health and social behavior may also need to be considered. The interior noises of concern may be air-conditioning systems, office equipment such as computers and copiers, conversations, or coffee makers. The external sound sources are usually associated with roads, rail traffic, aircraft, building or mechanical services involving pumps

or fans but not building construction, and other temporary or intermittent activities such as lawn mowing. The acoustical design of a building may also involve the impact, on neighboring buildings, of noise generated in or by the building being designed.

Design for noise in buildings can be considered under the usual three categories of source(s), path(s), and receiver(s). Where external noise sources are concerned, there is no opportunity for controlling noise at the source and very little opportunity for controlling noise at the receiver, and so noise control is predominantly by the building fabric. Building siting is important as noise problems can be caused to, as well as from, the local environment. For internal noise sources there is some possibility of source noise control, by the selection of mechanical plant, for instance, but again the control of noise is predominantly by the building fabric and the layout of the building (where sensitive and noisy spaces are located).

The approach to noise control then amounts to the determination of potential sound pressure levels from interior and exterior noise sources, the selection of appropriate noise criteria for the activities to be carried out in spaces in the building, and the design of the layout of the building and specification of materials, construction, and finishes in the building. One acoustical design approach is to estimate or measure the peak sound pressure levels at the building site and design the external envelope to reduce these to A-weighted levels about 5 dB below the background noise level caused by the air-conditioning system or the sound system designed to produce masking noise.

In the design procedure presented here, single-number criteria, sound pressure levels, and properties of materials and constructions are used. A frequency-dependent approach, such as in the music and media facilities, for instance, is beyond the scope of this chapter but is addressed in other texts, as are other design procedures.<sup>1–4</sup>

### 3 PLANNING NOISE CRITERIA

The siting of a building can be as important for producing a satisfactory sound environment (both inside and outside a building) as the design of the building itself. Whether this needs to be considered depends on the existing (and potential future) external noise sources, the sensitivity of the occupants, the activities in the building, and the budget for the building. It is always possible to design and construct buildings such as airport terminals and airport hotels for very noisy environments, but noise control comes at a price that tends to increase exponentially with the degree of noise control. It should be understood though that while it is possible to achieve a satisfactory internal sound environment in a building near a major airport or highway, this is unlikely if the building is to be naturally ventilated.

Often the most effective way of dealing with external noise is by way of site selection. In some countries there are standards and codes regulating or giving recommendations for the siting (and construction) of buildings in relation to major transportation noise sources.<sup>5,6</sup> Noise-sensitive buildings such as schools should generally not be sited on busy roads or under flight paths. Likewise, rooms that are noise sensitive should not be located near rooms in which the sound pressure level is expected to be high. For example, a plant room located directly above a CEO's office is not good planning.

There are many different planning criteria worldwide, and so it is difficult to give general coverage to this aspect of planning for noise and noise control. Here we give some recommended planning noise levels for Denmark<sup>7</sup> as it has some of the most stringent recommendations. In general Denmark follows World Health Organization and the Organization of Economic Cooperation and Development recommendations<sup>8,9</sup> and avoids using source-specific noise metrics. The Danish planning levels are of particular interest because they address the issue of different sound sources, of the times of occurrence of the noise, the character of the noise (low-frequency content and tonal and impulse corrections for some sources), and peak sound and vibration levels. Examples of the planning levels, which are not mandatory, are summarized in Table 1 for commercial and public buildings. Such criteria usually refer to sound pressure levels 1.2 m above the ground at the boundary of the nearest property and at least 2 m away from a building facade.

### 4 BUILDING NOISE CRITERIA

One of the most interesting aspects of designing buildings is the difficulty in dealing with multiple requirements that may be contradictory. Developing noise criteria is no exception and cannot be treated in isolation. For example, there is little point in specifying double glazing to control external noise if windows need to open for ventilation.

Theoretically (simplistically), it should only be necessary to set criteria based on acceptable internal sound pressure levels in spaces for the activities being

carried out in the building. In practice, it is usually necessary to specify the sound isolation performance of common walls between spaces, for example, the sound transmission class (STC), or weighted sound reduction index ( $R_w$ ) value of walls separating motel rooms, as well as reverberation times. The STC ( $R_w$ ) values are set because it is not possible to estimate what sound sources will be present in a building during its life, and, like other aspects of the environment, buildings can only be expected to moderate the external environmental conditions, such as noise events, rather than to produce constant sound pressure levels. Reverberation time is important for aural comfort as well as controlling sound pressure levels.

Much of the material on recommended sound levels in buildings has been developed over many years and should be considered as a mixture of practical and idealistic criteria. The interior sound pressure levels specified in Table 2 are for unoccupied spaces with air-conditioning and other services operating. The levels are assumed to be approximately steady, and so there is no need to specify a noise metric that accounts for temporal variations in the noise. For temporal variations of less than  $\pm 3$  dB an arithmetic average level can be assumed. For greater variations in level a metric such as  $L_{Aeq}$  should be used, but existing interior noise criteria should be considered as suitable for quasi-steady-state situations. There are other noise metrics used, for example, balanced noise criterion (NCB) and room criteria (RC)<sup>10,11</sup> besides the two common ones, noise criterion (NC) and  $L_{Aeq}$ , in Table 2. There are more comprehensive tabulations of indoor noise criteria.<sup>12,13</sup> Typical values of recommended sound isolation performances of walls in office buildings are given in Table 3.

There can be too little noise as well as too much noise, although this is rare. If the sound pressure levels in a building are too low, then minor activity noise can be disruptive and speech privacy cannot be achieved with economically viable constructions. If external sound pressure levels are low and a building is naturally ventilated, then again it may be difficult/expensive to achieve satisfactory speech privacy between workstations in open-plan offices or to control noise from the building affecting neighbors, for example, a school next to residential buildings.

An office building containing open-plan offices with many workstations is a special case where a compromise on background noise, screen, or partial-height partition attenuation values, speech level, and reverberation time must be considered to achieve adequate speech privacy and adequate speech intelligibility within a workspace (see also Chapter 109).

### 5 NOISE SOURCES

The noise sources that should be considered in commercial and public buildings can be considered in two categories: external and internal.

The major external noise sources are usually concerned with transportation: road traffic, aircraft, trains, and, occasionally, shipping. However, there are many other sources that may be significant at a given site.

**Table 1 Partial Summary of Danish Recommended Planning Sound Pressure Levels**

<b>a. Noise Limits from Commercial and Industrial Enterprises<sup>a</sup></b>			
Building location and use	Mon–Fri, 7 a.m.–6 p.m.,	Mon–Fri, 6–10 p.m., Sat, 2–10 p.m., Sun and public holidays, 7 a.m.–10 p.m.	All days, 10 p.m.–7 a.m.
Commercial and industrial areas	Sat, 7 a.m.–2 p.m. 70 dB	70 dB	70 dB
Mixed residential/commercial areas, urban centers	55 dB	45 dB	40 dB
<b>b. Recommended Limit Values for Use When the Enterprise and the Dwelling Are Located in the Same Building<sup>b</sup></b>			
	Day and evening, 7 a.m.–10 p.m.		Night, 10 p.m.–7 a.m.
Enterprises, apart from offices	50 dB		50 dB
Offices	40 dB		40 dB
Rooms in dwellings	30 dB		25 dB
<b>c. Recommended Road Traffic Noise Limits<sup>c</sup></b>			
Public institutions (hospitals, educational institutions, schools): 55 dB			
Service enterprises, (hotels, offices, etc.): 60 dB			
<b>d. Recommended Train Noise Limits<sup>d</sup></b>			
Public institutions (hospitals, schools, etc.): 60 dB			
Service enterprises (hotels, offices, etc.): 65 dB			
<b>e. Recommended Aircraft Noise Limits<sup>e</sup></b>			
Residential areas and noise-sensitive public institutions (schools, hospitals, nursing homes, etc.): 55 dB			
Service enterprises (hotels, offices, etc.): 60 dB			

<sup>a</sup>The noise limits in part (a) are A-weighted equivalent sound pressure levels ( $L_{Aeq}$ ), i.e., the energy averaged value over a specified period (8 h during the day, 1 h in the evening, and one-half hour at night). If the noise contains clearly audible tones or impulses, 5 dB must be added to the equivalent noise level to determine the noise rating level. The recommended noise limits refer to outdoor sound pressure levels.

<sup>b</sup>The recommended limit values in part (b), for noise from an enterprise, are indoor A-weighted equivalent sound pressure levels ( $L_{Aeq}$ ).

<sup>c</sup>Outdoor recommended limits in part (c) are 24-h  $L_{Aeq}$  values.

<sup>d</sup>The limits specified in part (d) are outdoor 24-h  $L_{Aeq}$  values. There are also requirements governing both the maximum sound and vibration levels at individual dwellings. The recommended maximum limit value is an A-weighted sound pressure level of 85 dB. To avoid vibrations, minimum planning distances have been laid down for the distance from a building to the center of the tracks.

<sup>e</sup>The recommendations quoted in part (e) are A-weighted equivalent sound pressure levels over a 24-h period ( $L_{Aeq}$ ), where 5 dB has been added to the sound pressure levels in the evening period (7–10 p.m.) and 10 dB to the sound pressure levels at night (10 p.m.–7 a.m.) for commercial and military aircraft.

Source: From Ref. 7.

**Table 2 Examples of Approximate Recommended Sound Pressure Levels (Unoccupied) and Reverberation Times<sup>a</sup>**

Room	A-weighted	NC	RT (s)
Private office	40	35	0.5
General office	45	40	0.5
Courtroom	40	35	0.8
Churches	35	30	1.0
Hospital ward	35	30	0.5
Hotel/motel bedroom	35	30	0.5
Restaurants	45	40	<1.0
Classroom/conference room	35	30	0.7

<sup>a</sup>Appropriate values in this table may depend on room size, amplification, and other factors.

Noise from industrial sites as well as sporting and cultural activities are occasionally significant. For schools the external sounds of children playing may be noise for classrooms. In public and commercial buildings noise sources such as fans and chillers in adjacent buildings and utilities such as transformers, sewage, and water pumps can be of concern, but these sources are usually controlled under environmental protection legislation. Construction site noise and alarms on buildings and vehicles can also be annoying sources, but these are infrequent events and are not designed for.

The major noise sources inside buildings besides people activity noises, such as conversations, footsteps, doors closing, sound systems, and music, are the heating, air-conditioning, and ventilation systems used.

**Table 3 Examples of Recommended Laboratory Measured STC ( $R_w$ ) Values to Achieve Adequate Sound Pressure Levels and Speech Privacy<sup>a</sup>**

Room	Adjacent Room	STC ( $R_w$ ) Value of Common Wall/Floor
General office	Corridor/lobby	45
	Plant room	60
Conference room	Conference room	50
	Office	50
	Toilet	55
	Plant room	60
Private office	Private office	50
	General office	45
	Corridor/lobby	50

<sup>a</sup>(These should be considered as approximate as published recommendations vary by about  $\pm$ STC 5 from the values listed in table.)

Other building services, such as lifts and plumbing, can also be important. External sound pressure levels can be measured at a site or can be estimated based on traffic usage of nearby roads, railroads, or aircraft flight paths, although whether these sound pressure levels will be maintained over the lifetime of the building is dubious.

### 5.1 Road Noise

There are many procedures for the estimation of road traffic noise<sup>14,15</sup> (see also Chapter 120) and recommendations for location of buildings based on noise metrics such as  $L_{A10}$  and  $L_{Aeq}$ . These methods take account of the vehicle flow rates, the mix of light and heavy vehicles, the speed of vehicles, whether the vehicles are freely flowing or not, the road gradient, the road surface, the topography of the surroundings, the distance to the road from the site under consideration, and the presence of roadside barriers or other buildings. Obviously, the noise will also depend on the make and model of vehicles and how well the vehicles are maintained.

An approximate estimate of the  $L_{Aeq}$  from a road over flat ground can be obtained from

$$L_{Aeq} = 55 + 10 \log(Q) + 0.3p - 20 \log(d) \quad \text{dB}$$

where  $Q$  is the vehicle flow rate in vehicles per hour,  $p$  is the percentage of heavy vehicles, and  $d$  is the distance in metres from the center of the nearside traffic flow. To achieve a value of  $L_{Aeq}$  of 55 dB with a traffic flow of 1000 vehicles per hour and 10% heavy vehicles would require a distance of approximately 50 m from the road.

### 5.2 Aircraft Noise

There are a bewildering number of aircraft noise metrics [e.g., maximum overpass sound pressure level ( $L_{max}$ ), noise and number index (NNI), noise exposure forecast (NEF), Australian noise exposure forecast (ANEF), and time above A-weighted sound pressure

level of 70 dB (TA70)] and an even larger number of aircraft types, movements, loadings, flight paths, weather conditions and other factors that can affect the sound pressure levels at a building site (see also Chapter 125). It is not possible to give approximate estimates of sound pressure levels experienced near airports, but data on at least one noise metric are often available from aviation authorities for specific airports and military airfields. This is in the form of noise contours, often averaged over a year. Approximate maximum sound pressure levels at a site can be estimated from the maximum pressure level of large commercial aircraft measured during takeoff: approximate A-weighted noise level of 110 dB at 150 m. For most commercial buildings aircraft noise should not be a problem if the building is more than 1 km to the side of a flight path. For public buildings this sideline distance may need to be more than 2 km.

### 5.3 Air-Conditioning Noise Sources and Control

The main noise sources in air-conditioning systems are the fans, chillers, cooling towers, airflows through ducts, grills and diffusers, and flanking transmission through ducts and plenums (see also Chapters 110 and 112). The control of these sources is largely by the appropriate siting and selection of mechanical equipment, silencers, duct sizes, and linings.<sup>16</sup>

### 5.4 Airborne and Structure-Borne Noise and Vibration Transmission in Commercial Buildings

In commercial buildings as in other buildings and structures, there are two basic forms of sound transmission between spaces: airborne and structure-borne or vibration transmission (see also Chapter 105). Airborne sound transmission, as the name suggests, is the transmission of acoustic energy through the air for all or part of its transmission. Structure-borne transmission involves the direct excitation of the structure by a services source such as a fan or pump or by activity in the building such as people walking on floors with hard surfaces or doors closing, or sporting activity such as a bouncing ball or water lapping against the sides of a swimming pool. Such sound transmission may not be noticeable to occupants of the room in which the source is located but can be annoying to occupants in other parts of the building.

The STC ratings of single-leaf walls, such as solid masonry walls, is wholly determined by the surface density of the wall. For a given type of composite construction, for example, gypsum board on metal studs, the STC value is still mainly dependent on the surface density of the wall, but other factors such as the size, spacing and gauge of the studs, the type and thickness of the absorbing material between the studs, and the use of resilient channels (vibration isolation) all influence the performance. Table 4 indicates approximate values of different constructions and more detailed information can be found elsewhere.<sup>17-19</sup>

Structure-borne sound transmission is dealt with by specifying the impact isolation class (IIC) of floors, the

vibration isolation required for different types of rotating machinery, its weight, its center of gravity and floor construction and span, and the vibration isolation of supply and waste pipes from the building structure.<sup>20</sup>

## 6 FLANKING TRANSMISSION

Transmission of sound that is not via the most direct path or the major dividing element between spaces is known as flanking transmission. Thus, sound that travels via an air-conditioning duct that services two adjacent rooms is considered to be flanking transmission because the direct transmission path (the shortest path) is through the common wall. Sound transmission is more likely to be affected by flanking transmission the greater the acoustic performance of the common wall is. Below STC ( $R_w$ ) 35 flanking transmission can usually be ignored. Above STC 55 flanking transmission usually dominates transmission due to poor sealing of joints within the wall or between the wall and other building elements such as other walls or the ceiling or in the air gaps around a door or through a suspended ceiling or return-air plenum or because of the chasing of electrical or hydraulic services within a wall.

There is one flanking transmission path that is often significant in commercial buildings: transmission of sound through suspended ceilings from one office to another. This type of transmission is important because office partitions are often built to the suspended ceiling and not the structural slab. This allows flexibility in office layout without the need to relocate services above the suspended ceiling. However, suspended ceilings often have low mass and hence low STC ratings.

A doorway through a high-performance wall is a sure way of degrading the acoustic performance of a wall, as is the use of return-air grills in doors. Operable walls such as folding and sliding doors tend to have poor acoustic performances partially because of the difficulty in sealing them. The fitting of lightweight partitions is also important.<sup>21</sup>

## 7 EFFECT OF CONSTRUCTION OF WALLS AND FLOORS BETWEEN INHABITED SPACES

Although there are sophisticated theoretical and empirical equations for calculating the transmission of sound through walls and floors, most of the data used for design purposes comes from laboratory tests. Simple theory based on the surface density of a wall is often adequate for single-leaf constructions. For masonry walls it gives STC values within about  $\pm$ STC 2, and there is little advantage in achieving greater accuracy because of wall material, construction, and flanking path variability. The simple model for random incidence sound transmission loss (TL) (also known as sound reduction index) is

$$TL(\text{dB}) = 20 \log(fm) - 47$$

where  $f$  is the frequency (in Hz) (using  $f = 500$  will give an estimate of the STC value) and  $m$  is the surface density (in  $\text{kg/m}^2$ ). Double-leaf constructions

and lightweight constructions require more complex analysis.<sup>22</sup>

Besides mass and frequency there are three major factors effecting the sound transmission through walls and floors:

- Whether the wall or floor is a single- or multiple-leaf construction
- Whether, in the case of double- or multiple-leaf construction, the wall-floor has sound-absorbing treatment in the cavity
- Whether, in the case of double- or multileaf construction, the wall-floor has structural isolation (e.g., staggered stud wall or floated floor)

There are many possible constructions for walls and windows and as well as combinations of these. For design purposes it is useful to have some examples. These are given in Table 4 for walls and Table 5 for floors with more comprehensive data available elsewhere.<sup>17-19</sup>

## 8 COMPOSITE CONSTRUCTIONS

It is often the case that walls in commercial and public buildings are not uniform in construction because of doors, windows, or vents. In such situations the values in Tables 4 and 5 may also be used to estimate the “effective” (or “apparent,” “composite,” or “resultant”) STC value due to the inclusion of these other elements. The effective STC value,  $STC_{\text{eff}}$ , of the wall will depend on the relative areas and one-third octave transmission loss (TL) values of the elements (including air gaps) that form the wall. The expression for calculating the effective transmission loss,  $TL_{\text{eff}}$ , at a given frequency, is given below. It is common practice to use the same expression for calculating the effective STC value of the common wall by substituting STC for TL.

$$TL_{\text{eff}} = 10 \log \left[ \sum A_i / \sum (A_i \times 10^{-0.1 TL_i}) \right]$$

where  $A_i$  is the area of the  $i$ th component of the wall (in  $\text{m}^2$ ) and  $TL_i$  is the transmission loss of the  $i$ th component.

**Example** A wall is composed of brick (STC of 50 and area of  $10 \text{ m}^2$ ) and a window (STC of 20 and area of  $1 \text{ m}^2$ ):

$$\begin{aligned} STC_{\text{eff}} &= 10 \log[11/(10 \times 10^{-5} + 1 \times 10^{-2})] \\ &= 10 \log(11 \times 10^2) \\ &= 30 \end{aligned}$$

## 9 USE OF SOUND-ABSORBING MATERIALS

The use of sound-absorbing materials in buildings is important for speech intelligibility, aural comfort, and controlling sound pressure levels from mechanical services or other sources. (see also Chapter 104) In

**Table 4 Representative Transmission Class (STC/ $R_w$ ) Data for Walls, Doors and Windows (to Nearest STC5)**

Construction	STC/ $R_w$
<b>24-g Metal Studs</b>	
16-mm GB <sup>a</sup> each side of 65-mm studs at 600-mm centers, no absorption	40
16-mm GB each side of 65-mm studs at 600-mm centers, 40-mm FG <sup>b</sup>	45
2- × 16-mm GB each side of 65-mm studs at 600-mm centers 40-mm FG	55
2- × 16-mm GB each side of 90-mm studs 600 o.c., <sup>c</sup> no absorption between studs	50
2 × 16-mm +1- × 16-mm GB on 65-mm studs 600 o.c., 80-mm FG between studs	55
2 × 16-mm GB each side of 90-mm studs 600 o.c., 80-mm FG between studs	55
3 × 16-mm GB each side of 90-mm studs 600 o.c., 80-mm FG between studs	60
<b>20-g Metal Studs</b>	
2- × 16-mm GB each side of 90-mm studs 600 o.c., 80-mm FG between studs	50
As above with resilient channels on one side	60
<b>Wood Studs</b>	
16-mm GB each side of 50- × 100-mm studs at 600-mm centers, no absorption	35
As above but with 80-mm FG and resilient channels on one side	50
As above but with 2- × 16-mm GB on each side of studs and 50-mm FG	60
<b>Brick</b>	
Single brick	45
Double brick	50
Cavity brick	55
<b>Concrete Block</b>	
100-mm hollow lightweight	45
As above with 13 mm render both sides	50
100-mm hollow lightweight with 16-mm GB on resilient channels	55
<b>Solid Concrete</b>	
150 mm thick	55
As above with 40-mm FG +16-mm GB on 50-mm wood furring	60
<b>Windows</b>	
3 mm, fixed glazing	25
6 mm, fixed glazing	30
10 mm, laminated, fixed	35
Double glazing (4-mm glass, 50-mm airspace, 4-mm glass)	40
<b>Doors</b>	
Hollow core, no seal/gasket	15
Solid (35 mm) without seals	20–25
Solid (35 mm) with seals	25–30

<sup>a</sup>GB = gypsum board or similar.<sup>b</sup>FG = fibreglass batt or similar.<sup>c</sup>On centerline.

commercial and public buildings absorbing materials are more likely to be of use in reducing reverberation time in large spaces such as courts, multipurpose halls, and landscaped offices. The reason why special

**Table 5 Representative Transmission Class (STC/ $R_w$ ) and Impact Isolation Class [IIC( $L_{nTw}$ )] Data for Floors**

Construction	STC/ $R_w$	IIC( $L_{nTw}$ )
Concrete slab		
150 mm thick	55	25(85)
150 mm thick with carpet and underlay	55	85(25)
150 mm thick with 50-mm slab on isolation pads	60	< 70(> 40)
150 mm thick with wood on furring on pads	60	65(45)

absorbing treatments on walls and ceilings are often of limited use for controlling noise is worth considering as such treatments can be an expensive exercise giving little return when a room is carpeted and has other sound-absorbing furnishings.

In most office spaces speech privacy and low sound pressure levels are aimed for, but these two requirements are, to a degree, mutually exclusive. [A quiet space is one in which conversations can be most easily overheard and where there are the greatest distractions. When the A-weighted sound pressure level exceeds 50 dB, the noise increasingly becomes distracting.] Lower sound pressure levels would result if a ceiling with a higher absorption (NRC\* value) were used but by how much? In general terms, if the existing amount of absorbing material in a room is  $A_1$  m<sup>2</sup> sabin ( $A_1 = \sum(A_i \times NRC_i)$  where  $A_i$  is the area of surface  $i$  of absorption  $NRC_i$ ) and the absorption is increased to  $A_2$  m<sup>2</sup> sabin, the reduction in sound pressure level in the reverberant field (there will be no reduction in sound pressure level in the direct field near the source) will be  $10 \log(A_2/A_1)$ , which, for a doubling of the average NRC value or area of absorbent, results in a 3-dB reduction in the sound pressure level. However, if there is already a carpet or an acoustic ceiling and absorbent furnishings such as upholstered chairs and curtains, it would be difficult to double the amount of absorbing material in the room, and so any change in the sound pressure level will be small. A doubling of the absorption in a room results in the halving of the reverberation time (reverberation time is inversely proportional to the total absorption), which could have a significant influence on the perception of noise in the room.

\*NRC is a commonly used single-figure rating system for materials used where speech is of major importance. It is an average absorption coefficient in the speech frequency range. An NRC rating of 0 means the material reflects all the sound and a value of 1 means it absorbs all the sound. NRC values do not tell the complete story. A high NRC value might be achieved even though the material absorbs sound poorly at low frequencies, for instance. In such a case a room would sound "boomy," and low-frequency absorption using panels of resonant absorbers may need to be used. See Table 6 and other references<sup>23–25</sup> for some examples of materials and their NRC values.

**Table 6 Representative Absorption Coefficients of Materials**

Material/Construction	NRC <sup>a</sup>
Masonry walls	
Clay brick (glazed or painted)	0.05
Concrete block (coarse)	0.30
Concrete block (painted)	0.05
Masonry plastered	0.05
Marble or glazed tiles	0.00
Sound-absorbing concrete blocks	0.50
Stud walls/panels	
Any gypsum board wall, e.g., 13-mm	0.05
GB on each side of 90-mm studs	
6-mm plywood with airspace behind	0.10
Floors	
Wood floor on joists	0.05
Concrete or terrazzo	0.00
Linoleum, rubber or vinyl tiles	0.05
Carpet	
3-mm pile	0.15
6-mm pile heavy, foam backed	0.25
	0.55
Glass	
3 mm	0.15
>6 mm	0.05
Ceilings	
12-mm gypsum board	0.05
Rigid mineral fibreboard suspended ceiling	0.60
Cellulose sprayed-on absorbent, 16 mm thick	0.55
Furnishings	
Curtains	
10 oz velour, straight	0.15
18 oz velour, 50% full	0.55
Fabric- or vinyl-covered fiberglass wall panels 50 mm thick	0.80
Fabric- or vinyl-covered fiberglass wall panels 100 mm thick	0.95
People	
On medium upholstered seats	0.80
On hard seats	0.55

<sup>a</sup>The NRC values of some of these finishes, e.g., ceiling panels, will depend on the mounting conditions.<sup>26</sup>

## 10 SOUND INSULATION AGAINST TRAFFIC AND AIRCRAFT NOISE

Where codes are available for the construction of buildings against road traffic and aircraft noise,<sup>5,6</sup> they should be referred to. A simple approach is given below, but it should be understood that the acoustic transmission of facades is more complex than this method would suggest. The spectrum, level, and direction of the sound can vary over the facade that will in turn affect the transmitted sound. While most external sound sources are somewhat different in spectrum to speech (for which the STC rating system was developed) and the angle of incidence is not random (random incidence is used for STC determinations), STC values are often used for outdoor–indoor

**Table 7 Outdoor–Indoor Transmission Class<sup>a</sup>**

Source	Room Furnishings <sup>b</sup>	Façade Area as % of Floor Area						
		20	30	40	60	80	100	160
Aircraft	Hard	−1	+1	+2	+4	+5	+6	+8
	Standard	−3	−1	0	+2	+3	+4	+6
	Soft	−5	−3	−2	0	+1	+2	+4
Road	Hard	+1	+3	+4	+6	+7	+8	+10
	Standard	−1	+1	+2	+4	+5	+6	+8
	Soft	−3	−1	0	+2	+3	+4	+6

<sup>a</sup>Correction to be added to the difference between outdoor and indoor sound pressure levels to obtain the required STC for the facade fenestration.

<sup>b</sup>“Hard” is typical of a kitchen or bathroom, “standard” is typical of a living room or dining room, and “soft” is typical of a bedroom.

acoustical design purposes. Where a higher level of accuracy is required the outdoor–indoor transmission class (OITC) can be used.<sup>27</sup>

For outdoor sources such as aircraft and road traffic that have strong low-frequency components, the perceived insulation tends to be less than indicated by STC ratings. Harris<sup>28</sup> gives a correction method based on the noise source, facade area, and room furnishings:

$$L_{\text{out}} - L_{\text{in}} = \text{STC}_{\text{eff}} - \text{correction} \quad (\text{see Table 7})$$

where  $L_{\text{out}}$  is the outside A-weighted sound pressure level,  $L_{\text{in}}$  is the inside A-weighted sound pressure level (e.g., criteria in Table 2), and  $\text{STC}_{\text{eff}}$  is the STC value of the composite facade (walls, windows, doors, roof, vents, etc.).

Given the uncertainties in sound levels, perception, and other factors, it can be seen from Table 7 that for facade areas about 20 and 50% of the floor area there is little point in using the OITC in other than exceptional circumstances.

There are also alternatives to the previous equation. The most common is

$$L_{\text{out}} - L_{\text{in}} = \text{STC}_{\text{eff}} - 10 \log(S/A) - 6$$

where  $S$  is the area of facade through which the sound is transmitted to a room having  $A$  m<sup>2</sup> sabin of absorption.

The effort to control external sound transmission through the exterior envelope of a building is usually concentrated on windows, roofs, doors, and vents as these are the weakest transmission paths with the windows often being more important in commercial and public buildings while roofs may be more important in residential buildings.

## 11 ANALYTICAL NOISE MODELS

In buildings, because of the limitations on accuracy of sound transmission predictions due to flanking paths, workmanship, angle of incidence of sound,



unknown noise sources and levels, it is rarely necessary to use sophisticated techniques such as statistical energy analysis (SEA) for high-frequency transmission, finite element analysis/boundary element method (FEM/BEM) for low- to mid-frequency transmission, and the Helmholtz method (for the full-frequency range) to design for noise transmission.<sup>29–32</sup> There are a number of simple empirical and analytical noise models that are useful, but generally buildings are designed using tabulated values of STC, IONR, IIC, and NRC values as indicated above.

## REFERENCES

1. D. Templeton, Ed., *Acoustics in the Built Environment*, Architectural Press, Oxford, 1997, Chapter 2.
2. W. J. Cavanaugh and J. A. Wilkes, Eds., *Architectural Acoustics Principles and Practice*, Wiley, New York, 1999, Chapter 3.
3. C. M. Harris, Ed., *Noise Control in Buildings*, McGraw-Hill, New York, 1994, Chapter 10.
4. M. J. Crocker, Ed., *Encyclopedia of Acoustics*, Wiley, New York, 1997, Chapter 96.
5. Standards Australia, Acoustics—Aircraft Noise Intrusion—Building Siting and Construction, AS 2021-2000, Sydney, 2000.
6. Standards Australia, Acoustics—Road Traffic Noise Intrusion—Building Siting and Construction, AS 3671-1989, Sydney, 1989.
7. <http://www.mst.dk/homepage/>.
8. B. Berglund and T. Lindvall, Eds., Community Noise, Document prepared for WHO, *Archives of the Centre for Sensory Research*, Vol. 2, Issue 1, Stockholm University and Karolinska Institute, 1995.
9. Organization for Economic Co-operation and Development, *Fighting Noise in the 1990s*, OECD Publications Service, Paris, 1991.
10. M. J. Crocker, Ed., *Encyclopedia of Acoustics*, Wiley, New York, 1997, Chapter 80.
11. American Society of Heating, Refrigeration, and Air-Conditioning Engineers, *Applications Handbook*, ASHRAE, New York, 1999, Chapter 46, p. 46.22.
12. American Society of Heating, Refrigeration, and Air-Conditioning Engineers, *Applications Handbook*, ASHRAE, New York, 1999, Chapter 46, p. 46.25.
13. Standards Australia/Standards New Zealand, Acoustics—Recommended Design Sound Levels and Reverberation Times for Building Interiors, AS/NZS 2107: 2000, Sydney/Wellington, 2002.
14. Department of Transport, *Calculation of Road Traffic Noise*, HMSO, London 1988.
15. Federal Highways Administration, Highway Traffic Noise Prediction Model, Report No. FHWA-RD-77-108, US Department of Transportation, Washington DC (update information at [http://www.fhwa.dot.gov/rnt4u/ti/traffic\\_noise.htm](http://www.fhwa.dot.gov/rnt4u/ti/traffic_noise.htm)).
16. American Society of Heating, Refrigeration, and Air-Conditioning Engineers, *Applications Handbook*, ASHRAE, New York, 1999, Chapter 46.
17. W. J. Cavanaugh and J. A. Wilkes, Eds., *Architectural Acoustics Principles and Practice*, Wiley, New York, 1999, Tables 2.3 and 2.4.
18. M. Mehta, J. Johnson, and J. Rocafort, *Architectural Acoustics Principles and Design*, Prentice Hall, Upper Saddle River, NJ, 1999, Appendices I and J.
19. C. M. Harris, Ed., *Noise Control in Buildings*, McGraw-Hill, New York, 1997, Appendices 5.1 to 5.5 and Table 6.1.
20. American Society of Heating, Refrigeration and Air-Conditioning Engineers, *Applications Handbook*, ASHRAE, New York, 1999, Chapter 46, Table 45, p. 46.39.
21. American Society for Testing Materials, Standard Practice for Installation of Fixed Partitions of Light Frame Type for the Purpose of Conserving Their Sound Insulation Efficiency, ASTM E 497-89(94), 1994.
22. D. A. Bies and C. H. Hansen, *Engineering Noise Control*, 3rd ed., Spon Press, London, 2003, Chapter 8.
23. C. M. Harris, Ed., *Noise Control in Buildings*, McGraw-Hill, New York, 1997, Appendices 3.1 to 3.10.
24. M. Mehta, J. Johnson, and J. Rocafort, *Architectural Acoustics Principles and Design*, Prentice Hall, Upper Saddle River, NJ, 1999, Appendix H.
25. W. J. Cavanaugh and J. A. Wilkes, Eds., *Architectural Acoustics Principles and Practice*, Wiley, New York, 1999, Tables 2.1 and 2.2.
26. American Society for Testing Materials, Standard Practices for Mounting Test Specimens During Sound Absorption Tests, ASTM E 795-93, 1993.
27. American Society for Testing Materials, Standard Classification for Determination of Outdoor-Indoor Transmission Class, ASTM E 1332-90, 1994.
28. C. M. Harris, Ed., *Noise Control in Buildings*, McGraw-Hill, New York, 1997, Table 10.5.
29. M. J. Sablik, Statistical Energy Analysis, Structural Resonances and Beam Networks, *J. Acoust. Soc. Am.*, Vol. 77, 1985, pp. 1038–1045.
30. M. J. Crocker, Ed., *Encyclopedia of Acoustics*, Wiley, New York, 1997, Chapter 15.
31. M. J. Crocker, Ed., *Encyclopedia of Acoustics*, Wiley, New York, Chapter 14.
32. G. H. Koopman and H. Benner, Method for Computing the Sound Power of Machines Based on the Helmholtz Integral, *J. Acoust. Soc. Am.*, Vol. 71, 1982, pp. 78–88.

# CHAPTER 116

## VIBRATION RESPONSE OF STRUCTURES TO FLUID FLOW AND WIND

Malcolm J. Crocker

Department of Mechanical Engineering

Auburn University

Auburn, Alabama

### 1 INTRODUCTION

Structures immersed in a moving fluid experience fluid loading forces. These forces are caused by several physical phenomena. The phenomena may be divided into three main categories: (1) steady incoming flow that impinges on the structure, (2) unsteady incoming flow, and (3) eddies (vortices) that form in the fluctuating wake flowing past the structure. The manner in which a structure responds to the flow forces is governed by several factors, the most important being: (1) its geometrical shape and dimensions; (2) its boundary conditions and rigidity (stiffness) and mass distributions, which govern its fundamental and higher natural frequencies; and (3) its vibration damping. The structures may be divided into two main types: (1) stiff structures that are relatively rigid and that have fundamental bending and torsional frequencies that are above the predominant fluctuation frequencies in the incoming flow and wake eddy formation rates and (2) flexible structures that have fundamental frequencies much lower than or that coincide with the frequencies of the fluctuating forces in the incoming flow and/or wakes from any neighboring structures upstream. Dynamic forces experienced by “rigid” structures can be divided into two main types: (1) longitudinal forces in the flow direction mostly caused by unsteady incoming flow and (2) lateral and torsional forces that are mainly caused by the vortex shedding in the structure’s own wake. Flexible structures can experience additional forces caused by motion of the structure itself in response to the flow forces. Motion of the structure, sometimes caused by aeroelastic effects, can alter the flow and result in self-generating feedback mechanisms known such as galloping, flutter, or vortex-generated motion resulting in increased vortex shedding.

In addition, aeroelastic effects associated with vortex shedding are also important since, when the vortex shedding frequency coincides with an eigenfrequency, feedback motion results in which the vortex-generated motion intensifies the vortex shedding.

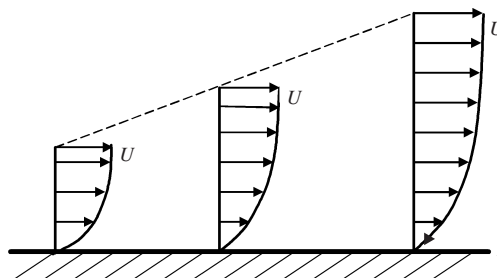
### 2 FLUID FLOWS

There is a considerable body of literature describing the vibration of structures caused by fluid flow. This chapter describes the response of structures to fluid flow forces and in particular the response of buildings, towers, and other structures to forces caused by

wind. The discussion includes reviews of the physical phenomena involved, methods of vibration prediction, human response to the vibration and methods of vibration reduction and control. In addition, references to the literature are provided for further reading, including books on wind effects on structures,<sup>1–6</sup> book chapters,<sup>7–9</sup> books of proceedings,<sup>10–13</sup> design guides,<sup>14–18</sup> and articles in journals.<sup>19–50</sup> There are many books covering the dynamic response of structures that are also useful in study of this topic.<sup>51</sup>

#### 2.1 Fluid Flow around a Body

When a fluid flow meets a structural body, the flow is perturbed as it travels around the structure. The flow behavior depends on several factors. In practice, the main fluid effects are due to the fluid’s *viscosity* and *inertia*. When a fluid flows near to the surface of a body, its viscosity causes it to adhere to the surface and to slow down near to the surface. The result is that a slowly moving layer of fluid exists near to the surface known as a boundary layer. Figure 1 shows the velocity profile of a typical boundary layer. In pipes and machinery elements containing fluid flow, boundary layers tend to grow in thickness with distance along the surface. In atmospheric wind the boundary layer is more or less constant in thickness, except that it differs in thickness depending upon the terrain roughness (e.g., whether the flow is over water, forests, suburbs, or over built-up city environments, etc.). The different flow speeds in the boundary layer cause flow shearing in the layer; after the fluid passes a body, it tends to rotate and at high enough speeds vortices can form, which are also known as eddies.<sup>1–6</sup>



**Figure 1** Growth of a typical two-dimensional boundary layer along a flat surface.

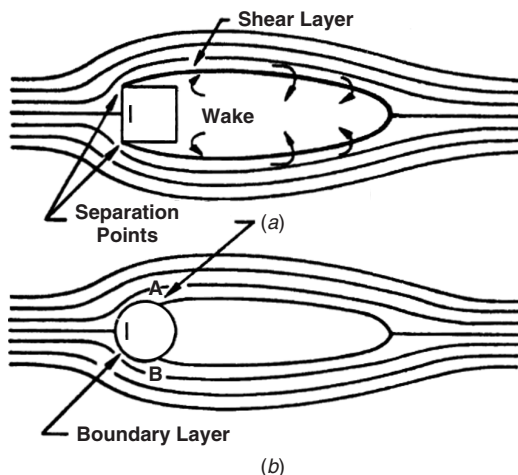
As the flow approaches a body in its path, it slows down on the upstream side, accelerates around the sides, and forms eddies in the downstream side. The collection of eddies is known as the *wake*. After traveling some distance downstream, the wake slowly disappears after the eddies disintegrate.<sup>1-6</sup> See Fig. 2.

When a fluid flow meets a structure, the flow is affected by its geometrical shape. Bodies that do not have a streamlined shape (i.e., bluff bodies) have a different effect on the fluid flow than those that do (i.e., streamlined bodies). Cables, wires, and cylindrical exhaust stacks and chimneys can be considered to be bluff bodies.<sup>1-9</sup> Some asymmetrical bodies such as aircraft wings, turbine blades, and some automobiles are essentially streamlined when the flow approaches in the design direction. But, if the flow approaches such bodies at an abrupt angle different from the design direction, they must be regarded as bluff bodies as well.

The feature that distinguishes the flow around bluff bodies from that around streamlined ones is that a significant wake is formed behind bluff bodies. (See Fig. 3.) The wake is separated from the rest of the



**Figure 2** Organized eddies in a flow that dissipate into a disorganized wake.



**Figure 3** Plan view of flow past a body, showing stagnation point (I) separation, and eddy formation: (a) square cylinder<sup>1</sup> and (b) circular cylinder. (From Ref. 1.)

flow by a shear layer. In the case of bluff bodies with sharp corners the shear layer begins at the corners as shown in Fig. 3a, and the flow separates from the body contour at these locations. With bluff bodies such as circular cylinders (Fig. 3b), flow separation is delayed. In the latter case a shear layer is formed first, which is known as the *boundary layer*, and then flow reversal in the boundary layer causes flow separation at locations such as A and B as shown in Fig. 3b, past which the boundary layer becomes a free shear layer.

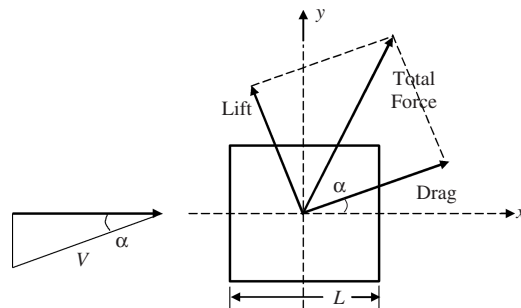
The exact location of these flow separation points depends on several factors including: (a) the intensity of the turbulence in the approaching flow, (b) the body shape and dimensions, (c) the surface roughness of the body, and (d) the Reynolds number.<sup>1-10</sup>

The static pressure (also known as the gauge pressure) in the flow depends upon the flow speed. Along any streamline, the pressure and flow velocity are related by the Bernoulli equation:

$$p_1 + \frac{1}{2}\rho U_1^2 = p_2 + \frac{1}{2}\rho U_2^2 = \text{constant} \quad (1)$$

where  $p_1$  and  $p_2$  are the static pressures at two points in the flow on a streamline,  $\rho$  is the fluid density, and  $U_1$  and  $U_2$  are the corresponding flow velocities at the two points 1 and 2. The quantity  $\frac{1}{2}\rho U^2$  is called the dynamic pressure denoted by  $q$ . At some upstream locations on the body the flow slows down, some of the dynamic head is lost, and the static pressure is increased according to Eq. (1). On the body's sides the flow velocity increases again, and the static pressure drops.

If the flow comes to a complete stop at any location, the point is known as a *stagnation point* (see, e.g., point 1 shown in Figs. 3a and 3b). The pressure is the sum of the static pressure and the dynamic pressure  $\frac{1}{2}\rho U^2$ . Further downstream from these locations the fluid stream can separate from the body forming regions of separated flow. The different static pressures around the body give rise to the well-known lift and drag forces, which are perpendicular to and in the same direction as the flow, respectively<sup>1,3</sup> (see Fig. 4). In Fig. 4 the flow approaches the body at an angle  $\alpha$  to the  $x$  axis. The angle  $\alpha$  is known



**Figure 4** Lift and drag forces on a body.

as the angle of incidence. In aeronautics, it is often called the angle of attack.

The viscous and inertia forces and their relationship to each other affect the characteristics of the flow around the body.<sup>1,7</sup> The ratio of the inertia and viscous forces can be shown to be the Reynolds number,  $Re$ , which is given by

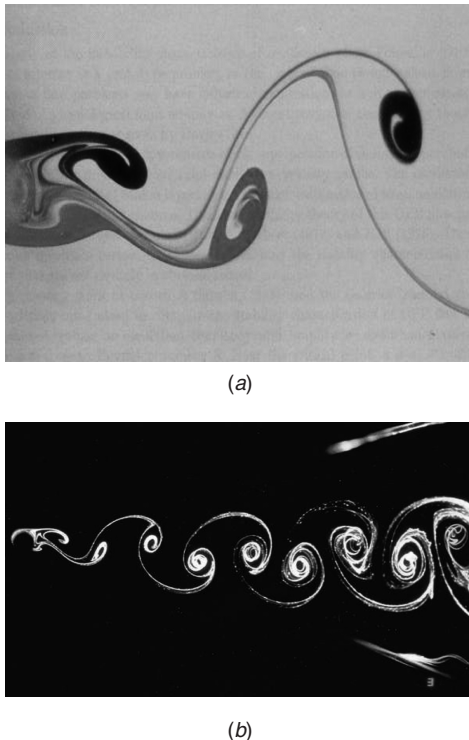
$$Re = \rho UL/\mu = UL/\nu, \quad (2)$$

where  $L$  is a typical body surface dimension,  $\mu$  is the fluid *dynamic viscosity*, and  $\nu = \mu/\rho$  is called the fluid *kinematic viscosity*.

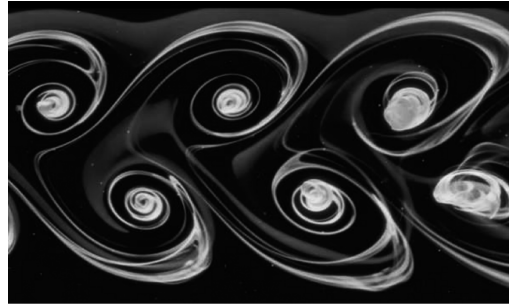
## 2.2. Vortex Formation

Long cylindrical structures such as machinery heat exchanger tubes, which the flow strikes perpendicularly, shed vortices (eddies) in the wake. The vortices are shed periodically and give rise to periodic lateral (lift) forces on the cylinders. This phenomenon is observed in the case of wind flow on slender circular cylindrical structures such as cables, chimney stacks, towers, masts, etc.<sup>1-9</sup> (see Fig. 5).

It also exists to a somewhat lesser degree on similar noncircular structures. (See Fig. 6.) Further discussion on eddy formation on circular cylinders follows.



**Figure 5** (a) Flow visualization of close wake behind a circular cylinder and (b) vortex street downstream of a circular cylinder. Copyright Onera (www.onera.fr), the French Aerospace Lab.



**Figure 6** Wake downstream of a thin plate immersed in a water flow. Copyright Onera (www.onera.fr), the French Aerospace Lab.

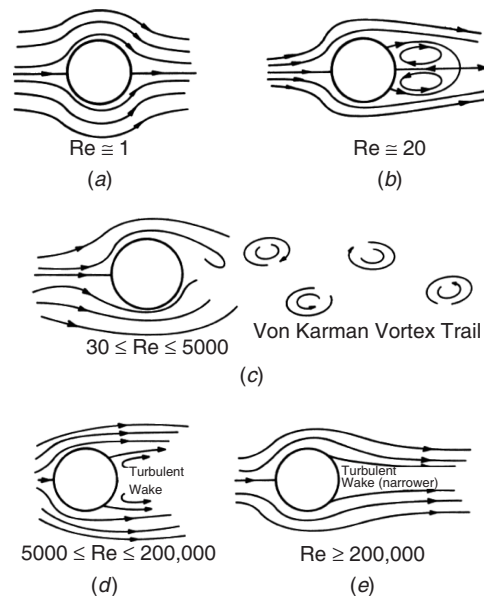
The Strouhal number  $S$  is defined as

$$S = nd/U \quad (3)$$

where  $n$  is the vortex shedding frequency (in Hz),  $d$  is the characteristic structural dimension (in m), and  $U$  is the flow velocity (in m/s). For a long slender cylinder, the characteristic dimension  $d$  is typically chosen to be its diameter.

Figure 7 shows, for smooth circular cylinders, the flow dependence on Reynolds number.<sup>1-9</sup>

In the case of noncircular slender prismatic structures, the Strouhal number is similarly defined; the characteristic dimension  $d$  is normally chosen to be the



**Figure 7** (a) Flow past circular cylinder  $Re \approx 1$ , (b) flow past circular cylinder  $Re \approx 20$ , (c) flow past circular cylinder  $30 \leq Re \leq 5000$ , (d) flow past circular cylinder  $5000 \leq Re \leq 200,000$ , and (e) flow past circular cylinder  $Re \geq 200,000$ . (From Ref. 1).

across-wind dimension. Table 1 gives Strouhal numbers for a selection of closed shapes (Table 1a) and for open and cylindrical shapes (Table 1b). It is seen that the Strouhal number for closed shapes depends not only on the across-flow dimension  $d$  but on the along-flow dimension  $B$  and the leading-edge radius  $r$  as well. The range of Reynolds number in which the Strouhal number is valid is also given in Table 1a.<sup>6</sup>

Using the characteristic dimension of the body and the flow velocity, the Strouhal number  $S$  can be used to predict the frequency of vortex shedding in the structure's wake. For cylindrical structures, the Strouhal number may be assumed to be about 0.2 and to be nearly independent of Reynolds number. The numbers given in Table 1 should be used for guidance only. Figure 8 shows some experimental results<sup>6</sup> for

**Table 1 Strouhal Numbers for (a) Closed Sectional Shapes and (b) for Open and Circular Sectional Shapes**

(a)

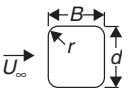
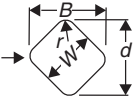
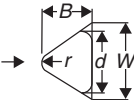
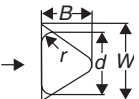
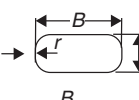
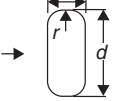
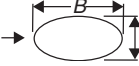
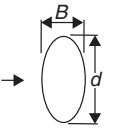
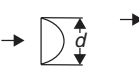


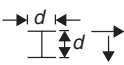
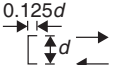
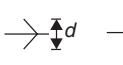
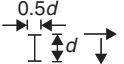
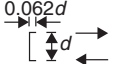

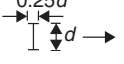
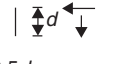

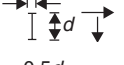
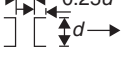
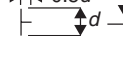
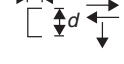
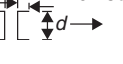
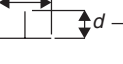
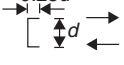
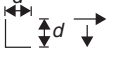
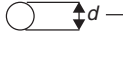
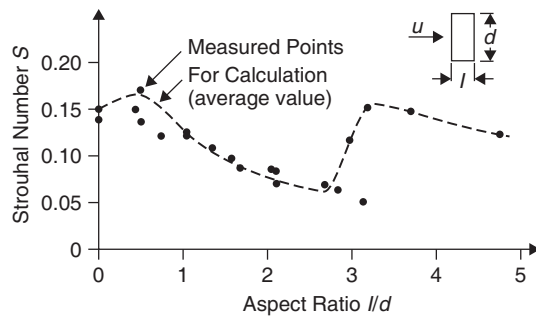
Shape of Cross Section	Strouhal Number $S = f \left( \frac{d_w}{U_\infty} \right)$	Valid Range of Reynolds Number
	$\frac{B}{d} = 1$ $\frac{r}{d} = \frac{1}{3}$	0.33 $2 \times 10^6 > Re > 4 \times 10^5$
	$\frac{B}{d} = 1$ $\frac{r}{w} = \frac{1}{4}$	0.2 → 0.35 $7 \times 10^5 Re > 4 \times 10^5$ 0.35 $2 \times 10^6 > Re > 7 \times 10^5$
	$\frac{B}{d} = 1$ $\frac{r}{w} = \frac{1}{4}$	0.2 $8 \times 10^5 > Re > 3 \times 10^5$ 0.3 $Re > 3 \times 10^5$
	$\frac{B}{d} = 1$ $\frac{r}{w} = \frac{1}{4}$	0.2 $5 \times 10^5 > Re > 3 \times 10^5$ 0.65 $1.6 \times 10^6 > Re > 6 \times 10^5$
	$\frac{B}{d} = 2$ $\frac{r}{d} = \frac{1}{2}$	0.4 $2.5 \times 10^6 > Re > 3 \times 10^5$
	$\frac{B}{d} = \frac{1}{2}$ $\frac{r}{d} = \frac{1}{4}$	0.2 → 0.35 $6 \times 10^5 > Re > 2 \times 10^5$ 0.35 $1 \times 10^6 > Re > 6 \times 10^5$
	Ellipse $\frac{B}{d} = 2$	0.12 $5 \times 10^5 > Re > 3 \times 10^5$ 0.60 $2 \times 10^6 > Re > 1 \times 10^6$
	Ellipse $\frac{B}{d} = \frac{1}{2}$	0.2 $7 \times 10^5 > Re > 1 \times 10^5$
		0.22 $Re > 8 \times 10^4$ 0.125 $Re > 5 \times 10^4$
		0.13 → 0.22 $Re = 0.3 + 1.4 \times 10^5$
		0.14 → 0.22 $Re > 0.8 \times 10^5$

Table 1 (continued)

(b)

Profile	Wind-direction	$S = f_w \left( \frac{d}{u_\infty} \right)$	Profile	Wind-direction	$S = f_w \left( \frac{d}{u_\infty} \right)$	Profile	Wind-direction	$S = f_w \left( \frac{d}{u_\infty} \right)$
	→	0.14 0.12		→	0.17 0.18		→	0.15
	→	0.14 0.18		→	0.18 0.18		→	0.12
	→	0.15		→	0.15 0.16		→	0.14
	→	0.18 0.16		→	0.18		→	0.11 0.15
	→	0.15 0.14 0.18		→	0.15		→	0.16
	→	0.17 0.15		→	0.14 0.15		→	0.20

Source: From H. Bachmann et al., Ref. 6. Reprinted, with permission.

**Figure 8** Strouhal numbers for rectangular sections. (From H. Bachmann et al., Ref. 6. Reprinted with permission).

the dependence of the Strouhal number for closed rectangular cross sections on the section aspect ratio  $l/d$ .

### 2.3 Added Fluid Mass

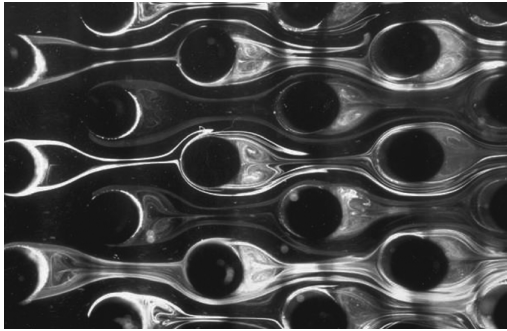
Structures immersed in moving fluids are exposed to a variety of dynamic forces that can cause vibration of the structures. However, it is well known that the fluid itself has an effect on the dynamics of structures. This effect is most pronounced in cases where the fluid density is comparable with the density of a structure. As a structure moves, it entrains some of the fluid, effectively increasing the structure's mass. The effect is independent of the fluid viscosity. The mass of the entrained fluid is normally termed the *added mass*. This added mass has the effect of reducing

the natural frequencies of the structure. It also has the effect of coupling together the modes of vibration of the structure and the vibration of structural elements situated near to each other in the fluid.<sup>7</sup>

The response of a structure to a dynamic force is related to its stiffness, damping, and effective mass. Extended structures have a low fundamental natural frequency and multiple higher natural frequencies. In many cases vibration in the fundamental frequency is dominant.<sup>3,6,51</sup> At a frequency below a natural frequency, the structural response is stiffness controlled. At or near to a natural frequency the response is damping controlled, and above a natural frequency it is mass (or inertia) controlled. Thus the added mass is seen to have most effect on the high-frequency vibration of light structures immersed in dense fluids. Proper modeling of the vibration of ship hulls in water, structural elements of pumps conveying dense liquids, and the dynamics of ship propellers, liquid heat exchanger tubes, and the like must always account for fluid mass loading and inertia effects.<sup>7</sup> It can be shown theoretically that the added mass is proportional to the mass of fluid displaced by the structural element.<sup>7</sup>

If two structures are situated close to each other, the added mass also becomes a function of the spacing between the structures and in addition inertial coupling will exist between them. Several books present tables of added mass for various structural geometries.<sup>3,7</sup> If the structure is axisymmetric, the added mass is easily calculated and the motion effects are symmetric about the length axis. If a structure is asymmetric, it can be shown that the added mass couples motion in the  $X$ - and  $Y$ -orthogonal directions and has an





**Figure 9** Flow in multitube heat exchangers of nuclear or thermal power stations. Copyright Onera (www.onera.fr), the French Aerospace Lab.

effect on torsional motion as well.<sup>7</sup> Figure 9 shows an experimental visualization of the flow in multitube assemblies such as those found in a heat exchanger in a nuclear or thermal power station. The interaction of the vortices in the wakes of upstream cylindrical structures with those downstream can be seen clearly. It can also be observed that the interaction between upstream and downstream cylinders varies with time as eddies are shed alternately from the top (right) and bottom (left) of the upstream cylinders.

For the theoretical case of a simple mass–spring–damper system, much above its natural frequency, the acceleration response of the structure to a given force is proportional to its mass. For real extended structures with multiple natural frequencies, the situation is more complicated, but at high frequency and for excitation that is not near to any natural frequency, the structure's mass is normally the dominant effect that governs its response. Thus the added mass effect is more important for light structures and at high frequency.

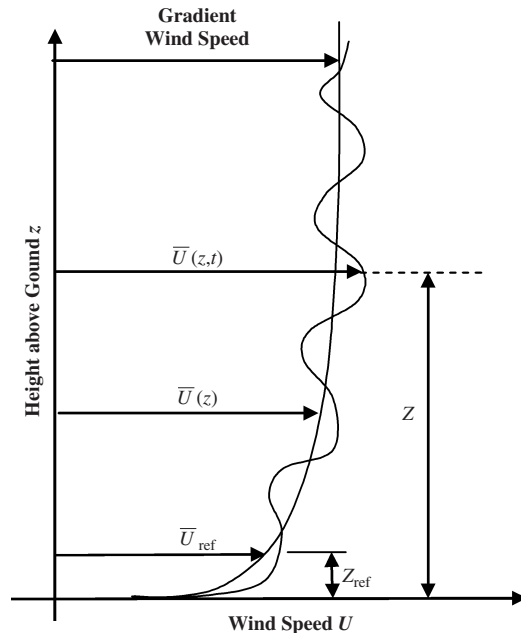
In cases where water or some dense liquid is the fluid medium, then mass loading effects are important and must be considered. However, for air or some other fluid medium such as natural gas, added mass effects can normally be ignored in practice. Since the rest of this chapter will be concerned mainly with the response of structures to wind forces, added mass will not be considered further.

### 3 WIND CHARACTERISTICS

The wind flow speed and direction normally continually change. The wind in most cases is highly turbulent, and its characteristics depend on a number of factors, the most important being: (a) the surface roughness of the terrain (which differs according to whether the surface is water, open terrain, suburban, or urban) and (b) the height above the ground.<sup>1–5</sup>

#### 3.1 Variation of Wind Velocity due to Height above Ground Level

Figure 10 represents the instantaneous velocity profile of wind with height above the ground,  $z$ . The wind



**Figure 10** Instantaneous wind profile  $U(z,t)$  with superimposed turbulence as a function of height,  $z$ .

flow velocity varies with height because of the addition of the turbulent flow to the mean flow. A time average of the flow is shown as the mean flow profile given in Fig. 10. The averaging time used must be significantly greater than the time of passage of the wind flow over the body  $d/U$ , where  $d$  is a characteristic dimension in the flow direction and  $U$  is the flow velocity.

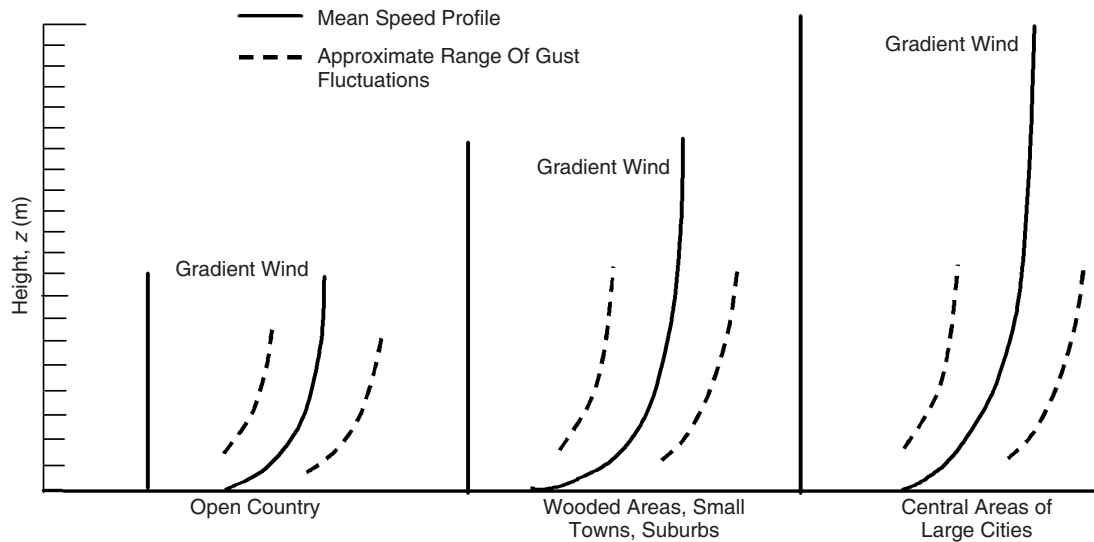
#### 3.2 Effect of Terrain

Buildings and other obstacles have the effect of slowing down the wind. This causes a large difference between low- and high-elevation wind velocities. In open country there is less difference between low- and high-level wind velocities. Figure 11 shows typical wind speed profiles in open country (rural), suburban, and city terrains. Both average (mean) speed profiles and an indication of the range of gust fluctuations are given. The gradient wind speed is the undisturbed wind speed expected at high elevation. The profiles can be predicted if the surface roughness factors expected for each terrain are known.<sup>1–5</sup>

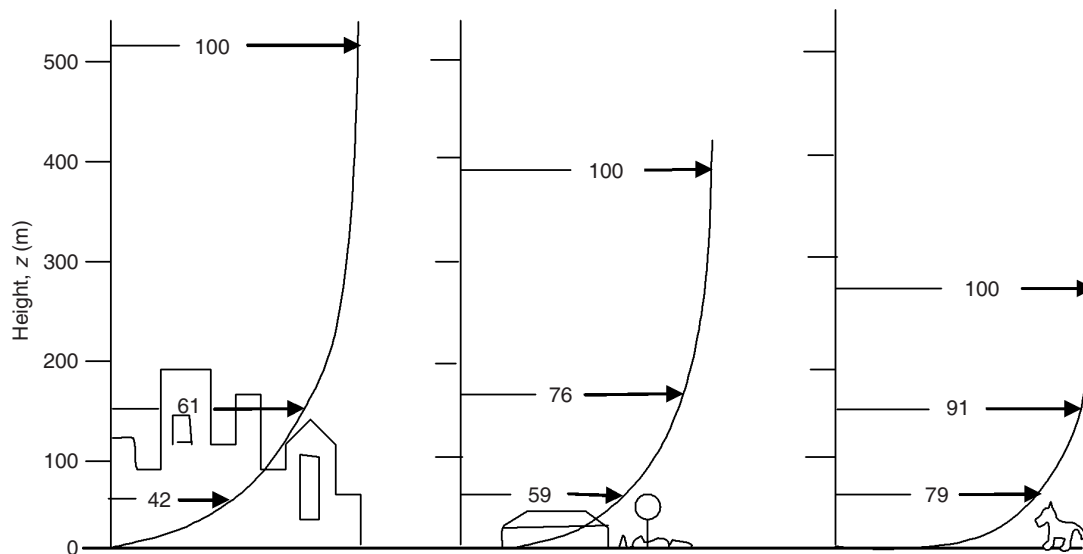
Figure 12 presents typical wind boundary layer velocity profiles for three different areas. The height,  $z$ , above the ground is given in the vertical scale in metres. Wind velocities are expressed on the horizontal scale as a percentage of the *gradient* (or upper level undisturbed) wind velocity.

#### 3.3 Wind Flow around Buildings

Wind speeds and profiles are typically referenced with respect to a standard height of 10 m (33 ft) above ground level. See Fig 13. It can maintain a fairly



**Figure 11** Vertical profiles of mean wind velocity for three typical terrains.



**Figure 12** Typical wind velocity profiles: town or city (*left*), suburban (*center*), and rural or open country (*right*) landscapes.

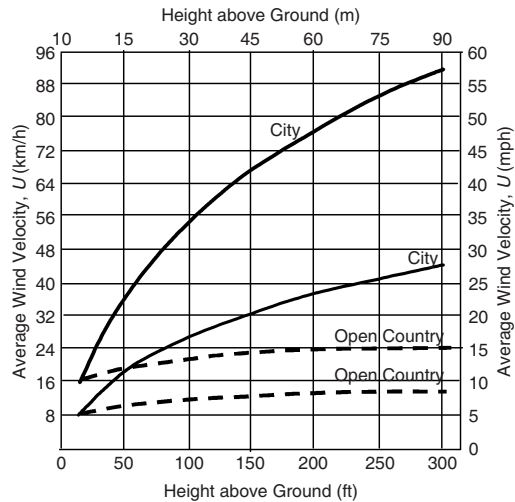
steady direction, but it can also change in speed and in direction (known as veering). When an obstruction such as a building is encountered, the flow pattern changes markedly. (See, e.g., Fig. 14.)

Buildings introduce distinct individual wind flow patterns. Near large buildings the wind can behave in a very complicated manner due to local flow accelerations, formation of eddies, and flow reversals. For example, winds can reverse direction and head downward in the “upwind roller” that can form in front

of a large tall building. The wind can also roll and flow upward behind such a building. (See Fig. 15.)

By watching the behavior of vegetation, birds in flight, flags flying, and the like near a building, it is possible to observe such wind flow patterns in real life. The use of scale-model buildings in wind tunnels makes it possible to reveal such wind flows by the use of flow visualization techniques (e.g., smoke). Wool or cotton tufts attached to the model building and ground surfaces are also used sometimes for flow visualization.





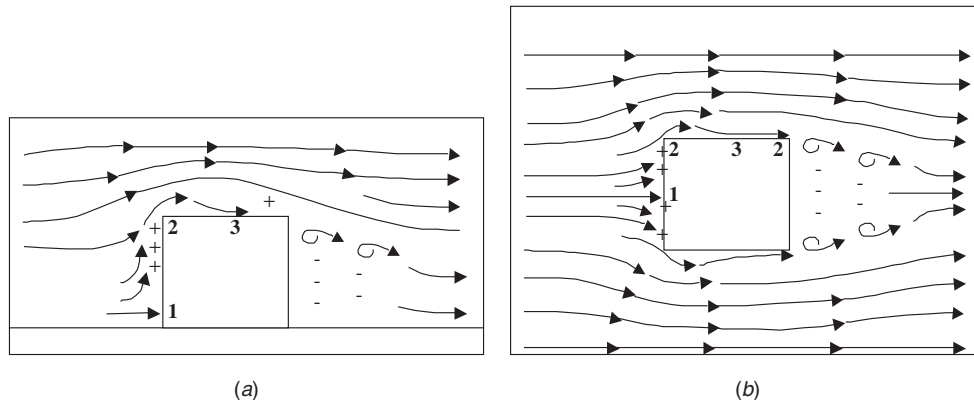
**Figure 13** Typical wind velocity profiles in city and open country regions with velocities of 8 km/h and 16 km/h referred to a height of 10 m.

Wind velocities vary widely in different parts of the world. For example, in England and Wales, large cities and towns rarely experience wind gusts that exceed 110 km/h (stagnation pressure  $p = 560$  Pa) (70 mph). Coastal areas can have gusts of up to 145 km/h (stagnation pressure  $p = 970$  Pa) (90 mph). Some areas in the north of England and Scotland can be subjected to gusts that exceed 160 km/h ( $p = 1185$  Pa) (100 mph.)

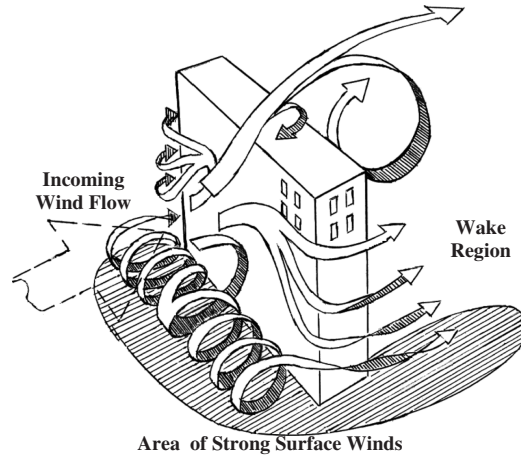
### 3.4 Wind Stagnation Pressure and Flow around Buildings

The stagnation pressure can be calculated from Eq. (4), which is based on the Bernoulli equation, Eq. (1)

$$p = 0.6U^2 \quad (4)$$



**Figure 14** Wind flow around a building. (a) section view and (b) plan view. (+) = Positive gauge pressure; (-) = negative gauge pressure. Flow normally separates at the sharp upstream corners of the building. Reattachment in some cases occurs before the wake is formed. (1 = stagnation point, 2 = separation points, and 3 = reattachment points).



**Figure 15** Schematic diagram of airflow patterns around a bluff-body or building.

The constant 0.6 is approximately half the specific mass of air, at 20°C and average relative humidity. For example, a strong gale-force wind blowing with a free stream velocity of 80 km/h (48 mph) could exert a maximum stagnation pressure of 296 Pa on a building:

As the air passes over and around the building, the static pressures are positive (relative to gauge pressure) on the upstream windward side and negative (relative to gauge pressure) on the downstream (leeward) or sheltered side. The negative pressures can cause the roofs to be “sucked off” buildings and windows out of walls. If the wind comes to a complete stop at a stagnation point, its dynamic pressure far upstream is fully converted into a static pressure.

The maximum wind force exerted on a building can be considerable. The wind force normally varies over a

building surface, and the total wind force usually does not exceed 80% of the maximum theoretically possible value.

**Example** Consider a building with 15-m wide  $\times$  6-m high wall exposed to 160 km/h gusts in an exposed coastal area in Scotland:

$$\text{Wind pressure} = 1185 \text{ Pa}$$

Actual force transmitted to building will be between 50 and 80% of theoretical maximum, depending on surface roughness of the building.

$$\begin{aligned} \text{Estimated maximum total force on building} \\ = 15 \times 6 \times 1185 \times 80\% \text{ N} = 87.7 \text{ tonnes} \end{aligned}$$

The Beaufort scale is used in some countries as a measure of wind strength. Table 2 shows Beaufort scale number ratings for several different wind descriptions and speeds, together with corresponding stagnation pressures.

### 3.5 Duration of Average Wind Speeds

Wind conditions vary from day to day and month to month in most parts of the world. Table 3 gives average wind speeds and the fraction of the time winds are above 8 and 16 km/h in the United Kingdom.

### 3.6 Wind Excitation of Buildings

The wind excitation forces on building structures may be divided into two main categories: (a) fluctuating forces in the wind direction on the structures caused by the turbulent pressure fluctuations that exist in the approaching wind flow and (b) fluctuating forces caused by turbulent eddies shed in the wake of the structure. These eddies (vortices) shed in the structure's wake mostly result in fluctuating forces

in the cross-wind direction and to a lesser extent in the torsional direction. Wind excitation forces and the building vibrations they cause may be further subdivided and are now described in more detail in the following sections in this chapter.<sup>1-9</sup>

As discussed already, the response of a building structure to wind depends not only on the wind characteristics but on the structure parameters as well. Very stiff structures deflect little in the wind, and their response can be treated as simple random forced response problems. However, flexible structures such as road signs, tall bridges, tall buildings, communication towers, and the like can respond appreciably and their movement can change the flow. The interaction of the structure motion and flow is known as an aeroelastic phenomenon. The calculation of the aeroelastic response of building structures is much more complicated than that of a pure forced response problem. Although many attempts have been made to calculate the response of rigid and flexible building structures to wind, many unknowns and variables in the wind flow, speed and direction with time, height above the ground, interactions with other structures, and complicated building geometries make calculations difficult.<sup>1-6,8,9</sup> In most cases, scale models need to be tested in wind tunnels to obtain reliable results.

Figure 16 shows a schematic of wind effects and building excitation effects.

**3.6.1 Turbulence-Induced Vibration (Gust or Buffeting)** Vibration of a structure may be caused by turbulence in the oncoming flow. The unsteady velocities and related pressure fluctuations in the approaching flow produce unsteady loading on the structure. The response of the structure caused by this unsteady loading is often termed *buffeting*. If the turbulence in the oncoming flow is associated mostly with turbulence in the wake of an upstream structure, the loading and structural response is usually called *wake buffeting*, although some refer to the phenomenon as *turbulence-induced vibration* or *gust-induced vibration*. The turbulent gusts cause fluctuating drag and lift forces on the structure and resulting inline, across-wind, torsional vibrations, and a combination of all three effects.<sup>1-6,8,9</sup>

**3.6.2 Wake-Induced Vibration (Buffeting)** If a structure is downstream of another structure, it will be subjected to the turbulent wake shed from the upstream structure. If the separation between the structures is only a few typical building dimensions, then the downstream building can be subjected to periodic excitation caused by the vortices shed alternately from the left and right sides of the upstream structure. (See Figs. 5, 6, and 9.) If the direction of the wind is such that only the vortices from one side of the upstream structure strike the downstream structure, the excitation frequency will be only half as much as in the case where vortices from both sides strike the downstream structure. If the wind is very turbulent and it veers in direction, then the vortices will strike the downstream structure aperiodically. Some of the time vortices may strike the downstream structure, and the

**Table 2 Beaufort Scale Ratings and Stagnation Pressures for Different Wind Conditions and Speeds**

Wind Speed			Wind Description	Beaufort Scale	Stagnation Pressure (Pa)
mph	km/h	m/s			
1	1.5	0.42	Calm	0	0.106
6	10	2.8	Light breeze	2	4.70
12	20	5.6	Gentle breeze	3	18.8
24	40	11.1	Fresh breeze	5	73.9
48	80	22.2	Fresh gale	8	296.0

**Table 3 Average Wind Speeds and Fraction of Time Winds Are above 8 and 16 km/h in the United Kingdom**

Under 8 km/h (5 mile/h)	Under 16 km/h (10 mile/h)	Situation
20%	45%	Coast
35%	55%	Rural
45%	75%	City suburbs
55%	95%	City centers

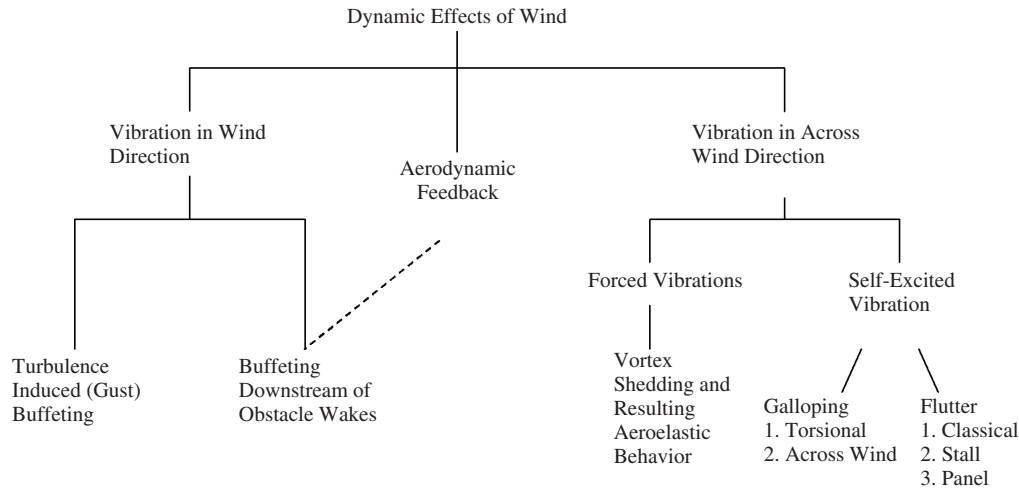


Figure 16 Classification of dynamic effects from wind.

rest of the time they may miss the structure completely, which may be in free flow conditions the rest of the time. At a considerable distance downstream, the wake will have become disorganized (see Fig. 2), and the excitation forces will become more random in nature. The wake effect depends also on the flow velocity, and, as Fig. 7 shows, it can be related more accurately to the Reynolds number. Methods for the calculation of the response of structure to inline buffeting are given in several recent publications.<sup>1-6,8,9,15</sup> The methods are too complicated to give in detail here.

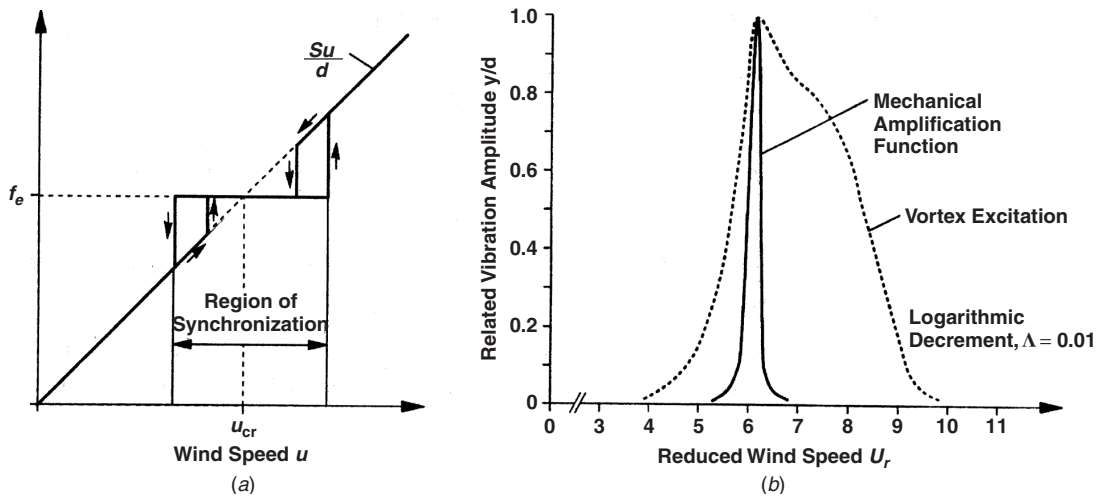
**3.6.3. Vortex-Induced Vibration** In the case of slender cylindrical structures such as chimneys, towers, and masts, vortices are shed alternately from the left and right of the structure in the wind direction in the wake. (See Figs. 5, 6, and 7.) This phenomenon gives rise to oscillating forces in the cross-wind (or lift) direction at the vortex shedding frequency,  $n$ . If the structure is very stiff, and the motion is negligibly small, then it can be regarded as forced motion. If the structure is extended as in the case of a tall flexible building, and the natural frequencies of the building are close to the Strouhal frequency, the structural motion can affect and significantly interact with the flow so that the motion of the body causes the eddies to be shed at the same frequency as the body vibration and this is no longer strictly related linearly to the wind speed. This important effect is known as *lock-in* and is observed experimentally to result in a considerable amplification of the structural motion. The motion can result in large vibration amplitudes, but not usually greater than half of the cross-wind dimension of the structure.<sup>1-6,8,9,15</sup> Theoretical analyses are not yet completely successful in predicting the full range of lock-in vibrations of flexible structures.<sup>2,6,15</sup> The motion is illustrated in Fig. 17.

Galloping is an aeroelastic phenomenon. It is more prevalent on slender structures such as ice-coated

power lines and slender flexible masts with rectangular cross sections and other open sections such as H, I, U, and so forth. See Table 1b. Galloping can occur in a variety of manners. One common form of galloping is *across-wind galloping*. Large motions of the structure can result in across-wind vibration with amplitudes up to 10 times or even more of the across-wind dimension of the structure. The motion can be explained physically as follows. As the structure moves, its velocity relative to the oncoming wind velocity increases the angle of incidence (sometimes also called angle of attack)  $\alpha$  of the wind to the structure. This increase in angle increases the lift forces on the structure. These increased forces cause further across-wind deflection and so on. The oscillatory motion is only limited when the structural velocity relative to the wind velocity no longer produces an increase in across-wind force with increase in the relative angle of attack. Some authors treat this motion as a nonlinear phenomenon and theories have been formulated to predict the effect and motion. Often the static lift and drag coefficients are used for first approximations of the lift and drag forces needed in a theoretical analysis.<sup>2,6</sup>

Across-wind galloping can occur at any wind speed. Surprisingly, galloping is often observed at low to moderate wind speeds. This is because with a low wind velocity, the structural velocity is appreciable compared to the wind velocity and causes a considerable change in the relative angle of attack  $\alpha$  of the structure to the wind. See Fig. 4.<sup>1-6,8,9,15</sup>

Torsional galloping is similar to across-wind galloping. With torsional galloping, torsional (twisting) vibration is involved in place of across-wind vibration. Such across-wind and torsional galloping motions are inherently unstable and can result in violent motions and even eventual structural failure.<sup>2</sup>



**Figure 17** Vortex resonance: (a) synchronization of vortex shedding and structure frequencies and (b) across-wind vibration amplitude ( $y/d$ ) referred to reduced wind speed  $U_r = u/df_e$ . (From H. Bachmann et al., Ref. 6. Reprinted with permission).

**3.6.4 Flutter** Flutter is similar to galloping, but here across-wind and torsional vibrations may be excited simultaneously. Like galloping, it is an aerodynamic instability. Unlike galloping, however, which is largely a single-degree-of-freedom phenomenon, flutter is a two-degree-of-freedom phenomenon. Vortex shedding is not involved. The torsional and the across-wind motions are coupled together.<sup>1,2</sup>

Several types of flutter have been observed.<sup>2</sup> *Classical flutter* is well known to aircraft designers, particularly with the wings themselves and the control elements on the wings (ailerons). If the structure has natural frequencies of vibration in the across-wind (lateral) and torsional modes, which are very close to each other, then with small changes in structural position or geometry, the two frequencies of vibration can be caused to coincide and flutter commences.

*Stall flutter* normally occurs when the wind is at an oblique incidence to the structure and when structural or airfoil stall is involved.<sup>1,2</sup> As the relative angle of attack increases, if the relative angle of attack is sufficient to reach and increase past the angle of stall, the lift force can be suddenly lost. Such flutter can result in very large vibration. Road signs mounted on a central cylindrical post are prone to such vibration. The vibration can be suppressed by increasing the stiffness of the supporting post and/or the structural damping.

*Panel flutter* is observed on aircraft and spacecraft fuselage and wing panel structures but can be observed on flexible building or bridge facings too, for instance, on sheet metal roofs. In such cases the motion is again self-excited, affects the fluid flow, and is unstable. It can be suppressed by geometrical redesign and/or increase in panel vibration damping.<sup>1-6,8,14,51</sup>

## 4 STRUCTURAL VIBRATION RESPONSE OF BUILDINGS AND TOWERS

Figure 18 presents a schematic that indicates the vibration amplitude responses of a building structure to the different types of excitation discussed in Sections 3.6.1 to 3.6.4 and as classified in Fig. 16.

### 4.1 Types of Building Vibrations

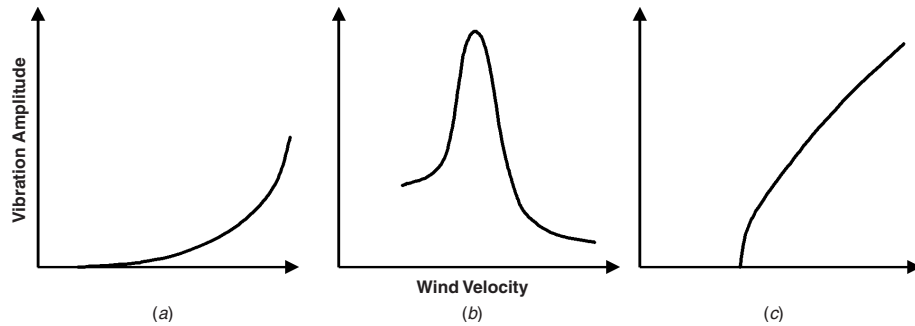
As already discussed in Section 3 of this chapter, fluid flow and wind forces are responsible for a variety of vibratory mechanisms in structures. In the case of inline buffeting, (Fig 18a), the vibration amplitudes generated increase nonlinearly and very rapidly with flow speed. This is because motion can be regarded as forced motion, and the turbulent flow forces involved are proportional to flow velocity squared. It is important to know the fundamental natural frequency of a structure if it is in forced motion since below the natural frequency the response is mostly stiffness controlled, at or near to the natural frequency is damping controlled, and above the natural frequency it is mass (or inertia) controlled.

In cross-wind vortex shedding motion (see Fig. 18b), again a knowledge of the structural fundamental natural frequency is needed since by careful building design, it may be possible to modify this frequency and change it so that it only becomes a problem at low wind speed at which excitation forces are minimal.

In cases of aerodynamic instability (galloping or flutter) such instabilities only begin at a critical wind speed, and again the natural frequencies of the structure are involved in the vibration as described before in Section 3.6 of this chapter.

### 4.2 Natural Frequencies of Building Structures

The natural frequencies of a building can be calculated from knowledge of its stiffness and mass distributions



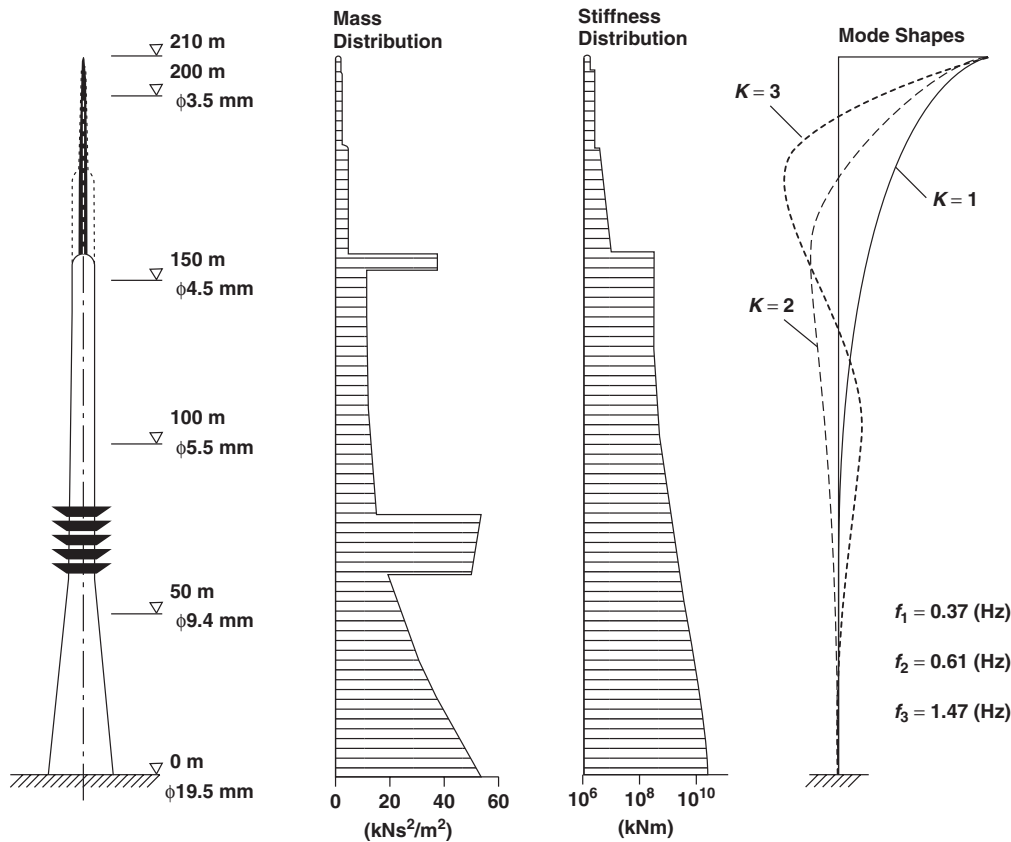
**Figure 18** Main types of wind-induced oscillations: (a) vibration due to turbulence, (b) vibration due to vortex shedding, and (c) self-excited vibration due to aerodynamic instability.

with a numerical program such as the finite element method (FEM). Figure 19 shows a schematic distribution of the mass and stiffness distributions of a 210-m telecommunications tower.<sup>6</sup>

The first three natural frequencies and mode shapes of vibration of the tower are shown in Fig. 19. These are seen to be very low, the first two being less

than 1 Hz. Often vibration in the fundamental natural frequency is dominant and most important.

Although FEM programs can be used to calculate the fundamental natural frequency, it has been found that the calculation is no more accurate than using an empirical calculation based on the height of the building alone and use of an approximate formula such



**Figure 19** Telecommunications tower with mass distribution, stiffness distribution, and natural modes of vibration. (From H. Bachmann et al., Ref. 6, Reprinted with permission).

as Eq. (5).<sup>6,31</sup>

$$f = 46/h \quad (5)$$

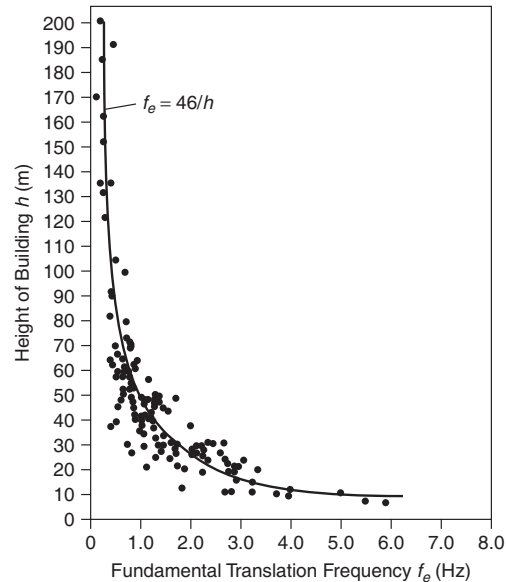
where  $h$  is the building height in metres.

The reason that the fundamental natural frequency is dominated by the building height appears to be that as the buildings grow taller they become more massive, and then stiffer supports must correspondingly be used to support the building's weight. Figure 20 shows measured experimental data for building height plotted against fundamental natural frequencies of a large number of tall buildings. Equation (5) is also plotted in Fig. 20. It is seen that this equation is a good fit to most of the experimental data.

Figure 21 shows that buildings of height even greater than those plotted in Fig. 20 have been constructed. The fundamental natural frequency of a building is of considerable importance, but so are several other building properties. Since there is a continuing trend to construct building structures of increasing height, wind-induced vibration of tall structures is a topic of increasing concern for structural engineers. The three most important properties of structures that are relevant to wind-induced vibration are: (1) shape, (2) stiffness (or flexibility), (3) fundamental natural frequency, and (4) damping. (See Fig. 22.)

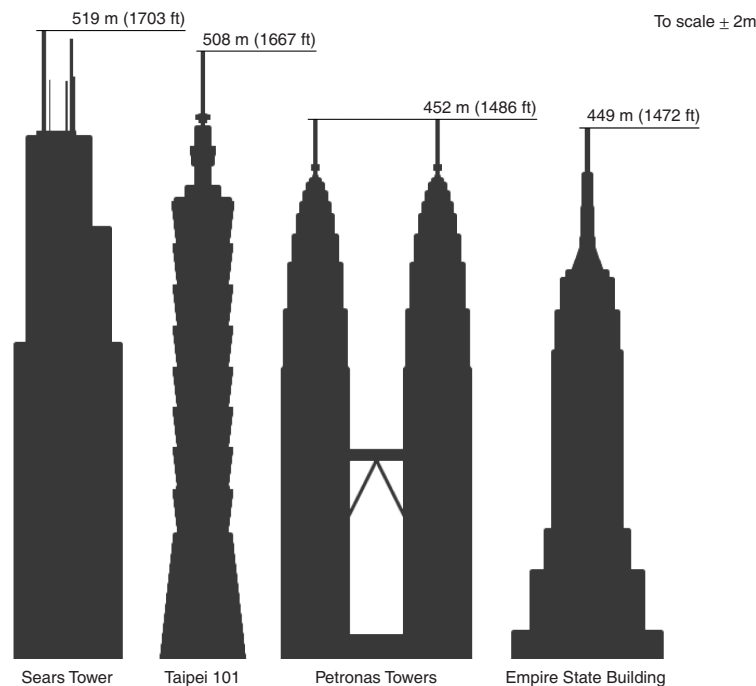
## 5 METHODS OF BUILDING STRUCTURE VIBRATION REDUCTION AND CONTROL

When structures are excited into motion, the forces opposing the motion are due to inertia, stiffness, and damping.

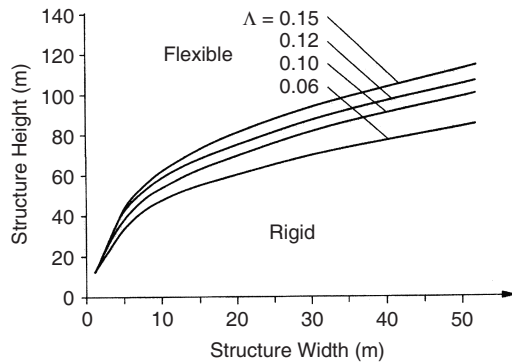


**Figure 20** Fundamental frequency  $f_e$  of tall buildings. (From H. Bachmann et al., Ref. 6. Reprinted with permission.)

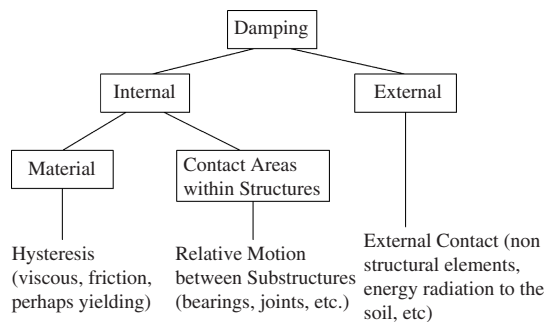
It is impractical to increase the mass of the building. Increasing the stiffness of a building can, in principle, reduce its deflection to wind forces, although often



**Figure 21** Telecommunication towers: (a) Hornigrsinde, Germany, (b) Munich, and (c) CN Tower, Toronto.



**Figure 22** Demarcation line between “flexible” and “rigid” structures ( $\Lambda$  = logarithmic decrement). (From H. Bachmann et al., Ref. 6. Reprinted with permission).

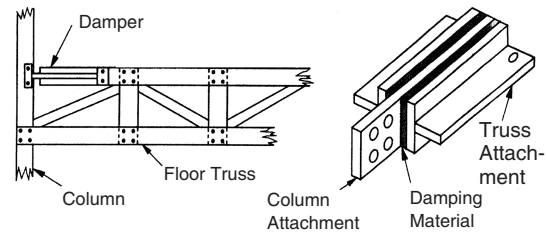


**Figure 23** Various types of damping.

there is a limit to the amount of stiffness increase that can be achieved. However, useful increases in stiffness can be achieved relatively easily in the case of masts, antennas in some cases by the use of guy wires and cables. The dynamics of guyed masts are complicated because tensioning of the guy cables is applied and the vibrations of the guy–mast system tend to be nonlinear in character. The guy cables themselves normally vibrate, resulting in some useful damping.<sup>6</sup> Various types of structural damping are illustrated in Fig. 23.

For wake buffeting, across-wind vortex-induced vibration, galloping, and flutter, damping forces become dominant in controlling vibration. Passive damping can be applied successfully in such cases. Different passive damping elements have been used in practice, and several new designs have been proposed. The World Trade Center in New York had about 10,000 passive “friction” dampers mounted in the truss structures. (See Fig. 24.)

Tuned vibration dampers (TMD) are also now used in many tall buildings. The first tall building to have such a device was the 280-m high Citicorp Center in New York City (Fig. 25). This employed a 270,000-kg concrete block “floated” on a hydrostatic support system. Springs are attached to the mass and tunes to

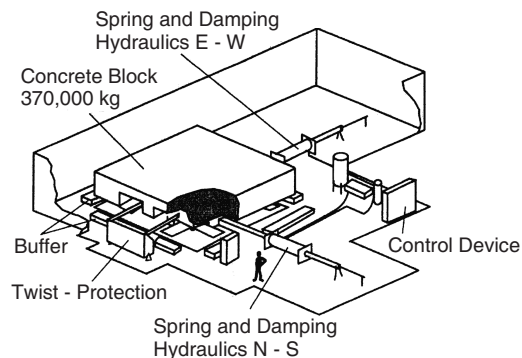


**Figure 24** Friction dampers used in the load-bearing structure of the now-destroyed World Trade Center towers (New York City).

give the TMD system a natural frequency the same as the fundamental vibration frequency of the building. In addition, hydraulic dampers are applied to dissipate the vibration energy. Stops must be provided to prevent excessive damaging motion of the floating mass during intense storms. A problem is that electrical power is needed to provide hydrostatic pressure for the oil suspension system. If the electrical power fails during a storm, then the TMD system becomes inoperative.

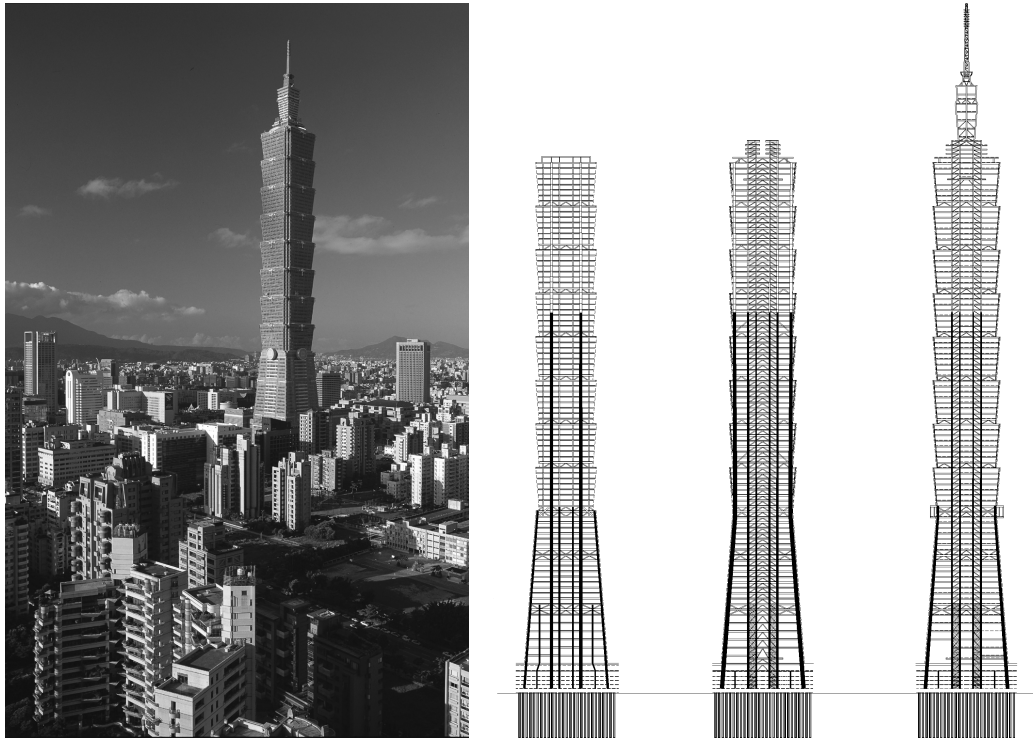
The principle of operation of the tuned mass damper is that as the building vibrates at its natural frequency, the tuned damper will also vibrate at the same frequency, but out of phase and thus applying forces opposing the motion of the building.

More recently, tall buildings have used TMDs made of large masses suspended by cables, rather like pendulums. The 500-m building in Taiwan opened in November 2004 has a 500,000-kg mass suspended on four cables near the top of the building between the 86th and 89th floors. See Figs. 26 and 27. As the building vibrates, the mass swings in an opposite direction, and pneumatic dampers are used to dissipate vibration energy. Excessive damaging vibration is prevented by the dampers. The system is mainly designed to reduce wind-induced vibrations by 35%, but it is said to also suppress earthquake vibrations. Since the building is situated only 1 km from a

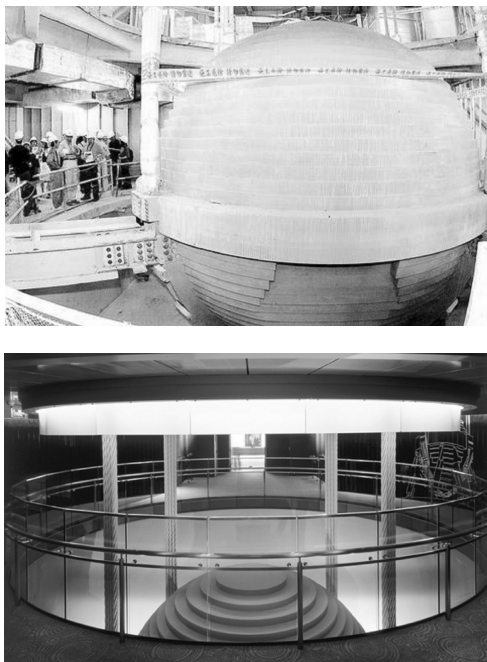


**Figure 25** Vibration absorber, Citicorp Center, New York. (From H. Bachmann et al., Ref. 6. Reprinted with permission).





**Figure 26** (a) Photograph and (b) construction drawing of Taipei 101 skyscraper in Taiwan.



**Figure 27** Photographs of tuned mass damper (TMD) ball in Skyscraper Taipei 101 in Taiwan.

fault line, earthquake damage is of concern. During construction in 2003, a 6.8-scale earthquake was experienced. The building survived the earthquake and the tuned mass system is said to have worked satisfactorily, although a construction crane fell from the 50th floor during the earthquake killing five construction workers.

Other types of damping systems have been proposed and in some cases implemented. Some such dampers rely on liquid motion inside rigid containers to absorb and dissipate the vibration energy. For example, nutation dampers have been investigated by Modi and Welf.<sup>52</sup> Tuned liquid dampers (TLD) and tuned liquid column dampers (TLCD) have been investigated for use in buildings by Sakai et al.<sup>53</sup> and Xu et al.<sup>38</sup> These dampers have been used successfully in spacecraft satellites and marine vessels by Amieux and Dureigne.<sup>54</sup> TLD and TLCD systems have some advantages over TMDs, including lower costs, less maintenance, and easier construction and handling.<sup>38</sup>

As discussed before, circular section structures, like chimneys, mast, and cooling towers are prone to across-wind vortex excitation. The vortex shedding can be reduced and suppressed to some degree by the use of strakes, shrouds, slats, and the like as shown in Fig. 28. The strakes, shrouds, and slats can reduce the coherence of the vortex shedding along the



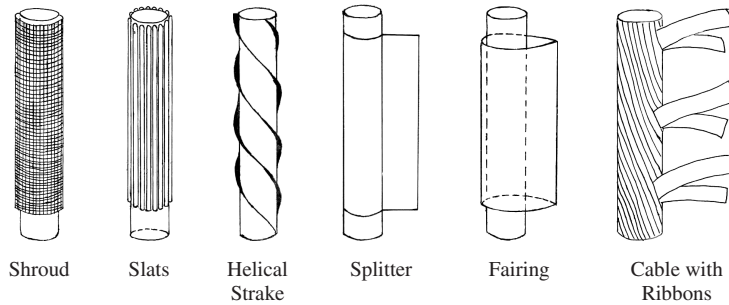


Figure 28 Methods of reducing vortex-induced vibration in cylindrical structures.

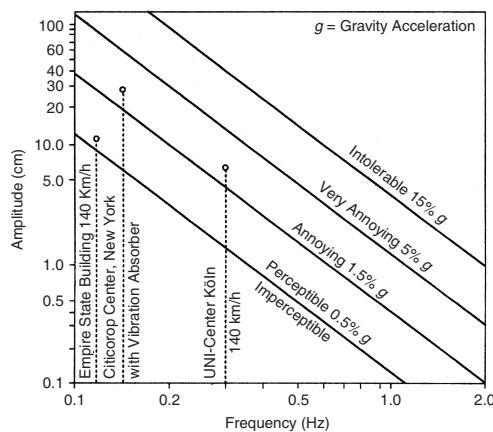


Figure 29 Human perception of building vibration due to wind. (See Ref. 50.)

cylindrical structure, but their effectiveness depends to some extent on the Reynolds number of the flow.<sup>1,4,6</sup>

## 6 HUMAN RESPONSE TO VIBRATION AND ACCEPTABILITY CRITERIA

In most cases, building vibration caused by wind is insufficient to cause structural damage, except in some cases to the superstructure or cladding. (See Fig. 29.) The vibration is, however, often unpleasant and worrying for occupants. The swaying of tall buildings particularly at the tops can be disconcerting for occupants to say the least. Most studies on acceptability of vibration have been for frequencies higher than those normally encountered in tall buildings. Some studies have been conducted with very low frequency vibration using vibration simulators. Other results have been obtained from extrapolations from high frequency to low frequency to arrive at criteria for acceptability of vibration at very low frequencies less than 1 Hz. Most subjects report that they cannot sense vibration with acceleration less than about 0.01  $g$ . If the vibration has an acceleration exceeding about 0.1  $g$ , most subjects find the vibration

Table 4 Human Acceleration Acceptability Criteria

Perception	Acceleration Limits
Imperceptible	$a < 0.005g$
Perceptible	$0.005g < a < 0.015g$
Annoying	$0.015g < a < 0.05g$
Very annoying	$0.05g < a < 0.15g$
Intolerable	$a > 0.15g$

Source: From Refs. 1, 6, and 50.

is becoming intolerable. Table 4 lists some human acceptability criteria.

## 7 USE OF WIND TUNNELS AND SCALE MODELS

In some cases, it is difficult to predict the wind flow around and forces on buildings from previous knowledge, published studies, and existing empirical prediction schemes and theoretical models. Such cases include building designs with complicated or unusual shapes, buildings in the downstream wake of other buildings or groups of buildings. In such cases, the testing of scale models in wind tunnels should be considered.

Since wind tunnel testing can be expensive (on the order of \$20,000 to \$100,000 in 2005), it is normally only considered for the design of larger buildings and structures where the cost savings is greater than the wind tunnel tests. Wind tunnel testing of model buildings and structures and model scaling and similarity laws for the flow are described in several publications.<sup>1,2,4,5,18</sup>

## REFERENCES

1. E. Simiu and R. Scanlan, *Wind Effects on Structures*, 3rd ed., Wiley, New York, 1996.
2. H. Liu, *Wind Engineering—A Handbook for Structural Engineers*, Prentice Hall, Englewood Cliffs, 1991.
3. R. D. Blevins, *Flow-Induced Vibration*, Van Nostrand Reinhold, New York, 1990.
4. P. Sachs, *Wind Forces in Engineering*, 2nd ed., Pergamon, Oxford, UK, 1977.
5. M. G. Melaragno, *Wind in Architectural and Environmental Design*, Van Nostrand Reinhold, New York, 1982.

6. H. Bachmann, W. J. Ammar, F. Deisch, and J. Eisenmann, *Vibration Problems in Structures—Practical Guidelines*, Birkhaeuser, Basel, 1995.
7. R. D. Blevins, Part I: Vibration of Structures, Induced by Fluid Flow, in *Shock and Vibration Handbook*, C. M. Harris, Ed., 4th ed., McGraw-Hill, New York, 1995, Chapter 29.
8. A. G. Davenport and M. Novak, Part II: Vibration of Structures, Induced by Wind, in *Shock and Vibration Handbook*, C. M. Harris, Ed., 4th ed., McGraw-Hill, New York, 1995, Chapter 29.
9. T. Kijewski, F. Hann, and A. Kareem, *Wind-Induced Vibrations*, in *Encyclopedia of Vibration*, Vol. III, S. Braun et al., Eds., Academic, London, 2002, pp. 1578–1587.
10. K. J. Eaton, Ed., *Wind Effects on Buildings and Structures*, Proceedings of the 4th International Conference on Wind Engineering, Heathrow, UK, 1975, Cambridge University Press, Cambridge, UK, 1975.
11. J. E. Cermak, Eds., *Wind Engineering*, Vols. 1 and 2, Proceedings of the 5th International Conference on Wind Engineering, Pergamon, Oxford, 1980.
12. C. Kramer and H. J. Gerhardt, Eds., *Advances in Wind Engineering*, Proceedings of the 7th International Conference on Wind Engineering, Parts 1, 2, and 3, Elsevier, Amsterdam, 1988.
13. R. E. A. Arndt et al., Eds., *Advancements in Aerodynamics. Fluid Mechanics and Hydraulics*, Proceedings of the Specialty Conference, American Society of Civil Engineers, New York, 1986.
14. H. Sockel, Damping Measures to Control Wind Induced Vibrations, CISM Courses and Lectures No. 335, Springer, Wien, New York, 1994.
15. American Society of Civil Engineers, *Wind Loading and Wind-Induced Structural Response*, American Society of Civil Engineers, Reston, VA, 1999.
16. American Society of Civil Engineers, Structural Division, *Minimum Design Loads for Buildings and Other Structures*, ASCE7-98, American Society of Civil Engineers, Reston, VA, 1999.
17. N. J. Cook, *The Designer's Guide to Wind Loading of Building Structures, Part 1*, Butterworths, London, 1985.
18. American Society of Civil Engineers, *Wind Tunnel Studies of Building and Structures*, ASCE Manuals and Reports on Engineering Practice, No. 67, American Society of Civil Engineers, Reston, VA, 1987.
19. J. E. Cermak, Aerodynamics of Buildings, *Ann. Rev. Fluid Mech.*, Vol. 8, 1976, pp. 75–106.
20. J. E. Cermak, Advances in Physical Modeling for Wind Engineering, *J. Eng. Mech.*, Vol. 113, No. 5, 1987, pp. 737–756.
21. A. Kareem, Wind Effects on Structures: A Probabilistic Viewpoint, *Prob. Eng. Mech.*, Vol. 2, No. 4, 1987, pp. 166–200.
22. T. Kijewski and A. Kareem, Dynamic Wind Effects: A Comparative Study of Provisions in Codes and Standards with Wind Tunnel Data, *Wind Structures*, Vol. 1, No. 1, 1998, pp. 77–109.
23. Vibrations: Building and Human Response, Building Research Establishment (UK), *BRE Digest*, Vol. 278, 1983.
24. Guide to Evaluation of Human Exposure to Vibration in Buildings (1 Hz to 80 Hz), British Standard BS 6472, 1984.
25. *Design Loads for Buildings; Imposed Loads; Windloads on Structures Unsusceptible to Vibration*, Norm DIN 1055 Blatt 4, Deutsches Institut für Normung, Beuth, Berlin, 1986; Aenderung 1, 1987.
26. *Structural Vibration in Buildings; Effects on Structures*, Norm DIN 4150 Teil 3, Deutsches Institut für Normung, Beuth, Berlin, 1986.
27. *Wind Actions on Structures*, ISO/DIS 4354, International Standard Organization, Geneva, 1991.
28. *Wind Loading (Static and Dynamic)*, ISO/TC98/SC3/WG2, International Standard Organization, Geneva, 1991.
29. V. Kolousek, M. Pimer, O. Fischer, and J. Naprstek, *Wind Effects on Civil Engineering Structures*, Academia, Praha, 1983.
30. H. Ruscheweyh, *Dynamische Windwirkung an Bauwerken (Dynamic Actions of Wind on Structures)*, Vols. I and II, Bauverlag, Berlin, 1982.
31. A. P. Jeary and B. R. Ellis, On Predicting the Response of Tall Buildings to Wind Excitation, *J. Wind Eng. Ind. Aerodyn.*, Vol. 13, 1983, pp. 173–182.
32. G. Hirsch, Practical Experiences in Passive Vibration Control of Chimneys, in *Structural Control*, Martinus Nijhoff, Dordrecht, 1987, pp. 278–296.
33. H. Ruscheweyh and G. Sedlacek, *Crosswind Vibrations of Steel Stacks—Critical Comparison Between Some Recently Proposed Codes*, *Advances in Wind Engineering, Part 3*, Elsevier, Amsterdam, 1988, pp. 173–184.
34. H. Ruscheweyh, Wind-Induced Vibrations of Towers and Stacks, Proceedings IUTAM-JAHR Symposium, Karlsruhe in *Practical Experiences with Flow Induced Vibrations*, Springer, Berlin, 1979, pp. 709–717.
35. A. Aschrafi and G. Hirsch, Control of Wind-Induced Vibrations of Cable-Stayed Bridges, *J. Wind Eng. Ind. Aerodyn.*, Vol. 14, 1983, pp. 235–246.
36. G. Hirsch, G. Nonhoff, and H. Volkmar, *Wind Induced Vibrations of Guyed Masts*, Vol. 1, Preprints EURO DYN '90, SFB 151 Ruhr-Universität Bochum, 1990, pp. 815–823.
37. T. G. Carne, Guy Cable Design and Damping for Vertical Axis Wind Turbines, Sandia National Laboratory, Division 5523, Albuquerque, NM, SAND 80–2669, 1981.
38. Y. L. Xu, B. Samali, and K. C. S. Kwok, Effect of Passive Damping Devices on Wind-Induced Response of Tall Buildings, in *National Conference Publication—Institution of Engineers, Australia*, No. 90, pt 9, *Vibration and Noise-Measurement Prediction and Control*, The Institution of Engineers, Australia, (National Office, Barton, ACT, Australia) 1990, pp. 127–132.
39. C. C. Chang, “Mass Dampers and Their Optimal Designs for Building Vibration Control, *Eng. Struct.*, Vol. 21, No. 5, May, 1999, pp. 454–463.
40. A. Kareem, T. Kijewski, and Y. Tamura, Mitigation of Motions of Tall Buildings with Specific Examples of Recent Applications, *Wind Structures*, Vol. 2, No. 3, 1999, pp. 201–251.
41. J. N. Yang, Y. Lei, S. Lin, and N. Huang, “Identification of Natural Frequencies and Dampings of in situ Tall Buildings Using Ambient Wind Vibration Data *J. Eng. Mech.*, Vol. 30, No. 5, May, 2004, pp. 570–577.
42. C. Winston and M. Q. Feng, Vibration Control of Super Tall Buildings Subjected to Wind Loads, *Int. J. Non-Linear Mech.*, Vol. 32, No. 4, Jul. 1997, pp. 657–668.

43. L.-S. Fur, H. T. Y. Yang, and S. Ankireddi, Vibration Control of Tall Buildings under Seismic and Wind Loads, *J. Struct. Eng.*, Vol. 122, No. 8, Aug. 1996, pp. 948–957.
44. S. Ankireddi and H. T. Y. Yang, Simple ATMD Control Methodology for Tall Buildings Subject to Wind Loads, *J. Struct. Eng.*, Vol. 122, No. 1, Jan. 1996, pp. 83–91.
45. Y. Zhou, T. Kijewski, and A. Kareem, Aerodynamic Loads on Tall Buildings: An Interactive Database, *J. Struct. Eng.*, ASCE, 2001.
46. J. A. Peterka, J. E. Cermak, and K. G. Medearis, *Wind Engineering Study of the Iterama Tower of the Sun*, Fluid Mechanics Program, Engineering Research Center, College of Engineering, Colorado State University, Fort Collins, CO, 1975.
47. T. T. Soong, Active Structural Control in Civil Engineering, *Eng. Struct.*, Vol. 10, 1988, pp. 74–84.
48. F. Y. Cheng and C. P. Pantelides, *Optimal Active Control of Wind Structures Using Instantaneous Algorithm*, American Society of Mechanical Engineers, Design Engineering Division (Publication) DE, Vol. 4, ASME, New York, 1987, pp. 21–28.
49. S. M. Hashemi and M. F. Golnaraghi, Active Control of Wind-Induced Building Vibration Using a Linear Coupling Strategy, Proceedings of the ASME Design Engineering Technical Conference, Vol. 6 A, 2001, pp. 987–994.
50. F. K. Chang, wind and Movement of Tall Buildings, *J. ASCE, Struct. Div.*, 1967, pp 70–72.
51. M. Paz, *Structural Dynamics—Theory and Computation*, 2nd ed., Van Nostrand Reinhold Company, New York, 1985.
52. V. Modi and F. Welt, Damping of Wind Induced Oscillations though Liquid Sloshing, *J. Wind Eng. Ind. Aerodyn.*, Vol. 30, 1988, pp. 85–94.
53. F. Sakai, S. Takaeda, and T. Tamaki, Tuned Liquid Column Dampers—New Type Device for Suppression of Building Vibrations, Proceedings of the International Conference on High Rise Buildings, Vol. 2, Nanjing, China, 1989, pp. 926–931.
54. J. Amieux and M. Dureigne, Analytical Design of Optimal Nutation Damper, *J. Spacecraft*, Vol. 9, No. 12, 1972, pp. 934–936.

# CHAPTER 117

## PROTECTION OF BUILDINGS FROM EARTHQUAKE-INDUCED VIBRATION

Andreas J. Kappos and Anastasios G. Sextos

Department of Civil Engineering  
Aristotle University of Thessaloniki  
Thessaloniki, Greece

### 1 INTRODUCTION

Earthquakes are generated wherever the accumulation of strain at geological *faults* leads to their rupture and slip, until a new stable state is reached. There are essentially two types of faults, those associated with horizontal (*strike-slip*) and those associated with vertical (*dip-slip*) movement. The waves generated propagate either by compression and dilation with the ground particle motion in the same direction as the propagation (*longitudinal* or *P waves*) or by shear (*transverse* or *S waves*); both types are referred to as *body waves*. When body waves reach the Earth's surface, they are reflected back into the crust, and a vibration of the surface is initiated, which propagates through *surface waves*. Surface waves, along with S waves, account for the strongest part of seismic motion, that is, these are the potentially more destructive. Protection of buildings from earthquake-induced vibration, therefore, is the process to estimate the amount of energy (often related to *magnitude*) that is expected with a specific probability to be released at the *source*, to establish methods for determining the *frequency content*, *duration*, and *intensity* of ground motion that finally excites the structure, and to define methods for calculating and optimizing the structural dynamic response to this vibration.

### 2 CONCEPT OF SEISMIC DESIGN OF STRUCTURES

Protection of buildings from earthquake-induced vibration is achieved through their *seismic design*. The goal of seismic design is to ensure that a structure behaves "satisfactorily" when subjected to earthquake loading. As is the case with most loading types, the anticipated behavior or performance levels for the structure are different for different levels of the loading. Ideally, and taking into account the large uncertainty associated with earthquake loading, several levels of performance should be considered in design, each one corresponding to a different probability of exceedance of the seismic loading. According to most current seismic codes, the structure should resist minor earthquakes (i.e., remain serviceable at its serviceability limit state) without significant damage, sustain moderate earthquakes (i.e., at its ultimate limit state) with repairable damage, while avoiding collapse during major earthquakes. This points to the need to design a structure for a set of performance objectives (limit states), recently referred to as performance-based design (PBD).<sup>1</sup> Through the

code-defined design procedure, therefore, the engineer is provided with the seismic loads that the structure should be able to withstand in order to meet the above objectives, the minimum design requirements and the detailing rules that ensure the desired performance as well as with the methods of structural analysis to be employed in order to determine the response of the structure under the design loads.

For a given level of seismic exposure, it can be generally claimed that structures built in industrialized countries aware of the seismic risk are in general adequately safe (less vulnerable), but the expected actual cost of damage inflicted, as well as the indirect cost resulting from business disruption, need for relocation, and the like can be significantly higher. As a result, the *seismic risk* of potential economic losses is in fact a qualitative product of *seismic hazard* (i.e., the level of seismic exposure), *structural vulnerability* (i.e., the level of expected damage), and *element value at risk* (defined by the importance of the structure). It has to be noted though that seismic risk modeling is a useful decision-making and risk management diagnostic tool that does not provide solutions alone; it is the code-prescribed design and assessment process that guarantees compliance with the structural performance criteria.

### 3 FUNDAMENTALS OF BUILDING RESPONSE TO EARTHQUAKE

#### 3.1 Single and Multiple-Degree-of-Freedom Systems

The simplest model of a structure that can be considered is a single-degree-of-freedom (SDOF) pendulum having its mass concentrated on top and vibrating laterally under base excitation, while its resistance is exclusively provided by the total stiffness  $k$  of its vertical elements (a one-story building or an elevated water tank are some typical examples). When a force that varies with time  $p(t)$  is applied on this structure with mass  $m$ , the resulting displacement, denoted by  $u(t)$ , is a function of the system damping force  $f_D$  and the stiffness-related resisting force  $f_s$ . Newton's second law of motion leads to the fundamental equation:

$$m\ddot{u} + c\dot{u} + ku = p(t) \quad (1)$$

which for the particular case of base excitation (due to earthquake) is written in the form:

$$m\ddot{u} + c\dot{u} + ku = -m\ddot{u}_g(t) \quad (2)$$

The solution of the above equation is obtained by adding the response of the SDOF system to the so-called effective earthquake force  $p_{\text{eff}}(t) = -m\ddot{u}_g(t)$  for all impulses up to the particular time  $t$ :

$$u(t) = \frac{1}{m\omega_n} \int_0^t p_{\text{eff}}(\tau) \sin[\omega_n(t - \tau)] d\tau \quad (3)$$

where  $\omega_n = \sqrt{k/m}$ . Equation (3) is known as *Duhamel's integral*, and it is a special form of the convolution integral.

For the case of multiple-degree of freedom systems (corresponding to the vast majority of engineering structures), nodal displacement is a vector that can be expressed in terms of particle modal contributions as

$$u(t) = \sum_{r=1}^N \phi_r q_r(t) = \Phi q(t) \quad (4)$$

where  $\phi_r$  are the modes of the system and  $q_r(t)$  the modal coordinates. Using this transformation, eq. (1) can be written in the form:

$$\sum_{r=1}^N m\phi_r \ddot{q}_r(t) + \sum_{r=1}^N c\phi_r \dot{q}_r(t) + \sum_{r=1}^N k\phi_r q_r(t) = p(t) \quad (5)$$

By multiplying each part of the equation by  $\phi_n^T$  and by substituting the *generalized mass*, *stiffness*, and *force* components being, respectively,  $M_n = \phi_n^T m \phi_n$ ,  $K_n = \phi_n^T k \phi_n$ , and  $P_n = \phi_n^T p \phi_n$ , the  $N$  equations expressed in Eq. (5) are summarized in matrix form:

$$\mathbf{M}\ddot{\mathbf{q}} + \mathbf{C}\dot{\mathbf{q}} + \mathbf{K}\mathbf{q} = \mathbf{P}(t) \quad (6)$$

where  $\mathbf{M}$  is the diagonal matrix of the generalized modal masses  $M_n$ ,  $\mathbf{K}$  is the diagonal matrix of the generalized modal stiffness  $K_n$ , and  $\mathbf{P}(t)$  is a column vector of the generalized modal forces  $P_n(t)$ .

### 3.2 Elastic Spectra and Design Spectra

A *response spectrum* is a plot of the peak response (to the aforementioned effective earthquake force) as a function of the natural period and can be derived by analyzing a series of SDOF systems, as can be seen in Fig. 1. It is explained in more detail in the literature.<sup>2-4</sup> The quantities typically plotted are the spectral pseudoacceleration  $S_{\text{pa}}$ , pseudovelocity  $S_{\text{pv}}$ , and displacement  $S_d$ , which are interrelated through the familiar expressions

$$S_{\text{pa}} = \omega S_{\text{pv}} = \omega^2 S_d \quad (7)$$

For design purposes,  $S_{\text{pa}}$  is more useful than the actual response acceleration since the former can be used to

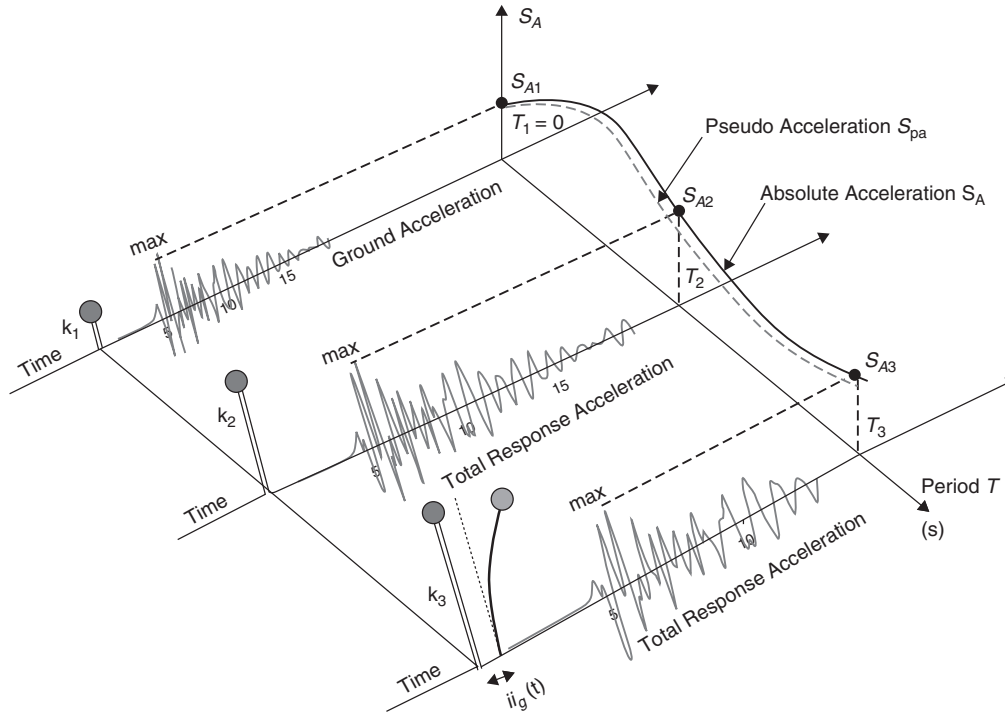
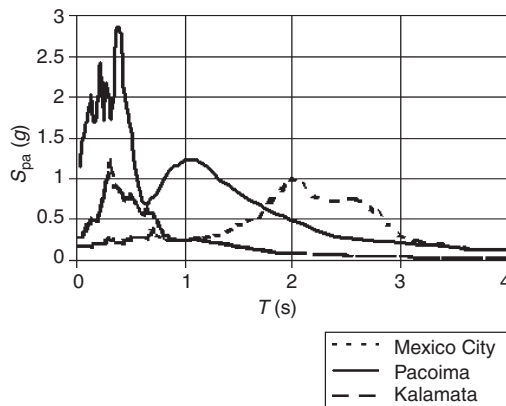


Figure 1 Pseudoacceleration and absolute acceleration response spectrum plots.



**Figure 2** 5% damped pseudoacceleration spectra for three different ground motions.

calculate directly the maximum forces on the structure. An important piece of information provided by a spectrum is the range of periods for which the response of a structure is peaking. A useful indicator of the damageability of a ground motion is  $S_{pv}$ , which is a direct measure of the seismic energy input, since for negligible damping the energy stored in an oscillator with mass  $m$  is equal to  $\frac{1}{2}mS_{pv}^2$ . On the other hand, recently developed *displacement-based design* and *assessment* procedures are based on the displacement spectrum. Despite those trends, current codes base their design forces on  $S_{pa}$  spectra (directly or indirectly), hence,  $S_{pv}$  and  $S_d$  curves can always be derived due to Eq. (7).

The significant differences in the shape of response spectra derived from different ground motions are illustrated in Fig. 2, which shows the 5% damped  $S_{pa}$  spectra for three accelerograms recorded in three different parts of the world. In particular, the Pacoima Dam (California) S16E and the Kalamata (Greece) N10W records are from earthquakes with similar magnitude (6.6 and 6.2) and very close to the recording station (epicentral distances of 3 and 15 km). It is seen that, although the amplitude is significantly larger for the Pacoima record, the shape of the two spectra is quite similar, with peaks occurring in the short period range. On the other hand the Mexico City 1985 transverse component, recorded at the SCT station during a magnitude 8.1 earthquake at a distance of 400 km, resulted in a significantly different spectral shape, wherein the critical period range is between 1.7 and 2.8 s. Bearing in mind that the fundamental natural period of a building frame is approximately equal to  $N/10$ , where  $N$  denotes the number of stories, it is seen that the Mexico City record with a peak ground acceleration (PGA) of only 0.17g, was more critical for high-rise buildings with  $T > 1.7$  s than the Pacoima record with a PGA of 1.17g.

For design purposes, it is clear that spectra smoother than those of Fig. 2 are required since a future motion is very unlikely to be identical to a previously recorded one, and also the exact periods

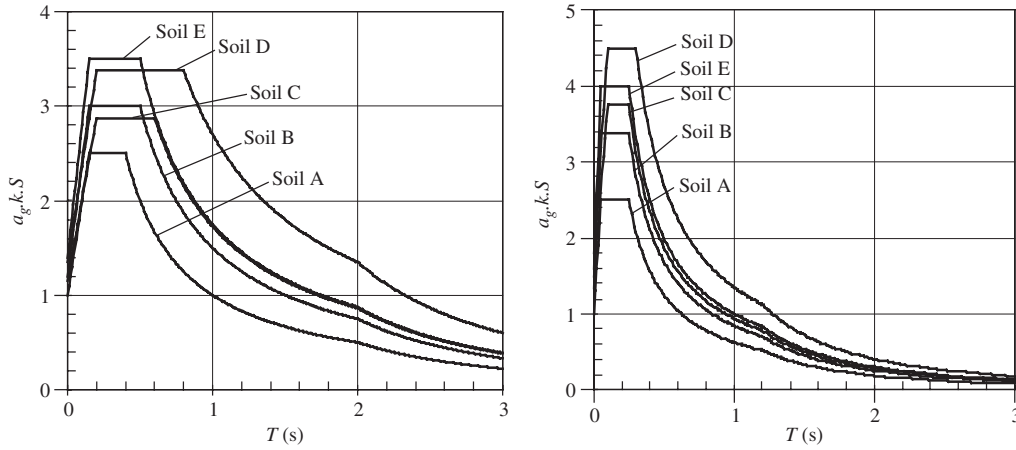
of a structure are difficult to assess in practical situations (e.g., when stiff cladding or partition elements are present in steel or reinforced concrete (R/C) frames). A smooth *design spectrum*, therefore, encompasses a family of ground motions and is derived from a statistical evaluation of actual spectra.

The *code spectrum* prescribed by the vast majority of modern seismic codes is a function of a number of parameters that define the target level of seismic excitation that is accepted for a structure and depends on:

- The seismo-tectonic environment of each geographical region and the corresponding exposure of structures to seismic hazard
- The foundation soil conditions that characterize the site of construction
- The importance of the structure
- The amount of damping due to a number of sources (material damping, damping at connections, etc.)
- The ability of the particular structural configuration to absorb seismic energy through stable cycles of inelastic response.

Seismic codes typically specify pseudoacceleration spectra only, consisting of a shape to be anchored to a (design) PGA, which is a function of the soil category that the foundation soil can be classified into: For softer materials, the spectrum is generally shifting rightwards representing a higher level of bedrock ground motion amplification that is expected to occur when higher period pulses propagate through the (relatively) loose soil profile. Moreover, the effect of the epicentral distance on the spectral amplification at particular period ranges (as seen in the Mexico and Pacoima response spectra) has been widely recognized in recent seismic codes (e.g., the American codes since 1997) through the specification of *near-source factors*. In the latest version of the American seismic code (*IBC 2000*)<sup>5</sup> the concept of spectral dependency remains intact, but the spectral acceleration is defined through the magnitude- and soil-dependent factors  $F_a$  and  $F_v$ . The latest version of the European Seismic Code, *Eurocode 8* (EN1998-1, 2003)<sup>6</sup> also accounts for the effect of earthquake magnitude by distinguishing to type 1 ( $M_s > 5.5$ ) and type 2 ( $M_s < 5.5$ ) spectra, as seen in Fig. 3.

Based on the above, it can be stated that the spectral values are a function of both foundation soil properties, distance from the source, and intensity of the event. However, there is a number of inherent uncertainties in the definition of the appropriate soil profile determination due to the difficulty to evaluate the overall dynamic response of the soil formations from the  $V_s$  profile of the uppermost 30 m as adopted in the U.S. codes. In fact, it has been extensively shown<sup>7</sup> that the dynamic material characteristics of soil profiles (described as a one-dimensional soil column) are often inadequate to depict the complex ("site effects"-related) nature and physics of the multilayered, nonlinear, three-dimensional and possibly inclined soil layers over a nonrigid bedrock.



**Figure 3** Recommended type 1 elastic response spectrum for soils A to E according to *Eurocode 8* (EN1998-1, CEN 2004).<sup>6</sup>

A typical example of a code-specified spectrum is shown in Fig. 3, where the 5% damped elastic pseudoacceleration spectrum of *Eurocode 8* (CEN 2004)<sup>6</sup> is plotted; it is calculated through the following set of expressions:

$$\begin{aligned}
 0 \leq T \leq T_B : S_C(T) &= a_g S \left[ 1 + \frac{T}{T_D} (\eta \cdot 2.5 - 1) \right] \\
 T_B \leq T \leq T_C : S_C(T) &= a_g S \eta \cdot 2.5 \\
 T_C \leq T \leq T_D : S_C(T) &= a_g S \eta \cdot 2.5 \left( \frac{T_C}{T} \right) \\
 T_D \leq T \leq 4s : S_C(T) &= a_g S \eta \cdot 2.5 \left( \frac{T_C T_D}{T^2} \right)
 \end{aligned} \quad (8)$$

where  $\alpha$  = effective peak ground acceleration normalized by gravity  
 $T$  = fundamental period of the structure  
 $T_A, T_B, T_C, T_D$  = corner (characteristic) period values depending on the corresponding subsoil class as described in Table 1  
 $\eta$  = factor accounting for damping other than 5% =  $\sqrt{5/\zeta}$  ( $\zeta$  being the critical damping ratio)  
 $S$  = soil amplification parameter varying from 1.0 to 1.6

It has to be noted that the values to be ascribed to periods  $T_B, T_C, T_D$ , and  $S$  for each ground type may be found in the National Annex of each country that will adopt the *Eurocode*. Although technically feasible, designing a normal structure to respond elastically to the design earthquake forces is believed to lead to disproportionately high construction cost. For this reason, seismic design codes allow inelastic response in plastic mechanisms that are considered as favorable in terms of seismic performance and

**Table 1** Soil Amplification Parameter and Corner Periods as a Function of Subsoil Class for Earthquake Type 1

Ground Type	$S$	$T_B$	$T_C$	$T_D$
A	1.0	0.15	0.40	2.00
B	1.20	0.15	0.50	2.00
C	1.15	0.20	0.60	2.00
D	1.35	0.20	0.80	2.00
E	1.40	0.15	0.50	2.00

maintain structural integrity. The relationship between elastic and design spectra, therefore, is inevitably related to the level of energy dissipation anticipated to take place through cycles of inelastic behavior and damage of the structural members.

Most of the seismic codes worldwide are influenced either by the American codes [mainly the Uniform Building Code (UBC) now replaced by the International Building Code (IBC)] or the *Eurocode*, and adopt the aforementioned concepts. An exception was Japan, which until recently was relying more on strength and much less on ductility, but this changed after the 1995 Great Hanshin (Kobe) earthquake, and stricter requirements regarding ductile detailing were introduced.

The reduction in the forces associated with the elastic spectra is usually made by dividing the elastic spectra by the “behavior factor”  $q$  (in the *Eurocodes*) or the “response modification factor”  $R$  (in the U.S. codes). It is noted that for an ordinary reinforced concrete building, the highest value according to *Eurocode 8* is less than 6, while the IBC provisions prescribe a top value of 8. It is therefore necessary, before proceeding to any comparative evaluation of code-defined spectra, to account for the different assumptions on the reduction of forces prescribed in different codes.



### 3.3 Design Situations

The design seismic action or the *design earthquake* is a ground motion or a set of ground motions defined in a way appropriate for the design of structures. Depending on its type and importance, the seismic action can be defined in terms of (a) a set of (equivalent) lateral forces, (b) a response spectrum, (c) a power spectrum, or (d) a set of acceleration time histories. The foregoing can be defined either on the basis of a seismic code (most common case) or by carrying out a site-specific seismic hazard analysis with due consideration of ground effects. The scope of each procedure can be appreciated by considering the following four situations that might be faced by an engineer in practical design (see Fig. 4):

- For many building structures, and also for some “small-scale” and *regular* (i.e., without abrupt changes in plan or height) civil engineering structures (such as small bridges, viaducts, etc., and typical geotechnical structures such as retaining walls), the *equivalent lateral force* procedure can be used. The procedure is well documented in most current seismic codes and will be described with specific reference to two major codes, *Eurocode 8* and *IBC 2000* code.<sup>5,6</sup>
- For buildings with configuration problems (*irregular* in plan and/or elevation), for many types of “medium” bridges, and for many of the structures falling beyond the scope of this chapter, an *elastic dynamic analysis* has to be

carried out, typically in the form of modal response spectrum analysis. The definition of the elastic spectrum, the aforementioned modifications due to site effects, and its reduction to an inelastic design spectrum, are some of the most important issues relating to seismic loading.

- In cases such as the design of very important structures, or structures clearly falling outside the limits of the existing codes (e.g., structures with very high fundamental natural periods), a full *time-history analysis*, typically in the inelastic range may be required. Note that there is no advantage in using this procedure for an elastic analysis of the structure which can be conveniently carried out (at essentially the same accuracy) using the modal superposition approach, the exception being structures where due to highly irregular geometry it is difficult to combine the modal contributions, or whenever the structural model includes critical frequency-dependent parameters.<sup>4</sup> An appropriate selection and scaling of natural and/or artificial records has then to be made. For *assessment* purposes, a *nonlinear static (pushover)* approach may also be performed in order to identify the expected plastic mechanism in a structure and to assess its actual capacity to resist earthquake loading.

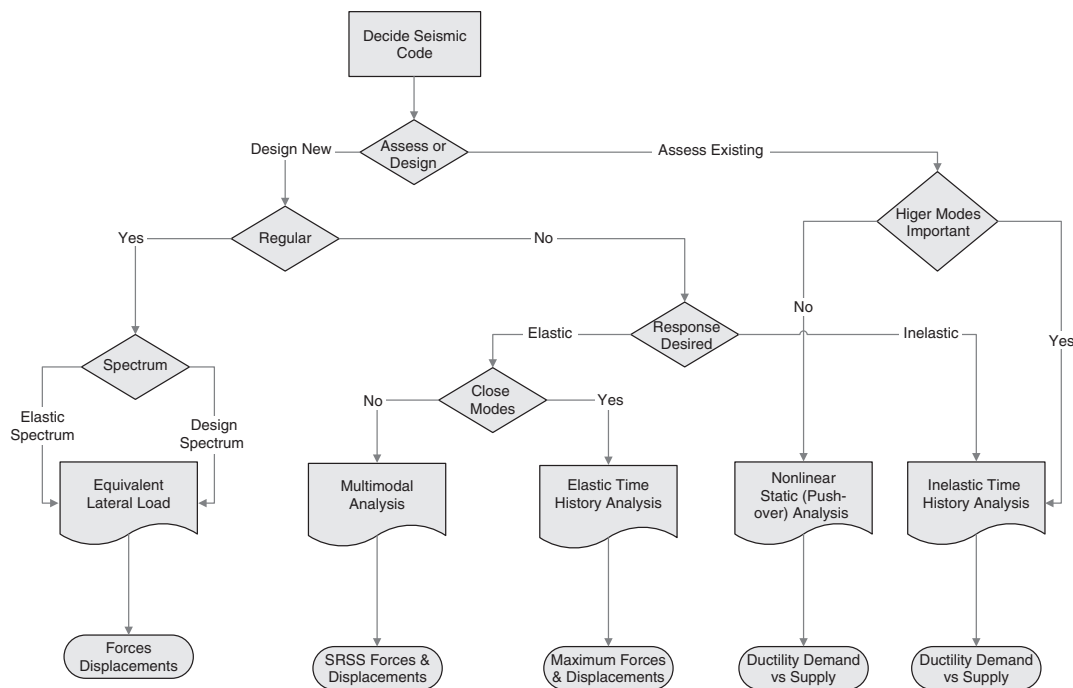


Figure 4 Overview of the alternative analysis approaches for the seismic design of structures.



### 3.4 Seismic Isolation and Passive Control

Designing a structure on the basis of inelastic spectra and capacity design means that for earthquakes that exceed the design event, damage to the structure could be substantial. Perhaps more importantly, formation of a favorable mechanism does not guarantee that interstory drifts and/or floor accelerations will be low enough to prevent extensive damage to the non-structural elements. These and other concerns have led to the development of alternative conceptual frameworks for seismic design, currently referred to as active and passive control of the seismic response of the structure. The devices used in *active control* introduce an energy (or force) source into the structure. Such systems<sup>8</sup> have been developed during the last two decades for reducing the response of buildings (particularly tall ones) to wind and earthquake loading. Nevertheless, despite the attractiveness of the concept and the high-quality interdisciplinary research carried out over the last two decades, the practical application of active control systems still remains very limited, mainly in full-scale demonstration projects.

As a result, by far the most practical approach, at least nowadays, is *passive control*, which incorporates the fundamental ideas of *seismic isolation* and provision of *supplemental damping*. There are two inter-related ideas behind developing a seismic isolation system: The first one is to make the structure much more flexible than it is, by altering the way it rests on the ground, hence shift it to the long period range of the response spectrum that is typically characterized by reduced accelerations (cf. Figs. 2 and 3) and consequently reduced inertial forces; the second is to introduce some kind of “fuse” between the structure and the ground, whereby the amount of base shear to be transferred from the shaking ground to the structure is controlled by the strength of the fuse. By making the structure more flexible, one might achieve lower seismic forces, but displacements tend to increase. It is therefore essential to also control the amount of horizontal displacement of the isolated structure and an efficient way to do this is by increasing its damping.

Currently, used isolation systems are based on the concept of flexible supports that can either remain essentially elastic (linear isolation) or enter the inelastic range (nonlinear isolation) upon exceeding a certain level of horizontal shear.<sup>9</sup> The basic elements included in a seismic isolation system are:

- Horizontally flexible supporting devices (*isolators*) located either between the structure and its foundation or at a higher level in the structure; in buildings the flexible supports are commonly located at the superstructure–foundation interface.
- A *supplemental damping* device (or energy dissipator) for reducing the relative horizontal displacement between the superstructure and substructure (i.e., the portion of the structure below the isolators). Such devices can be of different types: *Hysteretic* dampers, wherein energy dissipation is taking place by yielding of metals;

*lead–rubber bearings*, which are elastomeric bearings with a lead core that provides both damping (after yield) and resistance to service lateral loads; *viscous* dampers, such as the oil dampers commonly used in the motor industry; *frictional* dampers based on friction between different materials, that is, stainless steel and PTFE (Teflon).

- Some means for controlling displacements at service levels of lateral loading, that is, wind loading and serviceability limit state (SLS) or smaller earthquake loading.

A critical point in passive control systems is that whereas isolator damping is always reducing the displacements of the structure that are controlled by the fundamental mode, it tends to increase floor accelerations caused by higher modes. This might be very important in structures where protection of secondary systems (equipment and nonstructural elements) is the main reason for using seismic isolation. Seismic attack on secondary systems is frequency selective, and it is possible to design isolation systems that reduce the response of such systems more than that of the primary structural system. A related issue is that in nonlinear isolation systems (which are used in the majority of applications), control of the amount of base shear through the strength and the stiffness of the isolators does not guarantee control of the story shear distribution along the height of the building. Whenever higher mode response is not adequately controlled, “bulged” distributions of story shear can result and in extreme cases the shear in the upper half of the structure may exceed the base shear.<sup>9</sup> The foregoing are clear indications of the need for a reliable dynamic analysis when dealing with isolated structures.

A critical review of code provisions for seismic isolation can be found in Naeim and Kelly.<sup>10</sup> U.S. code provisions (*IBC 2000*)<sup>5</sup> include both the equivalent lateral force (section 1623.1.3.1) and the dynamic analysis (section 1623.1.3.4) procedures for seismically isolated buildings, but the restrictions for the former are such that in most practical cases the dynamic approach has to be applied. Two sets of verifications are required: The first one is for the design earthquake (10%/50-year probability), under which the structure is required to remain essentially elastic. The second one is a stronger event (10%/250-year probability) for which the isolation system should be designed and tested, while all building separations and utilities that cross the isolation interface should be designed to accommodate the forces and displacements associated with this seismic input. In Europe, provisions for seismic isolation of buildings have first been introduced in the final version of *Eurocode 8*.<sup>6</sup>

## 4 METHODS OF ANALYSIS UNDER EARTHQUAKE LOADING

### 4.1 Equivalent Lateral Force Procedures

The typical procedure in the equivalent static analysis method is the determination of an appropriate

value of the base shear in terms of the structure mass and the design earthquake intensity, properly reduced for inelastic effects, along the lines discussed in the previous section. The base shear is then used for estimating a set of lateral forces distributed along the structure following (more or less) the fundamental mode of vibration. Since the base shear itself is also calculated on the basis of the fundamental period, it is clear that the application of the equivalent lateral force method should be restricted to structures whose dynamic response is governed by the fundamental mode, that is, they are characterized by so-called *regularity* in height and plan.

**The Eurocode 8 and IBC 2000 Procedures** The method is referred to as *simplified modal response spectrum analysis* rather than as *equivalent static analysis*. The *base shear* (sum of horizontal loads) is calculated from

$$V_b = S_d(T_1)W \quad (9)$$

where  $S_d(T_1)$  is the ordinate of the design spectrum corresponding to the fundamental period  $T_1$  of the structure, and  $W$  is the gravity load contributing to inertial forces; this is taken as the permanent loading ( $G$ ) and a portion of the variable (live) loading  $Q$ . The fundamental period  $T_1$  can be estimated either from a proper eigenvalue analysis, or from Rayleigh's method, or from empirical formulas included in the code.

The *lateral forces* corresponding to the base shear of Eq. (9) are calculated assuming (conservatively) that the effective mass of the fundamental mode is the entire mass of the structure; hence

$$F_i = V_b \frac{s_i W_i}{\sum s_j W_j} \quad (10)$$

where  $F_i$  is the horizontal force acting on story  $i$ ,  $s_i$ ,  $s_j$  are the displacements of the masses  $m_i$ ,  $m_j$  in the fundamental mode shape, and  $W_i$ ,  $W_j$  are the weights corresponding to the previous masses.

According to the IBC 2000<sup>5</sup> provisions, the method is applicable to:

- All ordinary buildings in regions of moderate to slightly more severe ground motion potential
- Irregular structures in regions of moderate to slightly more severe ground motion potential having no more than five stories
- Other structures with plan or vertical irregularities but in areas primarily located on relatively stiff soil conditions and fundamental period less than 0.7 s

The design base shear as given in the following equation is the seismic response coefficient  $C_s$  times the effective seismic weight  $W$  of the structure, that is, *seismic dead load*, including the total dead load and applicable portions of other loads (partition load of at least 0.5 kN/m<sup>2</sup>, permanent equipment, etc.):

$$V_b = C_s W = \frac{S_{D1} I_E}{R T} W \leq \frac{S_{DS} I_E}{R} \quad (11)$$

where  $I_E$  is the importance factor,  $R$  the response modification factor,  $S_{D1}$  is the seismic coefficient, and  $S_{DS}$  is the minimum base shear coefficient illustrated in Fig. 5 and summarized in Table 2 as a function of the spectral response acceleration and the site class.

Two lower bounds to  $V_b$  are set in IBC 2000<sup>5</sup>:

- For all seismic zones

$$V_b \geq 0.44 S_{DS} I_E W \quad (12)$$

- For cases of seismic design conditions  $E$  and  $F$  where spectral acceleration  $S_1 > 0.6g$ :

$$V_b \geq \frac{0.5 S_1}{R/I_E} W \quad (13)$$

The fundamental period  $T_1$  is calculated using the same procedures as in Eurocode 8<sup>6</sup> [cf. Eq. (9)]. The distribution of lateral forces along the height of the structure is given by

$$F_i = \frac{(V_b - F_t) z_i W_i}{\sum z_j W_j} \quad (14)$$

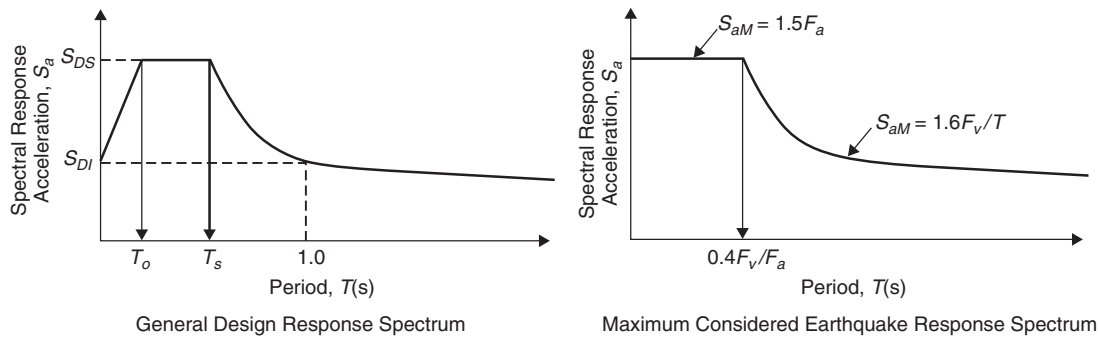


Figure 5 Design spectra according to IBC 2000.<sup>5</sup>

**Table 2 Minimum Base Shear Coefficient  $S_{DS}$  According to IBC 2000**

Site Class	Mapped Spectral Response Acceleration at Short Periods									
	$S_{DS}$	0.25 $V_{min}/W$ (%)	$S_{DS}$	0.50 $V_{min}/W$ (%)	$S_{DS}$	0.75 $V_{min}/W$ (%)	$S_{DS}$	1.00 $V_{min}/W$ (%)	$S_{DS}$	1.25 $V_{min}/W$ (%)
A	0.133	0.587	0.267	1.173	0.40	1.76	0.533	2.347	0.667	2.933
B	0.167	0.733	0.333	1.467	0.50	2.20	0.667	2.933	0.833	3.667
C	0.200	0.880	0.440	1.760	0.55	2.42	0.667	2.933	0.833	3.667
D	0.267	1.173	0.467	2.053	0.60	2.64	0.733	3.227	0.833	3.667
E	0.417	1.833	0.567	2.493	0.60	2.64	0.600	2.640	—	—

The top force  $F_t$  is a simple way of accounting for the effect of higher modes on the force pattern and is important for tall buildings only.

#### 4.2 Modal Analysis Procedures

For the purposes of seismic design the method is almost invariably applied in combination with the design response spectrum and is typically referred to as *modal response spectrum analysis*. Its field of applicability covers essentially cases where modes other than the fundamental one affect significantly the response of the structure. Detailed presentations of the modal response spectrum analysis can be found elsewhere.<sup>3,4,11</sup> In modal analysis involving lumped mass systems, the (elastic) force vector  $\mathbf{f}_n$  for the  $n$ th mode, calculated on the basis of the response spectrum, is

$$\mathbf{f}_n = \mathbf{m}\boldsymbol{\varphi}_n \pi \Phi \frac{L_n}{M_n} S_{pan} \quad (15)$$

where  $\mathbf{m}$  is the mass matrix,  $\boldsymbol{\varphi}_n$  is the  $n$ th mode shape vector,  $L_n$  is the earthquake excitation factor (depending on the mass distribution and the corresponding mode shape),  $M_n$  is the generalized mass, and  $S_{pan}$  is the spectral pseudoacceleration corresponding to the period  $T_n$  of the  $n$ th mode. Note that the forces  $f_{in}$  are acting on the (lumped) masses  $m_i$ ; in the common case of buildings with floor diaphragms,  $m_i$  is the mass of the  $i$ th story and  $f_{in}$  the  $n$ th mode force acting on this mass. The corresponding maximum *base shear* for the  $n$ th mode is given by

$$V_{0n} = \frac{L_n^2}{M_n} S_{pan} \quad (16)$$

The *displacements* for the  $n$ th mode can be calculated from

$$\mathbf{u}_n = \boldsymbol{\varphi}_n \frac{L_n}{M_n \omega_n^2} S_{pan} \quad (17)$$

where  $\omega_n = 2\pi/T_n$  is the circular frequency of the  $n$ th mode. Since the response of a structure results from the contribution of all modes, and since modal maxima generally do not occur simultaneously, it is customary to combine the action effects  $S_i$  from the individual modes in a statistical way. The most commonly adopted procedure is the *square root of the sum of squares* (SRSS) combination, that is,

$$S_{i,max} \cong \sqrt{S_{i1}^2 + S_{i2}^2 + S_{i3}^2 + \dots} \quad (18)$$

where  $S_{i,max}$  is the probable maximum value of the action effect (force or displacement), and the subscripts 1, 2, 3, ... refer to the 1st, 2nd, 3rd, ... mode; a sufficient number of modes should be considered in estimating  $S_{i,max}$ . Equation (18) gives reasonable values in many practical cases but is generally unconservative when two or more modes are closely spaced, that is, their periods are close to each other; this is often the case in three-dimensional structures susceptible to torsional effects. In these cases more refined combination rules, such as the *complete quadratic combination* (CQC)<sup>12</sup> or a time-history analysis are appropriate.

#### 4.3 Time-History Procedures

Time-history analysis is used for design purposes only as an exception and almost exclusively whenever non-linear effects are to be considered explicitly, rather than through the  $R$ -factor approach. When acceleration time histories are used for design, it is imperative that they actually correspond to the design earthquake for the site under consideration, which means that the envelope of the response spectra of the accelerograms used should reasonably match the *elastic* design spectrum for the site (no  $R$ -factor reduction). Several options are available for selecting a set of design accelerograms:

- Use of records from actual earthquakes, scaled to the design earthquake intensity
- Use of artificial accelerograms generated so as to match the (target) elastic response spectrum; this is sometimes referred to as the *engineering method*
- Use of simulated accelerograms generated by modeling the source and travel path mechanisms of the design earthquake (*seismological method*).

**Selection of Recorded Accelerograms** This can be the ideal solution whenever an extensive database of acceleration time histories is available, containing records from earthquakes with a broad range of characteristics. Then, a selection can be made of records matching the source parameters (focal mechanism and depth, distance from source), travel path, magnitude, peak ground motion parameters (A, V, D), and duration, for the site under consideration. In a practical context, the criteria for selecting ground motion

records are often related to the use of the A/V (i.e., peak ground acceleration over peak ground velocity, PGA/PGV) ratio,<sup>13</sup> which is a simple parameter, easy to calculate, and correlates well with the M–R (magnitude–distance) relationship as well as with the site conditions. Another possible criterion is to select ground motion records whose spectra ( $S_{pa}$  or, preferably,  $S_{pv}$ ) are peaking in the vicinity of the fundamental period of the structure under consideration, irrespective of their other characteristics.

**Scaling of Recorded Accelerograms** The most commonly applied scaling procedure is based on the PGA, that is, all records used for design are scaled to the same PGA but, as discussed in Section 3, the spectral ordinates are proportional to the PGA over the short period range only ( $T < 0.2$  s), whereas for longer periods (covering most of the usual civil engineering structures) they are proportional to the PGV, and for very long periods ( $T > 3.0$  s) they are proportional to the peak ground displacement (PGD). All these values are ground motion dependent only, that is, they are not correlated in any way to the characteristics of the structure to be designed.

A sensible choice of scaling parameters accounting for the characteristics of both the record and the structure are the spectral values, either those of the response spectrum or of the Fourier spectrum. An early (1952), but still quite popular, proposal is Housner's<sup>14</sup> *spectrum intensity*,  $SI_v$ , which is the area under the  $S_{pv}$  spectrum

$$SI_v = \int_{T_a}^{T_b} S_{pv}(T, \xi) dT \quad (19)$$

with  $T_a = 0.1$  s,  $T_b = 2.5$  s, and  $\zeta = 20\%$ . The reason for selecting these period limits is that they were deemed to represent the range of typical periods of buildings at the time; it is understood that  $SI_v$  is intended to be an overall measure of the “damageability” of a ground motion with respect to a population of structures. Whenever a particular structure is to be designed or assessed, a condensation of the limits suggested by Housner is appropriate. Kappos<sup>15</sup> suggested a modified Housner intensity based on  $T_a = 0.8T_1$  and  $T_b = 1.2T_1$ , where  $T_1$  is the fundamental period of the structure, calculated using the average of the SI values from the 5 and 10% velocity spectra.

**Use of Simulated Ground Motions** In the engineering method, artificial accelerograms are generated so as to match the (target) elastic response spectrum, hence they are typically called *spectrum-compatible motions*. In the seismological method, simulated accelerograms are generated by modeling the source and travel path mechanisms. All the aforementioned types of accelerograms are generally allowed as input for time-history analysis in *Eurocode 8*,<sup>6</sup> which, however, appears to promote the first. The duration of the records must be consistent with the characteristics (M, R, etc.) of the earthquake underlying the establishment of the design  $\alpha_g$ . A minimum

of five records is required for time-history analysis and additional rules are given in *Eurocode 8*,<sup>6</sup> regarding the allowable difference between the mean spectrum of these records and the code spectrum. IBC, on the other hand, recommends<sup>5</sup> the use of actual recorded accelerograms as input for time-history analysis; these should be selected from at least three different events, with due consideration of magnitude, source distance, and mechanisms, that should be consistent with the design earthquake. Simulated time histories are allowed whenever three appropriate recorded motions are not available. The design is based on the maximum response when three motions are used, while an average value can be used when the accelerograms used exceed seven.

## 5 DESIGN EXAMPLE

Consider the three-story, four-bay, moment resisting R/C frame building shown in Fig. 6, for which the base shear and its distribution along the height is to be determined. For such a frame, an approximate value for the fundamental period is given in *Eurocode 8*:<sup>6</sup>

$$T_1 = 0.075h^{3/4}$$

hence for  $h = 10.5$  m  $\Rightarrow T_1 = 0.44$  s.

The above approximate period value corresponds to the plateau ( $T_B < T < T_C$ ) of the elastic [see Eq.(8)], as well as of the design, spectrum given by *Eurocode 8*<sup>6</sup> for subsoil class B and corner periods:  $T_B = 0.15$ ,  $T_C = 0.50$ . Hence, the ordinate of the design spectrum can be calculated as follows:

$$S_d(T) = a_g S \frac{\beta_0}{q} = 0.24g \times 1.0 \times 2.5/3.9 = 0.153g$$

where  $a_g$  = effective peak ground acceleration  
= 0.24g

$S$  = soil parameter, which for the (assumed) subsoil class B is equal to 1.0

$\beta_0 = 2.5$

$q$  = behavior factor =  $q_0 K_W = 3.9 \times 1.0 = 3.9 > 1.50$

$q_0$  = basic value of the behavior factor, dependent on the type of the structural system and on regularity in elevation  
=  $3.0\alpha_u/\alpha_1 = 3.9$  (for a frame system and ductility class M, according to Table 5.1 of *Eurocode 8*)

$\alpha_u/\alpha_1 = 1.30$  for a multistory, multibay frame

$K_W$  = factor reflecting the prevailing failure mode in structural systems with walls  
= 1.0 for a frame system

The *total base shear* that acts on the frame is a function of its weight and is therefore derived as

$$V_b = S_d(T_1)W = 0.153g \times (3 \times 300) = 137.7 \text{ kN}$$

The *lateral forces* corresponding to the calculated base shear are derived according to (10), assuming that

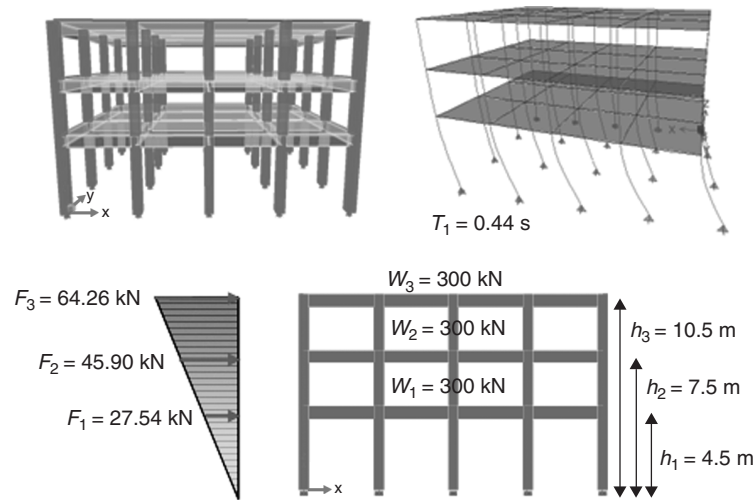


Figure 6 Calculation of the equivalent seismic forces of an RC frame.

the fundamental mode is increasing linearly with the building height, hence  $s_k$  are substituted by  $h_k$ , the heights of stories above the foundation level. As a result, Eq. (10) can be written as

$$F_i = V_b \frac{h_i W_i}{\sum h_j W_j}$$

and the forces  $F_i$  (as calculated in Table 3 and shown in Fig. 6) can then be used for a standard static analysis of the building.

## 6 CONCLUDING REMARKS

The goal of this chapter was to first present some fundamentals of earthquake engineering and then focus on different methods for the dynamic analysis of structures subjected to earthquakes. Subsequently, the most important features of *seismic design* (i.e., design of structures against earthquakes) were outlined, focusing on practical aspects of design regulations. However, since the scope of this short chapter was inevitably limited, the reader should make recourse to the more specialized literature (such as Chopra<sup>11</sup> and Kappos<sup>16</sup>) for a more detailed treatment of seismic analysis and design.

Table 3 Lateral Forces Acting on the Selected Frame

Story Level	$W_i$ (kN)	$h_i$ (m)	$h_i W_i$	$F_i$
0		0	0	
1	300	4.5	1350	27.54 kN
2	300	7.5	2250	45.90 kN
3	300	10.5	3150	64.26 kN
			<b>6750</b>	<b>137.70 kN</b>

## REFERENCES

1. P. Fajfar, and H. Krawinkler, Ed., *Seismic Design Methodologies for the Next Generation of Codes*, Proceedings of International Workshop held in Bled, Slovenia, June 1997, Balkema, 1997.
2. N. M. Newmark, and J. W. Hall, *Earthquake Spectra and Design*, EERI, Berkeley, 1982.
3. A. K. Gupta, *Response Spectrum Method in Seismic Analysis and Design of Structures*, Blackwell Scientific, Boston, 1990.
4. R. W. Clough, and J. Penzien, *Dynamics of Structures*, 2nd ed., McGraw-Hill, New York, 1993.
5. International Code Council, Inc. (ICC), *International Building Code 2000*, International Code Council, Falls Church, VA; 2000.
6. CEN (Comité Européen de Normalisation), *Eurocode 8: Design of Structures for Earthquake Resistance—Part 1: General Rules, Seismic Actions and Rules for Buildings* (EN 1998-1: 2004), Brussels, May 2004.
7. K. Pitilakis, Site Effects, in *Recent Advances in Earthquake Geotechnical Engineering & Microzonation*, A. Ansal, Ed., Kluwer, Norwell, MA, 2004, pp. 139–197.
8. T. T. Soong, S. F. Masri, and G. W. Housner, An Overview of Active Structural Control under Seismic Loads, *Earthquake Spectra*, Vol. 7, No. 3, 1991, pp. 483–505.
9. R. I. Skinner, W. H. Robinson, and G. H. McVerry, *An Introduction to Seismic Isolation*, Wiley, New York, 1993.
10. F. Naeim, and J. M. Kelly, *Design of Seismic Isolated Structures: From Theory to Practice*, Wiley, New York, 1999.
11. A. K. Chopra, *The Dynamics of Structures: Theory and Applications to Earthquake Engineering*, Prentice-Hall, Englewood Cliffs, NJ, 1995.
12. E. L. Wilson, A. Der Kiureghian, and E. P. Bayo, A Replacement for the SRSS Method in Seismic Analysis (Short communication), *Earthq. Eng. Struct. Dynamics*, Vol. 9, No. 2, 1981, pp. 187–194.

13. T. J. Zhu, W. K. Tso, and A. C. Heidebrecht, Effect of Peak Ground A/V Ratio on Structural Damage, *J. Struct. Eng., ASCE*, Vol. **114**, No. 5, 1988, pp. 1019–1037.
14. G. W. Housner, (1970) Strong Ground Motion, In *Earthquake Engineering*, (R. L. Wiegel Ed., Prentice-Hall, Englewood Cliffs, pp. 75–91.
15. A. J. Kappos, Analytical Prediction of the Collapse Earthquake for R/C Buildings: Suggested Methodology, *Earthq. Eng. and Struct. Dynamics*, Vol. **20**, No. 2, 1991, pp. 167–176.
16. A. J. Kappos, *Dynamic Loading and Design of Structures*, Spon Press, London, 2001.

# CHAPTER 118

## LOW-FREQUENCY SOUND TRANSMISSION BETWEEN ADJACENT DWELLINGS

Barry M. Gibbs

Acoustics Research Unit  
School of Architecture and Building Engineering  
University of Liverpool  
Liverpool, United Kingdom

Sophie Maluski

School of Computing, Science and Engineering  
University of Salford  
Greater Manchester, United Kingdom

### 1 INTRODUCTION

Low-frequency sound transmission between adjacent dwellings is causing an increase in noise nuisance. Reasons for this are the proliferation of hi-fi and home movie systems of high power and enhanced bass response and increased use of mechanical services in residential buildings and appliances within dwellings. Many of these sources generate significant low-frequency sound. In general, building elements that fail to satisfy sound insulation requirements and regulations do so at low frequencies. Lightweight cavity walls, for timber-frame housing and conversions, are least effective at low frequencies. Masonry walls and floors often fail in the frequency range of 50 to 400 Hz.

A major limitation in the implementation of present standard methods of test and prediction of wall and floor insulation at low frequencies results from the modal characteristic of the sound pressure fields generated in the rooms and of the vibration fields on the separating walls and floors. This causes large spatial and spectral variations in sound pressure level and the sound pressure level difference between rooms is strongly dependent on the room size and shape.

The standard methods for the measurement and prediction of sound insulation between dwellings should include a correction for the modal characteristics of the sound fields at low frequencies. Heavyweight and lightweight constructions must be treated differently and yield different corrections to the standard relationship between sound pressure level difference and sound reduction index.

### 2 LABORATORY AND FIELD PERFORMANCE INDICES

Although there has been a proliferation of sources of low-frequency noise in buildings,<sup>1,2</sup> the current standards<sup>3-6</sup> deal only with the frequency range of 100 to 3150 Hz. An annex to the International organization for Standardization (ISO) 140 standard for laboratory and field measurements deals with frequencies down to 50 Hz, but there is poor reproducibility

between laboratories below 100 Hz and a method of measurement has yet to be agreed. Eventually, it may be possible to achieve good reproducibility between laboratories using a universally acceptable measure of sound reduction index for frequencies below 100 Hz.<sup>7</sup> However, a fundamental question remains on how such laboratory measurements can be related to field performance of the separating wall, floor, or partition when in situ. Diffuse or neutral acoustic field conditions in test chambers do not correspond to the modal behavior of sound fields in small room volumes associated with dwellings at low frequencies.<sup>8</sup>

The standard expression for sound reduction index  $R$ , in laboratory test conditions, is<sup>4</sup>

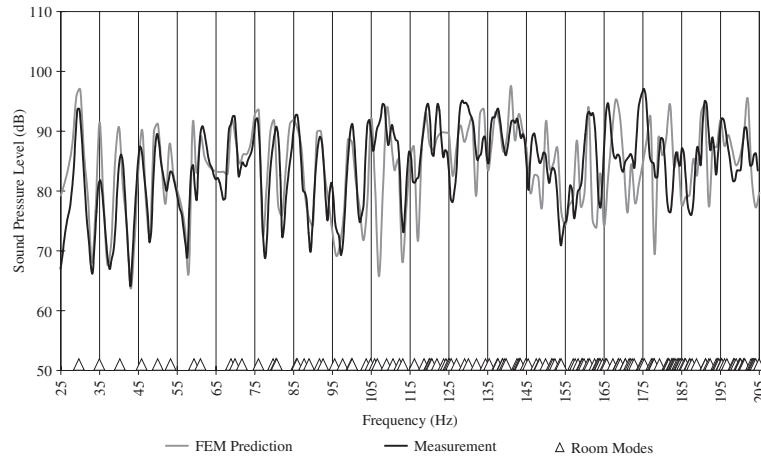
$$R = (L_1 - L_2) + 10 \log(S/A_2) \text{ dB} \quad (1)$$

where  $L_1$  and  $L_2$  is the average sound pressure level in the source and receiver rooms, respectively,  $S$  is the party wall area, and  $A_2$  is the total absorption of the receiving room. The performance of a partition in field conditions is given by the standardized level difference<sup>5</sup>:

$$D_{nT} = (L_1 - L_2) + 10 \log(T/0.5) \text{ dB} \quad (2)$$

where  $T$  is the reverberation time of the receiving room.

Procedures now are in place to relate the field performance of walls and floors to the laboratory measurements, including the effects of flanking transmission.<sup>9</sup> However, the relationships are based on the assumption of diffuse sound field conditions in the rooms. The sound fields in small rooms, at low frequencies, are not diffuse and exhibit large variations with source and receiver position and frequency. The maxima and minima in sound pressure level, at the room resonances, also are accentuated because room surfaces and contents are less effective absorbers at low frequencies than at mid and high frequencies.<sup>10</sup>



**Figure 1** Measured (heavy line) and finite element model predicted (light line) sound pressure level in a room of plastered brick walls and concrete floor and ceiling.

### 3 SOUND FIELDS IN ROOMS AT LOW FREQUENCIES

In addition to laboratory and field measurements, theoretical modal analysis and finite element methods have been used to demonstrate that the room dimensions exert a strong influence on sound pressure level difference between rooms at low frequencies.<sup>11–13</sup> Adjacent rooms of identical shape and size and thus of the same resonance frequencies are strongly acoustically coupled, and the resultant sound pressure level difference can deviate from the value, which would be obtained in diffuse field conditions.

For a rectangular room with hard walls, the sound pressure can be expressed in terms of normal modes<sup>14</sup>:

$$p = p_0 \cos \left[ \frac{\pi n_x x}{L_x} \right] \cos \left[ \frac{\pi n_y y}{L_y} \right] \cos \left[ \frac{\pi n_z z}{L_z} \right] \quad (3)$$

for  $0 \leq x \leq L_x$ ,  $0 \leq y \leq L_y$ ,  $0 \leq z \leq L_z$  where  $n_x$ ,  $n_y$ ,  $n_z$  are integers and  $p_0$  is the maximum pressure amplitude. The natural frequencies are given by

$$f_{n_x n_y n_z} = \left( \frac{c}{2} \right) \left[ \left( \frac{n_x}{L_x} \right)^2 + \left( \frac{n_y}{L_y} \right)^2 + \left( \frac{n_z}{L_z} \right)^2 \right]^{1/2} \quad (4)$$

where  $c$  is the velocity of sound.

In Figure 1 is shown the measured and predicted sound pressure level at one position in a rectangular ( $5.75 \times 4.88 \times 4.24$  m) chamber with a loudspeaker in a corner. The chamber is of plastered brick walls and concrete floor and ceiling. The peaks and dips are accentuated because of the low room absorption below 200 Hz. The predicted response was obtained from a finite element model,<sup>15</sup> which gave best agreement with measurement on assuming an average absorption coefficient of 0.02. The chamber volume of 120 m<sup>3</sup> is

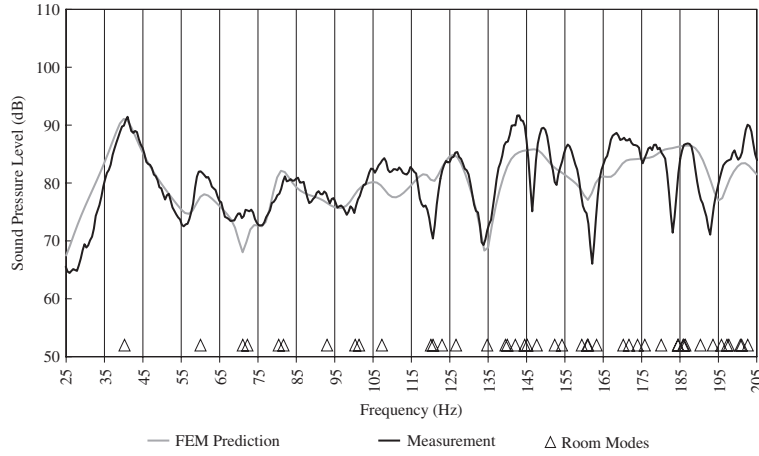
typical of acoustical test chambers, designed to give an even distribution of room modes and high modal density (see room modes indicated in Fig. 1) in order to approximate a diffuse field condition necessary for standard tests.

Rooms in dwellings generally are of small dimensions, and the sound field has a low modal density at frequencies below 200 Hz. In Figure 2 is the measured and predicted sound pressure level at one position in a room ( $4.24 \times 2.84 \times 2.40$  m) with a loudspeaker in a corner. The room modes are more separated than in the previous case (see room modes indicated in Fig. 2) with fluctuations in sound pressure level of the order of  $\pm 10$  dB about the average value. The room was constructed of plasterboard and timber-frame walls, timber floor, and ceiling. The finite element model prediction gives best agreement with measurement with an assumed average absorption coefficient of 0.15. This is because the lightweight construction acts partially as panel absorbers below 200 Hz and room damping is by modal reaction rather than local reaction.<sup>16</sup> In general, it has been found that the absorption of room contents, such as furnishing, has little effect on the spatial and spectral variation of sound pressure level at low frequencies.<sup>10</sup> Again, this is because porous absorbers are inefficient at low frequencies and also interact less with normal room modes than with tangential and oblique modes, which come into play at higher frequencies.

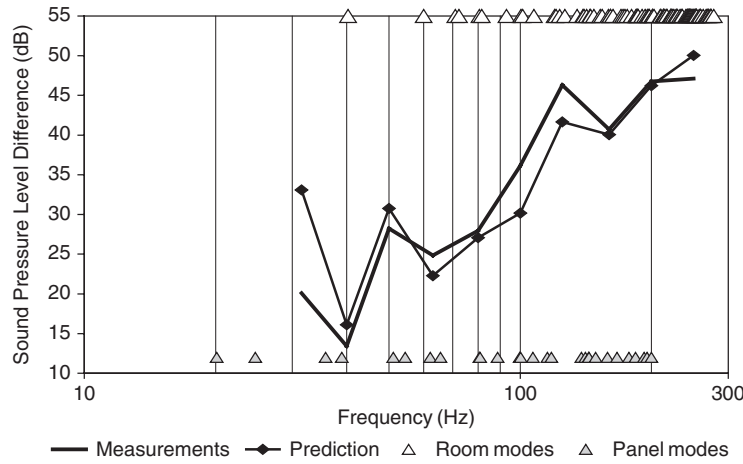
### 4 BENDING FIELDS ON WALLS AT LOW FREQUENCIES

So far, we have described the sound pressure field in a room in terms of normal modes as a prelude to discussing the modal interaction between two adjacent rooms. The generated bending field, on the wall separating the two rooms, also interacts with the room pressure fields. The bending wave field also can be expressed in terms of normal modes. If the wall is





**Figure 2** Measured (heavy line) and predicted (light line) sound pressure level in a room of timber-frame walls and timber floor and ceiling.



**Figure 3** Measured and predicted sound pressure level difference of a lightweight cavity wall.

modeled as a simply supported plate with bending stiffness  $B = Eh^3/12(1 - \nu^2)$  where  $E$  is Young's modulus and  $\nu$  is Poisson's ratio, then the bending vibration field takes the form<sup>17</sup>

$$v(y, z) = v_{n_y n_z} \sin(L_y/\pi n_y y) \sin(L_z/\pi n_z z) \quad (5)$$

$v_{n_y n_z}$  is the bending vibration amplitude,  $L_y$  and  $L_z$  are the wall dimensions,  $n_y$ ,  $n_z$  are integers, and  $0 \leq y \leq L_y$ ,  $0 \leq z \leq L_z$ . The natural frequencies of the wall are given by

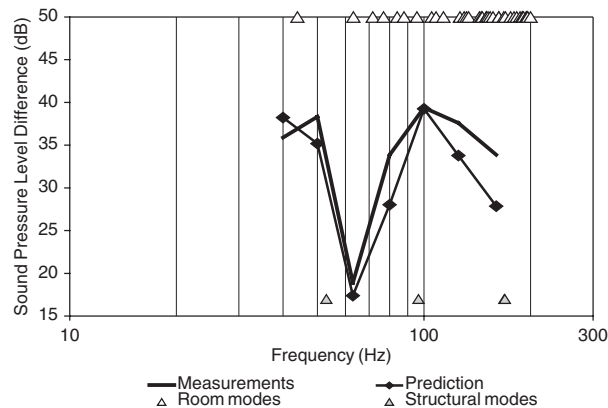
$$f_{n_y n_z} = \frac{\pi}{2} \left( \frac{B}{\rho_s} \right)^{1/2} \left[ \left( \frac{n_y}{L_y} \right)^2 + \left( \frac{n_z}{L_z} \right)^2 \right] \quad (6)$$

where  $\rho_s$  is the mass per unit area. If the natural frequencies of the wall bending field coincide with

those of the room pressure fields, then large variations in sound pressure level difference can be expected.

## 5 INTERACTION BETWEEN ROOM MODES AND WITH WALL MODES

Field surveys of low-frequency sound transmission across lightweight cavity walls and heavyweight masonry walls indicate large spatial and spectral variations in level difference. Figure 3 shows the measured and finite element model predicted one-third octave band sound pressure level difference across a lightweight cavity wall of area  $2.84 \times 2.4$  m. The wall was constructed from two leaves of 38-mm plasterboard, each on 50-mm timber frames and separated by a 200-mm cavity containing 50-mm mineral wool. The separated rooms were of equal



**Figure 4** Measured and predicted sound pressure level difference of a heavyweight cavity wall.

dimensions— $4.23 \times 2.84 \times 2.4$  m—and therefore had the same room modes, which are shown in Fig. 3.

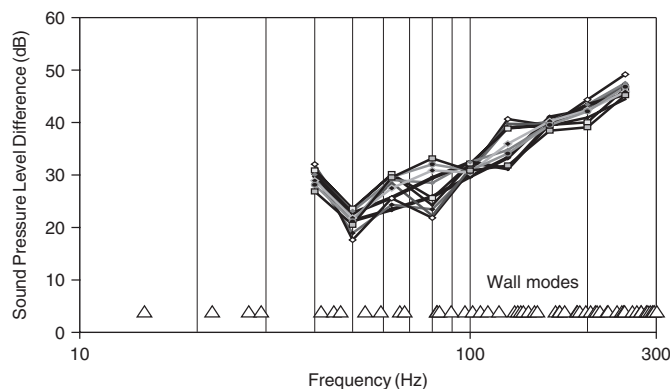
Both predicted and measured curves indicate a dip at 40 Hz, which is caused by the acoustic-acoustic coupling of the (1,0,0) mode in each room. Preliminary checks were made of the theoretical mass-spring-mass frequency  $f_{msm}$ . For the case shown,  $f_{msm} = 48$  Hz and did not coincide with the room mode coupling frequencies. In general, the mass-spring-mass resonance appeared to have little influence on room mode coupling. Also indicated in Fig. 3 are the wall modes, which onset at 20 Hz, below the first room modes. The wall modal density is relatively high, even below 100 Hz, and no single wall mode strongly influences room mode coupling.

Figure 4 shows the measured and finite element model predicted one-third octave band sound pressure level difference across a heavyweight cavity wall of area  $3.88 \times 2.38$  m. The wall was constructed from two leaves of 140-mm plastered brickwork, separated by a 75-mm cavity. The two rooms were of equal dimensions,  $2.7 \times 3.88 \times 2.38$  m. In the case shown

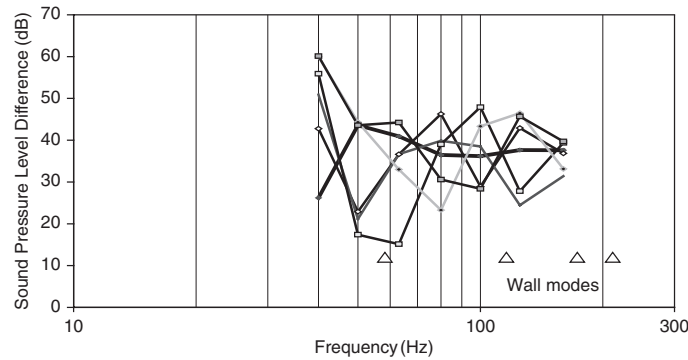
in Fig. 4, a significant dip in level difference occurs in the 63-Hz band, which is caused by the coupling of the room modes perpendicular to the separating wall [in this case the (0,1,0) modes], which also are in close proximity to the first (1,1) wall mode.

## 6 STATISTICAL SURVEY OF THE EFFECT OF ROOM DIMENSIONS

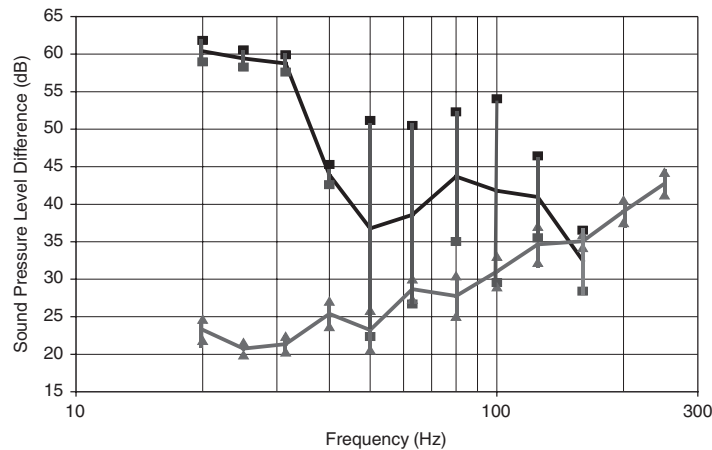
A field measurement survey of the influence of room dimensions on sound pressure level difference between rooms at low frequencies would be protracted and expensive. The survey would involve recording the room dimensions, construction details, location of loudspeakers, and microphone positions, and measurements would require a more refined frequency analysis than is presently available to the standard methods. However, an experimentally validated numerical model (in this discussion, a finite element model) of sound transmission between adjacent rooms can be employed in a survey of different room sizes, which allows the salient features to be identified and yields the likely statistical distributions.



**Figure 5** Sound pressure level difference of a lightweight cavity wall of plasterboard on timber frame of  $3.5 \times 2.5$ -m area for room volumes in the range of  $20 \text{ m}^3$  to  $50 \text{ m}^3$ .



**Figure 6** Sound pressure level difference of a  $3.5 \times 2.5$ -m heavyweight wall for room volumes in the range of  $20 \text{ m}^3$  to  $50 \text{ m}^3$ .



**Figure 7** Average sound pressure level difference and standard deviation for a lightweight cavity wall (lower curve) and a heavyweight wall (upper curve), between equal rooms for volumes ranging from  $25 \text{ m}^3$  to  $50 \text{ m}^3$ .

In Figure 5 are shown the predicted spatial average sound pressure level difference for a lightweight cavity wall of plasterboard on timber frame, between equal rooms where the room volumes have been varied from  $20$  to  $50 \text{ m}^3$ . The separating wall area is constant at  $3.5 \times 2.5 \text{ m}$ , and the room volumes were varied by altering the room dimension perpendicular to the separating wall (i.e., from  $2.3$  to  $5.7 \text{ m}$ ).

There are some dips in sound pressure level difference in the  $50$ -Hz third octave band and also in the  $80$ -Hz band, which correspond to the normal room modes perpendicular to the party wall. However, there also are some peaks in the  $80$ - and  $125$ -Hz band and, in general, the adverse dips are not pronounced because the wall modal densities are high and no single wall mode predominates.

In Figure 6 are shown results for the case of a heavyweight wall, of the same area and for the same range of room volumes. Here the variation in sound pressure level difference is much greater than for the

lightweight wall due to matching of both the room modes and the wall modes. The wall modes are few in number and therefore can be influential.

Figure 7 shows the mean sound pressure level difference and standard deviation for the two wall types: lightweight cavity and solid masonry. The values were obtained from 100 room pairs, ranging in volume from  $25$  to  $50 \text{ m}^3$ . The sound pressure level difference across lightweight cavity constructions shows a mass law trend with little statistical spread due to the effect of room volume. The standard deviation is of the order of  $2$  to  $3 \text{ dB}$ . This means that, although dips occur in sound pressure level difference, at frequencies dictated by the normal room modes perpendicular to the wall, they are of the order of  $5$  to  $10 \text{ dB}$  and “wash out” when all room volumes are considered in the population. Overall, the average sound insulation of a party wall of lightweight construction is lower than that of the heavyweight construction, below  $200 \text{ Hz}$ , as expected.

The sound pressure level difference across heavyweight walls is little affected by variations in room volume at frequencies below the onset of the first wall mode; in this case, below 50 Hz. Above this frequency, the sound pressure level difference is strongly dependent on room modes and thus on room dimensions, and the fluctuations are accentuated by the wall modes, which are well spaced in frequency. For the case considered, a 200 mm masonry wall, the standard deviation is 12 to 15 dB in the frequency range of 50 to 125 Hz.

## 7 PRACTICAL CONSIDERATIONS

Architects and builders naturally would be interested to know if dips in sound pressure level difference at low frequency could be predicted and possibly avoided. Such a prediction might be given as a correction to the standard relationship between sound pressure level difference and sound reduction index, expressed as a function of the room and wall modal distributions, in particular of the simultaneous occurrence of room and wall modes in the measurement band of interest.

However, the corrections should be simple. This is possible if the following is assumed: A standard laboratory method of measuring sound reduction index is possible for the frequency range of 50 to 100 Hz; the adjacent dwellings consist of rectangular room pairs of the same dimensions; the separating wall can be characterized as either lightweight cavity or heavyweight masonry; the associated flanking walls and floors are assumed to be of the same construction as the separating wall.

The first step is to estimate the third octave frequency band  $f_{1/3}$  where the dip in sound pressure level difference is likely to occur due to the coupling of room modes. This is when  $f_{1/3} = c/(2L)$ , where  $L$  is the room length perpendicular to the separating wall. It is not straightforward to estimate the natural frequencies of the wall bending vibration since the modes are strongly dependent on edge conditions, which cannot easily be assessed. The second step, therefore, assumes a worst-case condition, where a wall mode also occurs in the band  $f_{1/3}$  described above. A basic construction type is established, heavyweight or lightweight cavity, and the area of the separating wall also is considered.

For heavyweight walls of area less than 10 m<sup>2</sup>, subtract 20 dB from the value of level difference as follows:

$$L_1 - L_2 = R - 10 \log[S/(\alpha S_T)] - 20 \text{ dB} \quad (7)$$

where  $S$  is the wall area,  $S_T$  is the total room area, and  $\alpha = 0.02$ . For heavyweight walls of area greater than 10 m<sup>2</sup>, the correction to Eq. (7) is -10 dB. For lightweight cavity constructions, the correction to Eq. (7) is -5 dB, with  $\alpha = 0.15$ , irrespective of wall size.

Architects and builders should avoid pairing rooms of equal dimensions, if possible. The room dimensions perpendicular to the separating wall should differ by 0.5 to 1.0 m. It also is recommended that heavyweight walls should not be smaller than 10 m<sup>2</sup>. Where possible, the room shapes should be nonrectangular. These

recommendations will not eliminate low-frequency dips (and peaks) in sound pressure level difference between adjacent rooms but will reduce the variation in sound insulation by reducing the strength of the acoustic coupling between room modes and between room and wall modes.

## REFERENCES

1. J. R. Brooks and K. Attenborough, The Implication of Measured and Estimated Domestic Source Levels for Insulation Requirements, *Proc. Instit. Acoust.*, Vol. 11, 1989, pp. 19–27.
2. C. Grimwood, 1995 Complaints about Poor Sound Insulation between Dwellings, *Instit. Acoust., Acoust. Bull.*, Vol. 20, 1995, pp. 11–16.
3. *Control for Homes*, Building Research Establishment and Construction Industry Research and Information Association, London, 1993.
4. ISO 140: 1995: Acoustics—Measurements of Sound Insulation in Buildings and of Building Elements—Part 3: Laboratory Measurements of Airborne Sound Insulation of Building Elements.
5. ISO 140: 1998: Acoustics—Measurements of Sound Insulation in Buildings and of Building Elements—Part 4: Field Measurements of Airborne Sound Insulation of Building Elements.
6. ISO 717-1:1997: Acoustics—Rating of Sound Insulation in Buildings and of Building Elements.
7. D. B. Pedersen, J. Roland, G. Raabe, and W. Maysenholder, Measurement of the Low Frequency Sound Insulation of Building Components, *Acta Acust. (united with Acustica)*, Vol. 86, No. 3, 2000, pp. 495–505.
8. W. Kropp, A. Pietrzyk, and T. Kihlman, On the Meaning of the Sound Reduction Index at Low Frequencies, *Acta Acust.*, Vol. 2, 1994, pp. 379–392.
9. CEN12354-1: 2000: Building Acoustics—Estimation of Acoustic Performance in Buildings from the Performance of Elements—Part 1: Airborne Sound Insulation between Rooms.
10. S. Maluski and B. M. Gibbs, The Effect of Construction Material, Contents and Room Geometry on the Sound Fields in Dwellings at Low Frequencies, *Appl. Acoust.*, Vol. 65, No. 1, 2004, pp. 31 to 44.
11. L. Gargliardini, J. Roland, and J. L. Guyader, The Use of Functional Basis to Calculate Acoustic Transmission between Two Rooms, *J. Sound Vib.*, Vol. 145, No. 3, 1991, pp. 457–478.
12. A. Osipov, P. Mees, and G. Vermeir, Low Frequency Airborne Sound Transmission through Single Partitions in Buildings, *Appl. Acoust.*, Vol. 52, Nos. 3–4, 1997, pp. 273–288.
13. S. Maluski and B. M. Gibbs, Application of a Finite-Element Model to Low-Frequency Sound Insulation in Dwellings, *J. Acoust. Soc. Am.*, Vol. 108, No. 4, 2000, pp. 1741–1751.
14. H. Kuttruff, *Room Acoustics*, 4th ed., Spon Press, London, 1999.
15. Sysnoise, Numerical Integration Technologies, Leuven, Belgium, 1995.
16. J. Pan, S. J. Elliot, and K. H. Baek, Analysis of Low Frequency Acoustic Response in a Damped Rectangular Enclosure, *J. Sound Vib.*, Vol. 223, No. 4, 1999, pp. 543–566.
17. A. Leissa, *Vibration of Plates*, Acoustical Society of America, Woodbury, NY, 1993.

## **PART XI**

---

# **COMMUNITY AND ENVIRONMENTAL NOISE AND VIBRATION PREDICTION AND CONTROL**

# CHAPTER 119

## INTRODUCTION TO COMMUNITY NOISE AND VIBRATION PREDICTION AND CONTROL

Malcolm J. Crocker

Department of Mechanical Engineering  
Auburn University  
Auburn, Alabama

### 1 INTRODUCTION

The main sources of urban community noise are (a) road traffic, that is, trucks, cars, and motorcycles, (b) aircraft/airport noise, (c) railroads, (d) construction noise, (e) noise from light and heavy industry, and (f) noise from recreation activities. Road traffic noise is the most important of these and is discussed in this chapter in some detail. Aircraft/airport noise, although often cited as a major problem, is generally considered to be of less importance because, although it can be intense, it is mostly concentrated around major airports. However, from another point of view, aircraft noise is of extreme importance since strong public resistance to airport expansion in many countries is driven by aircraft noise complaints around airports. Railroad noise is a problem for residential strips situated along major rail lines, but it is much less pervasive than road traffic noise. Construction noise is often a problem too since in large cities there are normally some new building projects being undertaken; in addition, noise from the construction of new highways is a concern where heavy equipment contributes to the noise problem.

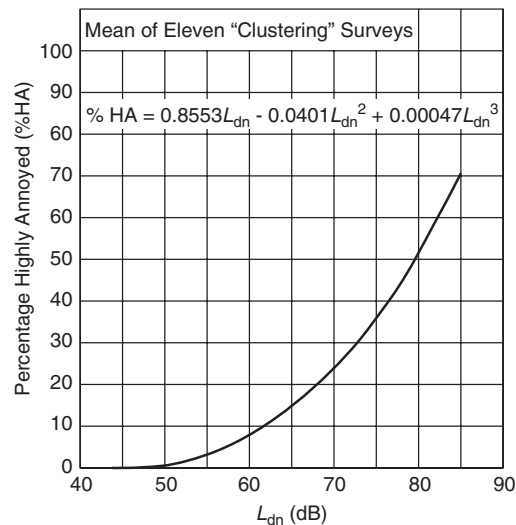
### 2 DISCUSSION

Several noise indicators and rating measures are in use. The equivalent sound pressure level  $L_{eq}$  is used in many countries for the assessment of road traffic noise, although the statistical 10% level  $L_{10}$  remains in use in Australia, Hong Kong, and the United Kingdom for target values and insulation regulations for new roads and planning values for new residential areas. The A-weighted day–night average sound pressure level, DNL is currently the main descriptor of community noise in the United States. With DNL, a penalty of 10 dB is added to noise made at night. In Europe the day–evening–night sound pressure level, LDEN is widely used. With LDEN, penalties of 5 dB are applied to noise in the evening and 10 dB at night. Chapter 34 discusses some of the descriptors that have been used. Chapter 127 describes the current practice of evaluating community noise problems in Europe, the United States, and several other countries. Coelho has written a review of community noise in Chapter 130 in which the different types of community noise ordinances are described.

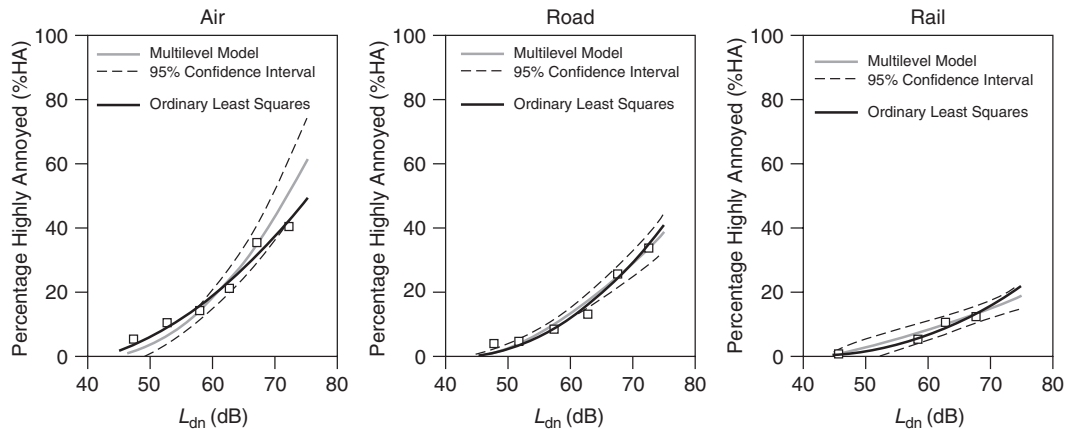
In the United States, the day–night average sound pressure level (DNL) has been in widespread use to assess community noise annoyance since its adoption

by several federal agencies in the mid-1970s. If the DNL of the community noise is below 70 dB, there is little danger of hearing loss. However, many people become highly annoyed, and there can be significant sleep disturbance in the community. In 1978, by evaluating the results of 11 clustering social surveys on noise annoyance in several countries, Schultz produced a curve relating the average annoyance response percentage of people highly annoyed with the day–night sound pressure level. See Fig. 1. The Schultz curve has been widely used since then, although in recent years considerable doubt has been expressed whether it can be applied with equal confidence to different sources of community noise, including road traffic, railroad, and aircraft.

As shown in Fig. 18 of Chapter 34, later studies sponsored by the U.S. Air Force in the early 1990s have indicated that people have a moderate, but a different, reaction to aircraft, traffic, and railway noise at the same day–night average sound pressure level.<sup>2</sup>



**Figure 1** Synthesis of all the clustering survey results. The mean of the “clustering surveys” data, shown here, is proposed as the best currently available estimate of public annoyance due to transportation noise of all kinds. It may also be applicable to community noise of other kinds.<sup>1</sup>



**Figure 2** Percentage highly annoyed persons (%HA) as a function of DNL. Two synthesis curves per mode of transportation, and the data points are shown. For the curves obtained with multilevel analysis the 95% confidence intervals are shown.<sup>3</sup>

One possible explanation may be that aircraft noise near a busy airport has a greater variation in level in time and has a different frequency content (generally higher) than road or rail traffic. Another explanation may be the inadequacy of the day-night sound pressure level measure itself, which does not make any allowance for level or, even more importantly, for loudness.

In a more recent study, Miedema and Vos<sup>3</sup> came to a similar conclusion as Finegold et al.,<sup>2</sup> although their results were slightly different in magnitude. At high values of DNL between 60 to 70 dB, the ranking of road traffic and railway noise differ a little from the earlier results of Finegold et al.<sup>2</sup> Their conclusions may be summarized as follows. Below a DNL of 40 to 45 dB, virtually no one is highly annoyed (HA). As the DNL increases, so does the percentage of the population who are highly annoyed (%HA). The rate of increase in the %HA is greater for aircraft noise than road traffic noise, which in turn has a greater rate of increase than railway noise.<sup>3</sup> Some of the results of this study are given in Fig. 2, which shows curves fitted to the data points by a least squares regression procedure. Since the 95% confidence limits for the three curves do not overlap, for the higher levels of DNL it can be concluded that the percentage of people that are highly annoyed, %HA, depends on the mode of transportation causing the noise.<sup>3</sup>

Equations fitting the data,<sup>3</sup> assuming zero annoyance at an A-weighted sound pressure level of 42 dB, are

$$\begin{aligned} \text{Aircraft : } \%HA &= 0.20(\text{DNL} - 42) \\ &\quad + 0.0561(\text{DNL} - 42)^2 \\ \text{Road traffic : } \%HA &= 0.24(\text{DNL} - 42) \\ &\quad + 0.0277(\text{DNL} - 42)^2 \\ \text{Rail : } \%HA &= 0.28(\text{DNL} - 42) \\ &\quad + 0.0085(\text{DNL} - 42)^2 \end{aligned}$$

More recently Fidel and Silvati have also found that aircraft noise is more annoying than noise from other forms of transportation at the same values of DNL.<sup>4</sup> In this study, the authors find 14% highly annoyed by aircraft noise at DNL of 55 dB and 5% highly annoyed at DNL of 50 dB, so that they estimate that the airport attitudinal survey data, when grouped in 5-dB wide "bins," will yield 12% highly annoyed at about 54 dB.<sup>4</sup> As a result of these and other more recent studies, many standards that continue to use A-weighted metrics such as LEQ, DNL, and LDEN have applied various penalties for aircraft noise in using the original Schultz curve (Fig. 1). The ISO standard<sup>5</sup> applies a 3- to 6-dB penalty, while the American National Standards Institute (ANSI) standard uses a 5-dB penalty.<sup>6</sup> The ANSI penalty is phased in between 55 and 60 dB as shown in Table 1.

Schomer et al. have questioned the continuing use of metrics such as DNL, which are based on A-weighting.<sup>7,8</sup> It is well known that the A-weighting filter is independent of the sound pressure level, while the apparent loudness of the sound is not. Since annoyance is obviously related strongly to loudness, then use of metrics based on A-weighting are likewise fraught with problems. Schomer et al.<sup>8</sup> have suggested instead that consideration should be given to the use of a loudness-level-weighted sound

**Table 1 Penalties for Aircraft Noise Applied by ANSI to Original Schultz Curve**

Measured Value of DNL	New Value of DNL
50	50
55	55
56	57
58	61
60	65
65	70

Source: From Ref. 7.

exposure level (LLSEL) and loudness-level-weighted equivalent level (LL-LEQ). They suggest that LLSEL and LL-LEQ can be used to assess the annoyance of environmental noise. They conclude from their annoyance studies that, compared with A-weighting, loudness-level weighting better orders and assesses transportation noise sources, and with the addition of a 12-dB adjustment, loudness-level weighting better orders and assesses highly impulsive sounds. Thus, they state that significant improvements can be made to the measurement and assessment of environmental noise without resorting to the large number of adjustments that are required when assessing sound using just the A-weighting.<sup>8</sup> Implementation of LLSEL and LL-LEQ capabilities on type 1, hand-held one-third octave band sound level meters would also be inexpensive.<sup>8</sup>

Some community noise ordinances and test codes or standards, such as those used to evaluate building site noise in Germany and the United Kingdom, require the intrusive noise to be compared with the ambient noise. If the noise is more than 10 dB above the ambient, it is deemed excessive, while if it is only 5 dB above, it may be tolerated. Fields claims that such a procedure is not supported by large amounts of noise data and surveys.<sup>9</sup> According to Fields, the results of 70,000 evaluations of 51 noise sources by over 45,000 residents show that there is no evidence to support the long-held assumption that the reactions of residents in a community to an intrusive noise is reduced when there are other environmental noises present.<sup>9</sup> In fact, Fields asserts that provided residents are able to ascertain a logical estimate of their long-term exposure to the actual noise levels of the intrusive events, the presence or absence of ambient noise does not affect their judgment of the amount of noise annoyance produced by the intrusive noise events.<sup>9</sup> This is an important finding since it suggests that noise limits should be given as an absolute number of decibels, rather than an amount exceeding the ambient noise. Of course, if DNL or the new European LDEN is used as the noise limit, different limits must be set for aircraft, road traffic, and railway noise.

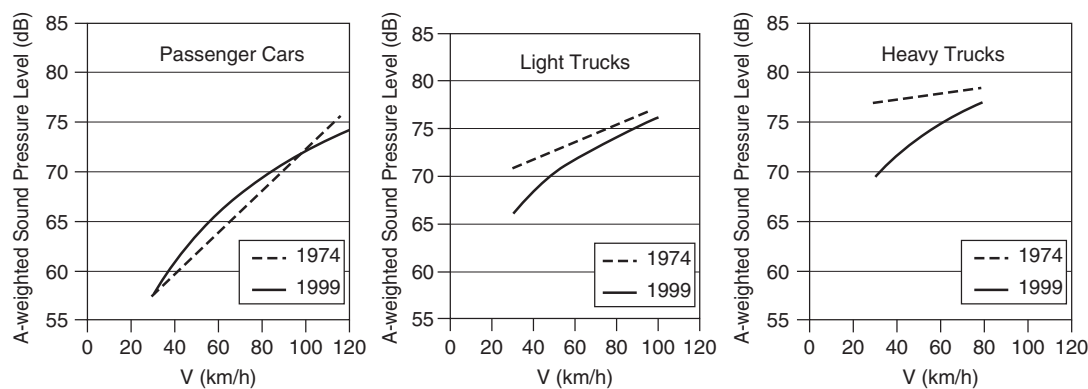
### 3 TRAFFIC NOISE PREDICTION AND CONTROL

There are several reasons for the emergence of traffic noise as the main source of community noise annoyance in most developed countries. The power-weight ratio of trucks and cars has been constantly increased to permit higher payloads and more speed and acceleration; the resulting higher power engines are usually noisier than the earlier lower power ones. The number of vehicles has increased dramatically in most countries over the last 20 or 30 years. This, combined with the movement of people from country to city and the natural increase in urban population, has exposed more and more people to more and more traffic noise. Chapter 120 discusses road traffic noise in more detail.

Although aircraft noise near airports is more intense than road traffic noise, the large number of vehicles in use and the fact that traffic noise is created in close proximity to residential housing ensures that it is a greater problem than aircraft and airport noise in most countries. The numbers of vehicles in use continues to increase. Studies in North America and Europe suggest that the external noise of many vehicles has not been significantly reduced in recent years. See Fig. 3, which shows the cruise-by noise levels of cars, light trucks, and heavy trucks over the period of 1974 to 1999.

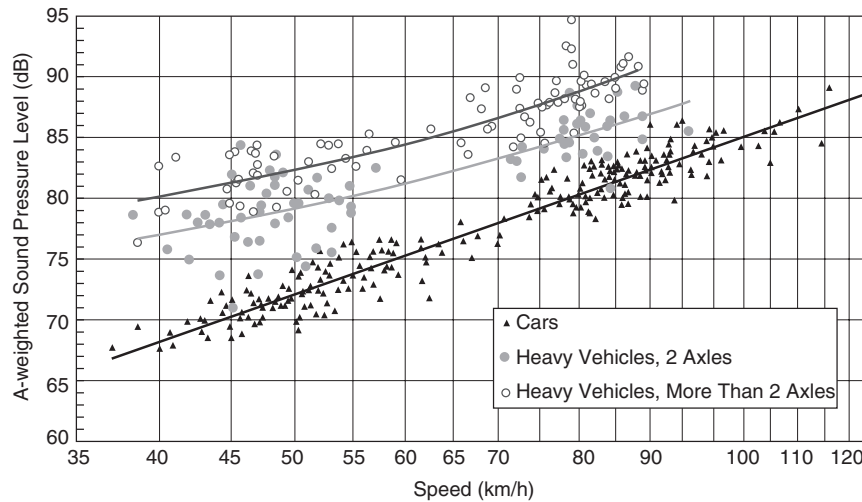
The main sources on vehicles include power plant (and power train) noise, tire-road interaction noise, and wind noise. The noise of cars is dominated by tire noise, except under accelerating conditions at low speed, during which power plant noise exceeds tire noise. With medium and heavy trucks, however, power plant noise is not exceeded normally until about 40 km/h or 50 km/h is reached. At very high speeds wind noise on cars and trucks can become a major source, but below about 130 km/h it normally does not exceed tire noise. See Chapters 83, 86, and 87.

The sound pressure levels generated by heavy vehicles exceed those of most cars by about 10 to 15 dB. See Fig. 4. Trucks are vastly outnumbered by



**Figure 3** A-weighted sound pressure levels of cars and light and heavy trucks measured at different speeds in 1974 and 1999.<sup>10</sup>





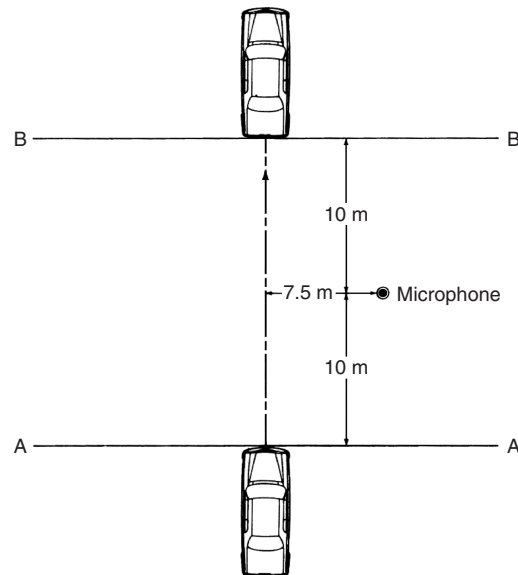
**Figure 4** Cruise by exterior A-weighted sound pressure levels measured at 7.5 m for cars, heavy vehicles with two axles, and vehicles with more than two axles.<sup>11</sup>

cars, but since they are normally in service for much longer periods than cars each day and they are so much noisier, they are a very important contributor to the overall road traffic noise problem. Noise levels near highways depend upon traffic flow rates and the mix of light and heavy vehicles with cars. Traffic noise tends to increase during mornings and evenings as people travel back and forth to work and other activities. Traffic noise is normally at a minimum during nighttime hours between about 1:00 and 4:00 a.m.

There are two main methods of evaluating vehicle noise. The first consists of measuring the passby noise of a vehicle at 7.5 or 15 m from the road centerline. The maximum A-weighted sound pressure level is recorded for single vehicles under controlled conditions normally on a special test track. See Chapter 120. Figure 4 is an example of the noise of individual vehicles traveling at constant speed, normally known as the “cruise-by” condition. For traffic noise prediction schemes, statistical passby measurements of randomly occurring vehicles are made near selected highways. The levels measured in the statistical passby approach are dependent on the mix of light and heavy vehicles with cars and are also dependent on the type of road surface.

The second type of test, normally used for regulatory purposes, consists of a full-throttle acceleration test performed on a vehicle, which approaches the measurement zone AA in Fig. 5 at a controlled speed. The measurement is again made at 7.5 or 15 m from the road centerline. The maximum A-weighted sound pressure level measured between lines A–A and B–B is recorded. See Fig. 5.

Traffic noise prediction schemes normally include statistical information on the numbers of vehicles, the vehicle mix, the noise characteristics of each vehicle, the road surfaces, and the shielding effects of



**Figure 5** Measurement positions used for cruise-by or acceleration noise tests.

residential buildings on the propagation of the sound to the prediction points. See Chapter 120.

Community noise surveys and the creation of noise maps are used in communities as a basis for checking results of some of these traffic noise prediction schemes. Also traffic noise prediction schemes and community noise surveys of the one-octave, one-third octave, and/or A-weighted sound pressure level generated by traffic are useful in deciding on noise abatement strategies. The most common traffic noise

abatement strategy employed is the construction of roadside barriers, although porous sound-absorbent road surfaces are coming into use in some countries, as discussed in Chapters 83 and 86. See Chapter 58 for a general discussion on barrier performance and Chapter 122 for a discussion on their use to control road and rail noise in the community.

Although well-established prediction schemes are available to predict environmental noise from road traffic in communities, it has been demonstrated that specific prediction schemes can be established, which are more reliable for individual cities during workday hours. Of course, such specific prediction schemes cannot be transferred to other cities.<sup>12</sup> There are many other studies of road traffic noise and its prediction in the community.<sup>13–19</sup>

#### 4 RAIL SYSTEM NOISE PREDICTION AND CONTROL

Railway noise is generally less of a problem than road traffic noise and aircraft/airport noise. This is because the numbers of rail vehicles are much smaller than road vehicles, and railroad noise generally adversely affects smaller regions of most cities. Rail system noise is, however, a major problem for communities situated near railroad routes.<sup>20–30</sup> The major sources on railway and rapid transit systems are (1) power plant noise, (2) wheel–rail interaction noise, and (3) aerodynamic noise. The main railway and rapid transit system power plants in use include (1) electric motors, (2) diesel engines, and (3) combined diesel–electric systems. See Chapter 121 for a detailed discussion on rail system noise sources and methods for their control.

Diesel power plants can be very noisy if the noise is not properly suppressed. Wheel–rail noise depends upon wheel–rail roughness and train speed. Wheel–rail roughness can be increased by the use of cast-iron brake systems. Disk brakes, which are coming into increasingly widespread use, have been found to reduce wheel–rail wear, roughness, and thus noise. Aerodynamic noise, although a problem inside rail vehicles at very high speeds, has not normally been found to be a major community noise problem, even at the very high speeds of 300 km/h as discussed in Chapter 121.

Community noise prediction schemes for railway noise must include data on the power plant and wheel–rail noise of the rail vehicles, the number of railcars in operation and the rail vehicle speeds. In addition, the prediction schemes must account for the attenuation caused by air and ground surface absorption and by the distance to the observation points. The screening caused by obstacles, including buildings, railway cuttings, embankments, and purpose-built noise barriers must also be included in the schemes. There is some evidence to suggest that railway noise causes less sleep disturbance than road traffic noise at the same noise level.<sup>26–31</sup> In the United Kingdom, an A-weighted sound pressure level differential in favor of railway noise has been used in the development of railway noise legislation, using the equivalent A-weighted sound pressure level and existing road traffic noise legislation as the base. Railway noise and

its effects continue to attract the attention of many researchers and authorities.<sup>26–31</sup>

#### 5 ATTENUATION PROVIDED BY BARRIERS, EARTH BERMS, BUILDINGS, AND VEGETATION

Noise barriers are being used increasingly to protect residential communities from road traffic and rail and rapid transit noise. Chapter 58 describes empirical formulas that can be used to predict barrier performance. Barriers are of limited use to protect residential areas from aircraft and airport noise, and construction site noise, with the possible exception of their use to offer protection from the noise caused by the testing of aircraft engines during ground run up. Likewise, the mobility and elevation of noise sources of construction equipment used on building sites and highway construction sites often make the use of barriers of limited use. Urban barriers must also be designed to be acceptable aesthetically. The formulas for barrier performance given in Chapter 58 are mostly based on idealized theoretical considerations or experimental studies conducted in the laboratory. Chapter 122 describes some of the practical considerations in the use of urban barriers.

The attenuation of a barrier is normally defined in two main ways. The first involves the barrier *attenuation*, which is defined as the difference between the sound pressure levels measured (or predicted) at a location and the sound pressure level at the same location under free-field conditions. The second definition involves the reduction in sound pressure level (known as *insertion loss*) at the receiving location achieved by the *insertion* of the barrier. The attenuation provided by a barrier is a function of frequency. More exactly it can be related to the difference between the two path lengths from the source to the receiver divided by the wavelength: (1) over the barrier and (2) straight through the barrier. This quantity is known as the Fresnel number, which is also used in optics. See Chapter 58.

The Fresnel number can also be related to the effective nondimensionalized height parameter of the barrier (defined as the ratio of barrier height perpendicular to the incident sound divided by its wavelength.) The effective height of the barrier increases with wavelength and so does the barrier attenuation. This means that a barrier of fixed height is more effective in attenuating high-frequency sound, and stronger shadows are created for high-frequency sound than low-frequency sound. A similarity can be observed with the behavior of light since an obstacle produces a stronger shadow for short-wavelength (high-frequency) violet light than long-wavelength (low-frequency) red light. See Chapter 58 for further discussion on barrier acoustics.

Theoretically, noise barriers can be shown to provide the same attenuation if placed at the same distance from the source or from the receiver. In practice, however, as common with other passive noise control measures, their placement nearer to the source is usually more effective. This is because receivers, such as the upper regions of high-rise buildings, can extend in height above a barrier placed near to them,

and thus sound is not blocked from reaching them and they are thus not protected.<sup>32</sup> However, single- or multiple-road and rail vehicles are normally located close to the ground, and barriers placed close to them block the sound better, which would otherwise be traveling to the multiple elevated receivers.

It is particularly important to ensure that barriers do not have holes or leaks that can degrade their performance and that they are constructed from material with an adequate transmission loss (sound reduction index) to sufficiently attenuate sound penetrating them and reaching the receivers directly in that manner. Urban barriers are sometimes made to absorb sound on the side facing the source so as to reduce the sound reflected back to the source. Care must then be made to ensure that the sound-absorbing material can survive the local environmental conditions and not become degraded too rapidly. Chapter 122 describes the use of sound-absorbing material with urban barriers. Chapter 58 presents formulas for predicting the attenuation of barriers, while Chapter 122 gives formulas and nomograms for predicting the attenuation of barriers used in urban situations. These formulas are now incorporated in commercial software. The sound attenuation of barriers with complicated shapes such as cantilever, parabolic barriers, or earth berms can now be predicted with boundary element method (BEM) approaches.

Unfortunately, when barriers are used in the field, the atmospheric effects of turbulence or wind and/or temperature gradients above the barriers normally degrade their attenuation and/or insertion loss performance. Chapter 122 describes factors that must be considered when barriers are used in practical situations to reduce road and rail traffic noise in the community. Wind is probably the main cause of the degradation of the acoustical performance of barriers. Wind has been found to have two main effects. First, the turbulence in the wind causes the sound waves to be scattered so that some of the sound energy propagates into the shadow zone behind the barrier. Second, wind gradients, which exhibit increasing wind speed with height above a barrier (with wind blowing in the same direction as the sound propagation), can bend the sound downward into the so-called shadow region of the barrier, thereby decreasing its attenuation. Temperature gradients in which the temperature increases with height (called temperature inversions) can have a similar effect in bending sound downward into the shadow zone behind a barrier. In practice, the attenuation of an urban barrier does not reach its theoretical value because of such environmental effects, and in real-use urban barriers normally have an upper attenuation limit of about 20 dB, unless they are of double construction, in which case the upper limit is about 25 dB. See Chapter 122.

## **6 GROUND-BORNE VIBRATION TRANSMISSION FROM ROAD AND RAIL SYSTEMS**

Vibration generated by road and rail vehicles, some industrial enterprises, and building sites is transmitted through the ground and into buildings nearby.

Vibration at frequencies up to 200 to 250 Hz can be transmitted at distances as far as about 200 m from roads or railway lines. Vibration at higher frequencies tends to be attenuated more rapidly with distance. The vibration caused in the buildings results in floor and wall vibrations, the movement of household or office objects, the rattling of doors and windows, and indirectly as reradiated noise. Vibration is annoying to people at frequencies up to 50 or 100 Hz because various body organs resonate at low frequencies. For example, the stomach and other internal organs resonate in the region of 8 to 10 Hz, and the eyes and head resonate at frequencies of about 20 to 40 Hz. The chest wall cavity resonates in the range of 50 to 100 Hz. Chapter 123 discusses some of these phenomena in more detail. Damage to buildings from vibration is unusual, although there are some cases where construction of new highways or railway lines has not been allowed because of the fear that the vibration they would cause could damage ancient historical buildings. Vibration of the ground or building foundations is normally measured in the vertical direction with velocity or acceleration transducers such as accelerometers. The quantities usually recorded consist of the maximum velocity or acceleration levels. The levels are normally measured in one-third octave frequency bands, and each band is weighted according to human response to vibration. Chapter 123 describes the procedures for measurement and prediction of these quantities. The chapter also discusses human response to vibration and suggests suitable vibration limits.

The sources of ground vibration from road vehicles include passage of the vehicle wheels over road irregularities such as bumps and holes. With rail vehicles, the source mechanisms are related to the travel of the wheels over the rail, which causes periodic and random forces. The periodic forces are created by the passage of the wheels over the spatially periodic supports of the rails and any discontinuities located at rail joints. The broadband random vibration is caused by unevenness or roughness in the rail and wheel contours. At high speed, vibration can also be caused when the vehicle speed exceeds either the Rayleigh surface wave speed in the ground or the bending wave speed in the rails, as described in Chapter 123.

Vibration is transmitted through the ground by various wave mechanisms. The wave motion is quite complicated and consists of three main types: dilatational or pressure waves, equivolume or shear waves, and free surface or Rayleigh waves, as described in Chapter 123. The main methods of protecting buildings from ground vibration include reduction of vibration at the source, such as better road and rail maintenance, the use of softer suspension systems for road and rail vehicles, resiliently mounted and better maintained rail tracks, and grinding of the wheels and rails to reduce roughness. Other methods to protect buildings include base isolation of the buildings themselves, as is described in Chapter 124.

Models exist for predicting the propagation of ground vibration from road and rail traffic.<sup>33,34</sup> The models are mainly different because of the different

input force mechanisms. With road vehicles, for the purpose of generating the wheel–road interface forces, the road itself can be considered to be rigid while the vehicle and its suspension are assumed to generate the dynamic forces in response to the road roughness. With rail vehicles, however, the excitation is different and is related to the unsprung mass of the wheel and axle combined with the mass of part of the rail system. Existing models range from mostly empirical to completely theoretical. Two-dimensional theoretical models are simpler but do not include the complete effects of fully three-dimensional models. Finite element (FEM) and coupled finite element/boundary element (FEM–BEM) models have been used and are becoming available in commercial software packages. Finite difference methods are also in use and have some advantages over FEM–BEM models since the computational code is simpler. Using those models to calculate absolute vibration level<sup>35</sup> requires significant modeling details. Greatest accuracy is achieved when making predictions of insertion loss, even with relatively simple models. See Chapters 123 and 124.

## 7 BASE ISOLATION OF BUILDINGS FOR CONTROL OF GROUND-BORNE VIBRATION

Road and rail traffic and some industrial and/or building operations cause ground vibration of a fairly continuous nature. Railways are usually the sources of most intense ground vibration since they often carry relatively heavy vehicles at high speeds, which results in significant rapidly created forces transmitted to the ground. Although it is possible to reduce the vibration at the source in some cases, there is some limit to the reduction that can be achieved economically.

When new buildings, particularly those of a sensitive nature, such as hospitals, auditoriums, and concert halls are to be constructed near to existing highways and railway lines, suppression of the building vibration and base isolation of the buildings themselves should be considered. See the discussion in Chapter 124. Some simple, relatively low cost measures are available for reducing building vibration, including (1) increasing the damping in the structure, (2) stiffening certain regions of the building to move natural frequencies away from forcing frequencies thereby avoiding resonances, and (3) the installation of floating floors in sensitive parts of the buildings.

In cases where the ground vibration is severe, such as where a building must be constructed near to a railway, it may be necessary to vibration isolate the complete building from the ground by means of base isolation, as described in Chapter 124. This may be essential only for sensitive buildings. The amount of vibration that is acceptable in the building will depend upon its use and other factors such as the duration and nature of the vibration. The principles of base isolation are similar to those used to protect buildings against earthquakes; however, the lower level of vibration experienced from road, rail, and some industrial sources compared with earthquakes, makes the design criteria somewhat different for each case studied. Each building design will be different

and building use, acceptable vibration limits, and other criteria will determine the design chosen. Typical isolation frequencies are in the range of 5 to 15 Hz.

There are two main types of isolators normally used for base isolation of buildings. These include (1) laminated rubber isolators and (2) helical steel spring isolators. The rubber isolators can either be made from natural rubber or from synthetic rubber. Steel spring isolators usually combine several helical springs in one unit. The rubber isolators normally have higher inherent damping than spring isolators. However, the spring isolators are sometimes made with additional damping elements to suppress internal coil resonances of the springs at high frequencies, and to limit vibration during the rapid vibration onset or vibration decay caused by passing trains or vehicles. Steel springs are expensive but can be manufactured to have precise stiffness values and long life. Rubber isolators are usually less expensive but have the drawback that they can be subject to degradation more rapidly than steel springs unless they are protected against any possible hostile environmental conditions, which could cause the degradation. If adequate protection is provided, however, rubber isolators can be made to have sufficient life in terms of both degradation and creep performance.

The design of vibration isolators is described in Chapters 54, 59, and 124. Their performance in buildings is normally measured in terms of the insertion loss they provide, as explained in Chapter 123, since this quantity describes the benefit obtained from the use of the isolators. Single-degree-of-freedom models are useful to give some approximate indication of the isolator performance, although building vibration is much more complicated, and more sophisticated vibration models must be used for better vibration predictions. With continuous excitation, which is almost steady state, such as is caused by passing trains, the vibration problem can be treated in the frequency domain. With some cases where the excitation is more impulsive in nature, such as is caused by some industrial applications, then a time-domain modeling approach is more convenient. More complicated building base models employ finite element methods. Studies on base isolations of buildings continue.<sup>36–42</sup> Various software programs are available commercially to create such sophisticated building vibration models. In some cases, simple two-dimensional numerical models are used to reduce computational demands. Three-dimensional approaches are more suitable to obtain more accurate building models, as discussed in Chapter 124.

## 8 AIRCRAFT AND AIRPORT NOISE PREDICTION AND CONTROL

Air travel is projected to continue increasing in the foreseeable future. These increases will require the expansion of existing major airports and the creation of new airports. Airport expansion provokes public resistance because of the annoyance, speech interference, and sleep interference caused by aircraft noise in nearby residential districts. Aircraft noise is a much more localized problem than surface transportation noise since it is significant primarily

around major airports. Most of the noise energy is produced by the operations of scheduled airliners, the contribution of the large numbers of general aviation aircraft being relatively small. See Chapter 125.

The introduction of early pure jet passenger aircraft in the late 1950s brought much higher noise levels during both takeoff and landing than the piston engine airliners that they replaced. The majority of piston engine propeller-driven airliners have now been phased out of service, although twin-engine prop-jet aircraft continue to be used on many low-density, short-range routes. Jet aircraft operate at much higher cruising speeds than do propeller ones, and the aerodynamic configuration necessary for them to achieve these results in higher takeoff and landing speeds. Required runway length is normally greater with jet than propeller aircraft, partly as a consequence of these higher speeds, and partly because jet engine thrust is reduced when an aircraft is stationary or nearly so. This naturally brings the airport noise closer to residential communities. The generally large size and inertia of long-range passenger jet aircraft, and their greater throttle response times compared with those of piston engine propeller-driven aircraft, require them to use long approach paths, resulting in more extensive low-level flight over surrounding neighborhoods. Moreover, jet aircraft normally use considerable amounts of power on approach to counteract the drag of their high-lift devices. The noise produced by jet powered aircraft is primarily from their engines. The aerodynamic noise produced by the passage of the aircraft through the air (termed airframe noise) is still normally insignificant in comparison. See Chapter 9 for a discussion on airframe noise.

In the early 1960s, the first fanjet engines (also known as turbofans or bypass jets) entered service. Although developed mainly to improve fuel economy, the fanjet engines were quieter than the first pure jet (or turbojet) engines of the same thrust. A fanjet engine can be regarded as essentially a ducted prop-jet engine, in which the propeller (called the fan) is ducted to improve efficiency. All long-range airliners and many medium-range airliners are now powered by fanjet engines. Such fanjet engines mostly produce broadband noise from their high-speed jet exhausts during takeoff, although with lower power conditions during landing approach, the tonal whine produced by the compressor stages usually becomes prominent. At a distance of 5 km, the A-weighted sound pressure level during a jet aircraft takeoff is of the order of 60 dB to 65 dB and is sufficient to interfere with speech. See Chapters 22, 34, and 125. Current wide-body fanjets (e.g., Boeing 717, 737, 767, 777, and 787 and Airbus A-300/310, A-318, A-320, A-330/340, A-350, and A-380) have considerable noise control technology built into their engines and are much quieter than the early pure jet and fanjet aircraft.

Some airliners have been particularly designed to have quiet operational characteristics. The BAe 146, first introduced in the 1980s, was an early, very quiet, four-engine jet airliner, which has special high-lift devices giving it short takeoff and landing capabilities

that make it able to operate from very short runways at small downtown airports. It is able to operate from downtown airports such as those at Mönchengladbach, Aspen, and at the London City Airport (a converted dock). In May 2006 landing and takeoff tests at the London City Airport of the newer Airbus A-318 has shown it can also use this downtown airport. Following evaluations by Airbus, London City Airport, and the UK airworthiness authorities, in March 2006, these authorities granted the A-318 a steep landing approach certification that enabled the airport compatibility tests to take place. With its very low noise characteristics, the A-318 makes it possible for it to use downtown airports such as the one in downtown London.

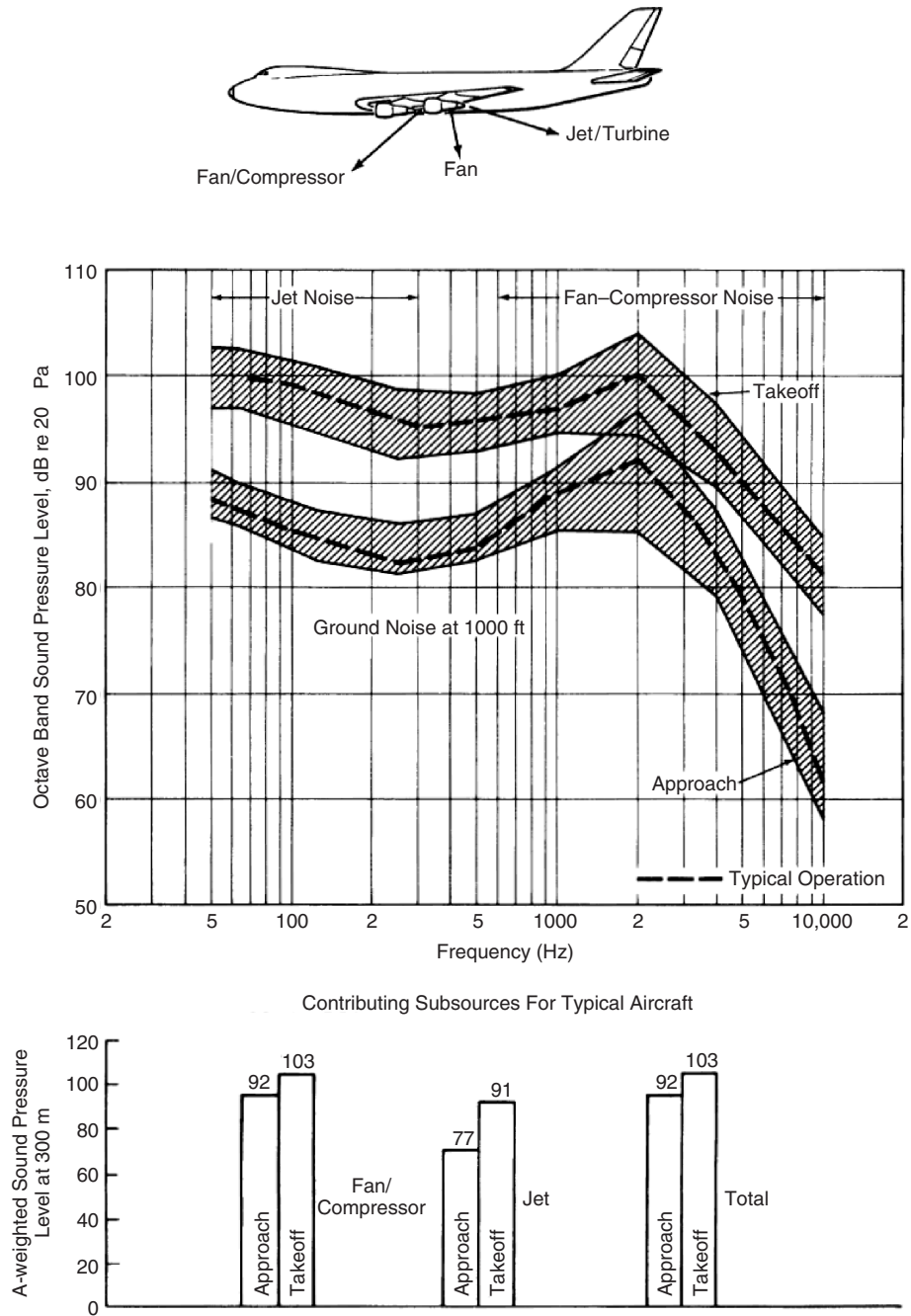
As discussed in more detail in Chapter 125, propeller-driven airliners are used on some medium-range and most short-range routes, and such aircraft are almost exclusively powered by gas turbine engines. Such turboprop aircraft, as they are commonly known, mainly produce tonal noise instead of the broadband jet noise. The noise of propellers is quite directional and is mostly radiated in the propeller plane. Helicopters are less commonly used than jet and turboprop aircraft, but they can be quite noisy and produce A-weighted sound pressure levels of about 60 dB at 1 km. Like propeller aircraft, the helicopter blade noise is very directional and is created both by the main rotor and the high-speed tail rotor.

Aircraft noise is evaluated for two main reasons: (1) for certification purposes and (2) to monitor the noise around airports. For certification, the noise of individual aircraft is measured using the effective perceived noise level (EPNL). For monitoring noise at airports it is normal to use a measure that accounts for many aircraft movements and the time of day that the noise is produced. In the European Union a composite measure known as day-evening-night sound pressure level (LDEN) is used. See Chapters 1, 34, and 125. The LDEN includes components for daytime, evening, and nighttime hours. During the evening, a 5-dB penalty is applied and at night a 10-dB penalty.

Figure 6 shows the noise levels and spectra of a fanjet aircraft both for takeoff and approach. Figure 7 shows the measurement locations used for certification of aircraft according to FAR Part 36 noise standards. See Chapter 34. Research on evaluating aircraft and airport noise and community annoyance continues.<sup>44–55</sup>

## 9 OFF-ROAD VEHICLE AND CONSTRUCTION EQUIPMENT EXTERIOR NOISE PREDICTION AND CONTROL

Off-road vehicles and heavy construction equipment are used for roadway and railway construction, earth moving and excavation, laying of pipes and cables, and construction of new buildings. They are responsible for high levels of environmental noise and cause annoyance, speech interference, and sleep disturbance in residential areas. In addition, there is the possibility they can cause hearing damage to people operating this equipment or people working in close proximity. A-weighted sound pressure levels can be as high as 75 to 90 dB at distances of 15 m. Sound pressure levels at

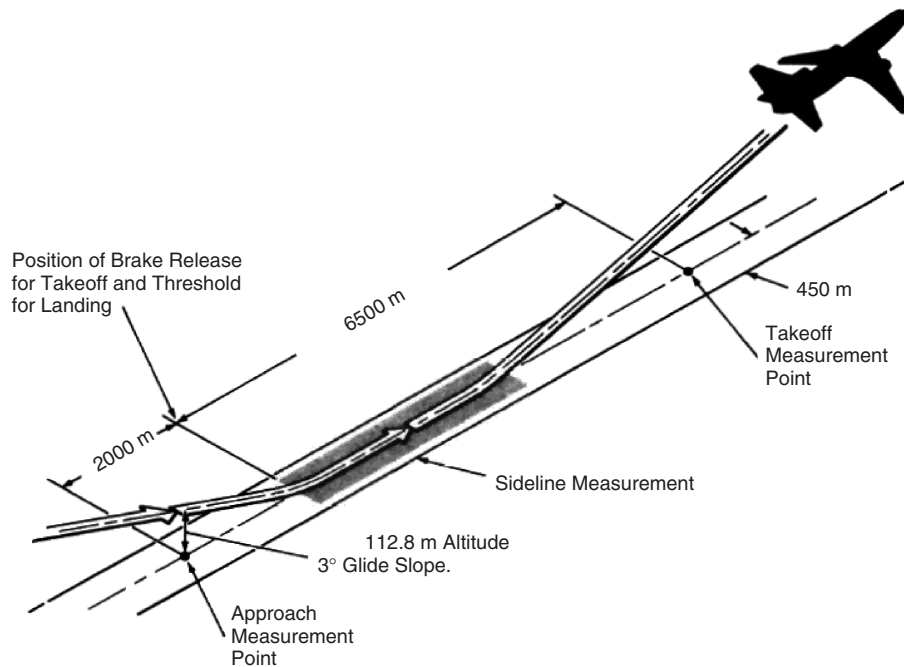


**Figure 6** Noise levels and spectra of wide-body fanjet aircraft (e.g., the Boeing 747).<sup>43</sup>

distances of several hundred metres can be of the order of 60 to 70 dB, which is above acceptable community noise limits.

The main noise sources on off-road vehicles and construction equipment consist of the engine, exhaust,

intake, cooling fans, and the tracked wheels. Mobile compressors are also significant noise contributors and are often used in conjunction with impulsive noise generators, such as pneumatic drills, cutters, and vibrating roller equipment.



**Figure 7** Measurement locations for certification testing of aircraft to FAR Part 36 noise standards.

In Europe, off-road vehicles and heavy construction equipment are required to have product labels giving their sound power outputs. Noise emission limitations are set by an EEC Directive. In the United States such equipment noise output is governed by community noise ordinances or state regulations. Mobile compressors are one exception since their noise output is regulated by the U.S. Environmental Protection Agency (EPA). Other countries do not seem to have uniform approaches to regulate the noise of off-road vehicle and construction equipment.

As described in Chapter 126, in Europe the sound power output of such equipment must be provided by display of a label. The sound power is normally determined through measurements of the sound pressure level at discrete microphone locations on a hemispherical surface as described in International Organization for Standardization (ISO) standards. Alternatively, the sound power can be determined with the use of sound intensity equipment.

Off-road vehicles and heavy construction equipment can be divided into three main categories as discussed in Chapter 126: (1) wheeled vehicles, including excavators, loaders, and graders, with which the engine is the dominant noise source, (2) tracked vehicles, in which the track noise is comparable to the engine noise, and (3) vibration and impact generating tools, including pneumatic drills and vibrating rollers, in which the noise is generated by the tool itself and no engine is involved.

The exterior noise can be reduced by a combination of passive means, including enclosures, vibration isolators, use of the vibration damping materials, sound-absorbing materials, and baffles and barriers. Enclosures can be very effective, particularly if absorbing materials are used inside and they are properly sealed. Unfortunately, this is not always possible because of the heat buildup created by most items of machinery, in particular the engine. The use of inlet and exhaust mufflers is essential on such equipment. Chapters 85 and 126 describe the design and use of such mufflers. Sound-absorbing material is sometimes placed inside the mufflers, although the material can lose its effectiveness because of contamination with moisture and carbon particles. Normally, for such reasons reactive mufflers are preferred. Chapter 126 gives an example of noise reduction on a mobile compressor. Other examples of mobile compressor noise control are given in Chapter 54. Compressor noise is discussed in detail in Chapter 74. Efforts continue on reducing interior and exterior noise and vibration of off-road vehicles.<sup>56-58</sup>

## 10 ENVIRONMENTAL NOISE IMPACT ASSESSMENT

Environmental noise impact assessments (sometimes known also as environmental noise impact statements) are used to balance the negative noise impact of a proposed development versus the benefits that that development, such as a new highway, industrial development area or recreation facility, could bring to a nearby community.<sup>59-63</sup> See Chapter 127.

Existing community noise exposure guidelines are consulted when preparing the assessments. These are based on the premise that there is a level of noise that is acceptable to the majority of the community. If this level is likely to be exceeded by a proposed development, appropriate mitigation measures need to be selected with due consideration of cost and technical feasibility. The mitigated noise impact is assessed for acceptability to the potentially affected community as well as the benefit of the development to the community as a whole. In Chapter 127 the terms *community noise* and *environmental noise* are used interchangeably.

## 11 INDUSTRIAL AND COMMERCIAL NOISE IN THE COMMUNITY

The annoyance produced by industrial and commercial noise is very similar to that produced by road traffic noise when the long-term energy equivalent sound pressure levels are the same.<sup>64–67</sup> However, as explained in Chapter 128, in most countries industrial noise is treated differently from road traffic noise. As explained in Chapter 130, it is common now for a city to have different districts zoned for noise. Normally, industrial enterprises are located in special zones in the city. It is desirable for the industrial zones to be separated from zones for residential housing. The separation in distance must not be too great; otherwise people will be inconvenienced by having to travel a long way to work. But the industrial and residential zones must not be situated too close to each other either. The noise created in residential areas from the sources in the industrial zones is normally predicted on the basis of the sound power outputs from the different noise source components in the industrial zone.

As explained in Chapter 128, industrial and commercial noise sources can be divided into two main categories. The first category includes steady noise sources that have little variation in level and character during the day and night. The second category includes intermittent noise resulting from different industrial production cycles and caused by vehicles coming and going to the industrial and commercial areas. Steady noise containing pure-tone and impulsive components is generally found to be less acceptable in residential areas compared with steady noise of the same long-term equivalent sound pressure level. This is particularly true when steady noise contains pure-tone components below 90 Hz, as discussed in Chapter 128. Impulsive noise is also known to be more annoying than steady noise of the same equivalent sound pressure level.

Chapter 128 describes a procedure for predicting the sound pressure levels in residential areas, which is based on knowledge of the sound power output per unit area of the industrial operation. Included in the procedure are adjustments for wind effects on the noise propagation. Such sound pressure level predictions are valuable in deciding whether new industrial operations should be permitted near residential communities and/or residential developments should be allowed near existing industry. It is important to monitor the noise levels produced by the industrial and commercial operations and make comparisons with those that

are predicted. Also in order to avoid community complaints, it is important to inform the public in the residential areas of such noise monitoring and also to provide details about all activities being undertaken to reduce noise from the industrial and commercial zones reaching the residential areas.<sup>68–78</sup>

## 12 CONSTRUCTION AND BUILDING SITE NOISE

Noise created on building sites in a city can interfere with speech, sleep, and other human activities.<sup>65–69</sup> The noise created comes from a variety of machinery and mechanical equipment and includes demolition of buildings, construction of new buildings, laying of pipelines, sewers, and cables, and construction of new roadways and railways. Some noise is impulsive in character, such as caused by pile driving. Other noise is more continuous in nature from sources such as compressors and heavy earth-moving equipment. Noise levels on building sites can be predicted from knowledge of the sound power output of the different items of machinery. Chapter 129 explains how predictions of the noise at different locations near a building site can be made. Normally the contributions from the different sources are added on an energy basis. In some countries the predicted or measured sound pressure level from all the sources is compared with the ambient noise level when none of the sources is acting. There are few standards or test codes for the prediction and control of noise from building sites. In 2006, the only such test codes were those in Germany and the United Kingdom. These test codes provide tools for the calculation of the daytime and nighttime rating levels. These are then compared to standard ambient-noise values for decisions on the acceptability of the building site noise. Transient noise peaks on the building site can also be considered in these assessments.

Local authorities sometimes are tolerant of intense noise on a building site in order to speed up construction for economic or political purposes or to limit disruptions to road and rail traffic and the operations of public utilities. If the A-weighted sound pressure levels caused by the sources are no more than 5 to 10 dB greater than the ambient levels, they may be allowed by some authorities. But levels that are greater than 10 dB above the ambient are normally determined to be excessive and require regulation and/or control.

Using city or national ordinances, some local authorities impose penalties for impulsive noise and/or noise containing prominent pure-tone components. Other local authorities restrict noise in certain city zones and others only during nighttime. In some cases noise control programs are initiated when repeated and/or frequent complaints are received. If noise control measures are found to be necessary, these should start with the noisiest sources and incorporate the normal source–path–receiver concepts as explained in Chapters 54 and 129. As discussed in Chapters 126 and 129, the European Union (EU) Directive 2000/14/EC requires construction equipment machinery used on building sites to be subject to noise labeling. This EU directive requires the manufacturer to



state the guaranteed sound power level in the operating instructions and on the machine itself with a label. The determination of the sound power level is usually carried out in accordance with ISO 3744. Some of these construction machines are subject to sound power level limits.

### 13 COMMUNITY NOISE ORDINANCES

The major sources of noise in the community are caused by surface transportation, aircraft/airports, industry, and construction.<sup>70-78</sup> As discussed in Chapter 130, the main contribution to community noise, in most countries, is caused by road and rail traffic. The annoyance caused by noise depends upon the level, duration, time of day, frequency content, and other factors. Road traffic noise depends upon the road surface, road inclination, traffic density and mix, and speed of automobiles and light and heavy trucks. Railroad noise depends upon vehicle speed, load, wheel and rail roughness, and other factors. Some of these sources can be controlled locally by regulation, such as with speed limits. Some factors are outside local control.

Community noise regulations and noise ordinances are of two main types: qualitative and quantitative. Qualitative types of noise ordinances prohibit excessive noise during certain hours of the day or night and/or prohibit some noisy activities during certain hours and in certain defined noise zones. The difficulty with such ordinances is that they are vague in nature and difficult to enforce. Quantitative noise ordinances, however, restrict noise generated and/or received. The levels allowed at the boundary where they are produced or the boundary where they are received are normally given as A-weighted sound pressure levels. These quantitative ordinances need trained staff for enforcement who can use calibrated measurement instruments to determine the sound pressure levels accurately. Since noise levels fluctuate in the community and vary during day, evening, and night periods, average levels are often used such as the equivalent sound pressure level. The A-weighted equivalent sound pressure level came into use in the United States in the 1970s, and recommendations have been published by the World Health Organization (WHO) for day and nighttime to protect people from becoming moderately or seriously annoyed. In the United States the day-night average sound pressure level is also widely used. This is calculated from the equivalent day time sound pressure level and the equivalent nighttime sound pressure level to which a 10-dB penalty is applied to sound occurring between 10 p.m. and 7 a.m.. In Europe the day-evening-night sound pressure level is now increasingly used. This is similar to the day-night average sound pressure level but is calculated from three periods with a 5-dB penalty applied during evening hours and a 10-dB penalty applied during nighttime.

Some noise ordinances specify different noise zones that are defined for the activities performed in the zones. Zones can be specified for heavy industry, light industry, residential, school, hospital, and other uses. Normally different noise zones are created with steps of 5 dB from noisiest to quietest zone with restrictions

on the maximum noise permitted in each zone. For instance, some activities such as construction may be prohibited in some zones. Obviously, enforcement is essential if the ordinance is to have any use at all. Fines and other financial penalties can be used for enforcement. In the United States, the Office of Noise Abatement and Control set limits for noise output of some sources such as heavy trucks and compressors on building sites and was active in producing a model community noise ordinance standard. Since 1980 centralized planning by the EPA Office of Noise Abatement and Control has largely been disbanded and taken up by different government agencies and local, citywide, or state authorities. In Europe, a different situation exists. European directives in recent years have required strategic noise maps to be created for major transportation facilities such as airports and railway stations and for large cities. Action plans are required to manage noise problems and recommend noise reduction if necessary. The goal is to harmonize noise criteria and noise zoning and limits among the different European member states. The experience in other countries such as Australia, Canada, China, and Japan is described in detail in Chapter 130. Further work and discussion on community noise evaluation and ordinances and regulations continues.<sup>70-78</sup>

### REFERENCES

1. T. J. Schultz, Synthesis of Social Surveys on Noise Annoyance, *J. Acoust. Soc. Am.*, Vol. 64, No. 2, Aug., 1978, pp. 377-405.
2. L. S. Finegold, S. C. Harris, and H. E. von Gierke, Community Annoyance and Sleep Disturbance: Updated Criteria for Assessing the Impacts of General Transportation Noise on People, *Noise Control Eng. J.*, Vol. 42, No. 1, Jan-Feb, 1994, pp. 25-30.
3. H. M. E. Miedema and H. Vos, Exposure-Response Relationships for Transportation Noise, *J. Acoust. Soc. Am.*, Vol. 104, No. 6, Dec., 1998, pp. 3432-3445.
4. S. Fidell and L. Silvati, Parsimonious Alternative to Regression Analysis for Characterizing Prevalence Rates of Aircraft Noise Annoyance, *Noise Control Eng. J.*, Vol. 52, No. 2, 2004, pp. 56-68.
5. International Organization for Standardization (ISO), ISO 1996-1 Acoustics—Description, Measurement and Assessment of Environmental Noise—Part 1: Basic Quantities and Assessment Procedures, Geneva, Switzerland, 2003.
6. ANSI S12.9 Part 4, American National Standard Quantities and Procedures for Description and Measurement of Environmental Sound—Part 4: Noise Assessment and Prediction of Long-Term Community Response, Acoustical Society of America, Melville NY, 2005.
7. Personal communication with P. D. Schomer, September 6, 2006.
8. P. D. Schomer, Y. Suzuki, and F. Saito, Evaluation of Loudness-Level Weightings for Assessing the Annoyance of Environmental Noise, *J. Acoust. Soc. Am.*, Vol. 110, No. 5, Pt. 1, Nov., 2001, pp. 2390-2397.
9. J. M. Fields, Reactions to Environmental Noise in an Ambient Noise Context in Residential Areas, *J. Acoust. Soc. Am.*, Vol. 104, No. 4, Oct., 1998, pp. 2245-2260.
10. D. F. de Graff, A Speed and Acceleration Limit in the Noise Type Approval of Vehicles Will Enable Silent

- Cars to Reveal Their Silence, Proceedings of Inter-noise 2001, The Hague, The Netherlands, 2001.
11. U. Sandberg and J. A. Ejsmont, *Tyre/Road Noise Reference Book*, Informex, Kisa, Sweden, 2002 (www.informex.info).
  12. M. Ausejo and M. Recuero, Study and Proposal of the Prediction Equation for Traffic Noise During Workable Days in Buenos Aires Downtown, Proceedings of the Thirteenth International Congress on Sound and Vibration, Vienna, Austria, 2006.
  13. C. Steele, A Critical Review of Some Traffic Noise Prediction Models, *Appl. Acoust.*, Vol. 62, No. 3, March, 2001, pp. 271–287.
  14. G. R. Watts, S. N. Chandler-Wilde, and P. A. Morgan, The Combined Effects of Porous Asphalt Surfacing and Barriers on Traffic Noise, *Appl. Acoust.*, Vol. 58, No. 3, Nov., 1999, pp. 351–377.
  15. Ö. Gündoğdu, M. Gökdağ, and F. Yüksel, A Traffic Noise Prediction Method Based on Vehicle Composition Using Genetic Algorithms, *Appl. Acoust.*, Vol. 66, No. 7, July, 2005, pp. 799–809.
  16. B. De Coensel, T. De Muer, I. Yperman, and D. Botteldooren, The Influence of Traffic Flow Dynamics on Urban Soundscapes, *Appl. Acoust.*, Vol. 66, No. 2, Feb., 2005, pp. 175–194.
  17. P. J. Thorsson, M. Ögren, and W. Kropp, Noise Levels on the Shielded Side in Cities Using a Flat City Model, *Appl. Acoust.*, Vol. 65, No. 4, April, 2004, pp. 313–323.
  18. D. S. Cho, J. H. Kim, T. M. Choi, B. H. Kim, and D. Manvell, Highway Traffic Noise Prediction Using Method Fully Compliant with ISO 9613: Comparison with Measurements, *Appl. Acoust.*, Vol. 65, No. 9, Sept., 2004, pp. 883–892.
  19. M. Tansatcha, P. Pamanikabud, A. L. Brown, and J. K. Affum, Motorway Noise Modelling Based on Perpendicular Propagation Analysis of Traffic Noise, *Appl. Acoust.*, Vol. 66, No. 10, Oct., 2005, pp. 1135–1150.
  20. E. Öhrström, Effects of Exposure to Railway Noise—A Comparison between Areas with and without Vibration, *J. Sound Vib.*, Vol. 205, No. 4, 28 August 1997, pp. 555–560.
  21. E. Öhrström and A.-B. Skånberg, A Field Survey on Effects of Exposure to Noise and Vibration from Railway Traffic, Part I: Annoyance and Activity Disturbance Effects, *J. Sound Vib.*, Vol. 193, No. 1, 30 May 1996, pp. 39–47.
  22. H. J. A. Van Leeuwen, Railway Noise Prediction Models: A Comparison, *J. Sound Vib.*, Vol. 231, No. 3, 30 March 2000, pp. 975–987.
  23. R. Makarewicz and M. Yoshida, Railroad Noise in an Open Space, *Appl. Acoust.*, Vol. 49, No. 4, Dec., 1996, pp. 291–306.
  24. C. C. Heng, Propagation of Train Noise in Housing Estates, *Appl. Acoust.*, Vol. 51, No. 1, May 1997, pp. 1–12.
  25. G. Xiaolan, Railway Environmental Noise Control in China, *J. Sound Vib.*, Vol. 293, Nos. 3–5, 13 June 2006, pp. 1078–1085.
  26. B. Griefahn, A. Marks, and S. Robens, Noise Emitted from Road, Rail and Air Traffic and Their Effects on Sleep, *J. Sound Vib.*, in press. Available online 27 March 2006.
  27. T. Yano, T. Yamashita, and K. Izumi, Comparison of Community Annoyance from Railway Noise Evaluated by Different Category Scales, *J. Sound Vib.*, Vol. 205, No. 4, 28 August 1997, pp. 505–511.
  28. C. Gore, Railway Noise: Principles for an EU Policy—The CER View, *J. Sound Vib.*, Vol. 193, No. 1, 30 May 1996, pp. 397–401.
  29. C. Lim, J. Kim, J. Hong, and S. Lee, The Relationship between Railway Noise and Community Annoyance in Korea, *J. Acoust. Soc. Am.*, Vol. 120, No. 4, 2006, pp. 2037–2042.
  30. B. Schulte-Werning, M. Beier, K.G. Degen, and D. Stiebel, Research on Noise and Vibration Reduction at DB to Improve the Environmental Friendliness of Railway Traffic, *J. Sound Vib.*, Vol. 293, Nos. 3–5, 13 June 2006, pp. 1058–1069.
  31. J. Oertli, Developing Noise Control Strategies for Entire Railway Networks, *J. Sound Vib.*, Vol. 293, Nos. 3–5, 13 June 2006, pp. 1086–1090.
  32. L. Godinho, J. António, and A. Tadeu, The Scattering of 3D Sound Sources by Rigid Barriers in the Vicinity of Tall Buildings, *Eng. Anal. Boundary Elements*, Vol. 26, No. 9, Oct., 2002, pp. 781–787.
  33. H. E. M. Hunt, Modelling of Rail Vehicles and Track For Calculation of Ground-Vibration Transmission into Buildings, *J. Sound Vib.*, Vol. 193, No. 1, 30 May 1996, pp. 185–194.
  34. F. Kirzhner, G. Rosenhouse, and Y. Zimmels, Attenuation of Noise and Vibration Caused by Underground Trains, Using Soil Replacement, *Tunnel. Underground Space Tech.*, Vol. 21, No. 5, Sept., 2006, pp. 561–567.
  35. A. B. Nagy, P. Fiala, F. Márki, F. Augusztinovicz, G. Degrande, S. Jacobs, and D. Brassinx, Prediction of Interior Noise in Buildings Generated by Underground Rail Traffic, *J. Sound Vib.*, Vol. 293, Nos. 3–5, 13 June 2006, pp. 680–690.
  36. C.-H. Loh and C.-H. Chao, Effectiveness of Active Tuned Mass Damper and Seismic Isolation on Vibration Control of Multi-Storey Building, *J. Sound Vib.*, Vol. 193, No. 4, 20 June 1996, pp. 773–792.
  37. A. Kareem, Modelling of Base-Isolated Buildings with Passive Dampers under Winds, *J. Wind Eng. Indust. Aerodynam.*, Vol. 72, Nov.-Dec., 1997, pp. 323–333.
  38. A. Vulcano, Comparative Study of the Earthquake and Wind Dynamic Responses of Base-Isolated Buildings, *J. Wind Eng. Indust. Aerodynam.*, Vols. 74–76, 1 April 1998, pp. 751–764.
  39. V. A. Matsagar and R. S. Jangid, Seismic Response of Base-Isolated Structures During Impact with Adjacent Structures, *Eng. Struct.*, Vol. 25, No. 10, Aug., 2003, pp. 1311–1323.
  40. I. Calì, M. Marletta, and F. Vinciprova, Seismic Response of Multi-storey Buildings Base-Isolated by Friction Devices with Restoring Properties, *Comput. Struct.*, Vol. 81, Nos. 28–29, Nov., 2003, pp. 2589–2599.
  41. A. Baratta and I. Corbi, Optimal Design of Base-Isolators in Multi-storey Buildings, *Comput. Struct.*, Vol. 82, Nos. 23–26, Sept.–Oct., 2004, pp. 2199–2209.
  42. V. A. Matsagar and R. S. Jangid, Influence of Isolator Characteristics on the Response of Base-Isolated Structures, *Eng. Struct.*, Vol. 26, No. 12, Oct., 2004, pp. 1735–1749.
  43. Wyle Laboratories, Transportation Noise and Noise from Equipment Powered by Internal Combustion Engines, EPA Report No. NTID 300.13, 1971.
  44. N. P. Miller, E. M. Reindel, D. A. Senzig, and R. D. Horonjeff, Low-Frequency Noise from Aircraft

- Start of Takeoff, Proceedings, INTERNOISE 1998, Christchurch, NZ, Nov., 1998.
45. G. Raman and D. K. McLaughlin, Highlights of Aeroacoustics Research in the U.S.—1998, *J. Sound Vib.*, Vol. 228, No. 3, 2 Dec. 1999, pp. 589–610.
  46. J. Clemente, E. Gaja, G. Clemente, and A. Reig, Sensitivity of the FAA Integrated Noise Model to Input Parameters, *Appl. Acoust.*, Vol. 66, No. 3, March 2005, pp. 263–276.
  47. C.-I. Hsu and P.-H. Lin, Performance Assessment for Airport Noise Charge Policies and Airline Network Adjustment Response, *Transport. Res. Part D: Transport and Environ.*, Vol. 10, No. 4, July 2005, pp. 281–304.
  48. J. Vogt, The Relative Impact of Aircraft Noise and Number in a Full-Factorial Laboratory Design, *J. Sound Vib.*, Vol. 282, Nos. 3–5, 22 April 2005, pp. 1085–1100.
  49. Per Kruppa, Research on Reduction of Aircraft Noise, Supported by the European Union, *Air Space Europe*, Vol. 2, No. 3, May–June 2000, pp. 18–19.
  50. F. Carlsson, E. Lampi, and P. Martinsson, The Marginal Values of Noise Disturbance from Air Traffic: Does the Time of the Day Matter? *Transport. Res. Part D: Transport Environ.*, Vol. 9, No. 5, Sept., 2004, pp. 373–385.
  51. D. P. McMillen, Airport Expansions and Property Values: The Case of Chicago O'Hare Airport, *J. Urban Econ.*, Vol. 55, No. 3, May, 2004, pp. 627–640.
  52. J. Ollerhead and B. Sharp, MAGENTA—Assessments of Future Aircraft Noise Policy Options, *Air Space Europe*, Vol. 3, Nos. 3–4, May–Aug., 2001, pp. 247–249.
  53. O. I. Zaporozhets and V. I. Tokarev, Predicted Flight Procedures for Minimum Noise Impact, *Appl. Acoust.*, Vol. 55, No. 2, Oct., 1998, pp. 129–143.
  54. R. Rylander and M. Björkman, Annoyance by Aircraft Noise around Small Airports, *J. Sound Vib.*, Vol. 205, No. 4, 28 Aug. 1997, pp. 533–537.
  55. G. M. Aasvang and B. Engdahl, Subjective Responses to Aircraft Noise in an Outdoor Recreational Setting: A Combined Field and Laboratory Study, *J. Sound Vib.*, Vol. 276, Nos. 3–5, 22 Sept. 2004, pp. 981–996.
  56. P. Kennes, J. Anthonis, L. Clijmans, and H. Ramon, Construction of a Portable Test Rig to Perform Experimental Modal Analysis on Mobile Agricultural Machinery, *J. Sound Vib.*, Vol. 228, No. 2, 25 Nov. 1999, pp. 421–441.
  57. I. Hostens and H. Ramon, Descriptive Analysis of Combine Cabin Vibrations and Their Effect on the Human Body, *J. Sound Vib.*, Vol. 266, No. 3, 18 Sept. 2003, pp. 453–464.
  58. K. Deprez, D. Moshou, and H. Ramon, Comfort Improvement of a Nonlinear Suspension Using Global Optimization and *in situ* Measurements, *J. Sound Vib.*, Vol. 284, Nos. 3–5, 21 June 2005, pp. 1003–1014.
  59. M. Arana and A. García, A Social Survey on the Effects of Environmental Noise on the Residents of Pamplona, Spain, *Appl. Acoust.*, Vol. 53, No. 4, April, 1998, pp. 245–253.
  60. S. Kurra, M. Morimoto, and Z. I. Maekawa, Transportation Noise Annoyance—A Simulated-Environment Study for Road, Railway and Aircraft Noises, Part 1: Overall Annoyance, *J. Sound Vib.*, Vol. 220, No. 2, 18 Feb. 1999, pp. 251–278.
  61. S. Kurra, M. Morimoto, and Z. I. Maekawa, Transportation Noise Annoyance—A Simulated-Environment Study for Road, Railway and Aircraft Noises, Part 2: Activity Disturbance and Combined Results, *J. Sound Vib.*, Vol. 220, No. 2, 18 Feb. 1999, pp. 279–295.
  62. J. M. Fields, R. De Jong, A. L. Brown, I. H. Flindell, T. Gjestland, R. F. S. Job, S. Kurra, P. Lercher, A. Schuemer-Kohrs, M. Vallet, and T. Yano, Guidelines for Reporting Core Information from Community Noise Reaction Surveys, *J. Sound Vib.*, Vol. 206, No. 5, 9 Oct. 1997, pp. 685–695.
  63. K. Minoura and K. Hiramatsu, On the Significance of an Intensive Survey in Relation to Community Response to Noise, *J. Sound Vib.*, Vol. 205, No. 4, 28 Aug. 1997, pp. 461–465.
  64. Y. Osada, T. Yoshida, K. Yoshida, T. Kawaguchi, Y. Hoshiyama and K. Yamamoto, Path Analysis of the Community Response to Road Traffic Noise, *J. Sound Vib.*, Vol. 205, No. 4, 28 Aug. 1997, pp. 493–498.
  65. D. Gottlob, Regulations for Community Noise, *Noise/News Int.*, Vol. 3, 1995, pp. 223–236.
  66. H. E. von Gierke and K. McK. Eldred, Effects of Noise on People, *Noise/News Int.*, Vol. 1, No. 2, 1993, pp. 67–89.
  67. E. A. G. Shaw, Noise Environments Outdoors and the Effects of Community Noise Exposure, *Noise Control Eng. J.*, Vol. 44, No. 3, 1996, pp. 109–120.
  68. ANSI S12.9–1996—Part 4, American National Standard Quantities and Procedures for Description and Measurement of Environmental Sound—Part 4: Noise Assessment and Prediction of Long-Term Community Response, Acoustical Society of America, New York, 1996.
  69. European Union, Future Noise Policy, European Commission Green Paper, European Union, Brussels, 1996.
  70. P. D. Schomer, Loudness-Level Weighting for Environmental Noise Assessment, *Acta Acust. (Stuttgart)*, Vol. 86, No. 1, Jan./Feb., 2000, pp. 49–61.
  71. Y. Suzuki, S. Kono, and T. Sone, An Experimental Consideration of the Evaluation of Environmental Noise with Tonal Components, *J. Sound Vib.*, Vol. 127, No. 3, Dec. 22, 1988, pp. 475–484.
  72. T. Sato, T. Yano, T. Morihara, and K. Masden, Relationships between Rating Scales, Question Stem Wording, and Community Responses to Railway Noise, *J. Sound Vib.*, Vol. 277, No. 3, 22 Oct. 2004, pp. 609–616.
  73. K. Hume, M. Gregg, C. Thomas, and D. Terranova, Complaints Caused by Aircraft Operations: An Assessment of Annoyance by Noise Level and Time of Day, *J. Air Transport Manage.*, Vol. 9, No. 3, May 2003, pp. 153–160.
  74. R. P. King and J. R. Davis, Community Noise: Health Effects and Management, *Int. J. Hygiene Environ. Health*, Vol. 206, No. 2, 2003, pp. 123–131.
  75. A. García, L. J. Faus, and A. M. García, The Community Response to Aircraft Noise around Six Spanish Airports, *J. Sound Vib.*, Vol. 164, No. 1, 8 June 1993, pp. 45–52.
  76. I. H. Knoepfel, A Framework for Environmental Impact Assessment of Long-Distance Energy Transport Systems, *Energy*, Vol. 21, Nos. 7–8, July–Aug., 1996, pp. 693–702.
  77. M. Omiya, K. Kuno, Y. Mishina, Y. Oishi, and A. Hayashi, Comparison of Community Noise Ratings by  $L_{50}$  And  $L_{\text{aeg}}$ , *J. Sound Vib.*, Vol. 205, No. 4, 28 Aug. 1997, pp. 545–554.
  78. H.G. Visser, Generic and Site-Specific Criteria in the Optimization of Noise Abatement Trajectories, *Transport. Res. Part D: Transport Environ.*, Vol. 10, No. 5, Sept., 2005, pp. 405–419.

# CHAPTER 120

## EXTERIOR NOISE OF VEHICLES – TRAFFIC NOISE PREDICTION AND CONTROL

**Paul R. Donovan**  
Illingworth and Rodkin  
Petaluma, California

**Richard Schumacher**  
R. S. Beratung LLC  
Fenton, Michigan

### 1 INTRODUCTION

Noise from motor vehicles is arguably the most pervasive of all environmental noises.<sup>1,2</sup> Although the noise levels of individual passenger cars, trucks, buses, and motorcycles are relatively low compared to airplanes and trains at equivalent distances, their shear numbers and close proximity to sensitive receptors more than offset their lower source levels. For this reason, considerable attention is given to controlling exterior motor vehicle noise at the source, abating noise from traffic flows, and planning appropriate land uses in the vicinity of highways. In this chapter, noise emissions from motor vehicles are examined individually and collectively in traffic flows. Because of their greater volumes, the noise from passenger cars and trucks tend to dominate traffic noise. Further, because trucks have in-service source levels that can be on the order of 10 dB higher than cars, the level of traffic noise is also strongly influenced by the mix of cars and trucks. To address the noise of individual vehicles, regulations are in place in most countries to limit the noise production by vehicle category. To address the noise from traffic flows, measurement protocols are available, as are various traffic noise models. These models typically not only predict traffic levels but are also used to assess different noise abatement strategies.

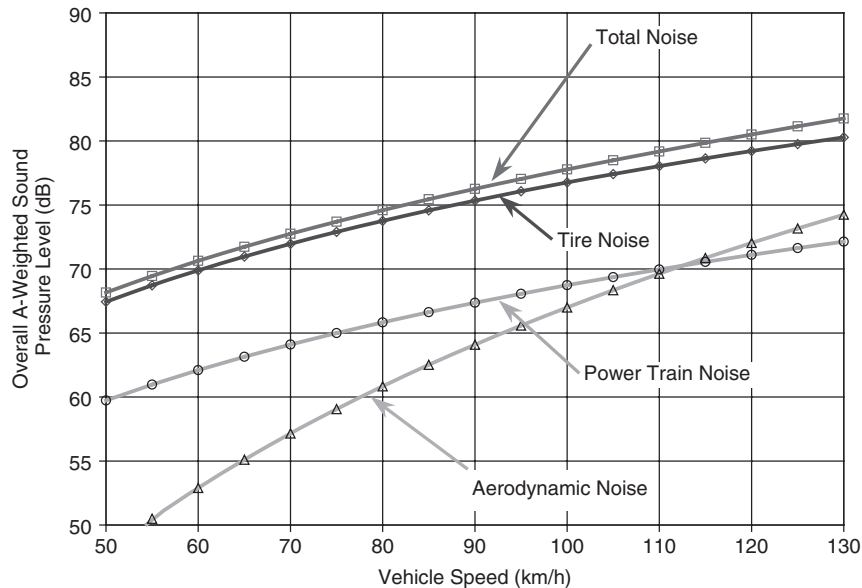
### 2 NOISE OF INDIVIDUAL VEHICLES

In the broadest sense, the sources of the exterior motor vehicle noise are considered in three categories: power train, tire–pavement, and aerodynamic noise. Power train noise is taken here to include all sources associated with vehicle propulsion, including noise from the engine, induction system, engine accessories, transmission and gears, cooling fan, and so forth. Also included in power train noise is exhaust outlet noise; however, this is often considered separately. Of the three categories, power train and aerodynamic noise are solely properties of the vehicle while tire–pavement noise is both a function of the vehicle (tires) and the pavement on which it operates. The contribution of these sources to the total exterior noise produced by a vehicle depends on the general type of motor vehicle, its operating condition, and its environment. Motor vehicles are typically

grouped as light vehicles (passenger cars, pickup trucks, sport utility vehicles, and passenger size vans), medium trucks, heavy trucks, buses, and motorcycles. In the United States, light vehicle are defined as being less than a gross vehicle weight (GVW) of 4500 kg, medium trucks have single-drive axles with a GVW of 4500 to 12,000 kg, and heavy trucks have multiple-drive axles with a GVW typically over 12,000 kg.<sup>3</sup> The operating conditions typically considered include acceleration, cruise, upgrade, deceleration, and idle. For modeling and assessing traffic noise, idle and deceleration are generally not considered with the possible exception of engine compression breaking of heavy trucks. The dependency of motor vehicle noise sources on environment is primarily due to pavement type; however, temperature is also generally acknowledged to have an effect on both power train and tire–pavement noise on the order of 1 dB/10°C.<sup>4–6</sup>

Each of the three noise source categories has its own typical dependency on vehicle operating parameters. Powertrain noise is dictated primarily by engine speed [revolutions/minute (rpm)] and load. Power train noise typically increases proportionally to 30 times log (rpm) and increases by about 2 to 3 dB for partial versus full throttle.<sup>7</sup> Power train noise does not show a constant relationship to vehicle speed, as the ratio between these is a function of gearing and gear selection. Tire–pavement noise is primarily a function of vehicle speed,  $V$ . Generally, tire–pavement noise increases proportionally to 30 to 35 times log( $V$ ), although a very wide range in the multiplier has been reported in the literature.<sup>8</sup> Tire–pavement noise is also known to depend on applied torque during acceleration. This effect can increase the noise produced by 0 to 8 dB, depending on the tire design and construction and on the applied torque.<sup>9</sup> Aerodynamic noise is also dictated by vehicle speed, typically proportionally to 60 times log( $V$ ). An example of how these sources combine based on these relationships and actual data<sup>9,10</sup> is shown in Fig. 1 for a composite of light vehicles operating under cruise, road-load conditions.

Two types of the test procedures are used for the measurement of individual vehicles. These are controlled passby tests, such as Society of Automotive Engineers



**Figure 1** Typical contribution of passenger car noise sources under cruise conditions as a function of speed.

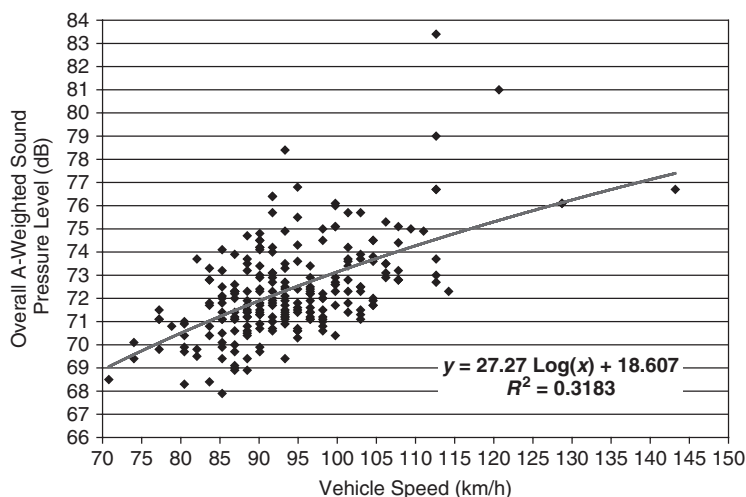
(SAE) J986<sup>11</sup> and International Organization for Standardization (ISO) 362,<sup>12</sup> and statistical passby tests, such as ISO 11819-1,<sup>13</sup> and those specified by the U.S. Federal Highway Administration (FHWA).<sup>14</sup> In controlled passby tests, a single test vehicle is driven by microphone(s) at a distance of 7.5 m and/or 15 m set at a height of 1.2 or 1.5 m (5 ft). The maximum A-weighted sound pressure level measured using a  $\frac{1}{8}$ -s (fast) exponential averaging time is reported. Operation of the vehicle is closely controlled, and often the tests are done on closed test tracks. These tests are typically used to determine differences between vehicles or tires with other variables held constant. In field situations, controlled passby tests are also used to isolate pavement effects for a vehicle(s) with specific test tires. Statistical passby tests are made of randomly occurring vehicles operating on public roadways. These tests are typically used to determine the range and average of noise levels within vehicle categories at one or more sites. Microphone placement and data measurement and reporting are the same as controlled passbys. Because vehicle speed is not controlled, the passby levels must be examined as a function of speed. The speed of each vehicle must be determined externally. Differences in the noise level–speed relationship are then used to compare site-specific issues such as pavement type or to compare noise from vehicle categories. Because of the variability of the noise from individual vehicles and the fact that vehicle speed is not controlled, statistical passby methods require many data points to achieve stable results.

Much has been done to characterize noise produced by various vehicle types in Europe and the United States using statistical passby methods. Under cruise conditions, these data typically show a large range in

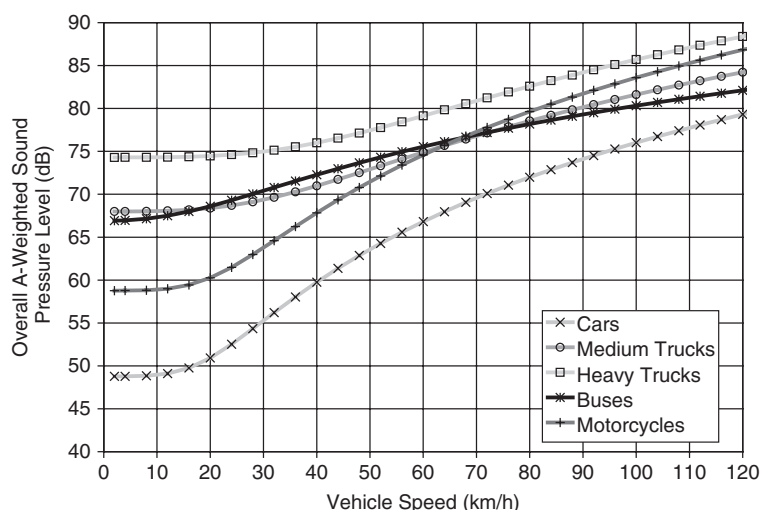
noise level for individual vehicles at any given speed and within a given vehicle category. Ranges for individual vehicles of 10 dB in each category are common across multiple sites in the speed range from 50 to 115 km/h. By segregating the sites by pavement type, this range is reduced by a few decibels, however, even for a single site, the typical range in individual vehicle noise level is typically 4 to 6 dB. Most of this variation can be accounted for by tire noise, which ranges by about 5 dB within a vehicle category. However, some variation is also due to higher noise levels generated by modified vehicles or ones with faulty exhaust systems. An example of statistical passby data for light vehicles taken at a single site only is shown in Fig. 2.

The largest and most recent database of statistical passby levels in the United States was reported by the U.S. Department of Transportation in 1995.<sup>3</sup> This data set consists of over 6000 individual passby events collected over 40 sites in different areas of the United States. Regression lines corresponding to the mean energy emission of five categories of vehicles are shown in Fig. 3 normalized to a distance of 15 m and averaged over all pavement types.

The data were also analyzed by pavement groupings of Portland cement concrete (PCC), dense graded asphalt concrete (DGAC), and open graded asphalt concrete (OGAC). The greatest effect of pavement was seen for automobiles and light trucks at speeds above 50 km/h where the averaged difference between PCC and OGAC reached about 4.5 dB. For medium and heavy trucks, this difference was about 2.5 dB above 65 to 80 km/h. Data from European studies display similar effects of vehicle and pavement type.<sup>15</sup> For



**Figure 2** Statistical passby test results for automobiles measured at 15 m from I-895.<sup>1</sup>



**Figure 3** Emission level comparison of various vehicle categories in the United States at a measurement distance of 15 m.<sup>1</sup>

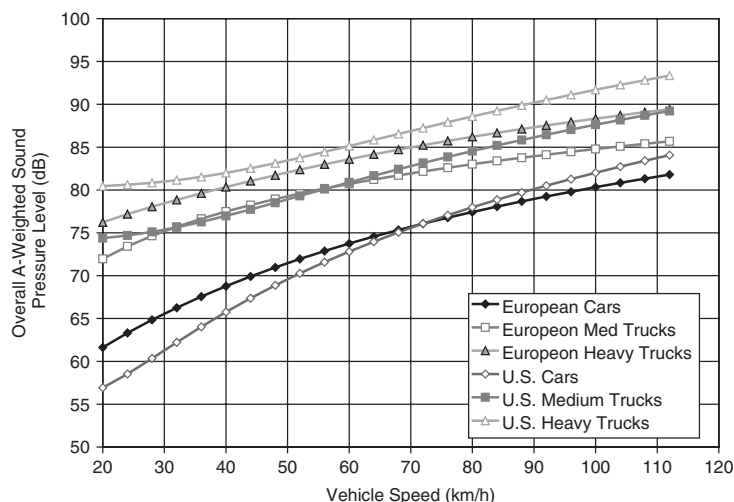
comparison, the average of mean energy emission levels taken from three European studies<sup>15-17</sup> have been energy averaged and compared to the U.S. levels in Fig. 4 as normalized to a distance of 7.5 m.

### 3 REGULATION OF MOTOR VEHICLE NOISE

Regulatory test procedures are an adaptation of the technical standard developed by an engineering body specializing in the measurement of product characteristics. The ISO dominates the regulatory procedures in European countries. In addition, other countries have procedures identical to the European countries or refer directly to a specific European regulation. In some

cases, the ISO procedures have been modified by the implementing country leading to a variety of similar but often different regulatory procedures.

The United States and Canada followed the development of procedures by the SAE. California, the first state to adopt a vehicle noise certification procedure, used the SAE J986 and SAE J366<sup>18</sup> for cars and trucks, respectively. The operating modes in ISO and SAE are similar, using acceleration from a stabilized approach speed around 50 km/h up to a higher speed but limit the engine speed to being equal to or less than the rated power engine speed. The SAE-based procedures



**Figure 4** Comparison of vehicle emission levels from the United States and average of European studies normalized to a measurement distance of 7.5 m. <sup>1,10-12</sup>

**Table 1** Exterior Motor Vehicle Noise Limits<sup>a</sup> in Overall A-weighted Sound Pressure Level, dB

Regulatory Group	Passenger Cars	Trucks and Buses	Motorcycles	Tires
Argentina	78–85	80–85	NR	NR
Australia	NR	81–85	80	NR
Brazil	79–81	84–87	80	NR
Canada	80	83	NR	NR
China	82–84	84–87	NR	NR
European Union	74	74–80	80	72–76
Japan	76	76–83	73	NR
Korea	76–82	79–82	77	NR
Mexico	81	84	89	NR
Saudi Arabia	78–82	79–85	NR	NR
South Africa	74	75–77	NR	NR
Taiwan	78	83	78	NR
United Nations	74	74–77	75–80	72–76
U.S. federal over 4535 kg	NR	80	80	NR
U.S. state and local	80	80–84	NR	NR

<sup>a</sup>Limits shown do not encompass the entire detailed variants based on mass, power on/off usage. NR indicates the jurisdiction listed does not have a regulation listed for the product.

required approximately twice the physical measurement area of the comparable ISO tests area with the measurement microphone 15 m from the driving lane for SAE versus 7.5 m for the ISO. The regulatory limits under these test procedures are given in Table 1 as of 2003. Static tests intended to monitor changes in the exhaust system performance or intentional modification are also in place in some jurisdictions. Both static and moving tests can identify a defective exhaust component, however, the no-load static tests are not otherwise correlated to passby tests.

The UN member countries have developed the 1998 Global Agreement, which modifies some of the mandatory requirements of 1958. Consequently, United Nations (UN) influence on noise procedures

and limits now includes most of the countries included in the 1958 agreement and also the United States, South Africa, China, and Russia as well as the major non-Western Europe areas that effectively make it a true global regulation. The consequences of this action are not yet known in many countries including the United States.

There has been some concern expressed about the effectiveness of new vehicle noise regulations in reducing noise levels in the community. The European Union 1995 Green Paper concluded the two decades of reductions of limits have not provided the desired improvement in the community exposure.<sup>19</sup> The reasons for the limited effectiveness were later identified to include slow exchange rate of older, noisier vehicles

to new, quiet ones; a trend toward bigger, more powerful trucks and light vehicles; lack of in-use controls; the underlying levels of tire–pavement noise; and a lack of a test procedure that represents actual vehicle operation.<sup>1</sup> Studies have shown the driving mode in the community is significantly less severe than the regulatory test. As a result, product design modifications are introduced for engine speeds higher than in use operation. In addition, the emphasis on power train noise conceals the contribution of tires that occurs even at the lower vehicle speeds near 30 km/h. Consequently, the ISO has embarked on developing a more representative urban rating that includes a power-train-dominated full-throttle mode and a tire-dominated constant speed. These are combined to yield a level that more closely represents the noise impact of urban traffic. The European regulations have also added a high-speed tire noise rolling test that addresses the highway noise problem. But the initial levels and step reductions along with the rate of vehicle exchange will delay any meaningful improvement for over a decade.

The U.S. consumer interest in vehicle noise regulation has been very limited. Early regulation reduced the initially higher exhaust levels, which was the public perception of vehicle noise problems. Although there is no conclusive noise data, trends in the United States support the notion of generally increasing traffic levels. The tire–pavement noise levels on U.S. freeways have led to residential complaints that have resulted in freeway noise barriers and the advent of major research on quiet highway surfaces. In 1968, when the first noise regulation was adopted in California, the average family of 3.4 people<sup>20</sup> owned one vehicle. Today, the average family of 2.7 people has two vehicles plus one recreational or off-road vehicle suggesting increased volumes of traffic.<sup>20</sup> In addition the predominance of sport-utility-styled vehicles has increased the tire noise component of the vehicle noise because of the more aggressive tires, which are intended for multiple season and recreational driving. Finally, the speed limits on the interstate system and regional highways are higher than 20 years ago. To address these trends, future test procedures must be developed to deal with the annoyance of the urban community, reflecting the manner in which vehicles are actually operated. Test procedures must rate the tire noise source as it impacts the urban and rural resident under a range of operating speeds from 60 km/h through 100 km/h. In addition, regulations must restrict the modification of vehicles to ensure that in-service vehicles continue to meet the design standard.

The international procedure groups must continue to be active in the development of tests that address the increasing range of products from the traditional internal combustion cars through the innovative electric vehicle with a variety of power sources. With the possible exception of motorcycles<sup>3</sup> all vehicles, regardless of the power source, have a significant tire component that becomes a more significant part of the total vehicle as the power train levels are reduced.

#### 4 VEHICLE NOISE IN TRAFFIC FLOWS

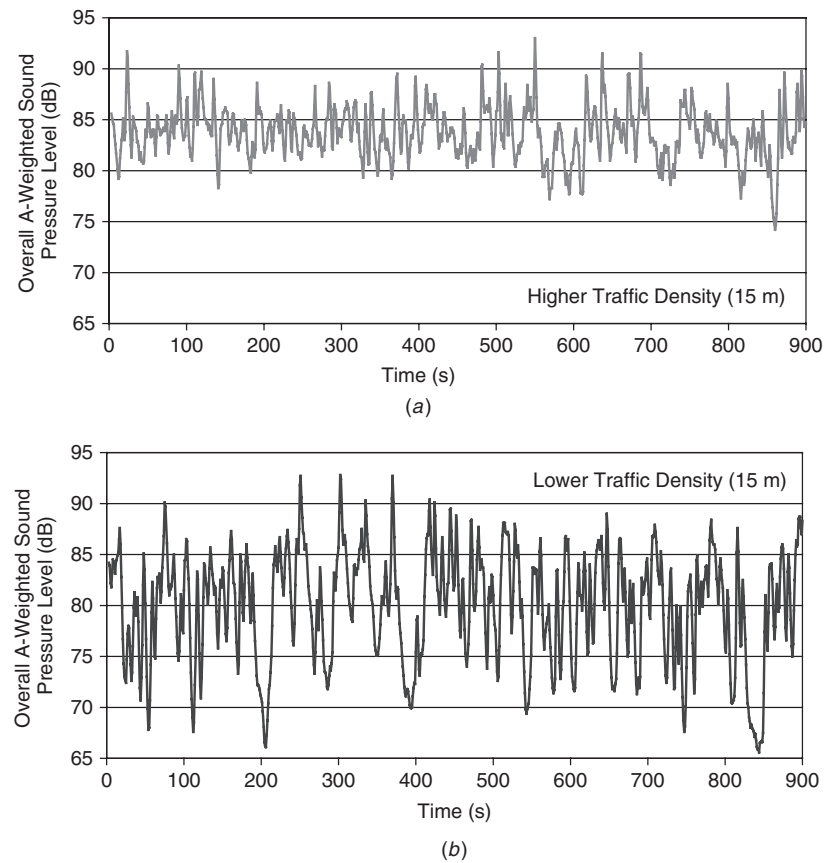
Because of the levels produced, traffic noise from freeways and multilane highways tends to be a primary source of concern for community noise. The basic parameters governing the noise generation from highways are average vehicle speed, traffic volume, mix of light vehicles and trucks, and pavement type. Above 80 km/h, the composite noise from a traffic flow of cars and trucks increases at about  $35 \log(V)$  (Fig. 3). At these speeds, since trucks are about 5 to 9 dB louder than light vehicles (Fig. 4), the traffic noise depends on the percentage of medium and heavy trucks as well as the total number of vehicles. Within each vehicle category, the noise level increases by 3 dB with each doubling of volume. The effects of pavement depend not only on the type of pavement present but also on the traffic mix. However, even with relatively high truck volumes, the pavement can cause differences in highway traffic noise of 6 dB or more.

The temporal nature of noise from highways also depends on traffic volume and mix as well as distance to the roadway. For higher volumes and/or further distances from the roadway, the short-term noise levels display little variation. At higher volumes, multiple individual vehicles determine the resultant noise so that there is little variation in noise from moment to moment. Similarly, at larger distances, more individual vehicles contribute to the noise because the distance to each vehicle is similar over a longer length of roadway. For lower traffic volumes and/or close distances, temporal variations of 30 to 40 dB or more can occur depending on background noise, the noise produced by an individual vehicle, and the distance away. An illustration of several measured temporal variations are given in Fig. 5 for different traffic volumes and distances from urban area freeways.

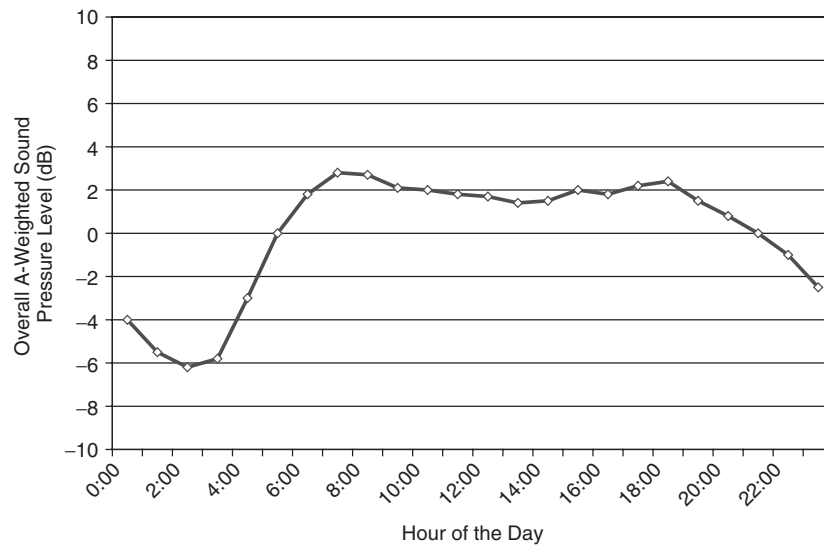
Reflecting the difference in day and nighttime traffic volumes, noise from major arterial roadways and highways often displays a consistent diurnal pattern for levels measured on an hourly basis.<sup>21</sup> Under this pattern, the lowest hourly levels characteristically occur in the early morning (1:00 to 3:00 a.m.) when traffic volumes are lower, rise rapidly to about 6:00 or 7:00 a.m., remain constant to after 6:00 p.m., and then fall off toward the early morning minimum. This pattern as measured for 28 different roadways is illustrated in Fig. 6. In congested areas, the hour of highest noise level and the hour of peak traffic volume are not necessarily the same due to reduced speeds at highest volumes.

For arterial roadways, the freeway diurnal noise pattern is also often present. In addition to the short-term temporal variations noted for highways, the presence of traffic control devices can also influence the temporal variation of noise from arterial roadways. Even away from intersections, traffic lights can create "platooning," where groups of vehicles pass by a location followed by long periods of no vehicles. At controlled intersections, the noise of the traffic is different both in terms of its temporal variation and character.<sup>22,23</sup> At traffic lights, there will be periods of time when vehicles are idling, producing relatively

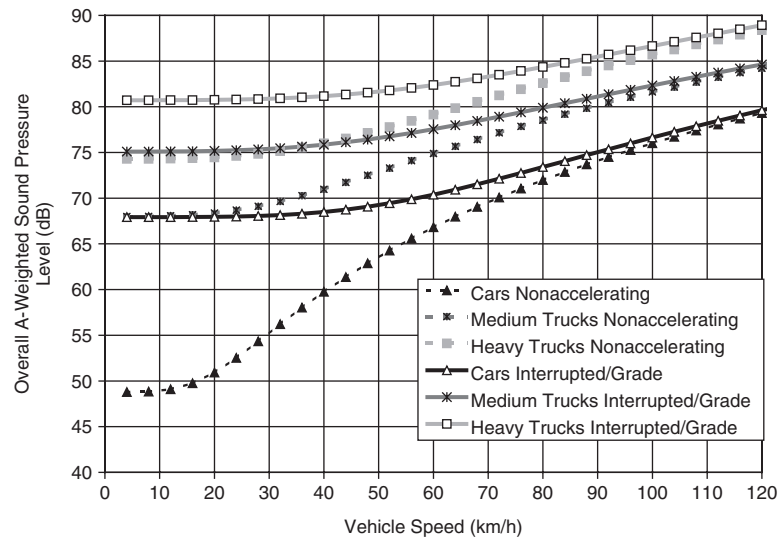




**Figure 5** Variation of overall A-weighted sound pressure level (slow response) over 15 min for heavy traffic and light traffic as measured at 15 m.



**Figure 6** Typical diurnal pattern of noise levels from roadway.<sup>17</sup>



**Figure 7** Vehicle noise emission levels for nonaccelerating and interrupted flow/grade operating conditions.<sup>1</sup>

low noise levels, followed by vehicles accelerating from rest and periods of cruise conditions. Unlike cruise where the noise emission is heavily influenced by tire–pavement noise, during acceleration, the noise emission is initially influenced by power train noise. Especially for trucks, the character of this sound is distinctive as the noise is very much a function of engine rpm, and noise will have a “saw-tooth” pattern as the truck uses several gears to gain speed.<sup>24,25</sup> Because of gearing differences and the prevalence of automotive transmissions, this characteristic is not as pronounced in light vehicles. However, the difference between low-speed cruise and acceleration is much greater for light vehicles than for trucks (Fig. 7).

Traffic noise is typically characterized using the equivalent sound pressure level ( $L_{eq}$ ) metric instead of maximum passby level. The time period over which the  $L_{eq}$  is determined can vary with the traffic density or temporal variation of the noise, however, a minimum of 2 min is specified for “steady” traffic noise and up to 30 min where the anticipated range in sound pressure level fluctuation is greater than 30 dB.<sup>14</sup> Three to six repetitions over the selected time period are also recommended. The details of measurement depend on the intent of the measurement. In cases where it is desired to assess the environmental noise impact at a specific location, measurements in hourly intervals over a 24-h period are typically made so that the day–night sound pressure level ( $L_{dn}$ ) or the community noise equivalent level (CNEL) values can be determined. Measurement locations are typically near the location for which the impact is to be assessed. Measurement of traffic speed and volume are not necessarily required and the measurements are often unattended. When the intent of the measurement is

to compare before and after levels when a roadway change is planned, or to compare the measurements to traffic model results, or to compare one site to another, additional documentation is required. In these cases, the noise measurements are typically shorter, lasting several hours, and are usually attended so that unusual occurrences and noises can be identified and removed. The measurement of traffic volume and average vehicle speed by category is also required. In addition, documentation of the site geometry and conditions, ground type and cover, and meteorological conditions are also needed. For before and after measurements, microphones are placed at standard locations or near sensitive receptors; however, a reference microphone 30 m or less from the center of the nearest travel lane is desirable. For comparison between sites or to traffic models, measurement sites should be flat and free from extraneous reflecting surfaces within at least 30 m of the traffic and microphone locations. One microphone is placed 15 m from the center of the near lane of vehicle travel at a height of 1.5 m above the plane of vehicle travel. Additional microphones at 7.5 m and 30 m are often used, as are microphones at greater heights than 1.5 m. Wind speed should not exceed 19 km/h (12 mph) during the measurements.<sup>14</sup> With these criteria, research-grade measurements are not possible in many situations.

## 5 PROPAGATION OF TRAFFIC NOISE

The underlying nature of sound propagation away from individual vehicles is that of a *point source* over a reflecting plane. This leads to a general behavior of spherical divergence or a 6-dB reduction in sound pressure level with each doubling of distance (DD) or as given by  $20 \log(r/r_o)$ . As a result, maximum

passby levels of individual vehicles falloff at a rate of about 6 dB/DD for propagation over acoustically hard, relatively flat ground for distances of 30 m or less. For traffic flows, the individual point sources are spread out into a continuous line of sources. In this case, the general behavior is that of cylindrical divergence or a 3-dB reduction in level with each doubling of distance [ $10 \log(r/r_0)$ ]. In urban settings, for propagation down a side street away from a traffic line source, the sound also decreases at about 3 dB/DD after about an initial 2-dB amplification due to reflections from the building surfaces.<sup>24</sup> For time-averaged metrics of vehicle passbys, such as the single event level (SEL), the averaged level also decreases at 3 dB/DD for open areas.

A number of different phenomena often occur to complicate the ideal propagation models discussed above. At distances close to the line of vehicle passby, constructive and destructive interference patterns occur, modifying the spectrum of the received sound and its overall A-weighted level. This interference is a function of the path length difference between the direct and reflected sound waves propagating from the vehicle and the impedance of the intervening ground. At farther distances, a number of other factors influence the sound propagation from vehicles and traffic flows. In open areas, these include temperature and wind gradients, propagation over acoustically "soft" ground, and atmospheric air absorption.<sup>26</sup> The net effect of these factors is to generally provide more sound attenuation than that predicted by the ideal spreading laws. As a result, applying the theoretical attenuation of 3 dB/DD for traffic flows or 6 dB/DD for individual vehicles tends to predict higher levels than those that actually occur. Of these factors, only attenuation by atmospheric absorption is generally considered not a source of noise level variation, although it is a function of relative humidity. Wind tends to be the most volatile in terms of effect on propagation due to its variation in both speed and direction. At distances as close as 30 m from a freeway, differences in noise due to wind changes can be as great as 5 to 6 dB even for relatively light wind conditions. For improved consistency in data, it is preferred to measure vehicle and traffic noise under conditions of virtually no wind or when the wind is in a cross direction between the roadway and measurement location or when the wind is in the direction from the roadway to the microphone (downwind). Upwind conditions should be avoided due to the potential for substantial excess attenuation in the resultant shadow zones.

In situations where other forms of excess attenuation exist, wind and temperature effects can reduce the effectiveness of the attenuation and result in higher levels than those normally occurring. When barriers, buildings, or topography provide the shielding between the traffic source and receiver, the downward bending of the sound rays with downwind propagation and temperature inversions can reduce the shielding provided by these obstacles. They can also nullify the effects of excess ground attenuation. As a result, for residences exposed to traffic noise, the received levels

can noticeably increase over what normally occurs in cases where excess attenuation is commonly present due to barriers and obstacles, ground attenuation, or prevailing wind conditions.

## 6 MODELING OF TRAFFIC NOISE

Modeling of traffic noise has several uses, including estimating current noise exposure along roadways, assessing the effect of roadway changes, and predicting the performance of noise abatement options. The basic elements of traffic noise modeling are the traffic source levels and the propagation or attenuation of sound between the traffic and the receiver. Typical source-related inputs to traffic noise models are the speed and volume of vehicle types, operating mode of the vehicles, and the length of roadway with line of sight to the receiver location. Propagation-related inputs include the acoustic characteristics of the ground, the number of lanes of travel, site geometry and topography, and the type and geometry of any barriers or buildings present. Most models also consider the type of pavement at the site in regard to tire-pavement noise generation, the prevailing wind and temperature conditions,<sup>27</sup> and interrupted traffic flows.<sup>22</sup> There are a number of resources that can be consulted for additional, detailed information about traffic noise prediction methods.<sup>26,28-30</sup>

Embedded in traffic noise prediction routines are some assumptions about the vertical distribution of source strength on the vehicles for the operating mode under consideration. Knowledge of source height is critical for predicting propagation effects and the effectiveness of the barriers. Under cruise conditions for properly maintained cars and trucks, tire-pavement noise typically begins to dominate power train noise at speeds above about 40 km/h.<sup>25</sup> For trucks, the speed is found to be more in the range of 50 to 60 km/h. At any speed in which tire-pavement noise dominates, the source is known to be very close to the ground, within about 100 mm.<sup>8</sup> At lower speeds, the distribution is skewed more to power train sources. For light vehicles, noise to the side of the vehicle comes from the underbody area and wheelwell areas near the engine compartment and from the exhaust outlet. These source regions are also relatively close to the ground, typically within one metre of the ground. For trucks, the engine compartments are higher, 1 to 2 m above the ground, and exhaust outlets may be as high as 4 m. Although there has been work completed worldwide on this subject,<sup>16,31</sup> the data are limited. As a result, traffic models often rely on partial data and/or assumed source heights.

Worldwide, there are many traffic noise models available. Many general sound-mapping software codes have some traffic noise prediction element. Also, many countries have their own accepted model for predicting traffic noise. In the United States, the new Federal Highway Administration (FHWA) Traffic Noise Model (TNM) is replacing the older STAMINA2.1. This new model features improved sound propagation prediction, particularly for barrier insertion loss and propagation over acoustically soft ground. Unlike the

older model, TNM uses one-third octave band levels in its calculations of sound propagation.<sup>32</sup> TNM has undergone and continues to undergo extensive validation. When a reference microphone position is used, the propagation algorithms typically provide superior results compared to older models.<sup>33</sup> Compared to STAMINA, TNM has been found to predict greater insertion loss by 1 to 3 dB.<sup>33,34</sup> Initial validation work by the U.S. Department of Transportation DOT indicates very good agreement between calibrated field measurements and TNM results with an average difference of 0.5 dB in open areas when strong winds were not present.<sup>35</sup> Although TNM has the provision for including the effects of pavement type, use of this feature is not currently allowed. As a result, on an absolute basis, TNM can overpredict traffic noise levels by as much as 5 dB in cases where the pavement is quieter than the average pavement assumed in the model.<sup>36</sup> To improve the absolute performance of TNM and other models, it is recommended to reference the model results to measurements of existing traffic noise representative of the site made at locations within 30 m (100 ft) of the roadway.<sup>35</sup>

## 7 ABATEMENT OF TRAFFIC NOISE

Abatement of traffic noise is driven by two distinct criteria. These are basically proactive and reactive. Proactively, for new highways or major alternations, such as adding lanes to an existing roadway, noise levels are predicted using traffic noise models. These levels are then compared to criteria that trigger the need for noise abatement to be considered. These criteria vary by country and jurisdiction. Within the European Union, 55  $L_{dn}$  is considered the goal for exterior noise levels, while 65  $L_{dn}$  is considered the limit of acceptable noise level.<sup>19</sup> Each country is then expected to develop plans to reduce the level down to the 55  $L_{dn}$  goal. In the United States, the FHWA identifies noise impact and need to consider noise abatement when the predicted levels from new highways or major alternations approach 67 dB for highest hourly  $L_{eq}$  level for noise-sensitive land uses.<sup>37</sup> States refine this criterion and commonly use hourly  $L_{eq}$  values ranging from 64 dB up to 67 dB as the threshold for considering noise abatement. At the local level, lower thresholds, such as 65  $L_{dn}$ , are common. These mixed metrics, maximum hour  $L_{eq}$  and  $L_{dn}$ , require some reconciliation in order to compare the various criteria. Using the data of Fig. 6, the highest hour  $L_{eq}$  values of 67 dB typically equate to an  $L_{dn}$  of about 70 dB, while an upper limit of  $L_{dn}$  of 65 then translates to a highest hour  $L_{eq}$  of 62 dB. At an  $L_{dn}$  of 70 dB, slightly more than 20% of the people exposed to the traffic noise would be expected to be highly annoyed (see Chapter 34). For existing highways, similar or higher criteria are often used to identify the need for noise abatement. In these cases, negative public reaction to the traffic noise can drive noise abatement even though the levels are at or below the criteria. Also, “minor” alternations to the pavement surface such as transverse tining of PCC can initiate

the need for abatement due to increased noise level and changes in noise character.<sup>38,39</sup>

Abatement of traffic noise can be considered using the traditional source–path–receiver analysis. In regard to the source, new vehicle noise emission standards are applicable as discussed previously. In-use noise levels, however, can be significantly higher due to poor maintenance or purposeful alternation. Although traffic noise levels could be significantly lowered by eliminating such vehicles from the traffic flow (refer to Fig. 2), in-use regulation and enforcement is not commonly done. Based on vehicle speed versus noise relationships (Fig. 3), traffic noise can also be reduced by lowering vehicle speed limits. Noisier vehicles, such as heavy trucks, can also be restricted on a roadway to reduce traffic noise levels. Quieter pavement surfaces are commonly used in Europe and Asia as a method of controlling noise at the source. Open graded (porous) and/or rubberized asphalt is beginning to be used in the United States for traffic noise abatement. Initially, such pavements have demonstrated the ability to reduce traffic noise up to 5 dB or more on highways and local roadways.<sup>36,40</sup>

In regard to the path, noise barriers are commonly used in many countries to shield sensitive receptors from traffic. In the United States, all but six states have constructed noise barriers along their highways. Although strictly voluntary, 22 of these states have constructed barriers for the sole purpose of abating existing noise levels.<sup>41</sup> Field performance of highway noise barriers typically provides a reduction in noise level in the range of 5 dB to 12 dB depending on the height of the barrier, the distance of the receptor location away from the barrier, and topography and acoustic characteristics of the site. Typically, noise reduction goals are established within the transportation agencies and if the stated goal is not feasible, the noise abatement project is not done. These goals commonly range from 5 to 10 dB. Noise barriers are not limited to major highways. Barriers are used for traffic noise abatement at the local level both by governmental bodies and developers when the levels along arterial streets warrant abatement. Most traffic noise models provide some algorithm for predicting barrier performance, which is used to specify barrier geometry and to predict performance. While other path-related traffic noise abatement methods include highway realignment, and acquiring land for buffer zones along the highway, these are seldom used.

In cases where the impact is severe and source–path abatement is not feasible, receiver-based abatement is considered. In this situation, air conditioning may be added to an existing building or house to reduce the need for open windows. Acoustically weaker elements of the building facade such as windows, doors, and vents may be replaced with units providing increased noise reduction. Finally, enhancement of the wall construction itself may be considered. Although not strictly abatement, noise levels experienced by sensitive receptors can be avoided through land-use planning and development. This is often done as a two-tier process where exterior noise criteria are applied as

the first level. If these cannot be met, development may still be allowed if it is demonstrated that interior criteria can be met through proper building sound insulation. These criteria are set on the state and local level.

In assessing traffic noise abatement methods to a specific application, a number of trade-off issues are involved. The use of barriers has been the long-standing method of choice. However, in some situations, barriers are not feasible because of site constraints and/or inability to produce a 5- to 10-dB reduction given the site geometry. Also, barriers may not be acceptable to the residents along a roadway due to blocking desired views and other aesthetic reasons. Use of barriers can also be restricted for safety, line-of-sight concerns. Abatement through the application of quieter pavement surface overlays has become an increasingly popular alternative. However, the effectiveness of quieter pavement surfaces depends on their improvement in noise performance relative to the original pavement and their continued noise performance over their life cycle. Although quieter pavement surfaces have been found to be cost effective in some countries and applications,<sup>42</sup> they are currently not eligible for federal funding or assistance in the United States as a noise abatement method.

## REFERENCES

1. U. Sandberg, Noise Emissions of Road Vehicles—Effectiveness of Regulations, Final Report from the Working Party on Noise Emissions of Road Vehicles, International Institute of Noise Control Engineering, The Hague, The Netherlands, July 2001.
2. W. Bowlby, Highway Noise Prediction and Control, in *Handbook of Acoustical Measurements and Noise Control*, C. Harris Ed., Acoustical Society of America, Melville, NY, 1998, pp. 48.1–48.23.
3. G. Fleming, A. Rapoza, and C. Lee, U.S. Department of Transportation, Report No. DOT-VNTSC-FHWA-96-2, Development of National Reference Energy Mean Emission Levels for the FHWA Traffic Noise Model (FHEA TNM), Version 1.0, Cambridge, MA, 1996.
4. R. Saville, The Effect of Temperature on Pass-by Noise, Paper No. 2001-01-1568, Proceedings of the Noise & Vibration Conference, Society of Automotive Engineers, Warrendale, PA, 2001.
5. B. Landsberger, J. DeMoss, and M. McNerney, Effects of Air and Road Surface Temperature on Tire Pavement Noise on an ISO 10844 Surface, Paper No. 2001-01-1598, Proceedings of the Noise & Vibration Conference, Society of Automotive Engineers, Warrendale, PA, 2001.
6. D. Morel, A Theoretical Approach to the Definition of a Type/Road Noise Level Temperature Correction of Passenger-Car Tyres, International Institute of Noise Control Engineering, Proceedings of Inter-Noise 94, Yokohama, Japan, 1994.
7. K. Plotkin, D. Pies, R. Helizon, and B. Sharp, Wyle Research Report WR 79-20, U.S. Environmental Protection Agency Contract No. 68-01-3518, *Light Vehicle Noise: Vol. III—Identification of Noise Source Components and Evaluation of Noise Reduction Techniques*, EPA, Washington, DC, 1979.
8. U. Sandberg and J. Ejsmont, Tyre/Road Noise Sources and Generation Mechanisms, in *Tyre/Road Noise Reference Book*, Informex, Kisa, Sweden, 2002, pp. 127–138, 147.
9. P. Donovan, Tire/Pavement Interaction Noise under Vehicle Operating Conditions of Cruise and Acceleration, Paper No. 931276, Proceedings of the Noise & Vibration Conference, Society of Automotive Engineers, Warrendale, PA, 1993.
10. P. Donovan, R. Schumacher, and J. Stott, Assessment of Tire/Pavement Interaction Noise under Vehicle Passby Test Conditions Using Sound Intensity Measurement Methods, The 16th International Congress on Acoustics and the 135th Meeting of the Acoustical Society of America, Seattle, WA, 1998.
11. SAE J986 Test Procedure: Measurement of Noise from Passenger Cars and Light Trucks, Society of Automotive Engineering, Warrendale, PA, May 1998.
12. ISO 362 Test Procedure: Measurement of Noise Emitted by Accelerating Road Vehicles, International Organization of Standardization, Geneva, Switzerland, 1998.
13. International Standard ISO 10844: 1994(E), Acoustics—Specification of Test Track for the Purpose of Measuring Noise Emitted by Road Vehicles, International Organization of Standardization, Geneva, Switzerland, 1994.
14. C. Lee, and G. Fleming, Measurement of Highway-Related Noise, Report No. DOT-VNTSC-FHWA-96-5, U.S. Department of Transportation, Washington, DC, 1996.
15. K. Heutschi, New Swiss Source Model for Road Traffic Noise, International Institute of Noise Control Engineering, Proceedings of Inter-Noise 2001, The Hague, The Netherlands, 2001.
16. J. van der Toorn, T. van den Dool, and W. van Vliet, Sound Emission by Motor Vehicles on Motorways in The Netherlands: 1974–2000, International Institute of Noise Control Engineering, Proceedings of Inter-Noise 2001, The Hague, The Netherlands, 2001.
17. H. Steven, Effects of Noise Limits for Powered Vehicles on Their Emissions in Real Operation, Paper No. 951257, Proceedings of the Noise & Vibration Conference, Society of Automotive Engineers, Warrendale, PA, 1995.
18. SAE J388 Test Procedure: Measurement of Noise from Medium and Heavy Trucks and Buses, Society of Automotive Engineering, Warrendale, PA.
19. Future Noise Policy, European Commission Green Paper, COM(96)540, issued by the Commission of the European Communities, Brussels, Belgium, 1996 (also see *Noise News Int.*, Vol. 5, No. 2, June, 1997).
20. U.S. Census and the National Household Travel Survey, U.S. Census Bureau, Washington, DC, June 2003.
21. M. Greene, Typical Diurnal Traffic Noise Patterns for a Variety of Roadway Types, International Institute of Noise Control Engineering, Proceedings of Inter-Noise 2002, Dearborn, MI, 2002.
22. R. Wayson, M. Martin, and A. Edwards, The AAMA Traffic Noise Model—A Better Approach, Paper No. 951336, Proceedings of the Noise & Vibration Conference, Society of Automotive Engineers, Warrendale, PA, 1995.
23. R. Makarewicz, M. Fujimoto, and P. Kokowski, “A Model of Interrupted Road Traffic Noise, *Appl. Acoust.*, Vol. 57, 1999, pp. 129–137.
24. B. Sharp and P. Donovan, Motor Vehicle Noise, in *Handbook of Noise Control*, 2nd ed., McGraw-Hill, New York, 1979, Chapter 32.

25. D. de Graaff, A Speed and Acceleration Limit in the Noise Type Approval of Vehicles Will Enable Silent Cars to Reveal Their Silence, International Institute of Noise Control Engineering, Proceedings of Inter-Noise 2001, The Hague, The Netherlands, 2001.
26. R. H. Lyon, *Lectures in Transportation Noise*, Grozier, Cambridge, MA, 1973, Chapters 15 and 16.
27. F. Besnard, H. Lefèvre, and V. Zouboff, Validation and Evolution of the Road Traffic Noise Prediction Model NMPB-96, International Institute of Noise Control Engineering, Proceedings of Inter-Noise 2001, The Hague, The Netherlands, 2001.
28. W. Bowlby, Highway Noise Prediction and Control, in *Handbook of Acoustical Measurements and Noise Control*, C. Harris, Ed., Acoustical Society of America, Melville, NY, 1998, pp. 48.1–48.23.
29. Technical Noise Supplemental, TeNs, A Technical Supplement to the Traffic Noise Analysis Protocol, California Department of Transportation, Sacramento, CA, 1998.
30. Braunstrein + Berndt, *User's Manual SoundPLAN®*, SoundPLAN, Backnang, Germany, 2004, Chapter 16.
31. R. Coulson, Report No. FL-ER-63-96, Vehicle Noise Source Heights & Sub-Source Spectra, Florida Atlantic University, Dept. of Ocean Engineering, Boca Raton, FL, 1996.
32. G. Anderson, C. Menge, and C. Rossano, The Federal Highway Administration's New Traffic Noise Model (FHWA TMN®) : Functionality, Input Types, and Computations, Proceedings of Noise-Con 96, Seattle, WA, October, 1996.
33. C. Menge, G. Anderson, and D. Barrett, Experiences with USDOT's Traffic Noise Model (TNM), International Institute of Noise Control Engineering, Proceedings of Inter-Noise 2001, The Hague, The Netherlands, 2001.
34. R. Wayson, J. McDonald, W. Arner, C. Corbisher, P. Tom, D. Srinivas, and B. Kim, Highway Traffic Noise Model Comparison Measured Data, Proceedings of Noise-Con 2001, Portland, ME, October, 2001.
35. J. Rochat and G. Fleming, Report No. DOT-VNTSC-FHWA-02-01, 2002, *Validation of FHWA's Traffic Noise Model® (TNM): Phase I*, U.S. Department of Transportation, Washington, DC, 2002.
36. California Department of Transportation, I-80 Davis OGAC Pavement Noise Study: Traffic Noise Levels Associated with an Aging Open Grade Asphalt Concrete Overlay, Environmental Program—Noise and Vibration Studies, Sacramento, CA, 2002.
37. Federal Highway Administration, Procedures for Abatement of Highway Traffic Noise and Construction Noise, *Federal-Aid Highway Program Manual*, U.S. Department of Transportation, Washington, DC, Vol. 7, Chapter 7, Section 3, 1982.
38. P. Burgé, Using FHWA TNM to Compare Acoustical Characteristics of Candidate Pavement Types, Institute of Noise Control Engineering USA, Proceedings of Noise-Con 2001, Portland, ME, 2001.
39. P. Donovan and L. Scofield, An Evaluation of the Effects of Different Portland Cement Concrete, Institute of Noise Control Engineering, Proceedings of Noise-Con 2003, Cleveland, OH, 2003.
40. P. Donovan, Pavement Rehabilitation and Traffic Noise Reduction along an Arterial Street, Institute of Noise Control Engineering, Proceedings of Noise-Con 2004, Baltimore, MD, 2004.
41. K. Polcak, Highway Traffic Noise Barriers in the U.S.—Construction Trends and Cost Analysis, *Noise News Int.*, Vol. 11, No. 3, September, 2003.
42. L. Larsen, and H. Bendtsen, Costs and Perceived Noise Reduction of Porous Asphalt Pavements, International Institute of Noise Control Engineering, Proceedings of Inter-Noise 2001, The Hague, The Netherlands, 2001.

# CHAPTER 121

## RAIL SYSTEM ENVIRONMENTAL NOISE PREDICTION, ASSESSMENT, AND CONTROL

**Brian Hemsworth**  
Noise Consultant  
Derby, United Kingdom

### 1 INTRODUCTION

The main purpose of any environmental noise prediction scheme is to determine whether the noise levels from the source in question exceed legislative limits (if they exist) or project-determined noise assessment criteria. This means that the noise prediction scheme is used to predict noise levels in terms of a noise descriptor that correlates with annoyance.

For railways this is the prediction of the equivalent sound pressure level ( $L_{eq}$ ), and there is a growing tendency for the simple 24-h  $L_{eq}$  noise level to be replaced by metrics that penalize night or evening/night traffic. The separation of the 24-h period into separate or aggregated time periods affects the detail of the operational information needed for accurate prediction but does not affect the basic prediction process.

It is more important to understand the principles on which prediction models can be developed than to attempt to provide prescriptive data for universal use in prediction models. These principles are appropriate to any surface rail system irrespective of the type of rolling stock used or the track designs. It is the role of the user to input the specific source levels and attenuation algorithms that are appropriate to the specific case under investigation.

### 2 PREDICTION PROCESS

A number of alternative  $L_{eq}$ -based criteria are used worldwide and are discussed in Chapters 25 and 34. For a series of individual events (such as train passages)  $L_{eq}$  can be derived from the following equation\*:

$$L_{eq} = 10 \log_{10} \left[ \sum_{i=1}^n 10^{SEL_i/10} \right] - 10 \log_{10} T \quad (1)$$

where  $SEL_i$  = SEL for the  $i$ th train passby  
 $T$  = assessment time period (in seconds)  
 $n$  = number of train passbys in period  $T$

\*A number of prediction schemes do not use SEL as the basic energy descriptor since SEL will invariably have a higher numerical value than the maximum A-weighted sound pressure level of the train passby and may be confusing to the general public. Alternative options such as  $L_{eq}/h$  are used<sup>1</sup> with the consequent change in  $T$  in Eq. (1), e.g., for 24-h  $L_{eq}$  from SEL,  $T = 86,400$ , for 24-h  $L_{eq}$  from hourly  $L_{eq}$ ,  $T = 24$ .

For a particular receiver position a train service can be considered as a number of repeated noise events ( $N_i$ ) and the summation equation for each train type is simplified to

$$L_{eq_i} = SEL_i + 10 \log_{10} N_i - 10 \log_{10} T \quad (2)$$

where the suffix  $i$  refers to types of trains with identical noise characteristics. Thus

$$L_{eq} = 10 \log_{10} \left[ \sum_{i=1}^m 10^{L_{eq_i}/10} \right] \quad (3)$$

where  $m$  is the number of types of trains.

It is therefore necessary to be able to predict the noise level caused by a single train passby ( $SEL_i$ ) from knowledge of its source characteristics and the propagation from the source to the receiver position.

Figure 1 shows a typical prediction flow diagram where the noise level (SEL in this example) is predicted for all trains on each track and summed over the relevant time period to give total  $L_{eq}$ . From a computational point of view the logic is for source noise to be summated for each track before entering a propagation loop, but this can be varied depending on whether it is important to identify which “train type” gives the highest noise level or the track which contributes most to the overall noise level.

In some prediction models the calculation process is in one-third octave or octave band levels. This does not alter the procedure described below but naturally requires more detailed information for each element of the calculation and a summation stage from frequency data into overall noise level. Each of the elements in the prediction process is summarized in the following sections.

### 3 SOURCE NOISE LEVELS

Three sources are considered:

- Rolling noise
- Power unit noise
- Aerodynamic noise

The first step in the process is to identify the free-field source related noise levels, before taking account of propagation effects. This is normally defined as a

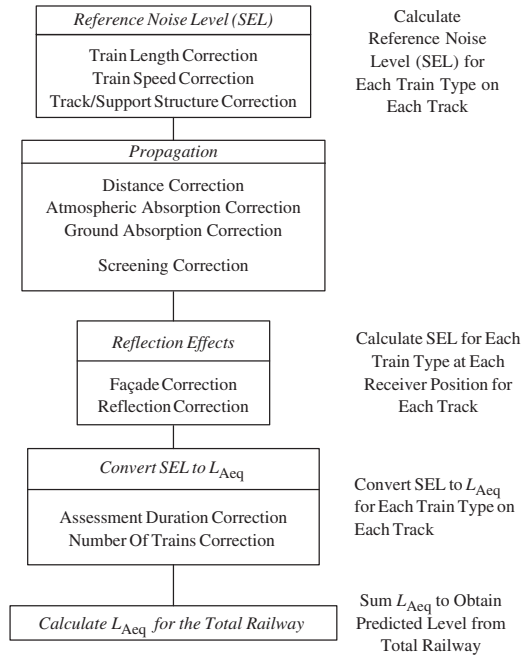


Figure 1 Railway noise prediction flow diagram.

noise level at a close distance from the track with the ground on the same level as the track. Different models use different reference distances, but the choice is not critical and the majority use a distance of 25 m relative to the track. This allows empirical data to be obtained for trains at all speeds without the danger of aerodynamic effects on microphones from high-speed trains.

### 3.1 Rolling Noise

Rolling noise is always present and must be included in any prediction model. Chapter 93 describes the background to rolling noise and identifies the major generation parameters as train speed and wheel–rail roughness.

Figure 2 shows the results of regression analysis of single-vehicle SEL [total SEL –  $10 \log N$  (where  $N$  = number of vehicles in train)] as a function of train speed for a number of passenger trains on continuously welded rail. This clearly demonstrates the difference in noise level between vehicles with cast-iron tread brakes and disk brakes.

The reason for this change in noise level is due to differences in wheel surface roughness produced by the different braking systems (see Chapter 93). The use of cast-iron tread brakes is reducing and has almost been completely replaced on passenger vehicles by disk brakes. Many freight vehicles in Europe are still braked using cast-iron tread brake blocks, but current initiatives involve replacement of these with tread brakes using brake blocks of composite materials. There is evidence to show reduced noise levels from

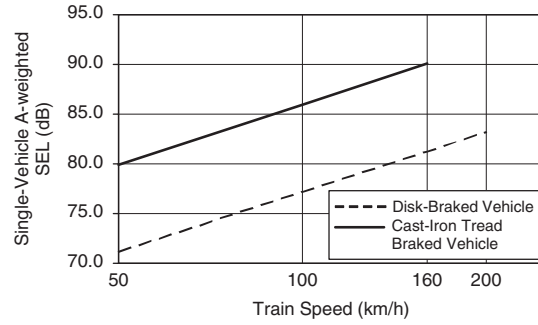


Figure 2 Example result of regression analysis for passenger vehicles.

these vehicles (again because of reduced wheel surface roughness levels) but comprehensive data on wheel roughness and noise levels are lacking, and it is currently believed that the noise characteristics of composition block tread braked trains are the same as disk braked trains. This needs to be confirmed, and it is therefore necessary that for new train designs, empirical data, similar to that shown in Fig. 2, is obtained for input to a prediction scheme to provide further information for “Train type” in Eq. 2.

Following normal convention, a speed function takes the form of

$$L_{Amax} = k \log(V) + C \quad (4)$$

where  $V$  is train speed and  $C$  is a constant; and it is commonly taken that  $k = 30$  can be used without serious loss of accuracy. This value will certainly be used in situations where data were obtained with insufficient speed range to provide a reliable regression analysis.

For a maximum passby noise speed function of  $30 \log(V)$ , it follows that noise energy (SEL) will have a speed function of  $20 \log(V)$ , and most prediction models include a  $20 \log(V)$  speed function for rolling noise SEL as is shown in Fig. 2. The usual modeling of rolling noise is to assume the train to be a line of incoherent dipoles. From this it can be assumed that for a receiver located approximately 25 m from the track, the maximum sound pressure level is independent of train length (for trains longer than say 50 m) since for these close distances the contribution from sources at the extremities of the line is negligible.

The length of the line source is, however, important in determining SEL since for a given train speed, train length will affect the duration of the noise signal. The correction term for train length is

$$10 \log(TL/TL_0) \quad (5)$$

where  $TL$  is train length and subscript 0 refers to an arbitrary reference.



It is more common to assess train length correction by the number of identical vehicles in the train since this information is likely to be a more readily available parameter. Thus it is necessary to provide an equation for SEL for a reference train length and modify this by Eq. (5) for the train in question.

Using the noise level versus speed relationships above, a doubling of speed gives a change in the A-weighted noise level  $L_{Amax}$  of 9 dB and 6 dB in the A-weighted SEL. The difference (at the same speed) in the A-weighted noise level between cast-iron tread-braked passenger vehicles and disk-braked passenger vehicles is about 10 dB in both  $L_{Amax}$  and A-weighted SEL. A train of disk-braked vehicles will therefore need to travel at approximately three times the speed of an identical train of cast-iron tread-braked vehicles to produce the same noise energy. Thus, for accurate prediction it is important to know the train speed and train type, particularly the form of braking utilized.

These reference levels are derived from measurements of the noise from train passbys. It is therefore important to define the measurement conditions that should be used. A number of standards exist, for example, Ref. 2, each with slight differences in detail. There are, however, a number of common features:

- Track to be good quality continuously welded rail, supported by concrete sleepers on ballasted track
- Free-field conditions
- Dry conditions
- Wind speed <5 m/s
- Wind direction from track to receiver

### 3.2 Diesel Locomotive on Power

The noise from a diesel locomotive on full power, and particularly at low speeds (see Chapters 93 and 97), needs to be treated separately from its rolling noise and is considered as an additional noise source. The maximum sound pressure level for this situation is usually independent of train speed, SEL will therefore reduce by  $10 \log(V)$  as speed increases because of the reduced duration of the noise event.

For older generation diesel locomotives, the UK prediction scheme<sup>3</sup> is based on a free-field maximum A-weighted sound pressure level of 90 dB at 25 m from the track. Using the modeling of a locomotive as a point source with cosine directivity gives the following relationship:

$$SEL = L_{Amax} + 10 \log(d/V) + 8.6 \quad (6)$$

where  $d$  is distance from track (m) and  $V$  train speed (km/h).

For the reference conditions of  $d = 25$  m, this becomes

$$SEL_0 = 112.6 - 10 \log(V) \quad (7)$$

In carrying out noise predictions it is therefore necessary to identify those locations where diesel locomotives will be regularly on power. Reference 4 suggests two

common situations as (a) a train accelerating with a heavy trailing load and (b) a train traversing an uphill gradient. One useful addition to a noise prediction suite would be to link the source noise data with train performance data. This would automatically give train speed by geographic location and identify those areas where the locomotive was generally on power.

### 3.3 Aerodynamic Noise

Classical aerodynamic noise is generated from fluctuations in the turbulent boundary layer, from flow over sharp edges and protuberances, cavities, and the wake. For trains the main sources have been identified as the leading bogie area and the pantograph.<sup>5</sup> Aerodynamic noise generation is dealt with in Chapters 9, 87, and 88.

As train speeds increase, there is the possibility that this source may become significant. The major problem, if it does occur, is that it will have a speed function approaching  $V^8$ , which is in excess of the other sources associated with train noise. Thus once aerodynamic noise becomes a major contributory noise source in a design, any attempt to increase speed without changing that design will give rise to higher noise levels than expected.

The speed at which aerodynamic noise becomes significant depends on a number of design factors, and it is not usually an issue for train speeds below 200 km/h. In Japan it can be the most important noise source at speeds in excess of 270 km/h.<sup>6</sup>

Aerodynamic noise may become significant at lower speeds when lineside noise barriers are used. If the aerodynamic A-weighted noise level is within say 10 dB of the total rolling noise level, because its source will be well above rail level, the barrier will attenuate that noise less than rolling noise. Then predictions using standard barrier formulas may overestimate that barrier's effectiveness because the barrier equation is likely to have been developed in the absence of aerodynamic noise.

Aerodynamic noise can be predicted from first principles, but it is more likely that total train noise will be measured to high speeds giving relationships similar to that shown in Fig. 2 but with a change in function of speed at the higher speeds.

## 4 PROPAGATION OF TRAIN NOISE

It is normal for the railway to be modeled as a series of straight-line segments, and the propagation of noise reflects this modeling.\* It is possible to derive an empirical relationship from measurements, but the final prediction will more than likely have to take into account the fact that some of the segments are of finite length. For this it is necessary to quantify the component parts that comprise total attenuation.

The prediction can be defined by the following equation:

$$L = L_0 - \Delta_{geo} - \Delta_{air} - \Delta_{grnd} - \Delta_{screen} + \Delta_{refl} \quad (8)$$

\*A segment is defined as the length of track over which the noise source and propagation characteristics are constant. Thus determination of segment extremities will consider train speed, train numbers, and propagation features, particularly the location of barriers to free propagation.

where  $L$  = noise level at the receiver

$L_0$  = train specific reference noise level for actual conditions of train and track (Section 2)

$\Delta_{\text{geo}}$  = attenuation due to geometric spreading

$\Delta_{\text{air}}$  = atmospheric absorption correction

$\Delta_{\text{grnd}}$  = ground absorption correction

$\Delta_{\text{screen}}$  = attenuation such as track in cutting, lineside noise barriers or housing development

$\Delta_{\text{refl}}$  = reflection corrections, including the effect of the facade

#### 4.1 Geometric Attenuation $\Delta_{\text{geo}}$

The geometric decay of noise energy (SEL) from a source of constant sound power, moving on an infinite straight line at uniform speed, can be shown to be

$$\Delta_{\text{geo}} = 10 \log(d/d_0)$$

where  $d$  = receiver distance

$d_0$  = reference distance

and distance is measured along a line normal to the straight-line trajectory of the source.

This relationship is valid for line and point sources and is independent of source directivity. Where the movement is over a finite path length, an angle of view correction is required. This is a function of source directivity, segment length, and distance between source and receiver.

#### 4.2 Air Attenuation $\Delta_{\text{air}}$

Sound propagation over relatively short distances in air involves slight losses that are frequency, temperature, and humidity dependent. Since the vehicle reference noise levels will have been obtained from measurement, with air attenuation, this correction will be zero at the reference distance. A linear function is normally taken with A-weighted attenuation values ranging from 0.5 dB to 1 dB per 100 m and each prediction model will have reviewed available data to include a value for air attenuation that is consistent with the way the propagation model has been defined.

The air absorption correction is not usually applied to the engine-generated noise from a diesel locomotive on full power because of its low-frequency content.

#### 4.3 Ground Attenuation $\Delta_{\text{grnd}}$

Two variables, distance from the track and mean propagation path height above ground level, are taken into account with the ground generally considered as either soft (to represent flat grassland) or hard (to represent concrete or water). As the height of the propagation path above the ground increases, the absorption of the propagating wave by that ground reduces, and for a mean path height greater than about 6 m it is often assumed to be zero.

Here again the location of the assumed source needs to be defined, and for diesel power noise, with the source taken to be 4 m above the rail level, the ground is predicted to have less influence on the received noise

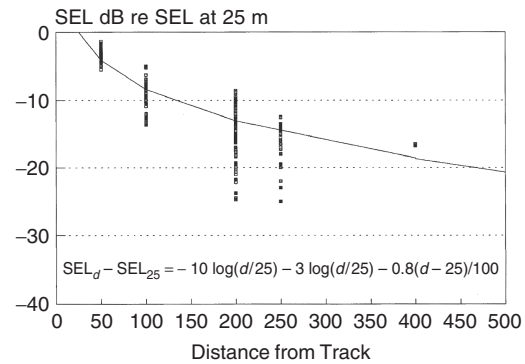


Figure 3 Decay of SEL with distance. (From Ref. 3.)

level. The maximum effect of the ground in Ref. 3 is taken as  $3 \log(d/25)$  for a mean path height less than 1 m. This decreases linearly to zero at a mean path height of 6 m. Thus at a distance of 300 m from the railway the maximum A-weighted ground attenuation will be slightly in excess of 3 dB.

Figure 3 compares the predicted effect of combining the above attenuation terms in Ref. 3 with measured data. This figure is derived from the difference in noise level between simultaneous measurements taken at the reference distance (in this case 25 m from the track) and the quoted distance for the same train. It indicates a reasonable fit and also shows the increased variability of noise as distance from the track increases even in the situation of only accepting data for low wind speeds (<5 m/s) in the direction from track to receiver. In this example the range in the A-weighted noise level measurements at 200 m from the track is in excess of 15 dB, indicating the difficulty in comparing the results obtained from a single measurement with predictions from a model aimed at determining an average noise level.

Traditionally, noise prediction models have aimed at predicting the *average worst case*, which was taken to be the situation with the wind in the direction from the source to receiver. The European Commission's Environmental Noise Directive<sup>7</sup> requires noise levels to be predicted in terms of  $L_{\text{den}}$  where the constituent parts ( $L_{\text{day}}$ ,  $L_{\text{evening}}$ , and  $L_{\text{night}}$ ) are the "A-weighted long term average sound pressure levels as defined in ISO 1996-2:1987, determined over all the day/evening/night periods of a year, . . . a year is a relevant year as regards the emission of sound and an average year as regards the meteorological circumstances."<sup>7</sup> This implies a need for assessing local meteorological conditions over a year period and including in the propagation model the effects of different meteorological conditions.

#### 4.4 Screening Attenuation $\Delta_{\text{screen}}$

Obstacles to free propagation occur in the form of railways in cuttings, the shoulders of embankments, solid station platforms, purpose-built noise barriers, or building development adjacent to the track. As with most other data that is used in the prediction model, the results for screening attenuation are generally

empirical. Discussion of the principles of attenuation from barriers is presented in Chapters 58 and 122.

It is common practice when assessing the performance of noise barriers to use the higher of the predicted barrier effect and ground attenuation. This has to be recognized when deriving a performance relationship from measured data. A number of screening algorithms can be found in the literature, but it is important to remember that a barrier prediction curve is only valid for the quoted source location, and the only way of comparing prediction equations with different source positions is to carry out predictions for specific source-barrier-receiver geometries.

Barrier design is also important in determining its effectiveness. It is likely that barriers will be built as close as 3 m to the rail (safety and track maintenance limitation will restrict the use of closer barriers), and this means that the effect of a reflected wave between the side of the rail vehicle and the barrier can be an influencing factor.<sup>8</sup> Barrier equations that attempt to quantify this effect are given in Ref. 3, which proposes a two-stage prediction for reflective barriers.

$$\Delta_{\text{barrier}} = \Delta_1 - \Delta_2$$

where  $\Delta_1$  = performance of an absorptive barrier and grass sided cuttings

$\Delta_2$  = reflective barrier correction

The following relationship is given for absorptive barriers:

$$\Delta_1 = 7.75 \log(5.2 + 203\delta) \quad \text{for } 0 < \delta < 2.5 \text{ m} \\ = 21 \quad \text{for } \delta > 2.5 \text{ m}$$

where  $\delta$  is the path difference (m) determined for a source at the head of the rail.

$$\Delta_2 = 0 \quad \text{for } D > 20 \text{ m} \\ = 5 - 0.25D \quad \text{for } 1 \text{ m} < D < 20 \text{ m} \\ = 4.8 \quad \text{for } D < 1 \text{ m}$$

where  $D$  is the distance between the relevant near rail and the barrier.

Housing development can also be a source of additional attenuation. These can be treated as a composite barrier.<sup>3</sup> Alternatively, some simple rules of thumb have been reported in Ref. 4 where an A-weighted noise level reduction of 8 dB is quoted for a row of semidetached houses. Subsequent rows provide an additional 4-dB reduction in noise level for each row.

High development near a railway line obviously provides shielding to other development behind it but creates other problems in that high stories overlook the railway and are difficult to shield with lineside barriers. Also in situations where such development is on both sides of the track, multiple reflections can give rise to problems.

#### 4.5 Reflection Correction $\Delta_{\text{refl}}$

Certain legislation requires prediction of the noise level at, or immediately in front of, the facade of a property.

This requires an additional correction due to the presence of the facade. Most models include a +3-dB correction relative to the free-field A-weighted noise level.

## 5 MODIFICATION TO REFERENCE NOISE LEVELS

The reference situation is a train operating on continuously welded rails supported by concrete sleepers on ballast. A number of variations to that reference situation are in use and their effect, which should be included in the reference noise level term, is discussed below.

### 5.1 Jointed Track

As the wheels traverse a joint, there will be an increase in noise level. The maximum passby A-weighted sound pressure level, when close to the track, will increase by approximately 5 dB. Since the noise profile will now consist of a number of "spikes," the effect will be less for A-weighted SEL, and an increase of about 2 dB is more appropriate. These increases can also apply in close proximity to switches and crossings. Jointed track will have no effect on the power unit noise from a diesel locomotive.

### 5.2 Wooden Sleepers

The effect of wooden sleepers appears to be within the variability of measured noise levels for supposedly identical conditions. No further corrections should be made for either rolling noise or diesel locomotive power noise.

### 5.3 Slab Track

This is an alternative track design where the ballast is replaced by a concrete slab to form the track foundation. It is not in common use on surface railways, but measurements have indicated an increase in A-weighted noise level relative to the reference condition of between 2 dB and 10 dB for rolling noise.

### 5.4 Elevated Structures

No change to the reference A-weighted noise level is required for a train on an embankment. Any change in received noise level compared to the flat site situation is a consequence of reduced attenuation by the ground. Surveys of concrete and steel structures have concluded that steel structures tend to be noisier than concrete structures, and the worst situation is for a steel structure with the track fastened directly to it, that is, there is no ballast. In this situation an enhancement in A-weighted noise level of up to 16 dB is possible relative to the reference situation. Where a concrete structure is used, direct fixation can give increases of up to 10 dB, but when the design includes ballasted track and a solid parapet (to act as a barrier) that increase may only be of the order of 1 dB. The addition to the A-weighted noise level results from the supporting structure acting as a secondary sound source.

## 6 RAIL SYSTEM NOISE ASSESSMENT

### 6.1 European Practice

A recent study,<sup>9</sup> funded by the European Commission, reviewed European national railway noise legislation and indicated an almost common use of external  $L_{\text{Aeq}}$

for assessing environmental noise from railways. Three Nordic countries use a 24-h value plus  $L_{Amax}$ , and the Nordic railway noise prediction model has been developed to predict both of these metrics.<sup>10</sup> The Netherlands uses a three-time-period (day, evening, night) assessment criteria and other countries use criteria based on a day–night split. It is common for those countries with railway noise legislation to have national railway noise prediction models. This is certainly the case for the United Kingdom, France, the Netherlands, Germany, and Switzerland.

The legislative limits *are not used* to determine a maximum level that must not be exceeded but are usually part of national noise insulation regulations for new infrastructure schemes where limits are set that, when exceeded at residential property adjacent to the railway, means that the property is eligible for additional sound insulation.

Each country has different limit values in its legislation, and where separate time periods are used these also differ from country to country. In order to obtain reliable statistics on noise exposure from transport in Europe an Environmental Noise Directive<sup>7</sup> requires mapping to be carried out in terms of the day–evening–night noise level  $L_{den}$ . No European country uses  $L_{den}$  as part of national legislation, therefore all member states will be required to introduce new prediction methodology to fulfill the requirements of the new European legislation.

European Union projects HARMONOISE<sup>11</sup> and IMAGINE<sup>12</sup> have been initiated to develop harmonized models for road, rail, and industrial noise. It is expected that models from these projects will eventually replace national models in preparation of the necessary maps.

## 6.2 Practice Elsewhere

In the United States noise impact estimates are made using either Federal Transit Administration (FTA) or American Public Transit Association (APTA) criteria. FTA criteria<sup>13</sup> are based on absolute  $L_{eq}$  values, whereas APTA guidelines<sup>14</sup> are written in terms of maximum passby A-weighted sound pressure level. Prediction models have been developed in Japan for the Shinkansen lines considering lower car parts, concrete bridge structures, and aerodynamic noise from the upper car and pantograph as separate noise sources.<sup>15</sup> It is common in Australia to assess railway noise in terms of both  $L_{eq}$  and  $L_{max}$ . The Nordic prediction model is used in these cases. More details on assessment criteria and legislative limits can be found in Chapters 25 and 34.

## 7 RAIL SYSTEM NOISE CONTROL OPTIONS

### 7.1 Noise Control at Source

Although received noise level ( $L_{eq}$ ) is dependent on number of trains, train speed, train length, and distance from the track, its change is not particularly sensitive to these parameters, especially when the considerations of a commercially competitive operating railway have to be taken into account. Effective noise control can

only be achieved by reducing the noise at source or by use of barriers to noise propagation.

Rolling noise, the main contributor to rail system noise, is the sum of wheel-radiated noise and track-radiated noise. The balance between these sources, given in the equation below, varies with detailed design of wheel and track and operating conditions:

$$L_{TOT} = 10 \log(10^{L_{WHEEL/10}} + 10^{L_{TRACK/10}})$$

where  $L_{TOT}$  = total rolling noise

$L_{WHEEL}$  = wheel-radiated noise

$L_{TRACK}$  = track-radiated noise

This relationship is important when considering the control of the A-weighted noise level. If

$$L_{WHEEL} - L_{TRACK} \geq 10 \text{ dB},$$

track treatments in isolation will be ineffective. If

$$L_{TRACK} - L_{WHEEL} \geq 10 \text{ dB},$$

wheel treatments in isolation will be ineffective.

The flowchart for rolling noise generation, discussed in Chapter 93, identifies areas where measures can be applied to reduce either both wheel and track noise (reduction of force in contact zone/increase propagation losses) or wheel and track noise separately by using low noise components in wheel and track designs. Chapter 93 has given an overview of noise mitigation options and these are summarized below.

**7.1.1 Smooth Wheels** Smooth wheels and rails can reduce both the wheel and track components of rolling noise. Wheel roughness is controlled by the type of braking used, and for some years the use of disk brakes on passenger vehicles has shown a reduction in A-weighted noise level of about 8 dB when compared to the noise from cast-iron tread braked vehicles at the same speed.

Brakes made of composite materials can give noise characteristics similar to disk-braked wheels on passenger vehicles, although because of higher wheel temperatures during braking, leading to higher residual stresses, wheel cross-section optimization will not be an option.

The general trend on mainland Europe is to use cast-iron tread brakes on freight vehicles; thus the wheels are considered to be “rough” and the vehicles “noisy.” An initiative currently being undertaken by the Union of International Railways (UIC) aims to replace those cast-iron brake blocks with ones made of composite materials.

The development of direct replacement composite brake blocks is the subject of a current EU 5th Framework Project.

Current knowledge is such that reduction of wheel roughness levels below those found on disk-braked wheels will not be achievable in the short to medium term. Therefore, where a vehicle design currently includes disk or composite brake blocks, any noise

benefit from a further reduction of wheel roughness should not be expected.

It should further be pointed out that where cast-iron tread brakes are used, the service roughness levels are achieved quickly and smoother surfaces to disk-braked wheel roughness levels are not achievable even through maintenance no matter how frequent.

**7.1.2 Smooth Rails** Smooth rails are essential for a low-noise railway, and the formation of corrugations can increase rolling A-weighted noise levels from disk-braked stock by up to 20 dB. There are no validated models for rail roughness growth, and rail roughness is usually controlled through maintenance by grinding. Rail roughness has to be higher than wheel roughness before noise reduction will result from grinding, and this is certainly the case with corrugated rail.

**7.1.3 Low-Noise Wheels** One of the objectives of the Silent Freight Project<sup>16</sup> (EU 4th Framework Brite Euram Project BE95-1238) was to develop cost-effective low-noise wheel designs. Options considered were:

- Optimization of the cross section to minimize axial response due to radial forces
- Reduction of wheel diameter
- Additional damping
- Screening of the web

The Silent Freight Project showed that when compared to the noise produced by a standard ORE/UIC 920-mm-diameter wheel, reductions in wheel-radiated A-weighted noise levels of about 7 dB (860-mm-diameter shape optimized wheel with tuned absorbers) and 9 dB (860-mm-diameter shape optimized wheel with shields on the web) could be obtained.

**7.1.4 Low-Noise Tracks** A parallel project Silent Track<sup>17</sup> (EU 4th Framework Brite Euram Project BE96-3017) developed a number of low-noise track designs incorporating:

- Use of stiff rail pads
- Rail-tuned absorbers
- Reduction of rail foot width
- Optimized sleeper

The Silent Track Project showed that compared to a track with standard soft rail pads a reduction in track-radiated A-weighted noise level of between 5 dB and 6 dB could be obtained from the use of tuned absorbers on the rail.

Because of the need to reduce dynamic fatigue loads in sleepers and track support structures, softer rail pads are becoming more common. Softer rail pads also limit rail roughness growth and are thus beneficial from that point of view. The desire for high rail pad stiffness for noise reasons is therefore in conflict with track fatigue requirements. Interestingly the absolute noise level when using tuned rail absorbers is virtually independent of the rail pad stiffness.

## 7.2 Bogie Shrouds and Low Trackside Barriers

As discussed in Chapter 93, where it is possible to achieve an overlap of the bottom of the shroud and top of the barrier, an A-weighted noise level reduction of up to 10 dB can be achieved.<sup>18</sup>

In a study as part of Silent Freight<sup>16</sup> and Silent Track,<sup>17</sup> where an overlap was not possible due to international gauging restrictions, this A-weighted noise level reduction was limited to 3 dB to 5 dB.

These forms of treatment can be effective, but there are a number of maintenance and inspection issues that need to be overcome before they can be implemented.

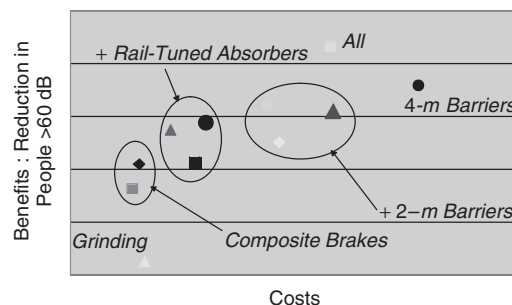
## 7.3 Noise Barriers

Section 3.4 of this chapter has indicated how the effectiveness of noise barriers can be incorporated into a noise prediction model. For a barrier to be effective, the receiver needs to be in the shadow zone, that is, below the straight line drawn from the source position through the top of the barrier.

Measurements indicate a maximum A-weighted noise level reduction for a plain vertical reflective barrier to be in the region of 15 dB, although this requires the barrier to have a height of 3 m more than the source. That benefit can be increased by about 5 dB with sound-absorbing material in the side of the barrier facing the railway. The European Rail Research Institute carried out a review of noise barrier design<sup>19</sup> and concluded that this was the most effective way of increasing the noise reduction of a plain vertical reflective barrier. At that time other changes to barrier design offered little effective benefit.

## 7.4 Cost-Effective Noise Mitigation

A software tool has been developed in the STAIRRS project (strategies and tools to assess and implement noise reducing measures for rail systems), which was funded through the EU's 5th Framework Competitive and Sustainable Growth Programme. Figure 4, taken from the final report,<sup>20</sup> shows a relative comparison of cost and effectiveness for a number of mitigation options when applied to the European network. This shows that noise reduction at source, as discussed above, can be more effective and less costly than



**Figure 4** Cost-effectiveness analysis of noise reduction options. (From Ref. 20.)

an option consisting of high barriers alone. Thus, it will be worthwhile to invest more time and effort into developing noise reduction at source to give designers more options in implementing low-noise railway systems.

## REFERENCES

1. Richtlinie zur Berechnung der Schallimmissionen von Schienenwagen, Schall 03 (Guidelines for the Calculation of Railway Noise Emission), Deutsche Bahn, Munich, 1990.
2. Draft prEN ISO 3095, Rail Application—Acoustics—Measurement of Noise Emitted by Railbound Vehicles (ISO/DIS 3095 2001), January 2001.
3. UK Department of Transport, *Calculation of Railway Noise 1995*, HMSO, London, 1995.
4. P. Nelson, Ed. *Transportation Noise Reference Book*, Butterworths, London, 1987, Chapter 15.
5. C. Talotte, P.-E. Gautier, D. J. Thompson, and C. Hanson, Identification, Modelling and Reduction Potential of Railway Noise Sources: A Critical Survey, *J. Sound Vib.*, Vol. 267, Issue 3, 23 Oct. 2003, pp. 447–468.
6. K. Nagakura, Localisation of Aerodynamic Sources of Shinkansen Trains, Paper to Eighth International Workshop on Railway Noise, Buxton, England, September 2004.
7. *Directive 2002/49/EC of the European Parliament and of the Council of 25 June 2003*, Relating to the Assessment and Management of Environmental Noise, Official Journal of the European Communities, Brussels, 2002.
8. B. Hemsworth and V. Webb, Noise Barriers for Fast Passenger Trains, *Proceedings of Internoise*, Zurich, 1977.
9. U. Danneskiold-Samsøe and U. Degn, A Study of European Priorities and Strategies for Railway Noise Abatement, Main Report, Report 01.980, Copenhagen, 2001.
10. M. Ringheim and H. L. Nielsen, *Railway Traffic Noise—Nordic Prediction Method*, Tema Nord 1996:524, Nordic Council of Ministers, Copenhagen, 1996.
11. HARMONOISE, EU 5th Framework IST Project, Harmonised Accurate and Reliable Methods for the EU Directive on the Assessment and Management of Environmental Noise IST-2000-28419, Brussels, 2001.
12. IMAGINE, EU 6th Framework Project, Improved Methods for the Assessment of the Generic Impact of Noise in the Environment, SSPI-CT-2003-503549, Brussels, 2003.
13. Federal Transit Administration (FTA), Transit Noise and Vibration Impact Assessment, U.S. Department of Transportation Report No. DOT-T-95-15, April 1995.
14. American Public Transit Association (APTA), 1981 Guidelines for Design of Rail Transit Facilities, Section 2–7, *Noise and Vibration*, 1979.
15. K. Nagakura and Y. Zenda, Prediction Model of Wayside Noise Level of Shinkansen, RTRI Report, September 2000.
16. B. Hemsworth (ERRI) and R. R. K. Jones (AEA Technology Rail Ltd), Silent Freight Project—Final Report, Report No. 5E0U15T1.DB, Dec. 2000.
17. B. Hemsworth (ERRI), Silent Track Project—Final Report, Report No. 00615/7/ERRI/T/A, Dec. 2000.
18. R. R. K. Jones (AEA Technology Rail Ltd), Railway Noise Control Using Combined Vehicle and Track Treatments, World Congress on Railway Noise Research, Paris, 1994.
19. P. de Vos, R. R. K. Jones, J. Colard, and P. van Tol, Railway Noise Barriers, State of the Art of Railway Noise Barriers in Europe, Report ERRI C163/RP20, Utrecht, July 1997.
20. B. Hemsworth (ERRI), STAIRRS Project—Final Technical Report, Report No. STR40TR181203ERRI, Dec. 2003.

# CHAPTER 122

## NOISE ATTENUATION PROVIDED BY ROAD AND RAIL BARRIERS, EARTH BERMS, BUILDINGS, AND VEGETATION

**Kirill Horoshenkov**

School of Engineering, Design and Technology  
University of Bradford  
Bradford, West Yorkshire, United Kingdom

**Yiu W. Lam**

Acoustics Research Centre  
School of Computing, Science and Engineering  
University of Salford  
Greater Manchester, United Kingdom

**Keith Attenborough**

Department of Engineering  
The University of Hull  
Hull, United Kingdom

### 1 INTRODUCTION

Noise barriers have become a very common feature of urban landscapes. For example, in the United States over 1200 miles of noise barriers were constructed in the year 2001 alone. Any form of solid obstacle between source and receiver can comprise a noise barrier. A barrier can reduce the noise in residential areas if it is well designed. Barriers should be impervious to sound without cracks or holes and of sufficient height to provide sufficient noise attenuation. Barriers are most effective if placed near to the source of noise or the receiver and are generally ineffective for low-frequency noise. In some instances, sound-absorbing material is placed on or in the source side of the barrier to reduce noise buildup there. The majority of barriers are installed in the vicinity of transportation and industrial noise sources to shield nearby residential properties. Unlike building insulation, noise barriers are designed to protect the external as well as the internal environment at a dwelling. Noise barriers are cost effective only for the protection of large areas including several buildings and are rarely used for the protection of individual properties. Noise barriers of usual height are generally ineffective in protecting the upper levels of multistory dwellings.

### 2 NOISE BARRIER PERFORMANCE INDICES

In the past two decades environmental noise barriers have become the subject of extensive studies, the results of which have been consolidated in the form of national and international standards and prediction models.<sup>1-5</sup> Some unresolved problems still remain, and these mainly relate to the degradation of the noise

barrier performance in the presence of wind and temperature gradients, atmospheric turbulence, temporal effects from moving traffic, vehicle composition and speed, aesthetic quality of barriers, and their environmental impact.<sup>6</sup> An extensive guide to the acoustical and visual design of noise barriers can be found in some textbooks and design manuals.<sup>7,8</sup>

The performance of a barrier in shielding a receiver from a noise source can be described by the term *barrier attenuation* (Att), which is defined by

$$\text{Att} = -10 \log_{10} \left( \frac{|p_{\text{bo}}|^2}{|p_{\text{ff}}|^2} \right) \text{ dB} \quad (1)$$

where  $p_{\text{ff}}$  is the sound pressure in free field at the receiver, and  $p_{\text{bo}}$  is the sound pressure in the presence of the infinite barrier in a semiinfinite configuration, that is, when there is no ground and the lateral length of the barrier is infinite. Therefore Att gives the most basic performance of a barrier in blocking the direct sound from reaching the receiver and is useful when comparing the performance of different barriers without the complications of influences from other propagation effects. The use of the negative sign in the right-hand side of the equation is based on the convention that a reduction in sound pressure level is defined as a positive attenuation.

Usually a barrier is placed on ground and is of finite length. Hence, a more practical performance index is the *excess attenuation* (EA):

$$\text{EA} = -10 \log_{10} \left( \frac{|p_b|^2}{|p_{\text{ff}}|^2} \right) \text{ dB} \quad (2)$$

where  $p_b$  is now the sound pressure at the receiver with the barrier in its actual configuration—erected above ground and of finite length.

The use of the free-field sound pressure  $p_{ff}$  as the reference in Att and EA is convenient for theoretical calculations. In practice, it is sometimes difficult to determine the free-field sound pressure. A more direct way of describing the performance of a barrier is to measure the reduction of the sound pressure level before and after the erection of the barrier. This is known as the *insertion loss* (IL):

$$IL = -10 \log_{10} \left( \frac{|p_b|^2}{|p_{w/o}|^2} \right) \quad \text{dB} \quad (3)$$

In this case the reference sound pressure  $p_{w/o}$  is the sound pressure at the receiver before the barrier is built. Usually, this includes the ground effect (see Chapter 5) and can be predicted using the models detailed in Chapter 58. IL is therefore a direct indicator of the actual benefit that a barrier could bring to a receiver in a specific site. Where there is no ground effect and the barrier is of infinite length, IL is equal to Att.

The above three indices are the preferred indices for barrier performance because they are consistent with indices used in other areas of acoustics. There are other terms that have also been used to describe barrier performance. Two common ones are *noise reduction* (NR) and *transmission loss* (TL). The noise reduction of a barrier is defined in a similar way to IL, but since the term is used also in building acoustics to describe the sound pressure level reduction provided by a partition between two rooms the use of noise reduction could cause confusion. The definition of transmission loss of a barrier can be even more confusing, since TL is used both in building acoustics to describe the reduction in sound intensity level through a partition made of particular materials, and also in outdoor sound propagation as the attenuation relative to the sound pressure at a reference position (usually 1 m) from the source. Hence the recommendation is to use Att, EA, and IL to describe barrier performance.

In 1996, the International Organization for Standardization (ISO) published ISO 9613-2<sup>1</sup> that describes a general method of calculation of attenuation of sound during propagation outdoors. This standard has been adopted widely for practical predictions of the noise barrier insertion loss using a modified form of the empirical formula:

$$IL = 10 \log_{10} \left[ 3 + \left( C_2 \frac{\delta_1}{\lambda} \right) C_3 K_{\text{met}} \right] \quad (4)$$

where  $C_2 = 20$  and includes the effect of ground reflections;  $C_2 = 40$  if ground reflections are taken into account elsewhere.  $C_3$  is a factor to take into account of a double diffraction or finite barrier effect,  $C_3 = 1$

for a single diffraction,  $\delta_1 = (r_s + r_r) - r_0$ , and

$$C_3 = \frac{\left[ 1 + \left( \frac{5\lambda}{w} \right)^2 \right]}{\left[ \frac{1}{3} + \left( \frac{5\lambda}{w} \right)^2 \right]}$$

for double diffractions,  $\delta_1 = (r_s + r_r + w) - r_0$ . In these expressions  $r_0$  is the direct distance from the source to the receiver in the absence of the barrier,  $r_s$  is the distance from the source to the top barrier edge,  $r_r$  is the distance from the top barrier edge to the receiver,  $w$  is the width of the barrier, and  $\lambda$  is the acoustic wavelength. The term  $K_{\text{met}}$  in Eq. (4) is a correction factor for average downwind meteorological effects, and is given by

$$K_{\text{met}} = \exp - \frac{1}{2000} \sqrt{\frac{r_s r_r r_0}{2\delta_1}} \quad \text{for } \delta_1 > 0$$

$$= 1 \quad \text{for } \delta_1 \leq 0$$

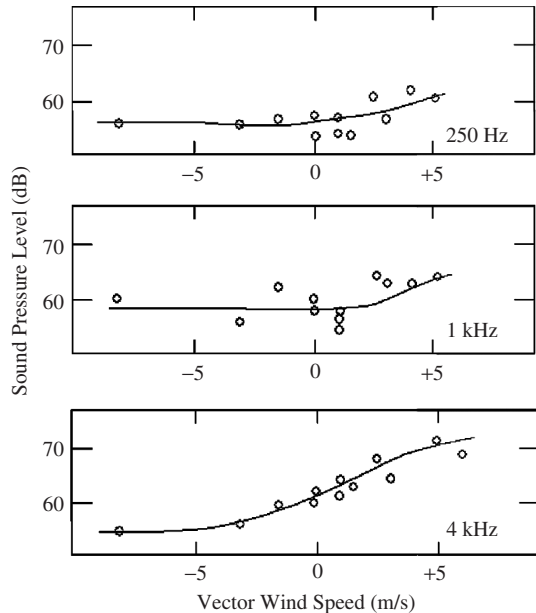
It can be seen that the formula reduces to the simple formula  $IL = 10 \log_{10}(3 + 20N_1)$  when the barrier is thin, there is no ground, and when meteorological effects are ignored. This formula is identical to that suggested by Tatge<sup>9</sup> and depends only on the Fresnel number,  $N_1 = 2\delta_1/\lambda$ , in which the path difference is  $\delta_1 = (r_s + r_r) - r_0$ .

### 3 ATMOSPHERIC EFFECTS ON NOISE BARRIER PERFORMANCE

The analytical and empirical formulas for barrier attenuation, which are presented in Chapter 58, are mostly derived from theoretical considerations or scale-model experimental data of edge diffraction under laboratory conditions. When barriers are used in the field, they are inevitably affected by the presence of ground and the meteorological condition of the atmosphere. Atmospheric turbulence, for example, can scatter substantial amount of sound energy into the shadow zone of a barrier. Generally, the field performance of a barrier is lower than predicted particularly at receivers where the predicted attenuation is high. In most standard calculation methods the barrier attenuation is limited to 20 dB for a single barrier and 25 dB for a double barrier.

The effect of ground on barrier insertion loss can be included by the methods introduced in Chapter 5. The effect of the meteorology is more difficult to account for, partly because of the complex theory involved but also because of the lack of detailed and rigorous enough meteorological data for the study. In most field studies, only simple meteorological data such as wind speed, direction, and temperature have been logged at a single position, and details of the position-dependent sound speed profile and turbulence structure were not determined. Scholes et al.<sup>10</sup> measured the effect of a full-size noise barrier under different weather



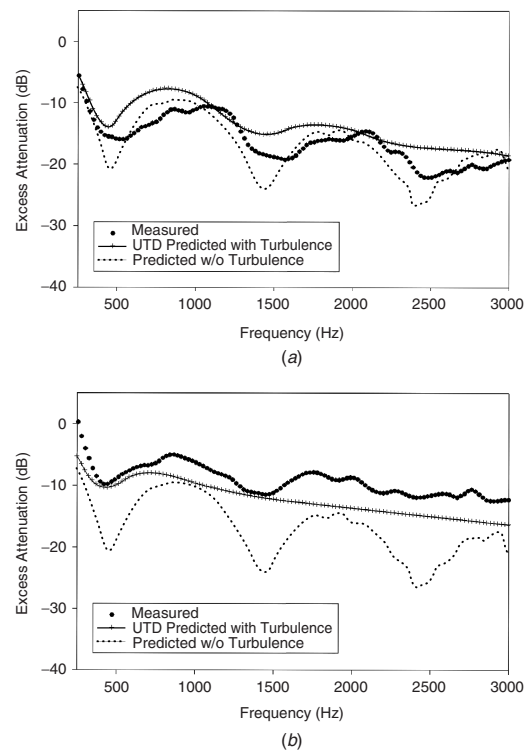


**Figure 1** Variation of sound pressure level behind a barrier in the field. (From Scholes et al.<sup>10</sup>)

conditions for the source height of 0.7 m. Although the meteorological data recorded was not sufficient to make the findings conclusive, the possible changes in field performance can still be seen when the measured sound pressure level behind the barrier was plotted against the recorded vector wind speed, as shown in Fig. 1. More than 15-dB variation can be seen at 4 kHz within a range of  $\pm 5$  m/s vector wind speed.

It should be noted that there are two influences of meteorological conditions on barrier attenuation. The first results from the refraction of the diffraction path due to the vertical sound speed gradient. If the gradient is positive, that is, sound speed increases with height, then the sound path will be refracted downward and the result is an effective reduction of the diffraction angle, and a corresponding reduction in the barrier attenuation. A simple empirical estimate of the effect of typical downward refraction condition is provided by the  $K_{\text{met}}$  factor, which is independent of frequency, in barrier attenuation formula (4).

The second influence is the scattering of the sound energy by atmospheric turbulence, such that higher level of sound energy penetrates the shadow zone than would be from diffraction alone. Both the sound speed profile and the atmospheric turbulence are dependent on the atmospheric temperature and wind. With typical sound speed profiles encountered outdoors, the refraction effect is generally small at a short range from the barrier. For example, with a 3-m high barrier, a source-to-barrier distance of 10 m, and a receiver-to-barrier distance of 100 m, the  $K_{\text{met}}$  correction gives a reduction of barrier attenuation of less than 1 dB. The atmospheric turbulence scattering



**Figure 2** Measure and predicted excess attenuation at a receiver 18 m from 2.44 m wide, 2.55 m high barrier showing the effect of atmospheric turbulence. Source is 8 m from barrier.

is, on the other hand, highly significant especially deep in the shadow zone where the diffracted energy is weak. Figure 2 shows the time-averaged excess attenuation EA (dB), taken from Forssén and Ögren, measured on a 2.44-m wide, 2.55-m high barrier under light turbulence (light wind, about 1 to 3 m/s) and strong turbulence (strong wind, about 4 to 7 m/s) conditions. The source is 8 m from one side of the barrier and 2.9 cm above ground. The receiver location chosen is 18 m on the other side of the barrier and 1.25 m above ground. The turbulence effect was predicted by means of a secondary source model.<sup>11</sup>

It can be seen clearly that the effect of turbulence is strongest at receivers where the attenuation is highest. Generally, the reduction in attenuation due to turbulence is stronger deeper into the shadow zone at higher frequencies and at longer ranges. Furthermore, with strong turbulence (wind 4 to 7 m/s), a reduction of more than 5 dB at a receiver 18 m away can be seen in the attenuation even at places where the no-turbulence attenuation is low. It should be noted that Fig. 2 shows the time-averaged values. Scattering by turbulence can produce large random variations of sound pressure level with time. Unfortunately, there is no reliable simple formula that can be used to estimate

the effect of turbulence on barrier attenuation. It should also be noted that although atmospheric turbulence is dependent on wind, it is equally dependent on temperature fluctuations in the atmosphere. Strong turbulence can still be found under no-wind situations because of large thermal buoyant instabilities. Hence measuring wind speed itself is not sufficient to fully characterise atmospheric turbulence.

The influence of uncertainties in ground characteristics and meteorological conditions can explain why, generally, the field performance of barriers, especially those with complex shapes, is found to be lower than predicted. For example, Watts<sup>12</sup> conducted an extensive field trial of a multiedge noise barrier at three motorway sites in the United Kingdom. Watts found that the improvement provided by the multiedge barrier in the field over a conventional thin barrier of the same height was close to that predicted when the A-weighted barrier attenuation is less than about 12 dB. The improvement in the field, however, was found to be insignificant for greater values of attenuation in contrast to the continuous improvement predicted by theory. More recent experiments by Watts<sup>13</sup> have demonstrated that  $\pm 2$ -m/s fluctuations in the wind velocity can result in 5 to 7 dB degradation in the spectral values of the insertion loss of a noise barrier for frequencies above 1000 Hz. In this work a source and receiver were installed on the opposite sides and 1.0 m away from the top of a 2.0-m T-shaped reflective noise barrier and the sound pressure levels and the wind speed were recorded for a period of time.

It is clear that the study of barriers, especially those with high performance, should also consider elements of outdoor sound propagation, including the barrier effects on the wind velocity profile, to obtain a reliable estimate of the performance of a barrier in the field.

#### 4 NOMOGRAMS AND COMPUTER PROGRAMS

The physical principles related to the diffraction of the sound by a noise barrier, discussed in detail in Chapter 58, form part of broader sound propagation prediction standards for specific types of noise sources, that is, road traffic, railway, airport, and industrial sources. Some of these formulas based on the Maekawa prediction method,<sup>14</sup> and on the method proposed by Kurze and Anderson.<sup>15</sup> Different predictive standards were adopted nationally, but increasingly these standards are showing some conformity and are condensing into smaller numbers with continental or worldwide acceptance.

An internationally adopted method of predicting the attenuation of noise barriers is given in the ISO 9613-2 (1996)<sup>1</sup> which is detailed in Section 2. Figure 3 plots the insertion losses as a function of the path length difference,  $\delta_1$ , calculated using the ISO 9613-2 for a single barrier (Fig. 3a) and for an earth berm of an equivalent height (Fig. 3b). In these calculations the top of the earth berm is assumed to be 1.0 m wide and the meteorological effects are ignored ( $K_{\text{met}} = 1$ ).

The formulas provided in this standard are incorporated in several software packages for community

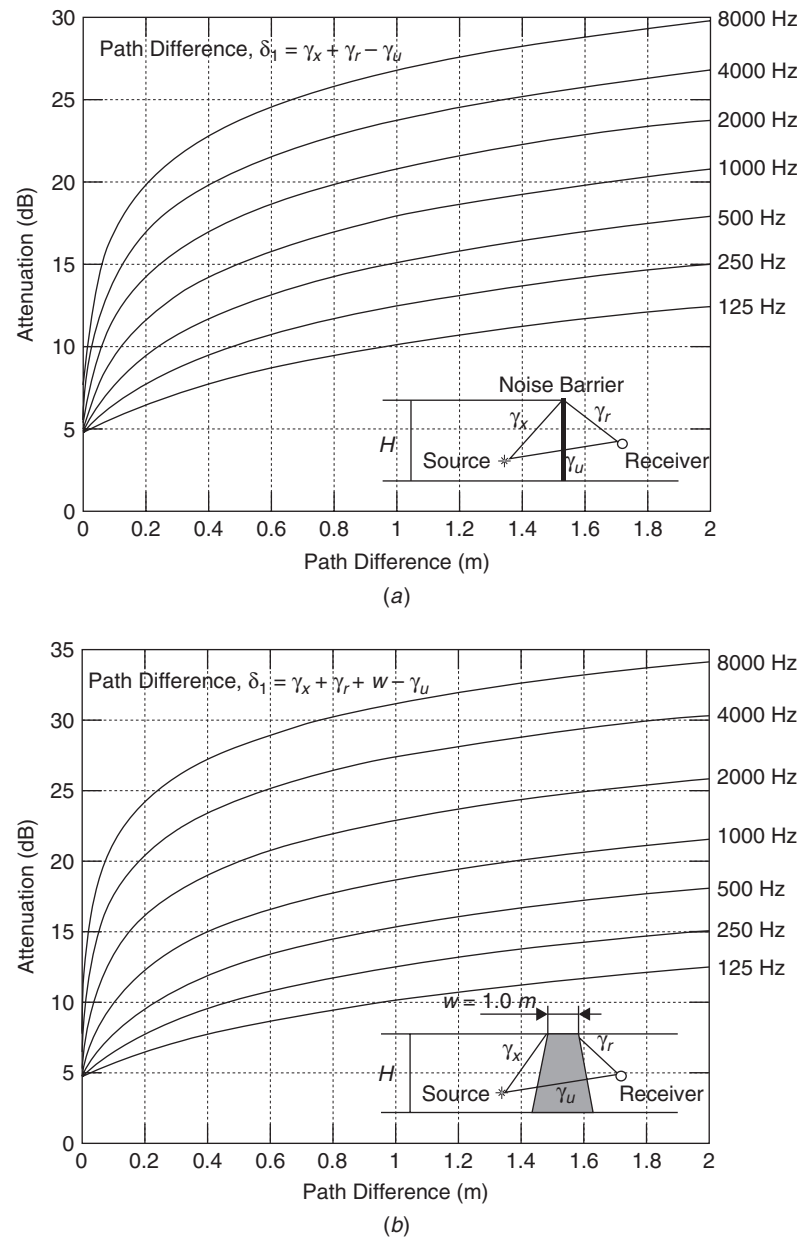
noise prediction, including Cadna-A<sup>16</sup> and SoundPLAN.<sup>17</sup> These products also include several national prediction models, for example, the American TNM, Scandinavian Nord 2000, British CRTN and CRN, French NMPB, and Japanese Road Model B, which also account for the noise barrier effect. A particular recent and comprehensive Nord 2000 method is based on the complete separation of sound emission and sound propagation phenomena. It accounts for the atmospheric and ground effects around a barrier and allows nonflat terrain profiles and nonstandard barrier shapes to be considered.<sup>18</sup>

In the last 20 years the boundary element method (BEM) has been used commonly to model the performance of noise barriers with the complex top edge and in the presence of absorbing/impedance surfaces. To date, it is only really effective, over the full frequency range of interest, for outdoor ground surfaces that are essentially one dimensional, meaning that there is some horizontal vector in which direction there is no change in surface elevation or in acoustical properties. The method requires the discretization of the noise barrier surfaces and the surfaces of nonuniform impedance. Practical applications of the method are limited to two-dimensional problems of several thousands elements. A typical size of the element is  $\lambda/10 - \lambda/5$ , where  $\lambda$  is the acoustic wavelength. Via conversion of the three-dimensional problem to a sequence of two-dimensional problems using a partial Fourier transform, the method can be used to produce predictions for a point or incoherent line source of sound.<sup>19</sup> (Duhamel, 1996). In its original form the boundary element method is limited to modeling homogeneous quiescent atmospheres, so that wind and temperature gradient effects are not modeled. A comprehensive summary of the existing BEM models and available software for the predictions has been compiled by Chandler-Wilde.<sup>20</sup>

Alternative methods for the prediction of noise barrier performance in the presence of wind and temperature gradients include the parabolic equation (PE) method and the fast field program (FFP) method. These methods are detailed in the textbook by Salomons.<sup>21</sup> The PE method is well-suited for medium- and long-range sound propagation predictions in the presence of slowly changing, realistic wind speed profiles. The original PE method is a one-way sound propagation method and does not include more complex interference effects, for example, the diffraction of sound around multiple edge noise barriers. The FFP method allows two-way propagation and is suitable for the prediction of sound propagation in vertically stratified media with piecewise constant sound speed profiles. Recently, this method has been combined with the BEM to model the complex diffraction effects.<sup>22</sup>

#### 5 NOISE BARRIER DESIGN

A major rule for the noise barrier design is to install it as close as possible to the noise source so that the distance to the source is less or equal to the barrier height  $r_s \leq H$  (see Fig. 3a). Alternatively, the barrier



**Figure 3** Predicted values of the attenuation provided by (a) a plane screen and (b) a 1 m wide earth berm. (From ISO 9613-2, section 7.4.<sup>1</sup>)

can be placed close to the receiver, but in this case the barrier will be effective only for low receiver heights. Where an earth berm or cutting is present in the vicinity of the source, any additional screen should be installed to ensure the maximum value of the path difference,  $\delta_1$ . The acoustical efficiency of such a noise barrier can be predicted using the procedures explained previously or determined in situ using the standard

methods detailed in ISO 10847:1997<sup>2</sup> or in American National Standards Institute (ANSI) S12.8-1998.<sup>3</sup>

### 5.1 Transmission of Sound through the Barrier Material

An essential criterion for selecting noise barrier material is to ensure that the noise contribution transmitted through the barrier material is insignificant

**Table 1 Categories for Airborne Sound Insulation Defined in EN1793-3:1997**

Category	$DL_R$ (dB)
B0	Not determined
B1	< 15
B2	15 to 24
B3	> 25

in comparison with the contribution from the sound diffracted over the barrier edges. The European standard EN 1793-3<sup>4</sup> defines the procedure for measuring the intrinsic characteristics of airborne sound insulation performance and specifies four categories B0 to B3, which are based on the value of single-number rating of airborne sound insulation performance,  $DL_R$ . These categories are summarized in Table 1.

A basic requirement for the material and structure of a noise barrier is that for a given noise source spectrum the difference between the broadband and sound pressure levels of the transmitted,  $L_t$ , and the diffracted,  $L_d$ , noise components should exceed 10 dB, that is,

$$L_d - L_t \geq 10 \text{ dB} \quad (5)$$

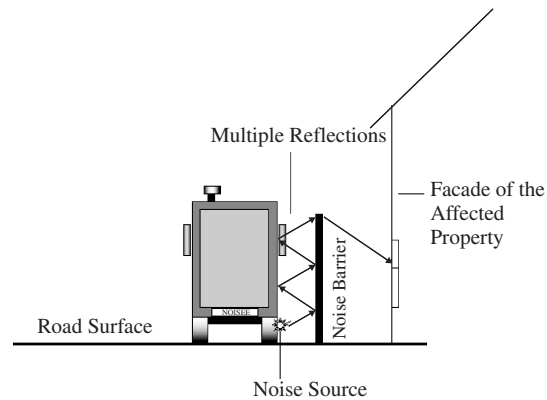
In the case of a long, continuous, impervious noise barrier assembly without any structural defects, ISO 9613-2<sup>1</sup> specifies a minimum surface density of 10 kg/m<sup>2</sup>. This is the minimum value required for any screening obstacle to be considered as a noise barrier. An alternative recommendation defines the minimum surface density ( $m$ ) of the noise barrier material<sup>23</sup> by

$$m = 3 \times 10^{\text{Att}-10/14} \text{ kg/m}^2 \quad (6)$$

where  $\text{Att} > 0$  dB is the predicted attenuation of the direct sound by a "massive barrier," that is, where there is only diffracted sound. The value of  $m$  predicted by expression (6) excludes the contribution from any structural elements and from the barrier foundation. According to expression (6) the minimum surface density required to achieve 20-dB attenuation is  $m = 15 \text{ kg/m}^2$ . The range of the surface densities of practical barrier materials varies from 4.4 kg/m<sup>2</sup> for a 1.59-mm aluminum sheet to 244 kg/m<sup>2</sup> for 100 mm of dense concrete. Typical barrier materials include metal, aluminum, pressure preservative treated timber, engineering bricks, or masonry blocks and their combinations. Almost half of the noise barriers constructed in North America until now are made of concrete. Transparent noise barriers are common in Europe and the Far East. These barriers are often made of Plexiglas, acrylic, or safety glass.

## 5.2 Absorption of Sound by the Barrier Material

In some applications the surface of a noise barrier is treated with an acoustically absorbing material to reduce the reflected acoustic energy. This requirement

**Figure 4** Effect of multiple reflections on the acoustical performance of a road noise barrier.

may be important if the barrier is close to the noise source, as illustrated in Fig. 4, or where two parallel noise barriers are closely installed. The absorbing barrier surface reduces the effect of multiple reflections. When high-sided vehicles, for example, lorries, buses, or trains, pass close to a barrier, multiple reflections increase the level of the diffracted component,  $L_d$ . The potential increase in the level of the diffracted component has been estimated in several studies.<sup>24-26</sup> In a particular case, where a rigid, 1.5-m high barrier was installed 1.0 m away from a passing railway carriage, the maximum predicted improvement in the average insertion loss due to the absorbing barrier treatment was 14 dB.<sup>25</sup> Another study by Watts and Godfrey<sup>26</sup> found that absorbing treatment on a 3.0-m high roadside noise barrier had an insignificant effect on barrier efficiency when the barrier was installed 5.6 m from the edge of a busy motorway. It should be generally understood that the value of the degradation can vary from site to site and would depend largely on the proximity of the barrier to the road, barrier elevation, position of the receiver, quality of the absorbing treatment, and the type of the ground near the barrier.

The quality of the absorbing treatment on noise barriers is regulated by the European standard EN1793-1.<sup>4</sup> The standard defines five categories, A0 to A4, which are related to the measured value of the single number rating of sound absorption performance,  $DL_{\alpha}$ . These categories are summarized in Table 2. It is generally accepted that noise barriers with high surface absorption offer superior performance only when the distance between a noise barrier and the source is less or comparable to the barrier height.

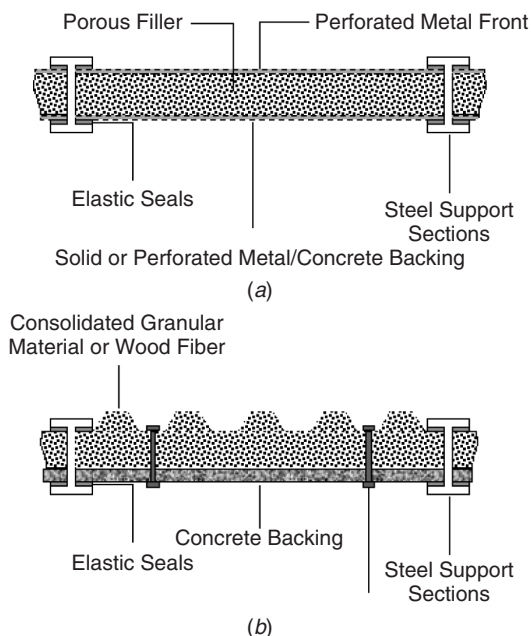
Examples of absorbing barrier assembly are illustrated in Fig. 5. Figure 5a shows a typical absorptive noise design consisting of prefabricated, perforated metal panels between two steel sections, which are secured into a solid concrete foundation. It is common to fill the panels with a mat of fibrous absorber (e.g., rockwool or fibreglass), the face of which is

**Table 2 Categories of Absorptive Performance Defined in EN 1793-1**

Category	$DL_{\alpha}$ (dB)
A0	Not determined
A1	< 4
A2	4 to 7
A3	8 – 11
A4	> 11

treated with a protective, hydrophobic porous membrane. A typical thickness of the mat is between 50 and 100 mm. Timber enclosures filled with fibrous absorbers can provide a cheaper alternative to the relatively expensive perforated metal panels.

In some countries it is common to use 50- to 150-mm slabs of consolidated granular materials or woodfibre as shown in Fig. 5b. The corrugated surface of the porous slabs improves the absorption and diffusion of sound at oblique angles of incidence. The slabs are securely fastened using steel bolts or threaded bars that can be cast into the concrete backing. A typical height of these barriers is largely determined by the site conditions and by the required value of insertion loss. Practical barrier heights tend to vary from 2 to 4 m, which are capable of achieving a 10- to 15-dB insertion loss at low receiver levels.



**Figure 5** Two types of absorbing treatment for barriers: (a) perforated panels filled with fibrous absorber and (b) slabs of consolidated granular material or wood fiber.

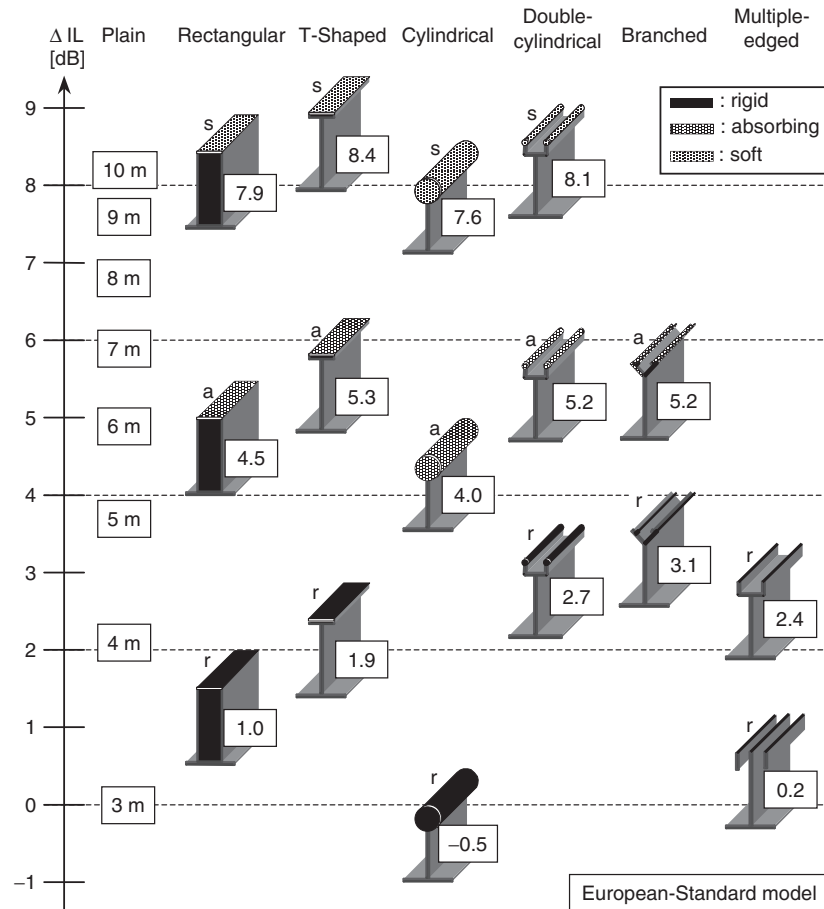
The length of a noise barrier should considerably exceed the barrier height. An empirical rule adopted by the U.S. Federal Highways Administration (FHA) suggests that a barrier should be long enough such that the distance between the receiver and a barrier end is at least four times the perpendicular distance from the receiver to the barrier along a line drawn between the receiver and the road. An alternative rule is to ensure that the angle subtended from the receiver to a barrier end should be at least 80 degrees, as measured from the perpendicular line from the receiver to the roadway.

### 5.3 Effect of the Barrier Shape

An improvement of the barrier efficiency can also be achieved by modifying the shape of the upper edge. The results of numerical modeling and full-scale tests, for example, Crombie et al.,<sup>27</sup> Duhamel,<sup>19</sup> Watts and Morgan,<sup>28</sup> and Ishizuka and Fujiwara,<sup>29</sup> suggest that T-shape barriers and multiple-edge noise barriers can provide a 2.0- to 2.5-dB improvement of the broadband insertion loss without apparent increase of the barrier height.<sup>28</sup> A comprehensive summary of the efficiency of noise barriers of different edge shapes can be found in the study by Ishizuka and Fujiwara.<sup>29</sup> This work shows that a complex noise barrier edge, for example, a Y-shape barrier or barrier with a cylindrical edge, can yield a 4.0 to 5.2-dB improvement in the insertion loss with respect to that for a plain barrier of the same height of 3.0 m. This is important when the increase in the barrier height is not practical or impossible. A useful diagram from this reference illustrating the change in the mean insertion loss relative to a standard 3 m high, plane screen noise barrier is provided in Fig. 6.<sup>29</sup>

In the Far East, particularly in Japan, cantilever barriers of parabolic shape are used widely to shield residential areas from noise emitted by elevated highways. These barriers curve inward over the roadway and are typically between 8.0 and 15.0 m in height, to maximize their efficiency (see Fig. 7). In a typical arrangement one barrier is made of a transparent material, for example, Perspex, to provide natural lighting conditions. All the internal surfaces of the nontransparent barrier are designed to be sound absorbing to control multiple reflections within the barrier corridor.

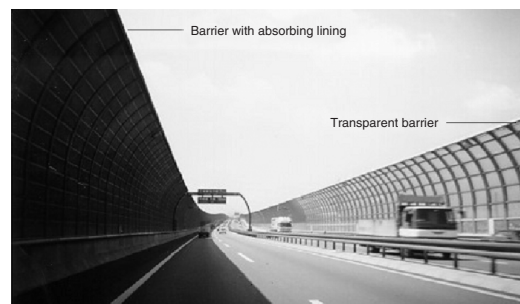
Earth berms (earth mounds) are used in rural and semirural locations as an alternative ecodesign to or in conjunction with noise barriers. These structures are attractive because they are easy to blend with the landscape and require little maintenance. However, earth berms require much more space than a vertical barrier of equivalent acoustical performance. The standard method of prediction of the acoustical efficiency of an earth berm is detailed in the ISO 9613-2.<sup>1</sup> The acoustical efficiency of a berm is determined by the path length difference between the noise source and receiver, the shape of the top edge, and by the effect of the porous soil of which the berm is constructed. It is generally agreed that when an absorbing surface is introduced to a wide earth berm, some improvement in insertion loss in the higher frequency range can be expected, particularly when the receiver and the source are in the proximity of the berm; see Daigle, page 146.<sup>7</sup>



**Figure 6** Comparison of acoustical performance of noise barriers of various shapes predicted using the source spectrum defined in EN 1793-3. The numerical labels indicate the relative change in the mean insertion loss relative to a 3-m plane screen. (From Ishizuka and Fujiwara.<sup>29</sup>)

This report suggests that the efficiency of the absorbing surface of the earth berm is reduced if the wedge angle of the berm is greater than  $45^\circ$ . The acoustical performance of the earth berm with a flat, grass-covered top can be similar to that of a plane rigid barrier of equivalent height.<sup>7</sup> Mounting of a plane barrier on the top of an earth berm may not offer any benefits due to lost positive effect of its absorbing surface.

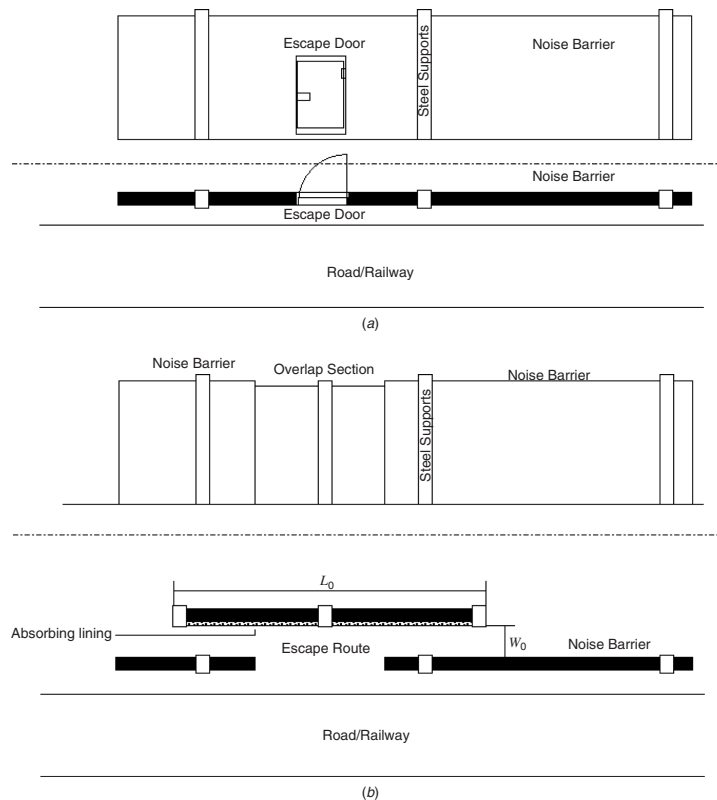
Alternative sustainable barrier designs (ecodesigns) include planting that has been used for many years, particularly in the Netherlands and Denmark, to blend a man-made barrier into the surrounding landscape. Present ecobarrier designs are based on successful combinations of living and man-made materials that include thatch barriers, willow-weave wall, and stack and crib biobarriers. Concrete, timber, masonry, and steel support structures can also be used to support vegetation including flowers and bushes. Some ecobarrier designs also incorporate porous absorbing materials that can control the reflections from the barrier surface. More



**Figure 7** Cantilever noise barrier system on a Japanese highway.

details of these can be found in the textbook by Kotzen and English.<sup>8</sup> Some of these barriers are designed to be self-sufficient, require little maintenance, and can have





**Figure 8** Typical arrangements of (a) the escape door and (b) a safety gap.

the life span of 25 years or more. An ecobarrier offers a 5- to 6-fold saving of space in comparison with the case of an earth berm and provides sustainable solutions to noise abatement, screening, and fencing, both in urban and rural situations.

#### 5.4 Air Gaps, Safety, and Maintenance

In addition to the basic requirements for the acoustical performance of a barrier, there are several non-acoustical characteristics that should be satisfied. These characteristics relate to wind and static loading, safety in collision, dynamic load from snow clearance, resistance to brush fire, danger of falling debris, light reflection, means of escape, transparency, and impact of flying stones. Relevant test methods are detailed in the EN 1794-1 and EN 1794-2.<sup>5</sup>

Long sections of noise barrier require regular access points for maintenance and emergencies. It is common to provide escape doors or gaps at intervals of a few hundred metres. The Highways Agency in the United Kingdom recommends the installation of safety doors or channels at intervals of not more than 200 m. The width of the access routes must be sufficient to enable delivery of the first aid equipment including stretchers. Examples of noise barrier escape routes are illustrated in Figs. 8a and 8b, respectively. Doors and frames must be accurately fitted and properly sealed to

minimize the leakage of noise through possible gaps. Escape channels should include an overlap section that is typically lined with acoustically absorbing material to ensure that the acoustical efficiency of the noise barrier is not compromised by the discontinuity. The length of the overlap is typically selected as a 2:1 or 3:1. To reduce line-of-sight propagation phenomena the overlap is designed so that the ratio of the overlap length,  $L_0$ , to the overlap width,  $W_0$  (see Fig. 8b), is typically 1:2 or 1:3.

The effects of gaps on barrier performance has been studied by Don et al.,<sup>30</sup> Watts,<sup>31</sup> and Herman and Clum.<sup>32</sup> Gaps in the continuous barrier surface can develop as a result of poor workmanship, degradation of the barrier material due to the weather and elements, vandalism, and as a result of road accidents. Watts demonstrated that the structural defects in wooden barriers could cause a 9-dB reduction in the predicted value of the insertion loss in the vicinity of the barrier.<sup>31</sup> Herman and Clum analyzed overlap barrier gaps both experimentally and numerically.<sup>32</sup> Their work shows that overlapping gaps between two reflective barriers can result in a 5- to 11-dB reduction in value of the insertion loss predicted immediately behind the barrier. Typically, a degradation of 1 to 5 dB can be expected in the performance of absorbing

barriers. The effects of the overlap gap tend to reduce and become negligible at distances from the barrier, which considerably exceed the width of the overlap. In countries with cold climates, for example, in Finland or Russia, controlled gaps are created deliberately at the bottom on a noise barrier to avoid the damage due to frost and snow. These gaps can cause a 3-dB degradation in the barrier insertion loss.<sup>8</sup> This value of degradation becomes negligible at greater receiver distances.

### 5.5 Effects of Traffic Type, Composition, and Speed

The traffic composition and speed can affect the broadband and spectral performance of a noise barrier as a result of the variation in the source spectrum, source type, and position. This detailed aspect of the performance of noise barriers is not well understood and is the subject of ongoing research. Although these factors have a marginal influence on the prediction of the barrier attenuation in terms of the time-dependent noise indices ( $L_{eq}$  and  $L_{10}$ ) used to assess environmental noise, there may be significant effects on the perception of the noise as a result of the influence on the spectrum at a receiver behind the barrier.

In the standard prediction schemes, complex traffic and railway noises are usually approximated by a line of coherent or incoherent monopoles. This type of source is assumed in several national and international standards, including the British CRTN<sup>33</sup> and CRN.<sup>34</sup> Improved analysis of continuous traffic noise can be achieved using a boundary element model based on the incoherent line source.<sup>19</sup> Improved analysis of railway noise can also be performed if the incoherent line source model includes a dipole-type radiation component. A 15/85 combination of monopole/dipole radiation contributions is suggested in the Austrian model ÖAL-Richtlinie.<sup>35</sup> The effect of such a combination has been investigated by Morgan et al.<sup>36</sup> In computer simulations (e.g., Jonasson and Storeheier<sup>18</sup>), it is common to assume a distribution of static or moving-point sources on the road or railway. In this way it is possible to calculate the different attenuation spectra from sources with oblique rays over the barrier and at different distances. This could have a significant effect on the time-dependent indices that are used, that is,  $L_{eq}$  and  $L_{10}$ . In this way, the effects of position, emission spectrum, directivity of source, and speed can be analyzed. This is not possible with the line source approach.

The broadband efficiency of a noise barrier can be predicted for a given traffic noise spectrum,  $L_0(f_n)$ , using the following expression:

$$IL_B = 10 \log_{10} \left( \sum_{n=1}^N 10^{L_0(f_n)/10} \right) - 10 \log_{10} \left( \sum_{n=1}^N 10^{[L_0(f_n) - IL_0(f_n)]/10} \right) \quad (7)$$

where  $IL_0(f_n)$  is the frequency-dependent insertion loss (dB) and  $N$  is the number of frequency bands,  $f_n$ ,

considered in the analysis. A representative traffic noise spectrum at the roadside is defined in EN 1793-3.<sup>4</sup> The increase in the proportion of heavy vehicles tends to affect the broadband sound pressure level, whereas its effect on the shape of the noise spectrum is relatively small. On the other hand, for railway noise, the shape of the noise spectrum and its broadband sound pressure level can experience a 20-dB fluctuation depending upon the train type, speed, and the train position with respect to the noise barrier. The effect of the railway noise spectra (see, e.g., Morgan et al.<sup>36</sup>) on the broadband efficiency of noise barriers has been studied by Horoshenkov et al.<sup>37</sup> While the efficiency of the plane screen is relatively unaffected by the spectral changes, the 4-dB to 7-dB variation of the noise efficiency of more exotic barrier designs, despite the higher insertion loss for the same height in terms of the A-weighted sound pressure level can be perceived as unacceptably high. Such fluctuations can be subjectively perceived to be more significant than the objectively measured gain of 1 dB to 2 dB in the average barrier performance.

### 6 INSERTION LOSS OF TREES AND SHIELDING CAUSED BY INTERVENING BUILDINGS

Often the insertion loss of tree belts alongside highways is considered relative to that over open grassland. An unfortunate consequence of the lower frequency ground effect observed in mature tree stands (see Chapter 5) is that the low-frequency destructive interference resulting from the relatively soft ground between the trees is associated with a constructive interference maximum at important frequencies (near 1 kHz) for traffic noise. Consequently, many narrow tree belts alongside roads do not offer much additional attenuation of traffic noise compared with the same distances over open grassland. A Danish study found relative attenuation of 3 dB in the A-weighted  $L_{eq}$  due to traffic noise for tree belts between 15 and 41 m wide.<sup>38</sup> Data obtained in the United Kingdom<sup>39</sup> indicates a maximum reduction of the A-weighted  $L_{10}$  due to traffic noise of 6 dB through 30 m of dense spruce compared with the same depth of grassland. This study found also that the effectiveness of the vegetation was greatest closest to the road. A relative reduction of 5 dB in the A-weighted  $L_{10}$  was found after 10 m of vegetation. For a narrow tree belt to be effective against traffic noise, it is important that (a) the ground effect is similar to that for grassland, (b) there is substantial reduction of coherence between ground-reflected and direct sound at frequencies of 1 kHz and above and (c) that the attenuation through scattering is significant.

If the belt is sufficiently wide, then the resulting greater extent of the ground effect dip can compensate for its low-frequency range. Through 100 m of red pine forest, Heisler et al.<sup>40</sup> have found 8-dB reduction in the A-weighted  $L_{eq}$  due to road traffic compared with open grassland. The edge of the forest was 10 m from the edge of the highway, and the trees occupied a gradual downward slope from the roadway extending about 325 m in each direction along the highway from the study site. Compared with open



grassland Huisman and Attenborough<sup>41</sup> have predicted an extra attenuation of 10 dB for road traffic noise through 100 m of pine forest. They remarked also that whereas downward-refracting conditions lead to higher A-weighted sound pressure levels over grassland, the levels in woodland are comparatively unaffected. This suggests that extra attenuation obtained through use of trees should be relatively robust to changing meteorology.

Defrance et al.<sup>42</sup> have compared results from both numerical calculations and outdoor measurements have been obtained for different meteorological situations. Their numerical method is based on a Green's fast parabolic equation (GFPE) method.<sup>21</sup> A two-dimensional GFPE code has been developed<sup>43</sup> and adapted to road traffic noise situations<sup>44</sup> where road line sources are modeled as a series of equivalent point sources of height 0.5 m. The data showed a reduction in A-weighted  $L_{eq}$  due to the trees of 3 dB during downward-refracting conditions, 2 dB during homogeneous conditions, and 1 dB during upward-refracting conditions. The numerical predictions suggest that in downward-refracting conditions, the extra attenuation due to the forest is between 2 dB and 6 dB with the receiver at least 100 m away from the road. In upward-refracting conditions and at large distances, the adapted GFPE model predicts that the forest may increase the received A-weighted sound pressure levels somewhat, but this is of less importance since levels at such distances are relatively low anyway. In homogeneous conditions, it is predicted that sound propagation through the forest is affected only by the scattering by trunks and foliage.

Defrance et al.<sup>42</sup> have concluded that a forest strip of at least 100 m wide appears to be a useful natural acoustical barrier. It should be noted that, in this study, both the data and numerical simulations were compared to A-weighted sound pressure levels without the trees present, that is, over ground from which the trees had simply been removed. This means that the ground effect both with and without trees would have been similar. This is rarely likely to be the case. ISO 9613-2<sup>1</sup> suggests a frequency-dependent foliage attenuation coefficient (see Fig. 8 in Chapter 5).

## 6.1 Buildings

For a single building, the double-diffraction calculations mentioned earlier could be used. For source or receiver situated in a built-up area, ISO 9613-2<sup>1</sup> proposes an empirical method for calculating the combined effects of screening and multiple reflections. The net attenuation  $A_{build}$  (<10 dB) is given by

$$\begin{aligned} A_{build} &= A_{build,1} + A_{build,2} \\ A_{build,1} &= 0.1Bd_0 \text{ dB} \\ A_{build,2} &= -10 \log[1 - (p/100)] \text{ dB} \end{aligned} \quad (8)$$

where  $B$  is the area density ratio of buildings (total plan area/total ground area) and  $d_0$  is the length of the refracted path from source to receiver that passes through buildings.  $A_{build,2}$  is intended to be used only

where there are well-defined rows of buildings near to a road or railway. For such cases,  $p$  is the percentage of the length of facades relative to the total length of the road or railway. The area density ratio and the percentage of the length of facades can also account for the effects of arcades and intermittent building arrangement along a busy road. As with barrier attenuation, the attenuation due to buildings is to be included only when it is predicted to be greater than that due to ground effect. The ISO scheme offers also a frequency-dependent attenuation coefficient (dB/m) for propagation of industrial noise through buildings on an industrial site.

## REFERENCES

1. ISO 9613-2 (1996), Acoustics—Attenuation of Sound During Propagation Outdoors—Part 2: General Method of Calculation, ISO 9613-2: 1996(E).
2. ISO 10847 (1997), Acoustics—In-situ Determination of Insertion Loss of Outdoor Noise Barriers of All Types, ISO 10847: 1997(E).
3. ANSI S12.8 (2003), Methods for Determination of Insertion Loss of Outdoor Noise Barriers, American National Standard ANSI S12.8-1998.
4. EN 1793 (1997), Road Traffic Noise Reducing Devices—Test Method for Determining the Acoustic Performance, European Standard EN 1793, Parts 1–5, 1997.
5. EN 1794 (1997), Road Traffic Noise Reducing Devices—Non-acoustic Performance, European Standard EN 1794, Parts 1 and 2, 1997.
6. EC Proposal COM (2000)468, Proposal for a Directive of the European Parliament and of the Council Relating to the Assessment and Management of Environmental noise, COM(2000), Brussels, 2000.
7. A. G. Daigle, Report by the International Institute of Noise Control Engineering Working Party on the Effectiveness of Noise Walls, *Noise/News International*, I-INCE, September 1999.
8. B. Kotzen and C. English, *Environmental Noise Barriers—A Guide To Their Acoustic and Visual Design*, E&F Spon, London, New York, 1999.
9. R. B. Tatge, Barrier-Wall Attenuation with a Finite Sized Source, *J. Acoust. Soc. Am.*, Vol. 1973, pp. 53, 1317–1319.
10. W. E. Scholes, A. C. Salvidge, and J. W. Sargent, Field Performance of a Noise Barrier, *J. Sound Vib.*, Vol. 16, 1971, pp. 627–642.
11. J. Forssén and M. Ögren, Thick Barrier Noise-Reduction in the Presence of Atmospheric Turbulence: Measurements and Numerical Modelling, *Appl. Acoust.*, Vol. 63, 2002, pp. 173–187.
12. G. R. Watts, Acoustic Performance of a Multiple Edge Noise Barrier Profile at Motorway Sites, *Appl. Acoust.*, Vol. 47, 1996, pp. 47–66.
13. G. R. Watts, Barriers—Quantification of Barrier Top Performance in Non-neutral Atmospheres, Transport Research Limited, Document HAR25MO-0310228-TRL02, Crowthorne, UK, July 2003.
14. Z. Maekawa, Noise Reduction by Screens, *Appl. Acoust.*, Vol. 1, 1968, pp. 157–173.
15. U. J. Kurze and G. S. Anderson, Sound Attenuation by Barriers, *Appl. Acoust.* Vol. 4, 1971, pp. 35–53.
16. CADNA, Datakustik GmbH, <http://www.datakustik.de>, 2004.

17. SoundPLAN, Braunstein + Berndt GmbH, <http://www.soundplan.com>, 2004.
18. H. G. Jonasson and S. Å. Storeheier, Nord 2000. New Nordic Prediction Method for Road Traffic Noise, SP Swedish National Testing and Research Institute, Purdue University, USA, 2001.
19. D. Duhamel, Efficient Calculation of the Three-Dimensional Sound Pressure Field around a Noise Barrier, *J. Sound Vib.*, Vol. 197, No. 5, 1996, pp. 547–571.
20. S. N. Chandler-Wilde, Tyndall Medal Lecture: The Boundary Element Method in Outdoor Noise Propagation, *Proc. Inst. Acoust.*, Vol. 19, No. 8, 1997, pp. 27–50.
21. E. M. Salomons, *Computational Atmospheric Acoustics*, Kluwer Academic, Dordrecht, The Netherlands, 2002.
22. S. Taherzadeh, K. M. Li, and K. Attenborough, A Hybrid BIE/FFP Scheme for Predicting Barrier Efficiency Outdoors, *J. Acoust. Soc. Am.*, Vol. 110, No. 2, 2001, pp. 918–924.
23. Department of Transport, Noise Barriers—Standards and Materials, Technical Memorandum H14/76, HMSO, London, 1976.
24. D. C. Hothersall and S. A. Tomlinson, Effects of High-Sided Vehicles on the Performance of Noise Barriers, *J. Acoust. Soc. Am.*, Vol. 102, No. 2, 1997, pp. 998–1003.
25. P. A. Morgan, D. C. Hothersall, and S. N. Chandler-Wilde, Influence of Shape and Absorbing Surface—A Numerical Study of Railway Noise Barriers, *J. Sound Vib.*, Vol. 217, No. 3, 1998, pp. 405–417.
26. G. R. Watts and N. S. Godfrey, Effects on Roadside Noise Levels of Sound Absorptive Materials in Noise Barriers, *Appl. Acoust.*, Vol. 58, No. 4, 1999, pp. 385–402.
27. D. H. Crombie, D. C. Hothersall, and S. N. Chandler-Wilde, Multiple-Edge Noise Barriers, *Appl. Acoust.*, Vol. 44, No. 4, 1995, pp. 353–367.
28. G. R. Watts and P. A. Morgan, Acoustic Performance of an Interference-Type Noise-Barrier Profile, *Appl. Acoust.*, Vol. 49, No. 1, 1996, pp. 1–16.
29. T. Ishizuka and K. Fujiwara, Performance of Noise Barriers with Variable Edge Shape and Acoustical Conditions, *Appl. Acoust.*, Vol. 65, 2004, pp. 125–141.
30. C. G. Don, G. G. Swenson, and M. Butyn, Investigation of Pulse Propagation through Slits in a Wide Barrier, *Proc. Inter-Noise 96, Int. Cong. Noise Cont. Eng.*, Liverpool, 30 July–2 August 1996, pp. 725–728.
31. G. R. Watts, Effects of Sound Leakage through Noise Barriers on Screening Performance, *Proc. Int. Cong. Sound Vib.*, Tech. Univ. Denmark, Lyngby, Copenhagen, 1999, pp. 2501–2508.
32. L. A. Herman, and C. M. Clum, Analysis of Noise Barrier Overlap Gaps, *J. Acoust. Soc. Am.*, Vol. 111, No. 4, 2002, pp. 1734–1742.
33. Department of Environment, *The Calculation of Road Traffic Noise*, HMSO, London, 1988.
34. Department of Environment, *The Calculation of Train Noise*, HMSO, London, 1995.
35. ÖAL-Richtlinie, No. 30, Calculation of the Sound Emission from Rail Traffic (in German), Vienna, Austria, 1990.
36. P. A. Morgan, D. C. Hothersall, and S. N. Chandler-Wilde, Influence of Shape and Absorbing Surface—A Numerical Study of Railway Noise Barriers, *J. Sound Vib.*, Vol. 217, No. 3, 1998, pp. 405–417.
37. K. V. Horoshenkov, S. Rehman, and S. J. Martin, The Variation of the Predicted Performance of Railway Noise Barriers, CD-ROM, Proceedings of the 5th European Noise Conference, Naples, Italy, 2003.
38. J. Kragh, Road Traffic Noise Attenuation by Belts of Trees and Bushes, Danish Acoustical Laboratory, Report No. 31, Lyngby, Denmark, 1982.
39. L. R. Huddart, the Use of Vegetation for Traffic Noise Screening, TRRL Research Report 238, Crowthorne, UK, 1990.
40. G. M. Heisler, O. H. McDaniel, K. K. Hodgdon, J. J. Portelli, and S. B. Glesson, Highway Noise Abatement in Two Forests, *Proc. NOISE-CON 87*, PSU, 1987.
41. W. H. T. Huisman and K. Attenborough, Reverberation and Attenuation in a Pine Forest, *J. Acoust. Soc. Am.*, Vol. 90, No. 5, 1991, pp. 2664–2667.
42. J. Defrance, N. Barrière, and E. Premat, Forest as a Meteorological Screen for Traffic Noise, CD-ROM, *Proc. 9th Int. Cong. Sound Vib.*, Orlando, FL, 2002.
43. N. Barrière and Y. Gabillet, Sound Propagation over a Barrier with Realistic Wind Gradients. Comparison of Wind Tunnel Experiments with GFPE Computations, *Acta Acust.*, Vol. 85, 1999, pp. 325–334.
44. N. Barrière, Theoretical and Experimental Study of Traffic Noise Propagation through Forest, Ph.D. Thesis, CSTB, Grenoble, France, 1999.

# CHAPTER 123

## GROUND-BORNE VIBRATION TRANSMISSION FROM ROAD AND RAIL SYSTEMS: PREDICTION AND CONTROL

**Hugh E. M. Hunt**  
Engineering Department  
Cambridge University  
Cambridge, United Kingdom

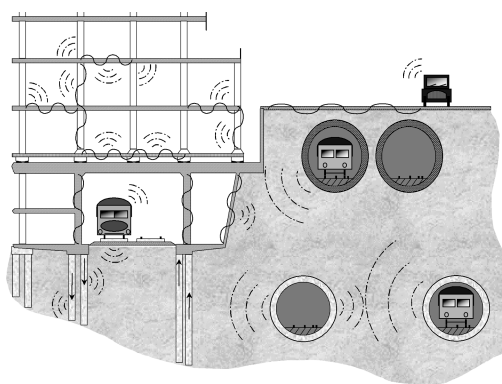
**Mohammed F. M. Hussein**  
School of Civil Engineering  
University of Nottingham  
Nottingham, United Kingdom

### 1 INTRODUCTION

Vibration is generated by road and rail traffic over a wide range of frequencies and amplitudes. Large-amplitude vibration can cause damage to track components, cracking of roadways, settlement of foundations, destabilization of embankments, and damage to nearby structures. But the focus of this chapter is on disturbance due to small-amplitude vibration. Vibration is perceptible at amplitudes several orders of magnitude below those generally required to cause damage to buildings. Regulations prescribe acceptable levels of vibration in the vicinity of new roads and railways and, in particular, near the tunnels of underground railway systems in cities. It is desirable to model accurately the generation and propagation of vibration because permission to build may only be granted if vibration can be shown to be within acceptable limits. There may also be restrictions applied if traffic patterns change, for instance, if nighttime freight trains are to be introduced on a line that normally carries only daytime passenger trains or if heavy bus traffic is to be increased on a residential road. This chapter addresses the issues confronting practicing engineers when asked to evaluate or mitigate ground vibration generated by road and rail traffic.

### 2 IMPACT OF GROUND-BORNE VIBRATION

Vibration generated by road vehicles and by trains can have significant environmental impact on nearby buildings. The general complexity of the problem is illustrated in Fig. 1. Inhabitants perceive vibration either directly as motion in floors and walls or indirectly as reradiated noise. A third and very significant source of disturbance is due to movement of household objects, especially mirrors, or by the rattling of window panes and glassware. In all these cases the problem of ground-borne vibration is important at frequencies typically up to 200 to 250 Hz.<sup>1</sup> Vibration at higher frequencies is generally attenuated rapidly with distance along the transmission path through the ground. Vibration can travel long distances from its



**Figure 1** Sources of ground vibration and their transmission paths. (Courtesy of J. P. Talbot, Atkins Consultants, UK.)

source. For a ground with soft clay or silt, ground-borne vibration may produce annoyance to people in buildings more than 200 m away from tracks.<sup>2</sup>

Many studies and standards address the effect of vibration on buildings, their occupants, and on equipment. The British standard BS 6472:1992<sup>3</sup> provides general guidance on human exposure to vibration in the frequency range 1 to 80 Hz. It provides curves for equal annoyance for humans plotted as root-mean-square acceleration versus frequency. The vibration dose value (VDV) is used as a vibration measure that takes into account the time history of the vibration (whether continuous or intermittent) for the day or the nighttime. The American National Standards Institute (ANSI) annoyance criteria due to vibration<sup>4</sup> are described by the maximum weighted acceleration level and are given in Table 1.

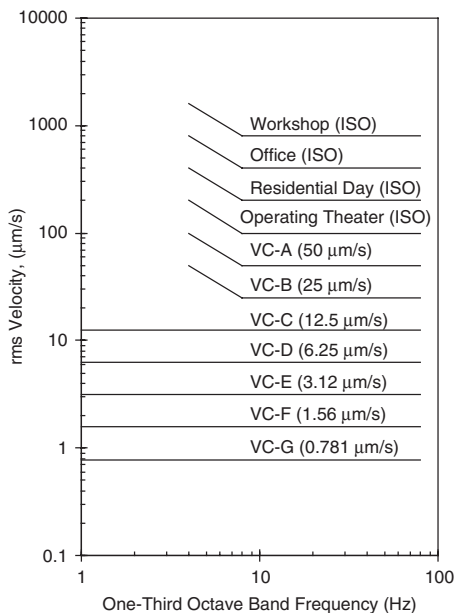
Experimental work by Duarte and Filho<sup>5</sup> shows that the sensitivity of people to a sinusoidal vibration decreases with frequency up to around 40 to 50 Hz. This is because the human head resonates around 20 to

**Table 1 ANSI Criteria for Annoyance due to Ground-Borne Vibration**

Building Use Category	Maximum Weighted Acceleration Level (dB re $10^{-6}$ g)
Hospital and critical areas	51
Residential (nighttime)	54
Residential (daytime)	57
Office	63
Factory	69

40 Hz, and hence it makes the person sensitive to even low amplitudes of vibration. Sensitivity increases again in the range between 50 and 100 Hz where the chest wall and ocular globe resonate. The work shows also that women are more sensitive to vibration than men.

Gordon<sup>6</sup> develops generic vibration criteria (VC curves) for vibration-sensitive equipment. These curves are plotted in a similar way to the International Organization for Standardization (ISO) 2631-2:2003 guidelines for the effects of vibration on people in buildings.<sup>7</sup> Vibration is expressed in terms of its root-mean-square velocity and is plotted as a one-third octave band. For a site to comply with a particular equipment category, the measured one-third octave band velocity must lie below the appropriate curve for the given category in Fig. 2.



**Figure 2** Generic vibration criterion (VC) curves for vibration-sensitive equipment showing also the ISO guidelines for people in buildings. [Courtesy of the Institute of Environmental Sciences and Technology (IEST), Rolling Meadows, Illinois; [www.iest.org](http://www.iest.org).]

Due to the increasing public sensitivity to noise and vibration,<sup>8</sup> railway companies must develop affordable vibration countermeasures and predictive tools to permit estimation of vibration levels in the early stages of planning for new railways. With increasing complaints about ground-borne vibration, many surveys are conducted to assess the vibration effect on buildings and their occupants and to help establish standards. In Nagoya, for example, the city authority conducts surveys about every 5 years to investigate the state of noise and vibration environment.<sup>9</sup>

A noise and vibration study by Fields<sup>10</sup> based on interviews with people who live near railway tracks finds a generally high level of dissatisfaction within 25 m of the track. People interviewed in the range 25 to 150 m from the track report rapidly diminishing levels of complaint, and for distances beyond 150 m there is a uniform and low level of complaint. The study shows that many factors affect perception such as the duration of vibration, the time of day, background vibration levels, and various psychological factors such as whether the railway is visible.

It is generally believed that damage to buildings is associated with vibration, but this is unlikely as vibration generated by road traffic or railway trains rarely approaches the threshold of architectural damage.<sup>11,12</sup> There are exceptions, and certain historic masonry structures are thought to have been damaged by traffic-induced vibration. Fear of damage to historic structures in Stockholm's medieval quarter Gamla Stan has been one of the obstacles to the building of a new track.<sup>13</sup> The fear is arguably justified in cases where vibration has the potential to cause compaction and differential settlement of foundations of buildings close to roads or railways. This has been put forward as an explanation for the road-ward inclination of cathedrals and other ancient buildings.<sup>14</sup>

Turunen-Rise et al.<sup>15</sup> and Klaboe et al.<sup>16</sup> present a new Norwegian standard NS8176 for vibration in buildings from road and rail traffic. The standard introduces a single quantity to describe the vibration in buildings. This quantity is the statistical value of maximum velocity or acceleration,  $v_{W,95}$  and  $a_{W,95}$ , respectively. These are calculated by recording the vibration for at least 15 passing trains or vehicles. For each record the third octave band frequency spectrum is calculated and weighted with weight values proportional to the human response at each band. Assuming a lognormal distribution of the root-mean-square values,  $v_{W,95}$  and  $a_{W,95}$  are calculated from the velocity and acceleration with a nonexceeding probability of 95%. In this standard vibration should be measured in a position and direction in the building that gives the highest vibration. A survey is conducted by questioning people who live in buildings where  $v_{W,95}$  and  $a_{W,95}$  were calculated using a prediction model developed by Madshus et al.<sup>2</sup> (see Section 5). According to the survey, it is found that there is no significant difference in reactions to vibration from different sources. Buildings are classified into four categories (A to D) according to the study, describing the building state in terms of vibration. In order to

provide a common answer format for sociovibrational studies and a better data exchange from future surveys to assess human perception of vibration in buildings, Klaboe et al.<sup>17</sup> present a methodology to standardize carrying out a survey.

Research on ground-borne vibration, especially from underground railways, has recently gained prominence on account of the need to establish new underground tunnels in cities. There is also pressure to put high-speed intercity lines underground near residential areas. A particular feature of underground trains is the widespread notion that once underground the problem of noise goes away. But pure vibration in the absence of noise can be unnerving and more disturbing than vibration from visible and audible surface trains. Also of concern is that underground tunnels may pass near building foundations causing significant structural vibration. To address these issues a program of research entitled CONVURT (control of vibration from underground rail traffic) was established under the fifth framework of the European Union (EU) program for research, technological developments, and demonstration. The project had four main objectives: The first was to create validated innovative and quantitative modeling tools to enable accurate prediction of ground-borne vibration transmission into buildings.<sup>18,19</sup> The second was to develop and evaluate new and cost-effective track and tunnel components to reduce ground-borne vibration and especially to develop devices capable of being retrofitted to existing track.<sup>20</sup> The third was to provide scientific input to allow the preparation of international standards. Finally, CONVURT has established guidelines of good practice for underground railway operation in order to maintain minimum vibration for the lifetime of operation.<sup>21</sup>

### 3 EXCITATION MECHANISMS

Vibration from road and rail vehicles derives from the inertia forces generated as vehicles pass over road and track irregularities. The nature of irregularities differs significantly between road and rail vehicles. For road vehicles much attention is given to potholes and speed cushions. A typical study is carried out by Watts<sup>22</sup> to assess the vibration levels generated by vehicle crossing speed control cushions and road humps finds that these speed control measures can produce perceptible levels of vibration, but it is very unlikely to cause even minor damage to buildings. In general the resilience offered by pneumatic tires helps to reduce the generation of high dynamic forces and so reduce the level of traffic-induced vibration in the vicinity of roads. By contrast the dynamic forces generated by heavy steel wheels rolling on steel rails are high, and the rest of this section will address excitation mechanisms for rail vehicles.

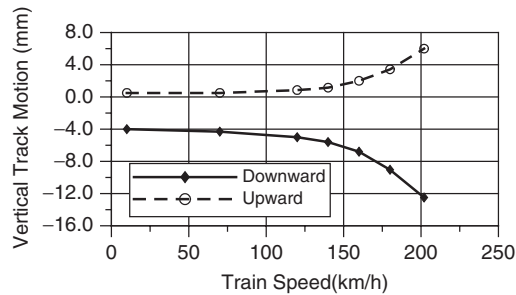
Significant vibration in buildings near railway tracks and subway tunnels is attributed to moving trains. There are five main mechanisms for the generation of vibration. The first is a *quasi-static* mechanism, and it is significantly close to a track where the passage of individual axles can be distinguished. The passage of a vehicle can be represented by the passage of a

number of discrete concentrated static forces applied to the rails. As each force passes by, the observer experiences an oscillatory motion even though the applied force is constant. This may be visualized by imagining a child riding a bicycle over a large mattress; the vertical applied force is a constant, yet oscillatory motion is induced in objects resting on the mattress. The quasi-static effect contributes significantly to the low-frequency response in the range 0 to 20 Hz.<sup>1,23</sup>

A second mechanism, known as *parametric excitation*, derives from the periodic support of rail by sleepers. The mechanism is similar to the quasi-static effect described above because vibration is generated when a constant wheel load moves along the rail at constant speed. The difference is that when it encounters variable rail support stiffness the resulting vertical motion of the wheel and axle cause dynamic forces to be applied to the rail. This is analogous to the same bicycle being influenced by individual springs in the mattress and the vertical applied force has an oscillatory component. Sleepers are uniformly spaced and excitation occurs at a frequency equal to the train velocity divided by the sleeper spacing (typically 25 Hz for low-speed trains and up to 150 Hz for high-speed trains). An investigation of this effect by Heckl et al.<sup>24</sup> gives results for the measured acceleration spectra near a railway track. It shows that peaks appear at some distinctive frequencies such as the sleeper-pass frequency, and also that the response can be large if the wheel track resonance coincides with one of the sleeper-pass harmonics.

A third mechanism occurs when wheels apply impulsive loading to the rail due to height differences at rail joints and crossings. This mechanism is becoming less important with the increasingly widespread use of continuously welded track, but the growth of surface unevenness is often more rapid in the vicinity of welds. Impulsive loading also occurs when the wheels have "flats" caused by skidding with locked brakes.

The fourth and generally most important source of vibration is that generated by rail and wheel unevenness or roughness. The unloaded rail profile is not smooth, and this is true even when the rail is new and has been recently installed. The reason is that the track and trackbed are never perfectly straight and flat. With time, ballast degrades and wheels and rails deteriorate so that rail roughness increases. Rail roughness contributes to vibration generation over a wide range of frequencies. Typical rail roughness has higher amplitudes for long wavelengths. An exception to this rule is that a major source of rail roughness is *corrugation* at wavelengths typically around 25 to 50 mm,<sup>25</sup> but for typical train speeds these short wavelengths generate vibration at frequencies well above 200 Hz. At low speeds (speed-restricted track and at the approaches to stations) dynamic forces due to corrugation are generally small in amplitude unless the track is badly corrugated. It is not generally necessary to consider corrugation when evaluating ground vibration from railways. Wheel roughness generally contributes to perceived roughness uniformly across the frequency range of interest to ground



**Figure 3** Average measured downward and upward vertical displacement of a track with different train velocities. (Reproduced from Ref. 28, by permission.)

vibration.<sup>26</sup> There is a good summary of the various factors contributing to rail roughness by Hunt.<sup>27</sup>

The fifth and final mechanism by which very large amplitudes of vibration can be generated occurs when train speeds approach or exceed either the speed of Rayleigh surface waves in the ground or the minimal phase velocity of bending waves in the track; see Fig. 3. In low-speed urban rail networks no attention need be given to this mechanism because the speed of trains is low compared with all critical wave propagation speeds. In recent years some attention has been given to this mechanism due to the increasing international trend toward higher speed trains; see, for example, Refs. 29 and 30. For the case of very soft soil, critical speed (often the Rayleigh wave speed) can be easily exceeded by modern trains. If the train velocity exceeds the Rayleigh wave speed, a ground vibration boom occurs. In a location near Ledsgard in Sweden the Rayleigh wave speed is around 45 m/s. An increase in train speed from about 38 to 50 m/s led to an increase of about 10 times in the generated ground vibration. If train speed increases further to the point where it reaches the minimal track phase velocity, larger deflections can occur with potential for train derailment. Vibration boom also occurs for underground trains if the speed reaches the velocity of shear waves in the ground.

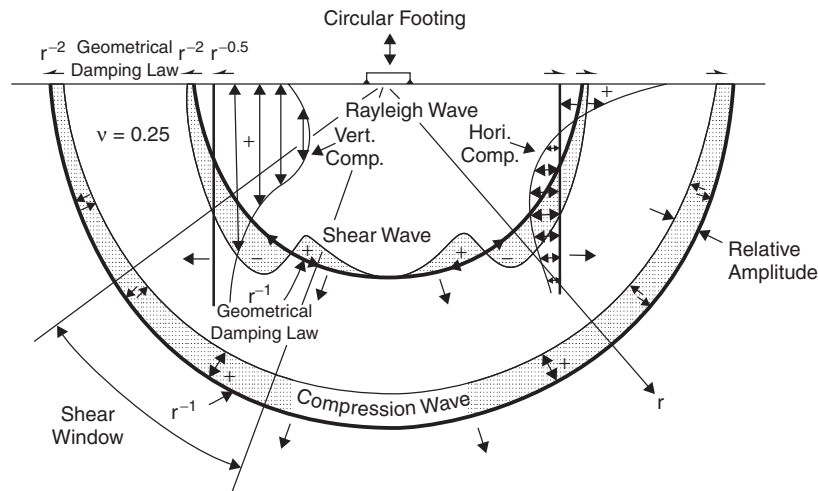
There are other special sources of vibration excitation in addition to the five mentioned above. For instance, vibration is generated when a train approaches a bridge due to the change of trackbed geometry and stiffness.<sup>31</sup> However, stiffness variation can be classified as a parametric excitation. There are also some avoidable sources of vibration, for instance, those due to static and dynamic out-of-balance of wheels, shafts, gearboxes, motors, and couplings aboard the train. Also there are disturbances that arise from tracking instability, cornering, flange contact, and gauge variation. These sources are generally of concern in older and poorly maintained track and are beyond the scope of this chapter.

#### 4 MODES OF PROPAGATION

Dynamic forces generated at the road-wheel or rail-wheel interface propagate as vibration through

the ground and into buildings, causing annoyance to people. Vibration waves in the ground are superficially like sound waves in air except that in solids many different kinds of waves exist depending on the nature of the medium and its boundaries. Even in an isotropic elastic full space (the simplest of solid media being an elastic solid infinite in all directions), two kinds of waves can propagate, and these are called the body waves, moving spherically away from a localized point of excitation. The first is a dilatational wave, or a *pressure* wave (known as the P-wave). This is a wave similar to compressive waves in air where the particles within the medium oscillate parallel to the direction of propagation of the wavefront. The second is the equivoluminal wave, or the *shear* wave (known as the S-wave). This is a transverse wave where particle motion is perpendicular to the direction of travel of the wavefront. There is no equivalent to the S-wave in air because air possesses no stiffness in shear. The situation becomes more complicated when one considers that an elastic full space has no free surface and is therefore unsuited to modeling wave propagation in the ground. It is more common to use models based on an elastic half-space (see Fig. 4) where a third kind of wave appears, confined to the free surface. This is the *Rayleigh* wave, also known as the R-wave, and the motion of particles is elliptical in a plane perpendicular both to the free surface and to the wavefront. Rayleigh waves are superficially similar to surface waves in water, but, whereas water waves are controlled by the action of gravity or surface tension, the Rayleigh wave is controlled by the elastic properties of the solid. This leads to very different characteristics. For instance, the particle motion for Rayleigh waves is *retrograde* while for waves in water particle motion is *prograde*, which means that the particles orbit in opposite directions. Also unlike water waves the vertical component of particle motion in a solid is greater than the horizontal component. Both components decay exponentially with depth so that most of the energy associated with Rayleigh waves is confined near the surface to a depth roughly equal to the wavelength.<sup>33</sup> From a practical point of view the implication is that R-waves will not be attenuated by barriers (natural or man-made) that are small compared with the wavelength, but more on this later.

Pioneering work of Lamb<sup>34</sup> on the response of an isotropic elastic half space to different kinds of impulsive and harmonic loads forms the basis of all contemporary understanding of wave propagation in elastic half space. All three types of waves (P-, S-, and R-waves) are nondispersive. This means that their wave speeds are each independent of the excitation frequencies. In the ground, the P-wave speed is the highest, typically 400 to 800 m/s. The S-wave is somewhat slower than the P-wave and only slightly faster than the R-wave, typically 200 to 300 m/s. For the frequency range of interest, the distribution of energy between the three different kinds of waves are calculated by Miller and Pursey<sup>35</sup> for an elastic half space excited by a vertically oscillating rigid disk on the surface. Of the total input energy, 67% radiates as



**Figure 4** Wave propagation in an elastic half space from a vertical surface load showing R-, S-, and P-waves. (Reproduced from Ref 32, by permission.)

R-waves, 26% as S-waves, and 7% P-waves. As P- and S-waves spread with hemispherical wavefronts in the ground, their decay rate is inversely proportional to the distance from the source. R-waves on the surface spread on a circular wavefront and with a decay rate inversely proportional to the square root of distance from the source. This reduction in amplitude with distance is called *geometric decay*. Material damping will also influence the rate at which energy decays with distance from the track, and to estimate this *material decay* it is necessary to use a model for damping.

For surface roads and railways and for buildings with reasonably shallow foundations, it is generally thought that the Rayleigh wave is chiefly responsible for vibration propagation. But this thinking is misguided in almost all situations due to the effects of layered media, wave reflections from bedrock, and the effects of building foundations. Some of these effects have analytical solutions. The Stoneley wave, for instance, appears at the discontinuous interface within an infinite solid formed by bonding two different half spaces. The Love wave (the fastest of all surface waves) moves within a surface layer bonded to a half space. The motion of particles is in a horizontal plane parallel to the free surface. Love waves can cause vibration to travel long distances from a source of disturbance. Practically speaking, real ground conditions are typified by continuous variation of soil properties with depth, and geological layers are generally inclined or discontinuous. Even if the dynamic loads applied to the track are purely vertical, the transfer of energy at the various tunnel-soil and soil-soil interfaces will cause all wave types to be excited. The depth of the water table is a further complicating and seasonally varying factor. Analytical solutions are unlikely to be of much use to practicing engineers, but an understanding of the underlying physics is useful for vibration propagation over long distances from the source. It

is useful to know that surface waves are of significance because they carry most of the energy and their geometric decay rate is low.

For propagation over long distances it is necessary to include a realistic model for damping. Modeling of damping is a matter of personal preference, and the most common approach is to use a material loss factor.<sup>36</sup> But given that many affected by vibration from railways live very close to the railway, it is not often necessary to be concerned about material decay. More important, however, are details of track components that may reduce the proportion of energy that enters the ground. For instance, energy that propagates along the rails may be dissipated before being transmitting into the ground. In tunnels the propagation process is more complicated due to interaction between the track, tunnel, and surrounding soil. It can readily be seen that vibration prediction from railways is not straightforward, but practicing engineers have evolved a number of methods for dealing with the various complications.

## 5 PREDICTION METHODS

There is increasing public sensitivity to noise and vibration, and transportation systems need to conform to increasingly stringent legislation. As a result engineers need accurate methods for predicting noise and vibration from road and rail systems. This section focuses on two prediction methods, while a good review of other methods can be found in the work of Leventhall<sup>11</sup> and Remington.<sup>12</sup>

The first is a method developed by Nelson and Saurenman.<sup>37</sup> It aims to estimate ground-borne noise and vibration from trains for a variety of building types, soil conditions, and track designs in the frequency range of 6.3 to 200 Hz in third octave bands. Design features such as resilient direct-fixation fasteners, floating slab track, resiliently supported sleepers,



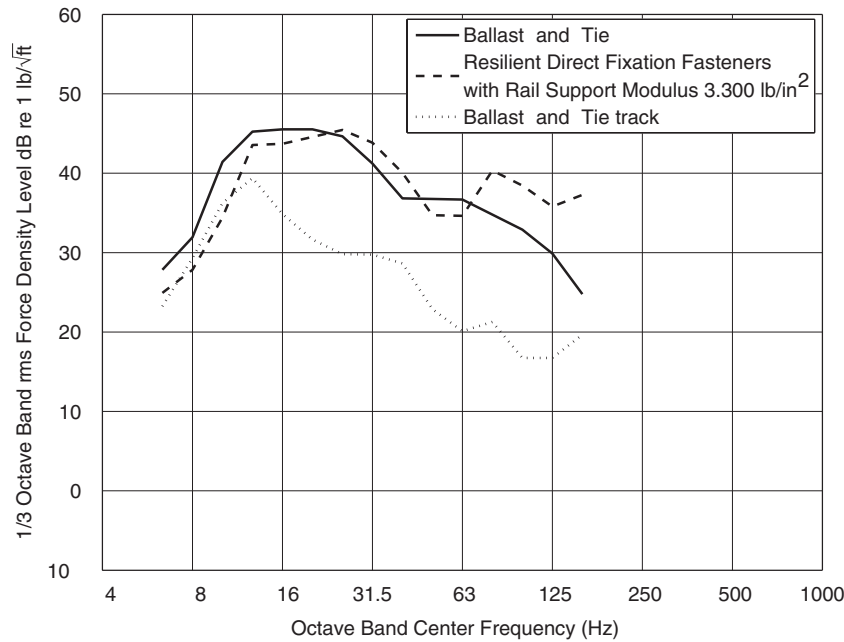


Figure 5 Force densities for heavy rail transit vehicles. (Reproduced from Ref. 37 with permission.)

continuous welded rails, vehicle suspensions, and others are considered. The method predicts the level of noise and vibration at a building (existing or proposed) at some distance from an existing or proposed surface railway or subway. The force density at trackbed, calculated from field measurements, are provided as a set of curves for different types of trains and track systems; see Fig. 5. The unit of force density is force divided by the square root of train length. The force density represents an incoherent line source at the trackbed. The curves may not correspond exactly to the actual train track system under consideration, in which case adjustments are provided for variations including floating slab, ballast mat, and primary suspension stiffness. The next step in the method is to conduct a field test procedure to determine the response due to a line source by measuring a point-to-point transfer mobility (Green's function) from the railway to the ground surface. The transfer mobility can be calculated by striking the ground or the subway invert with a hammer and measuring the input force and the resulting vibration on the ground.

For a proposed subway, the hammer is struck at the bottom of a borehole drilled to the depth of the proposed tunnel. The transfer mobility of a point source is numerically integrated over the train length to calculate the response due to a line source representing the train. This adjusted force density and the calculated response due to a line source are used to determine the vibration at the location of the building foundation as if the building were not present. A *coupling loss correction* is then used to calculate the vibration at the building foundation for the frequency range of

interest. The coupling loss gives the third octave band curve of the actual foundation vibration relative to the level of incident ground surface vertical vibration that would exist in the absence of the building and its foundation. The vibration at the foundation is corrected by means of *floor-to-floor attenuation* and *floor resonance amplification* to obtain the third octave band of vibration at the floor under consideration. These predictions can also be used to estimate room noise levels.

A second—and very different—method developed by Madshus et al.<sup>2</sup> predicts the vibration velocity from railway trains using the following formula:

$$V = F_V F_R F_B \quad (1)$$

where  $F_V = V_T F_S F_D$  is the basic vibration function.  $V_T$  is a train-type specific vibration level, defined as the vibration level on the ground at a reference distance of  $D_0 = 15$  m from the center of the track, when a train of the specified category passes at reference speed of  $S_0 = 70$  km/h on a standard track and embankment.  $F_S = (S/S_0)^A$  is a speed factor, which accounts for the effect of the train speed  $S$  and  $A$  is the train speed exponent.  $F_D = (D/D_0)^{-B}$  is a distance factor that accounts for the distance attenuation due to geometrical and hysteric damping.  $D$  is the distance from the center of the track to the receiver and  $B$  is the distance exponent.  $F_R$  is the track quality factor and  $F_B$  is the building amplification factor; it is used to transform the free-field ground vibration to floor vibration at the most unfavorable place.



**Table 2** Typical Parameters for Prediction Method

Ground Conditions	Train Type	$V_T$ (mm/s)	A	B
Soft clay	High speed	0.4–0.5	0.9–1.1	0.3–0.8
	Freight	0.7–0.8	0.9–1.1	0.3–0.4
Medium clay	High speed	0.1–0.15	0.9–1.1	0.9–1.0
	Freight	0.2–0.25	0.9–1.1	0.4–0.6

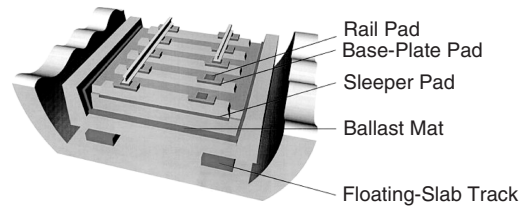
Source: From Ref. 2, reprinted by permission.

Equation (1) is used to predict one-third octave r.m.s values, with all factors being frequency dependent. Also a simplified version can be used at which all factors are frequency independent and directly related to the frequency-weighted root-mean-square (rms) velocity. The parameters of the model are computed based on a regression analysis. Typical parameters are given in Table 2.

There are other methods for predicting vibration from roads and railways. Examples are the prediction of loading and road response by Rudder<sup>38</sup> and the analytical-empirical ground vibration technique developed by Ungar and Bender.<sup>39</sup> These methods all have various merits. Individuals responsible for making vibration predictions will need to balance the need for accuracy against the resources (financial and computational) available. Some consultants will have access to an extensive database of vibration measurements from different sites, and their own experience will substantially enhance the usefulness of the predictive methods.

## 6 VIBRATION COUNTERMEASURES

Ballast in conventional railway track can act effectively to reduce vibration propagation. Generally, vibration countermeasures are required in confined spaces where ballast cannot be employed effectively. It is common to experience vibration problems where the rail is directly fixed to concrete or steel structures such as tunnels, bridges, and roadways. Vibration can also be controlled by careful attention to the detail of rail alignment, track foundation, widening of embankment (for surface railways), heavy tunnel structure, and increased tunnel depth.<sup>12,13,40</sup> Vibration can also be reduced by controlling rail and wheel roughness. This is generally considered a maintenance issue rather than a vibration countermeasure. One exception is that roughness growth can be controlled by the implementation of lubrication, especially at curves. In general, though, rail and wheel grinding are required to keep rail roughness under control. Moreover, all vibration countermeasures will require maintenance and inspection for their continued effectiveness, and some countermeasures require less maintenance than others. It must always be born in mind that any alteration to the track may render it more susceptible to corrugation growth, and this may more than outweigh the benefit of vibration countermeasures.<sup>25</sup> This can work both ways: Too high a rail support stiffness may not only give poor isolation but may contribute to excessive rail corrugation and thus excessive vibration and noise.<sup>37</sup>

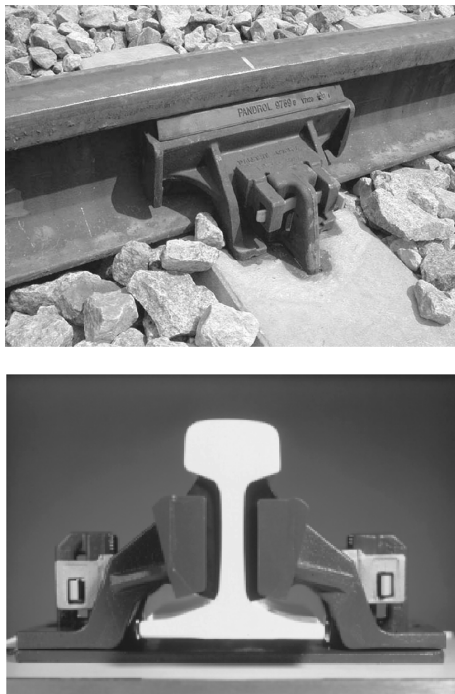


**Figure 6** Various rubber products used to reduce noise and vibration transmission from railways. (Courtesy of Getzner Werkstoffe GmbH, Bludenz, Austria.)

Vibration countermeasures fall into four categories. First, certain aspects of vehicle design will reduce dynamic force levels, for instance, by using low-stiffness vehicle suspension and a low unsprung mass (axle, axlebox, and wheel). Reducing the unsprung mass of a bogie can lead to a reduction of up to 10 to 15 dB in levels of ground-borne vibration.<sup>40</sup> Second, vibration can be isolated at the source by means of resiliently supported track (e.g., railpads and other resilient track support, resiliently mounted sleepers, ballast mat, embedded rail, and floating slab track) as illustrated in Fig. 6. Other in-track measures include reduced sleeper spacing and sleeper-mass redistribution.<sup>13</sup> Third, vibration propagation can be interrupted, for example, by digging a trench in the vibration path between the source and the receiver. This is an area of extensive study,<sup>32,41</sup> but two broad conclusions can be stated here. The performance of open trenches is better than that of concrete-filled trenches, and trench geometry has a clear effect on the isolation performance. Finally, vibration isolation can be achieved at the receiver by using rubber bearings or steel springs in the building foundations.

The most economic solution for vibration problems in old underground tunnels with directly fixed or ballasted track is likely to be resilient track support. The use of railpads does not raise the height of the rail significantly, which is an important consideration in small tunnels. A recent advance in resilient rail technology involves supporting the rail by the web and the underside of the head with large rubber wedges, leaving the foot of the rail suspended,<sup>20</sup> as shown in Fig. 7. This provides very low vertical dynamic stiffness while maintaining lateral stiffness required for vehicle and rail stability. The resilient bearing again has a low profile, and it can be installed and removed easily for maintenance. One possible disadvantage of using soft pads is that the level of noise radiated from the rail may be increased on account of the resiliently supported rail being less constrained by the base plates.<sup>13</sup>

Floating slab track is widely known as an effective measure of vibration isolation for underground tunnels. The track is mounted on a concrete slab that is fixed to the tunnel invert by means of rubber bearings or steel springs. The slab may be continuous or discrete (segmented). Continuous slab is cast in situ and segmented slab is constructed in discrete precast



**Figure 7** Resilient support of a rail, the Vanguard system. (Courtesy of Pandrol Ltd, UK.)

sections. Discrete slab is convenient in many situations: It has the advantage that vibration propagation along the track is interrupted, but there is potential for maintenance problems if the slab segments are to move relative to each other, affecting track alignment. Continuous slab has the advantage of structural integrity, but it permits vibration to propagate along the tunnel, and this may lead to greater levels of radiation from the tunnel. Examples of floating slab tracks are the 1.5-m slab in Toronto, the 3.4-m Eisenmann track in Munich and Frankfurt, the 7-m slab in the New York City subway, and the British VIPACT continuous-slab system.

In circumstances where ballast is used, as is generally the case for surface trains and in some tunnels, the use of ballast mats can be very effective. A ballast mat is simply a mat of resilient material (usually rubber, but sometimes rockwool inserted underneath the ballast). It is analogous to the use of floating-slab track in underground tunnels. An example of the use of ballast mats within a tunnel can be found in the MBTA Boston in the United States. Ballast mats are also used to improve electrical isolation, water drainage, or to reduce pulverization of the ballast.<sup>12</sup> The mechanism by which ballast mats attenuate vibration is not well understood. One view is that the ballast mat acts as a spring supporting the mass of ballast leading to vibration isolation.<sup>42</sup> An alternative view is that of the authors who believe that ballast mats are effective

on account of their ability to allow ballast to move under the application of axle loading. This prevents the ballast from “locking up.” The truth is, no doubt, a combination of these two effects.

In soft ground it may be necessary to improve the characteristics of the soil surrounding the track. Soil stabilization by means of injection grouting under and adjacent to the track is effective because it stiffens the soil structure, which reduces vibration propagation due the quasi-static effect.<sup>13</sup> This can be particularly important for high-speed trains where trans-Rayleigh effects can cause large-amplitude vibration.

A common theme that runs through all attempts to assess the performance of vibration countermeasures is that trends are difficult to identify. It is found, for instance, that measures effective for one site are less effective for another and that the effectiveness of in-track countermeasures is sometimes found to reduce with distance from the track. It is clear that detailed modeling is required to make sense of these observations and that accurate models can be used to drive the development of new countermeasures.

## 7 MODELING

The strategy for modeling ground vibration from road traffic differs from that for rail traffic mainly because of the difference in excitation mechanisms. For road vehicles the pavement can be considered to be rigid, and the vehicle suspension is responsible for controlling the dynamic forces generated in response to road roughness. This permits a decoupling of the excitation mechanism from the wave propagation mechanism, which simplifies modeling. However, for rail vehicles the unsprung mass of wheel and axle combine with the mass of that part of the rail within the deflection bowl to move in response to rail roughness. Decoupling is no longer possible. Nevertheless, the propagation mechanisms are largely common to both problems, and an understanding of wave propagation and modeling of the response of a half space under different kinds of loading is essential before embarking on any detailed modeling. Much of the fundamental work was discussed in Section 4, but there are some further fundamental issues that require discussion. These include: (1) the effects of moving loads, (2) random vibration theory, (3) track modeling, (4) tunnel modeling, and (5) ground modeling. For any realistic model of traffic-induced vibration, all these effects will need to be considered. Most can only be addressed through extensive use of mathematical techniques (Fourier, wavelet, and Floquet transforms) and through the use of computational techniques such as the finite element and boundary element methods (FEM–BEM). It is not possible here to do more than to identify the various techniques.

Early models for computing vibration generated from moving loads used a solution of moving constant force on elastic half space. More advanced developments were made possible by including the inertial effect of vehicles. Fryba<sup>43</sup> discusses lucidly several aspects of vibration of solids and structures under moving loads. Moving loads can be classified in three

ways depending on whether the speed is less than, equal to, or greater than the lowest wave speed in the structure—that is, the critical speed. Above the critical speed, waves analogous to shock waves are generated, producing large amplitudes in the structure. These large amplitudes are only to be expected in soft ground or on flexible structures; most readers need not concern themselves with the critical speed.

A theoretical analysis of the transmission of road-vehicle-induced vibration through the ground by Hunt<sup>44</sup> considers vibration as a Gaussian-distributed random process. Vehicles are modeled as single-axle two degrees of freedom. Power spectral expressions are calculated for the vertical ground acceleration away from a long straight road. Only a half-space model is used (i.e., no layering), and approximate methods are used to account for the effect of the bending stiffness of the road surface. A series of measurements is presented to validate the model, and a parametric survey demonstrates the sensitivity of traffic-induced ground vibration levels to ground properties, vehicle speed, traffic intensity, road roughness, and vehicle characteristics. This methodology is extended by Hunt<sup>45</sup> for the calculation of building vibration generated by railways using theory of random vibration and models of infinite length for both building and track.

The Winkler beam<sup>46</sup> (or *beam on elastic foundation*) is used extensively to model railway tracks. Discrete supports of rails can be assumed as an elastic foundation of Winkler type. The benefit of using Winkler beam theory to model railway track is that it is relatively easily coupled to models of the ground. But while Winkler beam methods are within the computational abilities of many engineers, they do not enable the beneficial effects of track resilience to be computed with any accuracy. It is not unusual for insertion loss performance figures of 30 dB or better to be quoted based on Winkler theory, but it is generally found that such performance cannot be achieved in practice. At any reasonable distance from the track, it is unrealistic to expect insertion loss of greater than 15 dB from even the best of vibration countermeasures.

A theoretical model for both the generation and propagation of vibration from freight trains is presented by Jones and Block.<sup>1</sup> The model accounts for both the rail roughness and the quasi-static effect of moving axles. The input to the model is taken from measurements by using a track recording coach. The predicted vibration agrees well with the measured vibration in the frequency range of 5 to 30 Hz. It is found that heavy freight trains emit ground vibration with predominant frequency component in the range of 4 to 30 Hz.

Sheng et al.<sup>23,47–49</sup> present a fully three-dimensional model of a railway track coupled to a multilayered half space. Both of the rails are modeled as a single Euler–Bernoulli beam, and railpads are modeled as a continuous resilient layer. Sleepers are modeled as a continuous beam with no bending stiffness, and ballast is modeled as a continuous layer of a linear spring with a consistent mass approximation. The results show a good agreement with measurements taken at three different

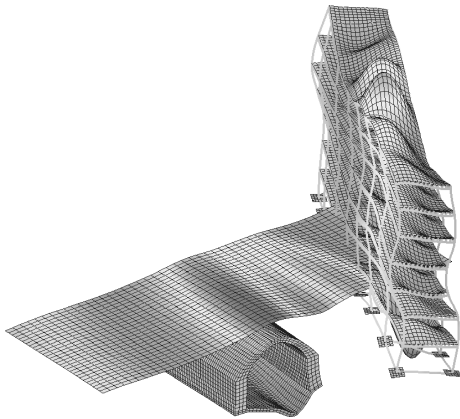
sites and demonstrate the dominance of the quasi-static effect near the track at low frequencies. The model is used to investigate the effect of track properties on ground-borne vibration.

Krylov<sup>50</sup> presents a model to investigate the effect of high-speed trains on ground vibration. The important feature of the model is that it accounts for sleeper spacing and the quasi-static forces of the moving train. This model is used by Krylov et al.<sup>29</sup> to predict the vibration generated by the French TGV and Eurostar high-speed trains along tracks built on soft soils. Degrande and Lombaert<sup>51</sup> use the Betti–Rayleigh dynamic reciprocity theorem to increase the efficiency of Krylov's model. Degrande and Schillemans<sup>51</sup> compare the results from this model with free-field vibration measurements during the passage of a Thalys high-speed train at various speeds. The model gives good predictions at low frequencies where the quasi-static response dominates and at high frequencies where sleeper-passing response dominates. At the mid-frequency range where other mechanisms, for example, rail roughness are important, the model underestimates the response. Another theoretical and experimental study on vibration from high-speed trains is presented by Kaynia et al.<sup>28</sup> where a good match is shown between the predicted and measured results.

A three-dimensional semianalytical model for a floating-slab track in a deep underground tunnel is presented by Hunt.<sup>53</sup> The model consists of Euler–Bernoulli beams to account for the rails and the track slab. The slab is coupled to the *pipe-in-pipe model*, which consists of a thin shell (the inner pipe) representing a tunnel, embedded within an infinite continuum with a cylindrical cavity (the outer pipe) representing the surrounding soil. Coupling is performed in the wavenumber–frequency domain. Three-dimensional numerical models are developed by some researchers to model vibration from underground railways. The main disadvantage of these models is that they are computationally expensive. Powerful numerical models are developed under CONVURT, where a coupled FEM–BEM is used. The FEM is used to model tunnel walls while the BEM is used to model the surrounding soil. Taking account of periodicity in the tunnel direction using Floquet transformation makes a significant improvement in the running time.<sup>54</sup>

Coupled FEM/BEM are also used to model road-traffic-induced vibration. An example is the work of Pyl et al.,<sup>55</sup> which incorporates a moving source and accounts for soil–structure interaction. A two-dimensional vehicle model is used on longitudinal road roughness to account for the source, and the input is calculated by assuming the vehicle response to be uncoupled from the road–soil response. The finite element method is used to model a building where the vibration is predicted, and the boundary element method is used to model the ground. An example of the power of coupled FEM/BEM methods is illustrated in Fig. 8.

A different numerical method is used by Sheng et al.<sup>56</sup> This method is the *discrete wavenumber*



**Figure 8** Example of boundary element modeling. Vibration of a building near a Metro tunnel in Paris. (Courtesy of D. Clouteau, École Centrale, Paris.)

*fictitious force* method and is used to model an underground tunnel embedded in a half space. The method depends on writing the boundary integral equations of only the displacement Green's function. This is an advantage over the BEM as the traction Green's function is not required. The finite difference method<sup>57</sup> may also be used to model the traffic-induced and rail-induced ground vibration. Its advantage is thought to be that the computational code is much simpler than conventional numerical methods such as BEM and FEM.

The methods described here are of limited use in practice for four reasons: First, they require substantial computational resources in addition to a working knowledge of some fairly high powered analytical tools. Second, a large quantity of input data is required for the models, and this may not be readily available. In particular, the variation of soil properties with depth is unlikely to be known to great accuracy, and the quality of predictions made can only be as good as the quality of the input data. Third, few of these models are validated over a wide range of different track and ground conditions. It may be more sensible to use an older and simpler predictive method that has stood the test of time. Finally, no models presently available take into account the nonlinearities of track elements and of soils. These are likely to be significant if accurate predictions are to be made.

## 8 CONCLUSION

There is no simple answer for the computation of vibration generated by road or rail traffic. Simple models do not work with sufficient accuracy and elaborate models are computationally expensive. Empirical models are valid only in certain simplified circumstances and experimental measurement of vibration is only really useful when there is the option of trying out various different methods. It is the view of the authors that substantial advances in vibration reduction will only occur when the computational tools are widely

available and in the hands of the engineers responsible for road, track, and tunnel design.

## REFERENCES

1. C. J. C. Jones and J. R. Block, Prediction of Ground Vibration from Freight Trains, *J. Sound Vib.*, Vol. 193, No. 1, 1996, pp. 205–213.
2. C. Madshus, B. Bessason, and L. Harvik, Prediction Model for Low Frequency Vibration from High Speed Railways on Soft Ground, *J. Sound Vib.*, Vol. 193, No. 1, 1996, pp. 195–203.
3. BS 6472:1992, Guide to Evaluation of Human Exposure to Vibration in Buildings (1 Hz to 80 Hz), 1992.
4. ANSI S3.29–1983, Guide to the Evaluation of Human Exposure to Vibration in Buildings, 1983.
5. M. L. M. Duarte and M. R. Filho, Perception Threshold of People Exposed to Sinusoidal Vibration, Proceedings of the Tenth International Congress on Sound and Vibration, Stockholm, Sweden, 2003, pp. 3791–3798.
6. C. G. Gordon, Generic Vibration Criteria for Vibration-Sensitive Equipment, *Proc. SPIE*, Vol. 3786, 1999, pp. 22–39.
7. ISO 2631-2:2003, Mechanical Vibration and Shock—Evaluation of Human Exposure to Whole-Body Vibration—Part 2: Vibration in Buildings (1 Hz to 80 Hz), 2003.
8. T. Maeda, Protecting the Tracks Environment, in *Railway Technology Today*, K. Wako, Ed., Japan Railway and Transport Review 22, December 1999, pp. 48–57.
9. Y. Okumura and K. Kuno, Statistical Analysis of Field Data of Railway Noise and Vibration Collected in an Urban Area, *Appl. Acoust.*, Vol. 33, 1991, pp. 263–280.
10. J. M. Fields, Railway Noise and Vibration Annoyance in Residential Areas, *J. Sound Vib.*, Vol. 66, No. 3, 1979, pp. 445–485.
11. H. G. Leventhall, Low-Frequency Traffic Noise and Vibration, in *Transportation Noise Reference Book*, P. M. Nelson, Ed., Butterworth, London, 1987, Chapter 12.
12. P. J. Remington, L. G. Kurzweil, and D. A. Towers, Low-Frequency Noise and Vibration from Trains, in *Transportation Noise Reference Book*, P. M. Nelson, Ed., Butterworth, London, 1987.
13. R. Hildebrand, Countermeasures against Railway Ground and Track Vibrations, Report at Department of Vehicle Engineering, Stockholm, 2001 ([www.lib.kth.se/Sammanfattningar/hildebrand011210.pdf](http://www.lib.kth.se/Sammanfattningar/hildebrand011210.pdf)).
14. J. H. A. Crockett, Some Practical Aspects of Vibration in Civil Engineering, in *Vibration in Civil Engineering*, Butterworths, London, 1966, pp. 267–272.
15. I. H. Turunen-Rise, A. Brekke, L. Harvik, C. Madshus, and R. Klaboe, Vibration in Dwellings from Road and Rail Traffic—Part I: A New Norwegian Measurement Standard and Classification System, *Appl. Acoust.*, Vol. 64, No. 1, 2003, pp. 71–87.
16. R. Klaboe, I. H. Turunen-Rise, L. Harvik, and C. Madshus, Vibration in Dwellings from Road and Rail Traffic—Part II: Exposure-Effect Relationships Based on Ordinal Logit and Logistic Regression Models, *Appl. Acoust.*, Vol. 64, No. 1, 2003, pp. 89–109.
17. R. Klaboe, E. Ohrstrom, I. H. Turunen-Rise, H. Bendtsen, and H. Nykanen, Vibration in Dwellings from Road and Rail Traffic—Part III: Towards a Common Methodology for Socio-vibrational Surveys, *Appl. Acoust.*, Vol. 64, No. 1, 2003, pp. 111–120.
18. D. Clouteau, R. Othman, M. Arnest, and H. Chebli, A Numerical Model for Ground-Borne Vibrations from

- Underground Railway Traffic Based on a Periodic FE-BE Formulation, Proceedings of the Eighth International Workshop on Railway Noise, No. 1, Buxton, UK, 2004, pp. 167–178.
19. M. F. M. Hussein and H. E. M. Hunt, A Power Flow Method for Evaluating Vibration from Underground Railways, Proceedings of the Eighth International Workshop on Railway Noise, No. 1, Buxton, UK, 2004, pp. 189–200.
  20. S. Cox, Installation and Testing of Vibration Reducing Track Fastening within the CONVURT Project, Proceedings of the Tenth International Congress on Sound and Vibration, Stockholm, Sweden, 2003, pp. 379–386.
  21. J. P. Talbot, H. E. M. Hunt, and M. F. M. Hussein, A Prediction Tool for Optimization of Maintenance Activity to Reduce Disturbance Due to Ground-Borne Vibration from Underground Railways, Proceedings of the Eighth International Workshop on Railway Noise, No. 2, Buxton, UK, 2004, pp. 409–420.
  22. G. R. Watts, Vehicle Generated Ground-Borne Vibration Alongside Speed Control Cushions and Road Humps, in *Ground Dynamics and Man-Made Processes: Prediction, Design, and Management*, B. O. Skipp, Ed., Thomas Telford, London, 1998, Chapter 6.
  23. X. Sheng, C. J. C. Jones, and D. J. Thompson, A Comparison of a Theoretical Model for Quasi-Static and Dynamically Induced Environmental Vibration from Trains with Measurements, *J. Sound Vib.*, Vol. 267, No. 3, 2003, pp. 621–635.
  24. M. Heckl, G. Hauk, and R. Wettschureck, Structure-Borne Sound and Vibration from Rail Traffic, *J. Sound Vib.*, Vol. 193, No. 1, 1996, pp. 175–184.
  25. J. C. O. Nielsen, Numerical Prediction of Rail Roughness Growth on Tangent Railway Track, *J. Sound Vib.*, Vol. 267, No. 3, 2003, pp. 537–548.
  26. G. Degrande, P. Chatterjee, W. V. Velde, P. Hoelscher, V. Hopman, A. Wang, N. Dadkah, and R. Klein, Vibrations Due to a Test Train at Variable Speeds in a Deep Bored Tunnel Embedded in London Clay, Proceedings of the Eleventh International Congress on Sound and Vibration, St. Petersburg, Russia, 2004, pp. 3055–3062.
  27. H. E. M. Hunt, Modelling of Rail Roughness for the Evaluation of Vibration-Isolation Measures, Proceedings of the Twelfth International Congress on Sound and Vibration, Lisbon, Portugal, 2005 (on CD-ROM).
  28. A. M. Kaynia, C. Madhus, and P. Zackrisson, Ground Vibration from High-Speed Trains: Prediction and Countermeasure, *J. Geotech. Geoenviron. Eng.*, Vol. 126, No. 6, 2001, pp. 531–537.
  29. V. V. Krylov, A. R. Dawson, M. E. Heelis, and A. C. Collop, Rail Movement and Ground Waves Caused by High-Speed Trains Approaching Track-Soil Critical Velocities, *Proc. Instn. Mech. Eng.*, Vol. 214, 2000, pp. 107–116.
  30. H. Takemiya, X. C. Bian, K. Yamamoto, and T. Asayama, High-Speed Train Induced Ground Vibrations: Transmission and Mitigation for Viaduct Case, Proceedings of the Eighth International Workshop on Railway Noise, No. 1, Buxton, UK, 2004, pp. 107–118.
  31. H. E. M. Hunt, Settlement of Railway Track Near Bridge Abutment, *Proc. Instn. Civ. Eng., Transp.*, Vol. 123, 1997, pp. 68–73.
  32. R. D. Woods, Screening of Surface Waves in Soils, *J. Soil Mech. Found. Div., Proc. Am. Soc. Civil Eng.*, SM4, 1968, pp. 951–979.
  33. K. F. Graff, *Wave Motion in Elastic Solids*, Oxford University Press, London, 1975.
  34. H. Lamb, On the Propagation of Tremors over the Surface of an Elastic Solid, *Phil. Trans. Roy. Soc., Ser. A*, CCIII 1, 1904, pp. 1–42.
  35. G. F. Miller and H. Pursey, On the Partition of Energy between Elastic Waves in a Semi-infinite Solid, *Proc. Royal Soc.*, Vol. 233, Series A, 1955, pp. 55–69.
  36. T. G. Gutowski and C. L. Dym, Propagation of Ground Vibration: A Review, *J. Sound Vib.*, Vol. 49, No. 2, 1976, pp. 179–193.
  37. J. T. Nelson and H. J. Saurenman, A Prediction Procedure for Rail Transportation Groundborne Noise and Vibration, Transportation Research Record, No. 1143, 1987, pp. 26–35.
  38. F. F. Rudder, Engineering Guidelines for the Analysis of Traffic Induced Vibrations, Report No. FHWA RD-78-167, U.S. Department of Transportation, Washington, DC, 1978.
  39. E. E. Ungar and E. K. Bender, Vibrations Produced in Buildings by Passage of Subway Trains: Parameter Estimation for Preliminary Design, Inter-Noise 75, Japan, 1975, pp. 491–498.
  40. G. P. Wilson, H. J. Saurenman, and J. T. Nelson, Control of Ground-Borne Noise and Vibration, *J. Sound Vib.*, Vol. 87, No. 2, 1983, pp. 339–350.
  41. S. E. Kattis, D. Polyzos, and D. E. Beskos, Modelling of Pile Wave Barriers by Effective Trenches and their Screening Effectiveness, *Soil Dynamics Earthquake Eng.*, Vol. 18, 1999, pp. 1–10.
  42. R. Wettschureck, Vibration and Structure-Borne Noise Insulation by Means of Cellular Polyurethane (PUR) Elastomers in Railway Track Applications, *Rail Eng. Int. Ed.*, Vol. 2, 1995, pp. 7–14.
  43. L. Fryba, *Vibration of Solids and Structures under Moving Loads*, Noordhoff Publishing, Groningen, 1972.
  44. H. E. M. Hunt, Stochastic Modelling of Traffic-Induced Ground Vibration, *J. Sound Vib.*, Vol. 144, No. 1, 1991, pp. 53–70.
  45. H. E. M. Hunt, Modelling of Rail Vehicles and Track for Calculation of Ground-Vibration Transmission into Buildings, *J. Sound Vib.*, Vol. 193, No. 1, 1996, pp. 185–194.
  46. L. Fryba, History of Winkler Foundation, *Vehicle Sys. Dynamics Suppl.*, Vol. 24, 1995, pp. 7–12.
  47. X. Sheng, C. J. C. Jones, and M. Petyt, Ground Vibration Generated by a Load Moving along a Railway Track, *J. Sound Vib.*, Vol. 228, No. 1, 1999, pp. 129–156.
  48. X. Sheng, C. J. C. Jones, and D. J. Thompson, A Theoretical Study on the Influence of the Track on Train-Induced Ground Vibration, *J. Sound Vib.*, Vol. 272, 2004, pp. 909–936.
  49. X. Sheng, C. J. C. Jones, and D. J. Thompson, A Theoretical Model for Ground Vibration from Trains Generated by Vertical Track Irregularities, *J. Sound Vib.*, Vol. 272, 2004, pp. 937–965.
  50. V. V. Krylov, Effects of Track Properties on Ground Vibrations Generated by High-Speed Trains, *Acta Acust.*, Vol. 84, 1998, pp. 78–90.
  51. G. Degrande and G. Lombaert, An Efficient Formulation of Krylov's Prediction Model for Train Induced Vibrations Based on the Dynamic Reciprocity Theorem, *J. Acoust. Soc. Am.*, Vol. 110, No. 3, 2001, pp. 1379–1390.
  52. G. Degrande and L. Schillemans, Freefield Vibrations During the Passage of a Thalys High-Speed Train at

- Variable Speed, *J. Sound Vib.*, Vol. 247, No. 1, 2001, pp. 131–144.
53. H. E. M. Hunt, Measures for Reducing Ground Vibration Generated by Trains in Tunnels, in *Noise and Vibration from High-Speed Trains*, V.V. Krylov, Ed., Thomas Telford, London, 2001.
54. D. Clouteau, M. Arnst, T.M. Al-Hussaini, and G. Degrande, Freefield Vibrations Due to Dynamic Loading on a Tunnel Embedded in a Stratified Medium, *J. Sound Vib.*, Vol. 283, Nos. 1–2, 2005, pp. 173–199.
55. L. Pyl, G. Degrande, and G. Lombaert, Numerical Modelling of Traffic Induced Vibrations in Buildings Based on a Dynamic Soil-Structure Interaction Formulation, 15th ASCE Engineering Mechanics Conference, New York, 2002.
56. X. Sheng, C. J. C. Jones, and D. J. Thompson, Ground Vibration Generated by a Harmonic Load Moving in a Circular Tunnel in a Layered Ground, Proceedings of the 10th International Meeting on Low Frequency Noise and Vibration and Its Control, York, UK, 2002, pp. 161–176.
57. R. M. Thornely-Taylor, The Prediction of Vibration, Ground-Borne and Structure-Radiated Noise from Railways Using Finite Difference Method—Part1—Theory, *Proc. Inst. Acoust.*, Vol. 26, No. 2, 2004, pp. 69–79.

# CHAPTER 124

## BASE ISOLATION OF BUILDINGS FOR CONTROL OF GROUND-BORNE VIBRATION

**James P. Talbot**  
Atkins Consultants  
Derby, United Kingdom

### 1 INTRODUCTION

There are many sources of ground-borne vibration in our cities. Some, such as the piling of a new building foundation, are short lived and relatively few people are affected. Others, such as the passage of vehicles on roads and railways, are a more permanent feature of the urban environment. These sources may cause daily disturbance to building occupants, with significant social and economic consequences.

Base isolation involves inserting isolation bearings between a building and its foundation in order to reduce internal levels of perceptible vibration and reradiated noise. Either rubber bearings or steel springs may be used. Since the introduction of base isolation techniques in the 1960s, they have become well established as one of the most effective means of controlling ground-borne vibration. These bearings are now used in residential buildings, office towers, concert halls, cinemas, and hospitals.

### 2 SOURCES OF GROUND-BORNE VIBRATION AND THEIR CONTROL

The dominant sources of urban ground-borne vibration fall into three categories: construction activity, roads, and railways. With the possible exception of certain construction activities, vibration levels are unlikely to cause damage to buildings. Typical levels due to road and rail traffic lie in the range from 0.1 to 1.0 mm/s and peak in the frequency range from 10 to 100 Hz. Such levels are significantly below those at which even light damage, such as the cracking of plaster, may be expected. Nevertheless, the daily disturbance caused to building occupants and the disruption caused in specialist buildings, such as hospitals and research facilities, can have significant social and economic consequences.

There are many examples of construction activity that generate ground-borne vibration: blasting, tunnelling, piling, and vibratory compaction can all cause disturbance in nearby buildings. These sources are usually short lived and relatively few people are affected. They are best controlled by careful design and management of the activities themselves.

In contrast, road and rail vehicles can cause disturbance to large numbers of people many times a day. In particular, railways carry heavy vehicles at high speed, often passing within a few metres of buildings and their foundations. They are generally regarded as the most significant source of ground-borne vibration. Railways may make use of vibration

control measures at source, and a variety of isolation systems are available for incorporation within the track. Further details may be found in Chapter 123.

Control at source is not always possible. For example, where new buildings are constructed near existing railways, it may be difficult and expensive to take retrospective measures with either the vehicles or the track. In such cases measures are usually restricted to the buildings themselves. A variety of straightforward cost-effective measures exist that may be sufficient to control low levels of ground-borne vibration. Damping treatments may be incorporated into the building structure, floating floors installed, or local stiffening undertaken to control structural resonances. However, in certain cases the level of ground-borne vibration may be considered large enough to justify the base isolation of a building. Figure 1 illustrates a typical example. In this case a multistory office building is isolated on spring bearings located in the basement car park.

### 3 DECISION TO BASE ISOLATE AND ITS IMPLICATIONS

The level of vibration within a building that is considered acceptable is dependent upon many factors, such as the duration and nature of the vibration, the type of building, the activities of its occupants, and what the occupants feel, hear, and see. More subjective factors may also be involved, such as what the occupants expect to experience, concerns over structural damage, and whether they believe anything could or would be done to improve the situation, such as reducing the vibration or awarding compensation, if they were to complain.

A number of standards aim to provide guidance on the acceptable levels of perceptible vibration in buildings, such as the British standard (BS) 6472<sup>1</sup> and the International Organization for Standardization (ISO) 2631-2.<sup>2</sup> Table 1 reproduces levels given in both these standards at which adverse reactions may be expected from people living and working in buildings. The levels are expressed as vibration dose values, a measure deemed appropriate for assessing transient vibration, such as that from a passing train. Further information may be found in Chapter 30. In some buildings, such as hospitals and research facilities, the acceptable level is determined by the nature of the equipment they contain.<sup>3,4</sup>

Audible noise radiated from the vibrating structure of a building can also cause disturbance. In the case



**Figure 1** Typical base-isolated building in the form of a multistory office. (Courtesy of GERB Schwingungsisolierungen GmbH & Co, Germany.) The entire building is isolated from its foundation by spring bearings located in the basement.

**Table 1** Vibration Dose Values ( $\text{m/s}^{1.75}$ ) Suggested in BS 6472 and ISO 2631-2 at Which Adverse Reactions May Be Expected from Building Occupants

Place	Low Probability of Adverse Comment	Adverse Comment Possible	Adverse Comment Probable
Critical working areas	0.1	0.2	0.4
Residential	0.2–0.4	0.4–0.8	0.8–1.6
Office	0.4	0.8	1.6
Workshops	0.8	1.6	3.2

of railway vibration, this *reradiated noise* manifests as a low-frequency rumble, which may be audible even when the vibration itself cannot be felt. The peak frequency component of the noise does not necessarily coincide with that of the vibration because it depends on the radiation efficiency of the structure concerned. It is typically most noticeable in the frequency range from 50 to 125 Hz. No standards currently exist specifically concerning internal reradiated noise, although

various guidelines exist, such as those produced by the American Federal Transit Administration (FTA).<sup>5</sup>

In practice, the decision on whether or not to base isolate a building is usually based on a series of vibration measurements. These are made either at the site in question, prior to any construction work, or on a similar building to the one being designed. The data collected may then be analyzed in light of previous experience and with the aid of the appropriate standards and theoretical models.

### 3.1 Practical Implications

There are practical design implications, not normally associated with a typical building project, that must be addressed once the requirement for base isolation has been established. A major implication is the reduction in structural stiffness and overall stability due to mounting the building on isolation bearings. Some tall buildings are constructed of floor slabs supported on columns and derive their stiffness from a service tower or lift shaft. Once such a building is mounted on bearings, the stiffness of the structure is often no longer adequate and additional stiffening is required. Additional horizontal stability may need to be provided by sets of horizontal bearings.

Additional consideration must be given to settlement of the building on its bearings, either during construction or subsequently through creep in the bearings, fire proofing of the bearings, and designing fail-safe measures for the unlikely event of a collapsed bearing. Care must also be taken not to “bridge” the isolation by, for example, staircases, building services, construction debris, or acoustical coupling. Suppliers of base isolation bearings are usually able to advise on these matters.

## 4 GENERIC DESIGN PRINCIPLES

The underlying principles of base isolation are similar to those used to protect buildings against earthquakes, although the practical implementation of isolation against ground-borne vibration differs due to the lower vibration amplitudes and the presence of higher frequencies. Seismic isolation of buildings is the subject of Chapter 117.

This chapter is concerned with *base*-isolated buildings and, usually, design considerations do indeed require the bearings to be located at the base of the building, such as on the pile caps or at basement level. In principle, it is possible to locate the bearings higher up the structure and isolate only the upper floors. However, this should be done with care as amplification of the ground vibration due to resonances of the unisolated structure below the bearings may reduce their performance.

No standards currently exist specifically governing the design of base-isolated buildings. In practice, design strategies are based on past experience and the requirements of the particular project. It is common practice to consider only vertical motion of the building: The horizontal component of ground motion is generally neglected on the assumption that the building’s inherent flexibility in this direction provides



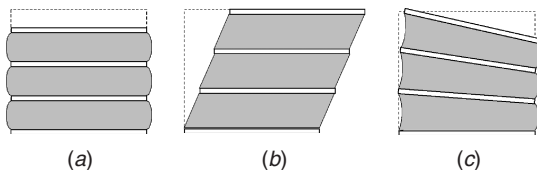
sufficient isolation. However, there is theoretical evidence to suggest that this may not always be the case.<sup>6</sup> It is now generally recognized that the structural elements at the base of a building exhibit a combination of vertical, horizontal, and rotational motion. It is, therefore, recommended that all three primary modes of deformation of an isolation bearing are accounted for during design, as illustrated in Fig. 2.

As originally proposed by Waller,<sup>7</sup> on the basis of vertical motion being dominant, base isolation systems are principally defined in terms of their *isolation frequency*. This is the resonance frequency of the building on its bearings assuming it behaves as a rigid mass on a spring. Note that effective isolation does not begin until frequencies somewhat higher than the isolation frequency, as discussed later. The isolation frequency must, therefore, lie sufficiently below the frequency range of the ground-borne vibration in order to avoid excessive low-frequency motion of the building.

Typical isolation frequencies lie in the range from 5 to 15 Hz, and a lower isolation frequency generally gives rise to more effective isolation. However, they should be quoted with care, primarily due to the limitations of the single-degree-of-freedom model. For example, the rocking modes of a building are likely to occur at frequencies significantly different from the vertical "bounce" frequency.

Isolation frequencies should be based on the dynamic stiffness of the bearings, which can depend on several factors, such as excitation frequency and static load. Allowance should also be made for secondary stiffnesses, such as those associated with seals between adjacent structures, and the mass should be based on the "unfactored" dead load of the building, including allowances for furniture, occupants, and equipment.

The level of inherent damping offered by bearings is also often quoted as an important design parameter. Base isolation relies on vibration isolation rather than energy dissipation, the basic requirement being a low dynamic stiffness. For maximum isolation, therefore, current designs are based on the inherent damping being as low as possible, provided that sufficient damping is present to control any internal resonances of the bearings themselves. It is generally true that sufficient damping is provided by structural elements within a building, and by vibration re-radiated into the foundation, so that the bearings themselves do not need to provide damping.



**Figure 2** Three primary modes of deformation associated with an isolation bearing: (a) vertical compression, (b) horizontal shear, and (c) rotation.

#### 4.1 Rubber Bearings and Steel Springs for Base Isolation

Despite many different types of isolation bearing having been tried in the past, the choice for modern buildings essentially lies between laminated rubber bearings and steel helical springs,<sup>8,9</sup> as illustrated in Fig. 3. Rubber bearings are available in two different types: either carbon-loaded natural rubber, reinforced and stiffened by laminating with steel plates, or synthetic rubber made more flexible by loading with cork particles and reinforced with layers of woven cloth. Spring bearings are supplied in units containing several steel helical springs. These may include additional damping elements to limit vibration transmission at the internal resonance frequencies of the bearing. Examples include the incorporation of "noise-stop pads," in the form of rubber pads inserted above or below the springs, or the use of auxiliary viscous dampers.

Some bearings are available precompressed between two steel plates, typically up to 80% of the



**Figure 3** Base isolation bearings are available as either laminated rubber bearings or steel helical springs. (Courtesy of CDM, Belgium and GERB Schwingungsisolierungen GmbH & Co, Germany.)

expected static load. This does not influence the isolation performance, but it does limit the static deflection of the building during construction. It also enables postconstruction adjustment of the bearings, should differential settlement be detected, for example.

In summary, when selecting a particular bearing design, the following primary characteristics should be considered.

- *Isolation frequency* This is the parameter commonly used for defining the vertical dynamic stiffness of the bearings for a particular application.
- *Horizontal and rotational stiffness* As well as influencing the isolation performance, these influence the horizontal stability of the building.
- *Dynamic/static stiffness ratio* The dynamic stiffness determines the isolation performance while the static stiffness controls the level of settlement during construction, or the level of precompression required to limit this. Dynamic stiffness is more difficult to measure than static stiffness and data may not be available for some materials.
- *Inherent damping* For a low dynamic stiffness this should be as low as possible, provided that sufficient damping is present to control any internal resonances of the bearings.

All of the above characteristics influence isolation performance to some extent and should be considered during design. The remainder of this chapter discusses the measurement and prediction of isolation performance in order to aid this process.

## 5 ISOLATION PERFORMANCE

No standard measures exist for assessing base isolation performance, although three categories of measure are encountered in practice: “green-field” site predictions, predictions given a particular source, and insertion gain. The first two are measures of *absolute* performance while the third is a measure of *insertion* performance.

### 5.1 Absolute Performance

The future occupants of a new building are interested in the absolute performance of the isolation, that is, what they will experience in the completed building. Engineers may satisfy this by predicting vibration levels within the isolated building given vibration data measured on the green-field site prior to any construction work. This approach often forms the basis of a decision on whether or not base isolation is necessary. Green-field site predictions require knowledge of the effects of the building and its foundation on the ground vibration field, as well as an understanding of the dynamic behavior of the building itself.

Alternatively, predictions of the vibration levels due to a particular source may be required. In this case, particular care must be taken as a detailed understanding of the entire vibration transmission path is required.

### 5.2 Insertion Performance

The client who pays for the additional cost of base isolation is interested in the insertion performance, that is, the benefit of inserting isolation bearings beneath a building. It is also of interest to the engineer who wishes to evaluate alternative types of bearing.

It is worth stressing that performance generally cannot be characterized by making in situ vibration measurements above and below bearings. Lower vibration levels above a bearing should not be regarded as indicative of isolation performance because such measurements concentrate on the forced response of only a small part of a complex structure. In addition, any difference in vibration levels across a bearing may be exaggerated by the existence of higher levels below the bearing than would otherwise exist if the building was unisolated. This is due to the decoupling of the building from its foundation and the consequent reduction in constraint at the base of the building.

In principle, if the building already exists, internal vibration measurements may be made before and after installation of the bearings. However, this can be difficult and expensive to achieve in practice, and, if attempted, an effective measurement program requires careful thought concerning the measurement locations, the quantity to be measured, and in what direction. A comprehensive evaluation of performance should account for the necessary structural changes associated with base isolation—the structure and foundation of an isolated building may be quite different from the unisolated design.

Given the difficulties associated with measurements, predictions of performance are essential in guiding design. A common measure of insertion performance is *insertion gain* (IG). This is the ratio, usually expressed in decibels, of the building response with bearings in position to that with no bearings at all:

$$IG = 20 \log_{10} \left( \frac{x_{\text{isol}}}{x_{\text{unisol}}} \right) \quad (1)$$

where  $x_{\text{isol}}$  and  $x_{\text{unisol}}$  are the responses of the building in the isolated and unisolated condition, respectively. Either the displacement, velocity, or acceleration response may be used because it is assumed that the behavior of the building is linear. Note that the reciprocal of IG is *insertion loss*, which, although a commonly used term, may be confusing because it defines a *loss* as a positive quantity.

Insertion gain is based on vibration amplitudes, and it is of limited use as a single measure of isolation performance due to the fact that it only accounts for vibration occurring in one direction and varies with position in a building. A more useful measure is *power flow insertion gain* (PFIG).<sup>6</sup> The principal behind PFIG is that the mean vibrational energy entering a building drives all internal noise and vibration, assuming there are no internal sources of either. A reduction in PFIG is therefore guaranteed to reduce

the average noise and vibration levels in a building:

$$\text{PFIG} = 10 \log_{10} \left( \frac{\bar{P}_{\text{isol}}}{\bar{P}_{\text{unisol}}} \right) \quad (2)$$

where  $\bar{P}_{\text{isol}}$  and  $\bar{P}_{\text{unisol}}$  are the total mean power flows entering a building in the isolated and unisolated cases, respectively.

Power flow IG has clear advantages over performance measures based on vibration amplitudes because it accounts for multidirectional vibration at multiple inputs and is insensitive to the spatial distribution of vibration levels within a building. It is useful in design because the variation in performance with frequency, for a particular set of design parameters, may be represented by a single curve. For the case of a single-input single-output system, PFIG can be shown to be directly equivalent to IG.

## 6 MODELING BASE-ISOLATED BUILDINGS

### 6.1 Single-Degree-of-Freedom Model

The single-degree-of-freedom (SDOF) model serves as a useful introduction to the principles behind base isolation. Figure 4 illustrates how a building may be represented as a rigid mass supported on a spring-damper element to represent the isolation bearings—in this example a viscous dashpot is used to model damping. Ground-borne vibration is represented by an imposed displacement amplitude  $X$  at the base of the spring-damper. The resulting motion of the building is described by the displacement amplitude of the mass  $Y$ .

The precise expression describing the variation in the ratio  $Y/X$  with frequency depends on the nature of the damping element,<sup>10</sup> but the essential features are the same in all cases: (1) the bearings act to amplify low-frequency vibration, and this is greatest at the

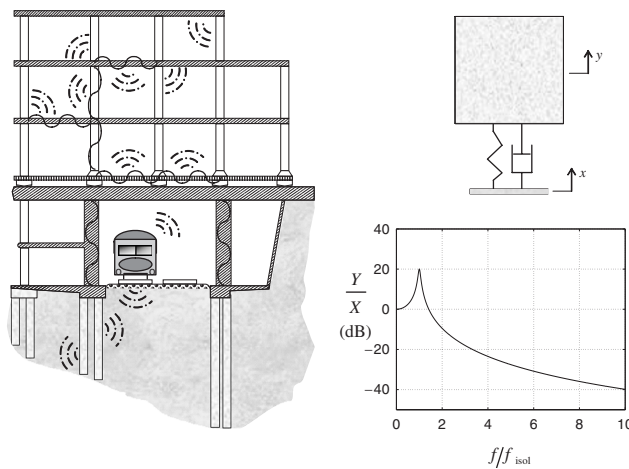
isolation frequency; (2) the bearings are only effective for frequencies greater than  $\sqrt{2}$  times the isolation frequency, above which the isolation improves with frequency; and (3) damping acts to limit the resonance amplitude but reduces the isolation performance.

These features of the SDOF model suggest some guiding design principles, but the model is too simplistic for making any useful predictions of isolation performance. For this, a more comprehensive representation of a building, its foundation, and the vibration source is required.

### 6.2 Modeling for the Prediction of Isolation Performance

Predictions of isolation performance may be obtained from empirical models, based on a database of measurements made on existing buildings. These can provide useful, as well as reasonably rapid, estimates of performance provided the database is sufficiently comprehensive to cover the possible combinations of source, transmission path, type of building, and the like. The disadvantage of empirical models is that they treat each part of the vibration transmission path separately, and the various factors and transfer functions are assumed to be independent. This does not represent the physical situation and cannot account for coupling between various parts of the system, such as that due to interaction between the building and its foundation.

An alternative is to use theoretical models based on physical laws. These are particularly useful during design as they may be tailored to the particular project and, in principle, include as much physical detail as necessary. The required level of detail depends on the particular application, but any model should include a representation of the building, its foundation, and the vibration source. Models may be formulated in either the time or frequency domains. The former is often



**Figure 4** principles of base isolation may be introduced by the single-degree-of-freedom model in which a building is represented as a rigid mass supported on a spring-damper element to represent the isolation bearings.

used for seismic analysis where peak vibration levels due to a transient, and often nonlinear, event are of interest. When dealing with ground-borne vibration, the response, particularly that due to railways, is of sufficient duration that the frequency domain is the most appropriate. The problem may also be treated as linear given the low strain amplitudes involved. In this case, irrespective of the particular methods employed, the modeling process may be broken down into the following steps. The entire process must be followed for each frequency of interest.

1. Calculate the foundation's frequency-response function (FRF) matrix  $\mathbf{H}_f^{11}$ . This relates vectors  $\mathbf{u}_{bf}$  and  $\mathbf{f}_{bf}$  containing the displacement and force amplitudes at various locations, or *nodes*, on the building-foundation interface.
2. Assemble a vector  $\mathbf{u}_{bf0}$  containing the displacement amplitudes at nodes on the building-foundation interface in the absence of the building. This represents the input to the final model. By considering equilibrium of forces and compatibility of displacements, the displacements of the building-foundation interface in the presence of the building may be obtained by superposition:

$$\mathbf{u}_{bf} = \mathbf{H}_f^{11} \mathbf{f}_{bf} + \mathbf{u}_{bf0} \quad (3)$$

3. Calculate the building's FRF matrix  $\mathbf{H}_b$ . This relates displacement and force amplitudes at nodes throughout the building model. Because the forces acting on the building are equal and opposite to those acting on the foundation, and no other external forces are assumed to act on the building,  $\mathbf{H}_b$  may be partitioned according to whether nodes lie on the building-foundation interface or elsewhere in the building:

$$\begin{bmatrix} \mathbf{u}_{bf} \\ \mathbf{u}_b \end{bmatrix} = \begin{bmatrix} \mathbf{H}_b^{11} & \mathbf{H}_b^{12} \\ \mathbf{H}_b^{21} & \mathbf{H}_b^{22} \end{bmatrix} \begin{bmatrix} -\mathbf{f}_{bf} \\ \mathbf{0} \end{bmatrix} \quad (4)$$

where  $\mathbf{u}_b$  contains displacements at nodes other than those located on the building-foundation interface. Eliminating  $\mathbf{f}_{bf}$  from Eqs. (3) and (4) gives

$$\mathbf{u}_{bf} = [\mathbf{I} + \mathbf{H}_f^{11} [\mathbf{H}_b^{11}]^{-1}]^{-1} \mathbf{u}_{bf0} \quad (5)$$

The interface displacements in the presence of the building may, therefore, be calculated from those in its absence.

4. The final stage is to calculate the building-foundation interface forces using Eq. (4):

$$\mathbf{f}_{bf} = -[\mathbf{H}_b^{11}]^{-1} \mathbf{u}_{bf} \quad (6)$$

These may then be used to calculate the remaining building displacements:

$$\mathbf{u}_b = -\mathbf{H}_b^{21} \mathbf{f}_{bf} \quad (7)$$

Depending on the intended use of the model, a variety of methods may be used to implement each of the above steps. Some of the most common methods are described below.

### 6.3 The Building Model

Any building model should represent, to some degree, the mass, stiffness, and damping of the building's primary structure. Accounting only for the mass—as in the SDOF model—is insufficient because the vibration modes of a building can result in a significant reduction in base isolation performance.<sup>11</sup> Comprehensive models should account for the essential dynamic behavior of a building's floors and columns, and the dynamic coupling between them.

The finite element method (FEM)<sup>12</sup> is now the most widely used numerical technique for engineering analysis and is a natural choice for modeling vibration of buildings. It has the advantage of being readily available commercially and may provide the most efficient means of generating comprehensive three-dimensional models. However, the FEM usually employs modal analysis and care must therefore be taken to ensure an adequate number of elements are used for the required accuracy over the frequency range of interest.

An alternative to the FEM is the dynamic stiffness method.<sup>13</sup> This is computationally efficient and particularly suited to producing two-dimensional portal frame models, although it may also be extended to three dimensions. The method is based on the analytical solutions of Euler beam theory and that describing an elastic bar. It is therefore exact within the limitations of the theory.

Statistical energy analysis (SEA) is another numerical technique for modeling noise and vibration transmission through structures. This includes buildings when the frequencies of interest lie within the audio range.<sup>14</sup> The problem with applying SEA to ground-borne vibration is that the frequencies of interest include only a few hertz, when the fundamental assumption of SEA—that of high modal density—does not apply. In addition, SEA elements for describing the interface between a foundation and the ground are not generally available in SEA codes. Despite its computational efficiency, SEA is therefore not recommended for modeling base-isolated buildings.

### 6.4 The Foundation Model

A building and its foundation are intimately coupled, and a significant degree of dynamic interaction occurs between them. The foundation and surrounding ground not only provide the transmission path from the vibration source, but they also act as a sink of vibration propagating in the building. The foundation model is

therefore an essential component of any model aimed at predicting isolation performance.

When modeling the semiinfinite extent of the ground, domain methods, such as the FEM or finite difference method,<sup>15</sup> suffer from a fundamental problem. The element mesh should extend toward infinity but in practice must be curtailed at a certain distance. The resulting artificial boundary leads to spurious wave reflections that can distort the solution. A simple solution to this problem is to use models large enough that insufficient wave energy reaches the model boundary. This approach is usually impractical given the computational requirements of the models. A solution available in some commercial FEM codes is to use non-reflecting boundaries or so-called infinite elements.<sup>16</sup> These help account for wave radiation to infinity but only approximately due to the difficulty of accounting for the different wave types.

One technique ideally suited to the modeling of ground-borne vibration is the boundary element method (BEM).<sup>17</sup> In contrast to the FEM, the BEM requires the discretization of only the domain boundaries, rather than the full domain. The governing equations are automatically satisfied, and the radiation of waves to infinity is automatically accounted for. As with the FEM, if necessary, the BEM enables the representation of different soil strata and inhomogeneous soils through the use of multiple BEM domains and appropriate fundamental solutions.

### 6.5 Note on Damping

Structural damping is the least well-understood aspect of structural dynamics and remains the subject of current research. In the frequency domain, material damping may be conveniently modeled by assuming viscoelastic behavior and replacing the standard elastic constants with suitable complex values.<sup>18</sup> Thus, for example, Young's modulus  $E$  becomes  $E(1 + i\eta_E)$ . In practice, damping is often found to be approximately hysteretic, that is, the damping loss factor  $\eta_E$  is approximately constant. Values ranging from 0.01 to 0.03 are representative of a wide range of construction materials.<sup>19</sup> However, these figures are inappropriate for an entire building where damping may be an order of magnitude greater than the inherent material damping due to energy dissipation at structural joints. An overall loss factor of 0.1 may be used for typical building structures.

The inherent damping of isolation bearings varies according to their design. Typical loss factors range from 0.01, corresponding to undamped steel springs, to 0.1 for high-hysteresis rubber bearings.

The hysteretic damping model is also suitable for many soils over the frequency range and amplitudes typical of ground-borne vibration.<sup>20</sup> However, in practice, the behavior of building foundations is generally dominated by radiation damping due to the geometric spreading of vibration wavefronts. It is therefore more important that models represent the unbounded nature of the soil, such that radiation damping is correctly accounted for, than the precise nature of the material damping.

### 6.6 Representing the Vibration Source

Following the modeling process outlined earlier, the vibration source is represented by the vector  $\mathbf{u}_{bf0}$ . This contains the displacement amplitudes at nodes on the building–foundation interface in the absence of the building. The advantage of expressing the input in this way is that it need only be defined once, even if several different building designs are subsequently modeled. Vector  $\mathbf{u}_{bf0}$  may be calculated using the foundation model, excited by either an incoming vibration field or an explicitly modeled source such as an underground railway tunnel. Alternatively, the displacements may be specified to represent a known distribution in vibration amplitudes across a particular site.

### 6.7 Two or Three Dimensions

It may be necessary to limit the size of a numerical model and a decision is often required on whether two or three dimensions should be considered. Two-dimensional models are simpler and less demanding on computational resources. The disadvantage is that they assume the modeled system to be invariant in the antiplane direction and, particularly with foundation models, this limits the ability to correctly model wave propagation. For example, vibration that in practice may propagate on spherical wavefronts is constrained to cylindrical wavefronts and, therefore, attenuates less rapidly with distance, and foundations such as piles are represented as infinitely long barriers around which waves can no longer diffract.

The decision between two and three dimensions must be made on a case-by-case basis. In the case of a building with a repeating structure and a slab foundation, it should be possible to identify a representative section. A two-dimensional model may then be acceptable for predicting insertion performance. In general, three-dimensional models are required if predictions of absolute performance are to be made.

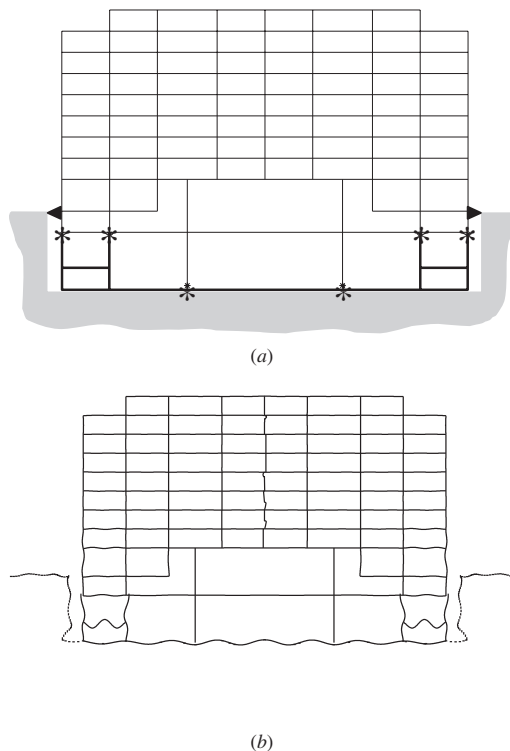
## 7 EXAMPLE CASE STUDY

This chapter concludes with an example case study concerning a new building that is to be constructed above an underground railway. Experience with an existing building on the neighboring site indicates that base isolation is necessary if the new building is to fulfill its intended function.

Here, attention is focused on the use of *side-restraint* bearings. The intention is to support the retaining walls of the basement cavity off the primary building structure, the aim of the side-restraint bearings being to minimize any “short-circuiting” of the base bearings. The objective of the modeling presented here is to predict the effect of the side-restraint bearings on the overall isolation performance.

### 7.1 Overview of Model

The building has a uniform repeating structure and a slab foundation in a substantially uniform soil. For this comparative study, a two-dimensional model is therefore deemed adequate, as illustrated in Fig. 5.



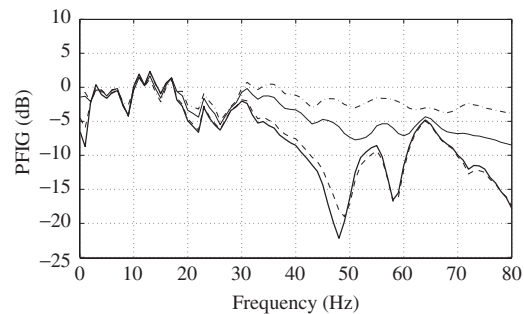
**Figure 5** Two-dimensional model for investigating the effect of side-restraint bearings: (a) the building is represented by a portal frame, isolated from a boundary element representation of the ground by six base bearings (\*) and two side-restraint bearings (>); and (b) the response of the building at 50 Hz to a buried harmonic force applied below the foundation slab.

The building is modeled using the dynamic stiffness method, which represents the primary structure as a series of coupled Euler beams and elastic columns. A finite element model would fulfill the same function provided care is taken to ensure an adequate number of elements are used. The isolation, which is designed to give an isolation frequency of 3.5 Hz, consists of six base bearings and two side-restraint bearings. Each one is modeled by three linear springs to account for its vertical, horizontal, and rotational stiffness.

The slab foundation is coupled to a boundary element representation of the ground, and the excitation from the underground railway is represented by a buried harmonic force. This is the simplest means of generating an incident vibration field that has the essential characteristics of the pressure and shear waves generated in practice.

## 7.2 Results

Following the process outlined earlier, the response of the building model may be calculated with and without isolation in place. The insertion performance may therefore be calculated for a system employing



**Figure 6** Effect of side-restraint bearings on the power flow insertion gain of a base-isolated building. The results correspond to side-bearing stiffnesses of 1.00 (chained), 0.30 (solid), and 0.10 (dashed) times the stiffness of the base bearings. The case corresponding to no side-restraint bearings is shown in bold.

only base bearings and one with the addition of side-restraint bearings. Here, PFIG is used to provide a single measure of the average isolation performance throughout the building. This is achieved by using the predicted axial and bending stresses and strains at the bases of the building columns to calculate the total mean power flows entering the building.<sup>10</sup>

Figure 6 shows the variation with frequency in the PFIG when the dynamic stiffness of the side-restraint bearings is varied from 1.00 to 0.30 and 0.10 times the stiffness of the base bearings. In this example, as a spatial average, the isolation performance is limited below approximately 18 Hz due to local vibration modes of the building and foundation. Above 30 Hz, the effect of the side-restraint bearings is significant and minimizing the stiffness of these bearings maximizes the overall isolation performance. In this example, it appears that the side-restraint bearings are ideally located to deliver additional vibrational power to the building, and this outweighs any benefit from power leaving the building to be dissipated in the soil.

## 8 CONCLUSION

Base isolation of buildings is now well established as a means of minimizing the disturbance caused by urban ground-borne vibration. Residential buildings, office towers, cinemas, concert halls, and hospitals have all been constructed on sites otherwise deemed unacceptable due to their proximity to vibration sources such as busy roads and railways.

Isolation designs vary from building to building, and there is no single approach that is guaranteed to provide adequate performance for all structures. Performance is very much influenced by construction details and local site characteristics. Although a number of generic principles exist, engineers are therefore advised to evaluate designs using a suitable dynamic model. This should account for the mass, stiffness, and damping of the building's primary structure, along with the essential behavior of the foundation and the vibration source. Such models

enable designs to be optimized by predicting measures of insertion performance, particularly those based on vibrational power flow.

## REFERENCES

1. British Standards Institution, BS 6472: Guide to Evaluation of Human Exposure to Vibration in Buildings (1 Hz to 80 Hz), 1992.
2. International Standards Organisation, ISO 2631-2: Mechanical Vibration and Shock—Evaluation of Human Exposure to Whole-Body Vibration—Part 2: Vibration in Buildings (1 Hz to 80 Hz), 2003.
3. E. E. Ungar, Vibration Criteria for Sensitive Equipment, *Proc. Internoise 92*, 1992, pp. 737–742.
4. E. E. Ungar, D. H. Sturz, and C. H. Amick, Vibration Control Design of High Technology Facilities, *J. Sound Vib.*, Vol. 24, 1990, pp. 20–27.
5. Federal Transit Administration, *Transit Noise and Vibration Impact Assessment*, U.S. Department of Transportation, Washington, DC, 1995.
6. J. P. Talbot and H. E. M. Hunt, Isolation of Buildings from Rail-Tunnel Vibration: A review, Invited Paper, *Building Acoustics*, Vol. 10, No. 4, 2003, pp. 177–192.
7. R. A. Waller, *Building on Springs*, Pergamon, Oxford, 1969.
8. A. H. Muhr, A Comparison of Rubber and Metal Springs for Vibration Isolation, *Plastics, Rubber Composites Proc. Appl.*, Vol. 18, 1992, pp. 3–7.
9. H. G. Wagner, Application of Steel Springs in the Support of Buildings, *Proc. Institute Acoust.*, Vol. 22, No. 2, 2000, pp. 221–230.
10. J. P. Talbot and H. E. M. Hunt, On the Performance of Base-Isolated Buildings, *Building Acoust.*, Vol. 7, No. 3, 2000, pp. 163–178.
11. D. E. Newlan and H. E. M. Hunt, Isolation of Buildings from Ground Vibration: A Review of Recent Progress, *Proc. IMechE, Part C: Mech. Eng. Sci.*, Vol. 205, No. 1, 1991, pp. 39–52.
12. O. C. Zienkiewicz and R. L. Taylor, *The Finite Element Method*, 5th ed., Butterworth-Heinemann, Oxford, UK, 2000.
13. H. E. M. Hunt, Modelling of Structures of Infinite Extent for Calculation of Vibration Transmission, in *New Advances in Modal Synthesis of Large Structures*, L. Jezequel, Ed., Balkema, Rotterdam, The Netherlands, 1995.
14. R. J. M. Craik, *Sound Transmission through Buildings Using Statistical Energy Analysis*, Gower, Aldershot, UK, 1996.
15. T. Wah and L. R. Calcote, *Structural Analysis by Finite Difference Calculus*, Van Nostrand Reinhold, New York, 1970.
16. P. Bettess, *Infinite Elements*, Penshaw Press, Sunderland, UK, 1992.
17. J. Dominguez, *Boundary Elements in Dynamics*, Computational Mechanics Publications and Elsevier Applied Science, New York, 1993.
18. D. R. Bland, *Theory of Linear Viscoelasticity*, Pergamon, Oxford, UK, 1960.
19. L. Cremer, M. Heckl, and E. E. Ungar, *Structure Borne Sound: Structural Vibrations and Sound Radiation at Audio Frequencies*, 2nd ed., Springer, Berlin, Germany, 1990.
20. B. Prange, Parameters Affecting Damping Properties, in *Dynamical Methods in Soil and Rock Mechanics I: Dynamic Response and Wave Propagation in Soils*, B. Prange, Ed., Balkema, Rotterdam, The Netherlands, 1977.



# CHAPTER 125

## AIRCRAFT AND AIRPORT NOISE PREDICTION AND CONTROL

**Nicholas P. Miller**  
Harris Miller Miller & Hanson Inc.  
Burlington, Massachusetts

**Eugene M. Reindel**  
Harris Miller Miller & Hanson Inc.  
Sacramento, California

**Richard D. Horonjeff**  
81 Liberty Square Road  
Boxborough, Massachusetts

### 1 INTRODUCTION

Demand for air travel is projected to increase in coming years. However, virtually all major proposed changes in airports or airspace can elicit significant public comment, scrutiny, and often political, if not litigation-based, resistance. Usually, concerns about the noise produced by aircraft are cited as the basis for this resistance. As a result, to develop a uniform and defensible approach to airport design and to smooth the process of developing increased capacity at their airports, more and more nations have established a variety of specific noise prediction, assessment, and mitigation procedures.

These procedures are designed to address the primary noise sources and the situations in which they may become issues. These sources and situations become issues for reasons of public health and welfare or because they provoke public resistance to changes or insistence on improvements. Consequently, all noise analysis requires not only metrics to quantify aircraft noise but also associated criteria or guidelines to assess the effects or impacts of this noise on people. The procedures that are in place include metrics and criteria, analysis methods, and approaches to mitigation or control of the specific types of aircraft noise. These procedures include specific noise control approaches to reduce noise at the source and to minimize noise and land-use incompatibilities in affected communities.

### 2 AIRCRAFT NOISE SOURCES

With the vast array of aircraft, and the ground-support equipment in use today, it is helpful to understand the acoustic noise-producing elements of each of these sources. Such understanding provides a basis for judging the effectiveness of aircraft noise control strategies, both now and in the future. The subsequent discussion is organized by type of aircraft: (1) jet turbine powered, (2) propeller with either turbine or reciprocating power plants, and (3) rotary wing helicopters. Noise-producing ground-support equipment for each aircraft type will be treated within the appropriate subsection.

### 2.1 Jet-Turbine-Powered Aircraft

At airports where they operate, jet-turbine-powered aircraft departures and arrivals are usually the primary contributors to the aircraft sound exposure produced in adjacent communities. Typical commercial jets in use today (2005) produce on departure maximum A-weighted sound pressure levels ranging from the mid-70 to mid-80 dB at about 3 miles from brake release to mid-60 to mid-70 at about 7 miles. At 3 miles, these levels produce speech interference outdoors (A-weighted levels exceed 60 dB) for about 20 to 30 s for each departure.

The primary noise-generating mechanisms are the high-velocity jet exhaust gases mixing with the still air surrounding the jet flow, and blade passage tones from the compressor stages of the engine inlet. The jet noise-generating mechanism is the formation of turbulent eddies at the boundary between the high-speed jet gasses and the surrounding still air. Sound levels produced by these eddies have been shown to be proportional to roughly the seventh power of the jet velocity. Hence, even moderate reductions in the exhaust velocity where it meets the still air can reduce the generated sound power. The rotating vanes of the compressor fan produce tones. These tones can emanate from both the front and rear of the engine: either out the inlet nacelle or out the compressor bypass airflow at the rear of the engine. Noise control at the source for jet engines has concentrated on reducing the velocity of the jet flow that mixes with the ambient air and adding absorption treatment for tones in the inlet nacelle and in the bypass air ducts leading to the rear of the engine.

For example, engine manufacturers have come to rely less and less on the combustion gasses for thrust and more on *bypass airflow*. Inlet turbine compressors are now designed to provide the air needed by the combustor as well as additional compressed air for thrust. The additional thrust is achieved by routing a portion of the compressed air around the engine core (i.e., bypassing the combustor) and exhausting this air in a ring around the outside of the higher velocity jet gasses. The bypass air is of lower velocity than the engine exhaust, thereby lowering the strength of



the turbulent eddies and associated noise levels. This increase in *bypass ratio* has been responsible for a 10-dB or more reduction of takeoff sound levels.

Turbulence produced by the airframe itself as it moves through the air is also another source of noise. This noise is produced by turbulent eddies created by the interaction of various parts of the airframe (fuselage, wings, engines, etc.) with the still air they encounter in flight. Presently, the only flight regime where this source is not completely dominated by other sources is during landing, where engine thrust is small compared with other flight regimes. In the future, as jet engines become yet quieter, this airframe noise may be the factor that limits how quiet jet aircraft can be.

Despite the usual dominance of departures and arrivals in producing noise in surrounding communities, ground operations can be of concern as well. Start of takeoff roll, while the aircraft is on the ground, reverse thrust after landing, taxi operations, and use of auxiliary power units (APU) can affect communities located close to the runways, taxiways, or gates. Start of takeoff noise is cited as producing "rumble," causing houses to vibrate and produce rattle of windows or objects inside. Though A-weighted sound levels are used almost universally to quantify aircraft noise (see Section 3.1), A-weighting is likely to be inadequate for describing start of takeoff noise because of the significant presence of low-frequency energy.<sup>1</sup> The A-weighting network's attenuation of 30 dB or more below 50 Hz significantly deemphasizes the region where most residential structural resonances occur.

Taxi noise can be dominated by tones from the engine compressor. During taxi, jet engines are usually operated at flight idle power except during startup from a standing stop. Although taxi sound levels are low compared with in-flight noise, several aircraft waiting their turn for departure clearance can produce a continuous din easily heard at close-by residences.

On the ground, while parked at the gate, yet another source of noise is often present: the APU. When the engines are shut down, an alternative source of power must be available to power on-board electrical equipment. In the early days APUs were cart-mounted generators powered by reciprocating engines. Engine noise associated with these units was low to the ground, and the sound of these units often attenuated by low buildings before reaching neighboring airport communities. Currently, APUs are installed in the aircraft themselves to eliminate dependence on the availability of ground-based carts, especially at smaller airports. These APUs are turbine powered, installed in the rear of the fuselage, and generally exhaust from the tail cone of the aircraft. For today's transport aircraft, the ramifications are (1) this sound source has been elevated to 20 to 30 ft above ground level, well above many naturally occurring sound barriers such as one- and two-story buildings, and (2) they operate almost continuously during the turnaround time between flights. This source of noise can be a particular issue at hub airports where large numbers of aircraft are on the ground for periods of 1 to 2 h, several times a day.

## 2.2 Propeller Aircraft

Propeller aircraft noise is generally of concern only when there are no or only occasional jet operations over the same areas, when there is a runway used exclusively by propeller aircraft, or when they fly at low altitudes (about 500 to 1500 ft above ground) over quiet residential areas, as during touch-and-go practice patterns or as air tours over park or wilderness areas. These aircraft fall into two categories, piston and turbine powered. The larger transport category aircraft are all turbine powered. The two primary noise-generating sources are the propeller and the turbine itself. For all practical purposes the propeller dominates the noise levels in all flight regimes (takeoff, cruise, and landing), as well as during taxi on the ground. The propeller is a highly directional source, with a phenomenon called *thickness noise* being quite prominent within  $\pm 10^\circ$  to  $15^\circ$  of the rotating plane of the propeller. Piston engine power plants are almost the exclusive province of private ownership, as well as some tour and transport operations serving very low demand markets. For piston-powered aircraft exhaust, tones can be a significant noise contributor in addition to the propeller.

## 2.3 Helicopters

Helicopters, also known as rotary wing aircraft, do not usually raise concerns when they operate from an airport with a mix of jet and propeller aircraft operations. Usually their operations are fewer and infrequent in comparison with the other aircraft operations at the airport. However, the obvious value of helicopters—their ability to fly into and out of constrained locations via arbitrary routes—can also be the source of public concern. At 1000 ft distance, they are about as loud as a large truck/lorry at 50 ft—A-weighted levels of 70 to 80 dB—so at lower altitudes, they can be easily heard in quiet residential areas, parks, and wildernesses and in the quieter areas of cities.

Helicopters fall into the same two categories as propeller aircraft, piston and turbine powered. In the case of helicopters, the main rotor supplies both the lift and forward thrust. The tail rotor provides directional stability and control. Both rotors are important noise contributors. As mentioned in the propeller aircraft discussion, rotating blades are highly directional sound sources. With the main rotor operating in the horizontal plane and the tail rotor in the vertical, helicopters can have highly complex, directional noise characteristics, in both the horizontal and vertical planes.

Although the main rotor produces a fundamental blade-vortex interaction tone of only 10 to 15 Hz, it is the higher harmonics of this tone that are audible to human observers. The sound is most pronounced within  $\pm 10^\circ$  to  $15^\circ$  of the plane of the rotor. As the aircraft approaches the observer, the main rotor can also produce a separate phenomenon called *blade slap* (the familiar whop-whop-whop sound). In general, the heavier the aircraft the more prominent this sound becomes. The blade slap sound, another blade-vortex

interaction phenomenon, is highly directional in the vertical plane and is only forward propagating. Once the aircraft passes overhead, the observer blade slap is generally no longer audible.

The tail rotor, which operates at higher speeds than the main rotor and has been often referred to as the “necessary evil of helicopter design,” is often the dominant noise source, especially when the aircraft is approaching the observer. In an effort to improve reliability and reduce noise, some newer helicopters have been designed with no tail rotors (NOTARs). For these aircraft the directional thrust of the tail rotor is replaced by compressed airflow. An air intake forward of the tail boom provides the air source; the main engine operates a fan that compresses this air down a long tube the length of the tail boom; and at the end of the boom the tube makes a right turn providing the required lateral thrust. NOTAR aircraft can be significantly quieter than the tail rotor design but can be more expensive to produce.

### 3 AIRCRAFT NOISE METRICS AND CRITERIA

All aircraft noise analysis procedures are based on metrics that quantify the aircraft-produced sound levels or sound exposure levels as experienced on the ground. A threshold value is derived above which adverse noise effects may be expected or below which no adverse effects should occur.

#### 3.1 Metrics or Indicators

There are two types of noise metrics used widely: one for the design and “certification” of specific aircraft types\* and one for analysis of aircraft operations noise and its effects on noise-sensitive land use. The former is a measure of a single aircraft operation, used to specify required noise emission design requirements for a new or derivative aircraft type, while the latter, sometimes referred to as an indicator, is generally an integrated measure that accumulates the sound energy of all aircraft operations and is generally accepted to correlate with the effects aircraft noise may have on people.

The metric used universally for aircraft certification is the effective perceived noise level, abbreviated EPNL, with units of effective perceived noise decibels, or EPNdB (as opposed to decibels, or dB, used for all other metrics). It is a tone- and duration-corrected measurement of a single aircraft flyover, computed from measured one-third octave band sound levels.<sup>2</sup>

The most common metric for effects on humans is a measure of energy-averaged sound exposure, generally with weightings for different periods of the day. Use of A-weighting is either explicitly stated or understood. Different metrics may be used to

define levels that protect hearing, classroom learning, minimize annoyance, sleep disturbance, or speech interference. The discussion of effects presented here is restricted to the metrics and criteria that address annoyance and sleep disturbance.

**3.1.1 European Union (EU)** The EU uses the day-evening-night level,  $L_{den}$ , in decibels (dB), which is defined by the following formula in the European Noise Directive (END)<sup>3</sup>:

$$L_{den} = 10 \log \frac{1}{24} (12 \times 10^{L_{day}/10} + 4 \times 10^{(L_{evening}+5)/10} + 8 \times 10^{(L_{night}+10)/10}) \quad (1)$$

where  $L_{day}$  = A-weighted long-term average sound level as defined in International Organization for Standardization (ISO) 1996-2: 1987, determined over all the day periods of a year  
 $L_{evening}$  = A-weighted long-term average sound level as defined in ISO 1996-2: 1987, determined over all the evening periods of a year  
 $L_{night}$  = A-weighted long-term average sound level as defined in ISO 1996-2: 1987, determined over all the night periods of a year

in which (a) the day is 12 h, the evening 4 h, and the night 8 h. Member states may shorten the evening period by 1 or 2 h and lengthen the day and/or the night period accordingly, provided that this choice is the same for all the sources and that they provide the commission with information on any systematic difference from the default option and (b) the start of the day (and consequently the start of the evening and the start of the night) shall be chosen by each member state (that choice shall be the same for noise from all sources); the default values are 07:00 to 19:00, 19:00 to 23:00, and 23:00 to 07:00 local time.

The EU also recognizes that some cases may benefit from the use of *supplementary noise indicators* and related limit values. Some examples for such use could be sources that operate for a small proportion of the time or that have unusual frequency characteristics, including tones, or that are impulsive in character.

**3.1.2 United States** In the United States, the primary metric for airport noise assessment is the day-night average sound level (or DNL, equation symbol  $L_{dn}$ ) as established by the Environmental Protection Agency (EPA) in 1974<sup>4</sup> and adopted by the Federal Aviation Administration (FAA) as interim in 1981 and finalized in December 1984.<sup>5</sup> The definition of the day-night average sound level is similar to the EU's  $L_{den}$  except it has two periods: Day is 07:00 to 22:00 and night is 22:00 to 07:00. The DNL metric adds a 10-dB penalty to the noise that occurs during the night hours. By definition, DNL is a 24-h metric.

Though not used directly by FAA procedures to assess aircraft noise effects, the FAA endorses

\*All aircraft that are permitted to fly must pass specific certification requirements. In terms of noise, these requirements are based on detailed sound level measurements made during specific departure and approach procedures. Section 5 discusses these requirements in more detail.

use of “supplemental metrics” other than DNL to “describe aircraft noise impacts for specific noise-sensitive locations or situations and to assist in the public’s understanding of the noise impact.”<sup>6</sup> These supplemental metrics may be measures of single-event levels or durations or integrated levels for periods shorter than 24 h. Their use may be for addressing effects such as sleep disturbance, speech interference, or audibility (e.g., for substantial restoration of natural quiet in Grand Canyon National Park).

**3.1.3 World Health Organization** For addressing annoyance and sleep disturbance, the World Health Organization (WHO) uses the “equivalent continuous sound pressure level,” which sums the “total energy over a selected time period ( $T$ )”<sup>7</sup> (equation symbol  $L_{Aeq,T}$ ). For daytime and evening annoyance assessment,  $T$  equals 16 h, while for sleep disturbance assessment,  $T$  equals 8 h. The WHO definition of  $L_{Aeq,T}$  is consistent with definitions of that quantity found in ISO 1996/1-1982(E) and the American National Standards Institute (ANSI) S1.1-1994. The guidelines also include use of A-weighted maximum (fast meter response<sup>8</sup>) for assessment of sleep.

**3.1.4 International Civil Aviation Organization** The International Civil Aviation Organization (ICAO) does not specify metrics but provides a method for computation of various metrics for use by the *contracting states*—the 188 states that have agreed to the ICAO constitution, drawn up in 1944.<sup>9</sup> See Section 5.

## 3.2 Effects or Impacts

Different countries/organizations have different approaches to determining the effects of aircraft noise on people. The term *impact* may have different meanings. In some cases, it identifies a threshold of unacceptable or undesirable effects, or it can mean that a threshold has been exceeded and specific actions to mitigate or alter the noise are required.

**3.2.1 European Union** The European Noise Directive provides for assessment of the harmful effects of noise as manifested by annoyance and sleep disturbance and offers dose–effect relations for this purpose.<sup>10</sup>

**Annoyance** Annoyance dose–effect relations have been developed for aircraft, road traffic, and railways and the results for aircraft are given in Table 1.<sup>11</sup> Member states may use the information as appropriate to their needs and some suggestions for use are provided. For example, three degrees of impact or acceptability might be developed. A highest level, which should not be exceeded or above which there should be no residential use, a middle range of conditional use suitable for goals of improvement, and a lowest level, which might serve as a target, or below which levels are completely acceptable and should be preserved. Values of Table 1 can be used to determine numbers of persons highly annoyed or

numbers annoyed when  $L_{den}$  is provided on maps of population distributions. Special sound insulation, shielding by buildings, differences in construction should be considered. Table 1 data are based on the responses of adult populations and are intended primarily for application to long-term stable situations. The relations are not recommended for use with taxiing noise.

**Sleep** The EU has also provided dose–effect relationships for assessing sleep disturbance.<sup>12</sup> The relationships are derived from surveys conducted in the Netherlands in which movement during sleep (motility), as determined by an actimeter worn on the wrist, is correlated with aircraft-produced noise events. This measured movement is found to correlate with change of sleep state, behavioral awakenings, and other measures of sleep disturbance, including responses to questions about sleep. Motility data were correlated with  $L_{night}$  yielding the relationship between maximum yearly noise-induced motilities,  $n_{max}$  and  $L_{night}$ :

$$n_{max} = N \times \left[ \begin{array}{l} 0.0001233(L_{night} + 70.2 - 10 \log N) \\ - L_{Diff1} - L_{Diff2} \\ -0.007415(L_{night} + 70.2 - 10 \log N) \\ - L_{Diff1} - L_{Diff2} + 0.0994 \end{array} \right] \quad (2)$$

In Eq. (2),  $N$  is the annual number of nighttime aircraft noise events above the effect threshold of an outdoor A-weighted level of 53 dB,  $L_{Diff1}$  is the difference between  $L_{night}$  (measured away from reflecting surfaces) and the  $L_{Aeq}$  measured at the exterior facade of the bedroom, and  $L_{Diff2}$  is the difference between the outdoor  $L_{Aeq}$  at the exterior facade of the bedroom and the interior  $L_{Aeq}$  in the bedroom during sleep. Figure 1 shows the relationships between  $n_{max}$  and  $L_{night}$  for different numbers of nighttime events. This figure is derived by assuming an energy average sound exposure level (SEL) for all events. It also assumes that  $L_{Diff1}$  is 0 dB, and  $L_{Diff2}$  is 21 dB, as recommended by the EU document.

**3.2.2 United States** In the United States, early studies conducted for the U.S. EPA recommended that to minimize annoyance and sleep disturbance, the outdoor day–night sound level should be less than

**Table 1 EU Recommended Relationships between Annoyance and Aircraft Noise**

Aircraft Produced $L_{den}$	Percent of Exposed Population	
	Annoyed at All	Highly Annoyed
45	11	1
50	19	5
55	28	10
60	38	17
65	48	26
70	60	37
75	73	49

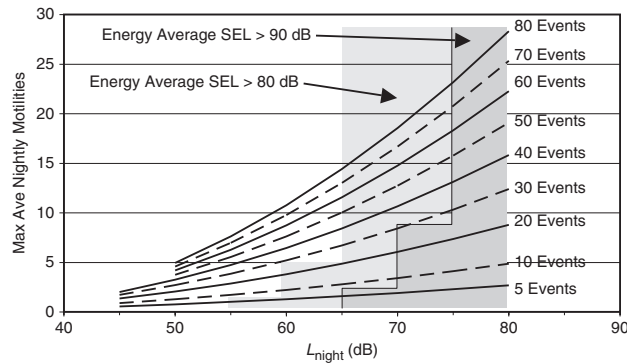


Figure 1 Average nightly noise-induced nighttime motilities.

60 dB.<sup>13</sup> The U.S. EPA used this information and added an “adequate margin of safety” and identified a day–night average sound level of 55 dB as protective of public health and welfare.<sup>14</sup>

**Annoyance** More recently the Federal Interagency Committee on Noise (FICON) provided additional guidance on determining aircraft noise effects in terms of annoyance. FICON researched recent work and provided an updated dose–response curve for annoyance as a function of DNL from any transportation noise source. Table 2 summarizes this updated information.<sup>14</sup>

**Sleep** The successor to FICON, the Federal Interagency Committee on Aviation Noise (FICAN) published a synthesis of the then available sleep disturbance data and recommended the relationship given by Fig. 2.<sup>15</sup> The FICAN 1992 curve of Fig. 2 represents the most conservative relationship for all the accumulated data—it is at or above the maximum percent awakening data at all points. Note that the sound levels on the horizontal axis are indoor levels. The awakening data are from on-site (as opposed to laboratory) studies that used either behaviorally confirmed awakening (the subject pressed a button when awakened) or

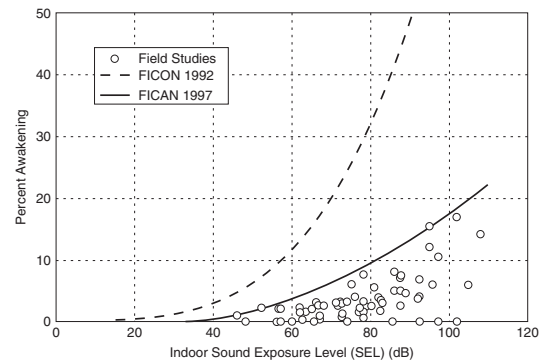


Figure 2 FICAN-recommended sleep disturbance dose–response curve.

motility within some specified latency from the noise event onset.

**Land-Use Compatibility** The FAA established guidelines for aircraft noise and land-use compatibility in 1981 for many land-use categories.<sup>16</sup> These guidelines show residential land use, other than mobile homes and transient lodgings as compatible with yearly day–night average sound level (DNL) below 65 dB. Residential land use at levels between DNL 65 and 75 dB may be determined by a community to be allowed if the outdoor-to-indoor *noise level reduction* is at least between 25 and 30 dB to achieve an interior level of DNL 45 dB. Note that these are identified as guidelines because FAR Part 150 clearly defines land-use compatibility as a state and local government responsibility.

In examining new actions, *significant noise impact* occurs if a noise-sensitive area is projected to experience an increase in noise of DNL 1.5 dB or more at or above DNL 65 dB.<sup>17</sup> Further, if such an increase occurs, noise-sensitive areas between DNL 60 and 65 dB should be examined for increases of 3 dB or more. If such increases occur, either above DNL 65 dB or between DNL 60 and 65 dB, additional analysis is

Table 2 FICON Recommended Relationship between Annoyance and Aircraft Noise

Aircraft Produced $L_{dn}$	Percent of Exposed Population	
	Annoyed at All <sup>a</sup>	Highly Annoyed
45	NA	1
50	NA	2
55	NA	3
60	NA	7
65	NA	12
70	NA	22
75	NA	37

<sup>a</sup> NA = not applicable.

required and mitigation measures should be considered for all areas of increase.

**3.2.3 World Health Organization** The WHO provides guidance for preventing critical health effects that can result from noise. Table 3 presents the guidance for dwellings. The levels shown, if not exceeded, are intended to prevent occurrence of the *critical health effect* for the most exposed receiver. The general WHO guidelines also note that, as suggested by the table, indicators based only on energy-type metrics (e.g.,  $L_{Aeq}$ ) are not sufficient to describe the protective noise environment. Such things as indoor reverberation time (for determining speech intelligibility), number and level of events, and low-frequency content should also be considered to fully describe the noise environment and to protect the critical health effect.

#### 4 NOISE ANALYSIS PROCEDURES

##### 4.1 Methods

Across the various organizations—the EU, the United States, and ICAO (the WHO does not examine the specifics of noise control)—the fundamental approach to analysis and management or control of aircraft noise is similar. All recommend a “balanced” approach that includes at least four ingredients: (1) noise control at the source (the aircraft), (2) land-use planning around airports, (3) noise abatement operating procedures for aircraft, (4) restrictions on operations.<sup>19–21</sup> In addition to these four categories, in the United States, the FAA includes (5) airport layout<sup>22</sup> and ICAO recognizes (6) noise charges.<sup>23</sup>

To pursue this balanced approach, specific tools are required. First, metrics or indicators of noise must be identified (Section 3.1), noise effects or impacts in relation to the indicators need to be defined (Section 3.2), and a method for computing the values of the metrics in communities around airports is required. The following subsection elaborates on the “balanced” approach, and the last subsection discusses the various computational methods.

##### 4.2 Balanced Approach

**4.2.1 European Union** The EU recognizes the balanced approach as defined by ICAO<sup>21</sup> but links it with a recognition that to be effective in achieving sustainable noise reduction, more stringent noise

standards for manufacture of aircraft, combined with action to take noisy aircraft out of service, will also be necessary. Specifically, Directive 2002/30/EC<sup>21</sup> provides guidance on “the establishment of rules and procedures with regard to the introduction of noise-related operating restrictions at Community airports.”

**4.2.2 United States** The Aviation Safety and Noise Abatement Act of 1979 (Public Law 96–193) authorized the FAA to award grants under the Airport Improvement Program (AIP) for noise mitigation projects. The FAA responded by promulgating 14 CFR Part 150, see discussion on FAR Part 150 below. As of the end of 2003, more than \$3.6 billion of AIP funding has been spent on developing and implementing Part 150 studies by more than 250 airports in the United States.

**Source Noise Control—Aircraft Certification and Phase Out** The FAA’s method for determining aircraft source levels and the phase out of the louder aircraft have been specified in federal regulations, 14 CFR Part 36 and Part 91. In 1990, the U.S. Congress passed the Airport Noise and Capacity Act (ANCA),<sup>24</sup> which set a schedule for phase out of all stage 2 aircraft weighing more than 75,000 lb by December 31, 1999 (all stage 1 aircraft having been previously prohibited from operation in the United States.). The phase-out schedule is codified in 14 CFR Part 91. Currently, there is no proposal to phase out stage 3 aircraft, although new stage 4 noise limits have already been established.

**FAR Part 150: Airport Noise Compatibility Planning** As part of the effort to encourage airport and land-use noise compatibility, the FAA makes funding available to airports for noise mitigation through its Part 150 Study program. In order to obtain federal monies for noise assessment, impact mitigation, and land-use compatibility, an airport is required to assess the existing and future noise environment through a Federal Aviation Regulation (FAR) Part 150 Study. Although airports are not required to conduct FAR Part 150 studies, many do in order to obtain this federal assistance. FAR Part 150 studies result in: (1) a noise exposure map (NEM), which documents the existing and future (minimum 5-year) noise exposure with no mitigation; (2) a noise compatibility program

**Table 3 WHO Guideline Values for Community Noise in Specific Environments<sup>18</sup>**

Specific Environment	Critical Health Effect	$L_{Aeq}$ [dB(A)]	Time Base (h)	$L_{Amax}$ Fast (dB)
Outdoor living area	Serious annoyance, day and evening	55	16	—
	Moderate annoyance, day and evening	50	16	—
Dwelling, indoors	Speech intelligibility & moderate annoyance, day and evening	35	16	
Inside bedrooms	Sleep disturbance, nighttime	30	8	45
Outside bedrooms	Sleep disturbance, window open (outdoor values)	45	8	60

Source: From Ref. 18.

(NCP), which identifies specific actions to minimize or eliminate the existing noise impacts in surrounding communities. In developing the NCP, the airport is to examine components that constitute the balanced approach and include land acquisition, construction of barriers, soundproofing, preferential runway use, flight procedures, and restrictions on the use of the airport. The NCP also includes the results of the program by providing an NEM with the recommended NCP measures in place.

#### 4.2.3 International Civil Aviation Organization

In 2001, the ICAO Assembly endorsed the concept of a balanced approach to aircraft noise management (see references in Ref. 20). Within ICAO, the Committee on Aviation Environmental Protection (CAEP) developed the requisite guidance material.<sup>25</sup> CAEP meets annually, and from each meeting, publications providing guidance are produced. (In terms of nomenclature, e.g., CAEP/5 indicates the fifth meeting of CAEP.) Some of this guidance and associated publications are summarized in the following paragraphs.

**Source Noise Control—Certification** Certification procedures and requirements are contained in Annex 16, Environmental Protection, Volume I, Aircraft Noise to the Convention on International Civil Aviation, while practical guidance to certifying authorities on implementation of the technical procedures of Annex 16 is contained in the Environmental Technical Manual on the Use of Procedures in the Noise Certification of Aircraft (Doc 9501). For ICAO, aircraft are designated as Chapter 1, not noise certified, Chapter 2, certified in accordance with the requirements of Annex 16, Volume 1, Chapter 2, and so forth for Chapter 3 and Chapter 4 aircraft. (These designations correspond with the U.S. FAA designations of stage 1, stage 2, stage 3, and stage 4.)

**Land-Use Planning** Land-use planning guidance can be found in Annex 16, Volume I, Part IV, and Airport Planning Manual, Part 2, Land Use and Environmental Control (Doc 9184). It is important that member states ensure that the potential reductions in noise levels to be gained from the introduction of quieter aircraft, particularly those complying with the new Chapter 4 standard, are not avoidably compromised by inappropriate land use or encroachment.

**Operational Procedures** Description of preferential runways and routes, as well as noise abatement procedures for takeoff, approach, and landing are contained in Annex 16, Volume I, Part V, and in Procedures for Air Navigation Services, Aircraft Operations (PANS-OPS, Doc 8168), Volume I, Flight Procedures, Part V. On the basis of recommendations made by CAEP/5, new noise abatement takeoff procedures became applicable in November 2001.

**Operating Restrictions** In the case of Chapter 2 aircraft, the ICAO Assembly in 1990 urged member states not to restrict aircraft operations without considering other possibilities first. It then provided a basis on which states wishing to restrict operations of

Chapter 2 aircraft may do so. States could start phasing out operations of Chapter 2 aircraft from April 1, 1995, and have all of them withdrawn from service by March 31, 2002. However, prior to the latter date, Chapter 2 aircraft were guaranteed 25 years of service after the issue of their first certificate of airworthiness. Thus, Chapter 2 aircraft that had completed less than 25 years of service on April 1, 1995, were not immediately affected by this requirement. Similarly, wide-body Chapter 2 aircraft and those fitted with quieter (high bypass ratio) engines were not immediately affected after April 1, 1995. Many countries including Australia, Canada, the United States, and many in Europe have nevertheless taken action on the withdrawal of operations of Chapter 2 aircraft at their airports, taking due account of the Assembly's resolution. This withdrawal has had a substantial effect in reducing noise levels at many airports. The benefits of removing Chapter 2 aircraft have now been largely achieved.

In the case of Chapter 3 aircraft, the ICAO Assembly in 2001 urged member states not to introduce any operating restrictions at any airport on Chapter 3 aircraft before fully assessing available measures to address the noise problem at the airport concerned in accordance with the balanced approach. The Assembly also listed a number of safeguards that would need to be met if restrictions are imposed on Chapter 3 aircraft. For example, restrictions should be based on the noise performance of the aircraft and should be tailored to the noise problem of the airport concerned, and the special circumstances of operators from developing countries should be taken into account (Appendix E of Assembly Resolution A33-7).

**Noise Charges** The ICAO's policy with regard to monetary noise charges was first developed in 1981 and is contained in ICAO's Policies on Charges for Airports and Air Navigation Services (Doc 9082/6). The ICAO recognizes that, although reductions are being achieved in aircraft noise at the source, many airports need to apply noise alleviation or prevention measures. The ICAO considers that the costs incurred may, at the discretion of states, be attributed to airports and recovered from the users. In the event that noise-related charges are levied, the ICAO recommends that they should be levied only at airports experiencing noise problems and should be designed to recover no more than the costs applied to their alleviation or prevention; and that they should be nondiscriminatory between users and not be established at such levels as to be prohibitively high for the operation of certain aircraft.

Practical advice on determining the cost basis for noise-related charges and their collection is provided in the ICAO Airport Economics Manual (Doc 9562), and information on noise-related charges actually levied is provided in the ICAO Manual of Airport and Air Navigation Facility Tariffs (Doc 7100).

#### 4.3 Airport Noise Modeling

Countries involved in aircraft noise analysis use or have developed and use computer programs that

combine the noise produced by all aircraft operations at an airport, generally to produce contours of equal noise exposure or level using the metric or indicator that is to be used for assessment, see Section 3. Figure 3 presents a typical contour set.

Typically, national or international organizations have developed the general guidelines and algorithms for aircraft noise computation. Then individual nations turn these guidelines into specific computer programs. ICAO provides guidance in its Circular 205,<sup>26</sup> the Society of Automotive Engineers (SAE) Committee A-21, Aircraft Noise Measurement, developed Aerospace Information Report 1845<sup>27</sup> and the EU recommends use of ECAC/CEAC Doc 29, Report on Standard Method of Computing Noise Contours around Civil Airports.<sup>28</sup> (Currently, all documents are undergoing review and updates.) The variables that must be included or input into one of the programs are considerable in number and can be found in one of the user manuals. The model output typically includes, at a minimum, contours of equal noise exposure, as mentioned. The models can also produce single-event noise metrics, and these are often computed to help the public understand the noise effects of the modeled operations or to compare with impact or health effect guidelines.

Each of these models requires an accurate account of the aircraft activity at the facility for which the model is to determine the noise exposure. It is critical that the modeler know the exact number of operations for every aircraft type operating at the facility and for each type of operation conducted, that is, arrival, departure, touch-and-go, runup, and so forth. Some states require this analysis be conducted for an annual average day. Therefore, it is imperative that data are collected for operations over a period of 1 year and

then the number of operations is divided by 365 days before inputting into the model.

## 5 NOISE CONTROL AT THE SOURCE

Aircraft noise control at the source has two components. First, for all manufacture of aircraft, specific noise testing or certification procedures and associated limits are defined. Second, the louder aircraft are phased out of operation over time.

### 5.1 Quieting of Aircraft

These procedures and limits apply at three specific measurement locations: one under a departure path, one laterally to the side of the departure path, and one under an arrival path. During measurements, weather and atmospheric conditions must fall within specific ranges, the aircraft must be operated in defined ways, and detailed methods are provided for computation of the required metric, EPNL (see references in Ref. 2).<sup>32</sup> Limits are specified by maximum gross takeoff weight and number of engines. Figure 4 presents the limits that define FAA's stage 1, stage 2, and stage 3 (ICAO's Chapter 1, Chapter 2, and Chapter 3) aircraft. Any aircraft above the stage 2 limit is stage 1.

There is also a stage/Chapter 4 certification for aircraft. On June 27, 2001, at its 163rd session, the ICAO unanimously approved the adoption of the new Chapter 4 noise standard in Annex 16. In the United States, the FAA also has accepted this certification limit. The new noise standard will apply to any application for new type designs submitted on or after January 1, 2006, for countries that use Annex 16 as its noise certification basis. Briefly, conformance with Chapter 4 has two basic components: (1) None of an airplane's maximum noise levels [flyover, lateral (sideline), and approach] may be greater than the maximum permitted

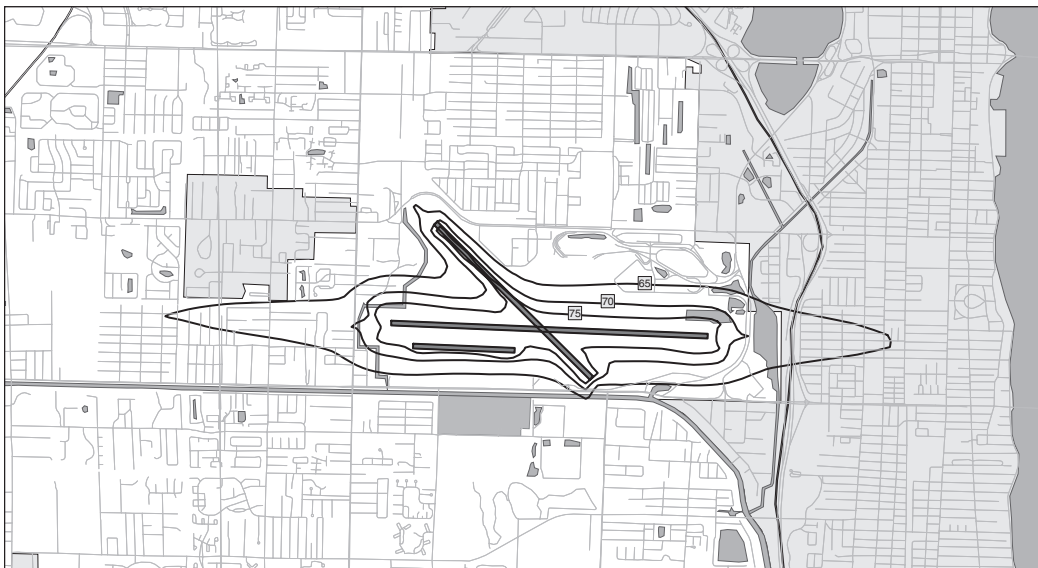


Figure 3 Typical noise contours for an airport.



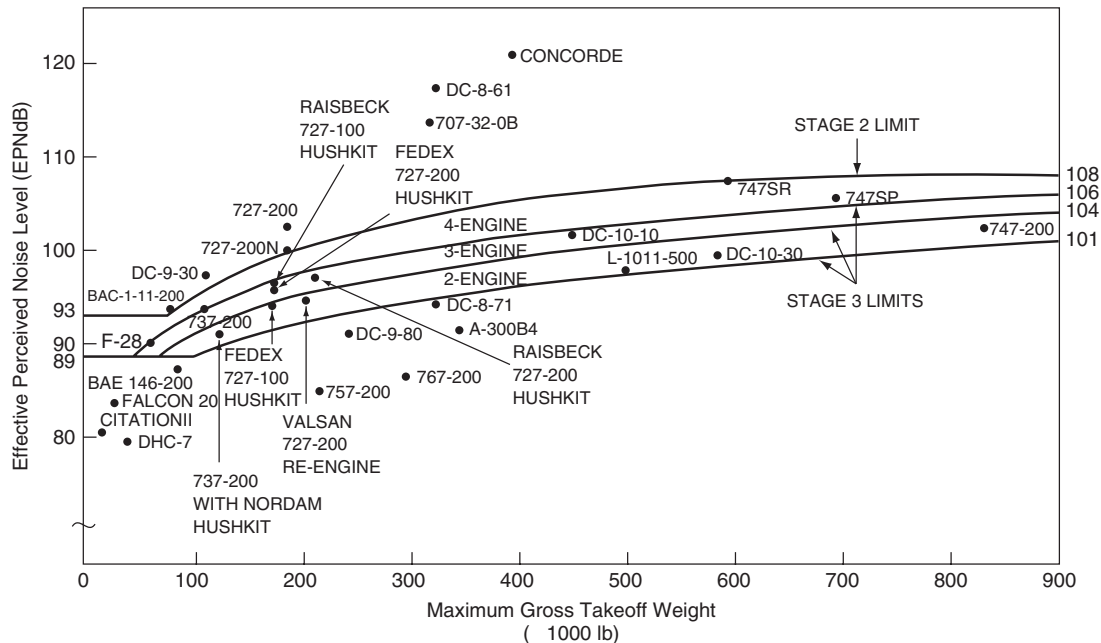


Figure 4 Certification limits for aircraft.

noise levels for Chapter 3 airplanes, as defined in Annex 16. (2) To determine stage 4 compliance, an airplane's maximum flyover, lateral and approach noise levels are each subtracted from the stage 3 maximum permitted noise levels. The differences obtained are the noise limit margins, to be used as follows:

1. When the three margins are added together, the total must be 10 EPNdB or greater.
2. When any two of the margins are added together, the sum must be 2 EPNdB or greater.

## 5.2 Phase Out of Louder Aircraft

The second component of noise control at the source is the phase out of the louder aircraft. To date (2005) stages/Chapters 1 and 2 aircraft have been completely phased out of operation in many countries and are being phased out in others.

## 6 AIRPORT-SPECIFIC NOISE CONTROL MEASURES

The balanced approach also includes land-use planning around airports, noise abatement operating procedures, restrictions on operations, and the airport layout. Additionally, monitoring systems and community outreach can aid in the efforts to reduce the effects of airport noise on communities.

### 6.1 Land-Use Strategies

Land-use strategies are directed at ensuring noise-compatible land use surrounds the airport. The most effective land-use strategies must include working with

local jurisdictions to deter and/or prohibit the development of incompatible noise-sensitive land uses within the airport environs. This strategy can include zoning and building code changes that either prevent incompatible uses or require that sufficient sound insulation be part of building design. Another strategy often employed by airports to eliminate future incompatibilities is the acquisition of vacant land in potentially incompatible areas. The strategies used for addressing existing incompatibilities are typically: (1) relocation of residents, business, and schools resulting in airport land acquisition after the relocations and (2) requiring remaining property owners sign an aviation easement allowing for the use of the airspace above the property. The second is often implemented in conjunction with sound insulation programs.

**6.1.1 Sound Insulation Programs** Residential sound insulation programs and institutional sound insulation programs, predominantly for schools, are intended to reduce the interior noise levels of structures to minimize speech and/or sleep disruption. Design goals are required for sound insulation. Goals for residences may be determined by speech interference or sleep disturbance criteria, such as those of Section 3.2 or by the requirements for a satisfactory teaching environment when sound-insulating schools. House construction varies with climate and local traditions, and premodification measurements and analysis are advisable to determine design, and postmodification measurements help ensure success.

**6.1.2 Noise Barriers** Noise barriers can be used to shield noise-sensitive land uses from aircraft



operations noise. See Chapter 58. Noise barriers are rarely built at airports since most of the noise exposure occurs when aircraft are above the ground and above any reasonably sized barrier. However, some communities are exposed to noise produced by ground operations of aircraft, such as start-of-takeoff roll, thrust reverse, taxi or ramp activities, and ground engine runups. One of the most successful uses of barriers in airport settings has been the installation of ground engine runup enclosures (GREs), which are provided by some airports for performance of maintenance engine runups.

## 6.2 Operational Procedures

Operational procedures for noise abatement are essentially ways for aircraft to use an airport that reduce the noise exposure of noise-sensitive areas. These procedures can include use of runways, specific cockpit procedures for arrival and/or departure, and routes or flight tracks flown for arrival and departure. Design of feasible, effective procedures requires full involvement by air traffic control personnel, pilots, use of modeling procedures and analysis to estimate effectiveness, and often a test period to determine if they are, in fact, practical and safe. Citizen involvement may be beneficial as well.

**6.2.1 Preferential Runway Use** Preferential runway use is designed to put aircraft operations on particular runways to minimize aircraft operations over populated areas. Design will require analysis of average wind conditions to determine maximum possible use of the various runways. Air traffic procedures used to determine which should be the active runway(s) may need modification to ensure maximum use of the preferred runway(s). Procedures for monitoring the ongoing runway use may also be desirable to determine the success of a preferential runway use program.

**6.2.2 Cockpit Procedures** Cockpit procedures are specific flight procedures designed to reduce the noise levels experienced on the ground. Specific noise abatement departure procedures (NADPs) have been developed by many airlines to address two different types of situations: one where the noise-sensitive areas are “close” to the airport and one where the noise-sensitive areas are “distant” from the airport. Usually, detailed modeling, including working with pilots or airlines to develop modeled approximations of the procedures, is required to understand the location and amount of the benefits provided. Cockpit procedures can also be used during aircraft arrival. Investigations have found that a *continuous descent approach*, or CDA—descending the aircraft at a nearly constant angle from a fairly high altitude (about 6000 ft above ground)—can reduce noise heard on the ground by eliminating the thrust changes used in the more common “stepped” approach. CDA procedures are still under investigation at this writing with regards to air traffic control implications.

**6.2.3 Flight Track Geometry and Flight Track Usage** Changes to flight track geometries and/or flight

track usage can be designed to move aircraft over less populated areas. Changing flight track corridors or use, however, requires full involvement of the air traffic controllers responsible for managing the airspace. Especially in congested airspace, maintaining minimum separations between the traffic flows is paramount for safety. Moving flight tracks can have a domino effect requiring other changes to the airspace, which may or may not be feasible. Modeling will provide estimates of benefits, and test periods may be necessary.

## 6.3 Airport Layout Improvements

Planning for major changes at an airport can provide an opportunity to consider layout improvements that would result in the reduction of noise exposure of sensitive areas. Generally, airport layout changes may be used to move aircraft operations (whether taxi, ground, departure, or arrival operations) away from noise-sensitive areas. For example, an airport may decide to lengthen a runway and displace the arrival and departure threshold at the other end of the runway. Start of takeoff and use of thrust reversal could be moved further onto airport property and away from noise-sensitive receivers near the runway end. Another change could be alteration of taxiways to move these ground operations away from adjacent residents. Design and placement of on-airport buildings could shield near-by communities from some types of aircraft ground operations noise.

## 6.4 Airport Use Restrictions

The European Union, the U.S. FAA, and ICAO documents all recognize there may be situations when restricting use of an airport by all or some aircraft types can be an important means to reduce noise exposure. All organizations caution that the costs, both to the traveling public and to individual aircraft operators, should be closely considered when developing any such restrictions. A rigorous approach would include clear determination of criteria for effects, analysis, and rank ordering of alternative methods, including restrictions, to reduce the effects and costs of the alternatives.

## 6.5 Aircraft Noise and Operations Monitoring Systems

Aircraft noise and operations monitoring systems (NOMS) have become increasingly common in recent years as citizens ask to have measured information about aircraft operations and noise levels, and as some airports regularly update their noise contours. These systems permit airports to continuously assess aircraft noise and operations and respond to citizen complaints. NOMS are used not only to assess airport noise but also can be used to educate the community about aircraft noise, respond to noise complaints, and monitor the implementation of noise mitigation measures.

The NOMS were first designed as aircraft noise measurement systems consisting of portable and permanent noise monitors strategically located throughout the airport environs. Flight tracking capability has been added by acquiring aircraft position data, usually from the local air traffic radar system. Flight tracking data

helps ensure that the noise captured by the noise monitors and identified as aircraft-produced noise is actually generated by an aircraft operation and not some other community noise source. Additionally, this flight track and flight identification information can be used to efficiently provide input to the aircraft noise modeling process. Airports can obtain integrated noise model (INM) preprocessors that will take the flight information and generate INM input files to compute daily, weekly, monthly, quarterly, and annual noise exposure contours for a relatively quick and efficient means of assessing the historical noise at their facility.

## 6.6 Community Outreach

Many airports have found community outreach, involvement, and education can be as effective and sometimes more effective than the measures discussed above. Outreach may take many different forms, but the most common avenues for providing this community involvement are: setting up and supporting an airport noise office with adequate and capable staff, acquiring a NOMS, setting up and being a member of a standing airport community noise committee or roundtable, and regularly reporting to the community the progress of the noise mitigation measures and the noise compatibility program.

## REFERENCES

1. N. P. Miller, E. M. Reindel, D. A. Senzig, and R. D. Horonjeff, Low-Frequency Noise from Aircraft Start of Takeoff, Proceedings, INTERNOISE 1998, Christchurch, NZ, November 1998.
2. The details of the measurement and computation procedures may be found in the ICAO publication Annex 16, Volume I, Aircraft Noise, or in the U.S. Code of Federal Regulations, Title 14, Part 36, Appendices A and B.
3. European Parliament and Council Directive 2002/49/EC, Annex I, 25 June 2002, OJ L 189, 18.7.2002, p. 12.
4. U.S. EPA, Information on Levels of Environmental Noise Requisite to Protect Public Health and Welfare with an Adequate Margin of Safety, NTIS PB-239 429, EPA Report No. 550/9-74-004, March 1974.
5. U.S. Code of Federal Regulations, Title 14, Part 150.
6. FAA Order 1050.1E, Appendix A, Section 14, June 8, 2004.
7. B. Berglund, T. Lindvall, and D. Schwela, Eds., *Guidelines for Community Noise*, World Health Organization, Geneva, 2000.
8. American National Standards Institute, S1.4-1983.
9. ICAO Circular 205-AN/1/25, Recommended Method for Computing Noise Contours Around Airports, March 1987.
10. Directive 2002/49/EC, Annex III, see Ref. 3.
11. H. Miedema and Working Group 2, European Commission, Noise Expert Network, Position Paper on Dose Response Relationships between Transportation Noise and Annoyance, 20 February 2002.
12. H. Miedema, W. Passchier-Vermeer, and H. Vos, Elements for a Position Paper on Night-time Transportation Noise and Sleep Disturbance, TNO Inro Report 2002-59, January 2003.
13. U.S. Environmental Protection Agency, Impact Characterization of Noise Including Implications of Identifying and Achieving Levels of Cumulative Noise Exposure (Final report), Washington, D.C., Office of Noise Abatement and Control, Report No.: EPA-NTID73.4 27 Jul 73.
14. Federal Interagency Committee on Noise, Federal Agency Review of Selected Airport Noise Analysis Issues, August 1992, Figure 3.1, p. 3-6, available at <http://www.fican.org/pages/reprt.html>.
15. Federal Interagency Committee on Aviation Noise, Effects of Aviation Noise on Awakenings from Sleep, July 1997; available at <http://www.fican.org/pages/sleepdst.html>.
16. See Table 1, Appendix A of U.S. Code of Federal Regulations, Title 14, Part 150.
17. FAA Order 1050.1E, Appendix A, Section 14, June 8, 2004.
18. B. Berglund, T. Lindvall, and D. Schwela, Eds., *Guidelines for Community Noise*, World Health Organization, Geneva, 2000.
19. European Parliament and Council Directive 2002/30/EC, 26 March 2002, OJ L 85, 28.3.2002, p. 40.
20. ICAO Assembly Resolution A33-7: Consolidated Statement of Continuing ICAO Policies and Practices Related to Environmental Protection, Appendix C, Policies and Programs Based on a "Balanced Approach" to Aircraft Noise Management, 2001.
21. US: 14 CFR (Code of Federal Regulations) Part 36, 14 CFR Part 91, 14 CFR Part 150.
22. 14 CFR Part 150.
23. ICAO, Policies on Charges for Airports and Air Navigation Services, Doc 9082/6.
24. P.L. 101-508.
25. CAEP, Guidance on the Balanced Approach to Aircraft Noise Management, Doc 9829.
26. ICAO, Recommended Method for Computing Noise Contours around Airports (Circular 205).
27. SAE Committee A-21, Aircraft Noise, Procedure for the Calculation of Airplane Noise in the Vicinity of Airports, SAE AIR 1845, March 1986.
28. European Directive 2002/49/EC (see Ref. 3) and Commission Recommendation (2003/613/EC) OJ L212, 22.8.2003, p. 49.

# CHAPTER 126

## OFF-ROAD VEHICLE AND CONSTRUCTION EQUIPMENT EXTERIOR NOISE PREDICTION AND CONTROL

Lyudmila Drozdova, Nickolay Ivanov, and Gennadiy H. Kurtsev  
Department of Environmental Engineering  
Baltic State Technical University  
St. Petersburg, Russia

### 1 INTRODUCTION

Off-road vehicles and construction equipment are used for earthmoving, road works, building and road construction, excavation, and the laying of pipes and cables. Off-road vehicles and equipment are normally powered by diesel engines and, in some cases, electric motors. Compressors provide compressed air for use on construction sites and can be mobile or stationary.

Off-road vehicles and construction equipment are significant environmental noise sources that cause annoyance, risks of hearing damage, and sleep disturbance in nearby residential areas. A-weighted sound pressure levels measured at a 15-m distance from an off-road vehicle during its operational cycle can reach 70 dB to 85 dB. Even at a short distance, the A-weighted noise levels emitted by off-road vehicles and construction equipment can be as much as 15 dB to 30 dB higher than permissible levels. Excessive noise levels are also noted at distances up to several hundred metres from working construction machinery. Off-road vehicles and construction equipment cause disturbance to people similar to that caused by automobiles, railways, and aircraft.

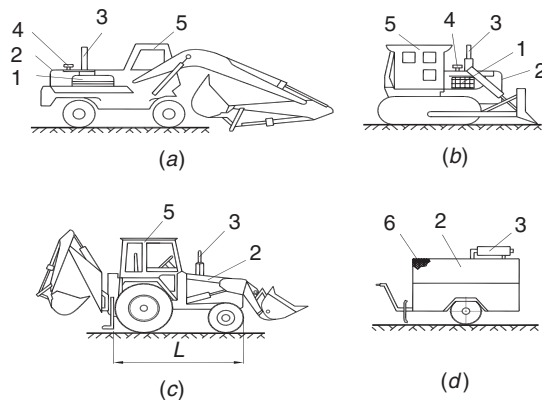
### 2 DESIGN FEATURES AND MAIN NOISE SOURCES

The outlines of most widely used off-road vehicles and construction equipment and main noise sources are represented in Fig. 1. Main noise sources of the off-road vehicles are an engine, exhaust and intake systems, tracks, engine cooling fans, hydraulic system, compressors of movable compressors and other noise, and vibration generating machinery (e.g., mill cutter, vibrating roller, and others). Table 1 gives the average acoustical characteristics of the main noise sources of construction vehicles and movable compressors.<sup>1</sup>

The contribution of a noise source into the noise generation process depends, first of all, on noise source acoustical characteristics but also on the distance from the noise source to the specific point (receiver), on the noise source size and its location at the machine, and on available noise reduction means and their effectiveness.

### 3 OFF-ROAD VEHICLES EXTERIOR NOISE EMISSIONS REQUIREMENTS

In most countries A-weighted sound power level emitted by a vehicle (in dB) is used as a standardized



**Figure 1** Schemes of off-road vehicles and construction equipment: (a) excavator, (b) tractor with dozer equipment, (c) backhoe loader, and (d) movable compressor; (1) engine, (2) enclosure, (3) muffler, (4) engine intake, (5) cab, and (6) sound absorption coating.

parameter. At the same time sound pressure levels are also used for normalization in some countries. For example, exterior noise limitation accepted in Russia and in the Commonwealth of Independent States is A-weighted sound pressure level of 85 dB measured at the distance of 7.5 m from a machine. In United States specific exterior sound requirements on off-road machines are related to state laws or community noise ordinances. The specific levels vary and are often expressed in terms of day and night sound pressure level. The European Community (EC) actual and expected noise limitations are declared in Directive 2000/14/EC of the European Parliament.<sup>2</sup> These limitations are presented in the Table 2.

In Germany, in addition to the European norms, the Federal Environmental Agency introduces the Environmental Label (Blue Angel) for off-road vehicle manufacturing companies (Table 3). This label may be awarded to products whose noise emissions are 10 dB or lower, on average, than EC Directive noise limitations.<sup>3</sup> Noise requirements of the Blue Angel label are the strongest among recently accepted limitations for off-road vehicles.<sup>4</sup>

**Table 1 Acoustical Characteristics of Main Noise Sources of Off-Road Vehicles and Movable Compressors**

Noise Source	A-Weighted Sound Power Level (dB)	Character of Noise Spectrum Emitted by the Noise Source
Engine body	100–110	High frequency <sup>a</sup>
Engine exhaust (with a muffler)	91–98	Low frequency <sup>b</sup>
Engine intake (with a muffler)	85–90	Low frequency
Engine cooling system fan	98–102	Medium frequency <sup>c</sup>
Tracks	89–92	Medium frequency
Vibrating roller	100–105	High frequency
Hydraulic motors and pumps	95–97	High frequency
Compressor	97–100	High frequency

<sup>a</sup>High-frequency components are dominant in the sound pressure level spectrum.

<sup>b</sup>Low-frequency components are dominant in the sound pressure level spectrum.

<sup>c</sup>Medium-frequency components are dominant in the sound pressure level spectrum.

As follows from the analysis, there is no uniform approach to be used in the exterior noise limits formulation throughout the world. Consideration of community noise limits may be applied to compare noise emissions of different off-road vehicles. In many countries community noise limits are declared in terms of equivalent continuous A-weighted sound pressure levels and are equal to 55 dB for daytime and 45 dB for nighttime.<sup>5</sup> Nowadays very few off-road vehicles meet these community noise limits, so machine manufactures in cooperation with acousticians have the challenge of finding innovative, state-of-the-art exterior noise reduction approaches.

#### 4 MEASUREMENT OF EXTERIOR NOISE EMITTED BY OFF-ROAD VEHICLES AND CONSTRUCTION EQUIPMENT

##### 4.1 Measurement of Exterior Noise Emitted by Off-Road Vehicles

Exterior noise measurement procedures are described in International Organization for Standardization (ISO) standards.<sup>6,7</sup> Measurements may be carried out in dynamic and stationary test conditions. The exterior noise is characterized by A-weighted sound power level ( $L_{WA}$ ) estimated based on measured equivalent continuous A-weighted sound levels averaged over the measurement surface over the whole measurement period.

Sound level measurements followed by determination of the emitted sound power level are carried out in six microphone positions at the hemispheric surface. The choice of the hemisphere radius depends on the basic machine length ( $L$ ). The hemisphere radius is determined as follows:

$r = 4$  m when  $L < 1.5$  m.

$r = 10$  m when  $L \geq 1.5$  m but less than 4 m.

$r = 16$  m when  $L > 4$  m.

The A-weighted sound power level,  $L_{WA}$ , emitted by a machine is determined as follows:

$$L_{WA} = \overline{L}_{pAeq,T} - K + 10 \log \frac{S}{S_0} \quad \text{dB} \quad (1)$$

$L_{pAeq,T}$  = equivalent A-weighted continuous sound pressure level averaged over the measurement surface, dB

$K$  = environmental correction

$S$  = area of the hemispherical measurement surface, in square metres, i.e.,  $S = 2\pi r^2$

$S_0 = 1 \text{ m}^2$

**Table 2 European Union Requirements on the Noise Emissions of Off-Road Vehicles and Construction Equipment**

Vehicle type	Net Installed Power $P$ (kW)	Permissible A-Weighted Sound Power Level (dB)	
		Stage I From 03.01.2002	Stage II From 03.01.2006
Compacting machines (vibrating rollers, vibratory plates, etc.)	$P \leq 8$	108	105
	$8 < P \leq 70$	109	106
Tracked dozers, loaders, excavator-loaders	$P > 70$	$89 + 11 \log P$	$86 + 11 \log P$
	$P \leq 55$	106	103
	$P > 55$	$87 + 11 \log P$	$84 + 11 \log P$
	$P \leq 55$	104	101
Wheeled dozers, loaders, excavator-loaders, mobile cranes, graders	$P > 55$	$85 + 11 \log P$	$82 + 11 \log P$
	–	$98 + \log P$	$96 + \log P$
Tower cranes	$P \leq 15$	99	97
	$P > 15$	$97 + 2 \log P$	$95 + 2 \log P$
Compressors	$P \leq 15$	96	93
	$P > 15$	$83 + 11 \log P$	$80 + 11 \log P$
Excavators	$P \leq 15$	96	93
	$P > 15$	$83 + 11 \log P$	$80 + 11 \log P$

**Table 3 Blue Angel Noise Criteria**

Machine Type	Category, Standardized Nominal Airflow ( $Q$ ), m <sup>3</sup> /min, Installed Power ( $P$ ), kW	Noise Emission Limits (A-Weighted Sound Power Level), dB
Track Vehicles, Except Excavators	$P \leq 60$	99
	$P > 60$	$80 + 11 \log P$ , but less than 101
Wheeled Dozers, Loaders	$P \leq 39$	97
	$P > 39$	$79 + 11 \log P$ , but less than 101
Compressors	$Q \leq 5$	88
	$5 < Q \leq 10$	89
	$10 < Q \leq 30$	91
	$Q > 30$	93
Excavators	$P \leq 14$	91
	$P > 14$	$78 + 11 \log P$ , but less than 101
Tower Cranes	$P < 15$	86
	$15 \leq P < 30$	88
	$P \geq 30$	90

Equivalent A-weighted continuous sound pressure level,  $L_{pAeq,T}$ , is estimated by the following equation:

$$\bar{L}_{pAeq,T} = 10 \log \left[ \frac{1}{N} \sum_{i=1}^N 10^{0.1 L_{pAeqi}} \right], \text{ dB} \quad (2)$$

$L_{pAeqi}$  = measured value of the equivalent A-weighted continuous sound level, dB, resulting from the  $i$ th point at the hemisphere (reference sound pressure is  $2 \times 10^{-5}$  Pa)

$N$  = is the number of microphone positions ( $N = 6$  for this test method)

The background noise level in each measurement position is supposed to be at least 10 dB lower than the noise level emitted by the machine under the test.

#### 4.2 Measurement of Exterior Noise Emitted by Movable Compressors

Methods of movable compressors exterior noise measurements are presented in the ISO standard.<sup>8</sup> Averaged octave sound pressure levels (dB) and A-weighted sound pressure levels (dB) measured at 7 m distance from a movable compressor are used as an acoustical characteristic of a compressor. Sound pressure levels are controlled in five microphone positions located in four main directions rectangular to the compressor side panels, and the fifth microphone location is chosen in the direction where controlled sound

pressure level is maximal. Measurement positions are located at 1.5 m distance from the underneath surface where the movable compressor is installed. Measurements are carried out in the free sound field. There shall not be any obstacle at 25 m distance from the compressor, whose size is comparable to the size of the movable compressor.

#### 5 ACOUSTICAL CHARACTERISTICS OF OFF-ROAD VEHICLES AND MOVABLE COMPRESSORS

Exterior noise emitted by off-road vehicles depends on their acoustical characteristics, on the number of noise sources, and on the composition and effectiveness of noise reduction means. Table 4 presents noise characteristics of some vehicles and tractors.<sup>1</sup>

All off-road vehicles considering their acoustical characteristics may be divided into three main groups. The first group consists of wheeled vehicles (excavators, loaders, graders) where the engine is the dominant noise source. These vehicles are characterized by the lowest sound power levels (among other off-road vehicles), and the difference between dynamic and stationary operating modes is not higher than 1 dB to 2 dB.

The second group consists of track vehicles in which the contributions of tracks and engine to exterior sound field are comparable. Noise level emitted by such machines in dynamic operating mode is 3 dB to 4 dB higher than in stationary mode because of increasing track contribution during dynamic cycles.

**Table 4 Exterior Noise Levels of Construction and Transportation Vehicles and Tractors**

Group Number	Vehicle Type	Operating Mode	A-Weighted Sound Power Level (dB)
1	Wheeled loaders, excavators, graders	Stationary	96–102
		Dynamic	97–105
2	Tracked tractors and dozers	Stationary	100–102
		Dynamic	103–106
3	Vibrating rollers	Stationary	97–99
		Dynamic	109–111

The third group consists of vehicles in which vibration or impact generation tools (e.g., vibrating rollers) or other noise-generating mechanical facilities are the dominant noise sources. Noise level emitted by such vehicles in stationary operating mode is 10 dB lower than noise emitted in dynamic mode. Spectrum of the first group is characterized by the dominance of the low- and medium-frequency components, the second group is characterized by dominant contributions in the high-frequency range, and the third group is characterized by the medium- and high-frequency spectrums.

Noise emitted by movable compressors depends on the type of a power plant—an engine (diesel or gas) or an electric motor—on the type of compressor (piston, membrane, rotation, blade, or screw type), and on the mode of operation since the power plant plays the main role in noise generation processes.

Movable compressors with volume flow rates varying from 2.5 m<sup>3</sup>/min up to 5 m<sup>3</sup>/min are the most widely applied (they are about 40% of the overall quantity of produced compressors). Movable compressors characterized by the volume flow rates varying in the range of 7.5 to 15 m<sup>3</sup>/min are only about 18% of the overall quantity of produced compressors.

Noise emitted by compressors with engine power plants is higher than noise emitted by compressors with electric motor power plants with the same volume flow rate. Thus A-weighted sound pressure level at 1 m distance is 101 dB for diesel-engine-driven compressors, and it is 96 dB for gas-engine-driven compressors, and it is 93 dB for electric-motor-driven compressors. Noise emitted by the diesel engine and electric-motor-driven compressors has high-frequency character and noise of gas compressors has low-frequency spectrum, mostly because of the contribution of the exhaust noise. Movable compressor noise also increases with an enhancement of the volume flow rate since the engine power consumed by the compressor is higher.

A-weighted sound pressure levels emitted by non-sound-protected compressors with volume flow rates up to 10 m<sup>3</sup>/min are usually in the range of 80 dB to 90 dB. Most of modern leading compressor manufacturing companies produce movable compressors in sound-protected varieties (Table 5).<sup>1</sup>

**Table 5 Acoustical Characteristics of Movable Compressors at 7-m Distance**

Movable Compressor Type	Drive Type	Volume Flow Rate (m <sup>3</sup> /min)	Sound Pressure Level (dB)
Non-sound-protected	Diesel	5.2	89
Non-sound-protected	Diesel	10.5	92
Non-sound-protected	Electric motor	5.2	80
Non-sound-protected	Electric motor	10.0	84
Non-sound-protected	Gas	5.2	86
Sound-protected	Diesel	5.0	70
Sound-protected	Diesel	10.6	75
Sound-protected	Electric motor	5.0	58

## 6 NOISE GENERATION PROCESSES AND PREDICTION OF EXTERIOR NOISE

An example of the calculation scheme of the exterior noise emitted by a tracked dozer is presented in Fig. 2. Main noise sources and noise propagation paths are as follows: track noise ( $L_{tr}$ ), engine body noise penetrating from the engine compartment through the enclosure walls ( $L_{eng\_enc}$ ), engine intake ( $L_{int}$ ), and exhaust noise ( $L_{exh}$ ).

The exterior noise field is formed by the total contributions of all above-mentioned noise sources and may be determined by the following equation<sup>1</sup>:

$$L^{ext} = 10 \log \left( 10^{0.1L_{eng\_enc}} + 10^{0.1L_{exh}} + 10^{0.1L_{int}} + 10^{0.1L_w} \right) \text{ dB} \quad (3)$$

The first term of Eq. (3) is estimated as follows<sup>1</sup>:

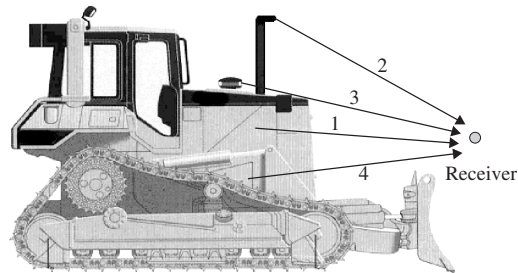
$$L_{eng\_enc} = L_{W_{enc}}^{total} + 10 \log \left( \frac{\chi_{enc}}{S_{enc\_total}} + \frac{4\psi_{enc}}{B_{enc}} \right) - 10 \log \frac{\sum_{i=1}^m S_{enc,i}}{\sum_{i=1}^m S_{enc,i} \times 10^{-0.1(SI_{enc,i} + t_{enc\_i})}} + 10 \log \frac{\sum_{i=1}^m S_{enc,i}}{S_{enc}} - 15 \log R_{enc} - x \text{ dB} \quad (4)$$

where  $L_{W_{enc}}^{total}$  = total acoustical power emitted within the enclosure, dB

$\chi_{enc}$  = coefficient of the effect of the near sound field of noise source (engine body)

$\psi_{enc}$  = is the coefficient of the sound field diffusivity violation under the enclosure;

$S_{enc\_total}$  = is the total area of inner structural panels of the enclosure (inside the engine compartment), m<sup>2</sup>



**Figure 2** Calculation scheme for tracked dozer exterior noise prediction: (1) engine body noise penetrating from the engine compartment through the enclosure walls, (2) internal combustion engine exhaust noise, (3) intake noise, (4) track noise.

$B_{\text{enc}}$  = is the acoustical enclosure constant,  $\text{m}^2$ , estimated by the following equation:

$$B_{\text{enc}} = \frac{A_{\text{enc}}}{1 - \bar{\alpha}_{\text{enc}}} \quad (5)$$

where  $A_{\text{enc}}$  = equivalent enclosure sound absorption area,  $\text{m}^2$ ;  $A_{\text{enc}} = \bar{\alpha}_{\text{enc}} S_{\text{enc}}$ ,  $\text{m}^2$

$\bar{\alpha}_{\text{enc}}$  = coefficient of average sound absorption under the enclosure

$S_{\text{enc}}$  = area of the enclosure structural panel surfaces through which sound penetrates,  $\text{m}^2$

$S_{\text{enc},i}$  = area of the  $i$ th enclosure panel,  $\text{m}^2$

$m$  = number of enclosure panels

$SI_{\text{enc},i}$  = sound isolation of the  $i$ th enclosure panel, dB

$t_{\text{enc},i}$  = addition to the enclosure panel sound isolation depending on panel arrangement relative to the specific point, dB

$R_{\text{enc}}$  = average distance from the enclosure to the receiver (specific point), m

$x$  = numerical correction equals to 5 dB if  $\Omega = \pi$ , or to 8 dB if  $\Omega = 2\pi$ , or to 11 dB if  $\Omega = 4\pi$  ( $\Omega$  is the noise source spatial angle of sound radiation; it is equal to  $4\pi$  when radiation is to the whole space,  $2\pi$  when radiation is to the half space, and  $\pi$  for the quarter space)

The exhaust noise contribution into the exterior sound field is estimated by the following equation<sup>1</sup>:

$$L_{\text{exh}} = L_{W_{\text{exh}}} - 20 \log R_{\text{exh}} + DI_{\text{exh}} - x \quad \text{dB}, \quad (6)$$

where  $L_{W_{\text{exh}}}$  = sound power of the exhaust, dB

$R_{\text{exh}}$  = average distance from the exhaust pipe to the specific point, m

$DI_{\text{exh}}$  = exhaust direction index, dB

$x$  = numerical correction described in Eq. (4)

The intake noise contribution is determined analogous to the exhaust noise component. The track noise contribution to the exterior sound field is calculated as follows<sup>1</sup>:

$$L_{\text{tr}} = L_{W_{\text{tr}}} - 10 \log R_{\text{tr}} - x \quad \text{dB} \quad (7)$$

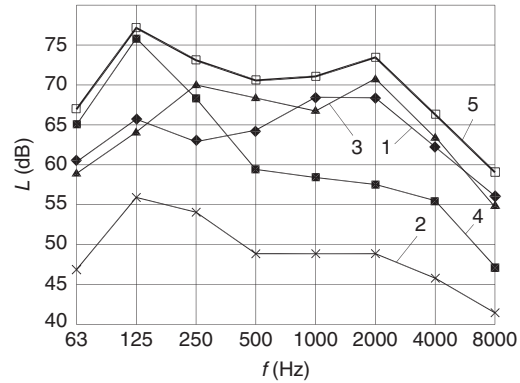
$L_{W_{\text{tr}}}$  = sound power emitted by tracks, dB

$R_{\text{tr}}$  = average distance from the tracks to the receiver (specific point) of the exterior field, m

$x$  = numerical correction described in Eq. (4)

Predicted tracked dozer noise contributions propagating to the receiver (specific point) located in the exterior sound field by various paths (in terms of A-weighted sound pressure levels, dB) are presented in the Fig. 3.

Analysis of the obtained results shows that intake noise does not affect exterior noise field, the contribution of track noise at medium and high frequencies is comparable with the contribution of the engine



**Figure 3** Predicted results of noise level source contributions penetrating by different paths into the exterior sound field of a tracked dozer (spectrum data): (1) engine compartment noise contribution, (2) intake noise contribution, (3) track noise contribution, (4) exhaust noise contribution, and (5) predicted total exterior noise.

compartment noise propagating through the enclosure. Low-frequency exterior noise is mostly formed by exhaust contribution. In the example under consideration the following paths of exterior noise reduction are formulated: attenuation of the track noise (e.g., with the help of acoustical baffles) and decrease of engine body noise (by an increase of enclosure panels' sound isolation, by closing of openings and slots, and by using of sound absorption lining within the enclosure).

## 7 EXTERIOR NOISE REDUCTION MEANS AND METHODS

### 7.1 Classification

Reduction of exterior noise emitted by off-road vehicles and construction equipment may be provided at the noise source or at the noise propagation path.<sup>1,9</sup> Main means of exterior noise reduction are the following: mufflers for aerodynamic (intake and exhaust) noise, sound-proofed enclosures (for reduction of engine body and fan noise), and acoustical baffles (for noise reduction in the source or to be used as additional noise reduction elements in sound-proofed enclosures). Effectiveness of the above-mentioned means depends on the noise source predominance.

For the first group of vehicles (specified in Section 4 of this chapter) decreasing the rotation velocity provides up to 3 dB to 4 dB of exterior A-weighted sound pressure level reduction, improvement of sound-proofed enclosure design may provides up to 4 dB to 5 dB of exterior noise reduction, and using of sound-absorbing materials within a sound-proofed enclosure yields reduction of exterior noise by 2 dB to 3 dB.

For the second group of vehicles isolation of tracks by application of acoustical baffles leads to the exterior A-weighted sound pressure level reduction by 3 dB to 5 dB, and the acoustical shield mounted on vibrating

roller may reduce exterior noise by 4 dB to 6 dB. Noise reduction by means of muffler application may reach 1 dB to 5 dB and depends on muffler effectiveness and on contributions of other noise sources.

## 7.2 Sound-Proofed Enclosures

The application of sound-proofed enclosures at the main noise source of off-road vehicles, the power plant, is a widely used technique of noise and vibration control in vehicles.

Enclosure effectiveness is determined by a number of factors: enclosure shape and size, stiffness of the shielding parts, area of the air holes and paths, average sound absorption coefficient, shielding devices for sound insulation, the damping of the enclosure parts, and so forth.

Extremely tight-fitting enclosures, providing effective sound insulation, result in a considerable air temperature rise within the enclosures that, in turn, may cause damage to or loss of performance of the power plant.

The major problem to be solved first is to provide normal heat transfer within the enclosure. This depends on the enclosure type, the total heat conductivity of enclosure walls, weather conditions, and the air temperature difference between the inside and the outside of the enclosure.

Enclosure tightness must provide necessary sound-proofing and at the same time produce no ill effects on the heat transfer from surfaces inside the enclosure. Being a universal technique to reduce noise in vehicles, an enclosure involves the addition of components to lower the propagation of airborne noise, structure-borne noise, and heat.

Enclosure walls, sound-reflecting baffles in the engine space, noise mufflers, packing units, and gaskets constitute the methods that can be used to reduce the airborne noise. Vibration isolation of the enclosed power plant and its enclosure, the vibration-absorbing enclosure wall components, the vibration-isolating packings and gaskets, the vibration dampers, antivibrators, and vibration-blocking masses hinder the structure-borne noise propagation.

The characteristic features of the vehicle engine enclosure are the following:

- Small air gap in the enclosure engine space when compared to the maximum enclosure dimensions
- Increased heat transfer into the enclosed engine airspace
- The passage of numerous engine piping systems and electric cables through the power plant enclosed space
- A number of openings, ventilation channels, and inspection windows necessary for the engine maintenance

Metal boards, transparent plastics, and sandwich (multilayer) constructions may be considered as basic construction materials for enclosure walls and surfaces.

Metal enclosures may be structural reinforced-frame constructions or structural non-reinforced-frame constructions, sectional and nonsectional, and two-wall or one-wall constructions. They usually have rectangular shape. Aluminum alloy is a preferable material for metal enclosures because this material is easily processed, has low density, and good heat reflection characteristics.

Enclosures from glass plastics in most cases are made as one-wall constructions and may have varied configurations. They are characterized by high values of sound insulation and resistance to corrosion. Application of transparent plastics reduces the metal content of an enclosure on average by 30 to 35% without degradation of structural strength or durability.

The outer layer of the sandwich (multilayer) type of construction materials consist of metal, plastics, and glass-plastics. Inner layer of sandwich-type constructions are usually made from vibration absorption material.

Inner surfaces of enclosures, as a rule, contain sound absorption and vibration absorption layers. A protection layer may also be used at the inner enclosure surface if necessary. A protection layer (a sound transparent film or a thin protection metal board) is used to prevent sound absorption material degradation caused by interference with oil, humidity, airflows, and other factors.

Sound-absorbing materials (SAM) have been found to be very useful in noise control of enclosures. Capacious fibrous and foam-type polymer materials are used as sound absorption materials in enclosures. Fibrous materials are characterized by higher sound absorption than foam-type polymer materials.

Vibration absorption coatings (VAC) are used to reduce spreading of oscillations emitted by construction elements of enclosures by means of transformation of oscillation energy into heat. Mastics, thin layers, and their combinations are used as vibration absorption coatings.

For instance, forced VAC are usually presented as combinations of dissipate layers of viscous elastic material and a thin (forced) metal layer. Shift deformation appears in the dissipate layer during bending of the construction. Vibration absorption happens in the coating due to these processes and due to material features. Various types of rubber, mastics, and other materials are used as the viscous elastic material for absorption of vibration.

Soft vibration absorption coatings consisting of a viscous elastic layer with low dynamic modulus of transverse elasticity or (and) by means of the air gap inclusions in the mastic massive cause increase of material compression ability. Mastic coating increases sound insulation of the damped wall of the enclosure by 1 dB to 2 dB in the medium and low frequencies and by 3 dB to 8 dB at the high-frequency range.

Adhesive thermos reactive glue or rigid vibration absorption coatings in the form of rigid plastics placed on the vibrating surfaces are mounted at one side of thin bitumen layers, which are used for vibration



absorption coatings. Deformation of this layer occurs when the layer is compressed or stretched.

Sound transparent films or thin protection metal boards (thickness less than 1 mm) attached to the inner enclosure surfaces may also be used as vibration protection materials. Most effective protection metal boards are made from aluminum alloys with perforation. Films covering the sound-absorbing materials reduce the coating sound absorption coefficient in the high-frequency range, thus resulting in some decrease of the enclosure effectiveness. At the same time film influence on sound absorption coefficient in the low-frequency range is negligible. Quite a different situation is observed for enclosures characterized by the presence of the enclosure underneath the opening. Their acoustical effectiveness is affected by the use of the protecting films only to a very small extent. A protecting metal board with a high-grade enclosure seal may be considered as an additional sound and heat radiation filter within the enclosure.

Acoustical effectiveness of a sound-proofed enclosure depends on the area of the SAM coating. With a coating of 15% of the enclosure inner protecting surfaces and a high degree of sealing, enclosure efficiency increases by 5 dB to 10 dB in the 125 to 8000 Hz frequency range. If the coating area is increased to 50%, an additional increase in efficiency of 4 dB to 6 dB is obtained, and a coating area of 100% increases the efficiency a further 7 dB to 13 dB, especially at the high-frequency range of 2000 to 8000 Hz (Fig. 4). Further increase of area of sound absorption coating also causes some increase of enclosure efficiency but not so significant. Such character of dependence of SAM area on the enclosure efficiency is confirmed only for closed enclosures (without an enclosure underneath the opening). The presence of an enclosure underneath the opening, ventilation channels, technological openings, slots, and the like influence sound distribution within the enclosure and change average sound absorption of the enclosure. These features yield changing

of dependence between the enclosure efficiency and sound absorption coating area.

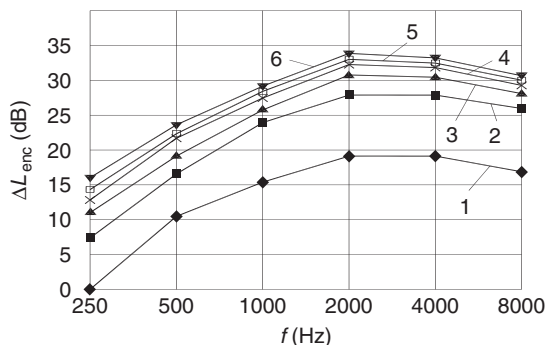
One of the main factors that negatively influence the enclosure effectiveness is the necessity of having ventilation channels or the presence of badly sealed holes in the enclosure. The leading part is played by the size and shape of the channels (holes, openings, slots). Depending on the relationship between the wavelength of the incident sound and the size of the hole or the slot width, the enclosure acoustical effectiveness with one and the same ventilation channel area may vary throughout a considerable range.

The substitution of a single-wall enclosure by a double-wall permits increase in the total surface density by more than twice (up to a value of 10 to 15 kg/m<sup>2</sup>), which makes it possible to increase the enclosure acoustical effectiveness by 7 dB to 13 dB in the whole frequency range. But if there are unprotected ventilation channels in the double-wall enclosure structure, its effectiveness becomes 5 dB to 12 dB lower, and it approaches the single-wall enclosure effectiveness.

Acoustical effectiveness of a sealed double-wall enclosure without a sound-absorbing coating is equal to that of a single-wall coated enclosure with exception of the low-frequency region in which the acoustical effectiveness of the double-wall enclosure is higher. Double-wall enclosures may be used for sound isolation of low-speed power plants. Application of sound-absorbing coatings increases the double-wall enclosure acoustical effectiveness in the whole frequency range, and the effectiveness at high frequencies can exceed 40 dB to 50 dB.<sup>1</sup>

There is certain dependence between the enclosure acoustical effectiveness and its shape. It is found that enclosure sound insulation increases at low frequencies is achieved with the reduction in the first resonance frequency of the enclosure due to the increase in the enclosure structure mechanical stiffness. This may be achieved by making the enclosure shielding structures with cylindrical or spherical shapes or by increasing the distance between the enclosure shielding surfaces and the power plant. The acoustical effectiveness of a spherically or hemispherically shaped enclosure at low frequencies is by 10 dB to 30 dB higher than of flat-walled ones with the same volume.

The spherical, hemispherical, or cylindrical enclosure shape in combination with an enclosure inner surface sound-absorbing coating and with an outer vibration damping coating permits an increase in sound insulation effect throughout the whole frequency range. At low frequencies, due to the greater stiffness of the enclosure, the sound insulation increases because of the resonance frequency shift toward the medium-frequency region, where the vibration damping coating effectiveness is high. In the medium-frequency range the vibration damping coating effect is equivalent to an enclosure dynamic stiffness increase. In the high-frequency region the enclosure sound insulation increases both due to the vibration damping coating, which increases the energy loss because of the enclosure shell vibration, and due to the use of a sound-absorbing coating.



**Figure 4** Dependence of the acoustical effectiveness of a coated enclosure on the area of sound-absorbing material (SAM): (1) area of SAM, 0%; (2) area of SAM, 20%; (3) area of SAM, 40%; (4) area of SAM, 60%; (5) area of SAM, 80%; and (6) area of SAM, 100%.

The relationship between the enclosure sound insulation of effectiveness and its dimensions is almost unpredictable: With increase of enclosure size and therefore with increase of the enclosed volume, the enclosure radiation surface area increases but at the same time the sound intensity on the enclosure inner walls decreases.

### 7.3 Engine Exhaust Noise Mufflers

Engine intake and exhaust noise mufflers are the significant noise control measures and play the most important role in the exterior noise reduction of noise sources with aerodynamic genesis. A-weighted sound pressure levels emitted by nonmuffled exhaust reaches 115 dB to 130 dB and may exceed noise of all other sources by 10 times. A-weighted sound pressure level of a nonmuffled intake is lower but also may reach 100 dB to 110 dB. Thus engine intake and exhaust noise mufflers are compulsory mounted on exhaust and intake systems of a vehicle engine.

Muffler functioning bases on two principles of sound intensity reduction by absorption or reflection (acoustical filters) and by decreasing the gas flow energy in the exhaust chamber (temperature, energy, gas flow velocity and pressure, smoothing of its pulsations) that leads to decreasing of sound energy effectiveness near the gas exits to the atmosphere.

The common classification of mufflers divides them into three classes in accordance with the principle of their operation:

- **Reactive** where the sound reflection takes place in the elements of expansion (contraction) in expansion chamber

- **Absorbing** where the sound energy transforms into the heat in soft fibrous coatings
- **Combined** which combines two preceding principles

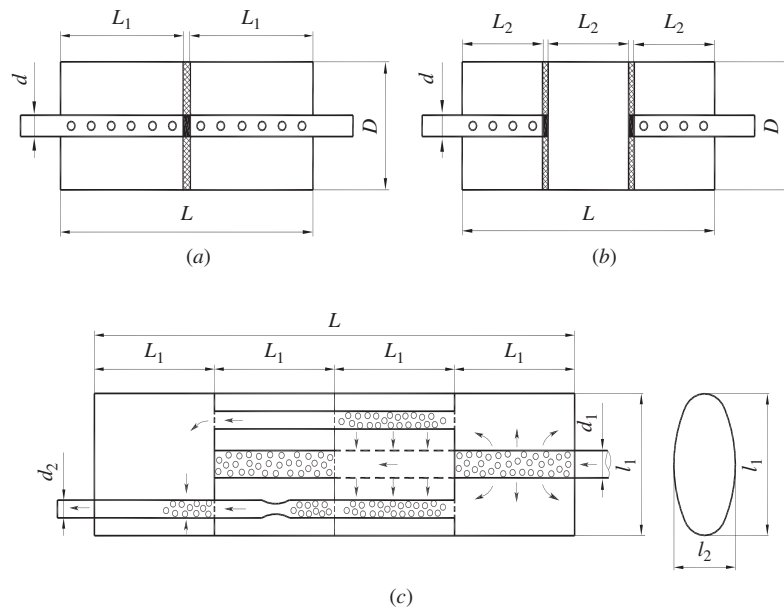
Mufflers as suppressors of the gas flow energy used in gas exhaust channels consist of the following elements: expansion chambers, perforated pipes and partitions connecting pipes, solid partitions and others. Such elements provide the expansion of gas flow, turning and smoothing what results in energy losses of the flow and noise reduction. Figure 5 shows some mufflers used in off-road vehicles and in movable compressors and their main elements.

Acoustical mufflers-filters are usually used for intake systems and may be either reactive (expansion chamber) or absorbing (chamber partly lined with a sound-absorbing material).

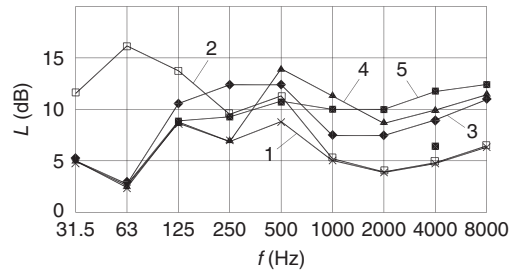
The influence of some basic muffler elements on the acoustical effectiveness of the muffler is shown in Fig. 6. From the presented results the extension of muffler volume increases its effectiveness at low frequencies.

Bend of the gas flow yields an increase of the muffler effectiveness in the medium- and high-frequency regions. Application of perforation in mufflers provides noise reduction in the wide frequency range. Use of sound absorption yields the effectiveness increase at the medium and high frequencies.<sup>1</sup>

Installation of the muffler in a gas channel provides increasing of pressure loss. For instance, pressure losses of 3000 to 5000 Pa (i.e., the common value for many exhaust noise mufflers) causes the fall of the



**Figure 5** Exhaust noise mufflers used for noise reduction in off-road vehicles and in movable compressors: (a) two-chamber reactive muffler, (b) three-chamber reactive muffler, and (c) four-chamber muffler.



**Figure 6** Noise spectra of muffler effectiveness depending on muffler construction: (1) empty chamber (a basic design for further comparison and analysis), (2) empty chamber of two times higher volume than the basic model muffler, (3) three-chamber muffler with two perforated partitions that volume is equal to the basic muffler, (4) empty chamber lined with sound-absorbing material, and (5) single-chamber muffler with right bend at the gas flow at the muffler outlet.

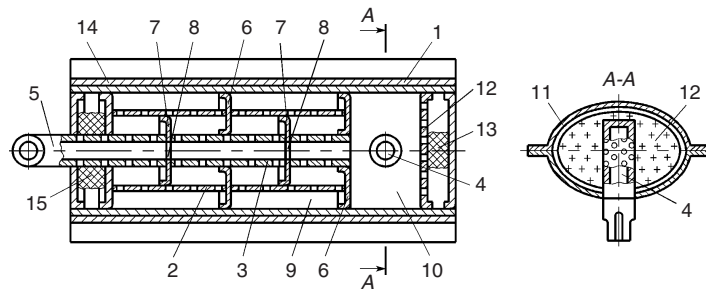
engine power by 1 to 1.5%. Thus, in most cases, design of an effective muffler is the compromise between providing necessary noise reduction and obtaining required pressure loss. Construction performance of modern mufflers tends to design complication and muffler enlargement. According to the newest exterior noise limitations, muffler structures have become more complicated because of the growth of the number of chambers, by introducing the elements provided multiple bends of gas flow, by using elements with large perforated areas, or with sound absorption lining.

An example of a muffler providing high effectiveness (up to 40 dB) and relatively low pressure loss (lower than 7000 Pa) is shown in Fig. 7. The feature of this muffler is the elliptical shape of the muffler body. The muffler consists of several internal pipes and partitions providing gas flow division into several jets with subsequent interference and extension of gas path through the muffler. Inlet flow turn and outlet sound-absorbing chamber are designed in the muffler. Described construction of the muffler allows providing high effectiveness of the muffler with minimal loss of the engine power. This muffler may be exploiting for the internal combustion engine with the power of 40 to 150 hp. Particular parameters of this muffler used in a movable compressor are the following: big axis of the ellipse is 300 mm; small axis of the ellipse is 170 mm; pressure loss is 500 mm H<sub>2</sub>O; and obtained acoustical effectiveness is 38 dB (23 dB to 52 dB in the frequency range of 63 to 8000 Hz). Details of effectiveness of the engine exhaust muffler are given in the Table 6.<sup>10</sup>

Active mufflers located in the gas exhaust systems are also used nowadays for exterior noise reduction. Such systems provide effectiveness of 5 dB to 15 dB at some low frequencies (lower than 200 Hz). Active mufflers are characterized by the presence of an artificial noise signal generated within the exhaust pipe in antiphase to the noise emitted by the vehicle exhaust system. Noise reduction is obtained due to the interference of two signals.

#### 7.4 Acoustical Baffles

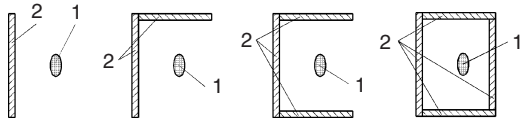
Acoustical baffles are the supporting sound-proofed constructions that may be installed near local noise



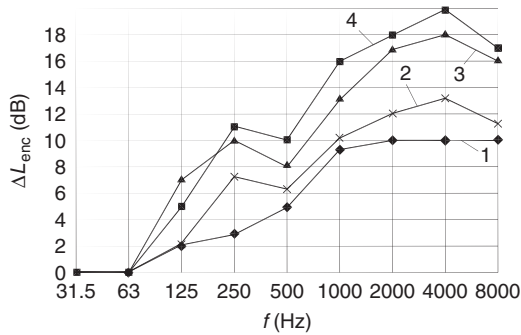
**Figure 7** Exhaust noise muffler for a movable compressor: (1) muffler body, (2) cylindrical tumbler, (3) central perforated pipe, (4) inlet pipe, (5) outlet pipe, (6) elliptical partition, (7) solid partition, (8) partition, (9) gas channels, (10) expansion chamber, (11) solid bottom, (12) perforated partition, (13) vibration-damping material, (14) solid partition, and (15) sound-absorption material.

**Table 6** Effectiveness of Exhaust Noise Muffler

Descriptor	Sound Pressure Levels and Enclosure Effectiveness (dB) in Octave Frequency Bands (Hz)							
	63	125	250	500	1000	2000	4000	8000
Exhaust without muffler	129	124	128	125	122	121	129	123
Exhaust with muffler	106	98	94	84	86	84	81	71
Effectiveness of the muffler	23	26	34	41	36	37	48	52



**Figure 8** Examples of acoustical baffle (2) shapes used for noise reduction of a local noise source (1).



**Figure 9** Dependence of the acoustical baffle effectiveness on baffle materials: (1) canvas baffle, (2) metal baffle without sound absorption, (3) soft sound-absorbing baffle, and (4) metal baffle with sound absorption.

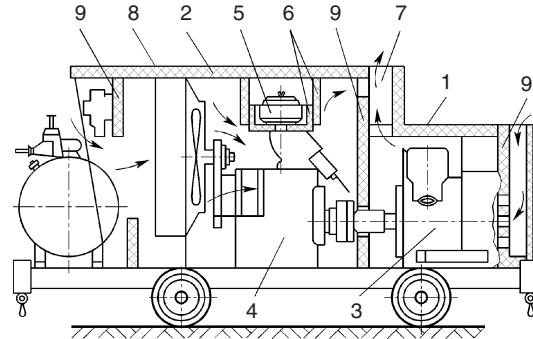
sources of the off-road vehicles (e.g., near the tracks, transmissions, hydraulic system, and others). Acoustical baffles may be used as noise protection in sound-proofed enclosures, for example, to partially cover an opening or an aperture in a sound-proofed enclosure. Acoustical baffles may be produced in various shapes (Fig. 8).<sup>11</sup>

Baffles may be rigid (metal, as a rule) or soft. It is necessary to use sound absorption for increasing acoustical baffle effectiveness (Fig. 9).<sup>11</sup>

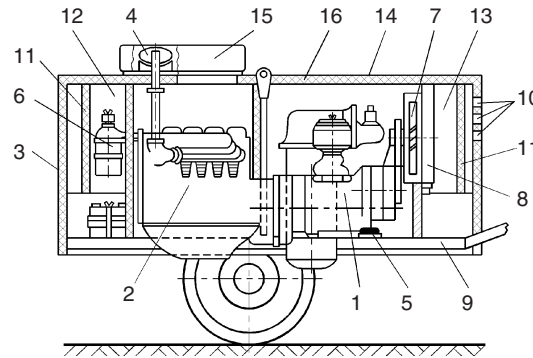
Acoustical baffles allow achieving up to 5 dB to 10 dB reduction of the exterior A-weighted sound pressure levels emitted by local noise sources. Baffles are expected to become a widely used measure for exterior noise reduction of the off-road vehicles.

## 8 EXAMPLES OF EXTERIOR NOISE REDUCTION USED IN OFF-ROAD VEHICLES AND CONSTRUCTION EQUIPMENT

Let us consider two noise reduction schemes used to decrease exterior noise emitted by a movable compressor. The first example describes a movable compressor with an electric motor drive (Fig. 10). A steel sound-proofed enclosure (1) of 1 mm thickness lined with sound-absorbing material (2) of 30 mm thickness was used for exterior noise reduction. The enclosure is divided into two chambers—one is for an engine (3) and another is for a compressor (4). Each chamber has an independent air intake system. The compressor intake filter (5) is covered with a light hood to avoid heating. This hood performs functions of an enclosure muffler (6) and the air duct at the same time. The heated air is released



**Figure 10** Sound-proofed movable compressor with an electric motor drive: (1) sound-proofed enclosure, (2) sound-absorbing material, (3) electric motor, (4) compressor, (5) intake filter, (6) enclosure muffler, (7) exhaust opening, (8) enclosure roof, (9) acoustical baffles.



**Figure 11** Sound-proofed movable compressor with a diesel engine: (1) compressor, (2) diesel engine, (3) sound-proofed enclosure, (4) engine exhaust muffler, (5) vibration isolators, (6) intake filter, (7) fan, (8) cooler, (9) frame, (10) exhaust slots, (11) acoustical baffles, (12) intake chamber, (13) exhaust chamber, (14) enclosure roof, (15) duct, (16) sound absorption coating.

through an exhaust opening (7) in the enclosure roof (8). Ventilation openings are protected with acoustical baffles (9). Described enclosure provides A-weighted sound pressure level reduction of 8 dB, and sound pressure level reduction of 5 dB to 11 dB in the frequency range of 500 to 8000 Hz.

Noise reduction equipment for a movable compressor (1) with a diesel engine (2) consists of a sound-proofed enclosure (3), engine exhaust muffler (4), and vibration isolators (5) for the engine-compressor unit (Fig. 11). The sound-proofed enclosure protects the engine with a turbofan, intake filter (6), fan (7), and cooler (8) installed on the frame (9). The enclosure has intake and exhaust slots (10) on its end and side panels. Inside the compressor enclosure, baffles, partitions, and an engine hood are installed. The wall faces of the main hood, partitions, and baffles (11) form the intake (12) and exhaust (13) chambers. On the main

enclosure of the roof (14), a duct (15) with an opening is installed. It is connected to the outer enclosure. An exhaust gas muffler is placed under the duct. Enclosure, partitions, and baffles are lined with a sound-absorbing material (16). The engine-compressor unit is mounted to the frame through the vibration isolators of the AKCC-160M type. The enclosure is made of 1.5-mm-thick steel. Elastic incombustible polyurethane of PPU-ET type is chosen as a sound-absorbing coating (with a layer of 40 mm thickness). Described noise control measures reduce sound pressure level by 6 dB to 17 dB in the frequency range of 250 to 8000 Hz.

## REFERENCES

1. M. J. Crocker, L. Drozdova, N. Ivanov, et al., in *Noise and Vibration Control in Vehicles*, M. J. Crocker and N. I. Ivanov, Eds., Politechnica, St. Petersburg, 1993.
2. Directive 2000/14/EC of the European Parliament and of the Council of 8 May 2000 on the Approximation of the Laws of the Member States Relating to the Noise Emission in the Environment by Equipment for Use Outdoors, *Official Journal of the European Communities*, 4.7.2000, L162.
3. EU Emission Requirements on Outdoor Equipment, *Noise News Int.*, Vol. 9, No. 2, 2001, pp. 102–104.
4. V. Irmer and E. Fischer-Sheikh Ali, Reduction of Noise Emission of Construction Machines Due to the “Blue Angel” Award, *Noise News Int.*, Vol. 7, No. 2, 1999, pp. 73–80.
5. D. Gottlob, Regulations for Community Noise, *Noise News Int.*, Vol. 3, No. 4, 1995, pp. 223–236.
6. ISO 6393, Acoustics—measurement of Exterior Noise Emitted by Earth-moving Machinery—Stationary Test Conditions.
7. ISO 6395, Acoustics—Measurement of Exterior Noise Emitted by Earth-moving Machinery—Dynamic Test Conditions.
8. ISO 2151 : 2004, Acoustics—Noise Test Code for Compressors and Vacuum Pumps—Engineering Method (Grade 2).
9. M. J. Crocker, Editor-in-Chief, *Handbook of Acoustics*, Willey New York, 1998.
10. L. Drozdova, N. Ivanov, and V. Potekhin, Design and Selection of exhaust Mufflers for Vehicles Internal-Combustion Engines, Proceedings of the First Joint CEAS/AIAA Aeroacoustics Conference, 12–15 June 1995, Munich, Germany, Vol. 2, pp. 773–776.
11. N. Tyurina and Yu. Elkin, Investigation of Efficiency of Vehicle Noise Reduction Providing by Shielding Constructions, Proceedings of the Eleventh International Congress on Sound and Vibration, 5–8 July 2004, St. Petersburg, Russia, Vol. 4, pp. 2177–2182.

# CHAPTER 127

## ENVIRONMENTAL NOISE IMPACT ASSESSMENT

Marion A. Burgess

Acoustics and Vibration Unit

University of New South Wales at the Australian Defence Force Academy  
Canberra, Australia

Lawrence S. Finegold

Finegold & So, Consultants

Centerville, Ohio

### 1 INTRODUCTION

Community noise sources, such as transportation modes, recreational activities, and commercial and industrial developments, can impact residential areas negatively. Environmental noise impact assessments provide a mechanism to investigate the balance between the negative noise impacts of a proposed development project versus the benefits that that development project is expected to bring to the community. Existing community noise exposure guidelines are consulted when preparing the assessments. These are based on the premise that there is a level of noise that is acceptable to protect most humans, animals, and structures. If this level is likely to be exceeded by a proposed development, appropriate mitigation measures need to be selected with due consideration of cost and technical feasibility. The mitigated noise impact is assessed for acceptability to the potentially affected community as well as the benefit of the development to the community as a whole. In this chapter the terms *community noise* and *environmental noise* are used interchangeably.

### 2 ENVIRONMENTAL NOISE DESCRIPTORS

The definition of environmental noise given in the recent European Commission Environmental Noise Directive<sup>1</sup> is: “unwanted or harmful sound created by human activity outdoors, including noise emitted by means of transport and from industrial sites or industrial buildings.”

Quantitative descriptors for environmental noise are generally based on the A-weighted decibel scale. The A-weighting is essentially a frequency filter that has a similar response to that of human hearing. As environmental noise is rarely constant in level, this time variation must be taken into consideration to provide a representative noise descriptor. A variety of such derived noise descriptors have been developed that incorporate time averaging of the sound pressure levels or integration of the energy within a sound over a defined period. Commonly used descriptors include:

- **Percentile Value,  $L_{An}$**  The A-weighted level exceeded for a percentage of a nominated time

period. The most commonly used are the  $L_{A10}$ , the level exceeded for 10% of the time period and so representative of the higher noise levels, and the  $L_{A90}$ , the level exceeded for 90% of the time period and considered representative of the background noise levels.

- **Equivalent Energy Level  $L_{Aeq}$**  The A-weighted sound pressure level for a continuous steady sound that has the same energy as the time-varying sound over the same time period. The  $L_{Aeq}$  is the basis for a number of derived descriptors discussed below.
- **Maximum Noise Level,  $L_{Amax}$**  The maximum noise level during the time period and often used as a criterion in conjunction with  $L_{Aeq}$  or  $L_{A10}$  to limit the highest noise levels in the noise.
- **Sound Exposure Level (SEL)** The noise level for a sound over a defined time period, such as 1s, that would have the same energy as the noise from a single event like a helicopter flyover or a train passby.
- **Perceived Noise Level (PNL)** The level of a sound that is considered to be equally noisy. It is calculated from the one-third octave band data.
- **Peak Noise Level,  $L_{Cpeak}$**  The peak C-weighted sound pressure level for impulse sound such as explosive noise. Note this environmental noise descriptor is not based on the A-weighting but is based on the C frequency weighting.

A number of derived noise descriptors are used for the assessment of noise impacts. The common ones include:

- **$L_{A10,18h}$**  The average of the hourly  $L_{A10}$  values between 06:00 and 24:00 and used for the assessment of noise from road traffic.
- **$L_{Aeq,Nh}$**  Average of  $L_{Aeq}$  over a defined number of hours such as 24 h, 9 h over a night, 15 h over a day, 1 h over a day, and so on, and used for wide range of environmental noises.



- **LDEN** The average of  $L_{Aeq}$  over the day with an adjustment to allow for the additional annoyance during the defined evening and night periods. The day period is 12 h and normally from 06:00 to 18:00, the evening 4 h normally from 18:00 to 22:00 with an adjustment of +5 dB, and the night 8 h with an adjustment of +10 dB. This derived descriptor is planned to be used in implementation of the new European Commission (EC) Directive on Environmental Noise.<sup>1</sup> The length of each period is given in hours, but the clock times can be changed to suit the lifestyle of the country.
- **DNL** The average of  $L_{Aeq}$  over the day with an adjustment of 10 dB to allow for the additional disturbances during the defined night period. DNL is commonly used in the United States. A comparison between the  $L_{DN}$  and  $L_{DEN}$  is provided in Miedema and Oudshoorn.<sup>2</sup> According to these authors, for specific types of noise the agreement is aircraft LDEN = DNL + 0.6, road traffic LDEN = DNL + 0.2, and railway LDEN = DNL.

As there are a large variety of descriptors for environmental noise, it is vital that the descriptor used for a criterion in regulations and guidelines be clearly stated to avoid any ambiguity. These details also need to be considered when comparing noise effects research findings and noise exposure criteria from various countries to ensure the validity of the comparison.

When there are particular frequency characteristics in the noise, such as from music or motor sports, it may be necessary to incorporate criteria based on the noise levels in particular frequency bands, in addition to the overall A-weighted level. These criteria generally use the  $L_{eq}$  descriptor.

### 3 REACTIONS TO ENVIRONMENTAL NOISE

The term environmental noise describes the noise generated by all the aspects of our society as it impinges on the usual activities of our daily lives, excluding occupational noise. It is only rarely that the level of environmental noise would be sufficient to produce permanent hearing damage. Transportation is a widespread source of noise and is heard to some extent by the majority of those living in urbanized areas and some of those living in rural areas. Other forms of environmental noise are related to activities associated with industry and mining, with commercial activities, with recreation, and with neighbors.

Annoyance, speech interference, and sleep disturbance are considered to be the main effects of environmental noise. Studies on nonauditory physiological health effects of those exposed to higher levels of environmental noise have shown some association with hypertension, cardiovascular, and digestive problems, for example, see the review by Stansfield and Lercher.<sup>3</sup> However, there are many confounding factors that can effect these reactions, and there is currently no clear relationship between a noise descriptor and particular physiological effects.

### 4 DOSE-RESPONSE RELATIONSHIPS

Important factors that lead to reactions to noise such as disturbance and annoyance include the noise level and character, the duration, the time at which it is occurring, and the activity of the person at that time. The difficulties in determining a quantitative assessment of noise annoyance are discussed in more detail in Chapter 25. There have been extensive studies (see discussions by Fields<sup>4,5</sup> and by Finegold and Finegold<sup>6</sup>) aimed at determining the relationship between some form of noise descriptor and reaction to environmental noise. These social surveys have typically led to dose-response relationships based on some form of quantitative descriptor for the noise and the percentage highly annoyed (%HA). The majority of these surveys have focused on reactions to transportation noise sources.

The first such curve to gain wide application was developed by Schultz.<sup>7</sup> In subsequent decades more surveys were undertaken and the older work reanalyzed, for example, by Fidell et al.<sup>8</sup> and Finegold et al.<sup>9</sup> It became apparent that there were differences in the relationships between the reactions to different types of transportation noise.<sup>9</sup> However, as there was not a clear 5-dB difference between the curves, the combined curve shown in Fig. 1 was adopted in an American National Standards Institute (ANSI) standard.<sup>10</sup> Since then, a more comprehensive database of community annoyance data has been compiled by The Netherlands Organisation for Applied Scientific Research (TNO) Division of Prevention and Health. Analysis of these data by TNO<sup>2,11,12</sup> led to separate dose-response relationships for noise from aircraft, road traffic, and railways, as shown in Figure 2. However, there is not universal acceptance of these three curves and the limitations have been discussed by Finegold,<sup>6</sup> concluding that there needs to be "more open dialog and debate concerning technical issues related to community annoyance research, along with freely sharing of data between researchers."

Both the International Organization for Standardization (ISO) and the ANSI are reconsidering the issue of the appropriate exposure-response relationship to

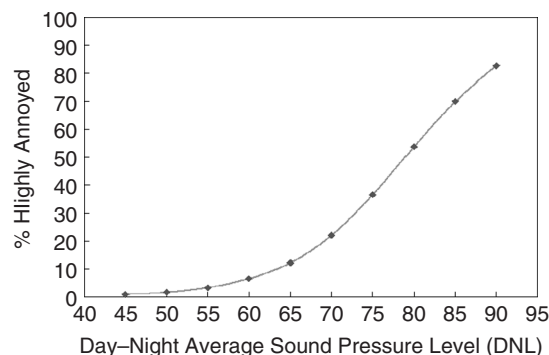


Figure 1 Dose annoyance curve. (From Finegold et al.<sup>9</sup>)

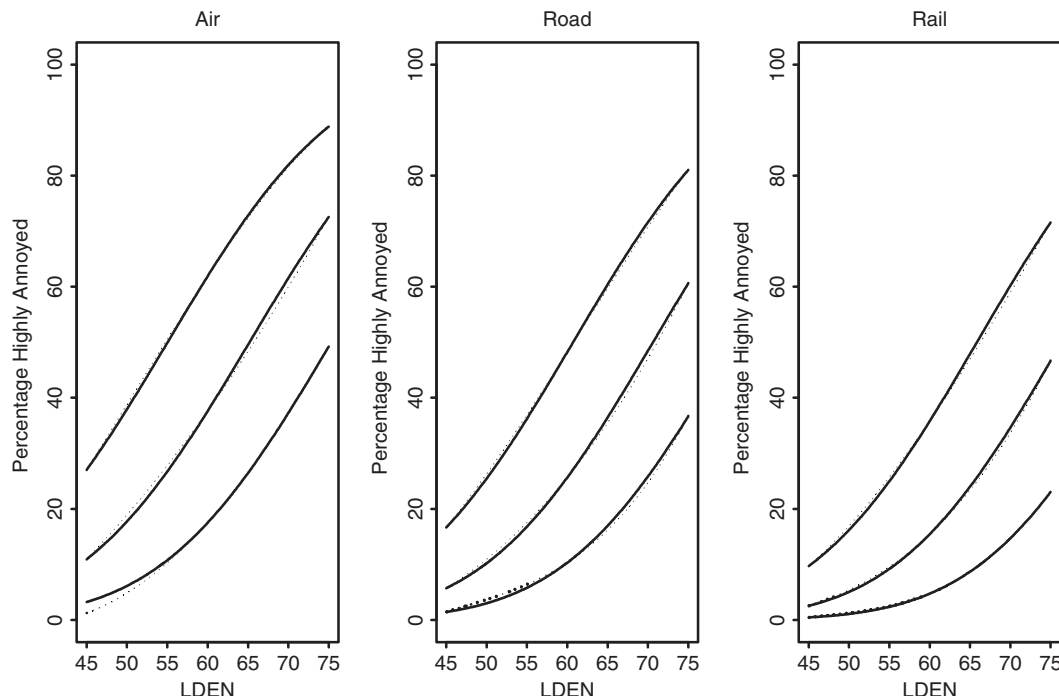


Figure 2 Dose annoyance curves. (From Miedema and Oudshoorn.<sup>2)</sup>)

use in their respective environmental noise standards and are reviewing a number of published curves. The recent revision of ISO 1996–1<sup>13</sup> recommends reverting to use of the original Schultz<sup>7</sup> community annoyance curve, but with adjustments for the type of noise source (road traffic, aircraft, and railways), special characteristics of the sound, and the time of day. In the United States, ANSI is considering making the same change, rather than the current use of the Finegold et al.<sup>9</sup> curve. In contrast, it appears that the European Commission will adopt the three separate curves developed by TNO. The World Health Organization has not advocated for adoption of any particular exposure–response curve.

#### 4.1 Sleep Disturbance

The most common metrics for assessing the impacts of community noise, such as DNL, already contain a strong 10-dB penalty for nighttime noises, and community noise exposure policies typically do not include separate criteria for sleep disturbance. However, there are circumstances where a separate analysis of the impacts of nighttime noise is warranted. There have been extensive studies of sleep disturbance using subjects sleeping in their homes and sleeping under laboratory conditions. The results of the studies are highly variable but, similar to the findings on community annoyance, there is clearly an increase in sleep disturbance with noise level. This topic is examined in detail in Chapter 24 and exposure–response relationships for sleep disturbance

may be found there. The World Health Organization (WHO)<sup>14</sup> has recommended that nighttime indoor sound pressure levels should not exceed approximately 45 dB  $L_{Amax}$  more than 10 to 15 times per night. For intermittent events similar to aircraft overflights, with an effective duration of 10 to 30 s, this corresponds to indoor A-weighted SEL values of 55 dB to 60 dB. According to WHO, either  $L_{Amax}$  or SEL may be used if the noise is not continuous. For total night exposure, a criterion of 30 dB  $L_{Aeq,8h}$  was recommended for use in combination with the single-event criterion ( $L_{Amax}$  or SEL). It needs to be pointed out, however, that the criteria recommended by WHO are long-term targets and do not take into consideration the cost or technical feasibility of meeting their recommended ideal maximum exposure levels. WHO intended that these criteria be used as part of a noise management decision-making process, for which environmental noise impact analysis is the central issue.

#### 4.2 Speech Interference

Speech interference is also an important part of the overall assessment of annoyance. For specific situations where the level of environmental noise is high, speech interference is possible inside buildings, such as schools or offices near busy roads or airports. There are national and international standard test procedures to determine quantitative measures of speech interference that have been designed for room acoustics (see Chapter 106 for more details of these methods).



## 5 METHODS FOR ASSESSMENT OF NOISE IMPACT

### 5.1 Assessment by Comparison with Background Noise Levels

Assessment of the acceptability of an environmental noise is necessary to judge if complaints about an existing noise source are justified or if a proposed development can proceed with or without mitigation measures. One approach involves comparison with background noise levels and is more applicable for assessment of industrial, commercial, or neighbor noise than for transportation noise. The aim is to limit the intrusiveness of the noise. This approach to assessment requires measurement of the noise level in the area before the proposed development, or if it is in response to a complaint, with the noise considered to be offensive turned off. If it is not possible to turn the noise source off, the background noise measurements can be made in a similar type of area. The background noise is usually measured in terms of  $L_{A90}$ , the A-weighted noise level exceeded for at least 90% of the time period. The background noise can vary during different times of the day so the measurements must be made during the time the noise may be considered to be annoying. The measurement of the background noise may need to be over a number of days in which case the 90% value of the  $L_{A90}$  can provide a good representation of the background noise level in the area.

After the background level of noise is determined, then either the noise from the existing source is measured or noise from the proposed development is predicted. This noise is generally either in terms of  $L_{A10}$ , the A-weighted noise level exceeded for 10% of the time period, or  $L_{Aeq}$ , the A-weighted equivalent noise level. Adjustments are then made to the noise level to allow for the additional annoyance because of the character of the noise. Objective and subjective methods for determining these adjustments are given in ISO 1996, Part 2.<sup>13,15</sup> However, it is essential to check local regulations as they may differ from the guidance in ISO 1996. Typically, values for adjustments to the measured noise levels are +5 dB for a prominent tonal component and for an impulse or impact noise. It is also common to allow for the criterion at the receptor to be increased when the comparison is made with a single event in any 24 h. This increase in criterion is related to the length of time of the event, and for an event with less than 1.5 min duration can be as high as 20 dB during daytime or 10 dB during nighttime.

The adjusted measured, or predicted, noise level is compared with the background noise level with an excess of +5 dB considered acceptable. This is based on the assumption that such small increases in noise level are not likely to cause a long-term significant increase in annoyance. A 5-dB increase is also often used to determine whether a full Environmental Impact Statement needs to be prepared. A general guide to the expected reactions to noise intrusion is given in Table 1.

The concept of assessment by comparison with background noise level is easy for the community to understand, but there are a number of disadvantages.

**Table 1 Guide to Reactions to Different Levels of Noise Intrusion for A-weighted Sound Pressure Levels**

Noise Intrusion	Likely Reaction
0–5 dB	Marginal
5–15 dB	Great concern
15–20 dB	Serious concern
20–25 dB	Extreme action

Source: Based on data from the U.S. Environmental Protection Agency<sup>16</sup> and the earlier report of Eldred.<sup>17</sup>

Background noise levels vary from day to day, so long-term noise monitoring is required to obtain a consistent value. Most modern measurement instruments allow for pausing of the data collection when extraneous noise is present, but often decisions need to be made “on the spot” if noise should be considered as part of the background noise in the area. Limits for the total noise must be established to avoid gradually increasing or “creeping” background noise as each new source is introduced. The assessment method does not encourage the overall reduction in environmental noise.

### 5.2 Assessment of Environmental Noise by Comparison with a Specified Criterion Level

This method involves defining criteria for acceptable noise levels in an area with the aim of maintaining the amenity of the environment. The estimated noise levels from proposed developments or the noise levels from current activities should not exceed these criteria. A number of factors are taken into consideration by the authority when selecting these criteria. Criteria often vary for the type of area and time of day. The types of activities plus the transportation such as roadways, railways, and airports all contribute to the overall ambient noise that constitutes a city area. In rural areas the expectations are for a quieter environment. Similarly higher noise levels during the day are more acceptable than during the night when they may cause sleep disturbance. The findings from surveys of noise annoyance are also taken into consideration but, as discussed above, these do not give a definite level that can be considered as acceptable to all.

This method has been commonly used for assessment of transportation noise but is also applicable for general environmental noise. There is an increasing trend to include an adjustment to take into consideration the increased annoyance to noise during the nighttime and the evening. Options for such criteria include:

- Different criteria for the average over specific time periods during the 24 h, that is, daytime, evening, and nighttime
- Average over a relevant time period for the adjacent land uses, that is, during the school day or the office hours
- Level that must not be exceeded during any one hour, or shorter time if applicable, for critical spaces such as hospitals

**Table 2 Guideline Values for Community Noise in Specific Environments**

Specific Environment	Critical Health Effect(s)	$L_{Aeq}$ (dB)	Time Base (h)	$L_{Amax,fast}$ (dB)
Outdoor living area	Serious annoyance, daytime and evening	55	16	—
	Moderate annoyance, daytime and evening	50	16	—
Dwelling, indoors	Speech intelligibility and moderate annoyance, daytime and evening	35	16	—
Inside bedrooms	Sleep disturbance, nighttime	30	8	45
Outside bedrooms	Sleep disturbance, window open (outdoor values)	45	8	60
School class rooms and preschools, indoors	Speech intelligibility, disturbance of information extraction, message communication	35	During class	—
Preschool bedrooms, indoors	Sleep disturbance	30	Sleeping time	45
School, playground outdoor	Annoyance (external source)	55	During play	—
Hospital, ward rooms, indoors	Sleep disturbance, nighttime	30	8	40
	Sleep disturbance, daytime and evenings	30	16	—
Hospitals, treatment rooms, indoors	Interference with rest and recovery	<sup>a</sup>		—
Outdoors in parkland and conservation areas	Disruption of tranquility	<sup>b</sup>		

<sup>a</sup>As low as practically possible.

<sup>b</sup>Existing quiet outdoor areas should be preserved and the ratio of intruding noise to natural background sound should be kept low.

Source: Extracted from Table 4.1 in WHO Guidelines.<sup>14</sup> The time base for the  $L_{Aeq}$  value varies as shown in the table.

- One value that is the average of the  $L_{Aeq}$  during the day and the night but with an adjustment of 10 dB added to the nighttime levels, that is,  $L_{DN}$ , as used in the United States
- One value that is the average of the  $L_{Aeq}$  during the day, the evening, and the night but with an adjustment of 5 and 10 dB, respectively, for the evening and the nighttime levels, that is,  $L_{DEN}$ , as used in the European Union (EU) directive on noise

The advantage of this method is that the criterion value is established so all involved with the assessment know what the goal is. Allowance must be made for transition areas between zones with different standards, such as a commercial area near a residential area. One management method is to apply the average of the zone criteria near to the boundary between the zones. If the existing noise level is in excess of the zone noise criterion, decisions need to be made.

### 5.3 Establishing Noise Exposure Criterion Levels

Studies on the reactions to environmental noise give a guide to reasonable criteria that the government authority can adopt. However, as discussed above, most of these

studies show that annoyance increases with noise level at different slopes for different types of noise, and there is no firm agreement about a level that clearly separates an acceptable from an unacceptable noise impact.

A robust dose–response relationship can give guidance to the authorities and others charged with making the decisions defining acceptable levels of noise. The WHO supported an extensive study of the available data, and the outcomes have been published for such guidance by Berglund et al.<sup>18</sup> The guidelines for environmental noise have been extracted from the table in the WHO document and are shown in Table 2. These have quickly become acknowledged worldwide as the goals for which authorities should aim for community noise criteria.

### 5.4 Interpretation and Use of Noise Exposure Criterion Levels

All environmental noise impact analyses should include comparison of the noise level at the receiver location with the applicable exposure criteria. These criteria are immission levels, that is, the noise that is received at a particular location and is the cumulative noise from all the sources in the area. When the immission noise level is in excess of the criterion, the first step should be to attempt to mitigate (reduce) the

emission noise at the source. As discussed in other chapters, there are many alternatives for the reduction of the emission noise at the source. Once the maximum reduction in emission noise has been achieved, other approaches to noise control, such as use of barriers or improving the noise reduction provided by buildings, can be applied to reduce the immission noise levels to meet the criteria. Of course, environmental noise should be considered at the land-use planning stage to minimize the occurrence of inappropriate land uses. This is very important for management of environmental noise at the community level. For example, great care should be taken to consider the noise impact prior to releasing land for residential use in areas that are potentially noisy such as in the vicinity of aircraft flight paths or near industrial estates. The potential impact should not just be considered at the time of the proposed development but into the future, 5, 10, 15, or even 20 years.

In the production of any environmental impact statement it is important to identify the status of the criteria that are being used in the assessment of acceptability. The WHO criteria in Table 2 are guidelines only and as such carry no legislative power and hence are not enforceable in law. Similarly criteria listed in standards such as those produced by ISO or by individual countries are also only guidelines. It is up to each jurisdiction to introduce regulations or similar legal instruments listing criteria with which compliance is then enforceable by law. The approach to legislation varies from country to country, and the regulations can be introduced at the local government level, at the state government level, or at the federal government level.

## 6 ASSESSMENT OF PROPOSED DEVELOPMENTS

### 6.1 Environmental Noise Impact Assessment

Environmental impact assessment (EIA) is just one term that is applied to the processes of establishing the extent of all impacts on the surrounding areas of a proposed development. Other terms that essentially mean the same are environmental effects statement, review of environmental effects, and the like. For most projects there are a number of stages in the EIA process. In some cases the EIA may only be assessed by the appropriate government authorities. Commonly a draft assessment is produced and released for a public comment period during which time community discussion sessions may be organized. The final EIA should then address all of the relevant issues that have been raised during that public comment period. The magnitude of the EIA is related to the size of the proposed development. An EIA for the construction of a new runway at an airport will comprise many volumes, while an EIA for a smaller project like a residential complex may be only one slender document. Noise is one component that must be considered as part of an EIA.

The basic elements for the first part of the noise assessment in an EIA include:

- Identification of all the noise-producing elements in the proposal
- Identification of all the noise-sensitive areas that could be affected by the proposal both currently and into the future, say 15 to 20 years
- Statement of the applicable criteria in the surrounding areas
- Estimation of the noise immission levels for all the noise-sensitive locations
- Comparison with the applicable criteria and determination of any excess

If there is an excess, the next steps are:

- Identification of cost-effective mitigation measures
- Comparison of the mitigated noise immission levels with the criteria

For equity, the onus of responsibility for the mitigation measures should rest with the proponent of the proposed development. Thus, a new or upgraded road development through a suburban area should include mitigation to meet the criteria as part of the road project. On the other hand, if land near an existing major road or an industry is rezoned from broad acre to residential, the responsibilities for mitigation should lie with the residential developer. The responsibility for mitigation can become more complex when there is not a clear rezoning but simply a change of use. For example, a commercial complex may include an entertainment venue that has been used only during the day and causing no problem to the surrounding residences. A change of tenant, still within the property zone allowances, may lead to a change of operations that may cause annoyance to the residents. If assessment on the basis of the criteria for the nature of the area and the time of day shows an excess, then the responsibility for mitigation is with the new leasee. However, if there is no excess, then any mitigation needs to be undertaken by the residents.

It is reasonable to consider the cost effectiveness of mitigation measures since complete mitigation of the noise may be beyond the current technical capabilities or may be prohibitively expensive for the proponent.

After this stage there is sufficient information for a community consultation period, which is aimed at advising members of the community and seeking their opinions. For smaller projects it may be sufficient to advise the community that the documentation is available for inspection on the Internet or at government offices. For larger and for controversial proposals it may be necessary to arrange for public displays, information sessions, and discussion groups.

If the noise criteria are met with mitigation measures that are acceptable to the community, a satisfactory conclusion has been achieved in terms of noise control. If either the mitigation measures are unacceptable or the mitigated noise levels are in excess of the criteria, a review of the EIA plus negotiation with the concerned community is required. Some changes to

the proposed mitigation measures to meet the community requirements may not change their effectiveness, for example, changing the material of barriers from opaque to transparent. Other changes may reduce the effectiveness of the measure, for example, reducing the height or location of a barrier wall, and negotiation will be required.

## 6.2 Negotiation Process

Achieving a satisfactory resolution involves the three main stakeholders—the proponent, the community, and the government authority. The economic and social benefits to the wider community need to be evaluated with regard to the undesirable noise impact for the affected proportion of the community. The proponent must be able to demonstrate that application of all the economically viable mitigation strategies has been considered. The EIA and supporting documents must provide the assessment and the evaluation in a form that can be understood by the community. An independent facilitator should assist with the negotiation to avoid accusations of bias by either the proponent or the government authority. Advances in noise simulation offer the opportunity to provide an audio demonstration of the expected noise in various areas. While this may assist the community to better understand the type of noise and the possible level, it does have some disadvantages and should be used only with caution. The inputs for the simulation model, the sound system, and the meeting venue can all affect the sound produced. There is also a possible psychological effect whereby intentionally listening to the sound produced by the simulation could lead to a different reaction than if the sound was superimposed on other sounds in a normal environment.

The basis of any agreement is that the community receives some benefits to offset the noise impact. Of course, these benefits have to comply with what is legally permitted under the jurisdiction. The benefits could be payments, improved noise insulation of the houses, improvements to the community infrastructure, and the like. Benefits could also involve a sharing of the noise impact, for example, the flight tracks for an airport could be changed so that a balance is achieved between high and low noise days. Agreement could be reached on a management control method that encouraged lower noise activities; for example, a motor sports facility or an outdoor concert venue could have an annual credit allowance whereby higher noise emission events would use more of the credits than low noise events.

It is not uncommon that there is initially not unanimous acceptance of the noise predicted from a proposed major development project. Adequate noise policies need to clearly identify the responsibilities and rights of all the involved government authorities, the local community, and the business arena for what is required for environmental noise decision making. An environmental noise impact analysis process, which would be required for all proposed major development projects to assess the expected noise impacts on the community, could be the central focus of the required

noise management program. The results of this process include decisions about acceptable noise exposure levels, noise mitigations measures, and the like. Once this agreement has been reached, it becomes binding on the community so that future new members of the community must accept the negotiated agreement. The final negotiated decisions are documented in a record of decision (ROD), and approval to proceed with the planned development project is granted, subject to the provisions of the ROD. If agreement cannot be reached between the government, the developers, and the community, a formal dispute resolution system could be used to settle the disagreements and finalize the noise-related decisions.

## 6.3 Interacting with the Public

It is important in the whole assessment process to provide information in a manner that can be understood by the community that is potentially affected. The various descriptors for noise are not necessarily easy for the community to understand. This is especially the case for descriptors that involve averages over long times, such as 24 h or even more. The community needs to understand that such criteria do not mean that the noise will not exceed the stated value at any time. Part of the assessment documentation should clearly identify what the variations in noise level may be yet still meet the criterion. For example, with aircraft noise assessment the documentation should show that while the operations may meet the criteria, there may also be a number of overflights for which the noise levels will exceed certain values. Work by Southgate<sup>19</sup> on aircraft noise assessment in Australia has indicated that communities seek information and are more accepting if they consider the proponent has clearly stated all the potential impacts as well as showing that specific criteria will be met. A responsive complaint management system has also been shown to be a quite useful public interaction tool in countries such as Japan.

## 6.4 Monitoring and Review

Permission to proceed with the proposed development should not be the end of the process. The government authority needs to ensure that noise monitoring is undertaken so that the actual noise levels are not in excess of those estimated and that the mitigation measures are maintained and are effective. Changes to the development should trigger a review of the EIA to ensure the noise levels do not increase. Guidelines as to what are considered substantial changes need to be carefully defined by the government authority.

## 7 SUMMARY

Environmental impact assessment for the noise from a proposed development requires assessment of the predicted noise level at the receiver and comparison with current acceptability criteria. These criteria differ for a variety of factors including the type of receiving location, the type of area, the time of day, the type of sound source, and the like. An environmental impact assessment should show that an appropriate noise management plan has been implemented to ensure that

the criteria are met. If it is not reasonable or feasible to meet the criteria, alternatives may be available to allow the development to proceed while minimizing the impact on the surrounding areas. It is important to remember that reaction and annoyance to noise varies greatly across the community, and establishment of criteria levels is based on an acceptance that there may still be a small proportion of the community who will experience annoyance or disturbance from the noise. The environmental noise impact process, especially with its receiver-oriented (immission) perspective, is a crucial part of an effective community noise management strategy.

## REFERENCES

1. European Commission, EU Directive on the Assessment and Management of Environmental Noise (END), The European Parliament and the Council of the European Union, Brussels, 2002; [http://europa.eu.int/eur-lex/pri/en/oj/dat/2002/l\\_189/l\\_18920020718en00120025.pdf](http://europa.eu.int/eur-lex/pri/en/oj/dat/2002/l_189/l_18920020718en00120025.pdf).
2. H. M. E. Miedema and C. G. M. Oudshoorn, Annoyance from Transportation Noise: Relationships with Exposure Metrics  $L_{dn}$  and  $L_{den}$  and Their Confidence Intervals, *Environmental Health Perspectives*, Vol. 109, No. 4, April 2001; <http://ehpnet1.niehs.nih.gov/members/2001/109p409-416miedema/miedema-full.html>.
3. S. A. Stansfield and P. Lercher, Nonauditory Physiological Effects of Noise: Five Year Review and Future Directions, Proceedings of ICBEN 2003, The Hague, Netherlands, 2003, pp. 84–90.
4. J. M. Fields, *An Updated Catalog of 360 Social Surveys of Residents Reactions to Environmental Noise (1943–1993)*, Georgia Institute of Technology, Atlanta, 1994.
5. J. M. Fields, A Review of an Updated Synthesis of Noise/Annoyance Relationships, NASA Contractor Report 194950, National Aeronautics and Space Administration, Langley Research Center, Hampton, VA, 1994.
6. L. S. Finegold and M. S. Finegold, Historical Development and Current Status of Exposure-Response Relationships between Transportation Noise and Community Annoyance, Proceedings INTER-NOISE 2003 (Paper N601), Jeju Island, Korea, 25–28 August, 2003.
7. T. J. Schultz, Synthesis of Social Surveys on Noise Annoyance, *J. Acoust. Soc. Am.*, Vol. 64, 1978, pp. 377–405.
8. S. Fidell, D. S. Barber, and T. J. Schultz, Updating a Dosage-Effect Relationship for the Prevalence of Annoyance Due to General Transportation Noise, *J. Acoust. Soc. Am.*, Vol. 89, 1991, pp. 221–233.
9. L. S. Finegold, C. S. Harris, and H. E. von Gierke, Community Annoyance and Sleep Disturbance: Updated Criteria for Assessing the Impacts of General Transportation Noise on People, *Noise Control Eng. J.*, Vol. 42, No. 1, 1994, pp. 25–30.
10. American National Standards Institute (ANSI), *Quantities and Procedures for Description and Measurement of Environmental Sound—Part 4: Noise Assessment and Prediction of Long-Term Community Response—Includes Errata (10/01/97)*, Acoustical Society of America, Melville, NY, 1996.
11. H. M. E. Miedema and H. Vos, Exposure-Response Relationships for Transportation Noise, *J. Acoust. Soc. Am.*, Vol. 104, 1998, pp. 3432–3445.
12. H. M. E. Miedema, Position Paper on Dose Response Relationships between Transportation Noise and Annoyance. European Commission, Brussels, 2002.
13. International Organization for Standardization, ISO 1996-1:2003, Acoustics—Description, Measurement and Assessment of Environmental Noise—Part 1: Basic Quantities and Assessment Procedures, ISO, Geneva, 2003.
14. World Health Organization, *Guidelines for Community Noise*, B. Berglund, T. Lindvall, D. Schwela, and K.T. Goh, Eds., World Health Organization, Geneva, 2000.
15. International Organization for Standardization, ISO 1996-2:1987, Acoustics—Description and Measurement of Environmental Noise, Part 2: Acquisition of Data Pertinent to Land Use (currently under revision as Draft International Standard ISO/DIS 1996-2, Acoustics—Description, Assessment and Measurement of Environmental Noise—Part 2: Determination of Environmental Noise Levels), ISO, Geneva, 1987 and 2003.
16. U.S. Environmental Protection Agency (EPA), *Information on Levels of Environmental Noise Requisite to Protect Public Health and Welfare with an Adequate Margin of Safety*, EPA, Washington, DC, March 1974.
17. K. M. Eldred, Community Noise, U.S. Environmental Protection Agency Report (NTID 300.3), EPA, Washington, DC, December 1971.
18. B. Berglund and T. Lindvall, *Community Noise*, Centre for Sensory Research, Stockholm (prepared for World Health Organization), 1995.
19. D. Southgate, Expanding Ways to Describe and Assess Aircraft Noise, Paper presented at EC Conference on Good Practice in Integration of Environment into Transport Policy, 1–10 October 2002, European Commission, Brussels, Belgium. Also published by the Australian Government Department of Transport and Regional Services, Canberra, March 2003.

# CHAPTER 128

## INDUSTRIAL AND COMMERCIAL NOISE IN THE COMMUNITY

Dietrich Kuehner  
de BAKOM  
Odenthal, Germany

### 1 INTRODUCTION

In most industrialized countries, the legal limiting values for industrial and commercial noise are different from those for road traffic noise. There is, however, a general consensus that the annoyance produced by road traffic is very similar to that produced by industrial or commercial noise if the long-term energy equivalent sound pressure levels are the same. However, this is considered to be true only if the noise is not tonal or low frequency or impulsive in character. There have been extensive studies of this problem in the United Kingdom.

Different zoning solutions have been developed to control the noise from light and heavy industry and commercial enterprises including retail outlets, restaurants, and warehouses. Enterprises categorized as industrial are designated to specific zones that have been created for numerous reasons, of which noise is just one. With this approach, a reasonable separation of residential areas from noise-producing activities can be ensured. Similarly, commercial enterprises are also allotted to areas that may be closer to residential areas under the assumption that the emission from such areas is less. To limit the emission from such areas, specific sound power levels are introduced in relation to the size of the area. It is often necessary to carry out noise measurements in order to obtain the necessary data to establish—if necessary—a mitigation scheme.

### 2 INDUSTRIAL ACTIVITIES AND LOCAL COMMUNITY REACTIONS

Industrial and commercial noise can be subdivided into two categories. Into the first category falls stationary noise with small variation during day and nighttime, and into the second falls the intermittently occurring noise resulting from transport, production cycles, impulses, and the like, including truck traffic to and from an industrial area.

The stationary part is generally accepted if no single-tone components are involved up to nighttime A-weighted long-term equivalent  $L_{eq}$  levels of 48 dB. Above this level, reactions from the neighborhood are frequently observed. Similarly, a 10-dB higher value is accepted for the daytime, even if the noise is nonstationary as long as it is not impulsive or tonal.

The reaction of the community to industrial and commercial noise is very similar to that of road traffic noise of typical roads in a community. Noise resulting from superhighways seems to be more annoying at comparable levels.<sup>1</sup> However, if the noise is tonal or

impulsive in character, including low-frequency noise (below 90 Hz), the reaction can be severe.

The extent of the problem can be derived from a survey performed by the UK Department of Environment, Food & Rural Affairs.<sup>2</sup> A questionnaire was sent to local authorities (LA) to obtain information about the range and composition of industrial noise sources.

In Fig. 1 the range of industries identified by the LA is given, which covers the range of industrial activities. The size of the slices expresses the frequency of occurrence in the response of the LA. The category “Others” includes airfields/airports, brickworks, bus depots, civic amenity centers, drycleaners, dyeworks, glassworks, motor speedways, gas stations, and train depots.

Furthermore, the questionnaire requested information regarding the characteristics of the noise. The result is shown in Table 1. The survey shows clearly that tonality and impulsiveness are a very important part of industrial and commercial noise in the communities. Tonality and impulsiveness can usually be reduced by available mitigation technologies. The result of the above survey means that the best available technologies (BAT) for noise reduction are frequently not applied. However, even if BAT is applied and tonality and impulsiveness are avoided, a necessity remains to separate residential areas from areas with commercial or industrial activities to ensure that acceptable reception noise levels are not transgressed.

### 3 PLANNING

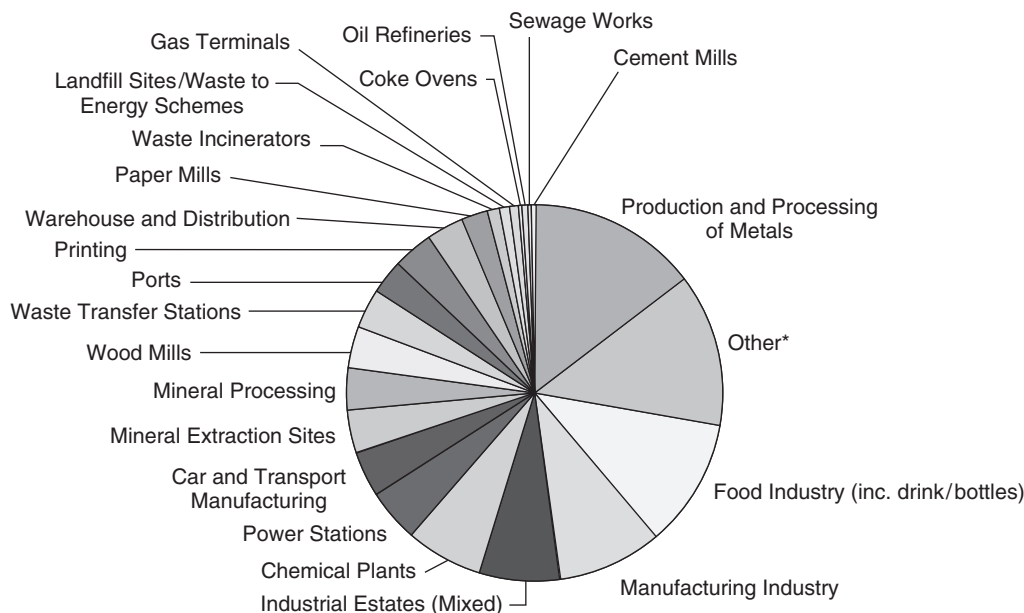
Communities are competing to obtain more and new enterprises to increase the number of jobs and tax revenues. Therefore, they design areas where potential investors may settle. To organize this such that the loudest plant is not directly positioned next to a residential neighborhood, a zoning of such areas is undertaken including the limitation of sound emission to the neighborhood. This limitation can be achieved by using the area related sound power level,  $L''_w$ .

The area-related sound power level is defined by

$$L''_w = 10 \log \left( \frac{I}{F} \frac{F_0}{I_0} \right) \text{ dB/m}^2$$

where  $I$  is the total sound power of the area under consideration of size,  $F$ ,  $F_0 = 1 \text{ m}^2$ , and  $I_0 = 10^{-12} \text{ W}$ . This concept is described in Ref. 3.

When using area-related sound power levels,  $L''_w$ , it should be noted that under this concept it is



\* "Other" includes Airfields/Airports, Brickworks, Bus Depots, Civic Amenity Centers, Dry Cleaners Dyeworks, Glassworks Motor Speedways, Petrol Stations, and Train Depots.

**Figure 1** Frequency and significance of industrial sources as given by local authorities in Great Britain.

**Table 1** Number and Percentages of Sites Identified with Various Acoustical Characteristics

Characteristics	Percentage
Tonal	51
Impulsive	38
Low frequency	37
None	22

formally assumed that no barrier effect or similar additional sound pressure level reducing factors are taken into account as long as the propagation path of the sound from each unit area to the neighborhood travels within the source area under consideration. Therefore, propagation calculation can be done simply by taking into account spatial spreading, air absorption, and ground effects as described, for example, in International Organization for Standardization (ISO) 9613-1 and ISO 9613-2 up to the nearest residential neighborhood.<sup>4</sup>

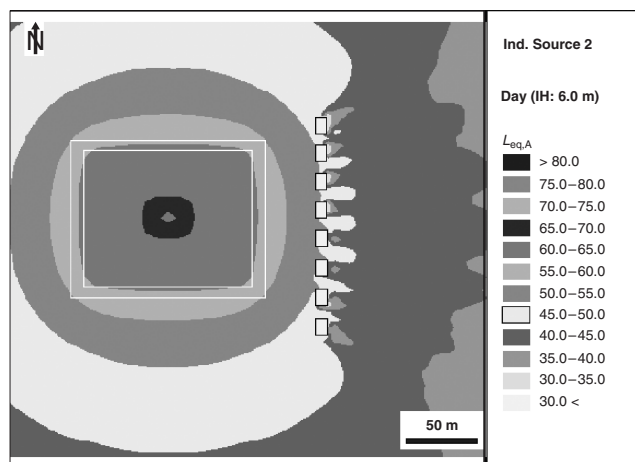
Commercially available propagation software allows to plant area-related sound sources into a specific topographical situation at a specific height above the ground. Using this, the long-term  $L_{eq}$  or the downwind  $L_{eq}$  of such sources can be calculated. Figure 2 shows such a case in a flat terrain with housing in the neighborhood (rectangles). The white line between the residential and the commercial area depicts the periphery of the zone over which the sound power has been

equally spread. It is assumed that the area within the two white lines is not used.

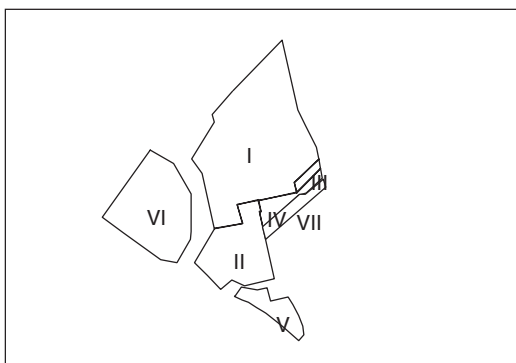
The total area is 12,000 m<sup>2</sup>; this means that a total A-weighted sound power level of approximately 101 dB can be installed. It is obvious that using a nonuniform distribution of the sound power level in a 1-ha area could lead to the installation of higher sound power levels. A point source on the opposite side of the residential neighborhood would lead to the highest value and a point source close to the boarder line of the neighborhood to the lowest value. This consideration shows that for one investor this type of planning is unnecessary, however, if more than one investor is considered, the above scheme is useful to avoid conflicts between the investors and the neighbors. In this context it should be noted that screening produced by buildings allows to increase the sound emission of those areas, which benefit from this.

In land use nonacoustical considerations are important in relation to the neighborhood and possible use. Therefore, a subdivision of an area under consideration is usually a must. In this case, different zones for different values of  $L''_w$  can be introduced. Such a case is shown in Fig. 3 for seven different areas.

In Table 2 the area-related sound power levels are listed. In Fig. 4 the nighttime situation is depicted in a nonflat topographic situation, including berms for noise protection. As this figure shows, the neighbors to the west will receive A-weighted noise levels up to 48 dB and those to the east 44 dB for the most exposed sites. Most of the neighbors to the west have A-weighted noise levels



**Figure 2** Reception A-weighted noise level distribution around an area-related source with A-weighted  $L''_W = 60$  dB/m<sup>2</sup>, 0.5 m above ground having a length of 120 m and a width of 100 m. The calculation is done for a receiver height of 1.5 m above ground. The diagram was calculated using LIMA, a product sold by Bruel & Kjaer.



**Figure 3** Planning with different area-related sound power levels.

**Table 2** List of Area-Related A-weighted Sound Power Levels

	$L''_W$ Night	$L''_W$ Day	
Area I, production	54	59	dB/m <sup>2</sup>
Area II, maintenance	47	59	dB/m <sup>2</sup>
Area III, storage area	45	59	dB/m <sup>2</sup>
Area IV, storage area	45	59	dB/m <sup>2</sup>
Area V, parking	44	50	dB/m <sup>2</sup>
Area VI, production	54	59	dB/m <sup>2</sup>
Area VII, <sup>a</sup> berms	30	30	dB/m <sup>2</sup>

<sup>a</sup>Just for berms for noise protection etc.

below 43 dB and to the east below 40 dB, which are the limiting values allotted to those areas for the nighttime.

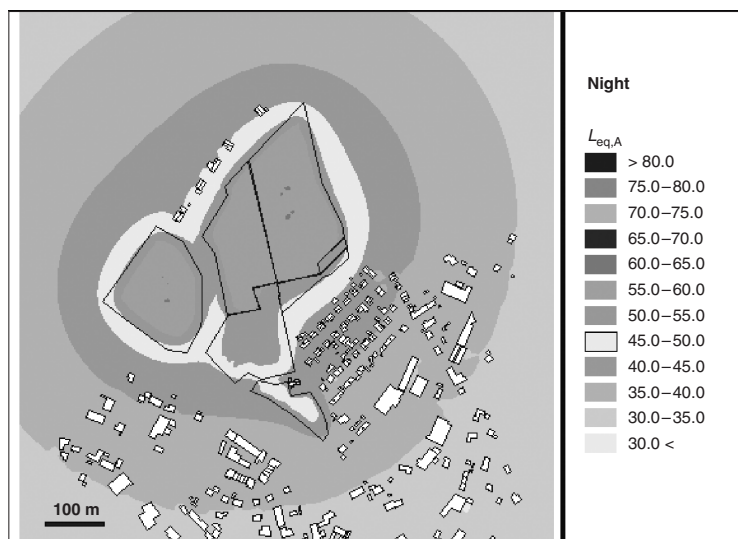
On the other hand, the area-related A-weighted sound power levels given in Table 2 show that only areas II and IV have nighttime values of 54 dB/m<sup>2</sup>; the rest of the area is well below those values. This separation means that the louder part of a production should be concentrated in these areas. Area VII is around the noise protection berms and the values of 30 dB/m<sup>2</sup> mean that absolutely no machinery should be installed there. The allocation and size of the areas have been chosen according to the landscape, transport roads, and the like. The purpose of this planning was to ensure that conflicts that occur at present can be reduced in the long term to an acceptable level for the neighborhood, which is mainly residential to the south east and mixed in the north and south.

#### 4 TYPICAL AREA-RELATED SOUND POWER LEVELS

The amount of sound power emitted from a typical plant such as a steel mill or a refinery depends strongly on the state of noise protection measures undertaken. It is, therefore, not possible to say a chemical plant of such a type has typically a specific sound power level. For practical purposes, it has turned out that it is sufficient to subdivide industrial and commercial noise sources into the following categories:

1. Open-air plants (e.g., petrochemical production, refineries, chemical plants, scrap yards, quarries)
2. Plants operating in buildings where parts of the process are outside (pharmaceutical production)
3. Plants in buildings, only auxiliary units such as cooling towers on the outside
4. Complete indoor production, only transport noise on the outside (e.g., car industry)





**Figure 4** Night situation in a nonflat topographic area including berms for noise protection 6 m above ground. North direction is to the top. The equivalent sound pressure levels given are A-weighted.

5. Logistic centers (transport and truck noise)
6. Machine working outdoor
7. Manufacturer
8. Shopping malls
9. Shops, repair shops, and trade companies
10. Small shops such as bakery, butcher, open-air restaurants (beer gardens)

Categories 1 to 5 deal with industrial and categories 6 to 10 deal with commercial noise.

In most countries, noise resulting from hotels, restaurants, and the like is considered to fall under commercial noise; however, the specific noise problems from these enterprises are usually dealt with on the basis of specific legal regulations.

In Table 3 area-related A-weighted sound power levels are given and the type of plants in which they occur. Commercial or industrial production with levels below 45 dB/m<sup>2</sup> is almost impossible. This can be

seen from a simple consideration. Assuming that 10 cars drive at night to and from the parking per hour lot of the premise under consideration. One parking per hour produces an area-related A-weighted sound power level of  $L''_W = 65$  dB/m<sup>25</sup>. Each parking lot has an area of 10 m<sup>2</sup> per car, which leads for 20 movements to an A-weighted sound power level of 88 dB per hour. The cars themselves have to be driven to the parking lot over a distance of 200 m at a speed of 30 km/h. Twenty movements per night lead to an A-weighted sound power level of 83 dB. In total, one obtains 89 dB or an average A-weighted sound power level of 80 dB per night. If this sound power level is spread over 3,000 m<sup>2</sup>, the 45 dB/m<sup>2</sup> are reached.

Typically, a fork lift has an A-weighted sound power level of 95 dB to 102 dB during operation. One fork lift continuously operating in an area of 100,000 m<sup>2</sup> or 10 ha will produce 45 to 52 dB/m<sup>2</sup> area-related A-weighted sound power levels. On the other hand, a front loader in a scrap yard typically

**Table 3** Type of Plants and Area-Related A-weighted Sound Power Levels

Area-Related A-weighted Sound Power Level (dB)	Plants
70–75	Open-air plants such as shipyards, refineries, open-air plants with few noise protection measures
65–70	Open-air plants such as refineries, integrated steel mills, chemical productions using state-of-the-art noise protection
60–65	Container terminal, louder equipment, steel mills, indoor, waste processing
55–60	Production mainly in buildings
50–55	All production in building, some transport noise, cooling towers
45–50	Indoor production without noticeable outdoor activities
35–45	No production. Warehouses with cooling etc. are possible

produces A-weighted sound power levels of 115 dB. A typical scrap yard has an area of 5 ha. If the front loader is operated for 4 h a day, the area related A-weighted sound power level is

$$\begin{aligned} L''_w &= 115 - 10 \log F/F_0 - 10 \log 4/16 \\ &= 62 \text{ dB/m}^2 \end{aligned}$$

A typical steel mill using BAT for noise reduction has an A-weighted sound power level of 123 dB during nighttime for a production of one million tonnes of steel per year, using an electric arc furnace and a rolling mill to produce specific products. If the area under consideration allows 60 dB/m<sup>2</sup>, an area of 100 ha is needed, if 65 dB/m<sup>2</sup> would be possible, only 33 ha would be needed.

These examples show that the concept of area-related sound power levels allows land-use planning on one side and gives possible investors a perspective whether or not a specific area is suitable for the production under consideration. Furthermore, it allows an estimation of whether or not investments in noise protection will be necessary to avoid complaints from the neighborhood, legal actions, and so forth.

## 5 MEASUREMENT OF COMMERCIAL AND INDUSTRIAL NOISE

### 5.1 General Considerations

There are two basic approaches for the measurement of industrial and commercial noise, depending on the size of the industrial or commercial activities under consideration. If the noise level for a small enterprise with few sources has to be established and the resulting rating level,  $L_r$ , to be compared with a legal limit, the measurements should be done for those sites in the neighborhoods that are of primary interest. If, however, a large number of complaints are observed and the enterprises consist of a larger number of sources, it is more suitable to measure the sound power level of all sources that might sufficiently contribute to noise in the neighborhood. This should cover all sources, which together contribute at least 90% of the A-weighted sound intensity received by the neighborhood. Additionally, all sources have to be measured, which are tonal or impulsive or of low frequency (less than 90 Hz) with respect to the definition of the rating level,  $L_r$ . For example, in Germany the daytime rating levels are calculated as the energy average over 16 h of the day, where the hours between 6 and 7 a.m. and those between 7 and 10 p.m. are rated with an addition of 6 dB. During nighttime the rating level of the noisiest hour is compared with the limiting value for the nighttime. This means that the hours during which certain sources appear have to be taken into account.

The sound power should be measured at least in octave bands. However, high-resolution sound power spectra are of great help to identify tonal sources and can easily be obtained using the Fast Fourier transform (FFT) algorithm. With commercially available software, which uses generally either A-weighted levels or

octave bands, the industrial source can realistically be modeled and noise maps can be calculated, from which the reception noise level and its rating level,  $L_r$ , at a specific height can be obtained, which allows to assess the noise at all possible sites in the neighborhood.

The additions necessary to express the impulsiveness and tonality can be included by adding them to the sound power of the source. It might be necessary to add higher values to obtain the proper rating levels. The advantage of this approach is that noise reduction measures can be quantified very precisely to reduce the rating levels below the legal limits.

### 5.2 Measurements at the Reception Site

In almost all cases where complaints are received with respect to industrial noise, the distance to the industrial source is less than 1000 m. Measurements should be performed under favorable sound propagation conditions (see, e.g., ISO 1996-2).<sup>6</sup> This can be expected for all situations where due to temperature and wind gradient the curvature of the sound wave is downward. During daytime and especially for situations with open sky, this situation may be assumed if the wind blows from the source to the receptor site at an angle up to 60°. At nighttime, especially for situations with open sky favorable conditions can be assumed if the wind speed is less than 0.5 m/s or at higher speeds and wind direction between ±120°. If the sky is clouded, downwind can be assumed for up to 90° (see, e.g., ISO 1996-2).<sup>6</sup>

Using three-dimensional wind meters, which measure the speed of sound in vertical and two horizontal directions, the temperature and wind gradient vector in the atmosphere can be estimated using methods from boundary layer meteorology<sup>7</sup> as a function of height for heights above ground of more than 100 m, which is sufficient for sound propagation. The respective software is provided with these instruments.

If the distance is less than 100 m, meteorological influences on sound propagation are small; for distances of more than 100 m measurements they should be performed under favorable sound propagation conditions. According to a large number of continuous acoustical monitoring measurements, the variance  $6\sigma$  of stationary industrial sources reaches at 1000-m values between 3 and 4 dB starting at 100 m with 1.5 to 2 dB and a measurement time of at least one hour. This variance means that repetitive measurements are necessary to ensure that sufficient precise results for favorable sound propagation situations are obtained.

If it is assumed that the limits of confidence for energy-averaged mean value  $\overline{L_{eq}}$  are similar as for the mean value of all levels that could be measured under favorable sound propagation conditions, the upper and lower limit of confidence  $L_{eq\pm}$  for  $\overline{L_{eq}}$  can then be approximated by

$$L_{eq\pm} = \overline{L_{eq}} \pm \frac{\sigma(r)}{\sqrt{n}} Z_\alpha$$

where  $Z_\alpha$  denotes the percentile  $\alpha$  of the normal distribution,  $n$  the number of independent measurements, and  $\sigma$  the variance as a function at distance  $r$

under downwind conditions;  $Z_\alpha = 1.96$  describes the coverage probability of 95%, which means that the true value of the  $L_{eq}$  falls with a probability of 95% within the above limits. The above relationship shows that for one measurement ( $n = 1$ ) at a distance of 1000 m the limits of confidence are between  $\pm 6$  and  $\pm 8$  dB and at a distance of 100 m between  $\pm 3$  and  $\pm 4$  dB. This means that repetitive measurements are usually necessary if measurements are taken at distances of 100 m and more.

It should be noted that the observed variance is produced by the variation of the propagation conditions, which tend to change from day to day and not from one hour to the next. This means that the time between two measurements has to be at least one day to ensure that the measurement results are independent.

To reach a limit of confidence between  $\pm 3$  and  $\pm 4$  dB for a measurement at 1000 m distance at least five independent measurements are necessary (see, e.g., DIN 45645-1).<sup>8</sup> It should be noted that the total measurement uncertainty has to include possible deviations produced by the measurement equipment (see Ref. 9).

Other statistical approaches may be used such as the assumption that the square of the sound pressure is lognormal distributed or equally distributed. These assumptions may lead to slightly different limits of confidence.

If the rating level,  $L_r$ , is defined as long-term  $L_{eq}$ , a correction for the frequency of occurrence of unfavorable sound propagation conditions may be used according to ISO 9613-2.<sup>4</sup> In this case the factor  $c_0$  in Eq. (8) of ISO 9613-2 may be chosen to be 2 dB at night-time and 5 dB during daytime and 3 dB for the evening and morning  $\pm 2$  h around sunrise and sunset. These corrections may produce additional deviations, which can be incorporated by an error calculus as described in ISO 3723 or GUM.<sup>9</sup>

In practical application, the rating level has to be compared with a limiting value  $X$ . In those cases where the measurements are done to prove that the situation is in compliance with the limiting value  $X$ , one has to prove that

$$X > \bar{L}_r + \frac{\sigma(r)Z_\alpha}{\sqrt{n}}$$

or if one has to prove that the noise levels are above the limiting value  $X$

$$X < \bar{L}_r - \frac{\sigma(r)Z_\alpha}{\sqrt{n}}$$

However, this leaves open the question what has to be done, if the limit  $X$  is within the range given by the limits of confidence  $L_{eq\pm}$ . If this range is smaller than 3 dB, one can assume that the situation under consideration does not deviate significantly from the legal limit.

### 5.3 Sound Power Levels

If model calculations are used to establish the rating level, the sound power of the relevant sources has to

be measured. The possible measurement errors result from the number of independent sources to be measured and modeled. If the standard deviation of the proposed measuring methods (see, e.g., ISO 8297, ISO 3744, and ISO 3746)<sup>10-12</sup> is  $\pm 3$  dB, the limit of confidence ( $Z_\alpha = 1.96$ ) reduces for 10 sources to  $\pm 2$  dB, if 100 sources are involved to approximately  $\pm 0.2$  dB if all sources have a comparable contribution at the reception site. If this is not the case, an error calculation has to be used that allows to weight the uncertainties with respect to the sound power of the sources.

The most frequently used standard for sound propagation calculation is ISO 9613-1 and -2.<sup>4</sup> Part 1 deals with air absorption and Part 2 with the other factors governing sound propagation. According to Table 8 in Part 2, the possible errors for a downwind calculation at a distance of 1000 m is 3 dB. This means together with the measurements errors of the sound power measurements a total error  $\Delta$ :

$$\Delta = \sqrt{3^2 + 3^2} = 4.24 \text{ dB}$$

for each source. For 10 sources one obtains the limit of confidence as follows:

$$L_{eq\pm} = L_{eq} \pm 1.34 \text{ dB}$$

a range comparable to those of measurements in the neighborhood. The only assumption is that the errors of the sound propagation model of ISO 9613-2 can be considered to be random and not systematic in nature.<sup>4</sup>

According to a large number of projects done to measure the sound power levels of up to 500 sources to evaluate the reception noise in the neighborhood of large industrial complexes, such as refineries, steel mills, and harbors, it could be shown that the deviation between long-term measurements up to 1 year and calculated levels falls well into a range of  $\pm 1$  dB. Judging from this, it can be assumed that for more than 10 sources the errors of the ISO 9613-2 sound propagation model behave randomly.<sup>4</sup> For smaller numbers this is not the case and control measurements at distances of about 100 m are recommended.

## 6 AVOIDING COMMUNITY REACTIONS

As can be seen from Fig. 1 and Table 1 in more than 70% of the cases, tonality, impulsiveness, and low-frequency noise seem to be the dominant cause of community reactions. The approach to reduce community reaction is simple—avoid these types of noise and avoid reducing the stationary sources to a level where the unavoidable intermittent sources can be heard in the neighborhood. If the legal limits are transgressed, noise reduction should concentrate on the intermittently audible sources. The reduction of the stationary part should be such that the intermittently occurring sources do not get more prominent. This is in line with numerous cases this author has been involved.

If there are complaints and the sources are known, few measurements and model calculations are sufficient to establish the situation and to find a technical

solution. However, in most cases the situation is more complicated. The company under consideration claims that the sometimes observed tonal, impulsive, or only very loud events are caused by something or someone else or are just the invention of neighbors. In these cases long-term measurements including the continuous recording of the sound is a sufficient method to establish whether or not such noises occur. According to this author's experience, in most cases complaints are well founded. The classical exceptions are tinnitus and psychological problems. The advantage of continuous monitoring is that the often heard complaints by neighbors can be excluded, that the auditor only appears when it is quiet, and that the company knows that he was coming. Especially if short-term very loud unknown activities are involved, continuous monitoring has proven to be a very efficient method to find the cause of complaints. The installation of long-term recording equipment leads to reductions of the emotional stress felt by both the company under investigation and the neighbors. Furthermore, the results are usually accepted by both sides, due to the fact that events, time, and impulses are well documented.

In cases where the limits are transgressed and a short-term technical solution is not possible, the acceptance by the neighbors can considerably be increased if the neighbors are invited to see the production during a day of open doors, which includes communication with the management on a casual basis. It also helps if the public and local community are regularly informed about measures taken and level reduction achieved, even if those reductions are well below 1 dB.

Of further help is if the neighbors obtain a telephone number to which they can talk at all times of the day. However, it is a must that the personal at the receiving side be trained to take those calls.

## REFERENCES

1. Health Council of the Netherlands, Assessing Noise Exposure for Public Health Purposes, No. 1997/23E, 1997.
2. DEFRA, Department of Environment, Food & Rural Affairs, Noise Mapping Industrial Sources, Final Report, Technical Report No. AT 5414/2 Rev 1, London, Research Contract, October 2003.
3. DIN 18005, Noise Abatement in Town Planning—Calculation Methods—Acoustic Orientation Values in Town Planning, 2003.
4. ISO 9613-1, Acoustics—Attenuation of Sound During Propagation Outdoors—Part 1: Calculation of the Absorption of Sound by the Atmosphere, 1993. ISO 9613-2, Acoustics—Attenuation of Sound During Propagation Outdoors—Part 2: General Method of Calculation, 1996.
5. Bayerisches Landesamt für Umweltschutz, *Parkplatzlärmstudie (Parking Lot Noise Study)*, Vol. 4, Auflage, Augsburg 2003.\*
6. ISO 1996-1, Acoustics—Description, Assessment and Measurement of Environmental Noise—Part 1: Basic Quantities and Procedures, April 2003. ISO 1996-2, Acoustics—Description and Measurement of Environmental Noise—Part 2: Acquisition of Data Pertinent to Land Use, April 1987.
7. R. B. Stull, *An Introduction to Boundary Layer Meteorology*, Kluwer Academic, Dordrecht, The Netherlands, 1988.
8. DIN 45645-1, Determination of Rating Levels from Measurement Data—Part 1: Noise Immission in the Neighbourhood, DIN Berlin, 1996.
9. ISO, GUM—Guide to the Expression of Uncertainties in Measurement, 1993 (rev. 1 June 1995).
10. ISO 8297, Acoustics—Determination of Sound Power Levels of Multisource Industrial Plants for Evaluation of Sound Pressure Levels in the Environment—Engineering Method, 1994.
11. ISO 3744, Acoustics—Determination of Sound Power Levels of Noise Sources Using Sound Pressure—Engineering Methods in an Essentially Free Field over a Reflecting Plane, 1995.
12. ISO 3746, Acoustics—Determination of Sound Power Levels of Noise Sources Using Sound Pressure—Survey Method Using an Enveloping Measurement Surface, 1995.

---

\*This study with the title *Parking Lot Noise Study* is written in German. However, there does not exist a comparable international study. The study can be ordered from Bayerisches Landesamt für Umweltschutz, Bürgermeister-Ulrich-Strasse 160, D-86179 Augsburg (e-mail: poststelle@lfu.bayern.de).

# CHAPTER 129

## BUILDING SITE NOISE

Uwe Trautmann  
ABIT Ingenieure Dr. Trautmann  
Teltow/Berlin, Germany

### 1 INTRODUCTION

Residents living near to inner-city building sites are frequently affected by the noise emitted by building sites, which disturbs sleep, mental concentration, and speech communication. The neighbors' right to rest is in conflict with the contractors' interest in performing building work in the shortest possible time and with intense utilization of the equipment and machinery. Local authorities may also take an interest in short construction times in order to limit disruptions to road and rail traffic and public utilities.

Although an inner-city building site may cause significant annoyance to the immediate neighbors, there are relatively few standards for the prediction of ambient noise, for example, from power plants. Some exceptions include test codes available for building site noise in Germany and the United Kingdom. These test codes provide tools for the calculation of the daytime and nighttime rating levels, which are compared to standard ambient-noise values. In addition, transient noise peaks can be considered.

### 2 GENERAL APPROACH, SOUND SOURCES

This chapter is mainly based on the practice in Germany and the United Kingdom. Conflicts must especially be avoided in the case of large-scale, long-term building projects. This calls for the following actions:

1. Preparation of a prediction of the expected ambient-noise values during the various building phases.
2. Assessment of ambient-noise values. Elaboration of a noise control program. Consideration of technical and organizational noise control measures.
3. Reconciliation/harmonization of the interests of builder-owner/contractor and neighbors in terms of an (administrative) special permit or a civil-law agreement. These documents may specify building technologies, machine utilizations, work hours, or maximum ambient-noise values.

The following are typical causes for inner-city building sites:

- Demolition of buildings including underground parts
- New constructions (foundation work, main works, facade, completion work, open areas)

- Road and rail construction
- Sewerage construction (open method, underground forcing)

Table 1 provides an overview of the most frequently used construction machines and their sound power levels during normal operation.

The characteristic noise emission value is the A-weighted sound power level averaged over the duration of several work cycles ( $L_{WAeq}$ ). For an assessment, the maximum level may also be required ( $L_{WAmax}$ ,  $L_{WA1\%}$ ); this level is usually determined by the process noise (effect of the construction material).

As per EU Directive 2000/14/EC, within the European Union many of the construction machines put on the market are subject to noise marking.<sup>6</sup> This means that the manufacturer must state the guaranteed sound power level in the operating instructions and on the machine. Operating conditions are given; alternatively, a machine-specific standard is cited (usually stipulating a simulation of a typical work cycle without construction material). Determination of the sound power is usually in accordance with ISO 3744.<sup>7</sup> Furthermore, some of these machines are subject to sound power limits (see Table 2).

The sound power radiated by a construction machine during actual operation on site is often less than that stated by the manufacturer.<sup>8</sup> On the one hand, this is a consequence of the standardized measurement conditions that stipulate maximum engine speed during the entire measurement; on the other hand, a penalty is added to the measured value declared so as to take into account the variance in noise emission between the individual machines (ISO 4871).<sup>9</sup> In some building technologies, the process noise may also be dominant (e.g., when sorting scrap metal). A database provides an extensive compilation of noise emission values for construction machines (standard and in-situ data).<sup>1</sup>

### 3 AMBIENT-NOISE PREDICTION

Figure 1 illustrates the general procedure of site noise prediction. To begin with, ambient-noise values due to individual building works, phases, or zones are calculated. Where the time schedule shows that building works are performed simultaneously, their contributions to the sound pressure level at the points of reception are summed up on an energy basis. The sound power levels of the machines in use can be found in Table 1 or measured values obtained in situ are used as a basis. Penalties for impulsiveness and

**Table 1 Selection of Construction Equipment and Construction Technologies Frequently Used on Inner-City Building Sites<sup>a</sup>**

Eurolist	Construction Equipment, Technology	$L_{WAeq}$ (dB)	p (%)
<b>A</b>	<b>Material Processing Equipment</b>		
	Crushers	113–119	80
	Power screens	112–116	80
<b>B</b>	<b>Equipment for Concrete Producing, Transport, and Distribution</b>		
	Concrete mixers	96–108	70
	Truck mixers	98–101	40
	Concrete pumps, truck mounted	104–107	40
	Screed mixers/pumps	98–104	40
	Electric concrete vibrators	100–108	60
	Concrete grinders (combustion engine)	110–115	40
<b>C</b>	<b>Lifting Equipment</b>		
	Tower cranes	95–103	20
	Mobile cranes	101–106	20
	Crawler cranes	102–108	20
	Material lifts	94–103	5
	Working platforms	80–85	5
	Fork lift trucks (combustion engine)	103–109	20
	Reach fork lift trucks (combustion engine)	102–106	20
<b>D</b>	<b>Equipment for Earthmoving and Soil Compacting</b>		
	Rope-operated crawler excavators earth moving/lifting	108–113	70/10
	Hydraulic crawler excavators earth moving/lifting	93–110	50/10
	Hydraulic excavators (wheeled) earth moving/lifting	93–102	50/10
	Excavator loaders (wheeled)	98–105	50
	Loaders (crawler tracked)	108–115	60
	Loaders (wheeled) earthmoving/auxiliary device	97–110	60/10
	Dozer	107–115	60
	Dumper	105–114	30
	Grader	104–109	40
	Vibratory rollers	106–112	50
	Vibratory plates	106–109	40
	Vibratory rammers	103–107	40
<b>E</b>	<b>Road Construction Equipment</b>		
	Paver	104–112	50
	Flat saws	112–116	30
	Road headers	101–112	50
	Road sweepers	99–108	10
<b>F</b>	<b>Railway Construction Equipment</b>		
	High-performance ballast screener	113–118	60
	Tamping machine	112–116	60
	Railway crane	108–112	10
	Screwing machines	100–103	20
<b>H</b>	<b>Tunneling Equipment</b>		
	Tunnel ventilator units	90–95	100
<b>J</b>	<b>Pile Drivers, Pile Pullers, Slurry Wall Equipment and Soil Injection Equipment</b>		
	Pile drivers	120–128	60
	Sheet piling presses	91–98	20
	Vibratory pile drivers	100–111	20
	Hydraulic hammers	110–126	30
	Mixing and grouting equipment	96–99	40

Table 1 (continued)

Eurolist	Construction Equipment, Technology	$L_{WAeq}$ (dB)	p (%)
<b>K</b>	<b>Drilling Equipment</b>		
	Drilling rigs (anchorage, injection)	110–115	30
	Hydraulic rotary drilling rigs	112–117	40
<b>P</b>	<b>Road Transportation Vehicles</b>		
	Pickup trucks (up to 3.5 tons)	75–80	20
	Dump trucks	98–106	20
<b>Q</b>	<b>Air Compressors and Pneumatic Tools</b>		
	Compressors (combustion eng., wheeled)	88–102	50
	Pneumatic hammers	106–111	30
<b>R</b>	<b>Equipment for Power Generation and Distribution</b>		
	Power generators	87–99	60
	Lighting equipment (power generator)	91–95	80
<b>T</b>	<b>Equipment For Pumping and Distribution of Fluids</b>		
	Water pump units (combustion engine)	96–106	50
<b>W</b>	<b>Workshop Equipment</b>		
	Hand-held motor hammers (electrically)	106–109	20
	Hand-held motor hammers (combust. eng.)	110–115	20
	Hand-held circular saws	102–113	15
	Circular saw benches	104–110	20
	Chain saws	103–105	10
	Brick saws	105–109	15
	Cut-off grinders	110–117	15

<sup>a</sup>A-weighted sound power levels  $L_{WAeq}$  for continuous work (declared resp. in situ measured values for typical working cycles). Acoustically effective time of use of construction machines (averaged) referred to time to be rated (p).

Source: From Refs. 1 to 5.

Table 2 Permissible Sound Power Levels as Laid Down in 2000/14/EC, Art. 12<sup>6</sup>

No.	Type of Equipment	Net Installed Power $P$ in kW, Electric Power $P_{el}$ in kW, or Mass $m$ in kg	Permissible A-weighted Sound Power Level (dB)	
			Stage I as from 03. 01.2002	Stage II as from 03.01.2006
1	Compaction machines (vibrating rollers, vibratory plates, vibratory rammers)	$P \leq 8$	108	105
		$8 < P \leq 70$	109	106
		$P > 70$	$89 + 11 \log P$	$86 + 11 \log P$
2	Tracked dozers, tracked loaders, tracked excavator-loaders	$P \leq 55$	106	103
		$P > 55$	$87 + 11 \log P$	$84 + 11 \log P$
3	Wheeled dozers, wheeled loaders, wheeled excavator-loaders, dumpers, graders, loader-type landfill compactors, combustion-engine-driven counterbalanced lift trucks, mobile cranes, compaction machines (nonvibrating rollers), paver-finishers, hydraulic powers packs	$P \leq 55$	104	101
		$P > 55$	$85 + 11 \log P$	$82 + 11 \log P$
4	Excavators, builders' hoists for the transport of goods, construction winches	$P \leq 15$	96	93
		$P > 15$	$83 + 11 \log P$	$80 + 11 \log P$

Table 2 (continued)

No.	Type of Equipment	Net Installed Power $P$ in kW, Electric Power $P_{el}$ in kW, or Mass $m$ in kg	Permissible A-weighted Sound Power Level (dB)	
			Stage I as from 03. 01.2002	Stage II as from 03.01.2006
5	Hand-held concrete breakers and picks	$m \leq 15$ $15 < m < 30$ $m > 30$	107 $94 + 11 \log m$ $96 + 11 \log m$	105 $92 + 11 \log m$ $94 + 11 \log m$
6	Tower cranes		$98 + \log P$	$96 + \log P$
7	Welding and power generators	$P_{el} \leq 2$ $2 < P_{el} \leq 10$ $P_{el} > 10$	$97 + \log P_{el}$ $98 + \log P_{el}$ $97 + \log P_{el}$	$95 + \log P_{el}$ $96 + \log P_{el}$ $95 + \log P_{el}$
8	Compressors	$P \leq 15$ $P > 15$	99 $97 + 2 \log P$	97 $95 + 2 \log P$

Source: From Ref. 6.

tonal character are added as specified in the relevant national regulations stipulating the determination of the rating level. Depending on the characteristic acoustical quantity, the penalty for impulsiveness may already be included in insitu values:

$$L_{WA,r} = L_{WA,eq} + \Delta I + \Delta T \quad (1)$$

where  $L_{WA,r}$  = rated sound power level for continuous operation of a construction machine

$L_{WA,eq}$  = equivalent continuous sound power level of a construction machine, e.g., during standard operation as specified<sup>6</sup>

$\Delta I, \Delta T$  = penalties for impulsiveness and tonal character, usually 0 dB to 6 dB

As a rule, none of the construction machines sustains uninterrupted acoustically significant operation throughout the time to be rated. Intermittent operation of the machines reduces their sound power as taken into account in the calculation of the rating level (time-average level):<sup>2,10,11</sup>

$$L_{WA,r,t} = L_{WA,r} + 10 \log(t/T) \quad \text{dB} \quad (2)$$

$$L_{WA,r,t} = L_{WA,r} + 10 \log(p/100) \quad \text{dB} \quad (3)$$

where  $L_{WA,r,t}$  = rated sound power level referred to actual time of use of a construction machine

$t$  = acoustically effective time of use of a construction machine during the time to be rated

$T$  = time to be rated (e.g., daytime 13 h, nighttime 11 h)

$p$  = percentage utilization rate of a construction machine,  $p = (t/T)$  100% (see also Table 1)

The specification of the position of use of a construction machine is not critical if the extent of the potential range of use during the time under consideration is

smaller than twice the distance to the nearest point of reception. As a rule, it will suffice to simulate the construction machine in terms of a stationary point source. The working range of a construction machine, or of a construction process, can also be represented as a two-dimensional or linear sound source:

$$L''_{WA,r,t} = L_{WA,r,t} - 10 \log(S) \quad \text{dB} \quad (4)$$

$$L'_{WA,r,t} = L_{WA,r,t} - 10 \log(l) \quad \text{dB} \quad (5)$$

where  $L''_{WA,r,t}$  = sound power level per unit area of a construction machine having  $L_{WA,r,t}$  (see above)

$L'_{WA,r,t}$  = sound power level per unit length of a construction machine having  $L_{WA,r,t}$  (see above)

$S$  = area of working range, in  $\text{m}^2$  (e.g., part of building zone)

$l$  = length of path traveled, in m (e.g., site road)

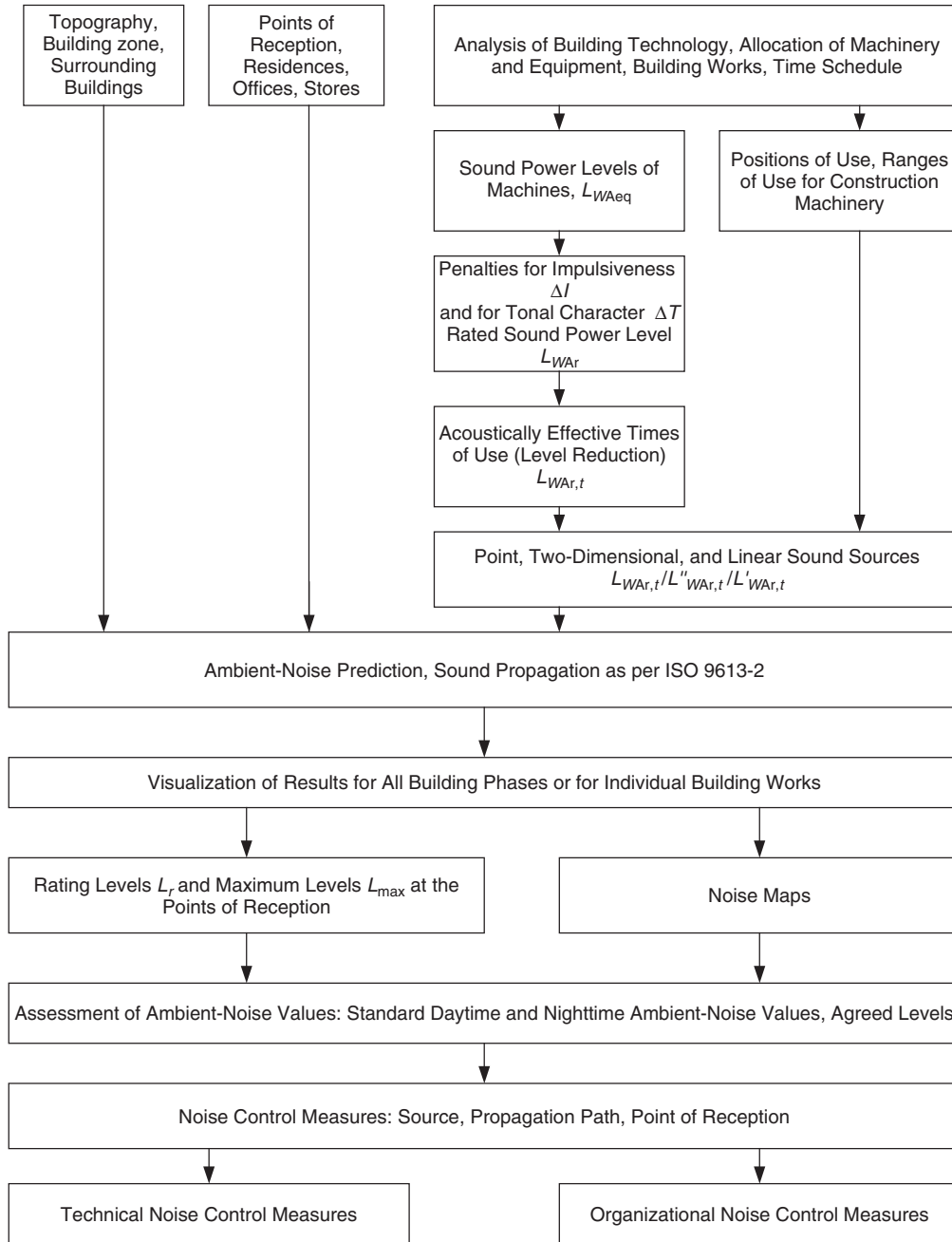
Energy-based summation allows to combine several construction machines to give one two-dimensional sound source, for example, for reinforced-concrete works: circular saw, hammer, crane, truck mixer, concrete pump, and internal vibrator.<sup>11</sup>

Commercially available computer software calculating sound propagation from the site to the points of reception on the basis of ISO 9613-2 determines the contributions of the construction machines/processes to the rating level, using  $L_{WA,r,t}$  and the pertinent distance ( $d$ ) to the point of reception in question.<sup>12</sup> With geometrical sound radiation (omnidirectional radiation over a sound reflecting plane), for distances  $d \lesssim 100$  m the sound pressure level is

$$L_{r,i} = L_{WA,r,t,i} - 20 \log(d) - 8 \quad \text{dB} \quad (6)$$

$$L_r = 10 \log \sum_i^n 10^{L_{r,i}/10} \quad \text{dB} \quad (7)$$





**Figure 1** Procedure of site noise prediction.

$L_{WA,r,t,i}$  = rated sound power level of construction machine no.  $i$   
 $L_{r,i}$  = contribution of rated sound pressure level of machine no.  $i$  at point of reception  
 $L_r$  = total rated sound pressure level at point of reception

$d$  = distance between construction machine and point of reception, in m  
 $n$  = number of construction machines

In addition, sound reflection (including absorption) and screening are taken into account. For the purpose

of sound propagation calculation, two-dimensional and linear sound sources are split up into point sources depending on their distance to the point of reception. The calculation of the maximum sound pressure levels at the point of reception is performed in an analogous way, albeit without time correction, assuming the maximum sound power  $L_{WAmax}$  or  $L_{WA1}$  %.

As a rule, ambient noise from building sites is calculated for the facade of the rooms requiring protection. In individual cases (especially in case of very high sound pressure levels), the indoor sound pressure level may be calculated and compared to standard levels (e.g., for living rooms and bedrooms, offices, and conference rooms). This is done on the basis of the sound insulation of the facade with windows closed. In order to ensure the minimum air exchange rates required by various room usages, ventilation intervals that increase the indoor rating level must be taken into account in buildings without ventilation system.

Usually the uncertainty of ambient-noise predictions for building sites lies in the range of  $\pm 3$  dB; no results are available of systematic investigations on the uncertainty. The predicted sound pressure level is mainly a function of the accuracy of the sound power ( $L_{WAeq}$ ,  $L_{WAr}$ ) and the assumed time of use ( $t$ ,  $p$ ) of the most noisy construction machines.

#### 4 MEASUREMENT OF SITE NOISE

As is the common procedure with ambient-noise control, measurements are usually carried out immediately at the points of reception or at substitute locations whose results are converted for the points of reception.<sup>10</sup> Extraneous noise not part of the site noise must be recorded separately for correction of the measured values or excluded during the measurements (e.g., traffic noise).<sup>13</sup>

The measurands (sound pressure levels) are stipulated by the laws and standards that are to be used for the assessment (e.g.,  $L_{AFeq}$ ,  $L_{Aeq}$ ,  $L_{AFTm5}$ ,  $L_{AFmax}$ ,  $L_{AF1\%}$ , and  $L_{AF10\%}$ ). Penalties for the calculation of a rating level ( $L_r$ ) are sometimes estimated (e.g.,  $\Delta L_f = 0$  to 6 dB).<sup>10</sup>

In the case of short-time measurements, the noise is recorded and averaged over a representative period. The rating level may then be calculated for the time to be rated by taking into account a level time correction (see Section 3). Extraneous noise can be identified and taken into account immediately.

In the case of continuous measurements, the levels of interest are recorded continuously over time. The rating levels for the times to be rated (e.g., daytime/nighttime) are calculated on this basis. Extraneous noise can only be identified by recording the time signal and subsequent "listening" to the recording (e.g., church bells, air traffic noise, or user noise at the point of reception).

Continuous sound pressure level measurements also allow good control of the compliance with work restrictions imposed on the building site (beginning and end of work hours, compliance with agreed rest

periods, restrictions to the use of machinery). Measurements on individual construction machines allow the determination of their sound power during use to be used as the basis for the predictive calculation ( $L_{WAeq}$ ,  $L_{WAr}$ ,  $L_{WAr,t}$ ).<sup>7</sup>

#### 5 ASSESSMENT OF SITE NOISE

The predicted or measured sound pressure levels at the points of reception are compared to the standard values stipulated in laws or standards or to sound pressure levels agreed upon in the noise control program. Limits for site noise do not exist on the international level, but they are available in Germany and some other countries. Standard ambient-noise values for site noise depend on the specific ambient-noise regulations in individual countries (e.g., rating levels for daytime and nighttime, additional limits for noise peaks during the night).

The disturbance caused by a building site lasting for a limited time only, ambient-noise values exceeding the standard ambient-noise values for stationary plants by 5 dB to 10 dB are admitted in some countries, depending on the duration of the building works (higher levels for shorter times).

The following arguments are usually taken into consideration in the assessment of site noise:

- In some cases, the use of construction machines may be limited depending on the type of machine and the legal ambient-noise classification of the area in question. Ambient-noise predictions may present reasons for exemptions.
- The approving authorities must enforce the neighbors' right to rest while also considering the builder-owners'/contractors' interests as well as public interest.
- Number of persons concerned.
- Intensity of exposure (difference between actual level and standard level, duration of noisy building works).
- Acoustical masking by other sound sources, for example, traffic noise.
- Reduction of overall duration of work, for example, where public traffic or commercial activities are impaired (nighttime building site required).
- Strong impairment of the quality of life and housing (night's sleep disturbed depending on the work and life rhythm, further annoyance caused by dust, exhaust gases, and vibrations).
- Neighbors' right to rest (especially night's sleep) to be pondered against technical necessity of the building methods.
- Right to working conditions as given in occupational health and safety regulations during daytime (offices, stores).
- Building contractor's or builder-owner's interest in an undisturbed progress of the building works (no interruptions due to complaints, lawsuits).

- Reduction of cost by two- or three-shift operation.

Special permits for site noise during the daytime may be granted, if

- The standard ambient-noise values are expected to be exceeded considerably.
- The contractor wishes to secure a legal basis for his interest in an undisturbed progress of the building works.

A special permit is required for the nighttime, if

- Modern building technologies call for continuous operation, making work during rest times unavoidable (as is the case, e.g., with high-pressure injections, large-scale concrete works).
- operation in at least two shifts (6 a.m. to 10 p.m.) is desirable for reasons of time and cost.
- work can only be performed during the nighttime because of the closing of roads or railways.

- Nighttime work causes less disturbance because the area is exclusively used for offices and stores.

## 6 NOISE CONTROL MEASURES

Establishing a noise control program is decisive for the effective functioning of noise control measures (acoustical and economic).<sup>3</sup> Noise control measures shall

- Start at the noisiest sources.
- Come into effect especially during rest periods.
- Be made known and explained to all those concerned (building contractor, authority, neighbors).

The noise control program should comprise the following steps:

1. Analysis of the building site. Where and when are noisy machines/processes used?
2. Ambient-noise prediction for the neighbors concerned (see Section 3).

**Table 3 Technical and Organizational Noise Control Measures for Building Sites**

No.	Measure	Note
<b>1</b>	<b>Noise control at source</b>	
1.1	Change building technology, use low-noise building methods; e.g., laying of prefab concrete parts, concrete works in limited areas using buckets instead of pump. Sawing, milling, or use of hydraulic tongs instead of demolition by pneumatic or hydraulic chipper. Pressing or vibrating, rather than pile-driving, of pit boards.	
1.2	Use low-noise construction machinery.	Strive for an acoustical balance. Noise control measures on construction machinery must, as a rule, be agreed with the manufacturer. Consider safety regulations where the reversing alarm is disabled.
1.3	Covering of toughs and filling holes with rubber. Damping of metal sheets.	
1.4	Restrictions (spatial, temporal) to the use of individual construction machines or processes.	Illustration of the ranges of use in the site plan, allocation of times of use.
1.5	Temporal and spatial organization of the site following the motto: Assign noisy building methods to noisy building phases/times, and low-noise building methods to low-noise building phases/times.	For example, plan on maximum use of machinery during daytime in order to ensure night's rest for neighbors.
1.6	Coordination of building times: Plan beginning and end in accordance with the legal ambient-noise classification (e.g., residential area, offices only, health resort area). Shifting or even exchanging daytime and nighttime works. Consideration of neighbors' typical rest times.	For example, in office-only areas: Noisy nighttime work is convenient (but consider sound propagation to remoter residential areas). Health resort areas often favor short overall building times (nighttime work, e.g., out of season).
1.7	Reduction of daily work time.	Unfavorable from building technology viewpoint, often causing excessive prolongation of overall building time.
1.8	Adaptation of running of construction machines with actual used power. Avoid idling especially during rest hours.	
1.9	Maintenance of construction machines.	Avoid vibration/rattling of cover sheets.
1.10	Instruction of employees on low-noise work. Avoid shouting. Use of radiotelephony for communication.	Use especially during rest hours. Use of tower crane loudspeakers only in case of emergency.

**Table 3 (continued)**

No.	Measure	Note
1.11	Supervision of building site (machines used, technology, work hours, work ranges).	Safety service.
<b>2</b>	<b>Measures taken on the sound propagation path</b>	
2.1	Increase distance between noisy building processes and points of reception. Allocate building zones in large-scale projects. Organize site traffic (delivery and disposal of construction material). Machine locations.	Give particular consideration to rest times, shift nighttime building activities to remote building zones.
2.2	Screening of construction machines/processes (installation of separate screens).	For example, formwork material, scaffold curtains, flexible materials, containers. Screens are only effective if placed close to the source. Consider all points of reception; those opposite the screen may be subject to an increase in sound pressure level! See also 2.2.
2.3	Use already erected building parts as acoustical screens.	
2.4	Enclosing or partial enclosing of machines and processes.	Sound insulation of the enclosure material, sound-absorbent cladding, proper sealing. Silencers on unavoidable openings (cooling air, exhaust gases). Orientation of partial enclosures, see also 2.2.
2.5	Avoid positioning of construction machines in front of sound reflecting surfaces.	
<b>3</b>	<b>Measures at point of reception</b>	
3.1	Inform neighbors, possibly in the form of a hearing prior to starting the building project, regular information about progress.	Unaddressed mailings, informative dioramas.
3.2	Improve sound insulation of windows.	Only effective as long as windows stay closed. Allow for ventilation: Ventilation system, sound-insulated ventilation elements. In the case of natural ventilation via the windows, consider ventilation intervals when calculating the rating level.
3.3	Provide substitute accommodation. For example, offer hotel accommodation for short-time building projects.	In case of short-time building projects, experience shows that neighbors tend to solve problems on their own by sleeping with windows closed. Accommodation may also be offered by relatives or acquaintances.
3.4	Agree on financial compensation (owner, landlord).	
3.5	Invite neighbors to social events (such as laying of foundation stone, ceremonies on completion of building pit/ceilings, topping out/dedication ceremonies).	
3.6	Inform the competent authority. Obtain special permit, agreement on special requirements. Inform the police precinct concerned.	The special permit can cover measures from rows 1 through 3.
3.7	Sample measurements or continuous monitoring of ambient-noise values. Regular information of neighbors, the authority, and the contractor about measurement results.	Continuous measurements allow to verify noise control measures (such as compliance with work hours, restrictions to use of machinery).
3.	Assessment of site noise (see Section 5).	
4.	Elaboration of technical and organizational noise control measures for all building phases, taking into account the acoustical effect and the cost.	
5.	Regular information of the neighbors about the work progress. Special information prior to noisy events (such as large-scale concrete work during nighttime).	
6.	Updating of the noise control program (repeat steps 1 through 5).	
Depending on the sound propagation conditions, noise control measures can be implemented at source, on the propagation path, and at the point of reception. Measures taken at source have the greatest acoustical effect in inner-city building sites, as many neighbors are affected by site noise at the same time. The most		

important measures for noise control are compiled in Table 3.

## REFERENCES

1. U. Trautmann, *Noise Emission Data of Construction Machines (Database)*, Wirtschaftsverlag NW Verlag für neue Wissenschaft, Bremerhaven, 2004.
2. BS 5228-1, Noise and Vibration Control on Construction and Open Sites—Part 1: Code of Practice for Basic Information and Procedures for Noise and Vibration Control, British Standards Institution, London, 1997.
3. E. Thalheimer, Construction Noise Control Program and Mitigation Strategy at the Central Artery/Tunnel Project, *Noise Control Eng. J.*, Vol. 48, No. 5, 2000, pp. 157–165.
4. G. Müller and M. Möser, *Taschenbuch der Technischen Akustik*, Springer, Berlin, Heidelberg, New York, 2004.
5. VDI 3765 (E), Characteristic Noise Emission Values of Technical Sources—Machinery and Equipment on Construction Sites, DIN Deutsches Institut für Normung, Berlin, 2005.
6. Directive 2000/14/EC of the European Parliament and of the Council of 8 May 2000 on the Approximation of the Laws of the Member States Relating to the Noise Emission in the Environment by Equipment for Use Outdoors, *Official Journal of the European Communities*, L 162/1, 03.07.2000.
7. ISO 3744, Acoustics—Determination of Sound Power Levels of Noise Sources Using Sound Pressure—Engineering Method in an Essentially Free Field over a Reflecting Plane, ISO, 1994.
8. M. Peters and U. Trautmann, Sound Power of Construction Machines: Declared Values vs. In-Situ Measurements, *Proceedings of the Joint Congress CFA/DAGA'04*, March 22–25, 2004, Strasbourg, France, (CD-ROM), DEGA, Oldenburg, 2004.
9. ISO 4871, Acoustics—Declaration and Verification of Noise Emission Values of Machinery and Equipment, ISO, 1996.
10. General Administrative Regulation for the Protection Against Construction Noise; Noise Immisions of 19.08.1970, *Federal Bulletin of FRG*, No. 160, 01.09.1970.
11. M. Pötter and U. Trautmann, Investigations into the Prediction of Construction Noise, *Proceedings of the Joint Congress CFA/DAGA'04*, March 22–25, 2004, Strasbourg, France, (CD-ROM), DEGA, Oldenburg, 2004.
12. ISO 9613-2, Acoustics—Attenuation of Sound During Propagation Outdoors—Part 2: General Method of Calculation, ISO, 1996.
13. ISO 1996-2, Acoustics—Description and Measurement of Environmental Noise—Part 2: Determination of Environmental Noise Levels, ISO, 2003.

# CHAPTER 130

## COMMUNITY NOISE ORDINANCES

**J. Luis Bento Coelho**  
CAPS—Instituto Superior Técnico  
Lisbon, Portugal

### 1 INTRODUCTION

Sound produced by human activities, transportation, machinery, and by nature itself is always present in a community. Such sounds, when unwanted, are perceived as noise. Each person perceives noise by taking into account a vast number of different factors including personal, cultural, economic, and societal. This makes the perception of noise very subjective.

Noise may be understood as an expression of human activity, but it can also be a source of annoyance. People make noise; however, noise is not a problem unless it becomes excessive, thereby hindering the community quality of life. This calls for each community and its government to set up policies for noise management and control and to devise and enforce strategies for noise abatement.

Community noise ordinances have been passed in most countries to address noise issues of all types, from neighborhood to transportation. They deal with noise limits at the receiver as well as with the quality of noise itself. Such ordinances can be qualitative or quantitative; they can be emission or receiver based. As part of the actions of a global noise policy, which includes sustainable development, community noise ordinances can be instrumental tools that ensure a noise-controlled environment.

### 2 COMMUNITY NOISE AS A PROBLEM

Community noise can be described as unwanted sound in a nonoccupational setting. Major sources of community noise are transportation systems, industry, construction, leisure activities, and neighborhood with transportation being the main contributor. Industry can contribute to the overall noise, especially in some suburban or rural areas. Leisure activities may account for a significant part of the noise in some areas of the community. Noise from equipment, either outdoors (construction, air conditioning, ventilation systems) or indoors (lifts, home appliances) is also a part of the overall noise.

Noise in a community must be addressed in terms of quantity and of quality. Once the quantity of noise is reduced, the quality becomes important. People usually have an expectation for the way different noise sources in the environment should sound. In quieter communities or in those where noise has already been reduced, this expected sound quality assumes a higher importance.

The larger and more complex a community is, the higher is the number of noise sources and the more difficult it is to act for noise abatement purposes. In a city, the complexity and intricacy of the human, economical, and social activities make urban noise management and control a difficult issue. Actions must

be devised and applied with the utmost care so as not to affect or disrupt the rhythm of life and the socioeconomic texture of the city.

Noise becomes a problem whenever the noise levels are high or when the number of complaints becomes relevant. The recognition of the noise problem must be followed by firm actions at the different levels of authority.

Noise was recognized as a problem in cities as early as the 1920s, although complaints from noise can be traced back to the Roman Empire due to the noise produced by the cart wheels on the pebble roads. With increasing population density, communities became noisier. In the last decades of the twentieth century, many cities in different parts of the world, namely in the United States, Europe, Japan, and Australia, for example, faced the problem of urban noise very seriously. Noise ordinances were promulgated and noise abatement became a prominent factor in urban planning and development.

### 3 NOISE ABATEMENT RESPONSIBILITIES

Success in the control of noise in a community can only be effectively achieved by a shared responsibility approach. Different levels of responsibilities can be established: local, regional, national, and federal. Community noise is a local problem. However, the solutions are not always necessarily local. Noise levels at a receiver are determined not only by local conditions but also by noise emissions whose limits or parameters are established above local or even national policies.<sup>1,2</sup> Noise from industry, for example, depends on the equipment and machinery noise power but also largely on factory layout and on installed noise control procedures and devices. This is basically a local problem. Road traffic noise depends on the road profile and on the type of pavement but mostly on traffic density and on vehicle emissions. However, limits for noise emissions by road vehicles, as by rail or aircraft, are established at national or federal level.

Noise regulations must then consider all levels of action, sharing the necessary responsibilities for each type of noise source as appropriate. The regulations at different levels must be coordinated and consistent. Provisions must also be made for the allocation of corresponding technical and financial resources for an effective enforcement at all levels.

### 4 COMMUNITY NOISE REGULATIONS

Community noise regulations are a fundamental part of a noise protection policy as they raise the awareness of citizens to noise and to noise effects and reduce

the production of noise in many circumstances. They establish the basic criteria for the acoustical quality of the environment and set the objective noise values that define the noise abatement purposes. These regulations require actions from lower levels of government, from transport authorities, and from other bodies responsible for noise sources and noise emissions. They establish law compliance mechanisms and penalties, making it a platform for the common citizen to be aware of his duties and to demand his rights.

Noise ordinances may define the excessive noise by its character or nature. They may prohibit certain activities, restrict activities to certain hours of the day, require permits or licenses for noisy activities, or merely define noise zones. These are qualitative ordinances. These ordinances do not include quantitative criteria and may therefore pose some difficulties such as vagueness, as they are generally subjective in nature. Community noise ordinances usually took this form in the past. They can be recommended as a first approach to raise the issues of self-regulation and noise control or for those communities where the noise problems are either not too severe or are caused by locally well-controlled noise sources. Costs associated with the enforcement of qualitative regulations are usually relatively low since the corresponding technical requirements do not have to be too sophisticated.

Quantitative ordinances, on the other hand, establish numerical values as limits for the noise levels produced or received. Criteria are defined and standards are required for measurement or prediction of noise. Maximum permitted noise levels are generally expressed in A-weighted sound pressure levels and may vary for different areas of the community and for different types of noise sources as appropriate. This type of ordinance is recommended for communities where the noise problems are more complex or where a more stringent management of noise must be met. Good results, though, require that technical facilities (know-how, acoustical technicians and engineers, measuring apparatus) either exist or are created, and such costs must be envisaged when the ordinance is being drafted. Qualitative and quantitative ordinances are both valuable, although a composition of both features usually prove to lead to the most effective noise ordinance contents.

Noise ordinances can be of two types: emission laws or receiver-based laws. Emission laws and regulations regulate noise at the source, by establishing limits to the amount of noise emitted by equipment. Maximum permissible noise levels are defined for each type of machinery, vehicle, transportation, or activity. Receiver-based laws regulate the noise levels received at a particular site. Limits are defined for the noise exposure at specific locations. These limits are usually related to the use of the property the sound is entering. These ordinances set zoning performance standards for new noise sources. Noise zoning is then used by local authorities for land-use planning.

In the 1990s, the World Health Organization (WHO) published guideline target values to be adopted for protection against noise.<sup>3,4</sup> The WHO recommended the following: (1) to protect the majority of people

from being moderately annoyed during the daytime, the outdoor A-weighted sound pressure level ( $L_{Aeq}$ ) should not exceed 50 dB, (2) to protect the majority of people from being seriously annoyed during the daytime in outdoor living areas the A-weighted sound pressure level ( $L_{Aeq}$ ) should not exceed 55 dB and (3) at nighttime outside sound pressure level should not exceed 45 dB in residential areas, so that the recommended A-weighted sound pressure level of 30 dB inside bedrooms with the windows open can be met. The WHO also suggests a limit of 60 dB for the maximum outdoor event A-weighted sound pressure level at night to protect people from sleep disruption.

These values were recommended in the European Green Paper on Future Noise Policy<sup>1</sup> as objective noise levels for all European Union (EU) member states. They have also been adopted in noise regulations in other parts of the world.<sup>5</sup> New guidelines for the exposure to noise at night have been prepared recently by the WHO. A final draft was approved in late 2006, and a final publication is expected in 2007.

## 5 COMMUNITY NOISE ORDINANCE COMPONENTS

A community noise ordinance can be a precious instrument for dealing with noise at a local level. The quality and the quantity of the overall noise are addressed, noisy activities are regulated, noise limits are set, and responsible bodies and cost-effective noise abatement policies are defined. It must first be determined, however, whether the local government concerned has enough authority to legislate on the noise matters, since its powers are delegated powers and its legislative authority is only that granted by statutory or constitutional provisions.

A well-written noise ordinance must cover a number of components in a concise, clear, and precise way so as to address the local noise issues in as comprehensive a manner as possible to avoid misinterpretation and litigation. Vagueness, indefiniteness, and uncertainty should be prevented.

A community noise ordinance starts by a declaration of policy, a comprehensive list of definitions of terms and technical references, and by establishing the powers and duties of the municipal agency or department having the lead responsibility for the ordinance (noise control officer).

The rating index and its assessment method must be very clearly defined. The metrics most widely used is the long-term A-weighted continuous equivalent sound pressure level,  $L_{Aeq}$ , since it yields a good correlation with noise effects.<sup>6</sup> The day-night average noise level,  $L_{dn}$ , is a 24-h A-weighted noise index used in the United States. It is calculated from the values of  $L_{Aeq}$  during daytime and during nighttime where a 10-dB penalty is applied to sound occurring between 10 p.m. and 7 a.m. The European Directive 2002/49/EC introduced the 24-h day-evening-night level,  $L_{den}$ , also calculated from the values of  $L_{Aeq}$  during the day period, during the evening period with a penalty of 5 dB and during the night period with a penalty of 10 dB, to be used by all EU member states in strategic noise mapping and action plans.<sup>7</sup> Other

indicators are used for the rating of road traffic noise or of aircraft noise in different countries. The ordinance must also refer to impulsive, narrow-band, or other relevant acoustical characteristics and establish any corresponding corrections to the rating index.

Measurement and calculation procedures are required to follow the applying standards. The recommendations and provisions set out in the International Organization for Standardization (ISO) 1996 standard<sup>8</sup> or equivalent [e.g., American National Standards Institute (ANSI)] are usual requisites. Noise assessment location (by measurement or calculation) and other relevant conditions (time intervals, emission or received noises) not covered by applying standards should be included in the text of the ordinance.

Reference time periods are defined, with their start and end hours clearly established, if not set at national level. Some countries consider only two reference periods, daytime and nighttime, whereas others consider a third one, a rest or evening period.

The noise ordinance usually defines noise zones according to the land uses and noise-sensitive activities. Corresponding noise limit values are stipulated for each reference time interval. The most stringent limits apply to residential, school, hospital, or leisure areas. It is recommended that different noise zones are created with noise limits in steps of 5 dB. Experiences with courser grades, with 10-dB steps, for example, have proved less practical and less effective.

Restrictions on noisy activities, musical instruments, and public address systems, construction, machine operation, traffic (e.g., heavy goods vehicles and aircraft) should be defined for the different noise-sensitive zones, together with criteria regarding the maximum permitted noise levels and the applicable hours. All such activities have to be clearly defined so as to avoid alternative interpretations and future litigation.

Restrictions are set for construction of some types of buildings (residence, school, hospital, or similar structure) and for land-use planning purposes so that the noise limits for each noise zone can be ensured. Similar types of restrictions are set for new outdoor or indoor recreational and leisure areas for the same reason. Plans for construction of new transportation systems or expansion of the capacity of existing ones in or near noise-sensitive zones may also be restricted, unless the necessary noise abatement measures are included to ensure that the noise levels in the zone will be within the prescribed limits.

The noise limits usually apply to the overall noise levels, but they may refer to noise from the different primary noise sources (industry, road traffic, railway traffic, and air traffic). Limits on noise emissions from machinery, construction work, and industry can be set since they can be well controlled at local level. These noisy activities are usually licensed by the municipalities. Limits on noise from transportation are usually set at the receiver. This is an area where coordination with transport authorities and with regulations at national level will prove most fruitful, given the limitations of the local legislative powers regarding

nationwide transport systems (e.g., airports, highways, and national railways).

Some restrictions (access traffic, activities) may have economic and societal prices, and the community should decide what level of cost-benefit is most appropriate. A number of experiences with severe traffic restrictions in some European cities have met with the opposition of residents who abandoned the area allegedly due to a decrease in economic activity and to the fear of a drop in real estate values.

Responsibilities for the measurement and assessment of noise should be set. Duties of the noise control agency or officer are defined to review the projects that may result in the production of sound, to inspect any place or situation suspected of violating any provision of the ordinance, and to investigate and pursue possible violations of the ordinance. Public education and information programs should be required or suggested. Participation of public-interest groups is mandatory in some countries and recommended in others. Noise mapping and noise action planning are usually required to integrate the land-use plans and long-term urban development plans where these instruments are operative.

Enforcement provisions must be clearly set out. The noise control officer or agency must rely on a well-trained team of municipal or county engineers who must be technically prepared and equipped to review relevant acoustical projects, to proceed with inspections, and to issue notices of violation and abatement orders (these are more effective if such orders include advice or recommendations on types of possible solutions or remedies). Although they do not need to be experts or even hold a college degree, some training on basic acoustics, sound radiation and propagation, and acoustical measurements should be provided to the technical staff. They must have a good knowledge of the existing measurement and calculation standards and of the measuring apparatus. The higher the quantitative nature of the ordinance, the higher is the technical requirement and the associated cost.

Fines and penalty actions must be well defined. The ordinance must state the explicit time criteria and goals for the full compliance of the regulations: hours of restrictions and periods of time to correct the violation or to implement the necessary remedies or abatement measures. Exceptions (e.g., emergencies) and variances (time to comply in specific conditions) should also be included.

The document *Model Community Noise Control Ordinance* issued by the U.S. Environmental Protection Agency (EPA) in the 1970s, describes a generic layout of a community noise ordinance to be adopted in U.S. communities.<sup>9</sup> Model noise ordinances were thereafter drafted in various U.S. states (e.g., Alaska, California, and New Jersey) aimed at their municipalities.

The community may publish, as a support to the noise ordinance, technical and information guides on community noise with more detailed definitions, basic explanations on noise production, noise sources, and effects of noise on practical measures and procedures to reduce it and on how the citizens can seek abatement orders. This has been followed in many cities of various countries with great success. Information regarding



noise and noise effects is never too much but should be provided at a level that can be fully understood by the target population, meaning that different brochures or documents, technical and nontechnical, may be required. Community noise ordinances have been instruments for the management and control of noise in local communities of many countries worldwide.

## 6 THE U.S. NOISE POLICY

The need for a noise policy in the United States was first recognized in 1967. In 1969, the National Environmental Policy Act (NEPA) was approved.<sup>10</sup> The NEPA is a basic national charter for protection of the environment in the United States. NEPA mandated the environmental impact assessment process, and noise is one of the many environmental attributes that must be considered.

In 1972, the Noise Control Act (NCA 72) was approved by the U.S. Congress.<sup>11</sup> The NCA 72 was passed specifically to address environmental noise. The NCA 72 stated that it is "the policy of the United States to promote an environment for all Americans free from noise that jeopardizes their health or welfare." In the act, the U.S. Congress recognized that the "primary responsibility for the control of noise rests with state and local governments" while "federal action is essential to deal with major noise sources."

The responsibility for implementing NCA 72 was assigned to the EPA.<sup>12</sup> This was to be the leading federal agency in charge of coordinating the programs of all federal agencies dealing with noise control. However, in the early 1980s EPA was no longer involved with noise control regulations.<sup>12,13</sup> About a dozen federal agencies have since been responsible for the development, formulation and implementation of the U.S. noise policies together with the corresponding bodies of state and local authorities. The policies of these agencies have not always been coordinated, leading to some lack of consistency in noise requirements, which usually apply separately to different noise source emissions.<sup>14</sup>

The aircraft noise policy of the Federal Aviation Administration (FAA), applicable to civilian-operated airports, has been very effective. The Aircraft Noise Abatement Act of 1968 (later modified by the NCA 72) directed the FAA to establish standards and regulations for aircraft noise.<sup>15</sup> Aircraft noise certification by FAA was required by the 1969 Federal Aviation Regulations.<sup>16</sup> This was followed by the 1976 Aviation Noise Abatement Policy<sup>17</sup> and by the Aviation Safety and Noise Abatement Act of 1979.<sup>18</sup> In 2000, the Aviation Noise Abatement Policy was revised and various issues from aviation noise assessment to promotion of compatible uses of impacted land were outlined. The FAA and the Department of Defense adopted the annual A-weighted day-night average sound pressure level of 65 dB as the level for action regarding aircraft noise abatement in residential areas near an airport.<sup>19</sup>

Road traffic noise has been regulated by the Federal Highway Administration (FHWA) since it was mandated by the Highway Federal Act of 1970 to develop noise standards for mitigating highway traffic

noise and by the NCA 72 to enforce the noise emission standards for vehicles that were to be defined by the EPA. A number of documents were published since the 1970s. The Procedures for Abatement of Highway Traffic Noise and Construction Noise set limits for levels of noise along highways and defined criteria and the responsible bodies for noise abatement procedures.<sup>20</sup> The FHWA criterion for action to protect residents near a federally funded highway project is the noise action level of 67 dB corresponding to the peak traffic hour  $L_{Aeq1h}$ . Land-use planning near highways is, however, left to state and local governments.

The U.S. EPA recommended in 1974 that the outdoor A-weighted day-night sound pressure level should be kept below 55 dB in residential areas. This value has also been adopted by the Federal Energy Regulatory Commission (FERC) to protect residents near some industrial installations.

The policy for noise protection is now basically defined at state or local level since it was recognized as a more efficient approach. Nevertheless, for communities impacted by a combination of different sources, the issue is a difficult one since a variety of limits and metrics apply. A large number of U.S. cities and towns have their own community noise ordinances.<sup>21</sup> The first known local noise ordinance regarding noise limits was adopted by Chicago around 1955. These were zoning regulations aimed primarily at industry and targeted at 61 dB for sound entering other business areas and 54 dB for sound entering residential areas during day or night. The New York City noise ordinance is currently undergoing a major revision. Most community noise ordinances in the United States now apply the general strategy set out in the EPA's Framework for Community-Based Environmental Protection.<sup>22</sup>

The need to revise the U. S. national noise policy is now being considered seriously.<sup>13,14,23,24</sup> There is a need to unify noise protection criteria at the national level and to reactivate a lead agency responsible for noise policy and control. A reformulation of the U.S. noise policy can be expected in the near future.<sup>21</sup>

## 7 THE EUROPEAN CHALLENGE

Noise regulations were passed in many European countries and cities since the late 1970s. They dealt with different aspects of noise from transportation, equipment, neighborhood, or leisure activities. Most defined noise-sensitive zones, depending on the different land uses, defined associated noise limits for day and for night periods, and established restrictions on traffic and on noise-producing activities.

Environmental noise is addressed at the European level through a wide range of instruments.<sup>25</sup> Various directives regarding noise emissions from different sources, such as motor vehicles, railway systems, aircraft, household appliances, and outdoor machinery, have been approved since the early 1970s.

Directive 86/594/EEC was passed in 1986 regarding noise labeling of household appliances.<sup>26</sup> Directive 2000/14/EC lays down noise provisions to reduce the noise emitted by outdoor equipment and requirements for harmonization of noise emission limits and standards,

of conformity assessment procedures, and of noise level marking.<sup>27</sup> Directive 2003/44/EC, which amends the previous recreational craft Directive 94/25/EC and took effect progressively from 2005, establishes requirements regarding noise emission limit values for recreational craft.<sup>28</sup>

The directives on noise emission from new motor vehicles have been a success story. The first European harmonized noise requirements for road vehicles were introduced in 1970 by Directive 70/157/EEC relating to the permissible noise level and the exhaust system of four-wheel motor vehicles.<sup>29</sup> Noise limits for new cars first defined in Directive 77/212/EEC were made increasingly more stringent until the most recent one, 92/97/EEC.<sup>29</sup> The decrease in the prescribed maximum allowed noise levels ranged from 6 dB for passenger cars to 10 dB for heavy trucks. Directive 97/24/EC<sup>30</sup> sets permissible noise levels for two- and three-wheel vehicles and their exhaust systems, and Directive 2001/43/EC<sup>31</sup> deals with tire rolling noise.

European legislation has addressed railway noise at source through directives on railway interoperability for high-speed rail (Directive 96/48/EC<sup>32</sup>) and for conventional rail (Directive 2001/16/EC<sup>33</sup>). Technical specifications were approved in 2002, setting out noise emission limits for high-speed trains at different speeds.

Noise emission limitations from civil aircraft have been in force since 1980 (Directive 80/51/EEC.<sup>34</sup>) Directive 92/14/EEC of 1992, based on standards of the International Civil Aviation Organization (ICAO), banned the noisiest aircraft (Chapter 2 of Annex 16 of ICAO) from European airports.<sup>35</sup> In 2002, Directive 2002/30/EC established rules and procedures with respect to the introduction of noise-related operating restrictions at EU airports.<sup>36</sup> It further required that results of the implementation of this directive be reported no later than 2007.

In the mid-1990s various studies were conducted as a starting point of a new directive on environmental noise. It was found<sup>37</sup> that about 20% of the European population was exposed to A-weighted sound pressure levels of 65 dB or above, mainly from transportation. In 1996, the European Commission produced the Green Paper on Future Noise Policy.<sup>1</sup> Following the publication of this document, a new framework for noise policy, based on shared responsibility between the European Union, national, and local authorities was defined.

The Environmental Noise Directive (END) 2002/49/EC was published in 2002 on the basis of the Green Paper recommendations to address noise issues and to define a "common approach for all European countries in order to avoid, prevent or reduce on a prioritized basis the harmful effects, including annoyance, due to exposure to environmental noise".<sup>7</sup> The END defines the basic principles of a harmonized European noise policy. It requires the assessment of the environmental noise, both overall and from major noise sources, such as transportation and industry, the number of people exposed to different noise levels, action plans for reduction of noise

exposure, communication with the public, and communication between the European Commission and the member states. No noise limits were included as this is left to each country or local community.

A noise expert network was set up in order to assist and provide advice to the European Commission prior to and after the publication of the END. Different working groups of experts from different member states were created to deal with emissions from noise sources and with noise effects and perception. Two working groups still meet regularly: Assessment of Exposure to Noise (WG-AEN) and Health and Socio-Economic Aspects (WG-HSEA).

The European Directive 2002/49/EC requires the competent authorities to draw strategic noise maps for the assessment of noise from major transport infrastructures and in communities with more than 100,000 inhabitants.<sup>7</sup> Action plans are required and should be designed to manage noise issues and effects, including noise reduction, if necessary. Two stages are defined. In the first stage, strategic noise maps for all agglomerations with more than 250,000 inhabitants, major airports with more than 50,000 movements per year, major roads with more than 6,000,000 vehicles per year, and railways with more than 60,000 passages per year must be completed by June 2007. The corresponding action plans must be finished by July 2008. The second stage corresponds to other agglomerations with more than 100,000 inhabitants, major roads with more than 3,000,000 vehicles per year, and railways with more than 30,000 passages per year. Strategic noise maps must be completed by June 2012 and action plans by July 2013. Noise maps and action plans are to be reviewed every 5 years.

All EU directives are transposed into national legislations of the European member states. Their own noise ordinances at national, regional, or municipal levels that address noise zoning, noise limits, and noise abatement<sup>38</sup> incorporate the growing harmonized noise criteria and procedures.

## 8 THE EXPERIENCE IN JAPAN

Environmental noise policies in Japan started in 1967, and in 1968 the first Noise Regulation Law was approved and later amended in 1995 and in 2000.<sup>39</sup> The Environmental Quality Standards for Noise<sup>40</sup> were first defined in May 1971, based on Article 9 of the Basic Law for Environmental Pollution Control. Limit noise values were stipulated for two types of areas: general areas and roadside areas. General limits for the A-weighted sound pressure level were established at 35 dB during nighttime for quiet neighborhoods and at 60 dB during daytime for areas with a considerable number of dwellings but which included commerce and industrial uses. Limits for roadside areas were 5 to 10 dB higher depending on various factors such as the number of road lanes. In accordance with the provisions of Article 16 of the Basic Environment Law (Law No. 91) of 1993, the noise limits were reviewed in 1998 and enforced in 1999.<sup>41</sup> Outdoor noise limits of 55 dB during daytime and of 45 dB during nighttime for residential areas

were then recommended. For areas with particularly noise-sensitive uses, the limits are 5 dB lower, whereas for areas with commerce and industry they are 5 dB higher. In areas facing roads with two or more lanes, another 5 dB were allowed.

The Noise Regulation Law required the local governments to proceed with noise zoning and classification. By the mid-1990s, more than 600 large cities and more than 850 small municipalities had their own noise ordinances.<sup>42</sup> That law also demanded the Environment Agency to establish the maximum permissible levels of noise produced by the operation of motor vehicles. Since they were first implemented in 1971, controls of running noise on new vehicles have been strengthened several times, namely in 1979, in 1986, and in 1992 when the document *The Future Policy for Motor Vehicle Noise Reduction* was approved.

The Environmental Quality Standards for Aircraft Noise were initially defined in 1973 and later revised and updated in 1993 to prevent aircraft noise pollution.<sup>43</sup> Maximum levels of the A-weighted equivalent continuous perceived noise level (WECPNL) (calculated from  $WECPNL = L_{Apeak} + 10 \log N - 27$  where  $L_{Apeak}$  is the mean level of all peaks that exceed the background noise by at least 10 dB in one day, and  $N$  is a time-weighted total number of aircraft) are prescribed as 70 dB for residential areas and 75 dB for other areas where normal living conditions should be preserved. A certification system banning the operation of aircraft whose noise exceeds prescribed levels has been in effect since 1975 and later strengthened in 1978, leading to the phasing out of the noisier aircraft at major airports as from 1988. In order to implement further aircraft noise countermeasures, a portion of the Civil Aeronautics Law was revised in 1994 pointing to the gradual restriction of operation of the noisier aircraft in Japan from 1995 and to their prohibition as from 2002.

Noise from the Shinkansen railway line is the subject of the Environmental Quality Standards for Shinkansen Superexpress Railway Noise, as originally issued in 1975 and revised and updated in 1993.<sup>44</sup> Noise limits are 70 dB for residential areas and 75 dB for areas with commerce and industry where normal living conditions should be preserved, measured as A-weighted peak sound pressure levels. These limits actually relate to noise emissions but not to the exposure of the population to noise since the number of trains is not accounted for. For conventional railway trains, noise standards have been under study.

Based on the noise standards, countermeasures have been implemented against all types of noise sources. Local government actions deriving from local community noise ordinances have been reportedly very effective. However, it has been recognized that the whole noise policy needs to be reconsidered and this seems to be underway.

## 9 THE AUSTRALIAN EXPERIENCE

In Australia, excessive noise is regulated in each state by environment protection acts and by environment protection policies. The environment protection policies set maximum permissible noise levels for certain types

of machines during specified times as well as for motor vehicles and control the maximum levels of noise exposure in areas with residential uses. Local governments, as regulatory authorities, are demanded to enforce the noise limit values.

In South Australia, for example, the Environment Protection (Industrial Noise) Policy 1994 established maximum permissible noise levels for both day and night in six different land zones.<sup>45</sup> Daytime A-weighted sound pressure level limits are 47 dB for a rural area or 52 to 58 dB for urban residential areas, depending on other existing uses. The corresponding limits for nighttime are 40 dB and 45 to 50 dB. Maximum noise levels are also defined for premises adjoining roadways carrying more than 100 vehicles/hour ranging from 54 to 76 dB with corrections for the distances to the road.

In New South Wales, local environmental noise issues are managed by the Protection of the Environment Operations Act 1997<sup>46</sup> and by the Protection of the Environment Operations (Noise Control) Regulation 2000. This document prescribes maximum noise levels for different classes of motor vehicles with specifications for testing procedures. The Environmental Noise Criteria for Road Traffic Noise set out criteria to be applied to residential areas with maximum A-weighted sound pressure levels of 55 dB to 60 dB during the day or 50 dB to 55 dB during the night, depending on the type of road and on new or redevelopment area.<sup>47</sup>

In Queensland, the Environmental Protection (Noise) Policy 1997, amended in 2003, prescribes rules for noise labeling of various products, for noise assessment to be used by the local authorities, and recommendations to get the communities involved in the protection of environmental noise.<sup>48</sup> Planning levels are defined. The A-weighted equivalent sound pressure levels in front of the most exposed facades of noise-sensitive buildings must not exceed 65 dB (87 dB maximum single event) near railways or 60 dB (80 dB maximum single event) near public roads. Near an airport,  $L_{max}$  must not exceed 70 dB.

## 10 OTHER EXPERIENCES

In Canada, provincial governments set their own noise policies. Ottawa's regulations are based on the Noise Control Guidelines of 1995.<sup>49</sup> The city new environmental plan prescribes maximum A-weighted sound pressure levels of 58 dB during the day and 53 dB during the night from roads, railways, or transitways. Criteria are established for the compatibility of land uses in the vicinity of airports. The Noise Control By-Law of the City of Vancouver of 1989, last amended in 2004, establishes noise limits for noise emissions in different noise zones. For a quiet zone, for example, the A-weighted sound pressure level limits vary between 55 dB and 60 dB during daytime and between 45 dB and 55 dB during nighttime, depending on from where the noise is emitted.<sup>50</sup>

In China, the first act concerned with noise was the National Environment Protection Act of 1979.<sup>51</sup> The Regulations on Prevention and Control of Environmental Noise were approved in 1989 and updated in 1996. Local governments were made responsible for the implementation of noise requirements. Maximum

noise emission levels for motor vehicles were approved in 1979. Other criteria and standards were defined together with noise zoning where noise limits were established for day and for night in 1993. Residential area A-weighted sound pressure level limits are 55 dB during daytime and 45 dB during the night. For quiet residential areas, the limits are 5 dB lower, and for mixed areas they are 5 dB higher. The criteria are implemented by national and local authorities.

In Hong Kong, the Noise Control Ordinance 1988 (with later amendments) is the basic regulation.<sup>52</sup> The Road Traffic Ordinance and the Civil Aviation (Aircraft Noise) Ordinance requires compliance with noise emission standards. New more stringent regulations have been under study.

In Brazil, the state of Rio de Janeiro approved in 2004 an ordinance on urban noise.<sup>53</sup> Of a qualitative nature, it demands the municipalities to implement noise assessment and noise abatement actions and sets the basis for a future environmental noise policy.

## 11 FINAL DISCUSSION

Community noise ordinances of different types have been promulgated in many cities and counties all over the world. They need to be coordinated and consistent with regulations at all other levels, namely regional and national, if an effective improvement in the quality of the sound environment is to be achieved. In a global policy, community noise ordinances act as self-regulation measures that are able to address noise at a local level in a way that citizens can be drawn closer to the actions and get more involved with their results.

Since much of the noise in a community is a local issue, local policies and actions can produce measurable results if a straightforward, practical, and economical approach is set up. Simply enacting a new noise ordinance, either of qualitative or quantitative nature, is not enough, though. The noise ordinance must address the noise problems in a clear and realistic way and must be reasonable. All technical issues such as metrics, standards, assessment, and inspection procedures must be well defined. Responsible bodies must be established together with their obligations and powers, ensuring a capable supervision and enforcement. Efficient enforcement measures and the allocation of adequate financial and technical resources are key issues for successful results. The provision of guides to help on the technical issues and of rules for dissemination of information has generally proved to be an advisable feature.

The maximum permitted noise levels defined in noise zoning for daytime and for nighttime in recent years are generally very close to those recommended by the WHO, in most cases referred to the A-weighted continuous equivalent sound pressure level.

Community noise ordinances and national noise policies are currently being revised in many parts of the world, generally incorporating more stringent noise limits and criteria. Although a reduction in noise emissions from road vehicles and aircraft has been achieved due to successful policies in the United States, Europe and Japan, for example, a corresponding reduction in receiver noise values has not been so

apparent given the rise in traffic.<sup>54</sup> The trend in the increase of population density in urban areas must be met with the growing citizen's requirements for a better quality of life. Community noise criteria and goals must be used as tools in land-use and transport planning.<sup>55</sup> Experience has shown that noise ordinances play a primary role in the community noise management and control policy.

## REFERENCES

1. European Commission, EU Future Noise Policy—European Commission Green Paper, Report COM(96)540, Brussels, November 1996.
2. W. W. Lang, Is Noise Policy a Global Issue, or Is It a Local Issue?, *Noise Control Eng. J.*, Vol. 49, No. 4, 2001 July–Aug, pp. 155–158.
3. B. Berglund and T. Lindvall, Eds., *Community Noise*, Archives of the Center for Sensory Research 2(1), Stockholm and Karolinska Institute (Document prepared for the World Health Organization), 1995.
4. B. Berglund, T. Lindvall, and D. H. Schwela, Eds., *Guidelines for Community Noise*, World Health Organization, Geneva, 1999.
5. D. Gottlob, Regulations for Community Noise, *Noise/News Int.*, Vol. 3, No. 4, 1995 December, pp. 223–236.
6. Commission of the European Communities, Directorate-General XI, Working Group on Noise Indicators, Position Paper on EU Noise Indicators, 1999.
7. Directive 2002/49/EC of the European Parliament and of the Council of 25 June 2002 Relating to the Assessment and Management of Environmental Noise, OJ L 189, 18.7.2002.
8. International Organization for Standardization, Acoustics—Description and Measurement of Environmental Noise, ISO, 1996.
9. U.S. Environmental Protection Agency, *The Environmental Protection Agency's Model Community Noise Control Ordinance*, EPA, Washington, DC,
10. U.S. Congress, National Environmental Policy Act of 1969 (Public Law 91–190).
11. U.S. Congress, Noise Control Act of 1972 (Public Law 92–574).
12. L. S. Finegold, M. S. Finegold, and G. C. Maling Jr., An Overview of U.S. Noise Policy, *Noise Control Eng. J.*, Vol. 51, No. 3, 2003 May–June, pp. 131–142.
13. L. L. Beranek and W. W. Lang, America Needs a New National Policy, *Noise Control Eng. J.*, Vol. 51, No. 3, 2003 May–June, pp. 123–130.
14. B. M. Brooks, The Need for a Unified Community Noise Policy, *Noise Control Eng. J.*, Vol. 51, No. 3, 2003 May–June, pp. 160–161.
15. U.S. Congress, Aircraft Noise Abatement Act of 1968 (Public Law 90–411).
16. Federal Aviation Administration (FAA), Federal Aviation Administration Noise Standards: Aircraft Type and Airworthiness Certification (14 CFR Part 36), 1969.
17. U.S. Congress, Airport and Airway Development Act Amendments of 1976 (Public Law 94–353).
18. U.S. Congress, Aviation Safety and Noise Abatement Act of 1979 (Public Law 96–193).
19. U.S. Department of Transportation, Federal Aviation Administration, *Noise Control and Compatibility Planning for Airports*, Advisory Circular AC 150/5020-1, 1983.

20. U.S. Department of Transportation, Federal Highway Administration, Title 23 of the United States Code of Federal Regulations Part 772 (23 CFR 772).
21. G. C. Maling and L. S. Finegold, A Review of United States Noise Policy, *Proc. Inter-Noise 2004*, 2004 Aug.
22. U.S. Environmental Protection Agency, *EPA's Framework for Community-Based Environmental Protection*, EPA 273-K-99-001, February 1999.
23. A. S. Harris, G. G. Fleming, W. W. Lang, P. D. Schomer, and E. W. Wood, Reducing the Impact of Environmental Noise on Quality of Life Requires an Effective National Noise Policy, *Noise Control Eng. J.*, Vol. 51, No. 3, 2003 May–June, pp. 151–154.
24. L. S. Finegold and M. S. Finegold, Updating the U.S. Environmental Noise Management Strategy, *Noise Control Eng. J.*, Vol. 51, No. 3, 2003 May–June, pp. 155–159.
25. Commission of the European Communities, Report from the Commission to the European Parliament and the Council Concerning Existing Community Measures Relating to Sources of Environmental Noise, Pursuant to Article 10.1 of Directive 2002/49/EC Relating to the Assessment and Management of Environmental Noise, Report COM(2004) 160 Final, Brussels, March 2004.
26. Council Directive 86/594/EEC of 1 December 1986 on Airborne Noise Emitted by Household Appliances, OJ L 344, 06/12/1986.
27. Directive 2000/14/EC of the European Parliament and of the Council of 8 May 2000 on the Approximation of the Laws of the Member States Relating to the Noise Emission in the Environment by Equipment for Use Outdoors, OJ L 162, 3.7.2000.
28. Directive 2003/44/EC of the European Parliament and of the Council of 16 June 2003 Amending Directive 94/25/EC on the Approximation of the Laws, Regulations and Administrative Provisions of the Member States Relating to Recreational Craft, OJ L 214, 26.8.2003.
29. Council Directive 70/157/EEC of 6 February 1970 on the Approximation of the Laws of the Member States Relating to the Permissible Sound Level and the Exhaust System of Motor Vehicles, OJ L 42, 23.2.1970 as subsequently amended, in particular by Council Directive 92/97/EEC of 10 November 1992, OJ L 371, 19.12.1992.
30. Directive 97/24/EC of the European Parliament and of the Council of 17 June 1997 on Certain Components and Characteristics of Two or Three-Wheel Motor Vehicles, OJ L 226, 18.8.1997.
31. Directive 2001/43/EC of the European Parliament and of the Council of 27 June 2001 Amending Council Directive 92/23/EEC Relating to Tyres for Motor Vehicles and Their Trailers and to Their Fitting, OJ L 211, 04/08/2001.
32. Council Directive 96/48/EC of 23 July 1996 on the Interoperability of the Trans-European High-Speed Rail System, OJ L 235, 17.9.1996.
33. Directive 2001/16/EC of the European Parliament and of the Council of 19 March 2001 on the Interoperability of the Trans-European Conventional Rail System OJ L 110, 20.4.2001.
34. Council Directive 80/51/EEC of 20 December 1979 on the Limitation of Noise Emissions from Subsonic Aircraft OJ L 018, 24/01/1980.
35. Council Directive 92/14/EEC of 2 March 1992 on the Limitation of the Operation of Aeroplanes Covered by Part II, Chapter 2, Volume 1 of Annex 16 to the Convention on International Civil Aviation, second edition (1988), OJ L 76, 23.3.1992, as amended by Council Directive 98/20/EC of 30 March 1998, O.J.L 107, 7.4.1998.
36. Directive 2002/30/EC of the European Parliament and of the Council of 26 March 2002 on the Establishment of Rules and Procedures with Regard to the Introduction of Noise-Related Operating Restrictions at Community Airports, OJ L 85, 28.3.2002.
37. J. Lambert and M. Vallet, Study Related to the Preparation of a Communication on a Future EC Noise Policy, Final Report, LEN Report No. 9420, INRETS, 1994.
38. *Noise Abatement in European Towns and Cities, Strategies, Concepts and Approaches for Local Noise Policy*, Ed. European Academy of the Urban Environment, Berlin, 1999.
39. Japan Ministry of the Environment, Noise Regulation Law, Law No. 98 of 1968, Latest Amendment by Law No. 91 of 2000.
40. Japan Ministry of the Environment, Environmental Quality Standards for Noise, Environmental Agency Notification No. 64, 1998.
41. K. Yamazaki and H. Tachibana, New Japanese Environmental Quality Standards for Noise, *Proc. Inter-Noise 99*, Vol. 3, pp. 1970–1974.
42. Japan Ministry of the Environment, Quality of the Environment in Japan 1995 (White Paper), 1995.
43. Japan Ministry of the Environment, Environmental Quality Standards for Aircraft Noise, Environmental Agency Notification No. 91, 1993.
44. Japan Ministry of the Environment, Environmental Quality Standards for Shinkansen Superexpress Railway Noise, Environmental Agency Notification No. 91, 1993.
45. *Environmental Protection (Industrial Noise) Policy*, Gov. Notice, Gaz. 27 October 1994, 1366.
46. New South Wales, Protection of the Environment Operations Act 1997 No. 156.
47. New South Wales, Environmental Protection Authority, *Environmental Criteria for Road Traffic Noise*, 1999.
48. Queensland, Environmental Protection Act 1994, Environmental Protection Policy (Noise) 1997, with amendments up to 2003 SL No. 73.
49. Regional Municipality of Ottawa-Carleton, Noise Control Guidelines for New Construction, Reconstruction and Widening of Regional Roads and Transitways, 1995.
50. City of Vancouver, British Columbia, Noise Control By-Law No. 6555, 1989 with latest amendment of 2004.
51. M. Cheng, Noise Legislation and Criteria in China, *Proc. Inter-Noise 94*, Vol. 3, 1994, pp. 2149–2152.
52. Hong Kong Environmental Protection Department, Environment Hong Kong 2000 (Resource Materials), pp. 71–84.
53. Parliament of the State of Rio de Janeiro, Guidelines for the Quality of the Acoustical Environment of the Population of the State of Rio de Janeiro, Law No. 4324, of May 12, 2004.
54. U. Sandberg, Noise Emissions of Road Vehicles—Effect of Regulations, Final Report 01-1 by the I-INCE Working Party on the Effect of Regulations on Road Vehicle Noise, *Noise/News Intl.*, Vol. 9. No. 3, 2001 September, pp. 147–206.
55. T. Kihlman and W. Kropp, City Traffic Noise—A Local or Global Problem?, *Noise Control Eng. J.*, Vol. 49, No. 4, 2001 July–Aug, pp. 165–169.

## REVIEWERS LIST

---

Kazem Abhary  
Maurice L. Adams, Jr.  
Syed R. Ahmed  
Schaia Akkerman  
Peter W. Alberti  
James J. Allen  
Basem Alzahabi  
David Anderton  
Jorge P. Arenas  
Pedro M. Arezes  
Francesco Asdrubali  
Marc Asselineau  
Torben Astrup  
Andy Farquhar Atkins  
Allan C. Aubert  
Frank Auer  
Paul Avan  
Francesca Avenati-Bassi  
Peter Baade  
Lorraine A. Babeu  
Sid P. Bacon  
R. Bannister  
Juan Miguel Barrigón Morillas  
David C Barton  
Hans D. Baumann  
Elliott H. Berger  
Warren E. Blazier  
Jonathan D. Blotter  
Yuri I. Bobrovnitskii  
Hans Bodén  
Hans-Georg Bosshardt  
David L. Bowen  
Luigi Bregant  
Norm Broner  
Mihai J. Bugaru  
Marion Burgess  
L. M. B. C. Campos  
Rosario Caracausi  
Eleonora Carletti  
Ted N. Carnes  
António P. O. Carvalho  
William J. Cavanaugh  
Sébastien Chaigne  
William W. Clark  
Kerry M. Cone  
Trevor J. Cox  
Mirko Čudina  
Joseph M. Cuschieri

Vicente Cutanda Henríquez  
Mohammad Daraei  
John Davy  
Alex de Bruijn  
Corné de Hoon  
Sergio De Rosa  
Gert De Sitter  
Filip Deblauwe  
Michael Dittrich  
Werner Dobrzynski  
Paul R Donavan  
Jeffrey J. Dosch  
Nelik Dreiman  
Maria Lúcia Machado Duarte  
David Eager  
Raghu Echempati  
Alexandre Carlos Eduardo  
Wolfgang Ellermeier  
Tamer Elnady  
Rodney D. Entwistle  
Ed Envia  
John Erdreich  
Haluk Erol  
David J. Evans  
Jack B. Evans  
Sanford Fidell  
Chris Field  
Jarosław Figwer  
Lawrence S. Finegold  
Raymond Fischer  
Gregory A. Flamme  
Neville H. Fletcher  
George T. Flowers  
Timothy J. Foulkes  
Fergus R. Fricke  
Glenn Frommer  
Howard Gaberson  
Svend Gade  
William J. Galloway  
W. S. Gan  
G. Garinther  
Joel Garrelick  
Julius L. Goldstein  
Michael J. Griffin  
Richard M. Guernsey  
Mark Hamilton  
Colin Hansen  
Jay C. Hardin

Maria A. Heckl  
 Martin Helfer  
 Detlef Helling  
 Paula P. Henry  
 David W. Herrin  
 Chad N. Himmel  
 Elmer L. Hixson  
 Ole Holst-Jensen  
 Robert M. Hoover  
 Carl Hopkins  
 Zdzislaw Hryniewicz  
 Dennis L. Huff  
 William O. Hughes  
 Mohammed F. M. Hussein  
 Mette Husted  
 Ronald G. Ingham  
 Dan Inman  
 Finn Jacobsen  
 Andreas Johansson  
 Sven Johansson  
 Nigel Johnston  
 Karl T. Kalveram  
 Max Kandula  
 Jian Kang  
 Zerhan Karabiber Yuksel  
 Chucris A. Kardous  
 Leif Kari  
 Stephen E. Keith  
 Frederick M. Kessler  
 Kwang-Joon Kim  
 D. C. Kim  
 Geon-Seok Kim  
 Howard F. Kingsbury  
 Leonard L. Koss  
 Charles M. Krousgrill  
 Victor Krylov  
 Frank R. Kuhn  
 Ard Kuijpers  
 Selma Kurra  
 Ulrich J. Kurze  
 Heinrich Kuttruff  
 Thomas L. Lagö  
 Joseph Lai  
 Nick Lalor  
 Conny Larsson  
 Gerald C. Lauchle  
 Jang Moo Lee  
 Sang-Kwon Lee  
 R. C. N. Leung  
 Geoff Leventhall  
 John Leverton  
 Serge Lewy  
 Zhuang Li  
 Torben R. Licht  
 Teik C. Lim  
 Zhong-Sheng (Simon) Liu  
 Mark E. Lutman  
 Tasos Lyrantzis  
 George C. Maling, Jr.  
 Douglas Manvell  
 Steffen Marburg  
 Ykä Marjanen

Glen K. Martin  
 Christian Maschke  
 Chris K. Mechefske  
 Rui Bettencourt Melo  
 Nicholas P. Miller  
 Henrik Møller  
 Peter Moretti  
 Philip J. Morris  
 M. L. Munjal  
 Preston V. Murphy  
 William J. Murphy  
 Ricardo E. Musafir  
 Konstantin Naugolnykh  
 Donald J. Nefske  
 James Tuman Nelson  
 David Oldham  
 Chandramouli Padmanabhan  
 Thomas L. Paez  
 Jie Pan  
 R. Parchen  
 Goran Pavic  
 Marek Pawelczyk  
 Francesca Pedrielli  
 Bart Peeters  
 B. A. T. Petersson  
 Maurice Petyt  
 Allan G. Piersol  
 Roger J. Pinnington  
 Mihai Valentin Predoi  
 Robert A. Putnam  
 Miloud Rahmoune  
 R. B. Randall  
 Jose Noé Razo Razo  
 Eugene I. Rivin  
 Jacques Roland  
 Oleg Rudenko  
 M. Saeki  
 Stephen Samuels  
 Ulf Sandberg  
 Dietrich Schwela  
 Andrew F. Seybert  
 Guillermo Silva-Pineda  
 Emil Simiu  
 Myles A. Simpson  
 Stan Skaistis  
 Joseph C. Slater  
 David O. Smallwood  
 Mark R. Stephenson  
 Paul J. R. Strange  
 Christian Svendsen  
 James Talbot  
 Kari M. J. Tammi  
 Jukka Tantari  
 T. ten Wolde  
 David Thompson  
 Rupert Thornely-Taylor  
 Henrik W. Thrane  
 Laszlo Timar Peregrin  
 Serguei Timouchev  
 Gregory C. Tocci  
 Jiri Tuma  
 Eric E. Ungar

**REVIEWERS LIST****1535**

Takashi Usuda  
Steve Vanlanduit  
Ian Veldman  
Jan W. Verheij  
Albert Visscher  
Hans-Jürgen von Martens  
Hiroshi Wada  
Peter Wagstaff  
Lily M. Wang  
Semyung Wang

Alf Warnock  
Simon Watkins  
Holger Waubke  
Ewart A. Wetherill  
John Wilby  
T. W. Wu  
John J. Yu  
George Zusman  
Subhash C. Sinha



# GLOSSARY

---

## REFERENCES

1. ISO Standards  
ISO 11201: Acoustics—Noise Emitted by Machinery and Equipment—Measurement of Emission Sound Pressure Levels at a Work Station and at Other Specified Positions Engineering Method in an Essentially Free Field over a Reflecting Plane  
ISO 11688: Acoustics—Recommended Practice for the Design of Low-Noise Machinery and Equipment.  
ISO 140: Acoustics—Measurement of Sound Insulation in Buildings and of Building Elements  
ISO 1996: Acoustics—Description, Measurement and Assessment of Environmental Noise  
ISO 1999: Acoustics—Determination of Occupational Noise Exposure and Estimation of Noise-Induced Hearing Impairment  
ISO 226: Acoustics—Preferred Frequencies  
ISO 354: Acoustics—Measurement of Sound Absorption in a Reverberation Room  
ISO 3741: Acoustics—Determination of Sound Power Levels of Noise Sources Using Sound Pressure—Precision Methods for Reverberation Rooms  
ISO 3744: Acoustics—Determination of Sound Power Levels of Noise Sources Using Sound Pressure—Engineering Method in an Essentially Free Field over a Reflecting Plane  
ISO 3745: Acoustics—Determination of Sound Power Levels of Noise Sources Using Sound Pressure—Precision Methods for Anechoic and Hemianechoic Rooms  
ISO 3751:1988  
ISO 389: Acoustics—Reference Zero for the Calibration of Audiometric Equipment  
ISO 4869: Acoustics—Hearing Protectors  
ISO 6081-1986 (replaced by ISO 11201-1995)  
ISO 7235: Acoustics—Laboratory Measurement Procedures for Ducted Silencers and Air-Terminal Units—Insertion Loss, Flow Noise and Total Pressure Loss  
ISO 7849: Acoustics—Estimation of Airborne Noise Emitted by Machinery Using Vibration Measurement  
ISO 80000-8: Quantities and Units—Part 8: Acoustics  
ISO 9053: Acoustics—Materials for Acoustical Applications—Determination of Airflow Resistance  
ISO 9614: Acoustics—Determination of Sound Power Levels of Noise Sources Using Sound Intensity
2. IEC Standards  
IEC 61043: Electroacoustics—Instruments for the Measurement of Sound Intensity—Measurements with Pairs of Pressure Sensing Microphones  
IEC 61260: Electroacoustics—Octave-Band and Fractional-Octave-Band Filters  
IEC 61672-1: Electroacoustics—Sound Level Meters—Part 1: Specifications
3. ANSI Standards  
ANSI S1.1-1994: Acoustical Terminology  
ANSI S1.11: Specification for Octave-Band and Fractional-Octave-Band Analog and Digital Filters  
ANSI S1.42: Design Response of Weighting Networks for Acoustical Measurements  
ANSI S12.12: Engineering Method for the Determination of Sound Power Levels of Noise Sources using Sound Intensity
4. ASTM Standards  
ASTM E336-97 Standard Test Method for Measurement of Airborne Sound Insulation in Buildings  
ASTM C384-04 Standard Test Method for Impedance and Absorption of Acoustical Materials by Impedance Tube Method  
ASTM C423-02 Standard Test Method for Sound Absorption and Sound Absorption Coefficients by the Reverberation Room Method  
ASTM C634-02: Standard Terminology Relating to Environmental Acoustics  
ASTM E413-87: Classification for Rating Sound Insulation  
ASTM E492-90: Standard Test Method for Laboratory Measurement of Impact Sound Transmission through Floor-Ceiling Assemblies Using the Tapping Machine  
ASTM E596-96 Standard Test Method for Laboratory Measurement of Noise Reduction of Sound-Isolating Enclosures  
ASTM E989-89: Standard Classification for Determination of Impact Insulation Class (IIC)
5. Christopher L. Morfey, *Dictionary of Acoustics*, Academic, London, 2001.
6. U.S Department of Labor, Occupational Safety and Health Administration, 1910.95 Appendix I—Definitions ([http://www.osha.gov/pls/oshaweb/owadisp.show\\_document&p\\_table=STANDARDSp\\_id=9744?](http://www.osha.gov/pls/oshaweb/owadisp.show_document&p_table=STANDARDSp_id=9744?)).

7. U.S. Department of Health and Human Services, 98–126, Occupational Noise Exposure (<http://www.cdc.gov/niosh/pdfs/98-126.pdf>).
8. Daniel N. Lapedes, Editor-in-Chief, *McGraw-Hill Dictionary of Physics and Mathematics*, McGraw-Hill, New York, 1978.
9. David Crystal, *A Dictionary of Linguistics and Phonetics*, 3rd ed., Blackwell, Oxford, UK, 1991.
10. Ingo R. Titze, *Principles of Voice Production*, 2nd printing, National Center for Voice and Speech, Denver, CO, 2000.
11. Douglas O'Shaughnessy, *Speech Communications: Human and Machine*, 2nd ed., IEEE Press, New York, 2000.
12. Vibration Institute, *Vibration Terminology* ([http://www.vibinst.org/vglos\\_a-e.htm](http://www.vibinst.org/vglos_a-e.htm)).
13. Brüel & Kjær's definitions. Brüel & Kjær, Naerum, Denmark.

## GLOSSARY

**A-weighted sound exposure** *See* Sound exposure.

**Absorption** Conversion of sound energy into another form of energy, usually heat, when passing through an acoustical medium or at a boundary.

**Absorption area** *See* Equivalent sound absorption area.

**Absorption factor, absorption coefficient, absorbance** Ratio of the dissipated and transmitted sound power to the incident sound power. In a specified frequency band, the absorption factor is a measure of the absorptive property of a material or surface. Also known as (*sound*) *absorption coefficient*. Unit: none. Symbol:  $\alpha$ . *See* Dissipation factor, Transmission factor, Reflection factor. *Note:* (1) The absorption factor equals the dissipation factor plus the transmission factor,  $\alpha = \delta + \tau$ , where  $\delta$  is the dissipation factor, and  $\tau$  is the transmission factor. (2) The summation of the dissipation, transmission, and reflection factors is unity,  $\delta + \tau + r = 1$ , where  $r$  is the reflection factor.

**Accelerance** A form of the frequency response function, which is the complex ratio of the acceleration to the excitation force. Units: (metre per square second) per newton [ $(\text{m/s}^2)/\text{N} = \text{kg}^{-1}$ ]. *See* Compliance, Mobility, Dynamic Mass. *Note:* The alternative term *inertance* is not recommended because it has a conflicting interpretation. Sometimes inertance is referred to as the reciprocal of acceleration.

**Acceleration** A vector quantity equal to the rate of change of velocity. Units: metre per square second ( $\text{m/s}^2$ ). *See* Displacement, Velocity, Jerk.

**Accelerometer** A transducer whose electrical output is proportional to acceleration in a specified frequency range.

**Acoustical holography** An inspection method using the phase interference between sound waves from an object and a reference signal to obtain an image of reflectors in the object under test.

**Acoustical trauma** Ear injury caused by a sudden and intense sound pressure that causes a degree of permanent or temporary hearing loss.

**Acoustic impedance** At a specified surface, the complex ratio of the average sound pressure over that surface to the sound volume flow rate through that surface. Units: pascal per (cubic metre per unit time) [ $\text{Pa}/(\text{m}^3/\text{s})$ ]. Symbol:  $Z_a$ . *See* Characteristic impedance, Mechanical impedance, Specific acoustic impedance. **Acoustic reactance** Imaginary part of acoustic impedance. Symbol:  $R_a$ . **Acoustic resistance** Real part of acoustic impedance. Symbol:  $X_a$ .

**Acoustic reactance** *See* Acoustic impedance.

**Acoustic resistance** *See* Acoustic impedance.

**Acoustics** Science of the production, control, transmission, reception, and effects of sound and of the phenomena of hearing.

**Action level** The cumulative work shift noise dose at which hearing conservation program is mandated by the Occupational Safety and Health Administration (OSHA). An 8-hour time-weighted average of 85 dB measured with A-weighting and slow response, or equivalently, a dose of 50 percent. *See* Hearing conservation Program, Noise dose.

**Active control** Of sound and vibration, the use of secondary sources of excitation to cancel, or reduce, the response of a system to given prime sources; also to suppress self-excitation oscillations of a system that is unstable.

**Active sound control** *See* Active control.

**Active sound field** A sound field in which the particle velocity is in phase with the sound pressure. All acoustic energy is transmitted; none is stored. A plane wave propagating in free field is an example of a purely active sound field.

**Active vibration control** *See* Active control.

**Admittance** The reciprocal of an impedance. *See* Acoustic impedance, Characteristic impedance, Mechanical impedance, Mobility.

**Airborne sound** Sound that propagates through air. *See* Liquid-borne sound, Structure-borne sound.

**Airflow resistance** A quantity defined by  $R = \Delta p / q_v$ , where  $\Delta p$  is the air pressure difference, in pascals, across the test specimen;  $q_v$  is the volumetric airflow rate, in cubic metres per second, passing through the test specimen. Units: pascal second per cubic metre ( $\text{Pa}\cdot\text{s}/\text{m}^3$ ). Symbol:  $R$ . *See* Specific airflow resistance.

**Airflow resistivity** If the material is considered as being homogenous, a quantity defined by  $r = R_s / d$ , where  $R_s$  is the specific airflow resistance, in pascal seconds per metre, of the test specimen;

$d$  is the thickness, in metres, of the test specimen in the direction of flow. Units: pascal second per square metre (Pa·s/m<sup>2</sup>). Symbol:  $r$ . *See* Specific airflow resistance.

**Aliasing error** An error in digital signal processing in which high-frequency signal energy is folded into lower frequency components due to inadequate sampling frequency that is less than twice the maximum frequency in the signal. *See* Sampling theorem, Antialiasing filter.

**Alignment** The fact of being in line or bringing into line. For rotating machinery, alignment refers to the axial continuity of machine components, such as shaft and bearings, during operation.

**Ambient noise** (1) Sound present in a given situation at a given time, in absence of that from sources of immediate concern, usually being composed of sound from many sources near and far. *See* Background noise. (2) In underwater acoustics, the naturally occurring acoustical environment in the ocean, caused by wave breaking, marine life, and other sources. (3) In sonar detection, the noise from all unwanted sources of sound, apart from those directly associated with the sonar equipment and the platform on which it is mounted.

**Amplitude distribution** A method of representing the amplitude (or level) variation of noise by indicating the percentage of time that the noise level occurs in a series of amplitude intervals.

**Analog-to-digital conversion (ADC)** The process of sampling an analog signal to convert it to a series of quantized numbers, a series that is a digital representation of the same signal. The sampling frequency must be at least twice as high as the highest frequency present in the signal to prevent aliasing errors. *See* Aliasing error, Nyquist frequency, Sampling theorem.

**Anechoic room** A test room whose surfaces absorb essentially all of the incident sound energy over the frequency range of interest, thereby approximating free-field conditions over a measurement surface. *See* Semianechoic room, Free field.

**Angular frequency** Frequency of a periodic quantity in units of radians per unit time (rad/s). Symbol:  $\omega$ . *See* Frequency.

**Angular repetency** *See* Wavenumber.

**Annoyance** A person's internal response to a noise. Is quantifiable (1) psychologically by rating or (2) technically by a physical noise descriptor, for example, the equivalent continuous A-weighted sound pressure level  $L_{Aeq,T}$ . For a given person, usually the correlation coefficient between descriptor and related ratings does not exceed 0.5 due to the influence of other factors in determining annoyance. *See* Noise, Rating, Equivalent continuous A-weighted sound pressure.

**Antialiasing filter** An analog low-pass filter applied to continuous analog signals prior to analog-to-digital conversion, to eliminate frequency components higher than one-half the sampling frequency (Nyquist frequency). *See* Aliasing error, Sampling theorem, Nyquist frequency.

**Antiresonance** A condition in forced vibration whereby a specific point has zero amplitude at a specific frequency of vibration. For a certain frequency response function (FRF), an antiresonance may correspond to a local minimum in the magnitude. For a point FRF, there must be an antiresonance between two resonances. However, different FRFs have different antiresonances. Some FRFs have no antiresonance. *See* Resonance.

**Apparent sound reduction index** *See* Sound reduction index.

**Argand diagram** A plot of a complex function in which the  $x$  and  $y$  coordinates denote the real and imaginary parts of the function. *See* Frequency response function, Nyquist diagram.

**Articulation index (AI)** A number that specifies the output intelligibility of a speech transmission channel, based on the signal-to-noise ratio at the listener. The articulation index takes values between zero (completely unintelligible) and unity (completely intelligible). *See* Intelligibility, Signal-to-noise ratio, Privacy index.

**Articulator** Any of the moveable parts in and around the vocal tract that can affect its shape, and therefore, the speech sounds generated. The tongue is the most important articulator; lips, teeth, and velum are others. *See* Vocal tract, Articulatory.

**Articulatory** An articulatory model or synthesizer uses parameters related to properties of the articulators: for example, position of tongue tip or tongue dorsum, degree of lip rounding, or length of the vocal tract. *See* Articulator.

**Attenuation coefficient** Coefficient  $\alpha$  in the spatial attenuation factor  $e^{-\alpha x}$ , which describes the amplitude reduction of a single-frequency progressive wave with distance  $x$ , in the propagation direction. Unit: reciprocal metre (m<sup>-1</sup>). Symbol:  $\alpha$ . *Note:* the quantity  $1/\alpha$  is called the *attenuation length*, and  $m = 2\alpha$  is called the *power attenuation coefficient*.

**Audibility threshold** The lowest sound pressure level, at a specified frequency, at which persons with normal hearing can hear. Sometimes also known as *hearing threshold*. *See* Hearing threshold.

**Audio frequency** Frequency of a sound in the range normally audible to humans. Unit: hertz (Hz). Audio frequencies range roughly from 20 Hz to 20 kHz.

**Autocorrelation Function** A statistical measure of the extent to which one part of a signal is related to

another part, offset by a given time, of the same signal. The Fourier transform of the autocorrelation function gives the autospectrum. *See* Cross-correlation function, Power spectrum.

**Autospectrum** Also known as *autospectral function, power spectrum*. *See* Power spectrum, Cross spectrum.

**A-weighted sound power level** *See* Sound power level.

**A-weighted sound pressure level** *See* Sound pressure level.

**Background noise** (1) Total of all interference from unwanted sound, independent of the sound source being studied. *See* Ambient noise. (2) Undesired signals that are always present in electrical or other systems, independent of whether or not the desired signal is present. Background noise may include contributions from airborne sound, structure-borne vibration, and electrical noise in instrumentation. *Note* According to ANSI S1.1 - 1994, ambient noise detected, measured, and recorded with the signal is part of the background noise.

**Balancing** The procedure of adjusting the mass distribution of a rotor to reduce the transverse vibration of the rotor.

**Band pressure level** *See* Sound pressure level.

**Bandwidth** (1) The difference between the upper and lower frequency limits of a frequency band. (2) Of a signal, the range of frequencies between the upper and lower frequency limits within which most of the signal energy is contained. (3) Of a linear system or transducer, the range of frequencies over which the system is designed to operate. (4) Of a bandpass filter, the difference in frequency between the upper and lower cutoff frequencies. *See* Critical bandwidth, Effective noise bandwidth, Half-power bandwidth.

**Bearing** A device that supports, guides, and reduces the friction of motion between fixed and moving machine parts. There are primarily two types, rolling-element bearings and fluid-film bearings. A rolling-element bearing consists of an inner race, an outer race, balls or rollers, and a cage to maintain the proper separation of the rolling elements. A fluid-film bearing supports the shaft on a thin film of oil or on a thin film of pressurized air. **Bearing misalignment** Misalignment that results when the bearings supporting a shaft are not aligned with each other. The bearings may not be mounted in parallel planes, cocked relative to the shaft, or distorted due to foundation settling or thermal growth.

**Beat** A phenomenon of slow amplitude modulation produced by interference between two simple harmonic signals, when the frequency difference is a small fraction of either frequency. **Beat frequency** The frequency of the amplitude modulation, equal to

the difference in frequency between the two original signals.

**Bel (B)** Unit of level in terms of logarithm to base 10, abbreviated as B. *See* Level, Decibel.

**Bode diagram, Bode plot** (1) A form of presentation of a complex function, such as a frequency response function, in two plots. One plot shows the magnitude of the complex function against frequency, plotted in decibels. The other plot shows the phase of the complex function against frequency. Both plots use the same logarithmic frequency scale on the horizontal axis. *See* Frequency response function, Argand diagram, Nyquist diagram. (2) Specifically for rotating machines, a pair of two plots displaying the magnitude and phase of a particular order component of a vibration vector. Both plots are in Cartesian format and use the same horizontal axis, which represents rotational speed or perturbation frequency. *See* Order analysis.

**Boundary element method** A numerical approach for solving a boundary integral equation in which the domain of integral is divided into subdomains referred to as elements. An advantage of the boundary element method is the reduction of dimensionality. The wave equation in a three-dimensional region can be rewritten as boundary integral equation on a two-dimensional surface. Unlike the finite element method, the boundary element method is based on the Green's function, which satisfies the governing differential equation exactly over the domain and solves the unknown nodal values that approximately satisfy the boundary conditions. *See* Finite element method.

**Bulk modulus** Of a fluid or solid, the slope of the curve of pressure plotted against the logarithm of the density, with either adiabatic or isothermal conditions imposed.

**Center frequency** The arithmetic center of a constant bandwidth filter or the geometric center (midpoint on a logarithmic scale) of a constant percentage filter. *See* Constant bandwidth filter, Constant percentage filter.

**Cepstrum** For a real signal, a nonlinear signal processing technique that involves the inverse Fourier transform of the logarithm of the power spectrum or the Fourier transform of the signal. Since both the Fourier transform and the inverse Fourier transform are complex processes, the cepstrum is complex if the phase information is preserved. The complex cepstrum has the corresponding inverse complex cepstrum. However, if the input of the inverse Fourier transform is real, for example, the power spectrum, or the magnitude of the Fourier transform of the signal, the cepstrum is real. Exact definitions vary across the literature.

**Characteristic equation** (1) Any equation that has a solution, subject to specified boundary conditions, only when a parameter occurring in it has certain

values. (2) Specifically, the equation  $A\mathbf{u} = \lambda\mathbf{u}$ , which can have a solution only when the parameter  $\lambda$  has certain values, where  $A$  can be a square matrix that multiplies the vector  $\mathbf{u}$ , or a linear differential or integral operator that operates on the function  $\mathbf{u}$ , or in general, any linear operator operating on the vector  $\mathbf{u}$  in a finite or infinite dimensional vector space. Also known as *eigenvalue equation*. (3) An equation that sets the characteristic polynomial of a given linear transformation on a finite dimensional vector space, or of its matrix representation, equal to zero. *See* Eigenvalue, Eigenvector.

**Characteristic impedance** Of a medium, at a point and for a plane progressive wave, the magnitude of the ratio of the sound pressure to the component of the sound particle velocity, in the direction of the wave propagation. Characteristic impedance is defined by  $Z_c = \rho c$ , where  $\rho$  is the density, in kilograms per cubic metre;  $c$  is the (phase) speed of sound, in metres per second. Units: pascal per metre per second [Pa/(m/s)]. Symbol:  $Z_c$ . *See* Acoustic impedance, Specific acoustic impedance, Mechanical impedance.

**Charge amplifier** An amplifier with a low input impedance whose output voltage is proportional to the output charge from a piezoelectric transducer.

**Close-proximity (CPX) method** A measurement method used for measuring noise properties of tires and/or road surfaces (pavements), utilizing either a trailer with a test tire or a regular vehicle such as an automobile, SUV, or van on which one of its tires constitutes the test tire. Generally, at least two microphones are placed close to the test tire. In case of a trailer, the test tire is often covered by an enclosure that protects the tire and the microphones from noise from other vehicles and from air turbulence noise. Attempts to standardize this procedure and to specify a couple of reference tires for the CPX method are made within the ISO as part of the ISO 11819 series of standards. *See* Tire/road noise, Statistical pass-by method.

**Coherence function** Of two time signals, a measure of the degree to which the two signals are linearly related at any given frequency. The coherence function takes values between zero and unity.

**Coincidence effect** For a panel or partition, a great reduction of the sound reduction index as a function of frequency when the trace wave speed (speed at which the incident wave propagates along the panel) and the speed of the flexural wave in the panel are the same. *See* Sound reduction index.

**Compliance** (1) The reciprocal of stiffness. Sometimes also known as *flexibility*. (2) A form of the frequency response function: the complex ratio of the displacement to the excitation force. Also known as *dynamic compliance*, or *receptance*. *See* Accelerance, Mobility.

**Condensation** In acoustics, the increase in the density of a material under stress, divided by the original density. *See* Density.

**Conductance** Real part of an admittance. *See* Admittance, Susceptance.

**Conductive hearing loss** *See* Hearing loss.

**Constant bandwidth filter** A filter that has a fixed-frequency bandwidth, regardless of center frequency.

**Constant percentage filter** A filter whose bandwidth is a fixed percentage of center frequency, for example, octave filter.

**Correlation coefficient** (1) Of two real signals,  $x(t)$  and  $y(t)$ , that are joint stationary with respect to time, the value of the covariance function at zero time delay  $C_{xy}(0)$ , normalized by the standard deviations of the two signals,  $\sigma_x$  and  $\sigma_y$ :

$$\rho_{xy} = \frac{C_{xy}(0)}{\sigma_x \sigma_y}.$$

*See* Cross-correlation coefficient. (2) Of two random variables  $X$  and  $Y$ , the normalized covariance, defined by

$$\rho_{XY} = \frac{\text{cov}(X, Y)}{\sigma_X \sigma_Y}.$$

**Critical bandwidth** The widest frequency band within which the perceived loudness of a band of continuously distributed random noise of constant bandwidth sound pressure level is independent of its bandwidth.

**Critical frequency, critical coincidence frequency** Of a panel or partition, the lowest frequency at which the coincidence effect occurs. If the panel is orthotropic or anisotropic, the critical frequency may vary with direction along the panel. Unit: hertz (Hz). Symbol:  $f_c$ . *See* Coincidence effect.

**Critical speed** Rotational speed of a rotating system that corresponds to a resonance frequency of that same system.

**Cross-correlation coefficient** Of two real signals that are joint stationary with respect to time, the normalized covariance function, defined by

$$\rho_{xy} = \frac{C_{xy}(\tau)}{\sigma_x \sigma_y}$$

where  $C_{xy}(\tau)$  is the covariance function of the two signals  $x(t)$  and  $y(t)$ , evaluated at time delay  $\tau$ , and  $\sigma_x$  and  $\sigma_y$  are the respective standard deviations. *See* Correlation coefficient.

**Cross-correlation function** The statistical correlation between two different signals as a function of relative time between the signals. The Fourier transform of

the cross-correlation function gives the cross spectrum. See Autocorrelation function, Cross spectrum.

**Cross spectrum, cross-power spectrum** A complex spectrum containing the product of the power spectra of two correlated signals. The Fourier transform of the cross-correlation function. If the two time signals are  $x(t)$  and  $y(t)$ , then the cross spectrum is  $G_{xy}(i\omega) = X^*(i\omega)Y(i\omega)$ , where  $*$  denotes complex conjugate. The cross spectrum is conjugate even. See Cross-correlation function, Power spectrum.

**Cumulative distribution** A method of representing time-varying noise by indicating the percentage of time that the noise level is present above (or below) a series of amplitude levels.

**Damped natural frequency** Frequency of free vibration of a damped linear system. Unit: hertz (Hz). See Natural frequency.

**Damping** (1) Any means of dissipating vibration energy within a vibrating system to reduce the amplitude of movement, or to shorten the decay time of free vibration. (2) Of an enclosure, removal of echoes and reverberation by the use of sound-absorbing materials. Also known as *sound proofing*. **Coulomb damping** Dissipation of energy that occurs when the motion of a vibrating system is resisted by a force whose magnitude is constant and independent of displacement and velocity, and whose direction is opposite to the direction of the velocity of the system. Also known as *dry friction damping*. **Critical damping** The minimum viscous damping that will allow a displaced system to return to its original position without oscillation. **Damping ratio** For a system with viscous damping, the ratio of viscous damping to critical damping. **Hysteretic damping, hysteresis damping** Damping of a vibrating due to energy dissipation through mechanical hysteresis. The area of the hysteresis loop is a measure of damping. Also sometimes called *structural damping*. **Viscous damping** Dissipation of energy that occurs when the motion of a vibrating system is resisted by a force that has a magnitude proportional to the magnitude of the velocity of the system and direction opposite to the direction of the velocity of the system. **Structural damping** An equivalent term for *hysteretic damping*.

**Day average sound pressure level** Time-average sound pressure level between 0700 and 2200 hours (15 hours). Unit: decibel (dB). Symbol:  $L_d$ . See Time-average sound pressure level, Day-night average sound pressure level.

**Day-night average sound pressure level** The 24-hour time-average sound pressure level for a given day, after addition of 10 dB to night levels from between 2200 and 0700 hours. Unit: decibel (dB). Symbol:  $L_{dn}$ . See Time-average sound pressure level, Day average sound pressure level.

**Decade** A unit of logarithmic frequency interval from  $f_1$  to  $f_2$ , defined as  $\log_{10}(f_2/f_1)$ . 1 decade = 3.322 octaves. See Octave.

**Decibel (dB)** The unit of measure for powerlike quantities in acoustics, noise, and vibration to denote level and level difference where the base of the logarithm is  $10^{1/10}$ . Abbreviated as dB. One tenth of a Bel. One decibel is equal to the ratio  $10^{1/10} = 1.26$ . Multiplying powerlike quantities (such as sound power or mean square sound pressure) by the factor  $10^{n/10}$  increases the level by  $n$  decibels. **Decibel scale** A linear numbering scale used to define a logarithmic amplitude scale, in units of decibels, thereby compressing a wide range of amplitude values to a small set of numbers.

**Degrees of freedom** The minimum number of independent coordinates required to define completely the positions of all parts of a mechanical system at any instant of time.

**Density** In continuum mechanics, the mass per unit volume of a material. Also known as *mass density*. Units: kilograms per cubic metre ( $\text{kg/m}^3$ ).

**Diffraction** A phenomenon by which the propagation direction and intensity of a sound wave are changed when it passes by an obstacle or through an aperture if the wavelength of the sound wave is the same size or greater than the size of the obstacle or aperture.

**Diffuse field** An idealized sound field in which the sound pressure level is the same everywhere and the flow of energy is equally probable in all directions.

**Diffuse sound** Sound that is completely random in phase; sound that appears to arrive uniformly from all directions.

**Dipole** An idealized sound source consisting of two closely spaced out-of-phase monopoles. See Monopole, Quadrupole.

**Directivity factor** (1) Of a sound source, the ratio of the far-field mean-square pressure at a given frequency and radius, in a specified direction from the source, to the average mean square pressure over a sphere of the same radius, centered on the source. (2) The ratio of the mean-square pressure (or intensity) on the axis of a transducer, at a certain distance, to the mean-square pressure (or intensity) that a monopole source radiating the same power would produce at that point.

**Directivity index** A measure of the extent to which a source radiates sound predominantly in one direction. The directivity index,  $DI_i$ , in the direction from a source to microphone position  $i$ , is defined as  $DI_i = L_{pi}^* - \bar{L}_p^*$ , where  $L_{pi}^*$  is the sound pressure level at microphone position  $i$ , corrected for background noise,  $\bar{L}_p^*$  is the sound pressure level averaged over the measurement surface, corrected for background noise. Unit: decibel (dB). Symbol: DI.

**Discrete Fourier transform (DFT)** A version of the Fourier transform applicable to a finite number of discrete samples. For a discrete sequence  $x[n]$ , its

discrete Fourier transform is

$$X[k] = \sum_{n=0}^N x[n] e^{-j(2\pi kn/N)}.$$

$X[k]$  is also discrete and has the same number of samples as does  $x[n]$ . The original sequence can be recovered from the inverse DFT:

$$x[n] = \frac{1}{N} \sum_{k=0}^N X[k] e^{j(2\pi kn/N)}$$

See Fourier transform, Fast Fourier transform.

**Displacement** A vector quantity that specifies the change of position of a body, usually measured from the rest or equilibrium position. Unit: metre (m). See Velocity, Acceleration, Jerk.

**Dissipation factor, dissipation** Ratio of the dissipated sound power to the incident sound power. Unit: none. Symbol:  $\delta$ . See Absorption factor, Reflection factor, Transmission factor.

**Doppler effect** Phenomenon evidenced by the shift in the observed frequency from the source frequency caused by relative motion between the source and the observer. The Doppler effect is described quantitatively by

$$f_r = f_s \frac{1 + v_r/c}{1 - v_s/c}$$

where  $f_r$  is the received frequency, in Hz;  $f_s$  is the source frequency, in Hz;  $v_r$  is the component of velocity relative to the medium of the receiving point toward source, in metres per second;  $v_s$  is the component of velocity relative to the medium of the source toward the receiving point, in metres per second;  $c$  is (phase) speed of sound in a stationary medium, in metres per second.

**Dose** See Noise dose.

**Dosimeter(s)** Noise dosimeters measure and store sound pressure levels (SPL) and, by integrating these measurements over time, provide a cumulative noise exposure reading for a given period. Dosimeters may also provide a time history of sound exposure that is useful in determining contributions to the cumulative noise exposure.

**Duct silencer** See Muffler.

**Dynamic capability index** Given by  $L_d = \delta_{pI_0} - K$ , where  $\delta_{pI_0}$  is the pressure-residual intensity index,  $K$  is selected according to the grade of accuracy required (see the table below). Unit: decibel (dB). Symbol:  $L_d$ . See Pressure-residual intensity index.

#### Bias Error Factor, $K$

Grade of Accuracy	Bias Error Factor (dB)
Precision (grade 1)	10
Engineering (grade 2)	10
Survey (grade 3)	7

**Dynamic mass** Ratio of applied force amplitude to resulting acceleration amplitude during simple harmonic motion. Reciprocal of accelerance magnitude. See Accelerance.

**Dynamic modulus** Ratio of stress to strain under vibratory conditions. Generally a complex quantity.

**Dynamic range** (1) Of a transducer, the ratio of the highest to the lowest input quantities within the linear range of the transducer, expressed in decibels. Unit: decibel (dB). (2) Of a spectrum analyzer, the maximum ratio of two signals simultaneously present at the input that can be measured to a specified accuracy, expressed in decibels. Unit: decibel (dB). (3) Of an acoustical variable, the ratio of the maximum and minimum mean-square values. Unit: decibel (dB).

**Dynamic stiffness** Of a point-excited mechanical system, the complex ratio of applied force to displacement. It is the reciprocal of dynamic compliance. Units: newton per metre (N/m). See Compliance.

**Eccentricity** Distance of the center of gravity of a revolving body from the axis of rotation.

**Effective noise bandwidth** Bandwidth of an ideal filter that would pass the same amount of power from a white noise source as the filter described. Used to define bandwidth of one-third octave and octave filters.

**Effective perceived noise level** A complex rating used to certify aircraft types for flyover noise. Includes corrections for pure tones and for duration of the noise. If  $L(t)$  denotes the tone-corrected perceived noise level as a function of time, the effective perceived noise (EPN) level is defined as

$$L_{EPN} = 10 \log_{10} \left[ \frac{1}{t_{\text{ref}}} \int 10^{L/10} dt \right]$$

The reference time used for normalization is  $t_{\text{ref}} = 10$  s. Unit: dB re  $(20 \mu\text{Pa})^2 \cdot 10$  s. Symbol:  $L_{EPN}$ . See Noise Exposure forecast.

**Eigenfrequency** An alternative term for *natural frequency*. See: Natural frequency, Eigenvalue.

**Eigenvalue** (1) Scalar  $\lambda$  such that  $T(v) = \lambda v$ , where  $T$  is a linear operator on a vector space, and  $v$  is an eigenvector. Specifically, of a square matrix, any scalar  $\lambda$  such that the determinant of  $\mathbf{A} - \lambda \mathbf{I}$  vanishes, where  $\mathbf{A}$  is the matrix concerned, and  $\mathbf{I}$  is the identity matrix of the same size. Also known as *characteristic number*, *characteristic root*, *characteristic value*. See Eigenvector. (2) Of an acoustical system, usually refers

to one of the values  $\kappa_n^2$  ( $n = 1, 2, 3, \dots$ ) for which the equation describing the acoustic pressure at a specified frequency, e.g., the Helmholtz equation  $(\nabla^2 + \kappa^2)p = 0$ , has a solution matching the boundary conditions. (3) Root of a characteristic equation. Specifically, in modal analysis, the eigenvalue of the characteristic equation of a dynamic system is related to the square of one of the natural frequencies of the system. *See* Characteristic equation, Modal analysis.

**Eigenvector** (1) Nonzero vector  $v$  whose direction is not changed by a given linear transformation  $T$ ; that is,  $T(v) = \lambda v$  for some scalar  $\lambda$ . Also known as *characteristic vector*. *See* Eigenvalue. (2) Specifically, in modal analysis an eigenvector of the characteristic equation of a dynamic system refers to a mode shape of the system.

**Equivalent continuous A-weighted sound pressure level** Value of the A-weighted sound pressure level of a continuous, steady sound that, within a specified time interval  $T$ , has the same mean-square sound pressure as a sound under consideration whose level varies with time. It is given by

$$L_{\text{Aeq},T} = 10 \log_{10} \left[ \frac{1}{t_2 - t_1} \int_{t_1}^{t_2} \frac{p_A^2(t)}{p_0^2} dt \right]$$

where  $p_A(t)$  is the instantaneous A-weighted sound pressure of the sound signal,  $p_0$  is the reference sound pressure (20  $\mu\text{Pa}$ ). Unit: decibel (dB). Symbol:  $L_{\text{Aeq},T}$ . *See* Equivalent continuous sound pressure level, Sound pressure.

**Equivalent continuous sound pressure level** Value of sound pressure level of a continuous steady sound that, within a measurement time interval  $T$ , has the same mean-square sound pressure as a sound under consideration which varies with time, given by

$$L_{\text{peq},T} = 10 \log_{10} \left[ \frac{1}{t_2 - t_1} \int_{t_1}^{t_2} \frac{p^2(t)}{p_0^2} dt \right]$$

where  $t_1$  and  $t_2$  are the starting and ending times for the integral,  $p(t)$  is the instantaneous sound pressure,  $p_0$  is the reference sound pressure (20  $\mu\text{Pa}$ ). Also known as *time-averaged sound pressure level*. Unit: decibel (dB). Symbol:  $L_{\text{peq},T}$ . If the equivalent continuous sound pressure level is A-weighted, then the symbol is  $L_{\text{pAeq},T}$ , which can be abbreviated as  $L_{\text{pA}}$ . In general the subscripts "eq" and "T" can be omitted. *See* Sound pressure level, Equivalent continuous A-weighted sound pressure level.

**Equivalent sound absorption area** (1) Of a room, the hypothetical area of a totally absorbing surface without diffraction effects that, if it were the only absorbing element in the room, would give the same reverberation time as the room under consideration.

Units: square metre ( $\text{m}^2$ ). Symbol:  $A_1$ , for the empty reverberation room;  $A_2$ , for the reverberation room containing a test specimen. *See* Sabin, Eyring absorption coefficient. (2) Of a test specimen, the difference between the equivalent sound absorption area of the reverberation room with and without the test specimen. Units: square metre ( $\text{m}^2$ ). Symbol:  $A$ .

**Equivalent threshold level** For monaural listening, at a specified frequency, for a specified type of transducer, and for a stated force of application of the transducer to the human head, the vibration level, or sound pressure level set up by that transducer in a specified coupler or artificial ear when the transducer is activated by that voltage that, with the transducer applied to the ear concerned, would correspond with the hearing threshold. Unit: decibel (dB). *See* Hearing threshold (1).

**Ergodic process** A stationary time-dependent stochastic process whose time average is equal to the ensemble average.

**Excitation** An external force or motion applied to a system that causes the system to respond in some way. **Force excitation** The excitation force is independent of the properties of the excited structures; an example of this is the effect of a light and flexible source on a relatively stiff and heavy structure. **Velocity excitation** The excitation velocity is independent of the properties of the excited structures; an example of this is a light and flexible structure excited by a relatively massive source.

**Eyring absorption coefficient** Sound absorption coefficient attributed to a surface according to the Eyring reverberation time equation

$$T = \frac{24V \ln 10}{-cS \ln(1 - \bar{\alpha})}$$

where  $V$  is the volume of the room, in cubic metres;  $c$  is the (phase) speed of sound in air, in metres per second;  $S$  is the total internal surface area of the room, in square metres. Unit: none. Symbol:  $\bar{\alpha}$ .

**Far field** Portion of the radiation field of a sound source in which the sound pressure level decreases by 3 dB for each doubling of the area of the measurement surface. This is equivalent to a decrease of 6 dB for each doubling of the distance from a point source. In the far field, the sound waves can be considered locally planar, and the mean-square pressure is proportional to the total sound power radiated by the source.

**Fast Fourier transform (FFT)** A rapid numerical technique for computing the discrete Fourier transform. *See* Discrete Fourier transform, Fourier transform.

**Fast Hilbert transform** A rapid numerical technique for computing the Hilbert transform. The Fourier



transform of the Hilbert transform of  $x(t)$  is  $H(f) = -j\text{sgn}(f)X(f)$ , where  $\text{sgn}(f)$  is a sign function, and  $X(f)$  is the Fourier transform of  $x(t)$ . So the fast Hilbert transform can be realized using the fast Fourier transform. *See* Hilbert transform, fast Fourier transform.

**Finite element method** A numerical approach for obtaining approximate solutions to variational problems. The domain of interest is divided into subdomains referred to as elements. The finite element method uses interpolation functions that satisfy the essential boundary conditions and solves the unknown nodal values that approximately satisfy the governing differential equation over the domain. *See* Boundary element method.

**Flanking transmission** Sound that travels between a source and a receiving room along paths other than through the partition dividing the two rooms.

**Flexibility** *See* Compliance.

**Force** Vector quantity that causes a massive body to accelerate, equal to the time rate of change of momentum of the body. *See* Newton.

**Force excitation** *See* Excitation.

**Forced vibration, forced oscillation** Response of a system caused by external excitation. *See* Free vibration.

**Formant** (1) Noun. A resonance of the vocal tract. The frequencies of the formants are determined in large part by the vocal tract shape; changes in the shape change the frequencies and so result in different speech sounds. *See* Vocal tract. (2) Adjective. A formant synthesizer uses parameters related to the formant frequencies and bandwidths of different speech sounds.

**Fourier transform** A mathematical operation for decomposing a time function  $x(t)$  into its frequency components (amplitude and phase) given by

$$X(f) = \int_{-\infty}^{\infty} x(t)e^{-j2\pi ft} dt$$

The inverse Fourier transform is

$$x(t) = \int_{-\infty}^{\infty} X(f)e^{j2\pi ft} df$$

*See* Discrete Fourier transform, Spectrum, Fast Fourier transform, Power spectrum.

**Free field** A sound field in a homogeneous, isotropic medium free of boundaries. In practice, it is a field in which reflections at the boundaries are negligible in the frequency range of interest. *See* Free field over a reflecting plane, Diffuse field.

**Free field over a reflecting plane** A sound field in a homogeneous, isotropic medium in the half-space above an infinite, rigid plane surface on which the source is located. *See* Free field.

**Free vibration, free oscillation** A phenomenon that occurs in a mechanical system when it vibrates in the absence of external excitation. Free vibration consists of natural modes of the system, each vibrating at a natural frequency. *See* Forced vibration, Natural frequency, Normal mode of vibration.

**Frequency** The number of cycles of a periodic phenomenon per unit time interval. It is the reciprocal of the period. Unit: hertz (Hz). Symbol:  $f$ . *See* Angular frequency, Period, Hz.

**Frequency response function (FRF)** Of a linear time-invariant system, the complex ratio of the Fourier transforms of the output signal to the input signal. Mathematically, the frequency response function is the Fourier transform of the impulse response function. By extension, the frequency response function can be used for any two linearly related signals. *See* Impulse response function, Transfer function.

**Frequency weighting** Modification of the spectrum of an acoustical signal by means of an analog or digital filter having one of the standardized response characteristics known as A, B, C, etc., defined in IEC 61672-1. The A-weighting filter is the one most commonly used. *See* Weighting network.

**Fundamental frequency** The lowest natural frequency of a dynamic system. *See* Natural frequency.

**Ground effect** In outdoor sound propagation, the influence of the sound reflected from a surface on horizontal propagation of sound traveling directly from source to receiver. Over distances of 25 m and above, this can be significant at audio frequencies, particularly when reflection at near-grazing angles is involved.

**Group speed of sound** Travel speed of the energy of a sound wave through a medium, given by  $c_g = d\omega/dk$ , where  $\omega$  is the angular frequency, in radians per second;  $k$  is the wavenumber, in reciprocal metre. Units: metre per unit time (m/s). Symbol:  $c_g$ . *See* Phase speed of sound.

**Half-power bandwidth** (1) Of a resonance response curve in which the squared gain factor of a linear system is plotted against frequency, the frequency separation between the 3-dB down points on the two sides of the resonance peak, at which the curve is at half of its peak value. (2) Of a signal with a peaked power spectrum, the frequency separation between the points on two sides of the spectral peak where the spectrum level is 3 dB less than the peak value. *See* Bandwidth.

**Hand-transmitted vibration** Vibration transmitted to the hand, often from powered hand tools.

**Harmonic** A frequency component whose frequency is an integer multiple of the fundamental frequency of a periodic quantity to which it is related.

**Hearing conservation program** A system to identify noise-exposed workers, and to monitor their exposure and audiometric function.

**Hearing loss** Increase in the threshold of audibility due to disease, injury, age, or exposure to intense noise. *See* Presbycusis. **Conductive hearing loss** Hearing loss caused either by blockage of the external ear or by disease or damage in the middle ear, so that the signal amplitude reaching the inner ear is reduced. **Noise-induced hearing loss (NIHL)** Cumulative hearing loss associated with repeated exposure to noise. **Sensorineural hearing loss** Hearing loss due to a lesion or disorder of the inner ear or of the auditory nervous system. **Nonoccupational hearing loss** Hearing loss that is caused by exposures outside of the occupational environment.

**Hearing threshold** (1) For a given listener and specific signal, the minimum sound pressure level that is capable of evoking an auditory sensation in a specified function of trials. Sound reaching the ears from other sources is assumed to be negligible. *See* Audibility threshold, Masking. (2) The level of a sound at which, under specified conditions, a person gives a predetermined percentage of correct detection responses on repeated trials.

**Hearing threshold level (HTL)** For a specified signal, amount in decibels by which the hearing threshold for a listener, for either one or two ears, exceeds a specified reference equivalent threshold level. Unit: decibel (dB). *See* Equivalent threshold level, Hearing threshold (1).

**Helmholtz resonator** Hollow, rigid-walled cavity filled with gas or liquid and having a small opening called the neck. Its fundamental frequency  $f_0$  is approximated by

$$f_0 = \frac{c}{2\pi} \sqrt{\frac{A}{LV}}$$

where  $c$  is the (phase) speed of sound, in metres per second,  $A$  and  $L$  are the cross-sectional area, in square metres and effective length, in metres, of the neck, and  $V$  is the cavity volume, in cubic metres. *See* Muffler.

**Hertz (Hz)** A unit of frequency measurement, representing cycles per second. *See* Frequency.

**Hilbert transform** A mathematical transform that shifts the phase of each frequency component of the instantaneous spectrum by  $90^\circ$  without affecting the magnitude. For a time signal  $x(t)$ , its Hilbert transform

is defined as

$$h(t) = H\{x(t)\} = \frac{1}{\pi} \int_{-\infty}^{+\infty} \frac{x(\tau)}{t - \tau} d\tau$$

*See* Fast Hilbert transform, Fourier transform.

**Ideal filter** A filter having a rectangularly shaped characteristic: unity amplitude transfer within its passband and zero transfer outside its passband.

**Impact** Excitation of a structure with a force pulse, for example, by using an impact hammer.

**Impact insulation class (IIC)** A single number representing 110 dB minus the normalized impact sound index. *See* Normalized impact sound index.

**Impact sound pressure level** In architectural acoustics, average sound pressure level in a specified frequency band in the receiving room under a test floor being excited by the standardized impact sound source specified in ASTM E492-90. Unit: decibel (dB). *See* Normalized impact sound index, Impact insulation class. **Normalized impact sound pressure level** For a specified frequency band, average sound pressure level in decibels due to the standardized impact sound source, plus 10 times the logarithm to the base 10 of the ratio of the Sabine absorption in the receiving room to the reference Sabine absorption of 10 metric sabins.

**Impedance tube** A uniform rigid-walled tube with a sound generation device, for example, loudspeaker, at one end to excite plane sound waves. When such a tube is terminated by a sample of material, the acoustic impedance (or the absorption factor) of the material can be determined using a traversing microphone or two fixed microphones. Also known as *standing-wave tube* or *Kundt's tube*.

**Impulse response function** Of a linear time-invariant system, the function that gives the system output when the input is an impulse function (Dirac's delta function) at time  $t = 0$ . Its Fourier transform is the frequency response function of the system. For any other type of input, the system output is determined by the convolution between the input and the impulse response function. *See* Frequency response function.

**Infrasound** Sound at frequencies below the audible range, generally below about 20 Hz.

**Insertion loss** (1) Of a silencer or other sound reduction element, in a specified frequency band, the decrease in sound pressure level, measured at the location of the receiver, when the sound reduction element is inserted in the transmission path between the source and the receiver. Unit: decibel (dB). (2) Of a silencer or other sound reduction element, in a specified frequency band, the decrease in sound power level, measured when the sound reduction element is

inserted in the transmission path between the source and the receiver. Unit: decibel (dB).

**Instantaneous sound intensity** Instantaneous rate of flow of sound energy per unit area in the direction of the local instantaneous acoustic particle velocity. This is a vector quantity that is equal to the product of the instantaneous sound pressure at a point and the associated particle velocity:  $\mathbf{I}(t) = p(t) \cdot \mathbf{u}(t)$ , where  $p(t)$  is the instantaneous sound pressure at a point, and  $\mathbf{u}(t)$  is the associated particle velocity. Units: watt per square metre ( $\text{W/m}^2$ ). Symbol:  $\mathbf{I}(t)$ . *See* Sound intensity. *Note:* The sound intensity is generally complex. The real part is the propagating part of the sound field (sometimes called the active part). The imaginary part is the nonpropagating part of the sound field (sometimes called the reactive part).

**Integrator** A device the output of which is the integrated input. For noise and vibration applications, the integrator is generally an electrical device, used to convert a signal proportional to a vibratory acceleration to one that is proportional to velocity or displacement, or to convert a signal proportional to a vibratory velocity to one that is proportional to displacement.

**Intelligibility, speech intelligibility** Of speech in a particular listening environment, a qualitative term that describes the ability of the acoustical environment to transmit speech intelligibly, usually expressed relative to perfect listening conditions. Intelligibility can be quantified for a particular speech sample by asking listeners to record their interpretation of what they hear and processing the data to obtain the percentage syllable articulation. *See* Percentage syllable articulation, Articulation index.

**Intensity** *See* Instantaneous sound intensity, Sound intensity.

**Isolation** Resistance to the transmission of sound or vibration by materials and structures. **Vibration isolation** Reduction, usually attained by the use of a resilient coupling, in the vibration of a system in response to mechanical excitation.

**Jerk** A vector quantity that specifies time rate of change of acceleration. Units: metre per second-cubed ( $\text{m/s}^3$ ). *See* Displacement, Velocity, Acceleration.

**Leakage** *See* Spectral leakage error.

**Level** Logarithm of the ratio of a powerlike quantity to a reference quantity of the same kind. The base of the logarithm, the reference quantity, and the kind of level shall be specified.

**Level difference** In architectural acoustics, in a specified frequency band, the difference in the space and time-average sound pressure levels produced in two rooms by one or more sound sources in one of them:  $D = L_1 - L_2$ , where  $L_1$  is the average sound pressure level in the source room,  $L_2$  is the average

sound pressure level in the receiving room. Also known as *noise reduction*. Unit: decibel (dB). Symbol:  $D$  or NR. *See* Sound reduction index. **Standardized level difference** The level difference corresponding to a reference value of the reverberation time in the receiving room, given by  $D_{nT} = D + 10 \log_{10}(T/T_0)$ , where  $D$  is the level difference,  $T$  is the reverberation time in the receiving room, and  $T_0$  is the reference reverberation time. Unit: decibel (dB). Symbol:  $D_{nT}$ . *Note:* For dwellings,  $T_0 = 0.5$  s. The standardizing of the level difference corresponding to the reverberation time in the receiving room of  $T_0 = 0.5$  s is equivalent to standardizing the level difference with respect to an equivalent absorption area of  $A_0 = 0.32V$ , where  $A_0$  is the equivalent absorption area, in square metres, and  $V$  is the volume of the receiving room, in cubic metres.

**Linearity** A characteristic that satisfies the superposition property. (1) Of a system, if two separate inputs  $x_1$  and  $x_2$  produce respective outputs  $y_1$  and  $y_2$ , then the combined input  $x_1 + x_2$  produces an output  $y_1 + y_2$ ; if input  $x$  produces output  $y$ , then input  $ax$  (where  $a$  is a constant) produces output  $ay$ . (2) Of an operator  $L$ , it satisfies  $L(x_1 + x_2) = L(x_1) + L(x_2)$  and  $L(ax) = aL(x)$ , where  $x_1$  and  $x_2$  are variables on which the operator  $L$  acts, and  $a$  is a constant. (3) Of an equation, two solutions can be added, or a solution can be multiplied by a constant, the result is also a solution. *See* Nonlinearity.

**Liquid-borne sound** Sound that propagates through a liquid. *See* Airborne sound, Structure-borne sound.

**Loss factor** A measure of the damping capability of a system. For viscous damping, the loss factor is twice the damping ratio. The loss factor may appear in different forms, for example, internal loss factor, radiation loss factor, or coupling loss factor. *See* Damping.

**Loudness** The attribute of auditory sensation in terms of which sounds may be ordered on a scale extending from soft to loud. *See* Sone, Rating, Magnitude scaling.

**Loudness level** Of a given sound, the sound pressure level of a reference sound, consisting of a sinusoidal plane progressive wave of frequency 1000 Hz coming from directly in front of the listener, which is judged by otologically normal person to be equally loud to the given sound. Unit: phon. *See* Phon.

**Magnitude scaling** A method to quantify psychological variables. Typically, a fixed physical stimulus is provided that evokes a perceptual strength to be taken as an internal standard (unit). The subject is requested to assess the ratio of the perceptual strength of an unknown stimulus with respect to that internal standard. *See* Rating, Loudness, Sone.

**Masking** (1) The process by which the threshold of audibility of one sound is raised by the presence of another (masking) sound. (2) The amount by which

the hearing threshold level is so raised, expressed in decibels.

**Mechanical impedance** (1) At a surface, the ratio of the total force on the surface to the component of the average sound particle velocity at the surface in the direction of the force. Called driving point impedance if force and velocity are measured at the same point and in the same direction, otherwise called transfer impedance. Units: newton per metre per second [N/(m/s)]. Symbol:  $Z_m$ . (2) A form of the inverse frequency response function, which is the complex ratio of the excitation force to the velocity response. *See* Acoustic impedance, Characteristic impedance, Specific acoustic impedance, Mobility.

**Microphone** Transducer that converts a sensed sound pressure signal to an electric output signal, with minimal distortion over its designed frequency range.

**Mobility** (1) An alternative term for *mechanical admittance*. (2) The ratio of the following complex quantities:

Mechanical mobility  $Z_M = \text{velocity across/}$   
force through

Rotational mobility  $Z_R = \text{angular velocity across/}$   
torque through

Acoustic mobility  $Z_A = \text{volume velocity across/}$   
sound pressure through

*See* Admittance, Accelerance, Compliance, Mechanical impedance, Acoustic impedance.

**Modal analysis** Process of determining the mode shapes and associated parameters, natural frequencies, and damping. **Modal mass** In modal analysis, of a particular mode of a dynamic system, an element in the generalized mass matrix. For mass-normalized mode shapes, the modal mass is unity. **Modal stiffness** In modal analysis, of a particular mode of a dynamic system, an element in the generalized stiffness matrix. For mass-normalized mode shapes, the modal stiffness is equal to the eigenvalue of the characteristic equation of the system. *See* Eigenvalue. **Mode shape** A pattern of vibration exhibited by a structure at a natural frequency. Generally, described as a vector of values, defining the relative displacement amplitudes and phases of each point on the structure at a specified natural frequency. *See* Eigenvector.

**Modal density** For a given system, the average number of modal resonances per unit interval of frequency. Unit: reciprocal hertz (1/Hz).

**Mode of vibration** Characteristic pattern assumed by a system undergoing vibration in which the motion of every particle is simple harmonic with the same frequency. *See* Normal mode of vibration.

**Mode shape** *See* Modal analysis.

**Monopole** An idealized sound source that is concentrated at a single point in space. A monopole can be

represented by a pulsating sphere producing spherical wave fronts. *See* Dipole, Quadrupole.

**Muffler, duct silencer** Device designed to reduce the level of sound transmitted along a duct system.

**Natural frequency** Frequency of free vibration of a system. If the system is damped, then the natural frequency is the damped natural frequency. Unit: hertz (Hz). *See* Damped natural frequency, Eigenvalue, Free vibration.

**Near field** The portion of the radiation field of a sound source that lies between the source and the far field. *See* Far field.

**Neper (Np)** A unit of level of a field quantity in terms of logarithm on the Napierian base  $e \approx 2.7183$ , and unit of level of powerlike quantity when the base of the logarithm is  $e^2$ .

**Newton (N)** A unit of force. The force of one newton accelerates a 1 kg mass at 1 m/s<sup>2</sup>. *See* Force, Acceleration.

**Night average sound pressure level** Time-average sound pressure level between 2200 and 0700 hours (9 hours). Unit: decibel (dB). *See* Day average sound pressure level, Day–night sound pressure level, Equivalent continuous sound pressure level.

**Node** (1) A point, curve, or surface, on a vibrating structure or in a fluid volume that remains stationary. *See* Standing wave. (2) A grid point in the discrete model of a structure.

**Noise** (1) Undesired, unpleasant sound. *See* Periodic noise, Random noise, Tonal noise, Pink noise, White noise. (2) Erratic, unwarranted disturbance, for example, electrical noise.

**Noise dose** (1) According to the definition given by Occupational Safety and Health Administration (OSHA), the ratio, expressed as a percentage of (1) the time integral, over a stated time or event, of the 0.6 power of the measured “S” (slow) exponential time-averaged, squared A-weighted sound pressure and (2) the product of the criterion duration (8 hours) and the 0.6 power of the squared sound pressure corresponding to the criterion sound pressure level (90 dB). (2) According to the definition given by the National Institute for Occupational Safety and Health (NIOSH), the percentage of actual exposure relative to the amount of allowable exposure, and for which 100 percent and above represent exposures that are hazardous. The noise dose is calculated using:  $D = \sum_{i=1}^n C_i / T_i \times 100\%$ , where  $C_i$  is the total time of exposure at a specified noise level, and  $T_i$  is the exposure time at which noise for this level becomes hazardous.

**Noise emission level** A-weighted sound pressure level measured at a specified distance and direction from a noise source, in an open environment,

above a specified type of surface. Generally follows the recommendation of a national or industry standard.

**Noise exposure forecast (NEF)** A complex criterion for predicting future noise impact of airports. The computation considers effective perceived noise level of each type of aircraft, flight profile, number of flights, time of day, etc. Generally used in plots of NEF contours for zoning control around airports. *See* Effective perceived noise level.

**Noise exposure level** The level given by  $L_{EX,8h} = L_{Aeq,T_e} + 10 \log_{10}(T_e/T_0)$ , where  $T_e$  is the effective duration of the working day, in hours;  $T_0$  is the reference duration (=8 hours);  $L_{Aeq,T_e}$  is the A-weighted equivalent sound pressure level during the time interval  $T_e$ . If  $T_e$  does not exceed 8 hours,  $L_{EX,8h}$  is numerically equal to  $L_{Aeq,8h}$ . Unit: decibel (dB). Symbol:  $L_{EX,8h}$ . *See* Equivalent continuous A-weighted sound pressure level, Sound exposure. *Note:* The noise exposure level  $L_{EX,8h}$  may be calculated from the A-weighted sound exposure  $E_{A,T_e}$ , in pascal-squared second ( $\text{Pa}^2 \cdot \text{s}$ ), using the following formula:

$$L_{EX,8h} = 10 \log_{10} \frac{E_{A,T_e}}{1.15 \times 10^{-5}}$$

where the reference sound exposure is  $1.15 \times 10^{-5} \text{ Pa}^2 \cdot \text{s}$ .

**Noise immission level (NIL)** A measure of cumulative A-weighted sound exposure during a person's lifetime, based on a modification of the noise exposure level concept. The reference sound exposure is chosen in such a way that after working for  $N$  years in an environment with a constant A-weighted sound pressure level  $L_A$ , a person who works a typical 1740 hours per year will have a cumulative noise immission level given by  $NIL = L_A + 10 \log_{10} N$ , assuming that person's leisure time exposure and previously cumulated work exposure are negligible. The equation implies a reference sound exposure of  $E_0 = 2.5 \times 10^{-3} \text{ Pa}^2 \cdot \text{s}$ , i.e., (1740/8) times the reference sound exposure used for noise exposure level. Unit: decibel (dB). Symbol: NIL. *See* Noise exposure level, Sound exposure level.

**Noise reduction coefficient (NRC)** Arithmetic average of the sound absorption coefficients of a material at 250, 500, 1000, and 2000 Hz.

**Noise reduction (NR)** An alternative term for *level difference*. *See* Level difference, Sound reduction index.

**Noise reduction rating (NRR)** A single-number rating that indicates the noise reduction capabilities of a hearing protector. Unit: decibel (dB).

**Noise-induced hearing loss (NIHL)** *See* Hearing loss.

**Nonlinearity** Characteristic that does not satisfy linearity. *See* Linearity.

**Normal mode of vibration** Mode of free vibration of an undamped system. *See* Eigenvector.

**Normal sound intensity** Component of the sound intensity in the direction normal to a measurement surface defined by the unit normal vector  $\mathbf{n}$ :  $I_n = \mathbf{I} \cdot \mathbf{n}$ . Units: watt per square metre ( $\text{W}/\text{m}^2$ ). Symbol:  $I_n$ . *See* Sound intensity.

**Normal sound intensity level** Logarithmic measure of the unsigned value of the normal sound intensity  $|I_n|$ , given by:  $L_{I_n} = 10 \log_{10} |I_n|/I_0$ , where  $I_0$  is the reference sound intensity and is  $10^{-12} \text{ W}/\text{m}^2$ . When  $I_n$  is negative, the level is expressed as  $(-)$  XX dB, except when used in the evaluation of residual intensity index. Unit: decibel (dB). Symbol:  $L_{I_n}$ . *See* Normal sound intensity, Sound intensity.

**Normalized impact sound index (NISI)** A single-number rating of normalized impact sound pressure level for 16 successive one-third octave bands from 100 to 3150 Hz inclusive. The calculation procedure is specified in ASTM E989-89. Unit: decibel (dB). *See* Impact sound pressure level, Impact insulation class.

**Normalized impact sound pressure level** *See* Impact sound pressure level.

**Noy** A linear unit of noisiness to quantify the annoyance potential of complex sound. *See* Perceived noisiness, Sone.

**Nyquist diagram, Nyquist plot** A plot of the real part versus the imaginary part of the frequency response function. For a single-degree-of-freedom system, the Nyquist plot is a circle. *See* Argand diagram, Bode diagram, Frequency response function.

**Nyquist frequency** One-half the sampling frequency in analog-to-digital conversion, which is the theoretical maximum frequency that can be correctly sampled. *See* Sampling theorem, Aliasing error.

**Octave** A unit of logarithmic frequency interval from  $f_1$  to  $f_2$ , defined as  $\log_2(f_2/f_1)$ . 1 octave = 0.301 decade. *See* Decade.

**Octave band** A frequency band whose upper and lower frequency limits are in the ratio of 2. *See* One-third octave band.

**Octave filter** A filter whose upper and lower passband limits are in the ratio of 2 and centered at one of the preferred frequencies given in ISO 266. Should meet the attenuation characteristic of IEC 61260 and ANSI S1.11-1986.

**One-third octave band** A frequency band whose upper and lower frequency limits are in the ratio of  $2^{1/3}$ .

**One-third octave filter** A filter whose upper and lower passband limits are in the ratio of  $2^{1/3}$  and centered at one of the preferred frequencies given in ISO 266. Should meet the attenuation characteristics of IEC 61260 and ANSI S1.11–1986.

**Order analysis** A form of frequency analysis, used with rotating machines where the amplitudes of signal frequency components are plotted as a function of multiples of the rotational speed. The frequency component with frequency of  $n$  times the rotational speed is called the  $n$ th order, generally symbolized as  $nX$ .

**Ototoxic chemical** Chemical that causes damage specifically to the cochlea, the auditory nerve, or vestibular system, which impairs the ability to hear. For example, organic solvents, lead, and mercury are ototoxic.

**Particle velocity** Velocity of a medium particle about its rest positions, usually due to a sound wave. Units: metre per second (m/s).

**Pascal (Pa)** A unit of pressure corresponding to a force of 1 newton acting uniformly upon an area of 1 square metre.  $1 \text{ Pa} = 1 \text{ N/m}^2$ .

**Passband** Of a filter, the frequency range over which the frequency response function has a magnitude close to unity.

**Perceived noise level (PNL)** A frequency-weighted sound pressure level obtained by a stated procedure that combines the sound pressure levels in the 24 one-third octave bands with midband frequencies from 50 Hz to 10 kHz. Unit: decibel (dB). Symbol:  $L_{PN}$ . See Perceived noisiness.

**Perceived noisiness, noisiness** Prescribed function of sound pressure levels in the 24 one-third octave bands with nominal midband frequencies from 50 Hz to 10 kHz that is used in the calculation of the perceived noise level. Unit: noy. See Noy.

**Percentage syllable articulation** In a given speech sample presented to a listener, the percentage of syllables that are heard correctly. See Intelligibility, Articulation index.

**Percentile level** A-weighted sound pressure level obtained by using time-weighting “F” (see IEC 61672-1) that is exceeded for  $N\%$  of the time interval considered. Unit: decibel (dB). Symbol:  $L_{AN,T}$ , for example,  $L_{A95,1h}$  is the A-weighted level exceeded for 95% of one hour.

**Period** The smallest interval (of time or distance) over which an oscillation repeats itself.

**Periodic noise** A noise event that is periodically repeated. Typical sources of periodic noise are gear wheels and piston machines.

**Periodic vibration** Oscillatory motion whose amplitude pattern is repeated after fixed increments of time.

**Permissible exposure level (PEL)** Regulatory limit of sound exposure. The OSHA (Occupational Safety and Health Administration) PEL is a noise dose of 1.0 based on 8-hour A-weighted sound exposure level at 90 dB with a 5 dB exchange rate. European PEL is generally 8-hour A-weighted sound exposure level at 85 dB with a 3-dB exchange rate.

**Phase speed of sound** Travel speed of the phase of a sound wave through a medium, given by  $c = \omega/k$ , where  $\omega$  is the angular frequency, in radians per second;  $k$  is the wavenumber, in reciprocal metre. Units: metre per second (m/s). Symbol:  $c$ . See Group speed of sound.

**Phon** Unit of loudness level of a sound. It is numerically equal to the sound pressure level of a 1-kHz free progressive wave that is judged by reliable listeners to be as loud as the unknown sound. See Loudness level.

**Phone** Acoustic realization of a phoneme. Phones can represent the variation in pronunciation of a phoneme, due to context, dialect, speaking style, or rate, that does not cause a change in meaning. See Phoneme.

**Phoneme** The minimal sound unit in a language that can change meaning of a word. Each language has its own set of phonemes, which vary both in number of phonemes, from 15 to over 100, and in the sounds included. See Phone.

**Pink noise** A broadband random noise whose power spectrum is inversely proportional to frequency ( $-3$  dB per octave or  $-10$  dB per decade), thus giving it a constant power spectrum per octave or one-third octave band. See Random noise, White noise.

**Power spectrum** Magnitude square of frequency spectrum. Also known as *autospectrum*. The power spectrum is real and even. See Autocorrelation function, Power spectrum density, Cross spectrum.

**Power spectrum density, power spectral density** Limit of the power of a signal (displacement, velocity, acceleration, etc.) divided by bandwidth, as the bandwidth approaches zero. See Power spectrum.

**Power spectrum level** The level of the power in a band 1 Hz wide referred to a given reference power.

**Power unit noise** Unwanted sound generated by the propulsion system of a road vehicle, except the tires; such sources including, e.g., engine, air intake, exhaust silencer, transmission, and fan. Other terms sometimes (but incorrectly and inconsistently) used for this include power train noise and drive train noise. Also known as *propulsion noise*. See Tire/road noise.

**Preferred frequencies** A set of standardized octave and one-third octave center frequencies defined by ISO 266, DIN 45 401, and ANSI S1.6–1967.

**Presbycusis, presbicusis** Progressive hearing impairment with age, in the absence of other identifiable causes. *See* Hearing loss.

**Pressure-residual intensity index** Of a sound intensity measurement device, the difference between the indicated sound pressure level  $L_p$  and the indicated sound intensity  $L_I$  when the device is placed and oriented in a sound field such that the sound intensity is zero:  $\delta_{pI_0} = L_p - L_I$ . Details for determining the pressure-residual intensity index are given in IEC 61043. Unit: decibel (dB). Symbol:  $\delta_{pI_0}$ . *See* Dynamic capability index.

**Privacy index, speech privacy index (PI)** A number that is a measure of speech privacy or lack of speech intelligibility. The privacy index is calculated from the articulation index (AI):  $PI = (1 - AI) \times 100\%$ . *See* Articulation index.

**Quadrupole** An idealized sound source consisting of four closely spaced monopoles with adjacent monopoles out-of-phase.

**Quality factor, Q factor** Of a lightly damped linear system, a measure of the sharpness of a peak in the frequency response, which is equal to the reciprocal of the loss factor of the corresponding vibration mode. *See* Loss factor, Half-power bandwidth.

**Radiation efficiency, radiation factor** The ratio of the sound power radiated by a vibrating surface, with a given time-mean-square velocity, to the sound power, which would be emitted as a plane wave by the same vibrating surface with the same vibration velocity. The radiation factor is given by the following equation:

$$\sigma = \frac{P_S}{\rho c S_S \bar{v}^2}$$

where  $P_S$  is the airborne sound power emitted by the vibrating surface,  $\rho c$  is the characteristic impedance of air,  $S_S$  is the area of the vibrating surface, and  $\bar{v}^2$  is the squared rms value of the vibratory velocity averaged over the area  $S_S$ . Unit: none. Symbol:  $\sigma$ . *See* Sound power, Characteristic impedance, Vibratory velocity.

**Radiation impedance** A generic term for the impedance presented to a vibrating surface by the adjacent acoustical medium. Units: newton per metre per second [N/(m/s)]. Symbol:  $Z_r$ . Also known as *fluid loading impedance*. Its real part is the *radiation resistance* from which the emitted sound power is obtained by multiplying it by the mean-square velocity of the body. Symbol:  $R_r$ . The imaginary part is called the *radiation reactance*. Symbol:  $X_r$ . *See* Acoustic impedance, Mechanical impedance.

**Random noise** Stationary noise whose instantaneous amplitude cannot be specified at any given instant of time. Instantaneous amplitude can only be defined statistically by an amplitude distribution function. *See* Pink noise, White noise.

**Random vibration** Vibration whose instantaneous amplitude cannot be specified at any given instant of time. The instantaneous amplitude can only be defined statistically by a probability distribution function that gives the fraction of the total time that the amplitude lies within specified amplitude intervals. Random vibration contains no periodic or quasi-periodic constituents. Pseudo, periodic, and burst random are special forms.

**Rating** A method to quantify psychological variables, such as annoyance, loudness, and others. Typically, the subject is requested to choose one out of several locations on a scale labeled, for instance, from 0 to 10, whereby the selected location indicates the strength of the internal response. *See* Annoyance, Loudness.

**Rayleigh's criterion** In thermoacoustics, a necessary condition for the onset of instability, in an irrotational flow at low Mach number that contains a compact heat source of time-varying output  $Q(t)$ . It states that oscillations can become unstable when the heat input is in phase with the local sound pressure  $p(t)$ , at any given frequency. A more precise statement applicable to nonlinear oscillation is that instability requires  $\oint p(t)Q(t) dt > 0$  (integral over one cycle).

**Reactance** The imaginary part of an impedance. *See* Acoustic impedance, Mechanical impedance, Resistance.

**Reactive sound field** Sound field in which the particle velocity is  $90^\circ$  out of phase with the pressure. An ideal standing wave is an example of this type of field, where there is no net flow of energy and constitutes the imaginary part of a complex sound field. *See* Standing wave.

**Receptance** An alternative term for *dynamic compliance*. *See* Compliance (2).

**Reflection coefficient** The ratio of the reflected sound pressure amplitude to the pressure amplitude of the sound wave incident on the reflecting object. Unit: none. Symbol:  $r_a$ .

**Reflection factor, reflectance** The ratio of the reflected sound power to the incident sound power. Unit: none. Symbol:  $r$ . *See* Absorption factor, Dissipation factor, Transmission factor.

**Refraction** A phenomenon by which the propagation direction of a sound wave is changed when a wavefront passes from one region into another region of different phase speed of sound.

**Repetency** *See* Wavenumber.

**Resistance** The real part of an impedance. *See* Acoustic impedance, Mechanical impedance, Radiation impedance, Reactance.

**Resolution** The smallest change or amount a measurement system can detect.

**Resonance** Conditions of peak vibratory response where a small change in excitation frequency causes a decrease in system response.

**Resonance frequency** Frequency at which resonance exists. Unit: Hz.

**Response** Motion or other output resulting from an excitation, under specified conditions. *See* Excitation.

**Reverberant sound field** Portion of the sound field in the test room over which the influence of sound received directly from the source is negligible.

**Reverberation** Persistence of sound in an enclosure after a sound source has stopped.

**Reverberation room** A room with low absorption and long reverberation time, designed to make the sound field therein as diffuse as possible.

**Reverberation time** Of an enclosure, for a given frequency or frequency band, the time required for the sound pressure level in an initially steady sound field to decrease by 60 dB after the sound source has stopped. Unit: second (s).

**Room constant** A quantity used to describe the capability of sound absorption of an enclosure, determined by  $R = S\bar{\alpha}/(1 - \bar{\alpha})$ , where  $S$  is the total internal surface area of the enclosure, in square metres;  $\bar{\alpha}$  is the average sound absorption coefficient of the enclosure. Units: square metre ( $\text{m}^2$ ). Symbol:  $R$ .

**Root mean square (rms)** The square root of the arithmetic average of a set of squared instantaneous values.

**Sabin, metric sabin** A measure of sound absorption of a surface. One metric sabin is equivalent to 1 square metre of perfectly absorptive surface. *See* Absorption, Equivalent sound absorption area.

**Sampling theorem** Theorem that states that if a continuous time signal is to be completely described, the sampling frequency must be at least twice the highest frequency present in the original signal. Also known as *Nyquist theorem*, *Shannon sampling theorem*.

**Scaling** *See* Magnitude scaling, Rating.

**Semianechoic field** *See* Free field over a reflecting plane.

**Semianechoic room** A test room with a hard, reflecting floor whose other surfaces absorb essentially all the incident sound energy over the frequency range of interest, thereby affording free-field conditions above a reflecting plane. *See* Anechoic room, Free field over a reflecting plane.

**Sensitivity** (1) Of a linear transducer, the quotient of a specified quantity describing the output signal by another specified quantity describing the corresponding input signal, at a given frequency. (2) Of a data acquisition device or spectrum analyzer, a measure of the device's ability to display minimum level signals. (3) Of a person, with respect to a noise, the extent of being annoyed.

**Sensorineural hearing loss** *See* Hearing loss.

**Shock** Rapid transient transmission of mechanical energy.

**Shock spectrum** Maximum acceleration experienced by a single-degree-of-freedom system as a function of its own natural frequency in response to an applied shock.

**Signal-to-noise ratio (SNR)** In a signal consisting of a desired component and an uncorrelated noise component, the ratio of the desired-component power to the noise power. For a signal  $x(t)$ , if  $x(t) = s(t) + n(t)$ , where  $s(t)$  is the desired signal, and  $n(t)$  is noise, then the signal-to-noise ratio is defined as  $\text{SNR} = 10 \log_{10} \langle s^2 \rangle / \langle n^2 \rangle$ , where  $\langle \rangle$  indicates a time average.

**Significant threshold shift** Shift in hearing threshold, outside the range of audiometric testing variability ( $\pm 5$  dB), that warrants followup action to prevent further hearing loss. The National Institute of Occupational Safety and Health (NIOSH), defines significant threshold shift as an increase in the hearing threshold level of 15 dB or more at any frequency (500, 1000, 2000, 3000, 4000, or 6000 Hz) in either ear that is confirmed for the same ear and frequency by a second test within 30 days of the first test. *See* Hearing threshold level.

**Silencer** Any passive device used to limit noise emission.

**Simple harmonic motion** Periodic motion whose displacement varies as a sinusoidal function of time.

**Single-event sound pressure level** Time-integrated sound pressure level of an isolated single sound event of specified duration  $T$  (or specified measurement time  $T$ ) normalized to  $T_0 = 1$  s. It is given by the formula:

$$L_{p,1s} = 10 \log_{10} \left[ \frac{1}{T_0} \int_0^T \frac{p^2(t)}{p_0^2} dt \right]$$

$$= L_{peq,T} + 10 \log_{10} \left( \frac{T}{T_0} \right) \text{ dB},$$

where  $p(t)$  is the instantaneous sound pressure,  $p_0$  is the reference sound pressure, and  $L_{peq,T}$  is the equivalent continuous sound pressure level. Unit: decibel (dB). Symbol:  $L_{p,1s}$ .

**Sone** A linear unit of loudness. One sone is the loudness of a pure tone presented frontally as a



plane wave of 1000 Hz and a sound pressure level of 40 dB, referenced to 20  $\mu\text{Pa}$ . *See* Loudness, Magnitude scaling.

**Sound** Energy that is transmitted by pressure waves in air or other materials and is the objective cause of the sensation of hearing. Commonly called noise if it is unwanted.

**Sound absorption coefficient** *See* Absorption factor.

**Sound energy density** Mean sound energy in a given volume of a medium divided by that volume. If the energy density varies with time, the mean shall be taken over an interval during which the sound may be considered statistically stationary. Units: joule per cubic metre ( $\text{J/m}^3$ ).

**Sound energy, acoustic energy** Total energy in a given volume of a medium minus the energy that would exist in that same volume with no sound wave present. Unit: joule (J).

**Sound exposure** Time integral of squared, instantaneous sound pressure over a specified interval of time,

given by  $E = \int_{t_1}^{t_2} p^2(t) dt$ , where  $p(t)$  is the instantaneous sound pressure,  $t_1$  and  $t_2$  are the starting and ending times for the integral. If the instantaneous sound pressure is frequency weighted, the frequency weighting should be indicated. Units: pascal-squared second ( $\text{Pa}^2\text{s}$ ). Symbol:  $E$ . *See* Sound pressure.

**A-weighted sound exposure** Exposure given by  $E_{A,T} = \int_{t_1}^{t_2} p_A^2(t) dt$ , where  $p_A(t)$  is the instantaneous A-weighted sound pressure of the sound signal integrated over a time period  $T$  starting at  $t_1$  and ending at  $t_2$ . *See* Frequency weighting.

**Sound exposure level (SEL)** Measure of the sound exposure in decibels, defined as  $L_E = 10 \log_{10}(E/E_0)$  dB, where  $E$  is sound exposure, and the reference value  $E_0 = 400 \mu\text{Pa}^2 \text{ s}$ . Unit: decibel (dB). Symbol:  $L_E$ . *See* Sound exposure, Single-event sound pressure level.

**Sound intensity** Time-averaged value of the instantaneous sound intensity  $\mathbf{I}(t)$  in a temporally stationary sound field:

$$\mathbf{I} = \frac{1}{t_1 - t_2} \int_{t_1}^{t_2} \mathbf{I}(t) dt$$

where  $t_1$  and  $t_2$  are the starting and ending times for the integral. Units: watt per square metre ( $\text{W/m}^2$ ). Symbol:  $\mathbf{I}$ . *See* Instantaneous sound intensity. *Note:* Sound intensity is generally complex. The symbol  $J$  is often used for complex sound intensity. The symbol  $I$  is used for active sound intensity, which is the real part of a complex sound intensity.

**Sound intensity level** A measure of the sound intensity in decibels, defined as  $L_I = 10 \log_{10}(I/I_0)$ , where  $I$  is the active sound intensity, and the reference value  $I_0 = 10^{-12} \text{W/m}^2 = 1 \text{ pW/m}^2$ . Unit: decibel (dB).

**Sound level** *See* Sound pressure level.

**Sound level meter** Electronic instrument for measuring the sound pressure level of sound in accordance with an accepted national or international standard. *See* Sound pressure level.

**Sound power** Power emitted, transferred, or received as sound. Unit: watt (W). *See* Sound intensity.

**Sound power level (SPL)** Ten times the logarithm to the base 10 of the ratio of a given sound power to the reference sound power, given by  $L_W = 10 \log_{10}(P/P_0)$ , where  $P$  is the rms value of sound power in watts, and the reference sound power  $P_0$  is 1 pW ( $= 10^{-12} \text{ W}$ ). Unit: decibel (dB). Symbol:  $L_W$ . The weighting network or the width of the frequency band used should be indicated. If the sound power level is A-weighted, then the symbol is  $L_{WA}$ . *See* Frequency weighting.

**Sound pressure** Dynamic variation in atmospheric pressure. Difference between the instantaneous pressure and the static pressure at a point. Unit: pascal (Pa). Symbol:  $p$ . **A-weighted sound pressure** The root-mean-square sound pressure determined by use of frequency weighting network A (see IEC 61672-1). Symbol:  $p_A$ .

**Sound pressure level (SPL)** Ten times the logarithm to the base 10 of the ratio of the time-mean-square sound pressure to the square of the reference sound pressure, given by  $L_p = 10 \log_{10}(p^2/p_0^2)$ , where  $p$  is the rms value (unless otherwise stated) of sound pressure in pascals, and the reference sound pressure  $p_0$  is 20  $\mu\text{Pa}$  ( $= 20 \times 10^{-6} \text{ N/m}^2$ ) for measurements in air. Unit: decibel (dB). Symbol:  $L_p$ . If  $p$  denotes a band-limited, frequency or time-weighted rms value, the frequency band used or the weighting shall be indicated. Frequency and time weightings are specified in IEC 61672-1. **A-weighted sound pressure level** Sound pressure level of A-weighted sound pressure, given by  $L_{pA} = 10 \log_{10}(p_A^2/p_0^2)$ , where  $p_A$  is the A-weighted sound pressure, and  $p_0$  is the reference sound pressure. Symbol:  $L_{pA}$ . *See* Sound pressure. **Band pressure level** The sound pressure level in a particular frequency band.

**Sound reduction index** Of a partition, in a specified frequency band, 10 times the logarithm to the base 10 of the reciprocal of the sound transmission coefficient, given by  $R = 10 \log_{10}(1/\tau) = 10 \log_{10}(W_1/W_2)$ , where  $\tau$  is the sound transmission coefficient,  $W_1$  is the sound power incident on the partition under test, and  $W_2$  is the sound power transmitted through the specimen. In practice, the sound reduction

index is evaluated from

$$R = L_1 - L_2 + 10 \log_{10} \frac{S}{A} = D + 10 \log_{10} \frac{S}{A}$$

where  $L_1$  and  $L_2$  are the average sound pressure levels in the source and receiving rooms,  $S$  is the area of the test specimen,  $A$  is the equivalent sound absorption area in the receiving room, and  $D$  is the level difference. Also known as *sound transmission loss*. Unit: decibel (dB). Symbol:  $R$ , or TL. *See* Sound transmission coefficient, Level difference, Equivalent sound absorption area, Coincidence effect. **Apparent sound reduction index** Ten times the logarithm to the base 10 of the ratio of the sound power  $W_1$ , which is incident on the partition under test to the total sound power transmitted into the receiving room if, in addition to the sound power  $W_2$  transmitted through the specimen, the sound power  $W_3$  transmitted by flanking elements or by other components, is significant:

$$R' = 10 \log_{10} \left( \frac{W_1}{W_2 + W_3} \right)$$

Unit: decibel (dB). Symbol:  $R'$ . *See* Flanking transmission.

**Sound source** Anything that emits acoustic energy into the adjacent medium.

**Sound transmission class (STC)** A single-number rating for describing sound transmission loss of a wall or partition. Unit: decibel (dB). The standardized method of determining sound transmission class is provided in ASTM E413-87. *See* Sound reduction index.

**Sound transmission loss** *See* Sound reduction index.

**Sound volume velocity** Surface integral of the normal component of the sound particle velocity over an area through which the sound propagates. Also known as *sound volume flow rate*. Units: cubic metre per second ( $\text{m}^3/\text{s}$ ). Symbol:  $q$  or  $q_v$ .

**Sound energy flux** Time rate of flow of sound energy through a specified area. Unit: watt (W).

**Specific acoustic impedance** Complex ratio of sound pressure to particle velocity at a point in an acoustical medium. Units: pascal per metre per second [ $\text{Pa}/(\text{m}/\text{s})$ ], or rayls ( $1 \text{ rayl} = 1 \text{ N} \cdot \text{s}/\text{m}^3$ ). *See* Characteristic impedance, Acoustic impedance, Mechanical impedance.

**Specific airflow resistance** A quantity defined by  $R_s = RA$ , where  $R$  is the airflow resistance, in pascal seconds per cubic metre, of the test specimen, and  $A$  is the cross-sectional area, in square metres, of the test specimen perpendicular to the direction of flow. Units: pascal second per metre ( $\text{Pa} \cdot \text{s}/\text{m}$ ). Symbol:  $R_s$ . *See* Airflow resistance.

**Spectral leakage error** In digital spectral analysis, an error that the signal energy concentrated at a particular frequency spreads to other frequencies. This phenomenon results from truncating the signal in the time domain. The leakage error can be minimized by applying a proper window to the signal in the time domain. *See* Window.

**Spectrum** Description of a signal resolved into frequency components, in terms of magnitude, and sometimes as well as phase, such as power spectrum, one-third octave spectrum. *See* Fourier transform, Power spectrum, Power spectrum density, Cross spectrum.

**Speech quality** Degree to which speech sounds normal, without regard to its intelligibility. Measurement is subjective and involves asking listeners about different aspects of speech such as naturalness, amount and type of distortion, amount and type of background noise.

**Standard threshold shift** Increase in the average hearing threshold of 10 dB or more at 2000, 3000, and 4000 Hz in either ear. *See* Hearing loss, Hearing threshold.

**Standardized level difference** *See* Level difference.

**Standing wave** Periodic wave motion having a fixed amplitude distribution in space, as the result of superposition of progressive waves of the same frequency and kind. Characterized by the existence of maxima and minima amplitudes that are fixed in space.

**Static pressure** Pressure that would exist in the absence of sound waves.

**Statistical pass-by (SPB) method** A measurement method used for measuring noise properties of road surfaces (pavements), utilizing a roadside microphone (7.5 m from the center of the road lane being measured) and speed measurement equipment. Vehicles passing by in the traffic are measured and classified according to standard types, provided no other vehicles influence the measurement. The measured values are treated statistically, by vehicle type; being plotted as noise level versus speed. Either the regression curve is determined or the noise level is read at one or a few reference speeds. The method is standardized as ISO 11819-1. *See* Tire/road noise, Close-proximity method.

**Stiffness** The ratio of the change in force to the corresponding change in displacement of an elastic element, both in specified direction.

**Structure-borne sound** Sound that propagates through a solid structure. *See* Airborne sound, Liquid-borne sound.

**Subharmonic** A frequency component whose frequency is an integer fraction of the fundamental frequency of a periodic quantity to which it is related. *See* Harmonic.

**Susceptance** The imaginary part of an admittance. *See* Admittance, Conductance.

**Swept sine** A test signal consisting of a sine wave whose frequency is changing according to a certain pattern, usually a linear or logarithmic progression of frequency as a function of time, or an exponential sweep.

**Thermoacoustical excitation** Excitation of sound wave by periodic heat release fluctuations of a reacting flow (flame). A necessary condition for thermoacoustical excitation is given by the Rayleigh criterion. *See* Rayleigh criterion.

**Time-averaged sound pressure level** An alternative term for *equivalent continuous sound pressure level*. *See* Equivalent continuous sound pressure level.

**Time-weighted average (TWA)** The averaging of different exposure levels during an exposure period. For noise, given an A-weighted 85-dB sound exposure level limit and a 3-dB exchange rate, the TWA is calculated using:  $TWA = 10 \log_{10}(D/100) + 85$ , where  $D$  is the noise dose. *See* Noise dose (2).

**Tire/road noise** Unwanted sound generated by the interaction between a rolling tire and the surface on which it is rolling. Also known as *tire/pavement noise*. *See* Close-proximity method, Statistical pass-by method.

**Tonal noise** Noise dominated by one or several distinguishable frequency components (tones).

**Transducer** A device designed to convert an input signal of a given kind into an output signal of another kind, usually electrical.

**Transfer function** Of a linear time-invariant system, the ratio of the Fourier or Laplace transform of an output signal to the same transform of the input signal. *See* Frequency response function.

**Transmissibility** The ratio of the response amplitude of a system in steady-state forced vibration to the excitation amplitude. The input and output are required to be of the same type, for example, force, displacement, velocity, or acceleration.

**Transmission factor, transmission coefficient, transmittance** The ratio of the transmitted sound power to the incident sound power. Unit: none. Symbol:  $\tau$ . *See* Absorption factor, Dissipation factor, Reflection factor.

**Transmission loss** (1) Reduction in magnitude of some characteristic of a signal between two stated points in a transmission system, such as a silencer. The characteristic is often some kind of level, such as power level or voltage level. Transmission loss is usually in units of decibels. It is imperative that the characteristic concerned (such as sound pressure level) be clearly identified because in all transmission

systems more than one characteristic is propagated. (2) An equivalent term for *sound transmission loss*. *See* Sound reduction index. (3) In underwater acoustics, between specified source and receiver locations, the amount by which the sound pressure level at the receiver lies below the source level. Also known as *propagation loss*.

**Turbulence** A fluid mechanical phenomenon that causes fluctuation in the local sound speed relevant to sound generation in turbo machines (pumps, compressors, fans, and turbines), pumping and air-conditioning systems, or propagation from jets and through the atmosphere.

**Ultrasound** Sound at frequencies above the audible range, i.e., above about 20 kHz.

**Velocity** A vector quantity that specifies time rate of change of displacement. Units: metre per second (m/s). *See* Displacement, Acceleration, Jerk, Particle velocity, Vibratory velocity.

**Velocity excitation** *See* Excitation.

**Vibration** (1) Oscillation of a parameter that defines the motion of a mechanical system. Vibration may be broadly classified as transient or steady state, with further subdivision into either deterministic or random vibration. (2) The science and technology of vibration. *See* Forced vibration, Free vibration.

**Vibration absorber** A passive subsystem attached to a vibrating machine or structure in order to reduce its vibration amplitude over a specified frequency range. At frequencies close to its own resonance, the vibration absorber works by applying a large local mechanical impedance to the main structure. Also known as *vibration neutralizer*, *tuned damper*.

**Vibration isolator** A resilient support that reduces vibration transmissibility. *See* Isolation, Transmissibility.

**Vibration meter** An instrument for measuring oscillatory displacement, velocity, or acceleration.

**Vibration severity** A criterion for predicting the hazard related to specific machine vibration levels.

**Vibratory velocity level, vibration velocity level** Velocity level given by the following formula  $L_v = 10 \log_{10}(v^2/v_0^2)$ , where  $v$  is the rms value of the vibratory velocity within the frequency band of interest,  $v_0$  is the reference velocity and is equal to  $5 \times 10^{-8}$  m/s (as specified in ISO 7849) or  $10^{-9}$  m/s (as specified in ISO 1683). Unit: decibel (dB). Symbol:  $L_v$ . *See* Vibratory velocity.

**Vibratory velocity, vibration velocity** Component of the velocity of the vibrating surface in the direction normal to the surface. The root-mean-square value of the vibratory velocity is designated by the symbol  $v$ . *See* Vibratory velocity level.

**Viscosity** Of a fluid, in a wide range of fluids the viscous stress is linearly related to the rate of strain; such fluids are called *newtonian*. The constant of proportionality relating fluid stress and rate of strain is called the viscosity. Units: pascal seconds (Pa·s).

**Vocal folds, vocal cords** Paired muscular folds of tissue layers inside the larynx that can vibrate to produce sound.

**Vocal tract** Air passage from the vocal folds in the larynx to the lips and nostrils. It can be subdivided into the pharynx, from larynx to velum, the oral tract, from velum to lips, and the nasal tract, from above the velum through the nasal passages to the nostrils. Its shape is the main factor affecting the acoustical characteristics of speech sounds. *See* Vocal folds.

**Voicing, voiced, voiceless, unvoiced, devoiced** Voicing is one of the three qualities by which speech sounds are classified; a sound with voicing is called voiced, which means that the vocal folds are vibrating and produce a quasi-periodic excitation of the vocal tract resonances. A phoneme that is normally voiced but is produced without voicing, or in which the voicing ceases, is devoiced. A phoneme that is intended not to be voiced is voiceless or unvoiced. *See* Vocal folds, Phoneme.

**Voltage preamplifier** A preamplifier that produces an output voltage proportional to the input voltage from a piezoelectric transducer. Input voltage depends upon cable capacitance.

**Volume velocity** (1) *See* Sound volume velocity. (2) For speech, a measure of flow rate in the absence of sound, as through a duct, including through the vocal tract. Units: cubic metre per second ( $\text{m}^3/\text{s}$ ).

**Wavefront** (1) For a progressive wave in space, the continuous surface that is a locus of points having the same phase at a given instant. (2) For a surface wave, the continuous line that is a locus of points having the same phase at a given instant.

**Wavelength** Distance in the direction of propagation of a sinusoidal wave between two successive points

where at a given instant of time the phase differs by  $2\pi$ . Equals the ratio of the phase speed of sound in the medium to the fundamental frequency.

**Wavenumber** At a specified frequency,  $2\pi$  divided by wavelength, or angular frequency divided by the phase speed of sound:  $k = 2\pi/\lambda = \omega/c$ , where  $\lambda$  is wavelength, in metres;  $\omega$  is angular frequency, in radians per second;  $c$  is the phase speed of sound, in metres per second. Unit: reciprocal metre (1/m). Symbol:  $k$ . *Notes:* (1) The ISO standards prefer to use the term *angular repetency* and *repetency*. A remark in ISO 8000 says that in English the names repetency and angular repetency should be used instead of wavenumber and angular wavenumber, respectively, since these quantities are not numbers. (2) Angular repetency is defined as the same as wavenumber. (3) Repetency: at a specified frequency, the reciprocal of wavelength:  $\sigma = 1/\lambda$ , where  $\lambda$  is wavelength. Unit: reciprocal metre (1/m). Symbol:  $\sigma$ .

**Weighting** (1) *See* Frequency weighting. (2) *See* Window. (3) Exponential or linear time weighting defined in IEC 61672-1.

**Weighting network** Electronic filter in a sound level meter that approximates under defined conditions the frequency response of the human ear. The A-weighting network is most commonly used. *See* Frequency weighting.

**White noise** A noise the power spectrum of which is essentially independent of frequency. *See* Pink noise.

**Whole-body vibration** Vibration of the human body as a result of standing on a vibrating floor or sitting on a vibrating seat. Often encountered near heavy machinery and on construction equipment, trucks, and buses.

**Window** In signal processing, a weighting function with finite length applied to a signal. Usually applied in the time domain, as a multiplying function applied to the time signal. For spectral analysis, Hanning, Hamming, triangle, Blackman, flat top, Kaiser windows are commonly used. Force and exponential windows are special for impact testing.

# INDEX

- Absorbing materials. *See* Sound absorbing materials
- Absorption coefficient. *See* Sound absorption coefficient; Statistical absorption coefficient
- Accelerance, 566, 679–680
- Acceleration, 11
- Acceleration, base, 213–216
- Acceleration level, 305, 420 *f*, 429, 503, 524, 627, 679, 1152, 1418
- weighted, 1458–1459, 1459
- Accelerogram(s), 219, 1395, 1400–1401
- Accelerometer, 790, 790 *f*, 792, 928, 1088, 1164, 1210
- piezoelectric, 1080
- resonance frequency, 864
- Acoustical baffles, 1494, 1498–1499, 1499 *f*
- Acoustical control, 781–783, 782 *f*, 1207, 1209 *f*, 1210, 1217
- Acoustical efficiency, 935, 936, 981
- Acoustical enclosure(s), 658
- close fitting, 663–665, 664 *f*, 665 *f*, 690–692, 691 *f*, 979
- insertion loss, 658–659, 688–692, 691 *f*
- leaks through, 660, 689, 692, 693, 694
- for machines, 659–660, 665–666
- noise reduction, 649–650, 658, 665–666, 692, 692 *t*, 693
- partial, 692, 692 *f*
- for personnel, 658–659
- Acoustical holography, 238, 417, 433, 598–610
- Acoustical leak, 1205
- Acoustical lumped elements, 41
- Acoustical modeling, 42, 101–113, 796–797, 1217–1218, 1217 *f*
- Acoustical privacy, 1152, 1310
- Acoustical standards. *See* Standards
- Acoustical terminology, 377–378, 1016
- Acoustical trauma, 334
- Acoustic disturbances, 8
- Acoustic impedance, 517–520, 518 *f*
- characteristic, 21, 29, 29 *f*, 54, 72, 249, 535, 670, 676, 699, 1047, 1252
- complex, 519, 708 *f*, 709
- specific, 61, 64, 698–699
- Acoustic reactance, 71, 699
- Acoustic resistance, 243, 250, 699, 792, 1046, 1254
- Action level, 346, 347 *f*, 384, 385, 1528
- Active headsets, 761, 768, 1155, 1207, 1210–1211, 1213
- Active machinery isolation, 651–655
- Active noise control
- of acoustic energy in enclosure(s), 761–769
- cancellation, 761–762, 761 *f*
- (effect of) modal overlap, 766–767, 767 *f*
- enclosed field, 764–766, 766 *f*
- free field radiation, 763–764
- wave transmission, 761
- Active sound control 762, 768
- Active sound field, 535
- Active vibration control, 770–783
- actuators, 770–774
- advanced, 772
- electrodynamic, 770–771
- error sensors, 772–774
- piezoelectric, 771–772
- control, 774–777
- feedback, 776–777
- feed forward, 775–776
- Active vibration isolation, 639, 770, 777–778
- Actuators
- electrodynamic, 451–452, 770–771
- electromagnetic, 451–452
- electrorheological fluid type, 453
- hydraulic, 223, 451
- magnetostrictive, 452–453
- piezoelectric, 453, 771–772
- pneumatic, 451
- structural, 454
- Adaptation, 286–291, 813, 1284–1294, 1357
- Added fluid mass, 1379–1380
- Admittance, 70–73, 103
- Aerodynamic noise, 128–155, 802, 838, 840, 935, 938, 966, 972, 980–981, 982–983, 1017–1018, 1019, 1021, 1417, 1427–1428, 1440
- Aerodynamic sound, 1072–1083
- generation, 1323–1327
- Affricatives, 294
- Air absorption, 1247–1248
- Air attenuation (of sound), 60, 1441
- Air-borne sound, 1056, 1162, 1237, 1257–1265
- Air compressor, 1004, 1332, 1347
- Aircraft noise, 128–155
- exterior noise, 1479–1489
- interior noise, 598–599, 668, 673, 674, 1198, 1200, 1203, 1204
- metrics, 317, 1481–1484
- Airflow resistance, 1252
- Airflow resistivity, 698
- Air jet noise, 987–988, 993, 1323
- Airport(s)
- land use planning, 1485
- layout, 1488
- noise, 1487–1488
- operational procedure(s), 1488
- preferential runway use, 1488
- Air spring(s), 1338
- Air terminal device(s), 1319–1320
- Aliasing, 496–497
- Ambient noise, 1225, 1237–1238, 1299, 1516–1523
- American National Standards Institute (ANSI), 286, 326, 368, 378, 386, 394, 456, 465, 505, 1267, 1270, 1300, 1305, 1414, 1451, 1458, 1482, 1502
- American Society of Heating, Refrigeration and Air-Conditioning Engineers (ASHRAE), 322, 401, 1270–1271, 1272, 1274, 1352
- American Society of Testing and Materials (ASTM), 1305
- Amplitude, 3–4
- Amplitude distribution, 859
- Gaussian, 209
- Analog-to-digital conversion (A/D) or (ADC), 493–496
- Analyzer(s), 470–485
- Anechoic chamber (anechoic room), 34 *f*, 265, 432, 621, 939, 1111
- Angular spectrum, 600, 604, 607–608
- Annoyance, 274, 303–304, 316–319, 320–324, 394–397, 408–410, 502–508
- complaints (about noise), 318–319
- percentage highly annoyed (%HA), 318, 408, 1414, 1414 *f*
- Anti-aliasing filter, 471, 476, 487, 496–497, 504, 671
- Anti-resonance, 183–184, 186–189–190, 297–299, 564, 569–570, 746, 950, 1142
- A-pillar, 1073, 1075–1076, 1079, 1084, 1160
- Apparent sound reduction index, 1286
- Architectural acoustics, 510, 511, 1297, 1298
- Area-related sound power level(s), 1511–1523
- Articulation Index (AI), 399–402, 1281, 1299–1300
- Artificial head, 805, 1080
- Aspiration, 294, 957, 1149, 1159–1162, 1160, 1160 *f*
- Asymptotic threshold shift (ATS), 327–331, 329 *f*, 331 *f*
- Atmospheric pressure, 7, 10, 20, 43, 61
- Atmospheric sound absorption, 67–68, 1111, 1248
- Atmospheric sound attenuation, 60, 1441. *See also* Atmospheric sound absorption

*Note:* An *f* following a page number indicates a citation in a figure on that page. A *t* indicates following a page number indicates a citation in a table on that page.

- Atmospheric turbulence, 74, 76  
 Attenuation  
   atmospheric, 60, 1441  
   by barrier(s), 70  
   by foliage, 74  
   outdoor, 67–70  
   by trees, 74  
 Audibility threshold, 277, 277*f*, 279, 297*f*  
 Audible range of hearing, 13–14, 14*f*, 274–275, 304, 326, 391, 458, 901  
 Audio frequency 559  
 Audiogram, 286, 320, 387, 388, 391–392, 391*f*, 392*f*  
 Audiometer, 287, 462  
 Audiometric test(s), 381, 385, 387  
 Auditory canal, 277–282, 278*f*, 281*f*  
 Auditory cortex, 283, 283*f*  
 Auditory ossicles, 277, 278, 278*f*, 279, 337  
 Auditory threshold, 339, 368  
 Autocorrelation function, 206–207, 206*f*, 263, 560–562  
 Automobile noise  
   exterior noise, 1427–1436  
   interior noise, 1149–1152  
 Auto spectrum, 477–480, 497–500, 562–563, 677, 1091*f*  
 A-wave, 326  
 A-weighted sound power level, 527–531, 1001–1009, 1143*f*, 1186–1187, 1490–1492, 1510, 1512–1513  
 A-weighted sound pressure level, 398*f*, 404*f*, 1267–1269, 1428*f*, 1429*f*, 1430*f*, 1432*f*, 1433*f*  
 Background noise  
   and speech intelligibility, 1300  
   and speech interference level, 399, 399*f*, 1268–1269, 1268*f*  
 Balanced noise criterion (BNC)  
   curves, 402–403, 402*f*, 1275–1276, 1276*f*  
 Balancing  
   influence coefficient method, 757–758  
   rotor(s)  
     flexible, 755–756  
     rigid, 754–755  
   unbalance  
     dynamic, 754–755  
     static, 753–754  
 Band sound pressure level, 842*f*, 1020*f*, 1273*f*, 1280, 1328, 1331, 1406, 1407  
 Bandwidth  
   half-power, 735, 1242  
   octave, 472–473, 473*f*, 556–558, 561  
 Bark, 811*f*, 812*f*, 818*f*, 819*f*  
 Barrier(s)  
   absorption, 717, 718  
   attenuation, excess, 1417–1418  
   design, 720–721, 721*f*  
   diffraction over, 68–70, 714–715  
   double, 720  
   finite, 718, 718*f*  
   Fresnel number, 68–69, 714, 716, 718, 1417  
   indoors, 716–717, 717*f*  
   insertion loss, 714–720  
   non-parallel, 718–719  
   for open plan offices 1300  
   outdoors, 717–718  
   performance, atmospheric effect(s)  
     (on), 1447–1449  
   rail, 722, 1444  
   reflection(s), 70, 719, 719*f*  
   road, 717, 719, 720, 721  
   shape, 720  
   theory, 1417–1418  
   thick, 719–720, 719*f*, 720*f*  
   transmission loss, 716  
 Base isolation (of buildings), 1419, 1470–1478  
 Basilar membrane, 271, 278, 278*f*, 280–283, 280*f*, 281*f*, 282*f*, 337  
 Bel, 11  
 Bearing(s), 832–833, 857–867  
   ball, 857, 952  
   clearance, 857, 863–865  
   defects, 865  
   diagnostics, 859–860  
   failure, 857–858  
   fatigue, 258  
   fixed, 857  
   floating, 857  
   frequencies, 857, 858–861  
   hydrostatic, 867  
   journal, 865, 866  
   lifetime, 857  
   misalignment, 863  
   monitoring  
     noise, 858  
     temperature, 858  
     vibration, 858–859  
   oil whip, 866–867  
   oil whirl, 866–867  
   roller, 861–862  
   rolling contact, 857  
   sliding, 862–863  
   sliding contact, 857  
   ultrasonic vibration, 860  
 Beat frequency, 475  
 Beaufort scale, 1383  
 Bending field, 1405–1406  
 Bending waves, 20, 35, 36, 38, 87, 594, 1257  
 Bernoulli equation, 192, 194, 202, 1376, 1382  
 Bias, 318  
 Bias error, 500, 540, 541, 543, 564  
 Blade-vortex interaction noise (of fans), 1120, 1125, 1127  
 Blowers. *See* Fan(s)  
 Blue Angel, 1490, 1492  
 Bode diagram, 864  
 Bogie(s), shrouds, 1444  
 Boundary conditions, 70, 119–121  
 Boundary element method (BEM) *See* Boundary element modeling  
 Boundary element modeling, 116–125  
   of gear housing, 117, 118*f*  
   of silencer transmission loss, 116–122  
   of sound power radiated from oil pan, 122  
 Boundary-layer (noise), 150–155  
 Boundary layer pressure fluctuation(s), 303, 1017, 1197, 1207, 1226  
 Brake(s)  
   disc, 1021, 1133, 1140, 1417, 1439  
   flutter, 1136  
   noise, 1133–1134  
   groan, 1134  
   judder, 1134  
   sprag-slip, 1135–1136  
   squeal, 1134, 1136–1137  
 Breakout noise, 1320  
   control, 1175–1176, 1316, 1322  
   prediction  
 Broadband noise, 163, 1219  
 Brownian motion, 7, 19  
 Buffeting, 1383–1384, 1384*f*  
 Building  
   codes, 1348–1353  
   natural frequencies, 1386–1388  
   site(s)  
     noise, 1423–1424, 1516–1524  
   vibration, 1238, 1385–1386, 1386*f*  
 Building Officials and Code Administrators International (BOCA), 1348  
 Built environment, 1267  
 Bulk modulus, 698, 951, 952  
 Bulldozer noise, 1186, 1189, 1189*f*, 1191, 1490–1494, 1490*f*, 1493*f*, 1580  
 Burner, 956–965  
   diffusion-flame, 957  
   nozzle-flame, 957  
   premix-flame, 957  
 B-wave, 326  
 By-pass ratio, 110, 128, 1096–1097, 1097*f*, 1101, 1102, 1480  
 Cabin noise, 1207–1215  
 Cab(s), 1189–1191, 1194–1196  
 Calibration methods  
   comparison methods, 616–617  
   coupler(s), 617  
   interferometry, 510, 629–630, 634–642  
   low frequency, 620  
   metrology, 620–621  
   microphone, 620, 621–622  
   on-site, 615–616  
   phase response, 618–620  
   reciprocity, 621*f*  
   secondary, 616  
   shock 624–626, 629–630  
   sound intensity, 542  
   sound pressure, 612–623  
   traceability, 633–645  
   vibration, 624–632  
 Calibrator, pistonphone, 616  
 California, 1349–1350  
 Casing radiated noise, 1321–1322  
 Causality, 390–392  
 Cavity flow (noise), 149, 1075  
 Ceiling absorption, 1301  
 Center frequency, 13, 14, 244, 247, 252, 272, 472, 481, 497, 810–811

- Central auditory nervous system, 283  
 Cepstrum analysis, 484, 498, 1092*f*  
 Characteristic equation, 187–188, 193, 198, 244  
 Characteristic impedance, 21, 29, 54, 72, 249, 535, 670, 676, 699, 1047, 1252  
 Charge amplifier, 429, 445, 450, 522, 627, 644, 644*f*  
 Chatter  
   control, 997–999  
   mechanisms, 995–997  
   prediction, 995–999  
 Chute, 988–989, 989*f*  
 Close fitting enclosure(s), 663, 665, 690–692, 691*f*  
 Close-Proximity (CPX) method, 1059–1060  
   Trailer, 1060  
 Cochlea, 271–271, 272*f*, 277–283, 277*f*, 278*f*, 280*f*, 337  
 Code spectrum (spectra), 1395, 1397*f*, 1401  
 Coherence, function, 498  
 Coincidence  
   dip, 1257–1258, 1259  
   effect, 35, 1257, 1258, 1259, 1261–1262  
   frequency, 95–96, 96*f*, 99, 1150, 1151, 1237  
 Combustion  
   active control, 963  
   oscillations, 960  
   resonator(s), 956–963  
 Combustion (system). *See* Burner; Furnace, burner  
 Community noise  
   criteria, 409–411  
   model code, 1348  
   noise rating (CNR), 403–405  
   noise regulations, 409–411  
   ordinances, 1424, 1525–1531  
 Community reaction (to noise), 1509, 1514–1515  
 Complex stiffness, 226–227, 679, 735, 736  
 Compliance, 1363–1364  
 Community noise exposure level (CNEL) 407, 1270, 1350  
 Composite noise rating (CNR), 403–405  
 Composite wall structures, 659, 688, 1237, 1299  
 Compressed air, 987–988  
 Compressional waves, 19–20  
 Compressor noise, 837, 910–931  
 Compressor(s)  
   axial, 911  
   centrifugal, 911, 915–916, 928–930, 929*f*  
   diaphragm, 913, 913*f*  
   dynamic, 911, 915, 928–930  
   ejector, 910  
   lobe (roots), 914, 914*f*  
   mode shape, 917, 923, 925  
   mount(s), 918, 923  
   muffler discharge, 917  
   muffler suction, 919–920, 920*f*, 921*f*  
   positive displacement, 910, 913  
   reciprocating, 913, 918–919, 918*f*, 919*f*  
   rolling piston, 915, 926  
   rotary, 925–926, 926*f*  
   screw, 913–914  
   scroll, 926–928  
   shell, sound radiation, 921–925  
   valve(s), 916–917  
     demand, 916–917  
     gate, 916–917  
     reed, 920–921  
 Computational fluid dynamics (CFD), 145, 148, 1018, 1072, 1116, 1164  
 Concrete  
   floors, 1263  
   slabs, 1263  
 Condensation, 20, 326, 1401  
 Condenser microphone(s), 422, 435–437, 435*f*, 436*f*, 456  
 Condition monitoring, 432, 575–583  
 Conductance, drive point, 242–243, 242*f*  
 Conductive hearing loss, 271  
 Consensus standard(s), 378  
 Constant bandwidth filter, 13, 472–473, 474*f*, 480, 559  
 Constant nonfluctuating force, 7  
 Constant percentage filter, 13, 473, 474*f*, 480–481, 484, 559–560, 583  
 Constrained layer(s), damping, 229, 252, 983, 990, 1154, 1154*f*, 1155*f*, 1184, 1184*f*, 1204, 1223  
 Construction equipment noise, 1007, 1420–1423, 1490–1500  
 Construction site noise, 1369, 1417, 1490  
 Control valve(s)  
   cavitation, 900, 900*f*, 902, 907–908, 948, 949–950, 1224, 1224*f*  
   globe, 908, 935, 936  
   hydrodynamic sound, 936–938  
   noise, 838  
   shock(s), 935, 936, 940  
   turbulence, 935–937  
 Convolution integral, 103, 176, 215, 1394  
 Cooling tower(s)  
   noise, 1006, 1329–1331  
 Correlation, 677, 877, 1105, 1201  
 Correlation coefficient, 143, 563  
 Correlation function  
   Cross-correlation function, 143–144, 207, 498, 560–562, 883  
 Coupling factor, 248–254  
 Coupling loss factor, 248–250  
 Crane(s), 1007–1008, 1186–1187, 1491, 1492, 1517, 1518, 1519  
 Crest factor, 304, 317, 326, 346, 484, 577  
 Critical band (critical bandwidth), 809–810, 810*f*  
 Critical distance (radius of reverberation), 34–35  
 Critical frequency (critical coincidence frequency), 35–36, 86–87, 87*f*, 94, 96, 99, 1257–1258, 1260–1262  
 Critical health effect(s), 1484, 1505  
 Critical speed, 575, 755–759, 1461, 1466  
 Cross-correlation function, 143–144, 498, 560–561, 883  
 Cross-over frequency, 1242–1243  
 Cross spectral density, 207–208, 497–498  
 Cross spectrum (cross power spectrum), 479–480, 562–563  
 Cumulative distribution, 327, 403  
 Cyclostationary signal(s), 561–562  
 Damping  
   Coulomb, 5, 174, 226, 261  
   critical damping ratio, 1396  
   hysteretic, 748–749  
   materials, 734–744  
   passive, 225–230  
   ratio, 5, 7, 180–181, 188, 213, 218–219, 225–230, 357, 651, 726, 727*f*, 734–735, 747–748, 748*f*, 749*f*, 765–766  
   shear, 743–744  
   structural, 125, 226, 227, 916, 967, 1149, 1153, 1476  
   treatments, 229–230, 744  
     add on, 1149–1150  
     tuned, 1204–1205, 1208  
   viscoelastic, 737–743  
   viscous damping, 227, 256  
 Damping materials, 734–744  
   behavior, 736–737  
   mechanisms, 734  
   viscoelastic, 737–743  
   coatings, 739–741  
   interlayers, 743  
 Damping ratio, 5, 7, 180–181, 188, 213, 218–219, 225–230, 357, 651, 726, 727*f*, 734–735, 747–748, 748*f*, 749*f*, 765–766  
 Data acquisition, 486–491  
 Data analysis  
   of deterministic signals, 470, 472–473  
   of random signals, 470–471, 475–478  
 Data processing, 430  
 Data retrieval, 496–497  
 Data storage, 496–497  
 Data window(s), 556–558  
 Day-night-evening sound pressure level, 15–16  
 Day-night rating level, 513  
 Day-night sound pressure level, 14–15, 403  
 Decade, 559–560  
 Decibel scale, 237, 1087, 1501  
 Degree(s) of freedom, 186–191, 227–229, 356–357, 729–730, 745–749, 1474  
 Demountable walls, 1299  
 Descriptor(s) (Noise). *See* Noise descriptor(s)  
 Design  
   for low noise, 794–804  
   of low noise road surfaces, 1060  
   spectrum, 1397, 1399–1401  
 Detector(s), 471–472, 471*f*, 472*f*, 474–476

- Diesel engine(s)  
 direct injection, 1025  
 indirect injection, 1025  
 noise, 1024–1032, 1182
- Diffraction, 29–30
- Diffuse field, 58–60, 96, 250, 617, 618, 622, 1236
- Diffuse sound, 58–59
- Digital-analog conversion, 497
- Dipole(s), 23–24, 49–50, 1073  
 aerodynamic, 49, 1125  
 directivity of, 27–28  
 sound power of, 24–26
- Dirac delta function, 87–88, 185
- Directivity, 27–28, 424
- Directivity factor, 27–28, 67, 717
- Directivity index (DI), 28, 67, 1224
- Directivity pattern, 56, 81, 1127
- Discrete Fourier transform (DFT), 476–478, 498, 554–555, 554*f*, 569, 585, 593
- Displacement, 913–915, 916–928
- Displacement-based design, 1395
- Dissipative silencer, 939, 944, 1043, 1318. *See also* Muffler(s)
- Door seals, 254, 1017, 1149
- Door slam, 317, 318, 1163, 1166
- Doppler effect, 144, 153, 625, 879, 1088
- Dose 385, 455
- Dose-response (relationship), 1502–1504
- Dosimeter, 430–432, 463–464, 465–469
- Double wall partitions, 1176, 1288
- Dozer noise. *See* Bulldozer noise
- Drop hammer noise, 992–994
- Duct acoustics, 1320–1321, 1323–1327
- Ducted system(s), 1316–1319
- Duct(s)  
 elbows, 929–930  
 lined, lining(s), 662, 1237, 1318  
 silencer (muffler), 1318  
 transmission loss (TL) of, 1318, 1320–1322
- Duffing's equation, 257
- Dummy head. *See* Artificial head
- Dynamic analysis, 241–246
- Dynamic capability index, 541–542
- Dynamic insertion loss. *See* Insertion loss
- Dynamic magnification factor (DMF), 6*f*, 7, 651, 653*f*
- Dynamic mass, 243–244
- Dynamic modulus, 1049
- Dynamic range, 419–420
- Dynamic vibration absorber. *See* Vibration absorber
- Dynamic viscosity, 1377
- Ear  
 auditory cortex, 283, 283*f*  
 basilar membrane, 271, 278, 278*f*, 280–283, 280*f*, 281*f*, 282*f*, 337  
 central auditory nervous system, 283  
 cochlea, 271–271, 272*f*, 277–283, 277*f*, 278*f*, 280*f*, 337  
 hair cells, 271, 277, 278, 278*f*, 280–283, 284, 284*f*  
 incus, 277*f*, 278, 278*f*, 280, 280*f*  
 inner, 277–278, 278*f*, 288  
 malleus, 277*f*, 278, 278*f*, 280, 280*f*  
 middle, 278–279, 278*f*  
 organ of Corti, 277, 278*f*, 281–282  
 ossicles, 278, 278*f*, 279, 337  
 outer (or external), 271, 272*f*, 278*f*, 286–287, 288, 337  
 Reissner's membrane, 278, 278*f*  
 semicircular canals, 277*f*  
 stapes, 277*f*, 278–280, 278*f*, 280*f*, 337, 338  
 tympanic membrane, 277–280, 277*f*, 278*f*, 279*f*, 280*f*, 286–287, 328, 337
- Earmuff(s), 306, 364–367, 365*f*, 369–370, 371–374, 373*f*
- Earth berm(s), 1417–1418, 1446–1456
- Earthquake(s), 1393–1402
- Eccentricity, 886–896
- Eddy, Eddies, 139, 148–150, 229–230, 238, 448
- Effective noise bandwidth, 472
- Effective Perceived Noise Level, 397, 398*f*
- Eigenfrequency, 52, 53, 121–122, 938–939, 1375
- Eigenvalue, 52–53, 54, 258–259, 566, 572–273, 1136, 1212
- Eigenvector, 187–188, 191, 228, 566, 573
- Elastic spectra, 1394–1397
- Electret microphone. *See* Microphone(s), prepolarized
- Electrical equipment, 835
- Electrical machine(s), 377, 433, 576
- Electric motor(s), 835, 885–896  
 asynchronous, 886–889  
 defects, 886  
 direct current (DC) machine(s), 892–896  
 noise, 835  
 rotor(s), 885–893  
 stator(s), 887–893  
 vibration diagnostics, 889–892
- Electronic sound masking system(s), 1299, 1302, 1304
- Electrostatic actuator, 617
- Element-normalized level difference, 1285
- Emission, 526–532
- Enclosure(s), 685–695  
 close fitting, 690–692  
 loose fitting, 658–659, 685, 688  
 machine, 685–686  
 partial, 692  
 personnel, 686
- Energy density. *See* Sound energy density
- Energy flow, 232–240, 241–251, 847
- Ensemble average, 243
- Ensemble averaging, 551, 600
- Envelope analysis, 484, 579, 1090–1091
- Environmental impact analysis, 308, 311–312
- Environmental impact statement, 303, 1506
- Environmental noise, 1233–1238
- Environmental Noise Directive (END), 1354, 1355, 1360, 1441, 1443, 1501, 1529
- Environmental noise impact statement, 1422
- Environmental Protection Agency of the United States (EPA), 368, 403, 405, 1269, 1349, 1422, 1481, 1527
- Equal energy hypothesis, 332–333
- Equal loudness contours, 286, 288, 288*f*, 395, 395*f*, 806–807, 807*f*
- Equivalent continuous A-weighted sound pressure level, 310–311, 312, 720, 1178, 1491
- Equivalent continuous sound pressure level, 403, 512
- Equivalent energy level, 1501
- Equivalent sound absorption area, 530, 532
- Equivalent sound pressure level, 14–15, 461
- Equivalent threshold level, 287
- Ergodic process, 205
- Ethernet, 488, 490
- Euler's Equation, 23–24, 534–535, 537–538, 606
- Eurocode(s), 1395–1399
- European (noise) directive (END), 310, 1355, 1360, 1481, 1529
- European Union (EU), 1007–1008
- Evanescent Waves, 607, 607*f*
- Excavator, 1517
- Exchange rate(s), 466
- Excitation  
 base, 1393  
 force excitation, 171, 266, 600, 672, 680, 748–749, 847, 852, 996
- Exhaust noise, 1015–1017, 1497–1498
- Expansion chamber (Muffler or Silencer), 1041–1042
- Eyring sound absorption coefficient, 60
- Fan-powered variable-air-volume (VAV) terminals, 1316, 1320
- Fan(s), 833–835  
 axial flow fan, 868, 874–876  
 propeller, 834  
 tube axial fan, 834  
 vane axial, 834  
 blade passing frequency, 835  
 centrifugal fan(s), 868–883  
 aerofoil, 834  
 backward curved, 834, 870–871  
 forward curved, 834  
 industrial (radial), 834  
 tubular, 834  
 cross-flow (tangential) fan, 868–869, 869*f*
- Far field, 31–34, 609–610
- Fast Fourier transform (FFT)  
 algorithm, 261, 263, 430, 464, 470, 478, 486, 498, 539, 549, 555, 629, 671, 1089, 1513  
 zoom FFT, 555–556



- Fast Hilbert transform, 577, 581, 1091, 1092–1093
- Fatigue, 858  
   damage, 210  
   failure, 210
- Fault detection, 582–583
- Federal Aviation Administration (FAA), 396, 1096, 1269, 1481, 1528
- Federal Highway Administration (FHWA), 720, 1269, 1427, 1434, 1435, 1528
- Federal Interagency Committee on Aviation Noise (FICAN), 1483
- Federal Interagency Committee on Noise (FICON), 311, 318, 1483
- Feedback control, 776–777
- Feed pump (noise), 1002, 1004
- Field Impact Insulation Class (FIIC), 1350
- Field incidence mass law, 688, 1247
- Field Sound Transmission Class (FSTC), 1278
- Filter analysis, 476  
   parallel, 476  
   stepped, 476  
   swept, 476
- Filter(s), 471–476  
   constant bandwidth, 13, 472–473, 474*f*, 480, 559  
   constant percentage, 13, 473, 474*f*, 480–481, 484, 559–560, 583  
   high pass, 472, 627  
   low pass, 472, 608–609, 627  
   pass band, 372, 472, 473*f*, 477  
   Tikhonov, 608–609
- Finite difference(s), 102–103, 149, 240
- Finite element analysis (FEA). *See* Finite element method (FEM)
- Finite element method (FEM), 101
- Finite element modeling, 101–114  
   duct transmission, 108–109, 108*f*
- Fire wire, 489–490
- First passage time, 210
- Flanking (flanking transmission), 1246, 1371
- Flanking path(s), 1260, 1298
- Flanking transmission, 1246, 1371
- Flat rooms, 1245–1246
- Flexibility, 189–190, 655, 961, 1299
- Flexible hose, 953–954, 954*f*
- Floating floor(s), 1263–1264
- Flow duct(s), 1323–1327
- Flow (generated) noise, 1324–1327
- Flow noise, 1321
- Flow resistance, 1252
- Flow ripple, 946–949, 947*f*, 948*f*
- Flow separation, 838, 879, 899–900, 938, 942, 1042, 1073, 1084, 1376
- Fluid-borne noise, 951–953, 951*f*  
   accumulator(s), 951, 952  
   damper(s), 951, 952  
   expansion chamber (muffler), 951, 952–953  
   Helmholtz resonator(s), 951, 952  
   side-branch (muffler), 951, 952
- Fluid loading, 79, 83, 90, 98, 245, 1218, 1375
- Fluid mass, added, 1379–1380
- Flutter, 1136, 1385
- Forced harmonic motion, 174
- Forced vibration  
   damped, 5–7  
   forced oscillation, 1195–1196
- Force excitation, 171, 266, 600, 672, 680, 748–749, 847, 852, 996, 1163*f*
- Force transmissibility, 7, 8*f*, 651, 652, 652*f*, 654, 654*f*, 655, 725
- Forging hammer, 843, 987, 992–993
- Formant, 275, 299
- Fourier integral, 185, 554*f*, 555, 556, 570
- Fourier series, 203, 553, 554*f*, 555, 558, 562, 570, 1048
- Fourier transform  
   discrete, 476–478  
   inverse, 103, 106, 207, 480, 498, 553, 554, 589, 605–606
- Free field, 32*f*, 457, 621–622
- Free field over a reflecting plane, 67
- Free vibration  
   damped, 4–5  
   free oscillation, 255  
   undamped, 4
- Frequency, 2  
   averages, 242–243  
   discrimination, 275–276  
   fundamental, 275–276  
   natural or resonance, 4, 7, 1379–1380, 1385–1388  
   response, 105, 207, 420–421, 421*f*, 479, 617–618  
   sweep testing, 484, 852, 854
- Frequency analysis, 13–14  
   aliasing error, 496–497  
   bandwidth (–3 dB), 473*f*, 620, 1236  
   bandwidth (effective noise), 472–473, 473*f*, 556–558, 561  
   center frequency, 13, 14, 244, 247, 252, 272, 472, 481, 497, 810–811  
   constant bandwidth filter, 13, 472–473, 474*f*, 480, 559  
   constant percentage filter, 13, 473, 474*f*, 480–481, 484, 559–560, 583  
   degrees of freedom, statistical, 186–191, 227–229, 356–357, 729–730, 745–749, 1474  
   detector, 471–472, 471*f*, 472*f*, 474–476  
   discrete Fourier Transform, 476–478, 498, 554–555, 554*f*, 569, 585, 593  
   exponential averaging, 455–456, 455*f*, 460, 461, 462, 463  
   fast Fourier Transform (FFT), 261, 263, 430, 464, 470, 478, 486, 498, 539, 549, 555, 629, 671, 1089, 1513  
   filter, 471–476  
   Fourier Transform, 497  
   Hanning weighting, 476*f*, 477, 478, 480, 595, 596*f*  
   ideal filter, 472, 473*f*  
   octave filter, 473, 481, 484  
   one-octave bands, 13–14  
   one-third-octave bands, 14, 368, 369, 395, 1292  
   order analysis, 1089, 1090  
   pass band, 372, 472, 473*f*, 477  
   pink noise, 273, 337, 484, 487, 707, 1258, 1285–1286  
   preferred frequencies, 176  
   sampling theorem, 487, 495, 1092  
   white noise, 337, 471, 472, 474, 487, 520, 561, 808–809
- Frequency domain analysis, 185, 1088–1090
- Frequency response, 105, 207, 420–421, 421*f*, 479, 617–618
- Frequency Response Function (FRF), 498, 563–564
- Frequency weightings, A, B, C, D, 14
- Fresnel number, 68–69, 714, 716, 718, 1417
- Fricatives, 293–297
- Fundamental frequency, 275–276
- Furnace, burner, 956–963
- Gain, 351*f*, 487
- Gas flow noise, 834, 914, 915, 918, 935, 1019, 1497–1498
- Gas turbine noise, 755, 956, 957, 959, 962, 962*f*, 963, 1002, 1334
- Gaussian amplitude distribution, 209
- Gearbox noise, 1018, 1086–1095
- Gear(s), 576–578, 831–832, 847–855  
   contact ratio, 849–850  
   entrapment, 849  
   housing, BEM model of, 852  
   involute, 831*f*  
   load, 832, 849, 850–851  
   lubricant, 849  
   noise, 832, 847–848, 849  
   non-parallel axes, 831  
     hypoid, 831, 832*f*, 851  
     spiral bevel, 831, 832*f*, 851  
     straight bevel, 831, 832*f*  
   parallel axes, 831, 849, 851  
     helical, 831, 832*f*, 850, 851, 851*f*  
     spur, 831, 831*f*, 832*f*, 849, 850, 851*f*  
   profile, 850  
   pump(s), 835–839  
   rattle, 853  
   tooth meshing frequency, 576, 848, 849, 851–852, 853*f*  
   transmission error, 576, 848, 849–851, 850*f*  
   troubleshooting, 577, 578*f*, 853–855  
   whine (excitation), 848–849, 852  
   worm, 851
- Geological fault(s), 1393
- Geometric attenuation (of sound), 1441
- Gradient wind speed, 1380
- Green's function, 80, 87–89, 118–119, 144, 151, 1467
- Ground attenuation (of sound), 73–74, 1112, 1434, 1441
- Ground (borne) vibration, 1418–1419, 1458–1467, 1470–1478
- Ground effect, 70, 71, 73, 74, 76, 1397, 1447, 1449, 1455–1456, 1510

- Ground vibration, 172, 1418–1419, 1458–1467, 1458 *f*, 1471, 1473
- Group speed, 244–245, 251
- Guideline(s) (for noise), 1307–1315, 1352
- Gypsum board, 657, 700, 708, 1244, 1257–1264, 1277, 1289, 1294, 1298–1299, 1301, 1320, 1322, 1370, 1372, 1373
- Hair cell(s), 271, 277, 278, 278 *f*, 280–283, 284, 284 *f*
- inner hair cells (IHC), 271, 277, 278, 278 *f*, 284, 337, 338
- outer hair cells (OHC), 271, 277, 278, 278 *f*, 281–284, 337–339
- Half power bandwidth, 766
- Half power points, 1242
- Hamilton's principle, 175, 191
- Hand-arm vibration syndrome, 349, 351
- Handheld tools, 985
- Hand-transmitted vibration, 343, 349–352
- Hearing, 13
- absolute threshold, 271 *f*, 272, 273, 344, 395 *f*
- asymptotic threshold shift (ATS), 327–331, 329 *f*, 331 *f*
- envelope, 143 *f*, 209–210, 210 *f*
- equal loudness contours, 286, 288, 288 *f*, 395, 395 *f*, 806–807, 807 *f*
- hearing conservation program (HCP), 307, 383–392
- hearing damage, 303, 304, 341, 1178, 1420, 1490, 1502
- hearing damage risk criteria
- continuous noise, 326–331, 333–334, 337, 339
- impulsive noise, 304, 326–332, 333–334, 337, 468
- hearing handicap, 284 *f*, 378, 387
- impairment, 305, 377, 378–379, 381, 383–384, 387, 390–391, 814, 895
- loudness adaptation, 290–291, 813
- minimum audible field (MAF), 286, 807 *f*
- permanent threshold shift, 290, 305, 327, 330–331, 330 *f*, 338, 379
- place theory, 271
- protective mechanisms, 304, 337–338
- protector devices (HPD), 306
- protector(s), 306
- attenuation measurements, 306
- attenuation of, 306
- comfort, 306
- earmuffs, 306
- earplugs, 306
- types, 306
- temporary threshold shift, 290, 304–305, 321, 338
- threshold, 286–291
- threshold level, HTL, 287, 378–379, 390, 462, 465, 644
- Hearing loss
- conductive, 271
- employer liability, 383–385
- noise-induced, 283–284, 337–341
- non-occupational, 392
- sensorineural, 271, 290, 350
- Heat exchanger, 1175, 1347, 1377, 1379, 1380, 1380 *f*
- Heating, Ventilation and Air Conditioning Systems (HVAC)
- breakout noise, 1175–1176, 1316, 1320, 1322
- Helicopter noise, 1021, 1120, 1121, 1130
- Helicopter rotor noise, 1021, 1120–1130
- blade-vortex, 1123–1125, 1127, 1480–1481
- blade-wake, 1021, 1122, 1125
- broadband, 1122–1123
- discrete, 1122
- impulsive, 1122, 1123–1124, 1125, 1127, 1129–1130
- kinematics, 1120–1122
- main rotor, 1021, 1120–1121, 1121–1125, 1121 *f*, 1127–1130, 1200, 1420, 1480–1481
- reduction, 745
- rotational, 1120, 1121, 1122, 1124, 1125, 1130
- volume, 1021, 1122, 1126
- Helmholtz equation, 102–103, 116, 606, 608–609
- Helmholtz resonator, sound absorbers, 951, 952
- Hemi-anechoic room (semi-anechoic room), 527, 528, 531, 678, 1088
- Hertz, 2, 129, 218, 219, 252, 550
- Hilbert transform, 577, 581, 1091, 1092
- Hologram noise, 599–600, 603, 608–609, 1134
- Holography. *See* Near-field acoustical holography (NAH)
- Hooke's law, 172, 191, 256
- Human body, resonances, 344
- Human response to noise, 394–411
- Human response to vibration, 1390
- Hydraulic actuator(s), 223, 451
- Hydraulic system(s)
- axial piston, 839 *f*, 898 *f*, 946–949, 946 *f*, 947 *f*
- cavitation, 900, 900 *f*, 902, 907–908, 948, 949–950, 1224, 1224 *f*
- flexible hoses, 953–954, 954 *f*
- flow ripple, 946–949, 947 *f*, 948 *f*
- gears, 576–578, 831–832, 847–855
- instability, 145, 258–259, 263, 264, 950
- noise, 838–839, 899–902, 946–955
- positive displacement, 836–839, 897, 900, 901, 903, 904, 906, 910–925, 946–949
- pulsation dampers, 839, 907, 951–953, 1205
- pump(s)
- piston, 839, 946–950
- water hammer, 159, 900, 901–902, 903, 908–909, 949, 950
- Imbalance (unbalance), 172, 320–322, 549, 575–576, 753–760, 885, 889, 901–907, 1159, 1208, 1219
- Immission, 1505–1506, 1508
- Impact
- hammer, 570, 679, 903, 923
- loading, 1143
- test, testing, 220, 222, 993
- Impact Insulation Class (IIC), 1237, 1262, 1280, 1281 *f*, 1350
- Field Impact Insulation Class (IIC)
- Impact isolation, 1280
- Impact noise, 304, 318, 326–334, 1143, 1422, 1501–1508
- Impact sound pressure level, 1292
- normalized impact sound pressure level, 1262, 1281 *f*, 1291
- Impact sound rating(s), 1262, 1358
- Impact sound transmission, 1237, 1257, 1262, 1352
- Impedance
- acoustic, 517–523
- specific acoustic, 46, 698–699
- of ground, 72–73
- mechanical, 344, 348, 422, 423, 436–437
- tube, 64, 65, 517, 519 *f*, 520–523, 707–709, 1250, 1250 *f*, 1276
- Impulse, 304, 326–332, 333–334, 337, 468
- Impulse response, 57–58, 57 *f*, 1049
- Impulse response function, 176, 185, 297, 475, 477, 480, 481, 484, 554, 563, 566, 571
- Incus, 277 *f*, 278, 278 *f*, 280, 280 *f*
- Industrial production machinery
- noise, 843, 987–994
- sound power level predictions, 843–844, 1001–1009
- Inertia base, 525, 726
- Inertia force(s), 172, 444, 1377, 1460
- Infrasound, 304, 320–324
- Initial phase angle, 2, 3 *f*, 553, 888, 891
- Insertion loss, 68, 368, 1016
- of barriers, 714–720
- of buildings, 1456
- of enclosures, 658–659, 662–665, 685, 687–693
- of mufflers, 920, 922 *f*, 1016–1017, 1016 *f*, 1035–1036
- of trees, 1455–1456
- Instantaneous sound intensity, 21, 534
- Intake noise, 1034–1051
- Integrating sound level meter, 403
- Integrator, 465, 493, 583
- Intelligibility, speech, 293–300, 399, 1305
- Intensity. *See* Sound intensity
- Internal combustion engine (ICE)
- noise, of diesel engines, 844, 1015, 1024–1032
- International Building Code (IBC), 1348, 1349, 1396
- International Civil Aviation Organization (ICAO), 397, 1096, 1482, 1485, 1529
- Ideal filter, 472, 473 *f*
- Image source(s), 56–57

- International Conference of Building Officials (ICHO), 1348
- International Electrotechnical Commission (IEC), 466, 505, 540, 612, 634, 816
- International Organization for Standardization (ISO), 286, 305, 340, 368, 378, 386, 395, 514, 526, 544, 568, 582, 627, 633, 717, 794, 985, 1054, 1171, 1185, 1217, 1247, 1258, 1283, 1354, 1422, 1427, 1447, 1459, 1470, 1491, 1502, 1510, 1516, 1527
- Inverse square law, 23, 675, 1077
- Isolation  
acoustical, noise, sound, 954, 1238, 1279, 1297, 1299, 1350  
efficiency, 348, 1195, 1337  
vibration, 725–733
- Isolators  
compressed glass fiber type, 1337, 1338, 1347  
neoprene pads type, 1337–1338  
steel spring type, 1337, 1338–1339, 1347, 1472–1473
- Isotropic 139, 142–143, 152
- Jerk, 1029
- Jet noise, 140–148, 1101–1103, 1105–1106, 1199
- Joint acceptance function, 79, 98–99
- Kinetic energy, 130–134, 139–140, 143, 144, 184, 192, 194, 195, 198, 250, 583, 773, 780, 781*f*, 911, 935, 1019, 1104
- Kirchhoff, 87–89, 150, 202, 714–715, 1046, 1104, 1120, 1125–1127
- Kronecker delta function, 133*n*
- Lagrange's equations, 175, 199–201, 203, 256
- Laminated glass damping, 1150, 1167, 1261–1262, 1279
- Laminated steel damping, 890, 1150
- Lateral quadrupole, 22*f*, 27*f*, 50–51, 50*f*, 51*f*
- Leakage, 368, 484, 987
- Leaks, 368*f*, 858*f*, 1173*f*, 1205, 1262
- Level  
sound pressure level, 11, 15–16, 398–399, 526–531, 1248  
standardized level difference, 1286, 1404
- Lighthill, Sir James, 128–145, 149–154
- Lilley, Geoffrey, 128, 130–138, 142–144, 154  
linearity, 130, 149
- Lined duct(s), 662, 1237, 1318
- Lined plenum(s), 1319
- Lined rectangular elbow(s), 1318
- Line source, 29
- Linings, liquid-borne sound, 951, 1046–1047
- Locally reacting boundary (surface), 65, 103
- Longitudinal wave(s), 19  
speed, 35, 430, 700, 943, 1230
- Loss factor, 184–185, 184*f*, 185*f*, 248–250
- Loudness  
adaptation, 290–291, 813  
level, 394–397, 395*f*
- Loudness level-weighted sound  
equivalent level (LL-LEQ), 1415
- Loudness level-weighted sound  
exposure level (LLSEL), 1415
- Low frequency noise (LFN), 304, 320–324
- Low frequency vibration, 348, 865, 887–889, 1474
- Lubrication, 832, 858, 861, 862, 863, 865, 902–903, 906, 914, 915, 1022, 1144, 1175, 1464
- Lumped element(s), 41, 1040
- Machinery condition monitoring  
(machinery health monitoring), 417, 575–583
- Machinery noise, 831–844, 966–973, 975–986  
low noise (machinery) design, 794–804  
concept(s), 794–795  
prototyping, 795, 799–802  
source identification, 802  
transmission paths, 802
- Machine tool  
chatter, 995–999  
noise, 843, 995–999
- Mach number, 128, 130–138, 136*f*, 140, 145, 148, 149, 150, 153, 154, 881, 936, 1039–1040, 1040*f*, 1045, 1050, 1073, 1114, 1115, 1123–1124, 1203, 1254
- Magnitude scaling, 272, 273
- Malleus, 277*f*, 278, 278*f*, 280, 280*f*
- Masking, 272, 807–813, 809*f*
- Masking sound spectrum, 1302–1303
- Mass law, 61, 254, 660*f*, 1237, 1257–1258, 1257*f*
- Material handling, 843, 967, 988–990
- Maximum noise level, 1501
- Mean flow, 110  
irrotational, 110
- Mean square sound pressure, 10, 12, 21, 23, 25, 28, 34, 250, 254, 535, 546, 685, 810, 1019
- Mean square velocity, 177, 250, 252, 676, 735
- Measurements, 354, 421–426, 430–433, 466–467, 501–525, 534–547, 598–610, 633–645, 1091–1093, 1110–1111, 1112, 1363–1364
- Measurement standard, 639–643
- Measuring instrument, 633–637, 635*f*, 642
- Mechanical equipment rooms, 1313, 1328, 1329, 1331, 1336, 1347
- Mechanical impedance, 344, 348, 422, 423, 436–437
- Mechanical power, 847, 877, 935, 936, 1018
- Membrane (sound) absorbers, 699–701
- Metal cutting, 966–973  
aerodynamic, 840, 966  
continuous, 840, 966  
drill, 840, 966  
grinding, 840, 843  
impact cutting, 967–972  
lathes, 966, 972  
milling, 966, 967, 972  
noise, 840–841  
shearing, 840, 966–970, 970*f*  
sheet dampers, 971, 971*f*, 972*f*  
structural vibrations, 840, 966–967  
tooling parameters, 968–969, 971, 973
- Metrology. *See* Calibration methods, metrology
- Microelectromechanical Systems (MEMS), 785–792  
accelerometers, 790  
fabrication, 788, 789, 790  
gyroscopes, 790–791  
piezoresistance, 789  
sensing, capacitance, 789–790  
sensors  
noise, 792  
pressure, 792  
vibration, 787, 790
- Microphone(s), 422–426, 435–442, 456–457, 612–622  
backplate, 435, 436, 439, 441, 442  
communication, 435  
condenser, 422, 435–437, 456–457  
diaphragm, 422, 426  
directional, 422, 438, 438*f*  
directivity, 424, 438  
dynamic, 437*f*  
dynamic range, 442–443  
electret. *See* Microphone(s), prepolarized  
free field, 422, 425, 439–440, 457  
piezoelectric, 423–424, 437–438  
prepolarized, 422–423  
pressure, 422, 439, 457  
random incidence, 422, 440–441, 457  
resonance, 423, 618  
static, 617
- Millington-Sette formula, 34, 1235
- Mobility, 242
- Modal analysis, 90–93, 432, 565–574  
experimental, 566–567  
global, 572–573  
mathematical model, 573  
multi-mode, 572  
parameter extraction, 571–574  
single mode, 572  
test planning, 567–568  
virtual test, 568
- Modal bandwidth, 766, 1242
- Modal damping, 1242
- Modal density, 243–246, 1242
- Modal mass, 79, 98, 242, 243, 734, 1394
- Modal overlap, 766–767, 767*f*, 1242.  
*See also* Active noise control; Active sound control
- Modal stiffness, 734, 1394
- Mode count, 243–246, 249
- Mode of vibration. *See* Normal mode (of vibration)

- Mode(s), normal. *See* Normal mode
- Mode shape, 36, 38–39, 90–91, 175, 187, 190–193, 228–229, 241–246, 566, 569, 573–574, 755–758, 772–774, 917, 959–960, 1030, 1240–1241, 1387, 1399, 1400
- Monopole, 22 *f*, 79, 1073
- Monte Carlo simulation, 208
- Muffler(s), 1034–1051  
absorption or absorptive, 963, 1034, 1034 *f*  
catalytic converter, 1045–1046  
design, 1015–1017, 1036  
dissipative, 1038  
expansion chamber(s), 1041–1046  
Helmholtz resonator(s), 951, 952, 1044  
insertion loss, 920, 922 *f*, 1016–1017, 1016 *f*, 1035–1036  
modeling, 1037–1038  
perforated, 1038–1040  
reactive, 1034–1035  
transmission loss (TL), 1035
- Multi-degree-of-freedom system (MDOFS), 186
- Multi-residential buildings, 1352
- Narrow band(s) (noise), 163, 209
- Nasal cavity, 294 *f*
- National Environmental Policy Act (NEPA), 1528
- National Institute of Occupational Safety and Health (NIOSH), 334
- National Research Council Committee on Hearing and Bioacoustics (CHABA), 378
- Natural angular frequency, 4, 5
- Natural frequency, 4, 7, 180–183, 650–655, 726–735
- Navier–Stokes equation(s), 131–133, 137, 140, 144, 149–150, 159, 167, 1080, 1104, 1126
- Near field, 23, 31–34
- Near-field acoustical holography (NAH), 598–610  
boundary element discretization, 601–603, 602 *f*  
characteristic eigenfunction expansion, 601, 601 *f*  
Helmholtz least squares (HELS), 601, 603–604  
planar, 598, 599, 601, 601 *f*, 604–606  
reconstruction theory, 600–604
- Near source factor, 1395
- Newton, Sir Isaac, 7
- Newton's law, 4, 172, 180, 213, 214, 227–228, 256, 537, 1091, 1393
- New York City, 1350
- Night average sound pressure level, 403, 1424
- Node, 101–102, 104, 104 *f*, 106–107, 111–113, 117, 118–120
- Noise, vibration and harshness (NVH), 1163, 1334
- Noise and Number Index (NNI), 405
- Noise charges, 1485
- Noise contour map(s), 1486, 1486 *f*, 1488
- Noise control  
commercial & public buildings, 1423  
community ordinance(s), 1424, 1525–1531  
multifamily dwellings, 1237–1238  
single family dwellings, 1237–1238
- Noise Control Act (of 1972), 1528
- Noise criteria, 399–402, 409–411, 1162–1163, 1351–1353, 1368
- Noise criteria (NC) curves, 400, 1270–1271
- Noise descriptor(s), 1501–1502
- Noise dose, 465–466
- Noise emission level, 1433 *f*, 1530–1531
- Noise exposure (criterion) level, 1505–1506
- Noise exposure forecast (NEF), 405
- Noise immission level (NIL), 1506
- Noise indicators, 1355, 1360, 1362, 1365, 1413, 1481
- Noise-induced hearing loss (NIHL), 283–284, 337–341
- Noise isolation class (NIC), 1279, 1297, 1299, 1350
- Noise map(s), 77, 801, 1360, 1416, 1424, 1526–1527, 1529
- Noise metrics, 317, 1481–1484
- Noise Pollution Level, 405–406
- Noise rating measures, 394–411
- Noise rating(s), 406, 1236  
Balanced Noise Criterion curve(s) (NCB), 1275  
curve(s) (NR), 400, 1270–1271  
Day-Night Average Sound Level (DNL), 1269  
Noise Criterion Rating (NC), 1236, 1270  
Speech Privacy Index (SPI), 1236
- Noise reduction coefficient (NRC). *See* Sound absorbing materials
- Noise reduction (NR), 35
- Noise reduction rating (NRR), 369–370
- Noisiness, 396–397
- Noisiness index, 396–397
- Nonlinear acoustics, 129–132, 159–167
- Nonlinearity, 167, 261, 419, 859
- Nonlinear vibration. *See* Vibration
- Normalized flanking level difference, 1285, 1291
- Normalized impact sound index (NIS), 1281, 1282
- Normalized impact sound pressure level, 1262, 1281 *f*, 1288, 1291–1293
- Normalized level difference, 1285, 1286, 1364
- Normal mode, 52–55, 105, 1240–1241
- Normal mode (of vibration), 187
- Normal sound intensity level, 11–12, 502
- Norris-Eyring equation, 1235, 1251, 1280
- Noy, 274, 396, 515
- Nozzle, 137, 139–142, 145–148
- Nyquist diagram, Nyquist plot, 572
- Nyquist frequency, 495, 496, 555, 556, 591, 594, 596
- Occupational injury, 383–384
- Occupational noise  
legislation, 377–382  
regulations, 377–382  
standards, 377–382
- Occupational Safety and Health Administration (OSHA), 290, 305, 324, 431–432, 460, 466, 935, 975
- Octave, 13
- Octave filter, 473, 481, 484, 559, 560
- Office work space(s), 1297–1306
- Off-road vehicle(s)  
measurement procedures, 1188  
noise, 1186–1196  
tracked, 1186, 1188, 1191
- Oil pan noise, 122, 670, 1030–1031, 1031 *f*, 1150
- One-octave bands, 13–14
- One-third octave bands, 14, 368, 369, 395, 1292
- One-third octave filter, 559, 560
- Open-plan office(s), 1297–1306
- Operating range, 461–462
- Order analysis, 1089–1090
- Order tracking, 482–483, 1087–1088
- Organ of Corti, 277, 278 *f*, 281–282
- Ossicles, 278, 278 *f*, 279, 337
- Outdoor-indoor transmission class (OITC), 1258, 1277, 1279–1280, 1373
- Overlap principle, 478–480, 766–767, 1209–1210, 1242–1243
- Overload indicator, 462
- Panel absorbers, of sound, 700, 702–704, 1254
- Parametric excitation, 172, 208, 575, 848, 1460, 1461
- Particle velocity, 10, 21, 23, 31–32, 39–40, 43–44, 46–47, 119–121, 160, 534–538, 616
- Pascal, 463, 600, 1326
- Pass band, 372, 472, 473 *f*, 477
- Passive damping, 225–230
- Passive noise control, 650–666, 1153–1155, 1203–1205
- Peak noise level, 397, 405, 468, 1087, 1501
- Peak value, 495, 532, 549, 552–553, 635–643
- Pendulum, 256–257, 732–733
- Perceived noise level (PNL), 512, 515, 1501  
tone corrected, 397
- Percentage highly annoyed persons (%HA). *See* Annoyance
- Percentile sound pressure level, 403, 1269
- Performance Based Design (PBD), 1393
- Period, 2
- Periodic noise, 498
- Periodic vibration, 356
- Permanent threshold shift, 290, 305, 327, 330–331, 330 *f*, 338, 379

- Permissible Exposure Level (PEL), 324, 384, 389
- Permissible Exposure Limits, 380
- Phase, 2
- Phase angle. *See* Initial phase angle
- Phase speed, 41, 175, 1045
- Phon, 273, 289, 806
- Phone, 286, 287
- Phoneme, 271, 275, 294, 299
- Physiological acoustics, 271
- Piezoelectric microphone(s), 423–424
- Pink noise, 273, 337, 484, 487, 707, 1258, 1285–1286
- Pistonphone, 616
- Pitch, 273
- Plane waves, 7–9, 20–21, 20 *f*
- Planning, 568, 799, 1484–1485, 1488, 1530
- Platform noise, 1224
- Point dipole, 49–50
- Point monopole, 46–50
- Point quadrupole, 50–51
- Polarity, 287
- Polyvinylidene difluoride (PVDF), 450
- Potential energy, 765–769
- Power spectrum, 876, 877–878
- Power spectrum density (power spectral density), 470–471, 495–497, 550, 558
- Power spectrum level, 1162, 1373
- Power train noise, 1013–1014, 1161–1163, 1427
- Power unit noise (propulsion noise), 1054–1055
- Prandtl number, 1037, 1047
- Preferred frequencies, 176
- Pressure drop, 296–297, 937–940, 1318–1320, 1326–1327
- Pressure loss coefficient, 1324–1325, 1325 *f*
- Pressure-residual intensity index, 541–543, 616
- Pressure wave. *See* P-wave(s)
- Privacy Index, speech privacy index (PI), 1300, 1304
- Privacy metric(s), 1299
- Probability density, 498, 552 *f*
- Probability distribution, 205
- Product sound quality, 805–825
- critical bands, 809–810, 810 *f*
- empirical loudness meter, 813–814
- fluctuation strength, 818–819
- frequency (bark), 811
- jury tests, 820–821
- category scaling, 815, 816 *f*
- magnitude estimation, 815
- paired comparison, 815
- random access ranking, 815
- semantic differential, 815, 815 *f*
- loudness, 806–807, 813
- Zwicker, 811–813
- masking, 807–809
- playback, 816–818
- earphones, 816
- loudspeakers, 816
- recording, 816–818
- roughness, 819
- sharpness, 818
- sound synthesis, 822–825
- Propeller noise, 1019–1020, 1109–1110, 1197–1199, 1223–1224
- control, 1116–1117
- loading, 1109–1110, 1113, 1115
- measurement(s), 1110–1111
- nonlinear, 1016, 1021, 1109–1110
- prediction, 1112–1116
- quadrupole, 1021, 1110, 1115
- thickness, 1109–1110, 1113, 1115
- Prop-fan noise, 1117
- Pseudohypacusis, 387–389
- Psychoacoustics, 271, 806. *See also* Psychological acoustics
- Psychological acoustics, 271–275, 1162. *See also* Product sound quality
- Pump(s), 835–839, 897–908, 898 *f*
- axial 897–908
- cavitation, 900–902, 907–908
- centrifugal, 899, 900 *f*, 901–904, 906, 908, 910
- external gear, 948–949
- internal gear, 949
- kinetic, 897
- noise, 906–908
- positive displacement, 897, 904
- sound power, 904
- special effects, 897, 899
- Punch press noise, 967, 968, 991, 991 *f*
- Pure tone threshold, 272, 286
- P-wave(s), 1461–1462
- Quadrupole, 22 *f*, 23, 1021, 1110, 1115
- Quality factor, Q-factor, 167
- Quantization, 486, 487
- Quiet seats, 1210, 1213
- Radiated noise, 79–99, 1030–1031, 1218–1231
- machinery, 1219–1223
- plate, 86–87, 90–99
- propeller, 1223–1224
- ship, 1218–1219, 1224–1227
- Radiation efficiency (radiation factor or radiation index or radiation ratio), 36–38, 47, 79, 80, 83–85, 94, 99, 249, 545–546, 676, 905, 1030, 1184
- Radiation factor. *See* Radiation efficiency
- Radiation impedance, 90–91, 91 *f*, 98
- Radiation index. *See* Radiation efficiency
- Railroad car noise, 1022, 1152–1153
- Railway(s)
- noise, 1178–1185, 1417
- traction motors, 1152, 1181–1182
- Random excitation, 600
- Random noise, 25, 164, 470, 498, 561, 571, 580, 599, 1022, 1111, 1138, 1249, 1319
- Random vibration, 205–210
- Rapid eye movement(s) (REM). *See* Sleep
- Rapid Speech Transmission Index (RaSTI), 1281
- Rapid transit system vehicle noise, 1152–1153
- Rating(s), 1267–1281, 1283–1296
- Rating(s) of noise. *See* Noise rating(s)
- Ray acoustics, 30–31
- Rayl, 25, 26, 698
- Rayleigh's principle, 175, 1399
- Rayleigh surface wave(s). *See* R-wave
- Reactive sound field, 535
- Receptance, 566
- Reciprocating compressor. *See* Compressor(s)
- Reciprocating engine(s), 1003, 1200, 1333–1334
- Reciprocating machine(s), 580–582. *See also* Machinery noise
- Reciprocity, 175, 248, 621
- Reference, 10–12
- displacement, 11
- sound intensity, 10, 11–12
- sound power, 10–11
- sound pressure, 10, 11
- sound source, 10, 12
- Reflection noise, 29–30
- coefficient, 29, 76, 517, 519–520, 709, 719, 1049, 1246, 1251, 1252
- Rotor balancing. *See* Balancing
- R-wave, 1461–1462
- Sabine, 33–34
- absorption coefficient, 34, 511, 717, 1244, 1245, 1247, 1248, 1249–1250, 1254, 1255 *f*, 1276
- enclosure, 1240
- reverberation time, 33–34, 1251–1252, 1280–1281, 1312
- Sampling
- error, 499–500
- rate, 487, 494, 495–496
- theorem, 487, 495, 1092
- Sandwich panel (or plate), 743, 1183
- Scaling, 140–145, 558–559, 788–789, 815, 1401
- Scanning, 543–544, 543 *f*
- Scattering, 29–30, 165, 1111, 1449
- Screech, 146–148, 148 *f*, 838–839
- Screens, 716–717, 801, 1299, 1301, 1523
- Seal(s), 254, 1017, 1149. *See also* Door seal(s)
- Seismic
- design, 1393
- induced vibration, 1393–1402
- isolation, 1398
- mass transducer, 427
- Semi-anechoic room (hemi-anechoic room), 527, 528, 531, 678, 1088
- Semicircular canals, 277 *f*
- Sensitivity, 277, 419, 524, 613, 616–617, 624, 626
- Sensorineural hearing loss, 271, 290, 350
- Shadow zone, 75, 665, 665 *f*, 714–717, 1418, 1434, 1444, 1447–1449
- Shaker, 220–221, 220 *f*, 451–453, 564, 1176, 1202, 1203

- Shape indicator, 1295–1296
- Shear flow, 138–140
- Shear layer, 137, 139, 145–147, 881, 1075–1078, 1101, 1102, 1103, 1111, 1376, 1376*f*
- Shear wave(s). *See* S-wave(s)
- Shielding, 803, 1111, 1185, 1191–1192, 1194–1196, 1455–1456, 1495–1496
- Shield(s), for noise control, 1031–1032
- Ship
- modeling, 202, 251–253, 251*f*, 252*f*, 253*f*
  - noise, 1218–1219, 1224–1227
- Shock
- isolation, 655
  - loading, 212, 214, 215
  - measurement, 633–645
  - mount(s), 625, 626, 627*f*, 628–629, 630, 631, 641
  - spectrum, 630, 641, 643
  - testing, 631–632
- Shock, mechanical effects on humans, 306, 354–362
- biodynamic models, 356–357, 359
  - comfort criteria, 359–360
  - injury risk, 360–361
  - criteria, 360
  - measurement(s), 354
  - metrics, 354
- Signal analysis, 430–432
- Signal processing, 13, 373, 374, 487, 491, 493–494, 501, 555, 599–602, 639, 643, 669, 671, 768, 772, 774, 817, 970, 1047, 1088
- Signal-to-noise ratio (SNR), 275, 299, 316, 317, 480, 495, 608, 1226, 1297–1298, 1302
- Silencer. *See* Muffler(s)
- Similarity spectrum, 142*f*
- Simple harmonic motion, 1–4, 1*f*, 2*f*, 3*f*, 427
- Single-degree-of-freedom system (SDOFS), 180, 213, 745
- Single event noise exposure level, 399, 1269
- Single-event sound pressure level, 526
- Sleep
- awakening from, 309–312
  - deprivation, 303, 309
  - rapid eye movement(s) (REM), 309
  - stages, 310, 407
- Sleep disturbance, 303, 308–313
- Sleeper(s), for rail tracks, 1139, 1140–1142, 1444, 1460, 1462–1464, 1466
- Sleep interference, 303, 307, 407–408, 1156, 1419
- Smart structure(s), 454, 783
- Snell's law, 140, 144
- Social survey(s), 317, 318, 408, 409, 1054, 1413, 1502. *See also* Survey(s)
- Sommerfeld radiation condition, 45, 103–104, 116
- Sonar, self-noise, 1224–1226
- Sone, 286, 288, 289, 395, 1268–1269
- Sound absorbers, 696–712
- Helmholtz resonator, 701–702, 951, 952
- perforated panel, 702–705, 705*f*
  - suspended, 704–705
- Sound absorbing materials
- acoustical plaster, 706
  - acoustic impedance, 698–699, 707–709
  - fibrous, 696–698
  - flow resistivity, 698–699
  - form factor, 698
  - Noise Reduction Coefficient (NRC), 696
  - porosity, 698
  - spray on, 705–706
  - volume coefficient, 698
- Sound absorption class, 1296
- Sound absorption coefficient, 696, 706, 711
- Sound analyzer, 1080, 1269
- Sound barrier, 254, 717, 954, 1480
- Sound classifications, of dwellings, 1360–1362
- Sound energy (acoustic energy), 534–536
- Sound energy density, 10, 59, 534, 1245
- Sound-energy flux, 144, 887, 888, 890
- Sound exposure
- A-weighted sound exposure, 306, 311, 408*f*
- Sound exposure level (SEL)
- A-weighted sound exposure level, 461, 512, 1268–1269, 1501
- Sound field, 54–55, 58–59, 535, 544–545, 612–613, 615–616, 618, 686–687, 1079–1080, 1182
- Sound insulation
- airborne, 1257–1265
  - impact, 1262–1263, 1288–1289
- Sound intensity, 10, 11, 23–24
- active sound field, 535
  - complex intensity, 534
  - dynamic capability, 541, 543
  - imaginary intensity, 536
  - measurement, 534–547
  - errors, 539–542
  - phase mismatch, 540–542
  - reactive sound field, 610
  - residual intensity, 540–541
  - residual intensity index, 541, 542–543
  - scanning, 543–544
  - supersonic, 601, 610
- Sound intensity level, 11–12, 535
- Sound intensity method, 534, 543–544, 546–547, 1060, 1203
- Sound level meter, 430, 455–464
- exponential averaging, 460
  - integrating averaging, 455–464
- Sound power, 10–11, 543–544
- Sound power level, 11, 526–532, 1001–1009
- Area-related. *See* Area-related sound power level(s)
  - A-weighted sound power level, 527–531, 1001–1009, 1143*f*, 1186–1187, 1490–1492, 1510, 1512–1513
  - band sound power level, 1001–1008, 1328–1330, 1333–1334
  - measurement uncertainty, 530–531
- Sound pressure, 10, 526
- instantaneous, 21, 534
  - peak, 397, 405, 468, 1087, 1501
  - reference, 11
  - root mean square (rms), 10, 497
- Sound pressure level, 11
- A-weighted (sound pressure level), 398*f*, 404*f*, 1267–1269, 1428*f*, 1429*f*, 1430*f*, 1432*f*, 1433*f*
  - band (sound pressure level), 842*f*, 1020*f*, 1273*f*, 1280, 1328, 1331, 1406, 1407
  - emission (sound pressure level), 526–532
- Sound-proofed enclosures, 1494–1497, 1499, 1499*f*
- Sound propagation, 7–10
- in atmosphere, 67–77
  - cylindrical, 67
  - energy density, 10, 59, 534, 1245
  - indoors, 52–66, 1240–1246
  - outdoors, 67–68, 74–75
  - particle velocity, 10, 21, 23, 31–32, 39–40, 43–44, 46–47, 119–121, 160, 534–538, 616
  - plane sound waves, 7–9, 20–21, 20*f*
  - in rooms, 52–65
  - sound intensity, 10
  - sound power, 10–11, 543–544
  - sound pressure, 10, 526
  - spherical, 19–25
- Sound quality. *See* Product sound quality
- Sound radiation, 35–36, 79–99, 763–764
- apparent sound reduction index, 1264
- Sound reduction index, (sound transmission loss), 546, 546*f*
- weighted, 1258, 1262, 1283, 1284, 1285, 1289, 1368
- Sound source(s), 43–51
- Sound transmission
- airborne, 1162, 1237
  - impact, 1237
  - structural, 1237
- Sound transmission class (STC), 1258, 1278–1279, 1297, 1336, 1368
- Sound transmission loss, 1182–1184, 1223, 1278, 1278*f*, 1279*f*
- Sound volume velocity, 27, 28, 41, 42, 46, 48, 296–299, 296*f*, 679, 681, 762, 763, 1037, 1038, 1043, 1045, 1047
- Source identification, 668–681
- change of excitation frequency, 672–673
  - coherence approach, 677
  - frequency analysis, 671–672
  - inverse numerical analysis, 680–681
  - numerical acoustics approach, 678–680
  - path blocking, 673
  - sound intensity approach, 677–678
  - transfer path analysis, 668, 678–680
  - wrapping, 670–671

- Source/path identification (source-path identification), 1201–1203
- Source power  
airborne, 1056, 1162, 1237, 1257–1265  
structure-borne, 1237
- Southern Building Code Congress International (SBCCI), 1348
- Spatial average, 243
- Specific acoustic impedance, 46, 698–699
- Spectral density, 141–144, 152, 185, 206–209, 236, 252, 550, 558, 677
- Spectral leakage error, 476, 479–480, 484, 498, 556, 558
- Speech intelligibility, 293–300, 1299, 1305, 1314
- Speech Intelligibility Index (SII), 399
- Speech interference, 1163, 1178, 1503–1504
- Speech interference level (SIL), 399, 399 *f*
- Speech perception, 275, 299–300
- Speech privacy, 1308, 1310–1312
- Speech privacy index, 1236–1237
- Speech privacy ratings, 1308, 1310–1311
- Speech quality, 299–300
- Speech reception threshold, 387
- Speech Transmission Index (STI), 1281
- Speed of sound, 7, 19–20, 29–30, 119, 129–132, 950–951, 1037–1038
- Spherical radiation, 46–47
- Spherical spreading, 73–75, 132, 166, 718, 1111, 1116
- Spherical wave(s), 45–46
- Splitters, 630, 639, 928, 963, 1327
- Spring isolator(s), 725–726, 728, 730–733, 1337  
elastomeric, 650, 732  
helical, 1419  
leaf, 732
- Spring mounts, 652, 923, 1339 *f*, 1340 *f*, 1341 *f*
- Stacked damping layers, 1154–1155
- Stagnation point, 1376, 1383
- Stagnation pressure, 1382–1383
- Stamping press(es), 991–992
- Standardized impact sound pressure level, 1292
- Standardized level difference, 1404
- Standards, noise, 377–382  
consensus, 378
- Standard threshold shift, 385, 388
- Standing wave(s), 36–40, 517–519
- Stapes, 277 *f*, 278–280, 278 *f*, 280 *f*, 337, 338
- Static pressure, 876 *f*, 900–901, 1376
- Statistical absorption coefficient, 1250–1254, 1254 *f*, 1276
- Statistical energy analysis (SEA), 1250–1254, 1254 *f*
- Statistical pass-by (SPB) method, 1059, 1060, 1061 *f*, 1065, 1066 *f*, 1067 *f*
- Statistical percentile level, 403–407
- Steady state, 54–55, 1243–1244
- Steam turbine noise, 1335, 1346–1347
- Stiffness, 731, 848, 1142–1143
- Strain gauge, resistive, 238, 428, 449–450, 449 *f*, 569, 627, 789, 919 *f*, 999
- Strouhal number, 131, 135, 140–141, 146 *f*, 152, 878–879, 1102, 1106 *f*, 1324–1326, 1325 *f*, 1377–1378, 1379 *f*
- Structural dynamics analysis, 565–566
- Structural intensity, 802
- Structure-borne sound, 1080, 1191–1194, 1377
- Sub harmonic, 260, 575, 864, 866, 1087
- Sump(s), noise from. *See* Oil pan noise
- Supersonic jet noise, 145–148
- Survey(s), 331, 350, 384, 389, 391, 405, 408–410, 721, 1054, 1060, 1406, 1413, 1413 *f*, 1415–1416, 1442, 1459–1460, 1502, 1504
- Suspended-ceiling normalized level difference, 1285
- S-wave(s)  
speed, 1461–1462
- Swept sine, 487, 599–600
- Synchronization, 488, 490, 988, 1207, 1211
- Synchronous averaging, 561, 1090
- Temperature gradient, in speed of sound, 74–75
- Temporary threshold shift (TTS), 290, 304–305, 321, 338
- Third-octave band. *See* One-third octave band(s)
- Three-dimensional equation of sound, 21–22
- Threshold  
of audibility, 277, 277 *f*, 279, 297 *f*  
of feeling, 13, 14 *f*, 350  
of hearing, 286–291  
of pain, 277, 321, 337, 806  
pure tone, 272, 286  
speech reception, 387
- Time-averaged sound pressure level (equivalent continuous sound pressure level), 403, 512
- Time constant(s), 460
- Time domain analysis, 560–561, 1090
- Time-synchronous averaging, 561
- Time weighted average (TWA), 305–306, 369, 385, 461, 467
- Timoshenko equation, 195, 196–199
- Tire/pavement noise. *See* Tire/road noise
- Tire/road noise, 1054–1069  
measurement method(s), 1017, 1056, 1059–1062  
close proximity (CPX), 1060–1061, 1067  
cruise-by, 1055 *f*, 1060  
drum, 1059  
sound intensity, 1060  
statistical pass-by, 1060  
mechanisms for sound generation, 1017, 1055–1056  
air pumping, 1056, 1069  
horn effect, 1055, 1056, 1069  
stick/slip, 1056  
texture impact, 1056, 1069  
tire resonance, 1056  
tread impact, 1056  
vibration, of belt/carcass, 1056  
modeling, 1056
- Tires  
composite wheel, 1068  
porous tread tire, 1068
- Tolerance limits, 458–459
- Tonal noise, 878–879, 881, 1219, 1270, 1420
- Tone(s), 272
- Tooth meshing frequency, 576, 848, 849, 851–852, 853 *f*
- Tort(s), 384
- Traceability, 633–645  
to national measurement standards, 612
- Track, 1438–1445  
barrier(s), 1444  
jointed, 1442  
low noise, 1444  
slab, 1442
- Traffic noise, 1427–1436  
abatement, 1435–1436  
control of, 1415–1417  
modeling, 1434–1435  
prediction of, 1415–1417  
propagation, 1433–1434
- Traffic Noise Index (TNI), 405
- Transducer, 418–421  
displacement, 419  
dynamic range, 419–420  
sensitivity, 419  
velocity, 418
- Transfer function, 176, 252, 254, 298–299, 519–520, 1203, 1222
- Transformer noise, 1003–1004, 1335–1336, 1347
- Transient response, 55, 106, 1244–1245
- Transient statistical energy analysis (Transient SEA), 1165–1166
- Transmissibility, 344, 726–728, 1194, 1336–1337
- Transmission coefficient (transmission factor or transmittance), 29, 248–251, 254, 658–659, 685–686, 688, 1262
- Transmission fault diagnostics, 1091
- Transmission Loss (TL)  
airborne, 673, 679, 680, 972, 1199, 1201, 1207  
structure-borne, 673, 678, 678 *f*, 1072, 1184, 1200, 1201, 1203, 1205, 1216, 1264, 1370
- Transmission noise. *See* Gearbox noise
- Transportation noise, 308–313, 1013–1022, 1149–1156
- Transverse wave(s), 20, 709, 1461
- Traveling waves, 39, 41, 146, 236, 250, 271, 280–283, 280 *f*, 1241
- Trees, insertion loss, 1455–1456
- Trend analysis, 582–583
- Triggering, 147, 488, 490
- Truck noise, 677, 1014, 1167, 1512
- Tuned damper(s), 1204–1205, 1208
- Tuned Liquid Column Damper(s) (TLCD), 1389
- Tuned Liquid Damper(s) (TLD), 1389

- Tuned vibration damper(s) (TMD), 998, 1208, 1388
- Turbine noise, 1103
- Turbofan engine(s), 1019
- by-pass ratio, 110, 128, 1096–1097, 1097*f*, 1101, 1102, 1480
- noise
- active control, 1155
  - combustor, 1103
  - compressor, 1103
  - core, 1106–1107
  - directivity, 1098
  - jet, 1101–1102, 1105–1106
  - turbine, 1103
- Turboshaft engine(s), 1096, 1097*f*
- Turbulence, 76–77, 131–154
- Turbulence-induced vibration, 1383
- Turbulence noise, 275, 293–294, 297, 299, 949, 981
- Tympanic membrane, 277–280, 277*f*, 278*f*, 279*f*, 280*f*, 286–287, 328, 337
- Ultrasound, 304, 320–324
- Uncertainty of measurement, 462, 507, 634, 641
- Uncertainty principle, 473, 580, 597
- Uncorrelated noise source(s), 12, 479–480, 483–484
- Underwater noise, 1217, 1218, 1231
- Unit impulse, 176
- Valve(s). *See also* Control valve(s)
- demand, 916
  - flutter, 916
  - gate, 916–917
  - impacts, 916–918
  - instability, 839, 946, 950
- Variable air volume (VAV)
- systems, 1316, 1319–1320
  - terminals, fan-powered, 1320
- Vector sound intensity, 48, 58, 83, 84
- Vehicle noise, 513–514, 1087–1088, 1149–1152, 1159, 1427–1436
- Velocity, 2–4, 10, 11
- Ventilation systems, 1324–1326, 1328–1347
- Vibration
- base excitation, 1393
  - bending, 39, 63, 82, 1405, 1409
  - flexural, 195–199, 234–236
  - lateral, 344, 756, 848, 852, 1141
  - longitudinal, 191–194
  - nonlinear, 255–266
    - chaotic oscillations, 261–263
    - forced, 260–261
    - instability, 258–259, 263–264
    - normal mode(s), 263
    - resonance, 259–260
    - sub harmonic, 260, 264–266
  - plates, 90–94, 199–202, 739–741
  - random, 205–210
  - seismic-induced. *See* Seismic, induced vibration
  - shells, 199, 202–203
- Vibration absorber (dynamic vibration neutralizer, or tuned damper)
- damped
    - hysteretic, 748–749, 749*f*, 1398
    - viscously, 747–748
  - design of, 742–743
  - single-degree of freedom, 745–749
  - undamped, 745–747
- Vibration damping. *See* Damping
- Vibration damping materials. *See* Damping materials
- Vibration discomfort, 344
- Vibration dose value(s), 346
- Vibration (human), 343–352
- in buildings, 345
  - cognitive effects, 346
  - discomfort, 344
  - hand-transmitted, 349–352
  - motion sickness, 348–349
  - standards for measurement, 351
  - transmissibility of the human body, 344
  - vision, effects on, 345
  - whole-body, 344–348
- Vibration isolation, 725–733, 954
- active. *See* Active vibration isolation
  - basic model, 725–728
  - force transmissibility, 651, 652, 652*f*, 654, 654*f*, 655, 725
  - horizontal stiffness, 731–732
  - inertia blocks, 654–655, 730, 731
  - theory, 650–651
  - three-dimensional masses, 730
  - transmissibility, 726–728
  - two-stage isolation, 728–729
  - vibration effectiveness, 726–728
- Vibration isolator(s), 650, 654–655, 694*f*, 725, 1195–1196
- Vibration (mechanical), 468
- multi-degree-of-freedom system, 186, 255
  - random vibration, 205–210
  - single-degree-of-freedom system, 180, 745
- Vibration severity, 343, 346, 348, 352, 582–583
- Vibration velocity (vibratory velocity), 80, 86, 89, 167, 233, 236, 447–448, 583, 680, 690, 796, 841, 859, 905, 1047, 1138, 1192, 1219
- Vibration velocity level (vibratory velocity level), 1192, 1221, 1222–1223
- Vibrator, 609, 790, 989–990
- Vibratory feeds, 989–990, 990*f*
- Vocal folds (vocal cords), 293–298, 294*f*
- Vocal tract, 272*f*, 275, 293–294, 294*f*, 297–299
- Voice
- devoiced, 297
  - unvoiced, 275
  - voiced, 275, 293–295, 297
  - voiceless, 293–297
  - voicing, 275, 293, 295–297, 298*f*
- Voltage preamplifier, 429, 627
- Volume velocity, 27–28, 41, 42, 46, 48, 296–299, 678–679, 762, 763, 1037, 1038, 1043, 1045, 1047, 1185
- Von Karman vortex trail, 1072, 1076, 1377*f*
- Vortex, Vortices, 1109–1111
- Vortex-induced vibration, 1384–1385
- Wake-induced vibration. *See* Buffeting
- Wake-structure interaction noise, 1200
- Walking noise, 1289–1290, 1293–1294
- Water hammer, 159, 900, 901–902, 903, 908–909, 949, 950
- Wave equation, 21–22, 43–47, 52, 102–103, 129–138, 150, 159–163, 173, 1104, 1113
- Wavefront(s), 9, 19, 30–31, 67, 71, 74–75, 144, 1461–1462, 1476
- Wavelength, 9, 20–21
- Wavelength parameter, 9
- Wavelet(s), 585–597
- algorithm, 586
  - Mallat's tree, 587, 587*f*
  - harmonic, 585–586, 588–589, 589*f*, 590*f*
- Malvar, 587–588, 588*f*
- maps
- mean-square, 591, 593, 594, 595
  - time-frequency, 591–596
- Meyer, 588
- transform(s)
- dilatational, 586–587, 586*f*
  - discrete harmonic, 589–590
  - orthogonal, 586
  - windowed, 593–594
- Wave motion, 19–20
- Wave number, 244–245, 249–251, 773
- Wave steepening, 159, 159*f*, 161*f*, 164
- Weighted apparent sound reduction index, 1286
- Weighted element-normalized level difference, 1285
- Weighted normalized flanking level difference, 1285, 1291
- Weighted normalized impact sound pressure level, 1288, 1291, 1292
- Weighted normalized level difference, 1286
- Weighted sound absorption coefficient, 1294–1295, 1296
- Weighted sound reduction index, 1258, 1262, 1283, 1284, 1285, 1289, 1368
- Weighted standardized impact sound pressure level, 1291
- Weighted standardized level difference, 1286
- Weighted suspended-ceiling normalized level difference, 1285
- Weighting function(s), 355–356, 477–478
- flat top, 477–478, 478*f*, 556, 557–558, 557*f*, 588
- Hanning, 476*f*, 477, 477*f*, 478, 478*f*, 480, 557*f*, 588, 595, 596
- Kaiser-Bessel, 477–478, 478*f*, 557, 557*f*, 558
- Rectangular, 476–478, 476*f*, 477*f*, 478*f*, 556–559, 557*f*, 588



- Weighting network, 457, 465, 1480
- Wheel
- damping, 1142
  - wheel modes, 1139–1140, 1144
- Wheel-rail interaction noise, 1022, 1138–144
- curve squeal, 1022, 1143–1144
  - impact, 1022, 1143
  - measurement method(s), 1141–1142
  - pad stiffness, 1141, 1142–1143
  - rail damping, 1022, 1142–1143
  - rolling, 1022, 1138–1139, 1142
  - roughness, 1022, 1138–1139, 1142
  - track damping, 1022
  - wheel sound radiation, 1022, 1138, 1139, 1141
- White fingers, 349–350
- White noise, 337, 471, 472, 474, 487, 520, 561, 808–809
- Whole body vibration, 344–348
- Wigner-Ville spectrum, 562, 581
- Wind gradient, in speed of sound, 30, 31, 1418, 1434, 1513
- Wind-induced vibration, 745, 1238, 1387, 1389
- Wind noise, 1159–1161, 1160*f*
- Windows, 556–559, 1161–1162
- Wind profile, 1380
- Wind tunnel(s), 1075, 1076–1079, 1078*f*, 1159, 1390
- Woodworking
- band saws, 980
  - chippers, 985
  - circular saws, 841, 980
  - collars, 841, 842*f*, 981–983, 982*f*, 983*f*
  - cutters
    - helical knife, 977
    - straight knife, 975, 975*f*, 976*f*, 977, 977*f*, 978*f*
  - enclosures, 977, 978–980, 982, 984, 984*f*
  - noise
    - aerodynamic, 980–981
    - blade vibration, 981–982
    - planers, 841, 976*f*, 977, 977*f*, 978, 980
- World Health Organization (WHO), 308, 312, 1368, 1424, 1482, 1484, 1503, 1526
- Young's modulus, 35, 87, 133, 136, 173, 191, 199, 220, 244, 689, 771, 788, 998, 1263, 1476
- Zone(s)
- noise, 1424, 1509, 1526, 1528, 1529, 1530, 1531
  - of silence, 1530
- Zoning, 1348, 1353, 1424, 1487, 1506, 1509, 1526, 1528, 1529, 1530, 1531
- Zoom, 555–556
- Zwicker, loudness, 811–813